Scientific and Technical Aerospace Reports

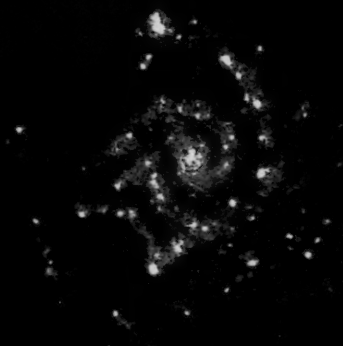

An Abstract Journal

Volume 32, Number 5
May 1994
N94-19800 to N94-22701

The NASA STI Program ... in Profile

Since its founding, NASA has been dedicated to the advancement of aeronautics and space science. The NASA Scientific and Technical Information (STI) Program plays a key part in helping NASA maintain this important role.

The NASA STI Program provides access to the NASA STI Database, the largest collection of aeronautical and space science STI in the world. The Program is also NASA's institutional mechanism for disseminating the results of its research and development activities.

Specialized services that help round out the Program's diverse offerings include creating custom thesauri, translating material to or from 34 foreign languages, building customized databases, organizing and publishing research results ... even providing videos.

For more information about the NASA STI Program, you can:

- **Phone** the NASA Access Help Desk at (301) 621-0390
- **Fax** your question to the NASA Access Help Desk at (301) 621-0134
- **E-mail** your question via the **Internet** to help@sti.nasa.gov
- **Write** to:

NASA Access Help Desk
NASA Center for AeroSpace Information
800 Elkridge Landing Road
Linthicum Heights, MD 21090-2934

Scientific and Technical Aerospace Reports

Scientific and Technical Aerospace Reports (STAR), is published each month as a major product of the NASA Scientific and Technical Information (STI) Program.

Inside this issue you will find:

- **Front Matter** containing a typical citation and abstract sample explaining the standard format, including codes for ordering reports
- **An Abstract Section** containing citations and abstracts of reports and publications that provide comprehensive coverage of worldwide aerospace-related topics including aeronautics and space science technology. *STAR* lists published and publicly available reports entered into the NASA STI Database during the four weeks preceding publication of this issue. These citations and abstracts are listed by subject categories.
- **An Index Section**
  - Subject
  - Personal author
  - Corporate source
  - Contract number
  - Report number
- **An Appendix** containing a guide for ordering cited reports, registering with the NASA STI Program, and using the available products and services. Additionally, price schedules, phone numbers, and addresses are included in this information packed section.

NASA also sponsors the companion journal, *NASA Open Volumes on Aerospace (NOVA)*, which lists abstracts of the open literature on aerospace subjects available worldwide. *NOVA* is for internal NASA use only, available from the NASA Center for AeroSpace Information (CASI).

Entries found in *STAR* are available through the NASA online retrieval service, RECON, and through DIALOG as the Aerospace Database.

The NASA STI Program gathers information through national and international agreements and exchanges and makes this information available to the NASA community and to the public in many forms through various outlets.

For additional information on the NASA STI Program, call the NASA Access Help Desk at (301) 621-0390, or write to:

NASA Center for AeroSpace Information
800 Elkridge Landing Road
Linthicum Heights, Maryland 21090-2934

US ISSN 0036-8741

This publication was prepared by the NASA Center for AeroSpace Information,
800 Elkridge Landing Road, Linthicum Heights, MD 21090-2934, (301) 621-0390.

Volume 32 Number 5 / May 1994

TABLE OF CONTENTS

AERONAUTICS For related information see also *Astronautics.*

01 AERONAUTICS (GENERAL) **1635**

02 AERODYNAMICS **1636**
Includes aerodynamics of bodies, combinations, wings, rotors, and control surfaces; and internal flow in ducts and turbomachinery. For related information see also *34 Fluid Mechanics and Heat Transfer.*

03 AIR TRANSPORTATION AND SAFETY **1641**
Includes passenger and cargo air transport operations; and aircraft accidents. For related information see also *16 Space Transportation* and *85 Urban Technology and Transportation.*

04 AIRCRAFT COMMUNICATIONS AND NAVIGATION **1642**
Includes digital and voice communication with aircraft; air navigation systems (satellite and ground based); and air traffic control. For related information see also *17 Space Communications, Spacecraft Communications, Command and Tracking* and *32 Communications and Radar.*

05 AIRCRAFT DESIGN, TESTING AND PERFORMANCE **1645**
Includes aircraft simulation technology. For related information see also *18 Spacecraft Design, Testing and Performance* and *39 Structural Mechanics.* For land transportation vehicles see *85 Urban Technology and Transportation.*

06 AIRCRAFT INSTRUMENTATION **1647**
Includes cockpit and cabin display devices; and flight instruments. For related information see also *19 Spacecraft Instrumentation* and *35 Instrumentation and Photography.*

07 AIRCRAFT PROPULSION AND POWER **1647**
Includes prime propulsion systems and systems components, e.g., gas turbine engines and compressors; and onboard auxiliary power plants for aircraft. For related information see also *20 Spacecraft Propulsion and Power, 28 Propellants and Fuels,* and *44 Energy Production and Conversion.*

08 AIRCRAFT STABILITY AND CONTROL **1650**
Includes aircraft handling qualities; piloting; flight controls; and autopilots. For related information see also *05 Aircraft Design, Testing and Performance.*

09 RESEARCH AND SUPPORT FACILITIES (AIR) **1650**
Includes airports, hangars and runways; aircraft repair and overhaul facilities; wind tunnels; shock tubes; and aircraft engine test stands. For related information see also *14 Ground Support Systems and Facilities (Space).*

ASTRONAUTICS For related information see also *Aeronautics.*

12 ASTRONAUTICS (GENERAL) **1652**
For extraterrestrial exploration see *91 Lunar and Planetary Exploration.*

13 ASTRODYNAMICS **1652**
Includes powered and free-flight trajectories; and orbital and launching dynamics.

14 GROUND SUPPORT SYSTEMS AND FACILITIES (SPACE) **1653**
Includes launch complexes, research and production facilities; ground support equipment, e.g., mobile transporters; and simulators. For related information see also *09 Research and Support Facilities (Air).*

15 LAUNCH VEHICLES AND SPACE VEHICLES **1653**
Includes boosters; operating problems of launch/space vehicle systems; and reusable vehicles. For related information see also *20 Spacecraft Propulsion and Power.*

16 SPACE TRANSPORTATION **1653**
Includes passenger and cargo space transportation, e.g., shuttle operations; and space rescue techniques. For related information see also *03 Air Transportation and Safety* and *18 Spacecraft Design, Testing and Performance.* For space suits see *54 Man/System Technology and Life Support.*

17 SPACE COMMUNICATIONS, SPACECRAFT COMMUNICATIONS, COMMAND AND TRACKING **1656**
Includes telemetry; space communications networks; astronavigation and guidance; and radio blackout. For related information see also *04 Aircraft Communications and Navigation* and *32 Communications and Radar.*

N.A.—No abstracts were assigned to this category for this issue.

18 SPACECRAFT DESIGN, TESTING AND PERFORMANCE **1657**
Includes satellites; space platforms; space stations; spacecraft systems and components such as thermal and environmental controls; and attitude controls. For life support systems see *54 Man/System Technology and Life Support.* For related information see also *05 Aircraft Design, Testing and Performance, 39 Structural Mechanics,* and *16 Space Transportation.*

19 SPACECRAFT INSTRUMENTATION **1666**
For related information see also *06 Aircraft Instrumentation* and *35 Instrumentation and Photography.*

20 SPACECRAFT PROPULSION AND POWER **1666**
Includes main propulsion systems and components, e.g., rocket engines; and spacecraft auxiliary power sources. For related information see also *07 Aircraft Propulsion and Power, 28 Propellants and Fuels, 44 Energy Production and Conversion,* and *15 Launch Vehicles and Space Vehicles.*

CHEMISTRY AND MATERIALS

23 CHEMISTRY AND MATERIALS (GENERAL) **1672**

24 COMPOSITE MATERIALS **1672**
Includes physical, chemical, and mechanical properties of laminates and other composite materials. For ceramic materials see *27 Nonmetallic Materials.*

25 INORGANIC AND PHYSICAL CHEMISTRY **1678**
Includes chemical analysis, e.g., chromatography; combustion theory; electrochemistry; and photochemistry. For related information see also *77 Thermodynamics and Statistical Physics.*

26 METALLIC MATERIALS **1687**
Includes physical, chemical, and mechanical properties of metals, e.g., corrosion; and metallurgy.

27 NONMETALLIC MATERIALS **1697**
Includes physical, chemical, and mechanical properties of plastics, elastomers, lubricants, polymers, textiles, adhesives, and ceramic materials. For composite materials see *24 Composite Materials.*

28 PROPELLANTS AND FUELS **1711**
Includes rocket propellants, igniters and oxidizers; their storage and handling procedures; and aircraft fuels. For related information see also *07 Aircraft Propulsion and Power, 20 Spacecraft Propulsion and Power,* and *44 Energy Production and Conversion.*

29 MATERIALS PROCESSING **1713**
Includes space-based development of products and processes for commercial application. For biological materials see *55 Space Biology:*

ENGINEERING For related information see also *Physics.*

31 ENGINEERING (GENERAL) **1713**
Includes vacuum technology; control engineering; display engineering; cryogenics; and fire prevention.

32 COMMUNICATIONS AND RADAR **1715**
Includes radar; land and global communications; communications theory; and optical communications. For related information see also *04 Aircraft Communications and Navigation* and *17 Space Communications, Spacecraft Communications, Command and Tracking.* For search and rescue see *03 Air Transportation and Safety,* and *16 Space Transportation.*

33 ELECTRONICS AND ELECTRICAL ENGINEERING **1748**
Includes test equipment and maintainability; components, e.g., tunnel diodes and transistors; microminiaturization; and integrated circuitry. For related information see also *60 Computer Operations and Hardware* and *76 Solid-State Physics.*

34 FLUID MECHANICS AND HEAT TRANSFER **1796**
Includes boundary layers; hydrodynamics; fluidics; mass transfer and ablation cooling. For related information see also *02 Aerodynamics* and *77 Thermodynamics and Statistical Physics.*

35 INSTRUMENTATION AND PHOTOGRAPHY **1806**
Includes remote sensors; measuring instruments and gauges; detectors; cameras and photographic supplies; and holography. For aerial photography see *43 Earth Resources and Remote Sensing.* For related information see also *06 Aircraft Instrumentation* and *19 Spacecraft Instrumentation.*

36 LASERS AND MASERS **1814**
Includes parametric amplifiers. For related information see also *76 Solid-State Physics.*

37 MECHANICAL ENGINEERING **1821**
Includes auxiliary systems (nonpower); machine elements and processes; and mechanical equipment.

38 QUALITY ASSURANCE AND RELIABILITY **1828**
Includes product sampling procedures and techniques; and quality control.

39 STRUCTURAL MECHANICS **1828**
Includes structural element design and weight analysis; fatigue; and thermal stress. For applications see *05 Aircraft Design, Testing and Performance* and *18 Spacecraft Design, Testing and Performance.*

GEOSCIENCES For related information see also *Space Sciences.*

42 GEOSCIENCES (GENERAL) **1836**

43 EARTH RESOURCES AND REMOTE SENSING **1837**
Includes remote sensing of earth resources by aircraft and spacecraft; photogrammetry; and aerial photography. For instrumentation see *35 Instrumentation and Photography.*

44 ENERGY PRODUCTION AND CONVERSION **1844**
Includes specific energy conversion systems, e.g., fuel cells; global sources of energy; geophysical conversion; and windpower. For related information see also *07 Aircraft Propulsion and Power, 20 Spacecraft Propulsion and Power,* and *28 Propellants and Fuels.*

45 ENVIRONMENT POLLUTION **1850**
Includes atmospheric, noise, thermal, and water pollution.

46 GEOPHYSICS **1854**
Includes aeronomy; upper and lower atmosphere studies; ionospheric and magnetospheric physics; and geomagnetism. For space radiation see *93 Space Radiation.*

47 METEOROLOGY AND CLIMATOLOGY **1864**
Includes weather forecasting and modification.

48 OCEANOGRAPHY **1881**
Includes biological, dynamic, and physical oceanography; and marine resources. For related information see also *43 Earth Resources and Remote Sensing.*

LIFE SCIENCES

51 LIFE SCIENCES (GENERAL) **1884**

52 AEROSPACE MEDICINE **1889**
Includes physiological factors; biological effects of radiation; and effects of weightlessness on man and animals.

53 BEHAVIORAL SCIENCES **1893**
Includes psychological factors; individual and group behavior; crew training and evaluation; and psychiatric research.

54 MAN/SYSTEM TECHNOLOGY AND LIFE SUPPORT **1895**
Includes human engineering; biotechnology; and space suits and protective clothing. For related information see also *16 Space Transportation.*

55 SPACE BIOLOGY **1897**
Includes exobiology; planetary biology; and extraterrestrial life.

MATHEMATICAL AND COMPUTER SCIENCES

59 MATHEMATICAL AND COMPUTER SCIENCES (GENERAL) **1897**

60 COMPUTER OPERATIONS AND HARDWARE **1898**
Includes hardware for computer graphics, firmware, and data processing. For components see *33 Electronics and Electrical Engineering.*

61 COMPUTER PROGRAMMING AND SOFTWARE **1902**
Includes computer programs, routines, algorithms, and specific applications, e.g., CAD/CAM.

62 COMPUTER SYSTEMS **1928**
Includes computer networks and special application computer systems.

63 CYBERNETICS **1938**
Includes feedback and control theory, artificial intelligence, robotics and expert systems. For related information see also *54 Man/System Technology and Life Support.*

64 NUMERICAL ANALYSIS **1949**
Includes iteration, difference equations, and numerical approximation.

65 STATISTICS AND PROBABILITY **1962**
Includes data sampling and smoothing; Monte Carlo method; and stochastic processes.

66 SYSTEMS ANALYSIS **1965**
Includes mathematical modeling; network analysis; and operations research.

67 THEORETICAL MATHEMATICS **1965**
Includes topology and number theory.

PHYSICS For related information see also *Engineering.*

70 PHYSICS (GENERAL) **1966**
For precision time and time interval (PTTI) see *35 Instrumentation and Photography*; for geophysics, astrophysics or solar physics see *46 Geophysics, 90 Astrophysics*, or *92 Solar Physics.*

71 ACOUSTICS **1967**
Includes sound generation, transmission, and attenuation. For noise pollution see *45 Environment Pollution.*

72 ATOMIC AND MOLECULAR PHYSICS **1969**
Includes atomic structure, electron properties, and molecular spectra.

73 NUCLEAR AND HIGH-ENERGY PHYSICS **1979**
Includes elementary and nuclear particles; and reactor theory. For space radiation see *93 Space Radiation.*

74 OPTICS **1983**
Includes light phenomena and optical devices. For lasers see *36 Lasers and Masers.*

75 PLASMA PHYSICS **1991**
Includes magnetohydrodynamics and plasma fusion. For ionospheric plasmas see *46 Geophysics.* For space plasmas see *90 Astrophysics.*

76 SOLID-STATE PHYSICS **2011**
Includes superconductivity. For related information see also *33 Electronics and Electrical Engineering* and *36 Lasers and Masers.*

77 THERMODYNAMICS AND STATISTICAL PHYSICS **2037**
Includes quantum mechanics; theoretical physics; and Bose and Fermi statistics. For related information see also *25 Inorganic and Physical Chemistry* and *34 Fluid Mechanics and Heat Transfer.*

SOCIAL SCIENCES

80 SOCIAL SCIENCES (GENERAL) **2038**
Includes educational matters.

81 ADMINISTRATION AND MANAGEMENT **2039**
Includes management planning and research.

82 DOCUMENTATION AND INFORMATION SCIENCE **2041**
Includes information management; information storage and retrieval technology; technical writing; graphic arts; and micrography. For computer documentation see *61 Computer Programming and Software.*

83 ECONOMICS AND COST ANALYSIS **2049**
Includes cost effectiveness studies.

84 LAW, POLITICAL SCIENCE AND SPACE POLICY ..... **N.A.**
Includes NASA appropriation hearings; aviation law; space law and policy; international law; international cooperation; and patent policy.

85 URBAN TECHNOLOGY AND TRANSPORTATION **2053**
Includes applications of space technology to urban problems; technology transfer; technology assessment; and surface and mass transportation. For related information see *03 Air Transportation and Safety, 16 Space Transportation,* and *44 Energy Production and Conversion.*

SPACE SCIENCES For related information see also *Geosciences.*

88 SPACE SCIENCES (GENERAL) ..... **N.A.**

89 ASTRONOMY **2054**
Includes radio, gamma-ray, and infrared astronomy; and astrometry.

90 ASTROPHYSICS **2080**
Includes cosmology; celestial mechanics; space plasmas; and interstellar and interplanetary gases and dust. For related information see also *75 Plasma Physics.*

91 LUNAR AND PLANETARY EXPLORATION **2088**
Includes planetology; and manned and unmanned flights. For spacecraft design or space stations see *18 Spacecraft Design, Testing and Performance.*

92 SOLAR PHYSICS **2147**
Includes solar activity, solar flares, solar radiation and sunspots. For related information see also *93 Space Radiation.*

93 SPACE RADIATION **2149**
Includes cosmic radiation; and inner and outer earth's radiation belts. For biological effects of radiation see *52 Aerospace Medicine.* For theory see *73 Nuclear and High-Energy Physics.*

GENERAL

Includes aeronautical, astronautical, and space science related histories, biographies, and pertinent reports too broad for categorization; histories or broad overviews of NASA programs.

99 GENERAL **2151**

SUBJECT INDEX **I-1**

PERSONAL AUTHOR INDEX **I-185**

CORPORATE SOURCE INDEX **I-211**

CONTRACT NUMBER INDEX **I-243**

REPORT NUMBER INDEX **I-249**

APPENDIX **A-1**

TYPICAL CITATION AND ABSTRACT

NASA SPONSORED
ON MICROFICHE

ACCESSION NUMBER → **N94-12270*#** United Technologies Corp., West Palm Beach, FL. ← CORPORATE SOURCE
Pratt and Whitney.

TITLE → **ADVANCED CONTROL FOR AIRBREATHING ENGINES, VOLUME 1: PRATT AND WHITNEY**

AUTHOR → J. A. Ralph Jul. 1993 83 p ← PUBLICATION DATE

CONTRACT OR GRANT → (Contract NAS3-25952; RTOP 505-62-61)

REPORT NUMBERS → (NASA-CR-189203; E-8006; NAS 1.26:189203) Avail: CASI HC A05/MF A01 ← AVAILABILITY SOURCE AND PRICE CODE

The application of advanced control concepts to air breathing engines may yield significant improvements in aircraft/engine performance and operability. Screening studies of advanced control concepts for air breathing engines were conducted by three major domestic aircraft engine manufacturers to determine the potential impact of concepts on turbine engine performance and operability. The purpose of the studies was to identify concepts which offered high potential yet may incur high research and development risk. A target suite of proposed advanced control concepts was formulated and evaluated in a two phase study to quantify each concept's impact on desired engine characteristics. To aid in the evaluation specific aircraft/engine combinations were considered: a Military High Performance Fighter mission, a High Speed Civil Transport mission, and a Civil Tiltrotor mission. Each of the advanced control concepts considered in the study are defined and described. The concept potential impact on engine performance was determined. Relevant figures of merit on which to evaluate the concepts are determined. Finally, the concepts are ranked with respect to the target aircraft/engine missions. A final report describing the screening studies was prepared by each engine manufacturer. Volume 1 of these reports describes the studies performed by Pratt & Whitney. Author (revised)

VOLUME 32 NUMBER 5 / May 1994

Scientific and Technical Aerospace Reports

A Monthly Publication of the National Aeronautics and Space Administration

01 AERONAUTICS (GENERAL)

N94-20035*# National Aeronautics and Space Administration. Ames Research Center, Moffett Field, CA.

SOME VTOL HEAD-UP DISPLAY DRIVE-LAW PROBLEMS AND SOLUTIONS

Vernon K. Merrick Nov. 1993 45 p

(RTOP 533-02-37)

(NASA-TM-104027; A-93090; NAS 1.15:104027) Avail: CASI HC A03/MF A01

A piloted simulation test was conducted on the Ames Research Center's vertical motion simulator (VMS) in support of the Phase 2A flight test of NASA's V/STOL systems research aircraft (VSRA). During the simulation several problems were found with the head-up display (HUD) symbol drive laws and the flightpath synthesis. These problems and the solutions devised to solve them are described. Most of the resulting HUD drive-law changes were implemented during the simulation and their effectiveness was verified. Subsequently both the HUD symbol drive-law and flightpath-synthesis changes were implemented in the VSRA and tested successfully in the Phase 2A flight tests. Author (revised)

N94-20191# Wichita State Univ., KS. National Inst. for Aviation Research.

AIAA TECHFEST 29 PROCEEDINGS

William H. Wentz, Jr., ed. and Jacqueline R. Luedtke, ed. 1993 217 p Conference held in Wichita, KS, 6-7 Nov. 1992

(NIAR-93-1) Avail: CASI HC A10/MF A03

Proceedings for the nineteenth annual techfest are accompanied by visual displays for selected topics. Selected topics in structures include limit-cycle oscillations of aircraft lifting surfaces; automated airframe monitoring; low-cost, high-performance target drone wing manufacturing process comparison; and elevated temperature testing considerations for various material systems. Experimental methods and instrumentation that were discussed included low-cost piloted flight simulation, and overview of doppler global velocimetry, and overview of the NIAR crash-dynamics lab, modernization of the Walter Beech Wind Tunnel, development of a PC-based real-time PCM display and analysis system. Topics in aerodynamics include axial flow fan research underway at the University of Kansas, axial agility and pitch agility of fighter aircraft revisited, an experimental and numerical investigation of a 70 degree delta wing at high angles of attack, and the adaptation of ACSYNT for business jet configuration synthesis. CASI

N94-20267* National Aeronautics and Space Administration, Washington, DC.

AERONAUTICAL ENGINEERING: A CONTINUING BIBLIOGRAPHY WITH INDEXES (SUPPLEMENT 294)

Aug. 1993 167 p

(NASA-SP-7037(294); NAS 1.21:7037(294)) Avail: CASI HC A08

This issue of Aeronautical Engineering - A Continuing Bibliography with Indexes lists 590 reports, journal articles, and other documents recently announced in the NASA STI Database. The coverage includes documents on the engineering and theoretical aspect of design, construction, evaluation, testing, operation, and performance of aircraft (including aircraft engines) and associated components, equipment, and systems. It also includes research and development in aerodynamics, aeronautics, and ground support equipment for aeronautical vehicles. The bibliographic series is compiled through the cooperative efforts of the American Institute of Aeronautics and Astronautics (AIAA) and the National Aeronautics and Space Administration (NASA). Seven indexes are included: subject, personal author, corporate source, foreign technology, contract number, report number, and accession number. Derived from text

N94-21194# Wright Lab., Wright-Patterson AFB, OH.

THE 1992 USAF STRUCTURAL INTEGRITY PROGRAM CONFERENCE Final Report

Thomas D. Cooper, John W. Lincoln, and Robert M. Bader Sep. 1993 894 p Conference held in San Antonio, TX, 1-3 Dec. 1992

(AD-A272876; WL-TR-93-4080) Avail: CASI HC A99/MF A10

Partial contents include the following: new developments in fatigue management of F-16 aircraft; quantifying accuracy of fatigue life prediction methodology; naval aircraft approach and landing data acquisition system; a diagnostic reasoning technology demonstrator for gas turbine engines; cost effective risk management in design and flight qualification; a preliminary study of fatigue durability in terms of crack growth; a fatigue analysis of panels with multiple site damage; probabilistic rotor design system; assessment of helicopter component statistical reliability computations; the effects of negative R ratio on fatigue crack growth; effect of microporosity on fatigue durability of thick 7050 aluminum plate; fatigue and residual strength characteristics of fiber metal laminates subjected to incidental damage; the role of nondestructive inspection in an F-15E wing spar structural integrity program; ultrasonic imaging system for F-4 lower torque box skin; acoustic emission monitoring of the CF116 (CF5) full-scale durability and damage tolerance test; vibratory characterization of integrally bladed rotors utilizing surrogate blade models; F-4 lower wing skin integral stiffener failure analysis; new aircraft lower wing skin trade study; C-141 composite material repairs to metallic airframe components; and repair of F-16 static discharge probes. DTIC

N94-21419# Aerospace Industries Association of America, Inc., Washington, DC.

AEROSPACE: FACTS AND FIGURES, 1992-1993

1992 177 p

(AD-A272571) Avail: CASI HC A09/MF A02

Contents of the document include the following: aerospace summary, aircraft production, missile programs, space programs, air transportation, research and development, foreign trade, employment, and finance. DTIC

N94-21490*# National Aeronautics and Space Administration. Ames Research Center, Moffett Field, CA.

THE MODERN ROTOR AERODYNAMIC LIMITS SURVEY: A REPORT AND DATA SURVEY

J. Cross, J. Brilla, R. Kufeld, and D. Balough Oct. 1993 261 p

(RTOP 505-59-36)

(NASA-TM-4446; A-91183; NAS 1.15:4446) Avail: CASI HC A12/MF A03

The first phase of the Modern Technology Rotor Program, the Modern Rotor Aerodynamic Limits Survey, was a flight test conducted by the United States Army Aviation Engineering Flight Activity for NASA Ames Research Center. The test was performed using a United States Army UH-60A Black Hawk aircraft and the United States Air Force HH-60A Night Hawk instrumented main-rotor blade. The primary purpose of this test was to gather high-speed, steady-state, and maneuvering data suitable for correlation purposes with analytical prediction tools. All aspects of the data base, flight-test instrumentation, and test procedures are presented

and analyzed. Because of the high volume of data, only select data points are presented. However, access to the entire data set is available upon request. Author (revised)

02 AERODYNAMICS

Includes aerodynamics of bodies, combinations, wings, rotors, and control surfaces; and internal flow in ducts and turbomachinery.

For related information see also *34 Fluid Mechanics and Heat Transfer.*

N94-19963# Air Force Inst. of Tech., Wright-Patterson AFB, OH. Foreign Aerospace Science and Technology Center.

EXPERIMENTAL STUDY ON INTERFERENCE AERODYNAMICS OF CLOSE-COUPLED CANARD CONFIGURATION

Yao-Bin Guo 20 Jul. 1993 19 p Transl. into ENGLISH from Hangkong Xuebao (China), v. 11, no. 12, 1990 p 528-533

(AD-A267760; FASTC-ID(RS)T-0730-92) Avail: CASI HC A03/MF A01

By using the canard-wing balance and the whole aircraft aerodynamic balance, which can measure the aerodynamic forces of the canard-wing part, experimental studies were conducted on interference aerodynamic forces on a canard-configuration model that can be assembled and disassembled. It was discovered that the interferences are destructive between the canard wing and the main wing when alpha is less than 20 deg, causing a reduction in the lift. When alpha is greater than 32 deg, the interferences turn increasingly beneficial. When alpha = 32 deg, the interference lift increases to 24 percent of total lift. If the main wing is a swept-forward wing, the aerodynamic properties of the canard configuration are better. Author

N94-20014*# Eloret Corp., Sunnyvale, CA.

EXPERIMENTAL INVESTIGATION OF NOZZLE/PLUME AERODYNAMICS AT HYPERSONIC SPEEDS Progress Research Report, 1 Dec. 1992 - 30 Jun. 1993

David W. Bogdanoff and Jean-Luc Cambier 30 Jun. 1993 32 p

(Contract NCC2-487)

(NASA-CR-194628; NAS 1.26:194628) Avail: CASI HC A03/MF A01

Work continued on the improvement of 16-Inch Shock Tunnel. This comprised studies of ways of improving driver gas ignition, an improved driver gas mixing system, an axial translation system for the driver tube, improved diaphragm materials (carbon steel vs. stainless steel), a copper liner for the part of the driven tube near the nozzle, the use of a buffer gas between the driver and driven gases, the use of N2O in the driven tube, the use of a converging driven tube, operation of the facility as a non-reflected shock tunnel and expansion tube, operation with heated hydrogen or helium driver gas, the use of detonations in the driver and the construction of an enlarged test section. Maintenance and developmental work continued on the scramjet combustor continued. New software which greatly speeds up data analysis has been written and brought on line. In particular, software which provides very rapid generation of model surface heat flux profiles has been brought on line. A considerable amount of theoretical work was performed in connection with upgrading the 16 Inch Shock Tunnel Facility. A one-dimensional Godunov code for very high velocities and any equation of state is intended to add viscous effects in studying the operation of the Shock Tunnel and also of two-stage light gas guns. Derived from text

N94-20043# Florida Atlantic Univ., Boca Raton.

THE FLUID MECHANICS OF VORTEX CUTTING BY A BLADE Final Report, 1 Aug. 1992 - 31 Jul. 1993

Jeffrey S. Marshall 25 Sep. 1993 31 p

(Contract DAAL03-92-G-0277)

(AD-A270932; ARO-30168.5-EG-YIP) Avail: CASI HC A03/MF A01

A study of the nonlinear response of a vortex to the approach of, and cutting by, a blade traveling in the plane normal to the vortex axis has been performed. Two different types of vortex forces on the blade are distinguished. For large values of the ratio of blade thickness T to vortex ambient core radius sigma(0), the force on the blade is primarily due to decreased pressure near the blade leading edge due to bending of the vortex about the blade. For values of T/sigma(0) of 0(1) or less, the vortex does not bend substantially during interaction with the blade and instead the blade passes through, or 'cuts', the vortex. In this case, the force on the blade is primarily due to formation of a vortex shock which propagates on the vortex away from the blade, and the subsequent difference in vortex core radius on opposite sides of the blade due to the vortex shock. This study was conducted based on analytical, computational and experimental studies, the results of which compared well in the regimes in which each are valid. DTIC

N94-20136*# National Aeronautics and Space Administration. Lewis Research Center, Cleveland, OH.

EXPERIMENTAL AND COMPUTATIONAL RESULTS FROM A LARGE LOW-SPEED CENTRIFUGAL IMPELLER

M. D. Hathaway (Army Research Lab., Cleveland, OH.), R. M. Chriss, J. R. Wood, and A. J. Strazisar Dec. 1993 12 p Presented at the 82nd Meeting of the AGARD Propulsion and Energetics Panel, Technology Requirements for Small Gas Turbine Engines, Montreal, Ontario, 4-6 October, 1993; sponsored by the Advisory Group for Aerospace Research and Development

(DA Proj. 1L1-61102-AH-45)

(NASA-TM-106421; E-8258; NAS 1.15:106421; ARL-TR-331) Avail: CASI HC A03/MF A01

An experimental and computational investigation of the NASA Low-Speed Centrifugal Compressor (LSCC) flow field has been conducted using laser anemometry and Dawes' 3D viscous code. The experimental configuration consists of a backswept impeller followed by a vaneless diffuser. Measurements of the three-dimensional velocity field were acquired at several measurement planes through the compressor. The measurements describe both the throughflow and secondary velocity field along each measurement plane and in several cases provide details of the flow within the blade boundary layers. The experimental and computational results provide a clear understanding of the development of the throughflow momentum wake which is characteristic of centrifugal compressors. Author

N94-20465# Lehigh Univ., Bethlehem, PA. Dept. of Mechanical Engineering and Mechanics.

A THEORETICAL INVESTIGATION OF UNSTEADY SEPARATION PHENOMENA RELATED TO DYNAMIC STALL Final Report, 11 Jan. 1990 - 30 Apr. 1993

J. D. Walker 30 Apr. 1993 15 p

(Grant AF-AFOSR-0069-91)

(AD-A271865; AFOSR-93-0822TR) Avail: CASI HC A03/MF A01

The objective of this research was to identify the principal cause and effect relationships in dynamic stall at large Reynolds numbers, as well as possible means for controlling the process. At high Reynolds numbers, it is demonstrated the formation of the dynamic stall vortex initiates for all airfoil shapes via an unsteady separation of the boundary layer near the leading edge. The stall vortex ultimately detaches from the upper surface by provoking an unsteady separation of the surface layer near midchord. At least two methods of controlling separation at various stages in the cycle have been identified, namely: (1) suction near the leading nose or at midchord; and (2) a moving portion of the surface. The present work shows how separation can be suppressed and makes significant contributions to the theory of unsteady boundary-layer separation. A general analysis of unsteady two-dimensional airfoil maneuvers was initiated and is currently under study as a possible third means of control. DTIC

N94-20486 Army Aviation Systems Command, Moffett Field, CA. Aeroflightdynamics Directorate.

AN EXPERIMENTAL INVESTIGATION OF THE DRAG MECHANISMS OF A HELICOPTER ROTOR IN HOVERING FLIGHT

M. Silva, D. Favier (Institut de Mecanique des Fluides de Marseille, France.), J. Ramos (Institut de Mecanique des Fluides de Marseille, France.), M. Nsi (Institut de Mecanique des Fluides de Marseille, France.), and E. Berton (Institut de Mecanique des Fluides de Marseille, France.) Sep. 1993 15 p Limited Reproducibility: More than 20% of this document may be affected by microfiche quality

(AD-A270201; Paper-C18) Avail: CASI HC A03

The present paper describes an experiment in which laser velocimetric methods are employed to investigate the drag mechanisms of a helicopter rotor in hover. Emphasis is on the development of a measurement technique capable of quantifying, the contribution of rotor profile drag to total power

required. The scheme devised employs a 2-D LV system to measure the axial and tangential velocity field in the vicinity of the rotor blade. Application of a combined Kutta and Momentum Equation (KME) along a closed contour surrounding the blade section provides a measure of the local sectional normal and shear forces. A detailed survey of the rotor blade's near wake region is then performed in an attempt to directly determine the streamwise, velocity deficit. Integration of the resulting velocity profiles provides a measure of the profile drag. Accuracy of the method is checked by performing measurements at conditions of very low lift and by introducing blade surface modifications which aggravate the profile drag with accompanying comparisons of the effect on sectional and global performance. DTIC

N94-20534*# National Aeronautics and Space Administration. Lewis Research Center, Cleveland, OH.

SOME PRACTICAL TURBULENCE MODELING OPTIONS FOR REYNOLDS-AVERAGED FULL NAVIER-STOKES CALCULATIONS OF THREE-DIMENSIONAL FLOWS

Trong T. Bui Nov. 1993 40 p Presented at the 24th Fluid Dynamics Conference, Orlando, FL, 6-9 Jul. 1993; sponsored by AIAA See also N93-48158

(RTOP 505-62-52)

(NASA-TM-106399; E-8231; NAS 1.15:106399; AIAA Paper 93-2964)

Avail: CASI HC A03/MF A01

New turbulence modeling options recently implemented for the 3-D version of Proteus, a Reynolds-averaged compressible Navier-Stokes code, are described. The implemented turbulence models include: the Baldwin-Lomax algebraic model, the Baldwin-Barth one-equation model, the Chien k-epsilon model, and the Launder-Sharma k-epsilon model. Features of this turbulence modeling package include: well documented and easy to use turbulence modeling options, uniform integration of turbulence models from different classes, automatic initialization of turbulence variables for calculations using one- or two-equation turbulence models, multiple solid boundaries treatment, and fully vectorized L-U solver for one- and two-equation models. Validation test cases include the incompressible and compressible flat plate turbulent boundary layers, turbulent developing S-duct flow, and glancing shock wave/turbulent boundary layer interaction. Good agreement is obtained between the computational results and experimental data. Sensitivity of the compressible turbulent solutions with the method of y(sup +) computation, the turbulent length scale correction, and some compressibility corrections are examined in detail. The test cases show that the highly optimized one-and two-equation turbulence models can be used in routine 3-D Navier-Stokes computations with no significant increase in CPU time as compared with the Baldwin-Lomax algebraic model.

Author

N94-20563*# National Aeronautics and Space Administration. Lewis Research Center, Cleveland, OH.

DEVELOPMENT OF PHASED TWIN FLIP-FLOP JETS

Ganesh Raman (Sverdrup Technology, Inc., Brook Park, OH.) and Edward J. Rice Nov. 1993 10 p Proposed for presentation at the ASME Winter Annual Meeting, New Orleans, LA, 28 Nov. - 3 Dec. 1993; sponsored by ASME

(Contract NAS3-25266; RTOP 505-62-52)

(NASA-TM-106404; E-7609; NAS 1.15:106404) Avail: CASI HC A02/MF A01

The flip-flop nozzle is a device that can produce an oscillating jet flow without any moving parts. There is now a renewed interest in such nozzles due to their potential for use as excitation devices in practical applications. An experiment aimed at developing twin flip-flop jets that operate at prescribed frequencies and phase differences was performed. The phasing was achieved using two different nozzle interconnection schemes. In one configuration the two jets flapped in-phase and in another they flapped out-of-phase with respect to each other. In either configuration the frequencies of oscillation of both jets were equal. When one of the jets was run at a constant high velocity and the velocity of the second jet was increased gradually, the higher velocity jet determined the frequency of oscillation of both jets. The two flip-flop jet configurations described could be used to excite a primary jet flow in either an anti-symmetric (sinuous) or a symmetric (varicose) mode. Author (revised)

N94-21054*# Old Dominion Univ., Norfolk, VA. Dept. of Aerospace Engineering.

PREDICTION AND CONTROL OF VORTEX-DOMINATED AND VORTEX-WAKE FLOWS Progress Report, 1 Dec. 1992 - 30 Nov. 1993

Osama Kandil Dec. 1993 123 p

(Grant NAG1-994)

(NASA-CR-194722; NAS 1.26:194722) Avail: CASI HC A06/MF A02

This progress report documents the accomplishments achieved in the period from December 1, 1992 until November 30, 1993. These accomplishments include publications, national and international presentations, NASA presentations, and the research group supported under this grant. Topics covered by documents incorporated into this progress report include: active control of asymmetric conical flow using spinning and rotary oscillation; supersonic vortex breakdown over a delta wing in transonic flow; shock-vortex interaction over a 65-degree delta wing in transonic flow; three dimensional supersonic vortex breakdown; numerical simulation and physical aspects of supersonic vortex breakdown; and prediction of asymmetric vortical flows around slender bodies using Navier-Stokes equations. CASI

N94-21411# Stanford Univ., CA. Dept. of Aeronautics and Astronautics.

AN EFFICIENT NUMERICAL METHOD FOR THREE-DIMENSIONAL HYPERSONIC FLOW Final Report, 15 Jan. 1987 - 15 Nov. 1992

Robert W. MacCormack Feb. 1993 40 p

(Contract F33615-86-C-3015; AF Proj. 2307)

(AD-A272506; WL-TR-93-3012) Avail: CASI HC A03/MF A01

The present paper presents an efficient algorithm for solving the unsteady Navier-Stokes equations. It is a line Gauss-Seidel relaxation implicit algorithm for three-dimensional flow. Such algorithms have shown very fast convergence properties for two-dimensional flow. The extension to three-dimensions has been troublesome. The proposed algorithm presented herein was developed to solve these difficulties. A computer program based upon this algorithm has been written to solve two-dimensional plane symmetric, axisymmetric or three-dimensional flow of a perfect gas, or a real gas model for air with five species (N2, 02, NO, N, 0) or seven species (N2, 02, NO, NO+, N, 0, e-). The program can simulate a gas in thermal equilibrium or in thermal nonequilibrium with two temperatures (Translational-Rotational and Vibrational) or three temperatures (Translational, Rotational, and Vibrational). Convergence to engineering accuracy is generally achieved in under a hundred time steps for both two- and three-dimensional flow. Provision is made within the program for a one or two equation turbulence model. Applications are presented to verify the code by comparison with experiment and flight tests. Finally, the numerically simulated flow about a hypersonic vehicle at Mach 25 in powered flight is presented. DTIC

N94-21569*# National Aeronautics and Space Administration. Langley Research Center, Hampton, VA.

INTERNAL PERFORMANCE OF A NONAXISYMMETRIC NOZZLE WITH A ROTATING UPPER FLAP AND A CENTER-PIVOTED LOWER FLAP

David J. Wing, Laurence D. Leavitt, and Richard J. Re Nov. 1993 59 p

(RTOP 505-62-30-01)

(NASA-TP-3385; L-17235; NAS 1.60:3385) Avail: CASI HC A04/MF A01

An investigation was conducted at wind-off conditions in the static-test facility of the Langley 16-Foot Transonic Tunnel to determine the internal performance characteristics of a single expansion-ramp nozzle with thrust-vectoring capability to 105 degrees. Thrust vectoring was accomplished by the downward rotation of an upper flap with adaptive capability for internal contouring and a corresponding rotation of a center-pivoted lower flap. The static internal performance of configurations with pitch thrust-vector angles of 0 degrees, 60 degrees, and 105 degrees each with two throat areas, was investigated. The nozzle pressure ratio was varied from 1.5 to approximately 8.0 (5.0 for the maximum throat area configurations). Results of this study indicated that the nozzle configuration of the present investigation, when vectored, provided excellent flow-turning capability with relatively high levels of internal performance. In all cases, the thrust vector angle was a function of the nozzle pressure ratio. This result is expected because the flow is bounded by a single expansion surface on both vectored- and unvectored-nozzle geometries. Author

N94-21591*# National Aeronautics and Space Administration. Lewis Research Center, Cleveland, OH.

A STUDY OF THE COMPRESSIBLE FLOW THROUGH A DIFFUSING S-DUCT

Steven R. Wellborn (Iowa State Univ. of Science and Technology, Ames.), Theodore H. Okiishi (Iowa State Univ. of Science and Technology, Ames.), and Bruce A. Reichert Dec. 1993 108 p Sponsored by NASA. Washington

(RTOP 505-62-52)

(NASA-TM-106411; E-8247; NAS 1.15:106411) Avail: CASI HC A06/MF A02

Benchmark aerodynamic data are presented for compressible flow through a representative S-duct configuration. A numerical prediction of the S-duct flow field, obtained from a subsonic parabolized Navier-Stokes algorithm, is also shown. The experimental and numerical results are compared. Measurements of the three-dimensional velocity field, total pressures, and static pressures were obtained at five cross-sectional planes. Aerodynamic data were gathered with calibrated pneumatic probes. Surface static pressure and surface flow visualization data were also acquired. All reported tests were conducted with an inlet centerline Mach number of 0.6. The Reynolds number, based on the inlet centerline velocity and duct inlet diameter, was 2.6 x 10(exp 6). Thin inlet turbulent boundary layers existed. The collected data should be beneficial to aircraft inlet designers and the measurements are suitable for the validation of computational codes. The results show that a region of streamwise flow separation occurred within the duct. Details about the separated flow region, including mechanisms which drive this complicated flow phenomenon, are discussed. Results also indicate that the duct curvature induces strong pressure driven secondary flows. The cross flows evolve into counter-rotating vortices. These vortices convect low momentum fluid of the boundary layer toward the center of the duct, degrading both the uniformity and magnitude of the total pressure profile. Author

N94-21776*# Teledyne Brown Engineering, Huntsville, AL.

CONCEPT REPORT: EXPERIMENTAL VECTOR MAGNETOGRAPH (EXVM) OPERATIONAL CONFIGURATION BALLOON FLIGHT ASSEMBLY Final Report

Dec. 1993 57 p

(Contract NAS8-38089; NASA Order H-07978-D)

(NASA-CR-194702; NAS 1.26:194702) Avail: CASI HC A04/MF A01

The observational limitations of earth bound solar studies has prompted a great deal of interest in recent months in being able to gain new scientific perspectives through, what should prove to be, relatively low cost flight of the magnetograph system. The ground work done by TBE for the solar balloon missions (originally planned for SOUP and GRID) as well as the rather advanced state of assembly of the EXVM has allowed the quick formulation of a mission concept for the 30 cm system currently being assembled. The flight system operational configuration will be discussed as it is proposed for short duration flight (on the order of one day) over the continental United States. Balloon hardware design requirements used in formulation of the concept are those set by the National Science Balloon Facility (NSBF), the support agency under NASA contract for flight services. The concept assumes that the flight hardware assembly would come together from three development sources: the scientific investigator package, the integration contractor package, and the NSBF support system. The majority of these three separate packages can be independently developed; however, the computer control interfaces and telemetry links would require extensive preplanning and coordination. A special section of this study deals with definition of a dedicated telemetry link to be provided by the integration contractor for video image data for pointing system performance verification. In this study the approach has been to capitalize to the maximum extent possible on existing hardware and system design. This is the most prudent step that can be taken to reduce eventual program cost for long duration flights. By fielding the existing EXVM as quickly as possible, experience could be gained from several short duration flight tests before it became necessary to commit to major upgrades for long duration flights of this system or of the larger 60 cm version being considered for eventual development. Derived from text

N94-21833*# Stanford Univ., CA. Dept. of Aeronautics and Astronautics.

NONLINEAR AERODYNAMICS AND THE DESIGN OF WING TIPS Final Report, 1 Apr. 1992 - 31 Mar. 1993

Ilan Kroo and Sean Wakayama Sep. 1993 14 p

(Contract NCC2-683)

(NASA-CR-194732; NAS 1.26:194732) Avail: CASI HC A03/MF A01

This contract began in April 1990 with studies on the effect of wingtip shape on induced drag. That work considered problems of determining induced drag from computational aerodynamic methods and examined effects of wake roll up on the induced drag of elliptical and crescent wings. The research contract was continued in April 1991 and again in April 1992 with scope augmented to include considerations other than induced drag. The idea was to develop methods for comparing wing tip shapes on the basis of their effects on total drag, structural weight, and high lift performance. To accomplish this, work was done to improve methods for multidisciplinary analysis and optimization of wings. This report describes results of research conducted from April 1992 through March 1993. The general objective was to improve an existing wing optimization method and apply the method to specific problems of interest. The method, while a valuable tool for wing tip design studies, can be applied to more general problems, and has been applied to some of these other problems during its development. Specific goals that were accomplished are listed below and are explained in more detail in attached reports: analysis methods were improved in the area of structural modeling; small improvements to the high lift model were made, and ideas were collected on how clean wing c(sub l(sub max)) should vary with sweep - these ideas should provide a guide for future examination of high lift with experiment or CFD; and a calculation for drag due to the loss of leading edge suction was added to the wing analysis. Derived from text

N94-22260# Technische Univ., Delft (Netherlands). Inst. for Wind Energy.

NEAR WAKE MEASUREMENTS ON A ROTOR MODEL WITH MIE-VANES IN THE DELFT OPEN JET TUNNEL

H. Imamura and N. J. Vermeer Aug. 1992 33 p See also PB92-202845 Prepared in cooperation with Mie Univ.

(PB93-215382; IW-92052R) Avail: CASI HC A03/MF A01

As a part of the international collaboration between Mie University and Delft University of Technology, near wake measurements behind a rotor model with Mie-vanes have been performed in the Delft open jet wind tunnel. Preceding these measurements, the performance measurements of this rotor model with Mie-vanes have already been carried out in Delft. In these measurements, the augmentation of rotor output power by application of Mie-vanes was not obtained. This can partly be contributed to higher optimal tip speed ratio of the Delft rotor model. NTIS

N94-22274*# National Aeronautics and Space Administration. Lewis Research Center, Cleveland, OH.

INSTABILITY MODES EXCITED BY NATURAL SCREECH TONES IN A SUPERSONIC RECTANGULAR JET

Ganesh Raman (Sverdrup Technology, Inc., Brook Park, OH.) and Edward J. Rice Dec. 1993 18 p Presented at the 15th AIAA Aeroacoustics Conference, Long Beach, CA, 25-27 Oct. 1993; sponsored by AIAA

(RTOP 505-62-52)

(NASA-TM-106409; E-8246; NAS 1.15:106409; AIAA Paper 93-4321)

Avail: CASI HC A03/MF A01

The evolution of hydrodynamic instability modes self-excited by harmonically related natural screech tones was experimentally investigated. A convergent rectangular nozzle with an aspect ratio of 9.63 was used to produce a supersonic shock containing jet. Measurements in the flow-field were made using standard hot-film probes positioned only in the subsonic (outer) portions of the flow. The hydrodynamic instability mode observed in the shear layer at the screech frequency was observed to be antisymmetric (sinuous) about the smaller dimension of the jet, whereas its harmonic was observed to be symmetric (varicose). In addition, the near-field noise measurements indicated that the radiated screech tone noise was out of phase on either side of the small jet dimension whereas its harmonic was in phase over the same region. To our knowledge such an observation on the nature of the harmonic has thus far gone unreported and therefore is the focus of the present work. The hydrodynamic instability modes occurring at the screech frequency and its harmonic satisfied the conditions for

resonance. Detailed measurements of the coherent wave evolution in the streamwise and spanwise directions indicated that strong spanwise variations were present beyond x/h = 8. Details of the screech noise radiated by the coherent instability modes are also presented in this paper.
Author (revised)

N94-22382 British Columbia Univ., Vancouver. Dept. of Mechanical Engineering.
MODELLING STALLED AIRFOILS Ph.D. Thesis
William Waihung Yeung Apr. 1990 166 p
(ISBN-0-315-59525-6; CTN-94-60891) Copyright Avail: Micromedia Ltd., Technical Information Centre, 240 Catherine Street, Suite 305, Ottawa, Ontario, K2P 2G8, Canada HC/MF

New applications of the wake source model, a two-dimensional incompressible potential flow model used for bodies experiencing flow separation, are presented. The body contour is conformally mapped to a circle, for which the problem is solved using source singularities to create free streamlines simulating the separating shear layers. In common with other inviscid theories, it generally requires the pressure in the separated flow region, and the location of separation if boundary layer controlled. Different mapping sequences and flow models have been constructed for the cases of trailing-edge stall for single element airfoils, flat plates with separation bubbles, separation bubbles upstream of spoilers with downstream wakes, spoiler/slotted flap combinations at which the spoiler inclination is arbitrary, and two-element airfoils near stall. Predictions of pressure distribution are compared with wind tunnel measurements, good agreement is found in the 1st and 5th cases, and results in the 2nd and 3rd cases are promising. Partial success was achieved for the 4th case, depending on spoiler inclination; the discrepancy diminishes as the spoiler angle decreases in the cases of higher incidences so that the wake boundary tugs away from the flap sooner. Author (CISTI)

N94-22586 Toronto Univ. (Ontario). Dept. of Aerospace Science and Engineering.
TRANSONIC FLOW CALCULATIONS: INTEGRAL METHOD M.S. Thesis
Marc Langlois 1993 110 p
(ISBN-0-315-83538-9; CTN-94-60948) Copyright Avail: Micromedia Ltd., Technical Information Centre, 240 Catherine Street, Suite 305, Ottawa, Ontario, K2P 2G8, Canada HC/MF

An integral equation (IE, or field panel) method has been developed to predict potential transonic flows around two-dimensional configurations, using the panel method approach. Compressibility is taken into account by a distribution of sources in the field. Shock waves are captured using type-dependent differencing in the evaluation of the field sources. Since no inflow or outflow boundary conditions need to be imposed and the sources' strength declines rapidly away from the airfoil(s), only a small computational domain is necessary. The method also has the advantage in that the field grid does not need to be body conforming, allowing use of a Cartesian mesh. The code was evaluated for subcritical and supercritical flows on the NACA 0012, NACA 64A010, RAE 2822, and Williams B airfoils. Subcritical results were found to be in very good agreement with other data from IE methods, although comparison with finite difference (FD) data shows a tendency to underpredict lift considerably. In comparison with FD transonic results, the location of shocks was predicted well, but these usually are weaker and more spread. Agreement with other IE methods for transonic flows is also very good. Author (CISTI)

N94-22597# Technische Univ., Berlin (Germany). Inst. fuer Luft- und Raumfahrt.
MEASUREMENT TECHNOLOGY FOR FLIGHT TESTS [MESSTECHNIK FUER FLUGVERSUCHE]
W. Nitsche, ed. and J. Szodruch, ed. May 1991 133 p In ENGLISH and GERMAN Presented at DGLR-Fachausschusstagung, Hamburg, Germany, 30-31 Jan. 1991 Original contains color illustrations
(ILR-Mitt-256(1991); ETN-94-95076) Avail: CASI HC A07/MF A02

In the framework of a German research program on fluid dynamics and thermodynamics tests, methodologies for flight tests are presented. The following topics were included: surface hot film measurements of ATTAS research aircraft laminar glove; testing of a multisensor hot film technique in wind channels and free flight; free flight experiments with a laminar wing glove; experiments with a fluid deicing system for cleaning laminar wings; measurement of the influence of deicing liquids on aircraft aerodynamics; implementation of lasers for air data measurements; hot wire anemometry--a versatile instrumentation used for predevelopment studies and flight testing of the Do-328 aircraft; riblet boundary layer measurements of an A320 aircraft fuselage with Pitot rakes; and image processing as a tool in flight testing evaluation and contributions to the development of flight test measurement techniques. For individual titles, see N94-22598 through N94-22607.

N94-22598# Deutsche Forschungsanstalt fuer Luft- und Raumfahrt, Goettingen (Germany). Inst. fuer Experimentelle Stromeungsmechanik.
SURFACE HOT FILM MEASUREMENTS AT ATTAS LAMINAR GLOVE [OBERFLAECHENHEISSFILMMESSUNGEN AM ATTAS-LAMINARHANDSCHUH] **c05**
H.-P. Kreplin and G. Hoehler *In* Tech. Univ. Berlin, Measurement Technology for Flight Tests May 1991 p 1-11 In GERMAN (For primary document see N94-22597 05-02)
Avail: CASI HC A03/MF A02

The surface hot film technique, which was used for free flight tests with the German research aircraft ATTAS, is described. The experiments were carried out in order to obtain criteria for the laminar turbulent boundary transition in swept wings in the framework of a research program on transonic laminar wings. The surface hot film technique was used for observing unstationary processes with high time resolution. V-shaped double sensors were used. The sensors are made of two nickel films on a thin plastic foil. Nine sensors were mounted in the middle section of the glove, and two sensors were located in internal and external glove sides on the nose. All were operated with constant temperature anemometers in the aircraft cabin. The probability distributions of laminar and turbulent signals amplitudes are shown to be similar to a Gaussian distribution. The intermittency factor could be evaluated considering the cumulative amplitude distribution function. It is concluded that the method is useful provided perturbations such as electronic noise do not influence the information.
ESA

N94-22599# Technische Hochschule, Aachen (Germany). Aerodynamisches Inst.
TESTING OF A MULTISENSOR HOT FILM TECHNIQUE IN WIND TUNNEL AND FREE FLIGHT [ERPROBUNG EINER NEUENTWICKELTEN MULTISENSOR-HEISSFILMTECHNIK IM WINDKANAL UND FREIFLUG]
M. Kornberger and F. Feyzi *In* Tech. Univ. Berlin, Measurement Technology for Flight Tests May 1991 p 12-20 In GERMAN (For primary document see N94-22597 05-02)
Avail: CASI HC A02/MF A02

A multisensor hot film measurement technique, which allows ninety-six sensors to be simultaneously operated on a polyimide foil and was used in free flight tests of laminar gloves, is described. The technique was also used for transition estimation in a low speed wind tunnel; angle of incidence and flow velocity were chosen as the experiment parameters. Each hot film was calibrated with a comparative measuring process for estimation of magnitude and direction of wall shear stress vector. The results were transferred to the multisensor technique as far as possible. Another calibration method, which is based on the solution of heat transfer balance equations for a hot film, was developed in order to take into account heat conduction, which was calculated for a rotation symmetric body. ESA

N94-22600# Technische Univ., Berlin (Germany). Inst. fuer Luft- und Raumfahrt.
FREE FLIGHT EXPERIMENT WITH A LAMINAR WING GLOVE [FREIFLUGEXPERIMENTE MIT EINEM LAMINARFLUEGEL-HANDSCHUH]
N. Weiser and W. Nitsche *In its* Measurement Technology for Flight Tests May 1991 p 21-34 In GERMAN (For primary document see N94-22597 05-02)
Avail: CASI HC A03/MF A02

The CPM3 (Computational Preston Tube) method and the piezo array technique are compared in terms of functionality for laminar turbulent boundary layer transition investigations. The CPM3 technique is based on static pressure measurement from three wall Pitot probes of differential pressure sensors; the local wall shear stress is obtained from measured velocities in correlation with the effective wall distance by adaptation of the proportionality factor between mixture length and wall distance.

Piezoelectric foils are used in multisensor arrays as electromagnetic converters for detection of wall pressure oscillations. Because of their high sensitivity and flexibility, they are particularly suited to examination of unstationary wall forces and can be mounted on an airfoil surface without perturbation. Wind tunnel measurements were carried out in order to establish static pressure probe reliability. Results of wall friction distributions with different angles of incidence are presented and compared with data calculated using the Eppler code. ESA

N94-22601# Deutsche Airbus G.m.b.H., Bremen (Germany).
EXPERIMENTS WITH A FLUID DEICING SYSTEM FOR CLEANING LAMINAR WINGS [EXPERIMENTE MIT EINEM FLUIDISCHEN ENTEISUNGSSYSTEM ZUR SAEUBERUNG VON LAMINARFLUEGELN] **c27**

R. Henke *In* Tech. Univ. Berlin, Measurement Technology for Flight Tests May 1991 p 35-56 In GERMAN (For primary document see N94-22597 05-02)
Avail: CASI HC A03/MF A02

The capability of a fluid deicing system for transonic laminar wing cleaning is tested with the ATTAS research aircraft. The ATTAS is a twin jet regional airplane. A panel of the original, coarsely porous deicing system was exchanged for a specially produced titanium plate with laser drilled holes, which were regularly located on the surface; an equivalent surface was defined as a reference panel and searchlight was mounted between both panels. A standard deicing liquid, made of 80 percent water and 20 percent glycol, was tested as well as three other liquids, with different additives which modify the viscosity. Testing free parameters were adjustable liquid quantity, flight velocity, and liquid viscosity as a function of temperature. All flights took place in low altitudes in order to obtain statistical distribution of dirtiness. The cleanliness results were measured with digital image processing and the residual dirtiness was estimated with roughness measurements. The tests are found to be reproducible and easily automatable. ESA

N94-22602# Deutsche Lufthansa A.G., Hamburg (Germany).
MEASUREMENT OF THE INFLUENCE OF DEICING LIQUIDS ON AIRCRAFT AERODYNAMICS [DIE MESSUNG DES EINFLUSSES VON ENTEISUNGSFLUESSIGKEITEN AUF DIE AERODYNAMIK DES FLUGZEUGES]

U. Rummelmann *In* Tech. Univ. Berlin, Measurement Technology for Flight Tests May 1991 p 57-63 In GERMAN (For primary document see N94-22597 05-02)
Avail: CASI HC A02/MF A02

Flight tests were carried out in the all engine operating case in order to determine the influence of four different deicing liquids on Boeing 737-200 aerodynamics. Two different slat/flap positions were considered in this investigation. For local film thickness a measuring process was developed. The process was based on laser sensors. The data were enhanced by video, photography, and movie recordings. The role of liquid density and temperature was examined. Drag resistance and lift variations were obtained using a high velocity PCM (Pulse Code Modulation) data acquisition facility; this system was used as the data source for the airborne data analysis and monitoring system, which allows data quality to be evaluated. The following data were obtained and studied: static and dynamic pressures, wind velocity and direction, ground proximity data, and trim angle of the tailplane. ESA

N94-22603# Airbus Industrie, Toulouse (France).
UTILIZATION OF LASERS FOR AIR DATA MEASUREMENTS [EINSATZ VON LASERN BEI LUFTDATENMESSUNGEN] **c36**

J. Hammer *In* Tech. Univ. Berlin, Measurement Technology for Flight Tests May 1991 p 64-81 In GERMAN (For primary document see N94-22597 05-02)
Avail: CASI HC A03/MF A02

The operating principles of the ALEV3 three axis laser Doppler anemometer, which was designed for flight tests with the A-320 and A-340 aircraft, are depicted. If mounted on the aircraft center of gravity, the ALEV-3 allows true flight velocity in three directions and angles of attack and sideslip to be directly measured with a very good accuracy, in particular flight areas such as limit buffeting, stall, high Mach numbers, or sideslip flights. Aircraft parameter estimation, calculation, and calibration results are presented. The accuracies of velocity, static pressure and aerodynamic angle measurements were compared with classical anemometers precisions. Flight tests results of the ALEV-1 one axis laser anemometer for A-320 are given as a reference. ESA

N94-22604# Dornier Luftfahrt G.m.b.H., Friedrichshafen (Germany).
HOT WIRE ANEMOMETRY: A VERSATILE INSTRUMENTATION USED FOR PREDEVELOPMENT STUDIES AND FLIGHT TESTING OF THE DO-328 AIRCRAFT [HITZDRAHTANEMOMETRIE: EIN VIELSEITIGES INSTRUMENTARIUM IM EINSATZ BEI VORENTWICKLUNG UND FLUGVERSUCH DER DO 328] **c35**

P. Dick *In* Tech. Univ. Berlin, Measurement Technology for Flight Tests May 1991 p 82-96 In GERMAN (For primary document see N94-22597 05-02)
Avail: CASI HC A03/MF A02

The qualities of hot wire anemometry measuring techniques for laboratory experiments, mock-ups, and flight tests are examined in the framework of the development of the Do-328 regional airliner. Probes for velocity measurements were calibrated in a small wind tunnel. The wind tunnel was designed to produce very low flow velocities. The method is shown to be particularly useful in the following cases: multichannel flowmeters for measuring the trim of air flux in tube systems; ventilation comfort indicators in an aircraft cabin; and test instruments for the flow configuration in free flow and boundary layers. ESA

N94-22605# Deutsche Airbus G.m.b.H., Bremen (Germany).
RIBLET BOUNDARY LAYER MEASUREMENTS OF AN A-310 FUSELAGE WITH PITOT COMBS [RIBLET-GRENZSCHICHTMESSUNGEN AN EINEM A320-RUMPF MIT PITOT - RECHEN]

F. X. Muench and R. Henke *In* Tech. Univ. Berlin, Measurement Technology for Flight Tests May 1991 p 97-110 In GERMAN (For primary document see N94-22597 05-02)
Avail: CASI HC A03/MF A02

Preparation, running, and results of global measurements for a flight test of riblet effects with the A-320 aircraft are presented. The following activities are reported: three dimensional boundary layer calculation for estimation of wall stream line direction, wall shear stress distribution and boundary layer thickness, choice of riblet location on the aircraft, and preparation of the local measurements of velocity profiles at some chosen parts of the aircraft. For the boundary layer measurements, two Pitot combs were mounted one behind the other on the fuselage upper side. Pressure values, Mach number, calibrated flight velocity, altitude, lift coefficient, angles of attack, and sideslip and vertical and lateral accelerations were recorded on magnetic tape. The method is found to be reproducible, insensitive to aircraft vibrations and useful for obtaining information about riblet effects. ESA

N94-22606# Saab-Scania, Linkoping (Sweden). Ground and Flight Testing Dept.
IMAGE PROCESSING AS A TOOL IN FLIGHT TESTING EVALUATION **c35**

Anders Kaelldahl *In* Tech. Univ. Berlin, Measurement Technology for Flight Tests May 1991 p 111-117 (For primary document see N94-22597 05-02)
Avail: CASI HC A02/MF A02

An advanced system for digitizing and automatically analyzing film and video images and its adaptation for specific purposes are described. A video camera of charge coupled devices type was installed in a Viggen test aircraft and flight tests of sensitivity for different wavelengths and measurable resolution were carried out. A video tape containing interesting runs was input into an image processing system in order to show that the video based system meets the specification for Head Up Display (HUD) evaluation. A market investigation was undertaken for an image processing system for HUD evaluation, with particular requirements on a high performance time base corrector in the video input unit, video disks, image processor, and display unit. A digital video disk system and a tracking algorithm based on correlation methods were chosen; the image processing system was completed with a film scanner for converting cinema films into a digital format. In addition to the HUD analysis technique, a photogrammetric system was used for testing microwave landing, radar altimeter, or third category landing system. It is concluded that this image processing system

provides evaluation time reduction, higher possibility for correct evaluation and higher accuracy since more points from each image are used. ESA

N94-22607# Office National d'Etudes et de Recherches Aerospatiales, Paris (France).
RECENT ONERA CONTRIBUTIONS TO THE DEVELOPMENT OF FLIGHT TEST MEASUREMENT TECHNIQUES
V. Schmitt, D. Arnal (Centre d'Etudes et de Recherches, Toulouse, France.), and J. J. Thibert *In* Tech. Univ. Berlin, Measurement Technology for Flight Tests May 1991 p 118-129 (For primary document see N94-22597 05-02)
Avail: CASI HC A03/MF A02

Activities in flight testing are summarized with an emphasis on particular requirements and specifications to achieve the required quality of the results. Some examples for both surface measurements and flow field measurement techniques are given. They were related to a variety of topics such as high lift investigations, transonic drag rise evaluation, riblet effects on boundary layers or wakes, and laminar flow research. These examples show that there is an increasing need for flow investigations in flight tests to validate wind tunnel or computer simulations. ESA

N94-21472*# National Technical Univ., Athens (Greece).
THE BLOCK ADAPTIVE MULTIGRID METHOD APPLIED TO THE SOLUTION OF THE EULER EQUATIONS
Nikos Pantelelis *In* NASA. Langley Research Center, The Sixth Copper Mountain Conference on Multigrid Methods, Part 2 Nov. 1993 p 465-479 (For primary document see N94-21464 05-64)
(Contract AERO-0018C)
Avail: CASI HC A03/MF A03

N94-21473*# National Aeronautics and Space Administration. Langley Research Center, Hampton, VA.
MULTIGRID SCHEMES FOR VISCOUS HYPERSONIC FLOWS
R. C. Swanson and R. Radespiel (Deutsche Forschungs- und Versuchsanstalt fuer Luft- und Raumfahrt, Brunswick, Germany.) *In its* The Sixth Copper Mountain Conference on Multigrid Methods, Part 2 Nov. 1993 p 481-495 (For primary document see N94-21464 05-64)
Avail: CASI HC A03/MF A03

03 AIR TRANSPORTATION AND SAFETY

Includes passenger and cargo air transport operations; and aircraft accidents.

For related information see also *16 Space Transportation* and *85 Urban Technology and Transportation.*

N94-19876 Naval Air Warfare Center, Indianapolis, IN. Aircraft Div.
GROUND PROXIMITY WARNING SYSTEM VOICE WARNING UNIT REQUIREMENTS STUDY Final Report
David L. Wampler 30 Aug. 1993 24 p Limited Reproducibility: More than 20% of this document may be affected by microfiche quality
(AD-A270541; NAWCADIND-TR-2481) Avail: CASI HC A03

This report provides a record of the engineering considerations driving the establishment of initial Ground Proximity Warning System (GPWS) Voice Warning Unit (VWU) requirements. The work was stopped before sections 4, 5, and 6 of appendix A could be completed. DTIC

N94-20189# Wichita State Univ., KS. National Inst. for Aviation Research.
AVIATION SAFETY RESEARCH AT THE NATIONAL INSTITUTE FOR AVIATION RESEARCH, WICHITA STATE UNIVERSITY
William H. Wentz, Jr., David Ellis, and Steve Hooper 1993 33 p
(NIAR-93-4) Avail: CASI HC A03/MF A01

In this National Institute for Aviation Research (NIAR) report to the FAA, goals included automatic target tracking to extract head motion during crash tests. Associated tasks included a crash analysis of aircraft seats and an analysis of commuter seat-type structures in a crash environment to study energy absorbing mechanics of seat structures subject to emergency landing conditions. One task was to evaluate and enhance the biodynamic analysis of the occupant responses for evaluation of aircraft crash safety. Another task was the bonded/fusion repair of aircraft structures to qualify a procedure for the assessment and repair of metallic and composite structures. The effects of mechanical paint removal on surface morphology and fatigue behavior of composite materials was studied. A test method was developed for the assessment of the integrity of bonded joints and composite materials; addressed features include cyclic loading and freeze/thaw moisture conditioning. With regards to regional/commuter aircraft flight loads, robotic assistance to aircraft inspection was studied and a robot was developed. Human factors in the cockpit were studied to improve the understanding of single pilot terminal area operations, with emphasis on flight guidance displays. There was also a task toward standardization of design procedures for turbine rotor containment. Proposals are included in the report with their goals, approach, and status. CASI

N94-20912 Rendzio (Robert J.), Ozark, AL.
ARMY AIRCRAFT FIRE-DETECTION SYSTEMS OPERATION AND RELIABILITY Final Report, Oct. 1988 - Sep. 1992
Robert J. Rendzio, Karla Flaherty, ed., and Frank Sisk 5 Oct. 1993 21 p Limited Reproducibility: More than 20% of this document may be affected by microfiche quality
(AD-A271327) Avail: CASI HC A03

This report evaluates the results of a five year study of fire indications onboard army aircraft. Specifically it evaluates the aircraft fire detection systems. The overall conclusion drawn from the report is that the fire detection systems are unreliable and do not meet the intent of the applicable specifications governing such devices. DTIC

N94-21030 Honeywell, Inc., Phoenix, AZ.
WINDSHEAR DETECTION FOR AIRCRAFT USING TEMPERATURE LAPSE RATE Patent
Terry L. Zweifel, inventor (to Honeywell, Inc.) 11 Feb. 1992 44 p Filed 2 Nov. 1988
(CA-Patent-1,295,736; Int-Patent-Class-G08B-31/00; CTN-93-60639)
Copyright Avail: Micromedia Ltd., Technical Information Centre, 165 Hotel de Ville, Place du Portage, Phase 2, Hull, Quebec J8X 3X2, Canada HC/MF

An on-board aircraft system is described that provides an indication of wind shear probability considerably before prior art systems. A measurement of temperature change with altitude (temperature lapse rate) is made, filtered to eliminate noise, and compared to the dry adiabatic temperature lapse rate: the latter being indicative of unstable air. When the measured or empirical temperature lapse rate is less than the dry adiabatic temperature lapse rate for a predetermined number of measurements, a cautionary message is relayed to the flight crew with a caution light. The same cautionary message may be transmitted to the landing airport to be used to caution other aircraft and may also be used to enhance the detection capability of existing on-board prior art systems. If a cautionary message has been generated and the aircraft enters a region of rapidly decreasing temperature as is usually present in the downflow of a microburst, a warning message is generated alerting the flight crew to take immediate action to exit the condition. The warning message may also be transmitted to the landing airport and used to warn other aircraft and/or used to enhance the detection capability of existing on-board prior art systems.
Author (CISTI)

N94-21428 Illinois Univ., Urbana-Champaign. Dept. of Community Health.
AVIATION SAFETY RESEARCH. VOLUME 1: LITERATURE REVIEW OF SOURCES OF AVIATION ACCIDENT AND INCIDENT DATA AND SELECTED FACTORS CONTRIBUTING TO ACCIDENTS
R. G. Mortimer and J. S. Hanson 7 May 1993 216 p Sponsored by Construction Engineering Research Lab. (Army), Champaign, IL Limited Reproducibility: More than 20% of this document may be affected by microfiche quality
(Contract DACA88-90-D-0028-28)
(PB93-202885; SAFETY RESEARCH-93-1-Vol-1) Avail: CASI HC A10

The report is Volume 1 in studies of aviation accidents. The emphasis is on general aviation, but Part 135 and 121 operations are also discussed. It is a review of the literature of sources of aviation accident and exposure data and of selected factors affecting safety in aviation. Among topics covered are: epidemiological studies, weather factors, induced pilot error, and the stall accident. It is believed that improved aerodynamic design, using available knowledge, could reduce stall/spin accidents by 10%.

Weather is a primary cause in about 18% of all accidents and in 32% of fatal accidents, and is a major contributor to accidents of general and commercial aviation. Alcohol is now involved in about 5% of pilots who are fatally injured, but about 12% have used therapeutic drugs and 3% illicit drugs. NTIS

N94-21590*# National Aeronautics and Space Administration. Lewis Research Center, Cleveland, OH.
USERS MANUAL FOR THE NASA LEWIS THREE-DIMENSIONAL ICE ACCRETION CODE (LEWICE 3D)
Colin S. Bidwell and Mark G. Potapczuk Dec. 1993 143 p Sponsored by NASA. Washington
(RTOP 505-68-10)
(NASA-TM-105974; E-7847; NAS 1.15:105974) Avail: CASI HC A07/MF A02

A description of the methodology, the algorithms, and the input and output data along with an example case for the NASA Lewis 3D ice accretion code (LEWICE3D) has been produced. The manual has been designed to help the user understand the capabilities, the methodologies, and the use of the code. The LEWICE3D code is a conglomeration of several codes for the purpose of calculating ice shapes on three-dimensional external surfaces. A three-dimensional external flow panel code is incorporated which has the capability of calculating flow about arbitrary 3D lifting and nonlifting bodies with external flow. A fourth order Runge-Kutta integration scheme is used to calculate arbitrary streamlines. An Adams type predictor-corrector trajectory integration scheme has been included to calculate arbitrary trajectories. Schemes for calculating tangent trajectories, collection efficiencies, and concentration factors for arbitrary regions of interest for single droplets or droplet distributions have been incorporated. A LEWICE 2D based heat transfer algorithm can be used to calculate ice accretions along surface streamlines. A geometry modification scheme is incorporated which calculates the new geometry based on the ice accretions generated at each section of interest. The three-dimensional ice accretion calculation is based on the LEWICE 2D calculation. Both codes calculate the flow, pressure distribution, and collection efficiency distribution along surface streamlines. For both codes the heat transfer calculation is divided into two regions, one above the stagnation point and one below the stagnation point, and solved for each region assuming a flat plate with pressure distribution. Water is assumed to follow the surface streamlines, hence starting at the stagnation zone any water that is not frozen out at a control volume is assumed to run back into the next control volume. After the amount of frozen water at each control volume has been calculated the geometry is modified by adding the ice at each control volume in the surface normal direction. Author (revised)

N94-21816*# Boeing Commercial Airplane Co., Seattle, WA. Payload Systems.
AIRCRAFT CABIN WATER SPRAY DISBENEFITS STUDY Final Report
Thomas L. Reynolds and Kent W. Porter Oct. 1993 137 p Sponsored in part by FAA
(Contract NAS1-18027)
(NASA-CR-194750; NAS 1.26:194750; DOT/FAA/CT-92/6) Avail: CASI HC A07/MF A02

The concept of utilizing a cabin water spray system (CWSS) as a means of increasing passenger evacuation and survival time following an accident has received considerable publicity and has been the subject of testing by the regulatory agencies in both the United States and Europe. A test program, initiated by the CAA in 1987, involved the regulatory bodies in both Europe and North America in a collaborative research effort to determine the benefits and 'disbenefits' (disadvantages) of a CWSS. In order to obtain a balanced opinion of an onboard CWSS, NASA, and FAA requested the Boeing Commercial Airplane Group to investigate the potential 'disbenefits' of the proposed system from the perspective of the manufacturer and an operator. This report is the result of a year-long, cost-sharing contract study between the Boeing Commercial Airplane Group, NASA, and FAA. Delta Air Lines participated as a subcontract study team member and investigated the 'return to service' costs for an aircraft that would experience an uncommanded operation of a CWSS without the presence of fire. Disbenefits identified include potential delays in evacuation, introduction of 'common cause failure' in redundant safety of flight systems, physiological problems for passengers, high cost of refurbishment for inadvertent discharge, and potential to negatively affect other safety systems. Author (revised)

N94-22055 Transportation Research Board, Washington, DC.
PUBLIC-SECTOR AVIATION ISSUES: GRADUATE RESEARCH AWARD PAPERS, 1991-1992
N. C. Kassabian, A. G. Tobias, L. Crayton, N. Solomon, and S. E. G. Brown 1993 50 p See also PB92-222629 Limited Reproducibility: More than 20% of this document may be affected by microfiche quality
(PB93-206258; TRB/TRR-1379,) Avail: CASI HC A03

Contents of the document are: robust control techniques for a commercial autoland system; response of U.S. air carriers to on-time disclosure rule; policy-level decision support for airport passenger terminal design; reexamination of stall and spin prevention training; and development of risk models for simultaneous instrument landing system approaches to closely spaced parallel runways. NTIS

N94-22373*# Miami Univ., Coral Gables, FL. Dept. of Management Science.
INTERVENTION STRATEGIES FOR THE MANAGEMENT OF HUMAN ERROR
Earl L. Wiener Aug. 1993 114 p
(Contract NCA2-441)
(NASA-CR-4547; A-93120; NAS 1.26:4547) Avail: CASI HC A06/MF A02

This report examines the management of human error in the cockpit. The principles probably apply as well to other applications in the aviation realm (e.g. air traffic control, dispatch, weather, etc.) as well as other high-risk systems outside of aviation (e.g. shipping, high-technology medical procedures, military operations, nuclear power production). Management of human error is distinguished from error prevention. It is a more encompassing term, which includes not only the prevention of error, but also a means of disallowing an error, once made, from adversely affecting system output. Such techniques include: traditional human factors engineering, improvement of feedback and feedforward of information from system to crew, 'error-evident' displays which make erroneous input more obvious to the crew, trapping of errors within a system, goal-sharing between humans and machines (also called 'intent-driven' systems), paperwork management, and behaviorally based approaches, including procedures, standardization, checklist design, training, cockpit resource management, etc. Fifteen guidelines for the design and implementation of intervention strategies are included. Author (revised)

04 AIRCRAFT COMMUNICATIONS AND NAVIGATION

Includes digital and voice communication with aircraft; air navigation systems (satellite and ground based); and air traffic control.

For related information see also *17 Space Communications, Spacecraft Communications, Command and Tracking* and *Communications and Radar.*

N94-20051# Systems Control Technology, Inc., Arlington, VA.
ROTORCRAFT LOW ALTITUDE IFR BENEFIT/COST ANALYSIS: CONCLUSIONS AND RECOMMENDATIONS Final Report
Robert K. Anoli, Robert B. Newman, and Edwin D. McConkey Oct. 1993 152 p
(Contract DTFA01-87-C-00014)
(DOT/FAA/RD-93/22; DOT/FAA/DS-89/11; SCT-92RR-8) Avail: CASI HC A08/MF A02

The Rotorcraft Master Plan advocates the establishment of additional communications, navigation, and surveillance (CNS) facilities, as well as the analysis and development of systems to satisfy the increasing demand for widespread instrument flight rules (IFR) rotorcraft operations within the National Airspace System (NAS). The objective of this study is to determine if there is an economic basis for improvement of these low altitude IFR services within the NAS in order to better support rotorcraft IFR operations. The findings of this study will aid FAA decision making in that regard. In view of prior implementation decisions on LORAN-C and GPS, the emphasis in this effort is on communications, surveillance, procedural changes, and

avionics. This report is the last of a series of three reports that address rotorcraft low altitude benefit/cost analysis. The other two are: Rotorcraft Low Altitude CNS Benefit/Cost Analysis: Operations Data, DOT/FAA/DS-89/9, and Rotorcraft Low Altitude IFR Benefit/Cost Analysis: Operations Analysis, DOT/FAA/RD-89/10. This final report reviews the operational requirements and constraints for specific rotorcraft missions identified in the previous reports in this series. It also reviews all of the alternatives identified for improving rotorcraft operations. The alternatives considered include additional communications and surveillance equipment, both existing equipment and future systems identified in the Aviation Systems Capital Investment Plan (CIP), and the air traffic control (ATC) procedural changes. A benefit/cost (B/C) analysis is conducted for each communication, surveillance, and procedural improvement identified. When site specific data is available, it is used to calculate actual B/C ratios. When no data exists, a break-even analysis is provided. Author

N94-20148*# Colorado Univ., Boulder. Center for Astrodynamical Research.

AUTOMATIC AVHRR IMAGE NAVIGATION SOFTWARE Final Report

Dan Baldwin and William Emery 1992 10 p

(Grant NAGw-3224)

(NASA-CR-194602; NAS 1.26:194602) Avail: CASI HC A02/MF A01

This is the final report describing the work done on the project entitled Automatic AVHRR Image Navigation Software funded through NASA-Washington, award NAGW-3224, Account 153-7529. At the onset of this project, we had developed image navigation software capable of producing geo-registered images from AVHRR data. The registrations were highly accurate but required a priori knowledge of the spacecraft's axes alignment deviations, commonly known as attitude. The three angles needed to describe the attitude are called roll, pitch, and yaw, and are the components of the deviations in the along scan, along track and about center directions. The inclusion of the attitude corrections in the navigation software results in highly accurate georegistrations, however, the computation of the angles is very tedious and involves human interpretation for several steps. The technique also requires easily identifiable ground features which may not be available due to cloud cover or for ocean data. The current project was motivated by the need for a navigation system which was automatic and did not require human intervention or ground control points. The first step in creating such a system must be the ability to parameterize the spacecraft's attitude. The immediate goal of this project was to study the attitude fluctuations and determine if they displayed any systematic behavior which could be modeled or parameterized. We chose a period in 1991-1992 to study the attitude of the NOAA 11 spacecraft using data from the Tiros receiving station at the Colorado Center for Astrodynamic Research (CCAR) at the University of Colorado. Derived from text

N94-20197 Department of the Navy, Washington, DC.

ALL-WEATHER PRECISION LANDING SYSTEM FOR AIRCRAFT IN REMOTE AREAS Patent

Gerald E. Hart, inventor (to Navy) 4 May 1993 16 p Filed 24 Jul. 1990

(AD-D015924; US-Patent-5,208,601; US-Patent-Appl-SN-556606) Avail: US Patent and Trademark Office

An all-weather aircraft landing system includes a plurality of ground based passive 90 deg dihedral reflectors for producing two-bounce reflected signals without ground reflections and an airborne radar system which may transmit and receive same sense circularly polarized radiation, while completely rejecting opposite sense polarization returns or else utilizing them to indicate weather conditions. Radar clutter from objects such as rain, buildings, and trees which produce opposite sense reflections are rejected by the same sense receiver or switched to an opposite sense receiver to provide weather/obstacle condition information. By properly orienting a plurality of 90 deg dihedral angle reflectors of a particular size in a predetermined array pattern and tilt-angle adjacent a runway, the reflections from airborne radar signals are processed and displayed to provide a visual means for determining glide slope deviation and approach vector of the landing aircraft. DTIC

N94-21037# Naval Postgraduate School, Monterey, CA.

A SOFTWARE ARCHITECTURE FOR A SMALL AUTONOMOUS UNDERWATER VEHICLE NAVIGATION SYSTEM M.S. Thesis

Clark D. Stevens Jun. 1993 153 p

(AD-A272322) Avail: CASI HC A08/MF A02

This thesis documents the development of an interim Small Autonomous Underwater Vehicle (AUV) Navigation System (SANS), a self-contained, externally mountable navigation package. The purpose of SANS is to determine the position of a submerged object of interest located by an AUV. The volume of SANS must not exceed 120 cubic inches and total system accuracy of 10.0 meters rms or better is required. An Inertial Navigation System (INS) is implemented to compute the ascent path during transit from an object of interest to the surface. INS hardware components include miniature spin gyroscopes, a compass, and a depth transducer interfaced through an analog to digital converter. Global Positioning System (GPS) is used to determine the AUV's location after reaching the surface. The reciprocal of the ascent vector is applied to the AUV's GPS position to accurately determine the location of the target of interest. A primarily object-oriented software architecture is implemented here with extensive software testing to verify the proper operation of key modules. The objective of this thesis is to quantify the adequacy of the selected components in meeting these requirements and to develop a breadboard design demonstrating the basic functions of the interim SANS. This research concludes that the components selected for the interim SANS meet the accuracy requirements provided the AUV maintains a climb angle which is equal to or steeper than 12 degrees from a typical mission depth of 20 meters. DTIC

N94-21606*# National Aeronautics and Space Administration. Ames Research Center, Moffett Field, CA.

DEVELOPMENT AND EVALUATION OF A PROFILE NEGOTIATION PROCESS FOR INTEGRATING AIRCRAFT AND AIR TRAFFIC CONTROL AUTOMATION

Steven M. Green, Wim denBraven (National Aerospace Lab., Amsterdam, Netherlands.), and David H. Williams (National Aeronautics and Space Administration. Langley Research Center, Hampton, VA.) Apr. 1993 23 p Presented at the RTCA 1991 Annual Assembly Meeting and Technical Symposium

(RTOP 505-64-13)

(NASA-TM-4360; A-92038; NAS 1.15:4360) Avail: CASI HC A03/MF A01

The development and evaluation of the profile negotiation process (PNP), an interactive process between an aircraft and air traffic control (ATC) that integrates airborne and ground-based automation capabilities to determine conflict-free trajectories that are as close to an aircraft's preference as possible, are described. The PNP was evaluated in a real-time simulation experiment conducted jointly by NASA's Ames and Langley Research Centers. The Ames Center/TRACON Automation System (CTAS) was used to support the ATC environment, and the Langley Transport Systems Research Vehicle (TSRV) piloted cab was used to simulate a 4D Flight Management System (FMS) capable aircraft. Both systems were connected in real time by way of voice and data lines; digital datalink communications capability was developed and evaluated as a means of supporting the air/ground exchange of trajectory data. The controllers were able to consistently and effectively negotiate nominally conflict-free vertical profiles with the 4D-equipped aircraft. The actual profiles flown were substantially closer to the aircraft's preference than would have been possible without the PNP. However, there was a strong consensus among the pilots and controllers that the level of automation of the PNP should be increased to make the process more transparent. The experiment demonstrated the importance of an aircraft's ability to accurately execute a negotiated profile as well as the need for digital datalink to support advanced air/ground data communications. The concept of trajectory space is proposed as a comprehensive approach for coupling the processes of trajectory planning and tracking to allow maximum pilot discretion in meeting ATC constraints. Author (revised)

N94-21629*# Lockheed Engineering and Sciences Co., Hampton, VA.

TECHNIQUES USED FOR THE ANALYSIS OF OCULOMETER EYE-SCANNING DATA OBTAINED FROM AN AIR TRAFFIC CONTROL DISPLAY

Daniel J. Crawford, Daniel W. Burdette, and William R. Capron Dec. 1993 184 p

(Contract NAS1-19000; RTOP 505-64-13-01)

(NASA-CR-191559; NAS 1.26:191559) Avail: CASI HC A09/MF A02

The methodology and techniques used to collect and analyze look-point position data from a real-time ATC display-format comparison experiment are documented. That study compared the delivery precision and controller workload of three final approach spacing aid display formats. Using an oculometer, controller lookpoint position data were collected, associated with gaze objects (e.g., moving aircraft) on the ATC display, and analyzed to determine eye-scan behavior. The equipment involved and algorithms for saving, synchronizing with the ATC simulation output, and filtering the data are described. Target (gaze object) and cross-check scanning identification algorithms are also presented. Data tables are provided of total dwell times, average dwell times, and cross-check scans. Flow charts, block diagrams, file record descriptors, and source code are included. The techniques and data presented are intended to benefit researchers in other studies that incorporate non-stationary gaze objects and oculometer equipment. Author (revised)

N94-22277*# Boeing Commercial Airplane Co., Seattle, WA.
PARALLEL RUNWAY REQUIREMENT ANALYSIS STUDY. VOLUME 1: THE ANALYSIS Final Report
Yaghoob S. Ebrahimi Dec. 1993 129 p
(Contract NAS1-18027; RTOP 505-66-41-04)
(NASA-CR-191549-Vol-1; NAS 1.26:191549-Vol-1) Avail: CASI HC A07/MF A02

The correlation of increased flight delays with the level of aviation activity is well recognized. A main contributor to these flight delays has been the capacity of airports. Though new airport and runway construction would significantly increase airport capacity, few programs of this type are currently underway, let alone planned, because of the high cost associated with such endeavors. Therefore, it is necessary to achieve the most efficient and cost effective use of existing fixed airport resources through better planning and control of traffic flows. In fact, during the past few years the FAA has initiated such an airport capacity program designed to provide additional capacity at existing airports. Some of the improvements that that program has generated thus far have been based on new Air Traffic Control procedures, terminal automation, additional Instrument Landing Systems, improved controller display aids, and improved utilization of multiple runways/Instrument Meteorological Conditions (IMC) approach procedures. A useful element to understanding potential operational capacity enhancements at high demand airports has been the development and use of an analysis tool called The PLAND—BLUNDER (PLB) Simulation Model. The objective for building this simulation was to develop a parametric model that could be used for analysis in determining the minimum safety level of parallel runway operations for various parameters representing the airplane, navigation, surveillance, and ATC system performance. This simulation is useful as: a quick and economical evaluation of existing environments that are experiencing IMC delays, an efficient way to study and validate proposed procedure modifications, an aid in evaluating requirements for new airports or new runways in old airports, a simple, parametric investigation of a wide range of issues and approaches, an ability to tradeoff air and ground technology and procedures contributions, and a way of considering probable blunder mechanisms and range of blunder scenarios. This study describes the steps of building the simulation and considers the input parameters, assumptions and limitations, and available outputs. Validation results and sensitivity analysis are addressed as well as outlining some IMC and Visual Meteorological Conditions (VMC) approaches to parallel runways. Also, present and future applicable technologies (e.g., Digital Autoland Systems, Traffic Collision and Avoidance System II, Enhanced Situational Awareness System, Global Positioning Systems for Landing, etc.) are assessed and recommendations made.
Derived from text

N94-22278*# Boeing Commercial Airplane Co., Seattle, WA.
PARALLEL RUNWAY REQUIREMENT ANALYSIS STUDY. VOLUME 2: SIMULATION MANUAL Final Report
Yaghoob S. Ebrahimi and Ken S. Chun Dec. 1993 51 p
(Contract NAS1-18027; RTOP 505-66-41-04)
(NASA-CR-191549-Vol-2; NAS 1.26:191549-Vol-2) Avail: CASI HC A04/MF A01

This document is a user manual for operating the PLAND—BLUNDER (PLB) simulation program. This simulation is based on two aircraft approaching parallel runways independently and using parallel Instrument Landing System (ILS) equipment during Instrument Meteorological Conditions (IMC). If an aircraft should deviate from its assigned localizer course toward the opposite runway, this constitutes a blunder which could endanger the aircraft on the adjacent path. The worst case scenario would be if the blundering aircraft were unable to recover and continue toward the adjacent runway. PLAND—BLUNDER is a Monte Carlo-type simulation which employs the events and aircraft positioning during such a blunder situation. The model simulates two aircraft performing parallel ILS approaches using Instrument Flight Rules (IFR) or visual procedures. PLB uses a simple movement model and control law in three dimensions (X, Y, Z). The parameters of the simulation inputs and outputs are defined in this document along with a sample of the statistical analysis. This document is the second volume of a two volume set. Volume 1 is a description of the application of the PLB to the analysis of close parallel runway operations.
Derived from text

N94-22427 Calgary Univ. (Alberta). Dept. of Geomatics Engineering.
A ROBUST QUALITY CONTROL SYSTEM FOR GPS NAVIGATION AND KINEMATIC POSITIONING Ph.D. Thesis
Goa Yang Sep. 1992 171 p
(ISBN-0-315-83148-0; CTN-94-60938) Copyright Avail: Micromedia Ltd., Technical Information Centre, 240 Catherine Street, Suite 305, Ottawa, Ontario, K2P 2G8, Canada HC/MF

The development and testing of a robust quality control system for global positioning system (GPS) navigation and kinematic positioning is described. The system is built upon the successful combination of well-known classical statistics with modern robust statistics. The theory of robust statistics was applied to make robust the standard Kalman filter and to formulate a robust failure signal generation function. Good performance in failure detection and failure identification, minimum implementation effort, and automation are the main criteria employed in the development of the system. Theoretical and numerical aspects of system modelling are presented along with the introduction of important concepts and the derivation of useful equations. Both the computational load and implementation effort were reduced to a minimum through various numerical techniques. The system was tested by applying it to integrity monitoring in GPS navigation and cycle slip detection and identification in GPS kinematic positioning. Results show that significant improvements have been achieved as compared to the conventional innovation based approach.
Author (CISTI)

N94-22134 Allied-Signal Aerospace Canada, Toronto (Ontario).
MLS SIGNAL-IN-SPACE CATEGORY 3 LANDING HAZARD ANALYSIS
R. J. Kelly *In* Engineering Inst. of Canada, Canadian Conference on Electrical and Computer Engineering, Volumes 1 and 2 1991 4 p
(For primary document see N94-22101 05-33)
Avail: Issuing Activity (Engineering Inst. of Canada, 2050 rue Mansfield, Suite 700, Montreal, PQ H3A 1Z2 Canada)

N94-22135 Transport Canada, Ottawa (Ontario).
APPLICATION OF SCATTERING BY ARRAYS OF CYLINDERS TO MLS SIGNAL PROPAGATION ERROR ESTIMATION
M. Z. El-Gamal and Do-Duy Hung *In* Engineering Inst. of Canada, Canadian Conference on Electrical and Computer Engineering, Volumes 1 and 2 1991 5 p (For primary document see N94-22101 05-33)
Avail: Issuing Activity (Engineering Inst. of Canada, 2050 rue Mansfield, Suite 700, Montreal, PQ H3A 1Z2 Canada)

N94-22136 Republic Electronic Industries Corp., Melville, NY.
TESTING OF DME/P EQUIPMENT PERFORMANCE FOR COMPLEX MLS PROCEDURES
J. F. Michaels *In* Engineering Inst. of Canada, Canadian Conference on Electrical and Computer Engineering, Volumes 1 and 2 1991 4 p
(For primary document see N94-22101 05-33)
Avail: Issuing Activity (Engineering Inst. of Canada, 2050 rue Mansfield, Suite 700, Montreal, PQ H3A 1Z2 Canada)

N94-22154 Micronav Ltd., Sydney (Nova Scotia).
MLS POINTING ANGLE ERROR SOURCES AND EFFECTS
David Babineau, Mike McAloney, and Maurice Meyer *In* Engineering Inst. of Canada, Canadian Conference on Electrical and Computer Engineering, Volumes 1 and 2 1991 4 p (For primary document see

N94-22101 05-33)
Avail: Issuing Activity (Engineering Inst. of Canada, 2050 rue Mansfield, Suite 700, Montreal, PQ H3A 1Z2 Canada)

N94-22155 Micronav Ltd., Sydney (Nova Scotia).
DEVELOPING SOFTWARE TO RTCA DO-178A
Ross Hooper, John Lord, and Kathy MacIntyre *In* Engineering Inst. of Canada, Canadian Conference on Electrical and Computer Engineering, Volumes 1 and 2 1991 3 p (For primary document see N94-22101 05-33)
Avail: Issuing Activity (Engineering Inst. of Canada, 2050 rue Mansfield, Suite 700, Montreal, PQ H3A 1Z2 Canada)

N94-22156 Ohio Univ., Athens.
A FLIGHT TEST SYSTEM DESIGN FOR THE MICROWAVE LANDING SYSTEM
D. B. Vickers *In* Engineering Inst. of Canada, Canadian Conference on Electrical and Computer Engineering, Volumes 1 and 2 1991 4 p (For primary document see N94-22101 05-33)
Avail: Issuing Activity (Engineering Inst. of Canada, 2050 rue Mansfield, Suite 700, Montreal, PQ H3A 1Z2 Canada)

N94-22219 Laval Univ. (Quebec). Dept. de Genie Electrique.
FM INTERFERENCE IN RADIO NAVIGATION RECEIVERS [INTERFERENCE MF DANS LES RECEPTEURS DE RADIO NAVIGATION]
H. T. Huynh, J. M. Vezin, and D. Angers *In* Engineering Inst. of Canada, Canadian Conference on Electrical and Computer Engineering, Volumes 1 and 2 1991 4 p In FRENCH (For primary document see N94-22101 05-33)
Avail: Issuing Activity (Engineering Inst. of Canada, 2050 rue Mansfield, Suite 700, Montreal, PQ H3A 1Z2 Canada)

05 AIRCRAFT DESIGN, TESTING AND PERFORMANCE

Includes aircraft simulation technology.

For related information see also *18 Spacecraft Design, Testing and Performance* and *39 Structural Mechanics*.For land transportation vehicles see *85 Urban Technology and Transportation*.

N94-19914 Aeronautical Research Labs., Melbourne (Australia).
DEVELOPMENT AND OPERATION OF THE F/A-18 MODEL CONTROL SURFACE ACTUATORS
S. S. Lam and Y. Y. Link Aug. 1993 29 p Limited Reproducibility: More than 20% of this document may be affected by microfiche quality
(AD-A271330; ARL-TN-29; DODA-AR-008-345) Avail: CASI HC A03

A series of test programs in the ARL 2.7m x 2.1m Low Speed Wind Tunnel of a 1/9th scale model of the F/A-18 required the development of a software package to drive the control surfaces. This software is written in VAX FORTRAN for a MicroVAX 2 computer. The software communicates with the model through a specially designed Actuator Module that responds to requests from the MicroVAX 2 computer. In order to establish the relationship between control surface angles and Linear Variable Differential Transformer readings a cubic spline interpolation method has been implemented. This report describes the development and operation of the control surface actuators' software and contains a detailed guide for its use. DTIC

N94-20040 Department of Defense, Arlington, VA. Office of Inspector General.
AUDIT REPORT. NAVY'S AIRCRAFT STRUCTURAL LIFE SURVEILLANCE PROGRAM DATA RECORDERS
12 Nov. 1992 15 p Limited Reproducibility: More than 20% of this document may be affected by microfiche quality
(AD-A270391; IG/DOD-93-022) Avail: CASI HC A03

We are providing this final report for your information and use. This audit was performed in response to a DoD Inspector General hotline allegation that the Navy's planned $188 million procurement of structural data recorders under the Navy's Aircraft Structural Life Surveillance Program duplicated existing Navy recorder systems. The recorder monitors the structural stress that an aircraft experiences during operation. Our objective was to evaluate the validity of this allegation. The effectiveness of applicable internal controls was also evaluated. The Navy's Aircraft Structural Life Surveillance Program data recorder does not duplicate any existing Navy recorder systems. The structural data recorder does duplicate functions of a similar Air Force system. However, it is no longer practicable or economical for the Navy and the Air Force to combine their structural recorder systems because both have already installed and integrated these recorder systems in substantial numbers of aircraft. DTIC

N94-20188# Wichita State Univ., KS. National Inst. for Aviation Research.
PROCEEDINGS OF THE TWENTIETH ANNUAL TECHNOLOGYFEST
1993 25 p Technologyfest held in Wichita, KS, 12-13 Nov. 1993; cosponsored by AIAA
Avail: CASI HC A03/MF A01

The program for the twentieth annual Techfest held November 12 - 13, 1993 is accompanied by abstracts of selected topics. Design topics include a supersonic oblique all-wing transport aircraft, an application of neural networks to airfoil design, aircraft nosewheel steering simulation, an alternative parameter airfoil optimization method, a high altitude long endurance aircraft with manufacturing considerations, and integrated design of controllers with bang bang and proportional control effectors. Structures topics include reducing structural loads, failure of aircraft structures due to internal blast, and geriatrics of commercial airplanes. Aerodynamics topics include visualization of the multiple supersonic jet oscillations by swept focused strobed schlieren technique, the near-wake flow behavior of an oscillating airfoil with modified trailing edge, full span flaperons for a biplane, an experimental investigation of helicopter rotor downwash and tail boom interaction at the WSU 7 x 10 foot wind tunnel, and incorporating biplane wing theory into a large subsonic all-cargo transport. CASI

N94-20561# Naval Postgraduate School, Monterey, CA.
CONTROL VANE GUIDANCE FOR A DUCTED-FAN UNMANNED AIR VEHICLE M.S. Thesis
Patrick J. Moran Jun. 1993 112 p
(AD-A271957) Avail: CASI HC A06/MF A02

Control of airborne vehicles was originally conceived to be done entirely by human pilots. Improvements in electronics in the last 50 years have allowed many flight control functions to become automated, with the pilot continuously monitoring flight parameters from within the vehicle cockpit. With the advent of small unmanned air vehicles (UAV's) which are limited in size and weight-carrying capacity, a pilot is now able to fly an airborne vehicle from a distant ground-fixed position. Miniature electronic instruments control or direct vehicle movements either through pilot commands or autonomously. In order to accomplish reliable, continuous control of a UAV, many sensors are necessary aboard the vehicle. This thesis designed and installed necessary hardware and developed software to guide a UAV's aerodynamic control vanes, with feedback from sensors aboard the vehicle, in order to facilitate ground-based pilot control. Previous thesis work accomplished on this project achieved control of a UAV, named Archytas, in one degree-of-freedom, roll, while mounted on a test stand. Umbilical-controlled guidance of Archytas' control vanes from a forward-mounted sensor pod was set as the goal for this phase of the Archytas project. This work focused on modification of hardware to generate and access required signals, programming of analog-to-digital (A/D) and counter/timer peripheral boards mounted in a personal computer to control electrical and signal flow, and implementation of single-input-single-output (SISO) control equations developed concurrently in another thesis. DTIC

N94-21051 Grumman Aerospace Corp., Bethpage, NY.
TORSION SPRING POWERED MISSILE WING DEPLOYMENT SYSTEM Patent
Arthur M. Frank, inventor (to Grumman Aerospace Corp.) 18 Aug. 1992 16 p Filed 28 May 1987
(CA-Patent-1,306,384; Int-Patent-Class-B64C-3/56;
Int-Patent-Class-F42B-10/18; CTN-93-60687) Copyright Avail: Micromedia Ltd., Technical Information Centre, 165 Hotel de Ville, Place du Portage, Phase 2, Hull, Quebec J8X 3X2, Canada HC/MF

A foldable wing deployment system is provided for a missile having a foldable wing section hinged to a fixed wing section. An overcenter linkage

connects the fixed and foldable wing section for securely deploying the foldable wing section to a coextensive position with the fixed wing section. A first torsion bar having a first end is connected to a first gear, and a hollow cylindrical torsion member is mounted over the torsion bar. A first end of the member is fixed and a second end is connected to a corresponding second end of the torsion bar. A second torsion bar is located in parallel proximity to the cylindrical torsion member and is connected to the overcenter linkage. A second gear is mounted on the second torsion bar and contacts the first gear for exerting supplementary bias on the overcenter linkage during its initial operation for ensuring a substantially linear actuating drive on the linkage, necessary for smooth and reliable wing deployment. CISTI

N94-21246# Aurora Flight Sciences Corp., Manassas, VA.
LOW-COST, DUAL-USE PLATFORMS FOR ENVIRONMENTAL SENSING, PHASE 1
Matthew G. Hutchison, John S. Langford, and Charles S. Preston 1993 47 p
(Contract N00014-93-C-0037)
(AD-A272951; AR-9305) Avail: CASI HC A03/MF A01

Recent advances in microelectronics, lightweight composite structures, and computational fluid mechanics have made possible a new generation of semi-autonomous, unmanned aircraft. Many of these unmanned aerial vehicles (UAV's) were originally conceived for purely military purposes, but the performance capabilities--in particular, the capacity for flights of extended range and endurance--have attracted the attention of the atmospheric and environmental research communities. While the application of UAV's to high-altitude research has been extensively investigated and documented, much less attention has been given to their potential role in low-altitude atmospheric studies. This report focuses on the application of unmanned aircraft to environmental sensing at low altitudes in the marine environment. There appear to be a number of missions in which a suitable UAV platform could provide unique opportunities for data collection that would greatly expand the current understanding of this vital region of the atmosphere. In addition to scientific contributions, the information collected at low altitude would also be of significant interest to the U.S. Navy for purposes varying from calibration of weapons guidance systems to initialization of computational models. DTIC

N94-21283# Naval Postgraduate School, Monterey, CA.
DESIGN, FABRICATION AND TEST OF A VERTICAL ATTITUDE TAKEOFF AND LANDING UNMANNED AIR VEHICLE M.S. Thesis
Robert B. Stoney Jun. 1993 234 p
(AD-A273003) Avail: CASI HC A11/MF A03

Future fleet needs for real-time intelligence require an unmanned platform capable of operations from small surface combatants without the need for extensive support personnel and equipment and without causing disruption to the operations of the ship from which it operates. A candidate must not only takeoff and land vertically but also be capable of high forward flight speeds and efficient on-station performance. The design and initial fabrication of a Vertical Attitude Takeoff and Landing (VATOL) Unmanned Air Vehicle (UAV) airframe was completed at the Naval Postgraduate School. The vehicle, called Archytas, was a combination of two existing UAV's--the AROD and Aquila--as well as locally manufactured components, including a canard and wing spar. The objective of creating Archytas was to provide a proof-of-concept platform for research to explore performance trade-offs and stability augmentation. A three-degree-of-freedom simulation was used as the focus of the design efforts, to validate design decisions made in the fields of propulsion, aerodynamics, structures and flight mechanics. Engine tests were conducted to determine thrust and control power. Structural components were designed, fabricated and then tested, making modifications where necessary to ensure sufficient airframe strength. A longitudinal control system was designed, validated by simulation, and tested structurally. DTIC

N94-21418# Naval Postgraduate School, Monterey, CA.
EFFECTS OF THRUST VECTOR CONTROL ON THE PERFORMANCE OF THE AEROBANG ORBITAL PLANE CHANGE MANEUVER M.S. Thesis
Richard E. Johnson Jun. 1993 76 p
(AD-A272532) Avail: CASI HC A05/MF A01

The aerobang maneuver, one of three types of aero-assisted orbital change methods, holds the possibility of reducing fuel consumption for orbital craft capable of atmospheric entry. It has been previously shown that different types of vehicles provide varying results over a constant heating rate trajectory. Further investigation into the optimization of the aerobang maneuver in this thesis includes the effects of using thrust vector control, the examination of the effects of increasing fuel mass fraction to increase orbital inclination changes, and the effects of that increase on both angle of attack and heating rate. The aerobang maneuver is shown to be capable of significant changes in orbital inclination in either a fixed heating rate or a fixed angle of attack mode for the Maneuverable Reentry Research Vehicle. DTIC

N94-21507# Quest Integrated, Inc., Kent, WA.
LOW-COST UNMANNED AIR VEHICLE (UAV) FOR OCEANOGRAPHIC RESEARCH Final Report, Apr. - Oct. 1993
J. J. Kolle Nov. 1993 26 p
(Contract N00014-93-C-0029)
(AD-A273103) Avail: CASI HC A03/MF A01

This Phase 1 study has demonstrated the feasibility of developing a low-cost unmanned air vehicle (UAV) designed for a range of oceanographic research missions, including photogrammetry, radiometry, video imaging, and atmospheric profiling, at altitudes of up to 3 km and a range of 300 km. The work included identification of a data link, control system, autopilot, automated launcher, and recovery parachute. These subsystems will allow straightforward programming of a wide range of mission profiles and instrumentation control and accurate aircraft positioning (including differential GPS positioning within 10 km of a ground station). We also demonstrated a low-cost radio-controlled aircraft capable of carrying a 4-kg instrument payload and an autopilot that minimizes the skill (or control algorithm complexity) required to fly the aircraft. We have estimated that a complete UAV system, including the ground station and all avionics, can be sold commercially for under $35K. DTIC

N94-21548# Naval Postgraduate School, Monterey, CA.
DATA LINK DEVELOPMENT FOR THE ARCHYTAS VERTICAL TAKEOFF AND LANDING TRANSITIONAL FLIGHT UNMANNED AERIAL VEHICLE M.S. Thesis
Frederick W. Reichert, Jr. 17 Jun. 1993 94 p
(AD-A272499) Avail: CASI HC A05/MF A01

The development of a data link for the Archytas, a vertical takeoff and landing, transitional flight unmanned aerial vehicle (UAV) prototype being built by the Aeronautics Department at the Naval Postgraduate School, is chronicled. Archytas is intended to be a proof-of-concept platform to satisfy the Navy's real-time, over-the-horizon intelligence mission with a UAV that could be launched and recovered from a small combatant ship. A history of the Archytas command and control data link development, a full description of the data link as delivered for use on the prototype, principles for near term enhancements, and future considerations for the data link should the Archytas concept be adapted for use in an operational combat environment are provided. DTIC

N94-21592*# National Aeronautics and Space Administration. Ames Research Center, Moffett Field, CA.
SURVEY OF LIFT-FAN AERODYNAMIC TECHNOLOGY
David H. Hickey and Jerry V. Kirk Sep. 1993 74 p
(NASA Order A-25364-D)
(NASA-CR-177615; A-93106; NAS 1.26:177615) Avail: CASI HC A04/MF A01

Representatives of NASA Ames Research Center asked that a summary of technology appropriate for lift-fan powered short takeoff/vertical landing (STOVL) aircraft be prepared so that new programs could more easily benefit from past research efforts. This paper represents one of six prepared for that purpose. The authors have conducted or supervised the conduct of research on lift-fan powered STOVL designs and some of their important components for decades. This paper will first address aerodynamic modeling requirements for experimental programs to assure realistic, trustworthy results. It will next summarize the results or efforts to develop satisfactory specialized STOVL components such as inlets and flow deflectors. It will also discuss problems with operation near the ground, aerodynamics while under lift-fan power, and aerodynamic prediction techniques. Finally, results of studies to reduce lift-fan noise will be presented. The paper will emphasize results from large scale experiments, where available, for reasons that will

be brought out in the discussion. Some work with lift-engine powered STOVL aircraft is also applicable to lift-fan technology and will be presented herein. Small-scale data will be used where necessary to fill gaps. Author

N94-21819*# Ohio State Univ., Columbus. Cognitive Systems Engineering Lab.
COGNITIVE ENGINEERING IN AEROSPACE APPLICATIONS Progress Report
David D. Woods Nov. 1993 5 p
(Contract NCC2-592; RF Proj. 767386/721951)
(NASA-CR-194782; NAS 1.26:194782) Avail: CASI HC A01/MF A01

The progress that was made with respect to the objectives and goals of the research that is being carried out in the Cognitive Systems Engineering Laboratory (CSEL) under a Cooperative Agreement with NASA Ames Research Center is described. The major objective of this project is to expand the research base in Cognitive Engineering to be able to support the development and human-centered design of automated systems for aerospace applications. This research project is in support of the Aviation Safety/Automation Research plan and related NASA research goals in space applications. Author (revised)

N94-22598# Deutsche Forschungsanstalt fuer Luft- und Raumfahrt, Goettingen (Germany). Inst. fuer Experimentelle Stromeungsmechanik.
SURFACE HOT FILM MEASUREMENTS AT ATTAS LAMINAR GLOVE [OBERFLAECHENHEISSFILMMESSUNGEN AM ATTAS-LAMINARHANDSCHUH]
H.-P. Kreplin and G. Hoehler *In* Tech. Univ. Berlin, Measurement Technology for Flight Tests May 1991 p 1-11 In GERMAN (For primary document see N94-22597 05-02)
Avail: CASI HC A03/MF A02

N94-22623*# National Aeronautics and Space Administration. Langley Research Center, Hampton, VA.
DEMONSTRATING DAMAGE TOLERANCE OF COMPOSITE AIRFRAMES
Clarence C. Poe, Jr. *In its* Computational Methods for Failure Analysis and Life Prediction Oct. 1993 p 323-345 (For primary document see N94-22608 05-39)
Avail: CASI HC A03/MF A03

06 AIRCRAFT INSTRUMENTATION

Includes cockpit and cabin display devices; and flight instruments.

For related information see also *19 Spacecraft Instrumentation* and *35 Instrumentation and Photography.*

N94-20053# Galaxy Scientific Corp., Pleasantville, NJ.
HANDBOOK. VOLUME 3: DIGITAL SYSTEMS VALIDATION BOOK PLAN Final Report
Joan Janowitz Jul. 1993 16 p
(Contract DTFA03-89-C-00043)
(DOT/FAA/CT-93/16-Vol-3) Avail: CASI HC A03/MF A01

The Digital Systems Validation Handbook is a tutorial series designed to provide certification engineers information on current topics related to digital avionics. The book plan lays the foundation for volume 3 of this series. The purpose of the handbook book plan is to identify technology and related issues that certification engineers are likely to encounter. Volume 3 of the handbook series will consist of approximately 20 chapters. Sixteen chapters are described in the book plan. Four were reserved for technologies or issues that might emerge during the course of the volume 3 life cycle. A list of potential handbook topics was derived from a survey of the literature, conference and seminar attendance, results of an informal questionnaire, and interviews with Federal Aviation Administration (FAA) National Resource Specialists, experts in the field of certification and digital avionics, National Aeronautics and Space Administration (NASA) officials, and persons in private industry. From this input, the list of potential topics was developed and refined into handbook chapters. In addition to the chapter list and descriptions, the handbook purpose, scope, and use is discussed. The unabridged list of topics is included in the book plan appendix. Author

N94-20343# Computer Resource Management, Inc., Pleasantville, NJ.
HANDBOOK. VOLUME 2: DIGITAL SYSTEMS VALIDATION. CHAPTER 18: AVIONIC DATA BUS INTEGRATION TECHNOLOGY
D. Elwell, L. Harrison, J. Hensyl, and N. VanSuetendael Nov. 1993 179 p
(Contract DTFA03-86-C-00042)
(DOT/FAA/CT-88/10-Vol-2) Avail: CASI HC A09/MF A02

As multiple digital avionic systems were introduced into aircraft, there arose a need for digital communications between systems. In the early 1970s, many different digital data bus designs were used to provide this communication. Because these digital systems proved to be reliable and cost effective, their popularity increased. Proliferation led to standardization, particularly in the air transport category of aircraft, which allowed communications between line replaceable units (LRU's) to become more complex. The LRU's began to rely more heavily on each other to reduce the amount of equipment required. Sensor data and systems data could be shared among multiple systems, rather than each system requiring its own private source. Integrated digital avionics are increasingly being used to implement essential and critical functions that cannot be sufficiently reproduced by conventional means. The safety of such aircraft is highly dependent upon the computer software, hardware, and data buses connecting the systems. The newest concerns relate to the problems that are unique to highly integrated systems. There is no standard with which to assess the possible impact of these bus-based systems on aircraft safety. These and other advanced avionic systems will result in specific safety assessment problems when the appropriate data packages are submitted to the Federal Aviation Administration during the certification process. Author

N94-21500# Air Univ., Maxwell AFB, AL. Airpower Research Inst.
OPERATIONAL TEST AND EVALUATION OF ELECTRONIC COMBAT SYSTEMS
Frederick L. Wright Aug. 1993 115 p
(AD-A273093; AU-ARI-92-2) Avail: CASI HC A06/MF A02

The current electronic combat (EC) test process lacks discipline and structure because there is no standardized operational test process used in evaluating EC systems. The purpose of this study is to describe a test process that incorporates discipline and structure into the operational test and evaluation (OT and E) of EC systems with the intent of providing needed information to the decision makers. DTIC

07 AIRCRAFT PROPULSION AND POWER

Includes prime propulsion systems and systems components, e.g., gas turbine engines and compressors; and onboard auxilliary power plants for aircraft.

For related information see also *20 Spacecraft Propulsion and Power, 28 Propellants and Fuels,* and *44 Energy Production and Conversion.*

N94-20042# Naval Academy, Annapolis, MD.
DESIGN OF A STATE-SPACE CONTROLLER FOR AN ADVANCED GAS TURBINE ENGINE
Karl F. Prigge 17 May 1993 50 p
(AD-A270859; USNA-TSPR-207) Avail: CASI HC A03/MF A01

A multi-input, multi-output (MIMO) controller for an advanced gas turbine has been developed and tested using a computer simulation. The engine modeled is a two-and-one-half spool gas turbine with both an intercooler and a regenerator. In addition, variable stator vanes are present in the free-power turbine. This advanced engine is proposed for future naval propulsion for both mechanical drive and electrical drive. The designed controller controls free-power turbine speed and turbine inlet temperature using fuel flow and angle of the stator vanes. The controller will also have four modes of operation to deal with over temperature and over speed conditions. An eight state reduced order controller was used with pole placement and LQR to arrive at control gains. Both these methods required considerable insight into the problem. This insight was provided by previous experience with controller design for a less complicated engine, and also by use of a polyhedral search model of the gas turbine engine. The difficulty with a MIMO controller was that both inputs affect both of the control variables. The classical resolution this problem is to have one

input control one variable at a fast time constant and the other input control the other variable at a slow time constant. The 'optimal' resolution of this problem is analyzed using the transient curves and basic control theory. DTIC

N94-21268# Martin Marietta Labs., Baltimore, MD.
APPLICABILITY AND PERFORMANCE BENEFITS OF XD (TRADENAME) TITANIUM ALUMINIDES TO EXPENDABLE GAS TURBINE ENGINES Final Report, 1 Oct. 1991 - 31 Mar. 1993
Pamela Sadler, K. S. Kumar, and John A. Green Aug. 1993 168 p
(Contract DAAL04-91-C-0034)
(AD-A272998; MML-TR-93-09; ARL-CR-61) Avail: CASI HC A08/MF A02

The purpose of this program was to produce XD-TiAl compressor rotors for the experimental P9005 gas turbine engine to be used in the Army's Integrated High Performance Turbine Engine Technology program. Specific tasks included the casting of XD-titanium aluminide, processing optimization, component design analysis modifications and final component machining to specifications. Specifically, an ingot of a Ti-45Al-2Mn-2V alloy containing 7 volume % TiB2 was cast and then HIPed to eliminate residual porosity. Eight cylinders were machined from the HIPed material and isothermally forged. Microstructural analysis and mechanical property evaluation were performed on representative forgings. Several heat treatment schedules were examined, and the resulting microstructures were characterized using x-ray diffraction, optical and scanning electron microscopy. From these analyses, heat treatments were identified. Tensile behavior as a function of temperature, fracture toughness at room and elevated temperatures, creep resistance and fatigue response were evaluated. Fracture surfaces were characterized. Based on the observed mechanical properties, heat-treatment schedules were identified for the remaining forgings intended to be machined into final components. Williams International performed a detailed design analysis for the rotor. A local vendor was identified to machine the final component. DTIC

N94-21433# Naval Postgraduate School, Monterey, CA.
OPTIMIZATION AND PERFORMANCE ANALYSIS OF A SUPERSONIC CONICAL-FLOW WAVERIDER FOR A DECK-LAUNCHED INTERCEPT MISSION M.S. Thesis
David R. Price Jun. 1993 81 p
(AD-A272498) Avail: CASI HC A05/MF A01

An aircraft configuration for a deck launched intercept mission was investigated. The mission requirements for the carrier-launched and recovered aircraft included Mach 6 cruise out to a 1000 nautical mile combat radius and 20 minutes of combat followed by return to the carrier. A conical-flow waverider served as the starting point for the aircraft configuration. A hydrocarbon scramjet was integrated with the waverider body. The aft end of the waverider was faired to decrease the base area thereby reducing the transonic base drag. A numerical optimization was then completed to maximize the product of L/D (lift to drag ratio) and I(sub sp) (specific impulse). Variables for the optimization included the cone shock angle (used to derive the conical flow waverider) and the geometry of both the waverider body and the integrated propulsion system. The vehicle was constrained to a minimum volume of 3240 cubic feet, a maximum span of 60 feet and a fixed length of 60 feet. The integrated propulsion system was constrained to produce a minimum contraction ratio of 12.0 and assurance that the cowl shock was within an acceptable distance of the inlet shoulder of the combustor. The optimum configuration met or exceeded all constraints. L/D comparisons were made between the integrated configuration (i.e., the subject of this study), pure Mach 6 optimized waveriders and historical trends. DTIC

N94-21563*# National Aeronautics and Space Administration. Lewis Research Center, Cleveland, OH.
THRUST AUGMENTATION OPTIONS FOR THE BETA 2 TWO-STAGE-TO-ORBIT VEHICLE
Christopher A. Snyder Dec. 1993 17 p Presented at the AIAA Aircraft Design, Systems and Operations Meeting, Monterey, CA, 11-13 Aug. 1993; sponsored by AIAA
(RTOP 505-70-00)
(NASA-TM-106448; E-8301; NAS 1.15:106448; AIAA Paper 93-4014)
Avail: CASI HC A03/MF A01

NASA LeRC is continuing to study propulsion concepts for a horizontal takeoff and landing, fully reusable, two-stage-to-orbit vehicle. This will be capable of launching and returning a 10,000 pound payload to a 100 nautical mile polar orbit using low-risk technology. The vehicle, Beta 2, is a derivative of the USAF/Boeing Beta vehicle which was designed to deliver a 50,000 pound payload to a similar orbit. Beta 2 stages at Mach 6.5 and about 100,000 ft altitude. The propulsion system for the booster is an over/under turbine bypass engine/ramjet configuration. In this paper, several options for thrust augmentation were studied in order to improve the performance of this engine where there was a critical need. Options studies were turbine engine overspeed in the transonic region, water injection at a various turbine engine locations also during the transonic region, and water injection at the turbine engine face during high speed operation. The methodology, constraints, propulsion performance, and mission study results are presented. Author (revised)

N94-21582*# General Motors Corp., Indianapolis, IN. Allison Gas Turbine Div.
FLOW INTERACTION EXPERIMENT. VOLUME 1: AEROTHERMAL MODELING, PHASE 1 Final Report
M. Nikjooy, H. C. Mongia, J. P. Sullivan (Purdue Univ., West Lafayette, IN.), and S. N. B. Murthy (Purdue Univ., West Lafayette, IN.) Nov. 1993 338 p Original contains color illustrations
(Contract NAS3-24350; RTOP 505-62-52)
(NASA-CR-189192-Vol-1; E-8177-Vol-1; EDR-16026; NAS 1.26:189192-Vol-1) Avail: CASI HC A15/MF A03; 16 functional color pages

An experimental and computational study is reported for the flow of a turbulent jet discharging into a rectangular enclosure. The experimental configurations consisting of primary jets only, annular jets only, and a combination of annular and primary jets are investigated to provide a better understanding of the flow field in an annular combustor. A laser Doppler velocimeter is used to measure mean velocity and Reynolds stress components. Major features of the flow field include recirculation, primary and annular jet interaction, and high turbulence. A significant result from this study is the effect the primary jets have on the flow field. The primary jets are seen to create statistically larger recirculation zones and higher turbulence levels. In addition, a technique called marker nephelometry is used to provide mean concentration values in the model combustor. Computations are performed using three levels of turbulence closures, namely k-epsilon model, algebraic second moment (ASM), and differential second moment (DSM) closure. Two different numerical schemes are applied. One is the lower-order power-law differencing scheme (PLDS) and the other is the higher-order flux-spline differencing scheme (FSDS). A comparison is made of the performance of these schemes. The numerical results are compared with experimental data. For the cases considered in this study, the FSDS is more accurate than the PLDS. For a prescribed accuracy, the flux-spline scheme requires a far fewer number of grid points. Thus, it has the potential for providing a numerical error-free solution, especially for three-dimensional flows, without requiring an excessively fine grid. Although qualitatively good comparison with data was obtained, the deficiencies regarding the modeled dissipation rate (epsilon) equation, pressure-strain correlation model, and the inlet epsilon profile and other critical closure issues need to be resolved before one can achieve the degree of accuracy required to analytically design combustion systems. Author (revised)

N94-21583*# General Motors Corp., Indianapolis, IN. Allison Gas Turbine Div.
FLOW INTERACTION EXPERIMENT. VOLUME 2: AEROTHERMALMODELING, PHASE 2 Final Report
M. Nikjooy, H. C. Mongia, J. P. Sullivan (Purdue Univ., West Lafayette, IN.), and S. N. B. Murthy (Purdue Univ., West Lafayette, IN.) Nov. 1993 307 p Original contains color illustrations
(Contract NAS3-24350; RTOP 505-62-52)
(NASA-CR-189192-Vol-2; E-8180-Vol-2; EDR-16026; NAS 1.26:189192-Vol-2) Avail: CASI HC A14/MF A03; 12 functional color pages

An experimental and computational study is reported for the flow of a turbulent jet discharging into a rectangular enclosure. The experimental configurations consisting of primary jets only, annular jets only, and a combination of annular and primary jets are investigated to provide a better understanding of the flow field in an annular combustor. A laser

Doppler velocimeter is used to measure mean velocity and Reynolds stress components. Major features of the flow field include recirculation, primary and annular jet interaction, and high turbulence. A significant result from this study is the effect the primary jets have on the flow field. The primary jets are seen to create statistically larger recirculation zones and higher turbulence levels. In addition, a technique called marker nephelometry is used to provide mean concentration values in the model combustor. Computations are performed using three levels of turbulence closures, namely k-epsilon model, algebraic second moment (ASM), and differential second moment (DSM) closure. Two different numerical schemes are applied. One is the lower-order power-law differencing scheme (PLDS) and the other is the higher-order flux-spline differencing scheme (FSDS). A comparison is made of the performance of these schemes. The numerical results are compared with experimental data. For the cases considered in this study, the FSDS is more accurate than the PLDS. For a prescribed accuracy, the flux-spline scheme requires a far fewer number of grid points. Thus, it has the potential for providing a numerical error-free solution, especially for three-dimensional flows, without requiring an excessively fine grid. Although qualitatively good comparison with data was obtained, the deficiencies regarding the modeled dissipation rate (epsilon) equation, pressure-strain correlation model, and the inlet epsilon profile and other critical closure issues need to be resolved before one can achieve the degree of accuracy required to analytically design combustion systems.

Author (revised)

N94-21586*# National Aeronautics and Space Administration. Lewis Research Center, Cleveland, OH.

BLADE ROW INTERACTION EFFECTS ON FLUTTER AND FORCED RESPONSE

Daniel H. Buffum Dec. 1993 19 p Presented at the 29th Joint Propulsion Conference, Monterey, CA, 28 Jun. - 1 Jul. 1993; cosponsored by AIAA, SAE, ASME, and ASEE See also A93-49911

(RTOP 505-62-10)

(NASA-TM-106438; E-8280; NAS 1.15:106438; AIAA Paper 93-2084)

Avail: CASI HC A03/MF A01

In the flutter or forced response analysis of a turbomachine blade row, the blade row in question is commonly treated as if it is isolated from the neigboring blade rows. Disturbances created by vibrating blades are then free to propagate away from this blade row without being disturbed. In reality, neighboring blade rows will reflect some portion of this wave energy back toward the vibrating blades, causing additional unsteady forces on them. It is of fundamental importance to determine whether or not these reflected waves can have a significant effect on the aeroelastic stability or forced response of a blade row. Therefore, a procedure to calculate intra-blade-row unsteady aerodynamic interactions was developed which relies upon results available from isolated blade row unsteady aerodynamic analyses. In addition, an unsteady aerodynamic influence coefficient technique is used to obtain a model for the vibratory response in which the neighboring blade rows are also flexible. The flutter analysis shows that interaction effects can be destabilizing, and the forced response analysis shows that interaction effects can result in a significant increase in the resonant response of a blade row. Author (revised)

N94-21758*# National Aeronautics and Space Administration. Lewis Research Center, Cleveland, OH.

COMPARISON OF MIXING CALCULATIONS FOR REACTING AND NON-REACTING FLOWS IN A CYLINDRICAL DUCT

V. L. Oechsle (General Motors Corp., Indianapolis, IN.), H. C. Mongia (General Motors Corp., Indianapolis, IN.), and J. D. Holdeman Jan. 1994 23 p Proposed for presentation at the 32nd Aerospace Sciences Meeting and Exhibit, Reno, NV, 10-13 Jan. 1994; sponsored by AIAA Original contains color illustrations

(RTOP 537-02-21)

(NASA-TM-106435; E-8277; NAS 1.15:106435; AIAA Paper 94-0865)

Avail: CASI HC A03/MF A01; 4 functional color pages

A production 3-D elliptic flow code has been used to calculate non-reacting and reacting flow fields in an experimental mixing section relevant to a rich burn/quick mix/lean burn (RQL) combustion system. A number of test cases have been run to assess the effects of the variation in the number of orifices, mass flow ratio, and rich-zone equivalence ratio on the flow field and mixing rates. The calculated normalized temperature profiles for the non-reacting flow field agree qualitatively well with the normalized conserved variable isopleths for the reacting flow field indicating that non-reacting mixing experiments are appropriate for screening and ranking potential rapid mixing concepts. For a given set of jet momentum-flux ratio, mass flow ratio, and density ratio (J, MR, and DR), the reacting flow calculations show a reduced level of mixing compared to the non-reacting cases. In addition, the rich-zone equivalence ratio has noticeable effect on the mixing flow characteristics for reacting flows. Author (revised)

N94-21759*# National Aeronautics and Space Administration. Lewis Research Center, Cleveland, OH.

OPTIONS FOR THRUST AUGMENTATION FOR THE BETA 2 TWO-STAGE-TO-ORBIT LAUNCH VEHICLE

Kenol Jules Dec. 1993 15 p

(RTOP 505-70-00)

(NASA-TM-106418; E-8255; NAS 1.15:106418) Avail: CASI HC A03/MF A01

A study to improve the performance of the NASA two-stage-to-orbit vehicle was undertaken. The NASA concept, a horizontal takeoff and landing, fully reusable, two-stage to orbit vehicle, will be capable of launching and returning a 10,000 pound payload to a 100 nmi polar orbit. The vehicle, Beta 2, is a derivative of the USAF/Boeing Beta vehicle which was designed to deliver a 50,000 pound payload to a similar orbit. Beta 2 stages at Mach 6.5 and about 100,000 feet altitude. The propulsion system for the booster is an over/under turbine engine/ramjet configuration. In this paper a study was performed for one of the candidate engines, the variable cycle engine, to assess its potential to meet the required performance needs of the Beta 2 vehicle. Several options for thrust augmentation were studied in order to improve the performance of the engine where there was a critical need. The methodology, constraints, propulsion performance, and mission study results are presented. Author (revised)

N94-21879*# National Aeronautics and Space Administration. Hugh L. Dryden Flight Research Facility, Edwards, CA.

ON THE ESTIMATION ALGORITHM USED IN ADAPTIVE PERFORMANCE OPTIMIZATION OF TURBOFAN ENGINES

Martin D. Espana and Glenn B. Gilyard Dec. 1993 34 p Presented at the AIAA Joint Propulsion Conference, Monterey, CA, 28 Jun. - 1 Jul. 1993 See also A93-49710

(RTOP 533-02-39)

(NASA-TM-4551; H-1908; NAS 1.15:4551; AIAA Paper 93-1823) Avail: CASI HC A03/MF A01

The performance seeking control algorithm is designed to continuously optimize the performance of propulsion systems. The performance seeking control algorithm uses a nominal model of the propulsion system and estimates, in flight, the engine deviation parameters characterizing the engine deviations with respect to nominal conditions. In practice, because of measurement biases and/or model uncertainties, the estimated engine deviation parameters may not reflect the engine's actual off-nominal condition. This factor has a necessary impact on the overall performance seeking control scheme exacerbated by the open-loop character of the algorithm. The effects produced by unknown measurement biases over the estimation algorithm are evaluated. This evaluation allows for identification of the most critical measurements for application of the performance seeking control algorithm to an F100 engine. An equivalence relation between the biases and engine deviation parameters stems from an observability study; therefore, it is undecided whether the estimated engine deviation parameters represent the actual engine deviation or whether they simply reflect the measurement biases. A new algorithm, based on the engine's (steady-state) optimization model, is proposed and tested with flight data. When compared with previous Kalman filter schemes, based on local engine dynamic models, the new algorithm is easier to design and tune and it reduces the computational burden of the onboard computer. Author (revised)

08 AIRCRAFT STABILITY AND CONTROL

Includes aircraft handling qualities; piloting; flight controls; and autopilots.

For related information see also *05 Aircraft Design, Testing and Performance.*

N94-19879 Naval Postgraduate School, Monterey, CA.

FSR BASED FORCE TORQUE TRANSDUCER DESIGN M.S. Thesis

Charles A. Gunzel, III Jun. 1993 135 p Limited Reproducibility: More than 20% of this document may be affected by microfiche quality

(AD-A271337) Avail: CASI HC A07

This thesis report discusses the design, construction and calibration of two force-torque transducers for use in a force control override of a rate control system. Pre-loaded force sensing resistors were used in a computer model to determine the number and location of sensors necessary to resolve three forces and three moments. An analysis was conducted on this full order model to determine redundancy limits. A reduced order model was then used to determine the sensor configuration required to resolve three forces and only one moment. Prototypes of the reduced order model were then built in two different sizes, and used to sense and display applied forces and moments. DTIC

N94-20524*# Massachusetts Inst. of Tech., Cambridge. Dept. of Aeronautics and Astronautics.

IMPROVEMENT OF HELICOPTER ATTITUDE STABILITY BY ACTIVE CONTROL OF THE CONVENTIONAL SWASH PLATE Final Report, Nov. 1986 - Dec. 1993

Norman D. Ham Dec. 1993 10 p

(Contract NCC2-447)

(NASA-CR-194786; NAS 1.26:194786; VTL-TR-198-6) Avail: CASI HC A02/MF A01

The Final Report on improvement of helicopter attitude stability by active control of the conventional swash plate covering the period from Nov. 1986 to Dec. 1993 is presented. A paper on the history, principles, and applications of helicopter individual-blade-control is included. CASI

N94-20556* National Aeronautics and Space Administration. Langley Research Center, Hampton, VA.

APPARATUS AND METHOD FOR IMPROVING SPIN RECOVERY ON AIRCRAFT Patent

H. Paul Stough, II, inventor (to NASA) 2 Nov. 1993 9 p Filed 21 Sep. 1992 Supersedes N93-20039 (31 - 7, p 1786)

(NASA-Case-LAR-14747-1; US-Patent-5,259,573;

US-Patent-Appl-SN-948057; US-Patent-Class-244-75R;

US-Patent-Class-244-87; Int-Patent-Class-B64C-9/02) Avail: US Patent and Trademark Office

Previous research on airplane spinning and recovery has shown that at potential spin conditions (high angles of attack with rotation) the horizontal tail, depending upon its location, can create a wake about the vertical tail and rudder which can adversely affect airplane spin and recovery characteristics. Many methods of altering the tail geometry to modify these interference effects were investigated for improving airplane spin and recovery characteristics. Examples of changes includes relocation of the horizontal tail, increasing control surface travel, and use of a 'flip tail' that can be rotated to extreme angles for spin recovery. A device is provided which improves the spin recovery characteristics of aircraft which involves attaching the horizontal tail of the aircraft to the aircraft such that a gap remains between the root end of each horizontal tail section and the fuselage or vertical tail of the aircraft. The gaps measure between about 15 and 30 percent of the tail semispan. The gaps may be covered by shields which are released should a spin occur.

Official Gazette of the U.S. Patent and Trademark Office

N94-21050 Honeywell, Inc., Phoenix, AZ.

OPTIMAL FLIGHT GUIDANCE FOR AIRCRAFT IN WINDSHEAR Patent

Terry L. Zweifel, inventor (to Honeywell, Inc.) and J. Rene Barrios, inventor (to Honeywell, Inc.) 15 Sep. 1992 28 p Filed 8 Dec. 1987

(CA-Patent-1,307,573; Int-Patent-Class-B64C-13/16; CTN-93-60686)

Copyright Avail: Micromedia Ltd., Technical Information Centre, 165 Hotel de Ville, Place du Portage, Phase 2, Hull, Quebec J8X 3X2, Canada HC/MF

An apparatus is provided for controlling the vertical flight path of an aircraft encountering a windshear condition. The apparatus provides guidance commands to optimize the resultant flight path of the aircraft and maximize time in the air and distance travelled. When operating in the presence of a tail windshear, a fixed flight path angle independent of the windshear magnitude is commanded that minimizes excitation of the aircraft's phugoid oscillatory mode while maintaining adequate clearance of hills and buildings that may be present around the airport. In the presence of a vertical wind component, the effect on the aircraft's flight path angle is computed and added to the fixed flight path angle command. The guidance command is limited in magnitude to preclude commands which would cause the aircraft to exceed the maximum allowable angle of attack. An angle of attack sensor provides a signal which is combined with a sensed pitch angle to derive a signal corresponding to the actual flight path angle. A command signal corresponding to a fixed flight path angle at a predetermined elevation is combined with a signal corresponding to the effective change in flight path angles due to a vertical windshear component and with the actual flight path angle to derive the pitch command signal. Author (CISTI)

N94-21742*# National Aeronautics and Space Administration. Lewis Research Center, Cleveland, OH.

A COMPARATIVE ROBUSTNESS EVALUATION OF FEEDFORWARD NEUROFILTERS

Terry Troudet (Sverdrup Technology, Inc., Brook Park, OH.) and Walter Merrill Dec. 1993 11 p Proposed for presentation at the 32nd Aerospace Sciences Meeting and Exhibit, Reno, NV, 10-13 Jan. 1994; sponsored by AIAA

(Contract NAS3-25266; RTOP 584-03-11)

(NASA-TM-106440; E-8282; NAS 1.15:106440; AIAA Paper 94-0397)

Avail: CASI HC A03/MF A01

A comparative performance and robustness analysis is provided for feedforward neurofilters trained with back propagation to filter additive white noise. The signals used in this analysis are simulated pitch rate responses to typical pilot command inputs for a modern fighter aircraft model. Various configurations of nonlinear and linear neurofilters are trained to estimate exact signal values from input sequences of noisy sampled signal values. In this application, nonlinear neurofiltering is found to be more efficient than linear neurofiltering in removing the noise from responses of the nominal vehicle model, whereas linear neurofiltering is found to be more robust in the presence of changes in the vehicle dynamics. The possibility of enhancing neurofiltering through hybrid architectures based on linear and nonlinear neuroprocessing is therefore suggested as a way of taking advantage of the robustness of linear neurofiltering, while maintaining the nominal performance advantage of nonlinear neurofiltering.

Author (revised)

09 RESEARCH AND SUPPORT FACILITIES (AIR)

Includes airports, hangars and runways; aircraft repair and overhaul facilities; wind tunnels; shock tubes; and aircraft engine test stands.

For related information see also *14 Ground Support Systems and Facilities (Space).*

N94-19880 Carnegie-Mellon Univ., Pittsburgh, PA. Software Engineering Inst.

STRUCTURAL MODELING: AN APPLICATION FRAMEWORK AND DEVELOPMENT PROCESS FOR FLIGHT SIMULATORS Final Report

Gregory D. Abowd, Len Bass, Larry Howard, and Linda Northrop Aug. 1993 35 p Limited Reproducibility: More than 20% of this document may be affected by microfiche quality

(Contract F19628-90-C-0003)

(AD-A271348; CMU/SEI-93-TR-14; ESC-TR-93-192) Avail: CASI HC A03

In this paper, we present the structural modeling approach, an application framework and development process for the construction of flight simulators. Structural modeling was developed to address functional, nonfunctional, and process requirements for flight simulators. It has been successfully used in the development of large scale (one million lines of Ada code) flight simulators for the United States Air Force. A structural model promotes a simple and coherent software architecture with a small number of specialized structural elements obeying a few system-wide coordination

strategies. It is this simplicity coherence of the software architecture that enables analysis to demonstrate the quality of the system. DTIC

N94-20011 Rome Lab., Griffiss AFB, NY.
THE AEROGEL MESH CONTAMINATION COLLECTOR Final Report, Oct. 1991 - Sep. 1992
Steven P. Hotaling Jul. 1993 99 p Limited Reproducibility: More than 20% of this document may be affected by microfiche quality
(AD-A270537; RL-TR-93-148) Avail: CASI HC A05

High performance optical and microelectronic components have ever tightening contamination specifications placed upon them. Contamination is now seen as a major reason for the degradation of space based optical systems and failure of high density integrated circuits used throughout industrial and military systems. To address this problem, contamination removal and collection techniques have been developed by Rome Laboratory (RL). However, some of these removal techniques create a flux of removed contaminants, which then may re-deposit on clean surfaces or be ejected into the environment. Current collection devices such as filters, charged metal plates or screens, and charged dielectric have collection efficiencies and capture radii incommensurate with the new nano-scale semiconductor devices and space optics system cleanliness requirements. Presented here is a new contamination collector (patent pending). The collector (Aerogel Mesh Contamination Collector) or AMCC, collects and contains particulate and molecular contaminants either passively or used in conjunction with contamination removal devices creating a synergistic contamination control system with prevention, removal, and collection capabilities. The system is applicable to both clean room and cryogenic-vacuum conditions such as spacecraft environments. DTIC

N94-20108 Air Force Systems Command, Brooks AFB, TX. Armstrong Lab. Directorate.
A FULL-COLOR, HIGH-RESOLUTION LASER PROJECTOR FOR A FLIGHT SIMULATOR VISUAL DISPLAY Final Report, Jan. - Jul. 1993
Philipp W. Peppler and J. C. Gainer Aug. 1993 22 p Limited Reproducibility: More than 20% of this document may be affected by microfiche quality
(AF Proj. 1123)
(AD-A270578; AL/HR-TR-1993-0120) Avail: CASI HC A03

Laser projection is a promising approach to solving many of the shortcomings associated with current flight simulator projection methods. The advantages of laser projection were investigated and are discussed. The characteristics of light valve, cathode-ray tube (CRT), liquid crystal display (LCD), and laser projectors are compared. It was found that laser projection offers many benefits over current projection technology. Laser projection promises an increased color gamut, higher luminance, zero persistence, and increased line rate. The technology required to develop an efficient, cost-effective laser projector was researched and is described. Recent advances in laser diodes, solid-state diodes, and other rapidly developing technologies and techniques promise new territory for laser projection. It is concluded that laser projection is a promising solution to the shortcomings of flight simulator visual displays and that the technology now exists to develop an efficient, cost effective laser projector. DTIC

N94-21239# Army Cold Regions Research and Engineering Lab., Hanover, NH.
NOTES ON ANTARCTIC AVIATION
Malcolm Mellor Aug. 1993 154 p
(AD-A273018; CRREL-93-14) Avail: CASI HC A08/MF A02

Antarctic aviation has been evolving for the best part of a century, with regular air operations developing over the past three or four decades. Antarctica is the last continent where aviation still depends almost entirely on expeditionary airfields and 'bush flying', but change seems imminent. This report describes the history of aviation in Antarctica, the types and characteristics of existing and proposed airfield facilities, and the characteristics of aircraft suitable for Antarctic use. It now seems possible for Antarctic aviation to become an extension of mainstream international aviation. The basic requirement is a well-distributed network of hard-surface airfields that can be used safely by conventional aircraft, together with good international collaboration. The technical capabilities already exist. DTIC

N94-21280# Deutsche Forschungsanstalt fuer Luft- und Raumfahrt, Goettingen (Germany). Hauptabt. Windkanaele.
DESCRIPTION AND ASSESSMENT OF A NEW OPTICAL PRESSURE MEASUREMENT SYSTEM (OPMS) DEMONSTRATED IN THE HIGH SPEED WIND TUNNEL IN GOETTINGEN (GERMANY)
R. H. Engler, K. Hartmann, I. Troyanovski (INTECO s.r.l., Frosione, Italy.), and A. Vollan (Omega G.m.b.H., Immenstaad, Germany.) Oct. 1992 66 p In GERMAN Original contains color illustrations
(DLR-FB-92-24; ETN-93-94868) Avail: CASI HC A04/MF A01; DLR, Wissenschaftliches Berichtswesen, VB-PL-DO, Postfach 90 60 58, 5000 Cologne 90, Germany

An assessment of a novel Optical Pressure Measurement System (OPMS) made in a high speed wind tunnel is reported. A model of a cropped delta wing was made available to demonstrate and assess OPMS. For this purpose pressure distributions were measured separately as well as simultaneously with both OPMS and a conventional technique via pressure taps for comparisons. Temperature variations on the model surface were determined by means of an infrared camera and thermocouples in order to assess a possible error caused by temperature changes. Surface oil flow visualizations were performed in order to get additional information on boundary layer transition, separation and reattachment lines as well as vortex positions. ESA

N94-22094 Technische Univ., Delft (Netherlands). Faculty of Aerospace Engineering.
SPACEPLANE FLIGHT SIMULATION: PROJECT DEFINITION
B. T. C. Zandbergen Jun. 1992 16 p Limited Reproducibility: More than 20% of this document may be affected by microfiche quality
(PB93-211399; M-661) Avail: CASI HC A03

In the report, a proposal is given for the development of a method allowing for the assessment of current and advanced technology on the mission performance of space launchers. In addition, for background information, a short overview is given on currently proposed launcher concepts and the available assessment method(s). NTIS

N94-22418 Carleton Univ., Ottawa (Ontario). Dept. of Civil Engineering.
PASSENGER TERMINAL LEVEL OF SERVICE MEASUREMENT: A UTILITY THEORETIC APPROACH M.S. Thesis
Khizer Farooq Omer May 1990 317 p
(ISBN-0-315-59037-8; CTN-94-60885) Copyright Avail: Micromedia Ltd., Technical Information Centre, 240 Catherine Street, Suite 305, Ottawa, Ontario, K2P 2G8, Canada HC/MF

The relationship between the existing space/service standards of various processors of an airport system is investigated, along with the user-perceived values of these space/service standards. The various processors include check-in, baggage claim, boarding lounge, and preliminary inspection line. The utility of these standards and the level of service of various airport subsystems are formulated. A utility theoretic approach is used to measure the airport landside level of service. Attitudinal surveys of airport users were conducted at Ottawa and Toronto international airports. For the airport processors mentioned above, the selected performance measures were studied to arrive at the individual as well as composite utility of those processors. Equations for the utility functions of those processors have been calculated and their application in developing airport landside level of service standards is discussed. The use of these individual and composite utility functions for each processor is described and recommendations are made for further research. Author (CISTI)

N94-22419 New Brunswick Univ., Fredericton. Dept. of Civil Engineering.
AN AIRPORT ECONOMIC IMPACT STUDY PROCEDURE FOR ATLANTIC CANADA M.S. Thesis
Terry Mark Mazerolle Aug. 1990 138 p
(ISBN-0-315-59445-4; CTN-94-60886) Copyright Avail: Micromedia Ltd., Technical Information Centre, 240 Catherine Street, Suite 305, Ottawa, Ontario, K2P 2G8, Canada HC/MF

A methodology was developed for economic impact studies suitable for the size of airport and economic conditions extant in Atlantic Canada. The methodology enables quantification of the net economic impact of an airport on the surrounding economy as an employer and as a consumer of goods and services. Three levels of airport dependent impacts were defined. Direct impacts are those economic activities derived from airport dependent

firms and from operation of the airport. Indirect impacts are the effect of the expenditures of airport dependent firms and the subsequent rounds of spending which occur in the local economy as a result. Induced impacts measure the effect of the wages of those employed by airport dependent firms. The airport's total impact is the sum of the direct, indirect, and induced impacts. The methodology of data collection described was explored with a case study at Fredericton Airport. The results showed that the airport is a far more valuable economic resource than was commonly perceived. It is concluded that a unique methodology was necessary to measure accurately the economic impact of an airport in the Atlantic region of Canada. Author (CISTI)

N94-22423 Waterloo Univ. (Ontario). Dept. of Civil Engineering.
PASSENGER TERMINAL SIMULATION MODEL Ph.D. Thesis
Jose Reynaldo Anselm Setti 1990 198 p
(ISBN-0-315-61113-8; CTN-94-60890) Copyright Avail: Micromedia Ltd., Technical Information Centre, 240 Catherine Street, Suite 305, Ottawa, Ontario, K2P 2G8, Canada HC/MF

A high-level computer program called TERMSIM has been developed to simulate passenger terminal operation in terms of number of passengers arriving, being served, and queueing at the various terminal facilities. It is assumed that passenger movements may be represented as a fluid flowing through a system of interconnected reservoirs corresponding to terminal components. Paxgraphs, functions describing passenger arrivals as a function of time before flight departure or after flight arrival, are used to generate passenger flows for user-defined discrete time intervals. The simulation analyzes passenger movement through the predetermined paths within the terminal. Operation of the terminal facilities is simulated by calculating output flows and queue lengths given input flows, queue lengths, and service characteristics at the end of discrete time intervals. Seven preprogrammed models have been developed to simulate terminal components, the passenger greeter and bag matching processes, and departure concourse and ancillary facilities. The capabilities of TERMSIM are demonstrated through a simulation of a typical day at Toronto International Airport, and results are shown to be similar to those produced by the Transport Canada simulation model. A guide to the use of TERMSIM is included. Author (CISTI)

N94-22425 Calgary Univ. (Alberta). Dept. of Civil Engineering.
A STUDY OF PARALLEL PIER FINGER AIRPORT TERMINAL CONFIGURATION M.S. Thesis
Ezekiel Sunday Dada Dec. 1992 167 p
(ISBN-0-315-83128-6; CTN-94-60936) Copyright Avail: Micromedia Ltd., Technical Information Centre, 240 Catherine Street, Suite 305, Ottawa, Ontario, K2P 2G8, Canada HC/MF

Taxiing, walking, baggage transport, and airport construction were studied to determine their effect on the geometry of pier finger terminals. The best terminal geometry based on taxiing alone is one with shorter fingers in the middle and longer ones at the ends. On the other hand, geometry that minimizes baggage transportation distance is the one with the longest pier at the center. Baggage transportation distance is affected both by the geometry of the terminal and the sorting room strategy adopted. Decentralized sorting gives a lower baggage tractor distance than centralized sorting. Walking distance has been studied extensively by others who found that pier finger terminals minimize walking. As far as the operations considered are concerned, the terminal with pier lengths decreasing with distance from the center gives the best combined optimal geometry. It also gives a lower number of piers than that found by others for walking only. Author (CISTI)

N94-20511*# National Aeronautics and Space Administration. Lewis Research Center, Cleveland, OH.
NEW TECHNIQUE FOR OIL BACKSTREAMING CONTAMINATION MEASUREMENTS
S. A. Alterovitz, H. J. Speier, R. M. Sieg (Cleveland State Univ., OH.), M. N. Drotos (Cleveland State Univ., OH.), and J. E. Dunning (Michigan State Univ., East Lansing.) *In its* Solid State Technology Branch of NASA Lewis Research Center: Fifth Annual Digest Aug. 1993 p 157-162 Repr. from American Inst. of Physics, Applied Physics Letter, v. 73, no. 4, 1 Jul./Aug. 1992 (For primary document see N94-20497 05-32)
Avail: CASI HC A02/MF A03

12 ASTRONAUTICS (GENERAL)

For extraterrestrial exploration see *91 Lunar and Planetary Exploration.*

N94-20765*# Geological Survey, Flagstaff, AZ.
CLEMENTINE: AN INEXPENSIVE MISSION TO THE MOON AND GEOGRAPHOS Abstract Only
Eugene M. Shoemaker and Stewart Nozette (Strategic Defense Initiative Organization, Washington, DC.) *In* Lunar and Planetary Inst., Twenty-Fourth Lunar and Planetary Science Conference. Part 3: N-Z 1993 p 1299-1300 (For primary document see N94-20636 05-91)
Avail: CASI HC A01/MF A06

N94-20829*# Jet Propulsion Lab., California Inst. of Tech., Pasadena.
MAGELLAN MISSION Abstract Only Progress Report
Thomas W. Thompson *In* Lunar and Planetary Inst., Twenty-Fourth Lunar and Planetary Science Conference. Part 3: N-Z 1993 p 1427-1428 (For primary document see N94-20636 05-91)
Avail: CASI HC A01/MF A06

N94-20850*# Science Applications International Corp., Washington, DC.
THE CLEMENTINE MISSION SCIENCE RETURN AT THE MOON AND GEOGRAPHOS Abstract Only
R. W. VorderBruegge, M. E. Davies (RAND Corp., Santa Monica, CA.), D. M. Horan (Naval Research Lab., Washington, DC.), P. G. Lucey (Hawaii Univ., Honolulu.), C. M. Pieters (Brown Univ., Providence, RI.), A. S. McEwen (Geological Survey, Flagstaff, AZ.), S. Nozette (Strategic Defense Initiative Organization, Washington, DC.), E. M. Shoemaker (Geological Survey, Flagstaff, AZ.), S. W. Squyres (Cornell Univ., Buffalo, NY.), and P. C. Thomas (Cornell Univ., Buffalo, NY.) *In* Lunar and Planetary Inst., Twenty-Fourth Lunar and Planetary Science Conference. Part 3: N-Z 1993 p 1469-1470 (For primary document see N94-20636 05-91)
Avail: CASI HC A01/MF A06

N94-21407 National Space Development Agency, Tokyo (Japan).
JAPANESE SPACE PROGRAM
Yoshiki Morino *In* CNES, Fifth International Symposium on Materials in a Space Environment Jun. 1993 p 513-515 (For primary document see N94-21367 05-18)
Copyright Avail: CEPADUES-Editions, 111, rue Nicolas-Vaquelin, 31100 Toulouse, France

13 ASTRODYNAMICS

Includes powered and free-flight trajectories; and orbital and launching dynamics.

N94-21224# Defence Research Agency, Farnborough (England).
A NEW PROCEDURE FOR ORBIT DETERMINATION BASED ON THREE LINES OF SIGHT: ANGLES ONLY Technical Report
R. H. Gooding Apr. 1993 66 p
(AD-A272937; DRA-TR-93004) Avail: CASI HC A04/MF A01

A new procedure has been developed for the general solution of the minimal angles-only problem in which an orbit is determined from three line-of-sight observations. The basis of the approach is a higher-order Newton correction of the assumed values for two of the unknown ranges, appeal being made to the author's (published) universal solution of Lambert's orbital boundary-value problem. The new procedure is free of the inherent limitations of the traditional methods of Laplace and Gauss, these methods being outlined in a summary of previous approaches to this classical problem. In particular, the observations are permitted to span several revolutions when the orbit is elliptic; multiple solutions can be obtained; and there is no restriction on the configuration of the three observing sites. The procedure has been carefully tested, some of the examples being taken from the literature. A number of test problems have been solved that would have failed by existing methods. DTIC

N94-22188 Department of Communications, Ottawa (Ontario).
INCLINED ORBITS AND INTERFERENCE TO STATIONARY SERVICE AND TO STATIONARY SERVICE BY SATELLITE [ORBITES INCLINEES ET BROUILLAGE AU SERVICE FIXE ET AU SERVICE FIXE PAR SATELLITE]
Michel Gaudreau and Vishnu Sahay *In* Engineering Inst. of Canada, Canadian Conference on Electrical and Computer Engineering, Volumes 1 and 2 1991 4 p In FRENCH (For primary document see N94-22101 05-33)
Avail: Issuing Activity (Engineering Inst. of Canada, 2050 rue Mansfield, Suite 700, Montreal, PQ H3A 1Z2 Canada)

14 GROUND SUPPORT SYSTEMS AND FACILITIES (SPACE)

Includes launch complexes, research and production facilities; ground support equipment, e.g., mobile transporters; and simulators.

For related information see also *09 Research and Support Facilities (Air).*

N94-20339* National Aeronautics and Space Administration. Lyndon B. Johnson Space Center, Houston, TX.
APPARATUS FOR SIMULATING AN EXOATMOSPHERIC STRUCTURE Patent
Robert Lynn Harvey, inventor (to NASA) 16 Nov. 1993 14 p Filed 17 Feb. 1993 Supersedes N93-22016 (31 - 8, p 2169)
(NASA-Case-MSC-21975-1; US-Patent-5,261,819;
US-Patent-Appl-SN-018844; US-Patent-Class-434-34;
Int-Patent-Class-G09B-9/08) Avail: US Patent and Trademark Office

Apparatus for simulating an exoatmospheric structure, such as a spin stabilized satellite, in an environment subject to gravitational forces is presented. The apparatus includes a floating structure which is pivotally and rotationally supported upon a gimballed bearing structure positioned adjacent to the center of mass of the floating structure and suspended upon a support structure. The floating structure is translatable in either vertical direction relative to the supporting structure upon a vertically movable suspension system connected to the supporting structure. The supporting structure is provided with bearing assemblies which are adapted to engage a supporting surface for permitting freedom of movement of the supporting structure over the supporting structure in any direction.

Official Gazette of the U.S. Patent and Trademark Office

N94-22588 Toronto Univ. (Ontario). Inst. for Aerospace Studies.
SYSTEM IDENTIFICATION OF THE DAISY LARGE SPACE STRUCTURE EMULATOR M.S. Thesis
Roberto Guccione 1992 138 p
(ISBN-0-315-83533-8; CTN-94-60950) Copyright Avail: Micromedia Ltd., Technical Information Centre, 240 Catherine Street, Suite 305, Ottawa, Ontario, K2P 2G8, Canada HC/MF

The Daisy structure consists of a central, gimbal-mounted hub and ten counterbalanced ribs interconnected with spring struts. All spring/inertia elements have been carefully sized so that Daisy exhibits the desired low natural frequencies and damping, and clustered modes of vibration, typical of large space structures. The eigensystem realization algorithm (ERA) is introduced to realize a mathematical model representative of the elastic vibrational modes of Daisy. The theory behind discrete state space systems, Markov parameters, and the ERA are presented, along with the implementation of the theory and the signal processing that was needed. Example systems and results are described to illustrate some of the characteristics of the realization algorithm, as well as the phenomenon of mode localization often encountered in closed periodic structures such as Daisy. The system natural frequencies, damping ratios, and mode shapes are identified for five-rib and ten-rib free cases, with the hub locked. A state space realization is investigated for a two-rib free case.

Author (CISTI)

N94-21370 Moscow State Univ. (Russia).
COMPLEX-2: LOW EARTH ORBITAL ENVIRONMENT SIMULATION FACILITY FOR MATERIALS DURABILITY EVALUATION
V. I. Titov, G. G. Solovyev, V. N. Chernik, Y. I. Tarasov, S. F. Naumov (Nauchno-Proizvodstvennoe Obedinenie Energomash, Khimki, USSR.), S. A. Demidov (Nauchno-Proizvodstvennoe Obedinenie Energomash, Khimki, USSR.), and A. H. Kutlaliyev (Nauchno-Proizvodstvennoe Obedinenie Energomash, Khimki, USSR.) *In* CNES, Fifth International Symposium on Materials in a Space Environment Jun. 1993 p 43-45 (For primary document see N94-21367 05-18)
Copyright Avail: CEPADUES-Editions, 111, rue Nicolas-Vaquelin, 31100 Toulouse, France

N94-21404 Centre National de la Recherche Scientifique, Odeillo (France).
HIGH TEMPERATURE SIMULATION CHAMBERS. PHYSICO-CHEMICAL AND THERMAL EFFECT OF ATMOSPHERIC REENTRY ON CERAMIC MATERIALS [ENCEINTES DE SIMULATION A HAUTE TEMPERATURE DES EFFETS THERMIQUES ET PHYSICO-CHIMIQUES DE LA RENTREE ATMOSPHERIQUE SUR DES MATERIAUX CERAMIQUES]
M. Balat, G. Flamant, B. Rivoire, M. Dudeck (Laboratoire d'Aerothermique du CNRS, Meudon, France.), and P. Lasgorceix (Laboratoire d'Aerothermique du CNRS, Meudon, France.) *In* CNES, Fifth International Symposium on Materials in a Space Environment Jun. 1993 p 475-488 In FRENCH (For primary document see N94-21367 05-18)
Copyright Avail: CEPADUES-Editions, 111, rue Nicolas-Vaquelin, 31100 Toulouse, France

15 LAUNCH VEHICLES AND SPACE VEHICLES

Includes boosters; operating problems of launch/space vehicle systems; and reusable vehicles.

For related information see also *20 Spacecraft Propulsion and Power.*

N94-20141*# National Aeronautics and Space Administration. Marshall Space Flight Center, Huntsville, AL.
TOTAL SYSTEMS DESIGN ANALYSIS OF HIGH PERFORMANCE STRUCTURES
V. Verderaime Washington Nov. 1993 65 p
(NASA-TP-3432; M-733; NAS 1.60:3432) Avail: CASI HC A04/MF A01

Designer-control parameters were identified at interdiscipline interfaces to optimize structural systems performance and downstream development and operations with reliability and least life-cycle cost. Interface tasks and iterations are tracked through a matrix of performance disciplines integration versus manufacturing, verification, and operations interactions for a total system design analysis. Performance integration tasks include shapes, sizes, environments, and materials. Integrity integrating tasks are reliability and recurring structural costs. Significant interface designer control parameters were noted as shapes, dimensions, probability range factors, and cost. Structural failure concept is presented, and first-order reliability and deterministic methods, benefits, and limitations are discussed. A deterministic reliability technique combining benefits of both is proposed for static structures which is also timely and economically verifiable. Though launch vehicle environments were primarily considered, the system design process is applicable to any surface system using its own unique filed environments.

Author (revised)

16 SPACE TRANSPORTATION

Includes passenger and cargo space transportation, e.g., shuttle operations; and space rescue techniques.

For related information see also *03 Air Transportation and Safety* and *18 Spacecraft Design, Testing and Performance.* For space suits see *54 Man/System Technology and Life Support.*

N94-20192*# National Aeronautics and Space Administration, Washington, DC.
SPACE SHUTTLE MISSION STS-61: HUBBLE SPACE TELESCOPE SERVICING MISSION-01 Press Kit
Dec. 1993 53 p
(NASA-TM-109344; NAS 1.15:109344) Avail: CASI HC A04/MF A01

This press kit for the December 1993 flight of Endeavour on Space

Shuttle Mission STS-61 includes a general release, cargo bay payloads and activities, in-cabin payloads, and STS-61 crew biographies. This flight will see the first in a series of planned visits to the orbiting Hubble Space Telescope (HST). The first HST servicing mission has three primary objectives: restoring the planned scientific capabilities, restoring reliability of HST systems and validating the HST on-orbit servicing concept. These objectives will be accomplished in a variety of tasks performed by the astronauts in Endeavour's cargo bay. The primary servicing task list is topped by the replacement of the spacecraft's solar arrays. The spherical aberration of the primary mirror will be compensated by the installation of the Wide Field/Planetary Camera-II and the Corrective Optics Space Telescope Axial Replacement. New gyroscopes will also be installed along with fuse plugs and electronic units. Derived from text

N94-20304* National Aeronautics and Space Administration. Lyndon B. Johnson Space Center, Houston, TX.

THERMALLY ACTIVATED RETAINER MEANS UTILIZING SHAPE MEMORY ALLOY Patent

Margaret E. Grimaldi, inventor (to NASA) and Leslie S. Hartz, inventor (to NASA) 19 Oct. 1993 8 p Filed 19 Apr. 1993 Supersedes N91-28186 (29 - 20, p 3289) Continuation of abandoned US-Patent-Appl-SN-731829, filed 15 Jul. 1991

(NASA-Case-MSC-21793-1; US-Patent-5,254,837; US-Patent-Appl-SN-049648; US-Patent-Appl-SN-731829; US-Patent-Class-219-200; US-Patent-Class-244-158A; US-Patent-Class-244-121; US-Patent-Class-411-909; US-Patent-Class-403-408.1; US-Patent-Class-403-404) Avail: US Patent and Trademark Office

A retainer member suitable for retaining a gap filler placed in gaps between adjacent tile members is presented. One edge of the retainer member may be attached to the gap filler and another edge may be provided with a plurality of tab members which in an intermediate position do not interfere with placement or removal of the gap filler between tile members. The retainer member may be fabricated from a shape memory alloy which when heated to a specified memory temperature will thermally activate the tab members to predetermined memory positions engaging the tile members to retain the gap filler in the gap. This invention has particular application to the thermal tiles on space vehicles such as the Space Shuttle Orbiter.

Official Gazette of the U.S. Patent and Trademark Office

N94-21429 Maxwell Labs., Inc., San Diego, CA. S-CUBED Div.

DATA ANALYSIS SUPPORT FOR THE SPREE INSTRUMENTS ON THE TSS-1 SHUTTLE FLIGHT Final Report, 29 Jun. 1992 - 14 Jun. 1993

I. Katz and M. J. Mandell 11 Aug. 1993 32 p Limited Reproducibility: More than 20% of this document may be affected by microfiche quality

(Contract F19628-90-C-0133)

(AD-A272445; SSS-DRF-93-14180; PL-TR-93-2180) Avail: Issuing Activity (Defense Technical Information Center (DTIC))

The objective of this contract is a scientific study of the interactions between the first flight of the Tethered Satellite System (TXX-1) and the ionosphere to increase understanding of the structure and current characteristics of high-voltage sheaths in the ionosphere. A paper describing the results of a review of the data sets for evidence of presheath heating around the subsatellite is included. DTIC

N94-21570*# National Aeronautics and Space Administration. Lewis Research Center, Cleveland, OH.

NEP EARLY FLIGHT PROGRAM: SYSTEM PERFORMANCE AND DEVELOPMENT CONSIDERATIONS

Michael P. Doherty and Jeffrey A. George Dec. 1993 9 p Presented at the 23rd International Electric Propulsion Conference, Seattle, WA, 13-16 Sep. 1993; sponsored by AIAA, DGLR, AIDAA, and JSASS Sponsored by NASA. Washington

(RTOP 506-49-00)

(NASA-TM-106415; IEPC-93-064; E-8252; NAS 1.15:106415) Avail: CASI HC A02/MF A01

A mission/system study of Nuclear Electric Propulsion (NEP) for early robotic planetary science mission applications has been conducted. Subject missions considered included a Mars orbiter with a Phobos and Deimos Rendezvous; a Comet Kopff Rendezvous; a Multiple Mainbelt Asteroid Rendezvous (MMBAR); an Asteroid (Vesta) Sample Return; a Trojan Asteroid (Odysseus) Rendezvous; and a Jupiter mini Grand Tour. The purpose of the study was to determine if 'near-term' NEP technology could be used on an early NEP flight to demonstrate the technologies while conducting a useful science mission. The analysis shows that, depending upon technology readiness date, the missions could be performed with low power NEP. The technology and system development costs associated with vehicle/stage development for a candidate mission are presented. The study assumed relatively mature space electric power and space electric propulsion technologies (more advanced technologies have been already shown by others to be enabling for many outer planetary missions). Thus, a very important first step in using NEP would be taken, which would contribute valuable solar system science, as well as reduce the risks associated with using NEP for more demanding outer planetary science mission applications. Author

N94-21790*# National Aeronautics and Space Administration. Lewis Research Center, Cleveland, OH.

THE 1992 SEALS FLOW CODE DEVELOPMENT WORKSHOP

Anita D. Liang and Robert C. Hendricks Oct. 1993 278 p Workshop held in Cleveland, OH, 5-6 Aug. 1992

(Contract NAS3-25644; RTOP 590-21-11)

(NASA-CP-10124; E-8172; NAS 1.55:10124) Avail: CASI HC A13/MF A03

A two-day meeting was conducted at the NASA Lewis Research Center on August 5 and 6, 1992, to inform the technical community of the progress of NASA Contract NAS3-26544. This contract was established in 1990 to develop industrial and CFD codes for the design and analysis of seals. Codes were demonstrated and disseminated to the user community for evaluation. The peer review panel which was formed in 1991 provided recommendations on this effort. The technical community presented results of their activities in the area of seals, with particular emphasis on brush seal systems. For individual titles, see N94-21791 through N94-21797.

N94-21791*# National Aeronautics and Space Administration. Lewis Research Center, Cleveland, OH.

BRUSH SEAL BRISTLE FLEXURE AND HARD-RUB CHARACTERISTICS c37

Robert C. Hendricks, Julie A. Carlile, and Anita D. Liang *In its* The 1992 Seals Flow Code Development Workshop Oct. 1993 p 95-115 (For primary document see N94-21790 05-16)

Avail: CASI HC A03/MF A03

The bristles of a 38.1-mm (1.5-in.) diameter brush seal were flexed by a tapered, 40-tooth rotor operating at 2600 rpm that provided sharp leading-edge impact of the bristles with hard rubbing of the rotor lands. Three separate tests were run with the same brush accumulating over 1.3 x 10(exp 9) flexure cycles while deteriorating 0.2 mm (0.008 in.) radially. In each, the test bristle incursion depth varied from 0.130 to 0.025 mm (0.005 to 0.001 in.) or less (start to stop), and in the third test the rotor was set 0.25 mm (0.010 in.) eccentric. Runout varied from 0.025 to 0.076 mm (0.001 to 0.003 in.) radially. The bristles wore but did not pull out, fracture, or fragment. Bristle and rotor wear debris were deposited as very fine, nearly amorphous, highly porous materials at the rotor groove leading edges and within the rotor grooves. The land leading edges showed irregular wear and the beginning of a convergent groove that exhibited sharp, detailed wear at the land trailing edges. Surface grooving, burnishing, 'whipping', and hot spots and streaks were found. With a smooth-plug rotor, post-test leakage increased 30 percent over pretest leakage. Author

N94-21792*# National Aeronautics and Space Administration. Lewis Research Center, Cleveland, OH.

INTEGRITY TESTING OF BRUSH SEAL IN A T-700 ENGINE c37

Robert C. Hendricks, Thomas A. Griffin, George A. Bobula, Robert C. Bill, and Harold W. Howe (Technetics, Inc., DeLand, FL.) *In its* The 1992 Seals Flow Code Development Workshop Oct. 1993 p 117-138 (For primary document see N94-21790 05-16)

Avail: CASI HC A03/MF A03

A split-ring brush seal was fabricated, installed between two labyrinth-honeycomb shroud seals, and tested in the fourth-stage turbine of a T-700 engine. The annealed Haynes 25 bristles rubbed directly against the nonconditioned, irregular Rene 80 turbine blade shroud surface. A total of 21 hr of cyclic and steady-state data were taken with surface speeds of 335 m/s (1100 ft/s) and shroud temperatures to 620 C (1150 F). Wear

appeared to be rapid initially, with an orange flash of hot brush fragments during the first engine startup, to minimal after 10 hr of operation. The brush survived the testing but experienced some bristle pullouts and severe bristle wear; some turbine interface wear and possible material transfer was noted. Future design concerns center on tribological behavior at the interface with or without lubricants. Author

N94-21793*# Air Force Systems Command, Wright-Patterson AFB, OH. Aero Propulsion and Power Directorate.

AIR FORCE BRUSH SEAL PROGRAMS **c37**

Connie Dowler *In* NASA. Lewis Research Center, The 1992 Seals Flow Code Development Workshop Oct. 1993 p 149-156 (For primary document see N94-21790 05-16)

Avail: CASI HC A02/MF A03

Aggressive pursuit of increased performance in gas turbine engines is driving the thermodynamic cycle to higher pressure ratios, bypass ratios, and turbine inlet temperatures. As these parameters increase, internal air system and resultant thermodynamic cycle losses increase. This conflict of reducing internal airflows while increasing thermodynamic efficiency and performance is putting more emphasis on improvements to the internal flow system. One improvement that has been and continues to be pursued by the Air Force for both man-rated and expendable turbine engine applications is the brush seal. This presentation briefly describes both past and current brush seal research and development programs and gives a summary of demonstrator and developmental engine testing of brush seals. Author

N94-21794*# Naval Air Warfare Center, Trenton, NJ. Aircraft Div.

NAVY GTE SEAL DEVELOPMENT ACTIVITY **c37**

Carl P. Grala *In* NASA. Lewis Research Center, The 1992 Seals Flow Code Development Workshop Oct. 1993 p 157-165 (For primary document see N94-21790 05-16)

Avail: CASI HC A02/MF A03

Under the auspices of the Integrated High Performance Turbine Engine Technology Initiative, the Naval Air Warfare Center conducts advanced development programs for demonstration in the next generation of air-breathing propulsion systems. Among the target technologies are gas path and lube oil seals. Two development efforts currently being managed by NAWCAD are the High Performance Compressor Discharge Film-Riding Face Seal and the Subsonic Core High Speed Air/Oil Seal. The High Performance Compressor Discharge Film-Riding Face Seal Program aims at reducing parasitic leakage through application of a film-riding face sea concept to the compressor discharge location of a Phase 2 IHPTET engine. An order-of-magnitude leakage reduction relative to current labyrinth seal configurations is expected. Performance goals for these seals are (1) 1200 F air temperature, (2) 800 feet-per-second surface velocity, and (3) 600 SPI differential pressure. The two designs chosen for fabrication and rig test are a spiral groove and a Rayleigh step seal. Rig testing is currently underway. The Subsonic Core High Speed Air/Oil Seal Program is developing shaft-to-ground seals for next-generation propulsion systems that will minimize leakage and provide full life. Significantly higher rotor speeds and temperatures will be experienced. Technologies being exploited include, hydrodynamic lift assist features, ultra light weight designs, and improved cooling schemes. Parametric testing has been completed; a final seal design is entering the endurance test phase. Author

N94-21795*# National Aeronautics and Space Administration. Lewis Research Center, Cleveland, OH.

COMPLIANT SEAL DEVELOPMENT **c37**

Robert C. Hendricks *In its* The 1992 Seals Flow Code Development Workshop Oct. 1993 p 171-173 (For primary document see N94-21790 05-16)

Avail: CASI HC A01/MF A03

The compliant metallic seal combines the noncontact feature of the labyrinth seal, the low leakage of a mechanical seal, and the compliant nature of the brush seal. It consists of several thin metallic elements or leaves mounted within a ring which is press fit into the housing, and in form, sort of resembles a lip seal sections wiping the shaft. A second set of overlapping cover leaves are placed on top of the shaft riding leaves which reduces leakage and provides stiffness. The leaves can be straight or angle cut. The shaft riding fingers are designed with mismatched curvature to provide lift off similar to the Rayleigh lift pads in mechanical seals with leading edge clearances nearly twice those of the trailing edge as as shown by Fleming to be optimal for gas flows in convergent seal passages. Leading edge clearances range from 300 to 500 microinches. Balance pockets beneath the leaves provide fluid film feed to the 'Rayleigh lift' surface and the proper balance ratio (mechanical seal) when combined with the static pressure and film pressure. The leaves flex in the radial direction and accommodate thermomechanical behavior as well as axial motion and angular misalignment. In the static mode, there is a net closing force on the leaves. The seals were tested to 70 psi at speeds to 16,000 rpm or surface speeds to 330 fps and temperatures from ambient to 440 F. A slow cycle through the rig critical at 10,000 rpm induced a radial vibration response of 0.004 to 0.005 inch were accommodated by the seal. Preliminary performance data are encouraging demonstrating hydrodynamic liftoff and noncontacting operation at pressure and speeds typical of gas turbine engines. The leakage performance data are significantly better than commercial labyrinth and brush seals which should be expected as this design incorporates the features of the low leakage face or mechanical seal along with the flexibility of the brush configuration. Author

N94-21796*# British Hydromechanics Research Association, Cranfield (England).

DYNAMICS OF FACE SEALS FOR HIGH SPEED TURBOMACHINERY **c37**

Simon Leefe *In* NASA. Lewis Research Center, The 1992 Seals Flow Code Development Workshop Oct. 1993 p 197-210 (For primary document see N94-21790 05-16)

Avail: CASI HC A03/MF A03

Face seals in rocket engine fuel and oxidizer turbopumps have been the subject of intense investigation for over 25 years. While advances have been made in the understanding of thin film lubrication between seal faces, valuable data has been produced on the friction and wear of material pairs in cryogenic environments; pioneering work has been done on the effect of lubricant phase change in seals, and many improvements have been made in mechanical seal design. Relatively superficial attention has been given to the vibrational dynamics of face seals in high-speed turbomachinery. BHR Group Ltd. (formerly BHRA) has recently completed the first stage of a study, commissioned by the European Space Agency, to investigate this area. This has involved the development of a two-dimensional adiabatic, turbulent lubrication model for thick gas film applications, the production of an integrated mathematical model of gas seal vibrational dynamics for thin film applications, implementation in software, the undertaking of an experimental program to validate software against variations in operating conditions and design variables, and suggestions for improved seal design. Author

N94-21797*# Columbia Univ., New York, NY. Dept. of Mechanical Engineering.

MODELING BRISTLE LIFT-OFF IN IDEALIZED BRUSH SEAL CONFIGURATIONS **c37**

Vijay Modi *In* NASA. Lewis Research Center, The 1992 Seals Flow Code Development Workshop Oct. 1993 p 217-232 (For primary document see N94-21790 05-16)

Avail: CASI HC A03/MF A03

We attempt in this paper to develop a model for the flow through brush seals and determine their elastic behavior in order to predict the dependence of brush/journal clearance on geometry and operating conditions. Several idealizations regarding brush seal configuration, flow conditions, and elastic behavior are made in the analysis in order to determine closed form parametric dependence. This formulation assumes that there is no initial interference between the bristle tip and the rotor. Also, interbristle, bristle-backing plate, and bristle-rotor friction is neglected. The bristle bundle or the brush seal as it is alternately called is assumed homogeneous and isotropic on a macroscopic scale so that a physical property like permeability is uniform. The fluid is assumed to be homogeneous, incompressible, viscous, and flowing under steady conditions. A schematic of a brush seal is shown. If the nominal bristle-shaft interference is absent then under static conditions the bristles may deflect axially due to the imposed pressure differential. This axial deflection may create a clearance permitting leakage flow in excess of that which occurs through the porous matrix formed by the bristle bundles. Under dynamic conditions the Couette flow created by shaft motion could be strong enough to

cause bristle deflection and once again a clearance may develop. The paper proposes a means to determine this clearance (or at least describe its parametric dependence on geometry and operating conditions) under static as well as dynamic conditions. Derived from text

N94-21813*# SUMMA Technology, Inc., Huntsville, AL.
SPECIALIZED DATA ANALYSIS FOR THE SPACE SHUTTLE MAIN ENGINE AND DIAGNOSTIC EVALUATION OF ADVANCED PROPULSION SYSTEM COMPONENTS Technical Progress Report
Nov. 1993 15 p
(Contract NAS8-39725)
(NASA-CR-194720; NAS 1.26:194720; TP042-121493-MS) Avail: CASI HC A03/MF A01

The Marshall Space Flight Center is responsible for the development and management of advanced launch vehicle propulsion systems, including the Space Shuttle Main Engine (SSME), which is presently operational, and the Space Transportation Main Engine (STME) under development. The SSME's provide high performance within stringent constraints on size, weight, and reliability. Based on operational experience, continuous design improvement is in progress to enhance system durability and reliability. Specialized data analysis and interpretation is required in support of SSME and advanced propulsion system diagnostic evaluations. Comprehensive evaluation of the dynamic measurements obtained from test and flight operations is necessary to provide timely assessment of the vibrational characteristics indicating the operational status of turbomachinery and other critical engine components. Efficient performance of this effort is critical due to the significant impact of dynamic evaluation results on ground test and launch schedules, and requires direct familiarity with SSME and derivative systems, test data acquisition, and diagnostic software. Detailed analysis and evaluation of dynamic measurements obtained during SSME and advanced system ground test and flight operations was performed including analytical/statistical assessment of component dynamic behavior, and the development and implementation of analytical/statistical models to efficiently define nominal component dynamic characteristics, detect anomalous behavior, and assess machinery operational condition. In addition, the SSME and J-2 data will be applied to develop vibroacoustic environments for advanced propulsion system components, as required. This study will provide timely assessment of engine component operational status, identify probable causes of malfunction, and indicate feasible engineering solutions. This contract will be performed through accomplishment of negotiated task orders. Author (revised)

N94-21859*# National Aeronautics and Space Administration. Marshall Space Flight Center, Huntsville, AL.
A SIMULATION MODEL FOR PROBABILISTIC ANALYSIS OF SPACE SHUTTLE ABORT MODES
R. T. Hage Nov. 1993 104 p
(NASA-TM-108432; NAS 1.15:108432) Avail: CASI HC A06/MF A02

A simulation model which was developed to provide a probabilistic analysis tool to study the various space transportation system abort mode situations is presented. The simulation model is based on Monte Carlo simulation of an event-tree diagram which accounts for events during the space transportation system's ascent and its abort modes. The simulation model considers just the propulsion elements of the shuttle system (i.e., external tank, main engines, and solid boosters). The model was developed to provide a better understanding of the probability of occurrence and successful completion of abort modes during the vehicle's ascent. The results of the simulation runs discussed are for demonstration purposes only, they are not official NASA probability estimates. Author (revised)

N94-21884*# National Aeronautics and Space Administration. John F. Kennedy Space Center, Cocoa Beach, FL.
DEBRIS/ICE/TPS ASSESSMENT AND INTEGRATED PHOTOGRAPHIC ANALYSIS FOR SHUTTLE MISSION STS-51 Report, 16 Jul. - 23 Sep. 1993
Gregory N. Katnik, Barry C. Bowen, and J. Bradley Davis Oct. 1993 153 p
(NASA-TM-109189; NAS 1.15:109189) Avail: CASI HC A08/MF A02

A debris/ice/thermal protection system (TPS) assessment and integrated photographic analysis was conducted for shuttle mission STS-51. Debris inspections of the flight elements and launch pad were performed before and after launch. Icing conditions on the external tank were assessed by the use of computer programs, nomographs, and infrared scanner data during cryogenic loading of the vehicle followed by on-pad visual inspection. High speed photography was analyzed after launch to identify ice/debris sources and evaluate potential vehicle damage and/or in-flight anomalies. This report documents the debris/ice/TPS conditions and integrated photographic analysis of Shuttle mission STS-51 and the resulting effect on the Space Shuttle Program. Author (revised)

17 SPACE COMM., SPACECRAFT COMM., COMMAND & TRACKING

Includes telemetry; space communications networks; astronavigation and guidance; and radio blackout.

For related information see also *04 Aircraft Communications and Navigation* and *32 Communications and Radar.*

N94-21581*# National Aeronautics and Space Administration. Lewis Research Center, Cleveland, OH.
ON-BOARD CLOSED-LOOP CONGESTION CONTROL FOR SATELLITE BASED PACKET SWITCHING NETWORKS
Pong P. Chu (Cleveland State Univ., OH.), William D. Ivancic, and Heechul Kim Dec. 1993 30 p Proposed for presentation at the 15th International Communications Satellite Systems Conference, San Diego, CA, 28 Feb. - 3 Mar. 1994; sponsored by AIAA
(Grant NAG3-1379; RTOP 235-01-04)
(NASA-TM-106446; E-8292; NAS 1.15:106446; AIAA Paper 94-1062)
Avail: CASI HC A03/MF A01

NASA LeRC is currently investigating a satellite architecture that incorporates on-board packet switching capability. Because of the statistical nature of packet switching, arrival traffic may fluctuate and thus it is necessary to integrate congestion control mechanism as part of the on-board processing unit. This study focuses on the closed-loop reactive control. We investigate the impact of the long propagation delay on the performance and propose a scheme to overcome the problem. The scheme uses a global feedback signal to regulate the packet arrival rate of ground stations. In this scheme, the satellite continuously broadcasts the status of its output buffer and the ground stations respond by selectively discarding packets or by tagging the excessive packets as low-priority. The two schemes are evaluated by theoretical queuing analysis and simulation. The former is used to analyze the simplified model and to determine the basic trends and bounds, and the later is used to assess the performance of a more realistic system and to evaluate the effectiveness of more sophisticated control schemes. The results show that the long propagation delay makes the closed-loop congestion control less responsive. The broadcasted information can only be used to extract statistical information. The discarding scheme needs carefully-chosen status information and reduction function, and normally requires a significant amount of ground discarding to reduce the on-board packet loss probability. The tagging scheme is more effective since it tolerates more uncertainties and allows a larger margin of error in status information. it can protect the high-priority packets from excessive loss and fully utilize the downlink bandwidth at the same time.
Author (revised)

N94-21852# Sandia National Labs., Albuquerque, NM.
REENTRY VEHICLE ADAPTIVE TELEMETRY
R. E. Kidner Sep. 1993 66 p
(Contract DE-AC04-76DP-00789)
(DE94-001168; SAND-93-1985) Avail: CASI HC A04/MF A01

In RF telemetry (TM) the allowable RF bandwidth limits the amount of data in the telemetered data set. Typically the data set is less than ideal to accommodate all aspects of a test. In the case of diagnostic data, the compromise often leaves insufficient diagnostic data when problems occur. As a solution, intelligence was designed into a TM allowing it to adapt to changing data requirements. To minimize the computational requirements for an intelligent TM, a fuzzy logic inference engine was developed. This reference engine was simulated on a PC and then loaded into a TM hardware package for final testing. DOE

N94-21980# Lawrence Livermore National Lab., CA.
A PACKET BASED, DATA DRIVEN TELEMETRY SYSTEM FOR AUTONOMOUS EXPERIMENTAL SUB-ORBITAL SPACECRAFT
J. R. Kalibjian 26 Apr. 1993 10 p Presented at the 29th Annual International Telemetering Conference, Las Vegas, NM, 25-28 Oct. 1993
(Contract W-7405-eng-48)
(DE94-000399; UCRL-JC-112636; CONF-9310131-6) Avail: CASI HC A02/MF A01

A data driven telemetry system is described that responds to the rapid nature in which experimental satellite telemetry content is changed during the development process. It also meets the needs of a diverse experiment which the many phases of a mission may contain radically different types of telemetry data. The system emphasizes mechanisms for achieving high redundancy of critical data. A practical example of such an implementation, Brilliant Pebbles Flight Experiment Three (FE-3), is cited. DOE

N94-21981# Lawrence Livermore National Lab., CA.
AUTOMATED ANALYSIS TOOLS FOR REDUCING SPACECRAFT TELEMETRY DATA
T. J. Voss 26 Apr. 1993 9 p Presented at the 29th Annual International Telemetering Conference, Las Vegas, NV, 25-28 Oct. 1993
(Contract W-7405-eng-48)
(DE94-000400; UCRL-JC-112639; CONF-9310131-3) Avail: CASI HC A02/MF A01

A practical description is presented of the methods used to reduce spacecraft telemetry data using a hierarchical toolkit of software programs developed for a UNIX environment. A project requiring the design, implementation, and test flight of small, lightweight spacecraft was recently conducted. This spacecraft development required hundreds of tests and integrations of subsystems on several special purpose testbeds, with each test creating large amounts of telemetered data. Focus is on the automated analysis and reduction of data which is telemetered from one of the key subsystems, the Probe. A typical telemetry stream from a testbed run averaged 50 Megabytes of raw data, containing over 1600 system variables. The large telemetry file (raw data) sent from the Probe was decoded and decomposed into a large number of smaller Break Out Files (BOF's) containing variables with timestamps, and image files. DOE

N94-21340*# National Aeronautics and Space Administration. Goddard Space Flight Center, Greenbelt, MD.
AN IN-DEPTH ANALYSIS AND MODELLING OF THE SHUTTLE TO MILA S-BAND TELEMETRY LINK
Armen Caroglanian, Fernando A. Pellerano, and Dale D. Shama (Loral AeroSys, Seabrook, MD.) *In its* Networks Technology Conference Nov. 1993 p 217-224 (For primary document see N94-21323 05-62)
Avail: CASI HC A02/MF A03

18 SPACECRAFT DESIGN, TESTING AND PERFORMANCE

Includes satellites; space platforms; space stations; spacecraft systems and components such as thermal and environmental controls; and attitude controls.

For life support systems see *54 Man/System Technology and Life Support.* For related information see also *05 Aircraft Design, Testing and Performance, 39 Structural Mechanics,* and *16 Space Transportation.*

N94-19863# Lawrence Livermore National Lab., CA.
POINTING CONTROL DESIGN FOR AUTONOMOUS SPACE VEHICLE APPLICATIONS
K. D. Young Mar. 1993 7 p Presented at the 12th International Federation of Automatic Control World Congress, Sydney, Australia, 19-23 Jul. 1993
(Contract W-7405-eng-48)
(DE93-019943; UCRL-JC-113458; CONF-930781-2) Avail: CASI HC A02/MF A01

This paper addresses the design of pointing control systems for autonomous space vehicles. The function of the pointing control system is to keep distant orbiting objects within the field-of-view of an on-board optical sensor. We outline the development of novel nonlinear control algorithms which exploit the availability of onboard sensors. Simulation results comparing the performance of the different pointing control implementations are presented. DOE

N94-19896# Naval Research Lab., Washington, DC.
THE NRL LACE PROGRAM Final Report
D. M. Horan, R. E. Perram, and R. E. Palma 27 Aug. 1993 37 p
(AD-A270861; NRL/FR/8121-93-9565) Avail: CASI HC A03/MF A01

The Naval Research Laboratory's Low-power Atmospheric Compensation Experiment (LACE) Program was established to provide and operate a satellite that could carry and support instruments to measure the intensity and distribution of low-energy laser beams transmitted from Earth; to image the ultraviolet emission from rocket plumes at high altitudes; and to measure the spectrum and distribution of terrestrial neutrons. The satellite was launched on 14 February 1990. It made many successful laser beam measurements; collected high-quality emission images from four rocket launches in four attempts; and made neutron background measurements almost continuously for 36 months. DTIC

N94-20173*# Michigan Univ., Ann Arbor. Dept. of Atmospheric, Oceanic and Space Science.
DYNAMICS EXPLORER 2: CONTINUED FPI AND NACS INSTRUMENT DATA ANALYSIS AND ASSOCIATED SCIENTIFIC ACTIVITY AT THE UNIVERSITY OF MICHIGAN Final Report, Dec. 1990 - 31 Jan. 1994
Alan Burns and T. L. Killeen 7 Dec. 1993 16 p
(Grant NAG5-465)
(NASA-CR-194689; NAS 1.26:194689) Avail: CASI HC A03/MF A01

The grant entitled 'Dynamics Explorer 2 - continued FPI and NACS instrument data analysis and associated scientific activity at the University of Michigan' is a continuation of a grant that began with instrument development for the Dynamics Explorer 2 (DE 2) satellite. Over the years, many publications and presentations at scientific meetings have occurred under the aegis of this grant. This present report details the progress that has been made in the final three years of the grant. In these last 4 years of the grant 26 papers have been published or are in press and about 10 more are in preparation or have been submitted. A large number of presentations have been made in the same time span: 36 are listed in Appendix 2. Evidence of the high educational utility of this research is indicated by the list of Ph. D. and M. S. theses that have been completed in the last 3 years that have involved work connected with NAG5-465. The structure of this report is as follows: a brief synopsis of the aims of the grant NAG5-465 is given in the next section; then there is a summary of the scientific accomplishments that have occurred over the grant period; last, we make some brief concluding remarks. Reprints of articles that have recently appeared in refereed journals are appended to the end of this document. Derived from text

N94-20235# European Space Agency. European Space Operations Center, Darmstadt (Germany). Spacecraft Operations Div.
THE EXOSAT OPERATIONAL EXPERIENCE
A. G. Parkes, P. T. Prior, and D. Heger Jun. 1993 93 p
(ESA-STM-248; ISBN-92-9092-357-1; ETN-93-94879) Copyright Avail: CASI HC A05/MF A01

The European X-ray Observatory Satellite (EXOSAT) system is reviewed. Those areas which gave rise to operational problems are highlighted. EXOSAT was launched on 26 May 1983 after definition, design, and development phases for both the space and ground systems and a number of launch delays. The planned mission lifetime was two years. This target was duly achieved, and the experiments continued to return scientific data until 9 Apr. 1986. Approximately one month later, on 6 May 1986, the orbit decayed and the spacecraft reentered the Earth's atmosphere. The wealth of scientific data received and the important and exciting scientific discoveries emerging from EXOSAT led to the mission being justifiably described within the scientific community as a 'great success.' ESA

N94-20367* National Aeronautics and Space Administration. Lyndon B. Johnson Space Center, Houston, TX.
SPACE STATION TRASH REMOVAL SYSTEM Patent
Andrew J. Petro, inventor (to NASA) 7 Sep. 1993 5 p Filed 22 May 1992 Supersedes N92-30315 (30 - 21, p 3588)
(NASA-Case-MSC-21723-1; US-Patent-5,242,134;

US-Patent-Appl-SN-887001; US-Patent-Class-244-158R; US-Patent-Class-244-160; Int-Patent-Class-B64G-1/22) Avail: US Patent and Trademark Office

A trash removal system for space stations is described. The system is comprised of a disposable trash bag member and an attached, compacted large, lightweight inflatable balloon element. When the trash bag member is filled, the astronaut places the bag member into space through an airlock. Once in the vacuum of space, the balloon element inflates. Due to the large cross-sectional area of the balloon element relative to its mass, the combined balloon element and the trash bag member are slowed by atmospheric drag to a much greater extent than the Space Station's. The balloon element and bag member lose altitude and re-enter the atmosphere, and the elements and contents are destroyed by aerodynamic heating. The novelty of this system is in the unique method of using the vacuum of space and aerodynamic heating to dispose of waste material with a minimum of increase in orbital debris.

Official Gazette of the U.S. Patent and Trademark Office

N94-20590* National Aeronautics and Space Administration. Lyndon B. Johnson Space Center, Houston, TX.

TETRAHEDRAL LANDER Patent

Michael L. Roberts, inventor (to NASA) 30 Nov. 1993 7 p Filed 3 Feb. 1993 Supersedes N94-15951 (32 - 3, p 886)
(NASA-Case-MSC-22082-1; US-Patent-5,265,829; US-Patent-Appl-SN-012839; US-Patent-Class-244-160; US-Patent-Class-244-138A; US-Patent-Class-244-100A; US-Patent-Class-244-110D; US-Patent-Class-244-113; US-Patent-Class-244-158A; US-Patent-Class-244-138R) Avail: US Patent and Trademark Office

An apparatus and method is disclosed for decelerating and absorbing impact of a re-entry vehicle suitable for payloads that are relatively light as well as payloads weighing several tons or more. The apparatus includes four inflatable legs displaced equidistantly from each other around a capsule or housing which contains a payload. The legs are inflated at a designated altitude after entering earth's atmosphere to slow the descent of the re-entry vehicle. Connected between each of the four legs are drag inducing surfaces that deploy as the legs inflate. The drag inducing surfaces are triangularly shaped with one such surface being connected between each pair of legs for a total of six drag inducing surfaces. The legs have drag inducing outer surfaces which act to slow the descent of the re-entry vehicle.

Official Gazette of the U.S. Patent and Trademark Office

N94-20617# Naval Research Lab., Washington, DC.

UVPI IMAGING FROM THE LACE SATELLITE: THE STARBIRD ROCKET PLUME

H. W. Smathers, D. M. Horan, J. G. Cardon, E. R. Malaret, and L. Perez 18 Aug. 1993 141 p
(AD-A271981; NRL/FR/8105-93-9546) Avail: CASI HC A07/MF A02

The Starbird rocket provides the second demonstration of the ability of the Ultraviolet Plume Instrument (UVPI) to observe missiles in flight above the atmosphere. The Starbird was launched from the Kennedy Space Center in Florida on 18 December 1990. The UVPI is a small, plume-tracking instrument flown on the Naval Research Laboratory's Low-power Atmospheric Compensation Experiment (LACE) satellite, launched in February 1990. The two cameras of the instrument, a tracker and a plume camera, use filters, image intensifiers, and CCD detectors to observe sources in the ultraviolet. The plume camera has a narrow field of view, 0.180 deg by 0.135 deg, and observes sources through any of the four filters with passbands of 195 to 295 nm, 200 to 300 nm, 235 to 350 nm, and 300 to 320 nm. The Starbird third and fourth stages, both of which used identical Orbus rocket motors, reached 90-km altitude and were successfully detected and tracked by the UVPI from a range of 596 to 483 km. The spectral radiance and intensities of the missile plumes were extracted from these images and made into contour plots. Spatial, temporal, and spectral characteristics of the plume are also provided. DTIC

N94-21041 Communications Satellite Corp., Clarksburg, MD.

METHOD OF ORIENTING A SYNCHRONOUS SATELLITE Patent

Lawrence H. Westerlund, inventor (to Communications Satellite Corp.) 28 Jul. 1992 63 p Filed 23 Aug. 1988
(CA-Patent-1,305,772; Int-Patent-Class-B64G-1/10; CTN-93-60690)

Copyright Avail: Micromedia Ltd., Technical Information Centre, 165 Hotel de Ville, Place du Portage, Phase 2, Hull, Quebec J8X 3X2, Canada HC/MF

A method is provided which has the objective of solving the problems involved in orienting a satellite in geosynchronous orbit. In a first embodiment, the method includes a step of orienting the spin axis of the satellite at orbit-normal. The direction angle is measured in a rotational direction from a first line which represents equatorial normal to a second line which represents orbit-normal, where the first and second lines intersect at the satellite's center of mass. In a second embodiment, the method includes a step of orienting the spin axis at orbit-normal plus a correction angle determined according to equations whose parameters include the elevation angle and latitude of the bore site target, and the inclination angle of the orbital plane with respect to the equatorial plane. In this embodiment, the direction angle is measured as in the first embodiment. The step of orienting the spin axis can be performed by firing thrusters. The method of the invention can be easily performed, and the advantage of vastly prolonging the useful life of a satellite by reducing or discontinuing north/south stationkeeping can be easily achieved, even with satellites already in orbit.

Author (CISTI)

N94-21147# Arizona Univ., Tucson. Optical Sciences Center.

LONG DURATION EXPOSURE FACILITY (LDEF) CONTAMINATION STUDY Final Report

Karen P. Scott Oct. 1993 16 p
(Contract N00014-90-J-4052)
(AD-A272419) Avail: CASI HC A03/MF A01

This report describes the optical measurements that were taken of LDEF surfaces during the deintegration of LDEF from February to April 1990. This project was one part of an overall effort conducted by Boeing Aerospace to determine and track contamination on LDEF. The purpose of this portion of the contamination project was to provide early documentation of the contamination level on LDEF experiments before shipment and disassembly by the principle investigators (PI). 35% of experiment trays located on all areas of LDEF were examined to, in particular, catalogue global differences in contamination depending on tray location. The optical measurements were performed with a Model BHMJ Nomarski microscope which had also darkfield and oblique lighting capabilities. The optical measurements were documented by video and 35-mm cameras that could be attached to the microscope. Approximately 15 hours of video and 17 rolls of film (24 exposure) were taken. A full list of all trays and experiments observed is presented in Appendix C. Due to the high volume of data, a short 10-min. video has been compiled to illustrate the different contamination processes observed on LDEF. DTIC

N94-21217# Naval Postgraduate School, Monterey, CA.

A CONCEPTUAL DATABASE DESIGN AND PERFORMANCE ANALYSIS OF THE MILSATCOM REQUIREMENTS DATABASE M.S. Thesis

Ronald G. Kearns Jun. 1993 87 p
(AD-A272672) Avail: CASI HC A05/MF A01

The Military Satellite Communications Decision Support System (MDSS) project for U.S. Space Command (USSPACECOM) is intended to provide decision makers an integrated information tool to effectively manage military satellite communication (MILSATCOM) resources while satisfying communications requirements. An important aspect of MDSS is the information provided by the MILSATCOM Requirements Database (MRDB). The objective of this thesis is twofold. First, it develops a new conceptual schema for the MRDB using the Entity Relationship Model and transforms it into a relational schema for implementation. Second, it conducts a comparative performance analysis to examine the tradeoffs between normalization and performance. This thesis concludes that a structured approach to designing the MRDB results in a normalized structure that is simple, easy to implement, and provides acceptable performance. A fully normalized database structure does not seem to have a significant impact on over-all MRDB retrieval performance. DTIC

N94-21251# Naval Postgraduate School, Monterey, CA.

DESIGN AND IMPLEMENTATION OF A PROTOTYPE PC BASED GRAPHICAL AND INTERACTIVE MILSATCOM REQUIREMENTS DATABASE SYSTEM M.S. Thesis

William M. Major Jun. 1993 137 p

(Contract MIPR-NS-93-76)
(AD-A272960) Avail: CASI HC A07/MF A02

This thesis develops a prototype PC based Military Satellite Communications (MILSATCOM) Requirements Database (MRDB) application for U.S. Space Command, using Microsoft's Access relational database management system (DBMS) for Windows. It demonstrates the advantages of using the proposed database system over the existing one and shows how U.S. Space Command can save both time and money by using a PC based interactive, graphical, and user friendly database system. A rapid prototyping approach in concert with a six phase database design process was used to develop the prototype. The first two chapters of the thesis provide a background of the application and describe database management systems in general and Microsoft Access in particular. The applications of Access - tables, queries, forms, reports, macros, and modules - to the design of the MRDB are then discussed in the succeeding five chapters. The conclusions describe the advantages and benefits of using the prototype MRDB database system and make recommendations for future improvements. DTIC

N94-21367 Centre National d'Etudes Spatiales, Toulouse (France).
FIFTH INTERNATIONAL SYMPOSIUM ON MATERIALS IN A SPACE ENVIRONMENT
Jun. 1993 500 p In ENGLISH and FRENCH Symposium held in Toulouse, France, Sep. 1991
(ISBN-2-85-428293-0; ETN-94-94968) Copyright Avail: CEPADUES-Editions, 111, rue Nicolas-Vaquelin, 31100 Toulouse, France

Results obtained from the Long Duration Exposure Facility (LDEF) and Mir Aragatz experiments are reviewed. Research in connection with atomic oxygen (effects, modeling, simulation, means of protection, etc.) is reported. The following are discussed: environment models (communication of the most recent use of the one best suited to the problem in hand); contamination and its effects (old problem/new data); ground testing (standardization/measurement standards); and functional deterioration of lubrication materials used in low orbit. For individual titles, see N94-21368 through N94-21408.

N94-21368 Centre d'Etudes et de Recherches, Toulouse (France). Space Technology Dept.
ORBITAL DEBRIS AND MICROMETEOROIDS: LDEF AND MIR DATA
J. C. Mandeville *In* CNES, Fifth International Symposium on Materials in a Space Environment Jun. 1993 p 15-25 (For primary document see N94-21367 05-18)
Copyright Avail: CEPADUES-Editions, 111, rue Nicolas-Vaquelin, 31100 Toulouse, France

Experiments devoted to the detection of cosmic dust in space are reported. One was located on the Long Duration Exposure Facility (LDEF) and one on the Soviet Mir Space Station. A variety of sensors and collecting devices made possible the study of the particles and their effects after recovery of exposed material. Flux mass distribution is expected to be derived with a good accuracy due to the large time area exposure. Understanding of the mechanism of impact process on materials currently used in space will be greatly improved after full analysis of data impacts on metals, fiberglass thermal covers, and quartz samples are reported. Remnants of particles suitable for chemical identification are found within impact craters. A discrimination between extraterrestrial particles and man-made orbital debris is expected. Preliminary examination of hypervelocity impact features gives valuable information on size distribution and nature of interplanetary dust particles in low earth orbit, within the 0.5 to 300 micrometer size range. So far, chemical investigation of craters found on LDEF clearly shows evidence of elements (Na, Mg, Si, S, Ca, and Fe) consistent with cosmic origin. It is suggested that thin foil detectors for chemical investigation of particle remnants within impact sites would be promising for future experiments. ESA

N94-21369 Centre National d'Etudes Spatiales, Toulouse (France).
FLIGHT AND LABORATORY TESTING OF MATERIALS IN LOW EARTH ORBIT **c23**
J. C. Guillaumon, J. Marco (Centre d'Etudes et de Recherches, Toulouse, France.), and A. Paillous (Centre d'Etudes et de Recherches, Toulouse, France.) *In its* Fifth International Symposium on Materials in a Space Environment Jun. 1993 p 27-42 (For primary document see N94-21367 05-18)
Copyright Avail: CEPADUES-Editions, 111, rue Nicolas-Vaquelin, 31100 Toulouse, France

Two experiments which evaluated the deterioration of materials in orbit and validated laboratory simulation techniques are reported. One was flown on the trailing edge of the Long Duration Exposure Facility (LDEF) and the other outside the Mir Space Station. Approximately 200 specimens of about 60 different materials were exposed in LEO (low earth orbit) conditions: their pre- and post-exposure properties were measured under laboratory conditions in air. The tested materials included thermal control coatings, polymers, protective layers against atomic oxygen, composite materials, and optical components. Most specimens were passively subjected to the space environment. Several sets of four identical specimens enabled investigation of the effects of the combined action of oxygen atoms and UV radiation and a comparison of these with the effects of solar UV radiation acting alone. Some samples were placed inside a canister which was opened and closed in orbit whereas others were submitted to the complete environment of the LDEF mission in order to evaluate possible contamination effects. The results provided valuable information on the performance of materials and the damage mechanisms experienced in orbit. Some typical material behavior examples are given. Particular emphasis is placed on the synergistic effects of the natural and induced components of the space environment. Some results of laboratory tests and in-flight tests can be compared. As a consequence the limitation of both flight and laboratory environment tests is examined. ESA

N94-21370 Moscow State Univ. (Russia).
COMPLEX-2: LOW EARTH ORBITAL ENVIRONMENT SIMULATION FACILITY FOR MATERIALS DURABILITY EVALUATION **c14**
V. I. Titov, G. G. Solovyev, V. N. Chernik, Y. I. Tarasov, S. F. Naumov (Nauchno-Proizvodstvennoe Obedinenie Energomash, Khimki, USSR.), S. A. Demidov (Nauchno-Proizvodstvennoe Obedinenie Energomash, Khimki, USSR.), and A. H. Kutlaliyev (Nauchno-Proizvodstvennoe Obedinenie Energomash, Khimki, USSR.) *In* CNES, Fifth International Symposium on Materials in a Space Environment Jun. 1993 p 43-45 (For primary document see N94-21367 05-18)
Copyright Avail: CEPADUES-Editions, 111, rue Nicolas-Vaquelin, 31100 Toulouse, France

The experimental facility design and measurement methods of Complex 2, which simulates the low earth orbit (LEO) environment by combined exposure of samples in asher low energy beams and solar radiation, are reported. The degradation of materials in a simulated LEO are evaluated in this facility which is equipped with a computer operated data system. The facility can be used to measure: mass loss by string low force converter or by torsion balance with threshold sensibility of 0.0001g and absorption spectra within the wave band of 0.35 to 2.5 micrometers. Results of fluoroplastic tests in air plasma flux are given. ESA

N94-21371 Centre National d'Etudes Spatiales, Toulouse (France).
RESULTS OF THE POST FLIGHT ANALYSES ON SYSTEM MATERIALS FOR THE LDEF-FRECOPA EXPERIMENT **c23**
Christian Durin and Irenee Alet *In its* Fifth International Symposium on Materials in a Space Environment Jun. 1993 p 47-74 (For primary document see N94-21367 05-18)
Copyright Avail: CEPADUES-Editions, 111, rue Nicolas-Vaquelin, 31100 Toulouse, France

Results of the successful FRECOPA (FREnch COoperative passive PAyload) experiment, which was attached to the Long Duration Exposure Facility (LDEF) satellite and which consisted of exposing structural materials, paints, ruled gratings, and components to the space environment and collecting microparticles present in orbit, are summarized. A comparison between the following materials after flight with those stored on the ground in laboratory conditions is given: DERLIN, Teflon, aluminized Mylar, Velcro, NOMEX thread, glues, rigid shields, canisters and their seals, electronics and wiring, and silver plated bolts. ESA

N94-21372* National Aeronautics and Space Administration. Lyndon B. Johnson Space Center, Houston, TX.
MEASURED SPACE ENVIRONMENTAL EFFECTS TO LDEF DURING RETRIEVAL
Carl R. Maag (Science Applications International Corp., Glendora, CA.), W. Kelly Linder, and Eugene N. Borson (Aerospace Corp., Los Angeles, CA.)

In CNES, Fifth International Symposium on Materials in a Space Environment Jun. 1993 p 75-90 (For primary document see N94-21367 05-18)

Copyright Avail: CEPADUES-Editions, 111, rue Nicolas-Vaquelin, 31100 Toulouse, France

Data gathered by the Interim Operational Contamination Monitor (IOCM) with regard to the effect of the space environment on the STS-32 Shuttle mission and on the Long Duration Exposure Facility (LDEF) are reported. IOCM measures the deposition of molecular and particulate contamination during all flight phases. It also measures the thermophysical properties of thermal control surfaces by calorimetry, the flux of the ambient atomic oxygen environment, the incident solar flux, and the absolute ambient pressure in the payload bay. The IOCM also provides a structure and sample holders for the exposure of passive material samples to the space environment. One of the more salient results from the STS-32 flight suggests that the LDEF emitted a large number of particulates after berthing into the Shuttle. The mission atomic oxygen fluence was also calculated. Although the fluence was low by normal standards, the Kapton (trademark) passive samples exhibited the onset of erosion. Orbital debris and micrometeoroid impacts also occurred during the retrieval mission. The average perforation diameter was approximately 1.25 micrometers. The largest perforation diameter was measured at 65 micrometers. ESA

N94-21373 Toronto Univ., Downsview (Ontario). Inst. for Aerospace Studies.

SPACE ENVIRONMENTAL EFFECTS ON POLYMER MATRIX COMPOSITES: THE UTIAS/LDEF EXPERIMENT **c27**

R. C. Tennyson, G. E. Mabson, W. D. Morison, and J. Kleiman *In* CNES, Fifth International Symposium on Materials in a Space Environment Jun. 1993 p 93-110 Sponsored by Ontario Inst. for Space and Terrestrial Science, Canada, and Ontario Center for Materials Research, Canada (For primary document see N94-21367 05-18)

Copyright Avail: CEPADUES-Editions, 111, rue Nicolas-Vaquelin, 31100 Toulouse, France

Results on the behavior of various polymer matrix composites containing carbon, boron, and aramid fibers after 70 months exposure in low earth orbit, from the UTIAS/LDEF (University of Toronto Institute for Aerospace Studies/Long Duration Exposure Facility), are reported. A data acquisition system provided information on the strain and temperature changes over the first 371 days in orbit. Data on dimensional changes, coefficients of thermal expansion, times to outgas, and erosion due to atomic oxygen is given. ESA

N94-21374 Centre National d'Etudes Spatiales, Toulouse (France).

RESIDUAL ATMOSPHERE IN THE FRECOPA EXPERIMENT AND DEGASSING OF MATERIALS [ATMOSPHERE RESIDUELLE DANS L'EXPERIENCE FRECOPA ET DEGAZAGE DES MATERIAUX] **c27**

J. Guillin *In its* Fifth International Symposium on Materials in a Space Environment Jun. 1993 p 111-118 In FRENCH (For primary document see N94-21367 05-18)

Copyright Avail: CEPADUES-Editions, 111, rue Nicolas-Vaquelin, 31100 Toulouse, France

Results of measures concerning the composition of residual gas and the pressure inside three of the containers of the FRECOPA (FREnch COoperative passive PAyload) experiment flown on the Long Duration Exposure Facility (LDEF) are reported. The deposition of contaminants on the diverse surfaces were also measured. A comparison between the weight losses of polymers in a vacuum flown in the experiment and those retained on the ground is made. ESA

N94-21375 European Space Agency. European Space Research and Technology Center, ESTEC, Noordwijk (Netherlands).

SOME RESULTS OF THE OXIDATION INVESTIGATION OF COPPER AND SILVER SAMPLES FLOWN ON LDEF **c26**

A. deRooij *In* CNES, Fifth International Symposium on Materials in a Space Environment Jun. 1993 p 119-129 (For primary document see N94-21367 05-18)

Copyright Avail: CEPADUES-Editions, 111, rue Nicolas-Vaquelin, 31100 Toulouse, France

Copper strips flown on the Long Duration Exposure Facility (LDEF) were partially exposed to the atomic oxygen environment present at the LDEF altitude. Depending on the sample position the copper strips show a surface darkening due to the presence of an oxide layer. The type of oxide is investigated as well as its thickness. The silver samples were part of an Ultra Heavy Cosmic Ray Experiment (UHCRE) thermal blanket. This thermal blanket consists of Teflon A-FEP (127 micrometers) + Silver (1600 A) + Inconel (400 A) + Black Paint Chemglaze Z306 (50 to 70 micrometers). The Teflon A-FEP was exposed to the space environment. After penetration of the Teflon A-FEP by a micrometeoroid, the underlying silver was oxidized, where the oxide manifested itself as circular rings around the micrometeoroid hole. An alternating pattern of oxygen and fluor was measured across these rings. ESA

N94-21376 Centre d'Etudes et de Recherches, Toulouse (France). Dept. d'Etudes et Recherches en Technologie Spatiale.

ARAGATZ PROJECT SAMPLES EXPERIMENT/MAPOL (POLYMER MATERIALS) EXPERIMENT: POSTFLIGHT EXPERT EVALUATION [PROJET AGRATZ EXPERIENCE ECHANTILLONS. EXPERIENCE MAPOL (MATERIAUX POLYMERES). COMPTE-RENDU DE L'EXPERIENCE D'APRES VOL] **c27**

C. Sable and J. Villaeys (Centre National d'Etudes Spatiales, Toulouse, France.) *In* CNES, Fifth International Symposium on Materials in a Space Environment Jun. 1993 p 131-136 In FRENCH (For primary document see N94-21367 05-18)

Copyright Avail: CEPADUES-Editions, 111, rue Nicolas-Vaquelin, 31100 Toulouse, France

Observations and measurements carried out during the MAPOL (French acronym for polymer materials) experiment which took place on the Space Station Mir during the french-Soviet Aragatz flight are reported. The aim was to evaluate the effect of the space environment on the mechanical and thermooptical properties of materials which could be used for different applications such as non-rigid space stations, and large dimension inflatable and rigidifiable masts. Different aramid materials were tested. These were exposed without protection, and with protective layers of polymers and fluorine-containing substances of different thicknesses. ESA

N94-21377* National Aeronautics and Space Administration. Lewis Research Center, Cleveland, OH.

THE IMPLICATIONS OF THE LDEF RESULTS ON SPACE STATION FREEDOM POWER SYSTEM MATERIALS

Bruce A. Banks, Sharon K. Rutledge, Kim K. deGroh, Michael J. Mirtich, Linda Gebauer (Cleveland State Univ., OH.), Raymond Olle (Cleveland State Univ., OH.), and Carol M. Hill (Ohio Aerospace Inst., Brook Park.) *In* CNES, Fifth International Symposium on Materials in a Space Environment Jun. 1993 p 137-154 (For primary document see N94-21367 05-18)

Copyright Avail: CEPADUES-Editions, 111, rue Nicolas-Vaquelin, 31100 Toulouse, France

Results and implications of Long Duration Exposure Facility (LDEF) exposure of materials relevant to the Space Station Freedom (SSF) power system materials are presented. Atomic oxygen interactions with potential synergistic UV effects on silicone materials on LDEF were shown to result in the deposition of a dark contaminant film on adjoining surfaces. Silicones associated with solar array construction have the potential for causing reduced solar illumination of the solar cells if such silicone molecular fragments are found to be surface mobile. Results of LDEF atomic oxygen protective coatings on polyimide Kapton indicated acceptable durability to the synergistic effects of atomic oxygen, UV, thermal cycling, and micrometecroid or debris impact. Results of combined atomic oxygen, UV radiation, thermal cycling, and micrometeoroid and debris impacts on LDEF high emittance radiator coatings indicate long term emittance and absorptance durability of Z 93 (zinc oxide pigment in a potassium silicate binder) coatings which have been selected for SSF radiator surfaces. ESA

N94-21378* Jet Propulsion Lab., California Inst. of Tech., Pasadena.

CALIBRATION OF A CALORIMETER FOR MEASURING THE PERFORMANCE OF THERMAL CONTROL SURFACES **c35**

John Houseman and Georg Siebes *In* CNES, Fifth International Symposium on Materials in a Space Environment Jun. 1993 p 155-168 (For primary document see N94-21367 05-18)

Copyright Avail: CEPADUES-Editions, 111, rue Nicolas-Vaquelin, 31100 Toulouse, France

The calibration to evaluate the heat leak in terms of the deviation from

a perfect calorimeter is described. A thermal vacuum test was carried out to characterize the performance of the calorimeter. The calorimeter was equipped with a heater to control the sample disc temperature and with specific instrumentation to measure the heat leak. The radiation sink temperature of the black cavity target was varied from -192 to +31C, while the heater power was varied from 0 to 311 milliwatts. A steady state thermal model was developed to correlate the results. The calorimeter performance was characterized in terms of the heat leak as a percentage of the ideal heat flow of the calorimeter disc. Large deviations from ideal performance occur at low sink temperatures. The effect of the use of the heater is discussed. The effects of transient conditions during low Earth orbit are discussed. It is concluded that heat leak calibrations are necessary for a wide range of conditions. ESA

N94-21379* National Aeronautics and Space Administration. Langley Research Center, Hampton, VA.

THERMAL STRESS ANALYSIS OF COMPOSITES IN THE SPACE ENVIRONMENT **c24**

David E. Bowles *In* CNES, Fifth International Symposium on Materials in a Space Environment Jun. 1993 p 171-186 (For primary document see N94-21367 05-18)

Copyright Avail: CEPADUES-Editions, 111, rue Nicolas-Vaquelin, 31100 Toulouse, France

A finite element micromechanics approach was utilized to investigate the thermally induced stress fields in continuous fiber reinforced polymer matrix composites at temperatures typical of spacecraft operating environments. The influence of laminate orientation was investigated with a simple global/local formulation. Thermal stress calculations were used to predict probable damage initiation locations, and the results were compared to experimentally observed damage in several epoxy matrix composites. The influence of an interphase region on the interfacial stress states was investigated. ESA

N94-21380 Academy of Sciences (USSR), Moscow. Inst. of Energy Problems of Chemical Physics.

THE SIMULATION OF ACTION OF SOME SPACE ENVIRONMENT FACTORS ON TEFLON AND ON RUBBER MATERIALS **c27**

V. E. Skurat, E. A. Barbashev, Y. I. Dorofeev, B. I. Khrushch, A. V. Milinchuk, and V. V. Sedov *In* CNES, Fifth International Symposium on Materials in a Space Environment Jun. 1993 p 187-196 (For primary document see N94-21367 05-18)

Copyright Avail: CEPADUES-Editions, 111, rue Nicolas-Vaquelin, 31100 Toulouse, France

The mechanical properties of Fluoroplast 4 Teflon (trademark) films with thickness 20 micrometers were measured after the irradiations: by sunlight in Low Earth Orbit (LEO); in the test chamber 'Sun' by light with wavelength longer than 220 nm; by light 147 nm from resonance Xe lamp; and by light from deuterium lamp with wavelength longer than 177 nm. The main contribution to the deterioration of mechanical properties of this polymer when irradiated by sunlight in LEO gives the VUV radiation with wavelength from 170 to about 200 to 220 nm. Light with longer and shorter wavelengths does not reproduce the efects of Sun irradiation. A method for screening the resistance of rubber materials to action of VUV, UV light and oxygen plasma is developed. The method is based on microscopic observations of surface of materials after their irradiation in stretched state. The deterioration of hermetic ability of rubber material is observable after a few minutes of exposition. This time is 30 to 50 times shorter than in usual techniques. ESA

N94-21381 National Research Council of Canada, Vancouver (British Columbia).

IN-VACUO SLIP TESTING OF MATERIALS FOR SSRMS FRICTION BRAKES **c27**

H. M. Hawthorne and S. Preston (Spar Aerospace Ltd., Weston, Ontario.) *In* CNES, Fifth International Symposium on Materials in a Space Environment Jun. 1993 p 197-208 (For primary document see N94-21367 05-18)

Copyright Avail: CEPADUES-Editions, 111, rue Nicolas-Vaquelin, 31100 Toulouse, France

An investigation involving the screening of potential materials to be used as friction pads on the Space Station Remote Manipulator System (SSRMS) brakes and clutch assemblies, and the intensive, long term (15 weeks) testing, under high vacuum, of the selected candidate materials, is reported. Screening tests identified ceramic/cermet materials which, after appropriate interface engineering to develop stable wear debris morphology, provide high friction in a vacuum environment, indefinitely. The first material selected, a refractory ceramic, successfully underwent slip testing during extended (15 weeks) exposure to high vacuum and at temperatures of -40 to 96 C, as well as ambient. Frictional stability and good wear resistance was demonstrated by this ceramic material, which makes it a viable choice for use as a friction element on the SSRMS brakes and clutch assemblies. ESA

N94-21382 Centre d'Etudes et de Recherches, Toulouse (France).

EFFECT OF GEOSTATIONARY ENVIRONMENT CONSTITUENTS ON SECONDARY ELECTRON EMISSION RATES

R. Reulet, J.-M. Siguier, L. Levy, and F. Levadou (European Space Agency. European Space Research and Technology Center, ESTEC, Noordwijk, Netherlands.) *In* CNES, Fifth International Symposium on Materials in a Space Environment Jun. 1993 p 209-219 (For primary document see N94-21367 05-18)

Copyright Avail: CEPADUES-Editions, 111, rue Nicolas-Vaquelin, 31100 Toulouse, France

Variations of Secondary Electron Emission (SEE) yield of a PST OSR type material covered with an ITO thin film, induced by geosynchronous orbit representative parameters, are shown. The following results were obtained: the simulated electrons and protons doses, corresponding to 6, 12 and 24 months duration in geosynchronous orbit, slightly modify the SEE yield of irradiated samples; in the same way, UV irradiation of 36 months has a slight influence on the SEE yield; protons + electrons and UV irradiations seem to modify SEE properties by their ability to fix on bombarded surfaces, residual gases, or particles of the chamber; the SEE yield is clearly decreased by increasing the RTV 566 contaminant thickness; an electron + proton or UV irradiation on a contamined surface has no detectable effect on the SEE yield. It is concluded that pollution seems to be the prominent factor on the SEE yield modification of treated surfaces, and Electron Spectroscopy for Chemical Analysis (ESCA) analysis confirm this hypothesis. ESA

N94-21383 Moscow State Univ. (Russia). Inst. de Physique Nucleaire.

ELECTROSTATIC CHARGING AND SECONDARY EFFECTS IN MATERIALS SUBMITTED TO RADIATION IN SPACE [DECHARGES ET EFFETS SECONDAIRES DANS LEX MATERIAUX SOUMIS AUX RAYONNEMENTS DANS L'ESPACE]

Y. Tutrin, A. Akichin, D. Ledyankin, and L. Novikov *In* CNES, Fifth International Symposium on Materials in a Space Environment Jun. 1993 p 221-228 In FRENCH (For primary document see N94-21367 05-18)

Copyright Avail: CEPADUES-Editions, 111, rue Nicolas-Vaquelin, 31100 Toulouse, France

A study to examine the nature and factors responsible for the accumulation of electrostatic charges on exposed materials in space is reported. The laboratory simulation of this charge accumulation on insulating materials exposed to radiation and bombarded by artificial micrometeoroids is reported. Secondary effects such as the emission of charged particles are brought about. A method of inciting the electrostatic charges using laser beams in optical glass exposed to radiation is described. The experimental data of the temporal properties of the provoked discharges are considered. ESA

N94-21384 European Space Agency. European Space Research and Technology Center, ESTEC, Noordwijk (Netherlands). Materials and Processes Div.

INTEGRITY AND TESTING CONCERNS OF THERMOSTRUCTURAL MATERIALS **c24**

R. Raynal *In* CNES, Fifth International Symposium on Materials in a Space Environment Jun. 1993 p 231-240 (For primary document see N94-21367 05-18)

Copyright Avail: CEPADUES-Editions, 111, rue Nicolas-Vaquelin, 31100 Toulouse, France

The current development status of ceramic matrix composites (CMC's) and the different problems related to their selection and utilization in space projects are discussed. In particular, the following subjects are addressed: determination of the physical properties which are of main importance for the heat and stress management of structures; concerns in relation to

mechanical testing at both ambient and high temperature and the need to establish standard methods; the correlation between tests performed on coupon samples and on engineered hardware; difficulties in simulating damaging processes which may occur during service; and the need to develop nondestructive test methods. Determination of thermal expansion and tensile mechanical behavior at high temperature are described. ESA

N94-21385* National Aeronautics and Space Administration. Langley Research Center, Hampton, VA.

SIMULATED SPACE ENVIRONMENTAL EFFECTS ON SOME EXPERIMENTAL HIGH PERFORMANCE POLYMERS **c27**

John W. Connell *In* CNES, Fifth International Symposium on Materials in a Space Environment Jun. 1993 p 241-253 (For primary document see N94-21367 05-18)

Copyright Avail: CEPADUES-Editions, 111, rue Nicolas-Vaquelin, 31100 Toulouse, France

High performance polymers for potential space applications were evaluated under simulated space environmental conditions. Experimental resins from blends of acetylene terminated materials, poly(arylene ether)s and low color polyimides were exposed to high energy electron and ultraviolet radiation in an attempt to simulate space environmental effects. Thin films, neat resin moldings, and carbon fiber reinforced composites were exposed, and the effect on certain polymer properties were determined. Recent research involving the effects of various radiation exposures on the physical, optical, and mechanical properties of several experimental polymer systems is reviewed. ESA

N94-21386 European Space Agency. European Space Research and Technology Center, ESTEC, Noordwijk (Netherlands).

MATERIALS EVALUATION AT ESA/ESTEC **c23**

G. Gourmelon, M. Froggatt, and D. Collins *In* CNES, Fifth International Symposium on Materials in a Space Environment Jun. 1993 p 255-272 (For primary document see N94-21367 05-18)

Copyright Avail: CEPADUES-Editions, 111, rue Nicolas-Vaquelin, 31100 Toulouse, France

A method of evaluating materials that are intended to be used in space is presented. The materials evaluated include thermal control coatings and films, conformal coatings, adhesives, adhesive tapes, primers and surface protection treatments, metals and solderless/mechanical electrical connection techniques. However, other materials or combination of materials can also be assessed by this method. The described evaluation program is divided into parts in order to provide a methodical and efficient procedure of test. The material evaluation should only pass to the following part if the material has satisfied the conditions of the previous part. This avoids waste of effort and expense on the more costly tests. Results of the following types of tests on ITO (indium tin oxide)/Kapton/VDA (vacuum deposited aluminum) and on McGHAN-NUSIL CV-1152 are given: outgassing, surface resistivity, chemical, humidity, thermal cycling, thermal shock, bend, adhesion, flammability, and offgassing. ESA

N94-21387 European Space Agency. European Space Research and Technology Center, ESTEC, Noordwijk (Netherlands).

COLUMBUS: MATERIALS FOR 30 YEARS HABITABILITY IN SPACE

D. Zanotti *In* CNES, Fifth International Symposium on Materials in a Space Environment Jun. 1993 p 273-290 (For primary document see N94-21367 05-18)

Copyright Avail: CEPADUES-Editions, 111, rue Nicolas-Vaquelin, 31100 Toulouse, France

A general assessment of the problem of the selection of materials to be used inside the Columbus habitable modules is provided. Basic safety requirements and system engineering considerations are described. Special emphasis was put on ground testing and materials screening, acceptance and ranking problems. Newly developed tests or original adaptation of existing ones are described. Some important relationships between the criteria for approval of materials, residual safety hazards, and design solutions are mentioned. The importance and complexity of the problems of the habitable environment in manned spacecraft that need to be addressed (toxicology, human factors engineering, microbiology, etc.) are emphasized. The need for a more systematic approach to materials selection which implies that the materials discipline shall become much more integrated into the design process, during all its phases, is stressed. ESA

N94-21388 MATRA Marconi Space, Toulouse (France).

METEOROIDS AND DEBRIS IMPACT RISK ASSESSMENT ON COLUMBUS AND HERMES USING A REALISTIC GEOMETRICAL ANALYSIS TOOL

J. Borde and G. Drolshagen (European Space Agency. European Space Research and Technology Center, ESTEC, Noordwijk, Netherlands.) *In* CNES, Fifth International Symposium on Materials in a Space Environment Jun. 1993 p 291-310 (For primary document see N94-21367 05-18)

Copyright Avail: CEPADUES-Editions, 111, rue Nicolas-Vaquelin, 31100 Toulouse, France

An enhanced three-dimensional (3D) numerical analysis tool for meteoroid/space debris risk evaluation was developed. It provides impact probabilities and resulting damage effects using realistic geometrical treatments and is based on presently available environment and particle/wall interaction models together with spacecraft shielding design. This tool is used for evaluating the risk of impacts on the Columbus Attached Pressurized Module (APM) and the Hermes Spaceplane. The more recent spacecraft geometry (ESABASE model), orbital parameters, pointing directions, environment models, and shielding configuration are employed. On each elementary surface of the spacecraft, the number of impacts, the number of failures, the mean velocity amplitude, the mean velocity elevation angle, and the percentage of cratered area are computed. This allows the critical parts of the spacecraft to be determined, i.e., the surfaces which require more shielding. For both spacecraft, some significant results and recommendations are provided. ESA

N94-21389 MATRA Marconi Space, Toulouse (France).

COMBINATION OF ON GROUND EXPERIMENTS AND ANALYSIS SOFTWARE FOR THE EVALUATION OF MATERIAL DEGRADATION IN SPACE (SILEX PROJECT) **c61**

P. Renard *In* CNES, Fifth International Symposium on Materials in a Space Environment Jun. 1993 p 311-320 (For primary document see N94-21367 05-18)

Copyright Avail: CEPADUES-Editions, 111, rue Nicolas-Vaquelin, 31100 Toulouse, France

An assessment study which combines analysis software for the prediction of atomic oxygen fluence and micrometeoroid impacts with laboratory tests to characterize the degradation they induce in the optical equipment of the optical intersatellite communications experiment SILEX, is presented. The software uses environment models and the ray tracing Monte Carlo technique. The laboratory tests assessed micrometeoroid impact both at the surface level and at the optical properties level, and some of the worst cases of damage were derived. ESA

N94-21390 Deutsche Forschungsanstalt fuer Luft- und Raumfahrt, Cologne (Germany).

GERMAN SPACE EXPERIMENTS ON SPACELAB D-2 AND EURECA-1 TO INVESTIGATE ATOMIC OXYGEN INTERACTION WITH MATERIALS **c25**

H. Hamacher and H. E. Richter *In* CNES, Fifth International Symposium on Materials in a Space Environment Jun. 1993 p 323-330 (For primary document see N94-21367 05-18)

Copyright Avail: CEPADUES-Editions, 111, rue Nicolas-Vaquelin, 31100 Toulouse, France

Two complementary passive space experiments to investigate atomic oxygen interactions with spacecraft materials, primarily those intended to be used for the Atomic Oxygen Sample Tray (AOST) to be flown on Eureca (European retrievable carrier) and the Atomic Oxygen Exposure Tray which is part of the German Spacelab D-2, are presented. The total atomic oxygen fluences of both missions are on the order of 10(exp 20) atoms/sq cm. The identical materials will be examined in both experiments to determine the material recession rate degradation for different exposure times and ambient atmospheres. The materials selected are mainly candidates for Columbus and other elements of the upcoming orbital infrastructure: fibers and matrix materials for composites; coatings, paints, and materials for thermal blankets; and electrical contacts. ESA

N94-21391* National Aeronautics and Space Administration. Lyndon B. Johnson Space Center, Houston, TX.

THE INTERNATIONAL TELECOMMUNICATIONS SATELLITE (INTELSAT) SOLAR ARRAY COUPON (ISAC) ATOMIC OXGYEN FLIGHT EXPERIMENT: TECHNIQUES, RESULTS AND SUMMARY **c44**

S. Koontz, G. King, A. Dunnet (International Telecommunications Satellite Organization, Washington, DC.), T. Kirkendahl (Communications Satellite Corp., Washington, DC.), R. Linton (National Aeronautics and Space Administration. Marshall Space Flight Center, Huntsville, AL.), and J. Vaughn (National Aeronautics and Space Administration. Marshall Space Flight Center, Huntsville, AL.) *In* CNES, Fifth International Symposium on Materials in a Space Environment Jun. 1993 p 331-348 (For primary document see N94-21367 05-18)

Copyright Avail: CEPADUES-Editions, 111, rue Nicolas-Vaquelin, 31100 Toulouse, France

Techniques and results of the ISAC flight experiment are presented, and comparisons between flight tests results and ground based testing are made. The ISAC flight experiment, one component of a larger INTELSAT 6 rescue program, tested solar array configurations and individual silver connects in ground based facilities and during STS-41 (Space Shuttle Discovery). In addition to the INTELSAT specimens, several materials, for which little or no flight data exist, were also tested for atomic oxygen reactivity. Dry lubricants, elastomers, polymeric materials, and inorganic materials were exposed to an oxygen atom fluence of 1.2 x 10(exp 20) atoms. Many of the samples were selected to support Space Station Freedom design and decision-making. ESA

N94-21392 Spar Aerospace Ltd., Toronto (Ontario).

DURABILITY OF THERMAL CONTROL AND ENVIRONMENTAL PROTECTIVE MATERIALS FOR THE SSRMS IN SIMULATED LEO ENVIRONMENT

S. K. Chang *In* CNES, Fifth International Symposium on Materials in a Space Environment Jun. 1993 p 349-367 Sponsored by Canadian Space Station Program (For primary document see N94-21367 05-18)

Copyright Avail: CEPADUES-Editions, 111, rue Nicolas-Vaquelin, 31100 Toulouse, France

Nine thermal control and environmental protection materials, selected on the basis of their space pedigree, thermal vacuum stability, and thermo-optical properties, were tested to determine their suitability for the Space Station Remote Manipulator System (SSRMS). The ground based testing was carried out to simulate the effects of atomic oxygen and thermal cycling in the Low Earth Orbit (LEO) environment. These factors are deemed most likely to cause degradation to the selected materials. With the exception of the urethane based coatings, the materials tested demonstrate sufficient resistance to atomic oxygen. The detrimental effect of thermal cycling on the adhesion of the silicate based coatings to aluminum substrate was found to depend on the pigment. A separate experiment on Beta-Cloth showed that its thermo-optical properties remained substantially unchanged as the Teflon coating was progressively removed in a plasma asher. ESA

N94-21393* National Aeronautics and Space Administration. Lyndon B. Johnson Space Center, Houston, TX.

ATOMIC OXYGEN INTERACTION WITH SPACECRAFT MATERIALS: RELATIONSHIP BETWEEN ORBITAL AND GROUND-BASED TESTING FOR MATERIALS CERTIFICATION **c25**

Jon B. Cross (Los Alamos National Lab., NM.), Steven L. Koontz, and Esther H. Lan (McDonnell-Douglas Space Systems Co., Huntington Beach, CA.) *In* CNES, Fifth International Symposium on Materials in a Space Environment Jun. 1993 p 369-384 (For primary document see N94-21367 05-18)

Copyright Avail: CEPADUES-Editions, 111, rue Nicolas-Vaquelin, 31100 Toulouse, France

The effects of atomic oxygen on boron nitride (BN), silicon nitride (Si3N4), Intelsat 6 solar cell interconnects, organic polymers, and MoS2 and WS2 dry lubricant, were studied in Low Earth Orbit (LEO) flight experiments and in a ground based simulation facility. Both the inflight and ground based experiments employed in situ electrical resistance measurements to detect penetration of atomic oxygen through materials and Electron Spectroscopy for Chemical Analysis (ESCA) analysis to measure chemical composition changes. Results are given. The ground based results on the materials studied to date show good qualitative correlation with the LEO flight results, thus validating the simulation fidelity of the ground based facility in terms of reproducing LEO flight results. In addition it was demonstrated that ground based simulation is capable of performing more detailed experiments than orbital exposures can presently perform. This allows the development of a fundamental understanding of the mechanisms involved in the LEO environment degradation of materials. ESA

N94-21394 Toronto Univ. (Ontario).

EVALUATION OF PLASMA-DEPOSITED PROTECTIVE COATINGS FOR SPACECRAFT APPLICATIONS **c27**

R. C. Tennyson, K. G. Balmain, M. R. Wertheimer (Ecole Polytechnique, Montreal, Quebec.), and D. G. Zimcik (Canadian Space Agency, Ottawa, Ontario.) *In* CNES, Fifth International Symposium on Materials in a Space Environment Jun. 1993 p 385-400 Sponsored by Natural Sciences and Engineering Research Council, Canada, and Ontario Inst. for Space and Terrestrial Science, Canada (For primary document see N94-21367 05-18)

Copyright Avail: CEPADUES-Editions, 111, rue Nicolas-Vaquelin, 31100 Toulouse, France

The results of evaluations of thin film protective layers applied to selected organic substrates (Kapton polyimide, graphite/epoxy, and amorphous carbon) that have been shown to be attacked by atomic oxygen are reported. These protective films, derived from volatile compounds via microwave glow discharge, include amorphous hydrogenated silicon, inorganic silicon compounds, and organosilicones. These materials were exposed to attack from atomic oxygen oxygen beam bombardment, while sensitive measurements of mass loss rate and total mass loss were made in situ using Quartz Crystal Microbalances (QCM's) coated with the candidate materials. The results of mass loss measurements show that the coatings provide excellent protection compared to unprotected specimens of the same materials. Results from high energy (20 keV) electron beam bombardment show that P-SiO2 and SiN coatings on Kapton prevent discharge occurrence while other coating substrate combinations result in discharge modification with respect to both peak current, and discharge frequency and duration. Mechanical loading and thermal stressing confirmed that the coatings adhere tightly to the substrate and remain intact up to the point of fracture of the underlying material. Thermal radiative property measurements are presented for protective films which show little change from the uncoated materials in the virgin state both before as well as after exposure to atomic oxygen attack. The results of space flight tests which corroborate the laboratory results are presented. ESA

N94-21395 Physical Sciences, Inc., Andover, MA.

FAST OXYGEN ATOM STUDIES RELATED TO LOW EARTH ORBIT ACTIVITIES Abstract Only

G. E. Caledonia, R. H. Krech, K. W. Holtzclaw, and D. Sonnenfroh *In* CNES, Fifth International Symposium on Materials in a Space Environment Jun. 1993 p 403 (For primary document see N94-21367 05-18)

Copyright Avail: CEPADUES-Editions, 111, rue Nicolas-Vaquelin, 31100 Toulouse, France

The technique of laser induced gas breakdown to develop a high flux pulsed source of fast oxygen atoms (v = 5 to 12 km/s) is considered. The technique is also used to produce high velocity beams of N/N2 mixtures and can be extended to produce beams of other species. The fast oxygen atoms are of particular current interest since this is the dominant atmospheric species encountered by spacecraft operating in Low Earth Orbit (LEO). The fast oxygen atom source has proven extremely versatile and is used to study a variety of gas-surface and gas-gas collision phenomena. The fast atom facility has reproducibly provided good comparison with LEO observations. Expanded programs involving material testing and measurement of O atom momentum and energy accommodation coefficients with surfaces are presently underway. ESA

N94-21396 European Space Agency. European Space Research and Technology Center, ESTEC, Noordwijk (Netherlands).

ATOMIC OXYGEN FLUENCE DETECTOR FOR BREMSAT: SCIENTIFIC AND TECHNICAL DESCRIPTION **c19**

G. Drolshagen and M. VanEesbeek *In* CNES, Fifth International Symposium on Materials in a Space Environment Jun. 1993 p 405-408 (For primary document see N94-21367 05-18)

Copyright Avail: CEPADUES-Editions, 111, rue Nicolas-Vaquelin, 31100 Toulouse, France

A detector which will be upgraded to proto-flight model to be flown on Bremsat and other future missions is presented. The detector basically consist of 2 carbon coated Quartz Crystal Microbalances (QCM) with the associated electronics and interfaces. A QCM measures frequency changes

due to mass change. It can be used both for mass deposition and erosion. The detector will be exposed to the direct O flux for about 5% of each Bremsat rotation period. Preliminary calculations show that this will correspond to some 1.9 times 10 to the 20th power O atoms/sq cm over the complete mission. After completion of the mission a detailed analysis will be performed comparing the measurements to the predictions obtained from the latest atmosphere models. ESA

N94-21397 Centre d'Etudes de Gramat (France).
HYPERVELOCITY IMPACT STUDIES AT CEG: EXPERIMENTAL AND NUMERICAL CAPABILITIES Abstract Only [LES MOYENS EXPERIMENTAUX ET NUMERIQUES DU CEG POUR LES ETUDES D'IMPACT HYPERVITESSE] **c39**
C. Loupias and B. Jimenez *In* CNES, Fifth International Symposium on Materials in a Space Environment Jun. 1993 p 409-410 In ENGLISH and FRENCH (For primary document see N94-21367 05-18)
Copyright Avail: CEPADUES-Editions, 111, rue Nicolas-Vaquelin, 31100 Toulouse, France

Experimental and numerical facilities to study hypervelocity impacts are addressed. The CEG (Centre d'Etudes de Gramat) experimental facilities mainly consist of a two stage light gas gun which can accelerate 1 to 5 grams projectiles up to 8 km/s, with full knowledge and repeatability of the impact conditions. The experimenter can choose the nature, shape and mass of the projectile, moreover he exactly knows the projectile state just before impact. For the diagnosis of hypervelocity impacts, specific instrumentation is associated with launcher: Lagrangian gauges, velocity interferometers, flash X-ray systems, infrared Crantz-Schardin camera, ultra high speed pyrometer. The numerical capabilities are also suited for numerical simulations of hypervelocity impacts: powerful computers, two dimensional and three dimensional codes (HULL, EPIC, etc.). This set of experimental and numerical capabilities can be used, on the one hand to characterize dynamic behavior of materials under hypervelocity impact and, on the other hand, to suggest and test new concepts of spacecraft bumper shields. ESA

N94-21398 Societe Europeenne de Propulsion, Vernon (France).
THERMOSTRUCTURAL MATERIAL COMPOSITES FOR SPACE APPLICATIONS Abstract Only [MATERIAUX COMPOSITES THERMOSTRUCTURAUX POUR APPLICATIONS SPATIALES] **c24**
F. Christin, P. Taveau, M. Cataldi, and M. Lacoste *In* CNES, Fifth International Symposium on Materials in a Space Environment Jun. 1993 p 411-412 In FRENCH (For primary document see N94-21367 05-18)
Copyright Avail: CEPADUES-Editions, 111, rue Nicolas-Vaquelin, 31100 Toulouse, France

The development, fabrication and space applications of Ceramic Matrix Composites (CMC's) reinforced by carbon or silicon carbon fibers are addressed. The CMC's used for the thermal protection of the Hermes Spaceplane are considered. Their resistance to solar radiation, fatigue and damage is described. Their space applications include thermal protection, thermal structures and high temperature antennas. ESA

N94-21399 Moscow State Univ. (Russia).
FORECASTING TECHNIQUE OF VARIATIONS OF THE OPTICAL ABSORPTIVITY OF THERMAL CONTROL COATINGS UNDER DIFFERENT SIMULTANEOUS RADIATIONS **c27**
A. P. Grashchenko and G. G. Soloviev *In its* Fifth International Symposium on Materials in a Space Environment Jun. 1993 p 413-426 (For primary document see N94-21367 05-18)
Copyright Avail: CEPADUES-Editions, 111, rue Nicolas-Vaquelin, 31100 Toulouse, France

Thermal control coatings with high reflectivity are considered with emphasis upon a model of the behavior of the integral optical absorptivity under different radiations. Since the change in the integral absorptivity of solar radiation is equal to the corresponding change in the reflectivity, the latter is discussed. Experimental results are presented. ESA

N94-21400 Centre National d'Etudes Spatiales, Toulouse (France).
THERMAL CONTROL COATINGS **c27**
Jean-Claude Guillaumon and Francoise Guerard (MAP S.A., Pamiers, France.) *In its* Fifth International Symposium on Materials in a Space Environment Jun. 1993 p 427-433 (For primary document see N94-21367 05-18)
Copyright Avail: CEPADUES-Editions, 111, rue Nicolas-Vaquelin, 31100 Toulouse, France

Thermal control coatings for space vehicles are presented. These can be divided into three groups: cold coatings (white paints), middle coatings (aluminum paints) and hot coatings (black paints). Conductive paints, which allow the evacuation of electrostatic charges, and non-conductive paints are considered. Since white conductive paints reduce or cancel the RF transparency a new generation of 'antistatic' white paints was developed to allow electrostatic charge evacuation without reducing RF transparency. A new generation of low outgassing aluminum paints and a new silicone varnish used to protect Kapton against atomic oxygen, are considered. Products under development are discussed. ESA

N94-21401 Nauchno-Proizvodstvennoe Obedinenie Energija, Kaliningrad (USSR).
STUDY OF SPACE FACTORS EFFECT ON MATERIALS FOR SPACECRAFT EXTERNAL SURFACES IN NPO ENERGIA PROGRAMS
V. P. Nikitskiy *In* CNES, Fifth International Symposium on Materials in a Space Environment Jun. 1993 p 435-437 (For primary document see N94-21367 05-18)
Copyright Avail: CEPADUES-Editions, 111, rue Nicolas-Vaquelin, 31100 Toulouse, France

The purpose and tasks of flight tests in near Earth orbits in the assessment of operating resistance of materials for spacecraft external materials are addressed. They include the determination of the strength and lifetime, verification under the conditions of flight of materials and coatings operationability recommended for perspective space vehicles; investigation of operational characteristics changes (thermal radiational, spectral, physical and mechanical, strength, mass, etc.) after long-term operation; procedures development to forecast materials operating characteristics changes for long-term operation. Specific instruments developed to perform these tests are listed. Different classes of thermal control coatings tested are considered. Experiments showed that the most effective way of material protection from atomic oxygen effect is application to its surfaces of thin coatings based on fluorine plastic materials, metals and silicon oxides. The tests of thermal control coating of the 'solar reflector' class proved their high endurance and allowed to predict their serviceability without further changes of thermal radiation characteristics for orbital service in near Earth orbits for up to 20 to 30 years. A platform, Sinus, developed to continue these experiments is addressed. ESA

N94-21402 Messerschmitt-Boelkow-Blohm G.m.b.H., Bremen (Germany). Columbus Mechanical Parts, Materials and Processes.
COLUMBUS PMP CRITICAL TECHNOLOGIES PROGRAM: APPROACH FOR MATERIALS LIFE TIME PREDICTION
Heinrich Baumann (Erno Raumfahrttechnik G.m.b.H., Bremen, Germany.) and Fabienne Dricot (Erno Raumfahrttechnik G.m.b.H., Bremen, Germany.) *In* CNES, Fifth International Symposium on Materials in a Space Environment Jun. 1993 p 441-455 (For primary document see N94-21367 05-18)
Copyright Avail: CEPADUES-Editions, 111, rue Nicolas-Vaquelin, 31100 Toulouse, France

An approach to resolve the verification of materials extended life time behavior for the Columbus elements is described. The combination of the 10 to 30 years life time requirement, on orbit maintenance and repair led to a new strategy in materials selection and verification. This strategy, introduced as the 'PMP (Parts, Materials and Processes) Critical Technologies Program' also considers the schedule and funding constraints which require adaptation to the minimum program needs and pragmatic approaches. ESA

N94-21403 European Space Agency. European Space Research and Technology Center, ESTEC, Noordwijk (Netherlands). Materials and Processes Div.
TOXICITY OF THERMAL DEGRADATION IN A MANNED SPACE ENVIRONMENT **c54**
M. D. Judd and D. Bryant *In* CNES, Fifth International Symposium on Materials in a Space Environment Jun. 1993 p 457-471 (For primary document see N94-21367 05-18)
Copyright Avail: CEPADUES-Editions, 111, rue Nicolas-Vaquelin, 31100 Toulouse, France

An overview of current thinking with regard to flammability and associated hazards pertinent to the special circumstances encountered in a manned space environment is given. The fire performance of materials needs to be assessed on a more comprehensive basis than the past and the first steps to achieving this are presented. More emphasis is necessary on the importance of understanding the toxicity of decomposition products, however difficult this is to quantify in practice. The extra safety problems associated with long term missions in space have to be tackled early in the design stage. The recent decision by the Space Station planners to choose an atmosphere of 30% O2 at 10.7 psi for facilitating EVA (Extravehicular Activity) will undoubtedly lead to a large amount of material testing since most current data is at 24.5% O2 normal pressure. ESA

N94-21404 Centre National de la Recherche Scientifique, Odeillo (France).
HIGH TEMPERATURE SIMULATION CHAMBERS. PHYSICO-CHEMICAL AND THERMAL EFFECT OF ATMOSPHERIC REENTRY ON CERAMIC MATERIALS [ENCEINTES DE SIMULATION A HAUTE TEMPERATURE DES EFFETS THERMIQUES ET PHYSICO-CHIMIQUES DE LA RENTREE ATMOSPHERIQUE SUR DES MATERIAUX CERAMIQUES] **c14**
M. Balat, G. Flamant, B. Rivoire, M. Dudeck (Laboratoire d'Aerothermique du CNRS, Meudon, France.), and P. Lasgorceix (Laboratoire d'Aerothermique du CNRS, Meudon, France.) *In* CNES, Fifth International Symposium on Materials in a Space Environment Jun. 1993 p 475-488 In FRENCH (For primary document see N94-21367 05-18)
Copyright Avail: CEPADUES-Editions, 111, rue Nicolas-Vaquelin, 31100 Toulouse, France

Two research facilities which use a microwave generator to produce high temperature, low pressure, and molecular or dissociated atmospheric conditions for the testing of ceramic materials are presented. These facilities simulate the conditions of atmospheric reentry. One simulator permits the testing of samples of small dimensions (40 by 40 mm) and the other for samples 500 by 500 mm. In the latter the plasma is of the arc blown type. Results of experiments carried out in the small chamber are presented. ESA

N94-21405 Centre National de la Recherche Scientifique, Odeillo (France).
A METHOD OF MEASURING THE THERMORADIATIVE PROPERTIES OF CERAMIC MATERIALS IN A SPACE ENVIRONMENT [METHODE DE MESURE DES PROPRIETES THERMORADIATIVES DE MATERIUX CERAMIQUES EN ENVIRONNEMENT SPATIAL] **c27**
M. Balat, C. Dupuy, D. Hernandez, J. F. Robert, and G. Olalde *In* CNES, Fifth International Symposium on Materials in a Space Environment Jun. 1993 p 489-496 In FRENCH (For primary document see N94-21367 05-18)
Copyright Avail: CEPADUES-Editions, 111, rue Nicolas-Vaquelin, 31100 Toulouse, France

A method to measure the thermoradiative properties of ceramic materials to be used for mechanical and thermal protection during reentry is considered. A method to measure emission suitable for space environment simulation devices was developed. A photonic system to measure temperature is described. The operating principle of the experimental device is outlined. Results showed that the emission of the ceramic spacecraft thermal protection materials depends principally on the temperature level, the type of thermal cycle and the surface state of the material, which is itself closely linked to oxidation phenomena at the time of treatment. ESA

N94-21406 Tsukuba Space Center (Japan).
R AND D TO HOPE AIRFRAME
Yoshiki Morino and Tadashi Matsushita *In* CNES, Fifth International Symposium on Materials in a Space Environment Jun. 1993 p 497-512 (For primary document see N94-21367 05-18)
Copyright Avail: CEPADUES-Editions, 111, rue Nicolas-Vaquelin, 31100 Toulouse, France

The status of research and development on the primary structure and Thermal Protection System (TPS) of the H2 Orbiting Plane (HOPE) is presented. Mechanical properties of graphite/polyimide composite, which is selected as first candidate material for the main structure, are reported under expected flight environments of HOPE and results of fabrication tests are also described. As for the TPS, design and manufacturing considerations of each TPS are outlined, and some data obtained from the research and development experiments so far are presented. ESA

N94-21407 National Space Development Agency, Tokyo (Japan).
JAPANESE SPACE PROGRAM **c12**
Yoshiki Morino *In* CNES, Fifth International Symposium on Materials in a Space Environment Jun. 1993 p 513-515 (For primary document see N94-21367 05-18)
Copyright Avail: CEPADUES-Editions, 111, rue Nicolas-Vaquelin, 31100 Toulouse, France

The organization and budget of Japanese space activities is outlined. There are two major performers: NASDA (National Space Development Agency) and ISAS (Institute of Space and Astronautical Sciences). The budget is roughly 1 billion dollars/year (1/10 of NASDA's budget), 70% goes to NASA, and 10% to ISAS. NASDA's space development programs, launch vehicles, NASDA's satellite programs, HOPE (H-2 Orbiting Plane) Project, scientific satellites of ISAS and NASDA's major facilities are described. ESA

N94-21408 Dassault Aviation, Balgnac (France).
MATERIAL PROPERTIES AND BEHAVIOR DURING SIMULATED ATMOSPHERIC REENTRY [PROPRIETES ET COMPORTEMENTS DES MATERIAUX LORS DE SIMULATION DE RENTREES ATMOSPHERIQUES]
B. Berton, G. Navarre, C. Chenet, and G. Bernhart *In* CNES, Fifth International Symposium on Materials in a Space Environment Jun. 1993 p 517-528 In FRENCH (For primary document see N94-21367 05-18)
Copyright Avail: CEPADUES-Editions, 111, rue Nicolas-Vaquelin, 31100 Toulouse, France

Specific test facilities were developed to characterize and validate the performance of thermal protection materials in this particular environment. Two classes of facilities are used: test facilities to determine surface properties which have a direct influence of the temperature of the parts (emissivity, catalycity), and test facilities for simulation of the atmospheric reentry, to study the evolution of materials during this flight phase (plasma torch, radiant facilities). The space plane induced environment is recalled and the operational and under development test facilities are described. Comparative results obtained on reference materials which were tested in those test facilities are presented. The comparative analysis shows a significant difference in behavior, especially in plasma arc jets. Ongoing activities which will be used to identify the most representative facilities are presented. ESA

N94-21420# Institute for Defense Analyses, Alexandria, VA.
ENTRY VELOCITIES AT MARS AND EARTH FOR SHORT TRANSIT TIMES Final Report, Dec. 1989 - Jul. 1991
Reinald G. Finke Jul. 1993 43 p
(AD-A272591; IDA-P-2602; IDA/HQ-91-37961; AD-E501719) Avail: CASI HC A03/MF A01

Propulsion systems composed of a Shuttle External Tank, appropriately modified for the purpose, with a rocket engine that is either an SSME or a NERVA could inject a gross personnel payload of 100,000 lb on a trans-Mars trajectory from Space Station Freedom with aerobraking at Mars with transit times of less that 70 days. Such transit times reflect a significant reduction from the 200-plus days generally considered. The 100,000-lb payload would include the mass of a hypothetical aerobrake for aerocapture at Mars. The entry velocities at Mars compatible with such transit times are greater that 21 km/sec, to be compared with previously stated constraints of 8.5 to 9.5 km/sec for nominal Mars entry velocity. Limits of current aerobrake technology are not well enough defined to determine the feasibility of an aerobrake to handle Mars-entry velocities for short-transit-time trajectories. Return from Mars to Earth on a mirror image of 70-days outbound trajectory (consistent with a stay time of about 12 days) would require a Mars-departure velocity increment more than twice as great as that at Earth departure and would require a correspondingly more capable propulsion system. The return propulsion system would preferably be pre-deployed at Mars by one or more separate minimum-energy, 0.5 to 1.1 Mlb gross payload cargo flights with the same outbound propulsion systems as the personnel flight, before commitment of the personnel flight. Aerobraking entry velocity at Earth after such a transit time would be about 16 km/sec, to be compared with constraints set at 12.5 to 16 km/sec. DTIC

N94-21864*# Sverdrup Technology, Inc., Brook Park, OH.
TROPIX PLASMA INTERACTIONS GROUP REPORT Final Report, Apr. - Jul. 1993
Joel L. Herr and Ricaurte Chock (National Aeronautics and Space Administration. Lewis Research Center, Cleveland, OH.) Oct. 1993 41 p
(Contract NAS3-25266; RTOP 506-41-52)
(NASA-CR-191149; E-8169; NAS 1.26:191149) Avail: CASI HC A03/MF A01

The purpose is to summarize the spacecraft charging analysis conducted by the plasma interactions group during the period from April 1993 to July 1993, on the proposed TROPIX spacecraft, and to make design recommendations which will limit the detrimental effects introduced by spacecraft charging. The recommendations were presented to the TROPIX study team at a Technical Review meeting held on 15 July 1993.
Author (revised)

N94-20864*# POD Associates, Inc., Albuquerque, NM.
A FRESH LOOK AT CRATER SCALING LAWS FOR NORMAL AND OBLIQUE HYPERVELOCITY IMPACTS Abstract Only
A. J. Watts, D. R. Atkinson, S. R. Rieco, J. B. Brandvold, S. L. Lapin, and C. R. Coombs *In* Lunar and Planetary Inst., Twenty-Fourth Lunar and Planetary Science Conference. Part 3: N-Z 1993 p 1497-1498 (For primary document see N94-20636 05-91)
Avail: CASI HC A01/MF A06

N94-20890*# Tokyo Univ. (Japan). Inst. for Cosmic Ray Research.
GEOMETRICAL ANALYSIS OF THE MICROCRATERS FOUND ON LDEF SAMPLES Abstract Only
Kazuo Yamakoshi, Hideo Ohashi, Motosaku Noma (Yamagata Univ., Japan.), Hirohisa Sakurai (Yamagata Univ., Japan.), Kazuo Nakashima (Yamagata Univ., Japan.), Kenichi Nogami (Dokkyo Univ., Tochigi, Japan.), and Rie Omori (Dokkyo Univ., Tochigi, Japan.) *In* Lunar and Planetary Inst., Twenty-Fourth Lunar and Planetary Science Conference. Part 3: N-Z 1993 p 1549-1550 (For primary document see N94-20636 05-91)
Avail: CASI HC A01/MF A06

N94-21338*# GTE Government Systems Corp., Las Cruces, NM.
ANALYSIS OF THE TDRS MULTIPLE ACCESS SYSTEM FOR POSSIBLE USE AS AN ATTITUDE CONTROL SYSTEM SENSOR
Bruce Allyn Blevins and Victor J. Sank (Herold, Fredrick and Associates, Inc., Greenbelt, MD.) *In* NASA. Goddard Space Flight Center, Networks Technology Conference Nov. 1993 p 195-207 (For primary document see N94-21323 05-62)
Avail: CASI HC A03/MF A03

19 SPACECRAFT INSTRUMENTATION

For related information see also *06 Aircraft Instrumentation* and *35 Instrumentation and Photography.*

N94-21780*# New Hampshire Univ., Durham. Office of Sponsored Research.
[A NEW INNOVATIVE INSTRUMENT FOR SPACE PLASMA INSTRUMENTATION] Final Report
Roy B. Torbert 6 Dec. 1993 50 p
(Grant NAGw-2043)
(NASA-CR-194736; NAS 1.26:194736) Avail: CASI HC A03/MF A01

The Faraday Ring Ammeter was the subject of this grant for a new innovative instrument for space plasma instrumentation. This report summarizes our progress in this work. Briefly, we have conducted an intensive series of experiments and trials over three years, testing some five configurations of the instrument to measure currents, resulting in two Ph.D. theses, supported by this grant, and two flight configurations of the instrument. The first flight would have been on a NASA-Air Force collaborative sounding rocket, but was not flown because of instrumental difficulties. The second has been successfully integrated on the NASA Auroral Turbulence payload which is to be launched in February, 1994.
Derived from text

N94-22275*# Lockheed Engineering and Sciences Co., Houston, TX.
SPACE GENERIC OPEN AVIONICS ARCHITECTURE (SGOAA) STANDARD SPECIFICATION
Richard B. Wray and John R. Stovall Dec. 1993 86 p Revised
(Contract NAS9-17900)
(NASA-CR-188269; NAS 1.26:188269; LESC-30354-B) Copyright Avail: CASI HC A05/MF A01

The purpose of this standard is to provide an umbrella set of requirements for applying the generic architecture interface model to the design of a specific avionics hardware/software system. This standard defines a generic set of system interface points to facilitate identification of critical interfaces and establishes the requirements for applying appropriate low level detailed implementation standards to those interface points. The generic core avionics system and processing architecture models provided herein are robustly tailorable to specific system applications and provide a platform upon which the interface model is to be applied.
Derived from text

N94-21086*# Jet Propulsion Lab., California Inst. of Tech., Pasadena. Very Large Scale Integrated Technology Group.
STRV RADMON: AN INTEGRATED HIGH-ENERGY PARTICLE DETECTOR
Martin Buehler, George Soli, Brent Blaes, and Gemma Tardio *In* New Mexico Univ., The Fifth NASA Symposium on VLSI Design 1993 11 p (For primary document see N94-21079 05-33)
Avail: CASI HC A03/MF A06

N94-21396 European Space Agency. European Space Research and Technology Center, ESTEC, Noordwijk (Netherlands).
ATOMIC OXYGEN FLUENCE DETECTOR FOR BREMSAT: SCIENTIFIC AND TECHNICAL DESCRIPTION
G. Drolshagen and M. VanEesbeek *In* CNES, Fifth International Symposium on Materials in a Space Environment Jun. 1993 p 405-408 (For primary document see N94-21367 05-18)
Copyright Avail: CEPADUES-Editions, 111, rue Nicolas-Vaquelin, 31100 Toulouse, France

N94-21733*# Jet Propulsion Lab., California Inst. of Tech., Pasadena.
LOW POWER, CMOS DIGITAL AUTOCORRELATOR SPECTROMETER FOR SPACEBORNE APPLICATIONS
Kumar Chandra and William J. Wilson *In* Idaho Univ., The 1992 4th NASA SERC Symposium on VLSI Design 1992 12 p (For primary document see N94-21694 05-33)
Avail: CASI HC A03/MF A04

20 SPACECRAFT PROPULSION AND POWER

Includes main propulsion systems and components, e.g., rocket engines; and spacecraft auxilliary power sources.

For related information see also *07 Aircraft Propulsion and Power, 28 Propellants and Fuels, 44 Energy Production and Conversion,* and *15 Launch Vehicles and Space Vehicles.*

N94-19818*# National Aeronautics and Space Administration. Ames Research Center, Moffett Field, CA.
BOOST-PHASE DISCRIMINATION RESEARCH Final Report, 26 Feb. 1990 - 25 Feb. 1993
Stephen R. Langhoff and William J. Feiereisen 7 Jul. 1993 15 p
(Contract MIPR-135-92)
(NASA-TM-109347; NAS 1.15:109347; AD-A270939; ARO-27469.1-EG-SDI)
Avail: CASI HC A03/MF A01

The final report describes the combined work of the Computational Chemistry and Aerothermodynamics branches within the Thermosciences Division at NASA Ames Research Center directed at understanding the signatures of shock-heated air. Considerable progress was made in determining accurate transition probabilities for the important band systems of NO that account for much of the emission in the ultraviolet region. Research carried out under this project showed that in order to reproduce the observed radiation from the bow shock region of missiles in their boost phase it is necessary to include the Burnett terms in the constituent equation, account for the non-Boltzmann energy distribution, correctly model the NO formation and rotational excitation process, and use accurate

transition probabilities for the NO band systems. This work resulted in significant improvements in the computer code NEQAIR that models both the radiation and fluid dynamics in the shock region. DTIC

N94-19847# Massachusetts Inst. of Tech., Cambridge. Dept. of Aeronautics and Astronautics.
PERFORMANCE POTENTIAL OF PLASMA THRUSTERS: ARCJET AND HALL THRUSTER MODELING Final Report, 1 May 1992 - 30 Apr. 1993
Manuel Martinez-Sanchez 17 Sep. 1993 66 p
(Grant AF-AFOSR-0256-91)
(AD-A271085; AFOSR-93-0753TR) Avail: CASI HC A04/MF A01

This is the second and final yearly Report on Grant 91-0256, for the period 5/1/92-4/30/93. The Report describes two recently completed and highly successful models for the internal physics and the performance of hydrogen arcjets and Hall thrusters, respectively. These are thought to represent the state-of-the-art in their respective topics. Also discussed is an equally significant theoretical model of MPD anode drops, which completes previously funded work. DTIC

N94-20015 Georgia Inst. of Tech., Atlanta. School of Aerospace Engineering.
INVESTIGATION OF FLAME DRIVING AND FLOW TURNING IN AXIAL SOLID ROCKET INSTABILITIES Final Report, 1 Mar. 1991 - 30 Jun. 1993
Ben T. Zinn, Brady R. Daniel, and Lawrence M. Matta 31 Aug. 1993 78 p Limited Reproducibility: More than 20% of this document may be affected by microfiche quality
(Grant AF-AFOSR-0160-91)
(AD-A271066; AFOSR-93-0776TR) Avail: CASI HC A05

An understanding of the processes responsible for driving and damping acoustic oscillations in solid rocket motors is necessary for developing practical design methods that eliminate or reduce the occurrence combustion instabilities. While state of the art solid rocket stability prediction methods generally account for the flow turning loss, the magnitude and characteristics of this loss have never been fully investigated. Results of an investigation of the role of the flow turning loss in the stability of solid rockets and its dependence upon motor design and operating parameters are described. A one dimensional acoustic stability equation that verifies that the flow turning loss term is appropriately included in the one dimensional stability formulation was derived for a chamber with a constant mean temperature and pressure by an approach independent from that of Culick. This study was extended providing the background and expressions needed to guide an experimental study of the flow turning loss in the presence of mean temperature and density gradients. This allows the study of combustion systems in which mean temperature gradients and heat losses are significant. The relevant conservation equations were solved numerically for the experimental configuration in order to predict the behavior of the flow turning loss and to assist in the analysis of experimental results. Experiments performed, with and without combustion, showed that the flow turning loss strongly depends upon the propellant burning rate and the location of the flow turning region relative to the standing pressure wave. DTIC

N94-20062*# National Aeronautics and Space Administration. Lewis Research Center, Cleveland, OH.
SYSTEM PERFORMANCE PREDICTIONS FOR SPACE STATION FREEDOM'S ELECTRIC POWER SYSTEM
Thomas W. Kerslake, Jeffrey S. Hojnicki, Robert D. Green, and Jeffrey C. Follo Nov. 1993 8 p Presented at the 28th Intersociety Energy Conversion Engineering Conference, Atlanta, GA, 8-13 Aug. 1993; sponsored by American Chemical Society
(RTOP 474-12-10)
(NASA-TM-106396; E-8221; NAS 1.15:106396) Avail: CASI HC A02/MF A01

Space Station Freedom Electric Power System (EPS) capability to effectively deliver power to housekeeping and user loads continues to strongly influence Freedom's design and planned approaches for assembly and operations. The EPS design consists of silicon photovoltaic (PV) arrays, nickel-hydrogen batteries, and direct current power management and distribution hardware and cabling. To properly characterize the inherent EPS design capability, detailed system performance analyses must be performed for early stages as well as for the fully assembled station up to 15 years after beginning of life. Such analyses were repeatedly performed using the FORTRAN code SPACE (Station Power Analysis for Capability Evaluation) developed at the NASA Lewis Research Center over a 10-year period. SPACE combines orbital mechanics routines, station orientation/pointing routines, PV array and battery performance models, and a distribution system load-flow analysis to predict EPS performance. Time-dependent, performance degradation, low earth orbit environmental interactions, and EPS architecture build-up are incorporated in SPACE. Results from two typical SPACE analytical cases are presented: (1) an electric load driven case and (2) a maximum EPS capability case. Author

N94-20068# Von Karman Inst. for Fluid Dynamics, Rhode-Saint-Genese (Belgium).
SPACECRAFT PROPULSION
1993 465 p Lecture series held in Rhode-Saint-Genese, Belgium, 25-29 Jan. 1993
(VKI-LS-1993-01; ETN-93-94444) Copyright Avail: CASI HC A20/MF A04

The principles of rocket propulsion and the advantages of the different schemes and propellant combinations are reviewed. The aim was to focus on the cryogenic types of propulsion units and the cycles on which they were based. A general overview of the main current engines is given. Specific items of propulsion or turbomachinery nature are included. The prospects of future applications are covered. The large cryogenic rocket engines and typical examples of the different cycles used in the design of advanced units currently in operation are summarized. Special turbomachinery problems such as the pump and turbine drive designs with their typical problems in the cryogenic environment are considered. Turbine nozzle and bucket design were reviewed. The high performance pump was exposed to the cavitation problems and an advanced analysis for the loss model was required using the distributed loss concept. For individual titles, see N94-20069 through N94-20080.

N94-20069# Massachusetts Inst. of Tech., Cambridge.
LIQUID ROCKET PROPULSION. THEORY
M. Martinez-Sanchez *In* VKI, Spacecraft Propulsion 1993 105 p (For primary document see N94-20068 05-20)
Copyright Avail: CASI HC A06/MF A04

The purpose is to introduce the fundamentals and the basic technology of liquid propellant rockets. Much of the material is derived from other courses on propulsion. The first lecture covers the foundations at the broad brush level. Starting from the functional requirements placed on the device, various types of rocket are examined. The missions for which liquid propellant rockets are the better choice are identified. An ideal gas examination of the essential performance parameters and their variation with basic controllable inputs is presented. The thermodynamics and the fluid mechanics of the reacting flows occurring in rocket combustors and nozzles are considered. The effects of propellant choices and the +/- 5 performance estimates are included. ESA

N94-20070# Rockwell International Corp., Canoga Park, CA. Rocketdyne Div.
SPACE SHUTTLE MAIN ENGINE. OVERVIEW
Eugene D. Jackson *In* VKI, Spacecraft Propulsion 1993 22 p (For primary document see N94-20068 05-20)
Copyright Avail: CASI HC A03/MF A04

An overview of the Space Shuttle Main Engine (SSME) is presented. The Space Shuttle propulsion system consists of two large solid booster motors, three SSME's, two orbital maneuvering system engines, and 44 reaction control system thrusters. The three SSME's burn liquid hydrogen and liquid oxygen from the external tank and are sequentially started at launch. Engine thrust is throttleable. The major components and some of their key features and operational parameters are outlined. The life and reliability being achieved by the SSME are presented. ESA

N94-20071# Rockwell International Corp., Canoga Park, CA. Rocketdyne Div.
ROCKETDYNE TURBOMACHINERY
Eugene D. Jackson *In* VKI, Spacecraft Propulsion 1993 19 p (For primary document see N94-20068 05-20)
Copyright Avail: CASI HC A03/MF A04

The four turbopumps used on the Space Shuttle Main Engine (SSME) highlighting key features of each, are described. The historical development

of liquid rocket engine turbopumps primarily using those from Rocketdyne as representatives is reviewed. The design of the SSME turbopumps required significantly extending the range of operation of key turbopump parameters. The SSME was the first staged combustion cycle, first reusable engine, and the turbopumps operated at much higher power densities, pressure levels, and speeds. Through the design process, the technical level of analysis had to be increased to handle the increased power densities and pressures and to address the longer life issues. The SSME turbopumps have not only achieved their mission of successfully performing on all flights to date but also have led to the state of the art technology that is applied to new turbopump designs today. ESA

N94-20072# Rockwell International Corp., Canoga Park, CA. Rocketdyne Div.

FUTURE TECHNICAL DIRECTIONS

Eugene D. Jackson and Munir Sindir *In* VKI, Spacecraft Propulsion 1993 20 p (For primary document see N94-20068 05-20)

Copyright Avail: CASI HC A03/MF A04

The areas of more recent technical advances are discussed. These are necessarily limited to those areas approved for public dissemination. The presentation is organized as follows: new directions in the Space Shuttle Main Engine (SSME); Computational Fluid Dynamics (CFD) advances; and other areas of technology advances. The advances in the SSME are focused on the continued support to reliable flights with additional benefits in lower cost and improved robustness. In the area of CFD, significant advances are made and emphasis is placed on further reductions in time and cost to perform the complex CFD in product design organizations. The need to better understand and analyze the reality of the environments and products that are designed are discussed. This includes emphasis on dynamic loads; probabilistic as well as deterministic loads, material properties, and hardware variations; and such real property effects as the existence of flaws. Each area represents significant challenges to the engineer of the future. ESA

N94-20073# Katholieke Univ. te Leuven (Belgium). Dept. of Physics.

PROPERTIES OF CRYOGENIC LIQUIDS **c28**

A. Dupre *In* VKI, Spacecraft Propulsion 1993 5 p (For primary document see N94-20068 05-20)

Copyright Avail: CASI HC A01/MF A04

The purpose of liquefaction is considered. The cooling processes of a gas and of a liquid are reviewed. The importance of heat conduction and radiation in the storage of cryogenic liquids is discussed. The properties of the following cryogenic liquids are summarized: oxygen, nitrogen, hydrogen, 4-helium, and 3-helium. Data on boiling points, heat of vaporization and density is given. ESA

N94-20074# Volvo Flygmotor A.B., Trollhaettan (Sweden). Space Propulsion.

A TUTORIAL ON THE AERO/THERMODYNAMICAL DESIGN OF LIQUID-PROPELLANT ROCKET ENGINE NOZZLES

Lars-Olaf Pekkari *In* VKI, Spacecraft Propulsion 1993 18 p (For primary document see N94-20068 05-20)

Copyright Avail: CASI HC A03/MF A04

The most basic aspects in the design of nozzles for liquid propellant rocket engines are presented. First the divergence loss and the optimizing of the nozzle contour are described. Second the flow separation and performance of sea level nozzles are discussed. Alternative sea level nozzle concepts are outlined. The heat transfer and basic concepts for the cooling of nozzles are presented. The tutorial examples are based on the simplest methods applicable to get a transparent description of each subject. ESA

N94-20075# Volvo Flygmotor A.B., Trollhaettan (Sweden). Space Propulsion.

TURBINE DESIGN

Per Andersson *In* VKI, Spacecraft Propulsion 1993 11 p (For primary document see N94-20068 05-20)

Copyright Avail: CASI HC A03/MF A04

Turbines for most space propulsion applications, such as the hydrogen and oxygen pump turbines for the Vulcain engine, are characterized by a high pressure ratio, a highly energetic working fluid, and a small size. Data on Vulcain turbines are given. The following topics are reviewed: turbine concept design and design tools; blade design; losses occurring in a blade which are due to friction, secondary flow, tip clearance and shock formation; and turbine testing. The purpose of any turbine is to provide power for other parts of an engineering system (compressors, electrical generators, pumps) or to drive mechanical components such as wheels or propellers to give propulsion to a vehicle. It should therefore always be the performance and cost effectiveness of this larger system and not of the isolated turbine that are the main objectives for the turbine design engineer. ESA

N94-20076# Central Inst. of Aviation Motors, Moscow (Russia).

CRYOGENIC PROPELLANT ROCKET ENGINE PROBLEMS

A. Roudakov *In* VKI, Spacecraft Propulsion 1993 106 p (For primary document see N94-20068 05-20)

Copyright Avail: CASI HC A06/MF A04

Modern achievements and the problems of powerful Liquid Rocket Engines (LRE) for launch system main propulsion units are shown. Results of LRE research and development carried out in Russia are included. LRE's have been used since the beginning of the forties. Many investigations were carried out on the design of high efficiency LRE's and the technology for engine development and production. Recent data and technology have led to the development of LRE's which have parameters that are close to the upper design limits. ESA

N94-20077# Societe Europeenne de Propulsion, Vernon (France).

THE VULCAIN CRYOGENIC ENGINE

J. Gastal and J. R. L. Barton *In* VKI, Spacecraft Propulsion 1993 23 p (For primary document see N94-20068 05-20)

Copyright Avail: CASI HC A03/MF A04

The Ariane 5 was developed for the purpose of serving as the next generation Ariane launcher. The Ariane 5 main stage is powered by the Vulcain cryogenic engine. The engine operation, its main technical characteristics, and its development activities are described. The features present due to the use of liquid oxygen and, especially, liquid hydrogen are emphasized: start up procedures; ignition of the combustion; materials; mastering liquid hydrogen leakages; and safety studies. A brief development status is given. 440 engines tests and more than 100,000 seconds are planned before the end of the development to ensure reliability and safety. ESA

N94-20078# Metraflu, Ecully (France).

DISTRIBUTED LOSS MODEL: APPLICATION TO A SPATIAL TURBOPUMP INDUCER

E. M. ElGhazzani, G. Bois, and F. Leboeuf (Ecole Centrale de Lyon, France.) *In* VKI, Spacecraft Propulsion 1993 51 p (For primary document see N94-20068 05-20)

Copyright Avail: CASI HC A04/MF A04

A three dimensional Euler flow computation in a spatial turbopump inducer with a distributed loss model at nominal flow rate is presented. The numerical results and the experimental ones are in good agreement. The loss model described uses a simple pitch averaged distribution of rotary stagnation pressure drop between hub and tip. A finely distributed loss model which can take into account global losses such as the effects of boundary layer on blades and the clearance gap ones is considered. Particular treatment of boundary conditions to simulate the rotation of the tip end wall is presented. One of the particularities of this method is to simulate back flow. The code CALECHE and the Clebsch-Hawthorne formulation are used. This code is also performed on a variety of isolate blade rows. ESA

N94-20079# Institut National Polytechnique, Grenoble (France). Centre de Recherches et d'Essais de Machines Hydrauliques de Grenoble.

CAVITATION MODELLING

J. L. Kueny *In* VKI, Spacecraft Propulsion 1993 26 p (For primary document see N94-20068 05-20)

Copyright Avail: CASI HC A03/MF A04

Improvements of cavitation modeling during the past years are reviewed. They are directly correlated to the development of the computers and above all to the development of cryogenic liquid propellant fed rocket engines. Cavitation is the evaporation of a liquid, caused by lowering its pressure. It occurs at locations where the pressure falls short of a critical value, roughly corresponding to the vapor pressure. In these areas of lowest pressure, vaporous cavities appear, that rest on walls or float within the liquid. New models are available for calculation of three dimensional

partial cavitation in pumps with steady state assumptions. Two dimensional unsteady cavitating flow modelization are in development. Promising results are obtained for the prediction of the thermodynamical effects on cavitation by using a coupled code of the external liquid and the internal vapor flow. ESA

N94-20080# Von Karman Inst. for Fluid Dynamics, Rhode-Saint-Genese (Belgium).

THREE DIMENSIONAL UNSTEADY FLOW CALCULATIONS IN RADIAL COMPONENTS **c34**

A. Fatsis *In its* Spacecraft Propulsion 1993 53 p (For primary document see N94-20068 05-20)

Copyright Avail: CASI HC A04/MF A04

A numerical model to predict the impeller response due to the downstream static pressure distortion caused by the volute when a centrifugal compressor works at off design conditions is presented. The three dimensional Euler equations are solved by a time marching technique allowing the evaluation of the unsteady flowfield using the finite volume space discretization and Runge-Kutta time stepping scheme. Phase lagged periodicity conditions were used in the computations of the unsteady flow upstream and downstream the blade channel. Reflecting and non-reflecting boundary conditions were tested. It was demonstrated that the latter result in faster convergence than the former. A cyclic variation of the impeller flowfield due to the donwstream static pressure non-uniform distribution is observed. ESA

N94-20102*# National Aeronautics and Space Administration. Langley Research Center, Hampton, VA.

POWER TRANSMISSION BY LASER BEAM FROM LUNAR-SYNCHRONOUS SATELLITE

M. D. Williams, R. J. DeYoung, G. L. Schuster, S. H. Choi, J. E. Dagle (Pacific Northwest Lab., Richland, WA.), E. P. Coomes (Pacific Northwest Lab., Richland, WA.), Z. I. Antoniak (Pacific Northwest Lab., Richland, WA.), J. A. Bamberger (Pacific Northwest Lab., Richland, WA.), J. M. Bates (Pacific Northwest Lab., Richland, WA.), and M. A. Chiu (Pacific Northwest Lab., Richland, WA.) et al Nov. 1993 32 p Sponsored by NASA. Washington

(RTOP 506-41-41-01)

(NASA-TM-4496; L-17243; NAS 1.15:4496) Avail: CASI HC A03/MF A01

The possibility of beaming power from synchronous lunar orbits (the L1 and L2 Lagrange points) to a manned long-range lunar rover is addressed. The rover and two versions of a satellite system (one powered by a nuclear reactor, the other by photovoltaics) are described in terms of their masses, geometries, power needs, missions, and technological capabilities. Laser beam power is generated by a laser diode array in the satellite and converted to 30 kW of electrical power at the rover. Present technological capabilities, with some extrapolation to near future capabilities, are used in the descriptions. The advantages of the two satellite/rover systems over other such systems and over rovers with onboard power are discussed along with the possibility of enabling other missions. Author (revised)

N94-20121 Department of the Navy, Washington, DC.

THRUST EXPANSION ENGINE Patent

Carl T. Zovko, inventor (to Navy) 16 Mar. 1993 9 p Filed 1 Jun. 1992

(AD-D015896; US-Patent-5,193,475; US-Patent-Appl-SN-891027; US-Patent-Class-114-20.2) Avail: US Patent and Trademark Office

Break-up activity of water by injection of hot propellant gas into channels of a thrust expansion engine is suppressed to prevent rapid cooling of the gas utilizing one or more methods including injection of a secondary inflow of the propellant gas and/or the water under lower pressures into the channels, injection of a viscosity enhancer and/or surfactant into the inflow stream of the water, and restricting outflow of the water from the channels by means of convergent nozzles. DTIC

N94-20226*# National Aeronautics and Space Administration, Washington, DC.

ROCKETS: PHYSICAL SCIENCE TEACHER'S GUIDE WITH ACTIVITIES

Gregory L. Vogt (National Aeronautics and Space Administration. Lyndon B. Johnson Space Center, Houston, TX.) and Carla R. Rosenberg, ed. Jul. 1993 47 p

(NASA-EP-291; NAS 1.19:291) Avail: CASI HC A03/MF A01

This guide begins with background information sections on the history of rocketry, scientific principles, and practical rocketry. The sections on scientific principles and practical rocketry are based on Isaac Newton's three laws of motion. These laws explain why rockets work and how to make them more efficient. The background sections are followed with a series of physical science activities that demonstrate the basic science of rocketry. Each activity is designed to be simple and take advantage of inexpensive materials. Construction diagrams, materials and tools lists, and instructions are included. A brief discussion elaborates on the concepts covered in the activities and is followed with teaching notes and discussion questions. The guide concludes with a glossary of terms, suggested reading list, NASA educational resources, and an evaluation questionnaire with a mailer. Derived from text

N94-20241# European Space Agency. European Space Research and Technology Center, ESTEC, Noordwijk (Netherlands). Power and Energy Conversion Div.

POWER STANDARD

Nov. 1992 63 p

(ESA-PSS-02-10-Vol-1-Issue-1; ETN-93-94881) Copyright Avail: CASI HC A04/MF A01

The power standard defines the requirements on electrical power systems to be applied by contractors and subcontractors to ESA spacecraft and associated equipment or payloads. The power standard consists of two volumes, which support two guideline specifications: the present document, volume 1, describes the standard itself, called the Power Standard (PS); volume 2 is a reference document, and is called Power standard Rationale (PR); it gives the rationale behind the requirements specified in volume 1. The guidelines for the establishment of a power supply subsystem specification and the guidelines for the establishment of an electrical unit specification are given. The applicable document contains test methods for the ESA power standard, which is not yet available, and defines the relevant test methods to be followed. ESA

N94-20370* National Aeronautics and Space Administration. Marshall Space Flight Center, Huntsville, AL.

LIQUID FUEL INJECTION ELEMENTS FOR ROCKET ENGINES Patent

George B. Cox, Jr., inventor (to NASA) 30 Nov. 1993 7 p Filed 27 Jan. 1993 Supersedes N93-29847 (31 - 11, p 3289)

(NASA-Case-MFS-28547-1; US-Patent-5,265,415; US-Patent-Appl-SN-010037; US-Patent-Class-60-258; US-Patent-Class-60-741; US-Patent-Class-137-853; US-Patent-Class-137-855; US-Patent-Class-239-410; US-Patent-Class-239-533.2; Int-Patent-Class-F02K-9/00) Avail: US Patent and Trademark Office

Thrust chambers for liquid propellant rocket engines include three principal components. One of these components is an injector which contains a plurality of injection elements to meter the flow of propellants at a predetermined rate, and fuel to oxidizer mixture ratio, to introduce the mixture into the combustion chamber, and to cause them to be atomized within the combustion chamber so that even combustion takes place. Evolving from these injectors are tube injectors. These tube injectors have injection elements for injecting the oxidizer into the combustion chamber. The oxidizer and fuel must be metered at predetermined rates and mixture ratios in order to mix them within the combustion chamber so that combustion takes place smoothly and completely. Hence tube injectors are subject to improvement. An injection element for a liquid propellant rocket engine of the bipropellant type is provided which includes tangential fuel metering orifices, and a plurality of oxidizer tube injection elements whose injection tubes are also provided with tangential oxidizer entry slots and internal reed valves. Official Gazette of the U.S. Patent and Trademark Office

N94-20496* National Aeronautics and Space Administration. Pasadena Office, CA.

SEGMENTED ION THRUSTER Patent

John R. Brophy, inventor (to NASA) (Jet Propulsion Lab., California Inst. of Tech., Pasadena.) 14 Dec. 1993 15 p Filed 25 Aug. 1992 Supersedes N94-15927 (32 - 3, p 925)

(NASA-Case-NPO-18192-1-CU; US-Patent-5,269,131;

US-Patent-Appl-SN-934988; US-Patent-Class-60-202;
Int-Patent-Class-H05H-1/00) Avail: US Patent and Trademark Office

Apparatus and methods for large-area, high-power ion engines comprise dividing a single engine into a combination of smaller discharge chambers (or segments) configured to operate as a single large-area engine. This segmented ion thruster (SIT) approach enables the development of 100-kW class argon ion engines for operation at a specific impulse of 10,000 s. A combination of six 30-cm diameter ion chambers operating as a single engine can process over 100 kW. Such a segmented ion engine can be operated from a single power processor unit.

Official Gazette of the U.S. Patent and Trademark Office

N94-21208# Naval Postgraduate School, Monterey, CA.
DUAL-BEAM MULTIPLE WAVELENGTH LIGHT TRANSMITTANCE MEASUREMENT FOR PARTICLE SIZING IN ROCKET MOTOR PLUMES M.S. Thesis
Kevin B. Taylor Jun. 1993 49 p
(AD-A272491) Avail: CASI HC A03/MF A01

A multiple-wavelength light transmittance measurement system previously used in a laboratory environment to study particles in solid rocket propellant exhaust plumes was modified for use in the field, where high levels of vibration can degrade the accuracy of data. The system was converted from a single light beam configuration to a dual beam configuration which was capable of obtaining a complete set of 1024 reference and scene measurements in 10.0 ms. Modifications included designing, building and testing a new analog-to-digital data converter trigger circuit, and a rotating-wheel light chopper. Optical components including beam splitters, lenses, and a fiber optic cable were installed, and existing data collection system software was modified. The new system was tested by measuring soot from an oxyacetylene torch to prove the design concept. Test results and system performance were documented. Recommendations for further modifications, improvements and applications are presented. DTIC

N94-21271*# Rockwell International Corp., Canoga Park, CA. Rocketdyne Div.
ADVANCED TRANSPORTATION SYSTEM STUDIES, TECHNICAL AREA 3. ALTERNATE PROPULSION SUBSYSTEM CONCEPTS: J-2S RESTART STUDY Final Report, Sep. 1992 - Apr. 1993
John Vilja and Daniel Levack Apr. 1993 179 p
(Contract NAS8-39210)
(NASA-CR-193874; NAS 1.26:193874; DCN-1-1-PP-02147) Avail: CASI HC A09/MF A02

The objectives were to assess what design changes would be required to remit late production of the J-2S engine for use as a large high energy upper stage engine. The study assessed design changes required to perform per the J-2S model specification, manufacturing changes required due to obsolescence or improvements in state-of-the-practice, availability issues for supplier provided items, and provided cost and schedule estimates for this configuration. The confidence that J-2S production could be reinitiated within reasonable costs and schedules was provided. No significant technical issues were identified in either the producibility study or in the review of previous technical data. Areas of potential cost reduction were identified which could be quantified to a greater extent with further manufacturing planning. The proposed schedule can be met with no foreseeable impacts. The results of the study provided the necessary foundation for the detailed manufacturing and test plans and non-recurring and recurring cost estimates that are needed to complete the effort to reinitiate production of the J-2S engine system. Author (revised)

N94-21565*# Sverdrup Technology, Inc., Brook Park, OH.
EVALUATION OF EXTERNALLY HEATED PULSED MPD THRUSTER CATHODES Final Report
Roger M. Myers, Matthew Domonkos (New Mexico Univ., Albuquerque.), and Alec D. Gallimore (Michigan Univ., Ann Arbor.) Dec. 1993 14 p
Presented at the 23rd International Electric Propulsion Conference, Seattle, WA, 13-16 Sep. 1993; sponsored by AIAA
(Contract NAS3-25266; RTOP 506-42-31)
(NASA-CR-191090; E-8293; NAS 1.26:191090) Avail: CASI HC A03/MF A01

Recent interest in solar electric orbit transfer vehicles (SEOTV's) has prompted a reevaluation of pulsed magnetoplasmadynamic (MPD) thruster systems due to their ease of power scaling and reduced test facility requirements. In this work the use of externally heated cathodes was examined in order to extend the lifetime of these thrusters to the 1000 to 3000 hours required for SEOTV missions. A pulsed MPD thruster test facility was assembled, including a pulse-forming network (PFN), ignitor supply and propellant feed system. Results of cold cathode tests used to validate the facility, PFN, and propellant feed system design are presented, as well as a preliminary evaluation of externally heated impregnated tungsten cathodes. The cold cathode thruster was operated on both argon and nitrogen propellants at peak discharge power levels up to 300 kW. The results confirmed proper operation of the pulsed thruster test facility, and indicated that large amounts of gas were evolved from the BaO-CaO-Al2O3 cathodes during activation. Comparison of the expected space charge limited current with the measured vacuum current when using the heated cathode indicate that either that a large temperature difference existed between the heater and the cathode or that the surface work function was higher than expected. Author

N94-21809*# National Aeronautics and Space Administration. Lewis Research Center, Cleveland, OH.
PRELIMINARY SP-100/STIRLING HEAT EXCHANGER DESIGNS
Paul Schmitz (Sverdrup Technology, Inc., Brook Park, OH.), Leonard Tower (Sverdrup Technology, Inc., Brook Park, OH.), Ronald Dawson (Aerospace Design and Fabrication, Inc., Brook Park, OH.), Brian Blue, and Pat Dunn Dec. 1993 11 p Proposed for presentation at the Eleventh Symposium on Space Nuclear Power and Propulsion, Albuquerque, NM, 10-14 Jan. 1994; sponsored by the Inst. for Space Nuclear Studies and ANS
(Contract NAS3-25266; RTOP 583-02-21)
(NASA-TM-106444; E-8288; NAS 1.15:106444) Avail: CASI HC A03/MF A01

Analytic modeling of several heat exchanger concepts to couple the SP-100 nuclear reactor primary lithium loop and the Space Stirling Power Convertor (SSPC) was performed. Four 25 kWe SSPC's are used to produce the required 100 kW of electrical power. This design work focused on the interface between a single SSPC and the primary lithium loop. Manifolding to separate and collect the four channel flow was not modeled. This work modeled two separate types of heat exchanger interfaces (conductive coupling and radiative coupling) to explore their relative advantages and disadvantages. The minimum mass design of the conductively coupled concepts was 18 kg or 0.73 kg/kWe for a single 25 kWe convertor. The minimum mass radiatively coupled concept was 41 kg or 1.64 kg/kWe. The direct conduction heat exchanger provides a lighter weight system because of its ability to operate the Stirling convertor evaporator at higher heat fluxes than those attainable by the radiatively coupled systems. Additionally the conductively coupled concepts had relatively small volumes and provide potentially simpler assembly. Their disadvantages were the tight tolerances and material joining problems associated with this refractory to superalloy interface. The advantages of the radiatively coupled designs were the minimal material interface problems. Author

N94-21824# Space Power, Inc., San Jose, CA.
SPACE-R THERMIONIC SPACE NUCLEAR POWER SYSTEM: DESIGN AND TECHNOLOGY DEMONSTRATION PROGRAM
May 1993 298 p
(Contract DE-AC03-92SF-19441)
(DE93-013969; DOE/SF-19441/T4) Avail: CASI HC A13/MF A03

This semiannual technical progress report summarizes the technical progress and accomplishments for the Thermionic Space Nuclear Power System (TI-SNPS) Design and Technology Demonstration Program of the prime contractor, Space Power Incorporated (SPI), its subcontractors, and supporting national laboratories during the first half of the government fiscal year (GFY) 1993. SPI's subcontractors and supporting national laboratories include: Babcock & Wilcox for the reactor core and externals; Space Systems/Loral for the spacecraft integration; Thermocore for the radiator heat pipes and the heat exchanger; INERTEK of CIS for the TFE, core elements, and nuclear tests; Argonne National Laboratories for nuclear safety, physics, and control verification; and Oak Ridge National laboratories for materials testing. Parametric trade studies are near completion. However, technical input from INERTEK has yet to be provided to determine some of the baseline design configurations. The INERTEK subcontract is expected to be initiated soon. The point design task has been initiated. The thermionic fuel element (TFE) is undergoing several design iterations. The reactor core vessel analysis and design has also been started. DOE

N94-21860*# National Aeronautics and Space Administration. Marshall Space Flight Center, Huntsville, AL.

PERFORMANCE ASSESSMENT OF LOW PRESSURE NUCLEAR THERMAL PROPULSION

H. P. Gerrish, Jr. and G. E. Doughty Dec. 1993 24 p

(NASA-TM-108433; NAS 1.15:108433) Avail: CASI HC A03/MF A01

A low pressure nuclear thermal propulsion (LPNTP) system, which takes advantage of hydrogen dissociation/recombination, was proposed as a means of increasing engine specific impulse (Isp). The effect of hydrogen dissociation/recombination on LPNTP Isp is examined. A two-dimensional computer model was used to show that the optimum chamber pressure is approximately 100 psia (at a chamber temperature of 3,000 K), with an Isp approximately 15 s higher than at 1,000 psia. At high chamber temperatures and low chamber pressures, the increase in Isp is due to both lower average molecular weights caused by dissociation and added kinetic energy from monatomic hydrogen recombination. Monatomic hydrogen recombination increases the Isp more then hydrogen dissociation. Variations in the mole fraction of monatomic hydrogen are similar to variations in static pressure along the axial nozzle position. Most recombination occurs close to the nozzle throat. Practical variations in nozzle geometry have minimal impact on recombination. Other models which can simulate a wider range of nozzle designs should be used in the future. The uncertainty of the hydrogen kinetic reaction rates at high temperatures (approximately 3,000 K) affects the accuracy of the analysis and should be verified with simple bench tests. Author (revised)

N94-21874*# Rockwell International Corp., Canoga Park, CA. Rocketdyne Div.

BRAYTON POWER CONVERSION SYSTEM PARAMETRIC DESIGN MODELLING FOR NUCLEAR ELECTRIC PROPULSION Final Report

Thomas L. Ashe (Allied-Signal Aerospace Co., Tempe, AZ.) and William D. Otting 21 Nov. 1993 160 p

(Contract NAS3-25808; RTOP 593-72-00)

(NASA-CR-191135; NAS 1.26:191135; Rept-93RC-010143) Avail: CASI HC A08/MF A02

The parametrically based closed Brayton cycle (CBC) computer design model was developed for inclusion into the NASA LeRC overall Nuclear Electric Propulsion (NEP) end-to-end systems model. The code is intended to provide greater depth to the NEP system modeling which is required to more accurately predict the impact of specific technology on system performance. The CBC model is parametrically based to allow for conducting detailed optimization studies and to provide for easy integration into an overall optimizer driver routine. The power conversion model includes the modeling of the turbines, alternators, compressors, ducting, and heat exchangers (hot-side heat exchanger and recuperator). The code predicts performance to significant detail. The system characteristics determined include estimates of mass, efficiency, and the characteristic dimensions of the major power conversion system components. These characteristics are parametrically modeled as a function of input parameters such as the aerodynamic configuration (axial or radial), turbine inlet temperature, cycle temperature ratio, power level, lifetime, materials, and redundancy. Author

N94-21882*# Florida Inst. of Tech., Melbourne.

MODEL-BASED REASONING FOR POWER SYSTEM MANAGEMENT USING KATE AND THE SSM/PMAD Final Report

Robert A. Morris, Avelino J. Gonzalez, Daniel J. Carreira, F. D. McKenzie, and Brian Gann Nov. 1993 65 p Prepared in cooperation with University of Central Florida, Orlando

(Contract NAS8-39385)

(NASA-CR-194716; NAS 1.26:194716) Avail: CASI HC A04/MF A01

The overall goal of this research effort has been the development of a software system which automates tasks related to monitoring and controlling electrical power distribution in spacecraft electrical power systems. The resulting software system is called the Intelligent Power Controller (IPC). The specific tasks performed by the IPC include continuous monitoring of the flow of power from a source to a set of loads, fast detection of anomalous behavior indicating a fault to one of the components of the distribution systems, generation of diagnosis (explanation) of anomalous behavior, isolation of faulty object from remainder of system, and maintenance of flow of power to critical loads and systems (e.g. life-support) despite fault conditions being present (recovery). The IPC system has evolved out of KATE (Knowledge-based Autonomous Test Engineer), developed at NASA-KSC. KATE consists of a set of software tools for developing and applying structure and behavior models to monitoring, diagnostic, and control applications. Author

N94-21979# Brookhaven National Lab., Upton, NY. Dept. of Advanced Technology.

TEMPERATURE AND DOPPLER COEFFICIENTS OF VARIOUS SPACE NUCLEAR REACTORS

Said F. Mughabghab, Hans Ludewig, and Eldon Schmidt 1993 5 p

(Contract DE-AC02-76CH-00016)

(DE94-001388; BNL-49463) Avail: CASI HC A01/MF A01

Temperature and Doppler feedback effects for a Particle Bed Reactor (PBR) designed to operate as a propulsion reactor are investigated. Several moderator types, fuel enrichments, and reactor sizes are considered in this study. From this study it could be concluded that a PBR can be configured which has a negative prompt feedback, zero coolant worth, and a small positive to zero moderator worth. This reactor would put the lowest demands on the control system. DOE

N94-22428*# Pennsylvania State Univ., University Park.

NASA PROPULSION ENGINEERING RESEARCH CENTER, VOLUME 1 Annual Report, 1 Nov. 1992 - 21 Oct. 1993

Nov. 1993 66 p

(Grant NAGw-1356)

(NASA-CR-194721-Vol-1; NAS 1.26:194721-Vol-1) Avail: CASI HC A04/MF A01

Over the past year, the Propulsion Engineering Research Center at The Pennsylvania State University continued its progress toward meeting the goals of NASA's University Space Engineering Research Centers (USERC) program. The USERC program was initiated in 1988 by the Office of Aeronautics and Space Technology to provide an invigorating force to drive technology advancements in the U.S. space industry. The Propulsion Center's role in this effort is to provide a fundamental basis from which the technology advances in propulsion can be derived. To fulfill this role, an integrated program was developed that focuses research efforts on key technical areas, provides students with a broad education in traditional propulsion-related science and engineering disciplines, and provides minority and other under-represented students with opportunities to take their first step toward professional careers in propulsion engineering. The program is made efficient by incorporating government propulsion laboratories and the U.S. propulsion industry into the program through extensive interactions and research involvement. The Center is comprised of faculty, professional staff, and graduate and undergraduate students working on a broad spectrum of research issues related to propulsion. The Center's research focus encompasses both current and advanced propulsion concepts for space transportation, with a research emphasis on liquid propellant rocket engines. The liquid rocket engine research includes programs in combustion and turbomachinery. Other space transportation modes that are being addressed include anti-matter, electric, nuclear, and solid propellant propulsion. Outside funding supports a significant fraction of Center research, with the major portion of the basic USERC grant being used for graduate student support and recruitment. The remainder of the USERC funds are used to support programs to increase minority student enrollment in engineering, to maintain Center infrastructure, and to develop research capability in key new areas. Significant research programs in propulsion systems for air and land transportation complement the space propulsion focus. The primary mission of the Center is student education. The student program emphasizes formal class work and research in classical engineering and science disciplines with applications to propulsion. Author (revised)

N94-20513*# National Aeronautics and Space Administration. Lewis Research Center, Cleveland, OH.

SPACE APPLICATIONS OF SUPERCONDUCTING MICROWAVE ELECTRONICS AT NASA LEWIS RESEARCH CENTER

R. F. Leonard, K. B. Bhasin, R. R. Romanofsky, C. D. Cubbage, and C. Z. Chorey (Sverdrup Technology, Inc., Cleveland, OH.) *In its* Solid State Technology Branch of NASA Lewis Research Center: Fifth Annual Digest Aug. 1993 p 173-179 Repr. from Applied Superconductivity, v. 1, no. 7-9, 1993 p 1341-1347 (For primary document see N94-20497 05-32) Avail: CASI HC A02/MF A03

23 CHEMISTRY AND MATERIALS (GENERAL)

N94-20540* National Aeronautics and Space Administration. Langley Research Center, Hampton, VA.
POLYBENZOXAZOLE VIA AROMATIC NUCLEOPHILIC DISPLACEMENT Patent
Paul M. Hergenrother, inventor (to NASA), John W. Connell, inventor (to NASA), and Joseph G. Smith, Jr., inventor (to NASA) 14 Dec. 1993 10 p Filed 10 Apr. 1992 Supersedes N93-23077 (31 - 8, p 2207)
(NASA-Case-LAR-14606-1-CU; US-Patent-5,270,432; US-Patent-Appl-SN-867864; US-Patent-Class-528-128; US-Patent-Class-528-125; US-Patent-Class-528-126; US-Patent-Class-528-167; US-Patent-Class-528-171; US-Patent-Class-528-172; US-Patent-Class-528-174) Avail: US Patent and Trademark Office

Polybenzoxazoles (PBO) are heterocyclic macromolecules which were first synthesized in a two-step process by the initial formation of aromatic diacid chlorides with bis(o-aminophenol)s through solution condensation of aromatic diacid chlorides with bis(o-aminophenol)s followed by thermal cyclodehydration. Since then several methods were utilized in their synthesis. The most common synthetic method for PBO involves a polycondensation of bis(o-aminophenol)s with aromatic diacid diphenyl esters. Another preparative route involves the solution polycondensation of the hydrochloride salts of bis(o-amino phenol)s with aromatic diacids in polyphosphoric acid. Another synthetic method involves the initial formation of poly(o-hydroxy amide)s from silylated bis(o-aminophenol)s with aromatic diacid chlorides followed by thermal cyclodehydration to PBO. A recent preparative route involves the reaction of aromatic bisphenols with bis(fluorophenyl) benzoxazoles by the displacement reaction to form PBO. The novelty of the present invention is that high molecular weight PBO of new chemical structures are prepared that exhibit a favorable combination of physical and mechanical properties.
Official Gazette of the U.S. Patent and Trademark Office

N94-21369 Centre National d'Etudes Spatiales, Toulouse (France).
FLIGHT AND LABORATORY TESTING OF MATERIALS IN LOW EARTH ORBIT
J. C. Guillaumon, J. Marco (Centre d'Etudes et de Recherches, Toulouse, France.), and A. Paillous (Centre d'Etudes et de Recherches, Toulouse, France.) *In its* Fifth International Symposium on Materials in a Space Environment Jun. 1993 p 27-42 (For primary document see N94-21367 05-18)
Copyright Avail: CEPADUES-Editions, 111, rue Nicolas-Vaquelin, 31100 Toulouse, France

N94-21371 Centre National d'Etudes Spatiales, Toulouse (France).
RESULTS OF THE POST FLIGHT ANALYSES ON SYSTEM MATERIALS FOR THE LDEF-FRECOPA EXPERIMENT
Christian Durin and Irenee Alet *In its* Fifth International Symposium on Materials in a Space Environment Jun. 1993 p 47-74 (For primary document see N94-21367 05-18)
Copyright Avail: CEPADUES-Editions, 111, rue Nicolas-Vaquelin, 31100 Toulouse, France

N94-21386 European Space Agency. European Space Research and Technology Center, ESTEC, Noordwijk (Netherlands).
MATERIALS EVALUATION AT ESA/ESTEC
G. Gourmelon, M. Froggatt, and D. Collins *In* CNES, Fifth International Symposium on Materials in a Space Environment Jun. 1993 p 255-272 (For primary document see N94-21367 05-18)
Copyright Avail: CEPADUES-Editions, 111, rue Nicolas-Vaquelin, 31100 Toulouse, France

24 COMPOSITE MATERIALS

Includes physical, chemical, and mechanical properties of laminates and other composite materials.

For ceramic materials see *27 Nonmetallic Materials.*

N94-19888# Ames Lab., IA.
QUANTITATIVE EVALUATION OF MATERIAL COMPOSITION OF COMPOSITES USING X RAY ENERGY-DISPERSIVE NDE TECHNIQUE Ph.D. Thesis
J. Ting 1 Sep. 1993 97 p
(Contract W-7405-eng-82)
(DE93-041157; IS-T-1640) Avail: CASI HC A05/MF A02

The technique described in this paper works well for determining the thickness and density of composite components having the higher linear attenuation coefficient; it accurately determines the thickness of epoxy-resin and Al metal, and the density of bone, to less than or equal to 4% in the graphite-epoxy, bone-plexiglass, and Al-Al corrosion composites. Accuracy is dictated by the magnitude and uncertainty of the linear attenuation coefficient. Use of Ge detector and multichannel analyzer is limited by inspection time (1 day for point measurement) and access limitation. Immediate development of a rapid in-service inspection tool is limited by the amplifier and MCA systems. The MCA should be replaced with a single-channel analyzer, and an electronic device should be built for monitoring the incoming signal for pile-up-rejection. DOE

N94-20010# Department of the Navy, Washington, DC.
PHTHALONITRILE PREPOLYMER AS HIGH TEMPERATURE SIZING MATERIAL FOR COMPOSITE FIBERS Patent Application
Teddy M. Keller, inventor (to Navy) 28 Jun. 1993 21 p
(AD-D015912; US-Patent-Appl-SN-082645; Navy-Case-74791) Avail: CASI HC A03/MF A01

Sized fibers, for use as reinforcements in high temperature polymeric composites, are prepared by coating the outside surface of the fibers with an amorphous, B-stage bisphthalonitrile prepolymer. The prepolymer may be prepared by curing a bisphthalonitrile monomer with an organic amine, an aromatic organic acid, a mineral acid, a Lewis acid or a salt of any of the above. Then, the fibers are coated by passage through an organic solution of the prepolymer. Either before or after completely curing the prepolymer coating on the fibers, the coated fibers are covered with a resin, for example, by passage through a solution or melt of a polyimide or bisphthalonitrile resin. If the phthalonitrile coating was incompletely cured prior to covering the phthalonitrile-coated fiber with the resin, the heat during the subsequent cure of the resin also completely cures the phthalonitrile coating. The resulting composite has excellent high temperature properties. In a preferred embodiment, the coated fibers are used to form a prepreg for usage in composite fabrication. DTIC

N94-20031# Elsevier Science Publishers Ltd., Barking (England).
THE SEVENTH INTERNATIONAL CONFERENCE ON COMPOSITE STRUCTURES, VOLUME 25, NUMBERS 1-4
I. H. Marshall Jul. 1993 611 p Conference held in United Kingdom, Jul. 1993
(Contract DAJA45-93-M-0343)
(AD-A269961; R/D-7145-AN-02) Avail: CASI HC A99/MF A06

Partial contents of papers presented at the Seventh Annual Conference on Composite Structures is as follows: The role of biaxial stresses in discriminating between meaningful and illusory composite failure theories; An evaluation of equivalent-single-layer and layerwise theories of composite laminates; The influence of trigger configurations and laminate lay-up on the failure mode of composite crush cylinders; Comparison between the short and long term behavior of fiber reinforced and unreinforced concrete beams; Examples of the multicriteria optimization of cement-based composites; A simplified tensile damage analysis method for composite laminates using a quasi-three-dimensional model; A reduced basis approach to quantifying damage dependent dynamic response of laminate composite structures; Free vibration of generally-laminated, shear-deformable, composite rectangular plates using a spline Rayleigh-Ritz method; Flutter analysis cantilevered curved composite panels; Weight change mechanism of randomly oriented GFRP panel immersed in hot water; The effects of environmental humidity after post care on the optimal temperature path of polymer composites; Artificial damage techniques for low velocity impact in

carbon fiber composites; and impact damage evaluation on advanced stitched composites by means of acoustics emission and image analysis. DTIC

N94-20064 Department of the Navy, Washington, DC.
METAL-GLASS COMPOSITE FIELD-EMITTING ARRAYS Patent
Jack D. Ayers, inventor (to Navy) 13 Apr. 1993 7 p Filed 10 Dec. 1991
(AD-D015942; US-Patent-5,202,602; US-Patent-Appl-SN-804558; US-Patent-Class-313-309) Avail: US Patent and Trademark Office

A field-emitting array is provided which comprises at least one thin wafer having electrically conducting filaments extending through a glass matrix between a first and second parallel surface of the wafer. At the first surface, the filaments extend beyond the plane of the glass matrix. The filaments extending beyond the first surface have an electron-emitting coating on their cylindrical surfaces. The coating extends beyond the filament end to create a shape that emits electrons when an electrical field is applied between the filaments and an anode. In an alternative embodiment, the filaments are recessed below the first surface and a conducting coating forms an extractor on that surface. DTIC

N94-20172*# Cincinnati Univ., OH. Dept. of Aerospace Engineering and Engineering Mechanics.
STRUCTURAL SIMILITUDE AND DESIGN OF SCALED DOWN LAMINATED MODELS
G. J. Simitses and J. Rezaeepazhand Dec. 1993 40 p
(Grant NAG1-1280)
(NASA-CR-194687; NAS 1.26:194687) Avail: CASI HC A03/MF A01

The excellent mechanical properties of laminated composite structures make them prime candidates for wide variety of applications in aerospace, mechanical and other branches of engineering. The enormous design flexibility of advanced composites is obtained at the cost of large number of design parameters. Due to complexity of the systems and lack of complete design based informations, designers tend to be conservative in their design. Furthermore, any new design is extensively evaluated experimentally until it achieves the necessary reliability, performance and safety. However, the experimental evaluation of composite structures are costly and time consuming. Consequently, it is extremely useful if a full-scale structure can be replaced by a similar scaled-down model which is much easier to work with. Furthermore, a dramatic reduction in cost and time can be achieved, if available experimental data of a specific structure can be used to predict the behavior of a group of similar systems. This study investigates problems associated with the design of scaled models. Such study is important since it provides the necessary scaling laws, and the factors which affect the accuracy of the scale models. Similitude theory is employed to develop the necessary similarity conditions (scaling laws). Scaling laws provide relationship between a full-scale structure and its scale model, and can be used to extrapolate the experimental data of a small, inexpensive, and testable model into design information for a large prototype. Due to large number of design parameters, the identification of the principal scaling laws by conventional method (dimensional analysis) is tedious. Similitude theory based on governing equations of the structural system is more direct and simpler in execution. The difficulty of making completely similar scale models often leads to accept certain type of distortion from exact duplication of the prototype (partial similarity). Both complete and partial similarity are discussed. The procedure consists of systematically observing the effect of each parameter and corresponding scaling laws. Then acceptable intervals and limitations for these parameters and scaling laws are discussed. In each case, a set of valid scaling factors and corresponding response scaling laws that accurately predict the response of prototypes from experimental models is introduced. The examples used include rectangular laminated plates under destabilizing loads, applied individually, vibrational characteristics of same plates, as well as cylindrical bending of beam-plates. Author

N94-20208# Bioelastics Research Ltd., Birmingham, AL.
DEVELOPMENT OF BIOELASTIC MATERIAL FOR ASPECTS OF WOUND REPAIR Training Progress Report, Jan. - Apr. 1993
Apr. 1993 5 p
(Contract N00014-90-C-0265)
(AD-A267832) Avail: CASI HC A01/MF A01

The broad goal of this contract is the synthesis and characterization of bioelastic materials designed for specific applications of wound healing. Specifically, for materials with possible use as wound coverings, control of the temperature of transition by changes in hydrophobicity will be examined. In addition, the rate of water passage through the matrix will be determined. The first application phase was concerned primarily with synthesis of the basic poly pentapeptide poly (VPGVG) and the analog with L-alanine substituted in position 3,poly (VPAVG) and mole fraction combinations thereof to achieve elastomeric matrices of varying elastic moduli. In the third year, poly pentapeptides containing chemical clocks are to be characterized for their rate of breakdown and their effects on drug release profiles. This document presents the goals, progress, and future plans of the current contract. Progress reported includes the transition temperatures of two bioelastic polymers and stress-strain curves for two matrices. CASI

N94-20327 American Society for Composites, Dayton, OH.
BIOTECHNOLOGY AND COMPOSITE MATERIALS Final Report, 1 Jun. 1990 - 31 May 1991
Barbara C. Woolsey, R. Narayan, and R. C. Schiavone Apr. 1993 43 p
Limited Reproducibility: More than 20% of this document may be affected by microfiche quality
(Grant AF-AFOSR-0293-90)
(AD-A264278; AFOSR-93-0249TR) Avail: CASI HC A03

As part of a meeting of the American Society of Composites, 10 - 13 June 1990, an Air Force supported session on 'Biotechnology and Composite Materials' was held. The titles of the presentations in this session were as follows: 'An Overview of Three Biotechnology Areas for the Development of Advanced Composite Materials and Structures'; 'Seashells as a Natural Model to Study Laminated Composites'; 'Recombinant Spider Silk Proteins for Composite Fibers'; 'Treatment of Graphite Fiber Surfaces with Gram-negative Aerobic Bacteria'; and 'Modeling the Effects of Aging on Bone Properties Using Composite Material Micromechanics.' DTIC

N94-20490# California Univ., Los Angeles. Dept. of Mechanical Aerospace and Nuclear Engineering.
THE EFFECTS OF PROCESSING AND CONSTITUENT MATERIALS ON COMPRESSIVE STRENGTH OF THICK COMPOSITE LAMINATES Annual Report
H. T. Hahn, E. A. Kempner, and J. Slaughter Aug. 1993 42 p
(Contract N00014-92-J-1846)
(AD-A271912) Avail: CASI HC A03/MF A01

The objectives of this study pertain to both the processing of thick composites and the constituent materials used. The main objectives of the research are to identify the processing conditions that are responsible for fiber wrinkling in thick, filament-wound cylinders and to develop a process simulation model for filament winding of thick cylinders. Analysis-experiment correlation will be used to aid model development. Also, the effect of constituent materials on compressive strength will be studied. This will be accomplished by identifying the fiber microstructure responsible for low compressive strength and developing an analytical model relating fiber microstructure to compressive strength. DTIC

N94-20539* National Aeronautics and Space Administration. Lewis Research Center, Cleveland, OH.
INTERCALATED HYBRID GRAPHITE FIBER COMPOSITE Patent
James R. Gaier, inventor (to NASA) 9 Nov. 1993 6 p Filed 25 Nov. 1991 Supersedes N92-17861 (30 - 8, p 1257)
(NASA-Case-LEW-15241-1; US-Patent-5,260,124; US-Patent-Appl-SN-798464; US-Patent-Class-428-257; US-Patent-Class-244-1A; US-Patent-Class-361-218; US-Patent-Class-428-260; US-Patent-Class-428-288; US-Patent-Class-428-289; US-Patent-Class-428-334) Avail: US Patent and Trademark Office

The invention is directed to a highly conductive lightweight hybrid material and methods of producing the same. The hybrid composite is obtained by weaving strands of a high strength carbon or graphite fiber into a fabric-like structure, depositing a layer of carbon onto the structure, heat treating the structure to graphitize the carbon layer, and intercalating the graphitic carbon layer structure. A laminate composite material useful for protection against lightning strikes comprises at least one layer of the hybrid material over at least one layer of high strength carbon or graphite fibers. The composite material of the present invention is compatible with matrix compounds, has a coefficient of thermal expansion which is the same as

underlying fiber layers, and is resistant to galvanic corrosion in addition to being highly conductive. These materials are useful in the aerospace industry, in particular as lightning strike protection for airplanes.
Official Gazette of the U.S. Patent and Trademark Office

N94-20550# Maryland Univ., College Park. Metallurgical Materials Lab.
STRENGTHENING OF NiAl MATRIX COMPOSITES Final Report, Oct. 1990 - Sep. 1993
Richard J. Arsenault Oct. 1993 32 p
(Contract N00014-91-J-1353)
(AD-A271491; MML-1993-1) Avail: CASI HC A03/MF A01

It has finally been concluded that none of the existing theories could account for the observed high temperature strengthening, nor could the models or theories that we considered. This led to the prediction that the strengthening at high temperatures was the result of an increase in strength in the intermediate temperature range where the yield stress is relatively independent of temperature. We believe that the increase in stress is due to an increase in the athermal component of the yield stress, a component of the yield stress which is not overcome by thermal fluctuations. A TEM investigation was undertaken of continuous filament Al2O3/NiAl composites to determine if dislocations were generated as a result of the relaxation of the thermal residual stress. The data indicates that dislocation generation did indeed occur and there is a possibility that dislocation generation also occurs in shot fiber Al2O3/NiAl composites. This data may produce an interesting paradox since in Al2O3/NiAl composites, as the size of the reinforcement gets larger the dislocation density increases, but in SiC/Al composites, as the size of the SiC increases the dislocation density decreases at a constant volume fraction. DTIC

N94-20574# Naval Air Warfare Center, Warminster, PA. Air Vehicle and Crew Systems Technology Dept.
INTERLEAVED BISMALEIMIDE COMPOSITES Final Report, Jul. 1989 - May 1991
Eileen Armstrong-Carroll and Thomas M. Donnellan 1 Dec. 1992 57 p
(AF Proj. RS3-4-AS-0)
(AD-A272233; NAWCADWAR-92102-60) Avail: CASI HC A04/MF A01

This report examines interleaving as a technique for the improvement of delamination resistance in composites. In particular, the influence of the deformation behavior of the interleaf film and film adhesion on composite fracture energy is studied. Teflon, E, and Kapton interleaf film materials are compared. Kapton and E films display predominantly brittle deformation behavior. Teflon exhibits substantial deformation before failure. All films are plasma treated to vary film-resin bond strengths. With the Kapton and Teflon films, plasma treatments are shown to increase film-resin adhesion and fracture energy. The effectiveness of Teflon as an interleaf material may be limited by the toughness of this film. Film-resin adhesion with the E film is determined to be optimized. Fracture energy is greatest with composites interleaved with the E film. DTIC

N94-20577# Army Research Lab., Watertown, MA. Materials Directorate.
BIAXIAL FLEXURAL TESTING OF A CARBON FIBER REINFORCED EPOXY COMPOSITE Final Report
Nikos Tsangarakis and Barmac K. Taleghani Oct. 1993 20 p
(AD-A271956; ARL-TR-221) Avail: CASI HC A03/MF A01

The response of a 3501-6 resin composite to biaxial flexural loading was assessed using disk specimens. The composite was cross-ply reinforced with continuous carbon fibers with a volume content of 60%. Under monotonic flexural loading, the formation of delaminations limited the useful range of the composite's deformation to a biaxial tensile strain of 0.0067. Under cyclic flexural loading and for a fatigue life of 10(6) cycles, the useful strain range was limited to 0.003. The latter strain is only 19% of the composite's uniaxial tensile strain to failure. Fatigue failure mechanisms included delaminations, matrix cracking, fiber, and possible fiber bundle debonds. Some delaminations were identified with ultrasonic C-scanning. DTIC

N94-20623# Cincinnati Univ., OH. Dept. of Materials Science and Engineering.
MICROSTRUCTURE EVOLUTION IN THE PRESENCE OF CONSTRAINTS AND IMPLICATIONS ON THE PROPERTIES OF Mg-Li AND Nb-Al CONSTRAINTS Final Report, 1 Jun. 1990 - 31 May 1993
J. A. Sekhar, L. Fabietti, D. Carr, L. Cantrell, and N. Dey 31 May 1993 358 p
(Grant AF-AFOSR-0308-90)
(AD-A272088; AFOSR-93-0812TR) Avail: CASI HC A16/MF A03

The objective of the research was to gain fundamental knowledge of solidification microstructure evolution in the presence of constraints and to apply this knowledge to relevant intermetallic composite designs. The work involved numerical modeling, transparent material solidification and the solidification of Mg-Li and Nb-Al composites. All work was completed and several novel findings are described in this report. This report is the first comprehensive document dealing with morphological evolution of solidification microstructure when constrained by diffusional barriers with different types of interface. First time report of non-directional dendrites and S/L interface strain energies leading to defect formation are disclosed. Development strategies and microstructure maps for particulate and fiber composites are reported. DTIC

N94-20950# Naval Surface Warfare Center, Bethesda, MD.
GRAPHITE/POLYURETHANE FLEXIBLE COMPOSITES: MECHANICAL AND VIBRATION DAMPING PROPERTIES
Roger M. Crane and Colin P. Ratcliffe Jul. 1993 66 p
(AD-A271608; CARDIVNSWC-TR-601-93/02) Avail: CASI HC A04/MF A01

Structures fabricated with advanced composite materials, such as graphite fibers in thermoset or thermoplastic resins, typically possess high stiffness. The material is elastic to failure, which occurs at strain levels which are relatively low, on the order of 2 to 5%, depending on fiber orientations. There are numerous naval applications in which systems are subjected to significantly large deformations due to the global deformation of the ship hull. To allow the subsystems to function while being subjected to these large global deformations, flexible couplings are often incorporated. These couplings must transfer in-plane loads and torque while allowing for dissimilar motion of each component. This paper describes such a structural configuration which is both flexible and structurally adequate to support significant mechanical loads. This flexible composite system consists of a braided graphite fiber preform infiltrated with a polyurethane, Adiprene, which has a modulus of 1100 psi and a strain to failure of 300%. This composite system possesses adequate structural characteristics of strength and stiffness, the capability to undergo large global deformations, while simultaneously dissipating significant levels of mechanical vibration energy. This paper discusses the fabrication and design of the flexible composite material, the mechanical characteristics and the damping that it provides.
Author

N94-21040 American Cyanamid Co., Stamford, CT.
FIBER REINFORCED THERMOSETTING RESIN COMPOSITION WITH COATED FIBERS FOR IMPROVED TOUGHNESS Patent
Arutun Maranci, inventor (to American Cyanamid Co.) 11 Aug. 1992 37 p Filed 21 Dec. 1987
(CA-Patent-1,306,320; Int-Patent-Class-C08J-5/06; Int-Patent-Class-C08G-59/50; CTN-93-60688) Copyright Avail: Micromedia Ltd., Technical Information Centre, 165 Hotel de Ville, Place du Portage, Phase 2, Hull, Quebec J8X 3X2, Canada HC/MF

Thermosettable resins are known to be useful in conjunction with fibrous reinforcing materials to form composite articles characterized by high strength to weight ratios for use in aircraft and aerospace industries, as well as in other commercial applications. A fiber-resin matrix composition is disclosed, comprised of reinforcing fibers precoated with a fiber- and matrix resin-reactive elastomeric material, forming a covalently bonded bridging layer between the fibers and the matrix resin, and a heat-curable resin composition comprising an epoxy prepolymer or combination of epoxy prepolymers having more than one epoxide group per molecule and an effective amount of an amine curing agent. The use of an elastomeric coating on the fiber surface in accordance with this invention results in improvements in the fracture resistance, in comparison with compositions and composite articles in which the fibers are not so coated. Moreover, this is accomplished while maintaining the hot-wet properties. Other facets of the invention comprise composite articles formed from the above mentioned compositions, structural members prepared from the composites, and processes for applying reactive elastomeric coatings to fibers, fiber tapes, fabrics, and rovings. Experiments are described to illustrate aspects of the invention. Author (CISTI)

N94-21176# University of Southern California, Los Angeles. Loker Hydrocarbon Research Inst.
COMPOSITE MATERIALS WITH IMPROVED PROPERTIES IN COMPRESSION Final Technical Report, 1 May 1989 - 30 Sep. 1993
William P. Weber 5 Nov. 1993 58 p
(Contract N00014-89-J-1961)
(AD-A272837) Avail: CASI HC A04/MF A01

Preparation of composite materials which have high strength in compression. The scientific approach is to prepare novel polymeric coupling agents. These will permit formation of multiple flexible covalent bonds between fibers as well as to matrix materials. In addition, these new coupling agents will possess elastomeric properties which may increase matrix toughness to fracture. DTIC

N94-21187# Dayton Univ., OH. Research Inst.
A STUDY OF THE INDUCTION HEATING OF ORGANIC COMPOSITES Interim Report, Oct. 1989 - Jun. 1992
G. W. Lawless and Ted Reinhart Feb. 1993 33 p
(Contract F33615-89-C-5643)
(AD-A272657; UDR-TR-92-146; WL-TR-93-4032) Avail: CASI HC A03/MF A01

This is a study of the application of induction heating to graphite-based composites, both thermoset and thermoplastic. Panels of IM-6/3501-6 and IM-6/PEEK were processed in magnetic fields of 450-kHz and 25-kHz frequencies. A 15.24-cm-diameter pancake-type induction coil was used with 10.2-cm x 10.2-cm, 16-ply specimens. Vacuum bagging provided the only consolidation pressure. Data include resin, fiber, void contents, 3-pt. and 4-pt. loading for mechanical properties evaluation, and thermal analysis (DSC and TMA). Comparisons are made to similar samples processed under a standard autoclave cycle. Additional variables studied and discussed include the use of various caul plate materials as field susceptors, effects of coil vibration, various prepreg lay-up orientations, and other sample thicknesses. A brief discussion of the overall field effects and value of induction heating for field repair is included. DTIC

N94-21191# Illinois Univ., Urbana. Dept. of Materials Science and Engineering.
PROPERTIES OF E-BEAM INTERACTIVE OXIDE FILMS FOR NANOMETER SCALE STRUCTURES Final Report, 1 Oct. 1988 - 1 Dec. 1993
R. C. Buchanan, J. L. Hollenbeck, and J. Kim 5 Nov. 1993 40 p
(Contracts N00014-88-K-0317; N00014-92-J-1868)
(AD-A272848) Avail: CASI HC A03/MF A01

E-beam generated ultrastructures on oxide film substrates have been investigated for high density memory and lithographic applications. In order to create the nanometer scale patterns (holes, lines, channels), a dedicated STEM has been used; it was also used for exposure studies, imaging, microdiffraction analysis, and monitoring the transmitted beam studies. Amorphous films of Al2O3, Y2O3, Sc2O3, 3Al2O3-2SiO2, and MgO-Al2O3 are deposited on to substrate at cryogenic temperature. Amorphous film structure is necessary to achieve rapid removal of material during e-beam exposure. Hole resolution in the sputtered oxide films of 5 nm holes on 8.1 nm centers was achieved with exposure times in the millisecond range, two to three orders of magnitude lower than produced by other technique. Deposition parameters and film thickness have been studied. The gas ambient on thin films electron dose are strongly related to the drilling speed. A possible mechanism for the exposure process is also developed. DTIC

N94-21431# Naval Postgraduate School, Monterey, CA.
A STUDY OF THE STRUCTURAL STABILITY OF AN UNBALANCED SANDWICH COMPOSITE CONFIGURATION M.S. Thesis
Mary C. Murphy Jun. 1993 60 p
(AD-A272496) Avail: CASI HC A04/MF A01

An unbalanced, sandwich composite structure consisting of Ti 6AL-4V and GRP (Glass Reinforced Plastic) skins with a phenolic honeycomb core is being considered for construction of a surface ship mast which will enclose critical shipboard equipment. Stability of the structure is one of the major concerns in the design process. This research focuses on analytical and experimental studies of an unbalanced composite sandwich beam subject to a compressive axial load. The limit load of each skin material separately, and two failure modes of the sandwich construction (general buckling and core shearing) are measured in the laboratory. An analytical model is developed for predicting the limit load of the unbalanced, sandwich composite configuration. DTIC

N94-21488*# National Aeronautics and Space Administration. Lewis Research Center, Cleveland, OH.
THERMAL STABILITY RELATIONSHIPS BETWEEN PMR-15 RESIN AND ITS COMPOSITES
Kenneth J. Bowles, Douglas Jayne (Case Western Reserve Univ., Cleveland, OH.), Todd A. Leonhardt (Sverdrup Technology, Inc., Brook Park, OH.), and Dennis Bors (Calspan Corp., Cleveland, OH.) Oct. 1993 24 p
Sponsored by NASA. Washington
(RTOP 510-01-50)
(NASA-TM-106285; E-8023; NAS 1.15:106285) Avail: CASI HC A03/MF A01

A study was conducted to investigate the relationship between the thermo-oxidative stability of PMR-15 matrix resin and the stability of graphite-fiber-reinforced composites that contain this resin as the matrix material. Three areas were investigated. The first was the effect of fiber/matrix interfacial bond strength on the isothermal aging weight loss of composites. By using type-A graphite fibers produced by Hercules, it was possible to study composites reinforced with fibers that were processed to receive different surface treatments. One of the fibers was untreated, a second fiber was treated by oxidation to enhance fiber/matrix bonding, and the third type of fiber was coated with an epoxy sizing. These treatments produced three significantly different interfacial bond strengths. The epoxy sizing on the third fiber was quickly oxidized from the bare fiber surfaces at 288, 316, and 343 C. The weight loss due to the removal of the sizing was constant at 1.5 percent. This initial weight loss was not observed in thermo-oxidative stability studies of composites. The PMR-15 matrix satisfactorily protected the reinforcemnt at all three temperatures. Author (revised)

N94-21504 Aeronautical Research Labs., Melbourne (Australia).
DAMAGE STATES AROUND FASTENER HOLES IN THICK GRAPHITE/EPOXY COMPOSITE LAMINATES
S. C. Galea, G. K. Deirmendjian, and D. S. Saunders Aug. 1993 46 p
Limited Reproducibility: More than 20% of this document may be affected by microfiche quality
(AD-A272613; ARL-RR-12; DODA-AR-006-673) Avail: CASI HC A03

This report presents qualitative studies of the development of damage around countersunk fastener holes in thick graphite/epoxy laminates which have been subjected to fatigue loading. The experiments have shown that damage at the hole bore surface produces sites for the nucleation of delaminations. The morphology of the delaminations and ply cracking was mapped extensively. This report discusses the methods used for the mapping of the damage and presents detailed maps of the damage for two loading conditions. In addition, several methods for the nondestructive monitoring of damage development and growth were investigated. These were load/displacement hysteresis measurements, fastener tilt measurements using shadow moire fringe techniques, and ultrasonic time-of-flight C-scanning. This report briefly discusses the possible mechanisms by which damage develops and grows around fastener holes. From the damage maps it was found that the volume of material around the fastener hole, damaged by the fatigue loading, adopted a characteristic shape; the volume of damaged laminate increased towards the faying surface of the laminate and metal fixture. This characteristic damage volume was generated by the fastener rocking under the fatigue loads. The growth of the delaminations has been shown to be preceded by intra-ply cracking and, as fatigue loading continued, more delaminations were generated at the hole bore surface. Author (revised)

N94-21530# Lawrence Livermore National Lab., CA.
MATERIALS SCIENCE AND ENGINEERING
D. R. Lesuer Jun. 1993 34 p
(Contract W-7405-eng-48)
(DE93-040497; UCRL-ID-112775-Rev-1) Avail: CASI HC A03/MF A01

Five papers are included: processing and characterization of laminated metal composites, casting process modeling, characterizing the failure of composite materials, fiber-optic Raman spectroscopy for cure monitoring of advanced polymor composites, and modeling superplastic materials. The papers have been processed separately for the data base. DOE

N94-21559# Seville Univ. (Spain).
DEFORMATION OF AN ALUMINA-ZIRCONIA-SILICON CARBIDE-WHISKER REINFORCED COMPOSITE
J. M. Calderon-Moreno, A. R. DeArellano-Lopez, A. Dominguez-Rodriguez, J. L. Routbort (Argonne National Lab., IL.), and T. Leasky (MER Corp., Tucson, AZ.) Apr. 1993 7 p Presented at the 3rd Conference of the European Ceramic Society, Madrid, Spain, 13-17 Sep. 1993
(Contract W-31-109-eng-38)
(DE93-040244; ANL/MSD/CP-79645; CONF-930927-2) Avail: CASI HC A02/MF A01

Alumina-zirconia composites (MERC) with the addition of 0 and 28 vol % of silicon carbide whiskers were deformed under compression at constant rate at 1450 C, in air. Mechanical results are compared with the behavior of a commercial alumina (ARCO) with analogous proportions of silicon carbide-whiskers (0 and 30 vol %), under the same testing conditions. Flow stresses are typically higher for ARCO materials than for MERC materials. The addition of SiC whiskers increases flow stresses in ARCO composites, and decreases them for MERC samples. Microstructural observations confirm that the change in flow stress is the result of the presence of a glass phase in the MERC samples. DOE

N94-21743*# Massachusetts Inst. of Tech., Cambridge. Dept. of Aeronautics and Astronautics.
MODELING OF OUTGASSING AND MATRIX DECOMPOSITION IN CARBON-PHENOLIC COMPOSITES Semiannual Progress Report, Jun. - Dec. 1993
Hugh L. McManus Dec. 1993 10 p
(Grant NAG8-295)
(NASA-CR-194741; NAS 1.26:194741) Avail: CASI HC A02/MF A01

A new release rate equation to model the phase change of water to steam in composite materials was derived from the theory of molecular diffusion and equilibrium moisture concentration. The new model is dependent on internal pressure, the microstructure of the voids and channels in the composite materials, and the diffusion properties of the matrix material. Hence, it is more fundamental and accurate than the empirical Arrhenius rate equation currently in use. The model was mathematically formalized and integrated into the thermostructural analysis code CHAR. Parametric studies on variation of several parameters have been done. Comparisons to Arrhenius and straight-line models show that the new model produces physically realistic results under all conditions. Derived from text

N94-21754# Brookhaven National Lab., Upton, NY.
PERFORMANCE OF CARBON-BASED HOT FRIT SUBSTRATES
R. Barletta, P. Vanier, J. Adams, J. Svandrlik, and J. R. Powell Jul. 1993 42 p
(Contract DE-AC02-76CH-00016)
(DE94-000509; BNL-49385) Avail: CASI HC A03/MF A01

Erosion tests were conducted on coated graphite and 2D and 3D carbon-carbons in 1 atm hydrogen at high temperatures. Refractory NbC and TaC coatings were used. It was found that the most effective combination of coating and substrate was TaC deposited by chemical vapor reaction method on AXF-5QI graphite. DOE

N94-21777*# Calspan-State Univ. of New York Joint Venture, Buffalo, NY. Dept. of Civil Engineering.
DEVELOPMENT OF BEM FOR CERAMIC COMPOSITES Final Technical Report
D. P. Henry, P. K. Banerjee, G. F. Dargush, D. A. Hopkins (National Aeronautics and Space Administration. Lewis Research Center, Cleveland, OH.), and R. K. Goldberg (National Aeronautics and Space Administration. Lewis Research Center, Cleveland, OH.) Dec. 1993 381 p
(Grant NAG3-888)
(NASA-CR-194718; NAS 1.26:194718) Avail: CASI HC A17/MF A03

BEST-CMS (boundary element solution technology - composite modeling system) is an advanced engineering system for the micro-analysis of fiber composite structures. BEST-CMS is based upon the boundary element program BEST3D which was developed for NASA by Pratt and Whitney Aircraft and the State University of New York at Buffalo under contract NAS3-23697. BEST-CMS presently has the capabilities for elastostatic analysis, steady-state and transient heat transfer analysis, steady-state and transient concurrent thermoelastic analysis, and elastoplastic and creep analysis. The fibers are assumed to be perfectly bonded to the composite matrix, or in the case of static or steady-state analysis, the fibers may be assumed to have spring connections, thermal resistance, and/or frictional sliding between the fibers and the composite matrix. The primary objective of this user's manual is to provide an overview of all BEST-CMS capabilities, along with detailed descriptions of the input data requirements. In the next chapter, a brief review of the theoretical background is presented for each analysis category. Then, chapter three discusses the key aspects of the numerical implementation, while chapter four provides a tutorial for the beginning BEST-CMS user. The heart of the manual, however, is in chapter five, where a complete description of all data input items is provided. Within this chapter, the individual entries are grouped on a functional basis for a more coherent presentation. Chapter six includes sample problems and should be of considerable assistance to the novice. Chapter seven includes capsules of a number of fiber-composite analysis problems that have been solved using BEST-CMS. This chapter is primarily descriptive in nature and is intended merely to illustrate the level of analysis that is possible within the present BEST-CMS system. Chapter eight contains a detail description of the BEST-CMS Neutral File which is helpful in writing an interface between BEST-CMS and any graphic post-processor program. Finally, all pertinent references are listed in chapter nine.
Derived from text

N94-21834*# National Aeronautics and Space Administration. Lyndon B. Johnson Space Center, Houston, TX.
COMPILATION OF REINFORCED CARBON-CARBON TRANSATLANTIC ABORT LANDING ARC JET TEST RESULTS Study/Test Results, Dec. 1987 - Mar. 1992
James D. Milhoan, Vuong T. Pham, and Eric H. Yuen Dec. 1993 334 p
(NASA-TM-104778; S-735; NAS 1.15:104778) Avail: CASI HC A15/MF A03

This document consists of the entire test database generated to support the Reinforced Carbon-Carbon Transatlantic Abort Landing Study. RCC components used for orbiter nose cap and wing leading edge thermal protection were originally designed to have a multi-mission entry capability of 2800 F. Increased orbiter range capability required a predicted increase in excess of 3300 F. Three test series were conducted. Test series #1 used ENKA-based RCC specimens coated with silicon carbide, treated with tetraethyl orthosilicate, sealed with Type A surface enhancement, and tested at 3000-3400 F with surface pressure of 60-101 psf. Series #2 used ENKA- or AVTEX-based RCC, with and without silicon carbide, Type A or double Type AA surface enhancement, all impregnated with TEOS, and at temperatures from 1440-3350 F with pressures from 100-350 psf. Series #3 tested ENKA-based RCC, with and without silicon carbide coating. No specimens were treated with TEOS or sealed with Type A. Surface temperatures ranged from 2690-3440 F and pressures ranged from 313-400 psf. These combined test results provided the database for establishing RCC material single-mission-limit temperature and developing surface recession correlations used to predict mass loss for abort conditions.
Author (revised)

N94-21889*# National Aeronautics and Space Administration. Goddard Space Flight Center, Greenbelt, MD.
OUTGASSING DATA FOR SELECTING SPACECRAFT MATERIALS
William A. Campbell, Jr. and John J. Scialdone Washington Sep. 1993 468 p Supersedes NASA-RP-1124-Rev-2, NASA-RP-1014, NASA-TN-D-7362, and NASA-TN-D-8008 This document will be available on disk from the NASA Center for AeroSpace Information
(RTOP 313-00-00)
(NASA-RP-1124-Rev-3; Rept-93E02432; NASA-RP-1124-Rev-2; NASA-RP-1014; NASA-TN-D-7362; NASA-TN-D-8008; NAS 1.61:1124-Rev-3) Avail: CASI HC A20/MF A04

This tenth compilation of outgassing data of materials intended for spacecraft use supersedes Reference Publication 1124, Revision 2, November 1990. The data were obtained at the Goddard Space Flight Center (GSFC), utilizing equipment developed at Stanford Research Institute (SRI) under contract to the Jet Propulsion Laboratory (JPL). SRI personnel developed an apparatus for determining the mass loss in vacuum and for collecting the outgassed products. The outgassing data have been presented in three different ways in order to facilitate material selection. In Section A, the materials are divided by category into the 18 probable uses, such as adhesives, greases, paints, potting compounds, and so forth. In Section

B, all the materials contained in Section A are listed in alphabetical order by the manufacturer's identification. In Section C, the only materials listed are those having 'Total Mass Loss' (TML) and Collected Volatile Condensable Materials (CVCM) equal to or lower than a maximum 1.0 percent TML and a maximum 0.10 percent CVCM. These are grouped by use, as in Section A. Derived from text

N94-21940# Argonne National Lab., IL.
MILLIMETER-WAVE IMAGING OF COMPOSITE MATERIALS
N. Gopalsami, S. Bakhtiari, S. L. Dieckman, A. C. Raptis, and M. J. Lepper 1993 9 p Presented at the 20th Annual Review of Progress in Quantitative Nondestructive Evaluation, Brunswick, ME, 1-6 Aug. 1993
(Contract W-31-109-eng-38)
(DE93-041160; ANL/ET/CP-79533; CONF-9308167-3) Avail: CASI HC A02/MF A01

This work addresses the application and evaluates the potential of mm-wave imaging in the W-band (75-110 GHz) using samples of low-loss dielectric and composite materials with artificial defects. The initial focus is on the measurement of amplitude changes in the back scattered and forward-scattered fields. The c-scan system employs a focused beam antenna to provide spatial resolution of about one wavelength. A plane-wave model is used to calculate the effective reflection (or transmission) coefficient of multilayer test sample geometry. Theoretical analysis is used to optimize the measurement frequency for higher image contrast and to interpret the experimental results. Both reflection and transmission images, based on back scattered and forward-scattered powers, were made with Plexiglas and Kevlar/epoxy samples containing artificially introduced defects such as subsurface voids and disbonds. The results clearly indicate that mm-wave imaging has high potential for non-contact interrogation of low-loss materials. DOE

N94-22022# Materials and Electrochemical Research Corp., Tucson, AZ.
FABRICATION OF WHISKER-TOUGHENED ALUMINA TUBES
Raouf O. Loutfy Sep. 1993 58 p Prepared in cooperation with Oak Ridge National Lab., TN
(Contract DE-AC05-84OR-21400)
(DE94-001012; ORNL/Sub-86-SE793C) Avail: CASI HC A04/MF A01

A process has been developed to fabricate whisker toughened alumina composites by slip casting dense colloidal suspensions of Al2O3-15% SiC(w). Optimum processing parameters for slip casting were developed with slip viscosity of 60-70 centipoise and solids content 78-79 wt %. Slip-cast parts with green densities 65 to 68% theoretical were achieved. Composite parts were pressureless sintered to 96-97% theoretical density with less than 1% open porosity. The composites exhibited strengths of 500 MPa, toughness of 6.5 MPa m(exp 1/2), and hardness of 17.26 GPa (1765 kg/mm(exp 2)). High temperature strength retention was maintained up to 1200 C. Good thermal shock resistance with (Delta)T(sub cr) = 500 C was also achieved. The process technology was transferred into pilot scale for producing prototype heat exchanger tubing up to 4 inches in diameter at the facilities of Vesuvius/McDanel. DOE

N94-22420 Montreal Univ. (Quebec). Dept. de Genie Mecanique.
CREEP DAMAGE OF CARBON FIBER REINFORCED PEEK M.S. Thesis [ENDOMMAGEMENT EN FLUAGE DU PEEK RENFORCE PAR DES FIBRES DE CARBONE]
Hamid OuldBrahim Jun. 1990 149 p In FRENCH
(ISBN-0-315-58962-0; CTN-94-60887) Copyright Avail: Micromedia Ltd., Technical Information Centre, 240 Catherine Street, Suite 305, Ottawa, Ontario, K2P 2G8, Canada HC/MF

The evolution of viscoelastic properties of a polyether ether ketone (PEEK)/carbon composite under creep loading in the transverse direction was investigated at various temperatures. Using the concept of effective stress, damage development was monitored through the measure of stiffness loss. Creep rupture is also discussed. Creep tests at four normalized stress levels were conducted on specimens of APC-2 until rupture occurred. Four temperatures in the glass transition zone were studied. After different periods of creep, static tests were performed and stiffness recorded. Results showed nonlinear creep behavior and an absence of the tertiary stage of creep. The strain at which the nonlinearity occurred decreased with increasing temperature. The creep behavior can be described by a power law function with an independent temperature exponent. The possibility of interpolation at intermediate temperatures was demonstrated. Damage progression was found to be linear and damage was linked to the nonlinear creep behavior. The stress and temperature was shown to influence damage. A temperature of 120 C appeared critical for the matrix-fiber interface. Kachanov's damage theory gave a good prediction of the time to failure, while the universality of Zhurkov's model was not confirmed. Author (CISTI)

N94-22587 Toronto Univ. (Ontario).
THE EFFECT OF DELAMINATION ON THE DYNAMIC RESPONSE OF COMPOSITE LAMINATES AS MEASURED BY EMBEDDED FIBER OPTIC MICHELSON SENSOR M.S. Thesis
Gao Peiliang 1993 139 p
(ISBN-0-315-83534-6; CTN-94-60949) Copyright Avail: Micromedia Ltd., Technical Information Centre, 240 Catherine Street, Suite 305, Ottawa, Ontario, K2P 2G8, Canada HC/MF

Inferring damage to composite materials from their acoustic emissions may pose some limitations to practical uses. The vibration method may be an alternative technique for detecting damage in composites. Delamination alters the dynamic behavior of structures made of composite materials. The effects of delaminations of various sizes in various locations on the dynamic response of a composite laminated beam structure was investigated experimentally. An embedded localized fiber optic Michelson sensor was employed to detect the dynamic response of the test specimen. The influence of embedded fiber sensors on the natural frequencies of the test specimens was also examined. Extensive experimental results are reported. Neither inside nor edge delamination was shown to affect the natural frequencies of the test sample, but through-width delamination and full edge delamination did affect the damping capacities of the samples. The analytical results based on the beam theory model are presented, which show good agreement with the experimental results. Author (CISTI)

N94-22589 Toronto Univ. (Ontario).
AN EMBEDDED FIBRE OPTIC FOR DAMAGE GROWTH MONITORING IN KEVLAR COMPOSITES M.S. Thesis
William Tsaw 1992 159 p
(ISBN-0-315-83501-X; CTN-94-60951) Copyright Avail: Micromedia Ltd., Technical Information Centre, 240 Catherine Street, Suite 305, Ottawa, Ontario, K2P 2G8, Canada HC/MF

The growth of damage in Kevlar composites was studied using embedded optical fibers in the specimens. It was found that the embedded optical fibers were able to detect and monitor damage growth from simple, one delamination interface layups to complex layups in the DeHavilland Dash-8 leading edge. Furthermore, the results reinforced the damage mechanics as suggested by Glossop (1988). In addition, the data also revealed that the damage mechanisms in the laminates were similar to those proposed by the K-Rule (Gosse et al, 1987, 1988) which describes the relationship between transverse cracks and delaminations. The use of image enhanced backlighting provided a useful nondestructive technique to verify the accuracy of the fracture of the optical fibers. The results also provided clues to the damage progression of thin plates subjected to low-velocity impacts.
Author (CISTI)

N94-21379* National Aeronautics and Space Administration. Langley Research Center, Hampton, VA.
THERMAL STRESS ANALYSIS OF COMPOSITES IN THE SPACE ENVIRONMENT
David E. Bowles *In* CNES, Fifth International Symposium on Materials in a Space Environment Jun. 1993 p 171-186 (For primary document see N94-21367 05-18)
Copyright Avail: CEPADUES-Editions, 111, rue Nicolas-Vaquelin, 31100 Toulouse, France

N94-21384 European Space Agency. European Space Research and Technology Center, ESTEC, Noordwijk (Netherlands). Materials and Processes Div.
INTEGRITY AND TESTING CONCERNS OF THERMOSTRUCTURAL MATERIALS
R. Raynal *In* CNES, Fifth International Symposium on Materials in a Space Environment Jun. 1993 p 231-240 (For primary document see N94-21367 05-18)
Copyright Avail: CEPADUES-Editions, 111, rue Nicolas-Vaquelin, 31100 Toulouse, France

N94-21398 Societe Europeenne de Propulsion, Vernon (France).
THERMOSTRUCTURAL MATERIAL COMPOSITES FOR SPACE APPLICATIONS Abstract Only [MATERIAUX COMPOSITES THERMOSTRUCTURAUX POUR APPLICATIONS SPATIALES]
F. Christin, P. Taveau, M. Cataldi, and M. Lacoste *In* CNES, Fifth International Symposium on Materials in a Space Environment Jun. 1993 p 411-412 In FRENCH (For primary document see N94-21367 05-18)
Copyright Avail: CEPADUES-Editions, 111, rue Nicolas-Vaquelin, 31100 Toulouse, France

N94-22622*# National Aeronautics and Space Administration. Langley Research Center, Hampton, VA.
DELAMINATION, DURABILITY, AND DAMAGE TOLERANCE OF LAMINATED COMPOSITE MATERIALS
T. Kevin OBrien *In its* Computational Methods for Failure Analysis and Life Prediction Oct. 1993 p 311-322 (For primary document see N94-22608 05-39)
Avail: CASI HC A03/MF A03

25 INORGANIC AND PHYSICAL CHEMISTRY

Includes chemical analysis, e.g., chromatography; combustion theory; electrochemistry; and photochemistry.

For related information see also *77 Thermodynamics and Statistical Physics.*.

N94-19839 Colorado School of Mines, Golden. Dept. of Physics.
SURFACE SCIENCE AT THE SOLID LIQUID INTERFACE Final Report, 1 May 1991 - 30 Apr. 1992
Thomas E. Furtak 6 Oct. 1993 87 p Limited Reproducibility: More than 20% of this document may be affected by microfiche quality
(Contract N00014-91-J-1688)
(AD-A271422) Avail: CASI HC A05

This report contains a summary of the Topical Conference on Surface Science at the Electrolyte - Solid Interface, held in conjunction with the 38th National Symposium of the American Vacuum Society on Nov. 11-12, 1991 in Seattle, Washington. DTIC

N94-19889# Lawrence Livermore National Lab., CA.
A DATABASE OF SELECTED TRANSPORT COEFFICIENTS FOR COMBUSTION STUDIES
L. D. Cloutman Aug. 1993 15 p
(Contract W-7405-eng-48)
(DE93-041278; UCRL-ID-115050) Avail: CASI HC A03/MF A01

COYOTE and similar combustion programs based on the multicomponent Navier-Stokes equations require the mixture viscosity, thermal conductivity, and species transport coefficients as input. This report documents a significant improvement to the calculation of these molecular transport coefficients in COYOTE and provides a self-contained and easy-to-use source of such data in a format suitable for use by such programs. The paper presents the data for various species in two forms. The first is a simple functional fit to the transport coefficients. The second is the use of tabulated Lennard-Jones parameters in simple theoretical expressions for the gas-phase transport coefficients. Tables are given for a number of chemical species. DOE

N94-19890# Altamira Instruments, Inc., Pittsburgh, PA.
DIRECT AROMATIZATION OF METHANE
30 Jun. 1993 10 p
(Contract DE-AC22-92PC-92109)
(DE93-040631; DOE/PC-92109/T1) Avail: CASI HC A02/MF A01

The design of the quench reactor was completed. A high temperature furnace, capable of reaching 1540 C was ordered. Thermodynamic equilibrium calculations were carried out in order to determine the maximum possible yields of various products from methane pyrolysis, assuming that the reaction could be quenched at C10 aromatics. Acetylene, benzene, and naphthalene were identified as the major products of such a process. Ethylene, propylene, cyclopentadiene, methylnaphthalene and toluene, vinylacetylene, butadiene, and propadiene were identified as minor products. The yields of benzene and naphthalene are highest in the temperature range between 1350-1550 K, with a maximum aromatic yield of ca. 45% (benzene + naphthalene) expected at about 1475 K (ca. 1200 C). DOE

N94-19924# Brookhaven National Lab., Upton, NY.
FEMTOSECOND RAMAN-INDUCED KERR EFFECT STUDY OF POLAR SOLVENT DYNAMICS: AMIDES
Yong Joon Chang and E. W. Castner, Jr. 1993 6 p Presented at the Time Resolved Vibrational Spectroscopy Conference, Berlin, Germany, 21-28 Jun. 1993
(Contract DE-AC02-76CH-00016)
(DE93-017563; BNL-49234; CONF-9306247-1) Avail: CASI HC A02/MF A01

We have measured the ultrafast pure solvent dynamics of highly power liquids, formamide (FA), N-methylformamide (NMF), N-methylacetamide (NMA), N-methylpropioamide (NMP) and N,N'-dimethylformamide (DMF) using femtosecond optical-heterodyne-detected Raman-induced Kerr effect spectroscopy (OHD-RIKES). The effects of deuteration and temperature-dependence were studied to characterize in detail both the inertial (or non-diffusive) and diffusive intermolecular motions in these liquids. DOE

N94-19953 Air Force Inst. of Tech., Wright-Patterson AFB, OH. School of Engineering.
PHOTOLUMINESCENCE SPECTROSCOPY OF ZINC GERMANIUM DIPHOSPHIDE (ZnGeP2) M.S. Thesis
Jack E. McCrae, Jr. 13 Sep. 1993 60 p Limited Reproducibility: More than 20% of this document may be affected by microfiche quality
(AD-A270705; AFIT/GAP/ENP/93S-01) Avail: CASI HC A04

Zinc germanium diphosphide (ZnGeP2) is a chalcopyrite semiconductor with strong nonlinear optical properties and potential application in Air Force interests. The characteristics of this material have been studied using photoluminescence (PL) spectroscopy. The PL spectrum is dominated by transitions from the conduction band to a deep acceptor level, and features in the spectrum suggest that more than one transition is being observed. The PL is partially polarized, and the degree of polarization appears to differ for each feature in the spectrum. The relative PL intensity of these features are seen to depend upon the wavelength of the excitation source in a fashion which suggests that the observed transitions may originate from three separate conduction bands. These experimentally observed results are found to agree qualitatively with the published band structure of ZnGeP2. DTIC

N94-20000 Louisiana State Univ., Baton Rouge. Dept. of Mechanical Engineering.
DEVELOPMENT OF A TECHNIQUE TO DETERMINE THE MORPHOLOGY AND DYNAMICS OF AGGLOMERATES IN CHEMICALLY REACTING FLOWS Annual Technical Report No. 1, 1 Aug. 1992 - 1 Aug. 1993
Tryfon Charalampopoulos 1 Aug. 1993 132 p Limited Reproducibility: More than 20% of this document may be affected by microfiche quality
(Contract F49620-92-J-0447)
(AD-A271160; AFOSR-93-0792TR) Avail: CASI HC A07

Analytical and experimental studies for the morphology and dynamics of agglomerated particulates in combustion systems were carried out. The analytical studies entailed the investigation of the validity of the approximate relations for scattering and absorption characteristics as well as predictions of the depolarized light scattering intensities for the agglomerates as functions of primary particle diameter, primary particle number density, scattering angle and optical properties of the particles. The approximate relations were found to be accurate to within 20% or better for agglomerates consisting of Rayleigh size primary particles and with optical properties typical of flame soot. It was found that the agglomerate structures encountered in typical flame systems and other agglomerates composed of metallic or dielectric spheres the reciprocity relations do not hold. Experiments were carried out utilizing latex spheres dispersions in distilled water. The results indicate that multiple scattering within the agglomerate may be the cause for the significant difference (up to 30% or more) of the depolarization ratio from the expected value of 1.0. DTIC

N94-20103# Pennsylvania Univ., Philadelphia.
CATALYTIC HYDROGENATION OF CARBON MONOXIDE

B. B. Wayland Dec. 1993 8 p
(Contract DE-FG02-86ER-13615)
(DE94-000881; DOE/ER-13615/7) Avail: CASI HC A02/MF A01

Focus of this project is on developing new approaches for hydrogenation of carbon monoxide to produce organic oxygenates at mild conditions. The strategies to accomplish CO reduction are based on favorable thermodynamics manifested by rhodium macrocycles for producing a series of intermediates implicated in the catalytic hydrogenation of CO. Metalloformyl complexes from reactions of H2 and CO, and CO reductive coupling to form metallo alpha-diketone species provide alternate routes to organic oxygenates that utilize these species as intermediates. Thermodynamic and kinetic-mechanistic studies are used in guiding the design of new metallospecies to improve the thermodynamic and kinetic factors for individual steps in the overall process. Electronic and steric effects associated with the ligand arrays along with the influences of the reaction medium provide the chemical tools for tuning these factors. Non-macrocyclic ligand complexes that emulate the favorable thermodynamic features associated with rhodium macrocycles, but that also manifest improved reaction kinetics are promising candidates for future development. DOE

N94-20111 Army Research Lab., Aberdeen Proving Ground, MD.
DETAILED STRUCTURE STUDY OF AN H2/N2O/Ar FLAME EMPLOYING MOLECULAR BEAM MASS SPECTROMETRY, LASER SPECTROSCOPY, AND MODELING Final Report, Jun. 1992 - Jan. 1993
Rosario C. Sausa, David C. Dayton, William R. Anderson, Cynthia M. Faust, and Stephen L. Howard Oct. 1993 56 p Limited Reproducibility: More than 20% of this document may be affected by microfiche quality
(DA Proj. 1L1-61102-AH-43)
(AD-A270720; ARL-TR-232) Avail: CASI HC A04

A combined experimental and detailed chemical modeling study has been performed on a 20-torr, stoichiometric H2/N2O/Ar burner stabilized flame. This study provides a check of part of the mechanism to be used in models for the combustion of solid nitramine propellants. Species concentration profiles were measured using molecular beam sampling with mass spectrometric detection and laser-induced fluorescence, while temperature profiles were measured with coated Pt/Pt-Rh(10%) thermocouples. The burned gases of the flame contain about 2 mole % of NO and H2, a concentration of approximately 10 times more than that of their equilibrium. This formation prevents full energy release of the systems within or near the flame zone. Experimental flame profiles of the major species, H2, N2O, N2, and H2O, as well as the minor species, NO, O2, OH, H, O, and NH, are presented and compared to calculated profiles generated by PREMIX, a one-dimensional premixed laminar flame code. The chemical mechanism used in the flame code was derived from a critical literature review and consists of 38 reactions and 14 species. Rate and sensitivity analyses performed reveal the intricacies of the mechanism as well as reactions important in the modeling of the experimental results. Several key reactions, including N2O + OH = HO2 + N2 = NO + NH, whose rate coefficients have been controversial, are discussed in detail. In addition, the importance of various collision partners in the key initiation step, N2O + M = N2 + O + M, is presented and discussed. DTIC

N94-20169*# Eloret Corp., Sunnyvale, CA.
COMPUTED POTENTIAL ENERGY SURFACES FOR CHEMICAL REACTIONS Periodic Research Report, 1 Jan. - 31 Aug. 1993
Stephen P. Walch and Eugene Levin 12 Oct. 1993 119 p
(Contract NCC2-478)
(NASA-CR-194600; NAS 1.26:194600) Avail: CASI HC A06/MF A02

A new global potential energy surface (PES) is being generated for O(P-3) + H2 yields OH + H. This surface is being fit using the rotated Morse oscillator method, which was used to fit the previous POL-CI surface. The new surface is expected to be more accurate and also includes a much more complete sampling of bent geometries. A new study has been undertaken of the reaction N + O2 yields NO + O. The new studies have focused on the region of the surface near a possible minimum corresponding to the peroxy form of NOO. A large portion of the PES for this second reaction has been mapped out. Since state to state cross sections for the reaction are important in the chemistry of high temperature air, these studies will probably be extended to permit generation of a new global potential for reaction. Derived from text

N94-20266# Westinghouse Savannah River Co., Aiken, SC.
HYDROGEN ISOTOPE SEPARATION EXPERIENCE AT THE SAVANNAH RIVER SITE
M. W. Lee 1993 5 p Presented at the Course and Workshop on Tritium Technology for Fusion Reactors, Varenna, Italy, 6-14 Sep. 1993
(Contract DE-AC09-89SR-18035)
(DE93-019832; WSRC-MS-93-255; CONF-930937-2) Avail: CASI HC A01/MF A01

Savannah River Site (SRS) is a sole producer of tritium for U.S. weapons program. SRS has built facilities, developed the tritium handling processes, and operated safely for the last forty years. Tritium is extracted from the irradiated reactor target, purified, mixed with deuterium, and loaded to the booster gas bottle in the weapon system for limited lifetime. Tritium is recovered from the retired bottle and recycled. Newly produced tritium is branded into the recycled tritium. One of the key processes is the hydrogen isotope separation that tritium is separated from deuterium and protium. Several processes have been used for the hydrogen isotope separation at SRS: thermal diffusion column (TD), batch cryogenic still (CS), and batch chromatography called fractional sorption (FS). TD and CS requires straight vertical columns. The overall system separation factor depends on the length of the column. These are three story building high and difficult to put in glove box. FS is a batch process and slow operation. An improved continuous chromatographic process called thermal cycling absorption process (TCAP) has been developed. It is small enough to be able to put in a glove box yet high capacity comparable to CS. The SRS tritium purification processes can be directly applicable to the fusion fuel cycle system of the fusion reactor. DOE

N94-20307# Sandia National Labs., Albuquerque, NM.
CHARACTERIZATION OF AMORPHOUS MATERIAL IN SHOCKED QUARTZ BY NMR SPECTROSCOPY
R. A. Assink, M. B. Boslough, and R. T. Cygan 1993 10 p Presented at the 14th International Conference of the International Association for the Advancement of High Pressure Science and Technology, Colorado Springs, CO, 27 Jun. - 2 Jul. 1993
(Contract DE-AC04-76DP-00789)
(DE93-019069; SAND-93-0441C; CONF-930676-34) Avail: CASI HC A02/MF A01

Nuclear magnetic resonance (NMR) analysis of the recovered products from a series of controlled explosive shock-loading experiments on quartz powders was performed to investigate shock-induced amorphization processes. Silicon-29 NMR spectroscopy is an excellent probe of the local bonding environment of silicon in minerals and is capable of detecting and characterizing amorphous and disordered components. NMR spectra obtained for the recovered material exhibit a narrow resonance associated with the shocked crystalline material, and a broad component consistent with an amorphous phase despite the absence of evidence for glass from optical microscopy. The NMR measurements were performed over a range of recycle times from 1 to 3 x 10(exp 5) S. Results demonstrate that the magnetization in both the crystalline and amorphous material following power-law behavior as a function of recycle time. The amorphous component dominates the spectra for short NMR recycle times due to its shorter relaxation time relative to the crystalline material. Fractal analysis of the power-law relations suggests a fractal dimension of 2 for the amorphous phase and 3 for the crystalline phase. DOE

N94-20319 Lawrence Livermore National Lab., CA.
STABILITY OF THE FACE-CENTERED-CUBIC PHASE OF HEAVY RARE GAS SOLIDS
F. H. Ree and Yumi Choi (Korea Advanced Inst. of Science and Technology, Taejon, Republic of Korea.) Jul. 1993 5 p Presented at the 14th International Conference of the International Association for the Advancement of High Pressure Science and Technology, Colorado Springs, CO, 27 Jun. - 2 Jul. 1993 Limited Reproducibility: More than 20% of this document may be affected by microfiche quality
(Contract W-7405-eng-48)
(DE93-019949; UCRL-JC-113296; CONF-930676-42) Avail: Issuing Activity (Department of Energy (DOE))

The authors' recent perturbation theory is applied to show that heavy rare gases solidify into a face-centered-cubic phase over a large temperature range near the melting lines. This paper investigates the static, harmonic,

and anharmonic contributions to the excess Helmholtz free energy and the stability to the face-centered-cubic phase. The observed stability is due to thermal contributions in the Helmholtz free energy. DOE

N94-20330 Purdue Univ., West Lafayette, IN. Dept. of Chemistry.
IN-SITU ELECTROCHEMICAL SURFACE SCIENCE
Michael J. Weaver and Xiao-Ping Gao Apr. 1993 67 p Limited Reproducibility: More than 20% of this document may be affected by microfiche quality
(Contract N00014-91-J-1409)
(AD-A265942; TR-137) Avail: Issuing Activity (Defense Technical Information Center (DTIC))

We consider here recent experimental findings taken primarily from three types of microscopic-level techniques which can yield direct structural information for both in-situ electrochemical and uhv-based surfaces. The first type, scanning probe microscopies, and in particular scanning tunneling microscopy (STM), has recently been shown to reveal remarkably detailed information on real-space atomic arrangements as well as larger-scale morphologies on ordered metal surfaces in solution as well as in uhv and gas-phase environments. The second class, x-ray synchrotron-based scattering techniques, provides accurate spatial structural information. Together, these methods are beginning to revolutionalize our appreciation of surface crystallography at in-situ electrochemical interfaces. The third category considered here, albeit more cursorily, is surface vibrational spectroscopy, specifically infrared reflection-absorption (IRAS) and surface-enhanced Raman (SERS) spectroscopies. While quite different in character and applicability, both these vibrational techniques can yield important insight into the chemical nature and bonding properties of electrochemical adsorbates, and the influences exerted by the local electrostatic and chemical environment. Derived from text

N94-20552# National Defence Research Establishment, Umea (Sweden). NBC-Defence Dept.
ZINC AND TITANIUM SMOKE: CHEMICAL COMPOSITION AND PHYSICAL CHARACTERISTICS [ZINK-OCH TITANROEK: KEMISK SAMMANSAETTNING OCH FYSIKALISKA EGENSKAPER]
Gudrun Cassel, Sten-Aake Fredriksson, and Ingrid Faengmark Oct. 1992 45 p In SWEDISH
(FOA-C-40277-4.9; ETN-93-93759) Avail: CASI HC A03/MF A01; National Defence Research Establishment, S-901 82 Umea, Sweden, HC

Smoke was generated from zinc/hexachloroethane and titanium dioxide/hexachloroethane pyrotechnical pictures in a closed space. The following parameters were investigated: smoke concentration, particle size distributions and chemical composition of the smoke. Zinc hydroxy acids, which are strong acids, are formed during combustion of the zinc munition. The titanium tetrachloride formed in smoke from the titanium dioxide munition will rapidly hydrolyze to hydrogen chrloride and titanium dioxide. Several chlorinated organic substances are formed from both types of smoke munitions during combustion. Some of these substances have well documented toxic and mutagenic effects, for example hexachlorobenzene, hexachlorobutadiene and chlorinated dibenzofurans and dibenzodioxins. The amount of byproducts formed is higher from the titanium dioxide/hexachloroethane munition than from the zinc munition. ESA

N94-20560 California Univ., Berkeley. Dept. of Chemistry.
APPLICATION OF THE REACTIVE FLUX FORMALISM TO STUDY WATER HYDROGEN BOND DYNAMICS Interim Report, Apr. 1992 - Oct. 1993
A. Luzar and D. Chandler Oct. 1993 2 p Limited Reproducibility: More than 20% of this document may be affected by microfiche quality
(Contract N00014-92-J-1361)
(AD-A271824; TR-3) Avail: CASI HC A01

We performed a molecular dynamics study of water at room temperature to examine the dynamics of hydrogen bond formation. It was carried out through an application of the reactive flux formalism. Computed long time relaxation functions are not consistent with a first-order process. Statistical (nondynamical) theories of hydrogen bond breaking, such as transition state theory with a single dividing surface, are found to be unsatisfactory. Further, our dynamical results indicate that at least two elementary processes contribute to hydrogen bond breaking. DTIC

N94-20566# Ehrlich Associates, Lexington, MA.
DIAGNOSTICS AND METHODS FOR REAL-TIME LASER MICROCHEMISTRY Final Report, 1 Apr. 1992 - 31 Mar. 1993
Daniel Ehrlich 31 Mar. 1993 7 p
(Contract F49620-92-C-0029)
(AD-A270871; AFOSR-93-0778TR) Avail: CASI HC A02/MF A01

Among the main goals of the program was the development of digital real-time microchemical processes and diagnostics. Further objective was the design of a stable platform, and the mechanical subsystems and electronic circuits to provide real-time machine control. These are the basis for the study of control and stabilization methods. Specific subassemblies designed were the massive 1.5-inch-thick steel plate, the mechanical frame support, the vibration isolators, and the sliding cell supports. In addition design of the main control circuits, including those for laser incident-light feed-back, laser reflected light, illumination control, opto-interrupt for vibration isolation and zoom magnification control, were completed. DTIC

N94-20584# Massachusetts Inst. of Tech., Cambridge. Dept. of Physics.
OPTICAL METROLOGY OF MAGNETICALLY TRAPPED HYDROGEN Final Report, 1 Jun. 1992 - 31 May 1993
Daniel Kleppner 19 Oct. 1993 4 p
(Contract F49620-92-J-0356)
(AD-A272110; AFOSR-93-0819TR) Avail: CASI HC A01/MF A01

Our goal is to carry out ultra-precise laser spectroscopy on trapped atomic hydrogen in the microkelvin regime, and to develop methods for measuring the 1S-2S transition frequency. The major effort during this past year was to perfect methods for carrying out ultraviolet laser spectroscopy in our cold hydrogen trap. We carried out extensive investigations on the absorption of UV light in various window materials, achieving values of a few percent. In addition, we developed a new method for dealing with the heat deposited in the window by controlling the helium film that lines the low temperature cell in which the experiment is performed. Other accomplishments include the development of improved instrumentation for spatially stabilizing and amplitude modulating the 243 nm laser beam, and improvements in the frequency control of the laser system. DTIC

N94-20934# Notre Dame Univ., IN. Dept. of Chemical Engineering.
TRANSIENT STUDIES OF LOW TEMPERATURE CATALYSTS FOR METHANE CONVERSION
E. E. Wolf 1993 7 p
(Contract DE-FG22-92PC-92529)
(DE93-041232; DOE/PC-92529/T3) Avail: CASI HC A02/MF A01

This report summarizes studies on the partial oxidation of methane on Li promoted vanadium phosphate, unsupported and supported on silica. Our previous report summarized the results on the unpromoted form of the same catalysts. However, we found that for the same level of conversion, Li promotion increased the formaldehyde selectivity in both the unsupported and silica supported forms. So we conducted further studies to determine the role of Li and the mechanism of promotion on these catalysts. DOE

N94-21145 Pittsburgh Univ., PA. Surface Science Center.
DIRECT IMAGES OF THERMAL DISORDER IN THE Cl-Si AND H-O-Si CHEMISORPTION BOND ON Si(100) Technical Report
Q. Gao, Z. Dohnalek, C. C. Cheng, W. J. Choyke, and J. T. Yates, Jr. 27 Oct. 1993 34 p Limited Reproducibility: More than 20% of this document may be affected by microfiche quality
(Contract N00014-82-0280)
(AD-A272386; TR-59) Avail: Issuing Activity (Defense Technical Information Center (DTIC))

The electron stimulated desorption ion angular distribution (ESDIAD) technique combined with a digital subtraction method have been employed to generate difference ESDIAD patterns between measurements made at 130K and 305K for both adsorbed Cl and OH on Si(100). The difference ESDIAD patterns reveal, in real space, images of the thermally excited vibrational amplitudes of the adsorbates. This permits a qualitative visualization of the potential energy surface associated with an adsorbate on its adsorption site. For Cl/Si(100), isotropic thermal broadening of the Cl(+) beams from 130K to 305K is observed. In contrast OH/Si(100) exhibits anisotropic thermal broadening of the H(+) beams on heating from 130K to 305K. These results are correlated with the vibrational frequencies of the surface oscillators. DTIC

N94-21165# Florida Univ., Gainesville.
A PROPOSED METHODOLOGY FOR COMBUSTION TOXICOLOGY TESTING OF COMBINED HALON REPLACEMENT AGENT/JET FUEL INTERACTION Final Report, Jun. - Sep. 1991
Charles J. Kibert Apr. 1993 67 p
(AF Proj. 6302)
(AD-A272695; AL/OET-TR-1993-0047) Avail: CASI HC A04/MF A01

An international consensus to remove chlorofluorocarbon (CFC) compounds from production and U.S. national policy to implement the resulting protocols has motivated the U.S. Air Force to embark on a program to find a suitable replacement for Halon 1211, currently used to extinguish flight line fires. This research addressed the feasibility of conducting a combustion toxicology (CT) program to assess the toxic products of the combustion interaction of JP-8 and the Group 1 or so-called Near Term candidate replacement agents for Halon 1211: HCFC's -123, -124, and -142b. A laboratory scale experiment benchmarked on large scale testing of a 150 sq ft pool fire was developed on the basis of Froude scaling of the full scale fire to a 15 x 15 cm pan fire. A prototype apparatus was developed and investigation into the use of animal behavior methods as an indicator of human incapacitation was conducted. The result is a new method which may potentially be utilized for future toxicity studies of the combustion interaction of current and future U.S. Air Force fuels with various fire extinguishants. DTIC

N94-21168# Colorado State Univ., Fort Collins. Dept. of Chemistry.
ELECTROCHEMICAL SYNTHESIS OF ULTRATHIN FILM COMPOSITE MEMBRANES Final Technical Report, 1 Jun. 1990 - 31 May 1993
C. R. Martin 27 Oct. 1993 23 p
(Grant AF-AFOSR-0282-90)
(AD-A272721; Rept-53-2380; AFOSR-93-0845TR) Avail: CASI HC A03/MF A01

Ultrathin film composite membranes consist of an ultrathin (less than 1,000 A-thickness) chemically-selective layer bonded to the surface of a microporous support membrane. Such composite membranes are important in electrochemical science because they can provide both high transport selectivity and low membrane resistance. This is possible because, while the chemically selective layer typically has high resistivity, its ultrathin nature insures that it has low resistance. We have been exploring new methods for synthesizing ultrathin film composite membranes, and we have been investigating the transport properties of the resulting composite membranes. This research effort has been extremely successful. DTIC

N94-21181# Delaware Univ., Newark. Dept. of Chemistry.
CHEMISTRY OF THE BURNING SURFACE Final Report, 1 Oct. 1989 - 30 Sep. 1993
Thomas B. Brill 12 Oct. 1993 202 p
(Grant AF-AFOSR-0521-89)
(AD-A272725; AFOSR-93-0840TR) Avail: CASI HC A10/MF A03

The objective of this project was to identify the dominant thermal decomposition and secondary reaction pathways that exist in the surface zone of a burning propellant. T-jump/FTIR spectroscopy and SMATCH/FTIR spectroscopy are new diagnostic techniques that were designed for this project. They enable a film of material to be heated at a high rate in such a manner as to simulate a thin volume element of the surface during combustion. The semiglobal thermal decomposition reactions and the first strongly exothermic secondary reaction of important oxidizers and monopropellants were identified. The compounds studied were nitramine (CL-20, HMX, RDX, DNNC), ammonium salts (AP, AN, ADN), and azide polymers (GAP, BAMO). DTIC

N94-21213# Massachusetts Inst. of Tech., Cambridge. Dept. of Mechanical Engineering.
REACTION ZONE MODELS FOR VORTEX SIMULATION OF TURBULENT COMBUSTION Annual Technical Progress Report, 1 Sep. 1992 - 31 Aug. 1993
Ahmed F. Ghoniem 1 Oct. 1993 113 p
(Contract F49620-92-J-0445)
(AD-A272723; AFOSR-93-0835TR) Avail: CASI HC A06/MF A02

During the first year of this effort, two related issues were investigated: (1) establishing the validity of the thin flame model when used to compute flow-combustion interactions in a turbulent shear layer; and (2) developing an efficient methodology to compute the unsteady strained flame structure when the flame thickness is much smaller than the flow scale. In the first effort, the transport element method was applied to compute (1) a reacting flow in which combustion proceeds according to a single-step, temperature dependent Arrhenius reaction, and (2) a mixing-limited model in which Schvab-Zeldovich variables are used to obtain the infinite speed chemistry results. The results of both computations showed that, at high Damkohler numbers, while there is a small error in the prediction of the total burning rate using the second approach, the second model accurately estimates the effect of combustion on the flow dynamics in terms of volumetric expansion and vorticity generation. Work on the second project resulted in a more efficient model to compute the flame structure under conditions of unsteady strain. The computational model is based on a series of mathematical transformations which reduce the governing equations to time-dependent reaction-diffusion equations. DTIC

N94-21216# Pennsylvania Univ., Philadelphia. Dept. of Chemistry.
INTEGRAL EQUATION CALCULATION OF SOLVENT ACTIVATION FREE ENERGIES FOR ELECTRON AND PROTON TRANSFER REACTIONS Technical Report, May 1993 - 1994
Indrani Bhattacharya-Kodali and Gregory Voth 4 Nov. 1993 22 p
(Contract N00014-92-J-1243)
(AD-A272665; TR-3) Avail: CASI HC A03/MF A01

The extended reference interaction site method (RISM) integral equation theory is applied to calculate the solvent activation free energy for the Fe(2+)/Fe(3+) electron transfer and a model proton transfer reaction in water. In the case of the electron transfer, the calculated free energy is found to be within a few percent of an existing computer simulation result. In the case of the proton transfer reaction, the agreement with simulation is not as good, but still reasonable. DTIC

N94-21226# Aerospace Corp., El Segundo, CA. Technology Operations.
CONVERSION OF LDEF EXPERIMENT M0003 SAMPLE OBSERVATION DATABASE TO MS-DOS FORMATS
B. C. Trotter, J. M. Coggi, and S. R. Gyetvay 1 Oct. 1993 51 p
(Contract F04701-88-C-0089)
(AD-A272945; TR-93(3935)-16; SMC-TR-93-55) Avail: CASI HC A04/MF A01

The four trays of the M0003 materials on the Long Duration Exposure Facility (LDEF) contained over 1200 samples from 20 subexperiments. The complete sample complement represented a broad range of materials, including thin-film optical coatings, paints, polymer sheets and tape, adhesives, and composites, for use in various spacecraft applications, including thermal control, structures, optics, and solar power. Since some subexperiments included duplicate samples exposed on the leading- and trailing-edge trays for 9-week, 19-week, 40-week, and 69-month durations, comparisons among samples provided a valuable time history of degradation. During the deintegration of the subexperiments from the M0003 trays, each sample was examined using bright-field, dark-field, and Nomarski-light microscopy techniques. Records of the condition of the samples and all available references of publication on postflight analyses on each sample were originally collected on a Macintosh computer database. In response to requests by the spacecraft community for a PC version of the database, two conversions were made: Paradox 4.0 and dBase IV. This report includes instructions for installation and use, including example searches and printouts, of each of these conversions. Copies of the electronic database are available on floppy disk by request in both IBM formats, as well as the original 4th Dimension for Macintosh version. DTIC

N94-21241# Defence Research Establishment Atlantic, Dartmouth (Nova Scotia).
ASBESTOS CHARACTERIZATION USING SCANNING ELECTRON MICROSCOPY/LIGHT ELEMENT X RAY SPECTROMETRY
G. C. Fisher and R. M. Morchat Sep. 1993 23 p
(AD-A271611; DREA-TM-93/206) Avail: CASI HC A03/MF A01

The Defence Research Establishment Atlantic (DREA) has traditionally used scanning electron microscopy (SEM) coupled with energy dispersive x-ray (EDX) spectrometry to identify asbestos fibers in solid insulating materials. This analysis typically utilizes fiber morphology to determine the presence of asbestiform fibers and EDX analysis to characterize asbestos type. The characterization is accomplished by comparison of the relative amounts of magnesium, silicon, and iron present in the fibers. The EDX detector traditionally used in asbestos characterization employs a protective

beryllium shield that effectively blocks the passage of low energy x-rays. Thus characteristic x-rays from 'light elements' (those below sodium in atomic weight) are not detected. Recently, DREA acquired a commercial EDX detector that employs a polymer shield that allows for detection of x-rays from elements as low as boron in atomic weight. This report summarizes results of a study on the effects of using a light element detector on characterization of both asbestos standards and commercial asbestos-containing insulating material. The study showed that 'light element' SEM/EDX can be used to characterize asbestos fibers in bulk insulations. DTIC

N94-21243# Aerodyne Research, Inc., Billerica, MA.
MODEL FOR LIQUID BORON OXIDE DROPLET GASIFICATION IN H/O/C/F COMBUSTION ENVIRONMENTS Final Report, 1-30 Oct. 1992
R. C. Brown, C. E. Kolb, R. A. Yetter, F. L. Dryer, and H. Rabitz 11 Nov. 1992 57 p
(Contract N00014-92-C-0225)
(AD-A272911; ARI-RR-1045) Avail: CASI HC A04/MF A01

A model for the gasification of liquid boron oxide droplet in high temperature H/O/C/F environments is presented. The model includes a detailed gas phase reaction mechanism, multi-component molecular diffusion, and heterogeneous gas-surface reactions. The gas phase reaction mechanism consists of 103 reversible reactions for H/O/C, B/H/O/C, and B/H/O/C/F combustion systems. The surface reactions include processes that are first order in gas phase reactants and are thermodynamically competitive with vaporization. Model results are presented that illustrate the effect of variations in droplet diameter, gas phase temperature, composition, and oxygen to fluorine mole ratio. In addition, the model calculations are analyzed with reaction flux and gradient sensitivity analysis to determine the fastest and rate-limiting steps. Model results for several calculations indicate that the addition of fluorine accelerates the gasification process relative to B/H/O/C systems. The degree of enhancement, however, depends upon the temperature and composition of the surrounding gas and the droplet diameter. DTIC

N94-21435 Army Research Lab., Fort Monmouth, NJ.
ANALYSIS OF SEMI-INSULATING BULK GaAs USING GLOW DISCHARGE MASS SPECTROMETRY
Andrew E. Souzis, Richard T. Lareau, and Richard Wittstruck Aug. 1993 23 p Limited Reproducibility: More than 20% of this document may be affected by microfiche quality
(AD-A273032; ARL-TR-69) Avail: CASI HC A03

The ability to perform sub-part per billion (ppb) analysis of semi-insulating (SI) GaAs substrate material is of critical importance for the development of electronic materials used in microelectronic device applications. Glow discharge mass spectrometry (GDMS) is commonly used to perform high sensitivity (part-per-trillion) measurements of metals and semiconductors. Since the sample is utilized as the cathode in a DC glow discharge, it must be conducting to some degree. Thus analysis of SI wafers presents major difficulties. Possible solutions include the use of a high purity mask or the mixing of pulverized sample material with high purity powder. Due to the finite purity of available materials, these methods have limitations. This study has resulted in the development of a novel method to perform maskless analysis of SI wafers with sub-ppb sensitivity across virtually the entire periodic table. This method has been utilized in various studies related to electronic device applications. DTIC

N94-21448# National Inst. of Standards and Technology, Gaithersburg, MD.
RADCAL: A NARROW-BAND MODEL FOR RADIATION CALCULATIONS IN A COMBUSTION ENVIRONMENT
W. L. Grosshandler Apr. 1993 57 p
(PB93-200889; NIST/TN-1402) Avail: CASI HC A04/MF A01

Radiation within a medium containing products of combustion is dependent upon the temperature and concentrations throughout the entire field. The energy is distributed across the infrared spectrum in a highly nonlinear fashion which greatly complicates modeling of the heat transfer within a burning environment. The report describes a numerical program, RADCAL, which predicts the radiant intensity leaving a nonisothermal volume containing nonuniform levels of carbon dioxide, water vapor, methane, carbon monoxide, nitrogen, oxygen, and soot. The absorption coefficient of the combined gases is calculated from a narrow-band model and a combination of tabulated spectral properties and theoretical approximations to the vibrational-rotational molecular bands. Soot is treated as a purely absorbing substance in the Rayleigh limit. Background on the development of the model, example calculations, and an explanation of input procedures are presented. NTIS

N94-21452# California Inst. of Tech., Pasadena. Graduate Aeronautical Labs.
COMBUSTION IN TURBULENT JETS AND BUOYANT FLAMES Final Report, 1 Jan. 1990 - 31 Dec. 1992
P. E. Dimotakis and J. E. Broadwell 6 Apr. 1993 61 p See also PB92-211481
(Contract GRI-5087-260-1467)
(PB93-202372; GRI-93/0108) Avail: CASI HC A04/MF A01

Results from an investigation of the mixing mechanisms in liquid-phase and gas-phase jets are reported. The investigation addressed the effects of molecular diffusion rates (Schmidt number) and combustion heat release on these mechanisms and incorporated these mechanisms into modeling and predictive techniques for practical natural gas flames. The gas-phase, chemically reacting jet experiments in the High Pressure Combustion Facility investigated the effects of Reynolds number on turbulent jet diffusion flame length, free of buoyancy and radiation effects. In a collaborative modeling effort with the SANDIA CRF at Livermore, CA, the authors have made progress in incorporating the effects of radiation and buoyancy in their description of turbulent jet diffusion flames and make comparisons between their model results and some recent NO(x) measurements. NTIS

N94-21574# Center for Mathematics and Computer Science, Amsterdam (Netherlands). Dept. of Numerical Mathematics.
A PROJECT ON PARAMETER IDENTIFICATION IN REACTION KINETICS
P. W. Hemker and J. Kok Jan. 1993 41 p Sponsored in part by AKZO Research Labs, Arnhem, Netherlands
(CWI-NM-R9301; ETN-94-94703) Copyright Avail: CASI HC A03/MF A01

A project to collect knowledge in parameter estimation, in order to be able to solve real life parameter estimation problems from chemical engineering is reported. A suitable method to solve these problems was found and a computer program was developed. These problems consist of a system of Ordinary Differential Equations (ODE's) or differential-algebraic equations containing parameters to be determined when experimental values are available that should fit the solution of the ODE's. By means of the program, several inverse problems for parameter estimation were solved. For the solution, the parameters and their range of probability were identified, and to what extent the information available from the experiments led to the possible identification of the parameters was determined. A summary of results is given and subjects for further research are identified. ESA

N94-21631# Brookhaven National Lab., Upton, NY.
THE ATOMIC WEIGHT AND ISOTOPIC COMPOSITION OF BORON AND THEIR VARIATION IN NATURE
N. E. Holden 1993 13 p Presented at the 37th International Union of Pure and Applied Chemistry (IUPAC) Meeting, Lisbon, Portugal, 5-12 Aug. 1993
(Contract DE-AC02-76CH-00016)
(DE93-019046; BNL-49333; CONF-9308148-2) Avail: CASI HC A03/MF A01

The boron isotopic composition and atomic weight value and their variation in nature are reviewed. Questions are raised about the previously recommended value and the uncertainty for the atomic weight. The problem of what constitutes an acceptable range for normal material and what should then be considered geologically exceptional is discussed. Recent measurements make some previous decisions in need of re-evaluation. DOE

N94-21789 Argonne National Lab., IL.
PLASMA-CHEMICAL CONVERSION OF HYDROGEN SULFIDE INTO HYDROGEN AND SULFUR
J. B. L. Harkness, R. D. Doctor, and E. J. Daniels 1993 8 p Presented at the 3rd World Congress on Engineering and Environment, Beijing, China, 12-14 Oct. 1993 Limited Reproducibility: More than 20% of this document may be affected by microfiche quality

(Contract W-31-109-eng-38)
(DE93-041167; ANL/ES/CP-80089; CONF-9310171-1) Avail: CASI HC A02/MF A01

A waste-treatment process that recovers both hydrogen and sulfur from hydrogen-sulfide-contaminated industrial wastes is being developed to replace the Claus technology, which recovers only sulfur. The proposed process is based on research reported in the Soviet technical literature and uses microwave (or radio-frequency) energy to initiate plasma-chemical reactions that dissociate hydrogen sulfide into elemental hydrogen and sulfur. In the plasma-chemical process, the gaseous stream would be purified and separated into streams containing the product hydrogen, hydrogen sulfide for recycle to the plasma reactor, and the process purge containing carbon dioxide and water. Since unconverted hydrogen sulfide is recycled to the plasma reactor, the plasma-chemical process has the potential for sulfur recoveries in excess of 99% without the additional tail-gas clean-up processes associated with the Claus technology. Laboratory experiments with pure hydrogen sulfide have confirmed that conversions of over 90% per pass are possible. Experiments with impurities typical of petroleum refinery and natural gas production acid gases have demonstrated that these impurities are compatible with the plasma dissociation process and do not appear to create new waste-treatment problems. Other experiments show that the cyclonic-flow pattern hypothesized by the Russian theoretical analysis of the plasma-chemical process can substantially decrease energy requirements for hydrogen sulfide dissociation while increasing conversion. This process has several advantages over the current Claus-plus-tail-gas-cleanup technology. The primary advantage is the potential for recovering hydrogen more cheaply than the direct production of hydrogen. The difference could amount to an energy savings of 40 x 10(exp 15) to 70 x 10(exp 15) J/yr in the refining industry, for an annual savings of $500 million to $1 billion. DOE

N94-21842# Brookhaven National Lab., Upton, NY.
FEMTOSECOND DYNAMICS IN HYDROGEN-BONDED SOLVENTS
E. W. Castner, Jr. and Y. J. Chang 1993 14 p Presented at the Royal Netherlands Academy of Sciences Colloquium on Femtosecond Reaction Dynamics, Amsterdam, Netherlands, 16-19 May 1993
(Contract DE-AC02-76CH-00016)
(DE93-019937; BNL-49140; CONF-9305270-1) Avail: CASI HC A03/MF A01

We present results on the ultrafast dynamics of pure hydrogen-bonding solvents. The resutls were obtained using femtosecond Fourier-transform optical-heterodyne-detected, Raman-induced Kerr effect spectroscopy. The solvent systems we have studied include the formamides, water, ethylene glycol, and acetic acid. Inertial and diffusive motions are clearly resolved. We comment on the effect that such ultrafast solvent motions have on chemical reactions in solution. DOE

N94-21947# California Univ., Berkeley. Lawrence Berkeley Lab.
WATER-ENHANCED SOLVATION OF ORGANICS Ph.D. Thesis
J. H. Lee Jul. 1993 73 p
(Contract DE-AC03-76SF-00098)
(DE93-040297; LBL-34410) Avail: CASI HC A04/MF A01

Water-enhanced solvation (WES) was explored for Lewis acid solutes in Lewis base organic solvents, to develop cheap extract regeneration processes. WES for solid solutes was determined from ratios of solubilities of solutes in water-saturated and low-water solvent; both were determined from solid-liquid equilibrium. Vapor-headspace analysis was used to determine solute activity coefficients as function of organic phase water concentration. WES magnitudes of volatile solutes were normalized, set equal to slope of log gamma(sub s) versus x(sub w)/x(sub s) curve. From graph shape, Delta(log gamma(sub s)) represents relative change in solute activity coefficient. Solutes investigated by vapor-headspace analysis were acetic acid; propionic acid; ethanol; 1,2-propylene glycol; and 2,3-butylene glycol. Monocarboxylic acids had largest decrease in activity coefficient with water addition followed by glycols and alcohols. Propionic acid in cyclohexanone showed greatest water-enhancement Delta (log gamma(sub acid))/Delta(x(sub w)/x(sub acid)) = -0.25. In methyl cyclohexanone, the decrease of the activity coefficient of propionic acid was -0.19. Activity coefficient of propionic acid in methyl cyclohexanone stopped decreasing once the water reached a 2:1 water to acid mole ratio, implying a stoichiometric relation between water, ketone, and acid. Except for 2,3-butanediol, activity coefficients of the solutes studied decreased monotonically with water content. Activity coefficient curves of ethanol, 1,2-propanediol, and 2,3-butanediol did not level off at large water/solute mole ratio. Solutes investigated by solid-liquid equilibrium were citric acid, gallic acid, phenol, xylenols, and 2-naphthol. Saturation concentration of citric acid in anhydrous butyl acetate increased from 0.0009 to 0.087 mol/L after 1.3 % (g/g) water co-dissolved into organic phase. Effect of water-enhanced solvation for citric acid is very large but very small for phenol and its derivatives. DOE

N94-21984# Energy Research Corp., Danbury, CT.
DEVELOPMENT OF AN ELECTROCHEMICAL HYDROGEN SEPARATOR
S. Abens, J. Fruchtman, and A. Kush 1993 16 p Presented at the Coal-Fired Power Systems 1993 Advances in IGCC and PFBC Review Meeting, Morgantown, WV, 28-30 Jun. 1993
(Contract DE-AC21-89MC-26040)
(DE93-019877; DOE/MC-26040/93/C0220; CONF-9306148-24) Avail: CASI HC A03/MF A01

The EHS is an electrochemical hydrogen separator based on the uniquely reversible nature of hydrogen oxidation reduction reactions in electrochemical systems. Hydrogen from the mixed gas stream is oxidized to H(+) ions, transported through a cation transport electrolyte membrane (matrix) under an applied electric field, and discharged in a pure hydrogen state on the cathode. The cation transfer electrolyte membrane provides a barrier between the feed and product gases. The EHS design is an off-shoot of phosphoric acid fuel cell development. Although any proton transfer electrolyte can be used, the phosphoric acid based system offers a unique advantage because its operating temperature of approximately 200 C makes it tolerant to trace CO and also closely matches the water-shift reactor exit gas temperature (approximately 250 C). Hydrogen containing streams in coal gasification systems have large carbon monoxide contents. For efficient hydrogen recovery, most of the CO must be converted to hydrogen by the low temperature water-shift reaction. Advanced coal gasification and gas separation technologies offer an important pathway to the clean utilization of coal resources. DOE

N94-22021# Idaho Univ., Moscow. Dept. of Chemistry.
COLUMN CHROMATOGRAPHIC SEPARATION OF Y(3+) FROM Sr(2+) BY POLYMERIC IONIZABLE CROWN ETHER RESINS
D. J. Wood, S. Elshani, C. M. Wai, R. A. Bartsch (Texas Technological Univ., Lubbock.), M. Huntley (Westinghouse Idaho Nuclear Co., Inc., Idaho Falls.), and S. Hartenstein (Westinghouse Idaho Nuclear Co., Inc., Idaho Falls.) 1993 22 p
(Contract DE-AC07-84ID-12435)
(DE94-000935; WINCO-11973) Avail: CASI HC A03/MF A01

Condensation polymers containing subunits of crown ether carboxylic acid monomers are effective stationary phases for the chromatographic separation of Y(3+) and Sr(2+). The pH range and metal loading capacities for the resins have been determined under equilibrium conditions. The resin can be regenerated for repeated use without losing its separation capability. Altering the molecular structure of the monomer (sym-dibenzo-16-crown-5-oxyacetic acid) by an alkyl substitution on the macrocyclic cavity decreases the loading capacity of the resin. DOE

N94-22031# Sandia National Labs., Albuquerque, NM.
INTERFACIAL REACTIONS BETWEEN TITANIUM AND BORATE GLASS
R. K. Brow, S. K. Saha (Lehigh Univ., Bethlehem, PA.), and J. I. Goldstein (Lehigh Univ., Bethlehem, PA.) 1992 6 p Presented at the Spring Meeting of the Materials Research Society, San Francisco, CA, 12-16 Apr. 1993
(Contract DE-AC04-76DP-00789)
(DE93-012847; SAND-92-2779C; CONF-930405-5) Avail: CASI HC A02/MF A01

Interfacial reactions between melts of several borate glasses and titanium were investigated by analytical scanning electron microscopy (ASEM) and x ray photoelectron spectroscopy (XPS). A thin titanium boride interfacial layer is detected by XPS after short (30 minutes) thermal treatments. ASEM analyses after longer thermal treatments (8-120 hours) reveal boron-rich interfacial layers and boride precipitates in the Ti side of the interface. DOE

N94-22046# Westinghouse Savannah River Co., Aiken, SC.
GAMMA RAY SPECTROMETRY OF LDEF SAMPLES: RESULTS OF 1992 ANALYSES
W. G. Winn Sep. 1993 19 p
(Contract DE-AC09-89SR-18035)
(DE94-001177; WSRC-TR-93-430) Avail: CASI HC A03/MF A01

In January 1990, NASA retrieved the Long Duration Exposure Facility (LDEF), which had orbited the Earth since April 1984. The satellite had become slightly radioactive due to cosmic exposure, and the SRTC Underground Counting Facility was used to analyze LDEF samples of Al and Ta for activations of Na-22, Lu-172, and Lu-173. Background steel trunnion samples, not irradiated in space, were analyzed for Co-60. This report summarizes results for 15 samples analyzed in 1992. DOE

N94-22395# Lawrence Livermore National Lab., CA.
THEORETICAL PHASE DIAGRAMS FOR SOLID H(SUB 2)
M. P. Surh and K. J. Runge Jul. 1993 6 p Presented at the 14th International Conference of the International Association for the Advancement of High Pressure Science and Technology, Colorado Springs, CO, 27 Jun. - 2 Jul. 1993
(Contract W-7405-eng-48)
(DE94-001049; UCRL-JC-113403; CONF-930676-58) Avail: CASI HC A02/MF A01

Possible phase diagrams for solid molecular para-hydrogen in the 0-200 GPa pressure regime are constructed on the basis of ab initio calculations. Structures for the broken symmetry phase (BSP) and H-A phase have recently been proposed under the assumption that the molecules are centered on sites of a hexagonal close-packed lattice with the ideal c/a ratio, i.e., only molecular orientational and electronic changes are allowed. Symmetry considerations then dictate the simplest phase diagrams consistent with experimental observations, although the possibility of additional transitions cannot be ruled out. A simple model is introduced to describe the BSP and H-A transitions. DOE

N94-20638*# Tokyo Univ. (Japan). Geological Inst.
EVAPORATION IN EQUILIBRIUM, IN VACUUM, AND IN HYDROGEN GAS Abstract Only
Hiroko Nagahara *In* Lunar and Planetary Inst., Twenty-Fourth Lunar and Planetary Science Conference. Part 3: N-Z 1993 p 1045-1046 (For primary document see N94-20636 05-91)
Avail: CASI HC A01/MF A06

N94-20640*# Academy of Sciences (USSR), Moscow. Inst. of Geochemistry and Analytical Chemistry.
THE EREVAN HOWARDITE: PETROLOGY OF GLASSY CLASTS AND MINERAL CHEMISTRY Abstract Only
M. A. Nazarov and A. A. Ariskin *In* Lunar and Planetary Inst., Twenty-Fourth Lunar and Planetary Science Conference. Part 3: N-Z 1993 p 1049-1050 (For primary document see N94-20636 05-91)
Avail: CASI HC A01/MF A06

N94-20642*# Academy of Sciences (USSR), Moscow. Inst. of Geochemistry and Analytical Chemistry.
CARBONACEOUS XENOLITHS FROM THE EREVAN HOWARDITE Abstract Only
M. A. Nazarov, F. Brandstaetter (Naturhistorisches Museum, Vienna, Austria.), and G. Kurat (Naturhistorisches Museum, Vienna, Austria.) *In* Lunar and Planetary Inst., Twenty-Fourth Lunar and Planetary Science Conference. Part 3: N-Z 1993 p 1053-1054 (For primary document see N94-20636 05-91)
Avail: CASI HC A01/MF A06

N94-20644*# Notre Dame Univ., IN. Dept. of Civil Engineering and Geological Sciences.
PETROGENESIS OF APOLLO 12 MARE BASALTS. PART 1: MULTIPLE MELTS AND FRACTIONAL CRYSTALLIZATION TO EXPLAIN OLIVINE AND ILMENITE BASALT COMPOSITIONS Abstract Only
Clive R. Neal and Lawrence A. Taylor (Tennessee Univ., Knoxville.) *In* Lunar and Planetary Inst., Twenty-Fourth Lunar and Planetary Science Conference. Part 3: N-Z 1993 p 1057-1058 (For primary document see N94-20636 05-91)
Avail: CASI HC A01/MF A06

N94-20645*# Notre Dame Univ., IN. Dept. of Civil Engineering and Geological Sciences.
PETROGENESIS OF APOLLO 12 MARE BASALTS. PART 2: AN OPEN SYSTEM MODEL TO EXPLAIN THE PIGEONITE BASALT COMPOSITIONS Abstract Only
Clive R. Neal and Lawrence A. Taylor (Tennessee Univ., Knoxville.) *In* Lunar and Planetary Inst., Twenty-Fourth Lunar and Planetary Science Conference. Part 3: N-Z 1993 p 1059-1060 (For primary document see N94-20636 05-91)
Avail: CASI HC A01/MF A06

N94-20652*# Bern Univ. (Switzerland). Physikalisches Inst.
DATING NATIVE GOLD BY NOBLE GAS ANALYSES Abstract Only
S. Niedermann, O. Eugster, B. Hofmann, Ch. Thalmann, and W. U. Reimold (Witwatersrand Univ., Johannesburg, South Africa.) *In* Lunar and Planetary Inst., Twenty-Fourth Lunar and Planetary Science Conference. Part 3: N-Z 1993 p 1073-1074 Sponsored by Swiss NSF (For primary document see N94-20636 05-91)
Avail: CASI HC A01/MF A06

N94-20664*# Deutsche Forschungs- und Versuchsanstalt fuer Luft- und Raumfahrt, Oberpfaffenhofen (Germany). Planetary Remote Sensing Section.
GONIOSPECTROMETRIC PROPERTIES OF A WHITE STANDARD Abstract Only
A. Oehler and A. Dummel *In* Lunar and Planetary Inst., Twenty-Fourth Lunar and Planetary Science Conference. Part 3: N-Z 1993 p 1097-1098 (For primary document see N94-20636 05-91)
Avail: CASI HC A01/MF A06

N94-20667*# Chicago Univ. Hospitals and Clinics, IL. Dept. of Geophysics Science.
TAMBO QUEMADO: EXTRAORDINARY CONCENTRATIONS OF REE AND REFRACTORY TRACE ELEMENTS CAUSED BY ARTIFICIAL HEATING Abstract Only
E. Olsen, I. Hutcheon (California Inst. of Tech., Pasadena.), and C. Moore (Arizona State Univ., Tempe.) *In* Lunar and Planetary Inst., Twenty-Fourth Lunar and Planetary Science Conference. Part 3: N-Z 1993 p 1103-1104 (For primary document see N94-20636 05-91)
Avail: CASI HC A01/MF A06

N94-20669*# California Inst. of Tech., Pasadena. Div. of Geological and Planetary Sciences.
SELF DIFFUSION OF ALKALINE-EARTH IN Ca-Mg-ALUMINOSILICATE MELTS: EXPERIMENTAL IMPROVEMENTS ON THE DETERMINATION OF THE SELF-DIFFUSION COEFFICIENTS Abstract Only
O. Paillat and G. J. Wasserburg *In* Lunar and Planetary Inst., Twenty-Fourth Lunar and Planetary Science Conference. Part 3: N-Z 1993 p 1107-1108 (For primary document see N94-20636 05-91)
Avail: CASI HC A01/MF A06

N94-20670*# New Mexico Univ., Albuquerque. Dept. of Earth and Planetary Sciences.
ORTHOPYROXENES AS RECORDERS OF DIOGENITE PETROGENESIS: MAJOR AND MINOR ELEMENT SYSTEMATICS Abstract Only
J. J. Papike, M. N. Spilde, G. W. Fowler, and C. K. Shearer *In* Lunar and Planetary Inst., Twenty-Fourth Lunar and Planetary Science Conference. Part 3: N-Z 1993 p 1109-1110 (For primary document see N94-20636 05-91)
(Grant NAG9-497)
Avail: CASI HC A01/MF A06

N94-20676*# Max-Planck-Inst. fuer Chemie, Mainz (Germany).
ABUNDANCE AND COMPOSITION OF SOLAR KR IN THE H3-H6 CHONDRITE ACFER111 Abstract Only
A. Pedroni *In* Lunar and Planetary Inst., Twenty-Fourth Lunar and Planetary Science Conference. Part 3: N-Z 1993 p 1121-1122 (For primary document see N94-20636 05-91)
Avail: CASI HC A01/MF A06

N94-20677*# First Inst. of Oceanography, Qingdao (China).
FIRST DISCOVERY OF THE ORGANIC MATERIALS IN DEEP-SEA IRON COSMIC SPHERULE Abstract Only
Peng Hanchang and Xu Peicang (Xian Inst. of Geology and Mineral Resources, China.) *In* Lunar and Planetary Inst., Twenty-Fourth Lunar and Planetary Science Conference. Part 3: N-Z 1993 p 1123-1124 (For primary document see N94-20636 05-91)
Avail: CASI HC A01/MF A06

N94-20679*# Harvard-Smithsonian Center for Astrophysics, Cambridge, MA.
LAMELLAR OLIVINE IN THE DIVNOE ACHONDRITE: EVIDENCE FOR HIGH-PRESSURE EXSOLUTION? Abstract Only
M. I. Petaev *In* Lunar and Planetary Inst., Twenty-Fourth Lunar and Planetary Science Conference. Part 3: N-Z 1993 p 1127-1128 (For primary document see N94-20636 05-91)
Avail: CASI HC A01/MF A06

N94-20684*# National Aeronautics and Space Administration. Lyndon B. Johnson Space Center, Houston, TX.
POST-IGNEOUS REDISTRIBUTION OF COMPONENTS IN EUCRITES Abstract Only
W. C. Phinney, D. J. Lindstrom, D. W. Mittlefehldt (Lockheed Engineering and Sciences Co., Houston, TX.), and R. R. Martinez (Lockheed Engineering and Sciences Co., Houston, TX.) *In* Lunar and Planetary Inst., Twenty-Fourth Lunar and Planetary Science Conference. Part 3: N-Z 1993 p 1137-1138 (For primary document see N94-20636 05-91)
Avail: CASI HC A01/MF A06

N94-20689*# Brown Univ., Providence, RI.
VISIBLE-INFRARED PROPERTIES OF CONTROLLED LABORATORY SOILS Abstract Only
C. M. Pieters, J. F. Mustard, S. F. Pratt, J. M. Sunshine, and Andrew Hoppin *In* Lunar and Planetary Inst., Twenty-Fourth Lunar and Planetary Science Conference. Part 3: N-Z 1993 p 1147-1148 (For primary document see N94-20636 05-91)
Avail: CASI HC A01/MF A06

N94-20695*# Washington Univ., Saint Louis, MO. Center for the Space Sciences.
ELEVATED INITIAL Sr-87/Sr-86 IN ORDINARY CHONDRITE METAL Abstract Only
F. A. Podosek, J. C. Brannon, C. Perron (National Museum of Natural History, Paris, France.), and P. Pellas (National Museum of Natural History, Paris, France.) *In* Lunar and Planetary Inst., Twenty-Fourth Lunar and Planetary Science Conference. Part 3: N-Z 1993 p 1159-1160 (For primary document see N94-20636 05-91)
Avail: CASI HC A01/MF A06

N94-20697*# California Univ., San Diego, La Jolla. Dept. of Chemistry.
LOW-ENERGY ION IMPLANTATION: LARGE MASS FRACTIONATION OF ARGON Abstract Only
K. V. Ponganis, Th. Graf, and K. Marti *In* Lunar and Planetary Inst., Twenty-Fourth Lunar and Planetary Science Conference. Part 3: N-Z 1993 p 1163-1164 (For primary document see N94-20636 05-91)
Avail: CASI HC A01/MF A06

N94-20701*# Geological Survey, Denver, CO.
U-Pb PROVENANCE AGES OF SHOCKED ZIRCONS FROM THE K-T BOUNDARY, RATON BASIN, COLORADO Abstract Only
W. R. Premo and G. A. Izett *In* Lunar and Planetary Inst., Twenty-Fourth Lunar and Planetary Science Conference. Part 3: N-Z 1993 p 1171-1172 (For primary document see N94-20636 05-91)
Avail: CASI HC A01/MF A06

N94-20702*# Geological Survey, Denver, CO.
U-Pb ISOTOPIC SYSTEMATICS OF FERROAN ANORTHOSITE 60025 Abstract Only
W. R. Premo and M. Tatsumoto *In* Lunar and Planetary Inst., Twenty-Fourth Lunar and Planetary Science Conference. Part 3: N-Z 1993 p 1173-1174 (For primary document see N94-20636 05-91)
Avail: CASI HC A01/MF A06

N94-20703*# Arizona State Univ., Tempe. Dept. of Geology.
THERMAL CONDUCTIVITY MEASUREMENTS OF PARTICULATE MATERIALS UNDER MARTIAN CONDITIONS Abstract Only
M. A. Presley and P. R. Christensen *In* Lunar and Planetary Inst., Twenty-Fourth Lunar and Planetary Science Conference. Part 3: N-Z 1993 p 1175-1176 (For primary document see N94-20636 05-91)
Avail: CASI HC A01/MF A06

N94-20717*# Chicago Univ., IL. Dept. of the Geophysical Sciences.
WAVELENGTH DISPERSIVE ANALYSIS WITH THE SYNCHROTRON X RAY FLUORESCENCE MICROPROBE Abstract Only
M. L. Rivers, K. S. Thorn, S. R. Sutton, K. W. Jones (Brookhaven National Lab., Upton, NY.), and S. Bajt *In* Lunar and Planetary Inst., Twenty-Fourth Lunar and Planetary Science Conference. Part 3: N-Z 1993 p 1203-1204 (For primary document see N94-20636 05-91)
(Contracts NAG9-106; DE-AC02-76CH-00016; DE-FG02-92ER-14244; NSF EAR-89-15699)
Avail: CASI HC A01/MF A06

N94-20727*# Brown Univ., Providence, RI. Dept. of Geological Sciences.
C-O VOLATILES IN APOLLO 15 AND APOLLO 17 PICRITIC GLASSES Abstract Only
Malcolm J. Rutherford and Robert A. Fogel (American Museum of Natural History, New York, NY.) *In* Lunar and Planetary Inst., Twenty-Fourth Lunar and Planetary Science Conference. Part 3: N-Z 1993 p 1223-1224 (For primary document see N94-20636 05-91)
Avail: CASI HC A01/MF A06

N94-20733*# Johns Hopkins Univ., Baltimore, MD.
THERMAL INFRARED REMOTE SENSING AND KIRCHHOFF'S LAW: 1. LABORATORY MEASUREMENTS Abstract Only
J. W. Salisbury, A. Wald, and D. M. DAria *In* Lunar and Planetary Inst., Twenty-Fourth Lunar and Planetary Science Conference. Part 3: N-Z 1993 p 1235-1236 (For primary document see N94-20636 05-91)
Avail: CASI HC A01/MF A06

N94-20745*# Brown Univ., Providence, RI. Dept. of Geological Sciences.
FURTHER ANALYSES OF RIO CUARTO IMPACT GLASS Abstract Only
Peter H. Schultz, T. E. Bunch (National Aeronautics and Space Administration. Ames Research Center, Moffett Field, CA.), C. Koeberl (Wien Univ., Austria.), and W. Collins *In* Lunar and Planetary Inst., Twenty-Fourth Lunar and Planetary Science Conference. Part 3: N-Z 1993 p 1259-1260 (For primary document see N94-20636 05-91)
Avail: CASI HC A01/MF A06

N94-20753*# Howard Univ., Washington, DC.
MAGNETIC PROPERTIES AND MOESSBAUER ANALYSES OF GLASS FROM THE K-T BOUNDARY, BELOC, HAITI Abstract Only
F. E. Senftle, A. N. Thorpe, L. May, A. Barkatt (Catholic Univ. of America, Washington, DC.), M. A. Adel-Hadadi (Catholic Univ. of America, Washington, DC.), G. S. Marbury (Catholic Univ. of America, Washington, DC.), G. Izett (Geological Survey, Washington, DC.), H. Sigurdsson (Rhode Island Univ., Kingston.), and F. J.-M. R. Maurasse (Florida International Univ., Miami.) *In* Lunar and Planetary Inst., Twenty-Fourth Lunar and Planetary Science Conference. Part 3: N-Z 1993 p 1275-1276 (For primary document see N94-20636 05-91)
Avail: CASI HC A01/MF A06

N94-20759*# New Mexico Univ., Albuquerque. Dept. of Earth and Planetary Sciences.
ORIGIN OF THE APOLLO 15 VERY LOW TI GREEN GLASS. A PERSPECTIVE FROM THE COMPOSITIONAL DIVERSITY IN THE VERY LOW TI GLASSES Abstract Only
C. K. Shearer and J. J. Papike *In* Lunar and Planetary Inst., Twenty-Fourth Lunar and Planetary Science Conference. Part 3: N-Z 1993 p 1287-1288 (For primary document see N94-20636 05-91)
(Grant NAG9-497)
Avail: CASI HC A01/MF A06

N94-20760*# New Mexico Univ., Albuquerque. Dept. of Earth and Planetary Sciences.
ORTHOPYROXENES AS RECORDERS OF DIOGENITE PETROGENESIS: TRACE ELEMENT SYSTEMATICS Abstract Only
C. K. Shearer, J. J. Papike, and G. D. Layne *In* Lunar and Planetary Inst., Twenty-Fourth Lunar and Planetary Science Conference. Part 3: N-Z 1993 p 1289-1290 (For primary document see N94-20636 05-91)
(Grant NAG9-497)
Avail: CASI HC A01/MF A06

N94-20761*# Alabama Univ., Huntsville. Dept. of Physics.
COMBINED BACKSCATTER MOESSBAUER SPECTROMETER/X RAY FLUORESCENCE ANALYZER (BaMS/XRF) FOR EXTRATERRESTRIAL SURFACES Abstract Only
T. D. Shelfer, E. L. Wills, D. G. Agresti, M. M. Pimperl, M. H. Shen, R. V. Morris (National Aeronautics and Space Administration. Lyndon B. Johnson Space Center, Houston, TX.), and T. Nguyen (Lockheed Engineering and Sciences Co., Houston, TX.) *In* Lunar and Planetary Inst., Twenty-Fourth Lunar and Planetary Science Conference. Part 3: N-Z 1993 p 1291-1292 (For primary document see N94-20636 05-91)
Avail: CASI HC A01/MF A06

N94-20794*# California Inst. of Tech., Pasadena. Div. of Geological and Planetary Sciences.
FINE RESOLUTION CHRONOLOGY BASED ON INITIAL Sr-87/Sr-86 Abstract Only
B. W. Stewart, D. A. Papanastassiou, R. C. Capo, and G. J. Wasserburg *In* Lunar and Planetary Inst., Twenty-Fourth Lunar and Planetary Science Conference. Part 3: N-Z 1993 p 1357-1358 (For primary document see N94-20636 05-91)
(Grant NAG9-43)
(Contrib-5230(794)) Avail: CASI HC A01/MF A06

N94-20804*# Tokyo Univ. (Japan). Dept. of Earth and Planetary Physics.
IMPLANTATION OF NITROGEN: EFFECTS OF HYDROGEN AND IMPLANTATION ENERGY Abstract Only
Naoji Sugiura, Tsuneji Futagami (Japan Atomic Energy Research Inst., Tokyo.), and Siro Nagai (Japan Atomic Energy Research Inst., Tokyo.) *In* Lunar and Planetary Inst., Twenty-Fourth Lunar and Planetary Science Conference. Part 3: N-Z 1993 p 1377-1378 (For primary document see N94-20636 05-91)
Avail: CASI HC A01/MF A06

N94-20805*# Brown Univ., Providence, RI. Dept. of Geological Sciences.
DETERMINING THE COMPOSITION OF OLIVINE ON ASTEROIDAL SURFACES Abstract Only
Jessica M. Sunshine and Carle M. Pieters *In* Lunar and Planetary Inst., Twenty-Fourth Lunar and Planetary Science Conference. Part 3: N-Z 1993 p 1379-1380 (For primary document see N94-20636 05-91)
(Grant NAGw-28)
Avail: CASI HC A01/MF A06

N94-20807*# Chicago Univ., IL. Dept. of Geophysical Sciences.
THE X RAY MICROPROBE DETERMINATION OF CHROMIUM OXIDATION STATE IN OLIVINE FROM LUNAR BASALT AND KIMBERLITIC DIAMONDS Abstract Only
S. R. Sutton, S. Bajt, M. L. Rivers, and J. V. Smith *In* Lunar and Planetary Inst., Twenty-Fourth Lunar and Planetary Science Conference. Part 3: N-Z 1993 p 1383-1384 (For primary document see N94-20636 05-91)
(Contract NAG9-106; DE-AC02-76CH-00016; NSF EAR-89-15699)
Avail: CASI HC A01/MF A06

N94-20808*# Chicago Univ., IL. Dept. of Geophysical Sciences.
MICROANALYSIS OF IRON OXIDATION STATE IN IRON OXIDES USING X RAY ABSORPTION NEAR EDGE STRUCTURE (XANES) Abstract Only
S. R. Sutton, J. Delaney (Rutgers Univ., New Brunswick, NJ.), S. Bajt, M. L. Rivers, and J. V. Smith *In* Lunar and Planetary Inst., Twenty-Fourth Lunar and Planetary Science Conference. Part 3: N-Z 1993 p 1385-1386 (For primary document see N94-20636 05-91)
(Contracts NAG9-106; NAG9-104; DE-FG02-92ER-14244; DE-AC02-76CH-00016; NSF EAR-89-15699)
Avail: CASI HC A01/MF A06

N94-20810*# Tokyo Univ. (Japan). Mineralogical Inst.
HYDROTHERMAL ALTERATION EXPERIMENTS OF OLIVINE WITH VARYING Fe CONTENTS: AN ATTEMPT TO SIMULATE AQUEOUS ALTERATION OF THE CARBONACEOUS CHONDRITES Abstract Only
Koichi Takatori, Kazushige Tomeoka (Kobe Univ., Japan.), Katsuhiro Tsukimura (Geological Survey of Japan, Tsukuba.), and Hiroshi Takeda *In* Lunar and Planetary Inst., Twenty-Fourth Lunar and Planetary Science Conference. Part 3: N-Z 1993 p 1389-1390 (For primary document see N94-20636 05-91)
Avail: CASI HC A01/MF A06

N94-20831*# Brown Univ., Providence, RI. Dept. of Geological Sciences.
OBJECTIVE DETERMINATION OF IMAGE END-MEMBERS IN SPECTRAL MIXTURE ANALYSIS Abstract Only
Stefanie Tompkins, John F. Mustard, Carle M. Pieters, and Donald W. Forsyth *In* Lunar and Planetary Inst., Twenty-Fourth Lunar and Planetary Science Conference. Part 3: N-Z 1993 p 1431-1432 (For primary document see N94-20636 05-91)
Avail: CASI HC A01/MF A06

N94-20851*# Battelle Northwest Labs., Richland, WA.
ALUMINUM-26 ACTIVITIES IN METEORITES Abstract Only
J. F. Wacker *In* Lunar and Planetary Inst., Twenty-Fourth Lunar and Planetary Science Conference. Part 3: N-Z 1993 p 1471-1472 (For primary document see N94-20636 05-91)
Avail: CASI HC A01/MF A06

N94-20852*# Washington Univ., Saint Louis, MO. Dept. of Earth and Planetary Sciences.
RARE EARTH ELEMENTS IN INDIVIDUAL MINERALS IN SHERGOTTITES Abstract Only
Meenakshi Wadhwa and Ghislaine Crozaz *In* Lunar and Planetary Inst., Twenty-Fourth Lunar and Planetary Science Conference. Part 3: N-Z 1993 p 1473-1474 (For primary document see N94-20636 05-91)
Avail: CASI HC A01/MF A06

N94-20853*# Massachusetts Inst. of Tech., Cambridge. Dept. of Earth, Atmospheric and Planetary Sciences.
ORIGIN OF HIGH-TI LUNAR ULTRAMAFIC GLASSES Abstract Only
T. P. Wagner and T. L. Grove *In* Lunar and Planetary Inst., Twenty-Fourth Lunar and Planetary Science Conference. Part 3: N-Z 1993 p 1475-1476 (For primary document see N94-20636 05-91)
Avail: CASI HC A01/MF A06

N94-20855*# Chicago Univ., IL. Dept. of the Geophysical Sciences.
DIFFUSION-CONTROLLED MAGNESIUM ISOTOPIC FRACTIONATION OF A SINGLE CRYSTAL FORSTERITE EVAPORATED FROM THE SOLID STATE Abstract Only
Jianhua Wang, Andrew M. Davis, Akihiko Hashimoto (Harvard-Smithsonian Center for Astrophysics, Cambridge, MA.), and Robert N. Clayton *In* Lunar and Planetary Inst., Twenty-Fourth Lunar and Planetary Science Conference. Part 3: N-Z 1993 p 1479-1480 (For primary document see N94-20636 05-91)
Avail: CASI HC A01/MF A06

N94-20868*# Arizona State Univ., Tempe. Dept. of Geology.
A STUDY OF CARBONATES, SULFATES, AND PHOSPHATES USING THERMAL EMISSION SPECTROSCOPY Abstract Only
M. L. Wenrich and P. R. Christensen *In* Lunar and Planetary Inst., Twenty-Fourth Lunar and Planetary Science Conference. Part 3: N-Z 1993 p 1505-1506 (For primary document see N94-20636 05-91)
Avail: CASI HC A01/MF A06

N94-20870*# National Aeronautics and Space Administration. Lyndon B. Johnson Space Center, Houston, TX.
PETROLOGY AND GEOCHEMISTRY OF VLT GLASSES FROM DOUBLE DRIVE TUBE 79001/2 Abstract Only
Susan J. Wentworth (Lockheed Engineering and Sciences Co., Houston, TX.), D. J. Lindstrom, R. R. Martinez (Lockheed Engineering and Sciences Co., Houston, TX.), and D. S. McKay *In* Lunar and Planetary Inst., Twenty-Fourth Lunar and Planetary Science Conference. Part 3: N-Z 1993 p 1509-1510 (For primary document see N94-20636 05-91)
Avail: CASI HC A01/MF A06

N94-21011*# Nebraska Univ., Lincoln. Dept. of Electrical Engineering.
FUNDAMENTALS AND APPLICATIONS OF VARIABLE ANGLE SPECTROSCOPIC ELLIPSOMETRY Abstract Only
John A. Woollam and Paul G. Snyder *In its* Materials, Structures, and Devices for High-Speed Electronics 1993 1 p Repr. from Materials Science and Engineering (Netherlands, Elsevier Sequoia), 1990 p 279-283 (For primary document see N94-20971 05-76)
Avail: CASI HC A01/MF A01

N94-21014*# Nebraska Univ., Lincoln. Dept. of Electrical Engineering.
VASE (VARIABLE ANGLE SPECTROSCOPIC ELLIPSOMETRY) Abstract Only
John A. Woollam and Paul G. Snyder *In its* Materials, Structures, and Devices for High-Speed Electronics 1993 1 p Presented 6 Jan. 1992 (For primary document see N94-20971 05-76)
Avail: CASI HC A01/MF A01

N94-21390 Deutsche Forschungsanstalt fuer Luft- und Raumfahrt, Cologne (Germany).
GERMAN SPACE EXPERIMENTS ON SPACELAB D-2 AND EURECA-1 TO INVESTIGATE ATOMIC OXYGEN INTERACTION WITH MATERIALS
H. Hamacher and H. E. Richter *In* CNES, Fifth International Symposium on Materials in a Space Environment Jun. 1993 p 323-330 (For primary document see N94-21367 05-18)
Copyright Avail: CEPADUES-Editions, 111, rue Nicolas-Vaquelin, 31100 Toulouse, France

N94-21393* National Aeronautics and Space Administration. Lyndon B. Johnson Space Center, Houston, TX.
ATOMIC OXYGEN INTERACTION WITH SPACECRAFT MATERIALS: RELATIONSHIP BETWEEN ORBITAL AND GROUND-BASED TESTING FOR MATERIALS CERTIFICATION
Jon B. Cross (Los Alamos National Lab., NM.), Steven L. Koontz, and Esther H. Lan (McDonnell-Douglas Space Systems Co., Huntington Beach, CA.) *In* CNES, Fifth International Symposium on Materials in a Space Environment Jun. 1993 p 369-384 (For primary document see N94-21367 05-18)
Copyright Avail: CEPADUES-Editions, 111, rue Nicolas-Vaquelin, 31100 Toulouse, France

26 METALLIC MATERIALS

Includes physical, chemical, and mechanical properties of metals, e.g., corrosion; and metallurgy.

N94-19802# Oak Ridge National Lab., TN.
INVESTIGATION OF AUSTENITIC ALLOYS FOR ADVANCED HEAT RECOVERY AND HOT GAS CLEANUP SYSTEMS
R. W. Swindeman 1993 16 p Presented at the 7th Annual Conference on Fossil Energy Materials, Oak Ridge, TN, 11-13 May 1993
(Contract DE-AC05-84OR-21400)
(DE93-017863; CONF-9305135-6) Avail: CASI HC A03/MF A01

Commercial and developmental alloys are evaluated in support of advanced steam cycle and combined cycle technology. Working with industrial groups, Grade 91 steel, which is a candidate for main steam line piping and superheater tubing in advanced steam cycle plants, is re-evaluated to examine metallurgical factors that influence long-time performance to 600 C. Deformation models and aging effect models are developed. Testing of corrosion-resistant filler metals for tubing is extended to times approaching 30,000 h. Good strengths are observed. Modified Type 310 stainless steels are examined to 927 C. It is found that these steels have up to twice the strength of standard Type 310H stainless steel. The behavior of aluminum-bearing alloys and high chromium alloys is examined for potential applications to 870 C. Thermal cycling of clad tubing is undertaken, and good performance is found. DOE

N94-19806# Argonne National Lab., IL.
ON THE EXPERIMENTAL DETERMINATION OF LOW ORDER STRUCTURE FACTORS IN TiAl BY ENERGY FILTERED CONVERGENT BEAM ELECTRON DIFFRACTION
S. Swaminathan (Ohio State Univ., Columbus.), H. L. Fraser (Ohio State Univ., Columbus.), I. P. Jones (Birmingham Univ., England.), N. J. Zaluzec, and D. M. Maher (North Carolina State Univ., Raleigh.) Apr. 1993 4 p Presented at the Annual Meeting of the Electron Microscopy Society of America, Cincinnati, OH, 1-6 Aug. 1993
(Contract W-31-109-eng-38)
(DE93-019521; ANL/MSD/CP-79660; CONF-930822-8) Avail: CASI HC A01/MF A01

It has been claimed that effective Peierls stresses and mobilities of some dislocations in TiAl are influenced by anisotropy of bonding charge densities. This paper describes experiments conducted to verify these calculations. The experiments involved recording convergent beam electron diffraction patterns from a number of reflections, with the sample oriented at the Bragg condition. The rocking curves were matched. The deformation electron charge density distribution map for the (001) section is in good agreement with theory. DOE

N94-19864# Sandia National Labs., Albuquerque, NM.
SEGREGATION OF Si TO THE SURFACE OF Fe-29Ni-17Co ALLOY
G. C. Nelson and R. W. Buttry 1993 17 p Presented at the Minerals, Metals, and Materials Society/American Society for Metals (TMS/ASM) Materials Week 1992, Chicago, IL, 2-5 Nov. 1992
(Contract DE-AC04-76DP-00789)
(DE93-040053; SAND-93-1911C; CONF-9211117-11) Avail: CASI HC A03/MF A01

The segregation of Si impurities from the bulk to the surface of a low Cr Lot of Kovar (Fe-29Ni-17Co) has been investigated in order to determine the effects on the quality of the braze of Cu to these altered surfaces. It is found that oxides of Si are formed on the surface during wet hydrogen firing. Kinetics of this segregation process have been measured. DOE

N94-19904# Sandia National Labs., Albuquerque, NM.
NEAR ATOMIC RESOLUTION MICROANALYSIS OF INTERFACES BY ANALYTICAL ELECTRON MICROSCOPY
A. D. Romig, Jr. and J. R. Michael 1993 2 p Presented at the 3rd National Congress for Materials Science, Cancun, Mexico, 27 Sep. - 2 Oct. 1993
(Contract DE-AC04-76DP-00789)
(DE93-019437; SAND-93-1756C; CONF-9309207-1) Avail: CASI HC A01/MF A01

High spatial resolution x-ray microanalysis in the analytical electron microscope (AEM) can be used to determine chemical composition on spatial scales of less than 50 nm. Simple scattering models have the drawback of being incapable of treating electron scattering in inhomogeneous specimens, such as at phase interfaces or grain boundary segregation. The best method for calculating electron scattering and x-ray generation function is by Monte Carlo methods. Two examples are discussed: a phase interface in an Fe-Ni-Cr alloy, and grain boundary segregation using a 0.3 nm Cu slab in a 25 nm Al film (the slab is parallel to incident electron beam). It is concluded that high spatial resolution x-ray microanalysis can achieve near atomic resolution, but that massively parallel Monte Carlo models for electron scattering and a well characterized electron beam are needed. DOE

N94-19922# Argonne National Lab., IL.
OXIDATION-REDUCTION INDUCED ROUGHENING OF PLATINUM (111) SURFACE
H. You and Z. Nagy Jun. 1993 8 p Presented at the 3rd International Conference on Surface X Ray and Neutron Scattering, Dubna, Russia, 24-29 Jun. 1993
(Contracts W-31-109-eng-38; DE-AC02-76CH-00016)

(DE93-017408; ANL/MSD/CP-80232; CONF-9306248-1) Avail: CASI HC A02/MF A01

Platinum (111) single crystal surface was roughened by repeated cycles of oxidation and reduction to study dynamic evolution of surface roughening. The interface roughens progressively upon repeated cycles. The measured width of the interface was fit to an assumed pow law, W approximately = t(exp beta), with beta = 0.38(l). The results are compared with a simulation based on a random growth model. The fraction of the singly stepped surface apparently saturates to 0.25 monolayer, which explains the apparent saturation to a steady roughness observed in previous studies. DOE

N94-19942# Westinghouse Savannah River Co., Aiken, SC.

RAPID HEATING TENSILE TESTING UPDATE: 304L STAINLESS STEEL

W. C. Mosley 1993 9 p Presented at the 1993 Meeting of the Interagency Manufacturing Operations Group on Mechanical Testing, Livermore, CA, 20-22 Jul. 1993
(Contract DE-AC09-89SR-18035)
(DE93-018770; WSRC-MS-93-404; CONF-9307121-1) Avail: CASI HC A02/MF A01

In stainless steel equipment exposed to tritium, embrittlement is thought to involve interactions between internal He and the complex triaxial stress state that arises when necking starts. Recent efforts have been directed at determining He concentration thresholds for this effect in several austenitic stainless steels. This report describes results of tests on 304L stainless steel containing low He-3 contents. 304L stainless steel containing 0.47 and 4.1 appm He-3 tested at 803-814 C had lower tensile properties than uncharged samples. Mechanical properties were not affected by 0.47 appm at 615 C but ductility was severely decreased at 810 C. DOE

N94-19944# Sandia National Labs., Albuquerque, NM.

SHOCK RESPONSE OF POROUS Al-2 + Fe2O3 POWDER MIXTURES

G. T. Holman, Jr., R. A. Graham, and M. U. Anderson 1993 4 p Presented at the 14th International Conference of the International Association for the Advancement of High Pressure Science and Technology, Colorado Springs, CO, 27 Jun. - 2 Jul. 1993
(Contract DE-AC04-76DP-00789)
(DE93-018851; SAND-93-0422C; CONF-930676-41) Avail: CASI HC A01/MF A01

Time-resolved pressure measurements have been conducted on Al-2 + Fe2O3 powder mixtures using the (PVDF) stress-rate gauge. These measurements were made on samples which were 53% of solid density. Measurements were made at pressures from 0.67 to more than 10 GPa utilizing both impact loading with a compressed gas gun and direct contact high explosive loading. The sample is pressed to the desired density in a copper capsule. PVDF gauges were positioned in front of and behind the powder sample in direct contact with the sample; they measure input and propagated stress-rate and are used for precise measurement of velocity through the 4 mm thick sample. In the case of high explosive loading, gauges are also installed on the explosive side and on the capsule side of a metal driver plate to measure the shock velocity through the driver so that the driver pressure can be determined. The response of Al-2 + Fe2O3 under shock compression appears to demonstrate a more complex behavior than other materials. At approximately 4.6 GPa, the material compresses to beyond solid density. There was no evidence of chemical reaction. DOE

N94-19957# Oak Ridge Y-12 Plant, TN.

INVESTIGATION OF CRACKING AND ERRATIC BEHAVIOR OF THE URANIUM-TITANIUM ALLOY

E. L. Bird Jul. 1993 17 p Presented at the International Metallographic Society Meeting, Charleston, SC, 18-21 Jul. 1993
(Contract DE-AC05-84OS-21400)
(DE93-018591; Y/DV-1227; CONF-9307118-1) Avail: CASI HC A03/MF A01

The uranium-0.8 wt % titanium (U-0.8 Ti) alloy is often used in weapon applications where high strength and fairly good ductility are necessary. Components are immersion quenched in water from the gamma phase to produce a martensitic structure that is amenable to aging. Undesirable conditions occur when a component occasionally cracks during the quenching process, and when tensile specimens fail prematurely during mechanical testing. These two failures prompted an investigative analysis and a series of studies to determine the causes of the cracking and erratic behavior observed in this alloy. Quench-related failures whereby components that cracked either during or immediately after the heat treatment/quenching operation were sectioned for metallographic examination of the microstructure to examine the degree of phase transformation. Examination of premature tensile specimen failures by scanning electron microscopy and x-ray imaging of fracture surfaces revealed pockets of inclusions at the crack origins. In addition, tests were conducted to evaluate the detrimental effects of internal hydrogen on ductility and crack initiation in this alloy. DOE

N94-19985# Oregon Univ., Eugene.

MICROSCOPIC ORIGINS OF METASTABLE EFFECTS IN a-Si:H AND DEEP DEFECT CHARACTERIZATION IN a-Si,Ge:H ALLOYS

J. D. Cohen Aug. 1993 23 p Prepared for Midwest Research Inst., Golden, CO
(Contract DE-AC02-83CH-10093)
(DE93-018205; NREL/TP-451-5737) Avail: CASI HC A03/MF A01

This report describes work to evaluate low-mobility-gap a-Si,Ge:H alloy films. Results are based on junction capacitance techniques of admittance spectroscopy, transient photocapacitance (and photocurrent), and drive-level capacitance profiling. Eight a-Si,Ge:H alloy samples grown by photo-CVD encompassed the range of optical gaps from 1.3 to 1.6 eV, and corresponding Ge fractions from about 20 to 60 at%. We employed junction capacitance techniques to determine deep defect energies and densities, Urbach band-tail energies, and (mu)(tau) products for holes. Electron microprobe analysis provided accurate Ge fractions for our samples, thus enabling us to establish clear trends in measured electronic properties vs Ge fraction. We concluded that these photo-CVD samples exhibited equal or superior properties in terms of band-tail widths and stable defect densities compared to any reported results on a-Si,Ge:H samples grown by glow discharge. By assigning defect energy levels from analysis of transient subband-gap photocapacitance and photocurrent spectra, we found clear evidence for two distinct defect subbands, one at roughly midgap and the other in the upper half of the gap. The trapping lifetime related (mu)(tau) products for holes decreased in direct proportion to the density of mid-gap defects in these samples. This appears to be the case regardless of whether we are dealing with stable defects or defects created by light-soaking. DOE

N94-19986# Lawrence Livermore National Lab., CA.

MAGNETIC CIRCULAR DICHROISM IN X RAY ABSORPTION AND CORE-LEVEL PHOTOEMISSION

J. G. Tobin, G. D. Waddill, T. H. Gouder, C. A. Colmenares, and D. P. Pappas (Naval Research Lab., Washington, DC.) 17 Mar. 1993 8 p Presented at the Spring Meeting of the Materials Research Society, San Francisco, CA, 12-16 Apr. 1993
(Contract W-7405-eng-48)
(DE93-019381; UCRL-JC-113366; CONF-930405-37) Avail: CASI HC A02/MF A01

Here is reported observation of magnetic circular dichroism in both x-ray absorption and core-level photoemission of ultra thin magnetic films using circularly polarized x-rays. Iron films (1 - 4 ML) grown on a Cu(001) substrate at 150 K and magnetized perpendicular to the surface show dramatic changes in the L(sub 2,3) branching ratio for different x-ray polarizations. For linearly-polarized x-rays perpendicular to the magnetic axis of the sample the branching ratio was 0.75. For films greater than or equal to 2 ML, this ratio varied from 0.64 to 0.85 for photon spin parallel and anti-parallel, respectively, to the magnetic axis. This effect was observed either by changing the x-ray helicity for a fixed magnetic axis or by reversing the magnetic axis for a fixed x-ray helicity. Our observation can be analyzed within a simple one-electron picture, if the raw branching ratios are normalized so that the linear value becomes statistical. Furthermore, warming the films to approximately 300 K eliminated this effect, indicating a loss of magnetization in the film over a temperature range of approximately 30 K. Finally, reversing the relative orientation of the photon spin and the magnetic axis from parallel to anti-parallel allowed measurement of the exchange splitting of the Fe 2p and 3p core levels which were found to be 0.3 eV and 0.2 eV, respectively. These results are consistent with earlier studies, but the use of off-plane circularly-polarized x-rays from a bending magnet monochromator offers approximately 2 orders of magnitude greater intensity than typical spin-polarization measurements. Finally, we have performed

preliminary x-ray absorption studies of UFe2, demonstrating the feasibilty of MCD measurements in 5f as well as 3D materials. DOE

N94-20019 Pennsylvania State Univ., University Park.
HIGH PERFORMANCE HEAVY ALLOYS BY ALLOYING AND PROCESS CONTROL Final Report, 15 Aug. 1991 - 14 May 1993
A. Belhadjhamida and R. M. German 22 Jun. 1993 35 p Limited Reproducibility: More than 20% of this document may be affected by microfiche quality
(Contract DAAL03-91-G-0309)
(AD-A271129; ARO-29326.14-MS) Avail: CASI HC A03

The kinetics and processing conditions of liquid phase sintering (LPS) have been addressed in the development of a novel heavy alloy, W-Ni-Mn. Solubility criteria were considered in the selection of manganese as an alloying element to the W-Ni system. The addition of manganese resulted in a depressed melting point of the matrix, and consequently, sintering in this system was achieved at temperatures 300 C lower than in the conventional heavy alloys. Concurrent with solubility criteria, the rearrangement stage in liquid phase sintering was treated. When capillary and viscous drag forces are accounted for, the time scales in rearrangement were found to be in the microseconds range for metal systems. On the other hand, heat transfer was found to be the rearrangement time limiting factor for metallic specimens with time scales in the range of seconds. Further, depending on the Green density and the system under consideration, there exists specific specimen dimensions where a transition from heat transfer to capillary control over the rearrangement time. These dimensions are, however, in the micrometer range. DTIC

N94-20027 SRI International Corp., Menlo Park, CA.
EVALUATION OF A DIFFUSION/TRAPPING MODEL FOR HYDROGEN INGRESS IN HIGH-STRENGTH ALLOYS Final Report, 15 Sep. 1991 - 14 Sep. 1993
Bruce G. Pound Oct. 1992 80 p Limited Reproducibility: More than 20% of this document may be affected by microfiche quality
(Contract N00014-91-C-0263)
(AD-A271328) Avail: CASI HC A05

Alloys developed to improve strength, weight, and corrosion resistance often remain susceptible to hydrogen embrittlement (HE). The objective of this research was to investigate hydrogen ingress in high performance alloys, particularly in terms of irreversible trapping, with a view to characterizing their susceptibility to HE. A technique referred to as hydrogen ingress analysis by potentiostatic pulsing (HIAPP) was applied to five unaged and aged B-Ti alloys (Beta-C, Ti-10-2-3, Ti-13-11-3, Ti-15-3, and Beta-21S), an alpha-beta Ti alloy (Ti-6-4), two Cu-Ni alloys (Marinel and Monel K-500), and a Ni-base alloy (UNS N07716). Anodic transients obtained in 1 mol/L HAc-l mol/L NaAc (Ac = acetate) were analyzed using a diffusion/trapping model to evaluate the trapping constant and hydrogen entry flux. Except for Ti-15-3, aging increases irreversible trapping in the B-Ti alloys, the increase parallels the decrease in their tolerance to hydrogen. Ti-13-11-3 is indicated to be the most susceptible to HE, followed by Beta-21S, Beta-C, Ti-10-2-3, and Ti-15-3, with the trapping constants apparently being determined by the degree of grain boundary alpha phase. The trapping constants for aged Marinel and alloy K-500 do not appear to differ significantly, but a lower flux for Marinel accounts, at least partly, for its higher resistance to HE. Likewise, a low flux for alloy 716 is consistent with it generally being resistant to cracking. DTIC

N94-20093# Oak Ridge National Lab., TN.
EFFECTS OF PROCESSING HISTORY ON THE CREEP STRENGTH OF Nb-1Zr
J. A. Horak and L. K. Egner 1993 6 p Presented at the Joint MMIJ/TMS International Conference on Processing Materials for Properties, Honolulu, HI, 7-10 Nov. 1993
(Contract DE-AC05-84OR-21400)
(DE93-015905; CONF-931103-1) Avail: CASI HC A02/MF A01

Power systems that are used to provide electrical power in space are designed to optimize conversion of thermal energy to electrical energy and to minimize the mass and volume that must be launched. Only refractory metals and their alloys have sufficient long-term strength for several years of uninterrupted operation at the temperatures required (e.g., greater than 1200 K). The high power densities and temperatures at which these reactors must operate require the use of liquid-metal coolants. The alloy Nb-1 wt % (Nb-1Zr), which exhibits excellent corrosion resistance to alkali liquid-metals at high temperatures, is being considered for the fuel cladding, reactor structural, and heat transport systems for current space exploration missions. Useful lifetimes of these power systems are limited by creep deformation in the reactor core. Nb-1Zr sheet procured to American Society for Testing and Materials (ASTM) specifications for reactor grade and commercial grade has been processed by several different cold work and annealing treatments to attempt to produce the grain structure (size, shape, and distribution of sizes) that provides the maximum creep strength of this alloy at temperatures from 1250 to 1450 K. The effects of grain size, differences in oxygen concentrations, tungsten concentrations, and electron beam and gas tungsten arc weldments on creep strength were studied. Grain size has a large effect on creep strength at 1450 K but much less of an effect at 1350 K. Differences in oxygen or tungsten concentrations did not affect creep strength, and the creep strengths of weldments were equal to, or greater than, those for base metal. DOE

N94-20100*# National Aeronautics and Space Administration. Marshall Space Flight Center, Huntsville, AL.
MICROSTRUCTURAL STABILITY OF WROUGHT, LASER AND ELECTRON BEAM GLAZED NARloy-Z ALLOY AT ELEVATED TEMPERATURES
J. Singh, G. Jerman, B. Bhat, and R. Poorman Nov. 1993 37 p Sponsored by NASA. Washington
(NASA-TM-108431; NAS 1.15:108431) Avail: CASI HC A03/MF A01

Microstructure of wrought, laser, and electron-beam glazed NARloy-Z(Cu-3 wt.% Ag-0.5 wt.% Zr) was investigated for thermal stability at elevated temperatures (539 to 760 C (1,100 to 1,400 F)) up to 94 h. Optical and scanning electron microscopy and electron probe microanalysis were employed for studying microstructural evolution and kinetics of precipitation. Grain boundary precipitation and precipitate free zones (PFZ's) were observed in the wrought alloy after exposing to temperatures above 605 C (1,120 F). The fine-grained microstructure observed in the laser and electron-beam glazed NARloy-Z was much more stable at elevated temperatures. Microstructural changes correlated well with hardness measurements. Author (revised)

N94-20180# Oak Ridge National Lab., TN.
ATOM PROBE FIELD ION MICROSCOPY CHARACTERIZATIONS OF VVER STEELS
M. K. Miller, R. Jayaram, P. J. Othen (Oxford Univ., England.), and G. Brauer (Zentralinstitut fuer Kernforschung, Rossendorf bei Dresden, German D.R..) 1993 12 p Presented at the 6th International Symposium on Environmental Degradation of Materials in Nuclear Power Systems: Water Reactors, San Diego, CA, 3-5 Aug. 1993
(Contract DE-AC05-84OR-21400)
(DE93-017864; CONF-930825-3) Avail: CASI HC A03/MF A01

An atom probe field ion microscopy (APFIM) characterization of Soviet types 15Kh2MFA Cr-Mo-V (VVER 440) and 15Kh2NMFA Ni-Cr-Mo-V (VVER 1000) pressure vessel steels has been performed. Field ion microscopy has revealed that the lath boundaries in unirradiated VVER 440 and VVER 1000 steels are decorated with a thin film of brightly-imaging molybdenum carbonitride precipitates and some coarser vanadium carbides. Atom probe analysis has revealed significant enrichments of phosphorous at the lath boundaries. DOE

N94-20182# Bettis Atomic Power Lab., Pittsburgh, PA.
HYDROGEN PICKUP AND REDISTRIBUTION IN ALPHA-ANNEALED ZIRCALOY-4
B. F. Kammenzind, D. G. Franklin, W. J. Duffin, and H. R. Peters (General Electric Co., Schenectady, NY.) Jul. 1993 31 p Presented at the Electric Power Research Institute Utility-industry Workshop on Pressurized-Water Reactor Fuel Rod Corrosion, Washington, DC, 28-30 Jul. 1993
(Contract DE-AC11-89PN-38014)
(DE93-018050; WAPD-T-3010; CONF-9307115-1) Avail: CASI HC A03/MF A01

Zircaloy-4, which is widely used as a core structural material in Pressurized-Water Reactors (PWR), picks up hydrogen during service. Hydrogen solubility in Zircaloy-4 is low and hydrides precipitate after the Zircaloy-4 matrix becomes slightly supersaturated with hydrogen. These hydrides embrittle the Zircaloy-4. To study hydrogen pickup and concentration

a postirradiation nondestructive radiographic technique for measuring hydrogen concentration was developed and qualified. Experiments on hydrogen pickup were conducted in the Advanced Test Reactor (ATR). Out-of-pile tests were conducted to determine the conditions for which hydrogen would migrate. Finally, a phenomenological model was built and indexed to the data. This presentation describes the experiments and the model, presents the results of experiments, and compares the model predictions to experimental results. DOE

N94-20183 Argonne National Lab., IL.
SOL-SPRAY PREPARATION, PARTICULATE CHARACTERISTICS, AND SINTERING OF ALUMINA POWDERS
H. K. Varma (Regional Research Lab., Thiruvananthapuram, India.), T. V. Mani (Regional Research Lab., Thiruvananthapuram, India.), A. D. Damodaran (Regional Research Lab., Thiruvananthapuram, India.), K. G. K. Warrier (Regional Research Lab., Thiruvananthapuram, India.), and U. Balachandran Jul. 1993 5 p Presented at the 3rd International Conference on Advanced Materials, Tokyo, Japan, 31 Aug. - 4 Sep. 1993 Limited Reproducibility: More than 20% of this document may be affected by microfiche quality
(Contract W-31-109-eng-38)
(DE93-018577; ANL/ET/CP-78942; CONF-9308122-2) Avail: CASI HC A01

Fine alumina powders of spherical morphology and narrow particle-size distribution have been synthesized by a technique that uses precipitation/peptization/spray drying of boehmite sol-prepared from aluminum nitrate. The spray-dried powder was further washed with solvents of varying polarities, such as acetone, isopropanol, and tert-butanol. This post-spray-drying treatment changed the powder's particle-size distribution, morphology, density, and compaction characteristics. Microstructure, dielectric properties, and effect of post-treatment on the boehmite-sol-derived alumina powders in reducing agglomeration are discussed. DOE

N94-20232# Oak Ridge National Lab., TN.
FUNDAMENTALS OF MECHANICAL BEHAVIOR IN STRUCTURAL INTERMETALLICS: A SYNTHESIS OF ATOMISTIC AND CONTINUUM MODELING
M. H. Yoo and C. L. Fu 1993 10 p Presented at the International Symposium on Structural Intermetallics, Champion, PA, 26-30 Sep. 1993
(Contract DE-AC05-84OR-21400)
(DE93-019166; CONF-930997-4) Avail: CASI HC A02/MF A01

After a brief account of the recent advances in computational research on mechanical behavior of structural intermetallics, currently unresolved problems and critical issues are addressed and the knowledge base for potential answers to these problems is discussed. As large-scale problems (e.g., dislocation core structures, grain boundaries, and crack tips) are treated by atomistic simulations, future development of relevant interatomic potentials should be made consistent with the results of first-principles calculations. The bulk and defect properties calculated for intermetallic compounds, both known and as yet untested, can furnish insights to alloy designers in search of new high-temperature structural intermetallics. DOE

N94-20233# Pacific Northwest Lab., Richland, WA.
PROPERTIES AND POTENTIAL OF HIGH-TEMPERATURE NIOBIUM BERYLLIDES
S. M. Bruemmer, J. L. Brimhall, C. H. Henager, Jr., and J. P. Hirth (Washington State Univ., Pullman.) Dec. 1992 6 p Presented at the 16th Materials Research Society Fall Meeting, Boston, MA, 30 Nov. - 5 Dec. 1992
(Contract DE-AC06-76RL-01830)
(DE93-019169; PNL-SA-21290; CONF-921101-137) Avail: CASI HC A02/MF A01

Recent research on the low- and high-temperature properties of two beryllium-niobium intermetallic compounds, Be12Nb and Be17Nb2, is reviewed and discussed. Strength (bend and compression), hardness and fracture toughness has been mapped as a function of test temperature up to 1200 C. Results for hot-isostatically-pressed Be12Nb and Be17Nb2 are highlighted illustrating the potential for reasonable strength at both low and high temperatures. Limitations for structural use of the beryllides are identified and discussed including low-temperature toughness, intermediate-temperature embrittlement, high-temperature creep strength and composite compatability. DOE

N94-20282# Oak Ridge National Lab., TN.
MICROSCOPIC EVALUATION OF LOW-TEMPERATURE EMBRITTLEMENT IN TYPE 308 STAINLESS STEEL WELDS
J. M. Vitek, S. A. David, and D. J. Alexander 1993 11 p Presented at the International Metallographic Society Meeting, Charleston, SC, 18-21 Jul. 1993
(Contract DE-AC05-84OR-21400)
(DE93-040266; CONF-9307118-2) Avail: CASI HC A03/MF A01

Effect of aging of type 308 stainless steel weld metal from 400 to 550 C on microstructure was examined. Microstructural development was correlated with earlier results on mechanical properties that showed the ferrite-containing welds were prone to severe embrittlement when aged in this temperature range. The embrittlement was manifested by an increase in the ductile-brittle transition temperature and a drop in the upper-shelf energy. It was found that although the embrittlement over this aging temperature range was comparable, the microstructural changes that were responsible for the embrittlement were different at different temperatures. Embrittlement was caused by a combination of spinodal decomposition of ferrite, precipitation of M23C6 carbide at the ferrite/austenite interface, and G-phase precipitation within the ferrite. Sigma phase formation at 550 C may also be a contributing factor to the embrittlement. DOE

N94-20288# Argonne National Lab., IL.
NEUTRAL COPPER CLUSTER SPUTTERING YIELDS: Ne(+), Ar(+) AND Xe(+) BOMBARDMENT
S. R. Coon, W. F. Calaway, and M. J. Pellin 1993 15 p Presented at the 15th International Conference on Atomic Collision in Solids, London, Ontario, 26-30 Jul. 1993
(Contract W-31-109-eng-38)
(DE93-019010; ANL/CHM/CP-80470; CONF-930712-3) Avail: CASI HC A03/MF A01

The sputtering of neutral metal clusters was investigated by measuring relative sputtering yields of copper clusters ejected from polycrystalline copper under 3.9 keV bombardment by Ne(+), Ar(+) and Xe(+) ions at normal incidence. Yields of clusters from Ne(+) bombardment were lower than those from Ar(+) bombardment, were lower than from Xe(+) bombardment. Sputtering yield ratios Ne(+)/Ar(+) and Xe(+)/Ar(+) were 0.56 and 1.08. Size distribution of sputtered clusters can be fit by a power law dependence with exponents of -8.1, -8.2 and -6.2 for Ne(+), Ar(+) and Xe(+), respectively. The similarity of the exponents of the Ne(+) and Ar(+) power law fits indicates that the sputtering yields for these two primary ions are similar while that for Xe(+) is substantially higher, in contrast to the sputtering yield ratio data. The difference between the two measurements can be explained by assuming a systematic uncertainty in the sputtering yield ratio measurements that makes the measured ratios lower than the true values. Assuming a value at the high end of the experimental Ne(+) sputtering yield range, the exponents of the power law fits exhibit a linear dependence on the total sputtering yield. DOE

N94-20301# Brookhaven National Lab., Upton, NY.
THE USE OF X RAY TECHNIQUES IN THE IN SITU STUDY OF CORROSION
H. S. Isaacs 1992 16 p Presented at the NATO Advanced Research Workshop, Maderia, Portugal, Dec. 1992
(Contract DE-AC02-76CH-00016)
(DE93-019845; BNL-49361; CONF-921277-2) Avail: CASI HC A03/MF A01

Applications of x-ray absorption and fluorescence techniques for in situ chemistry studies of passivity and localized corrosion have been described. X-ray absorption near edge structures showed that rapidly grown oxides on aluminum-chromium alloys incorporated chromium in the oxide. Repeated electrochemically induced changes between the chromium 3- and 6-valent state occurred without chromium dissolving. When the oxide was grown by small potential steps, the chromium dissolved when 6-valent chromate was formed. With iron-chromium alloys, dissolution of chromate took place, but 6-valent chromium was also incorporated in the oxide. The 6-valent state was reduced on exposing the iron alloy to air. X-ray fluorescence measurements, in conjunction with energy dispersive analysis, have been used to monitor iron, chromium, and nickel concentrationsin

solution. The concentrations and concentration gradients during localized corrosion of stainless steel were used to determine salt solubility and relative diffusion rates. DOE

N94-20313 Brookhaven National Lab., Upton, NY.
THE METALLIC BOND FOR MONOLAYER TRANSITION METAL LAYERS ON TRANSITION METAL SURFACES
M. Strongin, M. W. Ruckman, M. Weinert, R. E. Watson, and J. W. Davenport 1993 10 p Presented at the NATO Advanced Study Workshop on Metallic Alloys: Experimental and Theoretical Perspectives, Boca Raton, FL, 16-21 Jul. 1993 Limited Reproducibility: More than 20% of this document may be affected by microfiche quality
(Contract DE-AC02-76CH-00016)
(DE93-019060; BNL-49288; CONF-930759-1) Avail: CASI HC A02

This present work discusses changes in the electronic and chemical properties of some transition metal layers on transition metal substrates, and presents a simple framework for understanding the results. DOE

N94-20321 Los Alamos National Lab., NM.
TEMPERATURE DEPENDENCE OF 4f PES FEATURES AND HOLE OCCUPANCY IN YTTERBIUM HEAVY FERMIONS
A. B. Andrews, R. I. R. Blyth, and A. J. Arko et al 1993 8 p Presented at the International Conference on Strongly Correlated Electron Systems, La Jolla, CA, 16-19 Aug. 1993 Limited Reproducibility: More than 20% of this document may be affected by microfiche quality
(Contract W-7405-eng-36)
(DE93-040131; LA-UR-93-3014; CONF-930865-10) Avail: CASI HC A02

The authors have measured the temperature dependence between 80 and 300 K and spectral weight of the 4f features in clean single crystal Yb heavy fermions, cleaved in a vacuum of 5 x 10(exp -11) Torr. A small (approximately 10%) decrease in spectral weight differs substantially from the reported approximately 50% decrease over this range. All divalent features are much larger than expected, yielding n(sub f) values far too small. The intensity of the divalent features in YbAuCu4 is about two orders of magnitude larger than expected. DOE

N94-20478# Allied-Signal Aerospace Co., Kansas City, MO.
CRATERING EVALUATIONS AND RESULTS
J. R. Church Aug. 1993 29 p
(Contract DE-AC04-76DP-00613)
(DE93-040347; KCP-613-5111) Avail: CASI HC A03/MF A01

Investigations were performed on the 1-mil ultrasonic aluminum wire bonding process to determine how the interaction of the bonding parameters, ultrasonic power, time, force, and aluminum wire, contribute to cratering (cracking or damage to oxide/passivation layers). Investigations revealed that power, time, and force can interact at levels which can contribute to cratering. The age of the aluminum wire can also influence the quality of bonds. DOE

N94-20530# Technical Research Centre of Finland, Espoo. Metals Lab.
PRODUCTION OF NiAl AND TiAl INTERMETALLICS BY MECHANICAL ALLOYING [ALUMIINIYHDISTEIDEN VALMISTUS MEKAANISELLA SEOSTUKSELLA]
Jari Keskinen and Pekka Ruuskanen May 1992 34 p In FINNISH
(VTT-JULK-760; ISBN-951-38-4108-1; ETN-93-94468) Copyright Avail: CASI HC A03/MF A01

Mechanical alloying is a solid state process which can be used to synthesize various compounds. By mechanical alloying nanocrystalline, microcrystalline, crystalline, and amorphous materials can be produced. Wider solubility ranges can be obtained and the properties of materials can be varied more easily than by conventional methods. In addition, the process is less expensive and simpler than the methods that are used nowadays. It can be applied in producing new construction materials, magnets, copper alloys, hydrogen storage materials, and super conductors. The method makes the dispersion strengthening possible already during alloying. Also, the particle size can be controlled. The results of the alloying of nickel and titanium aluminum by mechanical alloying are presented. Aluminum alloys have many applications, for example in process industry and as tool materials because of their good corrosion resistance and excellent high temperature strength properties. They also offer good strength/weight ratio. Both nickel and titanium were alloyed with aluminum using many various concentration ratios. The alloys were examined by scanning electron microscope, X-ray diffractometer and differential scanning calorimeter. According to the X-ray diffraction both nickel and titanium aluminides were synthesized, i.e. the alloy consisted of chemical compound. Some samples were amorphous. The particle size varied in different samples. At smallest it was of the order of 1 micrometer. ESA

N94-21188# Dayton Univ. Research Inst., OH.
WELDALITE (TM) 049 (Al 2095-T8): ANISOTROPY EFFECTS AT CRYOGENIC CONDITIONS Interim Report, Aug. 1991 - Jun. 1993
John J. Ruschau and Kumar V. Jata Aug. 1993 36 p
(Contract F33615-90-C-5915)
(AD-A272658; UDR-TR-93-69; WL/ML-TR-93-4096) Avail: CASI HC A03/MF A01

Tensile, fracture, and FCGR testing was performed on a plate of the aluminum-lithium alloy Weldalite(TM) 049 (Al 2095-T8) over a temperature range from ambient to liquid helium (4K) conditions. Properties were developed on specimens removed from various orientations within a 12.7 mm (1/2 in) nominal thick plate to characterize anisotropy with respect to strength and toughness. Strength and FCGR properties are compared to the conventional aluminum alloy 2219-T87, developed for similar cryogenic applications. Results indicate a high degree of anisotropy with respect to strength and ductility, with the lowest strength/highest ductility occurring at 45-60 deg from the rolling direction. Decreases in test temperature led to higher strengths and similar anisotropic behavior, with little or no change in ductility. Fracture toughness measurements did not reveal any significant orientation effects, with toughness levels insensitive to the cryogenic temperatures examined. It was not possible to develop valid FCGR data on C(T) samples oriented in either the T-L or T-L plate directions due to out-of-plane cracking. Constant amplitude FCGR data generated on 45 deg oriented samples are comparable with reference data on similar Weldalite material for the T-L and L-T directions, though a slight degree of anisotropy appears to exist at lower values of Delta K. FCGR data obtained at liquid nitrogen and liquid helium test conditions were identical and only slightly lower than similar data developed under ambient conditions. DTIC

N94-21245# Cincinnati Univ., OH. Dept. of Chemistry.
SURFACE ELECTROCHEMISTRY OF METALS Final Report, 1 May 1990 - 30 Apr. 1993
Arthur T. Hubbard 30 Apr. 1993 36 p
(Grant AF-AFOSR-0281-90)
(AD-A272913; AFOSR-93-0839TR) Avail: CASI HC A03/MF A01

The essence of this Air Force Office of Scientific Research (AFOSR) project is to investigate the structure, composition, mode of attachment, and reactivity of the molecular species which form at the surfaces of metals in contact with fluids. Progress to date includes advances in investigative technology, 110 scientific articles, and useful findings as follows: a series of new findings, advances in investigative technology and 105 scientific articles have occurred thus far. These include (1) determination of molecular orientations and modes of attachment at electrode surfaces; (2) demonstration that mode of surface attachment affects electrochemical reactivity; (3) exploration of the structure and composition of electrodeposited metal monolayers and thin-films; (4) investigation of the nature of the species formed at electrode surfaces in ionic solutions; (5) adaptation of high-resolution electron energy-loss spectroscopy (HREELS) to measurement of vibrational spectra of species adsorbed at electrode surfaces; (6) systematic HREELS, Auger and electrochemical studies of families of adsorbates, including acids, alcohols, alkenes, amines, mercaptans, phenols, and pyridines; (7) demonstration of the stability of chemisorbates in vacuum; (8) development of techniques for measurement of complete Auger emission angular distributions potentially useful for structure probing of solid surfaces; (9) development of an infrared (IR) reflectance spectrometer capable of recording the vibrational spectra of typical adsorbed organic molecules; and (10) studies of the interaction of the polar solvent acetonitrile with solid electrode surfaces. DTIC

N94-21258# Naval Postgraduate School, Monterey, CA.
THE USE OF BACKSCATTERED ELECTRON IMAGING MODE TO ASSESS THE EFFECT OF FINE DISPERSIONS ON DEVELOPMENT OF SUPERPLASTIC MICROSTRUCTURE IN Al-Mg ALLOYS M.S. Thesis
Michael T. Coleman Jun. 1993 75 p
(AD-A272426) Avail: CASI HC A04/MF A01

Microstructural evolution during thermomechanical processing of several

Al-Mg alloys was studied using backscattered orientation contrast imaging in the scanning electron microscope. The microstructural evolution in AlMg8Zr(0.1) was characterized in three phases: in the initial stages, precipitation occurred on prior boundaries and microbands were observed in the grain interiors; during intermediate stages, higher order microbands were observed and precipitates formed throughout the microstructure on both lower- and higher-order microbands; and in the final stages, equiaxed regions appeared around larger particles suggesting particle stimulated nucleation of recrystallization. A higher Mg-content alloy (AlMg10Zr(0.1)) was compared at two stages and seen to provide a greater volume fraction of similar sized precipitate. A finer recrystallized microstructure and greater superplastic response was observed in the AlMg10Zr(0.1) alloy. DTIC

N94-21311 GKSS-Forschungszentrum Geesthacht (Germany). Inst. fuer Werkstofforschung.
EXAMINATIONS OF COMPOSITION AND DEFORMATION BEHAVIOR OF INTERMETALLIC PHASES ON THE BASIS OF Fe3(AlSi) Thesis - Technische Univ. [UNTERSUCHUNGEN DER KONSTITUTION UND ZUM VERFORMUNGSVERHALTEN VON INTERMETALLISCHEN PHASEN AUF DER BASIS VON FE3(ALSI)]
H. Bosse 12 Feb. 1992 292 p In GERMAN Limited Reproducibility: More than 20% of this document may be affected by microfiche quality
(GKSS-92/E/16; ETN-93-94186) Copyright Avail: CASI HC A13

The constitution of Fe3(AlSi) based alloys was examined by means of transmission electron microscopy and x ray powder diffraction on quenched samples. Critical temperatures for DO3-order as well as the ranges of the several miscibility gaps between the alpha solid solution and the ordered phases alpha' (B2 structure) alpha'' (DO3 structure) were determined in alloys with 80, 75, and 70 at% iron. The critical temperatures were used to calculate the interaction and antiphase boundary energies within the framework of thre Bragg-Williams approximation. The morphology of the two phase microstructures and the nucleation behavior in the ordered alloys are discussed. Additionally the dislocation structures in Fe70Al30 single crystals deformed at different temperatures were investigated by electron microscopy and the results were compared to existing models to explain the temperature dependence of the yield strength. ESA

N94-21320# McDonnell-Douglas Aerospace Information Services Co., Saint Louis, MO.
STRENGTH AND TOUGHNESS IMPROVEMENT OF SILICIDE INTERMETALLICS BY NANOPHASE AND MICROPHASE REINFORCEMENTS Final Report, 1 Apr. 1990 - 30 Apr. 1993
D. S. Schwartz, R. J. Lederich, D. A. Deuser, S. M. L. Sastry (Washington Univ., Saint Louis, MO.), and R. Suryanarayanan (Washington Univ., Saint Louis, MO.) 8 Oct. 1993 81 p
(Contract F49620-90-C-0030)
(AD-A272914; MDC-93B0465; AFOSR-93-0836TR) Avail: CASI HC A05/MF A01

The HIP processing of MoSi2 and MoSi2 + Nb powder, Nb wire, and Nb foil composites was optimized. The reaction between MOSi2 and Mo, W, Ta, and Nb reinforcements at 1700 C was examined. W, Ta, and Nb reinforcements formed complex, two layer reaction zones in contact with MoSi2. Reaction layer growth parameters were measured for Nb. Detailed HIP modeling and deformation mechanism mapping was carried out for MOSi2, MoSi2 + Nb, and MoSi2 + SiC. The results indicate 1400-1500 C to be optimal for producing greater than 98% dense material. A sensitivity analysis was developed and demonstrated for HIP modeling of TiAl and MOSi2. Bend strengths of MoSi2, MoSi2 + Nb powder, MOSi2 + 250 micrometer Nb wire, MoSi2 + 750 micrometers wire, and 200 micrometer Nb foil were measured between 20 and 1450 C in vacuum. Compositing with Nb significantly lowered elevated temperature strength. K(sub 1c) was measured at 20 C for each composite and significant improvements were observed. Reinforcement morphology had a strong effect on toughness. Reinforcement morphologies listed in order of increasing potency are: Nb powder, 250 micrometer Nb wire, 750 micrometer Nb wire, and Nb foil. Quantitative comparison was made between theory and measurement of the toughness increase, and poor agreement was found. HIP reaction of MoSi2 and Ti powder was explored. DTIC

N94-21525 Wright Lab., Wright-Patterson AFB, OH.
THE MECHANICAL PROPERTY DATA BASE FROM AN AIR FORCE/INDUSTRY COOPERATIVE TEST PROGRAM ON ADVANCED ALUMINUM ALLOYS: 2091 SHEET, PLATE, AND 8090 EXTRUSION Interim Report, Nov. 1988 - Dec. 1992
Mary A. Phillips and Steven R. Thompson Jun. 1993 170 p Limited Reproducibility: More than 20% of this document may be affected by microfiche quality
(AD-A273091; WL-TR-93-4076) Avail: Issuing Activity (Defense Technical Information Center (DTIC))

A mechanical property data base on Alcoa produced aluminum-lithium alloys 2091 Sheet, 2091 plate, and 8090 extrusion was developed. Mechanical property data consisted of tension, compression, bearing, shear, and fracture toughness. Fatigue, fatigue crack growth, and spectrum fatigue crack growth data were generated. DTIC

N94-21558# Argonne National Lab., IL.
LASER RAMAN AND X RAY SCATTERING STUDIES OF CORROSION FILMS ON METALS
C. A. Melendres Feb. 1993 10 p Presented at the 12th International Corrosion Congress, Houston, TX, 19-24 Sep. 1993
(Contract W-31-109-eng-38)
(DE93-040243; ANL/CMT/CP-79337; CONF-9309150-6) Avail: CASI HC A02/MF A01

Optical spectroscopic and x ray scattering techniques, coupled with electrochemical methods, are among the most useful in probing the structure of corrosion films on metals in-situ in aqueous environments. Laser Raman spectroscopy has been employed for a number of years to investigate composition of surface films on metals like iron, nickel, chromium, and stainless steel. Our work is illustrted by presenting some results of studies of composition of passive film on nickel, using surface enhanced Raman scattering (SERS) with an electrodeposited silver overlayer. It was found that both oxide and hydroxide species are present on the surface of Ni in the passive region. The utility of specular x ray reflection in providing complementary information on the physical structure of passivated metal surfaces was also demonstrated. Thickness of the corrosion films formed, density of surface layers, and development of surface and interface roughness on Cu electrodes were quantitatively monitored in-situ as a function of potential for the first time. DOE

N94-21604*# National Aeronautics and Space Administration. Lewis Research Center, Cleveland, OH.
EXPERIMENTAL STUDY OF VOID FORMATION DURING ALUMINUM SOLIDIFICATION IN REDUCED GRAVITY Ph.D. Thesis - Toledo Univ.
Francis Paul Chiaramonte, III Oct. 1993 78 p
(RTOP 674-24-05)
(NASA-TM-106190; E-7520-1; NAS 1.15:106190) Avail: CASI HC A05/MF A01

Void formation due to volumetric shrinkage and liquid/vapor reorientation during aluminum solidification was observed in real time by using a radiographic viewing system in normal and reduced gravity. An end-chill directional solidification furnace with water quench was designed and constructed to solidify aluminum samples during the approximately 16 sec of reduced gravity (+/-0.02g) achieved by flying an aircraft through a parabolic trajectory. In the first series of tests the aluminum was contained in a vacuum sealed, pyrolytic boron nitride crucible. An ullage space was present during each test. Void formation was recorded for two cases: a nonwetting system, and a wetting system where wetting occurred between the aluminum and the crucible lid. The void formation in the nonwetting case was similar in normal and reduced gravity, with a single vapor cavity forming at the top of the crucible. In the wetting case during reduced gravity surface tension caused two voids to form in the top corners of the crucible, but during normal gravity only one large void formed across the top. In the second series of tests the aluminum was contained in a pyrolytic boron nitride crucible that was placed in a stainless steel container and sealed in an environment of argon plus 4 percent hydrogen. An ullage space was present during each test. Void formation was recorded for two cases: a nonwetting system, and a wetting system where wetting occurred between the aluminum and one side wall and the lid. The void for nation in the nonwetting case was similar in normal and reduced gravity, with a single vapor cavity forming at the top of the crucible, although the meniscus became more convex in reduced gravity. In the wetting case the aluminum

did not climb up the corners in 1g, and one large symmetric void resulted at the top when the aluminum had solidified. In the wetting case during reduced gravity the molten aluminum was drawn up the wetted wall and partially across the lid by a capillary underpressure; however, on the nonwetting wall the aluminum moved down. One void resulted along the nonwetting side of the container continuing to the top on the same side.
Author (revised)

N94-21656# Lawrence Livermore National Lab., CA.
STATIC ULTRA-HIGH PRESSURE STUDY OF LANTHANIDE AND ACTINIDE METALS USING A DIAMOND-ANVIL CELL
J. Akella, G. S. Smith, and S. T. Weir 30 Jun. 1993 6 p Presented at the 14th International Conference of the International Association for the Advancement of High Pressure Science and Technology, Colorado Springs, CO, 27 Jun. - 2 Jul. 1993
(Contract W-7405-eng-48)
(DE94-000369; UCRL-JC-114166; CONF-930676-52) Avail: CASI HC A02/MF A01

Structural phase transformation in lanthanides and actinides were investigated as a function of pressure up to 300 GPa at room temperature. Except in Ce and Pr, no large volume changes were noticed for these metals as they went through several phase changes. The appearance of a bct ultra-high pressure phase in Ce, Sm, Th, and possibly in Np, raises the possibility that the ultimate high pressure structure for the 4f and 5f metals may be the bct structure. On the other hand, it is also possible that this is a precursor to another close-packed structure at even higher pressure.
DOE

N94-21771 Oak Ridge National Lab., TN.
EVALUATION OF THE FABRICABILITY OF ADVANCED IRON ALUMINIDE-CLAD AUSTENITIC STAINLESS STEEL TUBING
W. R. Mohn and M. J. Topolski Jul. 1993 42 p Prepared in cooperation with Babcock and Wilcox Co., Alliance, OH Limited Reproducibility: More than 20% of this document may be affected by microfiche quality
(Contract DE-AC05-84OR-21400)
(DE93-040598; ORNL/Sub-88-SB775/03) Avail: CASI HC A03

Researchers at Babcock & Wilcox Alliance Research Center have investigated methods to produce bimetallic tubing consisting of iron aluminide-clad austenitic stainless steel for practical use in fossil fueled energy equipment. In the course of this work, the compatibility of iron aluminide with four candidate austenitic stainless steel substrates was first evaluated using diffusion couples. Based on these results, a combination of iron aluminide and 304 stainless steel was selected for further development. Two composite billets of this combination were then prepared and extruded in separate trails at 2200 and 2000 F. Both extrusions yielded 2-inch OD clad tubes, each approximately 18 feet long. Results of the evaluation show that the tube extruded at 2000 F had a sound, integrally bonded clad layer throughout its entire length. However, the tube extruded at 2200 F exhibited regions of disbonding between the clad layer and the substrate. In supplement to this work, an assessment of the technical and economic merits of iron aluminide-clad austenitic stainless steel components in power generation systems was conducted by B&W Fossil Power Division. Future activities should include an investigation of lower extrusion processing temperatures to optimize the fabrication of high quality iron-aluminide clad tubing.
DOE

N94-21825 Argonne National Lab., IL.
SURFACE MODIFICATION FOR CORROSION RESISTANCE
K. Natesan Jun. 1993 12 p Presented at the Workshop on Materials for Coal Gasification Power Plant, Petten, Netherlands, 14-16 Jun. 1993 Limited Reproducibility: More than 20% of this document may be affected by microfiche quality
(Contract W-31-109-eng-38)
(DE93-017419; ANL/ET/CP-80044; CONF-9306246-1) Avail: CASI HC A03

The raw gas environments that arise from coal gasification have chemical compositions that are low in pO2 and moderate-to-high in pS2. Metallic materials for service in such an environment undergo predominantly sulfidation attack at temperatures of 400 to 700 C. Modification of alloy compositions in bulk can alter the scaling processes and lead to improvements in corrosion resistance, but the benefits can only be attained at temperatures much higher than the service temperatures of the components. Modification of surfaces of structural components by several of the coating techniques examined in this study showed substantial benefit in corrosion resistance when tested in simulated coal gasification environments. The paper presents several examples of surface modification and their corrosion performance.
DOE

N94-21843# Lawrence Livermore National Lab., CA.
DUCTILE-BRITTLE TRANSITION BEHAVIOR OF TUNGSTEN UNDER SHOCK LOADING CONDITIONS
D. H. Lassila and G. T. Gray, III (Los Alamos National Lab., NM.) Feb. 1993 16 p Presented at the 13th International Plansee Seminar, Triol, Austria, 24-28 May 1993
(Contract W-7405-eng-48)
(DE93-019945; UCRL-JC-112768; CONF-9305141-2) Avail: CASI HC A03/MF A01

In an effort to characterize the ductile-brittle transition behavior of warm forged tungsten under shock loading conditions, we have performed shock/soft-recovery experiments at 22 and 4000 C. Results at 22 C indicate that shock (19 GPa) induced strains appear to be accommodated by fracture processes, i.e. there were no indications of shock induced plastic deformation, and the test sample was reduced to rubble. At 400 C, the test sample was recovered intact and the shock induced plasticity caused deformation banding and an increase in the dislocation density of the material. For reasons that are unclear, almost no change in the post shock mechanical behavior was observed, despite the significant changes in the microstructure. The results of these experiments demonstrate the principal of a ductile-brittle transition behavior of tungsten under uniaxial shock loading conditions and indicate that explosively driven deformation of tungsten of this material will result in pulverization due to shock loading.
DOE

N94-21850 Oak Ridge National Lab., TN.
AN ASSESSMENT OF THE COST OF MICROWAVE SINTERING CERAMIC TILES FOR ARMOR APPLICATIONS
S. Das and T. R. Curlee Sep. 1993 32 p Limited Reproducibility: More than 20% of this document may be affected by microfiche quality
(Contract DE-AC05-84OR-21400)
(DE94-000978; ORNL/TM-12423) Avail: CASI HC A03 (US Sales Only)

The sintering component of a process cost model was used to estimate the cost of microwave sintering of alumina and Si carbide tiles. While the process cost model focuses only on cost of the sintering step, preliminary estimates of total cost of a microwave-sintered tile are also provided, assuming that costs of pre- and post-sintering steps will not be altered by adoption of microwave sintering. Base-case cost of microwave sintering alumina tiles is estimated to be $14.98 and $18.17/part for 2.45 and 28 GHz microwave power sources. Cost of microwave sintering is greater than 3 times the cost of conventional sintering, but microwave sintering is not expected to drastically increase the cost of ceramic tiles; the increase factor is only 1.3 times. For Si carbide tiles, the base-case cost of microwave sintering is lower than that of conventional sintering ($39.11 and $41.66/part for 2.45 and 28 GHz sources vs $106.14/part for conventional sintering). Labor is one of the largest sintering cost components in the case of alumina tiles, while for Si carbide tiles, material is the largest sintering cost component. Sensitivity analysis indicate that costs are particularly sensitive to changes in quantity of microwave energy required (kWh/lb) during sintering.
DOE

N94-21854# Minnesota Univ., Minneapolis. Corrosion Research Center.
FUNDAMENTAL STUDIES OF STRESS DISTRIBUTIONS AND STRESS RELAXATION IN OXIDE SCALES ON HIGH TEMPERATURE ALLOYS
D. A. Shores, J. H. Stout, and W. W. Gerberich Jun. 1993 45 p
(Contract DE-FG02-88ER-45337)
(DE94-001444; DOE/ER-45337/T5) Avail: CASI HC A03/MF A01

This report summarizes a three-year study of stresses arising in the oxide scale and underlying metal during high temperature oxidation and of scale cracking. In-situ XRD was developed to measure strains during oxidation over 1000 C on pure metals. Acoustic emission was used to observe scale fracture during isothermal oxidation and cooling, and statistical analysis was used to infer mechanical aspects of cracking. A microscratch technique was used to measure the fracture toughness of scale/metal

interface. A theoretical model was evaluated for the development and relaxation of stresses in scale and metal substrate during oxidation. DOE

N94-21921# Lawrence Livermore National Lab., CA.
MOLECULAR DYNAMICS MODELING OF THE MECHANICAL BEHAVIOR OF METALLIC MULTILAYERS
J. Belak and D. B. Boercker Jul. 1993 7 p Presented at the Spring Meeting of the Materials Research Society, San Francisco, CA, 12-16 Apr. 1993 Revised
(Contract W-7405-eng-48)
(DE93-019947; UCRL-JC-112347-Rev-1; CONF-930405-38-Rev-1) Avail: CASI HC A02/MF A01

Constant-stress molecular dynamics simulations are used to study the mechanical properties of equal concentration Cu-Ni (111) metallic multilayers of repeat lengths 0.4-5.0 nm. Uniaxial stress is applied along the close-packed 110 and perpendicular to the close-packed 112 directions within the (111) plane. The observed elastic modulus does not display a super-modulus effect as observed in experimental bulge tests for the biaxial modulus. However, both the average interlayer spacing and the out-of-plane Poisson ratio display anomalous effects for multilayer repeat lengths below about two nanometers. DOE

N94-21933# Oak Ridge National Lab., TN.
NI3AI ALUMINIDE ALLOYS
C. T. Liu 1993 13 p Presented at the International Symposium on Structural Intermetallics, Champion, PA, 26-30 Sep. 1993
(Contract DE-AC05-84OR-21400)
(DE94-000493; CONF-930997-6) Avail: CASI HC A03/MF A01

This paper provides a brief review of the recent progress in research and development of Ni3Al and its alloys. Emphasis has been placed on understanding low ductility and brittle fracture of Ni3Al alloys at ambient and elevated temperatures. Recent studies have resulted in identifying both intrinsic and extrinsic factors governing the fracture behavior of Ni3Al alloys. Parallel efforts on alloy design using physical metallurgy principles have led to properties for structural use. Industrial interest in these alloys is high, and examples of industrial involvement in processing and utilization of these alloys are briefly mentioned. DOE

N94-21937# Ames Lab., IA.
SULFUR-BONDED THIOPHENES IN ORGANOMETALLIC RHENIUM COMPLEXES AND ADSORPTION OF ISOCYANIDES ON GOLD Ph.D. Thesis
M. J. Robertson Aug. 1993 119 p
(Contract W-7405-eng-82)
(DE93-041126; IS-T-1645) Avail: CASI HC A06/MF A02

This dissertation contains results of research conducted in two different areas: (1) organometallic synthesis and reactivity, and (2) organometallic surface chemistry. In the synthesis and reactivity studies, sulfur coordination of thiophene and benzo(b)thiophene to the metal center in organometallic rhenium complexes is examined. In the surface chemistry studies, diffuse reflectance infrared Fourier transform spectroscopy (DRIFTS) is used to analyze the adsorption of several isocyanides on the surface of gold powder. Results are compared and contrasted to known organometallic chemistry. DOE

N94-21943# Lawrence Livermore National Lab., CA.
THE EFFECT OF MICROSTRUCTURAL EVOLUTION ON SUPERPLASTICITY IN NI3SI(V, Mo)
Susan L. Stoner and Amiya K. Mukherjee (California Univ., Davis.) Oct. 1992 14 p Presented at the Advances in Superplasticity and Superplastic Forming, Chicago, IL, 1-5 Nov. 1992
(Contract W-7405-eng-48)
(DE93-041320; UCRL-JC-112108; CONF-9211268-1) Avail: CASI HC A03/MF A01

To further the understanding of superplasticity in intermetallics, this paper presents results of experimental investigations on an intermetallic alloy based on nickel silicide. Specifically, the evolution of the microstructure and its influence on superplastic performance is discussed. In the duplex microstructure, one phase showed grain growth, and the other, grain refinement. Cavitation occurred at interphase boundaries and final failure was by interlinkage of these cavities. Annealing the material improved the homogeneity of the microstructure. The annealed material showed improved strain rate sensitivity values and enhanced superplasticity. Microstructural features and ductility were also influenced by changing the orientation of the tensile axis. Though a transverse orientation showed more cavitation than longitudinal, it yielded greater elongation. An increased resistance to cavity coalescence in the transverse direction played a role in the enhanced ductility. DOE

N94-21944# Lawrence Livermore National Lab., CA.
OBSERVATION OF X RAY ABSORPTION MAGNETIC CIRCULAR DICHROISM IN WELL-CHARACTERIZED IRON-COBALT-PLATINUM MULTILAYERS
A. F. Jankowski, G. D. Waddill, and J. G. Tobin Apr. 1993 7 p Presented at the Spring Meeting of the Materials Research Society, San Francisco, CA, 12-16 Apr. 1993
(Contract W-7405-eng-48)
(DE94-000303; UCRL-JC-113778; CONF-930405-42) Avail: CASI HC A02/MF A01

Magnetic circular dichroism in the Fe 2p x-ray absorption is observed in multilayers of(Fe9.5(Angstrom)/Pt9.5(Angstrom))(sub 92). The magnetization and helicity are both in the plane of this multilayer which is prepared by magnetron sputter deposition. This sample is part of a study to examine magnetization in the ternary multilayer system of FeCo/Pt. Lattice and layer pair spacings are measured using x-ray scattering. The atomic concentration profiles of the multilayer films are characterized using Auger electron spectroscopy coupled with depth profiling. Conventional and high resolution transmission electron microscopy are used to examine the thin film, growth morphology, and atomic structure. DOE

N94-21945# Oak Ridge National Lab., TN.
EFFECT OF POWDER CHARACTERISTICS ON GAS-PRESSURE SINTERING OF Si3N4 WITH RARE EARTH ADDITIVES
T. N. Tiegs, S. D. Nunn, C. A. Walls, D. Barker, C. Davisson, and P. J. Jones 1993 4 p Presented at the International Union of Materials Research Societies on Advanced Materials, Tokyo, Japan, 31 Aug. - 4 Sep. 1993
(Contract DE-AC05-84OR-21400)
(DE94-000330; CONF-9308122-8) Avail: CASI HC A01/MF A01

Several Si3N4 powders, synthesized by various methods and having different surface areas, oxygen contents and impurity levels, were examined. During early stage densification, all powders showed similar shrinkage with the diimide ederived powder exhibiting delayed (alpha)/(beta) transformation compared to the other powders. The diimide and gas-phase derived powders achieved the highest final densities. Improved densification was observed by increasing the oxygen content and this also resulted in high toughness for some materials with rare earth apatite additives. However, the increased oxygen resulted in reduced high temperature strength. Fracture toughnesses (K(sub Ic)) up to 10 MPa sq. root of m were obtained for some compositions. DOE

N94-21948# Oak Ridge National Lab., TN.
ALLOYING EFFECTS ON MECHANICAL AND METALLURGICAL PROPERTIES OF NiAl
C. T. Liu, J. A. Horton, E. H. Lee, and E. P. George Jun. 1993 31 p
(Contract DE-AC05-84OR-21400)
(DE93-040814; ORNL/TM-12200) Avail: CASI HC A03/MF A01

Alloying effects were investigated in near-stoichiometric NiAl for improving its mechanical and metallurgical properties. Ternary additions of 19 elements at levels up to 10 at. % were added to NiAl; among them, molybdenum is found to be most effective in improving the room-temperature ductility and high-temperature strength. Alloying with 1.0 +/- 0.6% molybdenum almost doubles the room-temperature tensile ductility of NiAl and triples its yield strength at 1000 C. The creep properties of molybdenum-modified NiAl alloys can be dramatically improved by alloying with up to 1% of niobium or tantalum. Because of the low solubilities of molybdenum and niobium in NiAl, the beneficial effects mainly come from precipitation hardening. Fine and coarse precipitates are revealed by both transmission electron microscopy (TEM) and electron microprobe analyses. Molybdenum-containing alloys possess excellent oxidation resistance and can be fabricated into rod stock by hot extrusion at 900 to 1050 C. This study of alloying effects provides a critical input for the alloy design of ductile and strong NiAl aluminide alloys for high-temperature structural applications. DOE

N94-21949# Oak Ridge National Lab., TN.
INVESTIGATION OF MOISTURE-INDUCED EMBRITTLEMENT OF IRON ALUMINIDES
A. Castagna and N. S. Stoloff (Rensselaer Polytechnic Inst., Troy, NY.) 15 Apr. 1993 11 p
(Contract DE-AC05-84OR-21400)
(DE93-040841; ORNL/Sub-90-SF521/01) Avail: CASI HC A03/MF A01

The effect in ambient air the tensile and fatigue behavior of an Fe3Al, Cr type intermetallic alloy is examined as a function of test temperature. Hydrogen due to moisture in the air is found to be a major cause of embrittlement. Rates and mechanisms of observed embrittlement appear to be temperature dependent. In addition, the alloy was found to have no notch sensitivity. DOE

N94-21964# Ames Lab., IA.
FIRST PRINCIPLES CALCULATIONS FOR ANALYSIS MARTENSITIC TRANSFORMATIONS
B. N. Harmon, G. L. Zhao, K. M. Ho, C. T. Chan, Y. Y. Ye, Y. Ding, and B. L. Zhang 1993 7 p Presented at the 3rd IUMRS International Conference, Tokyo, Japan, 31 Jul. - 4 Aug. 1993
(Contract W-7405-eng-82)
(DE94-000666; IS-M-761; CONF-9307142-1) Avail: CASI HC A02/MF A01

The change in crystal energy is calculated for atomic displacements corresponding to phonons, elastic shears, and lattice transformations. Anomalies in the phonon dispersion curves of NiAl and NiTi are analyzed and recent calculations for TiPd alloys are presented. DOE

N94-21976# Allied-Signal Aerospace Co., Kansas City, MO.
SHAPE MEMORY METALS
T. D. Dworak Sep. 1993 13 p
(Contract DE-AC04-76DP-00613)
(DE94-001373; KCP-613-5215) Avail: CASI HC A03/MF A01

The ability to define a manufacturing process to form, heat-treat, and join parts made of nickel-titanium and/or copper-zinc-aluminum shape memory alloys was investigated. The specific emphasis was to define a process that would produce shape memory alloy parts in the configuration of helical coils emulating the appearance of compression springs. In addition, the mechanical strength of the finished parts along with the development of a electrical lead attachment method using shape memory alloy wire was investigated. DOE

N94-21978# Allied-Signal Aerospace Co., Kansas City, MO.
EVALUATION OF NON-CHROMIUM-CONTAINING DEOXIDIZERS FOR ALUMINUM
T. L. Kempf and C. J. Stimetz Aug. 1993 31 p
(Contract DE-AC04-76DP-00613)
(DE94-001377; KCP-613-5255) Avail: CASI HC A03/MF A01

Environmental and regulatory pressures make it necessary to eliminate the use of hexavalent chromium wherever possible. This report discusses the evaluation of non-chromium deoxidizers as replacements for a hexavalent chromium dioxidizer. The current deoxidizer is used as a deoxidizer for anodizing aluminum and chromate conversion coating as well as a cleaner prior to welding. Performance of replacement deoxidizers was evaluated through salt spray testing, surface analysis, optical metallography, radiography and dye-penetrant analysis of welds, and a production simulation. DOE

N94-21986# Lawrence Livermore National Lab., CA.
STRENGTHENING AND TOUGHENING IN REFRACTORY METAL ALLOYS
J. Wadsworth, T. G. Nieh, and J. Wittenauer (Lockheed Missiles and Space Co., Palo Alto, CA.) Mar. 1993 16 p Presented at the Conference on Critical Issues in the Development of High Temperature Structural Materials, Kona, HI, 7-12 Mar. 1993
(Contract W-7405-eng-48)
(DE93-019942; UCRL-JC-113795; CONF-930317-2) Avail: CASI HC A03/MF A01

Development and application of refractory metal alloys for high temperature aerospace structures is reviewed. The use of refractory metals is often limited by poor room temperature properties, inadequate oxidation resistance at elevated temperatures, or difficulties associated with joining, welding, or forming. Materials selection criteria for high temperature structures are reviewed with an emphasis placed upon the distinctions between refractory metals and competing high temperature materials -- including carbon, ceramics, and intermetallics. Each class of materials has inherent limitations which govern application. In some cases, materials limitations are being solved through the use of engineered materials hybrids such as ceramic-coated refractory metals or ceramics roughened with a ductile refractory metal phase. For many applications, use of ceramics and intermetallics is limited by their technological immaturity. For example, current understanding and application of molybdenum-based materials is based upon nearly 40 years of application experience in high temperature structures. As an example of a materials development and qualification program, a brief synopsis of molybdenum alloy development is presented. Topics surveyed include recent advances in the understanding of the role of oxygen on the room temperature brittle behavior problem in molybdenum alloys. DOE

N94-21990# Los Alamos National Lab., NM.
MICROTEXTURAL CHARACTERIZATION OF ANNEALED AND DEFORMED COPPER
S. I. Wright and F. Heidelbach 1993 6 p Presented at the International Conference on Textures of Materials, Clausthal, Germany, 20-24 Sep. 1993
(Contract W-7405-eng-36)
(DE93-040144; LA-UR-93-3115; CONF-9309231-1) Avail: CASI HC A02/MF A01

Even though deformation produces material with preferred orientation it appears to randomize the grain boundary texture in copper. It appears that as dislocations move through the material the resulting lattice rotations serve to break down the twin structure in a stochastic manner. An effort was made to use the automatic BEKP data to search for dislocation cell wall structures. However, no evidence was found for such structure. This may be due, in part, to the resolution of the backscatter electron Kikuchidi diffraction pattern technique. Diffraction occurs from an area with mean diameter of approximately 0.5 mu m. DOE

N94-22023# Lawrence Livermore National Lab., CA.
TRANSFERABLE TIGHT-BINDING PARAMETERS: AN APPLICATION TO NI AND NI-AI ALLOYS
M. H. F. Sluiter and P. P. Singh Jul. 1993 12 p Presented at the NATO Advanced Study Workshop on Metallic Alloys: Experimental and Theoretical Perspectives, Boca Raton, FL, 16-21 Jul. 1993
(Contract W-7405-eng-48)
(DE94-001044; UCRL-JC-114779; CONF-930759-2) Avail: CASI HC A03/MF A01

Two approaches for obtaining tight-binding parameters for metallic alloys are compared and contrasted with special regard for the application to large scale simulations such as may occur in tight-binding molecular dynamics studies. DOE

N94-22024# Lawrence Livermore National Lab., CA.
SHOCK TEMPERATURE MEASUREMENTS OF IRON TO 350 GPa
C. S. Yoo, N. C. Holmes, M. Ross, and E. See Jul. 1993 6 p Presented at the 14th International Conference of the International Association for the Advancement of High Pressure Science and Technology, Colorado Springs, CO, 27 Jun. - 2 Jul. 1993
(Contract W-7405-eng-48)
(DE94-001058; UCRL-JC-113406; CONF-930676-54) Avail: CASI HC A02/MF A01

Shock temperatures of iron have been measured to 350 GPa, using high quality well-characterized iron films deposited on diamond substrates. The authors have found an inflection in the (P,T)-iron Hugoniot between 250 GPa and 300 GPa, indicating iron melting at 6,350 K and 6,720 K, respectively. An extrapolation yields the iron melting temperature of 6,870 (+/- 500) K at 330 GPa, the pressure of the Earth inner core-outer core boundary. In this paper, they present this new iron melting data together with a brief description of the experimental method to measure the shock temperatures of iron. DOE

N94-22025# Lawrence Livermore National Lab., CA.
INTERFACE SCIENCE OF CONTROLLED METAL/METAL AND METAL/CERAMIC INTERFACES PREPARED USING ULTRAHIGH VACUUM DIFFUSION BONDING
W. E. King, G. H. Campbell, A. W. Coombs, G. W. Johnson, B. E. Kelly, T. C. Reitz, S. L. Stoner, W. L. Wien, and D. M. Wilson Apr. 1993 7 p Presented at the Spring Meeting of the Materials Research Society, San Francisco, CA, 12-16 Apr. 1993
(Contract W-7405-eng-48)
(DE94-001066; UCRL-JC-113779; CONF-930405-46) Avail: CASI HC A02/MF A01

We have designed, constructed, and are operating a capability for production of controlled homophase and heterophase interfaces: an ultrahigh vacuum diffusion bonding machine. This machine is based on a previous design which is operating at the Max Planck Institut fuer Metallforschung, Institut fuer Werkstoffwissenschaft, Stuttgart, FRG. In this method, flat-polished single or polycrystals of materials with controlled surfaced topography can be heat treated up to 1500 C in ultrahigh vacuum. Surfaces of annealed samples can be sputter cleaned and characterized prior to bonding. Samples can then be precisely aligned crystallographically to obtain desired grain boundary misorientations. Material couples can then be bonded at temperatures up to 1500 C and pressures up to 10 MPa. Results are presented from initial work on Mo grain boundaries and Cu/Al2O3. DOE

N94-22034# Los Alamos National Lab., NM.
SURFACE MODIFICATION OF Ti3Al FOR IMPROVED OXIDATION RESISTANCE
R. U. Vaidya, A. K. Zurek, R. Castro, Y. W. Sin (Michigan State Univ., East Lansing.), and K. N. Subramanian (Michigan State Univ., East Lansing.) 1993 26 p Presented at the Fall Meeting of the Minerals, Metals and Materials Society: Physical Metallurgy and Materials in Conjunction With Materials Week and the Materials Applications and Services Exposition, Pittsburgh, PA, 17-21 Oct. 1993
(Contract W-7405-eng-36)
(DE93-018297; LA-UR-93-2686; CONF-931009-2) Avail: CASI HC A03/MF A01

Ti3Al has very attractive properties such as low density and high temperature mechanical strength for elevated temperature structural applications. Its major drawback however, is poor oxidation resistance at temperatures above 600 C. Potential use of Ti3Al in high temperature applications depends on its protection from excessive oxidation. To this effect, Al2O3 and Al3Ti were selected as coating materials chemically compatible with Ti3Al. Al2O3 acts as a protective layer on the surface of Ti3Al and is impervious to oxygen diffusion. Al3Ti is resistant to high temperatures and also protects the Ti3Al substrate by forming an oxide layer consisting primarily of Al2O3. In this study, Al2O3 was plasma sprayed onto the surface of Ti3Al, while the Al3Ti was applied by laser melting. Effectiveness of the coatings were investigated after 10 hours of cyclic oxidation. DOE

N94-22037# Pacific Northwest Lab., Richland, WA.
MICROSTRUCTURAL EVOLUTION OF NEUTRON-IRRADIATED Fe-Cr-Ni TERNARY ALLOYS AT HIGH HELIUM GENERATION RATES
N. Sekimura (Tokyo Univ., Japan.) and F. A. Garner Jul. 1993 21 p Presented at the 3rd Conference on Evolution of Microstructure in Metals During Irradiation, Chalk River, Canada, 29 Sep. - 2 Oct. 1992
(Contract DE-AC06-76RL-01830)
(DE93-018786; PNL-SA-20214; CONF-920970-9) Avail: CASI HC A03/MF A01

A series of Fe-Cr-Ni ternary alloys were irradiated to 12-14 dpa in the Oak Ridge Research Reactor (ORR). In this experiment, most of helium atoms were produced by the (58)Ni(n, gamma)(59)Ni(n, alpha)(56)Fe sequential reaction, and, therefore, the helium generation rate was almost proportional to the nickel content, ranging from 27 to 58 appm He/dpa in 20 to 45 wt.% Ni alloys. Irradiation temperatures were 330, 400, 500 and 600 C, and the specimen variables were the nickel level, the chromium level and cold working. The high levels helium, combined with details of the temperature history, were found to have dominated microstructural development, sometimes overwhelming and even reversing the action of a given material variable. Microscopy examination showed that there was an unprecedented refinement of cavity microstructure at all temperatures, which accounts for the substantial alterations in both swelling and mechanical properties observed in earlier studies. DOE

N94-22388# Los Alamos National Lab., NM.
THEORETICAL STUDIES OF STRUCTURAL PHASE TRANSITIONS IN ACTINIDE METALS
J. M. Wills, A. M. Boring, O. Eriksson (Uppsala Univ., Sweden.), and P. Soederlind (Uppsala Univ., Sweden.) 1993 14 p Presented at the Actinides 1993, Santa Fe, NM, 19-24 Sep. 1993
(Contract W-7405-eng-36)
(DE94-000796; LA-UR-93-3249; CONF-930905-3) Avail: CASI HC A03/MF A01

Accurate full-potential, relativistic, total energy electronic structure calculations have been carried out over a range of volumes for selected rare-earth and actinide elements in crystal structures experimentally observed in these elements. Correct zero temperature crystal structures are obtained, and calculated equilibrium properties are in reasonable agreement with experiment. Results of these calculations suggest that the unusual equilibrium crystal structures occurring in the light actinides are characteristic of narrow band metals in general and that the light actinides will exhibit structural phase transitions to high symmetry structures under compression. A balance between one-electron bandwidths and band fillings and the electrostatic energy of the crystal lattice produces a tendency toward high-symmetry structures at broad bandwidths and low-symmetry structures at narrow bandwidths. Allowing for expansion as well as contraction, simple metals, transition metals and actinides can be 'stabilized' in low- and high-symmetry crystal structures. DOE

N94-22394# Lawrence Livermore National Lab., CA.
TRANSMISSION ELECTRON MICROSCOPY STUDY OF THICK COPPER-304 STAINLESS STEEL MULTILAYERS
M. A. Wall, T. W. Barbee, Jr., and T. Weihs Jun. 1993 6 p Presented at the Spring Meeting of the Materials Research Society, San Francisco, CA, 12-16 Apr. 1993
(Contract W-7405-eng-48)
(DE94-001045; UCRL-JC-112054; CONF-930405-45) Avail: CASI HC A02/MF A01

Thick (10 to 25 micron), free-standing, equal layer thickness, Copper(Cu)-304 Stainless Steel(SS) multilayer foils, having periods of 1 to 100 nm, synthesized by magnetron sputter deposition, were examined by plan view and cross-sectional transmission electron microscopy. Multilayer growth morphology, individual layer structure and crystallographic phase orientation relationships were characterized in this study. Electron Energy Loss filtered imaging of a 20 nm period multilayer cross-section was also performed and showed that nickel had diffused into the Cu layers from the SS during synthesis. X-ray powder diffraction scans were performed and analyzed. A pure deposit of 304SS was synthesized and had a metastable BCC structure. Multilayer samples having periods of 20 nm were found to have a coherent layered Cu(FCC)SS(FCC) structure. At larger periods (50 and 100 nm) a bimodal Cu(FCC)-SS(FCC and BCC) structure was formed. These observations show that the 304SS will grow with a metastable BCC structure when sputter deposited. When layered with Cu(FCC) the 304SS has its equilibrium FCC structure at layer thicknesses up to 10nm as a result of epitaxy with the copper. At larger SS layer thicknesses, the SS appears to locally transform to the metastable BCC structure during synthesis, refining the grain structure of the depositing SS layer and the subsequent Cu layer. This transformation significantly increases the strength of the larger period multilayer. DOE

N94-22398# Lawrence Livermore National Lab., CA.
FIRST-PRINCIPLES PRESSURE-TEMPERATURE PHASE DIAGRAMS IN METALS
J. A. Moriarty Jul. 1993 6 p Presented at the 14th International Conference of the International Association for the Advancement of High Pressure Science and Technology, Colorado Springs, CO, 27 Jun. - 2 Jul. 1993
(Contract W-7405-eng-48)
(DE94-001056; UCRL-JC-113300; CONF-930676-55) Avail: CASI HC A02/MF A01

Using interatomic potentials derived from first-principles generalized pseudopotential theory, finite-temperature phase transitions in both simple and transition metals can be studied through a combination of analytic

statistical methods and molecular-dynamics simulation. In the prototype simple metal Mg, where volume and pair forces adequately describe the energetics, a complete and accurate phase diagram has thereby been obtained to 60 GPa. A rapidly temperature-dependent hcp-bcc phase line is predicted which ends in a triple point on the melting curve near 4 GPa. In central transition metals such as Mo or Fe, on the other hand, the energetics are complicated by d-state interactions which give rise to both many-body angular forces and enhanced electron-thermal contributions. We have made a detailed study of these phenomena and their impact on melting in the prototype case of Mo and a full melting curve to 2 Mbar has been obtained. In the case of Fe, we are examining the high-pressure phase diagram and the question of whether or not there exists a high-pressure, high-temperature solid bcc phase, as has been speculated. To date, we have shown that the bcc structure is both thermodynamically and mechanically unstable at high pressure and zero temperature, with a large and increasing bcc-hcp energy difference under compression. DOE

N94-22402# Lawrence Livermore National Lab., CA.
USING THE RULE OF MIXTURES TO EXAMINE THE HARDNESS OF Cu/Cu-Zr MULTILAYERS
T. P. Weihs, T. W. Barbee, Jr., and M. A. Wall Jun. 1993 8 p Presented at the Spring Meeting of the Materials Research Society, San Francisco, CA, 12-16 Apr. 1993
(Contract W-7405-eng-48)
(DE94-001068; UCRL-JC-114157; CONF-930405-44) Avail: CASI HC A02/MF A01

Cu/Cu-Zr multilayer foils were fabricated and indented to determine the degree to which multilayer hardness is enhanced by increasing the volume fraction of the harder phase. Using sputter deposition and thermal processing a series of foils was fabricated in which the thicknesses of the Cu layers remained fixed while the thicknesses of the alternate Cu-Zr layers varied. These samples were then indented both parallel and normal to their layering. In general hardness increased as the volume fraction of the harder Cu-Zr phase rose. When the films were loaded parallel to their layering, the measured hardnesses were higher and the dependencies on volume fraction of the Cu-Zr phase were stronger than when the films were loaded nominal to their layering. These results agree with predictions based on isostress and isostrain theories. The relations between hardness and volume fraction are used to compare the hardnesses of the Cu-Zr phases: amorphous Cu-Zr, Cu51Zr14 and Cu9Zr2, and to show that the hardness of the textured, as-deposited Zr layers is highly anisotropic. DOE

N94-22559# Oak Ridge National Lab., TN.
MINIATURIZED DISK-BEND TESTING, NANO-INDENTATION, AND THE MICROSTRUCTURE OF ION-IRRADIATED TITANIUM ALUMINIDES
N. L. Petouhoff (California Univ., Los Angeles.), A. J. Ardell (California Univ., Los Angeles.), W. C. Oliver, and B. N. Lucas 1993 10 p Presented at the International Symposium on Structural Intermetallics, Champion, PA, 26-30 Sep. 1993
(Contracts DE-AC05-84OR-21400; DE-FG03-86ER-45264; DE-AC05-76OR-00033)
(DE93-040600; CONF-930997-5) Avail: CASI HC A02/MF A01

Effect of ion irradiation on microstructures and mechanical properties of Ti-52Al (TiAl) and Ti-26Al (Ti3Al) were investigated. The alloys were irradiated with 2 MeV protons and Ar(+) ions at low temperatures (-175 to -135C) to max fluences of 4.5 x 10(exp 15) Ar(+)/cm(exp 2) and 2 x 10(exp 17) H(+)/cm(exp 2). Yield strengths of unirradiated TiAl and the fracture strength of unirradiated Ti3Al were 367 +/- 33 MPa and 536 +/- 30 MPa, respectively, in excellent agreement with published data. Yield strength of TiAl and fracture strength of Ti3Al increased as a result of irradiation. Strengths of both alloys were lowest for the samples irradiated to the highest Ar(+)-ion dose, but otherwise there was no correlation of strength with dose. The nanohardness of irradiated specimens generally increased with dose, but influence of dose on Young's modulus was erratic. Plate-shaped defects vacancy in character, and helical dislocations were observed in irradiated TiAl by TEM. The Ar(+)-ion irradiation-induced microstructure of Ti3Al contained defects producing mottled contrast at 1 dpa and black-spot contrast at 5 dpa. Irradiation-induced loss of long-range order was also observed in both alloys. Influence of these microstructural variables on mechanical behavior is discussed. DOE

N94-22571# Iowa State Univ. of Science and Technology, Ames. Center for Nondestructive Evaluation.
STRENGTH, ULTRASONIC AND METALLURGICAL EVALUATION OF DIFFUSION BONDS
G. C. Ojard, O. Buck, and D. K. Rehbein 1993 8 p Presented at the Annual Winter Meeting of the ASME, New Orleans, LA, 28 Nov. - 3 Dec. 1993
(Contract W-7405-eng-82)
(DE94-000665; IS-M-762; CONF-931121-24) Avail: CASI HC A02/MF A01

Diffusion bonding allows similar and dissimilar materials to be bonded together in near net shape. However, differentiation of almost perfect diffusion bonds, with little variation in their acoustic response, is of critical importance since relatively significant changes in bond strength may be a consequence. The challenge is to find ultrasonic techniques sensitive enough to detect small imperfections at interface. Diffusion bonds have been produced that show only a slight variation in a single frequency reflection measurement. The total energy, reflected from the bond line, can differentiate these diffusion bonds. This evaluation is based on Parseval's theorem which states that energy in time domain is proportional to energy in the frequency domain. This measurement takes advantage of presence of voids in the diffusion bonds as well as of the interdiffusion zone. Cu and Ni were chosen as the materials to be bonded due to the case of microstructural control. Diffusion bonds fabricated of Ti-6Al-4V are also discussed. DOE

N94-20724*# California Univ., Los Angeles. Inst. of Geophysics and Planetary Physics.
EUHEDRAL METALLIC-Fe-Ni GRAINS IN EXTRATERRESTRIAL SAMPLES Abstract Only
Alan E. Rubin *In* Lunar and Planetary Inst., Twenty-Fourth Lunar and Planetary Science Conference. Part 3: N-Z 1993 p 1217-1218 (For primary document see N94-20636 05-91)
Avail: CASI HC A01/MF A06

N94-21375 European Space Agency. European Space Research and Technology Center, ESTEC, Noordwijk (Netherlands).
SOME RESULTS OF THE OXIDATION INVESTIGATION OF COPPER AND SILVER SAMPLES FLOWN ON LDEF
A. deRooij *In* CNES, Fifth International Symposium on Materials in a Space Environment Jun. 1993 p 119-129 (For primary document see N94-21367 05-18)
Copyright Avail: CEPADUES-Editions, 111, rue Nicolas-Vaquelin, 31100 Toulouse, France

27 NONMETALLIC MATERIALS

Includes physical, chemical, and mechanical properties of plastics, elastomers, lubricants, polymers, textiles, adhesives, and ceramic materials.

For composite materials see *24 Composite Materials.*

N94-19809# Argonne National Lab., IL.
FREQUENCY AND TEMPERATURE DEPENDENCE OF HIGH DAMPING ELASTOMERS
R. F. Kulak and T. H. Hughes 1993 7 p Presented at the 12th Biennial Conference for the International Association for Structural Mechanics in Reactor Technology (SMIRT 12), Stuttgart, Germany, 16-26 Aug. 1993
(Contract W-31-109-eng-38)
(DE93-019539; ANL/RE/CP-78944; CONF-930803-22) Avail: CASI HC A02/MF A01

High damping steel-laminated elastomeric seismic isolation bearings are one of the preferred devices for isolating large buildings and structures. In the U.S., the current reference design for the Advanced Liquid Metal Reactor (ALMR) uses laminated bearings for seismic isolation. These bearings are constructed from alternating layers of high damping rubber and steel plates. They are typically designed for shear strains between 50 and 100% and are expected to sustain two to three times these levels for beyond design basis loading conditions. Elastomeric bearings are currently designed to provide a system frequency between 0.4 and 0.8 Hz and expected to operate between -20 and 40 C. To assure proper performance of isolation bearings, it is necessary to characterize the elastomer's response

under expected variations of frequency and temperature. The dynamic response of the elastomer must be characterized within the frequency range that spans the bearing acceptance test frequency, which may be as low as 0.005 Hz, and the design frequency. Similarly, the variation in mechanical characteristics of the elastomer must be determined over the design temperature range. This paper reports on the capabilities of a testing facility at ANL for testing candidate elastomers, the variation with frequency and temperature of the stiffness and damping of one candidate elastomer, and the effect of these variations on bearing acceptance testing criteria and on the choice of bearing design values for stiffness and damping. DOE

N94-19810# Lawrence Livermore National Lab., CA.
SUBSTRATE RECOVERY OF Mo-Si MULTILAYER COATED OPTICS
D. G. Stearns and S. L. Baker Jun. 1993 8 p Presented at the Optical Society of America Topical Meeting on Soft X Ray Projection Lithography, Monterey, CA, 10-12 May 1993
(Contract W-7405-eng-48)
(DE93-019610; UCRL-JC-114087; CONF-9305159-7) Avail: CASI HC A02/MF A01

Imaging optics in a soft x-ray projection lithography (SXPL) system must meet stringent requirements to achieve high throughput and diffraction limited performance. Errors in the surface figure must be kept to less than approximately 1 nm and the rms surface roughness must be less than 0.1 nm. The ML coatings must provide high reflectivity (greater than 60%) at wavelengths in the vicinity of 13 nm. The reflectivity bandpasses of the optics must be aligned within 0.05 nm. Each coating must be uniform across the surface of the optic to within 0.5%. These specifications challenge the limits of the current capabilities in optics fabrication and ML deposition. Consequently a set of qualified SXPL imaging optics is expected to be expensive, costing in the range of $100,000-$250,000. If the lifetime of the imaging optics is short, the replacement cost could significantly impact the economic competitiveness of the technology. The most likely failure modes for the imaging optics are mechanisms that degrade the ML coatings, but which leave the substrates intact. A potentially low cost solution for salvaging the imaging optics could be to strip the damaged ML coating to recover the substrate and then deposit a new coating. In this paper the authors report on the use of reactive ion etching (RIE) to remove Mo-Si ML coatings from precision optical substrates. The goal of this work is to characterize the etching process both in the ML film and at the substrate, and to determine the effects of the etching on the surface figure and finish of the substrate. DOE

N94-19830# Department of the Navy, Washington, DC.
CORROSION INHIBITION IN HIGH TEMPERATURE ENVIRONMENT Patent Application
Robert E. Jones, inventor (to Navy) 28 Jun. 1993 17 p
(AD-D015910; US-Patent-Appl-SN-082640; Navy-Case-75053) Avail: CASI HC A03/MF A01

This invention pertains to the use of tin oxide as a corrosion resistant material for preventing or inhibiting high temperature corrosion by molten sulfate-vanadate deposits and gaseous sulfur trioxide formed in engines or other high temperature apparatus which burn materials containing sodium, sulfur, and vanadium. DTIC

N94-19840 West Virginia Univ., Morgantown.
PROBLEMS RELATED TO CONSERVATION LAWS: PHASE TRANSITIONS AND VISCOELASTICITY Final Report, 15 Aug. 1989 - 14 Aug. 1993
Harumi Hattori 8 Sep. 1993 3 p Limited Reproducibility: More than 20% of this document may be affected by microfiche quality
(Contract DAAL03-89-G-0088)
(AD-A271429; ARO-27130.14-MA-SM) Avail: CASI HC A01

This is a final report of the project titled 'Problems Related to Conservation Laws: Phase Transitions and Viscoelasticity.' In this project I considered the dynamical aspects of a phase transitions problem and the stability issue of waves for viscoelastic materials with memory. DTIC

N94-19857# Allied-Signal Aerospace Co., Kansas City, MO.
CHARACTERIZATION STUDIES OF LOWER AND NON-TDI POLYURETHANE ENCAPSULANTS
M. H. Wilson Sep. 1993 32 p Presented at the Environmentally Conscious Manufacturing Congress, Arlington, VA, 30 Aug. - 1 Sep. 1993
(Contract DE-AC04-76DP-00613)
(DE93-041129; KCP-613-5282; CONF-9308150-6) Avail: CASI HC A03/MF A01

Polyurethane prepolymers containing toluene diisocyanate (TDI) are used within the nuclear weapons complex for many adhesive and encapsulation applications. As part of a program for minimizing hazards to workers and the environment, TDI will be eliminated. This report presents evaluation of alternative encapsulants. DOE

N94-19903# Sandia National Labs., Albuquerque, NM.
HYDRODYNAMIC COMPRESSIBILITY OF HIGH-STRENGTH CERAMICS
D. E. Grady 1993 11 p Presented at the Army Symposium on Solid Mechanics, Plymouth, MA, 17-19 Aug. 1993
(Contract DE-AC04-76DP-00789)
(DE93-019424; SAND-93-1640C; CONF-9308133-3) Avail: CASI HC A03/MF A01

In this study the author has developed the techniques to investigate the hydrodynamic response of high-strength ceramics by mixing these powders with copper powder, preparing compacts, and performing shock compression tests on these mixtures. Hydrodynamic properties of silicon carbide, titanium diboride, and boron carbide to 30 GPa are examined by this method, and hydrodynamic compression data for these ceramics are presented. It is concluded, however, that the measurement method is sensitive to sample preparation and uncertainties in shock wave measurements. Application of the experimental technique is difficult and further efforts are needed. DOE

N94-19938 Applied Research Associates, Inc., Albuquerque, NM.
EXPANDED POLYSTYRENE PROTECTIVE BARRICADE FULL-SCALE FIRE EXPOSURE TEST Final Report
J. H. Storm, B. R. Dees, and M. J. Wilson Nov. 1992 45 p Limited Reproducibility: More than 20% of this document may be affected by microfiche quality
(Contract F08635-88-C-0067)
(AD-A271450; AFESC/ESL-TR-92-53) Avail: CASI HC A03

This test program evaluated the burning characteristics of expanded polystyrene foam used as a munitions barricade in underground storage facilities. In accordance with nationally-accepted standards, a crib fire burning 30 pounds of wood was used as the ignition source. Standard sheet rock was evaluated as a protective material for the polystyrene barricades. Additionally, the two potential ignition sources present within munitions storage bays, an electrically overloaded light fixture and a 4 ounce paint spill, were evaluated for their ability to ignite the test polystyrene cell. While the sheet rock did protect the polystyrene from the fire and extend the time to failure, test results show that a large fire will melt the polystyrene material releasing the sand and extinguishing fire before a dangerous temperature is reached at the weapons location or serious damage is done. Therefore, a polystyrene barricade retrofit with a protective covering does not appear to be warranted. DTIC

N94-19947 Army Research Lab., Aberdeen Proving Ground, MD.
AB INITIO POTENTIAL ENERGY SURFACE FOR THE H + OCS REACTION Final Report, Feb. 1992 - 1993
Betsy M. Rice, Harry E. Cartland, and Cary F. Chabalowski Oct. 1993 35 p Limited Reproducibility: More than 20% of this document may be affected by microfiche quality
(DA Proj. 1L1-61102-AH-43)
(AD-A270577; ARL-TR-231) Avail: CASI HC A03

An ab initio MP4 study has been made of the potential energy surface of the H + OCS reaction, and saddle points leading to formation of OH + CS or SH + CO were found. Stationary points were located using the 6-31G** basis set at the ROHF and UMP2 levels of theory, with energy refinements at the MP4(SDTQ) level. Six minima corresponding to conformers of the HOCS system were calculated and transition states leading into and out of these minima were determined. This theoretical study, in conjunction with the recent experimental results of Boehmer, Mikhaylichenko, and Wittig, provides a mechanistic overview of the reactions of the H + OCS system. The results substantiate earlier experimental hypotheses of the existence of stable, four-body reaction intermediates, as well as tight four-body transition states leading to products. Our results also show that these transition states have nonlinear structures, contrary to assumptions made

in earlier experimental work. Our calculations provide the first set of structural data that detail the reaction mechanisms for H + OCS going to SH + CO or OH + CS. In addition, the feature of this potential energy surface suggest explanations for observed nonstatistical behavior in product energy distributions of the SH + CO channel, and the statistical behavior observed in the product energy distributions of the OH + CS channel. DTIC

N94-19960# Sandia National Labs., Albuquerque, NM.
SOLDER TECHNOLOGY IN THE MANUFACTURING OF ELECTRONIC PRODUCTS
P. T. Vianco 1993 72 p Presented at the 9th IEEE Pulsed Power Conference, Albuquerque, NM, 21-23 Jun. 1993
(Contract DE-AC04-76DP-00789)
(DE93-018842; SAND-93-1604C; CONF-930616-23) Avail: CASI HC A04/MF A01

The electronics industry has relied heavily upon the use of soldering for both package construction and circuit assembly. The solder attachment of devices onto printed circuit boards and ceramic microcircuits has supported the high volume manufacturing processes responsible for low cost, high quality consumer products and military hardware. Defects incurred during the manufacturing process are minimized by the proper selection of solder alloys, substrate materials, and process parameters. Prototyping efforts are then used to evaluate the manufacturability of the chosen material systems. Once manufacturing feasibility has been established, service reliability of the final product is evaluated through accelerated testing procedures. DOE

N94-19973# Brookhaven National Lab., Upton, NY.
OUTGASSING RATE OF REEMAY SPUNBONDED POLYESTER AND DUPONT DOUBLE ALUMINIZED MYLAR
R. J. Todd, D. Pate, and K. M. Welch Aug. 1993 8 p
(Contract DE-AC02-76CH-00016)
(DE93-040015; BNL-49345) Avail: CASI HC A02/MF A01

This paper presents the outgassing rates of two commercially available multi-layer insulation (MLI) materials commonly used in cryogenic applications. Both Reemay Spunbonded Polyester and DuPont Double Aluminized Mylar (DAM) were studied for outgassing species and respective rates, and the total amount of outgassed material. Measurements were made using a Fixed Aperture Technique. A sample was pumped on through an aperture of known size with a turbomolecular pump. Pressure vs. time was plotted for both Reemay and DAM, as well as the baseline system, and data conveniently extrapolated to approximately 1,000 hrs. A quadrupole residual gas analyzer was used to measure the outgassing species. DOE

N94-19975# Los Alamos National Lab., NM.
THERMAL BEHAVIOR OF NATURAL ZEOLITES
D. L. Bish 1993 22 p Presented at the Zeolite 1993: 4th International Conference on the Occurrence, Properties, and Utilization of Natural Zeolites, Boise, ID, 20-28 Jun. 1993
(Contract W-7405-eng-36)
(DE93-040091; LA-UR-93-2881; CONF-9306100-5) Avail: CASI HC A03/MF A01

Thermal behavior of natural zeolites impacts their application and identification and varies significantly from zeolite to zeolite. Zeolites evolve H2O upon heating, but recent data show that distinct 'types' of water (e.g., loosely bound or tightly bound zeolitic water) do not exist. Rather water is bound primarily to extra-framework cations with a continuum of energies, giving rise to pseudocontinuous loss of water accompanied by a dynamic interaction between remaining H2O molecules and extra-framework cations. These interactions in the channels of zeolites give rise to dehydration dependent on the extra-framework cation, in addition to temperature and water vapor pressure. The dehydration reaction and the extra-framework cation also affect the thermal expansion/contraction. Most zeolites undergo dehydration-induced contractions that may be anisotropic, although minor thermal expansion can be seen with some zeolites. Such contractions can be partially or completely irreversible if they involve modifications of the tetrahedral framework and/or if rehydration is sluggish. Thermally induced structural modifications are also driven initially by dehydration and the concomitant contraction and migration of extra-framework cations. Contraction is accommodated by rotations of structural units and tetrahedral cation-oxygen linkages may break. Thermal reactions that involve breaking of tetrahedral cation-oxygen bonds markedly irreversible and may be kinetically limited, producing large differences between short- and long-term heating. DOE

N94-20016 Florida Univ., Gainesville.
CHAIN PROPAGATION/STEP PROPAGATION POLYMERIZATION CHEMISTRY. THE PREPARATION OF SOLVENT RESISTANT WELL PHASE-SEPARATED THERMOPLASTIC ELASTOMERS Final Report, 16 Aug. 1989 - 15 Aug. 1993
Ken B. Wagener 30 Sep. 1993 13 p Limited Reproducibility: More than 20% of this document may be affected by microfiche quality
(Contract DAAL03-89-K-0103)
(AD-A271128; ARO-26441.5-CH) Avail: CASI HC A03

The essence of the research consists of synthesizing unsaturated, chlorofunctionalized carbosilanes or carbosiloxanes as a backbone polymer, and recent work with model compounds suggests that these syntheses will be successful. These chlorofunctionalized backbone polymers will be converted into either solvent resistant elastomers or high T(sub g) materials via nucleophilic grafting reactions, chemistry which is reminiscent of the work done with polyphosphazene backbones. Thus, the goals of this research are as follows: to synthesize a variety of unsaturated polycarbosilanes and carbosiloxanes functionalized with the silicon-chlorine bond, to graft low and high molecular weight sidechains on these backbones to tailor their physical behavior to specific needs, and, to demonstrate that these polymers can be recycled via depolymerization. As is normally the case, full structural characterization work will accompany all phases of this research. A successful effort will lead to the creation of recyclable materials for a variety of applications including lubricants, face masks, high performance engineering plastics, coatings, and self lubrication plastics. The final report summarized the research results. DTIC

N94-20017 Department of the Navy, Washington, DC.
MACHINABLE OXIDE CERAMIC Patent
Roy J. Rayne, inventor (to Navy), Louis E. Toth, inventor (to Navy), David Jones, inventor (to Navy), Robert J. Soulen, Jr., inventor (to Navy), and Barry A. Bender, inventor (to Navy) 1 Jun. 1993 4 p Filed 25 Jun. 1990
(AD-D015927; US-Patent-5,215,961; US-Patent-Appl-SN-543132; US-Patent-Class-505-1) Avail: US Patent and Trademark Office

A machinable high Tc ceramic superconductor is formed by weighing and mixing appropriate stoichiometric amounts of Bi2O3, SrCO3, CaCO3, and CuO (BSCCO), removing carbonates from the mixture, melting the mixture, casting the melted mixture into a mold, and inducing superconductivity and growth of randomly oriented platelets in the cast. DTIC

N94-20046# Cincinnati Univ., OH. Dept. of Chemistry.
POLYMER GELS AS PRECURSORS TO HIGH-PERFORMANCE MATERIALS Final Report, 1 Jun. 1990 - 31 May 1993
J. E. Mark 6 Jul. 1993 9 p
(Contract DAAL03-90-G-0131)
(AD-A270937; ARO-27373.10-MS) Avail: CASI HC A02/MF A01

The three types of materials covered in this investigation were (1) thermoreversible gels of organic polymers (such as polyethylene), (2) non-reversible gels obtained by the hydrolysis of organometallics and used as precursors to inorganic ceramics (silica and titania), and (3) hybrid composites prepared by having siloxane polymers present during the in-situ generation of the ceramic species. The kinetics of the gelation process were determined by measuring the shear moduli of the gels as a function of time for various compositions and catalyst concentrations. Of particular interest was the observed decreases in gelation time with increase in concentration of either catalyst (through increases in reaction rates) or polymer (through increases in the number of high molecular weight species necessary for gelation). Composites obtained by densification of the gels were characterized by NMR imaging, neutron and x-ray scattering, and impact strength measurements. The polymer components in the hybrid organic-inorganic composites was found to greatly increase their impact strengths. DTIC

N94-20047# National Inst. of Standards and Technology, Boulder, CO.
GROWTH MECHANISMS AND CHARACTERIZATION OF HYDROGENATED AMORPHOUS-SILICON-ALLOY FILMS

A. Gallagher, D. Tanenbaum, A. Laracuente, and E. Molenbroek Aug. 1993 25 p Prepared in cooperation with Midwest Research Inst., Golden, CO
(Contract DE-AC02-83CH-10093)
(DE93-018202; NREL/TP-411-5749) Avail: CASI HC A03/MF A01

Work performed to better understand the atomic-scale structure of glow-discharge-produced a-Si:H, a Ge:H, and a-Si:Ge:H films; its effect on film quality; and its dependence on deposition discharge conditions are described. Hydrogenated a-Si films are deposited from a silane rf discharge onto atomically flat crystal Si and GaAs substrates. The substrates are then transferred in vacuum to a scanning tunneling microscope, where the atomic-scale surface morphology is measured. The films were deposited at T(sub s) = 30 C and 250 C from a silane rf glow discharge using device-quality deposition conditions of 2.66 Pa (0.5 Torr) silane pressure, 1.7 Angstrom/s deposition rate, and small power/flow; IR absorption, sigma(sub L), and sigma(sub D) indicate high-quality intrinsic films. From the thickness dependence of the surface morphology, it was determined that the films initially conform smoothly to an atomically flat Si or GaAs substrate, but as the thickness increases the roughness steadily increases to approximately 10% of the length of the scanned region. The surface of 100-400 nm thick films is highly inhomogeneous, with steep hills and canyons in some areas and large atomically smooth regions in others. These unexpectedly large surface irregularities indicate severe and often connected void structures in the growing film, as well as relatively limited-range surface diffusion of the incorporating SiH3 radicals. On the other hand, large areas of atomically flat surface were occasionally found, indicating the possibility of growing a homogeneous and compact amorphous film if appropriate growth conditions could be discovered. DOE

N94-20057 Department of the Navy, Washington, DC.
SILVER LINED CERAMIC VESSEL Patent
William Ferrando, inventor (to Navy), Amarnath Divecha, inventor (to Navy), and James Kerr, inventor (to Navy) 27 Apr. 1993 3 p Filed 19 Feb. 1992
(AD-D015917; US-Patent-5,205,996; US-Patent-Appl-SN-838635;
US-Patent-Class-422-241) Avail: US Patent and Trademark Office

A reaction vessel comprising (1) a porous ceramic structure having interconnecting, open pores and (2) silver metal coating the inner ceramic surfaces of the reaction vessel and filling the interconnecting, open pores to form a strong bond between the porous ceramic structure and the silver coating. The reaction vessel can be produced by (1) coating the inner surface and infiltrating the continuous, open pores of an unglazed porous ceramic structure (or vessel) with molten AgNO3; (2) decomposing the AgNO3 to silver metal; and then (3) repeating steps (1) and (2) until all the pores are filled with silver metal. DTIC

N94-20195* National Aeronautics and Space Administration. Lewis Research Center, Cleveland, OH.
GUANIDINE BASED VEHICLE/BINDERS FOR USE WITH OXIDES, METALS, AND CERAMICS Patent
Warren H. Philipp, inventor (to NASA), Lisa C. Veitch, inventor (to NASA), and Martha H. Jaskowiak, inventor (to NASA) 26 Oct. 1993 7 p Filed 13 Mar. 1992 Supersedes N92-23461 (30 - 14, p 2354)
(NASA-Case-LEW-15314-1; US-Patent-5,256,451;
US-Patent-Appl-SN-842313; US-Patent-Class-427-374.2;
US-Patent-Class-427-383.1; US-Patent-Class-427-383.3;
US-Patent-Class-427-384; US-Patent-Class-427-383.5;
Int-Patent-Class-B05D-5/00) Avail: US Patent and Trademark Office

The use of guanidine salts of organic fatty acids (guanidine soaps) as vehicles and binders for coating substrate surfaces is disclosed. Being completely organic, the guanidine soaps can be burned off leaving no undesirable residue. Of special interest is the use of guanidine 2-ethyl hexanoate as the vehicle and binder for coating problematic surfaces such as in coating alumina fibers with platinum or zirconia. For this application, the guanidine soap is used as a melt. For applications, the guanidine soap may be use in a solution with a variety of solvents, the solution containing chlorometalates or powdered metals, refractories, or ceramics.
Official Gazette of the U.S. Patent and Trademark Office

N94-20265# Argonne National Lab., IL.
NEUTRON-SCATTERING STUDIES OF Yb-BEARING SILICATE GLASSES
A. J. G. Ellison, C. K. Loong, and J. Wagner 1993 14 p Presented at the 20th Rare Earth Research Conference, Monterey, CA, 12-17 Sep. 1993
(Contract W-31-109-eng-38)
(DE93-019768; ANL/MSD/CP-79820; CONF-9309142-1) Avail: CASI HC A03/MF A01

The static and dynamic magnetic responses of the Yb(3+) ions in 2Na2O center dot Yb2O3 center dot 6SiO2 glass and the isochemical crystalline silicate Na3YbSi3O9 are studied by neutron diffraction, inelastic magnetic-scattering, and magnetic susceptibility measurements. The rare earth sites in the glass have an average coordination number of 5.6 +/- 0.5 and give a mean rare earth-oxygen bond length of 2.23 Angstrom; average Si-O and O-O coordination numbers and bond distances are comparable to those in vitreous SiO2. The magnetic excitation spectrum of the Na3YbSi3O9 material is analyzed by a crystal-field model using a method of descending symmetry. The magnetic susceptibility and the excitation spectrum of the Yb glasses can be described by a distribution of ligand-field effects on the Yb(3+) ions that are similar to the nominal crystal field in crystalline Na3YbSi3O9. DOE

N94-20299# Meharry Medical Coll., Nashville, TN.
LATERAL DISTRIBUTION OF LIPIDS IN MEMBRANES AT HIGH PRESSURE Final Report, 1 Jul. 1991 - 30 Jun. 1993
Parkson L. Chong and Istvan P. Sugar 13 Jul. 1993 4 p
(Contract DAAL03-91-G-0228)
(AD-A271183; ARO-28657.3-LS-SAH) Avail: CASI HC A01/MF A01

This research is to study the lateral distribution of 1-palmitoyl-1-(10-pyreny)decanoyl)- sn-glycerol- 3-phosphatidylcholine (Pyr-PC) in dimyristoylphosphatidylcholine (DMPC) bilayer membranes. Fluorescence and statistical mechanics are employed. A series of dips were found in the plot of E/M (the ratio of excimer fluorescence to monomer fluorescence) vs. the mole fraction of Pyr-PC. The results can be interpreted in terms of the extended hexagonal super-lattice model. Based on this model, lipids in the Pyr-PC/DMPC binary mixtures are regularly distributed in the membrane. Pressure data further suggest that the bilayer membrane has more free volume at non-critical concentrations and more free volume when the regular distribution (as compared to the irregular region) reaches a local minimum. The computer simulation work further suggests that the area of regular arrangements have local maxima at the critical mole fractions if the repulsive interaction between Pyr-PC's is strong enough. DTIC

N94-20315 Sandia National Labs., Albuquerque, NM.
LIGHT SCATTERING STUDIES OF AN ELECTRORHEOLOGICAL FLUID
J. E. Martin and J. Odinek 1993 17 p Presented at the 2nd International Discussion Meeting on Relaxations in Complex Systems, Alicante, Spain, 28 Jun. - 8 Jul. 1993 Limited Reproducibility: More than 20% of this document may be affected by microfiche quality
(Contract DE-AC04-76DP-00789)
(DE93-019419; SAND-93-1844C; CONF-9306224-1) Avail: Issuing Activity (Department of Energy (DOE))

The authors report real-time, two-dimensional light scattering studies of the evolution of structure in an electrorheological fluid in the quiescent state and under shear. They find that when an electric field is applied to the quiescent fluid, particles chain along the electric field lines and cause strong light scattering lobes to appear at a finite scattering wave-vector q orthogonal to the field lines. These lobes then brighten as they move to q=O, indicating the existence of an unstable concentration fluctuation that signifies the segregation of chains into columns. In fact, the observed power law growth kinetics of the characteristic length, as well as the form of the structure factor, are qualitatively similar to two-dimensional spinodal decomposition in a system with a conserved order parameter. When the sample is subjected to shear, the authors find that the scattering pattern approaches a steady state, with lobes that are rotated in the direction of fluid vorticity. The angle of rotation is found to increase as the cube root of the shear rate, in agreement with a theoretical prediction of the steady state structure of fragmenting particle chains. DOE

N94-20328 Oregon Univ., Eugene.
THE MODIFICATION OF POLYMER SURFACES AND THE FABRICATION OF SUBMICRON-SCALE FUNCTIONALIZED STRUCTURES BY DEEP-UV AND ELECTRON BEAM LITHOGRAPHY Technical Report, Mar. 1992 - Jun. 1993

M. N. Wybourne, J. C. Wu, Ming-Di Yan, Sui X. Cai, and John F. Keana 10 Jun. 1993 18 p Limited Reproducibility: More than 20% of this document may be affected by microfiche quality
(Contract N00014-92-J-1412)
(AD-A265956; UO-JFWK-MNW-05) Avail: Issuing Activity (Defense Technical Information Center (DTIC))

We present a general technique to modify polymer surfaces using N-hydroxysuccinimide (NHS) functionalized perfluorophenyl azides (PFPA's). Thin polystyrene films are spin-coated with a solution containing the NHS PFPA ester and are either UV photolyzed with a dosage of 10 mJ cm(exp -2) or exposed with a 15 kV electron beam with a dosage between 1 and 75 (mu)m cm(exp -2). The NHS active ester groups become covalently attached to the polymer via photogenerated or electron beam generated, highly reactive nitrene intermediates derived form the PFPA. Using this technique we demonstrate that well-defined surface regions can be functionalized with a minimum observable feature size of 0.5 (mu)m and 0.2 (mu)m for UV and electron beam exposure, respectively. Through reaction of the functionalized surfaces with primary amine-containing reagents, we have installed biological molecules on the polymer and have measured the activity of an immobilized enzyme. DTIC

N94-20331 Department of the Navy, Washington, DC.
PLASMA CHEMICAL VAPOR DEPOSITION OF HALIDE GLASSES Patent
Lynda E. Busse, inventor (to Navy), Ishwar D. Aggarwal, inventor (to Navy), Kenneth J. Ewing, inventor (to Navy), and Barry B. Harbison, inventor (to Navy) 18 May 1993 6 p Filed 27 Jun. 1991
(AD-D015933; US-Patent-5,211,731; US-Patent-Appl-SN-722447; US-Patent-Class-65-3.12) Avail: US Patent and Trademark Office

A method for producing internally coated glass tube preforms for drawing Fiber optic conductors is presented. The internally coated glass tubes are halogen coated, preferably coated with metal fluorides, so that an optical fiber formed will have a halogen core which conveys light having a wavelength of about 2 to 4 microns, which is in the infrared region, with low attenuation. With one aspect of the method, a carrier gas and a halogenated alkoxide are introduced into a glass tube which has an inner wall and which is surrounded by a resonator for producing a plasma from the halogenated alkoxide in the tube. With another aspect of the method, a blend of a carrier gas, an organometallic compound, and a halogen-containing gas are introduced into a glass tube which has an inner wall and which is surrounded by a resonator for producing a plasma. DTIC

N94-20347*# Missouri Univ., Rolla. Dept. of Ceramic Engineering.
KINETICS OF PHASE TRANSFORMATIONS IN GLASS FORMING SYSTEMS Semiannual Progress Report No. 4, 16 May - 15 Nov. 1993
Chandra S. Ray 20 Nov. 1993 16 p
(Grant NAG8-898)
(NASA-CR-194270; NAS 1.26:194270) Avail: CASI HC A03/MF A01

In crystallization measurements of nonisothermal nucleation for Li2O.2SiO2 (LS2) glass, using DTA, the glass sample is scanned at different constant heating rates until it is crystallized. This means that the temperature range where nucleation can occur for the glass is scanned also at different rates which allows the glass to be nucleated for different time prior to crystallization. Consequently, the concentration of nuclei developed in the glass may be different for different heating rates and the DTA peak height which has shown to be sensitive to the number of nuclei present in the sample, is expected to change with heating rate. DTA peak height depends strongly on the overlap between the nucleation rate and growth rate curves, assuming the peak height is directly proportional to the total number of nuclei present in the glass sample under investigation, which, in turn, should be proportional to the volume or weight of the sample. To verify this assumption, DTA measurements were made using a LS2 glass to determine the peak height as a function of the sample weight. Using the DTA peak height technique, a nucleation rate like curve was determined for the BaO.2SiO2 (BS2) glass which showed that the temperature for nucleation ranged from 650 to 750 C for this glass and the temperature for maximum nucleation was approximately 705 C. These values are in excellent agreement with those determined by the conventional technique. There was international collaboration with Japan and Germany on this project. Derived from text

N94-20349 Department of the Navy, Washington, DC.
VOLATILE CVD PRECURSORS BASED ON COPPER ALKOXIDES AND MIXED GROUP 2A-COPPER ALKOXIDES Patent
Andrew Purdy, inventor (to Navy) 25 May 1993 3 p Filed 31 Jan. 1992
(AD-D015930; US-Patent-5,213,844; US-Patent-Appl-SN-828634; US-Patent-Class-427-248.1) Avail: US Patent and Trademark Office

Fluorinated alkoxy compounds of copper, copper-calcium, copper-strontium, and copper-barium having a certain structure in which 1 less than or equal to w less than or equal to 4; R is a fluorinated alkyl group; x greater than or equal to 1; Y is an alkoxy or alkyl group without beta-hydrogen; Y greater than or equal to 0; w less than or equal to (x+y) less than or equal to 2w; L is a Lewis base; 1 less than or equal to z less than or equal to 2w; M is Ca, Sr, or Ba; and 1 less than or equal to a less than or equal to 4; 1 less than or equal to b less than or equal to 4; (b + 2a) less than or equal to c less than or equal to 2(b+a), have exceptionally high volatilities, and hence low vaporization or sublimation temperatures, at 10(exp -5) torr. They are superior precursor compounds for chemical vapor deposition of thin films on substrates under vacuum, and for sol-gel processing. DTIC

N94-20352 Louisiana State Univ., Baton Rouge. Concurrent Computing Lab. for Materials Simulations.
EMBEDDED MICROCLUSTERS IN ZEOLITES AND CLUSTER BEAM SPUTTERING: SIMULATION ON PARALLEL COMPUTERS
P. Vashishta, R. K. Kalia, and D. Greenwell Sep. 1993 13 p Limited Reproducibility: More than 20% of this document may be affected by microfiche quality
(Contract DE-FG05-92ER-45477)
(DE94-000741; DOE/ER-45477/1) Avail: Issuing Activity (Department of Energy (DOE))

An optimal time-space multi-resolution approach has been designed to carry out large-scale molecular-dynamics (MD) simulations on distributed-memory MIMD (Multiple Instructions Multiple Data) machines. The multi-resolution MD approach was used to investigate structural correlations in porous silica. Structural parameters such as internal surface area and surface-to-volume ratio of pores, pore size distribution, fractal dimension, and mean particle size have been calculated over a wide range of densities. Simulation results are in accordance with structural measurements. Molecular-dynamics simulations were also performed to provide a microscopic understanding of recent pioneering high-pressure experiments on silica glasses at NSLS. The simulations reveal a structural transition to a new high-pressure amorphous phase with corner- and edge-sharing SiO6 octahedra. Parallel algorithms were designed for an initio quantum dynamics approach to materials simulations. With this approach, we have investigated the nature of electron transport in materials. We have also developed a tight-binding MD approach to investigate the influence of orientational disorder on structural correlations and phonon spectra of C60 solid. Results agree with neutron-scattering measurements. Currently, large-scale MD simulations (approximately 10(exp 6) atoms) are being performed to investigate the relation between structure, dynamics, and mechanical properties and the influence of environment, composition, and stress conditions on nanophase ceramics (Si3N4, SiC, TiO2, and Al2O3) and on silicates, aluminosilicates, and zeolites. DOE

N94-20359* National Aeronautics and Space Administration. Marshall Space Flight Center, Huntsville, AL.
BLADDER OPERATED ROBOTIC JOINT Patent
Glen A. Robertson, inventor (to NASA) 21 Sep. 1993 6 p Filed 13 Jul. 1992 Supersedes N92-29831 (30 - 20, p 3426)
(NASA-Case-MFS-28682-1; US-Patent-5,245,885; US-Patent-Appl-SN-912401; US-Patent-Class-74-479B; US-Patent-Class-92-48; US-Patent-Class-92-92; US-Patent-Class-294-119.3; US-Patent-Class-623-26; US-Patent-Class-901-22; US-Patent-Class-901-37) Avail: US Patent and Trademark Office

This invention is a robotic joint which is operated by inflatable bladders and which can be used in applications where it is desired to move or hold an object. A support block supports an elongated plate to which is pivotally attached a finger. A tension strip passes over a lever attached to the finger and is attached at its ends to the support block on opposite sides of the plate. Bladders positioned between the plate and the tension strip

on opposite sides of the plate can be inflated by pumps to pivot the finger, with one of the bladders being inflated while the other is being deflated. Official Gazette of the U.S. Patent and Trademark Office

N94-20373* National Aeronautics and Space Administration. Langley Research Center, Hampton, VA.

A PROCESS FOR PREPARING AN ASSEMBLY OF AN ARTICLE AND A SOLUBLE POLYIMIDE WHICH RESISTS DIMENSIONAL CHANGE, DELAMINATION, AND DEBONDING WHEN EXPOSED TO CHANGES IN TEMPERATURE Patent

Diane M. Stoakley, inventor (to NASA) and Anne K. St.Clair, inventor (to NASA) 28 Sep. 1993 6 p Filed 26 Jul. 1991 Supersedes N92-12121 (30 - 3, p 374)

(NASA-Case-LAR-14763-1; US-Patent-5,248,519;
US-Patent-Appl-SN-736667; US-Patent-Class-427-96;
US-Patent-Class-427-163; US-Patent-Class-427-385.5;
US-Patent-Class-427-388.1; Int-Patent-Class-B05D-1/00;
Int-Patent-Class-B05D-5/06; Int-Patent-Class-B05D-5/12) Avail: US Patent and Trademark Office

An assembly of an article and a polyimide is prepared. The assembly resists dimensional change, delamination, or debonding when exposed to changes in temperature. An article is provided. A soluble polyimide resin solution having a low coefficient of thermal expansion (CTE) was prepared by dissolving the polyimide in solvent and adding a metal ion-containing additive to the solution. Examples of the additive are: Ho(OOCCH3), Er(NPPA)3, TmCl3, and Er(C5H7O2)3. The soluble polyimide resin is combined with the article to form the assembly.

Official Gazette of the U.S. Patent and Trademark Office

N94-20374* National Aeronautics and Space Administration. Langley Research Center, Hampton, VA.

POLYIMIDES CONTAINING AMIDE AND PERFLUOROISOPROPYLIDENE CONNECTING GROUPS Patent

James F. Dezern, inventor (to NASA) 7 Sep. 1993 5 p Filed 28 Aug. 1991 Supersedes N92-17676 (30 - 8, p 1271)

(NASA-Case-LAR-14608-1; US-Patent-5,243,023;
US-Patent-Appl-SN-752246; US-Patent-Class-528-331;
US-Patent-Class-528-28; US-Patent-Class-528-41; US-Patent-Class-528-310;
US-Patent-Class-528-353; Int-Patent-Class-C08G-69/32;
Int-Patent-Class-C08G-73/10) Avail: US Patent and Trademark Office

New, thermooxidatively stable polyimides were prepared from the reaction of aromatic dianhydrides containing isopropylidene bridging groups with aromatic diamines containing amide connecting groups between the rings. Several of these polyimides were shown to be semi-crystalline as evidenced by wide angle x ray scattering and differential scanning calorimetry. Most of the polyimides form tough, flexible films with high tensile properties. These polyimide films exhibit enhanced solubility in organic solvents.

Official Gazette of the U.S. Patent and Trademark Office

N94-20377* National Aeronautics and Space Administration. Langley Research Center, Hampton, VA.

IMPROVED CERAMIC SLIP CASTING TECHNIQUE Patent

Gregory M. Buck, inventor (to NASA) and Peter Vasquez, inventor (to NASA) 30 Nov. 1993 3 p Filed 22 Sep. 1992 Supersedes N93-20041 (31 - 7, 1858)

(NASA-Case-LAR-14471-1; US-Patent-5,266,252;
US-Patent-Appl-SN-950580; US-Patent-Class-264-86;
US-Patent-Class-264-221; Int-Patent-Class-C04B-33/28) Avail: US Patent and Trademark Office

A primary concern in modern fluid dynamics research is the experimental verification of computational aerothermodynamic codes. This research requires high precision and detail in the test model employed. Ceramic materials are used for these models because of their low heat conductivity and their survivability at high temperatures. To fabricate such models, slip casting techniques were developed to provide net-form, precision casting capability for high-purity ceramic materials in aqueous solutions. In previous slip casting techniques, block, or flask molds made of plaster-of-paris were used to draw liquid from the slip material. Upon setting, parts were removed from the flask mold and cured in a kiln at high temperatures. Casting detail was usually limited with this technique -- detailed parts were frequently damaged upon separation from the flask mold, as the molded parts are extremely delicate in the uncured state, and the flask mold is inflexible. Ceramic surfaces were also marred by 'parting lines' caused by mold separation. This adversely affected the aerodynamic surface quality of the model as well. (Parting lines are invariably necessary on or near the leading edges of wings, nosetips, and fins for mold separation. These areas are also critical for flow boundary layer control.) Parting agents used in the casting process also affected surface quality. These agents eventually soaked into the mold, the model, or flaked off when releasing the case model. Different materials were tried, such as oils, paraffin, and even an algae. The algae released best, but some of it remained on the model and imparted an uneven texture and discoloration on the model surface when cured. According to the present invention, a wax pattern for a shell mold is provided, and an aqueous mixture of a calcium sulfate-bonded investment material is applied as a coating to the wax pattern. The coated wax pattern is then dried, followed by curing to vaporize the wax pattern and leave a shell mold of the calcium sulfate-bonded investment material. The shell mold is cooled to room temperature, and a ceramic slip is poured therein. After a ceramic shell of desired thickness has set up in the shell mold, excess ceramic slip is poured out. While still wet, the shell mold is peeled from the ceramic shell to expose any delicate or detailed parts, after which the ceramic shell is cured to provide a complete, detailed, precision ceramic article without parting lines.

Official Gazette of the U.S. Patent and Trademark Office

N94-20463 Massachusetts Inst. of Tech., Cambridge. Dept. of Chemical Engineering.

SPATIAL ORGANIZATION OF POLYMER CHAINS IN A CRYSTALLIZABLE DIBLOCK POLYETHYLENE AND POLYSTYRENE Technical Report No. 10

R. E. Cohen, A. Bellare, and M. Drzewinski 27 Oct. 1993 13 p Prepared in cooperation with Dept. of Chemical Engineering, Princeton Univ., Princeton, NJ and Enichem America, Inc., Monmouth, NJ Limited Reproducibility: More than 20% of this document may be affected by microfiche quality

(Contract N00014-91-J-1045)
(AD-A271862) Avail: CASI HC A03

A diblock copolymer containing polystyrene and linear polyethylene was synthesized using the anionic-to-Ziegler/Natta transformation reaction. Combined evidence from 2-D small angle X-ray scattering and wide angle x-ray pole figure analysis showed conclusively that the polyethylene chains crystallize within the heterogeneous structure in a manner which leaves the polyethylene chains (c-axis) parallel to the lamellar surfaces. DTIC

N94-20481# Oak Ridge National Lab., TN.

DEVELOPMENT OF IMPROVED PROCESSING AND EVALUATION METHODS FOR HIGH RELIABILITY STRUCTURAL CERAMICS FOR ADVANCED HEAT ENGINE APPLICATIONS, PHASE 1

V. K. Pujari (Norton Co., Northboro, MA.), D. M. Tracey (Norton Co., Northboro, MA.), M. R. Foley (Norton Co., Northboro, MA.), N. I. Paille (Norton Co., Northboro, MA.), P. J. Pelletier (Norton Co., Northboro, MA.), L. C. Sales (Norton Co., Northboro, MA.), C. A. Wilkens (Norton Co., Northboro, MA.), and R. L. Yeckley (Norton Co., Northboro, MA.) Aug. 1993 162 p

(Contract DE-AC05-84OR-21400)
(DE93-040528; ORNL/Sub-89-SB182/1) Avail: CASI HC A08/MF A02

The program goals were to develop and demonstrate significant improvements in processing methods, process controls and non-destructive evaluation (NDE) which can be commercially implemented to produce high reliability silicon nitride components for advanced heat engine applications at temperatures to 1,370 C. The program focused on a Si3N4-4% Y2O3 high temperature ceramic composition and hot-isostatic-pressing as the method of densification. Stage 1 had as major objectives: (1) comparing injection molding and colloidal consolidation process routes, and selecting one route for subsequent optimization, (2) comparing the performance of water milled and alcohol milled powder and selecting one on the basis of performance data, and (3) adapting several NDE methods to the needs of ceramic processing. The NDE methods considered were microfocus X-ray radiography, computed tomography, ultrasonics, NMR imaging, NMR spectroscopy, fluorescent liquid dye penetrant and X-ray diffraction residual stress analysis. The colloidal consolidation process route was selected and approved as the forming technique for the remainder of the program. The material produced by the final Stage 2 optimized process has been given the designation NCX 5102 silicon nitride. According to plan, a large

number of specimens were produced and tested during Stage 3 to establish a statistically robust room temperature tensile strength database for this material. Highlights of the Stage 3 process demonstration and resultant database are included in the main text of the report, along with a synopsis of the NCX-5102 aqueous based colloidal process. The R and D accomplishments for Stage 1 are discussed in Appendices 1-4, while the tensile strength-fractography database for the Stage 3 NCX-5102 process demonstration is provided in Appendix 5. DOE

N94-20526 State Univ. of New York, Buffalo. Dept. of Chemistry.
ADHESIVE ELECTROLESS METALLIZATION OF FLUOROPOLYMERIC SUBSTRATES Technical Report No. 1
Terrence G. Vargo, Jeffrey M. Calvert, Mu-San Chen, and Joseph A. Gardella, Jr. Sep. 1993 9 p Limited Reproducibility: More than 20% of this document may be affected by microfiche quality
(Contract N00014-93-310058)
(AD-A271858) Avail: CASI HC A02

A process for producing patterned metal deposits on fluoropolymeric substrates is described. A metal ion-chelating organosilane is chemisorbed by self-assembly onto a fluoropolymer surface after radio-frequency glow discharge plasma surface hydroxylation. Positional modulation of the surface hydrophobicity is illustrated by wetting. The silane covalently binds an aqueous palladium catalyst, and subsequent electroless deposition yields homogeneous or patterned metal deposits that exhibit excellent adhesion to the fluoropolymer. DTIC

N94-20529* National Aeronautics and Space Administration. Lewis Research Center, Cleveland, OH.
SINTERING SILICON NITRIDE Patent
Narottam P. Bansal, inventor (to NASA), Stanley R. Levine, inventor (to NASA), and William A. Sanders, inventor (to NASA) 26 Oct. 1993 4 p Filed 27 Nov. 1992 Supersedes N93-17062 (31 - 5, p 1126)
(NASA-Case-LEW-15489-1; US-Patent-5,256,610;
US-Patent-Appl-SN-982535; US-Patent-Class-501-97;
US-Patent-Class-501-96; Int-Patent-Class-C04B-35/58) Avail: US Patent and Trademark Office

Oxides having a composition of (Ba(1-x)Sr(x))O-Al2O3-2SiO2 are used as sintering aids for producing an improved silicon nitride ceramic material. The x must be greater than 0 to insure the formation of the stable monoclinic celsian glass phase.
Official Gazette of the U.S. Patent and Trademark Office

N94-20541* National Aeronautics and Space Administration. Marshall Space Flight Center, Huntsville, AL.
METHOD OF FABRICATING A ROCKET ENGINE COMBUSTION CHAMBER Patent
Richard R. Holmes, inventor (to NASA), Timothy N. McKechnie, inventor (to NASA), Christopher A. Power, inventor (to NASA), Ronald L. Daniel, Jr., inventor (to NASA), and Robert M. Saxelby, inventor (to NASA) 5 Oct. 1993 7 p Filed 27 Jan. 1993 Supersedes N93-30565 (31 - 11, p 3338)
(NASA-Case-MFS-28569-1; US-Patent-5,249,357;
US-Patent-Appl-SN-009908; US-Patent-Class-29-890.01;
US-Patent-Class-427-236; US-Patent-Class-427-270;
US-Patent-Class-427-455; Int-Patent-Class-B23P-15/00) Avail: US Patent and Trademark Office

A process for making a combustion chamber for a rocket engine wherein a copper alloy in particle form is injected into a stream of heated carrier gas in plasma form which is then projected onto the inner surface of a hollow metal jacket having the configuration of a rocket engine combustion chamber is described. The particles are in the plasma stream for a sufficient length of time to heat the particles to a temperature such that the particles will flatten and adhere to previously deposited particles but will not spatter or vaporize. After a layer is formed, cooling channels are cut in the layer, then the channels are filled with a temporary filler and another layer of particles is deposited.
Official Gazette of the U.S. Patent and Trademark Office

N94-20548# Ohio State Univ., Columbus.
DEVELOPMENT OF FUNDAMENTAL UNDERSTANDING OF FRICTION AND WEAR MECHANISMS BY ATOMIC-SCALE TRIBOLOGICAL STUDIES OF CERAMIC MATERIALS AND MULTILAYERED THIN FILMS Report, 1 Oct. 1992 - 30 Sep. 1993
Bharat Bhusham Oct. 1993 7 p
(Contract N00014-93-1-0067)
(AD-A271485) Avail: CASI HC A02/MF A01

The objective of the ongoing research program is to develop fundamental understanding of the friction and wear mechanisms through atomic-scale and micro-scale tribological studies of bulk ceramic materials and multilayered thin films in dry and boundary-lubricated conditions. We are studying the friction, scratching/wear and indentation behavior of engineering surfaces on atomic and microscales using on atomic force microscope (AFM)/ friction force microscope (FFM) and a nanoindenter. For comparisons, we are also conducting macro friction and wear tests on selected test specimens using a conventional pin-on-disk tribotester. Ceramics with various crystalline structures and multilayered thin films with a range of thicknesses and mechanical properties are planned for studies. Effect of thin layers of bonded and unbonded lubricant films on selected samples will be studied. A multiasperity contact model is being developed to predict the friction and wear for a multilayered solid in contact with another solid surface. The input to the model will be the measured micromechanical properties and 3-D surface topography statistics. DTIC

N94-20599# Ecole Centrale de Lyon (France).
THEORETICAL AND EXPERIMENTAL STUDY OF THE WINDING OF A THIN PLASTIC FILM: THE ROLE OF AERODYNAMIC EFFECTS Ph.D. Thesis [ETUDE THEORIQUE ET EXPERIMENTALE DE L'ENROULEMENT D'UN FILM PLASTIQUE MINCE: ROLE DES EFFETS AERODYNAMIQUES]
Franck Bouquerel 1993 175 p In FRENCH Sponsored by Rhone-Poulenc Films, France
(ECL-93-04; ETN-93-94602) Avail: CASI HC A08/MF A02

A theoretical model to specify the critical conditions which induce instability phenomena, such as wrinkles, in thin plastic films as they are wound around a core when used as a substrate or as magnetic recording tape, is proposed. The model is based on a physical approach of winding: critical conditions are supposed to be strongly connected with the internal stresses. These stresses depend on winding conditions and foil properties. A general and realistic model based on a global approach of phenomena involved is proposed. The effect of the surface topography on air exhaust and radial properties of the wound foil are taken into account. Under these assumptions, prediction of new parameters such as thicknesses of the entrapped, exhaust or residual air layer become possible. For a large set of winding conditions and foil properties, good agreement is obtained between the theoretical and experimental results. Typical variation of the air interlayer thickness and stress fields are presented. It was observed that effects of winding velocity, nip force, foil tension, and foil roughness are all of the same order of magnitude, which is consistent with industrial knowhow. These results justify the global approach of the model. The model allows the final stress state and the air interlayers thickness to be computed as functions of the winding conditions (velocity, foil tension, and nip force) and the foil properties (bulk mechanical and superficial). ESA

N94-20614# Naval Air Warfare Center, Warminster, PA. Air Vehicle and Crew Systems Technology Dept.
A COMPARISON OF SULFURIC ACID/BORIC ACID ANODIZE AND CHROMIC ACID ANODIZE PROCESSES Final Report, Mar. 1992 - Jun. 1993
Stephen J. Spadafora and Frank R. Pepe 22 Jun. 1993 22 p
(AD-A271933; NAWCADWAR-93042-60) Avail: CASI HC A03/MF A01

Chromic acid anodizing (CAA) is an aluminum surface pretreatment currently used on Navy aircraft and weapon systems. This anodize process forms a thick oxide film which provides protection against environmental degradation. This is particularly important due to the severely corrosive naval aviation operational environment. Chromium VI, however, is a carcinogen and its wide-spread use as a corrosion inhibitor in this process is being restricted. The Navy has targeted chromated maintenance operations for reduction of hazardous waste generation. Several alternative candidates have been identified: phosphoric acid anodizing, Boeing Aerospace Corp.'s boric-sulfuric acid anodize (SBAA), and thin film sulfuric acid anodizing.

The Boeing SBAA process was selected for optimization and service demonstration. The Naval Air Warfare Center Aircraft Division Warminster analyzed the performance properties of SBAA and CAA both sealed and unsealed on various substrates with and without standard Navy coatings. DTIC

N94-20946# Florida State Univ., Tallahassee.
MECHANICAL PROPERTIES AND RELIABILITY OF SEMI-CRYSTALLINE POLYMERS Final Report
Leo Mandelkern 1993 4 p
(Contract N00014-87-J-1185)
(AD-A271591) Avail: CASI HC A01/MF A01

The major effort of this project has been the study of the physical and mechanical properties of crystalline polymers and the changes that take place over long-time periods. The study of the long-time crystallization, at ambient temperature, of a series of linear and branched polyethylenes showed a slow but steady density increase with time that could be demonstrated to be due to a decrease in the content of the liquid-like region and an increase in the partially ordered interfacial region. Significantly, the core-crystallinity level remains unaffected by the long time density increase. A detailed study of the overall crystallization kinetics of a set of model random copolymers, the hydrogenated polybutadienes, that covered a wide range in molecular weight and count content was completed. A basic understanding of the crystallization process in random copolymers, and of the structural factors which control long-time crystallization from the melt was developed. For the first time it was possible to separate the influence of molecular weight and co-unit content as independent variables that govern crystallization. DTIC

N94-21143 Garrett Turbine Engine Co., Phoenix, AZ.
OXIDATION RESISTANT PROTECTIVE COATING SYSTEM FOR GAS TURBINE COMPONENTS AND PROCESS FOR PENETRATION THEREOF Patent
Thomas E. Strangman, inventor (to Garrett Turbine Engine Co.) and Steven J. Vonk, inventor (to Garrett Turbine Engine Co.) 14 Jan. 1992 34 p
Filed 24 Feb. 1987
(CA-Patent-1,294,155; Int-Patent-Class-C23C-30/00;
Int-Patent-Class-C22C-19/05; Int-Patent-Class-B32B-15/01; CTN-93-60672)
Copyright Avail: Micromedia Ltd., Technical Information Centre, 165 Hotel de Ville, Place du Portage, Phase 2, Hull, Quebec J8X 3X2, Canada HC/MF

An oxidation resistant coating system is provided for the protection of superalloy gas turbine components. The chemistry of the coating is modified from that of prior coatings to increase the adherence of the protective oxide scale and to increase the strength and diffusional stability of the coating, while maintaining adequate resistance to corrosion by ingested salts. The coating and substrate material may be optimized to provide increased performance and operating life of the gas turbine. The coating of the invention consists essentially of ingredients in substantially the following ranges, expressed in weight percent: Cr, 15-35; Al, 8-20; Ta, 0-10; Ta + Nb, 0-10; Si, 0.1-1.5; Hf, 0.1-1.5; Y, 0-1; Co, 0-10; and sufficient Ni to bring the total to 100 percent. Most preferably, a coating designed to protect superalloy turbine blades and vanes such as single crystal components consists essentially of ingredients in about the following amounts, in weight percent: Cr, 20; Al, 11; Ta, 7; Hf, 1; Si, 1; Nb, Si, and Y, zero to trace amounts; and the balance being Ni. The coatings can be applied to the substrates by any convenient means which minimizes oxidation or other degradation of the coating during application. Preferably the coating is applied as an overlay, for example by plasma spraying, electron beam deposition, or sputtering. Author (CISTI)

N94-21170# Harvard Univ., Cambridge, MA. Dept. of Chemistry.
ALUMOXANES: RATIONALIZATION OF BLACK BOX MATERIALS
Andrew R. Barron 18 May 1993 12 p
(Contract N00014-91-J-1934)
(AD-A272805) Avail: CASI HC A03/MF A01

Amorphous (Al2O3)x(SiO2)y thin films have been grown by atmospheric pressure metal-organic chemical vapor deposition using the single source precursor Al(OSiEt3)32. Characterization by x-ray photoelectron spectroscopy indicated that the films consisted of a mixture of Al2O3, SiO2, and an aluminosilicate. The relative amount of each species was dependent on the deposition temperature and the carrier gas composition. Use of NH3 as the carrier gas resulted in the increased volatility of the precursor by the in situ formation of the low melting Lewis acid-base adduct Al(OSiEt3)3(NH3), however, no nitrogen incorporation was observed in these deposited films. DTIC

N94-21184# Massachusetts Inst. of Tech., Cambridge. Dept. of Chemistry.
ROTATIONAL ISOMERS OF Mo(VI) ALKYLIDENE COMPLEXES AND Cis/TRANS POLYMER STRUCTURE: INVESTIGATIONS IN RING-OPENING METATHESIS POLYMERIZATION Technical Report
John H. Oskam and Richard R. Schrock 20 Oct. 1993 49 p
(Contract N00014-92-J-1433)
(AD-A272647) Avail: CASI HC A03/MF A01

In the last few years well-defined metathesis catalysts of the general type M(NR)(CHR)(OR')2 (M=Mo or W) have proven useful in a variety of olefin metathesis studies, in part because the activity of catalysts can be varied systematically by altering the electron-withdrawing ability of the alkoxides. Complexes containing t-butoxides (OCMe3 and OCMe(Cf3)2 in particular), an arylimido ligand (often NAr, where Ar= 2,6-i-Pr2C6H3), and molybdenum have been the most versatile. In the area of ring-opening metathesis polymerization (ROMP) molybdenum complexes have been employed most often to prepare polymers from a variety of norbornenes and norbornadienes. Molybdenum complexes appear to tolerate a wide range of functionalities, are stable and active in a variety of solvents,and have been shown to produce polymers that are virtually all trans and highly tactic or all cis with a tactic bias of approx. 75%. Alkylidene rotational isomers or rotamers (eq 1) are found for many high-oxidation state alkylidene complexes. DTIC

N94-21186# Massachusetts Inst. of Tech., Cambridge. Dept. of Chemistry.
POLYMERIZATION OF ENANTIOMERICALLY PURE 2,3-DICARBOALKOXY NORBORNADIENES AND 5,6-DISUBSTITUTED NORBORNENES BY WELL-CHARACTERIZED MOLYBDENUM ROMP CATALYSTS
Richard ODell, David H. McConville, Gretchen E. Hofmeister, and Richard R. Schrock 29 Oct. 1993 38 p
(Contract N00014-92-J-1433)
(AD-A272649; TR-22) Avail: CASI HC A03/MF A01

Preparing polymers with a regular primary structure is a prerequisite to ultimately controlling the properties of the bulk polymer in a systematic manner. Polymers prepared by ring-opening metathesis polymerization (ROMP) of norbornenes and norbornadienes employing classical metathesis catalysts are rarely regular. In contrast, it has been shown that 2,3-bis(trifluoromethyl) norbornadiene (NBDF6) and 2,3-dicarbomethoxy norbornadiene (DCMNBD) can be ring-opened with 'well-characterized' catalysts of the type Mo(CHCMe2R')(NAr)(OR)2 (R'= Me, Ph; Ar = 2,6-i-Pr2-C6H3) to give highly tactic (greater than 90%) high trans poly (NBDF6) and poly(DCMNBD) when OR = O-t-BU, and high cis poly (NBDF6) and poly (DCMNBD) with a tactic bias of approximately 75% (sigma m)c=0.75 when OR = OCMe(CF3)2. (The four possible regular structures of polymers of this type are shown in Scheme I.) It has been suggested that high trans poly (NBDF6) and high cis poly (NBDF6) prepared using the initiators mentioned above both have a syndiotactic bias (B and C, respectively) on the basis of the measurement of the value of the relaxed dielectric constant. DTIC

N94-21197# Norton Co., Northboro, MA. Advanced Ceramics.
MICROSTRUCTURAL MODELING AND TOUGHENING OF Si3N4 CERAMICS FOR HIGH TEMPERATURE ENGINE APPLICATIONS Final Report, 30 Aug. 1991 - 15 Oct. 1993
R. L. Yeckley Aug. 1993 30 p
(Contract DAAL04-91-C-0039)
(AD-A272897; ARL-CR-62) Avail: CASI HC A03/MF A01

R-curve behavior was achieved in hot isostatically pressed (HIP) silicon nitride with low additive levels. Two HIP densification processes which produced R-curve in HIP silicon nitride were demonstrated. The first densification process was extended soaks at 1840 deg C; the second included a pre-HIP sinter step. The strongest R-curve behavior was observed with the rare earth mixture of erbia-samaria, HIPed at 1840 deg C for 240 minutes. The fracture toughness approached 11 MPa-m(exp 1/2) at crack lengths of only 600 to 800 microns. Other rare earth combinations were

also evaluated. The final microstructure was influenced by the type of rare earths and silica content. The mixed rare earths resulted in a finer and higher aspect ratio microstructure than materials densified with yttria. The development work strongly suggests that HIP silicon nitride which combines the creep resistance of NT154 type materials with R-curve behavior is possible. DTIC

N94-21223# Queens Univ., Kingston (Ontario). Dept. of Chemistry.
EFFICIENCY OF REVERSIBLE OPTICAL STORAGE IN AZO POLYMERS Technical Report
P. Rochon, J. Mao, A. Natansohn, and S. Xie 15 Nov. 1993 9 p
(Contract N00014-93-1-0615)
(AD-A272923; TR-4) Avail: CASI HC A02/MF A01

Optical information can be stored, erased or overwritten on polymer thin films using polarized light. The information is in the power probe beam. We have measured the efficiency of the writing beam in a number of polymer and copolymer films containing azobenzene dyes as side groups. In this paper we compare the results amongst the polymers we have synthesized. Preliminary results indicate that copolymers may be optimized to allow for the preparation of efficient thick films for erasable optical recording. DTIC

N94-21225# Aerospace Corp., El Segundo, CA. Technology Operations.
THE USE OF SCREENING TESTS IN SPACECRAFT LUBRICANT EVALUATION
Chris Kalogeras, M. Hilton, D. Carre, S. Didziulis, and P. Fleischauer 15 Oct. 1993 38 p
(Contract F04701-88-C-0089)
(AD-A272943; TR-93(3935)-6; SMC-TR-93-50) Avail: CASI HC A03/MF A01

A lubricant screening test fixture has been devised to obtain lubricant performance data in a timely manner. This fixture has been used to perform short-term tests on potential lubricants for several spacecraft applications. The results of these tests have saved time by producing qualitative performance rankings of lubricant selections prior to life testing. To date, this test fixture has been used to test lubricants for three particular applications: an oscillating scanner bearing, a harmonic drive actuator mechanism, and a reaction wheel support bearing. The qualitative results from these tests have been verified by life test results and have provided insight into the function of various antiwear additives. DTIC

N94-21238# Queens Univ., Kingston (Ontario). Dept. of Chemistry.
THE 13C-NMR SPECTRA OF POLY (4-((2-(ACRYLOYLOXY) ETHYL) ETHYL AMINO)- 4-NITROAZOBENZENE-CO-METHYL METHACRYLATE) Technical Report No. 3
S. Xie and A. Natansohn 15 Nov. 1993 5 p
(Contract N00014-93-1-0615)
(AD-A273016; TR-3) Avail: CASI HC A01/MF A01

The C-13-NMR Spectra of the title copolymers reveal that the calculated triad distribution using high conversion equations adequately describes the sequence distribution in seven samples of copolymers with various composition. No tacticity information is available in the spectra. DTIC

N94-21259# Queens Univ., Kingston (Ontario). Dept. of Chemistry.
RECENT DEVELOPMENTS IN AROMATIC AZO POLYMERS RESEARCH Technical Report
S. Xie, A. Natansohn, and P. Rochon 15 Nov. 1993 28 p
(Contract N00014-93-1-0615)
(AD-A272966; TR-1) Avail: CASI HC A03/MF A01

The photochemical and thermal cis to trans isomerization of aromatic azo groups covalently bonded within polymers and its practical consequences as well as some other recent applications are reviewed. The kinetics and mechanism of the isomerization of azo polymers are briefly presented and then several recent developments in azo polymers research are discussed. They include liquid crystallinity, nonlinear optical properties, monolayer assemblies and the light induced birefringence and dichroism. Some of the phase transitions of liquid crystalline azo polymers can be induced photochemically by the azo groups isomerization. Second order optical nonlinearity can be obtained in polymers with donor and acceptor substituted azo groups. Using the Langmuir-Blodgett technique, azo polymer monolayers can be built and used as 'command surfaces' of liquid crystal films. The light induced birefringence is a reorientation phenomenon which is a consequence of the trans-cis-trans isomerization. Future possible applications for a variety of practical devices, such as display devices, optical modulators, optical waveguides, holography, and reversible optical storage are mentioned. DTIC

N94-21267# Queens Univ., Kingston (Ontario). Dept. of Chemistry.
AZO POLYMERS FOR OPTICAL STORAGE 3: EFFECT OF FILM THICKNESS ON NET PHASE RETARDATION AND WRITING SPEED Technical Report
P. Rochon, D. Bissonnette, A. Natansohn, and S. Xie 15 Nov. 1993 17 p
(Contract N00014-93-1-0615)
(AD-A272994; TR-5-ONR) Avail: CASI HC A03/MF A01

The optical writing phenomenon observed on azoaromatic containing polymer thin films exhibited a writing rate which was proportional to the intensity of the writing beam. This property of the mechanism for optically inducing dichroism and birefringence directly results in nonlinear optical behavior in the thin film. The net phase retardation obtainable and writing rates are functions of the thin film thickness which reflect this nonlinear behavior. DTIC

N94-21302# Army Research Lab., Watertown, MA. Materials Directorate.
STRESS-INDUCED CRACKING OF FLUOROCARBON RUBBER MTL-0002 AFTER EXPOSURE TO DS-2 Final Report
Karen M. Kinsley Sep. 1993 23 p
(AD-A271753; ARL-TR-219) Avail: CASI HC A03/MF A01

Fluorocarbon rubber 0002 (MTL-0002) was found to be susceptible to stress-induced cracking (SIC) when exposed to the standard decontaminant DS-2. In this report, several tensile tests were conducted upon this rubber and related fluorocarbon elastomers after exposure to DS-2 and its components. It was found that diethyl enetriamine, a DS-2 component, was responsible for the formation of cracks under tension. Of the vulcanizates tested, MTL-0002 was the most susceptible to SIC after a one-half hour immersion in DS-2, but I. B. Moore V7D failed at lower stress levels after 24 hours of immersion in DS-2. It is suggested that changing the proportion of magnesium oxide and calcium hydroxide in the recipe and altering the press curing temperature time may enhance the resistance to SIC of MTL-0002. DTIC

N94-21416# Clemson Univ., SC. Dept. of Ceramic Engineering.
INTELLIGENT PROCESSING OF FERROELECTRIC THIN FILMS Annual Report, 2 May 1992 - 31 Jul. 1993
Gene Haertling, Eric Skaar, Fei-Ling Wang, Joyti Guha, and David Dausch 3 Sep. 1993 242 p
(Contract N00014-91-J-1508)
(AD-A272518) Avail: CASI HC A11/MF A03

The work described in this report covers the second year of a three-year program involving intelligent processing of ferroelectric thin films and bulk materials. It is presented in seven parts dealing with automation, powder processing, bulk materials characterization, thin film fabrication and evaluation, electrooptic behavior of thin films, and published work. In regard to process automation and intelligence, the two-conductor ac resistance probe was tested for reading stability and response time. Both requirements were easily met, and simulated batching experiments were carried out. The fluid flow pattern for the batching system has required special attention and optimization. Programming of the device drivers which are needed to link the computer and its neural network has now been completed, thus paving the way for making the system totally operational. DTIC

N94-21425# SRI International Corp., Menlo Park, CA.
FABRICATION OF POROUS CERAMICS BY FREEZE-CASTING/FREEZE-DRYING Final Report, Apr. 1991 - Dec. 1992
S. M. Johnson and M. I. Gusman Apr. 1993 52 p
(Contract GRI-5091-260-2144)
(PB93-202513; GRI-93/0176; SRI-Proj.-2399) Avail: CASI HC A04/MF A01

Porous ceramics have many applications in the gas industry including gas separation, filtration, catalyst supports and substrates, lightweight insulation, and burners. The report explores the fabrication of porous ceramics by a new approach involving the use of cryogenic processing

techniques such as freeze-drying. This research was carried out in order to characterize the materials formed in this way and to evaluate the potential of the techniques for making porous ceramics for specific gas industry applications. NTIS

N94-21437# Air Force Inst. of Tech., Wright-Patterson AFB, OH. Foreign Aerospace Science and Technology Center.
EVALUATION OF ELECTROCONDUCTIVITY OF TWO SURFACE PAINTS FOR SPACECRAFT
Lu Yusun, Li Hua, Han Xiao-Wen, and Chen Wen-Ying 5 Nov. 1993 15 p Transl. into ENGLISH from Zhongguo Kongjian Kexue Jishu (China), v. 3, 1989 p 41-46
(AD-A273063; FASTC-ID(RS)T-0560-93) Avail: CASI HC A03/MF A01

This article briefly discusses the manufacturing process for two surface paints (used on spacecraft): No. 956 gray paint, and No. 956 green paint. Experimental studies were conducted on both paints at room temperatures in variations of electroconductivity in space environments: in a simulated space vacuum, under electron radiation and under solar radiation. From the experimental results, the states of both surface paints used in orbit can be predicted. In addition, the possibility of using such paints in high orbit is accepted. DTIC

N94-21460# Missouri Univ., Rolla. Dept. of Chemistry.
DYNAMICS OF ADSORBED, SWOLLEN BLOCK COPOLYMERS Interim Report, 1 Jan. 1991 - 31 Oct. 1993
Brijnaresh Sinha, Frank D. Blum, and Fredrick C. Schwab 20 Oct. 1993 25 p
(Contract N00014-91-J-1274)
(AD-A272013; UMR-FDB-32) Avail: CASI HC A03/MF A01

Deuterium NMR relaxation times of specifically deuterated block terpolymers of 2-vinyl pyridine (VP), styrene (S), and deuterostyrene (DS) were measured for the polymers in solution and on silica as a function of temperature and solvent. The block polymers were attached to the silica through the VP segments; the S and DS segments were extended into the solution. In a thermodynamically poor solvent, such as carbon tetrachloride, the relaxation times were consistent with the S segments on the surface-bound polymer being less mobile than their counterparts in solution. This is in contrast with their behavior in toluene (previously reported), where the styrene segments of the surface-bound polymer appeared to be more mobile than in solution. The results demonstrate that the solvent quality may have a dramatic effect on the dynamics of the chain segments of the surface-bound polymer. In a mixture of solvents, namely carbon tetrachloride and methanol, there was evidence for more mobile S segments in the surface-bound polymer, however, the VP units also had additional mobility due to the presence of the methanol. The relaxation times were also used, along with the model of Hall and Helfand, to determine the motional parameters and spectral densities for the polymers in the different s stems. DTIC

N94-21512# Lawrence Livermore National Lab., CA.
POLYMERIC NITROGEN
C. Mailhiot, L. H. Yang, A. K. McMahan, and T. W. Barbee, III Jul. 1993 6 p Presented at the 14th International Conference of the International Association for the Advancement of High Pressure Science and Technology, Colorado Springs, CO, 27 Jun. - 2 Jul. 1993
(Contract W-7405-eng-48)
(DE93-040544; UCRL-JC-110049-Rev-2; CONF-930676-50-Rev-2) Avail: CASI HC A02/MF A01

The equilibrium phase boundary between single-bonded, threefold-coordinated polymeric forms of nitrogen, and the observed, triple-bonded diatomic phases, is predicted to occur at relatively low (50 +/- minus) 15 GPa) pressure. This conclusion is based on extensive local-density functional total-energy calculations for polymeric structures (including that of black phosphorus, and another with all gauche dihedral angles) and diatomic structures (including that of the observed high-pressure epsilon-N2 phase). Our results suggest that the diatomic phase of nitrogen, observed up to 180 GPa and room temperature, is metastable at these conditions, and that such hysteresis enhances the prospects for the existence of a metastable polymeric form of nitrogen at ambient conditions. DOE

N94-21516# National Inst. of Standards and Technology, Gaithersburg, MD. Ceramics Div.
REVIEW OF CORROSION BEHAVIOR OF CERAMIC HEAT EXCHANGER MATERALS: CORROSION CHARACTERISTICS OF SILICON CARBIDE AND SILICON NITRIDE
R. G. Munro and S. J. Dapkunas 1993 103 p
(Contract DE-AI22-92PC-92179)
(DE93-041307; DOE/PC-92179/T1) Avail: CASI HC A06/MF A02

The present work is a review of the substantial effort that has been made to measure and understand the effects of corrosion with respect to the properties, performance, and durability of various forms of silicon carbide and silicon nitride. The review encompasses corrosion in diverse environments, usually at temperatures of 1000 C or higher. The environments include dry and moist oxygen, mixtures of hot gaseous vapors, molten salts, molten metals, and complex environments pertaining to coal ashes and slags. DOE

N94-21523# Queens Univ., Kingston (Ontario). Dept. of Chemistry.
OPTICALLY INDUCED BIREFRINGENCE IN COPOLYMERS AND BLENDS CONTAINING AZOBENZENE GROUPS Technical Report
D. Brown, A. Natansohn, P. Rochon, and S. Xie 15 Nov. 1993 7 p
(Contract N00014-93-1-0615)
(AD-A273085; TR-6) Avail: CASI HC A02/MF A01

The birefringence level in a copolymer or a blend containing disperse red 1 acrylate or methacrylate structural units depends not only on the molar fraction of the azo component, but also on the type of the next-neighbor on the chain. Copolymers behave quite differently from blends. Also, if a few azo groups are neighboring each other, the induced birefringence is more stable. DTIC

N94-21526 Sandia National Labs., Albuquerque, NM.
POLYIMIDE-BASED ELECTROOPTIC MATERIALS
P. A. Cahill, C. H. Seager, M. B. Meinhardt, A. J. Beuhler (Amoco Oil Co., Naperville, IL.), D. A. Wargowski (Amoco Oil Co., Naperville, IL.), K. D. Singer (Case Western Reserve Univ., Cleveland, OH.), T. C. Kowalczyk (Case Western Reserve Univ., Cleveland, OH.), and T. Z. Kosc (Case Western Reserve Univ., Cleveland, OH.) 1993 8 p Presented at the Annual Meeting of the Society of Photo-Optical Instrumentation Engineers (SPIE), San Diego, CA, 11-16 Jul. 1993 Limited Reproducibility: More than 20% of this document may be affected by poor print and microfiche quality
(Contract DE-AC04-76DP-00789)
(DE93-019416; SAND-93-0336C; CONF-930722-28) Avail: Issuing Activity (Department of Energy (DOE))

The properties of new, high temperature optical materials based on dye-doped Ultradel 9000D polyimides are presented. Ultradel 9000D is a soluble, pre-imidized, fluorinated polymer with properties optimized for integrated optical applications. When thermally or photochemically cross-linked, it has a Tg approaching 400 C and retains excellent optical transparency as measured by both waveguide loss spectroscopy (WLS) and photothermal deflection spectroscopy (PDS). The agreement between WLS and PDS data indicates that losses in polyimides are due to absorption, not scattering. Two thermally stable, donor-acceptor oxazole-based dyes were designed, synthesized, and doped into the polyimide at concentrations up to 25 percent by weight. The Tg of the doped polymers decreased from the neat polymer, but remained above 300 C. The effects of doping on the dielectric constant, refractive index, and coefficient of thermal expansion of the polyamide are presented. The oxazoles also photobleach and thereby, providean additional means of photodefining waveguides in these materials. DOE

N94-21542# Atominstitut der Oesterreichischen Hochschulen, Vienna.
TENSILE AND SHEAR FRACTURE BEHAVIOR OF FIBER REINFORCED PLASTICS AT 77K IRRADIATED BY VARIOUS RADIATION SOURCES
K. Humer, H. W. Weber, E. K. Tschegg (Technische Univ., Vienna, Austria.), Shigenori Egusa (Japan Atomic Energy Research Inst., Takasaki.), Robert C. Birtcher (Argonne National Lab., IL.), and Heiko Gerstenberg (Technische Univ., Munich, Germany.) Aug. 1993 10 p Presented at the International Cryogenic Engineering Conference and International Cryogenic Materials Conference, Albuquerque, NM, 12-16 Jul. 1993
(Contract W-31-109-eng-38)

(DE93-040280; ANL/MSD/CP-80610; CONF-930703-32) Avail: CASI HC A02/MF A01

Influence of radiation damage (gamma, electron, neutron) on mechanical properties of fiber reinforced plastics (FRP's) has been investigated. Different types of FRP's (two or three dimensional E-, S- or T-glass fiber reinforcement, epoxy or bismaleimide resin) have been irradiated at room temperature with 2 MeV electrons and Co-60 gamma-rays up to 1.8 x 10 exp 8 Gy as well as with different reactor spectra up to a fast neutron fluence of 5 x 10(exp 22) m(exp -2) (E greater than 0.1 MeV). Tensile and intralaminar shear tests were carried out on the irradiated samples at 77 K. Some samples were irradiated at 5 K and tested at 77 K with and without an annealing cycle to room temperature. Results on the influence of these radiation conditions and of warm-up cycles on the mechanical properties of FRP's are compared and discussed. DOE

N94-21546# Lawrence Livermore National Lab., CA.
SHOCK COMPRESSION OF LOW-DENSITY FOAMS
N. C. Holmes Jul. 1993 6 p Presented at the 14th International Conference of the International Association for the Advancement of High Pressure Science and Technology, Colorado Springs, CO, 27 Jun. - 2 Jul. 1993
(Contract W-7405-eng-48)
(DE93-040545; UCRL-JC-113766; CONF-930676-49) Avail: CASI HC A02/MF A01

Shock compression of very low density micro-cellular materials allows entirely new regimes of hot fluid states to be investigated experimentally. Using a two-stage light-gas gun to generate strong shocks, temperatures of several eV are readily achieved at densities of roughly 0.5-1 g/cm(exp 3) in large, uniform volumes. The conditions in these hot, expanded fluids are readily found using the Hugoniot jump conditions. We will briefly describe the basic methodology for sample preparation and experimental measurement of shock velocities. We present data for several materials over a range of initial densities. This paper explores the applications of these methods for investigations of equations of state and phase diagrams, spectroscopy, and plasma physics. Finally, we discuss the need for future work on these and related low-density materials. DOE

N94-21560# Los Alamos National Lab., NM.
ISSUES RELATED TO MECHANICAL PROPERTIES OF NEUTRON-IRRADIATED CERAMICS
F. W. Clinard, Jr., E. H. Farnum, and W. Dienst (European Atomic Energy Community, Karlsruhe, Germany.) 1993 27 p Presented at the 6th International Conference on Fusion Reactor Materials, Stresa, Italy, 27 Sep. - 1 Oct. 1993
(Contract W-7405-eng-36)
(DE93-040262; LA-UR-93-2820; CONF-930928-2) Avail: CASI HC A03/MF A01

Ceramics will be used for a number of applications in fusion devices, where their dielectric properties, high strength, refractoriness, or low activation characteristics are required. In all cases mechanical properties must be adequate for the use intended, and the material must tolerate irradiation damage without undue degradation. The damage response of four candidate ceramics is reviewed, major issues are identified, and recommendations are made for future studies. DOE

N94-21653# Oak Ridge National Lab., TN.
ELECTRON HOLOGRAPHY APPLIED TO THE STUDY OF CERAMIC MATERIALS
E. Voelkl, L. F. Allard, and T. A. Nolan 1993 11 p Presented at the 95th Annual Meeting of the American Ceramic Society, Cincinnati, OH, 18-22 Apr. 1993
(Contract DE-AC05-84OR-21400)
(DE94-000329; CONF-930438-29) Avail: CASI HC A03/MF A01

The experimental setup of a transmission electron microscope for electron holography is shown. Using a model system of small gold particles on amorphous germanium, capabilities of electron holography are demonstrated. These include nano-diffraction, energy filtering, correction of aberrations, and separate display of image amplitude and phase. The method of electron holography is then applied to the characterization of a grain boundary in a Si3N4 ceramic. DOE

N94-21822# Oak Ridge National Lab., TN.
CERAMIC TECHNOLOGY PROJECT Semiannual Progress Report, Apr. - Sep. 1992
D. R. Johnson Jul. 1993 442 p
(Contract DE-AC05-84OR-21400)
(DE94-001011; ORNL/TM-12363) Avail: CASI HC A19/MF A04

This project was developed to meet the ceramic technology requirements of the DOE Office of Transportation Systems' automotive technology programs. Significant progress in fabricating ceramic components for DOE, NASA, and DOE advanced heat engine programs show that operation of ceramic parts in high-temperature engines is feasible; however, additional research is needed in materials and processing, design, and data base and life prediction before industry will have a sufficient technology base for producing reliable cost-effective ceramic engine components commercially. A 5-year project plan was developed, with focus on structural ceramics for advanced gas turbine and diesel engines, ceramic bearings and attachments, and ceramic coatings for thermal barrier and wear applications in these engines. DOE

N94-21856# California Univ., Berkeley. Lawrence Berkeley Lab.
SWELLING EQUILIBRIA FOR CATIONIC 2-HYDROXYETHYL METHACRYLATE (HEMA)-BASED HYDROGELS
J. P. Baker, H. W. Blanch, and J. M. Prausnitz Aug. 1993 9 p
(Contract DE-AC03-76SF-00098)
(DE94-000728; LBL-34450) Avail: CASI HC A02/MF A01

Cationic HEMA-based hydrogels were synthesized by copolymerizing HEMA with (methacrylamido)propyl- trimethylammonium chloride (MAPTAC). Swelling equilibria were measured in pure water and in aqueous sodium chloride solutions. Hydrogel swelling is an increasing function of the MAPTAC content. A Flory-type swelling model using a concentration-dependent Flory (Chi) parameter semi-qualitatively describes poly(HEMA co-MAPTAC) hydrogel swelling in aqueous sodium chloride. DOE

N94-21890# Technical Research Centre of Finland, Espoo. Building Materials Lab.
SYMPOSIUM ON MICROSCOPY AND IMAGE ANALYSIS OF BUILDING MATERIALS
Paula Raivio, ed. 1993 53 p Symposium held in Espoo, Finland, 24 Jan. 1992 Original contains color illustrations
(VTT-SYMP-136; ISBN-951-38-4087-5; ETN-94-95245) Copyright Avail: CASI HC A04/MF A01

Six articles discussing specimen preparation, microstructure, composition and image analysis of building materials are presented. Focus is on concrete and mortar. The titles of the papers are as follows: preparation of concrete specimens for microstructural image analysis studies; optical air pore analysis; some experiments on using backscattered electron and energy dispersive X-ray imaging in determination of portland cement clinker phase composition; a quantitative scanning electron microscope image analysis of cement paste microstructure; determination of pore structure of concrete from thin sections by image analysis; and microstructure in mortar, a summary of a research project. For individual titles, see N94-21891 through N94-21896.

N94-21891# Technical Research Centre of Finland, Espoo. Building Materials Lab.
PREPARATION OF CONCRETE SPECIMENS FOR MICROSTRUCTURAL IMAGE ANALYSIS STUDIES
Paula Raivio *In its* Symposium on Microscopy and Image Analysis of Building Materials 1993 p 5-11 (For primary document see N94-21890 05-27)
Copyright Avail: CASI HC A02/MF A01

The preparation of concrete specimens for microstructural image analysis studies in incident light, transmission fluorescent light and backscattered electron imaging, is reported. The preparation of thick concrete sections for automatic air pore analysis in incident light is considered. For this the concrete should be solid with minor cracks and weak areas. The specimens are roughly 80 by 80 by 10 cu mm in size. The use of transmitted fluorescent light to study impregnated concrete sections requires thin samples. These are cut to roughly 30 by 50 by 10 cu mm. One side is treated with ethanol, after which it is glued onto a glass slide and impregnated with epoxy mixed with fluorescent dye. Polished section preparation, which

is similar to thin section preparation, is necessary to produce scanning electron microscope images. ESA

N94-21892# Technical Research Centre of Finland, Espoo. Building Materials Lab.

OPTICAL AIR PORE ANALYSIS

Erkki Vesikari *In its* Symposium on Microscopy and Image Analysis of Building Materials 1993 p 12-21 (For primary document see N94-21890 05-27)

Copyright Avail: CASI HC A02/MF A01

Methods for transforming direct measurement data into more refined data of the pore structure of concretes are discussed. The optical air pore analysis system considered consists of an optical microscope, an automatic microscope stage with control unit, a television (TV) camera, an image processing unit and TV monitor, a desk top computer with printer and a graphic plotter. A method for calculating real three dimensional pore size distribution and estimates for the total number of pores and average distance between pores is presented. A two dimensional distribution obtained by an optical air pore analysis can be made three dimensional by an automatic transformation process. A better estimate for the total number of pores can also be obtained. A measure for the average distance between pores based on improved estimation of the number of pores was developed. The average distance between pores showed a better coherence with freeze thaw resistance test results than did Power's spacing factor. ESA

N94-21893# Technical Research Centre of Finland, Espoo. Building Materials Lab.

SOME EXPERIMENTS ON USING BACKSCATTERED ELECTRON AND ENERGY DISPERSIVE X RAY IMAGING IN DETERMINATION OF PORTLAND CEMENT CLINKER PHASE COMPOSITION

Ludwik Hirvonen *In its* Symposium on Microscopy and Image Analysis of Building Materials 1993 p 22-27 (For primary document see N94-21890 05-27)

Copyright Avail: CASI HC A02/MF A01

The capabilities of a scanning electron microscope equipped with a backscatter electron detector and an energy dispersive X-ray spectrometer in determining the phase composition of portland cement clinker were examined. An image analyzer was used in acquiring, processing and calculating the data. ESA

N94-21894# Swedish Cement and Concrete Research Inst., Stockholm.

A QUANTITATIVE S.E.M. IMAGE ANALYSIS OF CEMENT PASTE MICROSTRUCTURE

Knut O. Kjellsen and Rachel J. Detwiler (Toronto Univ., Ontario.) *In* Technical Research Centre of Finland, Symposium on Microscopy and Image Analysis of Building Materials 1993 p 28-40 (For primary document see N94-21890 05-27)

Copyright Avail: CASI HC A03/MF A01

Image analysis was applied for quantification and verification of microstructural features of mature cement paste hydrated isothermally in the range 5 to 50 C. The image analysis provided quantitative information on the amount of unreacted cement, calcium hydroxide, other hydration products and pores above approximately 3500 A. It is shown from backscattered electron images that the hydration temperature influences the distribution of hydration products in the paste matrix. At the higher temperatures, dense hydration shells were formed around the hydrating grains, leaving an outer product phase of high capillary porosity. The image analysis showed that the temperature had a significant effect on the porosity. This can be attributed to the higher porosity of the outer product phase. In contrast to other reports, it could not be demonstrated that the hydration product formed at elevated temperatures contained less chemically bound water. ESA

N94-21895# Technical Research Centre of Finland, Espoo. Building Materials Lab.

DETERMINATION OF PORE STRUCTURE OF CONCRETE FROM THIN SECTIONS BY IMAGE ANALYSIS

Kai Tattari *In its* Symposium on Microscopy and Image Analysis of Building Materials 1993 p 41-46 (For primary document see N94-21890 05-27)

Copyright Avail: CASI HC A02/MF A01

A method was developed for analysis with an IMIX image analyzer of thin section images detected by a video camera and microscope. Image analysis was used for the determination of quantitative parameters characterizing microcracks and the air-void system of concrete. The analysis results were compared with those results from the reference images. Relative deviations were calculated for each pair of images. The parameters were the sum total of pores and cracks and the area fraction. The mean values and variances of the relative deviations were calculated so as to include each pair of images. In this way it was possible to find the best combination for the erosion and dilation. ESA

N94-21896# Lund Inst. of Tech. (Sweden). Div. of Building Materials.

MICROSTRUCTURE IN MORTAR: A SUMMARY OF A NEW PROJECT OF RESEARCH

Thomas Carlsson *In* Technical Research Centre of Finland, Symposium on Microscopy and Image Analysis of Building Materials 1993 p 47-50 (For primary document see N94-21890 05-27)

Copyright Avail: CASI HC A01/MF A01

A project aimed at the study of how different 'factors' influence the 'structure' and how the structure influences the 'qualities' of material and combinations of material within the field of render and masonary is summarized. The basic thought is that structural analysis will be able to forsee different qualities and consequences, especially long term. The project bases itself solely on microscope studies. Structure influencing factors that will be studied include air entraining agents in mortar, suction in the background at the moment of rendering/brick laying, frost load in mortar and brick. The structure dependent qualities which will be determined are frost resistance, strength and adhesion. ESA

N94-21954# Sandia National Labs., Albuquerque, NM.

TECHNIQUES FOR PRODUCING FREE-STANDING THIN FILMS ON FRAMES

J. H. Aubert and W. F. McNamara 1993 5 p Presented at the 9th Target Fabrication Specialists Meeting, Monterey, CA, 9 May 1993 (Contract DE-AC04-76DP-00789)

(DE93-041144; SAND-93-0998C; CONF-9305283-1) Avail: CASI HC A01/MF A01

The procedures of vapor-deposition polymerization, spin coating and orientation-dependent etching have been employed to make free-standing thin films of Parylene-N, Parylene-D, polystyrene, polycarbonate and perfluoro-dimethyl-dioxole / tetrafluoroethylene copolymer (Teflon(reg sign) AF-1600). The polymeric materials were vapor-deposited or spin-coated onto substrates of polished single-crystal silicon (wafers) and removed on frames of various shapes and sizes after application of adhesive and an etching process using potassium hydroxide. Thicknesses range from 2000 A to 12000 A. DOE

N94-21963# Sandia National Labs., Albuquerque, NM.

DYNAMIC PROPERTIES OF CERAMIC MATERIALS

D. E. Grady and J. L. Wise Sep. 1993 54 p

(Contract DE-AC04-76DP-00789)

(DE94-000654; SAND-93-0610) Avail: CASI HC A04/MF A01

Controlled impact methods have been employed to obtain dynamic response properties of armor materials. Experimental data have been obtained for high-strength ceramics. Continued analysis of time-resolved velocity interferometer measurements has produced systematic material-property data for Hugoniot and release response, initial and post-yield strength, pressure-induced phase transformation, and dynamic fracture strength. A new technique has been developed to measure hydrodynamic properties of ceramic through shock-wave experiments on metal-ceramic composites and data obtained for silicon carbide. Additional data on several titanium diboride ceramics and high-quality aluminum oxide ceramic have been acquired, and issues regarding the influence of microstructure on dynamic properties have emerged. Comparison of dynamic (Hugoniot elastic limit) strength and indentation hardness data has been performed and important correlations revealed. Innovative impact experiments on confined and unconfined alumina rods using axial and transverse VISAR diagnostics have been demonstrated which permit acquisition of multiaxial dynamic response data. Dynamic failure properties of a high-density aluminosilicate glass, similar in composition to the intergranular glassy phase of some aluminas, have been investigated with regard to yield, spall, and failure-wave propagation. DOE

N94-21970# Lawrence Livermore National Lab., CA.
THE OPTICAL CONSTANTS AND SPECTRAL SPECULAR REFLECTIVITY OF HIGHLY ORIENTED PYROLYTIC GRAPHITE (HOPG)
M. A. Havstad, M. A. Schildbach, and W. McLean, II Aug. 1993 26 p Presented at the National Conference and Exposition on Heat Transfer, Atlanta, GA, 8-11 Aug. 1993
(Contract W-7405-eng-48)
(DE93-040546; UCRL-JC-111969-Rev-1; CONF-930830-11-Rev-1) Avail: CASI HC A03/MF A01

Measurements of the specular reflectivity and the optical constants of highly ordered pyrolytic graphite (HOPG) have been made using two independent optical systems. The first measures reflectance (at 1.06 microns and 293 K) by comparing the intensity of a laser beam before and after reflecting off the sample. The second determines the complex index of raft-action (from 0.55 to 8.45 micron with sample temperatures of 293, 480, 900, and 1300 K) by ellipsometry. Agreement between the two methods is good. Moderate reflectivities are observed over the full spectral range of measurement: the spectral directional-hemispherical reflectivity at normal incidence varies from 0.41 at 0.55 micron to 0.74 at 8.45 microns. The components of the complex index of refraction increase smoothly with wavelength. The index of refraction increases from 3.10 at 0.55 micron to 7.84 at 8.45 microns. The extinction coefficient varies from 2.01 to 6.66 over the same range. DOE

N94-21982# Allied-Signal Corp., Des Plaines, IL.
HIGH TEMPERATURE SIZE SELECTIVE MEMBRANES
S. F. Yates and A. X. Swamikannu 1993 7 p Presented at the Coal-Fired Power Systems 1993 Advances in IGCC and PFBC Review Meeting, Morgantown, WV, 28-30 Jun. 1993
(Contract DE-AC21-92MC-29245)
(DE93-019865; DOE/MC-29245/93/C0205; CONF-9306148-19) Avail: CASI HC A02/MF A01

The high temperature membrane, capable of operation above 550 C, is designed to be a composite membrane composed of a thin layer of a size selective membrane supported by a microporous ceramic support. The kinetic diameters of H2 and CO2 are 2.96 A and 4.00 A. The thin layer will be made from carbon molecular sieve (CMS) whose pore size will be controlled to be less than 4 A. The membrane will be truly size selective and be impermeable to carbon dioxide. The membrane will have higher selectivity than membranes which operate on Knudsen diffusion mechanism. The ceramic support will be fabricated from Allied Signal's proprietary Blackglas (trademark) resin. The ceramic material, noted for its high thermal and oxidative resistance, has a coefficient of thermal expansion which matches closely that of CMS. The close match will insure mechanical integrity when the membrane is subjected to thermal cycles. The CMS layer will be produced by controlled pyrolysis of polymeric precursors. Pore size will be suitably modified by post-treatments to the carbon. The composite membrane will be tested for its permeation properties at 550 C or higher. Thermal, mechanical, and chemical stability of the membrane will be assessed. We have produced several samples of CMS from polymeric precursors. We have initiated work also on the preparation of microporous supports from Blackglas (trademark) resin. We have completed the design of the high temperature membrane pilot plant. The membrane cell was fabricated out of two kinds of stainless steel. The inner parts are made of SS 316 and the outer ring made of SS 420. The greater thermal expansion of the SS 316 will help obtain a leak free seal at the operating temperatures. DOE

N94-22008# Argonne National Lab., IL.
TENSILE STRENGTH OF FIBER REINFORCED PLASTICS AT 77K IRRADIATED BY VARIOUS RADIATION SOURCES
K. Humer, H. W. Weber (Atominstitut der Oesterreichischen Hochschulen, Vienna.), E. K. Tschegg (Technische Univ., Vienna, Austria.), and S. Egusa (Japan Atomic Energy Research Inst., Takasaki.) Aug. 1993 13 p Presented at the 6th International Conference on Fusion Reactor Materials, Stresa, Italy, 27 Sep. - 1 Oct. 1993
(Contract W-31-109-eng-38)
(DE93-040826; ANL/MSD/CP-79440; CONF-930928-5) Avail: CASI HC A03/MF A01

The influence of radiation damage on the mechanical properties of fiber reinforced plastics (FRP's), which are considered as candidate materials for the insulation of superconducting magnets for nuclear fusion reactors, has been investigated. Different types of FRP's (epoxies, bismaleimides; two- and three-dimensional reinforcement structures with E-, S-, or T-glass fibers) has been included in the test program. Three aspects of our present results are discussed in detail. The first is related to an assessment of the tensile strength and its radiation dependence under the influence of strongly varying radiation conditions. The second aspect refers to low temperature (approximately 5 K) reactor irradiation of selected materials. In this case, identical sets of tensile test samples were transferred into the tensile testing machine, one without warming-up to room temperature and the other after an annealing cycle to room temperature. Finally, a comparison between the radiation response of different materials is made. It turns out that the three-dimensionally reinforced bismaleimide shows the smallest degradation of its tensile properties under all irradiation conditions. DOE

N94-20518*# National Aeronautics and Space Administration. Lewis Research Center, Cleveland, OH.
MICROWAVE PROPERTIES AND CHARACTERIZATION OF CO-EVAPORATED BSCCO THIN FILMS
F. A. Miranda, C. M. Chorey (Sverdrup Technology, Inc., Brook Park, OH.), M. A. Stan (Kent State Univ., OH.), C. E. Nordgren (Case Western Reserve Univ., Cleveland, OH.), R. Y. Kwor (Colorado Univ., Colorado Springs.), and T. S. Kalkur (Colorado Univ., Colorado Springs.) *In its* Solid State Technology Branch of NASA Lewis Research Center: Fifth Annual Digest Aug. 1993 p 235-242 Repr. from U.S. Government, 1992 (For primary document see N94-20497 05-32)
Avail: CASI HC A02/MF A03

N94-20972*# National Aeronautics and Space Administration. Lewis Research Center, Cleveland, OH.
ELLIPSOMETRIC STUDIES OF SPUTTERED SILICON NITRIDE ON n-GaAs Abstract Only
Y. K. Peng (Nebraska Univ., Lincoln.), George H. Bu-Abbud (Nebraska Univ., Lincoln.), Samuel A. Alterovitz (Nebraska Univ., Lincoln.), John A. Woollam (Nebraska Univ., Lincoln.), B. Bayraktaroguiu (Universal Energy Systems, Inc., Dayton, OH.), Dieter Langer (Air Force Avionics Lab., Wright-Patterson AFB, OH.), David C. Liu, and E. Haugland *In* Nebraska Univ., Materials, Structures, and Devices for High-Speed Electronics 1993 1 p Repr. from Journal of Vacuum Science Technology (American Vacuum Society), v. 20, no. 3, Mar. 1982 p 713 (For primary document see N94-20971 05-76)
Avail: CASI HC A01/MF A01

N94-20973*# Air Force Avionics Lab., Wright-Patterson AFB, OH.
SURFACE STATES AT THE GaAs-GERMANIUM NITRIDE INTERFACE Abstract Only
Yeung Chung, Dieter W. Langer, H. P. Singh (ITT Advanced Technology Center, Shelton, CT.), and John A. Woollam (Nebraska Univ., Lincoln.) *In* Nebraska Univ., Materials, Structures, and Devices for High-Speed Electronics 1993 1 p Repr. from Thin Solid Films (Netherlands, Elsevier Sequoia), v. 103, 1983 p 75 (For primary document see N94-20971 05-76)
Avail: CASI HC A01/MF A01

N94-20975*# National Aeronautics and Space Administration. Lewis Research Center, Cleveland, OH.
STRUCTURAL AND CHEMICAL ANALYSIS OF A SILICON NITRIDE FILM ON GaAs BY NULL ELLIPSOMETRY Abstract Only
Samuel A. Alterovitz (Nebraska Univ., Lincoln.), George H. Bu-Abbud (Nebraska Univ., Lincoln.), John A. Woollam (Nebraska Univ., Lincoln.), and David C. Liu *In* Nebraska Univ., Materials, Structures, and Devices for High-Speed Electronics 1993 1 p Repr. from Phys. Stat. Sol, v. 85, no. 69, 1984 p 69 (For primary document see N94-20971 05-76)
Avail: CASI HC A01/MF A01

N94-20976*# National Aeronautics and Space Administration. Lewis Research Center, Cleveland, OH.
THIN FILM COMPOSITIONAL ANALYSIS USING NULL OR FIXED WAVELENGTH ELLIPSOMETRY Abstract Only
Samuel A. Alterovitz (Nebraska Univ., Lincoln.), George H. Bu-Abbud (Nebraska Univ., Lincoln.), John A. Woollam (Nebraska Univ., Lincoln.), and David C. Liu *In* Nebraska Univ., Materials, Structures, and Devices for High-Speed Electronics 1993 1 p Repr. from Applied Physics

Communications (Marcel Deller, Inc.), v. 4, no. 1, 1984 p 27-40 (For primary document see N94-20971 05-76)
Avail: CASI HC A01/MF A01

N94-20978*# Nebraska Univ., Lincoln. Electrical Materials Lab.
VARIABLE WAVELENGTH, VARIABLE ANGLE ELLIPSOMETRY INCLUDING A SENSITIVITIES CORRELATION TEST Abstract Only
George H. Bu-Abbud, N. M. Bashara, and John A. Woollam *In its* Materials, Structures, and Devices for High-Speed Electronics 1993 1 p Repr. from Thin Solid Films (Netherlands, Elsevier Sequoia), v. 138, 1986 p 27-41 (For primary document see N94-20971 05-76)
Avail: CASI HC A01/MF A01

N94-20979*# National Aeronautics and Space Administration. Lewis Research Center, Cleveland, OH.
InP MIS STRUCTURES WITH DIAMONDLIKE AMORPHOUS CARBON FILMS DEPOSITED BY ION-BEAM SPUTTERING AND FROM PLASMA Abstract Only
Jae E. Oh (Nebraska Univ., Lincoln.), Joel D. Lamb (Nebraska Univ., Lincoln.), Paul G. Snyder (Nebraska Univ., Lincoln.), John A. Woollam (Nebraska Univ., Lincoln.), and David C. Liu *In* Nebraska Univ., Materials, Structures, and Devices for High-Speed Electronics 1993 1 p Repr. from Solid-State Electronics (England, Pergamon Journals Ltd.), v. 29, no. 9, 1986 p 933-940 (For primary document see N94-20971 05-76)
Avail: CASI HC A01/MF A01

N94-20980*# Nebraska Univ., Lincoln. Dept. of Electrical Engineering.
INTERFACIAL PROPERTIES OF DIAMONDLIKE AMORPHOUS CARBON FILMS ON InP: METAL-INSULATOR-SEMICONDUCTOR STRUCTURES Abstract Only
Jae E. Oh, Joel D. Lamb, Paul G. Snyder, and John A. Woollam *In its* Materials, Structures, and Devices for High-Speed Electronics 1993 1 p Repr. from Journal of Vacuum Science Technology (American Vacuum Society), v. 4, no. 3, May - Jun. 1986 p 1022 (For primary document see N94-20971 05-76)
Avail: CASI HC A01/MF A01

N94-20981*# National Aeronautics and Space Administration. Lewis Research Center, Cleveland, OH.
THIN-FILM HERMETICITY: A QUANTITATIVE ANALYSIS OF DIAMONDLIKE CARBON USING VARIABLE ANGLE SPECTROSCOPIC ELLIPSOMETRY Abstract Only
S. Orzeszko (Nicolaus Copernicus Univ., Torun, Poland.), Bhola N. De (Nebraska Univ., Lincoln.), John A. Woollam (Nebraska Univ., Lincoln.), John J. Pouch, Samuel A. Alterovitz, and David C. Ingram (Universal Energy Systems, Inc., Dayton, OH.) *In* Nebraska Univ., Materials, Structures, and Devices for High-Speed Electronics 1993 1 p Repr. from Journal of Applied Physics (American Inst. of Physics), v. 64, no. 8, 15 Oct. 1988 p 4175 (For primary document see N94-20971 05-76)
Avail: CASI HC A01/MF A01

N94-20983*# Nebraska Univ., Lincoln. Dept. of Electrical Engineering.
ELLIPSOMETRIC MEASUREMENTS OF MOLECULAR-BEAM-EPITAXY-GROWN SEMICONDUCTOR MULTILAYER THICKNESSES: A COMPARATIVE STUDY Abstract Only
John A. Woollam, Paul G. Snyder, Anthony W. McCormick (Universal Energy Systems, Inc., Dayton, OH.), A. K. Rai (Universal Energy Systems, Inc., Dayton, OH.), David C. Ingram (Universal Energy Systems, Inc., Dayton, OH.), and Peter P. Pronko (Universal Energy Systems, Inc., Dayton, OH.) *In its* Materials, Structures, and Devices for High-Speed Electronics 1993 1 p Repr. from Journal of Applied Physics (American Inst. of Physics), v. 62, no. 12, 15 Dec. 1987 p 4867 (For primary document see N94-20971 05-76)
Avail: CASI HC A01/MF A01

N94-20984*# Nebraska Univ., Lincoln. Dept. of Electrical Engineering.
COMPARATIVE THICKNESS MEASUREMENTS OF HETEROJUNCTION LAYERS BY ELLIPSOMETRIC, RBS, AND XTEM ANALYSIS Abstract Only
John A. Woollam, Paul G. Snyder, Anthony W. McCormick (Universal Energy Systems, Inc., Dayton, OH.), A. K. Rai (Universal Energy Systems, Inc., Dayton, OH.), Peter P. Pronko (Universal Energy Systems, Inc., Dayton, OH.), and J. J. Geddes (Honeywell, Inc., Bloomington, MN.) *In its* Materials, Structures, and Devices for High-Speed Electronics 1993 1 p Repr. from Materials Research Society Symposium Proceedings, v. 77, 1987 p 755 Sponsored in part by Naval Air Systems Command (For primary document see N94-20971 05-76)
Avail: CASI HC A01/MF A01

N94-20986*# Nebraska Univ., Lincoln. Center for Microelectronic and Optical Materials Branch.
VARIABLE ANGLE SPECTROSCOPIC ELLIPSOMETRIC CHARACTERIZATION OF SURFACE DAMAGE IN CHEMICAL-MECHANICAL POLISHED GaAs Abstract Only
Yi-Ming Xiong and Paul G. Snyder *In its* Materials, Structures, and Devices for High-Speed Electronics 1993 1 p Repr. from Thin Solid Films (Elsevier Sequoia), v. 220, 1992 p 303-310 (For primary document see N94-20971 05-76)
Avail: CASI HC A01/MF A01

N94-20991*# National Aeronautics and Space Administration. Lewis Research Center, Cleveland, OH.
AMORPHOUS Ta-RICH Ta-Cu FILMS AS DIFFUSION BARRIERS BETWEEN Au AND GaAs Abstract Only
Jae E. Oh (Nebraska Univ., Lincoln.), John A. Woollam (Nebraska Univ., Lincoln.), John J. Pouch, Samuel A. Alterovitz, and David C. Ingram (Universal Energy Systems, Inc., Dayton, OH.) *In* Nebraska Univ., Materials, Structures, and Devices for High-Speed Electronics 1993 1 p Repr. from Journal of Vacuum Science Technology (American Vacuum Society), v. 6, no. 3, May - Jun. 1988 p 825 (For primary document see N94-20971 05-76)
Avail: CASI HC A01/MF A01

N94-21007*# Nebraska Univ., Lincoln. Dept. of Electrical Engineering.
THERMAL CHARACTERIZATION OF THIN FILMS BY PHOTOTHERMALLY INDUCED LASER BEAM DEFLECTION Abstract Only
Hassanayn Machlab, William A. McGahan, John A. Woollam, and Kevin Cole *In its* Materials, Structures, and Devices for High-Speed Electronics 1993 1 p Repr. from Thin Solid Films (Elsevier Sequoia), v. 224, 1993 p 22-27 Presented at the 19th International Conference on Metallurgical Coatings and Thin Films, San Diego, CA, 6-10 Apr. 1992 (For primary document see N94-20971 05-76)
Avail: CASI HC A01/MF A01

N94-21373 Toronto Univ., Downsview (Ontario). Inst. for Aerospace Studies.
SPACE ENVIRONMENTAL EFFECTS ON POLYMER MATRIX COMPOSITES: THE UTIAS/LDEF EXPERIMENT
R. C. Tennyson, G. E. Mabson, W. D. Morison, and J. Kleiman *In* CNES, Fifth International Symposium on Materials in a Space Environment Jun. 1993 p 93-110 Sponsored by Ontario Inst. for Space and Terrestrial Science, Canada, and Ontario Center for Materials Research, Canada (For primary document see N94-21367 05-18)
Copyright Avail: CEPADUES-Editions, 111, rue Nicolas-Vaquelin, 31100 Toulouse, France

N94-21374 Centre National d'Etudes Spatiales, Toulouse (France).
RESIDUAL ATMOSPHERE IN THE FRECOPA EXPERIMENT AND DEGASSING OF MATERIALS [ATMOSPHERE RESIDUELLE DANS L'EXPERIENCE FRECOPA ET DEGAZAGE DES MATERIAUX]
J. Guillin *In its* Fifth International Symposium on Materials in a Space Environment Jun. 1993 p 111-118 In FRENCH (For primary document see N94-21367 05-18)
Copyright Avail: CEPADUES-Editions, 111, rue Nicolas-Vaquelin, 31100 Toulouse, France

N94-21376 Centre d'Etudes et de Recherches, Toulouse (France). Dept. d'Etudes et Recherches en Technologie Spatiale.
ARAGATZ PROJECT SAMPLES EXPERIMENT/MAPOL (POLYMER MATERIALS) EXPERIMENT: POSTFLIGHT EXPERT EVALUATION [PROJET AGRATZ EXPERIENCE ECHANTILLONS. EXPERIENCE MAPOL (MATERIAUX POLYMERES). COMPTE-RENDU DE L'EXPERIENCE D'APRES VOL]
C. Sable and J. Villaeys (Centre National d'Etudes Spatiales, Toulouse, France.) *In* CNES, Fifth International Symposium on Materials in a Space Environment Jun. 1993 p 131-136 In FRENCH (For primary document see N94-21367 05-18)
Copyright Avail: CEPADUES-Editions, 111, rue Nicolas-Vaquelin, 31100 Toulouse, France

N94-21380 Academy of Sciences (USSR), Moscow. Inst. of Energy Problems of Chemical Physics.
THE SIMULATION OF ACTION OF SOME SPACE ENVIRONMENT FACTORS ON TEFLON AND ON RUBBER MATERIALS
V. E. Skurat, E. A. Barbashev, Y. I. Dorofeev, B. I. Khrushch, A. V. Milinchuk, and V. V. Sedov *In* CNES, Fifth International Symposium on Materials in a Space Environment Jun. 1993 p 187-196 (For primary document see N94-21367 05-18)
Copyright Avail: CEPADUES-Editions, 111, rue Nicolas-Vaquelin, 31100 Toulouse, France

N94-21381 National Research Council of Canada, Vancouver (British Columbia).
IN-VACUO SLIP TESTING OF MATERIALS FOR SSRMS FRICTION BRAKES
H. M. Hawthorne and S. Preston (Spar Aerospace Ltd., Weston, Ontario.) *In* CNES, Fifth International Symposium on Materials in a Space Environment Jun. 1993 p 197-208 (For primary document see N94-21367 05-18)
Copyright Avail: CEPADUES-Editions, 111, rue Nicolas-Vaquelin, 31100 Toulouse, France

N94-21385* National Aeronautics and Space Administration. Langley Research Center, Hampton, VA.
SIMULATED SPACE ENVIRONMENTAL EFFECTS ON SOME EXPERIMENTAL HIGH PERFORMANCE POLYMERS
John W. Connell *In* CNES, Fifth International Symposium on Materials in a Space Environment Jun. 1993 p 241-253 (For primary document see N94-21367 05-18)
Copyright Avail: CEPADUES-Editions, 111, rue Nicolas-Vaquelin, 31100 Toulouse, France

N94-21394 Toronto Univ. (Ontario).
EVALUATION OF PLASMA-DEPOSITED PROTECTIVE COATINGS FOR SPACECRAFT APPLICATIONS
R. C. Tennyson, K. G. Balmain, M. R. Wertheimer (Ecole Polytechnique, Montreal, Quebec.), and D. G. Zimcik (Canadian Space Agency, Ottawa, Ontario.) *In* CNES, Fifth International Symposium on Materials in a Space Environment Jun. 1993 p 385-400 Sponsored by Natural Sciences and Engineering Research Council, Canada, and Ontario Inst. for Space and Terrestrial Science, Canada (For primary document see N94-21367 05-18)
Copyright Avail: CEPADUES-Editions, 111, rue Nicolas-Vaquelin, 31100 Toulouse, France

N94-21399 Moscow State Univ. (Russia).
FORECASTING TECHNIQUE OF VARIATIONS OF THE OPTICAL ABSORPTIVITY OF THERMAL CONTROL COATINGS UNDER DIFFERENT SIMULTANEOUS RADIATIONS
A. P. Grashchenko and G. G. Soloviev *In its* Fifth International Symposium on Materials in a Space Environment Jun. 1993 p 413-426 (For primary document see N94-21367 05-18)
Copyright Avail: CEPADUES-Editions, 111, rue Nicolas-Vaquelin, 31100 Toulouse, France

N94-21400 Centre National d'Etudes Spatiales, Toulouse (France).
THERMAL CONTROL COATINGS
Jean-Claude Guillaumon and Francoise Guerard (MAP S.A., Pamiers, France.) *In its* Fifth International Symposium on Materials in a Space Environment Jun. 1993 p 427-433 (For primary document see N94-21367 05-18)
Copyright Avail: CEPADUES-Editions, 111, rue Nicolas-Vaquelin, 31100 Toulouse, France

N94-21405 Centre National de la Recherche Scientifique, Odeillo (France).
A METHOD OF MEASURING THE THERMORADIATIVE PROPERTIES OF CERAMIC MATERIALS IN A SPACE ENVIRONMENT [METHODE DE MESURE DES PROPRIETES THERMORADIATIVES DE MATERIUX CERAMIQUES EN ENVIRONNEMENT SPATIAL]
M. Balat, C. Dupuy, D. Hernandez, J. F. Robert, and G. Olalde *In* CNES, Fifth International Symposium on Materials in a Space Environment Jun. 1993 p 489-496 In FRENCH (For primary document see N94-21367 05-18)
Copyright Avail: CEPADUES-Editions, 111, rue Nicolas-Vaquelin, 31100 Toulouse, France

N94-21800# Technische Physische Dienst TNO-TH, Delft (Netherlands).
MODELING OF GLASS FABRICATION [MODELLERING VAN DE GLASFABRICAGE]
F. Simonis *In its* Activities Report of the Institute of Applied Physics 1990 p 23-25 In DUTCH (For primary document see N94-21798 05-70)
Avail: CASI HC A01/MF A01

N94-22601# Deutsche Airbus G.m.b.H., Bremen (Germany).
EXPERIMENTS WITH A FLUID DEICING SYSTEM FOR CLEANING LAMINAR WINGS [EXPERIMENTE MIT EINEM FLUIDISCHEN ENTEISUNGSSYSTEM ZUR SAEUBERUNG VON LAMINARFLUEGELN]
R. Henke *In* Tech. Univ. Berlin, Measurement Technology for Flight Tests May 1991 p 35-56 In GERMAN (For primary document see N94-22597 05-02)
Avail: CASI HC A03/MF A02

28 PROPELLANTS AND FUELS

Includes rocket propellants, igniters, and oxidizers; their storage and handling procedures; and aircraft fuels.

For related information see also *07 Aircraft Propulsion and Power, 20 Spacecraft Propulsion and Power,* and *44 Energy Production and Conversion.*

N94-19801 Department of the Navy, Washington, DC.
HIGH MELTING AMINO AROMATIC NITRATE ESTERS Patent
Michael E. Sitzmann, inventor (to Navy) 16 Mar. 1993 5 p Filed 15 Jun. 1992
(AD-D015929; US-Patent-5,194,659; US-Patent-Appl-SN-901618; US-Patent-Class-558-482) Avail: US Patent and Trademark Office

A nitrate ester is described which is 1,3-diamino-5 (hydroxyethyl-aminonitrate) 2,4,6-trinitrobenzene or 3-amino-3' (hydroxyethylamino-nitrate) 2,2',4,4',6,6'-hexanitrobiphenyl. DTIC

N94-19906# Materials Research Labs., Ascot Vale (Australia).
AGEING STUDIES ON A COMPOSITE PROPELLANT CONTAINING A NEW ORGANO-COPPER BURN RATE CATALYST
B.L. Hamshere and P. Rawson Jun. 1993 23 p
(AD-A271060; MRL-TN-627; DODA-AR-008-232) Avail: CASI HC A03/MF A01

The effect of a new organo-copper burn rate catalyst on the aging properties of an HTPB/AP based composite propellant has been studied and compared with a similar propellant containing copper chromite. The degradation of the propellant surface under conditions of thermo-oxidation was studied by monitoring oxygen uptake using a gravimetric technique. The oxidative induction times for the reaction were determined for a series of elevated temperatures and the data used to predict the storage life of the propellant at ambient temperatures using an Arrhenius plot. It was shown that the storage life of a copper chromite propellant was approximately 7.5 years at 20 C while the corresponding organo-copper propellant had a storage life of approximately 49 years. DTIC

N94-19984# Midwest Research Inst., Golden, CO.
BIOFUELS: PROJECT SUMMARIES
May 1993 117 p
(Contract DE-AC02-83CH-10093)
(DE93-010003; DOE/CH-10093/213) Avail: CASI HC A06/MF A02

Domestic transportation fuels are almost exclusively derived from petroleum and account for about two-thirds of total U.S. petroleum consumption. In 1990, more than 40% of the petroleum used domestically was imported. Because the United States has only 5% of the world's petroleum reserves, and the countries of the Middle East have about 75%, U.S. imports are likely to continue to increase. With our heavy reliance on oil and without suitable substitutes for petroleum-based transportation fuels, the United States is extremely vulnerable, both strategically and economically, to fuel supply disruptions. In addition to strategic and economic affairs, the environmental impacts of our use of petroleum are becoming increasingly evident and must be addressed. The U.S. Department of Energy's (DOE's) Office of Energy Efficiency and Renewable Energy (EE), through its Biofuels Systems Division (BSD), is addressing these issues. The BSD is aggressively pursuing research on biofuels-liquid and gaseous fuels produced from renewable domestic feedstocks such as forage grasses, oil seeds, short-rotation tree crops, agricultural and forestry residues, algae, and certain industrial and municipal waste streams. DOE

N94-20061 Department of the Navy, Washington, DC.
MONOPROPELLANT AQUEOUS HYDROXYL AMMONIUM NITRATE/FUEL Patent
Kurt F. Mueller, inventor (to Navy) and Manfred J. Cziesla, inventor (to Navy) 29 Jun. 1993 3 p Filed 28 Mar. 1969
(AD-D015922; US-Patent-5,223,057; US-Patent-Appl-SN-812567;
US-Patent-Class-149-45) Avail: US Patent and Trademark Office

This invention is a liquid monopropellant composition comprising the water solution of an hydroxylammonium nitrate and a compatible water soluble or water dispersible fuel. DTIC

N94-20122 Department of the Navy, Washington, DC.
N,N'-BIS(4,4,4-TRINITRO BUTYRYL) HYDRAZINE Patent
Michael E. Sitzmann, inventor (to Navy) 2 Feb. 1993 3 p Filed 15 Jun. 1992
(AD-D015897; US-Patent-5,183,938; US-Patent-Appl-SN-901620;
US-Patent-Class-564-151) Avail: US Patent and Trademark Office

N,N'-bis(4,4,4-trinitro butyryl) hydrazine is prepared by reacting 4,4,4-trinitro butyryl chloride with hydrazine in methanol at low temperature. This compound is sensitive enough to be used as an initiating explosive and thermally stable enough to be used in missile warheads. DTIC

N94-20551# Southwest Research Inst., San Antonio, TX. Fuels and Lubricants Research Facility.
COMPATIBILITY AND EFFICACY OF BIOCIDES QUALIFIED UNDER MILITARY SPECIFICATION MIL-S-53021 Interim Report, Oct. 1992 - Aug. 1993
S. R. Westbrook and M. L. Alexander Sep. 1993 24 p
(Contract DAAK70-92-C-0059; DA Proj. 1L2-63001-D-150)
(AD-A271496; BFLRF-282) Avail: CASI HC A03/MF A01

The Army has three fuel biocides qualified under specification MIL-S-53021. The military's aviation kerosene, JP-8, also contains an icing inhibitor additive that has some biocidal activity. The relative effectiveness and compatibility of these additives have never been investigated. This study was conducted to evaluate the efficacy of the individual biocides as well as the possible interactions (either synergistic or antagonistic) between these biocides and the icing inhibitor additive. Each of the qualified biocides was evaluated using standard microbiological techniques to determine additive efficacy and compatibility with other fuel additives. The relative effectiveness of the qualified additives was determined. The interactions of the biocides with the icing inhibitor additive in JP-8 were also investigated. DTIC

N94-20625 Denver Univ., CO. Dept. of Chemistry.
PHYSICAL CHEMISTRY OF ENERGETIC NITROGEN COMPOUNDS Final Report, 1 May 1991 - 31 Jul. 1993
Robert D. Coombe 1 Oct. 1993 52 p Limited Reproducibility: More than 20% of this document may be affected by microfiche quality
(Grant AF-AFOSR-0259-90)
(AD-A271819; AFOSR-93-0810TR) Avail: CASI HC A04

This research program produced detailed information concerning the reactions of atoms with azide radicals, amines, aminyl radicals, and isocyanates, These processes release substantial amounts of energy and are constrained (by angular momentum conservation) to substantial amounts of energy and are constrained (by angular momentum conservation) to transfer processes generate products in specific states. In addition, reactions and energy transfer processes involving excited nitrene radicals were studied and the rates and mechanisms of several such processes were determined. The information generated provides insight into the fundamental behavior of nitrogen-halogen systems, and is relevant to the development of new lasers. DTIC

N94-20927# Army Cold Regions Research and Engineering Lab., Fort Wainright, AK.
EVALUATION OF PRE-EXTRACTION ANALYTICAL HOLDING TIMES FOR NITROAROMATIC AND NITRAMINE EXPLOSIVES IN WATER Special Report
Clarence L. Grant, Thomas F. Jenkins, and Susan M. Golden Aug. 1993 18 p
(AD-A271547; Rept-93-24; ENAEC-TS-CR-93096) Avail: CASI HC A03/MF A01

A study was conducted to experimentally evaluate the maximum acceptable pre-extraction analytical holding times (MHT's) for three nitroaromatic compounds and two nitramines in water. Three fortified waters (reagent-grade water, ground water, and surface water) were utilized in the study. Analytes investigated were HMX, RDX, TNB, TNT, and 2,4-DNT, all at the low micrograms/L level. Subsamples of each water sample were held for periods of 0, 3, 7, 14, 28, and 70 days at either room temperature (22 C) or under refrigeration (2 C). Samples were analyzed by RPHPLC without preconcentration. The two nitramines, HMX and RDX, were stable over the entire period for all waters under both storage temperatures. For the three nitroaromatics (TNB, TNT, and 2,4-DNT) the results were very different. For the surface water, significant losses of TNB and TNT occurred in only a day or two, even under refrigeration. Loss of these analytes was accompanied by an increase in the concentration of their microbiological degradation products 3,5-dinitro aniline and 4-amino-2,6-dinitro toluene, respectively. The rate of loss of 2,4-DNT was much slower in the surface water than for either TNB or TNT. The rates of loss of the three nitroaromatics were much slower in the reagent-grade water and ground water than in the surface water. The recommended MHT for nitroaromatics and nitramines in relatively sterile water samples is 50 days under refrigeration. Surface water sample, or samples likely to have significant microbial activity, should be preserved in the field prior to shipment or analyzed on-site, or the loss of TNB and TNT is likely to be significant. DTIC

N94-21192# University of Southern California, Los Angeles. Dept. of Chemistry.
SURFACE SCIENCE AND MODELING STUDIES OF ENDOTHERMIC FUELS CATALYSIS Final Report, 1 Aug. 1990 - 31 Jul. 1993
Bruce E. Koel and Emily A. Carter 10 Oct. 1993 24 p
(Grant AF-AFOSR-0331-90)
(AD-A272850; AFOSR-93-0844TR) Avail: CASI HC A03/MF A01

A description is provided of experimental results from surface science studies and insight from theoretical and modeling studies for new catalysts for endothermic fuels. Our work has focused on providing fundamental information concerning the thermochemistry, kinetics, and mechanism of the dehydrogenation of methylcyclohexane (MCH) to toluene over Pt and Pt alloys or intermetallic compounds. Chemisorption and adsorption kinetics measurements reveal that alkali adatoms or alloys of Pt can promote selectivity in dehydrogenation reactions that yield benzene or toluene. In addition, a new apparatus with a reaction antechamber was constructed that allows catalytic reaction rates to be measured on surfaces that are thoroughly characterized by surface analytical methods. Ab-initio calculations were performed for simple models of alloy catalysts, e.g., Pt2, Pt3, PtZr, Pt3Zr, Zr-H, Pt-H, Zr-CH3, and Pt-CH3. Quasiempirical valence bond (QVB) calculations were done for the dehydrogenation of MCH on Pt. In addition, new tools were developed for treatments of electron correlation required for these bimetallic catalysts. Two computer programs were also developed

to predict accurately the barriers and calculate the pre-exponential factors that appear in the Arrhenius expression for the rate constant in order to predict kinetics from first principles. DTIC

N94-21760*# National Aeronautics and Space Administration. Lewis Research Center, Cleveland, OH.
POWDERED ALUMINUM AND OXYGEN ROCKET PROPELLANTS: SUBSCALE COMBUSTION EXPERIMENTS
Mike L. Meyer Dec. 1993 12 p Presented at the 30th JANNAF Combustion Subcommittee Meeting, Monterey, CA, 15-19 Nov. 1993; sponsored by the Joint Army-Navy-NASA-Air Force Combustion Subcommittee
(RTOP 232-01-OA)
(NASA-TM-106439; E-8281; NAS 1.15:106439) Avail: CASI HC A03/MF A01

Aluminum combined with oxygen has been proposed as a potential lunar in situ propellant for ascent/descent and return missions for future lunar exploration. Engine concepts proposed to use this propellant have not previously been demonstrated, and the impact on performance from combustion and two-phase flow losses could only be estimated. Therefore, combustion tests were performed for aluminum and aluminum/magnesium alloy powders with oxygen in subscale heat-sink rocket engine hardware. The metal powder was pneumatically injected, with a small amount of nitrogen, through the center orifice of a single element O-F-O triplet injector. Gaseous oxygen impinged on the fuel stream. Hot-fire tests of aluminum/oxygen were performed over a mixture ratio range of 0.5 to 3.0, and at a chamber pressure of approximately 480 kPa (70 psia). The theoretical performance of the propellants was analyzed over a mixture ratio range of 0.5 to 5.0. In the theoretical predictions the ideal one-dimensional equilibrium rocket performance was reduced by loss mechanisms including finite rate kinetics, two-dimensional divergence losses, and boundary layer losses. Lower than predicted characteristic velocity and specific impulse performance efficiencies were achieved in the hot-fire tests, and this was attributed to poor mixing of the propellants and two-phase flow effects. Several tests with aluminum/9.8 percent magnesium alloy powder did not indicate any advantage over the pure aluminum fuel. Author

N94-22033# Sandia National Labs., Albuquerque, NM.
CHARACTERISTICS OF SHOCK-COMPRESSED CONFIGURATION OF Ti AND Si POWDER MIXTURES
N. N. Thadhani (Georgia Inst. of Tech., Atlanta.), E. Dunbar (New Mexico Inst. of Mining and Technology, Socorro.), and R. A. Graham 1993 5 p Presented at the 14th International Conference of the International Association for the Advancement of High Pressure Science and Technology, Colorado Springs, CO, 27 Jun. - 2 Jul. 1993
(Contract DE-AC04-76DP-00789)
(DE93-018857; SAND-93-0510C; CONF-930676-36) Avail: CASI HC A01/MF A01

Shock-compression recovery experiments were performed on mixtures of Ti and Si powders of fine, medium, and coarse morphology, and packed at different initial densities, using the Sandia Momma and Poppa Bear fixtures with Baratol explosive. The shock-compressed configuration revealed characteristics typical of either chemically reacted material with fine equiaxed grains, or unreacted material with densely packed Ti and Si particles. The unreacted configuration showed that Ti particles were extensively deformed, irrespective of powder morphology and shock conditions generated by either fixture. In contrast Si particles showed different characteristics depending on the powder morphology, packing density, and shock conditions. The microstructural characteristics of unreacted configuration of Ti and Si powder mixtures were investigated. Mechanistic processes occurring prior to the inception of shock-induced chemical reactions in this system are described. DOE

N94-22091# New Energy and Industrial Technology Development Organization, Tokyo (Japan).
CURRENT SITUATION IN DEVELOPING PETROLEUM SUBSTITUTING ENERGY (THE UNITED KINGDOM)
Mar. 1993 72 p
(DE94-714897; NEDO-P-9203) Avail: CASI HC A04/MF A01

A survey was made to identify the trends in developing petroleum energy substitutes in the United Kingdom. The UK has abundant coal resources, produces petroleum and natural gas in addition, and is the only energy self-sustaining country in the EC. However, coal for power generation was replaced with coal imports and natural gas because of inferior price competitiveness. The coal mine close-down bill has turned to a social problem. Petroleum is also losing its price competitiveness as the oil reservoir beds go deeper and deeper. Demand for natural gas is increasing because of the new consolidation cycle type gas turbine power generation, but natural gas will be depleted in 30 years. Building new nuclear power plants has been discontinued. Government subsidies are sought for developing wave and wind power utilization to cope with the downward trend in energy self-sufficiency. With respect to harmony with environment, the government is attempting to solve the matter by applying the policies of energy conservation and renewable energy development. The energy saving policies are being promoted in power generation, power distribution, commerces and industries, buildings, and electric products. For renewable energies, the Non-Fossil Fuel Obligation taxation system has already been applied extensively. DOE

N94-20073# Katholieke Univ. te Leuven (Belgium). Dept. of Physics.
PROPERTIES OF CRYOGENIC LIQUIDS
A. Dupre *In* VKI, Spacecraft Propulsion 1993 5 p (For primary document see N94-20068 05-20)
Copyright Avail: CASI HC A01/MF A04

29 MATERIALS PROCESSING

Includes space-based development of products and processes for commercial applications.

For biological materials see *55 Space Biology.*

N94-20605# Missouri Univ., Rolla. Dept. of Ceramic Engineering and Graduate Center for Materials Research.
EVAPORATION OF A SODIUM TELLURITE MELT IN THE JAMIC LOW GRAVITY DROP SHAFT Final Report
Chandra S. Ray, Delbert E. Day, Masaki Makihara, and Junji Hayakawa 1 Oct. 1993 44 p
Avail: CASI HC A03/MF A01

A sodium-tellurite (Na2O.4TeO2) glass, fused to a platinum wire heating coil, was evaporated in low gravity in the JAMIC drop shaft. The primary objectives were to: gain a better understanding of the evaporation mechanism from a melt surface which could improve glass melting techniques presently used on earth, obtain information for the growth of solid particles from vapor, and study the feasibility of preparing chemically pure spherical particles (ranging from several nanometers to micrometers in size) which could have application in medicine (radiotherapy of malignant tumors), optical communications, and as advanced composite materials. A Na2O.4TeO2 glass was selected as a model glass for this investigation primarily for the reason that it melts at a relatively low temperature (less than 700 C) and, therefore, only a nominal amount of electrical power was needed to conduct these experiments. Also, the tellurite glasses possess unique optical and chemical properties which make them potential candidates for practical applications such as glass to metal seals, infrared optical fibers, laser hosts, paramagnetic generators, and optical shutters. The samples from each drop shaft experiment were returned to UMR for analysis. Interesting results on the growth of particles from the vapor phase and for the crystallization of a Na2O.4TeO2 melt in low gravity were obtained. Some of the results are surprising (unexpected) and additional experiments are recommended for verifying these preliminary results. Derived from text

31 ENGINEERING (GENERAL)

Includes vacuum technology; control engineering; display engineering; cryogenics; and fire prevention.

N94-19834# Army Research Lab., Adelphi, MD.
FOCUSED-ION-BEAM MATERIAL REMOVAL RATES Summary Report
Bruce Geil Sep. 1993 19 p
(AD-A270852; ARL-MR-114) Avail: CASI HC A03/MF A01

Focused-ion-beam milling is a tool used in failure analysis and production of integrated circuits. This technique uses a focused gallium beam to mill

away materials on a surface. Each material mills at a different rate, which must be experimentally determined. The data presented here for several materials used in standard integrated circuit processes will allow the user to determine the dose level needed to mill a certain amount of a given material. DTIC

N94-19946# Sandia National Labs., Tonopah, NV. Test Range Site Management Dept.
DIGITAL WIRELESS CONTROL SYSTEM
R. Smith Aug. 1993 28 p
(Contract DE-AC04-76DP-00789)
(DE93-040211; SAND-93-1612) Avail: CASI HC A03/MF A01 (US Sales Only)

The Digital Wireless Control System (DWCS) is designed to initiate high explosives safely while using a wireless remote control system. Numerous safety features have been designed into the fire control system to mitigate the hazards associated with remote initiation of high explosives. These safety features range from a telemetry (TM) fire control status system to mechanical timers and keyed power lockout switches. The environment, safety, and health (ES&H) Standard Operating Procedure (SOP) SP471970 is intended as a guide when working with the DWCS. This report describes the Digital Wireless Control System and outlines each component's theory of operation and its relationship to the system. DOE

N94-20099# Oak Ridge National Lab., TN.
ALTERNATIVE REFRIGERANTS AND REFRIGERATION CYCLES FOR DOMESTIC REFRIGERATORS
J. R. Sand, C. L. Rice, and E. A. Vineyard Dec. 1992 142 p
(Contract DE-AC05-84OR-21400)
(DE93-040481; ORNL/M-2270) Avail: CASI HC A07/MF A02

This project initially focused on using nonazeotropic refrigerant mixtures (NARM's) in a two-evaporator refrigerator-freezer design using two stages of liquid refrigerant subcooling. This concept was proposed and tested in 1975. The work suggested that the concept was 20% more efficient than the conventional one-evaporator refrigerator-freezer (RF) design. After considerable planning and system modeling based on using a NARM in a Lorenz-Meutzner (L-M) RF, the program scope was broadened to include investigation of a 'dual-loop' concept where energy savings result from exploiting the less stringent operating conditions needed to satisfy cooling of the fresh food section. A steady-state computer model (CYCLE-Z) capable of simulating conventional, dual loop, and L-M refrigeration cycles was developed. This model was used to rank the performance of 20 ozone-safe NARM's in the L-M refrigeration cycle while key system parameters were systematically varied. The results indicated that the steady-state efficiency of the L-M design was up to 25% greater than that of a conventional cycle. This model was also used to calculate the performance of other pure refrigerants relative to that of dichlorodifluoromethane, R-12, in conventional and dual-loop RF designs. Projected efficiency gains for these cycles were more modest, ranging from 0 to 10%. Individual compressor calorimeter tests of nine combinations of evaporator and condenser temperatures usually used to map RF compressor performance were carried out with R-12 and two candidate L-M NARM's in several compressors. Several models of a commercially produced two-evaporator RF were obtained as test units. Two dual-loop RF designs were built and tested as part of this project. DOE

N94-20278# Los Alamos National Lab., NM.
THE NATIONAL HIGH MAGNETIC FIELD LABORATORY, A USER FACILITY IN SUPPORT OF RESEARCH IN HIGH MAGNETIC FIELDS
J. E. Crow (Florida State Univ., Tallahassee.), H. J. Schneider-Muntau (Florida State Univ., Tallahassee.), D. Parkin, and N. S. Sullivan (Florida Univ., Gainesville.) 1993 10 p Presented at the International Cryogenic Engineering Conference and International Cryogenic Materials Conference, Albuquerque, NM, 12-16 Jul. 1993
(Contract W-7405-eng-36)
(DE93-040145; LA-UR-93-3120; CONF-930703-31) Avail: CASI HC A02/MF A01

The National High Magnetic Field Laboratory (NHMFL) develops and operates high magnetic field facilities at its main location at Florida State University, Tallahassee, as well as a pulsed magnetic field facility at Los Alamos National Laboratory. A number of specialized facilities are also available to collaborators at the University of Florida for research at ultra-low temperatures, advanced magnetic resonance imaging, and materials sciences. The NHMFL is supported by the United States National Science Foundation (NSF) and by the State of Florida. It is a user facility available to qualified users through a peer review proposal process. The facilities and staff support research and development at the extremes of parameter space. A part of its activities is devoted to the advancement of the state of the art of superconducting, pulsed, resistive, and hybrid magnets. This involves cryogenic materials research, the development of high strength, high conductivity conductors, and the development of low and ultra low temperature systems. DOE

N94-20355# Department of the Navy, Washington, DC.
ON DEMAND, NON-HALON, FIRE EXTINGUISHING SYSTEMS Patent Application
Bengamin D. Smith, inventor (to Navy) 23 Jun. 1993 26 p
(AD-D015957; US-Patent-Appl-SN-083403; Navy-Case-75238) Avail: CASI HC A03/MF A01

A system and process for on-demand generation of inert, nonflammable gases and water vapor to decrease the available atmospheric oxygen in the ullage of a hydrocarbon fuel storage tank to a level that will not support combustion of the hydrocarbon fuel, is disclosed. One, or more, of a variety of non-Halon, fire suppressor charges are selectively contained in one or more gas generating cartridges. The gas generating cartridge(s), when activated, cause release of these charges to promote rapid chemical reactions and supply inert, nonflammable gases and water vapor to the tank ullage. Activation is accomplished in aircraft by, either pilot action or, by pressure and temperature sensors contained within the hydrocarbon fuel tank. DTIC

N94-21426 Arizona State Univ., Tempe. Center for Energy Systems Research.
HEAT TRANSFER ADDITIVES FOR ABSORPTION COOLING SYSTEM FLUIDS Final Report, Oct. 1989 - Mar. 1993
B. D. Wood, N. S. Berman, K. Kim, and D. S. C. Chau Mar. 1993 349 p See also PB93-156859 Limited Reproducibility: More than 20% of this document may be affected by microfiche quality
(Contract GRI-5089-260-1874)
(PB93-202521; GRI-93/0149) Avail: Issuing Activity (National Technical Information Service (NTIS))

The work was directed towards developing a quantitative understanding of the phenomena that can enhance the heat and mass transfer in the absorber of an absorption chiller. Emphasis during the first year of a 3 year study was placed on compiling a comprehensive property data base and doing some exploratory experiments. During the second year experimental methods associated with heat and mass transfer in a falling film absorber were emphasized. All experiments used 2-ethyl-1-hexanal as the additive (surfactant) in an aqueous LiBr solution. The mass and heat transfer coefficients were found using the log mean averages based on the inlet and outlet properties. Significant accomplishments include: the onset of enhanced transfer was in the 2 to 200 ppm additive concentration range of surfactant and when 30 ppm was reached in the experiments the maximum enhancement was achieved. From 30 to 200 ppm additive concentration the enhancement remained the same. Visual observations of the experiments using the long absorber (85 cm) showed that chaotic flow was occurring only over the first half of the absorber. The majority of the tests were done with 100 ppm solutions of the surfactant. Tests as a function of absorber length showed that the mass transfer for 60% solution was about a factor of two. Tests on 50% LiBr showed an increase of a factor of 5.7 over the first 40 cm of length. NTIS

N94-21564*# National Aeronautics and Space Administration. Lewis Research Center, Cleveland, OH.
REDUCING THE COGNITIVE WORKLOAD: TROUBLE MANAGING POWER SYSTEMS
David B. Manner (Sverdrup Technology, Inc., Brook Park, OH.), Eugene M. Liberman (Sverdrup Technology, Inc., Brook Park, OH.), James L. Dolce, and Pamela A. Mellor Dec. 1993 7 p Presented at the Computing in Aerospace 9, San Diego, CA, 19-21 Oct. 1993; sponsored by AIAA
(Contract NAS3-25266; RTOP 476-14-10)
(NASA-TM-106413; E-8249; NAS 1.15:106413; AIAA Paper 93-4703-CP)
Avail: CASI HC A02/MF A01

The complexity of space-based systems makes monitoring them and

diagnosing their faults taxing for human beings. Mission control operators are well-trained experts but they can not afford to have their attention diverted by extraneous information. During normal operating conditions monitoring the status of the components of a complex system alone is a big task. When a problem arises, immediate attention and quick resolution is mandatory. To aid humans in these endeavors we have developed an automated advisory system. Our advisory expert system, Trouble, incorporates the knowledge of the power system designers for Space Station Freedom. Trouble is designed to be a ground-based advisor for the mission controllers in the Control Center Complex at Johnson Space Center (JSC). It has been developed at NASA Lewis Research Center (LeRC) and tested in conjunction with prototype flight hardware contained in the Power Management and Distribution testbed and the Engineering Support Center, ESC, at LeRC. Our work will culminate with the adoption of these techniques by the mission controllers at JSC. This paper elucidates how we have captured power system failure knowledge, how we have built and tested our expert system, and what we believe are its potential uses. Author

N94-21589*# National Aeronautics and Space Administration. Lewis Research Center, Cleveland, OH.

DESIGN AND IMPLEMENTATION OF A STATUS AT A GLANCE USER INTERFACE FOR A POWER DISTRIBUTION EXPERT SYSTEM

Eugene M. Liberman (Sverdrup Technology, Inc., Brook Park, OH.), David B. Manner (Sverdrup Technology, Inc., Brook Park, OH.), James L. Dolce, and Pamela A. Mellor Dec. 1993 7 p Presented at the AIAA Computing in Aerospace 9, San Diego, CA, 19-21 Oct. 1993; sponsored by AIAA

(Contract NAS3-25266; RTOP 476-14-10)

(NASA-TM-106412; E-8248; NAS 1.15:106412; AIAA Paper 93-4657) Avail: CASI HC A02/MF A01

Expert systems are widely used in health monitoring and fault detection applications. One of the key features of an expert system is that it possesses a large body of knowledge about the application for which it was designed. When the user consults this knowledge base, it is essential that the expert system's reasoning process and its conclusions be as concise as possible. If, in addition, an expert system is part of a process monitoring system, the expert system's conclusions must be combined with current events of the process. Under these circumstances, it is difficult for a user to absorb and respond to all the available information. For example, a user can become distracted and confused if two or more unrelated devices in different parts of the system require attention. A human interface designed to integrate expert system diagnoses with process data and to focus the user's attention to the important matters provides a solution to the 'information overload' problem. This paper will discuss a user interface to the power distribution expert system for Space Station Freedom. The importance of features which simplify assessing system status and which minimize navigating through layers of information will be discussed. Design rationale and implementation choices will also be presented. Author

32 COMMUNICATIONS AND RADAR

Includes radar; land and global communications; communications theory; and optical communications.

For related information see also *04 Aircraft Communications and Navigation* and *17 Space Communications, Spacecraft Communications, Command and Tracking.* For search and rescue see *03 Air Transportation and Safety,* and *16 Space Transportation.*

N94-19816# Scientific Studies Corp., Palm Beach Gardens, FL.

STATE-SPACE MODELS FOR MULTICHANNEL DETECTION Final Technical Report, Apr. 1993 - Jan. 1994

J. R. Roman and D. W. Davis Jul. 1993 138 p

(Contract F30602-92-C-0081)

(AD-A270608; SSC-TR-93-02; RL-TR-93-146) Avail: CASI HC A07/MF A02

In multichannel identification and detection (or model-based multichannel detection) problems the parameters of a model are identified from the observed channel process and the identified model is used to facilitate the detection of a signal in the observe process. A model-based multichannel detection algorithm was developed in the context of an innovations-based detection algorithm (IBDA) formulation for surveillance radar system applications. The state space model class was adopted to model the vector channel process because it is more general than the time series model class used in most analyses to date. An IBDA methodology was developed based on the canonical correlations algorithm which for state-space model identification offers performance advantages over alternative techniques. A computer simulation was developed to validate the methodology and the algorithm, and to carry out performance assessments. Simulation results indicate that the algorithm is capable of discriminating between the null hypothesis (clutter plus noise) and the alternative hypothesis (signal plus clutter plus noise). In summary, the applicability of the approach to radar system problems was established. DTIC

N94-19823 Kansas Univ. Center for Research, Inc., Lawrence. Radar Systems and Remote Sensing Lab.

RADAR BACKSCATTER MEASUREMENTS FROM SIMULATED SEA ICE DURING CRRELEX 1990

S. G. Beaven, S. P. Gogineni, A. Gow (Army Cold Regions Research and Engineering Lab., Hanover, NH.), A. Lohanick (Army Cold Regions Research and Engineering Lab., Hanover, NH.), and K. Jezek (Ohio State Univ., Columbus.) Jun. 1993 135 p Limited Reproducibility: More than 20% of this document may be affected by microfiche quality

(Contract N00014-89-J-1456)

(AD-A271034; RSL-TR-8243-2) Avail: CASI HC A07

Radar backscatter measurements were performed on artificially grown sea ice on an outdoor pond at the U.S. Army Cold Regions Research and Engineering Laboratory (CRREL) during the 1990 winter season. Measurements of microwave backscatter from simulated sea ice demonstrate that the dominant backscatter mechanism is the surface scatter. Both the co-polarized and cross-polarized measurements compare favorably with the predictions of surface scattering models at two frequencies. The surface parameters used in the models were measured directly from photographs of cross sections of the saline ice. Therefore, since two frequencies of backscatter measurements were predicted accurately by surface scatter models, the predominate backscatter must be from the surface. DTIC

N94-19874# Stanford Linear Accelerator Center, CA.

PERSISTENT WAKEFIELDS ASSOCIATED WITH WAVEGUIDE DAMPING OF HIGHER ORDER MODES

N. M. Kroll and X. Lin Apr. 1993 3 p Presented at the International Particle Accelerator Conference, Washington, DC, 17-20 May 1993

(Contract DE-AC03-76SF-00515)

(DE93-040973; SLAC-PUB-6144; CONF-930511-429) Avail: CASI HC A01/MF A01

By means of an analytic model and numerical simulations, it was demonstrated that the wake of a waveguide damped cavity contains a persistent component which decays as t(sup -3/2) and thus is dominant at sufficiently large values of t. Because there are scenarios for which the effect gives rise to unacceptable beam instability, it cannot be ignored, but it seems likely that such an outcome can be avoided with proper design. DOE

N94-19912# Jet Propulsion Lab., California Inst. of Tech., Pasadena.

MILLIMETER WAVE IMAGING TECHNOLOGY Final Report, 5 May 1989 - 4 May 1992

R. P. Smith, David Rutledge, and Neville Luhmann 6 Oct. 1993 9 p

(Contracts MIPR-137-91; MIPR-138-90)

(AD-A271257; ARO-27307.6-EL) Avail: CASI HC A02/MF A01

JPL/Caltech is pursuing millimeter-wave imaging technology for the Army Research Office because of the potential of penetrating smoke, fog, and darkness. During this reporting period, we made progress on varactor diode processing approaches appropriate for millimeter and submillimeter wave electronics, on fabricating and measuring diode grids for frequency multiplication and beam control, and especially in the area of grid amplifiers, which promise to deliver higher power at greatly reduced cost for millimeter-wave generation. DTIC

N94-19934# Georgia Inst. of Tech., Atlanta. School of Physics.
STUDY OF ELECTROMAGNETIC WAVE SCATTERING FROM CHARACTERIZED ROUGH SURFACES Final Report, 20 Feb. 1990 - 30 Jun. 1993
Kevin A. ODonnell 4 Aug. 1993 80 p
(Contract DAAL03-90-G-0041)
(AD-A270931; ARO-27485.9-GS) Avail: CASI HC A05/MF A01

In our experimental and theoretical research during our ARO grant, we have studied the optical scattering properties of rough conducting surfaces that have structure comparable to or slightly greater than the illumination wavelength. We theoretically and experimentally studied the diffuse scatter for surfaces with one-dimensional roughness, where we have seen backscattering enhancement and strong polarization effects. In the angular correlation functions associated with the scattered light, we clearly see the coherent effects that give rise to backscattering enhancement. Further experimental studies have considered backscattering enhancement from a surface with two dimensional roughness, and we have theoretically investigated the effects of finite stylus width in the contact profilometer methods that we have used in our experiments. DTIC

N94-19951 Naval Command, Control and Ocean Surveillance Center, San Diego, CA.
SPORADIC-E OBSERVATIONS DURING LoVHF TRANSIONOSPHERIC DIRECTION FINDER MEASUREMENTS
Robert B. Rose 1993 8 p Limited Reproducibility: More than 20% of this document may be affected by microfiche quality
(AD-A270619) Avail: CASI HC A02

A year long experimental program was conducted to measure refractive bending or how much the signal deviates from true line of sight, at low VHF (LoVHF) frequencies (29.5 MHz), and to determine whether this deviation or error could be predicted using large-scale ionospheric models such as the Ionospheric Conductivity and Electron Density (ICED) program. An experiment to directly measure the angle of arrival of a 29.5 MHz signal from an orbiting satellite was successfully completed. The satellite was in a circular orbit at an altitude of 1000 km. It was shown that refractive errors can be directly related to the electron density along the measurement slant range. The introduction of irregular patches of electron density occurring during sporadic-E events produced both horizontal and vertical gradients introducing large errors in both azimuth and elevation measurements. Nineteen test periods in May, June, July, and Aug. 1989 were affected by mid-latitude sporadic-E with the daytime E-region critical frequencies (foE's) reaching 13 MHz in one case. This paper will present examples of these effects. DTIC

N94-19964 Electronic Systems Div., Hanscom AFB, MA.
GROUND WAVE EMERGENCY NETWORK. FINAL OPERATIONAL CAPABILITY. ENVIRONMENTAL ASSESSMENT FOR SOUTH CENTRAL MONTANA RELAY NODE, SITE NO. RN8C925MT
11 Feb. 1993 102 p Limited Reproducibility: More than 20% of this document may be affected by microfiche quality
(AD-A267795) Avail: CASI HC A06

The Ground Wave Emergency Network (GWEN) is a radio communication system designed to relay emergency messages between strategic military areas in the continental United States. The proposed action covered by this Environmental Assessment (EA) includes construction and operation of a relay node of the GWEN in south central Montana. This relay node will provide essential connections with adjacent nodes in the network. The major features of a GWEN relay node and associated environmental impacts common to all sites are addressed in the Final Environmental Impact Statement (FEIS) for the Final Operational Capability (FOC) phase of GWEN. This EA is tiered from that FEIS and addresses site-specific conditions at the candidate GWEN sites (CGS's) for this particular site search area.
Derived from text

N94-19977 Massachusetts Inst. of Tech., Cambridge. Artificial Intelligence Lab.
ROBUST, HIGH-SPEED NETWORK DESIGN FOR LARGE-SCALE MULTIPROCESSING
Andre DeHon Sep. 1993 219 p Limited Reproducibility: More than 20% of this document may be affected by microfiche quality
(Contract N00014-91-J-1698)
(AD-A271003; AI-TR-1445) Avail: CASI HC A10

Large-scale multiprocessing remains an elusive, yet promising, paradigm for achieving high-performance computation. As machine size scales upward, there are two important aspects of multiprocessor systems which will generally get worse rather than better: (1) interprocessor communication latency will increase; and (2) the probability that some component in the system will fail will increase. Both of these problems can prevent us from realizing the potential benefits of large-scale multiprocessing. In this document we consider the problem of designing networks which simultaneously minimize communication latency while maximizing fault tolerance for large-scale multiprocessors. Using a synergy of techniques including connection topologies, routing protocols, signalling techniques, and packaging technologies, we assemble integrated, system-level solutions to this network design problem. In particular, we recommend the use of the following: multipath, multistage networks; simple, source-responsible routing protocols; stochastic fault-avoidance; dense three-dimensional packaging; low-voltage, series-terminated transmission line signalling; and scan based diagnostics and reconfiguration. DTIC

N94-20139*# Ohio State Univ., Columbus. Dept. of Electrical Engineering.
AN EXTENDED UTD ANALYSIS FOR THE SCATTERING AND DIFFRACTION FROM CUBIC POLYNOMIAL STRIPS Final Report
E. D. Constantinides and R. J. Marhefka Jan. 1993 54 p
(Grant NsG-1498)
(NASA-CR-194581; NAS 1.26:194581; Rept-725311-2) Avail: CASI HC A04/MF A01

Spline and polynomial type surfaces are commonly used in high frequency modeling of complex structures such as aircraft, ships, reflectors, etc. It is therefore of interest to develop an efficient and accurate solution to describe the scattered fields from such surfaces. An extended Uniform Geometrical Theory of Diffraction (UTD) solution for the scattering and diffraction from perfectly conducting cubic polynomial strips is derived and involves the incomplete Airy integrals as canonical functions. This new solution is universal in nature and can be used to effectively describe the scattered fields from flat, strictly concave or convex, and concave convex boundaries containing edges. The classic UTD solution fails to describe the more complicated field behavior associated with higher order phase catastrophes and therefore a new set of uniform reflection and first-order edge diffraction coefficients is derived. Also, an additional diffraction coefficient associated with a zero-curvature (inflection) point is presented. Higher order effects such as double edge diffraction, creeping waves, and whispering gallery modes are not examined. The extended UTD solution is independent of the scatterer size and also provides useful physical insight into the various scattering and diffraction processes. Its accuracy is confirmed via comparison with some reference moment method results.
Author (revised)

N94-20160*# Michigan Univ., Ann Arbor. Dept. of Electrical Engineering and Computer Science.
A COMPARATIVE STUDY OF AN ABC AND AN ARTIFICIAL ABSORBER FOR TRUNCATING FINITE ELEMENT MESHES
T. Oezdemir and John L. Volakis Dec. 1993 16 p
(Contract NCA2-839)
(NASA-CR-194275; NAS 1.26:194275; UMICH-031173-1-T) Avail: CASI HC A03/MF A01

The type of mesh termination used in the context of finite element formulations plays a major role on the efficiency and accuracy of the field solution. The performance of an absorbing boundary condition (ABC) and an artificial absorber (a new concept) for terminating the finite element mesh was evaluated. This analysis is done in connection with the problem of scattering by a finite slot array in a thick ground plane. The two approximate mesh truncation schemes are compared with the exact finite element-boundary integral (FEM-BI) method in terms of accuracy and efficiency. It is demonstrated that both approximate truncation schemes yield reasonably accurate results even when the mesh is extended only 0.3 wavelengths away from the array aperture. However, the artificial absorber termination method leads to a substantially more efficient solution. Moreover, it is shown that the FEM-BI method remains quite competitive with the FEM-artificial absorber method when the FFT is used for computing the matrix-vector products in the iterative solution algorithm. These conclusions are indeed surprising and of major importance in electromagnetic simulations based on the finite element method. Author (revised)

N94-20198 Department of the Navy, Washington, DC.
TARGET MOTION DETECTING IMPULSE DOPPLER RADAR SYSTEM Patent
Robert E. Jehle, inventor (to Navy) and David F. Hudson, inventor (to Navy) 15 Jun. 1993 7 p Filed 25 Mar. 1992
(AD-D015898; US-Patent-5,220,328; US-Patent-Appl-SN-857536; US-Patent-Class-342-21) Avail: US Patent and Trademark Office

Radiant energy intermittently emitted from a transmitter is reflected as echo pulses from a moving target being interrogated to produce Doppler signals by counting of photons of the echo pulses during time domain intervals between emission from the transmitter. Such counting of photons is limited to the time domain intervals by operational control of a laser pump through which a reference beam is generated at an energy level activating detectors irradiated by such beam to count the photons absorbed therein after capture or the photons by a receiving antenna. DTIC

N94-20207# Air Force Inst. of Tech., Wright-Patterson AFB, OH. Foreign Aerospace Science and Technology Center.
NEW ALGORITHM OF GROUND TRACK PROCESSING IN HIGH-FREQUENCY SKYWAVE OVER-THE-HORIZON-B RADAR
Jiao Peinan 6 Aug. 1993 19 p Transl. into ENGLISH from Dianzi Xuebao (China), v. 19, no. 1, 1991 p 1-6
(AD-A267821; FASTC-ID(RS)T-0853-92) Avail: CASI HC A03/MF A01

In this paper, the concept pattern of the recognition tracking coordinate transformation data processor in HF skywave OTH-B radar is described. A new algorithm to determine the ground distance of a moving object from the time delay transformation of HF radar is proposed. Just the probe data obtained from only a single radar station are needed; there is no need to know the midpoint ionospheric data. The calculated ground track is compared with the actual track and the results show that the mean deviation is less than four percent. DTIC

N94-20215# Rhode Island Univ., Kingston. Dept. of Electrical Engineering.
HIGH RESOLUTION SIGNAL PROCESSING Final Report, 13 Apr. 1990 - 12 Apr. 1993
Donald W. Tufts 19 Aug. 1993 6 p
(Contract DAAL03-90-G-0106)
(AD-A271181; ARO-27620.13-MA) Avail: CASI HC A02/MF A01

Motivated by the goal of efficient, effective, high-speed integrated-circuit realization, we have discovered an algorithm for high speed Fourier analysis called the Arithmetic Fourier Transform (AFT). It is based on the number-theoretic method of Mobius inversion, a method that is well suited for integrated-circuit realization. The computation of the AFT can be carried out in parallel, pipelined channels, and the individual operations are very simple to execute and control. Except for a single scaling in each channel, all the operations are additions or subtractions. Thus, it can reduce the required power, volume, and cost. Also, analog switched-capacitor realizations of the AFT have been studied. We have also analyzed the performance of a broad and useful class of data adaptive signal estimation algorithms. This in turn has led to our proposed improvements in the methods. We have used perturbation analysis of the rank-reduced data matrix to calculate its statistical properties. The improvements made have been demonstrated by computer simulation as well as by comparison with the Cramer-Rao Bound. DTIC

N94-20269*# Arizona State Univ., Tempe. Coll. of Engineering and Applied Science.
[RCS ANALYSIS OF PLATE GEOMETRIES, PARTS 1 AND 2] Semiannual Progress Report, 1 Feb. - 31 Jul. 1993
Constantine A. Balanis, Lesley A. Polka, and Anastasis C. Polycarpou 31 Jul. 1993 43 p
(Grant NAG1-562)
(NASA-CR-194173; NAS 1.26:194173; TRC-EM-CAB-9306-Pt-1/2) Avail: CASI HC A03/MF A01

High-frequency techniques for Radar Cross Section (RCS) prediction of plate geometries and a physical optics/equivalent currents model for the RCS of trihedral corner reflectors are addressed. In part 1, a Uniform Theory of Diffraction (UTD) model for the principal-plane radar cross section (RCS) of a perfectly conducting, rectangular plate coated on one side with an electrically thin, lossy dielectric is presented. In part 2, the scattering in the interior regions of both square and triangular trihedral corner reflectors are examined. For individual titles, see N94-20270 through N94-20271.

N94-20270*# Arizona State Univ., Tempe. Coll. of Engineering and Applied Science.
HIGH-FREQUENCY TECHNIQUES FOR RCS PREDICTION OF PLATE GEOMETRIES
Constantine A. Balanis and Lesley A. Polka *In its* RCS Analysis of Plate Geometries, Parts 1 and 2 31 Jul. 1993 p 2-21 (For primary document see N94-20269 05-32)
Avail: CASI HC A03/MF A01

A Uniform Theory of Diffraction (UTD) model for the principal-plane radar cross section (RCS) of a perfectly conducting, rectangular plate coated on one side with an electrically thin (t much less than lambda), lossy dielectric is presented. The incorporation of higher-order, multiple diffractions and of multiply diffracted surface-waves is discussed in detail. It is demonstrated that these terms are crucial to obtaining an accurate model. Approximations that are used in the model are discussed. Suggestions for improvements to the model are made. Validation is provided via comparison with experimental data and a physical optics (PO) model. Author (revised)

N94-20271*# Arizona State Univ., Tempe. Coll. of Engineering and Applied Science.
A PHYSICAL OPTICS/EQUIVALENT CURRENTS MODEL FOR THE RCS OF TRIHEDRAL CORNER REFLECTORS
Constantine A. Balanis and Anastasis C. Polycarpou *In its* RCS Analysis of Plate Geometries, Parts 1 and 2 31 Jul. 1993 p 22-41 (For primary document see N94-20269 05-32)
Avail: CASI HC A03/MF A01

The scattering in the interior regions of both square and triangular trihedral corner reflectors is examined. The theoretical model presented combines geometrical and physical optics (GO and PO), used to account for reflection terms, with equivalent edge currents (EEC), used to account for first-order diffractions from the edges. First-order, second-order, and third-order reflection terms are included. Calculating the first-order reflection terms involves integrating over the entire surface of the illuminated plate. Calculating the second- and third-order reflection terms, however, is much more difficult because the illuminated area is an arbitrary polygon whose shape is dependent upon the incident angles. The method for determining the area of integration is detailed. Extensive comparisons between the high-frequency model, Finite-Difference Time-Domain (FDTD) and experimental data are used for validation of the radar cross section (RCS) of both square and triangular trihedral reflectors. Author (revised)

N94-20329 Mission Research Corp., Albuquerque, NM.
CHARACTERIZATION OF ELECTROMAGNETIC FIELDS IN AN EXTENDED CHAMBER AT THE SHORT PULSE EXPERIMENTAL ELECTRON DEVICE (SPEED) SIMULATOR Final Report, May - Dec. 1992
Kenneth K. Hunt Apr. 1993 70 p Limited Reproducibility: More than 20% of this document may be affected by microfiche quality
(Contract F29601-89-C-0014)
(AD-A265955; PL-TR-92-1065; AD-E201456) Avail: Issuing Activity (Defense Technical Information Center (DTIC))

The electromagnetic (EM) fields present during testing in a large vacuum chamber at the Short Pulse Experimental Electron Device (SPEED) facility are observed and measured using B-dot and D-dot detectors. Because the cathode of the vacuum diode is exposed to the chamber, the EM fields are significant and could adversely affect nonfaraday-shielded experiments. The differential magnetic fields and electric fields are nearly isotopically distributed, build to a maximum at 100 - 200 ns of 7.9 x 10(exp 9) A/m-s and 9 x 10(exp 10) V/m-s, respectively, then decay for approximately 1000 ns. Fourier analysis of spectra gives primary frequencies (460, 550, and 60 MHz) characteristic of the dimensions of the chamber and of electrons rebounding between the target and the pulse generators. A collimated damper is designed which should eliminate most EM fields in future tests in this configuration. DTIC

N94-20333 Department of the Navy, Washington, DC.
PHOTONIC ELECTROMAGNETIC FIELD SENSOR APPARATUS Patent
Donald P. Hilliard, inventor (to Navy) and Dean L. Mensa, inventor (to

Navy) 7 Sep. 1993 13 p Filed 30 Sep. 1992
(AD-D015938; US-Patent-5,243,186; US-Patent-Appl-SN-958404;
US-Patent-Class-250-227.17) Avail: US Patent and Trademark Office

An electromagnetic field sensor apparatus which measures the amplitude, phase, frequency and polarization of an incoming electromagnetic field as well as the angle of arrival of an incident electromagnetic field is introduced. A Luneberg lens focuses an incoming electromagnetic wave entering on one side of the Luneberg lens onto a point on the opposite side of the lens. A pair of photonic sensor which may be electro-optic modulators or Pockel cells are positioned on the Luneberg lens at the point upon which the incident electromagnetic wave is focused. The sensing axis of one of the electro-optic modulators is perpendicular to the sensing axis of the other electro-optic modulator. Polarized light is provided to each photonic sensor along an optical path which passes through the sensor. Each photonic sensor modulates the polarized light passing therethrough when the photonic sensor detects the incident electromagnetic wave. DTIC

N94-20334 Department of the Navy, Washington, DC.
PHOTONIC ELECTROMAGNETIC FIELD SENSOR APPARATUS Patent
Donald P. Hilliard, inventor (to Navy) and Dean L. Mensa, inventor (to Navy) 6 Jul. 1993 8 p Filed 17 Aug. 1992
(AD-D015939; US-Patent-5,225,668; US-Patent-Appl-SN-932271;
US-Patent-Class-250-206.2) Avail: US Patent and Trademark Office

An electromagnetic field sensor apparatus which measures the field strength and phase of an incident electromagnetic field as well as the angle of arrival of an incident electromagnetic field is presented. The electromagnetic field sensor apparatus comprises a Luneberg lens which focuses an incoming planar electromagnetic wave entering on one side of the Luneberg lens onto a point on the opposite side of the lens. A photonic sensor is positioned on the Luneberg lens at the point upon which the electromagnetic wave is focused. A light source is located along an optical path which passes through the photonic sensor for transmitting polarized light through the sensor. The photonic sensor modulates the polarized light passing therethrough when the photonic sensor detects the incident electromagnetic wave. DTIC

N94-20368* National Aeronautics and Space Administration. Langley Research Center, Hampton, VA.
FLEXIBLE HEATING HEAD FOR INDUCTION HEATING Patent
Robert L. Fox, inventor (to NASA), Samuel D. Johnson, inventor (to NASA), Robert H. Coultrip, inventor (to NASA), and W. Morris Phillips, inventor (to NASA) 30 Nov. 1993 8 p Filed 31 Oct. 1991 Supersedes N92-31257 (30 - 22, p 3803)
(NASA-Case-LAR-14418-15-B; US-Patent-5,266,764;
US-Patent-Appl-SN-790723; US-Patent-Class-219-10.75;
US-Patent-Class-219-9.5; US-Patent-Class-219-10.77;
US-Patent-Class-219-10.79; US-Patent-Class-156-272.2;
US-Patent-Class-156-272.4; Int-Patent-Class-H05B-6/36) Avail: US Patent and Trademark Office

An induction heating head includes a length of wire having first and second opposite ends and being wound in a flat spiral shape to form an induction coil, a capacitor connected to the first and second ends of the wire, the induction coil and capacitor defining a tank circuit, and a flexible, elastomeric body molded to encase the induction coil. When a susceptor is placed in juxtaposition to the body, and the tank circuit is powered, the susceptor is inductively heated.
Official Gazette of the U.S. Patent and Trademark Office

N94-20403*# Jet Propulsion Lab., California Inst. of Tech., Pasadena.
PROGRESS IN ELECTROMAGNETICS RESEARCH SYMPOSIUM (PIERS) Abstracts Only
1993 900 p Third Symposium held in Pasadena, CA, 12-16 Jul. 1993
(Contract NAS7-918; RTOP 665-31-00-08-71)
(NASA-CR-194629; JPL-Publ-93-17; NAS 1.26:194629) Avail: CASI HC A99/MF A10

The third Progress In Electromagnetics Research Symposium (PIERS) was held 12-16 Jul. 1993, at the Jet Propulsion Laboratory, California Institute of Technology, Pasadena, California. More than 800 presentations were made, and those abstracts are included in this publication. For individual titles, see N94-20404 through N94-20461.

N94-20404*# Jet Propulsion Lab., California Inst. of Tech., Pasadena.
PROBE COMPENSATION IN CYLINDRICAL NEAR-FIELD SCANNING: A NOVEL SIMULATION METHODOLOGY Abstract Only
Ziad A. Hussein and Yahya Rahmat-Samii *In its* Progress In Electromagnetics Research Symposium (PIERS) 1993 p 21 (For primary document see N94-20403 05-32)
Avail: CASI HC A01/MF A10

Probe pattern compensation is essential in near-field scanning geometry, where there is a great need to accurately know far-field patterns at wide angular range. This paper focuses on a novel formulation and computer simulation to determine the precise need for and effect of probe compensation in cylindrical near-field scanning. The methodology is applied to a linear test array antenna and the NASA scatterometer radar antenna. The formulation is based on representing the probe by its equivalent tangential magnetic currents. The interaction between the probe equivalent aperture currents and the test antenna fields is obtained with the application of a reciprocity theorem. This allows us to obtain the probe vector output pickup integral which is proportional to the amplitude and phase of the electric field induced in the probe aperture with respect to its position to the test antenna. The integral is evaluated for each probe position on the required sampling point on a cylindrical near-field surface enclosing the antenna. The use of a hypothetical circular-aperture probe with a different radius permits us to derive closed-form expressions for its far-field radiation patterns. These results, together with the probe vector output pickup, allow us to perform computer simulated synthetic measurements. The far-field patterns of the test antenna are formulated based on cylindrical wave expansions of both the probe and test antenna fields. In the limit as the probe radius becomes very small, the probe vector output is the direct response of the near-field at a point, and no probe compensation is needed. Useful results are generated to compare the far-field pattern of the test antenna constructed from the knowledge of the simulated near-field with and without probe pattern compensation and the exact results. These results are important since they clearly illustrate the angular range over which probe compensation is needed. It has been found that a probe with an aperture radius of 0.25(lambda), 0.5(lambda), and 1(lambda) needs a little probe compensation, if any, near the test antenna main beam. In addition, a probe with low directivity may provide a better signal-to-noise ratio than a highly directive one. This is evident in test antenna patterns without probe compensation at wide angles. Author (revised)

N94-20405*# Jet Propulsion Lab., California Inst. of Tech., Pasadena.
ANALYSIS OF MICROSTRIP DIPOLES AND SLOTS TRANSVERSELY COUPLED TO A MICROSTRIP LINE USING THE FDTD METHOD Abstract Only
A. N. Tulintseff *In its* Progress In Electromagnetics Research Symposium (PIERS) 1993 p 32 (For primary document see N94-20403 05-32)
Avail: CASI HC A01/MF A10

Printed dipole elements and their complement, linear slots, are elementary radiators that have found use in low-profile antenna arrays. Low-profile antenna arrays, in addition to their small size and low weight characteristics, offer the potential advantage of low-cost, high-volume production with easy integration with active integrated circuit components. The design of such arrays requires that the radiation and impedance characteristics of the radiating elements be known. The FDTD (Finite-Difference Time-Domain) method is a general, straight-forward implementation of Maxwell's equations and offers a relatively simple way of analyzing both printed dipole and slot elements. Investigated in this work is the application of the FDTD method to the analysis of printed dipole and slot elements transversely coupled to an infinite transmission line in a multilayered configuration. Such dipole and slot elements may be used in dipole and slot series-fed-type linear arrays, where element offsets and interelement line lengths are used to obtain the desired amplitude distribution and beam direction, respectively. The design of such arrays is achieved using transmission line theory with equivalent circuit models for the radiating elements. In an equivalent circuit model, the dipole represents a shunt impedance to the transmission line, where the impedance is a function of dipole offset, length, and width. Similarly, the slot represents a series impedance to the transmission line. The FDTD method is applied to single dipole and slot elements transversely coupled to an infinite microstrip line using a fixed rectangular grid with Mur's second order absorbing boundary conditions. Frequency-dependent circuit and scattering parameters

are obtained by saving desired time-domain quantities and using the Fourier transform. A Gaussian pulse excitation is applied to the microstrip transmission line, where the resulting reflected signal due to the presence of the radiating element is used to determine the equivalent element impedance. Author (revised)

N94-20406*# National Aeronautics and Space Administration. Ames Research Center, Moffett Field, CA.

FD-TD MODELING OF 2-D DIELECTRIC WAVEGUIDES FOR PROPAGATION AND SCATTERING OF FEMTOSECOND OPTICAL SOLITONS Abstract Only

Rose Joseph (Northwestern Univ., Evanston, IL.), Peter Goorjian, and Allen Taflove (Northwestern Univ., Evanston, IL.) *In* JPL, Progress In Electromagnetics Research Symposium (PIERS) 1993 p 35 (For primary document see N94-20403 05-32)

Avail: CASI HC A01/MF A10

Experimentalists have produced all-optical switches capable of 100-fs responses. To adequately model such switches, nonlinear effects in optical materials (both instantaneous and dispersive) must be included. In principle, the behavior of electromagnetic fields in nonlinear dielectrics can be determined by solving Maxwell's equations subject to the assumption that the electric polarization has a nonlinear relation to the electric field. However, until our previous work, the resulting nonlinear Maxwell's equations have not been solved directly. Rather, approximations have been made that result in a class of generalized nonlinear Schrodinger equations (GNLSE) that solve only for the envelope of the optical pulses. In this paper, we present first-time calculations from the vector nonlinear Maxwell's equations of femtosecond soliton propagation and scattering, including carrier waves, in two-dimensional systems of dielectric waveguides exhibiting the Kerr and Raman quantum effects. We use the finite-difference time-domain (FD-TD) method in an extension of our 1-D work. There, in a fundamental innovation, we treated the linear and nonlinear convolutions for the electric polarization as new dependent variables. By differentiating these convolutions in the time domain, we derived an equivalent system of coupled, nonlinear second-order ODE's. These equations together with Maxwell's equations form the system that is solved to determine the electromagnetic fields in inhomogeneous nonlinear dispersive media. Backstorage in time is limited to only that needed by the time-integration algorithm for the ODE's, rather than that needed to store the time-history of the kernel functions of the convolutions (1000-10,000 time steps). Thus, a 2-D nonlinear optics model from Maxwell's equations is now feasible. Author (revised)

N94-20407*# Jet Propulsion Lab., California Inst. of Tech., Pasadena.

A GENERAL ROUGH-SURFACE INVERSION ALGORITHM: THEORY AND APPLICATION TO SAR DATA Abstract Only

M. Moghaddam *In its* Progress In Electromagnetics Research Symposium (PIERS) 1993 p 66 (For primary document see N94-20403 05-32)

Avail: CASI HC A01/MF A10

Rough-surface inversion has significant applications in interpretation of SAR data obtained over bare soil surfaces and agricultural lands. Due to the sparsity of data and the large pixel size in SAR applications, it is not feasible to carry out inversions based on numerical scattering models. The alternative is to use parameter estimation techniques based on approximate analytical or empirical models. Hence, there are two issues to be addressed, namely, what model to choose and what estimation algorithm to apply. Here, a small perturbation model (SPM) is used to express the backscattering coefficients of the rough surface in terms of three surface parameters. The algorithm used to estimate these parameters is based on a nonlinear least-squares criterion. The least-squares optimization methods are widely used in estimation theory, but the distinguishing factor for SAR applications is incorporating the stochastic nature of both the unknown parameters and the data into formulation, which will be discussed in detail. The algorithm is tested with synthetic data, and several Newton-type least-squares minimization methods are discussed to compare their convergence characteristics. Finally, the algorithm is applied to multifrequency polarimetric SAR data obtained over some bare soil and agricultural fields. Results will be shown and compared to ground-truth measurements obtained from these areas. The strength of this general approach to inversion of SAR data is that it can be easily modified for use with any scattering model without changing any of the inversion steps. Note also that, for the same reason it is not limited to inversion of rough surfaces, and can be applied to any parameterized scattering process. Author (revised)

N94-20408*# Jet Propulsion Lab., California Inst. of Tech., Pasadena.

VARIABLE-PERMITTIVITY LINEAR INVERSE PROBLEM FOR THE H(SUB z)-POLARIZED CASE Abstract Only

M. Moghaddam and W. C. Chew (Illinois Univ., Urbana-Champaign.) *In its* Progress In Electromagnetics Research Symposium (PIERS) 1993 p 77 (For primary document see N94-20403 05-32)

Avail: CASI HC A01/MF A10

The H(sub z)-polarized inverse problem has rarely been studied before due to the complicated way in which the unknown permittivity appears in the wave equation. This problem is equivalent to the acoustic inverse problem with variable density. We have recently reported the solution to the nonlinear variable-permittivity H(sub z)-polarized inverse problem using the Born iterative method. Here, the linear inverse problem is solved for permittivity (epsilon) and permeability (mu) using a different approach which is an extension of the basic ideas of diffraction tomography (DT). The key to solving this problem is to utilize frequency diversity to obtain the required independent measurements. The receivers are assumed to be in the far field of the object, and plane wave incidence is also assumed. It is assumed that the scatterer is weak, so that the Born approximation can be used to arrive at a relationship between the measured pressure field and two terms related to the spatial Fourier transform of the two unknowns, epsilon and mu. The term involving permeability corresponds to monopole scattering and that for permittivity to dipole scattering. Measurements at several frequencies are used and a least squares problem is solved to reconstruct epsilon and mu. It is observed that the low spatial frequencies in the spectra of epsilon and mu produce inaccuracies in the results. Hence, a regularization method is devised to remove this problem. Several results are shown. Low contrast objects for which the above analysis holds are used to show that good reconstructions are obtained for both permittivity and permeability after regularization is applied. Author (revised)

N94-20409*# National Aeronautics and Space Administration. Goddard Space Flight Center, Greenbelt, MD.

RELATING GROUND TRUTH COLLECTION TO MODEL SENSITIVITY Abstract Only

Faouzi Amar (Texas Univ., Arlington.), Adrian K. Fung (Texas Univ., Arlington.), Mostafa A. Karam, and Eric Mougin (Centre d'Etude Spatiale des Rayonnements, Toulouse, France.) *In* JPL, Progress In Electromagnetics Research Symposium (PIERS) 1993 p 161 (For primary document see N94-20403 05-32)

Avail: CASI HC A01/MF A10

The importance of collecting high quality ground truth before a SAR mission over a forested area is two fold. First, the ground truth is used in the analysis and interpretation of the measured backscattering properties; second, it helps to justify the use of a scattering model to fit the measurements. Unfortunately, ground truth is often collected based on visual assessment of what is perceived to be important without regard to the mission itself. Sites are selected based on brief surveys of large areas, and the ground truth is collected by a process of selecting and grouping different scatterers. After the fact, it may turn out that some of the relevant parameters are missing. A three-layer canopy model based on the radiative transfer equations is used to determine, before hand, the relevant parameters to be collected. Detailed analysis of the contribution to scattering and attenuation of various forest components is carried out. The goal is to identify the forest parameters which most influence the backscattering as a function of frequency (P-, L-, and C-bands) and incident angle. The influence on backscattering and attenuation of branch diameters, lengths, angular distribution, and permittivity; trunk diameters, lengths, and permittivity; and needle sizes, their angular distribution, and permittivity are studied in order to maximize the efficiency of the ground truth collection efforts. Preliminary results indicate that while a scatterer may not contribute to the total backscattering, its contribution to attenuation may be significant depending on the frequency. Author

N94-20410*# Jet Propulsion Lab., California Inst. of Tech., Pasadena.

MODIFICATIONS TO THE THREE-COMPONENT CLASSIFICATION ALGORITHM FOR SAR DATA Abstract Only

M. Moghaddam and A. Freeman *In its* Progress In Electromagnetics Research Symposium (PIERS) 1993 p 164 (For primary document see N94-20403 05-32)

Avail: CASI HC A01/MF A10

Previously, a scattering model was used to classify SAR data as due

to three mechanisms: surface or odd-bounce scattering; double-bounce scattering; and volume scattering. A Bragg rough-surface model was used for odd-bounce scattering, and two reflecting surfaces, as in a dihedral corner reflector, represented the double-bounce scattering mechanism. A random collection of infinitely thin cylinders was used to model the volume scattering contribution. It was assumed that the cylinders are uniformly oriented in all directions. In this work, modifications are made to the above model, which include specifying a preferred orientation for the cylinders representing branches and using thin cylinders of finite thickness as opposed to infinitely thin ones. In the first case, the preferred orientation is represented by a probability density function in the form of a dirac delta function. For the second case, small argument asymptotic expansions of Bessel functions are used to express the volume scattering contributions in terms of quantities containing the average radius of the cylinders. Since in each case the number of unknowns exceeds that of equations, simplifying assumptions are made. The solutions are applied to multifrequency polarimetric SAR data to obtain the new unknowns in addition to the relative contributions of each scattering mechanism. Several results are presented. It is found that the calculated percentage of each mechanism does not change significantly compared to the original model; however, additional information is gained about the scatterers. Author (revised)

N94-20411*# Jet Propulsion Lab., California Inst. of Tech., Pasadena.
DETERMINATION OF NOISE EQUIVALENT SIGMA(0) USING HIGHLY CORRELATED REPEAT-PASS SAR IMAGES Abstract Only
James Sun and Anthony Freeman *In its* Progress In Electromagnetics Research Symposium (PIERS) 1993 p 168 (For primary document see N94-20403 05-32)
Avail: CASI HC A01/MF A10

Noise equivalent sigma(sup 0) is a fundamental parameter in any synthetic aperture radar (SAR) measurement. Knowledge of the noise equivalent sigma(sup 0) allows the radar application scientist to band the error contributions due to noise present in his/her data. In this paper, a novel technique for determining noise equivalent sigma(sup 0) is presented. It has been observed that a pair of images obtained by a SAR over the same area in a nearly repeating orbit can demonstrate a high degree of correlation, depending on the baseline. If noise independence and signal power invariance are assumed, an estimate for the noise equivalent sigma(sup 0) for each image can be determined without any known ground targets. We examine the application of this technique to several images of different backscatter obtained by ERS-1. Author (revised)

N94-20412*# Jet Propulsion Lab., California Inst. of Tech., Pasadena.
ERS-1 AND SEASAT SCATTEROMETER MEASUREMENTS OF OCEAN WINDS: MODEL FUNCTIONS AND THE DIRECTIONAL DISTRIBUTION OF SHORT WAVES Abstract Only **c43**
Michael H. Freilich (Oregon State Univ., Corvallis.) and R. Scott Dunbar *In its* Progress In Electromagnetics Research Symposium (PIERS) 1993 p 186 (For primary document see N94-20403 05-32)
Avail: CASI HC A01/MF A10

Calculation of accurate vector winds from scatterometers requires knowledge of the relationship between backscatter cross-section and the geophysical variable of interest. As the detailed dynamics of wind generation of centimetric waves and radar-sea surface scattering at moderate incidence angles are not well known, empirical scatterometer model functions relating backscatter to winds must be developed. Less well appreciated is the fact that, given an accurate model function and some knowledge of the dominant scattering mechanisms, significant information on the amplitudes and directional distributions of centimetric roughness elements on the sea surface can be inferred. accurate scatterometer model functions can thus be used to investigate wind generation of short waves under realistic conditions. The present investigation involves developing an empirical model function for the C-band (5.3 GHz) ERS-1 scatterometer and comparing Ku-band model functions with the C-band model to infer information on the two-dimensional spectrum of centimetric roughness elements in the ocean. The C-band model function development is based on collocations of global backscatter measurements with operational surface analyses produced by meteorological agencies. Strengths and limitations of the method are discussed, and the resulting model function is validated in part through comparison with the actual distributions of backscatter cross-section triplets. Details of the directional modulation as well as the wind speed sensitivity at C-band are investigated. Analysis of persistent outliers in the data is used to infer the magnitudes of non-wind effects (such as atmospheric stratification, swell, etc.). The ERS-1 C-band instrument and the Seasat Ku-band (14.6 GHz) scatterometer both imaged waves of approximately 3.4 cm wavelength assuming that Bragg scattering is the dominant mechanism. Comparisons of the C-band and Ku-band model functions are used both to test the validity of the postulated Bragg mechanism and to investigate the directional distribution of the imaged waves under a variety of conditions where Bragg scatter is dominant. Author (revised)

N94-20413*# Jet Propulsion Lab., California Inst. of Tech., Pasadena.
Ku-BAND OCEAN RADAR BACKSCATTER OBSERVATIONS DURING SWADE Abstract Only **c43**
S. V. Nghiem, F. K. Li, S. H. Lou, and G. Neumann *In its* Progress In Electromagnetics Research Symposium (PIERS) 1993 p 188 (For primary document see N94-20403 05-32)
Avail: CASI HC A01/MF A10

We present results obtained by an airborne Ku-band scatterometer during the Surface Wave Dynamics Experiment (SWADE). The specific objective of this study is to improve our understanding of the relationship between ocean radar backscatter and near surface winds. The airborne scatterometer, NUSCAT, was flown on the NASA Ames C-130 over an instrumented oceanic area near 37 deg N and 74 deg W. A total of 10 flights from 27 Feb. to 9 Mar. 1991 were conducted. Radar backscatter at incidence angles of 0 to 60 deg were obtained. For each incidence angle, the NUSCAT antenna was azimuthally scanned in multiple complete circles to measure the azimuthal backscatter modulations. Both horizontal and vertical polarization backscatter measurements were made. In some of the flights, the cross-polarization backscatter was measured as well. Internal calibrations were carried out throughout each of the flights. Preliminary results indicate that the radar was stable to +/-0.3 dB for each flight. In this paper, we present studies of the backscatter measurements over several crossings of the Gulf Stream. In these crossings, large air-sea temperature differences were encountered and substantial changes in the radar cross section were observed. We summarize the observations and compare them to the changes of several wind variables across the Gulf Stream boundary. In one of the flights, the apparent wind near the cold side of the Gulf Stream was very low (less than 3 m/s). The behavior of the radar cross sections at such low wind speeds and a comparison with models are presented. A case study of the effects of swell on the absolute cross section and the azimuthal modulation pattern is presented. Significant wave heights larger than m were observed during SWADE. The experimentally observed effects of the swell on the radar backscatter are discussed. The effects are used to assess the uncertainties in wind retrieval due to underlying waves. A summary of azimuthal modulation from our ten-flight of NUSCAT data is given. Wind velocities, air and sea surface temperature, ocean spectrum, and other variables measured from aircraft and buoys are also shown. Author (revised)

N94-20414*# National Aeronautics and Space Administration. Wallops Flight Facility, Wallops Island, VA.
ANALYSIS OF Ku-BAND CROSS SECTION AT LOW INCIDENCE ANGLES Abstract Only
B. Chapron (Institut Francais de Recherche pour l'Exploitation de la Mer, Brest.) and D. Vandemark *In* JPL, Progress In Electromagnetics Research Symposium (PIERS) 1993 p 190 (For primary document see N94-20403 05-32)
Avail: CASI HC A01/MF A10

This study is using airborne Ku-band data to address questions which have implications for both model function development and for advancing our physical understanding of the sea surface. Concurrent measurements of ocean directional spectra, significant wave height, and mean surface roughness are made using the capabilities of the radar ocean wave spectrometer (ROWS). The NASA/GSFC's ROWS is a 15 GHz pulse compressed radar which is a radar sensor designed to measure the direction of the long wave components using spectral analysis of the tilt induced reflectively modulation. The ROWS are modified to cycle at 50 Hz for the scanning spectrometer antenna and a wide beamwidth nadir altimeter mode. This change allows the sensor to simultaneously measure directional wave spectra, wave height, mean square slope parameter, and small scale surface roughness. The surface stress caused by the wind is widely believed to be the predominant quantity related to the Ku-band radar cross section for a wide range of incidence angles. The complete coverage in the quasi specular

region provided by one sensor is essential to understand the uncertainties between the scattering model and what is happening on the surface. For this presentation, special attention is devoted to sort out some measurement of the anisotropy associated with the band of high frequencies. Using the other geophysical parameters, comparisons are then made with the classic spectral form currentlyused to describe the wind impact on the sea surface. Author (revised)

N94-20415*# Jet Propulsion Lab., California Inst. of Tech., Pasadena.
COMPARISON OF REMOTE SENSING MEASUREMENTS WITH A TWO-SCALE POLARIMETRIC EMISSION AND SCATTERING MODEL FOR SEA SURFACES Abstract Only **c43**
S. H. Yueh, S. V. Nghiem, R. Kwok, and F. K. Li *In its* Progress In Electromagnetics Research Symposium (PIERS) 1993 p 191 (For primary document see N94-20403 05-32)
Avail: CASI HC A01/MF A10

Recently, it has been observed that the brightness temperatures of sea surfaces correlate with the azimuth angle of the ocean wind vector, indicating that ocean wind direction can not only be retrieved from the microwave backscatter, but also from the brightness temperature measurements. In this paper, comparison of the theoretical result calculated from a two-scale emission and scattering model with the Seasat and SSM/I model functions and aircraft measurements is presented and potential applications of microwave polarimetry are discussed. In our two-scale model, the modified reflectivities of large scale surfaces are calculated by extending the small perturbation method to the second order for small scale perturbation with anisotropic directional spectrum. It was found that the modified reflectivities derived from the second-order scattered field agree excellently well with the results obtained from a Monte Carlo simulation technique which numerically calculates the polarimetric reflectivities of one-dimensional random rough surfaces with a power-law spectrum. Without the second-order correction, the modified reflectivities of the rough surfaces are significantly over-estimated and sign errors are observed in the third and fourth Stokes parameters for thermal emissions. The surface spectrum parameters and two-scale cutoff are selected so that the calculated scattering and emission signatures agree with the reported model functions for Seasat and SSM/I. Subsequently, the polarimetric signatures of sea surfaces are illustrated to indicate the possibility of reducing the number of azimuthal looks required for spaceborne sensors in the remote sensing of ocean wind by using the polarimetric information. Furthermore, it is found that contrary to the dependence of backscattering coefficients on incidence angles, polarimetric brightness temperatures display a stronger wind direction dependence in the near nadir-looking direction than away from nadir. Finally, we discuss the potential of a single-look polarimetric radiometer for wind retrieval. Author

N94-20416*# National Aeronautics and Space Administration. Goddard Inst. for Space Studies, New York, NY.
INTENSITY AND POLARIZATION OF LIGHT SCATTERED BY SIZE DISTRIBUTIONS OF RANDOMLY ORIENTED NONSPHERICAL PARTICLES Abstract Only
M. I. Mishchenko and L. D. Travis *In* JPL, Progress In Electromagnetics Research Symposium (PIERS) 1993 p 241 (For primary document see N94-20403 05-32)
Avail: CASI HC A01/MF A10

Calculations of light scattering by small particles are important in many diverse fields of science and engineering. In many cases of practical interest, scattering particles are nonspherical and are distributed over sizes and orientations. However, accurate light scattering computations for ensembles of nonspherical particles are difficult and time-consuming, and the literature in which such calculations are reported is rather scarce. In this paper, the T-matrix approach, as extended recently to randomly oriented particles, is used to calculate rigorously light scattering by size distributions of randomly oriented axially symmetric particles. To model the variation of particle sizes in real ensembles, we use a power law distribution typical of some terrestrial aerosols. Contour plots of intensity and degree of linear polarization for polydisperse prolate and oblate spheroids of different aspect ratios and effective equivalent-sphere size parameters from 0 to 10 are calculated and compared with calculations for equivalent spheres. The angular scattering behavior of nonspherical polydispersions is found to be greatly different from that of spheres, while the scattering properties of oblate and prolate spheroids of the same aspect ratio are similar. With increasing particle size, both intensity and polarization become more shape-dependent. In general, nonspherical particles are stronger side scatterers and weaker backscatterers than equivalent spheres. With increasing aspect ratio of nonspherical particles polarization tends to be predominantly positive. Possible effects of particle nonsphericity on optical remote sensing of atmospheric aerosols are discussed. Author

N94-20417*# Jet Propulsion Lab., California Inst. of Tech., Pasadena.
TOPOGRAPHIC MAPPING USING A MONOPULSE SAR SYSTEM Abstract Only **c43**
M. Zink (Deutsche Forschungsanstalt fuer Luft- und Raumfahrt, Oberpfaffenhofen, Germany.), H. Oettl (Deutsche Forschungsanstalt fuer Luft- und Raumfahrt, Oberpfaffenhofen, Germany.), and A. Freeman *In its* Progress In Electromagnetics Research Symposium (PIERS) 1993 p 256 (For primary document see N94-20403 05-32)
Avail: CASI HC A01/MF A10

Terrain height variations in mountainous areas cause two problems in the radiometric correction of SAR images: the first being that the wrong elevation angle may be used in correcting for the radiometric variation of the antenna pattern; the second that the local incidence angle used in correcting the projection of the pixel area from slant range to ground range coordinates may vary from that given by the flat earth assumption. We propose a novel design of a SAR system which exploits the monopulse principle to determine the elevation angle and thus the height at the different parts of the image. The key element of such a phase monopulse system is an antenna, which can be divided into a lower and upper half in elevation using a monopulse comparator. In addition to the usual sum pattern, the elevation difference pattern can be generated by a -pi phase shift on one half of the antenna. From the ratios of images radiometrically modulated by the difference and sum antenna pattern in cross-track direction, we can derive the appropriate elevation angle at any point in the image. Together with the slant range we can calculate the height of the platform above this point using information on the antenna pointing and the platform attitude. This operation, repeated at many locations throughout the image, allows us to build up a topographic map of the height of the aircraft above each location. Inversion of this map, using the precisely determined aircraft altitude and the accurate flight path, leads to the actual topography of the imaged surface. The precise elevation of one point in the image could also be used to convert the height map to a topographic map. In this paper, we present design considerations for a corresponding airborne SAR system in X-Band and give estimates of the error due to system noise and azimuth ambiguities as well as the expected performance and precision in topographic mapping. Author

N94-20418*# National Aeronautics and Space Administration. Langley Research Center, Hampton, VA.
INTEGRATED DISPLAY OF MULTI-SENSOR GEOPHYSICAL AND ELECTROMAGNETIC FLIGHT DATA Abstract Only
V. E. Delnore (Lockheed Engineering and Sciences Co., Hampton, VA.), E. M. Bracalente, S. D. Harrah, and C. L. Britt, Jr. (Research Triangle Inst., Hampton, VA.) *In* JPL, Progress In Electromagnetics Research Symposium (PIERS) 1993 p 259 (For primary document see N94-20403 05-32)
Avail: CASI HC A01/MF A10

Low-altitude wind shear has been identified by several aviation interests as a significant hazard to the safety of flying. The hazard may be greatest when the wind shear is due to an unpredicted and short-lived microburst occurring in the immediate flight path of an aircraft during takeoff or landing. Researchers from the NASA Langley Research Center have investigated wind shear by developing a suite of remote sensing instruments and then using these instruments in an airborne wind shear detection flight program. Among these instruments were a Doppler radar, a lidar, and an infrared sensor; these were supported by in situ measurements of aircraft and environmental parameters and by ground-based Doppler radars. The basic problem addressed was the airborne detection and measurement of meteorologically-induced wind shear sufficiently ahead of the aircraft to allow avoidance. If the remote measurements of the shear and its associated radar reflectivity did not exceed set limits, the airplane then continued through the wind shear so that in situ measurements could be made for comparison. Initial detection and vectoring to the wind shear was normally given from a ground-based Doppler weather radar and most of the wind shear events were due to microbursts, both wet and dry. This paper considers the problems of sampling the wind shear event, time and space

registration among the various sensors, coordination of the various sensors' beams and sampling volumes, and also various techniques for portraying the data, both for research and for presentation. Examples are given based on data from the 1991 and 1992 NASA/FAA wind shear flights, and the results and conclusions are generalized to other flight experiments involving multi-sensor electromagnetic data sets. Author

N94-20419*# National Aeronautics and Space Administration. Langley Research Center, Hampton, VA.
DESCRIPTION AND AVAILABILITY OF AIRBORNE DOPPLER RADAR DATA Abstract Only
S. D. Harrah, E. M. Bracalente, P. R. Schaffner, and E. G. Baxa (Clemson Univ., SC.) *In* JPL, Progress In Electromagnetics Research Symposium (PIERS) 1993 p 262 (For primary document see N94-20403 05-32)
Avail: CASI HC A01/MF A10

An airborne, forward-looking, pulse, Doppler radar has been developed in conjunction with the joint FAA/NASA Wind Shear Program. This radar represents a first in an emerging technology. The radar was developed to assess the applicability of an airborne radar to detect low altitude hazardous wind shears for civil aviation applications. Such a radar must be capable of looking down into the ground clutter environment and extracting wind estimates from relatively low reflectivity weather targets. These weather targets often have reflectivities several orders of magnitude lower than the surrounding ground clutter. The NASA radar design incorporates numerous technological and engineering achievements in order to accomplish this task. The basic R/T unit evolved from a standard Collins 708 weather radar, which supports specific pulse widths of 1-7 microns and Pulse Repetition Frequencies (PRF) of less than 1-10 kHz. It was modified to allow for the output of the first IF signal, which fed a NASA developed receiver/detector subsystem. The NASA receiver incorporated a distributed, high-speed digital attenuator, producing a range bin to range bin automatic gain control system with 65 dB of dynamic range. Using group speed information supplied by the aircraft's navigation system, the radar signal is frequency demodulated back to base band (zero Doppler relative to stationary ground). The In-phase & Quadrature-phase (I/Q) components of the measured voltage signal are then digitized by a 12-bit A-D converter (producing an additional 36 dB of dynamic range). The raw I/Q signal for each range bin is then recorded (along with the current radar & aircraft state parameters) by a high-speed Kodak tape recorder. Author

N94-20420*# Jet Propulsion Lab., California Inst. of Tech., Pasadena.
CLASSIFICATION OF SIMPLE VEGETATION TYPES USING POLSAR IMAGE DATA Abstract Only **c43**
A. Freeman *In its* Progress In Electromagnetics Research Symposium (PIERS) 1993 p 387 (For primary document see N94-20403 05-32)
Avail: CASI HC A01/MF A10

Mapping basic vegetation or land cover types is a fairly common problem in remote sensing. Knowledge of the land cover type is a key input to algorithms which estimate geophysical parameters, such as soil moisture, surface roughness, leaf area index or biomass from remotely sensed data. In an earlier paper, an algorithm for fitting a simple three-component scattering model to POLSAR data was presented. The algorithm yielded estimates for surface scatter, double-bounce scatter and volume scatter for each pixel in a POLSAR image data set. In this paper, we show how the relative levels of each of the three components can be used as inputs to simple classifier for vegetation type. Vegetation classes include no vegetation cover (e.g. bare soil or desert), low vegetation cover (e.g. grassland), moderate vegetation cover (e.g. fully developed crops), forest and urban areas. Implementation of the approach requires estimates for the three components from all three frequencies available using the NASA/JPL AIRSAR, i.e. C-, L- and P-bands. The research described in this paper was carried out by the Jet Propulsion Laboratory, California Institute of Technology under a contract with the National Aeronautics and Space Administration. Author

N94-20421*# Jet Propulsion Lab., California Inst. of Tech., Pasadena.
TWO MICROSTRIP ARRAYS FOR INTERFEROMETRIC SAR APPLICATIONS Abstract Only
J. Huang *In its* Progress In Electromagnetics Research Symposium (PIERS) 1993 p 396 (For primary document see N94-20403 05-32)
Avail: CASI HC A01/MF A10

Two types of C-band aircraft interferometric Synthetic Aperture Radar (SAR) are being developed at JPL to measure the ocean wave characteristics. Each type requires two identical antennas with each having a long rectangular aperture to radiate fan-shaped beam(s). One type of these radars requires each of its antennas to radiate a broadside beam that will measure the target's cross-track velocity. The other type, having each of its antennas to radiate two off-broadside pointed beams, will allow the measurement of both the cross-track and the along-track velocities of the target. Because flush mounting of the antenna on the aircraft fuselage is desirable, microstrip patch array is selected for these interferometric SAR antennas. To meet the radar system requirement, each array needs a total of 76 microstrip patches which are arranged in a 38 x 2 rectangular aperture with a physical size of 1.6m x 16.5cm. To minimize the insertion loss and physical real estate of this relatively long array, a combined series/parallel feed technique is used. Techniques to suppress cross-pol radiation and to effectively utilize the RF power are also implemented. Cross-pol level of lower than -30 dB from the co-pol peak and low insertion loss of 0.36 dB have been achieved for both types of arrays. For the type of radar that requires two off-broadside pointed beams, a simple phasing technique is used to achieve this dual-beam capability with adequate antenna gain (20 dBi) and sidelobe level (-14 dB). Both radar arrays have been flight tested on aircraft with excellent antenna performance demonstrated. Author

N94-20422*# National Aeronautics and Space Administration. Lewis Research Center, Cleveland, OH.
RECENT ACTIVITIES IN PRINTED ANTENNAS AT LeRC Abstract Only
Richard Q. Lee and Rainee N. Simons *In* JPL, Progress In Electromagnetics Research Symposium (PIERS) 1993 p 403 (For primary document see N94-20403 05-32)
Avail: CASI HC A01/MF A10

This paper will report two recent R&D efforts in printed antennas at NASA Lewis Research Center. These efforts are: (1) to enhance the current antenna performance in gain, bandwidth and pattern characteristics, and (2) to develop coplanar waveguide/aperture coupled feeding technique for dual excitation of a patch antenna. Research in area (1) has led to the development of a nonplanar linearly tapered slot antenna (LTSA) which has exhibited over 10 dB gain with broad bandwidth and excellent radiation patterns. This endfire antenna element is most suitable for use in MMIC arrays of 'brick' construction. A space power amplifier composed of active LTSA has been demonstrated and shown to have a gain of 30 dB at 20 GHz. In each of the antenna elements, a GaAs monolithic microwave integrated circuit (MMIC) three-stage power amplifier is integrated with two LTSA's. A single active LTSA has also been demonstrated and exhibited a power gain of 6.7 dB with the MMIC amplifier turned on. The aperture coupled feeding technique with coplanar waveguide feeds has demonstrated high coupling efficiency on both LTSA and patch antennas. Recent efforts have been focused on applying this technique for dual excitation (dual frequency and/or dual polarization) of a patch antenna. Preliminary results confirm the feasibility of this approach. Further development is required to improve the coupling efficiency and antenna radiation characteristics. Author

N94-20423*# Jet Propulsion Lab., California Inst. of Tech., Pasadena.
ANALYTICAL EVALUATION OF A SURFACE INTEGRAL EXPRESSING THE COUPLING BETWEEN INTERIOR AND EXTERIOR VOLUMES IN A FE-IE APPROACH Abstract Only
C. Zuffada, T. Cwik, and V. Jamnejad *In its* Progress In Electromagnetics Research Symposium (PIERS) 1993 p 446 (For primary document see N94-20403 05-32)
Avail: CASI HC A01/MF A10

Recently an approach which combines the finite element technique and an integral equation to determine the fields scattered by inhomogeneous bodies of complicated shape has been proposed. Basically, a mathematical surface which encloses the scatterers is introduced, thus dividing the space into an interior and an exterior volume, in which the finite element technique and an integral equation for EM scattering, respectively, are applied. The integral equation is set up for the tangential components of the fields at the surface, while the interior volume the unknowns are the total fields. Continuity of the tangential fields at the boundary, as required by Maxwell's equations, is imposed, thus coupling the two methods to obtain a consistent solution. The coupling term is expressed by a surface integral formed by the dot product of a FE basis function and an IE testing function, or

viceversa. By choosing the boundary to be a surface of revolution and by making a convenient selection of IE basis (testing) functions, it is possible to evaluate the integrals analytically on surfaces such as curved triangles, curved quadrilaterals and curved pentagons. We will illustrate the salient steps involved in setting up and carrying out these integrals and discuss what class of basis (testing) functions and analytic surfaces of revolution they are applicable to. Analytic calculations offer the advantage of better accuracy than purely numerical ones, and, when combined with them, often shed light on issues of numerical convergence and limiting values. Furthermore, they may reduce computation time and storage requirements. Author

N94-20424*# Jet Propulsion Lab., California Inst. of Tech., Pasadena.
ADVANCES IN SPACEBORNE RADAR REMOTE SENSING Abstract Only **c43**
C. Elachi *In its* Progress In Electromagnetics Research Symposium (PIERS) 1993 p 447 (For primary document see N94-20403 05-32)
Avail: CASI HC A01/MF A10

Radar sensors are being more commonly used for spaceborne sensing of Earth and Planetary surfaces and atmosphere. This is a result of advances in: better understanding wave/natural surface interaction mechanisms, measurement techniques, hardware development and data handling/visualization. A number of spaceborne radar systems are presently operational or will be launched in the next few years. In addition airborne instruments utilizing multispectral, polarmetric and interferometric capabilities are opening new vistas which will lead to major advances in radar sensing by the end of the decade. This paper is a review of recent developments and expected future advances. Author

N94-20425*# Jet Propulsion Lab., California Inst. of Tech., Pasadena.
DETECTION OF TRAVELING IONOSPHERIC DISTURBANCES INDUCED BY ATMOSPHERIC GRAVITY WAVES USING THE GLOBAL POSITIONING SYSTEM Abstract Only **c46**
Sassan Bassiri (Sharif Univ. of Technology, Tehran, Iran.) and George A. Hajj *In its* Progress In Electromagnetics Research Symposium (PIERS) 1993 p 452 (For primary document see N94-20403 05-32)
Avail: CASI HC A01/MF A10

Natural and man-made events like earthquakes and nuclear explosions launch atmospheric gravity waves (AGW) into the atmosphere. Since the particle density decreases exponentially with height, the gravity waves increase exponentially in amplitude as they propagate toward the upper atmosphere and ionosphere. As atmospheric gravity waves approach the ionospheric heights, the neutral particles carried by gravity waves collide with electrons and ions, setting these particles in motion. This motion of charged particles manifests itself by wave-like fluctuations and disturbances that are known as traveling ionospheric disturbances (TID). The perturbation in the total electron content due to TID's is derived analytically from first principles. Using the tilted dipole magnetic field approximation and a Chapman layer distribution for the electron density, the variations of the total electron content versus the line-of-sight direction are numerically analyzed. The temporal variation associated with the total electron content measurements due to AGW's can be used as a means of detecting characteristics of the gravity waves. As an example, detection of tsunami generated earthquakes from their associated atmospheric gravity waves using the Global Positioning System is simulated. Author

N94-20426*# Jet Propulsion Lab., California Inst. of Tech., Pasadena.
POLARIMETRIC BACKSCATTERING FROM SEA ICE Abstract Only **c48**
S. V. Nghiem, R. Kwok, and S. H. Yueh *In its* Progress In Electromagnetics Research Symposium (PIERS) 1993 p 477 (For primary document see N94-20403 05-32)
Avail: CASI HC A01/MF A10

Polarimetric backscattering from sea ice is presented. Theoretical models for backscattering are first presented for various ice types. Then, theoretical results are compared with experimental data for new thin ice, first-year ice, and multi-year ice. Sea ice is modeled as a layer medium containing random scatterers and rough interfaces. For multi-year sea ice with snow cover, the sea ice layer is modeled as an ice background with embedded spheroidal air bubbles and the snow layer as air with ice grains. The hummocky topography on multi-year ice is characterized by a Gaussian distribution which has an averaging effect on backscattering coefficients. First-year sea ice is described by an ice medium hosting ellipsoidal brine inclusions. These inclusions are oriented preferentially in the vertical direction due to the columnar structure of first-year sea ice. Azimuthally, the orientation of the brine pockets are random corresponding to the random c-axes in sea ice, unless the axes are oriented by sea currents. For thin ice in newly opened leads, it has been observed that there exists a thin brine layer with very high salinity on the top surface of the new ice. This brine layer is depicted as a medium with high permittivity which can significantly affect electromagnetic scattering signatures from the lower thin ice layer, with a higher fractional volume of brine inclusions due to higher salinity as compared to thick first-year sea ice. The rough medium interfaces are described as Gaussian rough surfaces characterized by root-mean-square heights and surface correlation lengths. The contribution from rough surface, calculated under the Kirchhoff approximation or small perturbation method, is assumed to be independent from volume scattering. The total loss including absorption and scattering losses in the scattering media is represented by the imaginary part of effective permittivity obtained from the strong fluctuation theory. The polarimetric scattering coefficients for different ice types are then derived under the distorted Born approximation. Author

N94-20427*# National Aeronautics and Space Administration. Goddard Space Flight Center, Greenbelt, MD.
OBSERVATION OF PRESSURE RIDGES IN SAR IMAGES OF SEA ICE: SCATTERING THEORY AND COMPARISON WITH OBSERVATIONS Abstract Only
J. F. Vesecky (Michigan Univ., Ann Arbor.), J. M. Daida (Michigan Univ., Ann Arbor.), R. A. Shuchman (Environmental Research Inst. of Michigan, Ann Arbor.), R. H. Onstott (Environmental Research Inst. of Michigan, Ann Arbor.), and J. C. Camiso *In* JPL, Progress In Electromagnetics Research Symposium (PIERS) 1993 p 479 (For primary document see N94-20403 05-32)
Avail: CASI HC A01/MF A10

Ridges and keels (hummocks and bummocks) in sea ice flows are important in sea ice research for both scientific and practical reasons. Sea ice movement and deformation is driven by internal and external stresses on the ice. Ridges and keels play important roles in both cases because they determine the external wind and current stresses via drag coefficients. For example, the drag coefficient over sea ice can vary by a factor of several depending on the fluid mechanical roughness length of the surface. This roughness length is thought to be strongly dependent on the ridge structures present. Thus, variations in ridge and keel structure can cause gradients in external stresses which must be balanced by internal stresses and possibly fracture of the ice. Ridging in sea ice is also a sign of fracture. In a practical sense, large ridges form the biggest impediment to surface travel over the ice or penetration through sea ice by ice-strengthened ships. Ridges also play an important role in the damage caused by sea ice to off-shore structures. Hence, observation and measurement of sea ice ridges is an important component of sea ice remote sensing. The research reported here builds on previous work, estimating the characteristics of ridges and leads in sea ice from SAR images. Our objective is to develop methods for quantitative measurement of sea ice ridges from SAR images. To make further progress, in particular, to estimate ridge height, a scattering model for ridges is needed. Our research approach for a ridge scattering model begins with a survey of the geometrical properties of ridges and a comparison with the characteristics of the surrounding ice. For this purpose we have used airborne optical laser (AOL) data collected during the 1987 Greenland Sea Experiment. These data were used to generate a spatial wavenumber spectrum for height variance for a typical ridge - the typical ridge is the average over 10 large ridges. Our first-order model radar scattering includes both the quasi-specular and Bragg resonant scatter mechanisms. This model is extended to include contributions from volume scatter and scatter from discrete objects. Geometrical characteristics from the AOL survey and model calculations imply that for radar wavelengths and observation geometries that are dominated by the quasi-specular scattering mechanism radar backscatter from a ridge is a measure of peak ridge height. We present scattering model results and compare them with ridges observed during the LEADEX experiment of March-April 1992 when both X, C, and L-band aircraft SAR and the ERS-1 satellite SAR observed a region in the Beaufort Sea near 86 deg N, 10 deg W. Data were also collected documenting ridge characteristics on the surface. The surface

data are used to generate a SAR signature via the scattering model described above. The predicted SAR signatures compare well with the SAR observations. Author

N94-20428*# Jet Propulsion Lab., California Inst. of Tech., Pasadena.
ON EVALUATING THE ACCURACY OF SAR SEA-ICE CLASSIFICATION USING MULTIFREQUENCY POLARIMETRIC AIRSAR DATA Abstract Only **c48**
Mark R. Drinkwater and Eric Rignot *In its* Progress In Electromagnetics Research Symposium (PIERS) 1993 p 480 (For primary document see N94-20403 05-32)
Avail: CASI HC A01/MF A10

We investigate how multifrequency and polarimetric synthetic aperture radar (SAR) imagery enhances present capability to discriminate different ice conditions in single-frequency, single-polarization satellite SAR data. Frequencies considered are C- (lambda = 5.6cm), L- (lambda = 24cm) and P- (lambda = 68cm) band. Radar backscatter characteristics of six radiometrically and polarimetrically distinct ice types are selected from a cluster analysis of the multifrequency polarimetric SAR data and used to classify SAR images. Validation of these ice conditions is based on information provided by aerial photos, weather and ice surface measurements acquired at an ice camp, together with airborne passive microwave imagery, and visual analysis of the SAR data. The six identified sea-ice types are: (1) multiyear sea-ice; (2) compressed first year ice; (3) first year rubble and ridges; (4) first year rough ice; (5) first year smooth ice; and (6) thin ice. Open water is absent in all analyzed data. Classification of the SAR imagery into those six ice types is performed using a Bayesian Maximum A Posteriori classifier. Two complete scenes acquired at different dates in different locations are classified. The scenes were chosen such that they are representative of typical ice conditions in the Beaufort Sea in March 1988 and because ancillary information is available for validating the segmentation of various ice surface conditions. Author

N94-20429*# Jet Propulsion Lab., California Inst. of Tech., Pasadena.
APPLICATION OF CLOUDE'S TARGET DECOMPOSITION THEOREM TO POLARIMETRIC IMAGING RADAR DATA Abstract Only
Jakob J. vanZyl *In its* Progress In Electromagnetics Research Symposium (PIERS) 1993 p 486 (For primary document see N94-20403 05-32)
Avail: CASI HC A01/MF A10

We apply Cloude's decomposition to imaging radar polarimetry. We derive the general expressions for the eigenvalues and eigenvectors for the case of terrain with reflection symmetry, and show in detail how the decomposition results can guide the interpretation of scattering from vegetated areas. For multi-frequency polarimetric radar measurements of a clear-cut area, the decomposition leads us to conclude that the vegetation is probably thin compared to even the C-band radar wavelength of 6 cm. For a forested area, we notice an increased amount of even number of reflection scattering at P-band and L-band, probably the result of penetration through the coniferous canopy resulting in trunk-ground double reflection scattering. The scattering for the forested area is still dominated by scattering from randomly oriented cylinders, however. It is found that these cylinders are thicker than in the case of clear-cut areas, leading us to conclude that scattering from the branches probably dominate in this case. Author

N94-20430*# Jet Propulsion Lab., California Inst. of Tech., Pasadena.
DIRECTION ANGLE SENSITIVITY OF AGRICULTURAL FIELD BACKSCATTER WITH AIRSAR DATA Abstract Only **c43**
Pascale C. Dubois, Eric Rignot, and Jakob J. vanZyl *In its* Progress In Electromagnetics Research Symposium (PIERS) 1993 p 488 (For primary document see N94-20403 05-32)
Avail: CASI HC A01/MF A10

This paper presents a study of the direction angle sensitivity of radar backscatter from agricultural fields. The direction angle is defined as the angle between the incident plane and the perpendicular to the field row direction. Previous studies have concentrated on comparing the backscatter of agricultural fields imaged with 0, 45, and 90 degree direction angles. In contrast, this study concentrates on the backscatter changes occurring when the direction angle is modified by a few degrees or even by fractions of a degree. This is possible by using the output of the NASA/JPL AIRSAR processor, in which sixteen independent frames are formed, each one corresponding to the same radar scene imaged with a slightly different squint angle. The studied data set is an agricultural area in La Mancha, Spain acquired in June and July 1991 during the EFEDA experiment. This paper describes the observed backscatter variations of the agricultural fields with direction angle measured at P, L, and C bands. As expected, the backscatter is maximum for a 0 degree direction angle. For several fields, the backscatter at P and L bands drops by more than 10 dB for a 5 degree change in direction angle. Furthermore, the sensitivity to the direction angle decreases with increasing vegetation. The variations in backscatter are compared with model predictions. One model, which agrees with scatterometer data, underestimates the observed backscatter variations with direction angle by more than 10 dB. It does not take into account the possible coherent component of the radar signal. We believe the strong direction sensitivity of agricultural field backscatter obtained with SAR data is due to a Bragg resonant effect, resulting in a strong coherent return when the direction angle is zero. The observations are then projected to the case of spaceborne SAR data. Author

N94-20431*# Jet Propulsion Lab., California Inst. of Tech., Pasadena.
TIME-DOMAIN ANALYSIS OF PLANAR MICROSTRIP DEVICES USING A GENERALIZED YEE-ALGORITHM BASED ON UNSTRUCTURED GRIDS Abstract Only
Stephen D. Gedney (Kentucky Univ., Lexington.) and Faiza Lansing *In its* Progress In Electromagnetics Research Symposium (PIERS) 1993 p 561 (For primary document see N94-20403 05-32)
Avail: CASI HC A01/MF A10

The generalized Yee-algorithm is presented for the temporal full-wave analysis of planar microstrip devices. This algorithm has the significant advantage over the traditional Yee-algorithm in that it is based on unstructured and irregular grids. The robustness of the generalized Yee-algorithm is that structures that contain curved conductors or complex three-dimensional geometries can be more accurately, and much more conveniently modeled using standard automatic grid generation techniques. This generalized Yee-algorithm is based on the the time-marching solution of the discrete form of Maxwell's equations in their integral form. To this end, the electric and magnetic fields are discretized over a dual, irregular, and unstructured grid. The primary grid is assumed to be composed of general fitted polyhedra distributed throughout the volume. The secondary grid (or dual grid) is built up of the closed polyhedra whose edges connect the centroid's of adjacent primary cells, penetrating shared faces. Faraday's law and Ampere's law are used to update the fields normal to the primary and secondary grid faces, respectively. Subsequently, a correction scheme is introduced to project the normal fields onto the grid edges. It is shown that this scheme is stable, maintains second-order accuracy, and preserves the divergenceless nature of the flux densities. Finally, for computational efficiency the algorithm is structured as a series of sparse matrix-vector multiplications. Based on this scheme, the generalized Yee-algorithm has been implemented on vector and parallel high performance computers in a highly efficient manner. Author

N94-20432*# Jet Propulsion Lab., California Inst. of Tech., Pasadena.
RETRIEVAL OF ICE THICKNESS FROM POLARIMETRIC SAR DATA Abstract Only **c48**
R. Kwok, S. H. Yueh, S. V. Nghiem, and D. D. Huynh *In its* Progress In Electromagnetics Research Symposium (PIERS) 1993 p 574 (For primary document see N94-20403 05-32)
Avail: CASI HC A01/MF A10

We describe a potential procedure for retrieving ice thickness from multi-frequency polarimetric SAR data for thin ice. This procedure includes first masking out the thicker ice types with a simple classifier and then deriving the thickness of the remaining pixels using a model-inversion technique. The technique used to derive ice thickness from polarimetric observations is provided by a numerical estimator or neural network. A three-layer perceptron implemented with the backpropagation algorithm is used in this investigation with several improved aspects for a faster convergence rate and a better accuracy of the neural network. These improvements include weight initialization, normalization of the output range, the selection of offset constant, and a heuristic learning algorithm. The performance of the neural network is demonstrated by using training data generated by a theoretical scattering model for sea ice matched to the database of interest. The training data are comprised of the polarimetric backscattering coefficients of thin ice and the corresponding input ice parameters to the scattering model. The retrieved ice thickness from the theoretical backscattering coefficients is compare with the input ice thickness

to the scattering model to illustrate the accuracy of the inversion method. Results indicate that the network convergence rate and accuracy are higher when multi-frequency training sets are presented. In addition, the dominant backscattering coefficients in retrieving ice thickness are found by comparing the behavior of the network trained backscattering data at various incidence angels. After the neural network is trained with the theoretical backscattering data at various incidence anges, the interconnection weights between nodes are saved and applied to the experimental data to be investigated. In this paper, we illustrate the effectiveness of this technique using polarimetric SAR data collected by the JPL DC-8 radar over a sea ice scene. Author

N94-20433*# Jet Propulsion Lab., California Inst. of Tech., Pasadena.
STUDIES OF GREENLAND USING THE SEASAT SCATTEROMETER Abstract Only **c48**
David G. Long (Brigham Young Univ., Provo, UT.) and Mark Drinkwater *In its* Progress In Electromagnetics Research Symposium (PIERS) 1993 p 575 (For primary document see N94-20403 05-32)
Avail: CASI HC A01/MF A10

We have used Ku-band (14.6 GHz) Seasat scatterometer (SASS) measurements to study changes in the backscatter of the Greenland ice sheet in response to seasonal changes in the surface and subsurface characteristics of the snow and glacial ice. To overcome the limitations imposed by the 50 km resolution of the SASS measurement, a resolution enhancement algorithm was used to generate 10 km resolution images of the backscatter response. To generate the images, the observed sigma(sup 0) (in dB) was modeled as a linear function of incidence angle theta, i.e., sigma(sup 0)(theta) = A + B(theta - 40 degrees) where theta epsilon (23 degrees, 55 degrees). The variable A can be thought of as the 'incidence angle-normalized sigma(sup 0)', while the gradient B describes the incidence angle dependence of sigma(sup 0). A time-series (one image every two weeks) of vertical and horizontally-polarized A and B was generated spanning a 100 day period between Julian Dates 180 and 280 (i.e. 29 June and 7 October) in 1978. This time series dramatically shows the effects of the summer melt and a clear transition with fall cooling and snowfall towards a typical winter scattering situation. The images also clearly delineate a number of principal snow and ice 'facies' which are identifiable on the surface. Author

N94-20434*# Jet Propulsion Lab., California Inst. of Tech., Pasadena.
RADAR BACKSCATTERING FROM SNOW FACIES OF THE GREENLAND ICE SHEET: RESULTS FROM THE AIRSAR 1991 CAMPAIGN Abstract Only **c48**
Eric Rignot, K. Jezek (Ohio State Univ., Columbus.), J. J. vanZyl, Mark R. Drinkwater, and Y. L. Lou *In its* Progress In Electromagnetics Research Symposium (PIERS) 1993 p 576 (For primary document see N94-20403 05-32)
Avail: CASI HC A01/MF A10

In June 1991, the NASA/JPL airborne SAR (AIRSAR) acquired C- (lambda = 5.6cm), L- (lambda = 24cm), and P- (lambda = 68m) band polarimetric SAR data over the Greenland ice sheet. These data are processed using version 3.55 of the AIRSAR processor which provides radiometrically and polarimetrically calibrated images. The internal calibration of the AIRSAR data is cross-checked using the radar response from corner reflectors deployed prior to flight in one of the scenes. In addition, a quantitative assessment of the noise power level at various frequencies and polarizations is made in all the scenes. Synoptic SAR data corresponding to a swath width of about 12 by 50 km in length (compared to the standard 12 x 12 km size of high-resolution scenes) are also processed and calibrated to study transitions in radar backscatter as a function of snow facies at selected frequencies and polarizations. The snow facies on the Greenland ice sheet are traditionally categorized based on differences in melting regime during the summer months. The interior of Greenland corresponds to the dry snow zone where terrain elevation is the highest and no snow melt occurs. The lowest elevation boundary of the dry snow zone is known traditionally as the dry snow line. Beneath it is the percolation zone where melting occurs in the summer and water percolates through the snow freezing at depth to form massive ice lenses and ice pipes. At the downslope margin of this zone is the wet snow line. Below it, the wet snow zone corresponds to the lowest elevations where snow remains at the end of the summer. Ablation produces enough meltwater to create areas of snow saturated with water, together with ponds and lakes. The lowest altitude zone of ablation sees enough summer melt to remove all traces of seasonal snow accumulation, such that the surface comprises bare glacier ice. Author

N94-20435*# Jet Propulsion Lab., California Inst. of Tech., Pasadena.
C-BAND RADAR BACKSCATTER OF SEA ICE IN THE WEDDELL SEA, ANTARCTICA DURING THE AUSTRAL WINTER OF 1992 Abstract Only
R. Hosseinmostafa (Kansas Univ. Center for Research, Inc., Lawrence.), Mark R. Drinkwater, S. P. Gogineni (Kansas Univ. Center for Research, Inc., Lawrence.), and W. Dierking (Alfred-Wegener-Inst. for Polar Research, Bremerhaven, Germany.) *In its* Progress In Electromagnetics Research Symposium (PIERS) 1993 p 578 (For primary document see N94-20403 05-32)
Avail: CASI HC A01/MF A10

A C-band ship-based scatterometer was used to measure the backscatter coefficient of sea ice in the Weddell Sea during June and July 1992. These are the first microwave scatterometer data ever to be collected in the Antarctic sea ice cover during the austral winter. The instrument was a frequency-modulated continuous-wave (FM-CW) radar altimeter modified by the University of Kansas Radar Systems and Remote Sensing Laboratory to perform backscatter measurements. Measurements were taken as part of a Jet Propulsion Laboratory experiment aboard the German ice research vessel F.S. Polarstern. Backscatter measurements were performed at incidence angles ranging from 17 to 65 degrees with VV and HV polarization as the Polarstern travelled from east to west across the central Weddell Sea. Backscatter measurements were made of several different types of ice sea including pancake, dark nilas, white nilas, grey, first-year and second-year ice. Periodic external calibrations were performed with the aid of a Luneberg Lens to enable absolute values of backscatter to be derived from the data. At each radar measurement location, in-situ measurements were made of snow and sea ice. Physical and chemical analyses of ice core and snow samples, together with high magnification photography of snow crystallography provide important information with which to develop physical models of the scattering systems. Meteorological information and oceanographic conditions were also recorded throughout the experiment. Many of the stations were chosen to coincide with periods of near-simultaneous or coincident imaging by the ERS-1 satellite Synthetic Aperture Radar (SAR). This enabled spaceborne imaging by the C-band SAR of areas of sea ice in which backscatter measurements were taken. This provides a valuable tool for interpretation of satellite SAR imagery from Antarctic sea ice in terms of the physical properties of the sea ice and snow. Preliminary results of the backscatter from the various ice types and their relation to the physical properties of sea ice are presented.
Author

N94-20436*# Jet Propulsion Lab., California Inst. of Tech., Pasadena.
AN EFFICIENT FORMULATION OF THE COUPLED FINITE ELEMENT-INTEGRAL EQUATION TECHNIQUE FOR SOLVING LARGE 3D SCATTERING PROBLEMS Abstract Only **c64**
T. Cwik, V. Jamnejad, and C. Zuffada *In its* Progress In Electromagnetics Research Symposium (PIERS) 1993 p 604 (For primary document see N94-20403 05-32)
Avail: CASI HC A01/MF A10

It is often desirable to calculate the electromagnetic fields inside and about a complicated system of scattering bodies, as well as in their far-field region. The finite element method (FE) is well suited to solving the interior problem, but the domain has to be limited to a manageable size. At the truncation of the FE mesh one can either impose approximate (absorbing) boundary conditions or set up an integral equation (IE) for the fields scattered from the bodies. The latter approach is preferable since it results in higher accuracy. Hence, the two techniques can be successfully combined by introducing a surface that encloses the scatterers, applying a FE model to the inner volume and setting up an IE for the tangential fields components on the surface. Here the continuity of the tangential fields is used bo obtain a consistent solution. A few coupled FE-IE methods have recently appeared in the literature. The approach presented here has the advantage of using edge-based finite elements, a type of finite elements with degrees of freedom associated with edges of the mesh. Because of their properties, they are better suited than the conventional node based elements to represent electromagnetic fields, particularly when inhomogeneous regions are modeled, since the node based elements impose an unnatural continuity of all field components across boundaries of mesh elements. Additionally,

our approach is well suited to handle large size problems and lends itself to code parallelization. We will discuss the salient features that make our approach very efficient from the standpoint of numerical computation, and the fields and RCS of a few objects are illustrated as examples. Author

N94-20437*# Jet Propulsion Lab., California Inst. of Tech., Pasadena.
MASSIVELY PARALLEL COMPUTATION OF RCS WITH FINITE ELEMENTS Abstract Only
Jay Parker *In its* Progress In Electromagnetics Research Symposium (PIERS) 1993 p 605 (For primary document see N94-20403 05-32)
Avail: CASI HC A01/MF A10

One of the promising combinations of finite element approaches for scattering problems uses Whitney edge elements, spherical vector wave-absorbing boundary conditions, and bi-conjugate gradient solution for the frequency-domain near field. Each of these approaches may be criticized. Low-order elements require high mesh density, but also result in fast, reliable iterative convergence. Spherical wave-absorbing boundary conditions require additional space to be meshed beyond the most minimal near-space region, but result in fully sparse, symmetric matrices which keep storage and solution times low. Iterative solution is somewhat unpredictable and unfriendly to multiple right-hand sides, yet we find it to be uniformly fast on large problems to date, given the other two approaches. Implementation of these approaches on a distributed memory, message passing machine yields huge dividends, as full scalability to the largest machines appears assured and iterative solution times are well-behaved for large problems. We present times and solutions for computed RCS for a conducting cube and composite permeability/conducting sphere on the Intel ipsc860 with up to 16 processors solving over 200,000 unknowns. We estimate problems of approximately 10 million unknowns, encompassing 1000 cubic wavelengths, may be attempted on a currently available 512 processor machine, but would be exceedingly tedious to prepare. The most severe bottlenecks are due to the slow rate of mesh generation on non-parallel machines and the large transfer time from such a machine to the parallel processor. One solution, in progress, is to create and then distribute a coarse mesh among the processors, followed by systematic refinement within each processor. Elimination of redundant node definitions at the mesh-partition surfaces, snap-to-surface post processing of the resulting mesh for good modelling of curved surfaces, and load-balancing redistribution of new elements after the refinement are auxiliary steps expected to result in a robust low i/o system for very large finite element problems. Author

N94-20438*# Jet Propulsion Lab., California Inst. of Tech., Pasadena.
NEAR GRAZING SCATTERING FROM NON-GAUSSIAN OCEAN SURFACES Abstract Only **c48**
Yunjin Kim and Ernesto Rodriguez *In its* Progress In Electromagnetics Research Symposium (PIERS) 1993 p 615 (For primary document see N94-20403 05-32)
Avail: CASI HC A01/MF A10

We investigate the behavior of the scattered electromagnetic waves from non-Gaussian ocean surfaces at near grazing incidence. Even though the scattering mechanisms at moderate incidence angles are relatively well understood, the same is not true for near grazing rough surface scattering. However, from the experimental ocean scattering data, it has been observed that the backscattering cross section of a horizontally polarized wave can be as large as the vertical counterpart at near grazing incidence. In addition, these returns are highly intermittent in time. There have been some suggestions that these unexpected effects may come from shadowing or feature scattering. Using numerical scattering simulations, it can be shown that the horizontal backscattering cannot be larger than the vertical one for the Gaussian surfaces. Our main objective of this study is to gain a clear understanding of scattering mechanisms underlying the near grazing ocean scattering. In order to evaluate the backscattering cross section from ocean surfaces at near grazing incidence, both the hydrodynamic modeling of ocean surfaces and an accurate near grazing scattering theory are required. For the surface modeling, we generate Gaussian surfaces from the ocean surface power spectrum which is derived using several experimental data. Then, weakly nonlinear large scale ocean surfaces are generated following Longuet-Higgins. In addition, the modulation of small waves by large waves is included using the conservation of wave action. For surface scattering, we use MOM (Method of Moments) to calculate the backscattering from scattering patches with the two scale shadowing approximation. The differences between Gaussian and non-Gaussian surface scattering at near grazing incidence are presented. Author

N94-20439*# Jet Propulsion Lab., California Inst. of Tech., Pasadena.
ROUGH SURFACE SCATTERING FROM MOVING OCEAN SURFACES AS AN INDICATOR OF SCATTERING MECHANISMS Abstract Only **c48**
Ernesto Rodriguez and Yunjin Kim *In its* Progress In Electromagnetics Research Symposium (PIERS) 1993 p 616 (For primary document see N94-20403 05-32)
Avail: CASI HC A01/MF A10

Ever since Crombie used the Doppler spectrum of RF signals scattered from the ocean surface to provide conclusive evidence for Bragg resonant scattering, scattering from the ocean surface has served as a testing ground for the identification of governing scattering mechanisms in rough surface scattering. The moving ocean surface has the advantage for rough surface scattering that, being a dispersive medium, features with different spatial scales the tendency to travel at different speeds. Thus, by looking at the temporal signature of the scattered field, one can try to isolate the scattering mechanism. This feature has been exploited by various authors. To give a recent example, we cite the work of Plant, who examined the Doppler spectrum of the return signal to infer the presence of two-scale scattering in scattering at medium incidence angles. The problem with restricting oneself to the examination of the Doppler spectrum, as has been done traditionally, is that one restricts the phenomena under investigation to temporally homogeneous phenomena: transient phenomena, which are localized in time, are not localized in frequency space. There is increasing evidence that this type of phenomena, due to specular scattering or breaking waves, may also play an important role in determining the scattering mechanism in ocean-like surfaces. To overcome this problem, we introduce the use of the Wavelet Transform to study the frequency-temporal signatures of the scattered field from moving ocean waves. We calculate this signature using various analytic scattering theories and show that the Wavelet Transform provides a useful tool for separating the different scattering mechanisms operating in scattering in ocean-like surfaces. Next we simulate realistic nonlinear moving ocean waves and calculate the temporal scattered field signature by using the method of moments and the stop-start approximation: the surface is assumed stationary during a scattering event, but moves between incident EM pulses. We compute and compare the Doppler frequency spectrum and the Wavelet Transform of the resulting signal for various types of surfaces and show how different scattering mechanisms may be isolated by this technique. Finally, we compare these numerical results against the analytical predictions in order to obtain the domain of applicability of various scattering theories for moving ocean surfaces which may include wave breaking and specular glints. Author

N94-20440*# Jet Propulsion Lab., California Inst. of Tech., Pasadena.
THE EFFECT OF DISSIPATIVE INHOMOGENEOUS MEDIUM ON THE STATISTICS OF THE WAVE INTENSITY Abstract Only
Sasan S. Saatchi *In its* Progress In Electromagnetics Research Symposium (PIERS) 1993 p 620 (For primary document see N94-20403 05-32)
Avail: CASI HC A01/MF A10

One of the main theoretical points in the theory of wave propagation in random medium is the derivation of closed form equations to describe the statistics of the propagating waves. In particular, in one dimensional problems, the closed form representation of the multiple scattering effects is important since it contributes in understanding such problems like wave localization, backscattering enhancement, and intensity fluctuations. In this the propagation of plane waves in a layer of one-dimensional dissipative random medium is considered. The medium is modeled by a complex permittivity whose real part is a constant representing the absorption. The one dimensional problem is mathematically equivalent to the analysis of a transmission line with randomly perturbed distributed parameters and a single mode lossy waveguide and the results can be used to study the propagation of radio waves through atmosphere and the remote sensing of geophysical media. It is assumed the scattering medium consists of an ensemble of one-dimensional point scatterers randomly positioned in a layer of thickness L with diffuse boundaries. A Poisson impulse process with density lambda is used to model the position of scatterers in the medium. By employing the Markov properties of this process an exact closed form equation of Kolmogorov-Feller type was obtained for the

probability density of the reflection coefficient. This equation was solved by combining two limiting cases: (1) when the density of scatterers is small; and (2) when the medium is weakly dissipative. A two variable perturbation method for small lambda was used to obtain solutions valid for thick layers. These solutions are then asymptotically evaluated for small dissipation. To show the effect of dissipation, the mean and fluctuations of the reflected power are obtained. The results were compared with a lossy homogeneous medium and with a lossless inhomogeneous medium and the regions where the effect of absorption is not essential were discussed. Author (revised)

N94-20441*# Jet Propulsion Lab., California Inst. of Tech., Pasadena.
POLARIMETRIC THERMAL EMISSION FROM ROUGH SURFACES Abstract Only

J. T. Johnson (Massachusetts Inst. of Tech., Cambridge.), J. A. Kong (Massachusetts Inst. of Tech., Cambridge.), R. T. Shin (Massachusetts Inst. of Tech., Cambridge.), D. H. Staelin (Massachusetts Inst. of Tech., Cambridge.), S. H. Yueh, S. V. Nghiem, R. Kwok, K. ONeill (Army Cold Regions Research and Engineering Lab., Hanover, NH.), and A. Lohanick (Army Cold Regions Research and Engineering Lab., Hanover, NH.) *In its* Progress In Electromagnetics Research Symposium (PIERS) 1993 p 671 (For primary document see N94-20403 05-32)

Avail: CASI HC A01/MF A10

Recent theoretical works have suggested the potential of passive polarimetry in the remote sensing of geophysical media. It was shown that the third Stokes parameter U of the thermal emission may become larger for azimuthally asymmetric fields of observation. In order to investigate the potential applicability of passive polarimetry to the remote sensing of ocean surface, measurements of the polarimetric thermal emission from a sinusoidal water surface and a numerical study of the polarimetric thermal emission from randomly rough ocean surfaces were performed. Measurements of sinusoidal water surface thermal emission were performed using a sinusoidal water surface which was created by placing a thin sheet of fiberglass with a sinusoidal profile in two dimensions extended infinitely in the third dimension onto a water surface. The theory of thermal emission from a 'two-layer' periodic surface is derived and the exact solution is performed using both the extended boundary condition method (EBC) and the method of moments (MOM). The theoretical predictions are found to be in good agreement with the experimental results once the effects of the radiometer antenna pattern are included and the contribution of background noise to the measurements is modeled. The experimental results show that the U parameter indicates the direction of periodicity of the water surface and can approach values of up to 30 K for the surface observed. Next, a numerical study of polarimetric thermal emission from randomly rough surfaces was performed. A Monte Carlo technique utilizing an exact method for calculating thermal emission was chosen for the study to avoid any of the limitations of the commonly used approximate methods in rough surface scattering. In this Monte Carlo technique, a set of finite rough surface profiles in two dimensions with desired statistics was generated and extended periodically. The polarimetric thermal emission from each surface of the set was then calculated using both the EBC and the MOM and the results were averaged. The surface statistics chosen were intended to model a wind perturbed ocean surface in the X to Ku band microwave region. The results indicate that the U parameter is sensitive to the azimuthal angle between the surface periodicity and the looking angle and to the rms height of the surface, and that the U parameter is fairly insensitive to variations in polar angle, permittivity, surface power law spectrum, and surface spectrum high frequency cutoff. These properties give further strength to the idea of using the U parameter to detect wind direction over the ocean. Author (revised)

N94-20442*# Jet Propulsion Lab., California Inst. of Tech., Pasadena.
OPTICAL BEAM FORMING TECHNIQUES FOR PHASED ARRAY ANTENNAS Abstract Only

Te-Kao Wu and C. Chandler *In its* Progress In Electromagnetics Research Symposium (PIERS) 1993 p 694 (For primary document see N94-20403 05-32)

Avail: CASI HC A01/MF A10

Conventional phased array antennas using waveguide or coax for signal distribution are impractical for large scale implementation on satellites or spacecraft because they exhibit prohibitively large system size, heavy weight, high attenuation loss, limited bandwidth, sensitivity to electromagnetic interference (EMI) temperature drifts and phase instability. However, optical beam forming systems are smaller, lighter, and more flexible. Three optical beam forming techniques are identified as applicable to large spaceborne phased array antennas. They are (1) the optical fiber replacement of conventional RF phased array distribution and control components, (2) spatial beam forming, and (3) optical beam splitting with integrated quasi-optical components. The optical fiber replacement and the spatial beam forming approaches were pursued by many organizations. Two new optical beam forming architectures are presented. Both architectures involve monolithic integration of the antenna radiating elements with quasi-optical grid detector arrays. The advantages of the grid detector array in the optical process are the higher power handling capability and the dynamic range. One architecture involves a modified version of the original spatial beam forming approach. The basic difference is the spatial light modulator (SLM) device for controlling the aperture field distribution. The original liquid crystal light valve SLM is replaced by an optical shuffling SLM, which was demonstrated for the 'smart pixel' technology. The advantages are the capability of generating the agile beams of a phased array antenna and to provide simultaneous transmit and receive functions. The second architecture considered is the optical beam splitting approach. This architecture involves an alternative amplitude control for each antenna element with an optical beam power divider comprised of mirrors and beam splitters. It also implements the quasi-optical grid phase shifter for phase control and grid amplifier for RF power. The advantages are no SLM is required for this approach, and the complete antenna system is capable of full monolithic integration. Author (revised)

N94-20443*# Jet Propulsion Lab., California Inst. of Tech., Pasadena.
SIMULATED RETRIEVAL OF LAND SURFACE PARAMETERS USING MULTICHANNEL SATELLITE MICROWAVE RADIOMETRY Abstract Only **c43**

Eni G. Njoku and Brian Rague *In its* Progress In Electromagnetics Research Symposium (PIERS) 1993 p 764 (For primary document see N94-20403 05-32)

Avail: CASI HC A01/MF A10

The current global change research emphasis on understanding water and energy fluxes at the land-atmosphere interface provided renewed interest in using passive microwave satellite data for land studies. Radiative transfer models of microwave emission and scattering in the soil-vegetation-atmosphere column, though still in the process of development, can be used to estimate the accuracies with which land surface parameters can be derived from satellite data. These parameters include surface soil moisture, surface temperature, vegetation water content, and atmospheric water content. A microwave radiative transfer model is used to develop linear and nonlinear versions of a multichannel retrieval algorithm to simulate retrievals of the surface and atmospheric parameters. These simulations include the effect of additive noise, and examine the effects of nonlinearities in the radiative transfer models. However, effects of spatial heterogeneity are not considered. Satellite data to which the retrieval algorithms may be applied include the SSMR and SSM/I, and in future will include the Multifrequency Imaging Microwave Radiometer (MIMR) to be launched as part of the Earth Observing System (EOS). The Scanning Multichannel Microwave Radiometer (SMMR) on the Nimbus-7 satellite provided data from 1978 to 1987 at five microwave frequencies between 6.6 and 37 GHz. The series of Special Sensor Microwave/Imager (SSM/I) instruments launched on the DMSP satellites provide data from 1987 to the present at four frequencies between 19.35 and 8.5 GHz. Spatial resolutions of the data range from approximately 12 to 120 km depending on the frequency. Examples using data from these sensors are shown to indicate the results of applying retrieval algorithms based on model simulations to real data. Author (revised)

N94-20444*# Jet Propulsion Lab., California Inst. of Tech., Pasadena.
SYNERGISM OF ACTIVE AND PASSIVE MICROWAVE DATA FOR ESTIMATING BARE SURFACE SOIL MOISTURE Abstract Only **c43**

Sasan S. Saatchi, Eni G. Njoku, and Urs Wegmueller (Bern Univ., Switzerland.) *In its* Progress In Electromagnetics Research Symposium (PIERS) 1993 p 769 (For primary document see N94-20403 05-32)

Avail: CASI HC A01/MF A10

Active and passive microwave sensors were applied effectively to the problem of estimating the surface soil moisture in a variety of environmental conditions. Research to date has shown that both types of sensors are

also sensitive to the surface roughness and the vegetation cover. In estimating the soil moisture, the effect of the vegetation and roughness are often corrected either by acquiring multi-configuration (frequency and polarization) data or by adjusting the surface parameters in order to match the model predictions to the measured data. Due to the limitations on multi-configuration spaceborne data and the lack of a priori knowledge of the surface characteristics for parameter adjustments, it was suggested that the synergistic use of the sensors may improve the estimation of the soil moisture over the extreme range of naturally occurring soil and vegetation conditions. To investigate this problem, the backscattering and emission from a bare soil surface using the classical rough surface scattering theory were modeled. The model combines the small perturbation and the Kirchhoff approximations in conjunction with the Peak formulation to cover a wide range of surface roughness parameters with respect to frequency for both active and passive measurements. In this approach, the same analytical method was used to calculate the backscattering and emissivity. Therefore, the active and passive simulations can be combined at various polarizations and frequencies in order to estimate the soil moisture more actively. As a result, it is shown that (1) the emissivity is less dependent on the surface correlation length, (2) the ratio of the backscattering coefficient (HH) over the surface reflectivity (H) is almost independent of the soil moisture for a wide range of surface roughness, and (3) this ratio can be approximated as a linear function of the surface rms height. The results were compared with the data obtained by a multi-frequency radiometer-scatterometer system working at frequencies between 3.0 GHz to 11.0 GHz. The data were acquired over bare soil surfaces with moisture variations due to freezing and thawing and roughness changes due to rain and erosion. The model predictions are shown to be in reasonable agreement with the data. In addition, it was shown that the same ratio when calculated from the data shows almost no dependence on the soil moisture. Finally, a simple technique which combines the backscattering coefficient at HH polarization (active sensing) with the emissivity at H polarization (passive sensing) is suggested for retrieving the soil moisture from bare soil surfaces.

Author (revised)

N94-20445*# Jet Propulsion Lab., California Inst. of Tech., Pasadena.

POLARIMETRIC THERMAL EMISSION FROM PERIODIC WATER SURFACES Abstract Only **c43**

S. H. Yueh, S. V. Nghiem, R. Kwok, W. J. Wilson, F. K. Li, J. T. Johnson (Massachusetts Inst. of Tech., Cambridge.), and J. A. Kong (Massachusetts Inst. of Tech., Cambridge.) *In its* Progress In Electromagnetics Research Symposium (PIERS) 1993 p 770 (For primary document see N94-20403 05-32)

Avail: CASI HC A01/MF A10

Experimental results and theoretical calculations are presented to study the polarimetric emission from water surfaces with directional features. For our ground-based Ku-band radiometer measurements, a water pool was constructed on the roof of a building in the Jet Propulsion Laboratory, and a fiberglass surface with periodic corrugations in one direction was impressed on the top of the water surface to create a stationary water surface underneath it. It is observed that the measured Stokes parameters of corrugated fiberglass-covered water surfaces are functions of azimuth angles and agree very well with the theoretical calculations. The theory, after being verified by the experimental data, was then used to calculate the Stokes parameters of periodic surfaces without fiberglass surface layer and with rms height of the order of wind-generated water ripples. The magnitudes of the azimuthal variation of the calculated emissivities at horizontal and vertical polarizations corresponding to the first two Stokes parameters are found to be comparable to the values measured by airborne radiometers and SSM/I. In addition, the third Stokes parameter not shown in the literature is seen to have approximately twice the magnitude of the azimuth variation of either T(sub h) or T(sub v), which may make it more sensitive to the row direction, while less susceptive to noises because the atmospheric and system noises tend to be unpolarized and are expected to be cancelled out when the third Stokes parameter is derived as the difference of two or three power measurements, as indicated by another experiment carried out at a swimming pool with complicated surroundings. The results indicate that passive polarimetry is a potential technology in the remote sensing of ocean wind vector which is a crucial component in the understanding of global climate change. Issues related to the application of microwave passive polarimetry to ocean wind are also discussed.

Author (revised)

N94-20446*# National Aeronautics and Space Administration. Goddard Space Flight Center, Greenbelt, MD.

MULTIPLE SCATTERING EFFECTS ON THE LINEAR DEPOLARIZATION RATIO (LDR) MEASURED DURING CaPE BY A Ka-BAND AIR-BORNE RADAR Abstract Only

Toshio Iguchi (Universities Space Research Association, Greenbelt, MD.) and Robert Meneghini *In* JPL, Progress In Electromagnetics Research Symposium (PIERS) 1993 p 774 (For primary document see N94-20403 05-32)

Avail: CASI HC A01/MF A10

Air-borne radar measurements of thunderstorms were made as part of the CaPE (Convection and Precipitation/Electrification) experiment in Florida in July 1991. The radar has two channels, X-band (10 GHz) and Ka-band (34.5 GHz), and is capable of measuring cross-polarized returns as well as co-polarized returns. In stratiform rain, the cross-polarized components can be observed only at the bright band region and from the surface reflection. The linear depolarization ratios (LDR's) measured at X-band and Ka-band at the bright band are nearly equal. In convective rain, however, the LDR in Ka-band often exceeds the X-band LDR by several dB, and sometimes by more than 10 dB, reaching LDR values of up to -5 dB over heavy convective rain. For randomly oriented hydrometeors, such high LDR values cannot be explained by single scattering from non-spherical scattering particles alone. Because the LDR by single backscatter depends weakly on the wavelength, the difference between the Ka-band and X-band LDR's suggests that multiple scattering effects prevail in the Ka-band LDR. In order to test this inference, the magnitude of the cross-polarized component created by double scattering was calculated using the parameters of the airborne radar, which for both frequencies has beamwidths of 5.1 degrees and pulse widths of 0.5 microsecond. Uniform rain beyond the range of 3 km is assumed.

Author (revised)

N94-20447*# Jet Propulsion Lab., California Inst. of Tech., Pasadena.

MULTI-BAND REFLECTOR ANTENNA WITH DOUBLE-RING ELEMENT FREQUENCY SELECTIVE SUBREFLECTOR Abstract Only

Te-Kao Wu and S. W. Lee (Illinois Univ., Urbana.) *In its* Progress In Electromagnetics Research Symposium (PIERS) 1993 p 788 (For primary document see N94-20403 05-32)

Avail: CASI HC A01/MF A10

Frequency selective subreflectors (FSS) are often employed in the reflector antenna system of a communication satellite or a deep space exploration vehicle for multi-frequency operations. In the past, FSS's have been designed for diplexing two frequency bands. For example, the Voyager FSS was designed to diplex S and X bands and the TDRSS FSS was designed to diplex S and Ku bands. Recently, NASA's CASSINI project requires an FSS to multiplex four frequency (S/X/Ku/Ka) bands. Theoretical analysis and experimental verifications are presented for a multi-band flat pannel FSS with double-ring elements. Both the exact formulation and the thin-ring approximation are described for analyzing and designing this multi-ring patch element FSS. It is found that the thin-ring approximation fails to predict the electrically wide ring element FSS's performance. A single screen double-ring element FSS is demonstrated for the tri-band system that reflects the X-band signal while transmitting through the S- and Ku-band signals. In addition, a double screen FSS with non-similar double-ring elements is presented for the Cassini's four-band system which reflects the X- and Ka-band signals while passing the S- and Ku-band signals. To accurately predict the FSS effects on a dual reflector antenna's radiation pattern, the FSS subreflector's transmitted/reflected field variation as functions of the polarization and incident angles with respect to the local coordinates was taken into account. An FSS transmission/reflection coefficient table is computed for TE and TM polarizations at various incident angles based on the planar FSS model. Next, the hybrid Geometric Optics (GO) and Physical Optics (PO) technique is implemented with linearly interpolating the FSS table to efficiently determine the FSS effects in a dual reflector antenna.

Author (revised)

N94-20448*# Jet Propulsion Lab., California Inst. of Tech., Pasadena.

SECOND ORDER DISTORTED BORN APPROXIMATION FOR BACKSCATTERING FROM A LAYER OF DISCRETE RANDOM MEDIUM Abstract Only

Roger H. Lang (George Washington Univ., Washington, DC.) and Sasan S. Saatchi *In its* Progress In Electromagnetics Research Symposium (PIERS) 1993 p 806 (For primary document see N94-20403 05-32)
Avail: CASI HC A01/MF A10

In recent years there has been increasing interest in scattering and depolarization characteristics of the vegetation canopies. Scattering models applied to the microwave remote sensing of vegetation canopies showed that multiple scattering effects can be important in simulating the backscattering coefficients correctly. In particular, in most applications, the cross-polarized backscattering coefficients are often underestimated by single scattering models. Recently, there have been concerted efforts to include the second order terms in the radiative transfer models of vegetation canopies in order to account for multiple scattering within the canopy. The coherent wave theory approach is extended to include multiple scattering effects to predict the coherent and incoherent backscattering contributions from a layer of vegetation canopy. The problem is initially formulated in terms of the exact equation for the correlation function of the field, i.e., the Bethe-Salpeter equation. Using fractional volume as a small parameter, a Foldy type approximation is made to obtain a more manageable correlation equation. This equation is iterated to obtain first and second order solutions. The iteration procedure assumes the variance of the field fluctuations are small compared to the coherent intensity. This assumption proved to be particularly successful in computing backscattering coefficients. First and second order backscattering coefficients are calculated from the iterants of the correlation equation. It is shown that the first order coefficients are the same as the distorted Born results used previously by the authors. These results contained enhancement terms in the direct-reflected contributions. The important contributions to second order backscattering are examined and interpreted in terms of scattering diagrams. Examples of situations in which second order backscattering coefficients are important are given.
Author (revised)

N94-20449*# Jet Propulsion Lab., California Inst. of Tech., Pasadena.
SYMMETRY IN POLARIMETRIC REMOTE SENSING Abstract Only **c43**
S. V. Nghiem, S. H. Yueh, and R. Kwok *In its* Progress In Electromagnetics Research Symposium (PIERS) 1993 p 807 (For primary document see N94-20403 05-32)
Avail: CASI HC A01/MF A10

Relationships among polarimetric backscattering coefficients are derived from the viewpoint of symmetry groups. For both reciprocal and non-reciprocal media, symmetry encountered in remote sensing due to reflection, rotation, azimuthal, and centrical symmetry groups is considered. The derived properties are general and valid to all scattering mechanisms, including volume and surface scatterings and their interactions, in a given symmetrical configuration. The scattering coefficients calculated from theoretical models for layer random media and rough surfaces are shown to obey the symmetry relations. Use of symmetry properties in remote sensing of structural and environmental responses of scattering media is also discussed. Orientations of spheroidal scatterers described by spherical, uniform, planophile, plagiothile, erectophile, and extremophile distributions are considered to derive their polarimetric backscattering characteristics. These distributions can be identified from the observed scattering coefficients by comparison with theoretical symmetry calculations. A new parameter is then defined to study scattering structures in geophysical media. Observations from polarimetric data acquired by the Jet Propulsion Laboratory airborne synthetic aperture radar over forests, sea ice, and sea surface are presented. Experimental evidences of the symmetry relationships are shown and their use in polarimetric remote sensing is illustrated. For forests, the coniferous forest in Mt. Shasta area (California) and mixed forest near Presque Isle (Maine) exhibit characteristics of the centrical symmetry at C-band. For sea ice in the Beaufort Sea, multi-year sea ice has a cross-polarized ratio e close to e(sub 0), calculated from symmetry, due to the randomness in the scattering structure. First-year sea ice has e much smaller than e(sub 0) due to the preferential alignment of the columnar structure of the ice. From polarimetric data of a sea surface in the Bering Sea, it is observed that e and e(sub 0) are increasing with incident angle and e is greater than e(sub 0) at L-band because of the directional feature of sea surface waves. Symmetry properties of geophysical media can also be used to calibrate polarimetric radars. Author (revised)

N94-20450*# National Aeronautics and Space Administration. Goddard Space Flight Center, Greenbelt, MD.
RELATIONSHIP OF ATTENUATION IN A VEGETATION CANOPY TO PHYSICAL PARAMETERS OF THE CANOPY Abstract Only **c43**
M. A. Karam and D. M. LeVine *In* JPL, Progress In Electromagnetics Research Symposium (PIERS) 1993 p 808 (For primary document see N94-20403 05-32)
Avail: CASI HC A01/MF A10

A discrete scatter model is employed to compute the radiometric response (i.e. emissivity) of a layer of vegetation over a homogeneous ground. This was done to gain insight into empirical formulas for the emissivity which have recently appeared in the literature and which indicate that the attenuation through the canopy is proportional to the water content of the vegetation and inversely proportional to wavelength raised to a power around unity. The analytical result assumes that the vegetation can be modeled by a sparse layer of discrete, randomly oriented particles (leaves, stalks, etc.). The attenuation is given by the effective wave number of the layer obtained from the solution for the mean wave using the effective field approximation. By using the Ulaby-El Rayes formula to relate the dielectric constant of the vegetation to its water content, it can be shown that the attenuation is proportional to water content. The analytical form offers insight into the dependence of the empirical parameters on other variables of the canopy, including plant geometry (i.e. shape and orientation of the leaves and stalks of which the vegetation is comprised), frequency of the measurement and even the physical temperature of the vegetation. Solutions are presented for some special cases including layers consisting of cylinders (stalks) and disks (leaves). Author

N94-20451*# Jet Propulsion Lab., California Inst. of Tech., Pasadena.
NUMERICAL MODELING FOR AN ELECTRIC-FIELD HYPERTHERMIA APPLICATOR Abstract Only **c52**
Te-Kao Wu, C. K. Chou (City of Hope Medical Center, Duarte, CA.), K. W. Chan (City of Hope Medical Center, Duarte, CA.), and J. McDougall (City of Hope Medical Center, Duarte, CA.) *In its* Progress In Electromagnetics Research Symposium (PIERS) 1993 p 824 (For primary document see N94-20403 05-32)
Avail: CASI HC A01/MF A10

Hyperthermia, in conjunction with radiation and chemotherapy for treatment of cancers, is an area of current concern. Experiments have shown that hyperthermia can increase the potency of many chemotherapy drugs and the effectiveness of radiation for treating cancer. A combination of whole body or regional hyperthermia with chemotherapy or radiation should improve treatment results. Conventional methods for inducing whole body hyperthermia, such as exposing a patient in a radiant cabinet or under a hot water blanket, conduct heat very slowly from the skin to the body core. Thus a more efficient system, such as the three-plate electric-field hyperthermia applicator (EHA), is developed. This three-plate EHA has one top plate over and two lower plates beneath the patient. It is driven at 27.12 MHz with 500 Watts through a matching circuit. Using this applicator, a 50 kg pig was successfully heated to 42 C within 45 minutes. However, phantom and animal studies have indicated non-uniform heating near the side of the body. In addition, changes in the size and distance between the electrode plates can affect the heating (or electromagnetic field) pattern. Therefore, numerical models using the method of moments (MOM) or the finite difference time domain (FDTD) technique are developed to optimize the heating pattern of this EHA before it is used for human trials. The accuracy of the numerical modeling has been achieved by the good agreement between the MOM and FDTD results for the three-plate EHA without a biological body. The versatile FDTD technique is then applied to optimize the EHA design with a human body. Both the numerical and measured data in phantom blocks will be presented. The results of this study will be used to design an optimized system for whole body or regional hyperthermia. Author (revised)

N94-20452*# Jet Propulsion Lab., California Inst. of Tech., Pasadena.
MAPPING OF TAIGA FOREST UNITS USING AIRSAR DATA AND/OR OPTICAL DATA, AND RETRIEVAL OF FOREST PARAMETERS Abstract Only **c43**
Eric Rignot, Cynthia Williams (Institute of Northern Forestry, Fairbanks, AK.), JoBea Way, and Leslie Viereck (Institute of Northern Forestry, Fairbanks, AK.) *In its* Progress In Electromagnetics Research Symposium

(PIERS) 1993 p 856 (For primary document see N94-20403 05-32)
Avail: CASI HC A01/MF A10

A maximum a posteriori Bayesian classifier for multifrequency polarimetric SAR data is used to perform a supervised classification of forest types in the floodplains of Alaska. The image classes include white spruce, balsam poplar, black spruce, alder, non-forests, and open water. The authors investigate the effect on classification accuracy of changing environmental conditions, and of frequency and polarization of the signal. The highest classification accuracy (86 percent correctly classified forest pixels, and 91 percent overall) is obtained combining L- and C-band frequencies fully polarimetric on a date where the forest is just recovering from flooding. The forest map compares favorably with a vegetation map assembled from digitized aerial photos which took five years for completion, and address the state of the forest in 1978, ignoring subsequent fires, changes in the course of the river, clear-cutting of trees, and tree growth. HV-polarization is the most useful polarization at L- and C-band for classification. C-band VV (ERS-1 mode) and L-band HH (J-ERS-1 mode) alone or combined yield unsatisfactory classification accuracies. Additional data acquired in the winter season during thawed and frozen days yield classification accuracies respectively 20 percent and 30 percent lower due to a greater confusion between conifers and deciduous trees. Data acquired at the peak of flooding in May 1991 also yield classification accuracies 10 percent lower because of dominant trunk-ground interactions which mask out finer differences in radar backscatter between tree species. Combination of several of these dates does not improve classification accuracy. For comparison, panchromatic optical data acquired by SPOT in the summer season of 1991 are used to classify the same area. The classification accuracy (78 percent for the forest types and 90 percent if open water is included) is lower than that obtained with AIRSAR although conifers and deciduous trees are better separated due to the presence of leaves on the deciduous trees. Optical data do not separate black spruce and white spruce as well as SAR data, cannot separate alder from balsam poplar, and are of course limited by the frequent cloud cover in the polar regions. Yet, combining SPOT and AIRSAR offers better chances to identify vegetation types independent of ground truth information using a combination of NDVI indexes from SPOT, biomass numbers from AIRSAR, and a segmentation map from either one. Author (revised)

N94-20453*# Jet Propulsion Lab., California Inst. of Tech., Pasadena.
APPLICATION OF THE TARGET DECOMPOSITION THEOREM TO A POLARIMETRIC RANDOM MEDIA MODEL Abstract Only
Sasan S. Saatchi and Jakob J. vanZyl *In its* Progress In Electromagnetics Research Symposium (PIERS) 1993 p 871 (For primary document see N94-20403 05-32)
Avail: CASI HC A01/MF A10

With advances in polarimetric radar measurements of land surfaces, the need for understanding the underlying scattering mechanisms and dominant target features has become the focus of many studies. In particular, the maximum use of the polarimetric information to identify and/or separate parameters related to the surface features such as vegetation thickness, structure, water content, and soil surface characteristics will enhance the possibility of using polarimetric radars for monitoring the earth's surface from space. In this paper, Cloude's decomposition theorem is applied to a polarimetric random media model to simulate the radar measurements of vegetated canopies. The vegetated canopies are modeled as a three layer discrete random medium with leaves and branches in the first layer, tree trunks in the second layer, and a half space of homogeneous ground with rough interface as the bottom layer. The distorted born approximation (DBA) has been used to compute full Mueller matrix of the canopy, using canonical dielectric objects such as thin discs and cylinders as leaves, branches, and trunks, respectively. The Mueller matrix and the derived covariance matrix contain information on the second order statistics of radar signals at various polarizations from the canopy. To decompose the covariance matrix to its constituent targets, the eigenvalues and eigenvectors of the covariance matrix are computed in terms of the physical parameters of the canopy. In addition, each eigenvector explicitly shows the scattering mechanisms such as odd and even reflections in the canopy. Cloude's decomposition theorem is applied using the Pauli spin matrices as a basis and an expression for the degree of disorder or the entropy for the vegetated surface is found. Then, the physical parameters estimated from in situ measurements are used in the random media to obtain realistic covariance matrices. As a result, the sensitivity of the eigenvalue spectrums and the coefficients resulting from the target decomposition theorem to the physical parameters of the canopy are examined and the possible use of Cloude's theorem to estimate vegetation and soil parameters is discussed. Author (revised)

N94-20454*# Jet Propulsion Lab., California Inst. of Tech., Pasadena.
A THEORETICAL AND NUMERICAL STUDY OF POLARIMETRIC SCATTERING AND EMISSION FROM RANDOM ROUGH SURFACES WITH ANISOTROPIC DIRECTIONAL SPECTRUM Abstract Only
S. H. Yueh and R. Kwok *In its* Progress In Electromagnetics Research Symposium (PIERS) 1993 p 873 (For primary document see N94-20403 05-32)
Avail: CASI HC A01/MF A10

In this paper, theoretical and numerical results of the polarimetric scattering and emission from random rough surfaces with anisotropic directional spectrum are presented for the remote sensing of ocean and soil surfaces. The polarimetric scattered field for rough dielectric surfaces is derived to the second order by the small perturbation method (SPM). It is found that the second-order scattered field is coherent in nature, and its coefficients for different polarizations present the lowest-order corrections to the Fresnel reflection coefficients of the surfaces. In addition, the cross-polarized (HV and VH) components of the coherent fields are reciprocal and not zero for surfaces with anisotropic directional spectrum when the azimuth angle of the incident direction is not aligned with the symmetry directions of surfaces. In order to verify the energy conservation condition of the theoretical results, which is important if the theory is to be applied to the passive polarimetry of rough surfaces, a Monte Carlo simulation is performed to numerically calculate the polarimetric reflectivities of one-dimensional random rough surfaces which are generated with a prescribed power-law spectrum in the spectral domain and transformed to the spatial domain by the FFT. The surfaces simulated by this approach are periodic with the period corresponding to the low-wavenumber cutoff. To calculate the scattering from periodic dielectric surfaces, the authors present a new numerical technique which applies the Floquet theorem to reduce the problem to one period and does not require the evaluation of one-dimensional periodic Green's function used in the conventional method of moment formulation. Once the scattering coefficients are obtained, the polarimetric Stokes vectors for the emission from the random surfaces are then calculated according to the Kirchhoff's law and are illustrated as functions of relative azimuth observation and row directions. The second-order SPM is also reduced to this one-dimensional case, and theoretical results for all four Stokes parameters are in excellent agreement with the numerical results obtained from the Monte Carlo simulation. Moreover, the second order coherent fields are found to be necessary for the theoretical evaluation of the third and fourth Stokes parameters. Without that, the reflectivities of random rough surfaces are significantly over-estimated, and the signs of the third and the fourth Stokes parameters are found to be incorrect, if calculated by using the first-order incoherent fields alone. Author (revised)

N94-20455*# Jet Propulsion Lab., California Inst. of Tech., Pasadena.
APPLICATION OF NEURAL NETWORK TO REMOTE SENSING OF SOIL MOISTURE USING THEORETICAL POLARIMETRIC BACKSCATTERING COEFFICIENTS Abstract Only **c43**
L. Wang (Massachusetts Inst. of Tech., Cambridge.), R. T. Shin (Massachusetts Inst. of Tech., Cambridge.), J. A. Kong (Massachusetts Inst. of Tech., Cambridge.), and S. H. Yueh *In its* Progress In Electromagnetics Research Symposium (PIERS) 1993 p 875 (For primary document see N94-20403 05-32)
Avail: CASI HC A01/MF A10

This paper investigates the potential application of neural network to inversion of soil moisture using polarimetric remote sensing data. The neural network used for the inversion of soil parameters is multi-layer perceptron trained with the back-propagation algorithm. The training data include the polarimetric backscattering coefficients obtained from theoretical surface scattering models together with an assumed nominal range of soil parameters which are comprised of the soil permittivity and surface roughness parameters. Soil permittivity is calculated from the soil moisture and the assumed soil texture based on an empirical formula at C-, L-, and P-bands. The rough surface parameters for the soil surface, which is described by the Gaussian random process, are the root-mean-square

(rms) height and correlation length. For the rough surface scattering, small perturbation method is used for the L-band frequency, and Kirchhoff approximation is used for the C-band frequency to obtain the corresponding backscattering coefficients. During the training, the backscattering coefficients are the inputs to the neural net and the output from the net are compared with the desired soil parameters to adjust the interconnecting weights. The process is repeated for each input-output data entry and then for the entire training data until convergence is reached. After training, the backscattering coefficients are applied to the trained neural net to retrieve the soil parameters which are compared with the desired soil parameters to verify the effectiveness of this technique. Several cases are examined. First, for simplicity, the correlation length and rms height of the soil surface are fixed while soil moisture is varied. Soil moisture obtained using the neural networks with either L-band or C-band backscattering coefficients for the HH and VV polarizations as inputs is in good agreement with the desired soil moisture. The neural net output matches the desired output for the soil moisture range of 16 to 60 percent for the C-band case. The next case investigated is to vary both soil moisture and rms height while keeping the correlation length fixed. For this case, C-band backscattering coefficients are not sufficient for retrieving two parameters because the Kirchhoff approximation gives the same HH and VV backscattering coefficients. Therefore, the backscattering coefficients at two different frequency bands are necessary to find both the soil moisture and rms height. Finally, the neural nets are also applied to simultaneously invert soil moisture, rms height, and correlation length. Overall, the soil moisture retrieved from the neural network agrees very well with the desired soil moisture. This suggests that the neural network shows potential for retrieval of soil parameters from remote sensing data. Author (revised)

N94-20456*# Jet Propulsion Lab., California Inst. of Tech., Pasadena.
THE BREWSTER ANGLE EFFECT IN SAR POLARIMETRY Abstract Only
B. Chapman *In its* Progress In Electromagnetics Research Symposium (PIERS) 1993 p 876 (For primary document see N94-20403 05-32)
Avail: CASI HC A01/MF A10

For the double bounce case, where the radar signal is reflected twice before returning to the radar antenna, some polarization effects may be observed related to the dielectric constant of the two surfaces causing the reflections. The most noticeable effect would be that the returned signal would be preferentially H polarized. In fact, it may be possible to discern the Brewster angle for both surfaces. The locations of the Brewster angle will depend on the dielectric constant and permittivity of each surface. If it is assumed that both reflections are in the same plane of incidence, and that both surfaces are smooth and flat, there is a straightforward relationship between the degree of linear polarization m and both the dielectric constants of the two reflecting surfaces and the angle of incidence of the illuminating wave: m carat = cos 2(arccot (square root of (R(sub v) / R(sub h)))) where R(sub v,h) are the V and H polarized Fresnel reflection coefficients for two surfaces perpendicular to each other. The degree of linear polarization may be calculated from AIRSAR compressed Stokes data and compared with the given equation. The degree of linear polarization may also be calculated using tree models and compared with AIRSAR data. With further work, it may be possible to use the degree of linear polarization to determine surface parameters of certain imaged areas. Author (revised)

N94-20457*# Jet Propulsion Lab., California Inst. of Tech., Pasadena.
MOBILE ANTENNA DEVELOPMENT AT JPL Abstract Only
J. Huang, V. Jamnejad, A. Densmore, A. Tulintseff, R. Thomas, and K. Woo *In its* Progress In Electromagnetics Research Symposium (PIERS) 1993 p 880 (For primary document see N94-20403 05-32)
Avail: CASI HC A01/MF A10

The Jet Propulsion Laboratory (JPL), under the sponsorship of NASA, has pioneered the development of land vehicle antennas for commercial mobile satellite communications. Several novel antennas have been developed at L-band frequencies for the Mobile Satellite (MSAT) program initiated about a decade ago. Currently, two types of antennas are being developed at K- and Ka-band frequencies for the ACTS (Advanced Communications Technology Satellite) Mobile Terminal (AMT) project. For the future, several hand-held antenna concepts are proposed for the small terminals of the Ka-band Personal Access Satellite System (PASS). For the L-band MSAT program, a number of omni-directional low-gain antennas, such as the crossed drooping-dipoles, the higher-order-mode circular microstrip patch, the quadrifilar helix, and the wrapped-around microstrip 'mast' array, have been developed for lower data rate communications. Several medium-gain satellite tracking antennas, such as the electronically scanned low-profile phased array, the mechanically steered tilted microstrip array, the mechanically steered low-profile microstrip Yagi array, and the hybrid electronically/mechanically steered low-profile array, have been developed for the MSAT's higher data rate and voice communications. To date, for the L-band vehicle application, JPL has developed the world's lowest-profile phased array (1.8 cm height), as well as the lowest-profile mechanically steered antenna (3.7 cm height). For the 20/30 GHz AMT project, a small mechanically steered elliptical reflector antenna with a gain of 23 dBi has recently been developed to transmit horizontal polarization at 30 GHz and receive vertical polarization at 20 GHz. Its hemispherical radome has a height of 10 cm and a base diameter of 23 cm. In addition to the reflector, a mechanically steered printed MMIC active array is currently being developed to achieve the same electrical requirements with a low profile capability. These AMT antenna developments, along with other Ka-band technologies, will lead to the development of several compact hand-held terminals for the PASS program. A few antenna concepts, such as the lap-top or desk-top terminal's printed array, the hand-held phased array, and the head-mounted low-profile array, have been proposed to achieve a future vision for the personal access communications system. Author

N94-20458*# Jet Propulsion Lab., California Inst. of Tech., Pasadena.
MOBILE TERMINAL ANTENNAS FOR HELICOPTERS Abstract Only
Te-Kao Wu, K. Farazian, N. Golshan, D. Divsalar, S. Hinedi, and K. Woo *In its* Progress In Electromagnetics Research Symposium (PIERS) 1993 p 885 (For primary document see N94-20403 05-32)
Avail: CASI HC A01/MF A10

In this paper, the feasibility of using an L-band low gain antenna (LGA) as a mobile terminal antenna for helicopters is described. The objective is to select the lowest cost antenna system which can be easily mounted on a helicopter and capable of communicating with a geosynchronous satellite. To ensure that all the antenna options are being considered, the steerable high gain reflector and medium gain array antennas as well as LGA are studied and compared in an exhaustive survey. The high gain reflector antenna in L-band is usually very large in size and heavy in weight. In addition, a bulky and expensive tracking system is needed to steer the antenna beam to the satellite direction. The medium gain antennas (including mechanically and electronically steered arrays) are also more expensive and less reliable than an LGA due to the addition of a beam steering system to track the satellite. The omni-directional LGA is simple, reliable, and inexpensive. It is typically ten times smaller than the medium gain antenna. This makes the position, selection, and mounting on the helicopter relatively easier. Therefore, the LGA is selected as a mobile terminal antenna for helicopters. Among the many LGA's (cross-dipole, helix, spiral, and slot antennas), the helix antenna is the most inexpensive. One can also change the size, shape, or pitch angle of the helix to optimize the gain in the desired direction. Therefore, the helix antenna is selected for further study. Both 2-arm and 4-arm helices are studied theoretically and experimentally to determine the antenna's performance and the scattering effects from the helicopter body and the blades. The multipath, Doppler, and Doppler rate issues as well as the periodic fading effects caused by the helicopter rotor blades will be briefly discussed in the paper. Author (revised)

N94-20459*# Jet Propulsion Lab., California Inst. of Tech., Pasadena.
TOPOGRAPHIC SLOPE FROM THE SAR INTERFEROMETRIC PHASE GRADIENT Abstract Only **c43**
Charles L. Werner (Zurich Univ., Switzerland.) and Paul A. Rosen *In its* Progress In Electromagnetics Research Symposium (PIERS) 1993 p 922 (For primary document see N94-20403 05-32)
Avail: CASI HC A01/MF A10

A new algorithm for the direct calculation of topographic slope maps from synthetic aperture radar (SAR) interferograms is presented. The algorithm derives slope maps without first requiring the creation of a digital elevational model (DEM) from the interferogram, thus obviating the need for high SNR in the interferogram and altitude calibration points for the scene. SAR data useful for interferometry has been collected by the Active Microwave Imager on board the ERS-1 satellite, when it was in a short period repeat orbit. Two passes of the radar sensor form a cross-track

interferometric baseline. For a point target at some position (x,y,h), the interferometric phase difference phi is proportional to the difference in path lengths for the two sensor positions to the scatterer. Given the phase difference as measured in the complex interferogram and an accurate baseline geometry, the position of the scatterer, most significantly the height h, can be determined through triangulation. The interferometric phase measurement however is known only modulo 2-pi, and hence it is necessary to determine the correct multiple of 2-pi to add to the phase at each point to obtain an estimate of the actual phase with respect to an absolute datum. This phase unwrapping process is required for creating DEM's, and is difficult or impossible for regions of low SNR or SAR image layover. The new algorithm described here derives slope maps without requiring phase unwrapping. Author (revised)

N94-20460*# Jet Propulsion Lab., California Inst. of Tech., Pasadena.
INTERFEROMETRIC DETECTION OF FREEZE-THAW DISPLACEMENTS OF ALASKAN PERMAFROST USING ERS-1 DATA Abstract Only c43
Charles L. Werner (Zurich Univ., Switzerland.) and Andrew K. Gabriel *In its* Progress In Electromagnetics Research Symposium (PIERS) 1993 p 923 (For primary document see N94-20403 05-32)
Avail: CASI HC A01/MF A10

The possibility of making large scale (50 km) measurements of motions of the earth's surface with high resolution (10 m) and very high accuracy (1 cm) from multipass SAR interferometry was established in 1989. Other experiments have confirmed the viability and usefulness of the method. Work is underway in various groups to measure displacements from volcanic activity, seismic events, glacier motion, and in the present study, freeze-thaw cycles in Alaskan permafrost. The ground is known to move significantly in these cycles, and provided that freezing does not cause image decorrelation, it should be possible to measure both ground swelling and subsidence. The authors have obtained data from multiple passes of ERS-1 over the Toolik Lake region of northern Alaska of suitable quality for interferometry. The data are processed into images, and single interferograms are formed in the usual manner. Phase unwrapping is performed, and the multipass baselines are estimated from the images using both orbit ephemerides and scene tie points. The phases are scaled by the baseline ratio, and a double-difference interferogram (DDI) is formed. It is found that there is a residual 'saddle-shape' phase error across the image, which is postulated to be caused by a small divergence (10(exp -2) deg.) in the orbits. A simulation of a DDI from divergent orbits confirms the shape and magnitude of the error. A two-dimensional least squares fit to the error is performed, which is used to correct the DDI. The final, corrected DDI shows significant phase (altitude) changes over the period of the observation.
Author (revised)

N94-20461*# Jet Propulsion Lab., California Inst. of Tech., Pasadena.
PERFORMANCE EVALUATION OF THE JPL TOPSAR SYSTEM: AN ACROSS-TRACK INTERFEROMETRIC SAR SYSTEM FOR TOPOGRAPHIC MAPPING Abstract Only c43
Soren N. Madsen, Howard A. Zebker, and Jan Martin *In its* Progress In Electromagnetics Research Symposium (PIERS) 1993 p 924 (For primary document see N94-20403 05-32)
Avail: CASI HC A01/MF A10

An across-track interferometric (XTI) SAR has the capability of determining the three dimensional target location from the recorded radar echos thus providing high spatial resolution both horizontally and vertically. The output of an XTI SAR will typically include both a radar backscatter map and a digital elevation model (DEM). The accuracy of the derived DEM is determined by factors such as data acquisition geometry, signal-to-noise ratio, knowledge of platform position and attitude as well as the accuracy of the processing system. In the summer of 1992 the authors acquired TOPSAR data over the Ft. Irwin area in California, a desert area with significant relief (height standard deviation 150 m). Very accurate DEM's have been derived for this area by the Topographic Engineering Center (TEC) using digital correlation methods on 1:20,000 scale digitized photographs. Corner reflectors were deployed in the area, and their locations were determined to cm accuracies by the Defense Mapping Agency (DMA) using differential GPS techniques. DEM's generated from the acquired radar data have been rotated and translated to overlay the reference DEM's provided by TEC. A detailed description of the errors and their characteristics will be given. The standard deviations of the radar data sets we acquired measured over a 5.6 by 7 km area were 1.9 and 2.3 m. The corresponding numbers for flat areas were 1.1 and 2.0 m and for mountain areas 3.3 and 2.2 m. Author (revised)

N94-20471 Naval Command, Control and Ocean Surveillance Center, San Diego, CA.
FOUR-CHANNEL HF RECEIVING ANTENNA ARRAY SIMULATOR Final Report, Jan. - Jul. 1992
K. C. Owens Aug. 1993 31 p Limited Reproducibility: More than 20% of this document may be affected by microfiche quality
(AD-A271876; NCCOSC/RDT/E-TD-2551) Avail: CASI HC A03

This document discusses the design, fabrication, and operation of an antenna array simulator, which is an integral part of the NRaD adaptive array evaluation facility. A brief introduction is provided to explain how adaptive receiving antenna arrays can improve Navy high-frequency communications and how this developmental work is supported at NRaD. The main body of the text encompasses both the software algorithms created to support computerized remote control and antenna phase-tuning operation and a detailed hardware description of the Simulator circuitry, which is suitable as a guide for maintenance and troubleshooting tasks.
DTIC

N94-20479# Los Alamos National Lab., NM.
LOCALIZATION FROM NEAR-SOURCE QUASI-STATIC ELECTROMAGNETIC FIELDS Ph.D. Thesis
J. C. Mosher Sep. 1993 148 p
(Contract W-7405-eng-36)
(DE93-040390; LA-12622-T) Avail: CASI HC A07/MF A02

A wide range of research has been published on the problem of estimating the parameters of electromagnetic and acoustical sources from measurements of signals measured at an array of sensors. In the quasi-static electromagnetic cases examined here, the signal variation from a point source is relatively slow with respect to the signal propagation and the spacing of the array of sensors. As such, the location of the point sources can only be determined from the spatial diversity of the received signal across the array. The inverse source localization problem is complicated by unknown model order and strong local minima. The nonlinear optimization problem is posed for solving for the parameters of the quasi-static source model. The transient nature of the sources can be exploited to allow subspace approaches to separate out the signal portion of the spatial correlation matrix. Decomposition techniques are examined for improved processing, and an adaptation of MUltiple SIgnal Characterization (MUSIC) is presented for solving the source localization problem. Recent results on calculating the Cramer-Rao error lower bounds are extended to the multidimensional problem here. This thesis focuses on the problem of source localization in magnetoencephalography (MEG), with a secondary application to thunderstorm source localization. Comparisons are also made between MEG and its electrical equivalent, electroencephalography (EEG). The error lower bounds are examined in detail for several MEG and EEG configurations, as well as localizing thunderstorm cells over Cape Canaveral and Kennedy Space Center. Time-eigenspectrum is introduced as a parsing technique for improving the performance of the optimization problem.
DOE

N94-20497*# National Aeronautics and Space Administration. Lewis Research Center, Cleveland, OH.
SOLID STATE TECHNOLOGY BRANCH OF NASA LEWIS RESEARCH CENTER: FIFTH ANNUAL DIGEST
Aug. 1993 273 p
(RTOP 506-72-1B)
(NASA-TM-106303; E-8004; NAS 1.15:106303) Avail: CASI HC A12/MF A03

The digest is a collection of papers written by the members of the Solid State Technology Branch of NASA Lewis Research Center from June 1992-June 1993. The papers cover a range of topics relating to superconductivity, monolithic microwave integrated circuits (MMIC's), coplanar waveguide, and material characterization. For individual titles, see N94-20498 through N94-20519.

N94-20498*# National Aeronautics and Space Administration. Lewis Research Center, Cleveland, OH.
AN X-BAND PEELED HEMT AMPLIFIER c33

Paul G. Young (Toledo Univ., OH.), Robert R. Romanofsky, Samuel A. Alterovitz, and Edwyn D. Smith (Toledo Univ., OH.) *In its* Solid State Technology Branch of NASA Lewis Research Center: Fifth Annual Digest Aug. 1993 p 7-13 Repr. from High-Speed Electronics and Optoelectronics, v. 1680, 1992 p 72-78 (For primary document see N94-20497 05-32)
(Grant NAG3-1226)
Avail: CASI HC A02/MF A03

A discrete peeled high electron mobility transistor (HEMT) device was integrated into a 10 GHz amplifier. The discrete HEMT device interconnects were made using photo patterned metal, stepping from the 10 mil alumina host substrate onto the 1.3 microns thick peeled GaAs HEMT layer, eliminating the need for bond wires and creating a fully integrated circuit. Testing of devices indicate that the peeled device is not degraded by the peel off step but rather there is an improvement in the quantum well carrier confinement. Circuit testing resulted in a maximum gain of 8.5 dB and a return loss minimum of -12 dB. Author (revised)

N94-20499*# National Aeronautics and Space Administration. Lewis Research Center, Cleveland, OH.
CHARACTERISTICS OF 0.8- AND 0.2-MICRONS GATE LENGTH In(x)Ga(1-x) As/In(0.52)Al(0.48)As/InP (0.53 LESS THAN OR EQUAL TO x LESS THAN OR EQUAL TO 0.70) MODULATION-DOPED FIELD-EFFECT TRANSISTORS AT CRYOGENIC TEMPERATURES c33
Richard Lai, Pallab K. Bhattacharya, David Yang, Timothy L. Brock, Samuel A. Alterovitz, and Alan N. Downey *In its* Solid State Technology Branch of NASA Lewis Research Center: Fifth Annual Digest Aug. 1993 p 15-22 Repr. from IEEE Transactions on Electron Devices, v. 39, no. 10, Oct. 1992 p 2206-2213 (For primary document see N94-20497 05-32)
Avail: CASI HC A02/MF A03

The performance characteristics of InP-based In(x)Ga(1-x)As/In(0.52)Al(0.48)As (0.53 is less than or equal to x is less than or equal to 0.70) pseudomorphic modulation-doped field-effect transistors (MODFET's) as a function of strain in the channel, gate, length, and temperature were investigated analytically and experimentally. The strain in the channel was varied by varying the In composition x. The temperature was varied in the range of 40-300 K and the devices have gate lengths L(sub g) of 0.8 and 0.2 microns. Analysis of the device was done using a one-dimensional self consistent solution of the Poisson and Schroedinger equations in the channel, a two-dimensional Poisson solver to obtain the channel electric field, and a Monte Carlo simulation to estimate the carrier transit times in the channel. An increase in the value of the cutoff frequency is predicted for an increase in In composition, a decrease in temperature, and a decrease in gate length. The improvements seen with decreasing temperature, decreasing gate length, and increased In composition were smaller than those predicted by analysis. The experimental results on pseudomorphic InGaAs/InAlAs MODFET's showed that there is a 15-30 percent improvement in cutoff frequency in both the 0.8- and 0.2-micron gate length devices when the temperature is lowered from 300 to 40 K.
Author (revised)

N94-20500*# National Aeronautics and Space Administration. Lewis Research Center, Cleveland, OH.
A COMPREHENSIVE THEORETICAL AND EXPERIMENTAL STUDY OF COPLANAR WAVEGUIDE SHUNT STUBS c33
Nihad I. Dib (Michigan Univ., Ann Arbor.), George E. Ponchak, and Linda P. B. Katehi (Michigan Univ., Ann Arbor.) *In its* Solid State Technology Branch of NASA Lewis Research Center: Fifth Annual Digest Aug. 1993 p 31-34 Repr. from IEEE MTT-S Digest, 1992 p 947-950 (For primary document see N94-20497 05-32)
(Grant NSF ECS-86-57951)
Avail: CASI HC A01/MF A03

A comprehensive theoretical and experimental study of straight and bent coplanar waveguide (CPW) shunt stubs is presented. In the theoretical analysis, the CPW is assumed to be inside a cavity, while, the experiments are performed on open structures. A hybrid technique was developed to analyze the CPW discontinuities which proved to be accurate since the theoretical and experimental results agree very well. The effect of the cavity resonances on the behavior of the stubs with and without air-bridges is investigated. In addition, the encountered radiation loss due to the discontinuities is evaluated experimentally. Author

N94-20501*# National Aeronautics and Space Administration. Lewis Research Center, Cleveland, OH.
A COMPARATIVE STUDY BETWEEN SHIELDED AND OPEN COPLANAR WAVEGUIDE DISCONTINUITIES c33
Nihad I. Dib (Michigan Univ., Ann Arbor.), W. P. Harokopus, Jr. (Texas Instruments, Inc., Dallas.), G. E. Ponchak, and L. P. B. Katehi (Michigan Univ., Ann Arbor.) *In its* Solid State Technology Branch of NASA Lewis Research Center: Fifth Annual Digest Aug. 1993 p 35-45 Repr. from Journal of Microwave and Milimeter-Wave Computer-Aided Engineering, v. 2, no. 4, 1992 (For primary document see N94-20497 05-32)
(Grant NSF ECS-86-57951)
Avail: CASI HC A03/MF A03

A comparative study between open and shielded coplanar waveguide (CPW) discontinuities is presented. The space domain integral equation method is used to characterize several discontinuities such as the open-end CPW and CPW series stubs. Two different geometries of CPW series stubs (straight and bent stubs) are compared with respect to resonant frequency and radiation loss. In addition, the encountered radiation loss due to different CPW shunt stubs is evaluated experimentally. The notion of forced radiation simulation is presented, and the results of such a simulation are compared to the actual radiation loss obtained rigorously. It is shown that such a simulation cannot give reliable results concerning radiation loss from printed circuits. Author (revised)

N94-20502*# National Aeronautics and Space Administration. Lewis Research Center, Cleveland, OH.
A THEORETICAL AND EXPERIMENTAL STUDY OF COPLANAR WAVEGUIDE SHUNT STUBS c33
Nihad I. Dib, George E. Ponchak, and Linda P. B. Katehi *In its* Solid State Technology Branch of NASA Lewis Research Center: Fifth Annual Digest Aug. 1993 p 47-53 Repr. from IEEE Transactions on Microwave Theory and Techniques, v. 41, no. 1, Jan. 1993 p 38-44 (For primary document see N94-20497 05-32)
Avail: CASI HC A02/MF A03

A comprehensive theoretical and experimental study of straight and bent coplanar waveguide (CPW) shunt stubs is presented. In the theoretical analysis, the CPW is assumed to be inside a cavity while, the experiments are performed on open structures. For the analysis of CPW discontinuities with air-bridges, a hybrid technique was developed which was validated through extensive theoretical and experimental comparisons. The effect of the cavity resonances on the behavior of the stubs with and without air-bridges is investigated. In addition, the encountered radiation loss due to the discontinuities is evaluated experimentally. Author (revised)

N94-20503*# National Aeronautics and Space Administration. Lewis Research Center, Cleveland, OH.
COPLANAR WAVEGUIDE RADIAL LINE STUB c33
R. N. Simons and S. R. Taub *In its* Solid State Technology Branch of NASA Lewis Research Center: Fifth Annual Digest Aug. 1993 p 55-56 Repr. from IEEE Electronics Letters, v. 29, no. 4, 18 Feb. 1993 p 412-413 (For primary document see N94-20497 05-32)
Avail: CASI HC A01/MF A03

A coplanar waveguide radial line stub resonator is experimentally characterized with respect to stub radius, sectoral angle, substrate thickness, and relative dielectric constant. A simple closed-form design equation which predicts the resonance radius of the stub is presented. Author (revised)

N94-20504*# National Aeronautics and Space Administration. Lewis Research Center, Cleveland, OH.
ATTENUATION OF EPSILON(SUB EFF) OF COPLANAR WAVEGUIDE TRANSMISSION LINES ON SILICON SUBSTRATES c33
Susan R. Taub and Paul G. Young *In its* Solid State Technology Branch of NASA Lewis Research Center: Fifth Annual Digest Aug. 1993 p 57-60 Repr. from the 11th Annual Benjamin Franklin Symposium on Antenna and Microwave Technology in the 1990s, May 1993 p 8-11 (For primary document see N94-20497 05-32)
Avail: CASI HC A01/MF A03

Attenuation and epsilon(sub eff) of Coplanar Waveguide (CPW) transmission lines were measured on Silicon substrates with resistivities ranging from 400 to greater than 30,000 ohm-cm, that have a 1000 angstrom coating of SiO2. Both attenuation and epsilon(sub eff) are given over the

frequency range 5 to 40 GHz for various strip and slot widths. These measured values are also compared to the theoretical values.
Author (revised)

N94-20505*# National Aeronautics and Space Administration. Lewis Research Center, Cleveland, OH.
LINEARLY TAPERED SLOT ANTENNA WITH DIELECTRIC SUPERSTRATE
Rainee N. Simons and Richard Q. Lee *In its* Solid State Technology Branch of NASA Lewis Research Center: Fifth Annual Digest Aug. 1993 p 73-80 Repr. from IEEE Antennas and Propagation Society International Symposium, Jun. 1993 p 1482-1485 (For primary document see N94-20497 05-32)
Avail: CASI HC A01/MF A03

The effect of dielectric superstrate on a linearly tapered slot antenna (LTSA) was investigated experimentally. It was observed that the dielectric superstrate improves the directivity but generally at the expense of higher sidelobe level. The dielectric superstrate could be used to reduce the physical length and to improve the radiation characteristics of the LTSA.
Author

N94-20506*# National Aeronautics and Space Administration. Lewis Research Center, Cleveland, OH.
SLOT-COUPLED PATCH ANTENNA WITH COPLANAR WAVEGUIDE FEED **c33**
Richard Q. Lee and Rainee N. Simons *In its* Solid State Technology Branch of NASA Lewis Research Center: Fifth Annual Digest Aug. 1993 p 89-92 Repr. from IEEE Antennas and Propagation Society International Symposium, Jul. 1992 p 1048-1051 (For primary document see N94-20497 05-32)
Avail: CASI HC A01/MF A03

Two slot-coupled feeding techniques for exciting a patch antenna with a coplanar waveguide (CPW) were experimentally investigated. In the first technique, a CPW with two notches on both sides of the slot lines is used to couple power to the antenna through a narrow rectangular slot. In the second technique, a grounded CPW with a series gap in the center strip conductor is used to couple power to the antenna through a 'dumbbell' slot. Results indicated that both techniques are feasible and yield high coupling efficiency.
Author

N94-20507*# National Aeronautics and Space Administration. Lewis Research Center, Cleveland, OH.
BANDWIDTH ENHANCEMENT OF DIELECTRIC RESONATOR ANTENNAS **c33**
Richard Q. Lee and Rainee N. Simons *In its* Solid State Technology Branch of NASA Lewis Research Center: Fifth Annual Digest Aug. 1993 p 93-96 Repr. from IEEE Antennas and Propagation Society International Symposium, Jun. 1993 p 1500-1503 (For primary document see N94-20497 05-32)
Avail: CASI HC A01/MF A03

An experimental investigation of bandwidth enhancement of dielectric resonator antennas (DRA) using parasitic elements is reported. Substantial bandwidth enhancement for the HE(sub 11delta) mode of the stacked geometry and for the HE(sub 13delta) mode of the coplanar collinear geometry was demonstrated. Excellent radiation patterns for the HE(sub 11delta) mode were also recorded.
Author (revised)

N94-20508*# National Aeronautics and Space Administration. Lewis Research Center, Cleveland, OH.
SPECTROSCOPIC ELLIPSOMETRY STUDIES OF HF TREATED Si (100) SURFACES **c33**
Huade Yao (Nebraska Univ., Lincoln.), John A. Woollam (Nebraska Univ., Lincoln.), and Samuel A. Alterovitz *In its* Solid State Technology Branch of NASA Lewis Research Center: Fifth Annual Digest Aug. 1993 p 129-131 Repr. from American Inst. of Physics, Applied Physics Letter, v. 62, no. 25, 21 Jun. 1993 (For primary document see N94-20497 05-32)
(Grant NAG3-154)
Avail: CASI HC A01/MF A03

Both ex situ and in situ spectroscopic ellipsometry (SE) measurements were employed to investigate the effects of HF cleaning on Si surfaces. The hydrogen-terminated (H-terminated) Si surface was modeled as an equivalent dielectric layer, and monitored in real time by SE measurements. The SE analyses indicate that after a 20-s 9:1 HF dip without rinse, the Si(100) surface was passivated by the hydrogen termination and remained chemically stable. Roughness of the HF-etched bare Si(100) surface was observed, in an ultrahigh vacuum (UHV) chamber, and analyzed by the in situ SE. Evidence for desorption of the H-terminated Si surface-layer, after being heated to approximately 550 C in the UHV chamber, is presented and discussed. This is the first use of an ex situ and in situ real-time, nondestructive technique capable of showing state of passivation, the rate of reoxidation, and the surface roughness of the H-terminated Si surfaces.
Derived from text

N94-20509*# National Aeronautics and Space Administration. Lewis Research Center, Cleveland, OH.
ELLIPSOMETRIC STUDY OF Si(0.5)Ge(0.5)/Si STRAINED-LAYER SUPERLATTICES **c76**
R. M. Sieg (Cleveland State Univ., OH.), S. A. Alterovitz, E. T. Croke (Hughes Research Labs., Malibu, CA.), and M. J. Harrell (Hughes Research Labs., Malibu, CA.) *In its* Solid State Technology Branch of NASA Lewis Research Center: Fifth Annual Digest Aug. 1993 p 135-137 Repr. from American Physics Inst., Applied Physics Letter, v. 62, no. 14, 5 Apr. 1993 (For primary document see N94-20497 05-32)
Avail: CASI HC A01/MF A03

An ellipsometric study of two Si(0.5)Ge(0.5)/Si strained-layer super lattices grown by MBE at low temperature (500 C) is presented, and results are compared with x ray diffraction (XRD) estimates. Excellent agreement is obtained between target values, XRD, and ellipsometry when one of two available Si(x)Ge(1-x) databases is used. It is shown that ellipsometry can be used to nondestructively determine the number of superlattice periods, layer thicknesses, Si(x)Ge(1-x) composition, and oxide thickness without resorting to additional sources of information. It was also noted that we do not observe any strain effect on the E(sub 1) critical point.
Author (revised)

N94-20510*# National Aeronautics and Space Administration. Lewis Research Center, Cleveland, OH.
SPECTROSCOPIC ELLIPSOMETRIC CHARACTERIZATION OF Si/Si(1-x)Ge(x) STRAINED-LAYER SUPERLATTICES **c76**
H. Yao (Nebraska Univ., Lincoln.), J. A. Woollam (Nebraska Univ., Lincoln.), P. J. Wang (International Business Machines Corp., Hopewell Junction, NY.), M. J. Tejwani (International Business Machines Corp., Hopewell Junction, NY.), and S. A. Alterovitz *In its* Solid State Technology Branch of NASA Lewis Research Center: Fifth Annual Digest Aug. 1993 p 139-143 Repr. from Applied Surface Science, v. 63, 1993 p 52-56 (For primary document see N94-20497 05-32)
(Grant NAG3-154)
Avail: CASI HC A01/MF A03

Spectroscopic ellipsometry (SE) was employed to characterize Si/Si(1-x)Ge(x) strained-layer superlattices. An algorithm was developed, using the available optical constants measured at a number of fixed x values of Ge composition, to compute the dielectric function spectrum of Si(1-x)Ge(x) at an arbitrary x value in the spectral range 17 to 5.6 eV. The ellipsometrically determined superlattice thicknesses and alloy compositional fractions were in excellent agreement with results from high-resolution x ray diffraction studies. The silicon surfaces of the superlattices were subjected to a 9:1 HF cleaning prior to the SE measurements. The HF solution removed silicon oxides on the semiconductor surface, and terminated the Si surface with hydrogen-silicon bonds, which were monitored over a period of several weeks, after the HF cleaning, by SE measurements. An equivalent dielectric layer model was established to describe the hydrogen-terminated Si surface layer. The passivated Si surface remained unchanged for greater than 2 h, and very little surface oxidation took place even over 3 to 4 days.
Author (revised)

N94-20511*# National Aeronautics and Space Administration. Lewis Research Center, Cleveland, OH.
NEW TECHNIQUE FOR OIL BACKSTREAMING CONTAMINATION MEASUREMENTS **c09**
S. A. Alterovitz, H. J. Speier, R. M. Sieg (Cleveland State Univ., OH.), M. N. Drotos (Cleveland State Univ., OH.), and J. E. Dunning (Michigan State Univ., East Lansing.) *In its* Solid State Technology Branch of NASA Lewis Research Center: Fifth Annual Digest Aug. 1993 p 157-162

Repr. from American Inst. of Physics, Applied Physics Letter, v. 73, no. 4, 1 Jul./Aug. 1992 (For primary document see N94-20497 05-32)
Avail: CASI HC A02/MF A03

Due to the large size and the number of diffusion pumps, space simulation chambers cannot be easily calibrated by the usual test dome method for measuring backstreaming from oil diffusion pumps. In addition, location dependent contamination may be an important parameter of the test. The backstreaming contamination in the Space Power Facility (SPF) near Sandusky, Ohio, the largest space simulation vacuum test chamber in the U.S.A. was measured. Small size clean silicon wafers as contamination sensors placed at all desired measurement sites were used. The facility used diffusion pumps with DC 705 oil. The thickness of the contamination oil film was measured using ellipsometry. Since the oil did not wet uniformly the silicon substrate, two analysis models were developed to measure the oil film: continuous, homogeneous film and islands of oil with the islands varying in coverage fraction and height. In both cases, the contamination film refractive index was assumed to be that of DC 705. The second model improved the ellipsometric analysis quality parameter by up to two orders of magnitude, especially for the low coverage cases. Comparison of the two models for our case shows that the continuous film model overestimates the oil volume by less than 50 percent. Absolute numbers for backstreaming are in good agreement with published results for diffusion pumps. Good agreement was also found between the ellipsometric results and measurements done by x ray photoelectron spectroscopy (XPS) and by scanning electron microscopy (SEM) on samples exposed to the same vacuum runs. Author (revised)

N94-20512*# National Aeronautics and Space Administration. Lewis Research Center, Cleveland, OH.

THE QUANTUM EFFICIENCY OF HgCdTe PHOTODIODES IN RELATION TO THE DIRECTION OF ILLUMINATION AND TO THEIR GEOMETRY **c33**

D. Rosenfeld and G. Bahir (Israel Inst. of Tech., Haifa.) *In its* Solid State Technology Branch of NASA Lewis Research Center: Fifth Annual Digest Aug. 1993 p 163-169 Repr. from American Inst. of Physics, Journal of Applied Physics, v. 72, no. 7, 1 Oct. 1992 (For primary document see N94-20497 05-32)
Avail: CASI HC A02/MF A03

A theoretical study of the effect of the direction of the incident light on the quantum efficiency of homogeneous HgCdTe photodiodes suitable for sensing infrared radiation in the 8-12 microns atmospheric window is presented. The probability of an excess minority carrier to reach the junction is derived as a function of its distance from the edge of the depletion region. Accordingly, the quantum efficiency of photodiodes is presented for two geometries. In the first, the light is introduced directly to the area in which it is absorbed (opaque region), while in the second, the light passes through a transparent region before it reaches the opaque region. Finally, the performance of the two types of diodes is analyzed with the objective of finding the optimal width of the absorption area. The quantum efficiency depends strongly on the way in which the light is introduced. The structure in which the radiation is absorbed following its crossing the transparent region is associated with both higher quantum efficiency and homogeneity. In addition, for absorption region widths higher than a certain minimum, the quantum efficiency in this case is insensitive to the width of the absorption region. Author (revised)

N94-20513*# National Aeronautics and Space Administration. Lewis Research Center, Cleveland, OH.

SPACE APPLICATIONS OF SUPERCONDUCTING MICROWAVE ELECTRONICS AT NASA LEWIS RESEARCH CENTER **c20**

R. F. Leonard, K. B. Bhasin, R. R. Romanofsky, C. D. Cubbage, and C. Z. Chorey (Sverdrup Technology, Inc., Cleveland, OH.) *In its* Solid State Technology Branch of NASA Lewis Research Center: Fifth Annual Digest Aug. 1993 p 173-179 Repr. from Applied Superconductivity, v. 1, no. 7-9, 1993 p 1341-1347 (For primary document see N94-20497 05-32)
Avail: CASI HC A02/MF A03

Since the discovery of high temperature superconductivity in 1987, NASA Lewis Research Center has been involved in efforts to demonstrate its advantages for applications involving microwave electronics in space, especially space communications. The program included thin film fabrication by means of laser ablation. Specific circuitry which was investigated includes microstrip ring resonators at 32 GHz, phase shifters which utilize a superconducting, optically activated switch, an 8x8 32 GHz superconducting microstrip antenna array, and an HTS-ring-resonator stabilized oscillator at 8 GHz. The latter two components are candidates for use in space experiments which are described in other papers. Experimental data on most of the circuits are presented as well as, in some cases, a comparison of their performance with an identical circuit utilizing gold or copper metallization. Author (revised)

N94-20514*# National Aeronautics and Space Administration. Lewis Research Center, Cleveland, OH.

Y-Ba-Cu-O SUPERCONDUCTING/GaAs SEMICONDUCTING HYBRID CIRCUITS FOR MICROWAVE APPLICATIONS **c33**

K. B. Bhasin, S. S. Toncich, C. M. Chorey (Sverdrup Technology, Inc., Brook Park, OH.), N. J. Rohrer (Ohio State Univ., Columbus.), and G. J. Valco (Ohio State Univ., Columbus.) *In its* Solid State Technology Branch of NASA Lewis Research Center: Fifth Annual Digest Aug. 1993 p 181-184 (For primary document see N94-20497 05-32)
Avail: CASI HC A01/MF A03

A two pole superconducting bandpass filter was combined with a packaged GaAs low noise amplifier, and a superconducting X-band oscillator was designed, fabricated, and tested. Both circuits were compared to normal metal circuits at 77K. The results of these experiments, technical issues, and potential applications are presented. Author (revised)

N94-20515*# National Aeronautics and Space Administration. Lewis Research Center, Cleveland, OH.

TEN GHz YBa2Cu3O(7-DELTA) SUPERCONDUCTING RING RESONATORS ON NdGaO3 SUBSTRATES **c76**

H. Y. To (Ohio State Univ., Columbus.), G. J. Valco (Ohio State Univ., Columbus.), and K. B. Bhasin *In its* Solid State Technology Branch of NASA Lewis Research Center: Fifth Annual Digest Aug. 1993 p 203-208 Repr. from Superconducting Scientific Technology, v. 5, 1992 p 421-426 (For primary document see N94-20497 05-32)
(Contract NCC3-197)
Avail: CASI HC A02/MF A03

YBa2Cu3O(7-delta) thin films were formed on NdGaO3 substrates by laser ablation. Critical temperatures greater than 89 K and critical current densities exceeding 2 x 10(exp 8) Acm(sub -2) at 77 K were obtained. The microwave performance of films patterned into microstrip ring resonators with gold ground planes was measured. An unloaded quality factor six times larger than that of a gold resonator of identical geometry was achieved. The unloaded quality factor decreased below 70 K for both the superconducting and gold resonators due to increasing dielectric losses in the substrate. The temperature dependence of the loss tangent of NdGaO3 was extracted from the measurements. Author (revised)

N94-20516*# National Aeronautics and Space Administration. Lewis Research Center, Cleveland, OH.

TlCaBaCuO HIGH Tc SUPERCONDUCTING MICROSTRIP RING RESONATORS DESIGNED FOR 12 GHz **c33**

G. Subramanyam (Cincinnati Univ., OH.), V. J. Kapoor (Cincinnati Univ., OH.), C. M. Chorey (Sverdrup Technology, Inc., Brook Park, OH.), and K. B. Bhasin *In its* Solid State Technology Branch of NASA Lewis Research Center: Fifth Annual Digest Aug. 1993 p 209-218 Repr. from Applied Superconductivity, v. 1, no. 10-12, 1993 p 1605-1614 (For primary document see N94-20497 05-32)
Avail: CASI HC A02/MF A03

Microwave properties of sputtered Tl-Ca-Ba-Cu-O thin films were investigated by designing, fabricating, and testing microstrip ring resonators. Ring resonators designed for 12 GHz fundamental resonance frequency, were fabricated and tested. From the unloaded Q values for the resonators, the surface resistance was calculated by separating the conductor losses from the total losses. The penetration depth was obtained from the temperature dependence of resonance frequency, assuming that the shift in resonance frequency is mainly due to the temperature dependence of penetration depth. The effective surface resistance at 12 GHz and 77 K was determined to be between 1.5 and 2.75 mOmega, almost an order lower than Cu at the same temperature and frequency. The effective penetration depth at 0 K is approximately 7000 A. Author (revised)

N94-20517*# National Aeronautics and Space Administration. Lewis Research Center, Cleveland, OH.

A 10 GHz Y-Ba-Cu-O/GaAs HYBRID OSCILLATOR PROXIMITY COUPLED TO A CIRCULAR MICROSTRIP PATCH ANTENNA **c33**

Norman J. Rohrer (Ohio State Univ., Columbus.), M. A. Richard (Case Western Reserve Univ., Cleveland, OH.), George J. Valco (Ohio State Univ., Columbus.), and Kul B. Bhasin *In its* Solid State Technology Branch of NASA Lewis Research Center: Fifth Annual Digest Aug. 1993 p 225-229 Repr. from IEEE Transactions on Applied Superconductivity, v. 3, no. 1, Mar. 1993 p 23-27 (For primary document see N94-20497 05-32)

Avail: CASI HC A01/MF A03

A 10 GHz hybrid Y-Ba-Cu-O / GaAs microwave oscillator proximity coupled to a circular microstrip antenna was designed, fabricated and characterized. The oscillator was a reflection mode type using a GaAs MESFET as the active element. The feedline, transmission lines, RF chokes, and bias lines were all fabricated from YBa2Cu3O(7-x) superconducting thin films on a 1 cm x 1 cm lanthanum aluminate substrate. The output feedline of the oscillator was wire bonded to a superconducting feedline on a second 1 cm x 1 cm lanthanum aluminate substrate, which was in turn proximity coupled to a circular microstrip patch antenna. Antenna patterns from this active patch antenna and the performance of the oscillator measured at 77 K are reported. The oscillator had a maximum output power of 11.5 dBm at 77 K, which corresponded to an efficiency of 10 percent. In addition, the efficiency of the microstrip patch antenna together with its high temperature superconducting feedline was measured from 85 K to 30 K and was found to be 71 percent at 77 4 increasing to a maximum of 87.4 percent at 30 K. Author (revised)

N94-20518*# National Aeronautics and Space Administration. Lewis Research Center, Cleveland, OH.

MICROWAVE PROPERTIES AND CHARACTERIZATION OF CO-EVAPORATED BSCCO THIN FILMS **c27**

F. A. Miranda, C. M. Chorey (Sverdrup Technology, Inc., Brook Park, OH.), M. A. Stan (Kent State Univ., OH.), C. E. Nordgren (Case Western Reserve Univ., Cleveland, OH.), R. Y. Kwor (Colorado Univ., Colorado Springs.), and T. S. Kalkur (Colorado Univ., Colorado Springs.) *In its* Solid State Technology Branch of NASA Lewis Research Center: Fifth Annual Digest Aug. 1993 p 235-242 Repr. from U.S. Government, 1992 (For primary document see N94-20497 05-32)

Avail: CASI HC A02/MF A03

An extensive characterization of Bi-Sr-Ca-Cu-O (BSCCO) thin films deposited by co-evaporation on LaAlO3 and SrTiO3 substrates was performed. The films had a T(sub c) (R = O) of approximately 78 K, and were predominantly c-axis oriented, with critical current densities (J(sub c)) at 4.5 K of 1.6 x 10(exp 6) and 1.1 x 10(exp 6) A cm(sup -2), for the samples on SrTiO3 and LaAlO3, respectively. The microwave properties of the films were examined by three techniques. The complex conductivity sigma(sub *) = sigma(sub 1) - j(sigma(sub 2)) and the magnetic penetration depth (A) were measured by power transmission at 30.6 GHz; the surface resistance (R(sub s)) was measured using a cavity resonator at 58.9 GHz, and the transmission line losses were determined by measuring the quality factor (Q) of a linear microstrip resonator at 10.4 and 20.2 GHz. The complex conductivity for the film on LaAlO3 was determined to be (2.0-j10) x 10(exp 5) S/m at 77 K. It was observed that in the superconducting state sigma(sub 1) deviates from both the Bardeen-Cooper-Schrieffer (BCS) theory and the two-fluid model. Values of lambda were found to be approximately 2.0 and 1.1 microns at 77 K and 20 K respectively, and were obtained for the film on LaAlO3. The value of lambda at 20 K was approximately three times larger than that of BSCCO single crystals. R(sub s) values of 865 and 1391 mOmega were obtained for the films on SrTiO3 and LaAlO3, respectively, at 77 K and 58.9 GHz. Unloaded Q factors at 20 K of approximately 1100 and 800 at 10.4 and 20.2 GHz respectively, were measured for the BSCCO resonator. Unloaded Q values of 290 and 405 at 20 K were obtained at 10.4 GHz and 20.2 GHz respectively, for an all gold (Au) resonator. Author (revised)

N94-20519*# National Aeronautics and Space Administration. Lewis Research Center, Cleveland, OH.

THE EFFECT OF FLUCTUATIONS ON THE ELECTRICAL TRANSPORT BEHAVIOR IN YBa2Cu3O(7-x) **c76**

Satish Vitta (Indian Inst. of Tech., Bombay.), S. A. Alterovitz, and M. A. Stan (Kent State Univ., OH.) *In its* Solid State Technology Branch of NASA Lewis Research Center: Fifth Annual Digest Aug. 1993 p 255-262 Repr. from Journal of Physics: Condens. Matter, v. 4, 1992 p 7891-7898 (For primary document see N94-20497 05-32)

(Grant NAG4-0751)

Avail: CASI HC A02/MF A03

The excess conductivity behavior of highly oriented YBa2Cu3O(7-x) thin films prepared by both coevaporation and laser ablation was studied in detail in the reduced-temperature range 9 x 10(exp -4) is less than t is less than 1. The excess conductivity in all the films studied was found to diverge sharply near T(sub c), in agreement with the conventional mean-field theory. However, the detailed temperature dependence could not be fitted to either the power-law or the logarithmic functional forms as predicted by the theory. The excess conductivity of all the films was found to be exponentially dependent on the temperature over nearly three decades for 9 x 10(exp -4) is less than t is less than 10(exp -1), in contradiction to the mean-field theory. Author (revised)

N94-20547# Boston Univ., MA. Dept. of Electrical Computer and Systems Engineering.

SEGMENT-BASED ACOUSTIC MODELS FOR CONTINUOUS SPEECH RECOGNITION Progress Report, 1 Oct. 1992 - 30 Sep. 1993

Mari Ostendorf and J. R. Rohlicek 8 Oct. 1993 12 p

(Contract N00014-92-J-1778; NSF IRI-89-02124)

(AD-A271483) Avail: CASI HC A03/MF A01

This research aims to develop new and more accurate stochastic models for speaker-independent continuous speech recognition by extending previous work in segment-based modeling and by introducing a new hierarchical approach to representing intra-utterance statistical dependencies. These techniques, which have high computational costs because of the large search space associated with higher order models, are made feasible through rescoring a set of HMM-generated N-best sentence hypotheses. We expect these different modeling techniques to result in improved recognition performance over that achieved by current systems, which handle only frame-based observations and assume that these observations are independent given an underlying state sequence. DTIC

N94-20570# Colorado Univ., Boulder. Dept. of Electrical and Computer Engineering.

SIGNAL PROCESSING IN THE LINEAR STATISTICAL MODEL Annual Report, 1 Oct. 1992 - 30 Sep. 1993

Louis L. Scharf and Clifford T. Mullis 20 Oct. 1993 5 p

(Contract N00014-89-J-1070)

(AD-A272114) Avail: CASI HC A01/MF A01

This research program has produced the following results: (1) a method of estimating power spectra using multiple orthogonal time-division windows; (2) an exact likelihood procedure for estimating frequencies and arrival angles for propagating plane waves that are detected by multisensor arrays; (3) a theory of oblique projections for solving estimation problems; (4) a method for designing matched subspace detectors for detecting subspace signals in subspace interference; (5) a method for designing data-adaptive and reduced-rank estimators for solving least squares problems; and (6) a method for bounding the probability of a subspace swap in SVD methods. Work is continuing on (1) general quadratic performance bounds for estimation; (2) complex exponential frames for modeling discrete-time sequences; (3) discrete wavelet frames and fitter banks; (4) projection operator decomposition of L2; and (5) representation and synthesis of periodically correlated time series using subband decompositions. DTIC

N94-20578# Naval Postgraduate School, Monterey, CA.

PROBABILITY OF DETECTION CALCULATIONS USING MATLAB M.S. Thesis

Yung-Chung Wei Jun. 1993 109 p

(AD-A271958) Avail: CASI HC A06/MF A02

A set of highly efficient computer programs based on the Marcum and Swerling's analysis on radar detection has been written in MATLAB to evaluate the probability of detection. The programs are based on accurate methods unlike the detectability method which is based on approximation. This thesis also outlines radar detection theory and target models as a background. The goal of this effort is to provide a set of efficient computer programs for student usage and teacher's aid. Programs are designed to be user friendly and run on personal computers. DTIC

N94-20582# Naval Command, Control and Ocean Surveillance Center, San Diego, CA. RDT and E Div.
AN INVERSE DWT FOR NONORTHOGONAL WAVELETS Final Report
M. J. Shensa Sep. 1993 58 p
(AD-A272064; NCCOSC/RDT/E-TR-1621) Avail: CASI HC A04/MF A01

Discrete nonorthogonal wavelet transforms play an important role in signal processing by offering finer resolution in time and scale than their orthogonal counterparts. The standard inversion procedure for such transforms is a finite expansion in terms of the analyzing wavelet. This approximation works quite well for many signals; however, for other signals, it fails to achieve good accuracy or requires an excessive number of scales. This paper proposes several algorithms that provide more adequate inversion and compares them in the case of Morlet wavelets. In the process, both practical and theoretical issues for the inversion of nonorthogonal wavelet transforms are discussed. DTIC

N94-20585# Rockwell International Science Center, Thousand Oaks, CA.
SPREAD SPECTRUM RANDOM ACCESS NETWORKS Final Report, 1 Sep. 1991 - 31 Aug. 1993
Ambatipudi R. Sastry Oct. 1993 78 p
(Contract N00014-91-C-0234)
(AD-A272280) Avail: CASI HC A05/MF A01

A new method of code allocation in Code Division Multiple Access is proposed, based on partitioned information 'classes' (CDMA-IC), that is particularly efficient in meeting multicasting needs. Transmitters choose spreading codes based on the types of messages they are transmitting, and receivers listen to codes corresponding to the types of messages they are interested in. The performance of this approach can exceed that of both the traditional receiver-directed codes or broadcast codes in environments where there are several multicast groups (in which a given message is of interest to more than one node), or where it is difficult to know what types of messages (out of a fixed set of message types) a receiver is interested in at any particular time. Performance is further enhanced when receivers can simultaneously attempt to correlate multiple spreading codes. A broad theoretical framework was developed for the CDMA-IC concept and numerical results through simulation were obtained and compared to receiver-directed and broadcasting scenarios. DTIC

N94-20592# Bertin et Cie., Plaisir (France).
OPTIMIZATION OF A SATELLITE LOCALIZATION AND MESSAGE SENDING SYSTEM [OPTIMISATION D'UN SYSTEME DE LOCALISATION ET DE MESSAGERIE PAR SATELLITE]
Fabienne Simon 1993 14 p In FRENCH Presented at 3rd Congres International on Valeur et Design dans le Management, Paris, France, 7-8 Apr. 1993
(ETN-93-94448) Avail: CASI HC A03/MF A01

The optimization and analysis of a localization and message transmission satellite system is described. The system is named TAOS which consists of five satellites and ground stations. The ground information processing centers provide messages to the customers and/or the localization of information with the help of mobile terminals. In order to improve the system performance a value analysis is carried out. The main purposes of the optimization were: to schedule the operations of TAOS; to allow validation of technical and economic choices made; and to homogenize the understanding of the TAOS mission to the customers. ESA

N94-20596# Admiralty Research Establishment, Gosport (England). Electronic Warfare Systems Dept.
THE APPLICATION OF SPACEBORNE SYNTHETIC APERTURE RADAR IN THE MARITIME ENVIRONMENT
C. J. Condley Oct. 1991 59 p Original contains color illustrations
(DRA-TM(AWE)-91013; BR317257; ETN-93-94970) Copyright Avail: CASI HC A04/MF A01

The principles of spaceborne Synthetic Aperture Radar (SAR) are given. Its application in the maritime environment is discussed, with reference to several specific systems. The requirement for calibration is discussed. Some of the more advanced techniques expected to be incorporated in future missions are summarized. Spaceborne SAR is a potentially powerful sensor in the maritime environment. Its active nature imparts an all weather, 24 hour imaging capability, limited only by orbit and power supply constraints. It is able to image a variety of ocean phenomena, leading to a range of applications in several fields. ESA

N94-20620# Naval Command, Control and Ocean Surveillance Center, San Diego, CA. RDT and E Div.
VLF HAROLD E. HOLT RADHAZ MEASUREMENTS Final Report
P. M. Hansen and J. Chavez Sep. 1993 71 p
(AD-A272018; NCCOSC/RDT/E-TR-1617) Avail: CASI HC A04/MF A01

This document details the radiation hazard (RADHAZ) measurements made at the very-low-frequency (VLF) Harold E. Holt (HEH) transmitting facility by personnel from U.S. Naval Command, Control and Ocean Surveillance Center (NCCOSC), Research, Development, Test and Evaluation Division (RDT&E Div.), the U.S. Naval Aerospace Medical Research Laboratory (NAMRL), the Australian Defence Force (ADF), and the Royal Australian Navy (RAN). The measurements were made to determine if hazardous levels of electromagnetic fields existed in locations normally accessed by personnel. NAMRL and ADF personnel were primarily responsible for the measurements on the ground and in and around the transmitter building; NRaD personnel were primarily responsible for measurements on the towers. DTIC

N94-20944# Massachusetts Inst. of Tech., Lexington. Lincoln Lab.
MASSACHUSETTS INSTITUTE OF TECHNOLOGY LINCOLN LABORATORY JOURNAL VOLUME 6, NUMBER 1, SPRING 1993 Special Report
1993 229 p
(AD-A272273) Avail: CASI HC A11/MF A03

In this article we introduce the subject of automatic target recognition (ATR). Interest in ATR is increasing in the defense community as the need for precision strikes in limited warfare situations becomes an increasingly important part of our defense posture. We discuss the difficulty of the ATR problem and we survey the variety of approaches that try to solve the problem. We conclude by introducing the other articles in this issue of the Lincoln Laboratory Journal. DTIC

N94-20949# Naval Undersea Warfare Center, Newport, RI.
HIGH FREQUENCY (HF) AND METEOR BURST COMMUNICATIONS IN A POLAR ENVIRONMENT Final Report
J. R. Katan 30 Sep. 1993 341 p
(AD-A271604; NUWC-NPT-TD-10375) Avail: CASI HC A15/MF A03

HF radio provides a low-cost, long-range communications alternative to satellite communication (SATCOM). In the polar environment, however, the frequent occurrence of dense sporadic E layers during summer in high-sunspot periods can prevent propagation in the HF band for the desired communications ranges. During solar storms, intense radiation may induce significant D-region absorption which further reduces the utility of HF radio. These phenomena cannot be defeated by the use of automatic link establishment (ALE) HF radio equipment because of the broadband nature of these effects. The use of VHF communication techniques, such as meteor scatter, provide a viable supplement to maintain connectivity when normal ALE HF radio is ineffective. This study combines the analysis of Scott Base Ionosonde data with computer predictions using A Stand-Alone Prediction Program (ASAPS) from the Australian Radio Prediction Service and IONCAP from the Institute for Telecommunications of the U.S. Department of Commerce to quantify the possibility of HF communications and suggest suitable radio system design parameters. Similarly, predictions of meteor burst (MF) link performance are provided for comparison with available measurements so that comparisons may be performed with actual link operations. Finally, an HF/VHF radio system design is envisioned to meet polar communications requirements and follow-on work to develop and verify design details is recommended. DTIC

N94-21031 Hazeltine Corp., Commack, NY.
PHASED ARRAY ANTENNA WITH COUPLERS IN SPATIAL FILTER ARRANGEMENT Patent
Alfred R. Lopez, inventor (to Hazeltine, Corp.) 18 Feb. 1992 49 p Filed 29 Dec. 1987
(CA-Patent-1,296,098; Int-Patent-Class-H01Q-3/34; CTN-93-60666)
Copyright Avail: Micromedia Ltd., Technical Information Centre, 165 Hotel de Ville, Place du Portage, Phase 2, Hull, Quebec J8X 3X2, Canada HC/MF

A lossless spatial filter is provided between the antenna input ports and the elements of an array antenna so that the effective element pattern associated with each input port is primarily within a selected angular region of space. The antenna elements are arranged along a predetermined path and each element is connected to only one output port of the spatial filter. A beam steering unit controls the direction of radiation and includes N phase shifters and means for controlling the phase shifters. Each phase shifter has an input port and an output port which is connected to only one input port of the spatial filter. The antenna also includes a supply means for supplying wave energy signals. The supply means includes a signal generator supplying a power divider having N output signal ports, each output port connected to only one phase shifter input port. In microwave landing systems, this invention provides a non-thinned or fully filled array which may be used to achieve linearity and minimize the field monitor distance for the glide path antenna. A synthesis procedure for a five level non-thinned spatial filter is included. Author (CISTI)

N94-21049 Hazeltine Corp., Commack, NY.
RADOME HAVING INTEGRAL HEATING AND IMPEDANCE MATCHING ELEMENTS Patent Application
Alfred R. Lopez, inventor (to Hazeltine Corp.) 4 Apr. 1992 21 p
(CA-Patent-Appl-SN-2,026,855; Int-Patent-Class-H01Q-1/42; CTN-93-60679)
Copyright Avail: Micromedia Ltd., Technical Information Centre, 165 Hotel de Ville, Place du Portage, Phase 2, Hull, Quebec J8X 3X2, Canada HC/MF

An antenna radome includes a dielectric member shaped to protect an antenna from environmental conditions, and a plurality of conductors fixed in relation to a major surface of the dielectric member in a predetermined pattern so that the member with the conductors provides a lower reflection coefficient to incident electromagnetic waves at the operating wavelength of the antenna than in the absence of the conductors. Means are provided for causing a desired heating current to flow through the conductors, thereby enabling sufficient heat to be generated in the dielectric member to de-ice the radome during severe weather conditions. A specific embodiment of the radome of the invention is described for use with an antenna of the type used in a microwave landing system. CISTI

N94-21073 Universiteit Twente, Enschede (Netherlands). Faculty of Applied Mathematics.
THE COMMUNICATION COMPLEXITY OF SET INTERSECTION PROBLEMS
Ulrich Faigle, Walter Kern, and Boris Spieker Sep. 1992 15 p Limited Reproducibility: More than 20% of this document may be affected by microfiche quality
(MEMO-1077; ETN-93-94117) Avail: CASI HC A03

The following is addressed: each of two players independently chooses one subset of a given set with n elements; how many bits of information must be communicated between the two players until at least one of them knows whether they have exactly t elements in common? Tamm showed that the trivial protocol is (up to one bit) optimal for deterministic communication of t-intersection. Nondeterministic communication is shown to also have the same order of complexity. ESA

N94-21182# Naval Postgraduate School, Monterey, CA.
DATA COMPRESSION BY USING WAVELET TRANSFORMS AND VECTOR QUANTIZATION M.S. Thesis
Alper Erdemir Jun. 1993 82 p
(AD-A272763) Avail: CASI HC A05/MF A01

This thesis proposes a new analysis/synthesis procedure for speech and image compression. The algorithm applies the discrete wavelet transform to subject data in order to obtain a set of multiresolution wavelet coefficients. The wavelet coefficients are then encoded by using the generalized Lloyd algorithm. The statistical properties of the wavelet coefficients are utilized to determine the number of resolution levels as well as the codebook size at each resolution level. Coding results show that the new procedure provides a significant improvement in the quality of the reproduced data. The tested data includes speech, image, and transient signals. DTIC

N94-21198# Naval Research Lab., Washington, DC.
NAVSPASUR SENSOR SYSTEM DIGITAL SIGNAL PROCESSING RECEIVER. VOLUME 1: HARDWARE AND SOFTWARE OVERVIEW Final Report, Oct. 1990 - Jul. 1993
Carl J. Morris, Carolyn F. Bryant, Marilyn P. Earl, and Tamara A. Myers 30 Sep. 1993 50 p
(AD-A272899; NRL/FR/8154-93-9577-Vol-1) Avail: CASI HC A03/MF A01

This is a system description of the Naval Space Surveillance (NAVSPASUR) Sensor System Digital Signal Processing Receiver (DSPR). The NAVSPASUR system began as an advanced research project in June 1958, was commissioned as an operational Naval command in February 1961, and is operated by the Naval Space Surveillance Center (NSSC) in Dahlgren, Virginia. The DSPR is a real-time radar data acquisition and analysis system. Its function is to detect, with no prior information, all space objects whose orbits cross the continental United States and to compute their subsequent orbits. It provides vital satellite information in support of national defense mission objectives of space intelligence, satellite attack warning, satellite intercept support, and space mission support. This system description was prepared as part of a modernization program that has replaced DSPR hardware for which parts are no longer available. Volume 1 (NRL/FR/8154--93-9577) describes the DSPR system in terms of current operation and hardware and software environment. Functions of the major subsystems and the relationship between them are discussed. Volume 2 (NRL/FR/8154--93-9578) discusses the function and capabilities of software and hardware components of the subsystems that provide the digital functions of the DSPR. For each subsystem, individual software modules and hardware components used primarily by that subsystem are described. DTIC

N94-21201# Federal Aviation Administration, Oklahoma City, OK. Civil Aeromedical Inst.
ATC/PILOT VOICE COMMUNICATIONS: A SURVEY OF THE LITERATURE Final Report
O. Veronika Prinzo and Thomas W. Britton Nov. 1993 38 p
(DOT/FAA/AM-93/20) Avail: CASI HC A03/MF A01

The first radio-equipped control tower in the United States opened at the Cleveland Municipal Airport in 1930. From that time to the present, voice radio communications have played a primary role in air safety. Verbal communications in air traffic control (ATC) operations have been frequently cited as causal factors in operational errors and pilot deviations in the FAA Operational Error and Deviation System, the NASA Aviation Safety Reporting System (ASRS), and reports derived from government sponsored research projects. Collectively, the data provided by these programs indicate that communications constitute a significant problem for pilots and controllers. Although the communications problem was well known the research literature was fragmented, making it difficult to appreciate the various types of verbal communications problems that existed and their unique influence on the quality of ATC/pilot communications. This is a survey of the voice radio communications literature. The 43 reports in the review represent survey data, field studies, laboratory studies, narrative reports, and reviews. The survey topics pertain to communications taxonomies, acoustical correlates and cognitive/psycholinguistic perspectives. Communications taxonomies were used to identify the frequency and types of information that constitute routine communications, as well as those communications involved in operational errors, pilot deviations, and other safety-related events. Acoustical correlate methodologies identified some qualities of a speaker's voice, such as loudness, pitch, and speech rate, which might be used potentially to monitor stress, mental workload, and other forms of psychological or physiological factors that affect performance. Cognitive/psycho-linguistic research offered an information processing perspective for understanding how pilots' and controllers' memory and language comprehension processes affect their ability to communicate effectively with one another. This analysis of the ATC/pilot voice radio communications literature was performed to provide an organized summary for the systematic study of interactive communications between controllers and pilots. Recommendations are given for new research initiatives, communications-based instructional materials, and human factors applications for new communications systems. Author

N94-21210# Massachusetts Inst. of Tech., Lexington. Lincoln Lab.
USE OF THE WEISS-WEINSTEIN BOUND TO COMPARE THE DIRECTION-FINDING PERFORMANCE OF SPARSE ARRAYS Technical Report
D. F. DeLong 16 Aug. 1993 62 p

(Contract F19628-90-C-0002)
(AD-A272582; TR-982; ESC-TR-93-244) Avail: CASI HC A04/MF A01

Weiss and Weinstein have recently derived a new lower bound on random parameter estimation error. This bound is used to develop a criterion for comparing two sparse array configurations. The arrays are first adjusted in size so that their direction-finding (DF) accuracies at high element signal-to-noise ratio (ESNR) are the same when averaged over all possible directions of arrival in the hemisphere. Then their threshold ESNR's are calculated using the Weiss-Weinstein bound. The array having the lower threshold ESNR is judged the better array. As an example of the application of the bound, three 7-element arrays, a circle, a spiral, and an L-shaped array are compared. The bound is also extended to the case of switched subarrays, where data are collected from several subarrays sequentially in time and processed as a unit. The purpose is to achieve DF accuracy approaching that of the full array while reducing the number of signal processing channels. An example, using five receivers on the 7-element spiral array, shows that this is indeed possible. DTIC

N94-21211# Massachusetts Inst. of Tech., Lexington. Lincoln Lab.
A COMPACT, PORTABLE EHF/SHF ANTENNA FOR ADVANCED SCAMP Technical Report
Joseph C. Lee 22 Sep. 1993 59 p
(Contract F19628-90-C-0002)
(AD-A272614; TR-981; ESC-TR-93-211) Avail: CASI HC A04/MF A01

The small, single-channel, antijam, man-portable (SCAMP) terminal is used for extremely high frequency (EHF) satellite communication. Since its development in 1987, it has repeatedly demonstrated successful communication through the EHF packages on the FLTSAT-7 and -8 Navy communication satellites. Advanced SCAMP is the second generation small terminal, highly elevated in performance and significantly reduced in weight. It is currently being developed at Lincoln Laboratory. Pertinent parameters are its 30-lb total weight, 75- to 2,400-bps data rate, and 24-in antenna aperture. Starting with the basic dual-band feed developed for another application, a compact, high-performance, EHF, dual-band ring-focus feed with an elliptical subreflector was developed for a displaced axis parabolic reflector. This reflector is made up of six lightweight deployable petals for portability. The feed weighs less than 1 lb, and the reflector weights 2.6 lb. The measured added loss due to imperfections of the petal reflector for the 44.5- and 20.7-GHz bands are 0.3 and 0.1 dB, respectively. An overall antenna efficiency of about 65% and 55% in the Q- and K-bands was achieved. Antenna and feed design considerations, measured performance, and other possible applications for this antenna are discussed. DTIC

N94-21218# Naval Research Lab., Washington, DC.
NAVSPASUR SENSOR SYSTEM DIGITAL SIGNAL PROCESSING RECEIVER. VOLUME 2: FUNCTION AND CAPABILITIES OF HARDWARE AND SOFTWARE COMPONENTS Final Report, Oct. 1990 - Jul. 1993
Carl J. Morris, Carolyn F. Bryant, Marilyn P. Earl, and Tamara A. Myers 30 Sep. 1993 50 p
(AD-A272900; NRL/FR/8154-93-9578-Vol-2) Avail: CASI HC A03/MF A01

This is a system description of the Naval Space Surveillance (NAVSPASUR) Sensor System Digital Signal Processing Receiver (DSPR). The NAVSPASUR system began as an advanced research project in June 1958, was commissioned as an operational Naval command in February 1961, and is operated by the Naval Space Surveillance Center (NSSC) in Dahlgren, Virginia. The DSPR is a real-time radar data acquisition and analysis system. Its function is to detect, with no prior information, all space objects whose orbits cross the continental United States and to compute their subsequent orbits. It provides vital satellite information in support of national defense mission objectives of space intelligence, satellite attack warning, satellite intercept support, and space mission support. This system description was prepared as part of a modernization program that has replaced DSPR hardware for which parts are no longer available. Volume 1 (NRL/FR/8154--93-9577) describes the DSPR system in terms of current operation and hardware and software environment. Functions of the major subsystems and the relationship between them are discussed. Volume 2 (NRL/FR/8154--93-9578) discusses the function and capabilities of software and hardware components of the subsystems that provide the digital functions of the DSPR. For each subsystem, individual software modules and hardware components used primarily by that subsystem are described. DTIC

N94-21235# Naval Command, Control and Ocean Surveillance Center, San Diego, CA. Research, Development, Test and Evaluation Div.
POLAR PROCESSING PROJECT Final Report, period ending 13 Jan. 1993
C. N. Tom, W. J. Davies, and J. F. Goycochea Sep. 1993 202 p
(AD-A271583; NCCOSC/RDT/E-TD-2565) Avail: CASI HC A10/MF A03

The purpose of this project was to explore the use of polar processing techniques in SIGINT-related signal processing applications. An investigation of ways to apply the CORDIC arithmetic algorithm to signal processing problems, and an application of the TMC2330 Coordinate Transformer chip in a coprocessor or accelerator board for a Sun workstation are covered. DTIC

N94-21240# Naval Command, Control and Ocean Surveillance Center, San Diego, CA. Research, Development, Test and Evaluation Div.
A NEW MATRIX FORMULATION OF CLASSICAL ELECTRODYNAMICS. PART 3: WAVE PROPAGATION THROUGH A MULTILAYER DIELECTRIC MEDIUM WITH PLANAR BOUNDARIES Final Report, period ending Sep. 1993
R. P. Bocker Oct. 1993 68 p
(AD-A271610; NCCOSC/RDT/E-TD-2569-Pt-3) Avail: CASI HC A04/MF A01

A new approach for solving electromagnetic wave propagation problems is currently being developed at the Naval Command, Control and Ocean Surveillance Center (NCCOSC), RDT and E Division (NRaD). This new approach is based upon an eight by eight matrix representation of the Maxwell field equations. In addition, a computer software package based on this matrix representation of electromagnetic theory is also being written and tested at NRaD to handle a variety of scenarios involving electromagnetic wave propagation through matter. This software package is referred to as the MATURE Program. MATURE is the acronym for matrix approach to understanding relativistic electrodynamics. The MATURE program is written in MATLAB code for use on a Sun 4 SPARCstation 2 workstation. Under Independent Research (IR) FY 92 funding, this matrix approach was successfully employed in solving problems dealing with electromagnetic wave propagation through dielectric, crystalline, linear electro-optic, and magneto-optic materials of infinite extent. Under the Office of Naval Research (ONR) FY 93 funding, this matrix formulation was extended to handle problems involving wave propagation through multilayer dielectric media with planar boundaries. Presented in this technical document is the underlying theory of this matrix approach. Several numerical examples, based on the use of the MATURE program, are also included to illustrate the use of the matrix approach in solving electromagnetic wave propagation problems. DTIC

N94-21244# Massachusetts Inst. of Tech., Lexington. Lincoln Lab.
DOWNLINK ACQUISITION AND TRACKING PROCEDURES FOR THE ASCAMP SATELLITE COMMUNICATIONS TERMINAL
Robert J. Figucia 14 Sep. 1993 58 p
(Contract F19628-90-C-0002)
(AD-A272912; ESC-TR-93-236) Avail: CASI HC A04/MF A01

The advanced single-channel antijam man portable (ASCAMP) terminal was developed at MIT Uncoin Laboratory as a proof of concept for the Army's SCAMP terminal. The ASCAMP terminal is a 30-lb, extremely high frequency (EHF) satellite communications terminal capable of operating from 75 to 2,400 bps with low inclination, geosynchronous FLTSAT EHF package and Milstar satellites. The terminal was designed to be carried, set up, and operated by a single user. In many instances the control algorithms were designed to compensate for simplifications made in the hardware to keep the terminal's size, weight, and power to a minimum. The procedures implemented in the ASCAMP terminal to locate the satellite and synchronize with its downlink are described. It contains descriptions of the timing and pointing requirements, the procedures for acquisition and tracking, and the measured performance. DTIC

N94-21264# Naval Postgraduate School, Monterey, CA.
MATHCAD COMPUTER APPLICATIONS PREDICTING ANTENNA PARAMETERS FROM ANTENNA PHYSICAL DIMENSIONS AND GROUND CHARACTERISTICS M.S. Thesis
Donald D. Gerry Jun. 1993 271 p
(AD-A272987) Avail: CASI HC A12/MF A03

This report provides the documentation for a set of computer applications for the evaluation of antenna parameters. The applications are written for the Mathcad personal computer software for various antenna types listed in the thesis index. Antenna dimensions and, in some cases, ground parameters are the only required inputs for each application. No new antenna parameter equations were developed as a part of this research. The chapters of this thesis are intended to provide Mathcad antenna application users with the background information necessary to readily use and interpret the software for each antenna type. Appendices are provided with examples of each antenna application. Each application has an introductory paragraph and a table of required inputs. The Mathcad software provides various numerical outputs and performance predictions, as well as a graphical representation of radiation patterns in the far-field. Mathcad application results are consistent with the predictions of applicable publications, as well as other antenna numerical analysis programs. DTIC

N94-21308 Naval Postgraduate School, Monterey, CA.
GOVERNMENT OPEN SYSTEMS INTERCONNECTION PROFILE (GOSIP) TRANSITION STRATEGY M.S. Thesis
Mark R. Laxen Sep. 1993 112 p Limited Reproducibility: More than 20% of this document may be affected by microfiche quality
(AD-A273005) Avail: Issuing Activity (Defense Technical Information Center (DTIC))

This thesis analyzes the Government Open Systems Interconnection Profile (GOSIP) and the requirements of the Federal Information Processing Standard (FIPS) Publication 146-1. It begins by examining the International Organization for Standardization (ISO) Open Systems Interconnection (OSI) architecture and protocol suites and the distinctions between GOSIP version one and two. Additionally, it explores some of the GOSIP protocol details and discusses the process by which standards organizations have developed their recommendations. Implementation considerations from both government and vendor perspectives illustrate the barriers and requirements faced by information systems managers, as well as basic transition strategies. The result of this thesis is to show a transition strategy through an extended and coordinated period of coexistence due to extensive legacy systems and GOSIP product unavailability. Recommendations for GOSIP protocol standards to include capabilities outside the OSI model are also presented. DTIC

N94-21352# Naval Postgraduate School, Monterey, CA.
TELECOMMUNICATIONS SERVICES FOR MULTIMEDIA DATA EXCHANGE SUPPORT M.S. Thesis
Paul C. Gibbons Jun. 1993 102 p
(AD-A271704) Avail: CASI HC A06/MF A02

Multimedia holds the promise of increased knowledge, creativity and productivity for virtually any application that can be imagined. The ability to present information in both an informative and entertaining way can lead to an enhanced quality of life for an increasingly larger segment of the world's population. However, information generated in a multimedia format presents special challenges for communication networks. This thesis is an attempt to understand the impact of multimedia computing as it relates to the transmission requirements to support large volume data exchange in a distributed computing environment. With a good understanding of these requirements one will be better equipped to evaluate the various physical transmission media and communication services available to meet the high transmission demands imposed by multimedia data exchange. DTIC

N94-21361 Microelectronics Center of North Carolina, Research Triangle Park.
FIELD EMITTER ARRAY RF AMPLIFIER DEVELOPMENT PROJECT, PHASE 1, OPTION 1 Quarterly R and D Status Report No. 8, 16 Jul. - 15 Oct. 1993
Gary E. McGuire 15 Oct. 1993 45 p Limited Reproducibility: More than 20% of this document may be affected by microfiche quality
(Contract MDA972-91-C-0028)
(AD-A272567) Avail: Issuing Activity (Defense Technical Information Center (DTIC))

Successful electrical testing was performed on 44,460 tip array. High-frequency testing is underway, both in-house and at Litton subprogram site. The first two runs of 2 microns column devices are finished. Arrays of 232,630 tips have been successfully fabricated and are being electrically tested. Two fabrication runs of 4 microns column devices have been started and are proceeding on a revised schedule after delays in the initial photolithography step. More rigorous uniformity requirements have resulted in modification of the initial photolithography steps. An in-situ cleaning system was installed and evaluated in the test chamber. Additional testing is needed to bring the cleaning process under control. Development of low work function and metal coatings has focused on the optimization of the deposition process for tantalum nitride, and the development of deposition processes for lanthanum hexaboride and zirconium carbide. The chemical composition, resistivity, and growth rate of the deposited films is being analyzed by several methods. A device serialization method was implemented to improve record keeping on field emitter device testing. DTIC

N94-21412# IIT Research Inst., Chicago, IL.
ELF COMMUNICATIONS SYSTEM ECOLOGICAL MONITORING PROGRAM Summary Report, 1982 - 1991
M. M. Abromavage Nov. 1992 107 p
(Contract N00039-88-C-0065)
(AD-A272507; IITRI-D06200-3) Avail: CASI HC A06/MF A02

The U.S. Navy initiated an ecological monitoring program in 1982 as a part of its environmental quality program for its extremely low frequency (ELF) radio transmitting stations in Wisconsin and Michigan. Investigators have completed and reported work each year through 1991. This report describes 13 projects comprising the ecological monitoring program and the findings through 1991. Studies in Wisconsin have been completed, with no indications that ecological relationships have been influenced by electromagnetic fields produced by the ELF radio transmitter in that state. Studies in Michigan are continuing. DTIC

N94-21436 Naval Postgraduate School, Monterey, CA.
MILITARY SATELLITE COMMUNICATIONS DECISION SUPPORT SYSTEM REQUIREMENTS ANALYSIS AND USER INTERFACE DESIGN M.S. Thesis
Hugh A. Henry Jun. 1993 88 p Limited Reproducibility: More than 20% of this document may be affected by microfiche quality
(AD-A273047) Avail: CASI HC A05

This research analyzed and decomposed U.S. Space Command missions to determine the requirements of a Military Satellite Communications Decision Support System (MDSS). Alternative functional architectures for an MDSS were evaluated and a graphical user interface prototype was developed. MDSS system requirements were derived through the combined use of the method of Critical Success Factors and the Representations, Operations, Memory Aids, and Controls method. The 'sandwich' architecture was suggested as the most suitable functional architecture for MDSS development. The user interface prototype allowed potential MDSS users to gain an appreciation of the look and feel of a potential system so they could more precisely articulate their specific requirements to MDSS builders. DTIC

N94-21518# Rome Lab., Griffiss AFB, NY.
HYBRID FINITE ELEMENT/WAVEGUIDE MODE ANALYSIS OF PASSIVE RF DEVICES Report, Jan. 1992 - Jan. 1993
Daniel T. McGrath Jul. 1993 88 p
(AF Proj. 2304)
(AD-A273074; RL-TR-93-130) Avail: CASI HC A05/MF A01

A numerical solution for time-harmonic electromagnetic fields in two-port passive radio frequency (RF) devices has been developed, implemented in a computer code, and validated. Vector finite elements are used to represent the fields in the device interior, and field continuity across waveguide apertures is enforced by matching the interior solution to a sum of waveguide modes. Consequently, the mesh may end at the aperture instead of extending into the waveguide. The report discusses the variational formulation and its reduction to a linear system using Galerkin's method. It describes the computer code, including its interface to commercial CAD software used for geometry generation. It presents validation results for waveguide

discontinuities, coaxial transitions, and microstrip circuits. They demonstrate that the method is an effective and versatile tool for predicting the performance of passive RF devices. DTIC

N94-21567*# National Aeronautics and Space Administration. Lewis Research Center, Cleveland, OH.

QPPM RECEIVER FOR FREE-SPACE LASER COMMUNICATIONS

J. M. Budinger, J. H. Mohamed, L. A. Nagy, P. J. Lizanich (Analex Corp., Brook Park, OH.), and D. J. Mortensen (Sverdrup Technology, Inc., Brook Park, OH.) Jan. 1994 12 p Proposed for presentation at the 15th International Communications Satellite Systems Conference, San Diego, CA, 28 Feb. - 3 Mar. 1994; sponsored by AIAA

(RTOP 506-72-21)

(NASA-TM-106424; E-8265; NAS 1.15:106424; AIAA Paper 94-1160) Avail: CASI HC A03/MF A01

A prototype receiver developed at NASA Lewis Research Center for direct detection and demodulation of quaternary pulse position modulated (QPPM) optical carriers is described. The receiver enables dual-channel communications at 325-Megabits per second (Mbps) per channel. The optical components of the prototype receiver are briefly described. The electronic components, comprising the analog signal conditioning, slot clock recovery, matched filter and maximum likelihood data recovery circuits are described in more detail. A novel digital symbol clock recovery technique is presented as an alternative to conventional analog methods. Simulated link degradations including noise and pointing-error induced amplitude variations are applied. The bit-error-rate performance of the electronic portion of the prototype receiver under varying optical signal-to-noise power ratios is found to be within 1.5-dB of theory. Implementation of the receiver as a hybrid of analog and digital application specific integrated circuits is planned. Author

N94-21684# Stanford Linear Accelerator Center, CA.

AN INTEGRO-ALGEBRAIC EQUATION FOR HIGH FREQUENCY WAKE FIELDS IN A TUBE WITH SMOOTHLY VARYING RADIUS

R. L. Warnock Jan. 1993 8 p Presented at the Computational Accelerator Physics Conference CAP 1993, Pleasanton, CA, 22-26 Feb. 1993

(Contract DE-AC03-76SF-00515)

(DE93-040940; SU-SLAC-Pub-6038; CONF-930269-23) Avail: CASI HC A02/MF A01

A technique to find the longitudinal wake field at frequencies above or below the tube cut-off is described. The round tube is infinite in length, and has an arbitrary, smooth variation of radius over a finite interval. A system of integro-algebraic equations enforces the boundary conditions on the wall and the outgoing wave condition at infinity. The first step in an iterative solution of the system, valid for variations of tube radius with small derivative, yields a convenient formula for the impedance as a double integral. At low frequencies the formula gives Yokoya's result plus corrections that can be large. For high frequencies in the case of several wall undulations it gives a sequence of finite-Q resonances. To avoid the limitations of the iterative method, a numerical solution of the system is carried out. DOE

N94-21783*# National Aeronautics and Space Administration. Goddard Space Flight Center, Greenbelt, MD.

APPLICATION GUIDE FOR UNIVERSAL SOURCE ENCODING FOR SPACE

Pen-Shu Yeh and Warner H. Miller Dec. 1993 35 p

(RTOP 310-20-46)

(NASA-TP-3441; 94B00028; NAS 1.60:3441) Avail: CASI HC A03/MF A01

Lossless data compression was studied for many NASA missions. The Rice algorithm was demonstrated to provide better performance than other available techniques on most scientific data. A top-level description of the Rice algorithm is first given, along with some new capabilities implemented in both software and hardware forms. Systems issues important for onboard implementation, including sensor calibration, error propagation, and data packetization, are addressed. The latter part of the guide provides twelve case study examples drawn from a broad spectrum of science instruments. Author (revised)

N94-21885*# Michigan Univ., Ann Arbor. Radiation Lab.

RADIATION AND SCATTERING FROM PRINTED ANTENNAS ON CYLINDRICALLY CONFORMAL PLATFORMS Final Report

Leo C. Kempel, John L. Volakis, and Sunil Bindiganavale Jan. 1994 115 p

(Grant NAG1-1478)

(NASA-CR-194703; NAS 1.26:194703; UM-030601-3-T) Avail: CASI HC A06/MF A02

The goal was to develop suitable methods and software for the analysis of antennas on cylindrical coated and uncoated platforms. Specifically, the finite element boundary integral and finite element ABC methods were employed successfully and associated software were developed for the analysis and design of wraparound and discrete cavity-backed arrays situated on cylindrical platforms. This work led to the successful implementation of analysis software for such antennas. Developments which played a role in this respect are the efficient implementation of the 3D Green's function for a metallic cylinder, the incorporation of the fast Fourier transform in computing the matrix-vector products executed in the solver of the finite element-boundary integral system, and the development of a new absorbing boundary condition for terminating the finite element mesh on cylindrical surfaces. For individual titles, see N94-21886 through N94-21888.

N94-21886*# Michigan Univ., Ann Arbor. Radiation Lab.

SCATTERING BY CAVITY-BACKED ANTENNAS ON A CIRCULAR CYLINDER

Leo C. Kempel and John L. Volakis *In its* Radiation and Scattering from Printed Antennas on Cylindrically Conformal Platforms Jan. 1994 p 1-35 (For primary document see N94-21885 05-32)

Avail: CASI HC A03/MF A02

Conformal arrays are popular antennas for aircraft, spacecraft, and land vehicle platforms due to their inherent low weight and drag properties. However, to date there has been a dearth of rigorous analytical or numerical solutions to aid the designer. In fact, it has been common practice to use limited measurements and planar approximations in designing such non-planar antennas. The finite element-boundary integral method is extended to scattering by cavity-backed structures in an infinite, metallic cylinder. In particular, the formulation specifics such as weight functions, dyadic Green's function, implementation details and particular difficulties inherent to cylindrical structures are discussed. Special care is taken to ensure that the resulting computer program has low memory demand and minimal computational requirements. Scattering results are presented and validated as much as possible. Author (revised)

N94-21887*# Michigan Univ., Ann Arbor. Radiation Lab.

RADIATION BY CAVITY-BACKED ANTENNAS ON A CIRCULAR CYLINDER

Leo C. Kempel, John L. Volakis, and Randy Sliva *In its* Radiation and Scattering from Printed Antennas on Cylindrically Conformal Platforms Jan. 1994 p 37-60 (For primary document see N94-21885 05-32)

Avail: CASI HC A03/MF A02

Conformal antenna arrays are popular antennas for aircraft, spacecraft and land vehicle platforms due to their inherent low weight, cost and drag properties. However, to date there has been a dearth of rigorous analytical or numerical solutions to aid the designer. In fact, it has been common practice to use limited measurements and planar approximations in designing such non-planar antennas. The finite element-boundary integral method is extended to radiation by cavity-backed structures in an infinite, metallic cylinder. The formulation is used to investigate the effect of cavity size on the radiation pattern for typical circumferentially and axially polarized patch antennas. Curvature effect on the gain, pattern shape, and input impedance is also studied. Finally, the accuracy of the FE-BI approach for a microstrip patch array is demonstrated. Author (revised)

N94-21888*# Michigan Univ., Ann Arbor. Radiation Lab.

USER MANUAL FOR EXCALIBUR: A FE-BI NUMERICAL LABORATORY FOR CAVITY-BACKED ANTENNAS IN A CIRCULAR CYLINDER, VERSION 1.2

Leo C. Kempel *In its* Radiation and Scattering from Printed Antennas on Cylindrically Conformal Platforms Jan. 1994 p 61-110 (For primary document see N94-21885 05-32)

Avail: CASI HC A03/MF A02

The Finite Element-Boundary Integral (FE-BI) technique was used to

analyze the scattering and radiation properties of cavity-backed patch antennas recessed in a metallic groundplane. A program, CAVITY3D, was written and found to yield accurate results for large arrays without the usual high memory and computational demand associated with competing formulations. Recently, the FE-BI approach was extended to cavity-backed antennas recessed in an infinite, metallic circular cylinder. EXCALIBUR is a computer program written in the Radiation Laboratory of the University of Michigan which implements this formulation. This user manual gives a brief introduction to EXCALIBUR and some hints as to its proper use. As with all computational electromagnetics programs (especially finite element programs), skilled use and best performance are only obtained through experience. However, several important aspects of the program such as portability, geometry generation, interpretation of results, and custom modification are addressed. Author (revised)

N94-22268# Bettis Atomic Power Lab., West Mifflin, PA.
IMPROVED APPROXIMATE FORMULAS FOR FLUX FROM CYLINDRICAL AND RECTANGULAR SOURCES
O. J. Wallace and S. A. Bokharee Mar. 1993 66 p
(Contract DE-AC11-88PN-38014)
(DE93-011390; WAPD-TM-1623) Avail: CASI HC A04/MF A01

This report provides two new approximate formulas for the flux at detector points outside the radial and axial extensions of a homogeneous cylindrical source and improved approximate formulas for the flux at points opposite rectangular surface sources. These formulas extend the range of geometries for which analytic approximations may be used by shield design engineers to make rapid scoping studies and check more extensive calculations for reasonableness. These formulas can be used to support skeptical, independent evaluations and are also valuable teaching tools for introducing shield designers to complex shield analyses. NTIS

N94-22279 Deutsche Forschungsanstalt fuer Luft- und Raumfahrt, Oberpfaffenhofen (Germany). Abt. Hochfrequenzsysteme.
A MOTION EXTRACTION METHOD FOR SYNTHETIC APERTURE RADARS Ph.D. Thesis - Technische Univ.
[BEWEGUNGSEXTRAKTIONSVERFAHREN FUER RADAR MIT SYNTHETISCHER APERTUR]
Joao Roberto Moreira-Neto Sep. 1992 129 p In GERMAN Limited Reproducibility: More than 20% of this document may be affected by poor print
(DLR-FB-92-31; ETN-93-94456) Avail: Issuing Activity (European Space Agency (ESA)); DLR, Zentrale Allgemeine Dienste, Versand, Postfach 90 60 58, 5000 Cologne 90, Germany, HC

A new method for motion error extraction for synthetic aperture radars (SAR), which is proved theoretically and experimentally, is presented. The new technique, called reflectivity displacement method (RDM), analyzes the frequency shift between two ground reflectivity functions of adjacent and strongly overlapping azimuth power spectra. It extracts the radar sensor's forward velocity and the displacement in the line of sight direction. The RDM removes the need for complex and expensive inertial navigation systems and greatly simplifies the design of high resolution SAR systems. Examples are given in order to show numerous usability opportunities of RDM, such as mountain region, sea surfaces, and calibration of the SAR system in a turbulent atmosphere. ESA

N94-22346 Technische Univ., Delft (Netherlands). Lab. of Electromagnetic Research.
EXTENDED RANGE MODIFIED GRADIENT TECHNIQUE FOR PROFILE INVERSION (EXTENDED VERSION OF REPORT Et/Em-1992-8)
R. E. Kleinman and P. M. VanDenBerg 1992 19 p See also PB93-137784 Limited Reproducibility: More than 20% of this document may be affected by microfiche quality
(PB93-215242; ET/EM-1992-26) Copyright Avail: CASI HC A03

A method for reconstructing the complex index of refraction of a bounded inhomogeneous object from measured scattered field data is presented. The index and the unknown fields within the object are simultaneously reconstructed in an iterative algorithm. The method is a refinement of earlier work which incorporates a more effective way to update the unknowns at each stage of the iteration. Considerable efficiency in the algorithm is achieved. Some numerical examples are given indicating the limits on the contrasts which can be reconstructed. These limits show that the range of contrasts that may be reconstructed is extended over that achievable with the earlier work. NTIS

N94-22347 Technische Univ., Delft (Netherlands). Lab. of Electromagnetic Research.
CONTINUOUS-TIME DISCRETIZED-SPACE APPROACH TO MODELING SHORT-PULSE PROPAGATION AND SCATTERING
A. G. Tijhuis 1992 12 p Limited Reproducibility: More than 20% of this document may be affected by microfiche quality
(PB93-215259; ET/EM-1992-22) Copyright Avail: Issuing Activity (National Technical Information Service (NTIS))

With the examples given in the paper, the author has described the building blocks for a new way of using integral equations to model the propagation and scattering of transient electromagnetic waves. Of each example, generalizations to more complicated scattering problems have already been realized. Mentioned in particular is the application of the marching-on in frequency method to the two dimensional transient scattering by conducting and dielectric obstacles. Applications to layered media include the excitation of a horizontally stratified dielectric slab by a point source and the excitation of a cylindrically symmetric borehole by a line or ring source. The next challenge is to combine these ideas so that realistic configurations can be handled. NTIS

N94-22348 Technische Univ., Delft (Netherlands). Lab. of Electromagnetic Research.
ELECTROMAGNETIC INTERFERENCE AND SHIELDING: AN INTRODUCTION (REVISED VERSION OF 1991-23)
A. T. deHoop and D. Quak 1992 66 p See also PB88-165410 Limited Reproducibility: More than 20% of this document may be affected by microfiche quality
(PB93-215275; ET/EM-1992-20) Copyright Avail: CASI HC A04

The basic equations of the electromagnetic field are summarized as far as they are needed in the theory of electromagnetic interference and shielding. Through the analysis of the planar electric current emitter, the propagation coefficient, attenuation coefficient, phase coefficient, wave-speed, wavelength, wave impedance, wave admittance, and power flow density of a wave are introduced. Next, the shielding effectiveness of a shielding plate and the shielding effectiveness of a shielding parallel-plate box are determined. In the latter, particular attention is given to the occurrence of internal resonance effects, which may degrade the shielding effectiveness. Further, a survey of some fundamental properties of a system of low frequency, multiconductor transmission lines is given. For a three conductor system with a plane of symmetry, the decomposition into the common mode and the differential mode of operation is discussed. Finally, expressions for the voltages and electric currents induced by external sources along a single transmission line are derived. NTIS

N94-22349 Technische Univ., Delft (Netherlands).
MODELLING SHORT BENT, GRADED INDEX DIELECTRIC SLAB WAVEGUIDES
Harrie J. M. Bastiaansen (PTT Research, Leidschendam, Netherlands.), Michiel V. D. Keur, and Hans Blok 3 Aug. 1992 37 p Limited Reproducibility: More than 20% of this document may be affected by microfiche quality
(PB93-215283; ET/EM-1992-19) Copyright Avail: CASI HC A03

Circularly short bent, graded index dielectric slab waveguides such as optical waveguides are mathematically modeled, using both a direct integration method and a source-type integral equation method. The former method is easy to implement, requiring only small amounts of computer time. The latter method has the possibility to be extended to a rigorous model for bent channel waveguides. Both homogeneous and inhomogeneous slab waveguide layers are considered. The mathematical models are validated through comparison of the numerical results with results obtained by the analytical resonance conditions. Numerous numerical examples are given. NTIS

N94-22408 Royal Military Coll. of Canada, Kingston (Ontario). Dept. of Electrical and Computer Engineering.
RADIO WAVE PROPAGATION STUDIES ALONG AN EARTH-SPACE SATELLITE LINK M.S. Thesis
Jacques Albert Mar. 1990 127 p

(ISBN-0-315-60627-4; CTN-94-60877) Copyright Avail: Micromedia Ltd., Technical Information Centre, 240 Catherine Street, Suite 305, Ottawa, Ontario, K2P 2G8, Canada HC/MF

The use of superhigh microwave frequencies for satellite communications has many advantages, but its major drawback lies in the effects of atmospheric hydrometeors on electromagnetic wave propagation. One research effort under way to investigate this problem is being conducted by the European Space Agency, which will launch the Olympus-1 communications satellite in June 1989. One of this satellite's four payloads is a 12.5/20/30 GHz beacon package which will enable 17 countries, including Canada, to conduct propagation experiments. The main objective of the Canadian participation is to study propagation during adverse weather conditions. The present thesis provides a model of the propagation path so that the system induced depolarization impurities can be removed from the received beacon signals. The overall system configuration and requirements are given. A system polarization matrix which incorporates all effects existing on the satellite link is described. Analyses needed to obtain the medium propagation characteristics from measured data at 12.5, 20, and 30 GHz are presented. The development of software to perform data acquisition and control of the equipment is reviewed and program listings are included. The preprocessing of the data using the mathematical model will be integrated into the software, as well as other needed mathematical analysis. Author (CISTI)

N94-22409 Royal Military Coll. of Canada, Kingston (Ontario). Dept. of Electrical and Computer Engineering.

APERTURE COUPLING OF CIRCULAR CYLINDRICAL DIELECTRIC RESONATOR ANTENNA M.S. Thesis

Joseph Theodore H. St-Martin Sep. 1990 169 p

(ISBN-0-315-60632-0; CTN-94-60878) Copyright Avail: Micromedia Ltd., Technical Information Centre, 240 Catherine Street, Suite 305, Ottawa, Ontario, K2P 2G8, Canada HC/MF

A new dielectric resonator antenna (DRA) configuration is proposed, based on a circular cylindrical dielectric resonator which is electromagnetically coupled to a microstrip feedline via an aperture in the ground plane separating them. This structure is studied both theoretically and experimentally to establish its feasibility. The theoretical approach develops the equivalent circuit model for the entire structure. The electromagnetic fields present are considered using their modal expansion. The links between the modal coefficients for the fields in the various parts of the structure are determined by examining the physical situation at hand and applying the principle of reciprocity to a volume in the feedline below the aperture. The resonant frequency for a particular resonator size was estimated assuming perfect conduction surfaces. The DRA radiation pattern was calculated assuming an infinite ground plane and then using an effective circular ground plane with a finite diameter. Experimental measurements are presented in the 12-16 GHz range. The results establish that the structure resonates as expected, its input impedance can be matched in a number of ways, and its radiation pattern is generally as expected. Author (CISTI)

N94-22410 Royal Military Coll. of Canada, Kingston (Ontario). Dept. of Mechanical Engineering.

A FEASIBILITY STUDY OF A PARALLAX-BASED PASSIVE MISSILE APPROACH WARNING SYSTEM M.S. Thesis

Erik Ronning May 1990 177 p

(ISBN-0-315-60640-1; CTN-94-60879) Copyright Avail: Micromedia Ltd., Technical Information Centre, 240 Catherine Street, Suite 305, Ottawa, Ontario, K2P 2G8, Canada HC/MF

A classical technique for measuring range uses two telescopes separated on a baseline to allow their optical fields of view to be matched and the resulting parallax angle measured to yield range and azimuth. This technique has been transferred to a high speed signal processing system. Computer programs have been developed to calculate the range and azimuth of a target. Atmospheric effects, such as turbulence, contrast degradation, and forward scattering on a practical system are discussed along with adverse effects caused by vibrations. The feasibility of finding the range and azimuth of a target has been demonstrated over a range of 700 cm and 3.5 deg field of view for a wavelength of 632.8 nm and source power of 10 mW. Range and azimuth values acquired are accurate to within 5 percent. Similar results over longer ranges may be obtained. Author (CISTI)

N94-22557# Westinghouse Hanford Co., Richland, WA.

INTERPRETATION OF GROUND PENETRATING RADAR DATA AT THE HANFORD SITE, RICHLAND, WASHINGTON

K. A. Bergstrom, T. H. Mitchell, and J. R. Kunk Jul. 1993 16 p Presented at the Advanced Ground Penetrating Radar: Technologies and Applications, Columbus, OH, 26-28 Oct. 1993

(Contract DE-AC06-87RL-10930)
(DE93-040409; WHC-SA-2018; CONF-9310160-1) Avail: CASI HC A03/MF A01

Ground Penetrating Radar (GPR) is being used extensively during characterization and remediation of chemical and radioactive waste sites at the Hanford Site in Washington State. Time and money for GPR investigations are often not included during the planning and budgeting phase. Therefore GPR investigations must be inexpensive and quick to minimize impact on already established budgets and schedules. An approach to survey design, data collection, and interpretation has been developed which emphasizes speed and budget with minimal impact on the integrity of the interpretation or quality of the data. The following simple rules of thumb can be applied: (1) Assemble as much pre-survey information as possible, (2) Clearly define survey objectives prior to designing the survey and determine which combination of geophysical methods will best meet the objectives, (3) Continuously communicate with the client, before, during and after the investigation, (4) Only experienced GPR interpreters should acquire the field data, (5) Use real-time monitoring of the data to determine where and how much data to collect and assist in the interpretation, (6) Always 'error' in favor of collecting too much data, (7) Surveys should have closely spaced (preferably 5 feet, no more than 10 feet), orthogonal profiles, and (8) When possible, pull the antenna by hand. DOE

N94-22576 Toronto Univ. (Ontario). Dept. of Electrical Engineering.

REAL-TIME STEP FREQUENCY RADAR M.S. Thesis

Chu Sunchun 1993 168 p

(ISBN-0-315-83588-5; CTN-94-60942) Copyright Avail: Micromedia Ltd., Technical Information Centre, 240 Catherine Street, Suite 305, Ottawa, Ontario, K2P 2G8, Canada HC/MF

Step frequency radar (SFR) offers advantages over impulse radar including better signal to noise ratio (SNR), better accuracy in locating targets composed of complex reflection coefficients, and flexibility. The slow processing speed of SFR has remained a major weakness of the system, imposing serious problems especially for airborne types of radar. A real-time SFR (RTSFR) design is proposed which can measure data at a rate of 30 Hz with 128 frequency steps. The RTSFR system is equivalent to an impulse radar that operates in the frequency domain. A series of ultrahigh frequency carrier waves that assemble a time domain impulse was transmitted. Each successive returned complex signal was coherently detected at an intermediate frequency of 200 kHz using a high speed digital phase detector. Collected data were then transmitted to the host computer for fast Fourier transform processing and display via a small computer systems interface bus. A software system was also developed which optimized the utilization of all available hardware using a parallel processing scheme. Program listings for the host and remote computers are included. The RTSFR exhibited a SNR of about 50 dB and was able to resolve targets that were 30 dB apart with the use of a Blackman window. Author (CISTI)

N94-20244# Max-Planck-Inst. for Psycholinguistics, Nijmegen (Netherlands).

MODELING THE HUMAN MENTAL LEXICON WITH SELF-ORGANIZING FEATURE MAPS

Peter Wittenburg and Uli H. Frauenfelder *In* Univ. Twente, Connectionism and Natural Language Processing Oct. 1992 p 5-15 (For primary document see N94-20242 05-63)

Copyright Avail: CASI HC A03/MF A02

N94-20245# Limburg State Univ., Maastricht (Netherlands). Dept. of Computer Science.

SPEECH SYNTHESIS WITH ARTIFICIAL NEURAL NETWORKS

Ton Weijters and Johan Thole *In* Univ. Twente, Connectionism and Natural Language Processing Oct. 1992 p 17-25 (For primary document see N94-20242 05-63)

Copyright Avail: CASI HC A02/MF A02

N94-20691*# Jet Propulsion Lab., California Inst. of Tech., Pasadena.
MAGELLAN VERTICAL POLARIZATION RADAR OBSERVATIONS Abstract Only
Jeffrey J. Plaut *In* Lunar and Planetary Inst., Twenty-Fourth Lunar and Planetary Science Conference. Part 3: N-Z 1993 p 1151-1152 (For primary document see N94-20636 05-91)
Avail: CASI HC A01/MF A06

N94-21091*# Alenia Spazio S.p.A., Rome (Italy).
DIGITAL RECEIVER FOR ON-BOARD FM/FSK-FM/BPSK DEMODULATION
G. Boscagli, M. C. Comparini, and M. Martone *In* New Mexico Univ., The Fifth NASA Symposium on VLSI Design 1993 13 p (For primary document see N94-21079 05-33)
Avail: CASI HC A03/MF A06

N94-21092*# Texas Instruments, Inc., Dallas. Semiconductor Group.
HIGH PERFORMANCE MPEG-AUDIO DECODER IC
M. Thorn, G. Benbassat, K. Cyr, S. Li, M. Gill, D. Kam, K. Walker, P. Look, C. Eldridge, and P. Ng *In* New Mexico Univ., The Fifth NASA Symposium on VLSI Design 1993 12 p (For primary document see N94-21079 05-33)
Avail: CASI HC A03/MF A06

N94-21099*# New Mexico Univ., Albuquerque. Dept. of Electrical and Computer Engineering.
ADAPTIVE ANALOG VIDEO SIGNAL CONDITIONER
Cheol-Ho Jeong, Brian Yu, Gregory Donohoe, and Robert Vitello *In its* The Fifth NASA Symposium on VLSI Design 1993 10 p (For primary document see N94-21079 05-33)
Avail: CASI HC A02/MF A06

N94-21100*# Nanyang Technological Inst. (Singapore). School of Applied Science.
VLSI MIXED SIGNAL PROCESSING SYSTEM
A. Alvarez and A. B. Premkumar *In* New Mexico Univ., The Fifth NASA Symposium on VLSI Design 1993 11 p (For primary document see N94-21079 05-33)
Avail: CASI HC A03/MF A06

N94-21102*# State Univ. of New York, Albany. Dept. of Computer Science.
COMPUTATION OF SIGNAL DELAYS IN RC NETWORKS
Juan Carlos Hidalgo, Paliath Narendran, and Seth Chaiken *In* New Mexico Univ., The Fifth NASA Symposium on VLSI Design 1993 11 p (For primary document see N94-21079 05-33)
Avail: CASI HC A03/MF A06

N94-21339*# Stanford Telecommunications, Inc., Seabrook, MD.
THE COMPOSITE ANALYTIC AND SIMULATION PACKAGE OR RFI (CASPR) ON A CODED CHANNEL
Jeff Freedman and Ted Berman *In* NASA. Goddard Space Flight Center, Networks Technology Conference Nov. 1993 p 209-215 (For primary document see N94-21323 05-62)
(Contract NAS5-31500)
Avail: CASI HC A02/MF A03

N94-21341*# Stanford Telecommunications, Inc., Seabrook, MD.
THE AUTOMATED CONFLICT RESOLUTION SYSTEM (ACRS)
Ted Kaplan, Andrew Musliner, and David Wampler *In* NASA. Goddard Space Flight Center, Networks Technology Conference Nov. 1993 p 225-233 (For primary document see N94-21323 05-62)
Avail: CASI HC A02/MF A03

N94-21344*# Stanford Telecommunications, Inc., Seabrook, MD.
SATELLITE COMMUNICATION HARDWARE EMULATION SYSTEM (SCHES)
Ted Kaplan *In* NASA. Goddard Space Flight Center, Networks Technology Conference Nov. 1993 p 253-263 (For primary document see N94-21323 05-62)
Avail: CASI HC A03/MF A03

N94-21345*# National Aeronautics and Space Administration. Goddard Space Flight Center, Greenbelt, MD.
A PACKET SWITCHED COMMUNICATIONS SYSTEM FOR GRO
Shabu Husain (Allied-Signal Aerospace Co., Seabrook, MD.), Wen-Hsing Yang (Allied-Signal Aerospace Co., Seabrook, MD.), Rani Vadlamudi (Allied-Signal Aerospace Co., Seabrook, MD.), and Joseph Valenti *In its* Networks Technology Conference Nov. 1993 p 265-274 (For primary document see N94-21323 05-62)
(Contract NAS5-27772)
Avail: CASI HC A02/MF A03

N94-21348*# Loral AeroSys, Seabrook, MD.
ARRAY SIMULATIONS PLATFORM (ASP) PREDICTS NASA DATA LINK MODULE (NDLM) PERFORMANCE
Allen David Snook *In* NASA. Goddard Space Flight Center, Networks Technology Conference Nov. 1993 p 309-327 (For primary document see N94-21323 05-62)
Avail: CASI HC A03/MF A03

N94-21349*# GTE Government Systems Corp., Las Cruces, NM.
CONVERSION OF THE PROPRIETARY ROLM (TM) INTER-NODE LINK FROM MULTIMODE TO SINGLEMODE OPERATION
Larry Boucher *In* NASA. Goddard Space Flight Center, Networks Technology Conference Nov. 1993 p 329-347 (For primary document see N94-21323 05-62)
Avail: CASI HC A03/MF A03

N94-21350*# Stanford Telecommunications, Inc., Seabrook, MD.
ADVANCED CODING AND MODULATION SCHEMES FOR TDRSS
Linda Harrell, Ted Kaplan, Ted Berman, and Susan Chang *In* NASA. Goddard Space Flight Center, Networks Technology Conference Nov. 1993 p 349-354 (For primary document see N94-21323 05-62)
Avail: CASI HC A02/MF A03

N94-22069# Academy of Sciences (USSR), Moscow. Automated Systems Inst.
IAS TELECOMMUNICATION INFRASTRUCTURE AND VALUE ADDED NETWORK SERVICES PROVIDED BY IASNET
Oleg L. Smirnov and Sergei Marchenko *In* Technical Research Centre of Finland, Information Technology and Economic Modelling 1992 p 101-119 (For primary document see N94-22056 05-83)
Copyright Avail: CASI HC A03/MF A03

N94-22076# Helsinki Univ. of Technology, Espoo (Finland).
CONTROLLING MULTISUPPLIER OPERATIONS BY INTELLIGENT EDI
Juha Eskelinen, Jyrki Kovanen, Miika Linna, Tero Mononen, and Reijo Sulonen *In* Technical Research Centre of Finland, Information Technology and Economic Modelling 1992 p 182-205 (For primary document see N94-22056 05-83)
Copyright Avail: CASI HC A03/MF A03

N94-22102 Concordia Univ., Montreal (Quebec). Center for Signal Processing and Communications.
ESTIMATION OF AR SIGNAL PATTERNS USING COMPETITIVE NEURAL NETWORKS
Keqin Gao, M. Omair Ahmad, and M. N. S. Swamy *In* Engineering Inst. of Canada, Canadian Conference on Electrical and Computer Engineering, Volumes 1 and 2 1991 4 p (For primary document see N94-22101 05-33)
Avail: Issuing Activity (Engineering Inst. of Canada, 2050 rue Mansfield, Suite 700, Montreal, PQ H3A 1Z2 Canada)

N94-22103 Maryland Univ., Princess Anne.
SIGNAL CLASSIFICATION AND NOISE FILTERING USING ARTIFICIAL NEURAL NETWORKS
Andrew M. Veronis and Demetri Michalopoulos (California State Univ., Fullerton.) *In* Engineering Inst. of Canada, Canadian Conference on Electrical and Computer Engineering, Volumes 1 and 2 1991 4 p (For primary document see N94-22101 05-33)
Avail: Issuing Activity (Engineering Inst. of Canada, 2050 rue Mansfield, Suite 700, Montreal, PQ H3A 1Z2 Canada)

N94-22110 Queens Univ., Kingston (Ontario). Dept. of Electrical Engineering.
VLSI ARCHITECTURES FOR THE NEW (T,L) ALGORITHM
P. A. Bengough and S. J. Simmons *In* Engineering Inst. of Canada, Canadian Conference on Electrical and Computer Engineering, Volumes 1 and 2 1991 4 p (For primary document see N94-22101 05-33)
Avail: Issuing Activity (Engineering Inst. of Canada, 2050 rue Mansfield, Suite 700, Montreal, PQ H3A 1Z2 Canada)

N94-22126 Concordia Univ., Montreal (Quebec). Dept. of Electrical and Computer Engineering.
IMPROVEMENTS IN ANTENNA COUPLING PATH ALGORITHMS FOR AIRCRAFT EMC ANALYSIS
Michael Bogusz and Stanley J. Kibina *In* Engineering Inst. of Canada, Canadian Conference on Electrical and Computer Engineering, Volumes 1 and 2 1991 4 p (For primary document see N94-22101 05-33)
Avail: Issuing Activity (Engineering Inst. of Canada, 2050 rue Mansfield, Suite 700, Montreal, PQ H3A 1Z2 Canada)

N94-22127 Laval Univ. (Quebec). Dept. Genie Electrique.
CALCULATION OF A DIFFRACTED ELECTRIC FIELD WITH THE AID OF THE METHOD OF EQUIVALENT CURRENTS (MEC) [CALCUL DU CHAMP ELECTRIQUE DIFFRACTE A L'AIDE DE LA METHODE DES COURANTS EQUIVALENTS (MEC)]
J. Raymond, G. Y. Delisle, J. Bedard (Defence Research Establishment Valcartier, Quebec.), and Y. deVilliers (Defence Research Establishment Valcartier, Quebec.) *In* Engineering Inst. of Canada, Canadian Conference on Electrical and Computer Engineering, Volumes 1 and 2 1991 4 p In FRENCH (For primary document see N94-22101 05-33)
Avail: Issuing Activity (Engineering Inst. of Canada, 2050 rue Mansfield, Suite 700, Montreal, PQ H3A 1Z2 Canada)

N94-22128 Concordia Univ., Montreal (Quebec). EMC Lab.
RCS OF SHIPS AND AIRCRAFT AT HF FREQUENCIES
C. W. Trueman, S. J. Kubina, S. R. Mishra (Canadian Space Agency, Ottawa, Ontario.), and C. Larose (Canadian Space Agency, Ottawa, Ontario.) *In* Engineering Inst. of Canada, Canadian Conference on Electrical and Computer Engineering, Volumes 1 and 2 1991 4 p (For primary document see N94-22101 05-33)
Avail: Issuing Activity (Engineering Inst. of Canada, 2050 rue Mansfield, Suite 700, Montreal, PQ H3A 1Z2 Canada)

N94-22137 McMaster Univ., Hamilton (Ontario). Communications Research Lab.
FULL WAVE NUMERICAL MODEL OF ARBITRARILY-SHAPED PROXIMITY COUPLED MICROSTRIP ANTENNAS
Ke-Li Wu, John Litva, Russ Fralich, and Chen Wu *In* Engineering Inst. of Canada, Canadian Conference on Electrical and Computer Engineering, Volumes 1 and 2 1991 4 p (For primary document see N94-22101 05-33)
Avail: Issuing Activity (Engineering Inst. of Canada, 2050 rue Mansfield, Suite 700, Montreal, PQ H3A 1Z2 Canada)

N94-22138 McMaster Univ., Hamilton (Ontario). Communications Research Lab.
MODELING OF COAXIAL-FED MICROSTRIP PATCH ANTENNA BY FINITE DIFFERENCE TIME DOMAIN METHOD
Chen Wu, Ke-Li Wu, Zhiqiang Bi, and John Litva *In* Engineering Inst. of Canada, Canadian Conference on Electrical and Computer Engineering, Volumes 1 and 2 1991 4 p (For primary document see N94-22101 05-33)
Avail: Issuing Activity (Engineering Inst. of Canada, 2050 rue Mansfield, Suite 700, Montreal, PQ H3A 1Z2 Canada)

N94-22139 Health and Welfare Canada, Ottawa (Ontario).
A BROADBAND V-ANTENNA FOR PULSED FIELD MEASUREMENTS: EXPERIMENTAL RESULTS
Karu P. Esselle and Stanislaw S. Stuchly (Ottawa Univ., Ontario.) *In* Engineering Inst. of Canada, Canadian Conference on Electrical and Computer Engineering, Volumes 1 and 2 1991 3 p (For primary document see N94-22101 05-33)
Avail: Issuing Activity (Engineering Inst. of Canada, 2050 rue Mansfield, Suite 700, Montreal, PQ H3A 1Z2 Canada)

N94-22140 Manitoba Univ., Winnipeg. Dept. of Electrical and Computer Engineering.
FORMULATION FOR NUMERICAL SOLUTION OF RADIATION AND TRANSMISSION FROM ARBITRARY APERTURES
H. Moheb and L. Shafai *In* Engineering Inst. of Canada, Canadian Conference on Electrical and Computer Engineering, Volumes 1 and 2 1991 4 p (For primary document see N94-22101 05-33)
Avail: Issuing Activity (Engineering Inst. of Canada, 2050 rue Mansfield, Suite 700, Montreal, PQ H3A 1Z2 Canada)

N94-22142 Defence Research Establishment, Ottawa (Ontario). Airborne Radar Section.
CFAR PROCESSING FOR AIRBORNE PULSE-DOPPLER RADARS
G. Vrckovnik and D. Faubert *In* Engineering Inst. of Canada, Canadian Conference on Electrical and Computer Engineering, Volumes 1 and 2 1991 4 p (For primary document see N94-22101 05-33)
Avail: Issuing Activity (Engineering Inst. of Canada, 2050 rue Mansfield, Suite 700, Montreal, PQ H3A 1Z2 Canada)

N94-22143 Raytheon Canada Ltd., Waterloo (Ontario).
SPACE-BASED RADAR FOR MOVING TARGET DETECTION
C. F. Weaver and A. W. Bridgewater (Defence Research Establishment, Ottawa, Ontario.) *In* Engineering Inst. of Canada, Canadian Conference on Electrical and Computer Engineering, Volumes 1 and 2 1991 4 p (For primary document see N94-22101 05-33)
Avail: Issuing Activity (Engineering Inst. of Canada, 2050 rue Mansfield, Suite 700, Montreal, PQ H3A 1Z2 Canada)

N94-22144 Defence Research Establishment, Ottawa (Ontario). Airborne Radar Section.
A DIGITAL DEMODULATION SCHEME FOR USE IN A HIGH DYNAMIC RANGE RADAR SYSTEM
Glen Rempel and George Haslam *In* Engineering Inst. of Canada, Canadian Conference on Electrical and Computer Engineering, Volumes 1 and 2 1991 4 p (For primary document see N94-22101 05-33)
Avail: Issuing Activity (Engineering Inst. of Canada, 2050 rue Mansfield, Suite 700, Montreal, PQ H3A 1Z2 Canada)

N94-22159 Defence Research Establishment, Ottawa (Ontario).
AN OVERVIEW OF SYNTHETIC APERTURE RADAR SIGNAL PROCESSING TECHNIQUES
M. R. Vant *In* Engineering Inst. of Canada, Canadian Conference on Electrical and Computer Engineering, Volumes 1 and 2 1991 7 p (For primary document see N94-22101 05-33)
Avail: Issuing Activity (Engineering Inst. of Canada, 2050 rue Mansfield, Suite 700, Montreal, PQ H3A 1Z2 Canada)

N94-22160 Laval Univ. (Quebec). Dept. Genie Electrique.
ADAPTIVE SYNTHESIS OF A RAY DIAGRAM FOR AN ANTENNA ARRAY [SYNTHESE ADAPTIVE D'UN DIAGRAMME DE RAYONNEMENT D'UNE ANTENNE RESEAU]
D. Grenier *In* Engineering Inst. of Canada, Canadian Conference on Electrical and Computer Engineering, Volumes 1 and 2 1991 4 p In FRENCH (For primary document see N94-22101 05-33)
Avail: Issuing Activity (Engineering Inst. of Canada, 2050 rue Mansfield, Suite 700, Montreal, PQ H3A 1Z2 Canada)

N94-22161 Defence Research Establishment, Ottawa (Ontario).
TARGET ANGULAR MOTION AND ITS EFFECTS ON SIMULATED SSAR SHIP IMAGES
A. Damini and G. E. Haslam *In* Engineering Inst. of Canada, Canadian Conference on Electrical and Computer Engineering, Volumes 1 and 2 1991 4 p (For primary document see N94-22101 05-33)
Avail: Issuing Activity (Engineering Inst. of Canada, 2050 rue Mansfield, Suite 700, Montreal, PQ H3A 1Z2 Canada)

N94-22162 Manitoba Univ., Winnipeg. Dept. of Electrical and Computer Engineering.
EFFECT OF ERRORS ON THE PHASE CENTRE AND POINTING ANGLE OF PHASED ARRAY ANTENNAS
H. Moheb, A. Helaly (Cairo Univ., Egypt.), A. Sebak, and L. Shafai *In* Engineering Inst. of Canada, Canadian Conference on Electrical and Computer Engineering, Volumes 1 and 2 1991 4 p (For primary document see N94-22101 05-33)
Avail: Issuing Activity (Engineering Inst. of Canada, 2050 rue Mansfield, Suite 700, Montreal, PQ H3A 1Z2 Canada)

N94-22170 Communications Research Centre, Ottawa (Ontario).
THE INFLUENCE OF LOWPASS FILTERING AND THE EFFECTS OF FADING ON THE GROUP DEMODULATION OF QPSK SIGNALS
Norman Secord, Shunkichi Isobe (Ministry of Posts and Telecommunications, Tokyo, Japan.), and Chun Loo *In* Engineering Inst. of Canada, Canadian Conference on Electrical and Computer Engineering, Volumes 1 and 2 1991 4 p (For primary document see N94-22101 05-33)
Avail: Issuing Activity (Engineering Inst. of Canada, 2050 rue Mansfield, Suite 700, Montreal, PQ H3A 1Z2 Canada)

N94-22171 Nippon Telegraph and Telephone Public Corp., Yokosuka (Japan). Radio Communication Systems Lab.
TDMA SATELLITE COMMUNICATION SYSTEMS FOR ISDN SERVICES
Katsuhiko Kawazoe, Masahiro Morikura, Shuji Kubota, Kiyoshi Enomoto, and Shuzo Kato *In* Engineering Inst. of Canada, Canadian Conference on Electrical and Computer Engineering, Volumes 1 and 2 1991 4 p (For primary document see N94-22101 05-33)
Avail: Issuing Activity (Engineering Inst. of Canada, 2050 rue Mansfield, Suite 700, Montreal, PQ H3A 1Z2 Canada)

N94-22172 Nippon Telegraph and Telephone Public Corp., Yokosuka (Japan). Radio Communication Systems Lab.
A CONSIDERATION OF THE INTEGRATION OF TERRESTRIAL AND SATELLITE MOBILE SYSTEMS
Masato Mori, Yasuki Nishi, and Hiraku Mishima *In* Engineering Inst. of Canada, Canadian Conference on Electrical and Computer Engineering, Volumes 1 and 2 1991 4 p (For primary document see N94-22101 05-33)
Avail: Issuing Activity (Engineering Inst. of Canada, 2050 rue Mansfield, Suite 700, Montreal, PQ H3A 1Z2 Canada)

N94-22187 Department of Communications, Ottawa (Ontario).
VISIBILITY CONSIDERATIONS IN FREQUENCY SHARING WITH LOW EARTH ORBIT SATELLITES
John W. Chang *In* Engineering Inst. of Canada, Canadian Conference on Electrical and Computer Engineering, Volumes 1 and 2 1991 4 p (For primary document see N94-22101 05-33)
Avail: Issuing Activity (Engineering Inst. of Canada, 2050 rue Mansfield, Suite 700, Montreal, PQ H3A 1Z2 Canada)

N94-22190 Concordia Univ., Montreal (Quebec). Dept. of Electrical and Computer Engineering.
THROUGHPUT, BLOCKING, AND INTERFERENCE IN PACKET RADIO NETWORKS
Han-Hua Ma and Marc Comeau *In* Engineering Inst. of Canada, Canadian Conference on Electrical and Computer Engineering, Volumes 1 and 2 1991 4 p (For primary document see N94-22101 05-33)
Avail: Issuing Activity (Engineering Inst. of Canada, 2050 rue Mansfield, Suite 700, Montreal, PQ H3A 1Z2 Canada)

N94-22196 Laval Univ. (Quebec). Dept. of Electrical Engineering.
AlGaAs LASER DIODE FM SPECTRUM: PHASED ARRAY ANTENNA APPLICATION
Martin Chamberland and Michel Tetu *In* Engineering Inst. of Canada, Canadian Conference on Electrical and Computer Engineering, Volumes 1 and 2 1991 4 p (For primary document see N94-22101 05-33)
Avail: Issuing Activity (Engineering Inst. of Canada, 2050 rue Mansfield, Suite 700, Montreal, PQ H3A 1Z2 Canada)

N94-22197 Ecole Polytechnique, Montreal (Quebec). Dept. de Genie Electrique et Genie Informatique.
NUMERICAL METHOD FOR COMPUTING THE ELECTRIC FIELD PRODUCED BY A MICROWAVE BEAM IN A STRATIFIED MEDIUM [METHODE POUR L'ETUDE DU CHAMP ELECTRIQUE PRODUIT PAR UN FAISCEAU HYPERFREQUENCE DANS UN MILIEU STRATIFIE]
Jean Montreuil *In* Engineering Inst. of Canada, Canadian Conference on Electrical and Computer Engineering, Volumes 1 and 2 1991 2 p In FRENCH (For primary document see N94-22101 05-33)
Avail: Issuing Activity (Engineering Inst. of Canada, 2050 rue Mansfield, Suite 700, Montreal, PQ H3A 1Z2 Canada)

N94-22198 Manitoba Univ., Winnipeg.
PERFORMANCE OF A SIMPLE CIRCULAR POLARIZATION SELECTIVE SURFACE
J. E. Roy, G. A. Morin (Defence Research Establishment, Ottawa, Ontario.), and L. Shafai *In* Engineering Inst. of Canada, Canadian Conference on Electrical and Computer Engineering, Volumes 1 and 2 1991 4 p (For primary document see N94-22101 05-33)
Avail: Issuing Activity (Engineering Inst. of Canada, 2050 rue Mansfield, Suite 700, Montreal, PQ H3A 1Z2 Canada)

N94-22203 Ottawa Univ. (Ontario). Dept. of Electrical Engineering.
BUFFER ALLOCATION IN AN ATM SWITCH WITH OUTPUT BUFFER AND SPEED CONSTRAINTS
Anil K. Gupta and N. D. Georganas *In* Engineering Inst. of Canada, Canadian Conference on Electrical and Computer Engineering, Volumes 1 and 2 1991 4 p (For primary document see N94-22101 05-33)
Avail: Issuing Activity (Engineering Inst. of Canada, 2050 rue Mansfield, Suite 700, Montreal, PQ H3A 1Z2 Canada)

N94-22204 Communications Research Centre, Ottawa (Ontario).
COMPARISON OF THEORETICAL AND SIMULATED PERFORMANCE RESULTS FOR SLOPPY-SLOTTED ALOHA SIGNALING
Stewart N. Crozier *In* Engineering Inst. of Canada, Canadian Conference on Electrical and Computer Engineering, Volumes 1 and 2 1991 4 p (For primary document see N94-22101 05-33)
Avail: Issuing Activity (Engineering Inst. of Canada, 2050 rue Mansfield, Suite 700, Montreal, PQ H3A 1Z2 Canada)

N94-22205 Concordia Univ., Montreal (Quebec). Dept. of Electrical and Computer Engineering.
NEURAL NETWORKS FOR OPTIMUM ROUTING IN PACKET-SWITCHED COMMUNICATIONS NETWORKS
Faouzi Kamoun and M. Mehmet Ali *In* Engineering Inst. of Canada, Canadian Conference on Electrical and Computer Engineering, Volumes 1 and 2 1991 4 p (For primary document see N94-22101 05-33)
Avail: Issuing Activity (Engineering Inst. of Canada, 2050 rue Mansfield, Suite 700, Montreal, PQ H3A 1Z2 Canada)

N94-22209 Ottawa Univ. (Ontario). Dept. of Electrical Engineering.
FILE TRANSFER PERFORMANCE IN LAN INTERCONNECTION THROUGH A SATELLITE CHANNEL
Xiao-Xiong Yao and Oliver W. W. Yang *In* Engineering Inst. of Canada, Canadian Conference on Electrical and Computer Engineering, Volumes 1 and 2 1991 4 p (For primary document see N94-22101 05-33)
Avail: Issuing Activity (Engineering Inst. of Canada, 2050 rue Mansfield, Suite 700, Montreal, PQ H3A 1Z2 Canada)

N94-22210 Quebec Univ., Verdun.
RECOGNIZING HESITATION PHENOMENA IN CONTINUOUS, SPONTANEOUS SPEECH
Douglas OShaughnessy *In* Engineering Inst. of Canada, Canadian Conference on Electrical and Computer Engineering, Volumes 1 and 2 1991 4 p (For primary document see N94-22101 05-33)
Avail: Issuing Activity (Engineering Inst. of Canada, 2050 rue Mansfield, Suite 700, Montreal, PQ H3A 1Z2 Canada)

N94-22211 Laval Univ. (Quebec). Dept. of Electrical Engineering.
A FRAMEWORK OF CONNECTIONIST NETWORK TOWARD SPEECH WAVEFORM CODING
Ying Cheng, Paul Fortier, and Denis Poussart *In* Engineering Inst. of

Canada, Canadian Conference on Electrical and Computer Engineering, Volumes 1 and 2 1991 4 p (For primary document see N94-22101 05-33)
Avail: Issuing Activity (Engineering Inst. of Canada, 2050 rue Mansfield, Suite 700, Montreal, PQ H3A 1Z2 Canada)

N94-22212 Carleton Univ., Ottawa (Ontario).
SEGMENTATION AND FREQUENCY DOMAIN ML PITCH ESTIMATION OF SPEECH SIGNALS
Salim A. Hanna *In* Engineering Inst. of Canada, Canadian Conference on Electrical and Computer Engineering, Volumes 1 and 2 1991 4 p (For primary document see N94-22101 05-33)
Avail: Issuing Activity (Engineering Inst. of Canada, 2050 rue Mansfield, Suite 700, Montreal, PQ H3A 1Z2 Canada)

N94-22213 Simon Fraser Univ., Burnaby (British Columbia). Communications Science Lab.
SPEAKER-INDEPENDENT ISOLATED-DIGIT RECOGNITION USING NEURAL NETWORKS AND HIDDEN MARKOV MODEL
Michael McGuire, Diane Ingraham, and Vladimir Cuperman *In* Engineering Inst. of Canada, Canadian Conference on Electrical and Computer Engineering, Volumes 1 and 2 1991 4 p (For primary document see N94-22101 05-33)
Avail: Issuing Activity (Engineering Inst. of Canada, 2050 rue Mansfield, Suite 700, Montreal, PQ H3A 1Z2 Canada)

N94-22217 Waterloo Univ. (Ontario). Dept. of Electrical and Computer Engineering.
ASYNCHRONOUS DETECTION OF SSB-SC DATA SIGNALS
T. R. Sommerville and J. V. Hanson *In* Engineering Inst. of Canada, Canadian Conference on Electrical and Computer Engineering, Volumes 1 and 2 1991 4 p (For primary document see N94-22101 05-33)
Avail: Issuing Activity (Engineering Inst. of Canada, 2050 rue Mansfield, Suite 700, Montreal, PQ H3A 1Z2 Canada)

N94-22223 Victoria Univ. (British Columbia). Dept. of Electrical and Computer Engineering.
CODED 64QAM USING A BINARY CONVOLUTIONAL CODE
Chintha Tellambura, Qiang Wang, and Vijay K. Bhargava *In* Engineering Inst. of Canada, Canadian Conference on Electrical and Computer Engineering, Volumes 1 and 2 1991 3 p (For primary document see N94-22101 05-33)
Avail: Issuing Activity (Engineering Inst. of Canada, 2050 rue Mansfield, Suite 700, Montreal, PQ H3A 1Z2 Canada)

N94-22224 Ottawa Univ. (Ontario). Dept. of Electrical Engineering.
CAPACITY COMPARISON BETWEEN DIRECT SEQUENCE PSK AND MFSK SPREAD SPECTRUM SYSTEMS IN CDMA APPLICATIONS
Jun Wang and Abbas Yongacoglu *In* Engineering Inst. of Canada, Canadian Conference on Electrical and Computer Engineering, Volumes 1 and 2 1991 4 p (For primary document see N94-22101 05-33)
Avail: Issuing Activity (Engineering Inst. of Canada, 2050 rue Mansfield, Suite 700, Montreal, PQ H3A 1Z2 Canada)

N94-22231 Nova Scotia Technical Coll., Halifax.
TRELLIS CODED MULTI-ORTHOGONAL MODULATION
Shalini Periyalwar, S. Fleisher, and Shou-Xing Qu *In* Engineering Inst. of Canada, Canadian Conference on Electrical and Computer Engineering, Volumes 1 and 2 1991 4 p (For primary document see N94-22101 05-33)
Avail: Issuing Activity (Engineering Inst. of Canada, 2050 rue Mansfield, Suite 700, Montreal, PQ H3A 1Z2 Canada)

N94-22232 Nova Scotia Technical Coll., Halifax.
QUADRATURE BIORTHOGONAL MODULATION
S. Fleisher, Shou-Xing Qu, and Shalini Periyalwar *In* Engineering Inst. of Canada, Canadian Conference on Electrical and Computer Engineering, Volumes 1 and 2 1991 4 p (For primary document see N94-22101 05-33)
Avail: Issuing Activity (Engineering Inst. of Canada, 2050 rue Mansfield, Suite 700, Montreal, PQ H3A 1Z2 Canada)

N94-22233 Laval Univ. (Quebec). Dept. de Genie Electrique.
ENCODING AND DECODING QUASI-SPHERICAL SIGNAL SETS
Paul Fortier *In* Engineering Inst. of Canada, Canadian Conference on Electrical and Computer Engineering, Volumes 1 and 2 1991 5 p (For primary document see N94-22101 05-33)
Avail: Issuing Activity (Engineering Inst. of Canada, 2050 rue Mansfield, Suite 700, Montreal, PQ H3A 1Z2 Canada)

N94-22234 Defence Research Establishment, Ottawa (Ontario).
THE APPLICATION OF SAMPLE VECTOR SELECTION TO ADAPTIVE NULLING: PERFORMANCE COMPARISON FOR TECHNIQUES COMBINING GRAM-SCHMIDT ORTHOGONALIZATION WITH AVERAGING
Mylene Toulgoat and Ross M. Turner *In* Engineering Inst. of Canada, Canadian Conference on Electrical and Computer Engineering, Volumes 1 and 2 1991 5 p (For primary document see N94-22101 05-33)
Avail: Issuing Activity (Engineering Inst. of Canada, 2050 rue Mansfield, Suite 700, Montreal, PQ H3A 1Z2 Canada)

N94-22237 Defence Research Establishment Valcartier (Quebec). Electro-Optics Div.
SIGNAL PROCESSING AND TARGET DISCRIMINATION ALGORITHMS FOR A ROSETTE SCAN TRACKER
Andre Morin *In* Engineering Inst. of Canada, Canadian Conference on Electrical and Computer Engineering, Volumes 1 and 2 1991 5 p (For primary document see N94-22101 05-33)
Avail: Issuing Activity (Engineering Inst. of Canada, 2050 rue Mansfield, Suite 700, Montreal, PQ H3A 1Z2 Canada)

N94-22238 Defence Research Establishment Valcartier (Quebec). Armament Div.
RADAR IMAGING OF MOVING TARGETS
Yves deVilliers *In* Engineering Inst. of Canada, Canadian Conference on Electrical and Computer Eng neering, Volumes 1 and 2 1991 4 p (For primary document see N94-22101 05-33)
Avail: Issuing Activity (Engineering Inst. of Canada, 2050 rue Mansfield, Suite 700, Montreal, PQ H3A 1Z2 Canada)

N94-22242 McGill Univ., Montreal (Quebec). Dept. of Electrical Engineering.
ARQ ON FADING CHANNELS
Patrick Beirouti, Harry Leib, and Salvatore D. Morgera *In* Engineering Inst. of Canada, Canadian Conference on Electrical and Computer Engineering, Volumes 1 and 2 1991 6 p (For primary document see N94-22101 05-33)
Avail: Issuing Activity (Engineering Inst. of Canada, 2050 rue Mansfield, Suite 700, Montreal, PQ H3A 1Z2 Canada)

N94-22250 McMaster Univ., Hamilton (Ontario). Communication Research Lab.
WIDEBAND SOURCE LOCATION IN TWO-DIMENSIONAL ARRAY PROCESSING
Jing-Yun Li and Patrick Yip *In* Engineering Inst. of Canada, Canadian Conference on Electrical and Computer Engineering, Volumes 1 and 2 1991 4 p (For primary document see N94-22101 05-33)
Avail: Issuing Activity (Engineering Inst. of Canada, 2050 rue Mansfield, Suite 700, Montreal, PQ H3A 1Z2 Canada)

N94-22252 Manitoba Univ., Winnipeg. Dept. of Electrical Engineering.
APPLICATIONS OF PLANAR NEAR-FIELD MEASUREMENTS TO ELECTROMAGNETIC RADIATION AND INTERFERENCE PROBLEMS
V. Betz, N. P. East, and A. Sebak *In* Engineering Inst. of Canada, Canadian Conference on Electrical and Computer Engineering, Volumes 1 and 2 1991 4 p (For primary document see N94-22101 05-33)
Avail: Issuing Activity (Engineering Inst. of Canada, 2050 rue Mansfield, Suite 700, Montreal, PQ H3A 1Z2 Canada)

N94-22253 McMaster Univ., Hamilton (Ontario). Communications Research Lab.
STUDY OF TE(1-DELTA) MODE IN OPEN DIELECTRIC RESONATORS BY A FINITE DIFFERENCE TIME DOMAIN METHOD
Ying Shen, Ke-Li Wu, Zhi-Qiang Bi, and John Litva *In* Engineering Inst.

of Canada, Canadian Conference on Electrical and Computer Engineering, Volumes 1 and 2 1991 4 p (For primary document see N94-22101 05-33)
Avail: Issuing Activity (Engineering Inst. of Canada, 2050 rue Mansfield, Suite 700, Montreal, PQ H3A 1Z2 Canada)

N94-22517*# Wisconsin Univ., Madison.
EFFICIENT TRANSFER OF IMAGES OVER NETWORKS Abstract Only
J. W. Percival and R. L. White (Space Telescope Science Inst., Baltimore, MD.) *In* NASA, Washington, Second Annual Conference on Astronomical Data Analysis Software and Systems. Abstracts 1992 p 86 (For primary document see N94-22438 05-89)
Avail: CASI HC A01/MF A02

N94-22526*# Rice Univ., Houston, TX.
DETECTOR NOISE STATISTICS IN THE NON-LINEAR REGIME Abstract Only
P. L. Shopbell and J. Bland-Hawthorn *In* NASA, Washington, Second Annual Conference on Astronomical Data Analysis Software and Systems. Abstracts 1992 p 95 (For primary document see N94-22438 05-89)
Avail: CASI HC A01/MF A02

33 ELECTRONICS AND ELECTRICAL ENGINEERING

Includes test equipment and maintainability; components, e.g., tunnel diodes and transistors; microminiaturization; and integrated circuitry.

For related information see also *60 Computer Operations and Hardware* and *76 Solid-State Physics.*

N94-19844# Sandia National Labs., Albuquerque, NM.
SPICE MACROMODEL FOR A 1-MEGAWATT POWER MOSFET SWITCH
C. Helms, M. Ackermann, T. Fischer, and M. Deveney 1993 13 p Presented at the 36th Midwest Symposium on Circuits and Systems, Detroit, MI, 16-18 Aug. 1993
(Contract DE-AC04-76DP-00789)
(DE93-019415; SAND-93-0298C; CONF-930854-3) Avail: CASI HC A03/MF A01

This paper presents a SPICE macromodel for a 1-megawatt high power electrical switch which uses power MOSFET's as the active switching elements. The model accurately predicts the time dependent switching current and provides a reasonable representation of the time dependent switch resistance and voltage drop across the switch. Techniques for extracting model parameters for commercial power MOSFET's are discussed along with suggestions for extending the model to spark gaps and other high power switches. DOE

N94-19884# Sandia National Labs., Albuquerque, NM.
EFFECT OF EXCITON LOCALIZATION AND DELOCALIZATION ON MAGNETIC-FIELD-DEPENDENT PHOTOLUMINESCENCE LINEWIDTHS IN SEMICONDUCTORS
S. K. Lyo, E. D. Jones, and S. R. Kurtz 1993 9 p Presented at the 9th International Conference on Luminescence and Optical Spectroscopy of Condensed Matter, Storrs, CT, 9-13 Aug. 1993
(Contract DE-AC04-76DP-00789)
(DE93-018860; SAND-93-0832C; CONF-930831-2) Avail: CASI HC A02/MF A01

Theory and data are presented for the photoluminescence linewidth in ordered and disordered semiconductor alloys (In(sub 0.48)Ga(sub 0.52)P) at low temperatures. In disordered (ordered) systems, the linewidth is due to exciton localization (exciton-impurity scattering) and increases (decreases) as a function of the field in agreement with the data. DOE

N94-19885# Argonne National Lab., IL.
ADVANCED BATTERIES FOR ELECTRIC VEHICLE APPLICATIONS: NONTECHNICAL SUMMARY
G. L. Henriksen 1993 4 p Presented at the 206th American Chemical Society National Meeting, Chicago, IL, 22-27 Aug. 1993
(Contract W-31-109-eng-38)
(DE93-019007; ANL/CMT/CP-79201; CONF-930802-13) Avail: CASI HC A01/MF A01

This paper provides an overview of the performance characteristics of the most prominent batteries under development for electric vehicles (EV's) and compares these characteristics to the USABC Mid-Term and Long-Term criteria, as well as to typical vehicle-related battery requirements. Most of the battery performance information was obtained from independent tests, conducted using simulated driving power profiles, for DOE and EPRI at Argonne National Laboratory. The EV batteries are categorized as near-term, mid-term, and long-term technologies based on their relative development status, as well as our estimate of their potential availability as commercial EV batteries. Also, the performance capabilities generally increase in going from the near-term to the mid-term and on to the long-term technologies. To date, the USABC has chosen to fund a few selected mid-term and long-term battery technologies. Derived from text

N94-19892# Department of the Navy, Washington, DC.
PROCESS TO FABRICATE THICK COPLANAR MICROWAVE ELECTRODE STRUCTURES Patent Application
R. W. McElhanon, inventor (to Navy), G. K. Gopalakrishnan, inventor (to Navy), and W. K. Burns, inventor (to Navy) 18 Jun. 1993 19 p
(AD-D015913; US-Patent-Appl-SN-077903; Navy-Case-74654) Avail: CASI HC A03/MF A01

A process for making thick metal structures on a substrate has the steps of: selectively exposing a thick layer of photoresist disposed on a substrate to ultraviolet radiation including the 350 nm to 450 nm portion of the spectrum of a mercury vapor lamp, where the photoresist layer is a heat-treated and hydrated photoresist layer, to fully pattern the substrate; developing the patterned substrate by contacting the photoresist layer with a photoresist developing solution; exposing the photoresist layer to a plasma for hardening the pattern against thermal flow; hardbaking the photoresist pattern on the substrate; and plating the metal onto the patterned substrate using a low current density (J) during at least part of the plating process, making a thick metal structure on the substrate. DTIC

N94-19902# Midwest Research Inst., Golden, CO.
CURRENT STATUS OF ENVIRONMENTAL, HEALTH, AND SAFETY ISSUES OF NICKEL METAL-HYDRIDE BATTERIES FOR ELECTRIC VEHICLES
D. Corbus, C. J. Hammel, and J. Mark Aug. 1993 87 p
(Contract DE-AC02-83CH-10093)
(DE93-017079; NREL/TP-463-5475) Avail: CASI HC A05/MF A01

This report identifies important environment, health, and safety issues associated with nickel metal-hydride (Ni-MH) batteries and assesses the need for further testing and analysis. Among the issues discussed are cell and battery safety, workplace health and safety, shipping requirements, and in-vehicle safety. The manufacture and recycling of Ni-MH batteries are also examined. This report also overviews the 'FH&S' issues associated with other nickel-based electric vehicle batteries; it examines venting characteristics, toxicity of battery materials, and the status of spent batteries as a hazardous waste. DOE

N94-19910 Maryland Univ., College Park. Dept. of Electrical Engineering.
MODELING FAILURE AND RELIABILITY IN NEW-GENERATION DEVICES Final Report, 2 May 1990 - 1 May 1993
Jeffrey Frey 31 Jul. 1993 6 p Limited Reproducibility: More than 20% of this document may be affected by microfiche quality
(Contract DAAL03-90-G-0120)
(AD-A271150; ARO-28004.1-EL) Avail: CASI HC A02

The physics of failure of semiconductor devices, and the means of simulating it, was studied in order to establish cost-effective methods to design two- and three-terminal semiconductor devices used in amplification, mixing, detection, and oscillation applications. An energy transport simulation code suitable for multi-layered two or three-terminal devices of Si, GaAs, and any other characterizable materials was written and its calculation speed continually enhanced using both physical approximation and numerical sophistication. Results were verified for submicronscale Si MOSFET's with hot-electron reliability problems and GaAs MESFET's with high-power microwave impingement problems. An effort to theoretically describe electron transport in hexagonal SiC and related crystals was also begun. DTIC

N94-20005# Allied-Signal Aerospace Co., Kansas City, MO.
AUTOMATED HMC ASSEMBLY
R. J. Blazek Aug. 1993 43 p
(Contract DE-AC04-76DP-00613)
(DE93-040641; KCP-613-5079) Avail: CASI HC A03/MF A01

An automated gold wire bonder was characterized for bonding 1-mil gold wires to gallium arsenide (GaAs) monolithic microwave integrated circuits (MMIC's) which are used in microwave radar transmitter-receiver (T/R) modules. Acceptable gold wire bond test results were obtained for the fragile, 5-mil-thick GaAs MMIC's with gold-metallized bond pads; and average wire bond pull strengths, shear strengths, and failure modes were determined. An automated aluminum wire bonder was modified to be used as a gold wire bonder so that a wedge bond capability was available for GaAs MMIC's in addition to the gold ball bond capability. DOE

N94-20012 Clemson Univ., SC.
PROCEEDINGS OF THE 8TH INTERNATIONAL SYMPOSIUM ON APPLICATIONS OF FERROELECTRICS Final Report, 1 Jan. 1992 - 30 Jun. 1993
M. Liu, A. Safari, A. Kingon, and G. Haertling 1 Feb. 1993 658 p Symposium held in Greenville, SC, 30 Aug. - 2 Sep. 1992 Limited Reproducibility: More than 20% of this document may be affected by microfiche quality
(Contract N00014-92-J-1474)
(AD-A270679) Avail: CASI HC A99

The eighth International Symposium on the Applications of Ferroelectrics was held in Greenville, SC, on August 30 to Sept 2, 1992. It was attended by approximately 260 scientists and engineers who presented nearly 200 oral and poster papers. The three plenary presentations covered ferroelectric materials which are currently moving into commercial exploitation or have strong potential to do so. These were (1) pyroelectric imaging, (2) ferroelectric materials integrated with silicon for use as micromotors and microsensors and (3) research activity in Japan on high permittivity materials for DRAM's. Invited papers covered such subjects as pyroelectric and electrooptic properties of thin films, photorefractive effects, ferroelectric polymers, piezoelectric transducers, processing of ferroelectrics, domain switching in ferroelectrics, thin film memories, thin film vacuum deposition techniques and the fabrication of chemically prepared PZT and PLZT thin films. The papers continued to reflect the large interest in ferroelectric thin films. It was encouraging that there have been substantial strides made in both the processing and understanding of the films in the last two years. It was equally clear, however, that much still remains to be done before reliable thin film devices will be available in the marketplace. DTIC

N94-20054# Sandia National Labs., Albuquerque, NM.
MEASURING LIQUID PROPERTIES WITH SMOOTH AND TEXTURED-SURFACE RESONATORS
S. J. Martin, K. O. Wessendorf, C. T. Gebert, G. C. Frye, R. W. Cernosek, L. Casaus, and M. A. Mitchell 1993 23 p Presented at the 1993 IEEE Frequency Control Symposium, Salt Lake City, UT, 2-4 Jun. 1993
(Contract DE-AC04-76DP-00789)
(DE93-019433; SAND-93-1565C; CONF-9306205-2) Avail: CASI HC A03/MF A01

The sensitivity of quartz resonators to surface mass accumulation enables their use in a number of sensing applications. The linear change in resonant frequency that occurs with mass accumulation allows the device to function as a general-purpose gravimetric detector or 'microbalance.' The device is easily instrumented as a sensor by incorporating it as the frequency-control element of an oscillator circuit. The response of thickness shear mode (TSM) resonators in liquids is examined. Smooth-surface devices, which viscously entrain a layer of contacting liquid, respond to the product of liquid density and viscosity. Textured-surface devices, which also trap liquid in surface features, exhibit an additional response that depends on liquid density alone. Combining smooth and textured resonators in a monolithic sensor allows simultaneous measurement of liquid density and viscosity. DOE

N94-20110 Illinois Univ., Urbana. Coordinated Science Lab.
VLSI DESIGN FOR RELIABILITY-CURRENT DENSITY Final Report, May 1991 - Sep. 1992
I. N. Hajj, P. Li, G. Kamath, G. Stamoulis, and H. Kriplani Jul. 1993 25 p Limited Reproducibility: More than 20% of this document may be affected by microfiche quality
(Contract F30602-91-C-0054)
(AD-A270719; RL-TR-93-129) Avail: CASI HC A03

This effort emphasizes the computation of the average and variance current density waveforms in the metal buses for estimating the mean time to failure (MTF) for electromigration effects. That effort is composed of two parts: the probabilistic simulation methods and software for computing the statistics of the current waveform at contact points to the buses, and the accurate extraction of the equivalent RC model of the bus for analyzing the bus currents. In addition, probabilistic methods have been applied to the calculation of the hot electron degradation in digital CMOS circuits and the problem of estimating the maximum current (as opposed to the average) in the bus for worst case voltage drop analysis. DTIC

N94-20120 Department of the Navy, Washington, DC.
LIGHTWEIGHT BATTERY ELECTRODE AND METHOD OF MAKING IT Patent
William A. Ferrando, inventor (to Navy) and Amarnath P. Divecha, inventor (to Navy) 30 Mar. 1993 8 p Filed 11 Jul. 1991
(AD-D015895; US-Patent-5,197,993; US-Patent-Appl-SN-728915; US-Patent-Class-29-2) Avail: US Patent and Trademark Office

A process for producing a lightweight electrode grid by exposing a heated mat of dense graphite fibers to Ni(CO)4 gas wherein the Ni(CO)4 decomposes upon contact with the graphite fibers depositing nickel metal coating on the graphic fibers is presented. The nickel coated graphite fibers are then sintered to form the grid. Nickel or cadmium electrodes are made by attaching a current collector to the grid and impregnating the grid with the appropriate nickel or cadmium active material. DTIC

N94-20166# Grenoble-1 Univ. (France). Techniques de l'Informatique, des Mathematiques, de la Microelectronique et de la Microscopie Quant.
EFFICIENT CHIP SIGNATURE CHECKING FOR DIAGNOSING BOUNDARY SCAN SYSTEMS
M. Lubaszewski, V. Castro-Alves, M. Nicolaidis, and B. Courtois Sep. 1992 22 p Sponsored in part by CAPES-COFECUB, Brazil
(RR-901-I; ETN-93-94991) Avail: CASI HC A03/MF A01

Off chip and on chip signature checking schemes suitable for Boundary Scan (BS) system testing are analyzed. The aim is to improve the diagnosis of onboard chip self testing at a negligible design effort. It is shown that an efficient off chip approach can reduce the memory requirements to store chip signatures. However, only a Built In Signature checking Circuit (BISC) can further improve diagnosis by reducing required memory and system scan time. Thus, based on the analysis of previous works and existing self checking approaches, the properties required for a BISC of general application are determined. A self testing BISC scheme which achieves these properties is proposed. The association of this BISC with an appropriate check of test data registers makes easier the task of embedding maximal diagnosis into a BS test controller chip. ESA

N94-20199 Department of the Navy, Washington, DC.
RESISTIVE GATE MAGNETIC FIELD SENSOR Patent
Francis J. Kub, inventor (to Navy) 4 May 1993 10 p Filed 31 Dec. 1990
(AD-D015923; US-Patent-5,208,477; US-Patent-Appl-SN-636348; US-Patent-Class-257-421) Avail: US Patent and Trademark Office

Described is an FET device for sensing a magnetic field, the FET device comprising: a semiconductor material having a source at a first position therein and receiving means at a second position therein for receiving charge carriers; bias voltage means for providing a bias voltage between the source and the receiving means to produce a movement of charge carriers between the source and the receiving means; a channel layer disposed within the semiconductor material between the source and the receiving means through which the charge carriers move as a function of the bias voltage and the magnetic field being sensed; a resistive gate disposed between the source and the receiving means and above the channel layer; a first resistive gate contact disposed in a first preselected position with respect to the source; a second resistive gate contact disposed in a second preselected position with respect to the receiving means; a resistive gate voltage means for providing a resistive gate bias voltage between the first and second resistive gate contacts to establish a longitudinal electric field in the channel layer; and output means disposed

in the semiconductor material for providing a signal related to the strength of the magnetic field sensed by the FET device. DTIC

N94-20218# Sandia National Labs., Albuquerque, NM.
A BREAKDOWN MODEL FOR THE BIPOLAR TRANSISTOR TO BE USED WITH CIRCUIT SIMULATORS
A. A. Keshavarz (Alliance Technologies Corp., Albuquerque, NM.), C. W. Raney, and D. C. Campbell 1993 22 p Presented at the 36th Midwest Symposium on Circuits and Systems, Detroit, MI, 16-18 Aug. 1993
(Contract DE-AC04-76DP-00789)
(DE93-019422; SAND-93-0241C; CONF-930854-2) Avail: CASI HC A03/MF A01

A breakdown model for the output characteristics of the bipolar transistor (bjt) has been developed. The behavioral modeling capability of PSPICE, a popular SPICE program (with emphasis on integrated circuits) was used to implement the macromodel. The model predicts bjt output characteristics under breakdown conditions. Experimental data was obtained to verify the macromodel. Good agreement exists between the measured and the simulated results. DOE

N94-20231# Lawrence Livermore National Lab., CA.
CHARACTERIZATION AND POSSIBLE REPAIR OF DEFECTS IN SOFT X RAY PROJECTION LITHOGRAPHY MASKS
A. M. Hawryluk Jul. 1993 6 p Presented at the Optical Society of America Topical Meeting on Soft X Ray Projection Lithography, Monterey, CA, 10-12 May 1993
(Contract W-7405-eng-48)
(DE93-019147; UCRL-JC-114416; CONF-9305159-4) Avail: CASI HC A02/MF A01

Soft X-ray Projection Lithography (SXPL) is one promising technique for the mass production of integrated circuits with minimum feature sizes below 100 nm. Mask fabrication, inspection and repair processes are critically important to all forms of lithography, including SXPL which requires a reflection mask (a substrate coated with a x-ray multilayer coating and patterned with thin metallization layer). Processes for the repair of defects in the metallization patterns have been developed, but at present, there exist no processes for the repair of defects in the multilayer coatings deposited in LLNL's magnetron sputter deposition facility, which produces state of the art x-ray multilayer mirrors. We also propose one possible process for the repair of defects in these multilayer coatings. DOE

N94-20257# Argonne National Lab., IL.
FUEL PROCESSING REQUIREMENTS AND TECHNIQUES FOR FUEL CELL PROPULSION POWER
R. Kumar, S. Ahmed, and M. Yu 1993 7 p Presented at the 206th American Chemical Society (ACS) National Meeting, Chicago, IL, 22-27 Aug. 1993
(Contract W-31-109-eng-38)
(DE93-019516; ANL/CMT/CP-79776; CONF-930802-9) Avail: CASI HC A02/MF A01

Fuels for fuel cells in transportation systems are likely to be methanol, natural gas, hydrogen, propane, or ethanol. Fuels other than hydrogen will need to be reformed to hydrogen on-board the vehicle. The fuel reformer must meet stringent requirements for weight and volume, product quality, and transient operation. It must be compact and lightweight, must produce low levels of CO and other byproducts, and must have rapid start-up and good dynamic response. Catalytic steam reforming, catalytic or noncatalytic partial oxidation reforming, or some combination of these processes may be used. This paper discusses salient features of the different kinds of reformers and describes the catalysts and processes being examined for the oxidation reforming of methanol and the steam reforming of ethanol. Effective catalysts and reaction conditions for the former have been identified; promising catalysts and reaction conditions for the latter are being investigated. DOE

N94-20294# Sandia National Labs., Albuquerque, NM.
PHOTOCONDUCTIVE SEMICONDUCTOR SWITCHES FOR PULSED POWER APPLICATIONS
G. M. Loubriel, F. J. Zutavern, G. J. Denison, W. D. Helgeson, D. L. McLaughlin, M. W. OMalley, and M. T. Buttram 1993 22 p Presented at the 9th IEEE Pulsed Power Conference, Albuquerque, NM, 21-23 Jun. 1993
(Contract DE-AC04-76DP-00789)
(DE93-019411; SAND-93-1630C; CONF-930616-31) Avail: CASI HC A03/MF A01

Photoconductive Semiconductor Switches (PCSS) are being used in, or tested for, many different pulsed power applications such as ultrawideband (UWB) transmitters and high current pulsers. Some aspects of the switches that are relevant to most of the applications are as follows: switch lifetime (longevity), switch opening time (related to the lifetime of carriers in the semiconductor), switching jitter, and the required laser energy. This paper will emphasize the results that we have obtained with Si switches for UWB applications. These include the following: measurement of switch longevity (a total of 80 Coulombs or 40 C/cm for a 2 cm wide switch and 18.4 Coulombs or 73 Coulombs/cm for a 0.25 cm wide switch), switching at high repetition rates (up to 540 Hz), measurement of carrier lifetime decay rates (a fast one of a few micro-s, and a slow one of about 330 micro-s), and measurements on the effect of neutron irradiation on carrier lifetimes. The total charge switched seems to be the highest ever reported for a PCSS. We have used these Si switches in a variety of circuits to produce: a monocycle with a period of about 10 ns corresponding to a center frequency of about 84 MHz, and ringing (many pulse) waveforms with periods of about 1 ns and 7.5 ns corresponding to center frequencies of 770 MHz and 133 MHz. We will also discuss recent studies on the switching properties of GaP. DOE

N94-20312 Sandia National Labs., Albuquerque, NM.
HIGH CURRENT DENSITY CONTACTS FOR PHOTOCONDUCTIVE SEMICONDUCTOR SWITCHES
A. G. Baca, H. P. Hjalmarson, G. M. Loubriel, D. L. McLaughlin, and F. J. Zutavern 1993 4 p Presented at the 9th IEEE Pulsed Power Conference, Albuquerque, NM, 21-23 Jun. 1993 Limited Reproducibility: More than 20% of this document may be affected by poor print
(Contract DE-AC04-76DP-00789)
(DE93-018837; SAND-93-1474C; CONF-930616-22) Avail: Issuing Activity (Department of Energy (DOE))

The current densities implied by current filaments in GaAs photoconductive semiconductor switches (PCSS) are in excess of 1 MA/cm(exp 2). As the lateral switches are tested repeatedly, damage accumulates at the contacts until electrical breakdown occurs across the surface of the insulating region. In order to improve the switch lifetime, the incorporation of n- and p-type ohmic contacts in lateral switches as well as surface geometry modifications are investigated. By using p-type AuBe ohmic contacts at the anode and n-type AuGe ohmic contacts at the cathode, contact lifetime improvements of 5-10x are observed compared to switches with n-type contacts at both anode and cathode. Failure analysis on samples operated for 1-1,000 shots show that extensive damage still exists for at least one contact on all switches observed and that temperatures approaching 500 C can be reached. However, the n-type AuGe cathode is often found to have no damage observable by scanning electron microscopy (SEM). The observed patterns of contact degradation indicate directions for future contact improvements in lateral switches. DOE

N94-20314 Fermi National Accelerator Lab., Batavia, IL.
CsI AND SOME NEW PHOTOCATHODES
D. F. Anderson, S. Kwan, and V. Peskov Jun. 1993 19 p Presented at the 1st Workshop on RICH Detectors, Bari, Italy, 1-5 Jun. 1993 Limited Reproducibility: More than 20% of this document may be affected by microfiche quality
(Contract DE-AC02-76CH-03000)
(DE93-019387; FNAL/C-93/128; CONF-9306188-2) Avail: CASI HC A03

A discussion of the possible sources of discrepancies in the measurements of the quantum efficiency of CsI photocathodes is presented. The authors propose that the major causes for disagreements in QE are due to the QE dependence on the current density extracted from the photocathode, on the electric field, and on the temperature of the photocathode. Preliminary results on TMAE enhanced GaAs and Si, plus TMAE protected CsTe and SbCs photocathodes, operated in gas, are also presented. DOE

N94-20325 EG and G Energy Measurements, Inc., Los Alamos, NM.
KINETIC THEORY OF RUNAWAY AIR-BREAKDOWN
R. A. Roussel-Dupre (Los Alamos National Lab., NM.), A. V. Gurevich

(Academy of Sciences, USSR, Moscow.), T. Tunnell, and G. M. Milikh (Maryland Univ., College Park.) 1993 36 p Limited Reproducibility: More than 20% of this document may be affected by microfiche quality
(Contract DE-AC08-93NV-11265)
(DE93-040731; EGG-11265-5007) Avail: CASI HC A03

The kinetic theory for a new air breakdown mechanism advanced in a previous paper is developed. The relevant form of the Boltzmann equation is derived and the particle orbits in both velocity space and configuration space are computed. A numerical solution of the Boltzmann equation, assuming a spatially uniform electric field, is obtained and the temporal evolution of the electron velocity distribution function is described. The results of our analysis are used to estimate the magnitude of potential x-ray emissions from discharges in thunderstorms. DOE

N94-20350 Department of the Navy, Washington, DC.
LAYERED THIN-EDGED FIELD-EMITTER DEVICE Patent
Henry F. Gray, inventor (to Navy) 25 May 1993 10 p Filed 8 Jun. 1990
(AD-D015932; US-Patent-5,214,347; US-Patent-Appl-SN-535612; US-Patent-Class-313-355) Avail: US Patent and Trademark Office

A field-emitter-array device includes layers of conductive material and intervening layers of insulating material. The lateral edges of the layers form a field-emitter array including a field emitter edge electrode interposed between a pair of control electrodes. The control electrode edges produce an electric field causing the flow of field emitted electrons to be substantially parallel to the plane of the control and field emitter edge electrodes. The direction of electron flow can be further controlled by additional electrodes in the form of additional conductive layers or external electrodes. A process for making the emitter device includes forming a plurality of planar first and second layers of insulating material alternately disposed between first, second and third layers of conductive material, forming a channel through the thickness of the layers and oriented perpendicular thereto, exposing the lateral edges of the layers of conductive and insulating materials adjacent to the channel to form a field emitter edge electrode interposed between a pair of control electrodes. Additional electrodes may be provided to form and deflect the electron flow. DTIC

N94-20354 Department of the Navy, Washington, DC.
HIGH-POWER GAS SWITCH WITH HYDRIDE ELECTRODES Patent
R. K. Hutcherson, inventor (to Navy) and Stuart L. Moran, inventor (to Navy) 3 Aug. 1993 6 p Filed 6 Nov. 1991
(AD-D015956; US-Patent-5,233,143; US-Patent-Appl-SN-788660; US-Patent-Class-200-144) Avail: US Patent and Trademark Office

A high-power, high-repetition-rate spark gap switch having metal-hydride electrodes is provided. The spark gap switch is configured with a trigger and two electrodes fabricated with metal hydrides. The hydride metals may be selected from a variety of alloys including iron, nickel, magnesium, and palladium based alloys. Use of these alloys for fabrication of the electrodes permits hydrogen to be absorbed into the electrode material at a density approximately that of liquid hydrogen. During operation of the switch, the increasing temperature causes hydrogen to be desorbed into cavity surrounding the switch. Whereas the increasing temperature lowers the breakdown voltage of the switch, the increasing pressure raises the breakdown voltage. The result is that the switch operates at a constant breakdown voltage independent of temperature. DTIC

N94-20483# Air Force Inst. of Tech., Wright-Patterson AFB, OH.
AN INVESTIGATION INTO THE INTEGRATION OF METER-LEVEL RANGE AND MILLIMETER-LEVEL PHASE DATA USING A MULTIMODE STIMULATION FOR OPTIMAL FILTER ESTIMATION SOFTWARE PACKAGE M.S. Thesis
Sharyn N. McWhorter Jun. 1993 140 p
(AD-A267955; AFIT/CI/CIA-93-115) Avail: CASI HC A07/MF A02

This is an investigation into the use of different types of Global Position System (GPS) data together with different types of bias sources. The intent was to examine their relative effect on the determination of the position of the receiver and the accuracy of the retrievable information. Selected inputs were processed through a simulation software package, Multimode Simulation for Optimal Filter Estimation (MSOF). GPS users and researchers continually attempt to analyze the effects of data and measurement biases to increase the quality of information gained from the system. Pseudorange and phase range data, together with various estimated and ignored measurement biases, were simulated and then processed through the optimal estimation software package. The output of the software-optimal estimations of the desired quantities provided insight into the consequence of virtually endless combinations of data.
Derived from text

N94-20553# Norwegian Defence Research Establishment, Kjeller.
TECHNICAL MANUAL PCDU MT 254 [TEKNISK HAANDBOK PCDU MT 254]
Kjetil Pettersen 10 Jun. 1992 90 p In NORWEGIAN
(FFI-92/7020; ETN-93-93769) Avail: CASI HC A05/MF A01

A detailed description of the MT254, Power Control and Distribution Unit (PCDU), which is a part of the MUNIN tactical electronic warfare system, is presented. ESA

N94-20555 Army Training and Doctrine Command, Fort Monroe, VA.
OPERATIONAL REQUIREMENTS DOCUMENT (ORD) FOR THE ALTERNATING CURRENT/DIRECT CURRENT (AC/DC) CLAMP-ON AMMETER, ME-563
14 Jul. 1993 12 p Limited Reproducibility: More than 20% of this document may be affected by microfiche quality
(AD-A271808; CARDS-ORD-16039) Avail: CASI HC A03

The ammeter shall operate in a frequency range of 45 Hertz (Hz) to 500 Hz with a resolution of no more than 100 mAMP on the low range scale and no more than 1 AMP on the high range scale. It will have a maximum AC current range to 300 AMP and a DC current range to 300 AMP. The clamp will encompass a conductor size up to 1.25 inches in diameter. DTIC

N94-20580# United Engineering Trustees, Inc., New York, NY.
HIGH SPEED/HIGH FREQUENCY OPTOELECTRONICS Final Report, 15 Mar. 1991 - 14 Nov. 1992
Charles Freiman 14 Nov. 1992 39 p Conference held in Palm Coast, FL, 17-22 Mar. 1991
(Grant AF-AFOSR-0187-91)
(AD-A271985; AFOSR-93-0814TR) Avail: CASI HC A03/MF A01

The attached program, and all available abstracts, cover the content of the conference. Areas showing remarkable advances, and possibilities for substantial further advances were: (1) high frequency modulation of multiple quantum well lasers on GaAs (especially strained InGaAs Q.W.'s); (2) high frequency photodetectors, including both surface-illuminated and travelling wave types; and (3) high frequency traveling-wave semiconductor modulators. DTIC

N94-20595# Ecole Centrale de Lyon (France). Lab. de Mecanique des Fluides et d'Acoustique.
TWO DIMENSIONAL SIMULATION OF THE ELECTRIC ARC BEHAVIOR IN A CUT-OFF DEVICE Ph.D. Thesis [SIMULATION BIDIMENSIONNELLE DU COMPORTEMENT D'UN ARC ELECTRIQUE DANS UN APPAREIL DE COUPURE]
Philippe Robin-Jouan 1992 189 p In FRENCH Original contains color illustrations
(ECL-92-41; ETN-93-94597) Avail: CASI HC A09/MF A02

The current cutoff in an electric circuit is followed by an electric arc between the contacts. The conducting media contains high intensity heat sources which induce very high temperature regions limited by boundaries of large temperature differences. Experimental tests are very hard to carry out under these conditions and simulations are needed. In order to perform the aerothermodynamic modeling, the dynamic, thermal, radiative, and electric effects have to be taken into account. A two dimensional calculation is performed by using parameters due to the influence of the wall at the horizontal surface between both electrodes. A thermal approach was applied and the importance of radiative parameters was stressed. The modeling of an electric arc was possible only for very short time delays and their strong dependence on magnetic forces was evidenced. Different front shapes, related to the structures of flow which form vortices, were characterized. ESA

N94-20628# Societe Suisse de Chronometrie, Neuchatel.
THE ONE-DAY WORKSHOP ON BATTERIES, STEPPING MOTORS, AND ELECTRONIC CLOCK DISPLAYS [ACTES DE LA JOURNEE D'ETUDE: PILES, MOTEURS PAS A PAS, AFFICHAGES DES MONTRES ELECTRONIQUES]
1991 48 p In FRENCH Workshop held in Neuchatel, Switzerland, 24 Oct. 1991
(ETN-93-94632) Avail: CASI HC A03/MF A01

The main topics were as follows: lithium and silver oxide batteries; performance tests of batteries and liquid crystal display devices; Lavet type stepping motors and the quality assurance tests applied; and the main characteristics of Lavet micromotors and of liquid crystal displays. For individual titles, see N94-20629 through N94-20635.

N94-20629# Ralston Energy Systems S.A., Geneva (Switzerland).
SILVER OXIDE BATTERIES: RECENT IMPROVEMENTS AND DEVELOPMENTS [PILES A L'OXYDE D'ARGENT: AMELIORATIONS ET DEVELOPPEMENTS RECENTS]
R. Dallenbach *In* Societe Suisse de Chronometrie, The One-Day Workshop on Batteries, Stepping Motors, and Electronic Clock Displays 1991 p 3-9 In FRENCH (For primary document see N94-20628 05-33)
Avail: CASI HC A02/MF A01

The main characteristics, the performance, and fabrication processes of silver oxide batteries are summarized. Since 1960, button type batteries have been commonly used as energy sources for electronic watches. Enormous progress concerning their lifetime, storage capacity, and leakage resistance was carried out. The principles of batteries and button batteries are reviewed. Particular attention is given to the miniature batteries. The main electrochemical systems and their applications are summarized. ESA

N94-20630# RENATA S.A., Itingen (Switzerland).
LITHIUM BATTERIES: FUTURE BATTERIES [PILES AU LITHIUM: PILES FUTURES]
Harald Reiche *In* Societe Suisse de Chronometrie, The One-Day Workshop on Batteries, Stepping Motors, and Electronic Clock Displays 1991 p 11-19 In FRENCH (For primary document see N94-20628 05-33)
Avail: CASI HC A02/MF A01

The main characteristics and applications of lithium batteries are reviewed. Miniature batteries for quartz crystal watches have been developed and fabricated in Switzerland since 1970. High technology systems like lithium batteries are largely used for their low auto-discharge during storage and for their high energy density. Two kinds of lithium batteries can be distinguished concerning their place in the watch: integrated batteries; and batteries placed between motion parts and the bottom of the watchcase. Lithium batteries are also used in pocket calculators, electronic modules for integrated circuits, telephone, control systems, electronic games, bank cards, and heart stimulators. ESA

N94-20631# ASULAB S.A., Neuchatel (Switzerland).
BATTERY TESTS [TEST DE PILES]
Roland W. Jeanmonod *In* Societe Suisse de Chronometrie, The One-Day Workshop on Batteries, Stepping Motors, and Electronic Clock Displays 1991 p 21-24 In FRENCH (For primary document see N94-20628 05-33)
Avail: CASI HC A01/MF A01

The reasons for performing battery tests are justified. The procedures and the required equipment are described. Examples of general rules which were found on the basis of a large amount of acquired data are given. The situation of standardization is summarized. Results of auto-discharges as a function of the height and the acceleration coefficient are given. ESA

N94-20632# ETA S.A., Grenchen (Switzerland).
LAVET TYPE STEPPING MOTORS AND ASSOCIATED CONTROLS [MOTEURS PAS A PAS HORLOGERS DU TYPE LAVET ET COMMANDES ASSOCIEES]
Yves Guerin *In* Societe Suisse de Chronometrie, The One-Day Workshop on Batteries, Stepping Motors, and Electronic Clock Displays 1991 p 25-30 In FRENCH (For primary document see N94-20628 05-33)
Avail: CASI HC A02/MF A01

The development of quartz crystals required new technologies such as miniature stepping motors. The construction of multiphase structure motors allowed two way operations for electronic regulation of time. The evolution steps of stepping motors and associated circuits are summarized. The main components and the operation principles of the motion are described. The rotor equilibrium position and power control and circuits are presented. ESA

N94-20633# ETA S.A., Grenchen (Switzerland).
TEST DEVICE FOR LAVET MOTORS [APPAREIL DE TEST POUR MOTEURS LAVET]
N. Perucchi *In* Societe Suisse de Chronometrie, The One-Day Workshop on Batteries, Stepping Motors, and Electronic Clock Displays 1991 p 31-36 In FRENCH (For primary document see N94-20628 05-33)
Avail: CASI HC A02/MF A01

The purpose of the test device is to provide the assembly and production lines with a tool to control and select, as a function of defects, the operation of a Lavet motor. Moreover this device can automatically perform the characterization of a given motor, either during the development phase, or during production phases. The theoretical bases on which the device was developed are summarized. The device operation modes and some results are presented. ESA

N94-20634# ASULAB S.A., Neuchatel (Switzerland).
LIQUID CRYSTAL DISPLAYS [LES AFFICHAGES A CRISTAUX LIQUIDES]
Naci Basturk *In* Societe Suisse de Chronometrie, The One-Day Workshop on Batteries, Stepping Motors, and Electronic Clock Displays 1991 p 37-46 In FRENCH (For primary document see N94-20628 05-33)
Avail: CASI HC A02/MF A01

Liquid crystals were discovered about a century ago. However, they were not industrially applied until 1970, when their properties of anisotropy were used in displays. The electro-optical properties of liquid crystals are presented under the following optical principles; light scattering; modulation of polarized light; light absorption by dichroic colorants. It must be noted that light scattering displays are no longer produced. ESA

N94-20635# ASULAB S.A., Neuchatel (Switzerland).
LCD DISPLAY TESTS [TEST D'AFFICHAGES LCD]
Roland-W. Jeanmonod *In* Societe Suisse de Chronometrie, The One-Day Workshop on Batteries, Stepping Motors, and Electronic Clock Displays 1991 p 47-50 In FRENCH (For primary document see N94-20628 05-33)
Avail: CASI HC A01/MF A01

The main characteristics of a display are discussed. The way in which a test procedure can be established is presented. Two kinds of tests procedures can be distinguished: certification tests and acceptance tests. The tests can be classified as reliability tests, storage tests, and mechanical resistance tests. Examples of results obtained are given. ESA

N94-20931 Naval Research Lab., Washington, DC.
AN 85 GHz QUASIOPTICAL GYROKLYSTRON EXPERIMENT Interim Report
Richard P. Fischer, Arne W. Fliflet, and Wallace M. Manheimer 29 Oct. 1993 197 p Limited Reproducibility: More than 20% of this document may be affected by microfiche quality
(AD-A272020; NRL/MR/6793-93-7387) Avail: CASI HC A09

The design and test of a new type of millimeter-wave tube called a quasioptical gyroklystron is reported. The device comprises a pair of quasioptical resonators separated by a drift region, which is powered by an annular electron beam with typical parameters 75 kV beam voltage, 6 A current, and an electron pitch angle of 1.9. The gyroklystron is operated as a free-running oscillator, a mode-primed oscillator, an amplifier, and a phase-locked oscillator. The output resonator is tilted by 2 deg relative to the plane perpendicular to the electron beam axis, which is predicted to increase the efficiency and operating region of stable, single-mode operation. Experimental measurements indicate that the output is single-moded over nearly all the gyroklystron operating parameter space. A new regime of operation has been studied called alpha priming, where the electron beam parameters are ramped to obtain higher power and efficiency. Peak electronic efficiencies of 22% are measured in a single mode with peak output powers up to 150 kW at 85.5 GHz in 13 microsecond pulses. A depressed collector is added to the experiment to increase the overall efficiency of

the tube to greater than 30%. Capacitive probes in the drift tube are used to measure the average pitch angle of the beam electrons and the results are compared to electron trajectory simulations. Experimental measurements of the output radiation are compared to time-dependent, multimode computer simulations, which demonstrate the advantages of mode priming by prebunching the electron beam and alpha priming. DTIC

N94-21021 Hahn-Meitner-Inst. fuer Kernforschung, Berlin (Germany).
A CONTRIBUTION TO DEVELOPMENT AND PARAMETER EXTRACTION OF SPICE COMPATIBLE MACROMODELS FOR DISCRETE BIPOLAR TRANSISTORS Ph.D. Thesis - Tech. Univ. Berlin [EIN BEITRAG ZUR ENTWICKLUNG UND PARAMETRISIERUNG SPICE-KOMPATIBLER MAKROMODELLE FUER DISKRETE BIPOLARTRANSISTOREN]
H. Krueger-Elencwajg Jul. 1992 159 p In GERMAN Limited Reproducibility: More than 20% of this document may be affected by microfiche quality
(HMI-B-499; ETN-93-93808) Avail: CASI HC A08

Based on the SPICE (Simulation Program with Integrated Circuit Emphasis) Gummel-Poon model for bipolar junction transistors, a macromodel which includes the influence of parasitic case elements, the effects of quasisaturation and the consequences of self heating due to power dissipation is described. A method for extracting the model parameters is given, using the results of S parameter measurements. The S parameters are measured at several operating points covering a very wide frequency range. The macromodel is built completely with SPICE standard elements to ensure full compatibility with this simulation program. ESA

N94-21064 Nationaal Inst. voor Kernfysica en Hoge Energiefysica, Amsterdam (Netherlands).
POWER SUPPLY AND CONTROLLER FOR THE SEXTUPOLE MAGNET OF AmPS [POWERSUPPLY EN CONTROLLER VOOR DE SEXTUPOLE MAGNEET VAN AMPS]
J. T. vanEs and J. H. vanTrigt 1992 14 p In DUTCH Limited Reproducibility: More than 20% of this document may be affected by microfiche quality
(DIGEL-1992-3; ETN-93-93306) Avail: CASI HC A03

A power supply was developed for the Sextupole magnet of the storage ring AmPS (Amsterdam Pulse Stretcher). The power supply consists of four units (Delta SM 7020) which are driven and controlled by a standard bit bus module via a specially designed interface printed ciruit. This circuit also contains LEDs (Light Emitting Diodes) which provide information about the status of the power supplies as well as status contact for external use. ESA

N94-21067# National Aerospace Lab., Amsterdam (Netherlands). Informatics Div.
THE ELECTRONICS TECHNOLOGY POLICY OF THE NLR INFORMATICS DIVISION: THE NLR ELECTRONICS CAE INFRASTRUCTURE [HET INFORMATICABELEID TEN AANZIEN VAN ELEKTRONISCHE TECHNOLOGIE: DE NLR INFRASTRUCTUUR VOOR CAE VAN ELEKTRONICA]
R. W. Mathijssen, L. J. Aartman, P. J. H. M. Manders, and H. Slot 17 Jan. 1991 63 p In DUTCH
(NLR-TP-91001-U; ETN-93-94335) Avail: CASI HC A04/MF A01

The NLR Infrastructure for Computer Aided Engineering (CAE) of Electronics (NICE) was introduced to solve problems due to the fact that CAE tools generally do not match mutually, with a view to the development of information systems for aerospace applications in which advanced electronics play an important role. CAE is used more and more to improve quality and reduce development time. Because most CAE tools generally do not match mutually, it is difficult to manage the design information present in the various tools and to exchange this information. NICE is based on an integrated set of local area networks, connected to the NLR computer network facilities. This is a basis for adding new tools for circuit simulation and analysis. Improved access to the tools and to the design information leads toward shorter development cycles of advanced electronics. ESA

N94-21079*# New Mexico Univ., Albuquerque. Space Engineering Research Center.
THE FIFTH NASA SYMPOSIUM ON VLSI DESIGN
1993 609 p Symposium held in Albuquerque, NM, 4-5 Nov. 1993; cosponsored by IEEE
(Grant NAGw-3293)
(NASA-CR-194644; NAS 1.26:194644) Avail: CASI HC A99/MF A06

The fifth annual NASA Symposium on VLSI Design had 13 sessions including Radiation Effects, Architectures, Mixed Signal, Design Techniques, Fault Testing, Synthesis, Signal Processing, and other Featured Presentations. The symposium provides insights into developments in VLSI and digital systems which can be used to increase data systems performance. The presentations share insights into next generation advances that will serve as a basis for future VLSI design. For individual titles, see N94-21080 through N94-21133.

N94-21080*# National Aeronautics and Space Administration. Goddard Space Flight Center, Greenbelt, MD.
AN ADAPTIVE, LOSSLESS DATA COMPRESSION ALGORITHM AND VLSI IMPLEMENTATIONS **c61**
Jack Venbrux (New Mexico Univ., Albuquerque.), Greg Zweigle (Advanced Hardware Architectures, Moscow, ID.), Jody Gambles (New Mexico Univ., Albuquerque.), Don Wiseman (New Mexico Univ., Albuquerque.), Warner H. Miller, and Pen-Shu Yeh *In* New Mexico Univ., The Fifth NASA Symposium on VLSI Design 1993 16 p (For primary document see N94-21079 05-33)
(Grant NAGw-3292)
Avail: CASI HC A03/MF A06

This paper first provides an overview of an adaptive, lossless, data compression algorithm originally devised by Rice in the early '70s. It then reports the development of a VLSI encoder/decoder chip set developed which implements this algorithm. A recent effort in making a space qualified version of the encoder is described along with several enhancements to the algorithm. The performance of the enhanced algorithm is compared with those from other currently available lossless compression techniques on multiple sets of test data. The results favor our implemented technique in many applications. Author

N94-21081*# Concordia Univ., Montreal (Quebec). Dept. of Computer Science.
AVOIDING AND TOLERATING LATENCY IN LARGE-SCALE NEXT-GENERATION SHARED-MEMORY MULTIPROCESSORS **c62**
David K. Probst *In* New Mexico Univ., The Fifth NASA Symposium on VLSI Design 1993 15 p Sponsored in part by MicroNet (For primary document see N94-21079 05-33)
(Grants NSERC-A3363; NSERC-MEF-0040121)
Avail: CASI HC A03/MF A06

A scalable solution to the memory-latency problem is necessary to prevent the large latencies of synchronization and memory operations inherent in large-scale shared-memory multiprocessors from reducing high performance. We distinguish latency avoidance and latency tolerance. Latency is avoided when data is brought to nearby locales for future reference. Latency is tolerated when references are overlapped with other computation. Latency-avoiding locales include: processor registers, data caches used temporally, and nearby memory modules. Tolerating communication latency requires parallelism, allowing the overlap of communication and computation. Latency-tolerating techniques include: vector pipelining, data caches used spatially, prefetching in various forms, and multithreading in various forms. Relaxing the consistency model permits increased use of avoidance and tolerance techniques. Each model is a mapping from the program text to sets of partial orders on program operations; it is a convention about which temporal precedences among program operations are necessary. Information about temporal locality and parallelism constrains the use of avoidance and tolerance techniques. Suitable architectural primitives and compiler technology are required to exploit the increased freedom to reorder and overlap operations in relaxed models. Author

N94-21082*# National Aeronautics and Space Administration. Goddard Space Flight Center, Greenbelt, MD.
RAD-HARD COMPUTER ELEMENTS FOR SPACE APPLICATIONS **c60**
G. S. Krishnan, Carl D. Longerot (Sandia National Labs., Albuquerque, NM.), and R. Keith Treece (Sandia National Labs., Albuquerque, NM.) *In* New Mexico Univ., The Fifth NASA Symposium on VLSI Design 1993

10 p (For primary document see N94-21079 05-33)
Avail: CASI HC A02/MF A06

Space Hardened CMOS computer elements emulating a commercial microcontroller and microprocessor family have been designed, fabricated, qualified, and delivered for a variety of space programs including NASA's multiple launch International Solar-Terrestrial Physics (ISTP) program, Mars Observer, and government and commercial communication satellites. Design techniques and radiation performance of the 1.25 micron feature size products are described. Author

N94-21083*# Prairie View Agricultural and Mechanical Coll., TX. Lab. for Radiation Studies.
DESIGN OF CMOS LOGIC GATES FOR TID RADIATION
John Okyere Attia and Maria L. Sasabo *In* New Mexico Univ., The Fifth NASA Symposium on VLSI Design 1993 9 p (For primary document see N94-21079 05-33)
(Grant NAG9-337)
Avail: CASI HC A02/MF A06

The rise time, fall time and propagation delay of the logic gates were derived. The effects of total ionizing dose (TID) radiation on the fall and rise times of CMOS logic gates were obtained using C program calculations and PSPICE simulations. The variations of mobility and threshold voltage on MOSFET transistors when subjected to TID radiation were used to determine the dependence of switching times on TID. The results of this work indicate that by increasing the size of P-channel transistor with respect to the N-channel transistors of the CMOS gates, the propagation delay of CMOS logic gate can be made to decrease with, or be independent of an increase in TID radiation. Author

N94-21084*# Phillips Lab., Kirtland AFB, NM.
EVALUATION OF RADIATION EFFECTS IN RE-OXIDIZED NITRIDED OXIDE DEVICES BY HOT CARRIER STRESSING AT 77 K c76
N. C. Das and V. Nathan *In* New Mexico Univ., The Fifth NASA Symposium on VLSI Design 1993 7 p Sponsored in part by AF Materiel Command and NSF (For primary document see N94-21079 05-33)
Avail: CASI HC A02/MF A06

An attempt has been made to understand the mechanisms of radiation induced degradation by using different types of hot carrier (HC) stressing experiments. The degradation of re-oxidized nitrided oxide gate dielectric due to irradiation and hot carriers are reported. The effect of electron and hole traps of the virgin device on radiation induced threshold voltage shift is discussed. Author

N94-21085*# Johns Hopkins Univ., Laurel, MD. Applied Physics Lab.
COMPARISON OF SINGLE EVENT UPSET RATES FOR MICROELECTRONIC MEMORY DEVICES DURING INTERPLANETARY SOLAR PARTICLE EVENTS c92
P. L. McKerracher, J. D. Kinnison, and R. H. Maurer *In* New Mexico Univ., The Fifth NASA Symposium on VLSI Design 1993 13 p (For primary document see N94-21079 05-33)
Avail: CASI HC A03/MF A06

Variability in the methods and models used for single event upset calculations in microelectronic memory devices can lead to a range of possible upset rates. Using heavy ion and proton data for selected DRAM and SRAM memories, we have calculated an array of upset rates in order to compare the Adams worst case interplanetary solar flare model to a model proposed by scientists at the Jet Propulsion Laboratory. In addition, methods of upset rate calculation are compared: the Cosmic Ray Effects on Microelectronics CREME code and a Monte Carlo algorithm developed at the Applied Physics Laboratory. The results show that use of a more realistic, although still conservative, model of the space environment can have significant cost saving benefits. Author

N94-21086*# Jet Propulsion Lab., California Inst. of Tech., Pasadena. Very Large Scale Integrated Technology Group.
STRV RADMON: AN INTEGRATED HIGH-ENERGY PARTICLE DETECTOR c19
Martin Buehler, George Soli, Brent Blaes, and Gemma Tardio *In* New Mexico Univ., The Fifth NASA Symposium on VLSI Design 1993 11 p (For primary document see N94-21079 05-33)
Avail: CASI HC A03/MF A06

The RADMON (Radiation Monitor) was developed as a compact device with a 4-kbit SRAM particle detector and two p-FET total dose monitors. Thus it can be used as a spacecraft radiation alarm and in situ total dose monitor. This paper discusses the design and calibration of the SRAM for proton, alpha, and heavy ion detection. Upset rates for the RADMON, based on a newly developed space particle flux algorithm, are shown to vary over eight orders of magnitude. On the STRV (Space Technology Research Vehicle) the RADMON's SRAM will be used to detect trapped protons, solar flares, and cosmic rays and to evaluate our ability to predict space results from ground tests. Author

N94-21087*# New Mexico Univ., Albuquerque. Space Engineering Research Center.
TEST RESULTS FOR SEU AND SEL IMMUNE MEMORY CIRCUITS
D. Wiseman, J. Canaris, S. Whitaker, J. Gambles, K. Arave, and L. Arave *In its* The Fifth NASA Symposium on VLSI Design 1993 11 p (For primary document see N94-21079 05-33)
Avail: CASI HC A03/MF A06

Test results for three SEU logic/circuit hardened CMOS memory circuits verify upset and latch-up immunity for two configurations to be in excess of 120 MeV cm(exp 2)/mg using a commercial, non-radiation hardened CMOS process. Test chips from three separate fabrication runs in two different process were evaluated. Author

N94-21088*# National Aeronautics and Space Administration. Goddard Space Flight Center, Greenbelt, MD.
SPACE QUALIFIED HIGH SPEED REED SOLOMON ENCODER c60
Jody W. Gambles (New Mexico Univ., Albuquerque.) and Tom Winkert *In* New Mexico Univ., The Fifth NASA Symposium on VLSI Design 1993 9 p (For primary document see N94-21079 05-33)
Avail: CASI HC A02/MF A06

This paper reports a Class S CCSDS recommendation Reed Solomon encoder circuit baselined for several NASA programs. The chip is fabricated using United Technologies Microelectronics Center's UTE-R radiation-hardened gate array family, contains 64,000 p-n transistor pairs, and operates at a sustained output data rate of 200 MBits/s. The chip features a pin selectable message interleave depth of from 1 to 8 and supports output block lengths of 33 to 255 bytes. The UTE-R process is reported to produce parts that are radiation hardened to 16 Rads (Si) total dose and 1.0(exp -10) errors/bit-day. Author

N94-21089*# Christopher Newport Coll., Newport News, VA.
AN ASIC MEMORY BUFFER CONTROLLER FOR A HIGH SPEED DISK SYSTEM c60
Robert F. Hodson and Steve Campbell *In* New Mexico Univ., The Fifth NASA Symposium on VLSI Design 1993 10 p Sponsored by NASA. Langley Research Center (For primary document see N94-21079 05-33)
Avail: CASI HC A02/MF A06

The need for large capacity, high speed mass memory storage devices has become increasingly evident at NASA during the past decade. High performance mass storage systems are crucial to present and future NASA systems. Spaceborne data storage system requirements have grown in response to the increasing amounts of data generated and processed by orbiting scientific experiments. Predictions indicate increases in the volume of data by orders of magnitude during the next decade. Current predictions are for storage capacities on the order of terabits (Tb), with data rates exceeding one gigabit per second (Gbps). As part of the design effort for a state of the art mass storage system, NASA Langley has designed a 144 CMOS ASIC to support high speed data transfers. This paper discusses the system architecture, ASIC design and some of the lessons learned in the development process. Author

N94-21090*# National Aeronautics and Space Administration. Goddard Space Flight Center, Greenbelt, MD.
MONGOOSE: CREATION OF A RAD-HARD MIPS R3000 c60
Dan Lincoln (LSI Logic Corp., Milpitas, CA.) and Brian Smith *In* New Mexico Univ., The Fifth NASA Symposium on VLSI Design 1993 9 p (For primary document see N94-21079 05-33)
Avail: CASI HC A02/MF A06

This paper describes the development of a 32 Bit, full MIPS R3000 code-compatible Rad-Hard CPU, code named Mongoose. Mongoose progressed from contract award, through the design cycle, to operational

silicon in 12 months to meet a space mission for NASA. The goal was the creation of a fully static device capable of operation to the maximum Mil-883 derated speed, worst-case post-rad exposure with full operational integrity. This included consideration of features for functional enhancements relating to mission compatibility and removal of commercial practices not supported by Rad-Hard technology. 'Mongoose' developed from an evolution of LSI Logic's MIPS-I embedded processor, LR33000, code named Cobra, to its Rad-Hard 'equivalent', Mongoose. The term 'equivalent' is used to infer that the core of the processor is functionally identical, allowing the same use and optimizations of the MIPS-I Instruction Set software tool suite for compilation, software program trace, etc. This activity was started in September of 1991 under a contract from NASA-Goddard Space Flight Center (GSFC)-Flight Data Systems. The approach affected a teaming of NASA-GSFC for program development, LSI Logic for system and ASIC design coupled with the Rad-Hard process technology, and Harris (GASD) for Rad-Hard microprocessor design expertise. The program culminated with the generation of Rad-Hard Mongoose prototypes one year later.

Author (revised)

N94-21091*# Alenia Spazio S.p.A., Rome (Italy).

DIGITAL RECEIVER FOR ON-BOARD FM/FSK-FM/BPSK DEMODULATION **c32**

G. Boscagli, M. C. Comparini, and M. Martone *In* New Mexico Univ., The Fifth NASA Symposium on VLSI Design 1993 13 p (For primary document see N94-21079 05-33)

Avail: CASI HC A03/MF A06

An all-digital demodulator FM/FSK-FM/BPSK is presented. The proposed architecture allows the 1-bit IF down-sampling technique with the hardware simplification of receiver analog section. The receiver exhibits great flexibility both in terms of signal demodulation (FSK or BPSK, subcarrier/ tone frequency, data rate) and interface capability. The demodulator is going to be realized in a VLSI chip (20 Kgate complexity). This paper describes the demodulator structure and its demodulation performances obtained with a breadboard based on programmable logic devices. The choice of a simple and effective scheme for frequency detection (FM and FSK demodulators) is suggested by system design considerations as well. Signal processing algorithms include also a Costas carrier phase recovery scheme in the case of BPSK signal and data transition tracking loop for the bit clock recovery. Test results address this solution as one of the most suitable for TT&C space application. Author

N94-21092*# Texas Instruments, Inc., Dallas. Semiconductor Group.

HIGH PERFORMANCE MPEG-AUDIO DECODER IC **c32**

M. Thorn, G. Benbassat, K. Cyr, S. Li, M. Gill, D. Kam, K. Walker, P. Look, C. Eldridge, and P. Ng *In* New Mexico Univ., The Fifth NASA Symposium on VLSI Design 1993 12 p (For primary document see N94-21079 05-33)

Avail: CASI HC A03/MF A06

The emerging digital audio and video compression technology brings both an opportunity and a new challenge to IC design. The pervasive application of compression technology to consumer electronics will require high volume, low cost IC's and fast time to market of the prototypes and production units. At the same time, the algorithms used in the compression technology result in complex VLSI IC's. The conflicting challenges of algorithm complexity, low cost, and fast time to market have an impact on device architecture and design methodology. The work presented in this paper is about the design of a dedicated, high precision, Motion Picture Expert Group (MPEG) audio decoder. Author (revised)

N94-21093*# Sandia National Labs., Albuquerque, NM. Failure Analysis Dept.

CORRECT CMOS IC DEFECT MODELS FOR QUALITY TESTING **c38**

Jerry M. Soden and Charles F. Hawkins (New Mexico Univ., Albuquerque.) *In* New Mexico Univ., The Fifth NASA Symposium on VLSI Design 1993 16 p (For primary document see N94-21079 05-33)

(Contract DE-AC04-76DP-00789)

Avail: CASI HC A03/MF A06

Leading edge, high reliability, and low escape CMOS IC test practices have now virtually removed the stuck-at fault model and replaced it with more defect-orientated models. Quiescent power supply current testing (I(sub DDQ)) combined with strategic use of high speed test patterns is the recommended approach to zero defect and high reliability testing goals. This paper reviews the reasons for the change in CMOS IC test practices and outlines an improved CMOS IC test methodology. Author (revised)

N94-21094*# Boeing Defense and Space Group, Seattle, WA.

COMPLEMENTARY HETEROJUNCTION FET TECHNOLOGY FOR SPACE APPLICATION

George LaRue *In* New Mexico Univ., The Fifth NASA Symposium on VLSI Design 1993 12 p (For primary document see N94-21079 05-33)

Avail: CASI HC A03/MF A06

A 32-bit serial integer multiplier was designed to investigate the yield and performance of complementary heterojunction FET (CHFET) technology. This is the largest reported CHFET logic circuit. The maximum operating frequency was 500 MHz. Very low power dissipation of 3 mW was obtained at 5 MHz operation. Single-event upset (SEU) characteristics of CHFET devices and latches were also measured and indicates the potential for SEU hard circuits for space and military applications. Author

N94-21095*# New Mexico Univ., Albuquerque. Biomedical Research.

NATURE'S CRUCIBLE: MANUFACTURING OPTICAL NONLINEARITIES FOR HIGH RESOLUTION, HIGH SENSITIVITY ENCODING IN THE COMPOUND EYE OF THE FLY, MUSCA DOMESTICA **c74**

Mike Wilcox *In its* The Fifth NASA Symposium on VLSI Design 1993 14 p (For primary document see N94-21079 05-33)

Avail: CASI HC A03/MF A06

The number of pixels per unit area sampling an image determines Nyquist resolution. Therefore, the highest pixel density is the goal. Unfortunately, as reduction in pixel size approaches the wavelength of light, sensitivity is lost and noise increases. Animals face the same problems and have achieved novel solutions. Emulating these solutions offers potentially unlimited sensitivity with detector size approaching the diffraction limit. Once an image is 'captured', cellular preprocessing of information allows extraction of high resolution information from the scene. Computer simulation of this system promises hyperacuity for machine vision.

Author (revised)

N94-21096*# New Mexico Univ., Albuquerque. Space Engineering Research Center.

PROTON RADIATION TESTING OF AN 18 BIT A/D CONVERTER **c60**

Donald C. Thelen and Don R. Wiseman *In its* The Fifth NASA Symposium on VLSI Design 9 p(SEE N94-21079 05-33) 1993 (For primary document see N94-21079 05-33)

Avail: CASI HC A02/MF A06

An 18-bit first order incremental analog to digital converter (ADC) has been constructed in a 2 mu commercial CMOS process. The ADC was exposed to energetic protons at the Harvard Cyclotron Laboratory to simulate latch-up and noise behavior in low earth orbits. Results of the test indicate no latch-up problems and only a small loss in accuracy while operating in proton radiation with energies similar to the South Atlantic Anomaly.

Author (revised)

N94-21097*# Idaho Univ., Moscow. Space Engineering Research Center.

USE OF SWITCHED CAPACITOR FILTERS TO IMPLEMENT THE DISCRETE WAVELET TRANSFORM

Kraig E. Kaiser and James N. Peterson *In* New Mexico Univ., The Fifth NASA Symposium on VLSI Design 1993 10 p (For primary document see N94-21079 05-33)

Avail: CASI HC A02/MF A06

This paper analyzes the use of IIR switched capacitor filters to implement the discrete wavelet transform and the inverse transform, using quadrature mirror filters (QMF) which have the necessary symmetry for reconstruction of the data. This is done by examining the sensitivity of the QMF transforms to the manufacturing variance in the desired capacitances. The performance is evaluated at the outputs of the separate filter stages and the error in the reconstruction of the inverse transform is compared with the desired results. Author (revised)

N94-21098*# Johns Hopkins Univ., Laurel, MD. Applied Physics Lab.

SILICON RETINA FOR OPTICAL TRACKING SYSTEMS **c74**

K. Strohbehn, R. E. Jenkins, X. Sun (Johns Hopkins Univ., Baltimore,

MD.), and A. G. Andreou (Johns Hopkins Univ., Baltimore, MD.) *In* New Mexico Univ., The Fifth NASA Symposium on VLSI Design 1993 12 p (For primary document see N94-21079 05-33)
Avail: CASI HC A03/MF A06

There are a host of position sensors, such as quadcells and CCD's, which are candidates for detecting optical position errors and providing error signals for a mirror positioning loop. We are developing a novel, very high bandwidth, biologically inspired position sensor for optical position tracking systems. We present recent test results and design issues for the use of biologically inspired silicon retinas for spaceborne optical position tracking systems. Author

N94-21099*# New Mexico Univ., Albuquerque. Dept. of Electrical and Computer Engineering.
ADAPTIVE ANALOG VIDEO SIGNAL CONDITIONER **c32**
Cheol-Ho Jeong, Brian Yu, Gregory Donohoe, and Robert Vitello *In its* The Fifth NASA Symposium on VLSI Design 1993 10 p (For primary document see N94-21079 05-33)
Avail: CASI HC A02/MF A06

This paper presents an adaptive analog video signal conditioner. This system supplements conventional irises and automatic gain controls to condition video signals for digitizing with a uniform analog-to-digital converter. Employing two degree of freedom, this circuit adjusts an analog gain and analog offset to increase the average information content of digitized images as defined by an entropy measure. The globally near-optimized implementation tracks smoothly to adapt to changing scene conditions. Author

N94-21100*# Nanyang Technological Inst. (Singapore). School of Applied Science.
VLSI MIXED SIGNAL PROCESSING SYSTEM **c32**
A. Alvarez and A. B. Premkumar *In* New Mexico Univ., The Fifth NASA Symposium on VLSI Design 1993 11 p (For primary document see N94-21079 05-33)
Avail: CASI HC A03/MF A06

An economical and efficient VLSI implementation of a mixed signal processing system (MSP) is presented in this paper. The MSP concept is investigated and the functional blocks of the proposed MSP are described. The requirements of each of the blocks are discussed in detail. A sample application using active acoustic cancellation technique is described to demonstrate the power of the MSP approach. Author (revised)

N94-21101*# Jet Propulsion Lab., California Inst. of Tech., Pasadena.
POWER OPTIMIZATION IN LOGIC ISOMERS **c60**
Ramesh Panwar (California Univ., Los Angeles.), David Rennels (California Univ., Los Angeles.), and Leon Alkalaj *In* New Mexico Univ., The Fifth NASA Symposium on VLSI Design 1993 11 p (For primary document see N94-21079 05-33)
(Contract N00014-91-J-1009)
Avail: CASI HC A03/MF A06

Logic isomers are labeled, 2-isomorphic graphs that implement the same logic function. Logic isomers may have significantly different power requirements even though they have the same number of transistors in the implementation. The power requirements of the isomers depend on the transition activity of the input signals. The power requirements of isomorphic graph isomers of n-input NAND and NOR gates are shown. Choosing the less power-consuming isomer instead of the others can yield significant power savings. Experimental results on a ripple-carry adder are presented to show that the implementation using the least power-consuming isomers requires approximately 10 percent less power than the implementation using the most power-consuming isomers. Simulations of other random logic designs also confirm that designs using less power-consuming isomers can reduce the logic power demand by approximately 10 percent as compared to designs using more power-consuming isomers. Author (revised)

N94-21102*# State Univ. of New York, Albany. Dept. of Computer Science.
COMPUTATION OF SIGNAL DELAYS IN RC NETWORKS **c32**
Juan Carlos Hidalgo, Paliath Narendran, and Seth Chaiken *In* New Mexico Univ., The Fifth NASA Symposium on VLSI Design 1993 11 p (For primary document see N94-21079 05-33)
Avail: CASI HC A03/MF A06

A model for signal delay computation in RC networks is presented. The strength of the paradigm is its generality and simplicity. The definition of delay is applicable to RC meshes with potential resistive attenuating paths to ground. The algorithms can also be applied to undriven circuits (static charge sharing) and circuits with initial charge. To compute the delays, each node in the network is explored locally to derive a system of sparse linear equations. The solutions of the system are delay values based on the Elmore time constant at each point in the circuit. Author (revised)

N94-21103*# Hewlett-Packard Co., Corvallis, OR. Integrated Circuit Business Div.
DELAY ANALYSIS OF COMBINATIONS OF PASS TRANSISTORS AND CLASSICAL LOGIC GATES
Jonathan S. Gibson *In* New Mexico Univ., The Fifth NASA Symposium on VLSI Design 1993 11 p (For primary document see N94-21079 05-33)
Avail: CASI HC A03/MF A06

Combinations of pass transistors and logic gates driving nonlinear capacitive loads are analyzed for the presence of characteristics that will permit easier and more accurate digital logic simulation. Accurate time delay models are developed by studying the nature of the response of simplified circuit models to variations of input waveform rise and fall times and output loading. The nonlinear effects of the CMOS logic devices are minimized to permit easier interpretation of the influence of nonlinear capacitive loads. The performance of a CMOS inverter with a complex nonlinear load consisting of a pass transistor that separates a range of capacitances is compared to the same inverter circuit with a linear capacitive load to develop an understanding of the unique requirements of modeling a nonlinear system. Several methods of modeling the delay of CMOS circuits are reviewed, and a multi-parameter linear model is described. General guidelines for designing CMOS circuits with complex load circuits are developed, emphasizing that the circuit output rise delays and fall delays must be separately analyzed. Author

N94-21104*# Jet Propulsion Lab., California Inst. of Tech., Pasadena.
MIXED VOLTAGE VLSI DESIGN
Ramesh Panwar (California Univ., Los Angeles.), David Rennels (California Univ., Los Angeles.), and Leon Alkalaj *In* New Mexico Univ., The Fifth NASA Symposium on VLSI Design 1993 12 p (For primary document see N94-21079 05-33)
(Contract N00014-91-J-1009)
Avail: CASI HC A03/MF A06

A technique for minimizing the power dissipated in a Very Large Scale Integration (VLSI) chip by lowering the operating voltage without any significant penalty in the chip throughput even though low voltage operation results in slower circuits. Since the overall throughput of a VLSI chip depends on the speed of the critical path(s) in the chip, it may be possible to sustain the throughput rates attained at higher voltages by operating the circuits in the critical path(s) with a high voltage while operating the other circuits with a lower voltage to minimize the power dissipation. The interface between the gates which operate at different voltages is crucial for low power dissipation since the interface may possibly have high static current dissipation thus negating the gains of the low voltage operation. The design of a voltage level translator which does the interface between the low voltage and high voltage circuits without any significant static dissipation is presented. Then, the results of the mixed voltage design using a greedy algorithm on three chips for various operating voltages are presented. Author (revised)

N94-21105*# Colorado State Univ., Fort Collins. Dept. of Electrical Engineering.
BRIDGING FAULTS IN BiCMOS CIRCUITS
Sankaran M. Menon, Yashwant K. Malaiya, and Anura P. Jayasumana *In* New Mexico Univ., The Fifth NASA Symposium on VLSI Design 1993 10 p Sponsored by Strategic Defense Initiative Organization (For primary document see N94-21079 05-33)
Avail: CASI HC A02/MF A06

Combining the advantages of CMOS and bipolar, BiCMOS is emerging as a major technology for many high performance digital and mixed signal applications. Recent investigations revealed that bridging faults can be a

major failure mode in IC's. Effects of bridging faults in BiCMOS circuits are presented. Bridging faults between logical units without feedback and logical units with feedback are considered. Several bridging faults can be detected by monitoring the power supply current (I(sub DDQ) monitoring). Effects of bridging faults and bridging resistance on output logic levels were examined along with their effects on noise immunity. Author (revised)

N94-21106*# New Mexico State Univ., Las Cruces. Dept. of Engineering Technology.

FAULT DETECTION IN DIGITAL AND ANALOG CIRCUITS USING AN I(DD) TEMPORAL ANALYSIS TECHNIQUE

J. Beasley, D. Magallanes, A. Vridhagiri, Hema Ramamurthy, and Mark DeYong (Intelligent Reasoning Systems, Inc., Las Cruces, NM.) *In* New Mexico Univ., The Fifth NASA Symposium on VLSI Design 1993 9 p (For primary document see N94-21079 05-33)

(Grant NSF HRD-92-53013)

Avail: CASI HC A02/MF A06

An i(sub DD) temporal analysis technique which is used to detect defects (faults) and fabrication variations in both digital and analog IC's by pulsing the power supply rails and analyzing the temporal data obtained from the resulting transient rail currents is presented. A simple bias voltage is required for all the inputs, to excite the defects. Data from hardware tests supporting this technique are presented. Author (revised)

N94-21107*# Allied-Signal Corp., Olathe, KS. General Aviation Avionics.

TEST PATTERN GENERATION FOR ILA SEQUENTIAL CIRCUITS

Yu Feng, James F. Frenzel (Idaho Univ., Moscow.), and Gary K. Maki (New Mexico Univ., Albuquerque.) *In* New Mexico Univ., The Fifth NASA Symposium on VLSI Design 1993 10 p (For primary document see N94-21079 05-33)

(Grant NAGw-3293)

Avail: CASI HC A02/MF A06

An efficient method of generating test patterns for sequential machines implemented using one-dimensional, unilateral, iterative logic arrays (ILA's) of BTS pass transistor networks is presented. Based on a transistor level fault model, the method affords a unique opportunity for real-time fault detection with improved fault coverage. The resulting test sets are shown to be equivalent to those obtained using conventional gate level models, thus eliminating the need for additional test patterns. The proposed method advances the simplicity and ease of the test pattern generation for a special class of sequential circuitry. Author (revised)

N94-21108*# Colorado State Univ., Fort Collins. Dept. of Electrical Engineering.

FAULTY BEHAVIOR OF ASYNCHRONOUS STORAGE ELEMENTS

Waleed K. Al-Assadi, Ding Lu, Anura P. Jayasumana, Yashwant K. Malaiya, and Carol Q. Tong *In* New Mexico Univ., The Fifth NASA Symposium on VLSI Design 1993 9 p Sponsored in part by Strategic Defense Initiative Organization (For primary document see N94-21079 05-33)

Avail: CASI HC A02/MF A06

It is often assumed that the faults in storage elements (SE's) can be modeled as output/input stuck-at-faults of the element. They are implicitly considered equivalent to the stuck-at faults in the combinational logic surrounding the SE cells. A more accurate higher level fault model for elementary SE's used in asynchronous circuits is presented. This model offers better representation of the physical failures. It is shown that the stuck-at model may be adequate if only modest fault coverage is desired. The enhanced model includes some common fault behaviors of SE's that are not covered by the stuck-at model. These include data-feed-through behaviors that cause the SE to be combinational. Fault models for complex SE cells can be obtained without a significant loss of information about the structure of the circuit. Author (revised)

N94-21109*# Utah Univ., Salt Lake City. Dept. of Computer Science.

TESTING SELF-TIMED CIRCUITS USING SCAN PATHS

Ajay Khoche and Erik L. Brunvand *In* New Mexico Univ., The Fifth NASA Symposium on VLSI Design 1993 11 p (For primary document see N94-21079 05-33)

Avail: CASI HC A03/MF A06

Testing is an essential part of any digital system design and one that can be made much easier if testing is considered during the design process rather than after the system is complete. There are a number of techniques for integrating testability into system design, but many of these traditional testing methods used for synchronous circuits are not directly applicable to non-clocked asynchronous circuits. As a result, many asynchronous circuits do not employ design for testability techniques. A method of using the familiar model of scan paths modified to test self-timed systems are presented. Specifically, circuits designed using a library of self-timed modules to assemble systems with two-phase transition control and bundled data paths are considered. The method involves modifying these self-timed modules such that circuits designed from them have a built-in scan path. Author (revised)

N94-21110*# Idaho Univ., Moscow. Dept. of Electrical Engineering.

DETECTION OF CMOS BRIDGING FAULTS USING MINIMAL STUCK-AT FAULT TEST SETS

Nabeel Ijaz and James F. Frenzel *In* New Mexico Univ., The Fifth NASA Symposium on VLSI Design 1993 10 p (For primary document see N94-21079 05-33)

Avail: CASI HC A02/MF A06

The performance of minimal stuck-at fault test sets at detecting bridging faults are evaluated. New functional models of circuit primitives are presented which allow accurate representation of bridging faults under switch-level simulation. The effectiveness of the patterns is evaluated using both voltage and current testing. Author (revised)

N94-21111*# Utah Univ., Salt Lake City. Dept. of Computer Science.

ROBUST NEURAL CLASSIFIER CIRCUITS USING ASYNCHRONOUS DESIGN

John F. Hurdle, Peter R. Conwell, and Erik L. Brunvand *In* New Mexico Univ., The Fifth NASA Symposium on VLSI Design 1993 11 p (For primary document see N94-21079 05-33)

Avail: CASI HC A03/MF A06

Aerospace neural circuits must be adaptive, offer a practical size-performance ratio, and be environmentally robust. Our approach to building such circuits combines asynchronous design with a new fuzzy/neural classifier model. Asynchronous circuits offer many design advantages for neural hardware and our hybrid fuzzy/neural model, using mainly min and max operators, promises a low circuit complexity. The general approach is described and a description of a use of rule-induction to further reduce circuit complexity is described. Author (revised)

N94-21112*# Idaho Univ., Moscow. Dept. of Electrical Engineering.

ACCELERATION-AUGMENTED LQG CONTROL OF AN ACTIVE MAGNETIC BEARING **c37**

Joseph J. Feeley *In* New Mexico Univ., The Fifth NASA Symposium on VLSI Design 1993 6 p (For primary document see N94-21079 05-33)

Avail: CASI HC A02/MF A06

A linear-quadratic-gaussian (LQG) regulator controller design for an acceleration-augmented active magnetic bearing (AMB) is outlined. Acceleration augmentation is a key feature in providing improved dynamic performance of the controller. The optimal control formulation provides a convenient method of trading-off fast transient response and force attenuation as control objectives. Author (revised)

N94-21113*# International Business Machines Corp., Research Triangle Park, NC.

MULTIPLE-FOLD CLUSTERED PROCESSOR MESH ARRAY

Gerald G. Pechanek, Stamatis Vassiliadis (International Business Machines Corp., Endicott, NY.), and Jose G. Delgado (State Univ. of New York, Binghamton.) *In* New Mexico Univ., The Fifth NASA Symposium on VLSI Design 1993 11 p (For primary document see N94-21079 05-33)

Avail: CASI HC A03/MF A06

The multiple-fold clustered processor mesh array is a triangular organization of clustered processing elements. This multiple-fold array maintains functional equivalence to the nearest neighbor mesh computer with uni-directional interprocessor communications, but with half the number of connection wires. In addition, the connectivity of the multiple-folded organization is superior to the standard square mesh due to the improved connectivity between the clustered processors. One of the primary application areas targeted is High Performance Architectures for image processing. Author

N94-21114*# University of Southern Illinois, Carbondale. Dept. of Electrical Engineering.
PRACTICAL ISSUES IN IMPLEMENTING ROVING SPARES IN VLSI SYSTOLIC ARRAYS
Rajendra Bandekar and Amitava Majumdar *In* New Mexico Univ., The Fifth NASA Symposium on VLSI Design 1993 12 p (For primary document see N94-21079 05-33)
Avail: CASI HC A03/MF A06

In this paper we address several unsolved problems in implementing roving spares as a methodology for on-line testing and reconfiguration of systolic arrays. An algorithm for distinguishing between permanent faults and intermittent/transient faults is proposed. A methodology for determining different parameter values for this algorithm is presented. Results characterizing an optimal switching structure are presented. A judicious partitioning of information (for distributed and central processing) allows design of simple switch controllers for implementing roving spares operation as well as reconfiguration in the presence of failures. Testability and self-checking capability is incorporated into these controllers using a few extra gates. Author (revised)

N94-21115*# Sri Venkateswara Univ., Tirupati (India). Dept. of Computer Science and Engineering.
A NOVEL VLSI PROCESSOR ARCHITECTURE FOR SUPERCOMPUTING ARRAYS **c60**
N. Venkateswaran, S. Pattabiraman, R. Devanathan, Ashaf Ahmed, S. Venkataraman, and N. Ganesh *In* New Mexico Univ., The Fifth NASA Symposium on VLSI Design 1993 11 p (For primary document see N94-21079 05-33)
Avail: CASI HC A03/MF A06

Design of the processor element for general purpose massively parallel supercomputing arrays is highly complex and cost ineffective. To overcome this, the architecture and organization of the functional units of the processor element should be such as to suit the diverse computational structures and simplify mapping of complex communication structures of different classes of algorithms. This demands that the computation and communication structures of different class of algorithms be unified. While unifying the different communication structures is a difficult process, analysis of a wide class of algorithms reveals that their computation structures can be expressed in terms of basic IP,IP,OP,CM,R,SM, and MAA operations. The execution of these operations is unified on the PAcube macro-cell array. Based on this PAcube macro-cell array, we present a novel processor element called the GIPOP processor, which has dedicated functional units to perform the above operations. The architecture and organization of these functional units are such to satisfy the two important criteria mentioned above. The structure of the macro-cell and the unification process has led to a very regular and simpler design of the GIPOP processor. The production cost of the GIPOP processor is drastically reduced as it is designed on high performance mask programmable PAcube arrays. Author (revised)

N94-21116*# Toledo Univ., OH. Dept. of Electrical Engineering.
SYNTHESIS ALGORITHM OF VLSI MULTIPLIERS FOR ASIC **c61**
O. H. Chua and A. G. Eldin *In* New Mexico Univ., The Fifth NASA Symposium on VLSI Design 1993 13 p (For primary document see N94-21079 05-33)
Avail: CASI HC A03/MF A06

Multipliers are critical sub-blocks in ASIC design, especially for digital signal processing and communications applications. A flexible multiplier synthesis tool is developed which is capable of generating multiplier blocks for word size in the range of 4 to 256 bits. A comparison of existing multiplier algorithms is made in terms of speed, silicon area, and suitability for automated synthesis and verification of its VLSI implementation. The algorithm divides the range of supported word sizes into sub-ranges and provides each sub-range with a specific multiplier architecture for optimal speed and area. The algorithm of the synthesis tool and the multiplier architectures are presented. Circuit implementation and the automated synthesis methodology are discussed. Author (revised)

N94-21117*# Brigham Young Univ., Provo, UT. Dept. of Electrical and Computer Engineering.
DESIGN AND IMPLEMENTATION OF GaAs HBT CIRCUITS WITH ACME
Brad L. Hutchings and Tony M. Carter (Utah Univ., Salt Lake City.) *In* New Mexico Univ., The Fifth NASA Symposium on VLSI Design 1993 10 p Sponsored by DARPA (For primary document see N94-21079 05-33)
Avail: CASI HC A02/MF A06

GaAs HBT circuits offer high performance (5-20 GHz) and radiation hardness (500 Mrad) that is attractive for space applications. ACME is a CAD tool specifically developed for HBT circuits. ACME implements a novel physical schematic-capture design technique where designers simultaneously view the structure and physical organization of a circuit. ACME's design interface is similar to schematic capture; however, unlike conventional schematic capture, designers can directly control the physical placement of both function and interconnect at the schematic level. In addition, ACME provides design-time parasitic extraction, complex wire models, and extensions to Multi-Chip Modules (MCM's). A GaAs HBT gate-array and semi-custom circuits have been developed with ACME; several circuits have been fabricated and found to be fully functional . Author (revised)

N94-21118*# Colorado Univ., Boulder. Dept. of Electrical and Computer Engineering.
EXPERIMENTS ON TECHNOLOGY MAPPING USING DIFFERENT CELL LIBRARIES
Enrico Macii (Politecnico di Torino, Italy.) and Massimo Poncino (Politecnico di Torino, Italy.) *In* New Mexico Univ., The Fifth NASA Symposium on VLSI Design 1993 9 p (For primary document see N94-21079 05-33)
Avail: CASI HC A02/MF A06

Technology mapping is one of the major steps in the synthesis process of integrated circuits. Efficient algorithms have been proposed in the recent past to optimize the number of cells required to implement a given design, but not enough effort has been spent in studying the relationship between the quality of the circuit produced by the logic synthesis tool and the cell library used to perform the mapping. In this paper we present experiments on technology mapping that show how the design of the cell library can influence the area and the delay of the synthesized circuit. Author

N94-21119*# Utah Univ., Salt Lake City. Dept. of Computer Science.
RELIABLE INTERFACE DESIGN FOR COMBINING ASYNCHRONOUS AND SYNCHRONOUS CIRCUITS
Lueli Josephson, Erik L. Brunvand, Ganesh Gopalakrishan, and John F. Hurdle *In* New Mexico Univ., The Fifth NASA Symposium on VLSI Design 1993 11 p (For primary document see N94-21079 05-33)
Avail: CASI HC A03/MF A06

In order to successfully integrate asynchronous and synchronous designs, great care must be taken at the interface between the two types of systems. Synchronizing asynchronous inputs with a free running clock can cause well-known problems with metastability in the synchronization circuits. Stretchable clocks allow a clock cycle to expand dynamically in response to the metastability effects of sampling asynchronous inputs. We use an interface organization where the special circuitry for detecting metastability and for stretching the clock that is delivered to the synchronous part of the system is encapsulated in a Q-flop-based interface. This provides a very convenient method for interfacing mixed systems, as the interface and clock generation circuitry are isolated into one special module, and neither the asynchronous nor the synchronous system need be modified internally to accommodate the interface. This is especially important when standard synchronous components are used as there is no opportunity to modify these parts. We show that this interface module is suitable for most mixed design needs and conclude with an example. Author

N94-21120*# Idaho Univ., Moscow. Dept. of Electrical Engineering.
DESIGN METHODS FOR FAULT-TOLERANT FINITE STATE MACHINES
Shailesh Niranjan and James F. Frenzel *In* New Mexico Univ., The Fifth NASA Symposium on VLSI Design 1993 10 p (For primary document see N94-21079 05-33)
Avail: CASI HC A02/MF A06

VLSI electronic circuits are increasingly being used in space-borne applications where high levels of radiation may induce faults, known as single event upsets. In this paper we review the classical methods of designing fault tolerant digital systems, with an emphasis on those methods which are particularly suitable for VLSI-implementation of finite state machines. Four methods are presented and will be compared in terms of

design complexity, circuit size, and estimated circuit delay.
Author (revised)

N94-21121*# Grand Valley State Coll., Allendale, MI. School of Engineering.
LOW-LATENCY DIGITAL FREQUENCY SYNTHESIZER USING THE RESIDUE NUMBER SYSTEM
William A. Chren, Jr. *In* New Mexico Univ., The Fifth NASA Symposium on VLSI Design 1993 10 p (For primary document see N94-21079 05-33)
Avail: CASI HC A02/MF A06

A low-latency frequency synthesizer using the Direct Digital Synthesis (DDS) technique has been designed. Called the Residue Assisted Frequency Synthesizer (RAFS), it exhibits frequency switching times which are reduced by more than 50 percent below previously published designs. The switching speed advantage is made possible by the use of the Residue Number System, which allows the pipeline lengths in the Phase Accumulator and other circuitry to be reduced significantly. Author

N94-21122*# Idaho Univ., Moscow. Dept. of Electrical Engineering.
USING CROSSCORRELATION TECHNIQUES TO DETERMINE THE IMPULSE RESPONSE OF LINEAR SYSTEMS
Michael J. Dallabetta, Harry W. Li, and Howard B. Demuth *In* New Mexico Univ., The Fifth NASA Symposium on VLSI Design 1993 10 p (For primary document see N94-21079 05-33)
(Grant NAGw-1406)
Avail: CASI HC A02/MF A06

A crosscorrelation method of measuring the impulse response of linear systems is presented. The technique, implementation, and limitations of this method are discussed. A simple system is designed and built using discrete components and the impulse response of a 'inear circuit is measured. Theoretical and software simulation results are presented.
Author (revised)

N94-21123*# Toledo Univ., OH. Dept. of Electrical Engineering.
AUTOMATED SYNTHESIS AND VERIFICATION OF CONFIGURABLE DRAM BLOCKS FOR ASIC'S
M. Pakkurti, A. G. Eldin, S. C. Kwatra, and M. Jamali *In* New Mexico Univ., The Fifth NASA Symposium on VLSI Design 1993 9 p (For primary document see N94-21079 05-33)
(Grant NAG3-799)
Avail: CASI HC A02/MF A06

A highly flexible embedded DRAM compiler is developed which can generate DRAM blocks in the range of 256 bits to 256 Kbits. The compiler is capable of automatically verifying the functionality of the generated DRAM modules. The fully automated verification capability is a key feature that ensures the reliability of the generated blocks. The compiler's architecture, algorithms, verification techniques and the implementation methodology are presented. Author

N94-21124*# Brigham Young Univ., Provo, UT. Lab. for Applied Logic.
CORRECTNESS PROPERTIES FOR ITERATED HARDWARE STRUCTURES
Phillip J. Windley *In* New Mexico Univ., The Fifth NASA Symposium on VLSI Design 1993 8 p (For primary document see N94-21079 05-33)
Avail: CASI HC A02/MF A06

Iterated structures occur frequently in hardware. This paper describes properties required of mathematical relations that can be implemented iteratively and demonstrates the use of these properties on a generalized class of adders. This work provides a theoretical basis for the correct synthesis of iterated arithmetic structures. Author

N94-21125*# New Mexico Univ., Albuquerque. Engineering Research Center.
PARTITION ALGEBRAIC DESIGN OF ASYNCHRONOUS SEQUENTIAL CIRCUITS
Gary K. Maki, Kristen Q. Chen, and Suresh K. Gopalakrishnan (Hewlett-Packard Co., Palo Alto, CA.) *In its* The Fifth NASA Symposium on VLSI Design 1993 13 p (For primary document see N94-21079 05-33)
Avail: CASI HC A03/MF A06

Tracey's Theorem has long been recognized as essential in generating state assignments for asynchronous sequential circuits. This paper shows that partitioning variables derived from Tracey's Theorem also has a significant impact in generating the design equations. Moreover, this theorem is important to the fundamental understanding of asynchronous sequential operation. The results of this work simplify asynchronous logic design. Moreover, detection of safe circuits is made easier. Author

N94-21126*# Boeing Defense and Space Group, Seattle, WA.
AUTOMATED RADIATION HARD ASIC DESIGN TOOL
Mike White, Bill Bartholet, and Mark Baze *In* New Mexico Univ., The Fifth NASA Symposium on VLSI Design 1993 8 p (For primary document see N94-21079 05-33)
Avail: CASI HC A02/MF A06

A commercial based, foundry independent, compiler design tool (ChipCrafter) with custom radiation hardened library cells is described. A unique analysis approach allows low hardness risk for Application Specific IC's (ASIC's). Accomplishments, radiation test results, and applications are described. Author

N94-21127*# Sri Venkateswara Univ., Tirupati (India). Dept. of Computer Science.
A UNIFIED APPROACH TO VLSI LAYOUT AUTOMATION AND ALGORITHM MAPPING ON PROCESSOR ARRAYS
N. Venkateswaran, S. Pattabiraman, and Vinoo N. Srinivasan *In* New Mexico Univ., The Fifth NASA Symposium on VLSI Design 1993 16 p (For primary document see N94-21079 05-33)
Avail: CASI HC A03/MF A06

Development of software tools for designing supercomputing systems is highly complex and cost ineffective. To tackle this a special purpose PAcube silicon compiler which integrates different design levels from cell to processor arrays has been proposed. As a part of this, we present in this paper a novel methodology which unifies the problems of Layout Automation and Algorithm Mapping. Author

N94-21128*# National Aeronautics and Space Administration. Goddard Space Flight Center, Greenbelt, MD.
A FIXED/VARIABLE BIT-RATE DATA COMPRESSION ARCHITECTURE **c60**
Gregary C. Zweigle (Advanced Hardware Architectures, Moscow, ID.), Jack Venbrux (New Mexico Univ., Albuquerque.), and Pen-Shu Yeh *In* New Mexico Univ., The Fifth NASA Symposium on VLSI Design 1993 9 p (For primary document see N94-21079 05-33)
(Grant NAGw-3292)
Avail: CASI HC A02/MF A06

A VLSI architecture for an adaptive data compression encoder capable of sustaining fixed or variable bit-rate output has been developed. There are three modes of operation: lossless with variable bit-rate, lossy with fixed bit-rate and lossy with variable bit-rate. For lossless encoding, the implementation is identical to the USES chip designed for Landsat 7. Obtaining a fixed bit-rate is achieved with a lossy DPCM algorithm using adaptive, nonuniform scalar quantization. In lossy mode, variable bit-rate coding uses the lossless sections of the encoder for post-DPCM entropy coding. The encoder shows excellent compression performance in comparison to other current data compression techniques. No external tables or memory are required for operation. Author

N94-21129*# Idaho Univ., Moscow. Microelectronics Research Center.
A CAM-BASED LZ DATA COMPRESSION IC **c61**
K. Winters, R. Bode (Advanced Hardware Architectures, Moscow, ID.), and E. Schneider (Video Lottery Consultants, Inc., Bozeman, MT.) *In* New Mexico Univ., The Fifth NASA Symposium on VLSI design 1993 8 p (For primary document see N94-21079 05-33)
Avail: CASI HC A02/MF A06

A custom CMOS processor is introduced that implements the Data Compression Lempel-Ziv (DCLZ) standard, a variation of the LZ2 Algorithm. This component presently achieves a sustained compression and decompression rate of 10 megabytes/second by employing an on-chip content-addressable memory for string table storage. Author

N94-21130*# New Mexico State Univ., Las Cruces. Center for Space Telemetering and Telecommunications Systems.
HIGH-SPEED VITERBI DECODING WITH OVERLAPPING CODE SEQUENCES **c61**
Michael D. Ross and William P. Osborne *In* New Mexico Univ., The Fifth NASA Symposium on VLSI Design 1993 8 p (For primary document see N94-21079 05-33)
Avail: CASI HC A02/MF A06

The Viterbi Algorithm for decoding convolutional codes and Trellis Coded Modulation is suited to VLSI implementation but contains a feedback loop which limits the speed of pipelined architecture. The feedback loop is circumvented by decoding independent sequences simultaneously, resulting in a 5-9 fold speed-up with a two-fold hardware expansion. Author

N94-21131*# New Mexico Univ., Albuquerque. Space Engineering Research Center.
ARITHMETIC IN LARGE GF(2(EXP n))
Kelly Cameron *In its* The Fifth NASA Symposium on VLSI Design 1993 11 p (For primary document see N94-21079 05-33)
Avail: CASI HC A03/MF A06

The decoding of Reed Solomon (BCH) codes usually requires large numbers of calculations using GF(2(exp n)) arithmetic. Though efficient algorithms and corresponding circuits for performing basic Galois field arithmetic are known, many of these techniques either become very slow or else require an inordinate amount of circuitry to implement when the size of the Galois field becomes much larger than GF(2(exp 8)). Consequently, most currently available Reed-Solomon decoders are built using small fields, such as GF(2(exp 8)) or GF(2(exp 10)), even though significant coding efficiencies could often be obtained if larger symbol sizes, such as GF(2(exp 16)) or GF(2(exp 32)), were used. Algorithms for performing the basic arithmetic required to decode Reed-Solomon codes have been developed explicitly for use in these large fields. They are discussed in detail. Author

N94-21132*# Sri Venkateswara Univ., Tirupati (India). Dept. of Computer Science and Engineering.
A COST-EFFECTIVE METHODOLOGY FOR THE DESIGN OF MASSIVELY-PARALLEL VLSI FUNCTIONAL UNITS **c62**
N. Venkateswaran, G. Sriram, and J. Desouza *In* New Mexico Univ., The Fifth NASA Symposium on VLSI Design 1993 16 p (For primary document see N94-21079 05-33)
Avail: CASI HC A03/MF A06

In this paper we propose a generalized methodology for the design of cost-effective massively-parallel VLSI Functional Units. This methodology is based on a technique of generating and reducing a massive bit-array on the mask-programmable PAcube VLSI array. This methodology unifies (maintains identical data flow and control) the execution of complex arithmetic functions on PAcube arrays. It is highly regular, expandable and uniform with respect to problem-size and wordlength, thereby reducing the communication complexity. The memory-functional unit interface is regular and expandable. Using this technique functional units of dedicated processors can be mask-programmed on the naked PAcube arrays, reducing the turn-around time. The production cost of such dedicated processors can be drastically reduced since the naked PAcube arrays can be mass-produced. Analysis of the the performance of functional units designed by our method yields promising results. Author

N94-21133*# Idaho Univ., Moscow. Dept. of Electrical Engineering.
BEHAVIORAL MODEL SIMULATION STUDIES OF AN IMAGE COMPRESSOR Thesis **c60**
Navid Madani and Sterling Whitaker *In* New Mexico Univ., The Fifth NASA Symposium on VLSI Design 1993 8 p (For primary document see N94-21079 05-33)
Avail: CASI HC A02/MF A06

The high initial cost of prototype Very Large Scaled Integrated (VLSI) parts requires that sufficient verifications be made to eliminate design errors before actually producing the prototypes. Logic simulation is the means by which the VLSI engineer can ensure that the design will function properly. The computer time required for logic simulation can be reduced through the use of behavioral models. Behavioral models, however, require time to write and verify and they do not always produce a dramatic speed up in logic simulation time. This paper presents a study of behavioral modeling aimed at discovering which circuit types benefit most from the use of behavioral models for logic simulation. Author

N94-21178 Communications Satellite Corp., Clarksburg, MD.
NON-DESTRUCTIVE SEMICONDUCTOR WAFER PROBING SYSTEM USING LASER PULSES TO GENERATE AND DETECT MILLIMETER-WAVE SIGNALS Patent Application
Thane Smith, inventor (to Communications Satellite Corp.), Ho-Chung Huang, inventor (to Communications Satellite Corp.) (Radio Corp. of America, Bethesda, MD.), and Chi H. Lee, inventor (to Communications Satellite Corp.) (Maryland Univ., College Park.) 10 Jan. 1992 54 p
(CA-Patent-Appl-SN-2,020,733; Int-Patent-Class-G01R-31/28; CTN-93-60667) Copyright Avail: Micromedia Ltd., Technical Information Centre, 165 Hotel de Ville, Place du Portage, Phase 2, Hull, Quebec J8X 3X2, Canada HC/MF

Monolithic microwave integrated circuits (MMIC's) are currently being developed for such applications as satellite communications, radar, and phased array systems. The conventional frequency domain approach for testing MMIC's is difficult and costly. A system is provided for nondestructive probing of MMIC's which overcomes the disadvantages of high cost and inconvenience of the prior art. According to the invention, both the electrical signal provided to the device under test and the sampling of that signal are performed using optical switching. In a preferred embodiment, optical pulses for triggering the input electrical signal and for use as sampling pulses are all derived from a single laser pulse via suitable beam splitters and adjustable delays. A set of samples at one value of delay between the input signal and each of the sample points is taken, and then the delays are adjusted for a further set of samples. This is repeated until enough samples are taken to completely reconstruct the signal waveform, and then a Fourier transform algorithm is used on the time domain waveforms to obtain amplitude and phase as a function of frequency. Author (CISTI)

N94-21221# Honeywell, Inc., Phoenix, AZ. Systems and Research Center.
MINIATURE COLOR DISPLAY, PHASE 4 Final Report, 1 Oct. 1992 - 31 May 1993
Henry Franklin May 1993 41 p
(Contract F33615-91-C-0534)
(AD-A272920; AL/CF-SR-1993-0009-Phase-4) Avail: CASI HC A03/MF A01

A 400 x 300-pixel miniature color display with a resolution of 300 pixels/inch, yielding a 1.3 x 1.0-inch active area, has been demonstrated for helmet-mount applications. The display uses active-matrix subtractive-crystal technology. This approach produces high luminance and full color at each pixel without the loss in addressable resolution that is associated with conventional additive-color displays. A stack of three active-matrix twisted-nematic liquid-crystal light valves, sandwiching cyan, magenta, and yellow color polarizers, is used to generate full color. By spectral tuning of the xenon arc-lamp backlight and the color polarizers, a color gamut comparable to that of a shadowmask color CRT is achieved. Four bits of grayscale are provided for each of the three color primaries, yielding a total availability of 4096 colors. The display produces a peak white luminance of 3500 fL and has an inherent (i.e., dark-field) contrast ratio of 50:1. The preceding figures are sufficient to achieve a 2:1 contrast ratio against a 10,000 fL ambient scene, using typical helmet-mounted display optics. The display refresh rate is 68 Hz. DTIC

N94-21229# California Univ., San Diego, La Jolla. Dept. of Electrical and Computer Engineering.
SYNTHESIS AND PROPERTIES OF MISMATCHED HETEROJUNCTION/SUBSTRATE INTERFACES Final Report, 27 Aug. 1991 - 16 Aug. 1993
H. H. Winder 8 Nov. 1993 35 p
(Contract N00014-91-K-2019)
(AD-A272904) Avail: CASI HC A03/MF A01

This report describes work performed at the University of California, San Diego, on the synthesis and characterization of molecular beam epitaxially-grown heterostructures of In(x)Ga(1-x)As and In(y)Al(1-y)As grown on GaAs substrates using a compositionally step-graded buffer layer which relaxes the mismatch strain between them by more than 90%. The electrical and the galvanomagnetic properties of the two dimensional electron gas

produced by modulation doping in such heterojunctions are related to the strain relaxation of the buffer, the impurity doping density, alloy scattering as a function of composition, and dislocation scattering at the heterojunction interfaces. DTIC

N94-21256# Illinois Univ., Urbana. Coordinated Science Lab.
VLSI DESIGN FOR RELIABILITY-HOT CARRIER EFFECTS Final Report, Jun. 1991 - Jun. 1992
S. Kang, I. Hajj, Y. Leblebici, C. Diaz, and P. Li Apr. 1993 74 p
(Contract F30602-91-C-0053)
(AD-A271586; RL-TR-93-25) Avail: CASI HC A04/MF A01

The accomplishments during the contract period (28 Jun. 1991 to 27 Jun. 1992) on the computer aided analysis of CMOS device and circuit degradation due to hot-carrier effects are described. The task involved four subtasks: (1) simulation of gate oxide degradation during long-term circuit operation; (2) determination of overall circuit performance after hot-electron stress; (3) probabilistic timing approach to hot-carrier-effect estimation; and (4) parametric macromodeling of hot-carrier-induced degradation in MOS VLSI circuits. The first two parts are continued subtasks while the latter two are new subtasks. In order to simulate the reliability of MOS circuits, both the detailed model and the macromodel are used; the detailed model is used for accurate analysis of small circuits and the macromodel is used for very large circuits for computational efficiency. Since the hot-carrier-induced aging of MOS circuits is input-pattern dependent, an important task is to develop a computationally efficient probabilistic timing approach to hot-carrier-effect estimation without resorting to the Monte Carlo simulation. A new probabilistic approach that accounts for cumulative effects of all input waveform combinations in a single run was developed. DTIC

N94-21257# North Carolina State Univ., Raleigh. Precision Engineering Center.
LONG RANGE FAST TOOL SERVO Final Report, 1 Jun. 1992 - 31 May 1993
G. M. Moorefield, II, Thomas A. Dow, Karl J. Falter, and Paul I. Ro 31 May 1993 19 p
(Contract N00014-92-J-4082)
(AD-A271614) Avail: CASI HC A03/MF A01

The PEC's MAC 100 Fast Tool Servo (FTS) System has demonstrated the efficacy of fabricating off-axis parabolic segments on axis by utilizing a fast tool motion to machine non-rotationally symmetric surfaces. The key to this technique was a servo for the tool motion that had a high-bandwidth coupled with a small range of motion. The Keck telescope, with its thirty-six (36) 1-meter diameter segments, would have been an excellent application for this technology. Since this technology was not available at the time of construction, each mirror segment was fabricated to its desired shape by loading it to a specified deformed shape and polishing it to a spherical contour, then removing the bending loads to allow the segment to relax to the desired asymmetric shape. If the segments of this optic had been constructed on axis with an FTS, the fabrication of the most extreme segment would have required only about 200 micrometers of non-rotational symmetry. However, the demand for larger displacement actuators is being driven by new applications with nonrotationally symmetric components in the millimeter range. This report describes the search for a suitable actuator for a long range fast tool servo system that would allow the fabrication of non-rotationally symmetric optical surfaces with a 1 mm range of servo motion. To allow cost-effective machining of these surfaces, the actuator must also possess a 50 Hz bandwidth (minimum) and 25 nanometer resolution. DTIC

N94-21275 Department of the Navy, Washington, DC.
WIRE ASSEMBLY FOR ELECTRICALLY CONDUCTIVE CIRCUITS Patent
Walter T. Schneider, inventor (to Navy) 5 Oct. 1993 4 p Filed 10 Apr. 1992 Supersedes AD-D015535
(AD-D015966; US-Patent-5,250,753; US-Patent-Appl-SN-866921; US-Patent-Class-174-36) Avail: US Patent and Trademark Office

A wire assembly for electrically conductive circuits is described. The wire assembly consists of the assembly comprising a circuit conductor wire having a coating of insulative material thereon, a shielding foil wrapped at least partially around the coating and having a leg portion extending outwardly from the coating, a shield conductor wire fixed to the shielding foil, and an insulative outer layer enclosing the shielding foil and the shield conductor wire. DTIC

N94-21282# Carnegie-Mellon Univ., Pittsburgh, PA. Dept. of Computer Science.
CMU VERY FAST RANGE-IMAGING SYSTEM
Shigeyuki Tada, Andrew Gruss, and Takeo Kanade 10 Oct. 1993 40 p
(Grants NSF MIP-89-15969; NSF MIP-90-47590; ARPA Order 7511)
(AD-A272057; CMU-CS-93-179) Avail: CASI HC A03/MF A01

We present a high-speed range-imaging system based on a VLSI computational sensor developed in the CMU Computer Science Department. The VLSI range sensor is a custom chip consisting of an array of cells which combine photo-sensing and computation. Unlike conventional 'step-and-repeat' light-stripe range finders, our sensor gathers range images in parallel as a scene is swept by a continuously moving, plane of light. A prototype range-finding system has been built using a second-generation sensor and is capable of acquiring a 32 x 32 point frame of 3-D measurements in a millisecond - two orders of magnitude faster than currently available range-finding systems. The accuracy and the repeatability of the acquired range data has been measured to be less than 0.2%. In this paper, we discuss the range-finding system and present experimental results that measure its performance. DTIC

N94-21532# Sandia National Labs., Albuquerque, NM.
MAGNETIC FORCE MICROSCOPY/CURRENT CONTRAST IMAGING: A NEW TECHNIQUE FOR INTERNAL CURRENT PROBING OF IC'S
A. N. Campbell, E. I. Cole, Jr., B. A. Dodd, and R. E. Anderson 1993 12 p Presented at the 4th European Conference on Electron and Optical Beam Testing of Electronic Devices, Zurich, Switzerland, 1-3 Sep. 1993
(Contract DE-AC04-76DP-00789)
(DE93-040754; SAND-93-1881C; CONF-9309130-1) Avail: CASI HC A03/MF A01

This invited paper describes recently reported work on the application of magnetic force microscopy (MFM) to image currents in IC conductors. A computer model for MFM imaging of IC currents and experimental results demonstrating the ability to determine current direction and magnitude with a resolution of approximately 1 mA dc and approximately 1 micro-A ac are presented. The physics of MFM signal generation and applications to current imaging and measurement are described. DOE

N94-21538 Technische Univ., Eindhoven (Netherlands). Electromechanics and Power Electronics Group.
DERIVATION OF A MODEL OF THE EXCITER OF A BRUSHLESS SYNCHRONOUS MACHINE
J. M. Vleeshouwers Jun. 1992 66 p Limited Reproducibility: More than 20% of this document may be affected by microfiche quality
(EUT-92-E-258; ISBN-9-06-144258-3; ETN-94-94765) Avail: Issuing Activity (European Space Agency (ESA))

The modeling of the brushless exciter for a machine used in a wind turbine is addressed. A brushless exciter reduces the susceptability of the machine to atmospheric conditions and therefore the need for maintenance compared to a synchronous machine equipped with brushes and sliprings. Furthermore, no large excitation winding power supply is needed. In large wind turbines which apply a synchronous machine, these advantages will be vital. A brushless exciter is usually constructed as a small synchronous machine with rectifier. According to manufacturers, exciters are designed to function as a current transformer. The method which has been developed in an earlier resarch project to model the synchronous machine with rectifier is concluded to be applicable to model the exciter, provided that the effect of resistances on the commutation may be neglected. This restricts the technique to modeling exciters of machines in the 100 kW range and larger. For smaller exciters the existing modeling approach is not applicable. Measurements of a small exciter (of a 37.5 kVa machine) show that higher harmonics in the exciter significantly contribute to its behavior. Based on experimental data a simple linear first order dynamic model was developed for the small exciter. The model parameters can be deduced from the steady state current gain and a simple dynamic experiment. ESA

N94-21566*# Sverdrup Technology, Inc., Brook Park, OH.
A LABORATORY SYSTEM FOR THE INVESTIGATION OF RAIN FADE COMPENSATION TECHNIQUES FOR Ka-BAND SATELLITES Final Report
James S. Svoboda and Brian A. Kachmar (Analex Corp., Brook Park, OH.) Dec. 1993 12 p Proposed for presentation at the 15th International Communications Satellite Systems Conference, San Diego, CA, 28 Feb. - 4 Mar. 1994
(Contracts NAS3-25266; NAS3-25776; RTOP 506-72-1E)
(NASA-CR-191200; E-8186; NAS 1.26:191200; AIAA Paper 94-0917)
Avail: CASI HC A03/MF A01

The design and performance of a rain fade simulation/counteraction system on a laboratory simulated 30/20 GHz, time division multiple access (TDMA) satellite communications testbed is evaluated. Severe rain attenuation of electromagnetic radiation at 30/20 GHz occurs due to the carrier wavelength approaching the water droplet size. Rain in the downlink path lowers the signal power present at the receiver, resulting in a higher number of bit errors induced in the digital ground terminal. The laboratory simulation performed at NASA Lewis Research Center uses a programmable PIN diode attenuator to simulate 20 GHz satellite downlink geographic rain fade profiles. A computer based network control system monitors the downlink power and informs the network of any power threshold violations, which then prompts the network to issue commands that temporarily increase the gain of the satellite based traveling wave tube (TWT) amplifier. After the rain subsides, the network returns the TWT to the normal energy conserving power mode. Bit error rate (BER) data taken at the receiving ground terminal serves as a measure of the severity of rain degradation, and also evaluates the extent to which the network can improve the faded channel. Author

N94-21620# Lawrence Livermore National Lab., CA.
ELECTROMECHANICAL BATTERY RESEARCH AND DEVELOPMENT AT THE LAWRENCE LIVERMORE NATIONAL LABORATORY
R. F. Post, D. E. Baldwin, D. A. Bender, and T. K. Fowler Jun. 1993 9 p Presented at the Conference on Zero Emission Vehicles: the Electric Hybrid and Alternative Fuels Challenge, Aachen, Germany, 13-17 Sep. 1993
(Contract W-7405-eng-48)
(DE93-019159; UCRL-JC-113905; CONF-930964-1) Avail: CASI HC A02/MF A01

The concepts undergirding a funded program to develop a modular electromechanical battery (EMB) at the Lawrence Livermore National Laboratory are described. Example parameters for EMB's for electric and hybrid-electric vehicles are given, and the importance of the high energy recovery efficiency of EMB's in increasing vehicle range in urban driving is shown. DOE

N94-21621# Lawrence Livermore National Lab., CA.
ELECTROMECHANICAL BATTERY RESEARCH AND DEVELOPMENT AT THE LAWRENCE LIVERMORE NATIONAL LABORATORY
R. F. Post, D. E. Baldwin, D. A. Bender, and T. K. Fowler 17 Jun. 1993 14 p Presented at the Project Energy 1993 Conference, Kansas City, MO, 21-23 Jun. 1993
(Contract W-7405-eng-48)
(DE94-000391; UCRL-JC-113905-Rev-1; CONF-9306204-2-Rev-1) Avail: CASI HC A03/MF A01

New materials and new design concepts are being incorporated in a new approach to an old idea - flywheel energy storage - to create an important alternative to the electrochemical storage battery for use in electric vehicles or for stationary applications, such as computer back-up power or utility load-leveling. DOE

N94-21632# Sandia National Labs., Albuquerque, NM.
RESULTS FROM LONG CONDUCTION TIME PLASMA OPENING SWITCH EXPERIMENTS AT SANDIA NATIONAL LABORATORIES
M. E. Savage, W. W. Simpson, and M. A. Usher (General Technology Corp., Albuquerque, NM.) 1993 6 p Presented at the 9th IEEE Pulsed Power Conference, Albuquerque, NM, 21-23 Jun. 1993
(Contract DE-AC04-76DP-00789)
(DE93-019063; SAND-93-0153C; CONF-930616-32) Avail: CASI HC A02/MF A01

Sandia National Laboratories is conducting research on Plasma Opening Switches (POS) with input current fluxing times of 200-250 nanoseconds. The opening switches that were studied at Sandia employ auxiliary magnetic fields to control the switch plasma. Results are presented from the latest series of experiments on the MITE pulser. Mite will presently deliver 650 kA in 250 ns to a short at the opening switch position. The MITE experiment is unique because it uses a 15 ns long (one-way) transmission line for the storage inductor. This is important for efficiency when the POS is used to transfer energy into an inductive load. The distributed storage inductor also allows pulse-shaping into resistive loads. The plasma injection methods used and the effects of the magnetic fields are discussed. Results from operation of the switch into electron beam loads at voltages from 2 to 3 megavolts are shown. The load voltage risetime 15 to 30 nanoseconds. Important to vacuum opening switch work is the electron flow downstream of the POS. Anode and cathode current measurements downstream of the switch are shown and how switch operation affects electron flow is discussed. DOE

N94-21634# Sandia National Labs., Albuquerque, NM.
ULTRAFAST GAS SWITCHING EXPERIMENTS
C. A. Frost, T. H. Martin, P. E. Patterson, L. F. Rinehart, G. J. Rohwein, L. D. Roose, J. F. Aurand, and M. T. Buttram 1993 5 p Presented at the 9th IEEE Pulsed Power Conference, Albuquerque, NM, 21-23 Jun. 1993
(Contract DE-AC04-76DP-00789)
(DE93-019071; SAND-93-0114C; CONF-930616-28) Avail: CASI HC A01/MF A01

Recent experiments which studied the physics of ultrafast gas breakdown under the extreme overvoltages which occur when a high pressure gas switch is pulse charged to hundreds of kV in 1 ns or less are described. The highly overvolted peaking gaps produce powerful electromagnetic pulses with risetimes less than 100 ps which can be used for ultrawideband radar systems, particle accelerators, laser drivers, bioelectromagnetic studies, electromagnetic effects testing, and for basic studies of gas breakdown physics. Pulses with 50 to 100 ps risetimes to peak levels of 75 to 160 kV at pulse repetition frequencies (PRF) to 1 kHz were produced and accurately measured. A unique gas switch was developed to hold off hundreds of kV with parasitic inductance less than 1 nH. An advanced diagnostic system using Fourier compensation was developed to measure single-shot risetimes below 35 ps. The complete apparatus is described and waveforms are presented. The measured data are compared with a theoretical model which predicts key features including dependence on gas species and pressure. This technology was applied to practical systems driving ultrawideband radiating antennas and bounded wave simulators. A thyristor/pulse transformer based system using a highly overvolted cable switch was developed. This pulser driving a Sandia-designed TEM cell, provides an ultra wideband impulse with less than 200 ps risetime to the test object at a PRF greater than 1 kHz at grater tha n 100 kV/m E field. DOE

N94-21636# Sandia National Labs., Albuquerque, NM.
LOCALIZATION OF PELLICLE-INDUCED OPEN CONTACTS USING CHARGE-INDUCED VOLTAGE ALTERATION
E. I. Cole, Jr. and J. M. Soden 1993 8 p Presented at the 1993 International Symposium on Testing and Failure Analysis, Los Angeles, CA, 15-19 Nov. 1993
(Contract DE-AC04-76DP-00789)
(DE93-019407; SAND-93-0456C; CONF-931191-1) Avail: CASI HC A02/MF A01

The recently developed Charge-Induced Voltage Alteration (CIVA) technique for localizing open metal conductors was used successfully to identify transistors with electrically open metal-1 contacts to silicon. The transistors were in the I/O port circuitry of a failing microcontroller and were completely covered by a metal-2 power bus. The root cause of the open contacts was a subtle scratch in the pellicle over the contact reticle. The scratch prevented full exposure of the photoresist, resulting in incomplete removal of the interlevel oxide in several contact windows. In addition to this powerful new application of CIVA, a number of failure analysis techniques utilizing both the electrical and physical properties of the failing microcontrollers were employed to identify and confirm the open contacts. These techniques are reviewed and recommendations are given for improved pellicle/reticle inspection. DOE

N94-21652# Allied-Signal Aerospace Co., Kansas City, MO.
PROCESS CHARACTERIZATION AND CONTROL OF HAND-SOLDERED PRINTED WIRING ASSEMBLIES
D. L. Cheray and R. G. Mandl Sep. 1993 42 p
(Contract DE-AC04-76DP-00613)
(DE93-041290; KCP-613-5258) Avail: CASI HC A03/MF A01

A designed experiment was conducted to characterize the hand soldering process parameters for manufacturing printed wiring assemblies (PWA's). Component tinning was identified as the most important parameter in hand soldering. After tinning, the soldering iron tip temperature of 700 degrees F and the choice of operators influence solder joint quality more than any other parameters. Cleaning and flux/flux core have little impact on the quality of the solder joint. The need for component cleaning prior to assembly must be evaluated for each component. DOE

N94-21654# Sandia National Labs., Albuquerque, NM.
IMPROVEMENT OF THE STABILITY OF THE PROCESS FOR SYNTHESIZING CHEMICALLY PREPARED VARISTOR POWDER
S. J. Lockwood and E. V. Thomas Aug. 1993 34 p
(Contract DE-AC04-76DP-00789)
(DE94-000345; SAND-92-1986) Avail: CASI HC A03/MF A01

Varistor material is currently supplied by a single commercial source. The chem-prep varistor process was developed as a backup/replacement. With the transfer of the process to the production facility, studies were made to verify that the process is stable in manufacturing. Process variables are the precursors oxalic acid, NaOH, and ZnCl2. Process stability was determined by comparing assay uncertainty region with precipitant/ZnCl2 compositional region meeting electrical and physical property specifications. Assay variability was assessed by conducting a round robin; standard deviations of repeated assays of the same sample was 0.1 wt% by the same labs; 0.1-0.4 wt% among laboratories. A mixture experiment was then conducted to assess the effects of the precipitants/ZnCl2 on breakdown field, nonlinearity coefficient, and bulk density. Results indicate that the chem-prep process can be stable; however the nominal target composition was on the edge of the composition region, and it was moved to the center of the large region with acceptable electrical and physical properties. Tests of unpotted component rods made from the new composition met all specifications. DOE

N94-21685# Stanford Linear Accelerator Center, CA.
SIMULATION OF TRAVELING-WAVE OUTPUT STRUCTURES FOR HIGH POWER RF TUBES
K. R. Eppley Apr. 1993 3 p Presented at the International Particle Accelerator Conference, Washington, DC, 17-20 May 1993
(Contract DE-AC03-76SF-00515)
(DE93-041005; SU-SLAC-Pub-6234; CONF-930511-435) Avail: CASI HC A01/MF A01

Travelling wave output structures can in principle provide higher efficiency and lower surface gradients than a single output cavity. We discuss simulations of TW structures designed for X-band klystrons to be used in the SLAC NLC. The PIC Code CONDOR calculated efficiency over 50 percent for one such circuit. When the circuit was built in the SLAC XC7 klystron, the match was so poor that it had to be modified. When tested, the tube produced less than half the efficiency calculated. We subsequently found significant differences between the field distribution calculated by CONDOR versus that from the 3-D code MAFIA. We have now developed a procedure which gives much better agreement between the 2D and 3-D models. We use a (pi)/2 disk-loaded structure, with the waveguide coupling to an output cavity through an iris, rather than directly to the drift tube as in the XC7. The disk radii are tapered to produce an approximately constant gradient. The output coupling is adjusted to match to a uniform structure replicating the cell before the waveguide. The simulations predict 75 MW, 49 percent efficiency, with peak surface fields of 73 MV/m from a 440 kV, 350 amp beam at 11.424 GHz. DOE

N94-21694*# Idaho Univ., Moscow. NASA Space Engineering Research Center.
THE 1992 4TH NASA SERC SYMPOSIUM ON VLSI DESIGN
Sterling R. Whitaker 1992 422 p Symposium held in Moscow, ID, 29-30 Oct. 1992
(Grant NAGw-3293)
(NASA-CR-194591; NAS 1.26:194591) Avail: CASI HC A18/MF A04

Papers from the fourth annual NASA Symposium on VLSI Design, co-sponsored by the IEEE, are presented. Each year this symposium is organized by the NASA Space Engineering Research Center (SERC) at the University of Idaho and is held in conjunction with a quarterly meeting of the NASA Data System Technology Working Group (DSTWG). One task of the DSTWG is to develop new electronic technologies that will meet next generation electronic data system needs. The symposium provides insights into developments in VLSI and digital systems which can be used to increase data systems performance. The NASA SERC is proud to offer, at its fourth symposium on VLSI design, presentations by an outstanding set of individuals from national laboratories, the electronics industry, and universities. These speakers share insights into next generation advances that will serve as a basis for future VLSI design. For individual titles, see N94-21695 through N94-21735.

N94-21695*# Cornell Univ., Ithaca, NY.
APPLICATIONS OF CORRELATOR CHIPS IN RADIO SCIENCE
John B. Hagen *In* Idaho Univ., The 1992 4th NASA SERC Symposium on VLSI Design 1992 6 p (For primary document see N94-21694 05-33)
Avail: CASI HC A02/MF A04

Spectral line observations in radio astronomy require simultaneous power estimation in many (often hundreds to thousands) frequency bins. Digital autocorrelation spectrometers, which appeared thirty years ago, are now being implemented in VLSI. The same architecture can be used to implement transversal digital filters. This was done at the Arecibo Observatory for pulse compression in radar observations of Venus. Author (revised)

N94-21696*# Johns Hopkins Univ., Laurel, MD. Applied Physics Lab.
SINGLE EVENT PHENOMENA: TESTING AND PREDICTION
James D. Kinnison *In* Idaho Univ., The 1992 4th NASA SERC Symposium on VLSI Design 1992 11 p (For primary document see N94-21694 05-33)
Avail: CASI HC A03/MF A04

Highly integrated microelectronic devices are often used to increase the performance of satellite systems while reducing the system power dissipation, size, and weight. However, these devices are usually more susceptible to radiation than less integrated devices. In particular, the problem of sensitivity to single event upset and latchup is greatly increased as the integration level is increased. Therefore, a method for accurately evaluating the susceptibility of new devices to single event phenomena is critical to qualifying new components for use in space systems. This evaluation includes testing devices for upset or latchup and extrapolating the results of these tests to the orbital environment. Current methods for testing devices for single event effects are reviewed, and methods for upset rate prediction, including a new technique based on Monte Carlo simulation, are presented. Author (revised)

N94-21697*# Rockwell International Science Center, Thousand Oaks, CA.
HETEROJUNCTION BIPOLAR TRANSISTOR TECHNOLOGY FOR DATA ACQUISITION AND COMMUNICATION
C. Wang, M. Chang, S. Beccue, R. Nubling, P. Zampardi, N. Sheng, and R. Pierson *In* Idaho Univ., The 1992 4th NASA SERC Symposium on VLSI Design 1992 14 p (For primary document see N94-21694 05-33)
(Contract N00014-83-C-0347)
Avail: CASI HC A03/MF A04

Heterojunction Bipolar Transistor (HBT) technology has emerged as one of the most promising technologies for ultrahigh-speed integrated circuits. HBT circuits for digital and analog applications, data conversion, and power amplification have been realized, with speed performance well above 20 GHz. At Rockwell, a baseline AlGaAs/GaAs HBT technology has been established in a manufacturing facility. This paper describes the HBT technology, transistor characteristics, and HBT circuits for data acquisition and communication. Author

N94-21698*# Idaho Univ., Moscow. NASA Space Engineering Research Center.
A NEW EDDY CURRENT MODEL FOR MAGNETIC BEARING CONTROL SYSTEM DESIGN c37
Joseph J. Feeley and Daniel J. Ahlstrom *In its* The 1992 4th NASA

SERC Symposium on VLSI Design 1992 8 p (For primary document see N94-21694 05-33)
(Grants NAGw-1406; NSF MIP-91-09618)
Avail: CASI HC A02/MF A04

This paper describes a new VLSI-based controller for the implementation of a Linear-Quadratic-Gaussian (LQG) theory-based control system. Use of the controller is demonstrated by design of a controller for a magnetic bearing and its performance is evaluated by computer simulation. Author

N94-21699*# Washington State Univ., Pullman.
DESIGN OF A NEW SQUARING FUNCTION FOR THE VITERBI ALGORITHM **c61**
Aria Eshraghi, Terri Fiez, Thomas Fischer, and Kel Winters (Advanced Hardware Architectures, Moscow, ID.) *In* Idaho Univ., The 1992 4th NASA SERC Symposium on VLSI Design 1992 8 p (For primary document see N94-21694 05-33)
Avail: CASI HC A02/MF A04

A new algorithm and hardware implementation of the Viterbi squaring function was developed. The use of an approximation squaring technique preserves the Viterbi performance as is demonstrated by Monte-Carlo simulations. Additionally, the 16-bit approximate squaring implementation is expected to require one-fourth the area and operate at three times the speed of the conventional squaring implementation. Author (revised)

N94-21700*# Standard Microsystems, CA.
A 20 MHz CMOS REORDER BUFFER FOR A SUPERSCALAR MICROPROCESSOR **c60**
John Lenell, Steve Wallace (California Univ., Irvine.), and Nader Bagherzadeh (California Univ., Irvine.) *In* Idaho Univ., The 1992 4th NASA SERC Symposium on VLSI Design 1992 11 p (For primary document see N94-21694 05-33)
Avail: CASI HC A03/MF A04

Superscalar processors can achieve increased performance by issuing instructions out-of-order from the original sequential instruction stream. Implementing an out-of-order instruction issue policy requires a hardware mechanism to prevent incorrectly executed instructions from updating register values. A reorder buffer can be used to allow a superscalar processor to issue instructions out-of-order and maintain program correctness. This paper describes the design and implementation of a 20MHz CMOS reorder buffer for superscalar processors. The reorder buffer is designed to accept and retire two instructions per cycle. A full-custom layout in 1.2 micron has been implemented, measuring 1.1058 mm by 1.3542 mm.
Author (revised)

N94-21701*# California Univ., Fullerton. Dept. of Electrical Engineering.
ANALOG/DIGITAL pH METER SYSTEM I.C. **c35**
Paul Vincent and Jea Park *In* Idaho Univ., The 1992 4th NASA SERC Symposium on VLSI Design 1992 10 p (For primary document see N94-21694 05-33)
Avail: CASI HC A02/MF A04

The project utilizes design automation software tools to design, simulate, and fabricate a pH meter integrated circuit (IC) system including a successive approximation type seven-bit analog to digital converter circuits using a 1.25 micron N-Well CMOS MOSIS process. The input voltage ranges from 0.5 to 1.0 V derived from a special type pH sensor, and the output is a three-digit decimal number display of pH with one decimal point.
Author (revised)

N94-21702*# Idaho Univ., Moscow. NASA Space Engineering Research Center.
AN 18 BIT 50 kHz ADC FOR LOW EARTH ORBIT **c60**
Donald C. Thelen *In its* The 1992 4th NASA SERC Symposium on VLSI Design 1992 11 p (For primary document see N94-21694 05-33)
Avail: CASI HC A03/MF A04

A fourth order incremental analog to digital converter (ADC) is proposed which performs 18 bit conversions at a 50 kHz rate on sampled and held data. A new self calibration scheme is presented which eases the matching requirements of capacitors, and the performance of the operational amplifiers in the ADC by changing coefficients in the digital postprocessing.
Author (revised)

N94-21703*# Idaho Univ., Moscow. NASA Space Engineering Research Center.
ON THE DECOMPOSITION OF SYNCHRONOUS STATE MECHINES USING SEQUENCE INVARIANT STATE MACHINES
K. Hebbalalu, S. Whitaker, and K. Cameron *In its* The 1992 4th NASA SERC Symposium on VLSI Design 1992 10 p (For primary document see N94-21694 05-33)
Avail: CASI HC A02/MF A04

This paper presents a few techniques for the decomposition of Synchronous State Machines of medium to large sizes into smaller component machines. The methods are based on the nature of the transitions and sequences of states in the machine and on the number and variety of inputs to the machine. The results of the decomposition, and of using the Sequence Invariant State Machine (SISM) Design Technique for generating the component machines, include great ease and quickness in the design and implementation processes. Furthermore, there is increased flexibility in making modifications to the original design leading to negligible re-design time. Author (revised)

N94-21704*# Nanyang Technological Inst. (Singapore). School of Electrical and Electronic Engineering.
HEURISTIC-BASED SCHEDULING ALGORITHM FOR HIGH LEVEL SYNTHESIS **c61**
Gulam Mohamed, Han-Ngee Tan, and Chew-Lye Chng *In* Idaho Univ., The 1992 4th NASA SERC Symposium on VLSI Design 1992 8 p (For primary document see N94-21694 05-33)
Avail: CASI HC A02/MF A04

A new scheduling algorithm is proposed which uses a combination of a resource utilization chart, a heuristic algorithm to estimate the minimum number of hardware units based on operator mobilities, and a list-scheduling technique to achieve fast and near optimal schedules. The schedule time of this algorithm is almost independent of the length of mobilities of operators as can be seen from the benchmark example (fifth order digital elliptical wave filter) presented when the cycle time was increased from 17 to 18 and then to 21 cycles. It is implemented in C on a SUN3/60 workstation.
Author (revised)

N94-21705*# Nanyang Technological Inst. (Singapore). School of Applied Sciences.
EVALUATION OF FLOATING-POINT SUM OR DIFFERENCE OF PRODUCTS IN CARRY-SAVE DOMAIN **c64**
A. Wahab, S. Erdogan, and A. B. Premkumar *In* Idaho Univ., The 1992 4th NASA SERC Symposium on VLSI Design 1992 9 p (For primary document see N94-21694 05-33)
Avail: CASI HC A02/MF A04

An architecture to evaluate a 24-bit floating-point sum or difference of products using modified sequential carry-save multipliers with extensive pipelining is described. The basic building block of the architecture is a carry-save multiplier with built-in mantissa alignment for the summation during the multiplication cycles. A carry-save adder, capable of mantissa alignment, correctly positions products with the current carry-save sum. Carry propagation in individual multipliers is avoided and is only required once to produce the final result. Author (revised)

N94-21706*# University of Southwestern Louisiana, Lafayette. Center for Advanced Computer Studies.
A STATISTICAL-BASED SCHEDULING ALGORITHM IN AUTOMATED DATA PATH SYNTHESIS **c61**
Byung Wook Jeon and Chidchanok Lursinsap *In* Idaho Univ., The 1992 4th NASA SERC Symposium on VLSI Design 1992 8 p (For primary document see N94-21694 05-33)
Avail: CASI HC A02/MF A04

In this paper, we propose a new heuristic scheduling algorithm based on the statistical analysis of the cumulative frequency distribution of operations among control steps. It has a tendency of escaping from local minima and therefore reaching a globally optimal solution. The presented algorithm considers the real world constraints such as chained operations, multicycle operations, and pipelined data paths. The result of the experiment shows that it gives optimal solutions, even though it is greedy in nature.
Author (revised)

N94-21707*# University of Southwestern Louisiana, Lafayette. Center for Advanced Computer Studies.

MICRO-ROLLBACK AND SELF-RECOVERY SYNTHESIS **c38**

Byung Wook Jeon and Chidchanok Lursinsap *In* Idaho Univ., The 1992 4th NASA SERC Symposium on VLSI Design 1992 12 p (For primary document see N94-21694 05-33)

Avail: CASI HC A03/MF A04

A new approach to high level synthesis with micro-rollback and self-recovery method is presented. The objective of this approach is to generate a reliable system from the behavioral descriptions. The approach is formulated as a rollback point insertion problem based on the probability function of being inserted rollback points after the given CDFG is scheduled. This function allows us not only to search the problem space efficiently but also to avoid the exhaustive search. Author (revised)

N94-21708*# Idaho Univ., Moscow. NASA Space Engineering Research Center.

NASA SERC DIGITAL CORRELATOR PROJECTS **c60**

John Canaris *In its* The 1992 4th NASA SERC Symposium on VLSI Design 1992 3 p (For primary document see N94-21694 05-33)

(Grants NAGw-1406; NAG5-1635)

Avail: CASI HC A01/MF A04

Interest in custom digital correlator processors is growing, in both the radio astronomy and earth sensing communities, as scientists realize that VLSI technology is available to them. This paper presents three digital correlator projects currently underway at the NASA SERC for VLSI Systems Design. The projects are as follows: a 60MHz chip for the ESTAR satellite; a 100MHz, 1024 channel autocorrelator; and a 64 MHz, VLSI system consisting of 8 32- channel complex crosscorrelators including phase rotators. Author (revised)

N94-21709*# Naval Ocean Systems Center, San Diego, CA. Research, Development, Test, and Evaluation Div.

FULLY-DEPLETED SILICON-ON-SAPPHIRE AND ITS APPLICATION TO ADVANCED VLSI DESIGN

Bruce W. Offord *In* Idaho Univ., The 1992 4th NASA SERC Symposium on VLSI Design 1992 7 p (For primary document see N94-21694 05-33)

Avail: CASI HC A02/MF A04

In addition to the widely recognized advantages of full dielectric isolation, e.g., reduced parasitic capacitance, transient radiation hardness, and processing simplicity, fully-depleted silicon-on-sapphire offers reduced floating body effects and improved thermal characteristics when compared to other silicon-on-insulator technologies. The properties of this technology and its potential impact on advanced VLSI circuitry will be discussed.

Author (revised)

N94-21710*# Johns Hopkins Univ., Laurel, MD. Applied Physics Lab.

DESIGN AND TEST OF FIELD PROGRAMMABLE GATE ARRAYS IN SPACE APPLICATIONS **c61**

Priscilla L. McKerracher, Russel P. Cain, Jon C. Barnett, William S. Green, and James D. Kinnison *In* Idaho Univ., The 1992 4th NASA SERC Symposium on VLSI Design 1992 2 p (For primary document see N94-21694 05-33)

Avail: CASI HC A01/MF A04

Field Programmable Gate Arrays (FPGAU's) offer substantial benefits in terms of flexibility and design integration. In addition to qualifying this device for space applications by establishing its reliability and evaluating its sensitivity to radiation, screening the programmed devices with Automatic Test Equipment (ATE) and functional burn-in presents an interesting challenge. This paper presents a review of the design, qualification, and screening cycle employed for FPGA designs in a space program, and demonstrates the need for close interaction between design and test engineers. Author (revised)

N94-21711*# Idaho Univ., Moscow. Dept. of Electrical Engineering.

DEFECT-SENSITIVITY ANALYSIS OF AN SEU IMMUNE CMOS LOGIC FAMILY

Erik H. Ingermann and James F. Frenzel *In its* The 1992 4th NASA SERC Symposium on VLSI Design 1992 10 p (For primary document see N94-21694 05-33)

(Grant NAGw-1406)

Avail: CASI HC A02/MF A04

Fault testing of resistive manufacturing defects is done on a recently developed single event upset immune logic family. Resistive ranges and delay times are compared with those of traditional CMOS logic. Reaction of the logic to these defects is observed for a NOR gate, and an evaluation of its ability to cope with them is determined. Author (revised)

N94-21712*# Idaho Univ., Moscow. NASA Space Engineering Research Center.

DIMENSION SCALING EFFECTS ON THE YIELD SENSITIVITY OF HEMT DIGITAL CIRCUITS

Jogendra C. Sarker and John E. Purviance *In its* The 1992 4th NASA SERC Symposium on VLSI Design 1992 12 p (For primary document see N94-21694 05-33)

Avail: CASI HC A03/MF A04

In our previous works, using a graphical tool, yield factor histograms, we studied the yield sensitivity of High Electron Mobility Transistors (HEMT) and HEMT circuit performance with the variation of process parameters. This work studies the scaling effects of process parameters on yield sensitivity of HEMT digital circuits. The results from two HEMT circuits are presented. Author (revised)

N94-21713*# New Mexico Univ., Albuquerque. NASA Space Engineering Research Center.

LINKS BETWEEN N-MODULAR REDUNDANCY AND THE THEORY OF ERROR-CORRECTING CODES **c61**

V. Bobin (Hewlett-Packard Co., Santa Clara, CA.), S. Whitaker, and G. Maki *In* Idaho Univ., The 1992 4th NASA SERC Symposium on VLSI Design 1992 11 p (For primary document see N94-21694 05-33)

(Grant NAGw-1406)

Avail: CASI HC A03/MF A04

N-Modular Redundancy (NMR) is one of the best known fault tolerance techniques. Replication of a module to achieve fault tolerance is in some ways analogous to the use of a repetition code where an information symbol is replicated as parity symbols in a codeword. Linear Error-Correcting Codes (ECC) use linear combinations of information symbols as parity symbols which are used to generate syndromes for error patterns. These observations indicate links between the theory of ECC and the use of hardware redundancy for fault tolerance. In this paper, we explore some of these links and show examples of NMR systems where identification of good and failed elements is accomplished in a manner similar to error correction using linear ECC's. Author (revised)

N94-21714*# New Mexico Univ., Albuquerque. Microelectronics Research Center.

REDUCTION OF BLOCKING EFFECTS FOR THE JPEG BASELINE IMAGE COMPRESSION STANDARD **c61**

Gregary C. Zweigle and Roberto H. Bamberger (Washington State Univ., Pullman.) *In* Idaho Univ., The 1992 4th NASA SERC Symposium on VLSI Design 1992 11 p (For primary document see N94-21694 05-33)

(Grant NSF MIPS-91-16683)

Avail: CASI HC A03/MF A04

Transform coding has been chosen for still image compression in the Joint Photographic Experts Group (JPEG) standard. Although transform coding performs superior to many other image compression methods and has fast algorithms for implementation, it is limited by a blocking effect at low bit rates. The blocking effect is inherent in all nonoverlapping transforms. This paper presents a technique for reducing blocking while remaining compatible with the JPEG standard. Simulations show that the system results in subjective performance improvements, sacrificing only a marginal increase in bit rate. Author (revised)

N94-21715*# Utah State Univ., Logan. Depts. of Electrical Engineering and Computer Science.

A NOVEL VISUAL HARDWARE BEHAVIORAL LANGUAGE **c61**

Xueqin Li and H. D. Cheng *In* Idaho Univ., The 1992 4th NASA SERC Symposium on VLSI Design 1992 12 p (For primary document see N94-21694 05-33)

Avail: CASI HC A03/MF A04

Most hardware behavioral languages just use texts to describe the

behavior of the desired hardware design. This is inconvenient for VLSI designers who enjoy using the schematic approach. The proposed visual hardware behavioral language has the ability to graphically express design information using visual parallel models (blocks), visual sequential models (processes) and visual data flow graphs (which consist of primitive operational icons, control icons, and Data and Synchro links). Thus, the proposed visual hardware behavioral language can not only specify hardware concurrent and sequential functionality, but can also visually expose parallelism, sequentiality, and disjointness (mutually exclusive operations) for the hardware designers. That would make the hardware designers capture the design ideas easily and explicitly using this visual hardware behavioral language. Author (revised)

N94-21716*# California Univ., Davis. Dept. of Computer Science.
A MECHANIZED PROCESS ALGEBRA FOR VERIFICATION OF DEVICE SYNCHRONIZATION PROTOCOLS **c61**
E. Thomas Schubert *In* Idaho Univ., The 1992 4th NASA SERC Symposium on VLSI Design 1992 13 p (For primary document see N94-21694 05-33)
(Contract NAS1-18586)
Avail: CASI HC A03/MF A04

We describe the formalization of a process algebra based on CCS within the Higher Order Logic (HOL) theorem-proving system. The representation of four types of device interactions and a correctness proof of the communication between a microprocessor and MMU is presented. Author (revised)

N94-21717*# Idaho Univ., Moscow. NASA Space Engineering Research Center.
HDL TO VERIFICATION LOGIC TRANSLATOR
J. W. Gambles and P. J. Windley *In its* The 1992 4th NASA SERC Symposium on VLSI Design 1992 12 p (For primary document see N94-21694 05-33)
(Grants NAGw-1406; NSF MIP-91-09618)
Avail: CASI HC A03/MF A04

The increasingly higher number of transistors possible in VLSI circuits compounds the difficulty in insuring correct designs. As the number of possible test cases required to exhaustively simulate a circuit design explodes, a better method is required to confirm the absence of design faults. Formal verification methods provide a way to prove, using logic, that a circuit structure correctly implements its specification. Before verification is accepted by VLSI design engineers, the stand alone verification tools that are in use in the research community must be integrated with the CAD tools used by the designers. One problem facing the acceptance of formal verification into circuit design methodology is that the structural circuit descriptions used by the designers are not appropriate for verification work and those required for verification lack some of the features needed for design. We offer a solution to this dilemma: an automatic translation from the designers' HDL models into definitions for the higher-ordered logic (HOL) verification system. The translated definitions become the low level basis of circuit verification which in turn increases the designer's confidence in the correctness of higher level behavioral models. Author (revised)

N94-21718*# Concordia Univ., Montreal (Quebec). Dept. of Computer Science.
A SIMPLE MODERN CORRECTNESS CONDITION FOR A SPACE-BASED HIGH-PERFORMANCE MULTIPROCESSOR **c60**
David K. Probst and Hon F. Li *In* Idaho Univ., The 1992 4th NASA SERC Symposium on VLSI Design 1992 10 p (For primary document see N94-21694 05-33)
(Grants NSERC-A3363; NSERC-A0921; NSERC-MEF0040121)
Avail: CASI HC A02/MF A04

A number of U.S. national programs, including space-based detection of ballistic missile launches, envisage putting significant computing power into space. Given sufficient progress in low-power VLSI, multichip-module packaging and liquid-cooling technologies, we will see design of high-performance multiprocessors for individual satellites. In very high speed implementations, performance depends critically on tolerating large latencies in interprocessor communication; without latency tolerance, performance is limited by the vastly differing time scales in processor and data-memory modules, including interconnect times. The modern approach to tolerating remote-communication cost in scalable, shared-memory multiprocessors is to use a multithreaded architecture, and alter the semantics of shared memory slightly, at the price of forcing the programmer either to reason about program correctness in a relaxed consistency model or to agree to program in a constrained style. The literature on multiprocessor correctness conditions has become increasingly complex, and sometimes confusing, which may hinder its practical application. We propose a simple modern correctness condition for a high-performance, shared-memory multiprocessor; the correctness condition is based on a simple interface between the multiprocessor architecture and a high-performance, shared-memory multiprocessor; the correctness condition is based on a simple interface between the multiprocessor architecture and the parallel programming system. Author (revised)

N94-21719*# Idaho Univ., Moscow. Dept. of Computer Science.
INSTRUCTION SET COMMUTIVITY **c61**
P. Windley *In its* The 1992 4th NASA SERC Symposium on VLSI Design 1992 11 p (For primary document see N94-21694 05-33)
(Contract MDA904-91-C-7054)
Avail: CASI HC A03/MF A04

We present a state property called congruence and show how it can be used to demonstrate commutivity of instructions in a modern load-store architecture. Our analysis is particularly important in pipelined microprocessors where instructions are frequently reordered to avoid costly delays in execution caused by hazards. Our work has significant implications to safety and security critical applications since reordering can easily change the meaning and an instruction sequence and current techniques are largely ad hoc. Our work is done in a mechanical theorem prover and results in a set of trustworthy rules for instruction reordering. The mechanization makes it practical to analyze the entire instruction set. Author (revised)

N94-21720*# Syracuse Univ., NY. Dept. of Electrical and Computer Engineering.
A MEAN FIELD NEURAL NETWORK FOR HIERARCHICAL MODULE PLACEMENT **c63**
M. Kemal Unaltuna and Vijay Pitchumani *In* Idaho Univ., The 1992 4th NASA SERC Symposium on VLSI Design 1992 9 p (For primary document see N94-21694 05-33)
Avail: CASI HC A02/MF A04

This paper proposes a mean field neural network for the two-dimensional module placement problem. An efficient coding scheme with only O(N log N) neurons is employed where N is the number of modules. The neurons are evolved in groups of N in log N iteration steps such that the circuit is recursively partitioned in alternating vertical and horizontal directions. In our simulations, the network was able to find optimal solutions to all test problems with up to 128 modules. Author

N94-21721*# Colorado State Univ., Fort Collins. Computer Science and Electrical Engineering Depts.
DETECTION OF FEED-THROUGH FAULTS IN CMOS STORAGE ELEMENTS
Waleed K. Al-Assadi, Yashwant K. Malaiya, and Anura P. Jayasumana *In* Idaho Univ., The 1992 4th NASA SERC Symposium on VLSI Design 1992 5 p Sponsored in part by SDIO/IST (For primary document see N94-21694 05-33)
Avail: CASI HC A01/MF A04

In testing sequential circuits, internal faults in the storage elements (SE's) are sometimes modeled as stuck-at faults in the combinational circuits surrounding the SE. The detection of some transistor-level faults that cannot be modeled as stuck-at are considered. These feed-through faults cause the cell to become either data-feed-through, which makes the cell combinational, or clock-feed-through, which causes the clock signal or its complement to appear at the output. Under such faults, the cell does not function as a memory element. Here it is shown that such faults may or may not be detected depending on delays involved. Conditions under which race-ahead occurs are identified. Author (revised)

N94-21722*# New Mexico Univ., Albuquerque. NASA Space Engineering Research Center.
SCHEMATIC DRIVEN LAYOUT OF REED SOLOMON ENCODERS
Kari Arave, John Canaris, Lowell Miles, and Sterling Whitaker *In* Idaho Univ., The 1992 4th NASA SERC Symposium on VLSI Design 1992

7 p (For primary document see N94-21694 05-33)
(Grants NAGw-1406; NSF MIP-91-09618)
Avail: CASI HC A02/MF A04

Two Reed Solomon error correcting encoders are presented. Schematic driven layout tools were used to create the encoder layouts. Special consideration had to be given to the architecture and logic to provide scalability of the encoder designs. Knowledge gained from these projects was used to create a more flexible schematic driven layout system.

Author

N94-21723*# Idaho Univ., Moscow. NASA Space Engineering Research Center.

INTERPOLATIVE MODELING OF GaAs FET S-PARAMETER DATA BASES FOR USE IN MONTE CARLO SIMULATIONS **c65**

L. Campbell and J. Purviance *In its* The 1992 4th NASA SERC Symposium on VLSI Design 1992 11 p (For primary document see N94-21694 05-33)
(Grants NAGw-1406; NSF MIP-91-09618)
Avail: CASI HC A03/MF A04

A statistical interpolation technique is presented for modeling GaAs FET S-parameter measurements for use in the statistical analysis and design of circuits. This is accomplished by interpolating among the measurements in a GaAs FET S-parameter data base in a statistically valid manner.

Author (revised)

N94-21724*# Texas Instruments, Inc., Lewisville.

BIT-SYSTOLIC ARITHMETIC ARRAYS USING DYNAMIC DIFFERENTIAL GALLIUM ARSENIDE CIRCUITS

Grant Beagles, Kel Winters (Advanced Hardware Architectures, Moscow, ID.), and A. G. Eldin (Toledo Univ., OH.) *In* Idaho Univ., The 1992 4th NASA SERC Symposium on VLSI Design 1992 11 p (For primary document see N94-21694 05-33)
Avail: CASI HC A03/MF A04

A new family of gallium arsenide circuits for fine grained bit-systolic arithmetic arrays is introduced. This scheme combines features of two recent techniques of dynamic gallium arsenide FET logic and differential dynamic single-clock CMOS logic. The resulting circuits are fast and compact, with tightly constrained series FET propagation paths, low fanout, no dc power dissipation, and depletion FET implementation without level shifting diodes.

Author

N94-21725*# Idaho Univ., Moscow. NASA Space Engineering Research Center.

A VLSI IMPLEMENTATION OF DCT USING PASS TRANSISTOR TECHNOLOGY

S. Kamath, Douglas Lynn, and Sterling Whitaker *In its* The 1992 4th NASA SERC Symposium on VLSI Design 1992 12 p (For primary document see N94-21694 05-33)
(Grants NAGw-1406; NSF MIP-91-09618)
Avail: CASI HC A03/MF A04

A VLSI design for performing the Discrete Cosine Transform (DCT) operation on image blocks of size 16 x 16 in a real time fashion operating at 34 MHz (worst case) is presented. The process used was Hewlett-Packard's CMOS26--A 3 metal CMOS process with a minimum feature size of 0.75 micron. The design is based on Multiply-Accumulate (MAC) cells which make use of a modified Booth recoding algorithm for performing multiplication. The design of these cells is straight forward, and the layouts are regular with no complex routing. Two versions of these MAC cells were designed and their layouts completed. Both versions were simulated using SPICE to estimate their performance. One version is slightly faster at the cost of larger silicon area and higher power consumption. An improvement in speed of almost 20 percent is achieved after several iterations of simulation and re-sizing.

Author (revised)

N94-21726*# New Mexico Univ., Albuquerque. NASA Space Engineering Research Center.

A HIGH SPEED CMOS A/D CONVERTER

Don R. Wiseman and Sterling R. Whitaker *In* Idaho Univ., The 1992 4th NASA SERC Symposium on VLSI Design 1992 13 p (For primary document see N94-21694 05-33)
(Grant NAGw-1406)
Avail: CASI HC A03/MF A04

This paper presents a high speed analog-to-digital (A/D) converter. The converter is a 7 bit flash converter with one half LSB accuracy. Typical parts will function at approximately 200 MHz. The converter uses a novel comparator circuit that is shown to out perform more traditional comparators, and thus increases the speed of the converter. The comparator is a clocked, precharged circuit that offers very fast operation with a minimal offset voltage (2 mv). The converter was designed using a standard 1 micron digital CMOS process and is 2,244 microns by 3,972 microns.

Author (revised)

N94-21727*# Colorado State Univ., Fort Collins. Dept. of Electrical Engineering and Computer Science.

BEHAVIOR OF FAULTY DOUBLE BJT BICMOS LOGIC GATES

Sankaran M. Menon, Yashwant K. Malaiya, and Anura P. Jayasumana *In* Idaho Univ., The 1992 4th NASA SERC Symposium on VLSI Design 1992 12 p Sponsored in part by SDIO/IST (For primary document see N94-21694 05-33)
Avail: CASI HC A03/MF A04

Logic Behavior of a Double BJT BiCMOS device under transistor level shorts and opens is examined. In addition to delay faults, faults that cause the gate to exhibit sequential behavior were observed. Several faults can be detected only by monitoring the current. The faulty behavior of Bipolar (TTL) and CMOS logic families is compared with BiCMOS, to bring out the testability differences.

Author (revised)

N94-21728*# Idaho Univ., Moscow. NASA Space Engineering Research Center.

ON FAST CARRY SELECT ADDERS

M. Shamanna and S. Whitaker *In its* The 1992 4th NASA SERC Symposium on VLSI Design 1992 8 p (For primary document see N94-21694 05-33)
(Grant NAGw-1406)
Avail: CASI HC A02/MF A04

This paper presents an architecture for a high-speed carry select adder with very long bit lengths utilizing a conflict-free bypass scheme. The proposed scheme has almost half the number of transistors and is faster than a conventional carry select adder. A comparative study is also made between the proposed adder and a Manchester carry chain adder which shows that the proposed scheme has the same transistor count, without suffering any performance degradation, compared to the Manchester carry chain adder.

Author

N94-21729*# Toledo Univ., OH. Electrical Engineering Dept.

A DRAM COMPILER ALGORITHM FOR HIGH PERFORMANCE VLSI EMBEDDED MEMORIES **c61**

A. G. Eldin *In* Idaho Univ., The 1992 4th NASA SERC Symposium on VLSI Design 1992 13 p (For primary document see N94-21694 05-33)
Avail: CASI HC A03/MF A04

In many applications, the limited density of the embedded SRAM does not allow integrating the memory on the same chip with other logic and functional blocks. In such cases, the embedded DRAM provides the optimum combination of very high density, low power, and high performance. For ASIC's to take full advantage of this design strategy, an efficient and highly reliable DRAM compiler must be used. The embedded DRAM architecture, cell, and peripheral circuit design considerations and the algorithm of a high performance memory compiler are presented .

Author (revised)

N94-21730*# Peradeniya Univ. (Sri Lanka).

A NOVEL CACHE MECHANISM **c61**

J. A. Gunawardena *In* Idaho Univ., The 1992 4th NASA SERC Symposium on VLSI Design 1992 12 p (For primary document see N94-21694 05-33)
Avail: CASI HC A03/MF A04

This cache mechanism is transparent but does not contain associative circuits. It does not rely on locality of reference of instructions or data. No redundant instructions or data are encached. Items in the cache are accessed without address arithmetic. A cache miss is detected by the simplest test; compare two bits. These features would result in faster access, higher hit rate, reduced chip area, and less power dissipation in comparison with associative systems of similar size.

Author (revised)

N94-21731*# Idaho Univ., Moscow. Dept. of Electrical Engineering.
A SET-ASSOCIATIVE, FAULT-TOLERANT CACHE DESIGN c61
Dan Lamet and James F. Frenzel *In its* The 1992 4th NASA SERC Symposium on VLSI Design 1992 5 p (For primary document see N94-21694 05-33)
(Grant NAGw-1406)
Avail: CASI HC A01/MF A04

The design of a defect-tolerant control circuit for a set-associative cache memory is presented. The circuit maintains the stack ordering necessary for implementing the Least Recently Used (LRU) replacement algorithm. A discussion of programming techniques for bypassing defective blocks is included. Author (revised)

N94-21732*# Spaceborn, Inc., La Canada, CA.
A 1 GHz SAMPLE RATE, 256-CHANNEL, 1-BIT QUANTIZATION, CMOS, DIGITAL CORRELATOR CHIP
C. Timoc, T. Tran, and J. Wongso *In* Idaho Univ., The 1992 4th NASA SERC Symposium on VLSI Design 1992 6 p (For primary document see N94-21694 05-33)
Avail: CASI HC A02/MF A04

This paper describes the development of a digital correlator chip with the following features: 1 Giga-sample/second; 256 channels; 1-bit quantization; 32-bit counters providing up to 4 seconds integration time at 1 GHz; and very low power dissipation per channel. The improvements in the performance-to-cost ratio of the digital correlator chip are achieved with a combination of systolic architecture, novel pipelined differential logic circuits, and standard 1.0 micron CMOS process. Author (revised)

N94-21733*# Jet Propulsion Lab., California Inst. of Tech., Pasadena.
LOW POWER, CMOS DIGITAL AUTOCORRELATOR SPECTROMETER FOR SPACEBORNE APPLICATIONS c19
Kumar Chandra and William J. Wilson *In* Idaho Univ., The 1992 4th NASA SERC Symposium on VLSI Design 1992 12 p (For primary document see N94-21694 05-33)
Avail: CASI HC A03/MF A04

A 128-channel digital autocorrelator spectrometer using four 32 channel low power CMOS correlator chips was built and tested. The CMOS correlator chip uses a 2-bit multiplication algorithm and a full-custom CMOS VLSI design to achieve low DC power consumption. The digital autocorrelator spectrometer has a 20 MHz band width, and the total DC power requirement is 6 Watts. Author (revised)

N94-21734*# Nanyang Technological Inst. (Singapore). School of Applied Science.
A REAL TIME CORRELATOR ARCHITECTURE USING DISTRIBUTED ARITHMETIC PRINCIPLES c60
A. Benjamin Premkumar and T. Srikanthan *In* Idaho Univ., The 1992 4th NASA SERC Symposium on VLSI Design 1992 5 p (For primary document see N94-21694 05-33)
Avail: CASI HC A01/MF A04

A real time correlator design based on the principles of Distributed Arithmetic (DA) is described. This design is shown to be more efficient in terms of memory requirement than the direct DA implementation, especially when the number of coefficients is large. Since the proposed architecture implements the sum of product evaluation, it can be easily extended to finite and infinite response filters. Methods to further reduce the memory requirements are also discussed. A brief comparison is made between the proposed method and different DA implementations. Author (revised)

N94-21735*# Jet Propulsion Lab., California Inst. of Tech., Pasadena.
LOW ENERGY CMOS FOR SPACE APPLICATIONS
Ramesh Panwar and Leon Alkalaj *In* Idaho Univ., The 1992 4th NASA SERC Symposium on VLSI Design 1992 15 p (For primary document see N94-21694 05-33)
Avail: CASI HC A03/MF A04

The current focus of NASA's space flight programs reflects a new thrust towards smaller, less costly, and more frequent space missions, when compared to missions such as Galileo, Magellan, or Cassini. Recently, the concept of a microspacecraft was proposed. In this concept, a small, compact spacecraft that weighs tens of kilograms performs focused scientific objectives such as imaging. Similarly, a Mars Lander micro-rover project is under study that will allow miniature robots weighing less than seven kilograms to explore the Martian surface. To bring the microspacecraft and microrover ideas to fruition, one will have to leverage compact 3D multi-chip module-based multiprocessors (MCM) technologies. Low energy CMOS will become increasingly important because of the thermodynamic considerations in cooling compact 3D MCM implementations and also from considerations of the power budget for space applications. In this paper, we show how the operating voltage is related to the threshold voltage of the CMOS transistors for accomplishing a task in VLSI with minimal energy. We also derive expressions for the noise margins at the optimal operating point. We then look at a low voltage CMOS (LVCMOS) technology developed at Stanford University which improves the power consumption over conventional CMOS by a couple of orders of magnitude and consider the suitability of the technology for space applications by characterizing its SEU immunity. Author (revised)

N94-21753# Lawrence Livermore National Lab., CA.
EFFECTS OF AQUEOUS SOLUTION COMPOSITIONS ON AEROCAPACITOR ENERGY DENSITY
S. T. Mayer, J. L. Kaschmitter, and R. W. Pekala May 1993 11 p Presented at the 183rd Electrochemical Society Meeting, Honolulu, HI, 16-21 May 1993
(Contract W-7405-eng-48)
(DE94-000385; UCRL-JC-112177-Rev-1; CONF-930571-12-Rev-1) Avail: CASI HC A03/MF A01

The Aerocapacitor is an electrochemical double-layer capacitor that uses carbon aerogels as electrodes. The method of fabrication, physical properties, associated electrochemical behavior, and the effects of electrolyte composition on capacitance of carbon aerogel electrodes are discussed. DOE

N94-21762 Los Alamos National Lab., NM.
MAGNETIC INSTABILITY OF KONDO INSULATORS
Ziqiang Wang, Xiao-Ping Li (Rutgers Univ., Piscataway, NJ.), and Dung-Hai Lee (International Business Machines Corp., Yorktown Heights, NY.) 1993 10 p Presented at the International Conference on Strongly Correlated Electron Systems, La Jolla, CA, 16-19 Aug. 1993 Limited Reproducibility: More than 20% of this document may be affected by microfiche quality
(Contract W-7405-eng-36)
(DE93-040064; LA-UR-93-2888; CONF-930865-3) Avail: CASI HC A02

We review a number of experiments on isoelectronic, isostructural ternary compounds CeTSn (T = Ni,Pd,Sn) and alloys CeNi(1-x)(Pd,Pt)(x)Sn, and propose a finite temperature phase diagram describing the evolution of a Kondo insulator to an antiferromagnetic Kondo state with decreasing hybridization or Kondo coupling. We then provide microscopic justifications for the phase diagram by analyzing the magnetic properties of the symmetric Kondo lattice model in two dimensions. DOE

N94-21770 Lawrence Livermore National Lab., CA.
HIGH POWER, ELECTRON-BEAM INDUCED SWITCHING IN DIAMOND
R. D. Scarpetti, W. W. Hofer, D. R. Kania, K. H. Schoenbach, R. P. Joshi, C. Molina, and R. P. Brinkmann (Old Dominion Univ., Norfolk, VA.) Jul. 1993 6 p Presented at the 9th IEEE Pulsed Power Conference, Albuquerque, NM, 21-23 Jun. 1993 Limited Reproducibility: More than 20% of this document may be affected by microfiche quality
(Contract W-7405-eng-48)
(DE93-040535; UCRL-JC-112023; CONF-930616-37) Avail: CASI HC A02

We are developing a high voltage, high average power, electron-beam controlled diamond switch that could significantly impact high power solid-state electronics in industrial and defense applications. An electron-beam controlled thin-film diamond could switch well over 100 kW average power at MHz frequencies, greater than 5 kV, and with high efficiency. This performance is due to the excellent thermal and electronic properties of diamond, the high efficiency achieved with electron beam control, and the demonstrated effectiveness of microchannel cooling. Our electron beam penetration depth measurements agree with our Monte-Carlo calculations. We have not observed electron beam damage in diamond for beam energies up to 150 keV. We describe our experimental and calculational results and research objectives. DOE

N94-21808*# National Aeronautics and Space Administration. Lewis Research Center, Cleveland, OH.

LINEARLY TAPERED SLOT ANTENNA CIRCULAR ARRAY FOR MOBILE COMMUNICATIONS

Rainee N. Simons (Sverdrup Technology, Inc., Cleveland, OH.), Eron Kelly (Princeton Univ., NJ.), Richard Q. Lee, and Susan R. Taub Dec. 1993 5 p Proposed for presentation at the International Conference on Millimeter and Submillimeter Waves and Applications, San Diego, CA, 10-14 Jan. 1994; sponsored by the Society of Photo-Optical Instrumentation Engineers

(Contract NAS3-25266; RTOP 506-44-2C)

(NASA-TM-106441; E-8188; NAS 1.15:106441) Avail: CASI HC A01/MF A01

The design, fabrication and testing of a conformal K-band circular array is presented. The array consists of sixteen linearly tapered slot antennas (LTSA). It is fed by a 1:16 microstrip line power splitter via electromagnetic coupling. The array has an omni-directional pattern in the azimuth plane. In the elevation plane the beam is displaced above the horizon.

Author (revised)

N94-21830 Oak Ridge National Lab., TN.

OPERATION OF A TEST BED AXIAL-GAP BRUSHLESS DC ROTOR WITH A SUPERCONDUCTING STATOR

J. W. McKeever, C. W. Sohns, S. W. Schwenterly, R. W. Young, Sr., V. W. Campbell, M. H. Hickey, G. W. Ott, and J. M. Bailey 1993 42 p Presented at the International Cryogenic Engineering and Materials Conference, Albuquerque, NM, 12-16 Jul. 1993 Limited Reproducibility: More than 20% of this document may be affected by microfiche quality

(Contract DE-AC05-84OR-21400)

(DE93-019167; CONF-930703-21) Avail: CASI HC A03

A variable-speed axial-gap motor with a stator consisting of four liquid helium cooled superconducting electromagnets (two pole pairs) was built and proof tested up to 608 rpm in November 1990 as a tool for joint industry-laboratory evaluation of coils fabricated from high temperature oxide superconductors. A second rotor was fabricated with improved material, winding configuration, and wire type, and the drive system was modified to eliminate current spiking. The modified motor was characterized to design speed, 188 rad/s (1800 rpm), to acquire a performance baseline for future comparison with that of high temperature superconducting (HIS) wire. As it becomes commercially available, HTS wire will replace the low temperature electromagnet wire in a stator modified to control wire temperatures between 4 K and 77 K. Measurements of the superconducting electromagnetic field and locked rotor torque as functions of cryocurrent and dc current through two phases of the rotor, respectively, provided data to estimate power that could be developed by the rotor. Back emf and parasitic mechanical and electromagnetic drag torques were measured as functions of angular velocity to calculate actual rotor power developed and to quantify losses, which reduce the motor's efficiency. A detailed measurement of motor power at design speed confirmed the developed power equation. When subsequently operated at the 33-A maximum available rotor current, the motor delivered 15.3 kW (20.5 hp) to the load. In a final test, the cryostat was operated at 2500 A, 200 A below its critical current. At rotor design current of 60 A and 2500 A stator current, the extrapolated developed power would be 44.2 kW (59.2 hp) with 94% efficiency. DOE

N94-21838# Lawrence Livermore National Lab., CA.

A FET-SWITCHED INDUCTION ACCELERATOR CELL

H. C. Kirbie, W. R. Cravey, S. A. Hawkins, M. A. Newton, and C. W. Ollis 10 Jun. 1993 6 p Presented at the 9th IEEE Pulsed Power Conference, Albuquerque, NM, 21-23 Jun. 1993

(Contract W-7405-eng-48)

(DE93-019604; UCRL-JC-112510; CONF-930616-34) Avail: CASI HC A02/MF A01

In this study, we limited our questions to ORNL discussing their models with almost a dozen staff members from four divisions. We collected some low-level data about the models, and we also tried to gain a sense of the philosophy of the modeler and how each model fit into the larger perspective of ORNL's and the scientific community's efforts. Time and budget prevented us from conducting any larger study, but we have no reason to suppose that conclusions about ORNL's models and modelers could not be extended to the larger scientific community. DOE

N94-21846# Los Alamos National Lab., NM.

SELF ASSEMBLY: AN APPROACH TO TERASCALE INTEGRATION

S. Singer 1993 15 p Presented at the 11th International Invitational Symposium on the Unification of Analytical, Computational, and Experimental Solution Methodologies, Danvers, MA, 18-20 Aug. 1993

(Contract W-7405-eng-36)

(DE93-040104; LA-UR-93-2957; CONF-9308138-2) Avail: CASI HC A03/MF A01

Surely one of the most remarkable accomplishments of modern times has been the miniaturization of electronic components starting with discrete transistors and leading to Very Large Scale Integrated (VLSI) Circuits which will soon contain almost 100 million components in a few square centimeters. It led to an information processing industry that fuels almost every aspect of industrial societies and that has brought manifold benefits to their citizens. Although continuation of the miniaturization process is likely to produce even greater benefits, many experts are concerned that extrapolation of traditional silicon VLSI techniques will meet with increasingly severe difficulties. Some of these are fundamental in nature, e.g., granularity and fluctuations in semiconductors and interconnects and proximity effects such as tunneling. The first major difficulty to be encountered will be a rising cost of products due to increased complexity and difficulty of manufacturing and assembly. Such difficulties are likely to be seen in about 10 years when minimum component sizes are expected to decrease below 0.15 - 0.2 microns. If alternatives to present VLSI techniques are to be available when needed, work on them must start now. At Los Alamos, we are exploring the feasibility of ultrasmall wires and switches that self-assemble themselves into computing elements and circuits. Their operation is based on the quantum properties of nanometer scale molecular clusters. This paper will describe our efforts in the development of these components and will summarize our work in four areas: (1) the development of conducting molecular wires; (2) conducting nanoparticle wires and switches based on the Coulomb Blockade principle; (3) the development of advanced architectures that benefit from the use of such components and that significantly advance the art of high performance computing; and (4) the development of novel methods for attaining sub-Angstrom 3-D non-destructive imaging. DOE

N94-21918# Sandia National Labs., Albuquerque, NM.

MICROMACHINED ACTUATOR AND SENSOR CAPABILITIES AT THE MICROELECTRONICS DEVELOPMENT LABORATORY

J. J. Sniegowski, M. G. Blain, J. G. Fleming, E. J. Garcia, D. R. Koehler, B. K. Smith, and J. H. Smith 1993 5 p Presented at the GOMAC 1993: Government Microcircuit Application Conference, New Orleans, LA, 1-4 Nov. 1993

(Contract DE-AC04-76DP-00789)

(DE93-019417; SAND-93-0816C; CONF-9311101-1) Avail: CASI HC A01/MF A01

This paper briefly summarizes micromachined actuator and sensor capabilities at the Microelectronics Development Laboratory (MDL) of Sandia National Laboratories. These include efforts utilizing either bulk or surface micromachining with silicon substrates. On going developmental projects utilizing both surface and bulk micromachining along with the MDL's effort to integrate a baseline CMOS process with micromachined elements are presented. The paper is broadly divided into three major headings: Surface Micromachined Projects, Bulk Micromachined Projects, and the CMOS/Micromachining Integration Project. DOE

N94-21959# Lawrence Livermore National Lab., CA.

MICROTECHNOLOGY: THE KEY TO THE TECHNICAL CHALLENGES OF THE 21ST CENTURY

N. M. Ceglio Aug. 1993 14 p Presented at the International Seminar on Planetary Emergencies, Erice, Italy, 19-24 Aug. 1993

(Contract W-7405-eng-48)

(DE94-000403; UCRL-JC-115147; CONF-9308168-2) Avail: CASI HC A03/MF A01

Through the ages each culture and civilization has expressed its values and world view in the form of monuments derived from its most advanced and valued technologies. From pyramids to cathedrals, skyscrapers and moon rockets, our technology has enabled us to leave our mark on the landscape and in the minds of our people. In the 21st century, the compelling technology will be that of the micro-world, enabling the fabrication of structures with features smaller than the wavelengths of light. Such structures

will allow us to monitor and control electrical, chemical, and optical phenomena in ways never before imagined. As in the past, we will continue to create monuments, but the technological monuments of the 21st century will likely be viewed through a microscope. This report provides a discussion of microtechnology in the 21st century. DOE

N94-22040# Sandia National Labs., Albuquerque, NM.
ACOUSTIC, FIBER OPTIC, AND SILICON MICROELECTRONIC MICROSENSORS RESEARCH AND DEVELOPMENT ACTIVITIES AT SANDIA NATIONAL LABORATORIES
J. J. Wiczer 1993 7 p Presented at the Sensors Expo Conference, Philadelphia, PA, 26-28 Oct. 1993
(Contract DE-AC04-76DP-00789)
(DE93-019075; SAND-93-1564C; CONF-9310146-1) Avail: CASI HC A02/MF A01

Sandia National Laboratories, an 8500+ person, multiprogram research and development facility operated for the US Department of Energy, has over 400 research, development and applications scientists and engineers working on sensor technologies. Sandia's 20 person Microsensors Research and Development Department has invented, developed and fielded sensor systems based on acoustic, fiber optic, and silicon microelectronic technologies. These sensors have been used for diverse applications inducting the monitoring of cleaning chemical concentrations in industrial process effluent streams, detection of explosive gas concentrations in aging industrial equipment, real-time measurements of fluid viscosity in equipment lubricants, and monitoring of contaminant concentration levels in ultrapure process gases. Representative sensor technologies available for technology transfer will be described including bulk acoustic wave resonators, surface acoustic wave devices, fiber optic micromirror sensors, and silicon microelectronic sensors. DOE

N94-22101 Engineering Inst. of Canada, Montreal (Quebec). Canadian Society for Electrical and Computer Engineering.
CANADIAN CONFERENCE ON ELECTRICAL AND COMPUTER ENGINEERING, VOLUMES 1 AND 2
1991 1402 p In ENGLISH and FRENCH Conference held in Quebec City, Quebec, 25-27 Sep. 1991; sponsored by CSECE and IEEE
(ISBN-0-9694170-2-0; CTN-94-60867) Avail: Issuing Activity (Engineering Inst. of Canada, 2050 rue Mansfield, Suite 700, Montreal, PQ H3A 1Z2 Canada)

A conference was held to facilitate exchange of information and research on various topics related to electrical and computer engineering. Papers were presented on neural networks, communications, power systems, computer vision, very large scale integration, software testing, computer architectures, signal processing, radar, electrical machines modelling and design, microwave landing systems, computer algorithms, antennas, artificial intelligence, permanent magnet machines, software development, power electronics applications, image processing, microwave circuits and components, computing systems, spectrum management, parallel processing, process control, resonant power supplies, speech processing, computer reliability and fault tolerance, industrial materials, coding, optical processing, digital modulation, biomedical applications, alternate energy, robotics, legal and administration issues, and electromagnetics. For individual titles, see N94-22102 through N94-22256.

N94-22102 Concordia Univ., Montreal (Quebec). Center for Signal Processing and Communications.
ESTIMATION OF AR SIGNAL PATTERNS USING COMPETITIVE NEURAL NETWORKS **c32**
Keqin Gao, M. Omair Ahmad, and M. N. S. Swamy *In* Engineering Inst. of Canada, Canadian Conference on Electrical and Computer Engineering, Volumes 1 and 2 1991 4 p (For primary document see N94-22101 05-33)
Avail: Issuing Activity (Engineering Inst. of Canada, 2050 rue Mansfield, Suite 700, Montreal, PQ H3A 1Z2 Canada)

The estimation of signals which are outputs of several unknown signal generating systems is investigated. The case of signals generated from autoregressive (AR) systems is discussed. A limited number of AR predictors are used to estimate the signals. Each of them is treated as a neuron in a competitive neural network. Competition is performed among the neurons to determine which neuron represents the current signal segment, and the weight vector of the winner is updated by an approximate gradient algorithm. The signal representation achieved with the neural network is in the parameter space of the signal model, while the inputs to the network are observed samples. Two advanced competitive algorithms, namely weighted initial competition and Kohonen's self-organizing map, are used in the current scheme. Simulation results are presented to illustrate the performance for various cases. Author (CISTI)

N94-22103 Maryland Univ., Princess Anne.
SIGNAL CLASSIFICATION AND NOISE FILTERING USING ARTIFICIAL NEURAL NETWORKS **c32**
Andrew M. Veronis and Demetri Michalopoulos (California State Univ., Fullerton.) *In* Engineering Inst. of Canada, Canadian Conference on Electrical and Computer Engineering, Volumes 1 and 2 1991 4 p (For primary document see N94-22101 05-33)
Avail: Issuing Activity (Engineering Inst. of Canada, 2050 rue Mansfield, Suite 700, Montreal, PQ H3A 1Z2 Canada)

An approach is presented for filtering and classifying communication signals using artificial neural networks. Two separate neural network topologies are used to accompliish the task. A recirculation network is employed to implement noise filtering and a probabilistic network to implement classification. An analysis is provided of the classification of signals in the presence of extensive noise. The communications signals used for data analysis were digitally reproduced amplitude-, frequency-, and phase-shift keying waveforms. The ability of a neural network to detect and identify imperfections characteristic of transmitter faults is also explored. The faults injected into the neural network system seek to simulate data from various stations, such that the neural network's ability to isolate a signal to a particular source is being modeled. Finally, suggestions for further enhancement are suggested. Author (CISTI)

N94-22104 Windsor Univ. (Ontario). Dept. of Electrical Engineering.
NOISE FILTERING USING MULTILAYER FEEDFORWARD NEURAL NETWORK
Hon-Keung Kwan *In* Engineering Inst. of Canada, Canadian Conference on Electrical and Computer Engineering, Volumes 1 and 2 1991 4 p (For primary document see N94-22101 05-33)
Avail: Issuing Activity (Engineering Inst. of Canada, 2050 rue Mansfield, Suite 700, Montreal, PQ H3A 1Z2 Canada)

A feedforward neural network for random noise filtering was developed, consisting of an N-input N-output L-layer feedforward structure. The number of neurons at each of its hidden layers can be flexible. The network is trained to recognize the original form of signal contaminated by random noise. After training, the network can be used to filter out a noisy signal. The learning algorithm used by the network is described and preliminary simulation results are presented of a two-layer feedforward network with nine inputs, nine hidden neurons, and nine output neurons. The results indicate that such a network can be used for filtering random noise. However, the effectiveness of the method depends very much on training, which is time-consuming. Author (CISTI)

N94-22105 Laval Univ. (Quebec). Lab. de Vision et Systemes Numeriques.
A 3-D VISION METHOD FOR ESTIMATING WORKSPACE OCCUPANCY OF A POWER-LINE MAINTENANCE ROBOT **c63**
Alain Croteau, Denis Laurendeau, and Jean Lessard (Institut de Recherche de l'Hydro-Quebec, Varennes.) *In* Engineering Inst. of Canada, Canadian Conference on Electrical and Computer Engineering, Volumes 1 and 2 1991 4 p (For primary document see N94-22101 05-33)
Avail: Issuing Activity (Engineering Inst. of Canada, 2050 rue Mansfield, Suite 700, Montreal, PQ H3A 1Z2 Canada)

A telerobotic system for power-line maintenance is equipped with a laser range-finder allowing it to perform an estimation of its workspace occupancy. The model used for describing space occupancy is described, along with the three dimensional computer vision method developed for extracting this information. The model consists in building an octree of the scene from several range images taken from various points of view. A calibration is performed using the first image in order to find the initial position of the camera relative to the scene. Successive three dimensional images are used to complete the model information until a satisfactory knowledge of the space occupancy is reached. Author (CISTI)

N94-22106 Toronto Univ. (Ontario). Dept. of Electrical Engineering.
DIRECTIONAL CODING OF MORPHOLOGICAL PYRAMIDAL REPRESENTATIONS **c61**
Zi-Heng Zhou and Anatasios N. Venetsanopoulos *In* Engineering Inst. of Canada, Canadian Conference on Electrical and Computer Engineering, Volumes 1 and 2 1991 4 p (For primary document see N94-22101 05-33)
Avail: Issuing Activity (Engineering Inst. of Canada, 2050 rue Mansfield, Suite 700, Montreal, PQ H3A 1Z2 Canada)

Morphological directional decomposition based image coding is a novel coding method for achieving high compression ratio while preserving spatial image features. A previous study is extended to focus on the structure and the analysis of the morphological direction filter bank used for directional feature decomposition. Four basic morphological filters are reviewed, and a multiresolution morphological representation called feature-width morphological pyramid is discussed. This pyramid is used for the extraction of image features at various resolutions. A more sophisticated 8-direction filter bank is introduced to replace the simple 4-direction bank, and its directional characteristics are analyzed. The directional decomposition coding method is then presented along with experimental results. The advantage of the new method is an additional 60 percent bit rate reduction achieved from feature coding. Author (CISTI)

N94-22107 Toronto Univ. (Ontario). Computer Integrated Manufacturing Lab.
OPTIMAL OBJECT MODELLING FOR AN ACTIVE-VISION SYSTEM **c63**
X. He, B. Benhabib, and K. C. Smith *In* Engineering Inst. of Canada, Canadian Conference on Electrical and Computer Engineering, Volumes 1 and 2 1991 4 p (For primary document see N94-22101 05-33)
Avail: Issuing Activity (Engineering Inst. of Canada, 2050 rue Mansfield, Suite 700, Montreal, PQ H3A 1Z2 Canada)

A new active-vision system is under development in order to develop an efficient three dimensional object recognition method for vision-based robotic assembly. In this system, objects are pre-marked with artificial markers in order to simplify the image analysis process. In this context, objects are represented in the vision model by a small set of their two dimensional perspective projections, referred to as standard-views, where each standard-view is defined by a corresponding marker. The optimal number of markers and their best locations on the objects must be determined a priori so that the objects can be efficiently modeled. A solution to this optimization problem is presented, where for a given set of objects the number of markers is minimized and the distinctiveness of the standard-views which are determined by these markers is maximized. An algorithm based on dynamic programming is developed to reach the solution. Author (CISTI)

N94-22108 Laval Univ. (Quebec). Lab. de Vision et Systemes Numeriques.
HIERARCHICAL SURFACE TRIANGULATION OF RANGE DATA **c61**
Marc Soucy and Denis Laurendeau *In* Engineering Inst. of Canada, Canadian Conference on Electrical and Computer Engineering, Volumes 1 and 2 1991 4 p (For primary document see N94-22101 05-33)
Avail: Issuing Activity (Engineering Inst. of Canada, 2050 rue Mansfield, Suite 700, Montreal, PQ H3A 1Z2 Canada)

A surface triangulation technique is presented which describes surfaces at different levels of resolution in a range image. A two-dimensional Delaunay triangulation of all points is first computed in the parametric grid of the range view. Then, a sequential optimization process removes, at each iteration, the point that minimizes the local retriangulation approximation error caused by its removal. The process can be stopped at any time to obtain a desired level of approximation error. Practical aspects of the implementation of the hierarchical triangulation algorithm are discussed. The data structures issued to represent a triangulation and control the sequential optimization process are described, and it is shown how these structures can be used to increase the speed of the algorithm. The retriangulation of a region after a point is removed from the triangulation is explained. Author (CISTI)

N94-22109 Concordia Univ., Montreal (Quebec). Dept. of Computer Science.
SEGMENTATION AND FITTING BY RESIDUAL CONSENSUS **c61**
Xin-Ming Yu, T. D. Bui, and A. Krzyzak *In* Engineering Inst. of Canada, Canadian Conference on Electrical and Computer Engineering, Volumes 1 and 2 1991 4 p (For primary document see N94-22101 05-33)
Avail: Issuing Activity (Engineering Inst. of Canada, 2050 rue Mansfield, Suite 700, Montreal, PQ H3A 1Z2 Canada)

A robust segmentation and surface fitting technique is presented which is very useful for computer vision based on range images. The method randomly samples appropriate image points and fits them into selected primitive types. From K samples, residual consensus is measured to choose a best fitting for a homogeneous surface patch. The residual consensus algorithm is not sensitive to outliers. A convergable histogram method is used to measure and compare residuals on various noise levels. The method segments data points of range images into first and second order primitives, and works very well even in smooth connected curve regions. Author (CISTI)

N94-22110 Queens Univ., Kingston (Ontario). Dept. of Electrical Engineering.
VLSI ARCHITECTURES FOR THE NEW (T,L) ALGORITHM **c32**
P. A. Bengough and S. J. Simmons *In* Engineering Inst. of Canada, Canadian Conference on Electrical and Computer Engineering, Volumes 1 and 2 1991 4 p (For primary document see N94-22101 05-33)
Avail: Issuing Activity (Engineering Inst. of Canada, 2050 rue Mansfield, Suite 700, Montreal, PQ H3A 1Z2 Canada)

Trellis coding techniques have seen much use in error correction codes for space and satellite applications. When long sequences of data are encoded, the number of possible paths through the trellis becomes great and a trellis search algorithm must be used to determine the path that best matches the received data sequence. The (T,L) algorithm is a new reduced complexity trellis search algorithm, applicable to data sequence estimation in digital communications, that adapts to changing channel conditions. Its simplicity and inherent parallelism suits it well for very large scale integration (VLSI) implementation. A number of alternative VLSI architectures are presented which can be used to realize this algorithm. While one uses a simple nonsorting structure, two other sorting designs based on parallel insertion and weavesorting algorithms are proposed. The area-time performance of the various architectures is compared. Author (CISTI)

N94-22111 Windsor Univ. (Ontario). Very Large Scale Integration Research Group.
AN IN-PLACE AND IN-ORDER ALGORITHM FOR THE DISCRETE COSINE TRANSFORM **c64**
Zhong-De Wang, G. A. Jullien, and J. J. Soltis *In* Engineering Inst. of Canada, Canadian Conference on Electrical and Computer Engineering, Volumes 1 and 2 1991 4 p (For primary document see N94-22101 05-33)
Avail: Issuing Activity (Engineering Inst. of Canada, 2050 rue Mansfield, Suite 700, Montreal, PQ H3A 1Z2 Canada)

An in place and in order algorithm for the discrete cosine transform (DCT) is introduced. The algorithm is based on the cosine factor fast cosine transform (CFFCT) algorithm which uses the Hadamard order for the indexing of the input sequence. A method to embed the unscrambling of the Hadamard ordering into the butterfly structure of the CFFCT leads to an in place and in order algorithm for the DCT. An in place and in order algorithm for the inverse DCT (IDCT) can be obtained simply by reversing the signal flowgraph, and the algorithm can be applied to both the DCT and the IDCT. Author (CISTI)

N94-22112 Waterloo Univ. (Ontario). Very Large Scale Integration Group.
FORMAL HARDWARE VERIFICATION IN MAPLE **c60**
F. Mavaddat *In* Engineering Inst. of Canada, Canadian Conference on Electrical and Computer Engineering, Volumes 1 and 2 1991 5 p (For primary document see N94-22101 05-33)
Avail: Issuing Activity (Engineering Inst. of Canada, 2050 rue Mansfield, Suite 700, Montreal, PQ H3A 1Z2 Canada)

A model is proposed for the Maple based specification of synchronous hardware, to aid in formal verification of several classes of hardware designs. Maple is an algebraic system for symbolic computation, and is also a programming language primarily used for algebraic computations. Given a Maple model (a program) of a design, the program is executed to derive

the system's symbolic behavior. The Maple model is also used to compare the derived and reference behaviors. The advantages of the Maple verification method are: (1) simplicity of the input language; (2) emphasis on arithmetic domain; and (3) strength of the methodology. The Maple based proof technique is applied to combinational circuits, sequential circuits and counters to illustrate the method. Author (CISTI)

N94-22113 Queens Univ., Kingston (Ontario). Dept. of Electrical Engineering.

SYSTEM LEVEL MODELLING USING PETRI NETS AND VHDL **c60**

A. C. Woo and L. E. Peppard *In* Engineering Inst. of Canada, Canadian Conference on Electrical and Computer Engineering, Volumes 1 and 2 1991 4 p (For primary document see N94-22101 05-33)

Avail: Issuing Activity (Engineering Inst. of Canada, 2050 rue Mansfield, Suite 700, Montreal, PQ H3A 1Z2 Canada)

Petri nets offer very large scale integration (VLSI) system designers a powerful modelling paradigm at the highest level of abstraction. Hardware description languages such as VHDL were created to capture designs at all levels of abstraction, but often require more detail than is available at preliminary stages of design. Four criteria for the translation of high level modelling paradigms into VHDL are: (1) the VHDL code must functionally model the behavior of the original system; (2) the resulting code should be efficient, both in execution and in the number of lines of code; (3) the VHDL code should be clear so that the original structure is evident; and (4) the amount of VHDL code should grow linearly with increasing complexity of the original description. To illustrate the process the dining philosophers problem is modeled with a petri net and translated into VHDL. Two aspects of VHDL, the lack of global variables and the lack of a random number generator, significantly increased the inefficiency of the simulation.

Author (CISTI)

N94-22114 Calgary Univ. (Alberta). Very Large Scale Integration and Verification Lab.

FORMAL VERIFICATION OF AN ALU **c60**

G. Birtwistle *In* Engineering Inst. of Canada, Canadian Conference on Electrical and Computer Engineering, Volumes 1 and 2 1991 4 p (For primary document see N94-22101 05-33)

Avail: Issuing Activity (Engineering Inst. of Canada, 2050 rue Mansfield, Suite 700, Montreal, PQ H3A 1Z2 Canada)

The formal verification of an adder based arithmetic logic unit (ALU) is outlined. The formal verification was undertaken using the HOL proof assistant and took 4 weeks. The proof was conducted from the bottom up and was partitioned as: (1) specifying and verifying the half adder and full adder; (2) specifying and verifying the ripple carry adder; (3) specifying and verifying the modified adder subsystem; (4) specifying and verifying the bank of input filters; and (5) completing the hierarchy by wiring together the modified adder subsystem and the bank of input filters, and proving that it meets specification. The formal verification was faster than that recorded for a similar verification using a more automated first order system, and was far quicker than would be possible using simulation. The proof methodology used the proof assistant itself to increase confidence in specifications by unfolding their definitions (symbolic simulation) and also proving some of their consequences. Author (CISTI)

N94-22115 Waterloo Univ. (Ontario). Dept. of Electrical and Computer Engineering.

IMPACT OF PARTITIONING ON PARALLEL DISCRETE EVENT SIMULATION OF LOGIC CIRCUITS

B. Nandy and W. M. Loucks *In* Engineering Inst. of Canada, Canadian Conference on Electrical and Computer Engineering, Volumes 1 and 2 1991 4 p (For primary document see N94-22101 05-33)

Avail: Issuing Activity (Engineering Inst. of Canada, 2050 rue Mansfield, Suite 700, Montreal, PQ H3A 1Z2 Canada)

The issue of partitioning for parallel discrete event simulation (PDES) of logic circuits is addressed. An analysis is performed to calculate the upperbound of the simulation performance improvement and the available concurrency in the circuit. An efficient iterative improvement algorithm similar to Fidducia-Mattheyse (1982) for effective partitioning of the logic circuit simulation is presented. The algorithm attempts to minimize the communication overhead and uniformly distribute the execution load among the processors. The partitioned circuit has been simulated on a transputer network. It shows that performance of conservative logic simulation can be improved with proper partitioning of circuits over random partition by 10-15 percent. Author (CISTI)

N94-22116 Ecole Polytechnique, Montreal (Quebec). Dept. de Genie Electrique.

TESTS OF LOGIC SPACES: A NEW STRATEGY FOR CERTIFYING THE ACCURACY OF PROGRAMS [TESTS DES ESPACES LOGIQUES: UNE NOUVELLE STRATEGIE POUR CERTIFIER L'EXACTITUDE DES PROGRAMMES] **c61**

Pierre Veronneau and Pierre-N. Robillard *In* Engineering Inst. of Canada, Canadian Conference on Electrical and Computer Engineering, Volumes 1 and 2 1991 4 p In FRENCH (For primary document see N94-22101 05-33)

Avail: Issuing Activity (Engineering Inst. of Canada, 2050 rue Mansfield, Suite 700, Montreal, PQ H3A 1Z2 Canada)

A new strategy applied to program testing is presented. The strategy certifies the absence of errors in the logic spaces of a program. Every program decomposes into a finite number of logic spaces. The output variables of a logic space aro modeled by vector, polynomial, or multinomial space. A finite number of tests are then required for certifying the absence of calculation errors in the logic space. The absence of errors is defined with respect to the requirements or real specifications of the program. Earlier research has demonstrated that the number of tests is finite for any program encountering this model. This test strategy is applied to payroll software having various types of data such as pointers, matrices, and data in dynamic memory. In addition, the strategy determines the extent and veracity of global predicates always with respect to the program requirements or specifications. The limits and possibilities of this strategy are discussed. Author (CISTI)

N94-22117 Bell-Northern Research Ltd., Ottawa (Ontario).

MODELING SOFTWARE SYSTEMS FOR DATA FLOW TESTING **c61**

Bo Yang and Hasan Ural (Ottawa Univ., Ontario.) *In* Engineering Inst. of Canada, Canadian Conference on Electrical and Computer Engineering, Volumes 1 and 2 1991 4 p (For primary document see N94-22101 05-33)

Avail: Issuing Activity (Engineering Inst. of Canada, 2050 rue Mansfield, Suite 700, Montreal, PQ H3A 1Z2 Canada)

Software modeling is very useful in software analysis and testing. Data flow testing requires selection of execution paths such that each individual, sequence, or group of data flow associations, known as definition-use pairs or du-pairs, captured in a program model are covered to a certain extent. For data flow testing, it is necessary to have a model which is capable of representing both control flow and data flow in a program. The well known def-use graph (DUG) is such a model. It is shown that DUG as well as some other program models are incapable of accurately representing inter-procedural data flow. DUG is then extended to overcome the problem. It is illustrated with a Pascal program that more accurate data flow testing can be achieved if the program is modeled by an extended DUG (EDUG). The EDUG consists of a DUG for each procedure, including the main procedure. The EDUG resolves many issues in modeling inter-procedural data flow and is capable of modeling control flow as well as both intra-procedural and inter-procedural data flow in a subprogram.

Author (CISTI)

N94-22118 Mitsubishi Electric Corp., Kamakura (Japan). Communication Systems Lab.

THE CONFORMANCE TESTING METHODOLOGY TO CTRON (COMMUNICATION AND CENTRAL TRON) EXTENDED OS **c61**

Yoshiaki Terashima, Hiroshi Matsuyama, Akira Otsuka, and Tsutomu Iwahashi *In* Engineering Inst. of Canada, Canadian Conference on Electrical and Computer Engineering, Volumes 1 and 2 1991 4 p (For primary document see N94-22101 05-33)

Avail: Issuing Activity (Engineering Inst. of Canada, 2050 rue Mansfield, Suite 700, Montreal, PQ H3A 1Z2 Canada)

A conformance testing methodology of communication softwares is presented. The test objective is to achieve portability not only in protocol service level but also in programming interface level. OSI was chosen as the protocol service level standard, and CTRON (communications and central TRON) was chosen as the programming interface level specification. OSI protocol standards have been studied to keep connectibility between different

implementations. The objective of the testing methodology is to determine whether implementations are conformed to the OSI protocol standards at the points of communication control block (CCB) specification. The methodology accords with OSI conformance testing methodology and framework in an abstract test level, and provides a method to carry out conformance tests in an execute level. Two tools are offered to support the methodology: a customization environment for a specific layer interface and a development environment of test scenario programs. The methodology was applied to PBX software development and its feasibility and efficiency were confirmed. Author (CISTI)

N94-22119 Concordia Univ., Montreal (Quebec). Dept. of Electrical Engineering.

A SHARED BUFFER MEMORY SWITCH WITH MAXIMUM QUEUE AND MINIMUM ALLOCATION **c60**

Xing Chen and Jeremiah F. Hayes *In* Engineering Inst. of Canada, Canadian Conference on Electrical and Computer Engineering, Volumes 1 and 2 1991 4 p (For primary document see N94-22101 05-33)

Avail: Issuing Activity (Engineering Inst. of Canada, 2050 rue Mansfield, Suite 700, Montreal, PQ H3A 1Z2 Canada)

Buffering is required in any type of packet switch structure in order to avoid packet loss whenever there are multiple input packets arriving for the same output. A shared buffer memory switch architecture is proposed. In this switch, a shared buffer pool and a dedicated buffer pool are properly handled for switching and buffering the packets. Being able to prevent monopolization of shared buffers and to secure a full utilization of all the N output channels, the sharing policy with maximum queue and minimum allocation provides good traffic characteristics especially under unbalanced or bursty traffic. The packet loss rate is examined under both balanced and unbalanced traffic. Author (CISTI)

N94-22120 Concordia Univ., Montreal (Quebec). Dept. of Electrical Engineering.

A ONE-SHOT ACCESS SCHEME FOR A MULTICAST SWITCH

Xing Chen, Jeremiah F. Hayes, and M. K. Mehmet Ali *In* Engineering Inst. of Canada, Canadian Conference on Electrical and Computer Engineering, Volumes 1 and 2 1991 4 p (For primary document see N94-22101 05-33)

Avail: Issuing Activity (Engineering Inst. of Canada, 2050 rue Mansfield, Suite 700, Montreal, PQ H3A 1Z2 Canada)

The capability of handling multipoint connections is essential for many communication needs. Input port queueing along with a contention resolution algorithm is used to resolve output request conflict. A study of the performance of a one-shot access scheme for a multicast packet switch is presented. The analysis is based on an assumption of random traffic, modeled by a Bernoulli process of packet arrival and Bernoulli trials of copy distribution patterns. Input port queueing along with random-selection policy is used to resolve the output request conflict. The primary performance measurement is the packet delay. A key assumption is that all copies of the same packet must be switched in the same slot. This one-shot discipline is easier to implement than one which disperses transmission over several time slots in small or medium size switching. Simulation results agree almost perfectly with the analysis. Author (CISTI)

N94-22121 Ecole Polytechnique, Montreal (Quebec). Dept. of Electrical and Computer Engineering.

SORTING NETWORK FOR THE PARTIAL SELECTION PROBLEM

Jean Belzile, Yvon Savaria, and David Haccoun *In* Engineering Inst. of Canada, Canadian Conference on Electrical and Computer Engineering, Volumes 1 and 2 1991 4 p (For primary document see N94-22101 05-33)

Avail: Issuing Activity (Engineering Inst. of Canada, 2050 rue Mansfield, Suite 700, Montreal, PQ H3A 1Z2 Canada)

Sorting networks and switching networks are widely used in the communication world. Partial selection networks have applications in areas where a single answer is desired but several paths are explored such as in suboptimal breadth-first tree searching algorithms. A technique is introduced which permits the evaluation of any network in terms of average selection and in terms of the number of elements that are always in the partial selection set. The Banyan network was examined using the method and it was found that the quality of the selection decreases as the size of the input set grows. It was also shown that the sorting networks such as the Banyan are not necessarily the best choices for selection problems. Networks which partially sort two sets and then compare the two sets together can achieve much better selection. These two types of network offer a higher number of guaranteed items than the Banyan network for all considered values of elements. Finally, it was noted that deterministic pre-ordering, if present, can also be used to configure a network. Author (CISTI)

N94-22122 Calcutta Univ. (India). Dept. of Applied Physics.

ADDITION OF DECIMAL NUMBERS IN OPTICAL COMPUTING ARCHITECTURE BY WALSH CODED DIGITS **c60**

Asit K. Datta and Sunit K. Sen *In* Engineering Inst. of Canada, Canadian Conference on Electrical and Computer Engineering, Volumes 1 and 2 1991 3 p (For primary document see N94-22101 05-33)

Avail: Issuing Activity (Engineering Inst. of Canada, 2050 rue Mansfield, Suite 700, Montreal, PQ H3A 1Z2 Canada)

In the addition of two numbers in optical computing, the need for a 'carry' limits the parallel operation unless some form of coding of numbers is taken into consideration. To overcome this difficulty and also retain the advantageous inherent parallel processing capabilities of optical computing architecture, a method of addition is proposed where the decimal numbers are represented by respective Walsh functions. Addition of Walsh functions is carried out bit-wise in an optical computing architecture where 1 is represented by the presence and 0 by the absence of light. Carry is accommodated by the addition of a carry Walsh wave which is selected according to an index sequence generated after 'shift to the left' operation. Author (CISTI)

N94-22123 McMaster Univ., Hamilton (Ontario). Dept. of Electrical and Computer Engineering.

IMPROVEMENTS ON THE DESIGN OF OPTIMUM SAW FILTERS WITH THE REMEZ EXCHANGE ALGORITHM

Peter M. Smith and Peter J. Edmonson (Mohawk Coll., Hamilton, Ontario.) *In* Engineering Inst. of Canada, Canadian Conference on Electrical and Computer Engineering, Volumes 1 and 2 1991 4 p (For primary document see N94-22101 05-33)

Avail: Issuing Activity (Engineering Inst. of Canada, 2050 rue Mansfield, Suite 700, Montreal, PQ H3A 1Z2 Canada)

Linear phase surface acoustic wave (SAW) devices are usually designed by using methods developed for digital filters. A method for improving the sidelobe suppression of surface acoustic wave filters designed with the Remez exchange algorithm is presented. The Remez exchange algorithm is a numerically intensive optimization method used in the transducer design, and has been shown to be directly applicable to the design of SAW single and multiple passband filters, SAW notch filters, and SAW spectral shaping filters. The algorithm iteratively performs a search for extremal frequencies and computes the corresponding frequency response until an equiripple response is obtained. By choosing the sampling rate in the output transducer such that the ripples in its frequency response misalign with those of the input transducer, improvements in suppression of up to 5 decibels are reported with no degradation in the passband response. Both theoretical and experimental results are presented. Author (CISTI)

N94-22124 Communications Research Centre, Ottawa (Ontario). Dept. of Communications.

SOFTWARE IMPLEMENTATION OF AN ADAPTIVE DIGITAL AUTOMATIC LEVEL CONTROL **c61**

Y. Jolly *In* Engineering Inst. of Canada, Canadian Conference on Electrical and Computer Engineering, Volumes 1 and 2 1991 4 p (For primary document see N94-22101 05-33)

Avail: Issuing Activity (Engineering Inst. of Canada, 2050 rue Mansfield, Suite 700, Montreal, PQ H3A 1Z2 Canada)

One of the problems encountered when implementing algorithms on a fixed point digital signal processor is the need to fully use the available dynamic range, in order to reduce the effects of quantization noise and the accumulation of roundoff error. The problem can be quite severe with speech applications, where the input signal level varies considerably, not only as a function of the speaker but also as a function of his position relative to the handset or microphone. An adaptive digital automatic level control (ALC) algorithm is described. It was designed to adapt the input level of various signals encountered in many applications, particularly toll quality speech. The algorithm enables better use to be made of the dynamic

range available on 16 and 32 bits fixed-point microprocessors. The implementation is done in software using a microprocessor, requiring a high resolution (12 bits and up) analog to digital converter and a few clock cycles from the processor. No delay is introduced in the signal path by the use of the algorithm. It can be added to most microprocessor based speech codes without any hardware modification. Author (CISTI)

N94-22125 Carleton Univ., Ottawa (Ontario). Dept. of Systems and Computer Engineering.

SUB-BAND ADAPTIVE NOISE CANCELLING

James G. Ryan and Rafik A. Goubran *In* Engineering Inst. of Canada, Canadian Conference on Electrical and Computer Engineering, Volumes 1 and 2 1991 4 p (For primary document see N94-22101 05-33)

Avail: Issuing Activity (Engineering Inst. of Canada, 2050 rue Mansfield, Suite 700, Montreal, PQ H3A 1Z2 Canada)

The technique of using sub-band adaptive filters for acoustic noise suppression is examined. Simulation results are presented for experimental systems trained with white noise and colored noise for both decimated and non-decimated sub-band signals. To illustrate the usefulness of the sub-band approach for a real application, the full band and sub-band noise cancellers were applied to car data. Estimates of the input and output power spectra for the different cases are presented. It is shown that the full-band noise canceller is unable to attenuate the noise in the higher frequencies due to the low input signal power in this region. The sub-band decomposition of the input signal can significantly increase the rate as compared to a full-band implementation under certain conditions. This increase in convergence speed is manifested as an increased noise attenuation in those regions of the input spectrum with relatively low amounts of power. In addition, the sub-band processing is seen to eliminate the noise enhancement phenomenon found in acoustic noise cancellers for mobile telephony. Author (CISTI)

N94-22126 Concordia Univ., Montreal (Quebec). Dept. of Electrical and Computer Engineering.

IMPROVEMENTS IN ANTENNA COUPLING PATH ALGORITHMS FOR AIRCRAFT EMC ANALYSIS **c32**

Michael Bogusz and Stanley J. Kibina *In* Engineering Inst. of Canada, Canadian Conference on Electrical and Computer Engineering, Volumes 1 and 2 1991 4 p (For primary document see N94-22101 05-33)

Avail: Issuing Activity (Engineering Inst. of Canada, 2050 rue Mansfield, Suite 700, Montreal, PQ H3A 1Z2 Canada)

The algorithms to calculate and display the path of maximum electromagnetic interference coupling along the perfectly conducting surface of a frustrum cone model of an aircraft nose are developed and revised for the Aircraft Inter-Antenna Propagation with Graphics (AAPG) electromagnetic compatibility analysis code. Analysis of the coupling problem geometry on the frustrum cone model and representative numerical test cases reveal how the revised algorithms are more accurate than their predecessors. These improvements in accuracy and their impact on realistic aircraft electromagnetic compatibility problems are outlined.

Author (CISTI)

N94-22127 Laval Univ. (Quebec). Dept. Genie Electrique.

CALCULATION OF A DIFFRACTED ELECTRIC FIELD WITH THE AID OF THE METHOD OF EQUIVALENT CURRENTS (MEC) [CALCUL DU CHAMP ELECTRIQUE DIFFRACTE A L'AIDE DE LA METHODE DES COURANTS EQUIVALENTS (MEC)] **c32**

J. Raymond, G. Y. Delisle, J. Bedard (Defence Research Establishment Valcartier, Quebec.), and Y. deVilliers (Defence Research Establishment Valcartier, Quebec.) *In* Engineering Inst. of Canada, Canadian Conference on Electrical and Computer Engineering, Volumes 1 and 2 1991 4 p In FRENCH (For primary document see N94-22101 05-33)

Avail: Issuing Activity (Engineering Inst. of Canada, 2050 rue Mansfield, Suite 700, Montreal, PQ H3A 1Z2 Canada)

The method of equivalent currents (MEC) is a technique for modelling the electric field diffracted by any target, applicable in the high frequency region. The method is based essentially on one or several contour integrals, according to the number of contours comprising the target, of different theoretical electric and magnetic currents generated along the target. These currents are determined starting from a mixture of the diffraction coefficients and the approximation of the field diffracted by a corner, deduced with the aid of the physical theory of diffraction. This method is independent of the directions of incidence and observation. The general concepts on which the MEC rests and some results are presented in the monostatic case during which a cylinder is irradiated by an electromagnetic wave polarized vertically. Author (CISTI)

N94-22128 Concordia Univ., Montreal (Quebec). EMC Lab.

RCS OF SHIPS AND AIRCRAFT AT HF FREQUENCIES **c32**

C. W. Trueman, S. J. Kubina, S. R. Mishra (Canadian Space Agency, Ottawa, Ontario.), and C. Larose (Canadian Space Agency, Ottawa, Ontario.) *In* Engineering Inst. of Canada, Canadian Conference on Electrical and Computer Engineering, Volumes 1 and 2 1991 4 p (For primary document see N94-22101 05-33)

Avail: Issuing Activity (Engineering Inst. of Canada, 2050 rue Mansfield, Suite 700, Montreal, PQ H3A 1Z2 Canada)

Coastal radar operating at high frequency (HF) has the potential of monitoring iceberg movement and ship and aircraft traffic over a wide area of ocean. The HF radar cross-section of an aircraft-like scatterer of simple geometry is investigated. At these frequencies, the aircraft size is comparable to the wavelength. The aircraft radar cross-section (RCS) is obtained both by computation and by direct measurement. It is demonstrated that at low frequencies in the HF range, the dorsal fin is the dominant scatterer, but at high HF the fuselage can scatter more strongly than the dorsal fin. Aircraft often carry wire antennas for HF communication, and it is shown that such wires can dramatically alter the RCS of the aircraft near the resonant frequencies of the wire. The RCS of a ship modelled as a parallelepiped with mast is 20-30 decibels larger than that of an aircraft, and is dominated at low HF by the contribution of the mast.

Author (CISTI)

N94-22129 Toronto Univ. (Ontario). Computer Integrated Manufacturing Lab.

THE CONCEPTUAL DESIGN OF A SHORT-RANGE DISTANCE SENSOR **c74**

S. Jacobi and B. Benhabib *In* Engineering Inst. of Canada, Canadian Conference on Electrical and Computer Engineering, Volumes 1 and 2 1991 4 p (For primary document see N94-22101 05-33)

Avail: Issuing Activity (Engineering Inst. of Canada, 2050 rue Mansfield, Suite 700, Montreal, PQ H3A 1Z2 Canada)

The conceptual design and analysis of an electro-optical, short-range distance sensor is presented. The sensor is based on the intensity measurement of modulated light signals reflected from the surface of an object whose distance is to be measured. In order to overcome the susceptibility to surface reflectivity of most range-finding sensors, which are based on light-intensity measurements, the proposed sensor uses two in-line detectors. The intensity of a reflected light beam is measured at two different distances from the illuminated surface. The combined information from the two detectors results in distance measurements robust to surface characteristics and surface inclination. The computer simulation of a mathematical model representation indicates acceptable accuracy levels of the computed distance in the range of 0 to 50 mm. This is achieved with surface inclination up to 30 deg with respect to the light beam direction, and with a variable nature of the illuminated surface. Author (CISTI)

N94-22130 Toronto Univ. (Ontario). Computer Integrated Manufacturing Lab.

SENSOR INTEGRATION AND DATA FUSION FOR OBJECT LOCALIZATION IN ROBOTIC WORKCELLS **c63**

I. Saban, K. C. Smith, and B. Benhabib *In* Engineering Inst. of Canada, Canadian Conference on Electrical and Computer Engineering, Volumes 1 and 2 1991 4 p (For primary document see N94-22101 05-33)

Avail: Issuing Activity (Engineering Inst. of Canada, 2050 rue Mansfield, Suite 700, Montreal, PQ H3A 1Z2 Canada)

A new approach to sensor integration and data fusion for location estimation of an object in a robotic workcell environment is presented. Integration of multiple sensors (both passive and active types) with a data fusion technique can significantly improve the accuracy of an object's estimated location. In the proposed scheme, the sensors are mounted on the robot's end-effector. The passive sensor is a single charge-coupled device (CCD) camera, while the active one is a range meter. By utilizing the mobility of the end-effector, the shape and magnitude of the sensor's hyperspheres can be controlled to achieve the desired performance. The objective is remote recognition of some features by both sensors, and

fusion of the acquired data. An application example of the proposed method, namely object identification and its subsequent grasping by a robotic end-effector is considered. Author (CISTI)

N94-22131 Quebec Univ., Montreal. Ecole de Technologie Superieure.
ULTRASONIC SENSOR VISION IN ROBOTICS [VISION PAR SENSEURS ULTRASONIQUES PAR LA ROBOTIQUE] **c63**
Michel Brule and Jean-Luc Dion (Quebec Univ., Trois-Riveres.) *In* Engineering Inst. of Canada, Canadian Conference on Electrical and Computer Engineering, Volumes 1 and 2 1991 5 p In FRENCH (For primary document see N94-22101 05-33)
Avail: Issuing Activity (Engineering Inst. of Canada, 2050 rue Mansfield, Suite 700, Montreal, PQ H3A 1Z2 Canada)

A vision system of very low resolution is proposed for the solution of the problem of locating and characterizing the form of an unknown surface, subject to constraints of cost, reliability, and availability of power. The system consists of sensors used in measurement of distances such as ultrasonic sensors. This permits estimation of the form of the visible surface of an object, its orientation and location. After a brief review of the fundamental elements of the sensor data processing method and its algorithms, new modules of analysis and calculation are presented which permit the graphical construction of a two-dimensional image of the shape, orientation, and location of that surface. Results of experimental investigations show that these methods have significant precision. Author (CISTI)

N94-22132 Ecole Polytechnique, Montreal (Quebec). Dept. of Electrical Engineering.
VLSI DESIGN OF A BIT SERIAL PARALLEL PROCESSING 4 EXTENDER CHIP FOR M-PATH CONVOLUTIONAL DECODING **c62**
Martin Chalifoux, Minh Nguyen, Steve Thiffault, Jean Belzile, Yvon Savaria, and David Haccoun *In* Engineering Inst. of Canada, Canadian Conference on Electrical and Computer Engineering, Volumes 1 and 2 1991 4 p (For primary document see N94-22101 05-33)
Avail: Issuing Activity (Engineering Inst. of Canada, 2050 rue Mansfield, Suite 700, Montreal, PQ H3A 1Z2 Canada)

Forward error correction (FEC) with convolutional codes is an efficient way of improving the reliability of communications systems. A bidirectional M-path decoding algorithm for covolutional codes as well as an architecture for its implementation were proposed at the Ecole Polytechnique de Montreal. An essential building block of this architecture is the extender. The design of a very large scale integration (VLSI) prototype which implements four extenders is described. The layout is largely made in a custom design style, incorporating standard cells for the irregular logic. This mix gives a good balance between area efficiency, design time and layout complexity. The result is a very fast chip with success at a 100 MHz clock rate, with a good core density of 2600 transistors per square milimeter, and is 100 percent testable. Author (CISTI)

N94-22133 McGill Univ., Montreal (Quebec). Research Center for Intelligent Machines.
DESIGN OF A FLOATING POINT CONVOLUTION PROCESSOR **c60**
J. Drolet, J. F. Panisset, and A. S. Molawany *In* Engineering Inst. of Canada, Canadian Conference on Electrical and Computer Engineering, Volumes 1 and 2 1991 4 p (For primary document see N94-22101 05-33)
Avail: Issuing Activity (Engineering Inst. of Canada, 2050 rue Mansfield, Suite 700, Montreal, PQ H3A 1Z2 Canada)

A specialized processor was designed which performs the convolution algorithm used in many signal processing applications. This processor operates on double precision floating point data to allow greater flexibility in the choice of filtering kernel coefficients. A full-custom very large scale integration device was designed to implement a systolic array architecture which can perform both one- and two-dimensional convolutions. Support circuitry handles data format conversion as well as data sequencing for the systolic array. The processor communicates with the memory of a host computer via a direct memory access interface to the computer's VMEbus. Author (CISTI)

N94-22134 Allied-Signal Aerospace Canada, Toronto (Ontario).
MLS SIGNAL-IN-SPACE CATEGORY 3 LANDING HAZARD ANALYSIS **c04**
R. J. Kelly *In* Engineering Inst. of Canada, Canadian Conference on Electrical and Computer Engineering, Volumes 1 and 2 1991 4 p (For primary document see N94-22101 05-33)
Avail: Issuing Activity (Engineering Inst. of Canada, 2050 rue Mansfield, Suite 700, Montreal, PQ H3A 1Z2 Canada)

The risks associated with a microwave landing system (MLS) signal-in-space and the information displayed to the pilot during approach and landing are large statistical guidance errors, loss of guidance information, and loss of signal integrity. MLS equipment specifications quantify these risks. An analysis is presented to identify the elements in the risk allocation process which formed the basis of MLS Category III specifications. Use of a hazard tree process uncovers the interrelationship between accuracy, continuity of service, and integrity in a way that shows the internal consistency of the MLS system design. The objective of this work is to develop a systems engineering methodology which identifies all the important factors contributing to an accident. As the analysis assumptions are confirmed by operational experience, the risk allocation tree can be updated and refined. Author (CISTI)

N94-22135 Transport Canada, Ottawa (Ontario).
APPLICATION OF SCATTERING BY ARRAYS OF CYLINDERS TO MLS SIGNAL PROPAGATION ERROR ESTIMATION **c04**
M. Z. El-Gamal and Do-Duy Hung *In* Engineering Inst. of Canada, Canadian Conference on Electrical and Computer Engineering, Volumes 1 and 2 1991 5 p (For primary document see N94-22101 05-33)
Avail: Issuing Activity (Engineering Inst. of Canada, 2050 rue Mansfield, Suite 700, Montreal, PQ H3A 1Z2 Canada)

Microwave landing systems (MLS) are collocated with approach light systems (ALS) and with existing instrument landing systems (ILS). Signals radiated from MLS are subject to unwanted reflections and shadowing from the ALS and ILS structures, as well as from the runway hump when it exists. The boundary discrete points method (BDP), originally developed to study the scattering of electromagnetic waves by multiple cylinders of different types, is applied to analyze the MLS signal scattering problem. The ILS localizer and ALS structures are represented by a number of cylinders or a combination of cylinders and spheres. A FORTRAN computer program was used to calculate scattered field. Initial results indicate that BDP is a simple but accurate technique that can be easily utilized to estimate the angle guidance error, path following error, control motion noise, and the power densities of signals from MLS antennas along the approach path of an aircraft and during the rollout for the humped-runway situation. Author (CISTI)

N94-22136 Republic Electronic Industries Corp., Melville, NY.
TESTING OF DME/P EQUIPMENT PERFORMANCE FOR COMPLEX MLS PROCEDURES **c04**
J. F. Michaels *In* Engineering Inst. of Canada, Canadian Conference on Electrical and Computer Engineering, Volumes 1 and 2 1991 4 p (For primary document see N94-22101 05-33)
Avail: Issuing Activity (Engineering Inst. of Canada, 2050 rue Mansfield, Suite 700, Montreal, PQ H3A 1Z2 Canada)

The performance of airborne distance measuring equipment needs to be tested and maintained to ensure that it can operate in its intended mode in a microwave landing system. The capabilities of the test and simulation equipment developed by Republic Electronics are described. The equipment comprises a microprocessor based system that can be used to test the airborne distance measuring equipment interrogation in a shop environment and in both the initial approach and final approach modes of operation. Distance information displayed on a separate display terminal is used to produce path following error and control motion noise calculations. Operator programmable parameters include range, range rate, range acceleration, overflight, radio frequency level, pulse spacing, reply efficiency, and echo. Calculations may also be performed to determine if the equipment is operating within the specified tolerances. Author (CISTI)

N94-22137 McMaster Univ., Hamilton (Ontario). Communications Research Lab.
FULL WAVE NUMERICAL MODEL OF ARBITRARILY-SHAPED PROXIMITY COUPLED MICROSTRIP ANTENNAS **c32**
Ke-Li Wu, John Litva, Russ Fralich, and Chen Wu *In* Engineering Inst. of Canada, Canadian Conference on Electrical and Computer Engineering, Volumes 1 and 2 1991 4 p (For primary document see N94-22101

05-33)
Avail: Issuing Activity (Engineering Inst. of Canada, 2050 rue Mansfield, Suite 700, Montreal, PQ H3A 1Z2 Canada)

An accurate analysis of an arbitrarily shaped microstrip antenna, electromagnetically coupled to a covered microstripline in a substrate superstrate configuration, is presented. The solution is based on the full-wave spectral-domain Green's functions for multilayer dielectric substrates and extended by incorporating the triangular finite element method. The antenna excitation is characterized by an equivalent impedance, and can be controlled by suitably selecting the offset of the antenna from the feed line. The theoretical results are in very good agreement with measurement results.
Author (CISTI)

N94-22138 McMaster Univ., Hamilton (Ontario). Communications Research Lab.
MODELING OF COAXIAL-FED MICROSTRIP PATCH ANTENNA BY FINITE DIFFERENCE TIME DOMAIN METHOD **c32**
Chen Wu, Ke-Li Wu, Zhiqiang Bi, and John Litva *In* Engineering Inst. of Canada, Canadian Conference on Electrical and Computer Engineering, Volumes 1 and 2 1991 4 p (For primary document see N94-22101 05-33)
Avail: Issuing Activity (Engineering Inst. of Canada, 2050 rue Mansfield, Suite 700, Montreal, PQ H3A 1Z2 Canada)

A direct three dimensional finite difference time-domain (FDTD) method is applied to the full-wave analysis of various coaxial-fed microstrip antennas. The model is shown to be an efficient and accurate tool for modeling coaxial-fed structures where, in this case, a transverse electromagnetic mode wave is excited by a source. The input impedance of the coaxial-fed microstrip antenna can be determined from the simulated time-domain wave that is reflected down the coaxial line. Two coaxial-fed microstrip antennas are used as examples, one a single element and the other a two-element stacked patch antenna. Excellent agreement over a wide frequency range is demonstrated in both cases between the measured and the FDTD-derived results. Author (CISTI)

N94-22139 Health and Welfare Canada, Ottawa (Ontario).
A BROADBAND V-ANTENNA FOR PULSED FIELD MEASUREMENTS: EXPERIMENTAL RESULTS **c32**
Karu P. Esselle and Stanislaw S. Stuchly (Ottawa Univ., Ontario.) *In* Engineering Inst. of Canada, Canadian Conference on Electrical and Computer Engineering, Volumes 1 and 2 1991 3 p (For primary document see N94-22101 05-33)
Avail: Issuing Activity (Engineering Inst. of Canada, 2050 rue Mansfield, Suite 700, Montreal, PQ H3A 1Z2 Canada)

A broadband receiving antenna was implemented using a resistively loaded thin-film V-monopole and a 500-ohm oscilloscope probe. The pulse-receiving performance of the antenna was evaluated using a time-domain antenna range. The antenna was also tested in a transverse electromagnetic mode cell, both in time and frequency domains. The antenna was found capable of receiving a 520-ps approximately Gaussian pulse, incident within 45 deg from the boresite direction, with good fidelity. The frequency domain receiving transfer function of the antenna is within -57 + or - 3 dB in the 22 MHz-1.1 GHz frequency range. Author (CISTI)

N94-22140 Manitoba Univ., Winnipeg. Dept. of Electrical and Computer Engineering.
FORMULATION FOR NUMERICAL SOLUTION OF RADIATION AND TRANSMISSION FROM ARBITRARY APERTURES **c32**
H. Moheb and L. Shafai *In* Engineering Inst. of Canada, Canadian Conference on Electrical and Computer Engineering, Volumes 1 and 2 1991 4 p (For primary document see N94-22101 05-33)
Avail: Issuing Activity (Engineering Inst. of Canada, 2050 rue Mansfield, Suite 700, Montreal, PQ H3A 1Z2 Canada)

A solution is offered to the general problem of a waveguide coupled to an arbitrary region through a rectangular aperture of arbitrary dimensions. An equivalence principle is used to reduce the original problem to two canonical problems, one for each side of the aperture. The only coupling is through the aperture, whose characteristics can be expressed by one aperture admittance matrix for each region. Application of the boundary conditions (the continuity of the tangential electric and magnetic fields) results in an integral equation, which can then be solved numerically for determining the equivalent magnetic current, which in turn is related to the tangential component of the electric field in the aperture. A moment method is then used to reduce the integral equation to a matrix equation to compute the current coefficients. The procedure is illustrated by considering the radiation from a waveguide fed aperture. Quantities computed are the transmission coefficient, the equivalent magnetic currents, and the gain pattern. Author (CISTI)

N94-22141 Laval Univ. (Quebec). Dept. d'Informatique.
LANGUAGE AS PRIMARY DIMENSION OF DISTRIBUTED AI SYSTEMS ACTIVITY **c63**
B. Chaib-Draa *In* Engineering Inst. of Canada, Canadian Conference on Electrical and Computer Engineering, Volumes 1 and 2 1991 3 p (For primary document see N94-22101 05-33)
Avail: Issuing Activity (Engineering Inst. of Canada, 2050 rue Mansfield, Suite 700, Montreal, PQ H3A 1Z2 Canada)

Research into the structures of multi-agent systems and the nature of multi-agent interactions is currently increasing, expecially for distributed applications such as robotic systems, air traffic control, and man-machine cooperation. A perspective based on language as action is introduced for distributed artificial intelligence systems. Language is described as a coordinated sequence of acts between participants, leading them to a mutual recognition of their mental states. If interacting plans are considered as mental plans binding agents' mental states (beliefs, desires, intentions, and commitments) to actions, the language/action must then facilitate building such plans. Author (CISTI)

N94-22142 Defence Research Establishment, Ottawa (Ontario). Airborne Radar Section.
CFAR PROCESSING FOR AIRBORNE PULSE-DOPPLER RADARS **c32**
G. Vrckovnik and D. Faubert *In* Engineering Inst. of Canada, Canadian Conference on Electrical and Computer Engineering, Volumes 1 and 2 1991 4 p (For primary document see N94-22101 05-33)
Avail: Issuing Activity (Engineering Inst. of Canada, 2050 rue Mansfield, Suite 700, Montreal, PQ H3A 1Z2 Canada)

Constant false alarm rate (CFAR) processors which may be used in airborne pulse-Doppler radar systems are described. Using radar parameters selected for an aircraft flying at Mach 1 and at up to 10 km altitude, a simulation using the ABRSIM airborne radar simulator reveals that a 70 dB clutter peak appears across all of the range gates and many of the Doppler bins, resulting in large CFAR losses with conventional CFAR processors. It is shown that by adaptively blanking the range-Doppler resolution cells which contain clutter, significant performance improvements may be achieved. An adaptive algorithm to determine which resolution cells should be blanked is derived and tested in conjunction with a cell-averaging CFAR processor. The adaptive blanking can be used with other types of CFAR, such as the ordered statistic or greatest-of processors. Author (CISTI)

N94-22143 Raytheon Canada Ltd., Waterloo (Ontario).
SPACE-BASED RADAR FOR MOVING TARGET DETECTION **c32**
C. F. Weaver and A. W. Bridgewater (Defence Research Establishment, Ottawa, Ontario.) *In* Engineering Inst. of Canada, Canadian Conference on Electrical and Computer Engineering, Volumes 1 and 2 1991 4 p (For primary document see N94-22101 05-33)
Avail: Issuing Activity (Engineering Inst. of Canada, 2050 rue Mansfield, Suite 700, Montreal, PQ H3A 1Z2 Canada)

A space-based radar intended for airborne target detection is studied from a signal processing perspective. Several antenna system concepts are used, including phased arrays and scanned reflectors. Promising signal processing techniques for use with a pulse-Doppler (P-D) approach are reviewed. Constraints and difficulties resulting from the unique nature of spaceborne systems are identified and mitigating techniques are suggested. Most of these problems result from the large satellite velocities which are experienced in low-altitude orbits. High PRF (pulse repetition frequency) and medium PRF waveforms are compared and a high PRF waveform is favored because of the advantages obtained from unambiguous velocity information. Non range eclipsing (NRE) and range eclipsing (RE) waveforms are also compared. The choice of NRE or RE waveform depends on the antenna and power system choice and on the minimization of power system weight. Approaches to clutter cancellation such as displaced phase center antennas (DPCA) and monopulse anomalous nulling are discussed. Generic

DPCA is compared with standard P-D processing and found to be better for the altitudes of interest in the phased array approach. Author (CISTI)

N94-22144 Defence Research Establishment, Ottawa (Ontario). Airborne Radar Section.

A DIGITAL DEMODULATION SCHEME FOR USE IN A HIGH DYNAMIC RANGE RADAR SYSTEM **c32**

Glen Rempel and George Haslam *In* Engineering Inst. of Canada, Canadian Conference on Electrical and Computer Engineering, Volumes 1 and 2 1991 4 p (For primary document see N94-22101 05-33)

Avail: Issuing Activity (Engineering Inst. of Canada, 2050 rue Mansfield, Suite 700, Montreal, PQ H3A 1Z2 Canada)

Digital demodulation is a technique whereby the positive frequency component of a narrowband signal is translated to baseband by digital means. With this technique, the dynamic range of some radar systems can be greatly increased. A digital demodulation scheme suitable for an airborne radar system is described, and some of the major design issues in its implementation are analyzed. The demodulation process first involves downconversion of the signal to an intermediate frequency (IF), filtering the resulting signal to reduce its frequency sidelobes, mixing the filtered signal to a second IF, digitizing the second IF signal, and filtering the digital signal with a lowpass finite impulse response filter. An expression for the optimal filter is derived, maximizing the ratio of the positive frequency clutter power to the negative frequency clutter plus noise power. Simulated input and output spectra are shown. The simulation results were validated by a simple experiment. Author (CISTI)

N94-22145 Defence Research Establishment Valcartier (Quebec).

MARINE BOUNDARY LAYER MODEL EVALUATION BY USING A HEIGHT GAIN MEASUREMENT TECHNIQUE IN THE INTERFERENCE REGION **c48**

Denis Dion *In* Engineering Inst. of Canada, Canadian Conference on Electrical and Computer Engineering, Volumes 1 and 2 1991 4 p (For primary document see N94-22101 05-33)

Avail: Issuing Activity (Engineering Inst. of Canada, 2050 rue Mansfield, Suite 700, Montreal, PQ H3A 1Z2 Canada)

Air refractivity is known to produce major effects on electromagnetic propagation in the radio and millimetric bands for paths above large water surfaces. Most of the time, a tropospheric duct is formed within which the energy is trapped. Fading zones may be found at certain elevations and the radiation pattern in the interference region is distorted. The most frequent type of duct is caused by the rapid exponential decrease of the moisture in the marine boundary layer (MBL) at the water surface. Reliable models of the MBL are required to study propagation effects on radar and communication systems. An approach is proposed for evaluating MBL models by comparing model predictions of the variation of the interference null elevation with respect to the refractivity conditions. Two models are considered: a model developed in San Diego called NOSCMBL and the recently issued WKDMBL model. In field tests using X-band radiation, the analysis of height gain and bulk meteorological measurements made over Lake Ontario showed better performances for WKDMBL; an average prediction error of 1.5 m was obtained for an observed null elevation course of about 15 m. Author (CISTI)

N94-22146 Concordia Univ., Montreal (Quebec). Centre for Pattern Recognition and Machine Intelligence.

THE LOCAL MEASUREMENT AND GLOBAL INTERPRETATION OF 3D MOTION FIELD GENERATED BY SEVERAL MOVING OBJECTS FROM RANGE IMAGE SEQUENCES **c43**

P. Y. Zhu, A. Krzyzak, and T. Kasvand *In* Engineering Inst. of Canada, Canadian Conference on Electrical and Computer Engineering, Volumes 1 and 2 1991 4 p (For primary document see N94-22101 05-33)

Avail: Issuing Activity (Engineering Inst. of Canada, 2050 rue Mansfield, Suite 700, Montreal, PQ H3A 1Z2 Canada)

A new approach is presented for the measurement and interpretation of three dimensional motion field generated by several moving objects from range image sequences. The approach includes six main modules: median filter, local measurement of three dimensional motion field, regularization of the three dimensional motion field, segmentation based on common motion, and determination of motion parameters for each moving part. Results of experiments tested on real and synthetic data with noise are given. Author (CISTI)

N94-22147 Hopital du Sacre-Coeur, Montreal (Quebec).

SEGMENTING THE OPTICAL FLOW DUE TO THE MOTION OF SEVERAL RIGID OBJECTS **c63**

Rita El-Nmeir and Guy Mailloux (Ecole Polytechnique, Montreal, Quebec.) *In* Engineering Inst. of Canada, Canadian Conference on Electrical and Computer Engineering, Volumes 1 and 2 1991 4 p (For primary document see N94-22101 05-33)

Avail: Issuing Activity (Engineering Inst. of Canada, 2050 rue Mansfield, Suite 700, Montreal, PQ H3A 1Z2 Canada)

Since real objects or observers move in three dimensional space, an important part of research in computer vision has been devoted to motion analysis. Motion information can generally be made computer accessible by serial digitization of each frame of a video recording of the scene to be analyzed. The interframe two dimensional velocity field, or optical flow, can then be computed provided there are enough contours in the images and that the interframe motion is not too fast. A method is presented for computing and segmenting the optical flow due to the motion of several moving rigid objects. Under orthographic projection, the components of the optical flow of a planar surface are describable by linear equations of three parameters each. This constraint is used both to compute the optical flow and to segment it using the generalized Hough transform. This method can be adapted for perspective projection. Author (CISTI)

N94-22148 Toronto Univ. (Ontario). Computer Integrated Manufacturing Lab.

ELLIPTICAL-SHAPE PARAMETER ESTIMATION FROM A SET OF NORMAL LINES **c61**

I. Tchoukanov, R. Safaee-Rad, B. Benhabib, and K. C. Smith *In* Engineering Inst. of Canada, Canadian Conference on Electrical and Computer Engineering, Volumes 1 and 2 1991 4 p (For primary document see N94-22101 05-33)

Avail: Issuing Activity (Engineering Inst. of Canada, 2050 rue Mansfield, Suite 700, Montreal, PQ H3A 1Z2 Canada)

A new method is proposed for elliptical shape parameter estimation, which does not require detection of the shape's boundary. The values of the parameters of an elliptical shape are estimated based on a set of normal lines to its boundary, computed by an edge detector. The essence of this approach is the use of the relationship between a set of normal lines to an ellipse and the Hough transform of its evolute. The evolute of an elliptical shape is an astroid represented by a shifted sinusoid in the Hough space. It is shown that the values of the elliptical shape parameters could be estimated by utilizing a certain geometrical property of ellipses (for center coordinates) and by analyzing the data in the Hough (parameter) space (for orientation angle, major and minor radii). Author (CISTI)

N94-22149 Regina Univ. (Saskatchewan).

SCALE-SPACE FILTERING AND THRESHOLD HIERARCHY FOR IMAGE SEGMENTATION **c61**

Neng-Quan Wang, Xue-Dong Yang, and L. R. Symes *In* Engineering Inst. of Canada, Canadian Conference on Electrical and Computer Engineering, Volumes 1 and 2 1991 4 p (For primary document see N94-22101 05-33)

Avail: Issuing Activity (Engineering Inst. of Canada, 2050 rue Mansfield, Suite 700, Montreal, PQ H3A 1Z2 Canada)

One common approach to image segmentation is to select thresholds by using local minimum points of the gray level histogram of the image. The histogram for an image is generally not smooth. Also, the use of the minimum values of the histogram as the thresholds is affected by the noise in the original image. The process of the threshold selection can be improved by the smoothing of the histogram. In an extension of Witkin's work on scale-space filtering, scale-space filtering is employed to smooth the original histogram of an image. Furthermore, a new, reliable and accurate method (threshold hierarchy) is presented for image segmentation. The interval tree is designed to display a concise and visible structure of the threshold hierarchy. Experimental results of segmented images with different threshold hierarchies are presented. Author (CISTI)

N94-22150 New Brunswick Univ., Fredericton. Faculty of Computer Science.

NEW ALGORITHM FOR THE DETECTION OF THE ORIENTATION OF A PLANAR LAMBERTIAN SURFACE IN 3D **c61**

Przemyslaw Pochec *In* Engineering Inst. of Canada, Canadian Conference

on Electrical and Computer Engineering, Volumes 1 and 2 1991 2 p (For primary document see N94-22101 05-33)
Avail: Issuing Activity (Engineering Inst. of Canada, 2050 rue Mansfield, Suite 700, Montreal, PQ H3A 1Z2 Canada)

A new image processing algorithm for the detection of the orientation of a planar surface is proposed. The algorithm relies on the ambient light array (ALA) representation of visual information, which is based on recording both the direction and intensity of light rays originating from points on objects in the scene. The algorithm is based on modelling the ALA imaging of a planar surface as a circular (Moebius) transformation - unit inversion. This class of linear-fractional transformations can describe the mapping of a plane to a sphere. In ALA domain, with a point light source close to the observer, the image of a Lambertian plane is a sphere. For the detection of orientation of a planar surface, the intensities of light reflected from only three points on the observed surface are needed. Author (CISTI)

N94-22151 Alberta Univ., Edmonton. Microelectronic Center.
SILICON MICROMACHINED THRESHOLD ACCELEROMETERS **c35**
Y. Loke, G. H. McKinnon, and M. J. Brett *In* Engineering Inst. of Canada, Canadian Conference on Electrical and Computer Engineering, Volumes 1 and 2 1991 4 p (For primary document see N94-22101 05-33)
Avail: Issuing Activity (Engineering Inst. of Canada, 2050 rue Mansfield, Suite 700, Montreal, PQ H3A 1Z2 Canada)

A threshold accelerometer, also known as a g-switch, was developed for sensing very high acceleration levels. The design follows the concept of a cantilever beam as the sensing element with a metal line running along its length. Under applied acceleration, the beam deflects upwards across a small gap and makes contact with a second electrode, thus closing a switch. The structural material chosen for the beam was silicon dioxide, due to its flexibility and ease in fabrication. The theory of the electrostatic and inertial forces are analyzed and a threshold acceleration level is derived. It is shown that this level is very sensitive to beam length. Fabrication steps are described, including chemical vapor deposition, chemical etching, and fabrication and assembly of the top glass plate. Electrostatic testing that involved voltages representative of threshold acceleration levels of 400 to 100,000 gravities was performed on over 150 beams. Under static centrifuge testing involving over 100 beams, threshold acceleration levels from 400 to 20,000 gravities were measured. Most of the experimental results are within the predicted tolerance limits set by the processing parameters. Author (CISTI)

N94-22152 Calgary Univ. (Alberta). Dept. of Electrical and Computer Engineering.
CHARGE INTEGRATING OPTICAL POSITION SENSOR **c35**
S. Balasubramanian, J. W. Haslett, and F. N. Trofimenkoff *In* Engineering Inst. of Canada, Canadian Conference on Electrical and Computer Engineering, Volumes 1 and 2 1991 4 p (For primary document see N94-22101 05-33)
Avail: Issuing Activity (Engineering Inst. of Canada, 2050 rue Mansfield, Suite 700, Montreal, PQ H3A 1Z2 Canada)

A modification to a recently described high-resolution optical position sensor increased its optical sensitivity by several orders of magnitude. The modification is based on charge transfer principles and was implemented in a 3-micrometer CMOS technology. One of the major applications of this device is to use it as the sensor in a telescope position control system for star tracking. The device can determine the precise position of the centroid of a diffuse light source focused on its surface, with integration times of a few milliseconds. Author (CISTI)

N94-22153 Ecole Polytechnique, Montreal (Quebec). Dept. of Electrical Engineering.
VLSI DESIGN OF A PARALLEL VIDEO OUTPUT INTERFACE
Eric Boisvert, Abdelhakim Khali, David Lachartre, Mario Larouche, Mohamed Nekili, Abdelmajid Bennani, and Yvon Savaria *In* Engineering Inst. of Canada, Canadian Conference on Electrical and Computer Engineering, Volumes 1 and 2 1991 4 p (For primary document see N94-22101 05-33)
Avail: Issuing Activity (Engineering Inst. of Canada, 2050 rue Mansfield, Suite 700, Montreal, PQ H3A 1Z2 Canada)

The design and integration of a very large scale integration (VLSI) video output interface (VOI) chip which allows building a scaleable speed VOI capable of extracting images in real time from a parallel machine of an adequate size is presented. The parallel VOI interfaces a massively parallel computer with a packet switched general purpose communication network and a wide range of video displays. Multiple copies of the VOI chip can be used to increase the rate at which results can be extracted from the parallel computer. It is thus possible to extract video images in real time with minimum impact on the performance of the parallel system. The architecture is highly flexible since it can be adapted to various image sizes, formats, number of ports, and throughputs. A VLSI chip based on the proposed architecture was designed and will be integrated in the near future. Extensive functional simulation will have to be carried out to validate the design. Author (CISTI)

N94-22154 Micronav Ltd., Sydney (Nova Scotia).
MLS POINTING ANGLE ERROR SOURCES AND EFFECTS **c04**
David Babineau, Mike McAloney, and Maurice Meyer *In* Engineering Inst. of Canada, Canadian Conference on Electrical and Computer Engineering, Volumes 1 and 2 1991 4 p (For primary document see N94-22101 05-33)
Avail: Issuing Activity (Engineering Inst. of Canada, 2050 rue Mansfield, Suite 700, Montreal, PQ H3A 1Z2 Canada)

Angle guidance for aircraft is one of the important functions performed by a microwave landing system. Identification of error sources is required by manufacturers of such systems in order to manage equipment error budgets. An analysis is presented of error sources internal to the angle guidance ground equipment which affect the angle accuracy measured at the aircraft. A straightforward approach for estimating the end effect for some of the error sources is given. The antenna components of the phased arrays typically used in microwave landing systems are divided into three types for the analysis: power divider, phase shifter, and waveguide. Error effects are divided into two categories: amplitude errors and phase errors. Other error sources discussed are those resulting from beam steering and from waveguide/frame parameters. The approach presented is a tool for reasonability checking and for initial design trade studies.
Author (CISTI)

N94-22155 Micronav Ltd., Sydney (Nova Scotia).
DEVELOPING SOFTWARE TO RTCA DO-178A **c04**
Ross Hooper, John Lord, and Kathy MacIntyre *In* Engineering Inst. of Canada, Canadian Conference on Electrical and Computer Engineering, Volumes 1 and 2 1991 3 p (For primary document see N94-22101 05-33)
Avail: Issuing Activity (Engineering Inst. of Canada, 2050 rue Mansfield, Suite 700, Montreal, PQ H3A 1Z2 Canada)

Software experiences during two development cycles of a microwave landing system (MLS) at Micronav International are presented. The MLS software was developed to Radio Technical Commission for Aeronautics standard/guideline DO-178A. The experiences and lessons which are described were learned over a three-year period where the software development methods were defined and formalized. Micronav's interpretation of the DO-178A phases of development and their impact are discussed. Particular emphasis is placed on the understanding of requirements definition, high level design, and verification and validation. Author (CISTI)

N94-22156 Ohio Univ., Athens.
A FLIGHT TEST SYSTEM DESIGN FOR THE MICROWAVE LANDING SYSTEM **c04**
D. B. Vickers *In* Engineering Inst. of Canada, Canadian Conference on Electrical and Computer Engineering, Volumes 1 and 2 1991 4 p (For primary document see N94-22101 05-33)
Avail: Issuing Activity (Engineering Inst. of Canada, 2050 rue Mansfield, Suite 700, Montreal, PQ H3A 1Z2 Canada)

The technical design of an aircraft true position (tracking) and data collection system to support flight tests of a microwave landing system (MLS) is reviewed. Key MLS characteristics and aircraft dynamics are analyzed in order to specify the minimum sampling rates for MLS and aircraft position data, the maximum allowable aircraft true position error in various regions of the MLS coverage volume, and the transformations and translations needed to achieve coincidence between MLS and true position coordinate systems. Existing and possible future implementations for determining the aircraft true position are discussed. Author (CISTI)

N94-22157 Paramax Electronic, Inc., Montreal (Quebec).
THE WHY, WHAT, AND HOW OF Ada SOFTWARE DEVELOPMENT **c61**

Paul D. Hamilton *In* Engineering Inst. of Canada, Canadian Conference on Electrical and Computer Engineering, Volumes 1 and 2 1991 4 p (For primary document see N94-22101 05-33)
Avail: Issuing Activity (Engineering Inst. of Canada, 2050 rue Mansfield, Suite 700, Montreal, PQ H3A 1Z2 Canada)

Ada is a programming language mandated for all developmental software by the US DOD, and the Canadian Department of National Defense is also moving in this direction. To respond to these requirements, the Paramax Ada Centre of Excellence was established. Specific defense programs currently targeted include the New Shipborne Aircraft Program, the New Search Helicopter Program, and the US Navy CP 901A Anti-Submarine Warfare Program for the P-3 aircraft. The Ada Centre is supporting the establishment and upgrading of the Ada Development Centre, which contains the necessary MIL-STD-2167A software development process. The underlying architecture is a heterogeneous local area network utilizing unshielded twisted-pair ethernet technology. Hardware includes a VAX 6310 computer and a Sun server supporting Sun, DEC, and Unisys workstations. The software tool of choice is Requirements Entry Allocation and Decomposition Support (READS), which was integrated with the CASE tool from IDE. The Centre also presents Ada training courses and has a technology transfer capability. Author (CISTI)

N94-22158 SD Scicon Public Ltd. Co., Cheadle (England).
FORMAL METHODS IN THE DESIGN OF CRITICAL SOFTWARE SYSTEMS **c61**

J. Burns and J. Spruce Riordon (AEPOS Technologies Corp., Hull, Quebec.) *In* Engineering Inst. of Canada, Canadian Conference on Electrical and Computer Engineering, Volumes 1 and 2 1991 4 p (For primary document see N94-22101 05-33)
Avail: Issuing Activity (Engineering Inst. of Canada, 2050 rue Mansfield, Suite 700, Montreal, PQ H3A 1Z2 Canada)

Software used in critical systems such as nuclear power station control, fly-by-wire aircraft, and data encryption should rigorously adhere to system specification. The technology of formal methods (FM) is an essential part of producing security and safety systems to the highest levels of assurance. A current deficiency in FM development is the lack of fully effective tools. In their absence, a pragmatic approach should be adopted and formal techniques applied judiciously. The OBJ/MALPAS methodology has proven to be a practical and effective route to code. FM techniques can be acquired by advanced software engineers without an excessive learning curve. An example is presented of FM techniques applied to a network security example. The OBJ specification equations are translated to an abstract version of the MALPAS intermediate language, and the output is successively refined. For each step in the refinement process it is necessary to show that the refined code meets the specifications of its predecessor. Implementation code is produced manually following the last stage of refinement, and is automatically translated back into the intermediate language and checked for compliance against the OBJ specification.
Author (CISTI)

N94-22159 Defence Research Establishment, Ottawa (Ontario).
AN OVERVIEW OF SYNTHETIC APERTURE RADAR SIGNAL PROCESSING TECHNIQUES **c32**

M. R. Vant *In* Engineering Inst. of Canada, Canadian Conference on Electrical and Computer Engineering, Volumes 1 and 2 1991 7 p (For primary document see N94-22101 05-33)
Avail: Issuing Activity (Engineering Inst. of Canada, 2050 rue Mansfield, Suite 700, Montreal, PQ H3A 1Z2 Canada)

The principles of synthetic aperture radar and its significance in a military and remote sensing context are reviewed. The signal processing operations required to convert the signal data into an image are described. These operations must accomplish two things: correction of the range migration, both walk and curvature; and compression or focusing of the cross-range portion of the signal. These operations include time-domain deramping, matched filtering, range-Doppler fast convolution, step transform processing, spotlight mode processing, and motion compensation. Processing problems specific to synthetic aperture radar signal processing are summarized and an example of synthetic aperture radar imagery is presented. Author (CISTI)

N94-22160 Laval Univ. (Quebec). Dept. Genie Electrique.
ADAPTIVE SYNTHESIS OF A RAY DIAGRAM FOR AN ANTENNA ARRAY [SYNTHESE ADAPTIVE D'UN DIAGRAMME DE RAYONNEMENT D'UNE ANTENNE RESEAU] **c32**

D. Grenier *In* Engineering Inst. of Canada, Canadian Conference on Electrical and Computer Engineering, Volumes 1 and 2 1991 4 p In FRENCH (For primary document see N94-22101 05-33)
Avail: Issuing Activity (Engineering Inst. of Canada, 2050 rue Mansfield, Suite 700, Montreal, PQ H3A 1Z2 Canada)

An algorithm is proposed which is capable of evaluating the optimal weighting of each of the elements of an antenna array. The algorithm has the objective of obtaining a radiation diagram predefined by samples marking the level of several principal lobes, all the while trying to increase the depth of the hollows between these lobes. The proposed algorithm uses the sum of the optimal weighting vectors which maximize the signal to interference ratio in the directions of the main lobes. The algorithm assumes that the signal emitted from each element of the network consists of the following: a useful signal whose azimuth and amplitude correspond to the angle and level of the lobe; a large number of interfering signals originating from many directions; and thermal noise. From several examples it is seen that the obtained solution does not always respect the starting data; nevertheless, the solution corresponds to the optimal solution in the least squares sense. Author (CISTI)

N94-22161 Defence Research Establishment, Ottawa (Ontario).
TARGET ANGULAR MOTION AND ITS EFFECTS ON SIMULATED SSAR SHIP IMAGES **c32**

A. Damini and G. E. Haslam *In* Engineering Inst. of Canada, Canadian Conference on Electrical and Computer Engineering, Volumes 1 and 2 1991 4 p (For primary document see N94-22101 05-33)
Avail: Issuing Activity (Engineering Inst. of Canada, 2050 rue Mansfield, Suite 700, Montreal, PQ H3A 1Z2 Canada)

Synthetic aperture radar (SAR) is an airborne radar mapping technique for generating high resolution images. Spotlight SAR is a mode of SAR in which the radar antenna is trained on the target area of interest. The dependence of the cross-range resolution achievable in spotlight SAR, both on the coherent integration time and the relative angular rotation rate between the radar and the target is described. The orientation of the image as a function of the relative angular motions is also examined. The type of motions experienced by an ocean-going vessel are expected to reduce the quality of a spotlight SAR image. Computer simulations of the radar returns from a spotlighted ocean-going vessel, and the processing of these returns to generate a spotlight SAR image of the ship, support this hypothesis. A fairly high sea state produces an image which is generally a vertical profile view through the target, while lower sea states produce a generally horizontal plan view of the target. Author (CISTI)

N94-22162 Manitoba Univ., Winnipeg. Dept. of Electrical and Computer Engineering.
EFFECT OF ERRORS ON THE PHASE CENTRE AND POINTING ANGLE OF PHASED ARRAY ANTENNAS **c32**

H. Moheb, A. Helaly (Cairo Univ., Egypt.), A. Sebak, and L. Shafai *In* Engineering Inst. of Canada, Canadian Conference on Electrical and Computer Engineering, Volumes 1 and 2 1991 4 p (For primary document see N94-22101 05-33)
Avail: Issuing Activity (Engineering Inst. of Canada, 2050 rue Mansfield, Suite 700, Montreal, PQ H3A 1Z2 Canada)

A mathematical model is developed to determine the antenna phase center and its uniqueness. The model is then used to investigate the phase center location for selected small phased array antennas and to determine its movement due to the beam scanning and various design or operational errors. It is shown that for an ideal antenna (the error-free case), the phase center coincides with its geometrical center. However, any deviation from the ideal conditions, due to design, fabrication or operational errors, due to the phase shifter quantization, or due to the scan angle algorithm, causes its non-uniqueness and movement from the antenna's geometrical center. Author (CISTI)

N94-22163 Laval Univ. (Quebec). Lab. de Vision et Systemes Numeriques.
A NEURAL NETWORK FOR MULTIRESOLUTION EDGE DETECTION **c63**

Richard Lepage and Denis Poussart *In* Engineering Inst. of Canada, Canadian Conference on Electrical and Computer Engineering, Volumes 1 and 2 1991 4 p (For primary document see N94-22101 05-33)
Avail: Issuing Activity (Engineering Inst. of Canada, 2050 rue Mansfield, Suite 700, Montreal, PQ H3A 1Z2 Canada)

A goal of computer vision is the construction of scene descriptions based on information extracted from one or more two-dimensional images. Edge detection makes explicit important information about the two-dimensional image but is scale dependent: edges are visible only over a range of scales. One needs multiple scale analysis of the input image in order to have a complete description of the edges. A compact pyramidal architecture is proposed for image representation at multiple spatial scales. A simple processing element (PE) is allocated at each pixel location at each level of the pyramid. A dense network of weighted links between each PE and PE's underneath is programmed to generate the levels of the pyramid. Lateral weighted links within a level compute edge localization and intensity gradient. Feedback between successive levels is used to reinforce and refine the position of true edges. Author (CISTI)

N94-22164 Laval Univ. (Quebec). Centre d'Optique Photonique et Laser.
IMPROVEMENT IN INVARIANT PATTERN RECOGNITION WITH NEURAL NETWORKS AND FOURIER-MELLIN FILTERS **c63**
Claude Lejeune and Yun-Long Sheng *In* Engineering Inst. of Canada, Canadian Conference on Electrical and Computer Engineering, Volumes 1 and 2 1991 4 p (For primary document see N94-22101 05-33)
Avail: Issuing Activity (Engineering Inst. of Canada, 2050 rue Mansfield, Suite 700, Montreal, PQ H3A 1Z2 Canada)

Fourier-Mellin filters are used to generate shift, rotation, and scale invariant pattern descriptors. The size of these descriptors is quite small compared to the original object that generated them. It has the added advantage of invariance that the original object has not. Their small size permits very fast training with a neural network. This approach is used with a training set of three aircraft. Once learning has taken place, the network is presented with a testing set consisting of those three aircraft and rotated versions of them. The network is able to learn and recognize the original objects as well as the rotated versions. Author (CISTI)

N94-22165 Laval Univ. (Quebec). Dept. of Electrical Engineering.
A MODIFIED MOMENT INVARIANTS TECHNIQUE FOR CLASSIFICATION OF NOISY OBJECTS **c61**
Halet Arezki, H. T. Huynh, and G. A. Lampropoulos *In* Engineering Inst. of Canada, Canadian Conference on Electrical and Computer Engineering, Volumes 1 and 2 1991 4 p (For primary document see N94-22101 05-33)
Avail: Issuing Activity (Engineering Inst. of Canada, 2050 rue Mansfield, Suite 700, Montreal, PQ H3A 1Z2 Canada)

With moment invariant methods for object classification, features are extracted by computing second and third order moments of the image, and combining them in a vector of seven numbers which is invariant under general linear transformation. These methods can be applied to the classification of binary or textured images, but result in features that are sensitive to noise. An improvement is proposed in which the magnitude of every one of the seven moments is used for normalization, with its power being equal to the order of the moments. These new moments are more steady in a noisy environment and give excellent results for classification of noisy images, as is demonstrated for the case of two types of images, human faces and military aircraft. Author (CISTI)

N94-22166 Waterloo Univ. (Ontario). Dept. of Electrical and Computer Engineering.
A NEURAL M-ARY TREE METHOD FOR DATA COMPRESSION
Zhi-Cheng Wang and J. Hanson *In* Engineering Inst. of Canada, Canadian Conference on Electrical and Computer Engineering, Volumes 1 and 2 1991 4 p (For primary document see N94-22101 05-33)
Avail: Issuing Activity (Engineering Inst. of Canada, 2050 rue Mansfield, Suite 700, Montreal, PQ H3A 1Z2 Canada)

A new version of a multilayer neural network, the self-learning neural model, is presented. This neural model can be used as adaptive nonparametric neural net clusters, which can be trained by unlabelled data. An M-ary decision tree structured vector code with the building blocks of this type of neural network is developed for data compression. The M-ary tree codes are systems of loosely coupled hybrid neural networks. They combine the traditional decision tree technique, artificial neural network technique, and hierarchical process in aspects of structure, training, and coding, resulting in new properties and good performance. The feedforward model learns coding without supervision and codes input in a parallel and sequential way. The model is smaller than the normal neural networks used for coding. Author (CISTI)

N94-22167 Windsor Univ. (Ontario). Dept. of Electrical Engineering.
CASCADED RECURSIVE ARTIFICIAL NEURAL NETWORKS **c63**
Hon-Keung Kwan *In* Engineering Inst. of Canada, Canadian Conference on Electrical and Computer Engineering, Volumes 1 and 2 1991 4 p (For primary document see N94-22101 05-33)
Avail: Issuing Activity (Engineering Inst. of Canada, 2050 rue Mansfield, Suite 700, Montreal, PQ H3A 1Z2 Canada)

The learning and recall algorithms of a cascaded recursive artificial neural network (CRANN) are presented. The network consists of L cascaded sections of M-layer feedforward structures with output delayed feedbacks. Simulation results on the use of the network as an auto-associator are compared to those of the multilayer feedforward neural network to illustrate the properties of the network. Comparisons show that the CRANN is generally capable of achieving higher recall accuracies while requiring less training epoches. Author (CISTI)

N94-22168 Concordia Univ., Montreal (Quebec). Dept. of Electrical and Computer Engineering.
CREIR: A MULTIACCESS PROTOCOL FOR ON-BOARD PROCESSING SATELLITE SYSTEMS **c60**
Le-Ngoc Tho and Yu-Dong Yao (Spar Aerospace Ltd., Sainte-Anne-de-Bellevue, Quebec.) *In* Engineering Inst. of Canada, Canadian Conference on Electrical and Computer Engineering, Volumes 1 and 2 1991 4 p (For primary document see N94-22101 05-33)
Avail: Issuing Activity (Engineering Inst. of Canada, 2050 rue Mansfield, Suite 700, Montreal, PQ H3A 1Z2 Canada)

Random access and reservation access protocols are studied for satellite communication systems with on-board processing. Explicit then implicit reservation, a protocol to accommodate long message transmissions and to reduce end-user buffer size effects, is introduced and its performance is compared with explicit reservation and implicit reservation performance. The combination of random access and explicit then implicit reservation access results in a new protocol called Combined Random/Explicit then Implicit Reservation (CREIR). The implementation of CREIR in an on-board satellite system is also discussed with reference to the handling of collision detection and data packet slot assignment. Author (CISTI)

N94-22169 Communications Research Centre, Ottawa (Ontario).
TIMING RECOVERY IN THE CHANNEL PROCESSOR OF A DIGITAL GROUP DEMODULATOR
Norman Secord *In* Engineering Inst. of Canada, Canadian Conference on Electrical and Computer Engineering, Volumes 1 and 2 1991 4 p (For primary document see N94-22101 05-33)
Avail: Issuing Activity (Engineering Inst. of Canada, 2050 rue Mansfield, Suite 700, Montreal, PQ H3A 1Z2 Canada)

In future generations of satellites, digital group demodulators will be used to regenerate frequency division multiple access (FDMA) / quadrature phase shift keying (QPSK) signals on board the satellite and convert them to a time division multiplexed stream for the return link. The group demodulator consists of a digital trans-multiplexer which separates out the individual FDMA/QPSK signals and a bank of per-channel processors which perform timing and carrier recovery for each channel. Timing recovery is examined within the channel processor of the group demodulator. The timing is adjusted using a finite impulse response filter that acts as an adaptive delay and also decimates the sample sequence to obtain a baud rate sequence from which decisions on the symbols can be made. The design of this adaptive rate control filter is discussed with emphasis on the influence of the tap length and filter response function in acquisition and tracking performance. Author (CISTI)

N94-22170 Communications Research Centre, Ottawa (Ontario).
THE INFLUENCE OF LOWPASS FILTERING AND THE EFFECTS OF FADING ON THE GROUP DEMODULATION OF QPSK SIGNALS **c32**
Norman Secord, Shunkichi Isobe (Ministry of Posts and Telecommunications, Tokyo, Japan.), and Chun Loo *In* Engineering Inst. of Canada, Canadian

Conference on Electrical and Computer Engineering, Volumes 1 and 2 1991 4 p (For primary document see N94-22101 05-33)
Avail: Issuing Activity (Engineering Inst. of Canada, 2050 rue Mansfield, Suite 700, Montreal, PQ H3A 1Z2 Canada)

The influence of the lowpass filter at the front end of a digital group demodulator on the number of usable satellite communication channels is discussed. A Monte Carlo simulation study was undertaken using a raised cosine filter as the lowpass filter response. The group demodulator was designed to accommodate 16 channels of quadrature phase shift keying data with a channel spacing equal to twice the symbol rate. In particular, it is shown that the proper design of this lowpass filter can provide several additional channels. The effects of fading and shadowing on the performance of a signal that is group demodulated are also discussed. The results indicate that the inter-channel interference that is present due to the close channel spacing of the signals combines with the fading to produce a severely distorted signal. This indicates that new receiver structures and the introduction of coding will be required to combat the fading, shadowing, and inter-channel interference for land mobile communications with on-board processing or group demodulation. Author (CISTI)

N94-22171 Nippon Telegraph and Telephone Public Corp., Yokosuka (Japan). Radio Communication Systems Lab.
TDMA SATELLITE COMMUNICATION SYSTEMS FOR ISDN SERVICES **c32**
Katsuhiko Kawazoe, Masahiro Morikura, Shuji Kubota, Kiyoshi Enomoto, and Shuzo Kato *In* Engineering Inst. of Canada, Canadian Conference on Electrical and Computer Engineering, Volumes 1 and 2 1991 4 p (For primary document see N94-22101 05-33)
Avail: Issuing Activity (Engineering Inst. of Canada, 2050 rue Mansfield, Suite 700, Montreal, PQ H3A 1Z2 Canada)

A time division multiple access (TDMA) satellite communication system is proposed, suitable for integrated satellite and terrestrial services covering both basic interface and primary interface services. To provide these services economically and efficiently, the proposed system employs demand assignment technology for each data burst and a transmitting and receiving transponder (carrier) hopping TDMA scheme. Moreover, to realize cost-effective transmission and subscriber lines and increase reliability of TDMA terminals, major functions of TDMA terminals have been implemented in various types of integrated circuits. The developed TDMA system which provides basic and primary subscriber transmission lines will be in commercial use from mid-1991. Author (CISTI)

N94-22172 Nippon Telegraph and Telephone Public Corp., Yokosuka (Japan). Radio Communication Systems Lab.
A CONSIDERATION OF THE INTEGRATION OF TERRESTRIAL AND SATELLITE MOBILE SYSTEMS **c32**
Masato Mori, Yasuki Nishi, and Hiraku Mishima *In* Engineering Inst. of Canada, Canadian Conference on Electrical and Computer Engineering, Volumes 1 and 2 1991 4 p (For primary document see N94-22101 05-33)
Avail: Issuing Activity (Engineering Inst. of Canada, 2050 rue Mansfield, Suite 700, Montreal, PQ H3A 1Z2 Canada)

Terrestrial communication systems can handle heavy traffic concentrated in a narrow urban area, but are uneconomic to handle light traffic distributed over a wide area. In satellite systems, communications are available wherever the satellite can be seen. However, such systems have channel capacity limitations which makes them unsuitable for intra-urban communications. The characteristics of each system can be effectively integrated to achieve an economical mobile communications system. A satellite mobile communications system is proposed which is network integrated into a terrestrial cellular system. The network is composed of a transit layer and a local switching layer, with several points of interface. The relationship between the optimum areas of coverage for the satellite system and the terrestrial system is discussed. The system will use the S band as the service link frequency for the multi-beam satellite system communicating with compact mobile terminals. Author (CISTI)

N94-22173 Laval Univ. (Quebec). Dept. de Genie Electrique.
CODING OF COLOR QUANTIZED IMAGES **c61**
Andre Zaccarin and Bede Liu (Princeton Univ., NJ.) *In* Engineering Inst. of Canada, Canadian Conference on Electrical and Computer Engineering, Volumes 1 and 2 1991 4 p (For primary document see N94-22101 05-33)
Avail: Issuing Activity (Engineering Inst. of Canada, 2050 rue Mansfield, Suite 700, Montreal, PQ H3A 1Z2 Canada)

Color images are usually compressed in a luminance chrominance coordinate space. Since the compression is done independently for each coordinate, the pixels of the decoded image can take any value in the full color space. If such a technique is applied to an image using a limited palette, the decoded image has to be quantized before it can be displayed with a limited palette. An approach for the compression of color images with limited palette is presented that does not require color quantization of the decoded image. The proposed technique restricts the pixels of the decoded image to take values only in the original palette. Thus, the decoded image can be readily displayed without having to be quantized. For comparable quality and bit rates, the proposed technique significantly reduces the decoder computational complexity. Author (CISTI)

N94-22174 Toronto Univ. (Ontario). Dept. of Electrical Engineering.
HIERARCHICAL MULTIRATE VECTOR QUANTIZATION FOR IMAGE CODING **c61**
P. Yu and A. N. Venetsanopoulos *In* Engineering Inst. of Canada, Canadian Conference on Electrical and Computer Engineering, Volumes 1 and 2 1991 4 p (For primary document see N94-22101 05-33)
Avail: Issuing Activity (Engineering Inst. of Canada, 2050 rue Mansfield, Suite 700, Montreal, PQ H3A 1Z2 Canada)

The hierarchical multirate vector quantization (HMVQ) is an improved form of vector quantization for digital image coding. The HMVQ uses block segmentation and a structure tree to divide an original image into several layers and sub-layers according to their grey scale contrast within blocks of a certain size. Variant bit rates are used for block coding of different layers with the same codebook. The codebook consists of several sub-codebooks which are generated separately from their respective layers. The HMVQ technique can provide high quality image reproduction with very low bit rates. The processing time for codebook generation is greatly shortened by using layer by layer optimization and a proper subsampling in low detail regions. The technique also demonstrates a flexibility in accurate reproduction in different detail regions. The accuracy for the recovery of different areas in an image can be adjusted by changing the thresholds, the number of layers, or the sizes of the relative codebooks.
Author (CISTI)

N94-22175 McMaster Univ., Hamilton (Ontario). Dept. of Electrical and Computer Engineering.
USING STREAM INTERLEAVING TO ELIMINATE THE NEED FOR INTERLOCKS IN DEEPLY PIPELINED PROCESSORS **c62**
Daniel C. McCrackin *In* Engineering Inst. of Canada, Canadian Conference on Electrical and Computer Engineering, Volumes 1 and 2 1991 6 p (For primary document see N94-22101 05-33)
Avail: Issuing Activity (Engineering Inst. of Canada, 2050 rue Mansfield, Suite 700, Montreal, PQ H3A 1Z2 Canada)

The performance of a practical multistream mechanism for achieving high utilization of deeply pipelined processors was investigated. The delay enforced multistreaming (DEMUS) mechanism circumvents both control hazards and data hazards in processors with an arbitrary number of pipeline stages. A novel dynamic stream interleaving technique is used to fill gaps in execution required for the correct operation of one stream with useful work for another stream. The control mechanism offers: potentially complete pipeline utilization, reduced performance loss due to data hazards and control hazards, no hardware interlocks, and no-overhead context switching for a hardware limited to a small number of streams. Sufficient delay is introduced after the dispatch of each instruction on each stream so that successive instructions cannot interfere with each other. The simulated performance of three simple stream dispatch mechanisms is presented.
Author (CISTI)

N94-22176 Defence Research Establishment Valcartier (Quebec).
THIN-FILM FABRICATION OF Pb-DOPED BiSrCaCuO SUPERCONDUCTOR **c76**
Linh Ngo Phong, Bruno Tremblay, Dominic Cote, Ishiang Shih (McGill Univ., Montreal, Quebec.), and Cindy X. Qiu (McGill Univ., Montreal, Quebec.) *In* Engineering Inst. of Canada, Canadian Conference on Electrical and Computer Engineering, Volumes 1 and 2 1991 4 p (For primary

document see N94-22101 05-33)
Avail: Issuing Activity (Engineering Inst. of Canada, 2050 rue Mansfield, Suite 700, Montreal, PQ H3A 1Z2 Canada)

Thin-film fabrication of superconductors is one of the most important fields in the development of advanced superconducting electronic and microwave devices. The processing details and properties are provided for Pb-doped BiSrCaCuO high temperature superconducting thin films. The fabrication processes included preparation of (Pb)BiSrCaCu oxide target in 2:2:2:2:3 cation ratio, deposition of amorphous films using single-target radio frequency magnetron sputtering, and annealing of the as-deposited films for oxygen-vacancy control. The substrates used for the film growth were (100)-oriented single-crystal MgO. The fabricated films, 1 micrometer thick, were a mixture of (001)-oriented 2212- and 2223- superconducting phases. The temperature dependent resistance of the thin films showed very sharp transition in the vicinity of 105 K. The current carrying capability of these films was established to be 3000 amperes per square centimeter at 77 K. Effects of the substrate materials, deposition geometries, and annealing conditions are described. Author (CISTI)

N94-22177 Communications Research Centre, Ottawa (Ontario).
CHARACTERIZATION AND MODELLING OF EXTREMELY HIGH FREQUENCY ENCLOSURES [CARACTERISATION ET MODELISATION DES BOITIERS HYPERFREQUENCES]
M. Gaudreault and M. Cuhaci *In* Engineering Inst. of Canada, Canadian Conference on Electrical and Computer Engineering, Volumes 1 and 2 1991 4 p In FRENCH (For primary document see N94-22101 05-33)
Avail: Issuing Activity (Engineering Inst. of Canada, 2050 rue Mansfield, Suite 700, Montreal, PQ H3A 1Z2 Canada)

The development of monolithic microwave integrated circuits has prompted the need to develop specific types of enclosures for these circuits. The choice of enclosure depends on the intended frequency of operation since the performance of enclosures is affected by parasitic effects related to their construction and physical characteristics. These effects are caused by transitions, the cavity volume, the effect of the cover, and the electromagnetic coupling between the metallic walls and the encapsulated circuit. Two types of transitions are studied in detail through tests on enclosures made by Technical Components Inc. and by the French company SOREP. Results of time domain measurements are presented showing effects of electromagnetic coupling, covers, and cavity resonance. Many of the effects depend on the enclosure dimensions and all the effects studied contribute to a degradation in performance. The transitions between interior and exterior are the greatest causes of this degradation and their equivalent circuit models have the topology of a low pass filter. Author (CISTI)

N94-22178 Communications Research Centre, Ottawa (Ontario).
MANUAL DESIGN TECHNIQUE FOR BROADBAND PASSIVE THIN-FILM ATTENUATORS USING THE SMITH CHART
H. Do Ky, M. Cuhaci, and A. Ittipiboon *In* Engineering Inst. of Canada, Canadian Conference on Electrical and Computer Engineering, Volumes 1 and 2 1991 3 p (For primary document see N94-22101 05-33)
Avail: Issuing Activity (Engineering Inst. of Canada, 2050 rue Mansfield, Suite 700, Montreal, PQ H3A 1Z2 Canada)

A manual design procedure for broadband passive thin film attenuators is described, in which the Smith chart is used to calculate attenuator dimensions. The procedure transforms a known terminating impedance to a real value, over a complex characteristic impedance transmission line. The proposed analysis of this transformation eliminates the need for using a complex numerical technique to solve for the input impedance of a resistive transmission line. Good agreement is found between the results from this manual procedure and those from running simulations using Mathematica. The design technique is verified with measured results of fabricated samples of these attenuators up to 26.5 GHz. Author (CISTI)

N94-22179 Calcutta Univ. (India). Inst. of Radio Physics and Electronics.
IMPROVEMENT OF THE PERFORMANCE OF IMPATT OSCILLATORS THROUGH APPROPRIATE MODIFICATION OF RESONANT-CAP ACTIVITY
Subal Kar and S. K. Roy *In* Engineering Inst. of Canada, Canadian Conference on Electrical and Computer Engineering, Volumes 1 and 2 1991 4 p (For primary document see N94-22101 05-33)
Avail: Issuing Activity (Engineering Inst. of Canada, 2050 rue Mansfield, Suite 700, Montreal, PQ H3A 1Z2 Canada)

A modified resonant-cap IMPATT oscillator has been developed at X band (8-12 GHz) by incorporating appropriately sized circumferential slots on the disc of the resonant-cap structure. The microwave power output of the optimally modified cap oscillator is almost doubled and the bandwidth of electronic tuning improved nearly four-fold compared to the optimized normal circular resonant-cap oscillator. A simple semi-quantitative understanding of these experimental results is outlined. The modified cap cavity has two effective values for the radius of the cap, with an operating frequency corresponding to the average of the two resultant resonant frequencies. This concept appears to be an attractive means of designing powerful solid-state sources of microwave energy with wide, electronically tunable bandwidth which may be useful for communication and radar systems. Author (CISTI)

N94-22180 Victoria Univ. (British Columbia). Lab. for Lightwave Electronics, Microwave and Communications.
A SIMPLIFIED METHOD FOR S-PARAMETER CALCULATIONS OF METAL SEPTUM WAVEGUIDE FILTERS
Kerry Zhenglian Cai, Danian Li (Beijing Normal Univ., China.), and Jens Bornemann *In* Engineering Inst. of Canada, Canadian Conference on Electrical and Computer Engineering, Volumes 1 and 2 1991 4 p (For primary document see N94-22101 05-33)
Avail: Issuing Activity (Engineering Inst. of Canada, 2050 rue Mansfield, Suite 700, Montreal, PQ H3A 1Z2 Canada)

A combined field theoretical and measurement oriented model is presented for the performance evaluation and design of waveguide E-plane filters with all-metal inserts. The analysis is based on both the variational method and general measurement techniques of scattering networks. Compared with previously published algorithms, this procedure is easy to program, uses less computer memory, and offers a better convergence behavior. The calculated scattering parameters include the interaction effects between the fundamental and higher-order modes at the waveguide to metal septum discontinuity. The method is verified by comparing computed data with measured results of three Ka-band filter prototypes. Due to the accurate predictions of the model, good agreement is obtained.
Author (CISTI)

N94-22181 Manitoba Univ., Winnipeg. Dept. of Electrical and Computer Engineering.
ON THE DISCOVERY OF APPROXIMATE ARITHMETIC RELATIONS BY BACKPROPAGATION NETWORKS **c63**
N. R. S. Simons and H. C. Card *In* Engineering Inst. of Canada, Canadian Conference on Electrical and Computer Engineering, Volumes 1 and 2 1991 4 p (For primary document see N94-22101 05-33)
Avail: Issuing Activity (Engineering Inst. of Canada, 2050 rue Mansfield, Suite 700, Montreal, PQ H3A 1Z2 Canada)

In this paper a backpropagation network is used to discover simple arithmetic relations. The first problem examined is that of determining an approximate value or range for the resistance of a wire given its length, cross-sectional area, and resistivity. The operation is performed in a discrete manner in that input and output values are lumped into low, medium, and high bins. In another problem the simpler operation of multiplication is examined to investigate some of the details regarding generalization and memorization, and to evolve improved multiplication rules. The multiplication problem is also re-examined using graded analog data rather than lumped data, and comparison with alternative approaches is made. In conclusion it is shown that an artificial neural network is capable of fitting a solution surface to a data set that is mathematically related. Although the relationships examined are simple examples, many of the conclusions are applicable to more complex arithmetic problems. Author (CISTI)

N94-22182 Manitoba Univ., Winnipeg. Dept. of Electrical and Computer Engineering.
LOGIC ORIENTED NEURAL NETWORKS **c63**
Robert V. Pelletier, Witold Pedrycz, Robert D. McLeod, and David C. Blight *In* Engineering Inst. of Canada, Canadian Conference on Electrical and Computer Engineering, Volumes 1 and 2 1991 4 p (For primary document see N94-22101 05-33)
Avail: Issuing Activity (Engineering Inst. of Canada, 2050 rue Mansfield, Suite 700, Montreal, PQ H3A 1Z2 Canada)

Logic networks are a special class of neural network that yield knowledge about the trained system more readily than conventional neural networks.

A new class of logic-based topologies based on mechanisms of fuzzy sets are studied. A detailed description of the proposed logical structure and learning scheme is presented. A number of experiments were performed to illustrate the practical operation of the logic networks. These experiments included: comparing the different methods described using a multi-valued version of the two-input XOR problem; determining the effects of modifying the learning rate and momentum on the convergence speed of the networks; and increasing the size of the network to a three-input XOR function with n=3 and m=4 for the logic networks. Methods other than the Lukasiewicz conjunction must be used for networks larger than two inputs, due to its discontinuous learning derivatives. Author (CISTI)

N94-22183 Concordia Univ., Montreal (Quebec). Dept. of Electrical and Computer Engineering.

A NEURAL NETWORK APPROACH TO THE MAXIMUM FLOW PROBLEM **c63**

M. Mehmet Ali and Faouzi Kamoun *In* Engineering Inst. of Canada, Canadian Conference on Electrical and Computer Engineering, Volumes 1 and 2 1991 4 p (For primary document see N94-22101 05-33)

Avail: Issuing Activity (Engineering Inst. of Canada, 2050 rue Mansfield, Suite 700, Montreal, PQ H3A 1Z2 Canada)

Neural network optimization techniques are applied to solve the maximum flow problem which is a traffic flow allocation problem with many applications in computer communication networks. Previous attempts to solve the network flow problem for the general multicommodity case have ended up with a linear programming formulation, in which the solution technique, based on the simplex algorithm, suffers from excessive storage and running time requirements especially for large networks. In order to solve the resulting linear programming problem in real time, using a neural network approach, an extended version of the Chau and Lin linear programming network is suggested. The computational power of the extended model is demonstrated through computer simulations. Author (CISTI)

N94-22184 McGill Univ., Montreal (Quebec). Dept. of Electrical Engineering.

A HOPFIELD NEURAL NET FOR DISCRETE FOURIER TRANSFORM CALCULATION **c63**

A. Cova, N. Kim, M. Petroni, and B. Zabawskij *In* Engineering Inst. of Canada, Canadian Conference on Electrical and Computer Engineering, Volumes 1 and 2 1991 4 p (For primary document see N94-22101 05-33)

Avail: Issuing Activity (Engineering Inst. of Canada, 2050 rue Mansfield, Suite 700, Montreal, PQ H3A 1Z2 Canada)

The discrete Fourier transform (DFT) is a valuable tool in signal processing being required in a wide variety of applications. For real-time tasks, fast calculation of the DFT is required. A practical implementation is presented of a modified Hopfield neural net for the computation of an N point DFT. The implementation is based on different configurations of operational transconductance amplifiers, biased in the active region. The use of the actively biased solution is limited to N less than or equal to 256 due to current power dissipation constraints. A drawback of the actively biased solution is its sensitivity to process fluctutations. An implementation in the sub-threshold region will likely find use when power dissipation is a major concern. The convergence time of the circuit is very fast compared to other reported implementations. Ideally, the computation time could decrease as the order of the transformation increases. An advantage of this method of DFT calculation over other processor-based implementations is its relative simplicity of architecture, despite its lack of modularity. Author (CISTI)

N94-22185 National Research Council of Canada, Ottawa (Ontario). Flight Research Lab.

EXPERIENCES IN AIRBORNE COMPUTING AT NRC FOR GEOPHYSICAL EXPLORATION APPLICATIONS **c60**

J. E. Jordan *In* Engineering Inst. of Canada, Canadian Conference on Electrical and Computer Engineering, Volumes 1 and 2 1991 4 p (For primary document see N94-22101 05-33)

Avail: Issuing Activity (Engineering Inst. of Canada, 2050 rue Mansfield, Suite 700, Montreal, PQ H3A 1Z2 Canada)

An experimental computing system has been installed in a Convair 580 aircraft at the National Research Center (Canada) Flight Research Laboratory. The system is used in a number of research projects in the fields of geophysics, oceanography, and meteorology. The characteristics and performance of this system are described, with a focus on its application in geophysical exploration. In its first configuration, a single centralized minicomputer was used. In this approach, all sensors, conversion equipment, and input-output devices were interfaced directly to the computer. Problems with interrupts, complex input/output structure, and development bottlenecks led to the decision to use front-end processors to perform low-level device handling and data acquisition functions. The resulting distributed computing system retained the main computer and a number of 16-bit microprocessors were added as front-end and auxiliary processors. Current work is aimed at upgrading the various components of the system. A local area network is also being considered to improve data communication in the system. Author (CISTI)

N94-22186 Carleton Univ., Ottawa (Ontario).

INTERFERENCE REDUCTION USING NEURAL NETWORKS **c63**

H. M. Hafez and G. K. Chan (Department of Communications, Ottawa, Ontario.) *In* Engineering Inst. of Canada, Canadian Conference on Electrical and Computer Engineering, Volumes 1 and 2 1991 4 p (For primary document see N94-22101 05-33)

Avail: Issuing Activity (Engineering Inst. of Canada, 2050 rue Mansfield, Suite 700, Montreal, PQ H3A 1Z2 Canada)

The feasibility of using neural networks in detecting binary data in the presence of inter-symbol interference and a strong co-channel interference is investigated. A generic model that combines co-channel and adjacent channel interference is explained and used as a basis for a numerical example demonstrating the strength of the neural network approach. A neural network processor views the data selection as a pattern classification problem. A back propagation algorithm is used to train the network off-line without additive noise. The trained network captures the statistics of the signal plus interference, establishes its own decision boundaries, and stores all the information in the values of the connecting weights. In the example considered, a three-layer neural network detector was trained and then tested in the recall phase for SIR (signal to interference ratios) of 3, 5, and 7 dB. In each test the signal to noise ratio was increased in 3-dB steps until no error could be detected. The bit error rate for the neural network detector at SIR of 7 dB or more was very close to that of binary phase shift keying in an ideal channel. Author (CISTI)

N94-22187 Department of Communications, Ottawa (Ontario).

VISIBILITY CONSIDERATIONS IN FREQUENCY SHARING WITH LOW EARTH ORBIT SATELLITES **c32**

John W. Chang *In* Engineering Inst. of Canada, Canadian Conference on Electrical and Computer Engineering, Volumes 1 and 2 1991 4 p (For primary document see N94-22101 05-33)

Avail: Issuing Activity (Engineering Inst. of Canada, 2050 rue Mansfield, Suite 700, Montreal, PQ H3A 1Z2 Canada)

Recent proposals in data-relay satellite systems indicate the use of multiple low earth orbit (LEO) satellites. These systems usually consist of many small satellites, each of which stays above the horizon for around 15 minutes in each 100-minute orbit. Allocation of frequency bands to this service sharing with existing services, with communication links between fixed points, will require additional considerations. In addition to interference assessment between the shared systems, parameters relating to probability of time exposure should be considered in the evaluation for sharing feasibility. The model used to estimate these parameters in sharing analyses is described. Author (CISTI)

N94-22188 Department of Communications, Ottawa (Ontario).

INCLINED ORBITS AND INTERFERENCE TO STATIONARY SERVICE AND TO STATIONARY SERVICE BY SATELLITE [ORBITES INCLINEES ET BROUILLAGE AU SERVICE FIXE ET AU SERVICE FIXE PAR SATELLITE] **c13**

Michel Gaudreau and Vishnu Sahay *In* Engineering Inst. of Canada, Canadian Conference on Electrical and Computer Engineering, Volumes 1 and 2 1991 4 p In FRENCH (For primary document see N94-22101 05-33)

Avail: Issuing Activity (Engineering Inst. of Canada, 2050 rue Mansfield, Suite 700, Montreal, PQ H3A 1Z2 Canada)

The maintenance of a communications satellite in a geosynchronous orbit requires the combustion of an on-board fuel. It can be of interest, in order to prolong the life of a satellite already in orbit or even to allow

lightening of a satellite at launch, to save onboard fuel by letting the satellite drift in a slightly inclined orbit. The mechanisms which govern the inclination of the orbit are reviewed, followed by the equations which describe the movement of the satellites and the service zones irradiated by their antennas. Once these parameters are defined, their impact on the management of the spectrum and of the orbit is evaluated through an analysis of the possibility of interference with other satellite radio communication systems or even systems in stationary service sharing the same frequency bands. Author (CISTI)

N94-22189 Concordia Univ., Montreal (Quebec). Dept. of Electrical and Computer Engineering.
THROUGHPUT AND BLOCKING IN CIRCUIT-SWITCHED INTERCONNECTION NETWORKS
Han-Hua Ma and M. Comeau *In* Engineering Inst. of Canada, Canadian Conference on Electrical and Computer Engineering, Volumes 1 and 2 1991 4 p (For primary document see N94-22101 05-33)
Avail: Issuing Activity (Engineering Inst. of Canada, 2050 rue Mansfield, Suite 700, Montreal, PQ H3A 1Z2 Canada)

Interconnection networks are applied in communications networks and high performance parallel computers. Contention is the central problem making performance analysis difficult, as it introduces statistical dependencies among the elements of the system. A Markov model is employed to determine throughput and blocking in circuit-switched interconnection networks. Internally nonblocking switches are considered and may be asymmetrically loaded. The model represents blocking at the ports as a relation to the circuits of the switch and yields a product form for the equilibrium distribution of the switch. The computational aspects of the model are greatly simplified for switches of a regular topology, resulting in simple recursions (over the dimensions of the switch) for throughput and blocking. Results are presented for symmetrically loaded networks. Author (CISTI)

N94-22190 Concordia Univ., Montreal (Quebec). Dept. of Electrical and Computer Engineering.
THROUGHPUT, BLOCKING, AND INTERFERENCE IN PACKET RADIO NETWORKS **c32**
Han-Hua Ma and Marc Comeau *In* Engineering Inst. of Canada, Canadian Conference on Electrical and Computer Engineering, Volumes 1 and 2 1991 4 p (For primary document see N94-22101 05-33)
Avail: Issuing Activity (Engineering Inst. of Canada, 2050 rue Mansfield, Suite 700, Montreal, PQ H3A 1Z2 Canada)

A model is described, extended, and applied to determine throughput, blocking, and interference in packet radio networks. Transmission interactions are systematically categorized for a class of channel access protocols yielding a product form Markov chain for the dynamics of the system. Nonpersistant CSMA, BTMA, and directional CSMA (D-CSMA) are modelled within the framework. In addition, two non-realizable protocols, collision-free multiple access (CFMA) and total capacity allocation protocol (TCAP), are introduced as capacity measures for networks with omnidirectional and directional transmission capabilities, respectively. A comparative study of CSMA, BTMA, and D-CSMA is conducted for various networks, using CFMA and TCAP to determine relative capacity utilization. Author (CISTI)

N94-22191 Queens Univ., Kingston (Ontario). Dept. of Electrical Engineering.
THE SCHUR BERLEKAMP-MASSEY ALGORITHM IS PARALLELIZABLE **c61**
Gordon Chan and Christopher Zarowski *In* Engineering Inst. of Canada, Canadian Conference on Electrical and Computer Engineering, Volumes 1 and 2 1991 4 p (For primary document see N94-22101 05-33)
Avail: Issuing Activity (Engineering Inst. of Canada, 2050 rue Mansfield, Suite 700, Montreal, PQ H3A 1Z2 Canada)

The Berlekamp Massey algorithm (BMA) is known for its applications in the decoding of error control codes, such as BCH codes. Unfortunately, the BMA does not run efficiently on a parallel computer. The Schur form of the BMA has been derived in order that the algorithm can run efficiently on a linearly connected parallel processor array. Interprocessor communication on the array is strictly local. Using the Schur BMA on a code capable of correcting N/2 errors requires an array of N processors and takes O(N) time to compute the error locator polynomial. The algorithm is superior in the sense that it is regular. That is, if the number of errors the code can correct increases, then more processors may be added to the array. Author (CISTI)

N94-22192 McGill Univ., Montreal (Quebec). Biorobotics Lab.
INTEGRATION OF PARALLEL PROCESSING STRUCTURES USING A MATRIX APPROACH **c62**
Sylvain Martel, Ian W. Hunter, and S. Lafontaine *In* Engineering Inst. of Canada, Canadian Conference on Electrical and Computer Engineering, Volumes 1 and 2 1991 4 p (For primary document see N94-22101 05-33)
Avail: Issuing Activity (Engineering Inst. of Canada, 2050 rue Mansfield, Suite 700, Montreal, PQ H3A 1Z2 Canada)

A novel interprocessor network is presented that can be gradually implemented and integrates several modern multiprocessor architectures. The network is particularly suitable for coarse-grain multiprocessor systems. It is also attractive in that many well known architectures requiring different resources from the present network system can be integrated with minimal bus or memory contention. Hardware and software interprocessor synchronization, interrupts, and DMA transfers can be supported. The interconnection system can in its full configuration support a number of processors in a fully interconnected network permitting parallel data exchanges without contention and minimum communication skew. The basic theory behind the approach is presented and examples of integration of parallel processing structures based on the network are given. The implementation and fabrication of the communications hardware are discussed. Author (CISTI)

N94-22193 McGill Univ., Montreal (Quebec). Biorobotics Lab.
SPECIFICATION AND FORMAL VERIFICATION OF THE SAFETY CRITERION IN THE ALTERNATING BIT PROTOCOL **c82**
Sylvain Martel, Ian W. Hunter, and Serge Lafontaine *In* Engineering Inst. of Canada, Canadian Conference on Electrical and Computer Engineering, Volumes 1 and 2 1991 4 p (For primary document see N94-22101 05-33)
Avail: Issuing Activity (Engineering Inst. of Canada, 2050 rue Mansfield, Suite 700, Montreal, PQ H3A 1Z2 Canada)

The alternating bit protocol is one of many protocols designed to transmit data reliably from a sender to a receiver over an unreliable channel. The Milner version of the alternating bit protocol is specified in HOL (the Cambridge higher order logic proof assistant) and checked for the desirable properties of a safe protocol (the order in which messages are given to the sender is the order in which they reach the receiver) and that the protocol is live (all messages given to the sender reach the receiver or the protocol aborts). A description is presented of the alternating bit protocol, expressing the protocol in HOL, and the proof structure. Author (CISTI)

N94-22194 Queens Univ., Kingston (Ontario). Dept. of Electrical Engineering.
MODELING AND ANALYSIS OF SECURE COMMUNICATION PROTOCOLS USING PETRI NET FORMALISM **c61**
Benjamin B. Nieh and Stafford E. Tavares *In* Engineering Inst. of Canada, Canadian Conference on Electrical and Computer Engineering, Volumes 1 and 2 1991 4 p (For primary document see N94-22101 05-33)
Avail: Issuing Activity (Engineering Inst. of Canada, 2050 rue Mansfield, Suite 700, Montreal, PQ H3A 1Z2 Canada)

The use of cryptographic techniques is essential for secure network communications. The security of such communication systems depends not only on the strength of the cryptographic algorithms employed, but also on the correctness and security of protocols based on these algorithms. A petri net based modelling and analysis methodology for secure communication protocol studies is presented. Ordinary petri nets, colored petri nets, and a modified petri net model are used to represent protocol entities as a hierarchical set of descriptions and to develop a corresponding intruder model. A security analysis is carried out of the Burns-Mitchell (B-M) protocol and security flaws are discussed. It is concluded that petri nets, a formalism with strong modelling power and theoretical foundation, are a useful tool in the study of security systems, and will play a role in the analysis and development of secure communications protocols. Author (CISTI)

N94-22195 Universite des Sciences et de la Technologie Houari Boumediene, Algiers (Algeria).

NON-LINEAR ANALYSIS OF THE ELECTRICAL PROPERTIES OF THE ACTIVE CIRCUITS OF HIGH-FREQUENCY OSCILLATORS [ANALYSE NON-LINEAIRE DES ELEMENTS ACTIFS DE L'OSCILLATEUR H.F. ACCORDE ELECTRIQUEMENT]

Salih Aidel, Andrei Szymczak, and Abdellatif Said (Constantine Univ., Algeria.) *In* Engineering Inst. of Canada, Canadian Conference on Electrical and Computer Engineering, Volumes 1 and 2 1991 4 p In FRENCH (For primary document see N94-22101 05-33)

Avail: Issuing Activity (Engineering Inst. of Canada, 2050 rue Mansfield, Suite 700, Montreal, PQ H3A 1Z2 Canada)

The parameters of active circuits incorporating high frequency wide-band semiconductors depend strongly on the amplitude of the high frequency signal supplied to it, and circuit analysis must take this fact into account. A new method for analyzing elementary microwave oscillator circuits is proposed, with the objective of predicting the output power of the high-frequency generator. The method is based on an examination of the retreat function of the visible reflectance at the level of the active gate as a function of the power supplied to the circuit of the oscillator in question. An example of an active circuit based on the HP3508238 transistor and a control circuit with the 2H703 varactor are used for illustration. The results obtained have contributed to the optimization of the structure of the oscillator. Author (CISTI)

N94-22196 Laval Univ. (Quebec). Dept. of Electrical Engineering.

AlGaAs LASER DIODE FM SPECTRUM: PHASED ARRAY ANTENNA APPLICATION **c32**

Martin Chamberland and Michel Tetu *In* Engineering Inst. of Canada, Canadian Conference on Electrical and Computer Engineering, Volumes 1 and 2 1991 4 p (For primary document see N94-22101 05-33)

Avail: Issuing Activity (Engineering Inst. of Canada, 2050 rue Mansfield, Suite 700, Montreal, PQ H3A 1Z2 Canada)

Preliminary results are presented on the use of an AlGaAs laser diode to generate microwave signals suitable for application with phased array antennas. The relative intensity noise (RIN) was measured under various operating conditions to give an indication of the frequency response limitation of the laser diode. The frequency response to intensity modulation was also measured directly at microwave frequencies. Finally, the FM spectrum was observed using a heterodyne technique and compared with an empirical model. The spectrum of intensity fluctuations shows a peak near the relaxation oscillation frequency. This is a good indication of the cutoff frequency for direct current modulation of the laser diode. The behavior of the modulated laser diode is well characterized by the simultaneous intensity and frequency modulation taking into account a phase difference between the two. Author (CISTI)

N94-22197 Ecole Polytechnique, Montreal (Quebec). Dept. de Genie Electrique et Genie Informatique.

NUMERICAL METHOD FOR COMPUTING THE ELECTRIC FIELD PRODUCED BY A MICROWAVE BEAM IN A STRATIFIED MEDIUM [METHODE POUR L'ETUDE DU CHAMP ELECTRIQUE PRODUIT PAR UN FAISCEAU HYPERFREQUENCE DANS UN MILIEU STRATIFIE] **c32**

Jean Montreuil *In* Engineering Inst. of Canada, Canadian Conference on Electrical and Computer Engineering, Volumes 1 and 2 1991 2 p In FRENCH (For primary document see N94-22101 05-33)

Avail: Issuing Activity (Engineering Inst. of Canada, 2050 rue Mansfield, Suite 700, Montreal, PQ H3A 1Z2 Canada)

Microwaves are often used in applications where they interact with stratified media, such as in high-frequency heating, microwave radiometry, and the study of soils and ice. To evaluate the electric fields in the strata, it is necessary to model the radiation from the antenna. A numerical method has been developed for evaluation of the electric field radiated by an antenna into a stratified medium. The radiation is modeled by a beam having a finite rather than infinite width. For several applications, this model is more appropriate and provides more accurate results than the ones based on a beam of infinite width. Author (CISTI)

N94-22198 Manitoba Univ., Winnipeg.

PERFORMANCE OF A SIMPLE CIRCULAR POLARIZATION SELECTIVE SURFACE **c32**

J. E. Roy, G. A. Morin (Defence Research Establishment, Ottawa, Ontario.), and L. Shafai *In* Engineering Inst. of Canada, Canadian Conference on Electrical and Computer Engineering, Volumes 1 and 2 1991 4 p (For primary document see N94-22101 05-33)

Avail: Issuing Activity (Engineering Inst. of Canada, 2050 rue Mansfield, Suite 700, Montreal, PQ H3A 1Z2 Canada)

A parametric analysis is presented of a simple circular polarization selective surface (CPSS) performed with the Numerical Electromagnetic Code NEC-2. The application envisaged is a Cassegrain reflector antenna in which the hyperboloidal subreflector is replaced by a flat CPSS in order to minimize the aperture blockage and thereby reduce the sidelobe level of the antenna. As the incidence angle varies from point to point on the subreflector surface, the effect of the incidence angle on the performance of the CPSS becomes of paramount importance. The operation of the unit cell and of an octagonal array made of 37 identical cells (operating frequency 1 GHz) is shown for variations in incidence angle, frequency, and cell size. Author (CISTI)

N94-22199 Communications Research Centre, Ottawa (Ontario).

MHMIC: TECHNOLOGY FOR THE INTEGRATION OF MICROWAVE SUB-ASSEMBLIES [MHMIC: TECHNOLOGIE D'INTEGRATION DES SOUS-ENSEMBLES HYPERFREQUENCES]

R. Douville, M. Cuhaci, and S. Meszaros *In* Engineering Inst. of Canada, Canadian Conference on Electrical and Computer Engineering, Volumes 1 and 2 1991 3 p In FRENCH (For primary document see N94-22101 05-33)

Avail: Issuing Activity (Engineering Inst. of Canada, 2050 rue Mansfield, Suite 700, Montreal, PQ H3A 1Z2 Canada)

A new technology for producing miniaturized microwave circuits is described. This technology is called miniature hybrid microwave integrated circuits (MHMIC) and is a technology which is intermediate between microwave integrated circuits (MIC) and monolithic microwave integrated circuits (MMIC). All the passive elements are produced during the different stages of fabrication, similar to MMIC's. The active devices are added at the end by assembly, using MIC techniques. The main difference between the MHMIC and MIC technologies is the utilization of metallized holes, air bridges, and dielectric layers in MHMIC. The advantages of integrating the passive elements are a significant reduction in assembly cost and in the number of elements to assemble. MHMIC technology gives the designer the choice of active device and allows the miniaturization of circuits while lowering the number of added components. In general, a thin-film technology is used in the fabrication of the various MHMIC elements. The choice of the substrate is generally determined by the final application. One of the first examples of the application of MHMIC is the development of balanced amplifier modules for 8-18 GHz. Some aerospace applications are also under development. Author (CISTI)

N94-22200 Laval Univ. (Quebec). Lab. de Vision et Systemes Numeriques.

A SOFTWARE ENVIRONMENT FOR THE EXPLOITATION OF THE MAR IMAGE SENSOR **c61**

F. Parent, M. Tremblay, D. Laurendeau, and D. Poussart *In* Engineering Inst. of Canada, Canadian Conference on Electrical and Computer Engineering, Volumes 1 and 2 1991 4 p (For primary document see N94-22101 05-33)

Avail: Issuing Activity (Engineering Inst. of Canada, 2050 rue Mansfield, Suite 700, Montreal, PQ H3A 1Z2 Canada)

The MAR (Multi-port Array Receptor) system combines optical sensing and integrated focal-plane processing capabilities. Its central element is a full custom, very large scale integrated circuit (VLSI) photosensor array with hexagonal tessellation and complex peripheral selection logic which provides parallel analog readout of a group of pixels over prescribed areas. The camera controller uses the information as feedback to perform edge tracking or area scanning. The principal characteristics of the MAR sensor and its controller are reviewed. The software environment is then described, followed by the results of tests performed on digital images.

Author (CISTI)

N94-22201 Sherbrooke Univ. (Quebec). Dept. de Mathematique et Informatique.

A PYRAMID NEURAL NETWORK ARCHITECTURE FOR STEREO FUSION **c63**

Shengrui Wang, Simon Gagne (Laval Univ., Quebec.), and Denis Poussart

(Laval Univ., Quebec.) *In* Engineering Inst. of Canada, Canadian Conference on Electrical and Computer Engineering, Volumes 1 and 2 1991 4 p (For primary document see N94-22101 05-33)
Avail: Issuing Activity (Engineering Inst. of Canada, 2050 rue Mansfield, Suite 700, Montreal, PQ H3A 1Z2 Canada)

A model for reconstruction of three dimensional representation from two dimensional images is proposed. The model is composed of three functional components. A pyramidal neural architecture is elaborated for multiscale edge detection. Important characteristics of the architecture include the introduction of an adaptive mechanism in a competitive neural network and an explicit modeling of multiscale processing. Also proposed is a neural network architecture for edge matching, whose design takes into account psychophysical contraints such as uniqueness and disparity gradient limit. The model is completed by a diffusive filling-in algorithm that can be used to estimate global disparity information by combining shading information (intensity gradient) and known disparities at edge points. Experimental results are provided to illustrate the performance of the model. Author (CISTI)

N94-22202 Centre National de la Recherche Scientifique, Paris (France).
TWO-DIMENSIONAL PERCEPTION BASED ON A LASER RANGEFINDER [PERCEPTION BIDIMENTIONNELLE A BASE D'UN TELEMETRE LASER] **c36**
G. Allegre and H. Clergeot *In* Engineering Inst. of Canada, Canadian Conference on Electrical and Computer Engineering, Volumes 1 and 2 1991 4 p In FRENCH (For primary document see N94-22101 05-33)
Avail: Issuing Activity (Engineering Inst. of Canada, 2050 rue Mansfield, Suite 700, Montreal, PQ H3A 1Z2 Canada)

A simple solution for obtaining a three dimensional vision system has been to add a plane sweep deviation system to a precision laser rangefinder. This system has allowed working with noncooperative targets at 12 m distance and at 50 kHz frequency with a precision often better than a millimeter. Coaxial send and receive optical beams enable deviation to be readily accomplished. A compromise is found between rapidity and precision for a given optical power received. Analysis of the causes of variation in signal level explained the observed dynamics, and procedures are suggested to limit these phenomena. Two other critical problems are related to the coupling between paths and to the phase derivatives of the measuring chain. A system of plane deviation offering a vision angle of +/- 30 deg and a maximum frequency of a dozen Hertz was developed using a galvanometric mirror. Dynamic testing of the profiling capability of the system was also conducted. For mobile robotics applications, it is proposed to simplify the system by determining a horizontal profile in two dimensions. This would be sufficient for many purposes and although one dimension would be lost, a significant improvement in response time is expected. Author (CISTI)

N94-22203 Ottawa Univ. (Ontario). Dept. of Electrical Engineering.
BUFFER ALLOCATION IN AN ATM SWITCH WITH OUTPUT BUFFER AND SPEED CONSTRAINTS **c32**
Anil K. Gupta and N. D. Georganas *In* Engineering Inst. of Canada, Canadian Conference on Electrical and Computer Engineering, Volumes 1 and 2 1991 4 p (For primary document see N94-22101 05-33)
Avail: Issuing Activity (Engineering Inst. of Canada, 2050 rue Mansfield, Suite 700, Montreal, PQ H3A 1Z2 Canada)

A synchronous nonblocking N times N switch for asynchronous transfer mode (ATM) networks or high speed packet switching networks transporting fixed length packets called cells is considered. Such a switch with output queuing achieves the optimal performance, however it requires the switch fabric to work at the speed of N. In practice the switch may operate L times faster than the input/output trunk. It is assumed that queues at each output port have a limited buffer space and whenever an output queue is full, the back-pressure is applied and the packets are retained at the head of the input queues. The upper bound on the packet loss probability at the input queues in such a switch are computed. To achieve a given packet loss rate, the switch with L equals 2 requires almost the same amount of input and output buffers as with L equals 4 up to 70 percent input load, but as the load increases beyond 70 percent the switch with L equals 4 would require more output buffers and less input buffers in comparison with a switch operating at L equals 2. The performance of a switch with L equals 3 is very similar to that for L equals 4 and is not considered. Author (CISTI)

N94-22204 Communications Research Centre, Ottawa (Ontario).
COMPARISON OF THEORETICAL AND SIMULATED PERFORMANCE RESULTS FOR SLOPPY-SLOTTED ALOHA SIGNALING **c32**
Stewart N. Crozier *In* Engineering Inst. of Canada, Canadian Conference on Electrical and Computer Engineering, Volumes 1 and 2 1991 4 p (For primary document see N94-22101 05-33)
Avail: Issuing Activity (Engineering Inst. of Canada, 2050 rue Mansfield, Suite 700, Montreal, PQ H3A 1Z2 Canada)

Sloppy-slotted Aloha refers to a form of random access signaling which allows slotted packets, with random timing errors, to spill over into adjacent slots. For the North American mobile satellite (MSAT) system, the two-way propagation delay variation is on the order of 40 milliseconds. The higher the signaling rate, or the shorter the packet length, the wider the timing error distribution, measured in packet lengths. With 192 transmission bits per packet, a 40 millisecond timing error corresponds to 2 packet lengths at 9600 bits per second. Approximate theoretical and simulated performance results are presented and compared for a mixed Gaussian discrete timing error distribution model. This model allows a fraction of the users to have corrected timing. It is found that the theoretical approximations are generally quite accurate. Where differences are observed, the theoretical approximations are always found to be pessimistic. The conclusion is that the theoretical approximations can be used with confidence as a conservative measure of performance. Author (CISTI)

N94-22205 Concordia Univ., Montreal (Quebec). Dept. of Electrical and Computer Engineering.
NEURAL NETWORKS FOR OPTIMUM ROUTING IN PACKET-SWITCHED COMMUNICATIONS NETWORKS **c32**
Faouzi Kamoun and M. Mehmet Ali *In* Engineering Inst. of Canada, Canadian Conference on Electrical and Computer Engineering, Volumes 1 and 2 1991 4 p (For primary document see N94-22101 05-33)
Avail: Issuing Activity (Engineering Inst. of Canada, 2050 rue Mansfield, Suite 700, Montreal, PQ H3A 1Z2 Canada)

A neural network solution is applied to the optimum routing problem in packet-switched communication networks, where the goal is to minimize the network-wide average time delay. Under appropriate assumptions it is shown that the optimum routing algorithm relies heavily on shortest path computations that have to be carried out in real time. For this purpose an efficient neural network shortest path algorithm, based on the Hopfield model, is proposed, which is an improved version of the previously suggested neural algorithms. The proposed model enables the routing algorithm to be implemented in real time and also to be adaptive to changes in link cost and network topology. Author (CISTI)

N94-22206 Manitoba Univ., Winnipeg. Dept. of Electrical and Computer Engineering.
ACCELERATION OF BACKPROPAGATION LEARNING USING A PARALLEL DSP MACHINE **c62**
Glenn K. Rosendahl, Robert D. McLeod, and Howard C. Card *In* Engineering Inst. of Canada, Canadian Conference on Electrical and Computer Engineering, Volumes 1 and 2 1991 4 p (For primary document see N94-22101 05-33)
Avail: Issuing Activity (Engineering Inst. of Canada, 2050 rue Mansfield, Suite 700, Montreal, PQ H3A 1Z2 Canada)

The backpropagation learning algorithm is of central importance to the field of artificial neural networks. Both analog and digital implementations are progressing, with digital being the most prevalent so far. However, digital implementations suffer from size limitions and long learning times imposed by inadequate computing resources restricting them to problems of primarily academic interest. By implementing the backpropagation algorithm on a parallel processor specifically designed for this task, the solution to larger problems associated with pattern recognition can be achieved. Speech processing, artificial vision systems, and robotic control problems are examples of tasks of practical interest. The overall parallel processor architecture is described, along with an initial implementation of the sigmoid transfer function on a 56000 digital signal processor. Comparisons are made to other high performance very large scale integration systems. Author (CISTI)

N94-22207 Alberta Univ., Calgary. Dept. of Electrical Engineering.
IMAGE CONVOLUTION USING THE MYRIAS SPS-2 PARALLEL COMPUTER **c62**

Kalpagam Krishnan, Werner B. Joerg, and Brian Minchau *In* Engineering Inst. of Canada, Canadian Conference on Electrical and Computer Engineering, Volumes 1 and 2 1991 5 p (For primary document see N94-22101 05-33)
Avail: Issuing Activity (Engineering Inst. of Canada, 2050 rue Mansfield, Suite 700, Montreal, PQ H3A 1Z2 Canada)

The implementation of an image convolution algorithm on the Myrias SPS-2 parallel computer (multiple instruction/multiple data type) is discussed. The architecture of the target system identifies an obvious preference for one of several parallelization schemes of interest. Two conceptually different schemes, namely instruction parallelism and image domain partitioning (a particular form of data parallelism) are considered. Performance studies show an efficiency of 91 percent with 16 processors in the case of instruction parallelism, with nearly linear speedup characteristics. The communication difficulties and the associated overheads are illustrated using the domain partitioning approach. It is observed that image convolution exhibits a processing structure compatible with instruction parallelism resulting in significant performance improvements on the SPS-2 and similar machines.
Author (CISTI)

N94-22208 Alberta Univ., Calgary. Dept. of Electrical Engineering.
PARALLELIZING A MAXIMUM ENTROPY IMAGE DECONVOLUTION ALGORITHM **c62**
Werner B. Joerg and Kalpagam Krishnan *In* Engineering Inst. of Canada, Canadian Conference on Electrical and Computer Engineering, Volumes 1 and 2 1991 5 p (For primary document see N94-22101 05-33)
Avail: Issuing Activity (Engineering Inst. of Canada, 2050 rue Mansfield, Suite 700, Montreal, PQ H3A 1Z2 Canada)

An image deconvolution algorithm based on the maximum entropy method (MEM) was implemented on the Myrias SPS-2 parallel computer, and its performance was studied. The application context of the deconvolution algorithm is the restoration of an unknown object from a known degraded input. The MEM algorithm is a nonlinear constrained optimization problem, solved iteratively using a relaxation scheme. For an image of size 256 by 256, the algorithm shows an efficiency of 78 percent for an optimum number of eight processors when implemented on the SPS-2. The implementation approach and the performance characteristics are discussed including the use of instruction parallelism and domain partitioning.
Author (CISTI)

N94-22209 Ottawa Univ. (Ontario). Dept. of Electrical Engineering.
FILE TRANSFER PERFORMANCE IN LAN INTERCONNECTION THROUGH A SATELLITE CHANNEL **c32**
Xiao-Xiong Yao and Oliver W. W. Yang *In* Engineering Inst. of Canada, Canadian Conference on Electrical and Computer Engineering, Volumes 1 and 2 1991 4 p (For primary document see N94-22101 05-33)
Avail: Issuing Activity (Engineering Inst. of Canada, 2050 rue Mansfield, Suite 700, Montreal, PQ H3A 1Z2 Canada)

The performance of transferring files from workstations in one local area network (LAN) to workstations in another LAN was studied. Satellite channels and associated gateway stations are used to interconnect these LAN's at different geographical locations. The file transfer performance was simulated using the QNAP2 simulation language. System performance according to delay and throughput criteria were evaluated against system parameters such as file sizes, window sizes, and the number of workstation pairs involved in transmission. Two traffic bottlenecks are identified: one due to the transmission control protocol/internet protocol flow control through its window size and the number of receive buffers; and one due to the queueing in the gateway of the system.
Author (CISTI)

N94-22210 Quebec Univ., Verdun.
RECOGNIZING HESITATION PHENOMENA IN CONTINUOUS, SPONTANEOUS SPEECH **c32**
Douglas OShaughnessy *In* Engineering Inst. of Canada, Canadian Conference on Electrical and Computer Engineering, Volumes 1 and 2 1991 4 p (For primary document see N94-22101 05-33)
Avail: Issuing Activity (Engineering Inst. of Canada, 2050 rue Mansfield, Suite 700, Montreal, PQ H3A 1Z2 Canada)

Spontaneous speech differs from read speech in speaking rate and hesitation. In natural, spontaneous speech, people often start talking and then think along the way; at times, this causes the speech to have hesitation pauses (both filled and unfilled) and restarts. Results are reported on all types of pauses in a widely-used speech database, for both hesitation pauses and semi-intentional pauses. A distinction is made between grammatical pauses (at major syntactic boundaries) and ungrammatical ones. Different types of unfilled pauses cannot be reliably separated based on silence duration, although grammatical pauses tend to be longer. In the prepausal word before ungrammatical pauses, there were few continuation rises in pitch, whereas 80 percent of the grammatical pauses were accompanied by a prior fundamental frequency rise of 10-40 kHz. Identifying the syntactic function of such hesitation phenomena can improve recognition performance by eliminating from consideration some of the hypotheses proposed by an acoustic recognizer. Results presented allow simple identification of filled pauses (such as uhh, umm) and their syntactic function.
Author (CISTI)

N94-22211 Laval Univ. (Quebec). Dept. of Electrical Engineering.
A FRAMEWORK OF CONNECTIONIST NETWORK TOWARD SPEECH WAVEFORM CODING **c32**
Ying Cheng, Paul Fortier, and Denis Poussart *In* Engineering Inst. of Canada, Canadian Conference on Electrical and Computer Engineering, Volumes 1 and 2 1991 4 p (For primary document see N94-22101 05-33)
Avail: Issuing Activity (Engineering Inst. of Canada, 2050 rue Mansfield, Suite 700, Montreal, PQ H3A 1Z2 Canada)

The application of a connectionist or neural network to speech waveform coding is investigated. A connectionist network, which was primarily based on the adaptive resonant theory principle, was built as a codebook generating machine. A three-layer/multi-layer perceptron learned to encode and decode the speech wave form. The connectionist network was tested in simulation experiments by implementing machines for both 4k bits/s and 8k bits/s at an 8 kHz sampling rate and vector dimensions of 8. During the training procedure, 6680 vectors (6680 ms of speech) contributed to the codebook generation, resulting in two codebooks of size 2(exp 7) and 2(exp 8). The recovered speech proved to be highly natural and legible for both the 4k and 8k machines.
Author (CISTI)

N94-22212 Carleton Univ., Ottawa (Ontario).
SEGMENTATION AND FREQUENCY DOMAIN ML PITCH ESTIMATION OF SPEECH SIGNALS **c32**
Salim A. Hanna *In* Engineering Inst. of Canada, Canadian Conference on Electrical and Computer Engineering, Volumes 1 and 2 1991 4 p (For primary document see N94-22101 05-33)
Avail: Issuing Activity (Engineering Inst. of Canada, 2050 rue Mansfield, Suite 700, Montreal, PQ H3A 1Z2 Canada)

The rate of oscillation of the vocal cords and its inverse value, the pitch period, are important speech features that are useful for speech analysis/synthesis, speech recognition, and speech coding. An automatic approach for the estimation of the pitch period in continuous speech is presented. The proposed approach considers the segmentation of the speech signal into homogeneous regions and the detection of segments that are generated by vocal cord oscillations prior to pitch estimation. The pitch period of voiced segments is estimated in the frequency domain using a maximum likelihood (ML) procedure. The estimated pitch period is chosen to maximize a likelihood function over the range of expected pitch periods. An efficient simplified realization of the generalized likelihood ratio segmentation method is also described.
Author (CISTI)

N94-22213 Simon Fraser Univ., Burnaby (British Columbia). Communications Science Lab.
SPEAKER-INDEPENDENT ISOLATED-DIGIT RECOGNITION USING NEURAL NETWORKS AND HIDDEN MARKOV MODEL **c32**
Michael McGuire, Diane Ingraham, and Vladimir Cuperman *In* Engineering Inst. of Canada, Canadian Conference on Electrical and Computer Engineering, Volumes 1 and 2 1991 4 p (For primary document see N94-22101 05-33)
Avail: Issuing Activity (Engineering Inst. of Canada, 2050 rue Mansfield, Suite 700, Montreal, PQ H3A 1Z2 Canada)

A speaker independent isolated-digit recognition system is described which incorporates neural networks for vector quantization (VQ) and postprocessing of VQ and hidden Markov model (HMM) decision information. Vector quantization was performed using word-based parameter specific codebooks generated with a frequency sensitive competitive learning (FSCL) training algorithm. A single-layer perceptron neural network was used to

increase recognition performance by postprocessing VQ distortion and HMM output probabilistic information. Experiments using both studio and telephone-line recorded databases demonstrate the FSCL VQ-HMM system without postprocessing achieves a recognition performance increase when compared to a previously developed VQ-HMM digit recognition system. With the addition of postprocessing to the FSCL VQ-HMM system, recognition performance was further increased. Author (CISTI)

N94-22214 Waterloo Univ. (Ontario). Dept. of Electrical and Computer Engineering.

TRENDS IN SOFTWARE RELIABILITY MODELING **c61**

Rudolph E. Seviora and Christian Brunelle (Bell Canada, Longueil, Quebec.) *In* Engineering Inst. of Canada, Canadian Conference on Electrical and Computer Engineering, Volumes 1 and 2 1991 4 p (For primary document see N94-22101 05-33)

Avail: Issuing Activity (Engineering Inst. of Canada, 2050 rue Mansfield, Suite 700, Montreal, PQ H3A 1Z2 Canada)

The state of reliability engineering is much less advanced for software than for hardware. Software reliability models used for estimation or prediction strive to either model the growth in the reliability of the product whose faults are being removed from its past failure history, or to forecast the reliability of the software product before any operational experience is available. The current state of software reliability estimation and prediction and possible future trends are described. The assumptions used in typical models are listed and discussed. Most estimation models have the underlying assumption that a fault, if not removed, would cause failures to occur according to a Poisson process; recent research has shown that this is true only for first-time failures. A major trend is the adjustment of models to pragmatic realities of failure data collection and software life cycle. For prediction models, one trend is towards models whose data requirements are lower (coarser granularity models). Author (CISTI)

N94-22215 Memorial Univ. of Newfoundland, Saint Johns.

A NEW CLASS OF MULTI-FUNCTION TWO-RAIL TOTALLY SELF-CHECKING BASIC BUILDING BLOCKS **c64**

Zhi-Jian Jiang and R. Venkatesan *In* Engineering Inst. of Canada, Canadian Conference on Electrical and Computer Engineering, Volumes 1 and 2 1991 4 p (For primary document see N94-22101 05-33)

Avail: Issuing Activity (Engineering Inst. of Canada, 2050 rue Mansfield, Suite 700, Montreal, PQ H3A 1Z2 Canada)

A new concept of strong morphic Boolean algebra is introduced. A new universal set of multi-function two-rail (TR) totally self-checking (TSC) basic building blocks (BBB) which implements a group of basic strong morphic operations is proposed. The proposed structures preserve the capabilities of fault indication (single or double error detection) and also facilitate normal logic operations. The logic representations of the TR error indication variable are 01 for logic 0, 10 for logic 1, and 00 or 11 for error indication. The new BBB are particularly useful and flexible in building TR-TSC logic functional circuits while they can still be used in building error correcting and/or error detecting circuits. Any arbitrary combinational logic can be implemented using the proposed BBB. As an example, a TR-TSC full adder with separate internal fault indication is presented. This cannot be achieved using the existing primitive operators. Author (CISTI)

N94-22216 Royal Military Coll. of Canada, Kingston (Ontario). Dept. of Electrical and Computer Engineering.

FAULT TOLERANCE FOR REAL-TIME MULTIPROCESSOR OPERATING SYSTEMS **c62**

Terry Shepard and Scott Knight *In* Engineering Inst. of Canada, Canadian Conference on Electrical and Computer Engineering, Volumes 1 and 2 1991 4 p (For primary document see N94-22101 05-33)

Avail: Issuing Activity (Engineering Inst. of Canada, 2050 rue Mansfield, Suite 700, Montreal, PQ H3A 1Z2 Canada)

Operating system mechanisms are explored which support system recovery from the failure of any one processor in a standard multiprocessor system. The mechanisms implemented allow existing operating system calls to be used. A history of messages is maintained for designated tasks. Only some tasks are backed up, so operation after a failure may be in a degraded mode. A synchronization operation limits the history which must be kept. A three-way atomic message protocol is needed to keep backups for both sender and receiver. A roll forward technique is used to recover the state of backed-up tasks. The design uses message passing primitives that support proprietors and administrators, which are useful abstractions for maintaining history and ensuring that variables shared between processors are protected and correctly updated for local access. A prototype based on the Harmony operating system was developed to demonstrate the major aspects of the design. Author (CISTI)

N94-22217 Waterloo Univ. (Ontario). Dept. of Electrical and Computer Engineering.

ASYNCHRONOUS DETECTION OF SSB-SC DATA SIGNALS **c32**

T. R. Sommerville and J. V. Hanson *In* Engineering Inst. of Canada, Canadian Conference on Electrical and Computer Engineering, Volumes 1 and 2 1991 4 p (For primary document see N94-22101 05-33)

Avail: Issuing Activity (Engineering Inst. of Canada, 2050 rue Mansfield, Suite 700, Montreal, PQ H3A 1Z2 Canada)

Single sideband (SSB) modulation is a special case of combined amplitude and phase modulation that results in suppresion of either the upper or lower sideband of the modulated signal. A study was carried out to combine the bandwidth efficiency of single sideband suppressed carrier transmission with the simplicity of detection offered by envelope detection as proposed by Hanson (1968). In the case of an analog message waveform this has been shown to be impossible, however for a digital data signal it is required only that the envelope have correct value at the sampling instant. Given this weaker constraint a data precoding/predistortion algorithm is proposed that may be applied in order to obtain a solution. The algorithm measures the squared error between the desired and predicted received levels for a given choice of transmitter inputs and determines a correction to the inputs based on the error gradient. The adaptive processor was able to achieve eye openings of up to 60 percent for single sideband suppressed carrier data signals. The best result used a table lookup to generate the initial input estimates, used two input streams, required knowledge of all data values affected by the block under optimization and considered error in the bits preceding and following the block under adaptation. Author (CISTI)

N94-22218 Queens Univ., Kingston (Ontario). Dept. of Electrical Engineering.

INTERSYMBOL INTERFERENCE EFFECTS IN DIGITAL MATCHED FILTERS

Norman C. Beaulieu and Colin C. Climie *In* Engineering Inst. of Canada, Canadian Conference on Electrical and Computer Engineering, Volumes 1 and 2 1991 4 p (For primary document see N94-22101 05-33)

Avail: Issuing Activity (Engineering Inst. of Canada, 2050 rue Mansfield, Suite 700, Montreal, PQ H3A 1Z2 Canada)

The performance of digital matched filters is evaluated in the presence of intersymbol interference and loss of desired signal energy caused by prefiltering. The optimum filter, in a probability of error sense, is sought with regards to filter bandwidth and number of samples per symbol. The degradation factor, based on average error probability, is derived for some common lowpass filter characteristics. It is shown that previous methods are ill-suited to the problem. In some cases, improvement over previous methods is as much as 2 dB when the analogue matched filter is used as a basis for comparison. Author (CISTI)

N94-22219 Laval Univ. (Quebec). Dept. de Genie Electrique.

FM INTERFERENCE IN RADIO NAVIGATION RECEIVERS [INTERFERENCE MF DANS LES RECEPTEURS DE RADIO NAVIGATION] **c04**

H. T. Huynh, J. M. Vezin, and D. Angers *In* Engineering Inst. of Canada, Canadian Conference on Electrical and Computer Engineering, Volumes 1 and 2 1991 4 p In FRENCH (For primary document see N94-22101 05-33)

Avail: Issuing Activity (Engineering Inst. of Canada, 2050 rue Mansfield, Suite 700, Montreal, PQ H3A 1Z2 Canada)

The azimuthal location receiver in an instrument landing system uses the 108-118 MHz frequency band which is adjacent to the FM broadcast band. With its low power (10 watts), the receiver would be strongly affected by the interference from the FM intermodulation provoked by two or three FM broadcast signals (interferences of type B1). Using a standard receiver with automatic gain control, the interference power/signal power ratio is computed at the interference threshold. The results show that the receiver is perfectly characterized only by its intermediate frequency stage bandwidth.

The worst case is noted when the intermodulation signal frequency coincides with the main carrier. The more the frequency difference increases, the more the system becomes tolerant. Author (CISTI)

N94-22220 Laval Univ. (Quebec). Centre d'Optique, Photonique et Laser.

ARCHITECTURES OF THE FREE SPACE OPTICAL INTERCONNECTS **c74**

Yun-Long Sheng *In* Engineering Inst. of Canada, Canadian Conference on Electrical and Computer Engineering, Volumes 1 and 2 1991 4 p (For primary document see N94-22101 05-33)

Avail: Issuing Activity (Engineering Inst. of Canada, 2050 rue Mansfield, Suite 700, Montreal, PQ H3A 1Z2 Canada)

Optical free space interconnects potentially offer high density, low power dissipation, flexibile solutions for pin out problems in very large scale integration (VLSI) chips. Two architectures of free space interconnects that are compatible with the VLSI environment are presented. One uses a retroreflective prism array to reduce the request for alignment accuracy and can be used for interconnections in a multichip module. Another uses integrated planar optics for intrachip interconnections. In the corner cube array the divergent signal beams from transmitters in the processing elements are colimated by a lens, reflected back by corner cubes, and converged into the photodetectors in the processing elements. Two optical elements useful for steering the signal beams in the integrated planar optical module are discussed: surface relief staircase profile gratings and micromirrors. The staircase profile surface relief gratings may be used for steering signals to zig-zag paths, and micromirrors made by mass transport procedures can provide array-to-array interconnections and large reflection angles. Author (CISTI)

N94-22221 National Research Council of Canada, Ottawa (Ontario). Inst. for Information Technology.

BALANCED ARROW MACH-ZEHNDER INTERFEROMETER **c35**

S. F. Yuen, J. Chrostowski, and B. A. Syrett *In* Engineering Inst. of Canada, Canadian Conference on Electrical and Computer Engineering, Volumes 1 and 2 1991 4 p (For primary document see N94-22101 05-33)

Avail: Issuing Activity (Engineering Inst. of Canada, 2050 rue Mansfield, Suite 700, Montreal, PQ H3A 1Z2 Canada)

A new integrated passive interferometer having balanced dissimilar arms is studied. One arm of the interferometer consists of a conventional rib waveguide while the other arm is made using an antiresonant reflecting optical waveguide (ARROW). The large wavelength dependent chromatic dispersion of the ARROW allows the two arms of the device to be built with the same optical pathlength at any one wavelength resulting in a device which is insensitive to changes in ambient temperature. The device can be used as a sensor, a multiplexer/demultiplexer in wavelength division multiplexing, and a filter in frequency division multiplexing. The interferometer is very useful in sensing applications where large temperature fluctuations are expected. The inferometer's usefulness in this situation is due to its temperature insensitivity. Author (CISTI)

N94-22222 National Research Council of Canada, Ottawa (Ontario). Inst. for Information Technology.

OPTICAL PROCESSING IN PHOTOREFRACTIVE MEDIA **c74**

S. A. Boothroyd, L. Chan, P. H. Beckwith, and J. Chrostowski *In* Engineering Inst. of Canada, Canadian Conference on Electrical and Computer Engineering, Volumes 1 and 2 1991 4 p (For primary document see N94-22101 05-33)

Avail: Issuing Activity (Engineering Inst. of Canada, 2050 rue Mansfield, Suite 700, Montreal, PQ H3A 1Z2 Canada)

A beam of light can be made to interact with other light beams through a nonlinear response of an optical medium. The potential of photorefractive media in optical processing is demonstrated using barium titanate. A novel method is described whereby input scenes can be processed within the photoreactive medium response time by image subtraction and feature enhancement. Results are presented showing the interference of two coherent images having both a controllable phase difference and pixel registration between them. The two images are written into the barium titanate crystal via a spatial light modulator. Four-wave mixing phase conjugation is used to effect a process output image showing image subtraction, spatial differentiation, and digital optical logic OR and XOR operations. Author (CISTI)

N94-22223 Victoria Univ. (British Columbia). Dept. of Electrical and Computer Engineering.

CODED 64QAM USING A BINARY CONVOLUTIONAL CODE **c32**

Chintha Tellambura, Qiang Wang, and Vijay K. Bhargava *In* Engineering Inst. of Canada, Canadian Conference on Electrical and Computer Engineering, Volumes 1 and 2 1991 3 p (For primary document see N94-22101 05-33)

Avail: Issuing Activity (Engineering Inst. of Canada, 2050 rue Mansfield, Suite 700, Montreal, PQ H3A 1Z2 Canada)

Trellis coding combined with Viterbi decoding can achieve asymptotic coding gains up to 6 decibels in AWGN channels; however each signal constellation requires a different code. The design of 64-CQAM (coded quadrature amplitude modulation) with binary convolutionary code having transmission efficiency of 5 bits/symbol is considered as an alternative approach using existing Viterbi decoding with punctured codes. The standard rate 1/2 v equals 7 convolutional code is used with puncturing to increase the code rate to 5/6. Code words are mapped into channel symbols using Gray codes. All permutations were considered, and the optimum were selected. Both analytical and Monte Carlo simulation results are presented. Channel cut-off rate is evaluated for both unquantized and quantized channels proving that the performance loss due to quantization is negligible. The asymptotic coding gain of 64CQAM over uncoded 32AMPM is found to be 3.0 decibels, which is somewhat less than Ungerbock's best with the same complexity. Author (CISTI)

N94-22224 Ottawa Univ. (Ontario). Dept. of Electrical Engineering.

CAPACITY COMPARISON BETWEEN DIRECT SEQUENCE PSK AND MFSK SPREAD SPECTRUM SYSTEMS IN CDMA APPLICATIONS **c32**

Jun Wang and Abbas Yongacoglu *In* Engineering Inst. of Canada, Canadian Conference on Electrical and Computer Engineering, Volumes 1 and 2 1991 4 p (For primary document see N94-22101 05-33)

Avail: Issuing Activity (Engineering Inst. of Canada, 2050 rue Mansfield, Suite 700, Montreal, PQ H3A 1Z2 Canada)

In most code division multiple access (CDMA) applications, the baseline system uses direct sequence (DS) phase shift keying (PSK) signals. Another possible direct sequence CDMA system which uses noncoherent orthogonal MFSK (frequency shift keying) signals has not received much attention. The capacities of direct sequence PSK and MFSK in spread spectrum (SS) systems are compared. Results show that for both systems, the asymptotic capacity at a certain value of bit error rate is inversely proportional to the required bit energy to noise density ratio. Since MFSK can be more power efficient than PSK, MFSK/DS-SS offers higher capacity when forward error correction (FEC) coding is not used. However, coherent PSK provides a larger capacity than MFSK when FEC coding is used. Author (CISTI)

N94-22225 Victoria Univ. (British Columbia). Dept. of Electrical and Computer Engineering.

APPLICATIONS OF A TWO-DIMENSIONAL NONLINEAR FILTERS TO IMAGE RESTORATION

C. M. Leung and W.-S. Lu *In* Engineering Inst. of Canada, Canadian Conference on Electrical and Computer Engineering, Volumes 1 and 2 1991 4 p (For primary document see N94-22101 05-33)

Avail: Issuing Activity (Engineering Inst. of Canada, 2050 rue Mansfield, Suite 700, Montreal, PQ H3A 1Z2 Canada)

The filter proposed by J.S. Lee in 1980 for image enhancement and noise filtering has been popular due to its adaptive nature associated with the use of the local statistics of the image. Two nonlinear extensions (quadratic and cubic) of the Lee filter are presented and used for noise filtering. The proposed nonlinear filters utilize higher moments of the available image and contain the Lee filters as a linear subclass. Sample image processing results are included. Author (CISTI)

N94-22226 Ecole Polytechnique, Montreal (Quebec). Dept. of Electrical and Computer Engineering.

AN APPROACH TO THE ESTIMATION OF GROUND STRUCTURE AND AIRCRAFT MOTION FROM AERIAL IMAGE SEQUENCES **c35**

Michel Audette, Ning Cui, Paul Cohen, and Ju-Yang Weng *In* Engineering Inst. of Canada, Canadian Conference on Electrical and Computer Engineering, Volumes 1 and 2 1991 4 p (For primary document see

N94-22101 05-33)
Avail: Issuing Activity (Engineering Inst. of Canada, 2050 rue Mansfield, Suite 700, Montreal, PQ H3A 1Z2 Canada)

An approach is described to the problem of building a three dimensional depth map of the ground sensed from an aircraft and computing the position of the sensing aircraft from a monocular sequence of aerial images. Specific solutions are presented for the aspects of camera calibration, image matching, and structure and motion estimation. Results from the calibration method show that correcting both radial and tangential distortions introduced by the lens system can bring about a substantial improvement. Image matching is performed by a region-based algorithm which is suitable for parallel implementation and produces dense displacement maps. Finally, the approach to the estimation problem is a so-called recursive-batch approach which is superior to conventional Kalmann filtering methods, while requiring only limited computational resources. Author (CISTI)

N94-22227 Applied Analytics Corp., Markham (Ontario).
A REAL-TIME INFRARED IMAGE PROCESSING TESTBED **c74**
E. Lithopoulos, J. Hodd, and E. Bender *In* Engineering Inst. of Canada, Canadian Conference on Electrical and Computer Engineering, Volumes 1 and 2 1991 4 p (For primary document see N94-22101 05-33)
Avail: Issuing Activity (Engineering Inst. of Canada, 2050 rue Mansfield, Suite 700, Montreal, PQ H3A 1Z2 Canada)

The development, implementation, and evaluation of an infrared target processor (TP) testbed is described. The testbed is capable of automatic real-time detection and tracking of targets in infrared imagery. Algorithms suitable for hardware implementation were first developed, tested, and evaluated in software and the ones with the best performance were implemented using Datacube's MaxVideo family of boards. The TP is capable of automatic target detection in infrared images, clutter/background target discrimination, target feature extraction and classification, and target tracking. A human interface allows the operator to bypass the TP and manually cue targets, and fully integrates all TP control functions and display in one station. The testbed is easily reconfigurable and capable of processing rates equivalent to thousands of millions of instructions per second.
Author (CISTI)

N94-22228 Defence Research Establishment Valcartier (Quebec). Electro-Optics Div.
MEMORY BASED VISION: A NEW CONCEPT **c63**
Martin P. Levesque and Auguste Blanchard *In* Engineering Inst. of Canada, Canadian Conference on Electrical and Computer Engineering, Volumes 1 and 2 1991 4 p (For primary document see N94-22101 05-33)
Avail: Issuing Activity (Engineering Inst. of Canada, 2050 rue Mansfield, Suite 700, Montreal, PQ H3A 1Z2 Canada)

The main goal of the memory based vision (MBV) paradigm is to provide a strategy to obtain the best knowledge and perception of an object of interest from every observation made of this object during the past and present. This requires a memory process that can compare the current observations with former ones. The purpose of this process is to build a representation of the selected object(s) and complete or update it using the current input. The application of MBV to a visualization problem results in a selective and associative vision system: selective because the system extracts only the information related to the object of interest, and associative because the system merges every available object observation into a coherent representation set. This leads to a system able to provide an updated object representation that contains more information than that only available in the current observation. Furthermore, it would be conceivable to extend the memory process to include observations done during other experiments and object models. Examples are presented of MBV applied to noise reduction, background suppression, super resolution, three dimensional estimation, and object removal. Author (CISTI)

N94-22229 Quebec Univ., Montreal. Ecole de Technologie Superieure.
AN ADAPTIVE CONTROL TO ENABLE A ROBOT TO FOLLOW CARTESIAN TRAJECTORIES [UNE COMMANDE ADAPTIVE DE SUIVI DE TRAJECTOIRES CARTESIENNES DE ROBOT] **c63**
L. Dessaint, M. Saad, K. Al-Haddad, and Y. Dube (Quebec Univ., Trois-Riveres.) *In* Engineering Inst. of Canada, Canadian Conference on Electrical and Computer Engineering, Volumes 1 and 2 1991 5 p In FRENCH (For primary document see N94-22101 05-33)
Avail: Issuing Activity (Engineering Inst. of Canada, 2050 rue Mansfield, Suite 700, Montreal, PQ H3A 1Z2 Canada)

An analysis is presented of an adaptive position control which allows a 4-axis SCARA robot to follow a trajectory expressed in Cartesian coordinates. The control stability is studied with the aid of a Liapunov function, which also allows deduction of a law of adaptation of the control parameters. A numerical simulation carried out utilizing the MATLAB program shows the precision of this adaptive control. A comparison with the precision obtained by a simple PD control shows the adaptive control's clear superiority.
Author (CISTI)

N94-22230 Concordia Univ., Montreal (Quebec). Dept. of Electrical and Computer Engineering.
A ROBUST ADAPTIVE CONTROL DESIGN FOR FLEXIBLE JOINT MANIPULATORS **c63**
K. Khorasani *In* Engineering Inst. of Canada, Canadian Conference on Electrical and Computer Engineering, Volumes 1 and 2 1991 4 p (For primary document see N94-22101 05-33)
Avail: Issuing Activity (Engineering Inst. of Canada, 2050 rue Mansfield, Suite 700, Montreal, PQ H3A 1Z2 Canada)

The problem of designing a robust adaptive control strategy for a flexible joint robot manipulator is considered. By utilizing the concept of integral manifolds, reduced-order models of the flexible system are obtained. This enables development of adaptive control schemes for the flexible full-order system at the reduced-order level, which otherwise would be difficult to obtain for the full-order system due to ill conditioning and the problem of dimensionality. Two common adaptive control strategies are examined: adaptive inverse dynamics, and the Slotine and Li algorithm (although any other algorithm can be treated similarly). It is shown how these standard rigid adaptive control techniques may be generalized and improved upon for successful application to a flexible joint manipulator. Author (CISTI)

N94-22231 Nova Scotia Technical Coll., Halifax.
TRELLIS CODED MULTI-ORTHOGONAL MODULATION **c32**
Shalini Periyalwar, S. Fleisher, and Shou-Xing Qu *In* Engineering Inst. of Canada, Canadian Conference on Electrical and Computer Engineering, Volumes 1 and 2 1991 4 p (For primary document see N94-22101 05-33)
Avail: Issuing Activity (Engineering Inst. of Canada, 2050 rue Mansfield, Suite 700, Montreal, PQ H3A 1Z2 Canada)

The trellis coding of quadrature frequency/phase modulated (QFPM) signal sets obtained from a multi-orthogonal modulation technique known as quadrature biorthogonal modulation (QBOM) is explored. Conventional trellis coded modulation (TCM) and multiple access TCM schemes are investigated for performance of the AWGN channel and the fading channel. A 2-N dimensional signal space is generated by the quadrature components at two orthogonal frequencies. Asymptotic coding gains are demonstrated over uncoded modulation and other trellis coded modulations of equivalent throughput rate. Author (CISTI)

N94-22232 Nova Scotia Technical Coll., Halifax.
QUADRATURE BIORTHOGONAL MODULATION **c32**
S. Fleisher, Shou-Xing Qu, and Shalini Periyalwar *In* Engineering Inst. of Canada, Canadian Conference on Electrical and Computer Engineering, Volumes 1 and 2 1991 4 p (For primary document see N94-22101 05-33)
Avail: Issuing Activity (Engineering Inst. of Canada, 2050 rue Mansfield, Suite 700, Montreal, PQ H3A 1Z2 Canada)

A digital modulation method based on quadrature carrier multiplexing of two N-dimensional biorthogonal signal sets is proposed. One embodiment of the proposed scheme, referred to as quadrature frequency/phase modulation (QFPM), is discussed in detail. QFPM results when two NFSK/2PSK (frequency shift keying/phase shift keying) signals are quadrature carrier multiplexed, and its bandwidth efficiency is doubled as compared to that of the constituent NFSK/2PSK signals. Quadrature PSK (QPSK) and recently proposed Q2PSK are special cases of QFPM when N=1 and N=2, respectively. It is shown that the bandwidth efficiency of QFPM under certain conditions (such as for a signal set size of M=16) is the same as that of quadrature amplitude modulation (QAM), while the power efficiency of the former is significantly better. These features,

combined with a constant-energy property and self-synchronization capability, suggest that the proposed modulation scheme is of practical interest.

Author (CISTI)

N94-22233 Laval Univ. (Quebec). Dept. de Genie Electrique.

ENCODING AND DECODING QUASI-SPHERICAL SIGNAL SETS **c32**

Paul Fortier *In* Engineering Inst. of Canada, Canadian Conference on Electrical and Computer Engineering, Volumes 1 and 2 1991 5 p (For primary document see N94-22101 05-33)

Avail: Issuing Activity (Engineering Inst. of Canada, 2050 rue Mansfield, Suite 700, Montreal, PQ H3A 1Z2 Canada)

Recent methods for coded modulation are based on multidimensional signal sets. Moreover, it is well known that a moderate gain can be achieved using specially shaped signal sets. A method for generating quasi-spherical signal sets to be used with coded modulation schemes is characterized. The method has the advantages of requiring a small number of computations. Shell construction is best used when the number of dimensions is about 20. The decoding procedure is described, as well as an alternative encoding procedure. Author (CISTI)

N94-22234 Defence Research Establishment, Ottawa (Ontario).

THE APPLICATION OF SAMPLE VECTOR SELECTION TO ADAPTIVE NULLING: PERFORMANCE COMPARISON FOR TECHNIQUES COMBINING GRAM-SCHMIDT ORTHOGONALIZATION WITH AVERAGING **c32**

Mylene Toulgoat and Ross M. Turner *In* Engineering Inst. of Canada, Canadian Conference on Electrical and Computer Engineering, Volumes 1 and 2 1991 5 p (For primary document see N94-22101 05-33)

Avail: Issuing Activity (Engineering Inst. of Canada, 2050 rue Mansfield, Suite 700, Montreal, PQ H3A 1Z2 Canada)

Adaptive antenna nulling is computationally demanding. New computationally efficient algorithms are presented for adaptive nulling based on the application of the Gram-Schmidt orthogonal ization to a selected set of data vectors which are in some sense the best vectors for estimating the jammer subspace. The performance of these algorithms is demonstrated as a function of the computational load versus the achieved output signal to noise plus jammer ratio and compared to the performance of the sampled matrix inversion technique. It is shown that the new algorithms perform better than the sampled matrix inversion method, requiring fewer computations when the ratio of the number of jammers to the array size is small. Author (CISTI)

N94-22235 Defence Research Establishment Valcartier (Quebec). Electro-Optics Div.

A FOUR-BAND INFRARED DATA ACQUISITION FACILITY FOR SIGNAL PROCESSING DEVELOPMENT **c74**

Benoit Montminy *In* Engineering Inst. of Canada, Canadian Conference on Electrical and Computer Engineering, Volumes 1 and 2 1991 4 p (For primary document see N94-22101 05-33)

Avail: Issuing Activity (Engineering Inst. of Canada, 2050 rue Mansfield, Suite 700, Montreal, PQ H3A 1Z2 Canada)

A four-band infrared data acquisition facility is reviewed, describing the internal operation of the multiband electro-optical scanner that collects the infrared scene radiation and the real-time computer that acquires the data. The data acquisition procedure and the format of the stored data are detailed and the use of the system as a tool for developing and demonstrating signal processing algorithms is discussed. An original experiment is introduced which will be made possible using the data acquisition facility. This experiment is the generation of false color infrared images for enhancing the target recognition capability of infrared systems. These images exhibit colors that depend on the ratio of the signal amplitude in different spectral bands, as opposed to the pseudocolor infrared images in which the intensity of the radiation is simply color coded.

Author (CISTI)

N94-22236 Defence Research Establishment Valcartier (Quebec).

TRAJECTORY COMPUTATIONS FOR AN IMPROVED CINETHEODOLITE TRACKING SYSTEM **c61**

Jean-Pierre Ardouin *In* Engineering Inst. of Canada, Canadian Conference on Electrical and Computer Engineering, Volumes 1 and 2 1991 4 p (For primary document see N94-22101 05-33)

Avail: Issuing Activity (Engineering Inst. of Canada, 2050 rue Mansfield, Suite 700, Montreal, PQ H3A 1Z2 Canada)

A new cinetheodolite tracking system has been developed for the Primrose Lake Evaluation Range in Alberta. This system improves the range's tracking abilities by providing different types of trajectories to slave the cinetheodolites in real time with new improved digital control algorithms. When the cinetheodolite operators need help, they can select any of these trajectories for slaving help and add corrections to them. The first type of trajectory is obtained by filtering radar coordinates with an alpha-beta filter. A second type of trajectory is based on a least squares solution of the cinetheodolites' pointing angles smoothed by an alpha-beta filter, and another type of trajectory is based on models of bombs or rockets. The different parts of the new tracking system are described, with emphasis on the trajectory computation algorithms. Some of the results obtained from the new system are illustrated to demonstrate its accuracy.

Author (CISTI)

N94-22237 Defence Research Establishment Valcartier (Quebec). Electro-Optics Div.

SIGNAL PROCESSING AND TARGET DISCRIMINATION ALGORITHMS FOR A ROSETTE SCAN TRACKER **c32**

Andre Morin *In* Engineering Inst. of Canada, Canadian Conference on Electrical and Computer Engineering, Volumes 1 and 2 1991 5 p (For primary document see N94-22101 05-33)

Avail: Issuing Activity (Engineering Inst. of Canada, 2050 rue Mansfield, Suite 700, Montreal, PQ H3A 1Z2 Canada)

A prototype of an infrared rosette scan tracker has been developed to evaluate the immunity of this type of tracker against decoys which can be deployed from a target aircraft. The performance of the tracker depends on the signal processing and the target discrimination algorithms employed to control the tracker. Because of the low resolution of the resulting target image, the rosette scanner does not have the ability to recognize the targets by their shape characteristics. In addition, targets which are too close appear simultaneously in the tracker instantaneous field of view. These targets are then detected in one single pulse signal. To prevent the tracker from breaking its lock onto its target, the transients in amplitude and width of the selected pulses are detected when decoys are deployed from the target. The occurrence of such transients initiates the computation of the drift between the estimated target position and the center of the pulse for the two axes to determine the direction in which the decoy was deployed. The performance of this processing technique is illustrated and some improvements are suggested. Author (CISTI)

N94-22238 Defence Research Establishment Valcartier (Quebec). Armament Div.

RADAR IMAGING OF MOVING TARGETS **c32**

Yves deVilliers *In* Engineering Inst. of Canada, Canadian Conference on Electrical and Computer Eng neering, Volumes 1 and 2 1991 4 p (For primary document see N94-22101 05-33)

Avail: Issuing Activity (Engineering Inst. of Canada, 2050 rue Mansfield, Suite 700, Montreal, PQ H3A 1Z2 Canada)

A radar technique utilizing frequency modulated continuous waves is being investigated as a means to identify in-flight targets. Special signal processing softwares were developed to obtain a radar image of the targets in free flight. The signal processing technique used to obtain the radar image is described. This technique can be divided into three parts. First, the program tracks the position of the target according to time. Secondly, the program computes the mean position, the mean velocity, and the mean acceleration of the center of gravity of the target. A correction of the displacement of the target is made from this information. Finally, the radar image is computed. This signal processing technique has been verified on real munitions in free flight. Radar images produced during that test are illustrated. Author (CISTI)

N94-22239 Laval Univ. (Quebec). Dept. of Computer Science.

AN ALGORITHM FOR THE INTERFERENCE DETECTION AMONG POLYGONAL SURFACES **c63**

Clemont Dupuis and Caroline Ricard *In* Engineering Inst. of Canada, Canadian Conference on Electrical and Computer Engineering, Volumes 1 and 2 1991 4 p (For primary document see N94-22101 05-33)

Avail: Issuing Activity (Engineering Inst. of Canada, 2050 rue Mansfield, Suite 700, Montreal, PQ H3A 1Z2 Canada)

The problem of avoiding collisions when operating on computer models of physical objects is central to model-based manipulation systems. A geometric component which can detect collisions between the manipulator and objects in the workspace and plan collision-free paths is essential in robotics. An efficient algorithm is presented for the detection of intersections among polygonal objects in fixed positions (static interference checking), based on the divide and conquer paradigm. A new mean is proposed to minimize the number of pairs of polygons which should be examined for intersection analysis. The proposed algorithm has been implemented, tested, and compared to the algorithm of Boyse (1979). Empirical evidence has confirmed its theoretical claim to efficiency. Author (CISTI)

N94-22240 Laval Univ. (Quebec). Dept. de Genie Mecanique.
STRATEGY FOR MOTION OF A MOVING BODY OF QUASI-POLYGONAL FORM WITHIN A POLYGONAL SPACE [STATEGIE DE MOUVEMENT D'UN FORME QUASI-POLYGONALE DANS UNE SCENE POLYGONALE] **c63**
Clement Gosselin and Moufid Karray *In* Engineering Inst. of Canada, Canadian Conference on Electrical and Computer Engineering, Volumes 1 and 2 1991 4 p In FRENCH (For primary document see N94-22101 05-33)
Avail: Issuing Activity (Engineering Inst. of Canada, 2050 rue Mansfield, Suite 700, Montreal, PQ H3A 1Z2 Canada)

An algorithm is presented for resolving the problem of the motion of a moving body within a space containing many polygonal obstacles. It is proposed to find, if it exists, a continuous trajectory connecting two positions of the moving body. Along this trajectory, the body must not interfere with an obstacle. The geometry of the moving body is rectangular with two circular ends. The algorithm reduces the study of the movement of this geometry to a study of the movement of a bar within a quasi-polygonal space. The obstacles are augmented to have a polygonal form with rounded corners. The critical curves corresponding to this type of obstacle are derived and their utilization in the planning of a trajectory is demonstrated with the aid of an example. The notion of a connection graph is finally introduced to aid in planning the trajectory, eliminating return paths, and removing useless movements. Author (CISTI)

N94-22241 Laval Univ. (Quebec). Dept. de Genie Mecanique.
ANALYTICAL REPRESENTATION OF WORKING ARTICULATION SPACE OF A PLANE MANIPULATOR IN AN ENCUMBERED ENVIRONMENT [REPRESENTATION ANALYTIQUE DE L'ESPACE DE TRAVAIL ARTICULAIRE D'UN MANIPULATEUR PLAN DANS UN ENVIRONNEMENT ENCOMBRE] **c63**
Ammar Hadj-Messaoud, Clement M. Gosselin, and Michel Guillot *In* Engineering Inst. of Canada, Canadian Conference on Electrical and Computer Engineering, Volumes 1 and 2 1991 4 p In FRENCH (For primary document see N94-22101 05-33)
Avail: Issuing Activity (Engineering Inst. of Canada, 2050 rue Mansfield, Suite 700, Montreal, PQ H3A 1Z2 Canada)

Analytic solutions are presented for the problem of planning trajectories for a certain type of robotic manipulator working in an environment encumbered by obstacles. The proposed method is based on obtaining analytic expressions describing the limits of the space attainable within the articulation space. These expressions will then render possible the detection of collisions while working directly in the articulation space, with the help of simple inequalities. A plane manipulator with two degrees of freedom is utilized as an example with the object of verifying the proposed method. Author (CISTI)

N94-22242 McGill Univ., Montreal (Quebec). Dept. of Electrical Engineering.
ARQ ON FADING CHANNELS **c32**
Patrick Beirouti, Harry Leib, and Salvatore D. Morgera *In* Engineering Inst. of Canada, Canadian Conference on Electrical and Computer Engineering, Volumes 1 and 2 1991 6 p (For primary document see N94-22101 05-33)
Avail: Issuing Activity (Engineering Inst. of Canada, 2050 rue Mansfield, Suite 700, Montreal, PQ H3A 1Z2 Canada)

A recursive procedure for obtaining a (2 to the power n)-state extended Gilbert-Elliott fading channel model suitable for n-bit block codes is described. The extended model may be used for numerical assessment of the throughput of a variety of popular automatic repeat-request schemes used over fading channels such as those encountered in mobile communications systems. Computationally efficient lower and upper performance bounds are also developed for low memory fading channels. It is found that the throughput of the stop-and-wait protocol exhibits a maximum; therefore, there exists an optimum codeword length for this automatic repeat-request scheme. Author (CISTI)

N94-22243 Carleton Univ., Ottawa (Ontario). Dept. of Systems and Computer Engineering.
SOME BEST RATE 1/p AND RATE (p-1)/p SYSTEMATIC QUASI-CYCLIC CODES OVER GF(3) AND GF(4) **c64**
T. Aaron Gulliver and Vijay K. Bhargava (Victoria Univ., British Columbia.) *In* Engineering Inst. of Canada, Canadian Conference on Electrical and Computer Engineering, Volumes 1 and 2 1991 4 p (For primary document see N94-22101 05-33)
Avail: Issuing Activity (Engineering Inst. of Canada, 2050 rue Mansfield, Suite 700, Montreal, PQ H3A 1Z2 Canada)

The class of quasi-cyclic (QC) codes has been proven to contain many good codes. To date the known QC codes are largely binary codes of the form 1/p and (p-1)/p constructed from circulant matrices. These results are extended to QC codes over GF(3) and GF(4). Good codes are constructed using integer linear programming and heuristic combinatorial optimization techniques. Many of these codes attain the best possible distance for any linear code with the same parameters, and several improve the maximum known minimum distances for linear codes. The link between power residue (PR) codes and QC codes is exploited as a means for constructing new QC codes and to initialize the construction algorithm. The minimum distance for the PR codes and the maximum known distance for the QC codes are tabulated. Author (CISTI)

N94-22244 Ottawa Univ. (Ontario). Dept. of Electrical Engineering.
PERFORMANCE OF RS CODES IN LOGNORMALLY SHADOWED RICIAN CHANNELS
Chokri Trabelsi and Abbas Yongacoglu *In* Engineering Inst. of Canada, Canadian Conference on Electrical and Computer Engineering, Volumes 1 and 2 1991 4 p (For primary document see N94-22101 05-33)
Avail: Issuing Activity (Engineering Inst. of Canada, 2050 rue Mansfield, Suite 700, Montreal, PQ H3A 1Z2 Canada)

The performance of Reed-Solomon (RS) codes with binary phase shift keying transmission is determined for a class of fading models for land mobile satellite communications. The fading model has the structure of a Rician model except that the line-of-sight component is subjected to a lognormal transformation. By exploiting the statistical characteristics of the multipath fading and shadowing, an effective coding/interleaving scheme is proposed. Author (CISTI)

N94-22245 Concordia Univ., Montreal (Quebec). Dept. of Electrical and Computer Engineering.
ON THE CAPACITY OF (T,U) PERMUTATION DECODING METHOD **c64**
Jia Ming, Anader Benyamin-Seeyar, and Le-Ngoc Tho *In* Engineering Inst. of Canada, Canadian Conference on Electrical and Computer Engineering, Volumes 1 and 2 1991 4 p (For primary document see N94-22101 05-33)
Avail: Issuing Activity (Engineering Inst. of Canada, 2050 rue Mansfield, Suite 700, Montreal, PQ H3A 1Z2 Canada)

Error-trapping decoding techniques are attractive due to their simple structure. Since 1962, several improved error-trapping methods have been devised in an effort to extend the capability and effectiveness in decoding multiple error correcting cyclic codes. Prange (1962) and MacWilliams (1964) introduced a (T,U) permutation group applied to this error-trapping decoding strategy by making use of a set of code-preserving permutation to obtain k error-free positions from which the rest of the code word could be reconstructed. Recently, exact lower bounds on the code length n for (n,k,t) cyclic codes have been found by using two-step and three-step (T,U) permutation groups. A study is presented on the relationship between the code parameters n, k, t, and the number of permutation steps. Equations representing the exact relations between the code parameters and the number of steps are derived. Some examples are given of the capability of (T,U) permutation decodable cyclic codes. Author (CISTI)

N94-22246 Ecole Polytechnique, Montreal (Quebec). Dept. de Genie Electrique et de Genie Informatique.

ADAPTIVE DECODING OF CONVOLUTIONAL CODES **c61**

Francois Chan and David Haccoun *In* Engineering Inst. of Canada, Canadian Conference on Electrical and Computer Engineering, Volumes 1 and 2 1991 4 p (For primary document see N94-22101 05-33)

Avail: Issuing Activity (Engineering Inst. of Canada, 2050 rue Mansfield, Suite 700, Montreal, PQ H3A 1Z2 Canada)

The adaptive decoding algorithm, which is a modification of the Viterbi algorithm (VA), is presented. Compared to the VA, the average number of survivors is reduced while the degradation in error performance is negligible. Just like the VA, this algorithm is self-synchronizing and can recover the transmitted path even if it is not among the survivors. It is shown that codes with a constraint length K up to 10 can be used while maintaining an average complexity similar to the VA with K = 7 but with an improved bit error performance. The distribution of the computational effort is exponential, leading to a modest size of the input buffer and hence, a small probability of outflow. Author (CISTI)

N94-22247 Ecole Polytechnique, Montreal (Quebec). Dept. of Electrical and Computer Engineering.

BIDIRECTIONAL ALGORITHMS FOR THE DECODING OF CONVOLUTIONAL CODES OVER MEMORYLESS CHANNELS **c61**

Jean Belzile and D. Haccoun *In* Engineering Inst. of Canada, Canadian Conference on Electrical and Computer Engineering, Volumes 1 and 2 1991 4 p (For primary document see N94-22101 05-33)

Avail: Issuing Activity (Engineering Inst. of Canada, 2050 rue Mansfield, Suite 700, Montreal, PQ H3A 1Z2 Canada)

New bidirectional multiple-path tree searching algorithms for the decoding of convolutional codes are presented. These suboptimal decoding algorithms, suited for long memory convolutional codes, use several paths, all of equal length, in a bidirectional breadth-first tree searching manner. Computer simulations using rate 1/2 codes with M = 32, 64, and 128 paths, show that a coding gain of 1 dB at a bit error probability of 10 to the minus 5 power can be achieved compared to Viterbi decoding using the same number of paths over a memoryless binary symmetric channel.

Author (CISTI)

N94-22248 Quebec Univ., Montreal. Ecole de Technologie Superieure.

AN ADAPTIVE METHOD FOR GROUP DELAY COMPENSATION USING SWITCHED CAPACITOR FILTERS

C. S. Gargour, F. Ramachandran (Concordia Univ., Montreal, Quebec.), N. Batani, and T. Wong *In* Engineering Inst. of Canada, Canadian Conference on Electrical and Computer Engineering, Volumes 1 and 2 1991 3 p (For primary document see N94-22101 05-33)

Avail: Issuing Activity (Engineering Inst. of Canada, 2050 rue Mansfield, Suite 700, Montreal, PQ H3A 1Z2 Canada)

The importance of linear phase and constant group delay filtering is well recognized in the processing of signals related to different types of applications such as telecommunications and image processing. An adaptive method for the approximate group delay compensation in the analog domain is presented. The method is best suited for switched capacitor implementation. A theoretical analysis relating to the proposed method is given which refers to transfer functions fulfilling certain conditions. The system used to carry out the method includes a filter having the specified frequency responses, a compensation filter with specified transfer functions, an analog signal processing block, and a delay unit. The system was built and tested for the previously determined transfer functions. The results indicate that the proposed method is best suited for group delay compensation over a narrow bandwidth of frequency components having a narrow magnitude spread. Author (CISTI)

N94-22249 Manitoba Univ., Winnipeg. Dept. of Electrical and Computer Engineering.

AN INSENSITIVE ALGORITHM FOR TEMPLATE MATCHING WITH CORRELATION **c61**

Zhen Mu, W. H. Lehn, and A. Wexler *In* Engineering Inst. of Canada, Canadian Conference on Electrical and Computer Engineering, Volumes 1 and 2 1991 4 p (For primary document see N94-22101 05-33)

Avail: Issuing Activity (Engineering Inst. of Canada, 2050 rue Mansfield, Suite 700, Montreal, PQ H3A 1Z2 Canada)

Template matching is an important approach used in image processing and computer vision to identify a certain pattern in a given image by comparing the grey levels between the selected pattern and a known pattern or template. An improved algorithm is presented for template matching with correlation to eliminate its sensitivities to scale and rotation of a segment. Comparisons are also made to template matching with Fourier transform. Tests demonstrate the efficiency and simplicity of the algorithm. The conditions and limitations of realizing insensitive algorithms for template matching with correlation are discussed. For segments of simple shape, the algorithm works quite efficiently and the correct results can be expected. For segments of complicated shape, this algorithm shows its low sensitivity in scale. The algorithm can be used when a segment and a template differ only in their scales and in the orientation of their main axes. Author (CISTI)

N94-22250 McMaster Univ., Hamilton (Ontario). Communication Research Lab.

WIDEBAND SOURCE LOCATION IN TWO-DIMENSIONAL ARRAY PROCESSING **c32**

Jing-Yun Li and Patrick Yip *In* Engineering Inst. of Canada, Canadian Conference on Electrical and Computer Engineering, Volumes 1 and 2 1991 4 p (For primary document see N94-22101 05-33)

Avail: Issuing Activity (Engineering Inst. of Canada, 2050 rue Mansfield, Suite 700, Montreal, PQ H3A 1Z2 Canada)

A method suitable for two-dimensional wideband source location is presented. The method has high resolution and is established on the basis of autoregressive spectral estimation. The algorithm relies on a two-dimensional frequency dependent vector model, which can be decomposed into two one-dimensional structures. The method is reviewed for the case of a linear array, and parameter estimators are determined for a two-dimensional array. The selection of basis functions and the procedures used for smoothing are then described, and some simulation results are included. The analysis shows that sine functions, as a set of basis functions, can generate less perturbation, simplify the frequency combination, and decrease the complexity of computation. In comparison with signal subspace methods, the proposed algorithm can work in the case of only one snapshot. Author (CISTI)

N94-22251 Ottawa Univ. (Ontario). Dept. of Electrical Engineering.

ON COEFFICIENT QUANTIZATION AND COMPUTATIONAL ROUNDOFF EFFECTS IN FREQUENCY INTERPOLATION FILTER BANKS

Gen-Zao Zhang and W. F. McGee *In* Engineering Inst. of Canada, Canadian Conference on Electrical and Computer Engineering, Volumes 1 and 2 1991 4 p (For primary document see N94-22101 05-33)

Avail: Issuing Activity (Engineering Inst. of Canada, 2050 rue Mansfield, Suite 700, Montreal, PQ H3A 1Z2 Canada)

Frequency interpolation filter banks have been presented as a new class of digital filter banks useful in speech and acoustics signal processing. The effects of filter coefficient quantization and computational roundoff on filter bank performance are studied for the case of fixed point arithmetic. The parameter sensitivity formulae of the filters in the bank are derived and discussed. The frequency response distortion and pole position change caused by finite word length implementation of the filter coefficients and zeroes of the bank are examined. White noise models are applied to analyze the effects of filter bank arithmetic roundoff, and the noise powers at filter outputs are calculated by numerical integration. Author (CISTI)

N94-22252 Manitoba Univ., Winnipeg. Dept. of Electrical Engineering.

APPLICATIONS OF PLANAR NEAR-FIELD MEASUREMENTS TO ELECTROMAGNETIC RADIATION AND INTERFERENCE PROBLEMS **c32**

V. Betz, N. P. East, and A. Sebak *In* Engineering Inst. of Canada, Canadian Conference on Electrical and Computer Engineering, Volumes 1 and 2 1991 4 p (For primary document see N94-22101 05-33)

Avail: Issuing Activity (Engineering Inst. of Canada, 2050 rue Mansfield, Suite 700, Montreal, PQ H3A 1Z2 Canada)

A simple system is described which finds the far-field radiation pattern of an antenna via the probe-corrected planar near to far-field transformation. An efficient method to obtain far-field data from near-field measurments based on a two-dimensional fast Fourier transform is presented. The practical aspects of the system, namely the type and quantity of field data required are discussed, as well as the design of the probe and data acquisition systems. The system is then used to find the far-field radiation patterns of

two antennas, a pyramidal horn and a planar microstrip array. Good agreement is obtained with patterns measured on a far-field range.
Author (CISTI)

N94-22253 McMaster Univ., Hamilton (Ontario). Communications Research Lab.
STUDY OF TE(1-DELTA) MODE IN OPEN DIELECTRIC RESONATORS BY A FINITE DIFFERENCE TIME DOMAIN METHOD **c32**
Ying Shen, Ke-Li Wu, Zhi-Qiang Bi, and John Litva *In* Engineering Inst. of Canada, Canadian Conference on Electrical and Computer Engineering, Volumes 1 and 2 1991 4 p (For primary document see N94-22101 05-33)
Avail: Issuing Activity (Engineering Inst. of Canada, 2050 rue Mansfield, Suite 700, Montreal, PQ H3A 1Z2 Canada)

The frequency resonant characteristics of axially symmetric dielectric resonators, the basic constituent elements of microwave integrated circuits, have previously been analyzed using several frequency domain approaches. The finite difference time domain (FDTD) method is proposed as an alternative approach. A numerical procedure based on the FDTD method and Mur's absorbing boundary condition is used to calculate the resonant frequencies of the TE(01-delta) mode for various open dielectric resonator structures. The calculated frequencies are compared with available experimental and published results. These comparisons demonstrate that the FDTD approach is a powerful tool for the modeling of arbitrary dielectric resonator structures with rotational symmetry. Author (CISTI)

N94-22254 East China Inst. of Tech., Nanjing.
ON THE RELATIONSHIP BETWEEN SPECTRAL DOMAIN APPROACH AND METHOD OF LINES **c64**
Da-Gang Fang, Hai-Qing Wu (Laval Univ., Quebec.), and Gilles Y. Delisle (Laval Univ., Quebec.) *In* Engineering Inst. of Canada, Canadian Conference on Electrical and Computer Engineering, Volumes 1 and 2 1991 4 p (For primary document see N94-22101 05-33)
Avail: Issuing Activity (Engineering Inst. of Canada, 2050 rue Mansfield, Suite 700, Montreal, PQ H3A 1Z2 Canada)

The method of lines was introduced to the field of microwave technology and was initially applied to the analysis of the dispersion characteristics of planar waveguide structures. This method can now be extended to include conductor thickness, dielectric, conductor losses, anisotropic substrates, and even non-rectangular boundaries. Some problems with the method of lines are discussed. First, a comparison is made between the two different methods introducing the method of lines, namely the separation of variables and the orthogonal transformation method. The agreement between the two methods yields the necessary knowledge to use the results in the method of lines. The relationship between the spectral domain approach and the method of lines is then presented. This relationship facilitates a better understanding of both methods and is helpful for transferring one technique to the other. As an example, the spectral domain immittance approach is introduced to the method of lines to provide a simple formulation and the theory is verified by comparison with the formulae developed by Nam, Ling, and Itoh (1989). Author (CISTI)

N94-22255 Thomson-CSF Systems Canada, Inc., Nepean (Ontario).
CONTROL OF MULTIPLE ROBOT MANIPULATORS WITH OPTIMAL FORCE DISTRIBUTION **c63**
S. Kalaycioglu *In* Engineering Inst. of Canada, Canadian Conference on Electrical and Computer Engineering, Volumes 1 and 2 1991 3 p (For primary document see N94-22101 05-33)
Avail: Issuing Activity (Engineering Inst. of Canada, 2050 rue Mansfield, Suite 700, Montreal, PQ H3A 1Z2 Canada)

The control aspects of multiple robot manipulators with optimal load distribution are investigated. An analysis of the load distribution problem for coordinating two PUMA 560 robots handling a single payload is carried out and an optimal load sharing algorithm is applied. In this algorithm, minimum (norm) joint torques and minimum contact forces are obtained by the minimization of a quadratic function associated with the joint torques and the force vectors of dual robot arms with the constraints of the robot system equations. The applied algorithm is not computationally intensive in comparison with the other existing algorithms described in the literature, and therefore, is very attractive for real-time applications. Author (CISTI)

N94-22256 Royal Military Coll. of Canada, Kingston (Ontario). Dept. of Mechanical Engineering.
OPTIMAL CONTROL OF THE TIP OF A FLEXIBLE ARM **c63**
Jean-Claude Piedboeuf, Denis Dochain (Ecole Polytechnique, Montreal, Quebec.), Richard Hurteau (Ecole Polytechnique, Montreal, Quebec.), and Kaouthar Benameur (McGill Univ., Montreal, Quebec.) *In* Engineering Inst. of Canada, Canadian Conference on Electrical and Computer Engineering, Volumes 1 and 2 1991 4 p (For primary document see N94-22101 05-33)
Avail: Issuing Activity (Engineering Inst. of Canada, 2050 rue Mansfield, Suite 700, Montreal, PQ H3A 1Z2 Canada)

The control of the tip position of a flexible robot is investigated. A linear optimal control law was selected and designed, based on a linear model obtained by linearization of a nonlinear model. The performance of the control method has been evaluated on the original nonlinear model, which has been found very useful to emphasize important flexible features and nonlinear characteristics of the system. Comparison was also made with a PID regulator. It was found that the optimal controller can overcome the difficulties encountered by the PID regulator, especially the control problems due to the inherent non-minimum phase behavior of the flexible arm. Author (CISTI)

N94-22380# Lawrence Livermore National Lab., CA.
SILICON MICROELECTRONIC FIELD-EMISSIVE DEVICES FOR ADVANCED DISPLAY TECHNOLOGY
J. D. Morse 29 Mar. 1993 12 p Presented at the National Center for Advanced Information Components Manufacturing Workshop, Albuquerque, NM, 30-31 Mar. 1993
(Contract W-7405-eng-48)
(DE94-000397; UCRL-JC-113483; CONF-9303198-6) Avail: CASI HC A03/MF A01

Field-emission displays (FED's) offer the potential advantages of high luminous efficiency, low power consumption, and low cost compared to AMLCD or CRT technologies. An LLNL team has developed silicon-point field emitters for vacuum triode structures and has also used thin-film processing techniques to demonstrate planar edge-emitter configurations. LLNL is interested in contributing its experience in this and other FED-related technologies to collaborations for commercial FED development. At LLNL, FED development is supported by computational capabilities in charge transport and surface/interface modeling in order to develop smaller, low-work-function field emitters using a variety of materials and coatings. Thin-film processing, microfabrication, and diagnostic/test labs permit experimental exploration of emitter and resistor structures. High field standoff technology is an area of long-standing expertise that guides development of low-cost spacers for FEDS. Vacuum sealing facilities are available to complete the FED production engineering process. Drivers constitute a significant fraction of the cost of any flat-panel display. LLNL has an advanced packaging group that can provide chip-on-glass technologies and three-dimensional interconnect generation permitting driver placement on either the front or the back of the display substrate. DOE

N94-22405# Sandia National Labs., Albuquerque, NM.
FLOW AND HEAT TRANSFER MODEL FOR A ROTATING CRYOGENIC MOTOR
R. C. Dykhuizen, R. G. Baca, and T. C. Bickel Aug. 1993 31 p
(Contract DE-AC04-76DP-00789)
(DE94-001151; SAND-93-1588) Avail: CASI HC A03/MF A01

Development of a high-temperature, superconducting, synchronous motor for large applications (greater than 1000 HP) could offer significant electrical power savings for industrial users. Presently 60% of all electric power generated in the United States is converted by electric motors. A large part of this power is utilized by motors 1000 HP or larger. The use of high-temperature superconducting materials with critical temperatures above that of liquid nitrogen (77 K) in the field winding would reduce the losses in these motors significantly, and therefore, would have a definite impact on the electrical power usage in the U.S. These motors will be 1/3 to 1/2 the size of conventional motors of similar power and, thus, offer potential savings in materials and floor space. The cooling of the superconducting materials in the field windings of the rotor presents a unique application of cryogenic engineering. The rotational velocity results in significant radial pressure gradients that affect the flow distribution of the cryogen. The internal pressure fields can result in significant nonuniformities in the

two-phase flow of the coolant. Due to the variable speed design, the flow distribution has the potential to change during operation. A multiphase-flow computer model of the cryogenic cooling is developed to calculate the boiling heat transfer and phase distribution of the nitrogen coolant in the motor. The model accounts for unequal phase velocities and nonuniform cooling requirements of the rotor. The unequal radial pressure gradients in the inlet and outlet headers result in a larger driving force for flow in the outer cooling channels. The effect of this must be accounted for in the design of the motor. Continuing improvements of the model will allow the investigation of the transient thermal issues associated with localized quenching of the superconducting components of the motor. DOE

N94-20498*# National Aeronautics and Space Administration. Lewis Research Center, Cleveland, OH.
AN X-BAND PEELED HEMT AMPLIFIER
Paul G. Young (Toledo Univ., OH.), Robert R. Romanofsky, Samuel A. Alterovitz, and Edwyn D. Smith (Toledo Univ., OH.) *In its* Solid State Technology Branch of NASA Lewis Research Center: Fifth Annual Digest Aug. 1993 p 7-13 Repr. from High-Speed Electronics and Optoelectronics, v. 1680, 1992 p 72-78 (For primary document see N94-20497 05-32)
(Grant NAG3-1226)
Avail: CASI HC A02/MF A03

N94-20499*# National Aeronautics and Space Administration. Lewis Research Center, Cleveland, OH.
CHARACTERISTICS OF 0.8- AND 0.2-MICRONS GATE LENGTH In(x)Ga(1-x) As/In(0.52)Al(0.48)As/InP (0.53 LESS THAN OR EQUAL TO x LESS THAN OR EQUAL TO 0.70) MODULATION-DOPED FIELD-EFFECT TRANSISTORS AT CRYOGENIC TEMPERATURES
Richard Lai, Pallab K. Bhattacharya, David Yang, Timothy L. Brock, Samuel A. Alterovitz, and Alan N. Downey *In its* Solid State Technology Branch of NASA Lewis Research Center: Fifth Annual Digest Aug. 1993 p 15-22 Repr. from IEEE Transactions on Electron Devices, v. 39, no. 10, Oct. 1992 p 2206-2213 (For primary document see N94-20497 05-32)
Avail: CASI HC A02/MF A03

N94-20500*# National Aeronautics and Space Administration. Lewis Research Center, Cleveland, OH.
A COMPREHENSIVE THEORETICAL AND EXPERIMENTAL STUDY OF COPLANAR WAVEGUIDE SHUNT STUBS
Nihad I. Dib (Michigan Univ., Ann Arbor.), George E. Ponchak, and Linda P. B. Katehi (Michigan Univ., Ann Arbor.) *In its* Solid State Technology Branch of NASA Lewis Research Center: Fifth Annual Digest Aug. 1993 p 31-34 Repr. from IEEE MTT-S Digest, 1992 p 947-950 (For primary document see N94-20497 05-32)
(Grant NSF ECS-86-57951)
Avail: CASI HC A01/MF A03

N94-20501*# National Aeronautics and Space Administration. Lewis Research Center, Cleveland, OH.
A COMPARATIVE STUDY BETWEEN SHIELDED AND OPEN COPLANAR WAVEGUIDE DISCONTINUITIES
Nihad I. Dib (Michigan Univ., Ann Arbor.), W. P. Harokopus, Jr. (Texas Instruments, Inc., Dallas.), G. E. Ponchak, and L. P. B. Katehi (Michigan Univ., Ann Arbor.) *In its* Solid State Technology Branch of NASA Lewis Research Center: Fifth Annual Digest Aug. 1993 p 35-45 Repr. from Journal of Microwave and Milimeter-Wave Computer-Aided Engineering, v. 2, no. 4, 1992 (For primary document see N94-20497 05-32)
(Grant NSF ECS-86-57951)
Avail: CASI HC A03/MF A03

N94-20502*# National Aeronautics and Space Administration. Lewis Research Center, Cleveland, OH.
A THEORETICAL AND EXPERIMENTAL STUDY OF COPLANAR WAVEGUIDE SHUNT STUBS
Nihad I. Dib, George E. Ponchak, and Linda P. B. Katehi *In its* Solid State Technology Branch of NASA Lewis Research Center: Fifth Annual Digest Aug. 1993 p 47-53 Repr. from IEEE Transactions on Microwave Theory and Techniques, v. 41, no. 1, Jan. 1993 p 38-44 (For primary document see N94-20497 05-32)
Avail: CASI HC A02/MF A03

N94-20503*# National Aeronautics and Space Administration. Lewis Research Center, Cleveland, OH.
COPLANAR WAVEGUIDE RADIAL LINE STUB
R. N. Simons and S. R. Taub *In its* Solid State Technology Branch of NASA Lewis Research Center: Fifth Annual Digest Aug. 1993 p 55-56 Repr. from IEEE Electronics Letters, v. 29, no. 4, 18 Feb. 1993 p 412-413 (For primary document see N94-20497 05-32)
Avail: CASI HC A01/MF A03

N94-20504*# National Aeronautics and Space Administration. Lewis Research Center, Cleveland, OH.
ATTENUATION OF EPSILON(SUB EFF) OF COPLANAR WAVEGUIDE TRANSMISSION LINES ON SILICON SUBSTRATES
Susan R. Taub and Paul G. Young *In its* Solid State Technology Branch of NASA Lewis Research Center: Fifth Annual Digest Aug. 1993 p 57-60 Repr. from the 11th Annual Benjamin Franklin Symposium on Antenna and Microwave Technology in the 1990s, May 1993 p 8-11 (For primary document see N94-20497 05-32)
Avail: CASI HC A01/MF A03

N94-20506*# National Aeronautics and Space Administration. Lewis Research Center, Cleveland, OH.
SLOT-COUPLED PATCH ANTENNA WITH COPLANAR WAVEGUIDE FEED
Richard Q. Lee and Rainee N. Simons *In its* Solid State Technology Branch of NASA Lewis Research Center: Fifth Annual Digest Aug. 1993 p 89-92 Repr. from IEEE Antennas and Propagation Society International Symposium, Jul. 1992 p 1048-1051 (For primary document see N94-20497 05-32)
Avail: CASI HC A01/MF A03

N94-20507*# National Aeronautics and Space Administration. Lewis Research Center, Cleveland, OH.
BANDWIDTH ENHANCEMENT OF DIELECTRIC RESONATOR ANTENNAS
Richard Q. Lee and Rainee N. Simons *In its* Solid State Technology Branch of NASA Lewis Research Center: Fifth Annual Digest Aug. 1993 p 93-96 Repr. from IEEE Antennas and Propagation Society International Symposium, Jun. 1993 p 1500-1503 (For primary document see N94-20497 05-32)
Avail: CASI HC A01/MF A03

N94-20508*# National Aeronautics and Space Administration. Lewis Research Center, Cleveland, OH.
SPECTROSCOPIC ELLIPSOMETRY STUDIES OF HF TREATED SI (100) SURFACES
Huade Yao (Nebraska Univ., Lincoln.), John A. Woollam (Nebraska Univ., Lincoln.), and Samuel A. Alterovitz *In its* Solid State Technology Branch of NASA Lewis Research Center: Fifth Annual Digest Aug. 1993 p 129-131 Repr. from American Inst. of Physics, Applied Physics Letter, v. 62, no. 25, 21 Jun. 1993 (For primary document see N94-20497 05-32)
(Grant NAG3-154)
Avail: CASI HC A01/MF A03

N94-20512*# National Aeronautics and Space Administration. Lewis Research Center, Cleveland, OH.
THE QUANTUM EFFICIENCY OF HgCdTe PHOTODIODES IN RELATION TO THE DIRECTION OF ILLUMINATION AND TO THEIR GEOMETRY
D. Rosenfeld and G. Bahir (Israel Inst. of Tech., Haifa.) *In its* Solid State Technology Branch of NASA Lewis Research Center: Fifth Annual Digest Aug. 1993 p 163-169 Repr. from American Inst. of Physics, Journal of Applied Physics, v. 72, no. 7, 1 Oct. 1992 (For primary document see N94-20497 05-32)
Avail: CASI HC A02/MF A03

N94-20514*# National Aeronautics and Space Administration. Lewis Research Center, Cleveland, OH.
Y-Ba-Cu-O SUPERCONDUCTING/GaAs SEMICONDUCTING HYBRID CIRCUITS FOR MICROWAVE APPLICATIONS
K. B. Bhasin, S. S. Toncich, C. M. Chorey (Sverdrup Technology, Inc.,

Brook Park, OH.), N. J. Rohrer (Ohio State Univ., Columbus.), and G. J. Valco (Ohio State Univ., Columbus.) *In its* Solid State Technology Branch of NASA Lewis Research Center: Fifth Annual Digest Aug. 1993 p 181-184 (For primary document see N94-20497 05-32)
Avail: CASI HC A01/MF A03

N94-20516*# National Aeronautics and Space Administration. Lewis Research Center, Cleveland, OH.
TlCaBaCuO HIGH Tc SUPERCONDUCTING MICROSTRIP RING RESONATORS DESIGNED FOR 12 GHz
G. Subramanyam (Cincinnati Univ., OH.), V. J. Kapoor (Cincinnati Univ., OH.), C. M. Chorey (Sverdrup Technology, Inc., Brook Park, OH.), and K. B. Bhasin *In its* Solid State Technology Branch of NASA Lewis Research Center: Fifth Annual Digest Aug. 1993 p 209-218 Repr. from Applied Superconductivity, v. 1, no. 10-12, 1993 p 1605-1614 (For primary document see N94-20497 05-32)
Avail: CASI HC A02/MF A03

N94-20517*# National Aeronautics and Space Administration. Lewis Research Center, Cleveland, OH.
A 10 GHz Y-Ba-Cu-O/GaAs HYBRID OSCILLATOR PROXIMITY COUPLED TO A CIRCULAR MICROSTRIP PATCH ANTENNA
Norman J. Rohrer (Ohio State Univ., Columbus.), M. A. Richard (Case Western Reserve Univ., Cleveland, OH.), George J. Valco (Ohio State Univ., Columbus.), and Kul B. Bhasin *In its* Solid State Technology Branch of NASA Lewis Research Center: Fifth Annual Digest Aug. 1993 p 225-229 Repr. from IEEE Transactions on Applied Superconductivity, v. 3, no. 1, Mar. 1993 p 23-27 (For primary document see N94-20497 05-32)
Avail: CASI HC A01/MF A03

N94-20985*# National Aeronautics and Space Administration. Lewis Research Center, Cleveland, OH.
CHARACTERIZATION OF MULTILAYER GaAs/AlGaAs TRANSISTOR STRUCTURES BY VARIABLE ANGLE SPECTROSCOPIC ELLIPSOMETRY Abstract Only
Kenneth G. Merkel (Air Force Wright Aeronautical Labs., Wright-Patterson AFB, OH.), Paul G. Snyder (Nebraska Univ., Lincoln.), John A. Woollam (Nebraska Univ., Lincoln.), Samuel A. Alterovitz, and A. K. Rai (Universal Energy Systems, Inc., Dayton, OH.) *In* Nebraska Univ., Materials, Structures, and Devices for High-Speed Electronics 1993 1 p Repr. from Japanese Journal of Applied Physics, v. 28, no. 6, Jun. 1989 (For primary document see N94-20971 05-76)
Avail: CASI HC A01/MF A01

N94-20988*# Nebraska Univ., Lincoln. Dept. of Electrical Engineering.
ELLIPSOMETRIC ANALYSIS OF BUILT-IN ELECTRIC FIELDS IN SEMICONDUCTOR HETEROSTRUCTURES Abstract Only
Paul G. Snyder, Jae E. Oh, John A. Woollam, and R. E. Owens (Colorado State Univ., Fort Collins.) *In its* Materials, Structures, and Devices for High-Speed Electronics 1993 1 p Repr. from Appl. Phys. Lett. (American Inst. of Physics), v. 51, no. 10, 7 Sep. 1987 p 770 (For primary document see N94-20971 05-76)
Avail: CASI HC A01/MF A01

N94-20989*# Nebraska Univ., Lincoln. Dept. of Electrical Engineering.
OPTICAL MEASUREMENT OF BUILT-IN AND APPLIED ELECTRIC FIELDS IN Al(x)Ga(1-x)As/GaAs HETEROSTRUCTURES Abstract Only
Paul G. Snyder, Kenneth G. Merkel, and John A. Woollam *In its* Materials, Structures, and Devices for High-Speed Electronics 1993 1 p Repr. from Spectroscopic Characterization Techniques for Semiconductor Technology 3 (Bellingham, WA, Society of Photo-Optical Instrumentation Engineers), v. 946, 1988 p 98 (For primary document see N94-20971 05-76)
Avail: CASI HC A01/MF A01

N94-21001*# National Aeronautics and Space Administration. Lewis Research Center, Cleveland, OH.
STUDY OF InGaAs-BASED MODULATION DOPED FIELD EFFECT TRANSISTOR STRUCTURES USING VARIABLE-ANGLE SPECTROSCOPIC ELLIPSOMETRY Abstract Only
Samuel A. Alterovitz, R. M. Sieg (Cleveland State Univ., OH.), Huade D. Yao (Nebraska Univ., Lincoln.), Paul G. Snyder (Nebraska Univ., Lincoln.), John A. Woollam (Nebraska Univ., Lincoln.), J. Pamulapati (Michigan Univ., Ann Arbor.), P. K. Bhattacharya (Michigan Univ., Ann Arbor.), and P. A. Sekula-Moise (Spire Corp., Bedford, MA.) *In* Nebraska Univ., Materials, Structures, and Devices for High-Speed Electronics 1993 1 p Repr. from Thin Solid Films (Lausanne, Switzerland, Elsevier Sequoia), v. 206, 1991 p 288-293 (For primary document see N94-20971 05-76)
Avail: CASI HC A01/MF A01

N94-21801# Technische Physische Dienst TNO-TH, Delft (Netherlands).
ELECTRONIC LOCKING SYSTEM [ELEKTRONISCH SLUITSYSTEEM]
E. Nieuwkoop *In its* Activities Report of the Institute of Applied Physics 1990 p 26-28 In DUTCH (For primary document see N94-21798 05-70)
Avail: CASI HC A01/MF A01

34 FLUID MECHANICS AND HEAT TRANSFER

Includes boundary layers; hydrodynamics; fluidics; mass transfer; and ablation cooling.

For related information see also *02 Aerodynamics* and *77 Thermodynamics and Statistical Physics.*

N94-19829# Los Alamos National Lab., NM.
CHEMICAL EQUILIBRIUM IN HIGH PRESSURE MOLECULAR FLUID MIXTURES
M. S. Shaw 1993 5 p Presented at the 14th International Conference of the International Association for the Advancement of High Pressure Science and Technology, Colorado Springs, CO, 27 Jun. - 2 Jul. 1993
(Contract W-7405-eng-36)
(DE93-040160; LA-UR-93-3185; CONF-930676-47) Avail: CASI HC A01/MF A01

The N(sub atoms)PT Monte Carlo simulation method has been reformulated to incorporate multiple species and chemical reactions with changes in total number of molecules. While maintaining a constant number of each type of atom, the number of molecules is changed by turning on and off the interactions of any particular molecular position with other molecules. Chemical reactions are allowed as a correlated move of atoms to different molecular locations. Equilibrium chemical composition is determined as an average over the simulation along with equation of state quantities. A large set of simulations has been made with the system N2 + O2 reversibly yields NO covering a wide range in P and T. Both Hugoniot states and the CJ point have been determined and are shown to be sensitive to the potentials between unlike species. DOE

N94-19913 California Univ., Davis.
PARTICLE DISPERSION IN TURBULENT SPRAYS Annual Report, 1 Aug. 1992 - 31 Jul. 1993
Ian M. Kennedy and Wolfgang Kollmann 20 Apr. 1993 37 p Limited Reproducibility: More than 20% of this document may be affected by microfiche quality
(Contract F49620-92-J-0418)
(AD-A271314; AFOSR-93-0791TR) Avail: CASI HC A03

Measurements of droplet dispersion and vaporization rates are carried out and compared with computational predictions. Droplet dispersion, mean axial velocity, and the axial autocorrelation function of the droplets are measured using a laser sheet technique. The experimental facility is modified to accommodate a true spray using an ultrasonic atomizer and droplets injected with a fluorescent dye. The computational part of the project is the development of a Large Eddy Simulation (LES) method for the turbulent jet. A LES-model for the unresolved scales of the flow is implemented into the Navier-Stokes solver. The results for filtered and unfiltered variables are compared to the experiments and improvement of the particle statistics due to the LES-model is found. DTIC

N94-19916# Lawrence Livermore National Lab., CA.
UNLIKE-PAIR INTERACTIONS AT HIGH PRESSURE AND HIGH TEMPERATURE
F. H. Ree and M. vanThiel Jul. 1993 8 p Presented at the 10th Detonation Symposium, Boston, MA, 12-16 Jul. 1993

(Contract W-7405-eng-48)
(DE93-019948; UCRL-JC-111524; CONF-930713-23) Avail: CASI HC A02/MF A01

Although there are more unlike-pairs than like-pairs in detonation products, information on unlike-pair interactions is scarce at present. We describe how unlike pair-interactions involving dissociation products of CO and CO2 can be derived by means of an accurate statistical mechanical theory of mixtures and recent shock wave data of CO and CO2. We then extend this complex study further by interpreting shock data of liquid NO and N2 + O2 mixture. It was done by constraining the resulting potentials to agree with all available Hugoniot data of chemical species occurring in detonation products in a self-consistent manner. DOE

N94-19936 TRW, Inc., Redondo Beach, CA. Space and Electronics Group.
INITIATION AND MODIFICATION OF REACTION BY ENERGY ADDITION: KINETIC AND TRANSPORT PHENOMENA Final Report, 1 Sep. 1990 - 1 Sep. 1993
Francis E. Fendell and Mau-Song Chou 1 Oct. 1993 27 p Limited Reproducibility: More than 20% of this document may be affected by microfiche quality
(Contract F49620-90-C-0070)
(AD-A271315; AFOSR-93-0788TR) Avail: CASI HC A03

Work has been pursued, by application of the fundamental principles of chemical kinetics and fluid transport, on a 'proof-of-principle' for a novel oblique-detonation-wave-engine (ODWE) as an alternative to a mixing-controlled supersonic combustor. The concept involves the nonintrusive stabilization of a conical detonation wave. Laser technology permits the rapidly repeated pulsed deposition of energy at a fixed site on the axis of symmetry of a supersonically flowing, combustible mixture. Each pulse suffices for the direct initiation of a radially-, outwardly-propagating, Chapman-Jouguet detonation wave. The interaction of the individual spherical waves, as the periodic train is convected by the flow, results in a nonintrusively stabilized conical wave as the time interval between the very brief pulses decreases. The detonated gas may be expanded in a supersonic nozzle (of practical length) for discharge at ambient pressure, such that thrust is generated. Author (DTIC)

N94-19974# Sandia National Labs., Albuquerque, NM.
WAVEFRONT SENSORS FOR OPTICAL DIAGNOSTICS IN FLUID MECHANICS: APPLICATION TO HEATED FLOW, TURBULENCE, AND DROPLET EVAPORATION
D. R. Neal, T. J. OHern, J. R. Torczynski, M. E. Warren, R. Shul, and T. S. McKechnie (POD Associates, Inc., Albuquerque, NM.) 1993 11 p Presented at the Annual Meeting of the Society of Photo-Optical Instrumentation Engineers (SPIE), San Diego, CA, 11-16 Jul. 1993
(Contract DE-AC04-76DP-00789)
(DE93-040060; SAND-93-0305C; CONF-930722-35) Avail: CASI HC A03/MF A01

Optical measurement techniques are extremely useful in fluid mechanics because of their non-invasive nature. However, it is often difficult to separate measurement effects due to pressure, temperature and density in real flows. Using a variation of a Shack-Hartmann wavefront sensor, we have made density measurements that have extremely large dynamic range coupled with excellent sensitivity at high temporal and spatial resolution. We have examined several classes of flow including volumetrically heated gas, turbulence and droplet evaporation. DOE

N94-19978# Illinois Univ., Urbana. Dept. of Mechanical and Industrial Engineering.
FLUID DYNAMIC MECHANISMS AND INTERACTIONS WITHIN SEPARATED FLOWS Final Report
J. C. Sutton and A. L. Addy 9 Aug. 1993 213 p
(Contract DAAL03-90-G-0021)
(AD-A271037; UILU-ENG-93-4019; ARO-27558.14-EG) Avail: CASI HC A10/MF A03

The significant results of a joint research effort investigating the fundamental fluid dynamic mechanisms and interactions within high-speed separated flows are presented in detail. The results were obtained through primary emphasis on experimental investigations of missile and projectile base flow-related configurations. The objectives of the research program focus on understanding the component mechanisms and interactions which establish and maintain high-speed separated flow regions. The experimental efforts considered the development and use of state-of-the-art laser Doppler velocimeter (LDV) and particle image velocimeter (PIV) systems for experiments with axisymmetric and planar, two-dimensional models in subsonic and supersonic flows. The LDV experiments yielded high quality, well documented mean and turbulence velocity data for a variety of high-speed separated flows including the near-wake region behind a cylindrical afterbody in supersonic flow. The PIV experiments studied the effect of a base cavity in a two-dimensional, subsonic base flow and the mechanism of drag reduction for this configuration. Another experimental study considered the interaction occurring when a supersonic stream is separated by means of a second stream impinging the first at an angle (plume-induced separation). The results of these various studies were carefully documented in a series of journal articles, conference proceedings papers, and theses. The full text of the papers and thesis abstracts are included as appendices. DTIC

N94-20033*# Institute for Computer Applications in Science and Engineering, Hampton, VA.
LINEAR AND NONLINEAR PSE FOR COMPRESSIBLE BOUNDARY LAYERS Final Report
Chau-Lyan Chang, Mujeeb R. Malik, Gordon Erlebacher, and M. Yousuff Hussaini Sep. 1993 47 p
(Contracts NAS1-18605; NAS1-19480; NAS1-18240; RTOP 505-90-52-01)
(NASA-CR-191537; NAS 1.26:191537; ICASE-93-70) Avail: CASI HC A03/MF A01

Compressible stability of growing boundary layers is studied by numerically solving the partial differential equations under a parabolizing approximation. The resulting parabolized stability equations (PSE) account for nonparallel as well as nonlinear effects. Evolution of disturbances in compressible flat-plate boundary layers are studied for freestream Mach numbers ranging from 0 to 4.5. Results indicate that the effect of boundary-layer growth is important for linear disturbances. Nonlinear calculations are performed for various Mach numbers. Two-dimensional nonlinear results using the PSE approach agree well with those from direct numerical simulations using the full Navier-Stokes equations while the required computational time is less by an order of magnitude. Spatial simulation using PSE were carried out for both the fundamental and subharmonic type breakdown for a Mach 1.6 boundary layer. The promising results obtained show that the PSE method is a powerful tool for studying boundary-layer instabilities and for predicting transition over a wide range of Mach numbers. Author

N94-20037*# Alabama Univ., Huntsville. Center for Microgravity and Materials Research.
STABILITY LIMITS AND DYNAMICS OF NONAXISYMMETRIC LIQUID BRIDGES Annual Report No. 1, 19 Nov. 1992 - 18 Nov. 1993
J. Iwan D. Alexander, Andy Resnik, and William F. Kaukler 1993 29 p
(Grant NAG3-1384)
(NASA-CR-194706; NAS 1.26:194706) Avail: CASI HC A03/MF A01

This program of theoretical and experimental ground-based and low gravity research is focussed on the understanding of the dynamics and stability limits of nonaxisymmetric liquid bridges. There are three basic objectives to the proposed work: (1) to determine the stability limits of nonaxisymmetric liquid bridges held between non-coaxially aligned disks; (2) to examine the dynamics of nonaxisymmetric bridges and nonaxisymmetric oscillations of initially axisymmetric bridges (some of these experiments require a low gravity environment and the ground-based research will culminate in a definitive flight experiment); and (3) to experimentally investigate the vibration sensitivity of liquid bridges under terrestrial and low gravity conditions. Author (revised)

N94-20094 Department of the Navy, Washington, DC.
THERMAL DILATION FIBER OPTICAL FLOW SENSOR Patent
Thomas G. Giallorenzi, inventor (to Navy) 4 May 1993 7 p Filed 30 Sep. 1991
(AD-D015926; US-Patent-5,208,650; US-Patent-Appl-SN-767189;
US-Patent-Class-356-345) Avail: US Patent and Trademark Office

A thermal dilation type optical flow sensor includes an optical heating source for heating a flowing fluid and a sensor disposed in a downstream direction from said heating source wherein the sensor includes a probe for varying a reflected light according to the temperature of the probe, a Michelson type interferometer for measuring the temperature of the probe

according to the phase of the reflected light, and a calculating device for determining the flow rate based on temperature of the probe, the distance between the heating source and the probe, and the amount of heat produced by the heating source. In an alternative embodiment, a thermal dilation type optical flow sensor includes a reflecting probe disposed in a flowing fluid for reflecting an incident light with a phase varied according to the probe temperature, an optical heater for heating the probe with a predetermined heat, and a calculating device for calculating a new rate based on the predetermined heat and the phase of the reflected light.
DTIC

N94-20101# Maryland Univ., College Park. Center for Environmental Energy Engineering.
EHD ENHANCEMENT OF POOL AND IN-TUBE BOILING OF ALTERNATE REFRIGERANTS
M. M. Ohadi, S. Dessiatoun, A. Singh, and M. A. Fanni Aug. 1993 44 p
(Contract DE-FG02-91CE-23810)
(DE94-000787; DOE/CE-23810/17) Avail: CASI HC A03/MF A01

The electrohydrodynamic (EHD) is an active heat transfer augmentation technique which utilizes the effect of secondary motions generated through the application of an electrostatic potential to a dielectric fluid. Net result is better momentum and heat transfer between the fluid and the heat transfer wall through destabilization of the thermal boundary layer and better mixing of the fluid adjacent to the heat transfer surface. EHD enhancement of refrigerant/refrigerant oil mixtures heat transfer using the electrohydrodynamic (EHD) technique is the subject of a three-year experimental investigation in a project funded by the U.S. Department of Energy, effective June 1, 1993. For the interim period between November 1992 and June 1993 when the DOE funds became available, the Air-Conditioning and Refrigeration Technology Institute (ARTI) provided partial funding for our EHD research program with the aim of accomplishing three major tasks: (1) conduct a comprehensive search of the literature on EHD-enhanced, in-tube and external boiling heat transfer enhancement of alternate refrigerants; (2) design, fabricate, and instrument an in-tube, EHD-enhanced boiling/condensation test rig and perform preliminary testing of the setup; and (3) conduct experiments and document new findings on EHD-enhanced external boiling of alternate refrigerants/refrigerant mixtures in an existing pool boiling test rig apparatus. Description of tasks performed are described and results are discussed.
DOE

N94-20104*# National Aeronautics and Space Administration. Ames Research Center, Moffett Field, CA.
A COMPARISON OF TWO INCOMPRESSIBLE NAVIER-STOKES ALGORITHMS FOR UNSTEADY INTERNAL FLOW
N. Lyn Willtberger, Stuart E. Rogers, and Dochan Kwak Nov. 1993 25 p Sponsored by NASA. Washington
(RTOP 505-10-01)
(NASA-TM-108794; A-94007; NAS 1.15:108794) Avail: CASI HC A03/MF A01

A comparative study of two different incompressible Navier-Stokes algorithms for solving an unsteady, incompressible, internal flow problem is performed. The first algorithm uses an artificial compressibility method coupled with upwind differencing and a line relaxation scheme. The second algorithm uses a fractional step method with a staggered grid, finite volume approach. Unsteady, viscous, incompressible, internal flow through a channel with a constriction is computed using the first algorithm. A grid resolution study and parameter studies on the artificial compressibility coefficient and the maximum allowable residual of the continuity equation are performed. The periodicity of the solution is examined and several periodic data sets are generated using the first algorithm. These computational results are compared with previously published results computed using the second algorithm and experimental data.
Author

N94-20145# Max-Planck-Inst. fuer Stroemungsforschung, Goettingen (Germany).
SHOCK INDUCED CONDENSATION IN FLUIDS OF HIGH MOLAR SPECIFIC HEAT: SHOCK STRUCTURE AND RELAXATION [STOSSSTRUKTUR UND RELAXATION BEI STOSSINDUZIERTER KONDENSATION IN SUBSTANZEN HOHER MOLARER SPEZIFISCHER WAERME]
Michael Hermann 1993 131 p In GERMAN
(MPIS-106/1993; ETN-93-94839) Avail: CASI HC A07/MF A02

The possible influence of nucleation on the thickness of a shock front which induces condensation of a retrograde gas in the mean flow of a shock tube is investigated. Measurements with and without condensation in the mean flow were performed using an optical method, which utilizes the dependence of the reflection of light from the shock front on its thickness. Condensation was monitored by means of scattering and extinction of laser light. As a test gas perfluoro-n-hexane was used, which, due to its high molar specific heat, exhibits retrograde behavior. For suitable conditions the gas reaches a supersaturated state within the shock, which gives rise to nucleation. Rotational and vibrational relaxation are very short; they are completed within the shock front. Following calculations presented in the literature, nucleation and subsequent condensation can cause a broadening of the shock. However, if the time scale for nucleation is much larger than those to reach thermodynamic equilibrium one can expect a relaxation tail behind the shock. In the range of the experiments depicted, no influence of nucleation on the shock thickness is observed. Within experimental accuracy all experiments can be described by an approximate continuum model, where the influence of vibrational relaxation is accounted for by introducing a bulk viscosity, which is assumed constant over the experimental range. The observed scattering and extinction of light in experiments with condensation can be examined by estimation of nucleation and droplet growth.
ESA

N94-20147 Technische Univ., Berlin (Germany). Inst. fuer Thermo- und Fluiddynamik.
PRINCIPLES AND APPLICATIONS OF OIL FILM INTERFEROMETRY FOR MEASURING WALL FRICTION FIELDS IN AIR FLOWS Ph.D. Thesis [UEBER DIE GRUNDLAGEN UND EINIGE ANWENDUNGEN DER OEFILMINTERFEROMETRIE ZUR MMSSUNG VON WANDREIBUNGSFELDERN IN LUFTSTROEMUNGEN]
Gerd Janke 1993 162 p In GERMAN Sponsored by DFG Limited Reproducibility: More than 20% of this document may be affected by microfiche quality
(ETN-93-95062) Avail: CASI HC A08

In the framework of thin layer interferences, it is shown that the optical components of oil film interferometry can be reduced to a simple experimental facility. A method for the presentation of interference fringe motion along wall streamlines in space time diagrams, which is based on a video camera and an image processing computer, is proposed. The partial differential equation for the deformation of oil film surface was derived with consideration of shear stresses, pressure gradients, gravity, and surface tensions and was considered by means of dimensional analysis and magnitude order estimations. For shear induced film motion a theory for analytical solution of the partial differential equation was developed, including film surface deformation with any initial conditions and wall shear stress distributions. Analogies between oil film and fluid motions were realized. Comparisons of measurements with Preston tube results show a very good agreement.
ESA

N94-20167*# National Aeronautics and Space Administration. Lewis Research Center, Cleveland, OH.
HEAD-ON COLLISION OF DROPS: A NUMERICAL INVESTIGATION
M. R. Nobari (Michigan Univ., Ann Arbor.), Y.-J. Jan (Michigan Univ., Ann Arbor.), and G. Tryggvason (Michigan Univ., Ann Arbor.) Nov. 1993 50 p
(Contract NCC3-233; NAG3-1317; RTOP 505-90-5K; NSF CTS-91-32140)
(NASA-TM-106394; ICOMP-93-45; E-8219; NAS 1.15:106394) Avail: CASI HC A03/MF A01

The head-on collision of equal sized drops is studied by full numerical simulations. The Navier-Stokes equations are solved for fluid motion both inside and outside the drops using a front tracking/finite difference technique. The drops are accelerated toward each other by a body force that is turned off before the drops collide. When the drops collide, the fluid between them is pushed outward leaving a thin later bounded by the drop surface. This layer gets progressively thinner as the drops continue to deform and in several of the calculations this double layer is artificially removed once it is thin enough, thus modeling rupture. If no rupture takes place, the drops always rebound, but if the film is ruptured the drops may coalesce permanently or coalesce temporarily and then split again.
Author (revised)

N94-20177*# National Aeronautics and Space Administration. Lewis Research Center, Cleveland, OH.

PRESSURIZATION AND EXPULSION OF A FLIGHTWEIGHT LIQUID HYDROGEN TANK

N. T. VanDresar and R. J. Stochl Dec. 1993 11 p Presented at the 29th Joint Propulsion Conference and Exhibit, Monterey, CA, 28-30 Jun. 1993; sponsored by AIAA, SAE, ASME, and ASEE See also A93-49814

(RTOP 506-42-73)

(NASA-TM-106427; E-8269; NAS 1.15:106427; AIAA Paper 93-1966) Avail: CASI HC A03/MF A01

Experimental results are presented for pressurization and expulsion of a flight-weight 4.89 cu m liquid hydrogen storage tank under normal gravity conditions. Pressurization and expulsion times are parametrically varied to study the effects of longer transfer times expected in future space flight applications. It is found that the increase in pressurant consumption with increased operational time is significant at shorter pressurization or expulsion durations and diminishes as the duration lengthens. Gas-to-wall heat transfer in the ullage is the dominant mode of energy exchange, with more than 50 percent of the pressurant energy being lost to tank wall heating in expulsions and the long duration pressurizations. Advanced data analysis will require a multidimensional approach combined with improved measurement capabilities of liquid-vapor interfacial transport phenomena.

Author (revised)

N94-20210*# North Carolina Agricultural and Technical State Univ., Greensboro. Dept. of Mechanical Engineering.

TURBULENCE MODELING FOR HIGH SPEED COMPRESSIBLE FLOWS Final Report, 16 May 1991 - 30 Jun. 1993

Suresh Chandra 1993 12 p

(Grant NAG1-1287)

(NASA-CR-194547; NAS 1.26:194547) Avail: CASI HC A03/MF A01

The following grant objectives were delineated in the proposal to NASA: to offer course work in computational fluid dynamics (CFD) and related areas to enable mechanical engineering students at North Carolina A&T State University (N.C. A&TSU) to pursue M.S. studies in CFD, and to enable students and faculty to engage in research in high speed compressible flows. Since no CFD-related activity existed at N.C. A&TSU before the start of the NASA grant period, training of students in the CFD area and initiation of research in high speed compressible flows were proposed as the key aspects of the project. To that end, graduate level courses in CFD, boundary layer theory, and fluid dynamics were offered. This effort included initiating a CFD course for graduate students. Also, research work was performed on studying compressibility effects in high speed flows. Specifically, a modified compressible dissipation model, which included a fourth order turbulent Mach number term, was incorporated into the SPARK code and verified for the air-air mixing layer case. The results obtained for this case were compared with a wide variety of experimental data to discern the trends in the mixing layer growth rates with varying convective Mach numbers. Comparison of the predictions of the study with the results of several analytical models was also carried out. The details of the research study are described in the publication entitled 'Compressibility Effects in Modeling Turbulent High Speed Mixing Layers,' which is attached to this report.

Derived from text

N94-20258# Argonne National Lab., Idaho Falls, ID.

A PARAMETRIC STUDY OF HEAT TRANSFER WITHIN A PLANAR THERMOSYPHON

R. Clarksean and G. Phillips 1993 11 p Presented at the National Conference and Exposition on Heat Transfer, Atlanta, GA, 8-11 Aug. 1993

(Contract W-31-109-eng-38)

(DE93-019546; ANL/FC/CP-78624; CONF-930830-28) Avail: CASI HC A03/MF A01

The results of a parametric study for a planar thermosyphon are presented. The thermosyphon consists of a 'U-shaped' geometry, with the center portion of the 'U' being a solid. The outer legs of the 'U' are the flow channels. One of the outer surfaces of a channel is held at a constant temperature. The remaining outer surfaces are considered adiabatic. The configuration described is characteristic of passive systems for radioactive waste storage and reactor safety systems. Parameters which are varied include the channel geometry, the thermal conductivity of the solid, and the Ra number. The average Nu number for the constant temperature surface decreases as the inlet channel width decreases, and as the thermal conductivity of the solid increases. A modified Ra number, defined as the Ra number divided by the length to gap ratio for the outer channel, is used in the paper. At low values of the modified Ra number, there is over an order of magnitude decrease in the average Nu number for a change in the inlet channel width from 1.0 to 0.25. But as the value of the modified Ra number increases for any inlet channel width, the average Nu number results approaches those of vertical parallel plates, independent of the inlet channel width and the thermal conductivity of the solid. The vertical parallel plate data is approached because the boundary layer flow near the heated plate is unaffected by the surface of the intervening solid.

DOE

N94-20263# Lawrence Livermore National Lab., CA.

A NOVEL SCHEME TO HANDLE HIGHLY PULSED LOADS WITH A STANDARD HELIUM REFRIGERATOR

D. S. Slack 30 Jun. 1993 9 p Presented at the International Cryogenic Engineering Conference and International Cryogenic Materials Conference, Albuquerque, NM, 12-16 Jul. 1993

(Contract W-7405-eng-48)

(DE93-019617; UCRL-JC-112599; CONF-930703-26) Avail: CASI HC A02/MF A01

Helium refrigerator performance degrades rapidly when it has to handle a varying or pulsed heat load. A novel scheme is presented to handle highly pulsed 4.5 K cryogenic loads with a standard helium refrigerator by isolating it from these pulses. The scheme uses a relatively simple arrangement of control valves, heat exchangers, and a storage dewar. Applications include pulsed tokamak machines such as TPX (Tokamak Physics Experiment) and ITER (International Thermonuclear Experimental Reactor). For example, the TPX (currently in the conceptual design phase in a DoE contract) requires an average 4.5 K refrigerator capacity of about 10 kW; however, pulsed loads caused by eddy current and nuclear heating will exceed 100 kW. The scheme presented here provides a method for handling these pulsed loads. Because of the simple and proven nature of the components involved and the thermodynamic properties of the helium, the system could be implemented for projects such as TPX or ITER with little or no development.

DOE

N94-20286# Los Alamos National Lab., NM.

EXPERIMENTAL STUDY OF A SHOCK ACCELERATED THIN GAS LAYER

J. W. Jacobs, D. G. Jenkins, D. L. Klein, and R. F. Benjamin 1993 9 p Presented at the 19th International Symposium on Shock Waves, Marseille, France, 26-30 Jul. 1993

(Contract W-7405-eng-36)

(DE93-018354; LA-UR-93-2449; CONF-930788-2) Avail: CASI HC A02/MF A01

Planar laser-induced fluorescence imaging is utilized in shock-tube experiments to visualize the development of a shock-accelerated thin gas layer. The Richtmyer-Meshkov instability of both sides of the heavy gas layer causes perturbations initially imposed on the two interfaces to develop into one of three distinct flow patterns. Two of the patterns exhibit vortex pairs which travel either upstream or downstream in the shock tube, while the third is a sinuous pattern that shows no vortex development until late in its evolution. The development of the observed patterns as well as the growth in the layer thickness is modeled by considering the dynamics of vorticity deposited in the layer by the shock interaction process. This model yields an expression for the layer growth which is in good agreement with measurements.

DOE

N94-20351 Duke Univ., Durham, NC. Dept. of Mathematics.

HIGH-RESOLUTION NUMERICAL METHODS FOR COMPRESSIBLE MULTI-PHASE FLOW IN HIERARCHICAL POROUS MEDIA

J. A. Trangenstein 15 Mar. 1993 12 p Limited Reproducibility: More than 20% of this document may be affected by microfiche quality

(Contract DE-FG05-92ER-25145)

(DE94-000740; DOE/ER-25145/1) Avail: Issuing Activity (Department of Energy (DOE))

This is the first year in the proposed three-year effort to develop high-resolution numerical methods for multi-phase flow in hierarchical porous media. There are three main issues being addressed in this research. The first issue is computational efficiency. Field-scale simulation of enhanced oil recovery, whether for energy production or aquifer remediation, is typically

highly under-resolved. This is because rock transport properties vary on many scales, and because current numerical methods have low resolution. The second issue is effective media properties. Since porous media are formed through complex geologic processes, they involve significant uncertainty and scale-dependence. Given this uncertainty, knowledge of ensemble averages of flow in porous media can be preferable to knowledge of flow in specific realizations of the reservoir. However, current models of effective properties do not represent the observed behavior very well. Relative permeability models present a good example of this problem. In practice, these models seldom provide realistic representations of hysteresis, interfacial tension effects or three-phase flow; there are no models that represent well all three effects simultaneously. The third issue is wave propagation. It is common in the petroleum industry to assume that the models have the same well-posedness properties as the physical system. An example of this fallacy is given by the three-phase relative permeability models; they were widely assumed by the petroleum community to produce hyperbolic systems for the Buckley-Leverett equations, but later the mathematics community proved that these models inherently produce local elliptic regions. Since numerical methods must use the models for computations, oscillations that develop could erroneously be attributed to numerical error rather than modeling difficulties. During this year, we have made significant progress on several tasks aimed at addressing these issues. DOE

N94-20361* National Aeronautics and Space Administration. Marshall Space Flight Center, Huntsville, AL.

SPIRAL FLUID SEPARATOR Patent

Glen A. Robertson, inventor (to NASA) 28 Sep. 1993 5 p Filed 9 Oct. 1992 Supersedes N93-17039 (31 - 5, p 1163)
(NASA-Case-MFS-28658-1; US-Patent-5,248,421;
US-Patent-Appl-SN-958843; US-Patent-Class-210-512.1;
US-Patent-Class-210-787; US-Patent-Class-209-144;
US-Patent-Class-209-211; US-Patent-Class-55-459.1;
Int-Patent-Class-B01D-21/26) Avail: US Patent and Trademark Office

A fluid separator for separating particulate matter such as contaminates is provided which includes a series of spiral tubes of progressively decreasing cross sectional area connected in series. Each tube has an outlet on the outer curvature of the spiral. As fluid spirals down a tube, centrifugal force acts to force the heavier particulate matter to the outer wall of the tube, where it exits through the outlet. The remaining, and now cleaner, fluid reaches the next tube, which is smaller in cross sectional area, where the process is repeated. The fluid which comes out the final tube is diminished of particulate matter.

Official Gazette of the U.S. Patent and Trademark Office

N94-20371* National Aeronautics and Space Administration. Ames Research Center, Moffett Field, CA.

COOLING APPARATUS AND COUPLINGS THEREFOR Patent

Curtis Lomax, inventor (to NASA) and Bruce Webbon, inventor (to NASA) 16 Nov. 1993 10 p Filed 21 May 1991 Supersedes N92-11286 (30 - 2, p 232)
(NASA-Case-ARC-11921-1; US-Patent-5,261,482;
US-Patent-Appl-SN-703649; US-Patent-Class-165-10;
US-Patent-Class-165-104.17; US-Patent-Class-165-78;
US-Patent-Class-62-59; US-Patent-Class-62-259.3; US-Patent-Class-62-299;
Int-Patent-Class-F28D-20/00) Avail: US Patent and Trademark Office

The present invention relates generally to the field of thermal transfer and, more specifically, to a direct-interface, fusible heat sink for non-venting, regenerable, and self-contained thermal regulation. A quick connect coupling includes a male and a female portion. The female portion is frozen in a container of solid-phase coolant fluid, i.e., water, so that passages in the housing are blocked by ice initially. The ice is melted by direct interface with liquid coolant fluid delivered from the male portion. The present invention has advantages in that the phase change material remains sealed at all times, including during regeneration. Also, it uses quick-disconnect couplings that allow the phase change material to completely fill the container and is easily handled in microgravity without spills, leakage, or handling of phase change material.

Official Gazette of the U.S. Patent and Trademark Office

N94-20466 Naval Undersea Warfare Center, New London, CT. New London Detachment.

THE EFFECT OF TRANSVERSE CURVATURE ON THE FLUCTUATING WALL PRESSURE AND STRUCTURE OF BOUNDARY LAYER TURBULENCE

Stephen R. Snarski 19 Aug. 1993 27 p Limited Reproducibility: More than 20% of this document may be affected by microfiche quality
(AD-A271868; NUWC-NPT-TD-10459) Avail: Issuing Activity (Defense Technical Information Center (DTIC))

This document consists of the text and viewgraphs of a paper presented at the ONR Workshop on Nonequilibrium Turbulence held at Arizona State University in Tempe, Arizona, from 10-12 Mar. 1993. This workshop was the first step of an ONR Accelerated Research Initiative (ARI) to establish the state-of-the-art for theory, computation, and experimentation relevant to turbulence in a nonequilibrium state, or, more generally, to turbulence in complex flows. The overall goal of the initiative is to understand the behavior of turbulence in such complex conditions in order to advance our prediction and control capabilities. When a cylinder in axial flow is sufficiently long and thin, the growth of the boundary layer results in its thickness exceeding the radius of the cylinder such that the three-dimensional effects due to transverse curvature cannot be neglected. With this condition, the wall of the cylinder provides less constraint on the outer flow and motion of eddies than is experienced in an equilibrium flat plate boundary layer introducing an avenue for enhanced inner-layer/outer-layer interaction and modified turbulence activity. In this paper, we present results of measurements of the fluctuating wall pressure and turbulent streamwise velocity in the turbulent boundary layer on a cylinder in axial flow to identify the coherent structures that contribute to the fluctuating pressure at the wall. Determining the influence of transverse curvature on the relationship between the wall pressure and velocity field allows examination of its effect on the structure of equilibrium boundary layer turbulence.

DTIC

N94-20495* National Aeronautics and Space Administration. Langley Research Center, Hampton, VA.

HEAT EXCHANGER WITH OSCILLATING FLOW Patent

Stephen J. Scotti, inventor (to NASA), Max L. Blosser, inventor (to NASA), and Charles J. Camarda, inventor (to NASA) 24 Aug. 1993 12 p Filed 24 Feb. 1992 Supersedes N92-30024 (30 - 20, p 3447) Division of US-Patent-Appl-SN-501909, filed 30 Mar. 1990
(NASA-Case-LAR-14033-2; US-Patent-5,238,056;
US-Patent-Appl-SN-843653; US-Patent-Appl-SN-501909;
US-Patent-Class-165-109.1; US-Patent-Class-165-97;
US-Patent-Class-165-104.31; US-Patent-Class-165-110;
US-Patent-Class-165-903; US-Patent-Class-165-913) Avail: US Patent and Trademark Office

Various heat exchange apparatuses are described in which an oscillating flow of primary coolant is used to dissipate an incident heat flux. The oscillating flow may be imparted by a reciprocating piston, a double action twin reciprocating piston, fluidic oscillators or electromagnetic pumps. The oscillating fluid flows through at least one conduit in either an open loop or a closed loop. A secondary flow of coolant may be used to flow over the outer walls of at least one conduit to remove heat transferred from the primary coolant to the walls of the conduit.

Official Gazette of the U.S. Patent and Trademark Office

N94-20533# Deutsche Forschungsanstalt fuer Luft- und Raumfahrt, Goettingen (Germany). Abt. Transition und Turbulenz.

NUMERICAL INVESTIGATION OF LAMINAR-TURBULENT TRANSITION IN TWO- AND THREE-DIMENSIONAL BOUNDARY LAYERS Ph.D. Thesis - Karslruhe Univ. [NUMERISCHE UNTERSUCHUNGEN ZUM LAMINAR-TURBULENTEN UEBERGANG IN ZWEI- UND DREIDIMENSIONALEN GRENZSCHICHTEN]

Michael Wagner Jul. 1992 114 p In GERMAN
(DLR-FB-92-36; ETN-93-94870) Avail: CASI HC A06/MF A02

Transition to turbulence in two and three dimensional boundary layers is investigated by temporal numerical simulations and linear stability analysis. Simulations which are adapted to a transition experiment reveal a marked influence of the relative initial amplitudes of stationary and fluctuating disturbances on the transition process. In the late stages of transition the stability characteristics of the deformed mean velocity profile differ significantly from the stability results obtained for the laminar flow. Temporal

simulation results could be related to the spatial disturbance development in the experiment and show a good agreement with measurements. Towards the end of transition the crossflow vortices, developing as a primary instability of the laminar flow, begin to break down. Comparably inexpensive simulations comprising only a few modes in the wall-parallel directions appear to be suitable for a quick preliminary transition estimation. ESA

N94-20542# Ecole Centrale de Lyon (France). Lab. de Mecanique des Fluides et d'Acoustique.

TWO-POINT LASER DOPPLER VELOCIMETRY MEASUREMENTS OF LENGTH-TURBULENT SCALES Ph.D. Thesis [MESURE DES ECHELLES TURBULENTES DE LONGUEUR PAR VELOCIMETRIE DOPPLER LASER EN DEUX POINTS]

Hafedh Belmabrouk 1992 188 p In FRENCH

(ECL-92-12; ETN-93-94412) Avail: CASI HC A09/MF A02

A method for measuring the space correlation between the flow velocity and the length-turbulent scales is proposed. The flow velocity simultaneous measurements at two distant points allow to calculate the space correlation coefficient. The next step is the calculation of integral and Taylor scales. The effect of optical and electronic adjusting parameters on the correlation is analyzed. The following parameters are found to be fundamental: the dimensions of the measurement volumes; and the need to adjust an osculate parabola near the origin by the least errors squares method. Two correlation models are applied: a Gaussian curve defined by the accurate Taylor scale data; and a model determined by both integral and Taylor scales. ESA

N94-20562# Oak Ridge National Lab., TN.

MULTI-CPU PLASMA FLUID TURBULENCE CALCULATIONS ON A CRAY Y-MP C90

V. E. Lynch, B. A. Carreras, J. N. Leboeuf, B. C. Curtis, and R. L. Troutman (National Energy Research Supercomputer Center, Livermore, CA.) 1993 32 p Presented at the Supercomputing Conference on High Performance Computing and Communications, Portland, OR, 15-19 Nov. 1993

(Contract DE-AC05-84OR-21400)

(DE93-015425; CONF-931115-6) Avail: CASI HC A03/MF A01

Significant improvements in real-time efficiency were obtained for plasma fluid turbulence calculations by microtasking the nonlinear fluid code KITE in which they are implemented on the CRAY Y-MP C90 at the National Energy Research Supercomputer Center (NERSC). The number of processors accessed concurrently scales linearly with problem size. Close to six concurrent processors have so far been obtained with a three-dimensional nonlinear production calculation at the currently allowed memory size of 80 Mword. With a calculation size corresponding to the maximum allowed memory of 200 Mword in the next system configuration, it is expected to be able to access close to nine processors of the C90 concurrently with a commensurate improvement in real-time efficiency. These improvements in performance are comparable to those expected from a massively parallel implementation of the same calculations on the Intel Paragon. DOE

N94-20588* National Aeronautics and Space Administration. Lewis Research Center, Cleveland, OH.

SYSTEM AND METHOD FOR CANCELLING EXPANSION WAVES IN A WAVE ROTOR Patent

Daniel E. Paxson, inventor (to NASA) 7 Dec. 1993 9 p Filed 26 May 1992 Supersedes N93-11172 (31 - 2, p 297)

(NASA-Case-LEW-15218-1; US-Patent-5,267,432;

US-Patent-Appl-SN-889003; US-Patent-Class-60-39.45;

US-Patent-Class-417-64; Int-Patent-Class-F02C-3/02) Avail: US Patent and Trademark Office

A wave rotor system that is comprised of a wave rotor coupled to first and second plates is described. Special ports are provided, one in each of the first and second end plates, to cancel expansion waves generated by the release of working fluid from the wave rotor. One of the expansion waves is reflected in the wave rotor from a reflecting portion and provided to the special port in the second end plate. Fluid present at the special port in the second end plate has a stagnation pressure and mass flow which is the same as that of the cells of the wave rotor communicating with such special port. This allows for cancellation of the expansion wave generated by the release of working fluid from the wave rotor. The special port in the second end plate has a first end corresponding to the head of the expansion wave and a second end corresponding to the tail of the expansion wave. Also, the special port is configured to continually change along the circumference of the second end plate to affect expansion wave cancellation. An expansion wave generated by a second release of working fluid from the wave rotor is cancelled in a similar manner to that described above using a special port in the first end plate. The cycle of operation of the wave rotor system is designed so that the stagnation pressure and mass flow of the fluid present at the special ports is the same so that the special ports may be connected by a common duct.

Official Gazette of the U.S. Patent and Trademark Office

N94-20597# Ecole Centrale de Lyon (France). Lab. de Mecanique des Fluides et d'Acoustique.

FINITE ELEMENT NUMERICAL SIMULATION OF THREE DIMENSIONAL TURBULENT FLOWS WITH DISPERSION: EULERIAN AND LAGRANGIAN APPROACHES Ph.D. Thesis [SIMULATION NUMERIQUE PAR ELEMENTS FINIS DES ECOULEMENTS TURBULENTS TRIDIMENSIONNELS AVEC DISPERSION: APPROCHES EULERIENNE ET LAGRANGIENNE]

Cesar Pinhobrasil, Jr. 1992 164 p In FRENCH Prepared in cooperation with Metraflu, Ecully, France Original contains color illustrations

(ECL-92-42; ETN-93-94598) Avail: CASI HC A08/MF A02

Turbulent models which can be applied for the investigation of industrial mixing system are studied. A three dimensional (3D) code is developed in this framework. The hydrodynamics of the turbulent flow is computed using the standard k-epsilon model. Some corrections of the standard model are also analyzed when a string rotation rate is imposed to the flow. For the scalar transport modeling two approaches are studied: the first one is the classical Eulerian first order closure, and the second one is a Lagrangian stochastic modeling based on the computation of scalar field using the statistic of fluid particle trajectories in the flow. In order to carry out computations into complex geometries a finite element method was applied. A set of test cases concerning both hydrodynamical and thermal problems is performed for which a great number of experimental data is given in the literature. More particularly, the case of a 3D turbulent jet normal to a cross flow is studied. ESA

N94-20601 Ecole Centrale de Lyon (France). Groupe Mecanique des Fluides Industriels.

MODELING OF PARTICLE DISPERSION IN A STATIONARY ISOTROPIC HOMOGENEOUS TURBULENCE BY LARGE SCALE NUMERICAL SIMULATION Ph.D. Thesis [DISPERSION DE PARTICULES DANS UNE TURBULENCE HOMOGENE ISOTROPE STATIONNAIRE CALCULEE PAR SIMULATION NUMERIQUE DIRECTE DES GRANDES ECHELLES]

Emmanuel Deutsche 1992 239 p In ENGLISH and FRENCH Original contains color illustrations

(ETN-93-94604) Avail: CASI HC A11/MF A03

A study aimed at improving the understanding of physical phenomena in the transport of discrete particles placed in a turbulent field, and aimed at validating certain closure hypotheses using a model with Eulerian transport equations for two phases is reported. In order to model the turbulence in the dispersed phase and the interfacial transfer terms between the phases, the Eulerian approach is based on the Lagrangian description of particle movement which enables the theoretical analysis of particle transport through a homogeneous turbulence. The model used to simulate the turbulence and the method used to maintain the stationary turbulent fields are described. The problem of simulating particle trajectories is considered. Results of simulations of particle clouds (25,000 to 100,000) in stationary homogenous turbulence are presented. ESA

N94-20915# Gough (Paul) Associates, Inc., Portsmouth, NH.

FORMULATION OF A NEXT-GENERATION INTERIOR BALLISTIC CODE Final Report, May - Dec. 1991

Paul S. Gough Oct. 1993 71 p

(Contract DAAA15-91-M-0073; DA Proj. 1L1-61102-AH-43)

(AD-A271539; PGA-TR-91-3; ARL-CR-68) Avail: CASI HC A04/MF A01

Two-phase flow interior ballistic codes, both one-dimensional and two-dimensional, have been developed over the last 20 years for the purpose of modeling the behavior of solid propellant gun propulsion systems. These codes have proven useful for explaining charge malfunctions and for studying possible remedies. Over the years, these codes have become

increasingly elaborate as more complex designs have been addressed and also as the depth of simulation has increased. However, charge designs involving liquid propellant or electrothermal-chemical propulsion remain largely outside the scope of the solid propellant codes and a number of separate codes have been developed for the simulation of these alternative propulsion schemes. As we look to the future, it is evident that the next generation of interior ballistic models will be required to address three-dimensional details of the flow inside the gun. Such models will be expensive to develop and it is, therefore, of great interest to assess the extent to which a single code can be formulated to treat all foreseeable propulsion schemes. In this report, we review the physical problems of current interest, as well as those anticipated in the foreseeable future. We review the models currently available to address these processes. We then discuss the architecture, of a possible next-generation code. This discussion addresses the formulation of the equations, the choice of solution algorithms, and the implications of the current trend toward massively parallel computing. DTIC

N94-20942# Argonne National Lab., IL.
CHEMICAL REACTION FOULING MODEL FOR SINGLE-PHASE HEAT TRANSFER
C. B. Panchal and A. P. Watkinson (British Columbia Univ., Vancouver.) 1993 16 p Presented at the National Conference and Exposition on Heat Transfer, Atlanta, GA, 8-11 Aug. 1993
(Contract W-31-109-eng-38)
(DE93-019556; ANL/ES/CP-79376; CONF-930830-25) Avail: CASI HC A03/MF A01

A fouling model was developed on the premise that the chemical reaction for generation of a precursor can take place in the bulk fluid, in the thermal boundary layer, or at the fluid/wall interface, depending upon the interactive effects of fluid dynamics, heat and mass transfer, and the controlling chemical reaction. The analysis was used to examine the experimental data for fouling deposition of polyperoxides produced by autoxidation of indene in kerosene. The effects of fluid and wall temperatures for two flow geometries were analyzed. The results showed that the relative effects of physical parameters on the fouling rate would differ for the three fouling mechanisms; therefore, it is important to identify the controlling mechanism in applying the closed-flow-loop data to industrial conditions. DOE

N94-21155# Stanford Univ., CA. Dept. of Mechanical Engineering.
INVESTIGATION OF THE PHYSICS OF THE TURBULENT BOUNDARY LAYER FOCUSING ON VORTEX STRUCTURES Final Report, 1 Sep. 1991 - 31 Jan. 1993
Steve Kline 31 Mar. 1993 12 p
(Grant AF-AFOSR-0364-91)
(AD-A272879; AFOSR-93-0843TR) Avail: CASI HC A03/MF A01

The report describes summary results of a community-wide assessment of our understanding of the structure and dynamics of turbulent boundary layers. It also summarizes the findings of an in depth numerical study of vortex structures in the boundary layer. DTIC

N94-21169# Lehigh Univ., Bethlehem, PA. Dept. of Mechanical Engineering and Mechanics.
COMPUTATIONAL AND ANALYTICAL METHODS IN NONLINEAR FLUID DYNAMICS Final Report, 1 Sep. 1989 - 28 Feb. 1993
James Walker Sep. 1993 30 p
(Grant AF-AFOSR-0487-89)
(AD-A272722; AFOSR-93-0846TR) Avail: CASI HC A03/MF A01

The central focus of the program was on the application and development of modern analytical and computational methods to the solution of nonlinear problems in fluid dynamics and reactive gas dynamics. The research was carried out within the Division of Engineering Mathematics in the Department of Mechanical Engineering and Mechanics and principally involved Professors P.A. Blythe, E. Varley and J.D.A. Walker. In addition, the program involved various international collaborations. Professor Blythe completed work on reactive gas dynamics with Professor D. Crighton FRS of Cambridge University in the United Kingdom. Professor Walker and his students carried out joint work with Professor F.T. Smith, of University College London, on various problems in unsteady flow and turbulent boundary layers. DTIC

N94-21193# Illinois Univ., Chicago. Dept. of Mechanical Engineering.
LIQUID-PHASE CIRCULATION AND MIXING IN MULTICOMPONENT DROPLETS VAPORIZING IN A LAMINAR CONVECTIVE ENVIRONMENT Final Report, 15 Aug. 1992 - 31 Jul. 1993
Constantine M. Megaridis and Joseph T. Hodges 15 Oct. 1993 93 p
(Contract F49620-92-J-0476)
(AD-A272851; AFOSR-93-0828TR) Avail: CASI HC A05/MF A01

A combined theoretical/experimental study of internal circulation induced by surface rotation of mm-sized pendant droplets was completed. The study consistently revealed predictable helical three-dimensional circulation patterns that bear little resemblance to the two-dimensional toroidal internal flows established within droplets under axisymmetric convective conditions. The observed complex flow patterns suggested substantially enhanced liquid mixing rates, thus indicating that droplet spinning may be very important in practical situations involving droplet convective transport. In a parallel study, charged droplets up to 100 micrometers in diameter were stably levitated and exposed to uniform air streams with Reynolds numbers up to three. The evaporation rate of levitated dodecanol droplets was measured under quiescent conditions and followed the familiar d squared law. No detailed information could be obtained on internal circulation of levitated droplets impregnated with scattering or fluorescent agents. DTIC

N94-21220# University of Southern California, Los Angeles. Dept. of Aerospace Engineering.
ESTABLISHING THE BASIS FOR VALIDATED PREDICTIONS OF HIGHLY NON-EQUILIBRIUM FLOWS (WITH 9 ATTACHMENTS) Final Report, 15 Feb. 1990 - 14 Feb. 1993
Dan Erwin, Joseph Kunc, and E. P. Muntz 14 Sep. 1993 277 p
(Grant AF-AFOSR-0170-90)
(AD-A272918; AFOSR-93-0842TR) Avail: CASI HC A13/MF A03

A unique iodine vapor hypersonic flow facility for the study of nonequilibrium reacting flows has been developed and used in initial experiments. An important new computationally efficient theoretical approach to describing the energy exchange of iodine and other molecules during collisions has been formulated and applied to iodine. The transport properties of dissociating diatomic molecules have been studied and a potentially very significant phenomena appearing when a gas is partially dissociated has been identified. A Ph.D. thesis has been completed on experiments with the iodine flow facility. Several journal articles and meeting papers on both the experimental and theoretical work have been prepared. A second Ph.D. thesis is nearly complete on the design of parallel flow nozzles for nonequilibrium dissociating, vibrationally active iodine flows. DTIC

N94-21261# Rensselaer Polytechnic Inst., Troy, NY. Center for Multiphase Research.
AN ANALYSIS OF POOL SURFACE DEFORMATION DUE TO A PLUNGING LIQUID JET Quarterly Report
F. Bonetto, D. A. Drew, and Richard T. Lahey, Jr. 31 Oct. 1993 49 p
(Contract N00014-91-J-1271)
(AD-A272970) Avail: CASI HC A03/MF A01

When a liquid jet impacts a pool containing the same liquid and surrounded by a still gas, a surface depression is produced. The surface shape is determined by the Weber number and the Bond number. In this work the shape of the surface is obtained as a function of the Weber number and Bond number by using a non-singular perturbation technique. DTIC

N94-21263# Wright Lab., Wright-Patterson AFB, OH.
CHARACTERISTIC BASED METHODS FOR THE TIME-DOMAIN MAXWELL EQUATIONS Final Report, Jun. 1990 - Feb. 1991
J. S. Shang 9 Aug. 1993 51 p
(AD-A272973; WL-TR-93-3080) Avail: CASI HC A04/MF A01

Numerical procedures for solving the time-domain Maxwell equations based on the theory of characteristics were successfully developed. Both explicit and implicit methods were formulated by the time-central and spatial-windward algorithm to better describe wave motion. A new trapezoidal consistent implicit scheme was shown to be unconditionally stable for the linear initial value system and was able to generate numerical solutions comparable to those of the established explicit method. The formulation of the three-dimensional system including generalized coordinate system was completed but not explored. The present 2-D results on Cartesian frame demonstrated a potential for numerical efficiency improvement. DTIC

N94-21417# Naval Postgraduate School, Monterey, CA.
MEASUREMENT AND PREDICTION OF THE FLOW THROUGH AN ANNULAR TURBINE CASCADE M.S. Thesis
Gregory D. Thomas 2 Jun. 1993 81 p
(AD-A272530) Avail: CASI HC A05/MF A01

An annular turbine cascade was designed and manufactured for laser Doppler velocimetry and probe measurements in a small-scale rig. The purpose of the experiment was to determine the limitations of these measurements in a confined annulus, and to compare the experimental results with numerical predictions. Downstream probe surveys were conducted at a Reynolds number of 500,000. Total pressure and temperature measurements were taken upstream of the test section, and hub static pressure was measured downstream of the cascade. A two-dimensional laser anemometer was used to obtain preliminary velocity field measurements for code validation. The two main problem areas identified were the type of seeding material used and the configuration of the optical access window. Flowfield characteristics were predicted using a three-dimensional viscous code, which were then compared to experimental measurements. The comparison showed that the numerical simulator predicted well the general features of the flow field that were measured in the experiment. Recommendations are made which would improve the mapping of the velocity field for a more complete code validation. DTIC

N94-21459# Clemson Univ., SC. Dept. of Mechanical Engineering.
LOW REYNOLDS-NUMBER TURBULENT BOUNDARY LAYERS Final Report, 14 Apr. 1989 - 30 Mar. 1993
Ting Wang 30 Jun. 1993 58 p
(Grant AF-AFOSR-0324-89)
(AD-A272011; AFOSR-93-0809TR) Avail: CASI HC A04/MF A01

An experimental investigation was performed to determine the Reynolds analogy factor and turbulent Prandtl number in the transitional and low-Reynolds-number turbulent boundary layer. A miniature three-wire probe was specially designed to measure the mean velocity and temperature profiles and the Reynolds stresses and heat fluxes. Tests were conducted over a heated flat wall with zero pressure gradient and three levels of streamwise acceleration: K = 0.07, 0.16, and 0.25 x 10(exp -6). Mean temperature profiles lagged in development compared to the mean velocity profiles and the values of the Reynolds analogy factor, 2St/Cf, in the late-transition and early-turbulent regions were lower than the values known to apply to the high-Reynolds-number turbulent flow. The profiles of Reynolds cross-stream heat flux showed negative values in the near wall region. The region of negative vt narrowed as the flow proceeded downstream. These negative values of vt in a flow with a negative mean temperature gradient result in negative eddy thermal diffusivity and negative Pr(sub t). It is speculated that the negative values might be caused by the size of the sensor and the three-dimensional behavior of transition. A conditional sampling technique was utilized to separate the flow into turbulent and non-turbulent portions. Detailed flow and thermal structures were investigated. DTIC

N94-21531# Lawrence Livermore National Lab., CA.
DIRECT SIMULATION OF SHOCK-INDUCED MIXING LAYER
J. A. Greenough and J. B. Bell Mar. 1993 12 p Presented at the 4th International Workshop on the Physics of Compressible Turbulent Mixing, Cambridge, United Kingdom, 29 Mar - 1 Apr. 1993
(Contract W-7405-eng-48)
(DE93-040498; UCRL-JC-112208; CONF-9303126-9) Avail: CASI HC A03/MF A01

The interaction of a shock wave with a dense fluid layer in three dimensions is investigated using direct numerical simulations. The underlying numerical method is a second-order Godunov scheme. This is coupled to an implementation of Adaptive Mesh Refinement which is used to manage the hierarchical grid structure. An anomalous shock refraction is formed as the initiating shock wave impinges on a quiescent thin dense gas layer. One of the two resulting centered waves from the refraction, the contact surface, serves as the site for initial deposition of primarily spanwise vorticity and represents the primary mixing layer instability. The other wave, the transmitted shock wave, through repeated interactions with the free-surface, forms a cellular structure within the dense layer. The initial interaction introduces three dimensional perturbations onto the slip surface. These perturbations are selectively enhanced, due to favorable velocity gradients over part of the cellular structures, and form large-scale counter-rotating streamwise vertical structures. The structures characterize the secondary instability of this mixing layer. These vortices are quite unstable and transition to small-scales within a distance spanned by two of the cellular structures behind the initiating shock. The transition location has been verified in physical experiments. The fine-scale structure contains evidence of hairpin vortices. The evolution of a conserved scalar is used to monitor mixing progress. Increases in the rate of mixing are directly tied to intensification events associated with the streamwise vortices. Overall the large-scale streamwise structures provide an efficient mechanism for mixing the light and dense fluids. Analysis of time-series data from the calculation shows evidence of what are termed energetic small scales. This is the characteristic signature of the hairpin vortices undergoing intensification. DOE

N94-21575# Center for Mathematics and Computer Science, Amsterdam (Netherlands). Dept. of Numerical Mathematics.
A NOTE ON SINGULARITIES CAUSED BY THE HYDRODYNAMIC DISPERSION TENSOR
Ron A. Trompert Jan. 1993 9 p Sponsored by Ministry of Economic Affairs, The Hague, Netherlands
(CWI-NM-R9302; ETN-94-94704) Copyright Avail: CASI HC A02/MF A01

A study showing that the equation describing transport in a porous medium is not uniquely defined in points of the domain where the velocity of the fluid is zero is presented. This is due to the fact that the hydrodynamic dispersion tensor is defined as a not sufficiently differentiable function of the fluid velocity. The implications of this non smoothness for the numerical simulation of fluid flow and transport in porous media is discussed. ESA

N94-21609 Center for Mathematics and Computer Science, Amsterdam (Netherlands). Dept. of Numerical Mathematics.
LOCAL UNIFORM GRID REFINEMENT AND BRINE TRANSPORT IN POROUS MEDIA WITH INHOMOGENEITIES
Ron A. Trompert Nov. 1992 33 p Sponsored by Ministry of Economic Affairs, The Hague, Netherlands Limited Reproducibility: More than 20% of this document may be affected by microfiche quality
(CWI-NM-R9224; ETN-94-94699) Copyright Avail: CASI HC A03

The application of an adaptive grid method is discussed for a mathematical model for unsteady flow, coupled with transport of brine in porous media with inhomogeneities in two space dimensions. When the concentration of salt is large, the salt concentration profile in brine transport problems can show locally large gradients in space and in time. For this reason an adaptive grid method was chosen to solve these problems. A method based on local uniform grid refinement, where integration takes place on a series of nested, local uniform finer and finer subgrids, is considered. These subgrids are created up to a level of refinement where sufficient spatial accuracy is reached and their location and shape is adjusted after each time step. The space domain is considered to be a rectangle and all grids in use are uniform and cartesian. The interfaces, caused by the inhomogeneities, are assumed to coincide with cell edges in the numerical approximation. Special conditions are applied, connecting the solutions on both sides of the interface. These interface conditions involve continuity of fluxes across the interfaces. The mesh refinement process and the variabe time stepsizes are controlled by heuristic error monitors. The performance of the method is illustrated by two example problems. ESA

N94-21651# Lawrence Livermore National Lab., CA.
SURFACE PATH LINES IN PLANE STOKES FLOW DRIVEN BY CAPILLARITY
R. W. Hopper 3 May 1993 11 p
(Contract W-7405-eng-48)
(DE93-041277; UCRL-ID-114105) Avail: CASI HC A03/MF A01

Consider the free creeping viscous plane flow in a region, bounded by a simple smooth closed curve and driven solely by surface tension. The shape evolution may in principle, and often in practice, be described by a time-dependent mapping z = Omega(zeta,t) of the unit circle, conformal on absolute value of zeta less than or equal to one. It is shown that the path lines of fluid elements at the surface are determined by a first-order ordinary differential equation involving Omega(zeta,t), together with an initial condition. Typically, this must be integrated numerically. Velocities are not needed. The analogous theory for maps from the half-plane imaginary part

of zeta greater than or equal to zero is presented. Surface path lines of a collapsing elliptic hole, in two reference frames, are calculated. DOE

N94-21748# Bettis Atomic Power Lab., West Mifflin, PA.
PARTICLE IMAGE VELOCIMETRY
B. B. Ibrahim Jun. 1993 12 p
(Contract DE-AC11-89PN-38014)
(DE93-040657; WAPD-TM-1629) Avail: CASI HC A03/MF A01

This document describes the development of a new flow visualization and measurement facility that incorporates a sheet of laser light and digital image enhancement and processing techniques. A simple bench test that was used to demonstrate the feasibility of such techniques is also described. This technique offers the advantages of real time visualization of flow and the ability to freeze the flow pattern at any instant in time. In this sense, the technique plays a role similar to that of large scale direct numerical simulation of flows on supercomputers. Therefore, it will provide a better basis for code qualification than we have today. In addition, quantitative information about the flow field (e.g., the velocity vectors), both instantaneous and time-averaged, can easily be extracted from the still or video image with a high level of accuracy and in considerably shorter testing time. This is considered to be a very powerful tool for use in future computer model qualification. Because of the capabilities of the cameras in magnifying the image, this technique is far superior to previous techniques when the test geometry is very small. DOE

N94-21765 Westinghouse Savannah River Co., Aiken, SC.
AN ANALYSIS OF PRESSURE DRIVEN CROSS-FLOW THROUGH A LONG SLOT CONNECTING TWO PARALLEL CHANNELS
M. A. Shadday, Jr. 1992 11 p Presented at the National Conference and Exposition on Heat Transfer, Atlanta, GA, 8-11 Aug. 1993 Limited Reproducibility: More than 20% of this document may be affected by microfiche quality
(Contract DE-AC09-89SR-18035)
(DE93-040181; WSRC-MS-92-396; CONF-930830-29) Avail: CASI HC A03

Cross-flow between two parallel channels that were connected by a long narrow slot has been measured. The data was presented primarily in terms of transverse resistance coefficients. This data has been analyzed with momentum balances applied to both the axial and transverse components of the slot flow. The importance of wall friction to the slot flow and the necessity of calculating the axial component of the slot flow is demonstrated. DOE

N94-21820*# Wisconsin Univ., Milwaukee. Dept. of Mechanical Engineering.
REWETTING OF MONOGROOVE HEAT PIPE IN SPACE STATION RADIATORS Annual Status Report, 15 Dec. 1992 - 14 Dec. 1993
S. H. Chan 14 Dec. 1993 20 p
(Grant NAG3-1381)
(NASA-CR-194781; NAS 1.26:194781) Avail: CASI HC A03/MF A01

The annual status report for the experimental work in progress regarding the rewetting of a monogroove heat pipe in a microgravity environment is presented. This report is divided into two sections. The first details improvements in the experimental apparatus, and the second reports the ground based and theoretical results. Author (revised)

N94-21861*# Institute for Computer Applications in Science and Engineering, Hampton, VA.
SIMULATIONS OF DIFFUSION-REACTION EQUATIONS WITH IMPLICATIONS TO TURBULENT COMBUSTION MODELING Final Report
Sharath S. Girimaji Sep. 1993 44 p Submitted for publication
(Contract NAS1-19480; RTOP 505-90-52-01)
(NASA-CR-191536; NAS 1.26:191536; ICASE-93-69) Avail: CASI HC A03/MF A01

An enhanced diffusion-reaction reaction system (DRS) is proposed as a statistical model for the evolution of multiple scalars undergoing mixing and reaction in an isotropic turbulence field. The DRS model is close enough to the scalar equations in a reacting flow that other statistical models of turbulent mixing that decouple the velocity field from scalar mixing and reaction (e.g. mapping closure model, assumed-pdf models) cannot distinguish the model equations from the original equations. Numerical simulations of DRS are performed for three scalars evolving from non-premixed initial conditions. A simple one-step reversible reaction is considered. The data from the simulations are used (1) to study the effect of chemical conversion on the evolution of scalar statistics, and (2) to evaluate other models (mapping-closure model, assumed multivariate beta-pdf model). Author (revised)

N94-21875*# Institute for Computer Applications in Science and Engineering, Hampton, VA.
NEW RESULTS ON THE REALIZABILITY OF REYNOLDS STRESS TURBULENCE CLOSURES Final Report
Charles G. Speziale (Boston Univ., MA.), Ridha Abid (National Aeronautics and Space Administration. Langley Research Center, Hampton, VA.), and Paul A. Durbin (Stanford Univ., CA.) Oct. 1993 51 p Submitted for publication
(Contract NAS1-19480; RTOP 505-90-52-01)
(NASA-CR-191548; NAS 1.26:191548; ICASE-93-76) Avail: CASI HC A04/MF A01

The realizability of Reynolds stress models in homogeneous turbulence is critically assessed from a theoretical standpoint. It is proven that a well known second-order closure formulated by Shih and Lumley using the strong realizability constraints of Schumann is, in fact, not a realizable model. The problem arises from the failure to properly satisfy the necessary positive second time derivative constraint when a principal Reynolds stress vanishes - a fatal flaw that becomes apparent when the non-analytic terms in their model are made single-valued as required on physical grounds. It is furthermore shown that the centrifugal acceleration generated by rotations of the principal axes of the Reynolds stress tensor can make the second derivative singular at the most extreme limits of realizable turbulence. This previously overlooked effect appears to make it impossible to identically satisfy the strong form of realizability in any version of the present generation of second-order closures. On the other hand, models properly formulated to satisfy the weak form of realizability - wherein states of one or two component turbulence are not accessible in finite time are found to be realizable. However, unlike the simpler and more commonly used second order closures, these models can be ill-behaved near the extreme limits of realizable turbulence due to the way that higher-degree nonlinearities are often unnecessarily introduced to satisfy realizability. Illustrative computations of homogeneous shear flows are presented to demonstrate these points which can have important implications for turbulence modeling. Author

N94-21880*# Institute for Computer Applications in Science and Engineering, Hampton, VA.
COMPUTATION OF THE SOUND GENERATED BY ISOTROPIC TURBULENCE
S. Sarkar (California Univ., San Diego.) and M. Y. Hussaini (National Aeronautics and Space Administration. Langley Research Center, Hampton, VA.) Oct. 1993 30 p
(Contract NAS1-19480; RTOP 505-90-52-01)
(NASA-CR-191543; ICASE-93-74; NAS 1.26:191543) Avail: CASI HC A03/MF A01

The acoustic radiation from isotropic turbulence is computed numerically. A hybrid direct numerical simulation approach which combines direct numerical simulation (DNS) of the turbulent flow with the Lighthill acoustic analogy is utilized. It is demonstrated that the hybrid DNS method is a feasible approach to the computation of sound generated by turbulent flows. The acoustic efficiency in the simulation of isotropic turbulence appears to be substantially less than that in subsonic jet experiments. The dominant frequency of the computed acoustic pressure is found to be somewhat larger than the dominant frequency of the energy-containing scales of motion. The acoustic power in the simulations is proportional to epsilon (M(sub t))(exp 5) where epsilon is the turbulent dissipation rate and M(sub t) is the turbulent Mach number. This is in agreement with the analytical result of Proudman (1952), but the constant of proportionality is smaller than the analytical result. Two different methods of computing the acoustic power from the DNS data bases yielded consistent results.
Author (revised)

N94-22027*# Eloret Corp., Palo Alto, CA.
THEORETICAL RESEARCH PROGRAM TO STUDY CHEMICAL REACTIONS IN AOTV BOW SHOCK TUBES Final Technical Report, 1 Nov. 1985 - 31 Aug. 1993

Peter R. Taylor 10 Dec. 1993 10 p
(Contract NCC2-371)
(NASA-CR-194710; NAS 1.26:194710) Avail: CASI HC A02/MF A01

The main focus was the development, implementation, and calibration of methods for performing molecular electronic structure calculations to high accuracy. These various methods were then applied to a number of chemical reactions and species of interest to NASA, notably in the area of combustion chemistry. Among the development work undertaken was a collaborative effort to develop a program to efficiently predict molecular structures and vibrational frequencies using energy derivatives. Another major development effort involved the design of new atomic basis sets for use in chemical studies: these sets were considerably more accurate than those previously in use. Much effort was also devoted to calibrating methods for computing accurate molecular wave functions, including the first reliable calibrations for realistic molecules using full CI results. A wide variety of application calculations were undertaken. One area of interest was the spectroscopy and thermochemistry of small molecules, including establishing small molecule binding energies to an accuracy rivaling, or even on occasion surpassing, the experiment. Such binding energies are essential input to modeling chemical reaction processes, such as combustion. Studies of large molecules and processes important in both hydrogen and hydrocarbon combustion chemistry were also carried out. Finally, some effort was devoted to the structure and spectroscopy of small metal clusters, with applications to materials science problems. Author (revised)

N94-22269# General Electric Co., Schenectady, NY. Atomic Power Lab.
MEASUREMENT OF THERMAL-HYDRAULIC PARAMETERS IN TWO-PHASE FLOW USING FLOW VISUALIZATION IMAGE ANALYSIS
T. A. Trabold Nov. 1992 65 p
(Contract DE-AC12-76SN-00052)
(DE93-006255; KAPL-4739) Avail: CASI HC A04/MF A01

Continued advances in thermal-hydraulic computer codes based on the two-fluid model formulation depend upon empirically derived constitutive relations that describe the two-phase flow field structure. A nonintrusive measurement technique, Flow Visualization Image Analysis (FVIA), has been developed to acquire some of the necessary data in test sections with visual access. The technique essentially consists of extracting quantitative information from digitized images of gas/liquid flow fields. The results of air/water experiments performed in a vertical 6.35-mm-thick duct indicate that full-field, transient, or time-averaged measurements of bubble size, shape factor, bubble number density, void fraction, and interfacial area concentration can be acquired using FVIA. Further studies are in progress to improve the associated spatial and temporal resolution, as well as to develop advanced illumination methods. NTIS

N94-22272 Institut des Hautes Etudes Scientifiques, Bures-sur-Yvette (France).
CANONICALLY COVARIANT FORMULATION OF LANDAU'S NEWTONIAN SUPERFLUID DYNAMICS
B. Carter (Centre National de la Recherche Scientifique, Meudon-Bellevue, France.) and I. M. Khalatnikov May 1993 31 p Limited Reproducibility: More than 20% of this document may be affected by microfiche quality
(PB93-221034; IHES/P/93/24) Avail: CASI HC A03

The classical Landau theory of perfect (i.e. conservative) two constituent superfluid dynamics in Newton spacetime is radically reformulated in a canonical presentation that helps to reveal symmetries and conservation properties (notably those of the thermal vorticity and helicity) that are obscured in the traditional treatment. This presentation uses a 4-dimensional terminology that is more concise and elegant than the traditional 3+1 description and that simplifies the description of transformation properties under the action of the Milne group (i.e. the nonlinear generalization of the Galilei group). NTIS

N94-22386# Science Applications International Corp., Albuquerque, NM.
F2D USERS MANUAL: A TWO-DIMENSIONAL COMPRESSIBLE GAS FLOW CODE
A. Suo-Anttila Aug. 1993 69 p Prepared for Sandia National Labs., Albuquerque, NM
(Contract DE-AC04-76DP-00789)
(DE94-000653; SAND-92-7343) Avail: CASI HC A04/MF A01

The F2D computer code is a general purpose, two-dimensional, fully compressible thermal-fluids code that models most of the phenomena found in situations of coupled fluid flow and heat transfer. The code solves momentum, continuity, gas-energy, and structure-energy equations using a predictor-corrector solution algorithm. The corrector step includes a Poisson pressure equation. The finite difference form of the equation is presented along with a description of input and output. Several example problems are included that demonstrate the applicability of the code in problems ranging from free fluid flow, shock tubes, and flow in heated porous media. DOE

N94-22417 Laval Univ. (Quebec).
MIXED FINITE ELEMENT AND FINITE VOLUME METHODS Ph.D. Thesis [METHODES D'ELEMENTS FINIS MIXTES ET VOLUMES FINIS]
Mohamed Farhloul Mar. 1991 148 p In FRENCH
(ISBN-0-315-63035-3; CTN-94-60884) Copyright Avail: Micromedia Ltd., Technical Information Centre, 240 Catherine Street, Suite 305, Ottawa, Ontario, K2P 2G8, Canada HC/MF

Two new mixed finite elements are presented, based on two mixed formulations of the Stokes problem in which the auxiliary variable sigma = grad u is introduced. For the two elements, it is attempted to reproduce a principal property of the finite volume method: local and consequently global conservation of mass and motion. This is done employing the Raviart-Thomas (1977) finite element as an approximation to certain unknowns of the problem. After elimination of certain variables in the algebraic equations generated by the approached problems, the same degrees of freedom for the two elements are obtained. Nevertheless, the two interpolations are different. The error estimates for the two elements are optimal. The second element has certain advantages over the first in the sense that the local conservation of motion and mass is assured by the second element, while for the first, a priori, only the mass is locally conserved. In addition, the generalization of the second element to higher degrees is immediate. The numerical results obtained (in the framework of incompressible Navier-Stokes equations) for the problems of the square cavity and flow across a step are entirely comparable with those existing in the literature. CISTI

N94-22556# Sandia National Labs., Albuquerque, NM.
COUPLING OF SMOOTH PARTICLE HYDRODYNAMICS WITH THE FINITE ELEMENT METHOD
S. W. Attaway, M. W. Heinstein, and J. W. Swegle 1993 10 p Presented at the IMPACT-4: Structural Mechanics in Reactor Technology Conference, Berlin, Germany, 23-24 Aug. 1993
(Contract DE-AC04-76DP-00789)
(DE93-019081; SAND-93-1806C; CONF-9308161-1) Avail: CASI HC A02/MF A01

A gridless numerical technique called smooth particle hydrodynamics (SPH) has been coupled to the transient dynamics finite element code, PRONTO. In this paper, a new weighted residual derivation for the SPH method will be presented, and the methods used to embed SPH within PRONTO will be outlined. Example SPH-PRONTO calculations will also be presented. One major difficulty associated with the Lagrangian finite element method is modeling materials with no shear strength; for example, gases, fluids and explosive bi-products. Typically these materials can be modeled for only a short time with a Lagrangian finite element code. Large distortions cause tangling of the mesh, which will eventually lead to numerical difficulties such as negative element area or 'bow tie' elements. Remeshing will allow the problem to continue for a short while, but the large distortions can prevent a complete analysis. Smooth particle hydrodynamics is a gridless Lagrangian technique. Requiring no mesh, SPH has the potential to model material fracture, large shear flows, and penetration. SPH computes the strain rate and the stress divergence based on the nearest neighbors of a particle, which are determined using an efficient particle sorting technique. Embedding the SPH method within PRONTO allows part of the problem to be modeled with quadrilateral finite elements while other parts are modeled with the gridless SPH method. SPH elements are coupled to the quadrilateral elements through a contact like algorithm. DOE

N94-22580 Toronto Univ. (Ontario). Dept. of Aerospace Science and Engineering.
ORTHOGONALIZATION METHOD FOR DETERMINATION OF BOUNDARY LAYER RECEPTIVITY COEFFICIENTS M.S. Thesis
Michele Susanne Titcombe 1993 103 p

(ISBN-0-315-83426-9; CTN-94-60954) Copyright Avail: Micromedia Ltd., Technical Information Centre, 240 Catherine Street, Suite 305, Ottawa, Ontario, K2P 2G8, Canada HC/MF

The determination of coupling coefficients is part of the receptivity problem, which is the study of the generation of instability waves in boundary layers. External disturbances such as free-stream acoustic waves couple with the instability waves and hence greatly affect laminar to turbulent transition. A semi-infinite flat plate in a viscous flow with an acoustic wave serving as an excitation is considered. The effects of compressibility are taken into account. The response of the boundary layer to external excitation consists of a forced response plus an intrinsic response in the form of an eigenfunction expression whose coefficients are termed coupling coefficients. A method is described for determining coupling coefficients by comparing the superposition of the forced and intrinsic responses. The intrinsic response, in the form of an asymptotic expansion, is orthogonalized using the Gram-Schmidt process to produce an orthogonal base. The coefficients can then be extracted with the numerical solution to the flow re-expanded in terms of the original base. Author (CISTI)

N94-20080# Von Karman Inst. for Fluid Dynamics, Rhode-Saint-Genese (Belgium).
THREE DIMENSIONAL UNSTEADY FLOW CALCULATIONS IN RADIAL COMPONENTS
A. Fatsis *In its* Spacecraft Propulsion 1993 53 p (For primary document see N94-20068 05-20)
Copyright Avail: CASI HC A04/MF A04

N94-21466*# Colorado Univ., Colorado Springs. Computational Mathematics Group.
FLOW TRANSITION WITH 2-D ROUGHNESS ELEMENTS IN A 3-D CHANNEL
Zhining Liu, Chaoquin Liu, and Stephen F. McCormick *In* NASA. Langley Research Center, The Sixth Copper Mountain Conference on Multigrid Methods, Part 2 Nov. 1993 p 377-391 (For primary document see N94-21464 05-64)
(Contract NAS1-19312)
Avail: CASI HC A03/MF A03

N94-21471*# National Aeronautics and Space Administration. Langley Research Center, Hampton, VA.
LOOKING FOR O(N) NAVIER-STOKES SOLUTIONS ON NON-STRUCTURED MESHES
Eric Morano and Alain Dervieux (Institut National de Recherche d'Informatique et d'Automatique, Valbonne, France.) *In its* The Sixth Copper Mountain Conference on Multigrid Methods, Part 2 Nov. 1993 p 449-463 See also N94-11277 Sponsored in part by DRET Group 6, INRIA and ICASE (For primary document see N94-21464 05-64)
Avail: CASI HC A03/MF A03

N94-21480*# National Aeronautics and Space Administration. Goddard Space Flight Center, Greenbelt, MD.
A SEMI-LAGRANGIAN APPROACH TO THE SHALLOW WATER EQUATION
J. R. Bates, Stephen F. McCormick (Colorado Univ., Boulder.), John Ruge (Colorado Univ., Boulder.), David S. Sholl (Colorado Univ., Boulder.), and Irad Yavneh (National Center for Atmospheric Research, Boulder, CO.) *In* NASA. Langley Research Center, The Sixth Copper Mountain Conference on Multigrid Methods, Part 2 Nov. 1993 p 593-604 (For primary document see N94-21464 05-64)
Avail: CASI HC A03/MF A03

N94-21481*# National Aeronautics and Space Administration. Lewis Research Center, Cleveland, OH.
MULTIGRID SOLUTION OF THE NAVIER-STOKES EQUATIONS ON HIGHLY STRETCHED GRIDS WITH DEFECT CORRECTION
Peter M. Sockol *In* NASA. Langley Research Center, The Sixth Copper Mountain Conference on Multigrid Methods, Part 2 Nov. 1993 p 605-619 (For primary document see N94-21464 05-64)
Avail: CASI HC A03/MF A03

N94-21485*# National Aeronautics and Space Administration. Langley Research Center, Hampton, VA.
MULTIGRID PROPERTIES OF UPWIND-BIASED DATA RECONSTRUCTIONS
Gary P. Warren and Thomas W. Roberts *In its* The Sixth Copper Mountain Conference on Multigrid Methods, Part 2 Nov. 1993 p 663-677 (For primary document see N94-21464 05-64)
Avail: CASI HC A03/MF A03

N94-21487*# Technische Hogeschool, Delft (Netherlands). Faculty of Technical Mathematics and Informatics.
NUMERICAL STUDY OF A MULTIGRID METHOD WITH FOUR SMOOTHING METHODS FOR THE INCOMPRESSIBLE NAVIER-STOKES EQUATIONS IN GENERAL COORDINATES
S. Zeng and P. Wesseling *In* NASA. Langley Research Center, The Sixth Copper Mountain Conference on Multigrid Methods, Part 2 Nov. 1993 p 691-708 (For primary document see N94-21464 05-64)
Avail: CASI HC A03/MF A03

35 INSTRUMENTATION AND PHOTOGRAPHY

Includes remote sensors; measuring instruments and gages; detectors; cameras and photographic supplies; and holography.

For aerial photography see *43 Earth Resources and Remote Sensing*. For related information see also *06 Aircraft Instrumentation*, and *19 Spacecraft Instrumentation*.

N94-19837 Aeronautical Research Labs., Melbourne (Australia).
AN ASSESSMENT OF COMSCAN, A COMPTON BACKSCATTER IMAGING CAMERA, FOR THE ONE-SIDED NON-DESTRUCTIVE INSPECTION OF AEROSPACE COMPONENTS
L. Sponder Jul. 1993 42 p Limited Reproducibility: More than 20% of this document may be affected by microfiche quality
(AD-A271331; ARL-TR-34; DODA-AR-008-346) Avail: CASI HC A03

This report presents some results obtained using a Compton backscatter imaging camera, developed by Philips Industries, which were obtained during a visit to the Defense Research Establishment Pacific (DREP) during May/June 1992. Compton backscatter imaging is an X-ray technique which can be used to non-destructively inspect the interior of both metallic and non-metallic structures and, unlike conventional X-ray methods, requires access to only one side of the part being inspected. DTIC

N94-19882 Department of the Navy, Washington, DC.
ELECTRODE ARRAY ELECTROMAGNETIC VELOCIMETER Patent Application
Rolf G. Kasper, inventor (to Navy) and Lee S. Langston, inventor (to Navy) 18 Mar. 1993 20 p Limited Reproducibility: More than 20% of this document may be affected by microfiche quality
(AD-D015950; US-Patent-Appl-SN-038598; Navy-Case-73185) Avail: CASI HC A03

A velocimeter for measuring the velocity field characteristics of a conductive fluid moving over a surface is provided. A magnet has a central axis that is aligned with a direction of fluid movement of interest such that a plurality of magnetic flux lines extend generally normal from the surface. A plurality of electrode pairs provide electrical output signals that are proportional to variations in the magnetic flux lines as the conductive fluid flows there-through in accordance with Lorentz forces. Each electrode pair is disposed symmetrically about the central axis of the magnet. The plurality of electrodes are mounted in a fixed relation with the magnet. The electrical output signals from the electrode pairs are processed and displayed as the velocity field characteristics of the fluid in the direction of interest. DTIC

N94-19920* Massachusetts Inst. of Tech., Cambridge. Artificial Intelligence Lab.
ROBUST PHOTO-TOPOGRAPHY BY FUSING SHAPE-FROM-SHADING AND STEREO
Clay M. Thompson Feb. 1993 171 p Limited Reproducibility: More than 20% of this document may be affected by microfiche quality
(Contracts NAS5-31352; N00014-91-J-4038)

(NASA-CR-194697; NAS 1.26:194697; AD-A270885; AI-TR-1411) Avail: CASI HC A08

Methods for fusing two computer vision methods are discussed and several example algorithms are presented to illustrate the variational method of fusing algorithms. The example algorithms solve the photo-topography problem; that is, the algorithms seek to determine planet topography given two images taken from two different locations with two different lighting conditions. The algorithms each employ a single cost function that combines the computer vision methods of shape-from-shading and stereo in different ways. The algorithms are closely coupled and take into account all the constraints of the phototopography problem. One such algorithm, the z-only algorithm, can accurately and robustly estimate the height of a surface from two given images. Results of running the algorithms on four synthetic test image sets of varying difficulty are presented. DTIC

N94-19987# Fermi National Accelerator Lab., Batavia, IL.
THERMAL INFORMATION REGARDING THE COOLDOWN AND OPERATION OF LIQUID ARGON CALORIMETERS
R. A. Rucinski, W. E. Cooper, K. D. Dixon, K. J. Krempetz, G. T. Mulholland, K. Primdahl, and J. B. Urbin Jul. 1993 10 p Presented at the International Cryogenic Engineering Conference and International Cryogenic Materials Conference, Albuquerque, NM, 12-16 Jul. 1993
(Contract DE-AC02-76CH-03000)
(DE93-019391; FNAL/C-93/222; CONF-930703-22) Avail: CASI HC A02/MF A01

Three liquid argon calorimeters were cooled down and operated as part of the D-Zero detector at Fermi National Accelerator laboratory. The largest vessel contains 248 metric tons of uranium and copper plates and 19 kL (5000 gal.) of liquid argon. The other two vessels are mirror images, each containing 185 metric tons of uranium and stainless steel plates and 12.1 kL (3200 gal.) of liquid argon. The cool down was accomplished by convection heat transfer between boiling liquid nitrogen filled finned heat exchangers and argon gas inside the vessels. Information regarding the general internal geometry of the calorimeters, cool down, operation, and steady state heat loads will be presented. DOE

N94-19990# Argonne National Lab., IL.
A CONCEPTUAL DESIGN FOR THE STAR ENDCAP ELECTROMAGNETIC CALORIMETER
E. Bielick, T. Fornek, H. Spinka, and D. G. Underwood Aug. 1993 49 p
(Contract W-31-109-eng-38)
(DE93-040801; ANL-HEP-TR-93-62) Avail: CASI HC A03/MF A01

In order to make measurements of the gluon spin or helicity distribution in the proton or the gluon spin average distribution in nuclei, both a barrel and an endcap electromagnetic calorimeter must be added to the STAR baseline detector. Information on the gluon will be obtained in inclusive direct-(gamma) + jet and jet + jet production. In order to be sensitive to the proper gluon kinematic regions, either the direct-(gamma) or the jet must be in the endcap electromagnetic calorimeter (EMC). However, the endcap EMC is not large enough to completely contain the jets, so that the barrel EMC is also needed. A conceptual design for the STAR endcap EMC is described. Constraints are imposed by the space available between the end of the time projection chamber (TPC) and the inside of the magnet pole tip iron. Severe constraints also occur near the absolute value of eta = 1, where the barrel and endcap EMC's meet. Cables from detectors inside the EMC, including those from the TPC, will exit from STAR near the absolute value of eta = 1. The constraints in this region have not yet been seriously studied since no decision on the detailed routing of these cables was available at the time this work was being done. Details of the conceptual design, analytical and finite element calculations of stresses in various structural members for the endcap EMC, and a preliminary cost estimate are included. DOE

N94-20114# Los Alamos National Lab., NM.
TECHNIQUES FOR REDUCING ERROR IN THE CALORIMETRIC MEASUREMENT OF LOW WATTAGE ITEMS
W. A. Sedlacek, S. S. Hildner, K. L. Camp, and T. L. Cremers 1993 4 p Presented at the 34th Annual Meeting of the Institute of Nuclear Materials Management, Scottsdale, AZ, 18-21 Jul. 1993
(Contract W-7405-eng-36)
(DE93-018472; LA-UR-93-2638; CONF-930749-59) Avail: CASI HC A01/MF A01

The increased need for the measurement of low wattage items with production calorimeters has required the development of techniques to maximize the precision and accuracy of the calorimeter measurements. An error model for calorimetry measurements is presented. This model is used as a basis for optimizing calorimetry measurements through baseline interpolation. The method was applied to the heat measurement of over 100 items and the results compared to chemistry assay and mass spectroscopy. DOE

N94-20115# Los Alamos National Lab., NM.
CALORIMETER MEASUREMENTS OF LOW WATTAGE ITEMS
T. L. Cremers, K. L. Camp, S. S. Hildner, and W. A. Sedlacek 1993 4 p Presented at the 34th Annual Meeting of the Inst. of Nuclear Materials Management, Scottsdale, AZ, 18-21 Jul. 1993
(Contract W-7405-eng-36)
(DE93-018473; LA-UR-93-2637; CONF-930749-58) Avail: CASI HC A01/MF A01

The transition of DOE facilities from production to decontamination and decommissioning has led to more measurements of waste, scrap, and other less attractive materials. The difficulty that these materials pose for segmented gamma scanning and neutron counting has increased the use of calorimetric assay for very low wattage items (less than 250 milliwatts). The authors have measured well characterized Pu-238 oxide ranging in wattage from 25 to 500 milliwatts in the calorimeters at the Los Alamos Plutonium Facility and report the error and the precision of the measurements. DOE

N94-20203# Naval Air Warfare Center, Patuxent River, MD. Aircraft Div.
ROTORWASH WIND SENSOR EVALUATION Final Report
Curtis L. Meyerhoff, Robert E. Lake, and Dennis N. Gordge Aug. 1993 30 p Original contains color illustrations
(Contract DTFA01-92-Y-02017)
(AD-A268987; DOT/FAA/RD-93/10) Avail: CASI HC A03/MF A01

This project's purpose was to assess and document the ability of the Qualimetrics, Inc. model 2132 wind sensor (a cup and vane type sensor) to measure a rotor wash flow field as compared to the TSI, Inc. model 204D ion beam deflection sensor. The tests concentrated on the sensor's ability to capture dynamic characteristics of a helicopter rotor wash flow field. The project was conducted from April to November 1992 and consisted of quantitative laboratory and field testing. The laboratory testing included 9.5 hours of wind tunnel test time, subjecting each sensor to three step input tests at velocities of 20 knots, 50 knots, and 80 knots. Field test data were collected during one hour of SH-60B helicopter hover time at heights of 15 and 25 feet above ground level at distances of 35 and 70 feet from the wind sensors. Aircraft gross weights ranged between 19,600 and 20,500 pounds. All field test data were obtained in ambient wind conditions of approximately 8 knots at 40 degrees relative to the aircraft nose, -40 feet pressure altitude in an ambient temperature of 85 F. Laboratory data analysis indicates the model 2132 cup and vane sensor's time constant values were significantly higher than those of the model 204D ion beam sensor and varied relative to wind tunnel velocity settings. This indicates the model 2132 sensor's ability to accurately capture oscillations in a dynamic flow field is significantly less than the model 204D sensor. The model 2132 sensor did detect periodic or pulsating velocity magnitudes, but failed to capture significant oscillations as compared to the model 204D sensor. Comparative analysis of all field test event data indicate the model 2132 sensor only detected frequencies below 1.5 Hz and only captured an average of 46 percent of the model 204D sensor's maximum amplitude pulse values that were below 1.5 Hz. The model 2132 sensor's inability to capture many of the maximum pulse amplitudes is evidence of the sensor's limited capability to capture velocity magnitude variations in a dynamic flow field. The model 2132 cup and vane sensor's average and minimum velocities for each test event were significantly higher than the model 204D ion beam sensor's values. This is additional evidence that the model 2132 sensor is slower to respond to rapid changes in a dynamic flow field. Compared to the TSI, Inc. model 204D ion beam sensor, the Qualimetrics, Inc. model 2132 cup and vane sensor failed to measure accurately a rotorwash flow field in terms of frequency, amplitude, frequency content, and velocity magnitude and thus is not recommended for helicopter rotorwash velocity data collection. Author

N94-20287# Los Alamos National Lab., NM.
MULTIPORT SOLID-STATE IMAGER CHARACTERIZATION AT VARIABLE PIXEL RATES
G. J. Yates, K. A. Albright, and B. T. Turko (California Univ., Berkeley. Lawrence Berkeley Lab.) 1993 19 p Presented at the Annual Meeting of the Society of Photo-Optical Instrumentation Engineers, San Diego, CA, 11-16 Jul. 1993
(Contract W-7405-eng-36)
(DE93-018366; LA-UR-93-2545; CONF-930722-18) Avail: CASI HC A03/MF A01

The imaging performance of an 8-port Full Frame Transfer Charge Coupled Device (FFT CCD) as a function of several parameters including pixel clock rate is presented. The device, model CCD-13, manufactured by English Electric Valve (EEV) is a 512 times 512 pixel array designed with four individual programmable bidirectional serial registers and eight output amplifiers permitting simultaneous readout of eight segments (128 horizontal times 256 vertical pixels) of the array. The imager was evaluated in Los Alamos National Laboratory's High-Speed Solid-State Imager Test Station at true pixel rates as high as 50 MHz for effective imager pixel rates approaching 400 MHz from multiporting. Key response characteristics measured include absolute responsivity, Charge-Transfer-Efficiency (CTE), dynamic range, resolution, signal-to-noise ratio, and electronic and optical crosstalk among the eight video channels. Preliminary test results and data obtained from the CCD-13 will be presented and the versatility/capabilities of the test station will be reviewed. DOE

N94-20297# Sandia National Labs., Albuquerque, NM.
DEVELOPMENT AND CHARACTERIZATION OF A TIME-, POSITION- AND ENERGY-RESOLVED X RAY DIAGNOSTIC FOR PBFA 2 TARGET EXPERIMENTS
M. S. Derzon, A. B. Filuk, J. Pantuso, R. J. Dukart, R. Olsen (EG and G Energy Measurements, Inc., Albuquerque, NM.), T. Barber (Ktech Corp., Albuquerque, NM.), and M. Bernard (Ktech Corp., Albuquerque, NM.) 1992 12 p Presented at the Annual Meeting of the Society of Photo-Optical Instrumentation Engineers (SPIE), San Diego, CA, 11-16 Jul. 1993
(Contract DE-AC04-76DP-00789)
(DE93-019429; SAND-92-2754C; CONF-930722-24) Avail: CASI HC A03/MF A01

A time-, position-, and energy-resolved soft x-ray (100-500 eV) diagnostic is being developed for PBFA 2 target experiments. The diagnostic provides measurements of hydrodynamic motion and thermal gradients in light-ion fusion targets. A slit-image of the source is imprinted onto thin sheets (20 microns) of organic scintillator to create a one-dimensional image. The scintillator light is then proximity-coupled to a linear array of fiber-optics that transports the light to a streak camera that is operated without an intensifier. The streak camera output is recorded on a charge-coupled-device (CCD) camera. We are characterizing the spatial and temporal resolutions of the systems. This is done by collecting data from as many as 90 individual fibers and correcting for variations in throughput and the effects of spatial resolution to roughly 5% standard deviation in their relative throughput. Spatial resolution of these systems at the source is approximately 0.4 mm. Timing resolution is nominally 2 ns and it is limited primarily by the scintillator response and dispersion in the 50-m-long fiber array. We describe the measurement techniques and the results of the characterization. DOE

N94-20930 Army Research Lab., Aberdeen Proving Ground, MD.
MULTISENSOR PINHOLE YAWSONDE Final Report, 1 Aug. - 30 Sep. 1990
Eugene M. Ferguson, David J. Hepner, and Wallace H. Clay Sep. 1993 29 p Limited Reproducibility: More than 20% of this document may be affected by microfiche quality
(DA Proj. 1L1-62618-AH-80)
(AD-A271715; ARL-TR-213) Avail: CASI HC A03

The yawsonde is a device used at the U.S. Army Research Laboratory (ARL) to investigate the in-flight behavior of spinning projectiles. The standard yawsonde consists of a pair of solar cells and slits that respond to solar rays. The sun is used as an inertial reference to measure the pitching and yawing motions of the projectile. An FM telemetry package transmits the sensor data to a ground receiving station for analysis. The standard yawsonde package is housed in an M577-type artillery fuse body. The spinning motion of the projectile serves as the sampling rate for the measurements. When the spin rate is not significantly higher than the yaw rate, multiple sets of sensors must be used to effectively increase the sampling rate. The multiple-sensor pinhole yawsonde was developed for projectiles that require multiple sets of sensors in a very limited space. This pinhole yawsonde consists of a number of sensors located behind pinholes placed around the projectile's circumference. Since each pinhole makes a yaw measurement, many measurements, or samples, are taken with each projectile spin revolution. More pinhole sensors may be added to increase the measurement sampling rate. One application of this yawsonde is to aid in evaluating the performance of tactical devices and inertial systems onboard projectiles with limited space for instrumentation. DTIC

N94-21167# Massachusetts Inst. of Tech., Cambridge. Artificial Intelligence Lab.
INTERNAL CAMERA CALIBRATION USING ROTATION AND GEOMETRIC SHAPES
Gideon P. Stein Feb. 1993 50 p
(Contract N00014-91-J-4038)
(AD-A272718; MIT-AI-TR-1426) Avail: CASI HC A03/MF A01

This paper describes a simple method for internal camera calibration for computer vision systems. It is intended for use with medium to wide angle camera lenses. With modification it can be used for longer focal lengths. This method is based on tracking image features through a sequence of images while the camera undergoes pure rotation. This method does not require a special calibration object. The location of the features relative to the camera or to each other need not be known. It is only required that the features can be located accurately in the image. This method can be used both for laboratory calibration and for self-calibration in autonomous robots working in unstructured environments. The method works when features can be located to single pixel accuracy, but subpixel accuracy should be used if available. DTIC

N94-21278 Department of the Navy, Washington, DC.
RECORDING SYSTEM USING MULTIPLEXED INPUTS TO A MULTICHANNEL RECORDER Patent
David M. Deveau, inventor (to Navy) and Victor A. Andersen, inventor (to Navy) 28 Sep. 1993 13 p Filed 7 Oct. 1991
(AD-D015971; US-Patent-5,249,085; US-Patent-Appl-SN-772186; US-Patent-Class-360-32) Avail: US Patent and Trademark Office

A system, or applique apparatus, for recording and reproducing large numbers of electrical signals on input channel limited recording devices is described. It is accomplished by time sequencing groups of pluralities of separate input signals to a plurality of recording units within a recorder, wherein each recording unit handles a separate group of input signals. The time sequence is provided by a multiplexer controller and is common to each group. The plurality of recording units after recording the signals provide them in the groups in which they were received to respective demultiplexers. A demultiplex controller that receives 2 timing signals from the multiplex controller via the recorder supplies timing signals to the plurality of demultiplexers for reconstruction of the original input signals. DTIC

N94-21441# California Univ., Berkeley. Lawrence Berkeley Lab.
DIFFRACTION AND HOLOGRAPHY OF PHOTOELECTRONS AND FLUORESCENT X RAYS
C. S. Fadley Apr. 1993 19 p Presented at the Spring Meeting of the Materials Research Society, San Francisco, CA, 12-16 Apr. 1993
(Contract DE-AC03-76SF-00098)
(DE93-019240; LBL-34374; CONF-930405-36) Avail: CASI HC A03/MF A01

Photoelectron diffraction is by now a powerful technique for studying surface structures, with special capabilities for resolving chemical and magnetic states of atoms and deriving direct structural information from both forward scattering and backscattering. Fitting experiment to theory can lead to structural accuracies in the 0.03 Angstrom range. Holographic inversions of such diffraction data also show considerable promise for deriving local three-dimensional structures around a given emitter with accuracies of 0.2-0.3 Angstrom. Resolving the photoelectron spin in some way and using circularly polarized radiation for excitation provide added dimensions for the study of magnetic systems and chiral experimental geometries. Synchrotron radiation with the highest brightness and energy

resolution, as well as variable polarization, is crucial to the full exploitation of these techniques. X-ray fluorescence holography also has promise for structural studies, but will require intense excitation sources and multichannel detection to be feasible. DOE

N94-21445# Carnegie-Mellon Univ., Pittsburgh, PA. Dept. of Computer Science.

EXPERIMENTS IN KNOWLEDGE REFINEMENT FOR A LARGE RULE-BASED SYSTEM

Wilson A. Harvey, Jr. and Milind Tambe Aug. 1993 16 p

(Contracts DACA76-92-C-0036; F49620-92-J-0318)

(AD-A272055; CMU-CS-93-195) Avail: CASI HC A03/MF A01

Knowledge-refinement is a central problem in the field of expert systems. For rule-based systems, refinement implies the addition, deletion, and modification of rules in the system so as to improve the system's overall performance. The goal of this research effort is to understand the methodology for refining large rule-based systems, as well as to develop tools that will be useful in refining such systems. The vehicle for our investigation is SPAM, a production system (rule-based system) for the interpretation of aerial imagery. Complex and computation-intensive systems like SPAM impose some unique constraints on knowledge refinement. More specifically, the credit/blame assignment problem for locating pieces of knowledge to refine becomes difficult. Given that constraint, we approach the problem in a bottom-up fashion, i.e., begin by refining portions of SPAM's knowledge base and then attempt to understand the interactions between them. We begin by identifying gaps and/or faults in the knowledge base by comparing SPAM's intermediate output to that of an expert, then modifying the knowledge base so that the system's output more accurately matches the expert's output. While this approach leads to some improvements, it also raises some interesting issues concerning the evaluation of refined knowledge at intermediate levels and of interaction between the refinements. This paper presents our initial efforts toward addressing these issues. DTIC

N94-21508# Aberdeen Proving Ground, MD. Edgewood Research Development and Engineering Center.

MIRROR VELOCITY SAMPLING ERRORS IN A MICHELSON INTERFEROMETER Final Report, Jun. 1992 - May 1993

R. J. Combs, R. B. Knapp, and P. E. Field Sep. 1993 43 p

(AD-A273105; ERDEC-TR-106) Avail: CASI HC A03/MF A01

Mirror velocity variations in a continuous mirror drive Michelson interferometer result in erroneous interferogram sampling. The effects of systematic and random mirror fluctuations are evaluated. Four methods of evaluation provide a means to quantify the importance of mirror velocity errors in the Fourier spectrometer's performance as a spectroradiometer. The four methods are time interval signal analysis, sine wave test, optical chopper modulation, and examination of consecutive interferograms. Examination of consecutive interferograms includes the monitoring of a constant blackbody infrared radiation source as well as an interposed ammonia sample cell for wavenumber axis registration. Each method furnishes a known input to the interferometer modulation equation (i.e., 2tm = f) and permits an internal validation of the interferometer mirror velocity evaluation results. DTIC

N94-21545# California Univ., Berkeley. Lawrence Berkeley Lab.

THE ENERGY PERFORMANCE OF PROTOTYPE HOLOGRAPHIC GLAZINGS

K. Papamichael, L. Beltran, R. Furler, E. S. Lee, S. Selkowitz, and M. Rubin Feb. 1993 28 p

(Contract DE-AC03-76SF-00098)

(DE93-040451; LBL-34367) Avail: CASI HC A03/MF A01

We report on the simulation of the energy performance of prototype holographic glazings in commercial office buildings in a California climate. These prototype glazings, installed above conventional side windows, are designed to diffract the transmitted solar radiation and reflect it off the ceiling, providing adequate daylight illumination for typical office tasks up to 10m from the window. In this study, we experimentally determined a comprehensive set of solar-optical properties and characterized the contribution of the prototype holographic glazings to workplane illuminance in a scale model of a typical office space. We then used the scale model measurements to simulate the energy performance of the holographic glazings over the course of an entire year for four window orientations (North, East, South and West) for the inland Los Angeles climate, using the DOE-2.ID building energy analysis computer program. The results of our experimental analyses indicate that these prototype holographic glazings diffract only a small fraction of the incident light. The results of this study indicate that these prototype holographic glazings will not save energy in commercial office buildings. Their performance is very similar to that of clear glass, which, through side windows, cannot efficiently illuminate more than a 4-6 m depth of a building's perimeter, because the cooling penalties due to solar heat gain are greater than the electric lighting savings due to daylighting. DOE

N94-21556# Sandia National Labs., Albuquerque, NM.

INITIAL LABORATORY EVALUATION OF COLOR VIDEO CAMERAS, PHASE 2

P. L. Terry Jul. 1993 51 p

(Contract DE-AC04-76DP-00789)

(DE93-040201; SAND-91-2579/2) Avail: CASI HC A04/MF A01

Sandia National Laboratories has considerable experience with monochrome video cameras used in alarm assessment video systems. Most of these systems, used for perimeter protection, were designed to classify rather than to identify intruders. The monochrome cameras were selected over color cameras because they have greater sensitivity and resolution. There is a growing interest in the identification function of security video systems for both access control and insider protection. Because color camera technology is rapidly changing and because color information is useful for identification purposes, Sandia National Laboratories has established an on-going program to evaluate the newest color solid-state cameras. Phase 1 of the Sandia program resulted in the SAND91-2579/1 report titled: Initial Laboratory Evaluation of Color Video Cameras. The report briefly discusses imager chips, color cameras, and monitors, describes the camera selection, details traditional test parameters and procedures, and gives the results reached by evaluating 12 cameras. In Phase 2 of the report, six additional cameras using traditional methods were tested. In addition, all 18 cameras were tested by newly developed methods. This Phase 2 report details those newly developed test parameters and procedures, and evaluates the results. DOE

N94-21607*# Physical Sciences, Inc., Andover, MA.

INSTANTANEOUS VELOCITY FIELD IMAGING INSTRUMENT FOR SUPERSONIC REACTING FLOWS Final Report

M. G. Allen, S. J. Davis, W. J. Kessler, H. H. Legner, K. R. McManus, P. A. Mulhall, T. E. Parker, and D. M. Sonnenfroh Cleveland, OH NASA Sep. 1993 101 p Original contains color illustrations

(Contract NAS3-26254; RTOP 324-02-00)

(NASA-CR-191162; E-8131; NAS 1.26:191162) Avail: CASI HC A06/MF A02; 2 functional color pages

The technical tasks conducted to develop and demonstrate a new gas velocity measurement technique for high enthalpy reacting flows is described. The technique is based on Doppler-shifted Planar Laser-induced Fluorescence (PLIF) imaging of the OH radical. The imaging approach permits, in principle, single-shot measurements of the 2-D distribution of a single velocity component in the measurement plane, and is thus a technique of choice for applications in high enthalpy transient flow facilities. In contrast to previous work in this area, the present program demonstrated an approach which modified the diagnostic technique to function under the constraints of practical flow conditions of engineering interest, rather than vice-versa. In order to accomplish the experimental demonstrations, the state-of-the-art in PLIF diagnostic techniques was advanced in several ways. Each of these tasks is described in detail and is intended to serve as a reference in supporting the transition of this new capability to the fielded PLIF instruments now installed at several national test facilities. Among the new results of general interest in LIF-based flow diagnostics, a detailed set of the first measurements of the collisional broadening and shifting behavior of OH (1,0) band transitions in H7-air combustion environments is included. Such measurements are critical in the design of a successful strategy for PLIF velocity imaging; they also relate to accurate concentration and temperature measurements, particularly in compressible flow regimes. Furthermore, the results shed new light on the fundamental relationship between broadening and energy transfer collisions in OH A(sup 2)Sigma(+)v(sup ') = 1. The first single-pulse, spectrally-resolved measurements of the output of common pulsed dye lasers were also produced during the course of this effort. As with the OH broadening

measurements, these data are a significant aspect of a successful velocity imaging strategy, and also have potential implications for many other LIF measurement techniques. Our results indicated the need to modify the commercially available laser cavity in order to accommodate the constraints imposed by typical SCRAMJET combustion characteristics as well as to increase the instrument's velocity dynamic range to span an intra-image range in excess of 2 km/s. The various technical efforts were brought together in a series of experiments demonstrating the applicability of the technique in a high pressure, high temperature H2-air combustion system. The resultant images were compared with 2-D flow simulations in order to determine the accuracy of the instrument. Mean velocity imaging in flows with an axis of symmetry was demonstrated with an accuracy of +/- 50 m/s out of an intra-image dynamic range of 1600 m/s, including reversed flow. A more complex configuration amenable to single-shot imaging in flows without an axis of symmetry was also demonstrated. Limitations imposed by available equipment resulted in an accuracy of about +/- 200 m/s out of 1750 m/s in these demonstrations. Minor modifications to the present configuration were suggested to improve this performance. Each technical task is described in detail, along with significance of the results for the overall imaging velocimeter configuration. This report should allow the user community to integrate this new measurement capability in their existing instrumentation platforms. Author (revised)

N94-21876*# Hawaii Univ., Honolulu. Inst. for Astronomy.
SOLAR IMAGING VECTOR MAGNETOGRAPH Final Technical Report, 1 Aug. 1988 - 31 Jul. 1993
Richard C. Canfield 15 Dec. 1993 7 p
(Grant NAGw-1454)
(NASA-CR-194729; NAS 1.26:194729) Avail: CASI HC A02/MF A01

This report describes an instrument which has been constructed at the University of Hawaii to make observations of the magnetic field in solar active regions. Detailed knowledge of active region magnetic structures is crucial to understanding many solar phenomena, because the magnetic field both defines the morphology of structures seen in the solar atmosphere and is the apparent energy source for solar flares. The new vector magnetograph was conceived in response to a perceived discrepancy between the capabilities of X ray imaging telescopes to be operating during the current solar maximum and those of existing magnetographs. There were no space-based magnetographs planned for this period; the existing ground-based instruments variously suffered from lack of sensitivity, poor time resolution, inadequate spatial resolution or unreliable sites. Yet the studies of flares and their relationship to the solar corona planned for the 1991-1994 maximum absolutely required high quality vector magnetic field measurements. By 'vector' measurements we mean that the observation attempts to deduce the complete strength and direction of the field at the measurement site, rather than just the line of sight component as obtained by a traditional longitudinal magnetograph. Knowledge of the vector field permits one to calculate photospheric electric currents, which might play a part in heating the corona, and to calculate energy stored in coronal magnetic fields as the result of such currents. Information about the strength and direction of magnetic fields in the solar atmosphere can be obtained in a number of ways, but quantitative data is best obtained by observing Zeeman-effect polarization in solar spectral lines. The technique requires measuring the complete state of polarization at one or more wavelengths within a magnetically sensitive line of the solar spectrum. This measurement must be done for each independent spatial point for which one wants magnetic field data. All the measurements need to be done in a time short compared to the time scale for changes of the solar features being observed. Were it possible, one would want to record all the needed data simultaneously, since temporal variation of atmospheric seeing degrades both the image and the polarization sensitivity. Since the measurements must span four dimensions, two spatial plus polarization and wavelength, we had some freedom to design the instrument to favor some dimensions over others in terms of simultaneity. Our earlier instrument, the Haleakala Stokes Polarimeter, records a range of wavelengths spanning two spectral lines in each reading, but requires two seconds to determine the polarization state and obtains spatial information only by assembling a long sequence of measurements at single locations on the sun. The new instrument sacrifices spectral detail and accuracy in favor of greatly improved imaging characteristics. The scientific goals for this instrument were to measure surface magnetic fields with enough accuracy to permit calculations of photospheric currents, but with a field of view covering an entire typical active region, high spatial resolution, and a fast enough temporal cadence for detecting flare-associated changes in magnetic structures.
Derived from text

N94-21950# Lawrence Livermore National Lab., CA.
PHOTOELECTRON HOLOGRAPHY OF PLATINUM (111)
B. L. Petersen (California Univ., Berkeley. Lawrence Berkeley Lab.), L. J. Terminello, and J. J. Barton Apr. 1993 5 p Presented at the Spring Meeting of the Materials Research Society, San Francisco, CA, 12-16 Apr. 1993
(Contract W-7405-eng-48)
(DE93-040856; UCRL-JC-113802; CONF-930405-41) Avail: CASI HC A01/MF A01

Platinum atoms near a (111) single-crystal face have been imaged using photoelectron holography. Electron angular intensity patterns were collected at equally spaced wavenumbers from 6 to 12 A(exp -1). Images of atoms near expected atomic positions are obtained from single-wavenumber analyses over the range of the data set. Positions are detected further from the emitter than we have seen previously, and symmetry assumptions are not required. We have also adopted a three dimensional means of representing the data in order to help understand the results. Twin image suppression and artifact reduction in the holographically reconstructed data are set are obtained when images at different wavenumbers are correctly phase-summed. We are assessing the capability of the technique for rendering true three-dimensional structural information for unknown systems. DOE

N94-21953# Oak Ridge National Lab., TN.
OTDR STRAIN GAUGE FOR SMART SKINS
S. W. Kercel Sep. 1993 67 p
(Contract DE-AC05-84OR-21400)
(DE93-041043; ORNL/TM-12383) Avail: CASI HC A04/MF A01

Optical time-domain reflectometry (OTDR) is a simple and rugged technique for measuring quantities such as strain that affect the propagation of light in an optical fiber. For engineering applications of OTDR, it is important to know the repeatable limits of its performance. The author constructed an OTDR-based, submillimeter resolution strain measurement system from off-the-shelf components. The systems repeatably resolves changes in time of flight to within +/- 2 ps. Using a 1-m, single-mode fiber as a gauge and observing the time of flight between Fresnel reflections, a repeatable sensitivity of 400 microstrains was observed. Using the same fiber to connect the legs of a 3-dB directional coupler to form a loop, a repeatable sensitivity of 200 microstrains was observed. Realizable changes to the system that should improve the repeatable sensitivity to 20 microstrains or less are discussed. DOE

N94-22000# Sandia National Labs., Albuquerque, NM.
FLUORESCENT MICROTHERMOGRAPHIC IMAGING
D. L. Barton 1993 32 p Presented at the 1993 International Symposium on Testing and Failure Analysis, Los Angeles, CA, 15-19 Nov. 1993
(Contract DE-AC04-76DP-00789)
(DE93-040332; SAND-93-1874C; CONF-931191-3) Avail: CASI HC A03/MF A01

In the early days of microelectronics, design rules and feature sizes were large enough that sub-micron spatial resolution was not needed. Infrared or IR thermal techniques were available that calculated the object's temperature from infrared emission. There is a fundamental spatial resolution limitation dependent on the wavelengths of light being used in the image formation process. As the integrated circuit feature sizes began to shrink toward the one micron level, the limitations imposed on IR thermal systems became more pronounced. Something else was needed to overcome this limitation. Liquid crystals have been used with great success, but they lack the temperature measurement capabilities of other techniques. The fluorescent microthermographic imaging technique (FMI) was developed to meet this need. This technique offers better than 0.01 C temperature resolution and is diffraction limited to 0.3 mircron spatial resolution. While the temperature resolution is comparable to that available on IR systems, the spatial resolution is much better. The FMI technique provides better spatial resolution by using a temperature dependent fluorescent film that emits light at 612 nm instead of the 1.5 to 12 micron range used by IR techniques. This tutorial starts with a review of blackbody radiation physics,

the process by which all heated objects emit radiation to their surroundings, in order to understand the sources of information that are available to characterize an object's surface temperature. The processes used in infrared thermal imaging are then detailed to point out the limitations of the technique but also to contrast it with the FMI process. The FMI technique is then described in detail, starting with the fluorescent film physics and ending with a series of examples of past applications of FMI. DOE

N94-22391# Argonne National Lab., IL. Energy Systems Div.
EXPERIMENTAL EVALUATION OF OXYGEN-ENRICHED AIR AND EMULSIFIED FUELS IN A SIX-CYLINDER DIESEL ENGINE
R. R. Sekar, W. W. Marr, R. L. Cole, T. J. Marciniak, and D. E. Longman (AutoResearch Labs., Inc., Chicago, IL.) Jan. 1993 356 p
(Contract W-31-109-eng-38)
(DE94-000907; ANL/ESD/TM-53) Avail: CASI HC A16/MF A03

The objectives of this investigation are to (1) determine the technical feasibility of using oxygen-enriched air to increase the efficiency of and reduce emissions from diesel engines, (2) examine the effects of water-emulsified fuel on the formation of nitrogen oxides in oxygen-enriched combustion, and (3) investigate the use of lower-grade fuels in high-speed diesel engines by emulsifying the fuel with water. These tests, completed on a Caterpillar model 3406B, six-cylinder engine are a scale-up from previous, single-cylinder-engine tests. The engine was tested with (1) intake-air oxygen levels up to 30%, (2) water content up to 20% of the fuel, (3) three fuel-injection timings, and (4) three fuel-flow rates (power levels). The Taguchi technique for experimental design was used to minimize the number of experimental points in the test matrix. Four separate test matrices were run to cover two different fuel-flow-rate strategies and two different fuels (No. 2 diesel and No. 6 diesel). A liquid-oxygen tank located outside the test cell supplied the oxygen for the tests. The only modification of the engine was installation of a pressure transducer in one cylinder. All tests were run at 1800 rpm, which corresponds to the synchronous speed of a 60-Hz generator. Test results show that oxygen enrichment results in power increases of 50% or more while significantly decreasing the levels of smoke and particulates emitted. The increase in power was accompanied by a small increase in thermal efficiency. Maximum engine power was limited by the test-cell dynamometer capacity and the capacity of the fuel-injection pump. Oxygen enrichment increases nitrogen-oxide emissions significantly. No adverse effects of oxygen enrichment on the turbocharger were observed. The engine operated successfully with No. 6 fuel, but it operated at a lower thermal efficiency and emitted more smoke and particulates than with No. 2 fuel. DOE

N94-22392# Westinghouse Idaho Nuclear Co., Inc., Idaho Falls.
PASSIVE CRYOGENIC SAMPLER
1993 3 p Presented at the 1993 Industry Technology, Kansas City, MO, 5-8 May 1993
(Contract DE-AC07-84ID-12435)
(DE94-000918; WINCO-11955; CONF-9305290-1) Avail: CASI HC A01/MF A01

Sampling is the key step in any analysis regime. Gaseous systems only magnify the critical nature of the sampling step. The Passive Cryogenic Gas Sampler provides a proven, cost-effective way to obtain high-quality samples. This report specifies some advantages and design specifications of the Passive Cryogenic Gas Sampler. DOE

N94-22430*# Lunar and Planetary Inst., Houston, TX.
MSATT WORKSHOP ON INNOVATIVE INSTRUMENTATION FOR THE IN SITU STUDY OF ATMOSPHERE-SURFACE INTERACTIONS ON MARS
Bruce Fegley, Jr., ed. and Heinrich Waenke, ed. 1992 25 p Workshop held in Mainz, Germany, 8-9 Oct. 1992
(Contract NASw-4574)
(NASA-CR-194584; NAS 1.26:194584; LPI/TR-92-07-Pt-1) Avail: CASI HC A03/MF A01

Papers accepted for the Mars Surface and Atmosphere Through Time (MSATT) Workshop on Innovative Instruments for the In Situ Study of Atmosphere-Surface Interaction of Mars, 8-9 Oct. 1992 in Mainz, Germany are included. Topics covered include: a backscatter Moessbauer spectrometer (BaMS) for use on Mars; database of proposed payloads and instruments for SEI missions; determination of martian soil mineralogy and water content using the Thermal Analyzer for Planetary Soils (TAPS); in situ identification of the martian surface material and its interaction with the martian atmosphere using DTA/GC; mass spectrometer-pyrolysis experiment for atmospheric and soil sample analysis on the surface of Mars; and optical luminescence spectroscopy as a probe of the surface mineralogy of Mars. For individual titles, see N94-22431 through N94-22437.

N94-22431*# National Aeronautics and Space Administration. Lyndon B. Johnson Space Center, Houston, TX.
A BACKSCATTER MOESSBAUER SPECTROMETER (BaMS) FOR USE ON MARS Abstract Only
D. G. Agresti (Alabama Univ., Birmingham.), R. V. Morris, E. L. Wills (Alabama Univ., Birmingham.), T. D. Shelfer (Alabama Univ., Birmingham.), M. M. Pimperl (Alabama Univ., Birmingham.), M.-H. Shen (Alabama Univ., Birmingham.), and T. Nguyen (Lockheed Engineering and Sciences Co., Houston, TX.) *In* Lunar and Planetary Inst., MSATT Workshop on Innovative Instrumentation for the In Situ Study of Atmosphere-Surface Interactions on Mars 1992 p 1 (For primary document see N94-22430 05-35)
Avail: CASI HC A01/MF A01

The use of Moessbauer spectroscopy for in situ analysis on the surface of Mars was proposed and the design and implementation of a backscatter Moessbauer spectrometer (BaMS) instrument suitable for planetary missions to the surfaces of Mars (MESUR), the Moon (Artemis and lunar outpost), asteroids, or other solid solar system objects is discussed. The BaMS instrument is designed to be capable of analysis of a sample for the mineralogy of its iron-bearing phases without any sample preparation. A requirement of lander missions to Mars is instrumentation for in situ mineralogical analyses. Such analyses provide data needed for primary characterization as to the type of surface materials present and by inference the processes that formed and subsequently modified them. For purposes of providing diagnostic information about naturally occurring materials, the element iron is particularly important because it is abundant and multivalent (primarily 0, +2, and +3 oxidation states). Knowledge of the oxidation state of iron and its distribution among iron-bearing mineralogies tightly constrains the types of materials present. The pivotal role of iron was already recognized in 1978 by COMPLEX, who recommended development of flight instruments that would identify mineralogy and the oxidation state of iron in planetary surface materials. The near-term U.S. strategy for the exploration of Mars is the MESUR (Mars Environmental SURvey) program, which entails emplacement of a network of small, long-lived surface landers. For the Moon, BaMS was recommended as part of a three-instrument landed payload for the Artemis missions, targeted for 1997. BaMS would prospect for ilmenite, an oxygen resource material, and provide data to assess the maturity of lunar soil. Because instrumental characteristics are low mass, low volume, and low power consumption, BaMS is suitable for implementation on even small landers and rovers, as are being envisioned in MESUR and Artemis concepts. In addition to providing highly diagnostic data, a BaMS analyzer is inherently simple and, as is highly desirable for remote operation, no sample preparation is required. Author (revised)

N94-22432*# National Aeronautics and Space Administration. Lyndon B. Johnson Space Center, Houston, TX.
DATABASE OF PROPOSED PAYLOADS AND INSTRUMENTS FOR SEI MISSIONS Abstract Only
N. G. Barlow *In* Lunar and Planetary Inst., MSATT Workshop on Innovative Instrumentation for the In Situ Study of Atmosphere-Surface Interactions on Mars 1992 p 2-3 (For primary document see N94-22430 05-35)
Avail: CASI HC A01/MF A01

A database of all payloads and instruments proposed for lunar and Mars missions was compiled by the author for the Exploration Programs Office at NASA's Johnson Sapce Center. The database is an outgrowth of the document produced by C. J. Budney et al. at the Jet Propulsion Laboratory in 1991. The present database consists not only of payloads proposed for human exploratory missions of the Moon and Mars, but also experiments selected or proposed for robotic precursor missions such as Lunar Scout, Mars Observer, and MESUR. The database consists of two parts: a written payload description and a matrix that provides a breakdown of payload components. Each payload description consists of the following information: (1) the rationale for why the instrument or payload package is being proposed for operation on the Moon or Mars; (2) a description of

how the instrument works; (3) a breakdown of the payload, providing detailed information about the mass, volume, power requirements, and data rates for the constituent pieces of the experiment; (4) estimates of the power consumption and data rate; (5) how the data will be returned to Earth and distributed to the scientific community; (6) any constraints on the location or conditions under which the instrument can or cannot operate; (7) what type of crew interaction (if any) is needed; (8) how the payload is to be delivered to the lunar or martian surface (along with alternative delivery options); (9) how long the instrument or payload package will take to set up; (10) what type of maintenance needs are anticipated for the experiment; (11) stage of development for the instrument and environmental conditions under which the instrument has been tested; (12) an interface required by the instrument with the lander, a rover, an outpost, etc.; (13) information about how often the experiment will need to be resupplied with parts or consumables, if it is to be resupplied; (14) the name and affiliation of a contact person for the experiment; and (15) references where further information about the experiment can be found.

Author (revised)

N94-22433*# National Aeronautics and Space Administration. Lyndon B. Johnson Space Center, Houston, TX.

DETERMINATION OF MARTIAN SOIL MINERALOGY AND WATER CONTENT USING THE THERMAL ANALYZER FOR PLANETARY SOILS (TAPS) Abstract Only

James L. Gooding, Douglas W. Ming, Judith H. Allton (Lockheed Engineering and Sciences Co., Houston, TX.), Terry B. Byers (Lockheed Engineering and Sciences Co., Houston, TX.), Robert P. Dunn (Lockheed Engineering and Sciences Co., Houston, TX.), Frank L. Gibbons (Lockheed Engineering and Sciences Co., Houston, TX.), Daniel B. Pate (Lockheed Engineering and Sciences Co., Houston, TX.), and Thomas M. Polette (Lockheed Engineering and Sciences Co., Houston, TX.) *In* Lunar and Planetary Inst., MSATT Workshop on Innovative Instrumentation for the In Situ Study of Atmosphere-Surface Interactions on Mars 1992 p 4-5 (For primary document see N94-22430 05-35)

Avail: CASI HC A01/MF A01

Physical and chemical interactions between the surface and atmosphere of Mars can be expected to embody a strong cause-and-effect relationship with the minerals comprising the martian regolith. Many of the minerals in soils and sediments are probably products of chemical weathering (involving surface/atmosphere or surface/hydrosphere reactions) that could be expected to subsequently influence the sorption of atmospheric gases and water vapor. Therefore, identification of the minerals in martian surface soils and sediments is essential for understanding both past and present interactions between the Mars surface and atmosphere. Clearly, the most definitive mineral analyses would be achieved with well-preserved samples returned to Earth-based laboratories. In advance of a Mars sample return mission, however, significant progress could be made with in situ experiments that fill current voids in knowledge about the presence or abundance of key soil minerals such as clays (layered-structured silicates), zeolites, and various salts, including carbonates. TAPS is intended to answer that challenge by providing first-order identification of soil and sediment minerals.

Author (revised)

N94-22434*# National Aeronautics and Space Administration. Ames Research Center, Moffett Field, CA.

IN SITU IDENTIFICATION OF THE MARTIAN SURFACE MATERIAL AND ITS INTERACTION WITH THE MARTIAN ATMOSPHERE USING DTA/GC Abstract Only

R. L. Mancinelli and M. R. White *In* Lunar and Planetary Inst., MSATT Workshop on Innovative Instrumentation for the In Situ Study of Atmosphere-Surface Interactions on Mars 1992 p 12-13 (For primary document see N94-22430 05-35)

Avail: CASI HC A01/MF A01

Little is known about the mineralogy of the martian surface material. Several techniques have been suggested as candidates for the in situ identification of the martian surface material. The most promising of these techniques include differential thermal analysis (DTA) coupled with gas chromatography (GC) and differential scanning calorimetry (DSC) coupled with either mass spectrometry (MS) or GC. Our studies showed that differential thermal analysis coupled with gas chromatography (DTA/GC) is a more appropriate analytical technique than DSC/MS or DSC/GC to identify the mineralogy of the martian surface material in situ. DTA/GC can be regarded as an advancement from pyrolytic GC analyses that were successfully flown on previous missions, but have supplied only limited mineralogical information.

Author (revised)

N94-22435*# National Aeronautics and Space Administration. Goddard Space Flight Center, Greenbelt, MD.

MASS SPECTROMETER-PYROLYSIS EXPERIMENT FOR ATMOSPHERIC AND SOIL SAMPLE ANALYSIS ON THE SURFACE OF MARS

Konrad Mauersberger (Minnesota Univ., Minneapolis.), Paul Mahaffy, and Hasso Niemann *In* Lunar and Planetary Inst., MSATT Workshop on Innovative Instrumentation for the In Situ Study of Atmosphere-Surface Interactions on Mars 1992 p 14 (For primary document see N94-22430 05-35)

Avail: CASI HC A01/MF A01

Results from the Viking mission will form the foundation for future in-depth investigations of atmosphere-surface interactions on Mars. The two Viking landers carried impressive instrumentation to obtain and analyze soil samples: the sites were observed by cameras, and the collector head was located on a long boom and allowed the collection of large samples at various depths. A selection of grain sizes was possible and a distribution system supplied a number of experiments with soil material. Despite stationary vehicles, a wide sampling field was reachable. The GCMS system, responsible for atmospheric as well as surface soil analysis, worked well on both landers. Atmospheric measurements resulted in the determination of the abundance of noble gases as well as of other molecular species. Isotopic composition measurements included the important ratios of C-13/C-12, N-15/N-14, and Ar-36/Ar-40. To verify these past results and to advance detailed studies of noble gas isotope ratios and minor constituents, better instrument sensitivities, higher precision, and lower background contributions are required in future Mars missions. Soil analysis during the Viking mission concentrated on organic material. Heating cycles were performed to 500 C and only water and carbon dioxide were identified. Higher pyrolysis temperatures are of primary importance to advance our understanding of the mineralogy and gas loading of surface material and atmospheric exchange.

Author (revised)

N94-22436*# National Aeronautics and Space Administration. Ames Research Center, Moffett Field, CA.

TEMPERATURE/PRESSURE AND WATER VAPOR SOUNDING WITH MICROWAVE SPECTROSCOPY Abstract Only

D. O. Muhleman (California Inst. of Tech., Pasadena.), M. A. Janssen (Jet Propulsion Lab., California Inst. of Tech., Pasadena.), R. T. Clancy (Washington Univ., Saint Louis, MO.), S. Gulkis (Jet Propulsion Lab., California Inst. of Tech., Pasadena.), D. J. McCleese (Jet Propulsion Lab., California Inst. of Tech., Pasadena.), R. Zurek (Jet Propulsion Lab., California Inst. of Tech., Pasadena.), R. M. Haberle, and M. Frerking (Jet Propulsion Lab., California Inst. of Tech., Pasadena.) *In* Lunar and Planetary Inst., MSATT Workshop on Innovative Instrumentation for the In Situ Study of Atmosphere-Surface Interactions on Mars 1992 p 14-15 (For primary document see N94-22430 05-35)

Avail: CASI HC A01/MF A01

Two intense microwave spectra lines exist in the martian atmosphere that allow unique sounding capabilities: water vapor at 183 GHz and the (2-1) rotational line of CO at 230 GHz. Microwave spectra line sounding is a well-developed technique for the Earth's atmosphere for sounding from above from spacecraft and airplanes, and from below from fixed surface sites. Two simple instruments for temperature sounding on Mars (the CO line) and water vapor measurements are described. The surface sounder proposed for the MESUR sites is designed to study the boundary layer water vapor distribution and the temperature/pressure profiles with vertical resolution of 0.25 km up to 1 km with reduced resolution above approaching a scale height. The water channel will be sensitive to a few tenths of a micrometer of water and the temperature profile will be retrieved to an accuracy between 1 and 2 K. The latter is routinely done on the Earth using oxygen lines near 60 GHz. The measurements are done with a single-channel heterodyne receiver looking into a 10-cm mirror that is canned through a range of elevation angles plus a target load. The frequency of the receiver is sweep across the water and CO lines generating the two spectra at about 1-hr intervals throughout the mission. The mass and power for the proposed instrument are 2 kg and 5-8 W continuously. The measurements are completely immune to the atmospheric dust and ice particle loads. It was felt that these measurements are the ultimate ones

to properly study the martian boundary layer from the surface to a few kilometers. Sounding from above requires an orbiting spacecraft with multichannel microwave spectrometers such as the instrument proposed for MO by a subset of the authors, a putative MESUR orbiter, and a proposed Discovery mission called MOES. Such an instrument can be built with less than 10 kg and use less than 15 W. The obvious advantage of this approach is that the entire atmosphere can be sounded for temperature and water vapor in a few hours with somewhat better than a scale height resolution. If a bigger mirror is used (greater than 30 cm) limb sounding geometry can be employed and half scale height resolution achieved to altitudes up to at least 60 km. Again, the measurements are immune to dust and ice loads. Water vapor sensitivity of 0.1 micrometer can be achieved (even with a nadir instrument) and temperature profiles retrieved to an accuracy of better than 2 K from the surface to about 60 km. Winds can be measured from the doppler shifts of CO lines in the limb sounding mode. Author (revised)

N94-22437*# National Aeronautics and Space Administration. Lyndon B. Johnson Space Center, Houston, TX.

OPTICAL LUMINESCENCE SPECTROSCOPY AS A PROBE OF THE SURFACE MINERALOGY OF MARS Abstract Only

A. H. Treiman *In* Lunar and Planetary Inst., MSATT Workshop on Innovative Instrumentation for the In Situ Study of Atmosphere-Surface Interactions on Mars 1992 p 17 (For primary document see N94-22430 05-35)

Avail: CASI HC A01/MF A01

Optical luminescence (OpL) spectroscopy is an attractive use of a visible-near-IR spectrometer on a Mars lander because mineral products of atmosphere-surface interactions on Mars will probably have characteristic OpL spectra. Optical luminescence spectra would be taken at night, when a spectrometer might otherwise sit idle. Also needed would be a source of exciting radiation, which could be shared with other experiments. Optical luminescence is emission of nonthermal optical photons (near-UV through near-IR) as a response to energy input. On absorption of energy, an atom (or ion) will enter an excited state. The favored decay of many such excited states involving valence-band electrons is emission of an optical photon. Optical luminescence spectra can be useful in determining mineralogy and mineral composition. Optical luminescence in crystals can arise from essential elements (or ions), trace-element substituents (activators), or defects. Common activators in salts of alkali and alkaline earth elements include Mn(2+)(VI), other transition metals, the rare earths, and the actinides. Trace substituents of other species can enhance or quench OpL (e.g., Pb(2+) vs. Fe(3+)). Optical luminescence can also arise from defects in crystal structures, including those caused by radiation and shock. Author (revised)

N94-20650*# Deutsche Forschungsanstalt fuer Luft- und Raumfahrt, Berlin (Germany). Inst. for Planetary Exploration.

THE HIGH RESOLUTION STEREO CAMERA (HRSC) FOR THE LUNAR SCOUT 1 MISSION Abstract Only

G. Neukum *In* Lunar and Planetary Inst., Twenty-Fourth Lunar and Planetary Science Conference. Part 3: N-Z 1993 p 1069 (For primary document see N94-20636 05-91)

Avail: CASI HC A01/MF A06

N94-20688*# Brown Univ., Providence, RI.

MinMap: AN IMAGING SPECTROMETER FOR HIGH RESOLUTION COMPOSITIONAL MAPPING OF THE MOON Abstract Only

C. M. Pieters, James W. Head, and T. B. McCord (SETS Technology, Inc., Honolulu, HI.) *In* Lunar and Planetary Inst., Twenty-Fourth Lunar and Planetary Science Conference. Part 3: N-Z 1993 p 1145-1146 (For primary document see N94-20636 05-91)

Avail: CASI HC A01/MF A06

N94-21346*# Herold (Fredrick) and Associates, Inc., Greenbelt, MD.

USING THE USCCS FOR SUB MICROSECOND SPACECRAFT CLOCK CALIBRATION

Victor J. Sank *In* NASA. Goddard Space Flight Center, Networks Technology Conference Nov. 1993 p 275-287 (For primary document see N94-21323 05-62)

Avail: CASI HC A03/MF A03

N94-21347*# Allied-Signal Aerospace Co., Columbia, MD. Data Systems Group.

A LOW COST ALTERNATIVE TO HIGH PERFORMANCE PCM BIT SYNCHRONIZERS

Bruce DeShong *In* NASA. Goddard Space Flight Center, Networks Technology Conference Nov. 1993 p 289-307 (For primary document see N94-21323 05-62)

Avail: CASI HC A03/MF A03

N94-21378* Jet Propulsion Lab., California Inst. of Tech., Pasadena.

CALIBRATION OF A CALORIMETER FOR MEASURING THE PERFORMANCE OF THERMAL CONTROL SURFACES

John Houseman and Georg Siebes *In* CNES, Fifth International Symposium on Materials in a Space Environment Jun. 1993 p 155-168 (For primary document see N94-21367 05-18)

Copyright Avail: CEPADUES-Editions, 111, rue Nicolas-Vaquelin, 31100 Toulouse, France

N94-21646*# National Aeronautics and Space Administration. Goddard Inst. for Space Studies, New York, NY.

MICHELSON INTERFEROMETER (MINT)

Andrew Lacis and Barbara Carlson *In its* Long-Term Monitoring of Global Climate Forcings and Feedbacks Sep. 1993 p 47-53 (For primary document see N94-21639 05-47)

Avail: CASI HC A02/MF A02; 13 functional color pages

N94-21701*# California Univ., Fullerton. Dept. of Electrical Engineering.

ANALOG/DIGITAL pH METER SYSTEM I.C.

Paul Vincent and Jea Park *In* Idaho Univ., The 1992 4th NASA SERC Symposium on VLSI Design 1992 10 p (For primary document see N94-21694 05-33)

Avail: CASI HC A02/MF A04

N94-22151 Alberta Univ., Edmonton. Microelectronic Center.

SILICON MICROMACHINED THRESHOLD ACCELEROMETERS

Y. Loke, G. H. McKinnon, and M. J. Brett *In* Engineering Inst. of Canada, Canadian Conference on Electrical and Computer Engineering, Volumes 1 and 2 1991 4 p (For primary document see N94-22101 05-33)

Avail: Issuing Activity (Engineering Inst. of Canada, 2050 rue Mansfield, Suite 700, Montreal, PQ H3A 1Z2 Canada)

N94-22152 Calgary Univ. (Alberta). Dept. of Electrical and Computer Engineering.

CHARGE INTEGRATING OPTICAL POSITION SENSOR

S. Balasubramanian, J. W. Haslett, and F. N. Trofimenkoff *In* Engineering Inst. of Canada, Canadian Conference on Electrical and Computer Engineering, Volumes 1 and 2 1991 4 p (For primary document see N94-22101 05-33)

Avail: Issuing Activity (Engineering Inst. of Canada, 2050 rue Mansfield, Suite 700, Montreal, PQ H3A 1Z2 Canada)

N94-22221 National Research Council of Canada, Ottawa (Ontario). Inst. for Information Technology.

BALANCED ARROW MACH-ZEHNDER INTERFEROMETER

S. F. Yuen, J. Chrostowski, and B. A. Syrett *In* Engineering Inst. of Canada, Canadian Conference on Electrical and Computer Engineering, Volumes 1 and 2 1991 4 p (For primary document see N94-22101 05-33)

Avail: Issuing Activity (Engineering Inst. of Canada, 2050 rue Mansfield, Suite 700, Montreal, PQ H3A 1Z2 Canada)

N94-22226 Ecole Polytechnique, Montreal (Quebec). Dept. of Electrical and Computer Engineering.

AN APPROACH TO THE ESTIMATION OF GROUND STRUCTURE AND AIRCRAFT MOTION FROM AERIAL IMAGE SEQUENCES

Michel Audette, Ning Cui, Paul Cohen, and Ju-Yang Weng *In* Engineering Inst. of Canada, Canadian Conference on Electrical and Computer Engineering, Volumes 1 and 2 1991 4 p (For primary document see N94-22101 05-33)

Avail: Issuing Activity (Engineering Inst. of Canada, 2050 rue Mansfield, Suite 700, Montreal, PQ H3A 1Z2 Canada)

N94-22510*# Massachusetts Inst. of Tech., Cambridge.
WILBUR: A LOW-COST CCD CAMERA SYSTEM FOR MDM OBSERVATORY Abstract Only
M. R. Metzger, G. A. Luppino (Istituto di Fisica dell Atmosfera, Rome, Italy.), and J. L. Tonry *In* NASA, Washington, Second Annual Conference on Astronomical Data Analysis Software and Systems. Abstracts 1992 p 79 (For primary document see N94-22438 05-89)
Avail: CASI HC A01/MF A02

N94-22604# Dornier Luftfahrt G.m.b.H., Friedrichshafen (Germany).
HOT WIRE ANEMOMETRY: A VERSATILE INSTRUMENTATION USED FOR PREDEVELOPMENT STUDIES AND FLIGHT TESTING OF THE DO-328 AIRCRAFT [HITZDRAHTANEMOMETRIE: EIN VIELSEITIGES INSTRUMENTARIUM IM EINSATZ BEI VORENTWICKLUNG UND FLUGVERSUCH DER DO 328]
P. Dick *In* Tech. Univ. Berlin, Measurement Technology for Flight Tests May 1991 p 82-96 In GERMAN (For primary document see N94-22597 05-02)
Avail: CASI HC A03/MF A02

N94-22606# Saab-Scania, Linkoping (Sweden). Ground and Flight Testing Dept.
IMAGE PROCESSING AS A TOOL IN FLIGHT TESTING EVALUATION
Anders Kaelldahl *In* Tech. Univ. Berlin, Measurement Technology for Flight Tests May 1991 p 111-117 (For primary document see N94-22597 05-02)
Avail: CASI HC A02/MF A02

36 LASERS AND MASERS

Includes parametric amplifiers.
For related information see also *76 Solid-State Physics*.

N94-19800 Department of the Navy, Washington, DC.
SUPPRESSION OF RELAXATION OSCILLATIONS IN FLASHPUMPED, TWO-MICRON TUNABLE SOLID STATE LASERS Patent
Leon Esterowitz, inventor (to Navy) and Joseph F. Pinto, inventor (to Navy) 27 Apr. 1993 15 p Filed 31 Jan. 1992
(AD-D015928; US-Patent-5,206,867; US-Patent-Appl-SN-829145; US-Patent-Class-372-20) Avail: US Patent and Trademark Office

A flashpumped, tunable, two-micron, solid state laser is disclosed in which laser spiking is suppressed. The solid state laser comprises: a laser cavity defined by a first reflective element and an output coupler reflective element to form a reflective path there between; a laser crystal disposed in the laser cavity, the laser crystal having a host material doped with preselected activator ions sufficient to produce a pulse or laser emission at a desired laser transition wavelength in a range between about 1.9 microns and about 2.1 microns when the crystal is optically excited to produce the laser emission; a pulsed flashlamp for optically exciting the laser crystal to produce a pulse of laser emission at the desired laser transition wavelength; a tuner disposed in the laser cavity between the laser crystal and one of the reflective elements for tuning the laser emission to the desired laser transition wavelength in the range of wavelengths between about 1.9 microns and about 2.1 microns; optical plates oriented at Brewster's angle in the reflective path for suppressing oscillation of undesired wavelengths within the laser cavity; and a nonlinear crystal disposed in the reflective path to enable the laser to emit through the output coupler reflective element a smooth, long pulse of laser emission without spiking at the desired laser transition wavelength. DTIC

N94-19828# Los Alamos National Lab., NM.
INITIAL PERFORMANCE OF LOS ALAMOS ADVANCED FREE ELECTRON LASER
D. C. Nguyen, R. H. Austin, K. C. D. Chan, C. Fortgang, W. J. D. Johnson, J. Goldstein, S. M. Gierman, J. Kinross-Wright, S. H. Kong, and K. L. Meier et al 1993 18 p Presented at the 15th International Free Electron Laser Conference, The Hague, Netherlands, 23-27 Aug. 1993
(Contract W-7405-eng-36)
(DE93-040158; LA-UR-93-3175; CONF-930855-3) Avail: CASI HC A03/MF A01

The Los Alamos compact Advanced FEL has lased at 4.7 and 5.2 micron with a 1-cm period wiggler and a high-brightness electron beam at 16.8 and 15.8 MeV, respectively. The measured electron beam normalized emittance is 1.7 pi mm mrad at a peak current of 100 A, corresponding to a beam brightness greater than 2 x 10(exp 12) A/sq m rad(exp 2). Initial results indicate that the AFEL small signal gain is approximately 8% at 0.3 nC (30 A peak). The maximum output energy is 7 mJ over a 2-micro-s macropulse. The AFEL performance can be significantly enhanced by improvements in the rf and drive laser stability. DOE

N94-19850 Electronics Research Lab., Salisbury (Australia).
DESIGN ASPECTS AND PARAMETRIC CHARACTERISATION OF A NEUTRAL RARE GAS LASER
Kenneth J. Grant May 1993 16 p Limited Reproducibility: More than 20% of this document may be affected by microfiche quality
(AD-A271100; ERL-0703-GD; DODA-008-148) Avail: Issuing Activity (Defense Technical Information Center (DTIC))

A neutral rare gas laser has been built and used to produce continuous wave output at several wavelengths in the mid-infrared region. The laser design is described and results are presented of a parametric study of its operating characteristics. Mixtures of He-Ar, He-Kr, and He-Xe were used. The output power at each wavelength was monitored as a function of the discharge parameters to determine the optimum working regimes. This General Document is a paper presented at the 8th Conference of the Australian Optical Society, held at the University of Sydney, NSW, in Feb. 1993. DTIC

N94-19851 Surveillance Research Lab., Salisbury (Australia).
EVALUATION OF A SINGLE STAGE OF THE LADS FILTER
R. S. Seymour, S. Rees, J. Staromlynska, J. Richards, and P. Wilson Nov. 1992 54 p Limited Reproducibility: More than 20% of this document may be affected by microfiche quality
(AD-A271101; SRL-0109-TR; DODA-008-107) Avail: Issuing Activity (Defense Technical Information Center (DTIC))

A tunable, large aperture, wide angle, narrowband filter, centered at 532 nm, has been developed to improve the signal to noise ratio in the Laser Airborne Depth Sounder. Several new concepts have been included in the design. DTIC

N94-19853 Smithsonian Astrophysical Observatory, Cambridge, MA.
MEASUREMENTS OF ATOMIC INTERACTIONS AND FREQUENCY STABILITY WITH A CRYOGENIC HYDROGEN MASER Final Report
Robert F. Vessot Aug. 1993 9 p Limited Reproducibility: More than 20% of this document may be affected by microfiche quality
(Grant AF-AFOSR-0282-91)
(AD-A271132; AFOSR-93-0780) Avail: CASI HC A02

With support from the Air Force Office of Scientific Research, we have developed a hydrogen maser that operates near 0.5 K using a high-cooling-power 3 He refrigerator. We have used this cryogenic hydrogen maser to study low temperature atomic hydrogen spin-exchange collisions and hydrogen-helium interactions and to investigate the performance of cryogenic hydrogen masers as possibly improved frequency standards. DTIC

N94-19865# Sandia National Labs., Albuquerque, NM.
SPATIAL PATTERNS IN SEMICONDUCTOR LASERS
G. Khitrova (Arizona Univ., Tucson.), F. BrowndeColstoun (Arizona Univ., Tucson.), C. W. Lowry (Arizona Univ., Tucson.), E. M. Wright (Arizona Univ., Tucson.), H. M. Gibbs (Arizona Univ., Tucson.), T. M. Brennan, and B. E. Hammons 1993 3 p Presented at the Institute of Electrical and Electronics Engineers/Lasers and Electro-Optics Society (IEEE/LEOS) Annual Meeting, San Jose, CA, 15-19 Nov. 1993
(Contract DE-AC04-76DP-00789)
(DE93-040056; SAND-93-1847C; CONF-931197-1) Avail: CASI HC A01/MF A01

Spatial solitons occur when an intense pulse propagates in a self-focusing semiconductor gain medium. Injecting light into a vertical-cavity surface-emitting laser causes dramatic modifications of the phase and transverse output intensity profiles, including the appearance of phase defects. DOE

N94-19867# Los Alamos National Lab., NM.
LASER AMPLIFIER DEVELOPMENTS AT MERCURY

E. A. Rose, J. P. Brucker, E. M. Honig, A. W. McCown, V. O. Romero, and G. W. York 1993 5 p Presented at the 9th IEEE Pulsed Power Conference, Albuquerque, NM, 21-23 Jun. 1993
(Contract W-7405-eng-36)
(DE93-040103; LA-UR-93-2961; CONF-930616-36) Avail: CASI HC A01/MF A01

Electron-beam pumped laser amplifiers have been modified to address the mission of krypton-fluoride excimer laser technology development. Methods are described for improving the performance and reliability of two pre-existing amplifiers at minimal cost and time. Preliminary performance data are presented to support the credibility of the approach. DOE

N94-19878# Northwestern Univ., Evanston, IL.
FIRST RESULTS ON InGaAsP SEPARATE CONFINEMENT HETEROSTRUCTURE DIODE LASERS Interim Technical Report, 15 Mar. - 9 Sep. 1993
M. Razeghi 9 Sep. 1993 31 p
(Contract DAAH04-93-G-0044)
(AD-A270849; ARO-31108.2-PH) Avail: CASI HC A03/MF A01

The first attempts of fabrication of InGaAsP/GaAs SCH-QW laser structures allowed to obtain laser diodes with threshold current densities as low as 47O A/sq cm and differential efficiencies as high as 0.7 W/A. Long-cavity (L approx. 1mm) laser diodes have low series resistances of 0.1-0.4 ohms. These diodes are suitable for testing of the properties of the Al-free material in continuous wave regime. At the same time, it is evident that further optimization of structure parameters is necessary to reach the ultimate performance expected for InGaAsP SCH QW lasers. DTIC

N94-19965# Air Force Inst. of Tech., Wright-Patterson AFB, OH. Foreign Aerospace Science and Technology Center.
CIRCULAR POLARIZING MIRRORS FOR HIGH POWER LASERS
Qing-Ming Chen, Feng-Qing Zhou, Ziao-Ping Li, Yong-Gui He, and Jin-Hua Wang 16 Jul. 1993 14 p Transl. into ENGLISH from unidentified Chinese language document p 193-196
(AD-A267820; FASTC-ID(RS)T-0101-93) Avail: CASI HC A03/MF A01

In this paper, the circular polarizing mirrors for high power lasers have been theoretically and experimentally studied, the circular polarizing mirror coated with multiple-film, which could induce 90 degrees phase retardation is prepared experimentally. Author

N94-20055 Department of the Navy, Washington, DC.
TUNABLE LASER FREQUENCY STABILIZING SYSTEM Patent
David F. Hudson, inventor (to Navy) 29 Jun. 1993 6 p Filed 27 May 1992
(AD-D015904; US-Patent-5,224,110; US-Patent-Appl-SN-888996; US-Patent-Class-372-32) Avail: US Patent and Trademark Office

Laser emissions are stabilized at a plurality of frequencies by passage through an absorbing medium pumped by light, merged therewith, to an excited energy state corresponding to pumping light frequencies. Error signals are generated in response to detection of intensity of radiation exiting the absorbing medium which deviates from that of the laser emissions at the stabilizing frequencies to correctively adjust resonant cavity length of the laser generator being frequency stabilized. DTIC

N94-20060 Department of the Navy, Washington, DC.
RESONANTLY PUMPED, ERBIUM-DOPED, GSGG, 2.8 MICRON, SOLID STATE LASER WITH ENERGY RECYCLING AND HIGH SLOPE EFFICIENCY Patent
Leon Esterowitz, inventor (to Navy) and Robert C. Stoneman, inventor (to Navy) 6 Apr. 1993 13 p Filed 14 May 1992
(AD-D015920; US-Patent-5,200,966; US-Patent-Appl-SN-883336; US-Patent-Class-372-71) Avail: US Patent and Trademark Office

This invention is a laser system and method for producing a laser emission at a wavelength of substantially 2.8 microns and having a quantum efficiency of at least unity and a slope efficiency of about 36%. In a preferred embodiment of the invention, the laser system comprises a laser cavity defined by first and second reflective elements with one of the reflective elements operating as an output coupler; a crystal disposed in the laser cavity and having a GSGG host material doped with a preselected percent concentration of erbium, the GSGG host material and preselected percent concentration of erbium being selected so as to provide a quantum efficiency of at least unity by the 4I13/2 + 4I13/2 right arrow 4I9/2 + 4I15/2 upconversion process and a slope efficiency of about 36% when the crystal is resonantly pumped; and a resonant pump laser for directly pumping the 4I11/2 upper laser state of the erbium with a pump beam to cause the crystal to produce a laser emission corresponding to the 4I11/2 right arrow 4I13/2 laser transition having a wavelength of substantially 2.8 microns. DTIC

N94-20223# Lawrence Livermore National Lab., CA.
COMPUTATIONAL MODEL OF A MAGNETIC MODULATOR FOR COPPER LASERS
C. D. Boley Apr. 1993 6 p Presented at the 9th IEEE Pulsed Power Conference, Albuquerque, NM, 21-23 Jun. 1993
(Contract W-7405-eng-48)
(DE93-019603; UCRL-JC-111938; CONF-930616-35) Avail: CASI HC A02/MF A01

A numerical model of a three-stage magnetic modulator for copper lasers is described. The model follows in detail the hysteresis behavior of the magnetic switches and a transformer. The laser is treated via a simple model of field diffusion. The calculated voltage across the laser and current through the laser are shown to compare favorably with experiment. DOE

N94-20259# Lawrence Livermore National Lab., CA.
APPLICATIONS AND SOURCE DEVELOPMENT FOR HIGH-REPETITION RATE X RAY LASERS
D. C. Eder, P. Amendt, and P. R. Bolton et al 30 Jul. 1993 9 p Presented at the Annual Meeting of the Society of Photo-Optical Instrumentation Engineers (SPIE), San Diego, CA, 11-16 Jul. 1993
(Contract W-7405-eng-48)
(DE93-019547; UCRL-JC-112493; CONF-930722-30) Avail: CASI HC A02/MF A01

Many applications in material science, chemistry, and atomic physics require an x-ray source that has a repetition rate of 1 Hz to a few kHz. In these fields, a very wide range of photon energies is of interest. One application is time-resolved surface photoelectron spectroscopy and microscopy where low energy (less than 1 micro-J) pulses are required to avoid space charge effects but high-repetition rates (approximately 1 kHz) provide the high average power which is needed to obtain the desired resolution. In pump-probe experiments, it is desirable to have the repetition rate of the x-ray source be comparable to the repetition rate of the corresponding IR, optical, or UV laser. The authors show that the very high-repetition rate of synchrotrons (1-1000 MHz) results in an inefficient use of x rays for these types of experiments and that a kHz repetition rate x-ray laser would be an excellent source for many experiments. For some applications, a slower repetition rate of order 1 Hz is adequate provided the energy per pulse is larger (approximately 1 mJ). For example, in photoelectron spectroscopy of free clusters, an x-ray laser can provide the required large number of nearly mono-energetic photons during the short time the clusters can be probed in each formation cycle. In the context of source development, the authors discuss conventional collisional x-ray laser schemes with mJ output pulses that can operate at Hz repetition rates using a high average power driving laser. The near term prospects for high-repetition rate x-ray lasing for photon energies below 100 eV are very good with higher energy capabilities expected in the future. In addition, prospects of table-top size x-ray lasers with kHz repetition rates are presented. DOE

N94-20272# Los Alamos National Lab., NM.
MEASUREMENT AND CORRECTION OF MAGNETIC FIELDS IN PULSED SLOTTED-TUBE MICROWIGGLERS
C. M. Fortgang and R. W. Warren 1993 10 p Presented at the 15th International Free Electron Laser Conference, The Hague, Netherlands, 23-27 Aug. 1993
(Contract W-7405-eng-36)
(DE93-040100; LA-UR-93-2924; CONF-930855-2) Avail: CASI HC A02/MF A01

Pulsed electromagnetic microwigglers are capable of creating stronger fields with shorter periods than conventional wigglers. Wiggler field parameters of 1 Tesla and 5-mm period are achieved by passing approximately 25 kA down a slotted 3 mm outer diameter copper tube. The taut-wire technique is used to measure the wiggler magnetic field in a small aperture (approximately 1.7 mm) with the required spatial (0.1 mm)

and temporal (approximately 5 microsecond) resolution. The absence of midplane symmetry, in contrast to permanent magnet wigglers, causes unique problems in our microwigglers. We have measured strong dipole (bending) and quadrupole (defocusing) field errors with both dc and time-dependent parts. The effects on the magnetic field of current redistribution caused by heating in the copper tube has been measured. We have identified causes for the various field errors and their sensitivities to fabrication tolerances. Improvements we have made towards meeting the required tolerances and our field-correction technique are discussed. DOE

N94-20277# Los Alamos National Lab., NM.
PERFORMANCE OF THE HIGH BRIGHTNESS LINAC FOR THE ADVANCED FREE ELECTRON LASER INITIATIVE AT LOS ALAMOS
R. L. Sheffield, R. H. Austin, K. D. C. Chan, S. M. Gierman, J. M. Kinross-Wright, S. H. Kong, D. C. Nguyen, S. J. Russell, and C. A. Timmer 1993 14 p Presented at the 15th International Free Electron Laser Conference, The Hague, Netherlands, 23-27 Aug. 1993
(Contract W-7405-eng-36)
(DE93-040141; LA-UR-93-3101; CONF-930855-1) Avail: CASI HC A03/MF A01

The AFEL accelerator has produced beams of greater than 2 x 10(exp 12) A/m(exp 2) at 1 nC (brightness = 2*I/(var epsilon)(exp 2), with I greater than 100 A and (var epsilon) of than 2(pi) mm-mrad normalized ms emittance). The 1300 MHz standing-wave accelerator uses on-axis coupling cells. The electron source is a photoinjector with a CsK2Sb photocathode. The photoinjector is an integral part of a single 11-cell accelerator structure. The accelerator operates between 12 and 18 MeV. The beam emittance growth in the accelerator is minimized by using a photoinjector, a focusing solenoid to correct the emittance growth due to space charge, and a special design of the coupling slots between accelerator cavities to minimize quadrupole effects. This paper describes the experimental results and compares those results with PARMELA simulation. The simulation code PARMELA was modified for this effort. This modified version uses SUPERFISH files for the accelerator cavity fields, MAFIA files for the fields due to the coupling slots in the accelerator cells, and POISSON files for the solenoid field in the gun region. DOE

N94-20298# Sandia National Labs., Albuquerque, NM.
PHOTOPUMPED X RAY LASER RESEARCH ON SATURN
T. J. Nash, R. B. Spielman, M. Vargas, and L. Ruggles 1993 11 p Presented at the Annual Meeting of the Society of Photo-Optical Instrumentation Engineers (SPIE), San Diego, CA, 11-16 Jul. 1993
(Contract DE-AC04-76DP-00789)
(DE93-019430; SAND-93-1639C; CONF-930722-25) Avail: CASI HC A03/MF A01

Using Saturn as a driver, we are pursuing both photoresonantly pumped and photoionization/recombination lasers. Our lasing targets are gas cells with thin windows that are pumped by a z pinch 2 cm away radiating 10 TW. In both schemes the lasant and gas fill is neon. We will present evidence for inversion in the sodium/neon photoresonant scheme, but we have yet to detect the lasing transition itself. To increase our chances of measuring this line we have introduced potassium into a sodium z-pinch and have eliminated oxygen from the gas cell windows. We have measured the spatial dependence of ionization balance across the gas cell, and this measurement is consistent with propagation of a shock front across the gas cell target. We have measured the Li-like neon 5f-3d transition to increase more rapidly with fill pressure than all other measured lines. Based on this result we have performed experiments emphasizing the photoionization/recombination laser scheme that use a flat-field grazing incidence spectrometer to provide good spatial resolution of the 4f-3d, 4d-3p, and 5f-3d lines of Li-like neon. We have attempted a gain length measurement by imaging parallel to a baffle that varies the length of the target illuminated. DOE

N94-20341*# Colorado Univ., Boulder. Cooperative Inst. for Research in the Environmental Sciences.
COHERENT LIDAR DESIGN AND PERFORMANCE VERIFICATION Annual Report, 1 Dec. 1992 - 1 Dec. 1993
Rod Frehlich 1993 97 p
(Grant NAG8-253)
(NASA-CR-193813; NAS 1.26:193813) Avail: CASI HC A05/MF A02

The verification of LAWS beam alignment in space can be achieved by a measurement of heterodyne efficiency using the surface return. The crucial element is a direct detection signal that can be identified for each surface return. This should be satisfied for LAWS but will not be satisfied for descoped LAWS. The performance of algorithms for velocity estimation can be described with two basic parameters: the number of coherently detected photo-electrons per estimate and the number of independent signal samples per estimate. The average error of spectral domain velocity estimation algorithms are bounded by a new periodogram Cramer-Rao Bound. Comparison of the periodogram CRB with the exact CRB indicates a factor of two improvement in velocity accuracy is possible using non-spectral domain estimators. This improvement has been demonstrated with a maximum-likelihood estimator. The comparison of velocity estimation algorithms for 2 and 10 micron coherent lidar was performed by assuming all the system design parameters are fixed and the signal statistics are dominated by a 1 m/s rms wind fluctuation over the range gate. The beam alignment requirements for 2 micron are much more severe than for a 10 micron lidar. The effects of the random backscattered field on estimating the alignment error is a major problem for space based lidar operation, especially if the heterodyne efficiency cannot be estimated. For LAWS, the biggest science payoff would result from a short transmitted pulse, on the order of 0.5 microseconds instead of 3 microseconds. The numerically errors for simulation of laser propagation in the atmosphere have been determined as a joint project with the University of California, San Diego. Useful scaling laws were obtained for Kolmogorov atmospheric refractive turbulence and an atmospheric refractive turbulence characterized with an inner scale. This permits verification of the simulation procedure which is essential for the evaluation of the effects of refractive turbulence on coherent Doppler lidar systems. The analysis of 2 micron Doppler lidar data from Coherent Technologies, Inc. (CTI) has demonstrated many of the advantages of doppler lidar measurements of boundary layer winds. The effects of wind shear and wind turbulence over the pulse volume are probably the dominant source of the reduced performance. The effects of wind shear and wind turbulence on the statistical description of doppler lidar data has been derived and calculated. Derived from text

N94-20480# Lawrence Livermore National Lab., CA.
LASER PROPAGATION IN UNDERDENSE PLASMAS: SCALING ARGUMENTS
J. C. Garrison May 1993 23 p
(Contract W-7405-eng-48)
(DE93-040439; UCRL-ID-114297) Avail: CASI HC A03/MF A01

The propagation of an intense laser beam in the underdense plasma is modelled by treating the plasma as a relativistic, zero temperature, charged fluid. For paraxial propagation and a sufficiently underdense plasma (omega p/(omega) much less than 1), a multiple-scales technique is used to expand the exact equations in powers of the small parameter theta equivalent to omega p/(omega). The zeroth order equations are used in a critical examination of previous work on this problem, and to derive a scaling law for the threshold power required for cavitation. DOE

N94-20484# Air Force Inst. of Tech., Wright-Patterson AFB, OH. Foreign Aerospace Science and Technology Center.
TACTICAL LASER WEAPONS AND OTHER DIRECTED-ENERGY WEAPONS
Rongrui Wang 30 Jul. 1993 17 p Transl. into ENGLISH from Laser and Infrared (China), v. 20, no. 5, 1990 p 26-29
(AD-A267961; FASTC-ID(RS)T-0124-93) Avail: CASI HC A03/MF A01

This paper briefly introduces the current development status of three directed-energy weapons: laser weapons, radio frequency/microwave weapons, and charged-particle-beam weapons. Among them, the tactical laser weapon may be the first to find application. Derived from text

N94-20546# Wright Lab., Wright-Patterson AFB, OH.
ANALYSIS AND DESIGN OF WEIGHT BALANCING SYSTEM FOR LASER VELOCIMETRY TRAVERSE Final Report, Jun. 1989 - Sep. 1993
Hsue-Fu Lee Sep. 1993 23 p
(AD-A271171; WL-TM-93-307) Avail: CASI HC A03/MF A01

This technical memorandum describes the process of designing the weight balancing system which is an in-house effort to extend the lifting capability of the vertical axis of the Anomatic II system. The Anomatic II system is a programmable three-dimensional positioning controller used as

a laser velocimetry traverse. The Anomatic II system is the prime mover and the weight balancing system is an add-on follower that derives its motion and speed in response to the Anomatic II system. The weight balancing system consists primarily of a pneumatic cylinder-steel cable mechanism which proves to be effective in lifting excessive weight, economic in construction and simple to operate. DTIC

N94-20583# Cornell Univ., Ithaca, NY. Dept. of Chemistry.
ROTATIONAL SPECTRUM OF A DARK STATE IN 2-FLUOROETHANOL USING MICROWAVE/RADIOFREQUENCY-INFRARED MULTIPLE RESONANCE
C. C. Miller and L. A. Philips 26 Oct. 1993 32 p
(Contract N00014-90-J-1971)
(AD-A272101; TR-10-ONR) Avail: CASI HC A03/MF A01

Microwave/radiofrequency-infrared multiple resonance has been used with an electric-resonance optothermal spectrometer to characterize a weak 21.6 MHz perturbation in the infrared spectrum of the v14 C-O stretching vibration of 2-fluoroethanol. The infrared spectrum of 2-fluoroethanol was recorded at a resolution of approximately 2 MHz using a tunable microwave-sideband CO2 laser. The spectrum is fit by an asymmetric-rotor Hamiltonian to a precision of 0.6 MHz, except for the transitions to the 4(13) upper state which are split into doublets by an interaction between the 4(13) level and a rotational level of a nearby background, or dark, vibrational state. DTIC

N94-20611# Naval Postgraduate School, Monterey, CA.
DEVELOPMENT OF A LIDAR FOR INTEGRATION WITH THE NAVAL POSTGRADUATE SCHOOL INFRARED SEARCH AND TARGET DESIGNATION (NPS-IRSTD) SYSTEM M.S. Thesis
Murray M. Regush Jun. 1993 103 p
(AD-A271847) Avail: CASI HC A06/MF A02

A lidar was designed and manufactured at the Naval Postgraduate School, Monterey, CA, to provide range information to atmospheric features, such as clouds. It is further planned to integrate the lidar with the NPS-IRSTD system at some future date. The NPS-IRSTD uses two vertical linear focal plane arrays for target detection and target direction can be determined very accurately but the system does not provide any useful range information. The lidar was proposed as the solution for this shortcoming. The lidar used a frequency-doubled Nd:YAG laser which had an energy output of 2 millijoules. The laser beam was expanded to 17.75 inches using a Dall-Kirkham telescope to operate within laser safety limitations. The theoretical analysis of the 'Klett' method for the inversion of lidar returns was derived and a MATLAB program was written to demonstrate the process. A daytime and nighttime maximum range equation for the lidar was developed. The considerations for integrating the lidar with the NPS-IRSTD were listed and a solution was proposed to obtain the mean extinction coefficient along the path in the infrared spectrum using the lidar inversion extinction coefficient profile at 532 nanometers. DTIC

N94-20939# Georgia Inst. of Tech., Atlanta. School of Physics.
STATISTICAL FLUCTUATIONS IN LASERS
R. Roy 31 Dec. 1992 20 p
(Contract DE-FG05-87ER-13708)
(DE94-000710; DOE/ER-13708/1) Avail: CASI HC A03/MF A01

We summarize here the progress made over the period 1 June 1990 to 31 May 1993 for the research supported by the grant DOE-FG05-87ER13708. Our research has encompassed four major areas: (1) Detection of Weak Signals; (2) Interaction of an Atom with Chaotic and Coherent Fields; (3) Four-Wave Mixing in Nonlinear Optical Media; and (4) Coherence and Dynamics of Laser Arrays. We outline in this report the progress made in each area of investigation. The papers in the Appendix provide a comprehensive report including details of the experimental and theoretical investigations. DOE

N94-21253# Environmental Research Inst. of Michigan, Ann Arbor.
LONG-RANGE LASER IMAGING Final Report, Jan. - Jul. 1993
Joseph C. Marron and Richard G. Paxman 30 Sep. 1993 63 p
(Contract DLA900-88-D-0392)
(AD-A273020; ERIM-246830-9-F) Avail: CASI HC A04/MF A01

This report summarizes a research program in which we evaluated the use of a Long-Range Laser Imaging (LRLI) system to perform the imaging tasks associated with laser target designation. The motivation for LRLI is to improve crew and aircraft survivability by increasing the standoff range and reducing the required time interval for air-based laser target designation. In this program, we analyzed the capabilities of LRLI systems. We considered the signal level and its impact on sensor field-of-view. This analysis includes laser selection, atmospheric transmission, target reflectivity, and optical system characteristics. It is shown that the laser signal level ultimately limits the number of target pixels. It is also shown that a pulsed system is required for background rejection. The impact of optical turbulence on system performance is also discussed. We evaluated the achievable resolution and considered the use of adaptive optics. It is shown, however, that severe anisoplanatism limits the utility of adaptive optics. We conclude that the most promising sensor design is based on conventional imaging and recommendations for proof-of-concept experiments are given. DTIC

N94-21284# Science Research Lab., Inc., Somerville, MA.
COMPACT LIGHTWEIGHT CO2 LASER FOR SDIO APPLICATION Final Report, 1 Jul. 1990 - 30 Jun. 1992
Stephen Fulghum and Jonah Jacob 15 Nov. 1993 50 p
(Contract N00014-90-C-0162)
(AD-A273010; SRL-12-F-1993) Avail: CASI HC A03/MF A01

SRL has combined two all-solid-state pulsed power generators based on SCR-commutated nonlinear magnetic pulse compressors with low-pressure, conduction-cooled, CO2 laser cavities in a program to produce high repetition rate laser systems without the weight penalty of flow loop cooling. The first CO2 system used a transverse discharge, rectangular slab geometry, laser amplifier matched to the 10 Hz, SRL COLD-I solid-state pulser. Visible interferometric probes of the slab geometry laser medium showed the characteristic cylindrical wavefront error expected of a uniformly heated slab cooled at its walls. Conduction cooling of the 2.4 cm slab was sufficient to dissipate the thermal energy deposited by a single pulse dissipated to below the measurement level within 100 ms (10 Hz). The second CO2 system used a longitudinal discharge, cylindrical geometry, laser amplifier combined with the new SSLAM-VIII pulser which produces 72 KV, 30 J pulses at up to 5 KHz. The longitudinal laser output power typically peaked at 50 Hz since the heat load from higher repetition rates could not be dissipated sufficiently rapidly from the 4 cm diameter discharge. Due to an impedance mismatch the maximum single pulse energy in steady state operation was 350 mJ (18 W average power). A circuit to provide proper matching has been designed but has not yet been implemented. DTIC

N94-21299# Lawrence Livermore National Lab., CA.
GENERATION OF INTENSE ULTRASHORT X RAY PULSES
D. C. Eder, R. A. London, M. D. Rosen, and G. L. Strobel (Georgia Univ., Macon.) Aug. 1993 11 p Presented at the Annual Meeting of the Society of Photo-Optical Instrumentation Engineers (SPIE), San Diego, CA, 11-16 Jul. 1993
(Contract W-7405-eng-48)
(DE93-019607; UCRL-JC-112492; CONF-930722-29) Avail: CASI HC A03/MF A01

Modeling of x-ray emission from targets heated by an ultrashort-pulse high-intensity optical laser is discussed. One application, using the emitted x rays, is pumping inner-shell photo-ionized x-ray lasers. Short wavelength lasing (lambda less than or equal to 15 Angstrom) requires fast rise-time 1-3 KeV x rays to ionize inner K-shell electrons. It was shown that structured targets, consisting of grooves on a solid material or a composite of clusters, have high absorption. Grooved targets are modeled as an ensemble of exploding foils finding that the rise time of x rays is rapid enough for pumping inner-shell x-ray lasers. It is shown that simple atomic models can overestimate the energy in x-ray emission bands. High-Z materials are found to have the highest conversion efficiency but mid-Z materials can be used to provide a band of emission at a particular energy. It is shown that the pondermotive inhibition of expansion has only a small effect on the x-ray emission. The emission of a Au plasma is found to be appropriate for pumping inner-shell lasing at 14.6 Angstrom in Ne. The required optical laser intensity is of order 10(exp 17) W/cm(sup 2) using a 100 fsec FWHM duration pulse. To produce a laser with a gain-length product of order 10 requires 5-15 J of optical energy. DOE

N94-21353# Naval Postgraduate School, Monterey, CA.
A THEORY FOR OPTICAL WAVELENGTH CONTROL IN SHORT PULSE

FREE ELECTRON LASER OSCILLATORS M.S. Thesis
Wade F. Wilkenson Jun. 1993 110 p
(AD-A271706) Avail: CASI HC A06/MF A02

The future safety of the U.S. Navy warship depends on the development of a directed energy self-defense system to keep pace with the ever-improving technology of anti-ship missiles. Two candidates are reviewed. The free electron laser (FEL) has the most advantages, but a chemical laser proposed by TRW is ready for installation on existing ships. Initial testing of issues related to directed energy use at sea can be conducted with the chemical laser. When the technology of the FEL matures, it can replace the chemical laser to provide the best possible defense in the shortest period of time. Continuous tunability is a key advantage of the FEL over the conventional laser. But since the output wavelength is dependent on electron energy, it is subject to random fluctuations originating from the beam source. At the Stanford University Superconducting (SCA) Free Electron Laser (FEL) Facility, the effects are minimized through negative feedback by changing the input electron energy proportional to the observed wavelength drift. The process is simulated by modifying a short pulse FEL numerical program to allow the resonant wavelength to vary over many passes. The physical effects behind optical wavelength control are explained. A theory for the preferential nature of the FEL to follow the resonant wavelength from longer to shorter wavelengths is presented. Finally, the response of the FEL to a rapidly changing resonant wavelength is displayed as a transfer function for the system. DTIC

N94-21509# Air Force Inst. of Tech., Wright-Patterson AFB, OH. Foreign Aerospace Science and Technology Center.
EFFECTS OF STIMULATED RAMAN SCATTERING ON LIGHT BEAM PROPERTIES DURING HIGH-POWER LASER BEAM LONG-PATH PROPAGATION
Lian Chien, Zhan Shui, Xiao-Min Zhang, Xiao-Feng Wei, and Xiao-Dong Yuan 3 Nov. 1993 19 p Transl. into ENGLISH from Qiongjiguang Yu Lizishu (China), v. 4, no. 2, May 1992 p 277-283
(AD-A273109; FASTC-ID(RS)T-0100-93) Avail: CASI HC A03/MF A01

Beginning from the third-order nonlinear polarization from the stimulation and induction of matter based on the semiclassical theory of stimulated Raman scattering (SRS), a theoretical model of coupling between the phase of a pump (transmission) laser beam and the phase of the Stokes beam intensity is established for the case of stimulated Raman scattering during long-path propagation of a high-power laser. The model clearly explains how the SRS effect influences the beam properties of the pump laser, including the physical regime and effective factors of time-domain properties and space-domain properties (light beam quality). The theoretical analysis is in fairly satisfactory agreement with the experimental results. In the experiments, measurements of time-domain properties were taken of the pump laser beam and the Stokes beam after transmission in a situation with various conversion efficiencies eta(sub s). As shown by the results, under conditions of low-conversion efficiencies, basically the time-domain properties of the pump laser beam are not affected by the SRS effect. But when the conversion efficiency eta(sub s) is greater than five percent, the pulse duration of the pump laser beam is gradually reduced as eta(sub s) is increased. DTIC

N94-21547# Lawrence Livermore National Lab., CA.
LASER DRIVEN HYDRODYNAMIC INSTABILITY EXPERIMENTS
B. A. Remington, S. V. Weber, S. W. Haan, J. D. Kilkenny, S. G. Glendinning, R. J. Wallace, W. H. Goldstein, B. G. Wilson, and J. K. Nash 17 Feb. 1993 23 p Presented at the Meeting of the Division of Plasma Physics of the American Physical Society, Seattle, WA, 16-20 Nov. 1992
(Contract W-7405-eng-48)
(DE93-040550; UCRL-JC-111286-Rev-1; CONF-921103-6-Rev-1) Avail: CASI HC A03/MF A01

An extensive series of experiments has been conducted on the Nova laser to measure hydrodynamic instabilities in planar foils accelerated by x-ray ablation. Single mode experiments allow a measurement of the fundamental growth rates from the linear well into the nonlinear regime. Two-mode foils allow a first direct observation of mode coupling. Surface-finish experiments allow a measurement of the evolution of a broad spectrum of random initial modes. DOE

N94-21554# Los Alamos National Lab., NM.
DEMONSTRATION OF ULTRAVIOLET LASING WITH A LOW ENERGY ELECTRON BEAM
P. G. OShea, S. C. Bender, D. A. Byrd, J. W. Early, D. W. Feldman, C. M. Fortgang, J. C. Goldstein, B. E. Newman, R. L. Sheffield, and R. W. Warren et al 10 Aug. 1993 10 p Presented at the 15th International Free Electron Laser Conference, The Hague, Netherlands, 23-27 Aug. 1993
(Contract W-7405-eng-36)
(DE93-040192; LA-UR-93-3039; CONF-930855-4) Avail: CASI HC A02/MF A01

We report on the design details of the first ultraviolet (UV) free-electron laser (FEL) oscillator driven by low-energy electrons from a radio-frequency linear accelerator. In our experiment we used a high-current, high brightness electron beam in combination with a wiggler of novel design to produce an FEL that lased at wavelengths from 369-380 nm using 45.9-45.2 MeV electrons. In addition we performed a proof-of principle experiment that demonstrated the first ever photolithography on a photoresist-coated silicon wafer using an FEL light source. DOE

N94-21817*# Virginia Univ., Charlottesville. Dept. of Electrical Engineering.
DETERMINING THE 3-D STRUCTURE AND MOTION OF OBJECTS USING A SCANNING LASER RANGE SENSOR Progress Report, 1 Sep. - 15 Dec. 1993
N. Nandhakumar and Philip W. Smith Dec. 1993 12 p
(Grant NGT-51055)
(NASA-CR-194745; NAS 1.26:194745; UVA/528476/EE94/101) Avail: CASI HC A03/MF A01

In order for the EVAHR robot to autonomously track and grasp objects, its vision system must be able to determine the 3-D structure and motion of an object from a sequence of sensory images. This task is accomplished by the use of a laser radar range sensor which provides dense range maps of the scene. Unfortunately, the currently available laser radar range cameras use a sequential scanning approach which complicates image analysis. Although many algorithms have been developed for recognizing objects from range images, none are suited for use with single beam, scanning, time-of-flight sensors because all previous algorithms assume instantaneous acquisition of the entire image. This assumption is invalid since the EVAHR robot is equipped with a sequential scanning laser range sensor. If an object is moving while being imaged by the device, the apparent structure of the object can be significantly distorted due to the significant non-zero delay time between sampling each image pixel. If an estimate of the motion of the object can be determined, this distortion can be eliminated; but, this leads to the motion-structure paradox - most existing algorithms for 3-D motion estimation use the structure of objects to parameterize their motions. The goal of this research is to design a rigid-body motion recovery technique which overcomes this limitation. The method being developed is an iterative, linear, feature-based approach which uses the non-zero image acquisition time constraint to accurately recover the motion parameters from the distorted structure of the 3-D range maps. Once the motion parameters are determined, the structural distortion in the range images is corrected. Author (revised)

N94-21829 Lawrence Livermore National Lab., CA.
IONIZATION OF H2(+) IN INTENSE LASER FIELDS
F. H. Mies (National Inst. of Standards and Technology, Gaithersburg, MD.), A. Giusti-Suzor (Laboratoire de Chimie-Physique, Orsay, France.), K. C. Kulander, and K. J. Schafer 1 Jan. 1993 13 p Presented at the North Atlantic Treaty Organization Workshop, Han-Sur-Lesse, Belgium, 8-14 Jan. 1993 Limited Reproducibility: More than 20% of this document may be affected by microfiche quality
(Contract W-7405-eng-48)
(DE93-019160; UCRL-JC-114023; CONF-9301119-2) Avail: CASI HC A03

The motivation for the present ionization calculations is to test the reliability of a recent study of H2(+) photodissociation which employed such a two electronic state model and neglected any competition with ionization. The photodissociation calculations indicate that in intense short pulsed laser fields appreciable populations of stable vibrational states can survive the pulse. This survival effect can be attributed to the trapping of portions of the initial vibrational wavepacket in transient laser-induced

potential wells at intermediate R approximately 3-4 au distances. Since the calculated ionization rates exhibit a marked decrease at short R, they already lend some credence to the vibrational trapping effect. Having accurate R-dependent rates enables us to estimate the competitive influence of the ionization on the stabilized population, and may ultimately allow us to predict the contribution of the Coulomb 'explosion' channel to observed proton kinetic energy distributions. In this paper we will demonstrate the effectiveness of the two-state length gauge model in interpreting the ionization rates that we extract from the numerically exact solutions of the time-dependent Schroedinger equation. A more elaborate presentation of the theory and the results for the full range of distances and wavelengths will be presented elsewhere. DOE

N94-21839# Rochester Univ., NY. Lab. for Laser Energetics.
STABILITY ANALYSIS OF UNSTEADY ABLATION FRONTS
R. Betti, R. L. McCrory, and C. P. Verdon Aug. 1993 10 p
(Contract DE-FC03-92SF-19460)
(DE93-019689; DOE/DP-40200-265) Avail: CASI HC A02/MF A01

The linear stability analysis of unsteady ablation fronts is carried out for a semi-infinite uniform medium. For a laser accelerated target, it is shown that a properly selected modulation of the laser intensity can lead to the dynamic stabilization or growth-rate reduction of a large portion of the unstable spectrum. The theory is in qualitative agreement with the numerical results obtained by using the two-dimensional hydrodynamic code ORCHID. DOE

N94-21844# Lawrence Livermore National Lab., CA.
HIGH-POWER COPPER VAPOR LASERS AND THEIR APPLICATION TO PRECISION DRILLING AND CUTTING
B. E. Warner and P. D. Weber 27 Jul. 1993 4 p Presented at the Institute of Electrical and Electronics Engineers/Lasers and Electro-Optics Society (IEEE/LEOS) Annual Meeting, San Jose, CA, 15-19 Nov. 1993
(Contract W-7405-eng-48)
(DE93-019951; UCRL-JC-113183; CONF-931197-2) Avail: CASI HC A01/MF A01

High-power copper vapor lasers (CVL's) have been under development at Lawrence Livermore National Laboratory (LLNL) for more than 15 years in support of the DOE's Program in Laser Isotope Separation. The technology is now quite mature having met many of its goals in system architecture, power, reliability, and maintainability. Over the past several years we have begun an effort to utilize this technology in other industrial applications, such as metals processing, and have found a number of unique processes. In this paper we describe briefly the general characteristics of the CVL, our recent progress in developing the laser as an industrial tool, and our progress in using the laser in precision drilling and cutting. DOE

N94-21872 Lawrence Livermore National Lab., CA.
SIMULATIONS OF SPECTRAL BROADENING BY CROSS-PHASE MODULATION (XPM) WITH CHAOTIC LIGHT PULSES
M. A. Henesian, S. N. Dixit, C. J. Chen, P. K. A. Wai, and C. R. Menyuk 25 May 1993 14 p Presented at the OE/LASE 1993 International Society for Optical Engineering Conference, Los Angeles, CA, 13-23 Jan. 1993 Limited Reproducibility: More than 20% of this document may be affected by microfiche quality
(Contract W-7405-eng-48)
(DE93-019623; UCRL-JC-112742; CONF-930159-55) Avail: CASI HC A03

Spectral broadening of single-frequency laser pulses by optical cross-phase modulation (XPM) with chaotic laser pulses in birefringent single-mode optical fibers is investigated numerically and results are compared with experiments. By this process we have generated laser pulses of variable bandwidth (1-25 A) at the fundamental wavelength (1053 nm) for amplification in high power solid-state Nd:glass lasers used for inertial confinement fusion research. Simulations indicate that a temporally smooth XPM pulse can be generated with intensity fluctuations of less than 10% and spectral width greater than 50 A using a short length (approximately 5 m) of special low dispersion and low birefringence fiber, e.g. D = 10 ps/nm-km (normal dispersion) and Delta-n = 2 x 10(exp -5). Readily available fibers of similar length, with parameters of D = 40 ps/nm-km and Delta-n = 6 x 10(exp -5), can give spectral widths exceeding 25 A, but the noise will range from 25 to 60%. Broadband laser pulses generated by XPM are now routinely used at Lawrence Livermore National Laboratory for active smoothing of the laser irradiance on targets by the technique of smoothing by spectral dispersion. DOE

N94-21873 Lawrence Livermore National Lab., CA.
SHATTERING THE MYTH OF THE RESONANTLY PHOTO-PUMPED NEON-LIKE TITANIUM LASER
J. Nilsen, B. J. MacGowan, L. B. DaSilva, J. C. Moreno, and J. A. Koch 1993 9 p Presented at the Annual Meeting of the Society of Photo-Optical Instrumentation Engineers, San Diego, CA, 11-16 Jul. 1993 Limited Reproducibility: More than 20% of this document may be affected by microfiche quality
(Contract W-7405-eng-48)
(DE93-019624; UCRL-JC-112554; CONF-930722-31) Avail: CASI HC A02

Several years ago neon-like titanium (Z = 22) was made to lase at 326 A on the 3p yields 3s (J = 0 yields 1) transition. At the time it was suggested that the lasing may be due to resonantly photo-pumping the neon-like titanium 2p yields 4d lines using 3s yields 2p and 3d yields 2p lines in carbon-like and nitrogen-like titanium which results in lasing on the 3p yields 3s transition in neon-like titanium. The strongest argument for this explanation was that adjacent elements (scandium and vanadium) did not lase while titanium was unique in having the above mentioned resonance. In addition a pre-pulse was required to make the titanium lase, suggestive of the formation of a low density plasma, and the plasma was very overstripped, so the above mentioned pump lines should be quite strong for photo-pumping. We have re-investigated this laser system and will present results which show lasing on the 3p yields 3s (J = 0 yields 1) transition in neon-like chromium (Z = 24), iron (Z = 26), and nickel (Z = 28) at 285, 255, and 231 A respectively. This destroys the myth of titanium being unique and makes highly unlikely that the previously mentioned photo-pumping mechanism is playing a significant role in the titanium laser. The chromium, iron, and nickel experiments all require a pre-pulse in order to lase and our calculations suggest that the pre-pulse is an exciting new way to create a uniform low density plasma when illuminating a thick slab target. This allows the proper conditions for gain and laser propagation for low Z neon-like ions and may also be applicable to other systems such as low Z nickel-like ions. We also will present experiments done on other low-Z materials and offer an explanation as to how the hyperfine effect is destroying the gain of neon-like ions with odd Z. DOE

N94-21920# Lawrence Livermore National Lab., CA.
EFFECT OF BANDWIDTH ON BEAM SMOOTHING AND FREQUENCY CONVERSION AT THE THIRD HARMONIC OF THE NOVA LASER
D. M. Pennington, M. A. Henesian, S. N. Dixit, H. T. Powell, C. E. Thompson, and T. L. Weiland May 1993 13 p Presented at the OE/LASE 1993: International Society for Optical Engineering (SPIE) Conference, Los Angeles, CA, 13-23 Jan. 1993
(Contract W-7405-eng-48)
(DE93-019917; UCRL-JC-111593; CONF-930159-56) Avail: CASI HC A03/MF A01

We present the results of experiments performed on the Nova laser system to determine the effect of bandwidth on third harmonic (3 omega) frequency conversion and beam smoothing by spectral dispersion (SSD). Our experiments utilized a wide bandwidth fiber optic cross-phase modulated (XPM) source and a narrower bandwidth microwave modulated (FM) source, each centered at 1053 nm (1 omega). The FM source produced approximately 2 cm(exp -1) of bandwidth, modulated at 3 GHz; the XPM bandwidth was varied from 5 to 15 cm(exp -1), modulated by the temporally noisy output of a multimode Nd:glass laser (less than or equal to 500 GHz). The FM beam showed no evidence of self-phase modulation in the laser chain produced by intensity fluctuations, and 1 omega bandwidth was tripled upon conversion to 3 omega (2-6 cm(exp -1)). The 1 omega XPM bandwidth increased by greater than or equal to 25% due to self-phase modulation in the laser chain (16-22 cm(exp -1)) due to it's relative noisy temporal structure. Over 50% of the 1 omega XPM bandwidth was transferred to the 3 omega beam (22-36 cm(exp -1)), yielding 0.13% bandwidth at 3 omega. The maximum intrinsic narrowband 3 omega frequency conversion obtained using a type-II/type-II KDP crystal array was 62%. The intrinsic efficiency obtained at the Nova 10-beam chamber is typically greater than 65%. We have developed broadband frequency conversion codes and broadband pulse simulations to model our results,

and have obtained good agreement with experiment. Using a random phase plate without bandwidth, we obtained a smoothing level, sigma/I approximately 0.79, defined by the rms variance normalized with respect to the average intensity. This is less than the theoretically expected value of one for an ideal speckle pattern, and could be evidence of polarization smoothing as a result of focus lens birefringence. With spectral dispersion and RPP we demonstrated an excellent level of smoothing with the XPM source. DOE

N94-21957# Oak Ridge National Lab., TN.
THE LASER AND ITS APPLICATIONS ON ENVIRONMENT AND BIOTECHNOLOGY RESEARCH
C. H. Chen and F. C. Chen 1993 4 p Presented at the 1993 Chinese American Academic and Professional Convention, Chicago, IL, 2-5 Jul. 1993
(Contract DE-AC05-84OR-21400)
(DE94-000376; CONF-930796-4) Avail: CASI HC A01/MF A01

During the past few years, researchers at ORNL have developed four new instruments involving the use of a laser for environmental and biotechnology research. They are: (1) a single atom detector, (2) a rare gas atom counter, (3) biopolymer mass spectrometer, and (4) a refrigerant ratiometer. Their basic principles and applications are briefly described. DOE

N94-21975# Indore Univ. (India).
GENERATION OF HARMONIC RADIATION USING THE MULTI-CAVITY FREE-ELECTRON LASER
S. Krishnagopal and A. M. Sessler (California Univ., Berkeley. Lawrence Berkeley Lab.) 18 Aug. 1993 15 p Presented at the 15th International Free Electron Laser Conference, The Hague, Netherlands, 23-27 Aug. 1993
(Contract DE-AC03-76SF-00098)
(DE94-001261; LBL-34015; CONF-930855-7) Avail: CASI HC A03/MF A01

A Free-Electron Laser (FEL) provides a convenient method of reaching short wavelengths by resonating with an input source at the fundamental wavelength while providing bunching at a harmonic of the fundamental. Recently schemes have been proposed that use two wiggler segments, one resonant at the fundamental to pre-bunch the beam, the other lasing at the desired (third) harmonic. A similar effect, with some advantages and some disadvantages, can be achieved using the Multi-Cavity FEL (MC/FEL). The MC/FEL employs several short cavities, operating in an oscillator-like manner, to achieve high output power. In this paper we consider the use of the MC/FEL as a means of generating harmonics. We investigate the competitiveness of this option in comparison with other harmonic generation schemes, in terms of the total wiggler length needed, the saturated power achieved, and the restrictions imposed by mirror reflectivity. DOE

N94-22020# Los Alamos National Lab., NM.
VARIABLE-FIELD PERMANENT MAGNET DIPOLE
D. B. Barlow, R. H. Kraus, Jr., and R. E. Meyer 1993 4 p Presented at the 13th International Conference on Magnet Technology, Victoria, Canada, 20-24 Sep. 1993
(Contract W-7405-eng-36)
(DE94-000800; LA-UR-93-3237; CONF-930926-5) Avail: CASI HC A01/MF A01

A new concept for a variable-field permanent-magnet dipole (VFPMD) has been designed, fabricated, and tested at Los Alamos. The VFPMD is a C-shaped sector magnet with iron poles separated by a large block of magnet material (SmCo). The central field can be continuously varied from 0.07 T to 0.3 T by moving an iron shunt closer or further away from the back of the magnet. The shunt is specially shaped to make the dependence of the dipole field strength on the shunt position as linear as possible. The dipole has a 2.8 cm high by 8 cm wide aperture with approximately 10 cm long poles. DOE

N94-22401# Lawrence Livermore National Lab., CA.
PHASE SCREENS FOR THE CONTROL OF THE FOCAL IRRADIANCE OF THE NOVA LASER
J. K. Lawson, S. N. Dixit, D. Eimerl, M. A. Henesian, K. R. Manes, A. J. Morgan, H. T. Powell, I. M. Thomas, J. B. Trenholme, and B. W. Woods 17 Sep. 1993 9 p Presented at the OE/LASE 1993 International Society for Optical Engineering Conference, Los Angeles, CA, 13-23 Jan. 1993
(DE94-001067; UCRL-JC-111445; CONF-930159-58) Avail: CASI HC A02/MF A01

The authors report on the design and fabrication of continuous contour (kinoform) phase plates for homogenizing the focal plane irradiance of high-power, inertial confinement fusion laser systems. These kinoform phase plates are designed using an iterative algorithm. They offer the flexibility of controlling the overall shape of the far-field irradiance profile and the ability to concentrate the energy within a central region of the focal profile. These properties make kinoforms superior to the conventional, binary random phase plates for many applications. Potential methods for fabrication of such kinoform phase plates are discussed. DOE

N94-22585# Los Alamos National Lab., NM.
INFRARED FEL PHOTOCHEMISTRY: MULTIPLE-PHOTON DISSOCIATION OF FREON GAS
B. E. Newnam, J. W. Early, and J. L. Lyman 1993 14 p Presented at the 15th International Free Electron Laser Conference, The Hague, Netherlands, 23-27 Aug. 1993
(Contract W-7405-eng-36)
(DE94-000817; LA-UR-93-3419; CONF-930855-8) Avail: CASI HC A03/MF A01

Wavelength tunability, synchrotron sidebands, and picosecond pulse structure are inherent FEL characteristics that should be advantageous for photochemistry involving infrared multiple-photon photodissociation. Tuned to an absorption resonance, the FEL sideband structure will overlap the broad, excited-state spectral absorption and should lead to enhanced dissociation. The Los Alamos APEX FEL was operated with and without sidebands to test this hypothesis on CFCl3 (Freon 11), an inert chlorofluorocarbon widely used in refrigeration systems and one of the gases implicated as depleting the ozone in the Earth's stratospheric layer. The FEL wavelength was set at the C-Cl stretch absorption resonance at 11.8-microns, the oscillator cavity length was detuned first to minimize and then to maximize the spectral bandwidth, and the beam was focused through a pair of test cells (1.0 Torr Freon + 1.7 Torr air). Comparison of final and initial absorbance spectra indicated the CFCl3 photodissociation yield was 1.2% for the cell exposed with sideband spectra (3% FWHM) and 9-ns micropulse separation. Negligible effect was seen without sidebands, albeit at lower total beam fluence. Although the result of this single experiment is not large enough to be conclusive, it does provide a basis for optimizing the FEL temporal and spectral parameters to attain higher photodissociation yield in future tests. DOE

N94-21006*# Nebraska Univ., Lincoln. Dept. of Electrical Engineering.
THERMAL DIFFUSIVITY MEASUREMENTS BY PHOTOTHERMAL LASER BEAM DEFLECTION (PTD): DATA ANALYSIS USING THE LEVENBERG-MARQUARDT ALGORITHM
Hassanayn Machlab, William A. McGahan, and John A. Woollam *In its* Materials, Structures, and Devices for High-Speed Electronics 1993 1 p Repr. from Thin Solid Films (Elsevier Sequoia), v. 215, 1992 p 103-107 (For primary document see N94-20971 05-76)
Avail: CASI HC A01/MF A01

N94-22202 Centre National de la Recherche Scientifique, Paris (France).
TWO-DIMENSIONAL PERCEPTION BASED ON A LASER RANGEFINDER [PERCEPTION BIDIMENTIONNELLE A BASE D'UN TELEMETRE LASER]
G. Allegre and H. Clergeot *In* Engineering Inst. of Canada, Canadian Conference on Electrical and Computer Engineering, Volumes 1 and 2 1991 4 p In FRENCH (For primary document see N94-22101 05-33)
Avail: Issuing Activity (Engineering Inst. of Canada, 2050 rue Mansfield, Suite 700, Montreal, PQ H3A 1Z2 Canada)

N94-22603# Airbus Industrie, Toulouse (France).
UTILIZATION OF LASERS FOR AIR DATA MEASUREMENTS [EINSATZ VON LASERN BEI LUFTDATENMESSUNGEN]
J. Hammer *In* Tech. Univ. Berlin, Measurement Technology for Flight Tests May 1991 p 64-81 In GERMAN (For primary document see N94-22597 05-02)
Avail: CASI HC A03/MF A02

37 MECHANICAL ENGINEERING

Includes auxiliary systems (nonpower); machine elements and processes; and mechanical equipment.

N94-19833# Nevada Univ., Las Vegas.
RESEARCH IN LIGHTWEIGHT ELASTIC ROBOTIC ARMS Final Report, 19 Nov. 1986 - 30 Jun. 1993
T. A. Nartker 10 Jun. 1993 23 p
(Contract DAAL03-87-G-0004)
(AD-A270846; ARO-24960.70-MA-REP) Avail: CASI HC A03/MF A01

The program involved a series of individual projects coordinated to develop controls for a flexible light weight robot arm. A hydraulically actuated 3-link robot arm was installed on a PRAB hydraulic base, and was designed of tubular steel. A PERT program chart was prepared (appendix B) on which various interrelated project milestones were projected. DTIC

N94-19859# EG and G Rocky Flats, Inc., Golden, CO.
THERMOCAPILLARY AND ARC PHENOMENA IN STAINLESS STEEL WELDS Ph.D. Thesis
S. W. Pierce 1993 140 p
(Contract DE-AC34-90RF-62349)
(DE94-000518; RFP-4768) Avail: CASI HC A07/MF A02

The goal of this paper is to study the effects of power level and distribution on thermocapillary induced weld shape and of arc factors on weld shape. Thermocapillarity is apparent in both conduction mode electron beam welds (EBW) and gas tungsten arc (GTA) welds, particularly in the former. A non-Gaussian arc distribution is suggested to account for the differences between the two welding processes. At higher current levels (200-300 A), plasma shear force also contributes to weld shape development. Evidence suggests that thermocapillary flow reversal is not a factor in normal GTA welds; EBW flow reversal occurs only at high power density levels where the keyhole mode is present. DOE

N94-19891# Oak Ridge National Lab., TN.
EVALUATION OF A SCANNING HARTMANN DEVICE FOR SINGLE POINT TURNING APPLICATIONS
Arthur C. Miller, Jr. and Tilman W. Stuhlinger (Talandic Research Corp., Tucson, AZ.) 1993 11 p Presented at the Annual Meeting of the Society of Photo-Optical Instrumentation Engineers, San Diego, CA, 11-16 Jul. 1993
(Contract DE-AC05-84OR-21400)
(DE93-019204; CONF-930722-21) Avail: CASI HC A03/MF A01

A new, machine mounted aspheric metrology device designed to measure a broad range of figures without the use of auxiliary optics is addressed. A prototype device, based on the classical Hartmann test, called a Hartmann Optical Surface Tester (HOST) was evaluated on a single point diamond turning machine. Design, initial testing, and validation data from reference spheres, and two types of aspheres are discussed. Results of a simulation model for estimating acceptable alignment errors for the HOST on the diamond turning machine are also presented. Peak-to-valley measurement uncertainty on the test optics was found to be better than 0.08 microns. DOE

N94-20021 Woods Hole Oceanographic Inst., MA.
DESIGN OF A CONTROLLABLE PITCH UNDERWATER THRUSTER SYSTEM M.S. Thesis
Robert W. Keefe Aug. 1993 114 p Limited Reproducibility: More than 20% of this document may be affected by microfiche quality
(AD-A271140) Avail: CASI HC A06

Control systems for underwater vehicles have reached the level of sophistication where they are limited by the dynamic performance of the thrust actuators. Standard fixed-pitch propellers have been shown to have very poor dynamic characteristics, particularly at low thrust levels. The dynamic response of a fixed-pitch propeller is dependent upon highly non-linear transients encountered while the shaft speed approaches its steady-state value. This thesis proposes the use of a controllable pitch propeller system to address this problem. A controllable pitch propeller varies the amount of thrust produced by varying the pitch angle of the blades at a constant shaft speed. The bandwidth of this type of thrust actuator would be dependent primarily on the speed at which the pitch angle of the blades are changed. A variable pitch propeller system suitable for retrofit into an ROV is designed and built. The system is designed for maximal pitch angle bandwidth with low actuator power consumption. DTIC

N94-20044*# North Carolina State Univ., Raleigh. Mars Mission Research Center.
TELEROBOTIC CONTROL OF A MOBILE COORDINATED ROBOTIC SERVER, EXECUTIVE SUMMARY Annual Technical Report
Gordon Lee 7 Dec. 1993 23 p
(Grant NAG1-1283)
(NASA-CR-194685; NAS 1.26:194685) Avail: CASI HC A03/MF A01

This interim report continues with the research effort on advanced adaptive controls for space robotics systems. In particular, previous results developed by the principle investigator and his research team centered around fuzzy logic control (FLC) in which the lack of knowledge of the robotic system as well as the uncertainties of the environment are compensated for by a rule base structure which interacts with varying degrees of belief of control action using system measurements. An on-line adaptive algorithm was developed using a single parameter tuning scheme. In the effort presented, the methodology is further developed to include on-line scaling factor tuning and self-learning control as well as extended to the multi-input, multi-output (MIMO) case. Classical fuzzy logic control requires tuning input scale factors off-line through trial and error techniques. This is time-consuming and cannot adapt to new changes in the process. The new adaptive FLC includes a self-tuning scheme for choosing the scaling factors on-line. Further the rule base in classical FLC is usually produced by soliciting knowledge from human operators as to what is good control action for given circumstances. This usually requires full knowledge and experience of the process and operating conditions, which limits applicability. A self-learning scheme is developed which adaptively forms the rule base with very limited knowledge of the process. Finally, a MIMO method is presented employing optimization techniques. This is required for application to space robotics in which several degrees-of-freedom links are commonly used. Simulation examples are presented for terminal control - typical of robotic problems in which a desired terminal point is to be reached for each link. Future activities will be to implement the MIMO adaptive FLC on an INTEL microcontroller-based circuit and to test the algorithm on a robotic system at the Mars Mission Research Center at North Carolina State University. Author (revised)

N94-20126* National Aeronautics and Space Administration. Goddard Space Flight Center, Greenbelt, MD.
SPLINE SCREW PAYLOAD FASTENING SYSTEM Patent
John M. Vranish, inventor (to NASA) 14 Sep. 1993 16 p Filed 21 Sep. 1992 Supersedes N94-15871 (32 - 3, p 1046)
(NASA-Case-GSC-13454-1; US-Patent-5,244,406;
US-Patent-Appl-SN-947612; US-Patent-Class-439-362;
Int-Patent-Class-H01R-13/00) Avail: US Patent and Trademark Office

A system for coupling an orbital replacement unit (ORU) to a space station structure via the actions of a robot and/or astronaut is described. This system provides mechanical and electrical connections both between the ORU and the space station structure and between the ORU and the ORU and the robot/astronaut hand tool. Alignment and timing features ensure safe, sure handling and precision coupling. This includes a first female type spline connector selectively located on the space station structure, a male type spline connector positioned on the orbital replacement unit so as to mate with and connect to the first female type spline connector, and a second female type spline connector located on the orbital replacement unit. A compliant drive rod interconnects the second female type spline connector and the male type spline connector. A robotic special end effector is used for mating with and driving the second female type spline connector. Also included are alignment tabs exteriorally located on the orbital replacement unit for berthing with the space station structure. The first and second female type spline connectors each include a threaded bolt member having a captured nut member located thereon which can translate up and down the bolt but are constrained from rotation thereabout, the nut member having a mounting surface with at least one first type electrical connector located on the mounting surface for translating with the nut member. At least one complementary second type electrical connector on the orbital replacement unit mates with at least one first type electrical connector on the mounting surface of the nut member. When the driver on the robotic end effector mates with the second female

type spline connector and rotates, the male type spline connector and the first female type spline connector lock together, the driver and the second female type spline connector lock together, and the nut members translate up the threaded bolt members carrying the first type electrical connector up to the complementary second type connector for interconnection therewith. Official Gazette of the U.S. Patent and Trademark Office

N94-20127* National Aeronautics and Space Administration. Goddard Space Flight Center, Greenbelt, MD.

AN IMPROVED PATCH FOR RADIATIVE COOLERS Patent

Vincent T. Bly, inventor (to NASA) 7 Sep. 1993 7 p Filed 25 Jan. 1993 Supersedes N94-15873 (32 - 3, p 1046)
(NASA-Case-GSC-13503-1; US-Patent-5,241,836;
US-Patent-Appl-SN-008427; US-Patent-Class-62-467;
US-Patent-Class-165-41; US-Patent-Class-165-904;
US-Patent-Class-244-158R; US-Patent-Class-244-158A;
US-Patent-Class-244-163; Int-Patent-Class-F25B-23/00) Avail: US Patent and Trademark Office

A unique structure for constructing the emissive patch of a spaceborne radiative cooler is shown. The structure has very high emissivity for all angles up to a designed-in maximum angle and near zero emissivity for greater angles. The structure also allows the use of high emissivity, nonconducting paints while fully complying with the NASA Electrostatic Discharge Susceptibility requirements for spacecraft. To accomplish these tasks, two previous disadvantages of prior art methods are addressed; eliminating background thermal radiation sources and problems concerning the high emissivity paints used in association with the black body radiator. A reflector consisting of an array of parabolic concentrators is separated from a black body element by an electrically conductive spacer. The concentrators serve to limit the field of view while the conductive spacer eliminates the need to use a conductive paint on the emissive element.
Official Gazette of the U.S. Patent and Trademark Office

N94-20146# Loughborough Univ. of Technology (England). Dept. of Mathematical Sciences.

A DESIGN OPTIMIZATION PROCEDURE FOR EPICYCLIC GEARS

J. D. Andrews Jun. 1993 29 p
(MATHS-Rept-A-188; ETN-93-94906) Avail: CASI HC A03/MF A01

A design optimization procedure to increase the working life of epicyclic gears units by minimizing the tensile fillet stresses experienced in the gear system components is described. An objective function is formulated together with 69 constraints which ensure that a functional system design is achieved. For the example presented, the optimum design was produced in only three iterations and reduced the maximum stress in any component by 54%. ESA

N94-20157 Technische Univ., Delft (Netherlands). Faculty of Technical Mathematics and Informatics.

THE CAUSES OF CONTACT NOISE [OVER DE OORZAKEN VAN CONTACTGELUID]

J. J. Kalker 1992 15 p In DUTCH Limited Reproducibility: More than 20% of this document may be affected by microfiche quality
(Rept-92-100; ETN-93-94289) Copyright Avail: CASI HC A03

The rolling contact noise of trains and trams was studied. The differences in the research methods for trains and trams are outlined. Some fundamentals of contact mechanics and elementary properties of rolling noise are introduced. The mechanisms of rolling and curve noise are explained using a computer simulation. ESA

N94-20356# Department of the Navy, Washington, DC.

DISENGAGABLE ADAPTER FOR AN OPTICAL FIBER CONNECTOR Patent Application

Gair D. Brown, inventor (to Navy) and Michael A. Richardson, inventor (to Navy) 18 Mar. 1993 18 p
(AD-D015959; US-Patent-Appl-SN-033223; Navy-Case-75029) Avail: CASI HC A03/MF A01

A disengagable adapter for mechanically coupling optical fibers is provided. The disengagable adapter separates into two complementary receptacle parts. Each receptacle part receives through a bore a single optical-fiber located within an optical-fiber connector plug. Each receptacle part attaches to and securely holds a different connector plug. The receptacle parts mate with each other in a complementary fashion and thereby connect the two optical fiber connector plugs together. These connector plugs accordingly align the two optical fibers located within the plugs. The optical fibers can be separated either by demating the complementary parts or by disconnecting one side of the adapter from its connector plug. Mounting the complementary parts to a plate facilitates multiple, simultaneous connections. DTIC

N94-20365* National Aeronautics and Space Administration. Langley Research Center, Hampton, VA.

SHAFT MOUNT FOR DATA COUPLER SYSTEM Patent

James R. Elliott, Jr., inventor (to NASA) and Mark T. Lord, inventor (to NASA) 16 Nov. 1993 5 p Filed 3 Oct. 1991 Supersedes N92-30097 (30 - 20, p 3480)
(NASA-Case-LAR-13805-1; US-Patent-5,261,757;
US-Patent-Appl-SN-770509; US-Patent-Class-403-344;
US-Patent-Class-403-24; US-Patent-Class-403-27; US-Patent-Class-403-6;
US-Patent-Class-416-61; Int-Patent-Class-F16B-3/06) Avail: US Patent and Trademark Office

A device for mounting a data transmission apparatus to a rotating, tapered, and instrumented shaft is provided. This device permits attachment without interfering with shaft rotation or the accuracy of data output, and prevents both radial and axial slippage of the data transmission apparatus. The mounting device consists of a sleeve assembly which is attached to the shaft by means of clamps that are situated at some distance removed from the instrumented area of the shaft. The data transmission device is secured to the sleeve such that the entire assembly rotates with the shaft. Shim adjustments between sleeve sections assure that a minimum compressive load is transferred to the instrumented area of the shaft and a rubber lining is affixed to a large portion of the interior surface of the sleeve to absorb vibration.
Official Gazette of the U.S. Patent and Trademark Office

N94-20369* National Aeronautics and Space Administration. Langley Research Center, Hampton, VA.

COUNTER-BALANCED, MULTIPLE CABLE CONSTRUCTION CRANE Patent

Martin M. Mikulas, Jr., inventor (to NASA) and Li-Farn Yang, inventor (to NASA) 19 Oct. 1993 16 p Filed 18 Nov. 1991 Supersedes N92-34212 (30 - 24, p 4189)
(NASA-Case-LAR-14565-1-CU; US-Patent-5,253,771;
US-Patent-Appl-SN-793974; US-Patent-Class-212-148;
US-Patent-Class-212-196; US-Patent-Class-212-262;
Int-Patent-Class-B66C-23/76) Avail: US Patent and Trademark Office

The invention is a counter-balanced, multiple cable construction crane. The apparatus for hoisting payloads comprises a crane having a lifting means, the lifting means comprising an end effector means and three suspension means or cables. One end of each cable attaches to a different winding means located on the lifting means, and the other end of each cable attaches to a different point on the end effector, such that the three cables have a theoretical point of convergence with this point corresponding to the center of mass of the payload. Three controls command rotation of the winding means to a predetermined position. Accordingly, the crane provides precise and autonomous positioning of the payload without human guidance. The crane further comprises a counter-balancing means. Two controls position the counter-balancing means to offset the overturning moment which arises during the lifting of heavy payloads.
Official Gazette of the U.S. Patent and Trademark Office

N94-20375* National Aeronautics and Space Administration. Lewis Research Center, Cleveland, OH.

THREE POINT LEAD SCREW POSITIONING APPARATUS FOR A CAVITY TUNING PLATE Patent

Frank S. Calco, inventor (to NASA) 7 Sep. 1993 7 p Filed 27 Jan. 1992 Supersedes N92-17678 (30 - 8, p 1307)
(NASA-Case-LEW-15216-1; US-Patent-5,243,310;
US-Patent-Appl-SN-826547; US-Patent-Class-333-233;
US-Patent-Class-315-5.54; Int-Patent-Class-H01P-7/06) Avail: US Patent and Trademark Office

Three lead screws are provided for adjusting the position of a traversing plate. Each of the three lead screws is threaded through a collar that is press fitted through the center of one of three pinion gears. A sun gear meshes with all three pinion gears and transversely moves the three lead

screws upon actuation of a drive gear. The drive gear meshes with the sun gear and is driven by a handle or servomotor. When the handle or servomotor rotates the drive gear, the sun gear rotates causing the three pinion gears to rotate, thus, causing transverse movement of the three lead screws and, accordingly, transverse movement of the transversing plate. When the drive gear rotates, the traversing plate is driven in and out of a microwave cavity. Thus, the length or size of the cavity can be tuned while maintaining the traversing plate in an exact parallel relationship with an opposing plate on another end of the cavity.

Official Gazette of the U.S. Patent and Trademark Office

N94-20379* National Aeronautics and Space Administration. Marshall Space Flight Center, Huntsville, AL.

MOLD BOLT AND MEANS FOR ACHIEVING CLOSE TOLERANCES BETWEEN BOLTS AND BOLT HOLES Patent

David L. Johnston, inventor (to NASA) and Phillip G. Bryant, inventor (to NASA) 30 Nov. 1993 5 p Filed 27 Jan. 1993 Supersedes N93-30567 (31 - 11, p 3447)

(NASA-Case-MFS-28720-1; US-Patent-5,265,994;
US-Patent-Appl-SN-009909; US-Patent-Class-411-82;
US-Patent-Class-411-258; US-Patent-Class-411-930;
US-Patent-Class-425-129.1; Int-Patent-Class-F16B-39/02;
Int-Patent-Class-F16B-39/00) Avail: US Patent and Trademark Office

In the space shuttle, a cargo bay storage rack was required which was to be manufactured from a metal-plastic composite and bolted to a cargo structure. Following completion, utilization of the rack was disallowed due to tolerances, that is, the size differences between the outside bolt diameter and the inside hole diameter. In addition to the space shuttle problem there are other close tolerance requirements for bolts. Such environments often benefit from close tolerance bolting. Frequently such fabrication is not cost effective. Consequently there is a need for means of achieving close tolerances between bolts and bolt holes. Such means are provided. After compressing the elements together a strong rigid plastic, ceramic, or ceramic plastic fluid is forced into a channel extending through the bolt.

Official Gazette of the U.S. Patent and Trademark Office

N94-20380* National Aeronautics and Space Administration. Marshall Space Flight Center, Huntsville, AL.

TURNTABLE MECHANISM Patent

William Neill Myers, inventor (to NASA) 19 Oct. 1993 7 p Filed 31 Jan. 1992 Supersedes N93-31313 (31 - 12, p 3734)

(NASA-Case-MFS-28522-1; US-Patent-5,254,173;
US-Patent-Appl-SN-828612; US-Patent-Class-118-728;
US-Patent-Class-118-500; US-Patent-Class-118-730;
US-Patent-Class-269-71; Int-Patent-Class-B05C-13/00) Avail: US Patent and Trademark Office

In vacuum plasma spraying a turntable must be provided which not only makes it possible to rotate and tilt a heavy workpiece, but to operate at vacuum plasma temperatures to do so. In the vacuum plasma coating of large parts such as combustion chambers of rocket engines, the workpiece must not only be rotated, but it must be tilted. Hence, the turntable must be capable not only of supporting heavy parts, but of angulating such heavy workpieces. And this must be done without drive means failure due to extremely high temperatures under which the turntable mechanism is operated. A turntable mechanism is provided which is capable of operating under such conditions. For cooling the turntable drive mechanism, internal cooling means are included.

Official Gazette of the U.S. Patent and Trademark Office

N94-20464 Georgia Inst. of Tech., Atlanta. School of Physics.

MICROSCOPIC MODELING OF TRIBOLOGICAL AND INTERFACIAL PHENOMENA Final Report, 1 Jan. 1990 - 31 Jul. 1993

Uzi Landman 31 Jul. 1993 108 p Limited Reproducibility: More than 20% of this document may be affected by microfiche quality

(Grant AF-AFOSR-0117-90)
(AD-A271864; AFOSR-93-0817TR) Avail: CASI HC A06

Atomic-scale energetics and structural and dynamical mechanisms underlying interfacial processes--in particular for systems when two materials are brought together, separated, or slide against each other--are of fundamental importance for basic science and technology in areas such as interfaces, confined fluids, adhesion, tribology, junctions, lubrication, wear, surface modifications, and nano technology. Our research is focused on the development and implementation of methods of atomistic molecular dynamics simulations and applications to tribological, lubrication and related interfacial phenomena. The main research results are as follows: Simulations of the consequences of tip-substrate interactions, adhesive junction formation, nano-indentation, and force versus distance hysteresis. These investigations motivated experimental studies yielding results in agreement with the theoretical predictions. Furthermore, the results permit critical evaluation and extension of continuum treatments. Investigations of structural and dynamical properties of confined model lubricants (alkanes); formation of liquid junctions, interfacial segregation in mixtures, atomistic mechanisms of cavitation and collapse, and dependence of lubricant rheology on molecular architecture. DTIC

N94-20494*# National Aeronautics and Space Administration. Goddard Space Flight Center, Greenbelt, MD.

CLIMBING ROBOT Patent

James J. Kerley, inventor (to NASA), Edward L. May, inventor (to NASA), and Wayne D. Ecklund, inventor (to NASA) 2 Nov. 1993 21 p Filed 10 Feb. 1992 Supersedes N92-23547 (30 - 14, p 2382)

(NASA-Case-GSC-13442-1; US-Patent-5,257,669;
US-Patent-Appl-SN-843861; US-Patent-Class-180-7.1;
US-Patent-Class-901-1; Int-Patent-Class-B62D-57/024;
Int-Patent-Class-B25J-5/00) Avail: US Patent and Trademark Office

A mobile robot for traversing any surface consisting of a number of interconnected segments, each interconnected segment having an upper 'U' frame member, a lower 'U' frame member, a compliant joint between the upper 'U' frame member and the lower 'U' frame member, a number of linear actuators between the two frame members acting to provide relative displacement between the frame members, a foot attached to the lower 'U' frame member for adherence of the segment to the surface, an inter-segment attachment attached to the upper 'U' frame member for interconnecting the segments, a power source connected to the linear actuator, and a computer/controller for independently controlling each linear actuator in each interconnected segment such that the mobile robot moves in a caterpillar like fashion.

Official Gazette of the U.S. Patent and Trademark Office

N94-20538*# Georgia Inst. of Tech., Atlanta. School of Mechanical Engineering.

ACTIVELY CONTROLLED SHAFT SEALS FOR AEROSPACE APPLICATIONS Semiannual Status Report, Jul. - Dec. 1993

Richard F. Salant Dec. 1993 36 p

(Grant NAG3-974)
(NASA-CR-194759; NAS 1.26:194759; E25-666) Avail: CASI HC A03/MF A01

An electronically controlled mechanical seal for use as the purge gas seal in a liquid oxygen turbo pump has been fabricated and tested under transient operating conditions. The thickness of the lubricating film is controlled by adjusting the coning of the carbon face. This is accomplished by applying a voltage to a piezoelectric actuator to which the carbon face is bonded. The seal has been operated with a closed-loop control system that utilizes either the leakage rate or the seal face temperature as the feedback. Both speed and pressure transients have been imposed on the seal. The transient tests have demonstrated that the seal is capable of maintaining low leakage rates while limiting the face temperatures.

Author (revised)

N94-20567 Advanced Materials, Inc., Metairie, LA.

COLD-START MINIDIESEL ENGINE DEVELOPMENT Final Report, Jul. 1991 - Mar. 1992

Conrad Collins Sep. 1993 32 p Limited Reproducibility: More than 20% of this document may be affected by microfiche quality

(Contract DAAK60-91-C-0093; DA Proj. 1L1-62786-AH-98)
(AD-A271064; Natick-TR-93/039) Avail: CASI HC A03

Military mission performance in a chemically contaminated environment necessitates the wearing of chemically impermeable protective garments. Soldiers encapsulated in these protective garments will succumb to heat stress in a hot environment. Consequently, a microclimate cooling system is being developed. In the design, a vapor compression cycle chills water which is then circulated over the body to absorb heat via a cooling garment. The engine, the prime mover in the system, is a major component. Commercially available engines of approximately 0.5 hp at 4000 rpm, the

required size, include model aircraft engines and small outdoor power equipment (string trimmer) engines. However, these engines do not run on JP-8 or diesel fuel, a requirement for military use. Design, evaluation, and results of three engines are detailed. These include: the potential of a high compression, carbureted, glow plug engine operating on diesel fuel; the potential of a high compression, spark assist, fuel injected engine operating on diesel fuel; and a true high compression, fuel injected engine operating on diesel fuel. DTIC

N94-20576# Naval Postgraduate School, Monterey, CA.
MATHEMATICAL MODEL AND ANALYSIS OF THE TACTICAL UNMANNED GROUND VEHICLE (TUGV) USING COMPUTER SIMULATION M.S. Thesis
Donald D. Cersovsky and Edward Kleinschmidt Jun. 1993 114 p
(AD-A272258) Avail: CASI HC A06/MF A02

The purpose of this thesis is to mathematically model the Tactical Unmanned Ground Vehicle (TUGV) in the Janus(A) Combat Model. The TUGV has three sensors, an optical, thermal, and acoustic sensor. Algorithms currently exist in Janus(A) for both optical and thermal sensors. An acoustic detection algorithm exists although not available to all Janus(A) system users. This thesis examines the TUGV prototype, explains the Janus(A) TUGV model, discusses existing acoustic detection algorithms, and tests the TUGV model in a scenario driven experiment. DTIC

N94-20587* National Aeronautics and Space Administration. Langley Research Center, Hampton, VA.
METHOD FOR REMOTELY POWERING A DEVICE SUCH AS A LUNAR ROVER Patent
Russell J. DeYoung, inventor (to NASA), Michael D. Williams, inventor (to NASA), Gilbert H. Walker, inventor (to NASA), Gregory L. Schuster, inventor (to NASA), and Ja H. Lee, inventor (to NASA) 9 Nov. 1993 13 p
Filed 6 Jan. 1992 Supersedes N92-30388 (30 - 21, p 3658)
(NASA-Case-LAR-14789-1; US-Patent-5,260,639;
US-Patent-Appl-SN-822457; US-Patent-Class-322-2R;
US-Patent-Class-244-1R; US-Patent-Class-372-43;
Int-Patent-Class-B64G-1/10) Avail: US Patent and Trademark Office

A method of supplying power to a device such as a lunar rover located on a planetary surface is provided. At least one, and preferably three, laser satellites are set in orbit around the planet. Each satellite contains a nuclear reactor for generating electrical power. This electrical power is converted into a laser beam which is passed through an amplifying array and directed toward the device such as a lunar rover. The received laser beam is then converted into electrical power for use by the device.
Official Gazette of the U.S. Patent and Trademark Office

N94-20589* National Aeronautics and Space Administration. Lyndon B. Johnson Space Center, Houston, TX.
HIGH-TEMPERATURE, HIGH-PRESSURE OXYGEN METERING VALVE Patent
Rollin C. Christianson, inventor (to NASA), Peter P. Lycou, inventor (to NASA), and James A. Daniel, inventor (to NASA) 12 Oct. 1993 9 p
Filed 14 Aug. 1992 Supersedes N93-14843 (31 - 4, p 891)
(NASA-Case-MSC-21823-1; US-Patent-5,251,663;
US-Patent-Appl-SN-929552; US-Patent-Class-137-876;
US-Patent-Class-251-214; US-Patent-Class-137-625.47;
Int-Patent-Class-F16K-5/04) Avail: US Patent and Trademark Office

A control valve includes a body defining a central cavity arranged between a fluid inlet and outwardly-diverging first and second fluid outlets respectively disposed in a common transverse plane. A valve member is arranged in the cavity for rotation between first and second operating positions where a transverse fluid passage through the valve member alternatively communicates the fluid inlet with one or the other of the fluid outlets. To minimize fluid turbulence when the valve member is rotated to an alternate operating position, the fluid passage has a convergent entrance for maintaining the passage in permanent communication with the fluid inlet as well as an oblong exit opening with spaced side walls for enabling the exit opening to temporarily span the first and second fluid outlets as the valve member is turned between its respective operating positions.
Official Gazette of the U.S. Patent and Trademark Office

N94-20594# Ecole Centrale de Lyon (France). Dept. de Machines Thermiques.
THE FLOW OF GAS ACROSS THE PISTON-SEGMENTS-CYLINDER INTERFACE Ph.D. Thesis [CONTRIBUTION A L'ETUDE DE L'ECOULEMENT DE GAZ AU TRAVERS DE L'INTERFACE PISTON-SEGMENTS-CYLINDRE]
Hassan Saghir 1992 228 p In FRENCH
(ECL-92-40; ETN-93-94596) Avail: CASI HC A11/MF A03

A study to create a computer model to predict the consequences of modifications to engine construction, and those of engine running conditions, on engine performance is reported. The results illustrate the complex interactions between engine components which the engineer must take into account. A kinematical and dynamical analysis of the piston/piston rings/cylinder wall system was coupled to an engine simulation model to develop a model of gas flow through the piston ring crevices. An analytical method to solve the equation for the axial movement of a piston ring, which the model uses to calculate the piston ring positions, is used. The oil flow around the piston rings was studied and an estimation of the flow rate of oil leaking into the combustion chamber is proposed. The experimental analysis was performed on a single cylinder spark ignition engine. The measured blowby gas measurements and the model predictions were compared, and were found to be in reasonable agreement over a wide range of engine operating conditions and ring sets. A simple statistical study of cyclic dispersion in the combustion chamber was also carried out, which enabled the effect of cyclic dispersion to be incorporated in numerical simulation. ESA

N94-21142# Societe Nationale Industrielle Aerospatiale, Paris (France).
PROCESS AND APPARATUS FOR THE RELEASE OF A PRESTRESS INITIALLY APPLIED TO A MECHANISM SUCH AS A BEARING ON BOARD A SPACE VEHICLE Patent Application
Jean-Pierre Schoeffter, inventor (to SNIA) 12 Jan. 1992 13 p
(CA-Patent-Appl-SN-2,020,909; Int-Patent-Class-F16C-23/00;
CTN-93-60669) Copyright Avail: Micromedia Ltd., Technical Information Centre, 165 Hotel de Ville, Place du Portage, Phase 2, Hull, Quebec J8X 3X2, Canada HC/MF

In space vehicles, mechanisms such as ball bearings are subject to an initial preload or prestress enabling them to withstand the vibrations caused by the launch and without leading to any clearance or play. A member made from a shape memory material, for example, makes it possible under the effect of its elongation to release the preload when the vehicle is in the operational mode. The control of the release can take place by means of a heating resistor, whose energization leads to the member clearing its shape change temperature and releasing the prestress. The heating can also be done by means of solar energy. The process and apparatus of this invention makes it possible in a particularly simple and non-constraining manner to release the prestress applied to a mechanism during launch without incurring any risk of deterioration to the mechanism during the launch phase and without the need to use a rigid member linked with a pyrotechnic control. Author (CISTI)

N94-21274 Department of the Navy, Washington, DC.
HEAT REGENERATIVE EXTERNAL COMBUSTION ENGINE Patent
Anthony W. Duva, inventor (to Navy) 19 Oct. 1993 7 p Filed 23 Mar. 1993
(AD-D015965; US-Patent-5,253,473; US-Patent-Appl-SN-035867;
US-Patent-Class-60-39.462) Avail: US Patent and Trademark Office

A heat regenerative external combustion engine is disclosed. The engine includes fuel inlet means which extends along the exhaust passage and/or combustion chamber in order to preheat the fuel, To provide for preheating by gases in both the combustion chamber and the exhaust passage, the combustion chamber is arranged annularly around the drive shaft and between the cylinders. This configuration also is advantageous in that it reduces the noise of combustion. The engine of the invention is particularly well-suited for use in a torpedo. DTIC

N94-21277 Department of the Navy, Washington, DC.
SELF LOCKING SET SCREW Patent
Michael A. Tucchio, inventor (to Navy) 14 Sep. 1993 4 p Filed 3 Feb. 1993
(AD-D015969; US-Patent-5,244,323; US-Patent-Appl-SN-012837;
US-Patent-Class-411-271) Avail: US Patent and Trademark Office

A threaded, locking set screw with standard outer dimensions having a threaded body, an expansion plug, and a retaining wedge is described. The threaded body has a tapered cavity at its bottom end. The expansion plug and retaining wedge are inserted into the cavity in the body. The base of the plug extends from the cavity, and the plug is held in place by a force fit between the wedge and a retaining slot in the body. When the set screw is tightened against a part, the plug is forced into the cavity. Because of a locking taper between the plug and the cavity, the plug exerts an outward force on the inner surface of the cavity causing the set screw body to expand radially, thus, locking the set screw in place. DTIC

N94-21297# Argonne National Lab., IL.
ANALYSIS OF A DIESEL-ELECTRIC HYBRID URBAN BUS SYSTEM
W. W. Marr, R. R. Sekar, and M. C. Ahlheim (Regional Transportation Authority, Chicago, IL.) 1993 6 p Presented at the 1993 SAE Future Transpotation Technology Conference, San Antonio, TX, 9-12 Aug. 1993
(Contract W-31-109-eng-38)
(DE93-019514; ANL/ES/CP-80046; CONF-9308143-4) Avail: CASI HC A02/MF A01

A hybrid bus powered by a diesel engine and a battery pack was analyzed over an idealized bus-driving cycle in Chicago. Three hybrid configurations, two parallel and one series, were evaluated. The results indicate that the fuel economy of a hybrid bus, taking into account the regenerative braking, is comparable with that of a conventional diesel bus. Life-cycle costs are slightly higher because of the added weight and cost of the battery. DOE

N94-21424# Pennsylvania State Univ., University Park. Center for Advanced Materials.
UTILIZATION OF METALS TO IMPROVE THE LUBRICATION OF CERAMIC LOAD-BEARING DEVICES Topical Report, 1 Sep. 1987 - 1 Dec. 1990
C. I. Chen, E. E. Klaus, and J. L. Duda Apr. 1993 109 p
(Contract GRI-5084-238-1302)
(PB93-202448; CAM-9302; GRI-93/0048) Avail: CASI HC A06/MF A02

The objective of the study is to determine which potential constituents can be incorporated into ceramic bearing surfaces in order to enhance rates of film formation at elevated temperatures (700 C). Tricresyl Phosphate (TCP) and Trimethylolpropane Triheptanoate (TMPTH) were chosen as the vapor-delivered lubricants, and a wide variety of metals were evaluated using the vapor deposition test. The results of the study indicate that a small amount of metal incorporated into the ceramic surface can promote the formation of a lubricating film. Also, it is possible that a lightly loaded ferrous alloy-bearing separator or retainer could be incorporated in a ceramic rolling element bearing as a source of catalytic activity for enhanced deposit formation. NTIS

N94-21450# Pennsylvania State Univ., University Park. Center for Advanced Materials.
LUBRICATED WEAR OF STEEL-CERAMIC AND CERAMIC-CERAMIC SYSTEMS Topical Report, 1 Jun. 1986 - 1 Sep. 1990
W. T. Wu, E. E. Klaus, and J. L. Duda Apr. 1993 255 p
(Contract GRI-5084-238-1302)
(PB93-202356; CAM-9303; GRI-93/0049) Avail: CASI HC A12/MF A03

The goals of the program were to develop methods of measuring wear in the four-ball wear tester using lubricants in the fully flooded, vapor phase with condensation and vapor phase procedures with a variety of lubricant types. The use of ceramic discs as a substitute for balls in the friction dynamometer was also developed in the program. These studies show that changes in bearing systems from steel-on-steel to steel-on-ceramic can be made without changing the lubricant-additive systems now used in natural gas fired engines. The studies also showed that vapor phase lubrication could be substituted for liquid lubricants without sacrifice in performance in the four-ball wear tester. NTIS

N94-21451# Pennsylvania State Univ., University Park. Center for Advanced Materials.
VAPOR-DELIVERED LUBRICATION OF STEEL-STEEL AND STEEL-CERAMIC SYSTEMS Topical Report, 1 Sep. 1988 - 31 Dec. 1990
H. Li, E. E. Klaus, and J. L. Duda Apr. 1993 242 p See also PB89-129530
(Contract GRI-5084-238-1302)
(PB93-202364; CAM-9301; GRI-93/0047) Avail: CASI HC A11/MF A03

Heavy-duty natural gas engines run hot and relatively dry. This provides lubricant and lubrication problems in the piston ring-cylinder and valve areas. A potential materials solution to this problem is the use of ceramic bearing surfaces. The objective of the project was the investigation of the wear characteristics and surface interactions of lubricants on ceramic bearing surfaces and to compare these results with the behavior of the same lubricants on steel surfaces. The temperature range of interest in these comparisons is 200 to 370 C using a four-ball wear tester. NTIS

N94-21544# Argonne National Lab., Idaho Falls, ID.
THE 13TH INTERNATIONAL CONFERENCE ON MAGNETICALLY LEVITATED SYSTEMS AND LINEAR DRIVES MAGLEV 1993
1993 463 p Conference held in Argonne, IL, 19-21 May 1993
(Contract W-31-109-eng-38)
(DE93-040381; ANL/ES/PROC-79713; CONF-930550) Avail: CASI HC A20/MF A04

This report contains short papers on research being conducted throughout the world on magnetically levitated systems, mainly consisting of trains, and magnetic linear drives. These papers have been index separately elsewhere on the data base. DOE

N94-21580*# National Aeronautics and Space Administration. Marshall Space Flight Center, Huntsville, AL.
DETAILED STUDY OF OXIDATION/WEAR MECHANISM IN LOX TURBOPUMP BEARINGS
T. J. Chase (National Academy of Sciences - National Research Council, Washington, DC.) and J. P. McCarty Dec. 1993 112 p
(NASA-TM-108434; NAS 1.15:108434) Avail: CASI HC A06/MF A02

Wear of 440C angular contact ball bearings of the phase 2 high pressure oxygen turbopump (HPOTP) of the space shuttle main engine (SSME) has been studied by means of various advanced nondestructive techniques (NDT) and modeled with reference to all known material, design, and operation variables. Three modes dominating the wear scenario were found to be the adhesive/sheer peeling (ASP), oxidation, and abrasion. Bearing wear was modeled in terms of the three modes. Lacking a comprehensive theory of rolling contact wear to date, each mode is modeled after well-established theories of sliding wear, while sliding velocity and distance are related to microsliding in ball-to-ring contacts. Microsliding, stress, temperature, and other contact variables are evaluated with analytical software packages of SHABERTH(TM)/SINDA(TM) and ADORE(TM). Empirical constants for the models are derived from NIST experiments by applying the models to the NIST wear data. The bearing wear model so established precisely predicts quite well the average ball wear rate for the HPOTP bearings. The wear rate has been statistically determined for the entire population of flight and development bearings based on Rocketdyne records to date. Numerous illustrations are given. Author (revised)

N94-21637# Argonne National Lab., IL.
SOME EVIDENCE ON DETERMINANTS OF FUEL ECONOMY AS A FUNCTION OF DRIVING CYCLE AND TEST TYPE
D. J. Santini and J. Anderson 1993 14 p Presented at the 1993 Society of Automotive Engineers (SAE) Future Transportation Technology Conference, San Antonio, TX, 9-12 Aug. 1993
(Contract W-31-109-eng-38)
(DE93-019511; ANL/ES/CP-78818; CONF-9308143-3) Avail: CASI HC A03/MF A01

Statistical methods are used with 107 vehicles whose fuel economy was presented and reported for five test types in a single publication by Consumers Union (CU) for 1986-1988 vehicles. Standard loglinear statistical formulations (i.e., multiplicative models of interactions) are used with data from this and supplementary sources to develop coefficients estimating the percent fuel economy gain per percent change in engine/vehicle design characteristic. The coefficients are developed for the five different test conditions evaluated by CU and are compared with each other on the basis of attributes of the tests. The insights of engineering models are used to develop expectations regarding the shift in size of coefficients as driving cycles change. In both the engineering models and the statistical model, the effect of weight is estimated to be higher in urban driving than in highway driving. For two test categories - field tests and dynamometer

tests - the benefits of weight reduction are statistically estimated to be greatest in urban driving conditions. The effect on idle fuel flow rate of designing vehicles to hold performance roughly constant by maintaining power per kilogram and/or displacement per kilogram is examined, and its implication for the size of the weight effect is simply approximated from Sovran's 1983 engineering model results. The fuel-economy-decreasing effect of the desire for performance is estimated to be somewhat larger in the statistical analysis than in the NAS study, when engine technology is held constant. DOE

N94-21756*# National Aeronautics and Space Administration. Lewis Research Center, Cleveland, OH.

THE RELATIVE NOISE LEVELS OF PARALLEL AXIS GEAR SETS WITH VARIOUS CONTACT RATIOS AND GEAR TOOTH FORMS

Raymond J. Drago (Boeing Helicopter Co., Philadelphia, PA.), Joseph W. Lenski, Jr. (Boeing Helicopter Co., Philadelphia, PA.), Robert H. Spencer (Boeing Helicopter Co., Philadelphia, PA.), Mark Valco (Army Research Lab., Cleveland, OH.), and Fred B. Oswald Dec. 1993 17 p Presented at the Fall Technical Meeting of the American Gear Manufacturers Association, Detroit, MI, 14-15 Oct. 1993

(DA Proj. 1L1-6211-A-47-A; RTOP 505-62-10)

(NASA-TM-106431; E-8273; NAS 1.15:106431; ARL-TR-318) Avail: CASI HC A03/MF A01

The real noise reduction benefits which may be obtained through the use of one gear tooth form as compared to another is an important design parameter for any geared system, especially for helicopters in which both weight and reliability are very important factors. This paper describes the design and testing of nine sets of gears which are as identical as possible except for their basic tooth geometry. Noise measurements were made at various combinations of load and speed for each gear set so that direct comparisons could be made. The resultant data was analyzed so that valid conclusions could be drawn and interpreted for design use. Author

N94-21938# Solar Turbines, Inc. San Diego, CA.

ADVANCED TURBINE SYSTEMS (ATS). PHASE 1: SYSTEM SCOPING AND FEASIBILITY STUDIES

D. J. White 15 Apr. 1993 11 p

(Contract DE-AC21-86MC-23166)

(DE93-041130; DOE/MC-23166/3414; SR-93-R-5278-115) Avail: CASI HC A03/MF A01

As part of this involvement, Solar intends to design and commercialize a unique gas turbine system that promises high cycle efficiencies and low exhaust emissions. This engine of approximately 12-MW will be targeted for the dispersed power markets both urban and rural. Goals of 50% thermal efficiency and 8 parts-per-million by volume (ppmv) nitrogen oxide emissions were established. Reliability, availability, and maintainability (RAM) will continue to be the most important factors in the competitive marketplace. The other major goal adopted was one of reducing the cost of power produced by 10%. This reduction is based on the cost of power (COP) associated with today's engines that lie in the same horsepower range as that targeted in this study. An advanced cycle based on an approximation of the Ericsson Cycle was adopted after careful studies of a number of different cycles. This advanced intercooled, recuperated engine when fired at 2450 F will be capable of meeting the 50% efficiency goal if the cooling air requirements do not exceed 7% of the total air flow rate. This latter qualification will probably dictate the use of ceramic parts for both the nozzle guide vanes and the turbine blades. Cooling of these parts will probably be required and the 7% cooling flow allowance is thought to be adequate for such materials. Analyses of the cost of power and RAM goals show that the installed cost of this advanced engine can be approximately 50% above today's costs. This cost is based on $4.00 per million Btu fuel and a COP reduction of 10% while maintaining the same RAM as today's engines. DOE

N94-21983# Department of Energy, Morgantown, WV. Energy Technology Center.

PERFORMANCE CALCULATIONS AND RESEARCH DIRECTION FOR A WATER ENHANCED REGENERATIVE GAS TURBINE CYCLE

L. H. Rogers and D. H. Archer (Carnegie-Mellon Univ., Pittsburgh, PA.) 1993 9 p Presented at the 28th Intersociety Energy Conversion Engineering Conference, Atlanta, GA, 8-13 Aug. 1993

(DE93-019866; DOE/METC-C/93/7097; CONF-930804-18) Avail: CASI HC A02/MF A01

A cycle has been conceived that combines compressor cooling, humidification, and regenerative air heating with the added enhancement of direct injection of water into the air flow. In this cycle it is proposed that a fine mist of water be injected into the compressor air stream and a spray or film of water into the regenerator air stream. Water injection into the compressor air flow realizes several benefits: it cools the air flow, reducing the power required for compression and increasing the potential for exhaust heat recovery; it adds mass to the air stream, increasing the power produced by expansion; and it reduces the amount of cooling bleed air required by increasing the specific heat and decreasing the temperature of the cooling air stream. The greatest benefit would be derived from spraying a fine mist of water directly into the existing air flow into or before the compressor so that cooling and compression would occur simultaneously. This may be accomplished by entraining the water droplets in the inlet air flow or by introducing the water in stages during compression. An alternative and less technically challenging approach is to extract the air stream to a saturation chamber and then reintroduce the air stream into the compressor. This approach is not as desirable because it would increase the equipment cost and add a significant pressure drop penalty. The second use of water in this cycle is in water-assisted regeneration. The heat capacity of the hot stream in regenerators is greater than the heat capacity of the cool stream because of the increased mass flow and specific heat of the combustion products. This imbalance leads to a less than ideal exhaust heat recovery since the cool air stream is unable to absorb all of the available heat. If water is injected into the cool stream in the regenerator, some of the available heat is used to vaporize the water, allowing additional heat recovery and also adding mass to the air flow. Also, the effectiveness of the heat exchanger can be increased, and the cost reduced, by injecting the water as early as possible in the flow, keeping the cool stream temperature low and thus maximizing the temperature difference across the regenerator. DOE

N94-22038 Pacific Northwest Lab., Richland, WA.

ACTIVE DAMPING OF OSCILLATIONS IN A LONG COMPLIANT MANIPULATOR LINK

C. P. Baker, M. S. Evans, D. J. Trudnowski, and D. P. Magee (Georgia Inst. of Tech., Atlanta.) Jul. 1993 9 p Presented at the 9th International Conference on Mathematical and Computer Modeling, Oxford, England, 26-29 Jul. 1993 Limited Reproducibility: More than 20% of this document may be affected by poor print

(Contract DE-AC06-76RL-01830)

(DE93-018878; PNL-SA-22414; CONF-9307126-1) Avail: Issuing Activity (Department of Energy (DOE))

A flexible manipulator test bed consisting of a fifteen foot long fixed-free compliant beam (representing a compliant manipulator link) with a Shilling Titan II dextrous manipulator mounted on its free end has been constructed at Pacific Northwest Laboratory (PNL). A comprehensive dynamic model which includes flexible body effects has been developed at PNL using a commercially available multibody dynamics code. A linearized version of the model is used to develop control strategies which use inertial forces generated by movements of the dextrous manipulator to damp out induced oscillations in the beam. These control strategies are tested on the model and shown to be feasible, and then implemented in the flexible manipulator testbed. Results from the hardware experiments are analyzed and compared with the model results. DOE

N94-22093 Environmental Protection Agency, Ann Arbor, MI.

COLD STARTING AN ALCOHOL-FUELED ENGINE WITH ULTRASONIC FUEL ATOMIZATION

R. I. Bruetsch and F. J. Hamady Mar. 1993 24 p See also PB89-230692 Limited Reproducibility: More than 20% of this document may be affected by microfiche quality

(PB93-206597; EPA/AA/TDG-93/02A) Avail: CASI HC A03/MF A01

A test program was devised at EPA's National Vehicle and Fuel Emissions Laboratory to evaluate a Tonen ultrasonic fuel atomizer system on a Honda B20 engine using both M85 (85% methanol, 15% hydrocarbons) and M100 (neat methanol) fuels to determine whether cold starting a premixed-charge port injected engine on alcohol fuels at low ambient temperatures can be improved. Modification to the engine's intake manifold was performed at

the Japanese Automotive Research Institute (JARI) in cooperation with the New Energy Development Organization (NEDO) to install heated injectors in close proximity to the ultrasonic atomizers. The engine is also equipped with the stock port injector system intact and functional. Successful M100 cold starts were obtained down to 20 F (-7 C). NTIS

N94-22390# Los Alamos National Lab., NM.
THE EFFECT OF COMPTON SCATTERING ON THE DOUBLE TO SINGLE IONIZATION RATIO IN HELIUM
R. J. Bartlett, M. Sagurton (SFA, Inc., Landover, MD.), J. A. R. Samson (Nebraska Univ., Lincoln.), and Z. X. He (Nebraska Univ., Lincoln.) 1993 15 p Presented at the Double Ionization in He, Argonne, IL, 4 Oct. 1993 (Contract W-7405-eng-36)
(DE94-000884; LA-UR-93-3426; CONF-9310190-1) Avail: CASI HC A03/MF A01

The ratio of double to single ionization in Helium produced by photon impact has been measured for photon energies from 2.1 to 5.5 keV. The measurements suggest that a significant contribution to the single ionization cross section is caused by Compton scattering for energies greater than approximately 3.8 keV. After accounting for the ionizing Compton scattering, the measured ratio is not inconsistent with recent calculations of the asymptotic limit of the ionization ratio caused by photoabsorption which predict a limit near 1.66%. DOE

N94-22421 Memorial Univ. of Newfoundland, Saint Johns.
DYNAMIC ANALYSES OF FLEXIBLE ROBOTIC MANIPULATORS M.S. Thesis
Parveen Kalra Sep. 1989 267 p
(ISBN-0-315-59251-6; CTN-94-60888) Copyright Avail: Micromedia Ltd., Technical Information Centre, 240 Catherine Street, Suite 305, Ottawa, Ontario, K2P 2G8, Canada HC/MF

Flexible dynamic analysis of robotic manipulators was conducted using orthogonal polynomials in the assumed-mode method. In the derivation of the system equations, kinematic parameters such as joint displacements, velocities, and accelerations also occur. This necessitates the kinematic analysis of rigid links. The kinetic and potential energy of a link segment are obtained using homogeneous transformation matrices which relate the link coordinate system to the global coordinate frame. These energies are then substituted in Lagrange's equation. The nonlinear dynamic equations are then solved to evaluate the actuator torques required for a prescribed trajectory. The dynamic analysis of flexible manipulators is also carried out by the finite element method where the elemental equations are derived for three different types of beams subjected to gross motion. The resulting nonlinear set of system equations are solved using an iterative numerical integration scheme. To study the effect of contribution of various modes, the nonsymmetric system matrices are diagonalized using the biorthogonality property of the mode shapes of the original and transposed systems. The expressions for the elemental matrices are obtained using a computer simulation package, program listings of which are included. Author (CISTI)

N94-22577 Toronto Univ. (Ontario). Dept. of Aerospace Science and Engineering.
THE OPTOHYDRAULIC SERVOVALVE: A NOVEL DEVICE FOR THE PRECISE OPTICAL CONTROL OF HYDRAULIC PRESSURE M.S. Thesis
Sonny Hanseng Chee 1992 154 p
(ISBN-0-315-83580-X; CTN-94-60943) Copyright Avail: Micromedia Ltd., Technical Information Centre, 240 Catherine Street, Suite 305, Ottawa, Ontario, K2P 2G8, Canada HC/MF

In the development of opto-fluidic systems for flight control, the main bottleneck has been the lack of a suitable optomechanical interface and actuator. A novel optomechanical actuator is proposed, the optohydraulic servovalve (OHS), which could have flight control applications. The device consists of the mating of an optomechanical interface, the optothermic gas cell (Ocell), with a jet pipe servovalve. A review is presented of known optical to mechanical transduction mechanisms; a qualitative and quantitative comparison indicates that the Ocell has superior characteristics for interfacing with a servovalve. The Ocell constitutive relations describing pressure, diaphragm displacement, and bandwidth with respect to input optical power were also developed and verified experimentally. Mathematical models developed for the OHS are described, and it is shown numerically that the OHS can be operated by as little as 10 mW of optical power. Some experimental Ocells were designed and constructed, and it was demonstrated that a pair of Ocells could replace the torque motor in a standard electrohydraulic servovalve and thereby result in a new device. Author (CISTI)

N94-22578 Toronto Univ. (Ontario). Dept. of Mechanical Engineering.
ROBOT LINK AND CONTACT SURFACE DYNAMIC INTERACTION: AN EXPERIMENTAL STUDY OF CONTACT INSTABILITY M.S. Thesis
Yuri Andrew Lawryshyn 29 Apr. 1993 154 p
(ISBN-0-315-83439-0; CTN-94-60952) Copyright Avail: Micromedia Ltd., Technical Information Centre, 240 Catherine Street, Suite 305, Ottawa, Ontario, K2P 2G8, Canada HC/MF

The stability of manipulators with structurally compliant links during contact with a surface that exhibits structural compliance is examined. An experimental robot was designed to perform contact task experiments under varying dynamics. The contact surface is part of the Variable Impedance Machine, whose dynamics can be arbitrarily varied to represent any mass spring damper system. A dynamic model of the experimental facility was developed which was programmed to simulate the facility. Results from simulation agreed well with those from experiments. Using singular perturbation theory, a stability formulation was presented in which three dynamic cases were considered: the robot links are much stiffer than the environment; the environment is much stiffer than the links; and the links and environment have equal stiffness. The theory predicted stability for the first case under certain assumptions but was inconclusive for the other two cases. Experiments and simulations showed stability for all three cases. Author (CISTI)

N94-21112*# Idaho Univ., Moscow. Dept. of Electrical Engineering.
ACCELERATION-AUGMENTED LQG CONTROL OF AN ACTIVE MAGNETIC BEARING
Joseph J. Feeley *In* New Mexico Univ., The Fifth NASA Symposium on VLSI Design 1993 6 p (For primary document see N94-21079 05-33)
Avail: CASI HC A02/MF A06

N94-21696*# Idaho Univ., Moscow. NASA Space Engineering Research Center.
A NEW EDDY CURRENT MODEL FOR MAGNETIC BEARING CONTROL SYSTEM DESIGN
Joseph J. Feeley and Daniel J. Ahlstrom *In its* The 1992 4th NASA SERC Symposium on VLSI Design 1992 8 p (For primary document see N94-21694 05-33)
(Grants NAGw-1406; NSF MIP-91-09618)
Avail: CASI HC A02/MF A04

N94-21791*# National Aeronautics and Space Administration. Lewis Research Center, Cleveland, OH.
BRUSH SEAL BRISTLE FLEXURE AND HARD-RUB CHARACTERISTICS
Robert C. Hendricks, Julie A. Carlile, and Anita D. Liang *In its* The 1992 Seals Flow Code Development Workshop Oct. 1993 p 95-115 (For primary document see N94-21790 05-16)
Avail: CASI HC A03/MF A03

N94-21792*# National Aeronautics and Space Administration. Lewis Research Center, Cleveland, OH.
INTEGRITY TESTING OF BRUSH SEAL IN A T-700 ENGINE
Robert C. Hendricks, Thomas A. Griffin, George A. Bobula, Robert C. Bill, and Harold W. Howe (Technetics, Inc., DeLand, FL.) *In its* The 1992 Seals Flow Code Development Workshop Oct. 1993 p 117-138 (For primary document see N94-21790 05-16)
Avail: CASI HC A03/MF A03

N94-21793*# Air Force Systems Command, Wright-Patterson AFB, OH. Aero Propulsion and Power Directorate.
AIR FORCE BRUSH SEAL PROGRAMS
Connie Dowler *In* NASA. Lewis Research Center, The 1992 Seals Flow Code Development Workshop Oct. 1993 p 149-156 (For primary document see N94-21790 05-16)
Avail: CASI HC A02/MF A03

N94-21794*# Naval Air Warfare Center, Trenton, NJ. Aircraft Div.
NAVY GTE SEAL DEVELOPMENT ACTIVITY

Carl P. Grala *In* NASA. Lewis Research Center, The 1992 Seals Flow Code Development Workshop Oct. 1993 p 157-165 (For primary document see N94-21790 05-16)
Avail: CASI HC A02/MF A03

N94-21795*# National Aeronautics and Space Administration. Lewis Research Center, Cleveland, OH.
COMPLIANT SEAL DEVELOPMENT
Robert C. Hendricks *In its* The 1992 Seals Flow Code Development Workshop Oct. 1993 p 171-173 (For primary document see N94-21790 05-16)
Avail: CASI HC A01/MF A03

N94-21796*# British Hydromechanics Research Association, Cranfield (England).
DYNAMICS OF FACE SEALS FOR HIGH SPEED TURBOMACHINERY
Simon Leefe *In* NASA. Lewis Research Center, The 1992 Seals Flow Code Development Workshop Oct. 1993 p 197-210 (For primary document see N94-21790 05-16)
Avail: CASI HC A03/MF A03

N94-21797*# Columbia Univ., New York, NY. Dept. of Mechanical Engineering.
MODELING BRISTLE LIFT-OFF IN IDEALIZED BRUSH SEAL CONFIGURATIONS
Vijay Modi *In* NASA. Lewis Research Center, The 1992 Seals Flow Code Development Workshop Oct. 1993 p 217-232 (For primary document see N94-21790 05-16)
Avail: CASI HC A03/MF A03

N94-22489*# Hawaii Univ., Honolulu.
THE UNIVERSITY OF HAWAII INSTITUTE FOR ASTRONOMY CCD CAMERA CONTROL SYSTEM Abstract Only
K. T. C. Jim, H. T. Yamada, G. A. Luppino, and R. J. Hlivak *In* NASA, Washington, Second Annual Conference on Astronomical Data Analysis Software and Systems. Abstracts 1992 p 58 (For primary document see N94-22438 05-89)
Avail: CASI HC A01/MF A02

38 QUALITY ASSURANCE AND RELIABILITY

Includes product sampling procedures and techniques; and quality control.

N94-20468 Logistics Management Inst., Bethesda, MD.
USING ELECTRONIC DATA INTERCHANGE TO REPORT PRODUCT QUALITY Final Report
Donald F. Egan and Donald T. Frank Mar. 1993 165 p Limited Reproducibility: More than 20% of this document may be affected by microfiche quality
(Contract MDA903-90-C-0006)
(AD-A271843; LMI-DL207R1) Avail: CASI HC A08

The Product Quality Deficiency Report (PQDR) is a Department of Defense form that identifies deficiencies in the manufacture, repair, or procurement of materiel. It may be used by DoD employees or contractors to identify defects at any point in the item's life. DoD generates nearly 75,000 such deficiency reports each year. In most cases, when a defect is identified, Standard Form (SF) 368 is completed and sent to the activity managing the contract under which the materiel was procured. That activity, usually in conjunction with the contractor, investigates the complaint, attempts to determine a cause and a corrective action, and must make some disposition of the defective materiel. The process is labor- and paper-intensive and time-consuming. Technology can reduce the costs of the process and at the same time improve timeliness by electronically exchanging discrepancy data between activities. Electronic data interchange (EDI) is one technology for electronically passing PQDR data. It is widely used in industry and increasingly within DoD. DMRD 941 defines DoD's commitment to use EDI and cites the PQDR and other discrepancy reports as early candidates for EDI. In this report, we describe how EDI can be linked to changes in PQDR processing practices to provide further improvements. DTIC

N94-21012*# Nebraska Univ., Lincoln. Dept. of Electrical Engineering.
NON-DESTRUCTIVE EVALUATION IN MANUFACTURING USING SPECTROSCOPIC ELLIPSOMETRY Abstract Only
John A. Woollam and Paul G. Snyder *In its* Materials, Structures, and Devices for High-Speed Electronics 1993 1 p Repr. from Review of Progress in Quantitative Nondestructive Evaluation (NY, Plenum Press), v. 10B, 1991 p 2185 (For primary document see N94-20971 05-76)
Avail: CASI HC A01/MF A01

N94-21093*# Sandia National Labs., Albuquerque, NM. Failure Analysis Dept.
CORRECT CMOS IC DEFECT MODELS FOR QUALITY TESTING
Jerry M. Soden and Charles F. Hawkins (New Mexico Univ., Albuquerque.) *In* New Mexico Univ., The Fifth NASA Symposium on VLSI Design 1993 16 p (For primary document see N94-21079 05-33)
(Contract DE-AC04-76DP-00789)
Avail: CASI HC A03/MF A06

N94-21324*# Computer Sciences Corp., Lanham, MD.
THE NCC PROJECT: A QUALITY MANAGEMENT PERSPECTIVE
Raymond H. Lee *In* NASA. Goddard Space Flight Center, Networks Technology Conference Nov. 1993 p 1-10 (For primary document see N94-21323 05-62)
Avail: CASI HC A02/MF A03

N94-21707*# University of Southwestern Louisiana, Lafayette. Center for Advanced Computer Studies.
MICRO-ROLLBACK AND SELF-RECOVERY SYNTHESIS
Byung Wook Jeon and Chidchanok Lursinsap *In* Idaho Univ., The 1992 4th NASA SERC Symposium on VLSI Design 1992 12 p (For primary document see N94-21694 05-33)
Avail: CASI HC A03/MF A04

N94-22616*# Southwest Research Inst., San Antonio, TX.
RECENT ADVANCES IN COMPUTATIONAL STRUCTURAL RELIABILITY ANALYSIS METHODS
Ben H. Thacker, Y.-T. Wu, Harry R. Millwater, Tony Y. Torng, and David S. Riha *In* NASA. Langley Research Center, Computational Methods for Failure Analysis and Life Prediction Oct. 1993 p 185-203 (For primary document see N94-22608 05-39)
Avail: CASI HC A03/MF A03

N94-22619*# National Aeronautics and Space Administration. Lewis Research Center, Cleveland, OH.
TIME-DEPENDENT RELIABILITY ANALYSIS OF CERAMIC ENGINE COMPONENTS
Noel N. Nemeth *In* NASA. Langley Research Center, Computational Methods for Failure Analysis and Life Prediction Oct. 1993 p 239-269 (For primary document see N94-22608 05-39)
Avail: CASI HC A03/MF A03

39 STRUCTURAL MECHANICS

Includes structural element design and weight analysis; fatigue; and thermal stress.

For applications see *05 Aircraft Design, Testing and Performance* and *18 Spacecraft Design, Testing and Performance.*

N94-19815 Elsevier Science Publishers Ltd., Barking (England).
STRUCTURAL CRASHWORTHINESS AND FAILURE
Norman Jones and Tomasz Wierzbicki 16 Apr. 1993 524 p Limited Reproducibility: More than 20% of this document may be affected by microfiche quality
(Contract DAJA45-92-M-0089)
(AD-A270429; R/D-6917-AN-02) Avail: CASI HC A22

Lectures presented at the Third International Symposium on Structural Crashworthiness held at the University of Liverpool, Liverpool, UK on 14-16 April 1993 are included. Topics covered are: failure in ductile material using finite element methods; modelling the process of failure in structures; criteria for the inelastic rupture of ductile metal beams subjected to large dynamic loads; strain localization and fracture in metal sheets and thin

walled structures; impact on metal tubes; indentation and perforation; composite strength and energy adsorption as an aspect of structural crash resistance; crash response of composite structures; dynamic compression of cellular structures and materials; elastic effects in the dynamic plastic response of structure; impact performance of aluminium structures; motorway impact attenuation devices: past, present and future; and grounding damage of ships. DTIC

N94-19824# Sandia National Labs., Albuquerque, NM.
DYNAMIC, MULTIAXIAL IMPACT RESPONSE OF CONFINED AND UNCONFINED CERAMIC RODS
J. L. Wise and D. E. Grady 1993 5 p Presented at the 14th International Conference of the International Association for the Advancement of High Pressure Science and Technology, Colorado Springs, CO, 27 Jun. - 2 Jul. 1993
(Contract DE-AC04-76DP-00789)
(DE93-040057; SAND-93-1703C; CONF-930676-45) Avail: CASI HC A01/MF A01

A new configuration for impact testing was implemented which yielded time-resolved measurements of the dynamic response of materials undergoing multiaxial strain. With this method, one end of an initially stationary rod (i.e., right circular cylinder) of test material was subjected to planar impact with a flat-faced projectile. The test rod was either free (unconfined) or mounted within a close-fitting sleeve which provided lateral confinement. Velocity interferometer diagnostics monitored the axial (longitudinal) velocity of the rod free end and the transverse (radial) velocity for one or more points on the periphery of the rod or confinement sleeve. Analysis of the resultant velocity records allowed assessment of material properties, such as wave speeds and compressive yield strength, without the requirement of intact recovery of the rod. Data were obtained for alumina (Coors AD-99.5) rods in a series of tests involving variations in confinement and peak impact stress. DOE

N94-19836 North Carolina State Univ., Raleigh.
SHOCK WAVE INTERACTIONS WITH EXOTHERMIC MIXTURES Final Report, Sep. 1989 - Jan. 1993
K. Iyer 10 Aug. 1993 6 p Limited Reproducibility: More than 20% of this document may be affected by microfiche quality
(Contract DAAL03-89-C-0037)
(AD-A271149; ARO-27364.2-MS) Avail: CASI HC A02

Instrumented high velocity impact recovery experiments were performed to study solid state reactions in mixtures of nickel and aluminum powders during the passage of shock waves. Excess pressure due to the release of energy from the exothermic reaction was measured for a range of impact velocities. An impact velocity threshold for the initiation of reaction at the reflected shock front was established, and this threshold value was found to be dependent on the particle size of the powder. Microscopic examination of the recovered specimens show features which corroborate the hypothesized extent of a reaction based on pressure measurements. DTIC

N94-19881 Phillips Lab., Kirtland AFB, NM.
AN EQUATION OF STATE FOR SHOCK IN HOMOGENEOUS MATERIALS AND COMPARISON TO SHOCK DATA Final Report, 1 May 1991 - 30 Aug. 1992
J. H. Shively (California State Univ., Northridge.), C. Stein, and R. Robertson Aug. 1993 38 p Limited Reproducibility: More than 20% of this document may be affected by microfiche quality
(AD-A271436; AD-E201663; PL-TR-92-1060) Avail: CASI HC A03

An evaluation of hypervelocity impact data for metals, ceramics, ionic, and polymer materials and water as it leads to an equation of state for solids, is presented. The results indicate that for shock induced pressure, the materials behave as if they are in corresponding states, so that a single equation relates pressure to particle velocity for the entire range of materials investigated. The relationship between shock velocity and particle velocity can be represented by a line with a single slope and with an intercept associated with the bulk sound velocity. Comparisons to solid state theory are made which permit a discussion regarding Grueneisen's constant. DTIC

N94-19927# Sandia National Labs., Albuquerque, NM.
TIME-RESOLVED SHOCK COMPRESSION OF POROUS RUTILE: WAVE DISPERSION IN POROUS SOLIDS
M. U. Anderson, R. A. Graham, and G. T. Holman 1993 4 p Presented at the 14th International Conference of the International Association for the Advancement of High Pressure Science and Technology, Colorado Springs, CO, 27 Jun. - 2 Jul. 1993
(Contract DE-AC04-76DP-00789)
(DE93-018848; SAND-93-0406C; CONF-930676-40) Avail: CASI HC A01/MF A01

Rutile (TiO2) samples at 60% of solid density have been shock-loaded from 0.21 to 6.1 GPa with sample thickness of 4 mm and studied with the PVDF piezoelectric polymer stress-rate gauge. The technique uses a copper capsule to contain the sample which has PVDF gauge packages in direct contact with front and rear surfaces. A precise measure is made of the compressive stress wave velocity through the sample, as well as the input and propagated shock stress. Initial density is known from sample preparation, and the amount of shock-compression is calculated from the measurement of shock velocity and input stress. Shock states and re-shock states are measured. Observed data are consistent with previously published high pressure data. It is observed that rutile has a 'crush strength' near 6 GPa. Propagated stress-pulse rise times vary from 234 to 916 nsec. Propagated stress-pulse rise times of shock-compressed HMX, 2Al + Fe2O3, 3Ni + Al, and 5Ti + 3Si are presented. DOE

N94-19937 Indiana Univ.-Purdue Univ., Indianapolis.
FINITE ELEMENT MESH GENERATION AND ANALYSIS OF SOLDER JOINTS FOR FATIGUE LIFE PREDICTIONS Final Report, 1 Jul. 1991 - 30 Jun. 1993
Nasser H. Paydar, Yihong Tong, Hasan U. Akay, and William Boehmer 30 Aug. 1993 177 p Limited Reproducibility: More than 20% of this document may be affected by microfiche quality
(Contract DAAL03-91-G-0187)
(AD-A271329; ARO-29042.1-MS) Avail: CASI HC A09

Tools for fatigue life prediction of solder joints are developed. This report consists of two parts. In part One, the creep and plastic deformations stored in a solder joint are calculated by implementing appropriate plastic and creep constitutive models in a nonlinear finite element program. The calculated damage in each cycle is then related to the life of the material using two failure criteria: strain-life and energy-partitioning. The importance of parameters affecting the fatigue life of solders are evaluated. In part Two, the finite element analysis is combined with x-ray and laser imaging systems, from which real solder joint geometries can be constructed. The approaches presented herein provides a useful tool in the design and manufacturing of surface-mount assemblies. DTIC

N94-19940# Sandia National Labs., Albuquerque, NM.
A BENCHMARK STUDY OF 2D AND 3D FINITE ELEMENT CALCULATIONS SIMULATING DYNAMIC PULSE BUCKLING TESTS OF CYLINDRICAL SHELLS UNDER AXIAL IMPACT
E. L. Hoffman and D. J. Ammerman 1993 6 p Presented at the 12th Biennial Conference for the International Association for Structural Mechanics in Reactor Technology (SMIRT 12), Stuttgart, Germany, 16-26 Aug. 1993
(Contract DE-AC04-76DP-00789)
(DE93-018859; SAND-93-0641C; CONF-930803-16) Avail: CASI HC A02/MF A01

A series of tests investigating dynamic pulse buckling of a cylindrical shell under axial impact is compared to several finite element simulations of the event. The purpose of the study is to compare the performance of the various analysis codes and element types with respect to a problem which is applicable to radioactive material transport packages, and ultimately to develop a benchmark problem to qualify finite element analysis codes for the transport package design industry. DOE

N94-19943# Sandia National Labs., Albuquerque, NM.
PVDF GAUGE CHARACTERIZATION OF HYPERVELOCITY-IMPACT-GENERATED DEBRIS CLOUDS
M. B. Boslough, L. C. Chhabildas, W. D. Reinhart, C. A. Hall, J. M. Miller, R. Hickman, S. A. Mullin (Southwest Research Inst., San Antonio, TX.), and D. L. Littlefield (Southwest Research Inst., San Antonio, TX.) 1993 5 p Presented at the 14th International Conference of the International Association for the Advancement of High Pressure Science and Technology,

Colorado Springs, CO, 27 Jun. - 2 Jul. 1993
(Contract DE-AC04-76DP-00789)
(DE93-018831; SAND-93-0397C; CONF-930676-38) Avail: CASI HC A01/MF A01

We have used PVDF gauges to determine time-resolved stresses resulting from interaction between hypervelocity-impact-generated debris clouds and various target gauge blocks. Debris clouds were generated from three different impact configurations: (1) steel spheres impacting steel bumper sheets at 4.5 to 6.0 km/s, (2) aluminum inhibited shaped-charge jets impacting aluminum bumper sheets at 11.4 km/s, and (3) titanium disks impacting titanium bumper sheets at 7.6 to 10.1 km/s. Additional data were collected from the various experiments using flash X-ray radiography, pulsed laser photography, impact flash measurements, time-resolved strain gauge measurements, and velocity interferometry (VISAR). Data from these various techniques are in general agreement with one another and with hydrocode predictions, and provide a quantitative and comprehensive picture of impact-generated debris clouds. DOE

N94-20001 Texas Univ., Austin. Electronic Materials Research Lab.
DURABILITY PREDICTIONS FOR ADHESIVELY BONDED JOINTS IN HUMID ENVIRONMENTS Final Report, 15 Jan. 1990 - 14 Jul. 1993
G. J. Rodin and K. M. Liechti 29 Sep. 1993 3 p Limited Reproducibility: More than 20% of this document may be affected by microfiche quality
(Contract DAAL03-90-G-0003)
(AD-A271177; EMRL-93-10; ARO-27315.3-EG) Avail: CASI HC A01

The research objective of this study was to develop an understanding of the cohesive failure of adhesively bonded joints under load in aggressive environments. Such an understanding could then be used to predict the durability of adhesively bonded joints in humid environments. The problem was to have been approached by first examining the diffusion kinetics and then modeling the deformation and failure behavior as a function temperature and moisture. Although only one adhesive was to have been considered in the study, the first adhesive had to be abandoned mid-way through the program (after its diffusion characteristics had been studied) when creep deformation experiments revealed an unacceptable degree of scatter due to random shear banding. After some development, a suitable second adhesive was found, but there was not enough time to completely characterize its diffusion, deformation, and failure behavior as a function of temperature and moisture. In the analytical portion of the project, finite element analyses were conducted to optimize various specimens employed in the experimental program. In addition, several thermo-mechanical models for rate-dependent materials with sensitivity to hydrostatic pressure were explored. An extended Prager Drucker plasticity model reproduced the data obtained to date. DTIC

N94-20036*# Washington Univ., Saint Louis, MO. Center for Computational Mechanics.
THE p-VERSION OF THE FINITE ELEMENT METHOD IN INCREMENTAL ELASTO-PLASTIC ANALYSIS
Stefan M. Holzer and Zohar Yosibash Dec. 1993 33 p
(Contract NAG9-622; F49620-93-1-0173)
(NASA-CR-194707; NAS 1.26:194707; WU/CCM-93/4) Avail: CASI HC A03/MF A01

Whereas the higher-order versions of the finite elements method (the p- and hp-version) are fairly well established as highly efficient methods for monitoring and controlling the discretization error in linear problems, little has been done to exploit their benefits in elasto-plastic structural analysis. Aspects of incremental elasto-plastic finite element analysis which are particularly amenable to improvements by the p-version is discussed. These theoretical considerations are supported by several numerical experiments. First, an example for which an analytical solution is available is studied. It is demonstrated that the p-version performs very well even in cycles of elasto-plastic loading and unloading, not only as compared to the traditional h-version but also in respect to the exact solution. Finally, an example of considerable practical importance - the analysis of a cold-worked lug - is presented which demonstrates how the modeling tools offered by higher-order finite element techniques can contribute to an improved approximation of practical problems. Author (revised)

N94-20159*# Virginia Polytechnic Inst. and State Univ., Blacksburg. Dept. of Aerospace and Ocean Engineering.
COMPRESSION STRENGTH OF COMPOSITE PRIMARY STRUCTURAL COMPONENTS Semiannual Status Report, 1 Nov. 1992 - 30 Apr. 1993
Eric R. Johnson Oct. 1993 35 p
(Grant NAG1-537)
(NASA-CR-194561; NAS 1.26:194561) Avail: CASI HC A03/MF A01

Two projects are summarized in this report. The first project is entitled 'Stiffener Crippling Initiated by Delamination', and the second is entitled 'Pressure Pillowing of an Orthogonally Stiffened Cylindrical Shell.' The objective of the first project is to develop a computational model of the stiffener specimens that includes the capability to predict the interlaminar stress response at the flange free edge in postbuckling. The objectives of the second project are to analyze the concentration of interacting loads at the stiffener intersection and to study the pillowing of the skin.
Derived from text

N94-20170*# National Aeronautics and Space Administration. Lewis Research Center, Cleveland, OH.
MULTI-DISCIPLINARY COUPLING EFFECTS FOR INTEGRATED DESIGN OF PROPULSION SYSTEMS
C. C. Chamis and S. N. Singhal (Sverdrup Technology, Inc., Brook Park, OH.) Apr. 1993 16 p Presented at the 76th AGARD Structures and Materials Panel, Workshop on Integrated Airframe Design Technology, Antalya, Turkey, 19-23 Apr. 1993; sponsored by the Advisory Group for Aerospace Research and Development
(RTOP 505-10-11)
(NASA-TM-106349; E-8125; NAS 1.15:106349) Avail: CASI HC A03/MF A01

Effective computational simulation procedures are described for modeling the inherent multi-disciplinary interactions which govern the accurate response of propulsion systems. Results are presented for propulsion system responses including multi-disciplinary coupling effects using coupled multi-discipline thermal, structural, and acoustic tailoring; an integrated system of multi-disciplinary simulators; coupled material behavior/fabrication process tailoring; sensitivities using a probabilistic simulator; and coupled materials, structures, fracture, and probabilistic behavior simulator. The results demonstrate that superior designs can be achieved if the analysis/tailoring methods account for the multi-disciplinary coupling effects. The coupling across disciplines can be used to develop an integrated coupled multi-discipline numerical propulsion system simulator.
Author (revised)

N94-20171*# National Aeronautics and Space Administration. Lewis Research Center, Cleveland, OH.
QUANTIFICATION OF UNCERTAINTIES IN THE PERFORMANCE OF SMART COMPOSITE STRUCTURES
Michael C. Shiao (Sverdrup Technology, Inc., Brook Park, OH.) and Christos C. Chamis Oct. 1993 21 p Presented at the 34th Structures, Structural Dynamics, and Materials Conference, La Jolla, CA, 19-21 Apr. 1993; cosponsored by AIAA, ASME, AHS, and ASC
(RTOP 210-02-12)
(NASA-TM-106335; E-8102; NAS 1.15:106335) Avail: CASI HC A03/MF A01

A composite wing with spars, bulkheads, and built-in control devices is evaluated using a method for the probabilistic assessment of smart composite structures. Structural responses (such as change in angle of attack, vertical displacements, and stresses in regular plies with traditional materials and in control plies with mixed traditional and actuation materials) are probabilistically assessed to quantify their respective scatter. Probabilistic sensitivity factors are computed to identify those parameters that have a significant influence on a specific structural response. Results show that the uncertainties in the responses of smart composite structures can be quantified. Responses such as structural deformation, ply stresses, frequencies, and buckling loads in the presence of defects can be reliably controlled to satisfy specified design requirements. Author

N94-20477# Sandia National Labs., Albuquerque, NM.
HIGH ACCURACY DIE MECHANICAL STRESS MEASUREMENT WITH THE ATC04 ASSEMBLY TEST CHIP
J. N. Sweet and D. W. Peterson 29 Jul. 1993 3 p Presented at the 1993 International Integrated Reliability Workshop, Lake Tahoe, CA, 24-27

Oct. 1993
(Contract DE-AC04-76DP-00789)
(DE93-019435; SAND-93-1837C; CONF-9310147-1) Avail: CASI HC A01/MF A01

We have designed and manufactured a new CMOS piezoresistive stress sensing chip, ATC04, with an advanced cell design which enables stress measurement to much higher accuracy and precision than any other known die. DOE

N94-20572# Phillips Lab., Kirtland AFB, NM.
NUMERICAL SIMULATIONS OF HYPERVELOCITY IMPACT EXPERIMENTS INVOLVING SINGLE WHIPPLE BUMPER SHIELDS Final Report, 8 Jun. - 3 Sep. 1992
David F. Medina and Scott R. Maethner Oct. 1993 67 p
(AF Proj. SNL-O)
(AD-A272123; PL-TR-93-1027) Avail: CASI HC A04/MF A01

Well-controlled hypervelocity impact experiments, conducted in support of the Space Station Shielding program, were numerically modeled using two sophisticated hydrocodes, the multidimensional hydrodynamics code (CTH), and the Smoothed Particle Hydrodynamics code (SPH). The experiments simulated the impact of space debris on single shields and single Whipple bumper shield plate configurations. Impact velocities on the order of 10 km/s were applied to gram-sized flier lates and spherical projectiles that struck thin aluminum, titanium, and steel plates. Computational predictions of the debris cloud dynamics and plate damage for these experiments were analyzed and correlated with the data obtained from pulsed laser photographs and high-speed x-ray photography. Computational results of both hydrocodes were compared to each other. DTIC

N94-20916# Army Engineer Waterways Experiment Station, Vicksburg, MS. Structures Lab.
TWO-DIMENSIONAL FINITE ELEMENT ANALYSIS OF POROUS MEDIA AT MULTIKILOBAR STRESS LEVELS Final Report
Stephen A. Akers Sep. 1993 105 p
(AD-A271540; WES/TR/SL-93-16) Avail: CASI HC A06/MF A02

A finite element (FE) code was developed to verify laboratory test results or to predict unavailable laboratory test data for porous media loaded to multikilobar stress levels. The FE code simulates quasi-static, axisymmetric, laboratory mechanical property tests, i.e., the laboratory tests are analyzed as boundary value problems. The code calculates strains, total and effective stresses, and pore fluid pressures for fully and partially saturated porous media. The time-dependent flow of the pore fluid is also calculated. An elastic-plastic strain-hardening cap model calculates the time-independent skeletal responses of the porous solids. This enables the code to model nonlinear irreversible stress-strain behavior and shear-induced volume changes. Fluid and solid compressibilities were incorporated into the code, and partially saturated materials were simulated with a 'homogenized' compressible pore fluid. Solutions for several verification problems are given as proof that the program works correctly, and numerical simulations of limestone behavior under drained and undrained boundary conditions are also presented. DTIC

N94-21153 Technische Univ., Berlin (Germany). Inst. fuer Luft- und Raumfahrt.
ADAPTATION OF MODEL PARAMETERS OF A RAIL MODEL AT MEASURED RAIL COMPLIANCES [ANPASSUNG DER MODELLPARAMETER EINES GLEISMODELLS AN GEMESSENE GLEISREZEPTANZEN]
B. Ripke Jan. 1992 37 p In GERMAN Limited Reproducibility: More than 20% of this document may be affected by microfiche quality
(ILR-Mitt-274(1992); ETN-93-94174) Avail: CASI HC A03

A method for calculation of unknown parameters of a rail model is presented. Measurements were carried out on a test rail of a locomotive factory by means of pulse excitation. Accelerations of the rail head in the vertical and laterial directions were measured with an accelerometer and dilatations were measured as a function of rail flexion with a piezo film. Input and transfer compliances were measured. The obtained data were controlled by means of a fast Fourier transformation analyzer and recorded on magnetic tapes. A model was developed with the finite element method by considering the rail as a Timoshinko beam. Stiffness and damping of bulkhead and tiebar were obtained. A variable threshold mass was introduced for model adaptation to the experiment results in low frequency area. ESA

N94-21219# Applied Research Associates, Inc., Albuquerque, NM.
DYNAMIC RESPONSE OF MULTIPHASE POROUS MEDIA Final Report, 1 Feb. 1989 - 31 May 1993
Daniel E. Chitty, Scott E. Blouin, Kwang J. Kim, and Alan F. Rauch 16 Jun. 1993 236 p
(Contract F49620-89-C-0037)
(AD-A272915; ARA-5535-3; AFOSR-93-0838TR) Avail: CASI HC A11/MF A03

This report presents the results of a three-year theoretical and experimental investigation of the response of multiphase porous media to strong dynamic loadings. A material element model was developed to automate the determination of parameter values for multiphase material models and to predict the response of saturated porous materials to arbitrary stress, strain and fluid flow boundary conditions. Laboratory tests to measure fluid flow through porous media were conducted over a wide range of pressure gradients in granular materials and porous rock. The results of those tests were used to develop a unified fluid friction model. A laboratory apparatus was constructed for the purpose of studying wave propagation through saturated porous media. A suite of dynamic tests was performed on a porous stainless steel specimen, and the results of those tests were compared with detailed multiphase numerical simulations. The simulations were in excellent agreement with the laboratory measurements. With guidance from simulations, it was possible to identify in the test data, the wave of the second kind. This disturbance, which propagates at a speed significantly lower than the compressional wave, appears to be associated with a surge of pore fluid within the porous skeleton, and has previously only been predicted by analysis. DTIC

N94-21249# Texas Univ., Austin. Inst. for Advanced Technology.
HYPERVELOCITY IMPACT Final Report, 17 - 20 Nov. 1992
Harry D. Fair, Thomas M. Kiehne, and Charles E. Anderson, Jr. Oct. 1993 903 p Proceedings of the 1992 Symposium held in Austin, TX, 17-19 Nov. 1992
(Contract DAAA21-90-D-0009)
(AD-A272957; IAT.R-0023) Avail: CASI HC A99/MF A10

The 1992 Hypervelocity Impact Symposium was held in Austin, Texas on November 17-20, 1992. The proceedings are published in three volumes. Seventy-six papers were unclassified, and published together as Volume 14, Numbers 1-4 of the International Journal of Impact Engineering, which can be obtained from Pergamon Press, Maxwell House, Fairview Park, Elmsford, NY 10523. Nine papers were selected for presentation and publication in the Classified Proceedings, and eight papers were selected for presentation and publication in the NOFORN Proceedings. DTIC

N94-21310# Naval Command, Control and Ocean Surveillance Center, San Diego, CA.
ADHESIVE BONDED JOINT WITH IMPROVED CYCLIC FATIGUE LIFE FOR ALUMINA-CERAMIC CYLINDERS AND HEMISPHERES: FOURTH GENERATION HOUSINGS Final Report
J. D. Stachiw Aug. 1993 118 p
(AD-A273061; NCCOSC/RDT/E-TR-1587) Avail: CASI HC A06/MF A02

A series of 20-inch-diameter monocoque cylinders of 94-percent alumina-ceramic were pressure tested to determine their structural performance under repeated pressurizations to 9,000 psi external design pressure when their ends are encapsulated in epoxy-filled Mod 1 titanium or aluminum end caps. Naval Ocean Systems Center (NOSC) Type Mod 1 titanium end caps provided an order-of-magnitude improvement in cyclic fatigue life for the ceramic cylinders over previously tested Mod 0 end caps. The cyclic fatigue life of 20-inch OD by 18.63-inch ID by 30-inch L by 0.685-inch t ceramic cylinders with 0.5-inch weight/displacement ratio, the ends of which were encapsulated with epoxy adhesive in Mod 1 titanium end caps, exceeded 400 cycles to 9,000 psi that generated inside the cylinder compressive membrane stresses of 136,000 psi magnitude in hoop and 68,000 psi in axial direction. At these stress levels, the shell of the monocoque cylinder can tolerate imperfections in the shape of spherical 0.063-inch) and oblong cavities (less than or equal to 0.063-inch by less than or equal to 0.187-inch) located below, or on the shell surface, provided that they are at least two inches away from the ends. The payload-carrying

ability of 94-percent alumina-ceramic monocoque cylinders with above dimensions is approximately four-times larger than rib-stiffened titanium cylinders with the same external dimensions and pressure rating. DTIC

N94-21421# Naval Postgraduate School, Monterey, CA.
NUMERICAL MODELING OF A PROPAGATING CRACK M.S. Thesis
Clifford Christy Jun. 1993 58 p
(AD-A272604) Avail: CASI HC A04/MF A01

In the numerical modeling of the crack propagation in dynamic fracture using stationary elements, a discrete and sudden release of node at the crack tip creates spurious oscillation in the kinetic and strain energy values. In order to reduce the oscillation, a moving node element was utilized. This element can model a continuous crack tip movement more closely. The moving node element is compatible with surrounding regular isoparametric elements and no remeshing is required during the crack propagation. In addition, two different central difference schemes were compared and their results were almost the same. DTIC

N94-21557# Sandia National Labs., Albuquerque, NM.
EXPERIMENTAL AND NUMERICAL STUDIES OF HIGH-VELOCITY IMPACT FRAGMENTATION
M. E. Kipp, D. E. Grady, and J. W. Swegle Aug. 1993 130 p
(Contract DE-AC04-76DP-00789)
(DE93-040205; SAND-93-0773) Avail: CASI HC A07/MF A02

Developments are reported in both experimental and numerical capabilities for characterizing the debris spray produced in penetration events. A series of high-velocity experiments specifically designed to examine the fragmentation of the projectile during impact were performed. High-strength, well-characterized steel spheres (6.35 mm diameter) were launched with a two-stage light-gas gun to velocities in the range of 3 to 5 km/s. Normal impact with PMMA plates, thicknesses of 0.6 to 11 mm, applied impulsive loads of various amplitudes and durations to the steel sphere. Multiple flash radiography diagnostics and recovery techniques were used to assess size, velocity, trajectory, and statistics of the impact-induced fragment debris. Damage modes to the primary target plate (plastic) and to a secondary target plate (aluminum) were also evaluated. Dynamic fragmentation theories, based on energy-balance principles, were used to evaluate local material deformation and fracture state information from CTH, a three-dimensional Eulerian solid dynamics shock wave propagation code. The local fragment characterization of the material defines a weighted fragment size distribution, and the sum of these distributions provides a composite particle size distribution for the steel sphere. The calculated axial and radial velocity changes agree well with experimental data, and the calculated fragment sizes are in qualitative agreement with the radiographic data. A secondary effort involved the experimental and computational analyses of normal and oblique copper ball impacts on steel target plates. High-resolution radiography and witness plate diagnostics provided impact motion and statistical fragment size data. CTH simulations were performed to test computational models and numerical methods.
DOE

N94-21624*# National Aeronautics and Space Administration. Langley Research Center, Hampton, VA.
RESULTS OF THE SECOND ROUND ROBIN ON OPENING-LOAD MEASUREMENT CONDUCTED BY ASTM TASK GROUP E24.04.04 ON CRACK CLOSURE MEASUREMENT AND ANALYSIS
E. P. Phillips Nov. 1993 38 p
(RTOP 50-63-50-04)
(NASA-TM-109032; NAS 1.15:109032) Avail: CASI HC A03/MF A01

A second experimental Round Robin on the measurement of the crack opening load in fatigue crack growth tests has been completed by the ASTM Task Group E24.04.04 on Crack Closure Measurement and Analysis. Fourteen laboratories participated in the testing of aluminum alloy compact tension specimens. Opening-load measurements were made at three crack lengths during constant Delta K, constant stress ratio tests by most of the participants. Four participants made opening-load measurements during threshold tests. All opening-load measurements were based on the analysis of specimens compliance behavior, where the displacement/strain was measured either at the crack mouth or the mid-height back face location. The Round Robin data were analyzed for opening load using two non-subjective analysis methods: the compliance offset and the correlation coefficient methods. The scatter in the opening load results was significantly reduced when some of the results were excluded from the analysis population based on an accept/reject criterion for raw data quality. The compliance offset and correlation coefficient opening load analysis methods produced similar results for data populations that had been screened to eliminate poor quality data. Author (revised)

N94-21757*# National Aeronautics and Space Administration. Lewis Research Center, Cleveland, OH.
PROBABILISTIC ASSESSMENT OF COMPOSITE STRUCTURES
Michael E. Shiao (Sverdrup Technology, Inc., Brook Park, OH.), Galib H. Abumeri (Sverdrup Technology, Inc., Brook Park, OH.), and Christos C. Chamis Dec. 1993 17 p Presented at the 34th Structures, Structural Dynamics and Materials Conference, La Jolla, CA, 19-23 Apr. 1993; sponsored by AIAA, ASME, ASCE, AHS, and ASC See also A93-33990
(RTOP 510-02-12)
(NASA-TM-106368; E-8173; NAS 1.15:106368) Avail: CASI HC A03/MF A01

A general computational simulation methodology for an integrated probabilistic assessment of composite structures is discussed and demonstrated using aircraft fuselage (stiffened composite cylindrical shell) structures with rectangular cutouts. The computational simulation was performed for the probabilistic assessment of the structural behavior including buckling loads, vibration frequencies, global displacements, and local stresses. The scatter in the structural response is simulated based on the inherent uncertainties in the primitive (independent random) variables at the fiber matrix constituent, ply, laminate, and structural scales that describe the composite structures. The effect of uncertainties due to fabrication process variables such as fiber volume ratio, void volume ratio, ply orientation, and ply thickness is also included. The methodology has been embedded in the computer code IPACS (Integrated Probabilistic Assessment of Composite Structures). In addition to the simulated scatter, the IPACS code also calculates the sensitivity of the composite structural behavior to all the primitive variables that influence the structural behavior. This information is useful for assessing reliability and providing guidance for improvement. The results from the probabilistic assessment for the composite structure with rectangular cutouts indicate that the uncertainty in the longitudinal ply stress is mainly caused by the uncertainty in the laminate thickness, and the large overlap of the scatter in the first four buckling loads implies that the buckling mode shape for a specific buckling load can be either of the four modes. Author (revised)

N94-21772 Argonne National Lab., IL.
SURFACE AND SUBSURFACE DEFECT DETECTION IN Si3N4 COMPONENTS BY LASER SCATTERING
J. S. Steckenrider and W. A. Ellingson 1993 23 p Presented at the 20th Annual Review of Progress in Quantitative Nondestructive Evaluation, Brunswick, ME, 1-6 Aug. 1993 Limited Reproducibility: More than 20% of this document may be affected by microfiche quality
(Contract W-31-109-eng-38)
(DE93-040829; ANL/ET/CP-79613; CONF-9308167-2) Avail: CASI HC A03

Lifetimes of Si3N4 components that experience contact fatigue (e.g., bearings) are affected by defects (voids, inclusions, etc.) at or near the surface (less than 200 microns). An optical technique was developed for rapid detection and quantification of defects in both surface and subsurfaces, as well as characterization of subsurface microstructure. This laser scattering technique was applied to various Si3N4 component shapes. Polarization techniques were used to independently analyze surface and subsurface material, and surface defects such as Vickers indent markings were detected at 10-50 microns; subsurface defects were also detected (simulated voids at depths up to 100 microns below surface). Subsurface microstructure (locally high porosity, grain orientation variations) has been characterized.
DOE

N94-21814*# Virginia Polytechnic Inst. and State Univ., Blacksburg. Dept. of Engineering Science and Mechanics.
IMPROVEMENTS TO A METHOD FOR THE GEOMETRICALLY NONLINEAR ANALYSIS OF COMPRESSIVELY LOADED STIFFENED COMPOSITE PANELS Final Technical Report, Feb. 1991 - Dec. 1993
Frederick Stoll 1993 128 p
(Grant NAG1-1215)
(NASA-CR-194715; NAS 1.26:194715) Avail: CASI HC A07/MF A02

The NLPAN computer code uses a finite-strip approach to the analysis of thin-walled prismatic composite structures such as stiffened panels. The code can model in-plane axial loading, transverse pressure loading, and constant through-the-thickness thermal loading, and can account for shape imperfections. The NLPAN code represents an attempt to extend the buckling analysis of the VIPASA computer code into the geometrically nonlinear regime. Buckling mode shapes generated using VIPASA are used in NLPAN as global functions for representing displacements in the nonlinear regime. While the NLPAN analysis is approximate in nature, it is computationally economical in comparison with finite-element analysis, and is thus suitable for use in preliminary design and design optimization. A comprehensive description of the theoretical approach of NLPAN is provided. A discussion of some operational considerations for the NLPAN code is included. NLPAN is applied to several test problems in order to demonstrate new program capabilities, and to assess the accuracy of the code in modeling various types of loading and response. User instructions for the NLPAN computer program are provided, including a detailed description of the input requirements and example input files for two stiffened-panel configurations.
Author (revised)

N94-21916# Sandia National Labs., Albuquerque, NM.
A THERMODYNAMIC THEORY OF DYNAMIC FRAGMENTATION
Ching H. Yew (Texas Univ., Austin.) and P. A. Taylor 1993 10 p Presented at the Annual Winter Meeting of the American Society of Mechanical Engineers, New Orleans, LA, 28 Nov. - 3 Dec. 1993
(Contract DE-AC04-76DP-00789)
(DE93-019066; SAND-93-0887C; CONF-931121-18) Avail: CASI HC A02/MF A01

We present a theory of dynamic fragmentation of brittle materials based on thermodynamic arguments. We recover the expressions for average fragment size and number as originally derived by Grady. We extend the previous work by obtaining descriptions of fragment size distribution and compressibility change due to the fragmentation process. The size distribution is assumed to be proportional to the spectral power of the strain history and a sample distribution is presented for a fragmentation process corresponding to a constant rate strain history. The description of compressibility change should be useful in computational studies of fragmentation. These results should provide insight into the process of fragmentation of brittle materials from hypervelocity impact. DOE

N94-21927# Argonne National Lab., IL.
A VIBRATION MODEL FOR CENTRIFUGAL CONTACTORS
R. A. Leonard, M. O. Wasserman, and D. G. Wygmans Nov. 1992 84 p
(Contract W-31-109-eng-38)
(DE93-040645; ANL-92/40) Avail: CASI HC A05/MF A01

Using the transfer matrix method, we created the Excel worksheet 'Beam' for analyzing vibrations in centrifugal contactors. With this worksheet, a user can calculate the first natural frequency of the motor/rotor system for a centrifugal contactor. We determined a typical value for the bearing stiffness (k(sub B)) of a motor after measuring the k(sub B) value for three different motors. The k(sub B) value is an important parameter in this model, but it is not normally available for motors. The assumptions that we made in creating the Beam worksheet were verified by comparing the calculated results with those from a VAX computer program, BEAM IV. The Beam worksheet was applied to several contactor designs for which we have experimental data and found to work well. DOE

N94-21956# Oak Ridge National Lab., TN.
MODAL COMBINATION IN RESPONSE SPECTRUM MODAL DYNAMIC ANALYSIS
C. R. Hammond and M. K. Singhal 1993 5 p Presented at the 4th Energy Natural Phenomena Hazards Mitigation Conference, Atlanta, GA, 19-22 Oct. 1993
(Contract DE-AC05-84OR-21400)
(DE94-000339; CONF-9310102-21) Avail: CASI HC A01/MF A01

UCRL-15910 does not give explicit requirements for combining the values of the response of individual modes in a response spectrum modal dynamic analysis. Since UCRL-15910 references ASE 4-86, modal combination methods given in ASCE 4-86 are described in this paper. Efficient use of typical dynamic analysis computer programs while complying with ASCE 4-86 is also described. DOE

N94-22001# General Electric Co., Schenectady, NY. Atomic Power Lab.
BENEFITS OF THREAD ROLLING PROCESS TO THE STRESS CORROSION CRACKING AND FATIGUE RESISTANCE OF HIGH STRENGTH FASTENERS
A. R. Kephart and S. Z. Hayden May 1993 14 p Presented at the 6th International Symposium on Environmental Degradation of Materials in Nuclear Power Systems: Water Reactors, San Diego, CA, 3-5 Aug. 1993
(Contract DE-AC12-76SN-00052)
(DE93-040438; KAPL-4759; CONF-930825-5) Avail: CASI HC A03/MF A01

Stress corrosion cracking (SCC) behavior of cut (machined) vice thread rolled Alloy X-750 and Alloy 625 fasteners in a simulated high temperature primary water environment has been evaluated. SCC testing at 360 and 338 C included 157 small and 40 large 60 degree thread studs. Thread rolled fasteners had improved resistance relative to cut fasteners. Tests of fatigue resistance in air at room temperature and both air and primary water at 315 C were conducted on smaller studs with both cut and rolled threads. Results showed rolled threads can have significantly improved fatigue lives over those of cut threads in both air and primary water. Fasteners produced by two different thread rolling methods, in-feed (radial) and through-feed (axial), revealed similar SCC initiation test results. Testing of thread rolled fasteners revealed no significant SCC or fatigue growth of rolling induced thread crest laps typical of the thread rolling process. While fatigue resistance differed between the two rolled thread supplier's studs, neither of the suppliers studs showed SCC initiation at exposure times beyond that of cut threads with SCC. In contrast to rolling at room temperature, warm rolled (427 C) threads showed no improvement over cut threads in terms of fatigue resistance. The observed improved SCC and fatigue performance of rolled threads is postulated to be due to interactive factors, including beneficial residual stresses in critically stressed thread root region, reduction of plastic strains during loading and formation of favorable microstructure. DOE

N94-22590 University of Western Ontario, London. Dept. of Mechanical Engineering.
RESPONSE STATISTICS OF SHELL STRUCTURES WITH GEOMETRICAL AND MATERIAL NONLINEARITIES, VOLUME 1 Ph.D. Thesis
Meilan Liu 1993 681 p
(ISBN-0-315-84006-4; CTN-94-60960) Copyright Avail: Micromedia Ltd., Technical Information Centre, 240 Catherine Street, Suite 305, Ottawa, Ontario, K2P 2G8, Canada HC/MF

A series of hybrid strain-based three-node flat triangular shell elements is developed for structural analyses. For linear analyses, the Hellinger Reissner (H-R) variational principle is employed. The elements are obtained by combining a triangular bending element and a plane stress element. For nonlinear analysis, the updated Lagrangian formulation and the incremental H-R variational principle are applied. The incremental second Piola Kirchhoff stress and the incremental Washizu strain are chosen as incremental stress and strain measures. Material nonlinearity is of the elastoplastic type with isotropic hardening. In all cases, explicit expressions for the stiffness and consistent mass matrices are obtained. The various shell structures studied show that the element formulations are accurate, effective, flexible, and applicable to thin to moderately thick shells with geometrical and material nonlinearities. In parallel, the stochastic central difference (SCD) method is applied to determine response statistics of general structures. The SCD method is extended to include a relatively general nonstationary random excitation comprising deterministic and stochastic components. It is applied to compute the random responses of general nonlinear shell structures. Numerical results employing the proposed methodologies are presented and their effectiveness is addressed.
Author (CISTI)

N94-22608*# National Aeronautics and Space Administration. Langley Research Center, Hampton, VA.
COMPUTATIONAL METHODS FOR FAILURE ANALYSIS AND LIFE PREDICTION
Ahmed K. Noor, comp. (Virginia Univ., Hampton.), Charles E. Harris, comp., Jerrold M. Housner, comp., and Dale A. Hopkins, comp. (National Aeronautics and Space Administration. Lewis Research Center, Cleveland, OH.) Washington Oct. 1993 334 p Workshop held in Hampton, VA, 14-15 Oct. 1992 Sponsored by NASA, Washington and Virginia Univ.

(RTOP 505-63-50-17)
(NASA-CP-3230; L-17321; NAS 1.55:3230) Avail: CASI HC A15/MF A03

This conference publication contains the presentations and discussions from the joint UVA/NASA Workshop on Computational Methods for Failure Analysis and Life Prediction held at NASA Langley Research Center 14-15 Oct. 1992. The presentations focused on damage failure and life predictions of polymer-matrix composite structures. They covered some of the research activities at NASA Langley, NASA Lewis, Southwest Research Institute, industry, and universities. Both airframes and propulsion systems were considered. For individual titles, see N94-22609 through N94-22623.

N94-22609*# Boeing Commercial Airplane Co., Seattle, WA. Advanced Composites Stress Group.

NONLINEAR AND PROGRESSIVE FAILURE ASPECTS OF TRANSPORT COMPOSITE FUSELAGE DAMAGE TOLERANCE

Tom Walker, L. Ilcewicz, Dan Murphy (Boeing Computer Services Co., Seattle, WA.), and Bernhard Dopker (Boeing Computer Services Co., Seattle, WA.) *In* NASA. Langley Research Center, Computational Methods for Failure Analysis and Life Prediction Oct. 1993 p 11-35 (For primary document see N94-22608 05-39)
Avail: CASI HC A03/MF A03

The purpose is to provide an end-user's perspective on the state of the art in life prediction and failure analysis by focusing on subsonic transport fuselage issues being addressed in the NASA/Boeing Advanced Technology Composite Aircraft Structure (ATCAS) contract and a related task-order contract. First, some discrepancies between the ATCAS tension-fracture test database and classical prediction methods is discussed, followed by an overview of material modeling work aimed at explaining some of these discrepancies. Finally, analysis efforts associated with a pressure-box test fixture are addressed, as an illustration of modeling complexities required to model and interpret tests. Author (revised)

N94-22610*# Jet Propulsion Lab., California Inst. of Tech., Pasadena.

PROJECTIONS ON STRUCTURES AND MATERIAL STRENGTH IN THE COMPUTATIONAL CONTEXT

Wolfgang G. Knauss *In* NASA. Langley Research Center, Computational Methods for Failure Analysis and Life Prediction Oct. 1993 p 37-51 (For primary document see N94-22608 05-39)
Avail: CASI HC A03/MF A03

The ideas associated with the subsequent viewgraphs are summarized. The primary motivation behind this presentation is to observe that certain macroscopic, microscopic, and submicroscopic phenomena are being understood that have basic influence on understanding the durability and high temperature sensitivity of polymers and polymer-based composites. This understanding covers important issues of long term stability with respect to residual stresses and deformations which can have very deleterious effects on structures used for long periods of time as a result of the heat-involving manufacturing process. Beyond this, important progress is being made in understanding the nonlinear material response of polymers in the fracture context, because the nonlinear mechanics of the material at the tip of a crack, either propagating or ready to do so, is being understood with increasing precision. Author (revised)

N94-22611*# Texas A&M Univ., College Station. Center for Mechanics of Composites.

A THERMODYNAMIC ANALYSIS OF PROPAGATING SUBCRITICAL CRACKS WITH COHESIVE ZONES

David H. Allen *In* NASA. Langley Research Center, Computational Methods for Failure Analysis and Life Prediction Oct. 1993 p 53-81 (For primary document see N94-22608 05-39)
Avail: CASI HC A03/MF A03

The results of the so-called energetic approach to fracture with particular attention to the issue of energy dissipation due to crack propagation are applied to the case of a crack with cohesive zone. The thermodynamic admissibility of subcritical crack growth (SCG) is discussed together with some hypotheses that lead to the derivation of SCG laws. A two-phase cohesive zone model for discontinuous crack growth is presented and its thermodynamics analyzed, followed by an example of its possible application. Author

N94-22612*# Stanford Univ., CA. Dept. of Aeronautics and Astronautics.

MODELING OF FAILURE AND RESPONSE TO LAMINATED COMPOSITES SUBJECTED TO IN-PLANE LOADS

Iqbal Shahid and Fu-Kuo Chang *In* NASA. Langley Research Center, Computational Methods for Failure Analysis and Life Prediction Oct. 1993 p 83-120 (For primary document see N94-22608 05-39)
Avail: CASI HC A03/MF A03

An analytical model was developed for predicting the response of laminated composites with or without a cutout and subjected to in-plane tensile and shear loads. Material damage resulting from the loads in terms of matrix cracking, fiber-matrix shearing, and fiber breakage was considered in the model. Delamination, an out-of-plane failure mode, was excluded from the model. Author (revised)

N94-22613*# National Aeronautics and Space Administration. Lewis Research Center, Cleveland, OH.

BRIEF SUMMARY OF THE EVOLUTION OF HIGH-TEMPERATURE CREEP-FATIGUE LIFE PREDICTION MODELS FOR CRACK INITIATION

Gary R. Halford *In* NASA. Langley Research Center, Computational Methods for Failure Analysis and Life Prediction Oct. 1993 p 121-150 (For primary document see N94-22608 05-39)
Avail: CASI HC A03/MF A03

The evolution of high-temperature, creep-fatigue, life-prediction methods used for cyclic crack initiation is traced from inception in the late 1940's. The methods reviewed are material models as opposed to structural life prediction models. Material life models are used by both structural durability analysts and by material scientists. The latter use micromechanistic models as guidance to improve a material's crack initiation resistance. Nearly one hundred approaches and their variations have been proposed to date. This proliferation poses a problem in deciding which method is most appropriate for a given application. Approaches were identified as being combinations of thirteen different classifications. This review is intended to aid both developers and users of high-temperature fatigue life prediction methods by providing a background from which choices can be made. The need for high-temperature, fatigue-life prediction methods followed immediately on the heels of the development of large, costly, high-technology industrial and aerospace equipment immediately following the second world war. Major advances were made in the design and manufacture of high-temperature, high-pressure boilers and steam turbines, nuclear reactors, high-temperature forming dies, high-performance poppet valves, aeronautical gas turbine engines, reusable rocket engines, etc. These advances could no longer be accomplished simply by trial and error using the 'build-em and bust-em' approach. Development lead times were too great and costs too prohibitive to retain such an approach. Analytic assessments of anticipated performance, cost, and durability were introduced to cut costs and shorten lead times. The analytic tools were quite primitive at first and out of necessity evolved in parallel with hardware development. After forty years more descriptive, more accurate, and more efficient analytic tools are being developed. These include thermal-structural finite element and boundary element analyses, advanced constitutive stress-strain-temperature-time relations, and creep-fatigue-environmental models for crack initiation and propagation. The high-temperature durability methods that have evolved for calculating high-temperature fatigue crack initiation lives of structural engineering materials are addressed. Only a few of the methods were refined to the point of being directly useable in design. Recently, two of the methods were transcribed into computer software for use with personal computers. Author (revised)

N94-22614*# National Aeronautics and Space Administration. Lewis Research Center, Cleveland, OH.

LIFE ASSESSMENT OF STRUCTURAL COMPONENTS USING INELASTIC FINITE ELEMENT ANALYSES

Vinod K. Arya (Toledo Univ., OH.) and Gary R. Halford *In* NASA. Langley Research Center, Computational Methods for Failure Analysis and Life Prediction Oct. 1993 p 151-163 (For primary document see N94-22608 05-39)
Avail: CASI HC A03/MF A03

The need for enhanced and improved performance of structural components subject to severe cyclic thermal/mechanical loadings, such as in the aerospace industry, requires development of appropriate solution technologies involving time-dependent inelastic analyses. Such analyses

are mandatory to predict local stress-strain response and to assess more accurately the cyclic life time of structural components. The NASA-Lewis Research Center is cognizant of this need. As a result of concerted efforts at Lewis during the last few years, several such finite element solution technologies (in conjunction with the finite element program MARC) were developed and successfully applied to numerous uniaxial and multiaxial problems. These solution technologies, although developed for use with MARC program, are general in nature and can easily be extended for adaptation with other finite element programs such as ABAQUS, ANSYS, etc. The description and results obtained from two such inelastic finite element solution technologies are presented. The first employs a classical (non-unified) creep-plasticity model. An application of this technology is presented for a hypersonic inlet cowl-lip problem. The second of these technologies uses a unified creep-plasticity model put forth by Freed. The structural component for which this finite element solution technology is illustrated, is a cylindrical rocket engine thrust chamber. The advantages of employing a viscoplastic model for nonlinear time-dependent structural analyses are demonstrated. The life analyses for cowl-lip and cylindrical thrust chambers are presented. These analyses are conducted by using the stress-strain response of these components obtained from the corresponding finite element analyses. Author (revised)

N94-22615*# Pratt and Whitney Aircraft, West Palm Beach, FL.
LIFE PREDICTION SYSTEMS FOR CRITICAL ROTATING COMPONENTS
Susan E. Cunningham *In* NASA. Langley Research Center, Computational Methods for Failure Analysis and Life Prediction Oct. 1993 p 165-184 (For primary document see N94-22608 05-39)
Avail: CASI HC A03/MF A03

With the advent of advanced materials in rotating gas turbine engine components, the methodologies for life prediction of these parts must also increase in sophistication and capability. Pratt & Whitney's view of generic requirements for composite component life prediction systems are presented, efforts underway to develop these systems are discussed, and industry participation in key areas requiring development is solicited. Author (revised)

N94-22616*# Southwest Research Inst., San Antonio, TX.
RECENT ADVANCES IN COMPUTATIONAL STRUCTURAL RELIABILITY ANALYSIS METHODS **c38**
Ben H. Thacker, Y.-T. Wu, Harry R. Millwater, Tony Y. Torng, and David S. Riha *In* NASA. Langley Research Center, Computational Methods for Failure Analysis and Life Prediction Oct. 1993 p 185-203 (For primary document see N94-22608 05-39)
Avail: CASI HC A03/MF A03

The goal of structural reliability analysis is to determine the probability that the structure will adequately perform its intended function when operating under the given environmental conditions. Thus, the notion of reliability admits the possibility of failure. Given the fact that many different modes of failure are usually possible, achievement of this goal is a formidable task, especially for large, complex structural systems. The traditional (deterministic) design methodology attempts to assure reliability by the application of safety factors and conservative assumptions. However, the safety factor approach lacks a quantitative basis in that the level of reliability is never known and usually results in overly conservative designs because of compounding conservatisms. Furthermore, problem parameters that control the reliability are not identified, nor their importance evaluated. A summary of recent advances in computational structural reliability assessment is presented. A significant level of activity in the research and development community was seen recently, much of which was directed towards the prediction of failure probabilities for single mode failures. The focus is to present some early results and demonstrations of advanced reliability methods applied to structural system problems. This includes structures that can fail as a result of multiple component failures (e.g., a redundant truss), or structural components that may fail due to multiple interacting failure modes (e.g., excessive deflection, resonate vibration, or creep rupture). From these results, some observations and recommendations are made with regard to future research needs. Author (revised)

N94-22617*# National Aeronautics and Space Administration. Lewis Research Center, Cleveland, OH.
AN OVERVIEW OF COMPUTATIONAL SIMULATION METHODS FOR COMPOSITE STRUCTURES FAILURE AND LIFE ANALYSIS
Christos C. Chamis *In* NASA. Langley Research Center, Computational Methods for Failure Analysis and Life Prediction Oct. 1993 p 205-223 (For primary document see N94-22608 05-39)
Avail: CASI HC A03/MF A03

Three parallel computational simulation methods are being developed at the LeRC Structural Mechanics Branch (SMB) for composite structures failure and life analysis: progressive fracture CODSTRAN; hierarchical methods for high-temperature composites; and probabilistic evaluation. Results to date demonstrate that these methods are effective in simulating composite structures failure/life/reliability. Author (revised)

N94-22618*# National Aeronautics and Space Administration. Langley Research Center, Hampton, VA.
ANALYSIS OF THERMAL MECHANICAL FATIGUE IN TITANIUM MATRIX COMPOSITES
W. Steven Johnson and Massoud Mirdamadi *In its* Computational Methods for Failure Analysis and Life Prediction Oct. 1993 p 225-238 (For primary document see N94-22608 05-39)
Avail: CASI HC A03/MF A03

Titanium metal matrix composites are being evaluated for structural applications on advanced hypersonic vehicles. These composites are reinforced with ceramic fibers such as silicon carbide, SCS-6. This combination of matrix and fiber results in a high stiffness, high strength composite that has good retention of properties even at elevated temperatures. However, significant thermal stresses are developed within the composite between the fiber and the matrix due to the difference in their respective coefficients of thermal expansion. In addition to the internal stresses that are generated due to thermal cycling, the overall laminate will be subjected to considerable mechanical loads during the thermal cycling. In order to develop life prediction methodology, one must be able to predict the stresses and strains that occur in the composite's constituents during the complex loading. Thus the purpose is to describe such an analytical tool, VISCOPLY. Author (revised)

N94-22619*# National Aeronautics and Space Administration. Lewis Research Center, Cleveland, OH.
TIME-DEPENDENT RELIABILITY ANALYSIS OF CERAMIC ENGINE COMPONENTS **c38**
Noel N. Nemeth *In* NASA. Langley Research Center, Computational Methods for Failure Analysis and Life Prediction Oct. 1993 p 239-269 (For primary document see N94-22608 05-39)
Avail: CASI HC A03/MF A03

The computer program CARES/LIFE calculates the time-dependent reliability of monolithic ceramic components subjected to thermomechanical and/or proof test loading. This program is an extension of the CARES (Ceramics Analysis and Reliability Evaluation of Structures) computer program. CARES/LIFE accounts for the phenomenon of subcritical crack growth (SCG) by utilizing either the power or Paris law relations. The two-parameter Weibull cumulative distribution function is used to characterize the variation in component strength. The effects of multiaxial stresses are modeled using either the principle of independent action (PIA), the Weibull normal stress averaging method (NSA), or the Batdorf theory. Inert strength and fatigue parameters are estimated from rupture strength data of naturally flawed specimens loaded in static, dynamic, or cyclic fatigue. Two example problems demonstrating proof testing and fatigue parameter estimation are given. Author (revised)

N94-22620*# National Aeronautics and Space Administration. Lewis Research Center, Cleveland, OH.
A HIGH TEMPERATURE FATIGUE LIFE PREDICTION COMPUTER CODE BASED ON THE TOTAL STRAIN VERSION OF STRAINRANGE PARTITIONING (SRP)
Michael A. McGaw and James F. Saltsman *In* NASA. Langley Research Center, Computational Methods for Failure Analysis and Life Prediction Oct. 1993 p 271-284 See also A93-31341 (For primary document see N94-22608 05-39)
Avail: CASI HC A03/MF A03

A recently developed high-temperature fatigue life prediction computer

code is presented and an example of its usage given. The code discussed is based on the Total Strain version of Strainrange Partitioning (TS-SRP). Included in this code are procedures for characterizing the creep-fatigue durability behavior of an alloy according to TS-SRP guidelines and predicting cyclic life for complex cycle types for both isothermal and thermomechanical conditions. A reasonably extensive materials properties database is included with the code. Author

N94-22621*# National Aeronautics and Space Administration. Langley Research Center, Hampton, VA.
NASA LANGLEY DEVELOPMENTS IN RESPONSE CALCULATIONS NEEDED FOR FAILURE AND LIFE PREDICTION
Jerrold M. Housner *In its* Computational Methods for Failure Analysis and Life Prediction Oct. 1993 p 285-310 (For primary document see N94-22608 05-39)
Avail: CASI HC A03/MF A03

NASA Langley developments in response calculations needed for failure and life predictions are discussed. Topics covered include: structural failure analysis in concurrent engineering; accuracy of independent regional modeling demonstrated on classical example; functional interface method accurately joins incompatible finite element models; interface method for insertion of local detail modeling extended to curve pressurized fuselage window panel; interface concept for joining structural regions; motivation for coupled 2D-3D analysis; compression panel with discontinuous stiffener coupled 2D-3D model and axial surface strains at the middle of the hat stiffener; use of adaptive refinement with multiple methods; adaptive mesh refinement; and studies on quantity effect of bow-type initial imperfections on reliability of stiffened panels. Author (revised)

N94-22622*# National Aeronautics and Space Administration. Langley Research Center, Hampton, VA.
DELAMINATION, DURABILITY, AND DAMAGE TOLERANCE OF LAMINATED COMPOSITE MATERIALS **c24**
T. Kevin OBrien *In its* Computational Methods for Failure Analysis and Life Prediction Oct. 1993 p 311-322 (For primary document see N94-22608 05-39)
Avail: CASI HC A03/MF A03

Durability and damage tolerance may have different connotations to people from different industries and with different backgrounds. Damage tolerance always refers to a safety of flight issue where the structure must be able to sustain design limit loads in the presence of damage and return to base safely. Durability, on the other hand, is an economic issue where the structure must be able to survive a certain life under load before the initiation of observable damage. Delamination is typically the observable damage mechanism that is of concern for durability, and the growth and accumulation of delaminations through the laminate thickness is often the sequence of events that leads to failure and the loss of structural integrity. Author (revised)

N94-22623*# National Aeronautics and Space Administration. Langley Research Center, Hampton, VA.
DEMONSTRATING DAMAGE TOLERANCE OF COMPOSITE AIRFRAMES **c05**
Clarence C. Poe, Jr. *In its* Computational Methods for Failure Analysis and Life Prediction Oct. 1993 p 323-345 (For primary document see N94-22608 05-39)
Avail: CASI HC A03/MF A03

Commercial transport aircraft operating in the United States are certified by the Federal Aviation Authority to be damage tolerant. On 28 April 1988, Aloha Airlines Flight 243, a Boeing 727-200 airplane, suffered an explosive decompression of the fuselage but landed safely. This event provides very strong justification for the damage tolerant design criteria. The likely cause of the explosive decompression was the linkup of numerous small fatigue cracks that initiated at adjacent fastener holes in the lap splice joint at the side of the body. Actually, the design should have limited the damage size to less than two frame spacings (about 40 inches), but this type of 'multi-site damage' was not originally taken into account. This cracking pattern developed only in the high-time airplanes (many flights). After discovery in the fleet, a stringent inspection program using eddy current techniques was inaugurated to discover these cracks before they linked up. Because of concerns about safety and the maintenance burden, the lap-splice joints of these high-time airplanes are being modified to remove cracks and prevent new cracking; newer designs account for 'multi-site damage'. Author (revised)

N94-20891*# Tokyo Univ. (Japan). Electro-Communications.
ANTIPODAL FRAGMENT VELOCITIES FOR POROUS AND WEAK TARGETS AT CATASTROPHIC IMPACTS Abstract Only
M. Yanagisawa and T. Itoi *In* Lunar and Planetary Inst., Twenty-Fourth Lunar and Planetary Science Conference. Part 3: N-Z 1993 p 1551-1552 Sponsored in part by ISAS (For primary document see N94-20636 05-91)
Avail: CASI HC A01/MF A06

N94-21397 Centre d'Etudes de Gramat (France).
HYPERVELOCITY IMPACT STUDIES AT CEG: EXPERIMENTAL AND NUMERICAL CAPABILITIES Abstract Only [LES MOYENS EXPERIMENTAUX ET NUMERIQUES DU CEG POUR LES ETUDES D'IMPACT HYPERVITESSE]
C. Loupias and B. Jimenez *In* CNES, Fifth International Symposium on Materials in a Space Environment Jun. 1993 p 409-410 In ENGLISH and FRENCH (For primary document see N94-21367 05-18)
Copyright Avail: CEPADUES-Editions, 111, rue Nicolas-Vaquelin, 31100 Toulouse, France

N94-22065# Technical Research Centre of Finland, Espoo.
THE PROGRAM SYSTEM FOR THE DIAGNOSTICS OF STRAINS AND FRACTURE PREDICTION OF SOLIDS
V. Z. Parton and V. Boriskovski *In* Technical Research Centre of Finland, Information Technology and Economic Modelling 1992 p 85 (For primary document see N94-22056 05-83)
Copyright Avail: CASI HC A01/MF A03

42 GEOSCIENCES (GENERAL)

N94-20936# Department of Energy, Washington, DC. Office of Energy Research.
RESEARCH IN PROGRESS: FY 1992
Aug. 1993 427 p
(DE94-000410; DOE/ER-0592(08-93)) Avail: CASI HC A19/MF A04

The Biological and Environmental Research (BER) Program of OHER has two main missions: (1) to develop the knowledge base necessary to identify, understand, and anticipate the long-term health and environmental consequences of energy use and development; and (2) to utilize the Department's unique scientific and technological capabilities to solve major scientific problems in medicine, biology, and the environment. These missions reflect a commitment to develop the beneficial uses of advanced energy technologies while at the same time assuring that any potentially adverse health and environmental impacts of the Nation's energy policies are fully identified and understood. The BER Program includes research in the following areas: atmospheric, marine, and terrestrial processes, including the linkage between the use in greenhouse gases, carbon dioxide, and regional and global climate change; in molecular and subcellular mechanisms underlying human somatic and genetic processes and their responses to energy-related environmental toxicants; in nuclear medicine, structural biology, the human genome, measurement sciences and instrumentation; and other areas that require the unique capabilities of the Department's laboratory system. The principal areas of research are Health Research and Environmental Research. DOE

43 EARTH RESOURCES AND REMOTE SENSING

Includes remote sensing of earth resources by aircraft and spacecraft; photogrammetry; and aerial photography.

For instrumentation see *35 Instrumentation and Photography.*

N94-20028# Naval Research Lab., Bay Saint Louis, MS. Remote Sensing Applications Branch.

GLOBAL AND REGIONAL COMPARATIVE PERFORMANCE OF LINEAR AND NONLINEAR SATELLITE MULTICHANNEL SEA SURFACE TEMPERATURE ALGORITHMS Final Report

Douglas A. May Sep. 1993 36 p

(NRL Proj. 0101)

(AD-A270475; NRL/MR/7240-93-7049) Avail: CASI HC A03/MF A01

This report summarizes investigations conducted at the Naval Research Laboratory on the accuracy of advanced very high resolution radiometer (AVHRR) satellite sea surface temperature (SST) retrieval techniques. Investigations focused on linear and nonlinear AVHRR atmospheric correction algorithms and their comparative performance relative to global drifting buoy in situ SST observations. Satellite retrievals were matched to drifting buoy SST's within two hours and ten kilometers from January to December 1990. Emphasis was placed on the bias and root-mean-square difference (rmsd) statistical accuracy of each algorithm for various global regions, atmospheric conditions, and seasonal time periods. Results demonstrate that the nonlinear sea surface temperature (NLSST) algorithm provides consistently better bias and rmsd accuracy statistics relative to the other algorithms tested. Given these results, it is recommended that global satellite SST retrieval processing should utilize the NLSST algorithm for operational retrieval generation. Recommendations are also provided for future algorithms. DTIC

N94-20205*# Maryland Univ., College Park.

MODELING OF INTERACTIONS BETWEEN BIOSPHERE AND ATMOSPHERE ON THE GLOBAL SCALE Final Report

Ferdinand Baer and Y. Mintz 20 Aug. 1990 4 p

(Grant NAG5-383)

(NASA-CR-193423; NAS 1.26:193423) Avail: CASI HC A01/MF A01

Simulations of weather and climate with general circulation models show that the circulation and rainfall are sensitive to the transfers of radiation, sensible heat, water vapor, and momentum across the atmosphere land surface interface. Because, in nature, these transfers depend in large measure on the morphological and physiological characteristics of the surface vegetation, an interactive biosphere is needed for GCM's. The simple model of the biosphere (SiB) that the authors have constructed is based on the recognized difference between ground cover vegetation (grasses and other herbaceous plants) and canopy vegetation (trees and shrubs), where the latter act like elevated blocks of porous material which efficiently extract momentum from the air that flows through them; by a large number of multiple reflections enhance the absorption of the incident solar radiation; when the canopy is wet, act like well ventilated psychrometers which extract sensible heat from the air and produce a negative Bowen ratio; and, in all of these ways, behave differently from ground cover vegetation. The complete set of governing equations of SiB, whereby the various allowable combinations of trees, ground covers, and bare ground, in interaction with the atmosphere, determine all of the vegetation dependent transfers at the land surface, have been presented and described. Derived from text

N94-20209# Office of Technology Assessment, Washington, DC.

THE FUTURE OF REMOTE SENSING FROM SPACE: CIVILIAN SATELLITE SYSTEMS AND APPLICATIONS

Jul. 1993 216 p Original contains color illustrations

(OTA-ISC-558; ISBN-0-16-041884-4) Avail: CASI HC A10/MF A03; SOD HC

Over the past decade, the United States and other countries have increasingly turned to satellite remote sensing to gather data about the state of earth's atmosphere, land, and oceans. Satellite systems provide the vantage point and coverage necessary to study our planet as an integrated, interactive physical and biological system. In particular, the data they provide, combined with data from surface and aircraft-based instruments, should help scientists monitor, understand, and ultimately predict the long term effects of global change. This report, the first of three in a broad OTA assessment of earth observation systems, examines issues related to the development and operation of publicly funded U.S. and foreign civilian remote sensing systems. It also explores the military and intelligence use of data gathered by civilian satellites. In addition, the report examines the outlook for privately funded and operated remote sensing systems. Despite the established utility of remote sensing technology in a wide variety of applications, the state of the U.S. economy and the burden of an increasing Federal deficit will force NASA, NOAA, and DoD to seek ways to reduce the costs of remote sensing systems. This report observes that maximizing the return on the U.S. investment in satellite remote sensing will require the Federal Government to develop a flexible, long-term interagency plan that would guarantee the routine collection of high-quality measurements of the atmosphere, oceans, and land over decades. Such a plan would assign the part each agency plays in gathering data on global change, including scientifically critical observations from aircraft- and ground-based platforms, as well as from space-based platforms. It would also develop appropriate mechanisms for archiving, integrating, and distributing data from many different sources for research and other purposes. Finally, it would assign to the private sector increasing responsibility for collecting and archiving remotely sensed data. Derived from text

N94-20284*# JJM Systems, Inc., Arlington, VA.

AN EXPERT SYSTEM SHELL FOR INFERRING VEGETATION CHARACTERISTICS Final Report, Mar. - Nov. 1993

P. Ann Harrison and Patrick R. Harrison Nov. 1993 145 p The Lisp and KEE code for this work is available on a Sun cartridge tape

(Contract NAS5-30127; RTOP 462-61-14)

(NASA-CR-194569; NAS 1.26:194569; C931033-U-2R00) Avail: CASI HC A07/MF A02

The NASA VEGetation Workbench (VEG) is a knowledge based system that infers vegetation characteristics from reflectance data. VEG is described in detail in several references. The first generation version of VEG was extended. In the first year of this contract, an interface to a file of unknown cover type data was constructed. An interface that allowed the results of VEG to be written to a file was also implemented. A learning system that learned class descriptions from a data base of historical cover type data and then used the learned class descriptions to classify an unknown sample was built. This system had an interface that integrated it into the rest of VEG. The VEG subgoal PROPORTION.GROUND.COVER was completed and a number of additional techniques that inferred the proportion ground cover of a sample were implemented. This work was previously described. The work carried out in the second year of the contract is described. The historical cover type database was removed from VEG and stored as a series of flat files that are external to VEG. An interface to the files was provided. The framework and interface for two new VEG subgoals that estimate the atmospheric effect on reflectance data were built. A new interface that allows the scientist to add techniques to VEG without assistance from the developer was designed and implemented. A prototype Help System that allows the user to get more information about each screen in the VEG interface was also added to VEG. Author (revised)

N94-20951*# San Diego State Univ., CA. Dept. of Geography.

MEASUREMENT OF EVAPOTRANSPIRATION WITH COMBINED REFLECTIVE AND THERMAL INFRARED RADIANCE OBSERVATIONS Final Report

Allen S. Hope 1993 150 p

(Grant NAG5-911)

(NASA-CR-194802; NAS 1.26:194802) Avail: CASI HC A07/MF A02

The broad goal of the research summarized in this report was 'To facilitate the evaluation of regional evapotranspiration (ET) through the combined use of solar reflective and thermal infrared radiance observations.' The specific objectives stated by Goward and Hope (1986) were to: (1) investigate the nature of the relationship between surface temperature (T(sub S)) and the normalized difference vegetation index (NDVI) and develop an understanding of this relationship in terms of energy exchange processes, particularly latent flux heat (LE); (2) develop procedures to estimate large area LE using combined T(sub S) and NDVI observations obtained from AVHRR data; and (3) determine whether measurements derived from satellite observations relate directly to measurements made at the surface or from aircraft platforms. Both empirical and modeling studies were used to develop an understanding of the T(sub S)-NDVI relationship. Most of the modeling was based on the Tergra model as originally proposed by Goward. This

model, and modified versions developed in this project, simulates the flows of water and energy in the soil-plant-atmosphere system using meteorological, soil and vegetation inputs. Model outputs are the diurnal course of soil moisture, T(sub S), LE and the other individual components of the surface energy balance. Derived from text

N94-20953# Instituto de Pesquisas Espaciais, Sao Jose dos Campos (Brazil).
THE 7TH BRAZILIAN REMOTE SENSING SYMPOSIUM, VOLUME 1 [7TH SIMPOSIO BRASILEIRO DE SENSORIAMENTO REMOTO, VOLUME 1]
Roberto PereiradaCunha, ed. and Luiz Alberto Vieira Dias, ed. 1993 188 p In ENGLISH and PORTUGUESE Symposium held in Curitiba, Brazil, 10-14 May 1993 Prepared in cooperation with Secretaria de Estadoddo Meio Ambiente, Parana, Brazil; Sociedad de Especialistas Latinoamericanos en Perception Remota, Chile; and Sociedade Brasileira de Cartografia, Geodesia, Fotogramtria e Sensoriamento Remoto Original contains color illustrations
Avail: CASI HC A09/MF A02

Papers presented at the 7th Brazilian Remote Sensing Symposium are included. Topics covered include: the use of satellite images in Amazonian Archeology: a case study in the Upper Rio Negro Basin; and application of SPOT to GIS/LIS in land capability evaluation for regional planning of JAICO semi-arid region of Piaui, Brazil. For individual titles, see N94-20954 through N94-20955.

N94-20954# Sao Paulo Univ. (Brazil). Museu de Arqueologia e Etnologia.
THE USE OF SATELLITE IMAGES IN AMAZONIAN ARCHAEOLOGY: A CASE STUDY IN THE UPPER RIO NEGRO BASIN
Eduardo G. Neves *In* INPE, The 7th Brazilian Remote Sensing Symposium, Volume 1 1993 p 112-118 (For primary document see N94-20953 05-43)
(Contract CNPq-203133/89.7; NSF DBS-92-23763)
Avail: CASI HC A02/MF A02

The preliminary results of an archaeological survey of the Middle Uaupes river, in the Upper Rio Negro basin are presented. The survey strategy is based on remote sensing, ethnographic, and geomorphological data. Author (revised)

N94-20955# Universidade Federal de Paraiba (Brazil).
APPLICATION OF SPOT TO GIS/LIS IN LAND CAPABILITY EVALUATION FOR REGIONAL PLANNING OF JAICO SEMI-ARID REGION OF PIAUI, BRAZIL
Harendra S. Teotia, Klaus A. Ulbricht (Deutsche Forschungsanstalt fuer Luft- und Raumfahrt, Wessling, Germany.), and Daniel L. Civco (Connecticut Univ., Storrs.) *In* INPE, The 7th Brazilian Remote Sensing Symposium, Volume 1 1993 p 144-154 (For primary document see N94-20953 05-43)
Avail: CASI HC A03/MF A02

Remote Sensing provides one or a few of the many data required in GIS/LIS for evaluation of various types of land capabilities, such as land capability for urban land use, agricultural use, and for forestry use. In northeastern Brazil, satellite data such as SPOT HRV and Landsat-TM were utilized to provide land use information for the semi-arid areas of the region. The present investigation was conducted over an area of approximately 700 Km(sup 2) in northeastern Brazil at JAICO and its environs located in the sul of the Piaui state. A Raster based Computer Mapping System-ERDAS (Earth Resources Data Analysis System) for a hybridized unsupervised-supervised classification (Maximum Likelihood) approach was used in order to extract 17 land use/land cover classes at the Level 2 of Anderson Classification. These classes were recoded in order to detect the 11 soil association classes in accordance with the Brazilian and USDA Systems which were then recoded into 9 land capability units using the Brazilian and American Systems. Finally, three maps were derived for the objectives of regional planning under this investigation: (1) Land use/Land cover map; (2) Soil Associations map; and (3) Land Capability Units map. This system is used to store information of various properties of land development for regional planning in NE Brazil. Comparison of digital interpretation with reference information indicated that digital interpretation, closely resembled field observation and the overall classification accuracy was observed 84.7 percent. Author (revised)

N94-20956# Instituto de Pesquisas Espaciais, Sao Jose dos Campos (Brazil).
THE 7TH BRAZILIAN REMOTE SENSING SYMPOSIUM, VOLUME 2 [7TH SIMPOSIO BRASILEIRO DE SENSORIAMENTO REMOTO, VOLUME 2]
Roberto PereiradaCunha, ed. and Luiz Alberto Vieira Dias, ed. 1993 489 p In ENGLISH and PORTUGUESE Symposium held in Curitiba, Brazil, 10-14 May 1993 Prepared in cooperation with Secretaria de Estadoddo Meio Ambiente, Parana, Brazil; Sociedad de Especialistas Latinoamericanos en Perception Remota, Chile; and Sociedade Brasileira de Cartografia, Geodesia, Fotogramtria e Sensoriamento Remoto Original contains color illustrations
Avail: CASI HC A21/MF A04

Papers presented at the 7th Brazilian Remote Sensing Symposium held at Curtibo, Brazil from 10-14 May 1993 are included. Topics covered include: change detection on land use and rainforest cover at Paragominas region, Brazilian Amazon; linear mixed model applied to Advanced Very High Resolution Radiometers (AVHRR) Local Area Coverage (LAC) data; and analysis of hyper-spectral Airborne Visible and Infrared Imaging Spectrometer (AVIRIS) image data. For individual titles, see N94-20957 through N94-20959.

N94-20957# Instituto Brasileiro do Meio Ambiente e dos Recursos Naturais Renovaveis, Rio de Janeiro.
CHANGE DETECTION ON LAND USE AND RAINFOREST COVER AT PARAGOMINAS REGION, BRAZILIAN AMAZON
Lisia Vamacor Barroso (Universidade Federal Fluminense, Niteroi, Brazil.), Daniel C. Nepstad (Universidade Federal Fluminense, Niteroi, Brazil.), I. Foster Brown (Universidade Federal Fluminense, Niteroi, Brazil.), and Paul A. Lefebvre (Universidade Federal Fluminense, Niteroi, Brazil.) *In* INPE, The 7th Brazilian Remote Sensing Symposium, Volume 2 1993 p 21-29 (For primary document see N94-20956 05-43)
Avail: CASI HC A02/MF A04

Paragominas region, at Eastern Para, is one of the oldest colonization centers of Amazonia. The objective was the change detection of land use in colonization settlements of that country, focusing forest cover, using LANDSAT satellite imagery. The methodology adopted included the examination of NDVI (normalized difference vegetation index), supervisioned classification (minimum distance), and the change detection technique. Results evidenced rainforest regeneration at Uraim Colony, a settlement that showed successful socio-economic characteristics. Author (revised)

N94-20958*# National Aeronautics and Space Administration. Goddard Space Flight Center, Greenbelt, MD.
LINEAR MIXING MODEL APPLIED TO AVHRR LAC DATA
Brent N. Holben and Yosio E. Shimabukuro (Instituto de Pesquisas Espaciais, Sao Jose dos Campos, Brazil.) *In* INPE, The 7th Brazilian Remote Sensing Symposium, Volume 2 1993 p 102-115 (For primary document see N94-20956 05-43)
Avail: CASI HC A03/MF A04

A linear mixing model was applied to coarse spatial resolution data from the NOAA Advanced Very High Resolution Radiometer. The reflective component of the 3.55 - 3.93 microns channel was extracted and used with the two reflective channels 0.58 - 0.68 microns and 0.725 - 1.1 microns to run a Constraine Least Squares model to generate vegetation, soil, and shade fraction images for an area in the Western region of Brazil. The Landsat Thematic Mapper data covering the Emas National park region was used for estimating the spectral response of the mixture components and for evaluating the mixing model results. The fraction images were compared with an unsupervised classification derived from Landsat TM data acquired on the same day. The relationship between the fraction images and normalized difference vegetation index images show the potential of the unmixing techniques when using coarse resolution data for global studies. Author (revised)

N94-20959*# Universities Space Research Association, Greenbelt, MD.
ANALYSIS OF HYPER-SPECTRAL AVIRIS IMAGE DATA OVER A MIXED-CONIFER FOREST IN MAINE
William T. Lawrence (Maryland Univ., College Park.), Yosio E. Shimabukuro (Instituto de Pesquisas Espaciais, Sao Jose dos Campos, Brazil.), and Bo-Cai Gao *In* INPE, The 7th Brazilian Remote Sensing Symposium,

Volume 2 1993 p 129-155 Sponsored by NASA. Goddard Space Flight Center (For primary document see N94-20956 05-43)
Avail: CASI HC A03/MF A04

An introduction to some of the potential uses of hyperspectral data for ecosystem analysis is presented. The examples given are derived from a digital dataset acquired over a sub-boreal forest in central Maine in 1990 by the NASA-JPL Airborne Visible and Infrared Imaging Spectrometer (AVIRIS) instrument gathers data from 400 to 2500 nm in 224 channels at bandwidths of approximately 10 nm. As a preview to the uses of the hyperspectral data, several products from this dataset were extracted. They range from the traditional false color composite made from simulated Thematic Mapper bands and the well known normalized difference vegetation index to much more exotic products such as fractions of vegetation, soil and shade based on linear spectral mixing models and estimates of the leaf water content at the landscape level derived using spectrum-matching techniques. Our research and that of many others indicates that the hyperspectral datasets carry much important information which is only beginning to be understood. This analysis gives an initial indication of the utility of hyperspectral data. Much work still remains to be done in algorithm development and in understanding the physics behind the complex information signal carried in the hyperspectral datasets. This work must be carried out to provide the fullest science support for high spectral resolution data to be acquired by many of the instruments to be launched as part of the Earth Observing System program in the mid-1990's. Author (revised)

N94-20960# Instituto de Pesquisas Espaciais, Sao Jose dos Campos (Brazil).
THE 7TH BRAZILIAN REMOTE SENSING SYMPOSIUM, VOLUME 3 [7TH SIMPOSIO BRASILEIRO DE SENSORIAMENTO REMOTO, VOLUME 3]
Roberto PereiradaCunha, ed. and Luiz Alberto Vieira Dias, ed. 1993 500 p In ENGLISH and PORTUGUESE Symposium held in Curitiba, Brazil, 10-14 May 1993 Prepared in cooperation with Secretaria de Estadoddo Meio Ambiente, Parana, Brazil; Sociedad de Especialistas Latinoamericanos en Perception Remota, Chile; and Sociedade Brasileira de Cartografia, Geodesia, Fotogramtria e Sensoriamento Remoto Original contains color illustrations
Avail: CASI HC A21/MF A04

Papers presented at the 7th Brazilian Remote Sensing Symposium held at Curitiba, Brazil from 10-14 May 1993 are included. Topics covered include: sun photometer network for monitoring aerosol properties in the Brazilian Amazon; predicting Landsat Multispectral Scanner System (MSS) endmember signatures from corresponding higher resolution Thematic Mapper fraction images; on the origin and evolution of circular forms observed in remote sensing images of the Rio de Janeiro State, Brazil; and evaluation of C-band Synthetic Aperture Radar (SAR) data from SAREX'92 (South American Radar Experiment): Tapajos study site. For individual titles, see N94-20961 through N94-20964.

N94-20961*# National Aeronautics and Space Administration. Goddard Space Flight Center, Greenbelt, MD.
SUNPHOTOMETER NETWORK FOR MONITORING AEROSOL PROPERTIES IN THE BRAZILIAN AMAZON Abstract Only
Brent N. Holben, T. F. Eck (ST Systems Corp., Greenbelt, MD.), A. Setzer (Instituto de Pesquisas Espaciais, Sao Jose dos Campos, Brazil.), Alfredo Pereira (Instituto de Pesquisas Espaciais, Sao Jose dos Campos, Brazil.), E. Vermote (Maryland Univ., College Park.), J. A. Reagan (Arizona Univ., Tucson.), Y. A. Kaufman, D. Tanre (Lille-1 Univ., Villeneuve-d'Asoq, France.), and I. Slutsker (Science Systems and Applications, Inc., Greenbelt, MD.) *In* INPE, The 7th Brazilian Remote Sensing Symposium, Volume 3 1993 p 54-55 (For primary document see N94-20960 05-43)
Avail: CASI HC A01/MF A04

Satellite platforms have provided a methodology for regional and global remote sensing of aerosols. New systems will significantly improve that capability during the EOS era; however, the voluminous 20 year record of satellite data has produced only regional snapshots of aerosol loading and have not yielded a data base of the optical properties of those aerosols which are fundamental to our understanding of their influence on climate change. The prospect of fully understanding the properties of the aerosols with respect to climate change is small without validation and augmentation by ancillary ground based observations. Sun photometry was demonstrated to be an effective tool for ground based measurements of aerosol optical properties from fire emissions. Newer technology has expanded routine sun photometer measurements to spectral observations of solar aureole and almucantar allowing retrievals of size distribution, scattering phase function, and refractive index. A series of such observations were made in Brazil's Amazon basin from a network of six simultaneously recording instruments deployed in Sep. 1992. The instruments were located in areas removed from local aerosol sources such that sites are representative of regional aerosol conditions. The overall network was designed to cover the counter clockwise tropospheric circulation of the Amazon Basin. Spectral measurements of sun, aureole and sky data for retrieval of aerosol optical thickness, particle size distribution, and scattering phase function as well as measurements of precipitable water were made during noncloudy conditions. Author (revised)

N94-20962*# National Aeronautics and Space Administration. Goddard Space Flight Center, Greenbelt, MD.
PREDICTING LANDSAT MSS ENDMEMBER SIGNATURES FROM CORRESPONDING HIGHER RESOLUTION TM FRACTION IMAGES
Yosio E. Shimabukuro (Instituto de Pesquisas Espaciais, Sao Jose dos Campos, Brazil.) and James A. Smith *In* INPE, The 7th Brazilian Remote Sensing Symposium, Volume 3 1993 p 117-128 (For primary document see N94-20960 05-43)
Avail: CASI HC A03/MF A04

The approach to predicting Landsat Multispectral Scanner System (MSS) endmember signatures from fraction images derived from high resolution Landsat Thematic Mapper (TM) data is presented. The purpose, conducted in the Mogi-Guacu study site located in Sao Paulo State, Brazil, was to determine if information derived from a mixture model applied to higher resolution TM data could serve as ground truth for the lower resolution MSS sensor. The Constrained Least Squares (CLS) method was used to generate vegetation, soil, and shade fraction images from the TM data. The resulting images were then used to estimate the endmember spectral response for MSS data by regressing each MSS spectral channel against the corresponding proportion values estimated for the same resolution cells from the TM mixture model. The evaluation of the predicted signatures was performed by comparing the corresponding fraction images derived from both the MSS and TM data acquired on 14 Sep. 1986. The techniques serves as a potential tool for integrating information in global studies where remote sensors with different spectral and spatial resolutions were used.
Author (revised)

N94-20963# Universidade Federal do Rio de Janeiro (Brazil).
ON THE ORIGIN AND EVOLUTION OF CIRCULAR FORMS OBSERVED IN REMOTE SENSING IMAGES OF THE RIO DE JANEIRO STATE, BRAZIL
Andre Calixto Vieira, Antonio Carlos J. deCastro, and Edgar Hans Brauer *In* INPE, The 7th Brazilian Remote Sensing Symposium, Volume 3 1993 p 385-394 (For primary document see N94-20960 05-43)
Avail: CASI HC A02/MF A04

The origin and evolution of circular, semi-circular, and stick-like forms identified in a selected area at the southwestern portion of the Rio de Janeiro State, Brazil, is related. Some of these 'morphological anomalies' were previously described either as igneous intrusions or as plutonic domes. A Tertiary tectonics of NW-SE compressional stress is known to be responsible for NE-SW movement of extense blocks. The tangential component of this movement caused the horizontal displacement and partition of pegmatites along the host-rock foliation. Conjugating the NW-SE compressional stress that acted upon the superior crust, with the tangential displacement of blocks situated over the underground, it is possible to suggest a model for the origin of the forms above mentioned. Remote sensing images of a target area were selected to identify the relation of several features with the morphological, structural, and drainage anomalies. Author (revised)

N94-20964*# Instituto de Pesquisas Espaciais, Sao Jose dos Campos (Brazil).
EVALUATION OF C-BAND SAR DATA FROM SAREX 1992: TAPAJOS STUDY SITE
Yosio Edemir Shimabukuro, Pedro Hernandez Filho, David Chung Liang Lee, F. J. Ahern (Canada Centre for Remote Sensing, Ottawa, Ontario.), Celio PaivadosSantosFilho (Instituto Brasileiro do Meio Ambiente e dos Recursos Naturais Renovaveis, Rio de Janeiro.), and Rionaldo

RolodeAlmeida (Instituto Brasileiro do Meio Ambiente e dos Recursos Naturais Renovaveis, Rio de Janeiro.) *In its* The 7th Brazilian Remote Sensing Symposium, Volume 3 1993 p 473-478 Sponsored by NASA. Goddard Space Flight Center (For primary document see N94-20960 05-43)
Avail: CASI HC A02/MF A04

As part of the SAREX'92 (South American Radar Experiment), the Tapajos study site, located in Para State, Brazil was imaged by the Canada Center for Remote Sensing (CCRS) Convair 580 SAR system using a C-band frequency in HH and VV polarization and 3 different imaging modes (nadir, narrow, and wide swath). A preliminary analysis of this dataset is presented. The wide swath C-band HH polarized image was enlarged to 1:100,000 in a photographic form for manual interpretation. This was compared with a vegetation map produced primarily from Landsat Thematic Mapper (TM) data and with single-band and color composite images derived from a decomposition analysis of TM data. The Synthetic Aperture Radar (SAR) image shows well the topography and drainage network defining the different geomorphological units, and canopy texture differences which appear to be related to the size and maturity of the forest canopy. Areas of recent clearing of the primary forest can also be identified on the SAR image. The SAR system appears to be a source of information for monitoring tropical forest which is complementary to the Landsat Thematic Mapper.
Author (revised)

N94-20965# Instituto de Pesquisas Espaciais, Sao Jose dos Campos (Brazil).
THE 7TH BRAZILIAN REMOTE SENSING SYMPOSIUM, VOLUME4 [7TH SIMPOSIO BRASILEIRO DE SENSORIAMENTO REMOTO, VOLUME 4]
Roberto PereiradaCunha, ed. and Luiz Alberto Vieira Dias, ed. 1993 479 p In ENGLISH and PORTUGUESE Symposium held in Curitiba, Brazil, 10-14 May 1993 Prepared in cooperation with Secretaria de Estadoddo Meio Ambiente, Parana, Brazil; Sociedad de Especialistas Latinoamericanos en Perception Remota, Chile; and Sociedade Brasileira de Cartografia, Geodesia, Fotogramtria e Sensoriamento Remoto Original contains color illustrations
Avail: CASI HC A21/MF A04

Papers presented at the 7th Brazilian Remote Sensing Symposium held at Curitiba, Brazil on 10-14 May 1993 are included. Topics covered include: drought early warning system for crop production; SIMA, an integrated environmental monitoring system; the development of remote sensing in Brazil and Canada: comparative case studies; rapid estimates of crop production using remote sensing: European experience; using Normalized Difference Vegetative Index/Advanced Very High Resolution Radiometer data for crop monitoring and forecasting. For individual titles, see N94-20966 through N94-20970.

N94-20966# Sao Paulo Univ. (Brazil). Dept. of Atmospheric Sciences.
DROUGHT EARLY WARNING SYSTEM FOR CROP PRODUCTION
William T. Liu *In* INPE, The 7th Brazilian Remote Sensing Symposium, Volume 4 1993 p 160-164 (For primary document see N94-20965 05-43)
Avail: CASI HC A01/MF A04

A new drought early warning system similar to the system developed by NOAA/NESDIS is suggested for implantation in Brazil. The proposed drought early warning system is based on three subsystems: agroclimatic index, satellite assessment, and crop yield forecast subsystems. Each subsystem contains several well developed assessment tools, derived from various data sources. Assessment tools produced by the drought early warning system include: NOAA satellite products such as vegetation index and vegetation condition index maps; vegetation index time-series and color-coded images; agroclimatic indices such as crop water use maps; crop risk index tables and maps; and crop yield forecast models including agrometeorological models, crop growth models, and vegetation index models. Short and long term weather forecast information should be incorporated in producing an assessment report. A geographic information system, which analyzes various data sources by overlaying, integrating and cross-checking between different assessment tools for consistency and convergence of information, should be used to produce a synthesized quantitative report.
Author

N94-20967# Paraiba Univ., Sao Jose dos Campos (Brazil).
SIMA: AN INTEGRATED ENVIRONMENTAL MONITORING SYSTEM
Merritt R. Stevenson (Instituto de Pesquisas Espaciais, Sao Jose dos Campos, Brazil.), Joao Antonio Lorenzzetti (Instituto de Pesquisas Espaciais, Sao Jose dos Campos, Brazil.), Jose Luiz Stech (Instituto de Pesquisas Espaciais, Sao Jose dos Campos, Brazil.), Paulo R. A. Arlino (Instituto de Pesquisas Espaciais, Sao Jose dos Campos, Brazil.), and Vladimir M. deCosta *In* INPE, The 7th Brazilian Remote Sensing Symposium, Volume 4 1993 p 300-310 (For primary document see N94-20965 05-43)
Avail: CASI HC A03/MF A04

During the past decade there has been a sharply increasing interest and need in obtaining environmental information related to the aquatic domain. The ability to receive serial information about current or recent weather, hydrological or environmental (quality) conditions, in a timely and reliable fashion is now recognized as the basis for any modern environmental monitoring system, whether the data are used for the protection of the environment, or to minimize the negative impact of extreme environmental conditions on the day-to-day safety of communities. Because the reliability of receiving such data via conventional telephone lines is often affected by the same adverse weather or environmental conditions being reported by the system, a modern system based on telemetry via satellite, that is, a system where the environment is remotely sensed, should be considered among the most reliable and desirable systems. The development of project SIMA, an integrated system for monitoring the aquatic environment, is presented. Because SIMA is based on the ARGOS system aboard the polar orbiting NOAA satellites, SIMA has no global limits for its 19+ million sq km regional coverage. The objective of this project is to design and develop a prototype system that can be used to monitor conditions in a coastal region where the possibility of oil spills exists, or in inland waters such as reservoirs and lakes, where the system can monitor changes in environmental parameters that may indicate the onset of floods, pollutants entering a reservoir, and so forth. Details of how SIMA functions, as well as its capabilties, are presented.
Author (revised)

N94-20968# Instituto de Pesquisas Espaciais, Sao Jose dos Campos (Brazil). Training Sector.
THE DEVELOPMENT OF REMOTE SENSING IN BRAZIL AND CANADA: COMPARATIVE CASE STUDIES
Tania Maria Sausen and Christine Nielsen (Ottawa Univ., Ontario.) *In its* The 7th Brazilian Remote Sensing Symposium, Volume 4 1993 p 431-436 (For primary document see N94-20965 05-43)
Avail: CASI HC A02/MF A04

The remote sensing programs of Brazil and Canada originated in late 1960's through participation in NASA's LANDSAT program. National governments of both countries have supported the development of remote sensing activities. Both countries have shared common interests in developing this technology in terms of large geographic areas and strong interests in natural resources exploration and management. Despite these similarities, the situation in the two countries are quite different today. There are between 3000 and 5000 remote sensing users in Canada. The majority are in the private sector. While there are approximately 3000 remote sensing users in Brazil, 85 percent of the users are in the public sector. Just few private companies are involved with remote sensing technology in Brazil, of these just two companies are 100 percent involved. There are many sectors of the economy that could benefit from remote sensing information; however, this large market remains undeveloped. One may conclude that more needs to be done if remote sensing technology is to be transferred successfully from the public to the private sector in Brazil. The purpose is to gain a better understanding of the evolution of remote sensing activities in Brazil and Canada over the past 25 years in order to further technology transfer/diffusion activities within the Brazilian context.
Author (revised)

N94-20969# SOTEMA, Ramonville Saint-Agne (France).
RAPID ESTIMATES OF CROP PRODUCTION USING REMOTE SENSING: EUROPEAN EXPERIENCE
Helene deBoissezon and M. Sharman (Joint Research Centre of the European Communities, Ispra, Italy.) *In* INPE, The 7th Brazilian Remote Sensing Symposium, Volume 4 1993 p 442-449 (For primary document see N94-20965 05-43)
Avail: CASI HC A02/MF A04

A technique in which high-resolution satellite imagery from SPOT and the Thematic Mapper is used in an operational way to provide rapid estimates of annual changes in area and production of various important crops in

Europe is described. The results, produced throughout the crop year, are transmitted to the Directorate General of Agriculture of the Commission of the European Communities and to the Statistical Office of European Communities, where they help to provide precise and up-to-date information on agricultural production. The agricultural information must be delivered rapidly in order to be of use. The Joint Research Center, which is responsible for this work, has set a target of 10 days from the date of acquisition to the date of delivery of the information. This tight schedule, and the number of sites (53) which are to be monitored, requires a novel and industrial approach to the image analysis. The operational implications of these requirements are examined and the fact that the Action 4 system is now fully operational is demonstrated. Author (revised)

N94-20970# Telespazio S.p.A., Rome (Italy). Earth Observation Dept.
USING NDVI/AVHRR DATA FOR CROP MONITORING AND FORECASTING IN SOUTH ITALY
Paolo Rossini *In* INPE, The 7th Brazilian Remote Sensing Symposium, Volume 4 1993 p 458-463 (For primary document see N94-20965 05-43)
Avail: CASI HC A02/MF A04

Crop monitoring, and in particular yield estimate and forecast, is considered very important for those Boards in charge to monitor agrarian season. Remote Sensing for its features and potentiality can contribute to these tasks in some new and interesting ways. The potential use of Advanced Very High Resolution Radiometer (AVHRR)/Normalized Difference Vegetation Index (NDVI) data from NOAA satellites for crop monitoring in South Italy within an interregional agrometeorological project is investigated. Over 1600 images in LAC format are processed from 1986 to date. Using previous results on NDVI correlation with plant photosynthetic capacity and efficiency during wheat Grain Filling Period Duration (GFPD), a simple linear regression model was derived for wheat yield estimate and forecast for each South Italy Agricultural Region. Estimated and forecasted values are compared with official ISTAT data. Author (revised)

N94-21015 Beleidscommissie Remote Sensing, Delft (Netherlands).
INFORMATION EXTRACTION FOR MULTISPECTRAL IMAGES USING RADIATION INTERACTION MODELS [INFORMATIE-EXTRACTIE UIT MULTISPECTRALE BEELDEN MET BEHULP VAN STRALINGSINTERACTIEMODELLEN]
W. Verhoef (National Aerospace Lab., Amsterdam, Netherlands.) Jul. 1992 49 p In DUTCH Limited Reproducibility: More than 20% of this document may be affected by microfiche quality
(BCRS-90-22; NLR-TP-90243-U; ISBN-9-05-411052-X; ETN-93-93312)
Avail: CASI HC A03

The possibilities of extraction of quantitative information from multispectral images of overgrown areas were investigated using radiation interaction models. Taking example by LANDSAT Thematic Mapper images it is shown that it is possible to construct reflection images and to extract reflection spectra of objects, using calibration and atmospheric correction. The usage of a vegetation reflection model in the interpretation of reflection spectra was started. ESA

N94-21017 Beleidscommissie Remote Sensing, Delft (Netherlands).
OCEAN MAPPING USING SATELLITE RADAR ALTIMETRY [OCEANEN IN KAART DOOR HOOGTEMETING MET SATELLIETRADAR]
Jun. 1992 4 p In DUTCH Limited Reproducibility: More than 20% of this document may be affected by microfiche quality
(ETN-93-93470) Avail: CASI HC A01

Sea surface altimetry using satellite radar is applied for the study of ocean topography and ocean circulation. The American satellite GEOS-3, Seasat and Geosat, and the European satellites ERS-1 and TOPEX/POSEIDON were used. Radar altimetry and ocean circulation data with very high precision were obtained and used as input for models, resulting in a better insight in the sea bottom topography and the Earth mantle structure under the oceans, which is important for science, offshore industry, and military use. A better knowledge of large ocean circulations and vortices is important for the study of environment and climate. ESA

N94-21068# World Meteorological Organization, Geneva (Switzerland).
SNOW COVER MEASUREMENTS AND AREAL ASSESSMENT OF PRECIPITATION AND SOIL MOISTURE
B. Sevruk, ed. 1992 299 p
(WMO-749; OHR-35; ISBN-9-26-310749-1; ETN-93-94841) Copyright
Avail: CASI MF A03; print copy available from WMO, Geneva, Switzerland

Recent developments in the field of areal estimation of precipitation, snow cover characteristics, and soil moisture, including remote sensing, are summarized. Numerous references and examples are provided along with annexes containing more detailed information on the following: snowfall estimation using radar, statistical estimation of snow cover fields, and semivariograms. The roles of precipitation, snow cover, and soil moisture in the water balance and for hydrological modeling are outlined. Some relevant physical properties of precipitation and soil required to understand the main topic are discussed. Methods of point and area measurement, in particular remote sensing techniques, are described. The general principles of the transformation of point values to mean areal values and the problem of representative point data are discussed. Emphasis is laid on the accuracy aspects of areal estimates, including systematic errors of point measurements and random errors originating from the local effects of measuring site and network density. The actual error of areal estimates can either be evaluated empirically by using the tables and diagrams enclosed or derived more objectively by using statistical analysis of spatial variability of particular hydrological variables. ESA

N94-21069# World Meteorological Organization, Geneva (Switzerland).
REMOTE SENSING FOR HYDROLOGY PROGRESS AND PROSPECTS
R. Kuttinen 1992 71 p
(WMO-773; OHR-36; ISBN-9-26-310773-9; ETN-93-94842) Copyright
Avail: CASI MF A01; print copy available from WMO, Geneva, Switzerland

The capability of satellite and aircraft based remote sensing techniques to meet the requirements of the World Meteorological Organization for operational hydrology programs at the present time and in the foreseeable future is discussed. The focus is on the application of remote sensing techniques to estimate hydrological variables and only limited information is provided on the technical aspects of the satellites, the sensors, and the data transmission and data interpretation devices. The observational requirements for operational hydrology are discussed. The technical aspects of sensors and data dissemination systems as well as the economic and practical aspects of remote sensing are considered. The applications for the measurement of precipitation, soil moisture and groundwater, evapotranspiration (including lake evaporation and evaporation from bare soils), snow, ice and frost, and surface water parameters are discussed. The use of remote sensing for the mapping of basic characteristics such as basin area, topography, soil types, vegetation, land use, and water courses is considered. Remotely sensed hydrological variables as inputs to hydrological models are discussed together with future trends in this field. Three appendices containing the observational requirements for operational hydrology and the assessed capability of remote sensing satellites and sensors relevant until 1995 as well as a list of LANDSAT and SPOT data distributors are provided. ESA

N94-21446 Office of Technology Assessment, Washington, DC.
DATA FORMAT STANDARDS FOR CIVILIAN REMOTE SENSING SATELLITES
May 1993 22 p Limited Reproducibility: More than 20% of this document may be affected by microfiche quality
(PB93-192920) Avail: CASI HC A03

The Office of Technology Assessment (OTA) was asked by the Senate Armed Services Committee to investigate the plethora of formats for remotely sensed Earth data. At a workshop held on 2 Oct. 1992, participants discussed the pros and cons of standardizing formats for remote-sensed data, the question of how many different standards are needed, with what else should remote-sensed data be compatible, and who should set the standards. It was clear from the workshop that data from different sources are largely provided in different formats and on different media. Moreover, formats, media, and recording hardware for the same system have often changed over time leading to situations where old data is virtually inaccessible. Creating order out of the current chaos will be a very difficult proposition and is likely to cause problems for many suppliers and users of data. Nevertheless, the payoff for doing so may be sufficiently great to warrant a major effort in that direction. NTIS

N94-21453 Aeronautical Research Labs., Melbourne (Australia).
DETECTING TOPOGRAPHICAL REGIONS IN DIGITAL TERRAIN MAPS

Sabrina Sestito, Simon Goss, and Terry Caelli Aug. 1993 25 p Limited Reproducibility: More than 20% of this document may be affected by microfiche quality
(AD-A272889; ARL-TR-53; DODA-AR-008-387) Avail: CASI HC A03

This report describes an application of Clustering and Differential Geometry to the characterization of digital terrain maps by different surface types and critical regions. Of particular interest is the determination of specific terrain types, where they occur, and describing them in ways which are invariant to viewing position. The development of robust and efficient segmentation and associated region characterization procedures is reported. Good results have been obtained for characterizing digital terrain maps. This work supports the development of techniques for generating optimal flight paths. DTIC

N94-21585*# Sterling Software, Inc., Palo Alto, CA.
PUBLICATION OF SCIENCE DATA ON CD-ROM: A GUIDE AND EXAMPLE
Gary Angelici and J. W. Skiles (Johnson Controls World Services, Cape Canaveral, FL.) Nov. 1993 62 p Sponsored by NASA. Washington (Contract NAS2-13210)
(NASA-CR-4560; A-94024; NAS 1.26:4560) Avail: CASI HC A04/MF A01

CD-ROM (Compact Disk-Read Only Memory) is becoming the standard media not only in audio recording, but also in the publication of data and information accessible on many computer platforms. Little has been written about the complicated process involved in creating easy-to-use, high quality, and useful CD-ROM's containing scientific data. This document is a manual designed to aid those who are responsible for the publication of scientific data on CD-ROM. All aspects and steps of the procedure are covered, from feasibility assessment through disk design, data preparation, disc mastering, and CD-ROM distribution. General advice and actual examples are based on lessons learned from the publication of scientific data for an interdisciplinary field experiment. Appendices include actual files from a CD-ROM, a purchase request for CD-ROM mastering services, and the disk art for the first disk published for the project. Author

N94-21855 International Bank for Reconstruction and Development, Washington, DC. Urban Management Programme.
URBAN APPLICATIONS OF SATELLITE REMOTE SENSING AND GIS ANALYSIS
B. Paulsson 1992 73 p
(PB93-202174; DP-9) Copyright Avail: Issuing Activity

The report serves as a practical guide to show how satellite remote sensing can be a useful source of urban management information and to demonstrate the benefits of geographical analysis of available data. It focuses on operational applications in cities in developing countries, based on a comprehensive review of recent reports and illustrated by experience from case studies and operational projects. It does not attempt to cover all possible urban applications of GIS technology or serve as a detailed manual for all possible applications of satellite remote sensing. Rather, it offers an introduction to the technologies, available range of products, and various methods of analysis offered by satellite remote sensing. NTIS

N94-22097 Technische Univ., Delft (Netherlands). Faculteit der Geodesie.
INFLUENCE OF GEOID MODEL UNCERTAINTY ON THE DETERMINATION OF OCEAN CIRCULATION WITH SATELLITE ALTIMETRY
Ina A. Elema Feb. 1993 109 p Limited Reproducibility: More than 20% of this document may be affected by microfiche quality
(PB93-219301) Avail: Issuing Activity (National Technical Information Service (NTIS))

The report contains the study of the inaccuracy in the determination of ocean circulation by satellite altimetry due to geoid errors. Chapter 2 gives a summary of the usefulness and applications of satellite altimetry. Chapter 3 gives some background of oceanography. The different types of ocean variations are described. In chapter 4, three methods to determine the geostrophic flow are described: the hydrographic method, the absolute method, and the integrated approach. The disadvantages and advantages of the methods are compared with each other. The problems in defining the geoid and its determination are presented in chapter 5. The accuracy of geoid models is briefly discussed. The influence of the accuracy of the earlier introduced geoid models on two test areas with varying parameters (such as maximum degree of expansion, zonals, tesserals) can be found in chapters 6 and 7. In chapter 8, conclusions from this investigation are drawn. Recommendations for further work concerning this topic are given in chapter 9. NTIS

N94-22265 Technische Univ., Delft (Netherlands). Faculteit der Geodesie.
ESTIMABILITY OF POLAR MOTION USING RANGE OBSERVATIONS TO SATELLITES
A. P. Kap Feb. 1993 83 p Limited Reproducibility: More than 20% of this document may be affected by microfiche quality
(PB93-219319) Avail: CASI HC A05

The purpose of the research has been to evaluate a model that gives a relation between, on one side, a range observation between an observation station on the Earth and a satellite, and the parameters that describe the motion of the Earth and the satellite on the other side. This evaluation was aimed at the estimability of the various parameters, possible rank deficiencies, and strong correlations, with special attention to the polar motion of the Earth. Contents include: Use of reference frames; Dynamics of a rigid body; Rotation of the Earth; Representation of the satellite orbit using Hill equations; The influence of the Earth's flattening on the satellite orbit; A model for the range observation; Testing of the model using singular value decomposition; Conclusions and recommendations. NTIS

N94-22345*# Sterling Software, Inc., Palo Alto, CA.
DATA MANAGEMENT FOR INTERDISCIPLINARY FIELD EXPERIMENTS: OTTER PROJECT SUPPORT
Gary Angelici, Lidia Popovici, and J. W. Skiles (Johnson Controls World Services, Cape Canaveral, FL.) Nov. 1993 23 p
(Contract NAS2-13210)
(NASA-CR-4559; A-94023; NAS 1.26:4559) Avail: CASI HC A03/MF A01

The ability of investigators of an interdisciplinary science project to properly manage the data that are collected during the experiment is critical to the effective conduct of science. When the project becomes large, possibly including several scenes of large-format remotely sensed imagery shared by many investigators requiring several services, the data management effort can involve extensive staff and computerized data inventories. The OTTER (Oregon Transect Ecosystem Research) project was supported by the PLDS (Pilot Land Data System) with several data management services, such as data inventory, certification, and publication. After a brief description of these services, experiences in providing them are compared with earlier data management efforts and some conclusions regarding data management in support of interdisciplinary science are discussed. In addition to providing these services, a major goal of this data management capability was to adopt characteristics of a pro-active attitude, such as flexibility and responsiveness, believed to be crucial for the effective conduct of active, interdisciplinary science. These are also itemized and compared with previous data management support activities. Identifying and improving these services and characteristics can lead to the design and implementation of optimal data management support capabilities, which can result in higher quality science and data products from future interdisciplinary field experiments. Author

N94-22374*# Universities Space Research Association, Huntsville, AL.
STUDIES IN REMOTELY SENSED GEOPHYSICAL PARAMETER RETRIEVAL AND ANALYSIS Final Progress Report No. 14, 31 Dec. 1990 - 31 Dec. 1993
Donald J. Perkey 31 Dec. 1993 8 p
(Contract NAS8-38769)
(NASA-CR-194768; NAS 1.26:194768) Avail: CASI HC A02/MF A01

This report describes Universities Space Research Association (USRA) activities in support of the Geophysical Parameter Retrieval and Analysis studies. Specifically it addresses personnel assigned to the effort, travel, consultant participants, technical progress, and contract spending.
Author (revised)

N94-22422 British Columbia Univ., Vancouver. Dept. of Forestry and Remote Sensing.
CHROMATICITY ANALYSIS OF LANDSAT MULTISPECTRAL SCANNER AND THEMATIC MAPPER IMAGERY OF CHILKO LAKE, BRITISH COLUMBIA, USING A THEORETICAL OPTICAL WATER QUALITY MODEL Ph.D. Thesis
Elizabeth Ann Gallie Jun. 1990 283 p
(ISBN-0-315-63832-X; CTN-94-60889) Copyright Avail: Micromedia Ltd., Technical Information Centre, 240 Catherine Street, Suite 305, Ottawa, Ontario, K2P 2G8, Canada HC/MF

Chromaticity analysis of LANDSAT multispectral scanner (MSS) imagery of Chilko Lake, British Columbia, reveals a locus whose shape has not been previously reported. To examine the cause of this and to gain knowledge of chromaticity analysis for MSS and Thematic Mapper (TM) data, an optical water quality model has been used. The model is composed of a reflectance model (R-model), an interface model, and an atmospheric model. The R-model was calibrated for Chilko Lake by determining the specific backscattering and absorption spectra for suspended minerals (SM), chlorophyll (C), and yellow substance (YS). The model reproduces the observed locus shape and indicates that it is primarily a function of SM. If brightness is used in combination with the chromaticity coordinate X, the model predicts that C and YS can be differentiated from SM at most SM concentrations. Furthermore, haze and wind gradients can be distinguished from the lower limb of MSS X-Y plots. Simulated chromaticity results were compared with results from actual images for which ground truth had been collected. Qualitative predictions regarding haze and water quality patchiness were confirmed. Modelling error is thought to originate in atmospheric assumptions which are not met. The study concludes that the model is qualitatively correct and that the use of brightness improves chromaticity analysis. Author (CISTI)

N94-22429 Calgary Univ. (Alberta). Dept. of Geomatics Engineering.
STAR-1 SAR ROAD EXTRACTION USING TEXTURE ANALYSIS AND MATHEMATICAL MORPHOLOGY Ph.D. Thesis
Elly Rasdiani Sudibjo Sep. 1992 172 p
(ISBN-0-315-83255-X; CTN-94-60939) Copyright Avail: Micromedia Ltd., Technical Information Centre, 240 Catherine Street, Suite 305, Ottawa, Ontario, K2P 2G8, Canada HC/MF

Synthetic aperture radar (SAR) images are becoming an important source of mapping information in many countries, especially where cloud cover is a major problem. Radar imagery is often used with other remote sensing imagery since these data are often the only source of mapping information. To correlate and use the data from different sensors, the data must be registered to each other, such as by using a linear feature as the registration feature. A methodology of road extraction was developed by a sequential procedure of smoothing, texture analysis, and mathematical morphology. The methodology was tested on a 250 by 250 pixel data set from a mountainous area covering about 1.5 by 1.5 km. Smoothing or noise reduction was applied before the texture analysis using six different filtering techniques, of which two were applicable for producing a filtered image. Texture analysis was investigated and an empirical evaluation was applied to four texture methods. For extracting the road network, thresholds were applied to texture values. To reconstruct the road network, a mathematical morphology dilation was implemented, using different sizes and patterns of structuring elements. With the proper choice of thresholds, roads could be detected and extracted, and the reconstruction procedures were able to connect the road network. Author (CISTI)

N94-20412*# Jet Propulsion Lab., California Inst. of Tech., Pasadena.
ERS-1 AND SEASAT SCATTEROMETER MEASUREMENTS OF OCEAN WINDS: MODEL FUNCTIONS AND THE DIRECTIONAL DISTRIBUTION OF SHORT WAVES Abstract Only
Michael H. Freilich (Oregon State Univ., Corvallis.) and R. Scott Dunbar *In its* Progress In Electromagnetics Research Symposium (PIERS) 1993 p 186 (For primary document see N94-20403 05-32)
Avail: CASI HC A01/MF A10

N94-20413*# Jet Propulsion Lab., California Inst. of Tech., Pasadena.
Ku-BAND OCEAN RADAR BACKSCATTER OBSERVATIONS DURING SWADE Abstract Only
S. V. Nghiem, F. K. Li, S. H. Lou, and G. Neumann *In its* Progress In Electromagnetics Research Symposium (PIERS) 1993 p 188 (For primary document see N94-20403 05-32)
Avail: CASI HC A01/MF A10

N94-20415*# Jet Propulsion Lab., California Inst. of Tech., Pasadena.
COMPARISON OF REMOTE SENSING MEASUREMENTS WITH A TWO-SCALE POLARIMETRIC EMISSION AND SCATTERING MODEL FOR SEA SURFACES Abstract Only
S. H. Yueh, S. V. Nghiem, R. Kwok, and F. K. Li *In its* Progress In Electromagnetics Research Symposium (PIERS) 1993 p 191 (For primary document see N94-20403 05-32)
Avail: CASI HC A01/MF A10

N94-20417*# Jet Propulsion Lab., California Inst. of Tech., Pasadena.
TOPOGRAPHIC MAPPING USING A MONOPULSE SAR SYSTEM Abstract Only
M. Zink (Deutsche Forschungsanstalt fuer Luft- und Raumfahrt, Oberpfaffenhofen, Germany.), H. Oettl (Deutsche Forschungsanstalt fuer Luft- und Raumfahrt, Oberpfaffenhofen, Germany.), and A. Freeman *In its* Progress In Electromagnetics Research Symposium (PIERS) 1993 p 256 (For primary document see N94-20403 05-32)
Avail: CASI HC A01/MF A10

N94-20420*# Jet Propulsion Lab., California Inst. of Tech., Pasadena.
CLASSIFICATION OF SIMPLE VEGETATION TYPES USING POLSAR IMAGE DATA Abstract Only
A. Freeman *In its* Progress In Electromagnetics Research Symposium (PIERS) 1993 p 387 (For primary document see N94-20403 05-32)
Avail: CASI HC A01/MF A10

N94-20424*# Jet Propulsion Lab., California Inst. of Tech., Pasadena.
ADVANCES IN SPACEBORNE RADAR REMOTE SENSING Abstract Only
C. Elachi *In its* Progress In Electromagnetics Research Symposium (PIERS) 1993 p 447 (For primary document see N94-20403 05-32)
Avail: CASI HC A01/MF A10

N94-20430*# Jet Propulsion Lab., California Inst. of Tech., Pasadena.
DIRECTION ANGLE SENSITIVITY OF AGRICULTURAL FIELD BACKSCATTER WITH AIRSAR DATA Abstract Only
Pascale C. Dubois, Eric Rignot, and Jakob J. vanZyl *In its* Progress In Electromagnetics Research Symposium (PIERS) 1993 p 488 (For primary document see N94-20403 05-32)
Avail: CASI HC A01/MF A10

N94-20443*# Jet Propulsion Lab., California Inst. of Tech., Pasadena.
SIMULATED RETRIEVAL OF LAND SURFACE PARAMETERS USING MULTICHANNEL SATELLITE MICROWAVE RADIOMETRY Abstract Only
Eni G. Njoku and Brian Rague *In its* Progress In Electromagnetics Research Symposium (PIERS) 1993 p 764 (For primary document see N94-20403 05-32)
Avail: CASI HC A01/MF A10

N94-20444*# Jet Propulsion Lab., California Inst. of Tech., Pasadena.
SYNERGISM OF ACTIVE AND PASSIVE MICROWAVE DATA FOR ESTIMATING BARE SURFACE SOIL MOISTURE Abstract Only
Sasan S. Saatchi, Eni G. Njoku, and Urs Wegmueller (Bern Univ., Switzerland.) *In its* Progress In Electromagnetics Research Symposium (PIERS) 1993 p 769 (For primary document see N94-20403 05-32)
Avail: CASI HC A01/MF A10

N94-20445*# Jet Propulsion Lab., California Inst. of Tech., Pasadena.
POLARIMETRIC THERMAL EMISSION FROM PERIODIC WATER SURFACES Abstract Only
S. H. Yueh, S. V. Nghiem, R. Kwok, W. J. Wilson, F. K. Li, J. T. Johnson (Massachusetts Inst. of Tech., Cambridge.), and J. A. Kong (Massachusetts Inst. of Tech., Cambridge.) *In its* Progress In Electromagnetics Research Symposium (PIERS) 1993 p 770 (For primary document see N94-20403 05-32)
Avail: CASI HC A01/MF A10

N94-20449*# Jet Propulsion Lab., California Inst. of Tech., Pasadena.
SYMMETRY IN POLARIMETRIC REMOTE SENSING Abstract Only
S. V. Nghiem, S. H. Yueh, and R. Kwok *In its* Progress In Electromagnetics Research Symposium (PIERS) 1993 p 807 (For primary document see N94-20403 05-32)
Avail: CASI HC A01/MF A10

N94-20450*# National Aeronautics and Space Administration. Goddard Space Flight Center, Greenbelt, MD.
RELATIONSHIP OF ATTENUATION IN A VEGETATION CANOPY TO PHYSICAL PARAMETERS OF THE CANOPY Abstract Only
M. A. Karam and D. M. LeVine *In* JPL, Progress In Electromagnetics Research Symposium (PIERS) 1993 p 808 (For primary document see N94-20403 05-32)
Avail: CASI HC A01/MF A10

N94-20452*# Jet Propulsion Lab., California Inst. of Tech., Pasadena.
MAPPING OF TAIGA FOREST UNITS USING AIRSAR DATA AND/OR OPTICAL DATA, AND RETRIEVAL OF FOREST PARAMETERS Abstract Only
Eric Rignot, Cynthia Williams (Institute of Northern Forestry, Fairbanks, AK.), JoBea Way, and Leslie Viereck (Institute of Northern Forestry, Fairbanks, AK.) *In its* Progress In Electromagnetics Research Symposium (PIERS) 1993 p 856 (For primary document see N94-20403 05-32)
Avail: CASI HC A01/MF A10

N94-20455*# Jet Propulsion Lab., California Inst. of Tech., Pasadena.
APPLICATION OF NEURAL NETWORK TO REMOTE SENSING OF SOIL MOISTURE USING THEORETICAL POLARIMETRIC BACKSCATTERING COEFFICIENTS Abstract Only
L. Wang (Massachusetts Inst. of Tech., Cambridge.), R. T. Shin (Massachusetts Inst. of Tech., Cambridge.), J. A. Kong (Massachusetts Inst. of Tech., Cambridge.), and S. H. Yueh *In its* Progress In Electromagnetics Research Symposium (PIERS) 1993 p 875 (For primary document see N94-20403 05-32)
Avail: CASI HC A01/MF A10

N94-20459*# Jet Propulsion Lab., California Inst. of Tech., Pasadena.
TOPOGRAPHIC SLOPE FROM THE SAR INTERFEROMETRIC PHASE GRADIENT Abstract Only
Charles L. Werner (Zurich Univ., Switzerland.) and Paul A. Rosen *In its* Progress In Electromagnetics Research Symposium (PIERS) 1993 p 922 (For primary document see N94-20403 05-32)
Avail: CASI HC A01/MF A10

N94-20460*# Jet Propulsion Lab., California Inst. of Tech., Pasadena.
INTERFEROMETRIC DETECTION OF FREEZE-THAW DISPLACEMENTS OF ALASKAN PERMAFROST USING ERS-1 DATA Abstract Only
Charles L. Werner (Zurich Univ., Switzerland.) and Andrew K. Gabriel *In its* Progress In Electromagnetics Research Symposium (PIERS) 1993 p 923 (For primary document see N94-20403 05-32)
Avail: CASI HC A01/MF A10

N94-20461*# Jet Propulsion Lab., California Inst. of Tech., Pasadena.
PERFORMANCE EVALUATION OF THE JPL TOPSAR SYSTEM: AN ACROSS-TRACK INTERFEROMETRIC SAR SYSTEM FOR TOPOGRAPHIC MAPPING Abstract Only
Soren N. Madsen, Howard A. Zebker, and Jan Martin *In its* Progress In Electromagnetics Research Symposium (PIERS) 1993 p 924 (For primary document see N94-20403 05-32)
Avail: CASI HC A01/MF A10

N94-20705*# DePauw Univ., Greencastle, IN. Dept. of Geology and Geography.
GEOLOGIC MAPPING OF HARMAKHIS AND REULL VALLES REGION, MARS: EVIDENCE FOR MULTIPLE RESURFACING AND DRAINAGE EVENTS Abstract Only
Katherine H. Price *In* Lunar and Planetary Inst., Twenty-Fourth Lunar and Planetary Science Conference. Part 3: N-Z 1993 p 1179 (For primary document see N94-20636 05-91)
Avail: CASI HC A01/MF A06

N94-20888*# Arizona State Univ., Tempe. Dept. of Geology.
CONVEX SET AND LINEAR MIXING MODEL Abstract Only
P. Xu and R. Greeley *In* Lunar and Planetary Inst., Twenty-Fourth Lunar and Planetary Science Conference. Part 3: N-Z 1993 p 1545-1546 (For primary document see N94-20636 05-91)
Avail: CASI HC A01/MF A06

N94-21645*# National Aeronautics and Space Administration. Goddard Inst. for Space Studies, New York, NY.
EARTH OBSERVING SCANNING POLARIMETER
Larry Travis *In its* Long-Term Monitoring of Global Climate Forcings and Feedbacks Sep. 1993 p 40-46 (For primary document see N94-21639 05-47)
Avail: CASI HC A02/MF A02; 13 functional color pages

N94-22073# Academy of Sciences (USSR), Moscow. Computer Center.
MULTICRITERIA OPTIMISATION PROBLEM IN THE AGRICULTURAL MODELLING
H. M. Stoliarova *In* Technical Research Centre of Finland, Information Technology and Economic Modelling 1992 p 148-161 (For primary document see N94-22056 05-83)
Copyright Avail: CASI HC A03/MF A03

N94-22146 Concordia Univ., Montreal (Quebec). Centre for Pattern Recognition and Machine Intelligence.
THE LOCAL MEASUREMENT AND GLOBAL INTERPRETATION OF 3D MOTION FIELD GENERATED BY SEVERAL MOVING OBJECTS FROM RANGE IMAGE SEQUENCES
P. Y. Zhu, A. Krzyzak, and T. Kasvand *In* Engineering Inst. of Canada, Canadian Conference on Electrical and Computer Engineering, Volumes 1 and 2 1991 4 p (For primary document see N94-22101 05-33)
Avail: Issuing Activity (Engineering Inst. of Canada, 2050 rue Mansfield, Suite 700, Montreal, PQ H3A 1Z2 Canada)

N94-22303*# National Aeronautics and Space Administration. Langley Research Center, Hampton, VA.
REMOTE SENSING OF MULTILEVEL CLOUDS DURING FIRE IFO 2
Bryan A. Baum, J. Titlow (Lockheed Engineering and Sciences Co., Hampton, VA.), V. Tovinkere (Lockheed Engineering and Sciences Co., Hampton, VA.), M. Poellot (North Dakota Univ., Grand Forks.), T. P. Ackerman (Pennsylvania State Univ., University Park.), J. Alvarez, T. Uttal (National Oceanic and Atmospheric Administration, Boulder, CO.), and J. Intrieri (Colorado Univ., Boulder.) *In its* The FIRE Cirrus Science Results 1993 Dec. 1993 p 40-43 (For primary document see N94-22292 05-47)
Avail: CASI HC A01/MF A03

N94-22319*# National Aeronautics and Space Administration. Ames Research Center, Moffett Field, CA.
GROUND-BASED PASSIVE REMOTE SENSING DURING FIRE IFO 2
Peter Pilewskie and Francisco P. J. Valero *In* NASA. Langley Research Center, The FIRE Cirrus Science Results 1993 Dec. 1993 p 115-116 (For primary document see N94-22292 05-47)
Avail: CASI HC A01/MF A03

44 ENERGY PRODUCTION AND CONVERSION

Includes specific energy conversion systems, e.g., fuel cells; global sources of energy; geophysical conversion; and windpower.

For related information see also *07 Aircraft Propulsion and Power, 20 Spacecraft Propulsion and Power,* and *28 Propellants and Fuels.*

N94-19803# Los Alamos National Lab., NM.
STATEMENT OF DAVID E. BALDWIN, ASSOCIATE DIRECTOR FOR ENERGY, LAWRENCE LIVERMORE NATIONAL LABORATORY AND JOHN C. CRAWFORD, VICE PRESIDENT, SANDIA NATIONAL LABORATORIES, CALIFORNIA, TO THE SUBCOMMITTEE ON RESEARCH AND DEVELOPMENT OF THE COMMITTEE ON ENVIRONMENT AND PUBLIC WORKS, US SENATE, WASHINGTON, DC, 22 MARCH 1993
D. E. Baldwin and J. C. Crawford (Sandia National Labs., Albuquerque,

NM.) 18 Mar. 1993 8 p Presented at the 1993 Federal Environmental Restoration Conference, Washington, DC, 25-27 Mar. 1993
(Contract W-7405-eng-48)
(DE93-017991; UCRL-JC-113664; CONF-9303105-2) Avail: CASI HC A02/MF A01

Testimony was submitted to the Senate on the environmental impacts of accelerated research and development of hydrogen-based energy systems. The advantages of hydrogen in transportation systems, in fuel cells for electric vehicles and power plants, and in energy storage from off-peak electricity production are described. The largest barrier to using hydrogen in the transportation sector is the on-board storage of enough fuel to provide an adequate driving range in an urban environment. Production methods and costs are also discussed. The authors believe a coordinated demonstration program with U.S. industry is needed to develop the best technologies for hydrogen-fueled vehicles. DOE

N94-19805# University of Southern California, Los Angeles.
HIGH EFFICIENCY EPITAXIAL OPTICAL REFLECTOR SOLAR CELLS
P. D. Dapkus and S. G. Hummel Aug. 1993 49 p Prepared in cooperation with Midwest Research Inst., Golden, CO
(Contract DE-AC02-83CH-10093)
(DE93-017115; NREL/TP-451-5591) Avail: CASI HC A03/MF A01

This report describes work to test the feasibility of a new solar cell concept -- the epitaxial optical reflector (EOR) solar cell. This cell concept alters current designs for high efficiency cells by changing the optical absorption efficiency of single cells. The change is introduced by the use an epitaxial multilayer reflector as an integral part of the cell to increase the optical path length of certain wavelengths of light in the cell. These changes are expected to increase the open circuit voltage at which power is extracted from the cell. The program is designed to test the feasibility of the use of a broadband epitaxial multilayer reflector grown as an integral part of the device structure to reflect the near-band-edge light back through the device for a second absorption pass. This second pass allows the design of a solar cell with a thinner base and the use of the epitaxial reflector as a heterojunction carrier-reflecting barrier at the rear of the device. The thinner cell design and altered carrier profile that results from the light- and carrier-reflecting barrier will decrease the carrier concentration gradient and increase the open circuit voltage. The program is structured to have three tasks: solar cell and reflector modeling, materials growth and optimization, and solar cell fabrication and characterization. DOE

N94-19921# Midwest Research Inst., Golden, CO.
WIND ENERGY: PROGRAM OVERVIEW, FY 1992
Jun. 1993 28 p
(Contract DE-AC02-83CH-10093)
(DE93-000056; DOE/CH-10093/191) Avail: CASI HC A03/MF A01

The DOE Wind Energy Program assists utilities and industry in developing advanced wind turbine technology to be economically competitive as an energy source in the marketplace and in developing new markets and applications for wind systems. This program overview describes the commercial development of wind power, wind turbine development, utility programs, industry programs, wind resources, applied research in wind energy, and the program structure. DOE

N94-19925# Georgia Inst. of Tech., Atlanta.
DEVELOPMENT OF HIGH-EFFICIENCY CdTe SOLAR CELLS
A. Rohatgi, H. C. Chou, A. K. Bhat, and S. Kamra Aug. 1993 52 p Prepared for Midwest Research Inst., Golden, CO
(Contract DE-AC02-83CH-10093)
(DE93-018206; NREL/TP-451-5650) Avail: CASI HC A04/MF A01

This report describes work to improve the basic understanding of the loss mechanisms in thin-film CdS/CdTe solar cells and to improve their efficiency by characterizing the properties of the films as well as the finished devices. To accomplish this, solar cells were fabricated on glass/SnO2CdS substrates by metal-organic chemical vapor deposition (MOCVD) growth of CdTe films and evaporation of Cu/Au contacts. The substrates were provided by Solarex Corporation and were recently grown in house on glass/SnO2 substrates using solution growth. Rapid thermal processing (RTP), still a relatively new technology with growing applications in the semiconductor industry, is being investigated in this program as an alternative to the conventional post-growth furnace annealing of the CdS/CdTe films. Consistent with the long-term goals of cost-effective, large-scale terrestrial applications of photovoltaics, we also made some preliminary investigations of a solution growth technique for depositing CdTe films. DOE

N94-20066*# Lamar Univ., Beaumont, TX. College of Engineering.
ABSORPTION HEAT PUMP FOR SPACE APPLICATIONS Final Report
Tuan Nguyen, William E. Simon, Gopinath R. Warrier, and Woranun Woramontri Dec. 1993 152 p
(Grant NAG9-613)
(NASA-CR-194693; NAS 1.26:194693) Avail: CASI HC A08/MF A02

In the first part, the performance of the Absorption Heat Pump (AHP) with water-sulfuric acid and water-magnesium chloride as two new refrigerant-absorbent fluid pairs was investigated. A model was proposed for the analysis of the new working pairs in a heat pump system, subject to different temperature lifts. Computer codes were developed to calculate the Coefficient of Performance (COP) of the system with the thermodynamic properties of the working fluids obtained from the literature. The study shows the potential of water-sulfuric acid as a satisfactory replacement for water-lithium bromide in the targeted temperature range. The performance of the AHP using water-magnesium chloride as refrigerant-absorbent pair does not compare well with those obtained using water-lithium bromide. The second part concentrated on the design and testing of a simple ElectroHydrodynamic (EHD) Pump. A theoretical design model based on continuum electromechanics was analyzed to predict the performance characteristics of the EHD pump to circulate the fluid in the absorption heat pump. A numerical method of solving the governing equations was established to predict the velocity profile, pressure - flow rate relationship and efficiency of the pump. The predicted operational characteristics of the EHD pump is comparable to that of turbomachinery hardware; however, the overall efficiency of the electromagnetic pump is much lower. An experimental investigation to verify the numerical results was conducted. The pressure - flow rate performance characteristics and overall efficiency of the pump obtained experimentally agree well with the theoretical model. Author (revised)

N94-20086 Hawaii Univ., Manoa.
ENERGY STORAGE AND CONVERSION IN SOLID HYDROGEN Final Report, 19 Sep. 1988 - 19 Mar. 1992
James R. Gaines and C. A. Vause Aug. 1993 27 p Limited Reproducibility: More than 20% of this document may be affected by microfiche quality
(Contract F04611-88-K-0048)
(AD-A271439; PL-TR-92-3019; AD-E201667) Avail: CASI HC A03

The trapping of unpaired atoms of hydrogen (H) in a solid hydrogen matrix (Hsub2) increases the energy available for propulsion applications, i.e. the specific impulse. The incremental increase in stored energy depends on the metastable atomic hydrogen concentration. To maintain a large atomic hydrogen concentration, recombination of atoms into molecules must be understood and suppressed. It was the purpose of this research to study both theoretical and experimental approaches to creating large atomic hydrogen concentrations. The theoretical considerations have lead to analytic procedures for calculating the atom diffusion times and the atomic recombination coefficients from statistical mechanics. The experimental studies have yielded numerical estimates of the atom density in solid tritium based on measurements of the ortho to para tritium conversion rate. The atom density expressed as a concentration approaches 1% near K. Such large atom densities lead to very unusual thermal response when the temperature of the host solid matrix is increased, resulting from the rapid recombination of the trapped atoms. In practice, this response provides a method of retrieving the stored energy from the host solid. DTIC

N94-20095# Solar Cells, Inc., Toledo, OH.
FABRICATION OF STABLE LARGE-AREA THIN-FILM CdTe PHOTOVOLTAIC MODULES
J. F. Nolan and P. V. Meyers Aug. 1993 24 p Prepared in cooperation with Midwest Research Inst., Golden, CO
(Contract DE-AC02-83CH-10093)
(DE93-018204; NREL/TP-413-5740) Avail: CASI HC A03/MF A01

This report highlights the progress made by Solar Cells, Inc. (SCI), in its program to produce 60-cm x 120-cm solar modules based on CdTe films. During the past year, confirmed efficiency has increased to 10.4% (active area) on a 1 sq cm cell, 9.8% (aperture area) on a 64 sq cm

8-cell submodule, and 6.6% (total area) on a 7200 sq cm module. A module measured in-house had a power output of 53 W, for a total-area efficiency of 7.4%. Average efficiency of modules produced is steadily increasing and standard deviation is decreasing; in a limited run of 12 modules, results were 6.3% +/- 0.2%. Field testing has begun; a nominal 1-kW array of 24 modules was set up adjacent to SCI's facilities. Analysis indicates that present modules are limited in efficiency by shunt resistance and optical absorption losses in the glass superstrate. Loss analysis of present devices allows us to project a module efficiency of 11.8%. A third generation deposition method, atmospheric pressure elemental vapor deposition (APEVD), has been brought on-line and has produced good quality CdTe. In addition, SCI is expanding its pro-active safety, health, environmental, and disposal program dealing with issues surrounding cadmium. DOE

N94-20151 Technische Univ., Berlin (Germany). Inst. Werkstoffe.
DEVELOPMENT OF A NUMERICAL SIMULATION MODEL FOR a-Si:H SOLAR CELLS AND APPLICATION TO THE ANALYSIS OF EXPERIMENTALLY OBTAINED SPECTRAL CHARACTERISTICS Ph.D. Thesis [DIE ENTWICKLUNG EINES NUMERISCHEN SIMULATIONSMODELLS FUER A-SI:H SOLARZELLEN UND SEINE ANWENDUNG ZUR ANALYSE EXPERIMENTELL ERMITTELTER SPEKTRALCHARAKTERISTIKEN]
Juergen Bruns 1993 134 p In GERMAN Limited Reproducibility: More than 20% of this document may be affected by microfiche quality
(ETN-93-95061) Avail: CASI HC A07

Solar cells for simulating the properties of thin layer cells for a-Si:H are modeled. A numerical simulation model, based on the finite difference method, is developed assuming that the amorphous material can be described by the semiconductor physics. The components were characterized by the transport equations, which were discretized and linearized in order to obtain a matrix with a tridiagonal structure for solving the partial differential equations. Properties of amorphous silicon were taken into account for the physical description of trapping and recombination processes. The distribution of localized states in motion holes was represented with two exponential tail states and two Gaussian distribution dangling bond states. A spectral measuring apparatus was built for examining the influence of the model parameters on the solar cell electrical characteristic line. The voltage dependence of photocurrent was observed with the quantum efficiency degree curve. A dispersive transition of primary to secondary photocurrent area is found, which is different for pin and nip solar cells. Spectral response simulation for both cell types show that this transition is caused by an exchange of drift and diffusion processes, which are compensated by photocurrent extinguishing. ESA

N94-20196* National Aeronautics and Space Administration. Lewis Research Center, Cleveland, OH.
SELF-DEPLOYING PHOTOVOLTAIC POWER SYSTEM Patent
Anthony J. Colozza, inventor (to NASA) 14 Sep. 1993 8 p Filed 2 Apr. 1992 Supersedes N92-24057 (30 - 14, p 2404)
(NASA-Case-LEW-15308-1; US-Patent-5,244,508;
US-Patent-Appl-SN-862113; US-Patent-Class-136-245;
US-Patent-Class-136-292; Int-Patent-Class-H01L-31/45) Avail: US Patent and Trademark Office

A lightweight flexible photovoltaic (PV) blanket is attached to a support structure of initially stowed telescoping members. The deployment mechanism comprises a series of extendable and rotatable columns. As these columns are extended the PV blanket is deployed to its proper configuration. Official Gazette of the U.S. Patent and Trademark Office

N94-20229*# Indiana Univ., Bloomington.
FLUID ABSORPTION SOLAR ENERGY RECEIVER Final Report, 1 May 1991 - 15 Apr. 1993
Edward J. Bair 1993 88 p
(Grant NAG3-1014)
(NASA-CR-194688; NAS 1.26:194688) Avail: CASI HC A05/MF A01

A conventional solar dynamic system transmits solar energy to the flowing fluid of a thermodynamic cycle through structures which contain the gas and thermal energy storage material. Such a heat transfer mechanism dictates that the structure operate at a higher temperature than the fluid. This investigation reports on a fluid absorption receiver where only a part of the solar energy is transmitted to the structure. The other part is absorbed directly by the fluid. By proportioning these two heat transfer paths the energy to the structure can preheat the fluid, while the energy absorbed directly by the fluid raises the fluid to its final working temperature. The surface temperatures need not exceed the output temperature of the fluid. This makes the output temperature of the gas the maximum temperature in the system. The gas can have local maximum temperatures higher than the output working temperature. However local high temperatures are quickly equilibrated, and since the gas does not emit radiation, local high temperatures do not result in a radiative heat loss. Thermal radiation, thermal conductivity, and heat exchange with the gas all help equilibrate the surface temperature. Derived from text

N94-21179*# Rockwell International Corp., Canoga Park, CA. Rocketdyne Div.
POWER CONDITIONING SYSTEM MODELLING FOR NUCLEAR ELECTRIC PROPULSION Final Report
Kenneth J. Metcalf Nov. 1993 164 p
(Contract NAS3-25808; RTOP 593-72-00)
(NASA-CR-191136; NAS 1.26:191136) Avail: CASI HC A08/MF A02

NASA LeRC is currently developing a Fortran based model of a complete nuclear electric propulsion (NEP) vehicle that would be used for piloted and cargo missions to the Moon or Mars. The proposed vehicle design will use either a Brayton or K-Rankine power conversion cycle to drive a turbine coupled with a rotary alternator. Two thruster types are also being studied, ion and magnetoplasmadynamic (MPD). In support of this NEP model, Rocketdyne developed a power management and distribution (PMAD) subroutine that provides parametric outputs for selected alternator operating voltages and frequencies, thruster types, system power levels, and electronics coldplate temperatures. The end-to-end PMAD model described is based on the direct use of the alternator voltage and frequency for transmitting power to either ion or MPD thrusters. This low frequency transmission approach was compared with dc and high frequency ac designs, and determined to have the lowest mass, highest efficiency, highest reliability and lowest development costs. While its power quality is not as good as that provided by a high frequency system, it was considered adequate for both ion and MPD engine applications. The low frequency architecture will be used as the reference in future NEP PMAD studies. Author (revised)

N94-21298# ERG International, Inc., Golden, CO.
BUILDING INTEGRATED PHOTOVOLTAIC SYSTEMS ANALYSIS
Aug. 1993 27 p Prepared for Midwest Research Inst., Golden, CO
(Contract DE-AC02-83CH-10093)
(DE93-018208; NREL/TP-472-5539) Avail: CASI HC A03/MF A01

The National Renewable Energy Laboratory (NREL) estimated that the deployment of photovoltaics (PV) in the commercial buildings sector has the potential to contribute as much as 40 gigawatts peak electrical generation capacity and displace up to 1.1 quads of primary fuel use. A significant portion of this potential exists for smaller buildings under 25,000 square feet (2,300 square meters) in size or two stories or less, providing a strong cross over potential for residential applications as well. To begin to achieve this potential, research is needed to define the appropriate match of PV systems to energy end-uses in the commercial building sector. Preliminary findings for a technical assessment of several alternative paths to integrate PV with building energy systems are presented. DOE

N94-21527# Morgantown Technology Center, WV.
MOLTEN CARBONATE FUEL CELL NETWORKS: PRINCIPLES, ANALYSIS, AND PERFORMANCE
J. G. Wimer, M. C. Williams, D. H. Archer (Carnegie-Mellon Univ., Pittsburgh, PA.), and J. F. Osterle (Carnegie-Mellon Univ., Pittsburgh, PA.) 1993 10 p Presented at the 28th Intersociety Energy Conversion Engineering Conference, Atlanta, GA, 8-13 Aug. 1993
(DE93-019872; DOE/METC-C/93/7100; CONF-930804-19) Avail: CASI HC A02/MF A01

Key to the concept of networking is multiple fuel cell stacks with regard to flow of reactant streams. In a fuel cell network, reactant streams are ducted so that they are fed and recycled through stacks in series. Stacks networked in series more closely approach a reversible process, which increases efficiency. Higher total reactant utilizations can be achieved by stacks networked in series. Placing stacks in series also allows reactant streams to be conditioned at different stages of utilization. Between stacks, heat can be consumed or removed, (methane injection, heat exchange)

which improves thermal balance. Composition of streams can be adjusted between stacks by mixing exhaust streams or by injecting reactant streams. Computer simulations demonstrated that a combined cycle system with MCFC stacks networked in series is more efficient than an identical system with MCFC stacks in parallel. DOE

N94-21540# Louisiana State Univ., Baton Rouge.
A CALCIUM OXIDE SORBENT PROCESS FOR BULK SEPARATION OF CARBON DIOXIDE
D. P. Harrison, C. Han, and A. Silaban 1993 12 p Presented at the Coal-Fired Power Systems 1993: Advances in IGCC and PFBC Review Meeting, Morgantown, WV, 28-30 Jun. 1993
(Contract DE-AC21-89MC-26366)
(DE93-019288; DOE/MC-26366/93/C0194; CONF-9306148-5) Avail: CASI HC A03/MF A01

Reaction conditions for those runs discussed in this paper are summarized. In tests O2, O3, and O4 the carbonation feed gas consisted of CO2 in N2 in order to establish the ability of the calcined dolomite sorbent to remove CO2 at conditions where the shift reaction could not occur. In the next group of tests (15, 16, 18), the carbonation feed gas contained only CO, H2O, and N2. Any change in feed gas composition would serve as proof that the shift reaction was occurring at the test conditions. CO2 formed by the shift reaction should be removed from the gas phase by reacting with the sorbent. Therefore, this series of tests involved both reactions even though the feed gas contained no CO2. Finally, the feed gas in test 19 contained all of the major components found in a sulfur-free coal-gas. CO2 in the reactor feed as well as that produced by the shift reaction was available for reacting with the sorbent. DOE

N94-21562# Midwest Research Inst., Golden, CO. National Renewable Energy Lab.
FIRST BIOMASS CONFERENCE OF THE AMERICAS: ENERGY, ENVIRONMENT, AGRICULTURE, AND INDUSTRY, VOLUME 2
1993 711 p Conference held in Burlington, VT, 30 Aug. - 2 Sep. 1993
(Contract DE-AC02-83CH-10093)
(DE94-000435; NREL/CP-200-5768-Vol-2; CONF-9308106-Vol-2) Avail: CASI HC A99/MF A06

This conference was designed to provide a national and international forum to support the development of a viable biomass industry. Although papers on research activities and technologies under development that address industry problems comprised part of this conference, an effort was made to focus on scale-up and demonstration projects, technology transfer to end users, and commercial applications of biomass and wastes. The conference was divided into these major subject areas: resource base, power production, transportation fuels, chemicals and products, environmental issues, commercializing biomass projects, biomass energy system studies, and biomass in latin america. The papers in this second volume cover transportation fuels, and chemicals and products. Transportation fuels topics include: biodiesel, pyrolytic liquids, ethanol, methanol and ethers, and commercialization. The chemicals and products section includes specific topics in: research, technology transfer, and commercial systems. Selected papers have been indexed separately for inclusion in the Energy Science and Technology Database. DOE

N94-21614# University of South Florida, Tampa.
ADVANCED PROCESSING TECHNOLOGY FOR HIGH-EFFICIENCY THIN-FILM CuInSe2 SOLAR CELLS
D. L. Morel, G. Attar, S. Karthikeyan, A. Muthaiah, and A. Zafar Aug. 1993 32 p Prepared for Midwest Research Inst., Golden, CO
(Contract DE-AC02-83CH-10093)
(DE93-010045; NREL/TP-451-5653) Avail: CASI HC A03/MF A01

This report describes work to develop novel fabrication for CuInSe2 (CIS) solar cells that will result in improved performance and cost effectiveness at the manufacturing level. The primary approach involves all solid-state processing for CIS. This was augmented by work to provide novel alternatives for the formation of the window layer/heterojunction contact. Inherent to the project was the need to develop a generic understanding of the relationship between processing and performance so that broad-based transfer to industry can be facilitated. We achieved good electronic quality CIS by the use of two selenization procedures for predeposited metal layers. We achieved good stoichiometry throughout the bulk of the film, attained grain sizes of up to 1 mu m, and measured electron mobilities of up to 60 cm(exp 2)/V-s. However, there is a complex relationship between grain size, adhesion, and performance. Our primary approach to characterization was to fabricate ZnO/CIS test devices and measure as many properties as possible in device format. We are also developing reactive sputtering of ZnO as an alternative window layer technology. DOE

N94-21616# Midwest Research Inst., Golden, CO.
PROCEEDINGS OF THE 1993 DOE/NREL HYDROGEN PROGRAM REVIEW
Aug. 1993 207 p Review held in Cocoa Beach, FL, 4-6 May 1993
(Contract DE-AC02-83CH-10093)
(DE93-018207; NREL/CP-470-5777; CONF-9305266) Avail: CASI HC A10/MF A03

The US Department of Energy has conducted programs of research and development in hydrogen and related technologies since 1975. The current program is conducted in accordance with the DOE Hydrogen Program Plan FY 1993-FY 1997 which was published in June 1992. The plan establishes program priorities and guidance for the allocation of funding. The core program, currently under the Office of Energy Management, supports projects in the areas of hydrogen production, storage, and systems research. A program review is held annually to evaluate each research project for technical quality, progress, and programmatic benefit. The evaluation is conducted by a panel of technical experts. This proceedings of the program review conducted in May 1993 is a compilation of all research projects supported by the Hydrogen Program during FY 1993. It is produced in the anticipation that it will serve as a useful technical reference for those interested in the status of hydrogen technologies. Selected papers have been indexed separately for inclusion in the Energy Science and Technology Database. DOE

N94-21650# Argonne National Lab., IL.
RESEARCH AND DEVELOPMENT OF ALTERNATIVE COMPONENTS AT ARGONNE NATIONAL LABORATORY FOR MOLTEN CARBONATE FUEL CELLS
M. Krumpelt, G. H. Kucera, M. Roche, and E. Indacochea 1993 7 p Presented at the Morgantown Energy Technology Center (METC) Contractors' Review Meeting, Morgantown, WV, 3-5 Aug. 1993
(Contract W-31-109-eng-38)
(DE93-019536; ANL/CMT/CP-80209; CONF-9308144-1) Avail: CASI HC A02/MF A01

The objective is to improve the lifetime of the molten carbonate fuel cell (MCFC). Doped LiFeO2 cathodes, Nb-doped CeO2 anodes, and a new CaCO3-Li2CO3-K2CO3 electrolyte were developed and tested. DOE

N94-21755# Department of Energy, Washington, DC. Office of Energy Research.
ADVANCED ENERGY PROJECTS, FY 1993 Research Summaries
Sep. 1993 83 p
(DE94-000539; DOE/ER-0596T) Avail: CASI HC A05/MF A01

AEP has been supporting research on novel materials for energy technology, renewable and biodegradable materials, new uses for scientific discoveries, alternate pathways to energy efficiency, alternative energy sources, innovative approaches to waste treatment and reduction, etc. The summaries are grouped according to projects active in FY 1993, Phase 1 SBIR projects, and Phase 2 SBIR projects. Investigator and institutional indexes are included. DOE

N94-21774 Argonne National Lab., IL.
MODELING OF POLYMER ELECTROLYTE FUEL CELL SYSTEMS
R. Kumar, R. Ahluwalia, H. K. Geyer, and M. Krumpelt 1993 6 p Presented at the 1993 Automotive Technology Development Contractors' Meeting, Dearborn, MI, 18-21 Oct. 1993 Limited Reproducibility: More than 20% of this document may be affected by microfiche quality
(Contract W-31-109-eng-38)
(DE93-041187; ANL/CMT/CP-80587; CONF-9310169-1) Avail: CASI HC A02

Propulsion systems based on the polymer electrolyte fuel cell (PEFC) are being developed. This paper reports an analysis undertaken to design improved PEFC systems. A reference system design with some variants were set up for a methanol-fueled PEFC propulsion system. Efficiency

improves from 38.4 to 44.1% as cell current density goes from 0.75 to 0.45 A/sq cm, while fuel cell efficiency increases from 52.6 to 60.0%; to get a net power output of 80 kWe, the active fuel cell area must increase from 18.8 to 27.3 sq m. Three parametric studies were conducted on the off-design performance of the reference system. DOE

N94-21823# Oak Ridge National Lab., TN.
PROCEEDINGS OF THE SEVENTH ANNUAL CONFERENCE ON FOSSIL ENERGY MATERIALS
N. C. Cole, comp. and R. R. Judkins, comp. Jul. 1993 402 p Conference held in Oak Ridge, TN, 11-13 May 1993
(Contract DE-AC05-84OR-21400)
(DE94-001091; ORNL/FMP-93/1; CONF-9305135) Avail: CASI HC A18/MF A04

The objective of the AR&TD Materials Program is to conduct research and development on materials for longer-term fossil energy applications as well as for generic needs of various fossil fuel technologies. The 37 papers are arranged into 3 sessions: ceramics, new alloys/intermetallics, and new alloys/advanced austenitics. Selected papers have been indexed separately for inclusion in the Energy Science and Technology Database. DOE

N94-21826# Midwest Research Inst., Golden, CO.
STABLE, HIGH-EFFICIENCY AMORPHOUS-SILICON SOLAR CELLS WITH LOW HYDROGEN CONTENT
S. S. Hegedus (Delaware Univ., Newark.) and J. E. Phillips (Delaware Univ., Newark.) Aug. 1993 60 p
(Contract DE-AC02-83CH-10093)
(DE93-018214; NREL/TP-451-5756) Avail: CASI HC A04/MF A01

This report describes a 21-month project to demonstrate amorphous-silicon (a-Si) solar cells with high stabilized conversion efficiency. The objective was to develop a research program spanning material issues (more stable a-Si and better a-SiGe alloys) and device issues (more stable a-Si-based solar cells) with the goal of high stabilized solar cell efficiency. The Institute of Energy Conversion (IEC) produced and analyzed the stability of a-Si films and solar cells with reduced hydrogen content (2-6%). A thermodynamic model of defect formation was developed that describes the high-temperature degraded state of a solar cell. An analysis of bi-facial current voltage and quantum efficiency results for a-SiGe p-i-n devices with transparent front and back contacts provided information about the influence of alloying and band-gap grading on hole and electron collection. IEC also studied the stability of graded and ungraded a-SiGe solar cells using bifacial devices to learn about the relative degradation of hole and electron collection, and concludes that degradation of the photoconductivity of a-SiGe materials does not agree with degradation observed in solar cells. DOE

N94-21827# Midwest Research Inst., Golden, CO. National Renewable Energy Lab.
THIN-FILM CdTe AND CuInSe2 PHOTOVOLTAIC TECHNOLOGIES
H. S. Ullal, K. Zweibel, and B. G. VonRoedern Aug. 1993 8 p Presented at the International Solar Energy Society World Congress, Budapest, Hungary, 23-27 Aug. 1993
(Contract DE-AC02-83CH-10093)
(DE93-018217; NREL/TP-413-5752; CONF-930838-1) Avail: CASI HC A02/MF A01

Total-area conversion efficiency of 15%-15.8% have been achieved for thin-film CdTe and CIS solar cells. Modules with power output of 5-53 W have been demonstrated by several groups world-wide. Critical processes and reaction pathways for achieving excellent PV devices have been elucidated. Research, development, and technical issues have been identified, which could result in potential improvements in device and module performance. A 1-kW thin-film CdTe array has been installed and is being tested. Multimegawatt thin-film CdTe manufacturing plants are expected to be completed in 1-2 years. DOE

N94-21870 Argonne National Lab., IL.
CATHODE MATERIALS FOR THE MOLTEN CARBONATE FUEL CELL
G. H. Kucera, A. P. Brown, M. F. Roche, E. J. Indacochea, M. Krumpelt, and K. M. Myles 1993 13 p Presented at the 206th ACS National Meeting, Chicago, IL, 22-27 Aug. 1993 Limited Reproducibility: More than 20% of this document may be affected by microfiche quality
(Contract W-31-109-eng-38)
(DE93-019515; ANL/CMT/CP-79775; CONF-930802-11) Avail: CASI HC A03

Both LiFeO2 and Li2MnO3 were stable in the cathode environment, had low solubility, and were nonprecipitating in the anode environment. Dopants were employed to enhance the electronic conductivity of both materials. Cobalt-doped LiFeO2 was a factor of 30 more conductive than the undoped LiFeO2; Nb-doped Li2MnO3 was a factor of 60 more conductive than its undoped form. However, only the Co-doped LiFeO2 exhibited the desired p-type conduction. Half- and full-cell tests with Co-doped LiFeO2 as the cathode material showed that its performance strongly depended on the oxygen partial pressure. Under simulated high-pressure conditions, where the O2 partial pressure was 70 kPa, the performance was good. LiCoO2 had low solubility and was a good electronic conductor undoped. In addition, it exhibited p-type conduction, and, when used as a cathode material, gave good cell performance. It precipitated as cobalt metal under reducing conditions in anode. However, neither rate of deposition nor conditions influencing deposition and location are known. DOE

N94-21942# Argonne National Lab., IL.
THE ELECTROCHEMICAL PERFORMANCE OF THIN-ELECTROLYTE SOLID OXIDE FUEL CELLS
D. Zurawski and T. Kueper 1993 3 p Presented at the 184th Meeting of the Electrochemical Society, New Orleans, LA, 10-15 Oct. 1993
(Contract W-31-109-eng-38)
(DE93-041184; ANL/CMT/CP-79617; CONF-931024-3) Avail: CASI HC A01/MF A01

Several benefits are realized by lowering the operating temperature of solid oxide fuel cells (SOFC's) from 1000C to temperatures in the 600 to 800C range. Among the advantages are decreased reaction between fuel cell components, shorter startup times, and the possibility of using metals in stack construction; however, the achievable power density in conventional SOFC's is too low. A strategy for overcoming this limitation is to decrease the thickness of this layer by approximately an order of magnitude. Thin (5 micron electrolyte SOFC's have recently been fabricated by Allied-Signal Aerospace Systems and Equipment Company (ASASE). The electrochemical performance of these cells has been studied and is discussed. DOE

N94-22012# Japan Machinery Federation, Tokyo.
THE FY1992 SURVEY ON MULTI-PURPOSE DAM AND ENERGY UTILIZATION SYSTEM BY THE WIND POWER GENERATION ERATION
Mar. 1993 204 p In JAPANESE
(DE94-707408; ETDE/JP-mf-94707408) Avail: CASI HC A10/MF A03

The wind power generation for power supply necessary for pumping for water-use works using underground dam which were pushed at Miyako Island, Okinawa is described. The survey aims to study economic effects of introduction of the wind power generation system by setting areas for irrigation. The field area, which is irrigable by three units of USW's 100kW wind power generator as a load follow-up system, is 100ha. Surplus power, when purchased by power companies, is appropriated for maintenance cost for irrigation and makes farmers' running cost nothing. Even though depreciation expenses and interest rates of the initial cost which is construction cost of the wind power generation system are borne, the system possibly pays. Since a public subsidy is expected to be given to the initial cost portion, burdens of farmers become much lighter. By using an inverter pump system, the number of operated pumps and the revolution number of the pump can be controlled so as to make all output of the wind turbine consume as power of the pump. So the system which is minimum in running cost can be obtained. DOE

N94-22013# New Energy and Industrial Technology Development Organization, Tokyo (Japan).
CURRENT SITUATION OF DEVELOPMENT OF PETROLEUM SUBSTITUTING ENERGIES (USA)
Mar. 1993 52 p In JAPANESE
(DE94-707492; NEDO-P-9201) Avail: CASI HC A04/MF A01

Trends in development of petroleum substituting energies in the U.S.A. are described. Among non-fossil fuel based energies currently available, nuclear power generation (7%), biomass power generation (4%), and hydraulic power generation (3%) account for a large part. The future for the nuclear energy is opaque. Biomasses are anticipated to be the largest

regenerative energy source. Solar energy was regarded to be a future energy source, but its cost effect is not still good. While geothermal power generation produces 0.1% of the entire energy, its future is bright. Ocean energies of all types of form such as sea water thermal energy conversion and wave energy were not treated as a substituting energy in the U.S.A. Multi-fuel vehicles using gasoline, methanol, and ethanol are estimated to account for 25% of vehicle operations in the U.S.A. by 2000. Electric vehicles for practical use would be a hybrid type combining electric motors and gasoline engines. DOE

N94-22014# New Energy and Industrial Technology Development Organization, Tokyo (Japan).
CURRENT SITUATION OF DEVELOPMENT OF PETROLEUM SUBSTITUTING ENERGIES (CANADA)
Mar. 1993 31 p In JAPANESE
(DE94-707493; NEDO-P-9202) Avail: CASI HC A03/MF A01

Trends in development of petroleum substituting energies in Canada are described. Those fuels being put into practical use as substituting fuels in the transportation sector are natural gas, propane gas, methanol, hydrogen, and electric power. An architectural energy technology improving project was inaugurated on air conditioning, ventilation, and illumination in buildings that consume 34% of the entire energy. The IERD program was implemented by the bureau of efficient substituting energy technologies of CANMET on the research and development in industrial areas. Since having been introduced in 1977, this project has extended assistance to about 80 cases in industrial areas, of which 50% have achieved technical successes and were commercialized. With respect to bio energies, methods for effectively utilizing wastes that are difficult to treat are drawing attention. Research and development are being moved forward to put into practical use the solar energy, wind power, and small-scale regenerative energies. DOE

N94-22015# Midwest Research Inst., Golden, CO. National Renewable Energy Lab.
ANNUAL REPORT, MATERIALS SCIENCE BRANCH, FY 1992
S. Padilla, ed. Oct. 1993 11 p
(Contract DE-AC02-83CH-10093)
(DE94-000204; NREL/TP-451-5733) Avail: CASI HC A03/MF A01

The progress of the Materials Science Branch of the National Renewable Energy Laboratory (NREL) from 1 Oct. 1991, through 30 Sep. 1992 is summarized. Six technical sections cover these main areas of NREL's in-house research: Crystal Growth, Amorphous Silicon, III-V High-Efficiency Photovoltaic Cells, Solid State Theory, Solid State Spectroscopy, and Program Management. Each section explains the purpose and major accomplishments of the work in the context of the US Department of Energy's National Photovoltaic Research Program plans. DOE

N94-22029# Japan Machinery Federation, Tokyo.
THE FY1992 SURVEY ON COMMERCIALIZATION OF STIRLING ENGINE UTILIZATION EQUIPMENT
Mar. 1993 103 p In JAPANESE
(DE94-707416; ETDE/JP-mf-94707416) Avail: CASI HC A06/MF A02

Problems on commercialization of Stirling engine heat pumps (SEHP) and the solution are studied. The Stirling engine is a small and fixed engine having a 30-40% thermal efficiency and a 1-100 kW output. It is a closed recipro type external combustion engine with non-condensable gas like helium as working fluid. Its theoretical efficiency agrees with that of the Carnot's cycle. This is because the Stirling engine is often called a dream engine. However, the Stirling engine is legally restricted from a viewpoint of ensuring safety because high pressure gas as working fluid is sealed into the Stirling engine. It is feared that this point will be a condition that restricts spread/promotion of the equipment which uses the engine. Therefore, by guidance of MITI and support of organizations/enterprises concerned, a committee was started in 1992FY and studied the safety of the Stirling engine and the related legal systems. DOE

N94-22030# New Energy and Industrial Technology Development Organization, Tokyo (Japan).
PRESENT STATUS OF DEVELOPING PETROLEUM-SUBSTITUTING ENERGY (EC)
Mar. 1993 58 p In JAPANESE
(DE94-707494; NEDO-P-9204) Avail: CASI HC A04/MF A01

The EC has had approximately 50% of its total energy demand supplied by imports from the exterior of the Community. Hence, it is getting important to develop oil-substituting renewable energy as well as to curtail the emission of carbon dioxide. In consideration of these situations, the results of investigation on the energy policy of the European Community are described. The policy comprises three courses: European Energy Charter, formation of an open European Community energy market, and environmental conservation. Particularly, concerning the reduction of carbon dioxide emission, the EC Council has decided to introduce carbon dioxide taxation so as to suppress the carbon dioxide emission in the year 2000 to the 1990 level. The arrangement for its introduction, however, encountered with difficulties because of the opposition of various countries other than the European Community and the industrial world of the European Community. Legislation of the investment promotion law for energy saving and the construction of infrastructure footing and an information network are ineffective due to the sluggish fuel price and economic recession. A plurality of EC member countries are advancing a comprehensive activity within the framework of the joint programs of research, development, and demonstration set for the renewable energy policy ensuring energy supply and environmental harmonization. DOE

N94-22043# New Energy and Industrial Technology Development Organization, Tokyo (Japan).
INVESTIGATION ON THE CHEMICALLY FIXING TECHNIQUE OF CARBON DIOXIDE UTILIZING SOLAR ENERGY
Mar. 1993 83 p
(DE94-714886; NEDO-GET-9208) Avail: CASI HC A05/MF A01

This report describes the results of an effective fixing technique of CO2 by utilizing solar energy. First of all, the investigation was directed to the technique for synthesizing ethylene, hydrocarbons, and alcohol by electrochemical reduction of CO2. The power required for this process is supplied by photovoltaic power generation. Development of an excellent electrode catalyst is needed because the reduction of CO2 requires a high overvoltage. It is desirable to enhance the selectivity of the reaction for specific material and improve the transport process in the electrolytic cell. Next, the designing of materials and the reaction of photocatalysts using semiconductor electrode and semiconductor particulate was examined. A semiconductor electrode made of FeS2 is inexpensive and is very efficient at collecting solar light. In the category of a photocatalysis system, a photocatalytic system in which semiconductor particles are embedded in a vesicle and a photocatalyst based on potassium niobate are noteworthy. As biosystem, the method of reducing CO2 by calcareous algae which simultaneously advances fixing and calcification of CO2 by photosynthesis is noteworthy. DOE

N94-22048# Massachusetts Inst. of Tech., Cambridge.
PHOTOCHEMICAL APPROACHES TO CONVERSION OF LIGHT TO ELECTRICITY OR FUEL
Mark S. Wrighton 1993 8 p
(Contract DE-FG02-88ER-13914)
(DE94-001650; DOE/ER-13914/16) Avail: CASI HC A02/MF A01

The objective is to understand photochemical and photophysical processes and to develop photochemical systems for converting light to electricity or fuel. Topics covered are orientation of multi-component redox polymers on surfaces, excited state electron transport in multi-component molecules prepared via ring opening metathesis polymerization, and molecular materials for solid state photovoltaics. Rhenium complexes were covered. DOE

N94-22052 New Energy and Industrial Technology Development Organization, Tokyo (Japan).
STUDY ON POSSIBILITY OF DEVELOPING ENERGY INTEGRATION TECHNOLOGY
Mar. 1993 154 p In JAPANESE Limited Reproducibility: More than 20% of this document may be affected by poor print and microfiche quality
(DE94-714903; NEDO-P-9220) Avail: Issuing Activity (Department of Energy (DOE))

Developments of conventional individual technologies were re-identified drastically and collectively to study the possibility of developing them as an energy integration technology. In addition, the theory for energy supplier side alone was eliminated, and the user side theory and considerations on

environments and human being were valued more importantly. In its bottom-up approaches, existing technologies are first identified transversely, their existing drawbacks are compensated, and other industrial technologies are introduced freely using the key technology as a nucleus. The present study has taken up diverse utilization of the inexhaustible solar energy and development of new energy storing technologies. In its top-down approaches, a proposition was set beginning with thinking what the ideal type could be for energy systems, and pursuits were made along stratified structures. The user side theory was emphasized to impart organic combined functions within the flows of supply and utilization. Energy conversion, storage, and transportation were assembled into one converged integrated function so that diversified energy supply sources may be dealt with efficiently. Non-thermal utilization of chemical energies remains a problem yet to be solved. DOE

N94-22092# New Energy and Industrial Technology Development Organization, Tokyo (Japan).
SURVEYS ON SPECIFIC PATTERNS OF FACILITY INTALLATION OF PHOTOVOLTAIC POWER GENERATING TECHNOLOGIES FOR INTERNATIONAL COOPERATION
Mar. 1993 161 p In JAPANESE
(DE94-714901; NEDO-P-9218) Avail: CASI HC A08/MF A02

The objective is to contribute to the international introduction of photovoltaic power generation. To do this, its load patterns, device constitution, land areas, and prices were rearranged and standardized so that design standardization and efficiency improvement may be achieved, and appropriate introduction patterns may be selected from climatic conditions at various sites. Areas dealt with are Africa, Asia, Oceania, and South and Central America. The basic design consists of combination of solar cells with storage batteries for DC load, whereas inverters were added for AC load. Facility capacities were designed so that they can be calculated by assuming general load menus comprising lighting, pumps, and electric appliances, as well as load patterns. Because of non-electrified areas requiring insolation to take care of all of the annual load, minimum monthly average insolation on slopes was used to calculate solar cell capacities. While storage battery capacities will be established upon investigating climatic conditions at proposed sites, arrangements were made on selecting charge controllers that can avoid overcharging and overdischarging due to variation in insolation. A design procedure document was prepared so that the basic design could be carried out efficiently. DOE

N94-22257# Advanced Photovoltaic Systems, Inc., Princeton, NJ.
RESEARCH ON STABLE, HIGH-EFFICIENCY AMORPHOUS SILICON MULTIJUNCTION MODULES
M. Ghosh, F. Kampas, and J. Xi Sep. 1993 11 p Prepared for Midwest Research Inst., Golden, CO
(Contract DE-AC02-83CH-10093)
(DE93-018220; NREL/TP-411-5760) Avail: CASI HC A03/MF A01

This report describes progress made in the first half of Phase 2 of a three-phase program to develop high-efficiency, same-band-gap, amorphous-silicon, tandem-junction modules. Results for both 1-cm(exp 2) devices and 0.3-m (0.09-m(exp 2)) modules are given. Considerable effort was devoted to finding a device structure and layer conditions that reconcile the conflicting requirements of a good 'tunnel junction' contact between the two stacks and a high-efficiency device. High-band-gap p(sub 2) layers, which enable good voltage and current from the second stack, were found to result in poor tunnel junctions. The best results were obtained by using a thin (1-nm-thick) p(sup +) layer (no carbon) between the n(sub 1) and p(sub 2) layers of the device. DOE

N94-21391* National Aeronautics and Space Administration. Lyndon B. Johnson Space Center, Houston, TX.
THE INTERNATIONAL TELECOMMUNICATIONS SATELLITE (INTELSAT) SOLAR ARRAY COUPON (ISAC) ATOMIC OXGYEN FLIGHT EXPERIMENT: TECHNIQUES, RESULTS AND SUMMARY
S. Koontz, G. King, A. Dunnet (International Telecommunications Satellite Organization, Washington, DC.), T. Kirkendahl (Communications Satellite Corp., Washington, DC.), R. Linton (National Aeronautics and Space Administration. Marshall Space Flight Center, Huntsville, AL.), and J. Vaughn (National Aeronautics and Space Administration. Marshall Space Flight Center, Huntsville, AL.) *In* CNES, Fifth International Symposium on Materials in a Space Environment Jun. 1993 p 331-348 (For primary document see N94-21367 05-18)
Copyright Avail: CEPADUES-Editions, 111, rue Nicolas-Vaquelin, 31100 Toulouse, France

45 ENVIRONMENT POLLUTION

Includes atmospheric, noise, thermal, and water pollution.

N94-19930# Pacific Northwest Lab., Richland, WA.
HEALTH EFFECTS OF GLOBAL WARMING: PROBLEMS IN ASSESSMENT
J. Longstreth Jun. 1993 11 p Presented at the International Conference on Comparative Risks Analysis of Air Pollution Issues and Priority Setting, Denver, CO, 6-11 Jun. 1993
(Contract DE-AC06-76RL-01830)
(DE93-040323; PNL-SA-22711; CONF-930656-1) Avail: CASI HC A03/MF A01

Global warming is likely to result in a variety of environmental effects ranging from impacts on species diversity, changes in population size in flora and fauna, increases in sea level, and possible impacts on the primary productivity of the sea. Potential impacts on human health and welfare have included possible increases in heat related mortality, changes in the distribution of disease vectors, and possible impacts on respiratory diseases including hayfever and asthma. Most of the focus thus far is on effects which are directly related to increases in temperature, e.g., heat stress or perhaps one step removed, e.g., changes in vector distribution. Some of the more severe impacts are likely to be much less direct, e.g., increases in migration due to agricultural failure following prolonged droughts. This paper discusses two possible approaches to the study of these less-direct impacts of global warming and presents information from on-going research using each of these approaches. DOE

N94-19941# State Univ. of New York, Albany. Atmospheric Sciences Research Center.
STUDY OF REGIONAL CLIMATE CHANGE
Wei-Chyung Wang 25 Jun. 1993 4 p
(Contract DE-FG02-92ER-61369)
(DE93-018926; DOE/ER-61369/2) Avail: CASI HC A01/MF A01

The research project includes GCM diagnosis, climate data preparation, climate data analysis, and the relationship between large- and regional-scale climates to address the following two scientific issues: the need for quality-assured climate data to study long term regional climate changes and to validate model simulated regional climate, and the need to understand the differences among GCM's in the simulations of present climate and climate changes due to increasing CO2 and other trace gases. This document consists of four sections: the project statement of work, the project progress for the period September 1, 1992 - June 25, 1993, the plan for the remaining period, and the plan for the next project year. DOE

N94-19976# Japan Machinery Federation, Tokyo.
TECHNOLOGY TO PREVENT GREENHOUSE EFFECT GASES Survey Report, FY 1992
Mar. 1993 100 p In JAPANESE
(DE94-707421; ETDE/JP-MF-94707421) Avail: CASI HC A05/MF A02

This paper makes studies on technology for CO2 deepsea storage, hydrate behavior, and CO2 biological effects. Accumulation and evaluation of more technical information/knowledge are required for CO2 transportation to the deepsea bottom in consideration of costs of CO2 separation/transportation and minimizing CO2 environmental effects. It is also required to accumulate thermodynamical property data and kinetic data on CO2/hydrates in the deepsea at temperatures of 1-4 C and at pressures over 30 MPa. Part of CO2 dissolves and diffuses into the ocean, and the rest forms solid particulate CO2/hydrates. The CO2 resultantly forms complicated solid-liquid mixed phase flows, which have serious effects on the mass transfer process. Investigation is made on the model predicting CO2 diffusion in the deepsea bottom. CO2 effects on deepsea organisms and possible ecosystem changes including food chain are also studied. It is difficult for higher organisms to survive in the liquid CO2 reservoir area, and pH becomes a problem in the diffusion area. A simulation model on the whole ecosystem is necessary to be made for elucidation. DOE

N94-19998 Rijksinstituut voor Volksgezondheid en Milieuhygieene, Bilthoven (Netherlands). Directorate-General for Environmental Protection.
MANUAL OF DRANC (RELEASE 1.1): A COMPUTER PROGRAM FOR THE DUTCH RISK ASSESSMENT OF NEW CHEMICAL SUBSTANCES
C. J. M. Visser and C. Toet 1992 29 p See also PB90-248980, PB93-102309, PB93-102317 and PB93-178184. Sponsored by Directorate-General for Environmental Protection, Leidschendam (Netherlands) Sponsored by Directorate-General for Environmental Protection, Leidschendam (Netherlands)
(PB93-194827; RIVM-679102010) Copyright Avail: Issuing Activity (National Technical Information Service (NTIS))

In the project, 'Evaluation System of New Substances', methods are developed to systematically predict and assess the hazards for man and environment related to the production and use of new chemical substances. Part of the project is the realization of a risk assessment system for new chemicals. Currently this system has the form of the computer program DRANC (Dutch Risk Assessment system for New Chemicals). The program is available for advisory tasks concerning the assessment of hazard and risk of new chemical substances (level 0, 1-100 ton/year). The manual describes the use of the program DRANC (version 1.1), which was developed using Turbo Pascal and can be run on all MS-DOS computers. NTIS

N94-20025 Aerospace Corp., Los Angeles, CA.
PARAMETERS AFFECTING HYDROGEN CHLORIDE MEASUREMENTS Final Report
L. R. Martin, N. A. Abul-Haj, Douglas M. Brenner, and Karl R. Westberg Jun. 1993 42 p Limited Reproducibility: More than 20% of this document may be affected by microfiche quality
(Contract F04701-85-C-0086)
(AD-A271326; AFESC/ESL-TR-89-23) Avail: CASI HC A03

The launching of solid rocket boosters releases numerous gases including hydrogen chloride. Monitoring the concentrations of these gases and predicting their atmospheric transport is required for safety reasons and for compliance with environmental laws. Monitoring of these gases is difficult because they are hydrophilic and tend to condense on atmospheric aerosols. Once such gases are condensed on the atmospheric aerosols, they will not appear on gas-phase sensors unless provision is made to evaporate the aerosols. Transport of the gases will also be governed by the chemistry in the aerosols and movement of the aerosols in the atmosphere, as opposed to the gas-phase chemistry alone. The objective of this project is to investigate the behavior of hydrogen chloride in the presence of atmospheric aerosols. The thermodynamics of HCl in the gas and liquid phase will be reviewed, and kinetics of mass transfer, diffusivity, and sticking coefficients on water of HCl will be measured. The evaporation of atmospheric aerosols will also be discussed. DTIC

N94-20116# Japan Machinery Federation, Tokyo.
TECHNOLOGY TO PREVENT GREENHOUSE EFFECT GASES Survey Report, FY 1992
Mar. 1993 193 p In JAPANESE
(DE94-707420; ETDE/JP-MF-94707420) Avail: CASI HC A09/MF A03

A direction to an environmental harmony type industrial technology system is proposed by grasping the total CO2 emission by linking the interindustry relations analysis and CO2 emissions from each industrial sector. Scenarios are made for fields of electricity, iron/steel, transportation, and residential/commercial use. In transportation and residential/commercial sectors where there is still room for energy conservation, energy conservation is set as a main theme of the scenario. In energy conversion, main themes of the scenario are energy conversion in demand fields which considers electrification increasingly adopted in lifestyle and the corresponding increase in a percentage of the nuclear power generation in a total power generation amount. As for industrial location, a scenario is made with dispersed location in the iron/steel industry as a model. Concerning CO2 reduction effects, CO2 can be reduced 9.8% if all the power plants to be newly installed are made nuclear power plants, 7.9% if all the fossil fuels consumed in automobile transportation and residential/commercial sectors are converted to electricity, 3.4% if energy conservation of 10% can be achieved in transportation and residential/commercial sectors, and 11.2% if iron-making processes in the iron/steel industry are dispersedly located. When CO2 emission in 2010 is maintained at the 1990 level, the economic growth rate will be 1.6%. To attain an economic growth rate of 2.5%, it is necessary to carry out the above-mentioned drastic policies. DOE

N94-20154 Cologne Univ. (Germany). Inst. fuer Geophysik und Meteorologie.
INTRUSION OF STRATOSPHERIC OZONE IN THE TROPOSPHERE THROUGH TROPOPAUSE FOLDING AND COLD AIR DROPLETS [INTRUSION STRATOSPHAERISCHEN OZONS IN DIE TROPOSPHAERE DURCH TROPOPAUSENFALTUNGEN UND KALTLUFTTROPFEN]
Andreas Oberreuter 1992 173 p In GERMAN Limited Reproducibility: More than 20% of this document may be affected by microfiche quality
(Rept-87; ETN-93-95065) Avail: CASI HC A08

The mutual exchange of ozone rich air from the stratosphere with ozone lean air from the troposhere is simulated using the EURAD (European Acid Deposition) model. Ozone concentrations in 22 model layers between Earth ground and 100 hPa were estimated. Vertical fluxes in several model heights, horizontal fluxes at lateral limits of model area, and dry deposition of ozone at Earth ground were investigated. The influence of a cold air droplet on the vertical flow of stratospheric ozone was separately examined. Clouds influence on ozone transport was also studied. A drop of ozone concentration above the tropopause and an increase under this one are found. It is noticed that dynamic processes are responsible for an enhancement of ozone flow through clouds appearing in the middle troposphere. ESA

N94-20948# Federal Aviation Administration, Washington, DC. Office of Environment and Energy.
EDMS MICROCOMPUTER POLLUTION MODEL FOR CIVILIAN AIRPORTS AND AIR FORCES BASES: USER'S GUIDE, SUPPLEMENT A
H. M. Segal Jul. 1993 28 p
(AD-A271596; DOT/FAA/EE-91-3-Suppl-A; AFESC/ESL-TR-91-31-Suppl-A) Avail: CASI HC A03/MF A01

This supplement announces the incorporation of the latest aircraft emission database (EPA, 1992) and the latest motor vehicle database (Mobile 5a) into the Emissions and Dispersion Modeling System (EDMS). (The Clean Air Act Amendments of 1990 requires that the latest emission information be used to establish the Conformity of an airport improvement project with the State Implementation Plan.) This supplement also documents the following model enhancements: (1) an expansion of the emissions inventory portion of the model to accommodate ground support equipment and airport spray painting facilities; (2) the condensation of the emissions report into a one page printout; (3) the summarizing of calculated concentrations into hourly average time periods associated with each pollutant; (4) the access of the dispersion output file (disperse.out) directly from the menu; (5) the addition of a gridding algorithm designed to permit the entry of up to 200 receptors into the model; (6) the expansion of the example problem procedure to accommodate gridding. DTIC

N94-21455 Norwegian Defence Research Establishment, Kjeller.
AIR TRANSPORT OF SAMPLES CONTAINING CHEMICAL WARFARE AGENTS
John Aasulf Toernes, Bjoern Johnsen, and Bjoern Pedersen 16 Apr. 1993 15 p Limited Reproducibility: More than 20% of this document may be affected by microfiche quality
(FFI-93/6005; ETN-93-94889) Avail: Issuing Activity (European Space Agency (ESA))

The ICAO/IATA (International Civil Aviation Organization/International Air Transport Association) regulations for transport of dangerous goods by air were reviewed, and a procedure for packing and transport of samples containing traces of chemical warfare agents was proposed. The shipping names poisonous liquids n.o.s. and poisonous solids n.o.s. with UN numbers 2810 and 2811 respectively should be used. The procedure was tested by trial transports of packages containing environmental samples containing traces of chemical warfare agents simulants. ESA

N94-21740# California Univ., Berkeley. Lawrence Berkeley Lab.
ROLE OF SURFACE CHARACTERISTICS IN URBAN METEOROLOGY AND AIR QUALITY Ph.D. Thesis
D. J. Sailor Aug. 1993 174 p
(Contract DE-AC03-76SF-00098)
(DE93-040929; LBL-34459) Avail: CASI HC A08/MF A02

Urbanization results in a landscape with significantly modified surface characteristics. The lower values of reflectivity to solar radiation, surface moisture availability, and vegetative cover, along with the higher values of anthropogenic heat release and surface roughness combine to result higher

air temperatures in urban areas relative to their rural counterparts. Through their role in the surface energy balance and surface exchange processes, these surface characteristics are capable of modifying the local meteorology. The impacts on wind speeds, air temperatures, and mixing heights are of particular importance, as they have significant implications in terms of urban energy use and air quality. This research presents several major improvements to the meteorological modeling methodology for highly heterogeneous terrain. A land-use data-base is implemented to provide accurate specification of surface characteristic variability in simulations of the Los Angeles Basin. Several vegetation parameterizations are developed and implemented, and a method for including anthropogenic heat release into the model physics is presented. These modeling advancements are then used in a series of three-dimensional simulations which were developed to investigate the potential meteorological impact of several mitigation strategies. Results indicate that application of moderate tree-planting and urban-lightening programs in Los Angeles may produce summertime air temperature reductions on the order of 4 C with a concomitant reduction in air pollution. The analysis also reveals several mechanisms whereby the application of these mitigation strategies may potentially increase pollutant concentrations. The pollution and energy use consequences are discussed in detail. DOE

N94-21787# Duke Univ., Durham, NC. Dept. of Botany.
MODELING THE RESPONSE OF ECOSYSTEMS TO CO2 AND CLIMATE CHANGE
J. F. Reynolds, P. R. Kemp, and J. Chen 19 Jun. 1993 39 p
(Contract DE-FG05-92ER-61493)
(DE94-000748; DOE/ER-61493/1) Avail: CASI HC A03/MF A01

In recognition of the role of plants in the bio-geosphere carbon cycle, the Department of Energy (OHER) initiated a research program: The Direct Effects of Increasing Carbon Dioxide on Vegetation. This report describes the continuing research that we are conducting as part of this program. The ultimate goal of our research is to develop computer models capable of predicting responses of plants and ecosystems to the direct and indirect effects of atmospheric levels of carbon dioxide that are approximately twice those of the pre-industrial period. The understanding of ecosystem responses to elevated CO2 necessarily depends on knowledge of responses of individual plants and their interactions with one another and their environment. Our research approach incorporates the study and modeling of response to CO2 at all levels of the plant-community-ecosystem hierarchy, in an effort to understand the linkages and translation of effects of CO2 from one level to another. The research results reported here focus at several different levels of this hierarchy, and are highlights of accomplishments for the period September 1992 to June 1993. DOE

N94-21969# Lawrence Livermore National Lab., CA.
GLOBAL EMISSIONS AND MODELS OF PHOTOCHEMICALLY ACTIVE COMPOUNDS
J. E. Penner, C. S. Atherton, and T. E. Graedel (Bell Telephone Labs., Inc., Murray Hill, NJ.) 20 May 1993 28 p Presented at the 1st International Global Atmospheric Chemistry Project Conference, Elat, Israel, 18-22 Apr. 1993
(Contract W-7405-eng-48)
(DE93-040490; UCRL-JC-112273; CONF-930443-1) Avail: CASI HC A03/MF A01

Anthropogenic emissions from industrial activity, fossil fuel combustion, and biomass burning are now known to be large enough (relative to natural sources) to perturb the chemistry of vast regions of the troposphere. A goal of the IGAC Global Emissions Inventory Activity (GEIA) is to provide authoritative and reliable emissions inventories on a 1 deg x 1 deg grid. When combined with atmospheric photochemical models, these high quality emissions inventories may be used to predict the concentrations of major photochemical products. Comparison of model results with measurements of pertinent species allows us to understand whether there are major shortcomings in our understanding of tropospheric photochemistry, the budgets and transport of trace species, and their effects in the atmosphere. Through this activity, we are building the capability to make confident predictions of the future consequences of anthropogenic emissions. This paper compares IGAC recommended emissions inventories for reactive nitrogen and sulfur dioxide to those that have been in use previously. We also present results from the three-dimensional LLNL atmospheric chemistry model that show how emissions of anthropogenic nitrogen oxides might potentially affect tropospheric ozone and OH concentrations and how emissions of anthropogenic sulfur increase sulfate aerosol loadings. DOE

N94-22004# Oak Ridge National Lab., TN.
ATMOSPHERIC SAMPLING GLOW DISCHARGE IONIZATION AND TRIPLE QUADRUPOLE TANDEM MASS SPECTROMETRY FOR EXPLOSIVES VAPOR DETECTION
S. A. McLuckey, D. E. Goeringer, K. G. Asano, K. J. Hart, G. L. Glish, B. C. Grant, and D. M. Chambers Aug. 1993 166 p
(Contract DE-AC05-84OR-21400)
(DE93-040593; ORNL/TM-12434) Avail: CASI HC A08/MF A02

The detection and identification of trace vapors of hidden high explosives is an excellent example of a targeted analysis problem. It is desirable to push to ever lower levels the quantity or concentration of explosives material that provides an analytical signal, while at the same time discriminating against all other uninteresting material. The detection system must therefore combine high sensitivity with high specificity. This report describes the philosophy behind the use of atmospheric sampling glow discharge ionization, which is a sensitive, rugged, and convenient means for forming anions from explosives molecules, with tandem mass spectrometry, which provides unparalleled specificity in the identification of explosives-related ions. Forms of tandem mass spectrometry are compared and contrasted to provide a summary of the characteristics to be expected from an explosives detector employing mass spectrometry/mass spectrometry. The instrument developed for the FAA, an atmospheric sampling glow discharge/triple quadrupole mass spectrometer, is described in detail with particular emphasis on the ion source/spectrometer interface and on the capabilities of the spectrometer. Performance characteristics of the system are also described as they pertain to explosives of interest including a description of an automated procedure for the detection and identification of specific explosives. A comparison of various tandem mass spectrometers mated with atmospheric sampling glow discharge is then described and preliminary studies with a vapor preconcentration system provided by the FAA are described. DOE

N94-22017 Los Alamos National Lab., NM.
THE USE OF LIDAR FOR THE EVALUATION OF TRAFFIC-RELATED URBAN POLLUTION
W. Eichinger, D. Cooper, W. Buttler, W. Cottingame, and L. Tellier 1993 11 p Presented at the Annual Meeting of the Society of Photo-Optical Instrumentation Engineers (SPIE), San Diego, CA, 11-16 Jul. 1993 Limited Reproducibility: More than 20% of this document may be affected by microfiche quality
(Contract W-7405-eng-36)
(DE94-000704; LA-UR-93-3437; CONF-930722-46) Avail: CASI HC A03

Lidar (Light Detection and Ranging) is demonstrated as a tool for the detection and tracking of sources of aerosol pollution. Existing elastic lidars have been used to demonstrate the potential of the application of this technology in urban areas. Data from several experiments is shown along with analysis methods used for interpretation of the data. The goal of the project is to develop a light-weight, low-cost, lidar system and data analysis methods which can be used by urban planners and local air quality managers. The ability to determine the sources, i.e. causes, of non-attainment may lead to more effective use of tax dollars. Future directions for the project are also discussed. DOE

N94-22044# New Energy and Industrial Technology Development Organization, Tokyo (Japan).
SURVEY ON CHEMICAL ENGINEERING TECHNOLOGIES FOR THE GLOBAL ENVIRONMENTAL PROTECTION
Mar. 1993 165 p In JAPANESE
(DE94-714887; NEDO-GET-9209) Avail: CASI HC A08/MF A02

The present paper suggests measures to suppress and reduce global greenhouse gases. Under the control of artificial environments such as bioreactors, hydroponics, and vegetable factories, a very high fixing rate of CO2 can be obtained, but CO2 generation as a byproduct of electric power consumption is also large. It is preferable to use methane as a resource by reforming reactions or selective oxidative reaction. In the recovery of fluorocarbons, 100% recovery is desirable. Techniques for decomposing recovered fluorocarbon and converting it to harmless material are the most immature ones. An understanding of the essential structural

relationship of coal is necessary for establishing combustion techniques for the reduction of N2O. An integrated power generation system composed of a solid electrolyte fuel cell, a coal gasification process, and a superheat pump system form the basis for a technology that imposes no burden on the global environment. Establishment of purification techniques for industrial- or living-related drainage to a closed water area system are discussed.
DOE

N94-22051# New Energy and Industrial Technology Development Organization, Tokyo (Japan).
SURVEY ON EVALUATION OF ENERGY TECHNOLOGY CONTRIBUTING TO PRESERVATION OF THE GLOBAL ENVIRONMENT. 2
Mar. 1993 289 p In JAPANESE
(DE94-714884; NEDO-GET-9205) Avail: CASI HC A13/MF A03

The analysis and evaluation are made on effectiveness of each of the energy technologies having large effects on control of greenhouse effect gas emissions. Details of the report based on the Framework Convention on Climate Change of the United Nations Conference on Environment and Development should essentially be made by efforts spontaneously exerted by countries now being in economic transition and development. The required database, however, has not necessarily been prepared. It is, therefore, necessary that developed countries should assist the countries in preparing methodology for estimating emission and absorption of greenhouse effect gases and methodology or know-how for working out domestic or regional plans. As for 'IPCC/EIS-IIASA International Workshop', discussions on the following are reported: energy-related greenhouse gases reduction and removal, analysis of factors affecting energy consumption and CO2 emissions and their regional and sectoral differences, and assessment of technologies for reducing CO2 emission. Also introduced is a report of the Eighth Session on the Inter-governmental Panel on Climate Change. DOE

N94-22090# New Energy and Industrial Technology Development Organization, Tokyo (Japan).
INVESTIGATION ON CONSTRUCTION OF THE DATABASE SYSTEM FOR RESEARCH AND DEVELOPMENT OF THE GLOBAL ENVIRONMENT INDUSTRY TECHNOLOGY
Mar. 1993 177 p In JAPANESE
(DE94-714890; NEDO-GET-9210-5) Avail: CASI HC A09/MF A02

This paper studies a concrete plan to introduce a new database system for the Research Institute of Innovative Technology for the Earth (RITE). RITE is necessary to promote the development of industrial technology that will bring about solutions to the global environmental problem. Specifications for the system introduction are concerned with maker selection, operating system, detailed schedule for introduction, etc. The RITE inhouse database has problems with its operating system and its maintenance cost, and it is apt to have a large construction cost in comparison with its utilization factor. Further study is made on its introduction. Information provided by the inhouse database is only the one owned by the organization, and information outside the organization is provided by the external database. The information is registered and selected by the registerer. The access network is set by personal computer network at the beginning and is set to transit to INTERNET in the future. For practical construction of the system, it is necessary to make the user's needs clear for the system design and to adjust functions between hardware systems.
DOE

N94-22258# New Energy and Industrial Technology Development Organization, Tokyo (Japan).
INVESTIGATIONS ON TRENDS IN GLOBAL ENVIRONMENT ADAPTIVE INDUSTRIAL TECHNOLOGIES
Mar. 1993 121 p In JAPANESE
(DE94-714888; NEDO-GET-9210-1) Avail: CASI HC A06/MF A02

This paper describes specific evaluations on measures to reduce carbon dioxide chemically, and measures to reduce non-carbon dioxide greenhouse gases. The former measures could reduce CO2 by 10% to 20% by improving energy utilization and using unutilized energy recovering technologies. The key to fixing CO2 through hydrogenation is how to ensure the hydrogen availability. During the coming two decades, the Japanese chemical industry is expected to reduce CO2 of about ten million tons, or about 10%. Use of CO2 oxidizing dehydrogenation process would be capable of reducing CO2 of about five million tons in Japan. For the latter measures, chemical technologies are available to recover and store methane as the greenhouse gas other than CO2. Promotion is urged in combustion technologies to suppress N2O generation, and technologies to treat waste gases from automotive tertiary catalysts and adipic acid processes. Fluorocarbon reduction requires development of technologies to synthesize, recover and treat new substitute materials. Positive measures are also called for to reduce CO, non-methane based hydrocarbons, and NO(x). DOE

N94-22259# London Univ. (England). School of Mathematics.
SURVEY ON UTILIZATION OF DATABASE FOR RESEARCH AND DEVELOPMENT OF GLOBAL ENVIRONMENTAL INDUSTRY TECHNOLOGY
Mar. 1993 99 p In JAPANESE
(DE94-714891; NEDO-GET-9213) Avail: CASI HC A05/MF A02

To optimize networks and database systems for promotion of the industry technology development contributing to the solution of the global environmental problem, studies are made on reusable information resource and its utilization methods. As reusable information resource, there are external database and network system for researchers' information exchange and for computer use. The external database includes commercial database and academic database. As commercial database, 6 agents and 13 service systems are selected. As academic database, there are NACSIS-IR and the database which is connected with INTERNET in the U.S. These are used in connection with the UNIX academic research network called INTERNET. For connection with INTERNET, a commercial UNIX network service called IIJ which starts service in April 1993 can be used. However, personal computer communication network is used for the time being.
DOE

N94-22384# Argonne National Lab., IL.
DEVELOPMENT OF ADVANCED CLOUD PARAMETERIZATIONS TO EXAMINE AIR QUALITY, CLOUD PROPERTIES, AND CLOUD-RADIATION FEEDBACK IN MESOSCALE MODELS
In-Young Lee 1993 7 p Presented at the 5th International Energy Conference, Seoul, Republic of Korea, 18-22 Oct. 1993
(Contract W-31-109-eng-38)
(DE93-041164; ANL/ER/CP-80454; CONF-9310173-2) Avail: CASI HC A02/MF A01

The distribution of atmospheric pollutants is governed by dynamic processes that create the general conditions for transport and mixing, by microphysical processes that control the evolution of aerosol and cloud particles, and by chemical processes that transform chemical species and form aerosols. Pollutants emitted into the air can undergo homogeneous gas reactions to create a suitable environment for the production by heterogeneous nucleation of embryos composed of a few molecules. The physicochemical properties of preexisting aerosols interact with newly produced embryos to evolve by heteromolecular diffusion and coagulation. Hygroscopic particles will serve as effective cloud condensation nuclei (CCN), while hydrophobic particles will serve as effective ice-forming nuclei. Clouds form initially by condensation of water vapor on CCN and evolve in a vapor-liquid-solid system by deposition, sublimation, freezing, melting, coagulation, and breakup. Gases and aerosols that enter the clouds undergo aqueous chemical processes and may acidity hydrometer particles. Calculations for solar and longwave radiation fluxes depend on how the respective spectra are modified by absorbers such as H2O, CO2, O3, CH4, N2O, chlorofluorocarbons, and aerosols. However, the flux calculations are more complicated for cloudy skies, because the cloud optical properties are not well defined. In this paper, key processes such as tropospheric chemistry, cloud microphysics parameterizations, and radiation schemes are reviewed in terms of physicochemical processes occurring, and recommendations are made for the development of advanced modules applicable to mesoscale models. DOE

N94-22569# Oak Ridge National Lab., TN.
ENVIRONMENTAL PROTECTION USING SOCIAL COSTING
R. Lee 1993 4 p Presented at the 1993 Chinese American Academic and Professional Convention, Chicago, IL, 2-5 Jul. 1993
(Contract DE-AC05-84OR-21400)
(DE94-000492; CONF-930796-5) Avail: CASI HC A01/MF A01

Emissions and other residual wastes come from industrial production, commercial and household activities, and transportation. These wastes damage the environment, including human health. As economies grow, so

does concern about balancing that growth with the desire for environmental protection. At issue is how much environmental protection we should have. We address this issue using the concept of social costing. The issue is discussed in the context of electric power generation. There is particular concern about the use of fossil fuels such as petroleum, the major fuel used in the Republic of China, and coal which is the most common fuel used in the U.S. Electric power generation is a major source of airborne pollutants such as SO2, NO(x) particulate matter, volatile organic compounds, CO, and CO2. It also results in liquid and solid wastes, and other effects such as changes in land use. To generate electric power, fuel (such as petroleum, coal or enriched uranium) or some other resource (e.g., wind or geothermal) is needed. A fuel cycle consists of a sequence of activities and processes involved in generating electric power. These activities include the following: fuel extraction, treatment, and processing; fuel conversion into electricity; transmission; waste disposal; and transportation of fuel and wastes between the different stages of the fuel cycle. Each stage results in emissions or other residuals. Several recent studies have been about the environmental costs of electricity. DOE

N94-20698*# Geo Eco Arc Research, La Canada, CA.
GLOBAL BLACKOUT FOLLOWING THE K/T CHICXULUB IMPACT: RESULTS OF IMPACT AND ATMOSPHERIC MODELING Abstract Only
K. O. Pope, A. C. Ocampo (Jet Propulsion Lab., California Inst. of Tech., Pasadena.), K. H. Baines (Jet Propulsion Lab., California Inst. of Tech., Pasadena.), and B. A. Ivanov (Academy of Sciences, USSR, Moscow.) *In* Lunar and Planetary Inst., Twenty-Fourth Lunar and Planetary Science Conference. Part 3: N-Z 1993 p 1165-1166 (For primary document see N94-20636 05-91)
Avail: CASI HC A01/MF A06

N94-22072# Helsinki Univ. of Technology, Espoo (Finland).
AN ECONOMIC ANALYSIS OF TRANSBOUNDARY AIR POLLUTION BETWEEN FINLAND AND THE SOVIET UNION Abstract Only
Veijo Kaitala, Matti Pohjola (Research Inst. of the Finnish Economy, Helsinki.), and Olli Tahvonen (Helsinki School of Economics and Business Administration, Finland.) *In* Technical Research Centre of Finland, Information Technology and Economic Modelling 1992 p 147 (For primary document see N94-22056 05-83)
(ETLA-Discussion-Paper-335) Copyright Avail: CASI HC A01/MF A03

46 GEOPHYSICS

Includes aeronomy; upper and lower atmosphere studies; ionospheric and magnetospheric physics; and geomagnetism.

For space radiation see *93 Space Radiation.*

N94-19820 Colorado School of Mines, Golden. Center for Wave Phenomena.
A KIRCHHOFF APPROACH TO SEISMIC MODELING AND PRESTACK DEPTH MIGRATION
Zhen-Yue Liu May 1993 22 p Limited Reproducibility: More than 20% of this document may be affected by microfiche quality
(Contract N00014-91-J-1267)
(AD-A271010) Avail: CASI HC A03

The Kirchhoff integral provides a robust method for implementing seismic modeling and prestack depth migration, which can handle lateral velocity variation and turning waves. With a little extra computation cost, the Kirchoff-type migration can obtain multiple outputs that have the same phase but different amplitudes, compared with that of other migration methods. The ratio of these amplitudes is helpful in computing some quantities such as reflection angle. I develop a seismic modeling and prestack depth migration method based on the Kirchhoff integral, that handles both laterally variant velocity and a dip beyond 90 degrees. The method uses a finite-difference algorithm to calculate travel times and WKBJ amplitudes for the Kirchhoff integral. Compared to ray-tracing algorithms, the finite-difference algorithm gives an efficient implementation and single-valued quantities (first arrivals) on output. In my finite difference algorithm, the upwind scheme is used to calculate travel times, and the Crank-Nicolson scheme is used to calculate amplitudes. Moreover, interpolation is applied to save computation cost. The modeling and migration algorithms require a smooth velocity function. I develop a velocity-smoothing technique based on damped least-squares to aid in obtaining a successful migration. DTIC

N94-19841 Boston Univ., MA.
CONVERGENCE OF THE HERMITE WAVELET EXPANSION Final Report, 1 Nov. 1988 - 31 Oct. 1992
G. H. Sandri Nov. 1992 38 p Limited Reproducibility: More than 20% of this document may be affected by microfiche quality
(Contract F19628-88-K-0017)
(AD-A271435; PL-TR-92-2325; AD-E201665) Avail: CASI HC A03

In this report we summarize the research carried out under this contract on the chaos dynamics analysis of the free sheared atmosphere. Our approach is to expand the fluid equations into finite energy modes rather than in the conventional Fourier analysis. We prove rigorously that our expansion method has the required convergence properties to ensure a satisfactory physical interpretation of the results. For the Taylor-Dyson atmosphere, our analysis, like the Fourier analysis, yields no unstable modes. DTIC

N94-19860# Surveillance Research Lab., Salisbury (Australia).
A GENERAL PURPOSE IONOSPHERIC RAY TRACING PROCEDURE
C. J. Coleman Aug. 1993 34 p
(AD-A271058; SRL-0131-TR; DODA-AR-008-171) Avail: CASI HC A03/MF A01

A general purpose ionospheric ray tracing procedure is developed. The procedure is based on a numerical solution to the Haselgrove ray tracing equations and includes calculations of ionospherically induced Doppler shift. The procedure can handle a wide variety of ionospheric descriptions and includes the effect of the Earth's magnetic field. DTIC

N94-19899# Pennsylvania State Univ., University Park. Dept. of Meteorology.
REFRACTIVE INDEX STRUCTURE IN THE LOWER ATMOSPHERE Final Report, 1 Jan. 1992 - 30 Jun. 1993
J. Wyngaard and D. Thomson Aug. 1993 34 p
(Contract DAAL03-92-G-0004)
(AD-A270935; ARO-29196.1-GS) Avail: CASI HC A03/MF A01

We develop a local scaling theory for structure-function parameters of refractive index and velocity fluctuations in the stably stratified atmospheric boundary layer. The theory relates them to the local values of vertical temperature flux and shearing stress. The theory agrees well with data from observations and from large-eddy simulations. The effects of flow unsteadiness, baroclinity, terrain slope, and breaking gravity waves are apt to cause vertical profiles of temperature flux and shear stress to vary strongly from case to case, making the profiles quite variable as well, but according to the theory the stress and heat flux profiles can generally be diagnosed from those of the structure parameters. DTIC

N94-19954 Wisconsin Univ., Madison. Dept. of Physics.
COLLISIONAL PROCESSES INVOLVING ATMOSPHERIC GASES Final Report, 1 Aug. 1992 - 31 Jul. 1993
Chun C. Lin 21 Sep. 1993 2 p Limited Reproducibility: More than 20% of this document may be affected by microfiche quality
(Contract F49620-92-J-0376)
(AD-A270729; AFOSR-93-0774TR) Avail: CASI HC A01

Optical emission cross section and excitation function for the D(exp 2)pi(sub g) yields A(exp 2)pi(sub u) bands of N2(+) produced by electron impact on N2 molecules have been measured. Analysis of the results indicates the difference in the production mechanisms for the N2(+)(D(exp 2)pi(sub g)) state as compared to the production mechanisms for the N2(+)(A(exp 2)pi(sub u)) and N2(+)(B(exp 2)sigma(sup +2)(sub u)) states. DTIC

N94-19955# Los Alamos National Lab., NM.
IONOSPHERIC TOMOGRAPHY USING THE FORTE SATELLITE
T. C. Murphy 1993 5 p Presented at the Committee on Space Research Colloquium on the Low-Altitude Ionospheric Physics, Taipei, China, 9-12 Nov. 1993
(Contract W-7405-eng-36)
(DE93-018545; LA-UR-93-2601; CONF-931196-1) Avail: CASI HC A01/MF A01

The possibility of obtaining ionospheric profile data via tomographic techniques has elicited considerable interest in recent years. The input data for the method is a set of total electron content measurements along intersecting lines of sight which form a grid. This can conveniently be provided by a fast-moving satellite with a VHF beacon which will generate the multiple paths needed for effective tomography. Los Alamos and Sandia National Laboratories will launch and operate the FORTE satellite for the U.S. Department of Energy, with launch scheduled in 1995. FORTE will provide such a beacon. Additionally, wideband VHF receivers aboard the satellite will allow corraborative measurements of ionospheric profile parameters in some cases. DOE

N94-20090 Phillips Lab., Hanscom AFB, MA.
PROCEEDINGS OF THE 15TH ANNUAL SEISMIC RESEARCH SYMPOSIUM Final Report
James F. Lewkowicz and Jeanne M. McPhetres 3 Aug. 1993 444 p Symposium held in Vail, CO, 8-10 Sep. 1993 Limited Reproducibility: More than 20% of this document may be affected by microfiche quality
(AF Proj. 2309)
(AD-A271458; AD-E201629; PL-TR-93-2160; ERP-1125) Avail: CASI HC A19

This Symposium represents the combined annual review for the seismic verification research programs. The scientific objectives of the research programs are to improve the Air Force's capability to seismically detect, locate, identify, and estimate the yield of underground nuclear explosions. The purpose of these Symposia is to provide the sponsoring agencies an opportunity to review research, particularly contractor research, accomplished during the preceding year and to outline areas of investigation for the coming year. For the researchers, it provides a forum for the exchange of scientific information to help achieve program goals, and an opportunity to meet PL, AFOSR, and NMRO staff to discuss results and future plans. The papers include studies of the identification and characterization of seismic explosion sources (discrimination), intelligent processing of regional seismic signals, the acquisition and processing of seismic data including data from the Commonwealth of Independent States, regional seismic wave propagation from both an empirical and theoretical viewpoint, yield estimation, and laboratory studies of rock properties appropriate to test sites. DTIC

N94-20132*# Michigan Univ., Ann Arbor. Dept. of Atmospheric, Oceanic, and Space Science.
REMOTE SOUNDING OF TROPOSPHERIC MINOR CONSTITUENTS Final Technical Report, Nov. 1990 - Oct. 1992
S. Roland Drayson, Paul B. Hays, and Jinxue Wang 3 Dec. 1993 49 p
(Grant NAG8-858)
(NASA-CR-194265; NAS 1.26:194265) Avail: CASI HC A03/MF A01

The etalon interferometer, or Fabry-Perot interferometer (FPI), with its high throughput and high spectral resolution was widely used in the remote-sensing measurements of the earth's atmospheric composition, winds, and temperatures. The most recent satellite instruments include the Fabry-Perot interferometer flown on the Dynamics Explorer-2 (DE-2) and the High Resolution Doppler Imager (HRDI) to be flown on the Upper Atmosphere Research Satellite (UARS). These instruments measure the Doppler line profiles of the emission and absorption of certain atmospheric species (such as atomic oxygen) in the visible spectral region. The successful space flight of DE-FPI and the test and delivery of UARS-HRDI demonstrated the extremely high spectral resolution and ruggedness of the etalon system for the remote sensing of earth and planetary atmospheres. Recently, an innovative FPI focal plane detection technique called the Circle-to-Line Interferometer Optical (CLIO) system was invented at the Space Physics Research Laboratory (SPRL). The CLIO simplifies the FPI focal plane detection process by converting the circular rings or fringes into a linear pattern similar to that produced by a conventional spectrometer, while retaining the throughput advantage of the etalon interferometer. CLIO makes the use of linear array detectors more practical and efficient with FPI, the combination of FPI and CLIO represents a very promising new technique for the remote sensing of the lower atmospheres of Earth, Mars, Venus, Neptune, and other planets. The Multiorder Etalon Spectrometer (MOES), as a combination of the rugged etalon and the CLIO, compares very favorably to other spaceborne optical instruments in terms of performance versus complexity. The feasibility of an advanced etalon spectrometer for the remote sensing of tropospheric trace species, particularly carbon monoxide (CO), nitrous oxide (N2O), and methane (CH4) was discussed. The etalon atmospheric spectroscopy techniques are described, instrument design and related technical issues are discussed. The primary objective is to establish the concept of atmospheric spectroscopy with the CLIO and etalon system and its applications for the measurements of tropospheric trace species analyze system requirements and performance, determine the feasibility of components and subsystem implementation with available technology, and develop inversion algorithm for retrieval simulation and data analysis. Author (revised)

N94-20155 Cologne Univ. (Germany). Inst. fuer Geophysik und Meteorologie.
INTERACTIONS OF FREE MODES, TIDES, AND GRAVITY WAVES IN THE MIDDLE ATMOSPHERE [WECHSELWIRKING FREIER MODEN, GEZEITEN UND SCHWEREWELLEN IN DER MITTLEREN ATMOSPHAERE]
Thomas Grollmann 1992 144 p In GERMAN Limited Reproducibility: More than 20% of this document may be affected by microfiche quality
(Contract DFG-Eb-56/9)
(Rept-84; ETN-93-95066) Avail: CASI HC A07

The effects of several wave types on wind and temperature field in mesosphere and lower thermosphere are studied using a global, fully nonlinear three dimensional circulation model of the middle atmosphere (0 to 150 km). Following results are presented: free mode propagation depends more strongly on mean flow with decreasing wave frequency while momentum deposition of normal modes in the mean flow modifies wind and temperature fields; normal modes, through propagation from Winter hemisphere to Summer hemisphere, cause a dynamic coupling of both hemispheres; thermal tides produce a strong easterly wind in the equatorial lower thermosphere by momentum transfer to the zonal mean flow, caused by dissipation of the diurnal tide near the equator; and thermal tides are generally damped by the nonlinear interaction of tides with normal modes which leads to an excitation of secondary waves and is modified if breaking gravity waves are taken into account. ESA

N94-20219# Naval Postgraduate School, Monterey, CA.
SCIENTIFIC DEVELOPMENT OF A MASSIVELY PARALLEL OCEAN CLIMATE MODEL
A. J. Semtner, Jr. and R. M. Chervin (National Center for Atmospheric Research, Boulder, CO.) May 1993 6 p
(Contract DE-AI05-91ER-61224)
(DE93-019446; DOE/ER-61224/2) Avail: CASI HC A02/MF A01

During the second year of CHAMMP funding to the principal investigators, progress has been made in the proposed areas of research, as follows: investigation of the physics of the thermohaline circulation; examination of resolution effects on ocean general circulation; and development of a massively parallel ocean climate model. DOE

N94-20220# Argonne National Lab., IL.
TROPOSPHERIC CHEMISTRY OF NATURAL HYDROCARBONS, ALDEHYDES, AND PEROXY RADICALS: THEIR CONNECTIONS TO SULFURIC ACID PRODUCTION AND CLIMATE EFFECTS
J. S. Gaffney and N. A. Marley May 1993 7 p Presented at the 28th Intersociety Energy Conversion Engineering Conference, Atlanta, GA, 8-13 Aug. 1993
(Contract W-31-109-eng-38)
(DE93-019525; ANL/ER/CP-78472; CONF-930804-16) Avail: CASI HC A02/MF A01

Recent work has shown that natural hydrocarbon emissions can significantly affect the levels of urban and regional tropospheric ozone. We report on the reactivities of these biogenic trace gases, particularly, isoprene, focusing on their importance in the production of aldehydes and peroxy radicals, leading to increased levels of hydrogen over regional forests. Hydrogen peroxide can lead to the wet oxidation of sulfur dioxide to acidic sulfate in aerosols, fogs, and clouds. In turn, acidic sulfate can act as a light scattering aerosol and a source of cloud condensation nuclei (CCN), potentially leading to global cooling. Aerosol sulfate and other dissolved organic and inorganic compounds can also play important roles as a greenhouse species in the lower troposphere. DOE

N94-20256 Commonwealth Scientific and Industrial Research Organization, Sydney (Australia). Div. of Atmospheric Research.
THE CSIRO 9-LEVEL ATMOSPHERIC GENERAL CIRCULATION MODEL

J. L. McGregor, H. B. Gordon, I. G. Watterson, M. R. Dix, and L. D. Rotstayn 1993 93 p
(CSIRO-TP-26; ISBN-0-643-05250-X) Copyright Avail: Issuing Activity

Numerical models of the general circulation of the atmosphere are an important tool in climate research. They have been used to investigate the dynamical and physical processes controlling the atmosphere. The incorporation of representations of the cryosphere and oceans into such a model allows it to be used for forecasting climate anomalies and climate change. The spectral 9-level Atmospheric General Circulation Model (AGCM) described was developed at the CSIRO Division of Atmospheric Research to provide the basis for the current greenhouse research project and for future research. The spectral method for modeling the general circulation of the atmosphere is now firmly established and was adopted at several major research centers including the National Center for Atmospheric Research (NCAR), the European Centre for Medium-range Weather Forecasting (ECMWF), and the Canadian Climate Center. It provides a cost effective means of atmospheric modeling which is essential for climate research. The version of the CSIRO9 model described was used to generate the implied ocean heat transports required to enable computation of sea temperatures by a slab ocean model rather than using prescribed temperatures. The inclusion of this simple 'mixed-layer' ocean into the model allows the lower boundary condition involving the land surfaces, the polar ice caps, and now the oceans to be self-determining. This form of the CSIRO9 model is currently being used for greenhouse research and will be documented elsewhere. This publication documents the formulation of CSIRO9 and is intended as a general guide to its contents and formulation. It does not give details of the model's computer coding as would be required by users wishing to modify the model. The description of the dynamical framework of the model was kept to a minimum since standard spectral techniques were used. On the other hand, the physical processes are comprehensively covered. Derived from text

N94-20362*# Massachusetts Inst. of Tech., Cambridge. Research Lab. of Electronics.
ATMOSPHERIC INFRARED SOUNDER Progress Report, 15 Jun. - 15 Dec. 1993
Philip W. Rosenkranz and David H. Staelin 29 Dec. 1993 11 p
(Contract NAS5-31376)
(NASA-CR-194814; NAS 1.26:194814) Avail: CASI HC A03/MF A01

Work continued on analysis of data from the TOGA-COARE experiment. The MIT Microwave Temperature Sounder was flown on NASA's ER-2 at Wallops Island in the CAMEX experiment during September and October. The preliminary version of the 'microwave first-guess' algorithm for temperature and moisture was delivered to JPL. In the iterative minimum-variance algorithm moisture retrievals from MHS make use of the retrieved temperature profile in calculation of weighting functions and in determining the saturation moisture capacity at each level. Simulations have been run to address the question of how important the temperature profile accuracy is to the moisture retrieval. Derived from text

N94-20485 Air Force Inst. of Tech., Wright-Patterson AFB, OH.
MODELING THE MINIMUM ENERGY STATE OF THE EARTH'S MAGNETOTAIL M.S. Thesis
Markus S. Sorrells Jun. 1993 140 p Limited Reproducibility: More than 20% of this document may be affected by microfiche quality
(AD-A267984; AFIT/CI/CIA-93-123) Avail: CASI HC A07

For a system that remains in thermodynamic equilibrium, stable equilibria are determined by minimizing an appropriate potential energy function such as the Gibb's free energy. However, when a system does not remain in thermodynamic equilibrium, one cannot use a potential function to derive a state of stable equilibrium. If we assume this is the case for the earth's magnetotail, then we must come up with another method to determine stable equilibrium. We conjecture that this will be a minimum total energy. By combining Poynting's theorem with the Lorentz force equation and Maxwell's equations, one can account for the energy advections into and out of a system containing a fully ionized plasma, as well as for the energy fluctuations caused by changing electric and magnetic fields. By minimizing the total energy equation representing an idealized model of the earth's magnetotail, one should be able to calculate its stable equilibrium state. Although the idealized minimum energy model presented in this paper depicts many trends observed in the earth's magnetotail, this thesis concludes that more modifications are needed before it becomes a useful tool for analyzing the earth's magnetotail. Author (revised)

N94-20537*# SRI International Corp., Menlo Park, CA. Geoscience and Engineering Center.
MODELING OF THE COUPLED MAGNETOSPHERIC AND NEUTRAL WIND DYNAMOS Semiannual Technical Status Report No. 1, 1 Apr. - 31 Oct. 1993
Jeff P. Thayer 15 Dec. 1993 10 p
(Grant NAGw-3508; SRI Proj. 4604)
(NASA-CR-194728; NAS 1.26:194728) Avail: CASI HC A02/MF A01

The solar wind interaction with the earth's magnetosphere generates electric fields and currents that flow from the magnetosphere to the ionosphere at high latitudes. Consequently, the neutral atmosphere is subject to the dissipation and conversion of this electrical energy to thermal and mechanical energy through Joule heating and Lorentz forcing. As a result of the mechanical energy stored within the neutral wind (caused in part by Lorentz--and pressure gradient--forces set up by the magnetospheric flux of electrical energy), electric currents and fields can be generated in the ionosphere through the neutral wind dynamo mechanism. At high latitudes this source of electrical energy has been largely ignored in past studies, owing to the assumed dominance of the solar wind/magnetospheric dynamo as an electrical energy source to the ionosphere. However, other researchers have demonstrated that the available electrical energy provided by the neutral wind is significant at high latitudes, particularly in the midnight sector of the polar cap and in the region of the magnetospheric convection reversal. As a result, the conclusions of a number of broad ranging high-latitude investigations may be modified if the neutral-wind contribution to high-latitude electrodynamics is properly accounted for. These include the following: studies assessing solar wind-magnetospheric coupling by comparing the cross polar cap potential with solar wind parameters; research based on the alignment of particle precipitation with convection or field aligned current boundaries; and synoptic investigations attributing seasonal variations in the observed electric field and current patterns to external sources. These research topics have been initiated by satellite and ground-based observations and have been attributed to magnetospheric causes. However, the contribution of the neutral wind to the high-latitude electric field and current systems and their seasonal and local time dependence has yet to be quantitatively evaluated. In this program, we are evaluating the coupled magnetospheric and neutral wind dynamos at high latitudes under various conditions. In addition to examining the impact of seasonal variations, we are investigating the consequences of the separate dynamos having pure current-source or voltage-source behaviors.
Author (revised)

N94-20607 Danish Meteorological Inst., Copenhagen. Solar-Terrestrial Physics Div.
NARSARSUAQ GEOPHYSICAL OBSERVATORY: MAGNETIC RESULTS, 1985 - 1990
1993 93 p
(Data-Rept-93-1; ETN-94-94965) Avail: Issuing Activity (Danish Meteorological Institute, Lyngbyvej 100, DK-2100 Copenhagen, Denmark)

The results of the geomagnetic measurements carried out at the Narsarsuaq (Greenland) Geophysical Observatory during the years 1985 to 1990 are presented. This observatory forms part of the Danish Meteorological Institutes magnetometer chains. The report is in two sections. Coordinates for the observatory are given and the instrumentation and methods of data reduction and distribution are described. Tables of monthly and annual mean values and plots of the secular variation for the different magnetic elements are presented. ESA

N94-20608 Danish Meteorological Inst., Copenhagen. Solar-Terrestrial Physics Div.
MAGNETIC RESULTS 1991: BRORFELDE, GODHAVN, THULE AND NARSARSUAQ Annual Report
1992 86 p
(Data-Rept-92-3; ETN-94-94966) Avail: Issuing Activity (Danish Meteorological Institute, Lyngbyvej 100, DK-2100 Copenhagen, Denmark)

Results of the geomagnetic measurements carried out at the four permanent observatories operated by the Danish Meteorological Institute, namely Brorfelde (Denmark) and Godhavn, Thule and Narsarsuaq (Greenland) are presented. The instrumentation and methods of data

reduction and distribution used for all four observatories are described. Relevant information for each individual observatory, such as observatory description, diary, tables and plots of adopted baseline values, and tables of monthly and annual mean values is given. Isomagnetic charts for Denmark and Greenland are shown. Topics relevant for the yearbook are presented in the appendix. ESA

N94-20609 Danish Meteorological Inst., Copenhagen. Solar-Terrestrial Physics Div.
THULE GEOPHYSICAL OBSERVATORY: MAGNETIC RESULTS 1985 - 1990
1992 98 p
(Data-Rept-92-4; ETN-94-94967) Avail: Issuing Activity (Danish Meteorological Institute, Lyngbyvej 100, DK-2100 Copenhagen, Denmark)

The results of the geomagnetic measurements carried out at the Thule (Greenland) Geophysical Observatory during the years 1985 to 1990 are presented. This observatory forms part of the Danish Meteorological Institute's magnetometer chains. The report is in two sections. Coordinates for the observatory are given and the instrumentation and methods of data reduction and distribution are described. Tables of monthly and annual mean values and plots of the secular variation for the different magnetic elements are presented. ESA

N94-21016 Beleidscommissie Remote Sensing, Delft (Netherlands).
MOBILITY OF SALT DOMES [MOBILITEIT VAN ZOUTKOEPELS]
J. H. A. Bosch (Rijks Geologische Dienst, Haarlem, Netherlands.) Aug. 1992 12 p In DUTCH Limited Reproducibility: More than 20% of this document may be affected by microfiche quality
(BCRS-92-08; ISBN-9-05-411046-5; ETN-93-93316) Avail: CASI HC A03

The mobility of salt domes in the northeast Netherlands was studied using LANDSAT Thematic Mapper and SPOT satellite pictures with a view to the underground storage of chemical and radioactive wastes. The detection of salt diapirism is important because it affects the water budget around a salt dome and hence the stability of the dome. However, the satellite picture did not allow determination of recent tectonic motion of the salt domes. In areas not overgrown with vegetation, several types of soil were identified which illustrate the recent geological history of these areas. ESA

N94-21044 GKSS-Forschungszentrum Geesthacht (Germany). Inst. fuer Physik.
EXAMINATIONS OF A THALLIUM ATOMIC VAPOR FILTER FOR A RAMAN TEMPERATURE LIDAR Thesis - Hamburg Univ. [UNTERSUCHUNGEN ZU EINEM THALLIUM-ATOMDAMPFFILTER FUER EIN RAMAN-TEMPERATUR-LIDAR]
D. Heimrath 24 Jan. 1992 84 p In GERMAN Limited Reproducibility: More than 20% of this document may be affected by microfiche quality
(GKSS-92/E/13; ETN-93-94184) Copyright Avail: CASI HC A05

In the remote measurement of tropospheric temperature with a rotational Raman lidar a perturbation of the Raman signal by elastic backscattering from molecules and aerosols occurs. This background is hard to suppress with conventional means such as gratings and filters because of the small spectral separation from the rotational Raman signal. An atomic vapor filter is a promising candidate for suppressing this background. It is obvious that this scheme can only be used if the lidar output wavelength coincides with the wavelength of a suitable atomic transition. The development and testing of narrow band filters made of atomic thallium vapor with and without the addition of argon is described. An application of a thallium atomic vapor filter may be the GKSS lidar project ATLAS (Advanced Temperature and humidity Lidar for Atmospheric Studies) with an output wavelength of 276.787 nanometer. A procedure for the preparation of thallium absorption cells made of fused silica is presented. Transmission spectra of two thallium filters, measured with a frequency doubled dye laser, show that the filter properties required for ATLAS are met by a thallium atomic vapor filter without argon. The addition of argon results in an undesired attenuation of the rotational Raman signal at high thallium temperatures. ESA

N94-21149 Bonn Univ. (Germany). Inst. fuer Physik.
MEASUREMENT OF MESOSPHERIC TURBULENCE IN THE FRAMEWORK OF THE METAL CAMPAIGN AND DEVELOPMENT OF A SENSOR FOR STATIC PRESSURE FREE MEASUREMENTS OF NEUTRAL AND ELECTRON DENSITY Thesis [MESSUNG MESOSPHAERISCHER TURBULENZ IM RAHMEN DER METAL-KAMPAGNE UND ENTWICKLUNG EINES SENSOREN ZUR STAUDRUCKFREIEN MESSUNG VON NEUTRAL- UND ELEKTRONENDICHTE]
Frank Foehner Nov. 1992 71 p In GERMAN Limited Reproducibility: More than 20% of this document may be affected by microfiche quality
(BONN-IR-92-45; ETN-93-93811) Avail: CASI HC A04

Six rocket borne ionization gages launched during the METAL campaign were employed to deduce profiles of turbulent energy dissipation rate (epsilon) in the polar mesosphere in Sep. and Oct. 1991. Very small activity of turbulence was found. The influence of epsilon on the energy budget of the polar mesosphere in Autumn is shown to be small in comparison to other heating and cooling effects. After METAL, a new gage for simultaneous measurements of electron and neutral densities was developed in order to improve the overall time constant of the instrument. The operational parameters of this instrument were optimized in the laboratory using vacuum facilities of the plasma chamber. The instrument allows spatial high resolution measurements of temperature and density with a strongly reduced time constant and its stability was proved by vibration tests in view of an implementation on a research rocket. ESA

N94-21189# Boston Univ., MA. Center for Space Physics.
THE EFFECTS OF MAGNETIC STORM PHASES ON F-LAYER IRREGULARITIES FROM AURORAL TO EQUATORIAL LATITUDES Quarterly Report, 1 Jul. - 30 Sep. 1993
Jules Aarons and Michael Mendillo 30 Sep. 1993 4 p
(Contract N00014-89-J-1754)
(AD-A272685) Avail: CASI HC A01/MF A01

Although the general pattern of equatorial F-layer irregularities as a function of latitude, longitude, and geophysical conditions is in hand, the day to day variations are still difficult to evaluate. The forcing functions for day to day variations appear to be neutral winds and electric field conditions. The data indicate that at times in 'the irregularity season', irregularities are produced day after day. However nights of irregularities are at other times followed by one or more nights with an absence of irregularities. For the equatorial region, using scintillation data at 136 MHz, we have correlated the occurrence of irregularities at several stations along a relatively narrow range of longitudes at various latitudes in the Pacific sector. The sites used are in the Philippines, Taiwan, and Korea. The correlation of daily occurrence was poor. For example at magnetically quiet times there are irregularities noted at a station such as Osan, Korea (dip latitude 30 deg) with little irregularity activity at Manila (dip latitude 5 deg), relatively close in longitude. For latitudes somewhat higher than the anomaly region, the problem arises of separating polewards effects of the equatorial plumes and the equatorwards motion of irregularity development originating in the auroral region during severe magnetic storms. A possibility exists for the generation of another class of F-layer irregularities at mid-latitudes with a body of data from Japan, Port Moresby, Osan, and Palehua, Hawaii. This is suggestive that at least in the Pacific region there is a low latitude generation of irregularities distinct from equatorial or auroral mechanisms. DTIC

N94-21202 Naval Postgraduate School, Monterey, CA.
IONOSPHERIC PHOTOELECTRONS MEASURED AT GEOSYNCHRONOUS ORBIT M.S. Thesis
John S. Laszakovits Jun. 1993 173 p Limited Reproducibility: More than 20% of this document may be affected by microfiche quality
(AD-A272431) Avail: Issuing Activity (Defense Technical Information Center (DTIC))

Measurements of ions and electrons were made by the Los Alamos National Laboratory instrument, the Magnetospheric Plasma Analyzer, onboard spacecraft 1989-046. Observations from five days indicated the presence of both field aligned electrons and equatorially trapped electrons. Correlation existed between occurrences and location in the magnetosphere. Field aligned electrons were measured in the plasmasphere during daylight. On two days, field aligned electrons were also noted in the midnight region of the magnetosphere. Field aligned electrons at energies between

1 and 50 eV were characterized. These electron's spectrum were shown to be similar in shape to the ionospheric photoelectron distribution. Conic distributions of photoelectrons were observed between 08:00 and 10:00 local time on days when both photoelectrons and equatorially trapped electrons were present. V(sub parallel) versus V(sub perpendicular) spectrograms clearly indicated that photoelectrons undergo perpendicular acceleration. Lack of any magnetic field measurements or collection of wave data prevented determining the source of the acceleration. DTIC

N94-21206 California Univ., Santa Cruz. Inst. of Tectonics.
ANALYSIS OF THE EFFECTS OF EURASIAN CRUSTAL AND UPPER MANTEL STRUCTURE ON REGIONAL PHASES USING BROADBAND SEISMIC DATA Final Report, Jul. 1990 - Mar. 1993
Jos Beckers, Susan Schwartz, and Thorne Lay 8 Jun. 1993 108 p Limited Reproducibility: More than 20% of this document may be affected by microfiche quality
(Contract F19628-90-K-0041)
(AD-A272446; PL-TR-93-2131) Avail: Issuing Activity (Defense Technical Information Center (DTIC))

The results of the second phase of a two-year effort to investigate the effects of upper mantle structure on the propagation of regional phases are presented. The first year investigation was directed at improving our understanding of the behavior of the PP phase at upper mantle distances, and developing methods to map large-scale variations in uppermost mantle velocity structure. During the second year investigation, the techniques developed to a dataset of 45 PP waveforms for paths traversing China were successfully applied. A first order P wave velocity model for the crust and upper mantle under China, which best explains the overall dataset, was determined. Next, the data was investigated on a path-by-path basis to constrain lateral deviations from this average model and to map large-scale variations in absolute velocities and velocity gradients in the uppermost mantle under China. Our final effort was directed at exploring the effect of our regionalized velocity models, on the propagation of the P(sub n) and L(sub g) regional phases to assess how variations in the velocity structure under China influence P(sub n)/L(sub g) ratios for earthquakes and explosion sources. DTIC

N94-21207# Institute for Defense Analyses, Alexandria, VA.
STANDARD ATMOSPHERES FOR ENGAGEMENT MODELING Final Report, Dec. 1991 - Nov. 1992
Ernest Bauer Jun. 1993 69 p
(Contract MDA903-89-C-0003)
(AD-A272447; IDA-D-1197; IDA/HQ-92-42146) Avail: CASI HC A04/MF A01

The use of model atmospheres for Ballistic Missile Defense (BMD) engagement modeling is reviewed. BMD engagement models simulate a ballistic missile attack from launch to interception. Model atmospheres are descriptions of atmospheric density and temperature as functions of altitude. However, BMD applications are not consistent in the choice of model atmosphere within a system application and, in fact, may employ more than one model atmosphere within an engagement model. The most widely used model atmospheres are the US-62 and US-76 models. These two differ significantly in the variable of solar activity. Thus, if engagement models run using both the US-62 and US-76 model atmospheres give the same result, the effect of the model atmosphere can probably be ruled out. It is recommended that to measure the effects of atmospheric variability on a particular BMD application, engagement models be run using both the US-62 and US-76 model atmospheres. If the results differ, more detailed examination of the physics of the atmosphere for the problem under consideration may be called for. DTIC

N94-21357# Naval Research Lab., Washington, DC.
MODELS OF REFRACTION IN THE MARINE ATMOSPHERE SURFACE LAYER
John S. Hornstein, Richard G. Priest, Edward H. Takken, and David Baukman 30 Sep. 1993 83 p
(NR Proj. RA1-1-M-16)
(AD-A271724; NRL/FR/7227-93-9547) Avail: CASI HC A05/MF A01

Models of near-surface refraction are compared with one another and are used to survey effects relevant to the design and use of optical and infrared sensors. DTIC

N94-21432# Naval Postgraduate School, Monterey, CA.
DETAILED ANALYSIS CASE STUDIES OF TRAPPED PLASMAS AT THE EARTH'S MAGNETIC EQUATOR M.S. Thesis
Eric S. Lantto Jun. 1993 154 p
(AD-A272497) Avail: CASI HC A08/MF A02

A previous statistical survey of data from the HPCE experiment on the AMPTE/CCE satellite established probability distributions for trapped ions and electrons. An extension of this survey for ions at 240 and 442 eV and for electrons at 340 and 770 eV confirmed these distributions. A further detailed analysis of the electron data from 13 individual data collection days also showed the trapped electron distribution to be concentrated in the dawn to noon region, centered at L=7. These trapped electron distributions can be described as a bi-Maxwellian distribution function and be characterized reasonably by the criteria that the flux has to exceed 5 x 10(exp 6) (sq cm s sr)(sup -1), the distribution has to be within 10 deg. of the magnetic equator, the ratio of the perpendicular temperature to the parallel temperature exceeds 3.0 and that the anisotropy exceeds 2.0 for 150 eV electrons and 4.4 for 340 eV electrons. DTIC

N94-21811*# Kansas Univ., Lawrence. Dept. of Electrical Engineering and Computer Science.
LOW-POWER MILLIMETER-WAVE RADAR OBSERVATIONS OF THE ATMOSPHERE Final Report
James F. Ronnau and S. Prasad Gogineni Dec. 1993 13 p Original contains color illustrations
(Grants NGT-50628; NSF ATM-89-22630)
(NASA-CR-194738; NAS 1.26:194738; RSL-TR-8750-1; RSL-TR-8920-1)
Avail: CASI HC A03/MF A01; 3 functional color pages

Historically, cloud structures, dynamics, and precipitation processes have been observed and measured with sensors from two different spatial resolutions. Laser-based sensors have volume resolutions on the order of 10(exp -4) to 10(exp -2) cubic meters for a 1-s sample. Radar systems operating at wavelengths between 1 and 10 cm have resolutions on the order of 10(exp 4) to 10(exp 7) cubic meters. The resolutions of micro-wave systems depend primarily on the system RF bandwidth and antenna bandwidth. Both resolution regimes were useful in the study of cloud structures and processes - the former for determining resolution on the individual cloud particle scale and the latter for studying the coarse characteristics of cloud dynamics and structure. There are, however, cloud processes and structures that occur on scales that lie between these two regimes: the process of entrainment, where outside air is brought within the cloud boundaries; the mixing of in-cloud particles with different histories; cloud particle coalescence; and ice formation. The use of mm-wave (30- to 300-GHz) radars offers an opportunity to observe cloud processes at these scales and determine their influence on precipitation development, cloud albedos, cloud lifetimes, chemical cycling of tract substances, aircraft icing, and other meteorological phenomena. To determine the usefulness of a 35-GHz radar for observing these precipitation and cloud processes, a research program was initiated. The objectives of this program are to develop a 35-GHz radar, to measure scattering from precipitation and clouds, and to develop a model to compute scattering from clouds using the finite-difference time-domain (FDTD) technique. Author (revised)

N94-21836*# Iowa Univ., Iowa City.
PHYSICS OF MAGNETOSPHERIC BOUNDARY LAYERS Semiannual Progress Report No. 1, 1 Jun. - 30 Nov. 1993
I. H. Cairns 20 Dec. 1993 6 p
(Grant NAGw-1483)
(NASA-CR-194725; NAS 1.26:194725) Avail: CASI HC A02/MF A01

The central ideas of this grant are that the magnetospheric boundary layers link disparate regions of the magnetosphere together, and the global behavior of the magnetosphere can be understood only by understanding the linking mechanisms. Accordingly the present grant includes simultaneous research on the global, meso-, and micro-scale physics of the magnetosphere and its boundary layers. These boundary layers include the bow shock, magnetosheath, the plasma sheet boundary layer, and the ionosphere. Analytic, numerical and simulation projects have been performed on these subjects, as well as comparison of theoretical results with observational data. Very good progress has been made, with four papers published or in press and two additional papers submitted for publication during the six month period 1 June - 30 November 1993. At least two projects are currently being written up. In addition, members of the group have given

papers at scientific meetings. The further structure of this report is as follows: section two contains brief accounts of research completed during the last six months, while section three describes the research projects intended for the grant's final period. Derived from text

N94-21928# California Univ., Berkeley. Lawrence Berkeley Lab.
ITERATIVE ELECTROMAGNETIC BORN INVERSION APPLIED TO EARTH CONDUCTIVITY IMAGING Ph.D. Thesis
D. L. Alumbaugh Aug. 1993 300 p
(Contract DE-AC03-76SF-00098)
(DE93-040668; LBL-34553) Avail: CASI HC A13/MF A03

This thesis investigates the use of a fast imaging technique to deduce the spatial conductivity distribution in the earth from low frequency (less than 1 MHz), cross well electromagnetic (EM) measurements. The theory embodied in this work is the extension of previous strategies and is based on the Born series approximation to solve both the forward and inverse problem. Nonlinear integral equations are employed to derive the series expansion which accounts for the scattered magnetic fields that are generated by inhomogeneities embedded in either a homogenous or a layered earth. A sinusoidally oscillating, vertically oriented magnetic dipole is employed as a source, and it is assumed that the scattering bodies are azimuthally symmetric about the source dipole axis. The use of this model geometry reduces the 3-D vector problem to a more manageable 2-D scalar form. The validity of the cross well EM method is tested by applying the imaging scheme to two sets of field data. Images of the data collected at the Devine, Texas test site show excellent correlation with the well logs. Unfortunately there is a drift error present in the data that limits the accuracy of the results. A more complete set of data collected at the Richmond field station in Richmond, California demonstrates that cross well EM can be successfully employed to monitor the position of an injected mass of salt water. Both the data and the resulting images clearly indicate the plume migrates toward the north-northwest. The plausibility of these conclusions is verified by applying the imaging code to synthetic data generated by a 3-D sheet model. DOE

N94-22006# Oak Ridge National Lab., TN.
POST-PALBOZOIC CRUSTAL RESPONSES TO THE CONTEMPORARY STRESS FIELD IN THE EASTERN UNITED STATES
W. P. Staub and H. K. Hardee Aug. 1993 7 p Presented at the 4th Energy Natural Phenomena Hazards Mitigation Conference, Atlanta, GA, 19-22 Oct. 1993
(Contract DE-AC05-84OR-21400)
(DE93-040604; CONF-9310102-17) Avail: CASI HC A02/MF A01

This paper summarizes the current state of knowledge with respect to post-Paleozoic tectonic features and their relationship to the contemporary stress field outside coastal plain regions of the eastern United States. Until the early 1970s, very little was known about such features. By the end of 1992 post-Paleozoic faults had been observed in at least five widely separated regions. Pleistocene-Holocene surface ruptures and liquefaction features had been observed over a steadily increasing area of the upper Mississippi embayment and adjacent regions. Ages of most recent ruptures on post-Paleozoic faults range from uncertain to Holocene and their senses of motion are compatible with the contemporary stress field. The cumulative amount of post-Paleozoic displacement on these faults is generally less than three meters. Fracture systems in Paleozoic rocks also are compatible with the contemporary stress field over a wide region of Indiana. DOE

N94-22018# National Academy of Sciences - National Research Council, Washington, DC.
THE BOARD ON EARTH SCIENCES AND RESOURCES
1993 16 p
(Contract DE-FG05-89ER-14061)
(DE94-000745; DOE/ER-14061/2) Avail: CASI HC A03/MF A01

During the past year, working groups of the committee have reviewed and reported on the status of regional networks, and wrote a report on the real-time warning of earthquakes. The field of seismology is going through revolutionary changes with new measurement capabilities, new analytical capabilities, and new understanding of earthquake processes at hand are still evolving. Earthquake 'gaps' are recognized as diagnostic elements for focusing on future large earthquakes; regional and national networks are under intense study, and future directions for them are emerging; and large scientific projects are under way in seismology which will bring new insights into earth structure, wave propagation, and earthquake processes. Ground motions and recurrence rates of earthquakes are major factors in the assessment of earthquake hazards, and improvements in both factors are badly needed. The Committee on Seismology will continue to review progress and needs for research on strong ground motions. DOE

N94-22026*# Michigan Univ., Ann Arbor. Dept. of Atmospheric, Oceanic, and Space Science.
MULTIORDER ETALON SOUNDER (MOES) DEVELOPMENT AND TEST FOR BALLOON EXPERIMENT Final Technical Report, 10 Jun. 1992 - 31 Dec. 1993
Paul B. Hays, Jinxue Wnag, and Jian Wu 14 Dec. 1993 38 p Original contains color illustrations
(Grant NAG8-919)
(NASA-CR-194730; NAS 1.26:194730) Avail: CASI HC A03/MF A01; 3 functional color pagaes

The Fabry-Perot interferometer (FPI), with its high throughput and high spectral resolution has been used in the remote-sensing measurements of the earth's atmospheric composition, winds, and temperatures. The most recent satellite instruments include the Fabry-Perot interferometer flown on the Dynamics Explorer-2 (DE-2), the High Resolution Doppler Imager (HRDI), and the Cryogenic Limb Array Etalon Spectrometer (CLAES) flown on the Upper Atmosphere Research Satellite (UARS). These instruments measure the Doppler line profiles of the emission and absorption of certain atmospheric species (such as atomic oxygen) in the visible and infrared spectral region. The successful space flight of DE-FPI, HRDI, and CLAES on UARS demonstrated the extremely high spectral resolution and ruggedness of the etalon system for the remote sensing of earth and planetary atmospheres. Recently, an innovative FPI focal plane detection technique called the Circle-to-Line Interferometer Optical (CLIO) system was invented at the Space Physics Research Laboratory. The CLIO simplifies the FPI focal plane detection process by converting the circular rings or fringes into a linear pattern similar to that produced by a conventional spectrometer, while retaining the throughput advantage of the etalon interferometer. The combination of FPI and CLIO allows the development of more sensitive Fabry-Perot interferometers in the infrared for the remote sensing of the lower atmospheres of Earth and possibly other planets. The Multiorder Etalon Sounder (MOES), a combination of the rugged etalon and the CLIO, compares very favorably to other space-borne optical instruments in terms of performance versus complexity. The new instrument is expected to be rugged, compact, and very suitable for an operational temperature and moisture sounder. With this technique, the contamination of radiance measurements by emissions of other gases is also minimized. At the Space Physics Research Laboratory (SPRL), the MOES concept and laboratory experiments were worked on for the past several years. Both theoretical studies and laboratory prototype experiments showed that MOES is very competitive compared with other high resolution sounders in terms of complexity and performance and has great potential as a compact and rugged high resolution atmospheric temperature and trace species sounder from the polar platform or the geostationary platform. The logical next step is to convert our laboratory prototype to a balloon instrument, so that field test of MOES can be carried out to prove the feasibility and capability of this new technology. Some of the activities related to the development of MOES for a possible balloon flight demonstration are described. Those research activities include the imaging quality study on the CLIO, the design and construction of a MOES laboratory prototype, the test and calibration of the MOES prototype, and the design of the balloon flight gondola. Author (revised)

N94-22036# Argonne National Lab., IL.
AREALLY AVERAGED ESTIMATES OF SURFACE HEAT FLUX FROM ARM FIELD STUDIES
R. L. Coulter, T. J. Martin, and D. R. Cook 1993 9 p Presented at the 3rd ARM Science Team Meeting, Norman, OK, 1-5 Mar. 1993
(Contract W-31-109-eng-38)
(DE93-018569; ANL/ER/CP-79787; CONF-9303122-6) Avail: CASI HC A02/MF A01

The determination of areally averaged surface fluxes is a problem of fundamental interest to the Atmospheric Radiation Measurement (ARM) program. The Cloud And Radiation Testbed (CART) sites central to the

ARM program will provide high-quality data for input to and verification of General Circulation Models (GCM's). The extension of several point measurements of surface fluxes within the heterogeneous CART sites to an accurate representation of the areally averaged surface fluxes is not straightforward. Two field studies designed to investigate these problems, implemented by ARM science team members, took place near Boardman, Oregon, during June of 1991 and 1992. The site was chosen to provide strong contrasts in surface moisture while minimizing the differences in topography. The region consists of a substantial dry steppe (desert) upwind of an extensive area of heavily irrigated farm land, 15 km in width and divided into 800-m-diameter circular fields in a close packed array, in which wheat, alfalfa, corn, or potatoes were grown. This region provides marked contrasts, not only on the scale of farm-desert (10-20 km) but also within the farm (0.1-1 km), because different crops transpire at different rates, and the pivoting irrigation arms provide an ever-changing pattern of heavy surface moisture throughout the farm area. This paper primarily discusses results from the 1992 field study. DOE

N94-22283# Max-Planck-Inst. fuer Meteorologie, Hamburg (Germany).
PROCEEDINGS OF THE WORKSHOP ON NEW GENERATION OF RADIATION BUDGET MEASUREMENTS FROM SPACE AND THEIR USE IN CLIMATE MODELLING AND DIAGNOSTIC STUDIES
L. Duemenil, ed. and E. Raschke, ed. (GKSS-Forschungszentrum Geesthacht, Germany.) Sep. 1992 34 p Workshop held in Hamburg, Germany, 11 Jun. 1992 Original contains color illustrations
(MPIM-90; ETN-94-93802) Avail: CASI HC A03/MF A01

Abstracts of papers presented at this workshop, whose aim was to bring together the research teams that are involved in the provision of satellite data from the ScaRaB (Scanner for Radiation Budget) project and potential users of these data in the climate modeling community, are presented. A continuation of spaceborne measurements of the planetary radiation budget is required in order to investigate the role of clouds and radiation within the climate system. Highly accurate measurements provided by the American ERBE (Earth Radiation Budget Experiment, 1984-1987) have proven to be excellent tools for the validation of climate model simulations. Experience gained with this data set is reported. It is proposed to employ a new radiation budget instrument, Scarab, to continue the monitoring of the required quantities from 1993 onwards. For individual titles, see N94-22284 through N94-22291.

N94-22284# GKSS-Forschungszentrum Geesthacht (Germany). Inst. fuer Physik.
SATELLITE MEASUREMENTS OF RADIATION BUDGET PARAMETERS
E. Raschke *In* Max-Planck-Inst. fuer Meteorologie, Proceedings of the Workshop on New Generation of Radiation Budget Measurements From Space and Their Use in Climate Modelling and Diagnostic Studies Sep. 1992 p 3-6 (For primary document see N94-22283 05-46)
Avail: CASI HC A01/MF A01

The uses of the Scarab (Scanner for Radiation Budget, to be launched on the Soviet Meteor 3 satellite) data outside the diagnostics of the Earth's radiation budget and its temporal changes, for example to inspect possible variation and trends in the Earth's climate system, are considered. Historical remarks about means of measurement and analyses of the Earth's radiative energy exchange with space are given and sampling problems are considered. The need for further measurements of the planetary radiation budget with Scarab, despite the fact that basic spectral data sets collected within the ISCCP (International Satellite Cloud Climatology Project) are available, is explained. A summary of the relative partition of energy fluxes in the climate system, when the Sun is the only source, is given. ESA

N94-22285# GKSS-Forschungszentrum Geesthacht (Germany).
ScaRaB AND ITS SUBSYSTEMS
Johannes Mueller *In* Max-Planck-Inst. fuer Meteorologie, Proceedings of the Workshop on New Generation of Radiation Budget Measurements From Space and Their Use in Climate Modelling and Diagnostic Studies Sep. 1992 p 7-12 (For primary document see N94-22283 05-46)
Avail: CASI HC A02/MF A01

The technical aspects of the ScaRaB (Scanner for Radiation Budget) radiometer to be launched on the Soviet Meteor 3 satellite are described. The instrument measures the radiance at the top of atmosphere in four channels (visible, solar, total, atmospheric window). The resolution is 48 by 48 mrad. Lamps and blackbodies are used for onboard calibration. These sources are calibrated themselves on ground before launch. ESA

N94-22286# GKSS-Forschungszentrum Geesthacht (Germany). Inst. fuer Physik.
THE USE OF ERBE DATA FOR CLIMATE STUDIES **c47**
R. Stuhlmann and M. Rieland (Deutscher Bundestag, Bonn, Germany.) *In* Max-Planck-Inst. fuer Meteorologie, Proceedings of the Workshop on New Generation of Radiation Budget Measurements From Space and Their Use in Climate Modelling and Diagnostic Studies Sep. 1992 p 13-18 (For primary document see N94-22283 05-46)
Avail: CASI HC A02/MF A01

The contribution of clouds to the shortwave radiation budget is discussed. In order to do this the concept of 'cloud radiative forcing' is applied to different satellite data sets to estimate the cloud forcing on the absorbed shortwave radiation at the top of the atmosphere, the surface, and within the atmosphere itself. All calculations for the top of the atmosphere are based entirely on measurements of the Earth Radiation Budget Experiment (ERBE). For the radiation budget at the surface, the incoming solar radiation at the surface is derived from Meteosat data and the surface albedo is calculated from ERBE clear sky planetary albedo measurements by applying an atmospheric correction scheme. The results are summarized. The dependence of cloud forcing on different cloud types, characterized by low, middle, and high level clouds, was investigated. The global shortwave radiation budget was assessed and results are summarized. ESA

N94-22287# Ecole Normale Superieure, Paris (France). Lab. de Meteorologie Dynamique.
SATELLITE VALIDATION OF GCM-SIMULATED ANNUAL CYCLE OF THE EARTH RADIATION BUDGET AND CLOUD FORCING
Sandrine Bony, Herve LeTreut, Jean-Philippe Duvel (Ecole Polytechnique, Palaiseau, France.), and Robert S. Kandel (Ecole Polytechnique, Palaiseau, France.) *In* Max-Planck-Inst. fuer Meteorologie, Proceedings of the Workshop on New Generation of Radiation Budget Measurements From Space and Their Use in Climate Modelling and Diagnostic Studies Sep. 1992 p 19-20 (For primary document see N94-22283 05-46)
Avail: CASI HC A01/MF A01

Earth Radiation Budget Experiment (ERBE) data are used to validate radiative fluxes and cloud radiative forcing simulated by the general circulation model (GCM). Regional and zonal distribution of actual and clear sky fluxes are considered to validate the general description of the earth radiation budget of the model. Tests to get more significant elements of comparison between models and observations are developed. These tests are applied to the actual radiation budget, to the clear sky fluxes, and to the cloud radiative forcing (CRF). ESA

N94-22288# Max-Planck-Inst. fuer Meteorologie, Hamburg (Germany).
THE SEASONAL VARIATION OF THE CLOUD RADIATIVE FORCING: COMPARISON OF ECHAM MODEL SIMULATIONS WITH ERBE DATA
Erich Roeckner *In its* Proceedings of the Workshop on New Generation of Radiation Budget Measurements From Space and Their Use in Climate Modelling and Diagnostic Studies Sep. 1992 p 21-24 (For primary document see N94-22283 05-46)
Avail: CASI HC A01/MF A01

The third generation atmospheric general circulation model ECHAM3, which was developed from an earlier version of the European Centre for Medium Range Weather Forecasts (ECMWF) medium range weather forecast model, is used for studying the impact of clouds on the radiation budget at the top of the atmosphere. The model was forced with observed sea surface temperatures between 1979 and 1988 so that there is a four year overlap with Earth Radiation Budget Experiment (ERBE) data (1985-1988). Results are presented for one year (Feb. 1985 - Jan. 1986) for which scanner measurements made by the ERBE and NOAA 9 satellites are available. It is shown that there is generally good agreement between the simulated and observed zonal mean cloud forcing for 1985. The seasonal variation of the zonal mean errors of the cloud forcing for 1985 are shown and discussed. The ERBE data can also be used to study the cloud variations due to internal temperature variations such as the El Nino southern oscillation cycle (ENSO) or the seasonal cycle. The response of the cloud forcing to seasonal temperature variations for July 1985 is shown. ESA

N94-22289# Max-Planck-Inst. fuer Meteorologie, Hamburg (Germany).
USE OF SATELLITE DATA FOR VALIDATION OF THE ECHAM MODELS
K. Arpe *In its* Proceedings of the Workshop on New Generation of Radiation Budget Measurements From Space and Their Use on Climate Modelling and Diagnostic Studies Sep. 1992 p 25 (For primary document see N94-22283 05-46)
Avail: CASI HC A01/MF A01

The validation of the ECHAM3 models, which are intended for use in simulating future climates, is considered. It is no longer sufficient to simply compare climatological means; the interannual variability also has to be investigated. In order to do this the impact of sea surface temperatures (SST) on the interannual variability in the model was investigated by running several experiments with different initial states but with the same observed SST. Results are given. The plan to use observation satellites to investigate this further is discussed. The use of geostationary satellites to provide information about the diurnal cycle is also considered. The use of satellite observations should give indications of changes in the albedo due to the aging of snow. ESA

N94-22290# Meteorological Office, Bracknell (England). Climate Prediction and Research Center.
SIMULATION OF CLEAR-SKY OUTGOING LONGWAVE RADIATION OVER THE OCEANS USING OPERATIONAL ANALYSIS **c47**
A. Slingo and M. J. Webb *In its* Proceedings of the Workshop on New Generation of Radiation Budget Measurements From Space and Their Use in Climate Modelling and Diagnostic Studies Sep. 1992 p 26-28 (For primary document see N94-22283 05-46)
Avail: CASI HC A01/MF A01

A system for the simulation and analysis of measurements from satellites using operational analyses (SAMSON) was developed. Simulations of clear sky outgoing longwave radiation (OLR) over the oceans are compared with data from the Earth Radiation Budget Experiment (ERBE). The calculations were performed with a Malkmus narrow band radiation scheme, including the effects of all the radiatively important gases. Sea surface temperatures were taken from the United Kingdom National Meteorological Center's blended analyses, and ozone data from the Nimbus 7 Solar Backscatter Ultraviolet experiment. Atmospheric temperatures and humidities came from operational analyses. Parallel simulations were performed with the analyses produced both by the European Center for Medium Range Weather Forecasts (ECMWF) and by the United Kingdom Meteorological Office (UKMO). Simulations for the period Feb. 1985 - Oct. 1986 were compared with ERBE data. ESA

N94-22291# European Centre for Medium-Range Weather Forecasts, Reading (England).
USE OF SATELLITE DATA FOR VALIDATION OF OPERATIONAL FORECAST MODELS AND OPERATIONAL ANALYSES **c47**
E. Klinker *In* Max-Planck-Inst. fuer Meteorologie, Proceedings of the Workshop on New Generation of Radiation Budget Measurements From Space and Their Use in Climate Modelling and Diagnostic Studies Sep. 1992 p 29 (For primary document see N94-22283 05-46)
Avail: CASI HC A01/MF A01

At the European Center for Medium Range Weather Forecasts (ECMWF), the operational forecast fluxes of radiation at the top of the atmosphere are monitored by comparing zonal and monthly means to the appropriate part of a fixed annual cycle of Earth Radiation Budget Experiment (ERBE) fluxes averaged in the same way. Some information on the general performance of the forecast model characteristics can be gained from scatter diagrams; one useful example is a scatter diagram of the greenhouse function over sea surface temperature. A synchronous comparison of ERBE and model fluxes for periods more than one to two years ago is only of limited use for the validation of the present model formulation. At ECMWF the data assimilation was repeated for a period when a good coverage of satellite data was available (Jul. and Aug. 1987). By using the model and analysis formulation of Jul. 1991 it was possible to evaluate the more recent changes in the parameterization of cloud radiation interaction. The synchronous comparison allows the validation of single circulation systems like the extra tropical cyclones, tropical cloud cluster, or tropical easterly waves. Additionally a comparison of observed and predicted monthly means and standard deviations of daily values give a good indication where the cloud-radiation interaction is still unsatisfactory. ESA

N94-22424 Calgary Univ. (Alberta). Dept. of Surveying Engineering.
VECTOR GRAVIMETRY BY A COMBINATION OF INERTIAL AND GPS SATELLITE MEASUREMENTS Ph.D. Thesis
Elfriede T. Knickmeyer Sep. 1990 173 p
(ISBN-0-315-61980-5; CTN-94-60892) Copyright Avail: Micromedia Ltd., Technical Information Centre, 240 Catherine Street, Suite 305, Ottawa, Ontario, K2P 2G8, Canada HC/MF

Vector gravimetry with inertial navigation systems (INS) has been successfully performed in semi-kinematic mode for several years. With advances in the kinematic use of the Global Positioning System (GPS), kinematic vector gravimetry has also come within reach. The problems of reducing the effect of INS sensor errors, determining the kinematic acceleration by means of GPS observations, and modelling the gravity vector in a state space setting are addressed. The requirements on INS and GPS observations are investigated in a covariance analysis. Different INS mechanizations, strapdown, platform, and rotating sensor unit are compared. It is shown that only the last two are suited for vector gravimetry. Subject to the principal limitations of the simulation study, the quantitative results show that current INS and GPS hardware should allow the determination of deflections of the vertical with an accuracy of 1 arcsecond. The determination of gravity anomalies with an accuracy of 10 micrometers per second squared, however, imposes very stringent requirements on the determination of the kinematic acceleration with GPS, which may possibly be met by high data rates and extensive filtering. Author (CISTI)

N94-22574 Calgary Univ. (Alberta). Dept. of Physics and Astronomy.
A COMPARISON OF A SIMPLE MODEL OF EUV DAYGLOW WITH VIKING DATA M.S. Thesis
Maurice Thomas Shevalier Feb. 1993 110 p
(ISBN-0-315-83258-4; CTN-94-60940) Copyright Avail: Micromedia Ltd., Technical Information Centre, 240 Catherine Street, Suite 305, Ottawa, Ontario, K2P 2G8, Canada HC/MF

A simple model of extreme ultraviolet dayglow was developed to determine the origin of double limbs observed by the Swedish Viking satellite, which had five instruments designed to investigate different regions of the auroral processes. A simple model was developed using results from previously published models. The shape and intensities of the calculated profiles match those that appear in the literature. The Viking altitude/intensity profiles show two peaks present which do not match published or modelled profiles. When the altitude of the upper peak was adjusted to match the modelled peak, the lower peak was decreased in altitude from 120 to 9 km, indicating a possible tropospheric source for the lower peak. The volume emission rate profiles obtained from the model and from altitude corrected inverted Viking data were very similar. The modelled column intensities were significantly larger than the Viking satellite's, so the normalized peak intensities were compared. The peaks have a similar shape with differences attributed to long wavelength leakage in the camera. Author (CISTI)

N94-22575 Calgary Univ. (Alberta). Dept. of Physics and Astronomy.
IMPLICATIONS OF VIKING DAYSIDE AURORAL MEASUREMENTS Ph.D. Thesis
Vo Hienbich Sep. 1992 293 p
(ISBN-0-315-83273-8; CTN-94-60941) Copyright Avail: Micromedia Ltd., Technical Information Centre, 240 Catherine Street, Suite 305, Ottawa, Ontario, K2P 2G8, Canada HC/MF

The ultraviolet images and other supporting data obtained by the Viking satellite were used to determine the general characteristics of dayside aurora. After defining a localized intensification in the auroral images, a statistical survey was made from a data set consisting of 60 Viking passes. Results indicate that the most probable region in which such features were found was 14-16 magnetic local time (MLT); this region often consists of more than one feature which have a spatial periodicity of 0.4 or 0.7 MLT. The source of the afternoon aurora was determined to be the low latitude boundary layer and colocated within a convection reversal region. Dayside aurora was determined to be a conjugate phenomenon which implied they are located on closed field lines. A strong dependence on the solar wind velocity was found for the active cases. All of this evidence suggests that afternoon auroras are caused by the Kelvin Helmholtz instability acting on the flank of the magnetosphere, as illustrated in a magnetosphere ionosphere coupling model. The results indicate that this viscous process

could play a main role in the interaction between the solar wind and the magnetosphere. Author (CISTI)

N94-20425*# Jet Propulsion Lab., California Inst. of Tech., Pasadena.
DETECTION OF TRAVELING IONOSPHERIC DISTURBANCES INDUCED BY ATMOSPHERIC GRAVITY WAVES USING THE GLOBAL POSITIONING SYSTEM Abstract Only
Sassan Bassiri (Sharif Univ. of Technology, Tehran, Iran.) and George A. Hajj *In its* Progress In Electromagnetics Research Symposium (PIERS) 1993 p 452 (For primary document see N94-20403 05-32)
Avail: CASI HC A01/MF A10

N94-20641*# Academy of Sciences (USSR), Moscow. Inst. of Geochemistry and Analytical Chemistry.
THE KOSHAK SECTION: EVIDENCE FOR ELEMENT FRACTIONATION AND AN OXIDATION EVENT AT THE K/T BOUNDARY Abstract Only
M. A. Nazarov, D. D. Badjukov, L. D. Barsukova, G. M. Kolesov, and D. P. Naidin (Moscow State Univ., Russia.) *In* Lunar and Planetary Inst., Twenty-Fourth Lunar and Planetary Science Conference. Part 3: N-Z 1993 p 1051-1052 (For primary document see N94-20636 05-91)
Avail: CASI HC A01/MF A06

N94-20649*# Academy of Sciences (USSR), Moscow. Inst. for Dynamics of Geospheres.
EFFECTS OF HYDRODYNAMICS AND THERMAL RADIATION IN THE ATMOSPHERE AFTER COMET IMPACTS Abstract Only
I. V. Nemchinov, M. P. Popova, L. P. Shubadeeva, V. V. Shuvalov, and V. V. Svetsov *In* Lunar and Planetary Inst., Twenty-Fourth Lunar and Planetary Science Conference. Part 3: N-Z 1993 p 1067-1068 (For primary document see N94-20636 05-91)
Avail: CASI HC A01/MF A06

N94-20668*# Ciudad Univ., Mexico City (Mexico). Inst. de Geofisica.
MODELLING THE GRAVITY AND MAGNETIC FIELD ANOMALIES OF THE CHICXULUB CRATER Abstract Only
C. Ortiz Aleman, M. Pilkington (Geological Survey of Canada, Ottawa, Ontario.), A. R. Hildebrand (Geological Survey of Canada, Ottawa, Ontario.), W. R. Roest (Geological Survey of Canada, Ottawa, Ontario.), R. A. F. Grieve (Geological Survey of Canada, Ottawa, Ontario.), and P. Keating (Geological Survey of Canada, Ottawa, Ontario.) *In* Lunar and Planetary Inst., Twenty-Fourth Lunar and Planetary Science Conference. Part 3: N-Z 1993 p 1105-1106 (For primary document see N94-20636 05-91)
Avail: CASI HC A01/MF A06

N94-20673*# Brown Univ., Providence, RI. Dept. of Geological Sciences.
THERMAL AND RHEOLOGICAL CONTROLS ON MAGMA MIGRATION IN DIKES: EXAMPLES FROM THE EAST RIFT ZONE OF KILAUEA VOLCANO, HAWAII Abstract Only
E. A. Parfitt, L. Wilson, and H. Pinkerton (Lancaster Univ., England.) *In* Lunar and Planetary Inst., Twenty-Fourth Lunar and Planetary Science Conference. Part 3: N-Z 1993 p 1115-1116 (For primary document see N94-20636 05-91)
Avail: CASI HC A01/MF A06

N94-20690*# Lancaster Univ. (England). Environmental Science Div.
A COMPARISON OF CALCULATED AND MEASURED RHEOLOGICAL PROPERTIES OF CRYSTALLISING LAVAS IN THE FIELD AND IN THE LABORATORY Abstract Only
Harry Pinkerton and Gill Norton *In* Lunar and Planetary Inst., Twenty-Fourth Lunar and Planetary Science Conference. Part 3: N-Z 1993 p 1149-1150 (For primary document see N94-20636 05-91)
Avail: CASI HC A01/MF A06

N94-20714*# Witwatersrand Univ., Johannesburg (South Africa). Economic Geology Research Unit.
KALKKOP CRATER, EASTERN CAPE: A NEW IMPACT CRATER IN SOUTH AFRICA Abstract Only
W. U. Reimold, F. G. LeRoux (Geological Survey of South-West Africa/Namibia, Windhoek.), C. Koeberl (Wien Univ., Austria.), and S. B. Shirey (Wien Univ., Austria.) *In* Lunar and Planetary Inst., Twenty-Fourth Lunar and Planetary Science Conference. Part 3: N-Z 1993 p 1197-1198 (For primary document see N94-20636 05-91)
Avail: CASI HC A01/MF A06

N94-20742*# Boeing Defense and Space Group, Seattle, WA.
PRESSURE VERSUS DRAG EFFECTS ON CRATER SIZE Abstract Only
R. M. Schmidt *In* Lunar and Planetary Inst., Twenty-Fourth Lunar and Planetary Science Conference. Part 3: N-Z 1993 p 1253-1254 (For primary document see N94-20636 05-91)
Avail: CASI HC A01/MF A06

N94-20744*# Brown Univ., Providence, RI. Dept. of Geological Sciences.
IMPACTOR CONTROL OF CENTRAL PEAK AND PEAK-RING FORMATION Abstract Only
Peter H. Schultz and D. E. Gault (Murphys Center of Planetology, CA.) *In* Lunar and Planetary Inst., Twenty-Fourth Lunar and Planetary Science Conference. Part 3: N-Z 1993 p 1257-1258 (For primary document see N94-20636 05-91)
Avail: CASI HC A01/MF A06

N94-20747*# Nevada Univ., Reno. School of Mines.
STRENGTH AND DEFORMATION PROPERTIES OF BASALTIC LAVA FLOWS ON PLANETARY SURFACES Abstract Only
Richard A. Schultz *In* Lunar and Planetary Inst., Twenty-Fourth Lunar and Planetary Science Conference. Part 3: N-Z 1993 p 1263-1264 (For primary document see N94-20636 05-91)
Avail: CASI HC A01/MF A06

N94-20757*# Lunar and Planetary Inst., Houston, TX.
CHICXULUB IMPACT BASIN: GRAVITY CHARACTERISTICS AND IMPLICATIONS FOR BASIN MORPHOLOGY AND DEEP STRUCTURE Abstract Only
Virgil L. Sharpton, Kevin Burke (Houston Univ., TX.), Stuart A. Hall (Houston Univ., TX.), Scott Lee, Luis E. Marin (Universidad Nacional Autonoma de Mexico, Mexico City.), Gerardo Suarez (Universidad Nacional Autonoma de Mexico, Mexico City.), Juan Manuel Quezada-Muneton (Universidad Nacional Autonoma de Mexico, Mexico City.), and Jaime Urrutia-Fucugauchi (Gerencia de Exploracion, Petroleos Mexicanos, Mexico City.) *In its* Twenty-Fourth Lunar and Planetary Science Conference. Part 3: N-Z 1993 p 1283-1284 (For primary document see N94-20636 05-91)
Avail: CASI HC A01/MF A06

N94-20766*# Geological Survey, Flagstaff, AZ.
RESEARCH PROGRAM ON THE MANSON IMPACT STRUCTURE, IOWA Abstract Only
E. M. Shoemaker, D. J. Roddy, and R. R. Anderson (Geological Survey, Iowa City, IA.) *In* Lunar and Planetary Inst., Twenty-Fourth Lunar and Planetary Science Conference. Part 3: N-Z 1993 p 1301-1302 (For primary document see N94-20636 05-91)
Avail: CASI HC A01/MF A06

N94-20767*# Pennsylvania State Univ., University Park.
PETROGRAPHY OF SHOCK FEATURES IN THE 1953 MANSON 2-A DRILL CORE Abstract Only
N. M. Short and D. P. Gold *In* Lunar and Planetary Inst., Twenty-Fourth Lunar and Planetary Science Conference. Part 3: N-Z 1993 p 1303-1304 (For primary document see N94-20636 05-91)
Avail: CASI HC A01/MF A06

N94-20776*# Tennessee Univ., Knoxville.
PRIMARY DIFFERENTIATION IN THE EARLY EARTH: Nd AND Sr ISOTOPIC EVIDENCE FROM DIAMONDIFEROUS ECLOGITES FOR BOTH OLD DEPLETED AND OLD ENRICHED MANTLE, YAKUTIA, SIBERIA Abstract Only
Gregory A. Snyder, Eric A. Jerde, Lawrence A. Taylor, Alex N. Halliday (Michigan Univ., Ann Arbor.), Vladimir N. Sobolev (Academy of Sciences, USSR, Novosibirsk.), Nickolai V. Sobolev (Academy of Sciences, USSR, Novosibirsk.), Robert N. Clayton (Chicago Univ., IL.), Toshiko K. Mayeda (Chicago Univ., IL.), and Peter Deines (Pennsylvania State Univ., University Park.) *In* Lunar and Planetary Inst., Twenty-Fourth Lunar and Planetary

Science Conference. Part 3: N-Z 1993 p 1321-1322 (For primary document see N94-20636 05-91)
Avail: CASI HC A01/MF A06

N94-20783*# New Brunswick Univ., Fredericton. Dept. of Geology.
DELIMITATION OF TERRESTRIAL IMPACT CRATERS BY WAY OF PSEUDOTACHYLYTIC ROCK DISTRIBUTION Abstract Only
John G. Spray *In* Lunar and Planetary Inst., Twenty-Fourth Lunar and Planetary Science Conference. Part 3: N-Z 1993 p 1335-1336 (For primary document see N94-20636 05-91)
Avail: CASI HC A01/MF A06

N94-20789*# Wyoming Univ., Laramie. Dept. of Geology/Geophysics.
TWO-POLARITY MAGNETIZATION IN THE MANSON IMPACT BRECCIA Abstract Only
M. B. Steiner and E. M. Shoemaker (Geological Survey, Flagstaff, AZ.) *In* Lunar and Planetary Inst., Twenty-Fourth Lunar and Planetary Science Conference. Part 3: N-Z 1993 p 1347-1348 (For primary document see N94-20636 05-91)
Avail: CASI HC A01/MF A06

N94-20798*# National Museum of Natural History, Paris (France).
THE AGE OF THE PRETORIA SALTPAN IMPACT CRATER, SOUTH AFRICA Abstract Only
Dieter Storzer, Christian Koeberl (Wien Univ., Austria.), and Wolf Uwe Reimold (Witwatersrand Univ., Johannesburg, South Africa.) *In* Lunar and Planetary Inst., Twenty-Fourth Lunar and Planetary Science Conference. Part 3: N-Z 1993 p 1365-1366 (For primary document see N94-20636 05-91)
Avail: CASI HC A01/MF A06

N94-20825*# Houston Univ., TX. Dept. of Geosciences.
ORIGINAL SIZE OF THE VREDEFORT STRUCTURE, SOUTH AFRICA Abstract Only
A. M. Therriault, A. M. Reid, and W. U. Reimold (Witwatersrand Univ., Johannesburg, South Africa.) *In* Lunar and Planetary Inst., Twenty-Fourth Lunar and Planetary Science Conference. Part 3: N-Z 1993 p 1419-1420 (For primary document see N94-20636 05-91)
Avail: CASI HC A01/MF A06

N94-20826*# Houston Univ., TX. Dept. of Geosciences.
ORIGIN OF THE VREDEFORT STRUCTURE, SOUTH AFRICA: IMPACT MODEL Abstract Only
A. M. Therriault, A. M. Reid (McMaster Univ., Hamilton, Ontario.), and W. U. Reimold (Witwatersrand Univ., Johannesburg, South Africa.) *In* Lunar and Planetary Inst., Twenty-Fourth Lunar and Planetary Science Conference. Part 3: N-Z 1993 p 1421-1422 (For primary document see N94-20636 05-91)
Avail: CASI HC A01/MF A06

N94-20833*# Arizona Univ., Tucson.
CORE FORMATION BY GIANT IMPACTS: CONDITIONS FOR INTACT MELT REGION FORMATION Abstract Only
W. B. Tonks and H. J. Melosh *In* Lunar and Planetary Inst., Twenty-Fourth Lunar and Planetary Science Conference. Part 3: N-Z 1993 p 1435-1436 (For primary document see N94-20636 05-91)
Avail: CASI HC A01/MF A06

N94-20843*# Universidad Nacional Autonoma de Mexico, Coyoacan. Inst. de Geofisica.
REVERSE POLARITY MAGNETIZED MELT ROCKS FROM THE CHICXULUB IMPACT STRUCTURE, YUCATAN PENINSULA, MEXICO Abstract Only
Jaime Urrutia-Fucugauchi, Luis E. Marin, Virgil L. Sharpton (Lunar and Planetary Inst., Houston, TX.), and Juan Manuel Quezada (Gerencia de Exploracion, Petroleos Mexicanos, Mexico City.) *In* Lunar and Planetary Inst., Twenty-Fourth Lunar and Planetary Science Conference. Part 3: N-Z 1993 p 1455-1456 (For primary document see N94-20636 05-91)
Avail: CASI HC A01/MF A06

N94-20878*# Brown Univ., Providence, RI. Dept. of Geological Sciences.
FORMATION OF PERCHED LAVA PONDS ON BASALTIC VOLCANOES: INTERACTION BETWEEN COOLING RATE AND FLOW GEOMETRY ALLOWS ESTIMATION OF LAVA EFFUSION RATES Abstract Only
L. Wilson and E. A. Parfitt *In* Lunar and Planetary Inst., Twenty-Fourth Lunar and Planetary Science Conference. Part 3: N-Z 1993 p 1525-1526 (For primary document see N94-20636 05-91)
Avail: CASI HC A01/MF A06

N94-20879*# Lancaster Univ. (England). Environmental Science Div.
A CLASSIFICATION SCHEME FOR THE MORPHOLOGY OF LAVA FLOW FIELDS Abstract Only
L. Wilson, H. Pinkerton, James W. Head (Brown Univ., Providence, RI.), and K. Magee Roberts (Brown Univ., Providence, RI.) *In* Lunar and Planetary Inst., Twenty-Fourth Lunar and Planetary Science Conference. Part 3: N-Z 1993 p 1527-1528 (For primary document see N94-20636 05-91)
Avail: CASI HC A01/MF A06

N94-20882*# Houston Univ., TX. Dept. of Geosciences.
CHARACTERIZATION OF THE MARQUEZ DOME BURIED IMPACT CRATER USING GRAVITY AND MAGNETIC DATA Abstract Only
A. M. Wong, A. M. Reid, S. A. Hall, and V. L. Sharpton (Lunar and Planetary Inst., Houston, TX.) *In* Lunar and Planetary Inst., Twenty-Fourth Lunar and Planetary Science Conference. Part 3: N-Z 1993 p 1533-1534 (For primary document see N94-20636 05-91)
Avail: CASI HC A01/MF A06

N94-20887*# Chinese Academy of Geological Sciences, Beijing. Inst. of Mineral Deposits.
SHOCK ATTENUATION AT THE SLATE ISLANDS REVISITED Abstract Only
S. Wu, P. B. Robertson (Geological Survey of Canada, Ottawa, Ontario.), and R. A. F. Grieve (Geological Survey of Canada, Ottawa, Ontario.) *In* Lunar and Planetary Inst., Twenty-Fourth Lunar and Planetary Science Conference. Part 3: N-Z 1993 p 1543-1544 (For primary document see N94-20636 05-91)
Avail: CASI HC A01/MF A06

N94-20889*# Rutgers Univ., New Brunswick, NJ. Dept. of Chemistry.
STABLE NI ISOTOPES AND Be-10 AND Al-26 IN METALLIC SPHEROIDS FROM METEOR CRATER, ARIZONA Abstract Only
S. Xue, G. F. Herzog, G. S. Hall, J. Klein (Pennsylvania Univ., Philadelphia.), R. Middleton (Pennsylvania Univ., Philadelphia.), and D. Juenemann (Pennsylvania Univ., Philadelphia.) *In* Lunar and Planetary Inst., Twenty-Fourth Lunar and Planetary Science Conference. Part 3: N-Z 1993 p 1547-1548 (For primary document see N94-20636 05-91)
Avail: CASI HC A01/MF A06

N94-20899*# Lehigh Univ., Bethlehem, PA. Dept. of Earth and Environmental Sciences.
AGE AND THERMOCHRONOLOGY OF K-FELDSPARS FROM THE MANSON IMPACT STRUCTURE Abstract Only
P. K. Zeitler and M. J. Kunk (Geological Survey, Reston, VA.) *In* Lunar and Planetary Inst., Twenty-Fourth Lunar and Planetary Science Conference. Part 3: N-Z 1993 p 1567-1568 (For primary document see N94-20636 05-91)
Avail: CASI HC A01/MF A06

N94-20904*# Smithsonian Institution, Washington, DC.
NUMERICAL SIMULATION OF LAVA FLOWS: APPLICATIONS TO THE TERRESTRIAL PLANETS Abstract Only
James R. Zimbelman, Bruce A. Campbell, Juliana Kousoum (Thomas Jefferson High School, Falls Church, VA.), and Derrick J. Lampkin (Ohio State Univ., Columbus.) *In* Lunar and Planetary Inst., Twenty-Fourth Lunar and Planetary Science Conference. Part 3: N-Z 1993 p 1577-1578 (For primary document see N94-20636 05-91)
Avail: CASI HC A01/MF A06

47 METEOROLOGY AND CLIMATOLOGY

Includes weather forecasting and modification.

N94-19852# Air Force Environmental Technical Applications Center, Scott AFB, IL.

AN ANALYSIS OF CLOUD-COVER REPORTING IN THE 1977 SURFACE OBSERVATION DATABASE

James G. Saccomando, Jr. Sep. 1993 14 p

(AD-A271102; USAFETAC/PR-93/002) Avail: CASI HC A03/MF A01

This document describes an analysis of the Air Force climatological surface weather observation database to determine global coverage and frequency of cloud-cover reports during the year 1977. The results of the analysis are depicted by cloud-cover reporting coverage and frequency plotted on global maps. DTIC

N94-19900 Colorado State Univ., Fort Collins. Dept. of Atmospheric Science.

CLOUDS: THEIR PREDICTION AND SIMULATION Annual Technical Report, 1 Apr. 1992 - 31 May 1993

W. R. Cotton and G. L. Stephens 30 Jun. 1993 12 p Limited Reproducibility: More than 20% of this document may be affected by microfiche quality

(Grant AF-AFOSR-0269-91)

(AD-A271161; AFOSR-93-0790TR) Avail: CASI HC A03

Mesoscale forecasts of several FIRE 2 cirrus events have been repeated using newly developed microphysics schemes. Boundary layer cloud fractional coverage schemes has been tested for one of the FIRE 1 stratocumulus cases in which there was a transition from solid stratocumulus to broken cumuli. RAMS ability to simulate ordinary deep convective clouds has been evaluated for one of the CaPE cases over the Kennedy Space Flight Center. New modules for cloud microphysics and radiation transfer have been written and the impacts of those schemes on cloud forecasting will be evaluated in the future. DTIC

N94-19908 Air Force Environmental Technical Applications Center, Scott AFB, IL.

WORLDWIDE FREQUENCY OF TEMPERATURES AT SELECTED ALTITUDES

James G. Saccomando, Jr. Sep. 1993 14 p Limited Reproducibility: More than 20% of this document may be affected by microfiche quality

(AD-A271111; USAFETAC/PR-93/003) Avail: CASI HC A03

This report provides maps that give frequency of occurrence of temperatures less than or equal to certain values at selected altitudes worldwide. Monthly data is plotted on world maps, with contours of probability. The analysis was performed using the Air Force Global Weather Central's HIRAS (High-Resolution Analysis) temperature and D-value data for 1985-1991. The analysis was accomplished for a 2.5 by 2.5 degree latitude/longitude global grid. The results of the analysis appear consistent with what meteorologists know about the atmosphere. The maps show USAFETAC's recently acquired data visualization capabilities. DTIC

N94-20088 Phillips Lab., Hanscom AFB, MA.

PREDICTING LIGHTNING EVENTS IN THE KSC AREA: A FEASIBILITY STUDY USING SINGLE STATION DATA Interim Report

Robert O. Berthel 8 Dec. 1992 32 p Limited Reproducibility: More than 20% of this document may be affected by microfiche quality

(AF Proj. 6670)

(AD-A271440; PL-TR-92-2333; ERP-1114) Avail: CASI HC A03

Surface observations and early-morning radiosonde measurements, taken on a regular daily basis in the KSC area during a late summer period, were scrutinized in an effort to form a correlation with subsequent lightning-related activity. Wind directions were the only measurements that could be directly associated. This study revealed that lightning activity, other than that associated with large-scale storm systems, developed in the 12-hr period following the morning radiosonde when both surface and upper-air (averaged between the 600-800 mb pressure levels) winds had directions that brought air off the ocean and moved it over lands towards KSC. The most basic explanation is the advection of oceanic water vapor, the elevation of the moisture through convergence and the transport of that moisture to KSC by upper-air winds. This premise was supported by the evidence of days having no lightning activity, presumably caused by the lack of advection and/or convergence or from elevated moisture being carried away from KSC. This investigation concludes that there is a good probability that the occurrence of daytime-lightning-related activity, local to the general KSC area, may be predicted from knowledge of the late-night to early-morning surface and upper wind directions. DTIC

N94-20138*# North Carolina State Univ., Raleigh. Dept. of Marine, Earth, and Atmospheric Sciences

MESO-BETA SCALE NUMERICAL SIMULATION STUDIES OF TERRAIN-INDUCED JET STREAK MASS/MOMENTUM PERTURBATIONS Semiannual Report

Yuh-Lang Lin and Michael L. Kaplan Nov. 1993 121 p

(Grant NAG5-1790)

(NASA-CR-194627; NAS 1.26:194627) Avail: CASI HC A06/MF A02

The Control-B simulation experiment was designed to improve on the Control-A experiment performed with the GMASS model. This experiment addressed several inadequacies with the first smooth terrain numerical simulation by including: (1) increased nested-grid resolution to better define the simulated gravity waves, (2) increased horizontal diffusion to remove outflow boundary condition noise, and (3) the use of reanalyzed rawinsonde data and surface observations in the initial state to increase the definition of the observed jet streak as well as other low-level features. A smoothed-terrain dry simulation with the nested-grid GMASS model has revealed many important aspects of the processes which resulted in the generation of gravity waves in the region and time when and where they were observed. However, the vertical structure, number, and characteristics of the waves are still quite different from observed waves as diagnosed thus necessitating future improved simulations. However, this control simulation has produced substantial insight into processes which occur on many spatial scales over a 30 hour time period thus allowing one to draw promising inferences as to the mechanisms for the complex process which occurred in nature during the CCOPE case study. The theoretical aspects of the project have focus on understanding the nature of the ageostrophic circulations which are produced in idealized models of the atmosphere in which the troposphere is modeled in one of two ways. The first model assumes that the lower atmosphere can be represented as a single layer of homogeneous fluid whose upper surface is free to exhibit vertical displacement. Two-dimensional internal convergence (divergence) occurring during the adjustment to an asymptotic equilibrium state from an ageostrophic initial state whose momentum structure is representative of a midlatitude localized zonal wind anomaly will cause the free upper surface of the homogeneous atmosphere to rise (fall), and therefore the response can be viewed as being physically three-dimensional. The second model assumes that the troposphere can be represented by an unbounded continuously stratified Boussinesq fluid of constant Brunt-Vaisala frequency N, where the vertical gradient of the basic state potential temperature profile allows for the existence of vertically propagating internal inertia-gravity waves.

Derived from text

N94-20186# Woods Hole Oceanographic Inst., MA.

THE MARINE LIGHT-MIXED LAYER EXPERIMENT CRUISE AND DATA REPORT: R/V ENDEAVOR CRUISE EN-224, MOORING DEPLOYMENT, 27 APRIL-1 MAY 1991: CRUISE EN-227, MOORING RECOVERY, 5-23 SEPTEMBER 1991

Albert J. Plueddemann, Robert A. Weller, Thomas D. Dickey, John Marra, and George H. Tupper May 1993 125 p

(Contract N00014-89-J-1683)

(AD-A271175; WHOI-93-33; UOP-93-4) Avail: CASI HC A06/MF A02

The Marine Light-Mixed Layer experiment took place in the sub-Arctic North Atlantic ocean, approximately 275 miles south of Reykjavik, Iceland. The field program included a central surface mooring to document the temporal evolution of physical, biological, and optical properties. The surface mooring was deployed at approximately 59 deg N, 21 deg W on 29 April 1991 and recovered on 6 September 1991. The Upper Ocean Processes Group of the Woods Hole Oceanographic Institution was responsible for design, preparation, deployment, and recovery of the mooring. The Group's contribution to the field measurements included four different types of sensors: a meteorological observation package on the surface buoy, a string of 15 temperature sensors along the mooring line, an acoustic Doppler current profiler, and four instruments for measuring mooring tension and accelerations. The observations obtained from the mooring are sufficient to describe the air-sea fluxes and the local physical response to surface

forcing. The objective in the analysis phase will be to determine the factors controlling this physical response and to work towards an understanding of the links among physical, biological, and optical processes. This report describes the deployment and recovery of the mooring, the meteorological data, and the subsurface temperature and current data. DTIC

N94-20239 Royal Netherlands Meteorological Inst., De Bilt. Ontwikkelingsafd. Wetenschappelijk Onderzoek.
ANALYSIS OF WIND OBSERVATION FROM TOWERS IN THE PERIOD 1977-1991 [ANALYSE VAN TORENWINDGEGEVENS OVER HET TIJDVAK 1977 TOT EN MET 1991]
Gertie Geertsema 1992 31 p In DUTCH
(KNMI-TR-148; ISBN-90-369-2027-2; ETN-94-94533) Avail: Issuing Activity (Royal Netherlands Meteorological Institute, Postbus 201, 3730 AE De Bilt, Netherlands)

Wind measurements performed on television broadcasting towers up to a height of about 200 m are analyzed with a view to meteorological support in case of calamities, such as the accidental release of radioactive or chemical substances. The emphasis is on the wind velocity. The error of the estimated wind direction depends strongly on the wind velocity. The error of the wind velocity can be significant. The mixing height is an important parameter in the distribution of air pollution. The choice of the wind direction measuring location is very important. ESA

N94-20309 Royal Netherlands Meteorological Inst., De Bilt.
SOIL TEMPERATURES [GRONDTEMPERATUREN]
P. C. vanderHoeven and W. N. Lablans 1992 64 p In DUTCH This supersedes KNMI-WR-74-14
(KNMI-WR-92-05; KNMI-WR-74-14; ISBN-9-03-692025-6; ETN-94-94537)
Avail: Issuing Activity (Royal Netherlands Meteorological Institute, Postbus 201, 3730 AE De Bilt, Netherlands)

Soil temperature measurements at nine stations in the south west of the Netherlands and at De Bilt in the period 1962-1973 were revised to study possible consequences of the Delta works on the regional climate. For De Bilt, Netherlands, monthly mean values and variances for the period 1961-1980 were also included. A number of practical problems and questions are discussed. The theory of heat transport in the soil is surveyed, including a 100 layer computer model for the calculation of soil temperature and heat flux response to an imposed temperature wave at the surface. ESA

N94-20332 Department of the Navy, Washington, DC.
ATMOSPHERIC MOISTURE COLLECTION DEVICE Patent
Norman P. Clarke, inventor (to Navy) 10 Aug. 1993 5 p Filed 12 Mar. 1992
(AD-D015935; US-Patent-5,233,843; US-Patent-Appl-SN-849866; US-Patent-Class-62-271) Avail: US Patent and Trademark Office

An apparatus for extracting moisture from the ambient air includes a desiccant pond for absorbing moisture from the air to produce a water rich desiccant, means for vaporizing the moisture in the water rich desiccant, mixing the vaporized moisture with ambient air to increase the dew point of the ambient air, condensing the vaporized moisture to form a potable water condensate and returning the water lean desiccant back to the desiccant pond. DTIC

N94-20353*# Purdue Univ., West Lafayette, IN. Dept. of Earth and Atmospheric Sciences.
THE LIFE CYCLES OF INTENSE CYCLONIC AND ANTICYCLONIC CIRCULATION SYSTEMS OBSERVED OVER OCEANS Semiannual Status Report, 1 Jul. - 31 Dec. 1993
Phillip J. Smith 31 Dec. 1993 12 p
(Grant NAG8-915)
(NASA-CR-194760; NAS 1.26:194760) Avail: CASI HC A03/MF A01

Full attention was now directed to the blocking case studies mentioned in previous reports. Coding and initial computational tests were completed for a North Atlantic blocking case that occurred in late October/early November 1985 and an upstream cyclone that developed rapidly 24 hours before block onset. This work is the subject of two papers accepted for presentation at the International Symposium on the Lifecycles of Extratropical Cyclones in Bergen, Norway, 27 June - 1 July 1994. This effort is currently highlighted by two features. The first is the extension of the Zwack-Okossi equation, originally formulated for the diagnosis of surface wave development, for application at any pressure level. The second is the separation of the basic large-scale analysis fields into synoptic-scale and planetary-scale components, using a two-dimensional Shapiro filter, and the corresponding partitioning of the Zwack-Okossi equation into synoptic-scale, planetary-scale, and synoptic/planetary-scale interaction terms. Preliminary tests suggest substantial contribution from the synoptic-scale and interaction terms. Author (revised)

N94-20482# Air Force Inst. of Tech., Wright-Patterson AFB, OH.
SPATIAL AND TEMPORAL VARIATIONS OF SATELLITE MICROWAVE MEASUREMENTS OF LATENT HEAT RELEASE IN TROPIC CYCLONES DUE TO ENVIRONMENTAL FORCING OBTAINED FROM A NUMERICAL MODEL M.S. Thesis
Derek A. West Mar. 1993 131 p
(AD-A267947; AFIT/CI/CIA-93-053) Avail: CASI HC A07/MF A02

Understanding tropical cyclone (TC) intensification is a problem that continues to intrigue researchers and forecasters. The objective of this case study was to investigate, by examination of the fields from a numerical model and satellite rain rate observation, the following: (1) the relationship between TC precipitation and intensity changes; and (2) the relationship between spatial and temporal changes in a TC's precipitation and large scale environmental tropospheric forcing. Author (revised)

N94-20487 University of Southern Mississippi, Hattiesburg. Center for Ocean and Atmospheric Modeling.
PROCESSING OF CLIMATOLOGICAL DATA FOR MODEL INITIALIZATION
Germana Peggion and Grace Foo Oct. 1993 43 p Limited Reproducibility: More than 20% of this document may be affected by microfiche quality
(Contract N00014-92-J-4112)
(AD-A271878; COAM-TM-2/94) Avail: CASI HC A03

This document describes and documents a numerical procedure to compile data sets to be applied in the North Atlantic (NA) basin-wide numerical simulations. The specific objectives are as follows: (1) to acquire climatological data sets for the NA and archive them in a data library; (2) to develop an interpolation procedure for 2-D and 3-D data fields from a regular grid into the generalized coordinate system adopted by the ocean models; and (3) to prepare plotting facilities for the display and presentation of the original and interpolated data sets. DTIC

N94-20532# Beleidscommissie Remote Sensing, Delft (Netherlands).
OFFSHORE DECISION SUPPORT SYSTEM: ERS-1 PILOT PROJECT WAVEWATCH
C. J. Calkoen (Delft Hydraulics Lab., Netherlands.), G. J. Wensink (Delft Hydraulics Lab., Netherlands.), A. J. M. vanderVlugt (Oceanor, Netherlands.), T. Coppens (Heeremac, Netherlands.), and H. J. Saetre (Shell Internationale Petroleum Maatschappij B.B., Netherlands.) Dec. 1992 33 p
(BCRS-92-09; ISBN-9-05-411047-3; ETN-93-94820) Avail: CASI HC A03/MF A01

A study whose aim was to implement an Offshore Decision Support system (ODS) for offshore operations is reported. The ODS needs easy access to wind wave and current forecasts, for which an offshore data storage and retrieval system will be installed. The ODS will be tested during actual offshore operations for a duration of 4 weeks in a period of 8 months. For periods in the operational phase of the project, wave hindcasts were generated with the help of a third generation wave model using data assimilation (WAVEWATCH subtask). During the evaluation, these results were compared with the standard forecasts used in the project. In this way, the impact of ERS-1 data to improve the safety of offshore operations was assessed. ESA

N94-20535*# Purdue Univ., West Lafayette, IN. Dept. of Earth and Atmospheric Sciences.
THE ANALYSIS OF GLOBAL CLOUD AND RADIATION DATA FOR THE STUDY OF CLOUD-CLIMATE INTERACTIONS Annual Report, 1 Jan. - 31 Dec. 1993
Harshvardhan 1993 41 p Proposed for presentation at the Eighth AMS Radiation Conference, Nashville, TN, Jan. 1994 Submitted for publication
(Grant NAGw-3150)
(NASA-CR-193388; NAS 1.26:193388) Avail: CASI HC A03/MF A01

During the past year, ISCCP C1 data has been analyzed for two regions,

the stratocumulus area off California and the tropical Atlantic. The first part of the study dealing with stratocumulus clouds is complete and the results form the technical portion of this report. A manuscript that has recently been prepared covering this subject is attached as an Appendix. The abstract describes the key finding that cloudy mean liquid water path (LWP) is invariant with cloud fraction for cloud cover between 20% - 80%. Similar conclusions are reached with ISCCP and LANDSAT data. This has important implications for General Circulation Models. A possible application is described in the Discussion section of the Appendix. An idea that has been proposed for dealing with GCM hydrology can be used.

Derived from text

N94-20557 Institut Franco-Allemand de Recherches, Saint-Louis (France).

LOW-ALTITUDE CROSS-WIND VELOCITY MEASUREMENTS USING PULSED VISIBLE FRINGE-TYPE LASER ANEMOMETRY

Eckhardt W. Sommer and Hans J. Pfeifer Jun. 1992 9 p Presented at the SPIE International Symposium and Exhibition on Optical Engineering and Photonics, Orlando, FL, 22-24 Apr. 1992 Sponsored by Ministry of Defence, Germany

(ISL-CO-216/92; ETN-94-95125) Avail: Issuing Activity (Fachinformationszentrum Karlsruhe, 7514 Eggenstein-Leopoldshafen 2, Germany)

A pulsed fringe type laser Doppler anemometer was developed during a feasibility study for remote wind velocity measurements. In contrast to conventional Doppler systems, this technique directly measures the cross components of the wind vector. Field measurements over a range of 100 m demonstrated successfully the performance of this method and showed eventual restricting atmospheric conditions. ESA

N94-20559 San Diego State Univ., CA. Center for Hydro-optics and Remote Sensing.

OPTICAL CLIMATOLOGY OF THE NORTHEAST PACIFIC OCEAN Final Report

James L. Mueller 3 Mar. 1993 127 p Limited Reproducibility: More than 20% of this document may be affected by microfiche quality

(Contracts N00014-87-C-6002; N00014-89-C-6007; DA Proj. R12-99) (AD-A271671; CHORS-001-93; NRL-CR/7410-93-0004) Avail: CASI HC A07

This report describes the results of a climatological study of optical variability in the upper 200 m of the Northeast Pacific Ocean. This work was supported by the Oceanographer of the Navy under NORDA/NOARL contracts N00014-87-C-6002 (SIO Visibility Lab., UCSD, La Jolla, CA) and N00014-89-C-6007 (SDSU CHORS, San Diego, CA), and this document constitutes our Final Report under those contracts. The project addressed two primary objectives. The first objective was to describe the two-dimensional spatial distribution and temporal variability of near-surface biooptical properties derived from satellite ocean color imagery, and to deliver the results in the form of a data base suitable for the developing new environmental products to support naval applications in the region. The second objective was to develop a model, with which the near-surface bio-optical properties derived from satellite data can be extrapolated downward to depths of interest for naval operations (i.e. 200 m). DTIC

N94-20565# Air Weather Service, Kessler AFB, MS. Detachment 5.

WEATHER TUTOR 1: STABILITY BASICS Interactive Training Package

Aug. 1993 19 p

(AD-A270758; AWS/ITP-93/001) Avail: CASI HC A03/MF A01

This is the first in a series of computer-based interactive packages produced by Air Weather Service for use by Air Force weather units. It consists of text (instructions for running and using the computer program) and three 3 1/2-inch diskettes containing program software that generate high-resolution graphic images, animation, and text. The training package is in three parts: the first familiarizes students with the relationships between atmospheric variables; the second correlates these variables to atmospheric stability using the parcel theory and the Equation of State; and the third and final part demonstrates the relationships of stability and moisture content with corresponding cloud scenes. An entry knowledge test is required before starting the lesson. DTIC

N94-20579# Naval Research Lab., Washington, DC.

A PARAMETRIC REPRESENTATION OF A THUNDERSTORM CELL Final Report

Gerard N. Vogel Sep. 1993 47 p

(AD-A271983; NRL/MR/7543-93-7209) Avail: CASI HC A03/MF A01

The TSTORM feature model, a simple parametric representation of a thunderstorm cell, is described. TSTORM is designed for use in simulations requiring an idealized magnitude and spatial distribution of significant meteorological parameters within a thunderstorm. A full description of the TSTORM algorithm, a test case demonstrating its capabilities, and a computer listing are provided. DTIC

N94-20600# Ecole Centrale de Lyon (France).

HYDROSTATIC/NONHYDROSTATIC COMPARISON WITH THE MERCURE CODE ON OROGRAPHIC FLOWS Ph.D. Thesis [COMPARAISON HYDROSTATIQUE/NON HYDROSTATIQUE AVEC LE CODE MERCURE SUR LES ECOULEMENTS OROGRAPHIQUES]

Ahmed Elkhalfi 1992 170 p In FRENCH

(ETN-93-94603) Avail: CASI HC A08/MF A02

A study of meteorologic flows over complex reliefs using the MERCURE model is reported. The analytic solution to the problem of simple mountain waves was first examined by finding out which conditions the models was capable of reproducing, and then nonlinear, and finally cases near to observation were examined. The equations used in the MERCURE model are presented. Different existing versions of the code were assembled into one single code and the use of the space memory and speed of calculation were improved. To avoid precision problems posed by the advection stage by the method of applied characteristics in cases of slight relief, a more simple schema of the advection type 'Euler backward' was developed, which enabled the validation of the model to be carried out on linear solutions of mountain waves. The numerical performance of the code during the three dimensional resolution of the pressure was improved. Besides the nonhydrostatic resolution of the pressure which already existed, a hydrostatic resolution was developed on the same version of the code MERCURE. This enabled the model to be used in the hydrostatic regime, as well as to address the convergence problems of the solver of pressure linked to the grid distortion. The two resolutions were compared for the simulation of flow over complex reliefs. The model was then applied to academic cases and finally to real situations. ESA

N94-20918 Utah State Univ., Logan. Center for Atmospheric and Space Sciences.

IMAGING RADAR STUDIES OF ATMOSPHERIC WINDS AND WAVES Final Report, 1 Mar. 1992 - 31 Aug. 1993

Kent L. Miller, R. G. Roper, G. W. Adams, and John W. Brosnahan 2 Sep. 1993 301 p Limited Reproducibility: More than 20% of this document may be affected by microfiche quality

(Contract F49620-92-J-0193)

(AD-A271672; CASS-93-3-01; AFOSR-93-0825TR) Avail: CASI HC A14

In this report, further analyses of data taken during the Arecibo Initiative in Dynamics of the Atmosphere (AIDA'89) campaigns are presented, concentrating on the third campaign (Scene III) from May 2-9, 1989. The major emphasis is on the comparison between the MAPSTAR Imaging Doppler Interferometry (IDI) radar and the Arecibo Observatory incoherent scatter (ISR) radar, but some comparisons with the Geospace Corporation meteor wind radar (MWR) and the Arecibo Observatory Fabry-Perot spectrometer (FPS) are also included. A re-analysis of four IDI - ISR - MWR comparisons show better agreement between all three techniques than previously reported. In general, better agreement was found between the daytime radar winds than that previously published for the April campaign, with the zonal winds agreeing better than the meridional. In contrast, the nighttime IDI - FPS comparisons showed better agreement in the meridional component and considerably better agreement after midnight than before.

DTIC

N94-21052 GKSS-Forschungszentrum Geesthacht (Germany). Inst. fuer Physik.

HOLOGRAPHIC MEASUREMENTS OF ICE CRYSTALS IN CIRRUS CLOUDS DURING INTERNATIONAL CIRRUS EXPERIMENT ICE Thesis - Cologne Univ. [HOLOGRAPHISCHE MESSUNGEN AN EISKRISTALLEN IN CIRRUSWOLKEN WAEHREND DES INTERNATIONALEN CIRRUS EXPERIMENTS ICE]

C. Krupp 31 Jan. 1992 144 p In GERMAN Limited Reproducibility: More than 20% of this document may be affected by microfiche quality
(GKSS-92/E/14; ETN-93-94185) Copyright Avail: CASI HC A07

An airborne holographic system is described. The system was employed during the International Cirrus Experiment in 1989. Ice particle concentration, size and shape were determined in three height levels in cirrus clouds and assigned to the surrounding temperature and humidity. Most of the particles were found to be smaller than 100 micrometers. Hexagonal columns, bullets, particles of irregular shape, and only a few hexagonal plates were detected. Nearly all particles larger than 200 micrometers showed a complex internal structure. Most of them were bullet rosettes and combinations of columns. Only one rimed column and one frozen big drop were found in the sampled data. The limitations and uncertainties of the holographic system were investigated and proposals for improvements are made. An improved system would be able to collect images of particles as small as 20 micrometers and determine their concentration and size. The development of a proposed new holographic system should be able to detect particles as small as 8 micrometers. The very labor intensive data extraction process outlines the need for the development of an automatic image analyzing system, which is also discussed. ESA

N94-21070# World Meteorological Organization, Geneva (Switzerland).
SIMULATED REAL-TIME INTERCOMPARISON OF HYDROLOGICAL MODELS
1992 256 p
(WMO-779; OHR-38; ISBN-9-26-310779-3; ETN-93-94843) Copyright
Avail: CASI MF A03; print copy available from WMO, Geneva, Switzerland

A study to compare the abilities of both rainfall runoff and snowmelt runoff models to forecast streamflow under simulated real time conditions is presented. The results of the study are reported, thus offering guidance through demonstrations of the models' abilities in various situations. Case studies from operators of real time hydrologic forecasting systems are reported, thus permitting inclusion of actual operational experiences not contained in the simulated real time exercise. The material prepared was disseminated to interested countries in order to encourage the adoption of such approaches to forecasting runoff and to assist countries that plan to use models for forecasting. ESA

N94-21146 Naval Postgraduate School, Monterey, CA.
INCORPORATION AND COMPARATIVE EVALUATION OF A NON-CONVECTIVE CLOUD PARAMETERIZATION SCHEME IN THE NAVAL RESEARCH LABORATORY WEST COAST MESOSCALE WEATHER PREDICTION MODEL M.S. Thesis
Damacene V. Ferandez Jun. 1993 83 p Limited Reproducibility: More than 20% of this document may be affected by microfiche quality
(AD-A272417) Avail: Issuing Activity (Defense Technical Information Center (DTIC))

This study describes the incorporation of the Sundqvist et al. (1989) explicit non-convective cloud liquid water scheme into the Naval Research Laboratory (NRL) limited area dynamical weather prediction model. Comparisons were made between model runs with the non-convective cloud water scheme and those without the scheme to evaluate mesoscale wind pattern, longwave radiation, temperature, and cloud simulations over the U.S. West Coast for the time period 0000 UTC 02 May 1990 to 1200 UTC 03 May 1990. The most significant improvement in the updated model was the more physically realistic horizontal and vertical non-convective cloud structures produced by the cloud liquid water fields. DTIC

N94-21212# Massachusetts Inst. of Tech., Lexington. Lincoln Lab.
A RETRIEVAL ERROR ANALYSIS TECHNIQUE FOR PASSIVE INFRARED ATMOSPHERIC SOUNDERS Technical Report
John P. Kerekes 8 Jul. 1993 50 p
(Contract F19628-90-C-0002)
(AD-A272618; TR-978; ESC-TR-92-204) Avail: CASI HC A03/MF A01

To support the design and analysis of passive infrared atmospheric sounding instruments, an analytical error analysis technique has been implemented. This technique is based on a linear approximation to the radiative transfer equation and uses a minimum variance estimation approach to atmospheric profile retrieval. As a result, once the proper matrices have been constructed an estimate of the retrieval error is computed through a single linear matrix equation. The solution vector is written with temperature and water vapor explicitly defined, thus producing the error vector for both simultaneously. Examples showing typical results are presented for a high spectral resolution sounder as well as for a lower resolution, filter-wheel type of instrument. DTIC

N94-21250# Air Force Inst. of Tech., Wright-Patterson AFB, OH. Foreign Aerospace Science and Technology Center.
ANALYSIS OF A SANDSTORM WEATHER PROCESS-TRANSLATION
Dongzhen Yang and Xiangming Ji 5 Nov. 1993 23 p Transl. into ENGLISH from Yici Huangsha Tianqi Guocheng Di Fenxi, Qixiang Xuebao Meteorology (China), v. 49, no. 3, Aug. 1991 p 334-342
(AD-A272959; FASTC-ID(RS)T-0331-93) Avail: CASI HC A03/MF A01

The favorable synoptic situation and climate background for a sandstorm process, which occurred in the period from the 9th to the 16th of April 1988, has been studied through analyzing weather maps, meteorological elements, satellite cloud pictures, and sandstorm trajectories. The sand dust origin area, the directions and the paths of sand dust transportation, and the extent the sand dust reached were also investigated. The results of measurements and analysis indicate that the concentration of sand dust particles is ten times greater than the normal. It is also shown that the elements in the sand dust are lithophile and come from natural source through the chemical composition analysis of the sand dust, so that the sand dust has not been seriously polluted by human activities. DTIC

N94-21307 Naval Postgraduate School, Monterey, CA.
LARGE-SCALE CIRCULATION REGIMES AND TROPICAL CYCLONE CHARACTERISTICS OVER THE WESTERN PACIFIC OCEAN Ph.D. Thesis
Patrick A. Harr Jun. 1993 300 p Limited Reproducibility: More than 20% of this document may be affected by microfiche quality
(AD-A273004) Avail: Issuing Activity (Defense Technical Information Center (DTIC))

The basic structure of the variability of the large-scale circulations over the tropical western North Pacific is investigated with respect to its influence on tropical cyclone characteristics. A vector empirical orthogonal function analysis and a fuzzy cluster algorithm are used to define six recurrent 700 mb circulation patterns that represent large-scale variabilities associated with the monsoon trough and subtropical ridge. Three circulation patterns are associated with an active monsoon trough, and two patterns represent an inactive monsoon trough. One pattern depicts small deviations from the long-term climatology. The 700 mb circulation patterns are shown to be physically consistent with outgoing longwave radiation anomalies and the 200 mb stream function and velocity potential anomalies. A seventh set of circulation patterns is defined to contain transition periods between the active, inactive, and small anomaly patterns. Transitions between recurrent circulation patterns may be within the active or the inactive patterns, or be transitions across the active/inactive boundary that are associated with major circulation changes. These significant transitions occur over a very limited set of paths, which are shown to be associated with interactions among tropical and midlatitude circulation systems. The recurrent circulation patterns and their transitions are shown to explain much of the observed intraseasonal variability in the occurrence and track types (recurving versus straight-moving) of tropical cyclones over the western North Pacific. DTIC

N94-21312 GKSS-Forschungszentrum Geesthacht (Germany). Inst. fuer Physik.
COMPUTERIZED SIMULATIONS WITH CELLULAR AUTOMATES FOR CLOUD FORMATION Thesis - Cologne Univ.
[COMPUTERSIMULATIONEN MIT ZELLULARAUTOMATEN FUER WOLKENBILDUNG]
K. Nagel 24 Feb. 1992 104 p In GERMAN Limited Reproducibility: More than 20% of this document may be affected by microfiche quality
(GKSS-92/E/22; ETN-93-94187) Copyright Avail: CASI HC A06

Starting from the phenomenology of cloud formation, a cellular automaton simulation model of the process is derived. The model turns out to have a strong resemblance to percolation based growth models; percolation plays an important role in the theory of random fractals. Projections of thereby produced clusters show a realistic fractal dimension of the perimeter, but only at or near the critical percolation threshold P(sub c). A mechanism based on the continuity equation is proposed and numerically tested which possibly explains why the atmosphere acts in fact near its critical threshold during cloud formation (self organizing criticality). Numerically, this is achieved

by a feedback of the number of 'active' sites on the occupation concentration p. ESA

N94-21356# Naval Command, Control and Ocean Surveillance Center, San Diego, CA. Research, Development, Test and Evaluation Div.
NOVAM EVALUATION UTILIZING ELECTRO-OPTICS AND METEOROLOGICAL DATA FROM KEY-90 Final Technical Report
S. G. Gathman, W. P. Hooper, J. E. James, H. E. Garber, and K. Davidson Sep. 1993 74 p
(AD-A271722; NRAD-TR-1608) Avail: CASI HC A04/MF A01

An experiment known as KEY-90 took place in the Straits of Florida, from 2 to 19 July 1990. The center of operations was the town of Marathon, which is in the center of the Florida Keys. The experiment's principal objective was to verify the Naval Oceanic Vertical Aerosol Model (NOVAM) and its kernel, the Navy Aerosol Model (NAM), in a tropical ocean scenario. The data collected during KEY-90 included aerosol particle-size distributions, lidar profiles, pertinent meteorological observations, and ocean surface parameters. Shore stations, a boat, buoys, radiosondes, and aircraft provided platforms to obtain these data. These measurements determined the structure of the atmospheric surface boundary layer. This report presents a general overview of these experiments, a description of the data available from KEY-90, and specific examples of these data for 14 July 1990. DTIC

N94-21427# National Oceanic and Atmospheric Administration, Boulder, CO. Forcast Systems Lab.
DEVELOPMENT AND TESTS OF A CLOUD PHYSICS PARAMETERIZATION FOR REAL-TIME AVIATION AND PUBLIC NUMERICAL WEATHER FORECASTING
P. Schultz Apr. 1993 48 p
(PB93-202711; NOAA-TM-ERL-FSL-6) Avail: CASI HC A03/MF A01

A package of FORTRAN subroutines for parameterizing condensation and precipitation processes in mesoscale models is described. The code is tailored to the requirements of operational weather forecasting for the aviation community and for public weather forecasting. As such, the emphasis is on computing efficiency, performance verification, simplicity of design (for rapid problem resolution), and regional tailorability. Results from preliminary testing are presented. A variety of procedures illustrate model attributes such as water mass conservation and physical realism, and some of the algorithm's limitations. NTIS

N94-21502 Air Force Inst. of Tech., Wright-Patterson AFB, OH.
THE SEA BREEZE CONVERGENCE ZONE AND ITS RELATIONSHIP TO FAIR WEATHER ELECTRICITY IN EAST CENTRAL FLORIDA M.S. Thesis
Sabrina Taijeron 1993 113 p Limited Reproducibility: More than 20% of this document may be affected by microfiche quality
(AD-A268511; AFIT/CI/CIA-93-121) Avail: Issuing Activity (Defense Technical Information Center (DTIC))

This research focused on the relationship between the fair weather electric field and the sea breeze convergence zone at the KSC/CCAFS. Wind sensor and electric field mill data from the CaPE project were analyzed. This study did not reveal any clear indication of a higher electric field during sea breeze convergence. The two phenomena exist, but their interactions appear to be weak. The expected interaction might be found in bigger data sets or through other types of analysis. DTIC

N94-21519# Federal Aviation Administration, Atlanta, GA.
NEXT GENERATION WEATHER RADAR (NEXRAD) PRINCIPAL USER PROCESSOR (PUP) OPERATIONAL TEST AND EVALUATION (OT/E) Operational Report
Baxter Stretcher Oct. 1993 38 p
(AD-A273075; DOT/FAA/CT-TN93/36) Avail: CASI HC A03/MF A01

This report details the results of the Operational Test and Evaluation (OT&E) Operational Test of the Next Generation Weather Radar (NEXRAD), Principle User Processor (PUP). The PUP was evaluated at the Leesburg, Virginia, and Houston, Texas, Air Route Traffic Control Centers (ARTCC) during the period 22 Mar. through 1 Apr. 1993. The objective of the OT&E Operational Test was to obtain the Central Weather Service Unit (CWSU) meteorologists' evaluation of the NEXRAD PUP. A questionnaire was used to obtain responses from the meteorologists. This report includes the meteorologists' evaluation of the quality and quantity of the products provided by the PUP, the workload, operational procedures, radar connections, and training. DTIC

N94-21605*# National Aeronautics and Space Administration. Goddard Space Flight Center, Greenbelt, MD.
A SYNOPTIC-SCALE OVERVIEW OF THE TOGA COARE INTENSIVE OBSERVING PERIOD NOVEMBER 1992 TO FEBRUARY 1993 BASED ON ANALYSES FROM US OPERATIONAL GLOBAL DATA ASSIMILATION SYSTEMS
M. Fiorino (Universities Space Research Association, Columbia, MD.), S. J. Lord (National Meteorological Center, Camp Springs, MD.), W. K.-M. Lau, P. A. Phoebus (Naval Research Lab., Monterey, CA.), and C. G. Strey (Fleet Numerical Oceanography Center, Monterey, CA.) Nov. 1993 270 p
(NASA-TM-104593; Rept-94B00015; NAS 1.15:104593) Avail: CASI HC A12/MF A03

The operational global analyses from the two major U.S. numerical weather prediction centers, the Navy's Fleet Numerical Oceanography Center and the National Meteorological Center, are used to describe the synoptic-scale features of the 1 Nov. 1992 to 28 Feb. 1993 TOGA COARE intensive observing period (IOP). TOGA COARE is an international field experiment in which a large number of research scientists from the Goddard Laboratory for Atmospheres (Code 910) and the Laboratory for Hydrospheres (Code 970) participated. Two high-amplitude intraseasonal (30-60 day) oscillations passed through the TOGA COARE observational network located in the equatorial western Pacific. Associated with the oscillations were two 6-10 day periods of persistent westerly surface winds at the equator or 'westerly wind bursts.' These events are depicted through time series and time-longitude cross sections of divergence/velocity potential, surface winds, precipitation, ocean mixed-layer depth, and sea surface temperature. The high and low frequency components of the flow in which the intraseasonal oscillations were embedded are shown using seasonal, monthly, and 5-day averages of the surface, 850 and 200 mb winds, precipitation, and sea-level pressure, and a time-longitude cross section of tropical cyclone activity. Independent verification of precipitation comes from near real-time satellite estimates, and a reference climatology is given based on 9 years of ECMWF analyses. Daily 00 UTC analyses of surface winds and sea-level pressure for the entire western Pacific and Indian Ocean are provided to trace the evolution of individual synoptic events. Author (revised)

N94-21639*# National Aeronautics and Space Administration. Goddard Inst. for Space Studies, New York, NY.
LONG-TERM MONITORING OF GLOBAL CLIMATE FORCINGS AND FEEDBACKS
J. Hansen, ed. (National Aeronautics and Space Administration. Goddard Space Flight Center, Greenbelt, MD.), W. Rossow, ed. (National Aeronautics and Space Administration. Goddard Space Flight Center, Greenbelt, MD.), and I. Fung, ed. (National Aeronautics and Space Administration. Goddard Space Flight Center, Greenbelt, MD.) Sep. 1993 101 p Workshop held in New York, NY, 3-4 Feb. 1992 Original contains color illustrations
(NASA-CP-3234; Rept-93E02369; NAS 1.55:3234) Avail: CASI HC A06/MF A02; 13 functional color pages

A workshop on Long-Term Monitoring of Global Climate Forcings and Feedbacks was held February 3-4, 1992, at NASA's Goddard Institute for Space Studies to discuss the measurements required to interpret long-term global temperature changes, to critique the proposed contributions of a series of small satellites (Climsat), and to identify needed complementary monitoring. The workshop concluded that long-term (several decades) of continuous monitoring of the major climate forcings and feedbacks is essential for understanding long-term climate change. For individual titles, see N94-21640 through N94-21648.

N94-21640*# National Oceanic and Atmospheric Administration, Princeton, NJ. Geophysical Fluid Dynamics Lab.
MONITORING ISSUES FROM A MODELING PERSPECTIVE
Jerry D. Mahlman *In* NASA. Goddard Inst. for Space Studies, Long-Term Monitoring of Global Climate Forcings and Feedbacks Sep. 1993 p 1-5
(For primary document see N94-21639 05-47)
Avail: CASI HC A01/MF A02; 13 functional color pages

Recognition that earth's climate and biogeophysical conditions are likely changing due to human activities has led to a heightened awareness

of the need for improved long-term global monitoring. The present long-term measurement efforts tend to be spotty in space, inadequately calibrated in time, and internally inconsistent with respect to other instruments and measured quantities. In some cases, such as most of the biosphere, most chemicals, and much of the ocean, even a minimal monitoring program is not available. Recently, it has become painfully evident that emerging global change issues demand information and insights that the present global monitoring system simply cannot supply. This is because a monitoring system must provide much more than a statement of change at a given level of statistical confidence. It must describe changes in diverse parts of the entire earth system on regional to global scales. It must be able to provide enough input to allow an integrated physical characterization of the changes that have occurred. Finally, it must allow a separation of the observed changes into their natural and anthropogenic parts. The enormous policy significance of global change virtually guarantees an unprecedented level of scrutiny of the changes in the earth system and why they are happening. These pressures create a number of emerging challenges and opportunities. For example, they will require a growing partnership between the observational programs and the theory/modeling community. Without this partnership, the scientific community will likely fall short in the monitoring effort. The monitoring challenge before us is not to solve the problem now, but rather to set appropriate actions in motion so as to create the required framework for solution. Each individual piece needs to establish its role in the large problem and how the required interactions are to take place. Below, we emphasize some of the needs and opportunities that could and should be addressed through participation by the theoreticians and modelers in the global change monitoring effort. Derived from text

N94-21641*# National Aeronautics and Space Administration. Goddard Inst. for Space Studies, New York, NY.

CLIMATE FORCINGS AND FEEDBACKS

James Hansen *In its* Long-Term Monitoring of Global Climate Forcings and Feedbacks Sep. 1993 p 6-12 (For primary document see N94-21639 05-47)

Avail: CASI HC A02/MF A02; 13 functional color pages

Global temperature has increased significantly during the past century. Understanding the causes of observed global temperature change is impossible in the absence of adequate monitoring of changes in global climate forcings and radiative feedbacks. Climate forcings are changes imposed on the planet's energy balance, such as change of incoming sunlight or a human-induced change of surface properties due to deforestation. Radiative feedbacks are radiative changes induced by climate change, such as alteration of cloud properties or the extent of sea ice. Monitoring of global climate forcings and feedbacks, if sufficiently precise and long-term, can provide a very strong constraint on interpretation of observed temperature change. Such monitoring is essential to eliminate uncertainties about the relative importance of various climate change mechanisms including tropospheric sulfate aerosols from burning of coal and oil smoke from slash and burn agriculture, changes of solar irradiance changes of several greenhouse gases, and many other mechanisms. The considerable variability of observed temperature, together with evidence that a substantial portion of this variability is unforced indicates that observations of climate forcings and feedbacks must be continued for decades. Since the climate system responds to the time integral of the forcing, a further requirement is that the observations be carried out continuously. However, precise observations of forcings and feedbacks will also be able to provide valuable conclusions on shorter time scales. For example, knowledge of the climate forcing by increasing CFC's relative to the forcing by changing ozone is important to policymakers, as is information on the forcing by CO2 relative to the forcing by sulfate aerosols. It will also be possible to obtain valuable tests of climate models on short time scales, if there is precise monitoring of all forcings and feedbacks during and after events such as a large volcanic eruption or an El Nino.

Derived from text

N94-21642*# National Aeronautics and Space Administration. Goddard Inst. for Space Studies, New York, NY.

ACCURACY REQUIREMENTS

Anthony DelGenio *In its* Long-Term Monitoring of Global Climate Forcings and Feedbacks Sep. 1993 p 13-19 (For primary document see N94-21639 05-47)

Avail: CASI HC A02/MF A02; 13 functional color pages

Satellite and surface measurements, if they are to serve as a climate monitoring system, must be accurate enough to permit detection of changes of climate parameters on decadal time scales. The accuracy requirements are difficult to define a priori since they depend on unknown future changes of climate forcings and feedbacks. As a framework for evaluation of candidate Climsat instruments and orbits, we estimate the accuracies that would be needed to measure changes expected over two decades based on theoretical considerations including GCM simulations and on observational evidence in cases where data are available for rates of change. One major climate forcing known with reasonable accuracy is that caused by the anthropogenic homogeneously mixed greenhouse gases (CO2, CFC's, CH4 and N2O). Their net forcing since the industrial revolution began is about 2 W/sq m and it is presently increasing at a rate of about 1 W/sq m per 20 years. Thus for a competing forcing or feedback to be important, it needs to be of the order of 0.25 W/sq m or larger on this time scale. The significance of most climate feedbacks depends on their sensitivity to temperature change. Therefore we begin with an estimate of decadal temperature change. Presented are the transient temperature trends simulated by the GISS GCM when subjected to various scenarios of trace gas concentration increases. Scenario B, which represents the most plausible near-term emission rates and includes intermittent forcing by volcanic aerosols, yields a global mean surface air temperature increase Delta Ts = 0.7 degrees C over the time period 1995-2015. This is consistent with the IPCC projection of about 0.3 degrees C/decade global warming (IPCC, 1990). Several of our estimates below are based on this assumed rate of warming. Derived from text

N94-21643*# National Aeronautics and Space Administration. Goddard Inst. for Space Studies, New York, NY.

CLIMSAT RATIONALE

James Hansen *In its* Long-Term Monitoring of Global Climate Forcings and Feedbacks Sep. 1993 p 26-35 (For primary document see N94-21639 05-47)

Avail: CASI HC A02/MF A02; 13 functional color pages

We summarize reasons for the Climsat proposition; we also stress the need for certain climate monitoring other than that supplied by Climsat, especially solar irradiance, and we stress the complementarity of Climsat monitoring to plans for detailed EOS measurements. Existing and planned observations will not provide measurements of most climate forcing and feedback parameters with the accuracy needed to measure plausible decadal changes. Stratospheric water vapor and aerosol requirements are not met, for example, even though the present SAGE II instrument on the ERBS spacecraft measures those two parameters accurately, because ERBS is not expected to last more than a few years and it does not provide global coverage. We stress the imminence of a potential data gap even of those parameters, such as solar irradiance and stratospheric aerosols, for which monitoring capability has been proven and currently is in place. We find that most of the missing global climate forcings and feedbacks can be measured by three small instruments, which would need to be deployed on two spacecraft to obtain adequate sampling and global coverage. The monitoring must be maintained continuously for at least two decades. Such continuity can be attained by replacing a satellite after it fails, the functioning satellite providing calibration transfer to the new satellite. Certain complementary monitoring data are also needed, including solar monitoring from space, in order to fully meet requirements for monitoring all the climate forcings and feedbacks. The complementary data needs are discussed toward the end of this section. We summarize the proposed Climsat measurements and compare the expected accuracies to those which are needed to analyze changes of the global thermal energy cycle on decadal time scales. We stress the need to get broader participation of the scientific community in the monitoring and analysis activity. Finally, we discuss related climate process and diagnostic measurements.

Derived from text

N94-21644*# National Aeronautics and Space Administration. Langley Research Center, Hampton, VA.

STRATOSPHERIC AEROSOL AND GAS EXPERIMENT (SAGE 3)

M. P. McCormick *In* NASA. Goddard Inst. for Space Studies, Long-Term Monitoring of Global Climate Forcings and Feedbacks Sep. 1993 p 36-39 (For primary document see N94-21639 05-47)

Avail: CASI HC A01/MF A02; 13 functional color pages

The proposed SAGE III instrument would be the principal source of

data for global changes of stratospheric aerosols, stratospheric water vapor, and ozone profiles, and a contributing source of data for upper tropospheric water vapor, aerosols, and clouds. The ability to obtain such data has been demonstrated by the predecessor instrument, SAGE II, but SAGE III will be substantially more capable, as discussed below. The capabilities for monitoring the profiles of atmospheric constituents have been verified in detail, including ground-based validations, for aerosol, ozone, and water vapor. Indeed, because of its self-calibrating characteristics, SAGE II was an essential component of the international ozone trend assessments, and SAGE II is now proving to be invaluable in tracking the aerosols from Mt. Pinatubo. Although SAGE profiles generally terminate at the height of the first tropospheric cloud layer, it has been found that the measurements extend down to 3 km altitude more than 40 percent of the time at most latitudes. Thus, useful information can also be obtained on upper tropospheric aerosols, water vapor, and ozone. Derived from text

N94-21645*# National Aeronautics and Space Administration. Goddard Inst. for Space Studies, New York, NY.

EARTH OBSERVING SCANNING POLARIMETER **c43**

Larry Travis *In its* Long-Term Monitoring of Global Climate Forcings and Feedbacks Sep. 1993 p 40-46 (For primary document see N94-21639 05-47)

Avail: CASI HC A02/MF A02; 13 functional color pages

Climate forcing by tropospheric aerosols is receiving increased attention because of the realization that the climate effects may be large, while our knowledge of global aerosol characteristics and temporal changes is very poor. Tropospheric aerosols cause a direct radiative forcing due simply to their scattering and absorption of solar radiation, as well as an indirect effect as cloud condensation nuclei which can modify the shortwave reflectivity of clouds. Sulfate aerosols tend to increase planetary albedo through both the direct and indirect effects; a cooling due to anthropogenic sulfate aerosols has been estimated of order 1 W/sq m, noting that this is similar in magnitude to the present anthropogenic greenhouse gas warming. Other aerosols, including those from biomass burning and wind-blown desert dust are also of potential climatic importance. At present, the only global monitoring of tropospheric aerosols is a NOAA operational product, aerosol optical thickness, obtained using channel-1 (0.58-0.68 mu m) radiances from the AVHRR. With this single channel radiance data, one must use an approach which is based on the inferred excess of reflected radiance owing to scattering by the aerosols over that expected from theoretical calculations. This approach is suited only for situations where the surface has a low albedo that is well known a priori. Thus, the NOAA operational product is restricted to coverage over the ocean at AVHRR scan angles well away from sun glint, and aerosol changes are subject to confusion with changes caused by either optically thin or subpixel clouds. Because optically thin aerosols have only a small effect on the radiance, accurate measurements for optical thickness less than 0.1 (which is a typical background level) are precluded. Moreover, some of the largest and most important aerosol changes are expected over land. The Earth Observing Scanning Polarimeter (EOSP) instrument, based upon design heritage and analysis techniques developed for planetary missions, will retrieve tropospheric aerosol characteristics from measurements of multispectral radiance and polarization. Moreover, the same radiance and polarization measurements will also provide very precise information on cloud properties and maps of surface characteristics for cloud-free regions. These capabilities also give EOSP the unique ability to discriminate aerosol from clouds and surface. Derived from text

N94-21646*# National Aeronautics and Space Administration. Goddard Inst. for Space Studies, New York, NY.

MICHELSON INTERFEROMETER (MINT) **c35**

Andrew Lacis and Barbara Carlson *In its* Long-Term Monitoring of Global Climate Forcings and Feedbacks Sep. 1993 p 47-53 (For primary document see N94-21639 05-47)

Avail: CASI HC A02/MF A02; 13 functional color pages

MINT is a Michelson interferometer designed to measure the thermal emission from the earth at high spectral resolution (2/cm) over a broad spectral range (250-1700/cm, 6-40 mu m) with contiguous 3-pixel wide (12 mrad, 8 km field of view) along-track sampling. MINT is particularly well suited for monitoring cloud properties (cloud cover, effective temperature, optical thickness, ice/water phase, and effective particle size) both day and night, as well as tropospheric water vapor, ozone, and temperature. The key instrument characteristics that make MINT ideally suited for decadal monitoring purposes are: high wavelength to wavelength precision across the full IR spectrum with high spectral resolution; space-proven long-term durability and calibration stability; and small size, low cost, low risk instrument incorporating the latest detector and electronics technology. MINT also incorporates simplicity in design and operation by utilizing passively cooled DTGS detectors and nadir viewing geometry (with target motion compensation). MINT measurement objectives, instrument characteristics, and key advantages are summarized in this paper. Derived from text

N94-21647*# Texas A&M Univ., College Station.

ORBIT AND SAMPLING REQUIREMENTS: TRMM EXPERIENCE

Gerald North *In* NASA. Goddard Inst. for Space Studies, Long-Term Monitoring of Global Climate Forcings and Feedbacks Sep. 1993 p 54-56 (For primary document see N94-21639 05-47)

Avail: CASI HC A01/MF A02; 13 functional color pages

The Tropical Rainfall Measuring Mission (TRMM) concept originated in 1984. Its overall goal is to produce datasets that can be used in the improvement of general circulation models. A primary objective is a multi-year data stream of monthly averages of rain rate over 500 km boxes over the tropical oceans. Vertical distributions of the hydrometers, related to latent heat profiles, and the diurnal cycle of rainrates are secondary products believed to be accessible. The mission is sponsored jointly by the U.S. and Japan. TRMM is an approved mission with launch set for 1997. There are many retrieval and ground truth issues still being studied for TRMM, but here we concentrate on sampling since it is the single largest term in the error budget. The TRMM orbit plane is inclined by 35 degrees to the equator, which leads to a precession of the visits to a given grid box through the local hours of the day, requiring three to six weeks to complete the diurnal cycle, depending on latitude. For sampling studies we can consider the swath width to be about 700 km. Derived from text

N94-21648*# National Aeronautics and Space Administration. Goddard Inst. for Space Studies, New York, NY.

SATELLITE ORBIT AND DATA SAMPLING REQUIREMENTS

William Rossow *In its* Long-Term Monitoring of Global Climate Forcings and Feedbacks Sep. 1993 p 57-67 (For primary document see N94-21639 05-47)

Avail: CASI HC A03/MF A02; 13 functional color pages

Climate forcings and feedbacks vary over a wide range of time and space scales. The operation of non-linear feedbacks can couple variations at widely separated time and space scales and cause climatological phenomena to be intermittent. Consequently, monitoring of global, decadal changes in climate requires global observations that cover the whole range of space-time scales and are continuous over several decades. The sampling of smaller space-time scales must have sufficient statistical accuracy to measure the small changes in the forcings and feedbacks anticipated in the next few decades, while continuity of measurements is crucial for unambiguous interpretation of climate change. Shorter records of monthly and regional (500-1000 km) measurements with similar accuracies can also provide valuable information about climate processes, when 'natural experiments' such as large volcanic eruptions or El Ninos occur. In this section existing satellite datasets and climate model simulations are used to test the satellite orbits and sampling required to achieve accurate measurements of changes in forcings and feedbacks at monthly frequency and 1000 km (regional) scale. Derived from text

N94-21862*# National Aeronautics and Space Administration. Goddard Space Flight Center, Greenbelt, MD.

EMPIRICAL WIND MODEL FOR THE MIDDLE AND LOWER ATMOSPHERE. PART 2: LOCAL TIME VARIATIONS

A. E. Hedin, E. L. Fleming (Applied Research Corp., Landover, MD.), A. H. Manson (Saskatchewan Univ., Saskatoon.), F. J. Schmidlin (National Aeronautics and Space Administration. Wallops Flight Center, Wallops Island, VA.), S. K. Avery (Colorado Univ., Boulder.), R. R. Clark (New Hampshire Univ., Durham.), S. J. Franke (Illinois Univ., Urbana.), G. J. Fraser (Canterbury Univ., Christchurch, New Zealand.), T. Tsuda (Kyoto Univ., Japan.), and F. Vial (Ecole Polytechnique, Palaiseau, France.) et al Washington Nov. 1993 101 p

(NASA-TM-104592; NAS 1.15:104592; Rept-94B00005) Avail: CASI HC A06/MF A02

The HWM90 thermospheric wind model was revised in the lower

thermosphere and extended into the mesosphere and lower atmosphere to provide a single analytic model for calculating zonal and meridional wind profiles representative of the climatological average for various geophysical conditions. Local time variations in the mesosphere are derived from rocket soundings, incoherent scatter radar, MF radar, and meteor radar. Low-order spherical harmonics and Fourier series are used to describe these variations as a function of latitude and day of year with cubic spline interpolation in altitude. The model represents a smoothed compromise between the original data sources. Although agreement between various data sources is generally good, some systematic differences are noted. Overall root mean square differences between measured and model tidal components are on the order of 5 to 10 m/s. Author (revised)

N94-22280 Deutsche Forschungsanstalt fuer Luft- und Raumfahrt, Oberpfaffenhofen (Germany). Abt. Wolkenphysik.

A DOCUMENTATION OF ICING RELEVANT CLOUD PHYSICAL PARAMETERS ON HORIZONTAL SOUNDINGS OF STRATIFORM CLOUDS (CONTINUATION) [EINE DOKUMENTATION VEREISUNGSRELEVANTER WOLKENPHYSIKALISCHER PARAMETER BEI HORIZONTALSONDIERUNGEN STRATIFORMER WOLKEN (FORTSETZUNG)]

Hans-Eberhard Hoffmann and Johann Demmel Aug. 1992 83 p In GERMAN Limited Reproducibility: More than 20% of this document may be affected by poor print

(DLR-Mitt-92-10; ETN-93-94458) Avail: Issuing Activity (European Space Agency (ESA)); DLR, Zentrale Allgemeine Dieste, Versand, Postfach 90 60 58, 5000 Cologne 90, Germany, HC

The results of 22 further horizontal soundings were arranged according to their synoptic conditions. Among the results were the following: in clouds of a high pressure area, on flight paths between 40 and 75 km and when the distance from the cloud base was constant, the total water content (TWC) fluctuated between approximately equal to 0.10 and approximately equal to 0.18 g/cu m and between approximately equal to 0.10 and approximately 0.25 g/cu m respectively. The value for the median volume diameter (MVD) was always small, between 8 and 20 micrometers. In the vicinity of cold and warm fronts or in flow from different directions, the value of TWC fluctuated between 0 and 0.10 g/cu m up to between 0 and 0.55 g/cu m on flight distances between 35 and 145 km. The value of MVD had small or large values on flight distances of different length or fluctuated between small values (8 to 50 micrometers) and larger values (up to 600 micrometers). ESA

N94-22292*# National Aeronautics and Space Administration. Langley Research Center, Hampton, VA.

THE FIRE CIRRUS SCIENCE RESULTS 1993

David S. McDougal, ed. Washington Dec. 1993 222 p Conference held in Breckenridge, CO, 14-17 Jun. 1993 Sponsored in part by NSF, NOAA, DOE, and ONR

(RTOP 460-42-90-70)

(NASA-CP-3238; L-17365; NAS 1.55:3238) Avail: CASI HC A10/MF A03

FIRE (First ISCCP (International Satellite Cloud Climatology Project) Regional Experiment) is a U.S. cloud-radiation research program that seeks to improve our basic understanding and parameterizations of cirrus and marine stratocumulus cloud systems and ISCCP data products. The FIRE Cirrus Science Conference was held in Breckenridge, CO, 14-17 Jun. 1993, to present results of cirrus research for the second phase of FIRE (1989-present) and to refine cirrus research goals and priorities for the next phase of FIRE (1994-future). This Conference Publication contains the text of short papers presented at the conference. The papers describe research analyses of data collected at the Cirrus Intensive Field Observations-2 field experiment conducted in Kansas, 13 Nov. - 7 Dec. 1991. For individual titles, see N94-22293 through N94-22344.

N94-22293*# National Center for Atmospheric Research, Boulder, CO.

OVERVIEW OF MICROPHYSICAL AND STATE PARAMETER MEASUREMENTS FROM FIRE 2

Andrew J. Heymsfield and Larry M. Miloshevich *In* NASA. Langley Research Center, The FIRE Cirrus Science Results 1993 Dec. 1993 p 1-4 (For primary document see N94-22292 05-47)

Avail: CASI HC A01/MF A03

In this article we present data collected by the NCAR King Air and Sabreliner aircraft in the FIRE 2 cirrus project over southeastern Kansas and northeastern Oklahoma in Nov. and Dec. of 1991. We present state parameter and microphysical measurements in summary form for the dates which have been selected by the FIRE Science Team for intensive analysis, 25 and 26 Nov. and 5 and 6 Dec. We will also evaluate the performance of 'key' aircraft instrumentation. Author (revised)

N94-22294*# Desert Research Inst., Reno, NV.

CIRRUS MICROPHYSICS OBSERVATIONS MADE DURING FIRE 2: SMALL PARTICLES, HIGH CONCENTRATIONS, AND PROBE COMPARISONS

W. P. Arnott, Y. Y. Dong, J. Hallett, and M. R. Poellot (North Dakota Univ., Grand Forks.) *In* NASA. Langley Research Center, The FIRE Cirrus Science Results 1993 Dec. 1993 p 5-8 (For primary document see N94-22292 05-47)

(Grant NAG1-1113)

Avail: CASI HC A01/MF A03

Aircraft observations of cirrus cloud microphysics were made near Coffeyville, Kansas during Nov. and Dec. 1991. Cloud microphysics measurements were made using both a PMS 2DC probe and an ice particle replicator, both were mounted on the UND Citation aircraft. Intercomparison is made of the size, area, and ice mass spectra determined from these probes. The PMS 2DC undercounts particles for D less than 70 microns and the replicator oversizes particles for D greater than 150 microns, at least when column rosettes are encountered. High concentrations of particles with D less than 50 microns are noted in selected portions of the 22 Nov. 91 replicator data set. Relations between the maximum dimension of a crystal and its shadow area (known as area dimensional relationships) are computed from the PMS data. Area and mass dimensional relationships are used to give a simple analytical expression for computing the wavelength dependent absorption coefficient averaged over a size bin. Calculations based upon the replicator data show that crystals with D less than 50 microns contribute significantly to the solar extinction and infrared absorption coefficients during some time intervals. Author (revised)

N94-22295*# National Oceanic and Atmospheric Administration, Boulder, CO. Wave Propagation Lab.

CIRRUS PROPERTIES DEDUCED FROM CO2 LIDAR OBSERVATIONS OF ZENITH-ENHANCED BACKSCATTER FROM ORIENTED CRYSTALS 00

Wynn L. Eberhard *In* NASA. Langley Research Center, The FIRE Cirrus Science Results 1993 Dec. 1993 p 9-12 (For primary document see N94-22292 05-47)

Avail: CASI HC A01/MF A03

Many lidar researchers have occasionally observed zenith-enhanced backscatter (ZEB) from middle and high clouds. The ZEB signature consists of strong backscatter when the lidar is pointed directly at zenith and a dramatic decline in backscatter as the zenith angle dips slightly off zenith. Mirror-like reflection from horizontal facets of oriented crystals (especially plates) is generally accepted as the cause. It was found during a 3-year observation program that approximately 50 percent of ice clouds had ZEB, regardless of cloud height. The orientation of crystals and the ZEB they cause are important to study and understand for several reasons. First, radiative transfer in clouds with oriented crystals is different than if the same particles were randomly oriented. Second, crystal growth depends partly on the orientation of the particles. Third, ZEB measurements may provide useful information about cirrus microphysical and radiative properties. Finally, the remarkable effect of ZEB on lidar signals should be understood in order to properly interpret lidar data. Author (revised)

N94-22296*# National Aeronautics and Space Administration. Goddard Space Flight Center, Greenbelt, MD.

BI-DIRECTIONAL REFLECTANCE AND OTHER RADIATION PARAMETERS OF CIRRUS FROM ER-2 OBSERVATIONS

James Spinhime *In* NASA. Langley Research Center, The FIRE Cirrus Science Results 1993 Dec. 1993 p 13-16 (For primary document see N94-22292 05-47)

Avail: CASI HC A01/MF A03

Passive and active remote sensing of cirrus were acquired from the ER-2 high altitude aircraft in the 1991 Cirrus Experiment. The observations include direct measurements of cirrus bi-directional reflectance from a new translinear scanning radiometer and the previously employed measurements

by lidar and visible-infrared imaging radiometers. For any cirrus radiative transfer application, it is necessary to know the appropriate model for visible reflectance in relation to angle and also the optical thickness and infrared emissivity of the clouds. At a more complicated level, for remote sensing and overall cloud effects it is ultimately required to understand effects from multiple cloud layers, broken clouds, and variable microphysics. Our overall data set from the scanning radiometers and lidar is intended to provide the necessary observations to investigate these problems.
Author (revised)

N94-22297*# National Aeronautics and Space Administration. Ames Research Center, Moffett Field, CA.
OPTICAL PROPERTIES OF CIRRUS DERIVED FROM AIRBORNE MEASUREMENTS DURING FIRE IFO 2
Francisco P. J. Valero, Peter Pilewskie, Anthony Bucholtz, and Steven Platnick *In* NASA. Langley Research Center, The FIRE Cirrus Science Results 1993 Dec. 1993 p 17-19 (For primary document see N94-22292 05-47)
Avail: CASI HC A01/MF A03

The Radiation Measurement System (RAMS) on board the NASA ER-2 was used to acquire several optical parameters of interest during the FIRE Cirrus IFO 2. In this abstract we present results from the 26 Nov. IFO when the ER-2 flew over the Coffeyville airport hub site. We show retrieved optical thickness and cloud temperature, along with optical thickness obtained from RAMS instruments on the NCAR Sabreliner and at the surface site B. Independent retrieval of optical thickness, from the ER-2 and at the surface, are in agreement during the overpasses. Cirrus optical depths, derived from each platform, ranged between 1 and 2.
Author (revised)

N94-22298*# National Aeronautics and Space Administration. Goddard Space Flight Center, Greenbelt, MD.
INTERCOMPARISON OF MAS, AVIRIS, AND HIS DATA FROM FIRE CIRRUS 2
Liam E. Gumley (Research and Data Systems, Inc., Greenbelt, MD.), Michael D. King, Si-Chee Tsay, Bo-Cai Gao, and G. Thomas Arnold (Applied Research Corp., Landover, MD.) *In* NASA. Langley Research Center, The FIRE Cirrus Science Results 1993 Dec. 1993 p 20-23 (For primary document see N94-22292 05-47)
Avail: CASI HC A01/MF A03

The NASA ER-2 flight on 5 Dec. 1991 is unique among the FIRE Cirrus 2 missions in that data were acquired simultaneously by the MODIS Airborne Simulator (MAS), the Airborne Visible/Infrared Imaging Spectrometer (AVIRIS), and the High Resolution Interferometer Sounder (HIS). These data represent a unique source of information about the spatial and spectral properties of cirrus clouds. The MAS is a new instrument which will aid in defining algorithms and building an understanding of the ability of the Moderate Resolution Imaging Spectroradiometer (MODIS) to remotely sense atmospheric conditions for assessing global change. In order to establish confidence in the absolute calibration accuracy of the MAS radiances, an inter-comparison of MAS radiances with AVIRIS and HIS has been undertaken.
Author (revised)

N94-22299*# National Aeronautics and Space Administration. Langley Research Center, Hampton, VA.
COMPARISON OF RADIATION AND CLOUD PARAMETERS DERIVED FROM SATELLITE AND AIRCRAFT MEASUREMENTS DURING FIRE 2 CIRRUS IFO
Patrick W. Heck (Lockheed Engineering and Sciences Co., Hampton, VA.), Shalini Mayor (Lockheed Engineering and Sciences Co., Hampton, VA.), David F. Young (Lockheed Engineering and Sciences Co., Hampton, VA.), Patrick Minnis, Yoshihide Takano (Utah Univ., Salt Lake City.), Kuo-Nan Liou (Utah Univ., Salt Lake City.), and James D. Spinhirne (National Aeronautics and Space Administration. Goddard Space Flight Center, Greenbelt, MD.) *In its* The FIRE Cirrus Science Results 1993 Dec. 1993 p 24-27 (For primary document see N94-22292 05-47)
Avail: CASI HC A01/MF A03

Meteorological satellite instrument pixel sizes are often much greater than the individual cloud elements in a given scene. Partially cloud-filled pixels can be misinterpreted in many analysis schemes because the techniques usually assume that all of the cloudy pixels are cloud filled. Coincident Landsat and Geostationary Operational Environmental Satellite (GOES) data and degraded-resolution Landsat data were used to study the effects of both sensor resolution and analysis techniques on satellite-derived cloud parameters. While extremely valuable for advancing the understanding of these effects, these previous studies were relatively limited in the number of cloud conditions that were observed and by the limited viewing and illumination conditions. During the First ISCCP Regional Experiment (FIRE) Phase 2 (13 Nov. - 7 Dec. 1991), the NASA ER-2 made several flights over a wide range of cloud fields and backgrounds with several high resolution sensors useful for a variety of purposes including serving as ground truth for satellite-based cloud retrievals. This paper takes a first look at utilizing the ER-2 for validating cloud parameters derived from GOES and NOAA-11 Advanced Very High Resolution Radiometer (AVHRR) data.
Author (revised)

N94-22300*# Oregon State Univ., Corvallis. College of Oceanic and Atmospheric Sciences.
CLOUD PROPERTIES FROM THE ANALYSIS OF AVHRR OBSERVATIONS FOR FIRE 2
Xijian Lin and James A. Coakley, Jr. *In* NASA. Langley Research Center, The FIRE Cirrus Science Results 1993 Dec. 1993 p 28-31 (For primary document see N94-22292 05-47)
Avail: CASI HC A01/MF A03

Preliminary results are presented for cloud properties from the analysis of AVHRR observations for FIRE 2. The properties were obtained from a combination of the spatial coherence method and a multispectral retrieval scheme. Geographically gritted fields for the number of cloud layers were produced. For single layered cloud systems, fractional cloud cover, cloud emission temperature, cloud emissivity, and particle size were retrieved. Statistics on the properties of upper-level clouds and the Coffeeville cloud conditions are presented.
Author (revised)

N94-22301*# National Aeronautics and Space Administration. Langley Research Center, Hampton, VA.
DEVELOPMENT OF METHODS FOR INFERRING CLOUD THICKNESS AND CLOUD-BASE HEIGHT FROM SATELLITE RADIANCE DATA
William L. Smith, Jr. (Lockheed Engineering and Sciences Co., Hampton, VA.), Patrick Minnis, Joseph M. Alvarez, Taneil Uttal (National Oceanic and Atmospheric Administration, Boulder, CO.), Janet M. Intrieri (Colorado Univ., Boulder.), Thomas P. Ackerman (Pennsylvania State Univ., University Park.), and Eugene Clothiaux (Pennsylvania State Univ., University Park.) *In its* The FIRE Cirrus Science Results 1993 Dec. 1993 p 32-35 (For primary document see N94-22292 05-47)
Avail: CASI HC A01/MF A03

Cloud-top height is a major factor determining the outgoing longwave flux at the top of the atmosphere. The downwelling radiation from the cloud strongly affects the cooling rate within the atmosphere and the longwave radiation incident at the surface. Thus, determination of cloud-base temperature is important for proper calculation of fluxes below the cloud. Cloud-base altitude is also an important factor in aircraft operations. Cloud-top height or temperature can be derived in a straightforward manner using satellite-based infrared data. Cloud-base temperature, however, is not observable from the satellite, but is related to the height, phase, and optical depth of the cloud in addition to other variables. This study uses surface and satellite data taken during the First ISCCP Regional Experiment (FIRE) Phase-2 Intensive Field Observation (IFO) period (13 Nov. - 7 Dec. 1991, to improve techniques for deriving cloud-base height from conventional satellite data.
Author (revised)

N94-22302*# National Aeronautics and Space Administration. Langley Research Center, Hampton, VA.
CLOUD FIELDS DERIVED FROM SATELLITE AND SURFACE DATA DURING FIRE CIRRUS PHASE 2
Patrick Minnis, William L. Smith, Jr. (Lockheed Engineering and Sciences Co., Hampton, VA.), David F. Young (Lockheed Engineering and Sciences Co., Hampton, VA.), and Patrick W. Heck (Lockheed Engineering and Sciences Co., Hampton, VA.) *In its* The FIRE Cirrus Science Results 1993 Dec. 1993 p 36-39 (For primary document see N94-22292 05-47)
Avail: CASI HC A01/MF A03

The interpretation of surface and aircraft measurements of cloud properties taken during field programs must take into account the large-scale cloud and meteorological conditions. Cloud properties are also required at

scales beyond the point and line data taken from ground and aircraft platforms. Satellite data can provide a quantitative description of these large-scale cloud properties. When derived from geostationary satellite data, the cloud fields constitute a unique source for evaluating the development and demise of a cloud system. Satellites, however, can only see the tops of clouds, so that cloud layers below the uppermost cloud deck may remain undetected resulting in a incomplete depiction of the cloud system. Some multilayer clouds are amenable to detection from satellites. Many, especially in midlatitude cyclonic systems, can only be observed from the surface. A combination of surface and satellite cloud observations should be the most complete quantification of large-scale cloudiness if there are sufficient surface measurements. During the First International Satellite Cloud Climatology Project (ISCCP) Regional Experiment Phase 2 (FIRE-2) Cirrus Intensive Field Observation (IFO) period (November 13 - December 7, 1991) conducted at Coffeyville, Kansas, cirrus observations were taken in a variety of conditions. The IFO area was selected for a variety of reasons including the relatively dense network of surface weather stations and special surface instrumentation sites. Thus, the FIRE-2 IFO presents an excellent opportunity to combine cloud observations from surface and satellite observations. This paper presents an analysis of cloud properties on a mesoscale grid using satellite cloud property retrievals, surface observer data, and rawinsonde temperature and humidity profiles.

Derived from text

N94-22303*# National Aeronautics and Space Administration. Langley Research Center, Hampton, VA.

REMOTE SENSING OF MULTILEVEL CLOUDS DURING FIRE IFO 2 c43

Bryan A. Baum, J. Titlow (Lockheed Engineering and Sciences Co., Hampton, VA.), V. Tovinkere (Lockheed Engineering and Sciences Co., Hampton, VA.), M. Poellot (North Dakota Univ., Grand Forks.), T. P. Ackerman (Pennsylvania State Univ., University Park.), J. Alvarez, T. Uttal (National Oceanic and Atmospheric Administration, Boulder, CO.), and J. Intrieri (Colorado Univ., Boulder.) *In its* The FIRE Cirrus Science Results 1993 Dec. 1993 p 40-43 (For primary document see N94-22292 05-47)

Avail: CASI HC A01/MF A03

An unresolved difficulty in the remote sensing of clouds concerns the inability of the cloud retrieval algorithms to adequately recognize and analyze scenes containing overlapping cloud layers. Most cloud retrieval schemes, such as that used by the International Satellite Cloud Climatology Project (ISCCP) assume that each picture element (pixel) contains a single cloud layer. The current study begins to address the complexities of multilayered cloud property retrieval through the application of a modified multispectral, multiresolution (MSMR) method, first detailed in Baum et al. (1992), which merges 1.1 -km (at nadir) spectral data from the Advanced Very High Resolution Radiometer (AVHRR) with 17.4-km (at nadir) High Resolution Infrared Radiometer Sounder (HIRS/2, henceforth HIRS). Both instruments are flown aboard the National Oceanic and Atmospheric Administration (NOAA) polar-orbiting platforms. An ideal case study for this investigation is provided by the NOAA-11 overpass at 20:48 UTC on November 28, 1991. At this time, a large-scale cirrostratus veil overlaid a low-level stratus deck over much of the IFO region. There were both surface lidar and radar observations of the clouds as well as University of North Dakota (UND) Citation aircraft measurements. The presence of overlapping cloud layers within a HIRS FOV is determined from colocated AVHRR spectral data through the use of a fuzzy logic expert system. Conventional algorithms such as spatial coherence and CO2 slicing are used to retrieve cloud pressure and height for each identified cloud layer. The results from the satellite cloud retrieval analysis are compared to results from both surface- and aircraft-based measurements. Derived from text

N94-22304*# Colorado Univ., Boulder. Cooperative Inst. for Research in Environmental Sciences.

MICROPHYSICAL PROPERTIES OF THE NOVEMBER 26 CIRRUS CLOUD RETRIEVED BY DOPPLER RADAR/IR RADIOMETER TECHNIQUE

Sergey Y. Matrosov, Robert A. Kropfli (National Oceanic and Atmospheric Administration, Boulder, CO.), Brad W. Orr (National Oceanic and Atmospheric Administration, Boulder, CO.), and Jack B. Snider (National Oceanic and Atmospheric Administration, Boulder, CO.) *In* NASA. Langley Research Center, The FIRE Cirrus Science Results 1993 Dec. 1993 p 44-47 (For primary document see N94-22292 05-47)

Avail: CASI HC A01/MF A03

Gaining information about cirrus cloud microphysics requires development of remote sensing techniques. In an earlier paper. Matrosov et al. (1992) proposed a method to estimate ice water path (IWP) (i.e., vertically integrated ice mass content IMC) and characteristic particle size averaged through the cloud from combined groundbased measurements of radar reflectivities and IR brightness temperatures of the downwelling thermal radiation in the transparency region of 10-12 mu m. For some applications, the vertically averaged characteristic particle sizes and IWP could be the appropriate information to use. However, vertical profiles of cloud microphysical parameters can provide a better understanding of cloud structure and development. Here we describe a further development of the previous method by Matrosov et al. (1992) for retrieving vertical profiles of cirrus particle sizes and IMC rather than their vertically averaged values. In addition to measurements of radar reflectivities, the measurements of Doppler velocities are used in the new method. This provides us with two vertical profiles of measurements to infer two vertical profiles of unknowns, i.e., particle characteristic sizes and IMC. Simultaneous measurements of the IR brightness temperatures are still needed to resolve an ambiguity in particle size-fall velocity relationships. Derived from text

N94-22305*# Colorado Univ., Boulder. Cooperative Inst. for Research in Environmental Sciences.

LIDAR AND RADAR DERIVED CIRRUS MICROPHYSICAL PROPERTIES FOR THE 26 NOVEMBER 1991 CASE STUDY

Janet M. Intrieri and Graham Feingold *In* NASA. Langley Research Center, The FIRE Cirrus Science Results 1993 Dec. 1993 p 48-51 (For primary document see N94-22292 05-47)

Avail: CASI HC A01/MF A03

The Wave Propagation Laboratory's CO2 lidar (lambda = 10.6 microns) and Ka-band radar (lambda = 8.66 mm) operate at widely separated wavelengths; the differences in how the transmitted waves interact with cloud targets can be exploited to provide information that neither sensor could provide alone. This can be as simple as overlapping the data sets to provide additional coverage on cloud geometry (see Uttal and Intrieri, 1993) or combining the measurements in a theoretical framework to provide cirrus cloud parameters of the size spectrum, i.e., characteristic particle size and number concentration. In this paper, the latter option is described and an example case study presented to illustrate the types of information available for cloud and radiation transfer models. Derived from text

N94-22306*# National Aeronautics and Space Administration. Langley Research Center, Hampton, VA.

COMPARISON OF CLOUD MICROPHYSICAL PARAMETERS DERIVED FROM SURFACE AND SATELLITE MEASUREMENTS DURING FIRE PHASE 2

David F. Young (Lockheed Engineering and Sciences Co., Hampton, VA.), Patrick Minnis, Jack Snider (National Oceanic and Atmospheric Administration, Boulder, CO.), Taneil Uttal (National Oceanic and Atmospheric Administration, Boulder, CO.), Janet M. Intrieri (Colorado Univ., Boulder.), and Sergey Matrosov (Colorado Univ., Boulder.) *In its* The FIRE Cirrus Science Results 1993 Dec. 1993 p 52-55 (For primary document see N94-22292 05-47)

Avail: CASI HC A01/MF A03

Cloud microphysical properties are an important component in climate model parameterizations of water transport, cloud radiative exchange, and latent heat processes. Estimation of effective cloud particle size, liquid or ice water content, and optical depth from satellite-based instrumentation is needed to develop a climatology of cloud microphysical properties and to better understand and model cloud processes in atmospheric circulation. These parameters are estimated from two different surface data sets taken at Coffeyville, Kansas, during the First ISCCP Regional Experiment (FIRE) Phase-2 Intensive Field Observation (IFO) period (November 13 - December 7, 1991). Satellite data can also provide information about optical depth and effective particle size. This paper explores the combination of the FIRE-2 surface and satellite data to determine each of the cloud microphysical properties. Derived from text

N94-22307*# Wisconsin Univ., Madison. Cooperative Inst. for Meteorological Satellite Studies.

CIMSS FIRE RESEARCH ACTIVITIES

W. L. Smith, S. A. Ackerman, R. O. Knuteson, X. L. Ma, and H. E. Revercomb *In* NASA. Langley Research Center, The FIRE Cirrus Science Results 1993 Dec. 1993 p 56-61 (For primary document see N94-22292 05-47)
Avail: CASI HC A02/MF A03

An overview of the Cooperative Institute for Meteorological Satellite Studies' FIRE research activities is presented. Emphasis is on the analysis of the High-Resolution Interferometer Sounder (HIS) made from the ER-2 as well as ground based measurements made by the Atmospheric Emitted Radiance Interferometer (AERI) prototype. Author (revised)

N94-22308*# National Oceanic and Atmospheric Administration, Boulder, CO. Wave Propagation Lab.
PROGRESS IN INTERPRETING CO2 LIDAR SIGNATURES TO OBTAIN CIRRUS MICROPHYSICAL AND OPTICAL PROPERTIES
Wynn L. Eberhard *In* NASA. Langley Research Center, The FIRE Cirrus Science Results 1993 Dec. 1993 p 63-66 (For primary document see N94-22292 05-47)
Avail: CASI HC A01/MF A03

One cloud/radiation issue at FIRE 2 that has been addressed by the CO2 lidar team is the zenith-enhanced backscatter (ZEB) signature from oriented crystals. A second topic is narrow-beam optical depth measurements using CO2 lidar. This paper describes the theoretical models we have developed for these phenomena and the data-processing algorithms derived from them. Author (revised)

N94-22309*# National Aeronautics and Space Administration. Langley Research Center, Hampton, VA.
A NUMERICAL TECHNIQUE FOR THE CALCULATION OF CLOUD OPTICAL EXTINCTION FROM LIDAR
J. M. Alvarez and M. A. Vaughan (Science Applications International Corp., Hampton, VA.) *In its* The FIRE Cirrus Science Results 1993 Dec. 1993 p 67-70 (For primary document see N94-22292 05-47)
Avail: CASI HC A01/MF A03

A simple numerical algorithm which calculates optical extinction from cloud lidar data is presented. The method assumes a two-component atmosphere consisting of 'clear air' and cloud particulates. 'Clear air' may consist of either molecules only or a mix of molecules and atmospheric aerosols. For certain clouds, the method may be utilized to provide an estimate of the cloud-atmospheric parameter defined as the ratio of the cloud volume backscatter coefficient to the cloud extinction coefficient divided by the atmospheric volume backscatter coefficient at a given altitude. The cloud-atmospheric parameter may be estimated only from cloud data from which the optical thickness may reliably be used as a constraint on the numerical solution. This constraint provides the additional information necessary to obtain the cloud-atmospheric parameter. Conversely, the method may be applied to obtain cloud extinction and optical thickness from lidar cloud soundings if an estimate of the cloud-atmospheric parameter is available. Author (revised)

N94-22310*# National Oceanic and Atmospheric Administration, Boulder, CO. Wave Propagation Lab.
BREAKING KELVIN-HELMHOLTZ WAVES AND CLOUD-TOP ENTRAINMENT AS REVEALED BY K-BAND DOPPLER RADAR
Brooks E. Martner and F. Martin Ralph *In* NASA. Langley Research Center, The FIRE Cirrus Science Results 1993 Dec. 1993 p 71-74 Sponsored in part by FAA and NOAA (For primary document see N94-22292 05-47)
Avail: CASI HC A01/MF A03

Radars have occasionally detected breaking Kelvin-Helmholtz (KH) waves under clear-air conditions in the atmospheric boundary layer and in the free troposphere. However, very few direct measurements of such waves within clouds have previously been reported and those have not clearly documented wave breaking. In this article, we present some of the most detailed and striking radar observations to date of breaking KH waves within clouds and at cloud top and discuss their relevance to the issue of cloud-top entrainment, which is believed to be important in convective and stratiform clouds. Aircraft observations reported by Stith suggest that vortex-like circulations near cloud top are an entrainment mechanism in cumuliform clouds. Laboratory and modeling studies have examined possibility that KH instability may be responsible for mixing at cloud top, but direct observations have not yet been presented. Preliminary analyses shown here may help fill this gap. The data presented in this paper were obtained during two field projects in 1991 that included observations from the NOAA Wave Propagation Laboratory's K-band Doppler radar (wavelength = 8.7 mm) and special rawinsonde ascents. The sensitivity (-30 dBZ at 10 km range), fine spatial resolution (375-m pulse length and 0.5 degrees beamwidth), velocity measurement precision (5-10 cm s-1), scanning capability, and relative immunity to ground clutter make it sensitive to non-precipitating and weakly precipitating clouds, and make it an excellent instrument to study gravity waves in clouds. In particular, the narrow beam width and short pulse length create scattering volumes that are cylinders 37.5 m long and 45 m (90 m) in diameter at 5 km (10 km) range. These characteristics allow the radar to resolve the detailed structure in breaking KH waves such as have been seen in photographic cloud images.
Derived from text

N94-22311*# National Oceanic and Atmospheric Administration, Boulder, CO. Wave Propagation Lab.
OBSERVATIONS OF MULTI-LAYERED CLOUDS USING K-BAND RADAR
Brooks E. Martner and Robert A. Kropfli *In* NASA. Langley Research Center, The FIRE Cirrus Science Results 1993 Dec. 1993 p 75-82 See also N93-23070 Sponsored in part by FAA, DOE, and NOAA (For primary document see N94-22292 05-47)
Avail: CASI HC A02/MF A03

Rudimentary ground-based K-band radars were once used by the U.S. Air Force to monitor clouds over air bases. The NOAA wave Propagation Laboratory has developed a significantly advanced dual-polarization Doppler K-band system that provides remarkably detailed visualizations of the structure and kinematics of nonprecipitating and weakly precipitating clouds. Unlike lidar and infrared radiometer systems, K-band radar can penetrate liquid water cloud layers and obtain measurements through moderate rainfall and heavy snowfall to reveal intricate cloud features including multiple layers of cloud. This is accomplished at less cost than would be possible with traditional longer wavelength weather radars. The radar's capabilities have been demonstrated in several recent cloud research field projects. In combination with measurements by other remote sensors, the radar can help detect aircraft icing hazards and infer microphysical properties of clouds. An automated, unattended version of the radar could provide a continuous, detailed depiction of the cloud environment in the vicinity of airports. Author (revised)

N94-22312*# National Aeronautics and Space Administration. Langley Research Center, Hampton, VA.
ATMOSPHERIC PARAMETERIZATION SCHEMES FOR SATELLITE CLOUD PROPERTY RETRIEVAL DURING FIRE IFO 2
James Titlow (Lockheed Engineering and Sciences Co., Hampton, VA.) and Bryan A. Baum *In its* The FIRE Cirrus Science Results 1993 Dec. 1993 p 83-86 (For primary document see N94-22292 05-47)
Avail: CASI HC A01/MF A03

Satellite cloud retrieval algorithms generally require atmospheric temperature and humidity profiles to determine such cloud properties as pressure and height. For instance, the CO2 slicing technique called the ratio method requires the calculation of theoretical upwelling radiances both at the surface and a prescribed number (40) of atmospheric levels. This technique has been applied to data from, for example, the High Resolution Infrared Radiometer Sounder (HIRS/2, henceforth HIRS) flown aboard the NOAA series of polar orbiting satellites and the High Resolution Interferometer Sounder (HIS). In this particular study, four NOAA-11 HIRS channels in the 15-micron region are used. The ratio method may be applied to various channel combinations to estimate cloud top heights using channels in the 15-mu m region. Presently, the multispectral, multiresolution (MSMR) scheme uses 4 HIRS channel combination estimates for mid- to high-level cloud pressure retrieval and Advanced Very High Resolution Radiometer (AVHRR) data for low-level (is greater than 700 mb) cloud level retrieval. In order to determine theoretical upwelling radiances, atmospheric temperature and water vapor profiles must be provided as well as profiles of other radiatively important gas absorber constituents such as CO2, O3, and CH4. The assumed temperature and humidity profiles have a large effect on transmittance and radiance profiles, which in turn are used with HIRS data to calculate cloud pressure, and thus cloud height and temperature. For large spatial scale satellite data analysis, atmospheric parameterization schemes for cloud retrieval algorithms

are usually based on a gridded product such as that provided by the European Center for Medium Range Weather Forecasting (ECMWF) or the National Meteorological Center (NMC). These global, gridded products prescribe temperature and humidity profiles for a limited number of pressure levels (up to 14) in a vertical atmospheric column. The FIRE IFO 2 experiment provides an opportunity to investigate current atmospheric profile parameterization schemes, compare satellite cloud height results using both gridded products (ECMWF) and high vertical resolution sonde data from the National Weather Service (NWS) and Cross Chain Loran Atmospheric Sounding System (CLASS), and suggest modifications in atmospheric parameterization schemes based on these results. Derived from text

N94-22313*# National Aeronautics and Space Administration. Langley Research Center, Hampton, VA.

AUTOMATED CLOUD CLASSIFICATION WITH A FUZZY LOGIC EXPERT SYSTEM

Vasanth Tovinkere (Lockheed Engineering and Sciences Co., Hampton, VA.) and Bryan A. Baum *In its* The FIRE Cirrus Science Results 1993 Dec. 1993 p 87-90 (For primary document see N94-22292 05-47)

Avail: CASI HC A01/MF A03

An unresolved problem in current cloud retrieval algorithms concerns the analysis of scenes containing overlapping cloud layers. Cloud parameterizations are very important both in global climate models and in studies of the Earth's radiation budget. Most cloud retrieval schemes, such as the bispectral method used by the International Satellite Cloud Climatology Project (ISCCP), have no way of determining whether overlapping cloud layers exist in any group of satellite pixels. One promising method uses fuzzy logic to determine whether mixed cloud and/or surface types exist within a group of pixels, such as cirrus, land, and water, or cirrus and stratus. When two or more class types are present, fuzzy logic uses membership values to assign the group of pixels partially to the different class types. The strength of fuzzy logic lies in its ability to work with patterns that may include more than one class, facilitating greater information extraction from satellite radiometric data. The development of the fuzzy logic rule-based expert system involves training the fuzzy classifier with spectral and textural features calculated from accurately labeled 32x32 regions of Advanced Very High Resolution Radiometer (AVHRR) 1.1-km data. The spectral data consists of AVHRR channels 1 (0.55-0.68 mu m), 2 (0.725-1.1 mu m), 3 (3.55-3.93 mu m), 4 (10.5-11.5 mu m), and 5 (11.5-12.5 mu m), which include visible, near-infrared, and infrared window regions. The textural features are based on the gray level difference vector (GLDV) method. A sophisticated new interactive visual image Classification System (IVICS) is used to label samples chosen from scenes collected during the FIRE IFO II. The training samples are chosen from predefined classes, chosen to be ocean, land, unbroken stratiform, broken stratiform, and cirrus. The November 28, 1991 NOAA overpasses contain complex multilevel cloud situations ideal for training and validating the fuzzy logic expert system. Derived from text

N94-22314*# National Aeronautics and Space Administration. Goddard Space Flight Center, Greenbelt, MD.

METEOROLOGICAL ANALYSIS OF THE DECEMBER 4-6 FIRE CIRRUS-2 CASE

David Starr and Andrew R. Lare (Applied Research Corp., Landover, MD.) *In* NASA. Langley Research Center, The FIRE Cirrus Science Results 1993 Dec. 1993 p 92-97 (For primary document see N94-22292 05-47)

Avail: CASI HC A02/MF A03

During the period 4-6 December 1991, three distinct and separate cirrus cloud systems were observed to move over the FIRE Cirrus-II field site at Coffeyville (COF) in southeastern Kansas. Meteorological analyses of the first and third events are presented here. These cases were well-sampled by the regional rawinsonde network, highly instrumented aircraft, and extensive ground-based remote sensors at COF. Our analyses are primarily based on the rawinsonde observations. Unfortunately, the intervening event was not well-observed by the regional rawinsonde network. Derived from text

N94-22315*# Wisconsin Univ., Madison. Cooperative Inst. for Meteorological Satellite Studies.

CIRRUS CLOUD RETRIEVALS FROM HIS OBSERVATIONS DURING FIRE 2

S. A. Ackerman, W. L. Smith, X. L. Ma, R. O. Knuetson, and H. E. Revercomb *In* NASA. Langley Research Center, The FIRE Cirrus Science Results 1993 Dec. 1993 p 98-102 (For primary document see N94-22292 05-47)

Avail: CASI HC A01/MF A03

This paper presents retrieval methods applied to HIS observations during FIRE II and doubling/adding model developed to simulate high-spectral resolution infrared radiances in a cloudy atmosphere. The capabilities of the retrieval methods and sensitivity studies of high-altitude aircraft based observations to cloud microphysical structure are conducted with the model. Author

N94-22316*# National Aeronautics and Space Administration. Goddard Space Flight Center, Greenbelt, MD.

ANALYSIS OF THE GOES 6.7 MICROMETER CHANNEL OBSERVATIONS DURING FIRE 2

B. J. Soden (Wisconsin Univ., Madison.), S. A. Ackerman (Wisconsin Univ., Madison.), and David Starr *In* NASA. Langley Research Center, The FIRE Cirrus Science Results 1993 Dec. 1993 p 104-106 (For primary document see N94-22292 05-47)

Avail: CASI HC A01/MF A03

Clouds form in moist environments. FIRE Phase II Cirrus Implementation Plan (August, 1990) noted the need for mesoscale measurements of upper tropospheric water vapor content. These measurements are needed for initializing and verifying numerical weather prediction models and for describing the environment in which cirrus clouds develop and dissipate. Various instruments where deployed to measure the water vapor amounts of the upper troposphere during FIRE II (e.g. Raman lidar, CLASS sonds and new cryogenic frost hygrometer on-board aircraft). The formation, maintenance and dissipation of cirrus clouds involve the time variation of the water budget of the upper troposphere. The GOES 6.7 mu m radiance observations are sensitive to the upper tropospheric relative humidity, and therefore proved extremely valuable in planning aircraft missions during the field phase of FIRE II. Warm 6.7 mu m equivalent black body temperatures indicate a relatively dry upper troposphere and were associated with regions generally free of cirrus clouds. Regions that were colder, implying more moisture was available may or may not have had cirrus clouds present. Animation of a time sequence of 6.7 mu m images was particularly useful in planning various FIRE missions. The 6.7 mu m observations can also be very valuable in the verification of model simulations and describing the upper tropospheric synoptic conditions. A quantitative analysis of the 6.7 mu m measurement is required to successfully incorporate these satellite observations into describing the upper tropospheric water vapor budget. Recently, Soden and Bretherton (1993) have proposed a method of deriving an upper tropospheric humidity based on observations from the GOES 6.7 mu m observations. The method is summarized in the next section. In their paper they compare their retrieval method to radiance simulations. Observations were also compared to ECMWF model output to assess the model performance. The FIRE experiment provides a unique opportunity to further verify the GOES upper tropospheric relative humidity retrieval scheme by providing (1) aircraft observations to cross-validate the calibration of the GOES 6.7 mu m channel, (2) accurate upper tropospheric water vapor concentrations for verification, and (3) veritical variability of upper tropospheric water vapor. Derived from text

N94-22317*# National Oceanic and Atmospheric Administration, Boulder, CO. Wave Propagation Lab.

COMPARISON OF CLOUD BOUNDARIES MEASURED WITH 8.6 mm RADAR AND 10.6 MICROMETER LIDAR

Taneil Uttal and Janet M. Intrieri (Colorado Univ., Boulder.) *In* NASA. Langley Research Center, The FIRE Cirrus Science Results 1993 Dec. 1993 p 107-110 (For primary document see N94-22292 05-47)

Avail: CASI HC A01/MF A03

One of the most basic cloud properties is location; the height of cloud base and the height of cloud top. The glossary of meteorology defines cloud base (top) as follows: 'For a given cloud or cloud layer, that lowest (highest) level in the atmosphere at which the air contains a perceptible quantity of cloud particles.' Our studies show that for a 8.66 mm radar, and a 10.6 micrometer lidar, the level at which cloud hydrometers become 'perceptible' can vary significantly as a function of the different wavelengths, powers, beamwidths and sampling rates of the two remote sensors. Author

N94-22318*# National Oceanic and Atmospheric Administration, Boulder, CO. Wave Propagation Lab.

CLOUD BOUNDARIES DURING FIRE 2

Taneil Uttal, Scott M. Shaver, Eugene E. Clothiaux (Pennsylvania State Univ., University Park.), and Thomas P. Ackerman (Pennsylvania State Univ., University Park.) *In* NASA. Langley Research Center, The FIRE Cirrus Science Results 1993 Dec. 1993 p 111-113 (For primary document see N94-22292 05-47)

(Contract NAG1-1095; DE-FG02-90ER-61071)

Avail: CASI HC A01/MF A03

To our knowledge, previous observations of cloud boundaries have been limited to studies of cloud bases with ceilometers, cloud tops with satellites, and intermittent reports by aircraft pilots. Comprehensive studies that simultaneously record information of cloud top and cloud base, especially in multiple layer cases, have been difficult, and require the use of active remote sensors with range-gated information. In this study, we examined a 4-week period during which the NOAA Wave Propagation Laboratory (WPL) 8-mm radar and the Pennsylvania State University (PSU) 3-mm radar operated quasi-continuously, side by side. By quasi-continuously, we mean that both radars operated during all periods when cloud was present, during both daytime and nighttime hours. Using this data, we develop a summary of cloud boundaries for the month of November for a single location in the mid-continental United States. Derived from text

N94-22319*# National Aeronautics and Space Administration. Ames Research Center, Moffett Field, CA.

GROUND-BASED PASSIVE REMOTE SENSING DURING FIRE IFO 2 c43

Peter Pilewskie and Francisco P. J. Valero *In* NASA. Langley Research Center, The FIRE Cirrus Science Results 1993 Dec. 1993 p 115-116 (For primary document see N94-22292 05-47)

Avail: CASI HC A01/MF A03

During the FIRE Cirrus IFO II, a set of passive radiometers were deployed at the Coffeyville, Kansas, Hub, site B, to compliment the Radiation Measurement System (RAMS) on board the NASA ER-2 and NCAR Sabreliner. The following three instruments were used at the surface: Narrow-field-of View IR Radiometer (NFOV); Total-Direct-Diffuse Radiometer (TDDR); and Near-Infrared Spectroradiometer (NIRS). Derived from text

N94-22320*# National Aeronautics and Space Administration. Ames Research Center, Moffett Field, CA.

COMPARISONS OF DOWNWELLING RADIATION TO MODEL PREDICTIONS BASED ON GROUNDBASED MEASUREMENTS DURING FIRE 1991

S. Kinne, R. Bergstrom, T. Ackerman (Pennsylvania State Univ., University Park.), and J. DeLuisi (National Oceanic and Atmospheric Administration, Boulder, CO.) *In* NASA. Langley Research Center, The FIRE Cirrus Science Results 1993 Dec. 1993 p 117-120 (For primary document see N94-22292 05-47)

Avail: CASI HC A01/MF A03

Surface radiation measurements and simultaneous ground-based measurements of the atmosphere during the FIRE'91 cirrus field experiment provided an opportunity to identify crucial measurements and parameterization deficiencies in current cloud-radiation models. Comparisons between measured and calculated broadband surface fluxes with only a small data subset already reveal these needs: accurate humidity and aerosol vertical profiles for clear cases, accurate vertical extinction profiles and dimensions for clouds, and understanding of the (solar) scattering properties of cirrus. Author

N94-22321*# Colorado State Univ., Fort Collins. Dept. of Atmospheric Science.

SPECTRAL VARIATION OF SCATTERING AND ABSORPTION BY CIRRUS

Paul F. Hein, John M. Davis, and Stephen K. Cox *In* NASA. Langley Research Center, The FIRE Cirrus Science Results 1993 Dec. 1993 p 121-124 (For primary document see N94-22292 05-47)

(Contract NAG1-1146; N00014-91-J-1422)

Avail: CASI HC A01/MF A03

The impact of cirrus clouds on the radiative budget of the earth depends on the microphysics and scattering properties of the clouds. Cirrus clouds have been especially difficult to observe because of their high altitude and complex tenuous structure. Observations by Abakumova et. al. (1991) show that the near infrared wavelengths are more sensitive to the cirrus cloud properties than the shorter ultraviolet wavelengths. Anikin (1991) was able to show that collimated spectral measurements can be used to determine an effective particle size of the cirrus clouds. Anikin (1991) also showed that the effect of scattering through cloud causes the apparent optical depth of a 10 degrees field of view pyrheliometer to be roughly half the actual optical depth. Stackhouse and Stephens (1991) have shown that the existence of small ice crystals do dramatically affect the radiative properties of the cirrus, though observations taken during the 1986 FIRE were not totally explained by their presence. Derived from text

N94-22322*# Colorado State Univ., Fort Collins.

SPECTRAL EMISSIVITY OF CIRRUS CLOUDS

Gordon H. Beck, John M. Davis, and Stephen K. Cox *In* NASA. Langley Research Center, The FIRE Cirrus Science Results 1993 Dec. 1993 p 125-128 (For primary document see N94-22292 05-47)

(Contract NAG1-1146; DE-FG02-90ER-60970)

Avail: CASI HC A01/MF A03

The inference of cirrus cloud properties has many important applications including global climate studies, radiation budget determination, remote sensing techniques and oceanic studies from satellites. Data taken at the Parsons Kansas site during the FIRE II project are used for this study. On November 26 there were initially clear sky conditions gradually giving way to a progressively thickening cirrus shield over a period of a few hours. Interferometer radiosonde and lidar data were taken throughout this event. Two techniques are used to infer the downward spectral emittance of the observed cirrus layer. One uses only measurements and the other involves measurements and FASCODE III calculations. FASCODE III is a line-by line radiance/transmittance model developed at the Air Force Geophysics Laboratory. Author

N94-22323*# Colorado Univ., Boulder. Cooperative Inst. for Research in Environmental Sciences.

CO2 LIDAR OBSERVATIONS OF MOUNT PINATUBO DEBRIS: FIRE 2 AND LONGER-TERM MEASUREMENTS

David H. Levinson, Madison J. Post (National Oceanic and Atmospheric Administration, Boulder, CO.), and Christian J. Grund (National Oceanic and Atmospheric Administration, Boulder, CO.) *In* NASA. Langley Research Center, The FIRE Cirrus Science Results 1993 Dec. 1993 p 130-133 (For primary document see N94-22292 05-47)

Avail: CASI HC A01/MF A03

The volcanic debris in the stratosphere from the June 1991 eruption of Mt. Pinatubo first appeared over the NOAA Wave Propagation Laboratory (WPL) field site near Boulder, Colorado (40.15 N, 105.23 W), in July of 1991. The presence of the Pinatubo cloud has allowed us to characterize both the tropospheric and stratospheric aerosol backscatter using the NOAA/WPL CO2 Doppler lidar. The lidar has measured vertical backscatter profiles at lambda = 10.59 mu m for over a decade. Analysis of this dense set of profiles reveals the effects of atmospheric and microphysical processes during the buildup and decay of Mt. Pinatubo's clouds. Further information on the NOAA lidar, specifically calibrations using a hard target, can be found in Post and Cupp (1990). We present results of those measurements for June 15, 1991, through December 31, 1992. During that period of longer-term measurements, WPL took part in FIRE II (First ISCCP (International Satellite Cloud Climatology Project) Regional Experiment II), from November 12 through December 8, 1991, measuring vertical backscatter profiles almost daily. One of the mechanisms for purging stratospheric aerosols is tropopause folding, which occurs in cold-core extratropical cyclones. Tropospheric mass loading occurs during folding events which can substantially increase the amount of ice nuclei in the upper troposphere, and may affect the formation of cirrus in that region. Spring and fall are prominent times for tropopause folding events because of the migration of the subtropical and polar jet streams during the transition seasons. Sassen has suggested that the volcanic aerosols from Pinatubo played a role in the formation of cirrus during FIRE II, particularly during a period of moist subtropical flow on December 5-6, 1991. Author

N94-22324*# National Aeronautics and Space Administration. Ames Research Center, Moffett Field, CA.

ANALYSIS OF THE TROPOSPHERIC WATER DISTRIBUTION DURING FIRE 2

Douglas L. Westphal *In* NASA. Langley Research Center, The FIRE Cirrus Science Results 1993 Dec. 1993 p 134-137 (For primary document see N94-22292 05-47)
(Contract DE-AI05-90ER-61074)
Avail: CASI HC A01/MF A03

The Penn State/NCAR mesoscale model, as adapted for use at ARC, was used as a testbed for the development and validation of cloud models for use in General Circulation Models (GCM's). This modeling approach also allows us to intercompare the predictions of the various cloud schemes within the same dynamical framework. The use of the PSU/NCAR mesoscale model also allows us to compare our results with FIRE-II (First International Satellite Cloud Climatology Project Regional Experiment) observations, instead of climate statistics. Though a promising approach, our work to date revealed several difficulties. First, the model by design is limited in spatial coverage and is only run for 12 to 48 hours at a time. Hence the quality of the simulation will depend heavily on the initial conditions. The poor quality of upper-tropospheric measurements of water vapor is well known and the situation is particularly bad for mid-latitude winter since the coupling with the surface is less direct than in summer so that relying on the model to spin-up a reasonable moisture field is not always successful. Though one of the most common atmospheric constituents, water vapor is relatively difficult to measure accurately, especially operationally over large areas. The standard NWS sondes have little sensitivity at the low temperatures where cirrus form and the data from the GOES 6.7 micron channel is difficult to quantify. For this reason, the goals of FIRE Cirrus II included characterizing the three-dimensional distribution of water vapor and clouds. In studying the data from FIRE Cirrus II, it was found that no single special observation technique provides accurate regional distributions of water vapor. The Raman lidar provides accurate measurements, but only at the Hub, for levels up to 10 km, and during nighttime hours. The CLASS sondes are more sensitive to moisture at low temperatures than are the NWS sondes, but the four stations only cover an area of two hundred kilometers on a side. The aircraft give the most accurate measurements of water vapor, but are limited in spatial and temporal coverage. This problem is partly alleviated by the use of the MAPS analyses, a four-dimensional data assimilation system that combines the previous 3-hour forecast with the available observations, but its upper-level moisture analyses are sometimes deficient because of the vapor measurement problem. An attempt was made to create a consistent four-dimensional description of the water vapor distribution during the second IFO by subjectively combining data from a variety of sources, including MAPS analyses, CLASS sondes, SPECTRE sondes, NWS sondes, GOES satellite analyses, radars, lidars, and microwave radiometers. Author (revised)

N94-22325*# Pennsylvania State Univ., University Park. Dept. of Meteorology.
EXAMINATION OF THE OBSERVED SYNOPTIC SCALE CIRRUS CLOUD ENVIRONMENT: THE DECEMBER 3-6 FIRE CIRRUS CASE STUDY
Gerald G. Mace and Thomas P. Ackerman *In* NASA. Langley Research Center, The FIRE Cirrus Science Results 1993 Dec. 1993 p 138-141 (For primary document see N94-22292 05-47)
(Contract NAG1-1095; NAG1-999; DE-FG02-90ER-61071)
Avail: CASI HC A01/MF A03

Recently, Sassen provided evidence for supercooled water droplets in cirrus uncinus cell heads at temperatures between 40 and -50 C. Chemistry related to volcanic aerosol of stratospheric origin was evoked as an explanation for this phenomenon. Sassen speculated that injections of sulfuric acid droplets into the upper troposphere were accomplished by tropopause folds associated with subtropical jet streams. He also postulated global climatic perturbations due to the effect of these cirrus microphysical perturbations on radiative fluxes. Using data processing and objective analysis techniques described by Mace and Ackerman, the synoptic scale environment was examined for evidence of tropopause folds that may have served as a source mechanism of stratospheric aerosol in the upper troposphere. Author (revised)

N94-22326*# National Aeronautics and Space Administration. Goddard Space Flight Center, Greenbelt, MD.
THE 5-6 DECEMBER 1991 FIRE IFO 2 JET STREAM CIRRUS CASE STUDY: THE INFLUENCE OF VOLCANIC AEROSOLS Abstract Only
Kenneth Sassen (Utah Univ., Salt Lake City.), Gerald G. Mace (Pennsylvania State Univ., University Park.), David Starr, Michael R. Poellot (North Dakota Univ., Grand Forks.), S. H. Melfi, Wynn L. Eberhard (National Oceanic and Atmospheric Administration, Boulder, CO.), James D. Spinhirne, E. W. Eloranta (Wisconsin Univ., Madison.), Donald E. Hagen (Missouri Univ., Rolla.), and John Hallett (Desert Research Inst., Reno, NV.) *In* NASA. Langley Research Center, The FIRE Cirrus Science Results 1993 Dec. 1993 p 142 (For primary document see N94-22292 05-47)
Avail: CASI HC A01/MF A03

In presenting an overview of the cirrus clouds comprehensively studied by ground-based and airborne sensors from Coffeyville, KS, during the 5-6 Dec. 1992 Project FIRE (First International Satellite Cloud Climatology Project Regional Experiment) IFO II case study period, evidence is provided that volcanic aerosols from the June 1991 Pinatubo eruptions significantly influenced the formation and maintenance of the cirrus. Following the local appearance of a spur of stratospheric volcanic debris from the subtropics, a series of jet streaks subsequently conditioned the troposphere through tropopause foldings with sulfur-based particles that became effective cirrus cloud-forming nuclei. Aerosol and ozone measurements suggest a complicated history of stratospheric-tropospheric exchanges embedded within the upper level flow, and cirrus cloud formation was noted to occur locally at the boundaries of stratospheric aerosol-enriched layers that became humidified through diffusion, precipitation, or advective processes. Apparent cirrus cloud alterations include abnormally high ice crystal concentrations (up to approximately 600 !(sup -1), small but complex radial ice crystal types, and relatively large haze particles in cirrus uncinus cell heads at temperatures between -40 to -50 C. Implications for volcanic-cirrus cloud climate effects, and usual (non-volcanic aerosol) jet stream cirrus cloud formation are discussed. Author (revised)

N94-22327*# National Aeronautics and Space Administration. Ames Research Center, Moffett Field, CA.
THREE DIMENSIONAL MODELING OF CIRRUS DURING THE 1991 FIRE IFO 2: DETAILED PROCESS STUDY Abstract Only
Eric J. Jensen, Owen B. Toon, and Douglas L. Westphal *In* NASA. Langley Research Center, The FIRE Cirrus Science Results 1993 Dec. 1993 p 143 (For primary document see N94-22292 05-47)
Avail: CASI HC A01/MF A03

A three-dimensional model of cirrus cloud formation and evolution, including microphysical, dynamical, and radiative processes, was used to simulate cirrus observed in the FIRE Phase 2 Cirrus field program (13 Nov. - 7 Dec. 1991). Sulfate aerosols, solution drops, ice crystals, and water vapor are all treated as interactive elements in the model. Ice crystal size distributions are fully resolved based on calculations of homogeneous freezing of solution drops, growth by water vapor deposition, evaporation, aggregation, and vertical transport. Visible and infrared radiative fluxes, and radiative heating rates are calculated using the two-stream algorithm described by Toon et al. Wind velocities, diffusion coefficients, and temperatures were taken from the MAPS analyses and the MM4 mesoscale model simulations. Within the model, moisture is transported and converted to liquid or vapor by the microphysical processes. The simulated cloud bulk and microphysical properties are shown in detail for the Nov. 26 and Dec. 5 case studies. Comparisons with lidar, radar, and in situ data are used to determine how well the simulations reproduced the observed cirrus. The roles played by various processes in the model are described in detail. The potential modes of nucleation are evaluated, and the importance of small-scale variations in temperature and humidity are discussed. The importance of competing ice crystal growth mechanisms (water vapor deposition and aggregation) are evaluated based on model simulations. Finally, the importance of ice crystal shape for crystal growth and vertical transport of ice are discussed. Author (revised)

N94-22328*# National Aeronautics and Space Administration. Goddard Space Flight Center, Greenbelt, MD.
METEOROLOGICAL ANALYSIS OF THE NOVEMBER 25 FIRE CIRRUS-2 CASE: A WELL-DEFINED RIDGE-CREST CIRRUS SYSTEM OVER OKLAHOMA
David Starr and Andrew R. Lare (Applied Research Corp., Landover, MD.) *In* NASA. Langley Research Center, The FIRE Cirrus Science Results 1993 Dec. 1993 p 144-147 (For primary document see N94-22292 05-47)
Avail: CASI HC A01/MF A03

On the morning of 25 Nov. 1991, a cirrus cloud system formed in a region extending eastward from the continental divide into central Oklahoma

and southwestern Kansas. The system moved slowly eastward during the day and maintained a relatively constant scale and shape. From the satellite perspective, this cloud system had a number of morphological similarities to the 27-28 Oct. FIRE (First International Satellite Cloud Climatology Project Regional Experiment) Cirrus-1 case analyzed by Starr and Wylie. By comparison, the present case had much better rawinsonde coverage. The rawinsonde network was much more extensive and the cloud system was relatively slow moving and well-located with respect to the enhanced sounding network and the National Weather Service (NWS) Wind Profiler Network. In addition to the rawinsonde soundings (1200 and 1800 UTC on 25 Nov. and 0000 and 0600 UTC on 26 Nov.) and satellite observations, four aircraft sorties were flown in the northern portion of this cirrus cloud system from mid-morning to mid afternoon. These included microphysical-radiation profiling missions by the NCAR Sabreliner near Tulsa (about midway between COF and OUN) and the NCAR King Air near Ponca City (about 80 km upwind of Tulsa), a microphysical profiling mission by the UND Citation near Tulsa, and a NASA ER-2 overflight. Thus, very good data are available for this case although, unfortunately, the cloud system remained south of the FIRE Hub site at Coffeyville (COF) where extensive ground-based remote sensor was located. The northern edge of the cloud system was visible from COF during most of the day. Given the wealth of available in situ and remote sensing observations, the similarity to the FIRE Cirrus-1 focal case study, and the particularly good match in scale and location of the cloud system with the rawinsonde and profiler networks, analysis of this case may yield very useful results on the life-cycle of this cirrus cloud system. The quality of the meteorological description for this case was assessed based on our preliminary analysis of the rawinsonde observations. Author (revised)

N94-22329*# Pennsylvania State Univ., University Park. Dept. of Meteorology.

CIRRUS CLOUD DEVELOPMENT IN A MOBILE UPPER TROPOSPHERIC TROUGH: THE NOVEMBER 26TH FIRE CIRRUS CASE STUDY

Gerald G. Mace and Thomas P. Ackerman *In* NASA. Langley Research Center, The FIRE Cirrus Science Results 1993 Dec. 1993 p 148-152 (For primary document see N94-22292 05-47)

(Contract NAG1-1095; NAG1-999; DE-FG02-90ER-61071)

Avail: CASI HC A01/MF A03

The period from 18 UTC 26 Nov. 1991 to roughly 23 UTC 26 Nov. 1991 is one of the study periods of the FIRE (First International Satellite Cloud Climatology Regional Experiment) 2 field campaign. The middle and upper tropospheric cloud data that was collected during this time allowed FIRE scientists to learn a great deal about the detailed structure, microphysics, and radiative characteristics of the mid latitude cirrus that occurred during that time. Modeling studies that range from the microphysical to the mesoscale are now underway attempting to piece the detailed knowledge of this cloud system into a coherent picture of the atmospheric processes important to cirrus cloud development and maintenance. An important component of the modeling work, either as an input parameter in the case of cloud-scale models, or as output in the case of meso and larger scale models, is the large scale forcing of the cloud system. By forcing we mean the synoptic scale vertical motions and moisture budget that initially send air parcels ascending and supply the water vapor to allow condensation during ascent. Defining this forcing from the synoptic scale to the cloud scale is one of the stated scientific objectives of the FIRE program. From the standpoint of model validation, it is also necessary that the vertical motions and large scale moisture budget of the case studies be derived from observations. It is considered important that the models used to simulate the observed cloud fields begin with the correct dynamics and that the dynamics be in the right place for the right reasons. Author (revised)

N94-22330*# Colorado State Univ., Fort Collins. Dept. of Atmospheric Science.

VERTICAL VELOCITY IN CIRRUS CASE OBTAINED FROM WIND PROFILER

Ran Song and Stephen K. Cox *In* NASA. Langley Research Center, The FIRE Cirrus Science Results 1993 Dec. 1993 p 153-156 (For primary document see N94-22292 05-47)

(Contract NAG1-1146; DE-FG02-90ER-60970)

Avail: CASI HC A01/MF A03

Cirrus clouds play an important role in the climate and general circulation because they significantly modulate the radiation properties of the atmosphere. However understanding the processes that govern their presence is made difficult by their high altitude, variable thickness, complex microphysical structure, and relatively little knowledge of the vertical motion field. In the FIRE 2 (First International Satellite Cloud Climatology Regional Experiment) experiment, a 404 MHz wind profiler was set up to provide continuous measurements of clear air wind field at Parsons, Kansas. Simultaneously, the NOAA wind profiler network supplied a wider spacial scale observation. On 26 Nov. 1991, the most significant cirrus cloud phenomena during the experiment with a jet streak at 250 Mb occurred. Analyses of the vertical wind velocity are made by utilizing different methods based on wind profiler data, among them the direct measurements from CSU wind profiler and NOAA network wind profilers, VAD (Velocity Azimuth Display) technique and the kinematic method. Author (revised)

N94-22331*# Colorado State Univ., Fort Collins. Dept. of Atmospheric Science.

MESOSCALE SIMULATIONS OF THE NOVEMBER 25-26 AND DECEMBER 5-6 CIRRUS CASES USING THE RAMS MODEL

J. L. Harrington, Michael P. Meyers, and William R. Cotton *In* NASA. Langley Research Center, The FIRE Cirrus Science Results 1993 Dec. 1993 p 158-161 (For primary document see N94-22292 05-47)

(Grants AF-AFOSR-0296-91)

Avail: CASI HC A01/MF A03

The Regional Atmospheric Modeling System (RAMS), developed at Colorado State University, was used during the First ISCCP (International Satellite Cloud Climatology Project) Regional Experiment (FIRE) 2 (13 Nov. through 6 Dec. 1991) to provide real time forecasts of cirrus clouds. Forecasts were run once a day, initializing with the 0000 UTC dataset provided by NOAA (Forecast Systems Laboratory (FSL) Mesoscale Analysis and Prediction System (MAPS)). In order to obtain better agreement with observations, a second set of simulations were done for the FIRE 2 cases that occurred on 25-26 Nov. and 5-6 Dec. In this set of simulations, a more complex radiation scheme was used, the Chen/Cotton radiation scheme, along with the nucleation of ice occurring at ice supersaturations as opposed to nucleation occurring at water supersaturations that was done in the actual forecast version. The runs using these more complex schemes took longer wall clock time (7-9 hours for the actual forecasts as compared to 12-14 hrs for the runs using the more complex schemes) however, the final results of the simulations were definitely improved upon. Comparisons between these two sets of simulations are given. Now underway are simulations of these cases using a closed analytical solution for the auto-conversion of ice from a pristine ice class (sizes less than about 50 microns in effective diameter) to a snow class (effective diameters on the order of several hundred microns). This solution is employed along with a new scheme for the nucleation of ice crystals due to Meyers et al and Demott et al. The scheme is derived assuming complete gamma distributions for both the pristine and snow classes. The time rate of change of the number concentration and mass mixing-ratio of each distribution is found by calculating either the flux of crystals that grow beyond a certain critical diameter by vapor deposition in an ice supersaturated regime or by calculating the flux of crystals that evaporate to sizes below that same critical effective diameter. Author (revised)

N94-22332*# National Aeronautics and Space Administration. Goddard Space Flight Center, Greenbelt, MD.

DYNAMICAL CHARACTERISTICS OF CIRRUS CLOUDS FROM AIRCRAFT AND RADAR MEASUREMENTS

I. Gultepe, David Starr, A. J. Heymsfield (National Center for Atmospheric Research, Boulder, CO.), M. Poellot (North Dakota Univ., Grand Forks.), T. Uttal (National Oceanic and Atmospheric Administration, Boulder, CO.), and T. Ackerman (Pennsylvania State Univ., University Park.) *In* NASA. Langley Research Center, The FIRE Cirrus Science Results 1993 Dec. 1993 p 162-165 (For primary document see N94-22292 05-47)

Avail: CASI HC A01/MF A03

Cirrus clouds play an important role in climate and in the development of other types of clouds. Although there are many studies of clouds within the boundary layer, cirrus clouds have been neglected up until the last decade. New tools and in-situ measurements of various physical and dynamical parameters permit us to now study cirrus clouds in much greater detail. Physical and dynamical structures of cirrus clouds were studied in

detail by Heymsfield using aircraft measurements. He emphasized the importance of interactions among physical and dynamical processes. Cirrus clouds often exhibit complex physical and dynamical structure. Upper tropospheric flows contain not only coherent structures, but also chaotic movements. The coherent structures (organized movements) transfer significant amounts of heat and momentum while their form, size, and intensity depend strongly on environmental instability. Various dynamical structures including cells, waves, and turbulence are studied in order to understand cirrus cloud formation and development. Author (revised)

N94-22333*# National Oceanic and Atmospheric Administration, Boulder, CO. Wave Propagation Lab.

ESTIMATION OF CIRRUS CLOUD PARTICLE FALLSPEEDS FROM VERTICALLY POINTING DOPPLER RADAR

Brad W. Orr and Robert A. Kropfli *In* NASA. Langley Research Center, The FIRE Cirrus Science Results 1993 Dec. 1993 p 166-168 Sponsored in part by NOAA (For primary document see N94-22292 05-47)
Avail: CASI HC A01/MF A03

The First ISCCP (International Satellite Cloud Climatology Project) Regional Experiment 2 (FIRE 2) was conducted in Coffeyville, Kansas in late 1991 to study the microphysical and radiative properties of cirrus clouds. A variety of active and passive remote sensors were employed, including an 8-mm-wavelength cloud-sensing Doppler radar developed at the Wave Propagation Laboratory (WPL). The radar, having excellent sensitivity to cloud particles (-30 dBZ at 10 km), good spatial resolution (37 m), and velocity precision (.05 ms -1), is an excellent tool for observing cirrus clouds. Having this radar directed toward the zenith for long periods of time during FIRE 2 permitted the reflectivity-weighted particle fallspeed to be related to reflectivity which allowed a separation of ice particle fallspeeds from vertical air motions. Additionally, such relationships proved useful in other multi-sensor techniques for determining vertical profiles of ice particle characteristic size and ice water content in cirrus clouds. The analysis method and the results of applying it to cirrus cloud reflectivity and velocity data collected during FIRE 2 are discussed. Author (revised)

N94-22334*# National Oceanic and Atmospheric Administration, Boulder, CO. Wave Propagation Lab.

NORMALIZED VERTICAL ICE MASS FLUX PROFILES FROM VERTICALLY POINTING 8-mm-WAVELENGTH DOPPLER RADAR

Brad W. Orr and Robert A. Kropfli *In* NASA. Langley Research Center, The FIRE Cirrus Science Results 1993 Dec. 1993 p 169-172 (For primary document see N94-22292 05-47)
Avail: CASI HC A01/MF A03

During the FIRE 2 (First International Satellite Cloud Climatology Project Regional Experiment) project, NOAA's Wave Propagation Laboratory (WPL) operated its 8-mm wavelength Doppler radar extensively in the vertically pointing mode. This allowed for the calculation of a number of important cirrus cloud parameters, including cloud boundary statistics, cloud particle characteristic sizes and concentrations, and ice mass content (imc). The flux of imc, or, alternatively, ice mass flux (imf), is also an important parameter of a cirrus cloud system. Ice mass flux is important in the vertical redistribution of water substance and thus, in part, determines the cloud evolution. It is important for the development of cloud parameterizations to be able to define the essential physical characteristics of large populations of clouds in the simplest possible way. One method would be to normalize profiles of observed cloud properties, such as those mentioned above, in ways similar to those used in the convective boundary layer. The height then scales from 0.0 at cloud base to 1.0 at cloud top, and the measured cloud parameter scales by its maximum value so that all normalized profiles have 1.0 as their maximum value. The goal is that there will be a 'universal' shape to profiles of the normalized data. This idea was applied to estimates of imf calculated from data obtained by the WPL cloud radar during FIRE II. Other quantities such as median particle diameter, concentration, and ice mass content can also be estimated with this radar, and we expect to also examine normalized profiles of these quantities in time for the 1993 FIRE II meeting. Author (revised)

N94-22335*# National Aeronautics and Space Administration. Goddard Space Flight Center, Greenbelt, MD.

A COMPARISON OF SMALL AND LARGER MESOSCALE LATENT HEAT AND RADIATIVE FLUXES: DECEMBER 6 CASE STUDY

I. Gultepe, David Starr, and A. J. Heymsfield (National Center for Atmospheric Research, Boulder, CO.) *In* NASA. Langley Research Center, The FIRE Cirrus Science Results 1993 Dec. 1993 p 173-176 (For primary document see N94-22292 05-47)
Avail: CASI HC A01/MF A03

Because of the small amounts of water vapor, the potential for rapid changes, and the very cold temperatures in the upper troposphere, moisture measuring instruments face several problems related to calibration and response. Calculations of eddy moisture fluxes are, therefore, subject to significant uncertainty. The purpose of this study is to examine the importance of latent heat (moisture) fluxes due to small and larger mesoscale circulations in comparison to radiative fluxes within cirrus. Scale separation is made at about 1 km because of significant changes in the structures within cirrus. Only observations at warmer than -40 C are used in this study. The EG&G hygrometer that is used for measuring dewpoint temperature (Td) is believed to be fairly accurate down to -40 C. On the other hand, Lyman-Alpha (L-alpha) hygrometer measurements of moisture may include large drift errors. In order to compensate for these drift errors, the L-alpha hygrometer is often calibrated against the EG&G hygrometer. However, large errors ensue for Td measurements at temperatures less than -40 C. The cryogenic hygrometer frost point measurements may be used to calibrate L-alpha measurements at temperatures less than -40 C. In this study, however, measurements obtained by EG&G hygrometer and L-alpha measurements are used for the flux calculations. Derived from text

N94-22336*# Desert Research Inst., Reno, NV.

IMPORTANCE OF AGGREGATION AND SMALL ICE CRYSTALS IN CIRRUS CLOUDS, BASED ON OBSERVATIONS AND AN ICE PARTICLE GROWTH MODEL

David L. Mitchell, Steven K. Chai, Yayi Dong, W. Patrick Arnott, and John Hallett *In* NASA. Langley Research Center, The FIRE Cirrus Science Results 1993 Dec. 1993 p 177-180 (For primary document see N94-22292 05-47)
(Grants NAG1-1113; NA16RC0118-01)
Avail: CASI HC A01/MF A03

The 1 November 1986 FIRE I case study was used to test an ice particle growth model which predicts bimodal size spectra in cirrus clouds. The model was developed from an analytically based model which predicts the height evolution of monomodal ice particle size spectra from the measured ice water content (IWC). Size spectra from the monomodal model are represented by a gamma distribution, N(D) = N(sub o)D(exp nu)exp(-lambda D), where D = ice particle maximum dimension. The slope parameter, lambda, and the parameter N(sub o) are predicted from the IWC through the growth processes of vapor diffusion and aggregation. The model formulation is analytical, computationally efficient, and well suited for incorporation into larger models. The monomodal model has been validated against two other cirrus cloud case studies. From the monomodal size spectra, the size distributions which determine concentrations of ice particles less than about 150 mu m are predicted. Derived from text

N94-22337*# Maryland Univ., College Park. Dept. of Meteorology.

CALIBRATION OF RADIATION CODES IN CLIMATE MODELS: COMPARISON OF CALCULATIONS WITH OBSERVATIONS FROM THE SPECTRAL RADIATION EXPERIMENT (SPECTRE)

R. G. Ellingson, W. J. Wiscombe, J. DeLuisi, H. Melfi, and W. Smith *In* NASA. Langley Research Center, The FIRE Cirrus Science Results 1993 Dec. 1993 p 181-184 (For primary document see N94-22292 05-47)
Avail: CASI HC A01/MF A03

The primary goal of SPECTRE is to: close the loopholes by which longwave radiation models have eluded incisive comparisons with measurements. Likewise, the experimental approach was quite simple in concept, namely: accurately measure the zenith infrared radiance at high spectral resolution while simultaneously profiling the radiatively important atmospheric properties with conventional and remote sensing devices. The field phase of SPECTRE was carried out as part of FIRE Cirrus II, and detailed spectra of the down welling radiance were obtained by several interferometers simultaneous to the measurement of the optical properties of the atmosphere. We are now well along in the process of analyzing the data and calibrating radiation codes so that they may be used more effectively in climate related studies. The calibration is being done with models ranging from the most detailed (line-by-line) to the broad-band parameterizations used in climate models. This paper summarizes our

progress in the calibration for clear-sky conditions. When this stage is completed, we will move on to the calibration for cirrus conditions.

Derived from text

N94-22338*# Phillips Lab., Hanscom AFB, MA. Atmospheric Sciences Div.

SSH-2 MEASUREMENTS OF CIRRUS AT 18-28 MICROMETERS FROM THE KING AIR DURING FIRE 2

Michael K. Griffin *In* NASA. Langley Research Center, The FIRE Cirrus Science Results 1993 Dec. 1993 p 185-188 (For primary document see N94-22292 05-47)

(Contract DE-AI06-91RL-12348)

Avail: CASI HC A01/MF A03

In November of 1991, the First ISCCP (International Satellite Cloud Climatology Project) Regional Experiment (FIRE) Phase II cirrus study took place at Coffeyville, Kansas. The field experiment incorporated instrumentation from surface, aircraft, and satellite to attempt to define the optical, radiative, and microphysical characteristics of these high altitude, predominantly ice clouds. The NCAR King Air research aircraft was outfitted with a variety of radiative and microphysical instrumentation for the FIRE II project. Included for this project was the SSH-2, a 16-channel passive radiometer. The SSH-2 was originally designed as a space-qualified infrared (IR) temperature and water vapor sounder for deployment onboard the Defense Meteorological Satellite Program (DMSP) series of environmental satellites. For this experiment, only those channels associated with the water vapor profiling function have been examined although downwelling radiance measurements were taken at all channels during the project. With supporting information from the aircraft telemetry observations it may be possible to relate these SSH-2 measurements to cloud radiative and microphysical properties. The following sections will describe the spectral characteristics of the instrument, the calibration scheme used to convert the raw measured counts into calibrated radiances, and the case studies that will be covered in this paper. This will be followed by a discussion of the results of this preliminary investigation and a description of future work to be done.

Derived from text

N94-22339*# Colorado State Univ., Fort Collins. Dept. of Atmospheric Science.

INVESTIGATION OF THE EFFECTS OF THE MACROPHYSICAL AND MICROPHYSICAL PROPERTIES OF CIRRUS CLOUDS ON THE RETRIEVAL OF OPTICAL PROPERTIES: RESULTS FOR FIRE 2

Paul W. Stackhouse, Jr. and Graeme L. Stephens *In* NASA. Langley Research Center, The FIRE Cirrus Science Results 1993 Dec. 1993 p 189-192 (For primary document see N94-22292 05-47)

Avail: CASI HC A01/MF A03

Due to the prevalence and persistence of cirrus cloudiness across the globe, cirrus clouds are believed to have an important effect on the climate. Stephens et al., (1990) among others have shown that the important factor determining how cirrus clouds modulate the climate is the balance between the albedo and emittance effect of the cloud systems. This factor was shown to depend in part upon the effective sizes of the cirrus cloud particles. Since effective sizes of cirrus cloud microphysical distributions are used as a basis of parameterizations in climate models, it is crucial that the relationships between effective sizes and radiative properties be clearly established. In this preliminary study, the retrieval of cirrus cloud effective sizes are examined using a two dimensional radiative transfer model for a cirrus cloud case sampled during FIRE Cirrus 11. The purpose of this paper is to present preliminary results from the SHSG model demonstrating the sensitivity of the bispectral relationships of reflected radiances and thus the retrieval of effective sizes to phase function and dimensionality.

Derived from text

N94-22340*# Colorado State Univ., Fort Collins. Dept. of Atmospheric Science.

EXTINCTION EFFICIENCIES FROM DDA CALCULATIONS SOLVED FOR FINITE CIRCULAR CYLINDERS AND DISKS

J. R. Withrow and S. K. Cox *In* NASA. Langley Research Center, The FIRE Cirrus Science Results 1993 Dec. 1993 p 193-196 (For primary document see N94-22292 05-47)

(Contracts NAG1-1146; N00014-91-J-1422; DE-FG02-90ER-60970)

Avail: CASI HC A01/MF A03

One of the most commonly noted uncertainties with respect to the modeling of cirrus clouds and their effect upon the planetary radiation balance is the disputed validity of the use of Mie scattering results as an approximation to the scattering results of the hexagonal plates and columns found in cirrus clouds. This approximation has historically been a kind of default, a result of the lack of an appropriate analytical solution of Maxwell's equations to particles other than infinite cylinders and spheroids. Recently, however, the use of such approximate techniques as the Discrete Dipole Approximation has made scattering solutions on such particles a computationally intensive but feasible possibility. In this study, the Discrete Dipole Approximation (DDA) developed by Flatau (1992) is used to find such solutions for homogeneous, circular cylinders and disks. This can serve to not only assess the validity of the current radiative transfer schemes which are available for the study of cirrus but also to extend the current approximation of equivalent spheres to an approximation of second order, homogeneous finite circular cylinders and disks. The results will be presented in the form of a single variable, the extinction efficiency.

Derived from text

N94-22341*# National Aeronautics and Space Administration. Goddard Space Flight Center, Greenbelt, MD.

SURFACE-INDUCED BRIGHTNESS TEMPERATURE VARIATIONS AND THEIR EFFECTS ON DETECTING THIN CIRRUS CLOUDS USING IR EMISSION CHANNELS IN THE 8-12 MICROMETER REGION

Bo-Cai Gao and W. J. Wiscombe *In* NASA. Langley Research Center, The FIRE Cirrus Science Results 1993 Dec. 1993 p 197-200 (For primary document see N94-22292 05-47)

Avail: CASI HC A01/MF A03

A method for detecting cirrus clouds in terms of brightness temperature differences between narrow bands at 8, 11, and 12 mu m has been proposed by Ackerman et al. (1990). In this method, the variation of emissivity with wavelength for different surface targets was not taken into consideration. Based on state-of-the-art laboratory measurements of reflectance spectra of terrestrial materials by Salisbury and D'Aria (1992), we have found that the brightness temperature differences between the 8 and 11 mu m bands for soils, rocks and minerals, and dry vegetation can vary between approximately -8 K and +8 K due solely to surface emissivity variations. We conclude that although the method of Ackerman et al. is useful for detecting cirrus clouds over areas covered by green vegetation, water, and ice, it is less effective for detecting cirrus clouds over areas covered by bare soils, rocks and minerals, and dry vegetation. In addition, we recommend that in future the variation of surface emissivity with wavelength should be taken into account in algorithms for retrieving surface temperatures and low-level atmospheric temperature and water vapor profiles.

Author (revised)

N94-22342*# National Aeronautics and Space Administration. Langley Research Center, Hampton, VA.

REMOTE SENSING ESTIMATES OF CIRRUS PARTICLE SIZE FOR TROPICAL AND MIDLATITUDE CIRRUS: HEXAGONAL CRYSTALS AND ICE SPHERES

Bruce A. Wielicki, Patrick Minnis, Robert Arduini (Lockheed Engineering and Sciences Co., Hampton, VA.), Lindsay Parker (Lockheed Engineering and Sciences Co., Hampton, VA.), Si-Chee Tsay (National Aeronautics and Space Administration. Goddard Space Flight Center, Greenbelt, MD.), Yoshihide Takano (Utah Univ., Salt Lake City.), and Kuo-Nan Liou (Utah Univ., Salt Lake City.) *In its* The FIRE Cirrus Science Results 1993 Dec. 1993 p 201-204 (For primary document see N94-22292 05-47)

Avail: CASI HC A01/MF A03

A large discrepancy exists in current estimates of a mean cirrus particle size appropriate for calculations of the effects of these ice clouds on solar and thermal infrared radiative fluxes. For spheres with large size parameter (x = (2 pi r / lambda) is greater than 30, where r is particle radius), and moderate absorption (n(sup i) x less than 1, where n(sup i) is imaginary index of refraction for ice), the optimal effective particle radius is given by: r(sub e) = integral of r(exp 3)n(r)dr / integral of r(exp 2)n(r)dr. For the remote sensing of cirrus particle size at wavelengths of 0.83, 1.65, and 2.21 mu m, a 50 mu m ice sphere would have a size parameter of about 200, and values of n(sup i) x of 0, 0.045, and 0.06, satisfying the above conditions. However, while r(sub e) is a well-defined parameter for spheres, this cross-section area-weighted particle radius can only be extended to non-spherical particles by defining some equivalent sphere, typically an equivalent volume or equivalent cross-section area sphere.

Using equivalent volume spheres, values of r(sub e) obtained over Lake Michigan on October 28, 1986, during FIRE phase I varied from 200 mu m (King Air 2D Imaging probes) to 60 mu m (Landsat reflectances at 0.83, 1.65, and 2.2 mu m), to 25 mu m (HIS spectrometer thermal emission between 8 and 12 mu m). Three major uncertainties were identified in this comparison: small ice particles missed by the 2D-C aircraft probes, uncertain ice refractive index, and uncertainties in the single scatter albedos and scattering phase functions used in the radiative calculations. Since the first FIRE cirrus results, advances have been made in all three areas. The present paper reports on improvements in the radiative modeling of ice particles at 0.83, 1.65, and 2.21 mu m wavelengths appropriate for comparisons to Landsat Thematic Mapper data. The paper also includes new results for Landsat observations of ice clouds in the eastern and western tropical Pacific. Derived from text

N94-22343*# Desert Research Inst., Reno, NV.
ARE TROPICAL CIRRUS BRIGHTER THAN MID-LATITUDE CIRRUS?
David L. Mitchell, W. Patrick Arnott, Kenneth Sassen (Utah Univ., Salt Lake City.), Yayi Dong, and John Hallett *In* NASA. Langley Research Center, The FIRE Cirrus Science Results 1993 Dec. 1993 p 205-208 (For primary document see N94-22292 05-47)
(Contract NAG1-1113; NA16RC0118-01)
Avail: CASI HC A01/MF A03

Recent measurements during FIRE II, in the tropics and elsewhere, support an emerging hypothesis about the role of stratospheric mixing in determining the microphysical and radiative properties of cirrus clouds. This is only a working hypothesis, and may change as new measurements become available. This report reviews the conditions under which certain types of ice crystals form. Derived from text

N94-22344*# National Aeronautics and Space Administration, Washington, DC.
AN OVERVIEW OF THE RADIATION COMPONENT OF THE NASA TOGA-COARE EXPERIMENT
Thomas Ackerman (Pennsylvania State Univ., University Park.) and John T. Suttles *In* NASA. Langley Research Center, The FIRE Cirrus Science Results 1993 Dec. 1993 p 209-211 (For primary document see N94-22292 05-47)
Avail: CASI HC A01/MF A03

During January and February, 1993, the Physical Climate Branch of NASA sponsored an aircraft program in support of the Tropical Ocean - Global Atmosphere (TOGA) Coupled Ocean-Atmosphere Response Experiment (COARE). The NASA program was integrated with and contributed directly to the COARE objectives, but had as its primary foci the measurement of convection and precipitation related to the Tropical Rainfall Measurement Mission (TRMM) and the measurement of the physical and radiative properties of tropical cirrus related to the International Satellite Cloud Climatology Project (ISCCP) and the First ISCCP Regional Experiment (FIRE). This brief overview will concentrate on the measurements associated with FIRE and ISCCP. Derived from text

N94-20699*# Oklahoma Univ., Norman.
SCHOOLS OF THE PACIFIC RAINFALL CLIMATE EXPERIMENT
Abstract Only
S. E. Postawko, M. L. Morrissey, G. J. Taylor, and P. Mouginis-Mark (Hawaii Univ., Honolulu.) *In* Lunar and Planetary Inst., Twenty-Fourth Lunar and Planetary Science Conference. Part 3: N-Z 1993 p 1167 (For primary document see N94-20636 05-91)
Avail: CASI HC A01/MF A06

N94-22286# GKSS-Forschungszentrum Geesthacht (Germany). Inst. fuer Physik.
THE USE OF ERBE DATA FOR CLIMATE STUDIES
R. Stuhlmann and M. Rieland (Deutscher Bundestag, Bonn, Germany.) *In* Max-Planck-Inst. fuer Meteorologie, Proceedings of the Workshop on New Generation of Radiation Budget Measurements From Space and Their Use in Climate Modelling and Diagnostic Studies Sep. 1992 p 13-18 (For primary document see N94-22283 05-46)
Avail: CASI HC A02/MF A01

N94-22290# Meteorological Office, Bracknell (England). Climate Prediction and Research Center.
SIMULATION OF CLEAR-SKY OUTGOING LONGWAVE RADIATION OVER THE OCEANS USING OPERATIONAL ANALYSIS
A. Slingo and M. J. Webb *In its* Proceedings of the Workshop on New Generation of Radiation Budget Measurements From Space and Their Use in Climate Modelling and Diagnostic Studies Sep. 1992 p 26-28 (For primary document see N94-22283 05-46)
Avail: CASI HC A01/MF A01

N94-22291# European Centre for Medium-Range Weather Forecasts, Reading (England).
USE OF SATELLITE DATA FOR VALIDATION OF OPERATIONAL FORECAST MODELS AND OPERATIONAL ANALYSES
E. Klinker *In* Max-Planck-Inst. fuer Meteorologie, Proceedings of the Workshop on New Generation of Radiation Budget Measurements From Space and Their Use in Climate Modelling and Diagnostic Studies Sep. 1992 p 29 (For primary document see N94-22283 05-46)
Avail: CASI HC A01/MF A01

48 OCEANOGRAPHY

Includes biological, dynamic, and physical oceanography; and marine resources.

For related information see also *43 Earth Resources and Remote Sensing.*

N94-19895# Woods Hole Oceanographic Inst., MA.
ON THE SOURCES OF NORTH ATLANTIC DEEP WATER
James Luyten, Michael McCartney, and Henry Stommel Aug. 1993 9 p
(Contracts N00014-90-J-1508; N00014-90-J-1425)
(AD-A270854; WHOI-CONTRIB-7943) Avail: CASI HC A02/MF A01

Because the volumetric census of deep and bottom water in the North Atlantic Ocean consists of three isolated linear ridges along which heat and salt flow through the main volumetric mode (and point of intersections), it is possible to deduce the expected ratio of heat flux and ratio of salt fluxes measured in the Denmark Strait overflow off Greenland and in the Antarctic Bottom Water near the equator. The weakly stratified layers of North Atlantic Deep Water fall on the nearly linear ridge at temperatures above that of the mode. There is an incompatibility between observed ratio and deduced ratio. It is predicted that a remeasurement of the flux of Antarctic Bottom Water near the equator will show that the previous determination of 4 deg N is unrepresentatively low. DTIC

N94-19905 Materials Research Labs., Ascot Vale (Australia).
DISTRIBUTION OF TURBIDITY IN AUSTRALIAN TROPICAL WATERS
P. J. Mulhearn Aug. 1993 27 p Limited Reproducibility: More than 20% of this document may be affected by microfiche quality
(AD-A271059; MRL-TN-688; DODA-AR-008-262) Avail: CASI HC A03

Data on underwater visibility in tropical Australian waters, in the form of Secchi disc depths and light attenuation coefficients were collected and are presented in the form of maps with Secchi depths grouped in the ranges: less than 5 m, 5 m to 10 m, and greater than 10 m. As one would expect there is a general trend for water turbidity to decrease (or Secchi depth to increase) with depth, and for turbidity to be high in areas with a large tidal range. It can be seen, from the maps, that high turbidity would not infrequently limit diver and remotely operated vehicle operations along Australia's northern coastal shipping routes and in major port approaches. DTIC

N94-19952 Naval Command, Control and Ocean Surveillance Center, San Diego, CA.
OCEANIC IN SITU FRAUNHOFER-LINE CHARACTERISTICS: FRAUNHOFER-LINE UNDERWATER EXPERIMENT (FLUX) Final Report, FY89 - FY91
M. G. Lovern, M. W. Roberts, S. A. Miller, and G. T. Kaye Sep. 1992 22 p Limited Reproducibility: More than 20% of this document may be affected by microfiche quality
(AD-A270659; NCCOSC/RDT/E-TR-1553) Avail: Issuing Activity (Defense Technical Information Center (DTIC))

Interest in making use of the existence of Fraunhofer lines to reduce

solar background noise for the Satellite Laser Communications (SLC) program prompted the requirement for making underwater in situ characterizations of five Fraunhofer lines in the blue-green spectrum. Recent papers that discuss and attempt to explain frequent occurrences of high measured values for underwater irradiance raised concerns about the persistence of Fraunhofer lines. The effect of an increased light field could significantly reduce (potentially eliminate) the absorption depth of Fraunhofer lines and reduce their solar-rejection benefits to optical communications. These characterizations were made from a surface ship off the coast of Hawaii in Aug. 1989. Fraunhofer lines at 420, 440, 486, 518, and 532 nm were characterized at the surface and at four discrete depths to a maximum depth of 90 m. These are the first known characterizations of Fraunhofer lines underwater. A high resolution scan from 450 to 550 nm was also made at a depth of 73 m. The results from this experiment showed no differences between the surface and underwater scans suggesting the effects of interwavelength scattering is less than originally proposed. DTIC

N94-19979# Naval Civil Engineering Lab., Port Hueneme, CA.
SIMBAT THEORETICAL MANUAL Final Report, Oct. 1986 - Sep. 1990
Leon E. Borgman, Warren A. Bartel, and David R. Shields Aug. 1993 81 p
(AD-A271063; NCEL-TR-941) Avail: CASI HC A05/MF A01

This manual develops the theory of the Conditional Ocean Wave Simulation Model (SIMBAT). SIMBAT is a high performance FORTRAN F77 based computer model that uses the Fast Fourier Transform (FFT) to produce ocean wave properties for ocean engineering applications. The model assumes the wave properties form a Gaussian stochastic process. SIMBAT may be used to perform a conditional or unconditional simulation. A conditional simulation uses a measured or existing input time series and forces the simulated wave properties to adhere to the input time series but also follow the laws of multivariate normal probability. An unconditional simulation uses a measured or created ocean wave spectra to randomly simulate the ocean wave properties. The program features include the following: creation of directional ocean wave spectra, water particle kinematic stretching, conditioning time series using an input time series less than or equal to the simulation length, use of Legendre orthogonal polynomials for post-creation of wave properties by program CKPOLY, and error checking. DTIC

N94-20131*# Massachusetts Inst. of Tech., Cambridge. Dept. of Earth, Atmospheric, and Planetary Sciences.
INVERSION OF GRAVITY AND BATHYMETRY IN OCEANIC REGIONS FOR LONG-WAVELENGTH VARIATIONS IN UPPER MANTLE TEMPERATURE AND COMPOSITION Final Report, 1 Jan. 1992 - 30 Jun. 1993
Sean C. Solomon and Thomas H. Jordan 17 Sep. 1993 5 p
(Grant NAGw-3036)
(NASA-CR-192272; NAS 1.26:192272) Avail: CASI HC A01/MF A01

Long-wavelength variations in geoid height, bathymetry, and SS-S travel times are all relatable to lateral variations in the characteristic temperature and bulk composition of the upper mantle. The temperature and composition are in turn relatable to mantle convection and the degree of melt extraction from the upper mantle residuum. Thus the combined inversion of the geoid or gravity field, residual bathymetry, and seismic velocity information offers the promise of resolving fundamental aspects of the pattern of mantle dynamics. The use of differential body wave travel times as a measure of seismic velocity information, in particular, permits resolution of lateral variations at scales not resolvable by conventional global or regional-scale seismic tomography with long-period surface waves. These intermediate scale lengths, well resolved in global gravity field models, are crucial for understanding the details of any chemical or physical layering in the mantle and of the characteristics of so-called 'small-scale' convection beneath oceanic lithosphere. In 1991 a three-year project to the NASA Geophysics Program was proposed to carry out a systematic inversion of long-wavelength geoid anomalies, residual bathymetric anomalies, and differential SS-S travel time delays for the lateral variation in characteristic temperature and bulk composition of the oceanic upper mantle. The project was funded as a three-year award, beginning on 1 Jan. 1992. Author

N94-20489# Massachusetts Univ., Amherst. Dept. of Electrical and Computer Engineering.
USE OF MICROWAVE POLARIMETRY TO ENHANCE SAR IMAGES OF THE OCEAN SURFACE Final Report
Robert E. McIntosh Sep. 1993 5 p
(Contract N00014-89-J-3230)
(AD-A271911) Avail: CASI HC A01/MF A01

The goal is to investigate the coherent backscatter of microwave signals from the ocean surface to better understand the effects of surface motion on synthetic aperture radar images. The objective is to analyze the behavior of coherent electromagnetic backscatter from the ocean surface for a dual frequency dual polarization radar. Frequency and polarization diversity provides a picture of the mechanisms involved in the microwave backscatter. In this study data were obtained from various UMass radar systems to obtain extensive radar observations of the ocean surface at the FPN research tower, in the North Sea, Germany. Some of the results were reported in the publications listed at the end of this report. DTIC

N94-20531# Institute of Oceanographic Sciences, Wormley (England). Deacon Lab.
SHIPBOARD ADCP OBSERVATIONS DURING RRS CHARLES DARWIN CRUISE 62
M. C. Hartman 1992 25 p
(IOS-298-1992; ETN-93-94561) Avail: CASI HC A03/MF A01

Shipboard Acoustic Doppler Current Profiler (ADCP) observations made during Aug. 1991 when RRS Charles Darwin Cruise 62 occupied Conductivity/Temperature/Depth (CTD) stations in a World Ocean Circulation Experiment (WOCE) control volume in the north Atlantic are reported. The 150 kHz ADCP was operating throughout producing data on water velocity and echo amplitude while the ship was under way and on station. A description of the set up and data processing route used is provided. A summary of the current velocity data collected from the instrument while on station is given as contour plots for each leg of the cruise. ESA

N94-20564# Quadrant Engineering, Inc., Hadley, MA.
FOUR-DIMENSIONAL REMOTE SENSING OF THE MARINE BOUNDARY LAYER WITH A DIGITAL BEAMFORMING RADAR WIND PROFILER Final Report, 1 Apr. - 30 Sep. 1993
James B. Mead 30 Sep. 1993 32 p
(Contract N00014-93-C-0042)
(AD-A270627) Avail: CASI HC A03/MF A01

Research performed by Quadrant Engineering is detailed. The purpose was to determine the feasibility of deploying a shipboard turbulent eddy profiling (TEP) radar system for studying the dynamics of the marine boundary layer. A similar system is currently being developed by the University of Massachusetts to study the atmospheric boundary over land. During the phase 1 study, Quadrant Engineering reviewed the design of the land based system, and determined that a slightly scaled down version of that system would be suitable for deployment on a large research vessel, such as the Knorr, operated by Woods Hole Oceanographic Institute. A design for the shipboard TEP system is presented and the particular requirements of installation on the Knorr are considered. The application of TEP to boundary layer research, especially in terms of complementing Large Eddy Simulation (LES) models, is also described. DTIC

N94-20581# Woods Hole Research Center, MA. Dept. of Geology and Geophysics.
SEAFLOOR CHARACTERIZATION/GALAPAGOS PROPAGATING RIFT Final Report
Martin C. Kleinrock, Peter R. Shaw, and Deborah K. Smith 1993 3 p
(Contract N00014-89-J-1021)
(AD-A272001) Avail: CASI HC A01/MF A01

Our goal is to better understand the system that produces the oceanic crust. Because the seafloor is a product of this system we believe that fundamental insight can be gained through the study of seafloor topography and the spatial variation in its characteristics. Our project has focused on applying and further developing our techniques for analyzing seafloor topography and combining our techniques for seafloor characterization with other data sources (e.g., seismicity) and models. DTIC

N94-20925 Naval Undersea Warfare Center, Newport, RI.
A SURVEY OF THE IMPACT ON ACOUSTIC PROPAGATION OF WARM CORE OCEAN EDDYS Final Report
David G. Browning, Joseph M. Monti, and Linda S. Petitpas 21 Sep. 1993 22 p Limited Reproducibility: More than 20% of this document may be affected by microfiche quality
(AD-A272188; NUSW-NPT-TD-10451) Avail: Issuing Activity (Defense Technical Information Center (DTIC))

Warm core eddys have been found throughout the oceans of the world. Most have a bowl-like shape extending down from the surface, which, along with an increased sound speed due to the warmer water core, causes more acoustic energy to be refracted toward the surface than would occur without an eddy present. However, the impact on acoustic propagation varies significantly from ocean to ocean, because of variations in eddy size and core temperature, as well as sound speed profile differences in the adjoining waters. Examples are given from the North and South Atlantic Oceans, North and South Pacific Oceans, Greenland and Norwegian Seas. DTIC

N94-21222# Naval Research Lab., Bay Saint Louis, MS.
ESTIMATING THE ROTATION RATE OF MESOSCALE OCEAN RINGS FROM SATELLITE ALTIMETRY Final Report
Theodore J. Bennett, Jr. 26 Oct. 1993 18 p
(AF Proj. 2008)
(AD-A272922; NRL/FR/7322-93-9443) Avail: CASI HC A03/MF A01

The mesoscale ocean environment has considerable impact on underwater acoustics. However, the ocean is such a data-sparse environment, especially at depth, that it is difficult to make effective ocean nowcasts and forecasts of the environment. A key input to nowcasts and forecasts is the rotation rate of mesoscale ocean rings. This report presents a technique for determining the rotation rate from satellite altimetry. The technique offers the prospect of a cost-effective system for monitoring this key ocean parameter. DTIC

N94-21358# Naval Research Lab., Washington, DC.
AIRBORNE SURFACE BACKSCATTERING STRENGTH MEASUREMENTS IN THE WESTERN ATLANTIC OCEAN Final Report
John P. Crockett, Peter M. Ogden, and Fred T. Erskine 17 Sep. 1993 38 p
(NR Proj. R03-5-B-03)
(AD-A271737; NRL/FR/7142-93-9563) Avail: CASI HC A03/MF A01

This report presents the results from a series of airborne, SUS-based acoustic surface backscattering strength tests conducted over the western Atlantic Ocean during April 1988. We describe the airborne technique used to gather the acoustic data and the environmental data (sound speed profiles and wind speed). Analysis provides information on sea surface acoustic backscattering strengths for mean grazing angles from 7 deg to 30 deg, wind speeds from 7 to 18 m/s, and frequencies from 50 to 800 Hz. The data analysis procedure is outlined, and the results are compared to first-order perturbation theory (air-water interface scatter), the Chapman-Harris empirical formula, and the Ogden-Erskine empirical algorithm. The absolute error in measured scattering strengths is approximately + or - 5 dB. The data comparison emphasizes the use of wind history as an environmental predictor of surface scattering. The results are summarized, and a list of the lessons learned concerning the experimental technique is provided. Brief analyses of the sound speed profiles and wind speed data are appended. DTIC

N94-21360 Woods Hole Oceanographic Inst., MA. Dept. of Physical Oceanography.
COMPARISON OF SATELLITE-DERIVED VELOCITY FIELDS IN THE COASTAL TRANSITION ZONE Final Report
26 Oct. 1993 3 p Limited Reproducibility: More than 20% of this document may be affected by microfiche quality
(Contract N00014-90-J-1808)
(AD-A272565) Avail: Issuing Activity (Defense Technical Information Center (DTIC))

Two methods of estimating surface velocity vectors from advanced very high resolution radiometer (AVHRR) data were applied to the same set of images and the results were compared with in situ and altimeter measurements. The first method used an automated feature-tracking algorithm and the second method used an inversion of the heat equation. The 11 images were from 3 days in July 1988 during the Coastal Transition field program and the in situ data included acoustic Doppler current profiler (ADCP) vectors and velocities from near-surface drifters. The two methods were comparable in their degree of agreement with the in situ data, yielding velocity magnitudes that were 30 - 50% less than drifter and ADCP velocities measured at 15 - 20 m depth, with rms directional differences of about 60 deg. These differences compared favorably with a baseline difference estimate between ADCP vectors interpolated to drifter locations within a well-sampled region. High correlations between the AVHRR estimates and the coincident Geosat geostrophic velocity profiles suggested that the AVHRR methods adequately resolved the important flow features. The flow field was determined to consist primarily of a meandering southward flowing current, interacting with several eddies, including a strong anticyclonic eddy to the north of the jet. Incorporation of sparse altimeter data into the AVHRR estimates gave a modest improvement in comparisons with in situ data. Author

N94-21366# Scripps Institution of Oceanography, La Jolla, CA.
ACOUSTIC MONITORING OF GLOBAL OCEAN VARIABILITY Final Report, 1 Nov. 1991 - 28 Feb. 1993
Walter H. Munk 10 Oct. 1993 39 p Prepared in cooperation with Washington Univ., Seattle
(Contract MDA972-92-C-0019)
(AD-A271998; UCSD-92-1070) Avail: CASI HC A03/MF A01

Oceanic circulation is known to be a central element in determining the present climate state and to be crucial in understanding how it might change in the future. However, our current understanding of the ocean is so primitive that forecasts of future climate states must be regarded as speculative. Central to the problem is the great difficulty associated with observing the state of the ocean today and of determining whether it is changing to any significant extent. The concept of Acoustic Thermometry of Ocean Climate as described by this document focuses on the critical role of the world's oceans in the process of global change. A research and engineering program to create a network of acoustic transmission paths represents the first step to measure long-term temperature change in the ocean (and hence by inference, atmospheric and climatic trends). This network can build on the results of The Heard Island Feasibility Test by using very long-range underwater sound transmissions to measure oceanic temperature on basin scales. It involves a multiyear program to monitor the ocean on a global basis by installing a system of acoustic sources and receives at sites that provide adequate spatial sampling, and are technically, politically, and logistically feasible. DTIC

N94-21423# Naval Postgraduate School, Monterey, CA.
OCEAN WAVE HEIGHT TRANSFORMATION MODEL USING SURFACE ROLLER THEORY M.S. Thesis
A. H. Brookins Jun. 1993 49 p
(AD-A272610) Avail: CASI HC A03/MF A01

A wave height transformation model is developed using surface roller theory. Roller energy production is included in the energy flux balance equation to predict rms wave height for randomly varying, irregular waves over arbitrary bathymetry. The dissipation function is defined using wave roller theory, where the area of the roller is defined from a simple bore analogy. The Rayleigh distribution is used to statistically describe wave heights as waves shoal, break, and dissipate. Model predictions are compared with data acquired on both barred and near planar beaches. The surface roller wave height transformation model predicts rms wave heights with an average rms error of 6.5% for a barred beach over three days, 3.0% for two planar beaches over four days, and 4.5% average error for all locations over seven days. The model has two free parameters, alpha representing the type of breaker and gamma a measure of breaking wave saturation, also a function of beach slope. Optimal values of both parameters are chosen by model fitting. The model is sensitive to gamma, but not sigma. The surface roller model improves the bore dissipation model by decreasing the average rms error by 40% while decreasing model sensitivity to input parameters. DTIC

N94-21443# Naval Research Lab., Washington, DC.
GREEN SHEET PROJECT: DYE SHEET EVOLUTION Interim Report, Dec. 1991 - Dec. 1992
C. L. Trump 30 Sep. 1993 54 p
(AD-A272019; NRL/MR/7340-93-7402) Avail: CASI HC A04/MF A01

A 300-kHz Acoustic Doppler Current Profiler (ADCP) was used aboard the USNS Bartlett as part of the Green Sheet 91 experiment during June 1991 in the Gulf of Mexico. The purpose of the experiment was to lay out a sheet of dye at the bottom of the mixed layer for later sampling by an airborne LIDAR system. Ship's tracks relative to targeted depths were calculated to reconstruct the dye deployment and sampling process. During the practice deployment, termed Dress Rehearsal, a small front was found between the second and third leg which adversely affected the location and geometry of the dye sheet. During the first LIDAR test, termed Flight One, currents rotating strongly in depth and weakly in the horizontal also adversely affected the character of the final dye sheet. A Shear-Advection model was developed, using ADCP data and concurrently recorded navigation data, to predict the dye sheet evolution. The results of the model helped understand the evolution of dye sheets and were in agreement with the results of the LIDAR sampling during Flight One. For future Green Sheet experiments the ADCP should be used to provide real-time ship's tracks relative to a given water depth to aid dye deployment. The Shear-Advection model should be used in near-real-time to aid the vectoring of the plane over the evolved dye sheet. DTIC

N94-21628*# National Aeronautics and Space Administration. Wallops Flight Facility, Wallops Island, VA.
PRESENTING THE RAIN-SEA INTERACTION FACILITY
Larry F. Bliven and Tonas M. Elfouhaily (Paris V Univ., France.) Nov. 1993 36 p Sponsored by NASA. Washington
(NASA-RP-1322; NAS 1.61:1322; Rept-94B00012) Avail: CASI HC A03/MF A01

The new Rain-Sea Interaction Facility (RSIF) was established at GSFC/WFF and the first finds are presented. The unique feature of this laboratory is the ability to systematically study microwave scattering from a water surface roughened by artificial rain, for which the droplets are at terminal velocity. The fundamental instruments and systems (e.g., the rain simulator, scatterometers, and surface elevation probes) were installed and evaluated during these first experiments - so the majority of the data were obtained with the rain simulator at 1 m above the water tank. From these initial experiments, three new models were proposed: the square-root function for NCS vs. R, the log Gaussian model for ring-wave elevation frequency spectrum, and the Erland probability density distribution for back scattered power. Rain rate is the main input for these models, although the coefficients may be dependent upon other factors (drop-size distribution, fall velocity, radar configuration, etc.). The facility is functional and we foresee collaborative studies with investigators who are engaged in measuring and modeling rain-sea interaction processes. Author (revised)

N94-20426*# Jet Propulsion Lab., California Inst. of Tech., Pasadena.
POLARIMETRIC BACKSCATTERING FROM SEA ICE Abstract Only
S. V. Nghiem, R. Kwok, and S. H. Yueh *In its* Progress In Electromagnetics Research Symposium (PIERS) 1993 p 477 (For primary document see N94-20403 05-32)
Avail: CASI HC A01/MF A10

N94-20428*# Jet Propulsion Lab., California Inst. of Tech., Pasadena.
ON EVALUATING THE ACCURACY OF SAR SEA-ICE CLASSIFICATION USING MULTIFREQUENCY POLARIMETRIC AIRSAR DATA Abstract Only
Mark R. Drinkwater and Eric Rignot *In its* Progress In Electromagnetics Research Symposium (PIERS) 1993 p 480 (For primary document see N94-20403 05-32)
Avail: CASI HC A01/MF A10

N94-20432*# Jet Propulsion Lab., California Inst. of Tech., Pasadena.
RETRIEVAL OF ICE THICKNESS FROM POLARIMETRIC SAR DATA Abstract Only
R. Kwok, S. H. Yueh, S. V. Nghiem, and D. D. Huynh *In its* Progress In Electromagnetics Research Symposium (PIERS) 1993 p 574 (For primary document see N94-20403 05-32)
Avail: CASI HC A01/MF A10

N94-20433*# Jet Propulsion Lab., California Inst. of Tech., Pasadena.
STUDIES OF GREENLAND USING THE SEASAT SCATTEROMETER Abstract Only
David G. Long (Brigham Young Univ., Provo, UT.) and Mark Drinkwater *In its* Progress In Electromagnetics Research Symposium (PIERS) 1993 p 575 (For primary document see N94-20403 05-32)
Avail: CASI HC A01/MF A10

N94-20434*# Jet Propulsion Lab., California Inst. of Tech., Pasadena.
RADAR BACKSCATTERING FROM SNOW FACIES OF THE GREENLAND ICE SHEET: RESULTS FROM THE AIRSAR 1991 CAMPAIGN Abstract Only
Eric Rignot, K. Jezek (Ohio State Univ., Columbus.), J. J. vanZyl, Mark R. Drinkwater, and Y. L. Lou *In its* Progress In Electromagnetics Research Symposium (PIERS) 1993 p 576 (For primary document see N94-20403 05-32)
Avail: CASI HC A01/MF A10

N94-20438*# Jet Propulsion Lab., California Inst. of Tech., Pasadena.
NEAR GRAZING SCATTERING FROM NON-GAUSSIAN OCEAN SURFACES Abstract Only
Yunjin Kim and Ernesto Rodriguez *In its* Progress In Electromagnetics Research Symposium (PIERS) 1993 p 615 (For primary document see N94-20403 05-32)
Avail: CASI HC A01/MF A10

N94-20439*# Jet Propulsion Lab., California Inst. of Tech., Pasadena.
ROUGH SURFACE SCATTERING FROM MOVING OCEAN SURFACES AS AN INDICATOR OF SCATTERING MECHANISMS Abstract Only
Ernesto Rodriguez and Yunjin Kim *In its* Progress In Electromagnetics Research Symposium (PIERS) 1993 p 616 (For primary document see N94-20403 05-32)
Avail: CASI HC A01/MF A10

N94-22145 Defence Research Establishment Valcartier (Quebec).
MARINE BOUNDARY LAYER MODEL EVALUATION BY USING A HEIGHT GAIN MEASUREMENT TECHNIQUE IN THE INTERFERENCE REGION
Denis Dion *In* Engineering Inst. of Canada, Canadian Conference on Electrical and Computer Engineering, Volumes 1 and 2 1991 4 p (For primary document see N94-22101 05-33)
Avail: Issuing Activity (Engineering Inst. of Canada, 2050 rue Mansfield, Suite 700, Montreal, PQ H3A 1Z2 Canada)

51 LIFE SCIENCES (GENERAL)

N94-19826 California Univ., Berkeley. Lawrence Berkeley Lab.
HIGH RESOLUTION ELECTRON CRYSTALLOGRAPHY OF PROTEIN MOLECULES
R. M. Glaeser and K. H. Downing Jun. 1993 21 p Presented at the John M. Crowley Symposium on Ultramicroscopy, Scottsdale, AZ, 5-8 Jan. 1993 Limited Reproducibility: More than 20% of this document may be affected by microfiche quality
(Contract DE-AC03-76SF-00098)
(DE93-040114; LBL-34224; CONF-9301114-3) Avail: Issuing Activity (Department of Energy (DOE))

Electron diffraction data and high resolution images can now be used to obtain accurate, three-dimensional density maps of biological macromolecules. These density maps can be interpreted by building an atomic-resolution model of the structure into the experimental density. The Cowley-Moodie formalism of dynamical diffraction theory was used to validate the use of kinematic diffraction theory, strictly the weak phase object approximation, in producing such 3-D density maps. Further improvements in the preparation of very flat specimens and in the retention of diffraction to a resolution of 0.2 nm or better could result in electron crystallography becoming as important a technique as x ray crystallography currently is for the field of structural molecular biology. DOE

N94-19866# Los Alamos National Lab., NM.
A COMPLEX SYSTEMS APPROACH TO COMPUTATIONAL MOLECULAR BIOLOGY
A. Lapedes 1993 24 p Presented at the Santa Fe Institute Workshop on Integrative Themes, Santa Fe, NM, 8-15 Aug. 1992

(Contract W-7405-eng-36)
(DE93-040062; LA-UR-93-2909; CONF-9208239-1) Avail: CASI HC A03/MF A01

The containing research program at Santa Fe Institute that applies complex systems methodology to computational molecular biology is reported. Two aspects stressed are the use of co-evolving adaptive neutral networks for determining predictable protein structure classifications, and the use of information theory to elucidate protein structure and function. A 'snapshot' of the current state of research in these two topics is presented, representing the present state of two major research thrusts in the program of Genetic Data and Sequence Analysis at the Santa Fe Institute. DOE

N94-21897*# National Aeronautics and Space Administration. Ames Research Center, Moffett Field, CA.
SELF-MOTION PERCEPTION AND MOTION SICKNESS Final Report, 1982 - 1991
Robert A. Fox (San Jose State Univ., CA.) 1991 150 p
(Contract NCC2-167)
(NASA-CR-194276; NAS 1.26:194276) Avail: CASI HC A07/MF A02

Motion sickness typically is considered a bothersome artifact of exposure to passive motion in vehicles of conveyance. This condition seldom has significant impact on the health of individuals because it is of brief duration, it usually can be prevented by simply avoiding the eliciting condition and, when the conditions that produce it are unavoidable, sickness dissipates with continued exposure. The studies conducted examined several aspects of motion sickness in animal models. A principle objective of these studies was to investigate the neuroanatomy that is important in motion sickness with the objectives of examining both the utility of putative models and defining neural mechanisms that are important in motion sickness. For individual titles, see N94-21898 through N94-21915.

N94-21898*# National Aeronautics and Space Administration. Ames Research Center, Moffett Field, CA.
CHANGES IN PLASMA VASOPRESSIN DURING MOTION SICKNESS IN CATS Abstract Only
Robert Fox (San Jose State Univ., CA.), L. Keil, Nancy G. Daunton, D. Thomsen (San Jose State Univ., CA.), M. Dictor (San Jose State Univ., CA.), and O. Chee (San Jose State Univ., CA.) *In its* Self-Motion Perception and Motion Sickness 1991 1 p Repr. from Neuroscience Abstracts, v. 6, 1980 p 656 (For primary document see N94-21897 05-51)
Avail: CASI HC A01/MF A02

Changes in levels of plasma vasopressin (AVP) and cortisol (C) have been shown to be correlated with motion sickness and nausea in man. As part of the research aimed at validation of the cat as an appropriate animal model for motion sickness research, levels of these hormones were investigated in the cat during motion sickness elicited by vertical linear acceleration of approximately 0.6 Hz and 1 +/- 0.6 G. In Study 1, 15 cats previously screened for susceptibility to motion sickness were prepared with indwelling jugular catheters to permit withdrawl of blood with minimal disruption of the stimulus and minimum stress to the animal. AVP and C were measured in blood samples obtained during exposure to vertical linear acceleration and during control sessions in which the animals were placed in the stationary apparatus. 10 min and 1 min prior to duration; 1, 5, 10, and 20 min after start of motion. Total duration of exposure to motion was 20 min. The data indicate that both AVP and C are elevated during exposure to motion if emesis occurs. AVP reaches maximum levels during or about the same time as emesis, while C increases gradually throughout the period of vertical acceleration. In Study 2, four cats were prepared with indwelling catheters and AVP was measured in blood withdrawn during exposure to the vertical linear acceleration. A single pre-motion sample consisting of three samples drawn 5 min prior to motion onset. Two series of samples consisting of three samples drawn at 3-min intervals were obtained during motion. The first series was initiated at emesis, and the second 25 min after emesis. Results show that levels of circulating AVP were elevated (2 to 27 times the control and pre-motion levels) in the samples taken during emesis and decreased, but remained 1 to 6 times above the pre-motion or control levels within 25 min. The results of these two studies indicate that AVP is elevated during motion-produced emesis than is C. These findings are in general agreement with those obtained from humans under motion sickness conditions, and indicate that it is appropriate to continue to use the cat in studies of hormone changes during motion sickness. Author

N94-21899*# National Aeronautics and Space Administration. Ames Research Center, Moffett Field, CA.
SUSCEPTIBILITY OF THE SQUIRREL MONKEY TO DIFFERENT MOTION CONDITIONS Abstract Only
Robert A. Fox (San Jose State Univ., CA.), Nancy G. Daunton, and J. Coleman (San Jose State Univ., CA.) *In its* Self-Motion Perception and Motion Sickness 1991 1 p Repr. from Neuroscience Abstracts, v. 8, 1982 p 698 (For primary document see N94-21897 05-51)
Avail: CASI HC A01/MF A02

The exact stimulus eliciting vomiting in animal studies of motion sickness is difficult to specify because the vestibular stimulation produced by many motion conditions is confounded by voluntary movements with animals. This is an important problem because experiments with animal models of motion sickness can provide useful information about antimotion sickness drugs or the role of neural mechanisms, only when animals are exposed to the same motion stimuli in each experimental session. A series of tests were conducted to determine the susceptibility of 15 adult squirrel monkeys to motion sickness in freely moving and restrained test conditions. Canal stimulation was varied by exposing the monkey in freely moving conditions to varying degrees of angular velocity (60, 90, 120, 150 deg/sec), and in restrained conditions to one angular velocity (150 deg/sec) and to cross-coupling effects of whole-body roll movements during rotation. Otolith stimulation was investigated by using sinusoidal vertical linear acceleration during free movement conditions, and off-vertical rotation and earth-horizontal (BBQ) rotation while restrained. The percentage of freely moving animal vomiting during vertical axis rotation was 27, 93, 86, and 92 for the angular velocities of 60, 90, 120, and 150 deg/sec respectively. None of the monkeys vomited during vertical axis rotation or cross-coupled rotation when restrained. Otolith stimulation appears to be a less provocative stimulus for the squirrel monkey as the percentage of animals vomiting were 13, 0, and 7 for the conditions of free movement during oscillation, restraint during off-vertical, and BBQ rotation respectively. Motion sickness to the point of vomiting occurred regularly only in conditions where self-motion was possible. Such effects could occur because voluntary movement during motion augments vestibular effects by producing self-inflicted cross-coupling, but the failure to elicit vomiting with experimenter-coupling cross-coupling argues against this interpretation. Alternatively, these results might imply that feedback from movement control mechanisms may play an important role in sensory conflict as suggested by Oman's sensory-motor conflict theory. Author

N94-21900*# National Aeronautics and Space Administration. Ames Research Center, Moffett Field, CA.
RELATIONSHIP OF AREA POSTREMA TO THREE PUTATIVE MEASURES OF MOTION SICKNESS Abstract Only
R. Sutton (San Jose State Univ., CA.), Robert A. Fox (San Jose State Univ., CA.), and Nancy G. Daunton *In its* Self-Motion Perception and Motion Sickness 1991 1 p Repr. from unidentified source (For primary document see N94-21897 05-51)
Avail: CASI HC A01/MF A02

Although the rat has an incomplete emetic reflex, several species-specific responses to motion were proposed as measures of 'motion sickness' in rats. The purpose was to determine the dependence of these responses on one of several neural structures known to be essential to motion-induced vomiting in species with a complete emetic reflex. The Area Postrema (AP) was shown to play an important role in the production of motion sickness in vomiting species. The effects of thermo-cautery ablations of the AP on three different responses supposedly reflecting motion sickness in the rat were compared: conditioned taste aversion (CTA); drinking suppression; and fecal boli. Efficacy of the ablations was determined by subjecting ablated, sham-operated, and unoperated control animals to a CTA test which is known to require a functional AP. Animals with AP ablations failed to form CTA when 0.15 M LiCl was paired with a 10 percent sucrose solution, while sham-operated control subjects conditioned as well as the unoperated control subjects. The extent of the ablations was evaluated histologically at the end of the experiment. To determine the effects of the ablations on the measures of motion sickness, all animals were subjected to rotation for 30 min or 90 min on a platform displaced 20 deg from earth horizontal. Results indicate that ablation of AP in the

rat has no effect on the formation of CTA to a 4 percent solution of cider paired with motion, on the suppression of drinking immediately after exposure to motion, or on the frequency of fecal boli during exposure to motion. This failure of AP ablations to eliminate the effects of motion on any of these responses discourages their use as equivalents of motion-induced vomiting. The appropriateness of other suggested measures, e.g., pica, remains untested but the dependence of such measures on stimulation more severe than commonly used in motion sickness research and the absence of a demonstration of their dependence on neural structures essential to motion sickness in vomiting species, suggest caution in the use of such responses. Further, until more is known about the neural structures underlying these putative measures, the rat will remain a questionable subject in which to study motion sickness. Author (revised)

N94-21901*# National Aeronautics and Space Administration. Ames Research Center, Moffett Field, CA.

REASSESSMENT OF AREA POSTREMA'S ROLE IN MOTION SICKNESS AND CONDITIONED TASTE AVERSION Abstract Only

Nancy G. Daunton, Kenneth R. Brizzee (Tulane Univ., Covington, LA.), Meryl Lee Corcoran, G. H. Crampton (Wright State Univ., Dayton, OH.), F. DAmelio, S. Elfar (San Jose State Univ., CA.), and Robert A. Fox (San Jose State Univ., CA.) *In its* Self-Motion Perception and Motion Sickness 1991 1 p Repr. from unidentified source (For primary document see N94-21897 05-51)

Avail: CASI HC A01/MF A02

On the basis of classical studies on the role of the area psotrema (AP) in motion-induced emesis it was generally accepted that the AP is an essential structure for the production of vomiting in response to motion. However, in more recent studies it has been demonstrated that vomiting induced by motion can still occur in animals in which the AP has been destroyed bilaterally. It was inferred from some of these more recent studies that the AP plays no role in motion-induced emesis. From the standpoint of the current understanding of central nervous system (CNS) plasticity, redundancy, remodeling, unmasking, regeneration, and recovery of function, however, it is important to realize the limitations of using ablation procedures to determine the functional role of a given neural structure in a highly integrated, adaptable central nervous system (CNS). For example, the results of our recent investigations in cat and squirrel monkey on the role of the AP in emesis and conditioned taste aversion induced by motion indicate that while AP lesions do not prevent motion-induced emesis when animals are tested 30 days or more after surgery, the lesions do change the latency to emesis. Thus, contradictory findings from lesion studies must be evaluated not only in terms of species difference, differences in lesioning techniques and extent of lesions, and in stimulus parameters, but also in terms of duration of the recovery period, during which significant recovery of function may take place. In our judgment, inadequate consideration of the foregoing factors could lead to erroneous inferences about given structure's role in the behavior of the intact, nonablated animal. Author (revised)

N94-21902*# National Aeronautics and Space Administration. Ames Research Center, Moffett Field, CA.

GAMMA-AMINOBUTYRIC ACID (GABA) AND NEUROPEPTIDES IN NEURAL AREAS MEDIATING MOTION-INDUCED EMESIS Abstract Only

F. DAmelio, Nancy G. Daunton, and Robert A. Fox *In its* Self-Motion Perception and Motion Sickness 1991 1 p Repr. from Chinese J. Physiological Sciences, v. 3, 1987, p 443-444 (For primary document see N94-21897 05-51)

Avail: CASI HC A01/MF A02

Immunocytochemical methods were employed to localize the neurotransmitter amino acid gamma-aminobutyric acid and the neuropeptides substance P and Met-enkephalin in the area postrema (AP), area subpostrema (ASP), nucleus of the tractus solitarius (NTS), dorsal motor nucleus of the vagus nerve (DMNV), and lateral vestibular nucleus (LVN). Glutamic acid decarboxylase immunoreactive (GAD-IR) terminals and fibers were observed in the AP and particularly in the ASP. A gradual decrease in the density of terminals was seen towards the solitary complex. The DMNV revealed irregularly scattered GAD-IR terminals within the neuropil or closely surrounding neuronal cell bodies. The LVN, particularly the dorsal division, showed numerous axon terminals which were mostly localize around large neurons and their proximal dendrites. Substance P immunoreactive (SP-IR) terminals and fibers showed high density in the solitary complex, in particular within the lateral division. The ASP showed medium to low density of SP-IR fibers and terminals. The AP exhibited a small number of fibers and terminals irregularly distributed. The DMNV revealed a high density of SP-IR terminals and fibers that were mainly concentrated in the periphery. Very few terminals were detected in the LVN. Met-enkephalin immunoreactive (Met-Enk-IR) fibers and terminals showed high density and uniform distribution in the DMNV. Scattered terminals and fibers were observed in the AP, ASP, and NTS (particularly the lateral division). The very few fibers were observed in the LVN surrounded the neuronal cell bodies. The present report is part of a study designed to investigate the interaction between neuropeptides and conventional neurotransmitters under conditions producing motion sickness and in the process of sensory-motor adaptation. Author (revised)

N94-21903*# National Aeronautics and Space Administration. Ames Research Center, Moffett Field, CA.

DETECTION OF EMETIC ACTIVITY IN THE CAT BY MONITORING VENOUS PRESSURE AND AUDIO SIGNALS Abstract Only

A. Nagahara (San Jose State Univ., CA.), Robert A. Fox (San Jose State Univ., CA.), Nancy G. Daunton, and S. Elfar *In its* Self-Motion Perception and Motion Sickness 1991 1 p Repr. from Neuroscience Abstracts, v. 12, Nov. 1986 (For primary document see N94-21897 05-51)

Avail: CASI HC A01/MF A02

To investigate the use of audio signals as a simple, noninvasive measure of emetic activity, the relationship between the somatic events and sounds associated with retching and vomiting was studied. Thoracic venous pressure obtained from an implanted external jugular catheter was shown to provide a precise measure of the somatic events associated with retching and vomiting. Changes in thoracic venous pressure monitored through an indwelling external jugular catheter with audio signals, obtained from a microphone located above the animal in a test chamber, were compared. In addition, two independent observers visually monitored emetic episodes. Retching and vomiting were induced by injection of xylazine (0.66mg/kg s.c.), or by motion. A unique audio signal at a frequency of approximately 250 Hz is produced at the time of the negative thoracic venous pressure change associated with retching. Sounds with higher frequencies (around 2500 Hz) occur in conjunction with the positive pressure changes associated with vomiting. These specific signals could be discriminated reliably by individuals reviewing the audio recordings of the sessions. Retching and those emetic episodes associated with positive venous pressure changes were detected accurately by audio monitoring, with 90 percent of retches and 100 percent of emetic episodes correctly identified. Retching was detected more accurately (p is less than .05) by audio monitoring than by direct visual observation. However, with visual observation a few incidents in which stomach contents were expelled in the absence of positive pressure changes or detectable sounds were identified. These data suggest that in emetic situations, the expulsion of stomach contents may be accomplished by more than one neuromuscular system and that audio signals can be used to detect emetic episodes associated with thoracic venous pressure changes. Author (revised)

N94-21904*# National Aeronautics and Space Administration. Ames Research Center, Moffett Field, CA.

RECOVERY OF THE VOMITING REFLEX FOLLOWING AREA POSTREMA ABLATION IN SQUIRREL MONKEYS

S. Elfar, Kenneth R. Brizzee (Tulane Univ., Covington, LA.), Robert A. Fox (San Jose State Univ., CA.), Meryl Lee Corcoran, Nancy G. Daunton, and J. Coleman (San Jose State Univ., CA.) *In its* Self-Motion Perception and Motion Sickness 1991 5 p Repr. from Neuroscience Abstracts, v. 12, Nov. 1986 (For primary document see N94-21897 05-51)

Avail: CASI HC A01/MF A02

The role of the area postrema (AP) in motion-induced emesis was re-assessed recently in several different species. In a few of these studies, the role of the AP in motion-induced conditioned taste aversion (CTA) was also addressed. The purpose was to extend this comparative study to the squirrel monkey, to evaluate further the role of AP in vomiting, and to investigate the dynamics of the recovery process. The AP was ablated bilaterally in 7 motion-susceptible squirrel monkeys which previously had been characterized in terms of their responses to various motion sickness-inducing stimuli. After recovery from surgery all animals were tested at 30-day intervals for a period of 11 months to determine the effects of AP ablations on susceptibility to the same sickness-inducing conditions. In

addition, the effectiveness of motion in producing CTA was evaluated. All pre-ablation motion tests involved stimulation for 30 min., while post-lesion tests were 60 min., in duration. All animals showed significant increases in latencies to vomiting after AP ablations. However, the latencies tended to decrease with time after ablation. All but one animal vomited on at least one of the 10 motion tests occurring after ablation of AP. In addition, CTA was produced by motion used in the conditioning sessions. These results suggest that structures other than AP, and processes other that those mediated through AP, may play an important role in motion-induced emesis. Author (revised)

N94-21905*# National Aeronautics and Space Administration. Ames Research Center, Moffett Field, CA.

MOTION SICKNESS ELICITED BY PASSIVE ROTATION IN SQUIRREL MONKEYS

Nancy G. Daunton and Robert A. Fox (San Jose State Univ., CA.) *In its* Self-Motion Perception and Motion Sickness 1991 2 p Repr. from Vestibular and Visual Control on Posture and Locomotion Equilibrium, 1983 p 164-169 (For primary document see N94-21897 05-51)
(Contract NCA2-OR-675-801; NIH-S06RR08192-02)
Avail: CASI HC A01/MF A02

Current theory and recent evidence suggest that motion sickness occurs under conditions of sensory input in which the normal motor programs for producing eye, head, and body movements are not functionally effective, i.e. under conditions in which there are difficulties in maintaining posture and controlling eye movements. Conditions involving conflicting or inconsistent visual-vestibular (VV) stimulation should thus result in greater sickness rates since the existing motor programs do not produce effective control of eye-head-body movements under such conditions. It is felt that the relationship of postural control to motion sickness is an important one and one often overlooked. The results are reported which showed that when postural requirements were minimized by fully restraining squirrel monkeys during hypogravity parabolic flight, no animals became motion sick, but over 80 percent of the same 11 animals became sick if they were unrestrained and maintained control of their posture.
Author (revised)

N94-21906*# National Aeronautics and Space Administration. Ames Research Center, Moffett Field, CA.

AREA POSTREMA ABLATIONS IN CATS: EVIDENCE FOR SEPARATE NEURAL ROUTES FOR MOTION- AND XYLAZINE-INDUCED CTA AND EMESIS Abstract Only

Meryl Lee Corcoran, Robert A. Fox (San Jose State Univ., CA.), Kenneth R. Brizzee (Tulane Univ., Covington, LA.), G. Crampton (Wright State Univ., Dayton, OH.), and Nancy G. Daunton *In its* Self-Motion Perception and Motion Sickness 1991 1 p Repr. from The Physiologist, v. 28., no. 4, Aug. 1985 (For primary document see N94-21897 05-51)
Avail: CASI HC A01/MF A02

Previous studies on the role of the area postrema (AP) in vomiting induced in the cat by motion and drugs have shown that the AP is not essential for motion-induced vomiting, but is necessary for vomiting to apomorphine and xylazine. To confirm these findings and to determine the role of the AP in the formation of Conditioned Taste Aversion (CTA), the AP was ablated bilaterally in 10 adult female cats. With one exception, the ablated cats continued to vomit to the same motion that elicited emesis before the ablation. Doses of xylazine and apomorphine that elicit emesis in intact cats, failed to induce emesis in the ablated cats. Histological examination indicated that 8 cats had complete lesions and 2 had partial lesions. Investigations of effects of AP ablations on CTA revealed that cats with complete lesions did not form CTA to flavored milk paired with xylazine-induced CTA. Seven of the eigth completely lesioned cats developed motion-induced CTA, even though emesis was not consistently elicited by motion. These results suggest that there are multiple routes for inducing CTA and the emetic reflex, that CTA can form without eliciting emesis, and that CTA may be a sensitive measure of sub-emetic motion sickness.
Author

N94-21907*# National Aeronautics and Space Administration. Ames Research Center, Moffett Field, CA.

EFFECT OF COPPER SULPHATE ON THE RATE OF AFFERENT DISCHARGE IN THE GASTRIC BRANCH OF THE VAGUS NERVE IN THE RAT

Akira Niijima (Niigata Univ., Japan.), Zheng-Yao Jiang (Niigata Univ., Japan.), Nancy G. Daunton, and Robert A. Fox (San Jose State Univ., CA.) *In its* Self-Motion Perception and Motion Sickness 1991 4 p Repr. from Neuroscience Letters, v. 80, 1987 p 71-74 (For primary document see N94-21897 05-51)
Avail: CASI HC A01/MF A02

The afferent nerve activity was recorded from a nerve filament isolated from the peripheral cut end of the gastric branch of the vagus nerve. The gastric perfusion of 4 ml of two different concentrations (0.04 percent and 0.08 percent) of CuSO4 solution provoked an increase in afferent activity. The stimulating effect of the 0.08 percent solution was stronger than that of the 0.04 percent solution, and lasted for a longer period of time. The observations suggest a possible mechanism by which CuSO4 elicits emesis. Author (revised)

N94-21908*# National Aeronautics and Space Administration. Ames Research Center, Moffett Field, CA.

CONDITIONED TASTE AVERSION INDUCED BY MOTION IS PREVENTED BY SELECTIVE VAGOTOMY IN THE RAT

Robert A. Fox (San Jose State Univ., CA.) and Susan McKenna (San Jose State Univ., CA.) *In its* Self-Motion Perception and Motion Sickness 1991 10 p Repr. from Behavioral and Neural Biology, v. 50, 1988 p 275-284 (For primary document see N94-21897 05-51)
(Contract NCC2-1421)
Avail: CASI HC A02/MF A02

The role of the vagus nerve in motion-induced conditioned taste aversion (CTA) was studied in hooded rats. Animals with complete, selective gastric vagotomy failed to form conditioned taste aversion after multiple conditioning sessions in which the conditioned stimulus (a cider vinegar solution) was drunk immediately before a 30-min exposure to vertical axis rotation at 150 deg/s. Results are discussed with reference to the use of CTA as a measure of motion-induced 'sickness' or gastrointestinal disturbance, and because motion-induced CTA requires that both the vagus nerve and the vestibular apparatus be intact, in light of the possible convergence of vegal and vestibular functions. Author (revised)

N94-21909*# National Aeronautics and Space Administration. Ames Research Center, Moffett Field, CA.

IMMUNOCYTOCHEMICAL LOCALIZATION OF GLUTAMIC ACID DECARBOXYLASE (GAD) AND SUBSTANCE P IN NEURAL AREAS MEDIATING MOTION-INDUCED EMESIS: EFFECTS OF VAGAL STIMULATION ON GAD IMMUNOREACTIVITY

F. DAmelio (San Jose State Univ., CA.), M. A. Gibbs, W. R. Mehler, Nancy G. Daunton, and Robert A. Fox (San Jose State Univ., CA.) *In its* Self-Motion Perception and Motion Sickness 1991 12 p Repr. from Basic and Applied Aspects of Vestibular Function, 1988 (For primary document see N94-21897 05-51)
Avail: CASI HC A03/MF A02

Immunocytochemical methods were employed to localize the neurotransmitter amino acid gamma-aminobutyric acid (GABA) by means of its biosynthetic enzyme glutamic acid decarboxylase (GAD) and the neuropeptide substance P in the area postrema (AP), area subpostrema (ASP), nucleus of the tractus solitarius (NTS), and gelatinous nucleus (GEL). In addition, electrical stimulation was applied to the night vagus nerve at the cervical level to assess the effects on GAD-immunoreactivity (GAR-IR). GAD-IR terminals and fibers were observed in the AP, ASP, NTS, and GEL. They showed pronounced density at the level of the ASP and gradual decrease towards the solitary complex. Nerve cells were not labelled in our preparations. Ultrastructural studies showed symmetric or asymmetric synaptic contracts between labelled terminals and non-immunoreactive dendrites, axons, or neurons. Some of the labelled terminals contained both clear- and dense-core vesicles. Our preliminary findings, after electrical stimulation of the vagus nerve, revealed a bilateral decrease of GAD-IR that was particularly evident at the level of the ASP. SP-immunoreactive (SP-IR) terminals and fibers showed varying densities in the AP, ASP, NTS, and GEL. In our preparations, the lateral sub-division of the NTS showed the greatest accumulation. The ASP showed medium density of immunoreactive varicosities and terminals and the AP and GEL displayed scattered varicose axon terminals. The electron microscopy revealed that all immunoreactive terminals contained clear-core vesicles which make symmetric or asymmetric synaptic contact with unlabelled dendrites. It is suggested that the GABAergic terminals might correspond to vagal afferent

projections and that GAD/GABA and substance P might be co-localized in the same terminal allowing the possibility of a regulated release of the transmitters in relation to demands. Author (revised)

N94-21910*# National Aeronautics and Space Administration. Ames Research Center, Moffett Field, CA.

THE EFFECTS OF AREA POSTREMA LESIONS AND SELECTIVE VAGOTOMY ON MOTION-INDUCED CONDITIONED TASTE AVERSION

Robert A. Fox (San Jose State Univ., CA.), R. L. Sutton (California Univ., Los Angeles.), and Susan McKenna (San Jose State Univ., CA.) *In its* Self-Motion Perception and Motion Sickness 1991 6 p Repr. from Basic and Applied Aspects of Vestibular Function, 1988 (For primary document see N94-21897 05-51)

Avail: CASI HC A02/MF A02

Conditioned taste aversion (CTA) is one of several behaviors which was suggested as a putative measure of motion sickness in rats. A review is made of studies which used surgical disruption of area postrema or the vagus nerve to investigate whether CTA and vomiting induced by motion may depend on common neural pathways or structures. When the chemoreceptive function of the area postrema (AP) is destroyed by complete ablation, rats develop CTA and cats and monkeys develop CTA and vomit. Thus the AP is not crucially involved in either CTA or vomiting induced by motion. However, after complete denervation of the stomach or after labyrinthectomy rats do not develop CTA when motion is used as the unconditioned stimulus. Studies of brainstem projections of the vagus nerve, the area postrema, the periaqueductal grey, and the vestibular system are used as the basis for speculation about regions which could mediate both motion-induced vomiting and behavioral food aversion. Author

N94-21911*# National Aeronautics and Space Administration. Ames Research Center, Moffett Field, CA.

EXPERIMENTAL STUDIES OF GASTRIC DYSFUNCTION IN MOTION SICKNESS: THE EFFECT OF GASTRIC AND VESTIBULAR STIMULATION ON THE VAGAL AND SPLANCHNIC GASTRIC EFFERENTS

A. Niijima (Niigata Univ., Japan.), Z. Y. Jiang (Niigata Univ., Japan.), Nancy G. Daunton, and Robert A. Fox (San Jose State Univ., CA.) *In its* Self-Motion Perception and Motion Sickness 1991 10 p Repr. from Basic and Applied Aspects of Vestibular Function, 1988 (For primary document see N94-21897 05-51)

Avail: CASI HC A02/MF A02

The experiments were conducted in anaesthetized rats. In the first part of the experiments, the effect of CuSO4 on the afferent activity in the gastric branch of the vagus nerve was investigated. Gastric perfusion of CuSO4 solution (0.04 percent and 0.08 percent) provoked an increase in afferent activity. In the second part of the experiments, the reflex effects of gastric perfusion of CuSO4 solution, repetitive stimulation of the gastric vagus nerve, and caloric stimulation of the right vestibular apparatus (5-18 C water) on gastric autonomic outflow were investigated. The results of these experiments showed that these three different types of stimulation caused an inhibition in efferent activity of the gastric vagus nerve and a slight activation of the splanchnic gastric efferents. The summation of the effect of each stimulation was also observed. These results, therefore, provide evidence for a possible integrative inhibitory function of the vagal gastric center as well as an excitatory function of gastric sympathetic motoneurons in relation to motion sickness. Author

N94-21912*# National Aeronautics and Space Administration. Ames Research Center, Moffett Field, CA.

ROLE OF THE AREA POSTREMA IN THREE PUTATIVE MEASURES OF MOTION SICKNESS IN THE RAT

Richard L. Sutton (San Jose State Univ., CA.), Robert A. Fox (San Jose State Univ., CA.), and Nancy G. Daunton *In its* Self-Motion Perception and Motion Sickness 1991 20 p Repr. from Behavioral and Neural Biology, v. 50, 1988 p 133-152 (For primary document see N94-21897 05-51)

Avail: CASI HC A03/MF A02

After thermal cauterization of the area postrema in rats, the absence of conditioned taste aversion of sucrose paired with lithium chloride (0.15M, 3.3 ml/kg) was used as a pharmacologic/behavioral index of area postrema damage. In a subsequent experiment the effects of area postrema lesions on three measures proposed as species-relevant measures of motion sickness were studied, using off-vertical rotation at 150 deg/s for either 30 or 90 min. Lesions of area postrema did not alter postrotational suppression of drinking or amount of defecation during motion. The initial acquisition of conditioned taste aversion to a novel cider vinegar solution paired with motion was not affected by lesioning of the area postrema, but these taste aversions extinguished more slowly in lesioned rats than in sham-operates or intact controls. Results are discussed in terms of proposed humoral factors which may induce motion sickness and in light of recent data on the role of the area postrema in similar measures in species possessing the complete emetic reflex. Author (revised)

N94-21913*# San Jose State Univ., CA.

INVESTIGATING MOTION SICKNESS USING THE CONDITIONED TASTE AVERSION PARADIGM

Robert A. Fox *In* NASA. Ames Research Center, Self-Motion Perception and Motion Sickness 1991 17 p Repr. from Motion and Space Sickness, 1990 (For primary document see N94-21897 05-51)

Avail: CASI HC A03/MF A02

The avoidance of foods which are associated with uncomfortable or aversive internal states has long been recognized. Many people are aware, either directly or via anecdotal reports, of individuals who avoid foods which were eaten just before the onset of sickness. Awareness of this phenomenon can be traced to the writings of John Locke. The disruption of diet during cancer therapy is sometimes ascribed to the attribution of an unpleasant quality to foods eaten preceding the sickness induced by therapy itself. In addition, it has long been recognized by the manufacturers of rodent poisons that animals avoid the injection of food treated with nonlethal doses of poison. An important part of the laboratory study of this phenomenon was directed toward studying the role learning plays in this type of avoidance behavior. Following the lead of Garcia and his associates, this avoidance has come to be interpreted as arising from a form of classical conditioning. In typical laboratory studies of this bahavior, a novel food is ingested just prior to exposure to some stimulus, commonly poisoning or irradiation, which produces illness. Following the terminology of classical conditioning, it is common to describe this procedure as one of 'pairing' a conditioned stimulus (CS), the novel food, with an unconditioned stimulus (US), the illness induced by toxicosis or irradiation. Avoidance of the food in succeeding feeding opportunities is viewed as a learned response or a conditioned taste aversion (CTA). Garcia et al. asserted that motion sickness could produce 'gustatory' aversions, but passive motion was first reported as an US to establish CTA by Green and Rachlin. The purpose is to review the manner in which CTA has been used to study motion sickness. Numerous reviews concentrating on other aspects of CTA are available in the existing literature. Readers are encouraged to consult the various papers and edited books for extensive information on other aspects of this literature. Author (revised)

N94-21914*# National Aeronautics and Space Administration. Ames Research Center, Moffett Field, CA.

CONDITIONED TASTE AVERSION AND MOTION SICKNESS IN CATS AND SQUIRREL MONKEYS

Robert A. Fox (San Jose State Univ., CA.), Meryl Lee Corcoran, and Kenneth R. Brizzee (Tulane Univ., Covington, LA.) *In its* Self-Motion Perception and Motion Sickness 1991 10 p Repr. from unidentified source (For primary document see N94-21897 05-51)

Avail: CASI HC A02/MF A02

The relationship between vomiting and conditioned taste aversion was studied in intact cats and squirrel monkeys and in cats and squirrel monkeys in which the area postrema was ablated by thermal cautery. In cats conditioned 7-12 months after ablation of the area postrema, three successive treatments with xylazine failed to produce either vomiting or conditioned taste aversion to a novel fluid. Intact cats, however, vomited and formed a conditioned aversion. In squirrel monkeys conditioned 6 months after ablation of the area postrema, three treatments with lithium chloride failed to produce conditioned taste aversion. Intact monkeys did condition with these treatments. Neither intact nor ablated monkeys vomited or evidenced other signs of illness when injected with lithium chloride. When the same ablated cats and monkeys were exposed to a form of motion that produced vomiting prior to surgery, conditioned taste aversion can be produced after ablation of the area postrema. The utility of conditioned taste aversion as a measure of subemetic motion sickness is discussed by examining agreement and disagreement between identifications of motion

sickness by conditioned taste aversion and vomiting. It is suggested that a convincing demonstration of the utility of conditioned taste aversion as a measure of nausea requires the identification of physiological correlates of nausea, and caution should be exercised when attempting to interpret conditioned taste aversion as a measure of nausea. Author

N94-21915*# San Jose State Univ., CA.
CURRENT STATUS: ANIMAL MODELS OF NAUSEA
Robert A. Fox *In* NASA. Ames Research Center, Self-Motion Perception and Motion Sickness 1991 10 p Repr. from Mechanisms and Control of Emesis, v. 223, 1992 p 341-350 (For primary document see N94-21897 05-51)
Avail: CASI HC A02/MF A02

The advantages, and possible benefits of a valid, reliable animal model for nausea are discussed, and difficulties inherent to the development of a model are considered. A principle problem for developing models arises because nausea is a subjective sensation that can be identified only in humans. Several putative measures of nausea in animals are considered, with more detailed consideration directed to variation in cardiac rate, levels of vasopressin, and conditioned taste aversion. Demonstration that putative measures are associated with reported nausea in humans is proposed as a requirement for validating measures to be used in animal models. The necessity for a 'real-time' measure of nausea is proposed as an important factor for future research; and the need for improved understanding of the neuroanatomy underlying the emetic syndrome is discussed.
Author (revised)

52 AEROSPACE MEDICINE

Includes physiological factors; biological effects of radiation; and effects of weightlessness on man and animals.

N94-19962# Air Force Inst. of Tech., Wright-Patterson AFB, OH. Foreign Aerospace Science and Technology Center.
ANALYSIS OF HEALTH STATUS FROM PRELIMINARY PHYSICAL EXAMINATION OF FLIGHT ACADEMY APPLICANTS
Zhi-Ying Zhou 30 Jul. 1993 15 p Transl. into ENGLISH from Chung-Hua Yu Fang i Hsueh Tsa Chih (China), v. 22, no. 4, Jul. 1988 p 241-244
(AD-A267759; FASTC-ID(RS)T-0732-92) Avail: CASI HC A03/MF A01

In March 1985, flight academy applicants selected from eight middle schools received physical examinations in Gong'an County. These male students' ages were between 16 and 19 years old. The overall disqualification percentage of the 416 persons, 64.18 percent were disqualified by the results of the physical examinations. 40.82 percent of the disqualifications were due to subnormal eye vision. In a follow-up investigation, it was found that in general there is substandard classroom lighting below normal illumination levels regulated by the Ministry of Public Health. These subnormal illumination levels have affected student visual acuity in varying degrees. Persons with scabies were amounted to 7.11 percent of all students, spread easily in most schools because of undesirable dormitory conditions. To improve student body constitution, schools should emphasize education in student health maintenance and public health by paying attention to keeping their eyes healthy as well as eye exercises. Derived from text

N94-19981# Air Force Inst. of Tech., Wright-Patterson AFB, OH. School of Engineering.
PHYSIOLOGICALLY BASED PHARMACOKINETIC MODELLING OF PERCUTANEOUSLY ABSORBED DIBROMOMETHANE UTILIZING MULTIPLE DERMAL SUB-COMPARTMENTS M.S. Thesis
Christopher R. McDaniel Sep. 1993 70 p
(AD-A271106; AFIT/ENC/GEE/93S-2) Avail: CASI HC A04/MF A01

The goal of this study was to develop a physiologically based pharmacokinetic (PBPK) model that predicts mammalian blood concentrations of dibromomethane following exposure by dermal absorption more accurately than a previously developed Homogeneous Dermal Model. The Homogeneous Dermal Model contains a dermal compartment with no dermal sub-compartments. The 1:1 Dermal Model developed in this research contains a dermal compartment with a stratum corneum and a composite dermal sub-compartment of equal volume. This model yields predictions which are 21.4 percent more accurate than the original homogeneous model. In order to represent skin anatomy more accurately, the 1:10 Dermal Model variation was developed. The 1:10 Dermal model contains a dermal compartment with a composite dermal sub-compartment ten times the volume of the stratum corneum sub-compartment. The 1:10 Dermal Model yields predictions which are 17.7 percent more accurate than the original model. Finally, the 1:3:7 Dermal Model was developed which contains a viable epidermis sub-compartment three times the volume of the stratum corneum sub-compartment and a composite dermal sub-compartment which is seven times the volume of the stratum corneum sub-compartment. This model yields predictions 27.7 percent more accurate than the original model. DTIC

N94-20022# Technische Univ., Berlin (Germany). Fachgruppe Computer Graphics.
A CONCEPT FOR IMPLEMENTING HYPERMEDIA TECHNOLOGY IN COMPUTER AIDED WORKPLACES IN MEDICINE Ph.D. Thesis [EIN KONZEPT FUER DEN EINSATZ DER HYPERMEDIATECHNIK AN COMPUTERGESTUETZTEN ARBEITSPLAETZEN IN DER MEDIZIN]
Michael Henke 1993 214 p In GERMAN
(ETN-93-95057) Avail: CASI HC A10/MF A03

A concept that allows medical personnel to structure the information about a patient is presented. It is assumed that the digital data is increasingly displacing the analog part and also that in addition to images, more and more other media (animation, video, text, graphics, charts etc.) will become an integral part of the digital patient folder. The result of the activities of the medical personnel that are involved in the patient's treatment is that there exists a strong relationship in the content of the documents which are created in that time. A report is related to medical images, a therapy plan is made on the basis of the diagnosis which refers to the reports and finally the results of the preliminary examination and the follow-up examination are compared for the purpose of therapy evaluation. Through a computer aided documentation of the relationship, that is by creating references between the documents of the patient folder, interdependencies will be easy to recognize and to duplicate later on. The aid that allows the connection of information in such a manner is realized with hypermedia technique. Through the application of the hypermedia technique, the structure of the patient folder results in a hypermedium. An expansion of this concept to several medical institutions gives additional advantages, such as comprehensive access to reference cases or the avoidance of repeated examinations. The success of the use of hypermedia techniques depends substantially on the design of the man machine communication. On the one hand new forms of interaction result from the demand to process multimedia data, on the other hand well designed user interfaces are needed to ensure an easy handling of the tools for creating and following up links. ESA

N94-20024 Technische Univ., Berlin (Germany). Fachbereich Elektrotechnik.
CALCULATION AND OPTIMIZATION OF ELECTROMAGNETIC FIELDS IN A PATIENT BY LOCAL HYPERTHERMIA UTILIZATION Ph.D. Thesis [BERECHNUNG UND OPTIMIERUNG ELEKTROMAGNETISCHER FELDER IM PATIENTEN BEI REGIONALEN HYPERTHERMIEANWENDUNGEN]
Jacek Nadobny 1993 168 p In GERMAN Sponsored by Deutschen Krebshilfe e.V., and Tech. Univ., Berlin, Germany Limited Reproducibility: More than 20% of this document may be affected by microfiche quality
(ETN-93-95059) Avail: CASI HC A08

Electric field intensities in an electrically inhomogeneous, lossy medium, near the source of the electromagnetic field, are calculated for estimation of the absorbed rate density distribution in human bodies. The volume surface integral equation formulation, in which a primary field is defined as the field put in the problem area, while the problem area is replaced by an inhomogeneous reference medium such as air is presented. Source distribution variations, due to reinstalled inhomogeneities, were defined as coupled sources and could be estimated as a problem part. The scatter field was defined as the difference between total and primary fields and was obtained as the sum of the fields generated by coupled sources and the polarization sources in the problem area. For numerical solution of equations, an iterative solver and a finite volume scheme were chosen. The method was tested from a medical point of view with an annular phased array, which creates an axially polarized electric field in the patient

tumor; temperature distributions were obtained by liquid crystal thermography and compared with calculations; the good agreement shows that the method is a useful tool for an optimized hypermedia treatment. ESA

N94-20045# East Carolina Univ., Greenville, NC. School of Medicine.
THE ROLE OF AXON-SCHWANN CELL INTERACTIONS IN NERVOUS SYSTEM IONIC HOMEOSTASIS Final Report, 1 May 1988 - 30 Apr. 1993
Edward M. Lieberman 8 Jun. 1993 5 p
(Contract DAAL03-88-K-0102)
(AD-A270936; ARO-25752.10-LS) Avail: CASI HC A01/MF A01

The long term goal of the research program of this laboratory is to reach an understanding of the physiological interactions between neurons and their associated glia that relate to their ability to cooperatively regulate the ionic and neurohumoral milieu of the perineural and/or periaxonal space. To this end we have been investigating the mechanisms by which axons and neurons generate the chemical signals during their excitation that signals the glia to activate their metabolic and uptake processes that inactivate neurotransmitters preventing their accumulation to toxic concentrations and the transport of potassium and of sodium to maintain appropriate amounts of each ion in the perineural space thereby preserving excitability properties of the neural elements of the nervous system. For these investigations we have used the intact nerve fiber Schwann cell preparations of crayfish and squid to study nerve-Schwann cell interactions in intact systems and the mammalian Schwann cell culture to determine the generality of our findings to mammalian systems. DTIC

N94-20112 California Inst. of Tech., Pasadena.
TOWARD A NEUROBIOLOGICAL THEORY OF VISUAL ATTENTION Annual Report, 1 Sep. 1992 - 31 Aug. 1993
Christof Koch 30 Sep. 1993 6 p Limited Reproducibility: More than 20% of this document may be affected by microfiche quality
(Contract F49620-92-J-0454)
(AD-A270724; AFOSR-93-0775TR) Avail: CASI HC A02

The investigators started the construction of a system-level simulation package incorporating the ideas of temporal tagging for attentional modulation of neuronal signals into a model of several interacting cortical and subcortical areas using video-camera acquired images. This simulation differs significantly from connectionist models, since the temporal structure of the neural signals plays a crucial role in the coding of attentional state. Thus, the simulation uses single neuron models with quasi-realistic temporal behavior. In particular, all models in which the activity of a neuron is measured only by average firing rate are excluded. Instead, the simulation assumes a spiking mechanism, and that the communication between neurons has to be accomplished by the exchange of potentials. DTIC

N94-20185# Tennessee Univ., Nashville. College of Engineering and Technology.
CENTER FOR NEURAL ENGINEERING Annual Progress Report, 15 May 1992 - 14 May 1993
Mohan J. Malkani Jul. 1993 27 p
(Contract N00014-91-J-1372)
(AD-A271164) Avail: CASI HC A03/MF A01

The main objectives of the Center for Neural Engineering are: (1) to advance the understanding of biologically-motivated neural network systems through inter-disciplinary basic research; (2) to develop the highest quality undergraduate and graduate curricula in neural computing and engineering that will serve as a role model for other institutions; (3) to provide pre-graduate and post-graduate training for students in a nationally and internationally recognized basic and applied research and development environment focusing on critical present and future technologies; and (4) to broaden educational and career development opportunities for minorities and women. DTIC

N94-20190# Wichita State Univ., KS. National Inst. for Aviation Research.
EVALUATION OF HEAD INJURY CRITERIA
Hamid M. Lankarani, Srinivas Reddy Malapati, and Rajiv Menon 1993 60 p
(NIAR-93-2) Avail: CASI HC A04/MF A01

Human safety is a major concern for those in airline industry and automobile industry. In order to improve the effectiveness and reduce the cost of vehicle safety, improved dummies and injury criteria are needed. A prerequisite for developing improved dummies is the development of injury tolerance of the human being to impacts like those caused in automobile accidents. One major problem of interest for aerospace and automotive designers is how to arrange seats, restraints and interior elements of a cockpit/cabin or a car to reduce the amount of passenger injury in specific types of collision situations. The use of Head Injury Criteria (HIC) in vehicle crash testing results in designing restraint systems. It is capable of predicting severity of human head injury. This knowledge can be applied to the development of improved design standards to reduce injuries in vehicle crash situations. According to the aerospace standards in designing seats, for civil rotor craft and transport airplanes HIC has to be evaluated during the tests on seats, and the results have to be included in the document. For these tests an anthropomorphic test dummy (ATD) shall be used to simulate each occupant. In this study an effort has been made to provide some details of the types of head injuries, the mechanisms associated with head injuries, some common definitions of terminologies related with head injuries, the historical development of various head injury criteria and their measures, some comparisons of the head injury criteria and computational aspects of head injury criteria. Derived from text

N94-20238 Royal Netherlands Meteorological Inst., De Bilt.
WIND CHILL: THE TEMPERATURE FEELING CAUSED BY THE WIND VELOCITY [WIND CHILL: DE DOOR DE WINDSNELHEID VEROORZAAKTE TEMPERATUURGEWAARWORDING]
B. Zwart Nov. 1992 42 p In DUTCH
(KNMI-TR-103a; ISBN-90-369-2029-9; ETN-94-94530) Avail: Issuing Activity (Royal Netherlands Meteorological Institute, Postbus 201, 3730 AE De Bilt, Netherlands)

The loss of heat of a body by the combination of low temperatures and high wind velocities was studied for the period around mid January 1987 when the weather conditions were extreme for the Netherlands. The concepts of sensory or apparent temperature and wind chill are introduced. The cooling speed of the body was determined with a Kata thermometer. The concepts of wind-chill equivalent and effective temperature are discussed. The effects of humidity and radiation on the apparent temperature are outlined. ESA

N94-20372* National Aeronautics and Space Administration. Lyndon B. Johnson Space Center, Houston, TX.
EXTRA-CORPOREAL BLOOD ACCESS, SENSING, AND RADIATION METHODS AND APPARATUSES Patent
Kent D. Castle, inventor (to NASA) 16 Nov. 1993 10 p Filed 16 Sep. 1991 Supersedes N92-11627 (30 - 2, p 289)
(NASA-Case-MSC-21775-1; US-Patent-5,261,874;
US-Patent-Appl-SN-760633; US-Patent-Class-604-4;
US-Patent-Class-604-28; Int-Patent-Class-A61M-1/03) Avail: US Patent and Trademark Office

The described invention is related to extra-corporeal blood access and radiation methods and apparatuses and, in particular, to subjecting flowing blood to energy in variety of forms, including radiation, electromagnetic force fields or atomic particles. It is directed to methods and apparatuses for accessing flowing blood and for subjecting the blood to electrical conductive, electrostatic or electromagnetic fields or for radiating the blood with some type of radiation, e.g., radio waves, ultrasonic or audio waves, microwaves, IR rays, visible light, UV radiation, x-rays, alpha, beta or gamma rays. An apparatus is employed which includes one or more access ports or windows for radiating blood and/or for sensing/analyzing blood. This invention is useful for killing viruses and bacteria in blood, monitoring blood for medical purposes, genetic modification of blood, and analyzing and/or treating blood components.
Official Gazette of the U.S. Patent and Trademark Office

N94-20462# Analytic Sciences Corp., Reading, MA.
OCULAR DAMAGE INDUCED BY ULTRASHORT LASER PULSES Interim Technical Report, Feb. - Jul. 1992
Joseph A. Zuclich, W. R. Elliott, Clarence P. Cain, Gary D. Noojin, and W. P. Roach Sep. 1993 34 p
(Contract F33615-92-C-0017)
(AD-A271859; AL/OE-TR-1993-0099) Avail: CASI HC A03/MF A01

A study has been conducted of interaction effects and damage mechanisms of ultrashort laser pulses in the eye. The preliminary results

reported here utilized rabbit subjects and ocular tissues isolated from the rabbit eye. Pulsewidths ranged from 4 ns down to 90 fs. In every case, a visible wavelength was used--either doubled Nd:YAG at 532 nm or the 580-nm output of a pumped dye laser. In the living subjects, we determined, for each pulsewidth, the threshold for minimally visible lesions (MVL's). In addition, we noted the energy doses required to induce hemorrhagic lesions relative to the corresponding MVL's and use these data to aid in the interpretation of the damage and energy dispersal mechanisms following absorption of ultrashort laser pulses. The ultrashort-pulse beam was directed through flat preparations of rabbit corneas and vitreous fluid and through intact rabbit lenses. Measurements were made to detect pulsewidth broadening or modulation, spectral broadening or white-light continuum generation, second-harmonic generation, and self-focussing or defocussing. These measurements, chosen as indicators of interactions as the ultrashort pulse passes through the ocular medium, were all negative. DTIC

N94-20615# Army Aeromedical Research Lab., Fort Rucker, AL.
CORONARY ANGIOGRAPHY OUTCOMES OF US ARMY AIRCREW WITH THE FINDING OF CORONARY ARTERY CALCIFICATIONS: AVIATION EPIDEMIOLOGY DATA REGISTER Final Report
Kevin T. Mason, Samuel G. Shannon, and Paul V. Celio Jul. 1993 38 p
(AD-A271968; USAARL-93-28) Avail: CASI HC A03/MF A01

U.S. Army aircrew with a history of coronary artery calcification were identified by cardiac fluoroscopy, followed by coronary angiography, in the U.S. Army Aviation Epidemiology Data Registry for the period 1 January 1988 to 1 August 1992. Eighty-two aircrew met these criteria. Their angiography outcomes are summarized. The positive predictive value of cardiac calcifications for predicting any degree of coronary artery occlusion was 82.9%. The Framingham Risk Index, total serum cholesterol, cholesterol/HDL-cholesterol ratio, and results of the graded exercise treadmill test and thallium scan were not significant factors in predicting the angiography outcome when coronary artery calcifications were present. Aircrew in coronary artery disease screening programs should be examined for coronary artery calcifications by cardiac fluoroscopy and referred for coronary angiography if calcifications are seen. DTIC

N94-20624# Minnesota Univ., Duluth.
STUDIES OF NEURAL AND COGNITIVE FUNCTION IN SUBJECTS EXPOSED TO THE MARINE-AIR INTERFACE, PHASES 1 AND 2 Final Report
Lorentz E. Wittmers, Jr. and Richard G. Hoffman 26 Oct. 1993 162 p
(Contract N00014-88-K-0582)
(AD-A272282) Avail: CASI HC A08/MF A02

In Phase 1 the effects of cold air (c), water (w), fatigue (f), and exercise (e) on physiological and psychological performance, and the effectiveness of several techniques for the suppression of shivering were investigated in 15 male subjects. Cold exposure was determined to be the most significant factor in reducing performance, causing significant reductions (p less than or equal to 0.05) in skin and rectal temperatures, temperature perceptions, shooting performance, grip strength, and dexterity both alone or when combined with any or all other factors. Cognitive performance, however was highest in the c/w/e/f, control, and c conditions, with the overall scores in the c/w, c/w/f and c/w/e conditions significantly lower than control and c/w/e/f. Shivering gradually increased throughout exposure in cold conditions but was delayed in conditions which included exercise. Rectal temperatures increased during exercise, but later fell to the same level as in the non-exercise conditions. After 2+ hours of exposure 4 shiver-suppression techniques were applied: voluntary relaxation (R), breath holding (B), mental arithmetic (M), and warm water ingestion (W). Shivering was significantly suppressed by R, B, and M. In Phase 2 analysis of evoked potentials and reaction times during central and peripheral cooling indicated that cooling methods have differing effects on physiological and physical function. DTIC

N94-20627 Wright State Univ., Dayton, OH. Dept. of Psychology.
PERCEPTION/ACTION: AN HOLISTIC APPROACH 2 Annual Technical Report, Aug. 1992 - Aug. 1993
John M. Flach 12 Oct. 1993 17 p Limited Reproducibility: More than 20% of this document may be affected by microfiche quality
(Contract F49620-92-J-0511)
(AD-A271822; WSU/TR/662238-39; AFOSR-93-0820TR) Avail: Issuing Activity (Defense Technical Information Center (DTIC))

A general systems approach was used to study the emergent properties of the human perception/action system. Two task domains, the control of locomotion and the recognition of objects from dynamic occlusion, were used to study human performance. The locomotion task involved the control of altitude. Experimental results indicate that conflicting results from studies of altitude perception can be explained when global optical flow rate is considered. Optical analyses of the structure of flow fields, empirical results from human performance studies, and control theoretical analyses of the state space all converge to indicate that altitude and speed are not independent with respect to the problem of controlling locomotion in low altitude flight. In the dynamic occlusion task, the effects of time delays, visual noise, training, and instructions have been evaluated. The results tend to support the hypothesis that information was the critical determinant of performance in the dynamic occlusion task. Mode (active versus passive observer) was only important to the extent that it made additional information available to the observer. This conclusion is consistent with research on adaptation where the 'reafference hypothesis,' in which mode played an important role, is being replaced by the 'information hypothesis.' DTIC

N94-20928 Army Aeromedical Research Lab., Fort Rucker, AL.
REVIEW OF USING CARDIAC FLUOROSCOPY IN SYMPTOMATIC AND ASYMPTOMATIC PATIENTS Final Report
Kevin T. Mason Aug. 1993 41 p Limited Reproducibility: More than 20% of this document may be affected by microfiche quality
(DA Proj. 3M1-62787-A-879)
(AD-A271690; USAARL-93-29) Avail: CASI HC A03

The history of methods to find coronary artery calcification is reviewed. Image-intensified cardiac fluoroscopy is the current method in general use for finding coronary artery calcifications. The technique of cardiac fluoroscopy is reviewed in detail. The findings of coronary angiography outcomes for symptomatic and asymptomatic populations with coronary artery calcifications are analyzed. There is a strong association between the finding of coronary artery calcification and the finding of anatomic coronary artery occlusions regardless of the patient's age or outcome of other cardiovascular disease tests. Patients with coronary artery calcifications are at a three-fold increased risk for premature mortality when followed over a five-year period. Clinicians should examine patients for coronary artery calcifications in stratified coronary artery disease screening programs. DTIC

N94-20935# Abcor, Inc., Wilmington, MA. Walden Research Div.
DEVELOPMENT AND DEMONSTRATION OF A PERSONAL MONITORING SYSTEM FOR EXPOSURE TO HYDROGEN FLUORIDE
M. S. Young and J. P. Monat 1993 98 p
(Contract DE-FG05-79EV-10249)
(DE93-041273; DOE/EV-10249/T1) Avail: CASI HC A05/MF A02

A good, functional Hydrogen Fluoride Gasbadge dosimeter has been developed for sampling of airborne HF vapor. The device is small (7.7 cm x 5.4 cm x 1.9 cm) and can easily and conveniently be worn on one's lapel. It consists of polyethylene and polypropylene parts and a triethanolamine-impregnated polyproylene collection element. It is completely self contained requiring no pumps, impingers, or sampling tubes. Subsequent to sampling, the collection element is analyzed quickly and easily with a fluoride selective-ion electrode. Laboratory tests were conducted to determine precision, linearity, interference effects, influences of temperature and humidity, and collection element stability over time. Results of the tests indicate that the Abcor Gasbadge HF dosimeter is an excellent passive HF monitor for work spaces, and that results obtained with it are accurate within +/- 25 percent. These results have been corroborated in a field study. DOE

N94-21035# Army Medical Center, Fort Gordon, GA.
NON-IONIC SURFACTANTS IN THE TREATMENT OF THIRD DEGREE BURNS Final Report, 1 Feb. 1990 - 31 Jul. 1993
James C. McPherson 1 Sep. 1993 35 p
(Contract MIPR-90-MM0544)
(AD-A271582) Avail: CASI HC A03/MF A01

Pluronic polyols are non-ionic surfactants developed in the 1950's. They are block co-polymers or the ABA type where A is made up of ethylene oxide polymers and B is propylene oxide polymers. They differ only in their molecular weight. The Pluronic polyols were shown to be non-toxic.

This protocol evaluates their effect on third degree scald burn in a rat model, pluronic polyols were administered 30 minutes following a third degree scald burn to the chest of 300-320 gram male rats. Histological evaluation documented this burn. The Pluronic polyol was administered intravenously at a concentration of 12mm/1 with a dose of 8ml/kg body weight. Animals were followed for four weeks (complete healing). DTIC

N94-21036# Army Research Inst. of Environmental Medicine, Natick, MA.

MAXIMUM TEAM LIFTING CAPACITY AS A FUNCTION OF TEAM SIZE

Marilyn A. Sharp, Valerie J. Rice, Bradley C. Nindl, and Tania L. Williamson Oct. 1993 70 p

(AD-A271642; USARIEM-T94-2) Avail: CASI HC A04/MF A01

The relationship between the sum of individual lifts and team lifting capacity in two-, three-, and four-person teams was examined. Twenty-three men and 17 women were assigned to single and mixed-gender teams of two, three, or four persons. A weight-lifting bar was used to measure individual deadlift, as square device for two- and four-person lifting and a triangular device for three-person lifting. Team lifting capacity increased with team size and with the number of males on the team. Team lifting capacity as a percent of the sum of deadlift strength (% sum) did not change with an increase in team size beyond two. The %sum for teams of men (87.3%) was less than for teams of women (91.1%, p less than .05), and the %sums for single gender teams were both greater (p less than .01) than for mixed-gender teams (80.2%). The limits for lift set by Military Standard 1472D (1989) are well below the capabilities demonstrated here, and there is ample evidence in the Military Occupational Classification Structure (1990) that soldiers are required to lift heavier loads than recommended. Since soldiers are capable of and required to lift more than the recommended loads, consideration could be given to increasing these design limits. DTIC

N94-21134 Technische Hochschule, Darmstadt (Germany). Fachbereich Mathematik.

A GEOMETRICAL PROCESS FOR THREE DIMENSIONAL OSTEOTOMY PLANNING Ph.D. Thesis [GEOMETRISCHE VERFAHREN ZUR DREIDIMENSIONALEN OSTEOTOMIEPLANUNG]

Matthias Eck 1991 139 p In GERMAN Limited Reproducibility: More than 20% of this document may be affected by microfiche quality

(ETN-93-93602) Avail: CASI HC A07

The possibilities of operation simulations with computer tomography before a bone operation are studied. An automatic algorithm was proposed for smoothing of digitalized datasets with an iterative formulation. Two algorithms are presented for data reduction, which are geometrical B-Spline curves and geometrical hermitian interpolation. Methods are described for bone surface reconstruction, which are based on Hardy multiquadrics. The well known implementation of experimental systems for planning of orthopedic operations were reviewed and two processes were developed in case of hip joint femur osteotomy, based on reconstructed computer tomography data, to estimate foreseeable member modifications before operations and to avoid or minimize them. ESA

N94-21141 Gesellschaft fuer Strahlen- und Umweltforschung m.b.H., Munich (Germany). Inst. fuer Strahlenschutz.

RADIOMETRY IN COMMERCIAL AIRCRAFT Final Report [STRAHLENMESSUNGEN IN VERKEHRSFLUGZEUGEN. ABSCHLUSSBEREICHT]

D. Regulla and J. David Nov. 1991 88 p In GERMAN Limited Reproducibility: More than 20% of this document may be affected by microfiche quality

(GSF-41/91; ETN-93-93458) Copyright Avail: CASI HC A05

Cosmic radiation exposure of pilots, aircrew, and passengers during commercial flights is studied as a function of flight altitude and geographic latitude. Radiation measurements were carried out aboard the German Lufthansa airlines with a mobile measuring laboratory equipped with photon and neutron radiation measuring instruments. Several routes were considered to examine pole, equator, and geomagnetism effects. A scintillation dosimeter was used for electron and photon detection and a Rem-counter was employed for neutron identification. Because measuring instruments were not calibrated under high radiation conditions, a tissue equivalent proportional counter was available. It is concluded that radiation exposure increases with altitude and geographic and geomagnetic latitude. ESA

N94-21209# Army Research Inst. of Environmental Medicine, Natick, MA.

HUMAN RESPONSES TO EXERCISE-HEAT STRESS Technical Report

Michael N. Sawka, C. Bruce. Wenger, and Kent B. Pandolf Nov. 1993 96 p

(AD-A272581; USARIEM-TR-T94-3) Avail: CASI HC A05/MF A01

A comprehensive overview of the normal human physiological responses to environmental and exercise-related heat stress, with emphasis placed on acute heat exposure and acclimation produced by repeated heat exposure is provided. In addition, biomedical factors that modify exercise-heat tolerance such as aerobic fitness, dehydration, circadian patterns and sleep loss and medications are reviewed. Also, thermoregulatory responses of special populations such as women, blacks, children, older adults and spinal cord injured populations are reviewed. DTIC

N94-21288* National Aeronautics and Space Administration, Washington, DC.

AEROSPACE MEDICINE AND BIOLOGY: A CONTINUING BIBLIOGRAPHY WITH INDEXES (SUPPLEMENT 383)

Jan. 1994 43 p

(NASA-SP-7011(383); NAS 1.21:7011(383)) Avail: CASI HC A03

This bibliography lists 100 reports, articles, and other documents introduced into the NASA Scientific and Technical Information System during Nov. 1992. Subject coverage includes the following topics: aerospace medicine and physiology, life support systems and man/system technology, protective clothing, exobiology and extraterrestrial life, planetary biology, and flight crew behavior and performance. Author (revised)

N94-21415# Louisville Univ., KY. Dept. of Surgery.

ENHANCEMENT OF WOUND HEALING BY BIOSYNTHETIC GROWTH FACTOR Midterm Report, 31 Jul. 1991 - 30 Jul. 1993

Gregory L. Brown and Gregory S. Schultz 30 Aug. 1993 147 p

(Contract DAMD17-91-C-1095)

(AD-A272517) Avail: CASI HC A07/MF A02

Our goal is to identify biological agents that play key roles in regulating normal healing, and using this knowledge, to develop methods to enhance wound healing. The major research focus has been centered on understanding the roles of peptide growth factors and proteases in normal wound healing. Fluids from healing human wounds contain extremely high levels of mitogenic activity; high levels of peptide growth factors including TGF-a, TGF-B, and IGF-I; and very low levels of proteolytic activity. In contrast, fluids from nonhealing ulcers contain low levels of mitogenic activity, low levels of growth factors, and very high levels of matrix metallo proteinases. Levels of EGF receptors also change during spontaneous healing of skin incisions. Thus, the molecular environment of healing wounds is radically different from the environment of chronic nonhealing wounds. We have utilized this knowledge to design rational combinations of growth factors and a new synthetic inhibitor of metallo proteinases (MMPI) that should improve healing of wounds. This combination of EGF and MMPI is undergoing testing in the pig skin graft model. If successful we will initiate a clinical trial with this formulation. We are also investigating TGF-B treatment to improve survival of irradiated skin flaps. DTIC

N94-21503# Bioelastics Research Ltd., Birmingham, AL.

DEVELOPMENT OF BIOELASTIC MATERIAL FOR ASPECTS OF WOUND REPAIR Triannual Progress Report, May - Aug. 1993

Aug. 1993 15 p

(Contract N00014-90-C-0265)

(AD-A272000) Avail: CASI HC A03/MF A01

For materials with possible use as wound coverings, control of the temperature of transition by changes in hydrophobicity will be examined. In addition, the rate of water passage through the matrix will be determined. The research approach is the stepwise coordination of the synthesis and characterization of the materials. The first application phase was concerned primarily with synthesis of the basic plypentapeptide poly(VPGVG) and the analog with L-alanine substituted in position 3, poly(VPAVG) and mole fraction combinations thereof to achieve elastomeric matrices of varying elastic moduli. And in the third year polypentapeptides containing chemical clocks are to be characterized for their rate of breakdown and their effects on drug release profiles. Derived from text

N94-21613# Department of Veterans Affairs, Washington, DC.
JOURNAL OF REHABILITATION RESEARCH AND DEVELOPMENT, VOLUME 30, NUMBER 1, 1993
1993 212 p
(AD-A272956) Avail: CASI HC A10/MF A03

The Journal of Rehabilitation Research and Development, published quarterly, is a scientific rehabilitation engineering, research, and development publication in the multidisciplinary field of disability rehabilitation. General priority areas are: prosthetics and orthotics; spinal cord injury and related neurological disorders; communication, sensory, and cognitive aids; and gerontology. The journal receives submissions from sources within the United States and throughout the world. Only original scientific rehabilitation engineering papers will be accepted. Technical notes describing preliminary techniques, procedures, or findings of original scientific research may also be submitted. Letters to the editor are encouraged. Books for review may be sent by authors or publishers. DTIC

N94-21863*# National Aeronautics and Space Administration. Lyndon B. Johnson Space Center, Houston, TX.
SPACEFLIGHT RADIATION HEALTH PROGRAM AT THE LYNDON B. JOHNSON SPACE CENTER
A. Steve Johnson (Krug Life Sciences, Inc., Houston, TX.), Gautam D. Badhwar, Michael J. Golightly, Alva C. Hardy, Andrei Konradi, and Tracy Chui-hsu Yang Dec. 1993 20 p
(NASA-TM-104782; S-742; NAS 1.15:104782) Avail: CASI HC A03/MF A01

The Johnson Space Center leads the research and development activities that address the health effects of space radiation exposure to astronaut crews. Increased knowledge of the composition of the environment and of the biological effects of space radiation is required to assess health risks to astronaut crews. The activities at the Johnson Space Center range from quantification of astronaut exposures to fundamental research into the biological effects resulting from exposure to high energy particle radiation. The Spaceflight Radiation Health Program seeks to balance the requirements for operational flexibility with the requirement to minimize crew radiation exposures. The components of the space radiation environment are characterized. Current and future radiation monitoring instrumentation is described. Radiation health risk activities are described for current Shuttle operations and for research development program activities to shape future analysis of health risk. Author

N94-20451*# Jet Propulsion Lab., California Inst. of Tech., Pasadena.
NUMERICAL MODELING FOR AN ELECTRIC-FIELD HYPERTHERMIA APPLICATOR Abstract Only
Te-Kao Wu, C. K. Chou (City of Hope Medical Center, Duarte, CA.), K. W. Chan (City of Hope Medical Center, Duarte, CA.), and J. McDougall (City of Hope Medical Center, Duarte, CA.) *In its* Progress In Electromagnetics Research Symposium (PIERS) 1993 p 824 (For primary document see N94-20403 05-32)
Avail: CASI HC A01/MF A10

53 BEHAVIORAL SCIENCES

Includes psychological factors; individual and group behavior; crew training and evaluation; and psychiatric research.

N94-20023 Southeastern Center for Electrical Engineering Education, Inc., Saint Cloud, FL.
DEVELOPMENT OF THE UTC-PAB NORMATIVE DATABASE Final Report, Jun. 1990 - May 1992
Robert E. Schlegel, Kirby Gilliland, and Mark S. Crabtree Oct. 1992 284 p Limited Reproducibility: More than 20% of this document may be affected by microfiche quality
(Contract F33615-88-D-0532)
(AD-A271319; AL-TR-1992-0145) Avail: CASI HC A13

This report summarizes the development of a comprehensive normative database for a large subset of tasks from the Unified Tri-Service Cognitive Performance Assessment Battery (UTC-PAB). Tasks were selected from the AGARD STRES, CTS, and Walter Reed batteries. Data were collected by the University of Oklahoma and Armstrong Laboratory. All data were analyzed at the University of Oklahoma to address issues related to task reliability, comparability of tasks across batteries, group vs. individual test administration, order of task presentation and battery sequence, test-retest time intervals, imposition of response deadlines, extended trial lengths, and the usefulness of psychometric state measures. With few exceptions, the data showed remarkable consistency across task batteries and within task types. Task reliability varied as a function of the dependent measure. CTS data showed good correspondence to a previous large-scale CTS database. Task presentation order and battery sequence did not influence task performance. Response deadlines provided a faster mean response time, but at the expense of more missed responses. Extended trial lengths had a more profound effect on continuous motor tasks such as Unstable Tracking. Changes in the psychometric state measures of sleepiness and mood were local reflections of time on task. DTIC

N94-20081# Oklahoma Univ. Health Sciences Center, Oklahoma City. Civil Aeromedical Inst.
PHYSIOLOGICAL CORRELATES OF STRESS-INDUCED DECREMENTS IN HUMAN PERCEPTUAL PERFORMANCE Final Report
Garnet A. McLean (Federal Aviation Administration, Oklahoma City, OK.), Landgrave T. Smith, Timothy J. Hill, and Carl J. Rubenstein Nov. 1993 13 p
(Contract DAMD17-83-C-3194)
(DOT/FAA/AM-93/19) Avail: CASI HC A03/MF A01

Stress-induced changes in human performance have been thought to result from alterations in the 'multidimensional arousal state' of the individual, as indexed by alterations in the physiological and psychological mechanisms controlling performance. Identification of such changes in substrate activities provide more complete descriptions of both the performance changes and the arousal state/mechanisms. Decrements in perceptual performance were produced by independent and combined administration of atropine, sleep loss, and exercise for both a visual aircraft identification task and an auditory vigilance task; measurements of performance changes were accompanied by state measures of cardiovascular function, pupillary diameter, sleep onset latency, and subject self reports. Observed performance changes were accompanied by monotonic increases in heart rate after atropine and exercise, but not sleep loss. Moderate exercise produced blood pressure changes indicative of physical workload, but only atropine increased diastolic blood pressure and pupillary diameter relative to performance effects. Atropine and sleep loss each reduced sleep onset times to less than 50 percent control values (p is less than .0001); when combined with exercise, sleep onset times were reduced further (p is less than .03). These reductions in general arousal were confirmed by subject self-reports of reduced attentiveness and competence. These state measures of organismic function were found to be discriminatively correlative, but not predictive, of the decrements in perceptual performance seen; however, practical combinations of appropriate real-time measurement techniques could be developed that would promote the telemetering of human physiological activity to signal performance breakdown. Author (revised)

N94-20168*# College of William and Mary, Williamsburg, VA.
INCONGRUITY, INCONGRUITY RESOLUTION, AND MENTAL STATES: THE MEASURE AND MODIFICATION OF SITUATIONAL AWARENESS AND CONTROL Final Report, 1 Jun. 1991 - 31 May 1993
Peter L. Derks and Lynn S. Gillikin 1 Jul. 1993 97 p
(Contract NCC1-160)
(NASA-CR-194568; NAS 1.26:194568) Avail: CASI HC A05/MF A02

The research reported here describes the process of induction of various mental states. Our goals were to measure and to manipulate both the behavioral and the neurological correlates of particular mental states that have previously been demonstrated to be either beneficial or deleterious to in-flight performance situations. The experimental paradigm involved developing a context of which the participants were aware, followed by the introduction of an incongruity into that context. The empirical questions involved how the incongruity was resolved and the consequent effects on mental state. The dependent variables were measures of both the short-term ERP changes and the longer-term brain mapping indications of predominant mental states. The mission of NASA Flight Management Division and Human/Automation Integration Branch centers on the understanding and improvement of interaction between a complex system and a human operator. Specifically, the goal is improved efficiency through better operative procedures and control strategies. More efficient performance in demanding

flight environments depends on improved situational awareness and replanning for fault management. Derived from text

N94-20467 New York Univ., New York.
COGNITION AND THE BRAIN: A CONTINUATION OF THE UNIVERSITY RESEARCH INITIATIVE AT NEW YORK UNIVERSITY Final Report, 15 Feb. 1990 - 14 Feb. 1993
Lloyd Kaufman 19 Oct. 1993 10 p Limited Reproducibility: More than 20% of this document may be affected by microfiche quality
(Grant AF-AFOSR-0221-90)
(AD-A271872; AFOSR-93-0818TR) Avail: Issuing Activity (Defense Technical Information Center (DTIC))

The main focus of this project was to make use of magneto-encephalographic (MEG) measures of brain activity to determine how the brain's neural resources are deployed during various cognitive tasks entailing different degrees of mental workload. Our laboratory pioneered this field, and the methods it devised are presently in wide use in clinical applications, as well as in other research laboratories. We initiated the use of a simple procedure to fit observed extracranial field patterns to fields that would be produced by equivalent current dipoles. The ideal dipole's position, orientation, and strength (current dipole moment) was adjusted until its field pattern matched that of the observed pattern. This is a primitive form of what we now refer to as Magnetic Source Imaging (MSI). It is still the basic method in clinical applications, but a more sophisticated form of MSI is now emerging, largely as a result of work on this project. DTIC

N94-20520# Rochester Univ., NY. Dept. of Computer Science.
HEAD-CENTERED ORIENTATION STRATEGIES IN ANIMATE VISION
Enrico Grosso and Dana H. Ballard Oct. 1992 25 p
(Grant NIH-1R24RRO6853)
(TR-442) Avail: CASI HC A03/MF A01

This paper is about orienting, that is, establishing and maintaining a spatial relation between a motorized pair of cameras (the eye-head system) and a static or a moving object tracked over time. Motivated by physiological evidence, the paper proposes a simple set of vision-based strategies aimed to perform head, eyes and body movements in a complex environment. Fixation is shown to be an essential feature in visual servoing, and it is used to decouple control on head rotational degrees of freedom, making possible a metric-less approach to the orientation problem. A running implementation of these strategies, using a binocular camera system mounted on a PUMA 700, demonstrates the electiveness of the approach. Author

N94-20610 Bolt, Beranek, and Newman, Inc., Cambridge, MA.
RESEARCH, DEVELOPMENT, TRAINING, AND EVALUATION (RDTE) SUPPORT DELIVERY ORDER 1: COMPUTATIONAL COGNITIVE MODELS Final Report, Mar. 1992 - Apr. 1993
Stephen E. Deutsch, Eva Hutlicka, Marilyn J. Adams, and Carl E. Feehrer Sep. 1993 82 p Limited Reproducibility: More than 20% of this document may be affected by microfiche quality
(Contract F33615-91-D-0009)
(AD-A271837; AL/HR-TR-1993-0072) Avail: CASI HC A05

This document reports on work associated with the three-phase development of a psychologically-based human performance process model that can be used in the assessment of system performance. The first phase produced a preliminary architecture consisting of two parts: a 'mass memory' composed of long term memory structures that supported associative activation, and a set of sensory, perceptual, cognitive, and motor agents that communicated via message passing - writing messages to or reading messages from the mass. Phase two produced a revised architecture in which the distinction between memory and process disappeared and the resulting structures became active processing elements in a data flow structure. The addition to model development, certain activities associated with enroute air traffic control were also decomposed in order to develop the basis for a scenario within which to prototype, program, and test aspects of the revised model. The activities selected provided an opportunity to model single and multitasking behaviors and performance. DTIC

N94-21237# Defense Systems Management School, Fort Belvoir, VA.
A DESCRIPTION OF PSYCHOLOGICAL TYPE AT THE DEFENSE SYSTEMS MANAGEMENT COLLEGE, 1993 EDITION
Carl Bryant, William H. Cummings, Daniel B. Chapla, Donald S. Fujii, and Mary-Jo Hall 1993 31 p
(AD-A271612) Avail: CASI HC A03/MF A01

This paper describes the psychological type, as measured by the Myers-Briggs Type Indicator, of a representative sample of more than 3,700 students who attended the Defense Systems Management College (DSMC) since 1985. This study addresses the contributions and potential pitfalls that personnel with each Myers-Briggs Type bring to an organization, and implications for leaders who must work in a possibly changing work force. This descriptive analysis may enable all who work in the defense acquisition environment to understand their coworkers better and, in this understanding, to enhance the overall acquisition process. DTIC

N94-21262# California Univ., Los Angeles.
PSYCHOMETRIC DEVELOPMENTS RELATED TO TESTS AND SELECTION
Bengt O. Muthen Aug. 1993 7 p
(Contract N00014-93-1-0619)
(AD-A272971) Avail: CASI HC A02/MF A01

Recent theoretical developments in the areas of latent variable modeling, random coefficient modeling, multilevel modeling, missing data theory, and empirical Bayes estimation provide interesting research opportunities for the psychometric modeling of the relationship between job performance and test performance. These developments suggest new approaches to the assessment of predictive validity of tests as well as to problems of selection and assignment. The purpose of the project is to use these theories as a basis for developing new psychometric methods that have the potential for better understanding the predictive validity of tests like the ASVAB and improving the selection and assignment of recruits for military jobs. DTIC

N94-21434 Navy Personnel Research and Development Center, San Diego, CA.
EXTRACTING INFORMATION FROM WRONG ANSWERS IN COMPUTERIZED ADAPTIVE TESTING Final Report, Oct. 1988 - Sep. 1991
J. B. Sympson Oct. 1993 32 p Limited Reproducibility: More than 20% of this document may be affected by microfiche quality
(AD-A272832; NPRDC-TN-94-1) Avail: Issuing Activity (Defense Technical Information Center (DTIC))

A brief review of the history of polychotomous (i.e., multi-category) item response models is provided. After describing a new polychotomous item response model (Model 8), examples of the Operating Characteristic Functions obtained when Model 8 is applied to real test data are given. In general, inspection of 'goodness-of-fit' plots indicates that Model 8 provides superior data fit and higher item information functions than the well-known 3-parameter logistic (dichotomous) item response model. A simulation of computerized adaptive testing (CAT) that used the actual item responses of applicants for military enlistment shows that Model 8 would be superior to the 3-parameter logistic model in a CAT environment. In this investigation, Model 8 increased test reliability by an amount that is equivalent to a 25% increase in test length. DTIC

N94-21510# American Inst. for Research, Washington, DC.
COMPATIBILITY EVALUATION AND RESEARCH ON THE COMPUTERIZED ADAPTIVE SCREENING TEST (CAST): USER AND PROGRAMMER'S GUIDE Final Report, Oct. 1989 - Jan. 1991
Randolph K. Park and Michael L. Dunn Oct. 1993 32 p
(Contract DAAL03-86-D-0001)
(AD-A273112; ARI-RN-94-01) Avail: CASI HC A03/MF A01

The Computerized Adaptive Screening Test (CAST) is used for predicting performance on the Armed Forces Qualification Test (AFQT). The goal of this project is to ensure CAST compatibility with the Electronic Information Delivery System (EIDS) now being fielded by the U.S. Army Recruiting Command. A number of software enhancements were implemented. Improvements were made in test item selection, reporting capability, experimental item selection, data storage capability, and software coordination. This report is a guide for users and programmers. DTIC

N94-21810*# Houston Univ., TX. Dept. of Psychology.
THE EFFECTS OF INSTRUCTIONAL SETS ON REACTIONS TO AND PERFORMANCE ON AN INTELLIGENT TUTORING SYSTEM Final Technical Report
Debra Steele Johnson 20 Dec. 1993 50 p
(Grant NAG9-555)
(NASA-CR-194739; NAS 1.26:194739) Avail: CASI HC A03/MF A01

The effects of a contextual factor, i.e., task instructions, on performance on and reactions to an Intellegent Tutoring System (ITS) training Remote Manipulator System (RMS) tasks were examined. The results supported the first prediction that task instructions could be used to successfully induce a mastery versus an achievement orientation. Previous research suggests that a mastery orientation can result in beneficial effects on learning and performance of complex tasks. Furthermore, the results supported the second prediction that a mastery orientation would have beneficial effects on learning and performance as well as affective and cognitive reactions to the ITS tasks. Moreover, the results indicated that a mastery orientation was especially beneficial for the more complex ITS tasks and later in task practice, i.e., when a task was performed for the second time. A mastery orientation is posited to have its beneficial effects by focusing more effort and attention on task performance. Conclusions are drawn with some caution due to the small number of subjects, although the results for these subjects were consistent across multiple trials and multiple measures of performance. ITS designers are urged to consider contextual factors such as task instructions and feedback in terms of their potential to induce a mastery versus an achievement orientation.
Author (revised)

54 MAN/SYSTEM TECHNOLOGY AND LIFE SUPPORT

Includes human engineering; biotechnology; and space suits and protective clothing.

For related information see also *16 Space Transportation.*

N94-19935# Dayton Univ., OH. Research Inst.
NIGHT VISION GOGGLE MODEL F4949 PREFLIGHT ADJUSTMENT/ASSESSMENT PROCEDURES Final Report, Mar. - Jun. 1993
Joseph C. Antonio and William E. Berkley Aug. 1993 21 p
(Contract F33615-90-C-0005)
(AD-A271079; AL/HR-TR-1993-0111) Avail: CASI HC A03/MF A01

Night vision goggles (NVG's) have been employed in a variety of aircraft for over twenty years. However, only recently has their application begun in fixed-wing fast movers. Research accomplished by the Night Vision Programs Office at the Aircrew Training Research Division of the USAF Armstrong Laboratory demonstrated the loss of NVG performance resulting from improper adjustments. This report describes correct adjustment procedures for the F4949 NVG system. The procedures described were developed so aircrews could take advantage of the adjustments available on the NVG's. Additionally, image descriptions are given to help aircrews evaluate NVG performance. Information on the proper equipment/space needed for proper evaluation is also included. DTIC

N94-20063*# Christopher Newport Coll., Newport News, VA. Dept. of Biology, Chemistry and Environmental Sciences.
SHIELDING FROM SPACE RADIATIONS Progress Report, 1 Jun. - 1 Dec. 1993
C. Ken Chang, Forooz F. Badavi, and Ram K. Tripathi 1 Dec. 1993 39 p
(Contract NCC1-178)
(NASA-CR-194683; NAS 1.26:194683) Avail: CASI HC A03/MF A01

This Progress Report covering the period of 1 June 1993 to 1 Dec. 1993 presents the development of an analytical solution to the heavy ion transport equation in terms of a one-layer Green's function formalism. The mathematical developments are recasted into an efficient computer code for space applications. The efficiency of this algorithm is accomplished by a nonperturbative technique of extending the Green's function over the solution domain. The code may also be applied to accelerator boundary conditions to allow code validation in laboratory experiments. Results from the isotopic version of the code with 80 isotopes present for a single layer target material, for the case of an iron beam projectile at 600 MeV/nucleon in water is presented. Author (revised)

N94-20137*# National Aeronautics and Space Administration. Ames Research Center, Moffett Field, CA.
QUINOA: AN EMERGING NEW CROP WITH POTENTIAL FOR CELSS
Greg Schlick and David L. Bubenheim Nov. 1993 9 p
(RTOP 199-61-12-28)
(NASA-TP-3422; A-93100; NAS 1.60:3422) Avail: CASI HC A02/MF A01

Chenopodium quinoa is being considered as a new crop for the Controlled Ecological Life Support System (CELSS) because of its high protein values (12 - 18%) and unique amino acid composition. Lysine, and essential amino acid that is deficient in many grain crops, is found in quinoa approaching Food and Agriculture Organization of the United Nations (FAO) standards set for humans. This 'new' crop, rich in protein and with desirable proportions of important amino acids, may provide greater versatility in meeting the needs of humans on long-term space missions. Initially, the cultivars CO407 x ISLUGA, CO407 Heat Tolerant Population 1, and Real' (a Bolivian variety) were examined. The first cultivar showed the most promise in greenhouse studies. When grown hydroponically in the greenhouse, with no attempt to maximize productivity, this cultivar produced 202 g m(exp -2) with a harvest index of 37%. None of the cultivars were greater than 70 cm in height. Initial results indicate that quinoa could be an excellent crop for CELSS because of the high concentration of protein, ease of use, versatility in preparation, and potential for greatly increased yields in controlled environments. Author

N94-20194* National Aeronautics and Space Administration. Lyndon B. Johnson Space Center, Houston, TX.
APPARATUS AND METHOD FOR MEASURING SUBJECT WORK RATE ON AN EXERCISE DEVICE Patent
William E. Thornton, inventor (to NASA) 7 Sep. 1993 19 p Filed 15 Oct. 1991 Supersedes N92-17910 (30 - 8, p 1335)
(NASA-Case-MSC-21752-1; US-Patent-5,242,339;
US-Patent-Appl-SN-775404; US-Patent-Class-482-8;
US-Patent-Class-482-54; US-Patent-Class-73-379.01;
Int-Patent-Class-A63B-22/02; Int-Patent-Class-A63B-71/00) Avail: US Patent and Trademark Office

Method and apparatus for accurately simulating locomotion in a weightless environment, especially to prevent atrophy of a subject's musculoskeletal and cardiorespiratory systems during space travel, are disclosed. Forces, including the vertical, horizontal, and lateral force generated by an individual during locomotion on a treadmill using a rigid belt with rigid transfer elements supported by low friction bogies, are measured by strain gauges sensitive in their respective direction. The vertical forces produced by securing the subject to the treadmill via bungee cords, in conjunction with the measured velocity of the treadmill and the mode of locomotion, are used to determine the subject's equivalent weight. The other horizontal and lateral forces are used to determine the external work produced by the subject when locomotion is performed on a nonlevel surface with an effective grade angle. The measured forces are related in such a way that the grade angle is easily determined. A motor and additional circuitry can be added to the apparatus to measure and force a subject to maintain a predetermined work rate associated with a preselected grade angle and tread velocity.
Official Gazette of the U.S. Patent and Trademark Office

N94-20338*# California Univ., Los Angeles. Dept. of Physiological Science.
COSMOS 2229 Final Report
V. Reggie Edgerton, Roland R. Roy, and John A. Hodgson Nov. 1993 17 p
(Contract NCC2-535; Proj. K-7-33)
(NASA-CR-194734; NAS 1.26:194734) Avail: CASI HC A03/MF A01

The 6 weeks preflight activities of the Cosmos project during 1993 included: modification of EMG connector to improve the reliability of EMG recording; 24 hour cage activity recording from all but two of the flight animals (monkeys); attempts to record from flight candidates during foot lever task; and force transducer calibrations on all flight candidate animals. The 4 week postflight recordings included: postflight recordings from flight

animals; postflight recordings on 3 control (non-flight) animals; postflight recalibration of force transducers on 1 flight and 4 control (non-flight) animals; and attempts to record EMG and video data from the flight animals during postflight locomotion and postural activity. The flight EMG recordings suggest that significant changes in muscle control may occur in spaceflight. It is also clear from recordings that levels of EMG recorded during spaceflight can attain values similar to those measured on earth. Amplifier gain settings should therefore probably not be changed for spaceflight. Derived from text

N94-20493* National Aeronautics and Space Administration. Marshall Space Flight Center, Huntsville, AL.

AUTOMATIC LOCKING ORTHOTIC KNEE DEVICE Patent

Bruce C. Weddendorf, inventor (to NASA) 7 Dec. 1993 8 p Filed 26 Dec. 1991 Supersedes N92-17866 (30 - 8, p 1335)

(NASA-Case-MFS-28633-1; US-Patent-5,267,950; US-Patent-Appl-SN-813629; US-Patent-Class-602-26; US-Patent-Class-602-16; US-Patent-Class-623-43; US-Patent-Class-623-44; Int-Patent-Class-A61F-5/00) Avail: US Patent and Trademark Office

An articulated tang in clevis joint for incorporation in newly manufactured conventional strap-on orthotic knee devices or for replacing such joints in conventional strap-on orthotic knee devices is discussed. The instant tang in clevis joint allows the user the freedom to extend and bend the knee normally when no load (weight) is applied to the knee and to automatically lock the knee when the user transfers weight to the knee, thus preventing a damaged knee from bending uncontrollably when weight is applied to the knee. The tang in clevis joint of the present invention includes first and second clevis plates, a tang assembly and a spacer plate secured between the clevis plates. Each clevis plate includes a bevelled serrated upper section. A bevelled shoe is secured to the tank in close proximity to the bevelled serrated upper section of the clevis plates. A coiled spring mounted within an oblong bore of the tang normally urges the shoes secured to the tang out of engagement with the serrated upper section of each clevic plate to allow rotation of the tang relative to the clevis plate. When weight is applied to the joint, the load compresses the coiled spring, the serrations on each clevis plate dig into the bevelled shoes secured to the tang to prevent relative movement between the tang and clevis plates. A shoulder is provided on the tang and the spacer plate to prevent overextension of the joint.

Official Gazette of the U.S. Patent and Trademark Office

N94-20606*# National Aeronautics and Space Administration. Lyndon B. Johnson Space Center, Houston, TX.

LOADS PRODUCED BY A SUITED SUBJECT PERFORMING TOOL TASKS WITHOUT THE USE OF FOOT RESTRAINTS

Sudhakar L. Rajulu (Lockheed Engineering and Sciences Co., Houston, TX.), Jeffrey Poliner (Lockheed Engineering and Sciences Co., Houston, TX.), and Glenn K. Klute Dec. 1993 38 p

(Contract NAS9-17900)

(NASA-TP-3424; S-744; NAS 1.60:3424) Avail: CASI HC A03/MF A01

With an increase in the frequency of extravehicular activities (EVA's) aboard the Space Shuttle, NASA is interested in determining the capabilities of suited astronauts while performing manual tasks during an EVA, in particular the situations in which portable foot restraints are not used to stabilize the astronauts. Efforts were made to document the forces that are transmitted to spacecraft while pushing and pulling an object as well as while operating a standard wrench and an automatic power tool. The six subjects studied aboard the KC-135 reduced gravity aircraft were asked to exert a maximum torque and to maintain a constant level of torque with a wrench, to push and pull an EVA handrail, and to operate a Hubble Space Telescope (HST) power tool. The results give an estimate of the forces and moments that an operator will transmit to the handrail as well as to the supporting structure. In general, it was more effective to use the tool inwardly toward the body rather than away from the body. There were no differences in terms of strength capabilities between right and left hands. The power tool was difficult to use. It is suggested that ergonomic redesigning of the power tool may increase the efficiency of power tool use. Author (revised)

N94-20914# Aerospace Medical Research Labs., Wright-Patterson AFB, OH. Crew Systems Directorate.

SYSTEM TEST RESULTS OF THE ADVANCED TECHNOLOGY ANTI-G SUIT (ATAGS) Final Report, Oct. 1991 - Nov. 1992

Larry J. Meeker, John H. Olhausen, and Grady L. Ripley Nov. 1992 10 p

(AF Proj. 2830)

(AD-A271535; AL/CF-TP-1993-0033) Avail: CASI HC A02/MF A01

Previous centrifuge and flight testing have shown that the ATAGS offers superior G endurance protection even when operated at lower pressures than the standard anti-G suit. All of the previous ATAGS testing was done, however, using human test subjects for the purpose of evaluating G protection. The purpose of the parametric tests was to provide basic system data such as volumes, fill rates and pressure differentials for the ATAGS. In order to allow direct comparison with data taken previously on the AF standard anti-G suit (CSU-13A/P), these tests were based on procedures detailed in SAM-TR-78-12, Engineering Test, and Evaluation During High G, VOL III: Anti-G Suits. ATAGS volumes were measured using pressure change during expansion from a known volume. The volumes of several suit sizes were taken, both with the suit unmounted and mounted on a mannequin to a proper fit. Total flow was measured with a flowmeter in the main fill hose. Differential pressure in various parts of the suit during rapid fill was measured at test points located on both sides of the abdominal bladder, on each thigh, and at the bottom of each leg. Preliminary data from these tests are presented. DTIC

N94-21154 Naval Air Warfare Center, Patuxent River, MD. Aircraft Div.

IN-FLIGHT MEASUREMENT OF AIRCREW BREATHING IN NAVY AIRCRAFT

Dennis N. Gordge 20 Sep. 1993 74 p Limited Reproducibility: More than 20% of this document may be affected by microfiche quality

(AD-A271811; NAWCADPAX-TM-93-59-SY) Avail: Issuing Activity (Defense Technical Information Center (DTIC))

A man-mounted, aircraft independent, self-contained recording system was developed for measuring the breathing flow rates of aircrew during all phases of flight. Breathing data of 41 Navy and Marine Corps aircrew operating F-14, F/A-18, A-7, A-6, and S-3 aircraft were measured during 51 flights including fleet combat exercises. The data were collected to validate current test and evaluation techniques and to modify oxygen system design and installation specifications. The data may also be used for designing future oxygen systems. The data generally show good correlation with previous studies, but also provide unique results for carrier operations and aerial combat maneuvering (ACM) conditions not previously reported. The results indicate that the current military oxygen system flow rate specifications are inadequate for tactical aircraft performing ACM. The results also suggest that current F-14 and F/A-18 oxygen systems may be inadequate for low altitude ACM. DTIC

N94-21247# Aerospace Medical Div., Brooks AFB, TX.

PHYSIOLOGICAL EFFICACY OF A LIGHTWEIGHT AMBIENT AIR COOLING UNIT FOR VARIOUS APPLICATIONS Final Report, Oct. 1988 - Sep. 1991

Yasu T. Chen, Susan H. Bomalaski, and Stefan H. Constable Oct. 1993 18 p

(AF Proj. 2729)

(AD-A272952; AL-TP-1993-0013) Avail: CASI HC A03/MF A01

In an attempt to further advance intermittent conditioned air cooling (IC) concept, a strategy of supplementing continuous air cooling (CC) was conceived. With this approach, ambient air cooling (AC) is added during work with conditioned air cooling delivered during rest periods. A compact, battery-powered belt-pack cooling unit (8.5 lb), designed and fabricated at the USAF Armstrong Laboratory, was used to deliver 12 cfm filtered ambient air during work cycles: 10 cfm to the body and 2 cfm to the face. Five experimental trials were completed in a thermally controlled chamber under warm conditions (32 deg C, 40% RH) consisting of no cooling (NC), IC, and CC during intermittent exercise, as well as NC and AC during continuous exercise. This study suggests that ambient air delivered during work by a lightweight portable unit can be applied in conjunction with conditioned air during rest to further improve personal comfort, reduce skin temperature, and decrease the cumulative fatigue seen over repeated work/rest cycles in selected military and industrial applications. DTIC

N94-21309# Acoustical Society of America, New York, NY.
U.S. TAG FOR ISO/TC 43, ACOUSTICS, IEC/TC 29 ELECTROACOUSTICS, AND ISO/TC 108/SC4 HUMAN EXPOSURE TO MECHANICAL VIBRATION AND SHOCK: MINUTES OF THE ACCREDITED STANDARDS COMMITTEE ON BIOACOUSTICS, S3
20 May 1993 108 p Meeting held in Ottawa, Canada, 20 May 1993
(AD-A273014; S3/368) Avail: CASI HC A06/MF A02

Presented are the minutes of the meeting of the Accredited Standards Committee on Bioacoustics, S3, held on November 3, 1992, as well as attachments containing summaries and correspondence on topics relating to ANSI standards on acoustics and human exposure. Included as attachments are S3 standards, working groups, and project status summaries. CASI

N94-21627*# National Aeronautics and Space Administration. Lyndon B. Johnson Space Center, Houston, TX.
STRENGTH CAPABILITIES AND LOAD REQUIREMENTS WHILE PERFORMING TORQUING TASKS IN ZERO GRAVITY
Jeffrey Poliner (Lockheed Engineering and Sciences Co., Houston, TX.), Robert P. Wilmington (Lockheed Engineering and Sciences Co., Houston, TX.), and Glenn K. Klute 1 Dec. 1993 22 p
(NASA-TP-3433; S-751; NAS 1.60:3433) Avail: CASI HC A03/MF A01

A generic examination of the loads produced by individuals performing maximal efforts with a torquing tool in zero gravity, to determine operator strength when performing torquing tasks; quantify the loads placed on foot restraints while performing these tasks; and examine effects of orientation and direction of tool rotation on strength effectiveness was conducted. The experiment was conducted aboard NASA's KC-135 reduced-gravity aircraft, using two force plates attached to a test stand, one with a foot restraint. Subjects used a wrench to apply maximum torques to various fittings, in different positions, in clockwise and counterclockwise directions. It was seen that these subjects could produce approximately 400 to 750 N of force, depending on the orientation of the tool and the direction of effort. The most force could be produced when pushing the tool upwards. A force effectiveness ratio (FER) defined as an indication of how much of the subjects' total effort actually went into performing the desired task. Values of FER ranged from 0.55 to 0.90, with the greatest FER occurring with UP and DOWN efforts, and the lowest with AWAY and LEFT efforts. Designers can use these results to set specifications for craft structures; tools can be developed based on the known strength of the tool users; and tasks can be developed to not exceed the crewmembers' capabilities. Author (revised)

N94-21812*# National Aeronautics and Space Administration. Lyndon B. Johnson Space Center, Houston, TX.
EVA TOOLS AND EQUIPMENT REFERENCE BOOK
R. K. Fullerton Nov. 1993 737 p Revised
(NASA-TM-109350; NAS 1.15:109350; JSC-20466-Rev-B) Avail: CASI HC A99/MF A06

This document contains a mixture of tools and equipment used throughout the space shuttle-based extravehicular activity (EVA) program. Promising items which have reached the prototype stage of development are also included, but should not be considered certified ready for flight. Each item is described with a photo, a written discussion, technical specifications, dimensional drawings, and points of contact for additional information. Numbers on the upper left-hand corner of each photo may be used to order specific pictures from NASA and contractor photo libraries. Points of contact were classified as either operational or technical. An operational contact is an engineer from JSC Mission Operations Directorate who is familiar with the basic function and on-orbit use of the tool. A technical contact would be the best source of detailed technical specifications and is typically the NASA subsystem manager. The technical information table for each item uses the following terms to describe the availability or status of each hardware item: Standard - Flown on every mission as standard manifest; Flight specific - Potentially available for flight, not flown every mission (flight certification cannot be guaranteed and recertification may be required); Reference only - Item no longer in active inventory or not recommended for future use, some items may be too application-specific for general use; and Developmental - In the prototype stage only and not yet available for flight. The current availability and certification of any flight-specific tool should be verified with the technical point of contact. Those tools built and fit checked for Hubble Space Telescope maintenance are program dedicated and are not available to other customers. Other customers may have identical tools built from the existing, already certified designs as an optional service. Author (revised)

N94-20665*# Colorado State Univ., Fort Collins. Center for Engineering Infrastructure and Sciences in Space.
CHARACTERIZATION OF MINNESOTA LUNAR SIMULANT FOR PLANT GROWTH Abstract Only
James P. Oglesby, Willard L. Lindsay, and Willy Z. Sadeh *In* Lunar and Planetary Inst., Twenty-Fourth Lunar and Planetary Science Conference. Part 3: N-Z 1993 p 1099 (For primary document see N94-20636 05-91)
Avail: CASI HC A01/MF A06

N94-21403 European Space Agency. European Space Research and Technology Center, ESTEC, Noordwijk (Netherlands). Materials and Processes Div.
TOXICITY OF THERMAL DEGRADATION IN A MANNED SPACE ENVIRONMENT
M. D. Judd and D. Bryant *In* CNES, Fifth International Symposium on Materials in a Space Environment Jun. 1993 p 457-471 (For primary document see N94-21367 05-18)
Copyright Avail: CEPADUES-Editions, 111, rue Nicolas-Vaquelin, 31100 Toulouse, France

55 SPACE BIOLOGY

Includes exobiology; planetary biology; and extraterrestrial life.

N94-20336*# Harvard Univ., Cambridge, MA.
WIDE-BANDWIDTH HIGH-RESOLUTION SEARCH FOR EXTRATERRESTRIAL INTELLIGENCE Semiannual Status Report, 15 Jun. - 15 Dec. 1993
Paul Horowitz 15 Dec. 1993 27 p
(Grant NAGw-2872)
(NASA-CR-194724; NAS 1.26:194724) Avail: CASI HC A03/MF A01

A third antenna was added to the system. It is a terrestrial low-gain feed, to act as a veto for local interference. The 3-chip design for a 4 megapoint complex FFT was reduced to finished working hardware. The 4-Megachannel circuit board contains 36 MByte of DRAM, 5 CPLDs, the three large FFT ASICs, and 74 ICs in all. The Austek FDP-based Spectrometer/Power Accumulator (SPA) has now been implemented as a 4-layer printed circuit. A PC interface board has been designed and together with its associated user interface and control software allows an IBM compatible computer to control the SPA board, and facilitates the transfer of spectra to the PC for display, processing, and storage. The Feature Recognizer Array cards receive the stream of modulus words from the 4M FFT cards, and forward a greatly thinned set of reports to the PC's in whose backplane they reside. In particular, a powerful ROM-based state-machine architecture has been adopted, and DRAM has been added to permit integration modes when tracking or reobserving source candidates. The general purpose (GP) array consists of twenty '486 PC class computers, each of which receives and processes the data from a feature extractor/correlator board set. The array performs a first analysis on the provided 'features' and then passes this information on to the workstation. The core workstation software is now written. That is, the communication channels between the user interface, the backend monitor program and the PC's have working software. Derived from text

59 MATHEMATICAL AND COMPUTER SCIENCES (GENERAL)

N94-21784*# Computer Sciences Corp., Mountain View, CA.
HIGHER ORDER BEZIER CIRCLES
Jin Chou Dec. 1993 20 p
(Contract NAS2-12961)

(NASA-CR-177633; A-94040; NAS 1.26:177633) Avail: CASI HC A03/MF A01

Rational Bezier and B-spline representations of circles have been heavily publicized. However, all the literature assumes the rational Bezier segments in the homogeneous space are both planar and (equivalent to) quadratic. This creates the illusion that circles can only be achieved by planar and quadratic curves. Circles that are formed by higher order rational Bezier curves which are nonplanar in the homogeneous space are shown. The problem of whether it is possible to represent a complete circle with one Bezier curve is investigated. In addition, some other interesting properties of cubic Bezier arcs are discussed. Author (revised)

60 COMPUTER OPERATIONS AND HARDWARE

Includes hardware for computer graphics, firmware, and data processing.

For components see *33 Electronics and Electrical Engineering.*

N94-19832# Massachusetts Inst. of Tech., Cambridge. Artificial Intelligence Lab.

A PARALLELIZING COMPILER BASED ON PARTIAL EVALUATION

Rajeev Surati Jul. 1993 55 p

(Contract N00014-92-J-4097)

(AD-A270838; AI-TR-1377) Avail: CASI HC A04/MF A01

This thesis demonstrates a compiler that uses partial evaluation to achieve outstandingly efficient parallel object code from very high-level source programs. The source programs are ordinary Scheme numerical programs, written abstractly, with no attempt to structure them for parallel execution. The compiler identifies and extracts parallelism completely automatically; nevertheless, it achieved by speed-ups equivalent to or better than the best observed results achieved by previous supercomputer compilers that require manual restructuring of code. DTIC

N94-19886# Lawrence Livermore National Lab., CA.

A PIPELINED SUPERCONDUCTING DIGITAL PROCESSOR

J. Spargo (TRW Systems Group, Redondo Beach, CA.), M. Lewis (TRW Systems Group, Redondo Beach, CA.), A. Silver (TRW Systems Group, Redondo Beach, CA.), S. Azevedo, J. Kaschmitter, and S. Whiteley (Conductus, Inc., Sunnyvale, CA.) Jul. 1993 2 p Presented at the International Superconductive Electronic Conference, Boulder, CO, 11-14 Aug. 1993

(Contract W-7405-eng-48)

(DE93-040852; UCRL-JC-114594; CONF-930863-2) Avail: CASI HC A01/MF A01

A team consisting of groups form TRW, Conductus, Stanford University, the University of California at Berkeley, and the National Institute of Standards & Technology (NIST) at Boulder, Colorado is building a high performance superconducting digital signal processor. This processor is based on advanced superconducting digital technology, low temperature semiconductor technology, optical communications technology, and multi-chip module packaging technlogy. This system, referred to as the hybrid Josephson Junction Digital Signal Processor (JJDSP) is described. This system was designed to maximize the benefits of Josephson Junctions (JJ) logic, while minimizing the restrictions imposed by its limitations. DOE

N94-20039*# California Polytechnic State Univ., San Luis Obispo.

REFERENCE MANUAL FOR A REQUIREMENTS SPECIFICATION LANGUAGE (RSL), VERSION 2.0

Gene L. Fisher and Gerald C. Cohen (Boeing Defense and Space Group, Seattle, WA.) Nov. 1993 30 p

(Contract NAS1-18586; RTOP 505-64-10-07)

(NASA-CR-191460; NAS 1.26:191460) Avail: CASI HC A03/MF A01

This report is a Reference Manual for a general-purpose Requirements Specification Language, RSL. The purpose of RSL is to specify precisely the external structure of a mechanized system and to define requirements that the system must meet. A system can be comprised of a mixture of hardware, software, and human processing elements. RSL is a hybrid of features found in several popular requirements specification languages and includes constructs for formal mathematical specification. Author (revised)

N94-20082 Technische Univ., Eindhoven (Netherlands). Dept. of Mathematics and Computing Science.

NOMINALIZATION, PREDICTION AND TYPE CONTAINMENT

F. Kamareddine (Glasgow Univ., Scotland.) and E. Klein (Edinburgh Univ., Scotland.) 1992 51 p Prepared in cooperation with Glasgow Univ. Limited Reproducibility: More than 20% of this document may be affected by microfiche quality

(PB93-191799; COMPUTING SCIENCE NOTES-92/23) Copyright Avail: Issuing Activity (National Technical Information Service (NTIS))

Type disciplines have featured prominently in formal approaches to natural language. The paper examines type-free theories of properties in order to accommodate the difficulties raised by nominalization and self-application. Historically, type disciplines for languages have developed in close association with intended models for interpretation. The proposals the authors shall make can also be construed in this way, inasmuch as they were inspired in part by the notion of a Frege structure, which is intended to provide a consistent formulation of Frege's logical notion of set. A system of types provides a classificatory scheme for the domain and range of functors. The type of an expression determines the domain in which that expression receives an interpretation. NTIS

N94-20085 Carnegie-Mellon Univ., Pittsburgh, PA. School of Computer Science.

A METHODOLOGY FOR FORMAL HARDWARE VERIFICATION, WITH APPLICATION TO MICROPROCESSORS Ph.D. Thesis

Derek L. Beatty, Randal E. Bryant, Edmund M. Clarke, Jr., Allan L. Fisher, and Carl-Johan H. Seger 29 Aug. 1993 355 p Limited Reproducibility: More than 20% of this document may be affected by microfiche quality

(Contract F33615-90-C-1465; ARPA Order 7597)

(AD-A270550; CMU-CS-93-190) Avail: CASI HC A16

Microprocessors are now ubiquitous, but their design is not without difficulties. Numerous microprocessors have been introduced only to find--sometimes years later--that they contain mistakes. The need for better ways of checking designs is clear. This research develops a methodology for formally verifying data-intensive circuits against abstract state machines defined by assertions and applies it to show that a microprocessor circuit implements its intended instruction set. 'Implementation' is a formal relation between input-output sequences: of an abstract state machine, and of a circuit. This simple abstract model of behavior is reconciled with concepts from digital-systems design including dynamic logic, pipelining, multi-phase clocks, and a separate memory system. The methodology structures proof of implementation using a series of decompositions. It exposes the internal system state. It dissects sequences into their component transitions (using a new formalism called marked strings to reason about overlapped operation). For processor verification it also abstracts away most of the memory state. DTIC

N94-20107 Carnegie-Mellon Univ., Pittsburgh, PA. School of Computer Science.

LIGHTWEIGHT RECOVERABLE VIRTUAL MEMORY

M. Satyanarayanan, Henry H. Mashburn, Puneet Kumar, David C. Steere, and James J. Kistler Aug. 1993 16 p Limited Reproducibility: More than 20% of this document may be affected by microfiche quality

(Contract F33615-90-C-1465; ARPA Order 7597)

(AD-A270576; CMU-CS-93-143) Avail: CASI HC A03

Recoverable virtual memory refers to regions of a virtual address spare on which transactional guarantees are offered. This paper describes RVM, an efficient, portable, and easily used implementation of recoverable virtual memory for UNIX environments. A unique characteristic of RVM is that it allows independent control over the transactional properties of atomicity, permanence, and serializability. This leads to considerable flexibility in the use of RVM, potentially enlarging the range of applications than can benefit from transactions. It also simplifies the layering of functionality such as nesting and distribution. The paper shows that RVM performs well over its intended range of usage even though it does not benefit from specialized operating system support. It also demonstrates the importance of intra- and inter-transaction optimizations. DTIC

N94-20357 Department of the Navy, Washington, DC.

M-DIMENSIONAL COMPUTER MEMORY WITH M-1 DIMENSIONAL HYPERPLANE ACCESS Patent

Allen D. Parks, inventor (to Navy), James C. Perry, inventor (to Navy), and

Albert P. Shuler, inventor (to Navy) 21 Sep. 1993 7 p Filed 9 Jul. 1990 Supersedes AD-D014615
(AD-D015960; US-Patent-5,247,630; US-Patent-Appl-SN-551103; US-Patent-Class-395-400) Avail: US Patent and Trademark Office

An m-dimensional memory with m-1 dimensional hyperplane access. Random access memory (RAM) circuits are arranged in a plurality of groups for storing data words corresponding to vertices of an m-dimensional lattice. Each vertex of the lattice is defined by an m-tuple. The minimum number of RAM circuits required to realize the memory architecture of the present invention is based upon the size of the lattice and the distribution of the data words in memory is based upon the m-tuples used to define the lattice. DTIC

N94-20469 University of Southern California, Los Angeles. School of Engineering.
CENTER FOR THE INTEGRATION OF OPTICAL COMPUTING Final Report, 15 Sep. 1990 - 14 Aug. 1993
A. A. Sawchuk and W. H. Steier 15 Oct. 1993 74 p Limited Reproducibility: More than 20% of this document may be affected by microfiche quality
(Grant AF-AFOSR-0133-90)
(AD-A271874; AFOSR-93-0826TR) Avail: CASI HC A04

Topics reviewed include the following: Optical interconnections, lenslet array processors, generalizable neural networks, spatial light modulators, MBE growth of quantum well structures, ultralow threshold arrays, charge transport optical nonlinearities, Ebium-doped amplifiers in optical switching systems, Optical computing, Laser arrays, Spatial modulators, Optical interconnections, and Optical neural interconnections. DTIC

N94-20476# Sandia National Labs., Albuquerque, NM.
DELIVERY OF VERY HIGH BANDWIDTH WITH ATM SWITCHES AND SONET
S. A. Gossage 1993 9 p Presented at the 29th Annual International Telemetering Conference, Las Vegas, NV, 25-28 Oct. 1993
(Contract DE-AC04-76DP-00789)
(DE93-019432; SAND-93-1686C; CONF-9310131-2) Avail: CASI HC A02/MF A01

To deliver high bandwidth, a ubiquitous inter-/intra-building cable plant consisting of single mode and multimode fiber as well as twisted pair copper is required. The selection of the 'glue' to transport and interconnect distributed LAN's with central facility resources over a pervasive cable plant is the focus of this paper. A description of the traditional problems that must be overcome to provide very high bandwidth beyond the narrow confines of a computer center is given. The applicability of Asynchronous Transfer Mode (ATM) switching (interconnection) and Synchronous Optical NETwork (SONET) (transport) for high bandwidth delivery is described using the environment and requirements of Sandia National Laboratories. Other methods for distributing high data rates are compared and contrasted. Sandia is implementing a standards based foundation utilizing a pervasive single mode fiber cable plant, SONET transport, and ATM switching to meet the goals of gigabit networking. DOE

N94-20549*# Jet Propulsion Lab., California Inst. of Tech., Pasadena.
TIME WARP OPERATING SYSTEM VERSION 2.7 INTERNALS MANUAL
Feb. 1992 233 p
(Contract NAS7-918)
(NASA-CR-194798; JPL-D-9516; NAS 1.26:194798; AD-A271489) Avail: CASI HC A11/MF A03

The Time Warp Operating System (TWOS) is an implementation of the Time Warp synchronization method proposed by David Jefferson. In addition, it serves as an actual platform for running discrete event simulations. The code comprising TWOS can be divided into several different sections. TWOS typically relies on an existing operating system to furnish some very basic services. This existing operating system is referred to as the Base OS. The existing operating system varies depending on the hardware TWOS is running on. It is Unix on the Sun workstations, Chrysalis or Mach on the Butterfly, and Mercury on the Mark 3 Hypercube. The base OS could be an entirely new operating system, written to meet the special needs of TWOS, but, to this point, existing systems have been used instead. The base OS's used for TWOS on various platforms are not discussed in detail in this manual, as they are well covered in their own manuals. Appendix G discusses the interface between one such OS, Mach, and TWOS. DTIC

N94-21177# Rochester Univ., NY. Dept. of Computer Science.
THE EFFECTS OF BLOCK SIZE ON THE PERFORMANCE OF COHERENT CACHES IN SHARED-MEMORY MULTIPROCESSORS Technical Report
Cezary Dubnicki May 1993 121 p
(Contract N00014-92-J-1801)
(AD-A272838; TR-462-ONR) Avail: CASI HC A06/MF A02

Several studies have shown that the performance of coherent caches depends on the relationship between the cache block size and the granularity of sharing and locality exhibited by the program. Large cache blocks exploit processor and spatial locality, but may cause unnecessary cache invalidations due to false sharing. Small cache blocks can reduce the number of cache invalidation, but increase the number of bus or network transactions required to load data into the cache. We use reference traces from a variety of parallel programs and detailed simulation of a scalable shared-memory multiprocessor to examine the effects of cache block size on the performance of coherent caches and quantify this impact with respect to the network bandwidth and latency. Our results suggest that, regardless of the available bandwidth or latency, applications with good spatial locality favor long cache lines, and for these applications the relative benefits of longer cache lines increase with the bandwidth and latency. DTIC

N94-21195# Carnegie-Mellon Univ., Pittsburgh, PA. Dept. of Statistics.
FAULT TOLERANT REAL-TIME SYSTEMS Annual Report, 1 Oct. 1992 - 30 Sep. 1993
John P. Lehoczky 30 Sep. 1993 12 p
(Contract N00014-92-J-1771)
(AD-A272878) Avail: CASI HC A03/MF A01

Over the last year, substantial progress was made on the integration of real-time scheduling with fault tolerance to create a theory of temporal redundancy. Temporal redundancy is an approach to real-time system dependability in which subtasks which are a part of tasks with real-time requirements but which fail their acceptance test can be executed again, the latter execution being scheduled so that, if successful, the task will meet its timing requirements, and the re-execution does not cause any other task to miss its deadline. The failures occur randomly, thus they create, in effect, a stream of periodic job requests. The job requests correspond to the time required to retry the subtask, or an alternative version of the subtask, and they have a deadline which is the same as the deadline of the failed task. The temporal redundancy problem, therefore, can be considered to be a special version of the problem of jointly scheduling hard deadline periodic tasks and aperiodic tasks. However, in this case, the aperiodic tasks also have hard deadlines, a problem which has never been addressed in the rate monotonic environment. The goal of this research is to develop methods to solve this new joint scheduling problem and to assess the efficacy of the algorithms produced in enhancing real-time system fault tolerance. Derived from text

N94-21230# Carnegie-Mellon Univ., Pittsburgh, PA.
REAL-TIME FAULT TOLERANT COMPUTER SYSTEMS Annual Report, 1 Oct. 1992 - 30 Sep. 1993
John P. Lehoczky, Lui Sha, Marc Bodson, and Ragunathan Rajkumar 30 Sep. 1993 9 p
(Contract N00014-92-J-1524)
(AD-A272909) Avail: CASI HC A02/MF A01

This project is designed to study a new approach to software fault tolerance called analytic redundancy. It has been widely acknowledged that software failures are the most important issue in large computer system reliability. The failure rate of software has risen to 9.4 times the failure rate of hardware, and software failures have captured substantial media attention in recent years. The problem of software reliability is especially difficult, because the major recognized approaches (recovery blocks and n-version programming) are known to have serious drawbacks, and do not protect against whole classes of errors such as specification or design errors. DTIC

N94-21252# Naval Postgraduate School, Monterey, CA.
SECURITY MANAGEMENT OF ELECTRONIC DATA INTERCHANGE

M.S. Thesis
Hua-Fu Pao Jun. 1993 139 p
(AD-A272962) Avail: CASI HC A07/MF A02

This thesis considers the security management issue of electronic data interchange (EDI) and the security tools that are used for secure EDI implementation. Management considerations of EDI are considered to be an integration of EDI and security services. The background of EDI is surveyed along with EDI implementation procedures and digital signature (DS) techniques. The security services that are being used today are discussed including the EDI-related security standards. Finally, a security management model is presented that may be used to improve the security of an EDI implementation. The model is based on the perceived threats and vulnerabilities to the EDI, and the availability of security services and mechanisms. Included in the model are the setting of security goals, the determination of security policies, the determination of priorities for EDI security, and the construction of security architecture and management activities. This thesis was written to survey the concepts of EDI and DS. The survey of EDI related security standards may provide an opportunity to understand security services and security mechanisms available when designing an EDI system. Also, the security management model may help to improve the security of an organization. DTIC

N94-21281# Rochester Univ., NY. Dept. of Computer Science.
SPACE-EFFICIENT DETERMINISTIC SIMULATION OF PROBABILISTIC AUTOMATA
Ioan I. Macarie Jul. 1993 19 p
(Grant NSF CDA-88-22724)
(TR-463) Avail: CASI HC A03/MF A01

Given a description of a probabilistic automaton (one-head probabilistic finite automaton or probabilistic Turing machine) and an input string x of length n, we ask how much space does a deterministic Turing machine need in order to decide the acceptance of an input string by that automaton? The question is interesting even in the case of one-head one-way probabilistic finite automata. We call (rational) stochastic languages (S(sup greater than)(sub rat)) the class of languages recognized by these devices with rational transition probabilities and rational cutpoint. The class S(sup greater than)(sub rat) contains context-sensitive languages that are not context free, but on the other hand there are context-free languages not included in S(sup greater than)(sub rat). Our main results are as follows: (1) The (proper) inclusion of S(sup greater than)(sub rat) in Dspace(log n), which is optimal. The previous upper bounds were Dspace(n), and, in a special case, Dspace(log n loglog n). (2) The inclusion of the languages recognized by S(n) belonging to o(loglog log n) space-bounded probabilistic Turing machines in Dspace(2(exp S(n))log n). The previous upper bound was Dspace(log n(S(n)+log log n)). (Note that this improvement is meaningful, based on Freivalds' result that probabilistic Turing machines do not have a space complexity gap below loglog n like their deterministic and nondeterministic counterparts) . We present a technique to compare numbers given in terms of their values modulo a sequence of primes, 3 less than or equal to (LE) p(sub 1) LE p(sub 2) LE ... LE p(sub n) = O(n(exp a)) (where a is some constant) in O(log n) deterministic space. The previous result was O(log n loglog n). Author

N94-21301# California Univ., Santa Barbara. Dept. of Electrical and Computer Engineering.
DECOUPLED COMPUTER ARCHITECTURES FOR VERY HIGH-SPEED TECHNOLOGIES Final Report, 1 Jul. 1988 - 30 Jun. 1992
Steven E. Butner and Stephen I. Long Oct. 1993 56 p
(ARPA Order 6356)
(AD-A271646; ECE-93-19) Avail: CASI HC A04/MF A01

The long-term goal of this project is to develop the capability to apply and effectively use emerging high-speed integrated circuit (IC) technologies such as gallium-arsenide. Success in this endeavor requires experience with circuits, packaging, and architecture, not only in the new technologies, but also in current MOS IC technologies. The fundamental problem addressed is that though GaAs systems can now (or soon) quite readily be built with 100-150 MHz clock rates, the scaling beyond that speed is greatly complicated due to two effects: (1) some subsystems within a computer can support faster clock rates without much special consideration, but there are subsystems (most notably memory and communications) that cannot readily be made to follow the faster clock rates; and (2) conventional computer architecture is not capable of effectively dealing with high latency operations. As clock rates for some (but not all) of the subsystems of a computer increase, the relative latency of the remaining subsystems grows. DTIC

N94-22100*# National Aeronautics and Space Administration. Langley Research Center, Hampton, VA.
INTRODUCTION TO THE LARC CENTRAL SCIENTIFIC COMPUTING COMPLEX
John N. Shoosmith Nov. 1993 55 p Revised
(RTOP 505-60-01-01)
(NASA-TM-104092-Rev-1; NAS 1.15:104092-Rev-1) Avail: CASI HC A04/MF A01

The computers and associated equipment that make up the Central Scientific Computing Complex of the Langley Research Center are briefly described. The electronic networks that provide access to the various components of the complex and a number of areas that can be used by Langley and contractors staff for special applications (scientific visualization, image processing, software engineering, and grid generation) are also described. Flight simulation facilities that use the central computers are described. Management of the complex, procedures for its use, and available services and resources are discussed. This document is intended for new users of the complex, for current users who wish to keep appraised of changes, and for visitors who need to understand the role of central scientific computers at Langley. Author (revised)

N94-21082*# National Aeronautics and Space Administration. Goddard Space Flight Center, Greenbelt, MD.
RAD-HARD COMPUTER ELEMENTS FOR SPACE APPLICATIONS
G. S. Krishnan, Carl D. Longerot (Sandia National Labs., Albuquerque, NM.), and R. Keith Treece (Sandia National Labs., Albuquerque, NM.) *In* New Mexico Univ., The Fifth NASA Symposium on VLSI Design 1993 10 p (For primary document see N94-21079 05-33)
Avail: CASI HC A02/MF A06

N94-21088*# National Aeronautics and Space Administration. Goddard Space Flight Center, Greenbelt, MD.
SPACE QUALIFIED HIGH SPEED REED SOLOMON ENCODER
Jody W. Gambles (New Mexico Univ., Albuquerque.) and Tom Winkert *In* New Mexico Univ., The Fifth NASA Symposium on VLSI Design 1993 9 p (For primary document see N94-21079 05-33)
Avail: CASI HC A02/MF A06

N94-21089*# Christopher Newport Coll., Newport News, VA.
AN ASIC MEMORY BUFFER CONTROLLER FOR A HIGH SPEED DISK SYSTEM
Robert F. Hodson and Steve Campbell *In* New Mexico Univ., The Fifth NASA Symposium on VLSI Design 1993 10 p Sponsored by NASA. Langley Research Center (For primary document see N94-21079 05-33)
Avail: CASI HC A02/MF A06

N94-21090*# National Aeronautics and Space Administration. Goddard Space Flight Center, Greenbelt, MD.
MONGOOSE: CREATION OF A RAD-HARD MIPS R3000
Dan Lincoln (LSI Logic Corp., Milpitas, CA.) and Brian Smith *In* New Mexico Univ., The Fifth NASA Symposium on VLSI Design 1993 9 p (For primary document see N94-21079 05-33)
Avail: CASI HC A02/MF A06

N94-21096*# New Mexico Univ., Albuquerque. Space Engineering Research Center.
PROTON RADIATION TESTING OF AN 18 BIT A/D CONVERTER
Donald C. Thelen and Don R. Wiseman *In its* The Fifth NASA Symposium on VLSI Design 9 p(SEE N94-21079 05-33) 1993 (For primary document see N94-21079 05-33)
Avail: CASI HC A02/MF A06

N94-21101*# Jet Propulsion Lab., California Inst. of Tech., Pasadena.
POWER OPTIMIZATION IN LOGIC ISOMERS
Ramesh Panwar (California Univ., Los Angeles.), David Rennels (California Univ., Los Angeles.), and Leon Alkalaj *In* New Mexico Univ., The Fifth NASA Symposium on VLSI Design 1993 11 p (For primary document

see N94-21079 05-33)
(Contract N00014-91-J-1009)
Avail: CASI HC A03/MF A06

N94-21115*# Sri Venkateswara Univ., Tirupati (India). Dept. of Computer Science and Engineering.
A NOVEL VLSI PROCESSOR ARCHITECTURE FOR SUPERCOMPUTING ARRAYS
N. Venkateswaran, S. Pattabiraman, R. Devanathan, Ashaf Ahmed, S. Venkataraman, and N. Ganesh *In* New Mexico Univ., The Fifth NASA Symposium on VLSI Design 1993 11 p (For primary document see N94-21079 05-33)
Avail: CASI HC A03/MF A06

N94-21128*# National Aeronautics and Space Administration. Goddard Space Flight Center, Greenbelt, MD.
A FIXED/VARIABLE BIT-RATE DATA COMPRESSION ARCHITECTURE
Gregary C. Zweigle (Advanced Hardware Architectures, Moscow, ID.), Jack Venbrux (New Mexico Univ., Albuquerque.), and Pen-Shu Yeh *In* New Mexico Univ., The Fifth NASA Symposium on VLSI Design 1993 9 p (For primary document see N94-21079 05-33)
(Grant NAGw-3292)
Avail: CASI HC A02/MF A06

N94-21133*# Idaho Univ., Moscow. Dept. of Electrical Engineering.
BEHAVIORAL MODEL SIMULATION STUDIES OF AN IMAGE COMPRESSOR Thesis
Navid Madani and Sterling Whitaker *In* New Mexico Univ., The Fifth NASA Symposium on VLSI Design 1993 8 p (For primary document see N94-21079 05-33)
Avail: CASI HC A02/MF A06

N94-21700*# Standard Microsystems, CA.
A 20 MHz CMOS REORDER BUFFER FOR A SUPERSCALAR MICROPROCESSOR
John Lenell, Steve Wallace (California Univ., Irvine.), and Nader Bagherzadeh (California Univ., Irvine.) *In* Idaho Univ., The 1992 4th NASA SERC Symposium on VLSI Design 1992 11 p (For primary document see N94-21694 05-33)
Avail: CASI HC A03/MF A04

N94-21702*# Idaho Univ., Moscow. NASA Space Engineering Research Center.
AN 18 BIT 50 kHz ADC FOR LOW EARTH ORBIT
Donald C. Thelen *In its* The 1992 4th NASA SERC Symposium on VLSI Design 1992 11 p (For primary document see N94-21694 05-33)
Avail: CASI HC A03/MF A04

N94-21708*# Idaho Univ., Moscow. NASA Space Engineering Research Center.
NASA SERC DIGITAL CORRELATOR PROJECTS
John Canaris *In its* The 1992 4th NASA SERC Symposium on VLSI Design 1992 3 p (For primary document see N94-21694 05-33)
(Grants NAGw-1406; NAG5-1635)
Avail: CASI HC A01/MF A04

N94-21718*# Concordia Univ., Montreal (Quebec). Dept. of Computer Science.
A SIMPLE MODERN CORRECTNESS CONDITION FOR A SPACE-BASED HIGH-PERFORMANCE MULTIPROCESSOR
David K. Probst and Hon F. Li *In* Idaho Univ., The 1992 4th NASA SERC Symposium on VLSI Design 1992 10 p (For primary document see N94-21694 05-33)
(Grants NSERC-A3363; NSERC-A0921; NSERC-MEF0040121)
Avail: CASI HC A02/MF A04

N94-21734*# Nanyang Technological Inst. (Singapore). School of Applied Science.
A REAL TIME CORRELATOR ARCHITECTURE USING DISTRIBUTED ARITHMETIC PRINCIPLES
A. Benjamin Premkumar and T. Srikanthan *In* Idaho Univ., The 1992 4th NASA SERC Symposium on VLSI Design 1992 5 p (For primary document see N94-21694 05-33)
Avail: CASI HC A01/MF A04

N94-22112 Waterloo Univ. (Ontario). Very Large Scale Integration Group.
FORMAL HARDWARE VERIFICATION IN MAPLE
F. Mavaddat *In* Engineering Inst. of Canada, Canadian Conference on Electrical and Computer Engineering, Volumes 1 and 2 1991 5 p (For primary document see N94-22101 05-33)
Avail: Issuing Activity (Engineering Inst. of Canada, 2050 rue Mansfield, Suite 700, Montreal, PQ H3A 1Z2 Canada)

N94-22113 Queens Univ., Kingston (Ontario). Dept. of Electrical Engineering.
SYSTEM LEVEL MODELLING USING PETRI NETS AND VHDL
A. C. Woo and L. E. Peppard *In* Engineering Inst. of Canada, Canadian Conference on Electrical and Computer Engineering, Volumes 1 and 2 1991 4 p (For primary document see N94-22101 05-33)
Avail: Issuing Activity (Engineering Inst. of Canada, 2050 rue Mansfield, Suite 700, Montreal, PQ H3A 1Z2 Canada)

N94-22114 Calgary Univ. (Alberta). Very Large Scale Integration and Verification Lab.
FORMAL VERIFICATION OF AN ALU
G. Birtwistle *In* Engineering Inst. of Canada, Canadian Conference on Electrical and Computer Engineering, Volumes 1 and 2 1991 4 p (For primary document see N94-22101 05-33)
Avail: Issuing Activity (Engineering Inst. of Canada, 2050 rue Mansfield, Suite 700, Montreal, PQ H3A 1Z2 Canada)

N94-22119 Concordia Univ., Montreal (Quebec). Dept. of Electrical Engineering.
A SHARED BUFFER MEMORY SWITCH WITH MAXIMUM QUEUE AND MINIMUM ALLOCATION
Xing Chen and Jeremiah F. Hayes *In* Engineering Inst. of Canada, Canadian Conference on Electrical and Computer Engineering, Volumes 1 and 2 1991 4 p (For primary document see N94-22101 05-33)
Avail: Issuing Activity (Engineering Inst. of Canada, 2050 rue Mansfield, Suite 700, Montreal, PQ H3A 1Z2 Canada)

N94-22122 Calcutta Univ. (India). Dept. of Applied Physics.
ADDITION OF DECIMAL NUMBERS IN OPTICAL COMPUTING ARCHITECTURE BY WALSH CODED DIGITS
Asit K. Datta and Sunit K. Sen *In* Engineering Inst. of Canada, Canadian Conference on Electrical and Computer Engineering, Volumes 1 and 2 1991 3 p (For primary document see N94-22101 05-33)
Avail: Issuing Activity (Engineering Inst. of Canada, 2050 rue Mansfield, Suite 700, Montreal, PQ H3A 1Z2 Canada)

N94-22133 McGill Univ., Montreal (Quebec). Research Center for Intelligent Machines.
DESIGN OF A FLOATING POINT CONVOLUTION PROCESSOR
J. Drolet, J. F. Panisset, and A. S. Molawany *In* Engineering Inst. of Canada, Canadian Conference on Electrical and Computer Engineering, Volumes 1 and 2 1991 4 p (For primary document see N94-22101 05-33)
Avail: Issuing Activity (Engineering Inst. of Canada, 2050 rue Mansfield, Suite 700, Montreal, PQ H3A 1Z2 Canada)

N94-22168 Concordia Univ., Montreal (Quebec). Dept. of Electrical and Computer Engineering.
CREIR: A MULTIACCESS PROTOCOL FOR ON-BOARD PROCESSING SATELLITE SYSTEMS
Le-Ngoc Tho and Yu-Dong Yao (Spar Aerospace Ltd., Sainte-Anne-de-Bellevue, Quebec.) *In* Engineering Inst. of Canada, Canadian Conference on Electrical and Computer Engineering, Volumes 1 and 2 1991 4 p (For primary document see N94-22101 05-33)
Avail: Issuing Activity (Engineering Inst. of Canada, 2050 rue Mansfield, Suite 700, Montreal, PQ H3A 1Z2 Canada)

N94-22185 National Research Council of Canada, Ottawa (Ontario). Flight Research Lab.
EXPERIENCES IN AIRBORNE COMPUTING AT NRC FOR GEOPHYSICAL EXPLORATION APPLICATIONS
J. E. Jordan *In* Engineering Inst. of Canada, Canadian Conference on Electrical and Computer Engineering, Volumes 1 and 2 1991 4 p
(For primary document see N94-22101 05-33)
Avail: Issuing Activity (Engineering Inst. of Canada, 2050 rue Mansfield, Suite 700, Montreal, PQ H3A 1Z2 Canada)

61 COMPUTER PROGRAMMING AND SOFTWARE

Includes computer programs, routines, alogorithms, and specific applications, e.g., CAD/CAM.

N94-19855 Stanford Univ., CA. Dept. of Operations Research.
SOME TOPICS IN REGENERATIVE STEADY-STATE SIMULATION
Peter W. Glynn May 1993 14 p Limited Reproducibility: More than 20% of this document may be affected by microfiche quality
(Contract DAAL03-91-G-0101)
(AD-A271145; SU-TR-93-5; ARO-29412.2-MA-SDI) Avail: CASI HC A03

This paper offers a short introduction to the regenerative method of steady-state simulation output analysis. The paper also contains several new results. In particular, it is shown that regenerative methods necessarily apply to steady-state simulations that are 'well-posed' in a certain precise sense. The paper also describes a bias-reduction algorithm that takes advantage of regenerative structure. DTIC

N94-19911 Electronics Research Lab., Salisbury (Australia).
PLANNING PROCESS SOFTWARE: A USER GUIDE FOR THE DMCA
J. Clothier and J. ONeill Aug. 1993 202 p Limited Reproducibility: More than 20% of this document may be affected by microfiche quality
(AD-A271252; ERL-0718-GD; DODA-AR-008-469) Avail: CASI HC A10

The Planning Process Software user guide was produced as supporting documentation to the element of the Operational Movements Planning System prototype addressing preference and constraint definition and tracking allocation of items to be moved to available transport assets. The User Guide was designed as an easy to use supplement to the Planning Process Software. For each user-computer interface in the software, a graphical display is shown. This is accompanied by a description of how the interface operates, what function is performed by the underlying software, and how the interface can be reached from elsewhere within the Software. DTIC

N94-19918 Carnegie-Mellon Univ., Pittsburgh, PA. School of Computer Science.
A COMPARISON OF DATA-PARALLEL ALGORITHMS FOR CONNECTED COMPONENTS
John Greiner 18 Aug. 1993 18 p Limited Reproducibility: More than 20% of this document may be affected by microfiche quality
(Contract F19628-91-C-0168; ARPA Order 8313)
(AD-A270551; CMU-CS-93-191) Avail: Issuing Activity (Defense Technical Information Center (DTIC))

This paper presents a pragmatic comparison of three parallel algorithms for finding connected components. Those being compared are two similar algorithms by Awerbuch and Shiloach and by Shiloach and Vishkin and a randomized contraction algorithm by Blelloch, based on algorithms by Reif and Phillips. Major improvements are given for the first two which significantly reduces the super-linear component of their work complexity. An improvement is also given for the randomized algorithm, and this algorithm is shown to be the fastest of those tested. These comparisons are presented with NESL data-parallel code as executed on a Connection Machine 2. DTIC

N94-19919 Carnegie-Mellon Univ., Pittsburgh, PA. School of Computer Science.
MODEL CHECKING, ABSTRACTION, AND COMPOSITIONAL VERIFICATION Ph.D. Thesis
David E. Long, Edmund M. Clarke, Randal E. Bryant, Stephen D. Brookes, and Orna Grumberg Jul. 1993 220 p Limited Reproducibility: More than 20% of this document may be affected by microfiche quality
(Contract F33615-90-C-1465; ARPA Order 7597)
(AD-A270552; CMU-CS-93-178) Avail: CASI HC A10

Because of the difficulty of adequately simulating large digital designs, there has been a recent surge of interest in formal verification, in which a mathematical model of the design is proved to satisfy a precise specification. Model checking is one formal verification technique. It consists of checking that a finite-state model of the design satisfies a specification given in temporal logic, which is a logic that can express properties involving the sequencing of events in time. One of the main drawbacks of model checking is the state explosion problem. This problem occurs in systems composed of multiple processes executing in parallel; the size of the state space generally grows exponentially with the number of components. This thesis considers two methods for avoiding the state explosion problem in the context of model checking: compositional verification and abstraction. DTIC

N94-19928# Argonne National Lab., IL.
AN INTRODUCTION TO GUGA IN THE COLUMBUS PROGRAM SYSTEM
R. Shepard 1992 7 p Presented at the Relativistic and Electron Correlation Effects in Molecules and Solids, Vancouver, Ontario, 9-22 Aug. 1992
(Contract W-31-109-eng-38)
(DE93-018994; ANL/CHM/CP-80472; CONF-9208237-1) Avail: CASI HC A02/MF A01

The COLUMBUS Program System is a collection of FORTRAN programs for performing general multiconfiguration self-consistent-field (MCSCF) and multireference single- and double-exicitation configuration interaction (MRSDCI) wave function optimization based on the graphical unitary group approach (GUGA). This paper describes at an introductory level how wave functions are specified and characterized in the COLUMBUS Program System in terms of the unitary group, and in particular, using the graphical representation proposed by Shavitt. DOE

N94-19932 Carnegie-Mellon Univ., Pittsburgh, PA. School of Computer Science.
IMPLEMENTATION OF A PORTABLE NESTED DATA-PARALLEL LANGUAGE
Guy E. Blelloch, Siddhartha Chatterjee, Jonathan C. Hardwick, Jay Sipelstein, and Marco Zagha Feb. 1993 30 p Limited Reproducibility: More than 20% of this document may be affected by microfiche quality
(Contract F33615-90-C-1465; ARPA Order 7597)
(AD-A270524; CMU-CS-93-112) Avail: CASI HC A03

This paper gives an overview of the implementation of NESL, a portable nested data-parallel language. This language and its implementation are the first to fully support nested data structures as well as nested data-parallel function calls. These features allow the concise description of parallel algorithms on irregular data structures, such as sparse matrices and graphs. In addition, they maintain the advantages of data-parallel languages: a simple programming model and portability. The current NESL implementation is based on an intermediate language called VCODE and a library of vector routines called CVL. It runs on the Connection Machines CM-2 and CM-5, the Cray C90, and serial workstations. We compare initial benchmark results of NESL with those of machine-specific code on these machines for three algorithms: least-squares line-fitting, median finding, and a sparse-matrix vector product. These results show that NESL's performance is competitive with that of machine-specific code for regular dense data, and is often superior for irregular data. DTIC

N94-19948 Carnegie-Mellon Univ., Pittsburgh, PA. School of Computer Science.
SET BASED ANALYSIS OF ML PROGRAMS
Nevin Heintze Jul. 1993 21 p Limited Reproducibility: More than 20% of this document may be affected by microfiche quality
(Contract F19628-91-C-0168; ARPA Order 8313)
(AD-A270597; CMU-CS-93-193) Avail: CASI HC A03

Reasoning about a program by treating program variables as sets of values leads to a simple, accurate, and intuitively appealing notion of program approximation. This paper presents such an approach for the

compile-time analysis of ML programs. To develop the core ideas of the analysis, we consider a simple untyped call-by-value functional language. Starting with an operational semantics for the language, we develop an approximate set based operational semantics which formalizes the intuition of treating program variables as sets. The key result of the paper is an O(n3) algorithm for computing the set based approximation of a program. We then show how the analysis can be extended in a natural way to deal with arrays, arithmetic, exceptions, and continuations. We also briefly describe results from an implementation of this analysis for ML programs. DTIC

N94-19959# Pacific Northwest Lab., Richland, WA.
GLOBAL COMBINE ON MESH ARCHITECTURES WITH WORMHOLE ROUTING
M. Barnett, R. Littlefield, D. G. Payne, and R. vandeGeijn Apr. 1993 8 p Presented at the 7th International Parallel Processing Symposium, Newport Beach, CA, 13-16 Apr. 1993
(Contract DE-AC06-76RL-01830)
(DE93-018792; PNL-SA-22002; CONF-9304200-1) Avail: CASI HC A02/MF A01

Several algorithms are discussed for implementing global combine (summation) on distributed memory computers using a two-dimensional mesh interconnect with wormhole routing. These include algorithms that are asymptotically optimal for short vectors (O(log(p)) for p processing nodes) and for long vectors (O(n) for n data elements per node), as well as hybrid algorithms that are superior for intermediate n. Performance models are developed that include the effects of link conflicts and other characteristics of the underlying communication system. The models are validated using experimental data from the Intel Touchstone DELTA computer. Each of the combine algorithms is shown to be superior under some circumstances. DOE

N94-19969 Air Force Inst. of Tech., Wright-Patterson AFB, OH. School of Engineering.
COMPARISON OF A DISTRIBUTED KALMAN FILTER VERSUS A CENTRALIZED KALMAN FILTER WITH FAULT DETECTION CONSIDERATIONS M.S. Thesis
Paul J. Lawrence, Jr. 30 Jul. 1993 280 p Limited Reproducibility: More than 20% of this document may be affected by microfiche quality
(AD-A270713; AFIT/GE/Eng/93S-06) Avail: Issuing Activity (Defense Technical Information Center (DTIC))

This project examined the results obtained by simulating an aircraft navigation system with a partial complement of a typical avionics sensor array. Two different techniques of estimation processes were utilized and compared: the conventional Kalman and the federated filter architectures. Areas of interest include error state estimation accuracy and overall performance, residual behavior under normal and induced sensor failure conditions, and potential for failure detection and isolation. Several simulations were accomplished for each filter design and the results were compared in order to verify the validity of the newly developed federated filter architecture. Comparison of the error state estimation accuracies of the two filter designs revealed excellent overall performances for both. The identification of failures showed a definite advantage in the federated filter design. Having sensor-dedicated local filters allowed for easy sensor failure identification for the federated filter, while the centralized filter design suffered from navigation solution corruption under the same circumstances. Once established as a valuable estimation technique, the federated filter will add significantly to the viable alternatives when choosing a particular filter architecture for current avionics modifications or future avionics implementations. DTIC

N94-19992 Technische Univ., Eindhoven (Netherlands). Dept. of Mathematics and Computing Science.
INTERVAL TIMED COLOURED PETRI NETS AND THEIR ANALYSIS
W. M. P. vanderAalst 1992 29 p See also PB92-200641 Limited Reproducibility: More than 20% of this document may be affected by microfiche quality
(PB93-191732; COMPUTING SCIENCE NOTES-92/17) Copyright Avail: Issuing Activity (National Technical Information Service (NTIS))

The paper presents the Interval Timed Colored Petri Net (ITCPN) model. An interval timed colored Petri net is a colored Petri net extended with time; time is in tokens, and transitions determine a delay for each produced token. The delay is specified by an upper and lower bound, i.e. an interval. The ITCPN model allows the modelling of the dynamic behavior of large and complex systems, without losing the possibility of formal analysis. In addition to the existing analysis techniques for colored Petri nets, the author proposes a new analysis method to analyze the temporal behavior of the net. This method constructs a reduced reachability graph and exploits the fact that delays are described by an interval. NTIS

N94-19993 Technische Univ., Eindhoven (Netherlands). Dept. of Mathematics and Computing Science.
TOTAL ORDER ASSUMPTION
J. C. M. Baeten 1992 19 p See also N91-25722 and N92-30178 Limited Reproducibility: More than 20% of this document may be affected by microfiche quality
(PB93-191740; COMPUTING SCIENCE NOTES-92/14) Copyright Avail: Issuing Activity (National Technical Information Service (NTIS))

The total order assumption (TOA) is the assumption that all execution sequences of observable actions or events are totally ordered by precedence. As long as in some cases TOA is to the point, total order and partial order semantics are both legitimate but lead to different theories. The author argues that TOA is a simplifying assumption and presents an example of a total order theory without interleaving and a partial order theory with interleaving. NTIS

N94-19994 Technische Univ., Eindhoven (Netherlands). Dept. of Mathematics and Computing Science.
PROGRAM DERIVATION IN ACYCLIC GRAPHS AND RELATED PROBLEMS
J. P. H. W. vandenEijnde 1992 92 p Limited Reproducibility: More than 20% of this document may be affected by microfiche quality
(PB93-191765; COMPUTING SCIENCE NOTES-92/04) Copyright Avail: Issuing Activity (National Technical Information Service (NTIS))

Several derivations of algorithms on acyclic graphs are presented. Acyclic graphs are shown to be important for the solution of a general form of recursive equations and, as such, appear everywhere in the practice of programming. The central problem of the paper concerns the computation of a general class of functions on the vertex set of an acyclic graph, defined by a particular form of recursive equation, which is shown to have a unique solution. Solving this problem gives rise to two interesting subproblems: graph inversion; and topological sorting. For these problems, compact derivations of algorithms are presented as well. The central problem is also solved for equations additionally satisfying a certain split property, leading to a more elegant algorithm. Finally, the practical applicability of the theory is demonstrated by means of a number of typical examples satisfying this split property. NTIS

N94-20020# Technische Univ., Berlin (Germany). Inst. fuer Angewandte Informatik.
EFFICIENT AND CORRECT TRANSLATION OF STRICT APPLICATIVE PROGRAMMING LANGUAGES Ph.D. Thesis [EFFIZIENTE UND KORREKTE UEBERSETZUNG STRIKTER APPLIKATIVER PROGRAMMIERSPRACHEN]
Wolfram Schulte 1992 119 p In GERMAN
(ETN-93-95056) Avail: CASI HC A06/MF A02

The applicative programming language OPAL is translated into the imperative programming language C; it is investigated whether the dynamic running of strict functional programs on sequential von Neumann machines is necessarily more inefficient than the running of imperative programs. The translation was divided into three parts: the analysis of structure and context conditions of OPAL in the extended lambda calculation was completed with pattern matching and structures parametrization was followed by operations parametrization; in the transformation phase, the code was sequentialized and normalized after functions are unfolded and specialized on the application level; for code production, iterative and linear recursive recursion were depicted on loops. The software was evaluated in terms of robustness, correctness, simplicity, portability, adaptability, and efficiency. The implementation of the translation system for its proper construction shows it is usable for bigger programs too and the integration of software in language C is possible with reduced costs. ESA

N94-20041# Massachusetts Inst. of Tech., Cambridge. Artificial Intelligence Lab.

ROBUST AND EFFICIENT 3D RECOGNITION BY ALIGNMENT

Tao D. Alter Sep. 1992 132 p

(Contracts N00014-85-K-0124; DACA76-85-C-0010)

(AD-A270839; AI-TR-1410) Avail: CASI HC A07/MF A02

Alignment is a prevalent approach for recognizing three-dimensional objects in two-dimensional images. Current implementations handle errors that are inherent in images in ad hoc ways. This thesis shows that these errors can propagate and magnify through the alignment computations, such that the ad hoc approaches may not work. In addition, a technique is given for tightly bounding the propagated error, which can be used to make the recognition robust while still being efficient. Further, the error bounds can be used to formally compute the likelihood that a set of hypothesized matches between model and image features is correct. The technique for bounding the propagated error makes use of a new solution to a fundamental problem in computer recognition, namely, the solution for 3D pose from three corresponding points under weak-perspective projection. The new solution is intended to provide a fast means of computing the error bounds. In deriving the new solution, this thesis gives a geometrical interpretation to the problem, from which the situations are inferred where the solution does not exist and is unstable. DTIC

N94-20049# Los Alamos National Lab., NM.

A WEIGHTED LEAST-SQUARES LUMP CORRECTION ALGORITHM FOR TRANSMISSION-CORRECTED GAMMA RAY NONDESTRUCTIVE ASSAY

T. H. Prettyman, J. K. Sprinkle, Jr., and G. A. Sheppard 1993 10 p Presented at the 34th Annual Meeting of the Institute of Nuclear Materials Management, Scottsdale, AZ, 18-21 Jul. 1993

(Contract W-7405-eng-36)

(DE93-018474; LA-UR-93-2632; CONF-930749-60) Avail: CASI HC A02/MF A01

With transmission-corrected gamma-ray nondestructive assay instruments such as the Segmented Gamma Scanner (SGS) and the Tomographic Gamma Scanner (TGS) that is currently under development at Los Alamos National Laboratory, the amount of gamma-ray emitting material can be underestimated for samples in which the emitting material consists of particles or lumps of highly attenuating material. This problem is encountered in the assay of uranium and plutonium-bearing samples. To correct for this source of bias, the authors have developed a least-squares algorithm that uses transmission-corrected assay results for several emitted energies and a weighting function to account for statistical uncertainties in the assay results. The variation of effective lump size in the fitted model is parameterized; this allows the correction to be performed for a wide range of lump-size distributions. It may be possible to use the reduced chi-squared value obtained in the fit to identify samples in which assay assumptions have been violated. The authors find that the algorithm significantly reduces bias in simulated assays and improves SGS assay results for plutonium-bearing samples. Further testing will be conducted with the TGS, which is expected to be less susceptible than the SGS to systematic source of bias. DOE

N94-20052# Sandia National Labs., Albuquerque, NM.

CTH: A SOFTWARE FAMILY FOR MULTI-DIMENSIONAL SHOCK PHYSICS ANALYSIS

E. S. Hertel, Jr., R. L. Bell, M. G. Elrick, A. V. Farnsworth, G. I. Kerley, J. M. McGlaun, S. V. Petney, S. A. Silling, P. A. Taylor, and L. Yarrington 1992 6 p Presented at the 19th International Symposium on Shock Waves, Marseille, France, 26-30 Jul. 1993

(Contract DE-AC04-76DP-00789)

(DE93-019428; SAND-92-2089C; CONF-930788-3) Avail: CASI HC A02/MF A01

CTH is a family of codes developed at Sandia National Laboratories for modeling complex multi-dimensional, multi-material problems that are characterized by large deformations and/or strong shocks. A two-step, second-order accurate Eulerian solution algorithm is used to solve the mass, momentum, and energy conservation equations. CTH includes models for material strength, fracture, porous materials, and high explosive detonation and initiation. Viscoplastic or rate-dependent models of material strength have been added recently. The formulations of Johnson-Cook, Zerilli-Armstrong, and Steinberg-Guinan-Lund are standard options within CTH. These models rely on using an internal state variable to account for the history dependence of material response. The implementation of internal state variable models is discussed and several sample calculations are presented. Comparison with experimental data is made among the various material strength models. The advancements made in modelling material response have significantly improved the ability of CTH to model complex, large-deformation, plastic-flow dominated phenomena. Detonation of energetic material under shock loading conditions has been of great interest. A recently developed model of reactive burn for high explosives (HE) has been added to CTH. This model along with newly developed tabular equations-of-state for the HE reaction by-products has been compared to one- and two-dimensional explosive detonation experiments. These comparisons indicate excellent agreement of CTH predictions with experimental results. The new reactive burn model coupled with the advances in equation-of-state modeling make it possible to predict multi-dimensional burn phenomena without modifying the model parameters for different dimensionality. Examples of the features of CTH are given. The simulations shown are compared with well characterized experiments covering key phenomena of shock physics. DOE

N94-20067# Rochester Univ., NY. Dept. of Computer Science.

A COMPUTATIONAL THEORY OF LEXICAL RELATEDNESS

Marc Light Feb. 1993 42 p

(Grant NSF IRI-90-13160)

(TR-421) Avail: CASI HC A03/MF A01

Lexicon coverage is often the limiting factor in natural language processing (NLP) systems. Recent work has attempted to remedy this situation by extracting information from machine readable dictionaries. Unfortunately, no NLP lexicon system or dictionary could possibly list all the potential words of English. However, humans are often able to interpret novel word forms (that is, words they have not seen before) without difficulty. One way we do this, if the word is complex (e.g. undecidability), is by using cues from the internal structure of the word. Relations in phonological form often correspond to relations in meaning. For example, if someone knows what the verb open means, a number of educated guesses can be made about the meaning of reopen. Exceptions abound in lexical data and any system that attempts to use lexical generalizations must be able to handle exceptions in a principled fashion. I describe the preliminary design of a system that uses relations in form to derive relations in meaning. For a new word, the system will produce meaning postulates that represent an educated guess about the meaning of the new word. These meaning postulates are written in Episodic Logic and the entire system will be a module of the TRAINS system. Author (revised)

N94-20091 Naval Postgraduate School, Monterey, CA. Dept. of Computer Science.

A SOFTWARE ARCHITECTURE FOR THE CONSTRUCTION AND MANAGEMENT OF REAL-TIME VIRTUAL WORLDS Ph.D. Thesis

David R. Pratt Jun. 1993 158 p Limited Reproducibility: More than 20% of this document may be affected by microfiche quality

(AD-A271465) Avail: CASI HC A08

As military budgets shrink, the Department of Defense (DoD) is turning to virtual worlds (VW) to solve problems and address issues that were previously solved by prototype or field exercises. However, there is a critical void of experience in the community on how to build VW systems. The Naval Postgraduate School's Network Vehicle Simulator (NPSNEI) was designed and built to address this need. NPSNET is a populated, networked, interactive, flexible, three dimensional (3D) virtual world system. This dissertation covers the construction and management of the VW in NPSNET. The system, which uses both standard and non-standard network message formats, is fully networked allowing multiple users to interact simultaneously in the VW. Commercial off the shelf (COTS), Silicon Graphics Incorporated (SGI) workstations hardware was used exclusively in NPSNET to ensure the usefulness and the portability of the system to many DoD commands. The core software architecture presented here is suitable for any VW. DTIC

N94-20097# California Univ., Berkeley. Lawrence Berkeley Lab.

QUALIFYING CODES UNDER SOFTWARE QUALITY ASSURANCE: TWO EXAMPLES AS GUIDELINES FOR CODES THAT ARE EXISTING OR UNDER DEVELOPMENT

D. Mangold May 1993 41 p
(Contract DE-AC03-76SF-00098)
(DE93-040452; LBL-34423) Avail: CASI HC A03/MF A01

Software quality assurance is an area of concern for DOE, EPA, and other agencies due to the poor quality of software and its documentation they have received in the past. This report briefly summarizes the software development concepts and terminology increasingly employed by these agencies and provides a workable approach to scientific programming under the new requirements. Following this is a practical description of how to qualify a simulation code, based on a software QA plan that has been reviewed and officially accepted by DOE/OCRWM. Two codes have recently been baselined and qualified, so that they can be officially used for QA level 1 work under the DOE/OCRWM QA requirements. One of them was baselined and qualified within one week. The first of the codes was the multi-phase multi-component flow code, TOUGH version 1, an already existing code, and the other was a geochemistry transport code, STATEQ, that was under development. The way to accomplish qualification for both types of codes is summarized in an easy-to-follow step-by-step fashion to illustrate how to baseline and qualify such codes through a relatively painless procedure. DOE

N94-20109 Norfolk State Univ., VA. Dept. of Computer Science.
A COMPREHENSIVE SOFTWARE ENGINEERING EDUCATIONAL EXPERIENCE
George C. Harrison 15 Aug. 1993 11 p Limited Reproducibility: More than 20% of this document may be affected by microfiche quality
(Contract MDA972-92-J-1024)
(AD-A270583) Avail: CASI HC A03

The original plan of the project outlined in the proposal in Aug. of 1991 was to experiment with possible solutions to the problems of offering a comprehensive software engineering course to undergraduates. The target student was assumed to be a junior computer science major with programming experience in Pascal through our CSC 260 (Computer Programming II) course. This course is analagous to the ACM designated CS2 course. Some of the problems with software engineering education to undergraduates were identified to be: (1) The inability to complete quality documents (user's manuals, requirements specifications, and detailed design) and implement the project during one 14 week semester; (2) Since the ARPA call for proposals included an Ada education component, I felt that it was impossible to have students without an Ada background to complete the implementation of the software engineering project; and (3) The lack of undergraduate experience in the use of CASE tools. DTIC

N94-20143# Rochester Univ., NY. Dept. of Computer Science.
MINT TUTORIAL AND USER MANUAL
Jack E. Veenstra May 1993 39 p
(Grant NSF CDA-88-22724)
(TR-452) Avail: CASI HC A03/MF A01

Mint, a MIPS code interpreter for parallel programs, is described. Mint generates memory reference traces that can be used to drive simulations of multiprocessor systems. Mint executes in a single address space and interprets MIPS R3000 object code programs. For faster interpretation, blocks of straight-line code in the object program are executed natively by creating functions at run-time. Unlike other memory tracers that compile the memory tracing calls into the simulated program, Mint does not require recompiling the simulated program. Interpreting the object program has the advantage that no source is needed, the simulator is independent of the object program, and a total program trace, including library references, is easily generated. Mint is a fast interpreter. When generating events for every memory reference, the overhead of Mint typically slows down a simulated program by a factor of 20 to 70 compared to its native execution time. Author (revised)

N94-20149*# Johnson Controls World Services, Cape Canaveral, FL.
DATA MANAGEMENT FOR SUPPORT OF THE OREGON TRANSECT ECOSYSTEM RESEARCH (OTTER) PROJECT
J. W. Skiles and Gary L. Angelici (Sterling Software, Inc., Palo Alto, CA.) Nov. 1993 48 p
(Contract NAS2-13712)
(NASA-CR-4557; A-94020; NAS 1.26:4557) Avail: CASI HC A03/MF A01

Management of data collected during projects that involve large numbers of scientists is an often overlooked aspect of the experimental plan. Ecosystem science projects like the Oregon Transect Ecosystem Research (OTTER) Project that involve many investigators from many institutions and that run for multiple years, collect and archive large amounts of data. These data range in size from a few kilobytes of information for such measurements as canopy chemistry and meteorological variables, to hundreds of megabytes of information for such items as views from multi-band spectrometers flown on aircraft and scenes from imaging radiometers aboard satellites. Organizing and storing data from the OTTER Project, certifying those data, correcting errors in data sets, validating the data, and distributing those data to other OTTER investigators is a major undertaking. Using the National Aeronautics and Space Administration's (NASA) Pilot Land Data System (PLDS), a Support mechanism was established for the OTTER Project which accomplished all of the above. At the onset of the interaction between PLDS and OTTER, it was not certain that PLDS could accomplish these tasks in a manner that would aid researchers in the OTTER Project. This paper documents the data types that were collected under the auspices of the OTTER Project and the procedures implemented to store, catalog, validate, and certify those data. The issues of the compliance of investigators with data-management requirements, data use and certification, and the ease of retrieving data are discussed. We advance the hypothesis that formal data management is necessary in ecological investigations involving multiple investigators using many data gathering instruments and experimental procedures. The issues and experience gained in this exercise give an indication of the needs for data management systems that must be addressed in the coming decades when other large data-gathering endeavors are undertaken by the ecological science community. Author

N94-20164# Grenoble-1 Univ. (France). Lab. ARTEMIS.
PREVAIL-DM: A FRAMEWORK-BASED ENVIRONMENT FOR FORMAL HARDWARE VERIFICATION
Flavio Rech Wagner Jul. 1992 32 p
(RR-899; ETN-93-94989) Avail: CASI HC A03/MF A01

The framework based PREVAIL-DM design environment for formal hardware verification is described. PREVAIL-DM integrates proof tools that are available in the PREVAIL environment around a common, Very Hardware Description Language (VHDL) based conceptual schema. Tools are encapsulated according to a black box approach. Design data are stored in a unique data base, and the environment offers a common main user interface, which gives access to design tools and methods and allows browsing through the database objects. Available methods to be applied on the design objects are oriented to the application semantics, thus helping to maintain all desired schema related integrity constraints. PREVAIL-DM is implemented upon the Cadlab framework and uses most of its main features. ESA

N94-20201# Grenoble-1 Univ. (France). Modelling and Computing Lab.
FAST SCALAR ALGORITHMS FOR MULTIVARIATE PARTIAL CORRELATIONS AND THEIR EMPIRICAL COUNTERPARTS
Dinh Tuan Pham Oct. 1992 27 p
(RR-903-M; ETN-93-94994) Avail: CASI HC A03/MF A01

Algorithms for computing the triangular partial correlation matrices and the scalar partial autocorrelation coefficients and their empirical counterparts, as well as for the conversion between the two types of partial correlations, are derived. Although these algorithms deal with multivariate time series, they work with scalars and vectors, avoiding any matrix operation, and hence are quite efficient computationally. ESA

N94-20228*# Information Science Inst., Marina del Rey, CA. Dept. of Contracts and Grants.
DISTRIBUTED VIRTUAL SYSTEM (DIVIRS) PROJECT Semiannual Progress Report No. 11
Herbert Schorr and B. Clifford Neuman Nov. 1993 23 p
(Contract NCC2-539)
(NASA-CR-194360; NAS 1.26:194360) Avail: CASI HC A03/MF A01

As outlined in the continuation proposal 92-ISI-50R (revised) on NASA cooperative agreement NCC 2-539, the investigators are developing software, including a system manager and a job manager, that will manage available resources and that will enable programmers to develop and execute parallel applications in terms of a virtual configuration of processors, hiding the mapping to physical nodes; developing communications routines that support

the abstractions implemented; continuing the development of file and information systems based on the Virtual System Model; and incorporating appropriate security measures to allow the mechanisms developed to be used on an open network. The goal throughout the work is to provide a uniform model that can be applied to both parallel and distributed systems. The authors believe that multiprocessor systems should exist in the context of distributed systems, allowing them to be more easily shared by those that need them. The work provides the mechanisms through which nodes on multiprocessors are allocated to jobs running within the distributed system and the mechanisms through which files needed by those jobs can be located and accessed. Author (revised)

N94-20276# Los Alamos National Lab., NM.
APPLYING THE INN MODEL TO THE MaxClique
T. Grossman 1993 13 p Presented at the 2nd Dimacs Challenge Conference, New Brunswick, NJ, 11-13 Oct. 1993
(Contract W-7405-eng-36)
(DE93-040137; LA-UR-93-3082; CONF-9310154-1) Avail: CASI HC A03/MF A01

Max-Clique is the problem of finding the largest clique in a given graph. It is not only NP-hard, but, as recent results suggest, even hard to approximate. Nevertheless, it is still very important to develop and test practical algorithms that will find approximate solutions for the maximum clique problem on various graphs stemming from numerous applications. Indeed, many different types of algorithmic approaches are applied to that problem. Several neural networks and related algorithms were applied recently to combinatorial optimization problems in general and to the Max-Clique problem in particular. These neural nets are dynamical system which minimize a cost (or computational 'energy') function that represents the optimization problem, the Max-Clique in our case. Therefore, they all belong to the class of integer programming algorithms surveyed in the Pardalos and Xue review. The work presented here is a development and improvement of a neural network algorithm that was introduced recently. In the previous work, we have considered two Hopfield type neural networks, the INN and the HcN, and their application to the Max-Clique problem. In this paper, I concentrate on the INN network and present an improved version of the t-A algorithm that was introduced in. The rest of this paper is organized as follows. In section 2, I describe the INN model and how it implements a given graph. In section 3, it is characterized in terms of graph theory. In particular, the stable states of the network are mapped to the maximal cliques of its underling graph. In section 4, I present the t-Annealing algorithm and an improved version of it, the Adaptive t-Annealing. Several experiments done with these algorithms on benchmark graphs are reported in section 5, and the efficiency of the new algorithm is demonstrated. I conclude with a short discussion. DOE

N94-20280# Sandia National Labs., Albuquerque, NM.
OBJECT-ORIENTED DFD MODELS TO PRESENT THE FUNCTIONAL AND BEHAVIORAL VIEWS
A. Maxted Jun. 1993 18 p
(Contract DE-AC04-76DP-00789)
(DE93-040206; SAND-93-0940) Avail: CASI HC A03/MF A01

An object-oriented methodology is presented that is based on two sets of Data Flow Diagrams (DFD's): one for the functional view, and one for the behavioral view. The functional view presents the information flow between shared objects. These objects map to the classes identified in the structural view (e.g., Information Model). The behavioral view presents the flow of information between control components and relates these components to their state models. Components appearing in multiple views provide a bridge between the views. The top-down hierarchical nature of the DFDs provide a needed overview or road map through the software system. DOE

N94-20281# Sandia National Labs., Albuquerque, NM.
A PROPOSAL FOR REVERSE ENGINEERING CASE TOOLS TO SUPPORT NEW SOFTWARE DEVELOPMENT
A. Maxted Jun. 1993 12 p
(Contract DE-AC04-76DP-00789)
(DE93-040207; SAND-93-0941) Avail: CASI HC A03/MF A01

Current CASE technology provides sophisticated diagramming tools to generate a software design. The design, stored internal to the CASE tool, is bridged to the code via code generators. There are several limitations to this technique: (1) the portability of the design is limited to the portability of the CASE tools, and (2) the code generators offer a clumsy link between design and code. The CASE tool, though valuable during design, becomes a hindrance during implementation. Frustration frequently causes the CASE tool to be abandoned during implementation, permanently severing the link between design and code. Current CASE stores the design in a CASE internal structure, from which code is generated. The technique presented herein suggests that CASE tools store the system knowledge directly in code. The CASE support then switches from an emphasis on code generators to employing state-of-the-art reverse engineering techniques for document generation. Graphical and textual descriptions of each software component (e.g., Ada Package) may be generated via reverse engineering techniques from the code. These reverse engineered descriptions can be merged with system over-view diagrams to form a top-level design document. The resulting document can readily reflect changes to the software components by automatically generating new component descriptions for the changed components. The proposed auto documentation technique facilitates the document upgrade task at later stages of development, (e.g., design, implementation and delivery) by using the component code as the source of the component descriptions. The CASE technique presented herein is a unique application of reverse engineering techniques to new software systems. This technique contrasts with more traditional CASE auto code generation techniques. DOE

N94-20311 Allied-Signal Aerospace Cc., Kansas City, MO.
FEATURE-BASED TOLERANCING FOR INTELLIGENT INSPECTION PROCESS DEFINITION
C. W. Brown Jul. 1993 13 p Presented at the Forum on Dimensional Tolerancing and Metrology, Dearborn, MI, 17-19 Jun. 1993 Limited Reproducibility: More than 20% of this document may be affected by microfiche quality
(Contract DE-AC04-76DP-00613)
(DE93-017984; KCP-613-5260; CONF-9306209-1) Avail: Issuing Activity (Department of Energy (DOE))

This paper describes a feature-based tolerancing capability that complements a geometric solid model with an explicit representation of conventional and geometric tolerances. This capability is focused on supporting an intelligent inspection process definition system. The feature-based tolerance model's benefits include advancing complete product definition initiatives (e.g., STEP - standard for exchange of product model data), supplying computer-integrated manufacturing applications (e.g., generative process planning and automated part programming) with product definition information, and assisting in the solution of measurement performance issues. A feature-based tolerance information model is developed based upon the notion of a feature's tolerance aspects and describes an object-oriented scheme for representing and relating tolerance features, tolerances, and datum reference frames. For easy incorporation, the tolerance feature entities are interconnected with STEP solid model entities. This schema will explicitly represent the tolerance specification for mechanical products, support advanced dimensional measurement applications, and assist in tolerance-related methods divergence issues. DOE

N94-20316 Lawrence Livermore National Lab., CA.
THREE-DIMENSIONAL DYNAMIC THERMAL IMAGING OF STRUCTURAL FLAWS BY DUAL-BAND INFRARED COMPUTED TOMOGRAPHY
N. K. DelGrande, K. W. Dolan, P. F. Durbin, M. R. Gorvad, B. T. Kornblum, D. E. Perkins, D. J. Schneberk, and A. B. Shapiro Apr. 1993 12 p Presented at the Society of Photo-Optical Instrumentation Engineers (SPIE) OE/Aerospace Science and Sensing Meeting, Orlando, FL, 11-16 Apr. 1993 Limited Reproducibility: More than 20% of this document may be affected by microfiche quality
(Contract W-7405-eng-48)
(DE93-019575; UCRL-JC-113744; CONF-930445-23) Avail: CASI HC A03

This paper discusses three-dimensional (3D) dynamic thermal imaging of structural flaws using dual-band infrared (DBIR) computed tomography. Conventional thermography provides single-band infrared images which are difficult to interpret. Standard procedures yield imprecise (or qualitative) information about sub-surface flaw sites which are typically masked by surface clutter. The authors use a DBIR imaging technique pioneered at

LLNL to capture the time history of surface temperature difference for flash-heated targets. They relate these patterns to the location, size, shape, and depth of subsurface flaws. The authors demonstrate temperature accuracies of 0.2 C, timing synchronizations of 3 ms (after onset of heat flash), and intervals of 42 ms, between images, during an 8 s cooling (and heating) interval characterizing the front (and back) surface temperature-time history of an epoxy-glue disbond site in a flash-heated aluminum lap joint. This type of disbond played a significant role in causing damage to the Aloha Aircraft fuselage on the aged Boeing 737 jetliner. By ratioing DBIR images (near 5 and 10 micron), the authors located surface temperature patterns (generated by weak heat flow anomalies at subsurface flaw sites) and removed the emissivity mask (from surface roughness variations). They compared measurements with calculations from the three-dimensional, finite element computer code TOPAZ3D. They combined infrared, ultrasound, and x-ray imaging methods to characterize the lap joint disbond site spatial, bond quality, and material differences. DOE

N94-20376*# Research Inst. for Computing and Information Systems, Houston, TX.
RESEARCH IN IMAGE MANAGEMENT AND ACCESS Report No. 3, 1 Apr. 1992 - 31 Mar. 1993
Raymond F. Vondran (University of North Texas, Denton.) and Billy J. Barron (University of North Texas, Denton.) 1993 155 p
(Contract NCC9-16; RICIS Proj. IR-02)
(NASA-CR-194797; NAS 1.26:194797) Avail: CASI HC A08/MF A02

Presently, the problem of over-all library system design has been compounded by the accretion of both function and structure to a basic framework of requirements. While more device power has led to increased functionality, opportunities for reducing system complexity at the user interface level have not always been pursued with equal zeal. The purpose of this book is therefore to set forth and examine these opportunities, within the general framework of human factors research in man-machine interfaces. Human factors may be viewed as a series of trade-off decisions among four polarized objectives: machine resources and user specifications; functionality and user requirements. In the past, a limiting factor was the availability of systems. However, in the last two years, over one hundred libraries supported by many different software configurations have been added to the Internet. This document includes a statistical analysis of human responses to five Internet library systems by key features, development of the ideal online catalog system, and ideal online catalog systems for libraries and information centers. Derived from text

N94-20492* National Aeronautics and Space Administration. Lyndon B. Johnson Space Center, Houston, TX.
RECONFIGURABLE FUZZY CELL Patent
George A. Salazar, inventor (to NASA) 2 Nov. 1993 32 p Filed 18 Sep. 1991 Supersedes N92-10331 (30 - 1, p 62)
(NASA-Case-MSC-21613-1; US-Patent-5,259,063;
US-Patent-Appl-SN-761566; US-Patent-Class-395-3;
US-Patent-Class-395-61; US-Patent-Class-395-900;
Int-Patent-Class-G06F-9/44; Int-Patent-Class-G05B-13/00) Avail: US Patent and Trademark Office

This invention relates to a reconfigurable fuzzy cell comprising a digital control programmable gain operation amplifier, an analog-to-digital converter, an electrically erasable PROM, and 8-bit counter and comparator, and supporting logic configured to achieve in real-time fuzzy systems high throughput, grade-of-membership or membership-value conversion of multi-input sensor data. The invention provides a flexible multiplexing-capable configuration, implemented entirely in hardware, for effectuating S-, Z-, and PI-membership functions or combinations thereof, based upon fuzzy logic level-set theory. A membership value table storing 'knowledge data' for each of S-, Z-, and PI-functions is contained within a nonvolatile memory for storing bits of membership and parametric information in a plurality of address spaces. Based upon parametric and control signals, analog sensor data is digitized and converted into grade-of-membership data. In situ learn and recognition modes of operation are also provided.
Official Gazette of the U.S. Patent and Trademark Office

N94-20521# Rochester Univ., NY. Dept. of Computer Science.
CLOSURE PROPERTIES OF STOCHASTIC LANGUAGES
Ioan Macarie Jan. 1993 27 p
(Grant NSF IRI-90-03841)
(TR-441) Avail: CASI HC A03/MF A01

The study of probabilistic one-way finite-state automata has been sparsely spread over at least thirty-three years, and across media that are not all readily accessible in the West at the present time. In a uniform setting, we present properties of the classes of languages specifiable by such automata. We present results found in a wide and nonhomogeneous literature together with original results. Along with probabilistic automata, we also study a clean generalized version. The classes of languages accepted by such automata are defined in terms of numerical cutpoints and the functions that these automata compute. Our main results are some closure properties for the classes and functions. We give a technique for proving stochasticity and we apply it in the case of some well known languages. Author

N94-20522# Rochester Univ., NY. Dept. of Computer Science.
EXPLANATION CLOSURE, ACTION CLOSURE, AND THE SANDEWALL TEST SUITE FOR REASONING ABOUT CHANGE
Lenhart K. Schubert Oct. 1992 22 p
(Contracts N00014-82-K-0193; F30602-91-C-0010)
(TR-440) Avail: CASI HC A03/MF A01

Explanation closure (EC) axioms were previously introduced as a means of solving the frame problem. This paper provides a thorough demonstration of the power of EC (combined with action closure) for reasoning about dynamic worlds, by way of Sandewall's recently compiled test suite of 12-or-so problems. The problems range from the 'Yale turkey shoot' (and variants) to the 'stuffy room' problem, and were intended as a test and challenge for nonmonotonic logics of action. The EC/AC-based solutions for the most part do not resort to nonmonotonic reasoning at all, yet fare much better in providing the intuitively warranted inferences than the best known nonmonotonic approaches. While there are good reasons for ultimately employing nonmonotonic or probabilistic logics--e.g., pervasive uncertainty and the qualification problem--this does show that the scope of monotonic methods has been underestimated. Subsidiary purposes of the paper are to clarify the intuitive status of EC axioms in relation to action effect axioms; and to show how EC, previously formulated within the situation calculus, can be applied within the framework of a temporal logic similar to Sandewall's 'discrete fluent logic,' with some gains in clarity. Author

N94-20525 Naval Postgraduate School, Monterey, CA.
A COMPARISON OF SOME OF THE MOST CURRENT METHODS OF IMAGE COMPRESSION M.S. Thesis
Robert T. Kay Jun. 1993 85 p Limited Reproducibility: More than 20% of this document may be affected by microfiche quality
(AD-A271841) Avail: CASI HC A05

In this report, commonly used lossless and lossy image compression algorithms are heuristically presented and then compared in terms of performance. The lossy algorithms, JPEG (Joint Photographic Experts Group) and Fractal compression, are compared in terms of their respective sensitivities between compression ratio and image fidelity. Compression algorithms based on the lossless models of Huffman, Adaptive Huffman, and arithmetic coding are compared in terms of compression ratio and compression/decompression time requirements. High fidelity image reconstructions of JPEG and fractal compressions are also included in the comparison. Results, for the images tested, indicate that if imperceptible losses in fidelity can be tolerated, then among the current versions of the algorithms tested, the JPEG results in higher compression with less process time. DTIC

N94-20536# Rochester Univ., NY. Dept. of Computer Science.
THRESHOLD COMPUTATION AND CRYPTOGRAPHIC SECURITY
Yenjo Han, Lane A. Hemachandra, and Thomas Thierauf (Ulm Univ., Germany.) 12 Nov. 1992 29 p
(Grants NSF CCR-89-57604; NSF CCR-90-57486)
(TR-443) Avail: CASI HC A03/MF A01

Threshold machines are Turing machines whose acceptance is determined by what portion of the machine's computation paths are accepting paths. Probabilistic machines are Turing machines whose acceptance is determined by the probability weight of the machine's accepting computation paths. Simon proved that for unbounded-error polynomial-time machines these two notions yield the same class, PP. Perhaps because Simon's result seemed to collapse the threshold and probabilistic modes of computation, the relationship between threshold and probabilistic computing

for the case of bounded error has remained unexplored. In this paper, we compare the bounded-error probabilistic class BPP with the analogous threshold class, BPP(sub path), and, more generally, we study the structural properties of BPP(sub path). We prove that BPP(sub path) contains both NP(sup BPP) and P(sup NP(log)), and that BPP(sub path) is contained in P(sup summation 2 to p of (log)), BPP(sup NP), and PP. We conclude that, unless the polynomial hierarchy collapses, bounded-error threshold computation is strictly more powerful than bounded-error probabilistic computation. We also formalize the natural notion of secure access to a database: an adversary who watches the queries should gain no information about the input other than perhaps its length. We show, for both BPP and BPP(sub path), that if there is any database for which this formalization of security differs from the security given by oblivious database access, then P not equal to PSPACE. It follows that if any set lacking small circuits can be securely accepted, then P not equal to PSPACE. Author

N94-20622# Carnegie-Mellon Univ., Pittsburgh, PA. Dept. of Computer Science.

STANDARD ML SIGNATURES FOR A PROTOCOL STACK

Edoardo Biagioni, Robert Harper, and Peter Lee Oct. 1993 18 p

(Contract F19628-91-C-0168; ARPA Order 8313)

(AD-A272060; CMU-CS-93-170) Avail: CASI HC A03/MF A01

This paper describes the design of a protocol stack implemented in Standard ML. Standard ML's signatures are a language construct which can be used to specify or constrain the interface of a module. The design includes both a generic signature which generalizes all the protocol modules, and individual signatures specific to each protocol module. The specific signatures all inherit from the generic signature. The implementation of each protocol is parametrized, so protocols can be composed into custom protocol stacks. The parameter to each protocol is constrained only by the generic signature, and this lets any protocol instance satisfying a specific signature be used as the parameter to any other protocol. As a result, the design and implementation are highly modular, and syntactic compatibility between modules is checked by the compiler. To provide some context for the discussion of the signatures, some of the details of the implementation are also presented. DTIC

N94-20917# General Accounting Office, Washington, DC. National Security and International Affairs Div.

TEST AND EVALUATION: DOD HAS BEEN SLOW IN IMPROVING TESTING OF SOFTWARE-INTENSIVE SYSTEMS

Sep. 1993 57 p

(AD-A271541; GAO/NSIAD-93-198) Avail: CASI HC A04/MF A01

Department of Defense (DoD) software cost total over $30 billion a year (estimated to be $42 billion by 1995), of which about two-thirds is for maintaining upgrading and modifying operational systems already in production. Today's major defense systems depend largely on the quality of this complex and increasingly costly software. In fact, many major weapon systems cannot operate if the software fails to function as required. Because software errors can cause a system to fail, possibly with life-threatening consequences, software-intensive systems need to be thoroughly tested before production. Since the early 1970's, GAO has reported problems in operational test and evaluation of defense acquisition programs. Senior DoD officials, as well as members of the Congress, are concerned that many of these problems continue today, particularly in software-intensive systems. Because of these concerns, GAO initiated this review to identify (1) the extent that software-related problems affect the performance of defense acquisition programs during operational test and evaluation, (2) pervasive barriers in the acquisition process that limit the effectiveness of the test and evaluation of software-intensive systems, and (3) DoD's effort to resolve software test and evaluation problems. Although GAO recognizes that inherently complex technical characteristics contribute to software problems, this report focuses more directly on nontechnical barriers that limit the effectiveness of operational test and evaluation and need management attention. DTIC

N94-20929 Massachusetts Inst. of Tech., Cambridge. Artificial Intelligence Lab.

CAUSAL RECONSTRUCTION

Gary C. Brochardt Feb. 1993 63 p Limited Reproducibility: More than 20% of this document may be affected by microfiche quality

(Contract N00014-91-J-4038)

(AD-A271692; AIM-1403) Avail: CASI HC A04

Causal reconstruction is the task of reading a written causal description of a physical behavior, forming an internal model of the described activity, and demonstrating comprehension through question answering. This task is difficult because written descriptions often do not specify exactly how referenced events fit together. This article characterizes the causal reconstruction problem; presents a representation called transition space, which portrays events in terms of transitions, or collections of changes expressible in everyday language; and describes a program called PATHFINDER, which uses the transition space representation to perform casual reconstruction on simplified English descriptions of physical activity. PATHFINDER works by identifying partial matches between the representations of events and using these matches to form causal chains, fill causal gaps, and merge overlapping accounts of activity. By applying transformations to events prior to matching, PATHFINDER is also able to handle a range of discontinuities arising from a writer's use of analogy or abstraction. DTIC

N94-20932# Oak Ridge National Lab., TN.

MEASURING THE EFFECTS OF THREAD PLACEMENT ON THE KENDALL SQUARE KSR1

T. D. Wagner, E. Smirni, A. W. Apon, M. Madhukar, and L. W. Dowdy Aug. 1993 29 p

(Contract DE-AC05-84OR-21400)

(DE93-040655; ORNL/TM-12462) Avail: CASI HC A03/MF A01

This paper describes a measurement study of the effects of thread placement on memory access times on the Kendall Square multiprocessor, the KSR1. The KSR1 uses a conventional shared memory programming model in a distributed memory architecture. The architecture is based on a ring of rings of 64-bit superscalar microprocessors. The KSR1 has a Cache-Only Memory Architecture (COMA). Memory consists of the local cache memories attached to each processor. Whenever an address is accessed, the data item is automatically copied to the local cache memory module, so that access times for subsequent references will be minimal. Experiments run on the KSR1 across a wide variety of thread configurations show that shared memory access is accelerated through strategic placement of threads which share data. The results indicate strategies for improving the performance of applications programs and illustrate that KSR1 memory access times can remain nearly constant even when the number of participating threads increases. DOE

N94-21020 Technische Hochschule, Darmstadt (Germany). Fachbereich Informatik.

AIDA: A GRAPHICAL INTERACTIVE SYSTEM, ADAPTED TO THE USER Ph.D. Thesis [AIDA: EIN AN DEN BENUTZER ANGEPASSTES GRAPHISCH-INTERAKTIVES SYSTEM]

Jairo Antonio CoteMunoz 1990 272 p In GERMAN Limited Reproducibility: More than 20% of this document may be affected by microfiche quality

(ETN-93-93792) Avail: CASI HC A12

The possibilities of improving man machine communication in a graphical interactive system are depicted with focus on the user support. The advantages of methods and technologies of artificial intelligence in such systems are examined. A tool for generation of user interfaces is presented: SIEMCAD is a user interface management system for integrating electronic and mechanical computer aided design. Models for better user support are presented: it was established, that user knowledge is an important influence factor on the mental user model. The AIDA model was developed with the theory of cognitive complexity, which takes into account user knowledge about technical graphics, computer graphics, and computer aided design systems. The AIDA model was examined from the point of view of tasks, semantics, and syntax. Strategies for the behavior of an adaptive system are presented. Architecture and implementation of AIDA are depicted. ESA

N94-21024 Center for Mathematics and Computer Science, Amsterdam (Netherlands). Dept. of Computer Science.

OPTIMAL SORTING IN LINEAR ARRAYS WITH MINIMUM GLOBAL CONTROL

Ferri Abolhassan (Saarland Univ., Saarbrucken, Germany.), Joerg Keller, and Dieter Scheerer (Saarland Univ., Saarbrucken, Germany.) Nov. 1992

9 p Sponsored in part by DFG Limited Reproducibility: More than 20% of this document may be affected by microfiche quality
(Contract NF-62-376)
(CWI-CS-R9244; ETN-94-94724) Copyright Avail: CASI HC A02

Linear sorting arrays with a single global control wire are investigated. The lower bound on the necessary time to sort n numbers in such an array is shown to be 2n, in contrast to 3n in arrays without global control. A two phase sorting algorithm for arrays with a global control wire that matches the time bound of 2n is presented. As 2n is a lower bound for sorting arrays with sequential input and output, this implies that further global control cannot lead to any improvements as long as sequential input/output is assumed. The algorithm needs an array of minimum length (n/2). The scheme can be easily extended to eliminate duplicate numbers. One possible application of the algorithm is in packet routing for algorithms that need presorted inputs. ESA

N94-21025# Center for Mathematics and Computer Science, Amsterdam (Netherlands). Dept. of Computer Science.
PROVING RUN-TIME PROPERTIES OF GENERAL PROGRAMS W.R.T. CONSTRUCTIVE NEGATION
Elena Marchiori Nov. 1992 31 p Sponsored in part by EEC
(CWI-CS-R9245; ETN-94-94725) Copyright Avail: CASI HC A03/MF A01

Run time properties of general programs with relation to constructive negation, that is, termination and properties of the form of the arguments of the literals selected during the execution, are studied. SLD-CNF resolution, resolution with constructive negation and arbitrary selection rule, and LD-CNF resolution, resolution with constructive negation and PROLOG selection rule, are considered. The class of programs which terminate for all ground goals for arbitrary (respectively, PROLOG) selection rule is shown to coincide with the so called acyclic (respectively, acceptable) programs, and SLD-CNF (respectively, LD-CNF) resolution is shown to be sound and complete with relation to Clark's semantics for bounded goals and acyclic (respectively, acceptable) programs. These results are applied to the study of run time properties of general programs: two proof methods are introduced and their soundness is proven with relation to SLD-CNF and LD-CNF resolution. ESA

N94-21026# Center for Mathematics and Computer Science, Amsterdam (Netherlands). Dept. of Computer Science.
A DECLARATIVE APPROACH FOR FIRST-ORDER BUILT-IN'S OF PROLOG
Krysztof R. Apt (Amsterdam Univ., Netherlands.), Elena Marchiori, and Catuscia Palamidessi (Genoa Univ., Italy.) Nov. 1992 48 p Sponsored in part by EEC
(Grant CNR-89.00036.69)
(CWI-CS-R9246; ETN-94-94726) Copyright Avail: CASI HC A03/MF A01

A framework for studying PROLOG programs with various 'built-ins' that include arithmetic operations, and such metalogical relations like 'var' and 'ground' is presented. To this end, a declarative semantics is proposed and completeness of the PROLOG computation mechanism with relation to this semantics is proved. This semantics is shown to be fully abstract in an appropriate sense. A method for proving termination of PROLOG programs with 'built-ins' which uses these semantics is provided. The method is shown to be modular and is illustrated by proving termination of a number of programs including the unify program of Sterling and Shapiro. ESA

N94-21028 Center for Mathematics and Computer Science, Amsterdam (Netherlands). Dept. of Computer Science.
EFFICIENT COMPARISON BASED STRING MATCHING
Dany Breslauer and Zvi Galil (Columbia Univ., New York, NY.) Dec. 1992 22 p Limited Reproducibility: More than 20% of this document may be affected by microfiche quality
(Grants NSF CCR-90-14605; CDA-90-24735)
(CWI-CS-R9249; ETN-94-94729) Copyright Avail: CASI HC A03

The exact number of symbol comparisons that are required to solve the string matching problem is studied and a family of efficient algorithms is presented. Unlike previous string matching algorithms, the algorithms in this family do not 'forget' results of comparisons, which makes their analysis much simpler. In particular, a linear time algorithm that finds all occurrences of a pattern of length m in a text of length n in $n + (((4 \log m + 2)/m)(n - m))$ comparisons is given. The pattern preprocessing takes linear time and makes at most 2m comparisons. This algorithm establishes that, in general, searching for a long pattern is easier than searching for a short one. It is shown that any algorithm in the family of the algorithms presented must make at least $n + ((\log m)((n - m)/m))$ symbol comparisons, for m 2 to the kth power - 1 and any integer k greater than or equal to 1. ESA

N94-21034# George Mason Univ., Fairfax, VA.
REPLICA CONTROL ALGORITHMS IN DISTRIBUTED DATABASES Final Report, 17 Jan. 1990 - 16 Jan. 1993
Sushil Jajodia Jul. 1993 3 p
(Grant AF-AFOSR-0135-90)
(AD-A271571; AFOSR-93-0787TR) Avail: CASI HC A01/MF A01

The effects of commutative transactions on distributed database performance was analyzed. The benefits were found to be insignificant unless the number of transactions was large. Two distributed algorithms for adaptive replication of data were developed, one which optimizes the communication cost objective function, and a second which optimizes communication time. A dynamic replication control algorithm was studied and showed improved performance over dynamic noting schemes. Concepts for using replicated data in multilevel secure databases showned the ability to guarantee one-copy serial ability using a small amount of trusted code. There were 14 articles published under this grant. DTIC

N94-21038# Naval Postgraduate School, Monterey, CA.
MULTIGRID APPROACH TO SOLVING THE LONG TRANSPORTATION PROBLEM ON A REGULAR GRID IN COST SPACE M.S. Thesis
Annette P. Cornett Jun. 1993 101 p
(AD-A272323) Avail: CASI HC A06/MF A02

Multigrid methods were developed to solve partial differential equations. Research has shown that these methods are applicable to a broader range of problems. This thesis investigates the application of multigrid techniques to minimal cost flow problems, specifically the long transportation problem. This research shows that multigrid techniques can be successfully applied to large-scale long transportation problems posed on a three-dimensional, regular grid in cost space. A V-cycle algorithm is developed for the long transportation problem. Analogies to the multigrid components of restriction, interpolation, and relaxation are detailed. Performance of the algorithm is discussed, and computational cost is analyzed. Future research is likely to include the development of more sophisticated restriction and interpolation schemes to provide integer-valued flows, and the development of a method to map an irregularly spaced problem to a regular grid, and to map the regular grid solution back to the original problem domain. DTIC

N94-21045 Universiteit Twente, Enschede (Netherlands). Tele-Informatics and Open Systems Group.
A SEMI-MARKOV MODEL OF A HOME NETWORK ACCESS PROTOCOL
Joost-Pieter Katoen 1992 10 p Sponsored by EEC Limited Reproducibility: More than 20% of this document may be affected by microfiche quality
(Memo-INF-92-71; TIOS-92/29; ETN-93-94113) Copyright Avail: CASI HC A02

Home networks provide a means for interconnecting consumer products in home environments. The performance characteristics of the medium access protocol (a slotted persistent CSMA/CD (Carrier Sense Multiple Access with Collision Detection) protocol) of a twisted pair home network are investigated. Using a dedicated semi Markov model throughput results are obtained by analyzing an overload situation. ESA

N94-21061 Nijmegen Univ. (Netherlands). Dept. of Informatics.
GWB: MANUAL FOR THE GRAMMAR WORKBENCH VERSION 1.5
C. Dekkers, C. H. A. Koster, M.-J. Nederhof, and A. vanZwol Jul. 1992 19 p Limited Reproducibility: More than 20% of this document may be affected by microfiche quality
(TR-92-14; ETN-93-93868) Avail: CASI HC A03

The manual of the Grammar Work Bench (GWB), an environment for the comfortable development of Affix Grammars in the AGFL formalism, is presented. Its purposes are to: allow the user to input, inspect and modify a grammar; perform consistency checks on a grammar; compute grammar

properties; generate example sentences; assist in performing grammar transformations. The GWB is not a computer game. Its user interface is not supposed to be self explanatory, but the user is supposed to have read this manual. In particular, the user is supposed to know the commands. The GWB was developed for use in the Natural Language Front End (NLFE) project, aimed at the construction of comprehensive and well validated grammars and efficient parsers for a number of European languages. ESA

N94-21062 Nijmegen Univ. (Netherlands). Dept. of Informatics.
A SIMPLIFIED TOKEN BUS PROTOCOL SPECIFIED USING LOTOS
Luc Rooijakkers and Mieke Massink Jan. 1991 124 p Limited Reproducibility: More than 20% of this document may be affected by microfiche quality
(TR-92-15; ETN-93-93869) Avail: CASI HC A06

The use of the formal description technique LOTOS (Language Of Temporal Ordering Specification) is explored to specify a token bus protocol which serves as a non-trivial specification problem. The development of four specifications in different styles is described. The specifications were simulated with the SEDOS 'hippo' simulator. Only two out of four specifications (the resource constraint oriented and the resource state oriented) could be proved (strong) bisimulation equivalent although all specifications are correct with respect to the informal specification. To be able to analyze the equivalence of the constraint oriented and the resource constraint oriented specifications, these specifications were annotated with state information and transformed into a specification in a state oriented style. In that form they could more easily be compared with each other and with the original state oriented specifications. This analysis revealed that the resource constraint oriented and the constraint oriented specification have a different deadlock behavior and were only trace equivalent. The same holds for the constraint oriented against the state oriented specification. The state oriented and resource state oriented specifications could not be proved (bisimulation) equivalent due to buffering problems. An evaluation of the use of LOTOS, the different specification styles and the use of the SEDOS 'hippo' simulator are given. ESA

N94-21063 Institut National de Recherche d'Informatique et d'Automatique, Valbonne (France). Programme 5: Traitement du Signal, Automatique et Productique.
COCOLOG: A CONDITIONAL OBSERVER AND CONTROLLER LOGIC FOR FINITE MACHINES
Peter E. Caines (McGill Univ., Montreal, Quebec.) and Suning Wang (Spar Aerospace Ltd., Sainte-Anne-de-Bellevue, Quebec.) Jun. 1992 30 p Limited Reproducibility: More than 20% of this document may be affected by microfiche quality
(Grant NSERC-A1329)
(INRIA-RR-1714; ETN-93-93913) Avail: CASI HC A03

The problem of observation and control for partially observed input-state-output machines is formulated in terms of a tree of first order logical theories. A set of first order languages for the description of the controlled evolution and state estimation of any given machine M is specified; further, conditional control axioms are formulated so that closed loop control actions occur when specified past observation dependent conditions are fulfilled. In particular, conditional control axioms may include commands that steer the system state from a current partially observed state (estimate) to a target state, if such a sequence of controls can be proved to exist. Starting from a general theory of M at the initial constant, observations on the input-output behavior of the system at any later instant are accepted by the system as new axioms; these are then used together with the previously generated theory to generate the current theory. The acronym COCOLOG is used to denote the family of first order Conditional Observer and Controller Logics for any given input-state-output system. A semantics is supplied for each COCOLOG in terms of interpretations of controlled transitions in a tree indexed by the possible sequences in input output observations. Extra-logical rules relating members of the family of theories of a COCOLOG are presented in the form of metalevel axioms and inference rules. Consistency and completeness of the first order theories in a COCOLOG family are established, decidability is obtained using a unique model property and examples of the operation of a COCOLOG logic control system are given. ESA

N94-21078 Center for Mathematics and Computer Science, Amsterdam (Netherlands). Dept. of Numerical Mathematics.
APPROXIMATE METHODS FOR N-COMPONENT SOLUTE TRANSPORT AND ION-EXCHANGE
P. M. C. Thoolen (Amsterdam Univ., Netherlands.) and P. W. Hemker (Amsterdam Univ., Netherlands.) Nov. 1992 20 p Limited Reproducibility: More than 20% of this document may be affected by microfiche quality
(CWI-NM-R9223; ETN-94-94698) Copyright Avail: CASI HC A03

The computation of ion exchange when an ambient groundwater of one uniform composition is displaced by an injection solution of a constant but differing composition is considered. The problem is to sort out the composition change from the initial to the injected compositions. An analytical method for the n dimensional homovalent system was described by Rhee, Aris, and Amundson. Conditions are given under which this method can be used to calculate an approximate solution to the plateau concentrations in the n dimensional heterovalent system. Two algorithms for the three component heterovalent system are derived from Chaberneau. A discretization method is introduced in which the concept of adaptive mesh refinement is applied. Such a method can be used in more complex situations and it still can represent sharp moving fronts. The results for the different approximate computations are compared for a real life problem. ESA

N94-21144# Army Armament Research, Development and Engineering Center, Picatinny Arsenal, NJ. Product Assurance.
THE READINESS GROWTH MODEL: A QUANTITATIVE ANALYSIS OF SOFTWARE RISK Final Report, 1990 - 1993
David R. Castellano, Paul E. Janusz, and Sharyn L. Tolochko Oct. 1993 26 p
(AD-A272383; ARPAD-TR-93003) Avail: CASI HC A03/MF A01

The readiness growth model (RGM) developed in 1990 is a methodology used to quantitatively assess software maturity and, in turn, software readiness for test. It is comprised of data from many low level metrics, and provides a 'bottom line' assessment which managers can use to track software progress throughout the lifecycle. RGM can be used to assess the quality of both the process and the product, can identify problematic areas, and can determine associated risk. All of this information is summarized quickly by means of its graphical output and metric data. RGM has been successfully implemented on various U.S. Army Armament Research, Development and Engineering Center systems, supporting executive software/system readiness and fielding decisions. It has received high level endorsement from the program managers, and the Army and Office of the Secretary of Defense leadership that have applied it to date. DTIC

N94-21152 Technische Univ., Berlin (Germany). Fachbereich Informatik.
DESIGN OF A COMPUTER ASSISTED TOOL FOR OBJECT ORIENTED ACQUISITION, MODELING AND SIMULATION OF KNOWLEDGE STRUCTURE Ph.D. Thesis [KONZEPTION EINES RECHNERGESTUETZTEN WERKZEUGES ZUR OBJEKTORIENTIERTEN ERFASSUNG, MODELLIERUNG UND SIMULATION VON WISSENSSTRUKTUREN]
Joerg Papke 1992 182 p In GERMAN Limited Reproducibility: More than 20% of this document may be affected by microfiche quality
(ETN-93-94183) Avail: CASI HC A09

The computer assisted tool STRUKTOR for object oriented acquisition, modeling, and simulation of knowledge structures is presented. STRUKTOR belongs to a new generation of object oriented knowledge acquisition tools which profit from the advantages and the power of object oriented technology and open a future oriented dimension for knowledge engineering. The tool is a synthesis of the areas of graphic oriented knowledge engineering and object oriented programming. The dimensions of knowledge engineering were examined by the analysis of the individual knowledge acquisition methods, which can be categorized to the conventional systems analysis area as well as to the knowledge-based area. The ideas, concepts, and organization models of object oriented programming are discussed and the relations between knowledge engineering and object-oriented technology are highlighted. The system is presented with emphasis on the description of the features of this tool, the representation of the complex architecture, the components, and the organizationl model, which organizes the use of the components. ESA

N94-21156# Center for Mathematics and Computer Science, Amsterdam (Netherlands). Dept. of Analysis, Algebra and Geometry.
THE ROBINSON-SCHENSTED AND SCHUETZENBERGER ALGORITHMS. PART 1: NEW COMBINATORIAL PROOFS
Marc A. A. vanLeeuwen Dec. 1992 47 p
(CWI-AM-R9208-Pt-1; ETN-0924-2953) Copyright Avail: CASI HC A03/MF A01

A self contained approach to the Robinson-Schensted and Schuetzenberger algorithms is given. The approach includes elementary proofs for many of their combinatorial properties and representations of the algorithms by graphical computations. An analog of the Robinson-Schensted algorithm for the hyper-octahedral groups instead of the symmetric groups and the relations of the algorithms with Schuetzenberger's theory of 'glissements' and the connection between the versions of the Robinson-Schensted algorithm defined by Robinson and Schensted, respectively, are described. ESA

N94-21157# Center for Mathematics and Computer Science, Amsterdam (Netherlands). Dept. of Analysis, Algebra and Geometry.
THE ROBINSON-SCHENSTED AND SCHUETZENBERGER ALGORITHMS. PART 2: GEOMETRIC INTERPRETATIONS
Marc A. A. vanLeeuwen Dec. 1992 23 p Sponsored in part by Schweizerische Nationalfonds, Switzerland
(CWI-AM-R9209-Pt-2; ETN-94-94709) Copyright Avail: CASI HC A03/MF A01

There is a correspondence of Young tableaux to irreducible components of the variety F(sub u) of flags fixed by some unipotent element u a member of GL(sub n) and a correspondence of permutations to relative positions pairs of flags. Using these, Steinberg has given an interpretation of the Robinson-Schensted algorithm; this interpretation is developed and a similar interpretation for the Schuetzenberger algorithm is derived. These interpretations clarify many of the key properties of those algorithms which were treated purely combinatorially in part 1 of the study. Interpretations of the individual insertion and extraction procedures used in the Robinson-Schensted algorithm, and of their transposed variants, are given. The use of these algorithms to obtain explicit information (even if incomplete in general) about the irreducible components of the intersections of unipotent conjugacy classes in GL(sub n) with a Borel subgroup, the so called orbital varieties, is described. ESA

N94-21180# Rochester Univ., NY. Dept. of Computer Science.
CLASSIFICATION IN FEATURE-BASED DEFAULT INHERITANCE HIERARCHIES
Marc Light Nov. 1993 32 p
(Contract N00014-92-J-1512; NSF IRI-90-13160)
(TR-473) Avail: CASI HC A03/MF A01

When one works with a system that utilizes inheritance hierarchies, the following problem often arises. A new object is introduced and it must be integrated into a hierarchy; under which classes in the hierarchy should the new object be positioned? I formalize this problem for feature-based default inheritance hierarchies. Since it turns out to be NP-complete, I present an approximation algorithm for it. I show that this algorithm is efficient and look at some of the possible problematic situations for the algorithm. Although more analysis and experimentation are needed, these preliminary results show that the algorithm warrants such efforts. Author (revised)

N94-21183# Georgia Southwestern Coll., Americus. Div. of Computer and Applied Sciences.
A PRACTICAL SOFTWARE ENGINEERING CURRICULUM: A PILOT STUDY Final Report
Arun P. Gupta, Weibin Zhu, Kimberly R. Brown, and Calvin Ezell 1993 15 p
(Contract MDA972-92-J-1035)
(AD-A272781) Avail: CASI HC A03/MF A01

This project identifies a problem in software engineering instruction and some approaches to overcome it. It is advocated that a software engineer must have at least one formal course in software engineering. Further, a course containing merely the concepts is not sufficient: additional course(s) complementing the formal course are required. A streamlined sequence of courses was developed that would help achieve the goals of software engineering. This report presents the course sequence and the observations for the project. It is hoped that other institutions can benefit from this study. DTIC

N94-21200# Rochester Univ., NY. Dept. of Computer Science.
ADVICE FROM NONADAPTIVE QUERIES TO NP
Yenjo Han and Thomas Thierauf (Ulm Univ., Germany.) Oct. 1993 14 p
(Grants NSF CCR-89-57604; NSF INT-91-16781)
(TR-470) Avail: CASI HC A03/MF A01

Consider the standard model of computation to decide a language that is bounded truth-table reducible to an NP set: on a given input, a polynomial-time Turing machine, called a generator, produces a constant number of queries to the NP oracle; then, a second polynomial-time Turing machine, called an evaluator, given the answers to the queries, determines the membership of the given input. In this paper, we investigate the classes of languages that are decided by bounded truth-table reductions to an NP set in which evaluators do not have full access to the answers to the queries but get only partial information such as the number of queries that are in the oracle set or even just this number modulo some constant. We also investigate the case in which evaluators are nondeterministic. We locate all these classes within levels of the boolean hierarchy, which allows us to compare the complexity of such classes. The result shows the various degrees to which the power of P or NP evaluators are affected as the partial information that the evaluators get from the answers to the queries produced by generators are changed. Author

N94-21203 Maryland Univ., Baltimore.
IMAGE DETECTION USING EDGE EXTRACTION ALGORITHMS Final Report, Sep. 1991 - Aug. 1992
Chein-I Chang Aug. 1993 74 p Limited Reproducibility: More than 20% of this document may be affected by microfiche quality
(Contract DAAA15-91-K-0002)
(AD-A272439) Avail: Issuing Activity (Defense Technical Information Center (DTIC))

Alternative time-domain image detection techniques that do not require statistical models are investigated. Two distinct methods are presented; multistage pulse code modulation (MPCM) and relative entropy-based image thresholding technique. The idea of MPCM is to expand the commonly used Pulse Code Modulation (PCM) to multistage quantization to decompose an image into multiple stages. Each stage represents an image description with different details. By virtue of this decomposition, MPCM can be regarded as a progressive edge detection technique and a top-down gray-level triangle method, respectively. For vapor cloud detection, interest is often in the detection of clouds. Without reconstructing the original image, progressive edge detection extracts edges of objects progressively from the most significant contours to the least important boundaries. The relative entropy-based approach adopts a different philosophy. It utilizes a co-occurrence matrix to efficiently segment objects from the background. It chooses an information theoretic criterion relative entropy as a thresholding technique which turns out to be a better approach than existing entropic thresholding methods in most test images. DTIC

N94-21204 Aberdeen Proving Ground, MD. Edgewood Research Development and Engineering Center.
METHOD FOR DESIGN ROTATION Final Report, Dec. 1991 - Jun. 1992
Ronald B. Crosier Aug. 1993 26 p Limited Reproducibility: More than 20% of this document may be affected by microfiche quality
(AD-A272440; ERDEC-TR-099) Avail: Issuing Activity (Defense Technical Information Center (DTIC))

All rotations of a response surface design can be obtained by making planar rotations in the set of planes defined by every pair of the coordinate axes. Standard multivariate optimization routines may then be used to optimize a criterion for the desirability of a rotation as a function of the set of planar angles. Criteria for the symmetry of the design (such as the same set of factor levels for all factors) and for the size of the design region (changed by rescaling after the rotation) are developed. The hexagon design, the two-factor central composite design, the four-factor complex number design of Hardin and Sloan, and the eight-factor uniform shell design are rotated to obtain a larger region, a symmetric treatment of the factors, or both. DTIC

N94-21205# Carnegie-Mellon Univ., Pittsburgh, PA. Software Engineering Inst.

AN INVESTIGATION INTO THE STATE OF THE PRACTICE OF CASE TOOL INTEGRATION Final Report

Jock Radar, Alan W. Brown, and Ed Morris Aug. 1993 35 p

(Contract F19628-90-C-0003)

(AD-A272441; CMU/SEI-93-TR-15; ESC-TR-93-192) Avail: CASI HC A03/MF A01

In the second half of 1992, a team of the SEI CASE Environments Project conducted a study into the state of the practice with respect to the operational use of integrated Computer-Aided Software Engineering (CASE) tools. After many false starts, a number of examples of large organizations with integrated CASE tools in operational use on software development projects were interviewed. Compared to the state of the art described in much of the literature, what was found might be considered modest. Compared to industry norms, it was quite impressive, representing significant commitment, ingenuity, and significant attention to end user needs. Our observations are detailed and the current state of the practice of CASE tool integration is analyzed. It also speculates on reasons for the modest state of the CASE tools. DTIC

N94-21227# Rochester Univ., NY. Dept. of Computer Science.

FAST MUTUAL EXCLUSION, EVEN WITH CONTENTION Technical Report

Maged M. Michael and Michael L. Scott Jun. 1993 16 p

(Contract N00014-92-J-1801)

(AD-A272947; TR-460) Avail: CASI HC A03/MF A01

The authors present a mutual exclusion algorithm that performs well both with and without contention, on machines with no atomic instructions other than read and write. The algorithm capitalizes on the ability of memory systems to read and write at both full- and half-word granularities. It depends on predictable processor execution rates, but requires no bound on the length of critical sections, performs only O(n) total references to shared memory when arbitrating among conflicting requests (rather than O(n (exp 2)) in the general version of Lamport's fast mutual exclusion algorithm), and performs only 2 reads and 4 writes (a new lower bound) in the absence of contention. We provide a correctness proof. We also investigate the utility of exponential backoff in fast mutual exclusion, with experimental results on the Silicon Graphics Iris multiprocessor and on a larger, simulated machine. With backoff in place, we find that Lamport's algorithm, our new algorithm, and a recent algorithm due to Alur and Taubenfeld all work extremely well, outperforming the native hardware locks of the Silicon Graphics machine, even with heavy contention. DTIC

N94-21255 Air Force Inst. of Tech., Wright-Patterson AFB, OH. Foreign Aerospace Science and Technology Center.

MATHEMATICIAN WANG JU

30 Jul. 1993 9 p Transl. into ENGLISH from Jiefangjun Huaboa (China), no. 3, 1992 p 24-25 Limited Reproducibility: More than 20% of this document may be affected by microfiche quality

(AD-A267882; FASTC-ID(RS)T-0831-92) Avail: Issuing Activity (Defense Technical Information Center (DTIC))

In the early seventies, exciting news was spread around the world: China had successfully launched an intercontinental ballistic missile. The person responsible for special ballistic designs for this major test was actually a 37 year old female engineer by the name of Wang Ju.

Author (DTIC)

N94-21265# Naval Postgraduate School, Monterey, CA. Dept. of Computer Science.

A GRAPHICAL USER-INTERFACE DEVELOPMENT TOOL FOR INTELLIGENT COMPUTER-ASSISTED INSTRUCTION SYSTEMS M.S. Thesis

Francius Suwono Sep. 1993 119 p

(AD-A272988) Avail: CASI HC A06/MF A01

An interactive graphical interface helps intelligent computer-assisted instruction systems, because many applications can be well represented by graphic objects. One approach is a facility whereby a teacher constructing a tutor can associate specific graphics with specific predicate-calculus expressions describing a state in a tutoring simulation. This further requires a specification of the arrangement of graphic objects on the screen, how graphic objects can change position with simulation states. It also requires a language for teachers to specify graphic objects. This thesis addresses both. We introduce a broader applications of cartoon animation modelling ideas to tutoring, that have been limited so far by the complexity of their implementation. The special tools provided help computer-inexperienced instructors to develop their own cartoon animation modelling tutor without the need of mathematical description of shapes or activities to be represented. The tutor generator used employes means-ends analysis, and the language for the teachers is built using Prowindows, a Prolog extension for object-oriented design. DTIC

N94-21273# Rochester Univ., NY. Dept. of Computer Science.

SELECTIVITY: REDUCTIONS, NONDETERMINISM, AND FUNCTION CLASSES

Lane A. Hemaspaandra, Albrecht Hoene (Technische Univ., Berlin, Germany.), Ashish V. Naik (State Univ. of New York, Buffalo.), Mitsunori Ogiwara (University of Electro-Communications, Tokyo, Japan.), Alan L. Selman (State Univ. of New York, Buffalo.), Thomas Thierauf (Ulm Univ., Germany.), and Jie Wang (North Carolina Univ., Greensboro.) Aug. 1993 43 p

(Grants NSF CCR-89-57604; NSF INT-91-16781; NSF CCR-90-02292; NSF CCR-91-08899)

(TR-469) Avail: CASI HC A03/MF A01

A set is P-selective if there is a polynomial-time semi-decision algorithm for the set - an algorithm that given any two strings decides which is 'more likely' to be in the set. Two natural generalizations of P-selectivity are studied: the NP-selective sets and the sets reducible or equivalent to P-selective sets via polynomial-time reductions. A strict hierarchy among the various reductions and equivalences to P-selective sets is established. It is shown that the NP-selective sets are in (NP intersect coNP)/poly, are extended low, and (those in NP) are Low(sub 2); it is also shown that NP-selective sets cannot be NP-complete unless NP = coNP. By studying more general notions of nondeterministic selectivity, it is concluded that all multivalued NP functions have single-valued NP refinements only if the polynomial hierarchy collapses to its second level. Author (revised)

N94-21285# Rochester Univ., NY. Dept. of Computer Science.

THRESHOLD COMPUTATION AND CRYPTOGRAPHIC SECURITY

Yenjo Han, Lane A. Hemaspaandra, and Thomas Thierauf (Ulm Univ., Germany.) Jun. 1993 29 p

(Grants NSF CCR-89-57604; NSF CCR-90-57486; NSF INT-91-16781)

(TR-461) Avail: CASI HC A03/MF A01

Threshold machines are Turing machines whose acceptance is determined by what portion of the machine's computation paths are accepting paths. Probabilistic machines are Turing machines whose acceptance is determined by the probability weight of the machine's accepting computation paths. Simon proved that for unbounded-error polynomial-time machines these two notions yield the same class, PP. Perhaps because Simon's result seemed to collapse the threshold and probabilistic modes of computation, the relationship between threshold and probabilistic computing for the case of bounded error has remained unexplored. In this paper, we compare the bounded-error probabilistic class BPP with the analogous threshold class, BPP(sub path), and, more generally, we study the structural properties of BPP(sub path). We prove that BPP(sub path) contains both NP(sup BPP) and P(sup NP(log)), and that BPP(sub path) is contained in P(exp summation from 2 to p of (log)), BPP(sup NP), and PP. We conclude that, unless the polynomial hierarchy collapses, bounded-error threshold computation is strictly more powerful than bounded-error probabilistic computation. We also consider the natural notion of secure access to a database: an adversary who watches the queries should gain no information about the input other than perhaps its length. We show, for both BPP and BPP(sub path), that if there is any database for which this formalization of security differs from the security given by oblivious database access, then P does not equal PSPACE. It follows that if any set lacking small circuits can be securely accepted, then P does not equal PSPACE.

Author (revised)

N94-21300# Cornell Univ., Ithaca, NY. Dept. of Computer Science.

A RESPONSE TO CHERITON AND SKEEN'S CRITICISM OF CASUAL AND TOTALLY ORDERED COMMUNICATION

Ken Birman Oct. 1993 33 p

(Contract N00014-92-J-1866)

(AD-A271486; CU-CSD-TR-93-1390) Avail: CASI HC A03/MF A01

In a paper to be presented at the 1993 ACM Symposium on Operating Systems Principles, Cheriton and Skeen offer their understanding of causal and total ordering as a communication property. I find their paper highly critical of Isis, and unfairly so, for a number of reasons. I present some responses to their criticism, and also explain why I find their discussion of causal and total communication ordering to be distorted and incomplete.
DTIC

N94-21313 Universiteit Twente, Enschede (Netherlands). Dept. of Computer Science.
BEHAVIOURAL SEMANTICS OF PARALLEL FUNCTIONAL PROGRAMMING LANGUAGES
Duco Fijma 21 Oct. 1992 22 p Limited Reproducibility: More than 20% of this document may be affected by microfiche quality
(Memo-INF-92-66; ETN-93-94108) Copyright Avail: CASI HC A03

The possibilities for using functional programming languages in the process of designing parallel algorithms are discussed. For this application of functional languages, the idea of 'independence of subtasks' must be formalized. This is done by presenting the behavioral semantics of such languages. This is done using a framework based on partially ordered sets of events. Annotations to express parallelism in functional languages are presented. The semantics of these annotations are defined using the same framework.
ESA

N94-21316# Rochester Univ., NY. Dept. of Computer Science.
THE MERCURY USER'S MANUAL
Leonidas Kontothanassis Aug. 1993 20 p
(TR-465) Avail: CASI HC A03/MF A01

It is common for parallel applications to require a large number of threads of control, often much larger than the number of processors provided by the underlying hardware. Using heavyweight (Unix style) processes to implement those threads of control is prohibitively expensive. Mercury is an environment for writing object-oriented parallel programs in C++ that provides the user with simple primitives for inexpensive thread creation and blocking and spinning synchronization. If required, Mercury primitives allow the user to control scheduling decisions in order to achieve good locality of reference in non uniform memory access (NUMA) multiprocessors. The basic Mercury primitives are described and examples of their use are provided.
Author (revised)

N94-21318# Rochester Univ., NY. Dept. of Computer Science.
BETA(SUB k)-COMPLETE PROBLEMS AND GREEDINESS
Robert Szelepcsenyi May 1993 26 p
(Grant NSF CCR-89-57604)
(TR-455) Avail: CASI HC A03/MF A01

Kintala and Fischer defined the limited nondeterminism hierarchy within NP, the so-called beta hierarchy. Beta(sub k) is the class of languages recognized by polynomial time bounded Turing machines making at most O(log(sup k) n) nondeterministic moves, where n is the length of the input. It was conjectured that 'By restricting the amount of nondeterminism in NP-complete problems, we do not seem to obtain complete problems for beta(sub k).' It was demonstrated that this statement is incorrect under what seems to us to be the natural interpretation of the term 'restricting the amount of nondeterminism.' The concept of limited nondeterminism-preserving reductions was developed and complete problems for beta(sub k) were obtained by restricting the amount of nondeterminism in NP-complete problems. The connections between beta hierarchy completeness and greedy algorithms were discussed; it was shown that using greediness we can define many complete problems for beta.
Author (revised)

N94-21364# Massachusetts Inst. of Tech., Cambridge. Artificial Intelligence Lab.
SOME EXTENSIONS OF THE k-MEANS ALGORITHM FOR IMAGE SEGMENTATION AND PATTERN CLASSIFICATION Memorandum Report
Jose L. Marroquin and Federico Girosi Jan. 1993 22 p
(Contracts N00014-91-J-1270; N00014-92-J-1879; N00014-91-J-4038; NSF ASC-92-17041)
(AD-A271691; AI-M-1390) Avail: CASI HC A03/MF A01

In this paper we present some extensions to the k-means algorithm for vector quantization that permit its efficient use in image segmentation and pattern classification tasks. It is shown that by introducing state variables that correspond to certain statistics of the dynamic behavior of the algorithm, it is possible to find the representative centers of the lower dimensional manifolds that define the boundaries between classes, for clouds of multi-dimensional, multi-class data; this permits one, for example, to find class boundaries directly from sparse data (e.g., in image segmentation tasks) or to efficiently place centers for pattern classification (e.g., with local Gaussian classifiers). The same state variables can be used to define algorithms for determining adaptively the optimal number of centers for clouds of data with space-varying density. Some examples of the application of these extensions are also given.
DTIC

N94-21365# Massachusetts Inst. of Tech., Cambridge. Artificial Intelligence Lab.
DATA AND MODEL-DRIVEN SELECTION USING PARALLEL-LINE GROUPS Memorandum Report
Syeda-Tanveer F. Mahmood May 1993 31 p
(Contracts N00014-91-J-4038; DACA76-85-C-0010; NSF IRI-89-00267)
(AD-A271702; AI-M-1399) Avail: CASI HC A03/MF A01

A key problem in model-based object recognition is selection, namely, the problem of isolating regions in an image that are likely to come from a single object. This isolation can be either based solely on image data (data-driven) or can incorporate the knowledge of the model object (model-driven). In this paper we present an approach that exploits the property of closely-spaced parallelism between lines on objects to achieve data and model-driven selection. Specifically, we present a method of identifying groups of closely-spaced parallel lines in images that generates a linear number of small-sized and reliable groups thus meeting several of the desirable requirements of a grouping scheme for recognition. The line groups generated form the basis for performing data and model-driven selection. Data-driven selection is achieved by selecting salient line groups as judged by a saliency measure that emphasizes the likelihood of the groups coming from single objects. The approach to model-driven selection, on the other hand, uses the description of closely-spaced parallel line groups on the model object to selectively generate line groups in the image that are likely to be the projections of the model groups under a set of allowable transformations and taking into account the effect of occlusions, illumination changes, and imaging errors. We then discuss the utility of line groups-based selection in the context of reducing the search involved in recognition, both as an independent selection mechanism, and when used in combination with other cues such as color. Finally, we present results that indicate a vast improvement in the performance of a recognition system that is integrated with parallel line groups-based selection.
DTIC

N94-21409 Naval Postgraduate School, Monterey, CA.
USE OF COMPUTERS IN THE INSTRUCTION OF INTEGRAL CALCULUS M.S. Thesis
Dennis A. Polaski Mar. 1993 165 p Limited Reproducibility: More than 20% of this document may be affected by microfiche quality
(AD-A272500) Avail: Issuing Activity (Defense Technical Information Center (DTIC))

One of the most difficult concepts in the area of integral multivariate calculus is finding the limits of integration. This thesis describes an interactive computer program designed to help students understand this important concept. The program shows how a given domain is plotted and teaches how to find the limits of integration when evaluating two-dimensional integrals. The program allows the user to enter any known information about a region and then evaluates the integral. The region is plotted; the limits of integration are given along with the area of the region. The program handles cartesian and polar coordinate, two-dimensional integral problems. This program could be used independently by the student and/or used by the calculus instructor in the classroom.
DTIC

N94-21413# Massachusetts Inst. of Tech., Cambridge. Artificial Intelligence Lab.
MAYGEN: A SYMBOLIC DEBUGGER GENERATION SYSTEM
Christine L. Tsien Jul. 1993 86 p
(Contract N00014-91-J-4038)
(AD-A272512; AI-TR-1429) Avail: CASI HC A05/MF A01

With the development of high-level languages for new computer architectures comes the need for appropriate debugging tools as well. One

method for meeting this need would be to develop, from scratch, a symbolic debugger with the introduction of each new language implementation for any given architecture. This, however, seems to require unnecessary duplication of effort among developers. Compilation technology has alleviated some duplication of effort in the development of compilers. Can similar ideas aid in the efficient development of symbolic debuggers as well? Maygen explores the possibility of making debugger development efficient by influencing the language and architecture development processes. Maygen is a debugger generation system, built upon the idea that symbolic debuggers can be divided into three components: a set of source language interface routines, a set of machine architecture interface routines, and a language-independent and architecture-independent debugger skeleton. Maygen then exploits this modularity: First, Maygen precisely defines as well as houses the language-independent and architecture-independent debugger skeleton. Second, Maygen defines the protocol for interface interaction among source language developers, machine architecture developers, and the general-purpose debugger skeleton. Finally, Maygen provides a framework in which the resident debugger skeleton is automatically developed into a stand-alone symbolic debugger; the resulting debugger is tailored to the specific provisions of a particular language group and a particular architecture group. DTIC

N94-21414# Naval Postgraduate School, Monterey, CA.
CONVERSION AND MAINTENANCE OF Co-oP FOR WINDOWS M.S. Thesis
Mai T. Orloff Dec. 1993 52 p
(AD-A272513) Avail: CASI HC A04/MF A01

The purpose of this thesis is four-fold: conduct a review of Co-oP to include its background and the multiple criteria decision making algorithms and group aggregation techniques implemented in the existing version of Co-oP; expand the model base to include ELECTRE 3; expand the group decision module to include the minimum-variance technique and a revised version of the min-max technique; and migrate Co-oP, using Visual Basic 2.0, onto a graphical user interface (GUI) environment that can be run with Microsoft Windows for Workgroup. DTIC

N94-21454 Universiteit Twente, Enschede (Netherlands). Tele-Informatics and Open Systems Group.
THE TERM PROCESSOR KIMWITU MANUAL AND COOKBOOK
Peter vanEijk and Axel Belinfante 1992 51 p Limited Reproducibility: More than 20% of this document may be affected by microfiche quality
(Memo-INF-92-67; TIOS-92/28; ETN-93-94109) Copyright Avail: CASI HC A04

A system that supports the construction of programs that use 'trees' or 'terms' as their main data structure is described. This system is a 'meta' tool in the development process of tools. Its 'input' is an abstract description of terms, annotated with implementation directives, plus a description of functions on these terms. The 'output' consists of a number of C-files that contain data structure definitions for the terms, a number of standard functions on those terms, and a translation (in C) of the function definitions in the input (for example, term rewriting). The standard functions can be used to create terms, compare them for equality, read and write them on files in various formats and do manipulations like list concatenation. The input format of the term processor is described and the output of the system is described: the C types and functions, the files, etc. The running of the system, and the relation with other software development tools, such as the UNIX tools make, yacc, lex, lint, and the Synthesizer Generator are detailed. Various techniques in which programs can be written over terms are discussed, thus giving examples of the concept of 'multi paradigm programming'. ESA

N94-21462*# Institute for Computer Applications in Science and Engineering, Hampton, VA.
A MULTI-LEVEL SOLUTION ALGORITHM FOR STEADY-STATE MARKOV CHAINS
Graham Horton (Erlangen-Nuremberg Univ., Germany.) and Scott T. Leutenegger Nov. 1993 32 p
(Contract NAS1-19480; RTOP 505-90-52-01)
(NASA-CR-191558; ICASE-93-81; NAS 1.26:191558) Avail: CASI HC A03/MF A01

A new iterative algorithm, the multi-level algorithm, for the numerical solution of steady state Markov chains is presented. The method utilizes a set of recursively coarsened representations of the original system to achieve accelerated convergence. It is motivated by multigrid methods, which are widely used for fast solution of partial differential equations. Initial results of numerical experiments are reported, showing significant reductions in computation time, often an order of magnitude or more, relative to the Gauss-Seidel and optimal SOR algorithms for a variety of test problems. The multi-level method is compared and contrasted with the iterative aggregation-disaggregation algorithm of Takahashi. Author (revised)

N94-21489*# Computer Sciences Corp., Mountain View, CA.
SUPERPATCH
Jin J. Chou and Francis Enomoto (National Aeronautics and Space Administration. Ames Research Center, Moffett Field, CA.) Oct. 1993 33 p Sponsored by NASA. Washington
(Contract NAS2-12961)
(NASA-CR-177627; A-94010; NAS 1.26:177627) Avail: CASI HC A03/MF A01

A design model geometry file format with topology information used for model geometry exchange in Computational Fluid Dynamics (CFD) grid generation is described. The first part describes the reason why this file format is necessary and what we want to achieve through the file format. The second part provides the information stored in the file format. The purpose of the publication is for broad dissemination of this file format and for the wide participation of testing. Author (revised)

N94-21495 Center for Mathematics and Computer Science, Amsterdam (Netherlands). Dept. of Computer Science.
PROCEDURAL DYNAMIC SEMANTICS, VERB-PHRASE ELLIPSIS, AND PRESUPPOSITION
D. Jan N. vanEijck (OTS, Utrecht, Netherlands.) and Nissim Francez (Technion - Israel Inst. of Tech., Haifa.) Feb. 1993 17 p Sponsored in part by Technion - Israel Inst. of Tech. and Haifa Univ. Limited Reproducibility: More than 20% of this document may be affected by microfiche quality
(CWI-CS-R9311; ETN-94-94740) Copyright Avail: Issuing Activity (European Space Agency (ESA))

Verb Phrase Ellipsis (VPE) is studied and its relationship to presupposition and its failure is shown. A representation of VPE by means of a dynamic semantics approach is used, using an extended version of Dynamic Predicate Logic which includes procedures, scope rules and functions. Focus is on the representation of the strict/sloppy ambiguity in connection with ellipsis constructs, which comes 'for free' in a procedural context. Independent justification for the representation of VPE in terms of procedure definitions and their invocations is provided. The relationship of VPE and presupposition sheds light on the arguments about the question whether VPE is syntactic or semantic in nature, as well as on the relative order of meaning determination and presupposition determination. ESA

N94-21496 Center for Mathematics and Computer Science, Amsterdam (Netherlands). Dept. of Computer Science.
REASONING ABOUT UPDATE LOGIC
D. Jan N. vanEijck and Fer-Jan deVries (OTS, Utrecht, Netherlands.) Feb. 1993 21 p Submitted for publication Limited Reproducibility: More than 20% of this document may be affected by microfiche quality
(CWI-CS-R9312; ETN-94-94741) Copyright Avail: Issuing Activity (European Space Agency (ESA))

Part of a larger scale enterprise to pursue the obvious parallel between information processing and imperative programming is presented. Logical tools from theoretical computer science are demonstrated to be relevant for the logic of information flow. More specifically, it is shown that the perspective of Hoare logic can be aplied to the conceptual simplification of information flow logics. In conclusion, it is argued that interpreting the dynamic statements of information logics as dynamic modal operators has much wider applicability. In fact, the method can be used to axiomatize quite a wide range of information logics. ESA

N94-21501# Air Force Inst. of Tech., Wright-Patterson AFB, OH. School of Engineering.
COMPUTING WITH BAYESIAN MULTI-NETWORKS
Eugene Santos, Jr. 16 Nov. 1993 18 p
(AD-A273106; AFIT/EN/TR93-10) Avail: CASI HC A03/MF A01

Existing probabilistic approaches to automated reasoning impose severe

restrictions on its knowledge representation scheme. Mainly, this is to ensure that there exists an effective inferencing algorithm. Unfortunately, this makes the application of these approaches to general domains quite difficult. In this paper, we present a new model called Bayesian multi-networks which uses a rule-based organization of knowledge quite natural for human experts modeling various domains. Furthermore, strong probabilistic semantics help quantify the knowledge. Combined with the rich structure of rule-based approaches, a general inference engine for Bayesian multi-networks is developed. DTIC

N94-21534 Center for Mathematics and Computer Science, Amsterdam (Netherlands). Dept. of Interactive Systems.

MINIFOLD: A KERNEL FOR A MANIFOLD-LIKE COORDINATION LANGUAGE

E. P. B. M. Rutten Dec. 1992 44 p Limited Reproducibility: More than 20% of this document may be affected by microfiche quality

(CWI-CS-R9252; ETN-94-94732) Copyright Avail: CASI HC A03

MINIFOLD is a kernel for a coordination language, following the MANIFOLD model. This model focuses on the coordination of processes, separated from their computation functionality. Processes are considered as black boxes, and their behavior is abstracted to their communications. MINIFOLD provides constructs to build up an environment of concurrent processes and to manage the communication between them. On one hand, a data flow mechanism can be used to build networks of streams, linking input and output ports of the processes, and carrying the units exchanged between them. On the other hand, an event broadcasting mechanism provides control on the dynamical modification of the data flow network. MINIFOLD is introduced in a constructive and incremental way. It is provided with an operational semantics; a model of its execution based on automata is proposed and illustrated by simple classical example. A study to explore models of the behavior of the MANIFOLD concept and to formalize its bare essentials is presented. It is intended that the MANIFOLD language can take advantage of this, as guidelines for formalisms underlying practical tools for program analysis, clarification of its structure and a basis for the comparison with other models. ESA

N94-21537 Center for Mathematics and Computer Science, Amsterdam (Netherlands). Dept. of Computer Science.

A LOWER BOUND ON WAIT-FREE COUNTING

Shlomo Moran (Technion - Israel Inst. of Tech., Haifa.) and Gadi Taubenfeld (Bell Telephone Labs., Inc., Murray Hill, NJ.) Feb. 1993 12 p Limited Reproducibility: More than 20% of this document may be affected by microfiche quality

(CWI-CS-R9307; ETN-94-94736) Copyright Avail: CASI HC A03

A counting protocol (mod m) consists of shared memory bits, referred to as the counter, and a procedure for incrementing the counter value by one (mod m). The procedure may be executed by many processes concurrently. It is required to satisfy a very weak correctness requirement, namely: the counter is required to show a correct value only in quiescent states (states in which no process is incrementing the counter). Special cases of counting protocols are 'counting networks' and 'concurrent counters.' The problem of implementing a wait-free counting protocol, assuming that the basic atomic operation of a process is a read-modify-write on a single bit, is considered. Let flip(Pr) be the maximum number of times a single increment operation changes the counter bits in a counting protocol Pr. The main result is: in any wait-free counting protocol Pr which counts modulo m, m divides 2(exp flip(Pr)). Thus, flip(Pr) is greater than or equal to log m and m is a power of two. This result provides interesting generalizations of lower bounds and impossibility results for counting and smoothing networks. ESA

N94-21539# Sandia National Labs., Albuquerque, NM.

COUPLING OF SMOOTH PARTICLE HYDRODYNAMICS WITH PRONTO

S. W. Attaway, M. W. Heinstein, F. J. Mello, and J. W. Swegle 1993 12 p Presented at the Annual Winter Meeting of the American Society of Mechanical Engineers, New Orleans, LA, 28 Nov. - 3 Dec. 1993

(Contract DE-AC04-76DP-00789)

(DE93-019080; SAND-93-1781C; CONF-931121-17) Avail: CASI HC A03/MF A01

A gridless numerical technique called smooth particle hydrodynamics (SPH) has been coupled to the transient dynamics finite element code, PRONTO. In this paper, a new weighted residual derivation for the SPH method is presented, and the methods used to embed SPH within PRONTO are outlined. Example SPH-PRONTO calculations are also presented. One major difficulty associated with the Lagrangian finite element method is modeling materials with no shear strength; for example, gases, fluids and explosive bi-products. Typically these materials can be modeled for only a short time with a Lagrangian finite element code. Large distortions cause tangling of the mesh, which will eventually lead to numerical difficulties such as negative element area or 'bow tie' elements. Remeshing will allow the problem to continue for a short while, but the large distortions can prevent a complete analysis. Smooth particle hydrodynamics is a gridless Lagrangian technique. Requiring no mesh, SPH has the potential to model material fracture, large shear flows, and penetration. SPH computes the strain rate and the stress divergence based on the nearest neighbors of a particle, which are determined using an efficient particle sorting technique. Embedding the SPH method within PRONTO allows part of the problem to be modeled with quadrilateral finite elements while other parts are modeled with the gridless SPH method. SPH elements are coupled to the quadrilateral elements through a contact like algorithm. DOE

N94-21551 Center for Mathematics and Computer Science, Amsterdam (Netherlands). Dept. of Computer Science.

CHANGING PREFERENCES

Johan vanBenthem (Amsterdam Univ., Netherlands.), Jan vanEijck (Amsterdam Univ., Netherlands.), and Alla Frolova (Amsterdam Univ., Netherlands.) Feb. 1993 19 p Limited Reproducibility: More than 20% of this document may be affected by microfiche quality

(CWI-CS-R9310; ETN-94-94739) Copyright Avail: CASI HC A03

An exploratory document for research in logical semantics emerging from several current developments in computer science is presented. Standard logic employs 'flat' unstructured sets of statements for its theories and unstructured classes of models for its semantic universes. Nowadays, however, there is an incipient literature on structured universes of models as well as structured theories, both employing 'preference relations', of some sort. This report aims: to propose a more systematic framework for this trend, while also connecting it up with some historical predecessors; to design some new logical systems bringing preferences out explicitly, thereby highlighting the theoretical properties of 'preferential reasoning' while raising some new kinds of technical question for further research; to link up with some current computational ideas (emerging also in the field of linguistics), by bringing in the general dynamic logic of procedures as well as logical systems providing suitable fine structure of information states. ESA

N94-21561# Allied-Signal Aerospace Co., Kansas City, MO.

COMPUTER-AIDED TEST EQUIPMENT GRAPHICS SYSTEM (CATEGS)

W. Fuller Sep. 1993 66 p

(Contract DE-AC04-76DP-00613)

(DE94-000383; KCP-613-5155) Avail: CASI HC A04/MF A01

This development effort evaluated existing CAD and emerging CAE technologies for implementing automated processes applicable to the design, documentation, fabrication, and maintenance of electrical test equipment. By developing designs in an electronic media and electronically moving those designs, a 2-to-1 productivity improvement was achieved over previous methods. Users and customers further identified value-added benefits of faster development of designs and improved quality of the definitions produced. DOE

N94-21584*# Institute for Computer Applications in Science and Engineering, Hampton, VA.

USING PARALLEL BANDED LINEAR SYSTEM SOLVERS IN GENERALIZED EIGENVALUE PROBLEMS Final Report

Hong Zhang (National Aeronautics and Space Administration. Langley Research Center, Hampton, VA.) and William F. Moss (Clemson Univ., SC.) Sep. 1993 20 p Submitted for publication

(Contract NAS1-19480; NSF CCR-91-03296; RTOP 505-90-52-01)

(NASA-CR-191540; NAS 1.26:191540; ICASE-93-71) Avail: CASI HC A03/MF A01

Subspace iteration is a reliable and cost effective method for solving positive definite banded symmetric generalized eigenproblems, especially in the case of large scale problems. This paper discusses an algorithm that makes use of two parallel banded solvers in subspace iteration. A shift is introduced to decompose the banded linear systems into relatively

independent subsystems and to accelerate the iterations. With this shift, an eigenproblem is mapped efficiently into the memories of a multiprocessor and a high speed-up is obtained for parallel implementations. An optimal shift is a shift that balances total computation and communication costs. Under certain conditions, we show how to estimate an optimal shift analytically using the decay rate for the inverse of a banded matrix, and how to improve this estimate. Computational results on iPSC/2 and iPSC/860 multiprocessors are presented. Author

N94-21587 Center for Mathematics and Computer Science, Amsterdam (Netherlands). Dept. of Computer Science.
TERMINATION AND CONFLUENCE OF RULE EXECUTION
M. H. Leonie vanderVoort and Arno P. J. M. Siebes Feb. 1993 17 p Limited Reproducibility: More than 20% of this document may be affected by microfiche quality
(CWI-CS-R9309; ETN-94-94738) Copyright Avail: CASI HC A03

A design theory for rule sets in an OODBMS (Object Oriented Data Base Management System) is developed. Two predicates, Terminate(n) and Independent, which imply respectively termination and confluency, are introduced. Both predicates are characterized under two kinds of rule execution semantics: set and instance based. The decidability of the predicates is proven and it is shown that set and instance based semantics coincide whenever the rule set is independent and terminates. Sufficient conditions of low algorithmic complexity for both Terminate(n) and Independent under both kinds of semantics are given. ESA

N94-21611# Center for Mathematics and Computer Science, Amsterdam (Netherlands). Dept. of Numerical Mathematics.
NUMERICAL MULTIGRID SOFTWARE (MGD5M): A PARALLEL MULTIGRID CODE WITH A TWISTED ILLU-RELAXATION
Margreet Louter-Nool Dec. 1992 14 p Sponsored by Cray Research, Inc., and Netherlands Organization for Scientific Research
(CWI-NM-R9226; ETN-94-94701) Copyright Avail: CASI HC A03/MF A01

The twisted LDU decomposition for tridiagnonal matrices is considered. This technique enables part parallelization of the Incomplete Line LU relaxation (ILLU). This relaxation method is applied as smoothing process for the multigrid method MGD5V. MGD5M, which is a multitasked code based on the twisted ILLU relaxation, is presented as a successor to MGD5V. The performance results of MGD5V and MGD5M as measured on a dedicated four processor Cray Y MP4/464 are compared. ESA

N94-21612# Center for Mathematics and Computer Science, Amsterdam (Netherlands). Dept. of Numerical Mathematics.
A PACKAGE FOR LONG INTEGER ARITHMETIC ON THE CRAY Y-MP
Dik T. Winter Dec. 1992 20 p Sponsored by Cray Research, Inc., and Netherlands Organization for Scientific Research
(CWI-NM-R9227; ETN-94-94702) Copyright Avail: CASI HC A03/MF A01

A package for arbitrary long integer arithmetic as it was implemented on the Cray Y-MP is described. The reasons and history for design decisions are detailed. The package is mostly written in C, but with support from Cray Assembler. Timing results are given and compared with the multiprecise integer arithmetic package of Buell and Ward. The contents of the long integer package are described. ESA

N94-21633# Sandia National Labs., Albuquerque, NM.
ADVANCED FAILURE ANALYSIS LABORATORY EQUIPMENT NETWORKING
C. L. Henderson and D. L. Barton 1993 9 p Presented at the 1993 Integrated Diagram Systems Users Conference, San Jose, CA, 24-26 Aug. 1993
(Contract DE-AC04-76DP-00789)
(DE93-019070; SAND-93-1748C; CONF-9308146-1) Avail: CASI HC A02/MF A01

Today's integrated circuits are so complex that it is often necessary to have access to the layouts and schematics when performing voltage contrast, cross sectioning, light emission, mechanical probing, optical beam induced current, and even simple SEM and Optical Examination. To deal with these issues, Sandia National Laboratories is developing an advanced failure analysis laboratory networking scheme to provide computer control, layout navigation, schematic navigation, and report generation on each of the major pieces of failure analysis equipment. This concept is known as an Integrated Diagnostic Environment or IDE. An integrated diagnostic environment is an environment where failure analysis equipment is computer-controlled and linked by a high speed network. The network allows CAD databases to be shared between instruments, improving the failure analyst's productivity on each analysis task. At Sandia, we are implementing this concept using SUN Sparcstation computers running Schlumberger's IDE software. To date, we have incorporated our electron beam prober and light emission system into the environment. We will soon add our scanning optical microscope and focused ion beam system and eventually add our optical microscope and microprobe station into the network. There are a number of issues to consider when implementing an Integrated Diagnostic Environment; these are discussed in detail. DOE

N94-21635# Sandia National Labs., Albuquerque, NM.
RHALE: A 3-D MMALE CODE FOR UNSTRUCTURED GRIDS
J. S. Peery, K. G. Budge, M. K. W. Wong, and T. G. Trucano 1993 16 p Presented at the Annual Winter Meeting of the American Society of Mechanical Engineers, New Orleans, LA, 28 Nov. - 3 Dec. 1993
(Contract DE-AC04-76DP-00789)
(DE93-019405; SAND-93-0178C; CONF-931121-19) Avail: CASI HC A03/MF A01

RHALE, a multi-material arbitrary Lagrangian-Eulerian (MMALE) shock physics code, is described. RHALE is the successor to CTH, Sandia's 3-D Eulerian shock physics code, and will be capable of solving problems that CTH cannot adequately address. The Lagrangian solid mechanics capabilities of RHALE, which include arbitrary mesh connectivity, superior artificial viscosity, and improved material models, are discussed. The MMALE algorithms that were extended for arbitrary grids in both two- and three-dimensions are discussed. The MMALE addition to RHALE provides the accuracy of a Lagrangian code while allowing a calculation to proceed under very large material distortions. Coupling an arbitrary quadrilateral or hexahedral grid to the MMALE solution facilitates modeling of complex shapes with a greatly reduced number of computational cells. RHALE allows regions of a problem to be modeled with Lagrangian, Eulerian or ALE meshes. In addition, regions can switch from Lagrangian to ALE to Eulerian based on user input or mesh distortion. For ALE meshes, new node locations are determined with a variety of element based equipotential schemes. Element quantities are advected with donor, van Leer, or Super-B algorithms. Nodal quantities are advected with the second order SHALE or HIS algorithms. Material interfaces are determined with a modified Young's high resolution interface tracker or the SLIC algorithm. RHALE was used to model many problems of interest to the mechanics, hypervelocity impact, and shock physics communities. Results of a sampling of these problems are presented. DOE

N94-21747# Los Alamos National Lab., NM.
A METHODOLOGY FOR QUANTIFYING UNCERTAINTY IN MODELS
M. D. McKay and R. J. Beckman 1993 4 p Presented at the Surety Technology Symposum, Chelyacinsk, Russia, 28 Sep. - 2 Oct. 1993
(Contract W-7405-eng-36)
(DE93-040154; LA-UR-93-3160; CONF-9309215-1) Avail: CASI HC A01/MF A01

This paper, condensed from McKay et al. (1992) outlines an analysis of uncertainty in the output of computer models arising from uncertainty in inputs (parameters). Uncertainty of this type most often arises when proper input values are imprecisely known. Uncertainty in the output is quantified in its probability distribution, which results from treating the inputs as random variables. The assessment of which inputs are important (sensitivity analysis) with respect to uncertainty is done relative to the probability distribution of the output. DOE

N94-21761 Sandia National Labs., Albuquerque, NM.
STOCHASTIC SIMULATION FOR IMAGING SPATIAL UNCERTAINTY: COMPARISON AND EVALUATION OF AVAILABLE ALGORITHMS
C. A. Gotway and B. M. Rutherford 1993 21 p Presented at the Workshop in English on Geostatistical Simulations, Fontainebleau, France, 27 May 1993 Limited Reproducibility: More than 20% of this document may be affected by microfiche quality
(Contract DE-AC04-76DP-00789)
(DE93-040058; SAND-93-0438C; CONF-9305268-1) Avail: CASI HC A03

Stochastic simulation has been suggested as a viable method for

characterizing the uncertainty associated with the prediction of a nonlinear function of a spatially-varying parameter. Geostatistical simulation algorithms generate realizations of a random field with specified statistical and geostatistical properties. A nonlinear function is evaluated over each realization to obtain an uncertainty distribution of a system response that reflects the spatial variability and uncertainty in the parameter. Crucial management decisions, such as potential regulatory compliance of proposed nuclear waste facilities and optimal allocation of resources in environmental remediation, are based on the resulting system response uncertainty distribution. Many geostatistical simulation algorithms have been developed to generate the random fields, and each algorithm will produce fields with different statistical properties. These different properties will result in different distributions for system response, and potentially, different managerial decisions. The statistical properties of the resulting system response distributions are not completely understood, nor is the ability of the various algorithms to generate response distributions that adequately reflect the associated uncertainty. This paper reviews several of the algorithms available for generating random fields. Algorithms are compared in a designed experiment using seven exhaustive data sets with different statistical and geostatistical properties. For each exhaustive data set, a number of realizations are generated using each simulation algorithm. The realizations are used with each of several deterministic transfer functions to produce a cumulative uncertainty distribution function of a system response. The uncertainty distributions are then compared to the single value obtained from the corresponding exhaustive data set. DOE

N94-21764 Los Alamos National Lab., NM.
GEOMETRIC OPTIMIZATION
P. Hinker and C. Hansen 1993 8 p Presented at the Visualization 1993, San Jose, CA, 25-29 Oct. 1993 Limited Reproducibility: More than 20% of this document may be affected by poor print and microfiche quality
(Contract W-7405-eng-36)
(DE93-040152; LA-UR-93-3140; CONF-931080-4) Avail: Issuing Activity (Department of Energy (DOE))

An algorithm is presented which describes an application independent method for reducing the number of polygonal primitives required to faithfully represent an object. Reducing polygon count without a corresponding reduction in object detail is important for: achieving interactive frame rates in scientific visualization, reducing mass storage requirements, and facilitating the transmission of large, multi-timestep geometric data sets. This paper shows how coplanar and nearly coplanar polygons can be merged into larger complex polygons and re-triangulated into fewer simple polygons than originally required. The notable contributions of this paper are: (1) a method for quickly grouping polygons into nearly coplanar sets, (2) a fast approach for merging coplanar polygon sets, and (3) a simple, robust triangulation method for polygons created by (1) and (2). The central idea of the algorithm is the notion of treating polygonal data as a collection of segments and removing redundant segments to quickly form polygon hulls which represent the merged coplanar sets. DOE

N94-21841# Lawrence Livermore National Lab., CA.
IMAGING VECTOR FIELDS USING LINE INTEGRAL CONVOLUTION
B. Cabral and L. C. Leedom 1 Mar. 1993 10 p Presented at the Computer Graphics (CG) Conference, Anaheim, CA, 1-6 Aug. 1992
(Contract W-7405-eng-48)
(DE93-019922; UCRL-JC-112935; CONF-9208240-1) Avail: CASI HC A02/MF A01

Imaging vector fields has applications in science, art, image processing, and special effects. An effective new approach is to use linear and curvilinear filtering techniques to locally blur textures along a vector field. This approach builds on several previous texture generation and filtering techniques. It is, however, unique because it is local, one-dimensional, and independent of any predefined geometry or texture. The technique is general and capable of imaging arbitrary two- and three-dimensional vector fields. The local one-dimensional nature of the algorithm lends itself to highly parallel and efficient implementations. Furthermore, the curvilinear filter is capable of rendering detail on very intricate vector fields. Combining this technique with other rendering and image processing techniques--like periodic motion filtering--results in richly informative and striking images. The technique can also produce novel special effects. DOE

N94-21851# Los Alamos National Lab., NM.
PROCEEDINGS OF THE IMOG (INTERAGENCY MANUFACTURING OPERATIONS GROUP) NUMERICAL SYSTEMS GROUP
G. J. Maes, comp. Oct. 1993 186 p Meeting on Numerical Systems held in Oak Ridge, TN, 9-10 Feb. 1993
(Contract W-7405-eng-36)
(DE94-001009; LA-12646-C; CONF-9302151) Avail: CASI HC A09/MF A02

This document contains the proceedings of the 62nd Interagency Manufacturing Operations Group (IMOG) Numerical Systems Group. Included are the minutes of the 61st meeting and the agenda for the 62nd meeting. Presentations at the meeting are provided in the appendices to this document. Presentations were as follows: 1992 NSG Annual Report to IMOG Steering Committee; Charter for the IMOG Numerical Systems Group; Y-12 Coordinate Measuring Machine Training Project; IBH NC Controller; Automatically Programmed Metrology Update; Certification of Anvil-5000 for Production Use at the Y-12 Plant; Accord Project; Sandia National Laboratories 'Accord;' Demo/Anvil Tool Path Generation 5-Axis; Demo/Video Machine/Robot Animation Dynamics; Demo/Certification of Anvil Tool Path Generation; Tour of the M-60 Inspection Machine; Distributed Numerical Control Certification; Spline Usage Method; Y-12 NC Engineering Status; and Y-12 Manufacturing CAD Systems. DOE

N94-21917 California Univ., Berkeley. Lawrence Berkeley Lab.
SURVEY AND ALIGNMENT ANALYSIS FOR THE ALS STORAGE RING USING COMPUTER SPREADSHEETS
R. Keller Jul. 1993 11 p Presented at the 3rd International Workshop on Accelerator Alignments, Annecy, France, 28 Sep. - 1 Oct. 1993 Limited Reproducibility: More than 20% of this document may be affected by microfiche quality
(Contract DE-AC03-76SF-00098)
(DE93-019254; LBL-34335; LSGN-143; CONF-9309204-2) Avail: CASI HC A03

The general survey and alignment concept for the ALS is based on a network of fixed, three-dimensional monuments installed in the building floor, to which all accelerator component positions are referred. The survey of these monuments is performed separately for horizontal and vertical coordinates, following the scheme imposed by the code PC-GEONET that is used for monument data analysis. For most of the accelerator objects the tasks of data acquisition, bundling, and transformations from observation-station into object coordinate-systems are being handled by the commercial software package ECDS rather than by PC-GEONET. This choice had to be made because no instrument stands are presently available at LBL that can be placed exactly over monuments and are high enough to permit observing the fiducials of installed magnets from above. Theodolites only are used with ECDS as observation instruments, and absolute scaling has to be provided by observing some object of precisely known length. To create ideal data and compute alignment values for all accelerator components, spreadsheets were developed by the author using the application EXCEL for Macintosh computers. Choice of a spreadsheet method rather than conventional programming techniques proved very convenient when in the course of this work the sheets had to be created and progressively modified under severe time pressure to include new effects and help redefine the observation procedures. With spreadsheets, varying input data formats coming from the survey crew could be easily accommodated, and adding numerous consistency checks as well as generating additional ideal data for special alignment tasks was possible with comparatively little effort. Dedicated spreadsheets were created for each of the 12 curved sectors of the storage ring. In this paper, the main features of the spreadsheets are presented, and the alignment results for lattice and corrector magnets are listed and discussed. DOE

N94-21923# Argonne National Lab., IL.
USER'S GUIDE FOR THE CASTING PROCESS SIMULATOR SOFTWARE CaPS-2D, VERSION 1.0
H. M. Domanus, R. C. Schmitt, and S. Ahuja Jul. 1993 104 p
(Contract W-31-109-eng-38)
(DE93-040398; ANL-93/14) Avail: CASI HC A06/MF A02

Most casting defects occur during initial pouring and therefore the design of the running system, which guides the metal from the ladle into the mold, is crucial. Traditionally, the running system and mold filling are designed by trial and error, which is tedious, time consuming, and expensive.

The uncertainties that remain can be overcome by a computer simulation that demonstrates the actual process of mold filling and subsequent solidification. Computer simulation of various processes has become more and more common in recent years. The cost-effectiveness of making flawless castings has made the foundry worker more aware of the process of mold filling, identification of hot spots, etc. The macroscopic Casting Process Simulator (CaPS) software combines heat transfer and fluid flow aspects and can describe a variety of solidification aspects, including mold filling. CaPS is a two-dimensional time-dependent computer code involving a finite volume formulation for the mass, momentum, and energy equations. CaPS has the following characteristics: CaPS uses the PATRAN geometric modeling package for constructing the geometry, generating a neutral file consisting of a list of named components, and post-processing of the simulation results; building the geometry independently of the mesh is a time-saving procedure. A structured mesh generator of structured regular cells is included and is interfaced with the neutral-file output of the solid geometric package. Visual user interfaces have been developed on the basis of the HOOPS package, which contains a hierarchical database of geometric information. The CaPS shell scripts interactively provide a step-by-step procedure to simulate the solidification process, thus making the software very user-friendly. DOE

N94-21924# Oak Ridge National Lab., TN.
AN EVALUATION OF INTEGRATION OF THE TRACE ASSERTION METHOD WITH THE BOX STRUCTURE METHOD FOR CODING IN C++
A. L. Bangs Aug. 1993 197 p
(Contract DE-AC05-84OR-21400)
(DE93-040480; ORNL/TM-12439) Avail: CASI HC A09/MF A03

The trace assertion method is a method for developing specifications for software modules. The nature of the method allows verification of consistency and completeness of the specification and provides a rigid structure to the designer. This method is extended to work with object-oriented designs for a C++ system involving a user interface. A number of object-oriented concepts which are not present in the original trace assertion method are incorporated into the method and demonstrated on two completely specified increments of the system being developed. In addition, the method is incorporated into a system wide view beyond the original modular scope of the method. Advantages of the adapted method and its problems are discussed. DOE

N94-21977# Allied-Signal Aerospace Co., Kansas City, MO.
ENHANCED SOFTWARE FOR THE GT1022 AUTOMATED GAGING SYSTEM
R. E. Hines Sep. 1993 28 p
(Contract DE-AC04-76DP-00613)
(DE94-001374; KCP-613-5153) Avail: CASI HC A03/MF A01

Several enhancements have been added to the gaging software of a microcomputer-controlled gaging system (GT1022) that is used to acquire and process dimensional product data from multiprobe rotary gages. Processing routines have been developed to inspect five additional feature types: dimension, least squares center, MMC position with datum diameter bonus, total indicator reading, and two-sided wall thickness. Mathematical alignment routines have been added that permit parts to be gaged in a misaligned condition and then have the measurements corrected relative to the part's datum axes. DOE

N94-22011# Lawrence Livermore National Lab., CA.
POST-EXPERIMENTAL PLOTS FOR HIGH SPEED DATA ACQUISITION PROGRAM
G. Koide (Hawaii Univ., Hilo.) and T. R. Metz Jul. 1993 12 p
(Contract W-7405-eng-48)
(DE94-000956; UCRL-ID-114808) Avail: CASI HC A03/MF A01

The post-experimental plot program allows the user to obtain hard copy outputs for the data acquisition program. Both single channel and multiple channels can be plotted for the customer. Another feature is the telescopic plots of any section of the given data. In addition, the user has a choice of papers, 8.5 x 11 inch or 11 x 17 inch and the graphs may be rotated by 90 degrees. Before making a plot, the experimental curves can be displayed on the screen. DOE

N94-22088# Oak Ridge National Lab., TN.
REVERSE AUTOMATIC DIFFERENTIATION OF MODULAR FORTRAN PROGRAMS
J. E. Horwedel 1993 5 p Presented at the Theory Institute on Combinatorial Challenges in Computational Differentiation Workshop, Argonne, IL, 24-26 May 1993
(Contract DE-AC05-84OR-21400)
(DE94-000336; CONF-9305285-1) Avail: CASI HC A01/MF A01

The calculation of derivatives necessary for sensitivity analysis or for the optimal solution of systems of nonlinear equations continues to be an important research objective. Several software systems were developed for implementing automatic differentiation of computer programs. The forward mode of automatic differentiation is efficient for calculating derivatives for a large number of dependent variables with respect to a few independent variables. As the number of independent variables increases, the computational complexity, as measured in execution time and memory requirements, renders the forward mode impractical. The reverse mode or adjoint approach is efficient for derivatives of a few dependent variables with respect to thousands of independent variables; however, available memory and disk storage generally limit the application of the reverse mode to problems with less than a few million floating point assignments. The fundamental problem with the reverse mode of automatic differentiation is that the accumulation of derivatives is required. A code that uses 3 minutes of execution time to perform 50 million floating point assignments could easily need more than one gigabyte to store the accumulated derivatives. DOE

N94-22098 Leiden Univ. (Netherlands). Dept. of Mathematics and Computer Science.
ALGORITHMS FOR MARKOV DECISION CHAINS WITH PARTIAL INFORMATION
J. A. Loeve 1993 14 p Limited Reproducibility: More than 20% of this document may be affected by microfiche quality
(PB93-220085; TW-92-14) Avail: Issuing Activity (National Technical Information Service (NTIS))

In this paper, the author considers Markov decision chains with partial state information. This means that the state space is partitioned, and at each decision moment the only information available on the state of the system is in which set of the partition it is contained. So the exact state is not known. The author presents several algorithms for this model. The author analyzes these and applies them on several examples, in particular on a special queueing model. NTIS

N94-22350*# National Aeronautics and Space Administration. Langley Research Center, Hampton, VA.
UNSTRUCTURED GRID GENERATION TECHNIQUES AND SOFTWARE
Mary-Anne K. Posenau, ed. Washington Sep. 1993 344 p Workshop held in Hampton, VA, 27-28 Apr. 1993; sponsored by NASA, Washington
(RTOP 505-90-53-02)
(NASA-CP-10119; NAS 1.55:10119) Avail: CASI HC A15/MF A03

The Workshop on Unstructured Grid Generation Techniques and Software was conducted for NASA to assess its unstructured grid activities, improve the coordination among NASA centers, and promote technology transfer to industry. The proceedings represent contributions from Ames, Langley, and Lewis Research Centers, and the Johnson and Marshall Space Flight Centers. This report is a compilation of the presentations made at the workshop. For individual titles, see N94-22351 through N94-22372.

N94-22351*# Computer Sciences Corp., Hampton, VA.
SOFTWARE SYSTEMS USED FOR UNSTRUCTURED GRID GENERATION AT NASA LANGLEY
Michael J. Bockelie *In* NASA. Langley Research Center, Unstructured Grid Generation Techniques and Software Sep. 1993 p 5-17 (For primary document see N94-22350 05-61)
Avail: CASI HC A03/MF A03

These viewgraphs provide an overview of grid generation system for 3D configurations (Euler Grids) and grid generators of viscous and inviscid flow, solution adaptive for steady and unsteady flow. The five systems presented are VGRID, FELISA, TETRA, NGP, and TGRID. CASI

N94-22352*# National Aeronautics and Space Administration. Ames Research Center, Moffett Field, CA.
NASA-AMES RESEARCH CENTER UNSTRUCTURED TECHNOLOGY DEVELOPMENT
William R. VanDalsem *In* NASA. Langley Research Center, Unstructured Grid Generation Techniques and Software Sep. 1993 p 19-41 (For primary document see N94-22350 05-61)
Avail: CASI HC A03/MF A03

These viewgraphs present an overview and highlights of Cartesian, Prismatic and Hybrid grid generators and flow solvers. Also presented is Tetrahedra grid generation (including surface modeling/gridding). CASI

N94-22353*# National Aeronautics and Space Administration. Lewis Research Center, Cleveland, OH.
UNSTRUCTURED GRID RESEARCH AND USE AT NASA LEWIS RESEARCH CENTER
Mark G. Potapczuk *In* NASA. Langley Research Center, Unstructured Grid Generation Techniques and Software Sep. 1993 p 43-55 (For primary document see N94-22350 05-61)
Avail: CASI HC A03/MF A03

Computational fluid dynamics applications of grid research at LRC include inlets, nozzles, and ducts; turbomachinery; propellers - ducted and unducted; and aircraft icing. Some issues related to internal flow grid generation are resolution requirements on several boundaries, shock resolution vs. grid periodicity, grid spacing at blade/shroud gap, grid generation in turbine blade passages, and grid generation for inlet/nozzle geometries. Aircraft icing grid generation issues include (1) small structures relative to airfoil chord must be resolved; (2) excessive number of grid points in far-field using structured grid; and (3) grid must be recreated as ice shape grows. Derived from text

N94-22354*# National Aeronautics and Space Administration. Marshall Space Flight Center, Huntsville, AL.
GRID GENERATION REQUIREMENTS AT MARSHALL SPACE FLIGHT CENTER
Larry Kiefling *In* NASA. Langley Research Center, Unstructured Grid Generation Techniques and Software Sep. 1993 p 57-67 (For primary document see N94-22350 05-61)
Avail: CASI HC A03/MF A03

These viewgraphs present three examples of structural grid generation from MSFC analysts. The propulsion systems components include high performance requirements and multi-curved surfaces. Grid generation or finite element meshing for structural and thermal analysis models is currently accomplished using interactive graphics based software on personal workstations. Derived from text

N94-22355*# National Aeronautics and Space Administration. Lyndon B. Johnson Space Center, Houston, TX.
JOHNSON SPACE CENTER CFD GRID GENERATION REQUIREMENTS
Fred Martin *In* NASA. Langley Research Center, Unstructured Grid Generation Techniques and Software Sep. 1993 p 69-78 (For primary document see N94-22350 05-61)
Avail: CASI HC A02/MF A03

Topics are presented in viewgraph form and include the following: heavy lift launch vehicles, space shuttles, space transportation system, grid generation, computational fluid dynamics, space station, and flow distribution. CASI

N94-22356*# National Aeronautics and Space Administration. Ames Research Center, Moffett Field, CA.
THE 3-D UNSTRUCTURED MESH GENERATION USING LOCAL TRANSFORMATIONS
Timothy J. Barth *In* NASA. Langley Research Center, Unstructured Grid Generation Techniques and Software Sep. 1993 p 79-85 (For primary document see N94-22350 05-61)
Avail: CASI HC A02/MF A03

The topics are presented in viewgraph form and include the following: 3D combinatorial edge swapping; 3D incremental triangulation via local transformations; a new approach to multigrid for unstructured meshes; surface mesh generation using local transforms; volume triangulations; viscous mesh generation; and future directions. CASI

N94-22357*# National Aeronautics and Space Administration. Langley Research Center, Hampton, VA.
STATUS OF VGRID/USM3D AERO ANALYSIS SYSTEM
Neal T. Frink, Paresh Parikh (Vigyan Research Associates, Inc., Hampton, VA.), and Shahyar Pirzadeh (Vigyan Research Associates, Inc., Hampton, VA.) *In its* Unstructured Grid Generation Techniques and Software Sep. 1993 p 87-105 (For primary document see N94-22350 05-61)
Avail: CASI HC A03/MF A03

The topics are presented in viewgraph form and include the following: grid generation; flow solver; graphic postprocessing; dissemination; customer applications; and plans. CASI

N94-22358*# National Aeronautics and Space Administration. Lewis Research Center, Cleveland, OH.
UNSTRUCTURED LOW-MACH NUMBER VISCOUS FLOW SOLVER
Philip C. E. Jorgenson *In* NASA. Langley Research Center, Unstructured Grid Generation Techniques and Software Sep. 1993 p 107-120 (For primary document see N94-22350 05-61)
Avail: CASI HC A03/MF A03

The topics are presented in viewgraph form and include the following: governing equations; grid generation; numerical approach; results; and conclusions. CASI

N94-22359*# Vigyan Research Associates, Inc., Hampton, VA.
ROBUST UNSTRUCTURED GRID GENERATION WITH VGRID
Shahyar Pirzadeh *In* NASA. Langley Research Center, Unstructured Grid Generation Techniques and Software Sep. 1993 p 121-136 (For primary document see N94-22350 05-61)
Avail: CASI HC A03/MF A03

The objective of this work is to develop a robust, user-oriented, unstructured grid-generation technique for fast generation of Euler/viscous grids around complex 2D and 3D configurations. To do this, two different approaches are employed: the advancing-front method for generation of Euler grids; and the advancing-layers method for generation of viscous grids. A discussion of these topics is presented in viewgraph form. Author (revised)

N94-22360*# Sverdrup Technology, Inc., Brook Park, OH.
THREE-DIMENSIONAL UNSTRUCTURED GRID METHOD APPLIED TO TURBOMACHINERY
Oh Joon Kwon and Chunill Hah (National Aeronautics and Space Administration. Lewis Research Center, Cleveland, OH.) *In* NASA. Langley Research Center, Unstructured Grid Generation Techniques and Software Sep. 1993 p 137-149 (For primary document see N94-22350 05-61)
Avail: CASI HC A03/MF A03

This work has three objectives: to develop a three-dimensional flow solver based on unstructured tetrahedral meshes for turbomachinery flows; to validate the solver through comparisons with experimental data; and to apply the solver for better understanding of the flow through turbomachinery geometries and design improvement. The work followed three different approaches: an existing external flow solver/grid generator (USM3D/VGRID) was extensively modified for internal flows; a three-dimensional, finite-volume solver based on Roe's flux-difference splitting and explicit Runge-Kutta time stepping; and three-dimensional unstructured tetrahedral mesh generation using an advancing-front technique. A discussion of these topics is presented in viewgraph form. Derived from text

N94-22361*# National Aeronautics and Space Administration. Langley Research Center, Hampton, VA.
DEVELOPMENT OF A GRIDLESS CFD METHOD
John T. Batina *In its* Unstructured Grid Generation Techniques and Software Sep. 1993 p 151-162 (For primary document see N94-22350 05-61)
Avail: CASI HC A03/MF A03

The objective of this paper is to stimulate ideas concerning alternative approaches to discretizing fluid flow problems, i.e., the so-called gridless approach. The gridless approach uses only clouds of points and does not require that the points be connected to form a grid as is necessary in conventional CFD algorithms. The governing equations are solved directly by performing local least-squares curve fits in each cloud of points and then analytically differentiating the resulting curve fits to approximate the

derivatives. A discussion of these topics is presented in viewgraph form.
Derived from text

N94-22362*# Institute for Computer Applications in Science and Engineering, Hampton, VA.
AN ADVANCING-FRONT DELAUNAY-TRIANGULATION ALGORITHM DESIGNED FOR ROBUSTNESS
D. J. Mavriplis *In* NASA. Langley Research Center, Unstructured Grid Generation Techniques and Software Sep. 1993 p 163-180 (For primary document see N94-22350 05-61)
Avail: CASI HC A03/MF A03

The following topics, which are associated with computational fluid dynamics, are discussed: unstructured mesh generation; the advancing front methodology; failures of the advancing front methodology; Delaunay triangulation; the Tanamua-Merriam algorithm; Yet Another Grid Generator (YAGG); and advancing front-Delaunay triangulation. The discussion is presented in viewgraph form. Author (revised)

N94-22363*# National Aeronautics and Space Administration. Ames Research Center, Moffett Field, CA.
DYNAMIC MESH ADAPTION FOR TRIANGULAR AND TETRAHEDRAL GRIDS
Rupak Biswas and Roger Strawn *In* NASA. Langley Research Center, Unstructured Grid Generation Techniques and Software Sep. 1993 p 181-192 (For primary document see N94-22350 05-61)
Avail: CASI HC A03/MF A03

The following topics are discussed: requirements for dynamic mesh adaption; linked-list data structure; edge-based data structure; adaptive-grid data structure; three types of element subdivision; mesh refinement; mesh coarsening; additional constraints for coarsening; anisotropic error indicator for edges; unstructured-grid Euler solver; inviscid 3-D wing; and mesh quality for solution-adaptive grids. The discussion is presented in viewgraph form.
Derived from text

N94-22364*# National Aeronautics and Space Administration. Lewis Research Center, Cleveland, OH.
CARTESIAN-CELL BASED GRID GENERATION AND ADAPTIVE MESH REFINEMENT
William J. Coirier and Kenneth G. Powell (Michigan Univ., Ann Arbor.) *In* NASA. Langley Research Center, Unstructured Grid Generation Techniques and Software Sep. 1993 p 193-201 (For primary document see N94-22350 05-61)
Avail: CASI HC A02/MF A03

Viewgraphs on Cartesian-cell based grid generation and adaptive mesh refinement are presented. Topics covered include: grid generation; cell cutting; data structures; flow solver formulation; adaptive mesh refinement; and viscous flow. CASI

N94-22365*# Lockheed Engineering and Sciences Co., Hampton, VA.
THE 2D AND 3D HYPERSONIC FLOWS WITH UNSTRUCTURED MESHES
Rajiv Thareja *In* NASA. Langley Research Center, Unstructured Grid Generation Techniques and Software Sep. 1993 p 203-221 (For primary document see N94-22350 05-61)
Avail: CASI HC A03/MF A03

Viewgraphs on 2D and 3D hypersonic flows with unstructured meshes are presented. Topics covered include: mesh generation, mesh refinement, shock-shock interaction, velocity contours, mesh movement, vehicle bottom surface, and adapted meshes. CASI

N94-22366*# Computer Sciences Corp., Hampton, VA.
UNSTRUCTURED SURFACE GRID GENERATION
Jamshid Samareh-Abolhassani *In* NASA. Langley Research Center, Unstructured Grid Generation Techniques and Software Sep. 1993 p 223-249 (For primary document see N94-22350 05-61)
Avail: CASI HC A03/MF A03

Viewgraphs on unstructured surface grid generation are presented. Topics covered include: requirements for curves, surfaces, solids, and text; surface approximation; triangulation; advancing; projection; mapping; and parametric curves. CASI

N94-22367*# National Aeronautics and Space Administration. Ames Research Center, Moffett Field, CA.
THE 3D EULER SOLUTIONS USING AUTOMATED CARTESIAN GRID GENERATION
John E. Melton, Francis Y. Enomoto, and Marsha J. Berger (New York Univ., New York.) *In* NASA. Langley Research Center, Unstructured Grid Generation Techniques and Software Sep. 1993 p 251-260 (For primary document see N94-22350 05-61)
Avail: CASI HC A02/MF A03

Viewgraphs on 3-dimensional Euler solutions using automated Cartesian grid generation are presented. Topics covered include: computational fluid dynamics (CFD) and the design cycle; Cartesian grid strategy; structured body fit; grid generation; prolate spheroid; and ONERA M6 wing. CASI

N94-22368*# National Aeronautics and Space Administration. Langley Research Center, Hampton, VA.
ACCURACY ASSESSMENT FOR GRID ADAPTATION
Gary P. Warren *In its* Unstructured Grid Generation Techniques and Software Sep. 1993 p 261-275 (For primary document see N94-22350 05-61)
Avail: CASI HC A03/MF A03

Viewgraphs on accuracy assessment for grid adaptation are presented. Topics covered include: uniform refinement, grid convergence, adapted grids, oblique shock wave, supersonic flow, and sonic flow. CASI

N94-22369*# Purdue Univ., West Lafayette, IN.
TIME-DEPENDENT GRID ADAPTATION FOR MESHES OF TRIANGLES AND TETRAHEDRA
Russ D. Rausch *In* NASA. Langley Research Center, Unstructured Grid Generation Techniques and Software Sep. 1993 p 277-290 (For primary document see N94-22350 05-61)
Avail: CASI HC A03/MF A03

This paper presents in viewgraph form a method of optimizing grid generation for unsteady CFD flow calculations that distributes the numerical error evenly throughout the mesh. Adaptive meshing is used to locally enrich in regions of relatively large errors and to locally coarsen in regions of relatively small errors. The enrichment/coarsening procedures are robust for isotropic cells; however, enrichment of high aspect ratio cells may fail near boundary surfaces with relatively large curvature. The enrichment indicator worked well for the cases shown, but in general requires user supervision for a more efficient solution. CASI

N94-22370*# National Aeronautics and Space Administration. Langley Research Center, Hampton, VA.
COMPUTATIONAL GEOMETRY ISSUES
Mary-Anne K. Posenau *In its* Unstructured Grid Generation Techniques and Software Sep. 1993 p 291-309 (For primary document see N94-22350 05-61)
Avail: CASI HC A03/MF A03

Presented in viewgraph format are some of the benefits of computational geometry for grid generation, including benefits to grid quality and algorithm efficiency. Many efficient algorithms are available, but it is concluded that high aspect ratio triangulations are not among them. Derived from text

N94-22371*# National Aeronautics and Space Administration. Ames Research Center, Moffett Field, CA.
NASA DATA EXCHANGE STANDARDS FOR COMPUTATIONAL FLUID DYNAMICS
Matthew Blake *In* NASA. Langley Research Center, Unstructured Grid Generation Techniques and Software Sep. 1993 p 311-321 (For primary document see N94-22350 05-61)
Avail: CASI HC A03/MF A03

This paper covers the following topics in viewgraph format: purpose of data exchange standards; data exchange in engineering analysis/CFD; geometry data exchange through existing product data exchange standards, NASA Data Exchange Committee, and NASA-IGES (Initial Graphics Exchange Specification); CFD grid and solution data exchange; and data exchange for multi-disciplinary engineering. Derived from text

N94-22372*# National Aeronautics and Space Administration. Ames Research Center, Moffett Field, CA.
SURFACE ACQUISITION THROUGH VIRTUAL MILLING

Marshal L. Merriam *In* NASA. Langley Research Center, Unstructured Grid Generation Techniques and Software Sep. 1993 p 323-337 (For primary document see N94-22350 05-61)
Avail: CASI HC A03/MF A03

Surface acquisition deals with the reconstruction of three dimensional objects from a set of data points. The most straightforward techniques require human intervention, a time consuming proposition. It is desirable to develop a fully automated alternative. Such a method is proposed in this paper. It makes use of surface measurements obtained from a 3-D laser digitizer - an instrument which provides the (x,y,z) coordinates of surface data points from various viewpoints. These points are assembled into several partial surfaces using a visibility constraint and a 2-D triangulation technique. Reconstruction of the final object requires merging these partial surfaces. This is accomplished through a procedure that emulates milling, a standard machining operation. From a geometrical standpoint the problem reduces to constructing the intersection of two or more non-convex polyhedra.
Author

N94-22375*# California Univ., Berkeley. Lawrence Berkeley Lab.
DATABASE COMPUTING IN HEP Abstract Only
C. T. Day, S. Loken, J. F. MacFarlane, E. May (Argonne National Lab., Idaho Falls, ID.), D. Lifka (Argonne National Lab., Idaho Falls, ID.), E. Lusk (Argonne National Lab., Idaho Falls, ID.), L. E. Price (Argonne National Lab., Idaho Falls, ID.), A. Baden (Maryland Univ., College Park.), R. Grossman (Chicago Univ., IL.), and X. Qin (Maryland Univ., College Park.) 1992 2 p
(Contracts NAG2-513; DE-FG02-92ER-25133; DE-AC03-76SF-00098)
(NASA-CR-194791; NAS 1.26:194791) Avail: CASI HC A01/MF A01

The major SSC experiments are expected to produce up to 1 Petabyte of data per year each. Once the primary reconstruction is completed by farms of inexpensive processors, I/O becomes a major factor in further analysis of the data. We believe that the application of database techniques can significantly reduce the I/O performed in these analyses. We present examples of such I/O reductions in prototypes based on relational and object-oriented databases of CDF data samples.
Author

N94-22376*# Illinois Univ., Chicago. Lab. for Advanced Computing.
A PROOF-OF-CONCEPT IMPLEMENTATION OF PERSISTENCE IN A HIERARCHICAL STORAGE SYSTEM Abstract Only
Robert Grossman, Xiao Qin, and Dave Lifka (Argonne National Lab., IL.) Oct. 1992 2 p
(Contract NAG2-513; DE-FG02-92ER-25133)
(NASA-CR-194790; NAS 1.26:194790) Avail: CASI HC A01/MF A01

The concept of providing transparent access to a collection of files in a mass storage system is a familiar one. The goal of this project was to investigate the feasibility of providing similar access to a collection of persistent, complex objects. We describe an architecture for interfacing a persistent store of complex objects to a hierarchical storage system. Persistent object stores support the uniform creation, storage, and access of complex objects, regardless of their lifetimes. In other words, a mechanism is provided so that persistent objects outlive the processes which create them and can be accessed in a uniform manner by other processes. We validated this architecture by implementing a proof-of-concept system and testing the system on two stores of data. These tests indicate that this architecture supports the creation, storage, and access of very large persistent object stores.
Author

N94-22383# Sandia National Labs., Albuquerque, NM.
A COMPARISON OF IDEF1X AND NIAM ISDM
J. K. Sharp 1993 13 p Presented at the 1993 Conference on Natural Language Information Analysis Methodology and Information System Design Methodology, Utrecht, 15-17 Sep. 1993
(Contract DE-AC04-76DP-00789)
(DE93-040899; SAND-93-2130C; CONF-9309238-1) Avail: CASI HC A03/MF A01

This paper describes the major differences in the IDEFIX and NIAM ISDM information modeling methodologies and presents the different philosophies behind these methodologies. The IDEFIX methodology base document comes from the Integrated Information Support System (IISS) project sponsored by the US Air Force. The IISS project office was contacted and they supplied the referenced document as the best base description of this methodology. The NIAM ISDM methodology base documents present the general NIAM methodology. IDEFIX is a variant of the entity-attribute-relationship (E-A-R) approach to data modeling and although many other variants exist, the comparison presented here covers the common aspects of entity-relationship approaches. This comparison identifies and illustrates the differences in the two methodologies.
DOE

N94-22406# Stanford Univ., CA. Systems Optimization Lab.
ALGORITHMIC ADVANCES IN STOCHASTIC PROGRAMMING
D. P. Morton Jul. 1993 116 p
(Contract DE-FG03-92ER-25116)
(DE94-001160; SU-SOL-93-6) Avail: CASI HC A06/MF A02

Practical planning problems with deterministic forecasts of inherently uncertain parameters often yield unsatisfactory solutions. Stochastic programming formulations allow uncertain parameters to be modeled as random variables with known distributions, but the size of the resulting mathematical programs can be formidable. Decomposition-based algorithms take advantage of special structure and provide an attractive approach to such problems. We consider two classes of decomposition-based stochastic programming algorithms. The first type of algorithm addresses problems with a 'manageable' number of scenarios. The second class incorporates Monte Carlo sampling within a decomposition algorithm. We develop and empirically study an enhanced Benders decomposition algorithm for solving multistage stochastic linear programs within a prespecified tolerance. The enhancements include warm start basis selection, preliminary cut generation, the multicut procedure, and decision tree traversing strategies. Computational results are presented for a collection of 'real-world' multistage stochastic hydroelectric scheduling problems. Recently, there has been an increased focus on decomposition-based algorithms that use sampling within the optimization framework. These approaches hold much promise for solving stochastic programs with many scenarios. A critical component of such algorithms is a stopping criterion to ensure the quality of the solution. With this as motivation, we develop a stopping rule theory for algorithms in which bounds on the optimal objective function value are estimated by sampling. Rules are provided for selecting sample sizes and terminating the algorithm under which asymptotic validity of confidence interval statements for the quality of the proposed solution can be verified. Issues associated with the application of this theory to two sampling-based algorithms are considered, and preliminary empirical coverage results are presented.
DOE

N94-21080*# National Aeronautics and Space Administration. Goddard Space Flight Center, Greenbelt, MD.
AN ADAPTIVE, LOSSLESS DATA COMPRESSION ALGORITHM AND VLSI IMPLEMENTATIONS
Jack Venbrux (New Mexico Univ., Albuquerque.), Greg Zweigle (Advanced Hardware Architectures, Moscow, ID.), Jody Gambles (New Mexico Univ., Albuquerque.), Don Wiseman (New Mexico Univ., Albuquerque.), Warner H. Miller, and Pen-Shu Yeh *In* New Mexico Univ., The Fifth NASA Symposium on VLSI Design 1993 16 p (For primary document see N94-21079 05-33)
(Grant NAGw-3292)
Avail: CASI HC A03/MF A06

N94-21116*# Toledo Univ., OH. Dept. of Electrical Engineering.
SYNTHESIS ALGORITHM OF VLSI MULTIPLIERS FOR ASIC
O. H. Chua and A. G. Eldin *In* New Mexico Univ., The Fifth NASA Symposium on VLSI Design 1993 13 p (For primary document see N94-21079 05-33)
Avail: CASI HC A03/MF A06

N94-21129*# Idaho Univ., Moscow. Microelectronics Research Center.
A CAM-BASED LZ DATA COMPRESSION IC
K. Winters, R. Bode (Advanced Hardware Architectures, Moscow, ID.), and E. Schneider (Video Lottery Consultants, Inc., Bozeman, MT.) *In* New Mexico Univ., The Fifth NASA Symposium on VLSI design 1993 8 p (For primary document see N94-21079 05-33)
Avail: CASI HC A02/MF A06

N94-21130*# New Mexico State Univ., Las Cruces. Center for Space Telemetering and Telecommunications Systems.
HIGH-SPEED VITERBI DECODING WITH OVERLAPPING CODE SEQUENCES

Michael D. Ross and William P. Osborne *In* New Mexico Univ., The Fifth NASA Symposium on VLSI Design 1993 8 p (For primary document see N94-21079 05-33)
Avail: CASI HC A02/MF A06

N94-21325*# Computer Sciences Corp., Lanham, MD.
LET YOUR FINGERS DO THE WALKING: THE PROJECTS MOST INVALUABLE TOOL
Deborah A. Zirk *In* NASA. Goddard Space Flight Center, Networks Technology Conference Nov. 1993 p 11-25 (For primary document see N94-21323 05-62)
Avail: CASI HC A03/MF A03

N94-21326*# Computer Sciences Corp., Lanham, MD.
SOFTWARE METRICS: THE KEY TO QUALITY SOFTWARE ON THE NCC PROJECT
Patricia J. Burns *In* NASA. Goddard Space Flight Center, Networks Technology Conference Nov. 1993 p 27-39 (For primary document see N94-21323 05-62)
Avail: CASI HC A03/MF A03

N94-21342*# Stanford Telecommunications, Inc., Seabrook, MD.
THE THREE-DIMENSIONAL EVENT-DRIVEN GRAPHICS ENVIRONMENT (3D-EDGE)
Jeffrey Freedman, Roger Hahn, and David M. Schwartz *In* NASA. Goddard Space Flight Center, Networks Technology Conference Nov. 1993 p 235-240 (For primary document see N94-21323 05-62)
(Contract NAS5-31500)
Avail: CASI HC A02/MF A03

N94-21389 MATRA Marconi Space, Toulouse (France).
COMBINATION OF ON GROUND EXPERIMENTS AND ANALYSIS SOFTWARE FOR THE EVALUATION OF MATERIAL DEGRADATION IN SPACE (SILEX PROJECT)
P. Renard *In* CNES, Fifth International Symposium on Materials in a Space Environment Jun. 1993 p 311-320 (For primary document see N94-21367 05-18)
Copyright Avail: CEPADUES-Editions, 111, rue Nicolas-Vaquelin, 31100 Toulouse, France

N94-21475*# Massachusetts Inst. of Tech., Cambridge. Research Lab. of Electronics.
OPTIMAL CONVOLUTION SOR ACCELERATION OF WAVEFORM RELAXATION WITH APPLICATION TO SEMICONDUCTOR DEVICE SIMULATION
Mark Reichelt *In* NASA. Langley Research Center, The Sixth Copper Mountain Conference on Multigrid Methods, Part 2 Nov. 1993 p 513-526 Sponsored in part by IBM (For primary document see N94-21464 05-64)
(Contract N00014-91-J-1698; NSF MIP-88-58764)
Avail: CASI HC A03/MF A03

N94-21483*# National Aeronautics and Space Administration. Langley Research Center, Hampton, VA.
MAPPING ROBUST PARALLEL MULTIGRID ALGORITHMS TO SCALABLE MEMORY ARCHITECTURES
Andrea Overman and John VanRosendale *In its* The Sixth Copper Mountain Conference on Multigrid Methods, Part 2 Nov. 1993 p 635-647 See also N93-32359 (For primary document see N94-21464 05-64)
(Contracts NAS1-19480; NAS1-18605)
Avail: CASI HC A03/MF A03

N94-21699*# Washington State Univ., Pullman.
DESIGN OF A NEW SQUARING FUNCTION FOR THE VITERBI ALGORITHM
Aria Eshraghi, Terri Fiez, Thomas Fischer, and Kel Winters (Advanced Hardware Architectures, Moscow, ID.) *In* Idaho Univ., The 1992 4th NASA SERC Symposium on VLSI Design 1992 8 p (For primary document see N94-21694 05-33)
Avail: CASI HC A02/MF A04

N94-21704*# Nanyang Technological Inst. (Singapore). School of Electrical and Electronic Engineering.
HEURISTIC-BASED SCHEDULING ALGORITHM FOR HIGH LEVEL SYNTHESIS
Gulam Mohamed, Han-Ngee Tan, and Chew-Lye Chng *In* Idaho Univ., The 1992 4th NASA SERC Symposium on VLSI Design 1992 8 p (For primary document see N94-21694 05-33)
Avail: CASI HC A02/MF A04

N94-21706*# University of Southwestern Louisiana, Lafayette. Center for Advanced Computer Studies.
A STATISTICAL-BASED SCHEDULING ALGORITHM IN AUTOMATED DATA PATH SYNTHESIS
Byung Wook Jeon and Chidchanok Lursinsap *In* Idaho Univ., The 1992 4th NASA SERC Symposium on VLSI Design 1992 8 p (For primary document see N94-21694 05-33)
Avail: CASI HC A02/MF A04

N94-21710*# Johns Hopkins Univ., Laurel, MD. Applied Physics Lab.
DESIGN AND TEST OF FIELD PROGRAMMABLE GATE ARRAYS IN SPACE APPLICATIONS
Priscilla L. McKerracher, Russel P. Cain, Jon C. Barnett, William S. Green, and James D. Kinnison *In* Idaho Univ., The 1992 4th NASA SERC Symposium on VLSI Design 1992 2 p (For primary document see N94-21694 05-33)
Avail: CASI HC A01/MF A04

N94-21713*# New Mexico Univ., Albuquerque. NASA Space Engineering Research Center.
LINKS BETWEEN N-MODULAR REDUNDANCY AND THE THEORY OF ERROR-CORRECTING CODES
V. Bobin (Hewlett-Packard Co., Santa Clara, CA.), S. Whitaker, and G. Maki *In* Idaho Univ., The 1992 4th NASA SERC Symposium on VLSI Design 1992 11 p (For primary document see N94-21694 05-33)
(Grant NAGw-1406)
Avail: CASI HC A03/MF A04

N94-21714*# New Mexico Univ., Albuquerque. Microelectronics Research Center.
REDUCTION OF BLOCKING EFFECTS FOR THE JPEG BASELINE IMAGE COMPRESSION STANDARD
Gregary C. Zweigle and Roberto H. Bamberger (Washington State Univ., Pullman.) *In* Idaho Univ., The 1992 4th NASA SERC Symposium on VLSI Design 1992 11 p (For primary document see N94-21694 05-33)
(Grant NSF MIPS-91-16683)
Avail: CASI HC A03/MF A04

N94-21715*# Utah State Univ., Logan. Depts. of Electrical Engineering and Computer Science.
A NOVEL VISUAL HARDWARE BEHAVIORAL LANGUAGE
Xueqin Li and H. D. Cheng *In* Idaho Univ., The 1992 4th NASA SERC Symposium on VLSI Design 1992 12 p (For primary document see N94-21694 05-33)
Avail: CASI HC A03/MF A04

N94-21716*# California Univ., Davis. Dept. of Computer Science.
A MECHANIZED PROCESS ALGEBRA FOR VERIFICATION OF DEVICE SYNCHRONIZATION PROTOCOLS
E. Thomas Schubert *In* Idaho Univ., The 1992 4th NASA SERC Symposium on VLSI Design 1992 13 p (For primary document see N94-21694 05-33)
(Contract NAS1-18586)
Avail: CASI HC A03/MF A04

N94-21719*# Idaho Univ., Moscow. Dept. of Computer Science.
INSTRUCTION SET COMMUTIVITY
P. Windley *In its* The 1992 4th NASA SERC Symposium on VLSI Design 1992 11 p (For primary document see N94-21694 05-33)
(Contract MDA904-91-C-7054)
Avail: CASI HC A03/MF A04

N94-21729*# Toledo Univ., OH. Electrical Engineering Dept.
A DRAM COMPILER ALGORITHM FOR HIGH PERFORMANCE VLSI EMBEDDED MEMORIES
A. G. Eldin *In* Idaho Univ., The 1992 4th NASA SERC Symposium on VLSI Design 1992 13 p (For primary document see N94-21694 05-33)
Avail: CASI HC A03/MF A04

N94-21730*# Peradeniya Univ. (Sri Lanka).
A NOVEL CACHE MECHANISM
J. A. Gunawardena *In* Idaho Univ., The 1992 4th NASA SERC Symposium on VLSI Design 1992 12 p (For primary document see N94-21694 05-33)
Avail: CASI HC A03/MF A04

N94-21731*# Idaho Univ., Moscow. Dept. of Electrical Engineering.
A SET-ASSOCIATIVE, FAULT-TOLERANT CACHE DESIGN
Dan Lamet and James F. Frenzel *In its* The 1992 4th NASA SERC Symposium on VLSI Design 1992 5 p (For primary document see N94-21694 05-33)
(Grant NAGw-1406)
Avail: CASI HC A01/MF A04

N94-22064# Academy of Sciences (USSR), Moscow. Computer Center.
COMPUTER-AIDED DESIGN SYSTEM FOR OBJECTS LOCATION AND RESERVOIR WITH DISPERSED RESOURCE EVOLUTION INVESTIGATION
S. V. Tuev *In* Technical Research Centre of Finland, Information Technology and Economic Modelling 1992 p 76-84 (For primary document see N94-22056 05-83)
Copyright Avail: CASI HC A02/MF A03

N94-22066# Algorithm Co. (Russia).
THE SOVIET SOFTWARE MARKET: CURRENT STATE AND ASPECTS OF DEVELOPMENT
Sergei A. Chizhov *In* Technical Research Centre of Finland, Information Technology and Economic Modelling 1992 p 86-92 (For primary document see N94-22056 05-83)
Copyright Avail: CASI HC A02/MF A03

N94-22067# Nokia Data, Helsinki (Finland).
APPLICATION DEVELOPMENT IN A PC/LAN ENVIRONMENT Abstract Only
Kurt Helenelund *In* Technical Research Centre of Finland, Information Technology and Economic Modelling 1992 p 93 (For primary document see N94-22056 05-83)
Copyright Avail: CASI HC A01/MF A03

N94-22068# All-Union Research Inst. on Computer and Informatics Problems, Moscow (Russia).
THE DISTRIBUTED CAD SYSTEM FOR LSI/VLSI DESIGN
V. G. Zacharov and V. A. Konyavsky *In* Technical Research Centre of Finland, Information Technology and Economic Modelling 1992 p 94-100 (For primary document see N94-22056 05-83)
Copyright Avail: CASI HC A02/MF A03

N94-22077# Academy of Sciences (USSR), Moscow. Computer Center.
APL-TECHNOLOGY OF COMPUTER SIMULATION
A. Y. Boozin *In* Technical Research Centre of Finland, Information Technology and Economic Modelling 1992 p 206-212 (For primary document see N94-22056 05-83)
Copyright Avail: CASI HC A02/MF A03

N94-22078# Technical Research Centre of Finland, Espoo.
APPLICATION OF THE STRUCTURES QUERY LANGUAGE OF APROS FOR SPECIFICATION OF INDUSTRIAL PROCESSES
Kaj Juslin *In its* Information Technology and Economic Modelling 1992 p 213-225 (For primary document see N94-22056 05-83)
Copyright Avail: CASI HC A03/MF A03

N94-22079# Academy of Sciences (USSR), Moscow.
THE COMBINATORIAL ALGORITHMS FOR LARGE SCALE DISCRETE OPTIMIZATION PROBLEMS
V. R. Khachaturov, I. H. Sigal, V. E. Veselovskii, and A. V. Zlotov *In* Technical Research Centre of Finland, Information Technology and Economic Modelling 1992 p 226-236 (For primary document see N94-22056 05-83)
Copyright Avail: CASI HC A03/MF A03

N94-22083# Academy of Sciences (USSR), Moscow. Automated Systems Inst.
THREE ORIGINAL PROGRAMMES FOR MANAGERS
Konstantin A. Antipov, Helen S. Bakanova, Sergei V. Letunovskiy, Sergei V. Marchenko, Sergei A. Orlov, Oleg L. Smirnov, and Vyacheslav Y. Smith *In* Technical Research Centre of Finland, Information Technology and Economic Modelling 1992 p 261-264 (For primary document see N94-22056 05-83)
Copyright Avail: CASI HC A01/MF A03

N94-22087# Academy of Sciences (USSR), Moscow. Computer Center.
METHOD AND SOFTWARE FOR DECISION MAKING IN PUBLIC PROBLEMS
Alexander Lotov, Vladimir Bushenkov (Institute of Technology, Helsinki, Finland.), George Kamenev, and Oleg Chernykh *In* Technical Research Centre of Finland, Information Technology and Economic Modelling 1992 p 293-308 (For primary document see N94-22056 05-83)
Copyright Avail: CASI HC A03/MF A03

N94-22106 Toronto Univ. (Ontario). Dept. of Electrical Engineering.
DIRECTIONAL CODING OF MORPHOLOGICAL PYRAMIDAL REPRESENTATIONS
Zi-Heng Zhou and Anatasios N. Venetsanopoulos *In* Engineering Inst. of Canada, Canadian Conference on Electrical and Computer Engineering, Volumes 1 and 2 1991 4 p (For primary document see N94-22101 05-33)
Avail: Issuing Activity (Engineering Inst. of Canada, 2050 rue Mansfield, Suite 700, Montreal, PQ H3A 1Z2 Canada)

N94-22108 Laval Univ. (Quebec). Lab. de Vision et Systemes Numeriques.
HIERARCHICAL SURFACE TRIANGULATION OF RANGE DATA
Marc Soucy and Denis Laurendeau *In* Engineering Inst. of Canada, Canadian Conference on Electrical and Computer Engineering, Volumes 1 and 2 1991 4 p (For primary document see N94-22101 05-33)
Avail: Issuing Activity (Engineering Inst. of Canada, 2050 rue Mansfield, Suite 700, Montreal, PQ H3A 1Z2 Canada)

N94-22109 Concordia Univ., Montreal (Quebec). Dept. of Computer Science.
SEGMENTATION AND FITTING BY RESIDUAL CONSENSUS
Xin-Ming Yu, T. D. Bui, and A. Krzyzak *In* Engineering Inst. of Canada, Canadian Conference on Electrical and Computer Engineering, Volumes 1 and 2 1991 4 p (For primary document see N94-22101 05-33)
Avail: Issuing Activity (Engineering Inst. of Canada, 2050 rue Mansfield, Suite 700, Montreal, PQ H3A 1Z2 Canada)

N94-22116 Ecole Polytechnique, Montreal (Quebec). Dept. de Genie Electrique.
TESTS OF LOGIC SPACES: A NEW STRATEGY FOR CERTIFYING THE ACCURACY OF PROGRAMS [TESTS DES ESPACES LOGIQUES: UNE NOUVELLE STRATEGIE POUR CERTIFIER L'EXACTITUDE DES PROGRAMMES]
Pierre Veronneau and Pierre-N. Robillard *In* Engineering Inst. of Canada, Canadian Conference on Electrical and Computer Engineering, Volumes 1 and 2 1991 4 p In FRENCH (For primary document see N94-22101 05-33)
Avail: Issuing Activity (Engineering Inst. of Canada, 2050 rue Mansfield, Suite 700, Montreal, PQ H3A 1Z2 Canada)

N94-22117 Bell-Northern Research Ltd., Ottawa (Ontario).
MODELING SOFTWARE SYSTEMS FOR DATA FLOW TESTING
Bo Yang and Hasan Ural (Ottawa Univ., Ontario.) *In* Engineering Inst. of

Canada, Canadian Conference on Electrical and Computer Engineering, Volumes 1 and 2 1991 4 p (For primary document see N94-22101 05-33)
Avail: Issuing Activity (Engineering Inst. of Canada, 2050 rue Mansfield, Suite 700, Montreal, PQ H3A 1Z2 Canada)

N94-22118 Mitsubishi Electric Corp., Kamakura (Japan). Communication Systems Lab.
THE CONFORMANCE TESTING METHODOLOGY TO CTRON (COMMUNICATION AND CENTRAL TRON) EXTENDED OS
Yoshiaki Terashima, Hiroshi Matsuyama, Akira Otsuka, and Tsutomu Iwahashi *In* Engineering Inst. of Canada, Canadian Conference on Electrical and Computer Engineering, Volumes 1 and 2 1991 4 p (For primary document see N94-22101 05-33)
Avail: Issuing Activity (Engineering Inst. of Canada, 2050 rue Mansfield, Suite 700, Montreal, PQ H3A 1Z2 Canada)

N94-22124 Communications Research Centre, Ottawa (Ontario). Dept. of Communications.
SOFTWARE IMPLEMENTATION OF AN ADAPTIVE DIGITAL AUTOMATIC LEVEL CONTROL
Y. Jolly *In* Engineering Inst. of Canada, Canadian Conference on Electrical and Computer Engineering, Volumes 1 and 2 1991 4 p (For primary document see N94-22101 05-33)
Avail: Issuing Activity (Engineering Inst. of Canada, 2050 rue Mansfield, Suite 700, Montreal, PQ H3A 1Z2 Canada)

N94-22148 Toronto Univ. (Ontario). Computer Integrated Manufacturing Lab.
ELLIPTICAL-SHAPE PARAMETER ESTIMATION FROM A SET OF NORMAL LINES
I. Tchoukanov, R. Safaee-Rad, B. Benhabib, and K. C. Smith *In* Engineering Inst. of Canada, Canadian Conference on Electrical and Computer Engineering, Volumes 1 and 2 1991 4 p (For primary document see N94-22101 05-33)
Avail: Issuing Activity (Engineering Inst. of Canada, 2050 rue Mansfield, Suite 700, Montreal, PQ H3A 1Z2 Canada)

N94-22149 Regina Univ. (Saskatchewan).
SCALE-SPACE FILTERING AND THRESHOLD HIERARCHY FOR IMAGE SEGMENTATION
Neng-Quan Wang, Xue-Dong Yang, and L. R. Symes *In* Engineering Inst. of Canada, Canadian Conference on Electrical and Computer Engineering, Volumes 1 and 2 1991 4 p (For primary document see N94-22101 05-33)
Avail: Issuing Activity (Engineering Inst. of Canada, 2050 rue Mansfield, Suite 700, Montreal, PQ H3A 1Z2 Canada)

N94-22150 New Brunswick Univ., Fredericton. Faculty of Computer Science.
NEW ALGORITHM FOR THE DETECTION OF THE ORIENTATION OF A PLANAR LAMBERTIAN SURFACE IN 3D
Przemyslaw Pochec *In* Engineering Inst. of Canada, Canadian Conference on Electrical and Computer Engineering, Volumes 1 and 2 1991 2 p (For primary document see N94-22101 05-33)
Avail: Issuing Activity (Engineering Inst. of Canada, 2050 rue Mansfield, Suite 700, Montreal, PQ H3A 1Z2 Canada)

N94-22157 Paramax Electronic, Inc., Montreal (Quebec).
THE WHY, WHAT, AND HOW OF Ada SOFTWARE DEVELOPMENT
Paul D. Hamilton *In* Engineering Inst. of Canada, Canadian Conference on Electrical and Computer Engineering, Volumes 1 and 2 1991 4 p (For primary document see N94-22101 05-33)
Avail: Issuing Activity (Engineering Inst. of Canada, 2050 rue Mansfield, Suite 700, Montreal, PQ H3A 1Z2 Canada)

N94-22158 SD Scicon Public Ltd. Co., Cheadle (England).
FORMAL METHODS IN THE DESIGN OF CRITICAL SOFTWARE SYSTEMS
J. Burns and J. Spruce Riordon (AEPOS Technologies Corp., Hull, Quebec.) *In* Engineering Inst. of Canada, Canadian Conference on Electrical and Computer Engineering, Volumes 1 and 2 1991 4 p (For primary document see N94-22101 05-33)
Avail: Issuing Activity (Engineering Inst. of Canada, 2050 rue Mansfield, Suite 700, Montreal, PQ H3A 1Z2 Canada)

N94-22165 Laval Univ. (Quebec). Dept. of Electrical Engineering.
A MODIFIED MOMENT INVARIANTS TECHNIQUE FOR CLASSIFICATION OF NOISY OBJECTS
Halet Arezki, H. T. Huynh, and G. A. Lampropoulos *In* Engineering Inst. of Canada, Canadian Conference on Electrical and Computer Engineering, Volumes 1 and 2 1991 4 p (For primary document see N94-22101 05-33)
Avail: Issuing Activity (Engineering Inst. of Canada, 2050 rue Mansfield, Suite 700, Montreal, PQ H3A 1Z2 Canada)

N94-22173 Laval Univ. (Quebec). Dept. de Genie Electrique.
CODING OF COLOR QUANTIZED IMAGES
Andre Zaccarin and Bede Liu (Princeton Univ., NJ.) *In* Engineering Inst. of Canada, Canadian Conference on Electrical and Computer Engineering, Volumes 1 and 2 1991 4 p (For primary document see N94-22101 05-33)
Avail: Issuing Activity (Engineering Inst. of Canada, 2050 rue Mansfield, Suite 700, Montreal, PQ H3A 1Z2 Canada)

N94-22174 Toronto Univ. (Ontario). Dept. of Electrical Engineering.
HIERARCHICAL MULTIRATE VECTOR QUANTIZATION FOR IMAGE CODING
P. Yu and A. N. Venetsanopoulos *In* Engineering Inst. of Canada, Canadian Conference on Electrical and Computer Engineering, Volumes 1 and 2 1991 4 p (For primary document see N94-22101 05-33)
Avail: Issuing Activity (Engineering Inst. of Canada, 2050 rue Mansfield, Suite 700, Montreal, PQ H3A 1Z2 Canada)

N94-22191 Queens Univ., Kingston (Ontario). Dept. of Electrical Engineering.
THE SCHUR BERLEKAMP-MASSEY ALGORITHM IS PARALLELIZABLE
Gordon Chan and Christopher Zarowski *In* Engineering Inst. of Canada, Canadian Conference on Electrical and Computer Engineering, Volumes 1 and 2 1991 4 p (For primary document see N94-22101 05-33)
Avail: Issuing Activity (Engineering Inst. of Canada, 2050 rue Mansfield, Suite 700, Montreal, PQ H3A 1Z2 Canada)

N94-22194 Queens Univ., Kingston (Ontario). Dept. of Electrical Engineering.
MODELING AND ANALYSIS OF SECURE COMMUNICATION PROTOCOLS USING PETRI NET FORMALISM
Benjamin B. Nieh and Stafford E. Tavares *In* Engineering Inst. of Canada, Canadian Conference on Electrical and Computer Engineering, Volumes 1 and 2 1991 4 p (For primary document see N94-22101 05-33)
Avail: Issuing Activity (Engineering Inst. of Canada, 2050 rue Mansfield, Suite 700, Montreal, PQ H3A 1Z2 Canada)

N94-22200 Laval Univ. (Quebec). Lab. de Vision et Systemes Numeriques.
A SOFTWARE ENVIRONMENT FOR THE EXPLOITATION OF THE MAR IMAGE SENSOR
F. Parent, M. Tremblay, D. Laurendeau, and D. Poussart *In* Engineering Inst. of Canada, Canadian Conference on Electrical and Computer Engineering, Volumes 1 and 2 1991 4 p (For primary document see N94-22101 05-33)
Avail: Issuing Activity (Engineering Inst. of Canada, 2050 rue Mansfield, Suite 700, Montreal, PQ H3A 1Z2 Canada)

N94-22214 Waterloo Univ. (Ontario). Dept. of Electrical and Computer Engineering.
TRENDS IN SOFTWARE RELIABILITY MODELING
Rudolph E. Seviora and Christian Brunelle (Bell Canada, Longueil, Quebec.) *In* Engineering Inst. of Canada, Canadian Conference on Electrical and Computer Engineering, Volumes 1 and 2 1991 4 p (For primary document see N94-22101 05-33)
Avail: Issuing Activity (Engineering Inst. of Canada, 2050 rue Mansfield, Suite 700, Montreal, PQ H3A 1Z2 Canada)

N94-22236 Defence Research Establishment Valcartier (Quebec).
TRAJECTORY COMPUTATIONS FOR AN IMPROVED CINETHEODOLITE TRACKING SYSTEM
Jean-Pierre Ardouin *In* Engineering Inst. of Canada, Canadian Conference on Electrical and Computer Engineering, Volumes 1 and 2 1991 4 p (For primary document see N94-22101 05-33)
Avail: Issuing Activity (Engineering Inst. of Canada, 2050 rue Mansfield, Suite 700, Montreal, PQ H3A 1Z2 Canada)

N94-22246 Ecole Polytechnique, Montreal (Quebec). Dept. de Genie Electrique et de Genie Informatique.
ADAPTIVE DECODING OF CONVOLUTIONAL CODES
Francois Chan and David Haccoun *In* Engineering Inst. of Canada, Canadian Conference on Electrical and Computer Engineering, Volumes 1 and 2 1991 4 p (For primary document see N94-22101 05-33)
Avail: Issuing Activity (Engineering Inst. of Canada, 2050 rue Mansfield, Suite 700, Montreal, PQ H3A 1Z2 Canada)

N94-22247 Ecole Polytechnique, Montreal (Quebec). Dept. of Electrical and Computer Engineering.
BIDIRECTIONAL ALGORITHMS FOR THE DECODING OF CONVOLUTIONAL CODES OVER MEMORYLESS CHANNELS
Jean Belzile and D. Haccoun *In* Engineering Inst. of Canada, Canadian Conference on Electrical and Computer Engineering, Volumes 1 and 2 1991 4 p (For primary document see N94-22101 05-33)
Avail: Issuing Activity (Engineering Inst. of Canada, 2050 rue Mansfield, Suite 700, Montreal, PQ H3A 1Z2 Canada)

N94-22249 Manitoba Univ., Winnipeg. Dept. of Electrical and Computer Engineering.
AN INSENSITIVE ALGORITHM FOR TEMPLATE MATCHING WITH CORRELATION
Zhen Mu, W. H. Lehn, and A. Wexler *In* Engineering Inst. of Canada, Canadian Conference on Electrical and Computer Engineering, Volumes 1 and 2 1991 4 p (For primary document see N94-22101 05-33)
Avail: Issuing Activity (Engineering Inst. of Canada, 2050 rue Mansfield, Suite 700, Montreal, PQ H3A 1Z2 Canada)

N94-22441*# European Southern Observatory, Munich (Germany).
A LOW-COST VECTOR PROCESSOR BOOSTING COMPUTE-INTENSIVE IMAGE PROCESSING OPERATIONS Abstract Only
Hans-Martin Adorf *In* NASA, Washington, Second Annual Conference on Astronomical Data Analysis Software and Systems. Abstracts 1992 p 10 (For primary document see N94-22438 05-89)
Avail: CASI HC A01/MF A02

N94-22443*# Rutherford Appleton Lab., Chilton (England).
MULTIFREQUENCY DATA ANALYSIS SOFTWARE ON STARLINK Abstract Only
P. M. Allan *In* NASA, Washington, Second Annual Conference on Astronomical Data Analysis Software and Systems. Abstracts 1992 p 12 (For primary document see N94-22438 05-89)
Avail: CASI HC A01/MF A02

N94-22456*# Dartmouth Coll., Hanover, NH.
A MULTIRESOLUTION WAVELET REPRESENTATION IN TWO OR MORE DIMENSIONS Abstract Only
B. C. Bromley *In* NASA, Washington, Second Annual Conference on Astronomical Data Analysis Software and Systems. Abstracts 1992 p 25 (For primary document see N94-22438 05-89)
Avail: CASI HC A01/MF A02

N94-22460*# Keck Observatory, Mauna Kea, HI.
THE KECK KEYWORD LAYER Abstract Only
A. R. Conrad and W. F. Lupton *In* NASA, Washington, Second Annual Conference on Astronomical Data Analysis Software and Systems. Abstracts 1992 p 29 (For primary document see N94-22438 05-89)
Avail: CASI HC A01/MF A02

N94-22461*# Smithsonian Astrophysical Observatory, Cambridge, MA.
PROS: AN IRAF BASED SYSTEM FOR ANALYSIS OF X RAY DATA Abstract Only
M. A. Conroy, J. DePonte, J. F. Moran, J. S. Orszak, W. P. Roberts, and D. Schmidt *In* NASA, Washington, Second Annual Conference on Astronomical Data Analysis Software and Systems. Abstracts 1992 p 30 (For primary document see N94-22438 05-89)
Avail: CASI HC A01/MF A02

N94-22464*# Kitt Peak National Observatory, Tucson, AZ.
NEW IRAF STELLAR PHOTOMETRY SOFTWARE Abstract Only
L. E. Davis *In* NASA, Washington, Second Annual Conference on Astronomical Data Analysis Software and Systems. Abstracts 1992 p 33 (For primary document see N94-22438 05-89)
Avail: CASI HC A01/MF A02

N94-22465*# Kitt Peak National Observatory, Tucson, AZ.
PHOTCAL: THE IRAF PHOTOMETRIC CALIBRATION PACKAGE Abstract Only
L. E. Davis and P. Gigoux (Cerro Tololo Inter-American Observatory, La Serena, Chile.) *In* NASA, Washington, Second Annual Conference on Astronomical Data Analysis Software and Systems. Abstracts 1992 p 34 (For primary document see N94-22438 05-89)
Avail: CASI HC A01/MF A02

N94-22470*# Space Telescope Science Inst., Baltimore, MD.
ENHANCEMENTS TO IRAF/STSDAS GRAPHICS Abstract Only
J. D. Eisenhamer and Z. G. Levay *In* NASA, Washington, Second Annual Conference on Astronomical Data Analysis Software and Systems. Abstracts 1992 p 39 (For primary document see N94-22438 05-89)
Avail: CASI HC A01/MF A02

N94-22471*# Applied Research Corp., Greenbelt, MD. Cosmology Data Analysis Center.
AN IDL-BASED ANALYSIS PACKAGE FOR COBE AND OTHER SKYCUBE-FORMATTED ASTRONOMICAL DATA Abstract Only
J. A. Ewing, Richard B. Isaacman, and J. M. Gales *In* NASA, Washington, Second Annual Conference on Astronomical Data Analysis Software and Systems. Abstracts 1992 p 40 (For primary document see N94-22438 05-89)
Avail: CASI HC A01/MF A02

N94-22474*# Kitt Peak National Observatory, Tucson, AZ.
SPPTOOLS: PROGRAMMING TOOLS FOR THE IRAF SPP LANGUAGE Abstract Only
M. Fitzpatrick *In* NASA, Washington, Second Annual Conference on Astronomical Data Analysis Software and Systems. Abstracts 1992 p 43 (For primary document see N94-22438 05-89)
Avail: CASI HC A01/MF A02

N94-22475*# Kitt Peak National Observatory, Tucson, AZ.
THE IRAF RADIAL VELOCITY ANALYSIS PACKAGE Abstract Only
M. Fitzpatrick *In* NASA, Washington, Second Annual Conference on Astronomical Data Analysis Software and Systems. Abstracts 1992 p 44 (For primary document see N94-22438 05-89)
Avail: CASI HC A01/MF A02

N94-22477*# Digital Equipment Corp., Cambridge, MA.
CRYSTAL BALL GAZING Abstract Only
Jim Gettys *In* NASA, Washington, Second Annual Conference on Astronomical Data Analysis Software and Systems. Abstracts 1992 p 46 (For primary document see N94-22438 05-89)
Avail: CASI HC A01/MF A02

N94-22478*# Space Telescope Science Inst., Baltimore, MD.
HST IMAGE RESTORATION: A COMPARISON OF PRE- AND POST-SERVICING MISSION RESULTS Abstract Only
R. J. Hanisch and J. Mo *In* NASA, Washington, Second Annual Conference on Astronomical Data Analysis Software and Systems. Abstracts 1992 p 47 (For primary document see N94-22438 05-89)
Avail: CASI HC A01/MF A02

N94-22480*# Ohio State Univ., Columbus.
WRITING INSTRUMENT INTERFACES WITH xf/tktcl Abstract Only
A. A. Henden *In* NASA, Washington, Second Annual Conference on

Astronomical Data Analysis Software and Systems. Abstracts 1992 p 49 (For primary document see N94-22438 05-89)
Avail: CASI HC A01/MF A02

N94-22481*# American National Standards Inst., New York, NY.
FORTRAN FOR THE NINETIES Abstract Only
J. T. Himer *In* NASA, Washington, Second Annual Conference on Astronomical Data Analysis Software and Systems. Abstracts 1992 p 50 (For primary document see N94-22438 05-89)
Avail: CASI HC A01/MF A02

N94-22482*# National Radio Astronomy Observatory, Green Bank, WV.
PROGRAMMABILITY IN AIPS++ Abstract Only
R. M. Hjellming *In* NASA, Washington, Second Annual Conference on Astronomical Data Analysis Software and Systems. Abstracts 1992 p 51 (For primary document see N94-22438 05-89)
Avail: CASI HC A01/MF A02

N94-22483*# Space Telescope Science Inst., Baltimore, MD.
TELESCOPE IMAGE MODELLING SOFTWARE IN STSDAS Abstract Only
P. E. Hodge, J. D. Eisenhamer, R. A. Shaw, and R. L. Williamson, II *In* NASA, Washington, Second Annual Conference on Astronomical Data Analysis Software and Systems. Abstracts 1992 p 52 (For primary document see N94-22438 05-89)
Avail: CASI HC A01/MF A02

N94-22484*# Space Telescope Science Inst., Baltimore, MD.
HOW IS WFPC FLAT FIELD MADE Abstract Only
J.-C. Hsu and C. E. Ritchie *In* NASA, Washington, Second Annual Conference on Astronomical Data Analysis Software and Systems. Abstracts 1992 p 53 (For primary document see N94-22438 05-89)
Avail: CASI HC A01/MF A02

N94-22485*# Space Telescope Science Inst., Baltimore, MD.
ASpect: A NEW SPECTRUM AND LINE ANALYSIS PACKAGE FOR IRAF Abstract Only
S. J. Hulbert, J. D. Eisenhamer, Z. G. Levay, and R. A. Shaw *In* NASA, Washington, Second Annual Conference on Astronomical Data Analysis Software and Systems. Abstracts 1992 p 54 (For primary document see N94-22438 05-89)
Avail: CASI HC A01/MF A02

N94-22486*# Massachusetts Inst. of Tech., Cambridge.
SPIKE: APPLICATION FOR ASTRO-D MISSION PLANNING Abstract Only
T. Isobe, M. Johnston, E. Morgan, and G. Clark *In* NASA, Washington, Second Annual Conference on Astronomical Data Analysis Software and Systems. Abstracts 1992 p 55 (For primary document see N94-22438 05-89)
Avail: CASI HC A01/MF A02

N94-22487*# National Aeronautics and Space Administration. Goddard Space Flight Center, Greenbelt, MD.
THE HEASARC GRAPHICAL USER INTERFACE Abstract Only
N. White, P. Barrett, P. Jacobs, and B. ONeel *In* NASA, Washington, Second Annual Conference on Astronomical Data Analysis Software and Systems. Abstracts 1992 p 56 (For primary document see N94-22438 05-89)
Avail: CASI HC A01/MF A02

N94-22488*# National Aeronautics and Space Administration. Goddard Space Flight Center, Greenbelt, MD.
FITS DATA CONVERSION EFFORTS AT THE COMPTON OBSERVATORY SCIENCE SUPPORT CENTER Abstract Only
D. G. Jennings, J. M. Jordan, T. A. McGlynn, N. G. Ruggiero, and T. A. Serlemitsos *In* NASA, Washington, Second Annual Conference on Astronomical Data Analysis Software and Systems. Abstracts 1992 p 57 (For primary document see N94-22438 05-89)
Avail: CASI HC A01/MF A02

N94-22491*# Space Telescope Science Inst., Baltimore, MD.
AN OBJECT-ORIENTED APPROACH FOR SUPPORTING BOTH X AND TERMINAL INTERFACES Abstract Only
J. Johnson *In* NASA, Washington, Second Annual Conference on Astronomical Data Analysis Software and Systems. Abstracts 1992 p 60 (For primary document see N94-22438 05-89)
Avail: CASI HC A01/MF A02

N94-22494*# Royal Observatory, Edinburgh (Scotland).
THE ADAM ENVIRONMENT AND TRANSPUTERS Abstract Only
B. D. Kelly, J. M. Stewart, and B. V. McNally *In* NASA, Washington, Second Annual Conference on Astronomical Data Analysis Software and Systems. Abstracts 1992 p 63 (For primary document see N94-22438 05-89)
Avail: CASI HC A01/MF A02

N94-22498*# Space Telescope Science Inst., Baltimore, MD.
HST PSF SIMULATION USING TINY TIM Abstract
J. E. Krist *In* NASA, Washington, Second Annual Conference on Astronomical Data Analysis Software and Systems. Abstracts 1992 p 67 (For primary document see N94-22438 05-89)
Avail: CASI HC A01/MF A02

N94-22501*# National Aeronautics and Space Administration. Goddard Space Flight Center, Greenbelt, MD.
GRO/EGRET DATA ANALYSIS SOFTWARE: AN INTEGRATED SYSTEM OF CUSTOM AND COMMERCIAL SOFTWARE USING STANDARD INTERFACES Abstract Only
N. A. Laubenthal, D. Bertsch, N. Lal, A. Etienne (Hughes STX, Inc., Greenbelt, MD.), L. McDonald (Hughes STX, Inc., Greenbelt, MD.), J. Mattox (Computer Sciences Corp., Greenbelt, MD.), P. Sreekumar (Universities Space Research Association, Greenbelt, MD.), P. Nolan (Stanford Univ., CA.), and J. Fierro (Stanford Univ., CA.) *In* NASA, Washington, Second Annual Conference on Astronomical Data Analysis Software and Systems. Abstracts 1992 p 70 (For primary document see N94-22438 05-89)
Avail: CASI HC A01/MF A02

N94-22505*# Kitt Peak National Observatory, Tucson, AZ.
INTERACTIVE SPECTRAL ANALYSIS AND COMPUTATION (ISAAC) Abstract Only
D. M. Lytle *In* NASA, Washington, Second Annual Conference on Astronomical Data Analysis Software and Systems. Abstracts 1992 p 74 (For primary document see N94-22438 05-89)
Avail: CASI HC A01/MF A02

N94-22506*# Kitt Peak National Observatory, Tucson, AZ.
THE NSO FTS DATABASE PROGRAM AND ARCHIVE (FTSDBM) Abstract Only
D. M. Lytle *In* NASA, Washington, Second Annual Conference on Astronomical Data Analysis Software and Systems. Abstracts 1992 p 75 (For primary document see N94-22438 05-89)
Avail: CASI HC A01/MF A02

N94-22507*# Smithsonian Astrophysical Observatory, Cambridge, MA. Center for Astrophysics.
AXAF USER INTERFACES FOR HETEROGENEOUS ANALYSIS ENVIRONMENTS Abstract Only
Eric Mandel, John Roll, and Mark S. Ackerman (Massachusetts Inst. of Tech., Cambridge.) *In* NASA, Washington, Second Annual Conference on Astronomical Data Analysis Software and Systems. Abstracts 1992 p 76 (For primary document see N94-22438 05-89)
Avail: CASI HC A01/MF A02

N94-22508*# Smithsonian Astrophysical Observatory, Cambridge, MA.
VERIFICATION OF THE PROS TIMING ANALYSIS PACKAGE
K. R. Manning, M. A. Conroy, J. DePonte, J. F. Moran, F. A. Primini, F. D. Seward, and B. Aschenbach (Max-Planck-Inst. fuer Extraterrestrische Physik, Garching, Germany.) *In* NASA, Washington, Second Annual Conference on Astronomical Data Analysis Software and Systems. Abstracts 1992 p 77 (For primary document see N94-22438 05-89)
Avail: CASI HC A01/MF A02

N94-22511*# Smithsonian Astrophysical Observatory, Cambridge, MA.
SKYMAP: EXPLORING THE UNIVERSE IN SOFTWARE Abstract Only
D. J. Mink *In* NASA, Washington, Second Annual Conference on Astronomical Data Analysis Software and Systems. Abstracts 1992 p 80 (For primary document see N94-22438 05-89)
Avail: CASI HC A01/MF A02

N94-22512*# Minnesota Univ., Minneapolis.
STARBASE: DATABASE SOFTWARE FOR THE AUTOMATED PLATE SCANNER Abstract Only
S. C. Odewahn, R. M. Humphreys, and P. Thurmes *In* NASA, Washington, Second Annual Conference on Astronomical Data Analysis Software and Systems. Abstracts 1992 p 81 (For primary document see N94-22438 05-89)
Avail: CASI HC A01/MF A02

N94-22513*# National Aeronautics and Space Administration. Goddard Space Flight Center, Greenbelt, MD.
XPI: THE XANADU PARAMETER INTERFACE Abstract Only
N. White, P. Barrett, B. ONeel, and P. Jacobs *In* NASA, Washington, Second Annual Conference on Astronomical Data Analysis Software and Systems. Abstracts 1992 p 82 (For primary document see N94-22438 05-89)
Avail: CASI HC A01/MF A02

N94-22515*# Eoetvoes Lorand Univ., Budapest (Hungary).
SOME PRACTICABLE APPLICATIONS OF QUADTREE DATA STRUCTURES/REPRESENTATION IN ASTRONOMY Abstract Only
L. Pasztor *In* NASA, Washington, Second Annual Conference on Astronomical Data Analysis Software and Systems. Abstracts 1992 p 84 (For primary document see N94-22438 05-89)
Avail: CASI HC A01/MF A02

N94-22516*# National Aeronautics and Space Administration. Goddard Space Flight Center, Greenbelt, MD.
DEVELOPMENT OF THE FITS TOOLS PACKAGE FOR MULTIPLE SOFTWARE ENVIRONMENTS Abstract Only
W. D. Pence and J. K. Blackburn *In* NASA, Washington, Second Annual Conference on Astronomical Data Analysis Software and Systems. Abstracts 1992 p 85 (For primary document see N94-22438 05-89)
Avail: CASI HC A01/MF A02

N94-22522*# Space Research Organization Netherlands, Groningen.
THE ISO SWS ON-LINE SYSTEM Abstract Only
P. R. Roelfsema, D. J. M. Kester, P. R. Wesselius, E. Wieprech, and N. Sym *In* NASA, Washington, Second Annual Conference on Astronomical Data Analysis Software and Systems. Abstracts 1992 p 91 (For primary document see N94-22438 05-89)
Avail: CASI HC A01/MF A02

N94-22523*# National Aeronautics and Space Administration. Goddard Space Flight Center, Greenbelt, MD.
KHOROS SOFTWARE SPECIFICATION FORMAT AND INTEROPERABILITY Abstract Only
A. H. Rots *In* NASA, Washington, Second Annual Conference on Astronomical Data Analysis Software and Systems. Abstracts 1992 p 92 (For primary document see N94-22438 05-89)
Avail: CASI HC A01/MF A02

N94-22524*# Smithsonian Astrophysical Observatory, Cambridge, MA.
SPATIAL REGION FILTERING IN IRAF/PROS Abstract Only
Eric Mandel, John Roll, Dennis Schmidt, Mike VanHilst (Washington Univ., Seattle.), and Richard Burg (Johns Hopkins Univ., Baltimore, MD.) *In* NASA, Washington, Second Annual Conference on Astronomical Data Analysis Software and Systems. Abstracts 1992 p 93 (For primary document see N94-22438 05-89)
Avail: CASI HC A01/MF A02

N94-22531*# Academy of Sciences (USSR), Moscow. Inst. of Astronomy.
A NEW PROGRAMMING METAPHOR FOR IMAGE PROCESSING PROCEDURES Abstract Only
O. M. Smirnov and N. E. Piskunov (Helsinki Univ., Finland.) *In* NASA, Washington, Second Annual Conference on Astronomical Data Analysis Software and Systems. Abstracts 1992 p 100 (For primary document see N94-22438 05-89)
Avail: CASI HC A01/MF A02

N94-22532*# Academy of Sciences (USSR), Moscow. Inst. of Astronomy.
PCIPS 2.0: POWERFUL MULTIPROFILE IMAGE PROCESSING IMPLEMENTED ON PCs Abstract Only
O. M. Smirnov and N. E. Piskunov (Helsinki Univ., Finland.) *In* NASA, Washington, Second Annual Conference on Astronomical Data Analysis Software and Systems. Abstracts 1992 p 101 (For primary document see N94-22438 05-89)
Avail: CASI HC A01/MF A02

N94-22533*# Academy of Sciences (USSR), Moscow. Inst. of Astronomy.
GUIDE STAR CATALOGUE DATA RETRIEVAL SOFTWARE 2 Abstract Only
O. M. Smirnov and O. Yu. Malkov *In* NASA, Washington, Second Annual Conference on Astronomical Data Analysis Software and Systems. Abstracts 1992 p 102 (For primary document see N94-22438 05-89)
Avail: CASI HC A01/MF A02

N94-22538*# Institute for Space and Terrestrial Science, Concord (Ontario). Space Astrophysics Lab.
TOOLS FOR THE IDL WIDGET SET WITHIN THE X-WINDOWS ENVIRONMENT Abstract Only
B. Turgeon and A. Aston *In* NASA, Washington, Second Annual Conference on Astronomical Data Analysis Software and Systems. Abstracts 1992 p 107 (For primary document see N94-22438 05-89)
Avail: CASI HC A01/MF A02

N94-22542*# Hughes STX, Inc., Greenbelt, MD.
DECONV-TOOL: AN IDL BASED DECONVOLUTION SOFTWARE PACKAGE Abstract only
F. Varosi and W. B. Landsman *In* NASA, Washington, Second Annual Conference on Astronomical Data Analysis Software and Systems. Abstracts 1992 p 111 (For primary document see N94-22438 05-89)
Avail: CASI HC A01/MF A02

N94-22543*# National Aeronautics and Space Administration. Goddard Space Flight Center, Greenbelt, MD.
MOSAIC: SOFTWARE FOR CREATING MOSAICS FROM COLLECTIONS OF IMAGES Abstract Only
F. Varosi and D. Y. Gezari *In* NASA, Washington, Second Annual Conference on Astronomical Data Analysis Software and Systems. Abstracts 1992 p 112 (For primary document see N94-22438 05-89)
Avail: CASI HC A01/MF A02

N94-22545*# Science Research Council, Slough (England).
THE STARLINK SOFTWARE COLLECTION Abstract Only
R. F. Warren-Smith and P. T. Wallace *In* NASA, Washington, Second Annual Conference on Astronomical Data Analysis Software and Systems. Abstracts 1992 p 114 (For primary document see N94-22438 05-89)
Avail: CASI HC A01/MF A02

N94-22549*# Kitt Peak National Observatory, Tucson, AZ.
TESTS OF A SIMPLE DATA MERGING ALGORITHM FOR THE GONG PROJECT Abstract Only
W. E. Williams and F. Hill *In* NASA, Washington, Second Annual Conference on Astronomical Data Analysis Software and Systems. Abstracts 1992 p 118 (For primary document see N94-22438 05-89)
Avail: CASI HC A01/MF A02

N94-22550*# Space Telescope Science Inst., Baltimore, MD.
REGISTERING AND RESAMPLING IMAGES IN STSDAS Abstract Only
R. L. Williamson, II *In* NASA, Washington, Second Annual Conference on Astronomical Data Analysis Software and Systems. Abstracts 1992 p 119 (For primary document see N94-22438 05-89)
Avail: CASI HC A01/MF A02

N94-22551*# National Optical Astronomy Lab. Tucson, AZ. Image Reduction Analysis Facility.
FIRST MEM TASK IRMEO IN IRAF Abstract Only
Nailong Wu *In* NASA, Washington, Second Annual Conference on Astronomical Data Analysis Software and Systems. Abstracts 1992 p 120 (For primary document see N94-22438 05-89)
Avail: CASI HC A01/MF A02

62 COMPUTER SYSTEMS

Includes computer networks and special application computer systems.

N94-19812# Superconducting Super Collider Lab., Dallas, TX.
PHYSICS DETECTOR SIMULATION FACILITY. PHASE 2: SYSTEM SOFTWARE DESCRIPTION
B. Scipioni, J. Allen, C. Chang, J. Huang, J. Liu, S. Mestad, J. Pan, M. Marquez, and P. Estep May 1993 8 p Presented at the 5th Annual International Industrial Symposium on the Super Collider and Exhibition, San Francisco, CA, 6-8 May 1993
(Contract DE-AC35-89ER-40486)
(DE93-019745; SSCL-Preprint-322; CONF-930537-99) Avail: CASI HC A02/MF A01

This paper presents the Physics Detector Simulation Facility (PDSF) Phase II system software. A key element in the design of a distributed computing environment for the PDSF has been the separation and distribution of the major functions. The facility has been designed to support batch and interactive processing and to incorporate the file and tape storage systems. By distributing these functions, it is often possible to provide higher throughput and resource availability. Similarly, the design is intended to exploit event-level parallelism in an open distributed environment. DOE

N94-19858# Sandia National Labs., Livermore, CA.
TCP PERFORMANCE ANALYSIS FOR WIDE AREA NETWORKS
H. Y. Chen, J. A. Hutchins, and N. Testi (Sandia National Labs., Albuquerque, NM.) Aug. 1993 29 p
(Contract DE-AC04-76DR-00789)
(DE94-000449; SAND-93-8243) Avail: CASI HC A03/MF A01

Even though networks have been getting faster, perceived throughput at the application level has not increased accordingly. In an attempt to identify many of the performance bottlenecks, the authors collected and analyzed data over a wide area network (WAN) at T3 (45 Mbps) bandwidth. The information gained will assist in designing new protocols and/or algorithms that are consistent with future high-speed requirements. DOE

N94-19877 Massachusetts Inst. of Tech., Cambridge. Artificial Intelligence Lab.
EXPLOITING THE PARALLELISM EXPOSED BY PARTIAL EVALUATION Memorandum Report
Andrew Berlin and Rajeev J. Surati Apr. 1993 14 p Limited Reproducibility: More than 20% of this document may be affected by microfiche quality
(Contract N00014-92-J-4093; NSF MIP-90-01651)
(AD-A270678) Avail: CASI HC A03

We describe an approach to parallel compilation that seeks to harness the vast amount of fine-grain parallelism that is exposed through partial evaluation of numerically-intensive scientific programs. We have constructed a compiler for the Supercomputer Toolkit parallel processor that uses partial evaluation to break down data abstractions and program structure, producing huge basic blocks that contain large amounts of fine-grain parallelism. We show that this fine-grain parallelism can be effectively utilized even on coarse-grain parallel architectures by selectively grouping operations together so as to adjust the parallelism grain-size to match the inter-processor communication capabilities of the target architecture. DTIC

N94-19950 Carnegie-Mellon Univ., Pittsburgh, PA. School of Computer Science.
SEGMENTED OPERATIONS FOR SPARSE MATRIX COMPUTATION ON VECTOR MULTIPROCESSORS
Guy E. Blelloch, Michael A. Heroux, and Marco Zagha Aug. 1993 25 p Prepared in cooperation with Cray Research, Inc. Limited Reproducibility: More than 20% of this document may be affected by microfiche quality
(Contract F33615-90-C-1465; ARPA Order 7597)
(AD-A270601; CMU-CS-93-173) Avail: CASI HC A03

In this paper we present a new technique for sparse matrix multiplication on vector multiprocessors based on the efficient implementation of a segmented sum operation. We describe how the segmented sum can be implemented on vector multiprocessors such that it both fully vectorizes within each processor and parallelizes across processors. Because of our method's insensitivity to relative row size, it is better suited than the Ellpack/Itpack or the Jagged Diagonal algorithms for matrices which have a varying number of non-zero elements in each row. Furthermore, our approach requires less preprocessing (no more time than a single sparse matrix-vector multiplication), less auxiliary storage, and uses a more convenient data representation (an augmented form of the standard compressed sparse row format). We have implemented our algorithm (SEGMV) on the Cray Y-MP C90 and have compared its performance with other methods on a variety of sparse matrices from the Harwell-Boeing collection and industrial application codes. Our performance on the test matrices is up to 3 times faster than the Jagged Diagonal algorithm and up to 5 times faster than Ellpack/Itpack method. Our preprocessing time is an order of magnitude faster than for the Jagged Diagonal algorithm. Also, using an assembly language implementation of SEGMV on a 16 processor C90, the NAS Conjugate Gradient benchmark runs at 3.5 gigaflops. DTIC

N94-19995 Technische Univ., Eindhoven (Netherlands). Dept. of Mathematics and Computing Science.
BOTTOM-UP ABSTRACT INTERPRETATION OF LOGIC PROGRAMS
M. Codish (Katholieke Univ. te Leuven, Belgium.), D. Dams, and E. Yardeni (Weizmann Inst. of Science, Rehovoth, Israel.) 1992 43 p Prepared in cooperation with Katholieke Univ. Limited Reproducibility: More than 20% of this document may be affected by microfiche quality
(PB93-191773; COMPUTING SCIENCE NOTES-92/24) Copyright Avail: Issuing Activity (National Technical Information Service (NTIS))

The paper presents a formal framework for the bottom-up abstract interpretation of logic programs which can be applied to approximate answer substitutions, partial answer substitutions, and call patterns for a given program and arbitrary initial goal. The framework is based on T(sub P)-like semantics defined over a Herbrand universe with variables which have previously been shown to determine the answer substitutions for arbitrary initial goals. The first part of the paper reconstructs this semantics to provide a more adequate basis for abstract interpretation. A notion of abstract substitution is introduced and shown to determine an abstract semantic function which for a given program can be applied to approximate the answer substitutions for an arbitrary initial goal. The second part of the paper extends the bottom-up approach to provide approximations of both partial answer substitutions and call patterns. This is achieved by applying Magic Sets and other existing techniques to transform a program in such a way that the answer substitutions of the transformed program correspond to the partial answer substitutions and call patterns of the original program. NTIS

N94-19996 Technische Univ., Eindhoven (Netherlands).
PROGRAMMING LOGIC FOR F OMEGA
E. Poll 1992 25 p Sponsored by Nederlandse Organisatie voor Wetenschappelijk Onderzoek, The Hague Limited Reproducibility: More than 20% of this document may be affected by microfiche quality
(PB93-191781; COMPUTING SCIENCE NOTES-92/25) Copyright Avail: Issuing Activity (National Technical Information Service (NTIS))

A programming logic is defined in which F sub omega programs can be specified and proven correct. Both the programming language and the logic are typed lambda calculi and can be defined as Pure Type Systems. Programs and correctness proofs, as well as types and specifications, are strictly separated. NTIS

N94-20009 Technische Univ., Eindhoven (Netherlands). Dept. of Mathematics and Computing Science.
SYSTEM AT THE CROSS-ROADS OF FUNCTIONAL AND LOGIC PROGRAMMING
F. Kamareddine 1992 45 p See also PB93-191815 Limited Reproducibility: More than 20% of this document may be affected by

microfiche quality
(PB93-191823; COMPUTING SCIENCE NOTES-92/15) Copyright Avail: Issuing Activity (National Technical Information Service (NTIS))

A system that combines polymorphism and higher order functions with logic is presented. The system is suitable for both the functional and the logical paradigms of programming as from the functional paradigms point of view. The system enables one to have all the polymorphism and higher order that exist in functional languages and much more. From the point of view of theorem proving, the system is expressive enough to allow self referential sentences and those sentences that lead to Russell's and Curry's paradoxes. However, the paradoxes do not hold due to the notion of circular types which contain the type of propositions. The system is implemented in Milner's ML and can be seen as extending ML in two important ways. First, it extends the part related to the functional paradigm in that it can type terms that could not be typed in ML; namely, those are the terms that contain self application such as the Y term above. Second, the system extends ML by adding logic to it in a consistent way. NTIS

N94-20084 Carnegie-Mellon Univ., Pittsburgh, PA. School of Computer Science.
MULTILIST SCHEDULING: A NEW PARALLEL PROGRAMMING MODEL Ph.D. Thesis
I-Chen Wu 30 Jul. 1993 150 p Limited Reproducibility: More than 20% of this document may be affected by microfiche quality
(Contract MDA972-90-C-0035; ARPA Order 7330)
(AD-A270549; CMU-CS-93-184) Avail: CASI HC A07

Parallel programming requires task scheduling to optimize performance; this primarily involves balancing the load over the processors. In many cases, it is critical to perform task scheduling at runtime. For example, in many parallel applications the task load cannot be accurately predicted a priori, and in a network-based multicomputer, the computational power of each processor may not remain constant. In order to support dynamic task scheduling, the programmer usually needs to design and implement a complex set of scheduling routines, e.g., routines for maintaining task lists and handling interprocessor communication for load balancing. Unfortunately, it is very difficult and time-consuming to write and debug all of these scheduling routines. This thesis proposes a new approach which can greatly reduce the effort of developing efficient dynamic task scheduling routines. In our new approach, we decompose task scheduling into two parts--the specification of scheduling policies and the implementation of supportive scheduling operations--and then hide the latter from the programmer. We call this approach multilist scheduling, because it is based on a uniform scheduling model involving the use of multiple scheduling lists. DTIC

N94-20124# Grenoble-1 Univ. (France). Lab. d'Informatique Fondamentale et d'Intelligence Artificielle.
BACK AND FORTH BISIMULATIONS ON PRIME EVENT STRUCTURES
Ferroudja Cherief May 1992 19 p
(RR-888-I-IMAG-124-LIFIA; ETN-93-94980) Avail: CASI HC A03/MF A01

A definition of back and forth bisimulation for event structures is proposed. It is shown that the proposal can be adapted in a uniform way to yield back and forth versions of step, partial word, and pomset bisimulations. These new equivalences are investigated and compared to other branching time semantics. ESA

N94-20144# Rochester Univ., NY. Dept. of Computer Science.
MEMORY CONTENTION IN SCALABLE CACHE-COHERENT MULTIPROCESSORS
Ricardo Bianchini, Mark E. Crovella, Leonidas Kontothanassis, and Thomas J. LeBlanc Apr. 1993 23 p
(Contract N00014-92-J-1801; NSF CDA-88-22724; ARPA Order 8930)
(TR-448) Avail: CASI HC A03/MF A01

Effective use of large-scale multiprocessors requires the elimination of all bottlenecks that reduce processor utilization. One such bottleneck is memory contention. It is shown that memory contention occurs in many parallel applications, when those applications are run on large-scale shared-memory multiprocessors. In our simulations of several parallel applications on a large-scale machine, it was observed that some applications exhibit near-perfect speedup on hundreds of processors when the effect of memory contention is ignored, and exhibit no speedup at all when memory contention is considered. As the number of processors is increased, many applications exhibit an increase in both the number of hot spots and in the degree of contention for each hot spot. In addition, it was observed that hot spots are spread throughout memory for some applications, and that eliminating hot spots on an individual basis can cause other hot spots to worsen. These observations suggest that modern multiprocessors require some mechanism to alleviate hot-spet contention. The effectiveness of two different mechanisms for dealing with hot-spot contention indirect-connected, distributed-shared-memory multiprocessors is evaluated: queueing requests at the memory module, which allows a memory module to be more highly utilized during period of contention, and increasing the effective bandwidth to memory by having the coherency protocol distribute the hot data to multiple memory modules. It is shown that queueing requires long queues at each memory module, and does not perform as well as our proposed coherency protocol, which essentially eliminates memory contention in the applications considered. Author (revised)

N94-20176# Grenoble-1 Univ. (France). Lab. de Genie Informatique.
PARALLEL LOGIC PROGRAMMING SYSTEMS
Jacques ChassindeKergommeaux and Phillippe Codognet (Institut National de Recherche d'Informatique et d'Automatique, Le Chesnay, France.) May 1992 46 p
(RR-891-I; ETN-93-94982) Avail: CASI HC A03/MF A01

Transparent exploitation of parallelism in existing logic programming languages such as PROLOG is focused upon and mature solutions to the problems to be solved in order to obtain efficient implementations are surveyed. These solutions have been implemented and the most efficient parallel logic programming systems reach effective speed-ups over state of the art sequential PROLOG implementations. Current and prospective research issues aiming to extend the applicability and the efficiency of existing systems, such as models merging the transparent parallelism and the concurrent logic languages approaches, combination of constraint logic programming with parallelism, and use of highly parallel architectures, are addressed. ESA

N94-20279# Los Alamos National Lab., NM.
FAST DATA PARALLEL POLYGON RENDERING
F. A. Ortega and C. D. Hansen 1993 13 p Presented at the Supercomputing Conference on High Performance Computing and Communications, Portland, OR, 15-19 Nov. 1993
(Contract W-7405-eng-36)
(DE93-040157; LA-UR-93-3173; CONF-931115-11) Avail: CASI HC A03/MF A01

This paper describes a parallel method for polygonal rendering on a massively parallel SIMD machine. This method, based on a simple shading model, is targeted for applications which require very fast polygon rendering for extremely large sets of polygons such as is found in many scientific visualization applications. The algorithms described in this paper are incorporated into a library of 3D graphics routines written for the Connection Machine. The routines are implemented on both the CM-200 and the CM-5. This library enables a scientists to display 3D shaded polygons directly from a parallel machine without the need to transmit huge amounts of data to a post-processing rendering system. DOE

N94-20472# Naval Command, Control and Ocean Surveillance Center, San Diego, CA. RDT and E Div.
UNDERSTANDING OPEN SYSTEMS INTERCONNECTION (OSI) Final Report, period ending Jan. 1993
G. B. Myers Aug. 1993 25 p
(AD-A271877; NCCOSC/RDT/E-TD-2499) Avail: CASI HC A03/MF A01

This document will serve as a guide for people who are new to the Open Systems Interconnection (OSI) concept. Described are concepts and defined are terminology important to achieving a better understanding of OSI. DTIC

N94-20571# Naval Surface Warfare Center, Silver Spring, MD.
DESIGN STRUCTURING AND ALLOCATION OPTIMIZATION (DESTINATION) PROTOTYPE LEVEL 1 USER'S MANUAL Interim Report, Sep. 1992 - Oct. 1993
My-Hanh N. Trinh and Cuong M. Nguyen 19 Oct. 1993 73 p
(AD-A272115; NSWCDD/TR-92/372) Avail: CASI HC A04/MF A01

The objective of the System Design Structuring and Allocation

Optimization (DESTINATION) Prototype Level 1 User's Manual is to help the systems engineers and systems analysts use the DESTINATION prototype Level 1 effectively. This manual specifies the system's installation requirements, each of the menus and commands in the prototype, and how to use specific menus and commands; it also gives troubleshooting procedures for handling error messages. DTIC

N94-21018 Technische Hochschule, Darmstadt (Germany). Fachbereich Informatik.

ANALYSIS AND EVALUATION OF CONFIGURING OF GRAPHICAL SYSTEMS ON MULTIPROCESSOR ARCHITECTURES Ph.D. Thesis [ANALYSE UND BEWERTUNG DER KONFIGURIERUNG VON GRAPHISCHEN SYSTEMEN AUF MEHRPROZESSOR-ARCHITEKTUREN]

Martin Goebel 1990 202 p In GERMAN Limited Reproducibility: More than 20% of this document may be affected by microfiche quality

(ETN-93-93618) Avail: CASI HC A10

Functional graphical systems for possible parallel processing and the requirements for an implementation on homogeneous multiprocessor systems are examined. Several models, such as standard computer graphics and visualization systems and function and architecture oriented models are considered. A configurating model was developed for data integration, system evaluation, code generation and implementation, installation, and testing. Software tools for configuration, such as data structures, specification interpretation, processor net, and typical structures for sequential, parallel, and pipeline adaptation are described. A multiprocessor prototype, which is available for installation of configurated graphical systems, is presented: a simple software achieves intercommunication and scheduling of current processes. A distributed implementation of the graphical kernel system, which supplies an optimal interprocessor communication between the processor modules, is proposed. ESA

N94-21023 Center for Mathematics and Computer Science, Amsterdam (Netherlands). Dept. of Computer Science.

REDUCTION OF NETWORK COST AND WIRING IN RANADE'S BUTTERFLY ROUTING

David Cross (California Univ., Berkeley.), Reinhard Drefenstedt (Saarland Univ., Saarbrucken, Germany.), and Joerg Keller Nov. 1992 9 p Submitted for publication Sponsored in part by DFG Limited Reproducibility: More than 20% of this document may be affected by microfiche quality

(Contract NF-62-376)

(CWI-CS-R9243; ETN-94-94723) Copyright Avail: CASI HC A02

The class of n-input butterfly networks is very important for the design of scalable parallel machines because of constant node degree, depth log n and the existence of routing algorithms capable of delivering n log n packets, forming a log n-relation (log n packets destined to each output), in time O(log n) with constant length buffers. Implementations, however, show ugly wiring. A method that, in comparison to the obvious implementation, reduces the number of chips and the number of links between chips in Ranade's butterfly routing by a factor of more than two is presented. The chips remain connected as a butterfly network. This reduction in space simplifies cooling, power supply, and allows for shorter links, thus, reducing wire delay. ESA

N94-21065*# Research Inst. for Computing and Information Systems, Houston, TX.

ADVANCED SOFTWARE DEVELOPMENT WORKSTATION: KNOWLEDGE BASE METHODOLOGY: METHODOLOGY FOR FIRST ENGINEERING SCRIPT LANGUAGE (ESL) KNOWLEDGE BASE

Kumar Peeris (Houston Univ., Clear Lake, TX.) and Michel Izygon (Barrios Technology, Inc., Houston, TX.) 31 May 1993 51 p

(Contract NCC9-16)

(NASA-CR-193643; NAS 1.26:193643) Avail: CASI HC A04/MF A01

This report explains some of the concepts of the ESL prototype and summarizes some of the lessons learned in using the prototype for implementing the Flight Mechanics Tool Kit (FMToolKit) series of Ada programs. Author

N94-21077 Center for Mathematics and Computer Science, Amsterdam (Netherlands). Dept. of Numerical Mathematics.

MGD1M: A PARALLEL MULTIGRID CODE WITH A FAST VECTORIZED ILU-RELAXATION

Margreet Louter-Nool Nov. 1992 17 p Sponsored by Cray Research, Inc., and Netherlands Organization for Scientific Research Limited Reproducibility: More than 20% of this document may be affected by microfiche quality

(CWI-NM-R9222; ETN-93-94697) Copyright Avail: CASI HC A03

MGD1M, a multigrid method which uses incomplete LU relaxation (ILU) as a smoothing process, is addressed. A straightforward ILU implementation leads to non-vectorizable recursive relations. By applying an alternative ordering of the grid points, proposed by Ashcraft et al., the ILU vectorizes and the overall execution time is reduced considerably. General techniques to improve the (vector) performance on the Cray Y-MP4, which are also suitable for other high performance machines, are considered. Parallelism was introduced by applying auto- and macrotasking. Performance results measured on a dedicated Cray Y-MP4/464 are discussed. ESA

N94-21161 Center for Mathematics and Computer Science, Amsterdam (Netherlands). Dept. of Operations Research, Statistics, and System Theory.

OPTIMIZATION OF STATIC TRAFFIC ALLOCATION POLICIES

M. B. Combe and O. J. Boxma Jan. 1993 31 p Sponsored in part by NFI, Netherlands Limited Reproducibility: More than 20% of this document may be affected by microfiche quality

(Grant CEC-DG-XIII-BRA-QMIPS)

(CWI-BS-R9302; ETN-94-94719) Copyright Avail: CASI HC A03

The traffic allocation problem is studied: customers in an arrival process have to be assigned to one of a group of servers. Such problems arise in distributed computer systems and flexible manufacturing networks. The aim is to optimize system performance measures, such as mean waiting time of a customer or total number of customers in the system, under a given static allocation policy. Two static policies are considered: probabilistic assignment and allocation according to a fixed pattern. For these two policies, general properties and optimization aspects are discussed. ESA

N94-21228# Rochester Univ., NY. Dept. of Computer Science.

SCHEDULING FOR LOCALITY IN SHARED-MEMORY MULTIPROCESSORS Technical Report

Evangelos Markatos May 1993 123 p

(Contract N00014-92-J-1801)

(AD-A272948; TR-457) Avail: CASI HC A06/MF A02

The last decade has produced enormous improvements in processor speed without a corresponding improvement in bus or interconnection network speeds. As a result, the relative costs of communication and computation in shared-memory multiprocessors have changed dramatically, and many parallel applications do not execute efficiently on today's multiprocessors. In this dissertation we quantify the effect of this trend-in architecture on parallel program performance, explain the implications of this trend on popular parallel programming models, and propose system software to efficiently map parallel programs and programming models to modern shared-memory multiprocessors. We propose new decomposition and scheduling algorithms that significantly reduce communication overhead. Our experiments over a wide variety of shared-memory multiprocessors demonstrate that the performance benefits of our scheduling-for-locality algorithms are significant, improving performance by up to 60% for some applications. We conclude that communication overhead need not dominate performance, given an appropriate programming model, multiprogramming scheduling policy, and user-level decomposition and scheduling algorithms. DTIC

N94-21234# Center for Mathematics and Computer Science, Amsterdam (Netherlands). Dept. of Operations Research, Statistics, and System Theory.

OPTIMAL REPAIRMAN ASSIGNMENT IN TWO MAINTENANCE MODELS WHICH ARE EQUIVALENT TO ROUTING MODELS WITH EARLY DECISIONS

Ger Koole Jan. 1993 11 p

(CWI-BS-R9301; ETN-94-94718) Copyright Avail: CASI HC A03/MF A01

Two maintenance models (a warm and a cold standby model) consisting of m parallel groups of identical components are considered. Components have exponentially distributed times to failure. There is a single repairman who can be assigned to the failed components. It is shown for both models that the repairman should be assigned to the group with the

smallest number of functioning components. The maintenance models are equivalent to routing models with delayed state information. The optimality results are obtained by adapting a method which proved to be successful in the study of routing models. ESA

N94-21272*# Rochester Univ., NY. Dept. of Computer Science.
SOFTWARE COHERENCE IN MULTIPROCESSOR MEMORY SYSTEMS
Ph.D. Thesis
William Joseph Bolosky May 1993 157 p Sponsored in part by NASA, Washington and DARPA
(NASA-CR-194696; NAS 1.26:194696; TR-456) Avail: CASI HC A08/MF A02

Processors are becoming faster and multiprocessor memory interconnection systems are not keeping up. Therefore, it is necessary to have threads and the memory they access as near one another as possible. Typically, this involves putting memory or caches with the processors, which gives rise to the problem of coherence: if one processor writes an address, any other processor reading that address must see the new value. This coherence can be maintained by the hardware or with software intervention. Systems of both types have been built in the past; the hardware-based systems tended to outperform the software ones. However, the ratio of processor to interconnect speed is now so high that the extra overhead of the software systems may no longer be significant. This issue is explored both by implementing a software maintained system and by introducing and using the technique of offline optimal analysis of memory reference traces. It finds that in properly built systems, software maintained coherence can perform comparably to or even better than hardware maintained coherence. The architectural features necessary for efficient software coherence to be profitable include a small page size, a fast trap mechanism, and the ability to execute instructions while remote memory references are outstanding. Author (revised)

N94-21323*# National Aeronautics and Space Administration. Goddard Space Flight Center, Greenbelt, MD.
NETWORKS TECHNOLOGY CONFERENCE
Keiji K. Tasaki, ed. Washington Nov. 1993 364 p Conference held in Greenbelt, MD, 9 Nov. 1993
(RTOP 535-00-00)
(NASA-CP-3241; Rept-94B00011; NAS 1.55:3241) Avail: CASI HC A16/MF A03

The papers included in these proceedings represent the most interesting and current topics being pursued by personnel at GSFC's Networks Division and supporting contractors involved in Space, Ground, and Deep Space Network (DSN) technical work. Although 29 papers are represented in the proceedings, only 12 were presented at the conference because of space and time limitations. The proceedings are organized according to five principal technical areas of interest to the Networks Division: Project Management; Network Operations; Network Control, Scheduling, and Monitoring; Modeling and Simulation; and Telecommunications Engineering. For individual titles, see N94-21324 through N94-21351.

N94-21324*# Computer Sciences Corp., Lanham, MD.
THE NCC PROJECT: A QUALITY MANAGEMENT PERSPECTIVE **c38**
Raymond H. Lee *In* NASA. Goddard Space Flight Center, Networks Technology Conference Nov. 1993 p 1-10 (For primary document see N94-21323 05-62)
Avail: CASI HC A02/MF A03

The Network Control Center (NCC) Project introduced the concept of total quality management (TQM) in mid-1990. The CSC project team established a program which focused on continuous process improvement in software development methodology and consistent deliveries of high quality software products for the NCC. The vision of the TQM program was to produce error free software. Specific goals were established to allow continuing assessment of the progress toward meeting the overall quality objectives. The total quality environment, now a part of the NCC Project culture, has become the foundation for continuous process improvement and has resulted in the consistent delivery of quality software products over the last three years. Author

N94-21325*# Computer Sciences Corp., Lanham, MD.
LET YOUR FINGERS DO THE WALKING: THE PROJECTS MOST INVALUABLE TOOL **c61**
Deborah A. Zirk *In* NASA. Goddard Space Flight Center, Networks Technology Conference Nov. 1993 p 11-25 (For primary document see N94-21323 05-62)
Avail: CASI HC A03/MF A03

The barrage of information pertaining to the software being developed for a project can be overwhelming. Current status information, as well as the statistics and history of software releases, should be 'at the fingertips' of project management and key technical personnel. This paper discusses the development, configuration, capabilities, and operation of a relational database, the System Engineering Database (SEDB) which was designed to assist management in monitoring of the tasks performed by the Network Control Center (NCC) Project. This database has proven to be an invaluable project tool and is utilized daily to support all project personnel.
Author (revised)

N94-21326*# Computer Sciences Corp., Lanham, MD.
SOFTWARE METRICS: THE KEY TO QUALITY SOFTWARE ON THE NCC PROJECT **c61**
Patricia J. Burns *In* NASA. Goddard Space Flight Center, Networks Technology Conference Nov. 1993 p 27-39 (For primary document see N94-21323 05-62)
Avail: CASI HC A03/MF A03

Network Control Center (NCC) Project metrics are captured during the implementation and testing phases of the NCCDS software development lifecycle. The metrics data collection and reporting function has interfaces with all elements of the NCC project. Close collaboration with all project elements has resulted in the development of a defined and repeatable set of metrics processes. The resulting data are used to plan and monitor release activities on a weekly basis. The use of graphical outputs facilitates the interpretation of progress and status. The successful application of metrics throughout the NCC project has been instrumental in the delivery of quality software. The use of metrics on the NCC Project supports the needs of the technical and managerial staff. This paper describes the project, the functions supported by metrics, the data that are collected and reported, how the data are used, and the improvements in the quality of deliverable software since the metrics processes and products have been in use. Author (revised)

N94-21327*# Computer Sciences Corp., Lanham, MD.
NCCDS CONFIGURATION MANAGEMENT PROCESS IMPROVEMENT **c81**
Kathy Shay *In* NASA. Goddard Space Flight Center, Networks Technology Conference Nov. 1993 p 41-52 (For primary document see N94-21323 05-62)
Avail: CASI HC A03/MF A03

By concentrating on defining and improving specific Configuration Management (CM) functions, processes, procedures, personnel selection/development, and tools, internal and external customers received improved CM services. Job performance within the section increased in both satisfaction and output. Participation in achieving major improvements has led to the delivery of consistent quality CM products as well as significant decreases in every measured CM metrics category.
Author (revised)

N94-21328*# Raytheon Service Co., Burlington, MA.
PROBLEM REPORTING MANAGEMENT SYSTEM PERFORMANCE SIMULATION **c81**
David S. VanNatta *In* NASA. Goddard Space Flight Center, Networks Technology Conference Nov. 1993 p 53-59 (For primary document see N94-21323 05-62)
Avail: CASI HC A02/MF A03

This paper proposes the Problem Reporting Management System (PRMS) model as an effective discrete simulation tool that determines the risks involved during the development phase of a Trouble Tracking Reporting Data Base replacement system. The model considers the type of equipment and networks which will be used in the replacement system as well as varying user loads, size of the database, and expected operational availability. The paper discusses the dynamics, stability, and application of the PRMS and addresses suggested concepts to enhance the service performance and enrich them. Author (revised)

N94-21329*# National Aeronautics and Space Administration. Goddard Space Flight Center, Greenbelt, MD.
ENHANCED NETWORKS OPERATIONS USING THE X WINDOW SYSTEM
Irving Linares *In its* Networks Technology Conference Nov. 1993 p 61-72 (For primary document see N94-21323 05-62)
Avail: CASI HC A03/MF A03

We propose an X Window Graphical User Interface (GUI) which is tailored to the operations of NASA GSFC's Network Control Center (NCC), the NASA Ground Terminal (NGT), the White Sands Ground Terminal (WSGT), and the Second Tracking and Data Relay Satellite System (TDRSS) Ground Terminal (STGT). The proposed GUI can also be easily extended to other Ground Network (GN) Tracking Stations due to its standardized nature. Author (revised)

N94-21330*# National Aeronautics and Space Administration. Goddard Space Flight Center, Greenbelt, MD.
THE AUTOMATED GROUND NETWORK SYSTEM c66
Miles T. Smith and Peter N. Militch (Allied-Signal Aerospace Co., Seabrook, MD.) *In its* Networks Technology Conference Nov. 1993 p 73-81 (For primary document see N94-21323 05-62)
Avail: CASI HC A02/MF A03

The primary goal of the Automated Ground Network System (AGNS) project is to reduce Ground Network (GN) station life-cycle costs. To accomplish this goal, the AGNS project will employ an object-oriented approach to develop a new infrastructure that will permit continuous application of new technologies and methodologies to the Ground Network's class of problems. The AGNS project is a Total Quality (TQ) project. Through use of an open collaborative development environment, developers and users will have equal input into the end-to-end design and development process. This will permit direct user input and feedback and will enable rapid prototyping for requirements clarification. This paper describes the AGNS objectives, operations concept, and proposed design.
Author (revised)

N94-21331*# Allied-Signal Aerospace Co., Seabrook, MD.
MISSION OPERATIONS SUPPORT AREA (MOSA) FOR GROUND NETWORK SUPPORT c66
Robert D. Woods and Susan A. Moser *In* NASA. Goddard Space Flight Center, Networks Technology Conference Nov. 1993 p 83-102 (For primary document see N94-21323 05-62)
Avail: CASI HC A03/MF A03

The Mission Operations Support Area (MOSA) has been designed utilizing numerous commercial off the shelf items allowing for easy maintenance and upgrades. At its inception, all equipment was at the forefront of technology. The system was created to provide the operator with a 'State of the Art' replacement for equipment that was becoming antiquated and virtually impossible to repair because new parts were no longer available. Although the Mini-NOCC provided adequate support to the Network for a number of years, it was quickly becoming ineffectual for higher data rate and non-standard missions. The MOSA will prove to be invaluable in the future as more and more missions require Ground Network support.
Author (revised)

N94-21332*# National Aeronautics and Space Administration. Goddard Space Flight Center, Greenbelt, MD.
SPACE NETWORK SCHEDULING BENCHMARK: A PROOF-OF-CONCEPT PROCESS FOR TECHNOLOGY TRANSFER c85
Karen Moe, Nadine Happell (Stanford Telecommunications, Inc., Reston, VA.), B. J. Hayden, and Cathy Barclay (Allied-Signal Aerospace Co., Seabrook, MD.) *In its* Networks Technology Conference Nov. 1993 p 103-120 (For primary document see N94-21323 05-62)
Avail: CASI HC A03/MF A03

This paper describes a detailed proof-of-concept activity to evaluate flexible scheduling technology as implemented in the Request Oriented Scheduling Engine (ROSE) and applied to Space Network (SN) scheduling. The criteria developed for an operational evaluation of a reusable scheduling system is addressed including a methodology to prove that the proposed system performs at least as well as the current system in function and performance. The improvement of the new technology must be demonstrated and evaluated against the cost of making changes. Finally, there is a need to show significant improvement in SN operational procedures. Successful completion of a proof-of-concept would eventually lead to an operational concept and implementation transition plan, which is outside the scope of this paper. However, a high-fidelity benchmark using actual SN scheduling requests has been designed to test the ROSE scheduling tool. The benchmark evaluation methodology, scheduling data, and preliminary results are described. Author (revised)

N94-21333*# Jet Propulsion Lab., California Inst. of Tech., Pasadena.
USING MANUFACTURING MESSAGE SPECIFICATION FOR MONITOR AND CONTROL AT VENUS c66
W. Randy Heuser, Richard L. Chen, and Michael H. Stockett *In* NASA. Goddard Space Flight Center, Networks Technology Conference Nov. 1993 p 121-135 (For primary document see N94-21323 05-62)
Avail: CASI HC A03/MF A03

The flexibility and robustness of a monitor and control (M&C) system are a direct result of the underlying interprocessor communications architecture. A new architecture for M&C at the Deep Space Communications Complexes (DSCC's) has been developed based on the Manufacturing Message Specification (MMS) process control standard of the Open System Interconnection (OSI) suite of protocols. This architecture has been tested both in a laboratory environment and under operational conditions at the Deep Space Network (DSN) experimental Venus station (DSS-13). The Venus experience in the application of OSI standards to support M&C has been extremely successful. MMS meets the functional needs of the station and provides a level of flexibility and responsiveness previously unknown in that environment. The architecture is robust enough to meet current operational needs and flexible enough to provide a migration path for new subsystems. This paper will describe the architecture of the Venus M&C system, discuss how MMS was used and the requirements this imposed on other parts of the system, and provide results from systems and operational testing at the Venus site. Author (revised)

N94-21334*# Computer Sciences Corp., Beltsville, MD.
PREDICTING SCHEDULING SUCCESS c81
Fredric Messing *In* NASA. Goddard Space Flight Center, Networks Technology Conference Nov. 1993 p 137-150 (For primary document see N94-21323 05-62)
Avail: CASI HC A03/MF A03

This paper provides an analytical formulation to predict scheduling success for a class of problems frequently referred to as activity scheduling. Space Network communications scheduling is an example of activity scheduling. The principal assumption is that the activity start times are randomly distributed over the available time in the time line. The formulation makes it possible to estimate how much of the demand can be scheduled as a function of the demand, number of resources, activity duration, and activity flexibility. The paper includes computed results for a variety of resource and demand conditions. The results demonstrate that even with highly flexible activities, it is difficult to schedule demand greater than 60 percent of resources without the use of optimization and conflict resolution capabilities in the scheduling system. Author

N94-21335*# National Aeronautics and Space Administration. Goddard Space Flight Center, Greenbelt, MD.
DISTRIBUTED INTELLIGENT CONTROL AND STATUS NETWORKING
Andre Fortin and Manoj Patel *In its* Networks Technology Conference Nov. 1993 p 151-161 (For primary document see N94-21323 05-62)
Avail: CASI HC A03/MF A03

Over the past two years, the Network Control Systems Branch (Code 532) has been investigating control and status networking technologies. These emerging technologies use distributed processing over a network to accomplish a particular custom task. These networks consist of small intelligent 'nodes' that perform simple tasks. Containing simple, inexpensive hardware and software, these nodes can be easily developed and maintained. Once networked, the nodes can perform a complex operation without a central host. This type of system provides an alternative to more complex control and status systems which require a central computer. This paper will provide some background and discuss some applications of this technology. It will also demonstrate the suitability of one particular technology for the Space Network (SN) and discuss the prototyping activities of Code 532 utilizing this technology. Author (revised)

N94-21336*# Computer Sciences Corp., Beltsville, MD.
GENERATING AND EVALUATING ALTERNATE SCHEDULES c81
Surender D. Reddy *In* NASA. Goddard Space Flight Center, Networks Technology Conference Nov. 1993 p 163-180 (For primary document see N94-21323 05-62)
Avail: CASI HC A03/MF A03

The demand for and availability of Space Network resources are subject to short-term fluctuations and long-term changes. Generation of acceptable schedules under changing demand and resource availability will require the use of different scheduling policies. This paper identifies several such scheduling policies. It defines metrics for evaluating schedules using the criteria directly related to these scheduling policies. Then it applies the metrics to compare several schedules generated for a scenario representative of 1998 SN demand and resources. Finally, the paper describes a method for using these metrics to evaluate schedules based on multiple criteria. Author

N94-21337*# National Aeronautics and Space Administration. Goddard Space Flight Center, Greenbelt, MD.
THE TEST ANALYSIS RETRIEVAL SYSTEM (TARS): MEETING THE CHALLENGES OF THE NETWORK'S TEST PROCESSES
Robert L. Stelmaszek and Douglas R. Lumsden (Loral AeroSys, Seabrook, MD.) *In its* Networks Technology Conference Nov. 1993 p 181-193 (For primary document see N94-21323 05-62)
Avail: CASI HC A03/MF A03

The Networks Systems Test Section (GSFC 531.4) is responsible for managing a variety of engineering and operational tests used to assess the status of the Network elements relative to readiness certification for new and ongoing mission support and for performance trending. To conduct analysis of data collected during these tests, to disseminate and share the information, and to catalog and create reports based on the analysis is currently a cumbersome and inefficient task due primarily to the manual handling of paper products and the inability to easily exchange information between the various Networks elements. The Test Analysis and Retrieval System (TARS) is being implemented to promote concise data analysis, intelligible reporting of test results, to minimize test duplication by fostering a broad sharing of test data, and perhaps most importantly, to provide significantly improved response to the Network's internal and external customers. This paper outlines the intended application, architecture, and benefits of the TARS. Author (revised)

N94-21338*# GTE Government Systems Corp., Las Cruces, NM.
ANALYSIS OF THE TDRS MULTIPLE ACCESS SYSTEM FOR POSSIBLE USE AS AN ATTITUDE CONTROL SYSTEM SENSOR c18
Bruce Allyn Blevins and Victor J. Sank (Herold, Fredrick and Associates, Inc., Greenbelt, MD.) *In* NASA. Goddard Space Flight Center, Networks Technology Conference Nov. 1993 p 195-207 (For primary document see N94-21323 05-62)
Avail: CASI HC A03/MF A03

A member of the constellation of TDR satellites (TDRS) has experienced a failure of its prime earth sensor. Failure of the remaining earth sensor could result in the inability of the satellite to control its attitude and provide user services. Loss of the satellite would be a serious event. The multiple access (MA) antenna array on the TDRS has been proposed for use as a backup sensor for the attitude control system. This paper describes our analysis of the performance of the MA array as an interferometer used for accurate attitude determination. A least squares fit of a plane to the MA phase information appears to represent the TDRS body roll and pitch within about 0.1 deg. This is sufficient for SGL pointing and MA and SSA user services. Analytic improvements that include ionospheric correction may yield sufficient accuracy for KSA user services. Author (revised)

N94-21339*# Stanford Telecommunications, Inc., Seabrook, MD.
THE COMPOSITE ANALYTIC AND SIMULATION PACKAGE OR RFI (CASPR) ON A CODED CHANNEL c32
Jeff Freedman and Ted Berman *In* NASA. Goddard Space Flight Center, Networks Technology Conference Nov. 1993 p 209-215 (For primary document see N94-21323 05-62)
(Contract NAS5-31500)
Avail: CASI HC A02/MF A03

CASPR is an analysis package which determines the performance of a coded signal in the presence of Radio Frequency Interference (RFI) and Additive White Gaussian Noise (AWGN). It can analyze a system with convolutional coding, Reed-Solomon (RS) coding, or a concatenation of the two. The signals can either be interleaved or non-interleaved. The model measures the system performance in terms of either the E(sub b)/N(sub 0) required to achieve a given Bit Error Rate (BER) or the BER needed for a constant E(sub b)/N(sub 0). Author (revised)

N94-21340*# National Aeronautics and Space Administration. Goddard Space Flight Center, Greenbelt, MD.
AN IN-DEPTH ANALYSIS AND MODELLING OF THE SHUTTLE TO MILA S-BAND TELEMETRY LINK c17
Armen Caroglanian, Fernando A. Pellerano, and Dale D. Shama (Loral AeroSys, Seabrook, MD.) *In its* Networks Technology Conference Nov. 1993 p 217-224 (For primary document see N94-21323 05-62)
Avail: CASI HC A02/MF A03

The S-Band radio frequency (RF) link between the Merritt Island (MILA) Tracking Station and the Space Shuttle launch pads is a critical communication path for prelaunch and launch operations. The proposed siting of the Center for Space Education (CSE) at the Visitor Center required a study to avoid RF line-of-sight blockage and reflection paths. The study revealed the trees near MILA's 9-meter (9-M) antennas are obstructing the optical line-of-sight. The studies found diffraction is the main propagation mechanism. This paper describes a link model based on the Geometric Theory of Diffraction. Author

N94-21341*# Stanford Telecommunications, Inc., Seabrook, MD.
THE AUTOMATED CONFLICT RESOLUTION SYSTEM (ACRS) c32
Ted Kaplan, Andrew Musliner, and David Wampler *In* NASA. Goddard Space Flight Center, Networks Technology Conference Nov. 1993 p 225-233 (For primary document see N94-21323 05-62)
Avail: CASI HC A02/MF A03

The Automated Conflict Resolution System (ACRS) is a mission-current scheduling aid that predicts periods of mutual interference when two or more orbiting spacecraft are scheduled to communicate with the same Tracking and Data Relay Satellite (TDRS) at the same time. The mutual interference predicted has the potential to degrade or prevent communications. Thus the ACRS system is a useful tool for aiding in the scheduling of Space Network (SN) communications. Author

N94-21342*# Stanford Telecommunications, Inc., Seabrook, MD.
THE THREE-DIMENSIONAL EVENT-DRIVEN GRAPHICS ENVIRONMENT (3D-EDGE) c61
Jeffrey Freedman, Roger Hahn, and David M. Schwartz *In* NASA. Goddard Space Flight Center, Networks Technology Conference Nov. 1993 p 235-240 (For primary document see N94-21323 05-62)
(Contract NAS5-31500)
Avail: CASI HC A02/MF A03

Stanford Telecom developed the Three-Dimensional Event-Driven Graphics Environment (3D-EDGE) for NASA GSFC's (GSFC) Communications Link Analysis and Simulation System (CLASS). 3D-EDGE consists of a library of object-oriented subroutines which allow engineers with little or no computer graphics experience to programmatically manipulate, render, animate, and access complex three-dimensional objects.
Author (revised)

N94-21343*# Booz-Allen and Hamilton, Inc., Seabrook, MD.
DEVELOPING A SPACE NETWORK INTERFACE SIMULATOR: THE NTS APPROACH c66
Gary E. Hendrzak *In* NASA. Goddard Space Flight Center, Networks Technology Conference Nov. 1993 p 243-251 (For primary document see N94-21323 05-62)
Avail: CASI HC A02/MF A03

This paper describes the approach used to redevelop the Network Control Center (NCC) Test System (NTS), a hardware and software facility designed to make testing of the NCC Data System (NCCDS) software efficient, effective, and as rigorous as possible prior to operational use. The NTS transmits and receives network message traffic in real-time. Data transfer rates and message content are strictly controlled and are identical to that of the operational systems. NTS minimizes the need for costly and time-consuming testing with the actual external entities (e.g., the Hubble Space Telescope (HST) Payload Operations Control Center (POCC) and

the White Sands Ground Terminal). Discussed are activities associated with the development of the NTS, lessons learned throughout the project's lifecycle, and resulting productivity and quality increases. Author (revised)

N94-21344*# Stanford Telecommunications, Inc., Seabrook, MD.
SATELLITE COMMUNICATION HARDWARE EMULATION SYSTEM (SCHES) **c32**
Ted Kaplan *In* NASA. Goddard Space Flight Center, Networks Technology Conference Nov. 1993 p 253-263 (For primary document see N94-21323 05-62)
Avail: CASI HC A03/MF A03

Satellite Communication Hardware Emulator System (SCHES) is a powerful simulator that emulates the hardware used in TDRSS links. SCHES is a true bit-by-bit simulator that models communications hardware accurately enough to be used as a verification mechanism for actual hardware tests on user spacecraft. As a credit to its modular design, SCHES is easily configurable to model any user satellite communication link, though some development may be required to tailor existing software to user specific hardware. Author (revised)

N94-21345*# National Aeronautics and Space Administration. Goddard Space Flight Center, Greenbelt, MD.
A PACKET SWITCHED COMMUNICATIONS SYSTEM FOR GRO **c32**
Shabu Husain (Allied-Signal Aerospace Co., Seabrook, MD.), Wen-Hsing Yang (Allied-Signal Aerospace Co., Seabrook, MD.), Rani Vadlamudi (Allied-Signal Aerospace Co., Seabrook, MD.), and Joseph Valenti *In its* Networks Technology Conference Nov. 1993 p 265-274 (For primary document see N94-21323 05-62)
(Contract NAS5-27772)
Avail: CASI HC A02/MF A03

This paper describes the packet switched Instrumenters Communication System (ICS) that was developed for the Command Management Facility at GSFC to support the Gamma Ray Observatory (GRO) spacecraft. The GRO ICS serves as a vital science data acquisition link to the GRO scientists to initiate commands for their spacecraft instruments. The system is ready to send and receive messages at any time, 24 hours a day and seven days a week. The system is based on X.25 and the International Standard Organization's (ISO) 7-layer Open Systems Interconnection (OSI) protocol model and has client and server components. The components of the GRO ICS are discussed along with how the Communications Subsystem for Interconnection (CSFI) and Network Control Program Packet Switching Interface (NPSI) software are used in the system. Author (revised)

N94-21346*# Herold (Fredrick) and Associates, Inc., Greenbelt, MD.
USING THE USCCS FOR SUB MICROSECOND SPACECRAFT CLOCK CALIBRATION **c35**
Victor J. Sank *In* NASA. Goddard Space Flight Center, Networks Technology Conference Nov. 1993 p 275-287 (For primary document see N94-21323 05-62)
Avail: CASI HC A03/MF A03

The Return Data Delay technique which requires knowledge of spacecraft range is commonly used for correlating a spacecraft clock against a ground time standard when millisecond accuracy is required. An analysis is presented that allows using the user spacecraft clock calibration system (USCCS) to correlate a spacecraft clock to better than one microsecond accuracy. The basic USCCS algorithm has been simplified and it is shown to result in about one microsecond accuracy without requiring orbital information. By considering the relative motion of the user satellite, the TDRS and the earth station about the center of the earth, a correction of almost two orders of magnitude can be made. Such accuracy is required for scientific investigations that require correlating coincident radiation or particle detection with a remote laboratory. Author (revised)

N94-21347*# Allied-Signal Aerospace Co., Columbia, MD. Data Systems Group.
A LOW COST ALTERNATIVE TO HIGH PERFORMANCE PCM BIT SYNCHRONIZERS **c35**
Bruce DeShong *In* NASA. Goddard Space Flight Center, Networks Technology Conference Nov. 1993 p 289-307 (For primary document see N94-21323 05-62)
Avail: CASI HC A03/MF A03

The Code Converter/Clock Regenerator (CCCR) provides a low-cost alternative to high-performance Pulse Code Modulation (PCM) bit synchronizers in environments with a large Signal-to-Noise Ratio (SNR). In many applications, the CCCR can be used in place of PCM bit synchronizers at about one fifth the cost. The CCCR operates at rates from 10 bps to 2.5 Mbps and performs PCM code conversion and clock regeneration. The CCCR has been integrated into a stand-alone system configurable from one to six channels and has also been designed for use in VMEbus compatible systems. Author

N94-21348*# Loral AeroSys, Seabrook, MD.
ARRAY SIMULATIONS PLATFORM (ASP) PREDICTS NASA DATA LINK MODULE (NDLM) PERFORMANCE **c32**
Allen David Snook *In* NASA. Goddard Space Flight Center, Networks Technology Conference Nov. 1993 p 309-327 (For primary document see N94-21323 05-62)
Avail: CASI HC A03/MF A03

Through a variety of imbedded theoretical and actual antenna patterns, the array simulation platform (ASP) enhanced analysis of the array antenna pattern effects for the KTx (Ku-Band Transmit) service of the NDLM (NASA Data Link Module). The ASP utilizes internally stored models of the NDLM antennas and can develop the overall pattern of antenna arrays through common array calculation techniques. ASP expertly assisted in the diagnosing of element phase shifter errors during KTx testing and was able to accurately predict the overall array pattern from combinations of the four internally held element patterns. This paper provides an overview of the use of the ASP software in the solving of array mis-phasing problems. Author (revised)

N94-21349*# GTE Government Systems Corp., Las Cruces, NM.
CONVERSION OF THE PROPRIETARY ROLM (TM) INTER-NODE LINK FROM MULTIMODE TO SINGLEMODE OPERATION **c32**
Larry Boucher *In* NASA. Goddard Space Flight Center, Networks Technology Conference Nov. 1993 p 329-347 (For primary document see N94-21323 05-62)
Avail: CASI HC A03/MF A03

Many NASA centers have selected ROLM(TM) Computerized Branch Exchanges (CBX's) as their standard telephone exchange. The ROLM 9751 CBX Model 70 with ROLM software release 9005 can inter-communicate as a 'multi-node' system over a multimode fiber optic link of 450 to 6,000 meters. Singlemode fiber installations are not supported by ROLM. Two New Mexico-based NASA satellite ground terminals were already connected via a 6 kilometer singlemode fiber optic link. The ROLM Inter-Node Link (INL) was converted from multimode LED transmitters to singlemode laser transmitters and two ROLM CBX systems were interconnected using the modified INL. On activation, the system operated normally and has done so for six months. System testing indicates sufficient margin to drive 45 kilometers of singlemode fiber, an important benefit for widely separated facilities. Author (revised)

N94-21350*# Stanford Telecommunications, Inc., Seabrook, MD.
ADVANCED CODING AND MODULATION SCHEMES FOR TDRSS **c32**
Linda Harrell, Ted Kaplan, Ted Berman, and Susan Chang *In* NASA. Goddard Space Flight Center, Networks Technology Conference Nov. 1993 p 349-354 (For primary document see N94-21323 05-62)
Avail: CASI HC A02/MF A03

This paper describes the performance of the Ungerboeck and pragmatic 8-Phase Shift Key (PSK) Trellis Code Modulation (TCM) coding techniques with and without a (255,223) Reed-Solomon outer code as they are used for Tracking Data and Relay Satellite System (TDRSS) S-Band and Ku-Band return services. The performance of these codes at high data rates is compared to uncoded Quadrature PSK (QPSK) and rate 1/2 convolutionally coded QPSK in the presence of Radio Frequency Interference (RFI), self-interference, and hardware distortions. This paper shows that the outer Reed-Solomon code is necessary to achieve a 10(exp -5) Bit Error Rate (BER) with an acceptable level of degradation in the presence of RFI. This paper also shows that the TCM codes with or without the Reed-Solomon outer code do not perform well in the presence of self-interference. In fact, the uncoded QPSK signal performs better than the TCM coded signal in the self-interference situation considered in this analysis. Finally, this paper shows that the E(sub b)/N(sub 0) degradation due to TDRSS hardware distortions is approximately 1.3 dB with a TCM coded signal or a rate 1/2

convolutionally coded QPSK signal and is 3.2 dB with an uncoded QPSK signal. Author (revised)

N94-21351*# Allied-Signal Aerospace Co., Columbia, MD.
NETWORK COMMAND PROCESSING SYSTEM OVERVIEW c66
Yon-Woo Nam and Lisa D. Murphy *In* NASA. Goddard Space Flight Center, Networks Technology Conference Nov. 1993 p 355-369 (For primary document see N94-21323 05-62)
(Contract NAS5-31000)
Avail: CASI HC A03/MF A03

The Network Command Processing System (NCPS) developed for the National Aeronautics and Space Administration (NASA) Ground Network (GN) stations is a spacecraft command system utilizing a MULTIBUS I/68030 microprocessor. This system was developed and implemented at ground stations worldwide to provide a Project Operations Control Center (POCC) with command capability for support of spacecraft operations such as the LANDSAT, Shuttle, Tracking and Data Relay Satellite, and Nimbus-7. The NCPS consolidates multiple modulation schemes for supporting various manned/unmanned orbital platforms. The NCPS interacts with the POCC and a local operator to process configuration requests, generate modulated uplink sequences, and inform users of the ground command link status. This paper presents the system functional description, hardware description, and the software design. Author (revised)

N94-21492# Center for Mathematics and Computer Science, Amsterdam (Netherlands). Dept. of Numerical Mathematics.
SOME EXPERIENCES OF SOLVING 1-D SEMICONDUCTOR DEVICE EQUATIONS ON A MATRIX COPROCESSOR BY A DOMAIN DECOMPOSITION METHOD
C.-H. Lai and H. J. J. teRiele Feb. 1993 20 p Sponsored in part by European Research Consortium for Informatics and Mathematics
(CWI-NM-R9304; ETN-94-94706) Copyright Avail: CASI HC A03/MF A01

The implementation of a domain decomposition technique for the numerical solution of 1-D (one dimensional) semiconductor device equations on a Cray S-MP System 500 Matrix Coprocessor with 28 processing elements is reported. A total work expression is constructed for comparison with the actual computing time of the parallel technique. The behavior of the numerical method is examined by using different configurations of the processing elements within the parallel machine. Experiments were performed on a number of devices including p-n junctions and thyristors. ESA

N94-21493# Center for Mathematics and Computer Science, Amsterdam (Netherlands). Dept. of Numerical Mathematics.
BUTCHER-KUNTZMANN METHODS FOR NONSTIFF PROBLEMS ON PARALLEL COMPUTERS
P. J. vanderHouwen and B. P. Sommeijer Mar. 1993 20 p
(CWI-NM-R9305; ETN-94-94707) Copyright Avail: CASI HC A03/MF A01

Nonstiff initial value problems are addressed and the possibility of introducing preconditioners into the iteration method is investigated. In particular, the iteration error was analyzed. By a number of numerical experiments the Butcher-Kuntzmann method, in combination with the preconditioned, parallel iteration scheme, is shown to perform much more efficiently than the best sequential methods. ESA

N94-21549# Center for Mathematics and Computer Science, Amsterdam (Netherlands). Dept. of Computer Science.
UNIFORM SELF-STABILIZING LEADER ELECTION. PART 1: COMPLETE GRAPH PROTOCOLS
Shlomi Dolev (Technion - Israel Inst. of Tech., Haifa.), Amos Israeli (Technion - Israel Inst. of Tech., Haifa.), and Shlomo Moran (Technion - Israel Inst. of Tech., Haifa.) Feb. 1993 20 p
(CWI-CS-R9308-Pt-1; ETN-94-94737) Copyright Avail: CASI HC A03/MF A01

A distributed system is self stabilizing if it can be started in any possible global state. Once started the system regains its consistency by itself, without any kind of an outside intervention. The self stabilization property makes the system tolerant to faults in which processors crash and then recover spontaneously in an arbitrary state. When the intermediate period in between one recovery and the next crash is long enough the system stabilizes. A distributed system is uniform if all processors with the same number of neighbors are identical. A study on uniform self stabilizing protocols for leader election under read/write atomicity is presented. The protocols use randomization to break symmetry. The si-game method for analyzing the performance of randomized distributed protocols is introduced and two protocols for the case where each processor in the system can communicate with all other processors are presented. Their performance is analyzed using the si-game technique. ESA

N94-21610 Center for Mathematics and Computer Science, Amsterdam (Netherlands). Dept. of Numerical Mathematics.
PARALLELIZING A HIGHLY VECTORIZED MULTIGRID CODE WITH ZEBRA RELAXATION
Walter M. Lioen Dec. 1992 19 p Sponsored by Cray Research, Inc., and Netherlands Organization for Scientific Research Limited Reproducibility: More than 20% of this document may be affected by microfiche quality
(CWI-NM-R9225; ETN-94-94700) Copyright Avail: CASI HC A03

An introduction to multigrid methods is given and the algorithmic choices in MGZEB, a parallelized highly vectorized multigrid code for the solution of linear systems resulting from the seven point discretization of general linear second order elliptic partial differential equations in two dimensions, are discussed. The minimization of the scalar operation count, the vector tuning on a vector register machine, and the parallelization of the already existing highly vectorized MGZEB code are described. At present, the same algorithm would be used with the same scalar operation count on a scalar uniprocessor. The overall parallel vector performance using autotasking on a Cray Y-MP4/464 is discussed. ESA

N94-21622# Los Alamos National Lab., NM.
A DATA DISTRIBUTED, PARALLEL ALGORITHM FOR RAY-TRACED VOLUME RENDERING
Kwan-Liu Ma, J. S. Painter, C. D. Hansen, and M. F. Krogh 30 Mar. 1993 35 p Presented at the Parallel Rendering Symposium, San Jose, CA, 25 Oct. 1993
(Contract W-7405-eng-36)
(DE93-040150; LA-UR-93-3138; CONF-9310153-1) Avail: CASI HC A03/MF A01

This paper presents a divide-and-conquer ray-traced volume rendering algorithm and its implementation on networked workstations and a massively parallel computer, the Connection Machine CM-5. This algorithm distributes the data and the computational load to individual processing units to achieve fast, high-quality rendering of high-resolution data, even when only a modest amount of memory is available on each machine. The volume data, once distributed, is left intact. The processing nodes perform local ray-tracing of their sub-volume concurrently. No communication between processing units is needed during this locally ray-tracing process. A sub-image is generated by each processing unit and the final image is obtained by compositing sub-images in the proper order, which can be determined a priori. Implementations and tests on a group of networked workstations and on the Thinking Machines CM-5 demonstrate the practicality of our algorithm and expose different performance tuning issues for each platform. We use data sets from medical imaging and computational fluid dynamics simulations in the study of this algorithm. DOE

N94-21745# Los Alamos National Lab., NM.
SIMULATED BEHAVIOUR OF LARGE SCALE SCI RINGS AND TORI
Ho-Jung Cha (Manchester Univ., England.), A. Knowles (Manchester Univ., England.), and R. Daniel, Jr. (Cambridge Univ., England.) 1993 10 p Presented at the 5th Institute of Electrical and Electronics Engineers (IEEE) Symposium on Parallel and Distributed Processing, Dallas, TX, 1-4 Dec. 1993
(Contract W-7405-eng-36)
(DE93-040149; LA-UR-93-3137; CONF-931220-2) Avail: CASI HC A02/MF A01

SCI (Scalable Coherent Interface) is a new IEEE standard for a high speed interconnect in parallel processors. It is attracting interest because of its high bandwidth (1 GB/sec/link) and low latency. The default SCI topology is a ring, which does not scale well to large numbers of processors. This paper uses stochastic and trace-driven simulations to compare the performance of SCI-based parallel computers with a ring topology to those based on a torus topology. We also look at the effects of varying some of the internals of the SCI components. DOE

N94-21746# Los Alamos National Lab., NM.
VISUALIZATION ON MASSIVELY PARALLEL COMPUTERS USING CM/AVS
M. F. Krogh and C. D. Hansen 1993 11 p Presented at the Advanced Visualization System (AVS) 1993 Users Group Meeting, Orlando, FL, 24-26 May 1993
(Contract W-7405-eng-36)
(DE93-040151; LA-UR-93-3139; CONF-9305168-6) Avail: CASI HC A03/MF A01

CM/AVS is a visualization environment for the massively parallel CM-5 from Thinking Machines. It provides a backend to the standard commercially available AVS visualization product. At the Advanced Computing Laboratory at Los Alamos National Laboratory, we have been experimenting and utilizing this software within our visualization environment. This paper describes our experiences with CM/AVS. The conclusions reached are applicable to any implementation of visualization software within a massively parallel computing environment. DOE

N94-21749# Lawrence Livermore National Lab., CA.
PERFORMANCE EVALUATION OF VIDEO ON ETHERNET
M. Pihlman and R. Farrell Aug. 1993 8 p
(Contract W-7405-eng-48)
(DE93-040696; UCRL-ID-115116) Avail: CASI HC A02/MF A01

The purpose of this project was to determine the feasibility of using an ethernet local area network (LAN) to support videoconferencing connections between CAMEO Macintosh desktop videoconferencing systems. The specific goals were to: (1) to ensure that CAMEO video could be transported-without protocol modification-via existing ethernet networks, and would do so without "bringing-down" the network; (2) to measure the effect of CAMEO video connections on ethernet traffic; (3) to evaluate qualitatively how generated ethernet traffic effects the CAMEO video; and (4) to evaluate qualitatively how multiple CAMEO connections work between two routered ethernet networks via a backbone. High quality CAMEO video can be transported on an ethernet network and between routered networks, via a backbone. The number of simultaneous video connections possible on an ethernet segment would probably be less than 45, since each connection uses 2.2% of the network and errors increase rapidly as video connections are made. However, the actual number of simultaneous video connections possible will depend upon your network implementation and the amount of 'normal' traffic present. The remainder of this report discusses the effect of CAMEO video on our networks. DOE

N94-21828 Lawrence Livermore National Lab., CA.
THE TRANSITION TO MASSIVELY PARALLEL COMPUTING WITHIN A PRODUCTION ENVIRONMENT AT A DOE ACCESS CENTER
M. G. McCoy Apr. 1993 14 p Presented at the Conference on High Speed Computing, Salisham, OR, Apr. 1993 Limited Reproducibility: More than 20% of this document may be affected by microfiche quality
(Contract W-7405-eng-48)
(DE93-019155; UCRL-JC-113508; CONF-9304159-2) Avail: CASI HC A03

In contemplating the transition from sequential to MP computing, the National Energy Research Supercomputer Center (NERSC) is faced with the frictions inherent in the duality of its mission. There have been two goals: the first has been to provide a stable, serviceable, production environment to the user base; the second to bring the most capable early serial supercomputers to the center to make possible the leading edge simulations. This seeming conundrum has in reality been a source of strength. The task of meeting both goals was faced before with the CRAY 1 which, as delivered, was all iron; so the problems associated with the advent of parallel computers are not entirely new, but they are serious. Current vector supercomputers, such as the C90, offer mature production environments, including software tools, a large applications base, and generality; these machines can be used to attack the spectrum of scientific applications by a large user base knowledgeable in programming techniques for this architecture. Parallel computers to date have offered less developed, even rudimentary, working environments, a sparse applications base, and forced specialization. They have been specialized in terms of programming models, and specialized in terms of the kinds of applications which would do well on the machines. Given this context, why do many service computer centers feel that now is the time to cease or slow the procurement of traditional vector supercomputers in favor of MP systems? What are some of the issues that NERSC must face to engineer a smooth transition? The answers to these questions are multifaceted and by no means completely clear. However, a route exists as a result of early efforts at the laboratories combined with research within the HPCC program. One can begin with an analysis of why the hardware and software appearing shortly should be made available to the mainstream, and then address what would be required in an initial production environment. DOE

N94-21853# Sandia National Labs., Albuquerque, NM.
EVALUATION OF DEC'S GIGAswitch FOR DISTRIBUTED PARALLEL COMPUTING
H. Chen, J. Hutchins, and J. Brandt Oct. 1993 30 p
(Contract DE-AC04-76DR-00789)
(DE94-001356; SAND-93-8013) Avail: CASI HC A03/MF A01

One of Sandia's research efforts is to reduce the end-to-end communication delay in a parallel-distributed computing environment. GIGAswitch is DEC's implementation of a gigabit local area network based on switched FDDI technology. Using the GIGAswitch, the authors intend to minimize the medium access latency suffered by shared-medium FDDI technology. Experimental results show that the GIGAswitch adds 16.5 microseconds of switching and bridging delay to an end-to-end communication. Although the added latency causes a 1.8% throughput degradation and a 5% line efficiency degradation, the availability of dedicated bandwidth is much more than what is available to a workstation on a shared medium. For example, ten directly connected workstations each would have a dedicated bandwidth of 95 Mbps, but if they were sharing the FDDI bandwidth, each would have 10% of the total bandwidth, i.e., less than 10 Mbps. In addition, they have found that when there is no output port contention, the switch's aggregate bandwidth will scale up to multiples of its port bandwidth. However, with output port contention, the throughput and latency performance suffered significantly. Their mathematical and simulation models indicate that the GIGAswitch line efficiency could be as low as 63% when there are nine input ports contending for the same output port. The data indicate that the delay introduced by contention at the server workstation is 50 times that introduced by the GIGAswitch. The authors conclude that the GIGAswitch meets the performance requirements of today's high-end workstations and that the switched FDDI technology provides an alternative that utilizes existing workstation interfaces while increasing the aggregate bandwidth. However, because the speed of workstations is increasing by a factor of 2 every 1.5 years, the switched FDDI technology is only good as an interim solution. DOE

N94-21919# Superconducting Super Collider Lab., Dallas, TX.
PHYSICS DETECTOR SIMULATION FACILITY (PDSF) ARCHITECTURE/UTILIZATION
B. Scipioni May 1993 9 p Presented at the 5th Annual International Industrial Symposium on the Super Collider and Exhibition, San Francisco, CA, 6-8 May 1993 Submitted for publication
(Contract DE-AC35-89ER-40486)
(DE93-019744; SSCL-Preprint-324; CONF-930537-100) Avail: CASI HC A02/MF A01

The current systems architecture for the SSCL's Physics Detector Simulation Facility (PDSF) is presented. Systems analysis data is presented and discussed. In particular, these data disclose the effectiveness of utilization of the facility for meeting the needs of physics computing, especially as concerns parallel architecture and processing. Detailed design plans for the highly networked, symmetric, parallel, UNIX workstation-based facility are given and discussed in light of the design philosophy. Included are network, CPU, disk, router, concentrator, tape, user and job capacities and throughput. DOE

N94-22032# Pacific Northwest Lab., Richland, WA.
EFFICIENT COMMUNICATION PRIMITIVES ON MESH ARCHITECTURES WITH HARDWARE ROUTING
M. Barnett (Idaho Univ., Moscow.), R. Littlefield, D. G. Payne (INTEL Corp., Beaverton, OR.), and R. vandeGeijn (Texas Univ., Austin.) Mar. 1993 6 p Presented at the 6th Society Industrial and Applied Math Conference on Parallel Processing for Scientific Computing, Newport Beach, CA, 22-24 Mar. 1993
(Contract DE-AC06-76RL-01830)

(DE93-018791; PNL-SA-22001; CONF-9303204-1) Avail: CASI HC A02/MF A01

Several algorithms are discussed for implementing global combine on distributed memory computers using a two-dimensional mesh interconnect with wormhole routing. These include algorithms that are asymptotically optimal for short vectors (O(log(p)) for p processors) and for long vectors (O(n) for n data elements per processor). Performance models are developed which include startup and transfer costs that can depend on the number of messages that each node must handle at once. The models are validated using experimental data from the Intel Touchstone DELTA computer.

DOE

N94-22042# Lawrence Livermore National Lab., CA.

MICROSCOPIC AND MACROSCOPIC DYNAMICS

W. G. Hoover, C. G. Hoover, A. J. DeGroot, and T. G. Pierce Jun. 1993 19 p Presented at the 2nd International Austrian Conference on Parallel Computing, Vienna, Austria, 4-8 Oct. 1993

(Contract W-7405-eng-48)

(DE93-019576; UCRL-JC-113895; CONF-9310161-1) Avail: CASI HC A03/MF A01

Atomistic Molecular Dynamics and Lagrangian Continuum Mechanics can be very similarly adapted to massively-parallel computers. Millions of degrees of freedom can be treated. The two complementary approaches, microscopic and macroscopic, are being applied to increasingly realistic flows of fluids and solids. The two approaches can also be combined in a hybrid simulation scheme. Hybrids combine the fundamental constitutive advantage of atoms with the size advantage of the continuum picture.

DOE

N94-22267# Oak Ridge National Lab., TN.

DISTRIBUTED PROCESSING USING ORACLE7 AND SQL*NET V2: AN IMPLEMENTATION STORY

J. P. Loftis and J. W. Grubb (Tennessee Univ., Knoxville.) 1993 9 p Presented at the 1993 International Oracle Users' Meeting, Orlando, FL, 26 Sep. - 1 Oct. 1993

(Contract DE-AC05-84OR-21400)

(DE94-000494; CONF-9309246-1) Avail: CASI HC A02/MF A01

The Army is successfully building on the Oracle7 system that includes a central data repository and decentralized processing hubs. One of the greatest challenges of this project is to connect multiple sites on the East, West, and Gulf Coasts with a database server and to distribute large volumes of data and messages between this database and Orcale7 nodes using SQL*Net. This presentation describes the problems we encountered, the solutions we found, and our success using Orcale7 and SQL*Net to provide global visibility of shipment cargo.

DOE

N94-22378# University of Southern California, Los Angeles. Dept. of Electrical Engineering.

DISTRIBUTED INPUT/OUTPUT PROCESSING IN DATA-DRIVEN MULTIPROCESSORS

P. Evripidou (Southern Methodist Univ., Dallas, TX.) and J. L. Gaudiot 1992 9 p Presented at the 2nd IEEE Symposium on Parallel and Distributed Processing, Dallas, TX, 9-13 Dec. 1990

(Contract DE-FG03-87ER-25043)

(DE94-000323; CONF-901221-2) Avail: CASI HC A02/MF A01

Data-flow principles of execution provide an elegant way to ensure at runtime that instructions can be executed asynchronously in a parallel environment. However, while the conventional von Neumann model of interpretation has a very rigid ordering of instructions, it is the very asynchronous character of the dataflow model of execution that introduces conflicts when 'state' tasks (such as I/O operations) must share common data objects. In order to execute I/O operations safely and in parallel, an algorithm to detect and classify cases of potential conflicts (hazards) has been developed; it is described in this paper. It is based upon localizing the effect of I/O operations by splitting the data-flow graph into two subgraphs: (1) the computation subgraph, and (2) the I/O subgraph. The scheme presented in this paper thus enables the creation and interaction of both subgraphs, which in turn yields a deterministic execution. Furthermore, the proposed scheme enables the distributed execution of I/O operations as permitted by data dependencies.

DOE

N94-22414*# Boeing Defense and Space Group, Seattle, WA.

TOWARDS THE FORMAL VERIFICATION OF THE REQUIREMENTS AND DESIGN OF A PROCESSOR INTERFACE UNIT: HOL LISTINGS

David A. Fura, Phillip J. Windley (Idaho Univ., Moscow.), and Gerald C. Cohen Nov. 1993 179 p

(Contract NAS1-18586; RTOP 505-64-10-07)

(NASA-CR-191466; NAS 1.26:191466) Avail: CASI HC A09/MF A02

This technical report contains the Higher-Order Logic (HOL) listings of the partial verification of the requirements and design for a commercially developed processor interface unit (PIU). The PIU is an interface chip performing memory interface, bus interface, and additional support services for a commercial microprocessor within a fault tolerant computer system. This system, the Fault Tolerant Embedded Processor (FTEP), is targeted towards applications in avionics and space requiring extremely high levels of mission reliability, extended maintenance-free operation, or both. This report contains the actual HOL listings of the PIU verification as it currently exists. Section two of this report contains general-purpose HOL theories and definitions that support the PIU verification. These include arithmetic theories dealing with inequalities and associativity, and a collection of tactics used in the PIU proofs. Section three contains the HOL listings for the completed PIU design verification. Section 4 contains the HOL listings for the partial requirements verification of the P-Port. Derived from text

N94-22558# Lawrence Livermore National Lab., CA.

PARALLEL FUNCTIONAL PROGRAMMING IN SISAL: FICTIONS, FACTS, AND FUTURE

J. R. McGraw 1 Jul. 1993 40 p Presented at the Programming Tools for Parallel Machines Workshop, Otranto, Italy, 22-26 Jun. 1993

(Contract W-7405-eng-48)

(DE93-040486; UCRL-JC-114360; CONF-9306250-1) Avail: CASI HC A03/MF A01

This paper provides a status report on the progress of research and development on the functional language Sisal. This project focuses on providing a highly effective method of writing large scientific applications that can efficiently execute on a spectrum of different multiprocessors. The paper includes sections on the language definition, compilation strategies, and programming techniques intended for readers with little or no background with Sisal. The section on performance presents our most recent results on execution speed for shared-memory multiprocessors, our findings using Sisal to develop codes, and our experiences migrating the same source code to different machines. For large programs, the execution performance of Sisal (with minimal supporting advice from the programmer) usually exceeds that of the best available automatic, vector/parallel Fortran compilers. Our evidence also indicates that Sisal programs tend to be shorter in length, faster to write, and clearer to understand than equivalent algorithms in Fortran. The paper concludes with a substantial discussion of common criticisms of the language and our plans for addressing them. Most notably, efficient implementations for distributed memory machines are lacking; an issue we plan to remedy.

DOE

N94-20253# University Coll., Dublin (Ireland). Dept. of Computer Science.

AN EXPLORATION OF CLAUSE BOUNDARY EFFECTS IN SRN REPRESENTATIONS

Ronan Reilly *In* Univ. Twente, Connectionism and Natural Language Processing Oct. 1992 p 97-102 (For primary document see N94-20242 05-63)

Copyright Avail: CASI HC A02/MF A02

N94-21081*# Concordia Univ., Montreal (Quebec). Dept. of Computer Science.

AVOIDING AND TOLERATING LATENCY IN LARGE-SCALE NEXT-GENERATION SHARED-MEMORY MULTIPROCESSORS

David K. Probst *In* New Mexico Univ., The Fifth NASA Symposium on VLSI Design 1993 15 p Sponsored in part by MicroNet (For primary document see N94-21079 05-33)

(Grants NSERC-A3363; NSERC-MEF-0040121)

Avail: CASI HC A03/MF A06

N94-21132*# Sri Venkateswara Univ., Tirupati (India). Dept. of Computer Science and Engineering.
A COST-EFFECTIVE METHODOLOGY FOR THE DESIGN OF MASSIVELY-PARALLEL VLSI FUNCTIONAL UNITS
N. Venkateswaran, G. Sriram, and J. Desouza *In* New Mexico Univ., The Fifth NASA Symposium on VLSI Design 1993 16 p (For primary document see N94-21079 05-33)
Avail: CASI HC A03/MF A06

N94-21468*# Princeton Univ., NJ. Dept. of Computer Science.
ANALYSIS OF MULTIGRID METHODS ON MASSIVELY PARALLEL COMPUTERS: ARCHITECTURAL IMPLICATIONS
Lesley R. Matheson and Robert E. Tarjan *In* NASA. Langley Research Center, The Sixth Copper Mountain Conference on Multigrid Methods, Part 2 Nov. 1993 p 405-421 (For primary document see N94-21464 05-64)
(Contract N00014-91-J-1463; NSF CCR-89-20505; NSF STC-88-09648)
Avail: CASI HC A03/MF A03

N94-22070# Nokia Data, Helsinki (Finland). Technology and Product Strategy.
INDUSTRY STANDARDS: KEY TO DISTRIBUTED COMPUTING
Ari Mikkola *In* Technical Research Centre of Finland, Information Technology and Economic Modelling 1992 p 120-133 (For primary document see N94-22056 05-83)
Copyright Avail: CASI HC A03/MF A03

N94-22132 Ecole Polytechnique, Montreal (Quebec). Dept. of Electrical Engineering.
VLSI DESIGN OF A BIT SERIAL PARALLEL PROCESSING 4 EXTENDER CHIP FOR M-PATH CONVOLUTIONAL DECODING
Martin Chalifoux, Minh Nguyen, Steve Thiffault, Jean Belzile, Yvon Savaria, and David Haccoun *In* Engineering Inst. of Canada, Canadian Conference on Electrical and Computer Engineering, Volumes 1 and 2 1991 4 p (For primary document see N94-22101 05-33)
Avail: Issuing Activity (Engineering Inst. of Canada, 2050 rue Mansfield, Suite 700, Montreal, PQ H3A 1Z2 Canada)

N94-22175 McMaster Univ., Hamilton (Ontario). Dept. of Electrical and Computer Engineering.
USING STREAM INTERLEAVING TO ELIMINATE THE NEED FOR INTERLOCKS IN DEEPLY PIPELINED PROCESSORS
Daniel C. McCrackin *In* Engineering Inst. of Canada, Canadian Conference on Electrical and Computer Engineering, Volumes 1 and 2 1991 6 p (For primary document see N94-22101 05-33)
Avail: Issuing Activity (Engineering Inst. of Canada, 2050 rue Mansfield, Suite 700, Montreal, PQ H3A 1Z2 Canada)

N94-22192 McGill Univ., Montreal (Quebec). Biorobotics Lab.
INTEGRATION OF PARALLEL PROCESSING STRUCTURES USING A MATRIX APPROACH
Sylvain Martel, Ian W. Hunter, and S. Lafontaine *In* Engineering Inst. of Canada, Canadian Conference on Electrical and Computer Engineering, Volumes 1 and 2 1991 4 p (For primary document see N94-22101 05-33)
Avail: Issuing Activity (Engineering Inst. of Canada, 2050 rue Mansfield, Suite 700, Montreal, PQ H3A 1Z2 Canada)

N94-22206 Manitoba Univ., Winnipeg. Dept. of Electrical and Computer Engineering.
ACCELERATION OF BACKPROPAGATION LEARNING USING A PARALLEL DSP MACHINE
Glenn K. Rosendahl, Robert D. McLeod, and Howard C. Card *In* Engineering Inst. of Canada, Canadian Conference on Electrical and Computer Engineering, Volumes 1 and 2 1991 4 p (For primary document see N94-22101 05-33)
Avail: Issuing Activity (Engineering Inst. of Canada, 2050 rue Mansfield, Suite 700, Montreal, PQ H3A 1Z2 Canada)

N94-22207 Alberta Univ., Calgary. Dept. of Electrical Engineering.
IMAGE CONVOLUTION USING THE MYRIAS SPS-2 PARALLEL COMPUTER
Kalpagam Krishnan, Werner B. Joerg, and Brian Minchau *In* Engineering Inst. of Canada, Canadian Conference on Electrical and Computer Engineering, Volumes 1 and 2 1991 5 p (For primary document see N94-22101 05-33)
Avail: Issuing Activity (Engineering Inst. of Canada, 2050 rue Mansfield, Suite 700, Montreal, PQ H3A 1Z2 Canada)

N94-22208 Alberta Univ., Calgary. Dept. of Electrical Engineering.
PARALLELIZING A MAXIMUM ENTROPY IMAGE DECONVOLUTION ALGORITHM
Werner B. Joerg and Kalpagam Krishnan *In* Engineering Inst. of Canada, Canadian Conference on Electrical and Computer Engineering, Volumes 1 and 2 1991 5 p (For primary document see N94-22101 05-33)
Avail: Issuing Activity (Engineering Inst. of Canada, 2050 rue Mansfield, Suite 700, Montreal, PQ H3A 1Z2 Canada)

N94-22216 Royal Military Coll. of Canada, Kingston (Ontario). Dept. of Electrical and Computer Engineering.
FAULT TOLERANCE FOR REAL-TIME MULTIPROCESSOR OPERATING SYSTEMS
Terry Shepard and Scott Knight *In* Engineering Inst. of Canada, Canadian Conference on Electrical and Computer Engineering, Volumes 1 and 2 1991 4 p (For primary document see N94-22101 05-33)
Avail: Issuing Activity (Engineering Inst. of Canada, 2050 rue Mansfield, Suite 700, Montreal, PQ H3A 1Z2 Canada)

N94-22454*# Center for Analysis, Newport Beach, CA.
SEEING THE FOREST FOR THE TREES: NETWORKED WORKSTATIONS AS A PARALLEL PROCESSING COMPUTER Abstract Only
J. O. Breen and D. M. Meleedy *In* NASA, Washington, Second Annual Conference on Astronomical Data Analysis Software and Systems. Abstracts 1992 p 23 (For primary document see N94-22438 05-89)
Avail: CASI HC A01/MF A02

63 CYBERNETICS

Includes feedback and control theory, artificial intelligence, robotics and expert systems.

For related information see also *54 Man/System Technology and Life Support.*

N94-19843 Department of the Navy, Washington, DC.
METRICS FOR SPECIFYING AND/OR TESTING NEURAL NETWORKS STATEMENT OF GOVERNMENT INTEREST Patent Application
Roger L. Woodall, inventor (to Navy) 18 Mar. 1993 35 p Limited Reproducibility: More than 20% of this document may be affected by microfiche quality
(AD-D015946; US-Patent-Appl-SN-033225; Navy-Case-73073) Avail: CASI HC A03

This invention relates generally to neural networks and, in particular, to methods and apparatus for testing the performance, and specifying the characteristics of, neural networks. DTIC

N94-19845 Carnegie-Mellon Univ., Pittsburgh, PA. School of Computer Science.
A DISTRIBUTED REINFORCEMENT LEARNING SCHEME FOR NETWORK ROUTING
Michael Littman and Justin Boyan Jul. 1993 7 p Limited Reproducibility: More than 20% of this document may be affected by microfiche quality
(Grant NSF IRI-92-14873)
(AD-A270600; CMU-CS-93-165) Avail: Issuing Activity (Defense Technical Information Center (DTIC))

In this paper we describe a self-adjusting algorithm for packet routing, in which a reinforcement learning module is embedded into each node of a switching network. Only local communication is used to keep accurate statistics at each node on which routing policies lead to minimal delivery times. In simple experiments involving a 36-node, irregularly connected network, this learning approach proves superior to a nonadaptive algorithm based on precomputed shortest paths. DTIC

N94-19875 Massachusetts Inst. of Tech., Cambridge. Artificial Intelligence Lab.

BUILDING BRAINS FOR BODIES

Rodney A. Brooks and Lynn A. Stein Aug. 1993 17 p Limited Reproducibility: More than 20% of this document may be affected by microfiche quality

(Contract N00014-91-J-4038)

(AD-A270531; AIM-1439) Avail: CASI HC A03

We describe a project to capitalize on newly available levels of computational resources in order to understand human cognition. We will build an integrated physical system including vision, sound input and output, and dextrous manipulation, all controlled by a continuously operating large scale parallel MIMD computer. The resulting system will learn to 'think' by building on its bodily experiences to accomplish progressively more abstract tasks. Past experience suggests that in attempting to build such an integrated system we will have to fundamentally change the way artificial intelligence, cognitive science, linguistics, and philosophy think about the organization of intelligence. We expect to be able to better reconcile the theories that will be developed with current work in neuroscience. DTIC

N94-19893 Massachusetts Inst. of Tech., Cambridge. Artificial Intelligence Lab.

WHY STEREO VISION IS NOT ALWAYS ABOUT 3D RECONSTRUCTION Memorandum Report

W. E. Grimson Jul. 1993 13 p Limited Reproducibility: More than 20% of this document may be affected by microfiche quality

(Contract N00014-91-J-4038; NSF IRI-89-00267)

(AD-A270522; AIM-1435) Avail: CASI HC A03

A common assumption of stereo vision researchers is that the goal of stereo is to compute explicit 3D information about a scene, to support activities such as navigation, hand-eye coordination and object recognition. This paper suggests reconsidering what is required of a stereo algorithm, in light of the needs of the task that uses its output. We show that very accurate camera calibration is needed to reconstruct accurate 3D distances, and argue that often it may be difficult to attain and maintain such accuracy. We further argue that for tasks such as object recognition, separating object from background is of central importance. We suggest that stereo can help with this task, without explicitly computing 3D information. We provide a demonstration of a stereo algorithm that supports separating figure from ground through attentive fixation on key features. DTIC

N94-19909 Stanford Univ., CA. Dept. of Operations Research.

LARGE DEVIATIONS BEHAVIOR OF COUNTING PROCESSES AND THEIR INVERSES

Peter W. Glynn and Ward Whitt Jul. 1993 29 p Limited Reproducibility: More than 20% of this document may be affected by microfiche quality

(Contract DAAL03-91-G-0101)

(AD-A271142; SU-TR-93-7; ARO-28809.14-MA-SDI) Avail: CASI HC A03

We show, under regularity conditions, that a counting process satisfies a large deviations principle in R, a sample-path large deviations principle in the function space D, or the Gartner-Ellis condition (convergence of the normalized logarithmic moment generating functions), if and only if, its inverse process does. We show, again under regularity conditions, that an embedded regenerative structure is sufficient for the counting process or its inverse process to have exponential asymptotics and thus satisfy the Gartner-Ellis condition. These results help characterize the small-tail asymptotic behavior of steady-state distributions in queueing models, e.g., the waiting time, workload, and queue length. DTIC

N94-20089*# National Aeronautics and Space Administration. Langley Research Center, Hampton, VA.

AN EXPERT SYSTEM EXECUTIVE FOR AUTOMATED ASSEMBLY OF LARGE SPACE TRUSS STRUCTURES

Cheryl L. Allen Nov. 1993 20 p Sponsored by NASA. Washington (RTOP 586-02-11)

(NASA-TM-4487; L-17189; NAS 1.15:4487) Avail: CASI HC A03/MF A01

Langley Research Center developed a unique test bed for investigating the practical problems associated with the assembly of large space truss structures using robotic manipulators. The test bed is the result of an interdisciplinary effort that encompasses the full spectrum of assembly problems - from the design of mechanisms to the development of software. The automated structures assembly test bed and its operation are described, the expert system executive and its development are detailed, and the planned system evolution is discussed. Emphasis is on the expert system implementation of the program executive. The executive program must direct and reliably perform complex assembly tasks with the flexibility to recover from realistic system errors. The employment of an expert system permits information that pertains to the operation of the system to be encapsulated concisely within a knowledge base. This consolidation substantially reduced code, increased flexibility, eased software upgrades, and realized a savings in software maintenance costs. Author

N94-20105 Massachusetts Inst. of Tech., Cambridge. Artificial Intelligence Lab.

APPLICATION OF CHANGE DETECTION TO DYNAMIC CONTACT SENSING Memorandum Report

Brian Eberman and J. K. Salisbury, Jr. Mar. 1993 21 p Limited Reproducibility: More than 20% of this document may be affected by microfiche quality

(Contracts N00014-91-J-4038; N00014-92-J-1814)

(AD-A270523; AIM-1421) Avail: CASI HC A03

The forces of contact during manipulation convey substantial information about the state of the manipulation. Textures, slip, impacts, grasping, and other contact conditions produce force and position signatures that can be used for identifying the state of contact. This paper addresses the fundamental problems of interpreting the force signals without any additional context on the state of manipulation. Techniques based on forms of the generalized sequential likelihood ratio test are used to segment individual strain signals into statistically equivalent pieces. The results of the segmentation are designed to be used in a higher level procedure which will interpret the results within a manipulation context. We report on our experimental development of the segmentation algorithm and on its results for detecting and labelling impacts, slip, changes in texture, and condition. The sequential likelihood ratio test is reviewed and some of its special cases and optimal properties are discussed. Finally, we conclude by discussing extensions to the techniques and lessons for sensor design. DTIC

N94-20135# Rochester Univ., NY. Dept. of Computer Science.

ROBOT SKILL LEARNING AND THE EFFECTS OF BASIS FUNCTION CHOICE

J. G. Schneider and C. M. Brown Sep. 1992 45 p

(Contract NSF IRI-89-20771; NSF CDA-88-22724; MDA972-92-J-1012)

(TR-437) Avail: CASI HC A03/MF A01

We present a computational, constructive theory of tunable, open loop trajectory skills. A skill is a controller whose outputs achieve any task in a space characterized by n parameters, n greater than 1. Throwing a ball at a target is a 3-dimensional task if the target may be anywhere within a 3-dimensional volume. Repetitious pick and place tasks are zero-dimensional, and thus not skills. Skills are performed open loop for speed reasons: we assume the entire command sequence is generated before any feedback can become available. We do not assume prior knowledge of plant or task models, so skills must be at least partly learned. A skill output is a vector of values -- in our work so far it is generated as the sum of a base vector and a weighted change vector whose weight accomplishes the tuning. Learning consists of a search for the best set of base and change vectors. An interpretation process maps skill outputs into sequences of commands for the plant by using basis functions (given a priori in this paper). The basis functions may be arbitrarily complex. We claim that appropriate basis functions can speed up the learning process and overcome the limitations of the linear trajectory tuning algorithm. This report describes a skill learning algorithm and experiments done with various basis functions and control methods for a one-dimensional throwing task. It concludes with a discussion of future work in learning basis functions, higher dimensional tasks, and comparisons against common learning and control algorithms. Author

N94-20212*# Houston Univ., TX. Dept. of Electrical Engineering.

SELF-ORGANIZATION VIA ACTIVE EXPLORATION IN ROBOTIC APPLICATIONS. PHASE 2: HYBRID HARDWARE PROTOTYPE Final Progress Report

Haluk Oegmen Dec. 1993 51 p Sponsored by NASA. Lyndon B. Johnson Space Center

(NASA-CR-194723; NAS 1.26:194723) Avail: CASI HC A04/MF A01

In many environments human-like intelligent behavior is required from robots to assist and/or replace human operators. The purpose of these robots is to reduce human time and effort in various tasks. Thus the robot should be robust and as autonomous as possible in order to eliminate or to keep to a strict minimum its maintenance and external control. Such requirements lead to the following properties: fault tolerance, self organization, and intelligence. A good insight into implementing these properties in a robot can be gained by considering human behavior. In the first phase of this project, a neural network architecture was developed that captures some fundamental aspects of human categorization, habit, novelty, and reinforcement behavior. The model, called FRONTAL, is a 'cognitive unit' regulating the exploratory behavior of the robot. In the second phase of the project, FRONTAL was interfaced with an off-the-shelf robotic arm and a real-time vision system. The components of this robotic system, a review of FRONTAL, and simulation studies are presented in this report. Derived from text

N94-20242# Universiteit Twente, Enschede (Netherlands). Dept. of Computer Science.

CONNECTIONISM AND NATURAL LANGUAGE PROCESSING

M. F. J. Drossaers, ed. and A. Nijholt, ed. Oct. 1992 143 p Proceedings of the 3rd Twente Workshop on Language Technology, Enschede, Netherlands, 12-13 May 1992; sponsored by Dutch Foundation on Neural Networks, Netherlands, and Dutch Foundation of Knowledge Based Systems

(Memo-INF-92-64; ETN-93-94528) Copyright Avail: CASI HC A07/MF A02

Current connectionist natural language research is presented. Topics include syntactic and semantic analysis, grammar learning, idiom representation, syllable segmentation, models for human word recognition, and models for speech synthesis. For individual titles, see N94-20243 through N94-20255.

N94-20243# Universiteit Twente, Enschede (Netherlands). Dept. of Electrical Engineering.

REPRESENTATION OF SPOKEN WORDS IN A SELF-ORGANIZING NEURAL NET

L. P. J. Veelenturf *In its* Connectionism and Natural Language Processing Oct. 1992 p 1-4 (For primary document see N94-20242 05-63)

Copyright Avail: CASI HC A01/MF A02

An algorithm for a two dimensional representation of the acoustic signal of spoken words is presented. Having such an algorithm, the result for different applications like speech recognition and machine control by voice can be used. If such a map from the domain of continuous speech signals to a two (or three) dimensional Euclidean space can be argued to be a reasonable model of the human speech processing system, then psycholinguistic phenomena can even be investigated with this model. The algorithm is in fact a shortcut for a self organizing artificial neural network as developed by Kohonen. ESA

N94-20244# Max-Planck-Inst. for Psycholinguistics, Nijmegen (Netherlands).

MODELING THE HUMAN MENTAL LEXICON WITH SELF-ORGANIZING FEATURE MAPS **c32**

Peter Wittenburg and Uli H. Frauenfelder *In* Univ. Twente, Connectionism and Natural Language Processing Oct. 1992 p 5-15 (For primary document see N94-20242 05-63)

Copyright Avail: CASI HC A03/MF A02

Recent efforts to model the remarkable ability of humans to recognize speech and words are described. Different techniques including the use of neural nets for representing phonological similarity between words in the lexicon with self organizing algorithms are discussed. Simulations using the standard Kohonen algorithm are presented to illustrate some problems confronted with this technique in modeling similarity relations of form in the human mental lexicon. Alternative approaches that can potentially deal with some of these limitations are sketched. ESA

N94-20245# Limburg State Univ., Maastricht (Netherlands). Dept. of Computer Science.

SPEECH SYNTHESIS WITH ARTIFICIAL NEURAL NETWORKS **c32**

Ton Weijters and Johan Thole *In* Univ. Twente, Connectionism and Natural Language Processing Oct. 1992 p 17-25 (For primary document see N94-20242 05-63)

Copyright Avail: CASI HC A02/MF A02

The application of neural nets to speech synthesis is considered. In speech synthesis, the main efforts so far have been to master the grapheme to phoneme conversion. During this conversion symbols (graphemes) are converted into other symbols (phonemes). Neural networks, however, are especially competitive for tasks in which complex nonlinear transformations are needed and sufficient domain specific knowledge is not available. The conversion of text into speech parameters appropriate as input for a speech generator seems such a task. Results of a pilot study in which an attempt is made to train a neural network for this conversion are presented. ESA

N94-20246# Tilburg Univ. (Netherlands).

GENERALIZATION PERFORMANCE OF BACKPROPAGATION LEARNING ON A SYLLABIFICATION TASK

Walter Daelemans and Antal vandenBosch *In* Univ. Twente, Connectionism and Natural Language Processing Oct. 1992 p 27-37 (For primary document see N94-20242 05-63)

Copyright Avail: CASI HC A03/MF A02

The generalization capabilities of backpropagation learning in feedforward and recurrent feedforward connectionist networks on the assignment of syllable boundaries to orthographic representations in Dutch (hyphenation) was investigated. This is a difficult task because phonological and morphological constraints interact, leading to ambiguity in the input patterns. The results are compared to different symbolic pattern matching approaches, and to an exemplar based generalization scheme, related to a k-nearest neighbor approach, but using a similarity metric weighed by the relative information entropy of positions in the training patterns. The results indicate that the generalization performance of backpropagation learning for this task is not better than that of the best symbolic pattern matching approaches, and of examplar based generalization. ESA

N94-20247# Tilburg Univ. (Netherlands). Inst. for Language Technology and Artificial Intelligence.

REPRESENTATION OF IDIOMS IN CONNECTIONIST MODELS

Erik-Jan vanderLinden and Wessel Kraaij *In* Univ. Twente, Connectionism and Natural Language Processing Oct. 1992 p 39-46 (For primary document see N94-20242 05-63)

Copyright Avail: CASI HC A02/MF A02

The resolution of the ambiguity between the nonidiomatic and the idiomatic reading of a phrase that is possibly idiomatic is discussed. A choice between these readings can be made using various kinds of linguistic information, but it is claimed that it can be made on the basis of the mere fact that one of the analyses is idiomatic, and that this choice does not have to be stipulated explicitly, but follows naturally from the architecture of the lexicon and the retrieval process, if an appropriate model of the lexicon is used. It is argued that a connectionist model is appropriate, and some comparisons with symbolic models are made, especially with hierarchical models of the lexicon. ESA

N94-20248# Amsterdam Univ. (Netherlands). Dept. of Computational Linguistics.

NEURAL DATA ORIENTED PARSING

Jan C. Scholtes *In* Univ. Twente, Connectionism and Natural Language Processing Oct. 1992 p 47-52 Sponsored by MSC Beheer BV, Netherlands (For primary document see N94-20242 05-63)

Copyright Avail: CASI HC A02/MF A02

Results of a hybrid parsing model that combines the speed of statistical and corpus based parsing methods with the disambiguation power of traditional production-rule systems are presented. Parsing consists of deriving the most probable structure (from fragments) that already exist in the corpus. The Data Oriented Parsing (DOP) paradigm uses statistical features of language in combination with a structured corpus. The derivation of the 'probabilities' and the storage of the corpus is done by means of a Kohonen feature map. The actual data oriented parsing is performed by a regular Von Neumann machine. The model can process incomplete sentences, wrong sentences and completely new sentences which contain a certain number of unknown words or structures. Implicit features of the Kohonen model turn the ranking of possible parses and the selection of the most probable one into a straightforward task. ESA

N94-20249# Groningen Rijksuniv. (Netherlands). Dept. of Computational Linguistics.

A CONNECTIONIST REPRESENTATION FOR PHRASE STRUCTURES **c82**

Erik F. TjongKimSang *In* Univ. Twente, Connectionism and Natural Language Processing Oct. 1992 p 53-55 (For primary document see N94-20242 05-63)

Copyright Avail: CASI HC A01/MF A02

Connectionist techniques are useful for modeling sentence comprehension because they allow competition between information of different sources to achieve a result. Present connectionist models of sentence comprehension are capable of assigning thematic roles to constituents which consist of simple lexical elements. A method which makes possible assignment of roles to constituents which consist of larger stuctures is described. ESA

N94-20250# Universiteit Twente, Enschede (Netherlands). Dept. of Computer Sciences.

HOPFIELD MODELS AS NEURAL-NETWORK ACCEPTORS

Marc F. J. Drossaers *In its* Connectionism and Natural Language Processing Oct. 1992 p 57-65 (For primary document see N94-20242 05-63)

Copyright Avail: CASI HC A02/MF A02

The first results of research into the use of neural networks for integrated linguistic analysis, a Hopfield model for syntactical analysis, are presented. A neural network is constructed as an implementation of a bounded push down automaton, which can accept context free languages with limited center embedding. The network's behavior can be predicted a priori, so the presented theory can be tested. The operation of the network as an implementation of the acceptor is probably correct. Furthermore a solution to the problem of spurious states in Hopfield models was found: they are used as dynamically constructed representations of sets of states of the implemented acceptor. The so called neural network acceptor proposed, is fast but large. ESA

N94-20251# British Telecom Research Labs., Ipswich (England). Speech and Language Technology Section.

A SINGLE LAYER HIGHER ORDER NEURAL NET AND ITS APPLICATION TO GRAMMAR RECOGNITION

Peter Wyard *In* Univ. Twente, Connectionism and Natural Language Processing Oct. 1992 p 67-85 (For primary document see N94-20242 05-63)

Copyright Avail: CASI HC A03/MF A02

A single layer Higher Order Dynamic Topology Neural Net (HODYNE) is described, targeted at natural language processing problems. HODYNE has an input layer of nodes containing concatenations of words from the input string, and grows nodes during training which are dependent on the training data. The training procedure also has some novel features. Results are presented on the problem of grammaticality determination. The results are encouraging, with almost perfect performance on unseen test sets derived from simple context free grammars, and promising performance of sentences taken from the LOB Corpus of British English. On the latter task, the performance of HODYNE is compared with that of a method based on the statistics of tag-pairs and with a multilayer perceptron. ESA

N94-20252# Exeter Univ. (England). Connection Science Center.

A MODULAR DESIGN FOR CONNECTIONIST PARSING

Noel E. Sharkey and Amanda J. C. Sharkey *In* Univ. Twente, Connectionism and Natural Language Processing Oct. 1992 p 87-96 Sponsored by British Telecom (For primary document see N94-20242 05-63)

Copyright Avail: CASI HC A02/MF A02

Research on network combination for natural language processing is reported. A modular parser is reported that utilizes three different connectionist architectures: a simple recurrent net, a feedforward net, and a recursive auto associative net. Each of these was trained individually on specialist tasks and then components of the architectures were linked to form an integrated system. The combination parser accepts sentences that are input sequentially, a word at a time, and produces a syntactic tree as output. As well as parsing the 1280 sentences for which the components had been trained, it correctly disambiguated 75.62% of a set of 320 novel structurally ambiguous sentences. This is impressive given that the system developed its own lexical rules and had no access to semantic or pragmatic information other than that implicit in the training sets. The results are discussed in terms of modular principles and the types of rules that the unified parser extracts from its modules. The kinds of operations that can be performed on compressed holistic connectionist representations are illustrated. ESA

N94-20253# University Coll., Dublin (Ireland). Dept. of Computer Science.

AN EXPLORATION OF CLAUSE BOUNDARY EFFECTS IN SRN REPRESENTATIONS **c62**

Ronan Reilly *In* Univ. Twente, Connectionism and Natural Language Processing Oct. 1992 p 97-102 (For primary document see N94-20242 05-63)

Copyright Avail: CASI HC A02/MF A02

A study carried out on the psychological plausibility of the language representations developed by Elman style Simple Recurrent Networks (SRN's) is described. These representations were discussed at length in Elman (1991) from the perspective of their capacity to represent complex structural relationships, and their ability to accommodate the open endedness of language within a fixed resource system. Although there is some suggestion that SRN representations have properties that make them psychologically plausible, this has not been put to a direct test. It is shown how two well known clause boundary memory effects are a consequence of the nature of SRN representations rather than an interaction with an external memory mechanism. ESA

N94-20254# Essex Univ., Colchester (England). Dept. of Electronic Systems Engineering.

SYNTACTIC NEURAL NETWORKS FOR NATURAL LANGUAGE PROCESSING

S. M. Lucas *In* Univ. Twente, Connectionism and Natural Language Processing Oct. 1992 p 103-114 (For primary document see N94-20242 05-63)

Copyright Avail: CASI HC A03/MF A02

An introduction to Syntactic Neural Networks (SNN) is given and the algebraic grammatical inference algorithm is presented. An SNN is a special modular neural architecture derived from the matrix method of parsing context free grammars. The special structure of the network gives it a head start over other types of neural architecture when dealing with problems requiring grammar based solutions, since general knowledge about how to parse is embedded in the network architecture, and need not be learned afresh for each new problem. An SNN comes preequipped to deal with grammars, it need only learn the details of the grammar from the training set, which is still very difficult. The algebraic inferencing method forms algebraic expressions for the net output for each input string, and performs constraint satisfaction to try and find an assignment to the variables (and hence a grammar) that will parse all the positive strings and none of the negative ones. Inferring non-stochastic grammars, only, is dealt with, but given a non-stochastic grammar it is much easier to infer the production probabilities than to infer these from some random startpoint. Hence, the method can greatly speed up the inference of stochastic grammars. The main limitation is the exponential growth with respect to pattern length. Nonetheless, results show how traditional toy problems such as parity and palindrome languages can be learned much more quickly than with previous methods. Ways of overcoming the exponential growth are discussed. ESA

N94-20255# Texas Univ., Austin. Dept. of Computer Sciences.

DISCERN: A DISTRIBUTED NEURAL NETWORK MODEL OF SCRIPT PROCESSING AND MEMORY

Risto Miikkulainen *In* Univ. Twente, Connectionism and Natural Language Processing Oct. 1992 p 115-124 Sponsored in part by ITA Foundation; Academy of Finland; Emil Aaltonen Foundation, Finland; Foundation for the Advancement of Technology; Alfred Kordelin Foundation, Finland (For primary document see N94-20242 05-63)

Copyright Avail: CASI HC A02/MF A02

DISCERN (Distributed Script processing and Episonic memory Network), a large scale natural language processing system built entirely from distributed neural networks, is addressed. DISCERN reads short narratives about stereotypical event sequences, stores them in episodic memory, generates fully expanded paraphrases of the narratives, and answers questions about them. Processing in DISCERN is based on hierarchically

organized backpropagation modules, communicating through a central lexicon of word representations. The lexicon is a double feature map system that transforms each orthographic word symbol in its semantic representation and vice versa. The episodic memory is a hierarchy of feature maps, where memories are stored 'one-shot' at different locations. Several high level phenomena emerge automatically from the special properties of distributed neural networks. DISCERN learns to infer unmentioned events and unspecified role fillers, and it generates expectations and defaults and exhibits plausible lexical access errors and memory interference behavior. Word semantics, memory organization, and appropriate script inferences are automatically extracted from examples. ESA

N94-20293# Sandia National Labs., Albuquerque, NM.
TELEOPERATION WITH VIRTUAL FORCE FEEDBACK
R. J. Anderson 1993 8 p Presented at the Society of Photo-Optical Instrumentation Engineer's (SPIE) International Symposium on Optical Tools for Manufacturing and Advanced Automation, Boston, MA, 7-10 Sep. 1993
(Contract DE-AC04-76DP-00789)
(DE93-019406; SAND-93-1914C; CONF-9309199-2) Avail: CASI HC A02/MF A01

In this paper we describe an algorithm for generating virtual forces in a bilateral teleoperator system. The virtual forces are generated from a world model and are used to provide real-time obstacle avoidance and guidance capabilities. The algorithm requires that the slaves tool and every object in the environment be decomposed into convex polyhedral Primitives. Intrusion distance and extraction vectors are then derived at every time step by applying Gilbert's polyhedra distance algorithm, which has been adapted for the task. This information is then used to determine the compression and location of nonlinear virtual spring-dampers whose total force is summed and applied to the manipulator/teleoperator system. Experimental results validate the whole approach, showing that it is possible to compute the algorithm and generate realistic, useful pseudo forces for a bilateral teleoperator system using standard VME bus hardware. DOE

N94-20360* National Aeronautics and Space Administration. Pasadena Office, CA.
ELECTRONIC NEURAL NETWORK FOR SOLVING TRAVELING SALESMAN AND SIMILAR GLOBAL OPTIMIZATION PROBLEMS Patent
Anilkumar P. Thakoor, inventor (to NASA) (Jet Propulsion Lab., California Inst. of Tech., Pasadena.), Alexander W. Moopenn, inventor (to NASA) (Jet Propulsion Lab., California Inst. of Tech., Pasadena.), Tuan A. Duong, inventor (to NASA) (Jet Propulsion Lab., California Inst. of Tech., Pasadena.), and Silvio P. Eberhardt, inventor (to NASA) (Jet Propulsion Lab., California Inst. of Tech., Pasadena.) 19 Oct. 1993 15 p Filed 8 Nov. 1991 Supersedes N92-29955 (30 - 20, p 3529) Continuation-in-part of US-Patent-Appl-SN-470664, filed 26 Jan. 1990
(NASA-Case-NPO-17807-2-CU; US-Patent-5,255,349;
US-Patent-Appl-SN-789567; US-Patent-Appl-SN-470664;
US-Patent-Class-395-27; US-Patent-Class-395-24;
Int-Patent-Class-G06F-15/46; Int-Patent-Class-G06G-7/12) Avail: US Patent and Trademark Office

This invention is a novel high-speed neural network based processor for solving the 'traveling salesman' and other global optimization problems. It comprises a novel hybrid architecture employing a binary synaptic array whose embodiment incorporates the fixed rules of the problem, such as the number of cities to be visited. The array is prompted by analog voltages representing variables such as distances. The processor incorporates two interconnected feedback networks, each of which solves part of the problem independently and simultaneously, yet which exchange information dynamically. Official Gazette of the U.S. Patent and Trademark Office

N94-20366* National Aeronautics and Space Administration. Lyndon B. Johnson Space Center, Houston, TX.
NEURAL NETWORK FOR PROCESSING BOTH SPATIAL AND TEMPORAL DATA WITH TIME BASED BACK-PROPAGATION Patent
James A. Villarreal, inventor (to NASA) and Robert O. Shelton, inventor (to NASA) 12 Oct. 1993 34 p Filed 26 Dec. 1991 Supersedes N92-30314 (30 - 21, p 3700)
(NASA-Case-MSC-21874-1; US-Patent-5,253,329;
US-Patent-Appl-SN-813556; US-Patent-Class-395-24;
US-Patent-Class-395-23; Int-Patent-Class-G06F-15/18) Avail: US Patent and Trademark Office

Neural networks are computing systems modeled after the paradigm of the biological brain. For years, researchers using various forms of neural networks have attempted to model the brain's information processing and decision-making capabilities. Neural network algorithms have impressively demonstrated the capability of modeling spatial information. On the other hand, the application of parallel distributed models to the processing of temporal data has been severely restricted. The invention introduces a novel technique which adds the dimension of time to the well known back-propagation neural network algorithm. In the space-time neural network disclosed herein, the synaptic weights between two artificial neurons (processing elements) are replaced with an adaptable-adjustable filter. Instead of a single synaptic weight, the invention provides a plurality of weights representing not only association, but also temporal dependencies. In this case, the synaptic weights are the coefficients to the adaptable digital filters. Novelty is believed to lie in the disclosure of a processing element and a network of the processing elements which are capable of processing temporal as well as spacial data.
Official Gazette of the U.S. Patent and Trademark Office

N94-20488# Air Force Inst. of Tech., Wright-Patterson AFB, OH. School of Engineering.
DEVELOPMENT AND TESTING OF A RELIABILITY PERFORMANCE INDEX FOR MODULAR ROBOTIC SYSTEMS Final Report
Dean L. Schneider, Delbert Tesar, and J. W. Barnes Oct. 1993 10 p
(AD-A271901; AFIT/EN/TR-93-08) Avail: CASI HC A02/MF A01

Using a probabilistic representation of manipulator kinematics and a reliability block diagram model of the manipulator system, a Reliability Performance Index (RPI) representing the probability of no hardware or software failure and the manipulator achieving a specified position and orientation is developed. The RPI is tested with a case study consisting of a three degree-of-freedom planar manipulator assembled from a choice of six joint modules of varying reliability and precision and a choice of six link module combinations of varying lengths and machining tolerances. A straight-line, square trajectory is specified and the RPI is calculated for each combination of joint modules and links, a total of 1296 different combinations. Using statistical testing, a 70% reduction in the module design space is achieved using the RPI. Optimization using other appropriate manipulator criteria can then be performed to generate the final configuration. Additional extensive case studies are needed to fully develop the RPI to a stage necessary for implementation into a computer-aided design system for modular robot configuration design. The RPI may also be useful in the quantification of the overall system reliability and performance of any system based upon measured error, such as control systems. DTIC

N94-20573# Oak Ridge National Lab., TN.
THE SEVENTH INTERNATIONAL SYMPOSIUM ON METHODOLOGIES FOR INTELLIGENT SYSTEMS (POSTER SESSION)
Karen S. Harbor 18 Jun. 1993 174 p Symposium held in Trondheim, Norway, 15-18 Jun. 1993
(AD-A272125; ORNL-TM-12375) Avail: CASI HC A08/MF A02

Contents: Implications in Vivid Logic; A Self-learning Bayesian Expert System (BEST); A Natural Language Generation System for a Heterogeneous Distributed Database System; 'Competence-Switching' Managed by Intelligent Systems; Strategy Acquisition by an Artificial Neural Network--Experiments in Learning to Play a Stochastic Game; Viewpoints Selective Inheritance in Object-Oriented Modeling; Multivariate Discretization of Continuous Attributes for Machine Learning; Utilization of the Case-Based Reasoning Method to Resolve Dynamic Problems; Formalization of an Ontology of Ceramic Science in CLASSIC; Linguistic Tools for Intelligent Systems; An Application of Rough Sets in Knowledge Synthesis and A Relational Model for Imprecise Queries. DTIC

N94-20621# Carnegie-Mellon Univ., Pittsburgh, PA. Dept. of Computer Science.
SIMULATING A USER'S PREFERENCES: TOWARDS AUTOMATED ARTIFICIAL EVOLUTION FOR COMPUTER GENERATED IMAGES
Shumeet Baluja, Dean Pomerleau, and Todd Jochem 14 Oct. 1993 31 p
(Contract N00014-93-1-0806)
(AD-A272058; CMU-CS-93-198) Avail: CASI HC A03/MF A01

In 1991, Karl Sims presented work on artificial evolution in which he used genetic algorithms to evolve complex structures for use in computer generated images and animations. The evolution of the computer generated images progressed from simple, randomly generated shapes to interesting images which the users interactively created. The evolution advanced under the constant guidance and supervision of the user. This paper describes attempts to automate the process of image evolution through the use of artificial neural networks. The central objective of this study is to learn the user's preferences, and to apply this knowledge to evolve aesthetically pleasing images which are similar to those evolved through interactive sessions with the user. This paper presents a detailed analysis of both the shortcomings and successes encountered in the use of five artificial neural network architectures. Further possibilities for improving the performance of a fully automated system are also discussed. DTIC

N94-20626 Princeton Univ., NJ.
ALGORITHM/ARCHITECTURE STUDY FOR ARTIFICIAL NEURAL NETS Final Report, 1 Sep. 1989 - 30 Nov. 1993
Sun-Yuan Kung 30 Nov. 1993 36 p Limited Reproducibility: More than 20% of this document may be affected by microfiche quality
(Grant AF-AFOSR-0501-89)
(AD-A271820; AFOSR-93-0811TR) Avail: CASI HC A03

Neural information processing has already helped catalyzed many potential opportunities of cross-fertilization, from which many diversified disciplines have benefited mutually. However, in order to substain a long-term impact, there must establish a fundamental and coherent theory for it. This project focuses on the development and understanding of the fundamental system theoretical basis for temporal dynamic networks. The main thrust of the research hinges on a thorough understanding of several key issues regarding temporal dynamical system modeling, including model unification, training efficiency, generalization performance, and hierarchical network structure. DTIC

N94-20920 Massachusetts Inst. of Tech., Cambridge. Artificial Intelligence Lab.
VISUAL TRACKING Memorandum Report
M. A. Taalebinezhaad Oct. 1992 16 p Limited Reproducibility: More than 20% of this document may be affected by microfiche quality
(Contract N00014-91-J-4038)
(AD-A271686; AIM-1382) Avail: CASI HC A03

A typical robot vision scenario might involve a vehicle moving with an unknown 3D motion (translation and rotation) while taking intensity images of an arbitrary environment. This paper describes the theory and implementation issues of tracking any desired point in the environment. This method is performed completely in software without any need to mechanically move the camera relative to the vehicle. This tracking technique is simple and inexpensive. Furthermore, it does not use either optical flow or feature correspondence. Instead, the spatio-temporal gradients of the input intensity images are used directly. The experimental results presented support the idea of tracking in software. The final result is a sequence of tracked images where the desired point is kept stationary in the images independent of the nature of the relative motion. Finally, the quality of these tracked images are examined using spatio-temporal gradient maps. DTIC

N94-20921 Massachusetts Inst. of Tech., Cambridge. Artificial Intelligence Lab.
RECOGNITION BY PROTOTYPES Memorandum Report
Ronen Basri Dec. 1992 19 p Limited Reproducibility: More than 20% of this document may be affected by microfiche quality
(Contract N00014-91-J-4038)
(AD-A271687; AIM-1391) Avail: CASI HC A03

A scheme for recognizing 3D objects from single 2D images is introduced. The scheme proceeds in two stages. In the first stage, the categorization stage, the image is compared to prototype objects. For each prototype, the view that most resembles the image is recovered and, if the view is found to be similar to the image, the class identity of the object is determined. In the second stage, the identification stage, the observed object is compared to the individual models of its class, where classes are expected to contain objects with relatively similar shapes. For each model, a view that matches the image is sought. If such a view is found, the object's specific identity is determined. The advantage of categorizing the object before it is identified is twofold. First, the image is compared to a smaller number of models, since only models that belong to the object's class need to be considered. Second, the cost of comparing the image to each model in a class is very low, because correspondence is computed once for the whole class. More specifically, the correspondence and object pose computed in the categorization stage to align the prototype with the image are reused in the identification stage to align the individual models with the image. As a result, identification is reduced to a series of simple template comparisons. The paper concludes with an algorithm for constructing optimal prototypes for classes of objects. DTIC

N94-20926 Naval Air Warfare Center, Warminster, PA. Air Vehicle and Crew Systems Technology Dept.
AN APPLICATION OF THE CEREBELLAR MODEL ARTICULATION CONTROLLER FOR A SWITCHED RELUCTANCE ROTOR POSITION ESTIMATOR
Jenifer M. Shannon Nov. 1992 53 p Limited Reproducibility: More than 20% of this document may be affected by microfiche quality
(AD-A271769; NAWCADWAR-93041-60) Avail: CASI HC A04

A method of estimating the rotor position of a switched reluctance machine without the need for a rotor-mounted position sensor has been developed. This method takes advantage of the information derived from known phase voltage and current waveforms. The information is fed as the inputs to a neural network, which after being trained, can correctly map the rotor position to its output. The most accurate mapping results were obtained using a Cerebellar Model Articulation Controller (CMAC) neural network. The performance of the neural network has been tested with measured waveforms from a three phase 120 HP switched reluctance motor. It successfully maps the rotor position with an average root mean square error of one tenth of a mechanical degree. DTIC

N94-20947# Logicon R and D Associates, Los Angeles, CA.
NEURAL NETWORK STUDIES Final Technical Report
Gregg Wilensky, Narbik Manukian, Joseph Neuhaus, and Natalie Rivetti Jul. 1993 121 p
(Contract N00014-89-C-0257; ARPA Order 7006)
(AD-A271593; RDA-TR-43-0005-001) Avail: CASI HC A06/MF A02

Research at Logicon RDA in neural networks under the ARPA contract includes three main areas: theoretical research in the fundamentals of neural networks, applications of neural networks to practical problems of interest, and the development of new and more powerful neural networks and techniques for solving these problems. The papers which follow are compendium of our research in these areas. The theoretical studies include an overview of the basic useful theorems and general rules which apply to neural networks (in 'Overview of Neural Network Theory'), studies of training time as the network is scaled to larger dimensions (in 'Scaling of Back-Propagation Training Time to Large Dimensions'), an analysis of the classification and function fitting capability of neural networks (in 'Classification and Function Fitting as a Function of Scale and Complexity'), a comparison of Bayes and k-nearest neighbor classifiers to neural networks (in 'A Comparison of Classifiers: The Neural Network, Bayes-Gaussian, and k-Nearest Neighbor Classifiers'), an analysis of fuzzy logic and its relationship to neural network (in 'Fuzzy Logic and the Relation to Neural Networks'), an analysis of the Reduced Coulomb Energy (RCE) network (in 'The Reduced Coulomb Energy Classifier'), radial basis functions (in 'Radial Basis Approximations'), and the Lynch-Granger models (in 'Lynch-Granger Model of Olfactory Cortex'). DTIC

N94-21032# Center for Mathematics and Computer Science, Amsterdam (Netherlands). Dept. of Operations Research, Statistics, and System Theory.
THE CORRELATED M/G/1 QUEUE
O. J. Boxma and M. B. Combe Jan. 1993 14 p Sponsored by NFI, Netherlands
(CWI-BS-R9303; ETN-94-94720) Copyright Avail: CASI HC A03/MF A01

A single server queue in which the service time of each customer depends on the length of the preceding interarrival interval is considered. The dependence structure corresponds to the situation where work arrives at a gate according to a process with independent increments, while at exponential intervals the gate is opened and, after the addition of an independent component, the work is delivered to the server as a single

customer. This model unifies and generalizes other recently studied M/G/1 queues with dependence between interarrival and service times. The main result is the joint steady state distribution of the waiting and service time of a customer. As a by-result, the sojourn time distribution is obtained; a decomposition for its Laplace-Stieltjes transform is presented and interpreted. ESA

N94-21033# Center for Mathematics and Computer Science, Amsterdam (Netherlands). Dept. of Operations Research, Statistics, and System Theory.

ROUTING OF FREEWAY TRAFFIC: A DISCRETE-TIME STATE SPACE MODEL AND ROUTING PROBLEMS

J. H. vanSchuppen Dec. 1992 22 p

(CWI-BS-R9232; ETN-94-94721) Copyright Avail: CASI HC A03/MF A01

An attempt to formulate an approach to routing of freeway traffic flow is presented. A state space model for traffic flow in a freeway network is proposed. The model consists of a control system in which the state variables are densities and average speeds in freeway sections. The routing problem is to synthesize a routing law that specifies the directions such that the travel cost of network users is minimized. Approaches to solve the routing problem by control theory are discussed. ESA

N94-21057 Technische Hochschule, Darmstadt (Germany). Fachbereich Informatik.

GRAPHICAL INTERACTIVE PLANNING OF ROBOTIC APPLICATIONS WITH SUPPORT OF INTEGRATED SIMULATION Ph.D. Thesis [GRAPHISCH-INTERAKTIVE PLANUNG VON ROBOTIKANWENDUNGEN MIT UNTERSTUETZUNG INTEGRIERTER SIMULATION]

Fan Dai 1991 184 p In GERMAN Limited Reproducibility: More than 20% of this document may be affected by microfiche quality

(ETN-93-93793) Avail: CASI HC A09

A general concept of a planning system in a graphical interactive environment is developed. An object model was used for describing work wells. The action model describes activities in a robot work cell as time dependent variations of the object properties. Operations are connected with one another through conditions. Graphical elements are used for general description of graphical information. Representation forms and manipulation features are taken into account. These models are attempted to guarantee the flexibility of the method. Abstract iterations describe, on the basis of object, classes, functional processes which are independent on work cells and can be performed by parameterization of actions of several work cells. The motion planning is considered as a part of the concrete operation planning. The simulation of planned processes is considered as a running operation and its integration is obtained in all phases of planning. The universal connection between planning components, needed for their integration, can be performed by using a knowledge basis, which contains descriptions of concrete objects. Visualization and manipulations of actions and objects are general functions, which can be integrated in the central interaction control. ESA

N94-21140 Universiteit Twente, Enschede (Netherlands). Faculty of Applied Mathematics.

INTERACTIVE SIMULATION PACKAGE FOR COUPLED BENDING AND TORSIONAL VIBRATIONS IN FLEXIBLE ROBOT ARMS

M. Vajta, Z. Pocz, and A. Bagchi Oct. 1992 9 p Presented at the 11th IASTED International Conference on Modelling, Identification and Control, Innsbruck, Austria, 10-12 Feb. 1992 Sponsored by IASTE Limited Reproducibility: More than 20% of this document may be affected by poor print

(MEMO-1089; ETN-93-94129) Avail: Issuing Activity (European Space Agency (ESA))

A dynamic model of coupled bending and torsional vibrations in flexible robot arms is described. Coupling is almost unavoidable due to the asymmetricity of the payload. The basic model is a Euler-Bernoulli beam with Voigt type of internal damping. Different damping coefficients were assumed in bending and in torsion, respectively. An interactive simulation package to analyze these vibrations is also described. Time domain analysis with different methods is detailed. Numerical examples of a beam used in laboratory experiments are also given. ESA

N94-21160# Center for Mathematics and Computer Science, Amsterdam (Netherlands). Dept. of Operations Research, Statistics, and System Theory.

ON THE OPTIMALITY OF FCFS FOR NETWORKS OF MULTI-SERVER QUEUES

Ger Koole Dec. 1992 15 p

(Grant CEC-DG-XIII-BRA-QMIPS)

(CWI-BS-R9235; ETN-94-94713) Copyright Avail: CASI HC A03/MF A01

Multiserver queues in which arriving customers can be assigned to different servers are considered. For three models the optimality of assigning customers to the server with smallest workload, FCFS (First Come First Served), is obtained. In the first two models, isolated queues are studied. The difference is that in the first the cost functions are related to the workload and in the second, the departure processes are compared. The third model is concerned with networks of multiserver queues. ESA

N94-21162 Springer-Verlag G.m.b.H. and Co. K.G., Heidelberg (Germany).

LECTURE NOTES IN ARTIFICIAL INTELLIGENCE 689: THE 7TH INTERNATIONAL SYMPOSIUM ON METHODOLOGIES FOR INTELLIGENT SYMPOSIUM (ISMIS 1993)

J. Komorowski, ed. and Z. W. Ras, ed. 18 Jun. 1993 664 p Symposium held in Trondheim, Norway, Apr. 1993 Limited Reproducibility: More than 20% of this document may be affected by microfiche quality

(Contract N00014-93-1-0244)

(AD-A271768) Avail: Issuing Activity (Defense Technical Information Center (DTIC))

This volume contains papers which were selected for presentation at the Seventh International Symposium on Methodologies for Intelligent Systems - ISMIS'93, held in Trondheim, Norway, 15-18 June 1993. The Organizing Committee selected the following major areas for ISMIS'93: approximate reasoning, constraint programming; expert systems; intelligent databases; knowledge representation; learning and adaptive systems; manufacturing; and methodologies. Derived from text

N94-21232# Center for Mathematics and Computer Science, Amsterdam (Netherlands). Dept. of Operations Research, Statistics, and System Theory.

N PARALLEL QUEUEING SYSTEMS WITH SERVER BREAKDOWN AND REPAIR

Pieter Wartenhorst Dec. 1992 35 p

(CWI-BS-R9236; ETN-94-94715) Copyright Avail: CASI HC A03/MF A01

A model that can be used to study the influence of machine breakdown and limited repair capacity on the performance of a system that has to provide service continuously is presented. A system consisting of N single server queueing stations, each serving its own stream of customers, is considered. The servers of the stations are subject to breakdown. Broken servers are repaired by a joint repair facility consisting of K parallel repairmen. Whenever K is less than N, the repair facility is causing interference between the N stations. The behavior of the queue length at a particular station (say station 1) is studied in the long run. By modeling station 1 as an M/M/1 queue in a Markovian environment, an exact matrix geometric solution for the marginal queue length distribution and for the distributions of the queue length at the beginning of an up (down) period of the server is obtained. Since the matrix geometric solution becomes rather time and memory consuming when N is large, approximating closed form expressions are also developed. By assuming the lengths of subsequent down periods to be independent, station 1 is approximated by an M/M/1 queue with independent interruptions. Stochastic decompositions are employed to obtain approximations for the queue length distributions. With this model several design issues can be investigated such as the number of repairmen that is needed to maintain a certain pool of machines, or the number of machines that can be assigned to a certain crew of repairmen. Several numerical examples illustrate how the queue at station 1 is afffected by breakdowns of server 1 and by the other stations due to congestion at the repair facility. ESA

N94-21233# Center for Mathematics and Computer Science, Amsterdam (Netherlands). Dept. of Operations Research, Statistics, and System Theory.
OPTIMIZATION OF FIXED TIME POLLING SCHEMES
S. C. Borst, O. J. Boxma, J. H. A. Harink, and G. B. Huitema (PTT Telecommunicatie, Groningen, Netherlands.) Dec. 1992 27 p
(Grant CEC-DG-XIII-BRA-QMIBS)
(CWI-BS-R9237; ETN-94-94716) Copyright Avail: CASI HC A03/MF A01

The problem of deriving efficient operational rules for polling queues according to a fixed time polling scheme is addressed. A fixed time polling scheme specifies the visit order of the queues, but also the starting times for each visit. This problem arose from the need to efficiently collect files with call records from telecommunication switches. Using a simple approximation for the mean waiting times in a polling system with a non-cyclic visit order of the queues, an approach to the problem of minimizing a weighted sum of the mean waiting times at the various queues is presented. This approach is tested via numerical experiments that are partly based on actual data for call records. ESA

N94-21269# Naval Postgraduate School, Monterey, CA.
AN EVALUATION OF ARTIFICIAL NEURAL NETWORK MODELING FOR MANPOWER ANALYSIS M.S. Thesis
Brian J. Byrne Sep. 1993 145 p
(AD-A273001) Avail: CASI HC A07/MF A02

This thesis evaluates the capabilities of artificial neural networks in forecasting the take-rates of the Voluntary Separations Incentive/Special Separations Benefit (VSI/SSB) programs for male, Marine Corps Enlisted Personnel in the grades of E-5 and E-6. The Artificial Neural Networks models are compared with the forecasting abilities of a classical regression model. The data are taken from the Headquarters Marine Corps Enlisted Master File which contains military and personal background on each enlisted member of the United States Marine Corps. The classical regression model is a casual model constructed based upon the theory of occupational job choice. The neural network models are presented with all available data elements. Empirical results indicate that artificial neural networks provide forecasting results at least as good as, if not better than, those obtained using classical regression techniques. However, artificial neural networks are limited in their usefulness for policy analysis. DTIC

N94-21305# Naval Postgraduate School, Monterey, CA.
IMPLEMENTING ELECTRONIC DATA INTERCHANGE (EDI) WITH SMALL BUSINESS SUPPLIERS IN THE PRE-AWARD ACQUISITION PROCESS M.S. Thesis
Robert B. Sergeson Jun. 1993 106 p
(AD-A271767) Avail: CASI HC A06/MF A02

This thesis examines the implementation of electronic data interchange (EDI) with small business suppliers in the pre-award acquisition process. The general history and concept of EDI is discussed along with the pre-award acquisition process. The results of a small business survey are analyzed to provide insight on the barriers and impediments to implementing EDI with small business concerns. Additionally, interviews and discussions with major corporations were conducted to identify common lessons learned by these corporations in their efforts to implement EDI with their small business supplier base. The major conclusion drawn is that DoD can successfully implement EDI with its small business supplier base in the preaward acquisition process. It was determined that the following key factors are crucial to successful implementation of EDI with small business: provide effective training; specifically direct grant funding to the Procurement Technical Assistance Centers; require the Small Business Administration to aggressively sponsor and implement EDI training; draft legislation to modify or eliminate restrictive laws and regulations; and foster the use of Value-Added Networks, Trading Partner Agreements, and EDI Service Bureaus. These efforts would provide the basic infrastructure to enable DoD to train, nurture, and help problem solve with small businesses once DoD becomes totally reliant upon EDI. DTIC

N94-21315# Rochester Univ., NY. Dept. of Computer Science.
GOAL-ORIENTED DYNAMIC VISION
Peter A. vonKaenel, Christopher M. Brown, and Raymond D. Rimey Aug. 1993 31 p
(Contract MDA972-92-J-1012; NSF CDA-88-22724; NSF IRI-89-20771)
(TR-466) Avail: CASI HC A03/MF A01

TEA-1 is a selective vision system that uses Bayes nets for representation and benefit-cost analysis for control of visual and nonvisual actions. TEA-1 solves T-world problems, a class of problems involving static two-dimensional scenes. For example, TEA-1 was demonstrated to answer questions about scenes of dinner tables. dTEA-1, an extension to TEA-1 that allow tasks to be performed on dynamic scenes, is presented. Currently, dTEA-1 successfully performs a task on a simulated train scene. The objects in the scene include a train on a track and a herd of cows, but the domain may be extended to include static objects and other classifications of moving objects. The task is to keep track of the locations of objects, and the system intelligently allocates its effort to keep uncertainty and cost to a minimum. Author (revised)

N94-21317# Rochester Univ., NY. Dept. of Computer Science.
HIGH DIMENSION ACTION SPACES IN ROBOT SKILL LEARNING
Jeff G. Schneider May 1993 22 p
(Contract MDA972-92-J-1012)
(TR-458) Avail: CASI HC A03/MF A01

Table lookup with interpolation is used for many learning and adaptation tasks. Redundant mappings capture the important concept of 'motor skill,' which is important in real, behaving systems. Few, if any, robot skill implementations have dealt with redundant mappings, in which the space to be searched to create the table has much higher dimensionality than the table itself. A practical method for inverting redundant mappings is important in physical systems with limited time for trials. The 'Guided Table Fill In' algorithm, which uses data already stored in the table to guide search through the space of potential table entries, is presented. The algorithm is illustrated and tested on a robot skill learning task both in simulation and on a robot with a flexible link. Our experiments show that the ability to search high dimensional action spaces efficiently allows skill learners to find new behaviors that are qualitatively different from what they were presented or what the system designer may have expected. Thus the use of this technique can allow researchers to seek higher dimensional action spaces for their systems rather than constraining their search space at the risk of excluding the best actions. Author (revised)

N94-21355# Naval Postgraduate School, Monterey, CA.
SIMULATION OF TRIPOD GAITS FOR A HEXAPOD UNDERWATER WALKING MACHINE M.S. Thesis
Charles A. Schue, III Jun. 1993 270 p
(AD-A271719) Avail: CASI HC A12/MF A03

This thesis develops the mathematical relationships necessary to implement alternating tripod gaits on the hexapod underwater walking machine, AquaRobot. Analysis of documentation and application of Denavit-Hartenberg kinematic modeling techniques determine the fundamental vehicle parameters. Smooth leg motion models following elliptical and cycloidal trajectories are devised. Gait planning algorithms, using the elliptical smooth leg motion model, are developed for both discrete and continuous body motion. Statically stable, alternating tripod gait simulations are implemented in the C + + programming language. A stick figure graphics display allows examination and testing of the gait algorithms prior to incorporation in follow-on 3D graphics simulations or in real-time operation. DTIC

N94-21430# Naval Postgraduate School, Monterey, CA.
APPLICATION OF A BACK-PROPAGATION NEURAL NETWORK TO ISOLATED-WORD SPEECH RECOGNITION M.S. Thesis
Chau G. Le Jun. 1993 44 p
(AD-A272495) Avail: CASI HC A03/MF A01

The primary objective of this research is to explore how a back-propagation neural network (BNN) can be applied to isolated-word speech recognition. Simulation results show that a BNN provides an effective approach for small vocabulary systems. The recognition rate reaches 100% for a 5-word system and 94% for a 10-word system. The general techniques developed can be further extended to other applications, such as sonar target recognition, missile seeking and tracking functions in modern weapon systems, and classification of underwater acoustic signals. DTIC

N94-21520# Naval Postgraduate School, Monterey, CA.
SECURITY EVALUATION OF UNIX NETWORKS M.S. Thesis

Thomas L. Brown Sep. 1993 127 p
(AD-A273076) Avail: CASI HC A07/MF A02

In recent years, computer networks have significantly increased in both complexity and number, and these networks are attractive targets for attack and intrusion. Unix networks being managed by the government and providing access to unclassified sensitive information are particularly vulnerable to attack. Ensuring the security of sensitive information will be one of the single most important management issues in computer/information security in the foreseeable future. Unfortunately, the number of automated security tools for Unix, as well as the number of computer security experts within DOD, has not increased sufficiently to keep up with the improvements in technology. The author proposes the concept of a security toolbox, containing a proposed standard set of automated security tools, to support Unix networks. The toolbox can be used to enhance system security automating many of the security related tasks required of the network administrator. Additionally, organizational changes will be necessary to improve the availability of computer security advice and assistance. It is recommended that a study of the function and organization of computer security expertise be conducted, so that access to and validation of security tools, along with consistent guidance for network administrators and security officers, can be accomplished effectively. The combination of a security toolbox and expert advice can then help bridge the gap in the development of computer security expertise. DTIC

N94-21550*# National Aeronautics and Space Administration. Lyndon B. Johnson Space Center, Houston, TX.
MODEL-BASED AUTOMATIC GENERATION OF GRASPING REGIONS
David A. Bloss 1 Dec. 1993 13 p
(NASA-TM-104785; S-745; NAS 1.15:104785) Avail: CASI HC A03/MF A01

The problem of automatically generating stable regions for a robotic end effector on a target object, given a model of the end effector and the object is discussed. In order to generate grasping regions, an initial valid grasp transformation from the end effector to the object is obtained based on form closure requirements, and appropriate rotational and translational symmetries are associated with that transformation in order to construct a valid, continuous grasping region. The main result of this algorithm is a list of specific, valid grasp transformations of the end effector to the target object, and the appropriate combinations of translational and rotational symmetries associated with each specific transformation in order to produce a continuous grasp region. Author (revised)

N94-21577# Center for Mathematics and Computer Science, Amsterdam (Netherlands). Dept. of Operations Research, Statistics, and System Theory.
TANDEM QUEUES WITH DETERMINISTIC SERVICE TIMES
O. J. Boxma and J. A. C. Resing (Technische Univ., Eindhoven, Netherlands.) Dec. 1992 20 p
(Grant CEC-DG-XIII-BRA-QMIPS)
(CWI-BS-R9238; ETN-94-94717) Copyright Avail: CASI HC A03/MF A01

A tandem queueing model for a sequence of multiplexers at the edge of an ATM (Asynchronous Transfer Mode) network is considered. All queues of the tandem queueing model have unit service times. Each successive queue receives the output of the previous queue plus some external arrivals. For the case of two queues in series, the end to end delay of a cell (customer) arriving at the first queue, and the covariance of its delay at both queues, are studied. The joint queue length process at all queues is studied in detail for the two and three queue cases and an approach to the case of an arbitrary number of queues in series is outlined. ESA

N94-21689 Stanford Linear Accelerator Center, CA.
A RELATIVISTIC CONSTITUENT QUARK MODEL
F. Schlumpf Aug. 1993 5 p Presented at the 14th European Conference on Few-Body Problems in Physics, Amsterdam, Netherlands, 22-27 Aug. 1993 Limited Reproducibility: More than 20% of this document may be affected by microfiche quality
(Contract DE-AC03-76SF-00515)
(DE93-041085; SU-SLAC-Pub-6335; CONF-9308164-2) Avail: CASI HC A01

We investigate the predictive power of a relativistic quark model formulated on the light-front. The nucleon electromagnetic form factors, the semileptonic weak decays of the hyperons and the magnetic moments of both baryon octet and decuplet are calculated and found to be in excellent agreement with experiment. DOE

N94-21845# Los Alamos National Lab., NM.
OPTIMIZATION AND CONTROL OF A SMALL ANGLE ION SOURCE USING AN ADAPTIVE NEURAL NETWORK CONTROLLER
S. K. Brown, W. C. Mead, P. S. Bowling, R. D. Jones, and C. W. Barnes 1993 17 p Presented at the 5th International Conference on Ion Sources, Peking, China, 31 Aug. - 4 Sep. 1993
(Contract W-7405-eng-36)
(DE93-040063; LA-UR-93-2908; CONF-9308136-3) Avail: CASI HC A03/MF A01

This project developed an automated controller based on an artificial neural network and evaluated its applicability in a real-time environment. This capability was developed within the context of a small angle negative ion source on the Discharge Test Stand at Los Alamos. The controller processes information obtained from the beam current waveform developing a figure of merit (fom) to determine the ion source operating conditions. The fom is composed of the magnitude of the beam current, the stability of operation, and the quietness of the beam. Using no knowledge of operating conditions, the controller begins by making a rough scan of the four-dimensional operating surface. This surface uses as independent variables the anode and cathode temperatures, the hydrogen flow rate, and the arc voltage. The dependent variable is the fom described above. Once the rough approximation of the surface has been determined, the network formulates a model from which it determines the best operating point. The controller takes the ion source to that operating point for a reality check. As real data is fed in, the model of the operating surface is updated until the neural network's model agrees with reality. The controller then uses a gradient ascent method to optimize the operation of the ion source. Initial tests of the controller indicate that it is remarkably capable. It has optimized the operation of the ion source on six different occasions bringing the beam to excellent quality and stability. DOE

N94-21925# Lawrence Livermore National Lab., CA.
ROBOTIC CONCEPTS FOR OPERATION IN BARREN TERRAIN
K. Dowling (Carnegie-Mellon Univ., Pittsburgh, PA.) Jan. 1993 24 p
(Contract W-7405-eng-48)
(DE93-040539; UCRL-CR-114855) Avail: CASI HC A03/MF A01

We have performed a series of studies and configurations for robots that are capable of operating in rough barren terrains. The environments we are targeting are like those of the moon or other planets in the roughness and starkness of the terrains, the loose and hard materials that range from sandy slopes to boulder fields, and the extremes of temperature that are encountered in such places. We present a mission scenario and requirements and then present and evaluate a mechanism design. Additional subsystem issues of power, communication, sensing, and computing are all addressed with respect to these requirements. DOE

N94-21929# Sandia National Labs., Albuquerque, NM.
AUTOMATING THE CONTROL OF ROBOTIC SYSTEMS IN UNSTRUCTURED ENVIRONMENTS
R. W. Harrigan 1993 9 p Presented at the 8th Institute of Electrical and Electronics Engineers (IEEE) International Symposium on Intelligent Control, Chicago, IL, 25-27 Aug. 1993
(Contract DE-AC04-76DP-00789)
(DE93-040753; SAND-93-1468C; CONF-9308171-1) Avail: CASI HC A02/MF A01

The US Department Energy's Office of Technology Development has sponsored the development of generic robotics technologies for application to a wide range of remote systems. Of primary interest is the development of technologies which enable faster, safer, and cheaper cleanup of hazardous waste sites than is possible using conventional human contact or remote manual approaches. The development of model-based sensor-directed robot control approaches supports these goals by developing modular control technologies which reduce the time and cost of development by allowing reuse of control system software. In addition, the use of computer models improves the safety of remote site cleanup by allowing automated errors detection and recovery while reducing the time for technology development. DOE

N94-22270*# National Aeronautics and Space Administration. Ames Research Center, Moffett Field, CA.
FUZZY AND NEURAL CONTROL
Hamid R. Berenji May 1992 24 p
(NASA-TM-108753; FIA-92-19; NAS 1.15:108753) Avail: CASI HC A03/MF A01

Fuzzy logic and neural networks provide new methods for designing control systems. Fuzzy logic controllers do not require a complete analytical model of a dynamic system and can provide knowledge-based heuristic controllers for ill-defined and complex systems. Neural networks can be used for learning control. In this chapter, we discuss hybrid methods using fuzzy logic and neural networks which can start with an approximate control knowledge base and refine it through reinforcement learning. Author

N94-22563# California Univ., Berkeley. Lawrence Berkeley Lab.
GENERAL ASYMMETRIC NEURAL NETWORKS AND STRUCTURE DESIGN BY GENETIC ALGORITHMS: A LEARNING RULE FOR TEMPORAL PATTERNS
S. Bornholdt (Heidelberg Univ., Germany.) and D. Graudenz Jul. 1993 14 p
(Contract DE-AC03-76SF-00098)
(DE94-001254; LBL-34384; HD-THEP-93-26) Avail: CASI HC A03/MF A01

This paper demonstrates that genetic algorithms provide a learning rule for general asymmetric neural nets which is suited for learning temporal patterns without any assumptions on the topology of the emerging network. The learning capability has been demonstrated with a five bit parity problem for a static diluted neural net. The successful training of a counting neural network shows the ability of the learning rule to choose the weights in a way that leads to feedback loops in the neural network that store the information necessary for counting. This mechanism turns out to be robust against asymmetric update of the neural network. Genetic algorithms are shown to be useful for training and choosing the weights of neural networks where standard learning rules fail. Derived from text

N94-22591 University of Western Ontario, London. Dept. of Computer Science.
MOBILE ROBOT PERCEPTION IN UNKNOWN AND UNSTRUCTURED DYNAMIC VOXEL ENVIRONMENTS Ph.D. Thesis
Zhang Yuefeng Jun. 1993 148 p
(ISBN-0-315-83951-1; CTN-94-60961) Copyright Avail: Micromedia Ltd., Technical Information Centre, 240 Catherine Street, Suite 305, Ottawa, Ontario, K2P 2G8, Canada HC/MF

The occupancy grid method (OGM), a probabilistic spatial modelling technique, was developed for handling a world where a robot is the only moving object. Since this method lacks the ability to predict the location of moving objects over time, the OGM was extended to handle objects moving at constant velocity. A four dimensional location velocity space is subdivided into cells, each of which is associated with a probability of an object existing at that location moving at that velocity. This probabilistic information is updated over time using the Bayesian reasoning formula. Two pieces of probabilistic information are considered in calculating such a probability: one indicating the likelihood that there are objects at that location and the other the likelihood that an object at a given location moves with a particular velocity. Methods are presented for deriving the probability for each cell in the extended occupancy grid by combining the original OGM with motion detection mechanisms such as the Hough transform. The latter approach is robust in the case of occlusion, and can be easily extended to handle other motions such as rotation and acceleration. Author (CISTI)

N94-21720*# Syracuse Univ., NY. Dept. of Electrical and Computer Engineering.
A MEAN FIELD NEURAL NETWORK FOR HIERARCHICAL MODULE PLACEMENT
M. Kemal Unaltuna and Vijay Pitchumani *In* Idaho Univ., The 1992 4th NASA SERC Symposium on VLSI Design 1992 9 p (For primary document see N94-21694 05-33)
Avail: CASI HC A02/MF A04

N94-22105 Laval Univ. (Quebec). Lab. de Vision et Systemes Numeriques.
A 3-D VISION METHOD FOR ESTIMATING WORKSPACE OCCUPANCY OF A POWER-LINE MAINTENANCE ROBOT
Alain Croteau, Denis Laurendeau, and Jean Lessard (Institut de Recherche de l'Hydro-Quebec, Varennes.) *In* Engineering Inst. of Canada, Canadian Conference on Electrical and Computer Engineering, Volumes 1 and 2 1991 4 p (For primary document see N94-22101 05-33)
Avail: Issuing Activity (Engineering Inst. of Canada, 2050 rue Mansfield, Suite 700, Montreal, PQ H3A 1Z2 Canada)

N94-22107 Toronto Univ. (Ontario). Computer Integrated Manufacturing Lab.
OPTIMAL OBJECT MODELLING FOR AN ACTIVE-VISION SYSTEM
X. He, B. Benhabib, and K. C. Smith *In* Engineering Inst. of Canada, Canadian Conference on Electrical and Computer Engineering, Volumes 1 and 2 1991 4 p (For primary document see N94-22101 05-33)
Avail: Issuing Activity (Engineering Inst. of Canada, 2050 rue Mansfield, Suite 700, Montreal, PQ H3A 1Z2 Canada)

N94-22130 Toronto Univ. (Ontario). Computer Integrated Manufacturing Lab.
SENSOR INTEGRATION AND DATA FUSION FOR OBJECT LOCALIZATION IN ROBOTIC WORKCELLS
I. Saban, K. C. Smith, and B. Benhabib *In* Engineering Inst. of Canada, Canadian Conference on Electrical and Computer Engineering, Volumes 1 and 2 1991 4 p (For primary document see N94-22101 05-33)
Avail: Issuing Activity (Engineering Inst. of Canada, 2050 rue Mansfield, Suite 700, Montreal, PQ H3A 1Z2 Canada)

N94-22131 Quebec Univ., Montreal. Ecole de Technologie Superieure.
ULTRASONIC SENSOR VISION IN ROBOTICS [VISION PAR SENSEURS ULTRASONIQUES PAR LA ROBOTIQUE]
Michel Brule and Jean-Luc Dion (Quebec Univ., Trois-Riveres.) *In* Engineering Inst. of Canada, Canadian Conference on Electrical and Computer Engineering, Volumes 1 and 2 1991 5 p In FRENCH (For primary document see N94-22101 05-33)
Avail: Issuing Activity (Engineering Inst. of Canada, 2050 rue Mansfield, Suite 700, Montreal, PQ H3A 1Z2 Canada)

N94-22141 Laval Univ. (Quebec). Dept. d'Informatique.
LANGUAGE AS PRIMARY DIMENSION OF DISTRIBUTED AI SYSTEMS ACTIVITY
B. Chaib-Draa *In* Engineering Inst. of Canada, Canadian Conference on Electrical and Computer Engineering, Volumes 1 and 2 1991 3 p (For primary document see N94-22101 05-33)
Avail: Issuing Activity (Engineering Inst. of Canada, 2050 rue Mansfield, Suite 700, Montreal, PQ H3A 1Z2 Canada)

N94-22147 Hopital du Sacre-Coeur, Montreal (Quebec).
SEGMENTING THE OPTICAL FLOW DUE TO THE MOTION OF SEVERAL RIGID OBJECTS
Rita El-Nmeir and Guy Mailloux (Ecole Polytechnique, Montreal, Quebec.) *In* Engineering Inst. of Canada, Canadian Conference on Electrical and Computer Engineering, Volumes 1 and 2 1991 4 p (For primary document see N94-22101 05-33)
Avail: Issuing Activity (Engineering Inst. of Canada, 2050 rue Mansfield, Suite 700, Montreal, PQ H3A 1Z2 Canada)

N94-22163 Laval Univ. (Quebec). Lab. de Vision et Systemes Numeriques.
A NEURAL NETWORK FOR MULTIRESOLUTION EDGE DETECTION
Richard Lepage and Denis Poussart *In* Engineering Inst. of Canada, Canadian Conference on Electrical and Computer Engineering, Volumes 1 and 2 1991 4 p (For primary document see N94-22101 05-33)
Avail: Issuing Activity (Engineering Inst. of Canada, 2050 rue Mansfield, Suite 700, Montreal, PQ H3A 1Z2 Canada)

N94-22164 Laval Univ. (Quebec). Centre d'Optique Photonique et Laser.
IMPROVEMENT IN INVARIANT PATTERN RECOGNITION WITH NEURAL NETWORKS AND FOURIER-MELLIN FILTERS
Claude Lejeune and Yun-Long Sheng *In* Engineering Inst. of Canada,

Canadian Conference on Electrical and Computer Engineering, Volumes 1 and 2 1991 4 p (For primary document see N94-22101 05-33)
Avail: Issuing Activity (Engineering Inst. of Canada, 2050 rue Mansfield, Suite 700, Montreal, PQ H3A 1Z2 Canada)

N94-22167 Windsor Univ. (Ontario). Dept. of Electrical Engineering.
CASCADED RECURSIVE ARTIFICIAL NEURAL NETWORKS
Hon-Keung Kwan *In* Engineering Inst. of Canada, Canadian Conference on Electrical and Computer Engineering, Volumes 1 and 2 1991 4 p (For primary document see N94-22101 05-33)
Avail: Issuing Activity (Engineering Inst. of Canada, 2050 rue Mansfield, Suite 700, Montreal, PQ H3A 1Z2 Canada)

N94-22181 Manitoba Univ., Winnipeg. Dept. of Electrical and Computer Engineering.
ON THE DISCOVERY OF APPROXIMATE ARITHMETIC RELATIONS BY BACKPROPAGATION NETWORKS
N. R. S. Simons and H. C. Card *In* Engineering Inst. of Canada, Canadian Conference on Electrical and Computer Engineering, Volumes 1 and 2 1991 4 p (For primary document see N94-22101 05-33)
Avail: Issuing Activity (Engineering Inst. of Canada, 2050 rue Mansfield, Suite 700, Montreal, PQ H3A 1Z2 Canada)

N94-22182 Manitoba Univ., Winnipeg. Dept. of Electrical and Computer Engineering.
LOGIC ORIENTED NEURAL NETWORKS
Robert V. Pelletier, Witold Pedrycz, Robert D. McLeod, and David C. Blight *In* Engineering Inst. of Canada, Canadian Conference on Electrical and Computer Engineering, Volumes 1 and 2 1991 4 p (For primary document see N94-22101 05-33)
Avail: Issuing Activity (Engineering Inst. of Canada, 2050 rue Mansfield, Suite 700, Montreal, PQ H3A 1Z2 Canada)

N94-22183 Concordia Univ., Montreal (Quebec). Dept. of Electrical and Computer Engineering.
A NEURAL NETWORK APPROACH TO THE MAXIMUM FLOW PROBLEM
M. Mehmet Ali and Faouzi Kamoun *In* Engineering Inst. of Canada, Canadian Conference on Electrical and Computer Engineering, Volumes 1 and 2 1991 4 p (For primary document see N94-22101 05-33)
Avail: Issuing Activity (Engineering Inst. of Canada, 2050 rue Mansfield, Suite 700, Montreal, PQ H3A 1Z2 Canada)

N94-22184 McGill Univ., Montreal (Quebec). Dept. of Electrical Engineering.
A HOPFIELD NEURAL NET FOR DISCRETE FOURIER TRANSFORM CALCULATION
A. Cova, N. Kim, M. Petroni, and B. Zabawskij *In* Engineering Inst. of Canada, Canadian Conference on Electrical and Computer Engineering, Volumes 1 and 2 1991 4 p (For primary document see N94-22101 05-33)
Avail: Issuing Activity (Engineering Inst. of Canada, 2050 rue Mansfield, Suite 700, Montreal, PQ H3A 1Z2 Canada)

N94-22186 Carleton Univ., Ottawa (Ontario).
INTERFERENCE REDUCTION USING NEURAL NETWORKS
H. M. Hafez and G. K. Chan (Department of Communications, Ottawa, Ontario.) *In* Engineering Inst. of Canada, Canadian Conference on Electrical and Computer Engineering, Volumes 1 and 2 1991 4 p (For primary document see N94-22101 05-33)
Avail: Issuing Activity (Engineering Inst. of Canada, 2050 rue Mansfield, Suite 700, Montreal, PQ H3A 1Z2 Canada)

N94-22201 Sherbrooke Univ. (Quebec). Dept. de Mathematique et Informatique.
A PYRAMID NEURAL NETWORK ARCHITECTURE FOR STEREO FUSION
Shengrui Wang, Simon Gagne (Laval Univ., Quebec.), and Denis Poussart (Laval Univ., Quebec.) *In* Engineering Inst. of Canada, Canadian Conference on Electrical and Computer Engineering, Volumes 1 and 2 1991 4 p (For primary document see N94-22101 05-33)
Avail: Issuing Activity (Engineering Inst. of Canada, 2050 rue Mansfield, Suite 700, Montreal, PQ H3A 1Z2 Canada)

N94-22228 Defence Research Establishment Valcartier (Quebec). Electro-Optics Div.
MEMORY BASED VISION: A NEW CONCEPT
Martin P. Levesque and Auguste Blanchard *In* Engineering Inst. of Canada, Canadian Conference on Electrical and Computer Engineering, Volumes 1 and 2 1991 4 p (For primary document see N94-22101 05-33)
Avail: Issuing Activity (Engineering Inst. of Canada, 2050 rue Mansfield, Suite 700, Montreal, PQ H3A 1Z2 Canada)

N94-22229 Quebec Univ., Montreal. Ecole de Technologie Superieure.
AN ADAPTIVE CONTROL TO ENABLE A ROBOT TO FOLLOW CARTESIAN TRAJECTORIES [UNE COMMANDE ADAPTIVE DE SUIVI DE TRAJECTOIRES CARTESIENNES DE ROBOT]
L. Dessaint, M. Saad, K. Al-Haddad, and Y. Dube (Quebec Univ., Trois-Riveres.) *In* Engineering Inst. of Canada, Canadian Conference on Electrical and Computer Engineering, Volumes 1 and 2 1991 5 p In FRENCH (For primary document see N94-22101 05-33)
Avail: Issuing Activity (Engineering Inst. of Canada, 2050 rue Mansfield, Suite 700, Montreal, PQ H3A 1Z2 Canada)

N94-22230 Concordia Univ., Montreal (Quebec). Dept. of Electrical and Computer Engineering.
A ROBUST ADAPTIVE CONTROL DESIGN FOR FLEXIBLE JOINT MANIPULATORS
K. Khorasani *In* Engineering Inst. of Canada, Canadian Conference on Electrical and Computer Engineering, Volumes 1 and 2 1991 4 p (For primary document see N94-22101 05-33)
Avail: Issuing Activity (Engineering Inst. of Canada, 2050 rue Mansfield, Suite 700, Montreal, PQ H3A 1Z2 Canada)

N94-22239 Laval Univ. (Quebec). Dept. of Computer Science.
AN ALGORITHM FOR THE INTERFERENCE DETECTION AMONG POLYGONAL SURFACES
Clemont Dupuis and Caroline Ricard *In* Engineering Inst. of Canada, Canadian Conference on Electrical and Computer Engineering, Volumes 1 and 2 1991 4 p (For primary document see N94-22101 05-33)
Avail: Issuing Activity (Engineering Inst. of Canada, 2050 rue Mansfield, Suite 700, Montreal, PQ H3A 1Z2 Canada)

N94-22240 Laval Univ. (Quebec). Dept. de Genie Mecanique.
STRATEGY FOR MOTION OF A MOVING BODY OF QUASI-POLYGONAL FORM WITHIN A POLYGONAL SPACE [STATEGIE DE MOUVEMENT D'UN FORME QUASI-POLYGONALE DANS UNE SCENE POLYGONALE]
Clement Gosselin and Moufid Karray *In* Engineering Inst. of Canada, Canadian Conference on Electrical and Computer Engineering, Volumes 1 and 2 1991 4 p In FRENCH (For primary document see N94-22101 05-33)
Avail: Issuing Activity (Engineering Inst. of Canada, 2050 rue Mansfield, Suite 700, Montreal, PQ H3A 1Z2 Canada)

N94-22241 Laval Univ. (Quebec). Dept. de Genie Mecanique.
ANALYTICAL REPRESENTATION OF WORKING ARTICULATION SPACE OF A PLANE MANIPULATOR IN AN ENCUMBERED ENVIRONMENT [REPRESENTATION ANALYTIQUE DE L'ESPACE DE TRAVAIL ARTICULAIRE D'UN MANIPULATEUR PLAN DANS UN ENVIRONNEMENT ENCOMBRE]
Ammar Hadj-Messaoud, Clement M. Gosselin, and Michel Guillot *In* Engineering Inst. of Canada, Canadian Conference on Electrical and Computer Engineering, Volumes 1 and 2 1991 4 p In FRENCH (For primary document see N94-22101 05-33)
Avail: Issuing Activity (Engineering Inst. of Canada, 2050 rue Mansfield, Suite 700, Montreal, PQ H3A 1Z2 Canada)

N94-22255 Thomson-CSF Systems Canada, Inc., Nepean (Ontario).
CONTROL OF MULTIPLE ROBOT MANIPULATORS WITH OPTIMAL FORCE DISTRIBUTION
S. Kalaycioglu *In* Engineering Inst. of Canada, Canadian Conference on

Electrical and Computer Engineering, Volumes 1 and 2 1991 3 p (For primary document see N94-22101 05-33)
Avail: Issuing Activity (Engineering Inst. of Canada, 2050 rue Mansfield, Suite 700, Montreal, PQ H3A 1Z2 Canada)

N94-22256 Royal Military Coll. of Canada, Kingston (Ontario). Dept. of Mechanical Engineering.
OPTIMAL CONTROL OF THE TIP OF A FLEXIBLE ARM
Jean-Claude Piedboueuf, Denis Dochain (Ecole Polytechnique, Montreal, Quebec.), Richard Hurteau (Ecole Polytechnique, Montreal, Quebec.), and Kaouthar Benameur (McGill Univ., Montreal, Quebec.) *In* Engineering Inst. of Canada, Canadian Conference on Electrical and Computer Engineering, Volumes 1 and 2 1991 4 p (For primary document see N94-22101 05-33)
Avail: Issuing Activity (Engineering Inst. of Canada, 2050 rue Mansfield, Suite 700, Montreal, PQ H3A 1Z2 Canada)

N94-22451*# Space Telescope Science Inst., Baltimore, MD.
A NEURAL NETWORK PROTOTYPING PACKAGE WITHIN IRAF Abstract Only
D. Bazell and I. Bankman (Johns Hopkins Univ., Baltimore, MD.) *In* NASA, Washington, Second Annual Conference on Astronomical Data Analysis Software and Systems. Abstracts 1992 p 20 (For primary document see N94-22438 05-89)
Avail: CASI HC A01/MF A02

N94-22492*# Space Telescope Science Inst., Baltimore, MD.
THE APPLICATION OF ARTIFICIAL INTELLIGENCE TO ASTRONOMICAL SCHEDULING PROBLEMS Abstract Only
Mark D. Johnston *In* NASA, Washington, Second Annual Conference on Astronomical Data Analysis Software and Systems. Abstracts 1992 p 61 (For primary document see N94-22438 05-89)
Avail: CASI HC A01/MF A02

64 NUMERICAL ANALYSIS

Includes iteration, difference equations, and numerical approximation.

N94-19838 General Electric Co., Schenectady, NY. Biological Sciences Lab.
REPRESENTATION AND RECOGNITION WITH ALGEBRAIC INVARIANTS AND GEOMETRIC CONSTRAINT MODELS Progress Report, 1 Mar. - 1 Jun. 1993
Joseph L. Mundy 7 Sep. 1993 9 p Limited Reproducibility: More than 20% of this document may be affected by microfiche quality
(Contract MDA972-91-C-0053; ARPA Order 8228)
(AD-A271395) Avail: CASI HC A02

This document reports progress on the subject project from 3/1/93 to 6/1/93. A new approach to epipolar calibration has been implemented which provides a coordinate framework for relating features across multiple views. The invariant object recognition system has been successfully demonstrated on RADIUS model board imagery. The approach reported last quarter for the extraction of Euclidean structure has been implemented and initial results are promising. DTIC

N94-19854 Stanford Univ., CA. Dept. of Operations Research.
STOCHASTIC OPTIMIZATION BY SIMULATION: NUMERICAL EXPERIMENTS WITH M/M/1 QUEUE IN STEADY-STATE
Peter W. Glynn, Nataly Giroux, and Pierre LEcuyer Jul. 1993 33 p Limited Reproducibility: More than 20% of this document may be affected by microfiche quality
(Contract DAAL03-91-G-0101)
(AD-A271143; SU-TR-93-13; ARO-28809.16-MA-SDI) Avail: CASI HC A03

This paper gives numerical illustrations of the behavior of stochastic approximation combined with different derivative estimation techniques, to optimize a steady-state system. It is a companion paper to L'Ecuyer and Glynn, which gives convergence proofs for most of the variants experimented with here. The numerical experiments are made with a simple M/M/1 queue, which while simple, serves to illustrate the basic convergence properties and possible pitfalls of the various techniques. DTIC

N94-19898# Minnesota Univ., Minneapolis. Dept. of Computer Science.
NUMERICAL SOLUTION OF DIFFERENTIAL-ALGEBRAIC EQUATIONS WITH ILL-CONDITIONED CONSTRAINTS
Linda R. Petzold, Yuhe Ren, and Timothy Maly Aug. 1993 34 p
(Contracts DAAL03-89-C-0038; DAAL03-92-G-0247)
(AD-A270934; TR-93-59; ARO-30980.2-MA) Avail: CASI HC A03/MF A01

In this paper we consider the numerical solution of higher-index differential algebraic equations with ill-conditioned or rank-deficient constraints. These types of problems arise for example in the solution of constrained mechanical systems, when a mechanism's trajectory passes through or near a kinematic singularity. We derive a class of methods for these problems which are based on minimization of the norm of the constraints. The new methods are analogous to trust-region methods of numerical optimization. We give error estimates and convergence and stability results for the new methods, and present SCM numerical experiments which illustrate their effectiveness. DTIC

N94-19907 Aeronautical Research Labs., Melbourne (Australia).
LITERATURE REVIEW OF THE ERRORS-IN-VARIABLES APPROACH TO THE PROBLEM OF SYSTEM IDENTIFICATION
Betty Emslie Jul. 1993 14 p Limited Reproducibility: More than 20% of this document may be affected by microfiche quality
(AD-A271098; ARL-TN-42; DODA-007-097) Avail: Issuing Activity (Defense Technical Information Center (DTIC))

The papers reviewed here deal with various aspects of the problem of system identification when all the observed variables are contaminated by noise errors. Theoretical issues of identifiability and practical methods for developing algorithms to estimate parameters of a dynamic system are considered. The total least squares approach and the Koopmans-Levin method are among the methods discussed. Both these methods are strongly based on matrix singular value decomposition, which is a computationally robust numerical technique. A book, which is a compilation of papers originating from a workshop on singular value decomposition and signal processing is included in the references. DTIC

N94-19997 Technische Univ., Eindhoven (Netherlands). Dept. of Mathematics and Computing Science.
ARE TYPES NEEDED FOR NATURAL LANGUAGE?
F. Kamareddine 1992 42 p See also PB93-191823 Limited Reproducibility: More than 20% of this document may be affected by microfiche quality
(PB93-191831; COMPUTING SCIENCE NOTES-92/20) Copyright Avail: Issuing Activity (National Technical Information Service (NTIS))

The type free lambda-calculus is powerful enough to contain all the polymorphic and self-referential nature of properties. Logic, however, due to the paradoxes, is absent from the type free lambda-calculus. This makes such a calculus an unsuitable device for Natural Language Semantics. Moreover, the problems that arise from mixing the type free Lambda-calculus with logic lead to type theory and hence formalization of Natural Language were carried out in a strictly typed framework. The paper embeds the typing system into one which gives an interpretation of Parsons system in a type free theory where logic is present. In other words, it takes the standpoint that type freeness is needed yet types are also indispensable. On this ground, by constructing types in the type free theory, it obtains a framework which can be seen as a formalization of Parsons' claim that Natural Language needs type freeness in order to accommodate self referentiality yet many sentences should be understood as implicitly typed. NTIS

N94-20006# Lawrence Livermore National Lab., CA.
STOCHASTIC DIFFERENTIAL EQUATIONS AND NUMERICAL SIMULATION FOR PEDESTRIANS
J. C. Garrison 27 Jul. 1993 33 p
(Contract W-7405-eng-48)
(DE93-040651; UCRL-ID-114856) Avail: CASI HC A03/MF A01

The mathematical foundation of the Ito interpretation of stochastic ordinary and partial differential equations is briefly explained. This provides

the basis for a review of simple difference approximations to stochastic differential equations. An example arising in the theory of optical switching is discussed. DOE

N94-20032# Technische Univ., Delft (Netherlands). Faculty of Technical Mathematics and Informatics.
MATHEMATICS B FOR THE STUDY DIRECTION VWO: A RECONNAISSANCE [WISKUNDE B VWO: EEN VERKENNING]
Annette Lievaart 1992 63 p In DUTCH
(Rept-92-80; ETN-93-94273) Copyright Avail: CASI HC A04/MF A01

The revised program Mathematics B for secondary schools (VWO) students who want a higher education in a technical or exact sciences direction is criticized. The aim is to improve the efficiency of the education of mathematics engineers by a better connection between the program of secondary schools and that of universities. The mathematics program of the VWO contains analysis and geometry and emphasizes calculation skills and not the theoretical background. The program is overloaded whereby too little time is left to refresh the basic knowledge from time to time. Theory and practice are not always in accordance. ESA

N94-20034*# Michigan Univ., Ann Arbor. Dept. of Electrical Engineering and Computer Science.
A NEW CONFORMAL ABSORBING BOUNDARY CONDITION FOR FINITE ELEMENT MESHES AND PARALLELIZATION OF FEMATS
A. Chatterjee, J. L. Volakis, J. Nguyen, M. Nurnberger, and D. Ross Dec. 1993 69 p
(Grant NAG2-866)
(NASA-CR-194740; NAS 1.26:194740; UMICH-031155-1-T) Avail: CASI HC A04/MF A01

Some of the progress toward the development and parallelization of an improved version of the finite element code FEMATS is described. This is a finite element code for computing the scattering by arbitrarily shaped three dimensional surfaces composite scatterers. The following tasks were worked on during the report period: (1) new absorbing boundary conditions (ABC's) for truncating the finite element mesh; (2) mixed mesh termination schemes; (3) hierarchical elements and multigridding; (4) parallelization; and (5) various modeling enhancements (antenna feeds, anisotropy, and higher order GIBC). Derived from text

N94-20087*# Institute for Computer Applications in Science and Engineering, Hampton, VA.
ON THE SPLINE-BASED WAVELET DIFFERENTIATION MATRIX Final Report
Leland Jameson Nov. 1993 38 p Submitted for publication
(Contracts NAS1-19480; N00014-91-C-4016; NSF DMS-92-11820; AF-AFOSR-0090-93; RTOP 505-90-52-01)
(NASA-CR-191557; NAS 1.26:191557; ICASE-93-80) Avail: CASI HC A03/MF A01

The differentiation matrix for a spline-based wavelet basis is constructed. Given an n-th order spline basis it is proved that the differentiation matrix is accurate of order $2n + 2$ when periodic boundary conditions are assumed. This high accuracy, or superconvergence, is lost when the boundary conditions are no longer periodic. Furthermore, it is shown that spline-based bases generate a class of compact finite difference schemes. Author (revised)

N94-20092*# Institute for Computer Applications in Science and Engineering, Hampton, VA.
SHAPE OPTIMIZATION GOVERNED BY THE EULER EQUATIONS USING AN ADJOINT METHOD Final Report
Angelo Iollo, Manuel D. Salas (National Aeronautics and Space Administration. Langley Research Center, Hampton, VA.), and Shlomo Taasan Nov. 1993 21 p Submitted for publication
(Contract NAS1-19480; RTOP 505-90-52-01)
(NASA-CR-191555; NAS 1.26:191555; ICASE-93-78) Avail: CASI HC A03/MF A01

A numerical approach for the treatment of optimal shape problems governed by the Euler equations is discussed. Focus is on flows with embedded shocks. A very simple problem is considered: the design of a quasi-one-dimensional Laval nozzle. A cost function and a set of Lagrange multipliers are introduced to achieve the minimum. The nature of the resulting costate equations is discussed. A theoretical difficulty that arises for cases with embedded shocks is pointed out and solved. Finally, some results are given to illustrate the effectiveness of the method. Author (revised)

N94-20125# Grenoble-1 Univ. (France). Lab. ARTEMIS.
ON MULTIFLOW PROBLEMS
Andras Frank (Bonn Univ., Germany.), Alexander Karzanov (Institute for System Studies, Moscow, USSR.), and Andras Sebo Apr. 1992 20 p Sponsored in part by Mairie de Grenoble, France
(RR-889-M; ETN-93-94981) Avail: CASI HC A03/MF A01

Some relationships between multicommodity flow problems are revealed. These are various versions of the multicommodity flow problems such as edge demand, node demand, maximization, and locking problems. With an unexpected use of Edmonds' polymatroid intersection theorem, a theorem of Karzanov and Lomonosov on multiflow maximization is derived. The approach gives rise to a combinatorial polynomial time algorithm to find the maximum in question. A certain weighted version of the maximization problem also becomes tractable. ESA

N94-20161# Grenoble-1 Univ. (France). Lab. ARTEMIS.
DETERMINING THE DISTANCE TO THE PERFECT MATCHING POLYTOPE OF A BIPARTITE GRAPH
Andras Frank (Bonn Univ., Germany.) and Alexander V. Karzanov Jun. 1992 10 p Sponsored by Mairie de Grenoble, France
(RR-895-M; ETN-93-94986) Avail: CASI HC A02/MF A01

The problem of finding the euclidean distance from the origin to the perfect matching polytope of a bipartite graph is considered. Being a quadratic program with linear constraints, this problem can be solved in polynomial time by use of a version of the ellipsoid method. A combinatorial algorithm which solves it in polynomial time is developed. The algorithm as well as the proof of its correctness uses ideas involved in the cancelling minimum mean circuit algorithm for the minimum cost circulation problem due to Goldberg and Tarjan. ESA

N94-20163# Grenoble-1 Univ. (France). Lab. de Structures Discretes et de Didactique.
LABEL-CONNECTED GRAPHS: AN OVERVIEW
Gustav Burosch (Rostock Univ., German D.R..) and Jean Marie Laborde Jul. 1992 43 p
(RR-898-M; ETN-93-94988) Avail: CASI HC A03/MF A01

An overview of some gossip problems is given: gossips with unique use of communication canal. It contains results about characterization of graphs G allowing such gossipings and about the NP completeness of the problem of whether G is of the required type. ESA

N94-20200# Grenoble-1 Univ. (France). Lab. de Modelisation et Calcul.
AFFINE AND NON-AFFINE BLOSSOMS
Marie-Laurence Mazure and Pierre-Jean Laurent Mar. 1993 30 p
(RR-913-M; ETN-93-94993) Avail: CASI HC A03/MF A01

The main properties of the blossom of a polynomial function are given. The main result is a theorem which gives an expression for the intersection of osculating flats. The notion of blossom is extended to spline curves and a proof of a result which is the direct generalization of the theorem to spline curves is given. It is shown that a notion of non-affine blossom can be defined for q spline curves. ESA

N94-20217# Stanford Univ., CA. System Optimization Lab.
ON THE NUMERICAL STABILITY OF QUASI-DEFINITE SYSTEMS
P. E. Gill, J. R. Shinnerl, and M. A. Saunders Jun. 1993 9 p
(Contract DE-FG03-92ER-25117)
(DE93-019404; SU-SOL-93-4) Avail: CASI HC A02/MF A01

The authors discuss the solution of sparse linear equations $Kd = r$, where K is a symmetric and specially structured indefinite matrix that often arises in numerical optimization. For such K, the indefinite factorization $K = LDL(\text{sup } T)$ is known to exist in exact arithmetic with 1 x 1 pivots and no row or column interchanges. It is shown that the stability of the $LDL(\text{sup } T)$ factorization of this matrix is naturally connected with the stability of the $LDM(\text{sup } T)$ factorization of a closely related unsymmetric positive-definite matrix. Conditions are given that allow the stable numerical solution of this system by Gaussian elimination without row and column interchanges. DOE

N94-20221# Argonne National Lab., IL.
PARALLEL BAND REDUCTION AND TRIDIAGONALIZATION
C. Bischof, X. Sun, and M. Marques (Texas Univ., Austin.) 1993 8 p Presented at the 6th Society for Industrial and Applied Mathematics (SIAM) Conference on Parallel Processing for Scientific Computing, Norfolk, VA, 21-24 Mar. 1993
(Contract W-31-109-eng-38)
(DE93-019566; ANL/MCS/CP-80518; CONF-930331-15) Avail: CASI HC A02/MF A01

This paper presents a parallel implementation of a blocked band reduction algorithm for symmetric matrices suggested by Bischof and Sun. The reduction to tridiagonal or block tridiagonal form is a special case of this algorithm. A blocked double torus wrap mapping is used as the underlying data distribution and the so-called WY representation is employed to represent block orthogonal transformations. Preliminary performance results on the Intel Delta indicate that the algorithm is well-suited to a MIMD computing environment and that the use of a block approach significantly improves performance. DOE

N94-20224# Texas Univ., Austin. Fusion Research Center.
NEOCLASSICAL KINETIC THEORY NEAR AN X-POINT: PLATEAU REGIME
E. R. Solano and R. D. Hazeltine Aug. 1993 11 p
(Contracts DE-FG05-88ER-53266; DE-FG05-89ER-53288)
(DE93-019825; DOE/ER-53266/45; FRCR-436) Avail: CASI HC A03/MF A01

Traditionally, neoclassical transport calculations ignore poloidal variation of the poloidal magnetic field. Near an X-point of the confining field of a diverted plasma, the poloidal field is small, causing guiding centers to linger at that poloidal position. We study how neoclassical transport is affected by this differential shaping. The problem is solved in general in the plateau regime, and a model poloidal flux function with an X-point is utilized as an analytic example to show that the plateau diffusion coefficient can change considerably (factor of 2 reduction). Ion poloidal rotation is proportional to the local value of B approaches pol, but otherwise it is not strongly affected by shaping. DOE

N94-20227# Institut National de Recherche d'Informatique et d'Automatique, Valbonne (France). Programme 5: Traitement du Signal, Automatique et Productique.
ASYMPTOTICS OF THE GLRT FOR THE DISORDER PROBLEM IN DIFFUSION PROCESSES
Fabien Campillo, Francois LeGland, and Yurii Kutoyants (Maine Univ., Le Mans, France.) Jul. 1992 26 p
(INRIA-RR-1735; ETN-93-94435) Avail: CASI HC A03/MF A01

The problem of detecting a change in the drift coefficient of a diffusion process (disorder problem), using the generalized likelihood ratio test (GLRT), is considered. Assuming that a change has occurred, the asymptotic behavior (consistency, asymptotic probability distribution) of the maximum likelihood estimate of the change time has already been investigated in the small noise asymptotics. This study addresses the asymptotics of the GLRT itself, i.e. the asymptotic behavior of both the probability of false alarm and the probability of miss detection. These probabilities are proven to go to zero with exponential rate, provided a simple detectability assumption is satisfied by the limiting deterministic system. The robustness of the GLRT with respect to model mis-specification, a very important property for practical implementation, is also investigated. Here, mis-specification means that some wrong expressions are used for either the drift coefficient (before change) or the change coefficient. Roughly the same behavior is obtained for the error probabilities, as in the correctly specified case, although the detectability assumption will include the requirement that the change to be detected is larger in some sense than the mis-specification error. ESA

N94-20237# Grenoble-1 Univ. (France). Lab. ARTEMIS.
TOTALLY STRONG AND STRONG GRAPHS [GRAPHES FORTS ET TOTALEMENT FORTS]
Brahim Chaourar and Andras Sebo Oct. 1992 16 p In FRENCH
(RR-902-I; ETN-93-94992) Avail: CASI HC A03/MF A01

The hilbertian base of graph trees, in particular totally strong graphs, in which all the trees are strong, and string graphs, in which each cone face of the trees contains a strong tree, is addressed. Definitions concerning the notion of hilbertian base as well as important open questions relative to this notion are given. The hilbertian base of trees is then focused upon. The lattice and cone facets of trees are characterized. ESA

N94-20302# Grenoble-1 Univ. (France). Lab. ARTEMIS.
HALF-INTEGRAL FLOWS IN A PLANAR GRAPH WITH FOUR HOLES
Alexander K. Karzanov Jun. 1992 53 p Sponsored by Mairie of Grenoble, France
(RR-894-M; ETN-93-94985) Avail: CASI HC A04/MF A01

Suppose that G = (VG, EG) is a planar graph embedded in the euclidean plane, that I, J, K, O are four of its faces (called holes in G), that s(sub 1),..., s(sub r), t(sub 1),..., t(sub r) are vertices of G such that each pair of the set s(sub i), t(sub i) belongs to the boundary of some I, J, K, O and that the graph (VG, EG union of the set of sets s(sub i), t(sub i),..., s(sub r), t(sub r)) is eulerian. It is proved that if the multi(commodity) flow problem in G with unit demands on the values of flows from s(sub i) to flows from s(sub i) to t(sub i), i = 1,...,r, has a solution then it has a half integral solution as well. In other words, there exist paths P(sub 1)(sup 1), P(sub 1)(sup 2), P(sub 2)(sup 2),..., P(sub r)(sup 1), P(sub r)(sup 2) in G such that each P(sub i)(sup j) connects s(sub i) and t(sub i), and each edge of G is covered at most twice by these paths. (It is known that in case of at most three holes there exist edge disjoint paths connecting s(sub i) and t(sub i), i = 1,...,r, provided that the corresponding multiflow problem has a solution, but this is, in general, false in case of four holes). ESA

N94-20358# Department of the Navy, Washington, DC.
SYSTEM FOR SOLVING BOOLEAN EQUATIONS USING OPTICAL LOOKUP TABLES Patent
Roy M. Reyes, inventor (to Navy) and Scott E. Spence, inventor (to Navy) 5 Oct. 1993 8 p Filed 2 Sep. 1992
(AD-D015962; US-Patent-5,251,052; US-Patent-Appl-SN-939229; US-Patent-Class-359-107) Avail: US Patent and Trademark Office

A reconfigurable digital optical lookup table for solving Boolean equations using in array of bistable optical devices is provided. A single light source is divided into a matrix of light beams using binary phase gratings and a lens system. This matrix of beams is modulated by a spatial light modulator symmetric self electro-optic effect device (S-SEED) according to the desired lookup table. The modulated light beams are used to set an S-SEED array with the lookup table. The rows and columns of the S-SEED array are then reset according to the inputs to the Boolean equation. Once all of the inputs have been processed, the S-SEED array will have only one member whose state has not been affected by the inputs, and the value of this S-SEED corresponds to the solution to the Boolean equation. The final result is output by using a matrix of equal intensity light beams and a mask to read out the state of one side of the S-SEEDs, and focusing the result onto a detector. DTIC

N94-20527 Maryland Univ., College Park. Inst. for Physical Science and Technology.
POLYNOMIAL INTERPOLATION OF REAL FUNCTIONS 1: INTERPOLATION IN AN INTERVAL Technical Note
Qi Chen (Sachs/Freeman Associates, Inc., Landover, MD.) and Ivo babuska Aug. 1993 31 p Sponsored in part by ARPA Limited Reproducibility: More than 20% of this document may be affected by microfiche quality
(Contract N00014-90-J-1030)
(AD-A272330; BN-1153) Avail: Issuing Activity (Defense Technical Information Center (DTIC))

This paper is the first in a series to analyze the accuracy of polynomial interpolation of functions and its dependence on the locations of the interpolation nodes. It surveys known results for polynomial interpolation in an interval. It also introduces the concept of the Minimal Interpolation Sets which are the 'optimal' interpolation sets. New results concerning the properties of the minimal sets as well as procedures for locating the minimal sets are presented. The table for the minimal sets in the L-norm is given. An adaptive scheme for determining the interpolation order is also presented. Examples show the efficacy of this approach. DTIC

N94-20545# Brown Univ., Providence, RI. Div. of Applied Mathematics.
DYNAMICAL SYSTEMS AND NONLINEAR PARTIAL DIFFERENTIAL EQUATIONS Final Report, Dec. 1989 - May 1993

Constantine M. Dafermos, John Mallet-Paret, Panagiotis E. Souganidis, and Walter Strauss 9 Sep. 1993 8 p
(Contract DAAL03-90-G-0012)
(AD-A271514; ARO-27403.8-MA) Avail: CASI HC A02/MF A01

The report describes work by several investigators on a number of projects in the general area of dynamical systems, nonlinear partial differential equations, delay equations and continuum physics. DTIC

N94-20568# Rensselaer Polytechnic Inst., Troy, NY. Dept. of Computer Science.
NUMERICAL METHODS FOR SINGULARLY PERTURBED DIFFERENTIAL EQUATIONS WITH APPLICATIONS Final Report, 1 Apr. 1990 - 31 Mar. 1993
Joseph Flaherty 31 Mar. 1993 24 p
(Grant AF-AFOSR-0194-90)
(AD-A272112; AFOSR-93-0807TR) Avail: CASI HC A03/MF A01

During the three-year period of this project, we conducted research on the development, analysis, and application of serial and parallel adaptive computational strategies for solving transient and steady partial differential systems. Concentrating on high-order methods and adaptive approaches that combine mesh refinement and coarsening (h-refinement, order variation (p-refinement), and occasionally, mesh motion (r-refinement), we addressed problems in combustion, materials science, and compressible fluid mechanics. Special spatially-discrete finite element Galerkin methods were considered for the parallel and adaptive solution of hyperbolic conservation laws. Improved solution-limiting and error-estimation strategies increased the accuracy and efficiency of these methods which are being applied to two- and three-dimensional compressible flow problems. Adaptive techniques for dissipative systems are being applied to problems in the manufacture of ceramic composite media. DTIC

N94-20613# Georgia Inst. of Tech., Atlanta.
GRAPH MINORS: STRUCTURE THEORY AND ALGORITHMS
Robin Thomas 1993 7 p
(Contract N00014-93-1-0325)
(AD-A271851) Avail: CASI HC A02/MF A01

There have been significant developments in graph theory over the last decade that imply the existence of polynomial time algorithms for a large class of problems. These results, however, guarantee the existence of polynomial-time algorithms to solve various problems, but give no hint how to find one. Yet another drawback of these algorithms is that even though they are theoretically fast (O(n squared) or O(n cubed)), the constant hidden in the O notation is so enormous that it makes the algorithms impractical. The purpose of this project is to further develop this theory and obtain more theoretical results, apply these results to the design of at least theoretically efficient algorithms, and turn these theoretically efficient algorithms into practical ones. DTIC

N94-20923 Clarkson Univ., Potsdam, NY. Inst. for Nonlinear Studies.
TWO-DIMENSIONAL NONLINEAR SCHRODINGER EQUATIONS AND THEIR PROPERTIES
D. J. Kaup and Ronald E. Kates Oct. 1993 22 p Limited Reproducibility: More than 20% of this document may be affected by microfiche quality
(AD-A272184; INS-241) Avail: Issuing Activity (Defense Technical Information Center (DTIC))

This paper studies a general class of two-dimensional systems of the cubic nonlinear Schrodinger type (2DNLS), defined by i del(sub t) q + O(1)q = pq and O(2)p = O(3)(q*q), where each O(sub n) is equated to D(sub ij)(sup n) del(sub i) del(sub j), n = 1,2,3, is a linear, second-order, operator with constant coefficients. This class generalizes the Djordjevic-Redekopp (DR) system, which has previously been encountered in the context of water waves. Integrability is characterized simply in terms of covariant conditions on the O(n). We obtain all integrable cases, including the known cases Davey-Stewartson I and II as well as other known integrable cases. All other regimes are modulationally unstable and have projections satisfying the ordinary (1D) NLS with soliton solutions, though in all known cases these 1D solitons are unstable with respect to transverse perturbations. The self-focusing regime is characterized by the eigenvalues of the D(sub ij)(sup n): O(1) and O(2) must both be elliptic, and for that choice of variables for which D(sub ij)(sup 1) and D(sub ij)(sup 2) both have positive signature, D(subij)(sup 3) must have at least one negative eigenvalue. The self-focusing regime is distinct from the modulationally stable regime and also from the integrable regime, while the integrable cases may be modulationally stable or unstable. There are no soliton solutions known in those integrable cases that are modulationally stable, whereas those integrable cases in which 2D solitons are known correspond to the modulational instability regime. DTIC

N94-21019 Technische Hochschule, Darmstadt (Germany). Fachbereich Mathematik.
ASYMPTOTIC BEHAVIOR OF FOURIER TRANSFORM OF SURFACE MEASURES ON CONVEX AND RADIAL HYPERSURFACES Ph.D. Thesis [UEBER DAS ASYMPTOTISCHE VERHALTEN DER FOURIERTRANSFORMIERTEN VON OBERFLAECHENMASSEN AUF KONVEXEN UND RADIALEN HYPERFLAECHEN]
Helmut Schulz 1991 74 p In GERMAN Limited Reproducibility: More than 20% of this document may be affected by microfiche quality
(ETN-93-93790) Avail: CASI HC A04

Smooth and convex hypersurfaces S of finite type with Lebesgue surface measure d-theta and function u defined on S were considered. Estimations were given for the asymptotic behavior of: absolute value of (F bracket (modules of K) to the zth power u d theta bracket). K is the Gauss curvature and z a complex number with a non negative real part. The structure of S and K are simple so that singularities do not disturb the calculations, which are given with dependence on local geometric structures of S. ESA

N94-21027 Center for Mathematics and Computer Science, Amsterdam (Netherlands). Dept. of Computer Science.
ON UPDATE LAST SCHEMES
John T. Tromp Nov. 1992 6 p Submitted for publication Sponsored in part by NFI, Netherlands Limited Reproducibility: More than 20% of this document may be affected by microfiche quality
(CWI-CS-R9247; ETN-94-94727) Copyright Avail: CASI HC A02

The notion of an Update-Last scheme as a method of distributing the identity of a 'last' among n objects over their labels is defined. A precise characterization of the possibility of such a scheme is given in terms of the number of values each level can assume. ESA

N94-21029 Center for Mathematics and Computer Science, Amsterdam (Netherlands). Dept. of Computer Science.
TIGHT COMPARISON BOUNDS FOR THE STRING PREFIX-MATCHING PROBLEM
Dany Breslauer, Livio Colussi (Padua Univ., Italy.), and Laura Toniolo (Padua Univ., Italy.) Dec. 1992 10 p Sponsored in part by European Research Consortium for Informatics and Mathematics Limited Reproducibility: More than 20% of this document may be affected by microfiche quality
(CWI-CS-R9250; ETN-94-94730) Copyright Avail: CASI HC A02

The exact complexity of the string prefix matching problem in the deterministic sequential comparison model is studied. The bounds do not account for comparisons made in a pattern preprocessing step. The following results are presented: a family of linear time string prefix matching algorithms that make at most (((2m - 1)/m)n) comparisons; a tight lower bound (((2m - 1)/m)n) comparisons for any string prefix matching algorithm. The special case when the pattern and the text strings are the same string and all comparisons are accounted is also considered. This problem, called the string self prefix problem, is similar to the failure function that is computed in the pattern preprocessing of the Knuth Morris Pratt string matching algorithm and used in several other comparison efficient algorithms. By using the lower bound for the string prefix matching problem the following is shown: a lower bound of 2m - (2 times the square root of m) comparisons for the self-prefix problem. ESA

N94-21042 Technische Univ., Berlin (Germany). Fachbereich Mathematik.
THEORETICAL AND NUMERICAL EXAMINATIONS OF NONLINEAR PARAMETER DEPENDENT ADVANCED DIFFERENTIAL DIFFERENCE EQUATIONS Ph.D. Thesis [THEORETISCHE UND NUMERISCHE UNTERSUCHUNGEN ZU NICHTLINEAREN PARAMETERABHAENGIGEN FORSTCHREITENDEN DIFFERENTIAL-DIFFERENZEN-GLEICHUNGEN]
Ulrik Haas 1992 99 p In GERMAN Limited Reproducibility: More than 20% of this document may be affected by microfiche quality
(ETN-93-93681) Avail: CASI HC A05

Mathematical models of excitation and propagation in nerves are developed, with reference to Hastings neurobiology models. Nonlinear differential difference equations, which described impulse transport in myelineated nerves, are examined. Two methods were used for modeling nonlinear terms: first, a nonlinear advanced differential-difference equation with three parameters in a model without recovery, and therefore an usual differential equation with five parameters in a model with recovery. Equations were discretized with finite differences and Sinc-Galerkin approximation method. A continuity process was developed for solving equations, which is based on the piecewise linear Newton method. Lemmas which guarantee existence and singleness of the solution are presented. The threshold values behavior for evaluating their conformity with physiology is discussed. ESA

N94-21046 Universiteit Twente, Enschede (Netherlands). Faculty of Applied Mathematics.

SYMMETRIES AND CONSERVATION LAWS OF THE SYSTEM: u(x)=vw(x), v(y)=uw(y), uv+w(xx)+w(yy)=0

T. vanBemmelen, P. K. Gragert, P. H. M. Kersten, and A. M. Sym (Warsaw Univ., Poland.) Sep. 1992 21 p Limited Reproducibility: More than 20% of this document may be affected by microfiche quality

(MEMO-1084; ETN-93-94124) Avail: CASI HC A03

The theory of local and nonlocal symmetries and conservation laws for systems of partial differential equations is discussed and results on these and the recursion operator are listed for the system of partial differential equations in the title. The methods of computation are explained. ESA

N94-21047 Universiteit Twente, Enschede (Netherlands). Faculty of Applied Mathematics.

ON THE CORE-STRUCTURE OF MINIMUM COST SPANNING TREE GAMES

Harry Aarts and Theo Driessen Oct. 1992 27 p Limited Reproducibility: More than 20% of this document may be affected by microfiche quality

(MEMO-1085; ETN-93-94125) Avail: CASI HC A03

It is a known result that Minimum Cost Spanning Tree (MCST) games possess nonempty cores and that some extreme points of the core can be deduced directly from the underlying network, that is, they can be described in terms of the costs of the edges (weight function) in the network. The determination of other extreme points of the core in this way is difficult because the precise connection between the core and the weight function is very complicated. Therefore there is still little known about the structure and the size of the core of MCST games. The connection between the core and the weight functions is studied. An adaptation of the weight function which does not change the core of the MCST game involved is introduced. For a special class of networks, this adaptation provides a useful description for the MCSTs in the various subnetworks. For this particular class, a second core invariant adaptation of the weight function is defined. The arising MCST games turn out to be exact games and the connection between the core and the (adapted) weights becomes much clearer. Many additional extreme points of the core can be deduced from the adapted network and a much better insight into the structure and the size of the core of these MCST games is obtained. The convexity of these games is investigated. ESA

N94-21048 Universiteit Twente, Enschede (Netherlands). Faculty of Applied Mathematics.

LONG CYCLES IN GRAPHS CONTAINING A 2-FACTOR WITH MANY ODD COMPONENTS

J. vandenHeuvel Oct. 1992 8 p Limited Reproducibility: More than 20% of this document may be affected by microfiche quality

(MEMO-1086; ETN-93-94126) Avail: CASI HC A02

A result on the length of a longest cycle in a graph on n vertices that contains a 2-factor and satisfies d(u) + d(v) + d(w) is greater than or equal to n + 2 for every triple u, v, w of independent vertices is proved. As a corollary, the following improvement of a conjecture of R. Haggkvist is obtained: let G be a 2-connected graph on n vertices where every pair of nonadjacent vertices has degree sum at least max (n - k, 2n/3 + 1) and assume G has a 2-factor with at least k - 1 odd components. Then G is hamiltonian. ESA

N94-21059 Technische Univ., Delft (Netherlands). Faculty of Technical Mathematics and Informatics.

ORTHOGONAL PAIRS AND ZEROS OF SOBOLEV-TYPE ORTHOGONAL POLYNOMIALS

H. G. Meijer 1992 24 p Limited Reproducibility: More than 20% of this document may be affected by microfiche quality

(Rept-92-46; ETN-93-93856) Copyright Avail: CASI HC A03

The following is presented: let the set (S(sup lambda)(sub n)) denote a set of polynomials orthogonal with respect to the Sobolev inner product (f, g) = integral upper limit b, lower limit a, f(x)g(x) d(psi)(sub 0)(x) + lambda integral upper limit b, lower limit a, f'(x)g'(x)d(psi)(sub 1)(x) where (d(psi)(sub 0)), (d(psi)(sub 1)) is a coherent pair as introduced by Iserles et al. and lambda is greater than or equal to 0. Let (K(sub n)) and (H(sub n)) denote sets of polynomials orthogonal with respect to d(psi)(sub 0) respectively d(psi)(sub 1). If lambda is sufficiently large, then S(sup lambda)(sub n) has n different, real zeros interlacing with the zeros of K(sub n - 1) and with those of H(sub n - 1). If (d(psi)(sub 0), d(psi)(sub 1)) is a symmetrically coherent pair the situation is somewhat more complicated and S(sup lambda)(sub n) may have a pair of complex zeros. ESA

N94-21060 Leiden Univ. (Netherlands). Div. of Applied Mathematics.

NUMERICAL RANGES AND STABILITY ESTIMATES

M. N. Spijker Sep. 1992 13 p Submitted for publication Limited Reproducibility: More than 20% of this document may be affected by microfiche quality

(TW-92-10; ETN-93-93866) Avail: CASI HC A03

The following is addressed: let A = (alpha(sub jk)) be a square matrix of order s, with complex entries alpha(sub jk); the set of all eigenvalues lambda of A is called the 'spectrum' of A. The so called 'numerical ranges' of A are addressed. Generalizations of the classical numerical range are studied and the relevance of these generalizations to stability questions is discussed. ESA

N94-21072 Universiteit Twente, Enschede (Netherlands). Faculty of Applied Mathematics.

EXPLICIT RESULTS ON gl(LAMBDA) AND sl(LAMBDA)

G. Post and N. W. vandenHijligenberg Aug. 1992 20 p Limited Reproducibility: More than 20% of this document may be affected by microfiche quality

(MEMO-1075; ETN-93-94116) Avail: CASI HC A03

The filtered algebras which are associated to the Poisson Lie subalgebra of even polynomials on the plane are discussed. Such algebras are 'parametrized' by lines through the origin in the set C(exp 2), leading to gl(lambda) for all lines but 1. It is also shown that gl(lambda)/C is simple if and only if lambda is not a member of the set (+/- 2, +/- 3, +/-4,...). ESA

N94-21074 Universiteit Twente, Enschede (Netherlands). Faculty of Applied Mathematics.

DEGREE SUMS, k-FACTORS AND HAMILTONIAN CYCLES IN GRAPHS

R. J. Faudree and J. vandenHeuvel (Memphis State Univ., TN.) Sep. 1992 15 p Sponsored in part by Netherlands Organization for Scientific Research Limited Reproducibility: More than 20% of this document may be affected by microfiche quality

(MEMO-1078; ETN-93-94118) Avail: CASI HC A03

A generalization of the following conjecture of R. Haggkvist is proved: let G be a 2-connected graph on n vertices where every pair of nonadjacent vertices has degree sum at least n - k and assume that G has a k-factor; then G is hamiltonian. This result is a common generalization of well known theorems of Ore and Jackson, respectively. ESA

N94-21075 Universiteit Twente, Enschede (Netherlands). Faculty of Applied Mathematics.

STOERMER-COWELL AND RELATED METHODS FOR THE NUMERICAL SOLUTION OF SECOND ORDER PERIODIC INITIAL VALUE PROBLEMS FOR ODE'S 2: NUMERICAL CHARACTERISTICS OF THE METHODS

Jan F. Frankena Sep. 1992 55 p Limited Reproducibility: More than 20% of this document may be affected by microfiche quality

(MEMO-1082; ETN-93-94122) Avail: CASI HC A04

Stiefel-Bettis' modification of the (Stormer-)Cowell method inspired many authors to find still better (that is, more stable and/or more accurate) methods for second order periodic initial value problems. A study which

compares the numerical characteristics of several sixth order methods is presented: Stormer-Cowell, Stiefel-Bettis, Lambert-Watson and the modified Numerov method as described by Van Daele-De Meyer-Vanden Berghe. Spijkers 'split' forms of these methods are also considered, together with the 'summed' counterparts of the Cowell method. The reason for this is the special interest in the summed Cowell methods that is shown by astronomers. ESA

N94-21137 Technische Hochschule, Darmstadt (Germany). Fachbereich Mathematik.
ADAPTIVE GRIDS FOR QUASILINEAR PARABOLIC SYSTEMS IN ONE SPACE DIMENSION Ph.D. Thesis [ADAPTIVE GITTER FUER QUASILINEARE PARABOLISCHE SYSTEME IN EINER RAUMDIMENSION]
Matthias Lappe 1990 95 p In GERMAN Limited Reproducibility: More than 20% of this document may be affected by microfiche quality
(ETN-93-93611) Avail: CASI HC A05

The problem of discretization for the numerical solution of partial differential equations is investigated with particular consideration to boundary conditions. Convergence issues with the method of lines were examined by considering Runge-Kutta processes of the semidiscrete problem. An algorithm for grid generation was achieved and applied to the linear heat conduction equation, the Burger equation, and a nonlinear system. The proposed method is particularly fitted for solving diffusion problem with Dirichlet boundary conditions. Existence and singleness of the solution were theoretically studied. ESA

N94-21158 Center for Mathematics and Computer Science, Amsterdam (Netherlands). Dept. of Analysis, Algebra and Geometry.
ON SEMISIMPLE COCOMMUTATIVE BIALGEBRAS
Michiel Hazewinkel Dec. 1992 7 p Limited Reproducibility: More than 20% of this document may be affected by microfiche quality
(CWI-AM-R9210; ETN-94-94710) Copyright Avail: CASI HC A02

It is well known that a semi-simple, finite dimensional commutative Hopf algebra over an algebraically closed field k is a group algebra. The standard proofs are rather deeply imbedded in the theory. This study aims to give a simple direct computational proof that also works in the infinite dimensional case and also gives results if there is no co-unit, or if the co-multiplication is not associative. ESA

N94-21159# Center for Mathematics and Computer Science, Amsterdam (Netherlands). Dept. of Analysis, Algebra and Geometry.
HILBERT 90 FOR POLYNOMIAL MATRICES
Michiel Hazewinkel Dec. 1992 6 p
(CWI-AM-R9211; ETN-94-94711) Copyright Avail: CASI HC A02/MF A01

A generalization of the 'Hilbert 90' theorem is proved for unimodular polynomial matrices. Let K/k be a finite Galois extension with Galois group Gamma = Gal(K/k). Let GL(sub n)(K z(sub 1),..., z(sub m)) be the group of polynomial unimodular n by n matrices over K, that is the group of n by n matrices M with entries that are polynomials in m variables over K and such that det(M) is a member of K the set(0). The group Gamma acts on GL(sub n)(K z(sub 1),..., z(sub m)) by acting on the coefficients of the matrix elements. The main theorem given says that the corresponding first cohomology group is zero. ESA

N94-21164# Yale Univ., New Haven, CT. Dept. of Computer Science.
FAST FOURIER TRANSFORMS FOR NONEQUISPACED DATA Ph.D. Thesis
Alok Dutt Aug. 1993 104 p
(Contract N00014-89-J-1527; NSF DMS-90-12751)
(AD-A272687) Avail: CASI HC A06/MF A01

Two groups of algorithms are presented generalizing the fast Fourier transform (FFT) to the case of non-integer frequencies and nonequispaced nodes on the interval (-pi, pi). These schemes are based on combinations of certain analytical considerations with the classical fast Fourier transform, and generalize both the forward and backward FFT's. The number of arithmetic operations required by each of the algorithms is proportional to N (dot) log N + N - log(1/epsilon), where epsilon is the desired precision of computations and N is the number of nodes. Several related algorithms are also presented, each of which utilizes a similar set of techniques from analysis and linear algebra. These include an efficient version of the Fast Multipole Method in one dimension and fast algorithms for the evaluation, integration, and differentiation of Lagrange polynomial interpolants. Several numerical examples are used to illustrate the efficiency of the approach, and to compare the performances of the two sets of nonuniform FFT algorithms. DTIC

N94-21173# Pittsburgh Univ., PA. Dept. of Mathematics and Statistics.
CLASSICAL AND GENERALIZED SOLUTIONS OF TIME-DEPENDENT LINEAR DIFFERENTIAL ALGEBRAIC EQUATIONS Technical Report
Patrick J. Rabier and Werner C. Rheinboldt 15 Oct. 1993 40 p
(Contract N00014-90-J-1025; NSF CCR-92-03488)
(AD-A272834; ICMA-93-183) Avail: CASI HC A03/MF A01

A reduction procedure is developed for linear time-dependent differential algebraic equations (DAE's) that transforms their solutions into solutions of smaller systems of ordinary differential equations (ODE's). The procedure applies to classical as well as distribution solutions. In the case of analytic coefficients, the hypotheses required for the reduction not only are necessary for the validity of the existence and uniqueness results, but they even allow for the presence of singularities. Straightforward extensions including undetermined systems and systems with non-analytic coefficients are also discussed. DTIC

N94-21174# Pittsburgh Univ., PA. Dept. of Mathematics and Statistics.
FINITE DIFFERENCE METHODS FOR TIME-DEPENDENT, LINEAR DIFFERENTIAL ALGEBRAIC EQUATIONS Technical Report
Patrick J. Rabier and Werner C. Reinboldt 27 Oct. 1993 10 p
(Contract N00014-90-J-1025; NSF CCR-92-03488)
(AD-A272835; ICMA-93-184) Avail: CASI HC A02/MF A01

Recently the authors developed a global reduction procedure for linear, time-dependent DAE that transforms their solutions into solutions of smaller, systems of ODE's. Here it is shown that this reduction allows for the construction of simple, convergent finite difference schemes for such equations. DTIC

N94-21199# Rochester Univ., NY. Dept. of Computer Science.
AN NP SET WITH NO CO-DP SPARSE SUBSET
Osamu Watanabe (Tokyo Inst. of Tech., Japan.) Oct. 1993 10 p
(Grant NSF INT-91-16781)
(TR-475) Avail: CASI HC A02/MF A01

An oracle is constructed relative to which there exists an NP set that has no infinite sparse subset in co-DP. Author

N94-21231# Center for Mathematics and Computer Science, Amsterdam (Netherlands). Dept. of Operations Research, Statistics, and System Theory.
FOURIER CALCULUS ON EVOLUTIONARY TREES
L. A. Szekely (Eoetvoes Lorand Univ., Budapest, Hungary.), M. A. Steel (Canterbury Univ., Christchurch, New Zealand.), and P. L. Erdoes (Hungarian Academy of Sciences, Budapest.) Dec. 1992 19 p Sponsored in part by Alexander von Humboldt Stiftung, Germany
(Contract N00014-91-J-1385)
(CWI-BS-R9234; ETN-94-94714) Copyright Avail: CASI HC A03/MF A01

A Fourier analysis approach to the reconstruction theory of evolutionary trees, one that is based on Kimura's model of molecular evolution, is described. The aim of the study is to develop the mathematical tools necessary for the spectral analysis/closest tree method for the reconstruction of evolutionary trees in Cavender's model and in Kimura's three parameter model. All sections of the study, apart from the last, can be read with no knowledge of biology. The last section explains the biological significance of the results from previous sections. The important tool in the work is the Fourier calculus over finite Abelian groups. ESA

N94-21314# Rochester Univ., NY. Dept. of Computer Science.
COMPUTING SOLUTIONS UNIQUELY COLLAPSES THE POLYNOMIAL HIERARCHY
Lane A. Hemaspaandra, Ashish V. Naik (State Univ. of New York, Buffalo.), Mitsunori Ogiwara (University of Electro-Communications, Tokyo, Japan.), and Alan L. Selman (State Univ. of New York, Buffalo.) 12 Aug. 1993 14 p Revised
(Grants NSF CCR-89-57804; NSF INT-91-16781; NSF CCR-90-02292)
(TR-467) Avail: CASI HC A03/MF A01

Is there a single-valued NP function that, when given a satisfiable formula as input outputs a satisfying assignment? That is, can a nondeterministic function cull just one satisfying assignment from a possibly exponentially large collection of assignments? It is shown that if there is such a nondeterministic function, then the polynomial hierarchy collapses to its second level. As the existence of such a function is known to be equivalent to the statement 'every multivalued NP function has a single-valued NP refinement,' our result provides the strongest evidence yet that multivalued NP functions cannot be refined. Our result is proved via theorems of independent interest. We say that a set A is NPSV-selective (NPMV-selective) if there is a 2-ary partial function in NPSV (NPMV, respectively) that decides which of its inputs (if any) is 'more likely' to belong to A; this is a nondeterministic analog of the recursion-theoretic notion of the semi-recursive sets and the extant complexity-theoretic notion of P-selectivity. Our hierarchy collapse follows by combining the easy observation that every set in NP is NPMV-selective with either of the following two theorems that proved: (1) If A is a member of NP is NPSV-selective, then A is a member of (NP intersection coNP)/poly; and (2) If A is a member of NP is NPSV-selective, then A is Low(sub 2). To wit, either result implies that if every set in NP is NPSV-selective, then the polynomial hierarchy collapses to its second level, NP(sup NP).

Author (revised)

N94-21359# Naval Postgraduate School, Monterey, CA.

ON A PROPOSED SYMBOLIC DYNAMICS FOR THE HENON MAP M.S. Thesis

Antonio P. Fontana Jun. 1993 169 p

(AD-A272514) Avail: CASI HC A08/MF A02

The utility of a computationally simple yet cryptologically robust rule for generating pseudorandom bitstreams cannot be overstated. In most applications we strive to detect and avoid chaotic behavior; here we embrace a particular chaotic discrete dynamical system to exploit its use as a driver for a pseudorandom number generator. The map from the Henon attractor to the binary domain (0,1) proposed by Forre/Heyman has been tested cryptologically and statistically with mixed results. In this thesis we mathematically evaluate this symbolic dynamics scheme and investigate more rigorously its utility as a pseudorandom number generator. Specifically, we demonstrate how the property of being one-to-one holds, but that the property of being onto does not.

DTIC

N94-21456# Rochester Univ., NY.

ON THE CLOSURE PROPERTIES OF #P IN THE CONTEXT OF PF OF #P

Mitsunori Ogiwara (University of Electro-Communications, Tokyo, Japan.), Thomas Thierauf (Ulm Univ., Germany.), Seinosuke Toda (University of Electro-Communications, Tokyo, Japan.), and Osamu Watanabe (Tokyo Inst. of Tech., Japan.) Dec. 1992 15 p

(Grants JSPS-ENGR-207; NSF CCR-90-02292; NSF CCR-89-57604; NSF INT-91-16781)

(TR-445) Avail: CASI HC A03/MF A01

For any operator tau, we say that #P is closed under tau in context PF of #P, if for every f belonging to #P, and for every h belonging to PF, h of tau(f) also belongs to PF of #P. For several operators tau on #P functions, it is shown that the closure property of #P with respect to tau in context PF of #P is closely related to the relation between P(sup #P(1)) and higher classes such as PH(sup PP) and PP(sup PP).

Author (revised)

N94-21464*# National Aeronautics and Space Administration. Langley Research Center, Hampton, VA.

THE SIXTH COPPER MOUNTAIN CONFERENCE ON MULTIGRID METHODS, PART 2

N. Duane Melson, ed., Steve F. McCormick, ed. (Colorado Univ., Denver.), and Thomas A. Manteuffel, ed. (Colorado Univ., Denver.) Washington Nov. 1993 342 p Workshop held in Copper Mountain, CO, 4-9 Apr. 1993; sponsored by NASA, AFOSR, DOE, and NSF

(RTOP 505-59-53-01)

(NASA-CP-3224-Pt-2; L-17275-Pt-2; NAS 1.55:3224-Pt-2) Avail: CASI HC A15/MF A03

The Sixth Copper Mountain Conference on Multigrid Methods was held on April 4-9, 1993, at Copper Mountain, Colorado. This book is a collection of many of the papers presented at the conference and so represents the conference proceedings. NASA Langley graciously provided printing of this document so that all of the papers could be presented in a single forum. Each paper was reviewed by a member of the conference organizing committee under the coordination of the editors. The multigrid discipline continues to expand and mature, as is evident from these proceedings. The vibrancy in this field is amply expressed in these important papers, and the collection clearly shows its rapid trend to further diversity and depth. For individual titles, see N94-21465 through N94-21487.

N94-21465*# Colorado Univ., Denver. Computational Mathematics Group.

OPTIMAL RESOLUTION IN MAXIMUM ENTROPY IMAGE RECONSTRUCTION FROM PROJECTIONS WITH MULTIGRID ACCELERATION

Mark A. Limber, Thomas A. Manteuffel, Stephen F. McCormick, and David S. Sholl (Colorado Univ., Boulder.) *In* NASA. Langley Research Center, The Sixth Copper Mountain Conference on Multigrid Methods, Part 2 Nov. 1993 p 361-375 (For primary document see N94-21464 05-64)

Avail: CASI HC A03/MF A03

We consider the problem of image reconstruction from a finite number of projections over the space L(sup 1)(Omega), where Omega is a compact subset of the set of Real numbers (exp 2). We prove that, given a discretization of the projection space, the function that generates the correct projection data and maximizes the Boltzmann-Shannon entropy is piecewise constant on a certain discretization of Omega, which we call the 'optimal grid'. It is on this grid that one obtains the maximum resolution given the problem setup. The size of this grid grows very quickly as the number of projections and number of cells per projection grow, indicating fast computational methods are essential to make its use feasible. We use a Fenchel duality formulation of the problem to keep the number of variables small while still using the optimal discretization, and propose a multilevel scheme to improve convergence of a simple cyclic maximization scheme applied to the dual problem.

Author

N94-21466*# Colorado Univ., Colorado Springs. Computational Mathematics Group.

FLOW TRANSITION WITH 2-D ROUGHNESS ELEMENTS IN A 3-D CHANNEL c34

Zhining Liu, Chaoquin Liu, and Stephen F. McCormick *In* NASA. Langley Research Center, The Sixth Copper Mountain Conference on Multigrid Methods, Part 2 Nov. 1993 p 377-391 (For primary document see N94-21464 05-64)

(Contract NAS1-19312)

Avail: CASI HC A03/MF A03

We develop a new numerical approach to study the spatially evolving instability of the streamwise dominant flow in the presence of roughness elements. The difficulty in handling the flow over the boundary surface with general geometry is removed by using a new conservative form of the governing equations and an analytical mapping. The numerical scheme uses second-order backward Euler in time, fourth-order central differences in all three spatial directions, and boundary-fitted staggered grids. A three-dimensional channel with multiple two-dimensional-type roughness elements is employed as the test case. Fourier analysis is used to decompose different Fourier modes of the disturbance. The results show that surface roughness leads to transition at lower Reynolds number than for smooth channels.

Author

N94-21467*# Colorado Univ., Denver. Computational Mathematics Group.

MULTILEVEL METHODS FOR TRANSPORT EQUATIONS IN DIFFUSIVE REGIMES

Thomas A. Manteuffel and Klaus Ressel *In* NASA. Langley Research Center, The Sixth Copper Mountain Conference on Multigrid Methods, Part 2 Nov. 1993 p 393-403 (For primary document see N94-21464 05-64)

Avail: CASI HC A03/MF A03

We consider the numerical solution of the single-group, steady state, isotropic transport equation. An analysis by means of the moment equations shows that a discrete ordinate S(sub N) discretization in direction (angle) with a least squares finite element discretization in space does not behave properly in the diffusion limit. A scaling of the S(sub N) equations is

introduced so that the least squares discretization has the correct diffusion limit. For the resulting discrete system a full multigrid algorithm was developed. Author

N94-21468*# Princeton Univ., NJ. Dept. of Computer Science.
ANALYSIS OF MULTIGRID METHODS ON MASSIVELY PARALLEL COMPUTERS: ARCHITECTURAL IMPLICATIONS **c62**
Lesley R. Matheson and Robert E. Tarjan *In* NASA. Langley Research Center, The Sixth Copper Mountain Conference on Multigrid Methods, Part 2 Nov. 1993 p 405-421 (For primary document see N94-21464 05-64)
(Contract N00014-91-J-1463; NSF CCR-89-20505; NSF STC-88-09648)
Avail: CASI HC A03/MF A03

We study the potential performance of multigrid algorithms running on massively parallel computers with the intent of discovering whether presently envisioned machines will provide an efficient platform for such algorithms. We consider the domain parallel version of the standard V cycle algorithm on model problems, discretized using finite difference techniques in two and three dimensions on block structured grids of size 10(exp 6) and 10(exp 9), respectively. Our models of parallel computation were developed to reflect the computing characteristics of the current generation of massively parallel multicomputers. These models are based on an interconnection network of 256 to 16,384 message passing, 'workstation size' processors executing in an SPMD mode. The first model accomplishes interprocessor communications through a multistage permutation network. The communication cost is a logarithmic function which is similar to the costs in a variety of different topologies. The second model allows single stage communication costs only. Both models were designed with information provided by machine developers and utilize implementation derived parameters. With the medium grain parallelism of the current generation and the high fixed cost of an interprocessor communication, our analysis suggests an efficient implementation requires the machine to support the efficient transmission of long messages, (up to 1000 words) or the high initiation cost of a communication must be significantly reduced through an alternative optimization technique. Furthermore, with variable length message capability, our analysis suggests the low diameter multistage networks provide little or no advantage over a simple single stage communications network. Author

N94-21469*# National Aeronautics and Space Administration. Langley Research Center, Hampton, VA.
TIME-ACCURATE NAVIER-STOKES CALCULATIONS WITH MULTIGRID ACCELERATION
N. Duane Melson, Harold L. Atkins, and Mark D. Sanetrik (Analytical Services and Materials, Inc., Hampton, VA.) *In its* The Sixth Copper Mountain Conference on Multigrid Methods, Part 2 Nov. 1993 p 423-437 (For primary document see N94-21464 05-64)
Avail: CASI HC A03/MF A03

A numerical scheme to solve the unsteady Navier-Stokes equations is described. The scheme is implemented by modifying the multigrid-multiblock version of the steady Navier-Stokes equations solver, TLNS3D. The scheme is fully implicit in time and uses TLNS3D to iteratively invert the equations at each physical time step. The design objective of the scheme is unconditional stability (at least for first- and second-order discretizations of the physical time derivatives). With unconditional stability, the choice of the time step is based on the physical phenomena to be resolved rather than limited by numerical stability which is especially important for high Reynolds number viscous flows, where the spatial variation of grid cell size can be as much as six orders of magnitude. An analysis of the iterative procedure and the implementation of this procedure in TLNS3D are discussed. Numerical results are presented to show both the capabilities of the scheme and its speed up relative to the use of global minimum time stepping. Reductions in computational times of an order of magnitude are demonstrated. Author

N94-21470*# General Electric Co., Moorestown, NJ. Advanced Tech Labs.
MGGHAT: ELLIPTIC PDE SOFTWARE WITH ADAPTIVE REFINEMENT, MULTIGRID AND HIGH ORDER FINITE ELEMENTS
William F. Mitchell *In* NASA. Langley Research Center, The Sixth Copper Mountain Conference on Multigrid Methods, Part 2 Nov. 1993 p 439-448 (For primary document see N94-21464 05-64)
Avail: CASI HC A02/MF A03

MGGHAT (MultiGrid Galerkin Hierarchical Adaptive Triangles) is a program for the solution of linear second order elliptic partial differential equations in two dimensional polygonal domains. This program is now available for public use. It is a finite element method with linear, quadratic or cubic elements over triangles. The adaptive refinement via newest vertex bisection and the multigrid iteration are both based on a hierarchical basis formulation. Visualization is available at run time through an X Window display, and a posteriori through output files that can be used as GNUPLOT input. In this paper, we describe the methods used by MGGHAT, define the problem domain for which it is appropriate, illustrate use of the program, show numerical and graphical examples, and explain how to obtain the software. Author

N94-21471*# National Aeronautics and Space Administration. Langley Research Center, Hampton, VA.
LOOKING FOR O(N) NAVIER-STOKES SOLUTIONS ON NON-STRUCTURED MESHES **c34**
Eric Morano and Alain Dervieux (Institut National de Recherche d'Informatique et d'Automatique, Valbonne, France.) *In its* The Sixth Copper Mountain Conference on Multigrid Methods, Part 2 Nov. 1993 p 449-463 See also N94-11277 Sponsored in part by DRET Group 6, INRIA and ICASE (For primary document see N94-21464 05-64)
Avail: CASI HC A03/MF A03

Multigrid methods are good candidates for the resolution of the system arising in Numerical Fluid Dynamics. However, the question is to know if those algorithms which are efficient for the Poissan equation on structured meshes will still apply well to the Euler and Navier-Stokes equations on unstructured meshes. The study of elliptic problems leads us to define the conditions where a Full Multigrid strategy has O(N) complexity. The aim of this paper is to build a comparison between the elliptic theory and practical CFD problems. First, as an introduction, we will recall some basic definitions and theorems applied to a model problem. The goal of this section is to point out the different properties that we need to produce an FMG algorithm with O(N) complexity. Then, we will show how we can apply this theory to the fluid dynamics equations such as Euler and Navier-Stokes equations. At last, we present some results which are 2nd-order accurate and some explanations about the behavior of the FMG process. Author

N94-21472*# National Technical Univ., Athens (Greece).
THE BLOCK ADAPTIVE MULTIGRID METHOD APPLIED TO THE SOLUTION OF THE EULER EQUATIONS **c02**
Nikos Pantelelis *In* NASA. Langley Research Center, The Sixth Copper Mountain Conference on Multigrid Methods, Part 2 Nov. 1993 p 465-479 (For primary document see N94-21464 05-64)
(Contract AERO-0018C)
Avail: CASI HC A03/MF A03

In the present study, a scheme capable of solving very fast and robust complex nonlinear systems of equations is presented. The Block Adaptive Multigrid (BAM) solution method offers multigrid acceleration and adaptive grid refinement based on the prediction of the solution error. The proposed solution method was used with an implicit upwind Euler solver for the solution of complex transonic flows around airfoils. Very fast results were obtained (18-fold acceleration of the solution) using one fourth of the volumes of a global grid with the same solution accuracy for two test cases. Author

N94-21473*# National Aeronautics and Space Administration. Langley Research Center, Hampton, VA.
MULTIGRID SCHEMES FOR VISCOUS HYPERSONIC FLOWS **c02**
R. C. Swanson and R. Radespiel (Deutsche Forschungs- und Versuchsanstalt fuer Luft- und Raumfahrt, Brunswick, Germany.) *In its* The Sixth Copper Mountain Conference on Multigrid Methods, Part 2 Nov. 1993 p 481-495 (For primary document see N94-21464 05-64)
Avail: CASI HC A03/MF A03

Several multigrid schemes are considered for the numerical computation of viscous hypersonic flows. For each scheme, the basic solution algorithm employs upwind spatial discretization with explicit multistage time stepping. Two-level versions of the various multigrid algorithms are applied to the two-dimensional advection equation, and Fourier analysis is used to determine their damping properties. The capabilities of the multigrid methods

are assessed by solving two different hypersonic flow problems. Some new multigrid schemes, based on semicoarsening strategies, are shown to be quite effective in relieving the stiffness caused by the high-aspect-ratio cells required to resolve high Reynolds number flows. These schemes exhibit good convergence rates for Reynolds numbers up to 200 x 10(exp 6). Author

N94-21474*# Technische Univ., Munich (Germany). Institut fuer Informatik.

LAYOUT OPTIMIZATION WITH ALGEBRAIC MULTIGRID METHODS

Hans Regler and Ulrich Ruede *In* NASA. Langley Research Center, The Sixth Copper Mountain Conference on Multigrid Methods, Part 2 Nov. 1993 p 497-511 Sponsored in part by Deutsche Forschungsgemeinschaft (DFG) (For primary document see N94-21464 05-64)

Avail: CASI HC A03/MF A03

Finding the optimal position for the individual cells (also called functional modules) on the chip surface is an important and difficult step in the design of integrated circuits. This paper deals with the problem of relative placement, that is the minimization of a quadratic functional with a large, sparse, positive definite system matrix. The basic optimization problem must be augmented by constraints to inhibit solutions where cells overlap. Besides classical iterative methods, based on conjugate gradients (CG), we show that algebraic multigrid methods (AMG) provide an interesting alternative. For moderately sized examples with about 10000 cells, AMG is already competitive with CG and is expected to be superior for larger problems. Besides the classical 'multiplicative' AMG algorithm where the levels are visited sequentially, we propose an 'additive' variant of AMG where levels may be treated in parallel and that is suitable as a preconditioner in the CG algorithm. Author

N94-21475*# Massachusetts Inst. of Tech., Cambridge. Research Lab. of Electronics.

OPTIMAL CONVOLUTION SOR ACCELERATION OF WAVEFORM RELAXATION WITH APPLICATION TO SEMICONDUCTOR DEVICE SIMULATION **c61**

Mark Reichelt *In* NASA. Langley Research Center, The Sixth Copper Mountain Conference on Multigrid Methods, Part 2 Nov. 1993 p 513-526 Sponsored in part by IBM (For primary document see N94-21464 05-64)

(Contract N00014-91-J-1698; NSF MIP-88-58764)

Avail: CASI HC A03/MF A03

In this paper we describe a novel generalized SOR (successive overrelaxation) algorithm for accelerating the convergence of the dynamic iteration method known as waveform relaxation. A new convolution SOR algorithm is presented, along with a theorem for determining the optimal convolution SOR parameter. Both analytic and experimental results are given to demonstrate that the convergence of the convolution SOR algorithm is substantially faster than that of the more obvious frequency-independent waveform SOR algorithm. Finally, to demonstrate the general applicability of this new method, it is used to solve the differential-algebraic system generated by spatial discretization of the time-dependent semiconductor device equations. Author (revised)

N94-21476*# Ghent Univ. (Belgium).

A MULTIGRID METHOD FOR STEADY EULER EQUATIONS ON UNSTRUCTURED ADAPTIVE GRIDS

Kris Riemslagh and Erik Dick *In* NASA. Langley Research Center, The Sixth Copper Mountain Conference on Multigrid Methods, Part 2 Nov. 1993 p 527-541 (For primary document see N94-21464 05-64)

Avail: CASI HC A03/MF A03

A flux-difference splitting type algorithm is formulated for the steady Euler equations on unstructured grids. The polynomial flux-difference splitting technique is used. A vertex-centered finite volume method is employed on a triangular mesh. The multigrid method is in defect-correction form. A relaxation procedure with a first order accurate inner iteration and a second-order correction performed only on the finest grid, is used. A multi-stage Jacobi relaxation method is employed as a smoother. Since the grid is unstructured a Jacobi type is chosen. The multi-staging is necessary to provide sufficient smoothing properties. The domain is discretized using a Delaunay triangular mesh generator. Three grids with more or less uniform distribution of nodes but with different resolution are generated by successive refinement of the coarsest grid. Nodes of coarser grids appear in the finer grids. The multigrid method is started on these grids. As soon as the residual drops below a threshold value, an adaptive refinement is started. The solution on the adaptively refined grid is accelerated by a multigrid procedure. The coarser multigrid grids are generated by successive coarsening through point removement. The adaption cycle is repeated a few times. Results are given for the transonic flow over a NACA-0012 airfoil. Author

N94-21477*# New York Univ., New York. Courant Inst.

TWO-LEVEL SCHWARTZ METHODS FOR NONCONFORMING FINITE ELEMENTS AND DISCONTINUOUS COEFFICIENTS

Marcus Sarkis *In* NASA. Langley Research Center, The Sixth Copper Mountain Conference on Multigrid Methods, Part 2 Nov. 1993 p 543-565 (For primary document see N94-21464 05-64)

(Contract NSF CCR-92-04255; DE-FG02-92ER-25127)

Avail: CASI HC A03/MF A03

Two-level domain decomposition methods are developed for a simple nonconforming approximation of second order elliptic problems. A bound is established for the condition number of these iterative methods, which grows only logarithmically with the number of degrees of freedom in each subregion. This bound holds for two and three dimensions and is independent of jumps in the value of the coefficients. Author

N94-21478*# Technion - Israel Inst. of Tech., Haifa. Dept. of Mathematics and Computer Science.

AN AUTOMATIC MULTIGRID METHOD FOR THE SOLUTION OF SPARSE LINEAR SYSTEMS

Yair Shapira, Moshe Israeli, and Avram Sidi *In* NASA. Langley Research Center, The Sixth Copper Mountain Conference on Multigrid Methods, Part 2 Nov. 1993 p 567-582 (For primary document see N94-21464 05-64)

Avail: CASI HC A03/MF A03

An automatic version of the multigrid method for the solution of linear systems arising from the discretization of elliptic PDE's is presented. This version is based on the structure of the algebraic system solely, and does not use the original partial differential operator. Numerical experiments show that for the Poisson equation the rate of convergence of our method is equal to that of classical multigrid methods. Moreover, the method is robust in the sense that its high rate of convergence is conserved for other classes of problems: non-symmetric, hyperbolic (even with closed characteristics) and problems on non-uniform grids. No double discretization or special treatment of sub-domains (e.g. boundaries) is needed. When supplemented with a vector extrapolation method, high rates of convergence are achieved also for anisotropic and discontinuous problems and also for indefinite Helmholtz equations. A new double discretization strategy is proposed for finite and spectral element schemes and is found better than known strategies. Author

N94-21479*# Texas A&M Univ., College Station. Inst. for Scientific Computation.

A MULTIGRID ALGORITHM FOR THE CELL-CENTERED FINITE DIFFERENCE SCHEME

Richard E. Ewing and Jian Shen *In* NASA. Langley Research Center, The Sixth Copper Mountain Conference on Multigrid Methods, Part 2 Nov. 1993 p 583-592 (For primary document see N94-21464 05-64)

(Contract DE-FG05-92ER-25143)

Avail: CASI HC A02/MF A03

In this article, we discuss a non-variational V-cycle multigrid algorithm based on the cell-centered finite difference scheme for solving a second-order elliptic problem with discontinuous coefficients. Due to the poor approximation property of piecewise constant spaces and the non-variational nature of our scheme, one step of symmetric linear smoothing in our V-cycle multigrid scheme may fail to be a contraction. Again, because of the simple structure of the piecewise constant spaces, prolongation and restriction are trivial; we save significant computation time with very promising computational results. Author

N94-21480*# National Aeronautics and Space Administration. Goddard Space Flight Center, Greenbelt, MD.

A SEMI-LAGRANGIAN APPROACH TO THE SHALLOW WATER EQUATION **c34**

J. R. Bates, Stephen F. McCormick (Colorado Univ., Boulder.), John Ruge

(Colorado Univ., Boulder.), David S. Sholl (Colorado Univ., Boulder.), and Irad Yavneh (National Center for Atmospheric Research, Boulder, CO.) *In* NASA. Langley Research Center, The Sixth Copper Mountain Conference on Multigrid Methods, Part 2 Nov. 1993 p 593-604 (For primary document see N94-21464 05-64)
Avail: CASI HC A03/MF A03

We present a formulation of the shallow water equations that emphasizes the conservation of potential vorticity. A locally conservative semi-Lagrangian time-stepping scheme is developed, which leads to a system of three coupled PDE's to be solved at each time level. We describe a smoothing analysis of these equations, on which an effective multigrid solver is constructed. Some results from applying this solver to the static version of these equations are presented. Author

N94-21481*# National Aeronautics and Space Administration. Lewis Research Center, Cleveland, OH.
MULTIGRID SOLUTION OF THE NAVIER-STOKES EQUATIONS ON HIGHLY STRETCHED GRIDS WITH DEFECT CORRECTION **c34**
Peter M. Sockol *In* NASA. Langley Research Center, The Sixth Copper Mountain Conference on Multigrid Methods, Part 2 Nov. 1993 p 605-619 (For primary document see N94-21464 05-64)
Avail: CASI HC A03/MF A03

Relaxation-based multigrid solvers for the steady incompressible Navier-Stokes equations are examined to determine their computational speed and robustness. Four relaxation methods with a common discretization have been used as smoothers in a single tailored multigrid procedure. The equations are discretized on a staggered grid with first order upwind used for convection in the relaxation process on all grids and defect correction to second order central on the fine grid introduced once per multigrid cycle. A fixed W(1,1) cycle with full weighting of residuals is used in the FAS multigrid process. The resulting solvers have been applied to three 2D flow problems, over a range of Reynolds numbers, on both uniform and highly stretched grids. In all cases the L(sub 2) norm of the velocity changes is reduced to 10(exp -6) in a few 10's of fine grid sweeps. The results from this study are used to draw conclusions on the strengths and weaknesses of the individual relaxation schemes as well as those of the overall multigrid procedure when used as a solver on highly stretched grids. Author

N94-21482*# Tokyo Univ. (Japan). Dept. of Information Science.
THE MULTIGRID PRECONDITIONED CONJUGATE GRADIENT METHOD
Osamu Tatebe *In* NASA. Langley Research Center, The Sixth Copper Mountain Conference on Multigrid Methods, Part 2 Nov. 1993 p 621-634 (For primary document see N94-21464 05-64)
Avail: CASI HC A03/MF A03

A multigrid preconditioned conjugate gradient method (MGCG method), which uses the multigrid method as a preconditioner of the PCG method, is proposed. The multigrid method has inherent high parallelism and improves convergence of long wavelength components, which is important in iterative methods. By using this method as a preconditioner of the PCG method, an efficient method with high parallelism and fast convergence is obtained. First, it is considered a necessary condition of the multigrid preconditioner in order to satisfy requirements of a preconditioner of the PCG method. Next numerical experiments show a behavior of the MGCG method and that the MGCG method is superior to both the ICCG method and the multigrid method in point of fast convergence and high parallelism. This fast convergence is understood in terms of the eigenvalue analysis of the preconditioned matrix. From this observation of the multigrid preconditioner, it is realized that the MGCG method converges in very few iterations and the multigrid preconditioner is a desirable preconditioner of the conjugate gradient method. Author

N94-21483*# National Aeronautics and Space Administration. Langley Research Center, Hampton, VA.
MAPPING ROBUST PARALLEL MULTIGRID ALGORITHMS TO SCALABLE MEMORY ARCHITECTURES **c61**
Andrea Overman and John VanRosendale *In its* The Sixth Copper Mountain Conference on Multigrid Methods, Part 2 Nov. 1993 p 635-647 See also N93-32359 (For primary document see N94-21464 05-64)
(Contracts NAS1-19480; NAS1-18605)
Avail: CASI HC A03/MF A03

The convergence rate of standard multigrid algorithms degenerates on problems with stretched grids or anisotropic operators. The usual cure for this is the use of line or plane relaxation. However, multigrid algorithms based on line and plane relaxation have limited and awkward parallelism and are quite difficult to map effectively to highly parallel architectures. Newer multigrid algorithms that overcome anisotropy through the use of multiple coarse grids rather than relaxation are better suited to massively parallel architectures because they require only simple point-relaxation smoothers. In this paper, we look at the parallel implementation of a V-cycle multiple semicoarsened grid (MSG) algorithm on distributed-memory architectures such as the Intel iPSC/860 and Paragon computers. The MSG algorithms provide two levels of parallelism: parallelism within the relaxation or interpolation on each grid and across the grids on each multigrid level. Both levels of parallelism must be exploited to map these algorithms effectively to parallel architectures. This paper describes a mapping of an MSG algorithm to distributed-memory architectures that demonstrates how both levels of parallelism can be exploited. The result is a robust and effective multigrid algorithm for distributed-memory machines. Author

N94-21484*# National Aeronautics and Space Administration. Langley Research Center, Hampton, VA.
UNSTRUCTURED MULTIGRID THROUGH AGGLOMERATION
V. Venkatakrishnan (National Aeronautics and Space Administration. Ames Research Center, Moffett Field, CA.), D. J. Mavriplis, and M. J. Berger (New York Univ., New York.) *In its* The Sixth Copper Mountain Conference on Multigrid Methods, Part 2 Nov. 1993 p 649-662 (For primary document see N94-21464 05-64)
Avail: CASI HC A03/MF A03

In this work the compressible Euler equations are solved using finite volume techniques on unstructured grids. The spatial discretization employs a central difference approximation augmented by dissipative terms. Temporal discretization is done using a multistage Runge-Kutta scheme. A multigrid technique is used to accelerate convergence to steady state. The coarse grids are derived directly from the given fine grid through agglomeration of the control volumes. This agglomeration is accomplished by using a greedy-type algorithm and is done in such a way that the load, which is proportional to the number of edges, goes down by nearly a factor of 4 when moving from a fine to a coarse grid. The agglomeration algorithm has been implemented and the grids have been tested in a multigrid code. An area-weighted restriction is applied when moving from fine to coarse grids while a trivial injection is used for prolongation. Across a range of geometries and flows, it is shown that the agglomeration multigrid scheme compares very favorably with an unstructured multigrid algorithm that makes use of independent coarse meshes, both in terms of convergence and elapsed times. Author

N94-21485*# National Aeronautics and Space Administration. Langley Research Center, Hampton, VA.
MULTIGRID PROPERTIES OF UPWIND-BIASED DATA RECONSTRUCTIONS **c34**
Gary P. Warren and Thomas W. Roberts *In its* The Sixth Copper Mountain Conference on Multigrid Methods, Part 2 Nov. 1993 p 663-677 (For primary document see N94-21464 05-64)
Avail: CASI HC A03/MF A03

The multigrid properties of two data reconstruction methods used for achieving second-order spatial accuracy when solving the two-dimensional Euler equations are examined. The data reconstruction methods are used with an implicit upwind algorithm which uses linearized backward-Euler time-differencing. The solution of the resulting linear system is performed by an iterative procedure. In the present study only regular quadrilateral grids are considered, so a red-black Gauss-Seidel iteration is used. Although the Jacobian is approximated by first-order upwind extrapolation, two alternative data reconstruction techniques for the flux integral that yield higher-order spatial accuracy at steady state are examined. The first method, probably most popular for structured quadrilateral grids, is based on estimating the cell gradients using one-dimensional reconstruction along curvilinear coordinates. The second method is based on Green's theorem. Analysis and numerical results for the two dimensional Euler equations show that data reconstruction based on Green's theorem has superior multigrid properties as compared to the one-dimensional data reconstruction method. Author

N94-21486*# Old Dominion Univ., Norfolk, VA. Dept. of Mechanical Engineering and Mechanics.
ON THE PREDICTION OF MULTIGRID EFFICIENCY THROUGH LOCAL MODE ANALYSIS
R. V. Wilson *In* NASA. Langley Research Center, The Sixth Copper Mountain Conference on Multigrid Methods, Part 2 Nov. 1993 p 679-689 (For primary document see N94-21464 05-64)
Avail: CASI HC A03/MF A03

A single grid local mode analysis is used to predict the smoothing properties of numerical schemes for solving the Navier-Stokes equations with factorization based on Stone's Strongly Implicit Method. Four difference approximations for the convection terms are considered, namely, hybrid, central, second-order upwind, and third-order upwind. Smoothing factors from the analysis are compared with practical convergence factors in a multigrid method for flow over a backward facing step and it is found that the local mode analysis correctly predicts the effects of Reynolds number and higher-order schemes. Author

N94-21487*# Technische Hogeschool, Delft (Netherlands). Faculty of Technical Mathematics and Informatics.
NUMERICAL STUDY OF A MULTIGRID METHOD WITH FOUR SMOOTHING METHODS FOR THE INCOMPRESSIBLE NAVIER-STOKES EQUATIONS IN GENERAL COORDINATES c34
S. Zeng and P. Wesseling *In* NASA. Langley Research Center, The Sixth Copper Mountain Conference on Multigrid Methods, Part 2 Nov. 1993 p 691-708 (For primary document see N94-21464 05-64)
Avail: CASI HC A03/MF A03

The performance of a linear multigrid method using four smoothing methods, called SCGS (Symmetrical Coupled GauBeta-Seidel), CLGS (Collective Line GauBeta-Seidel), SILU (Scalar ILU), and CILU (Collective ILU), is investigated for the incompressible Navier-Stokes equations in general coordinates, in association with Galerkin coarse grid approximation. Robustness and efficiency are measured and compared by application to test problems. The numerical results show that CILU is the most robust, SILU the least, with CLGS and SCGS in between. CLGS is the best in efficiency, SCGS and CILU follow, and SILU is the worst.
Author (revised)

N94-21524# Army Research Lab., Aberdeen Proving Ground, MD.
TOWARD A NEW METHOD OF DECODING ALGEBRAIC CODES USING GROEBNER BASES Final Report, Oct. 1991 - Sep. 1992
A. B. Cooper, III Oct. 1993 23 p
(AD-A273089; ARL-TR-293) Avail: CASI HC A03/MF A01

A binary BCH error control code is a vector subspace of binary N-tuples. Algebraically, the code is generated by a polynomial having binary coefficients and roots in GF(2(sup m)). It is decoded by computing a set of syndrome equations which are multivariate polynomials over GF(2(sup m)) and which exhibit a certain symmetry. If the number of transmission errors in a received word does not exceed a bound t for the code, the roots of the syndromes are the locations, in the received word, of those errors. These multivariate polynomials are taken as the basis for an ideal in the ring of polynomials in t variables over GF(2(sup m)). A celebrated algorithm by Buchberger produces a reduced Groebner basis of that ideal. It turns out that since the common roots of all the polynomials in the ideal are a set of isolated points, this reduced Groebner basis is in triangular form, and the univariate polynomial in that basis is the well known BCH error locator polynomial, the roots of which specify the error locations. Decoding is algorithmically complete when this polynomial is known.
DTIC

N94-21568*# Institute for Computer Applications in Science and Engineering, Hampton, VA.
RATIONAL TRIGONOMETRIC APPROXIMATIONS USING FOURIER SERIES PARTIAL SUMS Final Report
James F. Geer (State Univ. of New York, Binghamton.) Sep. 1993 34 p Submitted for publication
(Contract NAS1-19480; RTOP 505-90-52-01)
(NASA-CR-191535; NAS 1.26:191535; ICASE-93-68) Avail: CASI HC A03/MF A01

A class of approximations (S(sub N,M)) to a periodic function f which uses the ideas of Pade, or rational function, approximations based on the Fourier series representation of f, rather than on the Taylor series representation of f, is introduced and studied. Each approximation S(sub N,M) is the quotient of a trigonometric polynomial of degree N and a trigonometric polynomial of degree M. The coefficients in these polynomials are determined by requiring that an appropriate number of the Fourier coefficients of S(sub N,M) agree with those of f. Explicit expressions are derived for these coefficients in terms of the Fourier coefficients of f. It is proven that these 'Fourier-Pade' approximations converge point-wise to (f(x(exp +))+f(x(exp -)))/2 more rapidly (in some cases by a factor of 1/k(exp 2M)) than the Fourier series partial sums on which they are based. The approximations are illustrated by several examples and an application to the solution of an initial, boundary value problem for the simple heat equation is presented. Author

N94-21576# Center for Mathematics and Computer Science, Amsterdam (Netherlands). Dept. of Numerical Mathematics.
COMPARING QUASI-NEWTON METHODS FOR SOLVING SPARSE INTERFACE PROBLEMS
C.-H. Lai Jan. 1993 13 p Sponsored by European Research Consortium for Informatics and Mathematics
(CWI-NM-R9303; ETN-94-94705) Copyright Avail: CASI HC A03/MF A01

Quasi Newton methods for interface problems which arise from domain decomposition methods are examined. These interface problems are usually sparse systems of linear or nonlinear equations. Particular interest is the application of the methods to systems of linear equations where the Jacobian matrices cannot be calculated or it is not wished to calculate them. The suitability of implementing these algorithms on coarse grained parallel computers is examined. ESA

N94-21588*# National Aeronautics and Space Administration. Lewis Research Center, Cleveland, OH.
ORDER OF ACCURACY OF QUICK AND RELATED CONVECTION-DIFFUSION SCHEMES
B. P. Leonard Nov. 1993 32 p
(Contract NCC3-233; RTOP 505-90-5K)
(NASA-TM-106402; ICOMP-93-47; E-8236; NAS 1.15:106402) Avail: CASI HC A03/MF A01

This report attempts to correct some misunderstandings that have appeared in the literature concerning the order of accuracy of the QUICK scheme for steady-state convective modeling. Other related convection-diffusion schemes are also considered. The original one-dimensional QUICK scheme written in terms of nodal-point values of the convected variable (with a 1/8-factor multiplying the 'curvature' term) is indeed a third-order representation of the finite volume formulation of the convection operator average across the control volume, written naturally in flux-difference form. An alternative single-point upwind difference scheme (SPUDS) using node values (with a 1/6-factor) is a third-order representation of the finite difference single-point formulation; this can be written in a pseudo-flux difference form. These are both third-order convection schemes; however, the QUICK finite volume convection operator is 33 percent more accurate than the single-point implementation of SPUDS. Another finite volume scheme, writing convective fluxes in terms of cell-average values, requires a 1/6-factor for third-order accuracy. For completeness, one can also write a single-point formulation of the convective derivative in terms of cell averages, and then express this in pseudo-flux difference form; for third-order accuracy, this requires a curvature factor of 5/24. Diffusion operators are also considered in both single-point and finite volume formulations. Finite volume formulations are found to be significantly more accurate. For example, classical second-order central differencing for the second derivative is exactly twice as accurate in a finite volume formulation as it is in single-point. Author (revised)

N94-21655# Mound Lab., Miamisburg, OH.
OPERATIONAL EQUATIONS FOR THE FIVE-POINT RECTANGLE
G. L. Silver 15 Sep. 1993 36 p
(Contract DE-AC04-88DP-43495)
(DE94-000366; MLM-3787) Avail: CASI HC A03/MF A01

Two operational polynomials are demonstrated for the four-point rectangle with center point. The equations are exact on the points and the surfaces they describe ordinarily fit known monotonic surfaces better than the standard five-point equation, as judged by the L(sub 2) norm test. Equations for fitting the five-point rectangle by sines and cosines are presented. DOE

N94-21946# Los Alamos National Lab., NM.
THE ACCURACY-THROUGH-ORDER AND THE EQUIVALENCE PROPERTIES IN THE ALGEBRAIC APPROXIMANT
G. A. Baker, Jr. 1993 7 p Presented at the Nonlinear Numerical Methods and Rational Approximation, Antwerp, Belgium, 6-10 Sep. 1993
(Contract W-7405-eng-36)
(DE93-040188; LA-UR-93-3072; CONF-9309227-1) Avail: CASI HC A02/MF A01

In addition to the accuracy through order requirement that the defining polynomials not all be divisible by z, as required for Pade and integral approximants, there is the further problem of deficiency as pointed out by McInnes. The author proves a finite bound on the deficiency and also proves the accuracy through order property for algebraic approximants. In addition he proves the equivalence property for algebraic approximants. DOE

N94-21955# Oak Ridge National Lab., TN.
THE QUANTUM STRUCTURE OF MATTER GRAND CHALLENGE PROJECT: LARGE-SCALE 3-D SOLUTIONS IN RELATIVISTIC QUANTUM DYNAMICS
J. C. Wells, V. E. Oberacker, A. S. Umar, C. Bottcher, M. R. Strayer, J. Drake, and R. Flanery 1993 11 p Presented at the Supercomputing Conference on High Performance Computing and Communications, Portland, OR, 15-19 Nov. 1993
(Contract DE-AC05-84OR-21400)
(DE94-000328; CONF-931115-12) Avail: CASI HC A03/MF A01

We describe the numerical methods used to solve the time-dependent Dirac equation on a three-dimensional Cartesian lattice. Efficient algorithms are required for computationally intensive studies of nonperturbative relativistic quantum dynamics. Discretization is achieved through the lattice basis-spline collocation method, in which quantum-state vectors and coordinate-space operators are expressed in terms of basis-spline functions on a spatial lattice. All numerical procedures reduce to a series of matrix-vector operations which we perform on the Intel iPSC/860 hypercube, making full use of parallelism. We discuss our solutions to the problems of limited node memory and node-to-node communication overhead inherent in using distributed-memory, multiple-instruction, multiple-data stream parallel computers. DOE

N94-21966 Oak Ridge National Lab., TN.
A SHARP UPPER BOUND FOR DEPARTURE FROM NORMALITY
S. L. Lee Aug. 1993 18 p Limited Reproducibility: More than 20% of this document may be affected by microfiche quality
(Contract DE-AC05-84OR-21400)
(DE93-040457; ORNL/TM-12426) Avail: CASI HC A03

The departure from normality of a matrix is a real scalar that is impractical to compute if a matrix is large and its eigenvalues are unknown. A simple formula is presented for computing an upper bound for departure from normality in the Frobenius norm. This new upper bound is cheaper to compute than the upper bound derived by Henrici. Moreover, the new bound is sharp for Hermitian matrices, skew-Hermitian matrices, and, in general, any matrix with eigenvalues that are horizontally or vertically aligned in the complex plane. In terms of applications, the new bound can be used in computing bounds for the spectral norm of matrix functions or bounds for the sensitivity of eigenvalues to matrix perturbations. DOE

N94-21967# Oak Ridge National Lab., TN.
THE DESIGN OF LINEAR ALGEBRA LIBRARIES FOR HIGH PERFORMANCE COMPUTERS
J. J. Dongarra and D. W. Walker Aug. 1993 56 p
(Contract DE-AC05-84OR-21400)
(DE93-040458; ORNL/TM-12404) Avail: CASI HC A04/MF A01

This paper discusses the design of linear algebra libraries for high performance computers. Particular emphasis is placed on the development of scalable algorithms for MIMD distributed memory concurrent computers. A brief description of the EISPACK, LINPACK, and LAPACK libraries is given, followed by an outline of ScaLAPACK, which is a distributed memory version of LAPACK currently under development. The importance of block-partitioned algorithms in reducing the frequency of data movement between different levels of hierarchical memory is stressed. The use of such algorithms helps reduce the message startup costs on distributed memory concurrent computers. Other key ideas in our approach are the use of distributed versions of the Level 3 Basic Linear Algebra Subprograms (BLAS) as computational building blocks, and the use of Basic Linear Algebra Communication Subprograms (BLACS) as communication building blocks. Together the distributed BLAS and the BLACS can be used to construct higher-level algorithms and hide many details of the parallelism from the application developer. The block-cyclic data distribution is described and adopted as a good way of distributing block-partitioned matrices. Block-partitioned versions of the Cholesky and LU factorizations are presented, and optimization issues associated with the implementation of the LU factorization algorithm on distributed memory concurrent computers are discussed, together with its performance on the Intel Delta system. Finally, approaches to the design of library interfaces are reviewed. DOE

N94-21996# Lawrence Livermore National Lab., CA.
A FINITE ELEMENT FORMULATION AND ADAPTIVE SOLUTION APPROACH FOR LARGE-SCALE THERMOMECHANICAL PROBLEMS WITH COMPLEX CONTACT CONDITIONS
B. E. Engelmann, R. G. Whirley, and P. J. Raboin 31 Mar. 1993 14 p Presented at the 8th International Conference on Numerical Methods in Laminar and Turbulent Flow, Swansea, United Kingdom, 18-23 Jul. 1993
(Contract W-7405-eng-48)
(DE93-019605; UCRL-JC-112596; CONF-930785-3) Avail: CASI HC A03/MF A01

Traditional thermal stress analysis is based on an uncoupled approach in which the thermal problem is solved on a fixed geometry, and the resulting temperatures are then used to load a mechanical problem. In contrast, a fully coupled thermomechanical analysis solves the thermal problem on the deforming geometry and incorporates thermal loads into the mechanical problem. Thermal contact, in which heat flow paths depend on the mechanical deformations of adjacent surfaces, is a major component of many fully coupled thermomechanical analyses. This paper describes the development of a Lagrangian finite element thermomechanical contact methodology. The paper focuses on the formulation and implementation of thermal contact in two dimensions. The proposed approach accommodates arbitrarily large relative motions of contact surfaces, fully unstructured meshes, pressure-dependent contact resistance, conduction across small gaps, and approximate models for convection and radiation. The proposed thermal contact formulation has been implemented in the Lawrence Livermore National Laboratory public code PALM2D and has been used to solve a diverse set of thermomechanical problems. Examples frustrating the performance of this code on large deformation thermomechanical problems are presented and discussed. DOE

N94-22096 Technische Univ., Delft (Netherlands). Lab. of Electromagnetic Research.
TIME-LAPLACE-TRANSFORM-DOMAIN ANALYSIS OF WAVE PROPAGATION IN PLANAR WAVEGUIDES
K. F. I. Haak 1992 56 p Limited Reproducibility: More than 20% of this document may be affected by microfiche quality
(PB93-215226; ET/EM-1992-28) Copyright Avail: Issuing Activity (National Technical Information Service (NTIS))

The time-Laplace longitudinal-wavenumber analysis of the wave propagation along closed and open, possibly lossy, planar waveguiding structures leads to remarkable conclusions. For the closed waveguides, all of the solutions pertaining to the discrete infinite spectrum correspond to causal propagating guided waves. For the open waveguides however, a discrete spectrum that corresponds to a set of causal solutions does not exist. This implies that in an open electromagnetic waveguide there is no time-Laplace-domain equivalent of the frequency-domain concept of discrete propagating modes. NTIS

N94-22099 Vrije Univ., Amsterdam (Netherlands). Faculteit der Wiskunde en Informatica.
COLUMN REDUCED RATIONAL MATRIX FUNCTIONS WITH GIVEN NULL-POLE DATA IN THE COMPLEX PLANE
J. A. Ball, G. Groenewald, M. A. Kaashoek, and J. Kim Oct. 1992 38 p Limited Reproducibility: More than 20% of this document may be affected by microfiche quality
(PB93-220531; WS-402) Avail: CASI HC A03

Explicit formulas are given for rational matrix functions which have a prescribed null-pole structure in the complex plane and are column reduced

at infinity. A full parametrization of such functions is obtained. The results are specified and developed further for matrix polynomials. NTIS

N94-22263# Institut des Hautes Etudes Scientifiques, Bures-sur-Yvette (France).
VANISHING THEOREM ON ARITHMETIC SURFACES
C. Soule Jun. 1993 29 p
(PB93-215481; IHES/M-93/34) Avail: CASI HC A03/MF A01

In the paper, the author proves an analog for arithmetic surfaces of the Kodaira-Ramanujam vanishing theorem. It says that if L(bar) is a Hermitian line bundle on such a surface X which is positive on the associated Riemann surface and semi-positive on any divisor, the logarithm of the L(sup 2)-norm of any nontorsion element, e, in H(sup 1)(X,L(sup 1)) is bounded below by a multiple the arithmetic self-intersection of L(bar). The analogy with the classical geometric statement is explained. NTIS

N94-22264# Institut des Hautes Etudes Scientifiques, Bures-sur-Yvette (France).
NON COMMUTATIVE GEOMETRY AND PHYSICS
A. Connes Jun. 1993 142 p
(PB93-215499; IHES/M-93/32) Avail: CASI HC A07/MF A02

The set of lectures is an introduction to non-commutative geometry. The general purpose of non-commutative geometry is to adapt the traditional tools of geometry such as measure theory, topology, differential calculus and Riemannian geometry to spaces X which can no longer be comprehended as point sets because of their intrinisically quantum nature. The purpose of this course however, is not only to provide an introduction to non-commutative geometry, but also to survey the interplay between a selection of the latest developments with theoretical physics. In particular, one shall see how experimental physics leads us to accept not only the quantization of phase space, but also that of the Brillouin zone in solid state physics and even of space-time itself. Contents: (1) The involutive algebra of coordinates on a quantum space X; (2) Measure theory and representations; (3) C*-algebras and topology; (4) Vector bundles and cyclic cohomology; (5) The quantized calculus; (6) The metric aspect and classical matter fields; (7) The notion of manifold in non-commutative geometry; (8) Geometric interpretation of the standard model. NTIS

N94-22266 Vrije Univ., Amsterdam (Netherlands). Dept. of Mathematics and Computer Science.
MODULAR INTERVAL SPACES
H. J. Bandelt (Hamburg Univ., Germany.), M. VanDeVel, and E. Verheul Nov. 1992 32 p Limited Reproducibility: More than 20% of this document may be affected by microfiche quality
(PB93-220663; WS-404) Avail: CASI HC A03/MF A01

Modular interval spaces represent a common generalization of Banach spaces of type L(sub 1)(mu) or B(X), of hyperconvex metric spaces, modular lattices, modular graphs, and median algebras. It turns out that several types of structures are susceptible for a notion capturing essential features of modularity in lattices, e.g. semilattices, multilattices, metric spaces, ternary algebras, and graphs. There is no perfect correspondence between modular structures of various types unless the existence of a neutral point is imposed. Modular structures with neutral points embed in modular lattices. Particular modular interval spaces (e.g. median spaces, or more generally, modular spaces in which intervals are lattices) can be characterized by forbidden subspaces. NTIS

N94-22377# Institut des Hautes Etudes Scientifiques, Bures-sur-Yvette (France).
SEMI-STABILITY AND HEIGHTS OF CYCLES
J. B. Bost Jun. 1993 38 p
(PB93-215507; IHES/M-93/31) Avail: CASI HC A03/MF A01

The following, (pi): P(E) yields C, is a projective bundle over a projective curve. X is included in P(E) as a subvariety of dimension d flat over C. Extending the earlier work of Mumford and Vieweg, Cornalba and Harris proved that, if the Hilbert point of the generic fiber X(sub eta) included in P(E(Sub eta)) of (pi): X yields C is semi-stable in the sense of geometric invariant theory, then the intersection number C(sub 1)O(sub E)(1)(sup d)(small bullet)(in brackets: X) satisfies a non-trivial lower bound in terms of the degree deg E of the vector bundle E on C. In the paper the author proves an arithmetic analogue of this inequality and gives some applications. NTIS

N94-22379# Oak Ridge National Lab., TN.
HYPERSINGULAR INTEGRALS AT A CORNER
L. J. Gray and L. L. Manne 25 Mar. 1993 17 p Presented at the 15th Boundary Element Methods Conference, Worcester, MA, 10-12 Aug. 1993
(Contract DE-AC05-84OR-21400)
(DE94-000340; CONF-9308176-1) Avail: CASI HC A03/MF A01

For a smooth boundary, hypersingular integrals can be defined as a limit from the interior, the approach direction being taken, for convenience, normal to the surface. At a boundary corner, the limit process, with a necessarily non-normal approach direction, provides a valid definition of the hypersingular equation, as long as the direction is employed for all integrations. The terms which are potentially singular in the limit are shown to cancel, provided the function approximations at the corner are consistent. The analytical formulas for the singular integrals are more complicated than for a smooth surface, but are easily obtained using symbolic computation. These techniques have been employed to accurately solve the 'L-shaped domain' potential problem considered by Jaswon and Symm. DOE

N94-22381# Argonne National Lab., IL.
ASYMPTOTIC ANALYSIS. WORKING NOTE NO. 2, APPROXIMATION OF INTEGRALS
M. Garbey (Lyon-1 Univ., Villeurbanne, France.) and H. G. Kaper Jul. 1993 17 p
(Contract W-31-109-eng-38)
(DE94-000433; ANL/MCS-TM-180) Avail: CASI HC A03/MF A01

In this note we discuss the approximation of integrals that depend on a parameter. The basic tool is simple, namely, integration by parts. Of course, the power of the tool is evidenced in applications. The applications are numerous: Laplace integrals; generalized Laplace integrals; Fourier integrals; and Stokes' method of stationary phase for generalized Fourier integrals. These results illustrate beautifully Hardy's concept of applications of mathematics, that is, 'certain regions of mathematical theory in which the notation and the ideas of the method of integration by parts may be used systematically with a great gain in clearness and simplicity.' The notation differs slightly from Working Note No. 1, for reasons that are mainly historical. The asymptotic analysis of integrals originated in complex analysis, where the (real or complex) parameter, usually denoted by x, is usually introduced in such a way that the interesting behavior of the integrals occurs when x (yields) (infinity) in some sector of the complex plane. As there is nothing sacred about notation, and historical precedent is as good a guide as any, we follow convention and denote the parameter by x, focusing on the behavior of integrals as x (yields) (infinity) along the real axis or, if x is complex, in some sector of the complex plane. The connection with the notation of Working Note No. 1 is readily established by identifying the small parameter epsilon with 1/the absolute value of x. DOE

N94-22393# Argonne National Lab., IL.
ASYMPTOTIC ANALYSIS: BASIC CONCEPTS AND DEFINITIONS Working Note No. 1
M. Garbey (Lyon-1 Univ., Villeurbanne, France.) and H. G. Kaper Jul. 1993 16 p
(Contract W-31-109-eng-38)
(DE94-001000; ANL/MCS-TM-179) Avail: CASI HC A03/MF A01

We introduce the basic concepts of asymptotic analysis. After some comments of historical interest, we begin by defining the order relations O, o, and O(sup (number sign)), which enable us to compare the asymptotic behavior of functions of a small positive parameter (epsilon) as (epsilon) (down arrow) 0. Next, we introduce order functions, asymptotic sequences of order functions and more general gauge sets of order functions and define the concepts of an asymptotic approximation and an asymptotic expansion with respect to a given gauge set. This string of definitions culminates in the introduction of the concept of a regular asymptotic expansion, also known as a Poincare expansion, of a function f : (0, epsilon(sub o)) yields X, where X is a normed vector space of functions defined on a domain D is a member of the set R(sup N). We conclude the note with the asymptotic analysis of an initial value problem whose solution is obtained in the form of a regular asymptotic expansion. DOE

N94-20436*# Jet Propulsion Lab., California Inst. of Tech., Pasadena.
AN EFFICIENT FORMULATION OF THE COUPLED FINITE ELEMENT-INTEGRAL EQUATION TECHNIQUE FOR SOLVING LARGE 3D SCATTERING PROBLEMS Abstract Only
T. Cwik, V. Jamnejad, and C. Zuffada *In its* Progress In Electromagnetics Research Symposium (PIERS) 1993 p 604 (For primary document see N94-20403 05-32)
Avail: CASI HC A01/MF A10

N94-21705*# Nanyang Technological Inst. (Singapore). School of Applied Sciences.
EVALUATION OF FLOATING-POINT SUM OR DIFFERENCE OF PRODUCTS IN CARRY-SAVE DOMAIN
A. Wahab, S. Erdogan, and A. B. Premkumar *In* Idaho Univ., The 1992 4th NASA SERC Symposium on VLSI Design 1992 9 p (For primary document see N94-21694 05-33)
Avail: CASI HC A02/MF A04

N94-22111 Windsor Univ. (Ontario). Very Large Scale Integration Research Group.
AN IN-PLACE AND IN-ORDER ALGORITHM FOR THE DISCRETE COSINE TRANSFORM
Zhong-De Wang, G. A. Jullien, and J. J. Soltis *In* Engineering Inst. of Canada, Canadian Conference on Electrical and Computer Engineering, Volumes 1 and 2 1991 4 p (For primary document see N94-22101 05-33)
Avail: Issuing Activity (Engineering Inst. of Canada, 2050 rue Mansfield, Suite 700, Montreal, PQ H3A 1Z2 Canada)

N94-22215 Memorial Univ. of Newfoundland, Saint Johns.
A NEW CLASS OF MULTI-FUNCTION TWO-RAIL TOTALLY SELF-CHECKING BASIC BUILDING BLOCKS
Zhi-Jian Jiang and R. Venkatesan *In* Engineering Inst. of Canada, Canadian Conference on Electrical and Computer Engineering, Volumes 1 and 2 1991 4 p (For primary document see N94-22101 05-33)
Avail: Issuing Activity (Engineering Inst. of Canada, 2050 rue Mansfield, Suite 700, Montreal, PQ H3A 1Z2 Canada)

N94-22243 Carleton Univ., Ottawa (Ontario). Dept. of Systems and Computer Engineering.
SOME BEST RATE 1/p AND RATE (p-1)/p SYSTEMATIC QUASI-CYCLIC CODES OVER GF(3) AND GF(4)
T. Aaron Gulliver and Vijay K. Bhargava (Victoria Univ., British Columbia.) *In* Engineering Inst. of Canada, Canadian Conference on Electrical and Computer Engineering, Volumes 1 and 2 1991 4 p (For primary document see N94-22101 05-33)
Avail: Issuing Activity (Engineering Inst. of Canada, 2050 rue Mansfield, Suite 700, Montreal, PQ H3A 1Z2 Canada)

N94-22245 Concordia Univ., Montreal (Quebec). Dept. of Electrical and Computer Engineering.
ON THE CAPACITY OF (T,U) PERMUTATION DECODING METHOD
Jia Ming, Anader Benyamin-Seeyar, and Le-Ngoc Tho *In* Engineering Inst. of Canada, Canadian Conference on Electrical and Computer Engineering, Volumes 1 and 2 1991 4 p (For primary document see N94-22101 05-33)
Avail: Issuing Activity (Engineering Inst. of Canada, 2050 rue Mansfield, Suite 700, Montreal, PQ H3A 1Z2 Canada)

N94-22254 East China Inst. of Tech., Nanjing.
ON THE RELATIONSHIP BETWEEN SPECTRAL DOMAIN APPROACH AND METHOD OF LINES
Da-Gang Fang, Hai-Qing Wu (Laval Univ., Quebec.), and Gilles Y. Delisle (Laval Univ., Quebec.) *In* Engineering Inst. of Canada, Canadian Conference on Electrical and Computer Engineering, Volumes 1 and 2 1991 4 p (For primary document see N94-22101 05-33)
Avail: Issuing Activity (Engineering Inst. of Canada, 2050 rue Mansfield, Suite 700, Montreal, PQ H3A 1Z2 Canada)

65 STATISTICS AND PROBABILITY

Includes data sampling and smoothing; Monte Carlo method; and stochastic processes.

N94-19999 Stanford Univ., CA. Dept. of Operations Research.
STOCHASTIC OPTIMIZATION BY SIMULATION: CONVERGENCE PROOFS FOR THE G1/G/1 QUEUE IN STEADY-STATE
Peter W. Glynn and Pierre LEcuyer Jul. 1993 32 p Limited Reproducibility: More than 20% of this document may be affected by microfiche quality
(Contract DAAL03-91-G-0101)
(AD-A271141; SU-TR-93-12; ARO-28809.15-MA-SDI) Avail: CASI HC A03

Approaches like finite differences with common random numbers, infinitesimal perturbation analysis, and the likelihood ratio method, have recently drawn attention as ways of estimating the gradient of a performance measure with respect to continuous parameters in dynamic stochastic systems. In this paper, we study the use of such estimators in stochastic approximation algorithms, to perform so-called 'single-run optimizations' of steady-state systems. Under mild conditions, for an objective function that involves the mean system time in a G1/G/1 queue, we prove that many variants of these algorithms converge to the minimizer. In most cases, however, the simulation length must be increased from iteration to iteration; otherwise the algorithm may converge to the wrong value. One exception is a particular implementation of infinitesimal perturbation analysis, for which the single-run optimization converges to the optimum even with a fixed (and small) number of ends of service per iteration. As a by-product of our convergence proofs, we obtain some properties of the derivative estimators that could be of independent interest. DTIC

N94-20007 Technische Univ., Eindhoven (Netherlands). Dept. of Mathematics and Computing Science.
SET THEORY AND NOMINALISATION, PART 1
F. Kamareddine 1992 35 p See also Part 2, PB93-191831
(PB93-191807-Pt-1; COMPUTING SCIENCE NOTES-92/12) Copyright
Avail: Issuing Activity (National Technical Information Service (NTIS))

The paper argues that the basic problems of nominalization are those of set theory. The paper gives an overview of the problems of set theory, the various solutions, and assesses the influence on nominalization. It then discusses Aczel's Frege structures and compares them with Scott domains. Moreover, it sets the ground for the second part which demonstrates that Frege structures are a suitable framework for dealing with nominalization. NTIS

N94-20008 Technische Univ., Eindhoven (Netherlands). Dept. of Mathematics and Computing Science.
SET THEORY AND NOMINALISATION, PART 2
F. Kamareddine 1992 31 p See also Part 1, PB93-191807 Limited Reproducibility: More than 20% of this document may be affected by microfiche quality
(PB93-191815-Pt-2; COMPUTING SCIENCE NOTES-92/13) Copyright
Avail: Issuing Activity (National Technical Information Service (NTIS))

The paper meets the application of Scott domains to nominalization and explains its problem of predication. It claims that it is not possible to find a solution to such a problem within semantic domains without logic. Frege structures are more conclusive than a solution to domain equations and can be used as models for nominalization. Hence, it develops a type theory based on Frege structures and uses it as a theory of nominalization. NTIS

N94-20113 Massachusetts Inst. of Tech., Cambridge. Artificial Intelligence Lab.
STATISTICAL OBJECT RECOGNITION
William M. Wells, III Jan. 1993 180 p Limited Reproducibility: More than 20% of this document may be affected by microfiche quality
(Contracts N00014-85-K-0124; N00014-91-J-4038)
(AD-A270887; AI-TR-1398) Avail: CASI HC A09

To be practical, recognition systems must deal with uncertainty. Positions of image features in scenes vary. Features sometimes fail to appear because of unfavorable illumination. In this work, methods of statistical inference are combined with empirical models of uncertainty in order to evaluate and refine hypotheses about the occurrence of a known object in a scene.

Probabilistic models are used to characterize image features and their correspondences. A statistical approach is taken for the acquisition of object models from observations in images: mean edge images are used to capture object features that are reasonably stable with respect to variations in illumination. DTIC

N94-20162# Grenoble-1 Univ. (France). Lab. de Modelisation et Calcul.
PARTIAL EMPIRICAL AUTOCORRELATION OF A VECTORIAL CHRONOLOGICAL SERIES [AUTOCORRELATION PARTIELLE EMPIRIQUE D'UNE SERIE CHRONOLOGIQUE VECTORIELLE]
Serge Degerine Jul. 1992 27 p In FRENCH
(RR-896-M; ETN-93-94987) Avail: CASI HC A03/MF A01

Some supplements on the topic of partial autocorrelation function for a multivariate time series are given. Various sample estimators of this function are proposed and related to autoregressive estimation methods. ESA

N94-20165# Grenoble-1 Univ. (France). Techniques de l'Informatique, des Mathematiques, de la Microelectronique et de la Microscopie Quant.
STATISTICAL ANALYSIS OF A RECIPROCAL TRANSLOCATIONS DATA BASE [ANALYSE STATISTIQUE D'UNE BASE DE DONNEES DE TRANSLOCATIONS RECIPROQUES]
Christine Cans, Olivier Cohen, and Christian Lavergne Sep. 1992 63 p In FRENCH
(RR-900-I; ETN-93-94990) Avail: CASI HC A04/MF A01

Attempts made in using logistical regression analysis to predict the nonalternative segregation of the chromosomes of couples carrying reciprocal translocation babies are reported. One out of 600 babies have a reciprocal translocation which results in an exchange of a segment between two nonhomologous chromosomes. In 90% the segregation is alternative without serious consequences. In the other 10% of cases there is mental retardation. ESA

N94-20202# Grenoble-1 Univ. (France). Lab. de Genie Informatique.
DETERMINATION OF THE OPTIMAL STOCHASTIC UPPER BOUND OF A MARKOVIAN GENERATOR
Marc Tremolieres, Jean-Marc Vincent, and Brigitte Plateau Nov. 1992 18 p
(RR-906-I; ETN-93-94995) Avail: CASI HC A03/MF A01

An algorithm that computes a monotone Markovian infinitesimal generator that is stochastically greater than a given stochastic matrix A is proposed. This problem arises in the bounding of the marginal distributions of a continuous time Markov chain defined on a product space. The algorithm uses only basic algebraic operations, and it is shown that the matrix B constructed is optimal: any other monotone stochastic matrix C greater than A is also greater than B. Means of computing lower bounds are explained. ESA

N94-20913# Texas A&M Univ., College Station. Dept. of Statistics.
FUNCTIONAL STATISTICAL DATA ANALYSIS AND MODELING Final Report, 15 Mar. 1990 - 30 Sep. 1993
Emanuel Parzen Aug. 1993 8 p
(Contract DAAL03-90-G-0069)
(AD-A271520; ARO-27574.16-MA) Avail: CASI HC A02/MF A01

Our research during 1990-1993 was reported in 13 published papers and one Ph.D. thesis listed below. We regard our research as concerned with: (1) Change Analysis; (2) Functional Inference; (3) Time Series Analysis; (4) Statistical Culture and History; and (5) Supervision of Ph.D. theses. DTIC

N94-21022# Center for Mathematics and Computer Science, Amsterdam (Netherlands). Dept. of Operations Research, Statistics, and System Theory.
THE COMBINATORICS OF RECONSTRUCTING EVOLUTIONARY TREES
L. A. Szekely (Eoetvoes Lorand Univ., Budapest, Hungary.), P. L. Erdoes (Hungarian Academy of Sciences, Budapest.), and M. A. Steel (Canterbury Univ., Christchurch, New Zealand.) Dec. 1992 19 p Sponsored in part by Alexander von Humboldt Stiftung, Germany
(Contract N00014-91-J-1385)
(CWI-BS-R9233; ETN-94-94722) Copyright Avail: CASI HC A03/MF A01

Results and problems from the reconstruction Theory of evolutionary trees, which involve enumeration and inversion, are surveyed. Every bit of the aligned DNA (deoxyribonucleic acid) sequence is assumed to be one of four nucleotides, that is, insertions and deletions of nucleotides are neglected. A Fourier inverse pair depending on trees and Abelian groups is described, and Kimura's models of molecular evolution are set into this context. The spectral analysis/closest tree method is outlined. The construction of a complete set of invariants for Cavender's model and Kimura's three parameter model is described. Remarks on algorithmic and philosophical aspects are given. ESA

N94-21058 Universiteit Twente, Enschede (Netherlands). Tele-Informatics and Open Systems Group.
SPECIFICATION AND GENERATION OF MARKOV REWARD MODELS
Boudewijn R. Haverkort and Kishor S. Trivedi (Duke Univ., Durham, NC.) 10 Sep. 1992 38 p Sponsored in part by NSWC Limited Reproducibility: More than 20% of this document may be affected by microfiche quality
(Grant NSF CCR-91-08114)
(Memo-INF-92-60; TIOS-92-27; ETN-93-93838) Copyright Avail: CASI HC A03

A study on Markov Reward Models (MRM's) with emphasis on specification techniques is presented. This emphasis is done in an application independent way. Seven classes of specification techniques are distinguished: stochastic Petri nets, queueing networks, fault trees, production rule systems, communicating processes, specialized languages and hybrid techniques. For these classes, the main principles are discussed, examples are given, and software environments (tools) that support the use of these techniques are discussed. Earlier overviews were either only from a particular application area point of view or from a particular specification technique. The mapping of the high level specifications to the underlying MRM's, that is, the generation of the underlying MRM from the high level specification, is also addressed. Indications of important future research areas are given. ESA

N94-21066 Leiden Univ. (Netherlands). Div. of Applied Mathematics.
LINEAR PROGRAMMING FOR STANDARD AND NONSTANDARD MARKOVIAN CONTROL PROBLEMS. A SURVEY
L. C. M. Kallenberg 1993 66 p See also PB93-191930 Limited Reproducibility: More than 20% of this document may be affected by microfiche quality
(PB93-191948; TW-92-12) Avail: Issuing Activity (National Technical Information Service (NTIS))

An overview is given of linear programming methods for solving standard and nonstandard Markovian control problems. Standard problems are problems with the usual criteria such as expected total (discounted) rewards and average expected rewards. Also discussed is a particular class of stochastic games. In nonstandard problems there are additional considerations such as side constraints, multiple criteria, or mean-variance tradeoffs. Finally, it is shown that for some structured models, efficient algorithms exist. NTIS

N94-21076 Universiteit Twente, Enschede (Netherlands). Faculty of Applied Mathematics.
ON ESTIMATION AND TESTING IN POISSON REGRESSION MODELS WITH OVER-DISPERSION
Klaas Poortema Sep. 1992 17 p Limited Reproducibility: More than 20% of this document may be affected by microfiche quality
(MEMO-1083; ETN-93-94123) Avail: CASI HC A03

Poisson regression models with over-dispersion are considered. Over-dispersion is modeled by introducing stochastic variables Z(sub i) such that the dependent variable Y(sub i) given Z(sub i) = z(sub i) is Poisson distributed, with expectation mu(sub i)z(sub i) where mu(sub i) depends on covariates x(sub ij) through a link function g, g(mu(sub i)) = summation(sub j) beta(sub j) x(sub ij). The usual iteration procedure for estimation can be modified. Given square root of n consistent initial estimators for beta and lambda = var(Z(sub i)) one iteration step of the new procedure is needed for the desired asymptotic normality, under quite mild conditions. The construction of square root of n consistent initial estimators of beta and lambda is considered. For testing the null hypothesis that a number of elements of beta is zero, a Wald-statistic is proposed as test-statistic. ESA

N94-21139 Deutsche Forschungsanstalt fuer Luft- und Raumfahrt, Brunswick (Germany). Abt. Mathematische Verfahren und Datentechnik.
PARAMETER ESTIMATION WITH COST FUNCTION OF SECOND ORDER IN OUTPUT-ERROR-PROBLEM [PARAMETERSCHAETZUNGEN MIT QUADRATISCHER KOSTENFUNKTION BEI AUSGANGSFEHLER-PROBLEMEN]
Fro Hammelrath Jan. 1993 65 p In GERMAN Limited Reproducibility: More than 20% of this document may be affected by poor print
(DLR-FB-92-38; ETN-93-94457) Avail: Issuing Activity (European Space Agency (ESA))

A process for parameter estimation in output error problems which is derived from the maximum likelihood requirement with assumed normal distributions of measuring errors is presented. Parameter estimators are shown to be consistent under wide assumptions; with an incorrect model, the estimator converges in probability but may, in general, be biased. These results are valid for many problems with additional input noise. From consistency, it follows that in the case of sufficient smoothness the estimator may be linearized, and from this further results in asymptotic properties follow, for example influence and handling of previously filtered measurement data. This simplest case of stochastic dependency, Markovian correlation, is investigated in more detail. Additionally, it is shown that for output error problems efficient estimators exist only for linear models and Gaussian errors, and their cost functions are of second order. ESA

N94-21175# Army Research Lab., Aberdeen Proving Ground, MD.
CURRENT DIRECTIONS IN THE VULNERABILITY/LETHALITY PROCESS STRUCTURE Final Report, Jul. 1992 - 1993
James N. Walbert, Lisa K. Roach, and Mark D. Burdeshaw Oct. 1993 40 p
(DA Proj. 1L1-62618-AH-80)
(AD-A272836; ARL-TR-296) Avail: CASI HC A03/MF A01

An important aspect of the formulation of any scientific process is the definition of the mathematical framework within which that process is considered. This mathematical basis defines the limitations of the process, provides the means for conducting analyses, and helps ensure uniformity and consistency of results. It is quite common for analytical processes to evolve over a long period of time before the underlying mathematics is fully understood and illuminated. This is the case with Vulnerability/Lethality (V/L) analysis, long considered more an art than a science. In recent years, advances have been made in the rigorous mathematical treatment of certain areas of V/L analysis. In this report, the unifying mathematical framework for all V/L analysis is defined, demonstrating how each part of a well-known process fits into this framework, and illustrating the framework's growth potential. The Degraded States Vulnerability Methodology (DSVM) will be shown to provide an important example of the rigor with which one part of a vulnerability analysis may be conducted, specifically, the formulation of target capability measures from the damaged state. DTIC

N94-21215# Massachusetts Inst. of Tech., Cambridge. Artificial Intelligence Lab.
MEASURE FIELDS FOR FUNCTION APPROXIMATION Memo Report
Jose L. Marroquin Jun. 1993 22 p
(Contracts N00014-91-J-4038; N00014-92-J-1879)
(AD-A272660; MIT-AIM-1433) Avail: CASI HC A03/MF A01

The computation of a piecewise smooth function that approximates a finite set of data points may be decomposed into two decoupled tasks: first, the computation of the locally smooth models, and hence, the segmentation of the data into classes that consist on the sets of points best approximated by each model, and second, the computation of the normalized discriminant functions for each induced class (which may be interpreted as relative probabilities). The approximating function may then be computed as the optimal estimator with respect to this measure field. For the first step, we propose a scheme that involves both robust regression and spatial localization using Gaussian windows. The discriminant functions are obtained by fitting Gaussian mixture models for the data distribution in the boundary of each class. We give an efficient procedure for effecting both computations, and for the determination of the optimal number of components. Examples of the application of this scheme to image filtering, surface reconstruction, and time series prediction are presented as well. DTIC

N94-21322# Naval Surface Warfare Center, Bethesda, MD. Carderock Div.
TWO VISUALLY MEANINGFUL CORRELATION MEASURES FOR COMPARING CALCULATED AND MEASURED RESPONSE HISTORIES Final Report, 1 Apr. - 30 Jun. 1993
Benjamin Whang, William E. Gilbert, and Stephen Zilliacus Jun. 1993 64 p
(AD-A273044; CARDEROCKDIV-U-SSM-67-93/15) Avail: CASI HC A04/MF A01

Two visually meaningful correlation measures are proposed for comparing calculated and measured response histories. One is an error index which is a simplification of RSS (root-sum-square) error factor, and the other is an inequality index which is a simplification of Theil's inequality coefficient. The first compares the difference between the calculated and the measured histories to the measured history. The second compares the difference between the two histories to the sum of the two. The proposed correlation measures are compared to other existing measures, namely, Geer's Error Factors, RSS Error Factor, and Theil's Inequality Coefficient for ease of interpretation and visualization. DTIC

N94-21442# Harvard Univ., Cambridge, MA. Dept. of Statistics.
PAIRED COMPARISON MODELS WITH TIME-VARYING PARAMETERS
Mark E. Glickman May 1993 10 p
(Contract N00014-91-J-1005)
(AD-A272016; TR-ONR-C-14) Avail: CASI HC A02/MF A01

Paired comparison experiments involve comparisons among a set of objects, treatments, or competitors in blocks of size two to determine relative merits among the objects. Applications to tournament chess competition or team sports differ from the usual paired comparison framework in that competitors' abilities may change over time. A dynamic model is developed for the usual paired comparison experiment in which only a binary indicator of the preferred object is available (or trinary, if ties are allowed) and for alternative paired comparison experiments in which more information (perhaps the score) is available. Posterior distributions of the rating parameters and posterior prediction intervals for the results of future comparisons are obtained using methods that are closely related to the Kalman filter. The methodology is applied to the analysis of professional football game outcomes and to chess tournament results from the 1988-1989 World Cup. DTIC

N94-20881*# Purdue Univ., West Lafayette, IN. Dept. of Chemistry.
MULTIVARIATE STATISTICAL ANALYSIS: PRINCIPLES AND APPLICATIONS TO COORBITAL STREAMS OF METEORITE FALLS Abstract Only
S. F. Wolf and M. E. Lipschutz *In* Lunar and Planetary Inst., Twenty-Fourth Lunar and Planetary Science Conference. Part 3: N-Z 1993 p 1531-1532 (For primary document see N94-20636 05-91)
Avail: CASI HC A01/MF A06

N94-21723*# Idaho Univ., Moscow. NASA Space Engineering Research Center.
INTERPOLATIVE MODELING OF GaAs FET S-PARAMETER DATA BASES FOR USE IN MONTE CARLO SIMULATIONS
L. Campbell and J. Purviance *In its* The 1992 4th NASA SERC Symposium on VLSI Design 1992 11 p (For primary document see N94-21694 05-33)
(Grants NAGw-1406; NSF MIP-91-09618)
Avail: CASI HC A03/MF A04

N94-22458*# Observatoire de Strasbourg (France).
EXTRACTING GALACTIC STRUCTURE PARAMETERS FROM MULTIVARIATED DENSITY ESTIMATION Abstract Only
B. Chen, M. Creze, A. Robin (Observatoire de Besancon, France.), and O. Bienayme (Observatoire de Besancon, France.) *In* NASA, Washington, Second Annual Conference on Astronomical Data Analysis Software and Systems. Abstracts 1992 p 27 (For primary document see N94-22438 05-89)
Avail: CASI HC A01/MF A02

N94-22536*# Helsinki Univ. (Finland).
FACTOR ANALYSIS AS A TOOL FOR SPECTRAL LINE COMPONENT SEPARATION 21cm EMISSION IN THE DIRECTION OF L1780 Abstract Only
L. V. Toth, K. Mattila, L. Haikala, and L. G. Balazs (Konkoly Observatory, Budapest, Hungary.) *In* NASA, Washington, Second Annual Conference on Astronomical Data Analysis Software and Systems. Abstracts 1992 p 105 (For primary document see N94-22438 05-89)
Avail: CASI HC A01/MF A02

N94-22540*# Kitt Peak National Observatory, Tucson, AZ.
SPECFOCUS: AN IRAF TASK FOR FOCUSING SPECTROGRAPHS Abstract Only
F. Valdes *In* NASA, Washington, Second Annual Conference on Astronomical Data Analysis Software and Systems. Abstracts 1992 p 109 (For primary document see N94-22438 05-89)
Avail: CASI HC A01/MF A02

66 SYSTEMS ANALYSIS

Includes mathematical modeling; network analysis; and operations research.

N94-21463*# Institute for Computer Applications in Science and Engineering, Hampton, VA.
DEPENDABILITY AND PERFORMABILITY ANALYSIS Final Report
Kishor S. Trivedi (Duke Univ., Durham, NC.), Gianfranco Ciardo (College of William and Mary, Williamsburg, VA.), Manish Malhotra (Bell Telephone Labs., Inc., Holmdel, NJ.), and Robin A. Sahner (Gould, Inc., Urbana, IL.) Nov. 1993 28 p Repr. from Perf. Eval. of Comp. and Comm. Syst., Lect. Notes in Computer Science 729, Springer-Verlag, 1993 p 587-612
(Contract NAS1-19480; RTOP 505-90-52-01)
(NASA-CR-191565; NAS 1.26:191565; ICASE-93-85) Avail: CASI HC A03/MF A01

Several practical issues regarding specifications and solution of dependability and performability models are discussed. Model types with and without rewards are compared. Continuous-time Markov chains (CTMC's) are compared with (continuous-time) Markov reward models (MRM's) and generalized stochastic Petri nets (GSPN's) are compared with stochastic reward nets (SRN's). It is shown that reward-based models could lead to more concise model specifications and solution of a variety of new measures. With respect to the solution of dependability and performability models, three practical issues were identified: largeness, stiffness, and non-exponentiality, and a variety of approaches are discussed to deal with them, including some of the latest research efforts. Author (revised)

N94-22403# Los Alamos National Lab., NM.
HIGH-VELOCITY INTERCEPTORS FOR BOOST-PHASE INTERCEPTS
G. H. Canavan Nov. 1993 14 p
(Contract W-7405-eng-36)
(DE94-001077; LA-12300-MS) Avail: CASI HC A03/MF A01

Brilliant kill packages with existing booster technology, warning, and command and control could produce interceptors that could reduce the effectiveness of theater attacks in the boost phase. DOE

N94-21330*# National Aeronautics and Space Administration. Goddard Space Flight Center, Greenbelt, MD.
THE AUTOMATED GROUND NETWORK SYSTEM
Miles T. Smith and Peter N. Militch (Allied-Signal Aerospace Co., Seabrook, MD.) *In its* Networks Technology Conference Nov. 1993 p 73-81 (For primary document see N94-21323 05-62)
Avail: CASI HC A02/MF A03

N94-21331*# Allied-Signal Aerospace Co., Seabrook, MD.
MISSION OPERATIONS SUPPORT AREA (MOSA) FOR GROUND NETWORK SUPPORT
Robert D. Woods and Susan A. Moser *In* NASA. Goddard Space Flight Center, Networks Technology Conference Nov. 1993 p 83-102 (For primary document see N94-21323 05-62)
Avail: CASI HC A03/MF A03

N94-21333*# Jet Propulsion Lab., California Inst. of Tech., Pasadena.
USING MANUFACTURING MESSAGE SPECIFICATION FOR MONITOR AND CONTROL AT VENUS
W. Randy Heuser, Richard L. Chen, and Michael H. Stockett *In* NASA. Goddard Space Flight Center, Networks Technology Conference Nov. 1993 p 121-135 (For primary document see N94-21323 05-62)
Avail: CASI HC A03/MF A03

N94-21343*# Booz-Allen and Hamilton, Inc., Seabrook, MD.
DEVELOPING A SPACE NETWORK INTERFACE SIMULATOR: THE NTS APPROACH
Gary E. Hendrzak *In* NASA. Goddard Space Flight Center, Networks Technology Conference Nov. 1993 p 243-251 (For primary document see N94-21323 05-62)
Avail: CASI HC A02/MF A03

N94-21351*# Allied-Signal Aerospace Co., Columbia, MD.
NETWORK COMMAND PROCESSING SYSTEM OVERVIEW
Yon-Woo Nam and Lisa D. Murphy *In* NASA. Goddard Space Flight Center, Networks Technology Conference Nov. 1993 p 355-369 (For primary document see N94-21323 05-62)
(Contract NAS5-31000)
Avail: CASI HC A03/MF A03

N94-22075# Academy of Sciences (USSR), Moscow. Computer Center.
A MODEL OF NEGOTIATION IN AN EXTENSIVE FORM GAME
Ivan Menshikov *In* Technical Research Centre of Finland, Information Technology and Economic Modelling 1992 p 173-181 (For primary document see N94-22056 05-83)
Copyright Avail: CASI HC A02/MF A03

67 THEORETICAL MATHEMATICS

Includes topology and number theory.

N94-21286# Rochester Univ., NY. Dept. of Computer Science.
ON THE TOPOLOGICAL SIZE OF p-m-COMPLETE DEGREES
Marius Zimand May 1993 13 p
(Grant NSF CCR-89-57604)
(TR-459) Avail: CASI HC A03/MF A01

In this work we pursue the study of the topological size of some interesting classes of sets, focusing on complete degrees under the p-m-reduction. It is argued that neither the standard Cantor topology nor 'the next natural' superset topology are adequate for studying the topological size of classes inside NP. Instead, a combination of the two is proposed. Each finite string v belonging to Sigma(sup *) defines the basic open set U(sub v) = the set of all w belonging to Sigma(sup infinity) such that for every i less than or equal to the absolute value of v (v(i) = 1 implies w(i) = 1). Thus if we identify a set A contained in Sigma(sup *) with the binary infinite sequence w belonging to Sigma(sup infinity), representing its characteristic function, U(sub v) consists of all sets that extends the finite set encoded by v. A class of sets C contained in Sigma(sup infinity) is effectively nowhere dense if there is a recursive function f, called the witness function, such that for all v belonging to Sigma(sup *), v is a prefix of f(v) and U(sub f(v)) intersecting C = the null set. A class of sets C contained in Sigma(sup infinity) is effectively meagre (or effectively of the first category), if C is the countable union of some effectively nowhere dense sets, and is of the second category if it is not of the first category. It is shown that if P does not equal NP, then the class of NP complete sets under p-Turing reducibility is effectively meagre. In fact, by the same argument, one can show that if C is any class different from P, the class of C p-Turing complete sets is effectively meagre. In this work, we refine our tools, and admit witness functions with bounded resources. Thus if Gamma is a complexity class for functions, we say that C is Gamma-nowhere dense if the witness function is in Gamma, and we get the corresponding definitions for Gamma-meagre or Gamma-second category. The complexity class Gamma is a time complexity class, unless the word SPACE appears in the denomination of Gamma in which case Gamma is a space complexity class. We study the following question: what is the largest class Gamma such that the class of C p-m-complete sets is Gamma-second category, for different classes C. Derived from text

N94-21881*# Computer Sciences Corp., Mountain View, CA.
ACHIEVING HIGH DATA REDUCTION WITH INTEGRAL CUBIC B-SPLINES
Jin J. Chou Oct. 1993 17 p
(Contract NAS2-12961)
(NASA-CR-177628; A-94011; NAS 1.26:177628) Avail: CASI HC A03/MF A01

During geometry processing, tangent directions at the data points are frequently readily available from the computation process that generates the points. It is desirable to utilize this information to improve the accuracy of curve fitting and to improve data reduction. This paper presents a curve fitting method which utilizes both position and tangent direction data. This method produces G(exp 1) non-rational B-spline curves. From the examples, the method demonstrates very good data reduction rates while maintaining high accuracy in both position and tangent direction. Author (revised)

70 PHYSICS (GENERAL)

For precision time and time interval (PTTI) see *35 Instrumentation and Photography;* for geophysics, astrophysics or solar physics see *46 Geophysics, 90 Astrophysics,* or *92 Solar Physics.*

N94-19917 Kings Coll., London (England). Dept. of Physics.
NUMERICAL MODELING OF FRINGING FIELDS AND THEIR USE FOR COMPLEX PERMITTIVITY MEASUREMENTS AT HIGH FREQUENCIES Interim Report, Feb. 1991 - Jan. 1993
Camelia Gabriel Aug. 1993 28 p Limited Reproducibility: More than 20% of this document may be affected by microfiche quality
(Grant AF-AFOSR-0122-91)
(AD-A270478; AL/OE-TR-1993-0068) Avail: CASI HC A03

An accurate technique to measure the complex permittivity of materials based on a rigorous theoretical formulation of the admittance of an open-ended coaxial probe has been achieved. The technique was tested by measurements on standard solutions. The new technique was used to perform a comprehensive study of ionic solutions. The extensive data obtained led to the development of models to predict the dielectric parameters of ionic solutions at a given temperature as a function of concentration. The theoretical study and numerical techniques were extended to treat the case of a thin sample backed by a metallic plane. The technique was tested with standard solutions. Further analysis led to the development of expressions for the field in the sample adjacent to the probe. This enabled the pattern of power deposition to be determined and improved our understanding of the sampled volume. DTIC

N94-21511# Lawrence Livermore National Lab., CA.
ONE- AND MULTI-COMPONENT THEORIES OF MIXTURES
F. H. Ree Jul. 1993 6 p Presented at the 14th International Conference of the International Association for the Advancement of High Pressure Science and Technology, Colorado Springs, CO, 27 Jun. - 2 Jul. 1993
(Contract W-7405-eng-48)
(DE93-040543; UCRL-JC-113765; CONF-930676-48) Avail: CASI HC A02/MF A01

We describe one-component statistical mechanical theories and van der Waal's effective one-component mixture model. We then show how to apply them to mixtures (containing CO2) to extract reliable unlike-pair potential involving CO2 molecules as well as their dissociation products. A more fundamental approach will require the development of a perturbation or variational theory of mixtures based on a non-additive hard-sphere mixture reference system. Recent progresses made in this direction by means of an integral equation and computer simulations is described. DOE

N94-21798# Technische Physische Dienst TNO-TH, Delft (Netherlands).
[ACTIVITIES REPORT OF THE INSTITUTE OF APPLIED PHYSICS] Annual Report, 1990 [JAARVERSLAG 1990]
1990 39 p In DUTCH
(ETN-93-93749) Avail: CASI HC A03/MF A01

A scale model and a calculation model were developed to predict and reduce traffic noise of planned roads. A simulation model for the complete glass production process was developed. An electronic lock system was developed to replace the conventional mechanical door locks. For individual titles, see N94-21799 through N94-21801.

N94-21799# Technische Physische Dienst TNO-TH, Delft (Netherlands).
TRAFFIC NOISE IN A ROUNDABOUT WAY [VERKEERSLAWAAI VIA EEN OMWEG] **c71**
F. deRoo *In its* Activities Report of the Institute of Applied Physics 1990 p 20-22 In DUTCH (For primary document see N94-21798 05-70)
Avail: CASI HC A01/MF A01

A scale model and a calculation model were developed to predict traffic noise. The advantage of a scale model is that many different alternatives can be easily studied without high costs. The disadvantage is that materials properties have to be imitated according to fixed scaling rules and that the frequencies have to be increased by the scale factor. The scale model is very important in the planning of new roads and the reduction of noise, and for the improvement of calculation models. Legally prescribed calculation models were further improved in the sense that the sound waves are more closely followed. This model TOMAS is especially suited to study the interaction between the ground and noise screens. ESA

N94-21800# Technische Physische Dienst TNO-TH, Delft (Netherlands).
MODELING OF GLASS FABRICATION [MODELLERING VAN DE GLASFABRICAGE] **c27**
F. Simonis *In its* Activities Report of the Institute of Applied Physics 1990 p 23-25 In DUTCH (For primary document see N94-21798 05-70)
Avail: CASI HC A01/MF A01

A simulation model for the complete glass production process was developed. This model has a modular structure. The nucleus is a three dimensional model for the simulation of flows in the molten glass, to which specific models are coupled for the simulation of the melting process, resulting in a complete simulation model of the glass oven (melting kinetics, purification, interaction with the walls, residence time, heat transfer). ESA

N94-21801# Technische Physische Dienst TNO-TH, Delft (Netherlands).
ELECTRONIC LOCKING SYSTEM [ELEKTRONISCH SLUITSYSTEEM] **c33**
E. Nieuwkoop *In its* Activities Report of the Institute of Applied Physics 1990 p 26-28 In DUTCH (For primary document see N94-21798 05-70)
Avail: CASI HC A01/MF A01

An electronic locking system was developed to remove the disadvantages of conventional mechanical door locks. The electrolock has to replace existing locks. Therefore, the techniques of Surface Mount Technology and Application Specific Integrated Circuit were applied to overcome the space limitations. The key consists of a metal rod with grip equipped with a contactless chip. When the key is inserted in the lock, a magnetic field is generated in the cylinder which induces a voltage in the chip. Therefore a battery is not required. The chip then emits inductively a code which is unique for each key. The electrolock was successfully tested. ESA

N94-21958# Lawrence Livermore National Lab., CA.
PARAMETRIC INSTABILITIES IN PICOSECOND TIME SCALES
H. A. Baldis, W. Rozmus (Alberta Univ., Edmonton.), C. Labaune (Ecole Polytechnique, Palaiseau, France.), Ph. Mounaix (Ecole Polytechnique, Palaiseau, France.), D. Pesme (Ecole Polytechnique, Palaiseau, France.), S. Baton (Ecole Polytechnique, Palaiseau, France.), and V. Tikhonchuk (Academy of Sciences, USSR, Moscow.) 1 Mar. 1993 40 p Presented at the NATO/ASI Summer School: From Statistical Physics to Statistical Inference and Back, Cargese, France, 31 Aug. - 12 Sep. 1992
(Contract W-7405-eng-48)
(DE94-000384; UCRL-JC-113505; CONF-9208188-3) Avail: CASI HC A03/MF A01

The coupling of intense laser light with plasmas is a rich field of plasma physics, with many applications. Among these are inertial confinement fusion (ICF), x-ray lasers, particle acceleration, and x-ray sources. Parametric instabilities have been studied for many years because of their importance to ICF; with laser pulses with duration of approximately a nanosecond, and laser intensities in the range 10(exp 14)-10(exp 15)W/cm(exp 2) these instabilities are of crucial concern because of a number of detrimental

effects. Although the laser pulse duration of interest for these studies are relatively long, it has been evident in the past years that to reach an understanding of these instabilities requires their characterization and analysis in picosecond time scales. At the laser intensities of interest, the growth rate for stimulated Brillouin scattering (SBS) is of the order of picoseconds, and of an order of magnitude shorter for stimulated Raman scattering (SRS). In this paper, the authors discuss SBS and SRS in the context of their evolution in picosecond time scales. They describe the fundamental concepts associated with their growth and saturation, and recent work on the nonlinear treatment required for the modeling of these instabilities at high laser intensities. DOE

71 ACOUSTICS

Includes sound generation, transmission and attenuation.
For noise pollution see *45 Environmental Pollution.*

N94-19894 Texas Univ., Austin. Applied Research Lab.
NONLINEAR ACOUSTICS: PERIODIC WAVEGUIDE, FINITE-AMPLITUDE PROPAGATION IN A MEDIUM HAVING A DISTRIBUTION OF RELAXATION PROCESSES, AND PRODUCTION OF AN ISOLATED NEGATIVE PULSE IN WATER Annual Summary Report No. 5, 1 Oct. 1992 - 30 Sep. 1993
David T. Blackstock 24 Aug. 1993 26 p Limited Reproducibility: More than 20% of this document may be affected by microfiche quality
(Contract N00014-89-J-1109)
(AD-A270530; ARL-TR-93-17) Avail: CASI HC A03

Research on nonlinear acoustics has been performed during the 12-month period ending 30 September 1993. The following projects were completed: (1) propagation in a periodic waveguide, (2) finite-amplitude propagation in a medium having a distribution of relaxation processes, and (3) production of an isolated negative pulse in water. Public communication of the research was accomplished through three theses, four oral papers, one journal article published, four journal articles submitted, and one paper in a symposium proceedings. DTIC

N94-19949 Aerospace Corp., El Segundo, CA. Engineering and Technology Group.
ACOUSTIC MICROSCOPY AND NONLINEAR EFFECTS IN PRESSURIZED SUPERFLUID HELIUM
A. A. Moulthrop, M. S. Muha, G. C. Kozlowski, C. P. Silva, and B. Hadimioglu 31 Aug. 1993 29 p Limited Reproducibility: More than 20% of this document may be affected by microfiche quality
(Contract F04701-88-C-0089)
(AD-A270598; TR-0091(6925-02)-1) Avail: Issuing Activity (Defense Technical Information Center (DTIC))

The operation of an acoustic microscope having a resolution of 15 nm has been demonstrated. It uses as a coupling medium superfluid He-4 colder than 0.9 K and pressurized to greater than 20 bar. The microscope is now being used to image objects that show little or no contrast on a scanning electron microscope. In addition, the acoustic microscope is being used to study the properties of sound propagation in the coupling fluid. At low acoustic intensities, the coupling fluid has very low acoustic attenuation at the microscope's operating frequency (15.3 GHz), but near the focal point the acoustic intensity can be high enough that the helium behaves with extreme nonlinearity. In fact, this medium is capable of entering new regimes of nonlinear interaction. Plots of the received signal versus input power display a nearly complete pump depletion at certain input power levels and a reconversion to the pump frequency at higher power levels. Such behavior has never before been observed. We present arguments that the process underlying this nonlinear behavior is harmonic generation. DTIC

N94-20211*# Duke Univ., Durham, NC. Dept. of Mechanical Engineering.
ACOUSTIC RADIATION DAMPING OF FLAT RECTANGULAR PLATES SUBJECTED TO SUBSONIC FLOWS
Karen Heitman Lyle 1 Nov. 1993 118 p Sponsored in part by NASA
(NASA-TM-109382; NAS 1.15:109382) Avail: CASI HC A06/MF A02

The acoustic radiation damping for various isotropic and laminated composite plates and semi-infinite strips subjected to a uniform, subsonic and steady flow has been predicted. The predictions are based on the linear vibration of a flat plate. The fluid loading is characterized as the perturbation pressure derived from the linearized Bernoulli and continuity equations. Parameters varied in the analysis include Mach number, mode number and plate size, aspect ratio and mass. The predictions are compared with existing theoretical results and experimental data. The analytical results show that the fluid loading can significantly affect realistic plate responses. Generally, graphite/epoxy and carbon/carbon plates have higher acoustic radiation damping values than similar aluminum plates, except near plate divergence conditions resulting from aeroelastic instability. Universal curves are presented where the acoustic radiation damping normalized by the mass ratio is a linear function of the reduced frequency. A separate curve is required for each Mach number and plate aspect ratio. In addition, acoustic radiation damping values can be greater than or equal to the structural component of the modal critical damping ratio (assumed as 0.01) for the higher subsonic Mach numbers. New experimental data were acquired for comparison with the analytical results. Author

N94-20523*# Cornell Univ., Ithaca, NY. Dept. of Mechanical and Aerospace Engineering.
ROTORCRAFT NOISE: STATUS AND RECENT DEVELOPMENTS
Albert R. George, Ben Wei-C. Sim, and David R. Polak 27 Dec. 1993 28 p Submitted for publication
(Grant NAG2-554)
(NASA-CR-194761; NAS 1.26:194761) Avail: CASI HC A03/MF A01

This paper briefly reviews rotorcraft noise mechanisms and their approximate importance for different types of rotorcraft in different flight regimes. Discrete noise is due to periodic flow disturbances and includes impulsive noise produced by phenomena which occur during a limited segment of a blade's rotation. Broadband noise results when rotors interact with random disturbances, such as turbulence, which can originate in a variety of sources. The status of analysis techniques for these mechanisms are reviewed. Also, some recent progress is presented on the understanding and analysis of tilt rotor aircraft noise due to: (1) recirculation and blockage effects of the rotor flow in hover; and (2) blade-vortex interactions in forward and descending flight. Author (revised)

N94-21260# Naval Postgraduate School, Monterey, CA.
COMPARISON OF HIGHER ORDER MOMENT SPECTRUM ESTIMATION TECHNIQUES M.S. Thesis
Jeffrey F. McAloon Sep. 1993 123 p
(AD-A272967) Avail: CASI HC A06/MF A02

This thesis compares the detection performance of the 1-1/2 D instantaneous power spectrum (1-1/2 D (sub ips)), the bispectrum, the instantaneous higher-order moment slice (IHOMS) method, and the spectrogram for multi-component stationary signals, harmonically related stationary signals, and multi-component linear FM signals corrupted by additive white Gaussian noise. In addition, a determination of the relative processing gain between the 1-1/2 D(sub ips) method and the spectrogram is made for stationary signals in noise. The results of this thesis show that 1-1/2 D(sub ips) has a processing gain advantage over that of the spectrogram for a range of input SNR that depends upon the size of the data window. Under some conditions, the bispectrum can detect both harmonic coupling and phase coupling between the components of multi-component signals. IHOMS' ability to detect linear chirps in noise is limited to chirps having different slew rates, and the method has a significantly greater computational cost than both the spectrogram and 1-1/2 D(sub ips). DTIC

N94-21306 Defence Research Agency, Farnborough (England).
APPROXIMATION TO SOUND RADIATION AND SCATTERING BY SIMPLY SUPPORTED LAYERED CYLINDER Technical Memo
J. H. James Aug. 1993 21 p Limited Reproducibility: More than 20% of this document may be affected by microfiche quality
(AD-A272964; DRA-TM(USGR)93339) Avail: CASI HC A03

A theoretical approximation is obtained for calculating the acoustics of a finite multilayered anisotropic cylinder which is excited either by a mechanical force or by a plane wave at oblique incidence. The cylinder dynamics is obtained by a semi-analytical theory, and the far field acoustics by standard cylindrical baffle theory. A numerical example of steady state and transient sound radiation demonstrates an application of the model. DTIC

N94-21422# Naval Postgraduate School, Monterey, CA.
STABILITY CURVES FOR A THERMOACOUSTIC PRIME MOVER M.S. Thesis
Fan-Ming Kuo Jun. 1993 45 p
(AD-A272607) Avail: CASI HC A03/MF A01

The purpose of this thesis is to investigate the stability curves for and steady state waveforms in a helium filled prime mover for both the fundamental and second modes. The predicted and measured stability limits are in reasonable agreement for both modes at most mean pressures. There is, however, evidence that the stability of one mode is affected by the presence of the other. It is also observed that one mode can suppress the other. Measurements were also made on a prime mover modified such that the fundamental mode was selectively inhibited. Results indicate that the reduced fundamental amplitude allows the stability curve for the second mode to extend into the regions where the fundamental mode previously dominated. This produces a region where both modes are simultaneously excited. Analysis of the waveforms show that the resulting oscillations are quasiperiodic. DTIC

N94-21447 National Inst. of Standards and Technology, Boulder, CO.
SPEED OF SOUND DATA AND RELATED MODELS FOR MIXTURES OF NATURAL GAS CONSTITUENTS
B. A. Younglove, N. V. Frederick, and R. D. McCarty Jan. 1993 99 p Sponsored by Gas Research Inst. Limited Reproducibility: More than 20% of this document may be affected by microfiche quality
(PB93-200822; NIST/MONO-178) Avail: CASI HC A05

Sound speed data have been obtained for thirteen binary mixtures and four multicomponent mixtures of natural gas components using a cylindrical cavity. These data cover a temperature range from 250 to 350 K at pressures to 10 MPa. The uncertainty in the data is approximately 0.05 percent. The binary mixtures are primarily methane-rich, with ethane nitrogen, carbon dioxide, or propane as the second component. The multicomponent mixtures are representative of commercially available compositions in the United States and Europe. The data were used to develop and test mathematical models for prediction of the sound speed of natural gas mixtures, within an average uncertainty of 0.1 percent, over the ranges of pressure, temperature, and composition that encompass the major region of custody transfer for natural gas. NTIS

N94-21608*# United Technologies Research Center, East Hartford, CT.
ACTIVE CONTROL OF WAKE/BLADE-ROW INTERACTION NOISE THROUGH THE USE OF BLADE SURFACE ACTUATORS Final Report
Kenneth A. Kousen and Joseph M. Verdon Washington NASA Dec. 1993 39 p
(Contract NAS3-25425; RTOP 535-03-10)
(NASA-CR-4556; E-8227; NAS 1.26:4556) Avail: CASI HC A03/MF A01

A combined analytical/computational approach for controlling of the noise generated by wake/blade-row interaction through the use of anti-sound actuators on the blade surfaces is described. A representative two-dimensional section of a fan stage, composed of an upstream fan rotor and a downstream fan exit guide vane (FEGV), is examined. An existing model for the wakes generated by the rotor is analyzed to provide realistic magnitudes for the vortical excitations imposed at the inlet to the FEGV. The acoustic response of the FEGV is determined at multiples of the blade passing frequency (BPF) by using the linearized unsteady flow analysis, LINFLO. Acoustic field contours are presented at each multiple of BPF illustrating the generated acoustic response disturbances. Anti-sound is then provided by placing oscillating control surfaces, whose lengths and locations are specified arbitrarily, on the blades. An analysis is then conducted to determine the complex amplitudes required for the control surface motions to best reduce the noise. It is demonstrated that if the number of acoustic response modes to be controlled is equal to the number of available independent control surfaces, complete noise cancellation can be achieved. A weighted least squares minimization procedure for the control equations is given for cases in which the number of acoustic modes exceeds the number of available control surfaces. The effectiveness of the control is measured by the magnitude of a propagating acoustic response vector, which is related to the circumferentially averaged sound pressure level (SPL), and is minimized by a standard least-squares minimization procedure. Author (revised)

N94-21741*# Lockheed Engineering and Sciences Co., Hampton, VA.
EVALUATION OF A NONLINEAR METHOD FOR THE ENHANCEMENT OF TONAL SIGNAL DETECTION
Donald P. Garber Dec. 1993 27 p
(Contract NAS1-19000; RTOP 505-63-70-02)
(NASA-CR-191562; NAS 1.26:191562) Avail: CASI HC A03/MF A01

A method is presented for biasing spectral estimates to enhance detection of tonal signals against a background of broadband noise. In this method, a nonlinear average of an ensemble of individual spectral estimates is made where broadband noise energy is biased downward, pure tone energy is unbiased, and a mixture of the two is biased by an amount that depends on the ratio of tonal energy to broadband energy. The method is analyzed to provide estimates of the extent of tonal signal detection enhancement. Author

N94-21751# Sandia National Labs., Albuquerque, NM.
SURFACE ACOUSTIC WAVE SENSING OF VOC'S IN HARSH CHEMICAL ENVIRONMENTS
K. B. Pfeifer, S. J. Martin, and A. J. Ricco Jun. 1993 74 p
(Contract DE-AC04-76DP-00789)
(DE93-040721; SAND-93-0070) Avail: CASI HC A04/MF A01

The measurement of VOC concentrations in harsh chemical and physical environments is a formidable task. A surface acoustic wave (SAW) sensor has been designed for this purpose and its construction and testing are described in this paper. Included is a detailed description of the design elements specific to operation in 300 C steam and HCl environments including temperature control, gas handling, and signal processing component descriptions. In addition, laboratory temperature stability was studied and a minimum detection limit was defined for operation in industrial environments. Finally, a description of field tests performed on steam reforming equipment at Synthetica Technologies Inc. of Richmond, CA is given including a report on destruction efficiency of CCl4 in the Synthetica moving bed evaporator. Design improvements based on the field tests are proposed. DOE

N94-22003# Lawrence Livermore National Lab., CA.
THREE DIMENSIONAL ULTRASONIC IMAGING
G. H. Thomas, S. Benson, and S. Crawford Mar. 1993 12 p Presented at the Society of Photo-Optical Instrumentation Engineers (SPIE) OE/Aerospace Science and Sensing Meeting, Orlando, FL, 11-16 Apr. 1993
(Contract W-7405-eng-36)
(DE93-040549; UCRL-JC-113437; CONF-930445-25) Avail: CASI HC A03/MF A01

Ultrasonic nondestructive evaluation techniques interrogate components with high frequency acoustic energy. A transducer generates the acoustic energy and converts acoustic energy to electrical signals. The acoustic energy is reflected by abrupt changes in modulus and/or density which can be caused by a defect. Thus defects reflect the ultrasonic energy which is converted into electrical signals. Ultrasonic evaluation typically provides a two dimensional image of internal defects. These images are either planar views (C-scans) or cross-sectional views (B-scans). The planar view is generated by raster scanning an ultrasonic transducer over the component and capturing the amplitude of internal reflections. Depth information is generally ignored. The cross-sectional view is generated by scanning the transducer along a single line and capturing the amplitude and time of flight for each internal reflection. The amplitude and time of flight information is converted into an image of the cross section of the component where the scan was performed. By fusing the C-scan information with the B-scan information a three dimension image of the internal structure of the component can be produced. The three dimensional image can be manipulated by rotating and slicing to produce the optimal view of the internal structure. The high frequency ultrasonic energy requires a liquid coupling media and thus applications for imaging in liquid environments are well suited to ultrasonic techniques. Examples of potential ultrasonic imaging applications are Inside liquid filled tanks, inside the human body, and underwater. DOE

N94-22053 Harris, Miller, Miller and Hanson, Inc., Lexington, MA.
AIRCRAFT NOISE EFFECTS ON CULTURAL RESOURCES: RECOMMENDATION AND RATIONALE FOR FURTHER RESEARCH
Carl E. Hanson, Kenneth W. King (Interior Dept., Denver, CO.), Mary Ellen

Eagan, and Richard D. Horonjeff May 1993 15 p See also PB93-205318 and PB93-205334 Prepared in cooperation with National Park Service, Denver, CO Limited Reproducibility: More than 20% of this document may be affected by microfiche quality
(Contract NPS-CX-2000-0-0025)
(PB93-205326; HMMH-290940.04-2) Avail: CASI HC A03

The results are ultimately used to estimate the potential for damage to a wide variety of cultural resources from operations of commercial helicopters. Comparison of measured vibration levels with criteria for damage based on structural velocities will provide a family of restrictions on aircraft operations in the vicinity of sensitive structures. Such restrictions could take the form of minimum separation distances and prohibited maneuvers for helicopters. The results of the study would be presented in a report as a set of recommended procedures for helicopter operations to avoid damage to prehistoric, historic, sensitive, and conventional structures. NTIS

N94-22054 Harris, Miller, Miller and Hanson, Inc., Lexington, MA.
AIRCRAFT NOISE EFFECTS ON CULTURAL RESOURCES: ANNOTATED BIBLIOGRAPHY
C. E. Hanson and N. Peterson May 1993 24 p See also PB93-205326 and PB93-205318 Sponsored by National Park Service, Denver, CO Limited Reproducibility: More than 20% of this document may be affected by microfiche quality
(Contract NPS-CX-2000-0-0025)
(PB93-205334; HMMH-290940.04-3) Avail: Issuing Activity (National Technical Information Service (NTIS))

The scope of work required a review, critique, and analysis of the scientific literature to assess the nature and probable magnitude of the potential effects of aircraft overflights on historical and cultural resources in the National Park System. Excluded under this work order are such items as historical or cultural context or setting. NTIS

N94-22261# Technische Univ., Delft (Netherlands). Lab. of Electromagnetic Research.
INTERFACE REFLECTION OF SPHERICAL ACOUSTIC WAVES IN THE FIRST- AND SECOND-ORDER RATIONAL PARABOLIC APPROXIMATIONS AND THEIR ARTIFACTS
M. V. DeHoop and A. T. DeHoop 1992 48 p Prepared in cooperation with Koninklijke/Shell Exploratie en Produktie Lab., Rijswijk, Netherlands
(PB93-215424; ET/EM-1992-17) Copyright Avail: CASI HC A03/MF A01

The accuracy of the first- and second-order rational parabolic approximations of the 'vertical' slowness and the nature of the artifacts associated with them in the space-time solutions to the acoustic wave equations in a fluid medium are investigated. In particular, the reflection of an impulsive, point-source generated, spherical wave against the boundary with a medium with a higher wave speed is analyzed. From the space-time Green's functions in the relevant two-media configuration, evaluated with the aid of the modified Cagniard method, it is found that, instead of generating the real, physical head wave, the approximations generate artificial head-wavelike arrivals. The analysis makes explicit in which regions of space and in which time interval the artifacts show up and of what nature they are. Numerical results are presented. NTIS

N94-22262# Technische Univ., Delft (Netherlands). Lab. of Electromagnetic Research.
TRANSIENT ACOUSTIC WAVE MODELING: HIGHER-ORDER WKBJ ASYMPTOTICS AND SYMBOLICAL MANIPULATION (REVISED)
M. D. Verweij 1992 47 p
(PB93-215432; ET/EM-1992-18) Copyright Avail: CASI HC A03/MF A01

A combination of WKBJ asymptotics and the Cagniard-De Hoop method is used to determine the space-time domain acoustic wavefield in a continuously horizontally layered configuration. First, a Laplace transformation with a real and positive transform parameter is applied with respect to the time coordinate, followed by a two-dimensional Fourier transformation with respect to the horizontal coordinates. Using the integral equations of the resulting transform domain problem, a recurrence scheme is derived for the coefficients of the WKBJ asymptotic expansions of the transform domain solutions. This scheme is well-suited for implementation in a symbolical manipulation program. The transformation of the resulting higher order WKBJ asymptotic representations back to the space-time domain is performed with the aid of the Cagniard-De Hoop method, which is particularly efficient in this case. If both the source and the receiver are located in one homogeneous halfspace of the configuration, the Cagniard-De Hoop method allows for an almost completely analytical transformation back to the space-time domain. NTIS

N94-21799# Technische Physische Dienst TNO-TH, Delft (Netherlands).
TRAFFIC NOISE IN A ROUNDABOUT WAY [VERKEERSLAWAAI VIA EEN OMWEG]
F. deRoo *In its* Activities Report of the Institute of Applied Physics 1990 p 20-22 In DUTCH (For primary document see N94-21798 05-70)
Avail: CASI HC A01/MF A01

72 ATOMIC AND MOLECULAR PHYSICS

Includes atomic structure, electron properties, and molecular spectra.

N94-19804# Florida State Univ., Tallahassee. Dept. of Physics.
SIMULATING SUPERSYMMETRY WITH ISAJET 7.0/ISASUSY 1.0
H. Baer, F. E. Paige (Superconducting Super Collider Lab., Dallas, TX.), S. D. Protopopescu (Brookhaven National Lab., Upton, NY.), and X. Tata Apr. 1993 9 p Presented at the Workshop on Physics at Current Accelerators and the Supercollider, Argonne, IL, 2-5 Jun. 1993
(Contracts DE-FG05-87ER-40319; DE-AM03-76SF-00235)
(DE93-018266; FSU-HEP-930329; UH-511-764-93; CONF-9306176-3)
Avail: CASI HC A02/MF A01

This document reviews the physics assumptions and input embedded in ISAJET 7.0/ISASUSY 1.0 which is relevant for simulating fundamental processes within the framework of the Minimal Supersymmetric Model (MSSM) at p(bar p) and pp colliders. After a brief discussion of the underlying MSSM framework, the authors discuss event simulation and list the particle production processes and decay modes that have been incorporated into the calculations. They then describe how to set up and run an ISAJET/ISASUSY job, as well as the user input and output formats. The ISAJET program is sufficiently flexible that some non-miminal supersymmetry scenarios may be simulated as well. Finally, plans for future upgrades which include the extension to e(sup +)e(sup -) collisions are listed. DOE

N94-19813# Fermi National Accelerator Lab., Batavia, IL.
A SEARCH FOR NEW GAUGE BOSONS IN (BAR p)p COLLISIONS AT SQUARE ROOT OF s EQUALS 1.8 TeV IN THE DIELECTRON DECAY MODE
Aug. 1993 10 p Presented at the Symposium on Lepton and Photon Interactions, Ithaca, NY, 10-15 Aug. 1993
(Contract DE-AC02-76CH-03000)
(DE93-019901; FNAL/C-93/211-E; CONF-930823-5) Avail: CASI HC A02/MF A01

The authors have searched for the production of a neutral gauge boson (Z prime) with mass above 200 GeV/sq cm in (bar p)p collisions with the CDF detector. They present a 95% confidence level (CL) limit on the Z prime yields ee production cross section, assuming Standard Model coupling strengths. DOE

N94-19814# Fermi National Accelerator Lab., Batavia, IL.
MEASUREMENT OF THE B(+) AND B(0) LIFETIMES
Aug. 1993 17 p Presented at the Symposium on Lepton and Photon Interactions, Ithaca, NY, 10-15 Aug. 1993
(Contract DE-AC02-76CH-03000)
(DE93-019906; FNAL/C-93/198-E; CONF-930823-2) Avail: CASI HC A03/MF A01

The lifetimes of the B(sup +) and B(sup 0) have been measured using a sample of fully reconstructed B decays. Using approximately 19,000 J/psi yields mu(sup +) mu(sup -) decays recorded with the collider detector at Fermilab, 75 +/- 10 charged and 61 +/- 9 neutral B mesons have been reconstructed in the CDF silicon vertex detector. Unbinned likelihood fits to the proper lifetime distributions of these B mesons give tau(sup +/-) = 1.63 +/- 0.21 (stat) +/- 0.16 (sys) ps, tau(sup 0) = 1.54 +/-

0.2 (stat) +/- 0.10 (sys) ps, and tau(sup +/-)/tau(sup 0) = 1.06 +/- 0.20 (stat) +/- 0.12 (sys). DOE

N94-19822 Duke Univ., Durham, NC. Dept. of Physics.
UNCERTAINTY LIMITED ATOMIC POSITION MEASUREMENT USING OPTICAL FIELDS Final Report, 7 May 1990 - 30 Jun. 1993
J. E. Thomas 30 Jun. 1993 5 p Limited Reproducibility: More than 20% of this document may be affected by microfiche quality
(Contract DAAL03-90-G-0114)
(AD-A271013; ARO-27766.2-PH) Avail: CASI HC A01

Methods for position measurement of moving atoms with ultrahigh spatial resolution were developed, based on resonance imaging in a spatially varying potential with a steep gradient. Using a spatially light-shift due to an off-resonant focused optical field, spatial resolution of 200 nanometers, with a few percent linearity over several microns was obtained. Centroids of narrow spatial features, which are created and probed in the experiments, are determined with an accuracy of +/- 20 nanometers. Ultimately, with higher gradients and single atom detection, uncertainty principle limited spatial resolution of a few nanometers will be attainable. These methods will have applications in the characterization of atom-optical elements, and in the development of new methods of ultrahigh resolution neutral atom lithography. DTIC

N94-19868# Brookhaven National Lab., Upton, NY.
A SUMMARY OF STUDIES OF PARTICLE STABILITY AT RHIC
G. Parzen 1992 10 p Presented at the Workshop on the Stability of Particle Motion in Storage Rings, Upton, NY, 19-24 Oct. 1992
(Contract DE-AC02-76CH-00016)
(DE93-040173; BNL-49382; CONF-921077-12) Avail: CASI HC A02/MF A01

This paper summarizes some studies of particle stability done at RHIC. The topics reported on include: long-term tracking and the dynamic aperture; linear coupling effects and their correction; and tune spreads in the beam due to field multipoles in the magnets and their correction. DOE

N94-19870# Cornell Univ., Ithaca, NY.
ABSOLUTE TOTAL AND ONE AND TWO ELECTRON TRANSFER CROSS SECTIONS FOR Ar(8+) ON Ar AS A FUNCTION OF ENERGY
J. Vancura and V. O. Kostroun 1992 4 p Presented at the 6th International Conference on Physics of Highly Charged Ions, Manhattan, KS, 28 Sep. - 2 Oct. 1992
(Contract DE-FG02-86ER-13519)
(DE93-040283; CONF-920948-20) Avail: CASI HC A01/MF A01

The absolute total and one and two electron transfer cross sections for Ar(8+) on Ar were measured as a function of projectile laboratory energy from 0.090 to 0.550 keV/amu. The effective one electron transfer cross section dominates above 0.32 keV/amu, while below this energy, the effective two electron transfer starts to become appreciable. The total cross section varies by a factor over the energy range explored. The overall error in the cross section measurement is estimated to be +/- 15%. DOE

N94-19871# Cornell Univ., Ithaca, NY.
ENERGY GAIN SPECTROSCOPIC STUDY OF Ar(q+)-Ar COLLISIONS AT 40 qeV
J. Vancura and V. O. Kostroun 1992 3 p Presented at the 6th International Conference on Physics of Highly Charged Ions, Manhattan, KS, 28 Sep. - 2 Oct. 1992
(Contract DE-FG02-86ER-13519)
(DE93-040284; CONF-920948-18) Avail: CASI HC A01/MF A01

Energy gain spectra of Ar(q+)(8 less than or = q less than or = 16) on Ar at 40 qeV collision energy and 0.4 qeV energy resolution are presented. Capture into definite states of the projectile is observed which seems to exhibit a definite even-odd projectile charge state dependence. DOE

N94-19931# Brookhaven National Lab., Upton, NY.
ELECTRON REACTIONS IN NONPOLAR LIQUIDS: PRESSURE EFFECTS
R. A. Holroyd 1993 18 p Presented at the NATO Advanced Study Institute: Linking the Gaseous and Condensed Phases of Matter - the Behavior of Slow Electrons, Patras, Greece, 5-18 Sep. 1993
(Contract DE-AC02-76CH-00016)
(DE93-040328; BNL-49429; CONF-930993-2) Avail: CASI HC A03/MF A01

Theory predicts that electron energy levels in nonpolar molecular hydrocarbons should increase in energy with density/pressure increase, and therefore, electron attachment rates in solution should change with pressure. Studies of pressure effect on electron mobility show that some contraction occurs around trapped electrons, but more contraction occurs around ions in hydrocarbons. After a brief discussion of pressure effects on electron energy levels and mobility, this paper reports studies of electron attachment reactions of N2O, CO2, and n-C5F12 in tetramethylsilane, and of toluene, benzene, CO2, and 1,3-butadiene in several solvents. DOE

N94-19956# Argonne National Lab., IL.
ENCOUNTERS OF H AND D ATOMS WITH O2 IN WATER: RELATIVE DIFFUSION AND REACTION RATES
P. Han and D. M. Bartels 1993 14 p Presented at the Ultrafast Reaction Dynamics and Solvent Effects, Asnieres Sur Oise, France, 11-15 May 1993
(Contract W-31-109-eng-38)
(DE93-018587; ANL/CHM/CP-79706; CONF-9305254-1) Avail: CASI HC A03/MF A01

Diffusive encounters of H and D atoms with O2 in water are investigated with the time-domain EPR free induction decay attenuation technique. Given the paramagnetic triplet ground state of the O2 molecule, it is expected that all H-O2 encounters will contribute to spin dephasing, regardless of whether reaction to form HO2 occurs. In H2O the second-order spin-spin dephasing rate of H in the presence of O2 is 1.94 x 10(exp 10) M(exp -1) sec(exp -1) at 25 C, with an activation energy of 11.22 +/- 0.33 kJ/mole between 8 and 60 C. In a mixture of 90% D2O and 10% H2O, H atom dephasing is marginally slower in the same temperature range. Dephasing of D atoms in 90% D2O is about 5-10% slower than H, indicating that diffusion of D is slower than H. The results are analyzed in terms of other available data concerning H and O2 diffusion and the reaction rate in water. It seems clear that neither the Stokes Einstein hydrodynamic theory nor classical activated rate theory applies to the diffusion of light hydrophobic gases in water. The authors tentatively conclude that H-O2 spin exchange is slightly less efficient than can be predicted in the theoretical diffusion limit. DOE

N94-19958# University of Western Michigan, Kalamazoo. Dept. of Physics.
TESTING DOUBLE IONIZATION MECHANISMS WITH HIGHLY-CHARGED IONS
J. A. Tanis 1992 9 p Presented at the 6th International Conference on Physics of Highly Charged Ions, Manhattan, KS, 28 Sep. - 2 Oct. 1992
(Contract DE-FG02-87ER-13778)
(DE93-018750; CONF-920948-17) Avail: CASI HC A02/MF A01

Double ionization of He target atoms by intermediate- to high-velocity charged ions is considered in terms of two mechanisms: a two-step (TS) process in which both target electrons are removed in separate direct interactions with the projectile, and a one-step mechanism in which one electron is liberated in a single projectile-target interaction followed by subsequent 'shake-off' (SO) of the second electron. Measured double-to-single ionization ratios are used to exhibit and test the underlying mechanisms of double ionization. It is found that these ratios exhibit a high degree of universality as a function of v/q, where v is the velocity of the ion and q is its charge. The results strongly suggest that the important factor in determining the regions of validity for TS and SO is the ionic charge divided by the impact velocity and not just the impact velocity itself. DOE

N94-19971# Argonne National Lab., IL.
THE MULTICOMPONENT LINESHAPE OF THE ANHARMONIC A(1)(TO) PHONON IN PbTiO3
C. M. Foster, Z. Li, M. Grimsditch, S. K. Chan, and V. G. Karpov Jul. 1993 7 p Presented at the 8th International Meeting on Ferroelectricity, Gaithersburg, MD, 8-13 Aug. 1993
(Contract W-31-109-eng-38)
(DE93-018995; ANL/MSD/CP-78121; CONF-930852-1) Avail: CASI HC A02/MF A01

Detailed Raman studies of the optical phonons in single-crystal PbTiO3

indicate that the frequencies and symmetry assignments in the literature must be revised. In this study, all vector-k approximately equal to zero optical phonon modes are directly observed and are shown to rigorously obey Raman selection rules. The angular dependence of the phonon frequencies indicates that the energy of the lowest frequency A(sub 1)(TO) mode, which exhibits an anomalous anharmonisity-induced lineshape, is higher than the energy of the lowest frequency E(LO) mode at 300 K. DOE

N94-20030# Technische Hochschule, Darmstadt (Germany). Fachbereich Physik.

EXAMINATION OF LOW LEVEL MAGNETIC DIPOLE INTENSITIES IN THE TRANSITION NUCLEI Sm-148, Sm-150, Sm-152 AND Sm-154, WITH INELASTIC PHOTON SCATTERING AT S-DALINAC Ph.D. Thesis [UNTERSUCHUNG NIEDRIGLIEGENDER MAGNETISCHER DIPOLSTAERKE IN DEN UEBERGANGSKERNEN 148, 150, 152, 154SM MIT INELASTISCHER PHOTONENSTREUUNG AM S-DALINAC]

Wolfgang P. Ziegler 1990 95 p In GERMAN

(ETN-93-95069) Avail: CASI HC A05/MF A01

The intensities of magnetic dipole transitions in scissor mode excitation energy area are estimated for isotopes of vibration and rotation nuclei. Experiments were performed with the nuclear resonance fluorescence method at samarium isotopes, using a bremsstrahlung source and two germanium detectors, designed for a supraconductor linear accelerator. The results show a linear relation between the M1 sum intensity and the square of mass deformation; properties of mean excitation mode are examined in the framework of the neutron proton deformation model, in which separated neutron and proton deformation parameters were introduced. Sum intensities were calculated with the interacting free boson model and are found to be underestimated. The experimental value of median excitation energy is shown to agree with the predicted value in the monopole quadrupole pairing model. ESA

N94-20050# Argonne National Lab., IL.

COLLISIONS OF MOLECULES WITH CLUSTERS: A QUASICLASSICAL STUDY

J. Jellinek and Z. B. Guevenc 1993 15 p Presented at the European Research Conference in Physics: Fundamental Aspects of Clusters, Elounda, Greece, 26 May - 2 Jun. 1993

(Contract W-31-109-eng-38)

(DE93-018614; ANL/CHM/CP-79761; CONF-9305157-1) Avail: CASI HC A03/MF A01

Presented are results of a quasiclassical simulation study of processes induced by a collision of a D2 molecule with a Ni13 cluster. Focus is on the reactive channel, i.e., dissociative adsorption, of the molecule. Dependence on factors such as the collision energy, initial (quantized) rovibrational state of the molecule, and structure and temperature of cluster are analyzed. Direct and indirect (involving formation of transient complexes -- resonances) reaction pathways are considered and characterized quantitatively. The authors illustrate how multidimensional potential energy surfaces describing cluster-molecule interactions can be analyzed in terms of a reduced set of relevant degrees of freedom and the topologies of these surfaces correlated with dynamical phenomena extracted from the calculations. The complex problem of 'tuning' the cluster-molecule interaction potential using experimental data is addressed, and a specific example of such 'tuning' is given. It underscores the crucial role of the intimate interplay between theory and experiment, especially in the field of clusters where, because of the large number of degrees of freedom involved, first principle calculations are (and will remain) of limited feasibility. More generally, the analysis and the discussion presented show that the phenomena and problems relevant for cluster-molecule collisions -- a new research area by all accounts -- have much in common with those encountered in nucleus-nucleus, atom-atom, atom-molecule, and molecule-molecule collisions -- research fields with a considerable history. DOE

N94-20083 Rensselaer Polytechnic Inst., Troy, NY.

STUDY OF MECHANISMS FOR LONG WAVELENGTH SCHOTTKY-BARRIER INFRARED DETECTORS Final Technical Report

Leo J. Schowalter Jul. 1993 26 p Limited Reproducibility: More than 20% of this document may be affected by microfiche quality

(Contract F19628-91-K-0030)

(AD-A270538; RL-TR-93-135) Avail: CASI HC A03

We have studied ballistic electron transport across metal layers and metal/semiconductor interfaces using a scanning tunneling microscope to inject electrons with a controlled energy into a thin metal film, which allows measurements (with spatial resolution approaching 1 nm) of (1) the local Schottky barrier (SB) height, (2) ballistic mean free paths of energetic electrons (or holes), and (3) transmission probability of hot carriers across the metal/semiconductor interface. The attenuation length of hot electrons (1.5 eV above the Fermi level) in PtSi is measured as approximately 4 nm. We also used BEEM (Ballistic-electron-emission Microscopy) to observe the sharp onset of inelastic scattering mechanisms in Au/Si and PtSi. We observe that the derivative BEEM spectrum of Au/Si (001) n-type is rich with features which may correspond to either M/S interface states or to states in the semiconductor bandgap near the interface. We suggest that these interface scattering processes occur also for other M/S systems. Our experimental BEEM studies indicate that hot electron transport is diffusive in the sense that electrons will scatter elastically many times before an inelastic event will occur. We succeeded in constructing a low temperature (liquid nitrogen temperatures) BEEM head and have taken BEEM spectra of PtSi on P-type Si. DTIC

N94-20096# Lawrence Livermore National Lab., CA.

NEW RELATIVISTIC S-MATRIX RESULTS FOR SCATTERING -- BEYOND THE USUAL ANOMALOUS FACTORS/BEYOND IMPULSE APPROXIMATION

R. H. Pratt (Pittsburgh Univ., PA.), P. M. Bergstrom, Jr. (Pittsburgh Univ., PA.), and L. Kissel Aug. 1993 49 p Presented at the International Conference on Anomalous Scattering, Hamburg, Germany, 17-21 Aug. 1992

(Contract W-7405-eng-48)

(DE93-019148; UCRL-JC-114583; CONF-9208186-5) Avail: CASI HC A03/MF A01

The relativistic second-order S-matrix elements for photon-atom scattering have been successfully calculated with numerical methods within the independent particle approximation (IPA). This permits an assessment of the validity of simpler approximate predictions which are commonly used and it offers the possibility of improved tabulations of theoretical predictions. A variety of unresolved issues remain, some associated with the relativistic theory, some with IPA. The systematic use of the second-order S-matrix in calculations of Rayleigh scattering from isolated atoms has led to significant progress in understanding this process and to a wide range of agreement with experiment. The energy and angular dependence of anomalous factors and the importance of relativistic, higher-multipole and bound-bound contributions in their calculation is better understood. However correlation effects must also be included to obtain predictions for the near-edge region, such extensions of the present S-matrix calculation have been discussed but few results are available so far. Existing empirical approaches can be assessed in regard to their success in dealing with known IPA features. We have recently calculated the relativistic second-order S-matrix element for Compton scattering and have begun to try to understand this process in different regions. We can discuss this when the more complete calculation confirms the standard Compton peak. In the softer part of the spectrum impulse approximation fails. There can be resonant Raman peaks, and in the soft-photon region the spectrum is infrared divergent, proportional to the photoeffect angular distribution. This means the traditional incoherent scattering factor is undefined in the absence of a low-energy detector efficiency cutoff. DOE

N94-20119# Groningen Rijksuniv. (Netherlands). Kernfysisch Versneller Inst.

RELATIVISTIC CALCULATIONS OF THE SUPERHEAVY NUCLEUS (SUP 298)114

Hielke Freerk Boersma 19 Jan. 1993 8 p Submitted for publication

(KVI-969; ETN-93-94818) Avail: CASI HC A02/MF A01

Ground state properties of the superheavy nucleus with N = 184 and Z = 114, (sup 298)114 were investigated, using conventional relativistic mean field theory and density dependent mean field theory, which reproduces Dirac-Brueckner calculations in nuclear matter. There are strong indications that the next doubly magic nucleus beyond Pb-208 is (sup 298)114. The calculations provide support for N = 184 and Z = 114 being magic numbers. Density dependent mean field theory does not predict (sup 298)114 to be stable against beta decay. ESA

N94-20130*# Colorado Univ., Boulder. Joint Inst. for Lab. Astrophysics.
LABORATORY STUDIES OF LOW TEMPERATURE RATE COEFFICIENTS: THE ATMOSPHERIC CHEMISTRY OF THE OUTER PLANETS Final Report
Stephen R. Leone Dec. 1993 3 p
(Grant NAGw-2438)
(NASA-CR-193485; NAS 1.26:193485) Avail: CASI HC A01/MF A01

The objectives are to measure laboratory rate coefficients for key reactions of hydrocarbon molecules and radicals at low temperatures, which are relevant to the atmospheric photochemistry of Saturn, Jupiter, and Titan. Upcoming NASA planetary missions, such as Cassini, will probe the atmosphere of Titan in more detail, offering an excellent opportunity to test kinetic models and to establish fiducial standards for using kinetic models to interpret various parameters of the outer planets. Accurate low temperature kinetic data, which are presently lacking, may require crucial revisions to the rates of formation and destruction and are of utmost importance to the success of these efforts. In this program, several key reactions of ethynyl radicals (C2H) with acetylene (C2H2), methane (CH4), and oxygen (O2), down to temperatures of 170 K were successfully investigated. The experimental apparatus developed in our laboratory for measuring reaction kinetics at low temperatures consists of a laser photolysis/infrared probe laser setup. The rate measurements are carried out as a function of (low) temperature with a transverse flow cell designed specifically for these studies. A 193 nm argon fluoride pulsed excimer laser is used to photolyze a suitable precursor molecule, such as acetylene to produce C2H, and a high resolution, tunable infrared F-center laser (2.3-3.35 mu m) probes the transient concentrations of the radical species directly in absorption to extract the kinetic rate coefficients.
Author (revised)

N94-20181# Lawrence Livermore National Lab., CA.
TWO-DIMENSIONAL PARTICLE-IN-CELL SIMULATION ON TRANSPUTER ARRAYS
A. I. Dyachenko, A. N. Pushkarev (Landau Inst. for Theoretical Physics, Moscow, USSR.), M. A. Laypunov (Kurchatov, I. V. Inst. of Atomic Energy, Moscow, USSR.), E. A. Talnykin (Kurchatov, I. V. Inst. of Atomic Energy, Moscow, USSR.), and Yu. A. Omelchenko (Academy of Sciences, USSR, Moscow.) 3 May 1993 19 p Presented at the Supercomputing Conference on High Performance Computing and Communications, Portland, OR, 15-19 Nov. 1993
(Contract W-7405-eng-48)
(DE93-017977; UCRL-JC-113823; CONF-931115-8) Avail: CASI HC A03/MF A01

The authors have implemented a particle-in-cell method on a 32 transputer computing network. The tests have shown that the performance of this system reaches 1/8 of the equivalent one for the code optimized for a CRAY Y-MP/2E. The system performance analysis shows that this network remains cost-effective until expanded approximately up to 100 transputers. This transputer equipment has provided an efficient computational tool for investigating a novel physical phenomenon -- a collisionless mechanism for separation of different elements in colliding plasma beams. DOE

N94-20187# Argonne National Lab., IL.
NEUTRON AND PIMC DETERMINATION OF THE LONGITUDINAL MOMENTUM DISTRIBUTION OF HCP, BCC AND NORMAL LIQUID He-4
R. C. Blasdell, D. M. Ceperley, and R. O. Simmons (Illinois Univ. at Urbana-Champaign, Savoy.) Jul. 1993 6 p Presented at the 10th Sagamore Conference on Charge, Spin and Momentum Densities, Konstanz, Germany, 1-7 Sep. 1992
(Contracts W-31-109-eng-38; DE-FG02-91ER-45439)
(DE93-019009; ANL/XFD/CP-80438; CONF-9209267-5) Avail: CASI HC A02/MF A01

Deep inelastic neutron scattering has been used to measure the neutron Compton profile (NCP) of a series of condensed He-4 samples at densities from 28.8 atoms/nm(exp 3) (essentially the minimum possible density in the solid phase) up to 39.8 atoms/nm(exp 3) using a chopper spectrometer at the Argonne National Laboratory Intense Pulsed Neutron Source. At the lowest density, the NCP was measured along an isochore through the hcp, bcc, and normal liquid phases. Average atomic kinetic energies are extracted from each of the data sets and are compared to both published and new path integral Monte-Carlo (PIMC) calculations as well as other theoretical predictions. In this preliminary analysis of the data, account is taken of the effects of instrumental resolution, multiple scattering, and final-state interactions. Both our measurements and the PIMC theory show that there are only small differences in the kinetic energy and longitudinal momentum distribution of isochoric helium samples, regardless of their phase or crystal structure. DOE

N94-20225# Fermi National Accelerator Lab., Batavia, IL.
THE CROSS SECTION FOR THE PRODUCTION OF b(BAR-b) PAIRS IN p(BAR p) COLLISIONS AT THE SQUARE ROOT OF s EQUALS 1.8 TeV
Aug. 1993 16 p Presented at the Symposium on Lepton and Photon Interactions, Ithaca, NY, 10-15 Aug. 1993
(Contract DE-AC02-76CH-03000)
(DE93-019900; FNAL/C-93/199-E; CONF-930823-4) Avail: CASI HC A03/MF A01

The cross section for p(bar p) yields b(bar b)X is measured from high mass e(mu) events collected with the CDF detector during the 1988-1989 run of the Fermilab Tevatron. Comparisons are made between the data and next-to-leading order (NLO) Quantum Chromodynamics (QCD). DOE

N94-20230# Brookhaven National Lab., Upton, NY.
ANGULAR DISTRIBUTIONS OF HIGH-ORDER ATI
Baorui Yang, B. Walker, L. F. DiMauro, K. J. Schafer, K. C. Kulander (Lawrence Livermore National Lab., CA.), and P. Agostini (Commissariat a l'Energie Atomique, Gif-sur-Yvette, France.) 1993 4 p Presented at the 6th International Conference on Multiphoton Processes, Quebec City, Ontario, 25-30 Jun. 1993
(Contract DE-AC02-76CH-00016)
(DE93-019125; BNL-49362; CONF-9306125-3) Avail: CASI HC A01/MF A01

The above-threshold ionization (ATI), a strong-field behavior, can be studied using kilohertz lasers. This paper reports a study of electron angular distributions (AD) for Xe and Kr excited by a 50 ps, 1.05 micron strong field. AD's are presented for ATI orders up to 30 and show a new intensity-dependent structure. A physical picture is proposed that has its source in one-electron, and not two-electron, dynamics. DOE

N94-20264# Rochester Univ., NY. Lab. for Laser Energetics.
CHARGE COLLECTORS FOR THE OMEGA UPGRADE
B. Yaakobi Aug. 1993 11 p
(Contract DE-FC03-85DP-40200)
(DE93-019684; DOE/DP-40200/267) Avail: CASI HC A03/MF A01

Charge collectors placed at several distances from the target measure the current of ions resulting from target disassembly and expansion as a function of arrival time at the detector. Since the expanding plasma is neutral, comprising both electrons and ions moving together, the role of the charge collector is to separate out the electrons, so that the net ion current can be measured. The time-integrated current, or the total charge, can yield the total mass ablated from the target, provided the ionic charge Z is known. From the total ablated mass, the mass ablation rate during the target implosion can be estimated. This quantity provides a useful gauge of the combined effects of absorption, heat conduction, and hydrodynamic efficiency in target interactions. In principle, one charge collector can yield useful results because the author assumes spherical symmetry of the expansion (this question is addressed directly by the plasma calorimeters of which there are many around the target). In practice there will be four charge collectors, two at the tank wall (distance R from the target) and two in an extension tube, at a distance of about 2R from the target. The reason for the two different distances is to check that complete charge separation within the detector has been achieved. A signature of such separation will be to verify that the current falls off as I/R(exp 2) with distance from the target. Since the separation can be inadequate due to space charges within the detector, the farther detector, having smaller charge density, will be more reliable. The two pairs will be oriented at about 90 degrees with respect to each other (say, east and north) to give a rough idea on the isotropy. DOE

N94-20291# California Univ., Berkeley. Lawrence Berkeley Lab.
B PRODUCTION AT D0
T. G. Trippe Jun. 1993 4 p Presented at the 28th Conference on Quantum Chromodynamics and High Energy Hadronic Interactions, Les Arcs, France, 13-27 Mar. 1993

(Contract DE-AC03-76SF-00098)
(DE93-019250; LBL-34294; CONF-930363-6) Avail: CASI HC A01/MF A01

The D(0) detector is well suited for some aspects of B physics. The muon system is capable of triggering on muons with p(sub T) down to 3 GeV/c, is dense and compact to suppress backgrounds from punchthrough and decay in flight, and covers a large pseudorapidity range--the absolute value of eta is less than 3.3. This allows the study of B production in muon and multimuon channels over a wide p(sub T) and eta range, which should provide information about gluon densities at small x. The muon inclusive p(sub T) distribution is shown. Dimuon mass and charge correlations are analyzed to separate production and decay processes. B production in the inclusive B yields J/psi chi as well as J/psi and gamma production are discussed. B(bar-B) mixing is studied using like-sign dimuon events. DOE

N94-20306# Sandia National Labs., Albuquerque, NM.
TIME-OF-FLIGHT HEAVY ION BACKSCATTERING SPECTROMETRY
J. A. Knapp, J. C. Banks, and B. L. Doyle 1993 13 p Presented at the 11th International Conference on Ion Beam Analysis, Balatonfured, Hungary, 5-9 Jul. 1993
(Contract DE-AC04-76DP-00789)
(DE93-019067; SAND-93-0785C; CONF-930709-1) Avail: CASI HC A03/MF A01

A new time-of-flight (TOF) ion detection system for Heavy Ion Backscattering Spectrometry (HIBS) is described. Examples are also given of the use of the system for measuring low-level contamination on Si wafers. Currently, the TOF-HBIS system has a sensitivity of 1 x 10(exp 9)/sq cm for the heaviest of surface impurity atoms and a mass resolution capable of separating Fe from Cu. The sensitivity is expected to improve by an additional order of magnitude on a industrial TOF-HIBS system being constructed for SEMATECH. DOE

N94-20324 Brookhaven National Lab., Upton, NY.
HIGH ENERGY IONIZATION IN LIQUIDS: THE FREE ION YIELD
R. Holroyd 1993 16 p Presented at the NATO Advanced Study Institute: Linking the Gaseous and Condensed Phases of Matter - the Behavior of Slow Electrons, Patras, Greece, 5-18 Sep. 1993 Limited Reproducibility: More than 20% of this document may be affected by microfiche quality
(Contract DE-AC02-76CH-00016)
(DE93-040329; BNL-49430; CONF-930993-1) Avail: CASI HC A03

This paper considers some recent experimental results (n-hexane, neopentane, 2, 2, 4, 4-tetramethylpentane, 2, 2, 4-trimethylpentane) which show how G(sub fi) (number of ion pairs or free ions per 100 eV absorbed) depends on conditions. The results provide insight into factors which determine free ion yield: molecular structure, field, temperature, tracks, density. DOE

N94-20474# Florida State Univ., Tallahassee. Dept. of Physics.
MEASUREMENT OF THE STRANGE QUARK DISTRIBUTION FUNCTION IN W(+) CHARM QUARK EVENTS
U. Baur, S. Keller, F. Halzen (Wisconsin Univ., Madison.), K. Riesselmann (Wisconsin Univ., Madison.), and M. L. Mangano (Scuola Normale Superiore, Pisa, Italy.) 24 Jun. 1993 4 p
(Contracts DE-FG05-87ER-40319; DE-AC02-76ER-00881)
(DE93-018267; FSU-HEP-930608) Avail: CASI HC A01/MF A01

We investigate the prospects of measuring the strange quark distribution function at the Tevatron, using W plus charm quark events. The W plus charm quark signal produced by strange quark - gluon fusion, sg yields W-(c) and bar-sg yields W+(bar-c) is approximately 5% of the inclusive W + 1 jet cross section. We study the sensitivity of the W+ charm quark cross section to the parametrization of the strange quark distribution function, and evaluate the various background processes. The different prospects of tagging the charm quark with the CDF and D(theta) detectors are briefly discussed. DOE

N94-20612# Smithsonian Astrophysical Observatory, Cambridge, MA.
THEORETICAL INVESTIGATIONS OF METASTABILITY AND ENERGY STORAGE IN MOLECULAR SYSTEMS Final Report, Nov. 1989 - Nov. 1991
Kate P. Kirby 9 Mar. 1993 12 p
(Grant AF-AFOSR-0042-88)
(AD-A271849; AFOSR-93-0824TR) Avail: CASI HC A03/MF A01

A manuscript was completed describing the metastable vibrational levels of the D(sup 1) Delta and I(sup 1) Sigma(sup -) states of CO. Methods of population of these levels have been investigated. Work on binding in several high-spin multiplicity system, (sup 6)Sigma(sup +) states in CN and NO, is almost complete. DTIC

N94-20618 Cornell Univ., Ithaca, NY. Dept. of Chemistry.
HIGH RESOLUTION INFRARED SPECTROSCOPY OF FORMAMIDE AND DEUTERATED FORMAMIDE IN A MOLECULAR BEAM Technical Report
Christopher L. Brummel, Meihua Shen, Kevin B. Hewett, and Laura A. Philips 26 Oct. 1993 32 p Limited Reproducibility: More than 20% of this document may be affected by microfiche quality
(Contract N00014-90-J-1971)
(AD-A271986; TR-9) Avail: Issuing Activity (Defense Technical Information Center (DTIC))

High resolution infrared spectra of formamide and deuterated formamide (DCONH2) were collected using molecular beam optothermal spectroscopy. The spectrum of formamide was found to be perturbed such that each rotational transition was split into two peaks. The splitting was absent in the spectrum of deuterated formamide. The large splitting in the spectrum of formamide (approximately 0.7/cm) prevented an accurate deconvolution of the spectrum into zeroeth order bright and dark states. A list of the possible coupling modes is presented. The coupling, however, is not well represented as a simple coupling of two rigid rotors. DTIC

N94-20619# Cornell Univ., Ithaca, NY. Dept. of Chemistry.
HIGH RESOLUTION INFRARED SPECTROSCOPY OF CYCLOBUTANE: A STUDY OF VIBRATIONAL MODE COUPLING INVOLVING LARGE AMPLITUDE, LOW FREQUENCY MODES
H. Li, C. C. Miller, and Laura A. Philips 26 Oct. 1993 42 p
(Contract N00014-90-J-1971)
(AD-A271987; TR-11) Avail: CASI HC A03/MF A01

The high resolution IR spectrum of cyclobutane in a supersonic molecular beam was obtained for the region of 2981 to 2991/cm. The spectrum reveals four overlapping bands suggestive of vibrational mode coupling in the C-H stretching region. Ground state combination differences demonstrate that these bands originate from 2 different ground states, the symmetric and asymmetric ring puckering states. Evidence of vibrational mode coupling is present in all four bands. The coupling depends on both J and the symmetry of the puckering state. A model coupling scheme involving two qualitatively different types of couplings is developed to explain the observed spectrum. Symmetry restrictions and the interaction between molecular rotation and ring puckering qualitatively accounts for the dramatically different coupling behavior between the two ring puckering states. DTIC

N94-20938# California Univ., San Diego, La Jolla.
THEORETICAL PARTICLE PHYSICS
30 Sep. 1993 16 p
(Contract DE-FG03-90ER-40546)
(DE94-000538; DOE/ER-40546/2; UCSD-916904R) Avail: CASI HC A03/MF A01

This report discusses the following topics: Heavy Quark Physics; Chiral Perturbation Theory; Skyrmions; Large-N Limit; Weak Scale Baryogenesis; Supersymmetry; Rare Decays; Technicolor; Chiral Lattice Fermions; Pauli-Villars Regulator and the Higgs Mass Bound; Higgs and Yukawa Interactions; Gauge Fixing; and Quantum Beables. DOE

N94-21136 Technische Hochschule, Darmstadt (Germany). Fachbereich Physik.
F-SPIN CONCEPT AND g-BOSONS IN THE INTERCEDING BOSON MODEL Ph.D. Thesis [F-SPIN-KONZEPT UND G-BOSONEN IM MODELL WECHSELWIRKENDER BOSONEN]
Ottfried Engel 1990 96 p In GERMAN Limited Reproducibility: More than 20% of this document may be affected by microfiche quality
(ETN-93-93607) Avail: CASI HC A05

The F-spin concept is introduced in the interacting boson model to take into account fermion structure by considering bosons as fermion pairs. Majorana operator was designed as the quadratic Casimir operator, which

is diagonal on the subspaces of defined permutation symmetry and can energetically separate states of different permutation symmetry of the neutron-proton product wave function. Since the model is restricted to s and d bosons, mixed symmetry states must be defined. Excitation energies and boson densities were calculated and compared with experimental data. The validity of microscopic interpretation in the model was discussed from the point of view of particle freedom degree. ESA

N94-21185# Aberdeen Proving Ground, MD. Edgewood Research Development and Engineering Center.

APPLICATION OF MOLECULAR MODELING TO BIOLOGICAL PROCESSING Final Report, Jan. - Apr. 1992

Alfred H. Lowrey (Naval Research Lab., Washington, DC.), George R. Famini, and Charles Wick Jul. 1993 32 p

(AD-A272612; ERDEC-TR-029) Avail: CASI HC A03/MF A01

Detailed understanding of the molecular basis for biological processes is now available through computational modeling techniques. Advances in computational algorithms and technology allow applications to large biological macromolecules and permits the study of such problems as binding mechanisms, chemical reactivity, structural and conformational effects, and simulations of molecular motions. Recent crystallographic data provides access to detailed structural information that allows analysis and comparison of various computational techniques. Preliminary semiempirical studies on N-acetylneuraminic acid are presented as an example of computational studies on binding mechanisms. N-acetylneuraminic acid is a substituted carbohydrate, which is a recognition site for binding of proteins (i.e., cholera toxin). These calculations provide some insight into electronic effects on bin in a crystal complex and the effect of the molecular charge on hydrogen bonding the crystal complex. DTIC

N94-21461# SRI International Corp., Menlo Park, CA.

ELECTRONICALLY METASTABLE MOLECULES OF HIGH SYMMETRY Final Report, 16 Mar. 1990 - 15 Apr. 1993

Hanspeter Helm May 1993 131 p

(Contract F33615-90-C-2007)

(AD-A272015; MP-93-078; WL-TR-93-2079) Avail: CASI HC A07/MF A02

This project is part of the search for a novel propellant based on molecules with excess internal energy for use in the combustion process. Spectroscopic properties of neutral molecules of triatomic hydrogen, tetraoxygen, superexcited oxygen, and hydronium were investigated using laser ionization, laser photodissociation, and charge neutralization techniques. The neutrals were prepared in a fast beam by electron transfer from stationary gas targets to mass selected ions. Excited state lifetimes and electronic, vibrational, and rotational-structures were examined as well as the dissociation products and the effect that external electric fields have on the stability of the molecules. DTIC

N94-21515# Stanford Linear Accelerator Center, CA.

PARTON-PARTON ELASTIC SCATTERING AND RAPIDITY GAPS AT TEVATRON ENERGIES

V. DelDuca and Wai-Keung Tang Aug. 1993 3 p Presented at the 19th International Conference on Elastic and Diffractive Scattering (5th Blois Workshop), Providence, RI, 8-12 Jun. 1993

(Contract DE-AC03-76SF-00515)

(DE93-041024; SU-SLAC-Pub-6310; CONF-9306221-2) Avail: CASI HC A01/MF A01

The theory of the perturbative pomeron is used to compute the probability of observing parton-parton elastic scattering and rapidity gaps between jets in hadron collisions at Tevatron energies. DOE

N94-21543# Cornell Univ., Ithaca, NY. Ward Lab.

ELECTRON EMISSIONS IN LOW ENERGY Ar(q+)-Ar COLLISIONS

J. Vancura and V. O. Kostroun 1992 4 p Presented at the 6th International Conference on Physics of Highly Charged Ions, Manhattan, KS, 28 Sep. - 2 Oct. 1992

(Contract DE-FG02-86ER-13519)

(DE93-040285; CONF-920948-19) Avail: CASI HC A01/MF A01

The spectra of electrons emitted Ar(q+) on Ar (8 less than or = q less than or = 16) collisions at 2.3 q keV were measured in the 30 to 400 eV energy range. With the exception of Ar(8+) on Ar, the overall appearance of the electron spectra is quite similar, suggesting that the same mechanism is responsible for the observed features. One possible mechanism is the delocalization of the 3p and 3s target electrons during the collision. The resulting molecular state either deexcites by Auger transitions during the collision, or strands two or more electrons on the projectile in an excited state. This state in turn deexcites by Auger transitions. DOE

N94-21553# Los Alamos National Lab., NM.

PHOTOEMISSION AND THE ELECTRONIC PROPERTIES OF HEAVY FERMIONS: LIMITATIONS OF THE KONDO MODEL

J. J. Joyce, A. J. Arko, A. B. Andrews, R. I. R. Blyth, J. D. Thompson, D. Fisk, P. S. Riseborough, P. C. Canfield, C. G. Olson, and P. G. Benning 1993 13 p Presented at the International Conference on Strongly Correlated Electron Systems, La Jolla, CA, 16-19 Aug. 1993

(Contract W-7405-eng-36)

(DE93-040191; LA-UR-93-3041; CONF-930865-8) Avail: CASI HC A03/MF A01

The electronic properties of Yb-based heavy fermions have been investigated by means of high resolution synchrotron radiation photoemission and compared with predictions of the Kondo model. The Yb heavy fermion photoemission spectra show massive disagreement with the Kondo model predictions (as calculated within the Gunnarsson-Schonhammer computational method). Moreover, the Yb heavy fermion photoemission spectra give very strong indications of core-like characteristics and compare favorably to purely divalent Yb metal and core-like Lu 4f levels. The heavy fermions YbCu2Si2, YbAgCu4, and YbAl3 were measured and shown to have lineshapes much broader and deeper in binding energy than predicted by the Kondo model. The lineshape of the bulk component of the 4f emission for these three heavy fermion materials was compared with that from Yb metal and the Lu 4f levels in LuAl3; the heavy fermion materials show no substantive spectroscopic differences from simple 4f levels observed in Yb metal and LuAl3. Also, the variation with temperature of the 4f lineshape was measured for Yb metal and clearly demonstrates that phonon broadening plays a major role in 4f level lineshape analysis and must be accounted for before considerations of correlated electron resonance effects are presumed to be at work. DOE

N94-21657# Oak Ridge National Lab., TN.

HADRONIC MOLECULES AND SCATTERING AMPLITUDES FROM THE NONRELATIVISTIC QUARK MODEL

T. Barnes 1993 7 p Presented at the Conference on Hadron, Como, Italy, 21-25 Jun. 1993

(Contract DE-AC05-84OR-21400)

(DE94-000377; CONF-9306134-2) Avail: CASI HC A02/MF A01

This report summarizes recent calculations of low-energy hadron-hadron scattering amplitudes in the nonrelativistic quark potential model, which assume that the scattering mechanism is a single interaction (usually OGE) followed by constituent interchange. We refer to the scattering diagrams as 'quark Born diagrams.' For the cases chosen to isolate this mechanism, I=2 pi pi, I=3/2 K pi, KN and NN, the results are usually in good agreement with experimental S-wave scattering amplitudes given standard potential-model parameters. These calculations also lead to predictions of vector-vector bound states, one of which may be the theta(1710). This assignment can be tested by searches for K bar-K pi pi and phi pi(exp 0) gamma decay modes of the theta(1710). DOE

N94-21658# Oak Ridge National Lab., TN.

PHOTOABSORPTION AND COMPTON SCATTERING IN IONIZATION OF HELIUM AT HIGH PHOTON ENERGIES

L. R. Andersson (Tennessee Univ., Knoxville.) and J. Burgdoerfer (Tennessee Univ., Knoxville.) 1993 8 p Presented at the 18th International Conference on the Physics of Electronic and Atomic Collisions, Aarhus, Denmark, 21-27 Jul. 1993

(Contract DE-AC05-84OR-21400)

(DE94-000380; CONF-930711-12) Avail: CASI HC A02/MF A01

Production of singly and doubly charged helium ions by impact of keV photons is studied. The ratio R(sub ph) = sigma(sub ph)(sup ++)/sigma(sub ph)(sup +) for photoabsorption is calculated in the photon-energy range 2-18 keV using correlated initial- and final-state wave functions. Extrapolation towards asymptotic photon energies yields R(sub ph)(omega goes to infinity) = 1.66% in agreement with previous predictions.

Ionization due to Compton scattering, which becomes comparable to photoabsorption above omega approximately 3 keV, is discussed. DOE

N94-21693# Brookhaven National Lab., Upton, NY.
SEARCHING FOR HIGH BARYON DENSITY AT THE AGS WITH ARC
S. H. Kahana, T. J. Schlagel, and Y. Pang Aug. 1993 4 p Presented at the 10th International Conference on Ultra-Relativistic Nucleus-Nucleus Collisions, Borlenge, Sweden, 20-24 Jun. 1993
(Contract DE-AC02-76CH-00016)
(DE93-041155; BNL-49432; CONF-930636-1) Avail: CASI HC A01/MF A01

A relativistic cascade ARC is used to analyze heavy ion experiments at the AGS. In particular predictions from ARC for Au on Au at 11.6 GeV/c have proved to be remarkably accurate. Going to lower energies and inserting a phenomenological equation of state into the cascade should lead to information about the interesting region of high baryon density. DOE

N94-21766 Purdue Univ., West Lafayette, IN.
ELECTRON EMISSION FROM NANOMETER-SIZE METALLIC CLUSTERS: ELECTRONIC STATES AND STRUCTURAL STABILITY OF SUPPORTED Au CLUSTERS
M. E. Lin, A. Ramachandra, R. P. Andres, and R. Reifenberger 1992 12 p Presented at the North Atlantic Treaty Organization-ARW Meeting on Manipulation of Atoms Under High Fields and Temperatures, Lyon, France, 6-10 Jul. 1992 Limited Reproducibility: More than 20% of this document may be affected by microfiche quality
(Contract DE-FG02-84ER-45162)
(DE93-040184; CONF-9207218-1) Avail: CASI HC A03

Techniques developed to measure the thermodynamic and electronic properties of a single metallic cluster with nanometer-size dimensions are described. Using these techniques, experiments that resolve the quantized energy spectrum of electrons in a nanometer-size cluster of metallic atoms at room temperature have been performed. Studies on the stability of the electron emission current from an individual nanometer-size cluster supported on a tungsten tip have been performed to learn more about the intrinsic stability of these nanometer-size objects. The data show abrupt jumps between different emission states that are revisited as time progresses. This phenomenon is attributed to a rearrangement of the duster structure and/or orientation on the substrate and provides new evidence of multiple 'isomeric' structures for small clusters of metallic atoms. DOE

N94-21775# Fermi National Accelerator Lab., Batavia, IL.
SUMMARY OF THE HADRONIC WEAK INTERACTION SESSION
G. Bock, D. A. Bryman (British Columbia Univ., Vancouver.), and T. Numao (British Columbia Univ., Vancouver.) Jul. 1993 8 p Presented at the Future Directions in Particle and Nuclear Physics at Multi-GeV Hadron Beam Facilities, Upton, NY, 4-6 Mar. 1993
(Contract DE-AC02-76CH-03000)
(DE94-000592; FNAL/C-93/197; TRI-PP-93-68; CONF-930389-23) Avail: CASI HC A02/MF A01

We summarize and discuss present and future experiments on decays of light mesons and muons that were presented in the Hadronic Weak Interaction working group session of the Workshop on Future Directions in Particle and Nuclear Physics at Multi-GeV Hadron Facilities. Precise measurements and rare-decay searches, which sense mass scales in the 1-1000 TeV region, are discussed in the context of the standard model and beyond. DOE

N94-21785# Oak Ridge National Lab., TN.
SINGLE AND DOUBLE IONIZATION OF HELIUM BY HIGH-ENERGY PHOTON IMPACT
L. R. Andersson and J. Burgdoerfer 1993 19 p Presented at the 18th International Conference on the Physics of Electronic and Atomic Collisions, Aarhus, Denmark, 21-27 Jul. 1993
(Contract DE-AC05-84OR-21400)
(DE94-000381; CONF-930711-3) Avail: CASI HC A03/MF A01

Production of singly and doubly charged helium ions by impact of keV photons is studied. The ratio R(sub ph) = sigma(sub ph)(sup ++)/sigma(sub ph)(sup +) for photoabsorption is calculated in the photon-energy range 2-18 keV using correlated initial- and final-state wave functions. Extrapolation towards asymptotic photon energies yields R(sub ph)(omega approaches infinity) = 1.66% in agreement with previous predictions. Ionization due to Compton scattering, which becomes comparable to photoabsorption above omega approximately 3 keV, is discussed. DOE

N94-21786# Fermi National Accelerator Lab., Batavia, IL.
RECENT RESULTS ON TOP, BOTTOM AND EXOTIC PHYSICS AT THE TEVATRON
N. M. Shaw Aug. 1993 16 p Presented at the Workshop on Physics at Current Accelerators and the Supercollider, Argonne, IL, 2-5 Jun. 1993
(Contract DE-AC02-76CH-03000)
(DE94-000578; FNAL/C-93/263-E; CONF-9306176-6) Avail: CASI HC A03/MF A01

A summary of results from the recently concluded 1991-1993 Tevatron run is presented. Selected topics from b physics and exotic particle searches from the CDF and D0 collaborations are reviewed. Preliminary results from the CDF top search, using 12pb(exp -1) from the 1992-1993 run, are given. In particular, the lepton + b-tag and dilepton analyses are discussed. Preliminary results from the CDF dilepton analysis places a lower limit on the top quark mass of 108GeV/c(exp 2) at the 95% C.L. DOE

N94-21788 Stanford Linear Accelerator Center, CA.
SLAC MEASUREMENT OF THE NEUTRON SPIN STRUCTURE FUNCTION
E. Hughes Apr. 1993 6 p Presented at the 28th Conference on Quantum Chromodynamics and High Energy Hadronic Interactions, Les Arcs, France, 13-27 Mar. 1993 Limited Reproducibility: More than 20% of this document may be affected by microfiche quality
(Contract DE-AC03-76SF-00515)
(DE93-040998; SU-SLAC-PUB-6217; CONF-930363-9) Avail: CASI HC A02

A measurement of the nucleon spin asymmetries from deep inelastic scattering of polarized electrons by polarized He-3 has been performed. The neutron spin structure function g(sub 1)(exp n) is extracted and used to test the Bjorken sum rule. The neutron integral assuming a simple Regge theory extrapolation at low x is integral (sub 0)(sup 1)g(sub 1)(exp n)(x)dx = -0.022 (plus/minus) 0.011. Combined with the EMC proton results, the Bjorken sum rule predicts a neutron integral of integral(sub 0)(sup 1) g(sub 1)(exp n)(x)dx = -0.065 (plus/minus) 0.018. DOE

N94-21806# Fermi National Accelerator Lab., Batavia, IL.
MEASUREMENT OF THE B MESON AND b QUARK CROSS-SECTION IN (-p)p COLLISIONS AT THE SQUARE ROOT OF s = 1.8 TeV USING THE EXCLUSIVE DECAYS B(+) AND B(EXP 0) YIELDS J/PSIK*(EXP 0)
Aug. 1993 9 p Presented at the Symposium on Lepton and Photon Interactions, Ithaca, NY, 10-15 Aug. 1993
(Contract DE-AC02-76CH-03000)
(DE93-019907; FNAL/C-93/200-E; CONF-930823-8) Avail: CASI HC A02/MF A01

The production of b quarks in p(bar p) collisions in the Collider Detector at Fermilab (CDF), using the B meson decay channels B(+) yields J/(psi)K(+) and B(sup 0) yields J/(psi)K(*0), with J/(psi) yields mu(+)mu(-) and K(*0) yields K(+)pi(-), and their charge conjugates. Measurements of the B meson with b quark cross-sections integrated above minimum transverse momentum values in the rapidity range absolute value of y is less than 1 are described. The first fully differential B meson cross-section measurement in the same rapidity range is also reported. Comparison is made to previous CDF measurements and to the O(alpha(sub s)(sup 3)) theoretical calculations. DOE

N94-21840# Fermi National Accelerator Lab., Batavia, IL.
SEARCH FOR EXCITED QUARKS IN p(-p) COLLISIONS AT THE SQUARE ROOT OF s = 1.8 TeV
Aug. 1993 12 p Presented at the Symposium on Lepton and Photon Interactions, Ithaca, NY, 10-15 Aug. 1993
(Contract DE-AC02-76CH-03000)
(DE93-019910; FNAL/C-93/205-E; CONF-930823-9) Avail: CASI HC A03/MF A01

If quarks are composite particles, then excited states are expected in p(bar-p) collisions. Using the CDF detector we have searched for excited quarks (q*) which decay to common quarks by emitting a W boson (q*

yields qW) or a photon (q* yields q(gamma)). In the W + jet and photon + jet mass spectra we see no compelling evidence for a q* mass resonance. We set an upper limit on the q* cross section vs. mass, and using the simplest model of excited quark production, we exclude excited quarks in the mass range 90 less than M* less than 570 GeV at 95% confidence level. This analysis is preliminary and only statistical uncertainties have been included. DOE

N94-21847# Fermi National Accelerator Lab., Batavia, IL.
THE LEPTON CHARGE ASYMMETRY IN THE DECAY OF W BOSONS PRODUCED IN P(BAR P) COLLISIONS AT (RADICAL)S = 1.8 TeV
Aug. 1993 11 p Presented at the Symposium on Lepton and Photon Interactions, Ithaca, NY, 10-15 Aug. 1993
(Contract DE-AC02-76CH-03000)
(DE93-019903; FNAL/C-93/209-E; CONF-930823-6) Avail: CASI HC A03/MF A01

The charge asymmetry as a function of rapidity, A(y(sub l)), has been measured using the W decays to electrons and muons recorded by CDF during the 1992-93 run of the Tevatron Collider at Fermilab. The luminosity used, approximately 20 pb(sup -1), and detector improvements have lead to a six fold increase in statistics (in the plug region the increase is almost an order of magnitude) making discrimination between sets of parton distributions possible. Our data favors the most recent parton distributions and demonstrates the growing value of collider data in the measurement of the proton's structure. DOE

N94-21867# Fermi National Accelerator Lab., Batavia, IL.
RECENT FERMILAB RESULTS ON HADROPRODUCTION OF HEAVY FLAVORS
P. H. Garbincius Aug. 1993 29 p Presented at the Conference on Hadron, Como, Italy, 21-25 Jun. 1993
(Contract DE-AC02-76CH-03000)
(DE94-000595; FNAL/C-93/238; CONF-9306134-3) Avail: CASI HC A03/MF A01

Recent results from various Fermilab experiments on the hadroproduction of states containing charm, bottom, and top quarks are discussed. These include observation of the spectra, lifetime, and production characteristics of charmonium, open charm states, and bottom particle production with both high energy fixed target and (p bar)-p collider facilities. The status of the search for the top quark by the Fermilab collider experiments is updated. DOE

N94-21941# Argonne National Lab., IL.
STUDIES OF THE DEUTERON AT HIGH ENERGY AND MOMENTUM TRANSFER
R. J. Holt 1993 14 p Presented at the Workshop on Electron Nucleus Scattering, Elba, Italy, 5-10 Jul. 1993
(Contract W-31-109-eng-38)
(DE93-041162; ANL/PHY/CP-80703; CONF-9307145-1) Avail: CASI HC A03/MF A01

Measurements of the tensor analyzing power T(20) are in progress at the 2-GeV electron storage ring (VEPP-3) in Novosibirsk. Preliminary results from the second phase of this experiment will be presented along with a discussion of the theoretical implications of the existing data. Measurements of the (gamma)d yields pn reaction at photon energies above approximately 1 GeV were performed at SLAC during experiments NE8 and NE17. The results for experiment NE8 are final while those for NE17 are preliminary. The results appear to be consistent with the constituent scaling law near theta(sub CM) = 90 degrees, but inconsistent with the rule at a forward angle. DOE

N94-21951# Argonne National Lab., IL.
DIRECT DETECTION OF ATOMIC IONS FROM MOLECULAR PHOTOFRAGMENTATION DURING NONRESONANT MULTIPHOTON IONIZATION OF SPUTTERED SPECIES
S. R. Coon, W. F. Calaway, M. J. Pellin, J. W. Burnett (Ames Lab., IA.), and J. M. White 1993 17 p
(Contract W-31-109-eng-38)
(DE93-040886; ANL/CHM/PP-79176) Avail: CASI HC A03/MF A01

The photoionization of sputtered Cu, Al, and Ru atoms and dimers was investigated by measuring velocity distributions using both resonant and nonresonant photoionization. Nonresonant ionization produced an atomic distribution that peaked at the same velocity as the respective dimer distribution, indicating that virtually all the nonresonant atomic ion signal is from photofragmented dimers. Various mechanisms of dimer photofragmentation are discussed. Domination of the atomic photoion channel by molecule fragmentation appears to be a general phenomenon that must be accounted for in all gas-phase multiphoton nonresonant ionization experiments at easily achievable laser power densities (less than or equal to 10(exp 9) W/cm(exp 2)). DOE

N94-21961# Tennessee Univ., Knoxville.
SYMMETRY-DICTATED TRUCATION: SOLUTIONS OF THE SPHERICAL SHELL MODEL FOR HEAVY NUCLEI
M. W. Guidry (Oak Ridge National Lab., TN.) 1992 18 p Presented at the Workshop on Nuclear Physics in the Universe, Oak Ridge, TN, 24-26 Sep. 1992
(Contracts DE-AC05-84OR-21400; DE-FG05-93ER-40770)
(DE94-000482; CONF-9209239-8) Avail: CASI HC A03/MF A01

Principles of dynamical symmetry are used to simplify the spherical shell model. The resulting symmetry-dictated truncation leads to dynamical symmetry solutions that are often in quantitative agreement with a variety of observables. Numerical calculations, including terms that break the dynamical symmetries, are shown that correspond to shell model calculations for heavy deformed nuclei. The effective residual interaction is simple, well-behaved, and can be determined from basic observables. With this approach, we intend to apply the shell model in systematic fashion to all nuclei. The implications for nuclear structure far from stability and for nuclear masses and other quantities of interest in astrophysics are discussed. DOE

N94-21962# Fermi National Accelerator Lab., Batavia, IL.
TOWARD A QCD ANALYSIS OF JET RATES IN DEEP-INELASTIC MUON-PROTON SCATTERING
C. W. Salgado Aug. 1993 8 p Presented at the Workshop on Physics At Current Accelerators and the Supercollider, Argonne, IL, 2-5 Jul. 1993
(Contract DE-AC02-76CH-03000)
(DE94-000618; FNAL/C-93/251; CONF-9306176-7) Avail: CASI HC A02/MF A01

Measurements of multi-jet production rates in deep-inelastic Muon-Proton scattering at Fermilab-E665 are presented. Jet rates defined by the JADE clustering algorithm are compared to perturbative quantum chromodynamics (PQCD) and different Monte Carlo model predictions. The applicability of the jet-parton duality hypothesis is studied. We obtain hadronic jet rates which are approximately a factor of two higher than PQCD predictions at the parton level. Possible causes for this discrepancy are discussed. DOE

N94-21968# Lawrence Livermore National Lab., CA.
NON-ADIABATIC EFFECTS IN LOW-ENERGY ELECTRON-MOLECULE SCATTERING
T. N. Rescigno Jul. 1993 16 p Presented at the ICPEAC: Satellite Meeting on Electron Collision with Molecules, Clusters and Surfaces, London, England, 29-30 Jul. 1993
(Contract W-7405-eng-48)
(DE93-040485; UCRL-JC-114340; CONF-930717-1) Avail: CASI HC A03/MF A01

In this talk, I will show how the complex Kohn method which has been successfully applied to electronically elastic and inelastic electron scattering by both diatomic and polyatomic targets, can be modified to provide a computational tool for variational evaluation of the off-shell T-matrix in a completely general ab initio context. In the following section, I will give a brief outline of the theory. I will then illustrate the method by showing results we have recently obtained for vibrational excitation of both H2 and CH4 by low-energy electron impact. DOE

N94-21995# Los Alamos National Lab., NM.
INTERACTIONS OF SLOW H, H2, AND H3 WITH THIN FOILS
H. O. Funsten, B. L. Barraclough, and D. J. McComas 1993 12 p Presented at the ICACS 15th International Conference on Atomic Collision in Solids, London, Ontario, 26-30 Jul. 1993
(Contract W-7405-eng-36)

(DE93-040263; LA-UR-93-2790; CONF-930712-5) Avail: CASI HC A03/MF A01

Interaction processes resulting from the transit of incident 2-30 keV H(+), H2, and H3(+) through 1.2 to 2.5 mu-g/sq cm carbon foils are investigated by examining the charge state and angular scatter distributions of atomic and molecular species that exit the foils. A comparison of the scatter distributions of exiting H2(+) and H(0) show that H fragments from the same incident molecule that recombine to form H2 after transiting a foil scatter independently (i.e., not as a molecule) from foil atoms. The measured fractions of H2(+) from incident H2(+) and H3(+) are found to be dependent on the angular scatter half-width, but expected enhancements of this fraction for incident H3(+), due to the presence of an additional proton, are not observed within the experimental error. However, the observed fraction of H(0) is enhanced by approximately 2% for incident H2(+) and 4% for H3(+) relative to that observed using incident protons. This is evidence for a proximity effect at the exit surface of the foil in which the electron capture probability by one proton is enhanced by another proton in close proximity. DOE

N94-22009 Continuous Electron Beam Accelerator Facility, Newport New, VA.

PRODUCTION, COLLECTION AND UTILIZATION OF VERY LONG-LIVED HEAVY CHARGED LEPTONS

J. L. Goity, W. J. Kossler (College of William and Mary, Williamsburg, VA.), and M. Sher (College of William and Mary, Williamsburg, VA.) 1993 10 p Limited Reproducibility: More than 20% of this document may be affected by poor print

(Contract DE-AC05-84ER-40150)

(DE93-040867; DOE/ER-40150/238; CEBAF-TH-93-07) Avail: Issuing Activity (Department of Energy (DOE))

If a fourth generation of leptons exists, both the neutrino and its charged partner must be heavier than 45 GeV. We suppose that the neutrino is the heavier of the two, and that a global or discrete symmetry prohibits intergenerational mixing. In that case, non-renormalizable Planck scale interactions will induce a very small mixing; dimension five interactions will lead to a lifetime for the heavy charged lepton of O(1-100) years. Production of such particles is discussed, and it is shown that a few thousands can be produced and collected at a linear collider. The possible uses of these heavy leptons is also briefly discussed. DOE

N94-22049# Wisconsin Univ., Milwaukee.

INELASTIC ELECTRON SCATTERING FROM SURFACES

1993 26 p

(Contract DE-FG02-84ER-45076)

(DE94-001738; DOE/ER-45076/3) Avail: CASI HC A03/MF A01

This program is aimed at the quantitative study of surface dynamical processes (vibrational, magnetic excitations) in crystalline slabs, ultrathin-layered materials, and chemisorbed systems on substrates, and of the geometric structure connected to these dynamical excitations. High resolution electron energy loss spectroscopy (HREELS) is a powerful probe. Off-specular excitation cross sections are much larger if electron energies are in the LEED range (50-300 eV). The analyses has been used to study surfaces of ordered alloys (NiAl). Ab-initio surface lattice dynamical results were combined with phonon-loss cross sections to achieve a more accurate microscopic description. First-principles phonon eigenvectors and eigenfrequencies were used as inputs to electron energy loss multiple scattering cross section calculations. The combined microscopic approach was used to analyze EELS data of Cu(0001) and Ag(001) at two points. Positron diffraction is discussed as a structural and imaging tool. Future research plans are presented. DOE

N94-22271 Institut des Hautes Etudes Scientifiques, Bures-sur-Yvette (France).

PROOF OF STABILITY OF THE HYDROGEN MOLECULE

J.-M. Richard, J. Foehlich (Eidgenoessische Technische Hochschule, Zurich, Switzerland.), G. M. Graf (Eidgenoessische Technische Hochschule, Zurich, Switzerland.), and M. Seifert (Eidgenoessische Technische Hochschule, Zurich, Switzerland.) May 1993 11 p Limited Reproducibility: More than 20% of this document may be affected by microfiche quality

(PB93-221026; IHES/P/93/23) Avail: CASI HC A03

The authors sketch two rigorous proofs of the stability of the hydrogen molecule in quantum mechanics. The first one is based on an extrapolation of variational estimates of the ground state energy of a positronium molecule to arbitrary mass ratios. The second one is an extension of Heitler-London theory to nuclei of finite mass. NTIS

N94-22396# Lawrence Livermore National Lab., CA.

COMPUTER SIMULATION OF MOLECULAR RESPONSE AT A SHOCK FRONT

J. Belak Jul. 1993 6 p Presented at the 14th International Conference of the International Association for the Advancement of High Pressure Science and Technology, Colorado Springs, CO, 27 Jun. - 2 Jul. 1993

(Contract W-7405-eng-48)

(DE94-001050; UCRL-JC-113400; CONF-930676-60) Avail: CASI HC A02/MF A01

Molecular dynamics simulations of the response of small molecules at a shock front are presented. The simulations are performed in the reference frame of the shock and the results provide a unique insight into the sequence of states through which the material transforms during shock loading. The calculated up-pumping time (time for the translational and vibrational kinetic energy to equilibrate) for small molecules is quite fast, a few picoseconds for butane and about 10 ps for nitromethane. This is somewhat faster than the 100 ps suggested by a recent experiment. DOE

N94-22400# Lawrence Livermore National Lab., CA.

SMOOTHED-PARTICLE HYDRODYNAMICS AND NONEQUILIBRIUM MOLECULAR DYNAMICS

W. G. Hoover and C. G. Hoover Aug. 1993 14 p Presented at the Annual Winter Meeting of the ASME, New Orleans, LA, 28 Nov. - 3 Dec. 1993

(Contract W-7405-eng-36)

(DE94-001059; UCRL-JC-114311; CONF-931121-25) Avail: CASI HC A03/MF A01

Gingold, Lucy, and Monaghan invented a grid-free version of continuum mechanics 'smoothed-particle hydrodynamics,' in 1977. It is a likely contributor to 'hybrid' simulations combining atomistic and continuum simulations. We describe applications of this particle-based continuum technique from the closely-related standpoint of nonequilibrium molecular dynamics. We compare chaotic Lyapunov spectra for atomistic solids and fluids with those which characterize a two-dimensional smoothed-particle fluid system. DOE

N94-22416 Carleton Univ., Ottawa (Ontario). Dept. of Physics.

A MONTE CARLO STUDY OF THE SUDBURY NEUTRINO OBSERVATORY SMALL TEST DETECTOR EXPERIMENT M.S. Thesis

Alan B. Yeung 29 Jan. 1990 73 p

(ISBN-0-315-59056-4; CTN-94-60883) Copyright Avail: Micromedia Ltd., Technical Information Centre, 240 Catherine Street, Suite 305, Ottawa, Ontario, K2P 2G8, Canada HC/MF

A Monte Carlo study of the Sudbury Neutrino Observatory's small-scale prototype detector experiment is presented. This detector, called the Small Test Detector, consists of a cylindrical water-filled tank with 43 photomultiplier tubes arranged in a cylindrical array facing the center of the tank. Electrons are fired into the center of the tank at energies in the 2-11 MeV range and the responses of the photomultipliers are recorded for single electron events. The Monte Carlo simulation breaks down the electron's trajectory into small steps or cells; photons are simulated in a similar way to electrons. The modelling of the electromagnetic interactions that occur as a result of electrons entering the water (multiple scattering, bremsstrahlung, ionization energy loss, Cerenkov radiation, Compton scattering, and pair production by photons) is described. The simulated photoelectron yield as a function of incident electron energy, and the angular distributions of photomultiplier tube response for 3.0, 6.5, and 11.0 MeV electrons show excellent agreement with the experimental results. Author (CISTI)

N94-22572# Los Alamos National Lab., NM.

LIKELIHOOD ANALYSIS OF PARITY VIOLATION IN THE COMPOUND NUCLEUS

D. Bowman and E. Sharapov (Joint Inst. for Nuclear Research, Dubna, USSR.) 1993 11 p Presented at the International Workshop/Time Reversal Invariance and Parity Violation in Neutron Physics, Dubna, Russia, 4-7 May 1993

(Contract W-7405-eng-36)
(DE94-000671; LA-UR-93-3516; CONF-9305235-4) Avail: CASI HC A03/MF A01

We discuss the determination of the root mean-squared matrix element of the parity-violating interaction between compound-nuclear states using likelihood analysis. We briefly review the relevant features of the statistical model of the compound nucleus and the formalism of likelihood analysis. We then discuss the application of likelihood analysis to data on parity-violating longitudinal asymmetries. The reliability of the extracted value of the matrix element and errors assigned to the matrix element is stressed. We treat the situations where the spins of the p-wave resonances are not known and known using experimental data and Monte Carlo techniques. We conclude that likelihood analysis provides a reliable way to determine M and its confidence interval. We briefly discuss some problems associated with the normalization of the likelihood function. DOE

N94-22573# Ames Lab., IA.
INELASTIC NEUTRON SCATTERING OF (GAMMA)-IRON, AND THE DETERMINATION OF THE ELASTIC CONSTANTS BY LATTICE DYNAMICS
C. Stassis 1993 4 p Presented at the 14th International Conference of the Association for the Advancement of High Pressure Science and Technology, Colorado Springs, CO, 27 Jun. - 2 Jul. 1993
(Contract W-7405-eng-82)
(DE94-000694; IS-M-765; CONF-930676-57) Avail: CASI HC A01/MF A01

The physical properties of the various phases of iron have been the subject of numerous theoretical and experimental investigations. Of particular interest is the appearance of the fcc (gamma)-phase between approximately 1,200 K and 1,670 K. The authors were able to grow in situ single crystals of fcc iron of sufficient size to perform an inelastic neutron scattering study of the lattice dynamics of this phase of iron. The phonon dispersion curves along the (00(xi)), ((xi)(xi)0) and ((xi)(xi)(xi)) symmetry directions were measured at 1,428 K. A limited number of phonons were also measured at 1,227 K and 1,640 K to assess the temperature dependence of the phonon frequencies. The data collected at 1,428 K were used to evaluate the elastic constants, the phonon density of states and the lattice contribution to the specific heat. The measured dispersion curves of (gamma)-Fe are qualitatively similar to those of Ni (measured at 296 K) and Ni(0.3)Fe(0.7) (measured at 296 and 573 K). DOE

73 NUCLEAR AND HIGH-ENERGY PHYSICS

Includes elementary and nuclear particles; and reactor theory. For space radiation see *93 Space Radiation*.

N94-19856# Stanford Linear Accelerator Center, CA.
METHOD TO EVALUATE STEERING AND ALIGNMENT ALGORITHMS FOR CONTROLLING EMITTANCE GROWTH
C. Adolphsen and T. Raubenheimer Apr. 1993 3 p Presented at the International Particle Accelerator Conference, Washington, DC, 17-20 May 1993
(Contract DE-AC03-76SF-00515)
(DE93-041004; SLAC-PUB-6233; CONF-930511-436) Avail: CASI HC A01/MF A01

Future linear colliders will likely use sophisticated beam-based alignment and/or steering algorithms to control the growth of the beam emittance in the linac. In this paper, a mathematical framework is presented which simplifies the evaluation of the effectiveness of these algorithms. As an application, a quad alignment algorithm that uses beam data taken with the nominal linac optics, and with a scaled optics, is evaluated in terms of the dispersive emittance growth remaining after alignment. DOE

N94-19873# Stanford Linear Accelerator Center, CA.
A FIELD-BASED TECHNIQUE FOR THE LONGITUDINAL PROFILING OF ULTRARELATIVISTIC ELECTRON OR POSITRON BUNCHES DOWN TO LENGTHS OF LESS THAN OR EQUAL TO 10 MICRONS
R. Tatchyn May 1993 3 p Presented at the International Particle Accelerator Conference, Washington, DC, 17-20 May 1993
(Contract DE-AC03-76SF-00515)
(DE93-040954; SLAC-PUB-6105; SLAC/SSRL-0019; CONF-930511-419)
Avail: CASI HC A01/MF A01

Present and future generations of particle accelerating and storage machines are expected to develop ever-decreasing electron/positron bunch lengths, down to 100 microns and beyond. A method for measuring the longitudinal profiles of ultrashort (1000 microns - 10 microns) bunches, based on: (1) the extreme field compaction attained by ultrarelativistic particles, and (2) the reduction of the group velocity of a visible light pulse in a suitably-chosen dielectric medium, is outlined. DOE

N94-19945# Brookhaven National Lab., Upton, NY.
APERTURE DETERMINATION OF RHIC92 FROM RANDOMLY GENERATED INITIAL COORDINATES
G. F. Dell 1992 12 p Presented at the Workshop on the Stability of Particle Motion in Storage Rings, Upton, NY, 19-24 Oct. 1992
(Contract DE-AC02-76CH-00016)
(DE93-040174; BNL-49380; CONF-921077-13) Avail: CASI HC A03/MF A01

Results obtained by tracking 100 particles for 1,000 turns when initial coordinates are selected randomly, with the requirement that the total emittance be constant, are compared to results from 1,000-turn and 10(exp 6)-turn runs when initial coordinates satisfy epsilon(sub x)(i) = epsilon(sub y)(i) and X(sub i) prime = Y(sub i) prime = 0. For studies of ten distributions of magnetic field errors, the 100-particle results give apertures equivalent to those from 10(exp 6)-turn runs, have an aperture distribution of considerably less width, and yet require only one tenth the computer time. DOE

N94-19972# Fermi National Accelerator Lab., Batavia, IL.
A STUDY OF EVENTS WITH THE HIGHEST TOTAL TRANSVERSE ENERGY IN CDF
Aug. 1993 11 p Presented at the Symposium on Lepton and Photon Interactions, Ithaca, NY, 10-15 Aug. 1993
(Contract DE-AC02-76CH-03000)
(DE93-019904; FNAL/C-93/208-E; CONF-930823-3) Avail: CASI HC A03/MF A01

The properties of proton-antiproton interactions in which the total transverse energy exceeds 320 GeV are described. The events have been recorded at the Fermilab Tevatron collider operating at a center-of-mass energy of 1.8 TeV. The differential cross-section is in good agreement with the QCD predictions. DOE

N94-19983# Fermi National Accelerator Lab., Batavia, IL.
THE TWO-JET DIFFERENTIAL CROSS-SECTION AT CDF
Aug. 1993 11 p Presented at the Symposium on Lepton and Photon Interactions, Ithaca, NY, 10-15 Aug. 1993
(Contract DE-AC02-76CH-03000)
(DE93-019905; FNAL/C-93/201-E; CONF-930823-1) Avail: CASI HC A03/MF A01

Results for production of two or more hadronic jets at the square root of s = 1800 GeV at the Fermilab Tevatron are presented. The data are compared with the results predicted by perturbative quantum chromodynamics (QCD). Ratios of cross-sections are also given. DOE

N94-19988# Fermi National Accelerator Lab., Batavia, IL.
TOP SEARCH AT THE TEVATRON
Q. Li-Demarteau Jul. 1993 10 p Presented at the International Workshop on Physics and Instrumentation at Future Linear Colliders, Kona, HI, 26-30 Apr. 1993
(Contract DE-AC02-76CH-03000)
(DE93-019392; FNAL/C-93/223; CONF-930449-2) Avail: CASI HC A02/MF A01

Preliminary results on the top quark search at the TEVATRON are reported. The D(0) experiment, observing one candidate event in the e(mu) channel and combining the ee and e(mu) channel analyses, sets a lower limit of 103 GeV/sq c (99 GeV/sq c) for the top quark mass with (without) background subtraction at 95% confidence level. The CDF experiment, observing two candidate events, sets a top mass lower limit of 108 GeV/sq c at 95% confidence level for the ee, (mu)(mu) and e(mu) data combined, without background subtraction. Work is in progress at both experiments to reduce the backgrounds in the lepton + jets channel. DOE

N94-19989# California Univ., Berkeley. Lawrence Berkeley Lab.
STUDY OF TRANSVERSE COUPLED BUNCH INSTABILITIES BY USING NON-LINEAR TAYLOR MAPS FOR THE ADVANCED LIGHT SOURCE (ALS)
M. Meddahi and J. Bengtsson May 1993 3 p Presented at the International Particle Accelerator Conference, Washington, DC, 17-20 May 1993
(Contract DE-AC03-76SF-00098)
(DE93-040287; LBL-33226; ESG-219; CONF-930511-398) Avail: CASI HC A01/MF A01

To study coherent bunch instabilities for the third generation light source, ALS, it is insufficient to rely on a linear map with radiation damping for the lattice to obtain the correct dynamics. We have implemented a code for transverse bunch instabilities using a 4-dimensional map for the lattice and wake field expansions for cavities and resistive wall effects. This model has been used to study the injection process and to determine the needed performance of the proposed feedback system for the storage ring. DOE

N94-20117# Nationaal Inst. voor Kernfysica en Hoge Energiefysica, Amsterdam (Netherlands).
CONTROL AND READOUT OF THE EXTRACTION SEPTUM OF AmPS [BESTURING EN UITLEZING VAN HET EXTRACTIESEPTUM VAN AMPS]
J. T. VanEs, G. Luigjes, and J. H. VanTrigt 1993 21 p In DUTCH
(DIGEL-1993-2; ETN-93-94623) Avail: CASI HC A03/MF A01

The electronics used for the septum translation-rotation control system and for the control of the 100 kV power supply of the electrostatic septum of the storage ring AmPS (Amsterdam Pulse Stretcher) are described. The translation and rotation of the septum are performed by stepping motors controlled by LVDT's (Linear Variable Differential Transformers), which are controlled by a bitbus module which also controls the high voltage power supply. ESA

N94-20118# Nationaal Inst. voor Kernfysica en Hoge Energiefysica, Amsterdam (Netherlands).
NEW PREAMPLIFIERS FOR THE SEM SCANNER [NIEUWE PRE-AMPLIFIERS VOOR DE SEM-SCANNER]
H. Verkooijen 1993 4 p In DUTCH Revised
(DIGEL-1993-3; DIGEL-1979-5; ETN-93-94624) Avail: CASI HC A01/MF A01

Preamplifiers for the Secondary Emission Monitor (SEM) of the storage ring AmPS (Amsterdam Pulse Stretcher) are reported. The electron bundle causes secondary emission in the 20 aluminum foils composing the monitor. The magnitude of the secondary emission is a measure of the bundle current. The preamplifiers for the signals from the foils had to be modified because the bundle current was increased and the bundle pulse duration decreased. The existing design was taken into account as much as possible. ESA

N94-20123# Nationaal Inst. voor Kernfysica en Hoge Energiefysica, Amsterdam (Netherlands).
BUNDLE PROFILE MONITOR FOR AmPS [BUNDEL PROFIEL MONITOR VOOR AMPS]
M. G. VanBeuzekom and J. T. VanEs 1992 34 p In DUTCH
(DIGEL-1992-8; ETN-93-94903) Avail: CASI HC A03/MF A01

The Bundle profile monitor apparatus for the measurement of the profile of the electron bundle in the storage ring AmPS (Amsterdam Pulse Stretcher) is described. The monitors are used in the injection line of AmPS to determine the bundle profile before and after the injection septum. The circuitry of the preamplifier, the sampling electronics, and the control procedure of the preamplifier are described. ESA

N94-20216# Fermi National Accelerator Lab., Batavia, IL.
JET SHAPES IN HADRON AND ELECTRON COLLIDERS
N. Wainer May 1993 13 p Presented at the 1993 Rencontres de Physique de la Vallee d'Aoste, LaThuile, Italy, 8-13 Mar. 1993
(Contract DE-AC02-76CH-03000)
(DE93-019386; FNAL/C-93/122-E; CONF-9303172-3) Avail: CASI HC A03/MF A01

High energy jets are observed both in hadronic machines like the Tevatron and electron machines like LEP. These jets have an extended structure in phase space which can be measured. This distribution is usually called the jet shape. There is an intrinsic relation between jet variables, like energy and direction, the jet algorithm used, and the jet shape. Jet shape differences can be used to separate quark and gluon jets. DOE

N94-20222# Argonne National Lab., IL.
FACILITIES FOR IN SITU ION BEAM STUDIES IN TRANSMISSION ELECTRON MICROSCOPES
C. W. Allen, S. Ohnuki (Hokkaido Univ., Sapporo, Japan.), and H. Takahashi (Hokkaido Univ., Sapporo, Japan.) Aug. 1993 5 p Presented at the 3rd International Conference on Advanced Materials, Tokyo, Japan, 31 Aug. - 4 Sep. 1993
(Contract W-31-109-eng-38)
(DE93-019567; ANL/MSD/CP-79635; CONF-9308122-3) Avail: CASI HC A01/MF A01

Interfacing an ion accelerator to a transmission electron microscope (TEM) allows the analytical functions of TEM imaging and electron diffraction from very small regions to be employed during ion-irradiation effects studies. Presently, there are ten such installations in Japan, one in France, and one in the USA. General specifications of facilities which are operational in 1993 are summarized, and additional facilities which are planned or being proposed are briefly described. DOE

N94-20273# California Univ., Berkeley. Lawrence Berkeley Lab.
EMITTANCE MEASUREMENT AND MODELING OF THE ALS 50 MeV LINAC TO BOOSTER LINE
J. Bengtsson, W. Leemans, and T. Byrne May 1993 6 p Presented at the International Particle Accelerator Conference, Washington, DC, 17-20 May 1993
(Contract DE-AC03-76SF-00098)
(DE93-040116; LBL-33309; CONF-930511-396) Avail: CASI HC A02/MF A01

The Twiss parameters and emittance have been measured for the ALS LINAC through nonlinear chi(exp 2) fitting of the measured beam size (fixed location) vs. focal strength of a quadrupole triplet. The obtained values have been used to calculate the expected beam size and dispersion along the linac-to-booster transport line giving good agreement with measurements. The efforts resulted in superior injection into the booster. DOE

N94-20274# California Univ., Berkeley. Lawrence Berkeley Lab.
STUDY OF COUPLED-BUNCH COLLECTIVE EFFECTS IN THE PEP-2 B-FACTORY
J. Byrd May 1993 6 p Presented at the International Particle Accelerator Conference, Washington, DC, 17-20 May 1993
(Contract DE-AC03-76SF-00098)
(DE93-040117; LBL-33272; ESG-230; CONF-930511-397) Avail: CASI HC A02/MF A01

We present an overview of the calculated longitudinal and transverse coupled-bunch (CB) growth using the measured RF cavity higher order mode impedance and estimated resistive wall (RW) impedance for the proposed PEP-2 B-Factory, a dual-ring electron-positron collider. We also describe a visual method of representing the effective beam impedance and corresponding growth rates which is especially useful for understanding the dependence of growth rate on higher order mode frequency and Q, spread of HOM frequencies between cells, and for determining the requirements of the CB feedback systems. DOE

N94-20289# California Univ., Berkeley. Lawrence Berkeley Lab.
HIGH CURRENT INJECTOR FOR HEAVY ION FUSION
S. Yu, S. Eylon, and W. W. Chupp May 1993 14 p Presented at the International Symposium on Heavy Ion Fusion, Frascati, Italy, 25-28 May 1993
(Contract DE-AC03-76SF-00098)
(DE93-019241; LBL-33806; HIFAN-585; CONF-9305136-9) Avail: CASI HC A03/MF A01

A 2 MV, 800 mA, K(+) injector for heavy ion fusion studies is under construction. This new injector is a one-beam version of the proposed 4-beam ILSE injector. A new 36-module MARX is being built to achieve a 5 micro-s flat top. The high voltage generator is stiff (less than 5k Omega) to minimize effects of beam-induced transients. A large (approximately 7 in. diameter) curved hot alumina-silicate source emits a 1 micro-s long beam pulse through a gridless extraction electrode, and the ions are

accelerated to 1 MV in a diode configuration. Acceleration to 2 MV takes place in a set of electrostatic quadrupole (ESQ) units, arranged to simultaneously focus and accelerate the ion beam. Heavy shields and other protection devices have been built in to minimize risks of high voltage breakdown. Beam aberration effects through the ESQ have been studied extensively with theory, simulations, and scaled experiments. The design, simulations, experiments, and engineering of the ESQ injector will be presented. DOE

N94-20290# California Univ., Berkeley. Lawrence Berkeley Lab.
LONGITUDINAL INSTABILITY OF AN INDUCTION LINAC WITH ACCELERATION
L. Smith and E. P. Lee May 1993 7 p Presented at the International Particle Accelerator Conference, Washington, DC, 17-20 May 1993
(Contract DE-AC03-76SF-00098)
(DE93-019249; LBL-33288; HIFAN-573; CONF-930511-365) Avail: CASI HC A02/MF A01

The question arises as to what effect acceleration, which so far has been ignored, has on the longitudinal instability of an induction linac. The answer is not much for the anticipated acceleration rate (1-2 MeV/m) and minimum e-folding distance for the instability (50-500 m). However, total unstable growth is significantly reduced over distances which are long enough for appreciable acceleration to occur. The purpose of this note is to record a calculation of the instability including a constant acceleration rate. Some interesting features emerge--for example, the velocity of the head is a more convenient independent variable than axial position and, for an initial sinusoidal perturbation of velocity in time, the number of oscillations along the pulse is constant; however, as the pulse shortens in time the frequency increases. DOE

N94-20292# California Univ., Berkeley. Lawrence Berkeley Lab.
MEASUREMENT AND COMPUTATION OF THE HIGHER ORDER MODES OF THE ALS 500 MHz ACCELERATING CAVITIES
J. N. Corlett and J. M. Byrd May 1993 6 p Presented at the International Particle Accelerator Conference, Washington, DC, 17-20 May 1993
(Contract DE-AC03-76SF-00098)
(DE93-019256; LBL-33278; ESG-233; CONF-930511-372) Avail: CASI HC A02/MF A01

Higher order modes in the accelerating cavities are expected to drive coupled bunch instabilities in the ALS, which will be overcome by a bunch-by-bunch feedback system. Computations of the cavity higher order modes using the URMEL-T and MAFIA codes are presented. Damping of the higher order modes is achieved by filters in the high power feeder waveguide which is aperture coupled to the cavity. Measurements of the modes in an ALS 500 MHz cavity are presented and compared with computed values for an isolated, un-damped cavity. The resources of the Lambertson Beam Electrodynamics Laboratory of the Center for Beam Physics at LBL were used to perform these studies. DOE

N94-20295# Sandia National Labs., Albuquerque, NM.
OBSERVATION OF REFLECTED WAVES ON THE SABRE POSITIVE POLARITY INDUCTIVE ADDER MITL
M. E. Cuneo, J. W. Poukey, C. W. Mendel, S. E. Rosenthal, D. L. Hanson, J. R. Smith, J. E. Maenchen, D. F. Wenger, and M. A. Bernard 1993 5 p Presented at the 9th IEEE Pulsed Power Conference, Albuquerque, NM, 21-23 Jun. 1993
(Contract DE-AC04-76DP-00789)
(DE93-019413; SAND-92-2812C; CONF-930616-30) Avail: CASI HC A01/MF A01

We are studying the coupling of extraction applied-B ion diodes to Magnetically Insulated Transmission Lines (MITL's) on the SABRE (Sandia Accelerator and Beam Research Experiment, 6 MV, 300 kA) positive polarity inductive voltage adder. Our goal is to determine the conditions under which efficient coupling occurs. The best total power efficiency for an ideal ion diode load (i.e., without parasitic losses) is obtained by maximizing the product of cathode current and gap voltage. MITL's require that the load impedance be undermatched to the self-limited line operatingimpedance for efficient transfer of power to ion diodes, independent of transit time isolation, and even in the case of multiple cathode system with significant vacuum electron flow. We observe that this undermatched condition results in a reflected wave which decreases the line voltage and gap electron sheath current, and increases the anode and cathode current in a time-dependent way. The MITL diode coupling is determined by the flow impedance at the adder exit. We also show that the flow impedance increases along the extension MITL on SABRE. Experimental measurements of current and peak voltage are compared to analytical models and TWOQUICK 2.5-D PIC code simulations. DOE

N94-20300# Lawrence Livermore National Lab., CA.
ENERGY AND LUMINOSITY LIMITS OF HADRON SUPERCOLLIDERS
W. A. Barletta May 1993 6 p Presented at the International Particle Accelerator Conference, Washington, DC, 17-20 May 1993
(Contract DE-AC03-76SF-00098)
(DE93-019248; LBL-34068; CONF-930511-377) Avail: CASI HC A02/MF A01

Extending the frontiers of experimental high energy physics in a manner that maximizes discovery potential requires the building of accelerators of ever higher particle energies and luminosities. Both hadron and e(+)e(-) colliders have been proposed for this role. Based on a self-consistent computational model, this paper explores the features of hadron supercolliders beyond the SSC. The application of the presently available accelerator technologies embodied in the designs of the LHC and SSC to an ELOISATRON operating at 100 TeV per beam would yield a collider with a luminosity of 10(exp 34) cm(exp -2) s(exp -1). Even higher energies and luminosities are clearly possible. The paper concludes with an examination of the ultimate potential of synchrontron-based colliders to explore PeV energies. DOE

N94-20317 Fermi National Accelerator Lab., Batavia, IL.
DIRECT PHOTON RESULTS FROM CDF
Aug. 1993 22 p Presented at the Symposium on Lepton and Photon Interactions, Ithaca, NY, 10-15 Aug. 1993 Limited Reproducibility: More than 20% of this document may be affected by microfiche quality
(Contract DE-AC02-76CH-03000)
(DE93-019908; FNAL/C-93/202-E; CONF-930823-10) Avail: CASI HC A03

Results using isolated direct photons measured with the CDF detector during the 1992-1993 run of the Fermilab Tevatron are presented. Photon detection and background subtraction are described. Measurement of the inclusive photon cross section as well as photon-jet cross sections are discussed and compared to next-to-leading order QCD predictions. DOE

N94-20475# California Univ., Berkeley. Lawrence Berkeley Lab.
ELECTRON QUANTUM YIELDS FROM A BARIUM PHOTOCATHODE ILLUMINATED WITH POLARIZED LIGHT
M. E. Conde, S. Chattopadhyay, K. J. Kim, S. I. Kwon, K. N. Leung, and A. T. Young May 1993 5 p Presented at the International Particle Accelerator Conference, Washington, DC, 17-20 May 1993
(Contract DE-AC03-76SF-00098)
(DE93-019232; LBL-33303; ESG-236; CONF-930511-376) Avail: CASI HC A01/MF A01

Photoemission measurements with a barium photocathode and a nitrogen laser are reported. The cathode is prepared by evaporating barium onto a copper disc. Radiation from a nitrogen laser (337 nm, 10 ns) is polarized and strikes the cathode surface at variable angles. An electron quantum yield as high as 1 x 10(sup -3) is observed. The dependence of the quantum yield on the beam polarization and angle of incidence is investigated. The results indicate that higher quantum yields are achieved when the laser beam is incident at an angle of approximately 55 degrees and is polarized perpendicular to the plane of incidence. DOE

N94-20933# Texas A&M Univ., College Station. Dept. of Physics.
HIGH ENERGY PHYSICS PROGRAM AT TEXAS A/M UNIVERSITY
Dec. 1992 182 p
(Contract DE-AS05-81ER-40039)
(DE93-041089; DOE/ER-40039/99) Avail: CASI HC A09/MF A02

The Texas A&M experimental high energy physics program has been supported since its inception by DOE Contract DE-AS05-81ER40039. During that period we established a viable experimental program at a university which before this time had no program in high energy physics. In 1990, the experimental program was augmented with a program in particle theory. In the accompanying final report, we outline the research work accomplished during the final year of this contract and the program being proposed for

consideration by the Department of Energy for future grant support. Some of the particular areas covered are as follows: Collider detector at Fermilab program; the TAMU MACRO program; SSC R&D program; SSC experimental program; and theoretical physics program. DOE

N94-21439# California Univ., Berkeley. Lawrence Berkeley Lab.
LOW EMITTANCE 0.8A K(+) ION SOURCE FOR THE LBL INDUCTION LINAC SYSTEM EXPERIMENT (ILSE)
S. Eylon, E. Henestroza, W. W. Chupp, and S. Yu May 1993 14 p Presented at the International Symposium on Heavy Ion Fusion, Frascati, Italy, 25-28 May 1993
(Contract DE-AC03-76SF-00098)
(DE93-019237; LBL-33802; HIFAN-581; CONF-9305136-6) Avail: CASI HC A03/MF A01

A high current injector for heavy ion fusion presently under construction at Lawrence Berkeley Laboratory requires large sources of up to 17 cm in diameter and total potassium ion current of 790 mA with a low normalized transverse emittance of less than 0.5 mm-mr. A 1 in. diameter hot alumina silicate (zeolite) source was fabricated and tested in the injector setup of SBTE, an existing facility at LBL. Initial measurements showed a maximum space charge limited ion current of 95 mA. The corresponding density of 19 mA/sq cm was limited by the source diode optics and not by the source emission. The density required for the high current injector is 4 mA/sq cm. The normalized emittance was measured to be 0.06 mm-mrad, corresponding to a transverse temperature of 0.2 eV. Non-destructive life tests showed that the source can be operated under continuous operating conditions of the high current injector for more than a month (twenty eight-hour days, with 1 micro-s long pulses at 1 Hz). D.C. destructive life tests showed that approximately 30% of the total stored K can be ionized and extracted, allowing, in principle, for years of operation for the high current injector. Furthermore, we shall describe the extension of the fabricating technique to large diameter sources (up to 17 cm) and report on measured ion emission performance, measured surface temperature uniformity and heating power considerations. DOE

N94-21440# California Univ., Berkeley. Lawrence Berkeley Lab.
SIMULATION STUDIES OF SPACE-CHARGE-DOMINATED BEAM TRANSPORT IN LARGE APERTURE RATIO QUADRUPOLES
W. M. Fawley, L. J. Laslett, C. M. Celata, A. Faltens, and I. Haber (Naval Research Lab., Washington, DC.) May 1993 6 p Presented at the International Particle Accelerator Conference, Washington, DC, 17-20 May 1993
(Contracts DE-AC03-76SF-00098; DE-AI05-92ER-54177)
(DE93-019238; LBL-33282; HIFAN-566; CONF-930511-363) Avail: CASI HC A02/MF A01

For many cases of interest in the design of heavy-ion fusion accelerators, the maximum transportable current in a magnetic quadrupole lattice scales as alpha/L(sup 2) where alpha is the useful dynamic aperture and L is the half-lattice period. There are many cost benefits to maximizing the usable aperture which must be balanced against unwanted effects such as possible emittance growth and particle loss from anharmonic fringe fields. We have used two independent simulation codes to model space-charge dominated beam transport both in an azimuthally-pure quadrupole FODO lattice design and in a more conventional design. Our results indicate that careful matching will be necessary to minimize emittance growth and that (alpha/L) ratios of 0.2 or larger are possible for particular parameters. DOE

N94-21686# Stanford Linear Accelerator Center, CA.
MULTIBUNCH BEAM BREAK-UP IN DETUNED STRUCTURES
K. A. Thompson, C. Adolphsen, and K. L. F. Bane May 1993 3 p Presented at the International Particle Accelerator Conference, Washington, DC, 17-20 May 1993
(Contract DE-AC03-76SF-00515)
(DE93-041056; SU-SLAC-Pub-6153; CONF-930511-478) Avail: CASI HC A01/MF A01

A key problem in next-generation linear collider design utilizing multibunching is the control of multibunch beam break-up. One method of controlling the break-up is detuning, i.e., varying the frequency of the transverse deflecting modes by varying the cell dimensions within the accelerating structures. In this case, the beam breakup is sensitive to the resonances between the bunch frequency and some of the deflecting mode frequencies. It is also sensitive to errors in the fabrication and alignment of the accelerating structures. We examine these effects in the context of the SLAC NLC design. DOE

N94-21687# Stanford Linear Accelerator Center, CA.
SIMULATION AND COMPENSATION OF MULTIBUNCH ENERGY VARIATION IN NLC
K. A. Thompson and R. D. Ruth May 1993 3 p Presented at the International Particle Accelerator Conference, Washington, DC, 17-20 May 1993
(Contract DE-AC03-76SF-00515)
(DE93-041057; SU-SLAC-Pub-6154; CONF-930511-479) Avail: CASI HC A01/MF A01

The SLAC NLC design for a next-generation linear collider utilizes multibunching (acceleration of a train of bunches on each RF fill) to increase the luminosity and energy efficiency. It is necessary to control the energy spread of the beam, in order to minimize chromatic emittance dilution and be within the energy acceptance of the final focus. It is anticipated that the NLC may run with bunch trains having length equal to a substantial fraction of the filling time. Multibunch energy simulation methods and compensation schemes appropriate to this regime are presented. DOE

N94-21688# California Univ., Los Angeles.
PLASMA LENS EXPERIMENTS AT THE FINAL FOCUS TEST BEAM
B. Barletta, S. Chattopadhyay (California Univ., Berkeley. Lawrence Berkeley Lab.), P. Chen (Stanford Linear Accelerator Center, CA.), D. Cline, W. Craddock (Stanford Linear Accelerator Center, CA.), W. Gabella (Stanford Linear Accelerator Center, CA.), I. Hsu (National Tsing Hua Univ., Hsinchu, Taiwan.), T. Katsouleas (University of Southern California, Los Angeles.), P. Kwok, and P. Lau (University of Southern California, Los Angeles.) et al Apr. 1993 3 p Presented at the International Particle Accelerator Conference, Washington, DC, 17-20 May 1993
(Contract DE-AC03-76SF-00515)
(DE93-041081; SU-SLAC-Pub-6195; CONF-930511-432) Avail: CASI HC A01/MF A01

We intend to carry out a series of plasma lens experiments at the Final Focus Test Beam facility at SLAC. These experiments will be the first to study the focusing of particle beams by plasma focusing devices in the parameter regime of interest for high energy colliders, and is expected to lead to plasma lens designs capable of unprecedented spot sizes. Plasma focusing of positron beams will be attempted for the first time. We will study the effects of lens aberrations due to various lens imperfections. Several approaches will be applied to create the plasma required including laser ionization and beam ionization of a working gas. At an increased bunch population of 2.5 x 10(exp 10), tunneling ionization of a gas target by an electron beam -- an effect which has never been observed before -- should be significant. The compactness of our device should prove to be of interest for applications at the SLC and the next generation linear colliders. DOE

N94-21767 Los Alamos National Lab., NM.
A HIGH-INTENSITY He-JET PRODUCTION SOURCE FOR RADIOACTIVE BEAMS
D. J. Vieira, H. J. Kimberly, D. L. Grisham, W. L. Talbert, J. M. Wouters, D. Rosenauer, and Y. Bai 1993 6 p Presented at the 3rd International Conference on Radioactive Nuclear Beams, East Lansing, MI, 24-27 May 1993 Limited Reproducibility: More than 20% of this document may be affected by microfiche quality
(Contract W-7405-eng-36)
(DE93-040247; LA-UR-93-2759; CONF-930534-7) Avail: CASI HC A02

The use of a thin-target, He-jet transport system operating with high primary beam intensities is explored as a high-intensity production source for radioactive beams. This method is expected to work well for short-lived, non-volatile species. As such, the thin-target, He-jet approach represents a natural complement to the thick-target ISOL method in which such species are not, in general, rapidly released. Highlighted here is a thin-target, He-jet system that is being prepared for a 500(+) micro-A, 800-MeV proton demonstration experiment at LAMPF this summer. DOE

N94-21773 Stanford Linear Accelerator Center, CA.
THE PRESERVATION OF LOW EMITTANCE FLAT BEAMS
T. O. Raubenheimer Apr. 1993 5 p Presented at the International

Particle Accelerator Conference, Washington, DC, 17-20 May 1993 Limited Reproducibility: More than 20% of this document may be affected by microfiche quality
(Contract DE-AC03-76SF-00515)
(DE93-040964; SU-SLAC-PUB-6117; CONF-930511-406) Avail: CASI HC A01

Many future linear collider designs require beams with very small transverse emittances and large emittance ratios epsilon(sub x) (much greater than) epsilon(sub y). In this paper, we will discuss issues associated with the preservation of these small emittances during the acceleration of the beams. The primary sources of transverse emittance dilution in a high energy linear accelerator are the transverse wakefields, the dispersive errors, RF deflections, and betatron coupling. We will discuss the estimation of these effects and the calculation of tolerances that will limit the emittance dilution with a high degree of confidence. Since the six-dimensional emittance is conserved and only the projected emittances are increased, these dilutions can be corrected if the beam has not filamented (phase mixed). We discuss methods of correcting the dilutions and easing the tolerances with beam-based alignment and steering techniques, and non-local trajectory bumps. Finally, we discuss another important source of luminosity degradation; namely, pulse-to-pulse jitter. DOE

N94-21849# Los Alamos National Lab., NM.
LOW p(SUB T) PHENOMENA OBSERVED IN HIGH ENERGY NUCLEAR COLLISIONS
J. Simon-Gillo 1993 9 p Presented at the 10th International Conference on Ultra-Relativistic Nucleus-Nucleus Collisions, Borlaenge, Sweden, 20-24 Jun. 1993
(Contract W-7405-eng-36)
(DE94-000825; LA-UR-93-3429; CONF-930636-3) Avail: CASI HC A02/MF A01

For several decades, experiments have reported an enhancement in the pion invariant cross section at low p(sub T) (less than 300 MeV/c) when compared to a thermal fit or minimum bias pp results. Experimental results from pp reactions at the ISR to heavy ion collisions at CERN will be reviewed then compared to extract trends. Several theoretical explanations will be discussed. An emphasis will be placed on the role of resonances, and a comparison of data to models will be presented. DOE

N94-21866# Fermi National Accelerator Lab., Batavia, IL.
MEASUREMENT OF THE INCLUSIVE JET CROSS SECTION IN p(BAR-p) COLLISIONS AT CDF
Aug. 1993 10 p Presented at the Symposium on Lepton and Photon Interactions, Ithaca, NY, 10-15 Aug. 1993
(Contract DE-AC02-76CH-03000)
(DE94-000581; FNAL/C-93/204-E; CONF-930823-11) Avail: CASI HC A02/MF A01

The status of the CDF inclusive jet cross section measurement from the 1992-1993 run of the Fermilab Tevatron is described. The E(sub T) range of the jets extends from 15 to 420 GeV. Corrections are made to the measured cross section to obtain a true transverse energy spectrum. The corrected cross section is compared with next-to-leading order (NLO) quantum chromodynamics (QCD) calculations and to the 1989 CDF data. DOE

N94-21878*# Johns Hopkins Univ., Columbia, MD. Applied Physics Lab.
STUDIES OF ELECTROMAGNETIC ION CYCLOTRON WAVES USING AMPTE/CCE AND DYNAMICS EXPLORER Semiannual Report, 1 Jun. - 1 Dec. 1993
Robert E. Erlandson 1993 2 p
(Grant NAG5-1601)
(NASA-CR-194711; NAS 1.26:194711) Avail: CASI HC A01/MF A01

The principal activity during the past six months has involved the analysis of ion cyclotron waves recorded from DE-2 using the magnetic field experiment and electric field experiment. The results of this study have been published in the Geophysical Research Letters (GRL). The primary finding of this paper is that ion cyclotron waves were found to heat electrons, as observed in the DE-2 Langmuir probe data, through a Landau damping process. A second activity, which was started during the last six months, involves the study of large amplitude approximately one Hz electric and magnetic field oscillations recorded in the nightside auroral zone at substorm onset. Work is under way to determine the properties of these waves and investigate any association these waves may have with the substorm initiation process. A third activity under way involves a comprehensive study of ion cyclotron waves recorded at ionospheric altitudes by DE-2. This study will be an extension of the work reported in the GRL paper and will involve a larger sampling of wave events. This paper will focus on wave properties at ionospheric altitudes. A fourth activity involves a more in-depth analysis of the acceleration mechanisms and the resulting electron distributions based on the observations presented in the GRL paper. Derived from text

N94-21934# Fermi National Accelerator Lab., Batavia, IL.
STABILITY OF BEAM IN THE FERMILAB MAIN INJECTOR
C. S. Mishra and F. A. Harfoush Aug. 1993 5 p Presented at the International Particle Accelerator Conference, Washington, DC, 17-20 May 1993
(Contract DE-AC02-76CH-03000)
(DE94-000619; FNAL/C-93/229; CONF-930511-489) Avail: CASI HC A01/MF A01

The Fermilab Main Injector is a new 150 GeV protron synchrotron, designed to remove the limitations of the Main Ring in the delivery of high intensity protron and antiproton beams to the Tevatron. Extensive studies have been made to understand the performance of the Main Injector. In this paper, we present a study of the Main Injector lattice, which includes magnetic and misalignment errors. These calculations show the Main Injector's dynamical aperture is larger than its design value of 40 pi mm mradian at injection. DOE

N94-21952# Stanford Research Inst., Menlo Park, CA.
SLD RESULTS FROM THE STUDY OF POLARIZED Z(SUP 0) PRODUCED AT THE SLC
M. Piccolo (Istituto Nazionale di Fisica Nucleare, Frascati, Italy.) Jul. 1993 10 p Presented at the 1993 Rencontres De Physique De La Vallee D'Aoste, LaThuile, Italy, 8-13 Mar. 1993
(Contracts DE-AC03-76SF-00515; DE-FG03-92ER-40701; DE-FG03-91ER-40618; DE-FG02-91ER-40672; DE-FG02-91ER-40677; DE-FG02-91ER-40676; DE-FG02-91ER-40672)
(DE93-041020; SU-SLAC-Pub-6285; CONF-9303172-5) Avail: CASI HC A02/MF A01

The results obtained during the 1992 run of the SLD detector at the SLC are reviewed together with the general performances of the machine. The first measurement of the left-right asymmetry, the determination of the Z(sup 0) branching ratio to bottom quarks and the measurement of (alpha)(sub s) are presented. Current plans and expectations for the 1993 run, when high polarization (greater or equal to 60%) GaAs strained cathodes sources will be used, are described. DOE

N94-21974# California Univ., Berkeley. Lawrence Berkeley Lab.
MONTE CARLO CALCULATION OF MULTI-ELECTRON EFFECTS ON SYNCHROTRON RADIATION
C. Wang Jul. 1993 12 p Presented at the Annual Meeting of the SPIE, San Diego, CA, 11-16 Jul. 1993
(Contract DE-AC03-76SF-00098)
(DE94-001259; LBL-33355; CONF-930722-44) Avail: CASI HC A03/MF A01

The phase space distribution and time structure of an electron beam have fundamental influences on synchrotron radiation properties. These influences are due to the superposition of radiation from all electrons, each following a different trajectory. When the radiation wavelength is longer than the electron bunch length, coherent superposition occurs and results in the observed coherent synchrotron radiation. Usually the wavelength we use is much shorter, so incoherent superposition occurs and the emittance effect is the dominant multi-electron effect. The Monte Carlo simulation is a straightforward and generally valid approach to compute the multi-electron effects on synchrotron radiation. In this paper, we show how the Monte Carlo method can model these multi-electron effects systematically and discuss the statistical principles governing such simulation and their implication on the computing power requirement. We also describe the implementation of an efficient algorithm to calculate a single electron radiation spectrum, which is important to make the Monte Carlo simulation practical. Some calculated results are shown to demonstrate the methods. Comments on the usefulness and limitation of the Monte Carlo method are presented. DOE

74 OPTICS

Includes light phenomena; and optical devices.
For lasers see *36 Lasers and Masers.*

N94-19819 Massachusetts Inst. of Tech., Cambridge. Artificial Intelligence Lab.
RECOGNIZING 3-D OBJECTS USING 2-D IMAGES
David W. Jacobs May 1993 272 p Limited Reproducibility: More than 20% of this document may be affected by microfiche quality
(Contracts N00014-91-J-4038; N00014-85-K-0124)
(AD-A271005; AI-TR-1416) Avail: CASI HC A12

To visually recognize objects, the strategy of forming groups of image features with a bottom-up process, and then using these groups to index into a data base to find all of the matching groups of model features is adopted. This approach reduces the computation needed for recognition, since we only consider groups of model features that can account for these relatively large chunks of the image. To perform indexing, a group of 3-D model features are represented in terms of the 2-D images it can produce. Specifically, it is shown that the simplest and most space-efficient way of doing this for models consisting of general groups of 3-D point features is to represent the set of images each model group produces with two lines (1D subspaces), one in each of two orthogonal, high-dimensional spaces. These spaces represent all possible image groups so that a single image group corresponds to one point in each space. The effects of bounded sensing error on a set of image points, so that a robust and efficient indexing system may be built are determined. An optimal indexing method for more complicated features is also presented, and bounds on the space required for indexing in a variety of situations is presented. The representations of a model's images that are developed to analyze other approaches to matching were used. It is shown that there are no invariants of general 3-D models, and limitations in the use of non-accidental properties and in other approaches to reconstructing a 3-D scene from a single 2-D image are demonstrated. DTIC

N94-19846 Cape Cod Research, Buzzards Bay, MA.
COMPLEX AND STEREOREGULAR NONLINEAR OPTICAL MATERIALS Final Report, 15 Dec. 1992 - 14 Aug. 1993
Brian G. Dixon 20 Sep. 1993 26 p Limited Reproducibility: More than 20% of this document may be affected by microfiche quality
(Contract F49620-93-C-0006)
(AD-A271067; AFOSR-93-0757TR) Avail: CASI HC A03

This Phase 1 research program resulted in the synthesis and identification of a previously unknown set of aromatic phosphonic acid compounds, which possessed interesting thermal properties. There are very few phosphonate compounds reported that are liquid crystalline in nature. However, the non-linear optical properties of these compounds were determined to be unremarkable. Very probably, this is due to a relatively small dipole between the phosphonate moiety and a distal cyano group. DTIC

N94-19862# Lawrence Livermore National Lab., CA.
MULTIDIMENSIONAL SOLITONS IN FIBER ARRAYS
A. B. Aceves (New Mexico Univ., Albuquerque.), C. DeAngelis (New Mexico Univ., Albuquerque.), A. M. Rubenchik, and S. K. Turitsyn (Academy of Sciences, USSR, Novosibirsk.) 16 Aug. 1993 13 p Presented at the Annual Meeting of the Optical Society of America, Toronto, Ontario, 3-8 Oct. 1993
(Contract W-7405-eng-48)
(DE93-019923; UCRL-JC-114989; CONF-931057-1) Avail: CASI HC A03/MF A01

We demonstrate that nonlinear optical fiber arrays can support stable soliton-like pulses with finite energy. The bound state that we have found is localized both in time and in a spatial domain in the direction perpendicular to the pulse propagation. We have proved the boundedness of the Hamiltonian function for the array. Finally, numerical studies support our analytical conclusions. DOE

N94-19901 Duke Univ., Durham, NC. Dept. of Physics.
A MICROSCOPIC THEORY OF QUANTUM OPTICS AND NEW PHOTON-LOCKED BISTABLE STATES Final Report, 1 Sep. 1989 - 31 Jan. 1993
Mikael Ciftan 19 Jul. 1993 6 p Limited Reproducibility: More than 20% of this document may be affected by microfiche quality
(Contracts DAAL03-89-C-0034; DAAL03-89-D-0002)
(AD-A271250; ARO-27424.1-PH; ARO-28468.8-PH) Avail: Issuing Activity (Defense Technical Information Center (DTIC))

In order to explore the existence of spontaneous self-organization of states in quantum optics on a more concrete basis and to learn from known examples of many-body systems that show self-organization, we have taken up the study of Heisenberg Ferromagnetism. This is the magnetism of spherically symmetric spins interacting via the exchange Hamiltonian on two or three dimensional lattices. We have extracted the essential elements necessary for self-locking and the ensuing metastability of the system in the absence of any external field. Since the functional space of the Heisenberg ferromagnetic spins is homomorphic to the space of two level atoms, our recent results in magnetism will allow us to pass with great ease to the quantum optics case of self-locked bistable states and demonstrate their existence on a first-principles basis. DTIC

N94-19968 Massachusetts Inst. of Tech., Cambridge. Artificial Intelligence Lab.
ON GEOMETRIC AND ALGEBRAIC ASPECTS OF 3D AFFINE AND PROJECTIVE STRUCTURES FROM PERSPECTIVE 2D VIEWS Memorandum Report
Amnon Shashua Jul. 1993 16 p Limited Reproducibility: More than 20% of this document may be affected by microfiche quality
(Contracts N00014-91-J-1270; N00014-92-J-1879)
(AD-A270520; AIM-1405; CBCI-78) Avail: CASI HC A03

Part I of this paper investigates the differences conceptually and algorithmically - between affine and projective frameworks for the tasks of visual recognition and reconstruction from perspective views. It is shown that an affine invariant exists between any view and a fixed view chosen as a reference view. This implies that for tasks for which a reference view can be chosen, such as in alignment schemes for visual recognition, projective invariants are not really necessary. The projective extension is then derived, showing that it is necessary only for tasks for which a reference view is not available - such as happens when updating scene structure from a moving stereo rig. The geometric difference between the two proposed invariants are that the affine invariant measures the relative deviation from a single reference plane, whereas the projective invariant measures the relative deviation from two reference planes. The affine invariant can be computed from three corresponding points and a fourth point for setting a scale; the projective invariant can be computed from four corresponding points and a fifth point for setting a scale. Both the affine and projective invariants are shown to be recovered by remarkably simple and linear methods. DTIC

N94-20013 North Carolina State Univ., Raleigh. Dept. of Electrical and Computer Engineering.
OPTICAL SIGNAL PROCESSING Final Report, 5 Feb. 1990 - 30 Jun. 1993
A. VanderLugt 31 Jul. 1993 193 p Limited Reproducibility: More than 20% of this document may be affected by microfiche quality
(Contract DAAL03-90-G-0039)
(AD-A271036; ARO-27586.21-PH) Avail: CASI HC A09

A quasi-realtime adaptive processing system was used to correct the multipath distortion found in wideband digital radios. The measured power spectral density of the input signal was used to adaptively select one of eight equalization filters which reduce the residual distortion to less than 3.6 dB even for the most severe channel distortion. A related adaptive system was used for signal excision in which we removed narrowband interference from wideband signals with minimum signal distortion. An 8x8 acousto-optic switch in a multimode fiber-optic system was built. Insertion loss is approximately 2-4 dB, signal-to-crosstalk ratio is better than 25 dB, and the reconfiguration time is 880 nsec. Short pulses were detected by using the Fresnel transform. Pulses as short as the theoretical limit of 20 nanoseconds were detected for this system, and separated by as little as 60 nanoseconds or by as much as 17 nanoseconds. All possible acousto-optic scanning configurations were considered and classified into four basic types. A consistent set of design relationships for each of the scanning configurations was developed and presented in both tabular and graphic forms from which a preliminary design is obtained. DTIC

N94-20056 Department of the Navy, Washington, DC.
OPTICAL ENCODING OF IMAGING DATA Patent
Joseph P. Garcia, inventor (to Navy) 3 Aug. 1993 6 p Filed 16 Jul. 1990
(AD-D015915; US-Patent-5,233,440; US-Patent-Appl-SN-553058; US-Patent-Class-358-448) Avail: US Patent and Trademark Office

Optical imaging data sampled through a sensing array of spaced receiving end faces of optic fiber bundles, is encoded by the different signal delay lengths of the fibers forming the respective bundles. The geometry of such end faces in the array is such as to effect encoding in dependence on the angular orientation and position of sampled segments of the optical data relative to the end faces on which such sampled segments impinge. DTIC

N94-20059 Department of the Navy, Washington, DC.
OPTICAL SWITCHING DEVICES Patent
Michael E. Boyle, inventor (to Navy) and James S. Shirk, inventor (to Navy) 13 Apr. 1993 5 p Filed 12 Sep. 1991
(AD-D015918; US-Patent-5,202,786; US-Patent-Appl-SN-758143; US-Patent-Class-359-243) Avail: US Patent and Trademark Office

An optical switching device employs a rare earth bis-phthalocyanine having good third-order nonlinear susceptibilities. In a preferred optical switch, the rare earth bis-phthalocyanine is employed as a nonlinear optical material body that fills the space between two partially reflecting mirrors. When light incident on the switch is below a given intensity level, light passes through the switch and the switch is in an open state. When light is above a given intensity level, light is trapped in the nonlinear optical material and the switch is in a closed state. DTIC

N94-20065 Department of the Navy, Washington, DC.
FIBER OPTIC MICHELSON SENSOR AND ARRAYS WITH PASSIVE ELIMINATION OF POLARIZATION FADING AND SOURCE FEEDBACK ISOLATION Patent
Alan D. Kersey, inventor (to Navy) 27 Apr. 1993 15 p Filed 1 Sep. 1992
(AD-D015944; US-Patent-5,206,924; US-Patent-Appl-SN-937782; US-Patent-Class-385-24) Avail: US Patent and Trademark Office

A fiber optic Michelson interferometric sensor system with passive elimination of polarization fading and source feedback isolation is disclosed. In a preferred embodiment, an optical source provides light of a first polarization state to a polarization selective element. Output light from the polarization selective element passes through a length of optical fiber into a Michelson interferometric sensor which utilizes a Faraday rotator/mirror assembly, that is coupled to distal ends of sensing and reference arms of the Michelson interferometer, to provide for the passive elimination of polarization fading. The polarization selective element at the output of the optical source provides isolation of the optical source from the Michelson interferometer sensor. DTIC

N94-20128*# Alabama Univ., Huntsville. Physics Dept.
X RAY, EXTREME AND FAR ULTRAVIOLET OPTICAL THIN FILMS FOR SPACE APPLICATIONS
Muamer Zukic, Douglas G. Torr, and Jongmin Kim 1993 41 p
(Grant NAGw-2898)
(NASA-CR-194635; NAS 1.26:194635) Avail: CASI HC A03/MF A01

Far and extreme ultraviolet optical thin film filters find many uses in space astronomy, space astrophysics, and space aeronomy. Spacebased spectrographs are used for studying emission and absorption features of the earth, planets, sun, stars, and the interstellar medium. Most of these spectrographs use transmission or reflection filters. This requirement has prompted a search for selective filtering coatings with high throughput in the FUV and EUV spectral region. Important progress toward the development of thin film filters with improved efficiency and stability has been made in recent years. The goal for this field is the minimization of absorption to get high throughput and enhancement of wavelength selection. The Optical Aeronomy Laboratory (OAL) at the University of Alabama in Huntsville has recently developed the technology to determine optical constants of bulk and film materials for wavelengths extending from x-rays (0.1 nm) to the FUV (200 nm), and several materials have been identified that were used for designs of various optical devices which previously have been restricted to space application in the visible and near infrared. A new design concept called the Pi-multilayer was introduced and applied to the design of optical coatings for wavelengths extending from x-rays to the FUV. Section 3 of this report explains the Pi-multilayer approach and demonstrates its application for the design and fabrication of the FUV coatings. Two layer Pi-stacks have been utilized for the design of reflection filters in the EUV wavelength range from 70 - 100 nm. In order to eliminate losses due to the low reflection of the imaging optics and increase throughput and out-of-band rejection of the EUV instrumentation we introduced a self-filtering camera concept. In the FUV region, MgF2 and LiF crystals are known to be birefringent. Transmission polarizers and quarterwave retarders made of MgF2 or LiF crystals are commercially available but the performances are poor. New techniques for the design of the EUV and FUV polarizers and quarterwave retarders are described in Section 5. X- and gamma-ray detectors rely on a measurement of the electron which is effected when a ray interacts with matter. The design of an x- and gamma-ray telescope to operate in a particular region of the spectrum is, therefore, largely dictated by the mechanism through which the rays interact. Energy selection and the focusing of the incident high energy rays can be achieved with spectrally selective high reflective multilayers. The design and spectral performance of narrowband reflective x-ray Pi-multilayers are presented in section 6. Derived from text

N94-20140*# National Aeronautics and Space Administration. Lewis Research Center, Cleveland, OH.
SOLAR SIMULATOR FOR SOLAR DYNAMIC SPACE POWER SYSTEM TESTING
Kent S. Jefferies Nov. 1993 8 p Proposed for presentation at the 1994 ASME International Solar Energy Conference, San Francisco, CA, 27-30 Mar. 1994; sponsored by ASME
(RTOP 585-03-21)
(NASA-TM-106393; E-8218; NAS 1.15:106393) Avail: CASI HC A02/MF A01

Planned vacuum tank testing of a solar dynamic space power system requires a solar simulator. Several solar simulators were previously built and used for vacuum tank testing of various space systems. However, the apparent solar subtense angle, i.e., the angular size of the apparent sun as viewed from the experiment, of these solar simulators is too large to enable testing of solar dynamic systems. A new design was developed to satisfy the requirements of the solar dynamic testing. This design provides 1.8 kW/m(sup 2) onto a 4.5M diameter test area from a source that subtends only 1 deg, full cone angle. Key features that enable this improved performance are (1) elimination of the collimating mirror commonly used in solar simulators to transform the diverging beam into a parallel beam; (2) a redesigned lamp module that has increased efficiency; and (3) the use of a segmented reflective surface to combine beams from several individual lamp modules at the pseudosun. Each segment of this reflective surface has complex curvature to control the distribution of light. By developing a new solar simulator design for testing of the solar dynamic system instead of modifying current designs, the initial cost was cut in half, the efficiency was increased by 50 percent reducing the operating costs by one-third, and the volume occupied by the solar simulator was reduced by a factor of 10. Author (revised)

N94-20179# Jet Propulsion Lab., California Inst. of Tech., Pasadena.
DESIGN CONSIDERATIONS FOR A FIBER OPTIC COMMUNICATIONS NETWORK FOR POWER SYSTEMS
H. Kirkham, A. R. Johnston, and G. D. Allen (American Electric Power Service Corp., Columbus, OH.) 1993 8 p Presented at the IEEE Power Engineering Society Winter Meeting, Columbus, OH, 31 Jan. - 4 Feb. 1993
(Contract DE-AI05-79ET-29372)
(DE93-018404; CONF-930102-1) Avail: CASI HC A02/MF A01

The design of a fiber optic communication network for monitoring and control in power systems is discussed. It is shown that by appropriate choice of protocols, a fault-tolerant system can be built that operates in any arbitrary configuration. Since the network is based on fiber optics, it can be made fast enough for substation monitoring and control. In this application, a relatively small number of cables is required to implement a high reliability system. The network can also be used for distribution automation. In this application the network is required to reach all parts of the power system, and the fiber cable itself becomes a significant fraction of the cost of communications. However, since many applications can be supported at once, the cost per function can be reasonable. DOE

N94-20240* National Aeronautics and Space Administration. Goddard Space Flight Center, Greenbelt, MD.
ROTARY ENCODING DEVICE USING POLYGONAL MIRROR WITH DIFFRACTION GRATINGS ON EACH FACET Patent
Douglas B. Leviton, inventor (to NASA) 30 Nov. 1993 13 p Filed 3 Nov. 1992 Supersedes N94-15705 (32 - 3, p 1189)
(NASA-Case-GSC-13543-1; US-Patent-5,266,796;
US-Patent-Appl-SN-971035; US-Patent-Class-250-231.18;
US-Patent-Class-250-237G; Int-Patent-Class-G01D-5/34) Avail: US Patent and Trademark Office

A device for position encoding of a rotating shaft in which a polygonal mirror having a number of facets is mounted to the shaft and a monochromatic light beam is directed towards the facets. The facets of the polygonal mirror each have a low line density diffraction grating to diffract the monochromatic light beam into a number of diffracted light beams such that a number of light spots are created on a linear array detector. An analog-to-digital converter is connected to the linear array detector for reading the position of the spots on the linear array detector means. A microprocessor with memory is connected to the analog-to-digital converter to hold and manipulate the data provided by the analog-to-digital converter on the position of the spots and to compute the position of the shaft based upon the data from the analog-to-digital converter.
Official Gazette of the U.S. Patent and Trademark Office

N94-20262# JAYCOR, San Diego, CA.
OPTICS SURVIVABILITY SUPPORT, VOLUME 1
N. Wild, T. Simpson, A. Busdeker, and F. Doft Mar. 1993 86 p Prepared for Lawrence Livermore National Lab.
(Contract W-7405-eng-48)
(DE93-019616; UCRL-CR-114992-Vol-1) Avail: CASI HC A05/MF A01

This final report is a documentation of the activities and work performed by JAYCOR during the period from June 11, 1992 through March 10, 1993 to support Lawrence Livermore National Laboratory (LLNL) in the development of radiation tolerant optical subsystems and components for use under the Advanced Implementation Technology (AIT) effort. The work is primarily directed towards: performance of above-ground testing and analysis of the LLNL space-based LIDAR (Laser Illuminated Detection and Ranging) system and components, and compilation of a radiation effects data base for bulk optical materials, i.e., glasses. The objective is to support LLNL activities in the area of optics survivability and in engineering a radiation hardened LIDAR that can survive and operate through natural, as well as hostile, space environments (primary emphasis is on operation in electron, proton, and total dose environment). An analysis of the LIDAR design as developed by Kigre, Inc. for LLNL shows that the most susceptible components in terms of radiation susceptibility are the doubling crystal and laser rod materials. The radiation susceptibility analysis of the Kigre design (pulsed Q-switch mode) is performed using data obtained from above-ground testing of each individual component material. A passive Q-switch material is evaluated and found to degrade via a decrease in the amount of saturable absorption relative to an un-irradiated sample. Several different doubling crystal types (LBO, KTP, KD*P) are also evaluated for both total dose and high energy proton susceptibility. LBO is the least susceptible and KTP is the most affected by exposure to ionizing radiation. An analysis of the Kigre system response as a function of total dose is made, including the effects on thin film anti-reflection and band-pass filter coatings. DOE

N94-20283# JAYCOR, San Diego, CA.
OPTICS SURVIVABILITY SUPPORT, VOLUME 2
N. Wild, T. Simpson, A. Busdeker, and F. Doft Jan. 1993 194 p Prepared for Lawrence Livermore National Lab., CA
(Contract W-7405-eng-48)
(DE93-040310; J-204-93-0052/2789-Vol-2; UCRL-CR-114992-Vol-2) Avail: CASI HC A09/MF A03

This volume of the Optics Survivability Support Final Report contains plots of all the data contained in the computerized Optical Glasses Database. All of these plots are accessible through the Database, but are included here as a convenient reference. The first three pages summarize the types of glass included with a description of the radiation source, test date, and the original data reference. This information is included in the database as a macro button labeled 'LLNL DATABASE'. Following this summary is an Abbe chart showing which glasses are included and where they lie as a function of nu(sub d) and n(sub d). This chart is also callable through the database as a macro button labeled 'ABBEC'. DOE

N94-20303* National Aeronautics and Space Administration. Pasadena Office, CA.
OPTOELECTRONIC ASSOCIATIVE MEMORY Patent
Tien-Hsin Chao, inventor (to NASA) (Jet Propulsion Lab., California Inst. of Tech., Pasadena.) 16 Nov. 1993 6 p Filed 19 Aug. 1991 Supersedes N91-32925 (29 - 24, p 4103)
(NASA-Case-NPO-18278-1-CU; US-Patent-5,262,979;
US-Patent-Appl-SN-747059; US-Patent-Class-365-49;
US-Patent-Class-365-215; US-Patent-Class-359-561;
US-Patent-Class-382-42; Int-Patent-Class-G11C-15/00) Avail: US Patent and Trademark Office

An associative optical memory including an input spatial light modulator (SLM) in the form of an edge enhanced liquid crystal light valve (LCLV) and a pair of memory SLM's in the form of liquid crystal televisions (LCTV's) forms a matrix array of an input image which is cross correlated with a matrix array of stored images. The correlation product is detected and nonlinearly amplified to illuminate a replica of the stored image array to select the stored image correlating with the input image. The LCLV is edge enhanced by reducing the bias frequency and voltage and rotating its orientation. The edge enhancement and nonlinearity of the photodetection improves the orthogonality of the stored image. The illumination of the replicate stored image provides a clean stored image, uncontaminated by the image comparison process.
Official Gazette of the U.S. Patent and Trademark Office

N94-20305* National Aeronautics and Space Administration. Pasadena Office, CA.
FEEDBACK CONTROLLED OPTICS WITH WAVEFRONT COMPENSATION Patent
William G. Breckenridge, inventor (to NASA) (Jet Propulsion Lab., California Inst. of Tech., Pasadena.) and David C. Redding, inventor (to NASA) (Jet Propulsion Lab., California Inst. of Tech., Pasadena.) 23 Nov. 1993 13 p Filed 13 May 1991 Supersedes N91-32924 (29 - 24, p 4103)
(NASA-Case-NPO-18194-1-CU; US-Patent-5,265,034;
US-Patent-Appl-SN-700379; US-Patent-Class-364-525;
US-Patent-Class-364-559; US-Patent-Class-364-148;
US-Patent-Class-359-849; US-Patent-Class-250-201.1;
US-Patent-Class-250-201.9; Int-Patent-Class-G02B-5/10) Avail: US Patent and Trademark Office

The sensitivity model of a complex optical system obtained by linear ray tracing is used to compute a control gain matrix by imposing the mathematical condition for minimizing the total wavefront error at the optical system's exit pupil. The most recent deformations or error states of the controlled segments or optical surfaces of the system are then assembled as an error vector, and the error vector is transformed by the control gain matrix to produce the exact control variables which will minimize the total wavefront error at the exit pupil of the optical system. These exact control variables are then applied to the actuators controlling the various optical surfaces in the system causing the immediate reduction in total wavefront error observed at the exit pupil of the optical system.
Official Gazette of the U.S. Patent and Trademark Office

N94-20320 California Univ., Berkeley. Lawrence Berkeley Lab.
ULTRAFAST SCANNING MICROSCOPY
S. Weiss, D. Botkin, and D. S. Chemla Jan. 1993 5 p Presented at the Optical Society of America (OSA) Meeting on Ultrafast Optics and Optoelectronics, San Francisco, CA, 25-27 Jan. 1993 Limited Reproducibility: More than 20% of this document may be affected by microfiche quality
(Contract DE-AC03-76SF-00098)
(DE93-040121; LBL-34261; CONF-930150-2) Avail: Issuing Activity (Department of Energy (DOE))

The authors propose to combine ultrafast optical techniques with scanning probe microscopies to obtain, simultaneously, unprecedented temporal and spatial-resolution. DOE

N94-20345* National Aeronautics and Space Administration. Pasadena Office, CA.

WIDE-ANGLE IMAGING SYSTEM WITH FIBEROPTIC COMPONENTS PROVIDING ANGLE-DEPENDENT VIRTUAL MATERIAL STOPS Patent

Arthur H. Vaughan, inventor (to NASA) (Jet Propulsion Lab., California Inst. of Tech., Pasadena.) 30 Nov. 1993 16 p Filed 1 Nov. 1991 Supersedes N92-17892 (30 - 8, p 1368)

(NASA-Case-NPO-18146-1-CU; US-Patent-5,266,795; US-Patent-Appl-SN-786618; US-Patent-Class-250-227.2; US-Patent-Class-359-896; Int-Patent-Class-H01J-5/16) Avail: US Patent and Trademark Office

A strip imaging wide angle optical system is provided. The optical system is provided with a 'virtual' material stop to avoid aberrational effects inherent in wide angle optical systems. The optical system includes a spherical mirror section for receiving light from a 180 deg strip or arc of a target image. Light received by the spherical mirror section is reflected to a frustoconical mirror section for subsequent rereflection to a row of optical fibers. Each optical fiber transmits a portion of the received light to a detector. The optical system exploits the narrow cone of acceptance associated with optical fibers to substantially eliminate vignetting effects inherent in wide angle systems. Further, the optical system exploits the narrow cone of acceptance of the optical fibers to substantially limit spherical aberration. The optical system is ideally suited for any application wherein a 180 deg strip image need be detected, and is particularly well adapted for use in hostile environments such as in planetary exploration.

Official Gazette of the U.S. Patent and Trademark Office

N94-20378* National Aeronautics and Space Administration. Langley Research Center, Hampton, VA.

OPTICAL FIBERS AND FLUOROSENSORS HAVING IMPROVED POWER EFFICIENCY AND METHODS OF PRODUCING SAME Patent

Claudio O. Egalon, inventor (to NASA) and Robert S. Rogowski, inventor (to NASA) 16 Nov. 1993 8 p Filed 16 Sep. 1991 Supersedes N93-22008 (31 - 7, p 2069)

(NASA-Case-LAR-14525-1-CU; US-Patent-5,262,638; US-Patent-Appl-SN-761198; US-Patent-Class-250-227.14; US-Patent-Class-385-12; Int-Patent-Class-G01N-21/00) Avail: US Patent and Trademark Office

Optical fibers may have applications including fluorosensors which sense the concentration of an analyte. Like communication fibers, these fluorosensors are modeled using a weakly guiding approximation which is only effective when the difference between the respective refractive indices of the fiber core and surrounding cladding are minimal. An optical fiber fluorosensor is provided having a portion of a fiber core which is surrounded by an active cladding which is permeable by the analyte to be sensed and containing substances which emit light waves upon excitation. A remaining portion of the fiber core is surrounded by a guide cladding which guides these light waves to a sensor which detects the intensity of waves, which is a function of the analyte concentration. Contrary to conventional weakly guiding principles, the difference between the respective indices of refraction of the fiber core is surrounded by an active cladding which is thin enough such that its index of refraction is effectively that of the surrounding atmosphere, thereby the atmosphere guides the injective indices of the fiber core and the cladding results in an unexpected increase in the power efficiency of the fiber core.

Official Gazette of the U.S. Patent and Trademark Office

N94-20586* National Aeronautics and Space Administration. Langley Research Center, Hampton, VA.

OPTICAL FIBER SENSOR HAVING AN ACTIVE CORE Patent

Claudio Oliveira Egalon, inventor (to NASA) and Robert S. Rogowski, inventor (to NASA) 28 Sep. 1993 10 p Filed 18 Mar. 1992 Supersedes N92-30029 (30 - 20, p 3553) Continuation-in-part of US-Patent-Appl-SN-761198, filed 16 Sep. 1991

(NASA-Case-LAR-14607-1-SB; US-Patent-5,249,251; US-Patent-Appl-SN-855363; US-Patent-Appl-SN-761198; US-Patent-Class-385-123; US-Patent-Class-385-126; US-Patent-Class-385-127; US-Patent-Class-385-128; US-Patent-Class-385-142; US-Patent-Class-372-6) Avail: US Patent and Trademark Office

An optical fiber is provided. The fiber is comprised of an active fiber core which produces waves of light upon excitation. A factor ka is identified and increased until a desired improvement in power efficiency is obtained. The variable a is the radius of the active fiber core and k is defined as 2 pi/lambda wherein lambda is the wavelength of the light produced by the active fiber core. In one embodiment, the factor ka is increased until the power efficiency stabilizes. In addition to a bare fiber core embodiment, a two-stage fluorescent fiber is provided wherein an active cladding surrounds a portion of the active fiber core having an improved ka factor. The power efficiency of the embodiment is further improved by increasing a difference between the respective indices of refraction of the active cladding and the active fiber core.

Official Gazette of the U.S. Patent and Trademark Office

N94-20591* National Aeronautics and Space Administration. Goddard Space Flight Center, Greenbelt, MD.

CONICALLY SCANNED HOLOGRAPHIC LIDAR TELESCOPE Patent

Geary Schwemmer, inventor (to NASA) 19 Oct. 1993 9 p Filed 10 Mar. 1992 Supersedes N94-17321 (32 - 3, p 1194)

(NASA-Case-GSC-13462-1; US-Patent-5,255,065; US-Patent-Appl-SN-848885; US-Patent-Class-356-5; US-Patent-Class-359-17; US-Patent-Class-359-18; Int-Patent-Class-G01C-3/08; Int-Patent-Class-G02B-5/32) Avail: US Patent and Trademark Office

An optical scanning device utilizing a source of optical energy such as laser light backscattered from the earth's atmosphere or transmitted outward as in a lidar, a rotating holographic optical element having an axis of rotation perpendicular to the plane of its substrate, and having a stationary focus which may or may not be located on its axis of rotation, with the holographic optical element diffracting the source of optical energy at an angle to its rotation axis enabling a conical scanning area and a motor for supporting and rotating the rotating holographic optical element, is described. Official Gazette of the U.S. Patent and Trademark Office

N94-20922 Physical Optics Corp., Torrance, CA.

NOVEL N X N INTEGRATED CHANNEL WAVEGUIDE OPTICAL CROSSBARS FOR LARGE SCALE HIGH SPEED NON-BLOCKING DATA SWITCHING Final Report, 30 Sep. 1992 - 30 Mar. 1993

Michael Wang 31 May 1993 60 p Limited Reproducibility: More than 20% of this document may be affected by microfiche quality

(Contract F49620-92-C-0076)

(AD-A272065; AFOSR-93-0413TR) Avail: CASI HC A04

Physical Optics Corporation proposed a new structure for an optical crossbar based on a multi-wavelength ring resonator tuning/switching. To demonstrate its feasibility, in Phase I, we designed, analyzed, and demonstrated a basic ring resonator tuning/switching element for the crossbar. Two approaches for ring resonator tuning were identified: fiber-based ring resonator and waveguide-based ring resonator. For simplicity of the Phase I concept demonstration, we demonstrated a fiber ring resonator. At HeNe laser wavelengths of 632.8 and 611.9 nm, the fiber resonator demonstrated the desired wavelength selective switching operation. The finesse of the present unoptimized device was measured at about 19 under zero tap coupling, with a potential of exceeding 100. The device provided over 36% throughput with a potential for throughput efficiency of over 80%. The crosstalk was measured at -8 dB with a potential of better than -33 dB. Optimization is possible by reducing the coupler loss. Waveguide fabrication and fiber/waveguide pigtailing experiments were also conducted in Phase I to demonstrate pigtailing capability for crossbar applications. DTIC

N94-21043 Bonn Univ. (Germany). Inst. fuer Physik.

X RAY REFLECTION MASKS: MANUFACTURING, CHARACTERIZATION AND FIRST TESTS Thesis [ROETGENREFLEXIONSMASKEN: HERSTELLUNG, CHARAKTERISIERUNG UND ERSTE TESTS]

Stephen Rahn Sep. 1992 63 p In GERMAN Limited Reproducibility: More than 20% of this document may be affected by microfiche quality

(Bonn-IR-92-31; ETN-93-93809) Avail: CASI HC A04

SXPL (Soft X-ray Projection Lithography) multilayer mirrors are characterized, laterally structured and then used as reflection masks in a projecting lithography procedure. Mo/Si-multilayer mirrors with a 2d in the region of 14 nm were characterized by Cu-k(alpha) grazing incidence as well as soft X-ray normal incidence reflectivity measurements. The multilayer mirrors were patterned by reactive ion etching with CF4 using a photoresist as etch mask, thus producing X-ray reflection masks. The masks were

tested at the synchrotron radiation laboratory of the electron accelerator ELSA. A double crystal X-ray monochromator was modified so as to allow about 0.5 sq cm of the reflection mask to be illuminated by white synchrotron radiation. The reflected patterns were projected (with an energy of 100 eV) onto a resist and structure sizes down to 8 micrometers were nicely reproduced. Smaller structures were distorted by Fresnel-diffraction. The theoretically calculated diffraction images agree very well with the observed images. ESA

N94-21148 Bonn Univ. (Germany). Inst. fuer Physik.
EXAMINATION FOR OPTIMIZATION OF SYNCHROTRON RADIATION SPECTRUM FOR THE X RAY DEPTH LITHOGRAPHY Thesis [UNTERSUCHUNGEN ZUR OPTIMIERUNG DES SPEKTRUMS DER SYNCHROTRONSTRAHLUNG FUER DIE ROENTGENTIEFENLITHOGRAPHIE]
Raimund Dany Jun. 1992 72 p In GERMAN Limited Reproducibility: More than 20% of this document may be affected by microfiche quality
(BONN-IR-92-32; ETN-93-93810) Avail: CASI HC A04

The effect of reducing the vertical distribution of synchrotron radiation on its spectral distribution is examined through resin irradiation. The resulting filter effect is compared to that of absorption filters. Transmission coefficients of titanium, gold, and polyamide were calculated from linear absorption coefficients with the Beer law. The use of a diaphragm in X-ray depth lithography, which is the first step of the LIGA (Lithography Galvanoforming Molding) process, is discussed. A calorimetric device for determining the synchrotron radiation power and distribution was developed and tested. Measurements at the ELSA storage ring show a strong dependence of the vertical emittance on the electron current. ESA

N94-21163# Physical Optics Corp., Torrance, CA.
AN OPTICALLY-ASSISTED 3-D CELLULAR ARRAY MACHINE Final Report, 1 Apr. - 30 Sep. 1993
Freddie Lin 5 Nov. 1993 40 p
(Contract N00014-93-C-0021)
(AD-A272683) Avail: CASI HC A03/MF A01

In order to increase the real-time performance of next-generation image processing systems, Physical Optics Corporation (POC) explored a new architectural structure -- a hybrid optically-assisted 3-D cellular array machine. Three techniques are used in this architecture. An analog processing technique is used for front-end high-speed image preprocessing. A digital processing technique is employed for high-precision and highly programmable image processing. An optical interconnect technique is used for high-efficiency high-bandwidth data communication between the analog and digital processing layers. The combination of these three techniques yields a real-time image processing system in a compact 3-D system package with scalable expansion capability. DTIC

N94-21172# Sparta, Inc., Lexington, MA.
OBTAINING SURFACE OPTICAL PROPERTIES FROM SPACE-BASED LIDAR SYSTEMS Technical Report
John R. Hummel, James R. Jones, David R. Longtin, and Richard R. Zeoli 30 Mar. 1993 41 p
(Contract F19628-91-C-0093)
(AD-A272831; LTR93-004; PL-TR-93-2081; SR-5) Avail: CASI HC A03/MF A01

Space-based lidar systems are planned for a number of applications. One application being considered is to use a space-based lidar to infer information about the visibility near the surface from remote or inaccessible areas. This can be accomplished if one can obtain information about the optical properties near the surface. The concept would involve using a lidar on a space platform probing the atmosphere and underlying surface along its orbital path. The purpose of this research has two goals. The first is to determine if a unique relationship can be found at a suitable laser wavelength to relate the extinction coefficients near the surface to the visibility at the surface. The second goal is to determine if lidar backscatter measurements can be inverted in a reasonable fashion to obtain the extinction coefficient near the surface. If these goals can be met, then visibility can be obtained on a routine basis from space-based lidars. This paper presents the results from the study. In the study, a number of different lidar wavelengths have be studied to see if one is more suitable than the others. Also, an examination of the assumptions required to perform the inversion of the lidar equation has been made. DTIC

N94-21236# Naval Command, Control and Ocean Surveillance Center, San Diego, CA. Research, Development, Test and Evaluation Div.
OPTICAL PROPERTIES OF CHROMIUM AND NEODYMIUM IN ZIRCONIUM - BARIUM - LANTHANUM - ALUMINUM FLUORIDE GLASS Final Report, Oct. 1987 - Sep. 1988
F. E. Hanson and H. H. Caspers Aug. 1993 29 p
(AD-A271609; NCCOSC/RDT/E-TR-1623) Avail: CASI HC A03/MF A01

The optical properties are reported of chromium and neodymium doped in zirconium - barium - lanthanum - aluminum fluoride glass (ZBLA). The fluorescence of Cr(3+) and of co-doped Cr(3+), Nd(3+) glasses is investigated. Fluorescence decay rates of Cr(3+) and Nd(3+) are measured at various temperatures, and the excitation transfer efficiency between Cr(3+) and Nd(3+) is determined. The absorption spectrum of Nd(3+):ZBLA is characterized in terms of the Judd-Ofelt model of crystal field-induced electric-dipole transitions. The three phenomenological intensity parameters for Nd(3+) in ZBLA glass Omega(sub 2,4,6) are compared to those obtained for Nd(3+) in Y3Al5O12, Gd3S2Al3O12, and LHG-8 glass. DTIC

N94-21279 Department of the Navy, Washington, DC.
MODE TRANSITION MATRIX MEASURING SYSTEM Patent
Thomas J. Gryk, inventor (to Navy) 5 Oct. 1993 9 p Filed 25 Feb. 1992
(AD-D015973; US-Patent-5,251,002; US-Patent-Appl-SN-841105; US-Patent-Class-356-73.1) Avail: US Patent and Trademark Office

A mode transition matrix measuring system for nondestructively calculating mode-dependent losses and coupling of a multi-mode, graded-index, connectorized, passive fiber optic component is described as follows: the mode transition matrix measuring system comprising mode selective launcher means having a plurality of optical paths with varying launch conditions, input-output optic means having at least one reference optical path and at least one optical path for the passive fiber optic component under test, mode selective detection means having a plurality of optical paths with a variety of mode filters, and means for data storage and matrix calculation, wherein the mode transition matrix and the modal power vector are calculated using measurements of the optical power propagated through optical courses comprising the optical paths. DTIC

N94-21321# SRI International Corp., Menlo Park, CA.
IR MATERIALS PRODUCIBILITY Quarterly Report No. 5, 1 Aug. - 31 Oct. 1993
M. A. Berding 11 Nov. 1993 25 p
(Contract MDA972-92-C-0053; ARPA Order 8557)
(AD-A273031) Avail: CASI HC A03/MF A01

This quarter focus was on completing a paper containing the details of our calculations on the defect concentration in x = 0.2 Hg(1-x)Cd(x)Te. This involved the refinement of the calculations of all the defects. Our ideas about the formation and annihilation of tellurium precipitates in HgCdTe continue to be developed. Our work on dislocations and the reanalysis of the electronic band structure of narrow-gap HgCdTe was presented at the IRIS materials meeting in August and at the MCT Workshop in October. A paper on the electronic mobility in Hg(0.78)Cd(0.22)Te was submitted for publication in the Journal of Applied Physics. The calculations of the lithium vacancy and niobium antisite formation energies in LiNbO3 were completed and these energies are being incorporated into a thermodynamical analysis. Our calculations on the defect concentrations in ZnSe continue to be refined and preliminary predictions of the dominant defects in that system were made. DTIC

N94-21410 Naval Postgraduate School, Monterey, CA.
VALIDATION OF THE DESIGN OF A HIGH RESOLUTION ALL-REFLECTION MICHELSON INTERFEROMETER FOR ATMOSPHERIC SPECTROSCOPY M.S. Thesis
Scott M. Carlson Jun. 1993 85 p Limited Reproducibility: More than 20% of this document may be affected by microfiche quality
(AD-A272505) Avail: Issuing Activity (Defense Technical Information Center (DTIC))

The design of a high resolution plane grating all-reflection Michelson interferometer for ionospheric spectroscopy was analyzed using ray tracing

techniques. This interferometer produces an interference pattern whose spatial frequency is wavelength dependent. The instrument is intended for remote observations of the atomic oxygen triplet emission line profile at 1304 A in the thermosphere from sounding rocket or satellite platforms. The device was modeled using the PC-based ray tracing application, DART, and results analyzed through fourier techniques using the PC with Windows version of the Interactive Data Language (IDL). Through these methods, instrument resolution, resolving power, and bandpass were determined. An analysis of the effects of aperture size and shape on instrument performance was also conducted. DTIC

N94-21457# State Univ. of New York, Albany. Photonics Research Lab.
PHOTONICS AND NONLINEAR OPTICS WITH MOLECULAR MATERIALS AND POLYMERS Final Report, 1 Mar. 1990 - 28 Feb. 1993
Paras N. Prasad 28 Feb. 1993 35 p
(Contract F49620-90-C-0021)
(AD-A271747; AFOSR-93-0806TR) Avail: CASI HC A03/MF A01

We used a multidisciplinary approach to understand the structure-property relationship with an aim towards developing novel second-order and third-order nonlinear materials with enhanced performance for photonics applications. We used a combination of theoretical modeling and experimental measurement of nonlinearities in a group of systematically derivatized structures to understand the structure-property relationship. This approach was extremely useful in designing new structures with enhanced nonlinearities. We have incorporated organic second-order chromophores in sol-gel processed SiO2 and TiO2 composites which have been successfully electrically poled to form stable aligned structures. In-situ poling studies, while monitoring second harmonic generation and electro-optic modulation, were used to study the poling dynamics. The microstructures of sol-gel processed composites were investigated. A combination of optical Kerr-gate, transient absorption, and degenerate four-wave mixing was used along with appropriate theoretical development to understand the nature of resonant third-order optical nonlinearity. DTIC

N94-21491# Edgewood Arsenal, Aberdeen Proving Ground, MD. Research, Development and Engineering Center.
DOCUMENTATION FOR PCDIST, A FORTRAN SUBROUTINE TO CALCULATE POLLACK-CUZZI SCATTERING Final Report, Nov. 1992 - Mar. 1993
Jerold R. Bottiger Sep. 1993 25 p
(AD-A273070; ERDEC-TR-085) Avail: CASI HC A03/MF A01

This report documents a FORTRAN computer program (PCDIST), which may be used to calculate the light scattering phase function for a distribution of irregularly shaped particles. The subroutine also returns the average particle scattering and absorption cross-sections. PCDIST, which implements the semi-empirical theory of Pollack and Cuzzi, is called from a main program in which the user specifies particle characteristics via a construction called the parameter array. Examples demonstrating the use of the parameter array are given. DTIC

N94-21528# California Univ., Berkeley. Lawrence Berkeley Lab.
ADVANCED FAR INFRARED DETECTORS
E. E. Haller May 1993 43 p Presented at the Conference on Infrared Physics, Ascona, Switzerland, 21-26 Jun. 1993
(Contract DE-AC03-76SF-00098)
(DE93-040289; LBL-33575; CONF-9306235-1) Avail: CASI HC A03/MF A01

Recent advances in photoconductive and bolometric semiconductor detectors for wavelength 1 mm greater than lambda greater than 50 microns are reviewed. Progress in detector performance in this photon energy range has been stimulated by new and stringent requirements for ground based, high altitude, and space-borne telescopes for astronomical and astrophysical observations. The paper consists of chapters dealing with the various types of detectors: Be and Ga doped Ge photoconductors, stressed Ge:Ga devices, and neutron transmutation doped Ge thermistors. Advances in the understanding of basic detector physics and the introduction of modern semiconductor device technology have led to predictable and reliable fabrication techniques. Integration of detectors into functional arrays has become feasible and is vigorously pursued by groups worldwide. DOE

N94-21594# Technical Research Centre of Finland, Espoo. Photonics Section.
OPTICAL INTEGRATED STRUCTURES AND CIRCUITS ON SILICON Ph.D. Thesis - Helsinki Univ. of Technology
Jaakko Aarnio Jul. 1992 127 p Sponsored in part by Finnish National Fund for Research and Development; Technology Development Center, Finland; Vaisala, Finland; Nokia, Finland; PTT, Finland; Finnish Cultural Foundation; and EEC
(VTT-PUBS-106; ISBN-9-51-384224-X; ETN-93-94480) Copyright Avail: CASI HC A07/MF A02

Two types of integrated optical coupling elements were fabricated for fiberoptic sensor applications. This used a process which showed the feasibility of fabricating both optical and electronic functions on the same chip. A bidirectional method of measuring propagation losses from scattered light in a channel waveguide is presented. A new type of polarization splitter based on a Fresnel mirror is demonstrated using silicon nitride as a waveguide core. These circuits are designed to operate at a wavelength of 633 nm. Numerical scalar methods were applied to estimate the behavior of the polarization splitter, and 2, 4, and 16 channel wavelength division multiplexers based on the Fresnel mirror. The theoretical considerations are shown to be in good agreement with experimental data. The silica on silicon technology is studied for telecommunication applications and used for a new wide passband wavelength division multiplexer. For individual titles, see N94-21595 through N94-21603.

N94-21595# Technical Research Centre of Finland, Espoo. Semiconductor Lab.
A NOVEL SEMICONDUCTOR PROCESS FOR OPTOELECTRONIC APPLICATIONS ON SILICON SUBSTRATE
J. Aarnio, S. Honkanen, and M. Leppihalme *In its* Optical Integrated Structures and Circuits on Silicon Jul. 1992 4 p Repr. from 13th European Conference on Optical Communication, Helsinki, Finland, CPEF, v. 1, 1987 p 235-238 (For primary document see N94-21594 05-74)
Copyright Avail: CASI HC A01/MF A02

A semiconductor process for Si-optoelectronic integrated circuits (OEIC) applications is described. A significant simplicity and compatibility of waveguides and detectors with both types of complementary metal oxide semiconductors (CMOS) processes were achieved by careful consideration of different process steps and device geometry without having to degenerate the performance characteristics of single devices. ESA

N94-21596# Technical Research Centre of Finland, Espoo. Semiconductor Lab.
INTEGRATED OPTICAL COUPLING ELEMENT ON SILICON SUBSTRATE, APPENDIX 2
Jaakko Aarnio and Matti Leppihalme *In its* Optical Integrated Structures and Circuits on Silicon Jul. 1992 7 p Repr. from 5th European Conference on Integrated Optics, Paris, France, v. 1141, 1989 p 174-179 (For primary document see N94-21594 05-74)
Copyright Avail: CASI HC A02/MF A02

Two types of passive integrated optical coupling elements with same functions are proposed and demonstrated on silicon substrate. The elements can be hybridized along with semiconductor laser and coupled to a single intensity modulated optical fiber sensor. The reflective concept of a fiber sensor system is adopted in the designs. The comparison of switching properties of the two devices is made. Preliminary results show that an efficiency (100% back reflected to total signal ratio) of -3.2 dB can be obtained and that back reflected signal intensities lower than 0.34% (-24.7 dB) could be observed in on/off conditions. ESA

N94-21597# Technical Research Centre of Finland, Espoo. Semiconductor Lab.
BIDIRECTIONAL METHOD FOR OPTICAL CHANNEL WAVEGUIDE ATTENUATION MEASUREMENT BY DETECTORS INTEGRATED ON THE WAFER, APPENDIX 3
Jaakko Aarnio and Matti Leppihalme *In its* Optical Integrated Structures and Circuits on Silicon Jul. 1992 7 p Repr. from Integrated Optics and Optoelectronics Conference, Boston, MA, v. 1177, 1989 p 169-174 (For primary document see N94-21594 05-74)
Copyright Avail: CASI HC A02/MF A02

A new on-wafer bidirectional nondestructive measurement method is demonstrated for measuring losses in three dimensional integrated optical

waveguides. A thermally oxidized silicon wafer is used as substrate for silicon nitride multimode waveguides. The measurement is based on p-i-n photodetectors integrated near the waveguide. In order to eliminate the effect of different sensitivities of adjacent p-i-n detectors, the light is launched separately to both ends of the waveguide. The method can be applied to test structures in optoelectronic integrated circuits. ESA

N94-21598# Technical Research Centre of Finland, Espoo. Semiconductor Lab.

AN INTEGRATED-OPTIC POLARIZATION SPLITTER ON SILICON SUBSTRATE, APPENDIX 4

J. Aarnio *In its* Optical Integrated Structures and Circuits on Silicon Jul. 1992 4 p Repr. from 14th European Conference on Optical Communication, Brighton, England, v. 1, 1988 p 37-40 Sponsored by Technology Development Center, Finland (For primary document see N94-21594 05-74)

Copyright Avail: CASI HC A01/MF A02

A new type of integrated optic polarization splitter operating at the wavelength of 0.63 micrometers was proposed and demonstrated. The splitting device was fabricated by integrating a single mode silicon nitride input waveguide with a curved total reflecting grating consisting of small parts of ellipses. A preliminary measurement showed 11 dB extinction ratio for TE/TM-separation and 9 dB for TM/TE-separation. ESA

N94-21599# Commissariat a l'Energie Atomique, Grenoble (France).

FIBRE PIGTAILED SILICON BASED LOW COST PASSIVE OPTICAL COMPONENTS, APPENDIX 5

G. Grand, S. Valette, G. J. Cannell (Standard Telephones and Cables Ltd., Harlow, England.), J. Aarnio (Technical Research Centre of Finland, Espoo.), and M. delGiudice (Alcatel FACE Research Centre, Pomezia, Italy.) *In* Technical Research Centre of Finland, Optical Integrated Structures and Circuits on Silicon Jul. 1992 4 p Repr. from PTT Telecom, 16th European Conference on Optical Communication, Amsterdam, Netherlands, v. 1, 1990 p 525-528 Sponsored in part by EEC (For primary document see N94-21594 05-74)

Copyright Avail: CASI HC A01/MF A02

Some of the main achievements of an EEC program, RACE 1008, whose main objective was to demonstrate the potential of silica on silicon technology for fabrication of low cost passive optical components, are described. Reproducibility results of the silica on silicon technology are given for film refractive index and thickness, channel waveguides, and passive fiber waveguide alignmentstogether with details of the fabrication and results for a fiber pigtailed 4 channel wavelength multiplexer/demultiplexer. ESA

N94-21600# Technical Research Centre of Finland, Espoo. Semiconductor Lab.

BIREFRINGENCE CONTROL AND DISPERSION CHARACTERISTICS OF SILICON OXYNITRIDE OPTICAL WAVEGUIDES, APPENDIX 6

J. Aarnio, P. Heimala, M. delGiudice (Alcatel FACE Research Centre, Pomezia, Italy.), and F. Bruno (Alcatel FACE Research Centre, Pomezia, Italy.) *In its* Optical Integrated Structures and Circuits on Silicon Jul. 1992 2 p Repr. from Electronics Letters, v. 27, no. 25, 5 Dec. 1991 p 2317-2318 Sponsored in part by EEC (For primary document see N94-21594 05-74)

Copyright Avail: CASI HC A01/MF A02

The design, fabrication, and characterization of birefringent silicon oxynitride planar optical waveguides are described for applications at the wavelength of 1.54 micrometers. Form birefringence is attained by interposing a thin silicon nitride film in the waveguide stack and can be controlled by adjusting the nitride layer thickness. Dispersion characteristics of the oxynitride waveguides were measured and compared with theory. ESA

N94-21601# Technical Research Centre of Finland, Espoo. Semiconductor Lab.

REFRACTIVE INDEX BEHAVIOUR OF PHOSPHORUS-DOPED PLANAR SILICA WAVEGUIDES, APPENDIX 7

Paeivi Heimala and Jaakko Aarnio *In its* Optical Integrated Structures and Circuits on Silicon Jul. 1992 7 p Repr. from J. Phys. D: Appl. Phys., v. 25, 1992 p 733-739 (For primary document see N94-21594 05-74)

Copyright Avail: CASI HC A02/MF A02

The effect of annealing on the refractive index and the optical uniformity of undoped and phosphorus doped SiO2 films on silicon and quartz substrates is studied. The films are grown using low pressure chemical vapor deposition. Vertical homogeneity of the refractive index is shown to be a relevant measure upon optimizing the annealing treatment for the film. High temperature annealing results in a decrease of the refractive index and an increase in the inhomogeneity of the refractive index in the vertical direction. This is due to the outdiffusion of phosphorus as well as the reduction of compressive stresses in the films. Stresses were considered to be the main reason for the refractive index difference of the order of 0.001 between films grown on silicon and on quartz substrates. ESA

N94-21602# Technical Research Centre of Finland, Espoo. Semiconductor Lab.

WIDE PASSBAND WAVELENGTH MULTI/DEMULTIPLEXER AT 1.3/1.55 MICROMETERS BASED ON ETCHED FRESNEL MIRROR, APPENDIX 8

J. Aarnio, P. Heimala, and I. Stuns *In its* Optical Integrated Structures and Circuits on Silicon Jul. 1992 9 p Repr. from IEE Proceedings-J, v. 139, no. 3, Jun. 1992 p 228-236 (For primary document see N94-21594 05-74)

Copyright Avail: CASI HC A02/MF A02

The design, fabrication and analysis of the performance of an integrated optical wide passband multi/demultiplexer at 1.3 and 1.55 micrometers are presented. The device uses a large angle of incidence totally reflecting Fresnel mirror with average grating period of 44 micrometers to separate the wavelengths. The multi/demultiplexer is fabricated both on quartz and on silicon substrates using silica based waveguide technology. The 3 dB passbands exceed 60 nm with crosstalk below -20 dB. ESA

N94-21603# Technical Research Centre of Finland, Espoo. Semiconductor Lab.

PRECISION PRISM COUPLING SETUP APPLIED TO MEASURE PLANAR SILICA FILMS ON SILICON, APPENDIX 9

Paeivi Heimala, Jaakko Aarnio, and Simo Tammela *In its* Optical Integrated Structures and Circuits on Silicon Jul. 1992 30 p Repr. from Helsinki University, Report Series in Physics, 1992 28 p Sponsored in part by EEC and Technology Development Center, Finland (For primary document see N94-21594 05-74)

Copyright Avail: CASI HC A03/MF A02

A prism coupling set up with an absolute accuracy of 0.00006 in the refractive index determination and a relative accuracy of 0.00002 in the effective index measurement is reported. Ideas to improve the reference angle determination and the measurement accuracy of the coupling angle are included in the set up. The measurement accuracy of the refractive index of silica layer on silicon substrate is evaluated theoretically and experimentally. The effect of annealing atmosphere on the refractive index of films grown by different methods is studied. Applicability of the set up to measure refractive index uniformity, refractive index dispersion, and birefringence is shown. ESA

N94-21619# Lawrence Livermore National Lab., CA.

LASER GUIDE STAR ADAPTIVE OPTICS: PRESENT AND FUTURE

S. S. Olivier and C. E. Max 1 Mar. 1993 12 p Presented at the 158th International Astronomical Union (IAU) Symposium on Very High Angular Resolution Imaging, Sydney, Australia, 11-15 Jan. 1993 (Contract W-7405-eng-48)

(DE93-018642; UCRL-JC-113444; CONF-9301127-1) Avail: CASI HC A03/MF A01

Feasibility demonstrations using one to two meter telescopes have confirmed the utility of laser beacons as wavefront references for adaptive optics systems. Laser beacon architectures suitable for the new generation of eight and ten meter telescopes are presently under study. This paper reviews the concept of laser guide star adaptive optics and the progress that has been made by groups around the world implementing such systems. A description of the laser guide star program at LLNL and some experimental results is also presented. DOE

N94-21630# Lawrence Livermore National Lab., CA.

HIGH RESOLUTION, THREE DIMENSIONAL SOFT X RAY IMAGING

J. Trebes, J. Brase, R. Levesque, H. Szoke, T. Yorkey, E. Anderson (California Univ., Berkeley. Lawrence Berkeley Lab.), and C. Jacobsen (State Univ. of New York, Stony Brook.) 12 May 1993 5 p Presented

at the Workshop on Scientific Application of Short Wavelength Coherent Light Source, Stanford, CA, 21 Oct. 1992
(Contract W-7405-eng-48)
(DE93-018867; UCRL-JC-113429; CONF-9210278-2) Avail: CASI HC A01/MF A01

A long term goal of soft x ray imaging has been to make ultrahigh resolution images of unstained, unprepared, wet, live biological microstructures in physiological normal environments. This is now being accomplished with features as small as 300 Angstrom being observed in two dimensional x ray images. While this achievement is remarkable, most complex biological structures are three dimensional in nature and will require three dimensional images on the few hundred Angstrom scale for the structure-function studies required by modern biology. It was endeavored to achieve this three dimensional capability with soft x ray techniques. DOE

N94-21837# Argonne National Lab., IL.
MATERIAL OPTIMIZATION FOR HARD X RAY FRESNEL ZONE PLATES
J. Chrzas, W. Yun, B. Lai, D. Legnini, and Y. Xiao 1993 11 p Presented at the Annual Meeting of the Society of Photo-Optical Instrumentation Engineers (SPIE), San Diego, CA, 11-16 Jul. 1993
(Contract W-31-109-eng-38)
(DE93-019569; ANL/XFD/CP-80547; CONF-930722-26) Avail: CASI HC A03/MF A01

Fresnel zone plates have recently been used as the focusing optic for hard x-ray (5 - 11 keV) microscopy techniques. Fresnel zone plates used in the hard x-ray regime focus by constructive interference effects based on the phase modulation of the incident x-ray beam and have experimentally been shown to focus 20 - 30% of the incident photons to less than a one-micron focal spot. The materials of choice for these zone plates have been Al, Cu, Ni, and Au. The focus of this work is the theoretical optimization of the focusing efficiency of phase-modulating Fresnel zone plates in the hard x-ray regime by appropriate material selection. The optimal materials for three different energy ranges will be examined (1 - 5 keV, 5 - 20 keV, and greater than 20 keV), and a discussion of the selection criteria involved will be presented. The current zone plate fabrication techniques will be discussed as they pertain to the physical aspects of the zone plates such as thickness, finest zone width, and aspect ratio. DOE

N94-21868# California Univ., Berkeley. Lawrence Berkeley Lab.
CENTER FOR X-RAY OPTICS, 1992
Aug. 1993 27 p
(Contract DE-AC03-76SF-00098)
(DE94-000726; LBL-34462) Avail: CASI HC A03/MF A01

The following topics are discussed: Center for X Ray Optics; soft x ray imaging with zone plate lenses; biological x ray microscopy; extreme ultraviolet lithography for nanoelectronic pattern transfer; multilayer reflective optics; EUV/soft x ray reflectometer; photoemission microscopy with reflective optics; spectroscopy with soft x rays; hard x ray microprobe; coronary angiography; and atomic scattering factors. DOE

N94-21985# Lawrence Livermore National Lab., CA.
X RAY CHARACTERIZATION OF A THREE-ELEMENT CONDENSER SYSTEM FOR SOFT X RAY PROJECTION LITHOGRAPHY
D. P. Gaines (Brigham Young Univ., Provo, UT.), G. E. Sommargren, S. P. Vernon, and R. E. English 16 Jun. 1993 7 p Presented at the OSA Topical Meeting on Soft X Ray Projection Lithography, Monterey, CA, 10-12 May 1993
(Contract W-7405-eng-48)
(DE93-019916; UCRL-JC-114074; CONF-9305159-9) Avail: CASI HC A02/MF A01

A three-element condenser system has been fabricated and coated with multilayer reflectors designed to operate at a wavelength of 13.3 nm. The performance of the condenser system was evaluated by measuring the reflectance of the individual condenser mirrors at normal incidence and modeling the system transport efficiency. Although a transport efficiency of 17% should be attainable with this design, actual condenser performance will be reduced because of d-spacing variations on mirror C2 and surface roughness on mirror C3. Replacement mirrors C2 and C3 are being fabricated to recover system performance. DOE

N94-22002# Lawrence Livermore National Lab., CA.
DYNAMICS OF SURFACE THERMAL EXPANSION AND DIFFUSIVITY USING TWO-COLOR REFLECTION TRANSIENT GRATINGS
D. M. Pennington and C. B. Harris (California Univ., Berkeley. Lawrence Berkeley Lab.) Feb. 1993 14 p Presented at the OE/LASE 1993 International Society for Optical Engineering (SPIE) Conference, Los Angeles, CA, 13-23 Jan. 1993
(Contracts W-7405-eng-48; DE-AC03-76SF-00098)
(DE93-040547; UCRL-JC-111288; CONF-930159-57) Avail: CASI HC A03/MF A01

We report ultrafast measurements of the dynamic thermal expansion of a surface and the temperature dependent surface thermal diffusivity using a two-color reflection transient grating technique. Studies were performed on p-type, n-type, and undoped GaAs(100) samples at several temperatures. Using a 75 fs ultraviolet probe with visible excitation beams, the electronic effects that dominate single color experiments become negligible; thus, surface expansion due to heating and the subsequent contraction caused by cooling provide the dominant influence on the diffracted probe. The diffracted signal was composed of two components, thermal expansion of the surface and heat flow away from the surface, allowing the determination of the rate of expansion as well as the surface thermal diffusivity. At room temperature a signal rise due to thermal expansion was observed, corresponding to a maximum average displacement of approximately 1 A at 32 ps. Large fringe spacings were used; thus, the dominant contributions to the signal were expansion and diffusion perpendicular to the surface. Values for the surface thermal diffusivity of GaAs were measured and found to be in reasonable agreement with bulk values above 50 K. Below 50 K, the diffusivity at the surface was more than an order of magnitude slower than in the bulk due to increased phonon boundary scattering. Comparison of the results with a straightforward thermal model yields good agreement over a range of temperatures (12-300 K). The applicability and advantages of the transient grating technique for studying photothermal and photoacoustic phenomena are discussed. DOE

N94-22411 Laval Univ. (Quebec).
HOLOGRAPHIC OPTICAL ELEMENTS CORRECTING THE OFF-AXIS ABERRATIONS OF A PARABOLIC MIRROR M.S. Thesis [ELEMENT OPTIQUES HOLOGRAPHIQUES CORRIGEANT LES ABERRATIONS HORS AXE D'UN MIROIR PARABOLIQUE]
Guylain Lemelin Jul. 1990 142 p In FRENCH
(ISBN-0-315-57581-6; CTN-94-60880) Copyright Avail: Micromedia Ltd., Technical Information Centre, 240 Catherine Street, Suite 305, Ottawa, Ontario, K2P 2G8, Canada HC/MF

The technology of rotating liquid mirrors provides the potential for constructing reflecting telescopes of high optical quality at larger mirror diameters than those currently achievable using solid glass. However, such mirrors can only operate in a fixed position, and if they are used to observe objects off their optical axis, aberration of the image becomes more significant as the distance off the optical axis increases. Without the use of an optical correction device, the image can be degraded to the point where it is useless. It is proposed that a corrector as simple as a holographic optical element can carry out the necessary correction at a fixed angle of incidence. The theory of scalar diffraction of a monochromatic plane wave by a parabolic mirror is presented along with modeling of aberration phenomena at the mirror surface and at the telescope focus. The computer-aided generation of various types of numerical holographic correctors is presented and two are analyzed. Certain characteristics are put forward in evidence which allow expanding of the useful field of view. Computer program listings are included. CISTI

N94-22579 Toronto Univ. (Ontario). Dept. of Aerospace Science and Engineering.
DEMODULATION OF A FIBER FABRY-PEROT STRAIN ROSETTE USING WHITE LIGHT INTERFEROMETRY M.S. Thesis
Gary Louis Zuliani 1993 96 p
(ISBN-0-315-83427-7; CTN-94-60953) Copyright Avail: Micromedia Ltd., Technical Information Centre, 240 Catherine Street, Suite 305, Ottawa, Ontario, K2P 2G8, Canada HC/MF

Fiber optic sensors are starting to be used in specialty application areas where electrical sensors are usually found, such as in aircraft and spacecraft. Fiber optic sensor technology has advantages over its electronic counterparts including small size and weight, immunity to electromagnetic

interference, and ruggedness. The use of fiber interferometers as sensors is reviewed along with methods for demodulating their signals. The principles of path-matched differential interferometry and coherence multiplexing are demonstrated and applied to the design and construction of a system that simultaneously demodulates three fiber Fabry-Perot (FFP) interferometers. The FFP's formed the arms of a delta rosette which were bonded to the surface of an aluminum cantilevered beam and were illuminated with one broadband light source. The receiving interferometer consisted of a bulk Michelson interferometer with three distinct optical paths. A charge coupled device array was used as the detector allowing fringe shifts to be counted on a television monitor. Tensor measurements were made and found to be in good agreement when compared to those obtained from electrical strain gages. Author (CISTI)

N94-22581 Toronto Univ. (Ontario).
PHASE DEMODULATION OF INTERFEROMETRIC FIBER-OPTIC SENSORS M.S. Thesis
Thomas Gordon Beck Mason 1992 113 p
(ISBN-0-315-83425-0; CTN-94-60955) Copyright Avail: Micromedia Ltd., Technical Information Centre, 240 Catherine Street, Suite 305, Ottawa, Ontario, K2P 2G8, Canada HC/MF

A variety of interferometric fiber optic sensors is described and compared with a thorough development of their intensity transfer functions and phase strain models. Several different phase demodulation techniques are discussed, and the advantages of the pseudo heterodyne technique are explained. A review of the various types of tunable sources that can be used for pseudo heterodyne phase demodulation is conducted and several practical models are identified. The development of a complete sensor system is reported, and several iterations resulted in improved performance. Techniques for making temperature compensated strain measurements with the strain sensor system are examined, and a preferred technique is demonstrated. The development of a smart structure testbed with a two channel fiber Fabry-Perot sensing system designed to simulate a large space truss is documented. Results of tests with this structure are analyzed, and the sensor system performance is evaluated. Finally, an analysis of future sensing systems for absolute and acoustic sensing is performed on a practical and theoretical basis. Author (CISTI)

N94-20646*# Jet Propulsion Lab., California Inst. of Tech., Pasadena.
THE COHERENT BACKSCATTERING OPPOSITION EFFECT Abstract Only
R. M. Nelson, B. W. Hapke (Pittsburgh Univ., PA.), W. D. Smythe, V. Gharakanian, and P. Herrera *In* Lunar and Planetary Inst., Twenty-Fourth Lunar and Planetary Science Conference. Part 3: N-Z 1993 p 1061-1062 (For primary document see N94-20636 05-91)
Avail: CASI HC A01/MF A06

N94-21095*# New Mexico Univ., Albuquerque. Biomedical Research.
NATURE'S CRUCIBLE: MANUFACTURING OPTICAL NONLINEARITIES FOR HIGH RESOLUTION, HIGH SENSITIVITY ENCODING IN THE COMPOUND EYE OF THE FLY, MUSCA DOMESTICA
Mike Wilcox *In its* The Fifth NASA Symposium on VLSI Design 1993 14 p (For primary document see N94-21079 05-33)
Avail: CASI HC A03/MF A06

N94-21098*# Johns Hopkins Univ., Laurel, MD. Applied Physics Lab.
SILICON RETINA FOR OPTICAL TRACKING SYSTEMS
K. Strohbehn, R. E. Jenkins, X. Sun (Johns Hopkins Univ., Baltimore, MD.), and A. G. Andreou (Johns Hopkins Univ., Baltimore, MD.) *In* New Mexico Univ., The Fifth NASA Symposium on VLSI Design 1993 12 p (For primary document see N94-21079 05-33)
Avail: CASI HC A03/MF A06

N94-22129 Toronto Univ. (Ontario). Computer Integrated Manufacturing Lab.
THE CONCEPTUAL DESIGN OF A SHORT-RANGE DISTANCE SENSOR
S. Jacobi and B. Benhabib *In* Engineering Inst. of Canada, Canadian Conference on Electrical and Computer Engineering, Volumes 1 and 2 1991 4 p (For primary document see N94-22101 05-33)
Avail: Issuing Activity (Engineering Inst. of Canada, 2050 rue Mansfield, Suite 700, Montreal, PQ H3A 1Z2 Canada)

N94-22220 Laval Univ. (Quebec). Centre d'Optique, Photonique et Laser.
ARCHITECTURES OF THE FREE SPACE OPTICAL INTERCONNECTS
Yun-Long Sheng *In* Engineering Inst. of Canada, Canadian Conference on Electrical and Computer Engineering, Volumes 1 and 2 1991 4 p (For primary document see N94-22101 05-33)
Avail: Issuing Activity (Engineering Inst. of Canada, 2050 rue Mansfield, Suite 700, Montreal, PQ H3A 1Z2 Canada)

N94-22222 National Research Council of Canada, Ottawa (Ontario). Inst. for Information Technology.
OPTICAL PROCESSING IN PHOTOREFRACTIVE MEDIA
S. A. Boothroyd, L. Chan, P. H. Beckwith, and J. Chrostowski *In* Engineering Inst. of Canada, Canadian Conference on Electrical and Computer Engineering, Volumes 1 and 2 1991 4 p (For primary document see N94-22101 05-33)
Avail: Issuing Activity (Engineering Inst. of Canada, 2050 rue Mansfield, Suite 700, Montreal, PQ H3A 1Z2 Canada)

N94-22227 Applied Analytics Corp., Markham (Ontario).
A REAL-TIME INFRARED IMAGE PROCESSING TESTBED
E. Lithopoulos, J. Hodd, and E. Bender *In* Engineering Inst. of Canada, Canadian Conference on Electrical and Computer Engineering, Volumes 1 and 2 1991 4 p (For primary document see N94-22101 05-33)
Avail: Issuing Activity (Engineering Inst. of Canada, 2050 rue Mansfield, Suite 700, Montreal, PQ H3A 1Z2 Canada)

N94-22235 Defence Research Establishment Valcartier (Quebec). Electro-Optics Div.
A FOUR-BAND INFRARED DATA ACQUISITION FACILITY FOR SIGNAL PROCESSING DEVELOPMENT
Benoit Montminy *In* Engineering Inst. of Canada, Canadian Conference on Electrical and Computer Engineering, Volumes 1 and 2 1991 4 p (For primary document see N94-22101 05-33)
Avail: Issuing Activity (Engineering Inst. of Canada, 2050 rue Mansfield, Suite 700, Montreal, PQ H3A 1Z2 Canada)

75 PLASMA PHYSICS

Includes magnetohydrodynamics and plasma fusion.

For ionospheric plasmas see *46 Geophysics*. For space plasmas see *90 Astrophysics*.

N94-19872# Texas Univ., Austin.
FINITE LARMOR RADIUS FLUTE MODE THEORY WITH END LOSS
I. A. Kotelnikov (Academy of Sciences, USSR, Novosibirsk.) and H. L. Berk Aug. 1993 51 p
(Contract DE-FG05-80ET-53088)
(DE93-040914; DOE/ET-53088/620; IFSR-620) Avail: CASI HC A04/MF A01

The theory of flute mode stability is developed for a two-energy-component plasma partially terminated by a conducting limiter. The formalism is developed as a preliminary study of the effect of end-loss in open-ended mirror machines where large Larmor radius effects are important. DOE

N94-19883# Los Alamos National Lab., NM.
PARAMETRIC VARIATIONS OF ION TRANSPORT IN TFTR
S. D. Scott, C. W. Barnes, and D. Ernst (Massachusetts Inst. of Tech., Cambridge.) 18 Mar. 1993 33 p Presented at the US/Japan Workshop on Ion Temperature Gradient Driven Turbulent Transport, Austin, TX, 11-14 Jan. 1993
(Contract W-7405-eng-36)
(DE93-012653; LA-UR-93-1255; CONF-9301107-1) Avail: CASI HC A03/MF A01

This paper is divided into three roughly independent sections. The first is a historical review of the twenty year history of experimental ion heat transport measurements from many tokamaks. The second is a study of ion heat transport in Ohmic TFTR plasmas which shows that chi(sub i) is similar to chi(sub e) approximately equal to chi(sub i)(sup neo). Thus, ion heat transport is demonstrated to be strongly anomalous even the absence

of auxiliary heating. The third section describes the variation of chi(sub i) with local ion temperature in TFTR during auxiliary heating, with emphasis on characterizing the differences between transport in the L-mode and supershot regimes. The results are consistent with the conjecture that improved ion energy confinement in supershot plasmas is caused by a high ratio of T(sub 1)/T(sub e). DOE

N94-19887# Texas Univ., Austin. Inst. for Fusion Studies.
EFFECT OF LIMITER END LOSS IN FINITE LARMOR RADIUS THEORY
H. L. Berk and I. A. Kotelnikov (Academy of Sciences, USSR, Novosibirsk.) Aug. 1993 13 p
(Contract DE-FG05-80ET-53088)
(DE93-040913; DOE/ET-53088/619; IFSR-619) Avail: CASI HC A03/MF A01

The effect of incomplete line tying on the magnetohydrodynamic (MHD) flute mode with FLR (finite Larmor radius) effects was examined. It was shown that the combination of line tying and FLR effects can slow down MHD instability, but cannot produce complete stabilization. DOE

N94-19915# Lawrence Livermore National Lab., CA.
LONGITUDINAL BEAM DYNAMICS FOR HEAVY ION FUSION USING WARPrz
Debra A. Callahan, A. Bruce Langdon, Alex Friedman, and Irving Haber (Naval Research Lab., Washington, DC.) 22 Feb. 1993 10 p Presented at the 1993 Computational Accelerator Physics Conference, Pleasanton, CA, 22-26 Feb. 1993
(Contracts W-7405-eng-48; DE-AI05-92ER-54177; DE-AI05-83ER-40112)
(DE93-019154; UCRL-JC-112247; CONF-930269-20) Avail: CASI HC A02/MF A01

WARPrz is a 2.5 dimensional, cylindrically symmetric, electrostatic, particle-in-cell code. It is part of the WARP family of codes which has been developed to study heavy ion fusion driver issues. WARPrz is being used to study the longitudinal dynamics of heavy ion beams including a longitudinal instability that is driven by the impedance of the LINAC accelerating modules. This instability is of concern because it can enhance longitudinal momentum spread; chromatic abhoration in the lens system restricts the amount of momentum spread allowed in the beam in the final focusing system. The impedance of the modules is modeled by a continuum of resistors and capacitors in parallel in WARPrz. We discuss simulations of this instability including the effect of finite temperature and reflection of perturbations off the beam ends. We also discuss intermittency of axial confining fields ('ears' fields) as a seed for this instability. DOE

N94-19991# Lawrence Livermore National Lab., CA.
THE BEST OF GYMNOS: A USERS GUIDE
D. W. Hewett and D. J. Larson Aug. 1993 104 p
(Contract W-7405-eng-48)
(DE93-041275; UCRL-ID-110499) Avail: CASI HC A06/MF A02

The code GYMNOS is a 2.5D magnetostatic PIC code that is distinguished from the multitude of similar codes by its ability to handle boundary conditions and internal structures. This code was started during the period from December 1987 and the major sections were completed and in routine use by the end of 1990. The code is written in R-Z geometry (axisymmetric m=0 only) but could easily be modified to handle an X-Z configuration. The several competitors of this code, having similar (but we believe less general) capabilities, distinguish themselves in a different way: they have very formal, thick instruction manuals and usually command an army of people to maintain both the code and said manual. We are attempting to convince the reader that GYMNOS is better in these two regards. Offered is a description of a code with a great deal of physics capability coupled with no interactive graphics capability and very little system capability. These later two subjects contribute most of the complexity in both the code and manual in the competition! Expressed another way, the user will almost never be thwarted by unexpected system changes on Friday afternoon. The price extracted is that the user is required to monitor/babysit runs so that output is 'hand-delivered' to the output medium and properly archived to prevent loss. A further spinoff of this simplicity is that 'single pilot' operation is easy. And, the only manual is this modest document. DOE

N94-20003# General Atomic Co., San Diego, CA.
TRANSIENT THERMAL ANALYSIS OF CRYOCONDENSATION PUMP FOR JET
C. B. Baxi and W. Obert (Joint European Torus Project, Abingdon, England.) Aug. 1993 8 p Presented at the International Cryogenic Engineering Conference and International Cryogenic Materials Conference, Albuquerque, NM, 12-16 Jul. 1993
(Contract DE-AC03-89ER-51114)
(DE93-040372; GA-A-20941; CONF-930703-33) Avail: CASI HC A02/MF A01

A cryopump with pumping speed of 50,000 1/sec is to be installed in the Joint European Torus (JET) as part of the pumped divertor. The purpose of this pump is to control the plasma impurities. The pump consists of a helium panel cooled by supercritical helium and a nitrogen shield cooled by liquid nitrogen. This paper presents the following transient thermal flow analysis for this cryopump: (1) consequences of loss of torus vacuum on helium panel; and (2) cool down of the nitrogen shield form 300 K to 80 K. DOE

N94-20004# California Univ., Berkeley. Lawrence Berkeley Lab.
SPACE-CHARGE DOMINATED BEAM TRANSPORT IN MAGNETIC QUADRUPOLES WITH LARGE APERTURE RATIOS
W. F. Fawley Aug. 1993 20 p
(Contract DE-AC03-76SF-00098)
(DE93-040443; LBL-33608; HIFAN-614) Avail: CASI HC A03/MF A01

This memo summarizes the results of calculations of the usable aperture ratio for short period, magnetic quadrupoles for both ILSE magnet designs and the more general, heavy-ion fusion (HIF) 'driver' case. From both analytic decomposition of the magnetic field in a periodic lattice and particle code simulations of beam transport, we find that fringe field nonlinearities and associated emittance growth become quite large when the beam radius a(sub b) exceeds one-quarter or so of the half-lattice period L. For ILSE, there are a number of magnet designs which can transport the specified line charge without any significant difficulties, primarily because the ratio a(sub b)/L is of order 0.1 or less. For larger sized beams such as one might employ in the low energy part of a driver, there are problems with properly matching the beam to the transport lattice in both the macroscopic and microscopic sense as a(sub b)/L exceeds 0.2. For even larger aperture ratios, particle loss can occur, with the threshold in beam radius roughly scaling inversely with (sigma)(sub o), the single particle phase advance per lattice period. DOE

N94-20058# Oak Ridge National Lab., TN.
FAST ION BEHAVIOR DURING NEUTRAL BEAM INJECTION IN ATF
M. R. Wade, C. E. Thomas, R. J. Colchin, J. A. Rome, A. C. England, R. H. Fowler, and S. C. Aceto (Rensselaer Polytechnic Inst., Troy, NY.) 1993 8 p Presented at the 9th International Atomic Energy Agency Workshop on Stellarators, Garching, Germany, 10-14 May 1993
(Contract DE-AC05-84OR-21400)
(DE93-040267; CONF-9305210-3) Avail: CASI HC A02/MF A01

In stellarators, single-particle confinement properties can be more complex than in their tokamak counterparts. Fast-ion behavior in tokamaks has been well characterized through an abundance of measurements on various devices and in general has been shown to be consistent with classical slowing-down theory, although anomalous ion behavior has been observed during intense beam injection in ISX-B, during fishbone instabilities in PDX, and in experiments on TFR. In contrast, fast ion behavior in stellarators is not as well established experimentally with the primary experiments to date focusing on near-perpendicular or perpendicular neutral beam injection (NBI) on the Wendelstein 7-A stellarator and Heliotron-E. This paper addresses fast-ion confinement properties in a large aspect ratio, moderate shear stellarator, the Advanced Toroidal Facility, during tangential NBI. The primary data used in this study are the experimentally measured energy spectra of charge-exchange neutrals escaping from the plasma, using a two-dimensional scanning neutral particle analyzer. This diagnostic method is well established, having been used on several devices since the early 1970's. Various aspects of fast-ion behavior are investigated by comparing these data with computed theoretical spectra based on energetic ion distributions derived from the fast ion Fokker-Planck equation. Ion orbits are studied by computer orbit following, by the computation of J(sup *) surfaces, and by Monte Carlo calculations. DOE

N94-20156 Cologne Univ. (Germany). Inst. fuer Geophysik und Meteorologie.

RADIATION OF PLASMA WAVE WINGS THROUGH AN ELECTRODYNAMIC TETHER SATELLITE SYSTEM WITH ANY SHARP ANGLE GEOMETRY [ABSTRAHLUNG VON PLASMAWELLENFLUEGELN DURCH EIN ELEKTRODYNAMISCHES FESSELSATELLITENSYSTEM BEI BELIEBIGER SCHIEFWINKLIGER GEOMETRIE]

Andrea Luettgen 1992 110 p In GERMAN Limited Reproducibility: More than 20% of this document may be affected by microfiche quality
(Rept-85; ETN-93-95067) Avail: CASI HC A06

A model for the far field interaction between an electrodynamic tether satellite system and its ionospheric plasma environment is developed. The angles between cable orientation, plasma flow direction, and magnetic field were supposed to be different from 90 degrees. The charge exchange was assumed to regularly occur on a finite distance along the streamflow. Magnetic field was homogeneous and time constant; cold plasma approximation was used for the ionospheric plasma which only contained electrons and one ion species. Field parallel current density in Alfven wings, electric field in plasma and related impedence were calculated and their variations with magnetic field orientation were discussed. It is shown that frequency area, for which pure, nonevanescent wave propagation occurs, strongly varies with magnetic field orientation. It is found that current density in magnetic field direction has a stronger resolution of ideal Alfven wing structure by lower perturbation lengths and so by higher characteristic excitation frequency. Wave impedance was calculated with fixed magnetic field vector angle as a function of perturbation length; it can be concluded that oscillation area of impedance values drops with increasing perturbation lengths. ESA

N94-20234# California Univ., Berkeley. Lawrence Berkeley Lab.

HEAVY ION FUSION INJECTOR EXPERIMENTS

S. Eylon, E. Henestroza, H. Rutkowski, S. Yu, D. Grote, Y. J. Chen, and D. Hewett May 1993 15 p Presented at the International Symposium on Heavy Ion Fusion, Frascati, Italy, 25-28 May 1993
(Contract DE-AC03-76SF-00098)
(DE93-019188; LBL-33801; CONF-9305136-14) Avail: CASI HC A03/MF A01

We report on three experiments performed in connection with the 2 MV electrostatic quadrupole (ESQ) injector under construction at Lawrence Berkeley Laboratory. Scaled experiments have been conducted to study possible beam emittance growth due to beam aberrations in an ESQ injector. The experiment uses the SBTE (Single Beam Transport Experiment) accelerator system, quarter-scale ESQ setup and a potassium ion diode source. Measured emittance growth changes significantly with variations in current and diode energy, in good agreement with theoretical predictions. In addition, beam transport experiments were performed in a 1 MV axisymmetric electrostatic aperture column using a zeolite 1 inch diameter potassium ion source. Experimental measurements in good agreement with 2-1/2 D simulations showed that low emittance beams can be produced in axisymmetric structures. Finally, ESQ breakdown voltage tests without beam were performed at up to two times the quadrupole working voltage. DOE

N94-20261# Sandia National Labs., Albuquerque, NM.

OPTICAL DIAGNOSTIC INSTRUMENT FOR MONITORING ETCH UNIFORMITY DURING PLASMA ETCHING OF POLYSILICON IN A CHLORINE-HELIUM PLASMA

W. A. Hareland and R. J. Buss Jun. 1993 15 p
(Contract DE-AC04-76DP-00789)
(DE93-019582; SAND-93-0455) Avail: CASI HC A03/MF A01

Non-uniform etching is a serious problem in plasma processing of semiconductor materials and has important consequences in the quality and yield of microelectronic components. In many plasmas, etching occurs at a faster rate near the periphery of the wafer, resulting in nonuniform removal of specific materials over the wafer surface. This research investigates in situ optical diagnostic techniques for monitoring etch uniformity during plasma processing of microelectronic components. The authors measure 2-D images of atomic chlorine at 726 nm in a chlorine-helium plasma during plasma etching of polysilicon in a parallel-plate plasma etching reactor. The 3-D distribution of atomic chlorine is determined by Abel inversion of the plasma image. The experimental results show that the chlorine atomic emission intensity is at a maximum near the outer radius of the plasma and decreases toward the center. Likewise, the actual etch rate, as determined by profilometry on the processed wafer, is approximately 20% greater near the edge of the wafer than at its center. There is a direct correlation between the atomic chlorine emission intensity and the etch rate of polysilicon over the wafer surface. Based on these analyses, 3-D imaging would be a useful diagnostic technique for in situ monitoring of etch uniformity on wafers. DOE

N94-20326# General Atomic Co., San Diego, CA.

BETA-LIMITING INSTABILITIES IN D3-D DISCHARGES WITH LARGE BOOTSTRAP CURRENT

E. J. Strait, T. S. Taylor, A. D. Turnbull, M. S. Chu, J. R. Ferron, L. L. Lao, and T. H. Osborne May 1993 4 p Presented at the 20th European Conference on Controlled Fusion and Plasma Physics, Lisbon, Portugal, 26-30 Jul. 1993
(Contract DE-AC03-89ER-51114)
(DE93-015476; GA-A-21301; CONF-930720-10) Avail: CASI HC A01/MF A01

In reactor-relevant discharges with high beta and low collisionality, the beta limit may be reduced by the presence of a large bootstrap current density near the edge of the plasma. The combination of a large current density and a large pressure gradient may destabilize low-n ideal kink modes localized near the plasma edge. This hypothesis is consistent with the behavior of high-performance discharges in DIII-D, in which the ELM-free phase with good energy confinement often ends with a rapidly growing low-n MHD instability. A large bootstrap current density can occur near the edge of H-mode discharges, even at moderate values of volume-averaged beta, owing to the large pressure gradient associated with the H-mode transport barrier. In discharges with finite aspect ratio and low to moderate collisionality, the bootstrap current density is proportional to the pressure gradient rather than the density gradient and thus becomes large near the edge of high beta and H-mode discharges. A large bootstrap current density is found near the edge of low density H-mode and VH-mode discharges in DIII-D, as predicted by transport simulations and confirmed by equilibrium reconstructions. Derived from text

N94-20491* National Aeronautics and Space Administration. Lyndon B. Johnson Space Center, Houston, TX.

METHOD FOR ANISOTROPIC ETCHING IN THE MANUFACTURE OF SEMICONDUCTOR DEVICES Patent

Steven L. Koontz, inventor (to NASA) and Jon B. Cross, inventor (to NASA) 21 Dec. 1993 11 p Filed 12 Jul. 1991 Supersedes N91-32947 (29 - 24, p 4106)
(NASA-Case-MSC-21631-1; US-Patent-5,271,800;
US-Patent-Appl-SN-729107; US-Patent-Class-156-643;
US-Patent-Class-156-646; US-Patent-Class-156-668;
US-Patent-Class-156-662; US-Patent-Class-250-251;
US-Patent-Class-250-423R; US-Patent-Class-250-423P) Avail: US Patent and Trademark Office

Hydrocarbon polymer coatings used in microelectronic manufacturing processes are anisotropically etched by hyperthermal atomic oxygen beams (translational energies of 0.2 to 20 eV, preferably 1 to 10 eV). Etching with hyperthermal oxygen atom species obtains highly anisotropic etching with sharp boundaries between etched and mask protected areas.
Official Gazette of the U.S. Patent and Trademark Office

N94-20937# Yale Univ., New Haven, CT.

THEORETICAL AND NUMERICAL STUDIES IN MAGNETIC FUSION

1993 11 p
(Contract DE-FG02-86ER-53240)
(DE94-000536; DOE/ER-53240/5) Avail: CASI HC A03/MF A01

This past year has been devoted to the development of analytic and numerical kinetic theory for the edge physics problem in Tokamaks. For the charged particles the general formal problem involves the solution of the system of coupled drift-kinetic equations. Near a diverter, the set of equations must be supplemented by Boltzmann equations for the uncharged species, and the situation is complicated by wall chemistry and sheaths. The full problem is clearly beyond the ability of the current best in available analytic and numerical methods. Thus we have begun by considering simplified model kinetic theory models in order to explore phenomena and develop analytic and numerical techniques. The first effort was to use the kinetic equation of discharge theory, which while not quantitative, provides the easiest problem. Next we have completely solved a kinetic theory

problem using the Lorentz gas approximation for the collision term. This has provided analytic and computational tools for use in dealing with the kinetic equation including energy diffusion. In order to deal most simply with energy diffusion we have developed a simple model of the collision terms C(sub j) which conserves number and for self collisions, also conserves energy and momentum. It lends itself to rapid accurate computation. The associated solutions of the kinetic equation should be semiquantitative and provide a useful tool for the rapid exploration of edge phenomena and the development of first approximations required for the iterative solution of the full kinetic equation. DOE

N94-20940# Wisconsin Univ., Madison. Dept. of Electrical and Computer Engineering.
FUSION PLASMA THEORY GRANT. TASK 3: AUXILIARY RADIOFREQUENCY HEATING OF TOKAMAKS
J. E. Scharer Jun. 1993 11 p
(Contract DE-FG02-86ER-53218)
(DE94-000779; DOE/ER-53218/23) Avail: CASI HC A03/MF A01

The research performed under this grant during the past year has been concentrated on the following several key tokamak ICRF (Ion Cyclotron Range of Frequencies) coupling, heating, and current drive issues. We have made progress in developing a '3-D' cavity backed antenna array code to examine ICRF coupling to general plasma edge profiles. The effects of the finite antenna length and feeders as well as Faraday shield blade angle are being examined. We are also developing an analysis to examine large k(perpendicular)(rho) gyroradius interaction between alpha or beam particles and ICRF waves. This topic has important applications in the areas of ICRF heating for deuterium-tritium fusion plasmas, TAE modes, ash removal, and minority ion current drive. Research progress, publications, and conference and workshop presentations are summarized in this report. DOE

N94-20943# SFA, Inc., Landover, MD.
ENGINEERING DESIGN, FABRICATION, INSTALLATION, OPERATION, AND MAINTENANCE SERVICES IN SUPPORT OF RESEARCH ON LASER PLASMA PHYSICS Final Report, 22 Nov. 1991 - 8 May 1993
Kevin Smith, Mariano Sy, and Joseph Chow Sep. 1993 4 p
(Contract N00014-92-D-2000)
(AD-A272249; SFA-93/005) Avail: CASI HC A01/MF A01

SFA provided research support to the Naval Research Laboratory Beam Physics Branch by providing engineering layouts and modifications for the various high-power microwave and coherent radiation sources and laser plasma physics. SFA also reconfigured the feeds of the 12 resonant coils in the modified betatron to operate at a peak voltage as high as 55 kV. DTIC

N94-21039# Clemson Univ., SC. Dept. of Mathematical Sciences.
THREE-WAVE RESONANT INTERACTION IN A THIN LAYER
Aug. 1993 11 p Sponsored by ONR and AFOSR
(AD-A272331) Avail: CASI HC A03/MF A01

We analyze in detail conversion of a pump wave into two daughter waves (DW's) on an infinitely thin nonlinear layer, assuming that the conversion is initiated by weak seed pulses of the DW's. Three cases corresponding to different signs of the group velocities of the DW's are considered separately. In the case when both velocities are opposite to that of the pump wave, a threshold value of the 'strength' of the nonlinear layer is found, above which oscillations between the conversion and the inverse process of recombination set in. In the case when the DW group velocities have different signs, the shapes of the generated DW pulses do not depend upon shapes of the corresponding 'seed' pulses. In this case, multiple solutions are possible, provided the nonlinearity is strong enough. DTIC

N94-21053# College of Aeronautical Engineering, Risalpur Cantt (Pakistan). Dept. of Avionics.
IMPACT OF COPPER VAPOUR CONTAMINATION ON ARGON ARCS
Salim Akbar 1990 24 p Original contains color illustrations
Avail: CASI HC A03/MF A01

A fast, accurate, and comprehensive emission spectroscopic set up has been employed to study the impact of copper vapor on an Ar-Cu mixture plasma. Temperature profiles in the arc have been determined in the absence of Cu vapor and then in its presence, using the absolute line intensity method for an Ar spectral line; these profiles are compared with temperature profiles derived from relative intensities of Cu I lines. Temperature profiles derived from relative intensity of Cu I lines are used to calculate the radial density distribution of copper atoms in the arc. The following observations are made from the resulting atomic number densities: the copper vapor concentrates in the fringes of the arc, with atomic number densities up to 8.6 x 10(exp 11) cm(exp -3); and Cu atomic number densities in the core of the arc are small. Author (revised)

N94-21214# Ohio State Univ., Columbus. Dept. of Chemistry.
LASER DIAGNOSTICS OF RF HYDROGEN PLASMA REACTORS: APPLICATION TO THE PROCESSING OF III-V MATERIALS Final Report, Jul. 1989 - Sep. 1992
Bryan L. Preppernau, Angeliki Tserepi, Jim Dunlop, and T. A. Miller Feb. 1993 69 p
(Contract F33615-89-C-2921)
(AD-A272659; WL-TR-93-2046) Avail: CASI HC A04/MF A01

Two photon laser induced fluorescence (TALIF) has been developed as a convenient and reliable diagnostic of H atoms in plasma processing environments. It has high spatial and temporal resolution, good sensitivity, and the capability of absolute concentration measurements. Detailed diagnostics have been carried out in plasma reactors with and without semiconducting wafers. These measurements have led to a model that incorporates H atom production, diffusion, and surface recombination. This model has accurately predicted both the spatial and temporal behavior of the H-atom concentration in a plasma processing environment. DTIC

N94-21289*# Hampton Univ., VA. Dept. of Physics.
[RESEARCH ON PLASMA-PUFF INITIATION OF HIGH COULOMB TRANSFER SWITCHES] Final Technical Report, 1 Mar. 1989 - 30 Jun. 1993
Demetrius D. Venable and Kwang S. Han 1993 33 p
(Grant NAG1-970)
(NASA-CR-194371; NAS 1.26:194371) Avail: CASI HC A03/MF A01

The plasma-puff triggering mechanism based on hypocycloidal pinch geometry was investigated to determine the optimal operating conditions for an azimuthally uniform surface flashover which initiates plasma-puff under wide ranges of fill gas pressures of Ar, He and N2. Research is presented and resulting conference papers are attached. These papers include 'Characteristics of Plasma-Puff Trigger for an Inverse-Pinch Plasma Switch'; 'Ultra-High-Power Plasma Switch INPUTS for Pulse Power Systems'; 'Characteristics of Switching Plasma in an Inverse-Pinch Switch'; 'Comparative Study of INPIStron and Spark Gap'; and 'INPIStron Switched Pulsed Power for Dense Plasma Pinches.' For individual titles, see N94-21290 through N94-21294.

N94-21290*# Hampton Univ., VA.
PLASMA-PUFF INITIATION OF HIGH COULOMB TRANSFER SWITCHES
Kwang S. Han, Demetrius D. Venable, Ja H. Lee, Eun H. Choi, Y. K. Kim, J. H. Kim, and D. X. Nguyen *In its* Research on Plasma-Puff Initiation of High Coulomb Transfer Switches 1993 10 p (For primary document see N94-21289 05-75)
Avail: CASI HC A02/MF A01

The plasma-puff triggering mechanism based on a hypocycloidal pinch geometry was investigated to determine the optimal operating conditions for an azimuthally uniform surface flashover which initiates plasma-puff under wide ranges of fill gas pressures of Ar, He and N2. The optimal fill gas pressures for the azimuthally uniform plasma-puff were about 120 mTorr less than P(sub opt) less than 450 Torr for He and N2. For Argon 20 mTorr is less than P(sub opt) is less than 5 Torr. The inverse pinch switch was triggered with the plasma-puff and the switching capability under various electrical parameters and working gas pressures of Ar, He and N2 was determined. It was also shown that the azimuthally uniform switching discharges were dependent on the type of fill gas and its fill pressure. A new concept of plasma-focus driven plasma-puff was also discussed in comparison with hypocycloidal pinch plasma-puff triggering. The main discharge of the inverse pinch switch with the plasma-focus driven plasma-puff trigger is found to be more azimuthally uniform than that with the hypocycloidal pinch plasma-puff trigger in a gas pressure region between 80 mTorr and 1 Torr. In order to assess the effects of plasma current density on material erosion of electrodes, emissions from both an inverse-pinch plasma switch (INPIStron) and from a spark gap

switch under test were studied with an optical multichannel analyzer (OMA). The color temperature of the argon plasma was approximately 4,000 K which corresponded with the peak continuum emission near 750 nm. There are the strong line emissions of argon in the 650 - 800 nm range and a lack of line emissions of copper and other solid material used in the switch. This indicates that the plasma current density during closing is low and the hot spot or hot filament in the switch is negligible. This result also indicates considerable reduction of line emission with the INPIStron switch over that of a spark-gap switch. However, a strong carbon line emission exists due to vaporization of the plastic insulator used. In order to reduce the vaporization of the insulator, the plexiglass insulating material of INPIStron was replaced with Z-9 material. A comparative study of the INPIStron and a spark gap also reveals that the INPIStron, with a low impedance of Z = 9 ohms, can transfer a high voltage pulse with a superior pulse-shape fidelity over that of a spark gap with Z = 100 ohms. Author (revised)

N94-21291*# Hampton Univ., VA.
CHARACTERISTICS OF PLASMA-PUFF TRIGGER FOR A INVERSE-PINCH PLASMA SWITCH Abstract Only
Eun H. Choi, Demetrius D. Venable, Kwang S. Han, and Ja H. Lee *In its* Research on Plasma-Puff Initiation of High Coulomb Transfer Switches 1993 1 p (For primary document see N94-21289 05-75)
(Contract NAG1-970; DAAL03-89-G-0113)
Avail: CASI HC A01/MF A01

The plasma-puff triggering mechanism based on a hypocycloidal pinch geometry was investigated to determine the optimal operating conditions for the azimuthally uniform surface flashover which initiates plasma-puff under wide ranges of fill gas pressure of Ar, He and N2. The optimal fill-gas pressure range for the azimuthally uniform plasma-puff was about 120 mTorr less than or equal to P(sub op) less than or equal to 450 Torr for He and N2. For Argon 120 mTorr is less than or equal to P(sub op) is less than or equal to 5 Torr. The inverse-pinch switch was triggered with the plasma-puff and the switching capability under various electrical parameters and working gas pressures of Ar, He and N2 was determined. The azimuthally uniform switching discharges were dependent on the type of fill gas and its fill pressure. A new concept of plasma-focus driven plasma-puff will be discussed in comparison with the current hypocycloidal-pinch plasma-puff triggering. Author

N94-21292*# National Aeronautics and Space Administration. Langley Research Center, Hampton, VA.
CHARACTERISTICS OF SWITCHING PLASMA IN AN INVERSE-PINCH SWITCH
Ja H. Lee, Sang H. Choi, Demetrius D. Venable (Hampton Univ., VA.), Kwang S. Han (Hampton Univ., VA.), and Sang H. Nam (Source Tek., Inc., Poquoson, VA.) *In* Hampton Univ., Research on Plasma-Puff Initiation of High Coulomb Transfer Switches 1993 4 p Sponsored in part by ETDL, US Army LABCOM (For primary document see N94-21289 05-75)
(Contracts NAS1-970; DAAL03-89-G-0113)
Avail: CASI HC A01/MF A01

Characteristics of the plasma that switches on tens of giga volt-ampere in an inverse-pinch plasma switch (INPIStron) have been made. Through optical and spectroscopic diagnostics of the current carrying plasma, the current density, the motion of current paths, dominant ionic species have been determined in order to access their effects on circuit parameters and material erosion. Also the optimum operational condition of the plasma-puff triggering method required for azimuthally uniform conduction in the INPIStron has been determined. Author

N94-21293*# Hampton Univ., VA. Dept. of Physics.
COMPARATIVE STUDY OF INPIStron AND SPARK GAP
Kwang S. Han and Ja H. Lee *In its* Research on Plasma-Puff Initiation of High Coulomb Transfer Switches 1993 4 p (For primary document see N94-21289 05-75)
Avail: CASI HC A01/MF A01

An inverse pinch plasma switch, INPIStron, was studied in comparison to a conventional spark gap. The INPIStron is under development for high power switching applications. The INPIStron has an inverse pinch dynamics, opposed to Z-pinch dynamics in the spark gap. The electrical, plasma dynamics and radiative properties of the closing plasmas have been studied. Recently the high-voltage pulse transfer capabilities or both the INPIStron and the spark gap were also compared. The INPIStron with a low impedance Z = 9 ohms transfers 87 percent of an input pulse with a halfwidth of 2 mu s. For the same input pulse the spark gap of Z = 100 ohms transfers 68 percent. Fast framing and streak photography, taken with an TRW image converter camera, was used to observe the discharge uniformity and closing plasma speed in both switches. In order to assess the effects of closing plasmas on erosion of electrode material, emission spectra of two switches were studied with a spectrometer-optical multi channel analyzer (OMA) system. The typical emission spectra of the closing plasmas in the INPIStron and the spark gap showed that there were comparatively weak carbon line emission in 658.7 nm and copper (electrode material) line emissions in the INPIStron, indicating low erosion of materials in the INPIStron. Author

N94-21294*# Hampton Univ., VA.
INPIStron SWITCHED PULSED POWER FOR DENSE PLASMA PINCHES Abstract Only
Kwang S. Han and Ja H. Lee *In its* Research on Plasma-Puff Initiation of High Coulomb Transfer Switches 1993 1 p Meeting of the 9th International Pulsed Conference held in Albuquerque, NM, 21-23 Jun. 1993 (For primary document see N94-21289 05-75)
(Contract NAG1-970; N00014-89-J-1653)
Avail: CASI HC A01/MF A01

The inverse plasma switch INPIStron was employed for 10kJ/40kV capacitor bank discharge system to produce focused dense plasmas in hypocycloidal-pinch (HCP) devices. A single unit and an array of multiple HCP's were coupled as the load of the pulsed power circuit. The geometry and switching plasma dynamics were found advantageous and convenient for commutating the large current pulse from the low impedance transmission line to the low impedance plasma load. The pulse power system with a single unit HCP, the system A, was used for production of high temperature plasma focus and its diagnostics. The radially running down plasma dynamics, revealed in image converter photographs, could be simulated by a simple snow-plow model with a correction for plasma resistivity. The system B with an array of 8-HCP units which forms a long coaxial discharge chamber was used for pumping a Ti-sapphire laser. The intense UV emission from the plasma was frequency shifted with dye-solution jacket to match the absorption band of the Ti crystal laser near 500 nm. An untuned laser pulse energy of 0.6 J/pulse was obtained for 6.4 kJ/40 kV discharge, or near 103 times of the explosion limit of conventional flash lamps. For both systems the advantages of the INPIStron were well demonstrated: a single unit is sufficient for a large current (greater than 50 kA) without increasing the system impedance, highly reliable and long life operation and implied scalability for the high power ranges above I(sub peak) = 1 MA and V(sub hold) = 100 kV. Author

N94-21514# Texas Univ., Austin. Inst. for Fusion Studies.
SHEAR FLOW GENERATION BY REYNOLDS STRESS AND SUPPRESSION OF RESISTIVE g-MODES
H. Sugama (National Inst. for Fusion Science, Nagoya, Japan.) and W. Horton Aug. 1993 37 p
(Contract DE-FG05-80ET-53088)
(DE93-040911; IFSR-617; DOE/ET-53088/617) Avail: CASI HC A03/MF A01

Suppression of resistive g-mode turbulence by background shear flow generated from a small external flow source and amplified by the fluctuation-induced Reynolds stress is demonstrated and analyzed. The model leads to a paradigm for the low-to-high (L-H) confinement mode transition. To demonstrate the L-H transition model, single-helicity nonlinear fluid simulations using the vorticity equation for the electrostatic potential, the pressure fluctuation equation, and the background poloidal flow equation are used in the sheared slab configuration. The relative efficiency of the external flow and the Reynolds stress for producing shear flow depends on the poloidal flow damping parameter nu which is given by neoclassical theory. For large nu, the external flow is a dominant contribution to the total background poloidal shear flow and its strength predicted by the neoclassical theory is not enough to suppress the turbulence significantly. In contrast, for small nu, we show that the fluctuations drive a Reynolds stress that becomes large and suddenly, at some critical point in time, shear flow much larger than the external flow is generated and leads to an abrupt, order unity reduction of the turbulent transport just like that of the L-H transition in tokamak experiments. It is also found that, even in

the case of no external flow, the shear flow generation due to the Reynolds stress occurs through the nonlinear interaction of the resistive g-modes and reduces the transport. To supplement the numerical solutions we derive the Landau equation for the mode amplitude of the resistive g-mode taking into account the fluctuation-induced shear flow and analyze the opposite action of the Reynolds stress in the resistive g turbulence compared with the classical shear flow Kelvin-Helmholtz (K-H) driven turbulence. DOE

N94-21571# Institute of Plasma Physics, Prague (Czechoslovakia).
ON EFFECTS OF A LOCAL PLASMA DENSITY GROWTH DUE TO PONDEROMOTIVE FORCES AT FAST WAVE LAUNCHING IN TOKAMAKS
V. Petrzilka Dec. 1992 14 p
(IPPCZ-328) Avail: CASI HC A03/MF A01

Nonlinear changes of the reflection coefficient at fast wave launching by a waveguide array are computed also for the case of an eventual fast wave experiment on the FTU tokamak. In case of low plasma density gradients, the reflection coefficient may significantly change for the wave power in the range of several kilowatts per centimeter square due to the ponderomotive force effects. Author

N94-21572# Institute of Plasma Physics, Prague (Czechoslovakia).
ON ONE NUMERICAL APPROACH TO STEFAN PROBLEM
Pavel Kotalik Feb. 1993 10 p
(IPPCZ-330) Avail: CASI HC A02/MF A01

A one-dimensional Stefan problem for a spherical particle moving in a plasma jet is solved by approximating the enthalpy formulation of the problem by C(sup 0) piecewise linear finite elements in space combined with a semi-implicit scheme in time. Author (revised)

N94-21573# Institute of Plasma Physics, Prague (Czechoslovakia).
THE ANGULAR VELOCITY SPREAD OF REB INDUCED BY MAGNETIC FIELD DISCONTINUITY
P. Vrba and V. Piffl Mar. 1993 29 p
(IPPCZ-331) Avail: CASI HC A03/MF A01

The generation and propagation of relativistic electron beams (REB) through the thin foil into a plasma column was studied numerically. Two types of electron scattering on the anode foil were compared. The first one is multiple scattering of fast electrons with atomic nuclei. The second one arises when the magnetic field lines are discontinuous on vacuum-plasma boundary. It was pointed out, that these two types of scattering strongly affect the excitation of two stream instability. Author (revised)

N94-21593# Institute of Plasma Physics, Prague (Czechoslovakia).
RADIAL DIFFUSION OF TOROIDALLY TRAPPED PARTICLES INDUCED BY LOWER HYBRID AND FAST WAVES
L. Krlin Oct. 1992 7 p
(IPPCZ-327) Avail: CASI HC A02/MF A01

The interaction of RF field with toroidally trapped particles (bananas) can cause their intrinsic stochasticity diffusion both in the configuration and velocity space. In RF heating and/or current drive regimes, RF field can interact with plasma particles and with thermonuclear alpha particles. The aim of this contribution is to give some analytical estimates of induced radial diffusion of alphas and of ions. Author (revised)

N94-21752# Texas Univ., Austin. Inst. for Fusion Studies.
ON THE STABILITY OF SHEAR-ALFVEN VORTICES
D. Jovanovic and W. Horton Aug. 1993 23 p
(Contract DE-FG05-80ET-53088)
(DE93-040912; DOE/ET-53088/618; IFSR-618) Avail: CASI HC A03/MF A01

Linear stability of shear-Alfven vortices is studied analytically using the Lyapunov method. Instability is demonstrated for vortices belonging to the drift mode, which is a generalization of the standard Hasegawa-Mima vortex to the case of large parallel phase velocities. In the case of the convective-cell mode, short perpendicular-wavelength perturbations are stable for a broad class of vortices. Eventually, instability of convective-cell vortices may occur on the perpendicular scale comparable with the vortex size, but it is followed by a simultaneous excitation of coherent structures with better localization than the original vortex. DOE

N94-21769 Sandia National Labs., Albuquerque, NM.
PARTICLE BEHAVIOR IN AN ECR PLASMA ETCH TOOL
M. G. Blain, G. D. Tipton, W. M. Holber (International Business Machines Corp., Yorktown Heights, NY.), P. L. Westerfield, and K. L. Maxwell (SEMATECH, Austin, TX.) 1993 26 p Presented at the North Atlantic Treaty Organization Advanced Research Workshop, Toulouse, France, 30 Aug. - 3 Sep. 1993 Limited Reproducibility: More than 20% of this document may be affected by microfiche quality
(Contract DE-AC04-76DP-00789)
(DE93-040343; SAND-93-1981C; CONF-9308151-1) Avail: CASI HC A03

Sources of particles in a close-coupled electron cyclotron resonance (ECR) polysilicon plasma etch source include flaking of films deposited on chamber surfaces, and shedding of material from electrostatic wafer chucks. A large, episodic increase in the number of particles added to a wafer in a clean system is observed more frequently for a plasma-on than for a gas-only source condition. For polymer forming process conditions, particles were added to wafers by a polymer film which was observed to fracture and flake away from chamber surfaces. The presence of a plasma, especially when rf bias is applied to the wafer, caused more particles to be ejected from the walls and added to wafers than the gas-only condition; however, no significant influence was observed with different microwave powers. A study of effect of electrode temperatures on particles added showed that thermophoretic forces are not significant for this ECR configuration. Particles originating from the electrostatic chuck were observed to be deposited on wafers in much larger numbers in the presence of the plasma as compared to gas-only conditions. DOE

N94-21802# Stuttgart Univ. (Germany). Inst. fuer Plasmaforschung.
[ON PLASMA EDGE SPECTROSCOPY AND SPECTROSCOPIC STUDIES OF IMPURITY DENSITIES AND IMPURITY TRANSPORT]
K. Behringer Jun. 1992 32 p Presented at 4th Workshop on Magnetic Confinement Fusion: Diagnostics for Tokamaks and Stellarators, Santander, Spain, 22-24 Jun. 1992
(IPF-92-2; ETN-93-94207) Avail: CASI HC A03/MF A01

Atomic physics models for the interpretation of plasma edge spectroscopy measurements are discussed. Plasma edge spectroscopy is used to investigate atom and ion particle flux densities at the boundary of tokamaks or stellarators. Results are shown for oxygen, carbon and chromium in JET. Molecular particle fluxes, like H2, D2, and CH4 are considered. The interpretation of the shape and intensity of molecular band emission is explained, and results are presented with respect to chemical carbon production. The mechanisms of impurity screening at the plasma edge are investigated and respective mesurements are shown. Spectrometers and spectra, mainly from JET, are discussed with respect to diagnostic potential and calibration problems. Spatial scan facilities of multichord diagnostics are essential for transport investigations, and several possibilities are shown. For individual titles, see N94-21803 through N94-21804.

N94-21803# Stuttgart Univ. (Germany). Inst. fuer Plasmaforschung.
PLASMA EDGE SPECTROSCOPY
K. Behringer *In its* On Plasma Edge Spectroscopy and Spectroscopic Studies of Impurity Densities and Impurity Transport Jun. 1992 17 p
(For primary document see N94-21802 05-75)
Avail: CASI HC A03/MF A01

Atomic physics models for the interpretation of plasma edge spectroscopic measurements are discussed. Spectroscopy of the plasma edge, mainly in the visible range, provides information on hydrogen and impurity influxes, on impurity production measurements and on particle confinement. Some basic processes determining the population of excited levels are presented leading to the corona excitation balance and to collisional radiative models. These were discussed for the special case of helium. A first application of plasma edge spectroscopy is the investigation of atom and ion particle flux densities at the boundary of tokamaks or stellarators. Results are shown for oxygen, carbon and chromium in JET. Molecular particle fluxes, like H2, D2 and CH4 are then focused upon. The interpretation of the shape and intensity of molecular band emission is explained, and results are presented with respect to chemical carbon production. The mechanisms of impurity screening at the plasma edge are investigated and respective measurements are shown. ESA

N94-21804# Stuttgart Univ. (Germany). Inst. fuer Plasmaforschung.
SPECTROSCOPIC STUDIES OF IMPURITY DENSITIES AND IMPURITY TRANSPORT
K. Behringer *In its* On Plasma Edge Spectroscopy and Spectroscopic Studies of Impurity Densities and Impurity Transport Jun. 1992 15 p (For primary document see N94-21802 05-75)
Avail: CASI HC A03/MF A01

Spectrometers and spectra, mainly from JET, are discussed with respect to diagnostic potential and calibration problems. Spatial scan facilities or multichord diagnostics are essential for transport investigations, and several possibilities are shown. The interpretation of spectral line radiation usually requires the availability of impurity transport codes, which calculate the ionization balance in the presence of transport, the line emissivities and the total impurity radiation. Some atomic physics prerequisites of such codes are discussed. Theoretical and experimental approaches to the transport problem are investigated using ASDEX and JET results for anomalous transport. The occasional observation of neoclassical accumulation, for example after pellet injection, is presented and respective modeling is described. Some H mode transport phenomena are mentioned. ESA

N94-21816# Institute of Plasma Physics, Prague (Czechoslovakia).
EDGE PLASMA EXPERIMENTS ON CASTOR TOKAMAK
F. Zacek, J. Stockel, J. Badalec, K. Jakubka, P. Kletecka, L. Kryska, V. Kriha (Technical Univ. of Prague, Czechoslovakia.), V. Svoboda (Technical Univ. of Prague, Czechoslovakia.), J. Petrzilka (Karlova Univ., Prague, Czechoslovakia.), and I. Voitsekhovich (Kurchatov, I. V. Inst. of Atomic Energy, Moscow, USSR.) Apr. 1993 13 p Presented at the KFA-IPP-KFKI-RMKI Joint Workshop on the Use of Atomic Beams in Plasma Experiments, Budapest, 29 Mar. - 2 Apr. 1993
(IPPCZ-332) Avail: CASI HC A03/MF A01

The important role of the edge plasma in the global particle and energy balance in tokamaks is well recognized. However, the complexity of all processes involved in the particle and energy losses hinders to create an appropriate theoretical model of anomalous transport in tokamaks up to now. It seems to be evident only that the anomalous transport relies in the turbulent character of tokamak periphery. However, complete and exhaustive experimental data from the tokamaks periphery are still necessary. The main aim of the experimental research on tokamak CASTOR is focused to investigations of the edge plasma characteristics in the regimes with the improved confinement. Such regimes are reached in CASTOR with lower hybrid current drive or by plasma edge polarization. Results of these investigations indicate that the link between the global confinement and the level of edge fluctuations is more complex than it is generally assumed. The contribution brings a short survey of experimental activities undertaken on the tokamak CASTOR in this direction. Author (revised)

N94-21848 Lawrence Livermore National Lab., CA.
SPECTRAL CHARACTERIZATION OF LITHOGRAPHIC SOURCES
C. Cerjan Jun. 1993 20 p Presented at the Optical Society of America Topical Meeting on Soft X Ray Projection Lithography, Monterey, CA, 10-12 May 1993 Limited Reproducibility: More than 20% of this document may be affected by microfiche quality
(Contract W-7405-eng-48)
(DE93-019941; UCRL-JC-114072; CONF-9305159-8) Avail: CASI HC A03

Spectral data collected in recent laser-plasma experiments at LLNL for Sn are compared to simulation results in order to more fully characterize the plasma properties, especially electron temperature and density. These plasma conditions determine the ionization states achieved by the material and the consequent radiative emission. Synthetic spectra are produced using very detailed radiating line positions and oscillator strengths calculated from extensive multi-configuration Dirac-Fock computations. Better quantitative agreement with experimental conversion efficiencies in the laser intensity regime of interest to projection soft x-ray lithography is obtained using this atomic database. The spectral characterization thus validates the general reliability of the simulations. DOE

N94-21965# Los Alamos National Lab., NM.
A MOVING FINITE ELEMENT MODEL OF THE TOKAMAK SCRAPEOFF LAYER
A. H. Glasser and A. P. Kuprat 1993 10 p Presented at the 4th International Workshop on Plasma Edge Theory in Fusion Devices, Varenna, Italy, 4-6 Oct. 1993
(Contract W-7405-eng-36)
(DE94-000673; LA-UR-93-3502; CONF-931070-1) Avail: CASI HC A02/MF A01

Most numerical simulations of the tokamak scrapeoff layer use a mapping to flux coordinates and a piecewise equidistributed grid in those coordinates to resolve the multiple length scales and anisotropy characteristic of this problem. We have developed an alternative numerical method using simple cylindrical coordinates with a complex adaptive grid scheme. It is based on an understructured grid of traingles which move adaptively, aligning themselves with the magnetic field and concentrating in regions of sharp gradients. DOE

N94-21973# Texas Univ., Austin. Inst. for Fusion Studies.
A UNIFIED MONTE CARLO INTERPRETATION OF PARTICLE SIMULATIONS AND APPLICATIONS TO NONNEUTRAL PLASMAS
A. Y. Aydemir Sep. 1993 30 p
(Contract DE-FG05-80ET-53088)
(DE94-001231; DOE/ET-53088/602; IFSR-602) Avail: CASI HC A03/MF A01

Using a 'Monte Carlo interpretation' of particle simulations, a general description of low-noise techniques is developed in terms of well-known Monte Carlo variance reduction methods. These techniques are applied to linear and nonlinear studies of pure electron plasmas in cylindrical geometries, with emphasis on the generation and nonlinear evolution of electron vortices. Long-lived $l = 1$ and $l = 2$ vortices, and others produced by unstable diocotron modes in hollow profiles, are studied. It is shown that low-noise techniques make it possible to follow the linear evolution and saturation of even the very weakly unstable resonant diocotron modes. DOE

N94-21988# Los Alamos National Lab., NM.
MAGNETIC INSULATION OF SECONDARY ELECTRONS IN PLASMA SOURCE ION IMPLANTATION
D. J. Rej, B. P. Wood, R. J. Faehl, and H. H. Fleischmann (Cornell Univ., Ithaca, NY.) 1993 18 p Presented at the Workshop on Plasma-based Ion Implantation, Madison, WI, 4-6 Aug. 1993
(Contract W-7405-eng-36)
(DE93-040106; LA-UR-93-2950; CONF-9308156-1) Avail: CASI HC A03/MF A01

The uncontrolled loss of accelerated secondary electrons in plasma source ion implantation (PSII) can significantly reduce system efficiency and poses a potential x-ray hazard. This loss might be reduced by a magnetic field applied near the workpiece. The concept of magnetically-insulated PSII is proposed, in which secondary electrons are trapped to form a virtual cathode layer near the workpiece surface where the local electric field is essentially eliminated. Subsequent electrons that are emitted can then be re-absorbed by the workpiece. Estimates of anomalous electron transport from micro-instabilities are made. Insight into the process is gained with multi-dimensional particle-in-cell simulations. DOE

N94-21989# Los Alamos National Lab., NM.
A dc PENNING SURFACE-PLASMA SOURCE
H. V. Smith, Jr., P. Allison, C. Geisik, D. R. Schmitt, J. D. Schneider, and J. E. Stelzer 1993 15 p Presented at the 5th International Conference on Ion Sources, Peking, China, 31 Aug. - 4 Sep. 1993
(Contract W-7405-eng-36)
(DE93-040126; LA-UR-93-2990; CONF-9308136-5) Avail: CASI HC A03/MF A01

After developing a pulsed-8X source for H(-) beams, we are now testing a cooled, dc version. The design dc power density on the cathode surface is 900 W/sq cm, much higher than achieved in any previously reported Penning surface-plasma source (SPS). The source is designed to accommodate dc arc power levels up to 30 kW by cooling the electrode surfaces with pressurized hot water. After striking the arc using a 600-V pulser, a 350-V dc power supply is switched in to sustain the 100-V discharge. Now our tests are concentrating on arc pulse lengths less than or equal to one second. Ultimately, the discharge will be operated dc. The source is described and the initial arc test results are presented. DOE

N94-22019# Wisconsin Univ., Madison. Dept. of Nuclear Engineering and Engineering Physics.
FUSION PLASMA THEORY. TASK 1: MAGNETIC CONFINEMENT FUSION PLASMA THEORY
J. D. Callen 1993 10 p
(Contract DE-FG02-86ER-53218)
(DE94-000778; DOE/ER-53218/22) Avail: CASI HC A02/MF A01

The research performed under this grant during the current year has concentrated on few tokamak plasma confinement issues: applications of our new Chapman-Enskog-like approach for developing hybrid fluid/kinetic descriptions of tokamak plasmas; multi-faceted studies as part of our development of a new interacting island paradigm for the tokamak equilibrium and transport; investigations of the resolution power of BES and ECE diagnostics for measuring core plasma fluctuations; and studies of net transport in the presence of fluctuating surfaces. Recent progress and publications in these areas, and in the management of the NERSC node and the fusion theory workstations are summarized briefly. DOE

N94-22039# General Atomic Co., San Diego, CA.
ENHANCED CONFINEMENT REGIMES AND CONTROL TECHNOLOGY IN THE DIII-D TOKAMAK
J. Lohr, K. H. Burrell, S. Coda (Massachusetts Inst. of Tech., Cambridge.), J. R. Ferron, P. Gohil, R. J. Groebner, E. A. Lazarus (Oak Ridge National Lab., TN.), S. I. Lippmann, M. A. Mahdavi, and T. A. Osborne Jul. 1993 14 p Presented at the International Conference on Open Plasma Confinement Systems for Fusion, Novosibirsk (Russian Federation), 14-18 Jun. 1993
(Contracts DE-AC03-89ER-51114; DE-AC05-84OR-21400; DE-FG02-91ER-54109)
(DE93-019004; GA-A-21342; CONF-930655-1) Avail: CASI HC A03/MF A01

Advanced tokamak performance has been demonstrated in the DIII-D tokamak in a series of experiments which brought together developments in technology and improved understanding of the physical principles underlying tokamak operation. The achievement of greatly improved confinement coupled with development of new systems for real time plasma control have permitted investigation of the heretofore hidden or poorly controlled variables which together determine global confinement. These experiments, which included work in transport and control of the plasma boundary, point toward development of operationally and economically attractive reactors based on the tokamak. Some of these experiments are described. DOE

N94-22045# Oak Ridge National Lab., TN.
THE TST: A SMALL STEADY-STATE TOKAMAK FOR INTEGRATED DIVERTOR TESTING
Y. K. M. Peng, R. J. Colchin, D. W. Swain, B. E. Nelson, and J. F. Monday Sep. 1993 144 p
(Contract DE-AC05-84OR-21400)
(DE94-001016; ORNL/TM-12216) Avail: CASI HC A07/MF A02

This report discusses the following topics: the TST program; the TST physics basis; the TST auxiliary H&CD systems; the test divertors; the TST device; and ancillary systems. DOE

N94-22089# General Atomics Technologies Corp., San Diego, CA.
USE OF OPEN SYSTEMS FOR CONTROL, ANALYSIS, AND DATA ACQUISITION OF THE DIII-D TOKAMAK
P. A. Henline Oct. 1993 5 p Presented at the Symposium on Fusion Engineering, Hyannis, MA, 11-15 Oct. 1993
(Contract DE-AC03-89ER-51114)
(DE94-001101; GA-A-21403; CONF-931018-9) Avail: CASI HC A01/MF A01

For the past several years, it has been evident that the very old MODCOMP 16-bit computers being used at D3-D for control and data acquisition were no longer adequate to perform the services needed. In early 1992, the computer systems group began to look seriously into alternate systems to replace these aged MODCOMP systems. The decision was made to investigate 'OPEN' system computers and also to maintain the compatibility with the large usage of CAMAC equipment as the real-time hardware interface. Information about the needs for real-time capabilities and OPEN systems ability to meet these needs is discussed. The needs include hardware requirements, operating system software which has known response rates, and interconnectability and access of data from other workstations and computers. Some of the parameters and pitfalls of open systems are discussed as well as the advantages of OPEN systems for use in a real-time environment. The success of arriving at an OPEN systems solution is examined. DOE

N94-22389# Los Alamos National Lab., NM.
TIME EVOLUTION OF THE QUARK-GLUON PLASMA
F. Cooper, Y. Kluger, J. Dawson (New Hampshire Univ., Durham.), and H. Shepard (New Hampshire Univ., Durham.) 30 Aug. 1993 6 p Presented at the Pre-Equilibrium Parton Dynamics, Berkeley, CA, 23 Aug. - 3 Sep. 1993
(Contract W-7405-eng-36)
(DE94-000804; LA-UR-93-3227; CONF-9308181-1) Avail: CASI HC A02/MF A01

This report discusses the time evolution of the quark-gluon plasma. DOE

N94-22399# Lawrence Livermore National Lab., CA.
OPACITY MEASUREMENTS IN SHOCK-GENERATED ARGON PLASMAS
D. Erskine Jul. 1993 4 p Presented at the 14th International Conference of the International Association for the Advancement of High Pressure Science and Technology, Colorado Springs, CO, 27 Jun. - 2 Jul. 1993
(Contract W-7405-eng-48)
(DE94-001057; UCRL-JC-112349; CONF-930676-56) Avail: CASI HC A01/MF A01

Dense plasmas having uniform and constant density and temperature are generated by passage of a planar shock wave through gas. The opacity of the plasma is accurately measured versus wavelength by recording the risetime of emitted light. This technique is applicable to a wide variety of species and plasma conditions. Initial experiments in argon have produced plasmas with 2 eV temperatures, 0.004-0.04 g/cu cm densities, and coupling parameters Gamma approximately equal to 0.3-0.7. Measurements in visible light are compared with calculations using the HOPE code. An interesting peak in the capacity at 400 nm is observed for the first time and is identified with the 4s-5p transition in excited neutral argon atoms. DOE

N94-22560# Texas Univ., Austin. Inst. for Fusion Studies.
CONTINUUM DAMPING OF IDEAL TOROIDAL ALFVEN EIGENMODES
X.-D. Zhang, Y.-Z. Zhang, and S. M. Mahajan Aug. 1993 30 p
(Contract DE-FG05-80ET-53088)
(DE94-001233; DOE/ET-53088/621; IFSR-621) Avail: CASI HC A03/MF A01

A perturbation theory based on the two dimensional ballooning transform is systematically developed for ideal toroidal Alfven eigenmodes (TAE's). A formula, similar to the Fermi golden rule for decaying systems in quantum mechanics, is derived for the continuum damping rate of the TAE; the decay (damping) rate is expressed explicitly in terms of the coupling of the TAE to the continuum spectrum. Numerical results are compared with previous calculations. It is found that in some narrow intervals of the parameter m(circumflex epsilon) the damping rate varies very rapidly. These regions correspond precisely to the root missing intervals of the numerical solution by Rosenbluth et al. DOE

N94-22561# Texas Univ., Austin. Inst. for Fusion Studies.
KINETIC RESONANCE DAMPING RATE OF THE TOROIDAL ION TEMPERATURE GRADIENT MODE
J. Y. Kim, Y. Kishimoto, W. Horton, and T. Tajima Sep. 1993 35 p
(Contract DE-FG05-80ET-53088)
(DE94-001234; DOE/ET-53088/623; IFSR-623) Avail: CASI HC A03/MF A01

The linear damping rates of the toroidal ion temperature gradient (eta(sub i)) mode due to the toroidal resonance are calculated in the local kinetic limit. The well-known Landau contour method is generalized to treat the analytic continuation problem of the guiding center dispersion function in the toroidal resonance system where the resonance occurs from both the magnetic Delta B-curvature drift and the parallel ion transit drift. A detailed numerical analysis is presented for the dependence of the damping rate of the toroidal eta(sub i) mode on various parameters such as epsilon(sub n), kappa(sub y), and the trapped electron fraction. In addition, a consideration is presented on the decay problem of the ballistic response by the phase

mixing in the toroidal system, which is directly related to the present damping problem of the wave normal modes by the toroidal resonance.
DOE

N94-22562# Texas Univ., Bastrop. Inst. for Fusion Studies.
A TWO-DIMENSIONAL KINETIC MODEL OF THE SCRAPE-OFF LAYER
P. J. Catto and R. D. Hazeltine Sep. 1993 22 p
(Contracts DE-FG05-80ET-53088; DE-FG05-88ER-53267; DE-FG02-91ER-54109)
(DE94-001235; DOE/ET-53088/626; IFSR-626) Avail: CASI HC A03/MF A01

A two-dimensional (radius and poloidal angle), analytically tractable kinetic model of the ion (or energetic electron) behavior in the scrape-off layer of a limiter or divertor plasma in a tokamak is presented. The model determines the boundary conditions on the core ion density and ion temperature gradients, the power load on the limiter or divertor plates, the energy carried per particle to the walls, and the effective flux limit. The self-consistent electrostatic potential in the quasi-neutral scrape-off layer is determined by using the ion kinetic model of the layer along with a Maxwell-Boltzmann electron response that occurs because most electrons are reflected by the Debye sheaths (assumed to be infinitely thin) at the limiter or divertor plates.
DOE

N94-22566# California Univ., Berkeley. Electronics Research Lab.
FLUID SIMULATIONS OF DELTA T(SUB e)-DRIVEN TURBULENCE AND TRANSPORT IN BOUNDARY PLASMAS
X. Q. Xu 15 Dec. 1992 26 p
(Contract DE-FG03-90ER-54079)
(DE94-001304; UCB/ERL-M-92/147) Avail: CASI HC A03/MF A01

It is clear that the edge plasma plays a crucial role in global tokamak confinement. This paper is a report on simulations of a new drift wave type instability driven by the electron temperature gradient in tokamak scrape-off layers (SOL). A 2D fluid code has been developed in order to explore the anomalous transport in the boundary plasmas. The simulation consists of a set of fluid equations for the vorticity Delta(sub perpendicular)(exp 2) phi, the electron density n(sub c), and the temperature T(sub c) in a shearless plasma slab confined by a uniform, straight magnetic field B(sub z) with two divertor (or limiter) plates intercepting the magnetic field. The model has two regions separated by a magnetic separatrix: in the edge region inside the separatrix, the model is periodic along the magnetic field while in the SOL region outside the separatrix, the magnetic field is taken to be of finite length with model boundary conditions at diverter plates. The simulation results show that the observed linear instability agrees well with theory, and that a saturated state of turbulence is reached. In saturated turbulence, clear evidence of the expected long-wavelength mode penetration into the edge is seen; an inverse cascade of wave energy is observed. The simulation results also show that amplitudes of potential and the electron temperature fluctuations are somewhat above and the heat flux are somewhat below those of the simplest mixing-length estimates, and furthermore the large-scale radial structures of fluctuation quantities indicate that the cross-field transport is not diffusive. After saturation, the electron density and temperature profiles are flattened. A self-consistent simulation to determine the microturbulent SOL electron temperature profile has been done, the results of which reasonably agree with the experimental measurements.
DOE

N94-22567# California Univ., Berkeley. Electronics Research Lab.
THEORY AND SIMULATION OF PLASMA SHEATH WAVES
X. Q. Xu, G. DiPeso, V. Vahedi, and C. K. Birdsall 15 Dec. 1992 13 p
(Contract DE-FG03-90ER-54079)
(DE94-001305; UCB/ERL-M-92/148) Avail: CASI HC A03/MF A01

Sheath waves have been investigated analytically and with particle simulation for an unmagnetized two dimensional plasma slab with periodic boundary conditions in y and conducting walls at x = 0, L(sub x). Analytically treating the sheath as a vacuum layer, the sheath wave bears a resemblance to plasma vacuum surface waves. The simulations are in agreement with the theory for both bulk Bohm Gross waves and edge sheath waves, with some unanswered questions. Some waves that were expected did not show up, at least, where we thought they should be. Hence, improvements were made in the initialization (a better quiet start), in the diagnostics (especially the spectra in frequency), and in the excitation (ability to pulse). It has become clear that this problem, seeking both sheath (or surface) and body waves in a bounded system, needs far more attention, in analysis (non-uniform density included) and in simulation, especially in diagnostics. Hence, this report is to be treated as a start on the problem. The problem is not dropped, as the understanding of such waves (in 2D and 3D) is very important, for both basic sheath understanding and for applications, such as plasma control via excitation of sheath or pre-sheath waves.
DOE

N94-22568# Oak Ridge National Lab., TN.
EFFECTS OF MAGNETIC FIELD PERTURBATIONS IN THE ATF TORSATRON
R. J. Colchin, A. C. England, R. C. Isler, M. Murakami, D. A. Rasmussen, T. Uckan, J. B. Wilgen, S. C. Aceto, and J. J. Zielinski 1993 28 p
Presented at the 9th IAEA Workshop on Stellarators, Garching, Germany, 10-14 May 1993
(Contract DE-AC05-84OR-21400)
(DE94-000474; CONF-9305210-6) Avail: CASI HC A03/MF A01

The effects of errors in the magnetic fields of tokamaks on the plasma are quite different from those in stellarators. In tokamaks, field errors can cause disruptive locked modes through the nonlinear evolution of tearing modes acting on initially small error-induced islands. Scaling predictions for these effects indicate that the critical relative field error which can be tolerated becomes smaller as the tokamak size becomes larger. In stellarators, the effect is more benign, as field errors appear only to cause increased plasma transport in the vicinity of islands. Great care has been taken to minimize magnetic field errors in the most recent generation of stellarator-type magnetic plasma traps. In the past six years, several new and sensitive techniques have been developed to detect and map field errors. These methods all rely on the detection of electrons injected along magnetic field lines. During the commissioning of ATF, flux surfaces were mapped using the fluorescent screen technique. Field errors were discovered and traced to uncompensated dipoles in the helical current feeds. Prior to elimination of these errors, plasma discharges indicated centrally peaked plasma profiles. After correction of the uncompensated dipoles, flux surfaces were mapped a second time, and the island widths were found to be greatly reduced. Field errors were then deliberately introduced using a set of perturbation coils that had been added to ATF, and electron-beam mapping of the flux surfaces showed that islands several centimeters in width could easily be created by these coils. After elimination of the error fields, the measured plasma temperature and density profiles were much broader. The field-perturbation coils were then used to produce magnetic field asymmetries, and the measured plasma profiles were again shown to narrow as a result of islands.
DOE

N94-22595# California Univ., Berkeley. Electronics Research Lab.
VERIFICATION OF FREQUENCY SCALING LAWS FOR CAPACITIVE RF DISCHARGES USING TWO-DIMENSIONAL SIMULATIONS
V. Vahedi, C. K. Birdsall, M. A. Lieberman, G. DiPeso, and T. D. Rognlien 15 Dec. 1992 35 p
(Contracts DE-FG03-90ER-54079; W-7405-eng-48)
(DE94-001306; UCB/ERL-M-92/146) Avail: CASI HC A03/MF A01

Weakly ionized processing plasmas are studied in two-dimensions using a bounded particle-in-cell (PIC) simulation code with a Monte Carlo Collision (MCC) package. The MCC package models the collisions between charged and neutral particles, which are needed to obtain a self-sustained plasma and the proper electron and ion energy loss mechanisms. A two-dimensional capacitive RF discharge is investigated in detail. Simple frequency scaling laws for predicting the behavior of some plasma parameters are derived and then compared with simulation results, finding good agreements. We find that as the drive frequency increases, the sheath width decreases, and the bulk plasma becomes more uniform, leading to a reduction of the ion angular spread at the target and an improvement of ion dose uniformity at the driven electrode.
DOE

N94-22596# California Univ., Berkeley. Electronics Research Lab.
ELECTRON TEMPERATURE GRADIENT DRIVEN INSTABILITY IN THE TOKAMAK BOUNDARY PLASMA
X. Q. Xu, M. N. Rosenbluth, and P. H. Diamond 15 Dec. 1992 24 p
(Contracts DE-FG03-90ER-54079; DE-FG03-88ER-53275)
(DE94-001307; UCB/ERL-M-92/145) Avail: CASI HC A03/MF A01

A general method is developed for calculating boundary plasma fluctuations across a magnetic separatrix in a tokamak with a divertor or a

limiter. The slab model, which assumes a periodic plasma in the edge reaching the divertor or limiter plate in the scrape-off layer (SOL), should provide a good estimate, if the radial extent of the fluctuation quantities across the separatrix to the edge is small compared to that given by finite particle banana orbit. The Laplace transform is used for solving the initial value problem. The electron temperature gradient (ETG) driven instability is found to grow like t(sup -1/2)e(sup (gamma)mt). DOE

N94-22624# European Space Agency, Paris (France).
FOURTH INTERNATIONAL TOKI CONFERENCE ON PLASMA PHYSICS AND CONTROLLED NUCLEAR FUSION
H. T. Duc Guyenne, ed. and James J. Hunt, ed. Noordwijk, Netherlands May 1993 381 p The Satio Hayakawa Memorial Conference held in Toki, Japan, 17-20 Nov. 1992; sponsored by National Inst. for Fusion Science, Toki City, Fusion Science Association, and International School of Plasma Physics
(ESA-SP-351; ISBN-92-9092-246-X; ETN-94-94861) Copyright Avail: CASI HC A17/MF A03

The aim of the conference was to bring together the fusion, space and astro plasma physics. The main subjects are discussed: driven reconnection, turbulization of free shear flows, fusion plasmas, astrophysical plasmas, solar plasmas, planetary magnetosphere, dense plasmas, X-ray sources, gamma ray sources, relativistic plasmas, laboratory and space plasmas, and magnetohydrodynamic phenomena in star forming processes. For individual titles, see N94-22625 through N94-22701.

N94-22625# National Inst. for Fusion Science, Nagoya (Japan).
DRIVEN RECONNECTION AND SELF-ORGANIZATION
Tetsuya Sato, R. Horiuchi, T. Hayashi, K. Watanabe, and Kanya Kusano (Hiroshima Univ., Japan.) *In* ESA, Fourth International Toki Conference on Plasma Physics and Controlled Nuclear Fusion May 1993 p 17-2 (For primary document see N94-22624 05-75)
Copyright Avail: CASI HC A01/MF A03

The physical background and significance of magnetic reconnection are given. Magnetohydrodynamic self organization process is explained. Magnetic reconnection is believed to play a very important role in fusion, space and astronomical plasmas. Particular attention is paid to magnetic reconnection driven by a converging plasma flow which is called 'driven reconnection'. Magnetohydrodynamic self organization process is described where an ordered magnetic structure is created by changing the global magnetic topology and relaxing the magnetic energy in the magnetohydrodynamic time scale. ESA

N94-22626# Abastumani Astrophysical Observatory, Georgia (USSR).
TURBULIZATION OF FREE SHEAR FLOWS: 3D PERTURBATIONS
G. D. Chagelishvili, R. G. Chanishvili, Jumber G. Lominadze, and I. N. Segal *In* ESA, Fourth International Toki Conference on Plasma Physics and Controlled Nuclear Fusion May 1993 p 23-3 (For primary document see N94-22624 05-75)
Copyright Avail: CASI HC A02/MF A03

A theory of free smooth shear flows turbulization, that may be applied to other flows turbulized by finite amplitude perturbations, is proposed. Analytical calculations are performed for three dimensional perturbations. The proposed turbulization scenario is based on the specific evolution of the linear and nonlinear processes and it is an alternative to the Landau turbulization scenario. The mathematical formalism of the problem under examination is presented, together with analysis of the drift of the disturbance spatial Fourier harmonics in the space of the wave numbers. A case of two dimensional disturbances is discussed in order to expose the physics of the energy exchange between the main flow and disturbances at the linear stage in a free Couette flow. An analysis of the evolution of three dimensional disturbances is given. ESA

N94-22627# Kyoto Univ., Uji (Japan). Plasma Physics Lab.
MHD INSTABILITIES OF FUSION ORIENTED PLASMAS
Masahiro Wakatani *In* ESA, Fourth International Toki Conference on Plasma Physics and Controlled Nuclear Fusion May 1993 p 35-4 (For primary document see N94-22624 05-75)
Copyright Avail: CASI HC A02/MF A03

Several magnetically confined toroidal plasmas for developing a fusion reactor core are explained. Magnetohydrodynamic (MHD) equilibrium and stability theory is discussed, and MHD instabilities are characterized according to the free energy source. Several well known observations of MHD instabilities in tokamaks and helical systems are discussed, associated with theoretical models. Sawtooth oscillations are the most typical phenomena commonly observed in tokamaks. Recently the similar sawtooth type oscillations were observed in Heliotron E. The latter is a new phenomenon driven by pressure gradient. MHD phenomena induced by high energy ions are fishbone oscillations and TAE (Toroidal Alfven Eigenmode) in tokamaks. Recently loss of high energy particles induced by the sawtooth oscillations are also observed in Heliotron E. Future direction of MHD studies in fusion plasma research is mentioned. ESA

N94-22628# National Inst. for Fusion Science, Nagoya (Japan).
PHYSICS OF TRANSPORT PHENOMENA IN MAGNETIC CONFINEMENT PLASMAS
Kimitaka Itoh, Sanae-I. Itoh (Kyushu Univ., Fukuoka, Japan.), and Atsushi Fukuyama (Okayama Univ., Japan.) *In* ESA, Fourth International Toki Conference on Plasma Physics and Controlled Nuclear Fusion May 1993 p 41-4 Sponsored in part by Ministry of Education (For primary document see N94-22624 05-75)
Copyright Avail: CASI HC A02/MF A03

The phenomena caused by the transport of the plasma across the magnetic filed in toroidal devices are surveyed, and theoretical models are reviewed. The plasma structure in a steady state is discussed. The recent development of the theory on the plasma transport driven by the microscopic turbulence is explained. The sudden change in confinement, such as the H-mode transition in tokamaks, is discussed. The physics of the bifurcation of the edge plasma, based on the dynamics of the radial electric field, is studied. The role of the anomalous transport on the disruptive phenomena is reviewed. ESA

N94-22629# National Inst. for Fusion Science, Nagoya (Japan).
PLASMA HEATING IN TOROIDAL SYSTEMS
Masao Okamoto *In* ESA, Fourth International Toki Conference on Plasma Physics and Controlled Nuclear Fusion May 1993 p 47-5 (For primary document see N94-22624 05-75)
Copyright Avail: CASI HC A02/MF A03

The present status of plasma heating in toroidal systems, for astrophysical plasma scientists, is reviewed. The main method of plasma heating in toroidal systems or tori is to utilize fast ions. The maximum ion temperature of 38 keV was achieved at the plasma center by Neutral Beam Injections (NBI's) in the JT-60U tokamak. Ripple trapped losses of fast ions produced by NBI's were measured also in the JT-60U. The first tokamak discharges in deuterium-tritium fuelled mixtures were carried out successfully in the Jet European Torus (JET) tokamak. These experimental results are compared with the theoretical predictions based on the Coulomb collisions. The recent NBI experiments and the results are compared with theoretical predictions based on Coulomb collisions. Related to plasma heatings the current drive are discussed placing an emphasis on the neoclassical current (bootstrap current). ESA

N94-22630# Max-Planck-Inst. fuer Extraterrestrische Physik, Garching (Germany).
RESULTS FROM ROSAT **c89**
Joachim Truemper *In* ESA, Fourth International Toki Conference on Plasma Physics and Controlled Nuclear Fusion May 1993 p 55-6 (For primary document see N94-22624 05-75)
Copyright Avail: CASI HC A03/MF A03

Rosat is a German, U.S., United Kingdom project carrying a satellite borne X-ray telescope launched on 1 June 1990. One of the principal aims of the mission was to conduct a deep sky survey in the soft X-ray band. This was performed by scanning the sky in great circles in a plane perpendicular to the solar direction. The satellite carries two powerful coaligned grazing incidence telescopes observing in parallel in the soft X-ray and extreme ultraviolet bands. The X-ray telescope is equipped with position sensitive proportional counters and a channel plate detector while the extreme ultraviolet telescope, called wide field camera, has two redundant channel plate detectors in the focal plane. ESA

N94-22631# Osservatorio Astronomico, Turin (Italy).
JETS ASSOCIATED WITH ACTIVE GALACTIC NUCLEI **c90**
Attilio Ferrari (Turin Univ., Italy.) *In* ESA, Fourth International Toki

Conference on Plasma Physics and Controlled Nuclear Fusion May 1993 p 67-7 (For primary document see N94-22624 05-75)
Copyright Avail: CASI HC A02/MF A03

Some aspects of jet dynamics in connection with radiative effects are reviewed. Examples of the study of plasma physics of relativistic jets from Active Galactic Nuclei (AGN) are discussed. The common morphologies of jets at different scales can be summarized as follows: jets are collimated over very large distances, with aspect ratios up to 100; collimation begins in the very center of the associated AGN; jets remain collimated and dynamically stable even when there are signs of interaction with external environment and sharp bends; strong evidence exists that in many cases jets are relativistic, especially in the region near the core; correlation between jets and the optical activity of the associated galactic nucleus was found. An important fact for jets from active galactic nuclei, is that dynamics and radiation emission are combined in a peculiar way: the emission is just a tiny fraction of the total energy of the flow that is estimated by assuming that the general structure is produced by the central object, either continuously or in a single outburst. This means that the dynamics must be reconstructed observing its partial transformation in radiation. ESA

N94-22632# Tokyo Univ., Mitake (Japan). Inst. of Astronomy.
HIGHLIGHTS OF YOHKOH RESULTS **c92**
Saku Tsuneta *In* ESA, Fourth International Toki Conference on Plasma Physics and Controlled Nuclear Fusion May 1993 p 75-8 (For primary document see N94-22624 05-75)
Copyright Avail: CASI HC A02/MF A03

Data from the solar observation satellite Yohkoh, meaning sunbeam or sunlight, are presented with emphasis on the results from its Soft X-ray Telescope (SXT). The highly dynamical and transient nature of the coronal magnetic fields revealed by SXT is changing the views of the solar corona and behavior of magnetized plasma in general. Some of the initial discoveries are presented. The observations indicate that solar corona can be considered as a self organized critical system. SXT discovered numerous transient brightenings in active regions. SXT observations of solar flares are summarized. ESA

N94-22633# Nobeyema Solar Radio Observatory (Japan).
PRELIMINARY RESULTS OF OBSERVATIONS OF SOLAR FLARES WITH NOBEYAMA RADIOHELIOGRAPH **c92**
Hiroshi Nakajima, S. Enome, K. Shibasaki, M. Nishio, T. Takano, Y. Hanaoka, C. Torii, H. Sekiguchi, T. Bushimata, and S. Kawashima et al *In* ESA, Fourth International Toki Conference on Plasma Physics and Controlled Nuclear Fusion May 1993 p 85-8 (For primary document see N94-22624 05-75)
Copyright Avail: CASI HC A01/MF A03

Nobeyama Radioheliograph operates at 17 GHz and realizes high spatial and time resolution imaging capabilities of the whole Sun with high image quality. The objective of this instrument is to study various phenomena in the solar atmosphere, putting stress on active phenomena such as flares and active region evolution. From initial observations of solar flares, the following topics are presented: a thermal flare suggesting plasma heating through loop-loop interaction; prominence eruption followed by formation of arcade loops as evidence of energy release through magnetic reconnection; impulsive flares interpreted as production of nonthermal electron beams; and an intense flare initiated by preflare activities. ESA

N94-22634# Sydney Univ. (Australia). Research Center for Theoretical Astrophysics.
RADIATION FROM SOLAR FLARES **c92**
Don B. Melrose *In* ESA, Fourth International Toki Conference on Plasma Physics and Controlled Nuclear Fusion May 1993 p 91-9 (For primary document see N94-22624 05-75)
Copyright Avail: CASI HC A02/MF A03

Radiation from solar flares is reviewed. Particular attention is given to temporal variations that may give clues to the details of the energy release processes in flares. Hard X-ray and microwave bursts type III bursts and spike bursts are discussed. In each case, after a review of the observations, their standard interpretation is summarized. The present state of the theory of the energy release in solar flares is discussed, with emphasis on the implications of fine structures in the observed bursts. ESA

N94-22635# Cambridge Univ. (England).
NONTHERMAL PLANETARY RADIO EMISSIONS: THEORIES AND OBSERVATIONS **c91**
Abraham C.-L. Chian (Instituto de Pesquisas Espaciais, Sao Jose dos Campos, Brazil.) *In* ESA, Fourth International Toki Conference on Plasma Physics and Controlled Nuclear Fusion May 1993 p 101-104 Sponsored by Commission of the European Communities and CNPq (For primary document see N94-22624 05-75)
Copyright Avail: CASI HC A01/MF A03

Intense radio waves are emitted by several planets. A variety of Nonthermal Planetary Radio emissions (NPR) are observed. Recent theoretical research of NPR are reviewed covering: acceleration of particles by nonlinear potential structures, saturation of stimulated scattering by wave breaking or frequency shift of beam modes, and generation of plasma radiation by Langmuir turbulence. Theories and observations of nonthermal planetary radio emissions are summarized. A variety of NPR was observed by space and ground radio telescopes and the observed characteristics of five types of NPR are presented. The theories of generation mechanisms of NPR are discussed and recent theoretical research of NPR is summarized. ESA

N94-22636# Max-Planck-Inst. fuer Extraterrestrische Physik, Berlin (Germany).
CONSEQUENCES OF CHAOTIC PARTICLE MOTION FOR THE STABILITY OF SPACE PLASMA CURRENT SHEETS
Joerg Buechner and Antonius Otto (Alaska Univ., Fairbanks.) *In* ESA, Fourth International Toki Conference on Plasma Physics and Controlled Nuclear Fusion May 1993 p 105-110 (For primary document see N94-22624 05-75)
Copyright Avail: CASI HC A02/MF A03

The influence of a transition of thermal electrons to chaos and quasi adiabaticity on the large scale stability properties of collisionless plasma current sheets is investigated. A hybrid model which describes large scale plasma and field dynamics by a set of Magnetohydrodynamic (MHD) equations is developed, the non adiabatic response of particles in the neutral sheet is considered kinetically. Using the microscopic theory of chaotic particle motion the MHD is modified. The stability properties of two dimensional current sheet equilibria if the chaos parameter k(sub e) becomes unity are investigated. It is shown that even if electrons become chaotic the growth time of a collisionless tearing mode instability of thick current sheets is too large in order to explain substorm expansions in the Earth's magnetospheric tail. Critical thinning of the sheet is shown to lead to a quickly growing instability. ESA

N94-22637# Rochester Univ., NY. Dept. of Physics and Astronomy.
PHYSICAL PROPERTIES OF DENSE ASTROPHYSICAL PLASMAS
Hugh M. VanHorn *In* ESA, Fourth International Toki Conference on Plasma Physics and Controlled Nuclear Fusion May 1993 p 113-117 (For primary document see N94-22624 05-75)
(Grant NSF INT-90-16293)
Copyright Avail: CASI HC A01/MF A03

Calculations of stellar evolution require knowledge about the equation of state, transport properties, and nuclear reaction rates of plasmas at very high densities. Advances in each of these areas are highlighted, concentrating primarily on processes that are important for the structure and evolution of white dwarfs and neutron stars. The following topics are discussed: the equation of state, that is the pressure and entropy; the transport properties, such as the radiative Rosseland mean opacity and the conductive opacity; the nuclear reaction rates and neutrino emission rates of plasmas at very high densities. ESA

N94-22638# Sophia Univ., Tokyo (Japan). Dept. of Physics.
NEUTRINO EMISSION PROCESSES IN DENSE HIGH-TEMPERATURE PLASMAS
Naoki Itoh *In* ESA, Fourth International Toki Conference on Plasma Physics and Controlled Nuclear Fusion May 1993 p 119-122 (For primary document see N94-22624 05-75)
Copyright Avail: CASI HC A01/MF A03

The neutrino emission processes in dense high temperature plasmas are reviewed. The neutrino emission processes are key factors which decide the evolution of stars. Stellar evolution proceeds through the balance between the energy generation due to thermonuclear reactions and the

energy loss due to neutrino emission processes. Recent developments in the study of the four major neutrino emission processes are reviewed. The energy loss rates due to pair, photon, plasma and bremstrahlung neutrino processes are calculated using Weinberg-Salam theory. The screening effects, the ionic correlation effects, and the plasma effects are taken into account. ESA

N94-22639# Tokyo Univ., Sagamihara (Japan). Inst. of Space and Astronautical Science.
ACCRETION DISKS IN BRIGHT X RAY BINARIES **c89**
Hajime Inoue *In* ESA, Fourth International Toki Conference on Plasma Physics and Controlled Nuclear Fusion May 1993 p 125-130 (For primary document see N94-22624 05-75)
Copyright Avail: CASI HC A02/MF A03

X-ray observations of low mass X-ray binaries and black hole candidates are reviewed. In these sources, an accretion disk is considered to extend close to a neutron star or a black hole and to mainly govern the appearance of the X-ray emission. These sources show soft and hard spectral states, which possibly correspond to two interchangeable states of the inner part of the accretion disk. Similarities of active galactic nuclei to black hole candidates are discussed. X-ray observations of bright X-ray binaries in which an accretion disk is considered to extend close to the surface of the compact star are reported. Hereafter, X-ray binaries including a weakly magnetized neutron star are termed low mass X-ray binaries since they are the large majority of the bright low mass X-ray binaries. ESA

N94-22640# National Inst. for Fusion Science, Nagoya (Japan).
THERMAL PROPERTIES AND RADIATION PROCESSES IN ASTROPHYSICAL PLASMAS
Kuniaki Masai *In* ESA, Fourth International Toki Conference on Plasma Physics and Controlled Nuclear Fusion May 1993 p 131-136 (For primary document see N94-22624 05-75)
Copyright Avail: CASI HC A02/MF A03

Thermal properties of astrophysical plasmas are discussed in view of atomic processes responsible for thermal emission. The collisional ionization process in heating/recombining is described and a characteristic time scale for a plasma to reach an ionization equilibrium is derived. The case of shock heating by the interactions of supersonic stellar winds or supernovae with the ambient matter is considered. The case of ultraviolet or X-ray irradiated plasma is presented as examples of recombining condition. The effect of ionizing/recombining condition on iron K-line emission processes is described. The difference from a plasma nearly in an ionization equilibrium as in the case of solar flare or magneto confined plasmas is important for understanding the thermal properties of astrophysical plasmas or background physics. Thermal properties of various X-ray sources in view of emission processes are summarized. ESA

N94-22641*# Montana State Univ., Bozeman. Dept. of Physics.
PAIR PLASMAS IN THE CENTRAL ENGINE OF ACTIVE GALACTIC NUCLEI
Sachiko Tsuruta and B. G. Tritz *In* ESA, Fourth International Toki Conference on Plasma Physics and Controlled Nuclear Fusion May 1993 p 137-141 (For primary document see N94-22624 05-75)
(Grants NAGw-2208; NSF RII-89-21978)
Copyright Avail: CASI HC A01/MF A03

As the most promising model for the x-ray emission from a class of active galactic nuclei, represented by radio quiet quasars and Seyfert nuclei, a nonthermal pair cascade model, where soft photons are Comptonized by non thermal electron positron pair plasmas produced by gamma rays, is introduced. The simplest model of this kind, the 'homogeneous spherical cascade model', is presented. Many characteristics of this model are qualitatively similar to the homogeneous cascade model. An important difference is that gamma ray depletion is much more efficient in the surface cascade, and consequently this model satisfies the severe observational constraint imposed by the gamma ray background radiation. ESA

N94-22642# Max-Planck-Inst. fuer Extraterrestrische Physik, Garching (Germany).
COMPTON GAMMA RAY OBSERVATORY HIGHLIGHTS OF THE SKY SURVEY **c89**
Helmut Steinle *In* ESA, Fourth International Toki Conference on Plasma Physics and Controlled Nuclear Fusion May 1993 p 145-150 (For primary document see N94-22624 05-75)
Copyright Avail: CASI HC A02/MF A03

Gamma ray astronomy provides a diagnostic tool to study high energy processes in the Universe. NASA's Compton Gamma Ray Observatory completed the first full sky survey in gamma rays on 17 Nov. 1991. The highlights of this first observation period of Compton are presented. Special topics are the mysterious gamma ray bursts, the surprising large number of active galactic nuclei found, the 511 keV and 1.8 Mev line emissions from the galactic plane, the detection of the Co-57 line from supernova 1987A, some pulsar results and observations of gamma rays and neutrons from solar flares. Emphasis is given to present combined results of all four instruments on the Compton Gamma Ray Observatory. ESA

N94-22643# Academy of Sciences (USSR), Moscow. Inst. of Physics.
DARK MATTER: NEUTRON STAR HALO AND THE NATURE OF GAMMA-BURSTS **c90**
Alexander V. Gurevich, Vasily S. Beskin, Kirill P. Zybin, and Mikhail O. Ptitsyn *In* ESA, Fourth International Toki Conference on Plasma Physics and Controlled Nuclear Fusion May 1993 p 151-154 (For primary document see N94-22624 05-75)
Copyright Avail: CASI HC A01/MF A03

It is shown, that dark matter forms a halo around the Galaxy, with a power law density distribution rho = k/r(exp alpha). The size of the halo and the moment of its formation are respectively estimated to be R = 300 + 400 kpc and z = 4 + 5. The same halo is formed by relic neutron stars occurring in the protogalaxy as a result of supernova bursts which cause a change in the original chemical composition. The second component of the neutron stars which were born in the galactic disk and were pulsars at the early stage of their evolution, occurs much later. The statistical distribution of gamma bursts determined by both neutron star components is shown to be in good agreement with observations. A method of direct verificatcn of the model is proposed. ESA

N94-22644# Nagoya Univ. (Japan). Dept. of Physics.
GENERAL RELATIVISTIC WINDS IN A BLACK HOLE MAGNETOSPHERE **c90**
Akira Tomimatsu *In* ESA, Fourth International Toki Conference on Plasma Physics and Controlled Nuclear Fusion May 1993 p 157-160 (For primary document see N94-22624 05-75)
Copyright Avail: CASI HC A01/MF A03

Black hole driven magnetized winds in a stationary and axisymmetric magnestosphere are studied. Ingoing and outgoing winds are injected from a particle creation region around the black hole. This region is assumed to be a thin shell with a large poloidal current density. By using Ohm's law, the production of the mass flux and the heat flow is evaluated as a process of the Joule dissipation. A review of the well known results for the axisymmetric, stationary ideal magnetohydrodynamic system is given. The general relativistic effect becomes very important for ingoing winds near the black hole. The total energy carried by ingoing magnetized winds is found to be negative. This is a mechanism of energy extraction from a rotating hole. The particle creation region is considered to see the pair production of ingoing winds with negative energy and outgoing winds with positive energy. ESA

N94-22645# Tokyo Metropolitan Univ. (Japan). Dept. of Physics.
VERTICAL STRUCTURE OF ACCRETION DISKS **c90**
Toshiya Shimura and Fumio Takahara *In* ESA, Fourth International Toki Conference on Plasma Physics and Controlled Nuclear Fusion May 1993 p 161-164 (For primary document see N94-22624 05-75)
Copyright Avail: CASI HC A01/MF A03

Observationally, some active galactic nuclei show soft x-ray excess which suggests that spectrum deviates from black body. Attempts in calculating the emission spectrum for optically thick disk were made. Most investigations to date were made by adopting the given vertical structure which is obtained by assuming that radiation pressure dominates over gas pressure. However, this seems to be inadequate, because the effect of gas pressure is expected to be significant in determining the vertical structure near the surface where emission spectrum is formed. A detailed calculation, where radiative transfer and vertical structure are self-consistently solved, is performed. ESA

N94-22646*# Pennsylvania State Univ., University Park.
RELATIVISTICALLY EXPANDING PAIR PLASMAS AS BURSTING SOURCES OF COSMIC GAMMA RAYS **c93**
Peter Meszaros and M. J. Rees (Cambridge Univ., England.) *In* ESA, Fourth International Toki Conference on Plasma Physics and Controlled Nuclear Fusion May 1993 p 165-168 (For primary document see N94-22624 05-75)
(Grant NAGw-1522)
Copyright Avail: CASI HC A01/MF A03

High temperature shock heating of relativistically expanding plasmas produced in neutron star binary mergers provides a model for cosmic gamma ray burst sources. This requires the fireball resulting from the merger to have a very high entropy per baryon, mechanisms for which are discussed. The energy, temporal structure and spectrum produced by the blast wave and reverse shock as the fireball is decelerated in an external medium are comparable to those observed, as is the frequency of occurrence and the characteristics of the spatial distribution of the events. Difficulties common to all cosmological gamma ray burst scenarios concern the total amount of energy ultimately appearing at gamma ray energies, the time scales, the spectrum, and the great variety of time profiles. A very general mechanism which overcomes these problems is presented. Situations where the pair plasma is created in regions which are relatively free of baryons are discussed. The effect of the interaction of the expanding fireball with the external medium is considered. ESA

N94-22647# Osaka City Univ. (Japan). Dept. of Electrical Engineering.
LABORATORY RELATIONS BETWEEN THE SOLAR WIND DYNAMIC PRESSURE AND THE MAGNETOSPHERIC STRUCTURES OF THE EARTH AND COMETS **c92**
Shigeyuki Minami, T. Saito (Tohoku Univ., Sendai, Japan.), H. U. Rahman (California Univ., Riverside.), and R. S. White (California Univ., Riverside.) *In* ESA, Fourth International Toki Conference on Plasma Physics and Controlled Nuclear Fusion May 1993 p 171-176 (For primary document see N94-22624 05-75)
Copyright Avail: CASI HC A02/MF A03

Based on laboratory simulation of the Earth's and cometary magnetospheres, it is shown quantitatively how these configurations are controlled by the solar wind dynamic pressure without any effects of parameters. Laboratory relations between the size of contact surface of both magnetospheres and the dynamic pressure of the solar wind are analyzed and compared with the values calculated by a pressure balance equations. The quantitative result shows the dynamic pressure dependence on the size of the magnetopause. This result is applied to explain how the field lines change during the passage of the discontinuity of the dynamic pressure of the solar wind. The shrinking of the Earth's magnetosphere increases the current density in the tail and a reconnection in the tail occurs. It is suggested that this mechanism can exist even in the cometary tails resulting from the disconnection event. An evident chronological series of the solar terrestrial events of the cometary disconnection and the Earth's magnetospheric substorm due to single solar flare event is shown. ESA

N94-22648# Osaka City Univ. (Japan). Dept. of Electrical Engineering.
LABORATORY STRUCTURE OF THE HELIOPAUSE **c92**
Shigeyuki Minami *In* ESA, Fourth International Toki Conference on Plasma Physics and Controlled Nuclear Fusion May 1993 p 177-179 (For primary document see N94-22624 05-75)
Copyright Avail: CASI HC A01/MF A03

The size and structure of the heliopause, which is the hypothesized boundary separating the antiflowing solar wind from the interstellar medium, is discussed. The results of laboratory simulations found the existence of such a boundary as a highly asymmetrical and open structure not yet predicted. The heliopause is produced as a collisionless interaction between the supersonic plasma flow and another supersonic magnetized plasma flow flowing relative to the solar system. Earlier, a laboratory simulation of a cometary magnetosphere produced as an interaction between the solar wind plasma flow and a subsonic plasma flow was performed. Heliosphere is formed as a collisionless interaction between the magnetized plasma flow and the other supersonic plasma flow. ESA

N94-22649# Instituto de Pesquisas Espaciais, Sao Jose dos Campos (Brazil).
THEORY OF LEAKED AURORAL KILOMETRIC RADIATION **c93**
Maria Virginia Alves, Sergio R. Lopes, and Abraham C.-L. Chian (Cambridge Univ., England.) *In* ESA, Fourth International Toki Conference on Plasma Physics and Controlled Nuclear Fusion May 1993 p 181-183 Sponsored by FAPESP; CNPq; and Commission of the European Communities (For primary document see N94-22624 05-75)
Copyright Avail: CASI HC A01/MF A03

A variety of high frequency electromagnetic modes were observed in connection with the auroral kilometric radiation: extraordinary, ordinary, Z, and whistler mode. Large amplitude Langmuir, and Alfven waves are observed in the auroral region. The nonlinear decay process Langmuir to Whistler + Alfven is presented as a candidate to generate downward propagating auroral kilometric radiation along the auroral magnetic field lines, detected by satellites and rockets as well as on the ground level. Explicit expressions for the growth rate and threshold are obtained analytically. The relevance of this nonlinear wave-wave interaction process in the auroral plasma is discussed. ESA

N94-22650# Observatoire de Paris-Meudon (France).
COMPRESSIBLE MHD TURBULENCE IN THE INTERPLANETARY MEDIUM **c90**
Marco Velli and R. Grappin *In* ESA, Fourth International Toki Conference on Plasma Physics and Controlled Nuclear Fusion May 1993 p 185-188 (For primary document see N94-22624 05-75)
Copyright Avail: CASI HC A01/MF A03

Results from numerical simulations of the evolution of nonlinear waves and compressible Magnetohydrodynamic (MHD) turbulence in the solar wind are presented. The basic properties of the background flow, namely the solar wind expansion are taken into account. The evolution of a plasma parcel in a comoving frame of reference is studied. The main features of the expansion may be introduced in a cartesian geometry with periodic boundary conditions by expanding the equations in a small parameter, the angular dimensions of the box as viewed from the Sun. The box is seen to expand in the plane normal to the radial direction and the expansion is followed by using stretched coordinates in this plane. The expansion naturally introduces an anisotropic damping effect on velocity and magnetic field, as well as the Parker like rotation of the average magnetic fied. It is shown how this affects the evolution of an initially circularly polarized large amplitude Alfven wave in oblique propagation. Results for evolution in two dimensions and their relevance to solar wind in situ measurements are discussed. ESA

N94-22651# Tokyo Univ. (Japan). Dept. of Earth and Planetary Physics.
TANGENTIAL STRESS DUE TO KELVIN-HELMHOLTZ INSTABILITY AT THE MAGNETOSPHERIC BOUNDARY
Akira Miura *In* ESA, Fourth International Toki Conference on Plasma Physics and Controlled Nuclear Fusion May 1993 p 189-193 (For primary document see N94-22624 05-75)
Copyright Avail: CASI HC A01/MF A03

A two dimensional magnetohydrodynamic simulation of the Kelvin-Helmholtz instability at the terrestrial magnetospheric boundary was performed. The results show that finite thick velocity shear layer with super Alfvenic velocity jump at the magnetospheric boundary is unstable no matter how large the magnetosheath sonic Mach number. For all magnetosheath sonic Mach numbers, a velocity boundary layer is formed inside of the magnetospheric boundary due to tangential stress associated with the instability and a flow vortex is excited at the inner edge of the velocity boundary layer. The magnetospheric boundary is more highly nonlinearly corrugated by the instability for a smaller sonic Mach number. Tangential stress due to the instability at the boundary is mainly caused by Reynolds stress and is found to be large enough for exciting a residual plasma convection inside the terrestrial magnetosphere. ESA

N94-22652# Sydney Univ. (Australia). Research Center for Theoretical Astrophysics.
ENERGY RELEASE AT ALFVENIC FRONTS IN SOLAR FLARES **c92**
Jennifer Nicholls *In* ESA, Fourth International Toki Conference on Plasma Physics and Controlled Nuclear Fusion May 1993 p 195-197 (For primary document see N94-22624 05-75)
Copyright Avail: CASI HC A01/MF A03

An extension of the release of energy at Alfvenic fronts is presented. The Alfvenic fronts are created by the sudden switch on of a resistance, uniform across the flux tube, which is used to model the flare kernel. At

the fronts the current flowing in the flux tube is partially deflected to the surface of the tube, forming a singular surface current. In the models presented, the current density is partially deflected from smaller to larger radii within the flux tube, removing the singular surface current. It is found that for a significant amount of power released, the effective resistivity peaks in a thin sheath on the surface of the flux tube where the current drops to zero. The results show that various flare phenomena due to precipitating nonthermal electrons, accelerated in the regions of high resistivity, will be offset from the regions of peak vertical current density. ESA

N94-22653# National Inst. for Fusion Science, Nagoya (Japan).
NON-EQUILIBRIUM IONIZATION IN AN M CLASS SOLAR FLARE c92
Takako Kato, Kuniaki Masai, K. Sakimoto (Tokyo Univ., Sagamihara, Japan.), Y. Itikawa (Tokyo Univ., Sagamihara, Japan.), and T. Watanabe (Tokyo Astronomical Observatory, Mitaka, Japan.) et al *In* ESA, Fourth International Toki Conference on Plasma Physics and Controlled Nuclear Fusion May 1993 p 199-202 (For primary document see N94-22624 05-75)
Copyright Avail: CASI HC A01/MF A03

Time dependent Bragg crystal spectrometer x-ray spectra of Fe XXV and S XV during the flare of 21 Jan. 1992 from Yohkoh satellite are presented. The electron temperatures are derived from the intensity ratio of the dielectronic satellite lines to the resonance line from the spectra accumulated from one minute. The ion abundance ratios, n(Li)/n(He), n(Be)/n(He) and n(B)/n(He) of iron ions and n(H)/n(He) and n(Li)/n(He) of sulphur ions are obtained from the intensity ratios of the inner shell excited satellite lines to the resonance line. The electron temperatures derived from S XV begin to increase after the rise of that from Fe XXV. The values from S XV are always lower than those from Fe XXV. The derived ion ratios show a deviation from an ionization equilibrium toward an ionizing phase except for the ratio n(H)/n(He) of sulphur ions. The accuracy of atomic data was examined. ESA

N94-22654# Graduate Univ. for Advanced Studies (Japan). Dept. of Astronomical Science.
NUMERICAL SIMULATION OF MAGNETIC RECONNECTION ASSOCIATED WITH EMERGING FLUX IN THE SOLAR ATMOSPHERE c92
Takaaki Yokoyama and Kazumari Shibata (Tokyo Astronomical Observatory, Mitaka, Japan.) *In* ESA, Fourth International Toki Conference on Plasma Physics and Controlled Nuclear Fusion May 1993 p 203-206 (For primary document see N94-22624 05-75)
Copyright Avail: CASI HC A01/MF A03

The physical process of the magnetic reconnection associated with the emerging flux is discussed. The parameter dependence of the process is studied. A numerical simulation is performed with the two dimensional magnetohydrodynamic code. A two temperature layered plasma similar to the solar photosphere/chromosphere and corona in magnetostatic equilibrium is considered. The results show that magnetic flux in the photosphere emerges by magnetic buoyancy instability as rising loops. It is found that the magnetic reconnection is more violent, when the resistivity is smaller, or when the specific heat ratio gamma is smaller. It is also found that there are four types of jet like flow associated with the reconnection: hot jet along the magnetic field lines, slingshot jet, simple island ejection,and surge like cool jet. ESA

N94-22655# Tokyo Astronomical Observatory, Mitaka (Japan).
X RAY JETS IN THE SOLAR CORONA: OBSERVATIONS WITH YOHKOH SOFT X RAY TELESCOPE c92
Kazunari Shibata, Y. Ishido, L. Acton, K. Strong, T. Hirayama, Yutaka Uchida, A. McAllister, R. Matsumoto, Saku Tsuneta, and T. Shimizu et al *In* ESA, Fourth International Toki Conference on Plasma Physics and Controlled Nuclear Fusion May 1993 p 207-210 (For primary document see N94-22624 05-75)
Copyright Avail: CASI HC A01/MF A03

The discovery of x-ray jet like features using the soft x-ray telescope onboard Yohkoh satellite is reported. The origin of newly discovered x-ray jets and the relation to known solar jets at other wavelengths are discussed. The jets are associated with flare like bright points, flaring emerging flux regions, or flaring active regions. They appear to recur at the same place. The following characteristics are found: in some cases, a dark void appears after ejection at the footpoint of the jet; some jets show structure which suggests a helical magnetic field configuration along the jet; one of the jets associated with a flaring bright point was found to be identified as an H alpha surge. In this case, the x-ray bright point is situated just on H alpha bright point at the footpoint of the surge. The top of the surge is not bright in x-rays. ESA

N94-22656# Rikkyo Univ., Tokyo (Japan). Dept. of Physics.
YOHKOH GAMMA RAY SPECTRAL OBSERVATIONS (YGSO) c93
M. Yoshimori *In* ESA, Fourth International Toki Conference on Plasma Physics and Controlled Nuclear Fusion May 1993 p 211-214 (For primary document see N94-22624 05-75)
Copyright Avail: CASI HC A01/MF A03

The Yohkoh gamma ray flare data obtained from the flares on 27 Oct., 15 Nov., and 3 Dec. 1991 are reported. The data was acquired with the Yohkoh gamma ray spectral observations. The 27 Oct. flare (X6.1/3B) shows a strong gamma ray line emission, while the 3 Dec. flare (X2.0/2B) shows a strong bremsstrahlung continuum extending to 10 MeV. High energy protons and ions were produced in the former flare, while electrons were preferentially accelerated in the latter flare. The line to bremsstrahlung flux ratio is variable within flares. A line feature at 420 keV was observed from the 15 Nov. flare (X1.0/3B). The following problems are discussed on the basis of the gamma ray light curves and energy spectra observed with Yohkoh: timings of electron and proton acceleration, the proton energy spectra in the 10 to 200 MeV band, the angular distribution of accelerated He nuclei, and the production of positron annhilation line at 511 keV. ESA

N94-22657# Onagawa Magnetic Observatory (Japan). Astrogeophysics Inst.
LARGE-SCALE STRUCTURE OF THE SOLAR PLASMA CORONA: AN ANALYSIS OF YOHKOH SXT IMAGES c92
T. Saito, Shigeyuki Minami (Osaka City Univ., Japan.), Y. Kozuka (Nagoya Univ., Toyokawa, Japan.), T. Takahashi, H. Hudson (Hawaii Univ., Honolulu.), Saku Tsuneta (Tokyo Univ., Mitake, Japan.), and T. Watanabe (Nagoya Univ., Toyokawa, Japan.) *In* ESA, Fourth International Toki Conference on Plasma Physics and Controlled Nuclear Fusion May 1993 p 215-218 (For primary document see N94-22624 05-75)
Copyright Avail: CASI HC A01/MF A03

The Yohkoh Soft X-ray Telescope (SXT) images are analyzed. The large scale structure of the solar plasma corona is investigated. The clarified characteristics are as follows: preferred position of active regions and its possible mechanism, rules governing the coronal hole channel, a relation between the inner and outer corona, formation of the 4 sector structure, and the outer corona in pseudoaligned phase. These characteristics are in agreement with both the rotational reversing model and the triple dipole model on the structure and dynamics of the heliomagnetosphere. ESA

N94-22658# Hiroshima Univ. (Japan). Dept. of Materials Science.
MHD RELAXATION IN MAGNETIC LOOPS c92
Yoshio Suzuki, Kanya Kusano, Hiroko Kubo, Tetsuya Sato (National Inst. for Fusion Science, Nagoya, Japan.), and Kyoji Nishikawa *In* ESA, Fourth International Toki Conference on Plasma Physics and Controlled Nuclear Fusion May 1993 p 219-221 (For primary document see N94-22624 05-75)
Copyright Avail: CASI HC A01/MF A03

In order to reveal the solar flare mechanism, the dynamics, as well as the equilibria, in solar coronal magnetic loops and arcade are investigated using the numerical simulations. The main objectives are the following: to achieve the solution of Taylor's minimum energy state for the magnetic arcade; to investigate the two dimensional dynamics in a magnetic arcade by numerical simulations; and to investigate the three dimensional dynamics in magnetic loops by numerical simulations. A loop-loop interaction is observed when the magnetic energy and helicity are injected by a rotating motion on foot points of loops. ESA

N94-22659# Academy of Sciences, Potsdam (German D.R.). Astrophysical Inst.
PARTICLE ACCELERATION IN A FILAMENTARY CURRENT SHEET MODEL c92
Bernhard Kliem *In* ESA, Fourth International Toki Conference on Plasma Physics and Controlled Nuclear Fusion May 1993 p 223-228 (For

primary document see N94-22624 05-75)
(Contract DARA-50-QL-9208-5)
Copyright Avail: CASI HC A02/MF A03

The behavior of test particles in a filamentary current sheet, which was proposed as a model for fragmentary energy release, is investigated. An analytic current sheet model, with antiparallel external fields, is used, and a perpendicular electric field is added. It is demonstrated that the perpendicular electric field can accelerate particles efficiently and that the multiple X-line configuration permits higher particle energies than a single X-line configuration for similar plasma parameters. Taking typical plasma parameters of impulsive flare regions in the lower solar corona, many of the observed particle characteristics can be reproduced. The relevance of the considered process to particle acceleration in galactic and extragalactic plasmas requires further study. ESA

N94-22660*# Iowa Univ., Iowa City.
CURRENT LOOP COALESCENCE STUDIED BY 3-D ELECTROMAGNETIC PARTICLE CODE **c92**
Ken-Ichi Nishikawa, Jun-Ichi Sakai (Toyama Univ., Japan.), Shinji Koide (Toyama Univ., Japan.), O. Buneman (Stanford Univ., CA.), and T. Neubert (Michigan Univ., Ann Arbor.) *In* ESA, Fourth International Toki Conference on Plasma Physics and Controlled Nuclear Fusion May 1993 p 229-232 (For primary document see N94-22624 05-75)
(Contract NAS8-38772; NAGw-2350; NSF ATM-91-06639; NSF ATM-91-21116; ASR-ME-03640247)
Copyright Avail: CASI HC A01/MF A03

Solar flare plasma data from the Yohkoh satellite is analyzed. The interactions of current loops were observed in the active regions on the Sun. This observation pointed out the importance of the idea that the solar flare is generated by the coalescence of current loops. The three dimensional electromagnetic particle simulations are to help in understanding the global interaction between two current loops including the evolution of the twist of loops due to instabilities. Associated rapid dynamics of current loop coalescence such as reconnection, shock waves and associated kinetic processes such as energy transfer, acceleration of particles, and electromagnetic emissions are to be studied by the code to complement analytical theories and magnetohydrodynamic simulations of the current loop coalescence. The simulation results show the strong interactions between two current loops, beam and whistler instabilities, and associated parallel and perpendicular particle heating. ESA

N94-22661# Toyama Univ. (Japan). Plasma Astrophysics and Fusion Science Lab.
PROMPT HIGH-ENERGY PARTICLE ACCELERATION DURING TWO CURRENT LOOPS COLLISION **c92**
Jie Zhao, Bidzina Chargeishvili, and Jun-Ichi Sakai *In* ESA, Fourth International Toki Conference on Plasma Physics and Controlled Nuclear Fusion May 1993 p 233-236 (For primary document see N94-22624 05-75)
(Grant ASR-ME-03640247)
Copyright Avail: CASI HC A01/MF A03

A model of prompt high energy particle acceleration during two current loops collision is presented. A test of proton motion and a test of electron motion in the electromagnetic field derived from the magnetohydrodynamic equations is investigated. It is found that high energy particle acceleration occurs only in the case of Y type loop-loop collisions. The results are in strong dependence on plasma beta and initial position of the test particle. When plasma beta increases, the particle acceleration rate decreases. The particles near the edge of the collision region can be accelerated to higher energy than the ones inside it. It is shown that both the proton and electron can be maximally accelerated to approximately 10 GeV within 0.001 s and approximately 5 MeV within 0.000001 s respectively. In the case of Y type loop-loop collision, it may be expected that high energy gamma ray and neutrons will be generated under interaction between high energy particles and low atmospheric plasma. ESA

N94-22662# Toyama Univ. (Japan). Plasma Astrophysics and Fusion Science Lab.
FORMATION OF FAST MAGNETOSONIC SHOCK WAVES DURING TWO CURRENT LOOPS COLLISION IN SOLAR FLARE **c92**
Shinji Koide and Jun-Ichi Sakai *In* ESA, Fourth International Toki Conference on Plasma Physics and Controlled Nuclear Fusion May 1993 p 237-240 Sponsored in part by YKK Foundation (For primary document see N94-22624 05-75)
(Grant ASR-ME-03640247)
Copyright Avail: CASI HC A01/MF A03

A numerical simulation of fast magnetosonic shock wave formation during a two current loop collision is proposed. The magnetohydrodynamical model is used. It is shown that the rarefaction waves are generated in the initial stage when the two current loops start to collide. After the rarefaction waves propagate away from the exciting region, the fast magnetosonic waves with density enhancement can be produced for the case where the current strength of the loop is weak. When the current becomes strong enough, the magnetosonic shock waves can be generated in the direction perpendicular to that of two loops collision. ESA

N94-22663# Toyama Univ. (Japan). Plasma Astrophysics and Fusion Science Lab.
DYNAMICS OF PHYSICAL STATE DURING TWO CURRENT LOOPS COLLISION **c92**
Bidzina Chargeishvili (Abastumani Astrophysical Observatory, Georgia, USSR.), Jie Zhao, and Jun-Ichi Sakai *In* ESA, Fourth International Toki Conference on Plasma Physics and Controlled Nuclear Fusion May 1993 p 241-244 (For primary document see N94-22624 05-75)
(Grant ASR-ME-03640247)
Copyright Avail: CASI HC A01/MF A03

A model of the two current loops collision to explain the impulsive nature of solar flares is presented. From magnetohydrodynamic equations considering the gravity and resistivity effects, self consistent expressions and equations governing a behavior of all physical quantities just after a magnetic reconnection has taken place are found. Numerical simulations revealed that the most important parameters of the problem are the plasma beta and a ratio of initial values of pressure gradient in longitudinal and radial directions. Low plasma beta case during a Y type interaction shows a rapid pinch and simultaneous enhancement of all physical quantities. Plasma beta increase causes a weakening of pinch effect and decrease of extreme values of all physical quantities. For an X type collision, the increase of the plasma beta causes high velocity jet. For I type collision it shows neither jet production nor very strong enhancement of physical quantities. Direct and oblique collisions are considered taking into account both cases of partial and complete reconnection. ESA

N94-22664# Tohoku Univ., Sendai (Japan). Dept. of Electronic Engineering.
PLASMA STRUCTURE IN A PLASMA FLOW ALONG A MAGNETIC MIRROR FIELD
Seiji Ishiguro, Y. Kishi, and N. Sato *In* ESA, Fourth International Toki Conference on Plasma Physics and Controlled Nuclear Fusion May 1993 p 245-248 (For primary document see N94-22624 05-75)
Copyright Avail: CASI HC A01/MF A03

Using a two and a half dimensional electrostatic particle simulation code, the plasma structure in a plasma flow along a magnetic mirror field was investigated. A high speed plasma flow is injected along converging magnetic field lines. The plasma potential and density increase in the region of the converging magnetic field lines. The potential difference is greater than the ratio between the injected electron temperature and the electronic charge. The potential difference increases as the mirror ratio or the plasma flow speed increases and is accompanied by a gradual saturation. Twin potential peaks are generated at the edges of plasma flow in the region of the converging magnetic field lines. The peak potentials also increase as the mirror ratio or the plasma flow speed increases. Their positions move to the strong magnetic field region with an increase in the plasma flow speed. ESA

N94-22665# Beijing Normal Univ. (China). Dept. of Astronomy.
DYNAMO DRIVEN BY WEAK PLASMA TURBULENCE: THE EFFECT OF DIFFERENTIAL ROTATION
Yi Tong, Abraham C.-L. Chian, and Yang Su *In* ESA, Fourth International Toki Conference on Plasma Physics and Controlled Nuclear Fusion May 1993 p 249-252 Prepared in cooperation with INPE, Sao Jose dos Campos, Brazil; Cambridge Univ., England; and Academia Sinica, Beijing, China (For primary document see N94-22624 05-75)
Copyright Avail: CASI HC A01/MF A03

The effect of differential rotation on dynamo driven weak plasma

turbulence is discussed. Under the assumption that the rotational angular speeds of the celestial bodies vary with the altitude, the solutions modified by differential rotations of celestial bodies, which is applicable to the Sun and solar like stars, are found. It is discovered that there is a close relationship between plasma turbulence waves and rotations of celestial bodies, which is the cause of generating and maintaining the magnetic field. Using p-omega dynamo theory, the effect of uniform rotation of celestial bodies was researched and found to be very important; it is the requisite condition to produce the toroidal fields in the stars. ESA

N94-22666# Hiroshima Univ. (Japan). Dept. of Materials Science.
DOUBLE DIFFUSION CONVECTION IN A ROTATING SPHERICAL SHELL
Kanya Kusano, Tetsuya Sato (National Inst. for Fusion Science, Nagoya, Japan.), and Kyoji Nishikawa *In* ESA, Fourth International Toki Conference on Plasma Physics and Controlled Nuclear Fusion May 1993 p 253-254 (For primary document see N94-22624 05-75)
Copyright Avail: CASI HC A01/MF A03

The nonlinear dynamics of double diffusion convection in a rotating spherical shell is investigated. The simulation is carried out for the purely thermal convection. The drifting columnar convection aligning the rotating axis appears. The double diffusion convection, where the compositional buoyancy works as well as the thermal buoyancy, is studied. It is found that the columns drift to the opposite direction of the thermal convection. The highly nonlinear property of the double diffusion convection is studied. It is revealed that the nonlinear convection is complex, and different from the prediction of the linear property. ESA

N94-22667# Universidad de Los Andes, Merida (Venezuela). Programa de Postgrado en Astronomia y Astrofisica.
NON-LINEAR THERMAL INSTABILITY OF OPTICAL THIN MOLECULAR STRUCTURES
Antonio Parravano and S. Miguel H. Ibanez *In* ESA, Fourth International Toki Conference on Plasma Physics and Controlled Nuclear Fusion May 1993 p 255-257 Sponsored in part by Fundacion Polar (For primary document see N94-22624 05-75)
Copyright Avail: CASI HC A01/MF A03

The thermal stability of interstellar molecular structures in pressure equilibrium is examined. The numerical solution for steady structures is found, and the analytical study of the nonlinear stability of the trivial solution is performed. It is determined how the molecular gas is perturbed in order to develop supercritical stability, subcritical instability, superexponential instability, or asymptotic stability. Physical processes were included to understand the effect of the processes under consideration and as a guide in more complex models. ESA

N94-22668# Universidad de Los Andes, Merida (Venezuela). Programa de Postgrado en Astronomia y Astrofisica.
ON THE NONLINEAR INSTABILITY OF THERMAL STRUCTURES
S. Miguel H. Ibanez and Antonio Parravano *In* ESA, Fourth International Toki Conference on Plasma Physics and Controlled Nuclear Fusion May 1993 p 259-263 Sponsored in part by Fundacion Polar (For primary document see N94-22624 05-75)
Copyright Avail: CASI HC A01/MF A03

The thermal stability of symmetric structures with a given boundary temperature is analyzed. The structures are assumed to be heated, cooled, and have a thermal conduction coefficient depending only on the density and temperature of the constituting plasma. First order analytical solutions are found for plane, cylindrical, and spherical symmetries for the trivial solution. Explicit analytical criteria for supercritical stability, subcritical instability, asymptotic stability, and super exponential instability are reported. ESA

N94-22669# Kyushu Univ., Fukuoka (Japan). Dept. of Physics.
CONSEQUENCES OF PLASMA-MASER IN PLASMA ASTROPHYSICS
Mitsuhiro Nambu *In* ESA, Fourth International Toki Conference on Plasma Physics and Controlled Nuclear Fusion May 1993 p 265-268 (For primary document see N94-22624 05-75)
Copyright Avail: CASI HC A01/MF A03

The plasma-maser interactions are discussed and possible applications to astrophysical plasmas are presented. The total energy conservation relation between particles, kinetic energy, and wave energy is studied. The Manley-Rowe relation among plasma waves is violated, and as a result an efficient energy up conversion from the low frequency mode to the high frequency mode is possible even for a normal unreversed electrons population in plasma turbulence. The plasma-maser process always coexists with the quasilinear interaction and is important in interpreting observations in astrophysical plasmas. ESA

N94-22670# Nagoya Univ. (Japan). Plasma Science Center.
MEAN ELEMENTAL COMPOSITION AND He-3 ENRICHMENTS IN SOLAR ENERGETIC PARTICLES **c92**
M. Toida, T. X. Zhang, and Yukiharu Ohsawa *In* ESA, Fourth International Toki Conference on Plasma Physics and Controlled Nuclear Fusion May 1993 p 269-273 (For primary document see N94-22624 05-75)
Copyright Avail: CASI HC A01/MF A03

The following characteristics of solar energetic particles are investigated: the basic composition pattern of heavy ions which is similar to that of solar corona; He-3 rich events; and rapid ion acceleration to relativistic energies. It is found that large amplitude magnetosonic waves in a magnetohydrodynamic turbulence can produce high energy ions with elemental composition similar to that of background plasma. It is also shown that, in the presence of ion cyclotron waves or oblique ion acoustic waves with frequencies near the He-3 cyclotron frequency, magnetosonic waves can cause He-3 enrichments. ESA

N94-22671# Hawaii Univ., Honolulu. Inst. of Astronomy.
ENHANCED ABSORPTION OF p-MODES ON SUNSPOT AND PLAGE REGIONS **c92**
Barry J. LaBonte and Margarita Ryutova (Institute of Nuclear Physics, Novosibirsk, USSR.) *In* ESA, Fourth International Toki Conference on Plasma Physics and Controlled Nuclear Fusion May 1993 p 275-278 (For primary document see N94-22624 05-75)
Copyright Avail: CASI HC A01/MF A03

A mechanism for the enhanced absorption of p modes is presented. It is based on the idea that in sunspots the magnetic field has a fine filamentary structure. Magnetic regions on the Sun's surface are observed to absorb large fractions of the p mode (acoustic) wave power incident upon them. Strong gradients in the (perturbed) parameters of a wave propagating through such an inhomogeneous medium result in enhanced absorption of the wave power. The gradients in the wave parameters occur on the scale of the background flux tubes which is smaller than the wavelength. ESA

N94-22672# Kanagawa Univ., Yokahama (Japan). Inst. of Physics.
ACCELERATION OF SOLAR-FLARE PARTICLES AS VIEWED FROM THEIR CHEMICAL COMPOSITION **c92**
Kunitomo Sakurai *In* ESA, Fourth International Toki Conference on Plasma Physics and Controlled Nuclear Fusion May 1993 p 279-280 (For primary document see N94-22624 05-75)
Copyright Avail: CASI HC A01/MF A03

The mechanisms by which particles are accelerated in solar flares are investigated. To perform this task it is necessary to know the chemical composition of solar flare particles and gamma ray line emissions associated with flares. High energy quanta such as gamma rays and hard x rays are emitted in association with the acceleration of high energy protons and other nuclei in solar flares. They are called solar flare particles. Radio waves covering microwave to decametric frequencies are usually emitted from relativistic electrons. These electrons are accelerated in solar flares. The efficiency for these particles to be accelerated is shown to be dependent on the ratio of particle masses to their actual charges. ESA

N94-22673# Institut za Nuklearne Nauke Boris Kidric, Belgrade (Yugoslavia).
THE ONSET AND SPECTRA OF A MAGNETIZED LANGMUIR TURBULENCE
L. R. Hadzievski and Milos M. Skoric *In* ESA, Fourth International Toki Conference on Plasma Physics and Controlled Nuclear Fusion May 1993 p 281-284 Sponsored by Ministry of Science and Technology (For primary document see N94-22624 05-75)
Copyright Avail: CASI HC A01/MF A03

A two dimensional simulation of a soliton instability in a weakly magnetized plasma is performed. The Zakharov model of strong Langmuir turbulence is applied. Growth rate spectra are calculated. The suppression of magnetic

field effect with a growing soliton strength is shown. Nonlinear frequency shift and spectral broadening are observed, already in an early stage. A realistic vectorial form of the basic equations accounting for full ion dynamics valid for both small and large amplitude Langmuir solitons is applied. In order to check linear eigenvalue results, focus is put on the early exponentially growing instability stage. ESA

N94-22674*# Stanford Univ., CA.
SOLAR WIND-MAGNETOSPHERE INTERACTION AS SIMULATED BY A 3D, EM PARTICLE CODE **c92**
O. Buneman, Ken-Ichi Nishikawa (Iowa Univ., Iowa City.), and T. Neubert (Michigan Univ., Ann Arbor.) *In* ESA, Fourth International Toki Conference on Plasma Physics and Controlled Nuclear Fusion May 1993 p 285-288 (For primary document see N94-22624 05-75)
(Contract NAS8-38772; NAGw-2350; NSF ATM-91-06639; NSF ATM-91-21116)
Copyright Avail: CASI HC A01/MF A03

The results of simulating the solar wind-magnetosphere interaction with a three dimensional, electromagnetic (EM) particle code are presented. Hitherto such global simulations were done with magnetohydrodynamic (MHD) codes while lower dimensional particle or hybrid codes served to account for microscopic processes and such transport parameters as have to be introduced ad hoc in MHD. The kinetic model combines macroscopic and microscopic tasks. It relies only on the Maxwell curl equations and the Lorentz equation for particles. The preliminary results are for an unmagnetized solar wind plasma streaming past a dipolar magnetic field. The results show the formation of a bow shock and a magnetotail, the penetration of energetic particles into cusp and radiation belt regions, and dawn to dusk asymmetries. ESA

N94-22675# Academy of Sciences (USSR), Moscow. Inst. of Physics.
GAMMA RAY BURST AS A RESULT OF THE EXPLOSIVE INSTABILITY IN THE MAGNETOSPHERE OF OLD NEUTRON STAR **c93**
Y. N. Istomin and D. V. Mosyagin *In* ESA, Fourth International Toki Conference on Plasma Physics and Controlled Nuclear Fusion May 1993 p 291-295 (For primary document see N94-22624 05-75)
Copyright Avail: CASI HC A01/MF A03

The radio pulsars and the gamma bursts are considered phenomena of the same nature. As a result of rotation of the magnetic field the electron-positron plasma is generated in the magnetosphere. The slowly rotating neutron star is shown to work as the accumulator of the relativistic electron-positron plasma which is trapped by the strong magnetic field in the closed region of magnetosphere. The release of the energy will be at that time when the plasma energy density becomes equal to that of magnetic field. The frequency of the burst from one star is of 10 to 100 years. This conception agrees with observation if the old neutron stars are considered to form extended halo around our Galaxy. ESA

N94-22676# Osaka Univ., Toyonaka (Japan). Dept. of Earth and Space Science.
PROPERTIES OF X RAY EMISSION FROM X RAY NOVAE **c93**
Shunji Kitamoto *In* ESA, Fourth International Toki Conference on Plasma Physics and Controlled Nuclear Fusion May 1993 p 297-299 (For primary document see N94-22624 05-75)
Copyright Avail: CASI HC A01/MF A03

Some properties of x ray novae, considered to contain a black hole are described. 71% of the black hole candidates belong to x ray novae. From the spectral study of these novae, at the rising phase, the appearance of hard x rays beyond 100 keV is found. The origin of these hard x rays is described. The probability that a black hole candidate is an x ray nova is shown. The observation of a component comptonized by hot electrons around the soft x ray peak indicates the existence of nonthermal energetic phenomena at the early phase of the nova activity. A model including jet phenomena is discussed. ESA

N94-22677# Sydney Univ. (Australia). Research Center for Theoretical Astrophysics.
ELECTRON ACCELERATION IN AND RADIO EMISSION FROM SN1987A **c93**
Lewis Ball and J. G. Kirk (Max-Planck-Inst. fuer Kernphysik, Heidelberg, Germany.) *In* ESA, Fourth International Toki Conference on Plasma Physics and Controlled Nuclear Fusion May 1993 p 301-303 (For primary document see N94-22624 05-75)
Copyright Avail: CASI HC A01/MF A03

The radio emission from Supernova (SN) 1987A in Jul. 1990 is discussed. A model involving synchrotron radiation emitted by electrons undergoing diffusive acceleration at the supernova blast wave is discussed. This model involves reasonable assumptions concerning adiabatic losses and the magnetic field in the preexplosion stellar wind. The light curve and spectrum produced by a constant rate of particle injection occurring in a localized region of the shock front can be calculated from it. Observations indicate that at least two such clumps were found to date. The implications of the model and its application to the observations are discussed. ESA

N94-22678# Ecole Polytechnique, Palaiseau (France). Centre de Physique Theorique.
LANGMUIR MICROSTRUCTURES AND PULSAR RADIO EMISSION **c93**
Estelle Asseo *In* ESA, Fourth International Toki Conference on Plasma Physics and Controlled Nuclear Fusion May 1993 p 305-308 (For primary document see N94-22624 05-75)
Copyright Avail: CASI HC A01/MF A03

The simultaneous presence of relativistic particles and 'Langmuir microstructures' in pulsar magnetospheres is discussed. They result in the emission of electromagnetic waves in three different ways: the 'Langmuir microstructures', considered as an assembly of elementary structures, have an intrinsic electromagnetic radiation; the curvature radiation of the Langmuir microstructures, represented by elementary charges moving along dipolar magnetic field lines; the acceleration of relativistic particles in interaction with 'Langmuir microstructures' may also result in electromagnetic radiation. Implications of these mechanisms for the interpretation of pulsar radio emissions are considered. ESA

N94-22679# Institute of Physical and Chemical Research, Saitama (Japan).
STRUCTURE OF ACCRETION PLASMAS OF X RAY BINARY PULSARS IN MHD TURBULENCE **c93**
Masahiro Hoshino and Toshiaki Takeshima *In* ESA, Fourth International Toki Conference on Plasma Physics and Controlled Nuclear Fusion May 1993 p 309-312 (For primary document see N94-22624 05-75)
Copyright Avail: CASI HC A01/MF A03

The time variability of the x ray binary pulsars is discussed. It is found that the observed power spectral density of the aperiodic time variability of the x ray pulsar can be approximated by a power law spectrum which changes its slope at the coherent pulsation frequency. The indices of the observed spectra are respectively 1.4 to 2.0 above the pulsation frequency and 0 to 1.0 below the pulsation frequency. The density fluctuation spectra with inverse cascades in magnetohydrodynamic turbulence is studied. It is found that the observed x ray spectra can be interpreted as the density fluctuations in the accreting plasmas. It is shown that the structure of either disk fed or wind fed pulsar can be determined by comparing the observed x ray spectra with the theoretical density fluctuation spectra of two or three dimensional magnetohydrodynamic turbulence, respectively. ESA

N94-22680# Moscow Physical-Engineering Inst. (Russia).
VHE GAMMA RAY GENERATION BY RADIO PULSARS **c93**
Sergeii Vladimirovic Bogovalov (Institute of Physical and Chemical Research, Saitama, Japan.) and Y. D. Kotov *In* ESA, Fourth International Toki Conference on Plasma Physics and Controlled Nuclear Fusion May 1993 p 313-316 (For primary document see N94-22624 05-75)
Copyright Avail: CASI HC A01/MF A03

The Very High Energy (VHE) gamma ray generation due to inverse Compton scattering of relativistic electrons and positrons on soft thermal emission of a neutron star is discussed. Due to observations of Crab region there are no doubts that particles can be accelerated to energies of about 10 to the power of twelve eV near radio pulsars. Spectra and light curves of Crab, Vela, and Geminga are estimated. Comparison with observations is presented. It is shown that the periodically pulsed flux of TeV emission from the Crab pulsar is considerably smoothed in comparison with the signal in softer emission. ESA

N94-22681# Institute of Physical and Chemical Research, Saitama (Japan).
PARTICLE ACCELERATION ON THE ALFVEN SURFACE OF A PLASMA EJECTING AXISYMMETRIC ROTATOR
Sergeii Vladimirovic Bogovalov (Moscow Physical-Engineering Inst., Russia.) *In* ESA, Fourth International Toki Conference on Plasma Physics and Controlled Nuclear Fusion May 1993 p 317-320 (For primary document see N94-22624 05-75)
Copyright Avail: CASI HC A01/MF A03

The model of an axisymmetric magnetic rotator is considered in order to analyze the processes of particle acceleration in pulsar magnetosphere. The energetic losses of pulsars are shown to be transformed into the kinetic energy of the plasma on the Alfven surface of the magnetosphere. A general problem of dynamics of plasma and the structure of the magnetosphere of an axisymmetric rotator is considered. It is shown that the solution of the problem where the plasma flow continuously passes through slow, fast, and Alfven surfaces does not exist. The real flow has a discontinuity on the Alfven surface. On the outer side of the Alfven surface the azimuthal magnetic field goes to zero. A super fast magnetosound wind with power comparable with total energetic losses of the star is formed. ESA

N94-22682# Nagoya Univ. (Japan). Dept. of Physics.
ASYMPTOTIC STRUCTURE OF MAGNETICALLY DRIVEN MHD WIND **c90**
Shin-Ya Nitta *In* ESA, Fourth International Toki Conference on Plasma Physics and Controlled Nuclear Fusion May 1993 p 321-323 (For primary document see N94-22624 05-75)
Copyright Avail: CASI HC A01/MF A03

The asymptotic structure of plasma wind is discussed. By solving the special relativistic magnetohydrodynamic (MHD) equations for transfield force balance, an analytic self consistent solution is obtained for the steady and axisymmetric magnetically driven wind in the limit of viscousless, pressureless and resistiveless plasmas. In this solution, all the field lines are asymptotically conical. The inclination angle of each field line from the equatorial plane is determined. The thin jet solution as in radio loud active galactic nuclei or the equatorial wind solution can be obtained. ESA

N94-22683# Tokyo Metropolitan Univ. (Japan). Dept. of Physics.
HYDRODYNAMICAL WINDS FROM AN ACCRETION DISK **c90**
Rika Okada and Fumio Takahara *In* ESA, Fourth International Toki Conference on Plasma Physics and Controlled Nuclear Fusion May 1993 p 325-328 (For primary document see N94-22624 05-75)
Copyright Avail: CASI HC A01/MF A03

Numerical simulations of thermally driven winds originating in a disk round a compact object are performed. The disk is assumed to be geometrically thin, self similar under scaling in radius, and in a dynamical balance. A polytropic relation between density and pressure is assumed. Steady state solutions are obtained for appropriate boundary conditions. It is found that a cone where the density and the pressure become extremely low is formed around the rotation axis, if the disk has angular momentum. While a large portion of the flow is outgoing, gas originating in the inner disk falls into the central gravitating object. In order for the disk winds to blow, the pressure and density distributions at the disk are restricted in some range. ESA

N94-22684# Aichi Univ. of Education (Japan). Dept. of Physics and Astronomy.
MHD FLOWS FROM COMPACT OBJECTS: EFFECTS ON MAGNETIC FIELD CONFIGURATIONS
Masaaki Takahashi *In* ESA, Fourth International Toki Conference on Plasma Physics and Controlled Nuclear Fusion May 1993 p 329-332 (For primary document see N94-22624 05-75)
Copyright Avail: CASI HC A01/MF A03

Cold relativistic ideal magnetohydrodynamic (MHD) flows are studied in the stationary and axisymmetric magnetosphere of a rapidly rotating compact object. To obtain highly accelerated winds, MHD winds emanating from a geometrically thin disk and passing through smoothly both the Alfven and fast magnetosonic points for specified configuration of streamlines are examined. It is found that for a streamline converging toward the rotation axis the fast magnetosonic point always exists at a finite distance. For a straight configuration of streamlines the fast magnetosonic point can exist close to the Alfven point only if energy flux of a wind is sufficiently large. For a convex configuration a super fast wind solution is also possible. The solution stops at a finite distance and no solution reaches infinity. ESA

N94-22685# Sao Paulo Univ. (Brazil). Inst. Astronomico e Geofisico.
THREE-DIMENSIONAL SIMULATIONS OF COSMIC JETS EMPLOYING THE SMOOTHED PARTICLE HYDRODYNAMICS TECHNIQUE **c93**
Elisabete M. deGouveiaDalPino (Harvard-Smithsonian Center for Astrophysics, Cambridge, MA.) and Willy Benz (Arizona Univ., Tucson.) *In* ESA, Fourth International Toki Conference on Plasma Physics and Controlled Nuclear Fusion May 1993 p 333-336 (For primary document see N94-22624 05-75)
Copyright Avail: CASI HC A01/MF A03

Three dimensional simulations of supersonic jets performed with Cartesian smoothed particle hydrodynamics are presented. Jets are recognized as a common phenomena in astrophysics. Supersonic flows are observed to emerge from protostars and active nuclei of galaxies. The structure and evolution of both radiative cooling and adiabatic cosmic jets are compared. The development of nonaxisymmetric dynamic instabilities and thermal instabilities is also examined. The simulations show the presence of a dense cold shell formed by the cooling of the shock heated gas when q(sub S) = d(sub cool)/R(sub j) less than or equal to 1. ESA

N94-22686# National Inst. for Fusion Science, Nagoya (Japan).
HELICAL KINK INSTABILITY OF JETS FROM YOUNG STELLAR OBJECTS **c93**
Yasushi Todo *In* ESA, Fourth International Toki Conference on Plasma Physics and Controlled Nuclear Fusion May 1993 p 337-340 (For primary document see N94-22624 05-75)
Copyright Avail: CASI HC A01/MF A03

The results of three dimensional magnetohydrodynamic numerical simulations are described. They are applied to the behavior of the jets from young stellar objects under circumstances in which the ambient large scale interstellar magnetic field is twisted helically by the rotation of protostar and the protostellar disk through which this field threads. The calculations are continued until the bow shock propagates a distance 60 times as far as the initial jet radius. The case examined involves a jet with density 100 m(sub H)/cubic cm and velocity 100 km/s. It is shown that an azimuthal field B(sub phi) of strength 70 mu G drives a helical kink instability. The growth rate of this instability is large enough that significant morphological effects are expected to be visible during the typical lifetime of a Herbig-Haro (HH) object. ESA

N94-22687# Nagoya Univ. (Japan). Dept. of Astrophysics.
FRAGMENTATION OF MAGNETIZED FILAMENTARY INTERSTELLAR CLOUDS **c90**
Tomoyuki Hanawa, Fumitaka Nakamura, and Takenori Nakano (Nobeyema Solar Radio Observatory, Japan.) *In* ESA, Fourth International Toki Conference on Plasma Physics and Controlled Nuclear Fusion May 1993 p 341-344 (For primary document see N94-22624 05-75)
Copyright Avail: CASI HC A01/MF A03

Fragmentation of filamentary molecular clouds are calculated by one dimensional and two dimensional numerical simulations. It is shown by the two dimensional simulation that the high density clumps produced by fragmentation have different shapes depending on the magnetic field strength. When the magnetic field is weak, the high density clump is spherically symmetric. When the magnetic field is strong, a geometrically thin disk perpendicular to the axis is formed. A geometrically thin disk is unstable against further fragmentation, while a spherical cloud is not likely to fragment. Hierarchical fragmentation is expected in the case of strong magnetic fields. The one dimensional simulation showed that fragmentation propagates in a filamentary cloud. High density clumps are produced successively from one side to the other. ESA

N94-22688# Nagoya Univ. (Japan). Dept. of Astrophysics.
GRAVITATIONAL INSTABILITY OF MAGNETIZED FILAMENTARY CLOUDS. 1: HELICAL MAGNETIC FIELDS **c90**
Fumitaka Nakamura, Tomoyuki Hanawa, and Takenori Nakano (Nobeyema Solar Radio Observatory, Japan.) *In* ESA, Fourth International Toki Conference on Plasma Physics and Controlled Nuclear Fusion May 1993 p 345-348 (For primary document see N94-22624 05-75)
Copyright Avail: CASI HC A01/MF A03

The magnetohydrodynamical instability of self-gravitating magnetized filamentary clouds is investigated by means of a normal mode analysis. The density distribution in equilibrium is assumed to be a function of the radial distance from the axis. The magnetic field is assumed to have both longitudinal and azimuthal components. Dispersion relations are obtained numerically as a function of the strength and configuration of the magnetic field. The equilibrium model is described. The dispersion relation for axisymmetric and kink modes are obtained. The dependences of the dispersion relation on the magnetic field strength and configuration are shown. On the basis of the stability analysis, the application of the theory to observations is discussed. ESA

N94-22689# Nagoya Univ. (Japan). Dept. of Astrophysics.
GRAVITATIONAL INSTABILITY OF MAGNETIZED FILAMENTARY CLOUDS. 2: ROTATION **c90**
Tomoaki Matsumoto, Fumitaka Nakamura, and Tomoyuki Hanawa *In* ESA, Fourth International Toki Conference on Plasma Physics and Controlled Nuclear Fusion May 1993 p 349-352 (For primary document see N94-22624 05-75)
Copyright Avail: CASI HC A01/MF A03

Stability of filamentary molecular clouds against fragmentation was studied by means of a normal mode analysis. The model cloud is infinitely long along the axis and has an equilibrium density distribution. It rotates around the axis and is permeated with helical magnetic field strength. The dispersion relation was obtained as a function of rotation and magnetic fields. The model filamentary cloud is infinitely long and axisymmetric around the axis in equilibrium. It is supported against gravity by gas pressure, rotation, and magnetic force when in hydrodynamical equilibrium. The details of the model are described. The model with longitudinal magnetic fields and that with helical magnetic fields are discussed. ESA

N94-22690# Osaka Univ., Toyonaka (Japan). Dept. of Earth and Space Science.
TIME VARIATIONS OF X RAYS FROM BLACK HOLE CANDIDATES: CANONICAL TIME VARIATIONS IN HIGH AND LOW INTENSITY STATES **c90**
Sigenori Miyamoto, Shunji Kitamoto, Sayuri Iga, Yasuhide Kamodo, Kiyoshi Hayashida, Kentaro Terada, and Hitoshi Negoro *In* ESA, Fourth International Toki Conference on Plasma Physics and Controlled Nuclear Fusion May 1993 p 353-357 (For primary document see N94-22624 05-75)
Copyright Avail: CASI HC A01/MF A03

Time variations of X rays from a black hole candidate GS1124-683 are described and compared with other black hole candidates: Cyg X-1, GX339-4, GS2023+338, and a Z source of low mass binaries: GX5-1. In GS1124-683, the following states were recognized: a high flare state, a high quiet state, a high to low transition state, and a low state. Canonical time variations of X rays were observed not only in the low state but also in the high flare state. In the high state, the X rays consist of two components: a soft disk black body component and a power law component. These two components have different power spectrum density (PSD) functions: a flat top noise and a power law noise. In the low state, the X rays consist of a power law component. This component has a harder energy spectrum and shows different and larger time variations than those of the power law components in the high state. GS2023+338 in its flare state had a different normalized PSD and harder energy spectra than GS1124-683 in its high flare state. In the low state GS2023+338 had the same X ray energy spectrum and the same normalized PSD to the other black hole candidates. ESA

N94-22691# Commissariat a l'Energie Atomique, Saclay (France). Service d'Astrophysique.
PAIR PLASMAS IN THE GALACTIC CENTER REGION AND IN NOVA MUSCAE **c90**
Philippe Durouchoux and P. Wallyn *In* ESA, Fourth International Toki Conference on Plasma Physics and Controlled Nuclear Fusion May 1993 p 359-362 (For primary document see N94-22624 05-75)
Copyright Avail: CASI HC A01/MF A03

Accretion disks surrounding a compact object, which are able to produce a pair plasma, are investigated. The cooling down of positrons and their annihilation sites, in the light of the line observations, are evaluated. The model consists ofa black hole system, with an important accretion rate, fuelled by a companion star. The purpose is to emphasize that a search of features, mainly at 511 keV backscattered energies, as well as their relative intensities and timing evolution, might be a powerful tool in black hole searches. It is shown that backscattered features could provide a new set of signatures for black hole candidates. ESA

N94-22692# Nagoya Univ. (Japan). Dept. of Physics.
TIME VARIATION OF MHD ACCRETION ONTO A BLACK HOLE **c90**
Kouichi Hirotani, Akira Tomimatsu, and Masaaki Takahashi (Aichi Univ. of Education, Japan.) *In* ESA, Fourth International Toki Conference on Plasma Physics and Controlled Nuclear Fusion May 1993 p 363-366 (For primary document see N94-22624 05-75)
(Grant ASR-ME-04640268)
Copyright Avail: CASI HC A01/MF A03

Nonstationary and nonaxisymmetric perturbations of magnetohydrodynamic (MHD) accretion onto a Kerr black hole are studied. A small amplitude fluctuation of the electromagnetic field is regarded as a source of perturbations in a magnetosphere. How the plasma accretion will be affected by it along a flow line especially at the fast magnetosonic point in the short wave length limit is examined. A stationary black hole magnetosphere, in which the MHD interaction is so effective that typically ten of the fluid's rest mass energy will be transported to the magnetic field, is described. Adopting the magnetically dominated limit that the energy density of the magnetic field dominates the rest mass energy density of plasma particles, the electromagnetic perturbations are described. Using this result, it is shown that the fluid energy, angular momentum, and poloidal velocity become highly variable near the fast magnetosonic point in the magnetically dominated limit. This is because the radial variation of the meridional current becomes significant and causes large Lorentz force on the fluid. The observed short term variations of X ray emission from GBHCs (galactic black hole candidates) and/or active galactic nuclei are discussed. ESA

N94-22693# Tokyo Metropolitan Univ. (Japan). Dept. of Physics.
ACCRETION OF A HOT PLASMA ONTO THE CENTRAL BLACK HOLE: FOKKER-PLANCK FORMULATION **c90**
Fumiko Yabuki and Fumio Takahara *In* ESA, Fourth International Toki Conference on Plasma Physics and Controlled Nuclear Fusion May 1993 p 367-370 (For primary document see N94-22624 05-75)
Copyright Avail: CASI HC A01/MF A03

The accretion process of a hot plasma onto a central black hole is reported. The steady state distribution and consumption rate of particles orbiting a Schwarzschild hole are considered assuming the spherical symmetry. Only ion-ion Coulomb scattering is considered and the effects of electrons, except that they assure the charge neutrality, are neglected. It is assumed that diffusion approximation can be adopted. The relativistic Fokker-Planck equation in a general form is formulated and the Fokker-Planck coefficients are derived. ESA

N94-22694# Kyoto Univ. (Japan). Dept. of Astronomy.
MAGNETIC SUPERBUBBLES IN THE GALACTIC DISK AND HALO **c90**
S. Mineshige, Kazumari Shibata (Tokyo Astronomical Observatory, Mitaka, Japan.), and P. R. Shapiro (Texas Univ., Austin.) *In* ESA, Fourth International Toki Conference on Plasma Physics and Controlled Nuclear Fusion May 1993 p 371-374 Sponsored in part by Robert A. Welch Foundation (For primary document see N94-22624 05-75)
(Contract DE-FG05-80ET-53088)
Copyright Avail: CASI HC A01/MF A03

The evolution of the interstellar superbubbles arising from sequential supernova explosions or winds from OB associations in the galactic disk is studied. A two dimensional magnetohydrodynamics (MHD) code is used. It is found that in the presence of horizontal magnetic fields of strength comparable to that in the galactic disk, the vertical expansion of the superbubbles can, under some conditions, be significantly inhibited by the effect of a decelerating J by B force. The outermost effect of the disturbance actually propagates somewhat faster than in nonmagnetic cases, as an MHD fast shock or nonlinear wave. The implications of the results for the galactic fountain are discussed. ESA

N94-22695# Aichi Univ. of Education (Japan). Dept. of Physics and Astronomy.

GENERATION AND MAINTENANCE OF BISYMMETRIC SPIRAL MAGNETIC FIELDS IN DISK GALAXIES IN DIFFERENTIAL ROTATION **c90**

Takeyasu Sawa and M. Fujimoto (Nagoya Univ., Japan.) *In* ESA, Fourth International Toki Conference on Plasma Physics and Controlled Nuclear Fusion May 1993 p 375-378 (For primary document see N94-22624 05-75)

Copyright Avail: CASI HC A01/MF A03

The approximate dynamo equation, which yields asymptotic solutions for the large scale bisymmetric spiral (BSS) magnetic fields rotating rigidly over a large area of the galactic disk, is derived. The vertical thickness and the dynamo strength of the gaseous disk which are necessary to generate and sustain the BSS magnetic fields is determined. The globally BSS magnetic fields which propagate over the disk as a wave without being twisted more tightly are reproduced. A poloidal field configuration is theoretically predicted in the halo around the disk, and is observed in the edge-on galaxy NGC4631. Mathematical methods for the galactic dynamo are shown to be equivalent. Those methods give different growth rates between the BSS and the axisymmetric spiral (ASS) magnetic fields in the disk. Magnetohydrodynamical excitation is discussed between the BSS magnetic fields and the two armed spiral density waves. ESA

N94-22696# Waseda Univ., Tokyo (Japan). Dept. of Applied Physics.

THE RELAXED STATE AND ENTROPY PRODUCTION DUE TO THE ELECTRIC RESISTIVITY AND VISCOSITY OF PLASMA

Tomokazu Kato and Hideo Nagamori *In* ESA, Fourth International Toki Conference on Plasma Physics and Controlled Nuclear Fusion May 1993 p 379-382 (For primary document see N94-22624 05-75)

Copyright Avail: CASI HC A01/MF A03

The derivation of the relaxed state in reversed field pinch using the principle of the minimum entropy production is given. A sum of the entropy productions due to the electric resistivity and due to the viscosity of the plasma is considered. As the subsidiary conditions for the variational calculus, the helicity K and cross helicity M are taken. The F-theta curves obtained from these magnetic fields show slower decreasing functions of theta, compared with the Bessel function model. The gradient of these curves depend on the boundary values of velocity. Good agreement is obtained, provided a finite tangential relative velocity at the wall is assumed. The obtained magnetic field is expressed by a linear combination of solutions of the generalized force free equations with complex proportional constants beta, and its line of force B and current J are not exactly parallel to one another. ESA

N94-22697# Sydney Univ. (Australia). School of Physics.

MAGNETIC FIELDS IN SPIRAL GALAXIES **c90**

S. Spencer and Lawrence Cram *In* ESA, Fourth International Toki Conference on Plasma Physics and Controlled Nuclear Fusion May 1993 p 383-385 Sponsored in part by Australian Research Council and Science Foundation for Physics (For primary document see N94-22624 05-75)

Copyright Avail: CASI HC A01/MF A03

Recent investigations suggesting that amplification and regeneration of large scale magnetic fields can result from the combined action of galactic winds and magnetic diffusion are described. Observations of polarized radio emission from spiral galaxies imply the presence of magnetic fields organized with axisymmetric or bisymmetric structure on the scale of the whole galaxy. Such fields were explained previously either as a systematic patterning of primordial fields by differential rotation or as the result of dynamo generation of large scale components from non-mirror symmetric turbulence. A model for the phenomenon based on magnetic field regeneration by the interaction between turbulent diffusion and axially and radially sheared galactic winds is summarized. ESA

N94-22698# Commissariat a l'Energie Atomique, Saclay (France). Service d'Astrophysique.

SPIRAL ALFVEN INSTABILITY IN ACCRETION DISKS **c90**

Michel Tagger, R. Pellat (Ecole Polytechnique, Palaiseau, France.), and F. C. Coroniti (California Univ., Los Angeles.) *In* ESA, Fourth International Toki Conference on Plasma Physics and Controlled Nuclear Fusion May 1993 p 387-390 (For primary document see N94-22624 05-75)

Copyright Avail: CASI HC A01/MF A03

With the discovery that Alfven waves can be strongly unstable in a magnetized accretion disk, it can be expected to explain the turbulence necessary to drive accretion in these disks. The instability of non-axisymmetric Alfven waves is studied using analytical derivations and numerical simulations. An exact set of equations for the time evolution of the perturbations, giving a simple analytical result in the limit of very low beta, is derived. Using a Wentzel - Kramers - Brillouin approximation, the domain of existence and dominance of the set of modes corresponding to increasing values of n are found. A one dimensional linearized magnetohydrodynamic simulation is used to confirm these results and describe the time evolution of an initial perturbation in the disk. Pressure forces which can however be straightforwardly included are neglected. These forces are found negligible, even at high beta. ESA

N94-22699# Ibaraki Univ., Mito (Japan). Dept. of Physics.

SHOCK FORMATION IN MAGNETOHYDRODYNAMICAL ACCRETION ONTO A BLACK HOLE **c90**

Masayoshi Yokosawa *In* ESA, Fourth International Toki Conference on Plasma Physics and Controlled Nuclear Fusion May 1993 p 391-394 (For primary document see N94-22624 05-75)

Copyright Avail: CASI HC A01/MF A03

Magnetohydrodynamic (MHD) accretion onto a black hole is studied. The general relativistic MHD accretion was calculated by a numerical method. By using the new method of calculation, the angular momentum of the fluid generated by the black hole which is placed in the static medium with the uniform density and the uniform magnetic field is studied. The interaction between the magnetic field and the fluid matter in the rotating space time enhances the energy for the fluid and reduces the energy for the magnetic field. The rapidly rotating black hole produces the negative energy region in the distribution of the energy density for the magnetic field. The magnetic field transports the energy and the angular momentum from the stretched horizon to the outer atmosphere. The asymmetry of the flow increases the critical Mach number: M(sub AC) much greater than one. The MHD accretion with an initially uniform magnetic field produces the peaks of the magnetic stress near the event horizon. The perturbations at the peaks grow at M(sub AC) = 30. The gas energy density perturbs the MHD flow and generates the shock waves. The shock waves generated near the horizon may produce the large amount of X ray emission. The emission mechanism of the X ray radiation from the black hole candidates is discussed with the MHD accretion model. ESA

N94-22700# Universidade Federal do Rio Grande do Norte, Natal (Brazil). Dept. de Fisica.

MAGNETIC RECONNECTION IN EMISSION NEBULAE IN CLUSTERS OF GALAXIES **c90**

Luiz C. Jafelice and Amanacio C. S. Friaca (Sao Paulo Univ., Brazil.) *In* ESA, Fourth International Toki Conference on Plasma Physics and Controlled Nuclear Fusion May 1993 p 395-398 (For primary document see N94-22624 05-75)

Copyright Avail: CASI HC A01/MF A03

The effects of magnetic reconnection as a mechanism of excitation of filaments with optical emission lines observed in cooling flows in clusters of galaxies are studied. Hydrodynamical time dependent calculations to follow the evolution of cooling condensations until the phase of optical line emission are used. The results indicate that a much better agreement with observational results of emission line intensities and line ratios is attained when an active participation of the magnetic field through reconnection is included. ESA

N94-22701# Tokyo Univ. (Japan). Dept. of Astronomy.

MAGNETOHYDRODYNAMIC PHENOMENA IN STAR-FORMING PROCESSES AND THEIR ENVIRONMENT **c90**

Yutaka Uchida *In* ESA, Fourth International Toki Conference on Plasma Physics and Controlled Nuclear Fusion May 1993 p 401-407 (For primary document see N94-22624 05-75)

Copyright Avail: CASI HC A02/MF A03

The relevance of the magnetic field in the entire process of the star formation is studied. The investigation ranges from the initial contraction from the so called giant molecular cloud in the galaxy to the creation of high speed 'optical jets' in the final stage of star formation in and before the T Tauri stage of the new born stars. The results of magnetohydrodynamic (MHD) simulations made by using a modified MHD code developed for

axisymmetric problems, and by using a fourth order accuracy code developed for the upwind total variational diminishing code for the three dimensional astrophysical MHD situations, are reported. ESA

76 SOLID-STATE PHYSICS

Includes superconductivity.

For related information, see also *33 Electronics and Electrical Engineering* and *36 Lasers and Masers.*

N94-19807# Argonne National Lab., IL.
FERMIOLOGY AND DE HAAS-VAN ALPHEN EFFECT OF BETA-(ET)2IBr2
J. Wosnitza (Karlsruhe Univ., Germany.), G. W. Crabtree, K. D. Carlson, H. H. Wang, and J. M. Williams Apr. 1993 3 p Presented at the Conference of the International Union of Pure and Applied Physics on Low Temperature Physics (LT 20), Eugene, OR, 1-11 Aug. 1993
(Contract W-31-109-eng-38)
(DE93-019523; ANL/MSD/CP-79636; CONF-930801-10) Avail: CASI HC A01/MF A01

The Fermi surface of the organic superconductor beta-(ET)(sub 2)IBr(sub 2) investigated by measurements of the de Haas - van Alphen (dHvA) effect has been found to have the typical two-dimensional cylindrical form. A small amount of corrugation could be quantitatively determined by the distinctive angular dependence of beating nodes. The existence of up to four almost identical frequencies in the dHvA signal may be explained by magnetic interaction effects within the samples. Due to the 1/cos(Theta) behavior of the effective mass spin-splitting, zeros could be detected. DOE

N94-19808# Argonne National Lab., IL.
DYNAMICS OF VORTICES IN SUPERCONDUCTORS
E. Weinan 1992 11 p Presented at the World Congress of Nonlinear Analysts, Melbourne, FL, 19-26 Aug. 1992
(Contract W-31-109-eng-38)
(DE93-019535; ANL/MCS/CP-80512; CONF-920817-2) Avail: CASI HC A03/MF A01

This paper studies the dynamics of vortices in type-II superconductors from the point of view of time-dependent Ginzburg-Landau equations. The paper outlines a proof of existence, uniqueness, and regularity of strong solutions for these equations. It then derives reduced systems of ODE's governing the motion of the vortices in the asymptotic limit of large Ginzburg-Landau parameter. DOE

N94-19817# IBM Watson Research Center, Yorktown Heights, NY.
INVESTIGATION OF QUANTUM EFFECTS IN HETEROSTRUCTURES Final Report, Jun. 1990 - Apr. 1993
Emilio E. Mendez 20 Aug. 1993 16 p
(Contract DAAL03-90-C-0008)
(AD-A270938; ARO-27458.54-PH) Avail: CASI HC A03/MF A01

The most important results obtained are summarized. These results are: growth and characterization of a new class of III-V based diluted magnetic semiconductors; observation of one-dimensional conduction on surface channels of InAs; demonstration of Tamm states in semiconductor superlattices; realization of electric-field tunable stimulated emission; demonstration of resonant interband magnetotunneling in type II heterostructures; measurement of dynamic spin polarization in diluted magnetic semiconductor quantum wells. DTIC

N94-19821 Colorado State Univ., Fort Collins. Dept. of Chemical Engineering.
MATERIALS PROCESSING AND MANUFACTURING TECHNOLOGIES FOR DIAMOND SUBSTRATE MULTICHIP MODULES (DSMCM) Quarterly Technical Summary, 1 Jul. - 1 Oct. 1993
David S. Dandy 1 Oct. 1993 2 p Limited Reproducibility: More than 20% of this document may be affected by microfiche quality
(Contract N00014-93-1-2002)
(AD-A271011) Avail: CASI HC A01

Portions of a detailed surface kinetics mechanism developed in collaboration with Michael Coltrin of Sandia National Laboratories to describe the growth of diamond on a (100)-(2x1) surface were refined extensively during this period. Specifically, it was discovered that the molecular mechanics program employed to calculate the thermophysical properties of the diamond structures was not parameterized for use with radical species. After discussions with the program's author (N.L. Allinger, Univ. Georgia, Athens) and extensive testing with experimentally validated compounds, MM3(92) was re-applied to the 53 unique structures present in the surface mechanism to compute the temperature-dependent quantities enthalpy, entropy, and heat capacity for each structure. These thermodynamic properties were fit to polynomials over the temperature range 298.15 less than or equal to T less than or equal to 2000 K. The full mechanism is currently being incorporated into the stagnation flow model used to examine diamond deposition. DTIC

N94-19825# Department of Energy, Washington, DC. Office of Utility Technologies.
SUPERCONDUCTIVITY TECHNOLOGY PROGRAM FOR ELECTRIC POWER SYSTEMS: PROCEEDINGS
K. B. Marriott 1993 600 p Presented at the Annual Review Meeting for the US DOE Office of Utility Technologies, Washington, DC, 28-29 Jul. 1993
(DE93-040074; DOE/EE-0005; CONF-9307120) Avail: CASI HC A25/MF A06

Twenty-seven presentations are included in viewgraph form for the wire development panel, applications development panel, and thallium workshop. Topics covered include: critical currents and microstructure of high temperature superconductor materials, thallium conductor development, and thermomechanical processing of BSCCO conductors; the processing of HTS wires and tapes using electrodeposited Tl-oxide superconductors and alternative screen printing and thermomechanical processing of Tl-oxide superconductors; approaches to practical wire development using Tl-1223; thermomechanical processing of wire from Bi- and Tl-based superconductors; cryoprocessing (freeze drying) of precursor powders for development of commercially viable high-T(sub c) conductors; synthesis and processing of Tl-based thick films and tapes; practical conductor development for electric power systems; demonstration of magnetic refrigerator for HTS electric power applications; cryogenic design of a superconducting motor; prospects for thallium thick-film processing for wire applications; on the determination of thallium, hole concentration, and oxygen stoichiometry in thallium-cuprate superconductors. DOE

N94-19827# Los Alamos National Lab., NM.
CRYSTALLOGRAPHIC PHASE TRANSITIONS IN ACTINIDE METALS AS A FUNCTION OF PRESSURE
O. Eriksson, P. Soederlind, J. Melsen, R. Ahuja, B. Johansson (Uppsala Univ., Sweden.), J. M. Wills, and A. M. Boring 1993 37 p Presented at the 1993 Actinides, Santa Fe, NM, 19-24 Sep. 1993
(Contract W-7405-eng-36)
(DE93-040138; LA-UR-93-3086; CONF-930905-2) Avail: CASI HC A03/MF A01

The authors present first-principles calculations of the equilibrium volumes and crystal structures of the light actinides (Th-Pu). The calculated equilibrium volumes for fcc Th, bct Pu, alpha-U, and beta-Np are found to agree reasonably well with the experimental data, and when comparing the total energies of the bcc, fcc, bct, alpha-U, and beta-Np structures the authors obtain the correct crystal structures for all studied systems. Equilibrium volumes for Th-Pu, using a hypothetical fcc structure, have been calculated; although spin-orbit coupling is included in these calculations, the calculated equilibrium volume of Pu is smaller than for Np, in disagreement with experiment. Moreover, the calculated tetragonal elastic constant, C prime, is shown to be negative for bcc U, bcc Np, bcc Pu, and fcc Pu. Thus, the zero temperature calculations suggest that the bcc structure is unstable for these elements and that fcc Pu is also unstable. This is in conflict with experiment and the authors are led to the conclusion that temperature effects must be of crucial importance for stabilizing cubic structures in U, Np, and Pu. Further, as a function of decreasing volume the authors predict a crystal structure sequence fcc yields bct yields fcc in Th, a sequence alpha-U yields bct yields bcc in U, and a sequence beta-Np yields bct yields bcc in Np. Also, a sequence of transitions in Sc as a function of decreasing volume have been calculated, namely hcp yields fcc yields omega yields beta-Np yields bcc. DOE

N94-19835# SRI International Corp., Menlo Park, CA.
THEORY OF ENERGY-ASSISTED EPITAXY; THEORY OF ORDERED SEMICONDUCTOR ALLOYS: In(1-x)Tl(x)Sb AS A LONG-WAVE INFRARED MATERIAL Final Report, 27 Apr. 1988 - 1 Jul. 1993
M. A. Berding and A. Sher Oct. 1993 252 p
(Contract N00014-88-C-0096)
(AD-A271007) Avail: CASI HC A12/MF A03

We summarize research by SRI International on the theory of energy-assisted epitaxy and the properties of ordered semiconductor compounds. We include our published papers, and summarize the major conclusions from our work. We also report on our first year of work on the properties of InTlSb, a proposed new long-wave infrared detector material. We include a discussion of major aspects of our work, including the advantages of this material over HgCdTe and III-V superlattice and quantum-well devices. DTIC

N94-19842 McMaster Univ., Hamilton (Ontario). Dept. of Chemistry.
SYNTHESIS AND STRUCTURAL CHARACTERIZATION OF NEW LIGHT MOLECULAR WEIGHT INORGANIC OXIDIZERS AND RELATIVE DERIVATIVES, VOLUME 1 Final Report, 1 May 1991 - 30 Apr. 1992
G. J. Schrobilgen Feb. 1993 187 p Limited Reproducibility: More than 20% of this document may be affected by microfiche quality
(Contract F04611-91-K-0004)
(AD-A271437; PL-TR-93-3007-Vol-1; AD-E201668) Avail: CASI HC A09

The following annual report encompasses eleven areas of research. The basic philosophy underpinning this work has been to develop the technology for the synthesis, storage, and handling of new high-energy density materials. The importance of performing the 'easier' heavy element chemistry as the ground work to synthesizing the more challenging and potentially more useful lighter analogs has been stressed throughout much of this work. Where possible published or about to be published work is included in this report under each of the appropriate subheadings. DTIC

N94-19848 Brown Univ., Providence, RI. Dept. of Physics.
THE PROXIMITY EFFECT IN ULTRATHIN GRANULAR Pb FILMS
Shih-Ying Hsu, J. M. Valles, Jr., P. W. Adams, and R. C. Dynes 1992 2 p Limited Reproducibility: More than 20% of this document may be affected by microfiche quality
(Contract N00014-92-J-1344)
(AD-A271094) Avail: CASI HC A01

We present electron transport measurements that demonstrate that Pb films that are on the insulating side of the two dimensional superconductor to insulator transition can be made superconducting by depositing a normal metal, Ag, on them. DTIC

N94-19849 Brown Univ., Providence, RI. Dept. of Physics.
THE COULOMB ANOMALY IN STRONGLY DISORDERED FILMS Final Report
Shih-Ying Hsu and J. M. Valles, Jr. 1992 3 p Limited Reproducibility: More than 20% of this document may be affected by microfiche quality
(Contract N00014-92-J-1344)
(AD-A271095) Avail: CASI HC A01

Electron tunneling measurements of the Coulomb anomaly in the density of states in strongly disordered quench condensed granular films are presented. The strength of this anomaly grows with increasing sheet resistance, R(sub n), at low R(sub n) but saturates at high R(sub n). We suggest that the granular morphology of these films is responsible for the saturation. Author (DTIC)

N94-19861# Lawrence Livermore National Lab., CA.
FREQUENCY DEPENDENT ELECTRICAL PROPERTIES OF MINERALS AND PARTIAL-MELTS
J. J. Roberts and J. A. Tyburczy 14 Apr. 1993 40 p Presented at the 11th Workshop on Electromagnetic Induction in the Earth, Wellington, New Zealand, 26 Aug. - 2 Sep. 1992
(Contract W-7405-eng-48)
(DE93-019918; UCRL-JC-111340-Rev-1; CONF-9208215-1-Rev-1) Avail: CASI HC A03/MF A01

Methods have been developed that utilize the electrical and magnetic properties of rocks to explore the interior of the Earth. The electrical properties of minerals are strongly dependent on temperature, composition, point defect chemistry, and frequency at which the measurements were made. Complex impedance measurements aid understanding and interpretation of single frequency electrical properties measurements. This paper reviews the frequency dependent nature of the electrical response of minerals and partial-melts, with particular attention to the mineral olivine, an important mineral in the lower crust and upper mantle. DOE

N94-19869# Oak Ridge National Lab., TN.
FORMATION OF COLLOIDAL Ag PRECIPITATES IN FUSED SILICA BY MeV ION IMPLANTATION
C. W. White, D. S. Zhou, R. A. Zuhr, and R. H. Magruder (Vanderbilt Univ., Nashville, TN.) Aug. 1993 7 p Presented at the International Union of Materials Research Societies on Advanced Materials, Tokyo, Japan, 31 Aug. - 4 Sep. 1993
(Contract DE-AC05-84OR-21400)
(DE93-040268; CONF-9308122-5) Avail: CASI HC A02/MF A01

The formation of Ag nanoclusters in fused silica by MeV ion implantation has been studied. Size and size distributions of nanoclusters depend on dose. These nanoclusters give rise to strong absorption at the surface plasmon wavelength. Implantation at elevated temperatures results in the segregation of implanted Ag into the very near-surface region. Volume fractions for Ag nanoclusters up to approximately 5% have been obtained by MeV implantation. DOE

N94-19897# Rochester Univ., NY. Dept. of Electrical Engineering.
QUANTUM NOISE STUDIES WITH SUPERCONDUCTING TUNNEL JUNCTION MIXERS Final Report, 15 Mar. 1990 - 14 Mar. 1993
Mark F. Bocko 14 Mar. 1993 3 p
(Grant AF-AFOSR-0231-90)
(AD-A270897; AFOSR-93-0779TR) Avail: CASI HC A02/MF A01

We have completed our theoretical and experimental investigations of the noise properties of superconducting tunnel junction (SIS) mixers operated as both a phase insensitive linear amplifier and as a phase sensitive linear amplifier. We proposed a technique by which a SIS mixer could be operated as a phase sensitive linear amplifier, i.e., the gain and noise temperature of the amplifier are a function of the phase of the incoming signal. In this technique two phase coherent local oscillators at different frequencies are combined in the mixer simultaneously so both a phase preserving and phase conjugating mixing process occur resulting in a phase sensitive mixer. DTIC

N94-19923# Argonne National Lab., IL.
GENERAL INTRODUCTION TO MICROSTRUCTURAL EVOLUTION UNDER CASCADE DAMAGE CONDITIONS
H. Wiedersich Jun. 1993 25 p Presented at the International Workshop on Time Dependence of Radiation Damage Accumulation and Its Impact on Materials Properties, Montreux, Switzerland, 14-20 Oct. 1992
(Contract W-31-109-eng-38)
(DE93-017443; ANL/MSD/CP-80216; CONF-9210398-1) Avail: CASI HC A03/MF A01

A short overview of the processes that affect the evolution of the microstructure during irradiation is given. The processes include defect production with an emphasis on the effects of the dynamic cascade events, defect clustering, irradiation-enhanced diffusion, radiation-induced segregation, phase decompositions, and phase transformations. A simple model for the description of the development of the defect microstructure in a pure metal during cascade producing irradiation is also outlined which can provide, in principle, defect fluxes required for the description of the microstructural processes such as phase decomposition and irradiation-induced precipitation. DOE

N94-19926# Los Alamos National Lab., NM.
METASTABLE bcc PHASE FORMATION IN THE Nb-Cr SYSTEM
D. J. Thoma, R. B. Schwarz, J. H. Perepezko (Wisconsin Univ., Madison.), and D. H. Plantz (Coast Guard Academy, New London, CT.) 1993 14 p Presented at the 8th International Conference on Rapidly Quenched and Metastable Materials, Sendai, Japan, 22-27 Aug. 1993
(Contract W-7405-eng-36)
(DE93-018376; LA-UR-93-2500; CONF-9308140-1) Avail: CASI HC A03/MF A01

Extended metastable bcc solid solutions of Nb-X at.% Cr (X = 35, 50, 57, 77, 82, and 94) were synthesized by two-anvil splat-quenching. In addition, bcc (Nb-67 at.% Cr) was prepared by mechanically alloying mixtures

of niobium and chromium powders. The lattice parameters were measured by x-ray diffraction and the Young's moduli were measured by low-load microindentation. The composition dependence of the lattice parameters and elastic moduli show a positive deviation with respect to a rule of mixtures. During continuous heating at 15 C/min., the metastable precursor bcc phases decomposed at temperatures above 750 C to uniformly refined microstructures. DOE

N94-19929# Oak Ridge National Lab., TN.
PARTICLES ON SURFACES OF LASER ABLATED Y1Ba2Cu3O(7-DELTA) FILMS
X. Y. Zheng, S. Zhu, D. H. Lowndes, and R. J. Warmack 1993 7 p Presented at the 2nd International Conference on Laser Ablation: Mechanisms and Applications, Knoxville, TN, 19-22 Apr. 1993
(Contract DE-AC05-84OR-21400)
(DE93-040269; CONF-9304144-12) Avail: CASI HC A02/MF A01

Pulsed laser deposition of Y1Ba2Cu3O(7-delta) films grown at heater temperature of 720 and 800 C on SrTiO3 and MgO substrates with thickness ranging from a nominal 5 unit cells to 200 nm were studied by STM and SEM. Size and density of particles present in the films were found to depend on film thickness, growth, temperature, and substrate. STM images indicate a correlation between film growth mode and particle density: the onset of big particles comes after the growth mode changes from layer-like to island growth. DOE

N94-19933 Pennsylvania State Univ., University Park. Dept. of Physics.
INNOVATIVE ACOUSTIC TECHNIQUE FOR STUDYING NEW MATERIALS AND NEW DEVELOPMENTS IN SOLID STATE PHYSICS Annual Summary Report, 1 Nov. 1992 - 31 Oct. 1993
Julian D. Maynard 4 Oct. 1993 10 p Limited Reproducibility: More than 20% of this document may be affected by microfiche quality
(Contract N00014-92-J-1186)
(AD-A270540) Avail: CASI HC A02

The goals of this project involve the use of innovative acoustic techniques to study new materials and new developments in solid state physics, such as effects in mesoscopic electronic systems. Major accomplishments include (1) the preparation and publication of a number of major papers and chapters in books, (2) the comparison of the anisotropy of an aluminum alloy quasicrystal with that of its cubic approximant, (3) the measurement of the elastic constants of a diamond substitute material, TiB2, (4) the measurement of an extremely low (possibly the lowest) infrared optical-absorption coefficient, (5) the measurement of the effects of disorder on the propagation of a nonlinear pulse, and (6) the acquisition of initial data in an experiment on the onset of fracture. DTIC

N94-19939# Midwest Research Inst., Golden, CO.
RESEARCH ON DEFECTS AND TRANSPORT IN AMORPHOUS-SILICON-BASED SEMICONDUCTORS
E. A. Schiff, Qing Gu, and Qi. Wang Aug. 1993 14 p Prepared in cooperation with Syracuse Univ., NY
(Contract DE-AC02-83CH-10093)
(DE93-017117; NREL/TP-451-5651) Avail: CASI HC A03/MF A01

This report describes Phase 2 progress in two areas: (1) electron drift and conduction band tails in a-Si(1 - x)Ge(x):H and a-Si(1 - x)C(x):H alloys, and (2) optical bias effects on electron trapping and emission in a-Si:H. The authors completed a comprehensive study of electron drift in a-Si(1 - x)Ge(x):H alloys, including correlations of the drift parameters with 'blue' fill factor measurements and open-circuit voltages in solar cells. They began a study of electron and hole drift in a-Si(1 - x)C(x):H, but, at present, they have only confirmed that C alloying degrades the electron drift mobility in a-Si(1 - x)C(x):H. They completed a study of optical bias effects on transient photocharge measurements in a-Si:H, which clarified that optical bias effects found in earlier photocurrent transient measurements occur because deep trapping is suppressed by optical bias. DOE

N94-19961# Sandia National Labs., Albuquerque, NM.
PREPARATION AND PROPERTIES OF SOL-GEL DERIVED PZT THIN FILMS FOR DECOUPLING CAPACITOR APPLICATIONS
R. W. Schwartz, D. Dimos, S. J. Lockwood, and V. M. Torres 1993 12 p Presented at the International Symposium on Integrated Ferroelectrics, Colorado Springs, CO, 19-21 Apr. 1993
(Contract DE-AC04-76DP-00789)
(DE93-018853; SAND-93-1652C; CONF-9304197-1) Avail: CASI HC A03/MF A01

The use of ceramic thin films as decoupling capacitors offers the possibility of capacitor integration within the integrated circuit (IC) package and, potentially, directly onto the IC itself. Since these configurations minimize series inductance, higher operational speeds are possible. In the present study, the authors have investigated the dielectric and leakage characteristics of sol-gel PZT films. For compositions near the morphotropic phase boundary, dielectric constants of 1000, and loss tangents of about 0.02, are observed. The current-voltage behavior of the capacitors is characterized by a non-linear response, and significant asymmetry in both the leakage and breakdown characteristics as a function of bias sign is observed. Breakdown fields for PZT 53/47 thin films are typically approximately 800 kV/cm at 25 C. The authors have also studied the effects of La and Nb dopant additions and alternate firing strategies on film leakage characteristics. Donor doping at 2 - 5 mol % lowers leakage currents by a factor of 10(exp 3). For films prepared by a multilayering approach, firing each layer to crystallization results in leakage currents that are a factor of 10(exp 2) lower than films prepared by the standard process. DOE

N94-19966 Air Force Inst. of Tech., Wright-Patterson AFB, OH. School of Engineering.
A NOVEL METHOD FOR CHARACTERIZING THE ELECTRICAL PRIORITIES OF LEAD ZIRCONATE TITANATE (PZT) FERROELECTRIC FILMS AND MEMORY DEVICES Ph.D. Thesis
Robert D. Pugh Oct. 1993 173 p Limited Reproducibility: More than 20% of this document may be affected by microfiche quality
(AD-A270463; AFIT/DS/ENP/93-06) Avail: CASI HC A08

A novel technique for determining the electrical properties of lead zirconate titanate (PZT) ferroelectric-film memory devices is reported which eliminates a major systematic error discovered in other techniques. This novel technique measures the electrical response of a ferroelectric material (device) to an electrical signal that is similar in amplitude and frequency to the signals used in digital computers. The technique also provides a method for consistently converting the measured electrical response into polarization values. The ability to consistently process the data allows researchers to accurately compare the results of different measurements and to investigate the relationship changes in the operating characteristics of a ferroelectric memory device and changes in the electrical properties of the ferroelectric material. Ferroelectric aging in a PZT film was investigated using this new technique. The results of this investigation indicated that ferroelectric aging in PZT films is similar to ferroelectric aging in many bulk ferroelectric materials. Specifically, 'effective' internal electric fields increase linearly with the logarithm of the aging time. Additionally, the investigation revealed how earlier measurement techniques motivated investigators to believe that ferroelectric-film aging was different from bulk ferroelectric aging. DTIC

N94-19967 Materials Research Society, Pittsburg, PA.
COMMON THEMES AND MECHANISMS OF EPITAXIAL GROWTH, VOLUME 312
Paul Fuoss, Jeffrey Tsao, David W. Kisker, Andrew Zangwill, and Thomas Kuech 15 Apr. 1993 360 p Symposium held in San Francisco, CA, 13-15 Apr. 1993 Limited Reproducibility: More than 20% of this document may be affected by microfiche quality
(Contract N00014-93-1-0468)
(AD-A270513) Avail: CASI HC A16

Partial contents of these proceedings include: From Adatom Migration to Chemical Kinetics: Models for MBE, MOMBE and MOCVD; The Dynamical Transition to Step-Flow Growth During Homoepitaxy of GaAs (001); Evolution of Roughness on InP Layers Observed by Scanning Force Microscopy; Low Temperature Si Homoepitaxy: Effects of Impurities on Microstructure; Compositional Ordering in Semiconductor Alloys; Evolving Surface Cusps During Strained Layer Epitaxy; Effects of Minimizing the Driving Force for Epitaxy in the Ge/Si(001) System; A Comparison of Two Epitaxial Formation Mechanisms in the SiGe System; The Role of Vertical Exchange in the Growth of GaAs/AlAs Lateral and Vertical Superlattices; Surface Ordering of MBE Grown 001 Ga05A105As - A Theoretical Study; and Strain-Field Induced Crosshatch Formation During Molecular Beam Epitaxy of InGaAs/GaAs Films. DTIC

N94-19970# EG and G Energy Measurements, Inc., Idaho Falls.
SUPERCONDUCTING PROPERTY MEASUREMENTS IN TAPE GEOMETRY
K. L. Telschow 1993 8 p Presented at the 11th Symposium on Energy Engineering Sciences, Argonne, IL, 3-5 May 1993
(Contract DE-AC07-76ID-01570)
(DE93-018943; EGG-M-93181; CONF-9305134-2) Avail: CASI HC A02/MF A01

Fabrication of the new high Tc superconductor materials into useable long-length wires or tapes has proven difficult, often resulting in low critical currents. The ability to measure critical currents in high Tc superconducting tapes on a local scale can be valuable for assessing the microstructure resulting from the fabrication process. This paper describes the results of research on using induced currents from a small non-contacting electromagnetic probe to determine the critical current density in high Tc tapes on a local scale. The technique forces full-field penetration into the tape locally and infers the local critical current density from the 'critical state' model for flux penetration. Difficulties encountered with the tape geometry and demagnetization effects are overcome by an analysis procedure that provides comparative measurement of the critical current density with the contacting DC transport probe method. Results for several tapes with different critical currents are discussed. DOE

N94-19980# International Business Machines Corp., Yorktown Heights, NY.
ALE PROJECT Annual Report
S. M. Gates, F. J. Himpsel, S. S. Iyer, D. D. Koleske, and D. Lapiano-Smith Oct. 1993 60 p
(Contract N00014-91-C-0080)
(AD-A271080) Avail: CASI HC A04/MF A01

The general goal of this work is to identify the chemical species that are present at the surface during atomic layer epitaxy (ALE). Particularly interesting is the nature of the passivation layer that terminates the broken bonds at the semiconductor surface in the first ALE step. Likewise, we follow the removal of the passivating species in the second step by thermal decomposition, desorption, irradiation, or chemical reaction. We use mainly surface-sensitive photoelectron spectroscopy at our beam line at the National Synchrotron Light Source (NSLS) in Brookhaven. During the past year we have built a new beam line at the Advanced Light Source (ALS) in Berkeley, which will exhibit 10,000 times higher brightness than NSLS. We expect the ALS beam line to become operational late '93 or early '94. DTIC

N94-19982# Naval Academy, Annapolis, MD.
PHOTOCHEMICALLY INDUCED TRANSFORMATIONS OF TRANSITION COMPLEXES
James E. Brown 17 May 1993 136 p
(AD-A271112; USNA-TSPR-200) Avail: CASI HC A07/MF A02

Photolysis of the dinuclear complex ((n(sup 5)-C5H5)Fe(CO)2)2 in CHCl3 results in the formation of (n(sup 5)-C5H5)Fe(CO)2Cl through intermediate 17-electron radicals of the form (n(sup 5)-C5H5)Fe(CO)2. The photolyses of the related diphosphine-bridged compounds (n(sup 5)-C5H5)Fe(CO)2-u-DPPX, where DPPX = DPPM, DPPE, and DPPP and therefore are (Ph2P)2CH2, (Ph2P)2C2H, and (Ph2P)2C3H6 respectively, are described. The synthesis and photolysis of the analogous ruthenium DPPM dimer is also described. In contrast to the behavior of the simple iron dinuclear species, the DPPM and DPPE phosphine bridged compounds undergo photolysis in CHCl3 to yield products containing formyl substituted cyclopentadienyl rings. Details of the reactions studied and product characterizations using multinuclear NMR, IR, and single crystal X-ray diffraction techniques are described. A possible mechanism for the formation of the formyl derivatives is outlined. In the synthesis and purification of ((n(sup 5)-C5H5)Ru(CO))2-u-DPPM and the attempted synthesis of the ((n(sup 5)-C5H5)Ru(CO))2-u-DPPE, two ruthenium monomers of the form (n(sup 5)-C5H5)Ru(Cl)DPPX resulted. A possible reaction pathway for the synthesis of these two monomers as byproducts in the ruthenium phosphine dimer preparation is suggested. Full structural and spectral characterizations of the monomeric compounds are included. DTIC

N94-20002# Oak Ridge National Lab., TN.
SPIN-POLARON THEORY OF HIGH-(Tc) SUPERCONDUCTIVITY. 1: SPIN POLARONS AND HIGH (Tc) PAIRING
R. F. Wood Jun. 1993 18 p Presented at the International Symposium on High-Tc Superconductivity and its Applications, Cairo, Egypt, 4-16 Apr. 1993
(Contract DE-AC05-84OR-21400)
(DE93-019196; CONF-9304191-1) Avail: CASI HC A03/MF A01

The concept of a spin polaron is introduced and contrasted with the more familiar ionic polaron picture. A brief review of aspects of ionic bipolaronic superconductivity is given with particular emphasis on the real-space pairing and true Bose condensation characteristics. The formation energy of spin polarons is then calculated in analogy with ionic polarons. The spin-flip energy of a Cu spin in an antiferromagnetically aligned CuO2 plane is discussed. It is shown that the introduction of holes into the CuO2 planes will always lead to the destruction of long-range AF ordering due to the formation of spin polarons. The pairing of two spin polarons can be expected because of the reestablishment of local (short-range) AF ordering; the magnitude of the pairing energy is estimated using a simplified model. The paper closes with a brief discussion of the formal theory of spin polarons. DOE

N94-20018# Technische Univ., Berlin (Germany). Fachbereich Physik.
A GREEN FUNCTION METHOD FOR CALCULATION OF ATOMIC AND ELECTRONIC PROPERTIES OF ISOLATED ADSORBATE ATOMS Ph.D. Thesis [EINE GREEN-FUNKTIONSMETHODE ZUR BERECHNUNG ATOMARER UND ELEKTRONISCHER EIGENSCHAFTEN ISOLIERTER ADSORBATATOME]
Joerg Bormet 1992 140 p In GERMAN
(ETN-93-95055) Avail: CASI HC A07/MF A02

The calculation of the thermodynamic potential and the Hellman-Feynman forces of isolated adsorbates is theoretically described. A Green function method was used for the autoconsistent solving of the Kohn-Sham equation, assuming that the chemical potential is constant and the Fermi level of electrons is known. The system of electrons and nuclei was divided in two parts with a realistic atomic structure: the semi-infinite substrate with plane translation symmetry parallel to the surface as reference system and the adsorbate system. Provided both systems are known, all important physical quantities such as electron density, state density, and derived parameters were available. The binding geometry was estimated from the total energy calculation for the adsorbate system. Results were validated for hydrogen atom and silicon on Al(111). For the system Na/Al the nature of the binding of sodium on a metallic substrate was discussed. The binding is found to be clearly ionic for the limiting case where the surface is only poorly covered by sodium. Experimental results of raster tunnel microscopy for carbon on Al (111) were discussed in order to understand the adsorption of elements of the fourth group. ESA

N94-20026# Technische Hochschule, Darmstadt (Germany). Fachbereich Physik.
OPTICALLY INDUCED ROTATION DIFFUSION IN POLYMER LIQUID CRYSTALS: PHENOMENOLOGICAL THEORY AND EXPERIMENTAL VERIFICATION Ph.D. Thesis [OPTISCH INDUZIERTE ROTATIONSDIFFUSION IN POLYMEREN FLUESSIGKRISTALLEN: PHAENOMENOLOGISCHE THEORIE UND EXPERIMENTELLE VERIFIKATION]
Richard Birenheide 1991 132 p In GERMAN
(ETN-93-95068) Avail: CASI HC A07/MF A02

The physical processes involved in the light induced change of optical axis in polymer liquid crystals during cis/trans isomerization are investigated. Photostationary systems behavior in glass solid bodies such as azobenzol is mathematically formulated. The model was based on the assumption that a molecule can change its location in space during isomerization, while thermal motions are excluded because of glass state. The model predicts variations of orientation distribution function, and therefore of the optical axis, in the case of irradiation with polarized light; a biaxial distribution after irradiation with circular polarized light was ascertained. Ultraviolet dichroitic examinations were performed to assess these results; it is shown that during light exposure the thermal relaxation of cis molecules in glass is partially suppressed. The measured time profile of the refractive index allowed grid experiments to be interpreted and material qualities as a holographic accumulator to be evaluated. ESA

N94-20029# Full Circle Research, Inc., San Marcos, CA.
CMOS GATE ARRAY CHARACTERIZATION PROCEDURES Final Report, 8 May 1991 - 31 Mar. 1993

James P. Spratt Sep. 1993 44 p
(Contract DAAL02-91-C-0053)
(AD-A269943; ARL-CR-71) Avail: CASI HC A03

Present procedures are inadequate for characterizing the radiation hardness of gate array product lines prior to personalization because the selection of circuits to be used, from among all those available in the manufacturer's circuit library, is usually uncontrolled. (Some circuits are fundamentally more radiation resistant than others.) In such cases, differences in hardness can result between different designs of the same logic function. Hardness also varies because many gate arrays feature large custom-designed megacells (e.g., microprocessors and random access memories-MicroP's and RAM's). As a result, different product lines cannot be compared equally. A characterization strategy is needed, along with standardized test vehicle(s), methodology, and conditions, so that users can make informed judgments on which gate arrays are best suited for their needs. The program described developed preferred procedures for the radiation characterization of gate arrays, including a gate array evaluation test vehicle, featuring a canary circuit, designed to define the speed versus hardness envelope of the gate array. A multiplier was chosen for this role, and a baseline multiplier architecture is suggested that could be incorporated into an existing standard evaluation circuit chip. DTIC

N94-20152 Technische Univ., Berlin (Germany). Fachbereich Physik.
PHOTOELECTRON SPECTROSCOPY AT MODEL BOUNDARY SURFACES OF ENERGY CONVERTER SEMICONDUCTORS/ELECTROLYTE CONTACTS: ADSORPTION, COADSORPTION, AND TRIADSORPTION OF Br2, Na, AND H2O ON VAN DER WAALS SURFACES OF METAL CHALOCOGENIDE SEMICONDUCTORS Ph.D. Thesis
[PHOTOELEKTRONENSPEKTROSKOPIE AN MODELLGRENZFLAECHEN ENERGIEWANDELNDER HALBLEITER/ELEKTROLYT-KONTAKTE: ADSORPTION, KOADSORPTION UND TRIADSORPTION VON BR2, NA UND H2O AUF VAN-DER-WAALS-OBERFLAECHEN VON HALBLEITENDEN METALLCHALKOGENIDEN]
Thomas Mayer 1993 251 p In GERMAN Limited Reproducibility: More than 20% of this document may be affected by microfiche quality
(ETN-93-95063) Avail: CASI HC A12

The semiconductor/electrolyte interface is modeled in ultraviolet radiation through coadsorption of electrolyte components (Br2, Na, and H2O) on Van der Walls surfaces and analyzed by photoemission. By spectroscopy of valence band area and redox level, the line structures of substrate band adsorbate emissions, their energetic positions, and relative shifts were evaluated as a function of the adsorption mode (molecular or dissociative) and the electrical potential above the surface. It is found that Br2 does not adsorb on InSe but the reaction is activated by X-ray irradiation; in order to explain this difference, the electronic and spatial structure of substrate surfaces was discussed. It is concluded that Br2 acts on nonreactive substrates as an acceptor and increases electron affinity. It is observed that H2O molecularly adsorbs at 100K in WSe2, InSe, and GaSe; the coadsorption of Br2 and H2O shows that the acceptor character of Br2 is stronger than the donor character of H2O. ESA

N94-20184# Johns Hopkins Univ., Laurel, MD. Applied Physics Lab.
SINGLE-EVENT UPSET TESTING OF THE PERFORMANCE SEMICONDUCTOR 1750A CMOS/SOS CHIP SET
James D. Kinnison 30 Sep. 1993 16 p
(Contract N00039-91-C-0001)
(AD-A271158; JHU/APL-TG-1384) Avail: CASI HC A02/MF A01

Complex computer systems in space are vulnerable to many different environmental effects. One of the most difficult problems is survival under exposure to charged-particle radiation. Microelectronic devices are particularly sensitive to single-event upset-a change in the logic state of a dynamic node or memory cell due to interaction with cosmic rays. For reliable computing in satellite systems, designers must understand the sensitivity of the computer components to single-event upset. A description of tests performed on a MILSTD 1750A compliant microprocessor and peripherals is presented, and the results are used to estimate the single-event upset rate in space for each of the devices. DTIC

N94-20213# Tufts Univ., Medford, MA. Electro-Optics Technology Center.
SYNCHROTRON X RAY DIFFRACTION ANALYSIS OF PHOTOREFRACTIVE CRYSTALS AND THEIR GRATINGS Final Report, 1 May 1990 - 30 Apr. 1993
Mark Cronin-Golomb and Gerard Fogarty 26 Jul. 1993 39 p
(Contract DAAL03-90-G-0116)
(AD-A271176; ARO-27882.1-PH) Avail: CASI HC A03/MF A01

High-resolution synchrotron x-ray diffraction imaging was used to examine the state of crystal perfection in the photorefractive ferroelectric materials barium titanate and strontium barium niobate. Ferroelectric 180 degree domains, dislocations, striations, faceted growth remnants, and other lattice features were identified. The technique was also used to image the photorefractive space charge field profile in-situ. Measurements of the field were compared with numerical simulations of the standard model of the photorefractive effect, and simulations of the x-ray image formation process. DTIC

N94-20214# Massachusetts Univ., Amherst. Dept. of Electrical and Computer Engineering.
INTERINJECTION-LOCKED QUASIOPTICAL POWER COMBINERS AND PHASED ARRAYS Final Report, 1 Feb. 1989 - 30 Jun. 1993
Karl D. Stephen 16 Aug. 1993 16 p
(Contract DAAL03-89-K-0034)
(AD-A271178; ARO-26599.7-EL) Avail: CASI HC A03/MF A01

Monolithic integration of microwave and millimeter-wave circuits means new techniques for using high-frequency devices in monolithic circuits must be developed. This report describes a series of several studies that address this need. A biasing technique for negative-resistance devices using a low-impedance lossy transmission line was found to be very useful in the design of planar oscillator circuits. This technique can be applied to monolithic circuits. Mutual impedance between elements in a quasioptical power combiner is often hard to calculate. A simple technique is described for obtaining this quantity experimentally. Power combining experiments and noise measurements involving resonant-tunneling diodes conclude the report. DTIC

N94-20260# Brookhaven National Lab., Upton, NY.
NATIONAL SYNCHROTRON LIGHT SOURCE USER'S MANUAL: GUIDE TO THE VUV AND X RAY BEAMLINES
N. F. Gmuer, ed. Apr. 1993 105 p
(Contract DE-AC02-76CH-00016)
(DE93-019564; BNL-48724) Avail: CASI HC A06/MF A02

The success of the National Synchrotron Light Source is based, in large part, on the size of the user community and the diversity of the scientific and technical disciplines represented by these users. As evidence of this success, the VUV Ring has just celebrated its 10th anniversary and the X-ray Ring will do the same in 1995. In order to enhance this success, the NSLS User's Manual: Guide to the VUV and X-Ray Beamlines - Fifth Edition, is being published. This manual presents to the scientific community-at-large the current and projected architecture, capabilities, and research programs of the various VUV and X-ray beamlines. Also detailed is the research and computer equipment a general user can expect to find and use at each beamline when working at the NSLS. The manual is updated periodically in order to keep pace with the constant changes on these beamlines. DOE

N94-20275# Los Alamos National Lab., NM.
NON-FERMI-LIQUID AND MULTICHANNEL KONDO PHENOMENA IN Y(1-x)U(x)Pd3 AND RELATED ALLOYS
C. L. Seaman (California Univ., San Diego, La Jolla.) and M. B. Maple (California Univ., San Diego, La Jolla.) 1993 19 p Presented at the International Conference on Strongly Correlated Electron Systems, La Jolla, CA, 16-19 Aug. 1993
(Contracts W-7405-eng-36; DE-FG03-86ER-45230)
(DE93-040135; LA-UR-93-3025; CONF-930865-6) Avail: CASI HC A03/MF A01

A brief review of experimental results which reveal non-Fermi-liquid behavior in the low temperature properties of the M(1-x)U(x)Pd3 (M = rare earth or Th) Kondo alloy system is presented. Measurements of lattice parameters, electrical resistivity, magnetic susceptibility, low temperature specific heat, and magnetic neutron scattering are compared

to predictions of the multichannel Kondo model, and are generally consistent with a two-channel spin-1/2 quadrupoler Kondo effect. Possible deviations from the model due to crystalline electric field effects, interionic interactions, disorder, and Fermi-level tuning aspects are discussed. DOE

N94-20285# Florida State Univ., Tallahassee. Supercomputer Computations Research Inst.
STUDY OF (+-)J ISING SPIN GLASSES VIA MULTICANONICAL ENSEMBLE
Tarik Celik, Ulrich H. E. Hansmann, and Bernd Berg Mar. 1993 4 p Presented at the 6th Annual Workshop on Recent Developments in Computer Simulation Studies in Condensed Matter Physics, Athens, GA, 22-26 Feb. 1993
(Contracts DE-FG05-87ER-40319; DE-FC05-85ER-25000)
(DE93-018269; CONF-9302137-1; FSU-SCRI-93-31) Avail: CASI HC A01/MF A01

The authors performed numerical simulations of 2D and 3D Edwards-Anderson spin glass models by using the recently developed multicanonical ensemble. The ergodicity times increase with the lattice size approximately as V(sup 3). The energy, entropy and other physical quantities are easily calculable at all temperatures from a single simulation. Their finite size scalings and the zero temperature limits are also explored. DOE

N94-20296# Sandia National Labs., Albuquerque, NM.
OPTICALLY CONTROLLED CURRENT FILAMENTATION IN GaAs PHOTOCONDUCTIVE SEMICONDUCTOR SWITCHES
F. J. Zutavern, A. Baca, W. D. Helgeson, H. P. Hjalmarson, G. M. Loubriel, D. L. McLaughlin, and M. W. OMalley 1993 17 p Presented at the 9th IEEE Pulsed Power Conference, Albuquerque, NM, 21-23 Jun. 1993
(Contract DE-AC04-76DP-00789)
(DE93-019427; SAND-93-1629C; CONF-930616-29) Avail: CASI HC A03/MF A01

The use of focused laser beams and fiber optics to control the location and density of current filaments in GaAs photoconductive semiconductor switches (PCSS) is described in this paper. An intensified CCD camera is used to monitor the infrared photoluminescence of the filaments during fast initiation of high gain switching for several sizes of lateral GaAs PCSS (e.g. 0.5 x 5, 1 x 5, 2.5 x 5, 2 x 30, and 15 x 20 sq mm). The switches are triggered with either a focused, mode-locked, Nd:YAG laser (532 and 1064 nm) or fiber-optically coupled semiconductor laser diodes (approximately 900 nm). The dependencies of the size, location, and density of the current filaments on the optical trigger, switch voltage, and switch current will be discussed. The impact of optically controlled current filaments on device design and lifetime is emphasized. Electro-optical switching amplification is demonstrated using the high gain switching mode of GaAs (lock-on). A single semiconductor laser diode is used to trigger a small GaAs PCSS. This PCSS is used to drive a 15-element laser diode array. Both electrical and optical pulse compression, sharpening, and amplification are achieved. Estimates for electrical and optical power gains are 8000 and 750 respectively. DOE

N94-20318 Lawrence Livermore National Lab., CA.
PHONONS AND METASTABILITY IN COMPRESSED NITROGEN
T. W. Barbee, III Aug. 1993 6 p Presented at the 14th International Conference of the International Association for the Advancement of High Pressure Science and Technology, Colorado Springs, CO, 27 Jun. - 2 Jul. 1993 Limited Reproducibility: More than 20% of this document may be affected by microfiche quality
(Contract W-7405-eng-48)
(DE93-019913; UCRL-JC-113401; CONF-930676-43) Avail: CASI HC A02

The metastability of a recently proposed candidate for a polymeric structure of nitrogen is confirmed by using linear response theory to calculate the phonon dispersion throughout the Brillouin zone. It is found that the structure is mechanically stable for pressures below at least 360 GPa. Calculations of Raman and infrared-active phonon frequencies are presented for this metastable phase, and calculations of Raman frequencies for two molecular structures are compared with experimental data. DOE

N94-20322 Los Alamos National Lab., NM.
THE GEM SILICON TRACKING SYSTEM
G. B. Mills 1993 12 p Presented at the International Symposium on Development and Application of Semiconductor Tracking Detectors, Hiroshima, Japan, 22-24 May 1993 Limited Reproducibility: More than 20% of this document may be affected by microfiche quality
(Contract W-7405-eng-36)
(DE93-040133; LA-UR-93-3022; CONF-9305267-1) Avail: CASI HC A03

The GEM Collaboration has produced a baseline design for the GEM detector. The baseline design of the GEM Silicon Tracking System (STS) is discussed in this article. Mechanical and electrical engineering progress on the GEM STS is described. Results from simulations of detector performance and the implications on engineering issues are described. DOE

N94-20323 California Univ., Berkeley. Lawrence Berkeley Lab.
STUDY OF POSSIBLE ENERGY UPGRADE FOR THE ALS AND MODELING OF THE REAL LATTICE FOR THE DIAGNOSIS OF LATTICE PROBLEMS
M. Meddahi and J. Bengtsson May 1993 6 p Presented at the International Particle Accelerator Conference, Washington, DC, 17-20 May 1993 Limited Reproducibility: More than 20% of this document may be affected by microfiche quality
(Contract DE-AC03-76SF-00098)
(DE93-040286; LBL-33225; ESG-218; CONF-930511-393) Avail: CASI HC A02

We have studied change of expected performance of the Advanced Light Source storage ring at LBL for the (design) nominal and maximum energy of 1.5 and 1.9 GeV respectively. Furthermore, we have also studied a possible increase to 2.3 GeV by modeling the change of dynamical aperture caused by saturation of the magnets. Independently, we have also modeled the beam's trajectory at injection. Comparison with bpm data from early storage ring commissioning led to the diagnosis of a major lattice error due to a short in a quadrupole, which was rectified leading to stored beam of 60 turns. DOE

N94-20335# Los Alamos National Lab., NM.
NON-FERMI LIQUID AND SPIN-GLASS BEHAVIOR OF THE Sc(1-x)U(x)Pd3 SYSTEM
D. A. Gajewski, P. Allenspach, C. L. Seaman, and M. B. Maple 1993 11 p Presented at the International Conference on Strongly Correlated Electron Systems, La Jolla, CA, 16-19 Aug. 1993
(Contracts W-7405-eng-36; DE-FG03-86ER-45230)
(DE93-040134; LA-UR-93-3024; CONF-930865-5) Avail: CASI HC A03/MF A01

Previous electrical resistivity rho(T), magnetic susceptibility chi(T), and specific heat C(T) measurements on the Y(1-x)U(x)Pd3 system have revealed Kondo behavior for 0 less than x approximately less than 0.2 and spin-glass-like behavior for 0.3 approximately less than x approximately less than 0.5. The Kondo behavior is unusual and characterized by non-Fermi liquid behavior at low temperatures T much less than T(sub K), where T(sub K) is the Kondo temperature: rho(T)/rho(0) approximately equal to 1-T/(aT(sub K)), and C(T)/T approximately equal to -(1/T(sub K))ln(T) with evidence for a finite T = 0 residual entropy S(0) = (R/2)ln(2). The authors report measurements of rho(T), chi(T), and C(T) on the Sc(1-x)U(x)Pd3 system which reveal similar Kondo, non-Fermi liquid, and spin-glass behaviors. DOE

N94-20340*# StratEdge Corp., San Diego, CA.
QUARTZ/FUSED SILICA CHIP CARRIERS Final Report
15 Jan. 1992 82 p
(Contract NAS3-25870)
(NASA-CR-194154; NAS 1.26:194154) Avail: CASI HC A05/MF A01

The primary objective of this research and development effort was to develop monolithic microwave integrated circuit (MMIC) packaging which will operate efficiently at millimeter-wave frequencies. The packages incorporated fused silica as the substrate material which was selected due to its favorable electrical properties and potential performance improvement over more conventional materials for Ka-band operation. The first step towards meeting this objective is to develop a package that meets standard mechanical and thermal requirements using fused silica and to be compatible with semiconductor devices operating up to at least 44 GHz. The second step is to modify the package design and add multilayer and multicavity capacity to allow for application specific integrated circuits (ASIC's) to

control multiple phase shifters. The final step is to adapt the package design to a phased array module with integral radiating elements. The first task was a continuation of the SBIR Phase 1 work. Phase 1 identified fused silica as a viable substrate material by demonstrating various plating, machining, and adhesion properties. In Phase 2 Task 1, a package was designed and fabricated to validate these findings. Task 2 was to take the next step in packaging and fabricate a multilayer, multichip module (MCM). This package is the predecessor to the phased array module and demonstrates the ability to via fill, circuit print, laminate, and to form vertical interconnects. The final task was to build a phased array module. The radiating elements were to be incorporated into the package instead of connecting to it with wire or ribbon bonds. Derived from text

N94-20346*# Alabama Univ., Huntsville. Center for Microgravity and Materials Research.

GROWTH OF ZINC SELENIDE SINGLE CRYSTALS BY PHYSICAL VAPOR TRANSPORT IN MICROGRAVITY Semiannual Progress Report, 1 Apr. - 1 Oct. 1993

Franz Rosenberger 1 Oct. 1993 8 p
(Grant NAG8-767)
(NASA-CR-194679; NAS 1.26:194679) Avail: CASI HC A02/MF A01

The goals of this research were the optimization of growth parameters for large (20 mm diameter and length) zinc selenide single crystals with low structural defect density, and the development of a 3-D numerical model for the transport rates to be expected in physical vapor transport under a given set of thermal and geometrical boundary conditions, in order to provide guidance for an advantageous conduct of the growth experiments. In the crystal growth studies, it was decided to exclusively apply the Effusive Ampoule PVT technique (EAPVT) to the growth of ZnSe. In this technique, the accumulation of transport-limiting gaseous components at the growing crystal is suppressed by continuous effusion to vacuum of part of the vapor contents. This is achieved through calibrated leaks in one of the ground joints of the ampoule. Regarding the PVT transport rates, a 3-D spectral code was modified. After introduction of the proper boundary conditions and subroutines for the composition-dependent transport properties, the code reproduced the experimentally determined transport rates for the two cases with strongest convective flux contributions to within the experimental and numerical error. Derived from text

N94-20348 Department of the Navy, Washington, DC.

MONOCRYSTALLINE GERMANIUM FILM ON SAPPHIRE Patent

David J. Godbey, inventor (to Navy) and Syed B. Qadri, inventor (to Navy) 27 Apr. 1993 4 p Filed 1 Jun. 1990
(AD-D015925; US-Patent-5,205,871; US-Patent-Appl-SN-531720;
US-Patent-Class-148-33.3) Avail: US Patent and Trademark Office

A monocrystalline germanium film is grown on a sapphire substrate with a (l 102) orientation. The substrate is first pretreated to restructure the (1102) surface plane. Typically, restructuring is accomplished by either an anneal at high temperature or ion bombardment. A monocrystalline germanium layer is grown on the pretreated surface by a vapor deposition process such as molecular beam epitaxy or chemical vapor deposition.
DTIC

N94-20381* National Aeronautics and Space Administration. Lewis Research Center, Cleveland, OH.

PROCESS FOR THE HOMOEPITAXIAL GROWTH OF SINGLE-CRYSTAL SILICON CARBIDE FILMS ON SILICON CARBIDE WAFERS Patent

J. Anthony Powell, inventor (to NASA) 28 Sep. 1993 7 p Filed 12 Jun. 1991 Supersedes N91-26967 (29 - 18, p 3070)
(NASA-Case-LEW-15223-1; US-Patent-5,248,385;
US-Patent-Appl-SN-718314; US-Patent-Class-156-645;
US-Patent-Class-148-33; US-Patent-Class-148-DIG.148;
US-Patent-Class-156-646; US-Patent-Class-156-662;
US-Patent-Class-156-612; US-Patent-Class-156-DIG.64) Avail: US Patent and Trademark Office

The invention is a method for growing homoepitaxial films of SiC on low tilt angle vicinal (0001) SiC wafers. The invention proposes and teaches a new theoretical model for the homoepitaxial growth of SiC films on (0001) SiC substrates. The inventive method consists of preparing the growth surface of SiC wafers slightly off-axis (from less the 0.1 to 6 deg) from the (0001) plane, subjecting the growth surface to a suitable etch, and then growing the homoepitaxial film using conventional SiC growth techniques. Official Gazette of the U.S. Patent and Trademark Office

N94-20470 Michigan Univ., Ann Arbor. Ultrafast Science Lab.

TRANSPORT IN MICROSTRUCTURES IN THE MICROWAVE AND MILLIMETER-WAVE REGIME Final Report, 1 Apr. 1990 - 31 Mar. 1993

Theodore B. Norris, John F. Whitaker, and Gerard A. Mourou 22 Oct. 1993 238 p Limited Reproducibility: More than 20% of this document may be affected by microfiche quality
(Grant AF-AFOSR-0214-90)
(AD-A271875; Rept-026845-910719; AFOSR-93-0827TR) Avail: CASI HC A11

This report summarizes the work performed during a 3-year URI program on Transport in Microstructures in the Microwave and Millimeter-Wave Regime. It describes significant achievements in both basic investigations of transport physics and in applications to high-speed electronics and optoelectronics. Fundamental advances were made in measurements of transport in semiconductors under high-field conditions. A variety of ultrafast optical and optoelectronic techniques were used to perform the most comprehensive experimental study to date of the dynamics of high-field transport in semiconductors, including the first observations of the ballistic acceleration of electrons, of field-dependent velocity overshoot, and of the dynamics of impact ionization. Carrier dynamics in low-temperature-grown (LT) semiconductors and high-critical-temperature superconductors were investigated, and optimum materials growth conditions determined. The work on LT GaAs led to significant advances in high speed electronic measurement, including electro-optic network analysis up to 300 GHz bandwidth, and novel photoconductive probes with ps response, high spatial resolution, and microvolt sensitivity. LT GaAs MSM photodetectors were developed with bandwidths up to 375 GHz and both high sensitivity and large-signal capability, representing significant improvements over the prior state of the art. Novel femtosecond lasers were developed. This made possible the development of new high speed measurement techniques.
DTIC

N94-20528* National Aeronautics and Space Administration. Marshall Space Flight Center, Huntsville, AL.

METHOD FOR CONTROLLING PROTEIN CRYSTALLIZATION Patent

David A. Noever, inventor (to NASA) 26 Oct. 1993 4 p Filed 28 Aug. 1992 Supersedes N93-17043 (31 - 5, p 1323)
(NASA-Case-MFS-28688-1; US-Patent-5,256,241;
US-Patent-Appl-SN-936376; US-Patent-Class-156-600;
US-Patent-Class-156-621; US-Patent-Class-156-622;
US-Patent-Class-422-245; US-Patent-Class-23-295R;
Int-Patent-Class-C30B-7/02) Avail: US Patent and Trademark Office

A method and apparatus for controlling the crystallization of protein by solvent evaporation including placing a drop of protein solution between and in contact with a pair of parallel plates and driving one of the plates toward and away from the other plate in a controlled manner to adjust the spacing between the plates is presented. The drop of solution forms a liquid cylinder having a height dependent upon the plate spacing thereby effecting the surface area available for solvent evaporation. When the spacing is close, evaporation is slow. Evaporation is increased by increasing the spacing between the plates until the breaking point of the liquid cylinder. One plate is mounted upon a fixed post while the other plate is carried by a receptacle movable relative to the post and driven by a belt driven screw drive. The temperature and humidity of the drop of protein solution are controlled by sealing the drop within the receptacle and mounting a heater and dessicant within the receptacle.
Official Gazette of the U.S. Patent and Trademark Office

N94-20544# California Univ., Santa Barbara. Dept. of Chemistry.

MOLECULAR AND ATOMIC ARRAYS IN NANO- AND MESOPOROUS MATERIALS SYNTHESIS

G. D. Stucky, A. Monnier, F. Schueth, Q. Huo, and D. Margolese 14 Sep. 1993 17 p Revised
(Contract N00014-90-J-1159)
(AD-A271500) Avail: CASI HC A03/MF A01

A model is presented to explain the formation and morphologies of 3-D periodic surfactant-silicate mesostructures. The structures of lamellar, hexagonal tubular and a minimal surface cubic liquid crystal/silicate phase are described.
DTIC

N94-20554 Christopher Newport Coll., Newport News, VA.
OPTICAL AND TRANSPORT PROPERTIES OF METALLIC AND SEMICONDUCTOR NANOSTRUCTURES Final Technical Report, 1 Nov. 1992 - 31 Oct. 1993
Peter A. Knipp 26 Oct. 1993 17 p Limited Reproducibility: More than 20% of this document may be affected by microfiche quality
(Contract N00014-93-1-0140)
(AD-A271716) Avail: CASI HC A03

This final technical report covers the period from 11/92 to 10/93. The principal investigator studied theoretically the optoelectronic properties of quantum wire and dot systems. These studies included lateral quantization in barrier-modulated wires, optical absorption by dots, and electron-phonon coupling in wells, wires, and dots. DTIC

N94-20558 SFA, Inc., Landover, MD.
FABRICATION AND EVALUATION OF SUPERCONDUCTING AND SEMICONDUCTING MATERIALS Final Report, 30 Sep. 1989 - 15 Jun. 1993
William Lechter Sep. 1993 23 p Limited Reproducibility: More than 20% of this document may be affected by microfiche quality
(Contract N00014-89-C-2392)
(AD-A271645; SFA-93/003) Avail: CASI HC A03

SFA provided research support to the Naval Research Laboratory Material Physics Branch by conducting investigations into the properties of superconducting, magnetic, and other solid state materials. Studies were made with an assortment of experimental techniques, including sophisticated materials preparation, magnetic resonance, electrical resistivity, magnetic susceptibility, the Mossbauer effect, and a variety of other techniques that probe the physical state of matter. SFA also aided the Material Physics Branch in conducting research into applied problems such as the design of magnetic shielding and superconducting quantum interference device (SQUID) magnetometry detection of magnetic anomalies. SFA provided research assistance in the areas of bulk ceramic sample preparation, conversion electron Mossbauer spectrometry, ultra-high vacuum thin film deposition and characterization, sputter thin film deposition, and superconducting measurements. DTIC

N94-20569# University of Southern California, Los Angeles. Dept. of Electrical Engineering.
INVESTIGATION OF HETEROJUNCTIONS AND MULTIPLE QUANTUM WELL STRUCTURES USING CRYSTALLINE ORGANIC SEMICONDUCTORS Final Report, 1 Nov. 1990 - 31 Oct. 1992
Stephen R. Forrest 12 Oct. 1993 104 p
(Grant AF-AFOSR-0075-91)
(AD-A272113; AFOSR-93-0815TR) Avail: CASI HC A06/MF A02

A new class of engineered materials based on crystalline organic semiconductors grown by the ultrahigh vacuum process of organic molecular beam deposition is described. The objective of this program is to investigate these materials and the conditions which lead to ordered growth between highly lattice mismatched van der Waals crystals into novel 'quasi-epitaxial' structures. During the first year of the program, considerable progress has been made in understanding and exploiting this new class of materials. In particular, a simple model has been developed which describes the physical mechanisms underlying quasi-epitaxy. The electrical and optical properties of both single and multiple heterojunction structures grown using alternating layers of two different, lattice-mismatched organic molecules have been investigated in detail. It is found that the layers can be grown sufficiently thin (10 A) to result in exciton confinement in organic multiple quantum wells. These and other quasi-epitaxially grown structures can load to an entirely new family of optoelectronic devices with exciting new electronic and nonlinear optical characteristics. DTIC

N94-20575# Maine Univ., Orono. Lab. for Surface Science and Technology.
DIRECT IMAGING OF THE SURFACE MICROSTRUCTURE OF DIELECTRIC MATERIALS USING AN ATOMIC FORCE MICROSCOPE Final Technical Report
W. N. Unertl and R. J. Lad 24 Sep. 1993 11 p
(AF Proj. 3487)
(AD-A272251; AFOSR-93-0823TR) Avail: CASI HC A03/MF A01

An atomic force microscope was acquired and used to study the surface properties of polymers and ceramics. Studies of polymers included nanomachining, mechanical properties, wetting behavior of latex, and metallization. Studies of ceramics included faceting of TiO2 morphology of oxide fracture surfaces, heteroepitaxial oxide film growth, and oxidation of vanadium carbide. A prototype instrument for use in ultra-high vacuum was designed. DTIC

N94-20593# Ecole Centrale de Lyon (France). Dept. de Physico-Chimie des Interfaces.
STUDY OF THE UTILIZATION OF THIN OXIDES IN INDIUM PHOSPHIDES FOR THE REALISATION OF ELECTRON COMPONENTS Ph.D. Thesis [ETUDE DE L'UTILISATION DES OXYDES MINCES SUR LE PHOSPHURE D'INDIUM POUR LA REALISATION DE COMPOSANTS ELECTRONIQUES]
Pascal Louis 1992 166 p In FRENCH
(ECL-92-38; ETN-93-94595) Avail: CASI HC A08/MF A02

Theoretical principles describing the current in a Schottky diode are reviewed. The Bardeen model is applied and the theoretical electrical noise generated by this type of diode is investigated. Experimental techniques and layer characterization methods are presented. The X-ray photoelectron spectroscopy was applied to investigate the oxide growth and composition. The anodic oxides and the role of several parameters on the electric characteristics of diodes are investigated. The electric characterization of ultraviolet oxides is carried out. A model of the diode satisfying the data acquired, especially concerning noise, is described. The results show that the characteristics of a low pressure lamp are the best ones and that they can be described by a thermionic model. ESA

N94-20598# Ecole Centrale de Lyon (France). Lab. d'Electronique.
SURFACE TREATMENT OF InP AND CONTRIBUTION TO THE OPTIMIZATION OF THE InP(p)/InP(p) REGROWN INTERFACES GROWN BY GSMBE Ph.D. Thesis [TRAITEMENTS DE SURFACE D'INP ET CONTRIBUTION A L'OPTIMISATION DES INTERFACES DE REPRISES D'EPITAXIE INP(P)/INP(P) REALISEES PAR GSMBE]
Didier Gallet 1992 262 p In ENGLISH and FRENCH
(ECL-92-48; ETN-93-94599) Avail: CASI HC A12/MF A03

The performances of optoelectronic devices fabricated by Gas Source Molecular Beam Epitaxy (GSMBE) are critically dependent on the quality of the various interfaces of the initial vertical structure. Whereas continuously grown interfaces present very high quality, interfaces obtained after growth interruption, during which various technological processes can be performed (deposition, etching, etc.), are characterized by poor electrical properties. A carrier deletion layer is generally observed at the InP(p)/InP(p) regrown interface, on top of the mesa in laser Buried Ridge heteorostructures (BRS). The properties of regrown interfaces are closely dependent on the initial surfaces properties. Therefore, they directly depend on the surface treatment quality. In order to improve the quality of regrown interfaces, four various treatments were studied: an arsenic stabilization, a passivating sulfur treatment, an encapsulating process using oxidation, and an in situ hydrogen plasma treatment. The potentiality of each treatment was evaluated by measuring the resulting electrical interface properties. The interface electrical perturbations are induced by the presence of a strong density of interface dilectronic states which pin the interface Fermi level to a position close to the minimum of the conduction and intrinsic to InP. This density is associated to damaging bonds induced by various physicochemical perturbations (impurities, phosphorus vacancies, and structural defects) which contribute to the interface disorder by perturbating the local atomic order. ESA

N94-20616# Ibis Associates, Inc., Wellesley, MA.
ANALYSIS OF COST: CVD DIAMOND DEPOSITION Quarterly Report No. 3
1993 61 p
(Contract N00014-93-C-2044)
(AD-A271980) Avail: CASI HC A04/MF A01

IBIS Associates has updated its predictive spreadsheet models of the DC arcjet and microwave chemical vapor deposition (CVD) diamond technologies. This report presents the results obtained with the new models and revised sets of baseline inputs for diamond heat sink manufacture. The cost of producing 1,000 polished diamond wafers, 1 mm thick, is estimated in the long run to be $23.70 per square centimeter by the DC arcjet deposition technology (six inch diameter), and $8.49 per square centimeter by the microwave deposition technology (sixteen inch diameter).

Fifty-one percent of the DC arcjet cost is due to the deposition step, which consumes process gases and is capital intensive. Overall, the material cost of 31.2% and labor cost of 30.2% are significant factors in the total cost. DTIC

N94-20941# Argonne National Lab., IL.
DETERMINATION OF STRUCTURE FACTORS OF COPPER BY CONVERGENT BEAM ELECTRON DIFFRACTION
J. Mansfield, M. Saunders, D. Bird, and G. Burgess Apr. 1993 4 p Presented at the Annual Meeting of the Electron Microscopy Society of America, Cincinnati, OH, 1-6 Aug. 1993
(Contract W-31-109-eng-38)
(DE93-019520; ANL/MSD/CP-79659; CONF-930822-7) Avail: CASI HC A01/MF A01

Currently there is an interest in determining structure factors from convergent beam electron diffraction (CBED) patterns; the goal is to retrieve crystal structure by inverting a CBED pattern. In this paper, the zone-axis pattern fitting technique of Bird and Saunders is used to obtain structure factors for copper. DOE

N94-20971*# Nebraska Univ., Lincoln. Center for Microelectronic and Optical Materials Research.
MATERIALS, STRUCTURES, AND DEVICES FOR HIGH-SPEED ELECTRONICS Final Report, 1 Jan. 1981 - 31 Dec. 1992
John A. Woollam and Paul G. Snyder 1993 89 p
(Grant NAG3-154)
(NASA-CR-193177; NAS 1.26:193177) Avail: CASI HC A05/MF A01

The Final Report on materials, structures, and devices for high-speed electronics is presented. Topics studied include: Si3N4 on GaAs, null ellipsometry; diamondlike carbon films; variable angle spectroscopic ellipsometer (VASE); GaAs-AlGaAs heterostructures; Ta-Cu diffusion barrier films on GaAs; GaAs-AlGaAs superlattices and multiple quantum wells; superconductivity; in situ elevated temperature measurements of III-V's; optical constants of thermodynamically stable InGaAs; doping dependence of optical constants of GaAs; in situ ellipsometric studies of III-V epitaxial growth; photo-thermal spectroscopy; micro-ellipsometry; and Si passivation and Si/SiGe strained-layer superlattices. For individual titles, see N94-20972 through N94-21014.

N94-20972*# National Aeronautics and Space Administration. Lewis Research Center, Cleveland, OH.
ELLIPSOMETRIC STUDIES OF SPUTTERED SILICON NITRIDE ON n-GaAs Abstract Only **c27**
Y. K. Peng (Nebraska Univ., Lincoln.), George H. Bu-Abbud (Nebraska Univ., Lincoln.), Samuel A. Alterovitz (Nebraska Univ., Lincoln.), John A. Woollam (Nebraska Univ., Lincoln.), B. Bayraktarogulu (Universal Energy Systems, Inc., Dayton, OH.), Dieter Langer (Air Force Avionics Lab., Wright-Patterson AFB, OH.), David C. Liu, and E. Haugland *In* Nebraska Univ., Materials, Structures, and Devices for High-Speed Electronics 1993 1 p Repr. from Journal of Vacuum Science Technology (American Vacuum Society), v. 20, no. 3, Mar. 1982 p 713 (For primary document see N94-20971 05-76)
Avail: CASI HC A01/MF A01

A method for optimizing the sensitivity of ellipsometric measurements for thin dielectric films on semiconductors is described in simple physical terms. The technique is demonstrated for the case of sputtered silicon nitride films on gallium arsenide (GaAs). Author (revised)

N94-20973*# Air Force Avionics Lab., Wright-Patterson AFB, OH.
SURFACE STATES AT THE GaAs-GERMANIUM NITRIDE INTERFACE Abstract Only **c27**
Yeung Chung, Dieter W. Langer, H. P. Singh (ITT Advanced Technology Center, Shelton, CT.), and John A. Woollam (Nebraska Univ., Lincoln.) *In* Nebraska Univ., Materials, Structures, and Devices for High-Speed Electronics 1993 1 p Repr. from Thin Solid Films (Netherlands, Elsevier Sequoia), v. 103, 1983 p 75 (For primary document see N94-20971 05-76)
Avail: CASI HC A01/MF A01

Metal/insulator/semiconductor (MIS) structures were produced by reactive sputter deposition of germanium nitride onto n-GaAs. The electrical properties of the n-GaAs-germanium nitride interface were found to exhibit a strong dependence on the deposition process parameters and the annealing conditions. The interface density evaluated from conductance and capacitance measurements was on the order of 10(exp 11) /eV-sq cm at the mid gap and was improved by annealing in a hydrogen atmosphere before and after metallization. Because of a possible excess of germanium ions near the interface a counterclockwise hysteresis in the capacitance voltage curve was observed. The dependence of germanium nitride film properties on heat treatment at different temperatures in hydrogen and nitrogen gas was studied by X-ray diffraction analysis and ellipsometric measurements. The low interface state density found using low r.f. sputtering power establishes sputtering as a competitive deposition technique. Author (revised)

N94-20974*# Nebraska Univ., Lincoln. Electrical Materials Lab.
MULTIPLE-WAVELENGTH ANGLE-OF-INCIDENCE ELLIPSOMETRY: APPLICATION TO SILICON NITRIDE-GALLIUM ARSENIDE STRUCTURES Abstract Only
George H. Bu-Abbud, Samuel A. Alterovitz, N. M. Bashara, and John A. Woollam *In its* Materials, Structures, and Devices for High-Speed Electronics 1993 1 p Repr. from Journal of Vacuum Science Technology (American Vacuum Society), v. 1, no. 2, Apr. - Jun. 1983 p 619 (For primary document see N94-20971 05-76)
Avail: CASI HC A01/MF A01

In multiple angle-of-incidence (MAI) ellipsometry, measurements are taken at m angles of incidence at a single wavelength lambda. For systems with more than two unknown parameters, a least squares approximation is used. The paper discusses the application of MAI ellipsometry to silicon nitride-gallium arsenide structures. Author (revised)

N94-20975*# National Aeronautics and Space Administration. Lewis Research Center, Cleveland, OH.
STRUCTURAL AND CHEMICAL ANALYSIS OF A SILICON NITRIDE FILM ON GaAs BY NULL ELLIPSOMETRY Abstract Only **c27**
Samuel A. Alterovitz (Nebraska Univ., Lincoln.), George H. Bu-Abbud (Nebraska Univ., Lincoln.), John A. Woollam (Nebraska Univ., Lincoln.), and David C. Liu *In* Nebraska Univ., Materials, Structures, and Devices for High-Speed Electronics 1993 1 p Repr. from Phys. Stat. Sol, v. 85, no. 69, 1984 p 69 (For primary document see N94-20971 05-76)
Avail: CASI HC A01/MF A01

Multiple-wavelength-angle-of-incidence null ellipsometry, together with the effective medium approximation, are used to evaluate both the composition and the geometrical structure of an insulating film made of silicon nitride and silicon oxide on a GaAs substrate. The results are found to be in good agreement with AES measurements on the same film. Author (revised)

N94-20976*# National Aeronautics and Space Administration. Lewis Research Center, Cleveland, OH.
THIN FILM COMPOSITIONAL ANALYSIS USING NULL OR FIXED WAVELENGTH ELLIPSOMETRY Abstract Only **c27**
Samuel A. Alterovitz (Nebraska Univ., Lincoln.), George H. Bu-Abbud (Nebraska Univ., Lincoln.), John A. Woollam (Nebraska Univ., Lincoln.), and David C. Liu *In* Nebraska Univ., Materials, Structures, and Devices for High-Speed Electronics 1993 1 p Repr. from Applied Physics Communications (Marcel Deller, Inc.), v. 4, no. 1, 1984 p 27-40 (For primary document see N94-20971 05-76)
Avail: CASI HC A01/MF A01

In this paper we show how the chemical composition of an insulating film on a semiconducting substrate can be estimated using null or fixed wavelength ellipsometry. Multiple-wavelength angle-of-incidence (MAI) ellipsometry, together with the effective medium approximation, were used to evaluate both the composition and the geometrical structure of an insulating film made of silicon nitride and silicon oxide on a GaAs substrate. The general applicability of the technique for null or fixed wavelength ellipsometers is critically assessed and compared with the more commonly used fixed-angle-of-incidence spectroscopic ellipsometric method. Author (revised)

N94-20977*# Nebraska Univ., Lincoln. Dept. of Electrical Engineering.
ANALYTIC SOLUTIONS FOR OPTIMIZED ELLIPSOMETRIC MEASUREMENTS OF INTERFACES AND SURFACE LAYERS IN THIN FILM STRUCTURES Abstract Only
Samuel A. Alterovitz, George H. Bu-Abbud, and John A. Woollam *In its*

Materials, Structures, and Devices for High-Speed Electronics 1993 1 p Repr. from Thin Solid Films (Netherlands, Elsevier Sequoia), v. 123, 1985 p 183-195 (For primary document see N94-20971 05-76)
Avail: CASI HC A01/MF A01

The maximum experimental sensitivity in ellipsometric measurements for samples that include a composite (two-layer) film on a substrate is treated with mathematical generality. A detailed theoretical computation is made for a system consisting of a moderately thick film on a substrate and including either an interface layer between the film and substrate or a thin surface layer on top of the moderately thick film. Analytical conditions for the sensitivity of p or s wave suppression are determined. For the air/SiO2/Si system a numerical calculation is performed to determine the optimum sensitivity for interfacial layer studies. Author (revised)

N94-20978*# Nebraska Univ., Lincoln. Electrical Materials Lab.
VARIABLE WAVELENGTH, VARIABLE ANGLE ELLIPSOMETRY INCLUDING A SENSITIVITIES CORRELATION TEST Abstract Only **c27**

George H. Bu-Abbud, N. M. Bashara, and John A. Woollam *In its* Materials, Structures, and Devices for High-Speed Electronics 1993 1 p Repr. from Thin Solid Films (Netherlands, Elsevier Sequoia), v. 138, 1986 p 27-41 (For primary document see N94-20971 05-76)
Avail: CASI HC A01/MF A01

By combining variable wavelength and variable angle of incidence to assess solutions of the optical parameters of a system, a procedure is developed which provides more information on the optical parameters than methods where either the wavelength or the angle of incidence is held constant. This results in a reduction in the interdependence of the optical parameters and provides for more acceptable solutions. For a film on a substrate structure, if one knows the substrate optical parameters, the thickness and optical properties of the film can be characterized at each wavelength without the need for a dispersion equation, an independent measurement of the thickness, or any special requirements on the substrate optical properties. For a nearly transparent film on an absorbing substrate, all four parameters of the three-medium model (the substrate and film refractive indices, substrate extinction coefficient, and film thickness) can be determined. If, in addition, one uses a dispersion relation for the refractive index in a very weakly absorbing film, the optical properties of an absorbing substrate and the film can be determined unambiguously. As a second major feature of this paper we show that the sensitivity correlation matrix as well as the traditional parameter correlation matrix, should be calculated if one is to determine the independence of ellipsometric parameter solutions. An SiO2 film on silicon is used for illustration, but of course the analysis is recommended for more complicated materials systems.
Author (revised)

N94-20979*# National Aeronautics and Space Administration. Lewis Research Center, Cleveland, OH.
InP MIS STRUCTURES WITH DIAMONDLIKE AMORPHOUS CARBON FILMS DEPOSITED BY ION-BEAM SPUTTERING AND FROM PLASMA Abstract Only **c27**

Jae E. Oh (Nebraska Univ., Lincoln.), Joel D. Lamb (Nebraska Univ., Lincoln.), Paul G. Snyder (Nebraska Univ., Lincoln.), John A. Woollam (Nebraska Univ., Lincoln.), and David C. Liu *In* Nebraska Univ., Materials, Structures, and Devices for High-Speed Electronics 1993 1 p Repr. from Solid-State Electronics (England, Pergamon Journals Ltd.), v. 29, no. 9, 1986 p 933-940 (For primary document see N94-20971 05-76)
Avail: CASI HC A01/MF A01

The interfacial electronic properties of diamond-like carbon on both n-InP and p-InP were studied. These measurements include conductance and capacitance versus frequency or bias voltage for metal-insulator-semiconductor structures. Carbon was deposited by both ion-beam sputtering and from an rf plasma. We find that interface electronic state densities range from 10(exp 11) to 10(exp 13) states/eV sq cm, depending on sample and preparation procedures. Normalized conductance versus frequency data show an unusual behavior, namely, two loss peaks having greatly differing voltage dependencies. We speculate on the physical origins of the two peaks. Author (revised)

N94-20980*# Nebraska Univ., Lincoln. Dept. of Electrical Engineering.
INTERFACIAL PROPERTIES OF DIAMONDLIKE AMORPHOUS CARBON FILMS ON InP: METAL-INSULATOR-SEMICONDUCTOR STRUCTURES Abstract Only **c27**

Jae E. Oh, Joel D. Lamb, Paul G. Snyder, and John A. Woollam *In its* Materials, Structures, and Devices for High-Speed Electronics 1993 1 p Repr. from Journal of Vacuum Science Technology (American Vacuum Society), v. 4, no. 3, May - Jun. 1986 p 1022 (For primary document see N94-20971 05-76)
Avail: CASI HC A01/MF A01

In this paper, we report on the interfacial properties of diamond-like carbon films deposited on polished single crystal wafers of both n- and p-type indium phosphide. Here InP was chosen over GaAs because of its advantages for MISFET applications including higher drift field velocity, potentially higher current gain cutoff frequency, and good dielectric compatibility for MIS device fabrication. Author (revised)

N94-20981*# National Aeronautics and Space Administration. Lewis Research Center, Cleveland, OH.
THIN-FILM HERMETICITY: A QUANTITATIVE ANALYSIS OF DIAMONDLIKE CARBON USING VARIABLE ANGLE SPECTROSCOPIC ELLIPSOMETRY Abstract Only **c27**

S. Orzeszko (Nicolaus Copernicus Univ., Torun, Poland.), Bhola N. De (Nebraska Univ., Lincoln.), John A. Woollam (Nebraska Univ., Lincoln.), John J. Pouch, Samuel A. Alterovitz, and David C. Ingram (Universal Energy Systems, Inc., Dayton, OH.) *In* Nebraska Univ., Materials, Structures, and Devices for High-Speed Electronics 1993 1 p Repr. from Journal of Applied Physics (American Inst. of Physics), v. 64, no. 8, 15 Oct. 1988 p 4175 (For primary document see N94-20971 05-76)
Avail: CASI HC A01/MF A01

The purpose of this paper is twofold. First, we report on the successful application of variable angle spectroscopic ellipsometry (VASE) to quantitative thin-film hermeticity evaluation. Second, it is shown that under a variety of film preparations and moisture introduction conditions water penetrates only a very thin diamond-like carbon (DLC) top surface-roughness region. Thus DLC is an excellent candidate for use as protective coatings in adverse chemical and aqueous environments. Author (revised)

N94-20982*# National Aeronautics and Space Administration. Lewis Research Center, Cleveland, OH.
VARIABLE ANGLE OF INCIDENCE SPECTROSCOPIC ELLIPSOMETRIC STUDY OF SEMICONDUCTOR MULTILAYER STRUCTURES Abstract Only

Paul G. Snyder (Nebraska Univ., Lincoln.), John A. Woollam (Nebraska Univ., Lincoln.), and Samuel A. Alterovitz *In* Nebraska Univ., Materials, Structures, and Devices for High-Speed Electronics 1993 1 p Repr. from Materials Research Society Symposium Proceedings, v. 69, 1986 p 245 (For primary document see N94-20971 05-76)
Avail: CASI HC A01/MF A01

The sensitivity of spectroscopic ellipsometry data to multilayer model parameters is shown to be a strong function of the angle of incidence. A quantitative study for a GaAs-Al(x)Ga(1-x)As-GaAs structure shows that maximum sensitivity to layer thicknesses and ternary composition occurs near the wavelength-dependent principal angle. These results are verified by experimental measurements on two MBE-grown samples. Moderately high doping levels in the ternary layers are also found to strongly affect the data at photon energies below the ternary band gap. Null ellipsometry measurements at only two wavelengths are sufficient to determine layer thicknesses. Author (revised)

N94-20983*# Nebraska Univ., Lincoln. Dept. of Electrical Engineering.
ELLIPSOMETRIC MEASUREMENTS OF MOLECULAR-BEAM-EPITAXY-GROWN SEMICONDUCTOR MULTILAYER THICKNESSES: A COMPARATIVE STUDY Abstract Only **c27**

John A. Woollam, Paul G. Snyder, Anthony W. McCormick (Universal Energy Systems, Inc., Dayton, OH.), A. K. Rai (Universal Energy Systems, Inc., Dayton, OH.), David C. Ingram (Universal Energy Systems, Inc., Dayton, OH.), and Peter P. Pronko (Universal Energy Systems, Inc., Dayton, OH.) *In its* Materials, Structures, and Devices for High-Speed Electronics 1993 1 p Repr. from Journal of Applied Physics (American Inst. of Physics), v. 62, no. 12, 15 Dec. 1987 p 4867 (For primary document see

N94-20971 05-76)
Avail: CASI HC A01/MF A01

Variable angle of incidence spectroscopic ellipsometry, cross-sectional transmission electron microscopy, and Rutherford backscattering are used to measure heterojunction layer thickness in the same AlGaAs/GaAs sample. All three techniques yield the same thickness values within error limits. Two additional samples were implanted with 750-keV Ga ions to fluences of 5 x 10(exp 15) and 10(exp 16)/sq cm, respectively, and results of diagnostics measurements by the three techniques are compared. The three techniques are found to complement each other in providing useful information. Author (revised)

N94-20984*# Nebraska Univ., Lincoln. Dept. of Electrical Engineering.
COMPARATIVE THICKNESS MEASUREMENTS OF HETEROJUNCTION LAYERS BY ELLIPSOMETRIC, RBS, AND XTEM ANALYSIS Abstract Only **c27**
John A. Woollam, Paul G. Snyder, Anthony W. McCormick (Universal Energy Systems, Inc., Dayton, OH.), A. K. Rai (Universal Energy Systems, Inc., Dayton, OH.), David C. Ingram (Universal Energy Systems, Inc., Dayton, OH.), Peter P. Pronko (Universal Energy Systems, Inc., Dayton, OH.), and J. J. Geddes (Honeywell, Inc., Bloomington, MN.) *In its* Materials, Structures, and Devices for High-Speed Electronics 1993 1 p Repr. from Materials Research Society Symposium Proceedings, v. 77, 1987 p 755 Sponsored in part by Naval Air Systems Command (For primary document see N94-20971 05-76)
Avail: CASI HC A01/MF A01

Variable Angle of incidence Spectroscopic Ellipsometry (VASE), Rutherford Backscattering (RBS), and Cross-sectional Transmission Electron Microscopy (XTEM) are used to measure heterojunction layer thicknesses in an AlGaAs/GaAs sample. All three techniques yield the same thickness values within error limits. Author

N94-20985*# National Aeronautics and Space Administration. Lewis Research Center, Cleveland, OH.
CHARACTERIZATION OF MULTILAYER GaAs/AlGaAs TRANSISTOR STRUCTURES BY VARIABLE ANGLE SPECTROSCOPIC ELLIPSOMETRY Abstract Only **c33**
Kenneth G. Merkel (Air Force Wright Aeronautical Labs., Wright-Patterson AFB, OH.), Paul G. Snyder (Nebraska Univ., Lincoln.), John A. Woollam (Nebraska Univ., Lincoln.), Samuel A. Alterovitz, and A. K. Rai (Universal Energy Systems, Inc., Dayton, OH.) *In* Nebraska Univ., Materials, Structures, and Devices for High-Speed Electronics 1993 1 p Repr. from Japanese Journal of Applied Physics, v. 28, no. 6, Jun. 1989 (For primary document see N94-20971 05-76)
Avail: CASI HC A01/MF A01

Variable angle of incidence spectroscopic ellipsometry (VASE) has been implemented as a means of determining layer thickness alloy composition and growth quality of GaAs/AlGaAs samples composed of relatively thick layers as well as superlattices. The structures studied in this work contained GaAs/AlGaAs multilayers with a superlattice 'barrier' and were grown for later formation of modulation-doped field effect transistors (MODFET's). Sample modeling was performed by treating the superlattice as a bulk AlGaAs layer of unknown composition. Extremely good data fits were realized when five layer thicknesses and two alloy ratios were allowed to vary in a regression analysis. Room temperature excitonic effects associated with the e-hh(1) e-lh(1) and e-hh(2) transitions were observed in the VASE data. Author

N94-20986*# Nebraska Univ., Lincoln. Center for Microelectronic and Optical Materials Branch.
VARIABLE ANGLE SPECTROSCOPIC ELLIPSOMETRIC CHARACTERIZATION OF SURFACE DAMAGE IN CHEMICAL-MECHANICAL POLISHED GaAs Abstract Only **c27**
Yi-Ming Xiong and Paul G. Snyder *In its* Materials, Structures, and Devices for High-Speed Electronics 1993 1 p Repr. from Thin Solid Films (Elsevier Sequoia), v. 220, 1992 p 303-310 (For primary document see N94-20971 05-76)
Avail: CASI HC A01/MF A01

Variable angle spectroscopic ellipsometry (VASE) was applied to the quantitative characterization of surface and subsurface damage in GaAs, induced by conventional chemical-mechanical (CM) polishing. We show that the optimum selection of angle of incidence (75 degrees) and spectral range (greater than or equal to 430 nm) is of crucial importance for detecting and evaluating surface and subsurface quality. The measured VASE data from 249 to 789 nm were analyzed with several fitting models. A two-layer model, with a GaAs oxide over layer on a subsurface layer on a GaAs substrate, was found consistently to yield the best fits, suggesting the presence of subsurface damage in CM polished GaAs. In the model calculations, each composite layer was assumed, in the Bruggeman effective medium approximation, to be a simple physical mixture of the chosen constituents. The fitting results indicate that, typically, the thickness values were 2-3 nm of oxide overlayer and 15-40 nm of subsurface damage beneath it, consisting of about 1 percent-2 percent reduction in density. Independent atomic force microscopy (for surface characterization) and x-ray diffraction (for subsurface characterization) measurements were also made, for comparison with the VASE results. Consistent agreement was found. Author (revised)

N94-20987*# Nebraska Univ., Lincoln. Dept. of Electrical Engineering.
VARIABLE ANGLE OF INCIDENCE SPECTROSCOPIC ELLIPSOMETRIC MEASUREMENT OF THE FRANZ-KELDYSH EFFECT IN MODFET STRUCTURES Abstract Only
Paul G. Snyder, Jae E. Oh, and John A. Woollam *In its* Materials, Structures, and Devices for High-Speed Electronics 1993 1 p Repr. from Materials Research Society Symposium Proceedings, v. 77, 1987 p 761 (For primary document see N94-20971 05-76)
Avail: CASI HC A01/MF A01

It has been shown recently that variable angle-of-incidence spectroscopic ellipsometry (VASE) is a sensitive technique for determining semiconductor multilayer model parameters, e.g. layer thicknesses and ternary compositions. In this paper, we show that VASE is in addition sensitive to the Franz-Keldysh effect induced by band bending in the barrier layer of a GaAs-AlGaAs-GaAs (MODFET) structure. VASE measurements differ from electroreflectance and photoreflectance in that the internal heterojunction region electric field is directly probed without the application of a modulating field. The Franz-Keldysh effect appears in the VASE spectra near the AlGaAs band gap energy. Data for two samples with different doping profiles are quantitatively modeled to determine the internal electric field amplitudes. Author (revised)

N94-20988*# Nebraska Univ., Lincoln. Dept. of Electrical Engineering.
ELLIPSOMETRIC ANALYSIS OF BUILT-IN ELECTRIC FIELDS IN SEMICONDUCTOR HETEROSTRUCTURES Abstract Only **c33**
Paul G. Snyder, Jae E. Oh, John A. Woollam, and R. E. Owens (Colorado State Univ., Fort Collins.) *In its* Materials, Structures, and Devices for High-Speed Electronics 1993 1 p Repr. from Appl. Phys. Lett. (American Inst. of Physics), v. 51, no. 10, 7 Sep. 1987 p 770 (For primary document see N94-20971 05-76)
Avail: CASI HC A01/MF A01

Measurements of Franz-Keldysh (FK) effects in GaAs-Al(x)Ga(1-x)As heterostructures by variable angle of incidence spectroscopic ellipsometry are reported. The measured FK effects are due to the built-in band bending at the surface and heterointerfaces, with no externally applied bias or modulating voltage. The polarity of the FK line shape indicates whether the field is uniform or nonuniform (inhomogeneous) in the direction along the growth axis, while the line width is determined by the peak field strength. This information can be used to characterize the doping concentration in the Al(x)Ga(1-x)As layer. Author (revised)

N94-20989*# Nebraska Univ., Lincoln. Dept. of Electrical Engineering.
OPTICAL MEASUREMENT OF BUILT-IN AND APPLIED ELECTRIC FIELDS IN Al(x)Ga(1-x)As/GaAs HETEROSTRUCTURES Abstract Only **c33**
Paul G. Snyder, Kenneth G. Merkel, and John A. Woollam *In its* Materials, Structures, and Devices for High-Speed Electronics 1993 1 p Repr. from Spectroscopic Characterization Techniques for Semiconductor Technology 3 (Bellingham, WA, Society of Photo-Optical Instrumentation Engineers), v. 946, 1988 p 98 (For primary document see N94-20971 05-76)
Avail: CASI HC A01/MF A01

Variable angle spectroscopic ellipsometry (VASE) is used to study the built-in electric fields in Al(x)Ga(1-x)As/GaAs heterostructures. VASE data, obtained with no electrical contacts on the sample, contain Franz-Keldysh (FK) line shapes at the AlGaAs band gap energy, which are due to the

built-in field across the buried AlGaAs layer. Analysis of the line shapes, using the FK theory together with a multilayer model, yields the approximate field profile in the layer. This, combined with a numerical solution of Poisson's equation, provides the approximate doping concentration. In addition, measurements made on samples with electrical contacts are described.
Author

N94-20990*# National Aeronautics and Space Administration. Lewis Research Center, Cleveland, OH.
HIGH TEMPERATURE STABILITY OF AMORPHOUS Ta(x)Cu(1-x) DIFFUSION BARRIERS ON GaAs Abstract Only
Jae E. Oh (Nebraska Univ., Lincoln.), John J. Pouch, David C. Ingram (Universal Energy Systems, Inc., Dayton, OH.), Samuel A. Alterovitz, and John A. Woollam (Nebraska Univ., Lincoln.) *In* Nebraska Univ., Materials, Structures, and Devices for High-Speed Electronics 1993 1 p Repr. from Materials Research Society Symposium Proceedings, v. 77, 1987 p 563 (For primary document see N94-20971 05-76)
Avail: CASI HC A01/MF A01

The x value of the most thermally stable co-sputtered Ta(x)Cu(1-x) alloy films are found to correlate with measured maximum temperature coefficients of resistance as a function of alloy composition. To investigate the possible application of these materials as diffusion barriers for the AuGaAs system vacuum, annealing and infrared rapid thermal annealing are made over a wide temperature range. Resistivity changes, x-ray diffraction, Auger electron spectroscopy, and Rutherford backscattering measurements are performed to find the metallurgical stabilities of these materials at elevated temperatures. For high x values the reaction temperature for Ta(x)Cu(1-x) in contact with GaAs lies between 5OO and 700 C. For Au in contact with Ta(x)Cu(1-x), the Ta(x)Cu(1-x)/GaAs reaction occurs at about 600 C. Amorphous Ta93Cu7 exhibits uniform mixing with surrounding elements whereas Ta80Cu20 exhibits phase separation.
Author (revised)

N94-20991*# National Aeronautics and Space Administration. Lewis Research Center, Cleveland, OH.
AMORPHOUS Ta-RICH Ta-Cu FILMS AS DIFFUSION BARRIERS BETWEEN Au AND GaAs Abstract Only **c27**
Jae E. Oh (Nebraska Univ., Lincoln.), John A. Woollam (Nebraska Univ., Lincoln.), John J. Pouch, Samuel A. Alterovitz, and David C. Ingram (Universal Energy Systems, Inc., Dayton, OH.) *In* Nebraska Univ., Materials, Structures, and Devices for High-Speed Electronics 1993 1 p Repr. from Journal of Vacuum Science Technology (American Vacuum Society), v. 6, no. 3, May - Jun. 1988 p 825 (For primary document see N94-20971 05-76)
Avail: CASI HC A01/MF A01

The thermal stability of alloy films in the cosputtered amorphous Ta-Cu alloy systems have been found to be correlated with the measured maximum negative temperature coefficients of resistance as a function of alloy composition. From results of resistivity changes, x-ray diffraction, Auger electron spectroscopy, and Rutherford backscattering, reaction temperatures of Ta93Cu7 alloy films with Au overlayers and GaAs substrates were determined to be 600 and 700 C, respectively. Electrical measurements were performed with Schottky diodes formed on n-type GaAs. Amorphous Ta93Cu7/GaAs Schottky diodes were found to be electrically stable up to annealing temperatures of 400 C. Also rapid thermal annealing was applied to capitalize on its short processing time for possible application to self-aligned gate technology using this material.
Author

N94-20992*# Nebraska Univ., Lincoln. Dept. of Electrical Engineering.
MEASUREMENT OF SUPERLATTICE OPTICAL PROPERTIES BY VARIABLE ANGLE SPECTROSCOPIC ELLIPSOMETRY Abstract Only
Paul G. Snyder, Bhola N. De, Kenneth G. Merkel, John A. Woollam, Dieter W. Langer (Air Force Avionics Lab., Wright-Patterson AFB, OH.), C. E. Stutz (Air Force Avionics Lab., Wright-Patterson AFB, OH.), R. Jones (Air Force Avionics Lab., Wright-Patterson AFB, OH.), A. K. Rai (Universal Energy Systems, Inc., Dayton, OH.), and K. Evans (Universal Energy Systems, Inc., Dayton, OH.) *In its* Materials, Structures, and Devices for High-Speed Electronics 1993 1 p Repr. from Superlattices and Microstructures (Academic Press Ltd.), v. 4, no. 1, 1988 p 97 (For primary document see N94-20971 05-76)
Avail: CASI HC A01/MF A01

Variable angle of incidence spectroscopic ellipsometry is a sensitive nondestructive technique for determining optical constants, layer thicknesses, microstructure and other parameters. We have applied this technique to the study of AlAs-GaAs and Al(x)Ga(1-x)As-GaAs superlattices. For a sample with Al(0.5)Ga(0.5)As barrier layers and 20 periods, sharp spectroscopic features were observed at the first electron to heavy hole, e-hh(1), first electron to light hole, e-lh(1), and second electron to heavy hole, e-hh(2) transition energies. Cross sectional transmission electron microscopy (XTEM) showed this superlattice to be of good quality. Ellipsometric data for two other samples with AlAs barriers did not contain any sharp features due to quantized level transitions and XTEM of these samples revealed poor quality superlattice structure. An advantage of ellipsometry is that the complex refractive index can be obtained without Kramers-Kronig analysis. The effective refractive index for a 20 period superlattice was solved using ellipsometric data at three angles of incidence near 74 degrees. The real part is increased by about 2 percent at the e-hh(1) peak and the imaginary part (extinction coefficient) is increased by 0.05.
Author

N94-20993*# Nebraska Univ., Lincoln. Dept. of Electrical Engineering.
SUPERLATTICE OPTICAL PROPERTIES MEASURED BY VARIABLE ANGLE SPECTROSCOPIC ELLIPSOMETRY Abstract Only
Paul G. Snyder, Kenneth G. Merkel, Bhola N. De, John A. Woollam, Dieter W. Langer (Pittsburgh Univ., PA.), C. E. Stutz (Air Force Avionics Lab., Wright-Patterson AFB, OH.), R. Jones (Air Force Avionics Lab., Wright-Patterson AFB, OH.), A. K. Rai (Universal Energy Systems, Inc., Dayton, OH.), and K. Evans (Universal Energy Systems, Inc., Dayton, OH.) *In its* Materials, Structures, and Devices for High-Speed Electronics 1993 1 p Repr. from Materials Research Society Symposium, v. 102, 1988 p 165 (For primary document see N94-20971 05-76)
Avail: CASI HC A01/MF A01

Variable Angle of incidence Spectroscopic Ellipsometry (VASE) is a sensitive, nondestructive method of determining optical constants, layer thicknesses, alloy compositions and other parameters. We model the VASE data for a sample containing a 20 period Al(0.5)Ga(0.5)As-GaAs superlattice, to obtain the effective index of refraction (n) and extinction coefficient (k) of the superlattice layer. The room temperature VASE spectra contain strong, sharp features at the e-hh(1), e-lh(1) and e-hh(2) excitonic transition energies. In addition, VASE was used to characterize more complicated layered structures, which also contained superlattices.
Author

N94-20994*# National Aeronautics and Space Administration. Lewis Research Center, Cleveland, OH.
GaAs/AlGaAs SUPERLATTICE CHARACTERIZATION BY VARIABLE ANGLE SPECTROSCOPIC ELLIPSOMETRY Abstract Only
Kenneth G. Merkel (Nebraska Univ., Lincoln.), Paul G. Snyder (Nebraska Univ., Lincoln.), John A. Woollam (Nebraska Univ., Lincoln.), and Samuel A. Alterovitz *In* Nebraska Univ., Materials, Structures, and Devices for High-Speed Electronics 1993 1 p Repr. from Spectroscopic Characterization Techniques for Semiconductor Technology 3 (Bellingham, WA, Society of Photo-Optical Instrumentation Engineers), v. 946, 1988 p 105 (For primary document see N94-20971 05-76)
Avail: CASI HC A01/MF A01

Variable angle of incidence spectroscopic ellipsometry (VASE) was used to determine the thickness, alloy composition, and growth quality of multilayer samples. These samples contained a single quantum well grown on a GaAs/AlGaAs superlattice. The superlattice layers were modeled as a bulk AlGaAs layer of unknown composition and thickness. A data fitting procedure allowed the variation of five layer thicknesses and two alloy compositions in a regression analysis. Extremely good data fits of the ellipsometric parameters Psi and Delta were realized in the 1.55 to 3.54 eV spectral range. Computer generations of the ellipsometric parameters were performed, and were compared with experimental results. The e-hh(1), e-lh(1), and e-hh(2) exciton transitions were observed in the VASE data measured at room temperature. VASE has thus provided a nondestructive and highly effective technique for characterizing intricate multilayered structures.
Author

N94-20995*# Nebraska Univ., Lincoln. Dept. of Electrical Engineering.
CHARACTERIZATION OF AN ASYMMETRIC TRIANGULAR MULTIPLE QUANTUM WELL, BY VARIABLE ANGLE SPECTROSCOPIC ELLIPSOMETRY Abstract Only
Craig M. Herzinger, Paul G. Snyder, John A. Woollam, Keith Evans (Universal Energy Systems, Inc., Dayton, OH.), C. E. Stutz (Wright Research

Development Center, Wright-Patterson AFB, OH.), R. Jones (Wright Research Development Center, Wright-Patterson AFB, OH.), Kenneth G. Merkel (Wright Research Development Center, Wright-Patterson AFB, OH.), and D. C. Reynolds (Wright State Univ., Dayton, OH.) *In its* Materials, Structures, and Devices for High-Speed Electronics 1993 1 p Repr. from Materials Research Society Symposium Proceedings, v. 160, 1990 p 719 (For primary document see N94-20971 05-76)
Avail: CASI HC A01/MF A01

Variable angle spectroscopic ellipsometry (VASE) was used to characterize a 20 period GaAs/Al(x)Ga(1-x)As multiple quantum well structure grown by molecular beam epitaxy. The barriers were nominally 200A. Al(.25)Ga(.75)As and the well regions were grown to approximate a linearly graded composition, from x = 0 to x = 0.25, with total well width 200 A. VASE data in the E(sub 1), E(sub 1) + Delta(sub 1) region were analyzed using four different models. It was found that the dielectric function of the cap GaAs layer was shifted to higher energy with respect to the bulk GaAs dielectric function. Author

N94-20996*# Nebraska Univ., Lincoln. Dept. of Electrical Engineering.
POLARIZED-LIGHT REFLECTION MODE p-i-n MODULATORS WITH GaAs/AlGaAs MULTIPLE QUANTUM WELL ACTIVE LAYERS: DESIGN AND SIMULATION
Craig M. Herzinger and Paul G. Snyder *In its* Materials, Structures, and Devices for High-Speed Electronics 1993 1 p Repr. from Proceedings of the Second International Conference on Elec. Mats. (Materials Research Society), 1990 p 351 (For primary document see N94-20971 05-76)
Avail: CASI HC A01/MF A01

Recent developments in normal-incidence reflection mode modulators are extended in this investigation to the design and simulation of oblique-incidence polarized light modulators. The active element in the design is a 1OOA GaAs quantum well between Al(.3)Ga(.7)As barriers. A model for the optical properties of the quantum well is developed that accounts for quantum confinement, Stark shifts, excitons, and inhomogeneous broadening. Results of a simulation for an oblique-incidence intensity modulator, with two different input polarizations, are presented.
Author

N94-20997*# Nebraska Univ., Lincoln. Dept. of Electrical Engineering.
GaAs(100) SURFACE MODIFICATIONS AT ELEVATED TEMPERATURES, STUDIED BY IN-SITU SPECTROSCOPIC ELLIPSOMETRY Abstract Only
Huade D. Yao, Paul G. Snyder, and John A. Woollam *In its* Materials, Structures, and Devices for High-Speed Electronics 1993 1 p Repr. from Materials Research Society Symposium Proceedings, v. 202, 1991 p 339 (For primary document see N94-20971 05-76)
Avail: CASI HC A01/MF A01

Spectroscopic ellipsometric (SE) measurements of GaAs (100) were carried out in an ultrahigh vacuum (UHV) chamber, without arsenic over pressure, at temperatures ranging from room temperature (RT) to approximately 610 C. Surface changes induced at elevated temperatures were monitored by in-situ spectroscopic ellipsometry. The SE data clearly displayed in real time the process of desorption of the GaAs-surface-oxide overlayer at approximately 580 C. In addition, changes in the near-surface region were observed before and after the oxide desorption. The near-subsurface region (top 50-100 A) became less optically dense after being heated to 540 C or higher. For comparison, a pre-arsenic-capped molecular-beam-epitaxy (MBE)-grown GaAs surface was also studied. After the arsenic cap was evaporated off at approximately 350 C, this surface remained smooth and clean as it was heated to higher temperatures.
Author

N94-20998*# Nebraska Univ., Lincoln. Dept. of Electrical Engineering.
ELLIPSOMETRIC STUDY OF GaAs(100) SURFACE CHANGES INDUCED AT ELEVATED TEMPERATURES Abstract Only
Huade D. Yao, Paul G. Snyder, and John A. Woollam *In its* Materials, Structures, and Devices for High-Speed Electronics 1993 1 p Repr. from Proceedings of the Second International Conference on Elec. Mats (Materials Research Society), 1990 p 501 (For primary document see N94-20971 05-76)
Avail: CASI HC A01/MF A01

GaAs (100) samples were heated to temperatures as high as approximately 610 C in an ultrahigh vacuum (UHV) chamber without arsenic overpressure. In situ spectroscopic ellipsometry (SE) was used to monitor the surface changes induced at elevated temperatures. The SE measurements clearly displayed in real time the process of desorption of the GaAs-surface-oxide layer. In addition, the character of the near-subsurface region (top 50-100 A) was observed to change, apparently becoming less dense when heated to approximately 550 C or higher. The SE data also suggest that moisture is present in and on top of the oxide layer of a sample that has been exposed to air, and that the moisture desorbs in vacuum.
Author

N94-20999*# Nebraska Univ., Lincoln. Dept. of Electrical Engineering.
TEMPERATURE DEPENDENCE OF OPTICAL PROPERTIES OF AlAs, STUDIED BY IN-SITU SPECTROSCOPIC ELLIPSOMETRY Abstract Only
Huade D. Yao, Paul G. Snyder, Kathleen Stair (Amoco Oil Co., Naperville, IL.), and Thomas Bird (Amoco Oil Co., Naperville, IL.) *In its* Materials, Structures, and Devices for High-Speed Electronics 1993 1 p Repr. from Materials Research Society Symposium Proceedings, v. 242, 1992 p 481 (For primary document see N94-20971 05-76)
Avail: CASI HC A01/MF A01

The dielectric functions epsilon = epsilon(sub 1) + i(epsilon(sub 2)) of AlAs were determined from 1.5 eV to 5.0 eV, by spectroscopic ellipsometry (SE), from room temperature (RT) to approximately 577 C in an ultrahigh vacuum (UHV) chamber. Molecular beam epitaxy (MBE)-grown AlAs was covered by a thin GaAs layer, which was passivated by arsenic capping to prevent oxidation. The arsenic cap was desorbed inside the UHV chamber. SE measurements of the unoxidized sample were made at various temperatures. Temperature dependent optical constants of AlAs were obtained by mathematically removing the effects of the GaAs cap and substrate. Quantitative analyses of the variations of critical-point energies with temperature, by using the harmonic oscillator approximation (HOA), indicate that the E(sub 1) and E(sub 1) + Delta(sub 1) energies decrease approximately 350 MeV as temperature increases from RT to 500 C.
Author (revised)

N94-21000*# National Aeronautics and Space Administration. Lewis Research Center, Cleveland, OH.
DIELECTRIC FUNCTION OF InGaAs IN THE VISIBLE Abstract Only
Samuel A. Alterovitz, R. E. Sieg (Cleveland State Univ., OH.), Huade D. Yao (Nebraska Univ., Lincoln.), Paul G. Snyder (Nebraska Univ., Lincoln.), John A. Woollam (Nebraska Univ., Lincoln.), J. Pamulapati (Michigan Univ., Ann Arbor.), P. K. Bhattacharya (Michigan Univ., Ann Arbor.), and P. A. Sekula-Moise (Spire Corp., Bedford, MA.) *In* Nebraska Univ., Materials, Structures, and Devices for High-Speed Electronics 1993 1 p Repr. from Proceedings of the Second International Conference on Elec. Mats. (Materials Research Society), 1990 p 187 (For primary document see N94-20971 05-76)
Avail: CASI HC A01/MF A01

For the first time, measurements of the dielectric function of thermodynamically stable In(x)Ga(1-x)As in the composition range 0.3 less than or equal to x less than or equal to 0.7 are reported. The optically thick samples of InGaAs were made by molecular beam epitaxy (MBE) in the range 0.4 less than or equal to x less than or equal to 0.7 and by metal-organic chemical vapor deposition (MOCVD) for x = 0.3. The MBE made samples, usually 1 micron thick, were grown on semi-insulating InP and included a strain release structure. The MOCVD sample was grown on GaAs and was 2 microns thick. The dielectric functions were measured by variable angle spectroscopic ellipsometry in the range 1.55 eV to 4.4 eV. The data was analyzed assuming an optically thick InGaAs material with an oxide layer on top. The thickness of this layer was estimated by comparing our results for the InP lattice matched material, i.e. x = 0.53, with results published in the literature. The top oxide layer was removed mathematically for x = 0.3 and x = 0.53 to get the dielectric function of the bare InGaAs. In addition, the dielectric function of GaAs in vacuum, after a protective arsenic layer was removed, was measured. Our dielectric functions for x = 0, 0.3, and 0.53 were used together with the x = 1 result from the literature to evaluate an algorithm for calculating the dielectric function of InGaAs for an arbitrary value of x (0 less than or equal to x less than or equal to 1). Results of the dielectric function calculated using the algorithm were compared with experimental data. Author (revised)

N94-21001*# National Aeronautics and Space Administration. Lewis Research Center, Cleveland, OH.

STUDY OF InGaAs-BASED MODULATION DOPED FIELD EFFECT TRANSISTOR STRUCTURES USING VARIABLE-ANGLE SPECTROSCOPIC ELLIPSOMETRY Abstract Only **c33**

Samuel A. Alterovitz, R. M. Sieg (Cleveland State Univ., OH.), Huade D. Yao (Nebraska Univ., Lincoln.), Paul G. Snyder (Nebraska Univ., Lincoln.), John A. Woollam (Nebraska Univ., Lincoln.), J. Pamulapati (Michigan Univ., Ann Arbor.), P. K. Bhattacharya (Michigan Univ., Ann Arbor.), and P. A. Sekula-Moise (Spire Corp., Bedford, MA.) *In* Nebraska Univ., Materials, Structures, and Devices for High-Speed Electronics 1993 1 p Repr. from Thin Solid Films (Lausanne, Switzerland, Elsevier Sequoia), v. 206, 1991 p 288-293 (For primary document see N94-20971 05-76)

Avail: CASI HC A01/MF A01

Variable-angle spectroscopic ellipsometry was used to estimate the thicknesses of all layers within the optical penetration depth of InGaAs-based modulation doped field effect transistor structures. Strained and unstrained InGaAs channels were made by molecular beam epitaxy (MBE) on InP substrates and by metal-organic chemical vapor deposition on GaAs substrates. In most cases, ellipsometrically determined thicknesses were within 10 percent of the growth-calibration results. The MBE-made InGaAs strained layers showed large strain effects, indicating a probable shift in the critical points of their dielectric function toward the InP lattice-matched concentration. Author (revised)

N94-21002*# Nebraska Univ., Lincoln. Dept. of Electrical Engineering.

STUDY OF CONCENTRATION-DEPENDENT DIELECTRIC PROPERTIES OF n-TYPE GaAs USING VARIABLE ANGLE SPECTROSCOPIC ELLIPSOMETRY Abstract Only

Paul G. Snyder and Yi-Ming Xiong *In its* Materials, Structures, and Devices for High-Speed Electronics 1993 1 p Repr. from Surface and Interface Analysis, v. 18, 1992 p 107-112 (For primary document see N94-20971 05-76)

Avail: CASI HC A01/MF A01

The dielectric function epsilon spectra of Si-doped n-type GaAs crystals at room temperature (296 K) were determined between 1.53 and 5.01 eV, using variable angle spectroscopic ellipsometry (VASE). Samples with carrier concentrations ranging from 4.6 x 10(exp 17) to 3.3 x 10(exp 18) cm(sup -3) were measured. The effects of surface microscopic roughness, native oxide overlayer and the subsurface damage were mathematically removed with an appropriate multilayer model. The GaAs dielectric function spectra were modeled using the sum of seven harmonic oscillators, whose center energies, half-widths, and amplitudes were fitting parameters in the multilayer model. It was found that as the doping level increased, the E(sub 1) and E(sub 1) + Delta(sub 1), peak structures near 3 eV in the epsilon(sub 2) spectrum broadened considerably more than the E(sub 0)(sup prime) and E(sub 2) peak structures near 4.7 eV, while the amplitude of the E(sub 1) peak decreased with respect to that of the E(sub 1) + Delta(sub 1) peak. Other effects due to doping were a shift of the epsilon(sub 2) spectrum towards lower energies and a decrease in the amplitude of the E(sub 2) peak. Author (revised)

N94-21003*# Woollam (John A.) Co., Lincoln, NE.

IN-SITU SPECTROSCOPIC ELLIPSOMETRY FOR REAL TIME SEMICONDUCTOR GROWTH MONITOR Abstract Only

Blaine Johs, Duane Meyer, Gerald T. Cooney, Huade D. Yao (Nebraska Univ., Lincoln.), Paul G. Snyder (Nebraska Univ., Lincoln.), John A. Woollam (Nebraska Univ., Lincoln.), John L. Edwards (Arizona State Univ., Tempe.), and George N. Maracas (Arizona State Univ., Tempe.) *In* Nebraska Univ., Materials, Structures, and Devices for High-Speed Electronics 1993 1 p Repr. from Materials Research Society Symposium Proceedings, v. 216, 1991 p 459 (For primary document see N94-20971 05-76)

(Contracts DAAH01-89-C-0357; N00014-89-J-3120)

Avail: CASI HC A01/MF A01

A modular spectroscopic ellipsometer for in situ and ex situ materials analysis is described, and results for in situ Molecular Beam Epitaxy (MBE) growth of GaAs/AlGaAs are reported. Author (revised)

N94-21004*# Woollam (John A.) Co., Lincoln, NE.

REAL-TIME ANALYSIS OF IN-SITU SPECTROSCOPIC ELLIPSOMETRIC DATA DURING MBE GROWTH OF III-V SEMICONDUCTORS

Blaine Johs, John L. Edwards (Arizona State Univ., Tempe.), K. T. Shiralagi (Arizona State Univ., Tempe.), R. Droopad (Arizona State Univ., Tempe.), K. Y. Choi (Arizona State Univ., Tempe.), George N. Maracas (Arizona State Univ., Tempe.), Duane Meyer, Gerald T. Cooney, and John A. Woollam *In* Nebraska Univ., Materials, Structures, and Devices for High-Speed Electronics 1993 1 p (For primary document see N94-20971 05-76)

(Contract DAAH01-89-C-0357)

Avail: CASI HC A01/MF A01

A modular spectroscopic ellipsometer, capable of both in-situ and ex-situ operation, was used to measure important growth parameters of GaAs/AlGaAs structures. The ex-situ measurements provided layer thicknesses and compositions of the grown structures. In-situ ellipsometric measurements allowed the determination of growth rates, layer thicknesses, and high temperature optical constants. By performing a regression analysis of the in-situ data in real-time, the thickness and composition of an AlGaAs layer were extracted during the molecular beam epitaxy (MBE) growth of the structure. Author (revised)

N94-21005*# Arizona State Univ., Tempe. Dept. of Electrical Engineering.

IN-SITU SPECTROSCOPIC ELLIPSOMETRY IN MOLECULAR BEAM EPITAXY Abstract Only

George N. Maracas, John L. Edwards, K. Shiralagi, K. Y. Choi, R. Droopad, Blaine Johs (Woollam, John A. Co., Lincoln, NE.), and John A. Woollam (Woollam, John A. Co., Lincoln, NE.) *In* Nebraska Univ., Materials, Structures, and Devices for High-Speed Electronics 1993 1 p Repr. from Journal of Vacuum Science Technology (American Vacuum Society), v. 10, no. 4, Jul. - Aug. 1992 p 1832 (For primary document see N94-20971 05-76)

Avail: CASI HC A01/MF A01

Noninvasive, real-time material growth monitoring is becoming increasingly important as epitaxial layer structures become more complex and the thickness and alloy composition tolerances are reduced. The technique of spectroscopic ellipsometry was adapted to a commercial III-V semiconductor molecular beam epitaxy (MBE) system to monitor layer thickness, ternary alloy composition, and substrate temperature in real time during the growth of multilayer structures. Practical system considerations for reliably implementing the rotating analyzer ellipsometer in a hydride source MBE environment that contains a high pressure of dimeric group V species is discussed. Measurement of substrate temperature from room temperature to typical growth temperatures is then presented as well as in situ determination of alloy composition and thickness for efficient growth calibration. A growth run of GaAs/AlGaAs epitaxial layers is examined to observe surface smoothing upon group III pulse deposition and growth interruption at heterointerfaces. The growth of quantum well structures is then monitored and analyzed in attempts to extract heterojunction interface abruptness. Finally, a summary of epitaxial reactor design issues that need to be addressed to implement the spectroscopic ellipsometry (SE) technique in commercial systems is provided. Author (revised)

N94-21006*# Nebraska Univ., Lincoln. Dept. of Electrical Engineering.

THERMAL DIFFUSIVITY MEASUREMENTS BY PHOTOTHERMAL LASER BEAM DEFLECTION (PTD): DATA ANALYSIS USING THE LEVENBERG-MARQUARDT ALGORITHM **c36**

Hassanayn Machlab, William A. McGahan, and John A. Woollam *In its* Materials, Structures, and Devices for High-Speed Electronics 1993 1 p Repr. from Thin Solid Films (Elsevier Sequoia), v. 215, 1992 p 103-107 (For primary document see N94-20971 05-76)

Avail: CASI HC A01/MF A01

Photothermal laser beam deflection (PTD) is a powerful tool used to obtain the thermal diffusivities of bulk solids and thin films. PTD is of special interest for non-destructive evaluation of bulk, thin film, and composite materials anticipated for use in future space missions. Polycrystalline diamond thin films are expected to be useful as heat sinks and thermal conductors in space applications, and measurement of thermal diffusivity in these films is very important. One of the major problems in applying the PTD technique for diffusivity measurements (and hence the thermal conductivity, since heat capacities and densities are not difficult to measure and are frequently known) is that a numerical regression analysis must be performed to simultaneously determine several unknown parameters. Regression is done by matching experimental data with calculations based on analytic models such that an error function is minimized. The adaption of the

Levenberg-Marquardt algorithm for regression analysis to the determination of thermal diffusivity of bulk and thin film solids by PTD is described. The analytic theory is reviewed and the numerical analysis method is described. Experimental equipment for high signal-to-noise ratio data is described and data on bulk aluminum taken over a range of frequencies are presented. Regression analysis fits to the theory (performed in an inverse space reference frame) yield values for parameters of the experiment, including the thermal diffusivity. Author (revised)

N94-21007*# Nebraska Univ., Lincoln. Dept. of Electrical Engineering.
THERMAL CHARACTERIZATION OF THIN FILMS BY PHOTOTHERMALLY INDUCED LASER BEAM DEFLECTION Abstract Only **c27**
Hassanayn Machlab, William A. McGahan, John A. Woollam, and Kevin Cole *In its* Materials, Structures, and Devices for High-Speed Electronics 1993 1 p Repr. from Thin Solid Films (Elsevier Sequoia), v. 224, 1993 p 22-27 Presented at the 19th International Conference on Metallurgical Coatings and Thin Films, San Diego, CA, 6-10 Apr. 1992 (For primary document see N94-20971 05-76)
Avail: CASI HC A01/MF A01

The photothermal deflection technique, also known as the 'mirage effect,' is a powerful nondestructive means of evaluating the thermal properties of both bulk materials and thin films. In this experiment, the sample is heated by a modulated laser beam, and the deflection of a second laser beam passing through the heated region above the sample (parallel to the surface of the sample) is measured as a function of distance between the probe and heating beams. The temperature profile above the sample, and hence the beam deflections, are determined by the sample properties. These measurements can be analyzed to determine the thermal diffusivity of the sample. For multilayered samples it is often possible to find the thermal constants for a single layer if the properties of the other materials in the sample are previously measured or otherwise known. The authors have nonlinear regression software for the analysis of samples that may have any number of layers, based on a Green's function formalism with no approximations, for the calculation of beam deflections. They have applied this technique to a number of bulk and thin film systems, from which representative results are presented. Author (revised)

N94-21008*# Nebraska Univ., Lincoln. Dept. of Electrical Engineering.
MICRO-ELLIPSOMETRIC MEASUREMENTS OF STRAINED LAYER STRUCTURES Abstract Only
Yi-Ming Xiong and Paul G. Snyder *In its* Materials, Structures, and Devices for High-Speed Electronics 1993 1 p (For primary document see N94-20971 05-76)
Avail: CASI HC A01/MF A01

Ellipsometric measurements are extremely sensitive (on the monolayer scale) to layer thicknesses and surface or interfacial roughness. However, lateral resolution is poor because of the need for a highly collimated (less than or equal to 0.05 degrees) and therefore large diameter (typically 1 mm) optical beam. Many materials are inhomogeneous on a smaller lateral scale, in which case conventional ellipsometry simply measures some average value. Focusing the beam leads, for an incoherent light source, to an uncollimated beam and a consequential spread in the angle of incidence, which in turn degrades the sensitivity. This paper describes a technique for focusing a coherent, Gaussian laser beam to a minimum spot size of about 30 micron x 130 micron, while maintaining a negligible effective spread in angle of incidence. The technique is used to measure semi-insulating (S.I.) GaAs, laser annealed ion implanted GaAs, and In(x)Ga(1-x)As strained layer structures. Author (revised)

N94-21009*# National Aeronautics and Space Administration. Lewis Research Center, Cleveland, OH.
SPECTROSCOPIC ELLIPSOMETRIC CHARACTERIZATION OF Si/Si(1-x)Ge(x) STRAINED-LAYER SUPERLATTICES
Huade D. Yao (Nebraska Univ., Lincoln.), John A. Woollam (Nebraska Univ., Lincoln.), P. J. Wang (International Business Machines Corp., Hopewell Junction, NY.), M. J. Tejwani (International Business Machines Corp., Hopewell Junction, NY.), and Samuel A. Alterovitz *In* Nebraska Univ., Materials, Structures, and Devices for High-Speed Electronics 1993 1 p Repr. from Applied Surface Science (Netherlands, Elsevier Science Publishers B.V.), v. 63, 1993 p 52-56 (For primary document see N94-20971 05-76)
Avail: CASI HC A01/MF A01

Spectroscopic ellipsometry (SE) is employed to characterize Si/Si(1-x)Ge(x) strained-layer superlattices. An algorithm was developed, using the available optical constants measured at a number of fixed x values of Ge composition, to compute the dielectric function spectrum of Si(1-x)Ge(x) at an arbitrary x value in the spectral range 1.7 to 5.6 eV. The ellipsometrically determined superlattice thicknesses and alloy compositional fractions are in excellent agreement with results from high-resolution x ray diffraction studies. The silicon surfaces of the superlattices were subjected to a 9:1 HF cleaning prior to the SE measurements. The HF solution removed silicon oxides on the semiconductor surface and terminated the Si surface with hydrogen-silicon bonds, which were monitored over a period of several weeks, after the HF cleaning, by SE measurements. An equivalent dielectric layer model was established to describe the hydrogen-terminated Si surface layer. The passivated Si surface remained unchanged for greater than two hours, and very little surface oxidation took place even over three to four days. Author (revised)

N94-21010*# Nebraska Univ., Lincoln. Dept. of Electrical Engineering.
APPLICATIONS OF VARIABLE ANGLE SPECTROSCOPIC ELLIPSOMETRY IN SEMICONDUCTOR TECHNOLOGY Abstract Only
John A. Woollam and Paul G. Snyder *In its* Materials, Structures, and Devices for High-Speed Electronics 1993 1 p Presented at the Topical Conference on Metrology for Semiconductor Manufacturing, 21-22 Feb. 1990 (For primary document see N94-20971 05-76)
Avail: CASI HC A01/MF A01

Most semiconductor R&D laboratories use single wavelength ellipsometers for measuring SiO2 and/or Si3N4 film thicknesses and homogeneity. The purpose of this paper is to briefly review the enormous enhancement in semiconductor analysis capabilities obtainable using variable angle spectroscopic ellipsometry (VASE). The paper starts with a brief description of ellipsometry physics, then outlines several specific applications to semiconductor structures and processes. Author (revised)

N94-21011*# Nebraska Univ., Lincoln. Dept. of Electrical Engineering.
FUNDAMENTALS AND APPLICATIONS OF VARIABLE ANGLE SPECTROSCOPIC ELLIPSOMETRY Abstract Only **c25**
John A. Woollam and Paul G. Snyder *In its* Materials, Structures, and Devices for High-Speed Electronics 1993 1 p Repr. from Materials Science and Engineering (Netherlands, Elsevier Sequoia), 1990 p 279-283 (For primary document see N94-20971 05-76)
Avail: CASI HC A01/MF A01

Being able to accurately select the angle of incidence and spectral range for measurement makes ellipsometry a very powerful tool for materials, surface, and interface analysis. The technique is fast, is totally computer automated, and can be performed at atmospheric pressure. It is totally non-invasive and is sensitive to fractions of atom layer thicknesses. The paper illustrates the power of variable angle spectroscopic ellipsometry with three examples: optical coatings, surface roughness and wetting, and electric field effects in semiconductor studies. Author (revised)

N94-21012*# Nebraska Univ., Lincoln. Dept. of Electrical Engineering.
NON-DESTRUCTIVE EVALUATION IN MANUFACTURING USING SPECTROSCOPIC ELLIPSOMETRY Abstract Only **c38**
John A. Woollam and Paul G. Snyder *In its* Materials, Structures, and Devices for High-Speed Electronics 1993 1 p Repr. from Review of Progress in Quantitative Nondestructive Evaluation (NY, Plenum Press), v. 10B, 1991 p 2185 (For primary document see N94-20971 05-76)
Avail: CASI HC A01/MF A01

The manufacture of optical coatings, computer disks, as well as advanced electronic multilayered devices and circuit structures requires high precision in the measurement and control of thicknesses and interfacial and surface roughnesses. Variable angle spectroscopic ellipsometry (VASE) is non-destructive and monolayer sensitive. VASE uses polarized light, and the technique can be applied in nearly any ambient, including air, vacuum, or corrosive environment. Applications to coated window glass, space protective coatings, semiconductor device, as well as sputtered media computer disk manufacturing are discussed. At the present time these NDE measurements are mainly ex-situ, but in-situ (during deposition) applications are being rapidly developed. Derived from text

N94-21013*# Nebraska Univ., Lincoln. Dept. of Electrical Engineering.
IN-SITU AND EX-SITU ELLIPSOMETRIC CHARACTERIZATION FOR SEMICONDUCTOR TECHNOLOGY Abstract Only
John A. Woollam, Paul G. Snyder, Huade D. Yao, and Blaine Johs (Woollam, John A. Co., Lincoln, NE.) *In its* Materials, Structures, and Devices for High-Speed Electronics 1993 1 p Repr. from SPIE, v. 1678, 1992 p 246 Sponsored in part by DARPA (For primary document see N94-20971 05-76)
Avail: CASI HC A01/MF A01

The ellipsometric technique has been around since the end of the last century. However, until the introduction of computers in the 1960's, mainly nulling techniques were used. These were accurate, but extremely slow, and data analysis capabilities were limited. The use of personal computers permits rapid data acquisition and analysis. Thus the emphasis is now on ellipsometry for materials research and analysis. Ellipsometry is a unique tool in that it is totally non-destructive and can be performed in any ambient, including air, vacuum, high pressure, or liquid. In ellipsometry a polarized, collimated beam of monochromatic light is reflected at a preselected angle of incidence from the surface of a material, and the polarization state of the reflected beam is determined. For each wavelength and angle of incidence, one pair of numbers is obtained. These can be used to determine at most two materials parameters, such as the real and imaginary parts of the complex dielectric functions. Frequently, however, two or more variables are correlated and cannot be uniquely determined. This is an important caveat for ellipsometry: one always obtains numbers from the experiment, but they may not be correct. It is extremely important for the user to understand the basis of regression analysis and the possibility for correlated variables when using ellipsometry for any new materials system. To minimize this possibility, multiple angles of incidence and wavelength are used to maximize sensitivity and uniquely determine parameter values. In general, ellipsometry determines the real and imaginary part of the optical dielectric function or equivalently the index of refraction and extinction coefficient. For filmed materials systems, one can potentially determine film thickness (with monolayer sensitivity), void fraction (density), alloy fraction, interfacial and/or surface roughness, and other microstructural properties. To do these sophisticated levels of microstructural materials analysis requires spectroscopic and variable angle measurements, in order to minimize correlation, increase sensitivity, and maximize total information obtained. Derived from text

N94-21014*# Nebraska Univ., Lincoln. Dept. of Electrical Engineering.
VASE (VARIABLE ANGLE SPECTROSCOPIC ELLIPSOMETRY) Abstract Only **c25**
John A. Woollam and Paul G. Snyder *In its* Materials, Structures, and Devices for High-Speed Electronics 1993 1 p Presented 6 Jan. 1992 (For primary document see N94-20971 05-76)
Avail: CASI HC A01/MF A01

The technique of ellipsometry was introduced in the 1800s, but until computers became available, it was painfully slow to perform. Rapid advances in small computer technology have made ellipsometric data acquisition rapid and accurate. Most important, fast personal computers make possible quick and convenient analysis of data from complex material structures. Early work in ellipsometry focused on improving the technique, whereas attention now emphasizes applications to materials analysis. New uses continue to be found; however, ellipsometry traditionally has been used to determine film thicknesses (in the range 1-1000 nm), as well as optical constants. Common systems are oxide and nitride films on silicon wafers, dielectric films deposited on optical surfaces, and multilayer semiconductor structures. In ellipsometry a collimated polarized light beam is directed at the material under study, and the polarization state of the reflected light is determined using a second polarizer. To maximize sensitivity and accuracy, the angle that the light makes to the sample normal (the angle of incidence) and the wavelength are controlled. Ellipsometry is a very powerful, simple, and totally nondestructive technique for determining optical constants, film thicknesses in multilayered systems, surface roughness, and other microstructural properties. Derived from text

N94-21135 Technische Hochschule, Darmstadt (Germany). Fachbereich Physik.
THERMAL EXPANSION OF ELECTRONIC HIGHLY CORRELATED MATERIALS Ph.D. Thesis [THERMISCHE AUSDEHNUNG VON ELEKTRONISCH HOCHKORRELIERTEN MATERIALIEN]
Michael Lang 1991 148 p In GERMAN Limited Reproducibility: More than 20% of this document may be affected by microfiche quality (ETN-93-93605) Avail: CASI HC A07

Dilatometric examinations of electronically highly correlated materials were carried out, with special consideration of heavy fermion-superconductors CeCu2Si2 and of ceramic oxides of high temperature superconductors such as La(2-x)M(x)CuO4 and YBa2Cu3O(7-delta) to establish relationships between grid properties and superconduction in these systems. A capacitive measuring process was used, by which length variations of a specimen cause distance variations of electrodes in a plate condensator. A strongly anisotropic expansion behavior of CeCu2Si2 is noticed at superconducting phase transition. A thermodynamic analysis and specific heat measurements were carried out to show that the shortest Ce-Ce distance has an important influence on superconduction properties. A reduction of grid parameter is shown to increase the Kondo grid temperature. It is concluded that superconduction and magnetism in CeCu2Si2 appears to be narrowly linked. A grid anomaly is observed in systems La(2-x)Sr(x)CuO4, La(2-x)Ba(x)CuO4 and YBa2CuO7 which is assumed to lie in the CuO6 octahedron. ESA

N94-21151 Technische Univ., Berlin (Germany). Fachbereich Physik.
OPTICAL AMPLIFICATION AND THRESHOLD BEHAVIOR ON InGaAs/InGaAsP MULTIQUANTUM WELL STRUCTURES Ph.D. Thesis [OPTISCHE VERSTAERKUNG UND SCHWELLVERHALTEN VON INGAAS/INGAASP-MULTI-QUANTUM-WELL-STUKTUREN]
Martin Moehrle 1992 144 p In GERMAN Limited Reproducibility: More than 20% of this document may be affected by microfiche quality (ETN-93-94181) Avail: CASI HC A07

A systematic analysis of optical amplification, losses, and threshold current properties of optically or electrically pumped InGaAs/InGaAsP quantum well laser structures is carried out. Broad area and ridge waveguide laser elements were built from these structures for examination by electrical excitation. A theoretical model was achieved for calculation of structure optical amplification with focus on optical amplification maximal value dependence of charge carried density, which is established to be correctly described by a logarithmic relationship. The influence of barrier width and an additional optical wave guide on this dependence was examined. Threshold current densities of structrures and charge carrier injection by electrical excitation were studied and optical amplification by electrical and optical excitation was compared. Influence of optical losses, injection efficiency, and charge carrier lifetime in InGaAs/InGaAsP quantum well structures was estimated. It is shown that multiquantum well structures have a threshold current minimum for a characteristical resonator length and low threshold currents can be obtained by high resonator lengths with InGaAsP bulk lasers with thin active layer. ESA

N94-21190# North Carolina State Univ., Raleigh. Dept. of Materials Science and Engineering.
GROWTH, CHARACTERIZATION AND DEVICE DEVELOPMENT IN MONOCRYSTALLINE DIAMOND FILMS Quarterly Technical Report, 1 Jul. - 30 Sep. 1993
Robert F. Davis, Jeffrey T. Glass, and R. J. Nemanich Sep. 1993 35 p (Contract N00014-93-I-0437)
(AD-A272715) Avail: CASI HC A03/MF A01

For the heteroepitaxial deposition of diamond films, material selection criteria have been used to choose the closely lattice parameter matched substrate of Cu and the subsequent candidate interlayer materials of Ni, Si and Ti, the latter of which hold promise for both pseudomorphic matching to Cu and the promotion of the high density nucleation of diamond. Initial experiments of the Cu/Ti system have shown that a 20 A Ti layer can improve the particle density on Cu by nearly a factor of ten. Copper films have been evaporated under UHV conditions for examination as rectifying contacts. Atomic force microscopy indicated island growth of the Cu. Current-voltage measurements and UPS at 293 K revealed rectifying characteristics and a Phi approximately equal to 1.1 eV, respectively. In research regarding the negative electron affinity of the 2x1 diamond (100) surface, theoretical calculations indicate that it is associated with a monohydride terminated surface. DTIC

N94-21242# Columbia Univ., New York, NY. Dept. of Chemistry.
SCANNING TUNNELING MICROSCOPY INVESTIGATIONS OF METAL DICHALCOGENIDE MATERIALS Final Report, 1 Nov. 1989 - 30 Jun. 1993
Charles M. Lieber 25 Oct. 1993 44 p
(Grant AF-AFOSR-0029-90)
(AD-A272910; AFOSR-93-0841TR) Avail: CASI HC A03/MF A01

Scanning tunneling microscopy (STM) and atomic force microscopy (AFM) were used to characterize the atomic level structure of electronic properties, reactivity, and wear of metal dichalcogenide materials that are or have potential as solid state lubricants. Single crystals of MoS2, Ni(x)Mo(1-x)S2, MoS(2-x)Se(x), and MoS(2-x)Te(x) were prepared to determine how chemical modifications affect the local structure and electronic properties of this lubricant. STM images of Ni-doped MoS2 show localized electronic states due to the Ni atoms, while images of Se- and Te-doped materials indicate that anion substitution is electronically delocalized. AFM studies of Te-doped MoS2 show, however, that the tellurium dopants form atomic scale structural protrusions that may reduce sliding friction. AFM was also used to characterize nanometer scale wear and oxidation on MoS2 and NbSe2 surfaces. In atmosphere at room-temperature AFM studies showed that NbSe2 wears approximately three times faster than MoS2. Furthermore, oxidation studies demonstrated that NbSe2 was significantly more reactive than MoS2 with molecular oxygen. These results indicate that the intrinsic stability of the MoS2 surface make it an effective lubricant, AFM was also used to elucidate the growth of MoO3 on the surface Of MoS2 during oxidation, and to study wear properties of these MoO3 crystallites. The AFM tip was used to define lines with 10 nm resolution in MoO3 and to manipulate distinct MoO3 structures on the MoS2 surface. In addition, metal-substitution in TaS2 was studied systematically using STM and theoretical methods. DTIC

N94-21248# North Carolina State Univ., Raleigh. Dept. of Electrical and Computer Engineering.
SOLID-STATE DYNAMICS AND QUANTUM TRANSPORT IN NOVEL SEMICONDUCTOR NANOSTRUCTURES Annual Report, 1 Oct. 1992 - 30 Sep. 1993
K. W. Kim 30 Sep. 1993 51 p
(Contract N00014-90-J-1835)
(AD-A272955) Avail: CASI HC A04/MF A01

The objective of this research program is to study theoretically the underlying principles of solid-state dynamics and quantum mechanical transport of carriers in ultra-small novel semiconductor devices. The areas of research are: theory of phonon modes in reduced dimensions, effects of band structure on electronic and optical properties of heterostructures, and quantum transport in solids with special emphasis on non-perturbative role of high-electric fields and many-body effects in dynamical processes. The treatment of these problems is mainly analytical through the development of macroscopic and microscopic physical models with an emphasis on quantum mechanical principles. At the same time, numerical approaches has also been utilized for realistic solutions with accuracy. Specific subjects discussed in this report include the effects of confinement and localization on optical phonon modes, band mixing in tunneling, Bloch electron quantum transport theory under hot-electron conditions, and dielectric response function theory. DTIC

N94-21296# EG and G Energy Measurements, Inc., Las Vegas, NV.
X RAY ANALYSIS OF ALPHA MERCURIC IODIDE CRYSTAL STRUCTURE AND PROCESSING EFFECTS
L. Keller (CAMET Research, Inc., Goleta, CA.), E. X. Wang (CAMET Research, Inc., Goleta, CA.), and A. Y. Cheng (EG and G Energy Measurements, Inc., Goleta, CA.) 1993 6 p Presented at the 1993 Material Science Research (MRS) Spring Meeting, San Francisco, CA, 12-16 Mar. 1993
(Contract DE-AC08-88NV-10617)
(DE93-017620; EGG-10617-2184; CONF-9303206-1) Avail: CASI HC A02/MF A01

X-ray topography and rocking curve experiments were performed on (alpha)-mercuric iodide samples. As-grown crystals were examined for intrinsic defects and crystallinity. Orientation of certain defects depends on the direction of crystal growth. The propagation of as-grown crystalline features was documented. The extent of crystal damage introduced during various steps of device fabrication such as sawing, polishing, etching and contact deposition was explored. Coefficients of linear thermal expansion of alpha(sub 33) = 54 +/- 5 x 10(exp -6)/C along the tetragonal c-axis, (001) direction and alpha(sub 11) = 11 +/- 4 x 10(exp -6)/C in the (100) direction were measured. DOE

N94-21303# Army Research Lab., Watertown, MA. Materials Directorate.
INVESTIGATION OF THE EFFECT OF VARIOUS OXIDE AND FLUORIDE ADDITIVES ON THE MICROSTRUCTURE, ELECTRONIC PROPERTIES, AND PHASE SHIFTING ABILITY OF Ba(1-x)Sr(x)TiO3 Final Report
L. C. Sengupta, E. Ngo, S. Stowell, R. Lancto, and W. C. Drach Sep. 1993 27 p
(AD-A271756; ARL-TR-217) Avail: CASI HC A03/MF A01

A ceramic phase shifting device (used in phased array antenna systems) has been demonstrated using Ba(1-x)Sr(x)TiO3 (BSTO) ceramics. As a part of an effort to optimize the electronic device performance in the phase shifter, various dopants have been incorporated into BSTO. The effects of these additives on the Curie temperature, dielectric properties, tunability, hysteresis, and grain size have been investigated. The homogeneity of the doped materials has been verified using Curie-Weiss analysis. To further improve the electrical performance, some higher levels of doping have been attempted. A few of the latest results for these ceramic-ceramic composites will be presented. DTIC

N94-21304# Army Research Lab., Aberdeen Proving Ground, MD.
INFRARED ABSORPTION SPECTROSCOPY OF THE WEAKLY BONDED CO-Cl2 COMPLEX Final Report, Aug. 1990 - Aug. 1991
Steven W. Bunte, Jason B. Miller (Denison Univ., Granville, OH.), Zhi-Song S. Huang (Florida Univ., Gainesville.), Juan E. Verdasco (Universidad Complutense, Madrid, Spain.), Curt Wittig (California Univ., Los Angeles.), and Robert A. Beaudet (California Univ., Los Angeles.) Sep. 1993 23 p
(Contract DE-FG03-89ER-04053; DA Proj. 1L1-61192-SAH-43)
(AD-A271757; ARL-TR-202) Avail: CASI HC A03/MF A01

High-resolution rovibrational absorption spectra of the weakly bonded CO-Cl2 complex have been recorded in the 2143/cm region by exciting the CO chromophore with a tunable diode laser. The spectra indicate that CO-Cl2 is linear and semirigid. The distance between the CO and Cl2 centers of mass is approximately 4.78 A. The orientation of CO is not determined experimentally. However, Cl2 appears to act as a classical sigma electron acceptor, while CO behaves like a weak Lewis base donating charge from the carbon side via the weakly antibonding sigma orbital, thereby raising the CO vibrational frequency. DTIC

N94-21319# Applied Science and Technology, Inc., Woburn, MA.
MATERIALS PROCESSING AND MANUFACTURING TECHNOLOGIES FOR DIAMOND SUBSTRATE MULTICHIP MODULES Technical Report, Jul. - Sep. 1993
Evelio Sevillano 20 Oct. 1993 16 p
(Contract N00014-93-C-2026)
(AD-A271484; DARPA-BAA-92-20) Avail: CASI HC A03/MF A01

This quarter the first production of continuous diamond films in our 75kW reactor were seen. Our efforts concentrated on three fronts: improving reliability and capability of the reactor, understanding the diamond growth chemistry and how it compares to the prototype operation, and further modeling for refining the reactor design. On the first front, the reactor is regularly operated around the clock, and the power utilized in diamond growth as well as the design and thermal control of the substrate stage is steadily improved. On the second front, a series of deposition runs using a matrix of conditions to investigate the effects of gas composition and throughput on growth rate and diamond quality were initiated. These runs included real time pyrometry, emission spectroscopy, and residual gas analysis for comparison with prototype operation and modeling. Our first iteration yielded what we believe is a world record of over 350 mg/hr of CVD diamond at only 40 kW of microwave power. Our near term goals include: (1) production of free-standing 6 diameter films, (2) finishing the current iteration of chemistry matrix runs and understanding the similarities (and differences) with our 2.45 GHz prototype; and (3) further increasing power delivered to the plasma, and power removal capability of the substrate stage. DTIC

N94-21362# Emory Univ., Atlanta, GA.
DEPHASING PROCESSES IN III-V SEMICONDUCTORS Report, 1 Oct. 1992 - 30 Sep. 1993
Guy D. Gilliland Sep. 1993 153 p
(Contract N00014-92-J-1927)
(AD-A271677) Avail: CASI HC A08/MF A02

Our study has dealt with both experimental and theoretical studies of electronic 'dephasing' processes in a variety of model semiconductor systems, all based upon III-V materials and heterostructures. Attention has been primarily given to dephasing processes in excitonic systems, however, free-carrier dynamics have not been ignored. We have studied the following model systems: exciton-polaritons in GaAs, 3D bulk excitons in GaAs, quasi-2D interface excitons in GaAs/Al(x)Ga(1-x)As heterostructures, excitons and free-carriers in ordered In(x)Ga(1-x)P. Experimental techniques utilized include: photoluminescence (PL), PL-excitation, PL decay kinetics, time-resolved PL-excitation, resonant Raman scattering, time-resolved spectroscopics, resonant Brillouin scattering, and all optical carrier transport measurements. DTIC

N94-21438# Air Force Systems Command, Wright-Patterson AFB, OH. Foreign Aerospace Science and Technology Center.
SEMICONDUCTORS A(III)B(VI): TRANSLATION
G. A. Akhundov, G. B. Abdullaev, G. D. Guseynov, R. F. Mekhtiyev, and M. Kh. Aliyeva 3 Nov. 1993 16 p
(AD-A273064; FASTC-ID(RS)T-0579-93) Avail: CASI HC A03/MF A01

Semiconductors A(III) B(VI) crystallize in laminated or chain structures and contain nine valence electrons in each molecule. Connection in the layers and the chains is predominantly covalent, and Van der Waal between the layers and the chains. Calculated data of the energy spectrum of these compounds are absent, and the available experimental studies are insufficient for understanding of the zone structures. We have obtained and studied single crystals of GaS, GaSe, GaTe, InSe, and TiSe. DTIC

N94-21458# Maine Univ., Orono. Lab. for Surface Science and Technology.
STRUCTURE AND MORPHOLOGY OF Pd OVERLAYERS ON EPITAXIAL SnO2 FILMS STUDIES WITH THE ATOMIC FORCE MICROSCOPE
R. J. Lad, M. J. Matthews, M. D. Antonik, R. E. Cavicchi, and S. Semancik 1993 5 p Submitted for publication
(Grant AF-AFOSR-0258-90)
(AD-A271827; AFOSR-93-0803TR) Avail: CASI HC A01/MF A01

The structure and morphology of clean and Pd-doped epitaxial SnO2 films were studied with the atomic force microscope (AFM). The SnO2 films were grown by reactive sputter deposition on three different substrates yielding epitaxial orientations: (101) SnO2/r-cut sapphire, (100) SnO2/basal sapphire, and (110) SnO2/TiO2 (110). AFM imaging of monolayer amounts of Pd deposited onto the epitaxial SnO2 films shows that the Pd is dispersed at 300 K and forms clusters after annealing to 500 K in vacuum. DTIC

N94-21505 Surveillance Research Lab., Salisbury (Australia).
TECHNIQUES FOR THE FLUX GROWTH OF OPTICAL MATERIALS: GROWTH OF BETA-BARIUM BORATE Research Note
Janet B. Bedson, Robert W. Lawrence, and Philip J. Picone Jul. 1993 27 p Limited Reproducibility: More than 20% of this document may be affected by microfiche quality
(AD-A272717; SRL-0116-RN; DODA-AR-008-156) Avail: CASI HC A03

This report describes the method of flux growth of nonlinear optical single crystals and the techniques required to determine the flux choice. This is illustrated by the crystal growth of beta barium borate. These techniques are applicable to other optical materials. DTIC

N94-21506# North Carolina State Univ., Raleigh. Dept. of Materials Science and Engineering.
GROWTH, CHARACTERIZATION AND DEVICE DEVELOPMENT IN MONOCRYSTALLINE DIAMOND FILMS Final Technical Report, 10 Jan. 1990 - 31 Oct. 1993
Robert F. Davis 31 Oct. 1993 154 p
(Contract N00014-90-J-1604)
(AD-A273097) Avail: CASI HC A08/MF A02

The effects of hydrogen on cluster binding energy and resulting growth mode during chemical vapor deposition of diamond, the process parameters and the effect of substrates during bias enhanced nucleation, the growth of textured diamond films, and the characterization of these films using transmission electron microscopy, Raman spectroscopy, and photo-luminescence comprise the growth and thin film characterization research conducted during this grant. Additional work included determination of the surface properties including the negative electron affinity, the growth and characterization of SiGe contacts, and the modeling and characterization of electronic devices. The nucleation of diamond grains on unscratched Si(100) wafer is enhanced by four orders of magnitude relative to scratched substrates by using negative bias-enhanced microwave plasma CVD in a 2% methane/hydrogen plasma for an initial period. In vacuo surface analysis has revealed that the actual nucleation occurs on the amorphous C coating present on the thin SiC layer which forms as the product of the initial reaction with the Si surface. It is believed that the C forms critical clusters which are favorable for diamond nucleation. TEM of nucleation of diamonds on single crystal SiC showed that approximately half of the diamond nuclei were in epitaxial alignment with the SiC substrate. UV photoemission spectroscopy has revealed Schottky barrier heights of 1.0 +/- 0.2 eV and 1.5 +/- 0.2 for the Ti-diamond (111) and (100) interfaces. DTIC

N94-21517 Implant Sciences Corp., Wakefield, MA.
SINGLE CRYSTAL DIAMOND FILMS Final Report, 1 Aug. 1992 - 1 Mar. 1993
Stephen N. Bunker and Richard Sahagian 28 May 1993 27 p Limited Reproducibility: More than 20% of this document may be affected by microfiche quality
(Contract DAAL03-92-C-0030)
(AD-A266759; ARO-30461.1-MS-SBI) Avail: Issuing Activity (Defense Technical Information Center (DTIC))

Diamond films are important for radiation tolerant devices. However, fabrication of single crystal films has proven to be much more difficult than poolycrystalline deposites. A novel deposition process is proposed which can be used to deposit diamond on a seed crystal. The technique permits patterned deposites in islands and offers the potential of a new method for attempting to dope diamond semiconductors. DTIC

N94-21521# California Univ., Los Angeles. Dept. of Electrical Engineering.
HIGH TEMPERATURE SUPERCONDUCTING PLANAR CIRCUIT STRUCTURE FOR HIGH FREQUENCY APPLICATIONS Final Technical Report, 1 Jun. 1991 - 30 Sep. 1993
Tatsuo Itoh 1 Oct. 1993 11 p
(Contract N00014-91-J-1651)
(AD-A273083) Avail: CASI HC A03/MF A01

This document summarizes technical activities and accomplishments under the support of ONR in the area of electromagnetic analysis of planar circuit structures that contain high T(sub c) superconductors. Subjects discussed include the following: (1) pulse transmission along the superconducting transmission line; (2) the development of a new method for characterizing a transmission line made of a locally power dependent and hence nonlinear materials such as high T(sub c) superconductors; and (3) the enhancement of the finite difference time domain method. DTIC

N94-21541# Sandia National Labs., Albuquerque, NM.
SYNTHESIS AND CATALYTIC PROPERTIES OF METAL AND SEMICONDUCTOR NANOCLUSTERS
J. P. Wilcoxon, T. Martino, E. Klavetter, and A. P. Sylwester 1993 9 p Presented at the North Atlantic Treaty Organization (NATO) Advanced Study Meeting of Institute on Nanophas Materials, Corfu, Greece, 20 Jun. - 2 Jul. 1993
(Contract DE-AC04-76DP-00789)
(DE93-019418; SAND-93-1846C; CONF-9306223-1) Avail: CASI HC A02/MF A01

Synthesis of metal or semiconductor nanoclusters in microheterogeneous oil-continuous inverse micelle systems is discussed. We focus on synthesis and catalytic properties of palladium, iron, and iron sulfide nanoclusters. Cluster size-control is achieved by changing the micelle size which is determined by small angle neutron scattering (SANS) and chosen to produce cluster in size range of 1-20 nm. Cluster sizes were determined by either transmission electron microscopy (TEM) or small-angle x-ray scattering (SAXS). Cluster structure was determined by either x-ray or electron diffraction. In the case of Fe nanoclusters, the crystal structure depended

on the chemical nature of the surfactant micelle used in the synthesis, illustrating the important role of the surfactant during the growth process. Results of in-situ pyrene hydrogenation using size-selected Pd clusters show a significant increase in activity/total surface area as the size decreases. These clusters also proved effective as unsupported catalysts for direct coal hydropyrolysis, even at very low metal concentrations. Synthesis and optical features of a new semiconductor cluster material, FeS2, are discussed with regard to its use in photocatalysis. Application of FeS2 in coal hydrogenolysis reactions has improved yields of short chain hydrocarbons significantly compared to conventional FeS2 powders. DOE

N94-21552 Technische Univ., Eindhoven (Netherlands). Faculty of Electrical Engineering.

DEFECT MOTION AS THE ORIGIN OF THE 1/f CONDUCTANCE NOISE IN SOLIDS

V. B. Orlov (Gorky N. I. Lobachevsky State Univ., USSR.) Jun. 1992 75 p Limited Reproducibility: More than 20% of this document may be affected by microfiche quality

(EUT-92-E-259; ISBN-9-06-144259-1; ETN-94-94766) Avail: CASI HC A04

The nature of 1/f conductance fluctuations in solids is considered in models attributing this phenomenon to some kind of defect motion. Stochastic changes in the state of the system 'lattice defects' are treated as a noise source affecting the number and/or the mobility of charge carriers and providing the 1/f noise observed. In particular, the known model of Two Level Systems (TLS) and a more general approach of freely wandering defects within a randomized potential profile are discussed. Numerical estimations show that this noise model, previously established for metals, is relevant for semiconductors. The most basic properties of the 1/f conductance fluctuations in solids are described in this way: the bulk nature, the short range of spatial correlation, the detailed shape of the spectrum, and the thermoactivation. Experimental data are interpreted: correlation between the 1/f noise magnitude and the degree of crystal perfection, temperature dependence and field dependence in semiconductors, and 1/f noise in magnetoresistance. The possibility of characterization of defects by the noise spectroscopy is considered. ESA

N94-21555# Los Alamos National Lab., NM.

LOCAL STRUCTURE AND SUPERCONDUCTIVITY IN La(2-x)Ba(x)CuO4 FOR x=0.125 AND x=0.15

S. J. L. Billinge, G. H. Kwei, and H. Takagi (Tokyo Univ., Japan.) 1993 9 p Presented at the International Conference on Strongly Correlated Electron Systems, La Jolla, CA, 16-19 Aug. 1993

(Contract W-7405-eng-36)

(DE93-040193; LA-UR-93-3194; CONF-930865-9) Avail: CASI HC A02/MF A01

This paper reviews our recent work on characterizing the structural and electronic transitions in La(2-x)Ba(x)CuO4. This is a high-temperature superconductor which shows an interesting interrelationship between structure and atomic properties. We have used x-ray and neutron diffraction to characterize the structure and show that the current understanding of the structural phase transitions, and their relationship to the superconductivity, is incomplete. DOE

N94-21615# North Carolina State Univ., Raleigh.

FUNDAMENTAL STUDIES OF DEFECT GENERATION IN AMORPHOUS SILICON ALLOYS GROWN BY REMOTE PLASMA-ENHANCED CHEMICAL-VAPOR DEPOSITION

G. Lucovsky Aug. 1993 55 p Prepared for Midwest Research Inst., Golden, CO

(Contract DE-AC02-83CH-10093)

(DE93-017083; NREL/TP-451-5452) Avail: CASI HC A04/MF A01

This report describes research to reduce the intrinsic bonding defects in amorphous and microcrystalline Si alloys by controlling the bonding chemistry and the microstructure via the deposition process reactions. The specific approach was to use remote plasma-enhanced, chemical-vapor deposition (PECVD) and reactive magnetron sputtering to limit the multiplicity of deposition inaction pathways, and thereby gain increased control over the thin-film chemistry and microstructure. The research included the deposition of amorphous and microcrystalline Si alloy materials by the PECVD process and by reactive magnetron sputtering and the evaluation of the material properties of these films for potential applications in PV devices. The focus of the research was on gaining a fundamental understanding of the relationships between deposition reaction pathways, the bonding of dopant and alloy atoms, and the electrical properties of importance for PV applications. This involved studying the factors that contribute to defect generation and to defect removal and/or neutralization. In addition to the experimental studies, the research also included theoretical and modeling studies aimed at understanding the relationships between local atomic arrangements of Si and alloy atoms, and the electrical, optical, vibrational, and defect properties. DOE

N94-21617# Solarex Corp., Newtown, PA. Thin Film Div.

RESEARCH ON POLYCRYSTALLINE THIN-FILM SUBMODULES BASED ON CuInSe2 MATERIALS

R. Arya, J. Fogleboch, T. Lommasson, R. Podlesny, L. Russell, S. Skibo, S. Wiedeman, A. Rothwarf, and R. Birkmire Sep. 1993 64 p Prepared for Midwest Research Inst., Golden, CO

(Contract DE-AC02-83CH-10093)

(DE93-018223; NREL/TP-413-5759) Avail: CASI HC A04/MF A01

This report describes a 3-year, cost-shared research program at Solarex to develop all pertinent processes and technologies required to achieve the goal of 12% CIS submodule (with areas greater than 900 sq cm). The work is focused on four tasks: window layers, contacts, and substrate; CIS absorber layer; device structure; and submodule design and encapsulation. Each task addresses basic material improvements, fabrication and characterization of CIS solar cells, and scale up of processes to large-area substrates. DOE

N94-21649# Argonne National Lab., IL.

RELAXATION OF HYSTERESIS LOOP IN A SINGLE CRYSTAL OF YBa2Cu4O8

Ming Xu (Ames Lab., IA.), D. K. Finnemore (Ames Lab., IA.), G. W. Crabtree, V. M. Vinokur, D. G. Hinks, K. Zhang (Chicago Univ., IL.), and B. Dabrowski Apr. 1993 3 p Presented at the Conference of the International Union of Pure and Applied Physics on Low Temperature Physics (LT 20), Eugene, OR, 1-11 Aug. 1993

(Contract W-31-109-eng-38)

(DE93-019519; ANL/MSD/CP-79655; CONF-930801-9) Avail: CASI HC A01/MF A01

Magnetic relaxation has been studied for YBa2Cu4O8 in order to look for changes in the relaxation rates that arise because different pinning mechanisms dominate in different magnetic field regimes. In the low field regime where the Bean-Livingston surface barrier dominates, the vortices exit on a field decreasing branch with a relaxation rate about ten times faster than they enter on a corresponding field increasing branch. In high magnetic fields where bulk pinning dominates, the relaxation rates for field increasing and field decreasing are essentially the same. DOE

N94-21690# Sandia National Labs., Albuquerque, NM.

THE MILLING ASSISTANT, CASE-BASED REASONING, AND MACHINING STRATEGY: A REPORT ON THE DEVELOPMENT OF AUTOMATED NUMERICAL CONTROL PROGRAMMING SYSTEMS AT NEW MEXICO STATE UNIVERSITY

William Burd, David Culler (New Mexico State Univ., Las Cruces.), Tom Eskridge (New Mexico State Univ., Las Cruces.), Leon Cox (New Mexico State Univ., Las Cruces.), and Ted Slater (New Mexico State Univ., Las Cruces.) Aug. 1993 99 p

(Contract DE-AC04-76DP-00789)

(DE93-041101; SAND-93-1430) Avail: CASI HC A05/MF A02

The Milling Assistant (MA) programming system demonstrates the automated development of tool paths for Numerical Control (NC) machine tools. By integrating a Case-Based Reasoning decision processor with a commercial CAD/CAM software, intelligent tool path files for milled and point-to-point features can be created. The operational system is capable of reducing the time required to program a variety of parts and improving product quality by collecting and utilizing 'best of practice' machining strategies. DOE

N94-21691 Ames Lab., IA.

APPLICATION OF AN ELECTROCHEMICAL QUARTZ CRYSTAL MICROBALANCE TO THE STUDY OF ELECTROCATALYTIC FILMS Ph.D. Thesis

J. S. Gordon, Jr. 1 Sep. 1993 223 p Limited Reproducibility: More

than 20% of this document may be affected by microfiche quality
(Contract W-7405-eng-82)
(DE93-041124; IS-T-1670) Avail: CASI HC A10

The Electrochemical Quartz Crystal Microbalance (EQCM) was used to study the deposition and composition of electrodeposited pure PbO2 and Bi-doped PbO2 active toward anodic oxygen-transfer reactions. Within the doped films, Bi is incorporated as Bi(sup +5) in the form of BiO2A, where A is ClO4(-) or NO3(-). For deposition of these 2 materials, changes in hydration between the Au oxide and the depositing film resulted in higher mass-to-charge ratios. XRD and XPS were used to study the films; the rutile structure of PbO2 is retained even with the Bi doping. The EQCM was also used to study the formation and dissolution of Au oxide and preoxide structures formed on the Au substrate electrodes in acidic media. The preoxide structures were AuOH and increased the surface mass. For the formation of stable Au films on quartz wafers, Ti interlayers between Au and quartz was found to be very effective. DOE

N94-21744# California Univ., Berkeley. Lawrence Berkeley Lab.
SEMICONDUCTOR ISOTOPE ENGINEERING
E. E. Haller May 1993 10 p Presented at the GADEST 1993: Gettering and Defect Engineering in Semiconductors, Klingmuehle, Germany, 9-14 Oct. 1993
(Contract DE-AC03-76SF-00098)
(DE93-040119; LBL-34279; CONF-9310156-1) Avail: CASI HC A02/MF A01

Isotopic control of semiconductor crystals offers a wide range of scientific and technical opportunities. We review neutron transmutation doping of natural and isotopically controlled semiconductor structures, special properties of isotope superlattices, the effect of host isotopes on local vibrational modes of low mass impurities, and intrinsic properties which depend on isotope mass and isotopic composition of single crystals. DOE

N94-21763# California Univ., Berkeley. Lawrence Berkeley Lab.
IMPLANTATION OF CARBON IN GaAs AND COMPENSATING NATIVE DEFECTS
A. J. Moll, J. W. Ager, III, K. M. Yu, W. Walukiewicz, and E. E. Haller Jul. 1993 8 p Presented at the 17th International Conference on Defects in Semiconductors, Gmunden, Austria, 18-23 Jul. 1993
(Contract DE-AC03-76SF-00098)
(DE93-040122; LBL-34278; CONF-9307124-2) Avail: CASI HC A02/MF A01

The effects of co-implantation on the electrical activity of C acceptors have been studied using a series of elements as co-implants. A variety of electrical and structural techniques were used for characterization. It is found that although co-implantation with heavy ions improves the substitutionality of C atoms on As sites, a high electrical activity of the C(sub As) acceptors is attained only if the stoichiometry is maintained through co-implantation of group 3 atoms. DOE

N94-21768 Los Alamos National Lab., NM.
LOCAL STRUCTURE IN OXYGEN-DOPED La2CuO(4+DELTA)
P. C. Hammel, A. P. Reyes, E. T. Ahrens, D. E. MacLaughlin, J. D. Thompson, Z. Fisk, P. C. Canfield, S. W. Cheong, and J. E. Schirber (Sandia National Labs., Albuquerque, NM.) Aug. 1993 11 p Presented at the International Conference on Strongly Correlated Electron Systems, La Jolla, CA, 16-19 Aug. 1993 Limited Reproducibility: More than 20% of this document may be affected by microfiche quality
(Contract W-7405-eng-36)
(DE93-040248; LA-UR-93-2879; CONF-930865-7) Avail: CASI HC A03

Oxygen doped La2CuO(4+delta), due to the unusually large mobility of the oxygen ions at high temperatures, is the only cuprate which has macroscopic phase separation of doped holes. We discuss our studies of La2CuO(4+delta), including phase separation, distributed local structure whose onset coincides with-phase separation and the observation that in the presence of doped holes two distinct copper sites are generated, an observation which contrasts with results of diffraction studies. The superconducting transition temperature Tc in this material changes by over 10% in response to altered cooling history. Below a temperature T(sub f), the situation becomes similar to other cuprates since oxygen is no longer sufficiently mobile to allow further macroscopic phase separation. In this regime, the magnetic behavior of metallic La2CuO(4+delta) is conventional in context of cuprates. However La-139 NMR spectroscopy has shown the local structure of the La-O layer to be very sensitive to the presence of doped holes and to be strongly temperature dependent in this same regime. This sensitivity is evident in the CuO2 planes where, in the presence of doped holes a second, distinct copper site is present. This provides an opportunity to explore the relationship between local structure and the novel magnetic behavior of the cuprates. DOE

N94-21778*# Massachusetts Inst. of Tech., Cambridge. Dept. of Materials Science and Engineering.
CHARACTERIZATION OF CONVECTION RELATED DEFECTS IN II-VI COMPOUND SEMICONDUCTORS Final Report, 22 May - 30 Sep. 1992
August F. Witt Dec. 1993 13 p
(Grant NAG8-913)
(NASA-CR-194704; NAS 1.26:194704) Avail: CASI HC A03/MF A01

The research carried out under NAG8-913, 'Characterization of Convection Related Defects in II-VI Compound Semiconductors', was aimed at exploration of the potential of axial magnetic fields for melt stabilization when applied in Bridgman geometry to the growth of HgMnTe. The thrust of the work was directed at the experimental establishment of the limits of magnetic melt stabilization during crystal growth and at the analytical verification of the effects of stabilization on critical materials properties. The data obtained indicate noticeable stabilization effects, particularly as far as the formation of microscopic compositional inhomogeneities is concerned. The effects of magnetic fields on precipitate formation are found to be minor. Magnetic field effects were investigated for both 'Bridgman' and 'travelling heater' geometries. The research was conducted during the period from May 22 to September 30, 1992. Author (revised)

N94-21805 Illinois Univ., Urbana. Dept. of Electrical and Computer Engineering.
THE n-p(p(+))-n Al(yGa)(1-y) As-GaAs-In(x)Ga(1-x) AS QUANTUM WELL LASER WITH p(+)-n(+)GaAs-InGaAs TUNNEL CONTACT ON n GaAs
A. R. Sugg, E. I. Chen, T. A. Richard, S. A. Maranowski, and N. Holonyak, Jr. 17 May 1993 4 p Repr. from Applied Physics Letters, v. 62, no. 20, 17 May 1993 p 2510-2512 Limited Reproducibility: More than 20% of this document may be affected by microfiche quality
(Contract DAAL03-92-G-0264)
(AD-A271292; ARO-30090.3-EL) Avail: Issuing Activity (Defense Technical Information Center (DTIC))

Data are presented on the growth, by metalorganic chemical vapor deposition, and fabrication of n-p (n-up) AlGaAs-GaAs-InGaAs quantum-well heterostructure lasers using a p(+)-n(+) GaAs-InGaAs reverse-biased tunnel junction to contact the n-type GaAs substrate. The lasers operate continuously at 300 K with a threshold of approximately 37 mA for a 10-micrometer-wide native-oxide-defined gain-guided stripe (cavity length approximately 375 micrometers). Comparison tunnel junctions similar to those used in the diode lasers are also fabricated and exhibit low reverse-biased series resistances (approximately 2.2 ohms, area approximately 4.5 times larger). DTIC

N94-21807*# National Aeronautics and Space Administration. Marshall Space Flight Center, Huntsville, AL.
INITIAL DEVELOPMENT OF A HIGH-PRESSURE CRYSTAL GROWTH FACILITY: CENTER DIRECTOR'S DISCRETIONARY FUND Final Report
F. R. Szofran, S. L. Lehoczky, S. D. Cobb, and D. C. Gillies Nov. 1993 10 p
(NASA-TM-108430; NAS 1.15:108430) Avail: CASI HC A02/MF A01

A low-cost, flexible, high-pressure (600 psi) system for crystal growth and related thermophysical properties measurements was designed, assembled, and tested. The furnace system includes a magnetically coupled translation mechanism that eliminates the need for a high-pressure mechanical feedthru. The system is currently being used for continuing crystal growth experiments and thermophysical properties measurements on several material systems including Hg(1-x)Cd(x)Te, Hg(1-x)Zn(x)Te, and Hg(1-x)Zn(x)Se. Author (revised)

N94-21831# Oak Ridge National Lab., TN.
SPIN-POLARON THEORY OF HIGH-T(c) SUPERCONDUCTIVITY. 3: GAP FUNCTION AND CRITICAL TEMPERATURE
R. F. Wood Jun. 1993 18 p Presented at the International Symposium

on High-Tc Superconductivity and Its Applications, Cairo, Egypt, 4-16 Apr. 1993
(Contract DE-AC05-84OR-21400)
(DE93-019198; CONF-9304191-2) Avail: CASI HC A03/MF A01

Results from previous papers in this series are used to derive approximate expressions for the gap and T(sub c) within the framework of a Cooper-pairing approach. The possible symmetry types of the gap are discussed. It is shown how the proximity of the Fermi level to the Mott-Hubbard band edge and the interplay of O 2p-sigma and 2p-pi bands and/or localization effects can provide good fits to the variation of T(sub c) with x in La(2-x)Sr(x)CuO4 and YBa2Cu3O(7-x). It is concluded that the in-plane gap is either s- or d-like but anisotropic in either case. Other aspects and implications of the model and of the calculations are given and comparisons with Mott's spin-bipolaron model are made. DOE

N94-21857# Los Alamos National Lab., NM.
THEORETICAL STUDIES OF THE STRUCTURES AND ELECTRONIC PROPERTIES OF U(NH2)(SUB 3) AND Np(NH2)(SUB 3)
P. J. Hay and R. L. Martin 1993 10 p Presented at the Actinides 1993 Conference, Santa Fe, NM, 19-24 Sep. 1993
(Contract W-7405-eng-36)
(DE94-000768; LA-UR-93-3375; CONF-930905-12) Avail: CASI HC A02/MF A01

The electronic structure of the model compounds U(NH2)(sub 3) and Np(NH2)(sub 3) is investigated with the aid of ab initio electronic structure techniques. The electronic ground states and equilibrium geometries of these complexes are determined using multi-configuration SCF techniques. Comparisons are made to their counterparts U(CH3)(sub 3) and Np(CH3)(sub 3). DOE

N94-21869 Lawrence Livermore National Lab., CA.
ENERGY-RESOLVING X RAY DETECTORS WITH CHARGE AMPLIFICATION DUE TO MULTIPLE QUASIPARTICLE TUNNELING
C. A. Mears, S. E. Labov, and A. T. Barfknecht (Conductus, Inc., Sunnyvale, CA.) 1993 4 p Presented at the International Superconductive Electronic Conference, Boulder, CO, 11-14 Aug. 1993 Limited Reproducibility: More than 20% of this document may be affected by microfiche quality
(Contracts W-7405-eng-48; DE-FG02-91ER-81190)
(DE93-019506; UCRL-JC-114285; CONF-930863-1) Avail: CASI HC A01

A single 6 keV x ray absorbed in a superconductor produces more than a million electrons in excited states, called quasiparticles. The number of quasiparticles is proportional to the energy of the incident x ray and can be determined by measuring the increase in tunneling current through a thin oxide barrier between two superconducting layers. The energy resolution of an x ray detector based on such a measurement in principle could be limited only by the statistical variation in the number of quasiparticles produced. If this is the case, the resolution for 6 keV x rays absorbed in niobium (Delta = 1.5 meV) should be better than 5 eV. While high resolution has been achieved with superconducting tunnel junction detectors, the best resolution obtained is about ten times worse than this limit. The energy resolution of previous work was often limited by electronic noise produced in the charge amplification system. In order to minimize the effects of electronic noise, we developed a detector using a new geometry where each quasiparticle produced is trapped near the tunnel barrier and tunnels several times before it recombines into a Cooper pair, thus increasing the charge measured for a given x-ray. Because of this larger charge, the contribution of electronic noise to the energy resolution of the detector is minimized. DOE

N94-21871# Argonne National Lab., IL.
FULLERENE DERIVATIVES AND FULLERENE SUPERCONDUCTORS
H. H. Wang, J. A. Schlueter, and A. C. Cooper 1993 36 p Presented at the US/Japan Seminar on Physics and Chemistry of C(sub 60) and Related Compounds, Honolulu, HI, 10-23 Jul. 1993
(Contract W-31-109-eng-38)
(DE93-019568; ANL/CHM/CP-80106; CONF-9307123-1) Avail: CASI HC A03/MF A01

A series of 1:1 C60 cycloaddition adducts, C60A (A = anthracene, butadiene, cyclopentadiene, and methyl cyclopentadiene), has been synthesized. The products are cleanly separated and characterized by use of TGA, H-1 NMR, IR, and mass spectrometry. Among these adducts, C60(methyl cyclopentadiene) showed the highest thermal stability and was doped with three equivalents of rubidium. The resulting Rb3C60(MeCp) is a semiconductor but can be thermally converted to the superconducting Rb3C60 through a retro-Diels-Alder reaction. A one-step doping process to prepare Rb3C60 crystals has been developed. The optimal doping condition occurs at approximately 300 degrees C. High superconducting shielding fractions between 60 and 90% and sharp transition widths (Delta-T(sub 10-90) between 4 and 0.7 K) were measured for these samples. DOE

N94-21922# California Univ., Berkeley. Lawrence Berkeley Lab.
HYDROGEN IN COMPOUND SEMICONDUCTORS
E. E. Haller May 1993 10 p Presented at the 12th Record of Alloy Semiconductor Physics and Electronics Symposium, Izunagaoka, Japan, 14-16 Jul. 1993
(Contract DE-AC03-76SF-00098)
(DE93-040300; LBL-34395; CONF-9307139-1) Avail: CASI HC A02/MF A01

Progress in the understanding of hydrogen and its interactions in III/V and II/VI compound semiconductors is reviewed. Donor, acceptor, and deep level passivation is well established in III/V compounds based on electrical measurements and on spectroscopic studies. The hydrogen donor levels in GaAs and GaP are estimated to lie near E(sub v)+0.5 eV and E(sub v)+0.3 eV, respectively. Arsenic acceptors have been passivated by hydrogen in CdTe and the very first nitrogen-hydrogen local vibrational model spectra in ZnSe have been reported. This long awaited result may lead to an explanation for the poor activation of nitrogen acceptors in ZnSe grown by techniques which involve high concentrations of hydrogen. DOE

N94-21926# California Univ., Berkeley. Lawrence Berkeley Lab.
SPECIFIC HEAT OF YBa2Cu3O7
N. E. Phillips, J. P. Emerson, R. A. Fisher, B. F. Woodfield, D. A. Wright, and J. E. Gordon Aug. 1993 18 p Presented at the Physics and Chemistry of Molecular and Oxide Superconductors, Eugene, OR, 27-31 Jul. 1993
(Contract DE-AC03-76SF-00098)
(DE93-040640; LBL-34523; CONF-930710-2) Avail: CASI HC A03/MF A01

Specific heat measurements, including measurements in magnetic fields and at both low temperatures and near T(sub c), on a number of YBa2Cu3O7 samples have revealed several correlations among strongly sample dependent parameters. These correlations suggest that the sample dependence of the parameters reflects a sample dependence of the volume fraction of superconductivity, which is in turn correlated with a low concentration of Cu(2+) moments. The correlations give a criterion for recognizing the value of the parameters characteristic of the fully superconducting material. Preliminary results on effects of sample heat treatment are reported. New data on the 'linear term' is presented and discussed. DOE

N94-21930# Argonne National Lab., IL.
PHOTO- AND THERMAL-INDUCED ANTIFERROMAGNETIC INTERLAYER COUPLING IN Fe/(Fe-Si) SUPERLATTICES
J. E. Mattson, E. E. Fullerton, S. Kumar, S. R. Lee, C. H. Sowers, M. Grimsditch, S. D. Bader, and F. T. Parker (California Univ., San Diego, La Jolla.) Aug. 1993 20 p Presented at the Latin American Workshop on Magnetism, Guanujuato, Mexico, 23-28 Aug. 1993
(Contract W-31-109-eng-38)
(DE93-040822; ANL/MSD/CP-80646; CONF-9308175-1) Avail: CASI HC A03/MF A01

We have grown via sputtering, Fe - iron silicide superlattices that exhibit novel thermal and photomagnetic effects. For approximately 15 A nominal thickness of the silicide layer the superlattices are antiferromagnetically (AF) coupled at room temperature. Upon cooling below 100K, they gradually revert to ferromagnetic alignment, but the AF coupling is restored at low temperature by exposure to visible light off sufficient intensity (greater than 10 mW/mm(exp 2)). These effects are due to charge carriers in the silicide spacer layer which, when thermally or photo-generated, are capable of communicating spin information between the Fe layers. DOE

N94-21931# Argonne National Lab., IL.
DISKS OF YBa2Cu3O7 SHOCKED TO 10 GPa PRESSURES

W. J. Nellis, S. T. Weir, N. A. Hinsey, U. Balachandran, M. J. Kramer, and R. Raman (Ceracon, Inc., Sacramento, CA.) Aug. 1993 8 p Presented at the 14th International Conference of the International Association for the Advancement of High Pressure Science and Technology, Colorado Springs, CO, 27 Jun. - 2 Jul. 1993 Prepared in cooperation with LLNL, CA and Ames Lab., IA
(Contracts W-31-109-eng-38; W-7405-eng-48; W-7405-eng-82)
(DE94-000464; ANL/ET/CP-79207; UCRL-JC-113413; CONF-930676-53)
Avail: CASI HC A02/MF A01

The brittle superconducting oxide YBa2Cu3O7 was shocked to 6.6 and 10.3 GPa without macroscopic fracture. The melt-textured disk-shaped specimen was preferentially oriented and was shock-compressed at an angle of about 30 deg from the effective c axis of this orthorhombic-phase specimen. Subsequent anneals of the 6.6 GPa specimen in oxygen at 890 C produced a magnetic hysteresis which is enhanced relative to the initial unshocked state, as expected for shock-induced defects. DOE

N94-21932# Oak Ridge National Lab., TN.
STABILITY OF AN UNCOOLED SEGMENT OF A HIGH-TEMPERATURE SUPERCONDUCTOR
L. Dresner 1993 12 p Presented at the International Cryogenic Engineering Conference and International Cryogenic Materials Conference, Albuquerque, NM, 12-16 Jul. 1993
(Contract DE-AC05-84OR-21400)
(DE94-000476; CONF-930703-35) Avail: CASI HC A03/MF A01

If the level of a liquid cryogen inadvertently falls below the top of a magnet winding, it may expose a segment of the conductor. Depending on the length of the uncooled segment and on how the matrix resistivity varies with temperature, zero, one, or two steady normal states may be possible. The stability of the various steady states, the conditions under which they appear, their energies of formation, and the voltages they produce are studied in this paper. DOE

N94-21936# Iowa State Univ. of Science and Technology, Ames.
THE INCONGRUENT MELTING AND MELT TEXTURED SOLIDIFICATION PROCESS OF Bi2Sr2CaCu3O8 Ph.D. Thesis
J. Polonka 1993 118 p
(Contract W-7405-eng-82)
(DE93-041123; IS-T-1665) Avail: CASI HC A06/MF A02

The melting and solidification was studied using in-situ high temperature XRD from melting point to 900 C in 0.2, 0.1, 0.02 atm O2 and pure N2. The incongruent melting point of Bi2Sr2CaCu2O8 was lowered by decreasing the partial O2 pressure from 870 C (in .2 atm O2) to 830 C (in pure N2 atmosphere). As temperature was increased the incongruent melting of Bi2Sr2CaCu2O6 followed a phase sequence in which (Ca, Sr)CuO2 yields (Ca, Sr)CuO2 yields (Ca,Sr)O occur in presence of Bi-rich liquid. At 900 C, the only crystalline phase present in the melt was (Ca,Sr)O. This phase sequence remained the same for all four different partial O2 pressures. During the solidification of Bi2Sr2CaCuO8, from 10 C below the melting point to 760 C, the major phases that form depend on the partial O2 pressure. As partial O2 pressures was lowered from 0.2 to 0 atm, the major second phase formation out of the melt follows the sequence of (Ca, Sr)CuO2 yields (Ca,Sr)CuO2 Sr)CuO2 yields (Ca,Sr)O, respectively. At 0.1 atm partial O2 pressure and below, Bi2Sr2CaCu2O6 solidified out of the melt; at 0.2 atm of O2 Bi2Sr2CaCu2O6 forms instead. DOE

N94-21939# Sandia National Labs., Albuquerque, NM.
SIMPLE METHOD TO ESTIMATE MOS OXIDE-TRAP, INTERFACE-TRAP, AND BORDER-TRAP DENSITIES
D. M. Fleetwood, M. R. Shaneyfelt, and J. R. Schwank 1993 4 p Presented at the IEEE Semiconductor Interface Specialists Conference, Ft. Lauderdale, FL, 9-11 Dec. 1993
(Contract DE-AC04-76DP-00789)
(DE93-041138; SAND-93-1927C; CONF-931226-1) Avail: CASI HC A01/MF A01

Recent work has shown that near-interfacial oxide traps that communicates with the underlaying Si ('border traps') can play a significant role in determining MOS radiation response and long-term reliability. Thermally-stimulated-current 1/f noise, and frequency-dependent charge-pumping measurements have been used to estimate border-trap densities in MOS structures. These methods all require high-precision, low-noise measurements that are often difficult to perform and interpret. In this summary, we describe a new dual-transistor method to separate bulk-oxide-trap, interface-trap, and border-trap densities in irradiated MOS transistors that requires only standard threshold-voltage and high-frequency charge-pumping measurements. DOE

N94-21960# Lawrence Livermore National Lab., CA.
FABRICATION OF AMORPHOUS DIAMOND FILMS
S. Falabella, D. B. Boercker, and D. M. Sanders Apr. 1993 12 p Presented at the International Conference on Metallurgical Coatings and Thin Films, San Diego, CA, 19-23 Apr. 1993
(Contract W-7405-eng-48)
(DE94-000404; UCRL-JC-111960; CONF-930419-5) Avail: CASI HC A03/MF A01

Amorphous diamond (a:D) is a hard, electrically insulating, inert, and transparent form of carbon that has the sp3 bond character of crystalline diamond, but lacks a long-range ordered structure. Using our filtered cathodic arc system, we have produced a:D films at room temperature that demonstrate hardness above 8000 H(sub v), hydrogen content below 0.1%, density of 2.7 (plus or minus) 0.3 g/cc, and adhesion on tungsten carbide and silicon substrates above 10 kpsi. The fine structure of a:D was characterized by TEM and electron diffraction. TEM showed no evidence of any ordered structure down to 1 run. Unlike natural diamond or DLC, a:D has a flat transmission spectrum from 0.8 to over 50 which is due to its amorphous nature and the lack of hydrogen. Also, we determined the index of refraction of our a:D to be 2.47-2.57. The thermal diffusivity of a:D has been measured and reported for the first time. We have lowered the intrinsic stress in the films by the use of bias and the inclusion of impurity atoms, and produced films up to 8 gm thick on carbide tool bits. In addition, a molecular dynamics code has been used to model this material. DOE

N94-21972# Argonne National Lab., IL.
SPIN DYNAMICS AND IMPLICATIONS FOR SUPERCONDUCTIVITY: SOME PROBLEMS WITH THE d-WAVE SCENARIO
K. Levin (Chicago Univ., IL.), Y. Zha (Chicago Univ., IL.), R. J. Radtke (Chicago Univ., IL.), Q. Si (Rutgers Univ., Piscataway, NJ.), M. R. Norman, and H. B. Schuttler (Georgia Univ., Athens.) Sep. 1993 28 p Presented at the Physics and Chemistry of Molecular and Oxide Superconductors, Eugene, OR, 27-31 Jul. 1993
(Contract W-31-109-eng-38)
(DE94-001183; ANL/MSD/CP-80860; CONF-930710-3) Avail: CASI HC A03/MF A01

We review the spin dynamics of the normal state of the cuprates with special emphasis on neutron data in both the YBa2Cu3O(7-delta) and La(2-x)Sr(x)CuO4 systems. When realistic models of the Fermi surface shapes are incorporated, along with a moderate degree of spin fluctuations, we find good semi-quantiative agreement with experiment for both cuprates. Building on the success of this Fermi-liquid-based scheme, we explore the implications for d-wave pairing from a number of vantage points. We conclude that our present experimental and theoretical understanding is inadequate to confirm or refute the d-wave scenario. DOE

N94-21987# Los Alamos National Lab., NM.
MAGNETISM IN CeRu2Ge2 AND CeRh2Ge2 AND ITS PRESSURE DEPENDENCE
J. D. Thompson, T. Graf, Y. Uwatoko (Kumamoto Univ., Japan.), M. F. Hundley, D. Mandrus, C. Godart (Centre National de la Recherche Scientifique, Meudon-Bellevue, France.), L. C. Gupta (Centre National de la Recherche Scientifique, Meudon-Bellevue, France.), P. C. Canfield (Ames Lab., IA.), A. Migliori, and H. A. Borges 1993 14 p Presented at the International Conference on Strongly Correlated Electron Systems, La Jolla, CA, 16-19 Aug. 1993
(Contract W-7405-eng-36)
(DE93-040061; LA-UR-93-2919; CONF-930865-2) Avail: CASI HC A03/MF A01

We have studied magnetism in CeRu2Ge2 and CeRh2Ge2 through specific heat in zero and applied magnetic fields, dc magnetization, thermal expansion and electrical resistance measurements at pressures to 21 kbar. Both compounds have two transitions; although we argue that the higher one in CeRu2Ge2 is due to residual stress in the polycrystalline sample. The overall systematics are consistent with those found at ambient pressure in pseudoternaries formed with Si substitution for Ge. DOE

N94-21991# Los Alamos National Lab., NM.
TEMPERATURE DEPENDENCE OF MAGNETIC ORDER IN SINGLE-CRYSTALLINE UPdSn
R. A. Robinson, A. C. Lawson, J. W. Lynn, and H. Nakotte (Amsterdam Univ., Netherlands.) 1993 17 p Presented at the 38th Annual Conference on Magnetism and Magnetic Materials, Minneapolis, MN, 15-18 Nov. 1993
(Contract W-7405-eng-36)
(DE93-040153; LA-UR-93-3155; CONF-931133-1) Avail: CASI HC A03/MF A01

The noncollinear hexagonal antiferromagnet UPdSn exhibits two magnetic phase transitions, at 35.5 K and 23 K. The first transition is from a hexagonal paramagnetic state to a noncollinear antiferromagnetic state with a doubled unit cell (phase one). The second 23-K transition is to a monoclinic magnetic structure (phase two). Ever since these transitions were discovered, the question has been whether the moments simply rotate at 23 K, or whether the y- and z-components of the moment order at 35.5 K while the x-component orders out of incipient fluctuations at the lower 23-K transition. While previous powder studies were rather inconclusive on this point, we now present new single-crystal neutron diffraction results that show the second picture to be correct. In addition we discuss the structural distortions that accompany the change in symmetry and show that there is phase two type magnetic short range order between 23 K and 35.5 K. DOE

N94-21992# Argonne National Lab., IL.
SYNTHESIS AND CHARACTERIZATION OF CHARGE-SUBSTITUTED GARNETS YCaLnGa5O12 (Ln = Ce, Pr, Tb)
S. A. Gramsch and L. R. Morss 1993 15 p Presented at the 20th Rare Earth Research Conference, Monterey, CA, 12-17 Sep. 1993
(Contract W-31-109-eng-38)
(DE93-040227; ANL/CHM/CP-79242; CONF-9309142-4) Avail: CASI HC A03/MF A01

A low temperature method is described for the preparation of the new garnet compounds YCaLnGa5O12 (Ln=Ce, Pr, Tb). In this set of compounds Ca(2+) + Ln(4+) replaces 2 Y(3+) in the parent gallium based garnet Y3Ga5O12 in order to stabilize as effectively as possible the Ln(4+) species in the eight-coordinate 'A' site of the garnet structure. Characterization of the oxides by x-ray powder diffraction and thermogravimetric analysis is discussed with regard to the structural relationship of the substituted compound to the parent material. The tetravalent ions Pr(4+) and Tb(4+) exhibit increased thermal stability in reducing conditions as compared to the Ln(4+) states in the fluorite LnO2 and perovskite BaLnO3 type structures. This result is discussed with reference to the complex crystal chemistry of these systems. DOE

N94-21993# Argonne National Lab., IL.
CRYSTAL STRUCTURE AND SHORT-RANGE OXYGEN DEFECTS IN La- AND Nd-MODIFIED ZrO2
C. K. Loong, J. W. Richardson, Jr., M. Ozawa (Nagoya Inst. of Tech., Japan.), and M. Kimura (Toyota Central Research and Development Labs., Inc., Aichi, Japan.) 1993 11 p Presented at the 20th Rare Earth Research Conference, Monterey, CA, 12-17 Sep. 1993
(Contract W-31-109-eng-38)
(DE93-040229; ANL/IPNS/CP-79265; CONF-9309142-3) Avail: CASI HC A03/MF A01

The crystal structure of rare-earth modified zirconia and the associated oxygen defects were studied by neutron diffraction. A Rietveld analysis of the neutron powder patterns of heat treated samples of La- and Nd-10mol%-ZrO2 revealed the composition of a major tetragonal phase (space group P4(sub 2)/nmc) and a minor cubic phase (space group Fm3m). The short-range oxygen defects structure was examined by a Fourier-filtering technique. A real-space correlation function, obtained from a Fourier transform of the filtered residual diffuse scattering, showed evidence of static, oxygen-vacancy induced atomic displacements along the 111 and other directions of the pseudo-cubic cell. DOE

N94-21994 Argonne National Lab., IL.
MOCVD GROWTH AND STRUCTURE OF PbTiO3 THIN FILMS
Y. Gao (New Mexico Inst. of Mining and Technology, Socorro.), G. Bai, K. L. Merkle, H. L. M. Chang, and D. J. Lam Aug. 1993 7 p Presented at the Spring Meeting of the Materials Research Society, San Francisco, CA, 12-16 Apr. 1993 Limited Reproducibility: More than 20% of this document may be affected by poor print
(Contract W-31-109-eng-38)
(DE93-040230; ANL/MSD/CP-79239; CONF-930405-39) Avail: Issuing Activity (Department of Energy (DOE))

PbTiO3 thin films grown on (001)MgO and (110)MgO by MOCVD have been characterized by x-ray diffraction and transmission electron microscopy. The PbTiO3 films deposited on (001)MgO under the optimum conditions always show a bi-layer structure. The top layer of the films near the free surface is c-axis oriented with the orientation relationship (001) 100 PbTiO3 parallel (001) 100 MgO. The bottom layer of the films near the substrate is a-axis oriented with (100) 001 PbTiO3 parallel (001) 100 MgO. Ninety degree domains were observed, but only in the c-axis oriented layers. The thickness of the a-axis oriented layers near the substrate decreases with decreasing the cooling rate. PbTiO3 films deposited on (110) MgO, however, are single-layer, epitaxial films with (101) 001 PbTiO3 parallel (110) 001 MgO. DOE

N94-21997# Argonne National Lab., IL.
THE EFFECT OF CORRELATED AND POINT DEFECTS ON THE VORTEX LATTICE MELTING TRANSITION IN SINGLE CRYSTAL YBa2Cu3O(7-DELTA)
W. K. Kwok, S. Fleshler, U. Welp, J. Downey, G. W. Crabtree, and J. Fendrich Aug. 1993 31 p Presented at the Conference of the International Union of Pure and Applied Physics on Low Temperature Physics (LT 20), Eugene, OR, 1-11 Aug. 1993
(Contract W-31-109-eng-38)
(DE93-040277; ANL/MSD/CP-80634; CONF-930801-12) Avail: CASI HC A03/MF A01

The vortex melting transition T(sub m) in several untwinned and twinned crystals is measured resistively in fields up to 8 Tesla. A Lindemann criterion for vortex lattice melting is obtained in addition to a sharp hysteresis in the magnetoresistance at B(sub m) supporting a first order phase transition. The anisotropy of twin boundary pinning and its reduction of the 'kink' in (rho)(T) associated with the first order melting transition is discussed in samples with very dilute twin boundaries. We also report on direct suppression of melting transition by intrinsic pinning for H (parallel) ab and by electron-irradiation-induced point defects. DOE

N94-21998# Argonne National Lab., IL.
HIGH OXYGEN PRESSURE SYNTHESIS OF NEW COPPER OXIDE SUPERCONDUCTORS
B. Dabrowski, V. Zhang-MacCoy, Z. Wang, R. Hannon, J. D. Jorgensen, B. A. Hunter, D. G. Hinks, J. L. Wagner, and R. L. Hitterman Aug. 1993 10 p Presented at the Physics and Chemistry of Molecular and Oxide Superconductors, Eugene, OR, 27-31 Jul. 1993
(Contract W-31-109-eng-38)
(DE93-040278; ANL/MSD/CP-80635; CONF-930710-1) Avail: CASI HC A02/MF A01

The unique coordination of the copper ions in +1, +2, and +3 oxidation states which are stable in a range of oxygen partial pressure, 10(exp -6) less than P(O2) less than 10(exp 3) atm, makes possible the formation of a wide variety of distinct structures. By controlling the oxygen pressure during the synthesis and annealing, the distribution of metal- and oxygen ions can be modified on an atomic scale to optimize the structural and electronic properties. We present several examples of compounds for which the critical structural elements for superconductivity, i.e. the perfectly ordered CuO2-planes, have been obtained and doped with holes by means of high oxygen pressure, P(O2) greater than 1 atm. These materials, La22CuO(4+delta), La(2-x)Ca(x)CuO4 and YSr(2-x)La(x)Cu3O(7+delta) offer a unique opportunity to study the relationship between superconductivity and structural, magnetic, and chemical properties. DOE

N94-21999# Argonne National Lab., IL.
TEMPERATURE-DEPENDENT ION BEAM MIXING
L. E. Rehn and D. E. Alexander Aug. 1993 8 p Presented at the International Union of Materials Research Societies on Advanced Materials, Tokyo, Japan, 31 Aug. - 4 Sep. 1993
(Contract W-31-109-eng-38)
(DE93-040281; ANL/MSD/CP-78737; CONF-9308122-4) Avail: CASI HC A02/MF A01

Recent work on enhanced interdiffusion rates during ion-beam mixing

at elevated temperatures is reviewed. As discussed previously, the expected increase in ion-beam mixing rates due to radiation-enhanced diffusion (RED), i.e. the free migration of isolated vacancy and interstitial defects, is well documented in single-crystal specimens in the range of 0.4 to 0.6 of absolute melting temperature. In contrast, the increase often observed at somewhat lower temperatures during ion-beam mixing of polycrystalline specimens is not well understood. However, sufficient evidence is available to show that this increase reflects intracascade enhancement of a thermally-activated process that also occurs without irradiation. Recent evidence is presented which suggests that this process is Diffusion-induced Grain-Boundary Migration (DIGM). An important complementary conclusion is that because ion-beam mixing in single-crystal specimens exhibits no significant temperature dependence below that of RED, models that invoke only irradiation-specific phenomena, e.g., cascade-overlap, thermal-spikes, or liquid-diffusion, and hence which predict no difference in mixing behavior between single- or poly-crystalline specimens, cannot account for the existing results. DOE

N94-22005# Arizona Univ., Tucson.
A QUANTITATIVE MODEL FOR INTERPRETING NANOMETER SCALE HARDNESS MEASUREMENTS OF THIN FILMS
W. H. Poisl, B. D. Fabes, and W. C. Oliver (Oak Ridge National Lab., TN.) 1993 8 p Presented at the Spring Meeting of the Materials Research Society, San Francisco, CA, 12-16 Apr. 1993
(Contracts DE-AC05-84OR-21400; DE-AC05-76OR-00033)
(DE93-040601; CONF-930405-40) Avail: CASI HC A02/MF A01

A model was developed to determine hardness of thin films from hardness versus depth curves, given film thickness and substrate hardness. The model is developed by dividing the measured hardness into film and substrate contributions based on the projected areas of both the film and substrate under the indenter. The model incorporates constraints on the deformation of the film by the surrounding material in the film, the substrate, and friction at the indenter/film and film/substrate interfaces. These constraints increase the pressure that the film can withstand and account for the increase in measured hardness as the indenter approaches the substrate. The model is evaluated by fitting the predicted hardness versus depth curves obtained from titanium and Ta2O5 films of varying thicknesses on sapphire substrates. The model is also able to describe experimental data for Ta2O5 films on sapphire with a carbon layer between the film and the substrate by a reduction in the interfacial strength from that obtained for a film without an interfacial carbon layer. DOE

N94-22007# Sandia National Labs., Albuquerque, NM.
NMR STUDIES OF OXYGEN-DOPED La2CuO(4+DELTA)
P. C. Hammel, A. P. Reyes, E. T. Ahrens, D. E. MacLaughlin, J. D. Thompson, Z. Fisk, P. C. Canfield, S. W. Cheong (Los Alamos National Lab., NM.), and J. E. Schirber 11 Aug. 1993 14 p Presented at the International Conference on Strongly Correlated Electronic Systems, San Diego, CA, 15-19 Aug. 1993
(Contract DE-AC04-76DP-00789)
(DE93-040756; SAND-93-1979C; LA-UR-93-2879; CONF-9308173-1)
Avail: CASI HC A03/MF A01

The observation that the structure of this material is sensitive to levels of doping sufficient to produce superconductivity (T sub c approximately = 40 K) suggests an important role for structure in determining its electronic properties. We discuss unusual features of phase separation and studies of cooling rate dependence of the superconducting (T sub c) relevant to this proposition. DOE

N94-22016# Oak Ridge National Lab., TN.
LATTICE DAMAGE DURING ION IMPLANTATION OF SEMICONDUCTORS
T. E. Haynes Aug. 1993 6 p Presented at the International Union of Materials Research Societies on Advanced Materials, Tokyo, Japan, 31 Aug. - 4 Sep. 1993
(Contract DE-AC05-84OR-21400)
(DE94-000335; CONF-9308122-6) Avail: CASI HC A02/MF A01

The temperature dependence of the lattice damage created during ion implantation of Si, Ge, Si-Ge alloys, and various III-V compounds is reviewed and interpreted in terms of a transition between two different damage formation mechanisms. Implications of this transition for control of damage, annealing, and electrical activation are discussed, particularly in GaAs. DOE

N94-22028# Oak Ridge National Lab., TN.
TEMPERATURE DEPENDENCE OF CsI(Tl) GAMMA RAY EXCITED SCINTILLATION CHARACTERISTICS Ph.D. Thesis
1993 171 p
(Contracts DE-AC05-76OR-00033; DE-FG02-86NE-37969; DE-AC03-76SF-00098)
(DE94-000836; DOE/OR-00033/T542) Avail: CASI HC A08/MF A02

Gamma-ray excited emission spectrum, absolute scintillation yield, rise and decay time constants, and thermoluminescence emissions of CsI(Tl) were measured at -100 to +50 C, for crystals from 4 different vendors. The thermoluminescence glow curves were the only property that varied significantly from crystal to crystal; room temperature operation in current mode could be susceptible to temperature fluctuations. The CsI(Tl) emission spectrum has emission bands peaking around 400 and 560 nm; the former band disappears between -50 and -75 C. The RT absolute scintillation yield was calculated to be 65,500 +/- 4,100 photons/MeV. The two primary decay time constants increase exponentially with inverse temperature. An ultra-fast decay component was confirmed. Applications are discussed. DOE

N94-22035# Los Alamos National Lab., NM.
CRYSTAL ORIENTATION DEPENDENCE OF ELASTIC PRECURSOR STRENGTH IN PENTAERYTHRITOL TETRANITRATE
J. J. Dick, M. C. Whitehead, and A. R. Martinez 1993 5 p Presented at the 14th International Conference of the International Association for the Advancement of High Pressure Science and Technology, Colorado Springs, CO, 27 Jun. - 2 Jul. 1993
(Contract W-7405-eng-36)
(DE93-018340; LA-UR-93-2343; CONF-930676-23) Avail: CASI HC A01/MF A01

Elastic precursor shock strengths were measured using VISAR instrumentation on pentaerythritol tetranitrate crystals 2.9 to 6.4 mm thick. Input shock strength was 1.2 GPa. A factor of 3 difference in elastic shock strength and a factor of 2 difference in critical resolved shear stress were observed depending on the crystal orientation. The order of increasing elastic shock strength was (100), (101), (110), and (001). This is the same order as that obtained in our analysis for increasing steric hindrance to shear, indicating that the relative strength of different orientations of this molecular crystal under shock conditions is governed by steric hindrance to shear. DOE

N94-22041# California Univ., Berkeley. Lawrence Berkeley Lab.
QUANTITATIVE ANALYSIS OF SCANNING TUNNELING MICROSCOPY IMAGES FOR SURFACE STRUCTURE DETERMINATION: SULFUR ON Re(0001)
D. F. Ogletree, J. C. Dunphy, M. B. Salmeron, and P. Sautet (Ecole Normale Superieure, Lyon, France.) Feb. 1993 15 p Presented at the OE/LASE 1993 SPIE Conference, Los Angeles, CA, 13-23 Jan. 1993
(Contract DE-AC03-76SF-00098)
(DE93-019235; LBL-33786; CONF-930159-54) Avail: CASI HC A03/MF A01

Scanning Tunneling Microscopy (STM) images of adsorbed atoms and molecules on single crystal substrates provide important information on surface structure and order. In many cases images are interpreted qualitatively based on other information on the system. To obtain quantitative information, a theoretical analysis of the STM image is required. A new method of calculating STM images is presented that includes a full description of the STM tip and surface structure. This method is applied to experimental STM images of sulfur adsorbed on Re(0001). Effects of adsorption site, adsorbate geometry, tip composition and tunnel gap resistance on STM image contrast are analyzed. The chemical identity of tip apex atom and substrate subsurface structure are both shown to significantly affect STM image contrast. DOE

N94-22050# Lawrence Livermore National Lab., CA.
A SPHEROMAK IGNITION EXPERIMENT REUSING MIRROR FUSION TEST FACILITY (MFTF) EQUIPMENT
T. K. Fowler 28 Sep. 1993 36 p

(Contract W-7405-eng-48)
(DE94-001856; UCRL-ID-114696) Avail: CASI HC A03/MF A01

Based on available experimental results and theory, a scenario is presented to achieve ohmic ignition in a spheromak by slow (approximately 10 sec.) helicity injection using power from the Mirror Fusion Test Facility (MFTF) substation. Some of the other parts needed (vacuum vessel, coils, power supplies, pumps, shielded building space) might also be obtained from MFTF or other salvage, as well as some components needed for intermediate experiments for additional verification of the concept (especially confinement scaling). The proposed ignition experiment would serve as proof of principle for the spheromak DT fusion reactor design published by Hagenson and Krakowski, with a nuclear island cost about ten times less than a tokamak of comparable power. Designs at even higher power density and lower cost might be possible using Christofilos' concept of a liquid lithium blanket. Since all structures would be protected from neutrons by the lithium blanket and the tritium inventory can be reduced by continuous removal from the liquid blanket, environmental and safety characteristics appear to be favorable. DOE

N94-22273 Katholieke Univ., Nijmegen (Netherlands).
GROWTH AND MORPHOLOGY OF CRYSTALS: THEORY AND OBSERVATIONS Thesis
L. Vogels 1993 170 p Sponsored by Nederlandse Organisatie voor Wetenschappelijk Onderzoek, The Hague Limited Reproducibility: More than 20% of this document may be affected by microfiche quality
(PB93-221166; ISBN-90-9003857-4) Avail: Issuing Activity (National Technical Information Service (NTIS))

In the thesis, crystal growth and morphology, and the relationship between morphology and structure are investigated. Experimental observations and theoretical predictions on the growth and morphology of NH4N03, ((CH3)4N)2ZnCl(4-x)Br(x), and beta-triacyl-glycerol crystals based on the periodic bond chain approach are compared. The results of a study of in situ crystal growth of potassium hydrogenphthalate utilizing an on line digital imaging processing technique are presented. NTIS

N94-22385# Oak Ridge National Lab., TN.
SIMULATING THE EUCLIDEAN TIME SCHROEDINGER EQUATIONS USING AN INTEL IPSC/860 HYPERCUBE: APPLICATION TO THE t-J MODEL OF HIGH-T(SUB c) SUPERCONDUCTIVITY
M. D. Kovarik and T. Barnes 1993 14 p Presented at the 6th Annual Workshop on Recent Developments in Computer Simulation Studies in Condensed Matter Physics, Athens, GA, 22-26 Feb. 1993
(Contract DE-AC05-84OR-21400)
(DE94-000489; CONF-9302137-2) Avail: CASI HC A03/MF A01

We describe a Monte Carlo simulation of a dynamical fermion problem in two spatial dimensions on an Intel iPSC/860 hypercube. The problem studied is the determination of the dispersion relation of a dynamical hole in the t-J model of the high temperature superconductors. Since this problem involves the motion of many fermions in more than one spatial dimension, it is representative of the class of systems that suffer from the 'minus sign problem' of dynamical fermions which has made Monte Carlo simulation very difficult. We demonstrate that for small values of the hole hopping parameter one can extract the entire hole dispersion relation using the GRW Monte Carlo algorithm, which is a simulation of the Euclidean time Schroedinger equation, and present results on 4 x 4 and 6 x 6 lattices. Generalization to physical hopping parameter values will only require use of an improved trial wavefunction for importance sampling. DOE

N94-22387# Los Alamos National Lab., NM.
LOW TEMPERATURE ABSORPTION SPECTRA AND GROUND STATE ELECTRONIC STRUCTURE OF TETRAKIS(2,6-DI-TERT-BUTYLPHENOXIDE)URANIUM(IV)
J. M. Berg 1993 7 p Presented at the Actinides 1993, Santa Fe, NM, 19--24 Sep. 1993
(Contract W-7405-eng-36)
(DE94-000774; LA-UR-93-3333; CONF-930905-16) Avail: CASI HC A02/MF A01

The optical spectroscopy of the homoleptic U(IV) aryloxide compound U(O-2,6-t-Bu2C6H34 could give unique insight into actinide electronic structure because the complex has unusually high symmetry. Its synthesis and characterization were described in a recent paper. The characterization included presentation of several optical spectra in solution accompanied by a brief, qualitative discussion of the molecular properties that give rise to the observed features. This paper presents optical absorption data on microcrystalline solid samples at low temperature. Discussion of the data focuses generally on effect of the ligands on 5f2 electronic configuration of central U(IV) ion and specifically on properties of the ground state and the lowest lying electronic state. DOE

N94-22564# Argonne National Lab., IL.
ORIENTATIONALLY INDEPENDENT ANTIFERROMAGNETIC COUPLING IN EPITAXIAL Fe/Cr (211) AND (100) SUPERLATTICES
E. E. Fullerton, M. J. Conover, J. E. Mattson, C. H. Sowers, and S. D. Bader Sep. 1993 13 p Presented at the 38th Annual Conference on Magnetism and Magnetic Materials, Minneapolis, MN, 15-18 Nov. 1993
(Contract W-31-109-eng-38)
(DE94-001270; ANL/MSD/CP-79906; CONF-931133-3) Avail: CASI HC A03/MF A01

We present structural and magnetic characterization of epitaxial Fe/Cr (211) and Fe/Cr (100) superlattices grown simultaneously on MgO (110) and MgO (100) substrates by magnetron sputtering. The epitaxial orientation of the Fe/Cr (211) superlattice with the MgO (110) substrates is Fe/Cr 0 bar-1 1 // MgO 001 and the orientation of Fe/Cr (100) is Fe/Cr 001 // MgO 011. We find that for both orientations, the interlayer coupling oscillates in sign with a period of 18 A and, furthermore, that the strength and phase of the magnetic coupling are also nearly identical for these two orientations. DOE

N94-22565# Argonne National Lab., IL.
SPECTROSCOPIC STUDIES OF MAGNETIC TRANSITIONS IN TbPO4
G. K. Liu, C.-K. Loong, F. Trouw, M. M. Abraham (Oak Ridge National Lab., TN.), and L. A. Boatner (Oak Ridge National Lab., TN.) 1993 13 p Presented at the 38th Annual Conference on Magnetism and Magnetic Materials, Minneapolis, MN, 15-18 Nov. 1993
(Contracts W-31-109-eng-38; DE-AC05-84OR-21400)
(DE94-001274; ANL/CHM/CP-80906; CONF-931133-2) Avail: CASI HC A03/MF A01

Rare earth orthophosphates, RPO4 (R = Tb to Lu), crystallize in the tetragonal zircon structure in which R occupies sites of D(sub 2d) symmetry. The R = Tb, Dy, Ho compounds order antiferromagnetically at low temperature with the rare earth moments parallel to the crystallographic c-axis. In TbPO4 the magnetic transition is accompanied by a cooperative Jahn-Teller effect involving Tb ion-lattice coupling which induces a tetragonal to monoclinic distortion of the crystal lattice and a readjustment of the Tb electronic states as required by the lowering of the rare earth site symmetry. The laser excitation and emission spectra of TbPO4 and 0.1% Tb doped YPO4 single crystals were studied below and above the phase transition temperature. Line shapes of transitions in the stoichiometric compound are unusually broad and asymmetric whereas those for the dilute compound are sharp. The TbPO4 spectra show an anomalous temperature dependence near the phase transitions, indicating strong interactions of rare earth ions with environment. Comparison of the optical results with neutron scattering is made. DOE

N94-22570# Oak Ridge National Lab., TN.
TEST RESULTS OF TWO HIGH TEMPERATURE SUPERCONDUCTING SAMPLE COILS
J. W. Lue, S. W. Schwenterly, M. S. Lubell, J. N. Luton, C. H. Joshi, L. J. Masur, and E. R. Podtburg 1993 8 p Presented at the International Cryogenic Engineering and Material Conference, Albuquerque, NM, 12-16 Jul. 1993
(Contract DE-AC05-84OR-21400)
(DE94-000496; CONF-930703-36) Avail: CASI HC A02/MF A01

Electrical measurements have been performed on two high temperature superconducting coils made by American Superconductor Corporation. One coil measured 24-mm ID, 59-mm OD, 50-mm long, and used 85-m long Y-124 tape conductor. The other coil measured 29-mm ID, 44-mm OD, 43-mm long, and used 35-m long Bi-2223 tape conductor. V-I curves were measured from room to helium temperature in a variable temperature cryostat cooled by helium gas in external fields up to 5 T. Without external field, the better performing Bi-2223 coil had a critical current, I(sub c) of 14.1 A (2820 A/sq cm over the conductor) at 4.2 K and 1.8 A (360 A/sq cm) at 77 K. At 5 T, I(sub c) was 4.9 A (980 A/sq cm) at 4.2 K and 2.0 A (400 A/sq cm) at 50 K. Reduced critical current, I(sub c)(B)/I(sub c)(0) vs field

plots indicated that a single smooth curve could fit all the data of up to 50 K in temperature. The reduction in critical currents with external fields for the Y-124 coil was more than 80% at 1 T. For the Bi-2223 coil, it was about 38% at 1 T and about 61% at 5 T. DOE

N94-22582# Iowa State Univ. of Science and Technology, Ames.
MELT-SPIN PROCESSING OF HIGH (Tc) OXIDE SUPERCONDUCTORS
T. J. Folkerts, Hengning Wu, S. I. Yoo, B. D. Merkle, S. R. Arrasmith, K. W. Dennis, M. J. Kramer, and R. W. McCallum 1993 4 p Presented at the 122nd Annual Meeting of the Minerals, Metals and Materials Society, Denver, CO, 21-25 Feb. 1993
(Contracts W-7405-eng-82; DE-FG02-90ER-45427)
(DE94-000696; IS-M-766; CONF-9302103-6) Avail: CASI HC A01/MF A01

Containerless techniques offer distinct advantages for the melt processing of oxide superconductors. The majority of these materials form liquids which are highly reactive with standard crucible materials such as Al2O3 and Pt, resulting in non-negligible contamination. We have developed a containerless melt-spin processing technique wherein 50-400 micron particles of REBa2Cu3O(7-x) high temperature oxide superconductors are melted in free fall through a vertical tube furnace and quenched onto a copper wheel. Previously this method has been successful in producing glasses of NdBa2Cu3O(7-x) and GdBa2Cu3O(7-x). In this report we discuss the results for both stoichiometric and non-stoichiometric YBa2Cu3O(7-x) (Y123). Thermal, microstructural, and superconducting characterization of both the as-quenched and the annealed materials will be presented. DOE

N94-22583# Los Alamos National Lab., NM.
INITIAL OPERATION OF A LARGE-SCALE PLASMA SOURCE ION IMPLANTATION EXPERIMENT
B. P. Wood, I. Henins, R. J. Gribble, W. A. Reass, R. J. Faehl, M. A. Nastasi, and D. J. Rej 1993 20 p Presented at the Workshop on Plasma-Based Ion Implantation, Madison, WI, 4-6 Aug. 1993
(Contract W-7405-eng-36)
(DE94-000805; LA-UR-93-3216; CONF-9308156-2) Avail: CASI HC A03/MF A01

In Plasma Source Ion Implantation (PSII), a workpiece to be implanted is immersed in a weakly ionized plasma and pulsed to a high negative voltage. Plasma ions are accelerated toward the workpiece and implanted in its surface. Experimental PSII results reported in the literature have been for small workpieces. A large scale PSII experiment has recently been assembled at Los Alamos, in which stainless steel and aluminum workpieces with surface areas over 4 sq m have been implanted in a 1.5 m-diameter, 4.6 m-length cylindrical vacuum chamber. Initial implants have been performed at 50 kV with 20 micro-s pulses of 53 A peak current, repeated at 500 Hz, although the pulse modulator will eventually supply 120 kV pulses of 60 A peak current at 2 kHz. A 1,000 W, 13.56 MHz capacitively-coupled source produces nitrogen plasma densities in the 10(exp 15) m(exp -3) range at neutral pressures as low as 0.02 mtorr. A variety of antenna configurations have been tried, with and without axial magnetic fields of up to 60 gauss. Measurements of sheath expansion, modulator voltage and current, and plasma density fill-in following a pulse are presented. The authors consider secondary electron emission, x-ray production, workpiece arcing, implant conformality, and workpiece and chamber heating. DOE

N94-22584# Los Alamos National Lab., NM.
ALLOYING STUDIES IN U(1-x)Th(x)Pd2Al3 (0 (le) X (le) 1)
Y. Dalichaouch (California Univ., San Diego.) and M. B. Maple 1993 7 p Presented at the International Conference on Strongly Correlated Electronic Systems, San Diego, CA, 15-19 Aug. 1993
(Contracts W-7405-eng-36; DE-FG03-86ER-45230)
(DE94-000807; LA-UR-93-3143; CONF-9308173-3) Avail: CASI HC A02/MF A01

Measurements of temperature and concentration dependences of magnetic susceptibility and electrical resistivity for U(1-x)Th(x)Pd(2)Al(3) are presented. The magnetic susceptibility data scale with the concentration of U ions over large regions of x and T. The electrical resistivity shows a smooth evolution from the Kondo lattice regime to the single ion Kondo behavior as Th concentration x is increased. A lack of saturation in resistivity in the samples with x = 0.8 and 0.6, and a logarithmic divergence in (chi)(T) at low temperatures makes the U(1-x)Th(x)Pd2Al3 system a good candidate for a two-channel Kondo effect. DOE

N94-22594# Lawrence Livermore National Lab., CA.
POSITRON ANNIHILATION STUDY OF Sr DOPING IN La(2-x)Sr(x)CuO4
P. A. Sterne, R. H. Howell, M. J. Fluss, and J. H. Kaiser (Texas Univ., Arlington.) 22 Apr. 1993 10 p Presented at the Conference on Spectroscopies in Novel Superconductors, Santa Fe, NM, 17-19 Mar. 1993 (Contract W-7405-eng-48)
(DE94-000307; UCRL-JC-112045; CONF-930367-10) Avail: CASI HC A02/MF A01

A combined experimental and threshold study of effects of Sr doping on electronic structure of La(2-x)Sr(x)CuO(4) was presented. Electron-positron momentum distributions were measured to high statistical precision (greater than 4 x 10(exp 8) counts) at room temperature for samples with Sr concentrations of x = 0.0, 0.1, 0.13, and 0.2. Analysis of all four spectra reveal strong features due to electron-positron wavefunction overlap, in quantitative agreement with theoretical calculations. The Sr doped samples show discontinuities consistent with presence of a Fermi surface. The form and position of these features are in general agreement with the predictions of band theory. Correspondence between theory and experiment, as well as some differences, are revealed by a detailed study of the changes in electron-position momentum density with increasing Sr doping. DOE

N94-20509*# National Aeronautics and Space Administration. Lewis Research Center, Cleveland, OH.
ELLIPSOMETRIC STUDY OF Si(0.5)Ge(0.5)/Si STRAINED-LAYER SUPERLATTICES
R. M. Sieg (Cleveland State Univ., OH.), S. A. Alterovitz, E. T. Croke (Hughes Research Labs., Malibu, CA.), and M. J. Harrell (Hughes Research Labs., Malibu, CA.) *In its* Solid State Technology Branch of NASA Lewis Research Center: Fifth Annual Digest Aug. 1993 p 135-137 Repr. from American Physics Inst., Applied Physics Letter, v. 62, no. 14, 5 Apr. 1993 (For primary document see N94-20497 05-32)
Avail: CASI HC A01/MF A03

N94-20510*# National Aeronautics and Space Administration. Lewis Research Center, Cleveland, OH.
SPECTROSCOPIC ELLIPSOMETRIC CHARACTERIZATION OF Si/Si(1-x)Ge(x) STRAINED-LAYER SUPERLATTICES
H. Yao (Nebraska Univ., Lincoln.), J. A. Woollam (Nebraska Univ., Lincoln.), P. J. Wang (International Business Machines Corp., Hopewell Junction, NY.), M. J. Tejwani (International Business Machines Corp., Hopewell Junction, NY.), and S. A. Alterovitz *In its* Solid State Technology Branch of NASA Lewis Research Center: Fifth Annual Digest Aug. 1993 p 139-143 Repr. from Applied Surface Science, v. 63, 1993 p 52-56 (For primary document see N94-20497 05-32)
(Grant NAG3-154)
Avail: CASI HC A01/MF A03

N94-20515*# National Aeronautics and Space Administration. Lewis Research Center, Cleveland, OH.
TEN GHz YBa2Cu3O(7-DELTA) SUPERCONDUCTING RING RESONATORS ON NdGaO3 SUBSTRATES
H. Y. To (Ohio State Univ., Columbus.), G. J. Valco (Ohio State Univ., Columbus.), and K. B. Bhasin *In its* Solid State Technology Branch of NASA Lewis Research Center: Fifth Annual Digest Aug. 1993 p 203-208 Repr. from Superconducting Scientific Technology, v. 5, 1992 p 421-426 (For primary document see N94-20497 05-32)
(Contract NCC3-197)
Avail: CASI HC A02/MF A03

N94-20519*# National Aeronautics and Space Administration. Lewis Research Center, Cleveland, OH.
THE EFFECT OF FLUCTUATIONS ON THE ELECTRICAL TRANSPORT BEHAVIOR IN YBa2Cu3O(7-x)
Satish Vitta (Indian Inst. of Tech., Bombay.), S. A. Alterovitz, and M. A. Stan (Kent State Univ., OH.) *In its* Solid State Technology Branch of NASA Lewis Research Center: Fifth Annual Digest Aug. 1993 p 255-262 Repr. from Journal of Physics: Condens. Matter, v. 4, 1992 p

7891-7898 (For primary document see N94-20497 05-32)
(Grant NAG4-0751)
Avail: CASI HC A02/MF A03

N94-21084*# Phillips Lab., Kirtland AFB, NM.
EVALUATION OF RADIATION EFFECTS IN RE-OXIDIZED NITRIDED OXIDE DEVICES BY HOT CARRIER STRESSING AT 77 K
N. C. Das and V. Nathan *In* New Mexico Univ., The Fifth NASA Symposium on VLSI Design 1993 7 p Sponsored in part by AF Materiel Command and NSF (For primary document see N94-21079 05-33)
Avail: CASI HC A02/MF A06

N94-22176 Defence Research Establishment Valcartier (Quebec).
THIN-FILM FABRICATION OF Pb-DOPED BiSrCaCuO SUPERCONDUCTOR
Linh Ngo Phong, Bruno Tremblay, Dominic Cote, Ishiang Shih (McGill Univ., Montreal, Quebec.), and Cindy X. Qiu (McGill Univ., Montreal, Quebec.) *In* Engineering Inst. of Canada, Canadian Conference on Electrical and Computer Engineering, Volumes 1 and 2 1991 4 p (For primary document see N94-22101 05-33)
Avail: Issuing Activity (Engineering Inst. of Canada, 2050 rue Mansfield, Suite 700, Montreal, PQ H3A 1Z2 Canada)

77 THERMODYNAMICS AND STATISTICAL PHYSICS

Includes quantum mechanics; theoretical physics; and Bose and Fermi statistics.

For related information see also *25 Inorganic and Physical Chemistry* and *34 Fluid Mechanics and Heat Transfer.*

N94-19831 Army Research Lab., Aberdeen Proving Ground, MD.
FURTHER EXAMINATIONS ON THE THERMODYNAMIC STABILITY OF THE MIE-GRUENEISEN EQUATION OF STATE Final Report, Jan. 1991 - Jul. 1993
Steven B. Segletes Oct. 1993 28 p Limited Reproducibility: More than 20% of this document may be affected by microfiche quality
(DA Proj. 1L1-62618-AH-80)
(AD-A270526; ARL-TR-234) Avail: CASI HC A03

The Mie-Grueneisen equation of state (EOS) is further examined for restrictions upon the form of the Grueneisen parameter. Employing basic thermodynamic rules and applying them to the Mie-Grueneisen EOS, a more restrictive condition is offered for the Grueneisen parameter, which extends previous work on the subject. DTIC

N94-20178 International Centre for Theoretical Physics, Trieste (Italy).
ON THE TWISTED N=2 SUPERCONFORMAL STRUCTURE IN 2d GRAVITY COUPLED TO MATTER
S. Panda (Institute for Theoretical Physics, Groningen, Netherlands.) and S. Roy May 1993 Limited Reproducibility: More than 20% of this document may be affected by microfiche quality
(DE93-628627; IC-93/81; UG-3/93) Avail: CASI HC A01 (US Sales Only)

It is shown that the two dimensional gravity, described either in the conformal gauge (Liouville theory) or in the light cone gauge, when coupled to matter processes an infinite number of twisted N = 2 superconformal symmetries. The central charges of the N = 2 algebra for the two gauge choices are in general different. Further, it is argued that the physical states in the light cone gauge theory can be obtained from the Liouville theory by a field redefinition. DOE

N94-20473# IIT Research Inst., Bartlesville, OK.
THE THERMODYNAMIC PROPERTIES TO 700 K OF NAPHTHALENE AND 2,7-DIMETHYLNAPHTHALENE
R. D. Chirico, S. E. Knipmeyer, A. Nguyen, and W. V. Steele Aug. 1993 57 p
(Contract DE-FC22-83FE-60149)
(DE93-000160; NIPER-678) Avail: CASI HC A04/MF A01

Measurements leading to the calculation of the ideal-gas thermodynamic properties are reported for naphthalene and 2,7-dimethylnaphthalene. Experimental methods included adiabatic heat-capacity calorimetry, vibrating-tube densitometry, comparative ebulliometry, and differential-scanning calorimetry (d.s.c.). The critical temperature and critical density were determined experimentally for each compound and the critical pressures were derived from fitting procedures. Vapor-pressure measurements reported in the literature were compared with the results obtained in this research. Enthalpies of vaporization and sublimation were derived from the experimental measurements and compared with literature results. New self-consistent equations for the variation of sublimation pressure with temperature for naphthalene and 2,7-dimethylnaphthalene were derived. Literature values for entropies and enthalpies of the liquid phases and energies of combustion were combined with the present results to derive entropies, enthalpies, and Gibbs energies of formation for the ideal gases for selected temperatures between 298.15 K and 700 K. The ideal-gas properties for naphthalene were compared with values obtained using statistical mechanics with various fundamental vibrational frequency assignments available in the literature. A scheme to estimate the ideal-gas thermodynamic functions for alkylnaphthalenes was updated. The barrier to methyl-group rotation in 2,7-dimethylnaphthalene was shown to be of the same order of magnitude as that published for toluene. Values for ideal-gas entropies for 2-methylnaphthalene in the temperature range 300 K to 700 K were estimated. DOE

N94-20945# Aerospace Corp., El Segundo, CA. Technology Operations.
ON THE THEORY OF MORPHOLOGY-DEPENDENT RESONANCES: SHAPE RESONANCES, WIDTH FORMULAS, AND GRAPHICAL REPRESENTATIONS
B. R. Johnson 26 Oct. 1993 43 p
(Contract F040701-88-C-0089)
(AD-A272279; TR-92(2940)-3; SMC-TR-93-54) Avail: CASI HC A03/MF A01

The theory of morphology-dependent resonances of a spherical particle is developed in analogy with the theory of quantum mechanical shape resonances. Exact analytic formulas for predicting the widths of the resonances are developed. A useful graphical procedure for organizing and displaying data for a spectrum of resonances is demonstrated. DTIC

N94-21166# Pennsylvania Univ., Philadelphia. Dept. of Chemistry.
A FORMULATION OF QUANTUM STATISTICAL MECHANICS BASED ON THE FEYNMAN PATH CENTROID DENSITY 2 DYNAMICAL PROPERTIES Technical Report No. 6, May 1993 - 1994
Jianshu Cao and Gregory A. Voth 4 Nov. 1993 41 p
(Contract N00014-92-J-1243)
(AD-A272698) Avail: CASI HC A03/MF A01

The formulation of quantum dynamical time correlation functions is examined within the context of the path centroid variable in Feynman path integration. This study builds upon the centroid-based approach to equilibrium properties developed in the companion paper. The introduction of the centroid perspective into the calculation of real time position functions is outlined and intriguing quasiclassical role for the centroid variable in real time position correlation functions is identified. The centroid-based theory is then implemented in several different approaches to calculate general correlation functions. The theoretical results are illustrated and tested by representative numerical applications. DTIC

N94-21171# Pennsylvania Univ., Philadelphia. Dept. of Chemistry.
A FORMULATION OF QUANTUM STATISTICAL MECHANICS BASED ON THE FEYNMAN PATH CENTROID DENSITY 1: EQUILIBRIUM PROPERTIES Technical Report, May 1993 - 1994
4 Nov. 1993 44 p
(AD-A272809) Avail: CASI HC A03/MF A01

A formulation of quantum statistical mechanics is presented in which the Feynman path centroid density in Feynman path integration is recast as the central statistical distribution used to average equilibrium and dynamical quantities. In this formulation, the path integral centroid density occupies the same role as the Boltzmann density in classical statistical mechanics. Therefore, the statistical ensemble of imaginary time path centroid configurations provides the distribution which is used to average the appropriately formulated effective operators and imaginary time correlation functions. An accurate renormalized diagrammatic perturbation theory for the centroid density and centroid-constrained imaginary time

propagator is also described with a particular emphasis given to the mathematical advantages arising from the centroid-based formulation. The present paper is concerned with the calculation of equilibrium properties from the centroid perspective, while the companion paper describes a centroid-based formalism for calculating dynamical time correlation functions. DTIC

N94-21513# Continuous Electron Beam Accelerator Facility, Newport New, VA.
QUALITATIVE AND QUANTITATIVE ASPECTS OF THE QCD THEORY OF ELASTIC FORM FACTORS
A. V. Radyushkin (Old Dominion Univ., Norfolk, VA.) 1993 10 p
(Contract DE-AC05-84ER-40150)
(DE93-040864; DOE/ER-40150/242; CEBAF-TH-93-12) Avail: CASI HC A02/MF A01

A long-standing controversy about the early applicability of perturbative QCD to elastic form factors is reviewed with a particular emphasis on the qualitative and quantitative aspects of the modern QCD picture of hadronic structure. DOE

N94-21533 Center for Mathematics and Computer Science, Amsterdam (Netherlands). Dept. of Computer Science.
MATHEMATICAL THEORY OF THERMODYNAMICS OF COMPUTATION
Ming Li (Waterloo Univ., Ontario.) and Paul M. B. Vitanyi Dec. 1992 19 p Sponsored in part by Netherlands Organization for Applied Scientific Research Limited Reproducibility: More than 20% of this document may be affected by microfiche quality
(Grant NSERC-OGP-046506)
(CWI-CS-R9251; ETN-94-94731) Copyright Avail: CASI HC A03

The ultimate thermodynamic cost of computing from x to y is investigated. Such research has implications for future miniaturization of VLSI (Very Large Scale Integration) chips reducing the energy dissipation below kT (thermal noise) and the similarity problem in pattern recognition. The theory of thermodynamic cost of computation turns out to be possible to develop axiomatically. The theorem connects physics to mathematics and establishes optimal upper and lower bounds on the ultimate thermodynamic cost of computation. ESA

N94-21692# Brookhaven National Lab., Upton, NY.
LATTICE GAUGE THEORY: PRESENT STATUS
M. Creutz Sep. 1993 11 p Presented at the Conference on Hadron, Como, Italy, 21-25 Jun. 1993
(Contract DE-AC02-76CH-00016)
(DE93-041154; BNL-49465; CONF-9306134-1) Avail: CASI HC A03/MF A01

Lattice gauge theory is our primary tool for the study of non-perturbative phenomena in hadronic physics. In addition to giving quantitative information on confinement, the approach is yielding first principles calculations of hadronic spectra and matrix elements. After years of confusion, there has been significant recent progress in understanding issues of chiral symmetry on the lattice. DOE

N94-21935# Stanford Linear Accelerator Center, CA.
NEW PERSPECTIVES IN QUANTUM CHROMODYNAMICS
S. J. Brodsky Jul. 1993 53 p Presented at the Particle Physics At the Fermi Scale Workshop, Beijing, China, 27 May - 4 Jun. 1993
(Contract DE-AC03-76SF-00515)
(DE93-041021; SU-SLAC-Pub-6304; CONF-9305282-1) Avail: CASI HC A04/MF A01

In these lectures I will discuss three central topics in quantum chromodynamics: (1) the use of light cone quantization and Fock space methods to determine the long and short-distance structure of quark and gluon distributions within hadrons; (2) the role of spin, heavy quarks, and nuclei in unraveling fundamental phenomenological features of QCD; and (3) a new approach to understanding the scale and scheme dependence of perturbative QCD predictions. DOE

N94-21971# Stanford Linear Accelerator Center, CA.
ON THE CORRESPONDENCE LIMIT OF RELATIVISTIC QUANTUM MECHANICS
H. P. Noyes May 1993 6 p Presented at the 1993 Symposium on the Foundations of Modern Physics, Cologne, Germany, 1-6 Jun. 1993
(Contract DE-AC03-76SF-00515)
(DE93-040939; SU-SLAC-Pub-6010; CONF-9306255-1) Avail: CASI HC A02/MF A01

One of the many problems of second quantized relativistic field theory is that the 'correspondence limit' either in non-relativistic quantum mechanics for atomic systems or in non-relativistic quantum mechanics for strongly interacting nuclear systems or in classical relativistic particle mechanics is not well specified. In this paper we argue that by using a fully finite and discrete approach to relativistic quantum mechanics we can arrive at a theory which does not have these defects, yet reproduces many of the same empirical results which are conventionally accounted for in any elementary particle physics and the related physical cosmology. DOE

N94-22010# California Univ., Berkeley. Lawrence Berkeley Lab.
RESTORING LOCALITY WITH FASTER-THAN-LIGHT VELOCITIES
P. H. Eberhard 30 Aug. 1993 8 p Presented at the Waves and Particles in Light and Matter Conference, Trani, Italy, 24-30 Sep. 1992
(Contract DE-AC03-76SF-00098)
(DE93-040926; LBL-34575; CONF-9209407-1) Avail: CASI HC A02/MF A01

The idea of 'locality' is a deep rooted concept. It does not have to be abandoned even if 'loophole free' EPR experiments are performed and confirm the predictions of quantum theory. To satisfy locality, one can imagine that influences at a distance are exerted via mechanisms involving an ether and effects propagating in that ether a velocity V greater than c. Such model of physical phenomena is not Lorentz invariant but, with V large enough, the model can be made to reproduce the results of all experiments where quantum mechanics and Lorentz invariance have been verified. DOE

N94-22095 Institut des Hautes Etudes Scientifiques, Bures-sur-Yvette (France).
UNIVERSALITY IN BLOW-UP FOR NON LINEAR HEAT EQUATIONS
J. Bricmont and A. Kupiainen Jun. 1993 40 p Prepared in cooperation with Helsinki Univ., Finland Limited Reproducibility: More than 20% of this document may be affected by microfiche quality
(Contract SC1-CT91-0695; NSF DMS-89-03041)
(PB93-215465; IHES/P-93/30) Avail: Issuing Activity (National Technical Information Service (NTIS))

The authors consider the classical problem of the blowing-up of solutions of the nonlinear heat equation. The authors show that there exist infinitely many profiles around the blow-up point, and for each integer k, the authors construct a set of codimension 2k in the space of initial data giving rise to solutions that blow-up according to the given profile. NTIS

80 SOCIAL SCIENCES (GENERAL)

Includes educational matters.

N94-20129*# National Aeronautics and Space Administration, Washington, DC.
NASA'S EDUCATION PROGRAM
Sep. 1993 66 p
(NASA-EP-297; NAS 1.19:297) Avail: CASI HC A04/MF A01

NASA's current education programs, which will be examined under its Strategic Plan for Education are presented. It is NASA's first goal to maintain this base - revising, expanding, or eliminating programs as necessary. Through NASA's second goal, new education reform initiatives will be added which specifically address NASA mission requirements, national educational reform, and Federal Coordinating Council for Science, Engineering, and Technology (FCCSET) priorities. The chapters in this publication are divided by educational levels, with additional sections on programs to improve the technological competence of students and on an array of NASA published materials to supplement programs. The resource section lists NASA's national and regional Teacher Resource Centers and introduces the reader to NASA's Central Operation of Resources for Educators (CORE), which distributes materials in audiovisual format.
Derived from text

N94-20153 Technische Univ., Berlin (Germany). Inst. fuer Verkehrsplanung und Verkehrswegebau.
FEMALE SECURITY AS A GENERAL MOBILITY CONDITION Ph.D. Thesis [DIE SICHERHEIT VON FRAUEN ALS ALLGEMEINE MOBILITAETSBEDINGUNG]
Carola Jeschke 1993 227 p In GERMAN Limited Reproducibility: More than 20% of this document may be affected by microfiche quality
(ISBN-3-79-831536-1; ETN-93-95064) Avail: CASI HC A11

Female specific attitudes before jeopardy and threats and their influence on female mobility are examined from an engineering point of view. Feelings such as fear, anxiety, which women can experience, and their consequences on female behavior towards mobility, are reviewed with statistical information and enquiry results, and are examined from the viewpoint of traffic safety. The choice of limited mobility of women as a preventive measure was considered. Situations which influence subjective and objective security on the street or in collective transport vehicles and criteria of outer spaces for positive security feelings are depicted. Concepts for taking safety principles into account in the traffic planning are presented. Strategies for improvement of traffic conditions are proposed. ESA

N94-20364# Rochester Univ., NY. Dept. of Computer Science.
BELIEVING IN THE BASIS OF THE EVIDENCE
Henry E. Kyburg, Jr. Sep. 1992 29 p
(Grant NSF IRI-90-02659)
(TR-438) Avail: CASI HC A03/MF A01

Making a decision can be seen from both probabalistic and pragmatic views. Topics include the 'lottery paradox', subjective and evidential probability, decision making, practical certainty, evidence, and acceptance. It is concluded that the strongest argument in favor of accepting contingent statements, rather than assigning them probabilities, is a pragmatic argument based on efficiency. Derived from text

N94-20818*# Hawaii Univ., Honolulu. Dept. of Geology and Geophysics.
TUMULI AND TUBES: TEACHING SCIENTIFIC TECHNIQUES Abstract Only
Michelle J. Tatsumura, G. J. Taylor, and P. J. Mouginis-Mark *In* Lunar and Planetary Inst., Twenty-Fourth Lunar and Planetary Science Conference. Part 3: N-Z 1993 p 1405-1406 (For primary document see N94-20636 05-91)
(Grant NAGw-2955)
Avail: CASI HC A01/MF A06

N94-20819*# National Aeronautics and Space Administration. Lyndon B. Johnson Space Center, Houston, TX.
SPARKING YOUNG MINDS WITH MOON ROCKS AND METEORITES Abstract Only
G. Jeffrey Taylor (Hawaii Univ., Honolulu.) and Marilyn M. Lindstrom *In* Lunar and Planetary Inst., Twenty-Fourth Lunar and Planetary Science Conference. Part 3: N-Z 1993 p 1407 (For primary document see N94-20636 05-91)
Avail: CASI HC A01/MF A06

81 ADMINISTRATION AND MANAGEMENT

Includes management planning and research.

N94-20206# General Accounting Office, Washington, DC. National Security and International Affairs Div.
NASA PROPERTY: IMPROVING MANAGEMENT OF GOVERNMENT EQUIPMENT PROVIDED TO CONTRACTORS. REPORT TO THE CHAIRMAN, SUBCOMMITTEE ON INVESTIGATIONS AND OVERSIGHT, COMMITTEE ON SCIENCE, SPACE, AND TECHNOLOGY, HOUSE OF REPRESENTATIVES
Sep. 1993 56 p
(GAO/NSIAD-93-191; B-253482) Avail: CASI HC A04/MF A01; GAO, PO Box 6015, Gaithersburg, MD 20877 HC

NASA has provided billions of dollars of government-owned personal property to its contractors for use on research and development, production, and service contracts. The value of government personal property, especially general purpose equipment, provided to contractors has grown substantially in recent years despite the government policy to minimize providing equipment to contractors. The Chairman, Subcommittee on Investigations and Oversight, House Committee on Science, Space, and Technology, requested that the General Accounting Office (GAO) review NASA property management activities. Specifically, GAO's objectives were to determine NASA's compliance with federal regulations intended to minimize the amount of government-owned, contractor-held general purpose equipment; the effectiveness of government and contractor controls over equipment; and the adequacy of NASA's reporting of this equipment. Derived from text

N94-20236# General Accounting Office, Washington, DC. National Security and International Affairs Div.
NASA PROCUREMENT: PLANNING FOR PILOT TEST OF NEW PROCUREMENT PROCEDURES IS ADEQUATE. REPORT TO THE CHAIRMAN, COMMITTEE ON GOVERNMENTAL AFFAIRS, US SENATE
Nov. 1993 14 p
(GAO/NSIAD-94-67; B-254647) Avail: CASI HC A03/MF A01; also available from GAO, PO Box 6015, Gaithersburg, MD 20877 HC

This document reports on a review of the National Aeronautics and Space Administration's planning for a pilot test of new procedures for procurements with annual values between $25,000 and $500,000 and total 5-year values up to $2.5 million. NASA refers to these procurements as 'mid-range' procurements. The purpose of the pilot test is to determine if the new procedures will reduce the time and effort required to solicit offers and award contracts in this price range. As currently designed, each midrange acquisition of supplies or services shall be reserved exclusively for small business concerns. Specifically, the review covered the extent to which the pilot test procurement procedures differ from the Federal Acquisition Regulation (FAR); the development of key features of the pilot project, including the financial impact of using an electronic commerce system on those wanting to do business with NASA and how such a system would provide for amending solicitations; and NASA's plans for assessing the results of the pilot project. Derived from text

N94-21444# Pennsylvania State Univ., University Park. Dept. of Civil Engineering.
A GUIDE TO RESOLVING DISPUTES OVER CONTRACTOR DELAY ENTITLEMENTS M.S. Thesis
Michael J. Clark Dec. 1993 92 p
(AD-A272022) Avail: CASI HC A05/MF A01

This thesis presents criteria to resolve disputes over contractor entitlement for delay damages with a detailed examination of the enforceability of the no-damage-for-delay clause. Appellate case law identifies the rules applied by the courts in these disputes. These rules of application were organized into a flowchart format to give contract administrators and other construction professionals an understanding of how the no-damage-for-delay clause has been interpreted. The intent is for contract administrators to resolve their disputes without going to court. The thesis also states the rules of application for resolving disputes over site access delays prior to commencing construction. Finally, the thesis explains the significance of the time-is-of-the-essence clause, as it relates to delay disputes. DTIC

N94-21497*# National Aeronautics and Space Administration, Washington, DC.
ISSUES IN NASA PROGRAM AND PROJECT MANAGEMENT. SPECIAL REPORT: 1993 CONFERENCE
Ed Hoffman, ed. and Jenny S. Kishiyama, ed. 1993 52 p Presented at the Aerospace Management Issues from the Program/Project Management Conference, Hagerstown, MD, 20-23 Apr. 1993
(NASA-SP-6101(07); NAS 1.21:6101(07)) Avail: CASI HC A04/MF A01

This volume is the seventh in an ongoing series on aerospace project management at NASA. Articles in this volume cover the 1993 Conference: perspectives in NASA program/project management; the best job in aerospace; improvements in project management at NASA; strategic planning...mapping the way to NASA's future; new NASA procurement initiatives; international cooperation; and industry, government and university partnership. A section on resources for NASA managers rounds out the publication. Author

N94-21499*# National Aeronautics and Space Administration, Washington, DC.

ISSUES IN NASA PROGRAM AND PROJECT MANAGEMENT

Francis T. Hoban, ed. 1993 61 p

(NASA-SP-6101(06); NAS 1.21:6101(06)) Avail: CASI HC A04/MF A01

This volume is the sixth in an ongoing series on aerospace project management at NASA. Articles in this volume cover evolution of NASA cost estimating; SAM 2; National Space Science Program: strategies to maximize science return; and human needs, motivation, and results of the NASA culture surveys. A section on resources for NASA managers rounds out the publication. Author

N94-21623*# National Aeronautics and Space Administration, Washington, DC.

NASA PROCUREMENT REPORT, FY 1992 Semiannual Report, 1 Oct. 1991 - 31 Mar. 1992

1992 30 p

(NASA-TM-109390; NAS 1.15:109390) Avail: CASI HC A03/MF A01

This report presents summary data on all NASA procurement actions and detailed information on contracts, grants, agreements, and other procurements over $25,000 awarded by NASA during the first six months of Fiscal Year 1992. The dollar value on procurements over $25,000 amounted to 98 percent of the total dollar value of procurement actions completed during the first six months of Fiscal Year 1992. However, these larger procurements accounted for only 29 percent of the total actions. Procurement action, as used in this report, means contractual actions to obtain supplies, services, or construction which increase or decrease funds. A procurement action thus may be a new procurement, or modifications such as supplementary agreements, change orders, or terminations to a contract that change the total amount of funds obligated.

Derived from text

N94-21625*# National Aeronautics and Space Administration, Washington, DC.

NASA PROCUREMENT REPORT, FY 1993 Annual Report

1993 53 p

(NASA-TM-109393; NAS 1.15:109393) Avail: CASI HC A04/MF A01

Summary data on all NASA procurement actions and detailed information on contracts, grants, agreements, and other procurements over $25,000 awarded by NASA during fiscal year 1993. The dollar value on procurements over $25,000 amounted to 97 percent of the total dollar value of procurement actions completed during fiscal year 1993. However, these larger procurements accounted for only 29 percent of the total actions. Procurement action, as used in this report, means contractural actions to obtain supplies, services, or construction which increase or decrease funds. A procurement action thus may be a new procurement, or modifications such as supplemental agreements, change orders, or terminations to an existing contract that change the total amount of funds obligated. An obligation is a contractual commitment to pay for supplies or services that are specified in the contract. Derived from text

N94-21626# Federal Aviation Administration, Oklahoma City, OK. Civil Aeromedical Inst.

FACTORS ASSOCIATED WITH CONTINUANCE COMMITMENT TO FAA MATRIX TEAMS Final Report

Chan M. Hellman (Union Carbide Corp., La Mesa, CA.), Lawrence Alan Witt (Barnett Banks, Inc., OK.), and Thomas F. Hilton Nov. 1993 9 p

(DOT/FAA/AM-93/18) Avail: CASI HC A02/MF A01

Several organizations within the FAA employ matrix teams to achieve cross-functional coordination. Matrix team members typically represent different organizational functions required for project accomplishment (e.g., research and development, engineering, quality assurance, legal, acquisition, and customers). The matrix team strategy decentralizes decision-making to the level of a project leader, so that knowledge relevant to the decision can be collected and outcomes closely monitored. While there are several factors that influence productivity of matrix teams, member turnover can have a substantial impact. Thus, identifying the factors that affect a productive member's continued membership to the team is important. Data gathered as part of a research task initiated at the request of the Associate Administrator for NAS Development (AND-1) is summarized. Questionnaires were developed to evaluate how well existing AND matrix teams were functioning. These data will also serve as a baseline against which to gage future development of the matrix team program. Two issues were examined: the relationship between perceptions of the quality of member-team interactions and individual member commitment to remain on the team (continuance commitment) and, whether or not that relationship might be influenced by the degree to which a member identified with the team as opposed to his/her individual office, function, or profession. Results from 141 members of 22 FAA matrix teams indicated a significant relationship between the quality of member-team interactions and continuance commitment. Moreover, team identification moderated the magnitude of the relationship between interaction quality and continuance commitment. Specifically, regardless of team identification, when members perceived member-team interactions to be of high quality, they also reported commitment to continuing on the team. However, this relationship was particularly critical for those members whose identification with the team was weak. For them, the quality of interactions among team members was strongly related to continuance commitment. Based on these results, efforts by project leaders to increase the number of and quality of interactions between matrix team members and to encourage member identification with the team are likely to reduce unwanted turnover behaviors.

Author (revised)

N94-21638*# National Aeronautics and Space Administration, Washington, DC.

SUMMARY DATA ON ALL NASA PROCUREMENT ACTIONS Annual Procurement Report, FY 1992

1992 53 p

(NASA-TM-109392; NAS 1.15:109392) Avail: CASI HC A04/MF A01

This report presents summary data on all NASA procurement actions and detailed information on contracts, grants, agreements, and other procurements over $25,000 awarded by NASA during Fiscal Year 1992 (FY-92). The dollar value on procurements over $25,000 amounted to 97 percent of the total dollar value of procurement actions completed during FY-92. However, these larger procurements accounted for only 28 percent of the total actions. Procurement action, as used in this report, means contractual actions to obtain supplies, services, or construction which increase or decrease funds. A procurement action thus may be a new procurement or modifications such as supplemental agreements, change orders, or terminations to an existing contract that change the total amount of funds obligated. An obligation is a contractual commitment to pay for supplies or services that are specified in the contract. Author (revised)

N94-21821*# Massachusetts Inst. of Tech., Cambridge. Human-Machine Systems Lab.

MODELLING DECISION-MAKING BY PILOTS Progress Report

Nicholas J. M. Patrick 13 Dec. 1993 28 p

(Grant NAG2-729)

(NASA-CR-194767; NAS 1.26:194767) Avail: CASI HC A03/MF A01

Our scientific goal is to understand the process of human decision-making. Specifically, a model of human decision-making in piloting modern commercial aircraft which prescribes optimal behavior, and against which we can measure human sub-optimality is sought. This model should help us understand such diverse aspects of piloting as strategic decision-making, and the implicit decisions involved in attention allocation. Our engineering goal is to provide design specifications for (1) better computer-based decision-aids, and (2) better training programs for the human pilot (or human decision-maker, DM). Author (revised)

N94-21327*# Computer Sciences Corp., Lanham, MD.

NCCDS CONFIGURATION MANAGEMENT PROCESS IMPROVEMENT

Kathy Shay *In* NASA. Goddard Space Flight Center, Networks Technology Conference Nov. 1993 p 41-52 (For primary document see N94-21323 05-62)

Avail: CASI HC A03/MF A03

N94-21328*# Raytheon Service Co., Burlington, MA.

PROBLEM REPORTING MANAGEMENT SYSTEM PERFORMANCE SIMULATION

David S. VanNatta *In* NASA. Goddard Space Flight Center, Networks Technology Conference Nov. 1993 p 53-59 (For primary document see N94-21323 05-62)

Avail: CASI HC A02/MF A03

N94-21334*# Computer Sciences Corp., Beltsville, MD.
PREDICTING SCHEDULING SUCCESS
Fredric Messing *In* NASA. Goddard Space Flight Center, Networks Technology Conference Nov. 1993 p 137-150 (For primary document see N94-21323 05-62)
Avail: CASI HC A03/MF A03

N94-21336*# Computer Sciences Corp., Beltsville, MD.
GENERATING AND EVALUATING ALTERNATE SCHEDULES
Surender D. Reddy *In* NASA. Goddard Space Flight Center, Networks Technology Conference Nov. 1993 p 163-180 (For primary document see N94-21323 05-62)
Avail: CASI HC A03/MF A03

82 DOCUMENTATION AND INFORMATION SCIENCE

Includes information management; information storage and retrieval technology; technical writing; graphic arts; and micrography.

For computer documentation see *61 Computer Programming and Software.*

N94-19811# Superconducting Super Collider Lab., Dallas, TX.
SISSY: AN EXAMPLE OF A MULTI-THREADED, NETWORKED, OBJECT-ORIENTED DATABASED APPLICATION
B. Scipioni, D. Liu, and T. Song May 1993 8 p Presented at the 5th Annual International Industrial Symposium on the Super Collider and Exhibition, San Francisco, CA, 6-8 May 1993
(Contract DE-AC35-89ER-40486)
(DE93-019742; SSCL-Preprint-321; CONF-930537-101) Avail: CASI HC A02/MF A01

The Systems Integration Support System (SISSY) is presented and its capabilities and techniques are discussed. It is a fully automated data collection and analysis system supporting the SSCL's systems analysis activities as they relate to the Physics Detector and Simulation Facility (PDSF). SISSY itself is a paradigm of effective computing on the PDSF. It uses home-grown code (C++), network programming (RPC, SNMP), relational (SYBASE) and object-oriented (ObjectStore) DBMS's, UNIX operating system services (IRIX threads, cron, system utilities, shells scripts, etc.), and third party software applications (NetCentral Station, Wingz, DataLink) all of which act together as a single application to monitor and analyze the PDSF. DOE

N94-20038# BRTRC, Inc., Vienna, VA.
RDA-PC SYSTEM USER'S GUIDE
Jul. 1993 92 p
(Contract DAAK70-92-D-0003)
(AD-A270356) Avail: CASI HC A05/MF A01

The RDA-PC System was designed to provide: (1) a PC-based data entry tool for the Research, Development and Acquisition Annual Review System (RDAARS) which minimizes redundant data entry, performs data consistency checks immediately, and provides help screens to let users select from allowable entries; (2) a PC-based RDA budget planning and analysis system for managers, program analysts, and budget analysts, which provides enhanced 'What If' analysis capabilities and 1 to N reports, as well as links to other program management systems; (3) the capability to rapidly convert RDA data into other PC formats for use in analysis (e.g., LOTUS, DBase, RBase, etc.) and for reporting; (4) orderly control of the data among a System Administrator and various Users with 'Data Entry' and 'View Only' permissions, each working independently on separate PC's; and (5) a capability to handle classified data when installed on properly configured and controlled hardware. DTIC

N94-20106 Kaman Sciences Corp., Utica, NY.
DATA AND ANALYSIS CENTER FOR SOFTWARE Final Technical Report, Jun. 1989 - Aug. 1992
James J. Reed Aug. 1993 80 p Limited Reproducibility: More than 20% of this document may be affected by microfiche quality
(Contract F30602-89-C-0082)
(AD-A270571; RL-TR-93-163) Avail: CASI HC A05

This document discusses and describes the operation and maintenance of the Data and Analysis Center for Software (DACS), a Department of Defense (DoD) Information Analysis Center. The report outlines the core operations and technical area tasks performed. The enhanced activities and products and services provided to the DACS user community are discussed. DTIC

N94-20133*# University of Southern California, Marina del Rey. Information Sciences Inst.
EXPLAINABLE EXPERT SYSTEMS: A RESEARCH PROGRAM IN INFORMATION PROCESSING Final Report
Cecile L. Paris 1993 29 p
(Contract NCC2-520)
(NASA-CR-193422; NAS 1.26:193422) Avail: CASI HC A03/MF A01

Our work in Explainable Expert Systems (EES) had two goals: to extend and enhance the range of explanations that expert systems can offer, and to ease their maintenance and evolution. As suggested in our proposal, these goals are complementary because they place similar demands on the underlying architecture of the expert system: they both require the knowledge contained in a system to be explicitly represented, in a high-level declarative language and in a modular fashion. With these two goals in mind, the Explainable Expert Systems (EES) framework was designed to remedy limitations to explainability and evolvability that stem from related fundamental flaws in the underlying architecture of current expert systems. Author (revised)

N94-20134*# University of Southern California, Los Angeles. Information Sciences Inst.
A PROPOSED RESEARCH PROGRAM IN INFORMATION PROCESSING Final Technical Report, 1 Nov. 1987 - 30 Sep. 1992
Herbert Schorr 1992 10 p Sponsored in part by DOD and DARPA
(Contract NCC2-520)
(NASA-CR-194271; NAS 1.26:194271) Avail: CASI HC A02/MF A01

The goal of the Formalized Software Development (FSD) project was to demonstrate improvements productivity of software development and maintenance through the use of a new software lifecycle paradigm. The paradigm calls for the mechanical, but human-guided, derivation of software implementations from formal specifications of the desired software behavior. It relies on altering a system's specification and rederiving its implementation as the standard technology for software maintenance. A system definition for this paradigm is composed of a behavioral specification together with a body of annotations that control the derivation of executable code from the specification. Annotations generally achieve the selection of certain data representations and/or algorithms that are consistent with, but not mandated by, the behavioral specification. In doing this, they may yield systems which exhibit only certain behaviors among multiple alternatives permitted by the behavioral specification. The FSD project proposed to construct a testbed in which to explore the realization of this new paradigm. The testbed was to provide operational support environment for software design, implementation, and maintenance. The testbed was proposed to provide highly automated support for individual programmers ('programming in the small'), but not to address the additional needs of programming teams ('programming in the large'). The testbed proposed to focus on supporting rapid construction and evolution of useful prototypes of software systems, as opposed to focusing on the problems of achieving production quality performance of systems. Author (revised)

N94-20158*# Georgia Inst. of Tech., Atlanta. School of Electrical Engineering.
LOW BIT RATE CODING OF EARTH SCIENCE IMAGES
Faouzi Kossentini, Wilson C. Chung, and Mark J. T. Smith [1993] 10 p
(Grant NAG5-2187)
(NASA-CR-193729; NAS 1.26:193729) Avail: CASI HC A02/MF A01

In this paper, the authors discuss compression based on some new ideas in vector quantization and their incorporation in a sub-band coding framework. Several variations are considered, which collectively address many of the individual compression needs within the earth science community. The approach taken in this work is based on some recent advances in the area of variable rate residual vector quantization (RVQ). This new RVQ method is considered separately and in conjunction with sub-band image decomposition. Very good results are achieved in coding a variety of earth science images. The last section of the paper provides

some comparisons that illustrate the improvement in performance attributable to this approach relative the the JPEG coding standard.

Derived from text

N94-20193# Stockholm Univ. (Sweden). Dept. of Physics.
A SCSI-BUS DATA ACQUISITION SYSTEM FOR NUCLEAR SPECTROSCOPY EXPERIMENTS
B. Hovander, A. Johansson, G. Appelquist, and C. Bohm Sep. 1992 16 p
(USIP-92-03; ETN-93-94846) Avail: CASI HC A03/MF A01

An IBM-386 personal computer controlled data acquisition system which uses the Small Computer System Interface (SCSI) bus as a system bus is described. The SCSI bus choice makes it easy to attach commercially available mass storage devices such as Video-8 or Digital Audio Tape (DAT). The system was developed for nuclear physics applications but may be modified. The design is based on programmable components such as an embedded micro controller and a field programmable gate array. The data acquisition system serves in its present form 15 NIM standard Analog to Digital Converters (ADC's), but will be updated to accommodate more units. The data acqusition system is also equipped with a monitor function where the main data path to the storage device is diverted to a monitor interface in the system controller. Implementation details and flow charts are presented. ESA

N94-20268*# Alabama Univ., Huntsville. Earth System Science Lab.
[DEVELOPMENT OF A NAMING CONVENTION AND DATA MA NAGEMENT SYSTEM] Final Report, 24 Dec. 1987 - 15 Nov. 1992
Richard T. McNider, Michael Botts, Don Moss, Helen Conover, Evan Criswell, Sara Graves, and Danny Hardin 1993 107 p
(Contract NAS8-37139)
(NASA-CR-193860; NAS 1.26:193860) Avail: CASI HC A06/MF A02

This contract covered work in data management, acquisition, and analysis for the Earth Science and Applications Division (ESAD) of the Space Science Laboratory of MSFC. Under this contract, a naming convention and data management system were developed for ESAD data sets, data visualization, and standard data format issues were investigated, and specific data analysis and management needs were addressed for several ESAD projects and data sets. In the following sections, details of the research performed over the duration of this contract are summarized.

Author (revised)

N94-20308*# National Aeronautics and Space Administration, Washington, DC.
THE MANAGER'S GUIDE TO NASA GRAPHICS STANDARDS
[1980] 18 p
(NHB-1430.2; NAS 1.18:1430.2) Avail: CASI HC A03/MF A01

NASA managers have the responsibility to initiate and carry out communication projects with a degree of sophistication that properly reflects the agency's substantial work. Over the course of the last decade, it has become more important to clearly communicate NASA's objectives in aeronautical research, space exploration, and related sciences. Many factors come into play when preparing communication materials for internal and external use. Three overriding factors are: producing the materials by the most cost-efficient method; ensuring that each item reflects the vitality, knowledge, and precision of NASA; and portraying all visual materials with a unified appearance. This guide will serve as the primary tool in meeting these criteria. This publication spells out the many benefits inherent in the Unified Visual Communication System and describes how the system was developed. The last section lists the graphic coordinators at headquarters and the centers who can assist with graphic projects. By understanding the Unified Visual Communication System, NASA managers will be able to manage a project from inception through production in the most cost-effective manner while maintaining the quality of NASA communications.

Derived from text

N94-20310 Institute for Perception RVO-TNO, Soesterberg (Netherlands). Afd. Informatieverwerking.
HERMES, A REPORT GENERATOR FOR RESEARCH ON INFORMATION PROCESSING IN COMMAND POSTS: THE EFFECT OF MISSING INFORMATION Final Report [HERMES: EEN BERICHTENGENERATOR VOOR ONDERZOEK NAAR INFORMATIEVERWERKING IN COMMANDOPOSTEN; HET EFFECT VAN ONTBREKENDE INFORMATIE]
J. H. Kerstholt and J. E. T. Mathijssen Feb. 1993 24 p In DUTCH
(Contract A89/KL/309)
(IZF-1992-A-28; TD-92-2290; ETN-94-94925) Avail: Issuing Activity (TNO Institute for Perception, Kampweg 5, 3769 DE Soesterberg, Netherlands)

A computer program HERMES (Hierarchical Enemy Reports from Multiple Sensors), which can generate intelligence reports of sensors signaling vehicle movements within a prespecified range, is described. At present the messages are based on one sensor only. The simulator HERMES is designed for experimental purposes and offers the possibility to manipulate the output (for example the number of messages) of the simulation. Based on reports generated with HERMES the effects of missing information on the quality of recognizing the 'order of battle' was investigated. The results of previous research were replicated: on low command levels, less units were identified when 30% of the information was missing. On higher and more global performance levels, no effects of information reduction were found. It is concluded that HERMES can be used for further research, especially for the evaluation of man-computer systems in controlled, suboptimal task environments. ESA

N94-20363*# Southwest Research Inst., San Antonio, TX. Instrumentation and Space Research Div.
RECOMMENDATIONS RESULTING FROM THE SPDS COMMUNITY-WIDE WORKSHOP
1993 17 p Workshop held in Houston, TX, 1-3 Jun. 1993
(Grant NAG5-2264; SwRI Proj. 15-5659)
(NASA-CR-194684; NAS 1.26:194684) Avail: CASI HC A03/MF A01

The Data Systems Panel identified three critical functionalities of a Space Physics Data System (SPDS): the delivery of self-documenting data, the existence of a matrix of translators between various standard formats (IDFS, CDF, netCDF, HDF, TENNIS, UCLA flat file, and FITS), and a network-based capability for browsing and examining inventory records for the system's data holdings. The recommendations resulting from the workshop include the philosophy, funding, and objectives of a SPDS. Access to quality data is seen as the most important objective by the Policy Panel, with curation and information about the data being integral parts of any accessible data set. The Data Issues Panel concluded that the SPDS can supply encouragement, guidelines, and ultimately provide a mechanism for financial support for data archiving, restoration, and curation. The Software Panel of the SPDS focused on defining the requirements and priorities for SPDS to support common data analysis and data visualization tools and packages. Derived from text

N94-20919 Department of Defense, Washington, DC. Directorate for Information Operations and Reports.
LISTING OF APPROVED RECURRING INFORMATION REQUIREMENTS
1 Jul. 1993 109 p Supersedes AD-A267934 Limited Reproducibility: More than 20% of this document may be affected by microfiche quality
(AD-A271673; DOD-8910.1-L) Avail: CASI HC A06

This listing is issued under the authority of Department of Defense (DoD) Directive 8910.1, 'Management and Control of Information Requirements,' June 11, 1993. Its purpose is to identify DoD internal information requirements approved by the Office of the Secretary of Defense (OSD), interagency reporting requirements approved by the General Services Administration (GSA), and DoD public reports approved by the Office of Management and Budget (OMB). DTIC

N94-20924 Navy Personnel Research and Development Center, San Diego, CA.
AN ASSESSMENT OF THE STATISTICAL AND EDITORIAL OUTPUT OF TEXT ANALYSIS PROGRAMS Final Report, Feb. - Oct. 1992
Paul H. Radtke Oct. 1993 31 p Limited Reproducibility: More than 20% of this document may be affected by microfiche quality
(AD-A272185; NPRDC-TN-94-6) Avail: Issuing Activity (Defense Technical Information Center (DTIC))

This study assessed commercially available text analysis programs for their accuracy and usefulness to novice writers. Two topics were examined: the reliability and accuracy of scores and indicators, and the level and validity of the editorial comments. Six text analysis programs were assessed by comparing their output for two previously published Navy technical publications. The analyzers produced different word and sentence counts, and standard readability scales, suggesting that each uses different algorithms to analyze text material. The analyzers' statistical measures may be sensitive to the complexity and format of text samples, but not to their size. The analyzers varied on the number and level of comments, the validity of the comments, and the types of problems they detect. The text analyzers are able to detect problems of usage, sentence length, and other low-level mistakes. They are less able to detect problems involving the relationship between parts of sentences. Specific problems created by the unique characteristics of technical writing are identified (e.g., technical terminology, passive sentence forms, numbers). The analyzers assessed in this study are suitable to supplement, but not replace, traditional editing. If accompanied by additional guidance, they might be used as tutorial aids. DTIC

N94-21055*# Pennsylvania State Univ., University Park. Dept. of Astronomy and Astrophysics.

MULTI WAVE LINK: AN INTERACTIVE DATABASE FOR CO-ORDINATION OF MULTIWAVELENGTH PROGRAMS Final Report, 1 Oct. 1989 - 30 Sep. 1993

France Cordova 30 Sep. 1993 7 p

(Grant NAGw-1920)

(NASA-CR-194778; NAS 1.26:194778) Avail: CASI HC A02/MF A01

Multi Wave Link is an operational database used by the international astronomical community to plan and coordinate multiwavelength observational campaigns on various celestial objects. This facility has been and continues to be an essential tool for the organization of numerous simultaneous ground-based and satellite observations. The Multi Wave Link system has both an interactive component and an electronic mail alert notice component. The interactive portion contains a database of schedules from several of the world's larger observatories and orbiting satellites. Lists of observers, observatories, and their available instrumentation are additionally contained in the system. Another feature added to the software allows the user to search the Royal Greenwich Observatory e-mail listing of international astronomers. This capability is often used by astronomers to find the electronic address of colleagues for improved communication. However, the most productive aspect of the Multi Wave Link system appears to be one of the simplest parts of the system: the electronic mail alert notices for observing campaigns. Information useful in planning the structure of future astronomical databases can be obtained by studying patterns of use of the Multi Wave Link system. This paper analyzes 22 months of Multi Wave Link usage from Sep. 1991 - Jul. 1993. Derived from text

N94-21071 Universiteit Twente, Enschede (Netherlands). Dept. of Computer Science.

ON THE SELECTION OF INDICES IN RELATIONAL DATABASES

Sunil Choenni, Henk Blanken, and Thiel Chang (Gemeenschappelijk Administratiekantoor, Amsterdam, Netherlands.) 18 Nov. 1992 18 p Limited Reproducibility: More than 20% of this document may be affected by microfiche quality

(Memo-INF-92-72; ETN-93-94114) Avail: CASI HC A03

Topics relating to index selection in data bases are addressed. Intending to develop a tool which aims to support the physical design of relational data bases can not be done without considering the problem of index selection. Generally the problem is split into a primary and secondary index selection problem and the selection is done per table. Whereas much attention has been paid on the selection of secondary indices relatively less is known about the selection of a primary index and the relation between primary and secondary index selection. The primary index selection and secondary index selection problem are shown to be mutually independent. Two heuristic methods for solving the index selection problem are described and compared. Some rules of thumb used to determine candidate primary indices are evaluated. An attempt was made to improve existing heuristics. The methodology used in implementing the tool for supporting physical database design is described. ESA

N94-21254* National Aeronautics and Space Administration, Washington, DC.

NASA PATENT ABSTRACTS BIBLIOGRAPHY: A CONTINUING BIBLIOGRAPHY. SECTION 1: ABSTRACTS (SUPPLEMENT 44)

Jan. 1994 60 p

(NASA-SP-7039(44)-Sect-1; NAS 1.21:7039(44)-Sect-1) Avail: CASI HC A04

Abstracts are provided for 131 patents and patent applications entered into the NASA scientific and technical information system during the period Jun. 1993 through Dec. 1993. Each entry consists of a citation, an abstract, and in most cases, a key illustration selected from the patent or patent application. Author

N94-21266# Naval Postgraduate School, Monterey, CA.

PERFORMANCE MANAGEMENT SYSTEMS: A STATISTICAL ANALYSIS M.S. Thesis

James W. Kilby Sep. 1993 78 p

(AD-A272989) Avail: CASI HC A05/MF A01

This study assessed the performance management systems used by companies, in an effort to identify the evolution of new management techniques in corporations. The sample consisted of 119 individual survey respondents from 'high performing' entities. The data collected was part of a luger performance measurement study conducted by Euske, Lebas and McNair (1993). 'High performing' entities were identified by the management of companies included in this study. Companies selected for the study were identified by the CAM-I research consortia or directly identified by Euske, Lebas or McNair. DTIC

N94-21270*# Smithsonian Astrophysical Observatory, Cambridge, MA.

DEVELOPMENT AND OPERATIONS OF THE ASTROPHYSICS DATA SYSTEM Semiannual Report Nos. 1 and 2

S. S. Murray Nov. 1993 214 p

(Contract NCCw-24)

(NASA-CR-194691; NAS 1.26:194691) Avail: CASI HC A10/MF A03

The main effort in October 1992 was for the development and of the Astrophysics Data System (ADS) 3.1 graphical interface (GUI) and the preparation for its release. The beta-release for the GUI was made available to the nodes for testing. Development of the Abstract Server progressed satisfactorily. A test version was prepared for the ADASS meeting. Another major effort was the preparation for the user and nodes meetings on 5 and 6 November and for the ADASS conference on 2-4 November. February 1993 was highlighted by the preparation for the update release and its associated problems. We have the okay from the Commerce Department to export ADS. Foreign users can now sign on and receive the software. The main event during June was the AAS meeting. In the summer, the project decided on a new release schedule. The next major release is scheduled for January 1994 and will include major architectural improvements. In late spring 1994, a major release will include the new networking software. Derived from text

N94-21276 Department of the Navy, Washington, DC.

LIGHT UPDATE NOTIFICATION MECHANISM FOR SHARED DATA STRUCTURES Patent

Carlos M. Tavares, inventor (to Navy) 21 Sep. 1993 8 p Filed 3 Oct. 1991

(AD-D015967; US-Patent-5,247,684; US-Patent-Appl-SN-770207; US-Patent-Class-395-700) Avail: US Patent and Trademark Office

A system for updating and reading a data base utilizes a pair of counters working in conjunction with registers located within RAM to enable one upon reading the data base to know if a data base record has been added, deleted, or revised. The system also notifies if the data base is being updated on attempting a read process or during the reading. The updating is performed by a writer that is never inhibited from updating the data base. DTIC

N94-21287# Rochester Univ., NY. Dept. of Computer Science.

PROMISES AND FAULT-TOLERANT DATABASE ACCESS

Jin-Yi Cai (Princeton Univ., NJ.), Lane A. Hemachandra, and Jozef Vyskoc (Slovak Academy of Sciences, Bratislava, Czechoslovakia.) Apr. 1993 47 p

(Grants NSF CCR-90-57486; NSF CCR-89-57604; NSF INT-91-16781; NSF

STC-88-09648)
(TR-447) Avail: CASI HC A03/MF A01

This paper studies the power of access, especially fault-tolerant access, to probabilistic databases and to unambiguous databases . We study fault-tolerant access to probabilistic computation, and completely characterize the complexity classes R and ZPP in terms of fault-tolerant database access. We also show that consistent and inconsistent failure are in general interchangeable. We study the power of three types of access to unambiguous computation: nonadaptive access, fault-tolerant access, and guarded access. Though for NP it is known that nonadaptive access has exponentially terse adaptive simulations, we show that UP has no such relativizable simulations: there are worlds in which k + 1-truth-table access to UP is not subsumed by k-Turing access to UP, or even to NP machines that are unambiguous on the questions actually asked. Though fault-tolerant access (i.e., '1-helping' access) to NP is known to be no more powerful than NP itself, we give both structural and relativized evidence that fault tolerant access to UP suffices to recognize even sets beyond UP. Furthermore, we completely characterize, in terms of locally positive reductions, the sets that fault-tolerantly reduce to UP. In guarded access, Grollmann and Selman's natural notion of access to unambiguous computation, a deterministic polynomial-time Turing machine asks questions to a nondeterministic polynomial-time Turing machine in such a way that the nondeterministic machine never accepts ambiguously. In contrast to guarded access, the standard notion of access to unambiguous computation is that of access to a set that is uniformly unambiguous--even for queries that it never will be asked by its questioner, it must be unambiguous. We show that these notions, though the same for nonadaptive reductions, differ for Turing and strong nondeterministic reductions. Author (revised)

N94-21354# GKY and Associates, Inc., Springfield, VA.
INTEGRATION OPPORTUNITIES FOR COMPUTER MODELS, METHODS, AND GIS USED IN CORPS PLANNING STUDIES
Roger T. Kilgore, Joseph S. Krolak, and Mark P. Mistichelli Feb. 1993 114 p
(Contract DACW72-90-D-0001)
(AD-A271714; IWR-93-R-5) Avail: CASI HC A06/MF A02

The report surveys models, methods and geographic information systems (GIS) used in water resources planning by the Corps of Engineers and suggests opportunities for integrating these tools to improve planning and decision-making. Information on models, methods and GIS was gathered via completed planning studies, a literature survey and interviews with planners and researchers at Corps laboratories other technical centers and District offices. An inventory of planning tools discovered during the information-gathering process is included in the report. The report identifies several issues that will affect the integration of planning tools, including the difficulty of matching the needs of the user with the tool, data issues, hardware/software choices and organizational concerns. The report offers four strategies for approaching integration: (1) development of interfaces for existing models, methods and GIS; (2) incorporation of spatial functions into models; (3) incorporation of modeling functions into GIS; and (4) development of Spatial Decision Sup Systems (SDSS). Each strategy can be effective although the SDSS approach has considerable merit in addressing Corps planning problems. The report concludes with a description of general activities that should be undertaken by the Corps to facilitate the integration of planning tools for water resources decision-making. DTIC

N94-21363# Aerospace Medical Research Labs., Brooks AFB, TX. Occupational and Environmental Health Directorate.
PEGASUS, ELECTRONIC BULLETIN BOARD SYSTEM USER'S GUIDE Final Report
Paul T. Johnson Aug. 1993 49 p
(AD-A271679; AL/OE-TR-1993-0067) Avail: CASI HC A03/MF A01

At the request of HQ AFMOA/SGPA, an electronic bulletin board system was established and is maintained by Armstrong Laboratory/OEMO for the purpose of linking the Occupational and Environmental Health initiative worldwide. This guide is intended to assist remote users in maximizing bulletin board usage, using a mainframe terminal or microcomputer system. DTIC

N94-21449# Patent and Trademark Office, Washington, DC.
THE OFFICIAL GAZETTE OF THE UNITED STATES PATENT AND TRADEMARK OFFICE, VOL. 1145, NO. 4
22 Dec. 1992 647 p See also PB90-239237
(PB93-202240) Avail: CASI HC A99/MF A06

The Gazette contains a complete listing of patents granted for the week of 22 Dec. 1992. Also included is an index of patentees, as well as patent and trademark office notices. NTIS

N94-21494 Center for Mathematics and Computer Science, Amsterdam (Netherlands). Dept. of Computer Science.
CMIFed: A PRESENTATION ENVIRONMENT FOR PORTA BLE HYPERMEDIA DOCUMENTS
Guido vanRossum, Jack Jansen, K. Sjoerd Mullender, and Dick C. A. Bulterman Jan. 1993 14 p Presented at ACM Multimedia 1993 Conference Limited Reproducibility: More than 20% of this document may be affected by microfiche quality
(CWI-CS-R9305; ETN-94-94734) Copyright Avail: CASI HC A03

The architecture and implementation of CMIFed, an editing and presentation environment for hypermedia documents, are discussed. Typically such documents contain a mixture of text, images, audio, and video (and possibly other media), augmented with user interaction. CMIFed allows the author flexibility in specifying what is presented when by using multiple simultaneous output channels. Unlike systems that use a timeline or scripting metaphor to control the presentation, in CMIFed the user manipulates a collection of events and timing constraints among those events. Common timing requirements can be specified by grouping events together in a tree whose nodes indicate sequential and parallel composition. More general timing constraints between events can be added in the form of synchronization arcs. User interaction is supported in the form of hyperlinks. CMIFed is placed in the context of the CMIF (CWI Multimedia Interchange Format) model for hypermedia documents, which formalizes the properties of hypermedia presentations in a platform independent manner. ESA

N94-21529# Lawrence Livermore National Lab., CA.
ELECTRONIC RESOURCES FOR SECURITY RELATED INFORMATION: REFERENCE DOCUMENT
R. A. Feingold May 1993 40 p Presented at the Westinghouse Information Security Form Conference, Baltimore, MD, 13-14 May 1993
(Contract W-7405-eng-48)
(DE93-040488; UCRL-JC-113857; CONF-9305284-1) Avail: CASI HC A03/MF A01 (US Sales Only)

The quantity, quality, and availability of electronic resources is multiplying rapidly. Information technology security professionals must make timely and effective use of these resources if they are to contain the growing threats of globally networked attackers. This paper outlines the threats, including recent examples, and then provides multi-level descriptions of the abundant resources available to the information technology security community. These descriptions are valuable to everyone from a networking novice to a sophisticated expert. While the information is useful for the entire security community, this paper pays particular attention to Department of Energy requirements. DOE

N94-21535 Center for Mathematics and Computer Science, Amsterdam (Netherlands). Dept. of Computer Science.
STRUCTURED MULTIMEDIA AUTHORING
Lynda Hardman, Guido vanRossum, and Dick C. A. Bulterman Jan. 1993 15 p Presented at ACM Multimedia 1993 Conference Limited Reproducibility: More than 20% of this document may be affected by microfiche quality
(CWI-CS-R9304; ETN-94-94733) Copyright Avail: CASI HC A03

The user interface to the CMIF (CWI (Centrum voor Wiskunde en Informatica) Multimedia Interchange Format) authoring environment for constructing and playing multimedia presentations is presented. The CMIF authoring environment supports a rich hypermedia document model allowing structure based composition of multimedia presentations and the specification of synchronization constraints between constituent media items. An author constructs a multimedia presentation in terms of its structure and additional synchronization constraints, from which the CMIF player derives the precise timing information for the presentation. The advantages of a structured approach to authoring multimedia are discussed and facilities in the CMIF authoring environment for supporting this approach are described. The

authoring environment presents three main views of a multimedia presentation: the hierarchy view is used for manipulating and viewing a presentation's hierarchical structure; the channel view is used for managing logical resources and specifying and viewing precise timing constraints; and the player for playing the presentation. The authoring environment is presented in terms of a short example: constructing a walking tour of Amsterdam. ESA

N94-21536 Center for Mathematics and Computer Science, Amsterdam (Netherlands). Dept. of Computer Science.
THE AMSTERDAM HYPERMEDIA MODEL: EXTENDING HYPERTEXT TO SUPPORT REAL MULTIMEDIA
Lynda Hardman, Dick C. A. Bulterman, and Guido vanRossum Jan. 1993 19 p Submitted for publication Limited Reproducibility: More than 20% of this document may be affected by microfiche quality
(CWI-CS-R9306; ETN-94-94735) Copyright Avail: CASI HC A03

A model of hypermedia that allows the combination of 'hyperstructured' information with dynamic multimedia information is presented. The model is derived by extending the Dexter hypertext reference model and the CMIF (CWI Multimedia Interchange Format) multimedia model. The Amsterdam hypermedia model allows the following, in addition to the model provided by Dexter: the composition of multiple dynamic media, in order to specify a collection of time based media making up a complete multimedia presentation; the definition of 'channels' for specifying default presentation information allowing the specification of the presentation characteristics of nodes at a more general level than that for an individual node; the composition of existing presentations into larger presentations taking into account possible clashes of resource usage; the inclusion of temporal relations while maintaining the separation of structure and presentation information, where time based relationships are treated as presentation information; and the specification of 'context' for anchors, in order to determine whether on following a link a part, or the whole, of the presentation is replaced by the information at the destination of the link. The Amsterdam hypermedia model enables the description of structured multimedia documents, incorporating time at a fundamental level, and extending the hypertext notion of links to time based media and compositions of different media. The Dexter hypertext model and the CMIF multimedia model are summarized, and their limitations for use as a more general hypermedia model are discussed. The extensions included in the Amsterdam hypermedia model are described and a summary of the resulting model is given. ESA

N94-21750# Lawrence Livermore National Lab., CA.
ASSESSMENT OF THE ORGANIZATIONAL STRUCTURE AND SERVICES OF DOE NATIONAL LABORATORY LIBRARIES
Kathy Dieden (San Jose State Univ., CA.) 18 May 1993 27 p
(Contract W-7405-eng-48)
(DE93-040697; UCRL-ID-114069) Avail: CASI HC A03/MF A01

This fieldwork assignment was created to assess the library and information services at the National Laboratories and to understand their organizational structures and the role of the library within those structures. The author's goal was to collect the data and to evaluate the data and make appropriate recommendations for improving the quality of service at Lawrence Livermore National Laboratory Library. The objectives were: to develop a questionnaire which will be used in the reference interview; to contact a knowledgeable staff person at each facility and collect the information services data from that person; to identify innovative and unique services; to identify non-traditional methods of delivering information services to the scientific clientele; to obtain any user feedback on the services provided; and to identify the organization structure of each of the National laboratories and to determine the role of the library within those structures. DOE

N94-21865*# Mississippi State Univ., Bay Saint Louis. Center for Air Sea Technology.
DESIGN DOCUMENT AND DATABASE SPECIFICATIONS FOR THE NAVAL INTERACTIVE DATA ANALYSIS SYSTEM (NIDAS), VERSION 1.0
Dharmesh Krishnamagaru 29 Oct. 1993 60 p
(Contract NAS13-564)
(NASA-CR-194817; NAS 1.26:194817; AD-A273056; CAST-TN-01-94)
Avail: CASI HC A04/MF A01

The purpose of this document is to define and describe the structural framework and logical design of the software components/units which willbe integrated into the major computer software configuration item (CSCI) identified as the Naval Interactive Data Analysis System (NIDAS), Version 1.0. NIDAS provides interactive blending and overlaying capabilities for a broad range of environmental data types and formats. The final product output of NIDAS is three-dimensional gridded fields of temperature and salinity, constructed from data derived by the user internally within NIDAS and data obtained from external sources (numerical models, observations, and climatological databases). Derived from text

N94-22047# Oak Ridge K-25 Site, TN.
PROJECT RECORDS INFORMATION SYSTEM (PRIS): USER'S MANUAL
R. K. Schwarz, ed. Oct. 1993 72 p
(Contract DE-AC05-84OT-21400)
(DE94-001548; K/CSD/TM-93-Rev-2) Avail: CASI HC A04/MF A01

The Project Records Information System (PRIS) is an interactive system developed for the Information Services Division (ISD) of Martin Marietta Energy Systems, Inc., to perform indexing, maintenance, and retrieval of information about engineering project record documents for which they are responsible. This PRIS User's Manual provides instruction on the use of this system. Section 2.0 of this manual presents an overview of PRIS, describing the system's purpose; the data that it handles; functions it performs; hardware, software, and access; and help and error functions. Section 3.0 describes the interactive menu-driven operation of PRIS. Appendixes A, B, and C contain help screens, report descriptions, and the data dictionary, respectively. DOE

N94-22276 Universiteit Twente, Enschede (Netherlands). Dept. of Computer Science.
THE LOGISTIC MODEL: THE INTEGRATION OF BUSINESS PROCESS REDESIGN AND INFORMATION SYSTEMS DEVELOPMENT BASED ON LOGISTIC PRINCIPLES
F. Harmsen (Moret Ernst and Young Management Consultants, Utrecht, Netherlands.), M. Kraakman (Moret Ernst and Young Management Consultants, Utrecht, Netherlands.), S. Brinkkemper, N. Brand (Moret Ernst and Young Management Consultants, Utrecht, Netherlands.), and A. tenHarmsenvanderBeek (Moret Ernst and Young Management Consultants, Utrecht, Netherlands.) Nov. 1992 28 p Limited Reproducibility: More than 20% of this document may be affected by microfiche quality
(Memo-INF-92-70; ETN-93-94112) Copyright Avail: CASI HC A03

The concepts and notation of the Logistic Model, in relation with its background in logistics and information systems theory, are discussed. An account of the successful application of the Logistic Model in several business process redesign projects is given. The technique was completely, formally specified in metamodels and a modeling support tool is under development. Guidelines for the application of the Logistic Model in business redesign are presented. ESA

N94-22404# General Atomic Co., San Diego, CA.
ACCESS TO D3-D DATA LOCATED IN MULTIPLE FILES AND MULTIPLE LOCATIONS
B. B. McHarg, Jr. Oct. 1993 5 p Presented at the Symposium on Fusion Engineering, Hyannis, MA, 11-15 Oct. 1993
(Contract DE-AC03-89ER-51114)
(DE94-001104; GA-A-21404; CONF-931018-18) Avail: CASI HC A01/MF A01

The General Atomics DIII-D tokamak fusion experiment is now collecting over 80 MB of data per discharge once every 10 min, and that quantity is expected to double within the next year. The size of the data files, even in compressed format, is becoming increasingly difficult to handle. Data is also being acquired now on a variety of UNIX systems as well as MicroVAX and MODCOMP computer systems. The existing computers collect all the data into a single shot file, and this data collection is taking an ever increasing amount of time as the total quantity of data increases. Data is not available to experimenters until it has been collected into the shot file, which is in conflict with the substantial need for data examination on a timely basis between shots. The experimenters are also spread over many different types of computer systems (possibly located at other sites). To improve data availability and handling, software has been developed to allow individual computer systems to create their own shot files locally. The data interface routine PTDATA that is used to access DIII-D data has been modified so that a user's code on any computer can access data

from any computer where that data might be located. This data access is transparent to the user. Breaking up the shot file into separate files in multiple locations also impacts software used for data archiving, data management, and data restoration. DOE

N94-22407# Westinghouse Savannah River Co., Aiken, SC.
IMPLEMENTATION OF A LABORATORY INFORMATION MANAGEMENT SYSTEM FOR ENVIRONMENTAL REGULATORY ANALYSES
W. A. Spencer, H. B. Aiken, T. L. Spatz, W. F. Miles, and J. C. Griffin Sep. 1993 80 p Presented at the 34th ORNL/DOE Conference on Analytical Chemistry in Energy Technology, Gatlinburg, TN, 5-7 Oct. 1993
(Contract DE-AC09-89SR-18035)
(DE94-001198; WSRC-MS-93-390; CONF-931081-1) Avail: CASI HC A05/MF A01

The Savannah River Technology Center created a second instance of its ORACLE based PEN LIMS to support site Environmental Restoration projects. The first instance of the database had been optimized for R&D support and did not implement rigorous sample tracking, verification, and holding times needed to support regulatory commitments. Much of the R&D instance was transferrable such as the work control functions for backlog reports, work assignment sheets, and hazard communication support. A major enhancement of the regulatory LIMS was the addition of features to support a 'standardized' electronic data format for environmental data reporting. The electronic format, called 'AN92', was developed by the site environmental monitoring organization and applies to both onsite and offsite environmental analytical contracts. This format incorporates EPA CLP data validation codes as well as details holding time and analytical result reporting requirements. The authors support this format by using special SQL queries to the database. The data is then automatically transferred to the environmental databases for trending and geological mapping. DOE

N94-22413# Lawrence Livermore National Lab., CA.
EVERYTHING YOU MIGHT WANT TO KNOW ABOUT THE INTERNET BUT ARE AFRAID TO ASK!
E. Thiel 1993 301 p
(Contract W-7405-eng-48)
(DE93-041118; UCRL-MA-115210) Avail: CASI HC A14/MF A03

This document is a guide to accessing the internet and the services available on Internet. The document contains a short explanation of the Internet by E. Kroll and E. Hoffman, brief descriptions of the primary access tools, a glossary, answers to frequently asked questions about the Internet, J. Martin's 'Search for Internet Treasure,' and other helpful information. The data access tools discussed in this document include Gopher, World Wide Web, WAIS, ASTRA, ARCHIE, WHOIS, NETSERV, and TRICKLE. The file transfer tool discussed is BITFTP. The two communication services discussed are NETNEWS and LISTSERV. DOE

N94-20249# Groningen Rijksuniv. (Netherlands). Dept. of Computational Linguistics.
A CONNECTIONIST REPRESENTATION FOR PHRASE STRUCTURES
Erik F. TjongKimSang *In* Univ. Twente, Connectionism and Natural Language Processing Oct. 1992 p 53-55 (For primary document see N94-20242 05-63)
Copyright Avail: CASI HC A01/MF A02

N94-22057# Union Bank of Finland.
SYSTEM ARCHITECTURES FOR BANKING APPLICATIONS
Kalevi Kontinen *In* Technical Research Centre of Finland, Information Technology and Economic Modelling 1992 p 11-21 (For primary document see N94-22056 05-83)
Copyright Avail: CASI HC A03/MF A03

N94-22058# All-Union Research Inst. on Computer and Informatics Problems, Moscow (Russia).
SOVIET SOCIETY INFORMATIZATION: THE USSR STATE PROGRAM
V. G. Zacharov and M. I. Sinyukov *In* Technical Research Centre of Finland, Information Technology and Economic Modelling 1992 p 22-31 (For primary document see N94-22056 05-83)
Copyright Avail: CASI HC A02/MF A03

N94-22059# Helsinki Univ. of Technology, Espoo (Finland). Computers in Industrial Production Lab.
INFORMATION SCIENCES AND BUSINESS ENTERPRISES
Hans Andersin *In* Technical Research Centre of Finland, Information Technology and Economic Modelling 1992 p 32-38 (For primary document see N94-22056 05-83)
Copyright Avail: CASI HC A02/MF A03

N94-22063# Tampere Univ. of Technology (Finland).
INFORMATION AND DECISION STRUCTURE IN A JAPANESE TYPE OF MANAGEMENT WITH RESPECT TO QCC AND JUST-IN-TIME SYSTEMS
Ilari Tyrni *In* Technical Research Centre of Finland, Information Technology and Economic Modelling 1992 p 74-75 (For primary document see N94-22056 05-83)
Copyright Avail: CASI HC A01/MF A03

N94-22080# Nokia Data, Helsinki (Finland).
DATABASES IN DISTRIBUTED SYSTEMS
Tom Toernwall *In* Technical Research Centre of Finland, Information Technology and Economic Modelling 1992 p 237-249 (For primary document see N94-22056 05-83)
Copyright Avail: CASI HC A03/MF A03

N94-22082# Technical Research Centre of Finland, Espoo. Electrical and Automation Engineering.
MANUFACTURING AND INFORMATION TECHNOLOGY
Martin Ollus *In its* Information Technology and Economic Modelling 1992 p 253-260 (For primary document see N94-22056 05-83)
Copyright Avail: CASI HC A02/MF A03

N94-22193 McGill Univ., Montreal (Quebec). Biorobotics Lab.
SPECIFICATION AND FORMAL VERIFICATION OF THE SAFETY CRITERION IN THE ALTERNATING BIT PROTOCOL
Sylvain Martel, Ian W. Hunter, and Serge Lafontaine *In* Engineering Inst. of Canada, Canadian Conference on Electrical and Computer Engineering, Volumes 1 and 2 1991 4 p (For primary document see N94-22101 05-33)
Avail: Issuing Activity (Engineering Inst. of Canada, 2050 rue Mansfield, Suite 700, Montreal, PQ H3A 1Z2 Canada)

N94-22442*# European Southern Observatory, Munich (Germany).
ARCHIVING DATA FROM GROUND-BASED TELESCOPES Abstract Only
M. A. Albrecht *In* NASA, Washington, Second Annual Conference on Astronomical Data Analysis Software and Systems. Abstracts 1992 p 11 (For primary document see N94-22438 05-89)
Avail: CASI HC A01/MF A02

N94-22446*# National Aeronautics and Space Administration, Washington, DC.
THE COOL-STAR SPECTRAL CATALOG: A UNIFORM COLLECTION OF IUE SWP-LOs Abstract Only
T. Ayres (Colorado Univ., Boulder.), D. Lenz (Colorado Univ., Boulder.), R. Burton (Colorado Univ., Boulder.), and J. Bennett *In its* Second Annual Conference on Astronomical Data Analysis Software and Systems. Abstracts 1992 p 15 (For primary document see N94-22438 05-89)
Avail: CASI HC A01/MF A02

N94-22447*# Anglo-Australian Observatory, Epping.
AN OBJECT-ORIENTED DATA REDUCTION SYSTEM IN FORTRAN Abstract Only
J. Bailey *In* NASA, Washington, Second Annual Conference on Astronomical Data Analysis Software and Systems. Abstracts 1992 p 16 (For primary document see N94-22438 05-89)
Avail: CASI HC A01/MF A02

N94-22448*# Anglo-Australian Observatory, Epping.
A SELF-DEFINING HIERARCHICAL DATA SYSTEM Abstract Only
J. Bailey *In* NASA, Washington, Second Annual Conference on Astronomical Data Analysis Software and Systems. Abstracts 1992 p 17 (For primary document see N94-22438 05-89)
Avail: CASI HC A01/MF A02

N94-22449*# European Southern Observatory, Munich (Germany).
GUIs IN THE MIDAS ENVIRONMENT Abstract Only
P. Ballester *In* NASA, Washington, Second Annual Conference on Astronomical Data Analysis Software and Systems. Abstracts 1992 p 18 (For primary document see N94-22438 05-89)
Avail: CASI HC A01/MF A02

N94-22450*# National Aeronautics and Space Administration. Goddard Space Flight Center, Greenbelt, MD.
A STRUCTURED DATA TRANSFER PROTOCOL Abstract Only
P. Barrett and A. Rots *In* NASA, Washington, Second Annual Conference on Astronomical Data Analysis Software and Systems. Abstracts 1992 p 19 (For primary document see N94-22438 05-89)
Avail: CASI HC A01/MF A02

N94-22452*# Padua Univ. (Italy).
DATABASE ACTIVITY IN THE ITALIAN ASTRONET: DIRA 2 Abstract Only
L. Benacchio and M. Nanni (Bologna Univ., Italy.) *In* NASA, Washington, Second Annual Conference on Astronomical Data Analysis Software and Systems. Abstracts 1992 p 21 (For primary document see N94-22438 05-89)
Avail: CASI HC A01/MF A02

N94-22453*# Los Alamos National Lab., NM.
THE ALEXIS DATA PROCESSING PACKAGE: AN IDL BASED SYSTEM Abstract Only
J. J. Bloch, B. W. Smith, and B. C. Edwards *In* NASA, Washington, Second Annual Conference on Astronomical Data Analysis Software and Systems. Abstracts 1992 p 22 Sponsored in part by DOE (For primary document see N94-22438 05-89)
Avail: CASI HC A01/MF A02

N94-22455*# Smithsonian Astrophysical Observatory, Cambridge, MA.
VETA X RAY DATA ACQUISITION AND CONTROL SYSTEM Abstract Only
R. J. V. Brissenden, M. T. Jones, M. Ljungberg, D. T. Nguyen, and J. B. Roll, Jr. *In* NASA, Washington, Second Annual Conference on Astronomical Data Analysis Software and Systems. Abstracts 1992 p 24 Presented at the Conference ADASS, 1992 (For primary document see N94-22438 05-89)
Avail: CASI HC A01/MF A02

N94-22457*# Instituto de Pesquisas Espaciais, Sao Jose dos Campos (Brazil).
EXPERIMENTS WITH RECURSIVE ESTIMATION IN ASTRONOMICAL IMAGE PROCESSING Abstract Only
I. Busko *In* NASA, Washington, Second Annual Conference on Astronomical Data Analysis Software and Systems. Abstracts 1992 p 26 (For primary document see N94-22438 05-89)
Avail: CASI HC A01/MF A02

N94-22459*# California Univ., Berkeley. Center for EUV Astrophysics.
THE EUVE PROPOSAL DATABASE AND SCHEDULING SYSTEM Abstract Only
C. Christian, E. Olson, P. Jelinsky, and M. Samuel *In* NASA, Washington, Second Annual Conference on Astronomical Data Analysis Software and Systems. Abstracts 1992 p 28 (For primary document see N94-22438 05-89)
Avail: CASI HC A01/MF A02

N94-22462*# National Aeronautics and Space Administration. Goddard Space Flight Center, Greenbelt, MD.
ROSAT IMPLEMENTATION OF A PROPOSED MULTI-MISSION X RAY DATA FORMAT Abstract Only
M. Corcoran, W. Pence, R. White, and M. Conroy (Smithsonian Astrophysical Observatory, Cambridge, MA.) *In* NASA, Washington, Second Annual Conference on Astronomical Data Analysis Software and Systems. Abstracts 1992 p 31 (For primary document see N94-22438 05-89)
Avail: CASI HC A01/MF A02

N94-22463*# National Radio Astronomy Observatory, Green Bank, WV.
ON AIPS++, A NEW ASTRONOMICAL INFORMATION PROCESSING SYSTEM Abstract Only
G. A. Croes *In* NASA, Washington, Second Annual Conference on Astronomical Data Analysis Software and Systems. Abstracts 1992 p 32 (For primary document see N94-22438 05-89)
Avail: CASI HC A01/MF A02

N94-22468*# California Univ., Berkeley. Center for EUV Astrophysics.
THE EXTREME ULTRAVIOLET EXPLORER ARCHIVE Abstract Only
Jeremy J. Drake, Carl Dobson, and Elisha Polomski *In* NASA, Washington, Second Annual Conference on Astronomical Data Analysis Software and Systems. Abstracts 1992 p 37 (For primary document see N94-22438 05-89)
Avail: CASI HC A01/MF A02

N94-22469*# European Southern Observatory, Garching (Germany).
A DISTRIBUTED CLIENTS/DISTRIBUTED SERVERS MODEL FOR STARCAT Abstract Only
B. Pirenne, M. A. Albrecht, D. Durand (CADC, British Columbia.), and S. Gaudet (CADC, British Columbia.) *In* NASA, Washington, Second Annual Conference on Astronomical Data Analysis Software and Systems. Abstracts 1992 p 38 (For primary document see N94-22438 05-89)
Avail: CASI HC A01/MF A02

N94-22479*# Observatoire de Strasbourg (France).
ELECTRONIC PUBLISHING AND INTELLIGENT INFORMATION RETRIEVAL Abstract Only
A. Heck *In* NASA, Washington, Second Annual Conference on Astronomical Data Analysis Software and Systems. Abstracts 1992 p 48 (For primary document see N94-22438 05-89)
Avail: CASI HC A01/MF A02

N94-22490*# California Univ., Berkeley. Center for EUV Astrophysics.
QUALITY CONTROL OF EUVE DATABASES Abstract Only
L. M. John and J. Drake *In* NASA, Washington, Second Annual Conference on Astronomical Data Analysis Software and Systems. Abstracts 1992 p 59 (For primary document see N94-22438 05-89)
Avail: CASI HC A01/MF A02

N94-22493*# National Aeronautics and Space Administration. Goddard Space Flight Center, Greenbelt, MD.
A GENERIC ARCHIVE PROTOCOL AND AN IMPLEMENTATION Abstract Only
J. M. Jordan, D. G. Jennings, T. A. McGlynn, N. G. Ruggiero, and T. A. Serlemitsos *In* NASA, Washington, Second Annual Conference on Astronomical Data Analysis Software and Systems. Abstracts 1992 p 62 (For primary document see N94-22438 05-89)
Avail: CASI HC A01/MF A02

N94-22495*# Lick Observatory, Santa Cruz, CA.
CCD DATA ACQUISITION SYSTEMS AT LICK AND KECK OBSERVATORIES Abstract Only
R. I. Kibrick, R. J. Stover, and A. R. Conrad (Keck Observatory, Mauna Kea, HI.) *In* NASA, Washington, Second Annual Conference on Astronomical Data Analysis Software and Systems. Abstracts 1992 p 64 (For primary document see N94-22438 05-89)
Avail: CASI HC A01/MF A02

N94-22496*# National Aeronautics and Space Administration. Goddard Space Flight Center, Greenbelt, MD.
THE DIGITAL ARCHIVE OF THE INTERNATIONAL HALLEY WATCH Abstract Only
D. A. Klinglesmith, III, M. B. Niedner, E. Grayzeck (Maryland Univ., College Park.), M. Aronsson (Jet Propulsion Lab., Cape Canaveral, FL.), R. L. Newburn (Jet Propulsion Lab., Cape Canaveral, FL.), and A. Warnock, III (Hughes STX, Inc., Greenbelt, MD.) *In* NASA, Washington, Second Annual Conference on Astronomical Data Analysis Software and Systems. Abstracts 1992 p 65 (For primary document see N94-22438 05-89)
Avail: CASI HC A01/MF A02

N94-22497*# Space Telescope Science Inst., Baltimore, MD.
DECONVOLUTION OF HUBBLE SPACE TELESCOPE IMAGES USING SIMULATED POINT SPREAD FUNCTIONS Abstract Only
J. E. Krist and H. Hasan *In* NASA, Washington, Second Annual Conference on Astronomical Data Analysis Software and Systems. Abstracts 1992 p 66 (For primary document see N94-22438 05-89)
Avail: CASI HC A01/MF A02

N94-22499*# Smithsonian Institution, Cambridge, MA.
INTELLIGENT TEXT RETRIEVAL IN THE NASA ASTROPHYSICS DATA SYSTEM Abstract Only
M. J. Kurtz, T. Karakashian, C. P. Stern, G. Eichhorn, S. S. Murray, J. M. Watson, P. G. Ossorio (Ellery Systems, Inc., Boulder, CO.), and J. L. Stoner (Ellery Systems, Inc., Boulder, CO.) *In* NASA, Washington, Second Annual Conference on Astronomical Data Analysis Software and Systems. Abstracts 1992 p 68 (For primary document see N94-22438 05-89)
Avail: CASI HC A01/MF A02

N94-22500*# Hughes STX, Inc., Greenbelt, MD.
THE IDL ASTRONOMY USER'S LIBRARY Abstract Only
W. B. Landsman *In* NASA, Washington, Second Annual Conference on Astronomical Data Analysis Software and Systems. Abstracts 1992 p 69 (For primary document see N94-22438 05-89)
Avail: CASI HC A01/MF A02

N94-22502*# Observatoire de Strasbourg (France). Center de Donnees Astronomiques.
SIMBAD QUALITY-CONTROL Abstract Only
Soizick Lesteven *In* NASA, Washington, Second Annual Conference on Astronomical Data Analysis Software and Systems. Abstracts 1992 p 71 (For primary document see N94-22438 05-89)
Avail: CASI HC A01/MF A02

N94-22503*# California Univ., Berkeley. Center for EUV Astrophysics.
DATA INDEXING TECHNIQUES FOR THE EUVE ALL-SKY SURVEY Abstract Only
J. Lewis, V. Saba, and C. Dobson *In* NASA, Washington, Second Annual Conference on Astronomical Data Analysis Software and Systems. Abstracts 1992 p 72 (For primary document see N94-22438 05-89)
Avail: CASI HC A01/MF A02

N94-22504*# Keck Observatory, Mauna Kea, HI.
THE KECK TASK LIBRARY (KTL) Abstract Only
W. F. Lupton and A. R. Conrad *In* NASA, Washington, Second Annual Conference on Astronomical Data Analysis Software and Systems. Abstracts 1992 p 73 (For primary document see N94-22438 05-89)
Avail: CASI HC A01/MF A02

N94-22509*# National Aeronautics and Space Administration. Goddard Space Flight Center, Greenbelt, MD.
GammaCore: THE COMPTON OBSERVATORY RESEARCH ENVIRONMENT Abstract Only
T. A. McGlynn, D. G. Jennings, J. M. Jordan, N. Ruggiero, and T. A. Serlemitsos *In* NASA, Washington, Second Annual Conference on Astronomical Data Analysis Software and Systems. Abstracts 1992 p 78 (For primary document see N94-22438 05-89)
Avail: CASI HC A01/MF A02

N94-22514*# Leicester Univ. (England).
EVALUATION OF RDBMS PACKAGES FOR USE IN ASTRONOMY Abstract Only
C. G. Page and A. C. Davenhall *In* NASA, Washington, Second Annual Conference on Astronomical Data Analysis Software and Systems. Abstracts 1992 p 83 (For primary document see N94-22438 05-89)
Avail: CASI HC A01/MF A02

N94-22518*# European Southern Observatory, Munich (Germany).
THE EUROPEAN SOUTHERN OBSERVATORY-MIDAS TABLE FILE SYSTEM Abstract Only
M. Peron and P. Grosbol *In* NASA, Washington, Second Annual Conference on Astronomical Data Analysis Software and Systems. Abstracts 1992 p 87 (For primary document see N94-22438 05-89)
Avail: CASI HC A01/MF A02

N94-22519*# Smithsonian Astrophysical Observatory, Cambridge, MA.
AN X RAY ARCHIVE ON YOUR DESK: THE EINSTEIN CD-ROM'S Abstract Only
A. Prestwich, J. McDowell, D. Plummer, K. Manning, and M. Garcia *In* NASA, Washington, Second Annual Conference on Astronomical Data Analysis Software and Systems. Abstracts 1992 p 88 (For primary document see N94-22438 05-89)
Avail: CASI HC A01/MF A02

N94-22521*# European Space Research Organization, Noordwikj (Netherlands).
THE EXOSAT DATABASE AND ARCHIVE Abstract Only
A. P. Reynolds and A. N. Parmar *In* NASA, Washington, Second Annual Conference on Astronomical Data Analysis Software and Systems. Abstracts 1992 p 90 (For primary document see N94-22438 05-89)
Avail: CASI HC A01/MF A02

N94-22525*# Kitt Peak National Observatory, Tucson, AZ.
MANAGING AN ARCHIVE OF WEATHER SATELLITE IMAGES Abstract Only
R. L. Seaman *In* NASA, Washington, Second Annual Conference on Astronomical Data Analysis Software and Systems. Abstracts 1992 p 94 (For primary document see N94-22438 05-89)
Avail: CASI HC A01/MF A02

N94-22527*# Rice Univ., Houston, TX.
THE IRAF FABRY-PEROT ANALYSIS PACKAGE: RING FITTING Abstract Only
P. L. Shopbell, J. Bland-Hawthorn, and G. Cecil (North Carolina Univ., Chapel Hill.) *In* NASA, Washington, Second Annual Conference on Astronomical Data Analysis Software and Systems. Abstracts 1992 p 96 (For primary document see N94-22438 05-89)
Avail: CASI HC A01/MF A02

N94-22528*# Anglo-Australian Observatory, Sydney.
THE EVOLUTION OF THE FIGARO DATA REDUCTION SYSTEM Abstract Only
K. Shortridge *In* NASA, Washington, Second Annual Conference on Astronomical Data Analysis Software and Systems. Abstracts 1992 p 97 (For primary document see N94-22438 05-89)
Avail: CASI HC A01/MF A02

N94-22529*# Anglo-Australian Observatory, Sydney.
THE DATA ACQUISITION SYSTEM FOR THE ANGLO-AUSTRALIAN OBSERVATORY 2-DEGREE FIELD PROJECT Abstract Only
K. Shortridge, T. J. Farrell, and J. Bailey *In* NASA, Washington, Second Annual Conference on Astronomical Data Analysis Software and Systems. Abstracts 1992 p 98 (For primary document see N94-22438 05-89)
Avail: CASI HC A01/MF A02

N94-22530*# Space Telescope Science Inst., Baltimore, MD.
INTEGRATING A LOCAL DATABASE INTO THE StarView DISTRIBUTED USER INTERFACE Abstract Only
D. P. Silberberg *In* NASA, Washington, Second Annual Conference on Astronomical Data Analysis Software and Systems. Abstracts 1992 p 99 (For primary document see N94-22438 05-89)
Avail: CASI HC A01/MF A02

N94-22534*# National Aeronautics and Space Administration. Goddard Space Flight Center, Greenbelt, MD.
UIT SUPPORT OBSERVATIONS ARCHIVE Abstract Only
Eric P. Smith, Paul Hintzen, and Kwang-Ping Cheng *In* NASA, Washington, Second Annual Conference on Astronomical Data Analysis Software and Systems. Abstracts 1992 p 103 (For primary document see N94-22438 05-89)
Avail: CASI HC A01/MF A02

N94-22535*# Kitt Peak National Observatory, Tucson, AZ.
IRAF IN THE NINETIES Abstract Only

D. Tody *In* NASA, Washington, Second Annual Conference on Astronomical Data Analysis Software and Systems. Abstracts 1992 p 104 (For primary document see N94-22438 05-89)
Avail: CASI HC A01/MF A02

N94-22537*# National Aeronautics and Space Administration. Goddard Space Flight Center, Greenbelt, MD.
RECOMMENDATIONS FOR A SERVICE FRAMEWORK TO ACCESS ASTRONOMICAL ARCHIVES Abstract Only
J. J. Travisano and J. Pollizzi (Space Telescope Science Inst., Baltimore, MD.) *In* NASA, Washington, Second Annual Conference on Astronomical Data Analysis Software and Systems. Abstracts 1992 p 106 (For primary document see N94-22438 05-89)
Avail: CASI HC A01/MF A02

N94-22539*# Kitt Peak National Observatory, Tucson, AZ.
THE SPECTRAL WORLD COORDINATE SYSTEMS IN IRAF/NOAO Abstract Only
F. Valdes *In* NASA, Washington, Second Annual Conference on Astronomical Data Analysis Software and Systems. Abstracts 1992 p 108 (For primary document see N94-22438 05-89)
Avail: CASI HC A01/MF A02

N94-22541*# National Aeronautics and Space Administration. Goddard Space Flight Center, Greenbelt, MD.
NASA'S ASTROPHYSICS ARCHIVES AT THE NATIONAL SPACE SCIENCE DATA CENTER Abstract Only
M. E. VanSteenberg *In* NASA, Washington, Second Annual Conference on Astronomical Data Analysis Software and Systems. Abstracts 1992 p 110 (For primary document see N94-22438 05-89)
Avail: CASI HC A01/MF A02

N94-22544*# Hughes STX, Inc., Greenbelt, MD.
STELAR: AN EXPERIMENT IN THE ELECTRONIC DISTRIBUTION OF ASTRONOMICAL LITERATURE Abstract Only
A. Warnock, M. E. VanSteenburg (National Aeronautics and Space Administration. Goddard Space Flight Center, Greenbelt, MD.), L. E. Brotzman, J. Gass, and D. Kovalsky *In* NASA, Washington, Second Annual Conference on Astronomical Data Analysis Software and Systems. Abstracts 1992 p 113 (For primary document see N94-22438 05-89)
Avail: CASI HC A01/MF A02

N94-22546*# Jet Propulsion Lab., California Inst. of Tech., Pasadena.
SkICAT: A CATALOGING AND ANALYSIS TOOL FOR WIDE FIELD IMAGING SURVEYS Abstract Only
N. Weir (California Inst. of Tech., Pasadena.), U. M. Fayyad, S. G. Djorgovski (California Inst. of Tech., Pasadena.), and J. Roden *In* NASA, Washington, Second Annual Conference on Astronomical Data Analysis Software and Systems. Abstracts 1992 p 115 (For primary document see N94-22438 05-89)
Avail: CASI HC A01/MF A02

N94-22547*# National Radio Astronomy Observatory, Green Bank, WV.
THE VLBA CORRELATOR: REAL-TIME IN THE DISTRIBUTED ERA Abstract Only
D. C. Wells *In* NASA, Washington, Second Annual Conference on Astronomical Data Analysis Software and Systems. Abstracts 1992 p 116 (For primary document see N94-22438 05-89)
Avail: CASI HC A01/MF A02

N94-22548*# Space Telescope Science Inst., Baltimore, MD.
StarView: THE OBJECT ORIENTED DESIGN OF THE ST DADS USER INTERFACE Abstract Only
J. D. Williams and J. A. Pollizzi *In* NASA, Washington, Second Annual Conference on Astronomical Data Analysis Software and Systems. Abstracts 1992 p 117 (For primary document see N94-22438 05-89)
Avail: CASI HC A01/MF A02

N94-22553*# Space Telescope Science Inst., Baltimore, MD.
IRAF AND STSDAS UNDER THE NEW ALPHA ARCHITECTURE Abstract Only
N. R. Zarate *In* NASA, Washington, Second Annual Conference on Astronomical Data Analysis Software and Systems. Abstracts 1992 p 122 (For primary document see N94-22438 05-89)
Avail: CASI HC A01/MF A02

83 ECONOMICS AND COST ANALYSIS

Includes cost effectiveness studies.

N94-20098# Rochester Univ., NY. Dept. of Computer Science.
ELIMINATING AMORTIZATION: ON DATA STRUCTURES WITH GUARANTEED RESPONSE TIME Ph.D. Thesis
Rajeev Raman Oct. 1992 95 p
(Contract N00014-82-K-0193)
(TR-439) Avail: CASI HC A05/MF A01

An efficient amortized data structure is one that ensures that the average time per operation spent on processing any sequence of operations is small. Amortized data structures typically have very non-uniform response times; i.e., individual operations can be occasionally and unpredictably slow, although the average time over the sequence is kept small by completing most of the other operations quickly. This makes amortized data structures unsuitable in many important contexts, such as real-time systems, parallel programs, persistent data structures and interactive software. On the other hand, an efficient (single-operation) worst-case data structure guarantees that every operation will be processed quickly. The construction of worst-case data structures from amortized ones is a fundamental problem which is also of pragmatic interest. Progress has been slow so far, both because the techniques used were of a limited nature and because the resulting data structures had much larger hidden constant factors. Both these issues are addressed. Author (revised)

N94-22056# Technical Research Centre of Finland, Espoo. Electrical and Automation Engineering Lab.
INFORMATION TECHNOLOGY AND ECONOMIC MODELLING
Pentti Uuspaeae, ed. and Goeran Pulkkis, ed. (Helsinki Univ. of Technology, Espoo, Finland.) 1992 311 p Presented at Joint Finnish-Soviet Symposium, Helsinki, Finland, 20-22 Nov. 1990
(VTT-SYMP-135; ISBN-95-1384-086-7; ETN-93-94486) Copyright Avail: CASI HC A14/MF A03

Papers presented at a symposium to promote cooperation between Finnish and Soviet scientists, engineers, and economists by examining developments in information technology and economic modeling are presented. The papers are organized into the following working sessions: macroeconomic models, economic modeling, computer software and hardware, applied computing, economic modeling methods, operations research, data systems and technology, and economic evaluation. For individual titles, see N94-22057 through N94-22087.

N94-22057# Union Bank of Finland.
SYSTEM ARCHITECTURES FOR BANKING APPLICATIONS **c82**
Kalevi Kontinen *In* Technical Research Centre of Finland, Information Technology and Economic Modelling 1992 p 11-21 (For primary document see N94-22056 05-83)
Copyright Avail: CASI HC A03/MF A03

A discussion on system architectures for banking applications based on the experience of a Finnish bank is presented. In order to perform their society mission with quality and efficiency, banks need many resources and skills. Together with human competence and vision, data processing systems are the basis and key resource of modern banking. Production and development costs of information processing may exceed 15% of nonfinancial expenses of bank. Heavy investigating is no guarantee of success in data processing. Smarter, not larger spending makes the difference of good and mediocre systems. Right applications must be automated in the right way, buying the resources for the right price. Essential parts in the right way of doing things are the basic structural choices of systems and their architectures. ESA

N94-22058# All-Union Research Inst. on Computer and Informatics Problems, Moscow (Russia).
SOVIET SOCIETY INFORMATIZATION: THE USSR STATE PROGRAM **c82**
V. G. Zacharov and M. I. Sinyukov *In* Technical Research Centre of

Finland, Information Technology and Economic Modelling 1992 p 22-31 (For primary document see N94-22056 05-83)
Copyright Avail: CASI HC A02/MF A03

A discussion on informatization in Soviet society is presented. The program of informatization is oriented towards the transition to the regulated market economy as well as the creation of the conditions necessary to achieve social and economic development aims. An outline of what the program should provide is given. The state program of informatization includes the following sections: use of ITE (Information Technology Equipment) in national economy; informatization infrastructure; ITE development and production; organization and economic support of informatization processes; and macroeconomic indices of informatization. ESA

N94-22059# Helsinki Univ. of Technology, Espoo (Finland). Computers in Industrial Production Lab.
INFORMATION SCIENCES AND BUSINESS ENTERPRISES **c82**
Hans Andersin *In* Technical Research Centre of Finland, Information Technology and Economic Modelling 1992 p 32-38 (For primary document see N94-22056 05-83)
Copyright Avail: CASI HC A02/MF A03

The rationale for cooperation between the Soviet Union and Finland in the field of information sciences from the point of view of business enterprises is summarized. An example of a possible future field of cooperation, Computer Integrated Manufacturing (CIM), is given. CIM strategy and infrastructure are discussed and human roles in integration are considered. Reasons for CIM being a good candidate for future cooperation are outlined. ESA

N94-22060# Academy of Sciences (USSR), Moscow. Computer Center.
MATHEMATICAL MODELLING OF ECONOMIC SYSTEMS
Alexander A. Petrov *In* Technical Research Centre of Finland, Information Technology and Economic Modelling 1992 p 39-52 (For primary document see N94-22056 05-83)
Copyright Avail: CASI HC A03/MF A03

The main propositions of the general approach to mathematical description and analysis of economic systems are presented. This approach was developed in the U.S.S.R. as the system analysis of evolving economy. The basic equations of mathematical models in frames of the system analysis of evolving economy are displayed. The problem of closing this system of equations by means of modeling of goods production, exchange and distribution process control relations is discussed. Some results of market economy are also discussed. ESA

N94-22061# Technical Research Centre of Finland, Espoo.
AJKA: AN ECONOMETRIC MACROMODEL FOR FINLAND
Asko Korpela *In its* Information Technology and Economic Modelling 1992 p 53-63 (For primary document see N94-22056 05-83)
Copyright Avail: CASI HC A03/MF A03

The structure, utilization, performance, equations and data of the AJKA Keynesian demand oriented equilibrium econometric macromodel are outlined. AJKA is being employed on personal computers for forecasting and policy optimization in educational context. The model was found to be a well working backbone of an intermediate course in macroeconomics, allowing the students to become acquainted with the structural relationships of the national economy and the connection of basic theories and their empirical application. The model was also used in management training. ESA

N94-22062# Academy of Sciences (USSR), Moscow. Computer Center.
MACROMODEL OF CENTRALLY PLANNED ECONOMY
Alexander P. Krutov *In* Technical Research Centre of Finland, Information Technology and Economic Modelling 1992 p 64-73 (For primary document see N94-22056 05-83)
Copyright Avail: CASI HC A02/MF A03

A mathematical description of production, exchanges, distribution and consumption processes in the centrally planned economy is suggested. Information disposed by the planning center is described as well as planning procedures by it. Their influence on economic self adjustment mechanisms is analyzed. Some results of computer experiments are presented. ESA

N94-22063# Tampere Univ. of Technology (Finland).
INFORMATION AND DECISION STRUCTURE IN A JAPANESE TYPE OF MANAGEMENT WITH RESPECT TO QCC AND JUST-IN-TIME SYSTEMS **c82**
Ilari Tyrni *In* Technical Research Centre of Finland, Information Technology and Economic Modelling 1992 p 74-75 (For primary document see N94-22056 05-83)
Copyright Avail: CASI HC A01/MF A03

The requirements for the efficiency of Quality Control Circles (QCC) and Just-In-Time (JIT) systems are considered. The requirements of teamwork can be more generally considered instead of QCC for the proper organization of information and decision making systems. Even from the point of view of QCC and JIT, the optimal information and decision structure is not independent of the other structures of the firm. This is especially important with regard to the education and training of employees. Also the incentive structure (images, promotion, and other factors) must be such that it motivates QCC and JIT activities. ESA

N94-22064# Academy of Sciences (USSR), Moscow. Computer Center.
COMPUTER-AIDED DESIGN SYSTEM FOR OBJECTS LOCATION AND RESERVOIR WITH DISPERSED RESOURCE EVOLUTION INVESTIGATION **c61**
S. V. Tuev *In* Technical Research Centre of Finland, Information Technology and Economic Modelling 1992 p 76-84 (For primary document see N94-22056 05-83)
Copyright Avail: CASI HC A02/MF A03

A program intended for multiversional calculations of object location and reservoir evolution is reported. Objects are oriented for collection and manufacturing of resources dispersed on any reservoir. Reservoir evolution is also taken into account. The software is based on algorithms for representation of geographical information and dispersed resource distribution, algorithms giving information about the territory heterogeneity and its resources, algorithms solving a complex of objects allocation by distributed resource problems, and on algorithms analyzing the objects with dispersed resource (reservoir) evolution model. The expert can use the software to form effective projects of facility location. ESA

N94-22065# Technical Research Centre of Finland, Espoo.
THE PROGRAM SYSTEM FOR THE DIAGNOSTICS OF STRAINS AND FRACTURE PREDICTION OF SOLIDS **c39**
V. Z. Parton and V. Boriskovski *In* Technical Research Centre of Finland, Information Technology and Economic Modelling 1992 p 85 (For primary document see N94-22056 05-83)
Copyright Avail: CASI HC A01/MF A03

An expert system for fracture mechanics based assessment of structure lifetime is reported. The main design and operation features are outlined. The stress intensity factor computation for typical flaws is based on the weight function method. It allows the calculation efficiency to be improved and the numerous body configurations to be analyzed. In design, the part-through flaw shape is calculated (from the stable crack shapes). In service, the possibility is provided for the stress intensity factor computational and nominal stress assessment in the crack plane from discrete Crack Opening Displacement (COD) values at an essential distance from the crack tip. The J-, C*-, and COD-based fracture assessment methods are used in accordance with R6 standard. The failure assessment diagrams are derived with the use of a multiparametric approach. The crack growth prediction involves the evaluated criteria of transforming test results from standard specimens to structures with part-through cracks. The relationships of the so called small crack growth are also taken into account. Numerous applied problems for industry, power engineering, in particular, were solved. ESA

N94-22066# Algorithm Co. (Russia).
THE SOVIET SOFTWARE MARKET: CURRENT STATE AND ASPECTS OF DEVELOPMENT **c61**
Sergei A. Chizhov *In* Technical Research Centre of Finland, Information Technology and Economic Modelling 1992 p 86-92 (For primary document see N94-22056 05-83)
Copyright Avail: CASI HC A02/MF A03

A discussion on the market relations emerging from the transition of the Soviet economy to new mechanisms, including those of information

technology and software, is presented. The structure of the software market is explained. Recent changes in the situation are outlined. ESA

N94-22067# Nokia Data, Helsinki (Finland).
APPLICATION DEVELOPMENT IN A PC/LAN ENVIRONMENT Abstract Only **c61**
Kurt Helenelund *In* Technical Research Centre of Finland, Information Technology and Economic Modelling 1992 p 93 (For primary document see N94-22056 05-83)
Copyright Avail: CASI HC A01/MF A03

As the drive towards the desktop accelerates, the delivery of vertical business applications and mission critical applications on the desktop becomes critical. The networked systems will emerge as the main application platform not just for traditional personal productivity applications but also for workgroup solutions and corporate mission critical systems. The new generation of applications will be based on the client/server model, and they will use graphical user interfaces. Database servers using the SQL standard will emerge as the dominating information warehouse on PC LAN's (Personal Computer Local Area Networks). As the demand for easy to use applications increases, developers are faced with a situation where more and more time is spent on the design and implementation of the user interface. In most modern applications, a major part of the developed code is spent on the user interface with current technology. ESA

N94-22068# All-Union Research Inst. on Computer and Informatics Problems, Moscow (Russia).
THE DISTRIBUTED CAD SYSTEM FOR LSI/VLSI DESIGN **c61**
V. G. Zacharov and V. A. Konyavsky *In* Technical Research Centre of Finland, Information Technology and Economic Modelling 1992 p 94-100 (For primary document see N94-22056 05-83)
Copyright Avail: CASI HC A02/MF A03

Peculiarities of microelectronic CAD (Computer Aided Design) are conditioned by a wide assortment of design objects. Computer capacities necessary to carry on design processes vary with the class of the object (PLD's, Gate-Arrays, submicron technology custom VLSI (Very Large Scale Integration), etc.) as well as with design stages. For example, while performance of a PC (Personal Computer) is quite sufficient for circuit input or logical synthesis of nodes etc., a supercomputer's performance might not provide capacity for some technology simulation or circuitry modeling. This variety of requirements to be satisfied constrains the design of a distributed mode system. The structure of a distributed, multiple user CAD system for LSI/VLSI design is envisaged, while considering the demands to provide necessary peak capacities to perform variable information flow processing. Setting up a number of centers integrated into a regional computer net is envisaged by the USSR state informatization program to provide the structure implementation. Problems of hardware choice as well as those of choice of basic and application software are examined. ESA

N94-22069# Academy of Sciences (USSR), Moscow. Automated Systems Inst.
IAS TELECOMMUNICATION INFRASTRUCTURE AND VALUE ADDED NETWORK SERVICES PROVIDED BY IASNET **c32**
Oleg L. Smirnov and Sergei Marchenko *In* Technical Research Centre of Finland, Information Technology and Economic Modelling 1992 p 101-119 (For primary document see N94-22056 05-83)
Copyright Avail: CASI HC A03/MF A03

The topology of a packet switching network for the Soviet National Centre for Automated Data Exchange with Foreign Computer Networks and Databanks (NCADE) based on a design by the Institute for Automated Systems (IAS) is discussed. NCADE has partners all over the world: it is linked to East European countries via telephone lines while satellites are used for communication with remote partners, such as Cuba, Mongolia, and Vietnam. Moreover, there is a connection to the Austrian, British, Canadian, Finnish, French, U.S. and other western networks through which users can have access to databases on each network. At the same time, NCADE provides western customers with access to more than 70 Soviet databases. Software and hardware of IASNET use data exchange recommendations agreed with the International Standard Organization (ISO) and International Telegraph and Telephone Consultative Committee (CCITT). Technical parameters of IASNET are compatible with the majority of foreign networks such as DATAPAK, TRANSPAC, TELENET, and others. By means of IASNET, the NCADE provides connection of Soviet and foreign users to information and computer centers around the world on the basis of the CCITT X.25 and X.75 recommendations. Any information resources of IASNET and value added network services, such as computer teleconferences, E-mail, information retrieval system, intelligent support of access to databanks and databases, and others are discussed. The topology of the ACADEMNET connected to IASNET over an X.25 gateway is also discussed. ESA

N94-22070# Nokia Data, Helsinki (Finland). Technology and Product Strategy.
INDUSTRY STANDARDS: KEY TO DISTRIBUTED COMPUTING **c62**
Ari Mikkola *In* Technical Research Centre of Finland, Information Technology and Economic Modelling 1992 p 120-133 (For primary document see N94-22056 05-83)
Copyright Avail: CASI HC A03/MF A03

A major trend during the 1990's will be a continued downsizing and distribution of computing resources. This trend is fuelled by rapid development of PC (Personal Computer), workstation, and communications technologies which bring cost effective processing power on the desktop. An intelligent workstation is a user's window to the services of the entire distributed information system. Data stored in different computers is available to be shared by applications in other computers. The emphasis in distributed computing will be first on intracompany connectivity and access to public services and later on intercompany connectivity. Open industry standards play an important role. The standardization trends which are relevant to distributed computing in the areas of connectivity and interoperability, portability, and user access, are discussed. ESA

N94-22071# Academy of Sciences (USSR), Moscow. Computer Center.
MODELS OF TRANSIENT PROCESSES IN CENTRALLY PLANNED ECONOMY
I. Pospelov *In* Technical Research Centre of Finland, Information Technology and Economic Modelling 1992 p 134-146 (For primary document see N94-22056 05-83)
Copyright Avail: CASI HC A03/MF A03

Two models of centrally planned economics with free market elements are considered. The first model describes interaction of state and leased enterprises. The second gives some estimations of possible consequences of 'shock therapy' for the Soviet economy. All the models include the description of financial and planning systems. They also take into account the specific planned economy process of production of unused goods for the sake of fulfillment of plan. ESA

N94-22072# Helsinki Univ. of Technology, Espoo (Finland).
AN ECONOMIC ANALYSIS OF TRANSBOUNDARY AIR POLLUTION BETWEEN FINLAND AND THE SOVIET UNION Abstract Only **c45**
Veijo Kaitala, Matti Pohjola (Research Inst. of the Finnish Economy, Helsinki.), and Olli Tahvonen (Helsinki School of Economics and Business Administration, Finland.) *In* Technical Researh Centre of Finland, Information Technology and Economic Modelling 1992 p 147 (For primary document see N94-22056 05-83)
(ETLA-Discussion-Paper-335) Copyright Avail: CASI HC A01/MF A03

An evaluation of the net benefits to both parties of bilateral cooperation between Finland and the Soviet Union on reducing sulphur emissions is presented. The analysis is based on a sulphur transportation model and on estimated abatement cost functions. It is shown that efficient cooperation may entail financial transfers from Finland to the Soviet Union because it is cheaper to abate sulphur there. It is further demonstrated that the recently signed agreement aiming at reductions in air pollutants is not rational from the Soviet Union's viewpoint and may not, therefore, be carried out without monetary support from Finland. ESA

N94-22073# Academy of Sciences (USSR), Moscow. Computer Center.
MULTICRITERIA OPTIMISATION PROBLEM IN THE AGRICULTURAL MODELLING **c43**
H. M. Stoliarova *In* Technical Research Centre of Finland, Information Technology and Economic Modelling 1992 p 148-161 (For primary document see N94-22056 05-83)
Copyright Avail: CASI HC A03/MF A03

A multicriteria optimization problem concerning crop production is considered. Optimal strategies for winter wheat production (the principal

crop of the Stavropol region of the USSR) are determined on the base of the dynamic crop weather simulation models. Approximation of Pareto set for two criteria and different strategies of fertilizer application was constructed. As a result, reasonable compromising solutions were identified which could serve as a useful tool for agricultural planning in the Stavropol territory and in other semi arid regions. ESA

N94-22074# Academy of Sciences (USSR), Moscow. Computer Center.
ANALYSIS OF CONSUMER DEMAND STRUCTURE BY MEANS OF ECONOMIC INDEXES
A. A. Shananin *In* Technical Research Centre of Finland, Information Technology and Economic Modelling 1992 p 162-172 (For primary document see N94-22056 05-83)
Copyright Avail: CASI HC A03/MF A03

A nonparametric method for calculation of economic indexes, that are positive homogeneous utility function (index of product) and price index, is considered. The economic indexes calculated by this method reflect the structure of consumer demand functions and may be used for the solution of the following problems: to predict the changing of demand structure when prices change; to find the ratio of prices which is necessary to support some consumer demand structure. ESA

N94-22075# Academy of Sciences (USSR), Moscow. Computer Center.
A MODEL OF NEGOTIATION IN AN EXTENSIVE FORM GAME **c66**
Ivan Menshikov *In* Technical Research Centre of Finland, Information Technology and Economic Modelling 1992 p 173-181 (For primary document see N94-22056 05-83)
Copyright Avail: CASI HC A02/MF A03

Any game theoretical equilibrium is not effective as a social choice function. In general, the equilibrium is not Pareto optimal. So, it is reasonable to consider an improvement of the original game associated with negotiation. A comparison of several known approaches to game theoretical research of negotiation is presented. A problem of axiomatic characterization of a negotiation mechanism is discussed. The most attractive applications of this idea correspond to extensive form games. Re-negotiation of two different types is considered: talks at the initial position of the game and those at one of the next positions when, after disagreement, somebody makes a move in the original game. A number of unexpected features of that model are represented. ESA

N94-22076# Helsinki Univ. of Technology, Espoo (Finland).
CONTROLLING MULTISUPPLIER OPERATIONS BY INTELLIGENT EDI **c32**
Juha Eskelinen, Jyrki Kovanen, Miika Linna, Tero Mononen, and Reijo Sulonen *In* Technical Research Centre of Finland, Information Technology and Economic Modelling 1992 p 182-205 (For primary document see N94-22056 05-83)
Copyright Avail: CASI HC A03/MF A03

In modern CIM (Computer Integrated Manufacturing) environment, problems that can affect production should be discovered as soon as possible. This can be very difficult in multisupplier operations where problems outside one organization can remain undetected until they already have effects inside that organization. If Electronic Data Interchange (EDI) is used to control intercompany operations there is a better possibility to detect problems on logistic chain. Because these problems usually have some effects in the flow of EDI messages, they can be detected by controlling this flow. A Forget-Me-Not (FMN) system, which is a programmable message management system that can control the flow of EDI messages and detect exceptional situations is discussed. ESA

N94-22077# Academy of Sciences (USSR), Moscow. Computer Center.
APL-TECHNOLOGY OF COMPUTER SIMULATION **c61**
A. Y. Boozin *In* Technical Research Centre of Finland, Information Technology and Economic Modelling 1992 p 206-212 (For primary document see N94-22056 05-83)
Copyright Avail: CASI HC A02/MF A03

Advantages and disadvantages of the APL language usage for computer simulation are considered. The language was actively used in the computing center during the last 10 years for simulation of socio-economic systems. The original software package was developed with the aid of APL. This package makes the simulation researches easy and helps to get the results in graphical form. ESA

N94-22078# Technical Research Centre of Finland, Espoo.
APPLICATION OF THE STRUCTURES QUERY LANGUAGE OF APROS FOR SPECIFICATION OF INDUSTRIAL PROCESSES **c61**
Kaj Juslin *In its* Information Technology and Economic Modelling 1992 p 213-225 (For primary document see N94-22056 05-83)
Copyright Avail: CASI HC A03/MF A03

The development of a structured query language for specification of industrial processes is reported. The intention was to provide a tool for process design engineers for building a computerized model of the process studied, without having to learn how to solve differential equations, or without programming in any general simulation or high level language. This complies with the goals of the fifth generation software, to bring the user interface between hardware and user much closer to the concepts of user. The language has also proved to be useful in definition of the simulation experiments to be made, including model extent, initial conditions, duration of experiment, and variables to be plotted. ESA

N94-22079# Academy of Sciences (USSR), Moscow.
THE COMBINATORIAL ALGORITHMS FOR LARGE SCALE DISCRETE OPTIMIZATION PROBLEMS **c61**
V. R. Khachaturov, I. H. Sigal, V. E. Veselovskii, and A. V. Zlotov *In* Technical Research Centre of Finland, Information Technology and Economic Modelling 1992 p 226-236 (For primary document see N94-22056 05-83)
Copyright Avail: CASI HC A03/MF A03

Algorithms for three classes of NP complete problems are presented. The problems concern the multiextremum facility location problem, a network problem with discontinues cost functions, and the traveling salesman problem. ESA

N94-22080# Nokia Data, Helsinki (Finland).
DATABASES IN DISTRIBUTED SYSTEMS **c82**
Tom Toernwall *In* Technical Research Centre of Finland, Information Technology and Economic Modelling 1992 p 237-249 (For primary document see N94-22056 05-83)
Copyright Avail: CASI HC A03/MF A03

In a computer network data are stored at the different sites of the network. An application running in one computer can access data stored at a different site. The data thus constitute a distributed database. Many problems are faced when building and implementing such a distributed database. The structure of the database, that is, how the data are distributed, must be carefully planned. In order to do that, the interdependencies among data in a distributed system and the analysis of the particular data to be distributed must be understood. The most central issues encountered when planning a database in a distributed environment are discussed. ESA

N94-22081# Academy of Sciences (USSR), Moscow. Computer Center.
AN EXPERT SYSTEM OF ECONOMETRIC ANALYSIS
Y. P. Ivanilov *In* Technical Research Centre of Finland, Information Technology and Economic Modelling 1992 p 250-252 (For primary document see N94-22056 05-83)
Copyright Avail: CASI HC A01/MF A03

In the Computer Center of the USSR Academy of Sciences, an expert system for analysis of macroeconomics development, the production function tools (PFT) system, both for past and future was constructed and realized for IBM PC/XT/AT and compatibles. An outline of the system and its uses is presented. ESA

N94-22082# Technical Research Centre of Finland, Espoo. Electrical and Automation Engineering.
MANUFACTURING AND INFORMATION TECHNOLOGY **c82**
Martin Ollus *In its* Information Technology and Economic Modelling 1992 p 253-260 (For primary document see N94-22056 05-83)
Copyright Avail: CASI HC A02/MF A03

Different aspects of information technology in manufacturing automation are discussed. The architecture of automation is outlined and intelligence on local level and system level is discussed. Future development is outlined. ESA

N94-22083# Academy of Sciences (USSR), Moscow. Automated Systems Inst.
THREE ORIGINAL PROGRAMMES FOR MANAGERS **c61**
Konstantin A. Antipov, Helen S. Bakanova, Sergei V. Letunovskiy, Sergei V. Marchenko, Sergei A. Orlov, Oleg L. Smirnov, and Vyacheslav Y. Smith *In* Technical Research Centre of Finland, Information Technology and Economic Modelling 1992 p 261-264 (For primary document see N94-22056 05-83)
Copyright Avail: CASI HC A01/MF A03

The architecture, algorithms, and user friendly interface employed in three original programs for managers are described: SCAN MAN (optical character recognition system), Window eDitor (word processor system), and Teleman (business schedule system). Full time interval used to input and recognize one A4 page of 2000 character Russian/English test by MSF-300C scanner and 12 MHz PC/AT or compatible (without co-processor) using SCAN MAN program equals approximately one minute. In this case, the number of mistakes cannot exceed 0.5 as a rule. Window eDitor is a powerful and simple integrated system. Window eDitor has a compact executive module, easy command set, and powerful tools for block/windows operations. The following additional functions are used in the system: recoder; efficient file support subsystem; simultaneous use of several alphabets, for example Russian, English, and Georgian; simple and original storage and preparation of business papers; and pseudo multidimensional spreadsheet. Teleman includes the following subsystems: business schedule which makes it possible to itemize a task, to make an appointment or phone call for any day, and to review, correct, or print records; built-in structurized subscriber database; business card directories; and exchange of information with Casio B.O.S.S. pocket notebook, etc. ESA

N94-22084# Moscow State Univ. (Russia). Faculty of Computational Mathematics and Cybernetics.
MICRODYNAMIC MODEL OF REPRODUCTION: TAXATION AND CURRENCY ISSUE AS REGULATORS OF ECONOMY
A. V. Timokhov *In* Technical Research Centre of Finland, Information Technology and Economic Modelling 1992 p 265-277 (For primary document see N94-22056 05-83)
Copyright Avail: CASI HC A03/MF A03

A microdynamic model of social reproduction in decentralized economy with government regulation is introduced. The theory of regulation aimed at getting the system to the balanced stationary path is developed within the framework of the model. Exactly calculated profit tax rates and so called monetary mechanism of currency issue are main regulators here. Some results of computer experiments corroborating the theory are given. ESA

N94-22085# Ministry of Finance (Finland). Economics Dept.
USE OF ECONOMIC MODELS IN FINNISH ECONOMIC POLICY
Kauko Mannermaa *In* Technical Research Centre of Finland, Information Technology and Economic Modelling 1992 p 278-282 (For primary document see N94-22056 05-83)
Copyright Avail: CASI HC A01/MF A03

The history and background of economic policy and forecast modeling is described. The KESSU medium term model is discussed. Its economic structure is presented and the use of the model is described. ESA

N94-22086# Bank of Finland, Helsinki.
EXPERIENCES OF THE BANK OF FINLAND'S ECONOMETRIC SIMULATION MODEL
Juha Tarkka *In* Technical Research Centre of Finland, Information Technology and Economic Modelling 1992 p 283-292 (For primary document see N94-22056 05-83)
Copyright Avail: CASI HC A02/MF A03

Experiences on a simulation model of the Finnish economy consisting of about 270 equations are reported. The research team produces at least four business cycle forecasts each year and evaluates economic policy alternatives over a horizon of 3 to 10 years. It is seen to be of vital importance to ensure that the model is consistent and its structure well understood by the users. It is therefore useful to start the construction of a large model from a well defined set of first general principles and to work 'downwards' to practical solutions without breaking the a priori defined structure of the system. Second, it is necessary to keep the models sufficiently simple and quick to use. Although the models must of course evolve in parallel with the actual policy issues, the pressure to expand the size of the model too much with rarely needed detail must be resisted. Thirdly, the fact that the behavioral patterns of people and firms are not invariant over time must be considered. ESA

N94-22087# Academy of Sciences (USSR), Moscow. Computer Center.
METHOD AND SOFTWARE FOR DECISION MAKING IN PUBLIC PROBLEMS **c61**
Alexander Lotov, Vladimir Bushenkov (Institute of Technology, Helsinki, Finland.), George Kamenev, and Oleg Chernykh *In* Technical Research Centre of Finland, Information Technology and Economic Modelling 1992 p 293-308 (For primary document see N94-22056 05-83)
Copyright Avail: CASI HC A03/MF A03

An approach to public problems investigation is suggested. This approach provides conditions for discussions informing public opinion about potential results of the decision making. The approach presented is based on the so called generalized reachable sets (GRS) method. The method itself is quite universal and can be used for many purposes, but in the case when the economic system's performance indicators (objectives) are given the GRS method provides a tool for multi-objective evaluation of the system's potential possibilities. ESA

84 LAW, POLITICAL SCIENCE AND SPACE POLICY

Includes NASA appropriation hearings; aviation law; space law and policy; international law; international cooperation; and patent policy.

No abstracts in this category.

85 URBAN TECHNOLOGY AND TRANSPORTATION

Includes applications of space technology to urban problems; technology transfer; technology assessment; and surface and mass transportation.

For related information see also *03 Air Transportation and Safety, 16 Space Transportation,* and *44 Energy Production and Conversion.*

N94-21736* National Aeronautics and Space Administration, Washington, DC.
INDEX TO 1992 NASA TECH BRIEFS, VOLUME 16, NUMBERS 1-12
Apr. 1993 153 p
(NASA-TM-109377; NAS 1.15:109377) Avail: Issuing Activity (Technology Transfer Office, NASA Center for AeroSpace Information, 800 Elkridge Landing Road, Linthicum Heights, MD 21090-2934, please call (301)621-0245 or (410)859-5300x245)

Tech Briefs are short announcements of new technology derived from the R&D activities of the National Aeronautics and Space Administration. These briefs emphasize information considered likely to be transferrable across industrial, regional, or disciplinary lines and are issued to encourage commercial application. This index of Tech Briefs contains abstracts and four indexes: subject, personal author, originating center, and Tech Brief number. The abstract section is organized by the following subject categories: electronic components and circuits, electronic systems, physical sciences, materials, computer programs, life sciences, mechanics, machinery, fabrication technology, and mathematics and information sciences. CASI

N94-21737* National Aeronautics and Space Administration, Washington, DC.
INDEX TO 1991 NASA TECH BRIEFS, VOLUME 15, NUMBERS 1-12
Apr. 1992 141 p
(NASA-TM-109376; NAS 1.26:109376) Avail: Issuing Activity (Technology

Transfer Office, NASA Center for Aerospace Information, 800 Elkridge Landing Road, Linthicum Heights, MD 21090-2934, please call (301)621-0245 or (410)859-5300x245)

Tech Briefs are short announcements of new technology derived from the R&D activities of the National Aeronautics and Space Administration. These briefs emphasize information considered likely to be transferrable across industrial, regional, or disciplinary lines and are issued to encourage commercial application. This index of Tech Briefs contains abstracts and four indexes: subject, personal author, originating center, and Tech Brief number. The abstract section is organized by the following subject categories: electronic components and circuits, electronic systems, physical sciences, materials, life sciences, mechanics, machinery, fabrication technology, and mathematics and information sciences. CASI

N94-21738* National Aeronautics and Space Administration, Washington, DC.

CUMULATIVE INDEX TO NASA TECH BRIEFS, 1986-1990, VOLUMES 10-14

Apr. 1992 344 p

(NASA-TM-109378; NAS 1.15:109378) Avail: Issuing Activity (Technology Transfer Office, NASA Center for AeroSpace Information, 800 Elkridge Landing Road, Linthicum Heights, MD 21090-2934, please call (301)621-0245 or (410)859-5300x245)

Tech Briefs are short announcements of new technology derived from the R&D activities of the National Aeronautics and Space Administration. These briefs emphasize information considered likely to be transferrable across industrial, regional, or disciplinary lines and are issued to encourage commercial application. This cumulative index of Tech Briefs contains abstracts and four indexes (subject, personal author, originating center, and Tech Brief number) and covers the period 1986 to 1990. The abstract section is organized by the following subject categories: electronic components and circuits, electronic systems, physical sciences, materials, computer programs, life sciences, mechanics, machinery, fabrication technology, and mathematics and information sciences. CASI

N94-21739* National Aeronautics and Space Administration, Washington, DC.

SPINOFF, 1992

James J. Haggerty 1992 141 p Original contains color illustrations

(NASA-NP-201; NAS 1.83:201; ISBN-0-16-038211-4) Avail: Issuing Activity (Technology Transfer Office, NASA Center for AeroSpace Information, 800 Elkridge Landing Road, Linthicum Heights, MD 21090-2934, please call (301)621-0245 or (410)859-5300x245)

This publication is intended to foster the aim of the NASA Technology Transfer Program by heightening awareness of the NASA technology available for reapplication and its potential for public benefit. The publication is organized in three main sections. Section 1 outlines NASA's mainline effort, the major programs that generate new technology and therefore replenish and expand the bank of knowledge available for transfer. Section 2 contains a representative sampling of spinoff products that resulted from secondary application of technology originally developed to meet mainline goals. Section 3 describes the various mechanisms NASA employs to stimulate technology transfer and lists, in an appendix, contact sources for further information about the Technology Transfer Program.

Derived from text

N94-21332*# National Aeronautics and Space Administration. Goddard Space Flight Center, Greenbelt, MD.

SPACE NETWORK SCHEDULING BENCHMARK: A PROOF-OF-CONCEPT PROCESS FOR TECHNOLOGY TRANSFER

Karen Moe, Nadine Happell (Stanford Telecommunications, Inc., Reston, VA.), B. J. Hayden, and Cathy Barclay (Allied-Signal Aerospace Co., Seabrook, MD.) *In its* Networks Technology Conference Nov. 1993 p 103-120 (For primary document see N94-21323 05-62)

Avail: CASI HC A03/MF A03

88 SPACE SCIENCES (GENERAL)

No abstracts in this category.

89 ASTRONOMY

Includes radio, gamma-ray, and infrared astronomy, and astrometry.

N94-20142*# Lockheed Missiles and Space Co., Palo Alto, CA. Solar and Astrophysics Lab.

THE X RAY HALO OF AM HER Final Report

Richard C. Catura 4 Aug. 1993 6 p

(Contract NAS5-31223)

(NASA-CR-189310; NAS 1.26:189310) Avail: CASI HC A02/MF A01

The objective of this research was to study the halo surrounding the ROSAT image of the cataclysmic variable AM Her that is formed by scattering of x-rays by interstellar dust grains. AM Her was in a low state of x-ray emission during the 14,400 sec observation and thus an insufficient number of counts were obtained to detect the x-ray halo. Author

N94-20174*# Max-Planck-Inst. fuer Physik und Astrophysik, Garching (Germany). Inst. fuer Extraterrestrische Physik.

A DEEP X RAY SURVEY IN THE LOCKMAN HOLE AND THE SOFT X RAY LOG N - LOG S

G. Hasinger, R. Burg (Johns Hopkins Univ., Baltimore, MD.), R. Giacconi (Space Telescope Science Inst., Baltimore, MD.), G. Hartner, M. Schmidt (California Inst. of Tech., Pasadena.), J. Truemper, and G. Zamorani (Osservatorio Astronomico, Bologna, Italy.) Dec. 1992 35 p Submitted for publication

(Grants NAG5-1531; NAG8-794; NAG5-1649; NAGW-2508; ASI-91-RS-86)

(NASA-CR-194698; NAS 1.26:194698; MPE-Preprint-238; ETN-93-94918)

Copyright Avail: CASI HC A03/MF A01

The longest pointed observation (152 ksec) with the Rosat position sensitive proportional counter in the direction of the absolutely lowest neutral hydrogen column density is discussed. 26 shallower fields from the Rosat medium sensivity survey are analyzed. 1176 X-ray sources were detected in at least one Rosat energy band in these fields covering a total solid angle of 9.3 deg; 661 of these sources constitute a statistically complete sample detected in the hard band with 0.5 to 2 keV fluxes greater than 2.5 times 10 to the power of minus 15 erg/sq cm s. The faintest limiting flux of the survey is analyzed. Detailed simulations show that confusion effects and other selection biases are relatively small and can be corrected for in the sample. From an analysis in the Lockman field, a best fit slope of approximately 1.8 is found for the extrapolation of the differential X-ray counts below 2.5 times 10 to the power of minus 15 erg/sq cm s. On the basis of this analysis an upper limit of approximately 25% can be found for a truly diffuse background component in the Rosat hard band. ESA

N94-20175*# Max-Planck-Inst. fuer Physik und Astrophysik, Garching (Germany). Inst. fuer Extraterrestrische Physik.

X RAY ARCHEOLOGY IN THE COMA CLUSTER

Simon D. M. White (Arizona Univ., Tucson.), Ulrich G. Briel, and J. Patrick Henry (Hawaii Univ., Honolulu.) Jan. 1993 14 p Submitted for publication Sponsored in part by NASA and NATO

(NASA-CR-194799; NAS 1.26:194799; MPE-Preprint-246; ETN-93-94923)

Copyright Avail: CASI HC A03/MF A01

Images of X-ray emission from hot gas within the Coma cluster of galaxies are presented. These maps, made with the Rosat satellite, have high signal to noise ratio and allow cluster structure to be analyzed in unprecedented detail. They show greater structural irregularity than could be anticipated from earlier observations of Coma. Emission is detected from a number of bright cluster galaxies in addition to the two known previously. In four cases there is evidence that these galaxies lie at the center of an extended subconcentration within the cluster, possibly the remnant of their associated groups. For at least two galaxies the images

show direct evidence for ongoing disruption of their gaseous atmosphere. The luminosity associated with these galaxies is comparable to that detected around similar ellipticals in much poorer environments. Emission is easily detected and appears to become more regular at large radii. The data show that this archetype of a rich and regular galaxy cluster was formed by the merging of several distinct subunits which are not yet fully destroyed. ESA

N94-20204*# Space Telescope Science Inst., Baltimore, MD.
FOCUS HISTORY OF THE HUBBLE SPACE TELESCOPE: LAUNCH TO MAY 1993
H. Hasan, C. J. Burrows (European Space Agency, Washington, DC.), and D. J. Schroeder (Beloit Coll., WI.) 10 Sep. 1993 46 p
(Contract NAS5-26555)
(NASA-CR-194179; NAS 1.26:194179) Avail: CASI HC A03/MF A01

Since the launch of the Hubble Space Telescope (HST) the secondary mirror of the telescope has been moved several times in order to collimate the telescope and also to define a position of best focus. In addition to these moves the focus position changes over time because of water desorption by the graphite epoxy in the metering truss. The authors report here the focus history of the telescope based on a knowledge of the mirror moves made and an analysis of desorption monitoring data obtained by the Faint Object Camera (FOC) in the F/96 mode and of the routine calibration data obtained by the Wide Field and Planetary Cameras. Focus values are extracted using two different methods. In the first method the distance between the center of the point spread function (PSF) and the shadows of the pads supporting the HST primary mirror are related to the focus error. In the second method an analytical formula for the PSF with variable aberration coefficients is fitted to the data. Focus positions derived from the two methods show good agreement. The data show that a desorption of about 83 microns has taken place since Aug. 16, 1990. The desorption has clearly not leveled off as expected from the trend of the earlier data. Long term variations of the secondary mirror position of approximately 3-15 microns from the 'best' focus position have been observed. Variations of the order of 2-5 microns over an orbital period have also been noted. Focus changes resulting from secondary mirror movements greater than approximately 5 microns changes the point spread function significantly and makes deconvolution and quantitative measurements difficult. Author (revised)

N94-20344*# California Univ., Berkeley. Dept. of Physics.
STUDIES OF AN X RAY SELECTED SAMPLE OF CATACLYSMIC VARIABLES Ph.D. Thesis
Andrew D. Silber 1986 6 p
(Grant NAG8-691)
(NASA-CR-194773; NAS 1.26:194773) Avail: CASI HC A02/MF A01

Just prior to the thesis research, an all-sky survey in hard x rays with the HEAO-1 satellite and further observations in the optical resulted in a catalog of about 700 x-ray sources with known optical counterparts. This sample includes 43 cataclysmic variables, which are binaries consisting of a detached white-dwarf and a Roche lobe filling companion star. This thesis consists of studies of the x-ray selected sample of catalcysmic variables. Author (revised)

N94-20952*# Columbia Univ., New York, NY. Depts. of Astronomy and Physics.
HIGH-ENERGY ASTROPHYSICS: A THEORETICAL ANALYSIS OF THERMAL RADIATION FROM NEUTRON STARS Annual Status Report No. 2, 1 Apr. 1993 - 31 Mar. 1994
James H. Applegate Jan. 1994 37 p
(Grant NAGw-3075)
(NASA-CR-194808; NAS 1.26:194808; CAL-2151) Avail: CASI HC A03/MF A01

The unambiguous detection of thermal radiation from the surface of a cooling neutron star was one of the most anxiously awaited results in neutron star physics. This particular Holy Grail was found by Halpern and Holt, who used ROSAT to detect pulsed X-rays from the gamma-ray source Geminga and demonstrate that it was a neutron star, probably a radio pulsar beamed away from us. At an age of approximately 3.4 x 10(exp 5) years, Geminga is in the photon cooling era. Its surface temperature of 5.2 x 10(exp 5) K can be explained within the contexts of both the slow and fast cooling scenarios. In the slow cooling scenario, the surface temperature is too high unless the specific heat of the interior is reduced by extensive baryon pairing. In the fast cooling scenario, the surface temperature will be much too low unless the fast neutrino cooling is shut off by baryon pairing. Two other pulsars, PSR 0656+14 and PSR 1055-52, have also been detected in thermal X-rays by ROSAT. They are also in the photon cooling era. All of this research's neutron star cooling models to date have used the unmagnetized effective temperature-interior temperature relation for the outer boundary condition. Models are being improved by using published magnetic envelope calculations and assumed geometried for the surface magnetic field to determine local interior temperature-emitted flux relations for the surface of the star.
Derived from text

N94-21295*# Lockheed Missiles and Space Co., Palo Alto, CA. Solar and Astrophysics Lab.
THE X RAY HALO OF CEN X-3 Final Report, 24 Jun. 1992 - 23 Jul. 1993
Richard C. Catura 23 Jul. 1993 14 p
(Contract NAS5-31855)
(NASA-CR-189309; NAS 1.26:189309) Avail: CASI HC A03/MF A01

The objective of this research was to study the halo surrounding the ROSAT image of Cen X-3. The halo was formed by the scattering of x rays by interstellar dust grains. An X Ray Halo was observed and that comprised 11.5 percent of the total x rays detected in the central unscattered image. A void at the center of the halo, that was expected to form during eclipse, was not observed. It is likely the void is filled by x rays scattered from cirum-source matter, local to Cen X-3, during eclipse of the x ray source. Author (revised)

N94-21498*# Applied Research Corp., Landover, MD.
THE CIRCUMSTELLAR ENVIRONMENTS OF INTERMEDIATE MASS MAIN SEQUENCE STARS Final Report
Carol A. Grady 14 Jul. 1993 5 p
(Contract NAS5-32059)
(NASA-CR-189311; NAS 1.26:189311; ARC-R93-209) Avail: CASI HC A01/MF A01

Analysis of archival Infrared Astronomy Satellite (IRAS) and International Ultraviolet Explorer (IUE) data resulted in identification of accreting gas toward a 2.8 Myr post-Herbig Be star in the R CrA star formation region, and identification of accreting gas toward HD 93563, previously identified as a classical Be star. Accreting gas was also detected toward two B(e) stars of previously controversial evolutionary state, resulting in identification of these systems as pre-Main Sequence Herbig Be stars viewed edge-on to their circumstellar disks. In parallel with this effort, accreting gas was detected toward the Herbig Ae star HR 5999, resulting in development of identification criteria for edge-on PMS proto-planetary disk systems. The work on individual stars is described. Author (revised)

N94-21579*# Max-Planck-Inst. fuer Physik und Astrophysik, Garching (Germany). Inst. fuer Extraterrestrische Physik.
THE DISTRIBUTION OF DARK MATTER IN THE A2256 CLUSTER
J. Patrick Henry (Hawaii Univ., Honolulu.), Ulrich G. Briel, and Paul E. J. Nulsen (Wollongong Univ., Australia.) Jan. 1993 11 p Submitted for publication
(Grants NAG5-1789; NATO-CRG-910415)
(NASA-CR-194699; NAS 1.26:194699; MPE-Preprint-242; ETN-93-94922)
Copyright Avail: CASI HC A03/MF A01

Using spatially resolved X-ray spectroscopy, it was determined that the X-ray emitting gas in the rich cluster A2256 is nearly isothermal to a radius of at least 0.76/h Mpc, or about three core radii. These data can be used to measure the distribution of the dark matter in the cluster. It was found that the total mass interior to 0.76/h Mpc and 1.5/h Mpc is (0.5 +/- 0.1 and 1.0 +/- 0.5) x 10(exp 15)/h of the solar mass respectively where the errors encompass the full range allowed by all models used. Thus, the mass appropriate to the region where spectral information was obtained is well determined, but the uncertainties become large upon extrapolating beyond that region. It is shown that the galaxy orbits are midly anisotropic which may cause the beta discrepancy in this cluster.
ESA

N94-21779*# Columbia Univ., New York, NY. Depts. of Astronomy and Physics.

DUST CONTENT OF A HYDROGEN RICH, LOW SURFACE BRIGHTNESS GALAXY AND THE LUMINOSITY HISTORY OF 3C273 Annual Status Report, 1 Sep. 1992 - 31 Aug. 1993

Thomas T. Hamilton Dec. 1993 5 p

(Grant NAG5-2079)

(NASA-CR-194705; NAS 1.26:194705; CAL-2149) Avail: CASI HC A01/MF A01

This project consists of a 30,000 second PSPC observation of the Giovanelli-Haynes Cloud in an attempt to detect light emitted by 3C273 which has been reflected by the cloud, and incidentally search the cloud for other sources of X-ray emission. The observation was carried out by ROSAT on Dec. 25, 1992 and the data was received by the P.I. in late March of 1993. We have examined the data and determined that the observation's background level, astrometry, etc. are acceptable. We have also detected diffuse emission from the direction of the Giovanelli-Haynes Cloud. Determination of the origin of this emission, by examining its morphology in relation to that of the radio map and the object's geometric relation with 3C273, requires software implementation of specialized algorithms. However, the most dramatic observation in the field is a potentially new population of discrete soft X-ray sources associated with dwarf galaxies. Derived from text

N94-21835*# Colorado Univ., Boulder. Center for Astrophysics and Space Astronomy.

VVNRS: VARIABLE PHENOMENA IN VV CEPHEI Final Report, 1 Dec. 1991 - 30 Nov. 1993

Robert E. Stencel 1993 5 p

(Grant NAG5-1832)

(NASA-CR-194731; NAS 1.26:194731) Avail: CASI HC A01/MF A01

The current research project (VVNRS) involves VV Cephei, which is a binary system in which a 20 solar mass main sequence star orbits within the extended atmosphere of the 40 solar mass M-type supergiant primary. Although the period of the system is 20.3 years, the components are close enough for a stream of matter from the primary to form an accretion disk around the hot secondary. We had previously completed an ADP-sponsored study of twelve years of archival spectra of this system and were surprised to find intermittent changes in the line profiles of the chromosphere-like absorption spectrum. This we think may be related to the accretion process. The previously existing spectra were not closely spaced enough in time to clearly delineate the nature of these changes. Therefore, we proposed and were granted eleven half-shifts to obtain closely spaced IUE spectra during IUE's 14th year of operations (1991/1992). Derived from text

N94-22281*# Columbia Univ., New York, NY. Dept. of Astronomy and Physics.

A HIGH RESOLUTION LIQUID XENON IMAGING TELESCOPE FOR 0.3-10 MeV GAMMA RAY ASTROPHYSICS: CONSTRUCTION AND INITIAL BALLOON FLIGHTS Annual Status Report, 1 Jan. 1993 - 31 Dec. 1993

Elena Aprile 31 Dec. 1993 72 p

(Grant NAGw-2013)

(NASA-CR-194709; NAS 1.26:194709; CAL-2150) Avail: CASI HC A04/MF A01

The results achieved with a 3.5 liter liquid xenon time projection chamber (LXe-TPC) prototype during the first year include: the efficiency of detecting the primary scintillation light for event triggering has been measured to be higher than 85%; the charge response has been measured to be stable to within 0.1% for a period of time of about 30 hours; the electron lifetime has been measured to be in excess of 1.3 ms; the energy resolution has been measured to be consistent with previous results obtained with small volume chambers; X-Y gamma ray imaging has been demonstrated with a nondestructive orthogonal wires readout; Monte Carlo simulation results on detection efficiency, expected background count rate at balloon altitude, background reduction algorithms, telescope response to point-like and diffuse sources, and polarization sensitivity calculations; and work on a 10 liter LXe-TPC prototype and gas purification/recovery system. For individual title, see N94-22282.

N94-22282*# Columbia Univ., New York, NY. Dept. of Physics and Astrophysics Lab.

THE POLARIZATION SENSITIVITY OF THE LIQUID XENON IMAGING TELESCOPE

Elena Aprile, A. Bolotnikov, D. Chen, and R. Mukherjee *In its* A High Resolution Liquid Xenon Imaging Telescope for 0.3-10 MeV Gamma Ray Astrophysics: Construction and Initial Balloon Flights 31 Dec. 1993 18 p Presented at the INTEGRAL Workshop, Les Diableret, Switzerland, 2-5 Feb. 1993 Submitted for publication (For primary document see N94-22281 05-89)

Avail: CASI HC A03/MF A01

The properties and the expected performance of a liquid xenon (LXe) gamma ray imaging telescope, optimized for the MeV energy region, are presented. The unique potential of this telescope as a Compton polarimeter is particularly emphasized. Based on Monte Carlo simulations we show that the modulation factor is as high as 40 percent at 1 MeV with a detection efficiency close to 20 percent. These figures of merit combined with the excellent background suppression capability of the three dimensional position sensitive LXe detector yield sensitivity at the three sigma level to polarization fractions as small as a few percent for strong sources, even in a balloon flight. Author (revised)

N94-22412 Saint Mary's Univ., Halifax (Nova Scotia). Dept. of Astronomy.

SURFACE PHOTOMETRY OF THE SHELL GALAXY NGC 2865 M.S. Thesis

David Lee Wing Jul. 1990 111 p

(ISBN-0-315-60441-7; CTN-94-60881) Copyright Avail: Micromedia Ltd., Technical Information Centre, 240 Catherine Street, Suite 305, Ottawa, Ontario, K2P 2G8, Canada HC/MF

Independently calibrated charge coupled device surface photometry data were derived from 12 images of the shell galaxy NGC 2865 in the B, V, and R passbands. Short exposures were used to permit accurate sky subtraction. Mean isophotes were derived for each passband over the 3-60 second radial distance range. The isophotes are presented in the form of their best-fit ellipse parameters. The parameters for the best-fit de Vaucouleurs surface brightness law were determined for the mean profile in each passband, and deviations of the actual surface brightness profile from the r to the 1/4 power law are discussed in terms of the galaxy's shell structure. From the best-fit ellipse parameters, the amplitudes of the cosine(4 theta) component of the isophotes could be measured. It was found that they do not show the boxiness often observed in a galaxy which had experienced a recent merger. On the contrary, a peak amplitude of about +1 percent (2 sigma) over the 25-40 second interval suggests only the presence of a weak disk. If the disk is real it indicates NGC 2865 is an S0 galaxy. Both (B-V) and (B-R) color gradients were measured and show the galaxy becomes bluer with increasing radius. This may be explained in terms of a radial metallicity gradient in the sense that the metallicity decreases by about a factor of two per decade increase in distance. Author (CISTI)

N94-22415 Laval Univ. (Quebec). Ecole des Gradues.

AUTOMATED INVESTIGATION OF QUASARS AT A GALACTIC LATITUDE OF -45 DEG M.S. Thesis [RECHERCHE AUTOMATISEE DE QUASARS A UNE LATITUDE GALACTIQUE DE -45 DEG]

Steve Levesque Sep. 1989 210 p In FRENCH

(ISBN-0-315-57576-X; CTN-94-60882) Copyright Avail: Micromedia Ltd., Technical Information Centre, 240 Catherine Street, Suite 305, Ottawa, Ontario, K2P 2G8, Canada HC/MF

Within the framework of a long-term study of the large-scale structure of the universe, a study was conducted to compare the properties of homogeneity and isotropy for the distribution of quasars in the universe. Since examination of the entire sky was not possible, certain representative fields were chosen for comparison. Each field was surveyed with the aid of photographic plates to obtain the number of quasars per unit of surface and per unit of distance. Since the data obey a Poisson distribution, it is necessary to analyze a large number of plates to obtain significant information. The GRENS project analyzed 40 fields throughout the sky, and the present thesis undertakes the comparison of the characteristics of three photographic plates from field F at a galactic latitude of -45 deg. These plates are digitized and treated by various software in the GRENS unit, and data obtained on quasar distribution are then compared to those

in other fields using standard statistical tests. The GRENS software used to process the photographic images, correct spectral data, and select candidates for identification as quasars is described. Results of data processing and comparison of the F1, F2, and F3 fields are presented. The results have not allowed detecting any anisotropy in the candidate quasars. CISTI

N94-22438*# National Aeronautics and Space Administration, Washington, DC.
SECOND ANNUAL CONFERENCE ON ASTRONOMICAL DATA ANALYSIS SOFTWARE AND SYSTEMS. ABSTRACTS
1992 126 p Conference held in Boston, MA, 2-4 Nov. 1992; sponsored by NASA, National Optical Astronomy Observatories, NSF, Smithsonian Astrophsical Observatory, and Space Telescope Science Inst.
(NASA-TM-108245; NAS 1.15:108245) Avail: CASI HC A07/MF A02

Abstracts from the conference are presented. The topics covered include the following: next generation software systems and languages; databases, catalogs, and archives; user interfaces/visualization; real-time data acquisition/scheduling; and IRAF/STSDAS/PROS status reports. For individual titles, see N94-22439 through N94-22555.

N94-22439*# European Southern Observatory, Munich (Germany). Space Telescope-European Coordinating Facility.
RESTORATION OF HST IMAGES WITH MISSING DATA Abstract Only
Hans-Martin Adorf *In* NASA, Washington, Second Annual Conference on Astronomical Data Analysis Software and Systems. Abstracts 1992 p 8 (For primary document see N94-22438 05-89)
Avail: CASI HC A01/MF A02

Missing data are a fairly common problem when restoring Hubble Space Telescope observations of extended sources. On Wide Field and Planetary Camera images cosmic ray hits and CCD hot spots are the prevalent causes of data losses, whereas on Faint Object Camera images data are lossed due to reseaux marks, blemishes, areas of saturation and the omnipresent frame edges. This contribution discusses a technique for 'filling in' missing data by statistical inference using information from the surrounding pixels. The major gain consists in minimizing adverse spill-over effects to the restoration in areas neighboring those where data are missing. When the mask delineating the support of 'missing data' is made dynamic, cosmic ray hits, etc. can be detected on the fly during restoration. Author

N94-22440*# European Southern Observatory, Munich (Germany).
SCIENTIFIC COMPUTING IN THE 1990IES: AN ASTRONOMICAL PERSPECTIVE Abstract Only
Hans-Martin Adorf *In* NASA, Washington, Second Annual Conference on Astronomical Data Analysis Software and Systems. Abstracts 1992 p 9 (For primary document see N94-22438 05-89)
Avail: CASI HC A01/MF A02

The compute performance, storage capability, degree of networking, and usability of modern computer hardware have enormously progressed in the past decade. These hardware advances are not paralleled by an equivalent increase in software productivity. Among astronomers the need is gradually perceived to discuss questions such as whether we are prepared to meet the pending challenge of vector and massively parallel computers. Therefore, a moderated, time-limited and access-restricted, wide-area network discussion forum is proposed for having a first, broad-minded go at the question of whether our current software efforts are heading in the right direction. The main topics, goals, means, and form of the proposed discussion process are presented. Author

N94-22441*# European Southern Observatory, Munich (Germany).
A LOW-COST VECTOR PROCESSOR BOOSTING COMPUTE-INTENSIVE IMAGE PROCESSING OPERATIONS Abstract Only c61
Hans-Martin Adorf *In* NASA, Washington, Second Annual Conference on Astronomical Data Analysis Software and Systems. Abstracts 1992 p 10 (For primary document see N94-22438 05-89)
Avail: CASI HC A01/MF A02

Low-cost vector processing (VP) is within reach of everyone seriously engaged in scientific computing. The advent of affordable add-on VP-boards for standard workstations complemented by mathematical/statistical libraries is beginning to impact compute-intensive tasks such as image processing. A case in point in the restoration of distorted images from the Hubble Space Telescope. A low-cost implementation is presented of the standard Tarasko-Richardson-Lucy restoration algorithm on an Intel i860-based VP-board which is seamlessly interfaced to a commercial, interactive image processing system. First experience is reported (including some benchmarks for standalone FFT's) and some conclusions are drawn. Author

N94-22442*# European Southern Observatory, Munich (Germany).
ARCHIVING DATA FROM GROUND-BASED TELESCOPES Abstract Only c82
M. A. Albrecht *In* NASA, Washington, Second Annual Conference on Astronomical Data Analysis Software and Systems. Abstracts 1992 p 11 (For primary document see N94-22438 05-89)
Avail: CASI HC A01/MF A02

The scientific throughput of a particular observing facility has been demonstrated to be multiplied with the operation of a data archive and its corresponding retrieval system. A requisite to achieve such an exploitation is a well structured observations catalog, i.e. a catalog that includes all information necessary to reduce and analyze the data even many years after its acquisition. At the same time, an information system is required that allow users to browse through the catalog at different levels of detail, adapting the amount of information presented to the actual needs of the user. Archiving data acquired with ground-based telescopes is particularly difficult because of the relative short life-time of instruments and detectors in comparison to the expected life-time of the archive. This feature differentiates ground-based originated archives radically from its spaceborne counterparts. The organization of the observations catalog becomes highly dependent on the capability of the archive to deal with new instrumental configurations. We introduce in this paper, the concept of a catalog database as opposed to the static catalog design currently in use in many archiving facilities, as a method to deal with this problem. We also present a brief review of activities currently in progress in this area. Author

N94-22443*# Rutherford Appleton Lab., Chilton (England).
MULTIFREQUENCY DATA ANALYSIS SOFTWARE ON STARLINK Abstract Only c61
P. M. Allan *In* NASA, Washington, Second Annual Conference on Astronomical Data Analysis Software and Systems. Abstracts 1992 p 12 (For primary document see N94-22438 05-89)
Avail: CASI HC A01/MF A02

Although the STARLINK project was set up to provide image processing facilities to UK astronomers, it has grown over the last 12 years to the extent that it now provides most of the data analysis facilities for UK astronomers. One aspect of the growth of the STARLINK network is that it now has to cater for astronomers working in a diverse range of wavelengths. Since a given individual may be working with data obtained in a variety of wavelengths, it is most convenient if the data can be stored in a common format and the programs that analyze the data have a similar 'look and feel'. What is known as 'STARLINK software' is obtained from many sources: STARLINK funded programmers; astronomers; foreign projects such as AIPS; generally available shareware; and commercial sources when this proves cost effective. This means that the ideal situation of a completely integrated system cannot be realized in practice. Nevertheless, many of the major packages written by STARLINK application programmers and by astronomers do use a common data format, based on the Hierarchical Data System, so that interchange of data between packages designed separately from each other is simply a matter of using the same file names. For example, as astronomer might use KAPPA to read some optical spectra off a FITS tape, then use CCDPACK to debias and flat field the data (it is easy to set up an overnight batch job to do this if there is a lot of data), then use KAPPA to have a quick look at the data and then use Figaro to reduce the spectra. It is useful to divide data analysis packages into wavelength specific packages, or even instrument specific packages, and general purpose ones. Once the instrumental signature has been removed from some data, any appropriate general purpose package can be used to analyze te data. For example, the ASTERIX package deals with x-ray data reduction, but after dealing with all of the x-ray specific processing, an astronomer may well want to find the brightness of objects in a given frame. Since ASTERIX uses the standard STARLINK data format, the astronomer can use PHOTOM or DAOPHOT 2 to measure the brightness of the objects. Although DAOPHOT was written with optical astronomy in mind, it is useful for analyzing data from several wavelengths. The ability of DAOPHOT 2 to handle non-standard point spread functions can be especially useful in many areas of astronomy. Author

N94-22444*# Lawrence Livermore National Lab., CA.
HOW TO HANDLE 6GBytes A NIGHT AND NOT GET SWAMPED Abstract Only
R. Allsman, C. Alcock, T. Axelrod, D. Bennett, K. Cook, H.-S. Park, K. Griest (California Univ., Berkeley.), S. Marshall (California Univ., Berkeley.), S. Perlmutter (California Univ., Berkeley.), and C. Stubbs (California Univ., Berkeley.) et al *In* NASA, Washington, Second Annual Conference on Astronomical Data Analysis Software and Systems. Abstracts 1992 p 13 (For primary document see N94-22438 05-89)
Avail: CASI HC A01/MF A02

The Macho Project has undertaken a 5 year effort to search for dark matter in the halo of the Galaxy by scanning the Magellanic Clouds for micro-lensing events. Each evening's raw image data will be reduced in real-time into the observed stars' photometric measurements. The actual search for micro-lensing events will be a post-processing operation. The theoretical prediction of the rate of such events necessitates the collection of a large number of repeated exposures. The project designed camera subsystem delivers 64 Mbytes per exposure with exposures typically occurring every 500 seconds. An ideal evening's observing will provide 6 Gbytes of raw image data and 40 Mbytes of reduced photometric measurements. Recognizing the difficulty of digging out from a snowballing cascade of raw data, the project requires the real-time reduction of each evening's data. The software team's implementation strategy centered on this non-negotiable mandate. Accepting the reality that 2 full time people needed to implement the core real-time control and data management system within 6 months, off-the-shelf vendor components were explored to provide quick solutions to the classic needs for file management, data management, and process control. Where vendor solutions were lacking, state-of-the-art models were used for hand tailored subsystems. In particular, petri nets manage process control, memory mapped bulletin boards provide interprocess communication between the multi-tasked processes, and C++ class libraries provide memory mapped, disk resident databases. The differences between the implementation strategy and the final implementation reality are presented. The necessity of validating vendor product claims are explored. Both the successful and hindsight decisions enabling the collection and processing of the nightly data barrage are reviewed. Author

N94-22445*# Inter-University Centre for Astronomy and Astrophysics, Pune (India).
CCD SURFACE PHOTOMETRY OF GALAXIES Abstract Only
G. C. Anupama and A. K. Kembhavi *In* NASA, Washington, Second Annual Conference on Astronomical Data Analysis Software and Systems. Abstracts 1992 p 14 (For primary document see N94-22438 05-89)
Avail: CASI HC A01/MF A02

We present here the results based on analysis of broad band optical images of radio loud and radio quiet galaxies selected from a set of x-ray galaxies. Data reduction techniques, and surface photometry using the IRAF data reduction package are described. The radial surface brightness profile of each galaxy is obtained. The disc, bulge, and nucleus of the galaxy are modeled based on the estimated brightness profile. The model of the galaxy is constructed, which is subtracted from the observed image to enhance the small scale features in the galaxy. Color maps of the galaxy are obtained and compared with those of normal galaxies. The optical properties of the galaxy are compared with its x-ray and radio properties. Author

N94-22446*# National Aeronautics and Space Administration, Washington, DC.
THE COOL-STAR SPECTRAL CATALOG: A UNIFORM COLLECTION OF IUE SWP-LOs Abstract Only **c82**
T. Ayres (Colorado Univ., Boulder.), D. Lenz (Colorado Univ., Boulder.), R. Burton (Colorado Univ., Boulder.), and J. Bennett *In its* Second Annual Conference on Astronomical Data Analysis Software and Systems. Abstracts 1992 p 15 (For primary document see N94-22438 05-89)
Avail: CASI HC A01/MF A02

Over the past decade and a half of its operations, the International Ultraviolet Explorer has recorded low-dispersion spectrograms in the 1150-2000 A interval of more than 800 stars of late spectral type (F-M). The sub-2000 A region contains a number of emission lines that are key diagnostics of physical conditions in the high-excitation chromospheres and subcoronal 'transition zones' of such stars. Many of the sources have been observed a number of times, and the available collection of SWP-LO exposures in the IUE Archives exceeds 4,000. With support from the Astrophysics Data Program, we have assembled the archival material into a catalog of IUE far-UV fluxes of late-type stars. In order to ensure uniform processing of the spectra, we: (1) photometrically corrected the raw vidicon images with a custom version of the 1985 SWP ITF; (2) identified and eliminated, sharp cosmic-ray 'hits' by means of a spatial filter; (3) extracted the spectral traces with the 'optimal' (weighted-slit) strategy; and (4) calibrated them against a well-characterized reference source, the DA white dwarf G191-B2B. Our approach is similar to that adopted by the IUE Project for its 'Final Archive', but our implementation is specialized to the case of chromospheric emission-line sources. We measured the resulting SWP-LO spectra using a semi-autonomous algorithm that establishes a smooth continuum by numerical filtering, and then fits the significant emissions (or absorptions) by means of a constrained Bevington-type multiple-Gaussian procedure. The algorithm assigns errors to the fitted fluxes - or upper limits in the absence of a significant detection - according to a model based on careful measurements of the noise properties of the IUE's intensified SEC cameras. Here, we describe the 'visualization' strategies we adopted to ensure human-review of the semi-autonomous processing and measuring algorithms; the derivation of the noise model and the assignment of errors; and the structure of the final catalog as delivered to the Astrophysics Data System. Author

N94-22447*# Anglo-Australian Observatory, Epping.
AN OBJECT-ORIENTED DATA REDUCTION SYSTEM IN FORTRAN Abstract Only **c82**
J. Bailey *In* NASA, Washington, Second Annual Conference on Astronomical Data Analysis Software and Systems. Abstracts 1992 p 16 (For primary document see N94-22438 05-89)
Avail: CASI HC A01/MF A02

A data reduction system for the AAO two-degree field project is being developed using an object-oriented approach. Rather than use an object-oriented language (such as C++) the system is written in Fortran and makes extensive use of existing subroutine libraries provided by the UK Starlink project. Objects are created using the extensible N-dimensional Data Format (NDF) which itself is based on the Hierarchical Data System (HDS). The software consists of a class library, with each class corresponding to a Fortran subroutine with a standard calling sequence. The methods of the classes provide operations on NDF objects at a similar level of functionality to the applications of conventional data reduction systems. However, because they are provided as callable subroutines, they can be used as building blocks for more specialist applications. The class library is not dependent on a particular software environment thought it can be used effectively in ADAM applications. It can also be used from standalone Fortran programs. It is intended to develop a graphical user interface for use with the class library to form the 2dF data reduction system. Author

N94-22448*# Anglo-Australian Observatory, Epping.
A SELF-DEFINING HIERARCHICAL DATA SYSTEM Abstract Only **c82**
J. Bailey *In* NASA, Washington, Second Annual Conference on Astronomical Data Analysis Software and Systems. Abstracts 1992 p 17 (For primary document see N94-22438 05-89)
Avail: CASI HC A01/MF A02

The Self-Defining Data System (SDS) is a system which allows the creation of self-defining hierarchical data structures in a form which allows the data to be moved between different machine architectures. Because the structures are self-defining they can be used for communication between independent modules in a distributed system. Unlike disk-based hierarchical data systems such as Starlink's HDS, SDS works entirely in memory and is very fast. Data structures are created and manipulated as internal dynamic structures in memory managed by SDS itself. A structure may then be exported into a caller supplied memory buffer in a defined external format. This structure can be written as a file or sent as a message to another machine. It remains static in structure until it is reimported into SDS. SDS is written in portable C and has been run on a number of different machine architectures. Structures are portable between machines with SDS looking after conversion of byte order, floating point format, and alignment. A Fortran callable version is also available for some machines. Author

N94-22449*# European Southern Observatory, Munich (Germany).
GUIs IN THE MIDAS ENVIRONMENT Abstract Only **c82**

P. Ballester *In* NASA, Washington, Second Annual Conference on Astronomical Data Analysis Software and Systems. Abstracts 1992 p 18 (For primary document see N94-22438 05-89)
Avail: CASI HC A01/MF A02

MIDAS (Munich Image Data Analysis System) is the image processing system developed at ESO for astronomical data reduction. MIDAS is used for off-line data reduction at ESO and many astronomical institutes all over Europe. In addition to a set of general commands, enabling to process and analyze images, catalogs, graphics and tables, MIDAS includes specialized packages dedicated to astronomical applications or to specific ESO instruments. Several graphical interfaces are available in the MIDAS environment: XHelp provides an interactive help facility, and XLong and XEchelle enable data reduction of long-slip and echelle spectra. GUI builders facilitate the development of interfaces. All ESO interfaces comply to the ESO User Interfaces Common Conventions which secures an identical look and feel for telescope operations, data analysis, and archives.

Author

N94-22450*# National Aeronautics and Space Administration. Goddard Space Flight Center, Greenbelt, MD.
A STRUCTURED DATA TRANSFER PROTOCOL Abstract Only c82
P. Barrett and A. Rots *In* NASA, Washington, Second Annual Conference on Astronomical Data Analysis Software and Systems. Abstracts 1992 p 19 (For primary document see N94-22438 05-89)
Avail: CASI HC A01/MF A02

The transfer of data between different computers and programs can be a major obstacle during data analysis. We present a new data transfer protocol which is based on a simple structure containing a value, an error, and a unit. Each of these members can be arrays or another structure. The ability to nest structures allows for the concept of objects. When using an object-oriented language such as C++, reference can be made to the object name instead of each element explicitly. Prototype code has been written which implements the basic design with enhancements planned for the future.

Author

N94-22451*# Space Telescope Science Inst., Baltimore, MD.
A NEURAL NETWORK PROTOTYPING PACKAGE WITHIN IRAF Abstract Only c63
D. Bazell and I. Bankman (Johns Hopkins Univ., Baltimore, MD.) *In* NASA, Washington, Second Annual Conference on Astronomical Data Analysis Software and Systems. Abstracts 1992 p 20 (For primary document see N94-22438 05-89)
Avail: CASI HC A01/MF A02

We outline our plans for incorporating a Neural Network Prototyping Package into the IRAF environment. The package we are developing will allow the user to choose between different types of networks and to specify the details of the particular architecture chosen. Neural networks consist of a highly interconnected set of simple processing units. The strengths of the connections between units are determined by weights which are adaptively set as the network 'learns'. In some cases, learning can be a separate phase of the user cycle of the network while in other cases the network learns continuously. Neural networks have been found to be very useful in pattern recognition and image processing applications. They can form very general 'decision boundaries' to differentiate between objects in pattern space and they can be used for associative recall of patterns based on partial cures and for adaptive filtering. We discuss the different architectures we plan to use and give examples of what they can do.

Author

N94-22452*# Padua Univ. (Italy).
DATABASE ACTIVITY IN THE ITALIAN ASTRONET: DIRA 2 Abstract Only c82
L. Benacchio and M. Nanni (Bologna Univ., Italy.) *In* NASA, Washington, Second Annual Conference on Astronomical Data Analysis Software and Systems. Abstracts 1992 p 21 (For primary document see N94-22438 05-89)
Avail: CASI HC A01/MF A02

The development and utilization of informational archives and databases started, in the Italian Astronet Project, in the middle of 1983. In that year, a small group of astronomers and some more technical people met together in an Astronet working group, with a common, painful experience in managing astronomical catalogues and archives with computers. Nowadays, some years later, some software packages and the contents of both, a relative general database and several local databases represent the work and the effort of the group. The systems have been conceived and developed keeping in mind the original goal of the group: to allow the single atronomer to make a free use of original data. The main package (DIRA) was rewritten, after some years of use, to fully take advantage of the several suggestions of the astronomer that used it and gathered experiences in the astronomical catalog's management. A more technical goal was to install the whole system, born and developed in the vms environment, on unix and unix-like systems. This new version, DIRA2, has a new user interface, a query language with SQL style commands supporting numerical and character functions also and a set of commands to create new catalogues from existing data. The graphics commands are also more powerful with respect to the previous version. DIRA (and DIRA2 of course) philosophy and design are very simple and proved to be very appreciated by astronomers, namely, to normalize and homogenize, at minimum, astronomical catalogues, to collect satisfactory astronomical documentation on their contents and, finally, to allow an astronomical approach to the dialogue with the database. DIRA2 is currently used in most Italian astronomical institutes to retrieve data from a still growing database of about 140 well documented and controlled astronomical catalogues, for the identification of objects and the preparation of a 'medium size' survey, in astrometry and in the creation of new catalogues.

Author

N94-22453*# Los Alamos National Lab., NM.
THE ALEXIS DATA PROCESSING PACKAGE: AN IDL BASED SYSTEM Abstract Only c82
J. J. Bloch, B. W. Smith, and B. C. Edwards *In* NASA, Washington, Second Annual Conference on Astronomical Data Analysis Software and Systems. Abstracts 1992 p 22 Sponsored in part by DOE (For primary document see N94-22438 05-89)
Avail: CASI HC A01/MF A02

The Array of Low Energy X-ray Imaging Sensors (ALEXIS) experiment consists of a mini-satellite containing six wide angle EUV/ultrasoft x-ray telescopes. Its purpose is to map out the sky in three narrow (approximately 5 percent) bandpasses around 66, 71, and 93 eV. The 66 and 71 eV bandpasses are centered on intense Fe emission lines which are characteristic of million degree plasmas such as the one thought to produce the soft x-ray background. The 93 eV bandpass is not near any strong emission lines and is more sensitive to continuum sources. The mission will be launched on the Pegasus Air Launched Vehicle in the second half of 1992 into a 400-nautical-mile, high inclination orbit and will be controlled entirely from a small ground station located at Los Alamos. The project is a collaborative effort between Los Alamos National Laboratory, Sandia National Laboratory, and the University of California-Berkeley Space Sciences Laboratory. The six telescopes are arranged in three pairs. As the satellite spins twice a minute they scan the entire anti-solar hemisphere. Each f/1 telescope consists of a spherical, multilayer-coated mirror with a curved, microchannel plate detector located at the prime focus. The multilayer coatings determine the bandpasses of the telescopes. The field of view of each telescope is 30 degrees with a spatial resolution of 0.5 degree, limited by spherical aberration. The data processing requirements for ALEXIS are large. Each event is one of the six telescopes is telemetered to the ground with its time of arrival and position on the detector. This information must be folded with the aspect solution for the satellite to reconstruct the direction on the sky from which the photon came. Because of the way the six telescopes scan the sky, the effective exposure calculation is also very computationally intensive. ALEXIS may generate up to 100 megabytes of raw data per day, which are converted into a gigabyte per day of processed data. While the processing job for ALEXIS is sizable, the programming staff is small. To maximize programming efficiency, and to make the best use of tools available in the public domain, we chose IDL as our software development platform. IDL was used from the start of instrument development through flight. We use IDL as a top-level executive for the processing tasks (replacing Unix shell scripts), as a device independent graphics engine, as a database manager, and as a final data manipulator. IDL routines spawn special purpose C programs to perform detailed telemetry deconvolution and other specialized functions. We discuss the use of IDL and C within the processing and archiving strategy for the ALEXIS data anlaysis system as implemented on a SPARCstation platform. We also

show results from our End-to-End software simulation capability as processed by our analysis codes. Author

N94-22454*# Center for Analysis, Newport Beach, CA.
SEEING THE FOREST FOR THE TREES: NETWORKED WORKSTATIONS AS A PARALLEL PROCESSING COMPUTER Abstract Only **c62**
J. O. Breen and D. M. Meleedy *In* NASA, Washington, Second Annual Conference on Astronomical Data Analysis Software and Systems. Abstracts 1992 p 23 (For primary document see N94-22438 05-89)
Avail: CASI HC A01/MF A02

Unlike traditional 'serial' processing computers in which one central processing unit performs one instruction at a time, parallel processing computers contain several processing units, thereby, performing several instructions at once. Many of today's fastest supercomputers achieve their speed by employing thousands of processing elements working in parallel. Few institutions can afford these state-of-the-art parallel processors, but many already have the makings of a modest parallel processing system. Workstations on existing high-speed networks can be harnessed as nodes in a parallel processing environment, bringing the benefits of parallel processing to many. While such a system can not rival the industry's latest machines, many common tasks can be accelerated greatly by spreading the processing burden and exploiting idle network resources. We study several aspects of this approach, from algorithms to select nodes to speed gains in specific tasks. With ever-increasing volumes of astronomical data, it becomes all the more necessary to utilize our computing resources fully. Author

N94-22455*# Smithsonian Astrophysical Observatory, Cambridge, MA.
VETA X RAY DATA ACQUISITION AND CONTROL SYSTEM Abstract Only **c82**
R. J. V. Brissenden, M. T. Jones, M. Ljungberg, D. T. Nguyen, and J. B. Roll, Jr. *In* NASA, Washington, Second Annual Conference on Astronomical Data Analysis Software and Systems. Abstracts 1992 p 24 Presented at the Conference ADASS, 1992 (For primary document see N94-22438 05-89)
Avail: CASI HC A01/MF A02

We describe the X-ray Data Acquisition and Control System (XDACS) used together with the X-ray Detection System (XDS) to characterize the x-ray image during testing of the AXAF P1/H1 mirror pair at the MSFC X-ray Calibration Facility. A variety of x-ray data were acquired, analyzed, and archived during the testing including: mirror alignment, encircled energy, effective area, point spread function, system housekeeping, and proportional counter window uniformity data. The system architecture will be presented with emphasis placed on key features that include a layered UNIX tool approach, dedicated subsystem controllers, real-time X-window displays, flexibility in combining tools, network connectivity, and system extensibility. The VETA test data archive are also described. Author

N94-22456*# Dartmouth Coll., Hanover, NH.
A MULTIRESOLUTION WAVELET REPRESENTATION IN TWO OR MORE DIMENSIONS Abstract Only **c61**
B. C. Bromley *In* NASA, Washington, Second Annual Conference on Astronomical Data Analysis Software and Systems. Abstracts 1992 p 25 (For primary document see N94-22438 05-89)
Avail: CASI HC A01/MF A02

In the multiresolution approximation, a signal is examined on a hierarchy of resolution scales by projection onto sets of smoothing functions. Wavelets are used to carry the detail information connecting adjacent sets in the resolution hierarchy. An algorithm has been implemented to perform a multiresolution decomposition in n greater than or equal to 2 dimensions based on wavelets generated from products of 1-D wavelets and smoothing functions. The functions are chosen so that an n-D wavelet may be associated with a single resolution scale and orientation. The algorithm enables complete reconstruction of a high resolution signal from decomposition coefficients. The signal may be oversampled to accommodate non-orthogonal wavelet systems, or to provide approximate translational invariance in the decomposition arrays. Author

N94-22457*# Instituto de Pesquisas Espaciais, Sao Jose dos Campos (Brazil).
EXPERIMENTS WITH RECURSIVE ESTIMATION IN ASTRONOMICAL IMAGE PROCESSING Abstract Only **c82**
I. Busko *In* NASA, Washington, Second Annual Conference on Astronomical Data Analysis Software and Systems. Abstracts 1992 p 26 (For primary document see N94-22438 05-89)
Avail: CASI HC A01/MF A02

Recursive estimation concepts were applied to image enhancement problems since the 70's. However, very few applications in the particular area of astronomical image processing are known. These concepts were derived, for 2-dimensional images, from the well-known theory of Kalman filtering in one dimension. The historic reasons for application of these techniques to digital images are related to the images' scanned nature, in which the temporal output of a scanner device can be processed on-line by techniques borrowed directly from 1-dimensional recursive signal analysis. However, recursive estimation has particular properties that make it attractive even in modern days, when big computer memories make the full scanned image available to the processor at any given time. One particularly important aspect is the ability of recursive techniques to deal with non-stationary phenomena, that is, phenomena which have their statistical properties variable in time (or position in a 2-D image). Many image processing methods make underlying stationary assumptions either for the stochastic field being imaged, for the imaging system properties, or both. They will underperform, or even fail, when applied to images that deviate significantly from stationarity. Recursive methods, on the contrary, make it feasible to perform adaptive processing, that is, to process the image by a processor with properties tuned to the image's local statistical properties. Recursive estimation can be used to build estimates of images degraded by such phenomena as noise and blur. We show examples of recursive adaptive processing of astronomical images, using several local statistical properties to drive the adaptive processor, as average signal intensity, signal-to-noise and autocorrelation function. Software was developed under IRAF, and as such will be made available to interested users. Author

N94-22458*# Observatoire de Strasbourg (France).
EXTRACTING GALACTIC STRUCTURE PARAMETERS FROM MULTIVARIATED DENSITY ESTIMATION Abstract Only **c65**
B. Chen, M. Creze, A. Robin (Observatoire de Besancon, France.), and O. Bienayme (Observatoire de Besancon, France.) *In* NASA, Washington, Second Annual Conference on Astronomical Data Analysis Software and Systems. Abstracts 1992 p 27 (For primary document see N94-22438 05-89)
Avail: CASI HC A01/MF A02

Multivariate statistical analysis, including includes cluster analysis (unsupervised classification), discriminant analysis (supervised classification) and principle component analysis (dimensionlity reduction method), and nonparameter density estimation have been successfully used to search for meaningful associations in the 5-dimensional space of observables between observed points and the sets of simulated points generated from a synthetic approach of galaxy modelling. These methodologies can be applied as the new tools to obtain information about hidden structure otherwise unrecognizable, and place important constraints on the space distribution of various stellar populations in the Milky Way. In this paper, we concentrate on illustrating how to use nonparameter density estimation to substitute for the true densities in both of the simulating sample and real sample in the five-dimensional space. In order to fit model predicted densities to reality, we derive a set of equations which include n lines (where n is the total number of observed points) and m (where m: the numbers of predefined groups) unknown parameters. A least-square estimation will allow us to determine the density law of different groups and components in the Galaxy. The output from our software, which can be used in many research fields, will also give out the systematic error between the model and the observation by a Bayes rule. Author

N94-22459*# California Univ., Berkeley. Center for EUV Astrophysics.
THE EUVE PROPOSAL DATABASE AND SCHEDULING SYSTEM Abstract Only **c82**
C. Christian, E. Olson, P. Jelinsky, and M. Samuel *In* NASA, Washington, Second Annual Conference on Astronomical Data Analysis Software and Systems. Abstracts 1992 p 28 (For primary document see N94-22438

05-89)
Avail: CASI HC A01/MF A02

The proposal database and scheduling system for the Extreme Ultraviolet Explorer will be described. The proposal database has been implemented to take input for approved observations selected by the EUVE Peer Review Panel and output target information suitable for the scheduling system to digest. The scheduling system is a hybrid of the SPIKE program and EUVE software which checks spacecraft constraints, produces a proposed schedule and selects spacecraft orientations with optimal configurations for acquiring star trackers, etc. This system has been used to schedule the In Orbit Calibration activities that took place this summer, following the EUVE launch in early June 1992. The implemented strategy has implications for the selection of approved targets, which have impacted the Peer Review process. In addition, it will be discussed how the proposal database, founded on Sybase, controls the processing of EUVE Guest Observer data.
Author (revised)

N94-22460*# Keck Observatory, Mauna Kea, HI.
THE KECK KEYWORD LAYER Abstract Only **c61**
A. R. Conrad and W. F. Lupton *In* NASA, Washington, Second Annual Conference on Astronomical Data Analysis Software and Systems. Abstracts 1992 p 29 (For primary document see N94-22438 05-89)
Avail: CASI HC A01/MF A02

Each Keck instrument presents a consistent software view to the user interface programmer. The view consists of a small library of functions, which are identical for all instruments, and a large set of keywords, that vary from instrument to instrument. All knowledge of the underlying task structure is hidden from the application programmer by the keyword layer. Image capture software uses the same function library to collect data for the image header. Because the image capture software and the instrument control software are built on top of the same keyword layer, a given observation can be 'replayed' by extracting keyword-value pairs from the image header and passing them back to the control system. The keyword layer features non-blocking as well as blocking I/O. A non-blocking keyword write operation (such as setting a filter position) specifies a callback to be invoked when the operation is complete. A non-blocking keyword read operation specifies a callback to be invoked whenever the keyword changes state. The keyword-callback style meshes well with the widget-callback style commonly used in X window programs. The first keyword library was built for the two Keck optical instruments. More recently, keyword libraries have been developed for the infrared instruments and for telescope control. Although the underlying mechanisms used for inter-process communication by each of these systems vary widely (Lick MUSIC, Sun RPC, and direct socket I/O, respectively), a basic user interface has been written that can be used with any of these systems. Since the keyword libraries are bound to user interface programs dynamically at run time, only a single set of user interface executables is needed. For example, the same program, 'xshow', can be used to display continuously the telescope's position, the time left in an instrument's exposure, or both values simultaneously. Less generic tools that operate on specific keywords, for example an X display that controls optical instrument exposures, have also been written using the keyword layer.
Author

N94-22461*# Smithsonian Astrophysical Observatory, Cambridge, MA.
PROS: AN IRAF BASED SYSTEM FOR ANALYSIS OF X RAY DATA Abstract Only **c61**
M. A. Conroy, J. DePonte, J. F. Moran, J. S. Orszak, W. P. Roberts, and D. Schmidt *In* NASA, Washington, Second Annual Conference on Astronomical Data Analysis Software and Systems. Abstracts 1992 p 30 (For primary document see N94-22438 05-89)
Avail: CASI HC A01/MF A02

PROS is an IRAF based software package for the reduction and analysis of x-ray data. The use of a standard, portable, integrated environment provides for both multi-frequency and multi-mission analysis. The analysis of x-ray data differs from optical analysis due to the nature of the x-ray data and its acquisition during constantly varying conditions. The scarcity of data, the low signal-to-noise ratio and the large gaps in exposure time make data screening and masking an important part of the analysis. PROS was developed to support the analysis of data from the ROSAT and Einstein missions but many of the tasks have been used on data from other missions. IRAF/PROS provides a complete end-to-end system for x-ray data analysis: (1) a set of tools for importing and exporting data via FITS format -- in particular, IRAF provides a specialized event-list format, QPOE, that is compatible with its IMAGE (2-D array) format; (2) a powerful set of IRAF system capabilities for both temporal and spatial event filtering; (3) full set of imaging and graphics tasks; (4) specialized packages for scientific analysis such as spatial, spectral and timing analysis -- these consist of both general and mission specific tasks; and (5) complete system support including ftp and magnetic tape releases, electronic and conventional mail hotline support, electronic mail distribution of solutions to frequently asked questions and current known bugs. We will discuss the philosophy, architecture and development environment used by PROS to generate a portable, multimission software environment. PROS is available on all platforms that support IRAF, including Sun/Unix, VAX/VMS, HP, and Decstations. It is available on request at no charge.
Author (revised)

N94-22462*# National Aeronautics and Space Administration. Goddard Space Flight Center, Greenbelt, MD.
ROSAT IMPLEMENTATION OF A PROPOSED MULTI-MISSION X RAY DATA FORMAT Abstract Only **c82**
M. Corcoran, W. Pence, R. White, and M. Conroy (Smithsonian Astrophysical Observatory, Cambridge, MA.) *In* NASA, Washington, Second Annual Conference on Astronomical Data Analysis Software and Systems. Abstracts 1992 p 31 (For primary document see N94-22438 05-89)
Avail: CASI HC A01/MF A02

Until recently little effort has been made to ensure that data from X-ray telescopes are delivered in a format that reflects the common characteristics that most X-ray datasets share. Instrument-specific data-product design hampers the comparison of X-ray measurements made by different detectors and should be avoided whenever possible. The ROSAT project and the High Energy Astrophysics Science Archive Research Center (HEASARC) have defined a set of X-ray data products ('rationalized files') for ROSAT data that can be used for distribution and archiving of data from other X-ray missions. This set of 'rationalized files' has been defined to isolate instrument-independent and instrument-specific quantities using standards FITS constructs to ensure portability. We discuss the usage of the 'rationalized files' by ROSAT for data distribution and archiving, with particular emphasis on discrimination between instrument-independent and instrument-specific quantities, and discuss application of this format to data from other X-ray missions.
Author

N94-22463*# National Radio Astronomy Observatory, Green Bank, WV.
ON AIPS++, A NEW ASTRONOMICAL INFORMATION PROCESSING SYSTEM Abstract Only **c82**
G. A. Croes *In* NASA, Washington, Second Annual Conference on Astronomical Data Analysis Software and Systems. Abstracts 1992 p 32 (For primary document see N94-22438 05-89)
Avail: CASI HC A01/MF A02

The AIPS system that has served the needs of the radio astronomical community remarkably well during the last 15 years is showing signs of age and is being replaced by a more modern system, AIPS++. As the name implies, AIPS++ will be developed in a object oriented fashion and will use C++ as its main programming language. The work is being done by a consortium of seven organizations, with coordinated activities worldwide. After a review of the history of the project to this date from management, astronomical and technical viewpoints, and the current state of the project, the paper concentrates on the tradeoffs implied by the choice of implementation style and the lessons we have learned, good and bad.
Author

N94-22464*# Kitt Peak National Observatory, Tucson, AZ.
NEW IRAF STELLAR PHOTOMETRY SOFTWARE Abstract Only **c61**
L. E. Davis *In* NASA, Washington, Second Annual Conference on Astronomical Data Analysis Software and Systems. Abstracts 1992 p 33 (For primary document see N94-22438 05-89)
Avail: CASI HC A01/MF A02

A progress report on the IRAF stellar photometry package DIGIPHOT, with emphasis on algorithm enhancements and photometry catalog processing tools is presented. The IRAF implementation of Stetson's DAOPHOTII algorithms and improvements to the sky fitting algorithms is briefly discussed and results obtained with the new algorithms for NOAO direct imaging data are shown. New interactive photometry catalog examining and editing tool PEXAMINE, and plans for future photometry catalog analysis tools are discussed.
Author

N94-22465*# Kitt Peak National Observatory, Tucson, AZ.
PHOTCAL: THE IRAF PHOTOMETRIC CALIBRATION PACKAGE Abstract Only **c61**
L. E. Davis and P. Gigoux (Cerro Tololo Inter-American Observatory, La Serena, Chile.) *In* NASA, Washington, Second Annual Conference on Astronomical Data Analysis Software and Systems. Abstracts 1992 p 34 (For primary document see N94-22438 05-89)
Avail: CASI HC A01/MF A02

The IRAF photmetric calibration package PHOTCAL is discussed. PHOTCAL is a set of tasks designed to derive the transformation from the instrumental photometric system to the standard photometric system, and apply the transformation to the observations. The PHOTCAL package contains tasks for: (1) creating and/or editing standard star catalogs and observations catalogs, (2) creating, checking and editing the configuration file which specifies the format of the standard star and observations catalogs and the form of the transformation equations, (3) solving the transformation equations interactively or non-iteractively using non-linear least squares fitting routines, and (4) applying the transformation to the observations. PHOTCAL standard star and observations catalogs are simple text files, whose columns are delimited by whitespace, and whose first column contains the star names. This format makes it relatively easy to interface the output of non-IRAF photometry programs as well as the output of the IRAF APPHOT and DAOPHOT photometry packages to PHOTCAL. PHOTCAL maintains a standard star catalog directory for the convenience of the user, but users can easily create their own standard star catalogs and/or define their own standard star catalog directory. Separate observations files produced by APPHOT, DAOPHOT or a user program containing data for stellar fields taken through different filters, can be combined into observations catalogs using one of the PHOTCAL preprocessor tasks. The input configuration file required by PHOTCAL is a text file, consisting of a series of instructions written by the user in a mini-language understood by the PHOTCAL parser. These instructions: (1) assign names to the input data columns in the standard star and observations catalogs, (2) assign names and initial values to the parameters to be fit, (3) define and describe how to solve the transformation equations. The mini-language approach permits great flexibility in the format of the input catalogs and the form of the transformation equations. Author

N94-22466*# Smithsonian Astrophysical Observatory, Cambridge, MA.
DETECTION OF X RAY SOURCES IN PROS Abstract Only
J. DePonte and F. A. Primini *In* NASA, Washington, Second Annual Conference on Astronomical Data Analysis Software and Systems. Abstracts 1992 p 35 (For primary document see N94-22438 05-89)
Avail: CASI HC A01/MF A02

The problem of detecting discrete sources in x-ray images has much in common with the problem of automatic source detection at other wavelengths. In all cases, one searches for positive brightness enhancements exceeding a certain threshold, which appear consistent with what one expects for a point source, in the presence of a (possibly) spatially variable background. Multidimensional point spread functions (e.g., dependent on detector position and photon energy) are also common. At the same time, the problem in x-ray astronomy has some unique aspects. For example, for typical x-ray exposures in current or recent observatories, the number of available pixels far exceeds the number of actual x-ray events, so Poisson, rather than Gaussian statistics apply. Further, extended cosmic x-ray sources are common, and one often desires to detect point sources in the vicinity or even within bright, diffuse x-ray emission. Finally, support structures in x-ray detectors often cast sharp shadows in x-ray images making it necessary to detect sources in a region of rapidly varying exposure. We have developed a source detection package within the IRAF/PROS environment which attempts to deal with some of the problems of x-ray source detection. We have patterned our package after the successful Einstein Observatory x-ray source detection programs. However, we have attempted to improve the flexibility and accessibility of the functions and to provide a graphical front-end for the user. Our philosophy has been to use standard IRAF tasks whenever possible for image manipulation and to separate general functions from mission-specific ones. We will report on the current status of the package and discuss future developments, including simulation tasks, to allow the user to assess detection efficiency and source significance, tasks to determine source intensity, and alternative detection algorithms. Author

N94-22467*# Leiden Univ. (Netherlands).
DEEP NEAR-INFRARED SURVEY OF THE SOUTHERN SKY (DENIS) Abstract Only
E. Deul *In* NASA, Washington, Second Annual Conference on Astronomical Data Analysis Software and Systems. Abstracts 1992 p 36 (For primary document see N94-22438 05-89)
Avail: CASI HC A01/MF A02

DENIS (Deep Near-Infrared Survey of the Southern Sky) will be the first complete census of astronomical sources in the near-infrared spectral range. The challenges of this novel survey are both scientific and technical. Phenomena radiating in the near-infrared range from brown dwarfs to galaxies in the early stages of cosmological evolution, the scientific exploitation of data relevant over such a wide range requires pooling expertise from several of the leading European astronomical centers. The technical challenges of a project which will provide an order of magnitude more sources than given by the IRAS space mission, and which will involve advanced data-handling and image-processing techniques, likewise require pooling of hardware and software resources, as well as of human expertise. The DENIS project team is composed of some 40 scientists, computer specialists, and engineers located in 5 European Community countries (France, Germany, Italy, The Netherlands, and Spain), with important contributions from specialists in Australia, Brazil, Chile, and Hungary. DENIS will survey the entire southern sky in 3 colors, namely in the I band at a wavelength of 0.8 micron, in the 1.25 micron J band, and in the 2.15 micron K' band. The sensitivity limits will be 18th magnitude in the I band, 16th in the J band, and 14.5th in the K' band. The angular resolution achieved will be 1 arcsecond in the I band, and 3.0 arcseconds in the J and K' bands. The European Southern Observatory 1 m telescope on La Silla will be dedicated to survey use during operations expected to last four years, commencing in late 1993. DENIS aims to provide the astronomical community with complete digitized infrared images of the full southern sky and a catalogue of extracted objects, both of the best quality and in readily accessible form. This will be achieved through dedicated software packages and specialized catalogues, and with assistance from the Leiden and Paris Data Analysis Centers. The data will be mailed on DAT tapes from La Silla to the two Data Analysis Centers for further processing. Two centers are necessary because of the shear quantity of data and because of the complementary roles the Centers will develop, each exploiting its own particular expertise. The Leiden Data Analysis Center (LDAC) will extract objects, establish their parameters, and archive them into a source catalogue. The LDAC will collaborate with the Groningen Space Research group that has gained experience in infrared image handling from the IRAS satellite. The Paris Data Analysis Center (PDAC) will be responsible for archiving and preprocessing the raw data to provide a homogeneous set of data suitable for further reduction in both the Leiden and Paris data analysis streams. The PDAC will also extract and archive images for the sources flagged by the LDAC as extended, and create a catalogue of galaxies. In exploiting the DENIS data we foresee the collaboration with other data analysis centers, such as the Observatoire de Lyon where the relevant DENIS catalogue of galaxies can be incorporated into their extragalactic database. The Point Sources and the Small Extended Sources catalogues could be incorporated in the Late Type Star database at Montpellier, and in the SIMBAD database as CDS. At Groningen the IRAS Point Source catalogue and/or image data can be merged with the DENIS catalogues. At Meudon algorithms and software will be developed with main goal assessing the limits reachable for the homogeneity and intrinsic consistency between the ensemble of the images in the data base (flat-fielding, relative positioning of the fields, bootstrapped flux calibration) but also for the data analysis. Author

N94-22468*# California Univ., Berkeley. Center for EUV Astrophysics.
THE EXTREME ULTRAVIOLET EXPLORER ARCHIVE Abstract Only **c82**
Jeremy J. Drake, Carl Dobson, and Elisha Polomski *In* NASA, Washington, Second Annual Conference on Astronomical Data Analysis Software and Systems. Abstracts 1992 p 37 (For primary document see N94-22438 05-89)
Avail: CASI HC A01/MF A02

The Extreme Ultraviolet Explorer (EUVE) satellite was launched successfully at 12:400:00 EDT on June 7, 1992 from Cape Canaveral Air Force Station, Florida. The EUVE science payload consists of three scanning

telescopes carrying out an all-sky survey in the 70-760A spectral region, and a Deep Survey/Spectrometer telescope performing a deep survey in the 70-250A spectral region. This latter instrumentation will subsequently perform Guests Observer (GO) spectroscopic observations of individual targets. The EUVE public archive opened for business on July 17, 1992. The purpose of the archive is the storage and distribution of EUVE data and ancillary documentation, information and software which is in the public domain. As the mission proceeds, the all-sky survey, deep survey and spectroscopic data will become publicly available through a variety of interfaces to an archive system centered around an optical juke box. In this paper, we describe the current and future contents, the architecture, and the development plans for the archive. Author

N94-22469*# European Southern Observatory, Garching (Germany).
A DISTRIBUTED CLIENTS/DISTRIBUTED SERVERS MODEL FOR STARCAT Abstract Only **c82**
B. Pirenne, M. A. Albrecht, D. Durand (CADC, British Columbia.), and S. Gaudet (CADC, British Columbia.) *In* NASA, Washington, Second Annual Conference on Astronomical Data Analysis Software and Systems. Abstracts 1992 p 38 (For primary document see N94-22438 05-89)
Avail: CASI HC A01/MF A02

STARCAT, the Space Telescope ARchive and CATalogue user interface has been along for a number of years already. During this time it has been enhanced and augmented in a number of different fields. This time, we would like to dwell on a new capability allowing geographically distributed user interfaces to connect to geographically distributed data servers. This new concept permits users anywhere on the internet running STARCAT on their local hardware to access e.g., whichever of the 3 existing HST archive sites is available, or get information on the CFHT archive through a transparent connection to the CADC in BC or to get the La Silla weather by connecting to the ESO database in Munich during the same session. Similarly PreView (or quick look) images and spectra will also flow directly to the user from wherever it is available. Moving towards an 'X'-based STARCAT is another goal being pursued: a graphic/image server and a help/doc server are currently being added to it. They should further enhance the user independence and access transparency. Author

N94-22470*# Space Telescope Science Inst., Baltimore, MD.
ENHANCEMENTS TO IRAF/STSDAS GRAPHICS Abstract Only **c61**
J. D. Eisenhamer and Z. G. Levay *In* NASA, Washington, Second Annual Conference on Astronomical Data Analysis Software and Systems. Abstracts 1992 p 39 (For primary document see N94-22438 05-89)
Avail: CASI HC A01/MF A02

The IRAF graphics kernel, psikern, is a true encapsulated PostScript implementation, an improvement over the former SGI-based PostScript output available from IRAF. The psikern kernel implements many more capabilities of gio/gki such as cell arrays (grayscale images), color, filled area patterns and true PostScript fonts. Several of the general-purpose graphics tasks in STSDAS such as igi, sgraph, skymap, and wcslab have been modified to use these capabilities explicitly. Other graphics tasks not enhanced explicitly can also make use of new capabilities such as PostScript font support. We present an overview of psikern and several examples of output created by the enhanced STSDAS tasks. Author

N94-22471*# Applied Research Corp., Greenbelt, MD. Cosmology Data Analysis Center.
AN IDL-BASED ANALYSIS PACKAGE FOR COBE AND OTHER SKYCUBE-FORMATTED ASTRONOMICAL DATA Abstract Only **c61**
J. A. Ewing, Richard B. Isaacman, and J. M. Gales *In* NASA, Washington, Second Annual Conference on Astronomical Data Analysis Software and Systems. Abstracts 1992 p 40 (For primary document see N94-22438 05-89)
Avail: CASI HC A01/MF A02

UIMAGE is a data analysis package written in IDL for the Cosmic Background Explorer (COBE) project. COBE has extraordinarily stringent accuracy requirements: 1 percent mid-infrared absolute photometry, 0.01 percent submillimeter absolute spectrometry, and 0.0001 percent submillimeter relative photometry. Thus, many of the transformations and image enhancements common to analysis of large data sets must be done with special care. UIMAGE is unusual in this sense in that it performs as many of its operations as possible on the data in its native format and projection, which in the case of COBE is the quadrilateralized sphereical cube ('skycube'). That is, after reprojecting the data, e.g., onto an Aitoff map, the user who performs an operation such as taking a crosscut or extracting data from a pixel is transparently acting upon the skycube data from which the projection was made, thereby preserving the accuracy of the result. Current plans call for formatting external data bases such as CO maps into the skycube format with a high-accuracy transformation, thereby allowing Guest Investigators to use UIMAGE for direct comparison of the COBE maps with those at other wavelengths from other instruments. It is completely menu-driven so that its use requires no knowledge of IDL. Its functionality includes I/O from the COBE archives, FITS files, and IDL save sets as well as standard analysis operations such as smoothing, reprojection, zooming, statistics of areas, spectral analysis, etc. One of UIMAGE's more advanced and attractive features is its terminal independence. Most of the operations (e.g., menu-item selection or pixel selection) that are driven by the mouse on an X-windows terminal are also available using arrow keys and keyboard entry (e.g., pixel coordinates) on VT200 and Tektronix-class terminals. Even limited grey scales of images are available this way. Obviously, image processing is very limited on this type of terminal, but it is nonetheless surprising how much analysis can be done on that medium. Such flexibility has the virtue of expanding the user community to those who must work remotely on non-image terminals, e.g., via modem. Author

N94-22472*# Smithsonian Institution, Cambridge, MA. Center for Astrophysics.
VISUALIZING THE UNIVERSE, PART 2 Abstract Only **c90**
Emilio E. Falco, Michael J. Kurtz, and Mark Bajuk (National Center for Supercomputing Applications, Urbana, IL.) *In* NASA, Washington, Second Annual Conference on Astronomical Data Analysis Software and Systems. Abstracts 1992 p 41 (For primary document see N94-22438 05-89)
Avail: CASI HC A01/MF A02

It is now possible to create animated views of the universe that are realistic, physically relevant, and breathtaking. To demonstrate the point, we describe our efforts to navigate the CfA redshift survey. For our project, we selected several CCD images of spiral and elliptical galaxies, and placed them at their observed positions in redshift space. We demonstrate how, by choreographing aesthetically pleasing trajectories, we are able to develop our own and the viewer's intuition about the large-scale structures found in the CfA redshift survey. We show for instance that three-dimensional motion enhances significantly our perception of voids and sheets in the distribution of galaxies. Such sophistication happily has become possible with the 'coming of age' of observational cosmology, as data have grown to drive the field. Author

N94-22473*# Space Telescope Science Inst., Baltimore, MD.
C++, OBJECTED-ORIENTED PROGRAMMING, AND ASTRONOMICAL DATA MODELS Abstract Only
A. Farris *In* NASA, Washington, Second Annual Conference on Astronomical Data Analysis Software and Systems. Abstracts 1992 p 42 (For primary document see N94-22438 05-89)
Avail: CASI HC A01/MF A02

Contemporary astronomy is characterized by increasingly complex instruments and observational techniques, higher data collection rates, and large data archives, placing severe stress on software analysis systems. The object-oriented paradigm represents a significant new approach to software design and implementation that holds great promise for dealing with this increased complexity. The basic concepts of this approach will be characterized in contrast to more traditional procedure-oriented approaches. The fundamental features of objected-oriented programming will be discussed from a C++ programming language perspective, using examples familiar to astronomers. This discussion will focus on objects, classes and their relevance to the data type system; the principle of information hiding; and the use of inheritance to implement generalization/specialization relationships. Drawing on the object-oriented approach, features of a new database model to support astronomical data analysis will be presented. Author

N94-22474*# Kitt Peak National Observatory, Tucson, AZ.
SPPTOOLS: PROGRAMMING TOOLS FOR THE IRAF SPP LANGUAGE Abstract Only **c61**
M. Fitzpatrick *In* NASA, Washington, Second Annual Conference on

Astronomical Data Analysis Software and Systems. Abstracts 1992 p 43 (For primary document see N94-22438 05-89)
Avail: CASI HC A01/MF A02

An IRAF package to assist in SPP code development and debugging is described. SPP is the machine-independent programming language used by virtually all IRAF tasks. Tools have been written to aide both novice and advanced SPP programmers with development and debugging by providing tasks to check the code for the number and type of arguments in all calls to IRAF VOS library procedures, list the calling sequences of IRAF tasks, create a database of identifiers for quick access, check for memory which is not freed, and a source code formatter. Debugging is simplified since the programmer is able to get a better understanding of the structure of his/her code, and IRAF library procedure calls (probably the most common source of errors) are automatically checked for correctness. Author

N94-22475*# Kitt Peak National Observatory, Tucson, AZ.
THE IRAF RADIAL VELOCITY ANALYSIS PACKAGE Abstract Only **c61**

M. Fitzpatrick *In* NASA, Washington, Second Annual Conference on Astronomical Data Analysis Software and Systems. Abstracts 1992 p 44 (For primary document see N94-22438 05-89)
Avail: CASI HC A01/MF A02

The IRAF Radial Velocity Analysis package is described and future plans are presented. A discussion of the current strengths and weaknesses of the package is given along with an analysis of the accuracies that can be expected for a given data set. An overview of the cross-correlation task is presented along with atypical examples of it's use. Future plans for new tasks and algorithms are also described. Author

N94-22476*# Smithsonian Astrophysical Observatory, Cambridge, MA.
VISUALIZING THE UNIVERSE, PART 1 Abstract Only **c90**

M. J. Geller and J. P. Huchra *In* NASA, Washington, Second Annual Conference on Astronomical Data Analysis Software and Systems. Abstracts 1992 p 45 (For primary document see N94-22438 05-89)
Avail: CASI HC A01/MF A02

These decades are the first in which we can begin to map the universe. Recent surveys reveal patterns in the distribution of galaxies -- patterns coherent on scales of 150 million light years or more. These patterns contrast with the smoothness of the radiation background measured by the COBE satellite. Together these observations challenge our understanding of the origin of galaxies and large-scale structure in the universe. 'Visualizing the universe' is crucial for exploring the 3-dimensional maps, for analyzing them, for comparing the data with simulations, for designing instruments to make deeper maps with new large telescopes, and for sharing the excitement of discovery with the public. Author

N94-22477*# Digital Equipment Corp., Cambridge, MA.
CRYSTAL BALL GAZING Abstract Only **c61**

Jim Gettys *In* NASA, Washington, Second Annual Conference on Astronomical Data Analysis Software and Systems. Abstracts 1992 p 46 (For primary document see N94-22438 05-89)
Avail: CASI HC A01/MF A02

Over the last seven years, the CPU on my desk has increased speed by two orders of magnitude, from around 1 MIP to more than 100 MIPS; more important is that it is about as fast as any uniprocessor of any type available for any price, for compute bound problems. Memory on the system is also about 100 times as big, while disk is only about 10 times as big. Local network and I/O performance have increased greatly, though not quite at the same rate as processor speed. More important, I will argue, is that the CPU's address space is 64 bits, rather than 32 bits, allowing us to rethink some time honored presumptions. The Internet has gone from a few hundred machines to a million, and now have grown to span the entire globe, and wide area networks have now becoming commercial services. 'PC's' are now real computers, bringing what was top of the line computing capability to the masses only a few years behind the leading edge. So even a year or two from now, we can anticipate commonplace desktop machines running at speeds hundreds of MIPS, with main memories in the hundreds of megabytes to a gigabyte, able to draw millions of vectors/second, and all capable of some reasonable 3D graphics. And only a few years later, this will be the $1500 PC. So the 1990's certainly brings: 64 bit processors becoming standard; BIP/BFLOP class uniprocessors; large scale multiprocessors for special purpose applications; I/O as the most significant computer engineering problem; Hierarchical data servers in everyday use; routine access to archived data around the world; and what else? What do systems such as those we will have this decade imply to those building data analysis systems today? Many of the presumptions of the 1970's and 1980's need to be reexamined in the light of 1990's technology. Author

N94-22478*# Space Telescope Science Inst., Baltimore, MD.
HST IMAGE RESTORATION: A COMPARISON OF PRE- AND POST-SERVICING MISSION RESULTS Abstract Only **c61**

R. J. Hanisch and J. Mo *In* NASA, Washington, Second Annual Conference on Astronomical Data Analysis Software and Systems. Abstracts 1992 p 47 (For primary document see N94-22438 05-89)
Avail: CASI HC A01/MF A02

A variety of image restoration techniques (e.g., Wiener filter, Lucy-Richardson, MEM) have been applied quite successfully to the aberrated HST images. The HST servicing mission (scheduled for late 1993 or early 1994) will install a corrective optics system (COSTAR) for the Faint Object Camera and spectrographs and replace the Wide Field/Planetary Camera with a second generation instrument (WF/PC-II) having its own corrective elements. The image quality is expected to be improved substantially with these new instruments. What then is the role of image restoration for the HST in the long term? Through a series of numerical experiments using model point-spread functions for both aberrated and unaberrated optics, we find that substantial improvements in image resolution can be obtained for post-servicing mission data using the same or similar algorithms as being employed now to correct aberrated images. Included in our investigations are studies of the photometric integrity of the restoration algorithms and explicit models for HST pointing errors (spacecraft jitter). Author

N94-22479*# Observatoire de Strasbourg (France).
ELECTRONIC PUBLISHING AND INTELLIGENT INFORMATION RETRIEVAL Abstract Only **c82**

A. Heck *In* NASA, Washington, Second Annual Conference on Astronomical Data Analysis Software and Systems. Abstracts 1992 p 48 (For primary document see N94-22438 05-89)
Avail: CASI HC A01/MF A02

Europeans are now taking steps to homogenize policies and standardize procedures in electronic publishing (EP) in astronomy and space sciences. This arose from an open meeting organized in Oct. 1991 at Strasbourg Observatory (France) and another business meeting held late Mar. 1992 with the major publishers and journal editors in astronomy and space sciences. The ultimate aim of EP might be considered as the so-called 'intelligent information retrieval' (IIR) or better named 'advanced information retrieval' (AIR), taking advantage of the fact that the material to be published appears at some stage in a machine-readable form. It is obvious that the combination of desktop and electronic publishing with networking and new structuring of knowledge bases will profoundly reshape not only our ways of publishing, but also our procedures of communicating and retrieving information. It should be noted that a world-wide survey among astronomers and space scientists carried out before the October 1991 colloquium on the various packages and machines used, indicated that TEX-related packages were already in majoritarian use in our community. It has also been stressed at each meeting that the European developments should be carried out in collaboration with what is done in the US (STELLAR project, for instance). American scientists and journal editors actually attended both meetings mentioned above. The paper will offer a review of the status of electronic publishing in astronomy and its possible contribution to advanced information retrieval in this field. It will also report on recent meetings such as the 'Astronomy from Large Databases-2 (ALD-2)' conference dealing with the latest developments in networking, in data, information, and knowledge bases, as well as in the related methodologies. Author (revised)

N94-22480*# Ohio State Univ., Columbus.
WRITING INSTRUMENT INTERFACES WITH xf/tktcl Abstract Only **c61**

A. A. Henden *In* NASA, Washington, Second Annual Conference on Astronomical Data Analysis Software and Systems. Abstracts 1992

p 49 (For primary document see N94-22438 05-89)
Avail: CASI HC A01/MF A02

Tcl is an embedded control language written in C, running primarily under Unix and with an interpreted C look-and-feel. Tk is an X11 toolkit based on tcl. Xf is an application builder for tk. The entire package is public domain and available from sprite.berkeley.edu. This paper discusses the use of tk to develop a user interface for OSIRIS, an infrared camera/spectrograph now operational on the OSU Perkins 1.8m telescope. The good and bad features of the development process are described.
Author

N94-22481*# American National Standards Inst., New York, NY.
FORTRAN FOR THE NINETIES Abstract Only **c61**
J. T. Himer *In* NASA, Washington, Second Annual Conference on Astronomical Data Analysis Software and Systems. Abstracts 1992 p 50 (For primary document see N94-22438 05-89)
Avail: CASI HC A01/MF A02

Fortran has largely enjoyed prominence for the past few decades as the computer programming language of choice for numerically intensive scientific, engineering, and process control applications. Fortran's well understood static language syntax has allowed resulting parsers and compiler optimizing technologies to often generate among the most efficient and fastest run-time executables, particularly on high-end scalar and vector supercomputers. Computing architectures and paradigms have changed considerably since the last ANSI/ISO Fortran release in 1978, and while FORTRAN 77 has more than survived, it's aged features provide only partial functionality for today's demanding computing environments. The simple block procedural languages have been necessarily evolving, or giving way, to specialized supercomputing, network resource, and object-oriented paradigms. To address these new computing demands, ANSI has worked for the last 12-years with three international public reviews to deliver Fortran 90. Fortran 90 has superseded and replaced ISO FORTRAN 77 internationally as the sole Fortran standard; while in the US, Fortran 90 is expected to be adopted as the ANSI standard this summer, coexisting with ANSI FORTRAN 77 until at least 1996. The development path and current state of Fortran will be briefly described highlighting the many new Fortran 90 syntactic and semantic additions which support (among others): free form source; array syntax; new control structures; modules and interfaces; pointers; derived data types; dynamic memory; enhanced I/O; operator overloading; data abstraction; user optional arguments; new intrinsics for array, bit manipulation, and system inquiry; and enhanced portability through better generic control of underlying system arithmetic models. Examples from dynamical astronomy, signal and image processing will attempt to illustrate Fortran 90's applicability to today's general scalar, vector, and parallel scientific and engineering requirements and object oriented programming paradigms. Time permitting, current work proceeding on the future development of Fortran 2000 and collateral standards will be introduced.
Author (revised)

N94-22482*# National Radio Astronomy Observatory, Green Bank, WV.
PROGRAMMABILITY IN AIPS++ Abstract Only **c61**
R. M. Hjellming *In* NASA, Washington, Second Annual Conference on Astronomical Data Analysis Software and Systems. Abstracts 1992 p 51 (For primary document see N94-22438 05-89)
Avail: CASI HC A01/MF A02

AIPS++ is an Astronomical Information Processing System being designed and implemented by an international consortium of NRAO and six other radio astronomy institutions in Australia, India, the Netherlands, the United Kingdom, Canada, and the USA. AIPS++ is intended to replace the functionality of AIPS, to be more easily programmable, and will be implemented in C++ using object-oriented techniques. Programmability in AIPS++ is planned at three levels. The first level will be that of a command-line interpreter with characteristics similar to IDL and PV-Wave, but with an intensive set of operations appropriate to telescope data handling, image formation, and image processing. The third level will be in C++ with extensive use of class libraries for both basic operations and advanced applications. The third level will allow input and output of data between external FORTRAN programs and AIPS++ telescope and image databases. In addition to summarizing the above programmability characteristics, this talk will given an overview of the classes currently being designed for telescope data calibration and editing, image formation, and the 'toolkit' of mathematical 'objects' that will perform most of the processing in AIPS++.
Author (revised)

N94-22483*# Space Telescope Science Inst., Baltimore, MD.
TELESCOPE IMAGE MODELLING SOFTWARE IN STSDAS Abstract Only **c61**
P. E. Hodge, J. D. Eisenhamer, R. A. Shaw, and R. L. Williamson, II *In* NASA, Washington, Second Annual Conference on Astronomical Data Analysis Software and Systems. Abstracts 1992 p 52 (For primary document see N94-22438 05-89)
Avail: CASI HC A01/MF A02

The Telescope Image Modelling (TIM) system creates model point spread functions for optical systems based on ray-trace information. The original TIM runs only on VAX/VMS systems, but we are modifying the software to run under IRAF in the STSDAS package in order to make TIM more widely available. The current status of this project will be discussed. Initially the changes will be restricted to the user interface and replacing VAX-specific code. Soon thereafter the IMSL and NAG subroutines will be replaced by public-domain software, and some of the algorithms may be improved.
Author (revised)

N94-22484*# Space Telescope Science Inst., Baltimore, MD.
HOW IS WFPC FLAT FIELD MADE Abstract Only **c61**
J.-C. Hsu and C. E. Ritchie *In* NASA, Washington, Second Annual Conference on Astronomical Data Analysis Software and Systems. Abstracts 1992 p 53 (For primary document see N94-22438 05-89)
Avail: CASI HC A01/MF A02

An algorithm developed by the WFPC IDT to generate flat fields from Earth streak exposures is now implemented in STSDAS. We explain in detail how this algorithm works and possible deficiencies. We also present two associated tools which can be used to modify the flat field obtained from the standard procedure.
Author

N94-22485*# Space Telescope Science Inst., Baltimore, MD.
ASpect: A NEW SPECTRUM AND LINE ANALYSIS PACKAGE FOR IRAF Abstract Only **c61**
S. J. Hulbert, J. D. Eisenhamer, Z. G. Levay, and R. A. Shaw *In* NASA, Washington, Second Annual Conference on Astronomical Data Analysis Software and Systems. Abstracts 1992 p 54 (For primary document see N94-22438 05-89)
Avail: CASI HC A01/MF A02

We examined several publicly available spectral analysis software packages looking for one with enough functionality and versatility to meet the analysis needs of astronomers during the next decade. None of those examined can satisfactorily support the wide variety of panchromatic science programs that are now becoming possible. Furthermore, we concluded that none of these packages can be simply modified to include critical functions because of their original (limited) designs. During the next two years we will write a new spectral analysis package, ASpect, that will incorporate the latest analysis techniques for astronomical spectra in all wavelength domains. The ASpect package has several functional requirements. It must operate on spectra from a wide variety of ground-based and space-based instruments spanning wavelengths from radio to gamma rays. It must accommodate non-linear dispersion relations. It must provide a variety of functions, individually or in combination, with which to fit spectral features and the continuum. It is vitally important that known bad data be masked and that, uncertainties be propagated throughout the calculations in order for astronomers to evaluate the reliability of results. Finally, this new package must provide a powerful, intuitive graphical user interface to handle the burden of data input/output (I/O), on-line 'help,' selection of relevant features for analysis, plotting and graphical interaction, and data base management–all in a comprehensible environment. We anticipate that ASpect will take the form of an external package in IRAF (such as the NOAO and STSDAS packages) and will be layered upon the IRAF virtual Operating System to make it available on as many platforms as possible, while making it resistant to changes in operating systems and compilers. Our choice of IRAF is motivated by its portability, its wide use within the astronomical community, and its rich set of existing user applications.
Author (revised)

N94-22486*# Massachusetts Inst. of Tech., Cambridge.
SPIKE: APPLICATION FOR ASTRO-D MISSION PLANNING Abstract Only **c61**
T. Isobe, M. Johnston, E. Morgan, and G. Clark *In* NASA, Washington, Second Annual Conference on Astronomical Data Analysis Software and Systems. Abstracts 1992 p 55 (For primary document see N94-22438 05-89)
Avail: CASI HC A01/MF A02

SPIKE is a mission planning software system developed by a team of programmers at the STScI for use with the Hubble Space Telescope (HST). SPIKE has been developed for the purpose of automating observatory scheduling to increase the effective utilization and ultimately, scientific return from orbiting telescopes. High-level scheduling strategies using both rule-based and neural network approaches have been incorporated. Graphical displays of activities, constraints, and schedules are an important feature of the system. Although SPIKE was originally developed for the HST, it can be used for other astronomy missions including ground-based observatories. One of the missions that has decided to use SPIKE is ASTRO-D, a Japanese X-ray satellite for which the U.S. is providing a part of the scientific payload. Scheduled to fly in Feb. 1993, its four telescopes will focus X-rays over a wide energy range onto CCD's and imaging gas proportional counters. ASTRO-D will be the first X-ray imaging mission operating over the 0.5-12 keV band with high energy resolution. This combination of capabilities will enable a varied and exciting program of astronomical research to be carried out. ASTRO-D is expected to observe 5 to 20 objects per day and a total of several thousands per year. This requires the implementation of an efficient planning and scheduling system which SPIKE can provide. Although the version of SPIKE that will be used for ASTRO-D mission is almost identical to that used for the HST, there are a few differences. For example, ASTRO-D will use two ground stations for data downlinks, instead of the TDRSS system for data transmission. As a consequence ASTRO-D is constrained by limited on-board data storage capacity to schedule high data-rate observations during periods of frequent high bit rate observations accordingly. We will demonstrate the ASTRO-D version of SPIKE to show what SPIKE can provide and how efficiently it creates an observational schedule. Author (revised)

N94-22487*# National Aeronautics and Space Administration. Goddard Space Flight Center, Greenbelt, MD.
THE HEASARC GRAPHICAL USER INTERFACE Abstract Only **c61**
N. White, P. Barrett, P. Jacobs, and B. ONeel *In* NASA, Washington, Second Annual Conference on Astronomical Data Analysis Software and Systems. Abstracts 1992 p 56 (For primary document see N94-22438 05-89)
Avail: CASI HC A01/MF A02

An OSF/Motif-based graphical user interface has been developed to facilitate the use of the database and data analysis software packages available from the High Energy Astrophysics Science Archive Research Center (HEASARC). It can also be used as an interface to other, similar, routines. A small number of tables are constructed to specify the possible commands and command parameters for a given set of analysis routines. These tables can be modified by a designer to affect the appearance of the interface screens. They can also be dynamically changed in response to parameter adjustments made while the underlying program is running. Additionally, a communication protocol has been designed so that the interface can operate locally or across a network. It is intended that this software be able to run on a variety of workstations and X terminals.
Author

N94-22488*# National Aeronautics and Space Administration. Goddard Space Flight Center, Greenbelt, MD.
FITS DATA CONVERSION EFFORTS AT THE COMPTON OBSERVATORY SCIENCE SUPPORT CENTER Abstract Only **c61**
D. G. Jennings, J. M. Jordan, T. A. McGlynn, N. G. Ruggiero, and T. A. Seriemitsos *In* NASA, Washington, Second Annual Conference on Astronomical Data Analysis Software and Systems. Abstracts 1992 p 57 (For primary document see N94-22438 05-89)
Avail: CASI HC A01/MF A02

The Compton Gamma Ray Observatory (CGRO) is an active, earth orbiting satellite consisting of four gamma-ray telescopes. Each telescope is maintained by an independent principal investigator (PI) team, and each PI team has devised separate data formats to handle the needs of their particular instrument. As mandated by NASA, the Compton Observatory Science Support Center (COSSC) intends to archive and distribute PI data to the public in FITS (Flexible Image Transport System) format. To accomplish this task, we at COSSC have been developing a set of general purpose software tools that facilitate the transformation of non-FITS formatted data into FITS format. These tools, known as ToFU (To FITS Utilities), serve as the kernel of our CGRO data conversion software. This presentation describes the problems encountered in transcribing large amounts of data into a standard FITS form and the capabilities of the COSSC-built conversion software designed to perform the transformations.
Author (revised)

N94-22489*# Hawaii Univ., Honolulu.
THE UNIVERSITY OF HAWAII INSTITUTE FOR ASTRONOMY CCD CAMERA CONTROL SYSTEM Abstract Only **c37**
K. T. C. Jim, H. T. Yamada, G. A. Luppino, and R. J. Hlivak *In* NASA, Washington, Second Annual Conference on Astronomical Data Analysis Software and Systems. Abstracts 1992 p 58 (For primary document see N94-22438 05-89)
Avail: CASI HC A01/MF A02

The University of Hawaii Institute for Astronomy CCD Camera Control System consists of a NeXT workstation, a graphical user interface, and a fiber optics communications interface which is connected to a San Diego State University CCD controller. The UH system employs the NeXT-resident Motorola DSP 56001 as a real time hardware controller. The DSP 56001 is interfaced to the Mach-based UNIX of the NeXT workstation by DMA and multithreading. Since the SDSU controller also uses the DPS 56001, the NeXT is used as a development platform for the embedded control software. The fiber optic interface links the two DSP 56001's through their Synchronous Serial Interfaces. The user interface is based on the NeXTStep windowing system. It is easy to use and features real-time display of image data and control over all camera functions. Both Loral and Tektronix 2048 x 2048 CCD's have been driven at full readout speeds, and the system is intended to be capable of simultaneous readout of four such CCD's. The total hardware package is compact enough to be quite portable and has been used on five different telescopes on Mauna Kea. The complete CCD control system can be assembled for a very low cost. The hardware and software of the control system has proven to be quite reliable, well adapted to the needs of astronomers, and extensible to increasingly complicated control requirements. Author (revised)

N94-22490*# California Univ., Berkeley. Center for EUV Astrophysics.
QUALITY CONTROL OF EUVE DATABASES Abstract Only **c82**
L. M. John and J. Drake *In* NASA, Washington, Second Annual Conference on Astronomical Data Analysis Software and Systems. Abstracts 1992 p 59 (For primary document see N94-22438 05-89)
Avail: CASI HC A01/MF A02

The publicly accessible databases for the Extreme Ultraviolet Explorer include: the EUVE Archive mailserver; the CEA ftp site; the EUVE Guest Observer Mailserver; and the Astronomical Data System node. The EUVE Performance Assurance team is responsible for verifying that these public EUVE databases are working properly, and that the public availability of EUVE data contained therein does not infringe any data rights which may have been assigned. In this poster, we describe the Quality Assurance (QA) procedures we have developed from the approach of QA as a service organization, thus reflecting the overall EUVE philosophy of Quality Assurance integrated into normal operating procedures, rather than imposed as an external, post facto, control mechanism. Author (revised)

N94-22491*# Space Telescope Science Inst., Baltimore, MD.
AN OBJECT-ORIENTED APPROACH FOR SUPPORTING BOTH X AND TERMINAL INTERFACES Abstract Only **c61**
J. Johnson *In* NASA, Washington, Second Annual Conference on Astronomical Data Analysis Software and Systems. Abstracts 1992 p 60 (For primary document see N94-22438 05-89)
Avail: CASI HC A01/MF A02

While the X Window System is clearly becoming the dominant user interface between display system, there is still a continuing need to support character cell terminal devices. For a user interface application which must support both, it is desirable to be able to use them to their fullest extent, as opposed to simply providing a character-based display within an X window. An object-oriented application framework is presented here which

allows the full capabilities of each system to be used while minimizing and isolating the amount of device-dependent code. Every user interface application consists of two parts: the various components used to display information and accept user input, and the processing of the interaction between these components. Many user interfaces are built around a core set of components such as menus, text entry fields, and forms. For a given application, the interaction between these components is the same regardless of the display system in use. Our approach is to implement each component as an object, accessible via a single public interface. All of the code necesary to implement the component for the desired display system is completely encapsulated within the object. The application is then written as a collection of objects interacting in a device-independent manner with one another. If a display system provides additional capabilities, the application can be extended by adding objects (e.g. for image display in X). We are currently implementing StarView, the user interface to the HST science archive (STDADS) using this approach. StarView will be written in C++ and will use Vermont Views for the terminal interface and OSF/Motif for the X Window interface. Author (revised)

N94-22492*# Space Telescope Science Inst., Baltimore, MD.
THE APPLICATION OF ARTIFICIAL INTELLIGENCE TO ASTRONOMICAL SCHEDULING PROBLEMS Abstract Only **c63**
Mark D. Johnston *In* NASA, Washington, Second Annual Conference on Astronomical Data Analysis Software and Systems. Abstracts 1992 p 61 (For primary document see N94-22438 05-89)
Avail: CASI HC A01/MF A02

Efficient utilization of expensive space- and ground-based observatories is an important goal for the astronomical community; the cost of modern observing facilities is enormous, and the available observing time is much less than the demand from astronomers around the world. The complexity and variety of scheduling constraints and goals has led several groups to investigate how artificial intelligence (AI) techniques might help solve these kinds of problems. The earliest and most successful of these projects was started at Space Telescope Science Institute in 1987 and has led to the development of the Spike scheduling system to support the scheduling of Hubble Space Telescope (HST). The aim of Spike at STScI is to allocate observations to timescales of days to a week observing all scheduling constraints and maximizing preferences that help ensure that observations are made at optimal times. Spike has been in use operationally for HST since shortly after the observatory was launched in Apr. 1990. Although developed specifically for HST scheduling, Spike was carefully designed to provide a general framework for similar (activity-based) scheduling problems. In particular, the tasks to be scheduled are defined in the system in general terms, and no assumptions about the scheduling timescale are built in. The mechanisms for describing, combining, and propagating temporal and other constraints and preferences are quite general. The success of this approach has been demonstrated by the application of Spike to the scheduling of other satellite observatories: changes to the system are required only in the specific constraints that apply, and not in the framework itself. In particular, the Spike framework is sufficiently flexible to handle both long-term and short-term scheduling, on timescales of years down to minutes or less. This talk will discuss recent progress made in scheduling search techniques, the lessons learned from early HST operations, the application of Spike to other problem domains, and plans for the future evolution of the system. Author (revised)

N94-22493*# National Aeronautics and Space Administration. Goddard Space Flight Center, Greenbelt, MD.
A GENERIC ARCHIVE PROTOCOL AND AN IMPLEMENTATION Abstract Only **c82**
J. M. Jordan, D. G. Jennings, T. A. McGlynn, N. G. Ruggiero, and T. A. Serlemitsos *In* NASA, Washington, Second Annual Conference on Astronomical Data Analysis Software and Systems. Abstracts 1992 p 62 (For primary document see N94-22438 05-89)
Avail: CASI HC A01/MF A02

Archiving vast amounts of data has become a major part of every scientific space mission today. The Generic Archive/Retrieval Services Protocol (GRASP) addresses the question of how to archive the data collected in an environment where the underlying hardware archives may be rapidly changing. GRASP is a device independent specification defining a set of functions for storing and retrieving data from an archive, as well as other support functions. GRASP is divided into two levels: the Transfer Interface and the Action Interface. The Transfer Interface is computer/archive independent code while the Action Interface contains code which is dedicated to each archive/computer addressed. Implementations of the GRASP specification are currently available for DECstations running Ultrix, Sparcstations running SunOS, and microVAX/VAXstation 3100's. The underlying archive is assumed to function as a standard Unix or VMS file system. The code, written in C, is a single suite of files. Preprocessing commands define the machine unique code sections in the device interface. The implementation was written, to the greatest extent possible, using only ANSI standard C functions. Author (revised)

N94-22494*# Royal Observatory, Edinburgh (Scotland).
THE ADAM ENVIRONMENT AND TRANSPUTERS Abstract Only **c61**
B. D. Kelly, J. M. Stewart, and B. V. McNally *In* NASA, Washington, Second Annual Conference on Astronomical Data Analysis Software and Systems. Abstracts 1992 p 63 (For primary document see N94-22438 05-89)
Avail: CASI HC A01/MF A02

The ADAM environment is both used for data analysis by Starlink and for data acquisition by the UK-involved observatories in Australia, Hawaii, and the Canary Islands. ADAM was originally hosted under VAX/VMS but is now at an advanced stage of a Unix port. ADAM comprises a parameter system, hierarchical data system, noticeboard system, error handling system, and other components. Originally a multi-tasking single processor environment, it has been enhanced to a multiprocessor environment using local or wide area networking. The Royal Observatory Edinburgh is producing a transputer version of the ADAM kernel to allow instruments which make use of transputers for data acquisition/control to integrate more closely with the ADAM software running at the telescopes. Communication into the transputer system is based on Ethernet carrying TCP/IP, which eases development toward a network of mixed VMS/Unix/transputer Telescope systems. The transputer system is being applied to instruments under development for the UKIRT and JCMT telescopes. Author (revised)

N94-22495*# Lick Observatory, Santa Cruz, CA.
CCD DATA ACQUISITION SYSTEMS AT LICK AND KECK OBSERVATORIES Abstract Only **c82**
R. I. Kibrick, R. J. Stover, and A. R. Conrad (Keck Observatory, Mauna Kea, HI.) *In* NASA, Washington, Second Annual Conference on Astronomical Data Analysis Software and Systems. Abstracts 1992 p 64 (For primary document see N94-22438 05-89)
Avail: CASI HC A01/MF A02

This paper will describe and compare two distinct but related CCD data acquisition systems (DAS) currently under development at Lick and Keck Observatories. Although these two systems have a number of major architectural differences, they share a considerable amount of common hardware and software. Both of these new systems build on a large body of proven software that is the foundation of the existing CCD DAS currently in use at Lick Observatory. Both will provide support for reading up to four on-chip amplifiers per CCD and/or reading out mosaics of CCD chips. In addition, they will provide the capability for interactive, real-time adjustment of CCD waveforms for engineering purposes. Each of these two systems is composed of three major subsystems: (1) an instrument computer and its software; (2) a data capture computer and its software; and (3) a CCD/dewar controller and its software. The instrument computer is a Unix workstation, and the functions it provides include user interfaces, the interactive real-time display of CCD images, and the recording of image and FITS header data to disk and/or tape. The data capture computer is responsible for the packaging and high-speed transfer of the CCD pixel data stream into a bulk RAM, and the subsequent transfer of this data to the instrument computer. The CCD/dewar controller generates the waveforms for clocking the CCD, digitizes the pixel data, and transmits it via high-speed link to the data capture computer. It is also responsible for monitoring and controlling the dewar temperature and cryogen levels. Given the number of different types of processors and high-speed data links employed in both systems, a major emphasis of this paper will be on the various forms of interprocessor communications utilized for data transfer and distributed process synchronization. Author (revised)

N94-22496*# National Aeronautics and Space Administration. Goddard Space Flight Center, Greenbelt, MD.
THE DIGITAL ARCHIVE OF THE INTERNATIONAL HALLEY WATCH Abstract Only **c82**
D. A. Klinglesmith, III, M. B. Niedner, E. Grayzeck (Maryland Univ., College Park.), M. Aronsson (Jet Propulsion Lab., Cape Canaveral, FL.), R. L. Newburn (Jet Propulsion Lab., Cape Canaveral, FL.), and A. Warnock, III (Hughes STX, Inc., Greenbelt, MD.) *In* NASA, Washington, Second Annual Conference on Astronomical Data Analysis Software and Systems. Abstracts 1992 p 65 (For primary document see N94-22438 05-89)
Avail: CASI HC A01/MF A02

The International Halley Watch was established to coordinate, collect, archive, and distribute the scientific data from Comet P/Halley that would be obtained from both the ground and space. This paper describes one of the end products of that effort, namely the IHW Digital Archive. The IHW Digital Archive consists of 26 CD-ROM's containing over 32 gigabytes of data from the 9 IHW disciplines as well as data from the 5 spacecraft missions flown to comet P/Haley and P/Giacobini-Zinner. The total archive contains over 50,000 observations by 1,500 observers from at least 40 countries. The first 24 CD's, which are currently available, contain data from the 9 IHW disciplines. The two remaining CD's will have the spacecraft data and should be available within the next year. A test CD-ROM of these data has been created and is currently under review.
Author (revised)

N94-22497*# Space Telescope Science Inst., Baltimore, MD.
DECONVOLUTION OF HUBBLE SPACE TELESCOPE IMAGES USING SIMULATED POINT SPREAD FUNCTIONS Abstract Only **c82**
J. E. Krist and H. Hasan *In* NASA, Washington, Second Annual Conference on Astronomical Data Analysis Software and Systems. Abstracts 1992 p 66 (For primary document see N94-22438 05-89)
Avail: CASI HC A01/MF A02

Presented is a study of the use of simulated point spread functions (PSF's) to deconvolve Hubble Space Telescope images. We concentrate on images from the Wide Field and Planetary Camera (WFPC) and examine the affect of position dependence of the PSF and the telescope focus position on deconvolutions. Comparisons will be made to what will be expected from WFPC 2, which will include corrective optics. Since PSF's can be simulated for any specific observation, with the added advantage of being noise free and the ability to subsample them, they may be more suitable for deconvolution than observed ones in some cases. And since finding a suitable observed PSF may be difficult, simulated ones may be easier to use.
Author (revised)

N94-22498*# Space Telescope Science Inst., Baltimore, MD.
HST PSF SIMULATION USING TINY TIM Abstract **c61**
J. E. Krist *In* NASA, Washington, Second Annual Conference on Astronomical Data Analysis Software and Systems. Abstracts 1992 p 67 (For primary document see N94-22438 05-89)
Avail: CASI HC A01/MF A02

Tiny Tim is a program which simulates Hubble Space Telescope imaging camera PSF's. It is portable (written and distributed in C) and is reasonably fast. It can model the WFPC, WFPC 2, FOC, and COSTAR corrected FOC cameras. In addition to aberrations such as defocus and spherical, it also includes WFPC obscuration shifting, mirror zonal error maps, and jitter. The program has been used at a number of sites for deconvolving HST images. Tiny Tim is available via anonymous ftp on stsci.edu in the directory software/tinytim.
Author (revised)

N94-22499*# Smithsonian Institution, Cambridge, MA.
INTELLIGENT TEXT RETRIEVAL IN THE NASA ASTROPHYSICS DATA SYSTEM Abstract Only **c82**
M. J. Kurtz, T. Karakashian, C. P. Stern, G. Eichhorn, S. S. Murray, J. M. Watson, P. G. Ossorio (Ellery Systems, Inc., Boulder, CO.), and J. L. Stoner (Ellery Systems, Inc., Boulder, CO.) *In* NASA, Washington, Second Annual Conference on Astronomical Data Analysis Software and Systems. Abstracts 1992 p 68 (For primary document see N94-22438 05-89)
Avail: CASI HC A01/MF A02

In collaboration with the NASA Scientific and Technical Information System, the NASA Astrophysics Data System (ADS) is establishing a service to provide access to the literature abstracts relevant to astronomy in the NASA Scientific and Technical Aerospace Reports and the International Aerospace Abstracts (together also known as NASA RECON). The service will include several sophisticated retrieval methods, which may be combined. Included will be methods to perform relevancy ranking from natural language queries, synonym and misspelling recognition, author name translation (e.g. for multiple transliteration possibilities), and other features. The capabilities of the current release will be shown, and the plans for the near future will be discussed.
Author (revised)

N94-22500*# Hughes STX, Inc., Greenbelt, MD.
THE IDL ASTRONOMY USER'S LIBRARY Abstract Only **c82**
W. B. Landsman *In* NASA, Washington, Second Annual Conference on Astronomical Data Analysis Software and Systems. Abstracts 1992 p 69 (For primary document see N94-22438 05-89)
Avail: CASI HC A01/MF A02

IDL (Interactive Data Language) is a commercial programming, plotting, and image display language, which is widely used in astronomy. The IDL Astronomy User's Library is a central repository of over 400 astronomy-related IDL procedures accessible via anonymous FTP. The author will overview the use of IDL within the astronomical community and discuss recent enhancements at the IDL astronomy library. These enhancements include a fairly complete I/O package for FITS images and tables, an image deconvolution package and an image mosaic package, and access to IDL Open Windows/Motif widgets interface. The IDL Astronomy Library is funded by NASA through the Astrophysics Software and Research Aids Program.
Author (revised)

N94-22501*# National Aeronautics and Space Administration. Goddard Space Flight Center, Greenbelt, MD.
GRO/EGRET DATA ANALYSIS SOFTWARE: AN INTEGRATED SYSTEM OF CUSTOM AND COMMERCIAL SOFTWARE USING STANDARD INTERFACES Abstract Only **c61**
N. A. Laubenthal, D. Bertsch, N. Lal, A. Etienne (Hughes STX, Inc., Greenbelt, MD.), L. McDonald (Hughes STX, Inc., Greenbelt, MD.), J. Mattox (Computer Sciences Corp., Greenbelt, MD.), P. Sreekumar (Universities Space Research Association, Greenbelt, MD.), P. Nolan (Stanford Univ., CA.), and J. Fierro (Stanford Univ., CA.) *In* NASA, Washington, Second Annual Conference on Astronomical Data Analysis Software and Systems. Abstracts 1992 p 70 (For primary document see N94-22438 05-89)
Avail: CASI HC A01/MF A02

The Energetic Gamma Ray Telescope Experiment (EGRET) on the Compton Gamma Ray Observatory has been in orbit for more than a year and is being used to map the full sky for gamma rays in a wide energy range from 30 to 20,000 MeV. Already these measurements have resulted in a wide range of exciting new information on quasars, pulsars, galactic sources, and diffuse gamma ray emission. The central part of the analysis is done with sky maps that typically cover an 80 x 80 degree section of the sky for an exposure time of several days. Specific software developed for this program generates the counts, exposure, and intensity maps. The analysis is done on a network of UNIX based workstations and takes full advantage of a custom-built user interface called X-dialog. The maps that are generated are stored in the FITS format for a collection of energies. These, along with similar diffuse emission background maps generated from a model calculation, serve as input to a maximum likelihood program that produces maps of likelihood with optional contours that are used to evaluate regions for sources. Likelihood also evaluates the background corrected intensity at each location for each energy interval from which spectra can be generated. Being in a standard FITS format permits all of the maps to be easily accessed by the full complement of tools available in several commercial astronomical analysis systems. In the EGRET case, IDL is used to produce graphics plots in two and three dimensions and to quickly implement any special evaluation that might be desired. Other custom-built software, such as the spectral and pulsar analyses, take advantage of the XView toolkit for display and Postscript output for the color hard copy. This poster paper outlines the data flow and provides examples of the user interfaces and output products. It stresses the advantages that are derived from the integration of the specific instrument-unique software and powerful commercial tools for graphics and statistical evaluation. This approach has several proven advantages including flexibility, a minimum of development effort, ease of use, and portability.
Author (revised)

N94-22502*# Observatoire de Strasbourg (France). Center de Donnees Astronomiques.
SIMBAD QUALITY-CONTROL Abstract Only **c82**
Soizick Lesteven *In* NASA, Washington, Second Annual Conference on Astronomical Data Analysis Software and Systems. Abstracts 1992 p 71 (For primary document see N94-22438 05-89)
Avail: CASI HC A01/MF A02

The astronomical database SIMBAD developed at the Centre de donnees astronomiques de Strasbourg presently contains 760,000 objects (stellar and non-stellar). It has the unique characteristic of being structured specifically for astronomical objects. All types of heterogeneous data (bibliographic references, measurements, and sets of identification) are connected with each object. The attributes that define quality of the database include the following. Reliability: cross-identification should not rely upon just exact values object coordinates. It also means that information attached to one simple object should be consistent. The existing data must be controlled in order to start with a reliable base and to cross-identify new data assuring the quality as data grows. Exhaustivity: delays between publication of new informations and their inclusion in the database should be as short as possible. The integrity of the database has to be maintained as data accumulates. Taking the amount of data into consideration and the rate of new data production, it is necessary to use automatic methods. One of the possibilities is to use multivariate data analysis. The factor-space is a n-dimensional relevancy space which is described by the n-axes representing a set of n subject matter headings; the words and phrases can be used to scale the axes and the documents are then a vector average of the terms within them. The application reported herein is based on the NASA-STI bibliographical database. The selected data concern astronomy, astrophysics, and space radiation (102,963 references from 1975 to 1991 included 8070 keywords). The F-space is built from this bibliographical data. By comparing the F-space position obtained from the NASA-STI keywords with the F-space position obtained from the SIMBAD references, the authors will be able to show whether it is possible to retrieve information with a restricted set of words only. If the comparison is valid, this will be a way to enter bibliographic information in the SIMBAD quality control process. Furthermore, it is possible to connect the physical measurements of stars from SIMBAD to literature concerning these stars from the NASA-STI abstracts. The physical properties of stars (e.g. UBV colors) are not randomly distributed. Stars are distributed among different clusters in a physical parameter space. The authors will show that there are some relations between this classification and the literature concerning these objects clusters in a factor space. They will investigate the nature of the relationship between the SIMBAD measurements and the bibliography. These would be new relationships that are not pre-established by an astronomer. In addition, the bibliography could be neutral information that can be used in combination with the measured parameters.
Author (revised)

N94-22503*# California Univ., Berkeley. Center for EUV Astrophysics.
DATA INDEXING TECHNIQUES FOR THE EUVE ALL-SKY SURVEY Abstract Only **c82**
J. Lewis, V. Saba, and C. Dobson *In* NASA, Washington, Second Annual Conference on Astronomical Data Analysis Software and Systems. Abstracts 1992 p 72 (For primary document see N94-22438 05-89)
Avail: CASI HC A01/MF A02

This poster describes techniques developed for manipulating large full-sky data sets for the Extreme Ultraviolet Explorer project. The authors have adapted the quatrilateralized cubic sphere indexing algorithm to allow us to efficiently store and process several types of large data sets, such as full-sky maps of photon counts, exposure time, and count rates. A variation of this scheme is used to index sparser data such as individual photon events and viewing times for selected areas of the sky, which are eventually used to create EUVE source catalogs. Author (revised)

N94-22504*# Keck Observatory, Mauna Kea, HI.
THE KECK TASK LIBRARY (KTL) Abstract Only **c82**
W. F. Lupton and A. R. Conrad *In* NASA, Washington, Second Annual Conference on Astronomical Data Analysis Software and Systems. Abstracts 1992 p 73 (For primary document see N94-22438 05-89)
Avail: CASI HC A01/MF A02

KTL is a set of routines which eases the job of writing applications which must interact with a variety of underlying sub-systems (known as services). A typical application is an X Window user interface coordinating telescope and instruments. In order to connect to a service, application code specifies a service name--typically an instrument name--and a style, which defines the way in which the application will interact with the service. Two styles are currently supported: keyword, where the application reads and writes named keywords and the resulting inter-task message traffic is hidden; and message, where the application deals directly with messages. The keyword style is intended mainly for user interfaces, and the message style is intended mainly for lower-level applications. KTL applications are event driven: a typical application first connects to all its desired services, then expresses interest in specified events. The application then enters an event dispatch loop in which it waits for events and calls the appropriate service's event-handling routine. Each event is associated with a call-back routine which is invoked when the event occurs. Call-back routines may (and typically do) interact with other sub-systems and KTL provides the means of doing so without blocking the application (vital for X Window user interfaces). This approach is a marriage of ideas culled from the X window, ADAM, Keck instrument, and Keck telescope control systems. A novel feature of KTL is that it knows nothing about any services or styles. Instead it defines a generic set of routines which must be implemented by all services and styles (essentially open(), ioctl(), read(), write(), event(), and close()) and activates sharable libraries at run-time. Services have been implemented (in both keyword and message styles) for HIRES (the Keck high resolution echelle spectrograph built by Lick Observatory), LWS (the Keck long wavelength spectrometer built by UC San Diego), and the Keck telescope. Each of these implementations uses different underlying message systems: the Lick MUSIC system, RPC's, and direct sockets (respectively). Services for the remaining three front-line Keck instruments will be implemented over the next few months. Author (revised)

N94-22505*# Kitt Peak National Observatory, Tucson, AZ.
INTERACTIVE SPECTRAL ANALYSIS AND COMPUTATION (ISAAC) Abstract Only **c61**
D. M. Lytle *In* NASA, Washington, Second Annual Conference on Astronomical Data Analysis Software and Systems. Abstracts 1992 p 74 (For primary document see N94-22438 05-89)
Avail: CASI HC A01/MF A02

Isaac is a task in the NSO external package for IRAF. A descendant of a FORTRAN program written to analyze data from a Fourier transform spectrometer, the current implementation has been generalized sufficiently to make it useful for general spectral analysis and other one dimensional data analysis tasks. The user interface for Isaac is implemented as an interpreted mini-language containing a powerful, programmable vector calculator. Built-in commands provide much of the functionality needed to produce accurate line lists from input spectra. These built-in functions include automated spectral line finding, least squares fitting of Voigt profiles to spectral lines including equality constraints, various filters including an optimal filter construction tool, continuum fitting, and various I/O functions.
Author

N94-22506*# Kitt Peak National Observatory, Tucson, AZ.
THE NSO FTS DATABASE PROGRAM AND ARCHIVE (FTSDBM) Abstract Only **c61**
D. M. Lytle *In* NASA, Washington, Second Annual Conference on Astronomical Data Analysis Software and Systems. Abstracts 1992 p 75 (For primary document see N94-22438 05-89)
Avail: CASI HC A01/MF A02

Data from the NSO Fourier transform spectrometer is being re-archived from half inch tape onto write-once compact disk. In the process, information about each spectrum and a low resolution copy of each spectrum is being saved into an on-line database. FTSDBM is a simple database management program in the NSO external package for IRAF. A command language allows the FTSDBM user to add entries to the database, delete entries, select subsets from the database based on keyword values including ranges of values, create new database files based on these subsets, make keyword lists, examine low resolution spectra graphically, and make disk number/file number lists. Once the archive is complete, FTSDBM will allow the database to be efficiently searched for data of interest to the user and the compact disk format will allow random access to that data. Author (revised)

N94-22507*# Smithsonian Astrophysical Observatory, Cambridge, MA. Center for Astrophysics.

AXAF USER INTERFACES FOR HETEROGENEOUS ANALYSIS ENVIRONMENTS Abstract Only **c61**

Eric Mandel, John Roll, and Mark S. Ackerman (Massachusetts Inst. of Tech., Cambridge.) *In* NASA, Washington, Second Annual Conference on Astronomical Data Analysis Software and Systems. Abstracts 1992 p 76 (For primary document see N94-22438 05-89)

Avail: CASI HC A01/MF A02

The AXAF Science Center (ASC) will develop software to support all facets of data center activities and user research for the AXAF X-ray Observatory, scheduled for launch in 1999. The goal is to provide astronomers with the ability to utilize heterogeneous data analysis packages, that is, to allow astronomers to pick the best packages for doing their scientific analysis. For example, ASC software will be based on IRAF, but non-IRAF programs will be incorporated into the data system where appropriate. Additionally, it is desired to allow AXAF users to mix ASC software with their own local software. The need to support heterogeneous analysis environments is not special to the AXAF project, and therefore finding mechanisms for coordinating heterogeneous programs is an important problem for astronomical software today. The approach to solving this problem has been to develop two interfaces that allow the scientific user to run heterogeneous programs together. The first is an IRAF-compatible parameter interface that provides non-IRAF programs with IRAF's parameter handling capabilities. Included in the interface is an application programming interface to manipulate parameters from within programs, and also a set of host programs to manipulate parameters at the command line or from within scripts. The parameter interface has been implemented to support parameter storage formats other than IRAF parameter files, allowing one, for example, to access parameters that are stored in data bases. An X Windows graphical user interface called 'agcl' has been developed, layered on top of the IRAF-compatible parameter interface, that provides a standard graphical mechanism for interacting with IRAF and non-IRAF programs. Users can edit parameters and run programs for both non-IRAF programs and IRAF tasks. The agcl interface allows one to communicate with any command line environment in a transparent manner and without any changes to the original environment. For example, the authors routinely layer the GUI on top of IRAF, ksh, SMongo, and IDL. The agcl, based on the facilities of a system called Answer Garden, also has sophisticated support for examining documentation and help files, asking questions of experts, and developing a knowledge base of frequently required information. Thus, the GUI becomes a total environment for running programs, accessing information, examining documents, and finding human assistance. Because the agcl can communicate with any command-line environment, most projects can make use of it easily. New applications are continually being found for these interfaces. It is the authors' intention to evolve the GUI and its underlying parameter interface in response to these needs - from users as well as developers - throughout the astronomy community. This presentation describes the capabilities and technology of the above user interface mechanisms and tools. It also discusses the design philosophies guiding the work, as well as hopes for the future. Author (revised)

N94-22508*# Smithsonian Astrophysical Observatory, Cambridge, MA.

VERIFICATION OF THE PROS TIMING ANALYSIS PACKAGE **c61**

K. R. Manning, M. A. Conroy, J. DePonte, J. F. Moran, F. A. Primini, F. D. Seward, and B. Aschenbach (Max-Planck-Inst. fuer Extraterrestrische Physik, Garching, Germany.) *In* NASA, Washington, Second Annual Conference on Astronomical Data Analysis Software and Systems. Abstracts 1992 p 77 (For primary document see N94-22438 05-89)

Avail: CASI HC A01/MF A02

ROSAT observations of known pulsars are used to verify the functions of timing programs. The Crab Pulsar and PSR 0540-69, with 33 and 50 millisecond periods, are used to examine the fast Fourier transform and the epoch-folding task used to search for periodic signals. These fast pulsars provide a more vigorous test of the system than those with periods of a few seconds. Author (revised)

N94-22509*# National Aeronautics and Space Administration. Goddard Space Flight Center, Greenbelt, MD.

GammaCore: THE COMPTON OBSERVATORY RESEARCH ENVIRONMENT Abstract Only **c82**

T. A. McGlynn, D. G. Jennings, J. M. Jordan, N. Ruggiero, and T. A. Serlemitsos *In* NASA, Washington, Second Annual Conference on Astronomical Data Analysis Software and Systems. Abstracts 1992 p 78 (For primary document see N94-22438 05-89)

Avail: CASI HC A01/MF A02

The Compton Observatory Science Support Center (COSSC) is developing a coherent analysis environment for the analysis of Compton and other gamma-ray astronomy data. This environment, GammaCore, allows the astronomer to access the data analysis systems developed at the Principal Investigator (PI) sites for the four Compton Observatory instruments. In addition users have access to standard astronomical tools such as IRAF, IDL, and XANADU. The user interface of GammaCore is the AGCL (AnswerGarden Command Language), developed at the AXAF Science Center. The parameter interface supported by the AGCL allows GammaCore to access all PI software systems in a uniform fashion. These systems are quite different, having been developed independently on heterogeneous systems without much concern for general portability. The data kibitzer concept, where a window running in a specific PI environment is controlled by the AGCL, has been used extensively. Users can choose to view what is going on in the native environment, to use the window to control PI software directly, or to ignore the PI systems entirely and to work only through the homogeneous AGCL interface. Software developed at the COSSC is also integrated within GammaCore. Extensive facilities for conversions of PI data formats to and from FITS have been developed. Access to the Compton data archive and catalogs will also be completely integrated with the GammaCore. Users can retrieve any publicly available Compton data. This paper examines the issues that have arisen in attempting to meld these widely diverse systems. The advantages and limitations of the parameter interface and the kibitzer are discussed along with issues of data portability, documentation, and the feasibility of multi-instrument analysis. Limited capabilities are now available within GammaCore with significant enhancements planned over the coming year. An implementation including all PI systems will be available within that time. Instructions on how to access GammaCore and how to get more information are given.

Author (revised)

N94-22510*# Massachusetts Inst. of Tech., Cambridge.

WILBUR: A LOW-COST CCD CAMERA SYSTEM FOR MDM OBSERVATORY Abstract Only **c35**

M. R. Metzger, G. A. Luppino (Istituto di Fisica dell Atmosfera, Rome, Italy.), and J. L. Tonry *In* NASA, Washington, Second Annual Conference on Astronomical Data Analysis Software and Systems. Abstracts 1992 p 79 (For primary document see N94-22438 05-89)

Avail: CASI HC A01/MF A02

The recent availability of several 'off-the-shelf' components, particularly CCD control electronics from SDSU, has made it possible to put together a flexible CCD camera system at relatively low cost and effort. The authors describe Wilbur, a complete CCD camera system constructed for the Michigan-Dartmouth-MIT Observatory. The hardware consists of a Loral 2048(exp 2) CCD controlled by the SDSU electronics, an existing dewar design modified for use at MDM, a Sun Sparcstation 2 with a commercial high-speed parallel controller, and a simple custom interface between the controller and the SDSU electronics. The camera is controlled from the Sparcstation by software that provides low-level I/O in real time, collection of additional information from the telescope, and a simple command interface for use by an observer. Readout of the 2048(exp 2) array is complete in under two minutes at 5 e(sup -) read noise, and readout time can be decreased at the cost of increased noise. The system can be easily expanded to handle multiple CCD's/multiple readouts, and can control other dewars/CCD's using the same host software. Author (revised)

N94-22511*# Smithsonian Astrophysical Observatory, Cambridge, MA.

SKYMAP: EXPLORING THE UNIVERSE IN SOFTWARE Abstract Only **c61**

D. J. Mink *In* NASA, Washington, Second Annual Conference on Astronomical Data Analysis Software and Systems. Abstracts 1992 p 80 (For primary document see N94-22438 05-89)

Avail: CASI HC A01/MF A02

SKYMAP is a computer program which produces maps of arbitrary portions of the sky in a variety of projections and coordinate systems. Over the past ten years it has been used to produce finder charts for occultations by planets, display scan and image data from the Spacelab 2 Infrared Telescope, and make maps of fields for astronomical observations

at X-ray, optical, infrared, and radio wavelengths. It can display multiple source catalogs, including the HST Guide Star Catalog, as well as solar system objects with astrometric accuracy using the JPL DE-130 ephemeris or tabulated positions. SKYMAP can be tuned to a specific task using an ASCII parameter file which controls how information is displayed on any Tektronix-compatible graphics display. The program contains a variety of interactive graphic and image processing features and has been ported to a variety of computer systems. A recent project visually demonstrates source density variation in various commonly-used all-sky catalogs.

Author (revised)

N94-22512*# Minnesota Univ., Minneapolis.

STARBASE: DATABASE SOFTWARE FOR THE AUTOMATED PLATE SCANNER Abstract Only c61

S. C. Odewahn, R. M. Humphreys, and P. Thurmes *In* NASA, Washington, Second Annual Conference on Astronomical Data Analysis Software and Systems. Abstracts 1992 p 81 (For primary document see N94-22438 05-89)

Avail: CASI HC A01/MF A02

The Automated Plate Scanner (APS) of the University of Minnesota, a unique high speed 'flying spot' laser scanner, is currently being used to scan and digitize the 936 O and E plate pairs of the first epoch Palomar Sky Survey. The resultant database will be used to produce a catalog of approximately a billion stars and several million galaxies. The authors describe the ongoing development of a dedicated APS database management system which will be made available to the astronomical community via INTERNET. A specialized DBMS called STARBASE has been written to provide fast access to the hundreds of millions of images collected by the APS. This system provides an initial reduction mode for parameterizing APS images and classifying image types using a novel set of neural network image classifiers. A second analysis mode, which will be that commonly used by the general user, provides for searches of the database which may be constrained by any combination of physical and positional parameters. Through the use of pointer hash trees, the system has been optimized for extremely fast positional searches using either right ascension and declination on the sky or linear X and Y positions on the POSS field. In addition to fast data retrieval, the system provides a graphical interface for displaying scatter plots or histograms of the collected data. In addition, a specialized image display system is being developed to allow the user to view densitometric data for all objects classified as extended by the neural network system. Finally, STARBASE has a flexible programmable interface which allows other programs to access information in the database. This allows users to write applications suited to their particular needs to process APS data. Author (revised)

N94-22513*# National Aeronautics and Space Administration. Goddard Space Flight Center, Greenbelt, MD.

XPI: THE XANADU PARAMETER INTERFACE Abstract Only c61

N. White, P. Barrett, B. ONeel, and P. Jacobs *In* NASA, Washington, Second Annual Conference on Astronomical Data Analysis Software and Systems. Abstracts 1992 p 82 (For primary document see N94-22438 05-89)

Avail: CASI HC A01/MF A02

XPI is a table driven parameter interface which greatly simplifies both command driven programs such as BROWSE and XIMAGE as well as stand alone single-task programs. It moves all of the syntax and semantic parsing of commands and parameters out of the users code into common code and externally defined tables. This allows the programmer to concentrate on writing the code unique to the application rather than reinventing the user interface and for external graphical interfaces to interface with no changes to the command driven program. XPI also includes a compatibility library which allows programs written using the IRAF host interface (Mandel and Roll) to use XPI in place of the IRAF host interface.

Author

N94-22514*# Leicester Univ. (England).

EVALUATION OF RDBMS PACKAGES FOR USE IN ASTRONOMY Abstract Only c82

C. G. Page and A. C. Davenhall *In* NASA, Washington, Second Annual Conference on Astronomical Data Analysis Software and Systems. Abstracts 1992 p 83 (For primary document see N94-22438 05-89)

Avail: CASI HC A01/MF A02

Tabular data sets arise in many areas of astronomical data analysis, from raw data (such as photon event lists) to final results (such as source catalogs). The Starlink catalog access and reporting package, SCAR, was originally developed to handle IRAS data and it has been the principal relational DBMS in the Starlink software collection for several years. But SCAR has many limitations and is VMS-specific, while Starlink is in transition from VMS to Unix. Rather than attempt a major re-write of SCAR for Unix, it seemed more sensible to see whether any existing database packages are suitable for general astronomical use. The authors first drew up a list of desirable properties for such a system and then used these criteria to evaluate a number of packages, both free ones and those commercially available. It is already clear that most commercial DBMS packages are not very well suited to the requirements; for example, most cannot carry out efficiently even fairly basic operations such as joining two catalogs on an approximate match of celestial positions. This paper reports the results of the evaluation exercise and notes the problems in using a standard DBMS package to process scientific data. In parallel with this the authors have started to develop a simple database engine that can handle tabular data in a range of common formats including simple direct-access files (such as SCAR and Exosat DBMS tables) and FITS tables (both ASCII and binary).

Author (revised)

N94-22515*# Eoetvoes Lorand Univ., Budapest (Hungary).

SOME PRACTICABLE APPLICATIONS OF QUADTREE DATA STRUCTURES/REPRESENTATION IN ASTRONOMY Abstract Only c61

L. Pasztor *In* NASA, Washington, Second Annual Conference on Astronomical Data Analysis Software and Systems. Abstracts 1992 p 84 (For primary document see N94-22438 05-89)

Avail: CASI HC A01/MF A02

Development of quadtree as hierarchical data structuring technique for representing spatial data (like points, regions, surfaces, lines, curves, volumes, etc.) has been motivated to a large extent by storage requirements of images, maps, and other multidimensional (spatially structured) data. For many spatial algorithms, time-efficiency of quadtrees in terms of execution may be as important as their space-efficiency concerning storage conditions. Briefly, the quadtree is a class of hierarchical data structures which is based on the recursive partition of a square region into quadrants and sub-quadrants until a predefined limit. Beyond the wide applicability of quadtrees in image processing, spatial information analysis, and building digital databases (processes becoming ordinary for the astronomical community), there may be numerous further applications in astronomy. Some of these practicable applications based on quadtree representation of astronomical data are presented and suggested for further considerations. Examples are shown for use of point as well as region quadtrees. Statistics of different leaf and non-leaf nodes (homogeneous and heterogeneous sub-quadrants respectively) at different levels may provide useful information on spatial structure of astronomical data in question. By altering the principle guiding the decomposition process, different types of spatial data may be focused on. Finally, a sampling method based on quadtree representation of an image is proposed which may prove to be efficient in the elaboration of sampling strategy in a region where observations were carried out previously either with different resolution or/and in different bands.

Author (revised)

N94-22516*# National Aeronautics and Space Administration. Goddard Space Flight Center, Greenbelt, MD.

DEVELOPMENT OF THE FITS TOOLS PACKAGE FOR MULTIPLE SOFTWARE ENVIRONMENTS Abstract Only c61

W. D. Pence and J. K. Blackburn *In* NASA, Washington, Second Annual Conference on Astronomical Data Analysis Software and Systems. Abstracts 1992 p 85 (For primary document see N94-22438 05-89)

Avail: CASI HC A01/MF A02

The HEASARC is developing a package of general purpose software for analyzing data files in FITS format. This paper describes the design philosophy which makes the software both machine-independent (it runs on VAXs, Suns, and DEC-stations) and software environment-independent. Currently the software can be compiled and linked to produce IRAF tasks, or alternatively, the same source code can be used to generate stand-alone tasks using one of two implementations of a user-parameter interface library. The machine independence of the software is achieved by writing the source code in ANSI standard Fortran or C, using the machine-independent FITSIO subroutine interface for all data file I/O, and

using a standard user-parameter subroutine interface for all user I/O. The latter interface is based on the Fortran IRAF Parameter File interface developed at STScI. The IRAF tasks are built by linking to the IRAF implementation of this parameter interface library. Two other implementations of this parameter interface library, which have no IRAF dependencies, are now available which can be used to generate stand-alone executable tasks. These stand-alone tasks can simply be executed from the machine operating system prompt either by supplying all the task parameters on the command line or by entering the task name after which the user will be prompted for any required parameters. A first release of this FTOOLS package is now publicly available. The currently available tasks are described, along with instructions on how to obtain a copy of the software.

Author (revised)

N94-22517*# Wisconsin Univ., Madison.

EFFICIENT TRANSFER OF IMAGES OVER NETWORKS Abstract Only **c32**

J. W. Percival and R. L. White (Space Telescope Science Inst., Baltimore, MD.) *In* NASA, Washington, Second Annual Conference on Astronomical Data Analysis Software and Systems. Abstracts 1992 p 86 (For primary document see N94-22438 05-89)

Avail: CASI HC A01/MF A02

Effective remote observing requires sending large images over long distances. The usual approach to the transfer problem is to require high bandwidth transmission links, which are expensive to install and operate. An alternative approach is to use existing low-bandwidth connections, such as phone lines or the Internet, in a highly efficient manner by compressing the images. The combined use of existing low-cost infrastructure and standard networking software means that remote observing can be made practical even for small observatories with limited network resources. The authors have implemented such a scheme based on the H-transform compression method developed for astronomical images, which are often resistant to compression because they are noisy. The H-transform can be used for either lossy or lossless compression, and compression factors of at least 10 can be achieved with no noticeable losses in the astrometric or photometric properties of the compressed images. The H-transform allows us to organize the information in an image so that the 'useful' information can be sent first, followed by the noise, which makes up the bulk of the transmission. The receiver can invert a partially received set of H-coefficients, creating an image that improves with time. The H-transform is particularly well-suited to this style of incremental reconstruction, because the spatially localized nature of the basis functions of the H-transorm prevents the appearance of artifacts such as ringing around point sources and edges. The authors' implementation uses the WIYN Telescope Control System's TCP-based communications protocol. An 800x800 16-bit astronomical image was sent over a 2400 baud connection, which would normally take about 71 minutes; after only 60 seconds, the partially received H-transform produced an image that did not differ appreciably from the original. This poster presents a quantification of the efficiencies, as well as examples of images reconstructed from partial data. Author (revised)

N94-22518*# European Southern Observatory, Munich (Germany).

THE EUROPEAN SOUTHERN OBSERVATORY-MIDAS TABLE FILE SYSTEM Abstract Only **c82**

M. Peron and P. Grosbol *In* NASA, Washington, Second Annual Conference on Astronomical Data Analysis Software and Systems. Abstracts 1992 p 87 (For primary document see N94-22438 05-89)

Avail: CASI HC A01/MF A02

The new and substantially upgraded version of the Table File System in MIDAS is presented as a scientific database system. MIDAS applications for performing database operations on tables are discussed, for instance, the exchange of the data to and from the TFS, the selection of objects, the uncertainty joins across tables, and the graphical representation of data. This upgraded version of the TFS is a full implementation of the binary table extension of the FITS format; in addition, it also supports arrays of strings. Different storage strategies for optimal access of very large data sets are implemented and are addressed in detail. As a simple relational database, the TFS may be used for the management of personal data files. This opens the way to intelligent pipeline processing of large amounts of data. One of the key features of the Table File System is to provide also an extensive set of tools for the analysis of the final results of a reduction process. Column operations using standard and special mathematical functions as well as statistical distributions can be carried out; commands for linear regression and model fitting using nonlinear least square methods and user-defined functions are available. Finally, statistical tests of hypothesis and multivariate methods can also operate on tables.

Author (revised)

N94-22519*# Smithsonian Astrophysical Observatory, Cambridge, MA.

AN X RAY ARCHIVE ON YOUR DESK: THE EINSTEIN CD-ROM'S Abstract Only **c82**

A. Prestwich, J. McDowell, D. Plummer, K. Manning, and M. Garcia *In* NASA, Washington, Second Annual Conference on Astronomical Data Analysis Software and Systems. Abstracts 1992 p 88 (For primary document see N94-22438 05-89)

Avail: CASI HC A01/MF A02

Data from the Einstein Observatory imaging proportional counter (IPC) and high resolution imager (HRI) were released on several CD-ROM sets. The sets released so far include pointed IPC and HRI observations in both simple image and detailed photon event list format, as well as the IPC slew survey. With the data on these CD-ROMS's the user can perform spatial analysis (e.g., surface brightness distributions), spectral analysis (with the IPC event lists), and timing analysis (with the IPC and HRI event lists). The next CD-ROM set will contain IPC unscreened data, allowing the user to perform custom screening to recover, for instance, data during times of lost aspect data or high particle background rates. Author

N94-22520*# Astrophysical Inst., Potsdam (Germany).

ADAPTIVE FILTERING OF ECHELLE SPECTRA OF DISTANT QUASARS Abstract Only

A. Priebe, D.-E. Liebscher, H. Lorenz, and G.-M. Richter *In* NASA, Washington, Second Annual Conference on Astronomical Data Analysis Software and Systems. Abstracts 1992 p 89 (For primary document see N94-22438 05-89)

Avail: CASI HC A01/MF A02

The study of the Ly alpha - forest of distant (approximately greater than 3) Quasars is an important tool in obtaining a more detailed picture of the distribution of matter along the line of sight and thus of the general distribution of matter in the Universe and is therefore of important cosmological significance. Obviously, this is one of the tasks where spectral resolution plays an important role. The spectra used were obtained with the EFOSC at the ESO 3.6m telescope. Applying for the data reduction the standard Echelle procedure, as it is implemented for instance in the MIDAS-package, one uses stationary filters (e.g. median) for noise and cosmic particle event reduction in the 2-dimensional Echelle image. These filters are useful if the spatial spectrum of the noise reaches essentially higher frequencies then the highest resolution features in the image. Otherwise the resolution in the data will be degraded and the spectral lines smoothed. However, in the Echelle spectra the highest resolution is already in the range of one or a few pixels and therefore stationary filtering means always a loss of resolution. An Echelle reduction procedure on the basis of a space variable filter described which recognizes the local resolution in the presence of noise and adapts to it is developed. It was shown that this technique leads to an improvement in resolution by a factor of 2 with respect to standard procedures. Author (revised)

N94-22521*# European Space Research Organization, Noordwikj (Netherlands).

THE EXOSAT DATABASE AND ARCHIVE Abstract Only **c82**

A. P. Reynolds and A. N. Parmar *In* NASA, Washington, Second Annual Conference on Astronomical Data Analysis Software and Systems. Abstracts 1992 p 90 (For primary document see N94-22438 05-89)

Avail: CASI HC A01/MF A02

The EXOSAT database provides on-line access to the results and data products (spectra, images, and lightcurves) from the EXOSAT mission as well as access to data and logs from a number of other missions (such as EINSTEIN, COS-B, ROSAT, and IRAS). In addition, a number of familiar optical, infrared, and x ray catalogs, including the Hubble Space Telescope (HST) guide star catalog are available. The complete database is located at the EXOSAT observatory at ESTEC in the Netherlands and is accessible remotely via a captive account. The database management system was specifically developed to efficiently access the database and to allow the user to perform statistical studies on large samples of astronomical objects as well as to retrieve scientific and bibliographic

information on single sources. The system was designed to be mission independent and includes timing, image processing, and spectral analysis packages as well as software to allow the easy transfer of analysis results and products to the user's own institute. The archive at ESTEC comprises a subset of the EXOSAT observations, stored on magnetic tape. Observations of particular interest were copied in compressed format to an optical jukebox, allowing users to retrieve and analyze selected raw data entirely from their terminals. Such analysis may be necessary if the user's needs are not accommodated by the products contained in the database (in terms of time resolution, spectral range, and the finesse of the background subtraction, for instance). Long-term archiving of the full final observation data is taking place at ESRIN in Italy as part of the ESIS program, again using optical media, and ESRIN have now assumed responsibility for distributing the data to the community. Tests showed that raw observational data (typically several tens of megabytes for a single target) can be transferred via the existing networks in reasonable time.

Author (revised)

N94-22522*# Space Research Organization Netherlands, Groningen.

THE ISO SWS ON-LINE SYSTEM Abstract Only **c61**

P. R. Roelfsema, D. J. M. Kester, P. R. Wesselius, E. Wieprech, and N. Sym *In* NASA, Washington, Second Annual Conference on Astronomical Data Analysis Software and Systems. Abstracts 1992 p 91 (For primary document see N94-22438 05-89)

Avail: CASI HC A01/MF A02

The software which is currently being developed for the Short Wavelength Spectrometer (SWS) of the Infrared Space Observatory (ISO) is described. The spectrometer has a wide range of capabilities in the 2-45 micron infrared band. SWS contains two independent gratings, one for the long and one for the short wavelength section of the band. With the gratings a spectral resolution of approximately 1000 to approximately 2500 can be obtained. The instrument also contains two Fabry-Perault's yielding a resolution between approximately 1000 and approximately 20000. Software is currently being developed for the acquisition, calibration, and analysis of SWS data. The software is firstly required to run in a pipeline mode without human interaction, to process data as they are received from the telescope. However, both for testing and calibration of the instrument as well as for evaluation of the planned operating procedures the software should also be suitable for interactive use. Thirdly the same software will be used for long term characterization of the instrument. The software must work properly within the environment designed by the European Space Agency (ESA) for the spacecraft operations. As a result strict constraints are put on I/O devices, throughput etc. Author (revised)

N94-22523*# National Aeronautics and Space Administration. Goddard Space Flight Center, Greenbelt, MD.

KHOROS SOFTWARE SPECIFICATION FORMAT AND INTEROPERABILITY Abstract Only **c61**

A. H. Rots *In* NASA, Washington, Second Annual Conference on Astronomical Data Analysis Software and Systems. Abstracts 1992 p 92 (For primary document see N94-22438 05-89)

Avail: CASI HC A01/MF A02

Khoros defines formats for User Interface Specification (UIS) and Program Specification (PS) files. From such files, its code generator, Ghostwriter, creates source files and documentation. The great advantage of the system is that the code fragments that make up part of the PS file are purely generic. All Khoros-related code is created by the code generator; this includes all user interface code. As a matter of fact, both specification files are very generic in nature. Thus, one could imagine using it as the basis for other software systems. A case is made that writing a code generator that would create IRAF-compatible code from the Khoros UIS and PS files is fairly trivial. Another aspect of the Khoros system conventions concerns the way execution commands are generated by the user interface and the actual syntax of those commands. The protocols are such that interoperability at the level of executable modules is readily possible.

Author

N94-22524*# Smithsonian Astrophysical Observatory, Cambridge, MA.

SPATIAL REGION FILTERING IN IRAF/PROS Abstract Only **c61**

Eric Mandel, John Roll, Dennis Schmidt, Mike VanHilst (Washington Univ., Seattle.), and Richard Burg (Johns Hopkins Univ., Baltimore, MD.) *In* NASA, Washington, Second Annual Conference on Astronomical Data Analysis Software and Systems. Abstracts 1992 p 93 (For primary document see N94-22438 05-89)

Avail: CASI HC A01/MF A02

In order to analyze x ray data, it is nearly always necessary to extract source and background events from a data set. Typically, this is done by defining geometric spatial regions of the data set to describe the source and background. For example, one might wish to extract source events from a circular or elliptical region centered at a particular pixel, and background events from a circular or elliptical annulus whose inner radius matches the source region. At the same time, it might be necessary to exclude one or more nearby sources from the source or background region in question. Thus, it might be necessary to define a pie-shaped region or even an entirely irregularly-shaped region to exclude. A spatial filtering scheme called REGIONS was implemented in IRAF/PROS to support these and other types of spatial region extraction. It allows users to create a spatial mask by specifying one or more ASCII geometric shape descriptors (box, circle, ellipse, pie, point, annulus, and polygon) as regions to be included or excluded in the mask. In addition, two or more shapes can be combined using Boolean algebra to create an infinite variety of sophisticated regions. Each geometric shape has a specific set of parameters that describe that shape. For example, a circle is described by a center and a radius, while a box is described by a center, length, width, and rotation angle. These quantities can be specified in units of pixels or, in cases where the target image contains world coordinate system information, they can be described in units such as RA and Dec. Users can create region mask files by feeding an ASCII region descriptor to the IRAF/PROS picreate task. Temporary masks can also be created from ASCII region descriptors by individual applications that call the routines in the region creation library. This library implements a yacc-based region parser that compiles the ASCII descriptors into 'software CPU' instructions which are then executed to create the mask. The mask created from these region descriptors is a standard IRAF PLIO mask. It can be combined with other PLIO masks (e.g., exposure masks) to provide complete spatial filtering capabilities. The capabilities of the region filtering scheme are described. It also discusses the design philosophy guiding our work, as well as our plans for the future.

Author (revised)

N94-22525*# Kitt Peak National Observatory, Tucson, AZ.

MANAGING AN ARCHIVE OF WEATHER SATELLITE IMAGES Abstract Only **c82**

R. L. Seaman *In* NASA, Washington, Second Annual Conference on Astronomical Data Analysis Software and Systems. Abstracts 1992 p 94 (For primary document see N94-22438 05-89)

Avail: CASI HC A01/MF A02

The author's experiences of building and maintaining an archive of hourly weather satellite pictures at NOAO are described. This archive has proven very popular with visiting and staff astronomers - especially on windy days and cloudy nights. Given access to a source of such pictures, a suite of simple shell and IRAF CL scripts can provide a great deal of robust functionality with little effort. These pictures and associated data products such as surface analysis (radar) maps and National Weather Service forecasts are updated hourly at anonymous ftp sites on the Internet, although your local Atsmospheric Sciences Department may prove to be a more reliable source. The raw image formats are unfamiliar to most astronomers, but reading them into IRAF is straightforward. Techniques for performing this format conversion at the host computer level are described which may prove useful for other chores. Pointers are given to sources of data and of software, including a package of example tools. These tools include shell and Perl scripts for downloading pictures, maps, and forecasts, as well as IRAF scripts and host level programs for translating the images into IRAF and GIF formats and for slicing & dicing the resulting images. Hints for displaying the images and for making hardcopies are given.

Author (revised)

N94-22526*# Rice Univ., Houston, TX.

DETECTOR NOISE STATISTICS IN THE NON-LINEAR REGIME Abstract Only **c32**

P. L. Shopbell and J. Bland-Hawthorn *In* NASA, Washington, Second Annual Conference on Astronomical Data Analysis Software and Systems. Abstracts 1992 p 95 (For primary document see N94-22438 05-89)

Avail: CASI HC A01/MF A02

The statistical behavior of an idealized linear detector in the presence

of threshold and saturation levels is examined. It is assumed that the noise is governed by the statistical fluctuations in the number of photons emitted by the source during an exposure. Since physical detectors cannot have infinite dynamic range, our model illustrates that all devices have non-linear regimes, particularly at high count rates. The primary effect is a decrease in the statistical variance about the mean signal due to a portion of the expected noise distribution being removed via clipping. Higher order statistical moments are also examined, in particular, skewness and kurtosis. In principle, the expected distortion in the detector noise characteristics can be calibrated using flatfield observations with count rates matched to the observations. For this purpose, some basic statistical methods that utilize Fourier analysis techniques are described. Author (revised)

N94-22527*# Rice Univ., Houston, TX.
THE IRAF FABRY-PEROT ANALYSIS PACKAGE: RING FITTING Abstract Only **c82**
P. L. Shopbell, J. Bland-Hawthorn, and G. Cecil (North Carolina Univ., Chapel Hill.) *In* NASA, Washington, Second Annual Conference on Astronomical Data Analysis Software and Systems. Abstracts 1992 p 96 (For primary document see N94-22438 05-89)
Avail: CASI HC A01/MF A02

As introduced at ADASSI, a Fabry-Perot analysis package for IRAF is currently under development as a joint effort of ourselves and Frank Valdes of the IRAF group. Although additional portions of the package were also implemented, we report primarily on the development of a robust ring fitting task, useful for fitting the calibration rings obtained in Fabry-Perot observations. The general equation of an ellipse is fit to the shape of the rings, providing information on ring center, ellipticity, and position angle. Such parameters provide valuable information on the wavelength response of the etalon and the geometric stability of the system. Appropriate statistical weighting is applied to the pixels to account for increasing numbers with radius, the Lorentzian cross-section, and uneven illumination. The major problems of incomplete, non-uniform, and multiple rings are addressed with the final task capable of fitting rings regardless of center, cross-section, or completion. The task requires only minimal user intervention, allowing large numbers of rings to be fit in an extremely automated manner.
Author (revised)

N94-22528*# Anglo-Australian Observatory, Sydney.
THE EVOLUTION OF THE FIGARO DATA REDUCTION SYSTEM Abstract Only **c82**
K. Shortridge *In* NASA, Washington, Second Annual Conference on Astronomical Data Analysis Software and Systems. Abstracts 1992 p 97 (For primary document see N94-22438 05-89)
Avail: CASI HC A01/MF A02

The Figaro data reduction system originated at Caltech around 1983. It was based on concepts being developed in the U.K. by the Starlink organization, particularly the use of hierarchical self-defining data structures and the abstraction of most user-interaction into a set of 'parameter system' routines. Since 1984 it has continued to be developed at AAO, in collaboration with Starlink and Caltech. It was adopted as Starlink's main spectroscopic data reduction package, although it is by no means limited to spectra; it has operations for images and data cubes and even a few (very specialized) for four-dimensional data hypercubes. It continued to be used at Caltech and will be used at the Keck. It is also in use at a variety of other organizations around the world. Figaro was originally a system for VMS Vaxes. Recently it was ported (at Caltech) to run on SUN's, and work is underway at the University of New South Wales on a DecStation version. It is hoped to coordinate all this work into a unified release, but coordination of the development of a system by organizations covering three continents poses a number of interesting administrative problems. The hierarchical data structures used by Figaro allow it to handle a variety of types of data, and to add new items to data structures. Error and data quality information was added to the basic file format used, error information being particularly useful for infrared data. Cooperating sets of programs can add specific sub-structures to data files to carry information that they understand (polarimetry data containing multiple data arrays, for example), without this affecting the way other programs handle the files. Complex instrument-specific ancillary information can be added to data files written at a telescope and can be used by programs that understand the instrumental details in order to produce properly calibrated data files. Once this preliminary data processing was done the resulting files contain 'ordinary' spectra or images that can be processed by programs that are not instrument-specific. The structures holding the instrumental information can then be discarded from the files. Much effort has gone into trying to make it easy to write Figaro programs; data access subroutines are now available to handle access to all the conventional items found in Figaro files (main data arrays, error information, quality information etc), and programs that only need to access such items can be very simple indeed. A large number of Figaro users do indeed write their own Figaro applications using these routines. The fact that Figaro programs are written as callable subroutines getting information from the user through a small set of parameter routines means that they can be invoked in numerous ways; they are normally linked and run as individual programs (called by a small main routine that is generated automatically), but are also available linked to run under the ADAM data acquisition system and there is an interface that lets them be called as part of a user-written Fortran program. The long-term future of Figaro probably depends to a large extent on how successfully it manages the transition from being a VMS-only system to being a multi-platform system. Author (revised)

N94-22529*# Anglo-Australian Observatory, Sydney.
THE DATA ACQUISITION SYSTEM FOR THE ANGLO-AUSTRALIAN OBSERVATORY 2-DEGREE FIELD PROJECT Abstract Only **c82**
K. Shortridge, T. J. Farrell, and J. Bailey *In* NASA, Washington, Second Annual Conference on Astronomical Data Analysis Software and Systems. Abstracts 1992 p 98 (For primary document see N94-22438 05-89)
Avail: CASI HC A01/MF A02

The Anglo-Australian Observatory (AAO) is building a system that will provide a two-degree field of view at prime focus. A robot positioner will be used to locate up to 400 optical fibers at pre-determined positions in this field. While observations are being made using one set of 400 fibers, the robot will be positioning a second set of fibers in a background field that can be moved in to replace the first when the telescope is moved to a new position. The fibers feed two spectrographs each with a 1024 square CCD detector. The software system being produced to control this involves Vaxes for overall control and data recording, UNIX workstations for fiber configuration calculations and on-line data reduction, and VME systems running VxWorks for real-time control of critical parts such as the positioner robot. The system has to be able to interact with the observatory's present data acquisition systems, which use the ADAM system. As yet, the real-time parts of ADAM have not been ported to Unix, and so we are having to produce a smaller-scale system that is similar but inherently distributed (which ADAM is not). We are using this system as a testbed for ideas that we hope may eventually influence an ADAM II system. The system we are producing is based on a message system that is designed to be able to handle inter-process and inter-processor messages of any length, efficiently, and without ever requiring a task to block (i.e., be unresponsive to 'cancel' messages, enquiry messages), other than when deliberately waiting for external input - all of which will be through such messages. The essential requirement is that a message 'send' operation should never be able to block. The messages will be hierarchical, self-defining, machine-independent data structures. This allows us to provide very simple monitoring of messages for diagnostic purposes, and allows general purpose interface programs to be written without needing to share precise byte by byte message format definitions. Programs in this system have interfaces defined simply in terms of named actions and their parameters. Real-time control programs are required to be able to handle a number of such actions concurrently; data reduction programs will normally only need to handle one action at a time ('process an image', 'display a spectrum', etc). Author (revised)

N94-22530*# Space Telescope Science Inst., Baltimore, MD.
INTEGRATING A LOCAL DATABASE INTO THE StarView DISTRIBUTED USER INTERFACE Abstract Only **c82**
D. P. Silberberg *In* NASA, Washington, Second Annual Conference on Astronomical Data Analysis Software and Systems. Abstracts 1992 p 99 (For primary document see N94-22438 05-89)
Avail: CASI HC A01/MF A02

A distributed user interface to the Space Telescope Data Archive and Distribution Service (DADS) known as StarView is being developed. The DADS architecture consists of the data archive as well as a relational database catalog describing the archive. StarView is a client/server system in which the user interface is the front-end client to the DADS catalog and

archive servers. Users query the DADS catalog from the StarView interface. Query commands are transmitted via a network and evaluated by the database. The results are returned via the network and are displayed on StarView forms. Based on the results, users decide which data sets to retrieve from the DADS archive. Archive requests are packaged by StarView and sent to DADS, which returns the requested data sets to the users. The advantages of distributed client/server user interfaces over traditional one-machine systems are well known. Since users run software on machines separate from the database, the overall client response time is much faster. Also, since the server is free to process only database requests, the database response time is much faster. Disadvantages inherent in this architecture are slow overall database access time due to the network delays, lack of a 'get previous row' command, and that refinements of a previously issued query must be submitted to the database server, even though the domain of values have already been returned by the previous query. This architecture also does not allow users to cross correlate DADS catalog data with other catalogs. Clearly, a distributed user interface would be more powerful if it overcame these disadvantages. A local database is being integrated into StarView to overcome these disadvantages. When a query is made through a StarView form, which is often composed of fields from multiple tables, it is translated to an SQL query and issued to the DADS catalog. At the same time, a local database table is created to contain the resulting rows of the query. The returned rows are displayed on the form as well as inserted into the local database table. Identical results are produced by reissuing the query to either the DADS catalog or to the local table. Relational databases do not provide a 'get previous row' function because of the inherent complexity of retrieving previous rows of multiple-table joins. However, since this function is easily implemented on a single table, StarView uses the local table to retrieve the previous row. Also, StarView issues subsequent query refinements to the local table instead of the DADS catalog, eliminating the network transmission overhead. Finally, other catalogs can be imported into the local database for cross correlation with local tables. Overall, it is believe that this is a more powerful architecture for distributed, database user interfaces. Author (revised)

N94-22531*# Academy of Sciences (USSR), Moscow. Inst. of Astronomy.

A NEW PROGRAMMING METAPHOR FOR IMAGE PROCESSING PROCEDURES Abstract Only **c61**

O. M. Smirnov and N. E. Piskunov (Helsinki Univ., Finland.) *In* NASA, Washington, Second Annual Conference on Astronomical Data Analysis Software and Systems. Abstracts 1992 p 100 (For primary document see N94-22438 05-89)

Avail: CASI HC A01/MF A02

Most image processing systems, besides an Application Program Interface (API) which lets users write their own image processing programs, also feature a higher level of programmability. Traditionally, this is a command or macro language, which can be used to build large procedures (scripts) out of simple programs or commands. This approach, a legacy of the teletypewriter has serious drawbacks. A command language is clumsy when (and if) it attempts to utilize the capabilities of a multitasking or multiprocessor environment, it is but adequate for real-time data acquisition and processing, it has a fairly steep learning curve, and the user interface is very inefficient,. especially when compared to a graphical user interface (GUI) that systems running under XII or Windows should otherwise be able to provide. II these difficulties stem from one basic problem: a command language is not a natural metaphor for an image processing procedure. A more natural metaphor - an image processing factory is described in detail. A factory is a set of programs (applications) that execute separate operations on images, connected by pipes that carry data (images and parameters) between them. The programs function concurrently, processing images as they arrive along pipes, and querying the user for whatever other input they need. From the user's point of view, programming (constructing) factories is a lot like playing with LEGO blocks - much more intuitive than writing scripts. Focus is on some of the difficulties of implementing factory support, most notably the design of an appropriate API. It also shows that factories retain all the functionality of a command language (including loops and conditional branches), while suffering from none of the drawbacks outlined above. Other benefits of factory programming include self-tuning factories and the process of encapsulation, which lets a factory take the shape of a standard application both from the system and the user's point of view, and thus be used as a component of other factories. A bare-bones prototype of factory programming was implemented under the PcIPS image processing system, and a complete version (on a multitasking platform) is under development. Author (revised)

N94-22532*# Academy of Sciences (USSR), Moscow. Inst. of Astronomy.

PCIPS 2.0: POWERFUL MULTIPROFILE IMAGE PROCESSING IMPLEMENTED ON PCs Abstract Only **c61**

O. M. Smirnov and N. E. Piskunov (Helsinki Univ., Finland.) *In* NASA, Washington, Second Annual Conference on Astronomical Data Analysis Software and Systems. Abstracts 1992 p 101 (For primary document see N94-22438 05-89)

Avail: CASI HC A01/MF A02

Over the years, the processing power of personal computers has steadily increased. Now, 386- and 486-based PC's are fast enough for many image processing applications, and inexpensive enough even for amateur astronomers. PCIPS is an image processing system based on these platforms that was designed to satisfy a broad range of data analysis needs, while requiring minimum hardware and providing maximum expandability. It will run (albeit at a slow pace) even on a 80286 with 640K memory, but will take full advantage of bigger memory and faster CPU's. Because the actual image processing is performed by external modules, the system can be easily upgraded by the user for all sorts of scientific data analysis. PCIPS supports large format ID and 2D images in any numeric type from 8-bit integer to 64-bit floating point. The images can be displayed, overlaid, printed and any part of the data examined via an intuitive graphical user interface that employs buttons, pop-up menus, and a mouse. PCIPS automatically converts images between different types and sizes to satisfy the requirements of various applications. PCIPS features an API that lets users develop custom applications in C or FORTRAN. While doing so, a programmer can concentrate on the actual data processing, because PCIPS assumes responsibility for accessing images and interacting with the user. This also ensures that all applications, even custom ones, have a consistent and user-friendly interface. The API is compatible with factory programming, a metaphor for constructing image processing procedures that will be implemented in future versions of the system. Several application packages were created under PCIPS. The basic package includes elementary arithmetics and statistics, geometric transformations and import/export in various formats (FITS, binary, ASCII, and GIF). The CCD processing package and the spectral analysis package were successfully used to reduce spectra from the Nordic Telescope at La Palma. A photometry package is also available, and other packages are being developed. A multitasking version of PCIPS that utilizes the factory programming concept is currently under development. This version will remain compatible (on the source code level) with existing application packages and custom applications. Author (revised)

N94-22533*# Academy of Sciences (USSR), Moscow. Inst. of Astronomy.

GUIDE STAR CATALOGUE DATA RETRIEVAL SOFTWARE 2 Abstract Only **c61**

O. M. Smirnov and O. Yu. Malkov *In* NASA, Washington, Second Annual Conference on Astronomical Data Analysis Software and Systems. Abstracts 1992 p 102 (For primary document see N94-22438 05-89)

Avail: CASI HC A01/MF A02

The Guide Star Catalog (GSC), being the largest astronomical catalog to date, is widely used by the astronomical community for all sorts of applications, such as statistical studies of certain sky regions, searches for counterparts to observational phenomena, and generation of finder charts. It's format (2 CD-ROM's) requires minimum hardware and is ideally suited for all sorts of conditions, especially observations. Unfortunately, the actual GSC data is not easily accessible. It takes the form of FITS tables, and the coordinates of the objects are given in one coordinate system (equinox 2000). The included reading software is rudimentary at best. Thus, even generation of a simple finder chart is not a trivial undertaking. To solve this problem, at least for PC users, GUIDARES was created. GUIDARES is a user-friendly program that lets you look directly at the data in the GSC, either as a graphical sky map or as a text table. GUIDARES can read a sampling of GSC data from a given sky region, store this sampling in a text file, and display a graphical map of the sampled region in

projected celestial coordinates (perfect for finder charts). GUIDARES supports rectangular and circular regions defined by coordinates in the equatorial, ecliptic (any equinox) or galactic systems. Author (revised)

N94-22534*# National Aeronautics and Space Administration. Goddard Space Flight Center, Greenbelt, MD.
UIT SUPPORT OBSERVATIONS ARCHIVE Abstract Only c82
Eric P. Smith, Paul Hintzen, and Kwang-Ping Cheng *In* NASA, Washington, Second Annual Conference on Astronomical Data Analysis Software and Systems. Abstracts 1992 p 103 (For primary document see N94-22438 05-89)
Avail: CASI HC A01/MF A02

We are in the process of archiving the approximately 1.2Tbytes of imaging data acquired in support of UIT observations. The UIT is one of three telescopes comprising the ASTRO spacecraft and is a 38-cm f/9 Ritchey-Chretien telescope with wavelength coverage 1200 A to 3000 A and a 40 arcminute diameter field-of-view at 4 min FWHM resolution. During the ASTRO shuttle mission, there were 65 different pointings (some with multiple targets) of the UIT and hence 65 fields. Our support data of these fields were obtained with the KPNO and CTIO 0.9m telescopes and several of the 2048x2048 CCD's. Our images are typically about 20 acrminutes on a side and contain the entire UV target except for nearby galaxies, for which mosaiced images were created. All good quality images in the broadband and narrow band filters for every target are being archived. Though all of the UIT targets were well studied astronomical objects, these frames are many of the first large field format images of them and, when combined with the soon to be released UV frames, provide a unique dataset. These data were already used to address a wide variety of astronomical questions. Vacuum ultraviolet (VUV) observations were used to study star formation in a sample of nearby galaxies, since integrated VUV - optical colors provide the most sensitive available measure of the formation rate of massive stars. The blue stages later in stellar evolution are also being studied. These data allow more accurate determination of the helium and metallicities of hothorzontal branch stars. These data are being prepared to release to the public in CD-ROM format through the National Space Science Data Center. Author (revised)

N94-22535*# Kitt Peak National Observatory, Tucson, AZ.
IRAF IN THE NINETIES Abstract Only c82
D. Tody *In* NASA, Washington, Second Annual Conference on Astronomical Data Analysis Software and Systems. Abstracts 1992 p 104 (For primary document see N94-22438 05-89)
Avail: CASI HC A01/MF A02

The Interactive Data Reduction and Analysis Facility (IRAF) data reduction and analysis system has been around since 1981. Today it is a mature system with hundreds of applications, and is supported on all the major platforms. Many institutions, projects, and individuals around the US and around the world have developed software for IRAF. Some of these packages are comparable in size to the IRAF core system itself. IRAF is both a data analysis system, and a programming environment. As a data analysis system it can be easily installed by a user at a remote site and immediately used to view and process data. As a programming environment IRAF contains a wealth of high and low level facilities for developing new applications for interactive and automated processing of astronomical or other data. As important as the applications programs and user interfaces are to the scientist using IRAF, the heart of the IRAF system is the programming environment. The programming environment determines to a large extent the types of applications which can be built within IRAF, what they will look like, and how they will interact with one another and with the user. While applications can be easily added to or removed from a software system, the programming environment must remain fairly stable, with carefully planned evolution and growth, over the lifetime of a system. The IRAF programming environment is the framework on which the rest of the IRAF system is built. The IRAF programming environment as it exists in 1992, and the work currently underway to enhance the environment are discussed. The structure of the programming environment as a class hierarchy is discussed, with emphasis on the work being done on the image data structures, graphics and image display interfaces, and user interfaces. The new technologies which we feel IRAF must deal with successfully over the coming years are discussed. Finally, a preview of what IRAF might look like to the user by the end of the decade is presented. Author (revised)

N94-22536*# Helsinki Univ. (Finland).
FACTOR ANALYSIS AS A TOOL FOR SPECTRAL LINE COMPONENT SEPARATION 21cm EMISSION IN THE DIRECTION OF L1780 Abstract Only c65
L. V. Toth, K. Mattila, L. Haikala, and L. G. Balazs (Konkoly Observatory, Budapest, Hungary.) *In* NASA, Washington, Second Annual Conference on Astronomical Data Analysis Software and Systems. Abstracts 1992 p 105 (For primary document see N94-22438 05-89)
Avail: CASI HC A01/MF A02

The spectra of the 21cm HI radiation from the direction of L1780, a small high-galactic latitude dark/molecular cloud, were analyzed by multivariate methods. Factor analysis was performed on HI (21cm) spectra in order to separate the different components responsible for the spectral features. The rotated, orthogonal factors explain the spectra as a sum of radiation from the background (an extended HI emission layer), and from the L1780 dark cloud. The coefficients of the cloud-indicator factors were used to locate the HI 'halo' of the molecular cloud. Our statistically derived 'background' and 'cloud' spectral profiles, as well as the spatial distribution of the HI halo emission distribution were compared to the results of a previous study which used conventional methods analyzing nearly the same data set. Author (revised)

N94-22537*# National Aeronautics and Space Administration. Goddard Space Flight Center, Greenbelt, MD.
RECOMMENDATIONS FOR A SERVICE FRAMEWORK TO ACCESS ASTRONOMICAL ARCHIVES Abstract Only c82
J. J. Travisano and J. Pollizzi (Space Telescope Science Inst., Baltimore, MD.) *In* NASA, Washington, Second Annual Conference on Astronomical Data Analysis Software and Systems. Abstracts 1992 p 106 (For primary document see N94-22438 05-89)
Avail: CASI HC A01/MF A02

There are a large number of astronomical archives and catalogs on-line for network access, with many different user interfaces and features. Some systems are moving towards distributed access, supplying users with client software for their home sites which connects to servers at the archive site. Many of the issues involved in defining a standard framework of services that archive/catalog suppliers can use to achieve a basic level of interoperability are described. Such a framework would simplify the development of client and server programs to access the wide variety of astronomical archive systems. The primary services that are supplied by current systems include: catalog browsing, dataset retrieval, name resolution, and data analysis. The following issues (and probably more) need to be considered in establishing a standard set of client/server interfaces and protocols: Archive Access - dataset retrieval, delivery, file formats, data browsing, analysis, etc.; Catalog Access - database management systems, query languages, data formats, synchronous/asynchronous mode of operation, etc.; Interoperability - transaction/message protocols, distributed processing mechanisms (DCE, ONC/SunRPC, etc), networking protocols, etc.; Security - user registration, authorization/authentication mechanisms, etc.; Service Directory - service registration, lookup, port/task mapping, parameters, etc.; Software - public vs proprietary, client/server software, standard interfaces to client/server functions, software distribution, operating system portability, data portability, etc. Several archive/catalog groups, notably the Astrophysics Data System (ADS), are already working in many of these areas. In the process of developing StarView, which is the user interface to the Space Telescope Data Archive and Distribution Service (ST-DADS), these issues and the work of others were analyzed. A framework of standard interfaces for accessing services on any archive system which would benefit archive user and supplier alike is proposed.
Author (revised)

N94-22538*# Institute for Space and Terrestrial Science, Concord (Ontario). Space Astrophysics Lab.
TOOLS FOR THE IDL WIDGET SET WITHIN THE X-WINDOWS ENVIRONMENT Abstract Only c61
B. Turgeon and A. Aston *In* NASA, Washington, Second Annual Conference on Astronomical Data Analysis Software and Systems. Abstracts 1992 p 107 (For primary document see N94-22438 05-89)
Avail: CASI HC A01/MF A02

New tools using the IDL widget set are presented. In particular, a utility allowing the easy creation and update of slide presentations, XSlideManager, is explained in detail and examples of its application are shown. In addition

to XSlideManager, other mini-utilities are discussed. These various pieces of software follow the philosophy of the X-Windows distribution system and are made available to anyone within the Internet network. Acquisition procedures through anonymous ftp are clearly explained. Author (revised)

N94-22539*# Kitt Peak National Observatory, Tucson, AZ.
THE SPECTRAL WORLD COORDINATE SYSTEMS IN IRAF/NOAO Abstract Only **c82**
F. Valdes *In* NASA, Washington, Second Annual Conference on Astronomical Data Analysis Software and Systems. Abstracts 1992 p 108 (For primary document see N94-22438 05-89)
Avail: CASI HC A01/MF A02

The world coordinate system (WCS) for dispersion calibrated spectra used in the IRAF/NOAO spectroscopy packages is described. In particular, the image header keywords which define the coordinates in an 'image' pixel array. These keywords appear both as part of the IRAF image structure and map directly to FITS format. The types of spectra include multidimensional images with spectral dispersion as one axis, one dimensional images, and a special 'multispec' format consisting of multiple, semi-independent, one dimensional spectra in two or three dimensional images. The types of coordinate systems include multidimensional linear coordinates with individual keywords and one dimensional linear and nonlinear coordinates for the 'multispec' images stored in IRAF WCS attributes. The nonlinear world coordinate systems include polynomial, spline, sampled table, and look-up table function representations. Author

N94-22540*# Kitt Peak National Observatory, Tucson, AZ.
SPECFOCUS: AN IRAF TASK FOR FOCUSING SPECTROGRAPHS Abstract Only **c65**
F. Valdes *In* NASA, Washington, Second Annual Conference on Astronomical Data Analysis Software and Systems. Abstracts 1992 p 109 (For primary document see N94-22438 05-89)
Avail: CASI HC A01/MF A02

An IRAF task for measuring the point-spread function (PSF) along the dispersion and wavelength shifts across the dispersion in two dimensional arc spectra is described. In typical use, a set of spectra are obtained with various spectrograph focusing and alignment adjustments and the PSF information and shift information is derived and presented in tabular and graphical forms. Within each image the spectra may be divided into a number of samples along the dispersion and across the dispersion to investigate variations at different points in the detector at fixed focus settings. With many spectra and many samples interpreting the measurements is challenging. The task provides an interactive graphical interface to display the measurements in a number of interesting ways. The underlying algorithm for measuring the PSF and shifts in the auto/cross-correlation of spectral are samples. Author

N94-22541*# National Aeronautics and Space Administration. Goddard Space Flight Center, Greenbelt, MD.
NASA'S ASTROPHYSICS ARCHIVES AT THE NATIONAL SPACE SCIENCE DATA CENTER Abstract Only **c82**
M. E. VanSteenberg *In* NASA, Washington, Second Annual Conference on Astronomical Data Analysis Software and Systems. Abstracts 1992 p 110 (For primary document see N94-22438 05-89)
Avail: CASI HC A01/MF A02

NASA maintains an archive facility for Astronomical Science data collected from NASA's missions at the National Space Science Data Center (NSSDC) at Goddard Space Flight Center. This archive was created to insure the science data collected by NASA would be preserved and useable in the future by the science community. Through 25 years of operation there are many lessons learned, from data collection procedures, archive preservation methods, and distribution to the community. This document presents some of these more important lessons, for example: KISS (Keep It Simple, Stupid) in system development. Also addressed are some of the myths of archiving, such as 'scientists always know everything about everything', or 'it cannot possibly be that hard, after all simple data tech's do it'. There are indeed good reasons that a proper archive capability is needed by the astronomical community, the important question is how to use the existing expertise as well as the new innovative ideas to do the best job archiving this valuable science data. Author

N94-22542*# Hughes STX, Inc., Greenbelt, MD.
DECONV-TOOL: AN IDL BASED DECONVOLUTION SOFTWARE PACKAGE Abstract only **c61**
F. Varosi and W. B. Landsman *In* NASA, Washington, Second Annual Conference on Astronomical Data Analysis Software and Systems. Abstracts 1992 p 111 (For primary document see N94-22438 05-89)
Avail: CASI HC A01/MF A02

There are a variety of algorithms for deconvolution of blurred images, each having its own criteria or statistic to be optimized in order to estimate the original image data. Using the Interactive Data Language (IDL), we have implemented the Maximum Likelihood, Maximum Entropy, Maximum Residual Likelihood, and sigma-CLEAN algorithms in a unified environment called DeConv—Tool. Most of the algorithms have as their goal the optimization of statistics such as standard deviation and mean of residuals. Shannon entropy, log-likelihood, and chi-square of the residual auto-correlation are computed by DeConv—Tool for the purpose of determining the performance and convergence of any particular method and comparisons between methods. DeConv—Tool allows interactive monitoring of the statistics and the deconvolved image during computation. The final results, and optionally, the intermediate results, are stored in a structure convenient for comparison between methods and review of the deconvolution computation. The routines comprising DeConv—Tool are available via anonymous FTP through the IDL Astronomy User's Library. Author

N94-22543*# National Aeronautics and Space Administration. Goddard Space Flight Center, Greenbelt, MD.
MOSAIC: SOFTWARE FOR CREATING MOSAICS FROM COLLECTIONS OF IMAGES Abstract Only **c61**
F. Varosi and D. Y. Gezari *In* NASA, Washington, Second Annual Conference on Astronomical Data Analysis Software and Systems. Abstracts 1992 p 112 (For primary document see N94-22438 05-89)
Avail: CASI HC A01/MF A02

We have developed a powerful, versatile image processing and analysis software package called MOSAIC, designed specifically for the manipulation of digital astronomical image data obtained with (but not limited to) two-dimensional array detectors. The software package is implemented using the Interactive Data Language (IDL), and incorporates new methods for processing, calibration, analysis, and visualization of astronomical image data, stressing effective methods for the creation of mosaic images from collections of individual exposures, while at the same time preserving the photometric integrity of the original data. Since IDL is available on many computers, the MOSAIC software runs on most UNIX and VAX workstations with the X-Windows or Sun View graphics interface. Author

N94-22544*# Hughes STX, Inc., Greenbelt, MD.
STELAR: AN EXPERIMENT IN THE ELECTRONIC DISTRIBUTION OF ASTRONOMICAL LITERATURE Abstract Only **c82**
A. Warnock, M. E. VanSteenburg (National Aeronautics and Space Administration. Goddard Space Flight Center, Greenbelt, MD.), L. E. Brotzman, J. Gass, and D. Kovalsky *In* NASA, Washington, Second Annual Conference on Astronomical Data Analysis Software and Systems. Abstracts 1992 p 113 (For primary document see N94-22438 05-89)
Avail: CASI HC A01/MF A02

STELAR (Study of Electronic Literature for Astronomical Research) is a Goddard-based project designed to test methods of delivering technical literature in machine readable form. To that end, we have scanned a five year span of the ApJ, ApJ Supp, AJ and PASP, and have obtained abstracts for eight leading academic journals from NASA/STI CASI, which also makes these abstracts available through the NASA RECON system. We have also obtained machine readable versions of some journal volumes from the publishers, although in many instances, the final typeset versions are no longer available. The fundamental data object for the STELAR database is the article, a collection of items associated with a scientific paper - abstract, scanned pages (in a variety of formats), figures, OCR extractions, forward and backward references, errata and versions of the paper in various formats (e.g., TEX, SGML, PostScript, DVI). Articles are uniquely referenced in the database by journal name, volume number and page number. The selection and delivery of articles is accomplished through the WAIS (Wide Area Information Server) client/server models requiring only an Internet connection. Modest modifications to the server code have made it capable of delivering the multiple data types required by STELAR.

WAIS is a platform independent and fully open multi-disciplinary delivery system, originally developed by Thinking Machines Corp. and made available free of charge. It is based on the ISO Z39.50 standard communications protocol. WAIS servers run under both UNIX and VMS. WAIS clients run on a wide variety of machines, from UNIX-based Xwindows systems to MS-DOS and macintosh microcomputers. The WAIS system includes full-test indexing and searching of documents, network interface and easy access to a variety of document viewers. ASCII versions of the CASI abstracts have been formatted for display and the full test of the abstracts has been indexed. The entire WAIS database of abstracts is now available for use by the astronomical community. Enhancements of the search and retrieval system are under investigation to include specialized searches (by reference, author or keyword, as opposed to full test searches), improved handling of word stems, improvements in relevancy criteria and other retrieval techniques, such as factor spaces. The STELAR project has been assisted by the full cooperation of the AAS, the ASP, the publishers of the academic journals, librarians from GSFC, NRAO and STScI, the Library of Congress, and the University of North Carolina at Chapel Hill. Author (revised)

N94-22545*# Science Research Council, Slough (England).
THE STARLINK SOFTWARE COLLECTION Abstract Only **c61**
R. F. Warren-Smith and P. T. Wallace *In* NASA, Washington, Second Annual Conference on Astronomical Data Analysis Software and Systems. Abstracts 1992 p 114 (For primary document see N94-22438 05-89)
Avail: CASI HC A01/MF A02

The UK's STARLINK project based at the Rutherford Appleton Laboratory develops and distributes software applicable to a wide range of problems in Astronomy; it covers most wavebands, caters for a variety of instrumentation, and ranges from programming tools and libraries through to large package of applications. The facilities available and gives details of how they may be obtained are summarized. Recent developments and other features of particular interest are highlighted. Author

N94-22546*# Jet Propulsion Lab., California Inst. of Tech., Pasadena.
SkICAT: A CATALOGING AND ANALYSIS TOOL FOR WIDE FIELD IMAGING SURVEYS Abstract Only **c82**
N. Weir (California Inst. of Tech., Pasadena.), U. M. Fayyad, S. G. Djorgovski (California Inst. of Tech., Pasadena.), and J. Roden *In* NASA, Washington, Second Annual Conference on Astronomical Data Analysis Software and Systems. Abstracts 1992 p 115 (For primary document see N94-22438 05-89)
Avail: CASI HC A01/MF A02

We describe an integrated system, SkICAT (Sky Image Cataloging and Analysis Tool), for the automated reduction and analysis of the Palomar Observatory-ST ScI Digitized Sky Survey. The Survey will consist of the complete digitization of the photographic Second Palomar Observatory Sky Survey (POSS-II) in three bands, comprising nearly three Terabytes of pixel data. SkICAT applies a combination of existing packages, including FOCAS for basic image detection and measurement and SAS for database management, as well as custom software, to the task of managing this wealth of data. One of the most novel aspects of the system is its method of object classification. Using state-of-theart machine learning classification techniques (GID3* and O-BTree), we have developed a powerful method for automatically distinguishing point sources from non-point sources and artifacts, achieving comparably accurate discrimination a full magnitude fainter than in previous Schmidt plate surveys. The learning algorithms produce decision trees for classification by examining instances of objects classified by eye on both plate and higher quality CCD data. The same techniques will be applied to perform higher-level object classification (e.g., of galaxy morphology) in the near future. Another key feature of the system is the facility to integrate the catalogs from multiple plates (and portions thereof) to construct a single catalog of uniform calibration and quality down to the faintest limits of the survey. SkICAT also provides a variety of data analysis and exploration tools for the scientific utilization of the resulting catalogs. We include initial results of applying this system to measure the counts and distribution of galaxies in two bands down to Bj is approximately 21 mag over an approximate 70 square degree multi-plate field from POSS-II. SkICAT is constructed in a modular and general fashion and should be readily adaptable to other large-scale imaging surveys. Author (revised)

N94-22547*# National Radio Astronomy Observatory, Green Bank, WV.
THE VLBA CORRELATOR: REAL-TIME IN THE DISTRIBUTED ERA Abstract Only **c82**
D. C. Wells *In* NASA, Washington, Second Annual Conference on Astronomical Data Analysis Software and Systems. Abstracts 1992 p 116 (For primary document see N94-22438 05-89)
Avail: CASI HC A01/MF A02

The correlator is the signal processing engine of the Very Long Baseline Array (VLBA). Radio signals are recorded on special wideband (128 Mb/s) digital recorders at the 10 telescopes, with sampling times controlled by hydrogen maser clocks. The magnetic tapes are shipped to the Array Operations Center in Socorro, New Mexico, where they are played back simultaneously into the correlator. Real-time software and firmware controls the playback drives to achieve synchronization, compute models of the wavefront delay, control the numerous modules of the correlator, and record FITS files of the fringe visibilities at the back-end of the correlator. In addition to the more than 3000 custom VLSI chips which handle the massive data flow of the signal processing, the correlator contains a total of more than 100 programmable computers, 8-, 16- and 32-bit CPUs. Code is downloaded into front-end CPU's dependent on operating mode. Low-level code is assembly language, high-level code is C running under a RT OS. We use VxWorks on Motorola MVME147 CPU's. Code development is on a complex of SPARC workstations connected to the RT CPU's by Ethernet. The overall management of the correlation process is dependent on a database management system. We use Ingres running on a Sparcstation-2. We transfer logging information from the database of the VLBA Monitor and Control System to our database using Ingres/NET. Job scripts are computed and are transferred to the real-time computers using NFS, and correlation job execution logs and status flow back by the route. Operator status and control displays use windows on workstations, interfaced to the real-time processes by network protocols. The extensive network protocol support provided by VxWorks is invaluable. The VLBA Correlator's dependence on network protocols is an example of the radical transformation of the real-time world over the past five years. Real-time is becoming more like conventional computing. Paradoxically, 'conventional' computing is also adopting practices from the real-time world: semaphores, shared memory, light-weight threads, and concurrency. This appears to be a convergence of thinking. Author

N94-22548*# Space Telescope Science Inst., Baltimore, MD.
StarView: THE OBJECT ORIENTED DESIGN OF THE ST DADS USER INTERFACE Abstract Only **c82**
J. D. Williams and J. A. Pollizzi *In* NASA, Washington, Second Annual Conference on Astronomical Data Analysis Software and Systems. Abstracts 1992 p 117 (For primary document see N94-22438 05-89)
Avail: CASI HC A01/MF A02

StarView is the user interface being developed for the Hubble Space Telescope Data Archive and Distribution Service (ST DADS). ST DADS is the data archive for HST observations and a relational database catalog describing the archived data. Users will use StarView to query the catalog and select appropriate datasets for study. StarView sends requests for archived datasets to ST DADS which processes the requests and returns the database to the user. StarView is designed to be a powerful and extensible user interface. Unique features include an internal relational database to navigate query results, a form definition language that will work with both CRT and X interfaces, a data definition language that will allow StarView to work with any relational database, and the ability to generate adhoc queries without requiring the user to understand the structure of the ST DADS catalog. Ultimately, StarView will allow the user to refine queries in the local database for improved performance and merge in data from external sources for correlation with other query results. The user will be able to create a query from single or multiple forms, merging the selected attributes into a single query. Arbitrary selection of attributes for querying is supported. The user will be able to select how query results are viewed. A standard form or table-row format may be used. Navigation capabilities are provided to aid the user in viewing query results. Object oriented analysis and design techniques were used in the design of StarView to support the mechanisms and concepts required to implement these features. One such mechanism is the Model-View-Controller (MVC) paradigm. The MVC allows the user to have multiple views of the underlying database, while providing a consistent mechanism for interaction regardless of the

view. This approach supports both CRT and X interfaces while providing a common mode of user interaction. Another powerful abstraction is the concept of a Query Model. This concept allows a single query to be built form a single or multiple forms before it is submitted to ST DADS. Supporting this concept is the adhoc query generator which allows the user to select and qualify an indeterminate number attributes from the database. The user does not need any knowledge of how the joins across various tables are to be resolved. The adhoc generator calculates the joins automatically and generates the correct SQL query. Author (revised)

N94-22549*# Kitt Peak National Observatory, Tucson, AZ.
TESTS OF A SIMPLE DATA MERGING ALGORITHM FOR THE GONG PROJECT Abstract Only **c61**
W. E. Williams and F. Hill *In* NASA, Washington, Second Annual Conference on Astronomical Data Analysis Software and Systems. Abstracts 1992 p 118 (For primary document see N94-22438 05-89)
Avail: CASI HC A01/MF A02

The GONG (Global Oscillation Network Group) project proposes to reduce the impact of diurnal variations on helioseismic measurements by making long-term observations of solar images from six sites placed around the globe. The sun will be observed nearly constantly for three years, resulting in the acquisition of l+ terabyte of image data. To use the solar network to maximum advantage, the images from the sites must be combined into a single time series to determine mode frequencies, amplitudes, and line widths. Initial versions of combined, i.e., merged, time series were made using a simple weighted average of data from different sites taken simultaneously. In order to accurately assess the impact of the data merge on the helioseismic measurements, a set of artificial solar disk images was made using a standard solar model and containing a well known set of oscillation modes and frequencies. This undegraded data set and data products computed from it were used to judge the relative merits of various data merging schemes. The artificial solar disk images were subjected to various instrumental and atmospheric degradations, dependent on site and time, in order to create a set of images simulating those likely to be taken at the site. The degraded artificial solar disk images for the six observing sites were combined in various ways to form merged time series of images and mode coefficients. Various forms of a weighted average were used, including an equally-weighted average, an average with weights dependent upon air mass and averages with weights dependent on various quality assurance parameters. Both the undegraded solar disk image time series and several time series made up of various combinations of the degraded solar disk images from the six sites were subjected to standard helioseismic measurement processing. This processing consisted of coordinate remapping, detrending, spherical harmonic transformation, computation of power series for the oscillation mode coefficients, and mode frequency identification. Visual and statistical evaluation of the merged data sets themselves and differences between the merged and undegraded data set shows good agreement between the two data sets. Some slight differences in image scale and registration appear between the undegraded data set and the various merged data sets. In the set of power series made from the mode coefficients of the merged data sets, some power leakage is observed into the background and into slightly lower l-value modes, especially at higher l-value mode frequencies. The results of the comparison of time series and mode oscillation frequencies of the undegraded data with those of the data merged using weighted averages indicate that, at least for p-mode solar oscillations, a weighted average of either the detrended remapped images or the mode coefficients gives good determination of the mode frequencies and adequate-to-good determination of the amplitudes and widths of the mode frequency lines. This conclusion is most advantageous to the analysis of the massive amounts of data to be received by the GONG network. Author (revised)

N94-22550*# Space Telescope Science Inst., Baltimore, MD.
REGISTERING AND RESAMPLING IMAGES IN STSDAS Abstract Only **c61**
R. L. Williamson, II *In* NASA, Washington, Second Annual Conference on Astronomical Data Analysis Software and Systems. Abstracts 1992 p 119 (For primary document see N94-22438 05-89)
Avail: CASI HC A01/MF A02

Registering different images can be difficult, especially if the images to be registered are images at different wavelengths, where features in one image may look entirely different or be absent from the second image. Using two new packages soon to be added to the STSDAS package, REGISTER and RESAMPLE, this job is done automatically. The REGISTER package allows the user to determine the amount of translation, rotation, and/or magnification needed to make two images, spectra, or time series congruent. The methods implemented to compute the registration parameters use: a set of the pixel coordinates of the same features identified in two files, or the FITS coordinate transformation parameters in the headers of two data files, or a single feature identified as the peak of a cross-correlation between two vectors. The coefficients describing the registration are defined by the equations (for a two-dimensional image): $x = a + bx + cy$, $y = d + ex + fy$, where (X,Y) are the pixel coordinates of a feature in the reference image, (x,y) are the pixel coordinates of a feature in the secondary image, and the computed coefficients are a, b, c, d, e, and f. Results may be produced by linking the output of REGISTER to RESAMPLE in a command language procedure. The output from REGISTER and the input to RESAMPLE consists of a matrix of coefficients (a through f above) fully specifying the registration. The RESAMPLE package resamples simple vector or image data for a given amount of translation, rotation (images only), and magnification, or reflection of the science data. Specific options included are: image rotation about the FITS reference pixel; scale changes, i.e. magnification or demagnification (for images, independently on both axes); simple translation; reflection (for images, about one or both axes); and resampling and registration to a reference data set. Output from the RESAMPLE task is the resampled image which may then be displayed and compared with the reference image. Author (revised)

N94-22551*# National Optical Astronomy Lab. Tucson, AZ. Image Reduction Analysis Facility.
FIRST MEM TASK IRMEO IN IRAF Abstract Only **c61**
Nailong Wu *In* NASA, Washington, Second Annual Conference on Astronomical Data Analysis Software and Systems. Abstracts 1992 p 120 (For primary document see N94-22438 05-89)
Avail: CASI HC A01/MF A02

The first task for image restoration using the Maximum Entropy Method (MEM) in IRAF, called IRMEO, is described. The underlining algorithm is the approximate Newton method for optimization. The basic input images and parameters for deconvolution are described in some detail. Results of preliminary tests, including the number of iterations, required CPU time on a variety of computers, and deconvolved images are reported and compared with those from other deconvolution methods. The merits and limitations of this task are pointed out. The possible development of better MEM tasks on the basis of IRMEO is also discussed. Author

N94-22552*# Academia Sinica, Beijing (China).
SOLAR FULL-DISK MAGNETIC FIELD IMAGE RECEIVING SYSTEM AND OBSERVATION SOFTWARE Abstract Only
Yan Xu, Ming Chang-Rong, and Xing Rong *In* NASA, Washington, Second Annual Conference on Astronomical Data Analysis Software and Systems. Abstracts 1992 p 121 (For primary document see N94-22438 05-89)
Avail: CASI HC A01/MF A02

The paper introduces terminal hardware system of 10 cm high resolution full-disk magnetic field telescope among solar multi-channel telescope produced by Beijing Astronomical Observatory, and its software procedure by using imaging processing as well real time data collecting. These data were processed by Sun Workstation 470/4, including doing some spectrum analysis, the system is unique in the world now. It uses a set of CCD (1320 pixels plus 1035 pixels) of high resolution image explosion, also it has a set of fast and high resolution (1024 pixel plus 1024 pixel) image processor. Moreover, we can obtain higher time and space resolution about solar full-disk magnetic field and velocity field. This will provide excellent means in observation and studies of full-disk solar large-scale magnetic field and velocity field. Author

N94-22553*# Space Telescope Science Inst., Baltimore, MD.
IRAF AND STSDAS UNDER THE NEW ALPHA ARCHITECTURE Abstract Only **c82**
N. R. Zarate *In* NASA, Washington, Second Annual Conference on Astronomical Data Analysis Software and Systems. Abstracts 1992 p 122 (For primary document see N94-22438 05-89)
Avail: CASI HC A01/MF A02

Digital's next generation RISC architecture, known as ALPHA, presents

many IRAF system portability questions and challenges to both site managers and end users. DEC promises to support the ULTRIX, VMS, and OSF/1 operating systems, which should allow IRAF to be ported to the new architecture at either the program executable level (using VEST), or at the source level, where IRAF can be tuned for greater performance. These notes highlight some of the details of porting IRAF to OpenVMS on the ALPHA architecture. Author

N94-22554*# Academia Sinica, Beijing (China).
MIYUN 232 MHz SURVEY 1: FIELDS CENTERED AT: ALPHA:00(H)41(M), DELTA:41 DEG 12 MIN AND ALPHA: 07(H)00(M),DELTA:35 DEG 00 MIN Abstract Only
Xiz-Hen Zhang, Yi-Jia Zheng, Hong-Sheng Chen, and Shou-Guan Wang *In* NASA, Washington, Second Annual Conference on Astronomical Data Analysis Software and Systems. Abstracts 1992 p 123 (For primary document see N94-22438 05-89)
Avail: CASI HC A01/MF A02

A new meter-wave survey of sky region north of declination +30 deg is carried out with the Miyun 232 MHz Synthesis Radio Telescope (MSRT). The instrument, observation, and method of data reduction are briefly described. A preliminary catalog, first of a series, for two 8 deg. x 8 deg. regions centered respectively at 35 deg. is presented. On the average 4 - 5 sources per square degree are recorded with position accuracy of 5 sec. / S(Jy). BGPW scale is adopted for the flux density calibration. The accuracy of flux determination is limited by background fluctuation which is about 30 mJy. The catalog is complete for sources with flux larger than 0.25 Jy. The total number of sources listed in the paper amounts to 687. Several extended sources, sources with convex spectra, and one GPS source were found. Spectra of sources with flux larger than 0.5 Jy were also given. Author

N94-22555*# Max-Planck-Inst. fuer Extraterrestrische Physik, Garching (Germany).
ROSAT DATA ANALYSIS WITH EXSAS Abstract Only
H. U. Zimmermann, T. Belloni, C. Izzo, P. Kahabka, and O. Schwentker *In* NASA, Washington, Second Annual Conference on Astronomical Data Analysis Software and Systems. Abstracts 1992 p 124 (For primary document see N94-22438 05-89)
Avail: CASI HC A01/MF A02

For the x-ray observatory ROSAT, data from survey and pointed mission phases taken with different focal plane instruments and according to a complex mission timeline have to be handled. Data analysis therefore puts high demands on appropriate software tools. With EXSAS - the Extended Scientific Analysis System developed with an effort of 20 man years by the German ROSAT Scientific Data Center - a comfortable system for the reduction of data from the ROSAT x-ray and XUV instruments has been made available. EXSAS comprises a large collection of application modules as typically required in analyzing data of this wavelength regime and runs as a specific context in the wide-spread ESO-MIDAS environment. EXSAS, completely written in FORTRAN 77, takes full advantage of all the standards used in MIDAS and therefore, reflects the same portability (different UNIX installations and VMS). If required, the FORTRAN code also enables users to adapt the software in an easy way to their specific needs. To maintain independence from the specifics of different operating systems also on the data input side, all ROSAT data redistributed in the widely accepted FITS format. Although EXSAS has been developed specifically for data analysis of the ROSAT instruments, its structural design is sufficiently general to serve equally well also data from other X-ray and XUV instruments. EXSAS analysis modules are grouped into 4 application packages dealing with Data Preparation and Instrument Correction, Spatial Analysis, Spectral Analysis and Timing Analysis. A special EXSAS header, read and updated by each application, maintains the general information transfer on the origin, the history and the parameter space of the data stored in tables and images. About 100 genuine commands (most of which offer several additional options) allow to interactively explore the functionality of the system. Up to now 40 institutes all over the world have requested the EXSAS software. Maintenance and regular updates of the software and the comprehensive documentation are provided by the ROSAT Scientific Data Center at Garching. Author

N94-20880*# National Aeronautics and Space Administration. Lyndon B. Johnson Space Center, Houston, TX.
CERN-DERIVED ANALYSIS OF LUNAR RADIATION BACKGROUNDS Abstract Only
Thomas L. Wilson and Robert Svoboda (Louisiana State Univ., Baton Rouge.) *In* Lunar and Planetary Inst., Twenty-Fourth Lunar and Planetary Science Conference. Part 3: N-Z 1993 p 1529-1530 (For primary document see N94-20636 05-91)
Avail: CASI HC A01/MF A06

N94-22630# Max-Planck-Inst. fuer Extraterrestrische Physik, Garching (Germany).
RESULTS FROM ROSAT
Joachim Truemper *In* ESA, Fourth International Toki Conference on Plasma Physics and Controlled Nuclear Fusion May 1993 p 55-6 (For primary document see N94-22624 05-75)
Copyright Avail: CASI HC A03/MF A03

N94-22639# Tokyo Univ., Sagamihara (Japan). Inst. of Space and Astronautical Science.
ACCRETION DISKS IN BRIGHT X RAY BINARIES
Hajime Inoue *In* ESA, Fourth International Toki Conference on Plasma Physics and Controlled Nuclear Fusion May 1993 p 125-130 (For primary document see N94-22624 05-75)
Copyright Avail: CASI HC A02/MF A03

N94-22642# Max-Planck-Inst. fuer Extraterrestrische Physik, Garching (Germany).
COMPTON GAMMA RAY OBSERVATORY HIGHLIGHTS OF THE SKY SURVEY
Helmut Steinle *In* ESA, Fourth International Toki Conference on Plasma Physics and Controlled Nuclear Fusion May 1993 p 145-150 (For primary document see N94-22624 05-75)
Copyright Avail: CASI HC A02/MF A03

90 ASTROPHYSICS

Includes cosmology; celestial mechanics; space plasmas; and interstellar and interplanetary gases and dust.

For related information see also *75 Plasma Physics*.

N94-20337*# Pennsylvania State Univ., University Park. Dept. of Astronomy and Astrophysics.
PRE-MAIN SEQUENCE STARS IN THE CHAMAELEON CLOUD AND PRE-MAIN SEQUENCE STARS IN THE RHO OPHIUCHI CLOUD CORE Final Report
Eric D. Feigelson 15 Dec. 1993 3 p Submitted for publication
(Grant NAG5-1678)
(NASA-CR-194713; NAS 1.26:194713) Avail: CASI HC A01/MF A01

This grant funds two closely related studies of young stars under the ROSAT Guest Observer Program. A major paper on ROSAT discovery of X-ray emitting young stars in the Chamaeleon star forming cloud was published in the Astrophysical Journal. Two soft X-ray images of the Chamaeleon I star forming cloud obtained with the ROSAT Position Sensitive Proportional Counter are presented. Seventy reliable, and 19 possible additional, X-ray sources are found. Most are confirmed to be new weak T Tauri stars. A study of X-ray emitting stars in a deep ROSAT image of the rho Ophiuchi star forming cloud cores has been completed, and is being submitted for publication in the Astrophysical Journal. A list of X-ray sources, fluxes, signal-to-noise ratios and boresight-corrected positions has been compiled, and optical identification down to 22(exp m) are obtained. Of the 55 reliable ROSAT sources, virtually all are associated with embedded infrared-detected T Tauri stars. T Tauri X-rays may provide a crucial link in the photoionization self-regulation of star formation in the galaxy.
Derived from text

N94-20892*# National Inst. of Polar Research, Tokyo (Japan). Dept. of Antarctic Meteorites.
REGOLITH BRECCIA CONSISTING OF H AND LL CHONDRITE MIXTURE Abstract Only
Keizo Yanai and Hideyasu Kojima *In* Lunar and Planetary Inst.,

Twenty-Fourth Lunar and Planetary Science Conference. Part 3: N-Z 1993 p 1553-1554 (For primary document see N94-20636 05-91)
Avail: CASI HC A01/MF A06

Antarctic meteorite Yamato-8424 (Y-8424) is a regolith breccia that is homogenized mixture of H and LL chondrite components. The breccia consists mainly of a fine-grained material with mineral fragments of olivine, pyroxene, and Fe-Ni metal with traces of plagioclase. Author

N94-21138 Max-Planck-Inst. fuer Extraterrestrische Physik, Garching (Germany).
SPATIAL DISTRIBUTION OF NEAR INFRARED LINE RADIATION IN GALACTIC NUCLEI MEASURED WITH FABRY-PEROT SPECTROMETER FAST Thesis - Ludwig-Maximilians-Univ. [DIE RAEUMLICHE VERTEILUNG VON NAHINFRAROTLINIENSTRAHLUNG IN GALAKTISCHEN KERNEN GEMESSEN MIT DEM ABBILDENDEN FABRY-PEROT-SPEKTROMETER FAST]
Valentin Rotaciuc Jun. 1992 119 p In GERMAN Limited Reproducibility: More than 20% of this document may be affected by microfiche quality
(MPE-239; ETN-93-93680) Copyright Avail: CASI HC A06

A Fabri-Perot spectrometer for examination of astronomical objects with high spatial and spectral resolution is developed. Wide-band and circular variable filter were used for pre-decomposition. The measuring instrument was designed to be compatible with telescopes of varied aperture numbers and was equipped with a modular computer and cards for quick data transfer. The sensitivity was improved for optimization of surface detector representation methods. Results were obtained for the Seyfert-2 galaxy NGC 1068 and the Milky Way center, which supplied images of galactic nuclei in emission lines of varied atomic species. Seyfert-2 galaxy was recorded in Br-gamma recombination line of atomic hydrogen and of a quadrupole transfer of molecular hydrogen, whose emission has a cloud structure morphology. It can be concluded that galactic circumnuclear materials is aggregated in molecular clouds. A dozen compact sources were discovered in the Milky Way with broad helium emission lines. It can be deduced that luminosity is produced in galactic center through stars. ESA

N94-21578*# Max-Planck-Inst. fuer Physik und Astrophysik, Garching (Germany). Inst. fuer Astrophysik.
RADIATION DRIVEN WINDS OF HOT STARS: SOME REMARKS ON STATIONARY MODELS AND SPECTRUM SYNTHESIS IN TIME-DEPENDENT SIMULATIONS
Joachim Puls (Technische Univ., Munich, Germany.), Adalbert W. A. Pauldrach (Technische Univ., Munich, Germany.), Rolf-Peter Kudritzki (Technische Univ., Munich, Germany.), Stanley P. Owocki (Delaware Univ., Newark.), and Francisco Najarro (Technische Univ., Munich, Germany.) Dec. 1992 33 p Submitted for publication
(Grants NAGW-2624; NAG5-1657; DFG-Pu-117/1-1; DFG-Pa-477/1-1; DFG-SPA-112/1/90)
(NASA-CR-194691; NAS 1.26:194692; MPA-707; ETN-93-94914)
Copyright Avail: CASI HC A03/MF A01

The basic concept of some stationary models and the way in which these models are used for and in how far they influence the determination of stellar and wind parameters of massive hot stars are discussed. However, as follows directly from the assumption of stationarity, these models are inherently incapable of describing a number of additional observational features, which immediately show that the nonstationary aspects of the wind must be of significant importance. A number of these features are discussed: the soft X-ray emission; the discrete absorption components; the temporal variability of the wind lines, where the blue edges are varying most significantly while the red emission part remains relatively constant; the electron scattering wings of recombination lines in Wolf-Rayet stars; the black troughs in saturated P-Cygni profiles; the variability of optical lines; and the nonthermal radio emission observed in massive stars. The basic picture resulting from the present dynamical models is discussed. ESA

N94-21618# Lawrence Livermore National Lab., CA.
NEW PRODUCTION MECHANISMS FOR UNSTABLE NUCLEI IN STARS, SUPERNOVAE, AND THE BIG BANG
G. J. Mathews, M. B. Aufderheide, J. R. Wilson, G. M. Fuller (California Univ., San Diego, La Jolla.), K. Jedamzik (California Univ., San Diego, La Jolla.), and B. S. Meyer (Clemson Univ., SC.) May 1993 19 p Presented at the 3rd International Conference on Radioactive Nuclear Beams, East Lansing, MI, 24-27 May 1993
(Contract W-7405-eng-48)
(DE93-018627; UCRL-JC-114077; CONF-930534-4) Avail: CASI HC A03/MF A01

We overview three recently proposed sites for the formation of unstable nuclei in astrophysics. These include the development a new Urca-like process in the late stages of the evolution of massive stars; the development of unstable elements in the hot neutrino energized wind from the nascent neutron star in supernovae or gamma-ray burst models; and the formation and evolution of baryon inhomogeneities produced by cosmological phase transitions and expanded by neutrino induced heating during the big bang. In each of these environments the importance of unstable nuclei will be discussed and some useful measurements proposed. DOE

N94-22426 Calgary Univ. (Alberta). Dept. of Physics and Astronomy.
CIRCUMSTELLAR ENVIRONMENTS OF Be STARS AT INFRA-RED AND RADIO WAVELENGTHS Ph.D. Thesis
Sean Melbourne Dougherty Feb. 1993 107 p
(ISBN-0-315-83135-9; CTN-94-60937) Copyright Avail: Micromedia Ltd., Technical Information Centre, 240 Catherine Street, Suite 305, Ottawa, Ontario, K2P 2G8, Canada HC/MF

Circumstellar environments of Be stars are investigated via analysis of observations at near-infrared (IR) and radio wavelengths. Near-IR and quasi-simultaneous visual observations of Be and normal B-type stars were obtained. Intrinsic color relationships for B stars were derived. Excess IR emission is present for about 60% of Be stars. The excess color-color relationships are consistent with circumstellar envelopes of radius greater than 10 stellar radii and power law radial density distributions. The percentage of variable Be stars increases with wavelength, with 18% of the sample studied being identified as variables at K band. Variations are attributed to density variations in the circumstellar plasma. New multi-wavelength radio observations of six Be stars are presented, three of which appear to have variable radio emission. Emission from the Be star Psi Persei is resolved at 15 GHz. The radio emitting region has a major axis dimension of 111 milli arc seconds (mas) and the minor axis has an upper limit of 68 mas. The angular size of the major axis corresponds to a radius of 1,850 solar radii (SR). Using a radiative transfer disc model, it is shown that a truncated circumstellar disc cannot account for both the IR to radio spectrum of the excess emission and the observed radius of 1,850 SR. Author (CISTI)

N94-22592 University of Western Ontario, London. Dept. of Astronomy.
WHAT IS NORMAL AMONG THE A-TYPE STARS? Ph.D. Thesis
Grant Michael Hill Sep. 1993 156 p
(ISBN-0-315-83947-3; CTN-94-60962) Copyright Avail: Micromedia Ltd., Technical Information Centre, 240 Catherine Street, Suite 305, Ottawa, Ontario, K2P 2G8, Canada HC/MF

The abundances of 15 elements have been determined for 16 early A-type stars. Abundances were also determined for Sirius, a hot Am star, and lambda Boo, the prototypical member of its class. Spectrum synthesis was used to determine the abundances; it is shown to be reliable and capable of application to even broader lined stars. Despite the fact that 14 of the stars are classified as normal, they exhibit a considerable range of abundances. The abundances of most elements scale, at least roughly, with those of Fe, which ranges over more than 0.7 dex among supposedly normal stars. Carbon is probably anti-correlated with Fe while Ca exhibits a more complex behavior. Helium seems constant and slightly under-abundant with respect to the sun. Elements heavier than Fe generally show an enhancement with respect to the sun. Correlations of the abundances with various stellar parameters are studied. For some elements, such as Fe, the average abundance is roughly solar; for others, such as the heavy elements, it is not. The range of abundances exhibited by most elements is wide enough that there seems to be a continuous distribution of abundances from those of the Am stars through the normal stars. The lambda Boo stars may be the low abundance tail of this distribution. Author (CISTI)

N94-22593 University of Western Ontario, London. Dept. of Astronomy.
THE FORMATION OF MASSIVE STARS: A 30 Mo CASE STUDY Ph.D. Thesis
Martin Beech Jul. 1993 148 p

(ISBN-0-315-83944-9; CTN-94-60963) Copyright Avail: Micromedia Ltd., Technical Information Centre, 240 Catherine Street, Suite 305, Ottawa, Ontario, K2P 2G8, Canada HC/MF

Pre-main sequence evolutionary tracks have been calculated for a series of massive star models under Hayashi's canonical theory and Stahler's mass accretion paradigm. Canonical pre-main sequence tracks for 15-60 solar mass (SM) stars were calculated with both Cox-Stewart (CS) and Rogers-Iglesias (RI) opacities. The differences between the two sequences were systematically explored. The final pre-main sequence phase of the canonical evolution and the onset of central hydrogen burning is discussed. Arrival of a massive star on the zero age main sequence (ZAMS) is defined and the characteristics of the upper ZAMS models are determined. A systematic investigation of pre-main sequence tracks revealed a boundary in the central density versus central temperature plane, beyond which the models always had a central convective core. In a study of a sequence of accretion models, beyond about 17 SM their characteristics became increasingly more luminous and cooler compared to the same-mass canonical ZAMS models. In the main sequence phase, the accretion build model evolved at essentially the same effective temperature as the canonical model but at a lower luminosity. An upper stellar birthline is proposed, defining a boundary in the Hertzsprung Russell diagram beyond which massive stars first become optically visible. Author (CISTI)

N94-20639*# Kobe Univ. (Japan). Dept. of Earth Sciences.
REE AND OTHER TRACE LITHOPHILES IN MAC88177, LEW88280 AND LEW88763 Abstract Only
N. Nakamura and N. Morikawa *In* Lunar and Planetary Inst., Twenty-Fourth Lunar and Planetary Science Conference. Part 3: N-Z 1993 p 1047-1048 (For primary document see N94-20636 05-91)
Avail: CASI HC A01/MF A06

N94-20643*# Academy of Sciences (USSR), Moscow. Inst. of Geochemistry and Analytical Chemistry.
IGNEOUS ROCK FROM SEVERNYI KOLCHIM (H3) CHONDRITE: NEBULAR ORIGIN Abstract Only
M. A. Nazarov, F. Brandstaetter (Naturhistorisches Museum, Vienna, Austria.), and G. Kurat (Naturhistorisches Museum, Vienna, Austria.) *In* Lunar and Planetary Inst., Twenty-Fourth Lunar and Planetary Science Conference. Part 3: N-Z 1993 p 1055-1056 (For primary document see N94-20636 05-91)
Avail: CASI HC A01/MF A06

N94-20647*# Academy of Sciences (USSR), Moscow. Inst. for Dynamics of Geospheres.
ON MAGNETODYNAMIC EFFECTS INITIATED BY A HIGH-SPEED IMPACT OF A LARGE COSMIC BODY UPON THE EARTH'S SURFACE Abstract Only
I. V. Nemchinov, P. E. Alexandrov, V. I. Artemiev, V. I. Bergelson, and V. A. Rybakov *In* Lunar and Planetary Inst., Twenty-Fourth Lunar and Planetary Science Conference. Part 3: N-Z 1993 p 1063-1064 (For primary document see N94-20636 05-91)
Avail: CASI HC A01/MF A06

N94-20648*# Academy of Sciences (USSR), Moscow. Inst. for Dynamics of Geospheres.
DETERMINATION OF COSMIC BODIES SIZE-VELOCITY DISTRIBUTION BY OBSERVATION OF CURRENT IMPACTS ON MARS Abstract Only
I. V. Nemchinov, A. A. Perelomova, and V. V. Shuvalov *In* Lunar and Planetary Inst., Twenty-Fourth Lunar and Planetary Science Conference. Part 3: N-Z 1993 p 1065-1066 (For primary document see N94-20636 05-91)
Avail: CASI HC A01/MF A06

N94-20653*# Minnesota Univ., Minneapolis. School of Physics and Astronomy.
HELIUM IN INTERPLANETARY DUST PARTICLES Abstract Only
A. O. Nier and D. J. Schlutter *In* Lunar and Planetary Inst., Twenty-Fourth Lunar and Planetary Science Conference. Part 3: N-Z 1993 p 1075-1076 (For primary document see N94-20636 05-91)
Avail: CASI HC A01/MF A06

N94-20658*# California Univ., Berkeley. Space Sciences Lab.
EXPOSURE AGES OF CARBONACEOUS CHONDRITES, 1
K. Nishiizumi, J. R. Arnold (California Univ., San Diego, La Jolla.), M. W. Caffee (Lawrence Livermore National Lab., CA.), R. C. Finkel (Lawrence Livermore National Lab., CA.), J. R. Southon (Lawrence Livermore National Lab., CA.), H. Nagai (Nihon Univ., Tokyo, Japan.), M. Honda (Nihon Univ., Tokyo, Japan.), P. Sharma (Rochester Univ., NY.), M. Imamura (Tokyo Univ., Japan.), and K. Kobayashi (Tokyo Univ., Japan.) *In* Lunar and Planetary Inst., Twenty-Fourth Lunar and Planetary Science Conference. Part 3: N-Z 1993 p 1085-1086 (For primary document see N94-20636 05-91)
Avail: CASI HC A01/MF A06

N94-20659*# Washington Univ., Saint Louis, MO. Center for the Space Sciences and Physics Dept.
IDENTIFICATION OF AN INTERSTELLAR OXIDE GRAIN FROM THE MURCHISON METEORITE BY ION IMAGING Abstract Only
L. R. Nittler, R. M. Walker, E. Zinner, P. Hoppe (Bern Univ., Switzerland.), and R. S. Lewis (Chicago Univ., IL.) *In* Lunar and Planetary Inst., Twenty-Fourth Lunar and Planetary Science Conference. Part 3: N-Z 1993 p 1087-1088 (For primary document see N94-20636 05-91)
Avail: CASI HC A01/MF A06

N94-20678*# Office National d'Etudes et de Recherches Aeronautiques, Paris (France).
C/O ATOMIC RATIOS IN MICROMETER-SIZE CRUSHED GRAINS FROM ANTARCTIC MICROMETEORITES AND TWO CARBONACEOUS METEORITES Abstract Only
M. Perreau, C. Engrand (Centre de Spectrometrie Nucleaire et de Spectrometrie de Masse, Orsay, France.), Michel Maurette (Centre de Spectrometrie Nucleaire et de Spectrometrie de Masse, Orsay, France.), G. Kurat (Naturhistorisches Museum, Vienna, Austria.), and Th. Presper (Naturhistorisches Museum, Vienna, Austria.) *In* Lunar and Planetary Inst., Twenty-Fourth Lunar and Planetary Science Conference. Part 3: N-Z 1993 p 1125-1126 (For primary document see N94-20636 05-91)
Avail: CASI HC A01/MF A06

N94-20680*# Harvard-Smithsonian Center for Astrophysics, Cambridge, MA.
OPAQUE-RICH LITHOLOGY IN THE DIVNOE ACHONDRITE: PETROLOGY AND ORIGIN Abstract Only
M. I. Petaev *In* Lunar and Planetary Inst., Twenty-Fourth Lunar and Planetary Science Conference. Part 3: N-Z 1993 p 1129-1130 (For primary document see N94-20636 05-91)
Avail: CASI HC A01/MF A06

N94-20681*# Harvard-Smithsonian Center for Astrophysics, Cambridge, MA.
CHAUNSKIJ: THE MOST HIGHLY METAMORPHOSED, SHOCK-MODIFIED AND METAL-RICH MESOSIDERITE Abstract Only
M. I. Petaev, R. S. Clarke, Jr. (Smithsonian Institution, Washington, DC.), E. J. Olsen (Chicago Univ., IL.), E. Jarosewich (Smithsonian Institution, Washington, DC.), A. M. Davis (Chicago Univ., IL.), I. M. Steele (Chicago Univ., IL.), M. E. Lipschutz (Purdue Univ., West Lafayette, IN.), M.-S. Wang (Purdue Univ., West Lafayette, IN.), R. N. Clayton (Chicago Univ., IL.), and T. K. Mayeda (Chicago Univ., IL.) et al *In* Lunar and Planetary Inst., Twenty-Fourth Lunar and Planetary Science Conference. Part 3: N-Z 1993 p 1131-1132 (For primary document see N94-20636 05-91)
Avail: CASI HC A01/MF A06

N94-20694*# Jet Propulsion Lab., California Inst. of Tech., Pasadena.
GRAVITY INVESTIGATION OF THE MANSON IMPACT STRUCTURE, IOWA Abstract Only
J. B. Plescia *In* Lunar and Planetary Inst., Twenty-Fourth Lunar and Planetary Science Conference. Part 3: N-Z 1993 p 1157-1158 (For primary document see N94-20636 05-91)
Avail: CASI HC A01/MF A06

N94-20704*# Naturhistorisches Museum, Vienna (Austria).
ELEMENTAL DEPLETIONS IN ANTARCTIC MICROMETEORITES AND ARCTIC COSMIC SPHERULES: COMPARISON AND RELATIONSHIPS Abstract Only

T. Presper, G. Kurat, C. Koeberl (Wien Univ., Austria.), H. Palme (Max-Planck-Inst. fuer Chemie, Mainz, Germany.), and Michel Maurette (Centre de Spectrometrie Nucleaire et de Spectrometrie de Masse, Orsay, France.) *In* Lunar and Planetary Inst., Twenty-Fourth Lunar and Planetary Science Conference. Part 3: N-Z 1993 p 1177-1178 (For primary document see N94-20636 05-91)
Avail: CASI HC A01/MF A06

N94-20708*# American Museum of Natural History, New York, NY. Dept. of Mineral Science.
OXYGEN ISOTOPIC RELATIONSHIPS BETWEEN THE LEW85332 CARBONACEOUS CHONDRITE AND CR CHONDRITES Abstract Only
M. Prinz, M. K. Weisberg, R. N. Clayton (Chicago Univ., IL), and T. K. Mayeda (Chicago Univ., IL.) *In* Lunar and Planetary Inst., Twenty-Fourth Lunar and Planetary Science Conference. Part 3: N-Z 1993 p 1185-1186 (For primary document see N94-20636 05-91)
Avail: CASI HC A01/MF A06

N94-20715*# New Mexico Univ., Albuquerque. Dept. of Earth and Planetary Sciences.
MICROMETEORITE DYNAMIC PYROMETAMORPHISM: NONSTOICHIOMETRIC CLINOENSTATITE (CLEN) Abstract Only
Frans J. M. Rietmeijer *In* Lunar and Planetary Inst., Twenty-Fourth Lunar and Planetary Science Conference. Part 3: N-Z 1993 p 1199-1200 (For primary document see N94-20636 05-91)
Avail: CASI HC A01/MF A06

N94-20716*# New Mexico Univ., Albuquerque. Dept. of Earth and Planetary Sciences.
MICROMETEORITE DYNAMIC PYROMETAMORPHISM: OBSERVATION OF A THERMAL GRADIENT IN IRON-NICKEL SULFIDE Abstract Only
Frans J. M. Rietmeijer *In* Lunar and Planetary Inst., Twenty-Fourth Lunar and Planetary Science Conference. Part 3: N-Z 1993 p 1201-1202 (For primary document see N94-20636 05-91)
Avail: CASI HC A01/MF A06

N94-20721*# Geological Survey, Flagstaff, AZ.
THE MANSON IMPACT CRATER: ESTIMATION OF THE ENERGY OF FORMATION, POSSIBLE SIZE OF THE IMPACTING ASTEROID OR COMET, AND EJECTA VOLUME AND MASS Abstract Only
D. J. Roddy, E. M. Shoemaker, and R. R. Anderson (Geological Survey, Iowa City, IA.) *In* Lunar and Planetary Inst., Twenty-Fourth Lunar and Planetary Science Conference. Part 3: N-Z 1993 p 1211-1212 (For primary document see N94-20636 05-91)
Avail: CASI HC A01/MF A06

N94-20726*# Open Univ., Milton (England). Dept. of Geological Sciences.
A CARBON AND NITROGEN ISOTOPE STUDY OF CARBONACEOUS VEIN MATERIAL IN UREILITE METEORITES Abstract Only
S. S. Russell, J. W. Arden, I. A. Franchi, and C. T. Pillinger *In* Lunar and Planetary Inst., Twenty-Fourth Lunar and Planetary Science Conference. Part 3: N-Z 1993 p 1221-1222 (For primary document see N94-20636 05-91)
Avail: CASI HC A01/MF A06

N94-20729*# Planetary Science Inst., Tucson, AZ.
ASTEROID COLLISIONS: TARGET SIZE EFFECTS AND RESULTANT VELOCITY DISTRIBUTIONS Abstract Only
Eileen V. Ryan *In* Lunar and Planetary Inst., Twenty-Fourth Lunar and Planetary Science Conference. Part 3: N-Z 1993 p 1227-1228 (For primary document see N94-20636 05-91)
Avail: CASI HC A01/MF A06

N94-20735*# Moscow State Univ. (Russia).
PRELIMINARY ESTIMATION OF TAGAMITE COOLING CONDITIONS (PUCHEZH-KATUNKI ASTROBLEME, RUSSIA) Abstract Only
L. Sazonova, V. Feldman, and N. Korotaeva *In* Lunar and Planetary Inst., Twenty-Fourth Lunar and Planetary Science Conference. Part 3: N-Z 1993 p 1239-1240 (For primary document see N94-20636 05-91)
Avail: CASI HC A01/MF A06

N94-20741*# California Univ., Los Angeles. Inst. of Geophysics and Planetary Physics.
IRIDIUM IN SEDIMENTS CONTAINING LARGE ABUNDANCES OF AUSTRALASIAN MICROTEKTITES FROM DSDP HOLE 758B IN THE EASTERN INDIAN OCEAN AND FROM DSDP HOLE 769A IN THE SULU SEA Abstract Only
Gerhard Schmidt, Lei Zhou, and John T. Wasson *In* Lunar and Planetary Inst., Twenty-Fourth Lunar and Planetary Science Conference. Part 3: N-Z 1993 p 1251 (For primary document see N94-20636 05-91)
(Grant NSF EAR-91-19065)
Avail: CASI HC A01/MF A06

N94-20746*# Maryland Univ., College Park. Dept. of Astronomy.
C2, CN AND DUST IN COMET WILSON (1987VII) Abstract Only
R. Schulz, M. F. AHearn, P. V. Birch (Perth Observatory, Australia.), C. Bowers (Perth Observatory, Australia.), M. Kempin (Perth Observatory, Australia.), and R. Martin (Perth Observatory, Australia.) *In* Lunar and Planetary Inst., Twenty-Fourth Lunar and Planetary Science Conference. Part 3: N-Z 1993 p 1261-1262 (For primary document see N94-20636 05-91)
Avail: CASI HC A01/MF A06

N94-20749*# Hawaii Univ., Honolulu. Dept. of Geology and Geophysics.
POST-METAMORPHIC BRECCIATION IN TYPE 3 ORDINARY CHONDRITES Abstract Only
E. R. D. Scott, T. J. McCoy, and K. Keil *In* Lunar and Planetary Inst., Twenty-Fourth Lunar and Planetary Science Conference. Part 3: N-Z 1993 p 1267-1268 (For primary document see N94-20636 05-91)
Avail: CASI HC A01/MF A06

N94-20750*# Arkansas Univ., Fayetteville. Cosmochemistry Group.
CATHODOLUMINESCENCE OBSERVATIONS OF IN SITU AQUEOUS DESTRUCTION OF CHONDRULES IN THE MURCHISON CM CHONDRITE Abstract Only
Derek W. G. Sears, Paul H. Benoit, Lu Jie, and Andrew S. R. Sears *In* Lunar and Planetary Inst., Twenty-Fourth Lunar and Planetary Science Conference. Part 3: N-Z 1993 p 1269-1270 (For primary document see N94-20636 05-91)
Avail: CASI HC A01/MF A06

N94-20752*# Academy of Sciences (USSR), Moscow. Inst. of Geochemistry and Analytical Chemistry.
LUNAR BASALT METEORITE EET 87521: PETROLOGY OF THE CLAST POPULATION Abstract Only
A. S. Semenova, M. A. Nazarov, and N. N. Kononkova *In* Lunar and Planetary Inst., Twenty-Fourth Lunar and Planetary Science Conference. Part 3: N-Z 1993 p 1273-1274 (For primary document see N94-20636 05-91)
Avail: CASI HC A01/MF A06

N94-20756*# Centre d'Etudes de Limeil-Valenton, Villeneuve Saint-Georges (France). Commissariat a L'Energie Atomique.
MOLECULAR EQUILIBRIA AND CONDENSATION SEQUENCES IN CARBON RICH GASES Abstract Only
C. M. Sharp and G. J. Wasserburg (California Inst. of Tech., Pasadena.) *In* Lunar and Planetary Inst., Twenty-Fourth Lunar and Planetary Science Conference. Part 3: N-Z 1993 p 1281-1282 (For primary document see N94-20636 05-91)
Avail: CASI HC A01/MF A06

N94-20764*# National Science Museum, Tokyó (Japan).
THE CHONDRITE MIHONOSEKI: NEW OBSERVED FALL Abstract Only
Masako Shima, A. Okada (Okayama Univ., Japan.), and K. Nagao (Okayama Univ., Japan.) *In* Lunar and Planetary Inst., Twenty-Fourth Lunar and Planetary Science Conference. Part 3: N-Z 1993 p 1297-1298 (For primary document see N94-20636 05-91)
Avail: CASI HC A01/MF A06

N94-20768*# Scripps Institution of Oceanography, La Jolla, CA.
FE-60 AND THE EVOLUTION OF EUCRITES Abstract Only
A. Shukolyukov and G. W. Lugmair *In* Lunar and Planetary Inst.,

Twenty-Fourth Lunar and Planetary Science Conference. Part 3: N-Z 1993 p 1305-1306 (For primary document see N94-20636 05-91)
Avail: CASI HC A01/MF A06

N94-20770*# Chicago Univ., IL. Dept. of Geophysical Sciences.
PETROGRAPHY AND ORIGIN OF REFRACTORY INCLUSIONS FROM THE MURRAY AND MURCHISON C2 CHONDRITES Abstract Only
S. B. Simon, L. Grossman, and A. Hsu (Illinois Mathematics and Science Academy, Aurora.) *In* Lunar and Planetary Inst., Twenty-Fourth Lunar and Planetary Science Conference. Part 3: N-Z 1993 p 1309-1310 (For primary document see N94-20636 05-91)
Avail: CASI HC A01/MF A06

N94-20773*# Oberlin Coll., OH. Dept. of Geology.
SIZE DISTRIBUTIONS AND AERODYNAMIC EQUIVALENCE OF METAL CHONDRULES AND SILICATE CHONDRULES IN ACFER 059 Abstract Only
William R. Skinner and James M. Leenhouts (Arizona Univ., Tucson.) *In* Lunar and Planetary Inst., Twenty-Fourth Lunar and Planetary Science Conference. Part 3: N-Z 1993 p 1315-1316 (For primary document see N94-20636 05-91)
Avail: CASI HC A01/MF A06

N94-20788*# Chicago Univ., IL. Dept. of Geophysical Sciences.
Fe/Mn IN OLIVINE OF CARBONACEOUS METEORITES Abstract Only
Ian M. Steele *In* Lunar and Planetary Inst., Twenty-Fourth Lunar and Planetary Science Conference. Part 3: N-Z 1993 p 1345-1346 (For primary document see N94-20636 05-91)
Avail: CASI HC A01/MF A06

N94-20790*# Muenster Univ. (Germany). Inst. of Physikalisches.
MULTIELEMENT ANALYSIS OF INTERPLANETARY DUST PARTICLES USING TOF-SIMS Abstract Only
T. Stephan, W. Kloeck, E. K. Jessberger (Max-Planck-Inst. fuer Kernphysik, Heidelberg, Germany.), H. Rulle, and J. Zehnpfenning *In* Lunar and Planetary Inst., Twenty-Fourth Lunar and Planetary Science Conference. Part 3: N-Z 1993 p 1349-1350 (For primary document see N94-20636 05-91)
Avail: CASI HC A01/MF A06

N94-20793*# California Inst. of Tech., Pasadena.
VOLATILE LOSS FROM ACCRETING ICY PROTOPLANETS Abstract Only
D. J. Stevenson *In* Lunar and Planetary Inst., Twenty-Fourth Lunar and Planetary Science Conference. Part 3: N-Z 1993 p 1355-1356 (For primary document see N94-20636 05-91)
Avail: CASI HC A01/MF A06

N94-20795*# California Inst. of Tech., Pasadena. Div. of Geological and Planetary Sciences.
THE Sm-Nd SYSTEMATICS OF SILICATE INCLUSIONS IN IRON METEORITES: RESULTS FROM CADDO (IAB) Abstract Only
Brian W. Stewart, D. A. Papanastassiou, and G. J. Wasserburg *In* Lunar and Planetary Inst., Twenty-Fourth Lunar and Planetary Science Conference. Part 3: N-Z 1993 p 1359-1360 (For primary document see N94-20636 05-91)
(Grant NAG9-43)
(Contrib-5241(804)) Avail: CASI HC A01/MF A06

N94-20812*# Tokyo Univ. (Japan). Mineralogical Inst.
TI-BEARING OXIDE MINERALS IN LUNAR METEORITE Y793169 WITH THE VLT AFFINITY Abstract Only
Hiroshi Takeda, Tomoko Arai, and Kazuto Saiki *In* Lunar and Planetary Inst., Twenty-Fourth Lunar and Planetary Science Conference. Part 3: N-Z 1993 p 1393-1394 (For primary document see N94-20636 05-91)
Avail: CASI HC A01/MF A06

N94-20813*# National Aeronautics and Space Administration. Lyndon B. Johnson Space Center, Houston, TX.
A NEW ANTARCTIC METEORITE WITH CHROMITE, ORTHOPYROXENE AND METAL WITH REFERENCE TO A FORMATION MODEL OF S ASTEROIDS Abstract Only
Hiroshi Takeda (Tokyo Univ., Japan.), Kazuto Saiki (Tokyo Univ., Japan.), Mayumi Otsuki (Tokyo Univ., Japan.), and Takahiro Hiroi *In* Lunar and Planetary Inst., Twenty-Fourth Lunar and Planetary Science Conference. Part 3: N-Z 1993 p 1395-1396 (For primary document see N94-20636 05-91)
Avail: CASI HC A01/MF A06

N94-20817*# Baylor Univ., Waco, TX. Dept. of Physics.
DETERMINATION OF PARAMETERS FOR HYPERVELOCITY DUST GRAINS ENCOUNTERED IN NEAR-EARTH SPACE Abstract Only
William G. Tanner, Carl R. Maag (Science Applications International Corp., Glendora, CA.), W. Merle Alexander, and Patricia Sappenfield *In* Lunar and Planetary Inst., Twenty-Fourth Lunar and Planetary Science Conference. Part 3: N-Z 1993 p 1403-1404 (For primary document see N94-20636 05-91)
Avail: CASI HC A01/MF A06

N94-20823*# Belorussian State Univ., Minsk (Belarus).
THE SAND BAG MODEL OF THE DISPERSION OF THE COSMIC BODY IN THE ATMOSPHERE Abstract Only
A. V. Teterev and I. V. Nemchinov (Academy of Sciences, USSR, Moscow.) *In* Lunar and Planetary Inst., Twenty-Fourth Lunar and Planetary Science Conference. Part 3: N-Z 1993 p 1415-1416 (For primary document see N94-20636 05-91)
Avail: CASI HC A01/MF A06

N94-20824*# Belorussian State Univ., Minsk (Belarus).
ATMOSPHERIC BREAKUP OF A SMALL COMET IN THE EARTH'S ATMOSPHERE Abstract Only
A. V. Teterev, N. I. Misychenko, L. V. Rudak, G. S. Romanov (Institute of Heat and Mass Transfer, Minsk, Belarus.), A. S. Smetannikov (Institute of Heat and Mass Transfer, Minsk, Belarus.), and I. V. Nemchinov (Academy of Sciences, USSR, Moscow.) *In* Lunar and Planetary Inst., Twenty-Fourth Lunar and Planetary Science Conference. Part 3: N-Z 1993 p 1417-1418 (For primary document see N94-20636 05-91)
Avail: CASI HC A01/MF A06

N94-20827*# Cologne Univ. (Germany).
SYNOPTIC OBSERVATIONS OF NEAR SURFACE PROCESSES OF AN INSOLATED ICE-DUST BODY UNDER SPACE CONDITIONS: THE CASE OF KOSI 9 AND 10 Abstract Only
K. Thiel, G. Koelzer, E. Lorenz (Deutsche Forschungsanstalt fuer Luft- und Raumfahrt, Berlin, Germany.), H. Kochan (Deutsche Forschungsanstalt fuer Luft- und Raumfahrt, Cologne, Germany.), J. Gebhard (Max-Planck-Inst. fuer Kernphysik, Heidelberg, Germany.), and E. Gruen (Max-Planck-Inst. fuer Kernphysik, Heidelberg, Germany.) *In* Lunar and Planetary Inst., Twenty-Fourth Lunar and Planetary Science Conference. Part 3: N-Z 1993 p 1423-1424 (For primary document see N94-20636 05-91)
Avail: CASI HC A01/MF A06

N94-20828*# National Aeronautics and Space Administration. Lyndon B. Johnson Space Center, Houston, TX.
COMETARY INTERPLANETARY DUST PARTICLES? AN UPDATE ON CARBON IN ANHYDROUS IDPS Abstract Only
K. L. Thomas (Lockheed Engineering and Sciences Co., Houston, TX.), L. P. Keller, G. E. Blanford (Houston Univ., TX.), and D. S. McKay *In* Lunar and Planetary Inst., Twenty-Fourth Lunar and Planetary Science Conference. Part 3: N-Z 1993 p 1425-1426 (For primary document see N94-20636 05-91)
Avail: CASI HC A01/MF A06

N94-20834*# Geological Survey, Denver, CO.
THE U-Th-Pb, Sm-Nd, AND Ar-Ar ISOTOPIC SYSTEMATICS OF LUNAR METEORITE YAMATO-793169 Abstract Only
Noriko Torigoye, Keji Misawa, G. Brent Dalrymple (Geological Survey, Menlo Park, CA.), and Mitsunobu Tatsumoto *In* Lunar and Planetary Inst., Twenty-Fourth Lunar and Planetary Science Conference. Part 3: N-Z 1993 p 1437-1438 (For primary document see N94-20636 05-91)
Avail: CASI HC A01/MF A06

N94-20836*# Lockheed Engineering and Sciences Co., Houston, TX.
THE PARENT MAGMA OF THE NAKHLA (SNC) METEORITE: RECONCILIATION OF COMPOSITION ESTIMATES FROM MAGMATIC INCLUSIONS AND ELEMENT PARTITIONING Abstract Only
A. H. Treiman *In* Lunar and Planetary Inst., Twenty-Fourth Lunar and Planetary Science Conference. Part 3: N-Z 1993 p 1441-1442 (For primary document see N94-20636 05-91)
Avail: CASI HC A01/MF A06

N94-20837*# Jet Propulsion Lab., California Inst. of Tech., Pasadena.
INTACT CAPTURE OF HYPERVELOCITY PARTICLES ON SHUTTLE Abstract Only
P. Tsou, D. E. Brownlee (Washington Univ., Seattle.), and A. L. Albee (California Inst. of Tech., Pasadena.) *In* Lunar and Planetary Inst., Twenty-Fourth Lunar and Planetary Science Conference. Part 3: N-Z 1993 p 1443-1444 (For primary document see N94-20636 05-91)
Avail: CASI HC A01/MF A06

N94-20840*# Arizona State Univ., Tempe. Dept. of Geology.
IMPACT-INDUCED DEVOLATILIZATION OF CaSO4 ANHYDRITE AND IMPLICATIONS FOR K-T EXTINCTIONS: PRELIMINARY RESULTS Abstract Only
James A. Tyburczy and Thomas J. Ahrens (California Inst. of Tech., Pasadena.) *In* Lunar and Planetary Inst., Twenty-Fourth Lunar and Planetary Science Conference. Part 3: N-Z 1993 p 1449-1450 (For primary document see N94-20636 05-91)
Avail: CASI HC A01/MF A06

N94-20841*# European Space Research Organization, Noordwikj (Netherlands). Dept. of Space Science.
MEASUREMENTS OF THE DIELECTRIC PROPERTIES OF SIMULATED COMET MATERIAL AS PART OF THE KOSI 10 EXPERIMENT Abstract Only
S. Ulamec, H. Svedhem, and H. Kochan (Deutsche Forschungsanstalt fuer Luft- und Raumfahrt, Cologne, Germany.) *In* Lunar and Planetary Inst., Twenty-Fourth Lunar and Planetary Science Conference. Part 3: N-Z 1993 p 1451-1452 (For primary document see N94-20636 05-91)
Avail: CASI HC A01/MF A06

N94-20844*# Academy of Sciences (USSR), Moscow. Inst. of Geochemistry and Analytical Chemistry.
ON MODELLING NUCLEAR REACTIONS IN METEORITES Abstract Only
G. K. Ustinova and A. K. Lavrukhina *In* Lunar and Planetary Inst., Twenty-Fourth Lunar and Planetary Science Conference. Part 3: N-Z 1993 p 1457-1458 (For primary document see N94-20636 05-91)
Avail: CASI HC A01/MF A06

N94-20845*# Jet Propulsion Lab., California Inst. of Tech., Pasadena.
IMPS ALBEDO AND DIAMETER FOR ASTEROID 243 IDA Abstract Only
G. J. Veeder and E. F. Tedesco (Mission Research Corp., Santa Barbara, CA.) *In* Lunar and Planetary Inst., Twenty-Fourth Lunar and Planetary Science Conference. Part 3: N-Z 1993 p 1459-1460 (For primary document see N94-20636 05-91)
Avail: CASI HC A01/MF A06

N94-20846*# Open Univ., Milton (England).
ARE THE C DELTA LIGHT NITROGEN AND NOBLE GASES LOCATED IN THE SAME CARRIER? Abstract Only
A. B. Verchovsky, S. S. Russell, C. T. Pillinger, A. V. Fisenko (Academy of Sciences, USSR, Moscow.), and Yuri A. Shukolyukov (Academy of Sciences, USSR, Moscow.) *In* Lunar and Planetary Inst., Twenty-Fourth Lunar and Planetary Science Conference. Part 3: N-Z 1993 p 1461-1462 (For primary document see N94-20636 05-91)
Avail: CASI HC A01/MF A06

N94-20848*# National Aeronautics and Space Administration. Lyndon B. Johnson Space Center, Houston, TX.
COMPARISON OF VISIBLE AND NEAR-INFRARED REFLECTANCE SPECTRA OF CM2 CARBONACEOUS CHONDRITES AND PRIMITIVE ASTEROIDS Abstract Only
F. Vilas, T. Hiroi, and M. E. Zolensky *In* Lunar and Planetary Inst., Twenty-Fourth Lunar and Planetary Science Conference. Part 3: N-Z 1993 p 1465-1466 (For primary document see N94-20636 05-91)
Avail: CASI HC A01/MF A06

N94-20849*# Academy of Sciences (USSR), Moscow. Inst. of Physics of the Earth.
RECONDENSATION IN THE EARLY SOLAR SYSTEM: PHYSICAL CONDITIONS AND SOURCE MATERIAL Abstract Only
A. V. Vityazev, V. A. Dorofeyeva, and A. B. Makalkin *In* Lunar and Planetary Inst., Twenty-Fourth Lunar and Planetary Science Conference. Part 3: N-Z 1993 p 1467-1468 (For primary document see N94-20636 05-91)
Avail: CASI HC A01/MF A06

N94-20854*# Maryland Univ., College Park. Dept. of Geology.
RHENIUM-OSMIUM ISOTOPE SYSTEMATICS OF ORDINARY CHONDRITES AND IRON METEORITES Abstract Only
R. J. Walker, J. W. Morgan (Geological Survey, Reston, VA.), M. F. Horan (Geological Survey, Reston, VA.), and J. N. Grossman (Geological Survey, Reston, VA.) *In* Lunar and Planetary Inst., Twenty-Fourth Lunar and Planetary Science Conference. Part 3: N-Z 1993 p 1477-1478 (For primary document see N94-20636 05-91)
Avail: CASI HC A01/MF A06

N94-20857*# National Aeronautics and Space Administration. Lyndon B. Johnson Space Center, Houston, TX.
CONSORTIUM STUDY OF LUNAR METEORITES YAMATO-793169 AND ASUKA-881757: GEOCHEMICAL EVIDENCE OF MUTUAL SIMILARITY, AND DISSIMILARITY VERSUS OTHER MARE BASALTS Abstract Only
Paul H. Warren (California Univ., Los Angeles.) and Marilyn M. Lindstrom *In* Lunar and Planetary Inst., Twenty-Fourth Lunar and Planetary Science Conference. Part 3: N-Z 1993 p 1483-1484 (For primary document see N94-20636 05-91)
Avail: CASI HC A01/MF A06

N94-20858*# National Aeronautics and Space Administration. Goddard Space Flight Center, Greenbelt, MD.
MAGNETIC RECORD IN CHONDRITE METEORITES Abstract Only
P. J. Wasilewski, J. L. Faris, and M. V. OBryan *In* Lunar and Planetary Inst., Twenty-Fourth Lunar and Planetary Science Conference. Part 3: N-Z 1993 p 1485-1486 (For primary document see N94-20636 05-91)
Avail: CASI HC A01/MF A06

N94-20860*# California Univ., Los Angeles. Inst. of Geophysics and Planetary Physics.
MULTIPLICITY OF CHONDRULE HEATING EVENTS AND THE COARSENING OF CHONDRULE TEXTURES Abstract Only
John T. Wasson *In* Lunar and Planetary Inst., Twenty-Fourth Lunar and Planetary Science Conference. Part 3: N-Z 1993 p 1489-1490 (For primary document see N94-20636 05-91)
Avail: CASI HC A01/MF A06

N94-20861*# National Aeronautics and Space Administration. Lyndon B. Johnson Space Center, Houston, TX.
EQUILIBRIUM AND FRACTIONAL CRYSTALLIZATION OF A PRIMITIVE SHERGOTTITE COMPOSITION Abstract Only
L. E. Wasylenki (California Inst. of Tech., Pasadena.), J. H. Jones, L. Le (Lockheed Engineering and Sciences Co., Houston, TX.), and A. J. G. Jurewicz (Lockheed Engineering and Sciences Co., Houston, TX.) *In* Lunar and Planetary Inst., Twenty-Fourth Lunar and Planetary Science Conference. Part 3: N-Z 1993 p 1491-1492 (For primary document see N94-20636 05-91)
Avail: CASI HC A01/MF A06

N94-20865*# Arizona Univ., Tucson. Planetary Science Inst.
COAGULATION OF GRAINS IN STATIC AND COLLAPSING PROTOSTELLAR CLOUDS Abstract Only
S. J. Weidenschilling and T. V. Ruzmaikina (Academy of Sciences, USSR, Moscow.) *In* Lunar and Planetary Inst., Twenty-Fourth Lunar and Planetary Science Conference. Part 3: N-Z 1993 p 1499-1500 (For primary

document see N94-20636 05-91)
(Contract NASw-4616)
Avail: CASI HC A01/MF A06

N94-20866*# American Museum of Natural History, New York, NY. Dept. of Mineral Sciences.
THE FORMATION OF FeO-RICH PYROXENE AND ENSTATITE IN UNEQUILIBRATED ENSTATITE CHONDRITES: A PETROLOGIC-TRACE ELEMENT (SIMS) STUDY Abstract Only
M. K. Weisberg, M. Prinz, R. A. Fogel, and N. Shimizu (Woods Hole Oceanographic Inst., MA.) *In* Lunar and Planetary Inst., Twenty-Fourth Lunar and Planetary Science Conference. Part 3: N-Z 1993 p 1501-1502 (For primary document see N94-20636 05-91)
Avail: CASI HC A01/MF A06

N94-20869*# National Aeronautics and Space Administration. Lyndon B. Johnson Space Center, Houston, TX.
WEATHERING FEATURES AND SECONDARY MINERALS IN ANTARCTIC SHERGOTTITES ALHA77005 AND LEW88516 Abstract Only
Susan J. Wentworth (Lockheed Engineering and Sciences Co., Houston, TX.) and James L. Gooding *In* Lunar and Planetary Inst., Twenty-Fourth Lunar and Planetary Science Conference. Part 3: N-Z 1993 p 1507-1508 (For primary document see N94-20636 05-91)
Avail: CASI HC A01/MF A06

N94-20871*# Carnegie Institution of Washington, DC.
VARIETY IN PLANETARY SYSTEMS Abstract Only
George W. Wetherill *In* Lunar and Planetary Inst., Twenty-Fourth Lunar and Planetary Science Conference. Part 3: N-Z 1993 p 1511-1512 (For primary document see N94-20636 05-91)
Avail: CASI HC A01/MF A06

N94-20877*# Carnegie Institution of Washington, DC.
EQUILIBRIUM MODELS OF MASS DISTRIBUTION AND COLLISIONAL LIFETIMES OF ASTEROIDS Abstract Only
David R. Williams and George Wetherill *In* Lunar and Planetary Inst., Twenty-Fourth Lunar and Planetary Science Conference. Part 3: N-Z 1993 p 1523-1524 (For primary document see N94-20636 05-91)
Avail: CASI HC A01/MF A06

N94-20884*# California State Univ., Fullerton.
LREE VARIABILITY IN CM MATRICES: ANOTHER LOOK AT METEORITE COMPACTION AGES Abstract Only
Dorothy S. Woolum, Karen Poelstra, C. Alexander (Washington Univ., Saint Louis, MO.), and T. Ireland (Australian National Univ., Canberra.) *In* Lunar and Planetary Inst., Twenty-Fourth Lunar and Planetary Science Conference. Part 3: N-Z 1993 p 1537-1538 (For primary document see N94-20636 05-91)
Avail: CASI HC A01/MF A06

N94-20885*# Open Univ., Milton (England). Dept. of Earth Sciences.
THE CARBON COMPONENTS IN SNC METEORITES OF FELDSPATHIC HARZBURGITE COMPOSITION Abstract Only
I. P. Wright, C. Douglas, and C. T. Pillinger *In* Lunar and Planetary Inst., Twenty-Fourth Lunar and Planetary Science Conference. Part 3: N-Z 1993 p 1539-1540 (For primary document see N94-20636 05-91)
Avail: CASI HC A01/MF A06

N94-20886*# Open Univ., Milton (England). Dept. of Earth Sciences.
FURTHER CARBON ISOTOPE MEASUREMENTS OF LEW 88516 Abstract Only
I. P. Wright, C. Douglas, and C. T. Pillinger *In* Lunar and Planetary Inst., Twenty-Fourth Lunar and Planetary Science Conference. Part 3: N-Z 1993 p 1541-1542 (For primary document see N94-20636 05-91)
Avail: CASI HC A01/MF A06

N94-20893*# National Aeronautics and Space Administration. Lyndon B. Johnson Space Center, Houston, TX.
CONSORTIUM REPORTS ON LUNAR METEORITES YAMATO 793169 AND ASUKA 881757, A NEW TYPE OF MARE BASALT Abstract Only
Keizo Yanai (National Inst. of Polar Research, Tokyo, Japan.), Hiroshi Takeda (Tokyo Univ., Japan.), M. M. Lindstrom, M. Tatsumoto (Geological Survey, Denver, CO.), N. Torigoe (Geological Survey, Denver, CO.), K. Misawa (National Inst. of Polar Research, Tokyo, Japan.), P. H. Warren (California Univ., Los Angeles.), G. W. Kallemeyn (California Univ., Los Angeles.), C. Koeberl (Wien Univ., Austria.), and H. Kojima (National Inst. of Polar Research, Tokyo, Japan.) et al *In* Lunar and Planetary Inst., Twenty-Fourth Lunar and Planetary Science Conference. Part 3: N-Z 1993 p 1555-1556 (For primary document see N94-20636 05-91)
Avail: CASI HC A01/MF A06

N94-20894*# Lehigh Univ., Bethlehem, PA. Dept. of Materials Science and Engineering.
PRELIMINARY AEM STUDY OF THE MICROSTRUCTURE AND COMPOSITION OF METAL PARTICLES IN ORDINARY CHONDRITES Abstract Only
C. W. Yang, D. B. Williams, and J. I. Goldstein *In* Lunar and Planetary Inst., Twenty-Fourth Lunar and Planetary Science Conference. Part 3: N-Z 1993 p 1557-1558 (For primary document see N94-20636 05-91)
Avail: CASI HC A01/MF A06

N94-20895*# European Space Research Lab., Noordwijk (Netherlands). Space Science Dept.
MICROMETEORITE PRE-SOLAR DIAMONDS FROM GREENLAND CRYOCONITE? Abstract Only
P. D. Yates *In* Lunar and Planetary Inst., Twenty-Fourth Lunar and Planetary Science Conference. Part 3: N-Z 1993 p 1559-1560 (For primary document see N94-20636 05-91)
Avail: CASI HC A01/MF A06

N94-20897*# Chicago Univ., IL. Dept. of the Geophysical Sciences.
TRACE ELEMENT COMPOSITIONS OF SPINEL-RICH REFRACTORY INCLUSIONS FROM THE MURCHISON METEORITE Abstract Only
S. Yoneda, P. J. Sylvester, S. B. Simon, L. Grossman, and A. Hsu (Illinois Mathematics and Science Academy, Aurora.) *In* Lunar and Planetary Inst., Twenty-Fourth Lunar and Planetary Science Conference. Part 3: N-Z 1993 p 1563-1564 (For primary document see N94-20636 05-91)
Avail: CASI HC A01/MF A06

N94-20898*# Tsukuba Univ. (Japan). Inst. of Geoscience.
INTER- AND INTRA-CRYSTALLINE OXYGEN ISOTOPE DISTRIBUTION OF FASSAITES IN ALLENDE CAI Abstract Only
Hisayoshi Yurimoto, Hiroshi Nagasawa (Gakushuin Univ., Tokyo, Japan.), and Yoshiharu Mori (National Lab. for High Energy Physics, Ibaraki, Japan.) *In* Lunar and Planetary Inst., Twenty-Fourth Lunar and Planetary Science Conference. Part 3: N-Z 1993 p 1565-1566 (For primary document see N94-20636 05-91)
Avail: CASI HC A01/MF A06

N94-20901*# Arkansas Univ., Fayetteville. Cosmochemistry Group.
LEWIS CLIFF 87057: A NEW METAL-RICH E3 CHONDRITE WITH SIMILARITIES TO MT. EGERTON, SHALLOWATER AND HAPPY CANYON Abstract Only
Y. Zhang, P. H. Benoit, and D. W. G. Sears *In* Lunar and Planetary Inst., Twenty-Fourth Lunar and Planetary Science Conference. Part 3: N-Z 1993 p 1571-1572 (For primary document see N94-20636 05-91)
(Grant NAG9-81)
Avail: CASI HC A01/MF A06

N94-20902*# Chicago Univ., IL. Dept. of Geophysical Sciences.
CHEMICAL ZONING AND DIFFUSION OF Ca, Al, Mn, AND Cr IN OLIVINE OF SPRINGWATER PALLASITE Abstract Only
Y. Zhou and Iah M. Steele *In* Lunar and Planetary Inst., Twenty-Fourth Lunar and Planetary Science Conference. Part 3: N-Z 1993 p 1573-1574 (For primary document see N94-20636 05-91)
Avail: CASI HC A01/MF A06

N94-20905*# Max-Planck-Inst. fuer Chemie, Mainz (Germany).
CHEMICAL COMPOSITION OF NEW ACAPULCOITES AND LODRANITES Abstract Only
J. Zipfel and H. Palme *In* Lunar and Planetary Inst., Twenty-Fourth Lunar and Planetary Science Conference. Part 3: N-Z 1993

p 1579-1580 (For primary document see N94-20636 05-91)
Avail: CASI HC A01/MF A06

N94-20906*# National Aeronautics and Space Administration. Lyndon B. Johnson Space Center, Houston, TX.
DIFFUSE REFLECTANCE SPECTRA OF ORTHOPYROXENE, OLIVINE, AND PLAGIOCLASE AS A FUNCTION OF COMPOSITION AND STRUCTURE Abstract Only
M. E. Zolensky, L. Le (Lockheed Engineering and Sciences Co., Houston, TX.), C. Galindo (Lockheed Engineering and Sciences Co., Houston, TX.), R. Morris, V. Lauer (Lockheed Engineering and Sciences Co., Houston, TX.), and F. Vilas *In* Lunar and Planetary Inst., Twenty-Fourth Lunar and Planetary Science Conference. Part 3: N-Z 1993 p 1581-1582 (For primary document see N94-20636 05-91)
Avail: CASI HC A01/MF A06

N94-20907*# National Aeronautics and Space Administration. Lyndon B. Johnson Space Center, Houston, TX.
MINERALOGY OF DARK CLASTS IN PRIMITIVE VERSUS DIFFERENTIATED METEORITES Abstract Only
M. E. Zolensky, M. K. Weisberg (American Museum of Natural History, New York, NY.), R. A. Barrett (Lockheed Engineering and Sciences Co., Houston, TX.), and M. Prinz (American Museum of Natural History, New York, NY.) *In* Lunar and Planetary Inst., Twenty-Fourth Lunar and Planetary Science Conference. Part 3: N-Z 1993 p 1583-1584 (For primary document see N94-20636 05-91)
Avail: CASI HC A01/MF A06

N94-22472*# Smithsonian Institution, Cambridge, MA. Center for Astrophysics.
VISUALIZING THE UNIVERSE, PART 2 Abstract Only
Emilio E. Falco, Michael J. Kurtz, and Mark Bajuk (National Center for Supercomputing Applications, Urbana, IL.) *In* NASA, Washington, Second Annual Conference on Astronomical Data Analysis Software and Systems. Abstracts 1992 p 41 (For primary document see N94-22438 05-89)
Avail: CASI HC A01/MF A02

N94-22476*# Smithsonian Astrophysical Observatory, Cambridge, MA.
VISUALIZING THE UNIVERSE, PART 1 Abstract Only
M. J. Geller and J. P. Huchra *In* NASA, Washington, Second Annual Conference on Astronomical Data Analysis Software and Systems. Abstracts 1992 p 45 (For primary document see N94-22438 05-89)
Avail: CASI HC A01/MF A02

N94-22631# Osservatorio Astronomico, Turin (Italy).
JETS ASSOCIATED WITH ACTIVE GALACTIC NUCLEI
Attilio Ferrari (Turin Univ., Italy.) *In* ESA, Fourth International Toki Conference on Plasma Physics and Controlled Nuclear Fusion May 1993 p 67-7 (For primary document see N94-22624 05-75)
Copyright Avail: CASI HC A02/MF A03

N94-22643# Academy of Sciences (USSR), Moscow. Inst. of Physics.
DARK MATTER: NEUTRON STAR HALO AND THE NATURE OF GAMMA-BURSTS
Alexander V. Gurevich, Vasily S. Beskin, Kirill P. Zybin, and Mikhail O. Ptitsyn *In* ESA, Fourth International Toki Conference on Plasma Physics and Controlled Nuclear Fusion May 1993 p 151-154 (For primary document see N94-22624 05-75)
Copyright Avail: CASI HC A01/MF A03

N94-22644# Nagoya Univ. (Japan). Dept. of Physics.
GENERAL RELATIVISTIC WINDS IN A BLACK HOLE MAGNETOSPHERE
Akira Tomimatsu *In* ESA, Fourth International Toki Conference on Plasma Physics and Controlled Nuclear Fusion May 1993 p 157-160 (For primary document see N94-22624 05-75)
Copyright Avail: CASI HC A01/MF A03

N94-22645# Tokyo Metropolitan Univ. (Japan). Dept. of Physics.
VERTICAL STRUCTURE OF ACCRETION DISKS
Toshiya Shimura and Fumio Takahara *In* ESA, Fourth International Toki Conference on Plasma Physics and Controlled Nuclear Fusion May 1993 p 161-164 (For primary document see N94-22624 05-75)
Copyright Avail: CASI HC A01/MF A03

N94-22650# Observatoire de Paris-Meudon (France).
COMPRESSIBLE MHD TURBULENCE IN THE INTERPLANETARY MEDIUM
Marco Velli and R. Grappin *In* ESA, Fourth International Toki Conference on Plasma Physics and Controlled Nuclear Fusion May 1993 p 185-188 (For primary document see N94-22624 05-75)
Copyright Avail: CASI HC A01/MF A03

N94-22682# Nagoya Univ. (Japan). Dept. of Physics.
ASYMPTOTIC STRUCTURE OF MAGNETICALLY DRIVEN MHD WIND
Shin-Ya Nitta *In* ESA, Fourth International Toki Conference on Plasma Physics and Controlled Nuclear Fusion May 1993 p 321-323 (For primary document see N94-22624 05-75)
Copyright Avail: CASI HC A01/MF A03

N94-22683# Tokyo Metropolitan Univ. (Japan). Dept. of Physics.
HYDRODYNAMICAL WINDS FROM AN ACCRETION DISK
Rika Okada and Fumio Takahara *In* ESA, Fourth International Toki Conference on Plasma Physics and Controlled Nuclear Fusion May 1993 p 325-328 (For primary document see N94-22624 05-75)
Copyright Avail: CASI HC A01/MF A03

N94-22687# Nagoya Univ. (Japan). Dept. of Astrophysics.
FRAGMENTATION OF MAGNETIZED FILAMENTARY INTERSTELLAR CLOUDS
Tomoyuki Hanawa, Fumitaka Nakamura, and Takenori Nakano (Nobeyema Solar Radio Observatory, Japan.) *In* ESA, Fourth International Toki Conference on Plasma Physics and Controlled Nuclear Fusion May 1993 p 341-344 (For primary document see N94-22624 05-75)
Copyright Avail: CASI HC A01/MF A03

N94-22688# Nagoya Univ. (Japan). Dept. of Astrophysics.
GRAVITATIONAL INSTABILITY OF MAGNETIZED FILAMENTARY CLOUDS. 1: HELICAL MAGNETIC FIELDS
Fumitaka Nakamura, Tomoyuki Hanawa, and Takenori Nakano (Nobeyema Solar Radio Observatory, Japan.) *In* ESA, Fourth International Toki Conference on Plasma Physics and Controlled Nuclear Fusion May 1993 p 345-348 (For primary document see N94-22624 05-75)
Copyright Avail: CASI HC A01/MF A03

N94-22689# Nagoya Univ. (Japan). Dept. of Astrophysics.
GRAVITATIONAL INSTABILITY OF MAGNETIZED FILAMENTARY CLOUDS. 2: ROTATION
Tomoaki Matsumoto, Fumitaka Nakamura, and Tomoyuki Hanawa *In* ESA, Fourth International Toki Conference on Plasma Physics and Controlled Nuclear Fusion May 1993 p 349-352 (For primary document see N94-22624 05-75)
Copyright Avail: CASI HC A01/MF A03

N94-22690# Osaka Univ., Toyonaka (Japan). Dept. of Earth and Space Science.
TIME VARIATIONS OF X RAYS FROM BLACK HOLE CANDIDATES: CANONICAL TIME VARIATIONS IN HIGH AND LOW INTENSITY STATES
Sigenori Miyamoto, Shunji Kitamoto, Sayuri Iga, Yasuhide Kamodo, Kiyoshi Hayashida, Kentaro Terada, and Hitoshi Negoro *In* ESA, Fourth International Toki Conference on Plasma Physics and Controlled Nuclear Fusion May 1993 p 353-357 (For primary document see N94-22624 05-75)
Copyright Avail: CASI HC A01/MF A03

N94-22691# Commissariat a l'Energie Atomique, Saclay (France). Service d'Astrophysique.
PAIR PLASMAS IN THE GALACTIC CENTER REGION AND IN NOVA MUSCAE
Philippe Durouchoux and P. Wallyn *In* ESA, Fourth International Toki Conference on Plasma Physics and Controlled Nuclear Fusion May 1993

p 359-362 (For primary document see N94-22624 05-75)
Copyright Avail: CASI HC A01/MF A03

N94-22692# Nagoya Univ. (Japan). Dept. of Physics.
TIME VARIATION OF MHD ACCRETION ONTO A BLACK HOLE
Kouichi Hirotani, Akira Tomimatsu, and Masaaki Takahashi (Aichi Univ. of Education, Japan.) *In* ESA, Fourth International Toki Conference on Plasma Physics and Controlled Nuclear Fusion May 1993 p 363-366 (For primary document see N94-22624 05-75)
(Grant ASR-ME-04640268)
Copyright Avail: CASI HC A01/MF A03

N94-22693# Tokyo Metropolitan Univ. (Japan). Dept. of Physics.
ACCRETION OF A HOT PLASMA ONTO THE CENTRAL BLACK HOLE: FOKKER-PLANCK FORMULATION
Fumiko Yabuki and Fumio Takahara *In* ESA, Fourth International Toki Conference on Plasma Physics and Controlled Nuclear Fusion May 1993 p 367-370 (For primary document see N94-22624 05-75)
Copyright Avail: CASI HC A01/MF A03

N94-22694# Kyoto Univ. (Japan). Dept. of Astronomy.
MAGNETIC SUPERBUBBLES IN THE GALACTIC DISK AND HALO
S. Mineshige, Kazumari Shibata (Tokyo Astronomical Observatory, Mitaka, Japan.), and P. R. Shapiro (Texas Univ., Austin.) *In* ESA, Fourth International Toki Conference on Plasma Physics and Controlled Nuclear Fusion May 1993 p 371-374 Sponsored in part by Robert A. Welch Foundation (For primary document see N94-22624 05-75)
(Contract DE-FG05-80ET-53088)
Copyright Avail: CASI HC A01/MF A03

N94-22695# Aichi Univ. of Education (Japan). Dept. of Physics and Astronomy.
GENERATION AND MAINTENANCE OF BISYMMETRIC SPIRAL MAGNETIC FIELDS IN DISK GALAXIES IN DIFFERENTIAL ROTATION
Takeyasu Sawa and M. Fujimoto (Nagoya Univ., Japan.) *In* ESA, Fourth International Toki Conference on Plasma Physics and Controlled Nuclear Fusion May 1993 p 375-378 (For primary document see N94-22624 05-75)
Copyright Avail: CASI HC A01/MF A03

N94-22697# Sydney Univ. (Australia). School of Physics.
MAGNETIC FIELDS IN SPIRAL GALAXIES
S. Spencer and Lawrence Cram *In* ESA, Fourth International Toki Conference on Plasma Physics and Controlled Nuclear Fusion May 1993 p 383-385 Sponsored in part by Australian Research Council and Science Foundation for Physics (For primary document see N94-22624 05-75)
Copyright Avail: CASI HC A01/MF A03

N94-22698# Commissariat a l'Energie Atomique, Saclay (France). Service d'Astrophysique.
SPIRAL ALFVEN INSTABILITY IN ACCRETION DISKS
Michel Tagger, R. Pellat (Ecole Polytechnique, Palaiseau, France.), and F. C. Coroniti (California Univ., Los Angeles.) *In* ESA, Fourth International Toki Conference on Plasma Physics and Controlled Nuclear Fusion May 1993 p 387-390 (For primary document see N94-22624 05-75)
Copyright Avail: CASI HC A01/MF A03

N94-22699# Ibaraki Univ., Mito (Japan). Dept. of Physics.
SHOCK FORMATION IN MAGNETOHYDRODYNAMICAL ACCRETION ONTO A BLACK HOLE
Masayoshi Yokosawa *In* ESA, Fourth International Toki Conference on Plasma Physics and Controlled Nuclear Fusion May 1993 p 391-394 (For primary document see N94-22624 05-75)
Copyright Avail: CASI HC A01/MF A03

N94-22700# Universidade Federal do Rio Grande do Norte, Natal (Brazil). Dept. de Fisica.
MAGNETIC RECONNECTION IN EMISSION NEBULAE IN CLUSTERS OF GALAXIES
Luiz C. Jafelice and Amanacio C. S. Friaca (Sao Paulo Univ., Brazil.) *In* ESA, Fourth International Toki Conference on Plasma Physics and Controlled Nuclear Fusion May 1993 p 395-398 (For primary document see N94-22624 05-75)
Copyright Avail: CASI HC A01/MF A03

N94-22701# Tokyo Univ. (Japan). Dept. of Astronomy.
MAGNETOHYDRODYNAMIC PHENOMENA IN STAR-FORMING PROCESSES AND THEIR ENVIRONMENT
Yutaka Uchida *In* ESA, Fourth International Toki Conference on Plasma Physics and Controlled Nuclear Fusion May 1993 p 401-407 (For primary document see N94-22624 05-75)
Copyright Avail: CASI HC A02/MF A03

91 LUNAR AND PLANETARY EXPLORATION

Includes planetology; and manned and unmanned flights.
For spacecraft design or space stations see *18 Spacecraft Design, Testing and Performance.*

N94-20048*# Iowa Univ., Iowa City. Dept. of Physics and Astronomy.
A STUDY OF SATURN'S E-RING PARTICLES USING THE VOYAGER 1 PLASMA WAVE INSTRUMENT
D. Tsintikidis, W. S. Kurth, D. A. Gurnett, and D. D. Barbosa (California Univ., Los Angeles.) Sep. 1993 50 p
(Contract JPL-959193)
(NASA-CR-194694; NAS 1.26:194694; U-of-Iowa-93-19) Avail: CASI HC A03/MF A01

The flyby of Voyager 1 at Saturn resulted in the detection of a large variety of plasma waves, e.g., chorus, hiss, and electron cyclotron harmonics. Just before the outbound equator crossing, at about 6.1 R(sub s), the Voyager 1 plasma wave instrument detected a strong, well-defined low-frequency enhancement. Initially it was suggested that plasma waves might be responsible for the spectral feature but more recently dust was suggested as at least a partial contributor to the enhancement. In this report we present evidence which supports the conclusion that dust contributes to the low-frequency enhancement. A new method has been used to derive the dust impact rate. The method relies mainly on the 16-channel spectrum analyzer data. The few wide band waveform observations available (which have been used to study dust impacts during the Voyager 2 ring plane crossing) were useful for calibrating the impact rate from the spectrum analyzer data. The mass and, hence, the size of the dust particles were also obtained by analyzing the response of the plasma wave spectrum analyzer. The results show that the region sampled by Voyager 1 is populated by dust particles that have rms masses of up to few times 10(exp -11) g and sizes of up to a few microns. The dust particle number density is on the order of 10(exp -3) m(exp 3). The optical depth of the region sampled by the spacecraft is 1.04 x 10(exp -6). The particle population is centered about 2500 km south of the equatorial plane and has a north-south thickness of about 4000 km. Possible sources of these particles are the moons Enceladus and Tethys whose orbits lie within the E-ring radial extent. These results are in reasonable agreement with photometric studies and numerical simulations. Author

N94-20382*# Lunar and Planetary Inst., Houston, TX.
WORKSHOP ON THE MARTIAN NORTHERN PLAINS: SEDIMENTOLOGICAL, PERIGLACIAL, AND PALEOCLIMATIC EVOLUTION Abstracts Only
Jeffrey S. Kargel, ed. (Geological Survey, Flagstaff, AZ.), Jeffrey Moore, ed. (National Aeronautics and Space Administration. Goddard Space Flight Center, Greenbelt, MD.), and Timothy Parker, ed. (Jet Propulsion Lab., California Inst. of Tech., Pasadena.) 1993 29 p Workshop held in Fairbanks, AK, 12-14 Aug. 1993; sponsored by MSATT Study Group and Alaska Univ.
(Contract NASw-4574)
(NASA-CR-194831; NAS 1.26:194831; LPI-TR-93-04-Pt-1) Avail: CASI HC A03/MF A01

Papers that have been accepted for presentation at the Workshop on the Martian Northern Plains: Sedimentological, Periglacial, and Paleoclimatic Evolution, on 12-14 Aug. 1993 in Fairbanks, Alaska are included. Topics covered include: hydrological consequences of ponded water on Mars; morphological and morphometric studies of impact craters in the Northern Plains of Mars; a wet-geology and cold-climate Mars model: punctuation of

a slow dynamics approach to equilibrium; the distribution of ground ice on Mars; and stratigraphy of the Martian Northern Plains. For individual titles, see N94-20383 through N94-20402.

N94-20383*# Arizona Univ., Tucson. Dept. of Geosciences.
HYDROLOGICAL CONSEQUENCES OF PONDED WATER ON MARS Abstract Only
V. R. Baker *In* Lunar and Planetary Inst., Workshop on the Martian Northern Plains: Sedimentological, Periglacial, and Paleoclimatic Evolution 1993 p 1-2 (For primary document see N94-20382 05-91)
Avail: CASI HC A01/MF A01

Although geomorphological evidence for ancient highly active water cycling has long been obvious for Mars, geochemical analyses have only recently been found to be consistent with this fact. One approach to understanding the geomorphological evidence has been to estimate the total volume of the Martian hydrosphere. I will discuss an approach focused on the history of changing water processes on the planet, and on the understanding of those processes in a global sense. Author (revised)

N94-20384*# Lunar and Planetary Inst., Houston, TX.
MORPHOLOGIC AND MORPHOMETRIC STUDIES OF IMPACT CRATERS IN THE NORTHERN PLAINS OF MARS Abstract Only
N. G. Barlow *In its* Workshop on the Martian Northern Plains: Sedimentological, Periglacial, and Paleoclimatic Evolution 1993 p 2-3 (For primary document see N94-20382 05-91)
Avail: CASI HC A01/MF A01

Fresh impact craters in the northern plains of Mars display a variety of morphologic and morphometric properties. Ejecta morphologies range from radial to fluidized, interior features include central peaks and central pits, fluidized morphologies display a range of sinuosities, and depth-diameter ratios are being measured to determine regional variations. Studies of the martian northern plains over the past five years have concentrated in three areas: (1) determining correlations of ejecta morphologies with crater diameter, latitude, and underlying terrain; (2) determining variations in fluidized ejecta blanket sinuosity across the planet; and (3) measurement of depth-diameter ratios and determination of regional variations in this ratio. Author (revised)

N94-20385*# Alaska Univ., Fairbanks. Dept. of Geology and Geophysics.
CALDERAS PRODUCED BY HYDROMAGMATIC ERUPTIONS THROUGH PERMAFROST IN NORTHWEST ALASKA Abstract Only
J. E. Beget *In* Lunar and Planetary Inst., Workshop on the Martian Northern Plains: Sedimentological, Periglacial, and Paleoclimatic Evolution 1993 p 3 (For primary document see N94-20382 05-91)
Avail: CASI HC A01/MF A01

Most hydromagmatic eruptions on Earth are generated by interactions of lava and ground or surface water. This eruptive process typically produces craters 0.1-1 km in diameter, although a few as large as 1-2 km were described. In contrast, a series of Pleistocene hydromagmatic eruptions through 80-100-m-thick permafrost on the Seward Peninsula of Alaska produced four craters 3-8 km in diameter. These craters, called the Espenberg maars, are the four largest maars known on Earth. The thermodynamic properties of ground ice influence the rate and amount of water melted during the course of the eruption. Large quantities of water are present, but only small amounts can be melted at any time to interact with magma. This would tend to produce sustained and highly explosive low water/magma (fuel-coolant) ratios during the eruptions. An area of 400 km(sub 2) around the Alaskan maars shows strong reductions in the density of thaw lakes, ground ice, and other surface manifestations of permafrost because of deep burial by coeval tephra falls. The unusually large Espenberg maars are the first examples of calderas produced by hydromagmatic eruptions. These distinctive landforms can apparently be used as an indicator of the presence of permafrost at the time of eruption. Author (revised)

N94-20386*# Alaska Univ., Fairbanks. Dept. of Geology and Geophysics.
MILANKOVITCH INSULATION FORCING AND CYCLIC FORMATION OF LARGE-SCALE GLACIAL, FLUVIAL, AND EOLIAN LANDFORMS IN CENTRAL ALASKA Abstract Only
J. E. Beget *In* Lunar and Planetary Inst., Workshop on the Martian Northern Plains: Sedimentological, Periglacial, and Paleoclimatic Evolution 1993 p 3 (For primary document see N94-20382 05-91)
Avail: CASI HC A01/MF A01

Continuous marine and ice-core proxy climate records indicate that the Earth's orbital geometry modulates long-term changes. Until recently, little direct evidence has been available to demonstrate correlations between Milankovitch cycles and large-scale terrestrial landforms produced during worldwide glaciations. In central Alaska large areas of loess and sand fill valleys and basins near major outwash streams. The streams themselves are bordered by sets of outwash terraces, and the terraces grade up valley into sets of moraines. The discovery of the Stampede tephra (approximately 175,000 yr ago) reworked within push moraines of the Lignite Creek glaciation suggests that this event correlates with the glaciation of marine isotope stage 6. A new occurrence of the Old Crow tephra (approximately 140,000 yr ago) on the surface of the oldest outwash terrace of the Tanana River, correlated with Delta glaciation, suggests this event also occurred at this time. The penultimate Healy glaciation apparently correlates with marine isotope stage 4, while radiocarbon dates indicate the latest Pleistocene moraines correlate with marine isotope stage 2. Recognition of the importance of orbital forcing to the cyclical formation of glacial landforms and landscapes can help in interpretations of remotely sensed glacial and proglacial land forms. Author (revised)

N94-20387*# Geological Survey, Menlo Park, CA.
THE FATE OF WATER DEPOSITED IN THE LOW-LYING NORTHERN PLAINS Abstract Only
M. H. Carr *In* Lunar and Planetary Inst., Workshop on the Martian Northern Plains: Sedimentological, Periglacial, and Paleoclimatic Evolution 1993 p 3-4 (For primary document see N94-20382 05-91)
Avail: CASI HC A01/MF A01

Many large outflow channels terminate in the low-lying northern plains. If the outflow channels formed by running water, as appears likely, then standing bodies of water must have accumulated at the ends of the channels. Most of the observed channels, and hence the bodies of water, are post-Noachian. They formed after the period for which we have the most abundant evidence of climate change. While it has been speculated that the post-Noachian period has experienced large, episodic, climatic excursions, this paper takes the more conservative view that the climatic conditions on Mars, at least from mid-Hesperian onward, were mostly similar to the climatic conditions that prevail in the present epoch. Thus obliquity variations are taken into account, but massive climate changes induced by the floods are considered so improbable that they are ignored. Author (revised)

N94-20388*# Geological Survey, Flagstaff, AZ.
EVIDENCE FOR AN ICE SHEET/FROZEN LAKE IN UTOPIA PLANITIA, MARS Abstract Only
M. G. Chapman *In* Lunar and Planetary Inst., Workshop on the Martian Northern Plains: Sedimentological, Periglacial, and Paleoclimatic Evolution 1993 p 4-5 (For primary document see N94-20382 05-91)
Avail: CASI HC A01/MF A01

Previous workers noted evidence for a lacustrine basin in Utopia Planitia, Mars. Geomorphic features within the basin that collectively suggest that water or ice may once have been present include channels within the basin, channels peripheral to the basin, etched basin floor, 'thumbprint' terrain (whorled patterns), polygonal outlines, smooth floors (infilled), shoreline indicators (terraces, platforms, lineaments), and small cratered cones (pseudo craters or pingos). The authors interpret these data to suggest that the basin may have been the locus of a large paleolake in the northern lowlands of Mars. Alternatively, the area was proposed to be part of an ancient circumpolar ocean. The hypothetical paleolake was probably frozen to some depth. In fact, features now present at its boundaries suggest that the edges may have been frozen solid. Plains units at the southwestern boundary of Utopia Planitia show ridges that were compared with those that form at the mouths of Antarctic ice streams, thumbprint terrain, and young, high deposits having lobate margins that suggest mudflows. Thumbprint terrains were interpreted as recessional moraines, ice-pushed ridges, or subglacially eroded tunnel valleys with eroded eskers. At the east boundary of Utopia Planitia, geologic mapping at 1:500,000 scale of the Granicus Valles area (MTM quadrangles 30227, 30222, and 25227) indicates the presence of a basal scarp around the northwest flank

of Elysium that formed the east boundary of an ancient ice sheet.
Author (revised)

N94-20389*# Geological Survey, Flagstaff, AZ.
A WET-GEOLOGY AND COLD-CLIMATE MARS MODEL: PUNCTUATION OF A SLOW DYNAMIC APPROACH TO EQUILIBRIUM Abstract Only
J. S. Kargel *In* Lunar and Planetary Inst., Workshop on the Martian Northern Plains: Sedimentological, Periglacial, and Paleoclimatic Evolution 1993 p 5-7 (For primary document see N94-20382 05-91)
Avail: CASI HC A01/MF A01

It was suggested that Mars may have possessed a relatively warm humid climate and a vigorous hydrological cycle involving meteoric precipitation, oceans, and continental ice sheets. Baker hypothesized that these geologically active conditions may have been repeated several times; each of these dynamic epochs was followed by a collapse of the climate and hydrologic cycle of Mars into essentially current conditions, completing what is termed a 'Baker cycle'. The purpose is to present an endmember possibility that Martian glacial landscapes, including some that were previously considered to have formed under warm climatic conditions, might be explained by processes compatible with an extremely cold surface. Two aspects of hypothesized Martian glacial terrains were cited as favoring a warm climate during Baker cycles: (1) the formation of some landscapes, including possible eskers, tunnel channels, drumlins, and outwash plains, appears to have required liquid water, and (2) a liquid-surfaced ocean was probably necessary to feed the glaciers. The requirement for liquid water, if these features were correctly interpreted, is difficult to avoid; it is entirely possible that a comparatively warm climate was involved, but it is not clear that formation of landforms by wet-based glaciers actually requires a warm climate. Even less certain is the supposed requirement for liquid oceans. Formation of glaciers only requires a source of water or ice to supply an amount of precipitation that exceeds losses due to melting and sublimation. At Martian temperatures precipitation is very low, but so are melting and sublimation, so a large body of ice that is unstable with respect to sublimation may take the role of Earth's oceans in feeding the glaciers. Recent models suggest that even current Martian polar caps, long thought to be static bodies of ice and dust, might actually be slow-moving, cryogenic continental glaciers. Is it possible that subglacial processes beneath cryogenic (but wetbased) ice sheets formed the hypothesized Martian glacial landscapes? Author (revised)

N94-20390*# Geological Survey, Flagstaff, AZ.
POSSIBLE OCCURRENCE AND ORIGIN OF MASSIVE ICE IN UTOPIA PLANITIA Abstract Only
J. S. Kargel and F. M. Costard (Centre National de la Recherche Scientifique, Caen, France.) *In* Lunar and Planetary Inst., Workshop on the Martian Northern Plains: Sedimentological, Periglacial, and Paleoclimatic Evolution 1993 p 7-8 (For primary document see N94-20382 05-91)
Avail: CASI HC A01/MF A01

F. M. Costard recently discovered a large field of possible thermokarst depressions near latitude 45 deg N, longitude 270 deg, in western Utopia Planitia. Oval to circular pits are typically 300-1000 m across and approximately 25 m deep; larger depressions, 3-5 km across, are compound and seem to have formed by coalescence of smaller pits. Small domical hills occur on the floors of two pits. These depressions characteristically have steep, scalloped edges and one or more inner benches. Truncation relations of the benches suggest a discontinuous, lenslike stratification of the material in which the pits are developed. Based on a close analogy in form and scale with coalesced thawlake basins (alases) on Earth, the Martian pits may have formed by thermophysical interactions of pooled water with ice-rich permafrost. This interpretation is not unique; sublimation of ice-rich permafrost or possibly even eolian processes acting on ice-free material might have formed the pits. However, the regional setting contains many other indications of massive ice. Some of these features are examined. Author (revised)

N94-20391*# Geological Survey, Flagstaff, AZ.
ICE IN THE NORTHERN PLAINS: RELIC OF A FROZEN OCEAN? Abstract Only
B. K. Lucchitta *In* Lunar and Planetary Inst., Workshop on the Martian Northern Plains: Sedimentological, Periglacial, and Paleoclimatic Evolution 1993 p 9-10 (For primary document see N94-20382 05-91)
Avail: CASI HC A01/MF A01

Viking images revealed many features in the northern plains and along their boundary that early investigators believed to be formed by ice-related processes. The features are possible pingos, pseudocraters, table mountains and moberg ridges, thermokarst depressions, moraines, patterned ground, and lobate aprons that suggest viscous flow such as that of ice or rock glaciers. More recently, many of these features were reinterpreted as related to sedimentation in hypothetical former polar lakes, oceans, or alluvial plains or as shoreline features of associated water bodies. Some evidence that points toward the existence of former bodies of standing water in the northern plains, but is also consistent with the idea that these bodies were ice covered or completely frozen is reviewed. Author (revised)

N94-20392*# Lowell Observatory, Flagstaff, AZ.
OBSERVED CLIMATIC ACTIVITY PERTAINING TO THE EVOLUTION OF THE NORTHERN PLAINS Abstract Only
L. J. Martin and P. B. James (Toledo Univ., OH.) *In* Lunar and Planetary Inst., Workshop on the Martian Northern Plains: Sedimentological, Periglacial, and Paleoclimatic Evolution 1993 p 10 Sponsored in part by Space Telescope Inst. (For primary document see N94-20382 05-91)
(Grants NAGw-2257; NAGw-3311)
Avail: CASI HC A01/MF A01

Although most of the landforms observed by Viking were probably formed long before the advent of present climatic conditions, it is possible that some modifications occurred more recently and may continue to the present. Also, present climate activity provides another dataset for hypothesizing earlier climatic conditions. Observations of climatic activity in the northern plains from 1905 to 1993 are summarized. Data from Earthbound telescopes and from spacecraft, including the Hubble Space Telescope (HST), were used. Author (revised)

N94-20393*# Massachusetts Univ., Amherst. Dept. of Geology and Geography.
A MODEL FOR THE ORIGIN OF MARTIAN POLYGONAL TERRAIN Abstract Only
G. E. McGill *In* Lunar and Planetary Inst., Workshop on the Martian Northern Plains: Sedimentological, Periglacial, and Paleoclimatic Evolution 1993 p 10-12 (For primary document see N94-20382 05-91)
Avail: CASI HC A01/MF A01

Extensive areas of the Martian northern plains in Utopia and Acidalia Planitiae are characterized by 'polygonal terrain.' Polygonal terrain consists of material cut by complex troughs defining a pattern resembling mudcracks, columnar joints, or frost-wedge polygons on the Earth. However, the Martian polygons are orders of magnitude larger than these potential Earth analogs, leading to severe mechanical difficulties for genetic models based on simple analogy arguments. Stratigraphic studies show that the polygonally fractured material in Utopia Planitia was deposited on a land surface with significant topography, including scattered knobs and mesas, fragments of ancient crater rims, and fresh younger craters. Sediments or volcanics deposited over topographically irregular surfaces can experience differential compaction producing drape folds. Bending stresses due to these drape folds would be superposed on the pervasive tensile stresses due to desiccation or cooling, such that the probability of fracturing is enhanced above buried topographic highs and suppressed above buried topographic lows. Thus it was proposed that the scale of the Martian polygons is controlled by the spacing of topographic highs on the buried surface rather than by the physics of the shrinkage process. Author (revised)

N94-20394*# Colorado Univ., Boulder.
THE DISTRIBUTION OF GROUND ICE ON MARS Abstract Only
M. T. Mellon and B. M. Jakosky *In* Lunar and Planetary Inst., Workshop on the Martian Northern Plains: Sedimentological, Periglacial, and Paleoclimatic Evolution 1993 p 12 (For primary document see N94-20382 05-91)
Avail: CASI HC A01/MF A01

A wealth of geologic evidence indicates that subsurface water ice has played an important role in the evolution of Martian landforms. Theoretical models of the stability of ground ice show that in the near-surface regolith ice is currently stable at latitudes poleward of about +/- 40 deg and below a depth of a few centimeters to a meter, with some variations with longitude. If ice is not previously present at a particular location where it is stable, atmospheric water will diffuse into the regolith and condense as ice, driven by the annual subsurface thermal oscillations. The lower boundary

of this ice deposit is found to occur at a depth (typically a few meters) where the annual thermal oscillations give way to the geothermal gradient. In the equatorial regions near-surface ice is currently not stable, resulting in the sublimation of any existing ice and subsequent loss to the atmosphere. However, subliming ice might be maintained at a steady-state depth, where diffusion and loss to the atmosphere are balanced by resupply from a possible deeper source of water (either deeper, not yet depleted, ice deposits or ground water). This depth is typically a few tens to hundreds of meters and depends primarily on the surface temperature and the nature of the geothermal gradient, being deeper for a higher surface temperature and a lower geothermal gradient. Such an equatorial deposit is characterized by the regolith ice content being low nearer the surface and increasing with depth in the deposit. Oscillations in the orbit will affect this picture of ground ice in two ways: by causing periodic changes in the pattern of near-surface stability and by producing subsurface thermal waves that may be capable of driving water ice deeper into the regolith. Author (revised)

N94-20395*# University of Southern California, Los Angeles.
A MARINE SEDIMENTARY MODEL FOR THE EVOLUTION OF THE NORTHERN PLAINS Abstract Only
T. J. Parker and D. S. Gorsline *In* Lunar and Planetary Inst., Workshop on the Martian Northern Plains: Sedimentological, Periglacial, and Paleoclimatic Evolution 1993 p 12-14 (For primary document see N94-20382 05-91)
Avail: CASI HC A01/MF A01

For the purpose of focusing the following discussion, we begin with the reasonable assumption that landforms interpreted to be shorelines can be considered to be as diagnostic of former water levels within the northern plains of Mars as lava flows are of former volcanism. Once (or if) this interpretation of these features becomes more generally accepted and the compositional and topographic datasets for Mars improve, their distribution can be used to make valuable independent estimates of the planet's water budget by providing quantitative measures of surface reservoir volumes at specific instances in Martian history. The problem is approached from a consideration of the basin's volume and its implied requirement on juvenile water sources and channel discharges, rather than the other way around. Author (revised)

N94-20396*# Geological and Geophysical Surveys, Fairbanks, AK.
CRYOPLANATION TERRACES OF INTERIOR AND WESTERN ALASKA Abstract Only
R. D. Reger *In* Lunar and Planetary Inst., Workshop on the Martian Northern Plains: Sedimentological, Periglacial, and Paleoclimatic Evolution 1993 p 14-15 (For primary document see N94-20382 05-91)
Avail: CASI HC A01/MF A01

Cryoplanation terraces are step- or table like residual landforms consisting of a nearly horizontal bedrock surface covered by a thin veneer of rock debris and bounded by ascending or descending scarps or both. Among examples studied, rubble-covered scarps range in height from 3 to 76 m and slope from 9 deg to 32 deg; nearly vertical scarps exist where bedrock is exposed or thinly buried. Simple transverse nivation hollows, which are occupied by large seasonal snow banks, commonly indent the lower surfaces of sharply angular ascending scarps. Terrace treads slope from 1 deg to 10 deg and commonly cut across bedrock structures such as bedding, rock contacts, foliation, joints, faults, and shear zones. Debris on terrace treads is generally 0.8-2.5 m thick. Permafrost table is generally present from 0.5 to 2 m below the tread surface. Permafrost is shallowest in the floors of nivation hollows and deepest in the well-drained margins of terrace treads. Side slopes of cryoplanation terraces are shallowly buried bedrock surfaces that are littered with a variety of mass-movement deposits. Author (revised)

N94-20397*# National Aeronautics and Space Administration. Goddard Space Flight Center, Greenbelt, MD.
THE THUMBPRINT TERRAIN: WHAT WILL MARS OBSERVER TELL US? Abstract Only
M. W. Schaefer *In* Lunar and Planetary Inst., Workshop on the Martian Northern Plains: Sedimentological, Periglacial, and Paleoclimatic Evolution 1993 p 15 Prepared in cooperation with Maryland Univ., College Park (For primary document see N94-20382 05-91)
Avail: CASI HC A01/MF A01

Some of the more puzzling features seen on Mars are those known as curvilinear features or 'thumb print' terrain, types of patterned ground found in the northern plains. The thumbprint terrain, named for its resemblance to the lines of a human thumbprint is found on what appears to be level, relatively low-lying ground near the crustal dichotomy boundary. It is often found near the termini of large channels. There are three types of thumbprint terrain in the classification of Rossbacher and Judson. The first consists of ridges and depressions about a kilometer wide, separated by a few kilometers, and with an apparent relief of 40-100 m. The second consists of steep-sided, flat-floored depressions about a kilometer wide, separated by a few kilometers, and with an apparent relief of 10-290 m. The third consists only of albedo markings, with a typical scale of about a kilometer. Many models were proposed to explain the origin of this terrain. It was suggested that it was caused by lava flows, removal of debris mantles, glaciers, or karst. However, the most popular models at present involve the action of subsurface ice to form such thermokarst features as striped ground, solifluction lobes, and/or linear, ice-cored ridges. There are several instruments on the Mars Observer spacecraft that will be able to provide us with information useful in distinguishing between these models. Author (revised)

N94-20398*# Geological Survey, Flagstaff, AZ.
STRATIGRAPHY OF THE MARTIAN NORTHERN PLAINS Abstract Only
K. L. Tanaka *In* Lunar and Planetary Inst., Workshop on the Martian Northern Plains: Sedimentological, Periglacial, and Paleoclimatic Evolution 1993 p 15-17 (For primary document see N94-20382 05-91)
Avail: CASI HC A01/MF A01

The northern plains of Mars are roughly defined as the large continuous region of lowlands that lies below Martian datum, plus higher areas within the region that were built up by volcanism, sedimentation, tectonism, and impacts. These northern lowlands span about 50 x 10(exp 6) km(sup 2) or 35 percent of the planet's surface. The age and origin of the lowlands continue to be debated by proponents of impact and tectonic explanations. Geologic mapping and topical studies indicate that volcanic, fluvial, and eolian deposition have played major roles in the infilling of this vast depression. Periglacial, glacial, fluvial, eolian, tectonic, and impact processes have locally modified the surface. Because of the northern plains' complex history of sedimentation and modification, much of their stratigraphy was obscured. Thus the stratigraphy developed is necessarily vague and provisional: it is based on various clues from within the lowlands as well as from highland areas within and bordering the plains. The results are summarized. Author (revised)

N94-20399*# Lunar and Planetary Inst., Houston, TX.
SEISMIC-TRIGGERING HISTORY OF THE CATASTROPHIC OUTFLOWS IN THE CHRYSE REGION OF MARS Abstract Only
S. M. Clifford and K. L. Tanaka (Geological Survey, Flagstaff, AZ.) *In its* Workshop on the Martian Northern Plains: Sedimentological, Periglacial, and Paleoclimatic Evolution 1993 p 17-18 (For primary document see N94-20382 05-91)
Avail: CASI HC A01/MF A01

Much attention was recently focused on the Chryse outflow channels as the source for an ocean or large lakes in the northern plains of Mars. A critical question is whether the channels formed quickly and in concert or sporadically. Crosscutting relations demonstrate multiple episodes of channel formation for some of the channels; however, for most channels, the absence of high precision in the densities of superposed impact craters prevents precise reconstruction of the duration and sequence of channeling history. Another approach to addressing the groundwater discharge history is to evaluate the hypothetical storage of the Chryse aquifer system and its recharge and triggering histories. How outflow breakouts may have been triggered by relatively frequent, large marsquakes caused by faulting and impact is discussed. Author (revised)

N94-20400*# Arizona State Univ., Tempe.
A FORMATIONAL MODEL FOR THE POLYGONAL TERRAINS OF MARS: TAKING A CRACK AT THE GENESIS OF THE MARTIAN POLYGONS Abstract Only
M. L. Wenrich and P. R. Christensen *In* Lunar and Planetary Inst., Workshop on the Martian Northern Plains: Sedimentological, Periglacial, and Paleoclimatic Evolution 1993 p 19-21 (For primary document see N94-20382 05-91)
Avail: CASI HC A01/MF A01

The mechanism for the genesis of the polygonal terrains in Acidalia and Utopia Planitia has long been sought: however, no completely satisfying model was put forth that characterizes the evolution of these complexly patterned terrains. The polygons are roughly hexagonal but some are not entirely enclosed by fractures. These polygonal features range in widths from approximately 5 to 20 km. Several origins were proposed that describe the polygon borders as desiccation cracks, columnar jointing in a cooled lava, or frost-wedge features. These tension-induced cracking hypotheses were addressed by Pechmann, who convincingly disputes these mechanisms of formation based on scale magnitude difficulties and morphology. Pechmann suggests instead that the cracks delineating the 5-20-km-wide polygons on the northern plains of Mars are graben resulting from deep-seated, uniform, horizontal tension. The difficulty with this hypothesis is that no analogous polygonal forms are known to have originated by tectonism on Earth. McGill and Hills propose that the polygonal terrains on Mars resulted from either rapid desiccation of sediments or cooling of volcanics coupled with differential compaction of the material over a buried irregular topographic surface. They suggest that fracturing was enhanced over the areas of positive relief and was suppressed above the topographic lows. McGill and Hills suggest that the spacing of the topographic highs primarily controls the size of the Martian polygons and the physics of the shrinkage process is a secondary concern. Ray et. al. conducted a terrestrial study of patterned ground in periglacial areas of the U.S. to determine the process responsible for polygonal ground formation. They developed a model for polygon formation in which convection of seasonal melt water above a permafrost layer, driven by an unstable density stratification, differentially melts the permafrost interface, causing it to become undulatory. Author (revised)

N94-20401*# West (Frederick R.), Hanover, PA.
BALLOON EXPLORATION OF THE NORTHERN PLAINS OF MARS NEAR AND NORTH OF THE VIKING 2 LANDING SITE Abstract Only
Frederick R. West *In* Lunar and Planetary Inst., Workshop on the Martian Northern Plains: Sedimentological, Periglacial, and Paleoclimatic Evolution 1993 p 21 (For primary document see N94-20382 05-91)
Avail: CASI HC A01/MF A01

The next stage of exploratory surveying of the northern plains of Mars after the Mars Observer mission may best be done by Mars Balloon Exploration Vehicles (MBEV's) deployed in the atmosphere above the northern plains near and north of the Viking 2 lander (VL-2) landing site. This region of Mars is favorable for exploration by MBEV's for the following reasons: (1) the low surface elevation (approximately 2km, lower than the standard (zero) elevation of the Martian surface) provides atmospheric pressure sufficient to allow a MBEV to successfully operate and explore this region at the present stage of MBEV design and development; and (2) the relatively smooth nature of the northern plains terrain (few mountains, ridges, valleys, and craters) indicated so far by Mariner 9 and Viking Orbiter data seems adequate for operation of a MBEV when its SNAKE extension is in contact with the surface of one of these plains. The science objectives are presented. Author (revised)

N94-20402*# National Air and Space Museum, Washington, DC. Center for Earth and Planetary Studies.
GEOMORPHIC EVIDENCE FOR AN EOLIAN CONTRIBUTION TO THE FORMATION OF THE MARTIAN NORTHERN PLAINS Abstract Only
J. R. Zimbelman *In* Lunar and Planetary Inst., Workshop on the Martian Northern Plains: Sedimentological, Periglacial, and Paleoclimatic Evolution 1993 p 21-23 (For primary document see N94-20382 05-91)
Avail: CASI HC A01/MF A01

The northern plains of Mars have many morphologic characteristics that are uncommon or absent on the rest of the planet. Mariner 9 and Viking images obtained north of latitude 30 deg N revealed 'smooth' and 'mottled' plains of an uncertain origin. Some or all of the northern plains were interpreted to consist of lava plains intermixed with eolian and volcanic materials thick eolian mantles that buried portions of the mid latitudes periglacial deposits resulting from the presence of ground ice and as water-transported sediments derived from fluvial runoff, lacustrine deposition in standing bodies of water, or glacial runoff. The highest-resolution Viking images show many intriguing details that may provide clues to the origin of this complex and distinctive terrain. Some of the informative features present in the best Viking images, comparing the observations to what may be expected from various hypotheses of formation, are reviewed. While the results are not conclusive for any single hypothesis, eolian processes have played a major role in the erosion (and possibly deposition) of the materials that make up the surface exposures in the Martian northern plains. Author (revised)

N94-20636*# Lunar and Planetary Inst., Houston, TX.
TWENTY-FOURTH LUNAR AND PLANETARY SCIENCE CONFERENCE. PART 3: N-Z Abstracts Only
1993 631 p Conference held in Houston, TX, 15-19 Mar. 1993
(Contract NASw-4579)
(NASA-CR-193149; NAS 1.26:193149) Avail: CASI HC A99/MF A06

Papers from the conference are presented, and the topics covered include the following: planetary geology, meteorites, planetary composition, meteoritic composition, planetary craters, lunar craters, meteorite craters, petrology, petrography, volcanology, planetary crusts, geochronology, geomorphism, mineralogy, lithology, planetary atmospheres, impact melts, K-T Boundary Layer, volcanoes, planetary evolution, tectonics, planetary mapping, asteroids, comets, lunar soil, lunar rocks, lunar geology, metamorphism, chemical composition, meteorite craters, planetary mantles, and space exploration. For individual titles, see N94-20637 through N94-20911.

N94-20637*# Southwest Research and Development Co., Las Cruces, NM.
SO2 ON VENUS: IUE, HST AND GROUND-BASED MEASUREMENTS, AND THE ACTIVE VOLCANISM CONNECTION Abstract Only
C. Y. Na, E. S. Barker (Texas Univ., Austin.), S. A. Stern, and L. W. Esposito (Colorado Univ., Boulder.) *In* Lunar and Planetary Inst., Twenty-Fourth Lunar and Planetary Science Conference. Part 3: N-Z 1993 p 1043-1044 (For primary document see N94-20636 05-91)
Avail: CASI HC A01/MF A06

Magellan images have shown that the volcanic features are widespread over the surface of Venus. The question of whether there is active volcanism is important for understanding both the atmospheric and the geological processes on Venus. The thick cloud cover of Venus precludes any direct observation of active volcanoes even if they exist. The only means of monitoring the active volcanism on Venus at present seems to be remote sensing from Earth. Continuous monitoring of SO2 is important to establish the long term trend of SO2 abundance and to understand the physical mechanism responsible for the change. Derived from text

N94-20638*# Tokyo Univ. (Japan). Geological Inst.
EVAPORATION IN EQUILIBRIUM, IN VACUUM, AND IN HYDROGEN GAS Abstract Only **c25**
Hiroko Nagahara *In* Lunar and Planetary Inst., Twenty-Fourth Lunar and Planetary Science Conference. Part 3: N-Z 1993 p 1045-1046 (For primary document see N94-20636 05-91)
Avail: CASI HC A01/MF A06

Evaporation experiments were conducted for SiO2 in three different conditions: in equilibrium, in vacuum, and in hydrogen gas. Evaporation rate in vacuum is about two orders of magnitude smaller than that in equilibrium, which is consistent with previous works. The rate in hydrogen gas changes depending on hydrogen pressure. The rate at 10 exp -7 bar of hydrogen pressure is as small as that of free evaporation, but at 10 exp -5 bar of hydrogen pressure it is larger than that in equilibrium. In equilibrium and in vacuum, the evaporation rate is limited by decomposition of SiO2 on the crystal surface, but it is limited by a diffusion process for evaporation in hydrogen gas. Therefore, evaporation rate of minerals in the solar nebula can be shown neither by that in equilibrium nor by that in vacuum. The maximum temperature of the solar nebula at the midplane at 2-3 AU where chondrites are believed to have originated is calculated to be as low as 150 K, 1500 K, or in between them. The temperature is, in any case, not high enough for total evaporation of the interstellar materials. Therefore, evaporation of interstellar materials is one of the most important processes for the origin and fractionation of solid materials. The fundamental process of evaporation of minerals has been intensively studied for these several years. Those experiments were carried out either in equilibrium or in vacuum; however, evaporation in the solar nebula is in hydrogen (and much smaller amount of helium) gas. In order to investigate evaporation rate and compositional (including isotopic) fractionation during evaporation, vaporization experiments for various minerals in various conditions are conducted. At first, SiO2 was adopted for a starting material, because

thermochemical data and its nature of congruent vaporization are well known. Experiments were carried out in a vacuum furnace system.
Derived from text

N94-20639*# Kobe Univ. (Japan). Dept. of Earth Sciences.
REE AND OTHER TRACE LITHOPHILES IN MAC88177, LEW88280 AND LEW88763 Abstract Only **c90**
N. Nakamura and N. Morikawa *In* Lunar and Planetary Inst., Twenty-Fourth Lunar and Planetary Science Conference. Part 3: N-Z 1993 p 1047-1048 (For primary document see N94-20636 05-91)
Avail: CASI HC A01/MF A06

In order to investigate the petrogenesis of primitive achondrites, we have carried out precise isotope dilution analyses of REE, Sr, Ba, Rb, K, Li, Ca, Mg, and Fe for three new meteorites: (Lodranites) MAC88177, LEW88280, (Brachinite) LEW88763, together with analyses for Acapulco. Present results are compared with those of other primitive achondrites previously reported by us and others. Derived from text

N94-20640*# Academy of Sciences (USSR), Moscow. Inst. of Geochemistry and Analytical Chemistry.
THE EREVAN HOWARDITE: PETROLOGY OF GLASSY CLASTS AND MINERAL CHEMISTRY Abstract Only **c25**
M. A. Nazarov and A. A. Ariskin *In* Lunar and Planetary Inst., Twenty-Fourth Lunar and Planetary Science Conference. Part 3: N-Z 1993 p 1049-1050 (For primary document see N94-20636 05-91)
Avail: CASI HC A01/MF A06

The Erevan howardite is a polymict regolith breccia containing xenoliths of carbonaceous chondrites. In this work, we studied glassy clasts, which could be considered as primary quenched melts, and mineral chemistry of the breccia. The study reveals that the Erevan howardite consists of common rocks of the HED suite. However, unique glassy clasts, which are present in some eucritic melts, were identified. The mineral chemistry and the simulation of crystallization of the melts suggest that the compositions of the melts reflect those of some primary lithologies of EPB.
Derived from text

N94-20641*# Academy of Sciences (USSR), Moscow. Inst. of Geochemistry and Analytical Chemistry.
THE KOSHAK SECTION: EVIDENCE FOR ELEMENT FRACTIONATION AND AN OXIDATION EVENT AT THE K/T BOUNDARY Abstract Only **c46**
M. A. Nazarov, D. D. Badjukov, L. D. Barsukova, G. M. Kolesov, and D. P. Naidin (Moscow State Univ., Russia.) *In* Lunar and Planetary Inst., Twenty-Fourth Lunar and Planetary Science Conference. Part 3: N-Z 1993 p 1051-1052 (For primary document see N94-20636 05-91)
Avail: CASI HC A01/MF A06

The Koshak site is a new K/T section located about 125 km EEN of the Fort Shevchenko city, Mangyshlak, Kazakhstan. In this paper, we report results of geochemical and mineralogical studies of this section which indicate a deep element fractionation and an oxidation event at the K/T boundary.
Derived from text

N94-20642*# Academy of Sciences (USSR), Moscow. Inst. of Geochemistry and Analytical Chemistry.
CARBONACEOUS XENOLITHS FROM THE EREVAN HOWARDITE Abstract Only **c25**
M. A. Nazarov, F. Brandstaetter (Naturhistorisches Museum, Vienna, Austria.), and G. Kurat (Naturhistorisches Museum, Vienna, Austria.) *In* Lunar and Planetary Inst., Twenty-Fourth Lunar and Planetary Science Conference. Part 3: N-Z 1993 p 1053-1054 (For primary document see N94-20636 05-91)
Avail: CASI HC A01/MF A06

Preliminary studies of the Erevan howardite showed that the meteorite is a polymict breccia. We report on our study of CM-type carbonaceous xenoliths. All of these clasts are enriched in tochilinite and carbonate inclusion as compared to CM chondrites. They also contain a new, P-rich sulphide beside pentlandite. The P-rich sulphide represents a new type of P-bearing phases. It indicates a chalcophile behavior of P under certain nebular conditions.
Derived from text

N94-20643*# Academy of Sciences (USSR), Moscow. Inst. of Geochemistry and Analytical Chemistry.
IGNEOUS ROCK FROM SEVERNYI KOLCHIM (H3) CHONDRITE: NEBULAR ORIGIN Abstract Only **c90**
M. A. Nazarov, F. Brandstaetter (Naturhistorisches Museum, Vienna, Austria.), and G. Kurat (Naturhistorisches Museum, Vienna, Austria.) *In* Lunar and Planetary Inst., Twenty-Fourth Lunar and Planetary Science Conference. Part 3: N-Z 1993 p 1055-1056 (For primary document see N94-20636 05-91)
Avail: CASI HC A01/MF A06

The discovery of lithic fragments with compositions and textures similar to igneous differentiates in unequilibrated ordinary chondrites (UOC's) and carbonaceous chondrites (CC's) has been interpreted as to suggest that planetary bodies existed before chondrites were formed. As a consequence, chondrites (except, perhaps CI chondrites) cannot be considered primitive assemblages of unprocessed nebular matter. We report about our study of an igneous clast from the Severnyi Kolchim (H3) chondrite. The results of the study are incompatible with an igneous origin of the clast but are in favor of a nebular origin similar to that of chondrules.
Derived from text

N94-20644*# Notre Dame Univ., IN. Dept. of Civil Engineering and Geological Sciences.
PETROGENESIS OF APOLLO 12 MARE BASALTS. PART 1: MULTIPLE MELTS AND FRACTIONAL CRYSTALLIZATION TO EXPLAIN OLIVINE AND ILMENITE BASALT COMPOSITIONS Abstract Only **c25**
Clive R. Neal and Lawrence A. Taylor (Tennessee Univ., Knoxville.) *In* Lunar and Planetary Inst., Twenty-Fourth Lunar and Planetary Science Conference. Part 3: N-Z 1993 p 1057-1058 (For primary document see N94-20636 05-91)
Avail: CASI HC A01/MF A06

Mare basalts returned by the Apollo 12 mission have been divided into 4 groups on the basis of mineralogy and whole-rock chemistry: olivine basalts; pigeonite basalts; ilmenite basalts; and feldspathic basalts. James and Wright and Rhodes et al. concluded that the olivine and pigeonite groups were co-magmatic and that the within group variations are due to fractional crystallization of olivine and minor Cr-spinel, with pigeonite replacing olivine in the pigeonite basalts. Rhodes et al. concluded that the parental compositions for these suites were probably represented by the vitrophyres, and the olivine basalts are comprised essentially of cumulates and the pigeonites of evolved end-members. However, Neal et al. have demonstrated, using trace-element considerations, that the Apollo 12 olivine and pigeonite suites are not related. The ilmenite basalts were studied extensively by Dungan and Brown who noted that both cumulates and evolved fractionates were present within this group. In their modeling, Dungan and Brown used the vitrophyre compositions as parents. Neal et al. demonstrated that the feldspathic suite was probably comprised of only one member - 12038. Herein, the ilmenite and olivine basalts are demonstrated to be the products of several non-modal partial melting events of a single source followed by closed-system fractional crystallization.
Derived from text

N94-20645*# Notre Dame Univ., IN. Dept. of Civil Engineering and Geological Sciences.
PETROGENESIS OF APOLLO 12 MARE BASALTS. PART 2: AN OPEN SYSTEM MODEL TO EXPLAIN THE PIGEONITE BASALT COMPOSITIONS Abstract Only **c25**
Clive R. Neal and Lawrence A. Taylor (Tennessee Univ., Knoxville.) *In* Lunar and Planetary Inst., Twenty-Fourth Lunar and Planetary Science Conference. Part 3: N-Z 1993 p 1059-1060 (For primary document see N94-20636 05-91)
Avail: CASI HC A01/MF A06

Original petrogenetic models suggested that the pigeonite basalts were the evolved equivalents of the olivine basalts. Rhodes et al. concluded that the olivine and pigeonite basalts were co-magmatic, but Neal et al. have demonstrated that these two basaltic groups are distinct and unrelated. The pigeonite suite is comprised of porphyritic basalts with a fine-grained ground mass and range continuously to coarse-grained microgabbros with ophitic to graphic textures. Although it was generally recognized that the pigeonite basalts were derived from the olivine basalts by olivine + minor Cr-spinel fractionation, the compositional gap between these groups is difficult to reconcile with such a model. Indeed, Baldridge et al. concluded that these two basaltic groups could not have been co-magmatic. In this paper, we suggest an open system AFC model for pigeonite basalt

petrogenesis. The assimilant is lunar anorthositic crust and the r value used is 0.6. While the choice of assimilant composition is difficult to constrain, the modeling demonstrates the feasibility of this model. Derived from text

N94-20646*# Jet Propulsion Lab., California Inst. of Tech., Pasadena.
THE COHERENT BACKSCATTERING OPPOSITION EFFECT Abstract Only **c74**
R. M. Nelson, B. W. Hapke (Pittsburgh Univ., PA.), W. D. Smythe, V. Gharakanian, and P. Herrera *In* Lunar and Planetary Inst., Twenty-Fourth Lunar and Planetary Science Conference. Part 3: N-Z 1993 p 1061-1062 (For primary document see N94-20636 05-91)
Avail: CASI HC A01/MF A06

We have measured the opposition effect, the nonlinear surge in reflectance seen in particulate materials as phase angle approaches zero degrees, in a suite of materials of varying particle size and reflectance. These samples were illuminated by linearly and circularly polarized monochromatic radiation at two wavelengths, 0.442 and 0.633 microns. By measuring the linear and circular polarization ratios for each sample, we have found that in highly reflective materials the behavior of the reflected radiation is consistent with the coherent backscattering process which has recently been proposed to explain the opposition surge that is seen in such media. The size and width of the coherent backscattering opposition peak vary as a function of reflectance of the sample. The opposition effect has been observed in particulate materials studied in the laboratory and it is also observed in the radiation reflected from solar system bodies which present a regolith to the earth based observer. The traditional explanation of the opposition effect, the shadow-hiding hypothesis, is that it was caused by the elimination of mutual shadows cast between the regolith grains as the phase angle of the observation became smaller. This shadow-hiding hypothesis, however, is unable to explain the opposition effect seen in highly reflective materials such as magnesium oxide and barium sulfate powders. This is because highly reflective media will multiply scatter the incident radiation between the regolith grains. This causes the shadows to be eliminated. We have measured the angular scattering properties of a suite of materials of different reflectivity. We have observed polarization ratios in reflective particulates that are consistent with coherent backscattering as the principal process which causes the opposition surge. Derived from text

N94-20647*# Academy of Sciences (USSR), Moscow. Inst. for Dynamics of Geospheres.
ON MAGNETODYNAMIC EFFECTS INITIATED BY A HIGH-SPEED IMPACT OF A LARGE COSMIC BODY UPON THE EARTH'S SURFACE Abstract Only **c90**
I. V. Nemchinov, P. E. Alexandrov, V. I. Artemiev, V. I. Bergelson, and V. A. Rybakov *In* Lunar and Planetary Inst., Twenty-Fourth Lunar and Planetary Science Conference. Part 3: N-Z 1993 p 1063-1064 (For primary document see N94-20636 05-91)
Avail: CASI HC A01/MF A06

The impact of a large cosmic body with typical size R approximately = 1 km (mass M approximately = 4-10 Gt for a stony or icy body) moving with velocity V approximately = 50-70 km/s (kinetic energy of the order of 10 exp 21 J or 10 exp 6 Mt of TMT) on the Earth's surface leads to a full vaporization of a body and of a significant part of substance of the upper layers of the Earth and even to the ionization of this vapor cloud. As a result, a hypersonic jet of air and erosion plasma is formed. The kinetic energy E sub J is far above the total energy of the geomagnetic field of the Earth (approximately equivalent to the energy of 100 Mt) and the total mass of a fast-moving part of the jet M sub j approximately = 10 exp 12 kg is far above the mass of atmosphere in the jet expansion cone. Thus, the jet will propagate practically inertially with the constant mean velocity U approximately = 10-20 km/s and even higher. The interaction of this plasma jet with the Earth's magnetic field causes magnetodynamic effects similar to those which are produced by cosmic nuclear explosions but of a larger scale. The preliminary results of experimental and numerical modeling of the plasma jet-magnetosphere interaction are presented. Derived from text

N94-20648*# Academy of Sciences (USSR), Moscow. Inst. for Dynamics of Geospheres.
DETERMINATION OF COSMIC BODIES SIZE-VELOCITY DISTRIBUTION BY OBSERVATION OF CURRENT IMPACTS ON MARS Abstract Only **c90**
I. V. Nemchinov, A. A. Perelomova, and V. V. Shuvalov *In* Lunar and Planetary Inst., Twenty-Fourth Lunar and Planetary Science Conference. Part 3: N-Z 1993 p 1065-1066 (For primary document see N94-20636 05-91)
Avail: CASI HC A01/MF A06

Collisions of cosmic bodies with terrestrial planets involve many physical processes such as deceleration and ablation during their flight through an atmosphere, the impact at a surface accompanied by cratering, melting and evaporation of surface material, generation of shock waves, etc. If body velocity is high enough then a thermal radiation is very important. All these processes on Mars proceed differently than on the other planets because of the low density of its atmosphere. In particular, this leads to the fact that smaller bodies of sizes of the order of 0.1-10 m strike the planet surface without being decelerated and perform some effects which may be detected by equipment placed on a board of artificial satellites, by a network of stations at the surface of Mars and even from the Earth. These observations can be used to determine size-velocity distribution of such bodies in the Solar System. Numerical simulation of the impacts at the surface of Mars have been carried out using two-dimensional gas dynamic code with detailed consideration of the thermal radiative transfer. This work is an extension of our previous paper. We have expanded a range of projectile sizes up to r sub 0 = 100 m. For such a large-scale body, the initial stage of the impact, involving crate ring and ejection of surface material, is very important. Thus, these effects have been taken into account. Derived from text

N94-20649*# Academy of Sciences (USSR), Moscow. Inst. for Dynamics of Geospheres.
EFFECTS OF HYDRODYNAMICS AND THERMAL RADIATION IN THE ATMOSPHERE AFTER COMET IMPACTS Abstract Only **c46**
I. V. Nemchinov, M. P. Popova, L. P. Shubadeeva, V. V. Shuvalov, and V. V. Svetsov *In* Lunar and Planetary Inst., Twenty-Fourth Lunar and Planetary Science Conference. Part 3: N-Z 1993 p 1067-1068 (For primary document see N94-20636 05-91)
Avail: CASI HC A01/MF A06

Radiation phenomena in the atmosphere after impacts of cosmic bodies have special features in comparison with the surface nuclear explosions. First, initial concentration of energy after the impact is lower, and second, a wake after the passage of the meteoroid through the atmosphere has a dramatic effect on the atmospheric flow and radiation transfer. Consequently, scaling laws can not be employed for prediction of the flow in the atmosphere and the light flux on the Earth's surface. If a density of high-velocity impactor is low relative to the ground, as in a case of a comet impact on rocks, a major part of the kinetic energy is converted to internal energy of dense hot vapors. But radiation effects can be essential even for fairly low velocities of the impactor. To clarify this issue we have undertaken calculations of 100-Mt explosions at the Earth's surface caused by small comets with velocities from 10 to 70 km/sec. That is, the initial concentration of energy has been varied. The calculations have shown that for velocities of the comet greater or about 20 km/sec a portion of energy emitted from the fireball exceeds 20% of the total energy of the explosion and this quantity does not change very much with the velocity. Other aspects of this investigation are discussed. Derived from text

N94-20650*# Deutsche Forschungsanstalt fuer Luft- und Raumfahrt, Berlin (Germany). Inst. for Planetary Exploration.
THE HIGH RESOLUTION STEREO CAMERA (HRSC) FOR THE LUNAR SCOUT 1 MISSION Abstract Only **c35**
G. Neukum *In* Lunar and Planetary Inst., Twenty-Fourth Lunar and Planetary Science Conference. Part 3: N-Z 1993 p 1069 (For primary document see N94-20636 05-91)
Avail: CASI HC A01/MF A06

The High Resolution Stereo Camera (HRSC) is a planetary imaging system developed by the German Aerospace Research Establishment (DLR) with the involvement of the German Space Industry under the leadership of the German Space Agency (DARA) for the Russian Mars 94 and Mars 96 missions. The same instrument, virtually unmodified, is ideal for imaging

the Moon. If flown on a Lunar Scout spacecraft, the HRSC will be operated so that it will produce data suitable for generation of a global lunar geodetic net, a global stereo image data set (both data sets produced at an orbit altitude of 200 kms approximately) and high resolution stereo imagery of areas of interest to the scientific community from an orbit altitude of 100 kms (resolution is a function of orbit altitude). All data will be digital.

Derived from text

N94-20651*# New Mexico Univ., Albuquerque. Dept. of Earth and Planetary Sciences.

CORE FORMATION IN THE MOON: THE MYSTERY OF THE EXCESS DEPLETION OF Mo, W AND P Abstract Only

H. E. Newsom and S. A. Maehr *In* Lunar and Planetary Inst., Twenty-Fourth Lunar and Planetary Science Conference. Part 3: N-Z 1993 p 1071-1072 (For primary document see N94-20636 05-91)

Avail: CASI HC A01/MF A06

We have evaluated siderophile element depletion models for the Moon in light of our improved statistical treatment of siderophile element abundance data and new information on the physics of core formation. If core formation occurred in the Moon at the large degrees of partial melting necessary for metal segregation, according to recent estimates, then a significant inconsistency (not seen in the eucrite parent body) exists in the depletion of the incompatible siderophile elements Mo, W, and P, compared to other siderophile elements in the Moon. The siderophile data, with the exception of Mo, are most consistent with terrestrial initial siderophile abundances and segregation of a very small core in the Moon. Our improved abundance estimates and possible explanations for these discrepancies are discussed.

Derived from text

N94-20652*# Bern Univ. (Switzerland). Physikalisches Inst.

DATING NATIVE GOLD BY NOBLE GAS ANALYSES Abstract Only **c25**

S. Niedermann, O. Eugster, B. Hofmann, Ch. Thalmann, and W. U. Reimold (Witwatersrand Univ., Johannesburg, South Africa.) *In* Lunar and Planetary Inst., Twenty-Fourth Lunar and Planetary Science Conference. Part 3: N-Z 1993 p 1073-1074 Sponsored by Swiss NSF (For primary document see N94-20636 05-91)

Avail: CASI HC A01/MF A06

Our recent work on He, Ne, and Ar in Alpine gold samples has demonstrated that gold is extremely retentive for He and could thus, in principle, be used for U/Th-He-4 dating. For vein-type gold from Brusson, Northern Italy, we derived a U/Th-He-4 age of 36 Ma, in agreement with the K-Ar formation age of associated muscovites and biotites. However, in placer gold from the Napf area, Central Switzerland, we observed large excesses of both He-4 and radiogenic Ar-40 (Ar-40 sub rad, defined as Ar-40-295.5-Ar-.36). The gas release systematics indicate two distinct noble gas components, one of which is released below about 800 C and the other one at the melting point of gold (1064 C). We now present results of He and Xe measurements in a 1 g placer gold sample from the river Kruempelgraben, as well as He and Ar data for Brusson vein-type gold and for gold from the Lily Gold Mine, South Africa. We calculate reasonable U/Th-He-4 as well as U-Xe ages based on those gases which are released at approximately 800 C. Probably the low-temperature components represent in-situ-produced radiogenic He and fission Xe, whereas the gases evolving when gold melts have been trapped during gold formation. Therefore, only the low-temperature components are relevant for dating purposes.

Derived from text

N94-20653*# Minnesota Univ., Minneapolis. School of Physics and Astronomy.

HELIUM IN INTERPLANETARY DUST PARTICLES Abstract Only **c90**

A. O. Nier and D. J. Schlutter *In* Lunar and Planetary Inst., Twenty-Fourth Lunar and Planetary Science Conference. Part 3: N-Z 1993 p 1075-1076 (For primary document see N94-20636 05-91)

Avail: CASI HC A01/MF A06

Helium and neon were extracted from fragments of individual stratosphere-collected interplanetary dust particles (IDP's) by subjecting them to increasing temperature by applying short-duration pulses of power in increasing amounts to the ovens containing the fragments. The experiment was designed to see whether differences in release temperatures could be observed which might provide clues as to the asteroidal or cometary origin of the particles. Variations were observed which show promise for elucidating the problem.

Derived from text

N94-20654*# Moscow State Univ. (Russia). Dept. of Geology.

GEOLOGIC MAPPING OF NORTHERN ATLA REGIO ON VENUS: PRELIMINARY DATA Abstract Only

A. M. Nikishin and G. A. Burba (Academy of Sciences, USSR, Moscow.) *In* Lunar and Planetary Inst., Twenty-Fourth Lunar and Planetary Science Conference. Part 3: N-Z 1993 p 1077-1078 (For primary document see N94-20636 05-91)

Avail: CASI HC A01/MF A06

The Northern part of Atla Regio within the frame of C1-formate Magellan photo map 15N197 was mapped geologically at scale 1:8,000,000. This is a part of Russia's contribution into C1 geologic mapping efforts. The map is reproduced here being reduced about twice. The map shows that the Northern Atla area is predominantly a volcanic plain with numerous volcanic features: shield volcanoes, domes and hills with various morphology, corona-like constructions, radar bright and dark spots often with flow-like outlines. Relatively small areas of tessera occurred in the area are mainly semi-flooded with the plain material. Tesserae are considered to be the oldest terrains within the map sheet. There are many lineated terrains in the region. They are interpreted as the old, almost-buried tesserae (those with crossed lineaments) or partly buried ridge belts (those with parallel lineaments). These lineated terrains have an intermediate age between the young volcanic plains and the old tessera areas. Two prominent high volcanic shields are located within the region - Ozza Mons and Sapas Mona. The most prominent structure in Northern Atla is Ganis Chasma rift. The rift cuts volcanic plain and is considered to be under formation during approximately the same time with Ozza Mons shield. Ganis Chasma rift valley is highly fractured and bounded with fault scarps. Rift shoulder uplifts are typical for Ganis Chasma. There are few relatively young volcanic features inside the rift valley. The analysis of fracturing and rift valley geometry shows the rift originated due to 5-10 percent crustal extention followed by the crustal subsidence. The age sequence summary for the main terrain types in the region is (from older to younger ones): tesserae; lineated terrains with crossed lineaments; lineated terrains with parallel lineaments; volcanic plains; and prominent volcanic shields and Ganis Chasma rift valley. The geologic structure of Atla Regio as it appeared now with the Magellan high resolution images is very close to that of Beta Regio. Such conclusion coincide with the earlier ones based on the coarser data.

Derived from text

N94-20655*# Moscow State Univ. (Russia). Dept. of Geology.

BETA REGIO RIFT SYSTEM ON VENUS: GEOLOGIC INTERPRETATION OF MAGELLAN IMAGES

A. M. Nikishin, N. N. Bobina (Academy of Sciences, USSR, Moscow.), V. K. Borozdin (Academy of Sciences, USSR, Moscow.), and G. A. Burba (Academy of Sciences, USSR, Moscow.) *In* Lunar and Planetary Inst., Twenty-Fourth Lunar and Planetary Science Conference. Part 3: N-Z 1993 p 1079-1080 (For primary document see N94-20636 05-91)

Avail: CASI HC A01/MF A06

Magellan SAR images and altimetric data were used to produce a new geologic map of the Northern part of Beta Regio within the frames of C1-30N279 mapsheet. It was part of our contributions into C1-formate geologic mapping efforts. The original map is at 1:8,000,000 scale. The rift structures are typical for Beta Regio on Venus. There are many large uplifted tessera areas on Beta upland. They occupy areas of higher topography. These tessera are partly burried by younger volcanic cover of plain material. These observations show that Beta upland was formed mainly due to lithospheric tectonical uplifting, and only partly was constructed by volcanic activity. A number of rift valleis traverse Beta upland and spread to the surrounding lowlands. The largest rift crosses Beta N to S. Typical width of rifts is 40 to 160 km. Rift valleis in this region are structurally represented by crustal grabens and half-grabens. There are symmetrical and asymmetrical rifts. A lot of them have shoulder uplifts with the relative high up to 0.5-1 km and width 40 to 60 km. Preliminary analysis of the largest rift valley structural cross-sections leads to the conclusion that it originated due to a 5-10 percent crustal extension. The prominent shield volcano - Theia Mons - is located at the center of Beta rift system. It could be considered as the surface manifestation of the upper mantle hot spot. Most of the rift belts are located radially to Theia Mons. The set of these data leads to conclusion that Beta rift system has

an 'active-passive' origin. It was formed due to the regional tectonic lithospheric extension. Rifting was accelerated by the upper mantle hot spot located under the center of passive extension (under Beta Regio).
Derived from text

N94-20656*# Moscow State Univ. (Russia). Dept. of Geology.
BETA REGIO - PHOEBE REGIO ON VENUS: GEOLOGIC MAPPING WITH THE MAGELLAN DATA Abstract Only
A. M. Nikishin, V. K. Borozdin (Academy of Sciences, USSR, Moscow.), N. N. Bobina (Academy of Sciences, USSR, Moscow.), and G. A. Burba (Academy of Sciences, USSR, Moscow.) *In* Lunar and Planetary Inst., Twenty-Fourth Lunar and Planetary Science Conference. Part 3: N-Z 1993 p 1081-1082 (For primary document see N94-20636 05-91)
Avail: CASI HC A01/MF A06

The geologic maps of C1-15N283 and C1-00N283 sheets were produced (preliminary versions) with Magellan SAR images. This work was undertaken as a part of Russia's contribution into C1 geologic mapping efforts. The scale of the original maps is 1:8,000,000, and the maps are reproduced here at a reduced size.
Derived from text

N94-20657*# Academy of Sciences (USSR), Moscow.
LARGEST IMPACT FEATURES ON VENUS: NON-PRESERVED OR NON-RECOGNIZABLE? Abstract Only
Olga V. Nikolaeva *In* Lunar and Planetary Inst., Twenty-Fourth Lunar and Planetary Science Conference. Part 3: N-Z 1993 p 1083-1084 (For primary document see N94-20636 05-91)
Avail: CASI HC A01/MF A06

Conventional explanation of a lack of impact craters with diameters greater than 300 km on Venus is that they formed during the intense bombardment era and had lunar-like morphology, but they are not preserved now because of rapid viscous relaxation of their topograpy and/or high endogenous reworking of surface. Other explanation invokes failure to recognize these larger craters because of their non-lunar-like morphology from the moment of formation, since larger gravity of Venus relatively to the Moon results in that largest craters on Venus may form within the mass of shock melted material while comparably sized lunar craters would be still almost 'dry'. To test this hypothesis, morphologies and rim-crest diameters of the largest peak-ring and Orientale-type basins and all larger impact features on Moon, Mercury, Mars, and Venus were compiled and compared to rim crest diameters of model craters with different melt volume/transient-cavity volume ratios. Results show that the final diameters of model craters formed at depth of melting about twice of transient cavity depth correspond to changeover from a planet-similar morphology of all the smaller basins on any terrestrial planet to a planet-specific morphology of all the larger basins on the Moon, Mercury, and Mars. On Venus, these largest impact features are not found and instead, a Venus-specific morphology of the largest concentric coronae appears in this size range. The coronae were suggested to form over sites of mantle upwelling and modified by subsequent volcanism and gravitational relaxation. The results here suggest that mantle upwelling - the first and necessary step of the corona formation models - may be induced by impact event (as a result of transient cavity collapse) and operated under cover of hot, slowly cooled impact melt in the areas of thinned crust and/or thermally active regions.
Author (revised)

N94-20658*# California Univ., Berkeley. Space Sciences Lab.
EXPOSURE AGES OF CARBONACEOUS CHONDRITES, 1 c90
K. Nishiizumi, J. R. Arnold (California Univ., San Diego, La Jolla.), M. W. Caffee (Lawrence Livermore National Lab., CA.), R. C. Finkel (Lawrence Livermore National Lab., CA.), J. R. Southon (Lawrence Livermore National Lab., CA.), H. Nagai (Nihon Univ., Tokyo, Japan.), M. Honda (Nihon Univ., Tokyo, Japan.), P. Sharma (Rochester Univ., NY.), M. Imamura (Tokyo Univ., Japan.), and K. Kobayashi (Tokyo Univ., Japan.) *In* Lunar and Planetary Inst., Twenty-Fourth Lunar and Planetary Science Conference. Part 3: N-Z 1993 p 1085-1086 (For primary document see N94-20636 05-91)
Avail: CASI HC A01/MF A06

The recent exposure histories of carbonaceous chondrites have been investigated using cosmogenic radionuclides. Our results may indicate a clustering of exposure ages of C1 and C2 chondrites into two peaks, 0.2 My and 0.6 My, perhaps implying two collisional events of Earth-crossing parent bodies. Among carbonaceous chondrites are some having short exposure ages which Mazor et al. hypothesized cluster into a small number of families. This hypothesis is based on spallogenic Ne-21 exposure ages, which in some instances are difficult to determine owing to the large amounts of trapped noble gases in carbonaceous chondrites. Also, since Ne-21 is stable, it integrates a sample's entire exposure history, so meteorites with complex exposure histories are difficult to understand using exclusively Ne-21. Cosmogenic radionuclides provide an alternative means of determining the recent cosmic ray exposure duration. To test the hypothesis of Mazor et al. we have begun a systematic investigation of exposure histories of Antarctic and non-Antarctic carbonaceous chondrites especially C2s.
Derived from text

N94-20659*# Washington Univ., Saint Louis, MO. Center for the Space Sciences and Physics Dept.
IDENTIFICATION OF AN INTERSTELLAR OXIDE GRAIN FROM THE MURCHISON METEORITE BY ION IMAGING Abstract Only c90
L. R. Nittler, R. M. Walker, E. Zinner, P. Hoppe (Bern Univ., Switzerland.), and R. S. Lewis (Chicago Univ., IL.) *In* Lunar and Planetary Inst., Twenty-Fourth Lunar and Planetary Science Conference. Part 3: N-Z 1993 p 1087-1088 (For primary document see N94-20636 05-91)
Avail: CASI HC A01/MF A06

We report here the first use of a new ion-imaging system to locate a rare interstellar aluminum oxide grain in a Murchison acid residue. While several types of carbon-rich interstellar grains, including graphite, diamond, SiC, and TiC, have previously been found, isotopically anomalous interstellar oxide grains have proven more elusive. We have developed an ion imaging system which allows us to map the isotopic composition of large numbers of grains relatively quickly and is, thus, ideally suited to search for isotopically exotic subsets of grains. The system consists of a PHOTOMETRICS CCD camera coupled to the microchannel plate/fluorescent screen of the WU modified CAMECA IMS-3F ion microprobe. Isotopic images of the sample surface are focused on the CCD and digitized. Subsequent image processing identifies individual grains in the images and determines isotopic ratios for each. For the present work, we have imaged in O-16 and O-18; negligible contributions of (17)OH(-) and (16)OH2(-) signals to the O-18 signal allow the use of low mass resolution, simplifying the measurements. Repeated imaging runs on terrestrial corundum particles showed that the system measures isotopic ratios reproducibly to about +/- 40%. Each imaging run took about six minutes to complete, and for this study there were on average 5-15 grains in each image. We have conducted imaging searches in 2-4 micron size separates of both Orgueil and Murchison.
Derived from text

N94-20660*# Hawaii Univ., Honolulu. Dept. of Geology and Geophysics.
FRAGMENTS OF ANCIENT LUNAR CRUST: FERROAN NORITIC ANORTHOSITES FROM THE DESCARTES REGION OF THE MOON Abstract Only
M. D. Norman, C. Alibert (Australian National Univ., Canberra.), and M. T. McCulloch (Australian National Univ., Canberra.) *In* Lunar and Planetary Inst., Twenty-Fourth Lunar and Planetary Science Conference. Part 3: N-Z 1993 p 1089-1090 (For primary document see N94-20636 05-91)
Avail: CASI HC A01/MF A06

Noritic anorthosite clasts from breccia 67016 have bulk compositions similar to that of the upper crust of the Moon and petrogenetic affinities with pristine ferroan anorthosites. Rb-Sr and Sm-Nd isotopic compositions of mineral separates from one of these clasts suggest very old (greater than or = 4.4 Ga) ages, but interpretation of these data is complicated by the multi-stage history of the clasts which involved magmatic crystallization, brecciation, subsolidus recrystallization, and sulfide metasomatism. These clasts record some of the earliest events on the Moon, including early crust formation, accretionary bombardment, and degassing of the lunar interior. Modal analyses of these clasts show they are now composed of about 70 percent plagioclase, 28 percent pyroxene, 2 percent troilite, and minor amounts of ilmenite and chromite. No metallic iron, phosphates, or other trace phases were observed. Olivine is very rare, occurring only as relicts within secondary troilite+pyroxene intergrowths which may reflect reaction of olivine with sulfurous vapors. PIXE proton microprobe analyses of the sulfides show that the metasomatism was accompanied by enrichments of Cu, Zn, Ni, Se, and Sb. The clasts have been only mildly shocked since the observed texture was established. Major and minor element mineral compositions are very homogeneous and strikingly similar

to those of pristine ferroan anorthosites. Pyroxene compositions indicate equilibration temperatures of 850-900 C. Except for the sulfide and chalcophile element metasomatism, these clasts appear to be essentially monomict and probably represent a noritic member of the ferroan anorthosite suite. Their low Ni contents and Ni/Co ratios are consistent with the interpretation of these clasts as igneous rocks which have escaped mixing with meteoritic material. Derived from text

N94-20661*# Hawaii Univ., Honolulu. Dept. of Geology and Geophysics.

VOLATILITY IN THE LUNAR CRUST: TRACE ELEMENT ANALYSES OF LUNAR MINERALS BY PIXE PROTON MICROPROBE Abstract Only

M. D. Norman, W. L. Griffin (Commonwealth Scientific and Industrial Research Organization, North Ryde, Australia.), and C. G. Ryan (Commonwealth Scientific and Industrial Research Organization, North Ryde, Australia.) *In* Lunar and Planetary Inst., Twenty-Fourth Lunar and Planetary Science Conference. Part 3: N-Z 1993 p 1091-1092 (For primary document see N94-20636 05-91)

Avail: CASI HC A01/MF A06

In situ determination of mineral compositions using microbeam techniques can characterize magma compositions through mineral-melt partitioning, and be used to investigate fine-grained or rare phases which cannot be extracted for analysis. Abundances of Fe, Mn, Sr, Ga, Zr, Y, Nb, Zn, Cu, Ni, Se, and Sb were determined for various mineral phases in a small number of lunar highlands rocks using the PIXE proton microprobe. Sr/Ga ratios of plagioclase and Mn/Zn ratios of mafic silicates show that the ferroan anorthosites and Mg-suite cumulates are depleted in volatile lithophile elements to about the same degree compared with chondrites and the Earth. This links the entire lunar crust to common processes or source compositions. In contrast, secondary sulfides in Descartes breccia clasts are enriched in chalcophile elements such as Cu, Zn, Ni, Se, and Sb, and represent a potential resource in the lunar highlands. Derived from text

N94-20662*# Georgia Univ., Athens. Dept. of Geology.

IMPACT GLASSES FROM THE ULTRAFINE FRACTION OF LUNAR SOILS Abstract Only

J. A. Norris, L. P. Keller (National Aeronautics and Space Administration. Lyndon B. Johnson Space Center, Houston, TX.), and D. S. McKay (National Aeronautics and Space Administration. Lyndon B. Johnson Space Center, Houston, TX.) *In* Lunar and Planetary Inst., Twenty-Fourth Lunar and Planetary Science Conference. Part 3: N-Z 1993 p 1093-1094 (For primary document see N94-20636 05-91)

Avail: CASI HC A01/MF A06

The chemical compositions of microscopic glasses produced during meteoroid impacts on the lunar surface provide information regarding the various fractionation processes which accompany these events. To learn more about these fractionation processes, we studied the compositions of submicrometer glass spheres from two Apollo 17 sampling sites using electron microscopy. The majority of the analyzed glasses show evidence for varying degrees of impact induced chemical fractionation. Among these are HASP glasses (High-Al, Si-Poor) which are believed to represent the refractory residuum left after the loss of volatile elements (e.g. Si, Fe, N) from the precursor material. In addition to HASP-type glasses, we also observed a group of VRAP glasses (volatile-rich, Al-poor) that represent condensates of vaporized volatile constituents and are complementary to the HASP compositions. High-Ti glasses were also found during the course of the study, and are documented here for the first time.

Derived from text

N94-20663*# National Aeronautics and Space Administration. Lyndon B. Johnson Space Center, Houston, TX.

THE Sm-(146,147)-Nd-(142,143) FORMATION INTERVAL FOR THE LUNAR MANTLE AND IMPLICATIONS FOR LUNAR EVOLUTION Abstract Only

L. E. Nyquist, C.-Y. Shih (Lockheed Engineering and Sciences Co., Houston, TX.), H. Wiesmann (Lockheed Engineering and Sciences Co., Houston, TX.), and B. M. Bansal (Lockheed Engineering and Sciences Co., Houston, TX.) *In* Lunar and Planetary Inst., Twenty-Fourth Lunar and Planetary Science Conference. Part 3: N-Z 1993 p 1095-1096 (For primary document see N94-20636 05-91)

Avail: CASI HC A01/MF A06

Small anomalies in the isotopic abundance of Nd-142 have been measured for two A17 high-Ti basalts, ilmenite basalt 12056, olivine-pigeonite basalt 12039, feldspathic basalt 12038, and two KREEP basalts. These anomalies correlate with Sm-147/Nd-144 for the basalt source regions as calculated from initial Nd-143/Nd-144 ratios in the basalts, and are interpreted to be from decay of Sm-146 (t sub 1/2 = 103 Ma) in distinct lunar mantle reservoirs. A three-stage model for evolution of Nd-143/Nd-144 and Nd-142/Nd-144 yields reservoir Sm-147/Nd-144 ratios which, with the Nd-142/Nd-144 ratios in the basalts, form a 'mantle isochron' giving a lunar mantle formation interval of 94+2230 Ma (2c(rho)). Calculated reservoir Sm/Nd ratios are in the range expected from some earlier models of basalt petrogenesis. The isochron value of Nd-142/Nd-144 at Sm-147/Nd-144 sub CHUR = 0.1967 is within error limits of the average Nd-142/Nd-144 measured for an L6 chondrite, an H5 chondrite, and the Orgueil carbonaceous chondrite. Evolution of Nd-143 and Nd-142 for high-Ti basalt 70135 was modeled precisely, starting from chondritic relative REE and Nd-isotopic abundances and using the initial (Sm-146/Sm-144) sub 0 ratio inferred from a previous study of angrite LEW86010 as the initial solar system value of this parameter. We infer that the initial Sm/Nd ratio in precursor lunar materials was very nearly chondritic (within approximately 8 percent) prior to lunar differentiation. Derived from text

N94-20664*# Deutsche Forschungs- und Versuchsanstalt fuer Luft- und Raumfahrt, Oberpfaffenhofen (Germany). Planetary Remote Sensing Section.

GONIOSPECTROMETRIC PROPERTIES OF A WHITE STANDARD Abstract Only c25

A. Oehler and A. Dummel *In* Lunar and Planetary Inst., Twenty-Fourth Lunar and Planetary Science Conference. Part 3: N-Z 1993 p 1097-1098 (For primary document see N94-20636 05-91)

Avail: CASI HC A01/MF A06

Reflection spectroscopy is one of the fundamental tools in planetary remote sensing. Most of the laboratory work is done in terms of bidirectional reflectance R in the wavelength range of reflected sunlight (250 nm - 2500 nm). Bidirectional reflectance R is defined as the radiance of a surface relative to the radiance of an ideal Lambertian reflector, identically illuminated (radiance coefficient). For quantitative laboratory work the absolute scale of R has to be known. In addition, for many purposes it is necessary to know the dependence of R from phase angle for a large range of geometries. In many cases, this can only be achieved if the goniospectrometric properties of the white standard that is used are known with high precision. For a long time Halon has been used as a white standard by most laboratories. Because Halon is no more available we have now analyzed the goniospectrometric properties of Spectralon SRS-99 with the DLR-goniospectrometer. Derived from text

N94-20665*# Colorado State Univ., Fort Collins. Center for Engineering Infrastructure and Sciences in Space.

CHARACTERIZATION OF MINNESOTA LUNAR SIMULANT FOR PLANT GROWTH Abstract Only c54

James P. Ogiesby, Willard L. Lindsay, and Willy Z. Sadeh *In* Lunar and Planetary Inst., Twenty-Fourth Lunar and Planetary Science Conference. Part 3: N-Z 1993 p 1099 (For primary document see N94-20636 05-91)

Avail: CASI HC A01/MF A06

Processing of lunar regolith into a plant growth medium is crucial in the development of a regenerative life support system for a lunar base. Plants, which are the core of such a system, produce food and oxygen for humans and, at the same time, consume carbon dioxide. Because of the scarcity of lunar regolith, simulants must be used to infer its properties and to develop procedures for weathering and chemical analyses. The Minnesota Lunar Simulant (MLS) has been identified to date as the best available simulant for lunar regolith. Results of the dissolution studies reveal that appropriately fertilized MLS can be a suitable medium for plant growth. The techniques used in conducting these studies can be extended to investigate the suitability of actual lunar regolith as a plant growth medium. Dissolution experiments were conducted using the MLS to determine its nutritional and toxicity characteristics for plant growth and to develop weathering and chemical analysis techniques. Two weathering regimes, one with water and one with dilute organic acids simulating the root rhizosphere microenvironment, were investigated. Elemental concentrations were measured using inductively-coupled-plasma (ICP) emission spectrometry and ion chromatography (IC). The geochemical speciation

model, MINTEQA2, was used to determine the major solution species and the minerals controlling them. Acidification was found to be a useful method for increasing cation concentrations to meaningful levels. Initial results indicate that MLS weathers to give neutral to slightly basic solutions which contain acceptable amounts of the essential elements required for plant nutrition (i.e., potassium, calcium, magnesium, sulfur, zinc, sodium, silicon, manganese, copper, chlorine, boron, molybdenum, and cobalt). Elements that need to be supplemented include carbon, nitrogen, and perhaps phosphorus and iron. Trace metals in solution were present at nontoxic levels. Derived from text

N94-20666*# California Inst. of Tech., Pasadena. Experimental Geophysics Lab.

DYNAMICS OF LARGE SCALE IMPACTS ON VENUS AND EARTH Abstract Only

John D. OKeefe and Thomas J. Ahrens *In* Lunar and Planetary Inst., Twenty-Fourth Lunar and Planetary Science Conference. Part 3: N-Z 1993 p 1101-1102 (For primary document see N94-20636 05-91)
Avail: CASI HC A01/MF A06

Large scale impacts are a key aspect of the accretion and growth of the planets, the evolution of their atmospheres, and the viability of their life forms. We have performed an extensive series of numerical calculations that examined the mechanics of impacts over a broad range of conditions and are now extending these to account for the effects of the planetary atmosphere. We have examined the effects of large scale impacts in which the trapping and compression of an atmosphere during impact is a significant factor in the transfer of energy to the atmosphere. The various energy transfer regimes and where conventional drag and trapping and subsequent compression of atmosphere between the bolide and planetary surface are significant are shown. Derived from text

N94-20667*# Chicago Univ. Hospitals and Clinics, IL. Dept. of Geophysics Science.

TAMBO QUEMADO: EXTRAORDINARY CONCENTRATIONS OF REE AND REFRACTORY TRACE ELEMENTS CAUSED BY ARTIFICIAL HEATING Abstract Only c25

E. Olsen, I. Hutcheon (California Inst. of Tech., Pasadena.), and C. Moore (Arizona State Univ., Tempe.) *In* Lunar and Planetary Inst., Twenty-Fourth Lunar and Planetary Science Conference. Part 3: N-Z 1993 p 1103-1104 (For primary document see N94-20636 05-91)
Avail: CASI HC A01/MF A06

Buchwald examined samples of the IIIB iron Tambo Quemado (TAMQ) cut from the 130 kg main mass. He determined it had been artificially heated, at some time prior to being reported, in an attempt to obtain metal from it. Although the Widmanstatten structure appears relatively unaffected under macroscopic examination, microscopic study of etched sections reveals the effect of the heating. Taenite and plessite area boundaries are indistinct due to high temperature diffusion. Schreibersite, once present in significant amounts, has been melted. Schreibersites in the interior have resolidified in fine-grained eutectic textures surrounded by dark-etching metal rims supersaturated with phosphorus. Buchwald states that phosphate minerals were probably present originally, because graftonite, and its polymorph sarcopside (both essentially Fe3(PO4)2), are common in irons of the IIIB groups. Based on his metallographic study Buchwald estimates TAMQ was heated to 1000 C for about one hour. An interior sample from TAMQ was examined in order to determine what effect this unintended heating 'experiment' had upon the phosphate phases. Derived from text

N94-20668*# Ciudad Univ., Mexico City (Mexico). Inst. de Geofisica.

MODELLING THE GRAVITY AND MAGNETIC FIELD ANOMALIES OF THE CHICXULUB CRATER Abstract Only c46

C. Ortiz Aleman, M. Pilkington (Geological Survey of Canada, Ottawa, Ontario.), A. R. Hildebrand (Geological Survey of Canada, Ottawa, Ontario.), W. R. Roest (Geological Survey of Canada, Ottawa, Ontario.), R. A. F. Grieve (Geological Survey of Canada, Ottawa, Ontario.), and P. Keating (Geological Survey of Canada, Ottawa, Ontario.) *In* Lunar and Planetary Inst., Twenty-Fourth Lunar and Planetary Science Conference. Part 3: N-Z 1993 p 1105-1106 (For primary document see N94-20636 05-91)
Avail: CASI HC A01/MF A06

The approximately 180-km-diameter Chicxulub crater lies buried by approximately 1 km of sediment on the northwestern corner of the Yucatan Peninsula, Mexico. Geophysical, stratigraphic and petrologic evidence support an impact origin for the structure and biostratigraphy suggests that a K/T age is possible for the impact. The crater's location is in agreement with constraints derived from proximal K/T impact-wave and ejecta deposits and its melt-rock is similar in composition to the K/T tektites. Radiometric dating of the melt rock reveals an age identical to that of the K/T tektites. The impact which produced the Chicxulub crater probably produced the K/T extinctions and understanding the now-buried crater will provide constraints on the impact's lethal effects. The outstanding preservation of the crater, the availability of detailed gravity and magnetic data sets, and the two-component target of carbonate/evaporites overlying silicate basement allow application of geophysical modeling techniques to explore the crater under most favorable circumstances. We have found that the main features of the gravity and magnetic field anomalies may be produced by the crater lithologies. Author

N94-20669*# California Inst. of Tech., Pasadena. Div. of Geological and Planetary Sciences.

SELF DIFFUSION OF ALKALINE-EARTH IN Ca-Mg-ALUMINOSILICATE MELTS: EXPERIMENTAL IMPROVEMENTS ON THE DETERMINATION OF THE SELF-DIFFUSION COEFFICIENTS Abstract Only c25

O. Paillat and G. J. Wasserburg *In* Lunar and Planetary Inst., Twenty-Fourth Lunar and Planetary Science Conference. Part 3: N-Z 1993 p 1107-1108 (For primary document see N94-20636 05-91)
Avail: CASI HC A01/MF A06

Experimental studies of self-diffusion isotopes in silicate melts often have quite large uncertainties when comparing one study to another. We designed an experiment in order to improve the precision of the results by simultaneously studying several elements (Mg, Ca, Sr, Ba) during the same experiment thereby greatly reducing the relative experimental uncertainties. Results show that the uncertainties on the diffusion coefficients can be reduced to 10 percent, allowing a more reliable comparison of differences of self-diffusion coefficients of the elements. This type of experiment permits us to study precisely and simultaneously several elements with no restriction on any element. We also designed an experiment to investigate the possible effects of multicomponent diffusion during Mg self-diffusion experiments by comparing cases where the concentrations of the elements and the isotopic compositions are different. The results suggest that there are differences between the effective means of transport. This approach should allow us to investigate the importance of multicomponent diffusion in silicate melts. Derived from text

N94-20670*# New Mexico Univ., Albuquerque. Dept. of Earth and Planetary Sciences.

ORTHOPYROXENES AS RECORDERS OF DIOGENITE PETROGENESIS: MAJOR AND MINOR ELEMENT SYSTEMATICS Abstract Only c25

J. J. Papike, M. N. Spilde, G. W. Fowler, and C. K. Shearer *In* Lunar and Planetary Inst., Twenty-Fourth Lunar and Planetary Science Conference. Part 3: N-Z 1993 p 1109-1110 (For primary document see N94-20636 05-91)
(Grant NAG9-497)
Avail: CASI HC A01/MF A06

As a part of our research to better understand magmatic processes in the Eucrite Parent Body, we have initiated an ambitious program of study of major, minor and trace elements in orthopyroxene from diogenites. This paper reports preliminary results for major and minor elements in orthopyroxenes for a suite of 13 diogenites: Aioun El Atrouss, ALH 84001, ALH A 77256, EET 87530, Ellemeet, Garland, Ibbenburen, Johnstown, Manegoan, peckelsheim, Roda, Shalka, and Tatahouine. A companion paper by Shearer et al. reports new trace element data for ALH 84001, ALH A 77256, Ibbenburen, and Tatahouine. We have presently collected over 800 high quality pyroxene microprobe analyses for Si, Al, Ca, Na, Mn, Fe, Mg, Cr, and Ti. The chemical systematics observed for these orthopyroxenes reflect original magmatic mineral/melt partitioning plus later trapped liquid/mineral equilibration, subsolids, exsolution, and mineral/mineral metamorphic reactions. We have therefore avoided, at this point, any attempt to use statistical analysis to group (e.g. factor or cluster analysis) these orthopyroxenes chemically. Derived from text

N94-20671*# Arizona State Univ., Tempe.

STRUCTURAL EVIDENCE FOR REORIENTATION OF MIRANDA ABOUT A PALEO-POLE Abstract Only

R. Pappalardo and R. Greeley *In* Lunar and Planetary Inst., Twenty-Fourth Lunar and Planetary Science Conference. Part 3: N-Z 1993 p 1111-1112 (For primary document see N94-20636 05-91)
Avail: CASI HC A01/MF A06

Two structural arguments support the premise that Miranda has reoriented with respect to Uranus over its geologic history. Orientations of major extensional and compressional features are consistent with a major satellite reorientation similar to that previously suggested based on cratering asymmetry. Furthermore, structures within Elsinore Corona provide supporting evidence that this reorientation took place about a paleo-pole located near (-75 deg, 80 deg), suggesting a second minor reorientation of Miranda.
Derived from text

N94-20672*# Brown Univ., Providence, RI. Dept. of Geological Sciences.
FORMATION AND EVOLUTION OF RADIAL FRACTURE SYSTEMS ON VENUS Abstract Only
E. A. Parfitt and James W. Head *In* Lunar and Planetary Inst., Twenty-Fourth Lunar and Planetary Science Conference. Part 3: N-Z 1993 p 1113-1114 (For primary document see N94-20636 05-91)
Avail: CASI HC A01/MF A06

A survey of approximately 90 percent of the surface of Venus using Magellan data has been carried out to locate all radial fracture systems and to assess their association with other features such as volcanic edifices and coronae. Squyres et al. and Stofan et al. have discussed the association of radial fracture features in relation to coronae features, our approach was to assess the associations of all of the fracture systems. These fracture systems have two broad types of form - some fracture systems are associated with updomed topography, radiate from a point and have relatively uniform fracture lengths while others have a wider range of fracture lengths and radiate from the outer edge of a central caldera. Squyres et al. and Stofan et al. have interpreted both types of feature as reflecting tectonic fracturing resulting from uplift of the surface as a mantle plume impinges upon the crust. While it is true that a number of features are related to uplift and that such uplift will induce stresses consistent with radial fracturing, we explore the possibility that these fractures are not exclusively of tectonic origin. Purely tectonic fracturing will tend to generate a few main fractures/faults along which most of the stresses due to uplift will be accommodated leading to the triple-junction form common for terrestrial updoming. Though this type of feature is observed on Venus (e.g., feature located at 34S86), the majority of radial fracture systems display much more intensive fracturing than this through a full 360 degrees; this is difficult to explain by purely tectonic processes. The association of many of the fractures with radial lava flows leads us to interpret these fractures as reflecting dike emplacement: the form of the fractures being consistent with primarily vertical propagation from the head of a mantle plume. In the case of the second type of fracture system (those radiating from a central caldera), an even stronger case can be made that the fractures are not of tectonic origin. These features are not as commonly associated with updoming of the surface and where they are, the fractures extend out well beyond the edge of the topographic rise - an observation which is not consistent with the fractures being of tectonic uplift origin. Furthermore the fractures have a distribution of lengths (many short, fewer long) which is characteristic of dike swarms, and show direct associations with calderas and lava flows consistent with a volcanic origin. In addition, the longest fractures have a radial pattern only close to the center of the system but bend with distance to align themselves with the regional stress field - this behavior is very difficult to explain on purely tectonic grounds but is a pattern commonly seen for terrestrial dikes. For these reasons, we argue that many, if not the majority, of radial fracture systems found on Venus are the surface reflection of dike swarms, those associated with positive topography reflecting vertical emplacement and those radiating from calderas reflecting lateral propagation.
Derived from text

N94-20673*# Brown Univ., Providence, RI. Dept. of Geological Sciences.
THERMAL AND RHEOLOGICAL CONTROLS ON MAGMA MIGRATION IN DIKES: EXAMPLES FROM THE EAST RIFT ZONE OF KILAUEA VOLCANO, HAWAII Abstract Only **c46**
E. A. Parfitt, L. Wilson, and H. Pinkerton (Lancaster Univ., England.) *In* Lunar and Planetary Inst., Twenty-Fourth Lunar and Planetary Science Conference. Part 3: N-Z 1993 p 1115-1116 (For primary document see N94-20636 05-91)
Avail: CASI HC A01/MF A06

Long-lived eruptions from basaltic volcanoes involving episodic or steady activity indicate that a delicate balance has been struck between the rate of magma cooling in the dike system feeding the vent and the rate of magma supply to the dike system from a reservoir. We describe some key factors, involving the relationships between magma temperature, magma rheology, and dike geometry that control the nature of such eruptions.
Author

N94-20674*# Universal Analytics, Inc., Los Angeles, CA. Dept. of Geological Sciences.
CONSTRAINTS ON THE RATE OF DISCHARGE AND DURATION OF THE MANGALA VALLES FLOOD Abstract Only
T. J. Parker and D. S. Gorsline *In* Lunar and Planetary Inst., Twenty-Fourth Lunar and Planetary Science Conference. Part 3: N-Z 1993 p 1117-1118 (For primary document see N94-20636 05-91)
Avail: CASI HC A01/MF A06

Interest in Mangala Valles remains high within the planetary science community. This is justified because the survey mission images provide us with nearly complete coverage of the system at high resolution. Upcoming high resolution topography from the Mars Observer Laser Altimeter will enable the application of flood discharge models with an unprecedented level of detail. Previous work on the Mangala Valles problem has relied on the available low resolution topography. This has limited the ability of workers to constrain discharge calculations to only within several-order-of-magnitude estimates. Local determinations of channel depths via shadow length measurements and photoclinometric profiling are much more accurate, but can only be applied to steep slopes (and/or low sun elevations) in the case of shadow measurements, or across relatively short distances (to avoid changes in albedo along asymmetric photoclinometric profiles). We are taking stereo parallax measurements from medium resolution Viking Orbiter images, which provide a valuable intermediate check of the topography between those measurements made thus far and the upcoming Mars Observer data. The images used are from orbits 034A and 637A, and cover Mangala Valles from the source graben in Memnonia Fossae to the beginning of the bifurcated reach (at 9.5 deg lat., 151.5 deg lon.). These images are about 300 m/pixel and 250 m/pixel, respectively. Both sets of images were orthographically projected to 250 m/pixel. The separation angle between left-right pairs is approximately 52 degrees. This results in a vertical accuracy on the order of plus or minus 260 m. Though this is still somewhat coarse, the channel relief is clearly resolved. Preliminary profiles across Mangala Valles and the large topographic ridge to the east are shown on the following page. An east-west regional tilt that resulted from slight scaling differences in the digital data has been 'removed' by visually estimating a regional datum on the stereo pairs. North-south variations in scale have not yet been adjusted for, so the zero datum for each profile was simply taken to be the high water line of the channel itself. Our depth measurement for the source breach of about 750 m agrees reasonably well with values of 700-1000 m determined from shadow measurements.
Author

N94-20675*# Brown Univ., Providence, RI. Dept. of Geological Sciences.
MIXING OF A CHEMICALLY BUOYANT LAYER AT THE TOP OF A THERMALLY CONVECTING FLUID: IMPLICATIONS FOR MANTLE DYNAMICS WITH APPLICATION TO VENUS Abstract Only
E. M. Parmentier, P. C. Hess, and C. Sotin (Paris Univ., France.) *In* Lunar and Planetary Inst., Twenty-Fourth Lunar and Planetary Science Conference. Part 3: N-Z 1993 p 1119-1120 (For primary document see N94-20636 05-91)
Avail: CASI HC A01/MF A06

Partial melting to generate the crust of a planet can create a buoyant residual layer at the top of the mantle which may have important implications for episodic planetary evolution. However, the rate of mixing of such a chemically buoyant layer with a thermally convecting mantle is an important unresolved question. Except for a few laboratory and numerical studies designed to address questions related to convection in the Earth's mantle, previous studies have generally treated on the mixing of passive tracers. The inhibiting role of chemical buoyancy on mixing is intuitively obvious but not fully understood quantitatively. In this study, we examine the dynamics

of an intrinsically buoyant fluid layer at the top of a deeper, thermally convecting, infinite Prandtl number fluid that is heated from below.
Derived from text

N94-20676*# Max-Planck-Inst. fuer Chemie, Mainz (Germany).
ABUNDANCE AND COMPOSITION OF SOLAR KR IN THE H3-H6 CHONDRITE ACFER111 Abstract Only **c25**
A. Pedroni *In* Lunar and Planetary Inst., Twenty-Fourth Lunar and Planetary Science Conference. Part 3: N-Z 1993 p 1121-1122 (For primary document see N94-20636 05-91)
Avail: CASI HC A01/MF A06

He/Ne, Ne/Ar, and Ar/Kr abundance ratios of solar gases extracted by stepped heating, stepped oxidation, and stepped etching of lunar and meteoritic regoliths are significantly lower than ratios measured directly or predicted by model estimates. Of these, the differences in the He/Ne and Ne/Ar ratios are explained to be owing to diffusive fractionation losses from the host minerals. In contrast, it remains controversial if the Ar/Kr and Kr/Xe ratios were fractionated prior to or after the implantation of the gases into the minerals. In the H3-H6 chondritic regolith breccia ACFER 111, measured He/Ne and Ne/Ar ratios appear to be of nearly unfractionated solar composition. The Ar/Kr ratio of ACFER 111, might thus be also unfractionated. We examined by stepped etching a metal sample of ACFER 111 and obtained an average solar 36Ar/84Kr = 3150 plus or minus 300 which is in agreement with the model predictions. The isotopic composition of solar Kr was observed to change in the course of the etching in a way very similar to that report for lunar ilmenites by the Zurich group. This can be interpreted as a change of the mixing ratio of Solar Wind (SW) and Solar Energetic Particles (SEP). The isotopic composition of the SEP component obtained from our Kr data, however, is distinct from that reported by the Zurich group. Derived from text

N94-20677*# First Inst. of Oceanography, Qingdao (China).
FIRST DISCOVERY OF THE ORGANIC MATERIALS IN DEEP-SEA IRON COSMIC SPHERULE Abstract Only **c25**
Peng Hanchang and Xu Peicang (Xian Inst. of Geology and Mineral Resources, China.) *In* Lunar and Planetary Inst., Twenty-Fourth Lunar and Planetary Science Conference. Part 3: N-Z 1993 p 1123-1124 (For primary document see N94-20636 05-91)
Avail: CASI HC A01/MF A06

The dust impact mass analyzer (PUMA) carried by the spacecraft Vega 1, Vega 2 and Giotto has provided the first direct measurements of the physical and chemical properties of cometary dust. The results indicate that most of the cometary dust particles are rich in light elements such as H, C, N, and O, suggesting the validity of models that describe the cometary dust as including organic material. Up to now, there were none found with the organic material from the deep-sea cosmic spherules. We have determined this from the deep-sea iron cosmic spherules collected from the North Pacific. An iron cosmic spherule (382 microns in diameter) was determined by the Laser Raman Microprobe. Derived from text

N94-20678*# Office National d'Etudes et de Recherches Aeronautiques, Paris (France).
C/O ATOMIC RATIOS IN MICROMETER-SIZE CRUSHED GRAINS FROM ANTARCTIC MICROMETEORITES AND TWO CARBONACEOUS METEORITES Abstract Only **c90**
M. Perreau, C. Engrand (Centre de Spectrometrie Nucleaire et de Spectrometrie de Masse, Orsay, France.), Michel Maurette (Centre de Spectrometrie Nucleaire et de Spectrometrie de Masse, Orsay, France.), G. Kurat (Naturhistorisches Museum, Vienna, Austria.), and Th. Presper (Naturhistorisches Museum, Vienna, Austria.) *In* Lunar and Planetary Inst., Twenty-Fourth Lunar and Planetary Science Conference. Part 3: N-Z 1993 p 1125-1126 (For primary document see N94-20636 05-91)
Avail: CASI HC A01/MF A06

Antarctic micrometeorites (AMM's) have similarities (but also differences) with primitive meteorites, such as unequilibrated mineral assemblages. To further assess such similarities, we have measured the carbon content of micrometeorites and meteorites (Orgueil and Murchison), as determined in a random selection of micrometer-size crushed grain, with an analytical transmission electron microscope. Such analyses yield the C/O atomic ratio, the major and minor elements contents, and the textural features of the grains on a scale of approx. equal to 100 nanometers. An important proportion of micrometeorites from both the 100-400 micron and the 50-100 micron size fractions contains much more carbon than CI chondrite Orgueil. The average C-content of all micrometeorites in these two size fractions amount to approximately 1.8 x CI, and approximately 0.8 x CI, respectively (CI refers to the bulk C-content of Orgueil, of about 3.5 percent by weight). Carbon is usually not homogeneously distributed in the micrometeorite but is concentrated in C-rich grains. So far, most of these grains are amorphous, and seem to be associated with an oxidized Fe-rich phase (possibly a variety of 'dirty' magnetite). About 5 percent of them have the composition of 'COPS', a phase additionally enriched in O, P, and S.
Derived from text

N94-20679*# Harvard-Smithsonian Center for Astrophysics, Cambridge, MA.
LAMELLAR OLIVINE IN THE DIVNOE ACHONDRITE: EVIDENCE FOR HIGH-PRESSURE EXSOLUTION? Abstract Only **c25**
M. I. Petaev *In* Lunar and Planetary Inst., Twenty-Fourth Lunar and Planetary Science Conference. Part 3: N-Z 1993 p 1127-1128 (For primary document see N94-20636 05-91)
Avail: CASI HC A01/MF A06

The olivine-rich Divnoe achondrite contains numerous large olivine grains which have a lamellar or banded appearance in back-scattered electron images, caused by minor compositional differences. One such grain, viewed in transmitted light, displays a system of lamellae with the same orientation and scale as the compositional banding. The only process known to produce such structure and chemical variability in olivine grains is high-pressure transformations between alpha-, beta- and gamma-olivines, but in other meteorites and in experimental products the structure is approximately 100 times finer than the Divnoe lamella. Author

N94-20680*# Harvard-Smithsonian Center for Astrophysics, Cambridge, MA.
OPAQUE-RICH LITHOLOGY IN THE DIVNOE ACHONDRITE: PETROLOGY AND ORIGIN Abstract Only **c90**
M. I. Petaev *In* Lunar and Planetary Inst., Twenty-Fourth Lunar and Planetary Science Conference. Part 3: N-Z 1993 p 1129-1130 (For primary document see N94-20636 05-91)
Avail: CASI HC A01/MF A06

An opaque-rich lithology (ORL) makes up to approximately 9 vol. percent of the Divnoe achondrite. It is characterized by enrichment of troilite and pyroxene, compared to the bulk Divnoe, and by the presence of tiny remnants of olivine in low-CA pyroxene and low minor element concentrations in pyroxene. The ORL was formed by local reaction between gaseous sulfur and olivine in the Divnoe. The Divnoe meteorite is an olivine-rich achondrite with subchondritic chemistry and mineralogy. It has a granoblastic coarse-grained olivine groundmass (CGL: coarse-grained lithology) with relatively large (2-10 mm) poikilitic patches (PP) of pyroxene and, rarely, plagioclase. The groundmass also contains an opaque-rich fine-grained lithology (ORL) which comprises approximately 9 vol. percent of the meteorite, displays reaction boundaries with the groundmass, and differs in mineral chemistry from it. Numerous micron- to mm-thick veins of troilite and, rarely, metal cross all the lithologies found in the meteorite. The Divnoe itself appears to represent a sample of an igneous source region. Author

N94-20681*# Harvard-Smithsonian Center for Astrophysics, Cambridge, MA.
CHAUNSKIJ: THE MOST HIGHLY METAMORPHOSED, SHOCK-MODIFIED AND METAL-RICH MESOSIDERITE Abstract Only **c90**
M. I. Petaev, R. S. Clarke, Jr. (Smithsonian Institution, Washington, DC.), E. J. Olsen (Chicago Univ., IL.), E. Jarosewich (Smithsonian Institution, Washington, DC.), A. M. Davis (Chicago Univ., IL.), I. M. Steele (Chicago Univ., IL.), M. E. Lipschutz (Purdue Univ., West Lafayette, IN.), M.-S. Wang (Purdue Univ., West Lafayette, IN.), R. N. Clayton (Chicago Univ., IL.), and T. K. Mayeda (Chicago Univ., IL.) et al *In* Lunar and Planetary Inst., Twenty-Fourth Lunar and Planetary Science Conference. Part 3: N-Z 1993 p 1131-1132 (For primary document see N94-20636 05-91)
Avail: CASI HC A01/MF A06

The 1990 g Chaunskij meteorite was found in 1985 and classified as an anomalous ungrouped iron. It contains approximately 10 vol. percent mono- and polymineralic troilite-phosphate-silicate inclusions, microns to centimeters in size. We proposed its affinity with mesosiderites; here we

present mineralogical, chemical, and isotopic data establishing that Chaunskij is the most highly metamorphosed, shock-modified, and metal-rich of the mesosiderites. The most striking manifestation of metamorphism in Chaunskij is the presence in it of a cordierite-bearing assemblage substituting for basalt lithology. Derived from text

N94-20682*# Hawaii Univ., Honolulu. Dept. of Planetary Geosciences.
SPECTRAL REFLECTANCE STUDIES OF THE HUMORUM BASIN REGION Abstract Only
C. A. Peterson, B. R. Hawke, P. G. Lucey, G. J. Taylor, D. T. Blewett, and P. D. Spudis (Lunar and Planetary Inst., Houston, TX.) *In* Lunar and Planetary Inst., Twenty-Fourth Lunar and Planetary Science Conference. Part 3: N-Z 1993 p 1133-1134 (For primary document see N94-20636 05-91)
Avail: CASI HC A01/MF A06

A portion of the mare-bounding (MB) ring of Humorum Basin is composed of pure anorthosite while other parts of the ring are composed of noritic anorthosite. An episode of mare volcanism emplaced basaltic units in the region northwest of the MB ring after the Humorum impact event. Subsequently, large impacts emplaced a veneer of highlands material atop the basalt flows. Some mare material could have been mixed with this highlands debris either by local mixing by secondary craters or by vertical mixing. Spectra for most other highlands units in the region indicate a noritic anorthosite lithology. Spectra of mare basalts in Mare Humorum and nearby mare flooded craters show relatively deep absorption bands due to the presence of abundant high-Ca pyroxene. An analysis of spectra for a small number of craters in the highlands west of the outer ring of Humorum reveals the presence of high-Ca pyroxene. This suggests the possible presence of an extensive gabbroic province. Author

N94-20683*# Washington Univ., Saint Louis, MO. Dept. of Earth and Planetary Sciences.
VENUS MAGMATIC AND TECTONIC EVOLUTION Abstract Only
R. J. Phillips and V. L. Hansen (Southern Methodist Univ., Dallas, TX.) *In* Lunar and Planetary Inst., Twenty-Fourth Lunar and Planetary Science Conference. Part 3: N-Z 1993 p 1135-1136 (For primary document see N94-20636 05-91)
Avail: CASI HC A01/MF A06

Two years beyond the initial mapping by the Magellan spacecraft, hypotheses for the magmatic and tectonic evolution of Venus have become refined and focused. We present our view of these processes, attempting to synthesize aspects of a model for the tectonic and magmatic behavior of the planet. The ideas presented should be taken collectively as an hypothesis subject to further testing. The quintessence of our model is that shear and buoyancy forces in the upper boundary layer of mantle convection give rise to a spatially and temporally complex pattern of strain in a one-plate Venusian lithosphere and modulate the timing and occurrence of magmatism on a global basis. Derived from text

N94-20684*# National Aeronautics and Space Administration. Lyndon B. Johnson Space Center, Houston, TX.
POST-IGNEOUS REDISTRIBUTION OF COMPONENTS IN EUCRITES Abstract Only **c25**
W. C. Phinney, D. J. Lindstrom, D. W. Mittlefehldt (Lockheed Engineering and Sciences Co., Houston, TX.), and R. R. Martinez (Lockheed Engineering and Sciences Co., Houston, TX.) *In* Lunar and Planetary Inst., Twenty-Fourth Lunar and Planetary Science Conference. Part 3: N-Z 1993 p 1137-1138 (For primary document see N94-20636 05-91)
Avail: CASI HC A01/MF A06

In our analyses, we utilize a microdrilling technique that removes 40 to 100 micron diameter cores from mineral grains in thin sections analyzed by microprobe. The cores are then analyzed by INAA using the technique of Lindstrom. Three eucrites were selected for application of this analytical technique: monomict breccias Pasamonte and Stannern and unbrecciated EET90020. Pasamonte is among the most unequilibrated of the eucrites on the basis of zoning in pyroxenes and is considered to be an igneous rock not significantly affected by metamorphism. Stannern has igneous texture but its pyroxenes indicate some re-equilibration, although little, if any, recrystallization. EET90020 has a granulite texture and has been substantially recrystallized. Our sample of Pasamonte contains several clasts of different grain sizes ranging from glass to fine grained with diabasic texture containing lathy plagioclase, unexsolved pigeonite, and mesostasis. Cores were taken of the glass and from minerals and mesostases in six lithic clasts which normally allowed sampling of more than one phase per clast. Our sample of Stannern is also a breccia but with little difference in grain size between clasts and matrix. The plagioclase and pigeonite are blocky, twinned, and exsolved and coexist with a bit of mesostasis. Cores were taken of plagioclase and pigeonite with no attempt to distinguish separate clasts. EET90020 is a granular mixture of twinned plagioclase and pigeonite having rather uniform size and many triple junctions. Several cores were taken of both phases. Both clear and cloudy grains of plagioclase and pyroxene were sampled in all three eucrites. Derived from text

N94-20685*# Arizona Univ., Tucson. Planetary Image Research Lab.
WAVELENGTH DEPENDENCE OF LIMB-DARKENING OF MARS FROM VISIBLE AND NEAR-IR TELESCOPIC SPECTRAL IMAGING Abstract Only
E. Pierazzo and R. B. Singer *In* Lunar and Planetary Inst., Twenty-Fourth Lunar and Planetary Science Conference. Part 3: N-Z 1993 p 1139-1140 (For primary document see N94-20636 05-91)
Avail: CASI HC A01/MF A06

We are investigating the photometric properties of Mars using Earthbased telescopic spectral imaging obtained during 1988. Each spatial pixel consists of 300 spectral channels from 0.44 to 1.02 microns, calibrated to radiance factor (r(sub F)) through a careful procedure involving standard star observations in 1988 and 1990. Calibrated data include 3 spectral images with solar phase angle (g) of 12 degrees and 4 images with g of 4 degrees. Pixels near the sub-Earth point have a spatial footprint of about 280 x 150 km. Preliminary work using Hapke photometric function reveals a dependence of both single-scattering albedo and roughness parameter on wavelength. The former is in agreement with observed spectra of the martian surface, but the latter is unexpected. Derived from text

N94-20686*# Brown Univ., Providence, RI.
COMPOSITIONAL DIVERSITY OF THE LUNAR NORTH POLE: PRELIMINARY ANALYSES OF GALILEO SSI DATA Abstract Only
C. M. Pieters, M. Belton (Kitt Peak National Observatory, Tucson, AZ.), James W. Head, R. Greeley (Arizona State Univ., Tempe.), A. McEwen (Geological Survey, Flagstaff, AZ.), E. M. Fischer, J. M. Sunshine, K. Klaasen (Jet Propulsion Lab., California Inst. of Tech., Pasadena.), J. Plutchak, and G. Neukum (Deutsche Forschungsanstalt fuer Luft- und Raumfahrt, Oberpfaffenhofen, Germany.) et al *In* Lunar and Planetary Inst., Twenty-Fourth Lunar and Planetary Science Conference. Part 3: N-Z 1993 p 1141-1142 (For primary document see N94-20636 05-91)
Avail: CASI HC A01/MF A06

In December 1992, the Galileo spacecraft passed through the Earth-Moon system for its final gravity assist to Jupiter. The SSI camera obtained several 6-color mosaics of the lunar north polar region and the sunlit nearside and eastern limb at approximately 1.3 km/pixel. Initial analyses have concentrated on the north polar areas to assess the composition of the crust in that region. Representative 6-color calibration SSI spectra (typically 5 x 5 pixels) are shown. Photometric corrections have not yet been applied, and all spectra are scaled to unity at 0.56 microns. The data were first calibrated relative to MS2, a standard are in Mare Serenitatis (18.7 deg N, 21.5 deg E), and the top four plots of highlands, highland craters, maria, and mare craters are displayed relative to MS2. SSI spectra of areas measured with telescopic data (mare MT1/MS2 and mare crater MSA/MS2) agree well with previous data, confirming that the calibration procedures and SSI data are spectrally accurate. The bottom three plots of craters/sun have been calibrated to reflectance using previously obtained telescopic spectra of Apollo 16/MS2 (shown with Highlands/MS2) and laboratory spectra of mature Apollo 16 soil (shown for reference with the Highland Craters/Sun). Although some variations in these spectra mimic previously observed spectra of lunar terrains, several characteristics are unusual. Familiar and unfamiliar properties are observed in these northern latitudes and both types merit further investigation in their geologic context. Derived from text

N94-20687*# Brown Univ., Providence, RI.
OPTICAL EFFECTS OF SPACE WEATHERING ON LUNAR SOILS AND THE ROLE OF THE FINEST FRACTION Abstract Only
C. M. Pieters, E. M. Fischer, O. D. Rode (Academy of Sciences, USSR, Moscow.), and A. Basu (Indiana Univ., Bloomington.) *In* Lunar and Planetary Inst., Twenty-Fourth Lunar and Planetary Science Conference.

Part 3: N-Z 1993 p 1143-1144 (For primary document see N94-20636 05-91)
(Grants NAG9-184; NAGw-748)
Avail: CASI HC A01/MF A06

Lunar soils represent a cumulative product of space weathering and as such they exhibit distinct optical alteration. In comparison to the optical properties of similar rock powders, lunar soils are darker, have weaker diagnostic absorption bands, and exhibit a characteristic red continuum slope between 0.3 and 4.5 microns. Well-developed (mature) lunar soils have a mean grain size of about 60 microns and may contain more than 50 percent agglutinates (complex, glass-welded aggregates) which were previously believed to be the principal carriers of optical alteration resulting from space weathering. A detailed analysis of the spectral reflectance properties of the bulk soil, size separates, and agglutinate separates of several Apollo and Luna soils has been undertaken to evaluate the validity of the agglutinate paradigm for optical effects of space weathering. The data and results are summarized here which indicate that the finest fraction of natural lunar soils, rather than larger complex agglutinates, carries the principal effects of optical alteration. Bidirectional reflectance spectra were obtained using the small sample configuration of the RELAB facility, which accommodates 5-30 mg of material. Spectra are displayed with the labels for individual samples listed in order of brightness. Derived from text

N94-20688*# Brown Univ., Providence, RI.
MinMap: AN IMAGING SPECTROMETER FOR HIGH RESOLUTION COMPOSITIONAL MAPPING OF THE MOON Abstract Only **c35**
C. M. Pieters, James W. Head, and T. B. McCord (SETS Technology, Inc., Honolulu, HI.) *In* Lunar and Planetary Inst., Twenty-Fourth Lunar and Planetary Science Conference. Part 3: N-Z 1993 p 1145-1146 (For primary document see N94-20636 05-91)
Avail: CASI HC A01/MF A06

MinMap has been selected by the Lunar Scout program to characterize and map the mineral composition of the Moon. The instrument will be built as a collaborative effort between Brown University, SETS Technology Inc., and Ball Aerospace Corp. MinMap is a visible to near-infrared imaging spectrometer that contains 192 spectral channels from 0.35-2.4 microns with signal to noise greater than 200 and 256 cross-track spatial elements. The spectrometer design has a 6 deg field of view (FOV) and utilizes grating dispersive elements and two dimensional detectors (no moving parts). An 'image cube' of data is produced that contains two dimensions of spatial information and one dimension of spectral information. All spectral channels and cross-track spatial elements are recorded simultaneously with spacecraft motion scanning the second spatial dimension. The high spectral resolution and continuous spectral range of MinMap are designed to measure the diagnostic absorption features of principal lunar minerals and their lithologic mixtures. Since the optical properties of lunar materials change in a regular manner upon exposure to the space environment, this spectral range is also quite sensitive to variations in exposure history (soil maturity). Nominal measurement stragegy is to obtain full global data of the Moon at 180 m/pixel from a 450 km polar orbit during the first month or two of operation. A 100 km orbit is anticipated for the remaining part of a 1 year mission allowing higher resolution data (approx. 80 m/pixel) to be obtained for targeted regions. MinMap exceeds LE x SWG's measurement recommendations and will provide the highest spatial resolution compositional map of lunar rocks and soils currently planned for orbital missions. Since all spectral channels are co-registered and obtained simultaneously, 'image cube' data swaths will be available for analysis almost immediately.
Derived from text

N94-20689*# Brown Univ., Providence, RI.
VISIBLE-INFRARED PROPERTIES OF CONTROLLED LABORATORY SOILS Abstract Only **c25**
C. M. Pieters, J. F. Mustard, S. F. Pratt, J. M. Sunshine, and Andrew Hoppin *In* Lunar and Planetary Inst., Twenty-Fourth Lunar and Planetary Science Conference. Part 3: N-Z 1993 p 1147-1148 (For primary document see N94-20636 05-91)
Avail: CASI HC A01/MF A06

Almost all surfaces available for remote observation consist of particulate materials or soils. The distribution of mean particle sizes depend on the original material and physical and chemical processes that have acted on the surface over time. It is well known that the optical and infrared spectral properties of materials depends on the particle size. There has been little detailed study, however, of natural soils, namely particulate materials with a range of particle sizes. Current models for intimate mixing typically use an average particle size in calculations and are most successful when the particle size is constrained by known sieve fractions. Preliminary results of a study in which soils were prepared with a known composition and range of particle sizes are reported. This discussion presents the overall visible to infrared properties of these synthetic soils and evaluates the mid-infrared properties. Derived from text

N94-20690*# Lancaster Univ. (England). Environmental Science Div.
A COMPARISON OF CALCULATED AND MEASURED RHEOLOGICAL PROPERTIES OF CRYSTALLISING LAVAS IN THE FIELD AND IN THE LABORATORY Abstract Only **c46**
Harry Pinkerton and Gill Norton *In* Lunar and Planetary Inst., Twenty-Fourth Lunar and Planetary Science Conference. Part 3: N-Z 1993 p 1149-1150 (For primary document see N94-20636 05-91)
Avail: CASI HC A01/MF A06

Models of most magmatic processes, including realistic models of planetary lava flows require accurate data on the rheological properties of magma. Previous studies suggest that field and laboratory rheological properties of Hawaiian lavas can be calculated from their physico-chemical properties using a non-Newtonian rheology model. The present study uses new measurements of the rheological properties of crystallizing lavas to show that this is also true for lavas from Mount Etna. Rheological measurements on quenched Etna basalts were made in a specially designed furnace using a Haake Rotovisco viscometer attached to a spindle which has been designed to eliminate slippage at the melt-spindle interface. Using this spindle, we have made measurements at lower temperatures than other workers in this field. From these measurements, Mount Etna lavas are Newtonian at temperatures above 1120 C and they are thixotropic pseudoplastic fluids with a yield strength at lower temperatures. The close agreement between calculated and measured rheology over the temperature range 1084 - 1125 C support the use of the non-Newtonian rheology model in future modeling of planetary lava flows. Derived from text

N94-20691*# Jet Propulsion Lab., California Inst. of Tech., Pasadena.
MAGELLAN VERTICAL POLARIZATION RADAR OBSERVATIONS Abstract Only **c32**
Jeffrey J. Plaut *In* Lunar and Planetary Inst., Twenty-Fourth Lunar and Planetary Science Conference. Part 3: N-Z 1993 p 1151-1152 (For primary document see N94-20636 05-91)
Avail: CASI HC A01/MF A06

The Magellan high-gain radar antenna system was designed to transmit and receive signals in a pure linear polarization state. The nominal mapping configuration placed this linear polarization direction parallel to the surface of Venus, providing SAR image data in the HH polarization (horizontal transmit and receive) and radiothermal emission data in the H (horizontal - receive only) polarization. During Magellan's extended mission (cycles 2 and 3), two brief experiments were conducted in which the spacecraft was rotated 90 degrees along the axis of the antenna boresight, producing SAR data in the VV polarization and emission data in the V polarization. This study focuses on the SAR results from the first experiment, which included portions of the highly reflective Beta Regio highlands. Theoretical models of polarimetric backscatter, along with experimental data from terrestrial surfaces, predict VV backscatter cross section values to be higher than HH values for most natural surfaces. Randomly polarized ('depolarized') backscatter from rough surfaces is expected in equal amounts for either incident polarization. Roughness differences will therefore be more pronounced in HH measurements than in VV, because the depolarized random component makes up a proportionately larger fraction of the HH backscatter. In addition, HH cross section values are observed to fall off more rapidly than VV values with increasing incidence angle. Slope-related backscatter differences will, therefore, be more pronounced in HH images. The small perturbation polarimetric scattering model also predicts higher VV to HH ratios for surfaces of high dielectric constant. Author

N94-20692*# Jet Propulsion Lab., California Inst. of Tech., Pasadena.
ERUPTION HISTORY OF THE THARSIS SHIELD VOLCANOES, MARS Abstract Only
J. B. Plescia *In* Lunar and Planetary Inst., Twenty-Fourth Lunar and Planetary Science Conference. Part 3: N-Z 1993 p 1153-1154 (For

primary document see N94-20636 05-91)
Avail: CASI HC A01/MF A06

The Tharsis Montes volcanoes and Olympus Mons are giant shield volcanoes. Although estimates of their average surface age have been made using crater counts, the length of time required to build the shields has not been considered. Crater counts for the volcanoes indicate the constructs are young; average ages are Amazonian to Hesperian. In relative terms; Arsia Mons is the oldest, Pavonis Mons intermediate, and Ascreaus Mons the youngest of the Tharsis Montes shield; Olympus Mons is the youngest of the group. Depending upon the calibration, absolute ages range from 730 Ma to 3100 Ma for Arsia Mons and 25 Ma to 100 Ma for Olympus Mons. These absolute chronologies are highly model dependent, and indicate only the time surficial volcanism ceased, not the time over which the volcano was built. The problem of estimating the time necessary to build the volcanoes can be attacked in two ways. First, eruption rates from terrestrial and extraterrestrial examples can be used to calculate the required period of time to build the shields. Second, some relation of eruptive activity between the volcanoes can be assumed, such as they all began at a speficic time or they were active sequentially, and calculate the eruptive rate. Volumes of the shield volcanoes were derived from topographic/volume data. Derived from text

N94-20693*# Jet Propulsion Lab., California Inst. of Tech., Pasadena.
GEOLOGY OF BIBLIS PATERA, ULYSSES PATERA, AND JOVIS THOLUS, MARS Abstract Only
J. B. Plescia *In* Lunar and Planetary Inst., Twenty-Fourth Lunar and Planetary Science Conference. Part 3: N-Z 1993 p 1155-1156 (For primary document see N94-20636 05-91)
Avail: CASI HC A01/MF A06

There are a variety of constructional volcanic features in Tharsis. These features range from Olympus Mons and the Tharsis Montes shields, to the small low shields and fissure eruptions that characterize much of the volcanic plains, to the smaller volcanic constructs in the northeast and western parts of Tharsis. I describe the geology of the western group, which includes Biblis Patera, Ulysses Patera, and Jovis Tholus. Each of these volcanoes has had a unique, and complex geologic history. Biblis Patera is located at 2.3 deg. N, 123.8 deg. The volcano is elongate in a northwesterly direction and has a large, faulted caldera complex. The flanks of the volcano and adjacent plains are characterized by lava flows, northwest-trending graben and troughs, and caldera-concentric graben and troughs. Biblis Patera is approximately 66 x 127 km with an oval 51 x 56 km caldera; the summit elevation is approximately 2 km above the surrounding plains. The constrcut has an estimated volume of 8-22 x 10(exp 3) cu km. Ulysses Patera is located at 2.7 deg. N, 121.3 deg. W and stands approx. 2-3 km above the surrounding plain; flank slopes are approximately 7 deg. to 12 deg. The caldera floor is quite deep, lying 1.8 to 2.2 km below the caldera rim. The caldera has a void volume of approximately 5000 cu km, the total solid mass volume of the volcano is 7-16 x 10(exp 3) cu km. Jovis Tholus is centered at 18.3 deg N; 117.5 deg W; it is a low relief, volcano with gentle flank slopes of between 3 and 8 deg. The construct is dominated by a series of inset calderas which make up the largest fraction of the area. The caldera complex is offset to the southwest side. Total shield dimensions are approximately 77 km (e-wt) by 62 km (n-s); the caldera complex is approximately 44 x 34 km. The shield is embayed on all sides by younger Amazonian age volcanics. Total relief, relative to the surrounding plains, is probably approximately 2 km. The total volume of Jovis Tholus is estimated to be approximately 2-5 x 10(exp 3) cu km. Derived from text

N94-20694*# Jet Propulsion Lab., California Inst. of Tech., Pasadena.
GRAVITY INVESTIGATION OF THE MANSON IMPACT STRUCTURE, IOWA Abstract Only **c90**
J. B. Plescia *In* Lunar and Planetary Inst., Twenty-Fourth Lunar and Planetary Science Conference. Part 3: N-Z 1993 p 1157-1158 (For primary document see N94-20636 05-91)
Avail: CASI HC A01/MF A06

The Manson crater, of probable Cretaceous/Tertiary age, is located in northwestern Iowa (center at 42 deg. 34.44 min N; 94 deg. 33.60 min W). A seismic reflection profile along an east west line across the crater and drill hole data indicate a crater about 35 km in diameter having the classic form for an impact crater, an uplifted central peak composed of uplifted Proterozoic crystalline bedrock, surrounded by a 'moat' filled with impact produced breccia and a ring graben zone composed of tilted fault blocks of the Proterozoic and Paleozoic country rocks. The structure has been significantly eroded. This geologic structure would be expected to produce a significant gravity signature and study of that signature would shed additional light on the details of the crater structure. A gravity study was undertaken to better resolve the crustal structure. The regional Bouguer gravity field is characterized by a southeastward decreasing field. To first order, the Bouguer gravity field can be understood in the context of the geology of the Precambrian basement. The high gravity at the southeast corner is associated with the mid-continent gravity high; the adjacent low to the northwest results from a basin containing low-density clastic sediments shed from the basement high. Modeling of a simple basin and adjacent high predicts much of the observed Bouguer gravity signature. A gravity signature due to structure associated with the Manson impact is not apparent in the Bouguer data. To resolve the gravity signature of the impact, a series of polynomial surfaces were fit to the Bouguer gravity field to isolate the small wavelength residual anomalies. The residual gravity obtained after subtracting a 5th- or 6th-order polynomial seems to remove most of the regional effects and isolate local anomalies. The pattern resolved in the residual gravity is one of a gravity high surrounded by gravity lows and in turn surrounded by isolated gravity highs. The central portion of the crater is characterized by two positive anomalies having amplitudes of about plus 4 mGal separated by a gentle saddle located approximately at the crater center. Derived from text

N94-20695*# Washington Univ., Saint Louis, MO. Center for the Space Sciences.
ELEVATED INITIAL Sr-87/Sr-86 IN ORDINARY CHONDRITE METAL Abstract Only **c25**
F. A. Podosek, J. C. Brannon, C. Perron (National Museum of Natural History, Paris, France.), and P. Pellas (National Museum of Natural History, Paris, France.) *In* Lunar and Planetary Inst., Twenty-Fourth Lunar and Planetary Science Conference. Part 3: N-Z 1993 p 1159-1160 (For primary document see N94-20636 05-91)
Avail: CASI HC A01/MF A06

The metal phase of ordinary chondrites has been found to contain a complex assemblage of non-metal phases, evidently formed when elements such as Si, Cr and P, originally dissolved in the metal, were subsequently oxidized and exsolved. We have investigated the Rb-Sr isotopic system in samples of H-chondrite metal, finding small but nontrivial amounts of Sr, apparently concentrated toward the surface of metal grains, and characterized by pronounced excesses of Sr-87/Sr-86 in chondritic metal can plausibly account for the characteristically elevated initial Sr-87/Sr-86 found in ordinary chondrite phosphates, but it remains unclear when and where the metal experienced the high Rb/Sr environment needed to account for such high Sr-87/Sr-86. We have previously reported Rb-Sr data for separated metal from Dhajala (H3), Forest Vale (H4) and Estacado (H6). Here we report data for two size fractions (80-160 and 280-450 microns) of separated metal from the H4 chondrite Ste. Marguerite. These samples were etched twice (.5N HCl for one hour) before dissolution (6N HCl). Aliquots of the solutions were spiked for Fe, Ca and Rb + Sr. The results for Ste. Marguerite metal are presented; errors are two-sigma and elemental concentrations are stated in terms of total sample weight.
Derived from text

N94-20696*# Geological Survey, Reston, VA.
CRATER DESTRUCTION ON THE VENUSIAN HIGHLANDS BY TECTONIC PROCESSES Abstract Only
Howard A. Pohn and Gerald G. Schaber (Geological Survey, Flagstaff, AZ.) *In* Lunar and Planetary Inst., Twenty-Fourth Lunar and Planetary Science Conference. Part 3: N-Z 1993 p 1161-1162 (For primary document see N94-20636 05-91)
Avail: CASI HC A01/MF A06

It is apparent that few, if any, craters as old, or highly modified as Imbrian craters on the surface of the moon are present on the Venusian highlands, or indeed anywhere on the planet's surface. Degraded craters such as those seen on the Moon, Mercury, or Mars are conspicuously absent. Furthermore, virtually all the impact craters on the Venusian surface show modification only by extensional tectonics, whereas the Venusian highlands show modification by compression, strike-slip movement, and finally by extension. Presumably at an earlier time, the surface of Venus resembled the surfaces of the other inner planets. The relatively recent

resurfacing event that produced the plains units may be a mechanism for covering the older craters in the plains, but these vast outpourings of lava cannot be invoked as a mechanism for covering the craters on the Venusian highlands. If the plains units had covered the highlands, the entire Venusian surface would appear to be as smooth as the plains units that are embayed by and, therefore, postdate the highlands. The last major tectonic events to affect the highlands such as those seen on Ovda Regio appear to be thrust faulting with consequent folding, followed by at least three episodes of strike-slip faulting and finally extensional faulting. To test whether such tectonic movements could have destroyed highlands crater, a preliminary experiment was conducted by using a Lunar Orbiter mosaic of the lunar uplands as an analog for the ancient Venusian highlands.

Derived from text

N94-20697*# California Univ., San Diego, La Jolla. Dept. of Chemistry.

LOW-ENERGY ION IMPLANTATION: LARGE MASS FRACTIONATION OF ARGON Abstract Only **c25**

K. V. Ponganis, Th. Graf, and K. Marti *In* Lunar and Planetary Inst., Twenty-Fourth Lunar and Planetary Science Conference. Part 3: N-Z 1993 p 1163-1164 (For primary document see N94-20636 05-91)

Avail: CASI HC A01/MF A06

The isotropic signatures of noble gases in the atmospheres of the Earth and other planets are considerably evolved when compared to signatures observed in the solar wind. The mechanisms driving the evolution of planetary volatiles from original compositions in the solar accretion disk are currently poorly understood. Modeling of noble-gas compositional histories requires knowledge of fractionating processes that may have operated through the evolutionary stages. Since these gases are chemically inert, information on noble-gas fractionation processes can be used as probes. The importance of understanding these processes extends well beyond 'noble-gas planetology.' Trapped argon acquired by low-energy implantation (approximately less than 100 eV) into solids is strongly mass fractionated (approximately greater than or equal to 3 percent/amu). This has potential implications for the origin and evolution of terrestrial planet atmospheres.

Derived from text

N94-20698*# Geo Eco Arc Research, La Canada, CA.

GLOBAL BLACKOUT FOLLOWING THE K/T CHICXULUB IMPACT: RESULTS OF IMPACT AND ATMOSPHERIC MODELING Abstract Only **c45**

K. O. Pope, A. C. Ocampo (Jet Propulsion Lab., California Inst. of Tech., Pasadena.), K. H. Baines (Jet Propulsion Lab., California Inst. of Tech., Pasadena.), and B. A. Ivanov (Academy of Sciences, USSR, Moscow.) *In* Lunar and Planetary Inst., Twenty-Fourth Lunar and Planetary Science Conference. Part 3: N-Z 1993 p 1165-1166 (For primary document see N94-20636 05-91)

Avail: CASI HC A01/MF A06

Several recent studies have suggested that shock decomposition of anhydrite (CaSO4) target rocks during the K/T Chicxulub impact would have ejected tremendous amounts of sulfur gas into the stratosphere. One of the many potential biospheric effects of this sulfur gas is the generation of a sulfuric acid (H2SO4) aerosol layer capable of causing darkness and severe disruption of photosynthesis for periods of years. In this paper we report the preliminary results of our modeling of shock pressures within the anhydrites and of light attenuation by the H2SO4 aerosol cloud. These models indicate that earlier studies over-estimated the amount of sulfur gas produced, but that more than enough was produced to extend global blackout conditions 4-6 times longer than the approximately 3 month predictions for silicate dust alone.

Derived from text

N94-20699*# Oklahoma Univ., Norman.

SCHOOLS OF THE PACIFIC RAINFALL CLIMATE EXPERIMENT Abstract Only **c47**

S. E. Postawko, M. L. Morrissey, G. J. Taylor, and P. Mouginis-Mark (Hawaii Univ., Honolulu.) *In* Lunar and Planetary Inst., Twenty-Fourth Lunar and Planetary Science Conference. Part 3: N-Z 1993 p 1167 (For primary document see N94-20636 05-91)

Avail: CASI HC A01/MF A06

The SPaRCE program is a cooperative rainfall climate field project involving high school and college level students and teachers from various Pacific island and atoll nations. The goals of the SPaRCE program are: (1) to foster interest and increase understanding among Pacific-area students and teachers of climate and climate change; (2) to educate the students and teachers as to the importance of rainfall in the Pacific area to climate studies; (3) to provide the students and teachers an opportunity of making a major contribution to the global climate research effort by collecting and analyzing Pacific rainfall data; and (4) to incorporate collected rainfall observations into a comprehensive Pacific daily rainfall data base to be used for climate research purposes. Schools participating in SPaRCE have received standard raingauges with which to measure rainfall at their sites. Students learned to site and use their raingauges by viewing a video produced at the University of Oklahoma. Four more videos will be produced which will include information on Earth's atmosphere, global climate and climate change, regional climate and implications of climate change, and how to analyze and use the rainfall data they are collecting. The videos are accompanied by workbooks which summarize the main points of each video, and contain concrete learning activities to help the student better understand climate and climate change. Following each video, interactive sessions are held with the students using the PEACESAT (Pan-Pacific Education And Communication Experiments by Satellite) satellite radio communication system.

Derived from text

N94-20700*# Geological Survey, Denver, CO.

U-Pb ISOTOPIC AGES AND CHARACTERISTICS OF ANCIENT (GREATER THAN 4.0 Ga) LUNAR HIGHLAND ROCKS Abstract Only

W. R. Premo *In* Lunar and Planetary Inst., Twenty-Fourth Lunar and Planetary Science Conference. Part 3: N-Z 1993 p 1169-1170 (For primary document see N94-20636 05-91)

Avail: CASI HC A01/MF A06

A review of the present (and certainly sparse) U-Pb isotopic database for ancient (greater than 4.0 Ga) lunar highland rocks indicates that both early-forming anorthosites and high-Mg suite rocks were formed from sources with a wide variety of U-238/Pb-204(mu) values as early as 4.44 Ga. The U-Pb data from Apollo 16 anorthosites 67075, 60025, and 62337 indicate source-mu values between approximately 55 and approximately 350; whereas values for high-Mg suite rocks are tentatively considered to be over 500, similar to KREEP sources. At present, I interpret the data to indicate that either early cumulates were formed slowly in a magma environment that allowed isotopic reequilibration or mixing over a long period of crystallization, or these cumulates formed from rapidly-evolving (both geochemically and isotopically) residual liquids. It is possible that an early bombardment period played a role in the mixing process.

Author

N94-20701*# Geological Survey, Denver, CO.

U-Pb PROVENANCE AGES OF SHOCKED ZIRCONS FROM THE K-T BOUNDARY, RATON BASIN, COLORADO Abstract Only **c25**

W. R. Premo and G. A. Izett *In* Lunar and Planetary Inst., Twenty-Fourth Lunar and Planetary Science Conference. Part 3: N-Z 1993 p 1171-1172 (For primary document see N94-20636 05-91)

Avail: CASI HC A01/MF A06

U-Pb isotopic systematics from analyses of single zircons identify at least two provenance ages, approximately 575 Ma and approximately 330 Ma, for zircons from the impact layer of the K-T boundary, Raton Basin, Colorado. These data are a preliminary confirmation of results reported from the same layer. The zircon provenance ages provide a unique signature for identification of the source crater since igneous rocks of these ages (or sedimentary rocks derived from them) must characterize part of the impact stratigraphy.

Author

N94-20702*# Geological Survey, Denver, CO.

U-Pb ISOTOPIC SYSTEMATICS OF FERROAN ANORTHOSITE 60025 Abstract Only **c25**

W. R. Premo and M. Tatsumoto *In* Lunar and Planetary Inst., Twenty-Fourth Lunar and Planetary Science Conference. Part 3: N-Z 1993 p 1173-1174 (For primary document see N94-20636 05-91)

Avail: CASI HC A01/MF A06

Preliminary U-Pb isotopic data from separates of ferroan anorthosite 60025 confirm its antiquity at approximately 4.42 Ga. Three Pb-Pb isochron ages involving different sets of mineral separates vary by only 20 million years, but indicate derivation of the sets from isotopically distinct magma sources. If this anorthosite was a monomict cumulate product formed during the Moon's early primary differentiation stage, then residual liquids of crystallizing magmas were evolving isotopically, even at the cm-scale, over the duration of the crystallization period. Another explanation is that this

sample is simply a polymict breccia and that the Pb isotopic results are a result of subsequent mechanical mixing of mineral assemblages from various cumulate piles formed coevally at approximately 4.42 Ga from isotopically distinct magma sources. In our ongoing search for early lunar Pb isotopic compositions, we have analyzed Apollo 16 anorthosites 67075 and 62337 and Apollo 17 high-Mg suite cumulates (troctolite 76535, norite 78235, and dunite 72415). The U-Pb isotopic systematics have been better behaved in the high-Mg suite rocks than in the anorthosites that have shown evidence of mineral assemblages of mixed parentage. Our aim in analyzing anorthosite 60025 was to avoid or minimize this problem as it had been considered essentially monomict, although recent work has shown that not only is 60025 polymict, but shows textual evidence of at least two episodes of deformation. Of five splits studied by James, Lindstrom and McGee, the four mineral splits appeared monomict, whereas the whole-rock split was considered polymict. Previous isotopic work indicate that this anorthosite was quite primitive, a claim that was apparently confirmed by the U-Pb isotopic age of 4.51 +/- .01 Ga on three plagioclase separates. However, a Sm-Nd internal isochron age of 4.44 +/- 0.02 Ga was determined using plagioclase, olivine, and mafic mineral separates, creating some doubt about the anorthosite's true age. It was pointed out that the use of slightly evolved initial Pb values (corresponding to a source-micron value of approximately 35) to correct the U-Pb data can result in an U-Pb age of 4.44 Ga. The need to resolve the age and isotopic nature of this anorthosite is paramount to furthering our understanding of processes of ferroan anorthosite formation as well as the magmatic history of the early Moon.

Derived from text

N94-20703*# Arizona State Univ., Tempe. Dept. of Geology.

THERMAL CONDUCTIVITY MEASUREMENTS OF PARTICULATE MATERIALS UNDER MARTIAN CONDITIONS Abstract Only **c25**

M. A. Presley and P. R. Christensen *In* Lunar and Planetary Inst., Twenty-Fourth Lunar and Planetary Science Conference. Part 3: N-Z 1993 p 1175-1176 (For primary document see N94-20636 05-91)

Avail: CASI HC A01/MF A06

The mean particle diameter of surficial units on Mars has been approximated by applying thermal inertia determinations from the Mariner 9 Infrared Radiometer and the Viking Infrared Thermal Mapper data together with thermal conductivity measurement. Several studies have used this approximation to characterize surficial units and infer their nature and possible origin. Such interpretations are possible because previous measurements of the thermal conductivity of particulate materials have shown that particle size significantly affects thermal conductivity under martian atmospheric pressures. The transfer of thermal energy due to collisions of gas molecules is the predominant mechanism of thermal conductivity in porous systems for gas pressures above about 0.01 torr. At martian atmospheric pressures the mean free path of the gas molecules becomes greater than the effective distance over which conduction takes place between the particles. Gas particles are then more likely to collide with the solid particles than they are with each other. The average heat transfer distance between particles, which is related to particle size, shape and packing, thus determines how fast heat will flow through a particulate material.The derived one-to-one correspondence of thermal inertia to mean particle diameter implies a certain homogeneity in the materials analyzed. Yet the samples used were often characterized by fairly wide ranges of particle sizes with little information about the possible distribution of sizes within those ranges. Interpretation of thermal inertia data is further limited by the lack of data on other effects on the interparticle spacing relative to particle size, such as particle shape, bimodal or polymodal mixtures of grain sizes and formation of salt cements between grains. To address these limitations and to provide a more comprehensive set of thermal conductivities vs. particle size a linear heat source apparatus, similar to that of Cremers, was assembled to provide a means of measuring the thermal conductivity of particulate samples. In order to concentrate on the dependence of the thermal conductivity on particle size, initial runs will use spherical glass beads that are precision sieved into relatively small size ranges and thoroughly washed.

Derived from text

N94-20704*# Naturhistorisches Museum, Vienna (Austria).

ELEMENTAL DEPLETIONS IN ANTARCTIC MICROMETEORITES AND ARCTIC COSMIC SPHERULES: COMPARISON AND RELATIONSHIPS Abstract Only **c90**

T. Presper, G. Kurat, C. Koeberl (Wien Univ., Austria.), H. Palme (Max-Planck-Inst. fuer Chemie, Mainz, Germany.), and Michel Maurette (Centre de Spectrometrie Nucleaire et de Spectrometrie de Masse, Orsay, France.) *In* Lunar and Planetary Inst., Twenty-Fourth Lunar and Planetary Science Conference. Part 3: N-Z 1993 p 1177-1178 (For primary document see N94-20636 05-91)

Avail: CASI HC A01/MF A06

Antarctic micrometeorites (MM's) and Arctic cosmic spherules (CS's) have bulk compositions comparable to those of chondritic meteorites. However, abundance of Na, Ca, Mn, Ni, Co, and S are commonly lower in MM's and CS's as compared to chondrites. Our SEM, EMP, and INAA studies suggest that these elemental depletions in unmelted MM's are likely to be due to leaching of soluble components from the MM's in the upper atmosphere and the melt ice water. Depletions in CS's appear to be mainly due to volatilization during melting in the atmosphere or to sampling bias during aggregate formation or parent rock break-up.

Derived from text

N94-20705*# DePauw Univ., Greencastle, IN. Dept. of Geology and Geography.

GEOLOGIC MAPPING OF HARMAKHIS AND REULL VALLES REGION, MARS: EVIDENCE FOR MULTIPLE RESURFACING AND DRAINAGE EVENTS Abstract Only **c43**

Katherine H. Price *In* Lunar and Planetary Inst., Twenty-Fourth Lunar and Planetary Science Conference. Part 3: N-Z 1993 p 1179 (For primary document see N94-20636 05-91)

Avail: CASI HC A01/MF A06

Numerous mesas and irregular, channel-cut escarpments south of Harmakhis and Reull Valles suggesting at least two resurfacing events with subsequent periods of erosion are revealed from detailed geologic mapping of three adjacent 1:500,000-scale quadrangles (MTM-40262, -40267, -40272). Also, two distinct episodes of surface water runoff, each from different styles of water release, are evident. Geologic mapping is based on 1:500,000-scale photomosaics of the Harmakhis vallis region, and is an outgrowth of preliminary regional geologic mapping on a 1:2,000,000-scale on the east rim of Hellas Basin. Derived from text

N94-20706*# Princeton Univ., NJ. Dept. of Geological and Geophysical Sciences.

SOME DEFORMATION TRENDS AND TOPOGRAPHIC CHARACTERISTICS OF TESSERAE ON VENUS Abstract Only

Maribeth Price and John Suppe *In* Lunar and Planetary Inst., Twenty-Fourth Lunar and Planetary Science Conference. Part 3: N-Z 1993 p 1181-1182 (For primary document see N94-20636 05-91)

Avail: CASI HC A01/MF A06

Mapping of dominant trends of deformation and topographic analysis of tesserae reveal that (1) consistant patterns of deformation exist between individual tesserae; (2) regional deformation associated with coronae and rifts commonly overprints tesserae fabrics; (3) normalized area frequency plots of tesserae display a strongly bimodal distribution between -70 to 70 degrees latitude; and (4) the relief at tessera margins is relatively constant and independent of tessera elevation. We are continuing to expand these observations and test their implications for the formation of tesserae and for global models of deformation on Venus.

Author (revised)

N94-20707*# Princeton Univ., NJ. Dept. of Geological and Geophysical Sciences.

STUDYING VENUS USING A GIS DATABASE Abstract Only

Maribeth Price and John Suppe *In* Lunar and Planetary Inst., Twenty-Fourth Lunar and Planetary Science Conference. Part 3: N-Z 1993 p 1183-1184 (For primary document see N94-20636 05-91)

Avail: CASI HC A01/MF A06

A Geographic Information System (GIS) can significantly enhance geological studies on Venus because it facilitates concurrent analysis of many sources of data, as demonstrated by our work on topographic and deformation characteristics of tesserae. We are creating a database of structures referenced to real-world coordinates to encourage the archival of Venusian studies in digital format and to foster quantitative analysis of many combinations of data. Contributions to this database from all aspects of Venusian science are welcome.

Author

N94-20708*# American Museum of Natural History, New York, NY. Dept. of Mineral Science.
OXYGEN ISOTOPIC RELATIONSHIPS BETWEEN THE LEW85332 CARBONACEOUS CHONDRITE AND CR CHONDRITES Abstract Only **c90**
M. Prinz, M. K. Weisberg, R. N. Clayton (Chicago Univ., IL.), and T. K. Mayeda (Chicago Univ., IL.) *In* Lunar and Planetary Inst., Twenty-Fourth Lunar and Planetary Science Conference. Part 3: N-Z 1993 p 1185-1186 (For primary document see N94-20636 05-91)
Avail: CASI HC A01/MF A06

LEW85332, originally described as a unique C3 chondrite, was shown to be a C2 chondrite with important linkages to the CR clan. An important petrologic aspect of LEW85332 is that it contains anhydrous chondrules and hydrated matrix, and new oxygen isotopic data on chondrules, matrix and whole rock are consistent with the petrology. Chondrules fall on the equilibrated chondrite line (ECL), with a slope near 1, which goes through ordinary chondrite chondrules. This contrasts with the CR chondrule line which has a lower slope due to hydrated components. LEW85332 chondrules define a new carbonaceous chondrite chondrule line, parallel to the anhydrous CV chondrule line (CCC), consistent with the well-established concept of two oxygen isotopic reservoirs. Matrix and whole rock fall on the CR line. The whole rock composition indicates that the chondrite is dominated by chondrules, and that most of them contain light oxygen similar to that of anhydrous olivine and pyroxene separates in the Renazzo and Al Rais CR chondrites. Author (revised)

N94-20709*# Academy of Sciences (USSR), Moscow. Inst. for Dynamics of Geospheres.
IMPACT DISTURBANCE OF THE VENUS ATMOSPHERE Abstract Only
A. A. Provalov and B. A. Ivanov *In* Lunar and Planetary Inst., Twenty-Fourth Lunar and Planetary Science Conference. Part 3: N-Z 1993 p 1187-1188 (For primary document see N94-20636 05-91)
Avail: CASI HC A01/MF A06

Experimental simulations of the atmosphere-surface interaction during high-velocity impact are presented. At Venus an atmospheric vortex, generated with impact, may interact with a local wind. Some surface features, observed on Magellan images may be related with the simulated effect. Author

N94-20710*# Oulu Univ. (Finland). Dept. of Astronomy.
CHOCOLATE TABLET ASPECTS OF CYTHEREAN MESHKENET TESSERA Abstract Only
J. Raitala *In* Lunar and Planetary Inst., Twenty-Fourth Lunar and Planetary Science Conference. Part 3: N-Z 1993 p 1189-1190 (For primary document see N94-20636 05-91)
Avail: CASI HC A01/MF A06

Meshkenet Tessera structures were mapped from Magellan data and several resemblances to chocolate tablet boudinage were found. The complex fault sets display polyphase tectonic sequences of a few main deformation phases. Shear and tension have contributed to the areal deformation. Main faults cut the 1600-km long Meshkenet Tessera highland into bar-like blocks which have ridge and groove pattern oriented along or at high angles to the faults. The first approach to the surface block deformation is an assumption of initial parallel shear faulting followed by a chocolate tablet boudinage. Major faults which cut Meshkenet Tessera into rectangular blocks have been active repetitively while two progressive or superposed boudinage set formations have taken place at high angles during the relaxational or flattening type deformation of the area. Chocolate tablet boudinage is caused by a layer-parallel two-dimensional extension resulting in fracturing of the competent layer. Such structures, defined by two sets of boudin neck lines at right angles to each other, have been described by a number of authors. They develop in a flattening type of bulk deformation or during superposed deformation where the rock is elongated in two dimensions parallel to the surface. This is an attempt to describe and understand the formation and development of structures of Meshkenet Tessera which has complicated fault structures. Derived from text

N94-20711*# Oulu Univ. (Finland). Dept. of Astronomy.
RIDGE BELT-RELATED SCARPS AND TROUGHS: COMPRESSIONAL CRUSTAL BENDING ON VENUS Abstract Only
J. Raitala, T. Toermaenen, K. Kauhanen, and T. Tokkonen *In* Lunar and Planetary Inst., Twenty-Fourth Lunar and Planetary Science Conference. Part 3: N-Z 1993 p 1191-1192 (For primary document see N94-20636 05-91)
Avail: CASI HC A01/MF A06

Cytherean ridge arcs resulted in crustal shortening in places with either the strongest compression or weakest surface layers. Arcuate scarps on or close to the edge of the ridge arcs were compressional fronts formed by overthrust over or subduction of adjacent lowland. These ridge arcs became wider due to the propagation of new ridge formation close to previous one(s). As this process repeated itself with time, the crust became thicker and the foreland was bent either due to the excess load, overthrust or subduction event. The Salme Dorsa arc measures 100 km in width and 600 km in length. It consists of a horseshoe-like set of ridges and grooves on a gently sloping lowland. The westward arcuate ridge belt indicates lateral compressional stresses and crustal deformation from SE against the southern Ishtar Terra foreland plain. The trough on the western side of the ridge belt and tensional grabens close to the crest of the bulge to the west of the trough are due to the crustal bending and indicate effects of the load and thrust. Compression and relative movement from southeast against and over the foreland planitia have resulted in ridge belt, trough and bulge formation. The load- and/or stress-induced bending of the uppermost crust allows some estimations of the uppermost elastic lithosphere thickness. Repeated folding and thrust faulting of surface layers due to compression are indicated by four more ridge belts located close to Salme Dorsa. The northeasternmost one has short ridges located in troughs. The west-opening arcuate ridge belt interlocks with the Salme Dorsa horseshoe. Derived from text

N94-20712*# National Aeronautics and Space Administration. Lyndon B. Johnson Space Center, Houston, TX.
SCR NEON AND ARGON IN KAPOETA FELDSPAR: EVIDENCE FOR AN ACTIVE ANCIENT SUN Abstract Only **c92**
M. N. Rao, D. H. Garrison, and D. D. Bogard *In* Lunar and Planetary Inst., Twenty-Fourth Lunar and Planetary Science Conference. Part 3: N-Z 1993 p 1193-1194 (For primary document see N94-20636 05-91)
Avail: CASI HC A01/MF A06

From etched feldspar size-fractions of Kapoeta, we determine a significant excess of cosmogenic Ne-21 and Ar-38 over that produced by galactic cosmic rays. This excess component is attributed to early production by energetic solar protons and suggest that the energetic proton flux from the ancient Sun was several hundred times more intense than that of the contemporary Sun. Author (revised)

N94-20713*# Los Alamos National Lab., NM.
COSMOGENIC-RADIONUCLIDE PROFILES IN KNYAHINYA: NEW MEASUREMENTS AND MODELS Abstract Only **c93**
R. C. Reedy, J. Masarik, K. Nishiizumi (California Univ., La Jolla.), J. R. Arnold (California Univ., La Jolla.), R. C. Finkel (Lawrence Livermore National Lab., CA.), M. W. Caffee (Lawrence Livermore National Lab., CA.), J. Southon (Lawrence Livermore National Lab., CA.), A. J. T. Jull (Arizona Univ., Tucson.), and D. J. Donahue (Arizona Univ., Tucson.) *In* Lunar and Planetary Inst., Twenty-Fourth Lunar and Planetary Science Conference. Part 3: N-Z 1993 p 1195-1196 (For primary document see N94-20636 05-91)
Avail: CASI HC A01/MF A06

Cosmic-ray-produced nuclides measured in samples taken from known locations on a big slab of the large (R approximately equals to 45 cm) L5-chondrite Knyahinya provide good depth-vs-concentration profiles to develop and test models for the production of cosmogenic nuclides in meteorites. We report new profiles for Be-10, Al-26, Cl-36 in metallic and non-magnetic phases of 8 documented samples from Knyahinya and for C-14 in bulk samples from 7 Knyahinya samples. These new measured profiles are very similar to profiles calculated with particle fluxes from the LAHET Monte Carlo production and transport code system and with cross sections for major reactions. Derived from text

N94-20714*# Witwatersrand Univ., Johannesburg (South Africa). Economic Geology Research Unit.
KALKKOP CRATER, EASTERN CAPE: A NEW IMPACT CRATER IN SOUTH AFRICA Abstract Only **c46**
W. U. Reimold, F. G. LeRoux (Geological Survey of South-West Africa/Namibia, Windhoek.), C. Koeberl (Wien Univ., Austria.), and S. B.

Shirey (Wien Univ., Austria.) *In* Lunar and Planetary Inst., Twenty-Fourth Lunar and Planetary Science Conference. Part 3: N-Z 1993 p 1197-1198 (For primary document see N94-20636 05-91)
Avail: CASI HC A01/MF A06

Reimold et al. suggested that the 640 m diameter Kalkkop crater, at 32 deg 43 min S/24 deg 34 min E in the Eastern Cape Province (South Africa), could possibly be of impact origin. This idea was based on the circularity of this structure, its regional uniqueness, lack of recent igneous activity in the region, and descriptions of drillcore indicating that the crater is not underlain by a salt dome and is partially filled with a breccia layer of a thickness which would agree with the dimensions expected for an impact structure of this size. Unfortunately the old drillcore was no longer available for detailed study, and in the absence of sufficient surface exposure only drilling could provide the evidence needed to solve the problem of the origin of Kalkkop. For this reason and to study the crater fill from a paleoenvironmental point of view, the S. African Geological Survey decided to sponsor a new research drilling project at the Kalkkop site. First petrographic and isotopic results from Kalkkop drill core studies confirming, without doubt, that this crater is of impact origin are presented.
Author (revised)

N94-20715*# New Mexico Univ., Albuquerque. Dept. of Earth and Planetary Sciences.
MICROMETEORITE DYNAMIC PYROMETAMORPHISM: NONSTOICHIOMETRIC CLINOENSTATITE (CLEN) Abstract Only **c90**
Frans J. M. Rietmeijer *In* Lunar and Planetary Inst., Twenty-Fourth Lunar and Planetary Science Conference. Part 3: N-Z 1993 p 1199-1200 (For primary document see N94-20636 05-91)
Avail: CASI HC A01/MF A06

Polymorphs of enstatite are common phases in many meteorites. They contain clues on their formation and the thermal evolution of their host rock which includes shock metamorphism. Rare, micron-sized, CLEN whickers and thin platelets in chondritic porous micrometeorites were interpreted as solar nebula condensates that remained unaffected during atmospheric entry flash-heating. This CLEN formed by protoenstatite (PEN) inversion whereby the surface energy of the micron-sized PEN crystals aided the OREN-CLEN transformation or by metastable growth. Ca-poor, Mg,Fe-pyroxene with unequilibrated, intraparticle, Mg/(Mg+Fe) distributions occur in most chondritic micrometeorites. These distributions are a parent body signature that survived dynamic pyrometamorphism because the duration of the thermal spike during atmospheric entry is too short but this conclusion does not consider the ultrafine grain size of micrometeorites. The maximum temperature and duration of the heating event will depend on the kinetic energy and entry angle of the incoming micrometeorite. But lacking detailed petrological data for an individual particle, its thermal profile during atmospheric entry can not be deduced from its mass alone as a function of entry angle. In order to constrain dynamic pyrometamorphism in unmelted micrometeorites, I determined the petrological composition and silicate mineralogy in non-chondritic micrometeorites L2005T13, L2005E40, and L2006A28. Author (revised)

N94-20716*# New Mexico Univ., Albuquerque. Dept. of Earth and Planetary Sciences.
MICROMETEORITE DYNAMIC PYROMETAMORPHISM: OBSERVATION OF A THERMAL GRADIENT IN IRON-NICKEL SULFIDE Abstract Only **c90**
Frans J. M. Rietmeijer *In* Lunar and Planetary Inst., Twenty-Fourth Lunar and Planetary Science Conference. Part 3: N-Z 1993 p 1201-1202 (For primary document see N94-20636 05-91)
Avail: CASI HC A01/MF A06

Dynamic pyrometamorphism describes the mineralogical changes in a micrometeorite that occur in response to flash-heating during atmospheric entry. Mineral reactions during this event will be endothermic and act as local sinks for thermal energy which delays a uniform temperature distribution in decelerating micrometeorites. The most common pyrometamorphic reaction is formation of magnetite nanocrystal decorations on Mg,Fe-silicate grains and magnetite or (partial) maghemite rims. Constituent silicates also respond to this thermal event and show formation of olivine-maghemite symplectites and growth of garnet and partial laihunitisation. In continued effort to constrain dynamic pyrometamorphism of unmelted interplanetary dust particles (IDP's), I determined the mineralogical composition, and Fe,Ni-sulfide chemistry, in the sulfide-rich particles L2005C39, L2005E40, and L2006A28 using a JEOL 2000FX analytical electron microscope equipped with a TN5500 energy dispersive spectrometer for in situ microanalysis. Sulfide compositions in these three IDP's are distinctly different from those in silicate-rich particle L2005T13 which might suggest a delicate balance of the fO2/fS2 ratios during dynamic pyrometamorphism.
Author (revised)

N94-20717*# Chicago Univ., IL. Dept. of the Geophysical Sciences.
WAVELENGTH DISPERSIVE ANALYSIS WITH THE SYNCHROTRON X RAY FLUORESCENCE MICROPROBE Abstract Only **c25**
M. L. Rivers, K. S. Thorn, S. R. Sutton, K. W. Jones (Brookhaven National Lab., Upton, NY.), and S. Bajt *In* Lunar and Planetary Inst., Twenty-Fourth Lunar and Planetary Science Conference. Part 3: N-Z 1993 p 1203-1204 (For primary document see N94-20636 05-91)
(Contracts NAG9-106; DE-AC02-76CH-00016; DE-FG02-92ER-14244; NSF EAR-89-15699)
Avail: CASI HC A01/MF A06

A wavelength dispersive spectrometer (WDS) was tested on the synchrotron x ray fluorescence microprobe at Brookhaven National Laboratory. Compared to WDS spectra using an electron microprobe, the synchrotron WDS spectra have much better sensitivity and, due to the absence of bremsstrahlung radiation, lower backgrounds. The WDS spectrometer was successfully used to resolve REE L fluorescence spectra from standard glasses and transition metal K fluorescence spectra from kamacite.
Author

N94-20718*# Harvard-Smithsonian Center for Astrophysics, Cambridge, MA.
SUBDUCTION ON THE MARGINS OF CORONAE ON VENUS: EVIDENCE FROM RADIOTHERMAL EMISSIVITY MEASUREMENTS Abstract Only
C. A. Robinson *In* Lunar and Planetary Inst., Twenty-Fourth Lunar and Planetary Science Conference. Part 3: N-Z 1993 p 1205-1206 (For primary document see N94-20636 05-91)
Avail: CASI HC A01/MF A06

Retrograde subduction has been suggested to occur at three coronae on Venus: Latona, Artemis, and Eithinoha. Using the mineralogical arguments of Klose to explain surface emissivity, a study of radio thermal emissivity of Venus coronae showed that emissivity changes associated with Latona, Artemis, and Ceres imply the same crustal movements predicted by the subduction model of Sandwell and Schubert. Author (revised)

N94-20719*# Hawaii Univ., Hilo. Planetary Geosciences.
PRELIMINARY RESULTS FROM MARINER 10: HIGH RESOLUTION IMAGES OF THE MOON Abstract Only
Mark S. Robinson, B. Ray Hawke, Kay Edwards (Geological Survey, Flagstaff, AZ.), Paul G. Lucey, and Beth E. Clark *In* Lunar and Planetary Inst., Twenty-Fourth Lunar and Planetary Science Conference. Part 3: N-Z 1993 p 1207-1208 (For primary document see N94-20636 05-91)
Avail: CASI HC A01/MF A06

In November of 1973 the Mariner 10 spacecraft acquired high resolution images of both the Earth and the Moon as it began its voyage to Venus and then Mercury. The best images had a resolution of approximately 1 km and were taken from an unusual viewpoint, above the lunar North Pole. At this time the Moon was illuminated such that the eastern limb, including approximately 30 degrees of the farside, was visible. Two high resolution mosaics were acquired during this period which provide excellent views of regions of the Moon poorly seen from the Earth. These include the Frigoris, Humboldtianum, Marginis, and Smythii regions. These images also covered expanses of highlands not visible from the Earth. These data were unique in that they were the only useful robotic spacecraft images of the Moon; and they remained so until December of 1990 when the Galileo spacecraft made its first encounter with the Moon. These Mariner 10 lunar images were acquired and are currently being used in conjunction with Earth-based telescopic spectra as well as Apollo and Lunar Orbiter photographic data to investigate the nature of deposits comprising the Northeast Nearside of the Moon. These Mariner 10 frames have proved useful for photogeologic, photometric, and photoclinometric analyses; they were also used in support of the second Galileo lunar encounter of December 1992.
Author (revised)

N94-20720*# Hawaii Univ., Hilo. Planetary Geosciences.
CHRONOLOGY, ERUPTION DURATION, AND ATMOSPHERIC CONTRIBUTION OF APOLLINARIS PATERA, MARS Abstract Only
M. S. Robinson, P. J. Mouginis-Mark, J. R. Zimbelman (Smithsonian Institution, Washington, DC.), and S. S. C. Wu (Geological Survey, Flagstaff, AZ.) *In* Lunar and Planetary Inst., Twenty-Fourth Lunar and Planetary Science Conference. Part 3: N-Z 1993 p 1209-1210 (For primary document see N94-20636 05-91)
Avail: CASI HC A01/MF A06

Geologic mapping from Viking image data of the Martian volcano Apollinaris Patera allowed identification of 6 major events that shaped its current morphology. Derivation of new topographic data allowed accurate estimates of the volume of erupted products from which estimates of an eruption duration are presented for the edifice and its corresponding atmospheric water contribution. Topographic data were acquired using stereophotogrammetric (Viking picnos 603A42, 639A92) techniques in both profiling and contouring modes (1 km contour). The profiling mode results in a more precise measurement than the contouring mode, but is limited in its areal coverage. The contour data are used in a more general sense to provide synoptic coverage for the volcano. These new stereophotogrammetric measurements constrain the topography to an accuracy of approximately 800 m vertically and approximately 1000 m horizontally. Conversion of the derived contour map to a raster based digital elevation model (DEM) was done by a growing contours interpolation. An ambiguity arises in this volume calculation due to an uncertainty regarding the actual base of the volcano relative to the pre-existing topography. Thus, the volume estimate was bracketed by using the 100 m and the 750 m elevations, which generally correspond to the lower and upper portions of the circumferential basal scarp, respectively. The resulting volumes are 103,000 cu km and 97,000 cu km; therefore the total volume of Apollinaris Patera is estimated to be approximately 100,000 cu km.
Author (revised)

N94-20721*# Geological Survey, Flagstaff, AZ.
THE MANSON IMPACT CRATER: ESTIMATION OF THE ENERGY OF FORMATION, POSSIBLE SIZE OF THE IMPACTING ASTEROID OR COMET, AND EJECTA VOLUME AND MASS Abstract Only **c90**
D. J. Roddy, E. M. Shoemaker, and R. R. Anderson (Geological Survey, Iowa City, IA.) *In* Lunar and Planetary Inst., Twenty-Fourth Lunar and Planetary Science Conference. Part 3: N-Z 1993 p 1211-1212 (For primary document see N94-20636 05-91)
Avail: CASI HC A01/MF A06

A research program on the Manson impact structure has substantially improved our knowledge of the detailed features of this eroded crater. As part of our structural studies, we have derived a value of 21 km for the diameter of the final transient cavity formed during crater excavation. With this information, we can estimate the energy of formation of the Manson crater and the possible size of the impacting asteroid or comet. In addition, we have estimated the near- and far-field ejecta volumes and masses.
Author

N94-20722*# Centre National d'Etudes Spatiales, Toulouse (France).
COMPARATIVE HYPSOMETRIC ANALYSIS OF BOTH EARTH AND VENUS TOPOGRAPHIC DISTRIBUTIONS Abstract Only
P. Rosenblatt, P. C. Pinet, and E. Thouvenot *In* Lunar and Planetary Inst., Twenty-Fourth Lunar and Planetary Science Conference. Part 3: N-Z 1993 p 1213-1214 (For primary document see N94-20636 05-91)
Avail: CASI HC A01/MF A06

Previous studies have compared the global topographic distribution of both planets by means of differential hypsometric curves. For the purpose of comparison, the terrestrial oceanic load was removed, and a reference base level was acquired. It was chosen on the basis of geometric considerations and reflected the geometric shape of the mean dynamical equilibrium figure of the planetary surface in both cases. This reference level corresponds to the well-known sea level for the Earth; for Venus, given its slow rate of rotation, a sphere of radius close to the mean, median and modal values of the planetary radii distribution were considered and the radius value of 6051 km arbitrarily taken. These studies were based on the low resolution (100 x 100 sq km) coverage of Venus obtained by the Pioneer Venus altimeter and on the 1 deg x 1 deg terrestrial topography. But, apart from revealing the distinct contrast existing between the Earth's bimodal and Venus' strong unimodal topographic distribution, the choice of such a reference level is inadequate and even misleading for the comparative geophysical understanding of the planetary relief distribution. The present work reinvestigates the comparison between Earth and Venus hypsometric distribution on the basis of the high-resolution data provided, on one hand, by the recent Magellan global topographic coverage of Venus' surface, and on the other hand, by the detailed NCAR 5 x 5 ft. grid topographic database currently available for the Earth's surface.
Author (revised)

N94-20723*# National Aeronautics and Space Administration. Ames Research Center, Moffett Field, CA.
DERIVATION OF THE MIDINFRARED (5.0-25.0 MICRON) OPTICAL CONSTANTS OF HYDROUS CARBONATE AND SULFATE Abstract Only
Ted L. Roush, James B. Orenberg, and James B. Pollack *In* Lunar and Planetary Inst., Twenty-Fourth Lunar and Planetary Science Conference. Part 3: N-Z 1993 p 1215-1216 Sponsored by NASA. Washington (For primary document see N94-20636 05-91)
(Grant NAGw-2212; RTOP 199-70-22-11)
Avail: CASI HC A01/MF A06

There is ample theoretical and observational evidence suggesting liquid water was once stable at the surface of Mars. Because water is essential to the evolution of life, it is important to understand the types of environments in which the liquid water was present. For example, if water were present early in Mars' history, then this raises the possibility that biological activity may have evolved only to eventually become extinct as liquid water became scarce. Alternatively, if liquid water were stable only later in Mars' history, then it becomes problematic to envision mechanisms by which biological activity evolved and remained viable without water until more favorable conditions existed. Even without biological activity, atmospheric carbon dioxide dissolved in water can assist the chemical weathering of primary igneous minerals producing common secondary phases such as hydartes, carbonates, and sulfates. While the identification of hydrates, carbonates, and sulfates on Mars cannot provide direct evidence of biological activity, it can provide significant information regarding the presence and duration of an environment that would support the presence of liquid water at the surface. The specific mineralogy of these secondary phases can provide insight into the environments of their formation. For example, the slow precipitation that occurs in large standing bodies of water, e.g. oceans or lakes, commonly results in the formation of calcite, magnesite, dolomite, siderite, and rhodochrosite. Rapid precipitation that occurs in ephemeral bodies of water, e.g. hypersaline lakes or playas, can result in the formation of all of the above phases as well as aragonite, vaterite, hydrated carbonates, alkali carbonates, bicarbonates, and other poorly ordered phases. Absorption features identified in recent near-infrared spectra of Mars have been interpreted as being due to bicarbonate and bisulfate located in the mineral scaplite. Spectral data returned by the Mariner 6 and 7 spacecraft have been inerpreted as remaining consistent with the presence of hydrated carbonates. Additional, airborne thermal infrared spectra of Mars have been interpreted as implying the presence of carbonates, sulfates, and hydrates. Modeling of the thermal infrared data relied upon the optical constants of calcite anhydrite and a mixture of water in basalt because of their availability. The derived abundances of carbonate and sulfate were 1-3 percent and 10-15 percent by volume. However, the observed complexity and positions of the bands suggested other carbonate-, and sulfate-bearing species. We have already derived optical constants for hydrous and anhydrous silicates, and we are now applying these techniques to the derivation of the optical constants of hydrous carbonate and sulfate. Author (revised)

N94-20724*# California Univ., Los Angeles. Inst. of Geophysics and Planetary Physics.
EUHEDRAL METALLIC-Fe-Ni GRAINS IN EXTRATERRESTRIAL SAMPLES Abstract Only **c26**
Alan E. Rubin *In* Lunar and Planetary Inst., Twenty-Fourth Lunar and Planetary Science Conference. Part 3: N-Z 1993 p 1217-1218 (For primary document see N94-20636 05-91)
Avail: CASI HC A01/MF A06

Metallic Fe-Ni is rare in terrestrial rocks, being largely restricted to serpentinized peridotites and volcanic rocks that assimilated carbonaceous material. In contrast, metallic Fe-Ni is nearly ubiquitous among extraterrestrial samples (i.e., meteorites, lunar rocks, and interplanetary dust particles). Anhedral grains are common. For example, in eucrites and lunar basalts,

most of the metallic Fe-Ni occurs interstitially between silicate grains and thus tends to have irregular morphologies. In many porphyritic chondrules, metallic Fe-Ni and troilite form rounded blebs in the mesostasis because their precursors were immiscible droplets. In metamorphosed ordinary chondrites, metallic Fe-Ni and troilite form coarse anhedral grains. Some of the metallic Fe-Ni and troilite grains has also been mobilized and injected into fractures in adjacent silicate grains where local shock-reheating temperatures reached the Fe-FeS eutectic (988 C). In interplanetary dust particles metallic Fe-Ni most commonly occurs along with sulfide as spheroids and fragments. Euhedral metallic Fe-Ni grains are extremely rare. Several conditions must be met before such grains can form: (1) grain growth must occur at free surfaces, restricting euhedral metallic Fe-Ni grains to systems that are igneous or undergoing vapor-deposition; (2) the metal (+/-) sulfide assemblage must have an appropriate bulk composition so that taenite is the liquidus phase in igneous systems or the stable condensate phase in vapor-deposition systems; and (3) metallic Fe-Ni grains must remain underformed during subsequent compaction, thermal metamorphism, and shock. Because of these restrictions, the occurrence of euhedral metallic Fe-Ni grains in an object can potentially provide important petrogenetic information. Despite its rarity, euhedral metallic Fe-Ni occurs in a wide variety of extraterrestrial materials. Some of these materials formed in the solar nebula; others formed on parent body surfaces by meteoroid impacts. Author (revised)

N94-20725*# Geological Survey, Flagstaff, AZ.
NAMED VENUSIAN CRATERS Abstract Only
Joel F. Russell and Gerald G. Schaber *In* Lunar and Planetary Inst., Twenty-Fourth Lunar and Planetary Science Conference. Part 3: N-Z 1993 p 1219-1220 (For primary document see N94-20636 05-91)
Avail: CASI HC A01/MF A06

Schaber et al. compiled a database of 841 craters on Venus, based on Magellan coverage of 89 percent of the planet's surface. That database, derived from coverage of approximately 98 percent of Venus' surface, has been expanded to 912 craters, ranging in diameter from 1.5 to 280 km. About 150 of the larger craters were previously identified by Pioneer Venus and Soviet Venera projects and subsequently formally named by the International Astronomical Union (IAU). Altogether, the crater names submitted to the IAU for approval to date number about 550, a little more than half of the number of craters identified on Magellan images. The IAU will consider more names as they are submitted for approval. Anyone--planetary scientist or layman--may submit names; however, candidate names must conform to IAU rules. The person to be honored must be deceased for at least three years, must not be a religious figure or a military or political figure of the 19th or 20th century, and, for Venus, must be a woman. All formally and provisionally approved names for Venusian impact craters, along with their latitude, longitude, size, and origin of their name, will be presented at LPSC and will be available as handouts. Author (revised)

N94-20726*# Open Univ., Milton (England). Dept. of Geological Sciences.
A CARBON AND NITROGEN ISOTOPE STUDY OF CARBONACEOUS VEIN MATERIAL IN UREILITE METEORITES Abstract Only **c90**
S. S. Russell, J. W. Arden, I. A. Franchi, and C. T. Pillinger *In* Lunar and Planetary Inst., Twenty-Fourth Lunar and Planetary Science Conference. Part 3: N-Z 1993 p 1221-1222 (For primary document see N94-20636 05-91)
Avail: CASI HC A01/MF A06

The ureilite meteorite group is known to be rich in carbon in the form of graphite/diamond veins that are associated with planetary type noble gases. This paper reports preliminary data from a systematic study of the carbon and nitrogen isotopic composition of this carbonaceous vein material. A previous study focused on the whole rock signatures and reported that the carbon inventory appeared to be dominated by the graphitic/diamond intergrowths, whereas the nitrogen was clearly composed of several distinct components including one that was isotopically light, possibly associated with the carbonaceous material. Recent studies have demonstrated that diamonds in the solar system formed in many different environments. C and N measurements from ureilitic diamond made in a similar way would be a useful addition to this overall study. The methods used for isolating diamonds of possible presolar origin from primitive meteorites are equally applicable to the processing of carbon bearing components in the ureilite group so that their stable isotopic composition can be determined. Herein we discuss conjoint C and N stepped combustion measurements made on crushed whole rock ureilite samples that have been treated with 1M HCl/9M HF to dissolve silicate and free metal. In addition, two samples have been further treated with oxidizing acids to leave a diamond rich residue. Author (revised)

N94-20727*# Brown Univ., Providence, RI. Dept. of Geological Sciences.
C-O VOLATILES IN APOLLO 15 AND APOLLO 17 PICRITIC GLASSES Abstract Only **c25**
Malcolm J. Rutherford and Robert A. Fogel (American Museum of Natural History, New York, NY.) *In* Lunar and Planetary Inst., Twenty-Fourth Lunar and Planetary Science Conference. Part 3: N-Z 1993 p 1223-1224 (For primary document see N94-20636 05-91)
Avail: CASI HC A01/MF A06

A15 and A17 primitive picritic glasses have been examined by FTIR for the presence of dissolved C-O species to determine the role of C-O gasses on driving lunar fire-fountains. A15 green and yellow glasses were extensively studied and found to be free of dissolved C species down to FTIR detection limits (10-100 ppm; species and sample specific). Preliminary data on A17 orange glasses are similarly devoid of FTIR detectable C-O species. Re-analyses of the C-O driving mechanism theory for mare volcanism demonstrates the need to determine the fO2 of the lunar interior; the factor that most critically determined the role of C gasses in the fire-fountaining events. Oxygen fugacities equivalent to IW-0.5 and above imply dissolved CO3(=) in the primitive glasses at levels above FTIR detection. The f02's below IW-0.5 imply concentrations of CO3(=) below FTIR detection. Recent data suggesting lunar mantle fO2's of IW-2 or less, strongly mitigate against finding FTIR measurable dissolved CO3(=) consistent with the findings of this study. Author (revised)

N94-20728*# Arizona Univ., Tucson. Lunar and Planetary Lab.
FORMATION OF THE LOW-MASS SOLAR NEBULA **c92**
T. V. Ruzmaikina, I. V. Khatuncev (Academy of Sciences, USSR, Moscow.), and T. V. Konkina (Academy of Sciences, USSR, Moscow.) *In* Lunar and Planetary Inst., Twenty-Fourth Lunar and Planetary Science Conference. Part 3: N-Z 1993 p 1225-1226 (For primary document see N94-20636 05-91)
Avail: CASI HC A01/MF A06

We study an accretional stage of the formation and early evolution of the solar nebula with relatively small angular momentum. We investigate the evolution of the disk and its vertical structure, particularly the shock front between disk and infalling material. Calculations start at a moment when a low-mass star-like core surrounded by small embryo disk have been formed at the center of the presolar nebula and the bulk of mass remained in the envelope. The forming solar nebula is approximated as a thin viscous disk surrounded by accreting envelope. The distribution of temperature in the infalling envelope is determined by solving spherically symmetric equations of radiative transfer. As the energy source, we take into account all energy released within the centrifugal radius of the infalling matter. Other aspects of this study are discussed. Derived from text

N94-20729*# Planetary Science Inst., Tucson, AZ.
ASTEROID COLLISIONS: TARGET SIZE EFFECTS AND RESULTANT VELOCITY DISTRIBUTIONS Abstract Only **c90**
Eileen V. Ryan *In* Lunar and Planetary Inst., Twenty-Fourth Lunar and Planetary Science Conference. Part 3: N-Z 1993 p 1227-1228 (For primary document see N94-20636 05-91)
Avail: CASI HC A01/MF A06

To study the dynamic fragmentation of rock to simulate asteroid collisions, we use a 2-D, continuum damage numerical hydrocode which models two-body impacts. This hydrocode monitors stress wave propagation and interaction within the target body, and includes a physical model for the formation and growth of cracks in rock. With this algorithm we have successfully reproduced fragment size distributions and mean ejecta speeds from laboratory impact experiments using basalt, and weak and strong mortar as target materials. Using the hydrocode, we have determined that the energy needed to fracture a body has a much stronger dependence on target size than predicted from most scaling theories. In addition, velocity distributions obtained indicate that mean ejecta speeds resulting from large-body collisions do not exceed escape velocities. Derived from text

N94-20730*# Washington Univ., Seattle. Dept. of Geological Sciences.
DETECTABILITY OF CRYSTALLINE FERRIC AND FERROUS MINERALS ON MARS Abstract Only
Donald E. Sabol, Jr., James F. Bell, III (National Aeronautics and Space Administration. Ames Research Center, Moffett Field, CA.), and John B. Adams *In* Lunar and Planetary Inst., Twenty-Fourth Lunar and Planetary Science Conference. Part 3: N-Z 1993 p 1229-1230 (For primary document see N94-20636 05-91)
Avail: CASI HC A01/MF A06

Telescopic and spacecraft spectroscopic and geochemical data have been used to constrain the surface mineralogy of Mars and to yield clues about past and present Mars surface weathering/alteration scenarios. Based primarily on their visible to near-IR reflectance properties, several terrestrial iron-bearing minerals have been either identified on Mars or proposed as Mars spectral analogs. Among these are crystalline hematite, pyroxenes, as well as poorly crystalline materials like nonophase hematite and palagonite. Other iron-bearing minerals include nontronite, magnetite, jarosite, and goethite and the have been proposed as Mars surface constituents based on Viking Lander measurements or geochemical modeling. If present on Mars, these materials likely appear as spectral mixtures at the coarse spatial resolution of remotely sensed data. The detectability of any of these components must be evaluated relative to the other components with which they occur. The primary goal of this study is to determine how much of any given mineral would have to be present for it to be detectable in remotely-sensed data. Here, the detectability of iron-bearing minerals was evaluated using detection threshold analysis (DTA), an analytical technique based on spectral mixture analysis. Derived from text

N94-20731*# Sahuaro High School, Tucson, AZ.
DISTRIBUTION OF SMALL VOLCANIC CONES ON THE SURFACE OF VENUS BY SIZE AND ELEVATION: IMPLICATIONS FOR DIFFERENTIAL DEPOSITION OF VOLCANIC FEATURES Abstract Only
J. F. Lockwood, Mike Ellison, J. Johnson (Arizona Univ., Tucson.), and G. Kamatsu (Arizona Univ., Tucson.) *In* Lunar and Planetary Inst., Twenty-Fourth Lunar and Planetary Science Conference. Part 3: N-Z 1993 p 1231-1232 Prepared in cooperation with Evergreen High School, Vancouver, WA (For primary document see N94-20636 05-91)
Avail: CASI HC A01/MF A06

It appears that volcanic features are not evenly distributed on the surface of Venus. Head et. al. theorizes that the sparcity of volcanic features in the lowlands may be due to an altitude dependent inhibition of volatile exsolution and the resulting products of neutral buoyancy zones sufficient to form magma reservoirs and favoring flood lavas at lower elevation. The astronomy research classes of Evergreen and Sahuaro High Schools surveyed a cross-section of different elevation topography to investigate size and distribution of small volcanic cones by elevation. The results from this survey are presented. Derived from text

N94-20732*# Johns Hopkins Univ., Baltimore, MD. Dept. of Earth and Planetary Sciences.
VENUS PANCAKE DOME FORMATION: MORPHOLOGIC EFFECTS OF A COOLING-INDUCED VARIABLE VISCOSITY DURING EMPLACEMENT Abstract Only
S. E. H. Sakimoto and M. T. Zuber *In* Lunar and Planetary Inst., Twenty-Fourth Lunar and Planetary Science Conference. Part 3: N-Z 1993 p 1233-1234 (For primary document see N94-20636 05-91)
Avail: CASI HC A01/MF A06

The distinctive steep-sided 'pancake' domes discovered in the Magellan images of Venus have morphologies that suggest formation by a single continuous emplacement of a high viscosity magma. A resemblance of the venusian domes to much smaller terrestrial rhyolite and dacite volcanic domes has prompted some authors to suggest that the domes on Venus also have high silica compositions and thus, high viscosities. However, viscosity is a function of crystallinity as well as silica content in a magma, and thus increases as a result of magmatic cooling. To investigate the effect of a cooling-induced viscosity increase on dome morphology, we have modeled the domes as radial viscous gravity currents that cool during emplacement. Various aspects of the investigation are discussed.
Derived from text

N94-20733*# Johns Hopkins Univ., Baltimore, MD.
THERMAL INFRARED REMOTE SENSING AND KIRCHHOFF'S LAW: 1. LABORATORY MEASUREMENTS Abstract Only **c25**
J. W. Salisbury, A. Wald, and D. M. DAria *In* Lunar and Planetary Inst., Twenty-Fourth Lunar and Planetary Science Conference. Part 3: N-Z 1993 p 1235-1236 (For primary document see N94-20636 05-91)
Avail: CASI HC A01/MF A06

Kirchoff's Law, as originally conceived, applies only to samples in thermal equilibrium with their surroundings. Most laboratory measurements of emissivity only approach this condition and it never applies in remote sensing applications. In particular, the background is often much cooler than the radiating sample, and this has led to a long controversy about the applicability of Kirchhoff's Law under such conditions. It has also led to field and laboratory measurement techniques that use some form of the 'emissivity box' approach, which surrounds the sample with a background as close as possible to the sample temperature. In our experiments, we have heated soil samples in air on a hot plate in the laboratory to a much higher temperature than the room temperature background. Spectral emissivity was measured, except the known emissivities of both the primary and secondary Christiansen features were used, instead of assuming an emissivity of unity at these wavelengths. The results from this investigation are discussed in brief. Derived from text

N94-20734*# Jet Propulsion Lab., California Inst. of Tech., Pasadena.
MAGELLAN AT VENUS: SUMMARY OF SCIENCE FINDINGS Abstract Only
R. S. Saunders, E. R. Stofan, J. J. Plaut, and D. A. Senske *In* Lunar and Planetary Inst., Twenty-Fourth Lunar and Planetary Science Conference. Part 3: N-Z 1993 p 1237-1238 (For primary document see N94-20636 05-91)
Avail: CASI HC A01/MF A06

A brief summary of the principal science findings of the Magellan Mission and plans for future data acquisition are presented. This includes high resolution gravity data from a nearly circular orbit and atmospheric drag and occultation experiments. Derived from text

N94-20735*# Moscow State Univ. (Russia).
PRELIMINARY ESTIMATION OF TAGAMITE COOLING CONDITIONS (PUCHEZH-KATUNKI ASTROBLEME, RUSSIA) Abstract Only **c90**
L. Sazonova, V. Feldman, and N. Korotaeva *In* Lunar and Planetary Inst., Twenty-Fourth Lunar and Planetary Science Conference. Part 3: N-Z 1993 p 1239-1240 (For primary document see N94-20636 05-91)
Avail: CASI HC A01/MF A06

The velocities and initial temperatures of crystallization from super-heated shocked melts have been estimated as a result of the investigation of the structures and mineral association in impact melt rocks of Puchezh-Katunki astrobleme. The dependence of these parameters vs. the body thickness of impact melt rocks have been found. Derived from text

N94-20736*# Geological Survey, Flagstaff, AZ.
VENUS' IMPACT-CRATER DATABASE: UPDATE TO APPROXIMATELY 98 PERCENT OF THE PLANET'S SURFACE Abstract Only
Gerald G. Schaber and David J. Chadwick *In* Lunar and Planetary Inst., Twenty-Fourth Lunar and Planetary Science Conference. Part 3: N-Z 1993 p 1241-1242 (For primary document see N94-20636 05-91)
Avail: CASI HC A01/MF A06

A total of 912 impact craters between 1.5 and 280 km in diameter have now been identified on about 98% of Venus' surface. This total includes an additional 71 craters (mostly in the southern hemisphere) not in the crater inventory given in Schaber et al. for 89% of the planet. (Extrapolated to 100% of the surface, the inventory should consist of 930 craters greater than 1.5 km in diameter.) The total crater inventory for 98% of the planet is only slightly larger (912 versus 882) than that extrapolated from the inventory of 135 craters when only 15% of the planet had been mapped by Magellan. The remarkably consistent density of about 2.02 impact craters per 10(exp 6) sq km emphasizes the completely random nature of the crater population's distribution. About 400 craters recognized from Magellan mapping have been assigned names.
Derived from text

N94-20737*# Maryland Univ., College Park.
LOCAL TOPOGRAPHY OF MARS AND ITS RELATIONSHIP TO SURFACE WEATHERING PROCESSES Abstract Only
M. W. Schaefer *In* Lunar and Planetary Inst., Twenty-Fourth Lunar and Planetary Science Conference. Part 3: N-Z 1993 p 1243-1244 (For primary document see N94-20636 05-91)
Avail: CASI HC A01/MF A06

There is a growing body of evidence in favor of the importance of aqueous sedimentary processes on Mars. It is important to understand the role that surface weathering processes have played in the development of the present morphology of the Martian surface. Such an understanding is important not only for its relevance to the study of volatile sources and sinks on Mars through time, but also for its relevance to Martian geologic and tectonic history. Starting in the fall of this year, the Mars Observer Laser Altimeter will begin sending back to Earth data on the topography of Mars that is of a higher quality than most of the topography data available for the Earth. This data will be invaluable, not only for understanding global and large-scale regional processes and landforms on Mars, but also for the study of local and smaller-scale regional processes and landforms. Digital topography is an important part of geologic and geomorphic studies, useful in distinguishing between different lithologies and between different types of weathering. Digital topography data may be used to study a wide variety of local and regional-scale landforms, including valleys, sand dunes, lava flows, landslides, and slopes. Topography data are also essential to the analysis of spectral response patterns, especially in areas of high topographic relief. Geomorphic classification can be significantly improved by the addition of topographic information. Derived from text

N94-20738*# Lunar and Planetary Inst., Houston, TX.
DIAPIRS AND CANTALOUPES: LAYERING AND OVERTURN OF TRITON'S CRUST Abstract Only
P. Schenk and M. P. A. Jackson (Texas Univ., Austin.) *In its* Twenty-Fourth Lunar and Planetary Science Conference. Part 3: N-Z 1993 p 1245-1246 (For primary document see N94-20636 05-91)
Avail: CASI HC A01/MF A06

It has recently been proposed that cantaloupe terrain formed as a result of instability and overturn (i.e., diapirism) of Triton's crust. Morphologic evidence implicates compositional layering within Triton's crust as the driving mechanism for the overturn. Here, we review the morphologic evidence for this origin and evaluate some of the implications. Derived from text

N94-20739*# Lunar and Planetary Inst., Houston, TX.
GEOLOGY OF THE SOUTHERN HEMISPHERE OF TRITON: NO POLAR CAP Abstract Only
P. Schenk and J. M. Moore (National Aeronautics and Space Administration. Ames Research Center, Moffett Field, CA.) *In its* Twenty-Fourth Lunar and Planetary Science Conference. Part 3: N-Z 1993 p 1247-1248 (For primary document see N94-20636 05-91)
Avail: CASI HC A01/MF A06

The bright southern hemisphere, comprising Uhlanga Regio, is perhaps the most poorly understood geologic province on Triton. The entire bright southern hemisphere has been described as a bright polar 'cap', implying a seasonal origin, or as a permanent geologic terrain distinct from the equatorial terrains. Also, thermal models have predicted seasonal migration of frosts and ices from the presently sun-lit south latitudes to the dark northern latitudes. The distribution of frosts and geologic history of this region must be determined observationally. We reexamine the geology of this terrain with the goal of answering these questions. Derived from text

N94-20740*# Lunar and Planetary Inst., Houston, TX.
THE 3-D MOONS: THE VOYAGER STEREO ATLAS OF THE OUTER SOLAR SYSTEM Abstract Only
P. Schenk and J. M. Moore (National Aeronautics and Space Administration. Ames Research Center, Moffett Field, CA.) *In its* Twenty-Fourth Lunar and Planetary Science Conference. Part 3: N-Z 1993 p 1249-1250 (For primary document see N94-20636 05-91)
Avail: CASI HC A01/MF A06

Comprehension and analysis of geologic features on any planet is enhanced manyfold by a clear perception between albedo and topography. On many of the icy satellites significant albedo contrasts due to mixtures of dark rocky and bright icy materials can be associated with topographic features. Subtle topographic features can be masked by albedo variation and under high solar illumination albedo and topography can be difficult to separate. To this end we are compiling an atlas of stereo image pairs of the outer solar system based on Voyager imaging for the investigation of various geologic problems and for general use. For the icy satellites, general perceptions of topography are usually gleaned from shape-from-shading information in the images processed by the human brain (i.e. visual inspection). With few exceptions, actual topography has been measured on a spot-by-spot basis using shadow heights or photoclinometry, or along limb profiles (where geographic context may be unavailable). Shadow heights are limited to regions within approximately 10 deg of the terminator and images with resolution better than approximately 1 km/pixel. Photoclinometric scans can be used more widely but are subject to a variety of errors, primarily uncertain assumptions of uniform scene albedo or poorly understood photometry. Stereoscopic analysis, where available, has the potential for greatly expanding topographic perception. Derived from text

N94-20741*# California Univ., Los Angeles. Inst. of Geophysics and Planetary Physics.
IRIDIUM IN SEDIMENTS CONTAINING LARGE ABUNDANCES OF AUSTRALASIAN MICROTEKTITES FROM DSDP HOLE 758B IN THE EASTERN INDIAN OCEAN AND FROM DSDP HOLE 769A IN THE SULU SEA Abstract Only **c90**
Gerhard Schmidt, Lei Zhou, and John T. Wasson *In* Lunar and Planetary Inst., Twenty-Fourth Lunar and Planetary Science Conference. Part 3: N-Z 1993 p 1251 (For primary document see N94-20636 05-91)
(Grant NSF EAR-91-19065)
Avail: CASI HC A01/MF A06

Excess Ir found in sediments at the Cretaceous/Tertiary (K/T) boundary and in other (e.g., Pliocene) sediments from deep sea drilling cores is widely interpreted as evidence of major impact events. The Australasian tektites originated in an impact event approximately 0.77 Ma ago; microtektites have been found in deep-sea sediment cores throughout the Indian Ocean, the Philippine Sea, and western Pacific Ocean, but Ir has not been previously reported in these horizons. The deep-sea record of tektites is of particular interest, because in contrast to most continental occurrences, the stratigraphy preserves the original depositional position. Recently several cores having exceptionally high contents of Australasian microtektites have been investigated, Glass and Wu found shocked quartz associated with the microtektites. We used neutron activation to determine concentrations of Ir and other elements in two cores bearing microtektites, one from Deep Sea Drilling Project (DSDP) hole 758B in the Eastern Indian Ocean and one from DSDP hole 769A in the Sulu Sea (near Mindanao, Philippines). The sedimentation age for the microtektite layers in core 758B lies between 0.73 - 0.78 Ma and agrees well with the mean laser-fusion Ar-40/Ar-39 age of Australasian tektites of 0.77 +/- 0.02 Ma by Izett et al. We are able to resolve a small positive Ir enhancement in 758B. Core 769A shows too much scatter to allow resolution of an Ir peak. Derived from text

N94-20742*# Boeing Defense and Space Group, Seattle, WA.
PRESSURE VERSUS DRAG EFFECTS ON CRATER SIZE Abstract Only **c46**
R. M. Schmidt *In* Lunar and Planetary Inst., Twenty-Fourth Lunar and Planetary Science Conference. Part 3: N-Z 1993 p 1253-1254 (For primary document see N94-20636 05-91)
Avail: CASI HC A01/MF A06

The topic of atmospheric effects on crater formation is very complex because it includes not only pressure effects on excavation, but also drag effects on ejecta placement. Experiments have to be designed very carefully to allow isolation of the two phenomena. Historically, numerous investigators have shown an influence of atmospheric pressure. However, none have identified the scaling that correctly isolates pressure from drag effects. On-going work in explosive cratering has produced scaling paradigms for deeply buried explosive charges where drag effects are negligible. Here it was found that increased pressure caused significant induced strength effects that impeded crater excavation. The effect is more pronounced with increasing burial depth and less pronounced with increased yield.
Author (revised)

N94-20743*# Brown Univ., Providence, RI. Dept. of Geological Sciences.
SEARCHING FOR ANCIENT VENUS Abstract Only

Peter H. Schultz *In* Lunar and Planetary Inst., Twenty-Fourth Lunar and Planetary Science Conference. Part 3: N-Z 1993 p 1255-1256 (For primary document see N94-20636 05-91)
Avail: CASI HC A01/MF A06

The cratering record on Venus provides one of the few available remote chronometers for establishing relative age. Because the dense atmosphere shields the surface from smaller impactors, the most statistically significant fraction of the cratering record is incomplete at best and indeterminate at worst. Larger craters represent survivors of entry but occur too infrequently for delineating statistically significant ages on a local scale. This contribution reconsiders processes affecting the statistical cratering record and argues that the globally averaged age approaches 2-3 billion years with isolated relict surfaces dating back to 3-4 billion years. Author (revised)

N94-20744*# Brown Univ., Providence, RI. Dept. of Geological Sciences.
IMPACTOR CONTROL OF CENTRAL PEAK AND PEAK-RING FORMATION Abstract Only **c46**
Peter H. Schultz and D. E. Gault (Murphys Center of Planetology, CA.) *In* Lunar and Planetary Inst., Twenty-Fourth Lunar and Planetary Science Conference. Part 3: N-Z 1993 p 1257-1258 (For primary document see N94-20636 05-91)
Avail: CASI HC A01/MF A06

The relation between the depth and diameter of excavation for impacts typically is assumed to be proportional. Such an assumption is consistent with the constant aspect ratio (diameter:depth) observed for simple craters found in a wide range of planetary settings and crater-scaling laws derived from laboratory experiments. Although complex craters exhibit evidence for floor uplift and rim collapse of a transient profile, they are typically thought to resemble initially smaller, simple craters. At large scales, however, early-time processes consume a greater fraction of crater growth and the assumption of late-time equivalence of energy release as a point source becomes inappropriate. The authors propose instead that crater diameter, depth, and impactor penetration represent separable dependent variables that underscore the fundamental difference between impact and point-source explosion excavation processes. An important consequence of this perspective is that central pits, peaks, and rings may represent contrasting target responses to impactor penetration and could provide an important indicator of impactor dimensions. Author (revised)

N94-20745*# Brown Univ., Providence, RI. Dept. of Geological Sciences.
FURTHER ANALYSES OF RIO CUARTO IMPACT GLASS Abstract Only **c25**
Peter H. Schultz, T. E. Bunch (National Aeronautics and Space Administration. Ames Research Center, Moffett Field, CA.), C. Koeberl (Wien Univ., Austria.), and W. Collins *In* Lunar and Planetary Inst., Twenty-Fourth Lunar and Planetary Science Conference. Part 3: N-Z 1993 p 1259-1260 (For primary document see N94-20636 05-91)
Avail: CASI HC A01/MF A06

Initial analyses of the geologic setting, petrology, and geochemistry of glasses recovered from within and around the elongate Rio Cuarto (RC) craters in Argentina focused on selected samples in order to document the general similarity with impactites around other terrestrial impact craters and to establish their origin. Continued analysis has surveyed the diversity in compositions for a range of samples, examined further evidence for temperature and pressure history, and compared the results with experimentally fused loess from oblique hypervelocity impacts. These new results not only firmly establish their impact origin but provide new insight on the impact process. Author

N94-20746*# Maryland Univ., College Park. Dept. of Astronomy.
C2, CN AND DUST IN COMET WILSON (1987VII) Abstract Only **c90**
R. Schulz, M. F. AHearn, P. V. Birch (Perth Observatory, Australia.), C. Bowers (Perth Observatory, Australia.), M. Kempin (Perth Observatory, Australia.), and R. Martin (Perth Observatory, Australia.) *In* Lunar and Planetary Inst., Twenty-Fourth Lunar and Planetary Science Conference. Part 3: N-Z 1993 p 1261-1262 (For primary document see N94-20636 05-91)
Avail: CASI HC A01/MF A06

Column density profiles in C2 and CN as well as in blue and red continuum (BC and RC) were constructed from two dimensional images of the coma of Comet Wilson (1987VII). The authors' analysis showed that the continuum profiles decrease with the nuclear distance rho as 1/rho. From the C2 and CN profiles the authors determined the parent and the daughter lifetimes as well as the production rates in terms of the vectorial model. Author (revised)

N94-20747*# Nevada Univ., Reno. School of Mines.
STRENGTH AND DEFORMATION PROPERTIES OF BASALTIC LAVA FLOWS ON PLANETARY SURFACES Abstract Only **c46**
Richard A. Schultz *In* Lunar and Planetary Inst., Twenty-Fourth Lunar and Planetary Science Conference. Part 3: N-Z 1993 p 1263-1264 (For primary document see N94-20636 05-91)
Avail: CASI HC A01/MF A06

Basaltic rocks are thought to constitute a volumetrically significant rock type on the Moon, Mercury, Mars, and Venus, in addition to the Earth. Spacecraft images of surfaces with known or suspected basaltic composition on these bodies, particularly on Venus, indicate that these rocks have been deformed in the brittle regime to form faults and perhaps dilatant cracks, in addition to folding and more distributed types of deformation. Predictions of brittle fracture or other types of deformation are made by comparing calculated stresses from a tectonic model to some criterion for rock strength. Common strength criteria used in the planetary science literature for near-surface deformation include a Griffith tensile-strength criterion for intact rock, a Mohr envelope for intact basalt, and a brittle strength envelope based on Byerlee's law of rock frictional resistance. However, planetary terrains of basaltic composition consist of much more than just intact basaltic rock. The aggregate basaltic material, termed the 'rock mass,' consists of both the intact rock and the associated fracture, faults, lithologic contacts, and other discontinuous surfaces. A basaltic rock mass is the relevant material for which strength properties must be defined and calculated model stresses must be compared to in order to more accurately predict brittle deformation. For example, the various strengths of a rock mass are less than that of intact material of the same composition. This means that tectonic models which compare stresses to intact failure strengths overestimate the stresses required for fracture and so underestimate the extent and magnitude of brittle deformation predicted in these models. On the other hand, rock mass shear strength can be greater than that predicted from Byerlee's law. The concept of rock mass strength is central to many engineering design studies in which calculated stresses are used to predict brittle fracture, and this experience indicates that brittle strength envelopes which assume properties for intact rock (Griffith parabolas) or sliding along a single, continuous surface (Byerlee's law) inadequately characterize the tensile, compressive, and shear strengths of rock masses. The criterion adopted here to relate stresses to rock mass fracture is based on a Griffith-type curve for tensile normal stress and a concave downward curve for compressive normal stress. It is the only available criterion that explicitly considers the weakening effects of discontinuities within the rock mass on the stress state required for fracture. Author (revised)

N94-20748*# Geological Survey, Flagstaff, AZ.
MARS: NEW EVIDENCE FOR ORIGIN OF SOME VALLES MARINERIS LAYERED DEPOSITS Abstract Only
David H. Scott *In* Lunar and Planetary Inst., Twenty-Fourth Lunar and Planetary Science Conference. Part 3: N-Z 1993 p 1265-1266 (For primary document see N94-20636 05-91)
Avail: CASI HC A01/MF A06

The discovery of layered deposits in the walls of a deep trough in Lunae Planum has implications for the origin of similar-appearing deposits in some canyons of Valles Marineris. Although layering is visible in the competent, cliff-forming upper walls of the canyons, the dissimilarity in appearance between canyon walls and soft rounded hills of layered deposits on canyon floors, as well as their contrasting patterns of erosion, has been considered strong evidence that their modes of origin were different. Most workers agree that the wall rocks are volcanic flows derived from fissure vents and other volcanic sources in the region. However, several hypotheses have been advanced to account for the softer-appearing stratified floor deposits. Chief among them is the proposal that the floor deposits are waterlaid sediments that accumulated in large lakes within the canyons and include materials eroded from canyon walls, eolian deposits, and subaqueous volcanic eruptives. Author

N94-20749*# Hawaii Univ., Honolulu. Dept. of Geology and Geophysics.
POST-METAMORPHIC BRECCIATION IN TYPE 3 ORDINARY CHONDRITES Abstract Only **c90**
E. R. D. Scott, T. J. McCoy, and K. Keil *In* Lunar and Planetary Inst., Twenty-Fourth Lunar and Planetary Science Conference. Part 3: N-Z 1993 p 1267-1268 (For primary document see N94-20636 05-91)
Avail: CASI HC A01/MF A06

Type 3.1-3.9 ordinary chondrites can be divided into two kinds: those in which the compositions of chondrule silicates are entirely consistent with metamorphism of type 3.0 material, and those in which the computational heterogeneity appears to be too extreme for in situ metamorphism. We present petrologic data for three LL3 chondrites of the second kind--Ngawi, ALH A77278 (both type 3.6), and Hamlet (type 3.9)--and compare these data with results for the first kind of LL3-4 chondrites. Given that chondrules form in the nebula and that metamorphic equilibration occurs in asteroids, our new data imply that Ngawi, A77278, Hamlet, and many other type 3 ordinary chondrites are post-metamorphic breccias containing materials with diverse metamorphic histories; they are not metamorphic rocks or special kinds of 'primitive breccias.' We infer also that metamorphism to type 3.1-3.9 levels produces very friable material that is easily remixed into breccias and lithified by mild shock. Thus, petrologic types and subtypes of chondrites indicate the mean metamorphic history of the ingredients, not the thermal history of the rock. The metamorphic history of individual type 1 or 2 porphyritic chondrules in type 3 breccias is best derived from olivine and pyroxene analyses and the data of McCoy et al. for unbrecciated chondrites. The new chondrule classification schemes of Sears, DeHart et al., appears to provide less information about the original state and metamorphic history of individual porphyritic chondrules and should not replace existing classification schemes. Author (revised)

N94-20750*# Arkansas Univ., Fayetteville. Cosmochemistry Group.
CATHODOLUMINESCENCE OBSERVATIONS OF IN SITU AQUEOUS DESTRUCTION OF CHONDRULES IN THE MURCHISON CM CHONDRITE Abstract Only **c90**
Derek W. G. Sears, Paul H. Benoit, Lu Jie, and Andrew S. R. Sears *In* Lunar and Planetary Inst., Twenty-Fourth Lunar and Planetary Science Conference. Part 3: N-Z 1993 p 1269-1270 (For primary document see N94-20636 05-91)
Avail: CASI HC A01/MF A06

A low-power cathodoluminescence (CL) mosaic of a 1x2 cm section of the Murchison CM chondrite contains chondrules of two types: one contains olivines with red CL and is thought to be the equivalent of group A chondrules of Sears et.; and one without observable CL, which is probably equivalent to their group B chondrules. Both types of chondrule contain dust mantles with a characteristic uniform red CL due to very fine-grained forsterites, but the mantles of group A chondrules have a complex internal structure and are much thicker than the relatively thin rims on the group B chondrules. The variety of internal textures and the progressive integration of the objects with the surrounding matrix suggests to us that these features are large group A chondrules in the process of being destroyed by aqueous alteration. Prior to aqueous alteration, group A chondrules in CM chondrites were larger than group B chondrules, which is contrary to the situation in ordinary chondrites and were apparently destroyed more rapidly than group B chondrules by aqueous alteration. Author (revised)

N94-20751*# Arizona Univ., Tucson. Dept. of Planetary Science.
DIFFUSIVE REDISTRIBUTION OF WATER VAPOR IN THE SOLAR NEBULA REVISITED Abstract Only **c92**
William D. Sears *In* Lunar and Planetary Inst., Twenty-Fourth Lunar and Planetary Science Conference. Part 3: N-Z 1993 p 1271-1272 (For primary document see N94-20636 05-91)
Avail: CASI HC A01/MF A06

Stevenson and Lunine presented a model for enhancing the abundance of solid material in the region of the solar nebula at the water condensation point. This was used to provide a means to produce a much more rapid formation of Jupiter than the standard solar nebula models. However, they underestimated the drag induced sun-ward radial drift of the planetesimals of interest. Reanalysis reveals that these particles would spread over the inner solar system and might influence the formation of the asteroids. Author (revised)

N94-20752*# Academy of Sciences (USSR), Moscow. Inst. of Geochemistry and Analytical Chemistry.
LUNAR BASALT METEORITE EET 87521: PETROLOGY OF THE CLAST POPULATION Abstract Only **c90**
A. S. Semenova, M. A. Nazarov, and N. N. Kononkova *In* Lunar and Planetary Inst., Twenty-Fourth Lunar and Planetary Science Conference. Part 3: N-Z 1993 p 1273-1274 (For primary document see N94-20636 05-91)
Avail: CASI HC A01/MF A06

The Elephant Moraine meteorite EET 87521 was classified as a lunar mare basalt breccia which is composed mainly of VLT basalt clasts. Here we report on our petrological study of lithic clasts and monomineralic fragments in the thin sections EET 87521,54 and EET 87521,47,1, which were prepared from the meteorite. The results of the study show that EET 87521 consists mainly of Al-rich ferrobasalt clasts and olivine pyroxenite clasts. The bulk composition of the meteorite can be well modelled by the mixing of these lithic components which appear to be differentiates of the Luna 25 basalt melt. KREEP and Mg-rich gabbro components are minor constituents of EET 87521. Author (revised)

N94-20753*# Howard Univ., Washington, DC.
MAGNETIC PROPERTIES AND MOESSBAUER ANALYSES OF GLASS FROM THE K-T BOUNDARY, BELOC, HAITI Abstract Only **c25**
F. E. Senftle, A. N. Thorpe, L. May, A. Barkatt (Catholic Univ. of America, Washington, DC.), M. A. Adel-Hadadi (Catholic Univ. of America, Washington, DC.), G. S. Marbury (Catholic Univ. of America, Washington, DC.), G. Izett (Geological Survey, Washington, DC.), H. Sigurdsson (Rhode Island Univ., Kingston.), and F. J.-M. R. Maurasse (Florida International Univ., Miami.) *In* Lunar and Planetary Inst., Twenty-Fourth Lunar and Planetary Science Conference. Part 3: N-Z 1993 p 1275-1276 (For primary document see N94-20636 05-91)
Avail: CASI HC A01/MF A06

The experimental magnetic susceptibility, the temperature-independent component of the magnetic susceptibility, the magnetization, and the Curie constant have been measured for a number of specimens of glass from the K-T boundary found at Beloc, Haiti, and the results are compared with those of similar measurements of tektites. Because the Fe(3+)/Fe(2+) ratio is needed to calculate the magnetic parameters, Moessbauer spectroscopic measurements were also made. The data were consistent with the classification of the Beloc glasses as tektites. Author (revised)

N94-20754*# Jet Propulsion Lab., California Inst. of Tech., Pasadena.
RIFTING AT DEVANA CHASMA, VENUS: STRUCTURE AND ESTIMATION OF THE EFFECTIVE THICKNESS OF THE ELASTIC LITHOSPHERE Abstract Only
D. A. Senske *In* Lunar and Planetary Inst., Twenty-Fourth Lunar and Planetary Science Conference. Part 3: N-Z 1993 p 1277-1278 (For primary document see N94-20636 05-91)
Avail: CASI HC A01/MF A06

To understand the relationship between extension and sites on Venus interpreted to be associated with mantle upwelling, the characteristics of the northern part of Devana Chasma in Beta Regio are examined. The structure of this rift is compared to that of terrestrial continental rifts. To ascertain the degree to which the lithosphere at Beta might be thinned, estimates of lithospheric thickness are calculated using a plate flexure model. These values are compared to those determined for other parts of the planet. Author (revised)

N94-20755*# Jet Propulsion Lab., California Inst. of Tech., Pasadena.
VOLCANIC RISES ON VENUS: GEOLOGY, FORMATION, AND SEQUENCE OF EVOLUTION Abstract Only
D. A. Senske, E. R. Stofan, D. L. Bindschadler (California Univ., Los Angeles.), and S. E. Smrekar *In* Lunar and Planetary Inst., Twenty-Fourth Lunar and Planetary Science Conference. Part 3: N-Z 1993 p 1279-1280 (For primary document see N94-20636 05-91)
Avail: CASI HC A01/MF A06

Large centers of volcanism on Venus are concentrated primarily in the equatorial region of the planet and are associated with regional topographic rises. Analysis of both radar images and geophysical data suggest that these uplands are sites of mantle upwelling. Magellan radar imaging provides a globally contiguous data set from which the geology of these regions is evaluated and compared. In addition, high resolution gravity data currently

being collected provide a basis to assess the relationship between these uplands and processes in the planet's interior. Studies of the geology of the three largest volcanic highlands (Beta Regio, Atla Regio, Western Eistla Regio) show them to be distinct, having a range of volcanic and tectonic characteristics. In addition to these large areas, a number of smaller uplands are identified and are being analyzed (Bell Regio, Imdr Regio, Dione Regio (Ushas, Innini, and Hathor Montes), and Themis Regio). To understand better the mechanisms by which these volcanic rises form and evolve, we assess their geologic and geophysical characteristics.
Author (revised)

N94-20756*# Centre d'Etudes de Limeil-Valenton, Villeneuve Saint-Georges (France). Commissariat a L'Energie Atomique.
MOLECULAR EQUILIBRIA AND CONDENSATION SEQUENCES IN CARBON RICH GASES Abstract Only **c90**
C. M. Sharp and G. J. Wasserburg (California Inst. of Tech., Pasadena.) *In* Lunar and Planetary Inst., Twenty-Fourth Lunar and Planetary Science Conference. Part 3: N-Z 1993 p 1281-1282 (For primary document see N94-20636 05-91)
Avail: CASI HC A01/MF A06

Chemical equilibria in stellar atmospheres have been investigated by many authors. Lattimer, Schramm, and Grossman presented calculations in both O rich and C rich environments and predicted possible presolar condensates. A recent paper by Cherchneff and Barker considered a C rich composition with PAH's included in the calculations. However, the condensation sequences of C bearing species have not been investigated in detail. In a carbon rich gas surrounding an AGB star, it is often assumed that graphite (or diamond) condenses out before TiC and SiC. However, Lattimer et al. found some conditions under which TiC condenses before graphite. We have performed molecular equilibrium calculations to establish the stability fields of C(s), TiC(s), and SiC(s) and other high temperature phases under conditions of different pressures and C/O. The preserved presolar interstellar dust grains so far discovered in meteorites are graphite, diamond, SiC, TiC, and possibly Al2O3. Author (revised)

N94-20757*# Lunar and Planetary Inst., Houston, TX.
CHICXULUB IMPACT BASIN: GRAVITY CHARACTERISTICS AND IMPLICATIONS FOR BASIN MORPHOLOGY AND DEEP STRUCTURE Abstract Only **c46**
Virgil L. Sharpton, Kevin Burke (Houston Univ., TX.), Stuart A. Hall (Houston Univ., TX.), Scott Lee, Luis E. Marin (Universidad Nacional Autonoma de Mexico, Mexico City.), Gerardo Suarez (Universidad Nacional Autonoma de Mexico, Mexico City.), Juan Manuel Quezada-Muneton (Universidad Nacional Autonoma de Mexico, Mexico City.), and Jaime Urrutia-Fucugauchi (Gerencia de Exploracion, Petroleos Mexicanos, Mexico City.) *In its* Twenty-Fourth Lunar and Planetary Science Conference. Part 3: N-Z 1993 p 1283-1284 (For primary document see N94-20636 05-91)
Avail: CASI HC A01/MF A06

The K-T-aged Chicxulub Impact Structure is buried beneath the Tertiary carbonate rocks of the Northern Yucatan Platform. Consequently its morphology and structure are poorly understood. Reprocessed Bouguer (onshore) and Free Air (offshore) gravity data over Northern Yucatan reveal that Chicxulub may be a 200-km-diameter multi-ring impact basin with at least three concentric basin rings. The positions of these rings follow the square root of 2 spacing rule derived empirically from analysis of multi-ring basins on other planets indicating that these rings probably correspond to now-buried topographic basin rings. A forward model of the gravity data along a radial transect from the southwest margin of the structure indicates that the Chicxulub gravity signature is compatible with this interpretation. We estimate the basin rim diameter to be 204 +/- 16 km and the central peak ring diameter (D) is 104 +/- 6 km. Author (revised)

N94-20758*# New Mexico Univ., Albuquerque. Dept. of Earth and Planetary Sciences.
BASALTIC MAGMATISM ON THE MOON. A PERSPECTIVE FROM VOLCANIC PICRITIC GLASSES Abstract Only
C. K. Shearer and J. J. Papike *In* Lunar and Planetary Inst., Twenty-Fourth Lunar and Planetary Science Conference. Part 3: N-Z 1993 p 1285-1286 (For primary document see N94-20636 05-91)
(Grant NAG9-497)
Avail: CASI HC A01/MF A06

It is widely accepted that basaltic magmas are products of partial fusion of peridotite within planetary mantles. As such they provide valuable insights into the structure and processes of planetary interiors. Those compositions which approach primary melt compositions provide both a clearer vision of planetary interiors and a starting point at which to understand basaltic evolution. Within the collection of lunar samples returned by the Apollo and Luna missions are homogeneous, picritic glass beads of volcanic origin. These glass beads provide a unique perspective concerning the origin of mare basalts, the characteristics of the lunar interior, and processes culminating in the early differentiation of the moon. In this presentation, we report our ion microprobe derived trace element data from all picritic glasses previously identified. We place this trace element data and literature isotopic and experimental data on the picritic glasses with the framework of mare basaltic magmatism. Author (revised)

N94-20759*# New Mexico Univ., Albuquerque. Dept. of Earth and Planetary Sciences.
ORIGIN OF THE APOLLO 15 VERY LOW TI GREEN GLASS. A PERSPECTIVE FROM THE COMPOSITIONAL DIVERSITY IN THE VERY LOW TI GLASSES Abstract Only **c25**
C. K. Shearer and J. J. Papike *In* Lunar and Planetary Inst., Twenty-Fourth Lunar and Planetary Science Conference. Part 3: N-Z 1993 p 1287-1288 (For primary document see N94-20636 05-91)
(Grant NAG9-497)
Avail: CASI HC A01/MF A06

The very low Ti green glasses from the Apollo 15 site have intrigued scientists for over 20 years. Their primitive composition has been used to understand magmatic processes and the structure of the moon. The compositional variability observed in the Apollo 15 glass population has long been a point of debate. Initial studies did not recognize the compositional diversity in the glasses. Stolper et al. documented the major element variability and concluded it could not be produced by magmatic processes and therefore concluded that these glasses must be of impact origin. Subsequent studies confirmed a volcanic origin for the glass population and attempted to elucidate magmatic processes to account for its compositional variability. Models that have been proposed for these glasses include the following: (1) the crystallization of single or multiple phases (olivine, pyroxene, Fe metal, immiscible sulfide); (2) the incompatible behavior of Ni and Co during multiple phase crystallization at extremely low fO2; and (3) magma or source mixing. All of these models have problems. Type (1) models appear not to be consistent with recent trace element studies on the glasses; model (2) is dependent on the debatable incompatible behavior of Ni and Co, and, in models of type (3), the origin and nature of mixing models are somewhat unconstrained. This study compares the Apollo 15 green glasses with the very low Ti picritic glasses from other landing sites. Author (revised)

N94-20760*# New Mexico Univ., Albuquerque. Dept. of Earth and Planetary Sciences.
ORTHOPYROXENES AS RECORDERS OF DIOGENITE PETROGENESIS: TRACE ELEMENT SYSTEMATICS Abstract Only **c25**
C. K. Shearer, J. J. Papike, and G. D. Layne *In* Lunar and Planetary Inst., Twenty-Fourth Lunar and Planetary Science Conference. Part 3: N-Z 1993 p 1289-1290 (For primary document see N94-20636 05-91)
(Grant NAG9-497)
Avail: CASI HC A01/MF A06

Eucrite, howardite, and diogenite members of the achondrites are considered, by many, to be genetically related. Therefore, each provide a piece of the puzzle for reconstructing magmatic processes on the eucrite parent body (EPB). The relationship between eucrites and diogenites can be viewed within the context of two distinctly different models: (1) fractional crystallization; and (2) partial melting. In fractional crystallization models, eucrites and diogenites represent a complementary continuum of planetary fractional crystallization products in which the diogenites represent crystal accumulations during the crystallization of eucritic magmas at shallow to deep levels in the EPB. Alternatively, experimental studies may be interpreted as indicating eucrites represent peritectic partial melts of a primitive, chondritic EPB mantle. Within this type of model, the diogenites are also generally considered to be cumulates; however, their petrogenetic relationship to the eucrites is less clear. Sack et al. proposed that the olivine diogenites represent residua from the partial melting events that produced eucritic liquids. Initial trace element studies of orthopyroxene (OPX) are consistent with this model. However, this trace element modeling

of the olivine diogenites is nonunique. As a further test of these models, we did the following three things: (1) analyzed OPX from cumulate diogenites to compare with the olibine diogenite data; (2) improved ion microprobe analytical techniques for the analysis of elements critical to our interpretations; and (3) selected more relevant Kd's for OPX-eucritic melt. Author (revised)

N94-20761*# Alabama Univ., Huntsville. Dept. of Physics.
COMBINED BACKSCATTER MOESSBAUER SPECTROMETER/X RAY FLUORESCENCE ANALYZER (BaMS/XRF) FOR EXTRATERRESTRIAL SURFACES Abstract Only **c25**
T. D. Shelfer, E. L. Wills, D. G. Agresti, M. M. Pimperl, M. H. Shen, R. V. Morris (National Aeronautics and Space Administration. Lyndon B. Johnson Space Center, Houston, TX.), and T. Nguyen (Lockheed Engineering and Sciences Co., Houston, TX.) *In* Lunar and Planetary Inst., Twenty-Fourth Lunar and Planetary Science Conference. Part 3: N-Z 1993 p 1291-1292 (For primary document see N94-20636 05-91)
Avail: CASI HC A01/MF A06

We have designed and tested a prototype combined backscatter Moessbauer spectrometer and x-ray fluorescence analyzer (BaMS/XRF). A space qualified instrument based on this design would be suitable for in-situ use on planetary missions to the surfaces of the Moon (Artemis and lunar outpost), Mars (MESUR), asteroids, or other solid solar system objects. The BaMS/XRF instrument is designed to be capable of concurrent sample analyses for the mineralogy of iron-bearing phases and elemental composition without the need for sample preparation. Author

N94-20762*# Washington Univ., Saint Louis, MO. Center for the Space Sciences.
THE ROUGHNESS OF THE MARTIAN SURFACE: A SCALE DEPENDENT MODEL Abstract Only
M. K. Shepard, E. A. Guinness, and R. E. Arvidson *In* Lunar and Planetary Inst., Twenty-Fourth Lunar and Planetary Science Conference. Part 3: N-Z 1993 p 1293-1294 (For primary document see N94-20636 05-91)
Avail: CASI HC A01/MF A06

In the coming decade, several lander missions to Mars are planned (e.g., MESUR Pathfinder, MESUR). One of the dangers facing planners of these missions is the rough topography observed at both Viking Lander sites. Both landing sites are ubiquitously covered with meter-scale boulders. Objects of this size pose obvious threats to soft landers, especially at Mars where the distance from Earth causes prohibitive time lags between the transmission of commands and feedback from the spacecraft. An obvious solution is to scout for a 'smooth' site prior to the landing. However, the best resolutions realizable on current and future missions (i.e., Mars Observer) are on the order of several meters. Even at this scale, boulders of 1-2 meters in size are unresolvable. Additionally, the amount of time and spacecraft resources required to search even a small area of the planet are unrealistic given other mission objectives. An alternative is to determine the 'roughness' of the surface at a subpixel scale using bidirectional reflectance observations. Much larger areas of the planet can be searched, and much of the search can easily be automated. The morphology of the martian plains observed by the Viking Landers is physically simple. The surface is covered with a layer (approximately flat lying) of aeolian sediment from which numerous outcrops of bedrock and boulders protrude. This morphology, while simple, will be difficult to characterize from orbit using traditional bidirectional reflectance models for two reasons. First, modeling the surface as facets with Gaussian or exponential slope distributions is not realistic given the morphology described above. Second, the roughness parameter is an 'average' of the roughness at scales ranging from the wavelength of light being scattered to the pixel size of the observation. Thus, there is no definite scale of roughness that can be extracted from the Hapke roughness parameter. Using the concepts of geometric and boolean models developed by several workers, we have developed a model for the bidirectional reflectance of a surface morphology comparable to that observed at the Viking Lander sites. Author (revised)

N94-20763*# Lockheed Engineering and Sciences Co., Houston, TX.
CHRONOLOGY OF LUNAR GRANITE 12033,576: RESETTING OF Rb-Sr AND K-Ca ISOCHRONS Abstract Only
C.-Y. Shih, H. Wiesmann, D. H. Garrison, L. E. Nyquist (National Aeronautics and Space Administration. Lyndon B. Johnson Space Center, Houston, TX.), and D. D. Bogard (National Aeronautics and Space Administration. Lyndon B. Johnson Space Center, Houston, TX.) *In* Lunar and Planetary Inst., Twenty-Fourth Lunar and Planetary Science Conference. Part 3: N-Z 1993 p 1295-1296 (For primary document see N94-20636 05-91)
Avail: CASI HC A01/MF A06

Lunar granite 12033,576 is a subsample of the 'large' (approximately 1 g) felsite 12033,507 which was identified from a collection of 4-10 mm particles from the 12033 soil sampled from the north rim of Head Crater in the eastern part of Oceanus Procellarum. Discordant ages of approximately 3.6, approximately 0.8, approximately 3.9, and approximately 2.2 Ga for this lunar granite were obtained, respectively, by the K-Ca, Ar-39/Ar-40, and U-Pb zircon methods in previous studies and by the Rb-Sr method is this study. Assuming the granite crystallized approximately 3.9 Ga ago (zircon age) and was shocked by meteoritic impacts at 0.8 Ga ago (Ar-39-Ar-40 age), the intermediate apparent ages by the Rb-Sr and K-Ca methods can be interpreted as reset by diffusion of the parent and daughter nuclides. The Rb-Sr age is less resistant to resetting than the K-Ca age, but more resistant that the Ar-39/Ar-40 age. Author

N94-20764*# National Science Museum, Tokyo (Japan).
THE CHONDRITE MIHONOSEKI: NEW OBSERVED FALL Abstract Only **c90**
Masako Shima, A. Okada (Okayama Univ., Japan.), and K. Nagao (Okayama Univ., Japan.) *In* Lunar and Planetary Inst., Twenty-Fourth Lunar and Planetary Science Conference. Part 3: N-Z 1993 p 1297-1298 (For primary document see N94-20636 05-91)
Avail: CASI HC A01/MF A06

On 10 Dec. 1992, 21:00 hours Japanese standard time, a stone weighing 6.385kg, struck a two-story house in Mihonoseki-machi, Yatsuka-gun, Shimane-ken, Japan, 35 deg 34.1 min N, 133 deg 13.2 min E. Through petrographical and mineralogical examination and rare gas analysis, the meteorite was classified as an L6 chondrite. The preatmospheric chondrite is rather small in size (Ne-22/Ne-21 = 1.180 and extremely low Co-60 activity), and shocked features are not distinct. Cosmic-ray exposure ages obtained from He-3, Ne-21, and Ar-38 are 61 m.y., and K-40/Ar-40 age is 4.41 b.y. Measurements of cosmogenic radioactive nuclides and chemical analyses are now proceeding. Author (revised)

N94-20765*# Geological Survey, Flagstaff, AZ.
CLEMENTINE: AN INEXPENSIVE MISSION TO THE MOON AND GEOGRAPHOS Abstract Only **c12**
Eugene M. Shoemaker and Stewart Nozette (Strategic Defense Initiative Organization, Washington, DC.) *In* Lunar and Planetary Inst., Twenty-Fourth Lunar and Planetary Science Conference. Part 3: N-Z 1993 p 1299-1300 (For primary document see N94-20636 05-91)
Avail: CASI HC A01/MF A06

The Clementine Mission, a joint project of the Strategic Defense Initiative Organization (SDIO) and NASA, has been planned primarily to test and demonstrate a suite of lightweight sensors and other lightweight spacecraft components under extended exposure to the space environment. Although the primary objective of the mission is to space-qualify sensors for Department of Defense applications, it was recognized in 1990 that such a mission might also be designed to acquire scientific observations of the Moon and of Apollo asteroid (1620) Geographos. This possibility was explored jointly by SDIO and NASA, including representatives from NASA's Discovery Program Science Working Group, in early 1991. Besides the direct return of scientific information, one of the benefits envisioned from a joint venture was the development of lightweight components for possible future use in NASA's Discovery-class spacecraft. In Jan. 1992, SDIO informed NASA of its intent to fly a 'Deep Space Program Science Experiment,' now popularly called Clementine; NASA then formed an advisory science working group to assist in the early development of the mission. The Clementine spacecraft is being assembled at the Naval Research Laboratory, which is also in charge of the overall mission design and mission operations. Support for mission design is being provided by GSFC and by JPL. NASA's Deep Space Network will be utilized in tracking and communicating with the spacecraft. Following a recommendation of the COMPLEX committee of the Space Science Board, NASA will issue an NRA and appoint a formal science team in early 1993. Clementine is a 3-axis stabilized, 200 kg (dry weight) spacecraft that will be launched on a refurbished Titan-2G. One of the goals has been to build two spacecraft, including the sensors,

for $100M. Total time elapsed from the decision to proceed to the launch will be two years. Author (revised)

N94-20766*# Geological Survey, Flagstaff, AZ.
RESEARCH PROGRAM ON THE MANSON IMPACT STRUCTURE, IOWA Abstract Only c46
E. M. Shoemaker, D. J. Roddy, and R. R. Anderson (Geological Survey, Iowa City, IA.) *In* Lunar and Planetary Inst., Twenty-Fourth Lunar and Planetary Science Conference. Part 3: N-Z 1993 p 1301-1302 (For primary document see N94-20636 05-91)
Avail: CASI HC A01/MF A06

At or near the end of the Cretaceous, at least two large impact events occurred in the western hemisphere. One impact formed the 180-km diameter Chicxulub crater on the northern tip of the Yucatan peninsula. Another formed the 35-km diameter Manson structure in western Iowa. Several lines of evidence, including the chemical and isotopic composition of glass found in the K/T boundary layer at sites in the Gulf of Mexico and Caribbean region, the regional variation in thickness and the size of spherules in the K/T boundary layer, and indications at and near the boundary of disturbance and deposition of beds by giant waves in the Gulf of Mexico, point to Chicxulub as a major source of K/T boundary material, including a lower layer of clay at K/T boundary sites in western North America. The size, abundance, and mineral and lithic composition of shocked grains from an upper K/T boundary layer found at western North American sites, on the other hand, point to Manson as a possible source crater. More than one impact seems to be indicated by the K/T boundary stratigraphy in western North America, and present constraints on the age of the Manson structure suggest that it, as well as Chicxulub, may be a K/T boundary crater. Multiple craters produced over a relatively short interval of time are much more likely to have been formed by impact of comets rather than by impact of asteroids. Among likely mechanisms that could have produced multiple craters at or near the time of the K/T boundary are as follows: (1) splitting of a comet shortly before impact with Earth (impacts may have been spaced over about an hour), (2) fragmentation of a very large, Sun-grazing, periodic comet to form a compact stream of comets that intercepted the Earth's orbit (impacts may have been spread over about a century), and (3) perturbation of the Oort comet cloud by a passing massive object to form a comet shower in the inner solar system (impacts may have been spread over about a million years). Only in the first two cases are the impacts likely to have been close enough in time to contribute to the observed K/T boundary layers. All mechanisms could have produced many more than two craters. Author (revised)

N94-20767*# Pennsylvania State Univ., University Park.
PETROGRAPHY OF SHOCK FEATURES IN THE 1953 MANSON 2-A DRILL CORE Abstract Only c46
N. M. Short and D. P. Gold *In* Lunar and Planetary Inst., Twenty-Fourth Lunar and Planetary Science Conference. Part 3: N-Z 1993 p 1303-1304 (For primary document see N94-20636 05-91)
Avail: CASI HC A01/MF A06

Drilling of Nx core in late 1953 into an anomalous zone of disturbed rocks northwest of Manson, Iowa disclosed presence of extensive breccias including crystalline rocks brought to the surface from depths of 4 km or more. Hole 2-A penetrated breccias dominated by leucocratic igneous and metamorphic lithologies, later interpreted to be part of a general ringed peak complex within a 35 km wide impact structure produced about 65 Ma ago. Proof of this origin was given in 1966 by NMS through recognition of shock metamorphic features in 2-A materials during a cursory examination of samples provided by R.A. Hoppin, University of Iowa. A detailed study of this material now underway has revealed that most breccia clasts in 2-A show abundant and varied evidence of shock damage, including extensive planar deformation features (PDF) in quartz, K-feldspar, plagioclase, and a pyroxene and varying degrees of isotropization and incipient melting in feldspars. Author

N94-20768*# Scripps Institution of Oceanography, La Jolla, CA.
FE-60 AND THE EVOLUTION OF EUCRITES Abstract Only c90
A. Shukolyukov and G. W. Lugmair *In* Lunar and Planetary Inst., Twenty-Fourth Lunar and Planetary Science Conference. Part 3: N-Z 1993 p 1305-1306 (For primary document see N94-20636 05-91)
Avail: CASI HC A01/MF A06

We have recently presented evidence for the existence of live Fe-60 in the early solar system. This evidence comes from observations of 2.4 to 50 epsilon unit (1 part in 10(exp 4)) relative excesses of Ni-60 measured in samples from the eucrite Chervony Kut (CK). These isotopic excesses have been produced by the decay of the short-lived radionuclide Fe-60 (T(sub 1/2) = 1.5 Ma). Because CK originates from a planetesimal which was totally molten and its high Fe/Ni ratio is due to a planet-wide Fe-Ni fractionation during metal-silicate segregation, the presence of the Fe-60 decay product indicates the large scale abundance of Fe-60 in the early solar system and its presence during differentiation of this planetesimal. The observed variable Ni-60 excesses in different bulk samples and mineral separates from CK can only be understood if some Fe-60 was still alive at the time when basaltic magma had solidified on the eucrite parent body. The lack of a correlation between Ni-60 and the respective Fe/Ni ratios in different mineral fractions from CK indicates a metamorphic remobilization of Ni after essentially all Fe-60 has decayed. However, Ni-60 from three bulk samples from different locations within the meteorite appears to correlate reasonably well with the respective Fe/Ni ratios. If we regard this correlation as an isochron then its slope yields a Fe-60/Fe-56 ratio f (3.9 +/- 0.6) x 10(exp -9) and an initial Ni-60 of 3.2 plus or minus 0.9 epsilon units at the time of crystallization of CK. Estimates based on these values and a approximately 10 Ma time interval between CK solidification and formation of the earliest condensates in the solar system followed by rapid accretion of planetary bodies indicate that the decay of Fe-60 could produce sufficient heat to melt these planetesimals. If Al-26 was present on a planetary scale as Fe-60 and at abundances close to values observed in Allende inclusions then melting of small early formed planets is inevitable. As an attempt to further explore the Fe-60/Ni-60 isotope system as an early solar system chronometer we studied another noncumulate eucrite, Juvinas (JUV) (sample USNM 1051), which belongs to the same subgroup as CK. Author (revised)

N94-20769*# Massachusetts Inst. of Tech., Cambridge. Dept. of Earth, Atmospheric, and Planetary Sciences.
GEOID, TOPOGRAPHY, AND CONVECTION-DRIVEN CRUSTAL DEFORMATION ON VENUS Abstract Only
Mark Simons, Bradford H. Hager, and Sean C. Solomon (Carnegie Institution of Washington, DC.) *In* Lunar and Planetary Inst., Twenty-Fourth Lunar and Planetary Science Conference. Part 3: N-Z 1993 p 1307-1308 (For primary document see N94-20636 05-91)
Avail: CASI HC A01/MF A06

High-resolution Magellan images and altimetry of Venus reveal a wide range of styles and scales of surface deformation that cannot readily be explained within the classical terrestrial plate tectonic paradigm. The high correlation of long-wavelength topography and gravity and the large apparent depths of compensation suggest that Venus lacks an upper-mantle low-viscosity zone. A key difference between Earth and Venus may be the degree of coupling between the convecting mantle and the overlying lithosphere. Mantle flow should then have recognizable signatures in the relationships between the observed surface topography, crustal deformation, and the gravity field. Therefore, comparison of model results with observational data can help to constrain such parameters as crustal and thermal boundary layer thicknesses as well as the character of mantle flow below different Venusian features. We explore in this paper the effects of this coupling by means of a finite element modelling technique. Author (revised)

N94-20770*# Chicago Univ., IL. Dept. of Geophysical Sciences.
PETROGRAPHY AND ORIGIN OF REFRACTORY INCLUSIONS FROM THE MURRAY AND MURCHISON C2 CHONDRITES Abstract Only c90
S. B. Simon, L. Grossman, and A. Hsu (Illinois Mathematics and Science Academy, Aurora.) *In* Lunar and Planetary Inst., Twenty-Fourth Lunar and Planetary Science Conference. Part 3: N-Z 1993 p 1309-1310 (For primary document see N94-20636 05-91)
Avail: CASI HC A01/MF A06

By freeze-thaw disaggregation, we have recovered a total of 47 refractory inclusions. New discoveries include the following: a hibonite-pyroxene spherule from Murray; a CaAl4O7-bearing spherule from Murchison; and a Sc-fassaite-bearing ultrarefractory inclusion from Murchison. Freeze-thaw disaggregation, combined with density separation and hand-picking as described is a proven method for recovering rare objects from carbonaceous chondrites. This method is especially effective on C2's due to their porosity and typically results in the discovery of new types of refractory inclusions.

Because few refractory inclusions from Murray have been described, we studied this meteorite, although only a small amount of material (730 mg) was available for disaggregation. Many refractory inclusions from Murchison have been described, and we disaggregated a larger amount (approximately 18 g) of Murchison in an attempt to find new types of refractory inclusions, especially corundum-bearing ones. Author (revised)

N94-20771*# Stanford Univ., CA. Center for Radar Astronomy.
SCATTERING BY VENUS' SURFACE Abstract Only
R. A. Simpson, G. L. Tyler, M. J. Maurer, E. Holmann, and P. B. Wong *In* Lunar and Planetary Inst., Twenty-Fourth Lunar and Planetary Science Conference. Part 3: N-Z 1993 p 1311 (For primary document see N94-20636 05-91)
Avail: CASI HC A01/MF A06

During 1992, Magellan altimetry echoes were processed to yield scattering functions sigma(sub o)(phi) over near-nadir angles phi less than or equal to 10 deg from some 2000 Venus orbits. SAR image strips acquired simultaneously at oblique angles were also reduced to give scattering functions but over a few deg of incidence angle in the range 15 less than or equal to phi less than or equal to 45 deg. By sorting, the altimetry and SAR results can be combined to give composite scattering functions for much of Venus' surface. The data in hand should allow definition of such composite functions for 70-80 percent of Venus at resolutions of 20 km--approximately one million separate functions. Author (revised)

N94-20772*# Jet Propulsion Lab., California Inst. of Tech., Pasadena.
VENUS GRAVITY: NEW MAGELLAN LOW ALTITUDE DATA Abstract Only
W. L. Sjogren, Konopliv. A. S., N. Borderies, M. Batchelder (Telos Aerospace Systems, CA.), J. Heirath (Sterling Software, Inc., Palo Alto, CA.), and R. N. Wimberly (Sterling Software, Inc., Palo Alto, CA.) *In* Lunar and Planetary Inst., Twenty-Fourth Lunar and Planetary Science Conference. Part 3: N-Z 1993 p 1313-1314 (For primary document see N94-20636 05-91)
Avail: CASI HC A01/MF A06

Acquisition of a new high quality gravity data set has begun. The data set presently covers one third of the Venusian longitude. Better spatial resolution is obtained from a 60th degree and order spherical harmonic solution. Plans for aerobraking in May 1993 into a near circular orbit will provide excellent data for higher latitude regions. Author (revised)

N94-20773*# Oberlin Coll., OH. Dept. of Geology.
SIZE DISTRIBUTIONS AND AERODYNAMIC EQUIVALENCE OF METAL CHONDRULES AND SILICATE CHONDRULES IN ACFER 059 Abstract Only **c90**
William R. Skinner and James M. Leenhouts (Arizona Univ., Tucson.) *In* Lunar and Planetary Inst., Twenty-Fourth Lunar and Planetary Science Conference. Part 3: N-Z 1993 p 1315-1316 (For primary document see N94-20636 05-91)
Avail: CASI HC A01/MF A06

The CR2 chondrite Acfer 059 is unusual in that the original droplet shapes of metal chondrules are well preserved. We determined separate size distributions for metal chondrules and silicate chondrules; the two types are well sorted and have similar size distributions about their respective mean diameters of 0.74 mm and 1.44 mm. These mean values are aerodynamically equivalent for the contrasting densities, as shown by calculated terminal settling velocities in a model solar nebula. Aerodynamic equivalence and similarity of size distributions suggest that metal and silicate fractions experienced the same sorting process before they were accreted onto the parent body. These characteristics, together with depletion of iron in Acfer 059 and essentially all other chondrites relative to primitive CI compositions, strongly suggest that sorting in the solar nebula involved a radial aerodynamic component and that sorting and siderophile depletion in chondrites are closely related. Author (revised)

N94-20774*# National Aeronautics and Space Administration. Goddard Space Flight Center, Greenbelt, MD.
GMM-1: A 50 DEGREE AND ORDER GRAVITATIONAL FIELD MODEL FOR MARS Abstract Only
D. E. Smith, F. J. Lerch, R. S. Nerem, M. T. Zuber (Johns Hopkins Univ., Baltimore, MD.), G. B. Patel (Hughes STX, Inc., Lanham, MD.), S. K. Fricke (RMS Technologies, Inc., Landover, MD.), and F. G. Lemoine *In* Lunar and Planetary Inst., Twenty-Fourth Lunar and Planetary Science Conference. Part 3: N-Z 1993 p 1317-1318 (For primary document see N94-20636 05-91)
Avail: CASI HC A01/MF A06

Knowledge of the gravitational field, in combination with surface topography, provides one of the principal means of inferring the internal structure of a planetary body. The highest resolution gravitational field for Mars published thus far was derived from Doppler tracking data from the Mariner 9 and Viking 1 and 2 spacecraft and is complete to degree and order 18 corresponding to a half wavelength resolution of approximately 600 km. This field, which is characterized by a spatial resolution that is slightly better than that of the highest resolution (16x16) topographic model, has been utilized extensively in analyses of the state of stress and isostatic compensation of the Martian lithosphere. However, the resolution and quality of current gravity and topographic fields are such that the origin and evolution of even the major physiographic features on Mars, such as the hemispheric dichotomy and Tharsis rise, are not well understood. We have re-analyzed the Viking and Mariner data sets and have derived a new gravitational field, which we designated GMM-1 (Goddard Mars Model-1). This model is complete to spherical harmonic degree and order 50 with a corresponding (half wavelength) spatial resolution of 200-300 km where the data permit. In contrast to previous models, GMM-1 was solved to as high degree and order as necessary to nearly exhaust the attenuated gravitational signal contained in the tracking data. Author (revised)

N94-20775*# Jet Propulsion Lab., California Inst. of Tech., Pasadena.
RESPONSE OF THE TOPOGRAPHY AND GRAVITY FIELD ON VENUS TO MANTLE UPWELLING BENEATH A CHEMICAL BOUNDARY LAYER Abstract Only
Suzanne E. Smrekar and E. Marc Parmentier (Brown Univ., Providence, RI.) *In* Lunar and Planetary Inst., Twenty-Fourth Lunar and Planetary Science Conference. Part 3: N-Z 1993 p 1319-1320 (For primary document see N94-20636 05-91)
Avail: CASI HC A01/MF A06

The long wavelength correlation of the gravity and topography and the large apparent depths of compensation (approximately 150-300 km) for large highland regions on Venus require significant differences between the interior structure of Earth and Venus. The morphology, geologic history, and large apparent depths of compensation for many highlands have been interpreted to indicate areas of mantle upwelling. A large apparent depth of compensation at a mantle upwelling is generally interpreted to indicate the base of the thermal boundary layer of convection. A boundary layer thickness of 150-300 km implies that the interior of Venus is presently much colder than Earth and thus tectonically less active. The recent Magellan mission has provided contradictory evidence regarding the present level of tectonic activity on Venus, prompting considerable debate. In this study, we investigate the possibility that a chemical boundary layer acts together with a thermal boundary layer to produce large apparent depths of compensation, or equivalently, large geoid-to-topography-ratios (GTR's). The crust of a planet forms through partial melting of mantle materials. Both the melt and the residuum are lower in density than unmelted (or undepleted) mantle. In the absence of vigorous plate tectonics, a thick layer of buoyant residuum, or depleted mantle, may collect beneath the lithosphere. In this scenario, the thermal lithosphere does not need to be thick and cold to match the GTR's. Cooling of the depleted layer may lead to overturn of the upper mantle and episodic resurfacing with time scales on the order of 300-500 MY, consistent with the resurfacing age of Venus.
Author (revised)

N94-20776*# Tennessee Univ., Knoxville.
PRIMARY DIFFERENTIATION IN THE EARLY EARTH: Nd AND Sr ISOTOPIC EVIDENCE FROM DIAMONDIFEROUS ECLOGITES FOR BOTH OLD DEPLETED AND OLD ENRICHED MANTLE, YAKUTIA, SIBERIA Abstract Only **c46**
Gregory A. Snyder, Eric A. Jerde, Lawrence A. Taylor, Alex N. Halliday (Michigan Univ., Ann Arbor.), Vladimir N. Sobolev (Academy of Sciences, USSR, Novosibirsk.), Nickolai V. Sobolev (Academy of Sciences, USSR, Novosibirsk.), Robert N. Clayton (Chicago Univ., IL.), Toshiko K. Mayeda (Chicago Univ., IL.), and Peter Deines (Pennsylvania State Univ., University Park.) *In* Lunar and Planetary Inst., Twenty-Fourth Lunar and Planetary Science Conference. Part 3: N-Z 1993 p 1321-1322 (For primary

document see N94-20636 05-91)
Avail: CASI HC A01/MF A06

Ancient, stable, continental cratons possess thick, subcontinental-lithospheric mantle 'keels' which favor particularly the emplacement of diamondiferous kimberlites and included peridotites and eclogites. These refractory mantle samples of the roots provide hard constraints on the theories of formation, growth, and evolution of these cratons. Xenoliths containing only primary garnet and clinopyroxene (eclogites), although rare in most kimberlites, can retain the geochemical signatures of their parent protoliths (e.g., subducted oceanic crust, ancient mantle) thus offering the opportunity to address mantle processes which may have taken place at earlier times in the Earth's history. In fact, it has been postulated that some eclogites are residues from the accretion of the early Earth. Nd and Sr isotopic data are presented which may be interpreted as evidence of an early (greater than 4 Ga) mantle differentiation event. The kimberlites of Yakutia are located both marginal and central to the Siberian craton, and a wide variety of xenoliths are present within them. The Siberian mantle samples have received little attention in the western world, largely because suitable suites of Yakutian samples have not been readily available. Importantly, there is evidence that metasomatism of the Siberian lithosphere has been considerably less intense or extensive than for the Kaapvaal craton. Therefore, it should be considerably easier to elicit the igneous/metamorphic histories of Siberian kimberlitic xenoliths. One of the notable features of the Siberian eclogites is the common appearance of diamonds, especially in the Mir and Udachnaya pipes. In all, eight eclogite samples (eight garnet separates and eight clinopyroxene separates) have been analyzed to date on the Udachnaya pipe, seven from our group. Author (revised)

N94-20777*# Tennessee Univ., Knoxville. Dept. of Geological Sciences.
CHRONOLOGY AND GENESIS OF HIGH-TI MARE VOLCANISM: MELTING OF COGENETIC DEPLETED AND ENRICHED RESERVOIRS Abstract Only
Gregory A. Snyder, Lawrence A. Taylor, and Alex N. Halliday (Michigan Univ., Ann Arbor.) *In* Lunar and Planetary Inst., Twenty-Fourth Lunar and Planetary Science Conference. Part 3: N-Z 1993 p 1323-1324 (For primary document see N94-20636 05-91)
Avail: CASI HC A01/MF A06

An understanding of the chronology and petrogenesis of volcanic rocks is paramount to unravelling the complexities of the composition and structure of the mantle of the Moon. High-Ti mare basalts represent the best-sampled suite of lunar volcanic rocks and likely represent melts of the uppermost mantle of the Moon. Compiled Nd and Sr isotopic data for high-Ti basalts, combined with weighted average ages determiend by various techniques, yield a complex melting history for the high-Ti mantle source. Melting occurred during three distinct episodes (3.84 Ga, 3.75-3.69 Ga, and 3.56 Ga) separated by hiatuses of 100 Ma or more. The first episode included the melting of a relatively trapped liquid (KREEPy)-rich source beneath the A-11 landing site. Later melting of this source produced magmas which were relatively trapped liquid-free at the A-11 site. Synchronous melting at the A-17 landing site produced magmas with variable proportions of this evolved trapped liquid component. The final phase of volcanism occurred at the A-11 site and involved the assimilation of an evolved 'neuKREEP' component. Continued melting of a similar source, which was nearly exhausted of its ilmenite component, beneath the A-12 landing site may have lead to production of magmas parental to the A-12 ilmenite basalts. Author (revised)

N94-20778*# Tennessee Univ., Knoxville. Dept. of Geological Sciences.
GEOCHRONOLOGY AND PETROGENESIS OF THE WESTERN HIGHLANDS ALKALI SUITE: RADIOGENIC ISOTOPIC EVIDENCE FROM APOLLO 14 Abstract Only
Gregory A. Snyder, Lawrence A. Taylor, and Alex N. Halliday (Michigan Univ., Ann Arbor.) *In* Lunar and Planetary Inst., Twenty-Fourth Lunar and Planetary Science Conference. Part 3: N-Z 1993 p 1325-1326 (For primary document see N94-20636 05-91)
Avail: CASI HC A01/MF A06

Several rocks of alkalic affinity, from the western highlands of the Moon, have been analyzed for their Nd and Sr isotopic compositions. One sample yields a Sm-Nd mineral isochron of 4110 = 41 Ma. This age, in conjunction with U-Pb zircon ages on two other alkalic rocks from the Apollo 14 landing site suggests a distinct western highlands 'event' which was approximately 100 Ma in duration. Since the last dregs of the lunar magma ocean likely crystallized prior to 4.3 Ga, this alkalic 'event' may have included the re-melting of evolved plutons or the remobilization of urKREEP trapped liquid from upper mantle cumulates. Alkalic lithologies such as granites and felsites have been known from the Moon since the earliest days of the Apollo lunar sample returns. However, not until 1977 were alkali-rich rocks recognized from typical highlands suites such as ferroan anorthosites (FAN) and norites and Mg-suite rocks. In the intervening years, several other alkali suite samples have been discovered and characterized, mostly through labor-intesive breccia pull-apart studies of clasts and analyses of coarse-fine fractions of soils. We will speculate on the origins of this suite of lunar highlands rocks. Author (revised)

N94-20779*# Tennessee Univ., Knoxville. Dept. of Geological Sciences.
MAGNESIAN ANORTHOSITES FROM THE WESTERN HIGHLANDS OF THE MOON: ISOTOPE GEOCHEMISTRY AND PETROGENESIS Abstract Only
Gregory A. Snyder, Lawrence A. Taylor, and Alex N. Halliday (Michigan Univ., Ann Arbor.) *In* Lunar and Planetary Inst., Twenty-Fourth Lunar and Planetary Science Conference. Part 3: N-Z 1993 p 1327-1328 (For primary document see N94-20636 05-91)
Avail: CASI HC A01/MF A06

Breccias from the Apollo 14 landing site have provided a wealth of information on the genesis of the lunar highlands. Various pristine rock-types have been discovered in relative abundance including rare ferroan anorthosites and alkali-suite and magnesian-suite rocks. Mineral-chemical and radiogenic isotopic data are reported here for a newly discovered Mg-suite anorthosite from Apollo 14, sample 14303,347. Meyer et al. reported U-Pb zircon analyses of Mg-suite highlands rocks from the western limb of the Moon. We have compiled these ages and generated a weighted average age of 4211 = 6 Ma; some 200 Ma younger than ferroan anorthosites. Utilizing this age for Mg-anorthosite 14303,347, our data results in an initial epsilon(sub Nd) value of -1.0 and initial Sr-87/Sr-86 of 0.69915. Based on trace-element, isotopic, and mineral-chemical data, the western highlands Mg-suite is interpreted to be crustal precipitates of a picritic magma, which assimilated KREEPy trapped liquid from upper-mantle cumulates during its transport to the crust. Author (revised)

N94-20780*# California Inst. of Tech., Pasadena. Div. of Geological and Planetary Sciences.
DIFFERENTIATION OF MAGMA OCEANS AND THE THICKNESS OF THE DEPLETED LAYER ON VENUS Abstract Only
V. S. Solomatov and D. J. Stevenson *In* Lunar and Planetary Inst., Twenty-Fourth Lunar and Planetary Science Conference. Part 3: N-Z 1993 p 1329-1330 (For primary document see N94-20636 05-91)
Avail: CASI HC A01/MF A06

Various arguments suggest that Venus probably has no asthenosphere, and it is likely that beneath the crust there is a highly depleted and highly viscous mantle layer which was probably formed in the early history of the planet when it was partially or completely molten. Models of crystallization of magma oceans suggest that just after crystallization of a hypothetical magma ocean, the internal structure of Venus consists of a crust up to about 70 km thickness, a depleted layer up to about 500 km, and an enriched lower layer which probably consists of an undepleted 'lower mantle' and heavy enriched accumulates near the core-mantle boundary. Partial or even complete melting of Venus due to large impacts during the formation period eventually results in differentiation. However, the final result of such a differentiation can vary from a completely differentiated mantle to an almost completely preserved homogeneous mantle depending on competition between convection and differentiation: between low viscosity ('liquid') convection and crystal settling at small crystal fractions, or between high viscosity ('solid') convection and percolation at large crystal fractions. Author (revised)

N94-20781*# Carnegie Institution of Washington, DC. Dept. of Terrestrial Magnetism.
A TECTONIC RESURFACING MODEL FOR VENUS Abstract Only
Sean C. Solomon *In* Lunar and Planetary Inst., Twenty-Fourth Lunar and Planetary Science Conference. Part 3: N-Z 1993 p 1331-1332 (For primary document see N94-20636 05-91)
Avail: CASI HC A01/MF A06

Two remarkable aspects of the population of impact craters on Venus

are as follows: that craters at all sizes are indistinguishable from a random population; and that the vast majority of craters have not been significantly modified by tectonic strain or by volcanic flows external to the crater rim, despite evidence from Magellan images that volcanic and tectonic features are widespread on Venus. One interpretation of these observations is that most of the surface dates from the end of a catastrophic global resurfacing event that ceased about 500 My ago, and that the small fraction of craters volcanically embayed or modified by deformation indicates that volcanic and tectonic activity subsequent to that time has been at much lower levels. An alternative model, in which resurfacing occurs episodically in patches a few hundred kilometers in extent and there is a wider spectrum of surface ages, also appears to be consistent with the characteristics of impact craters on Venus. A number of potential mechanisms for catastrophic resurfacing of Venus have been proposed ranging from geologically sudden convective destabilization of the global lithosphere to strongly time-dependent heat flux and melt generation in the underlying mantle. In most of these geophysical models, resurfacing occurs implicitly or explicitly by volcanism. We explore here the hypothesis that, at least in the geologically recent history of Venus, the primary resurfacing mechanism has been tectonic deformation rather than volcanism. We show how such a hypothesis provides at least as good an explanation of a wide range of observations as do volcanic resurfacing models. Finally, we explore the implications of the tectonic resurfacing hypothesis for the controversy over the recent resurfacing history of the planet. Author (revised)

N94-20782*# City Univ. of New York, Flushing. Dept. of Geology.
THE MISSING IMPACT CRATERS ON VENUS Abstract Only
D. H. Speidel *In* Lunar and Planetary Inst., Twenty-Fourth Lunar and Planetary Science Conference. Part 3: N-Z 1993 p 1333-1334 (For primary document see N94-20636 05-91)
Avail: CASI HC A01/MF A06

The size-frequency pattern of the 842 impact craters on Venus measured to date can be well described (across four standard deviation units) as a single log normal distribution with a mean crater diameter of 14.5 km. This result was predicted in 1991 on examination of the initial Magellan analysis. If this observed distribution is close to the real distribution, the 'missing' 90 percent of the small craters and the 'anomalous' lack of surface splotches may thus be neither missing nor anomalous. I think that the missing craters and missing splotches can be satisfactorily explained by accepting that the observed distribution approximates the real one, that it is not craters that are missing but the impactors. What you see is what you got. The implication that Venus crossing impactors would have the same type of log normal distribution is consistent with recently described distribution for terrestrial craters and Earth crossing asteroids. Author (revised)

N94-20783*# New Brunswick Univ., Fredericton. Dept. of Geology.
DELIMITATION OF TERRESTRIAL IMPACT CRATERS BY WAY OF PSEUDOTACHYLYTIC ROCK DISTRIBUTION Abstract Only **c46**
John G. Spray *In* Lunar and Planetary Inst., Twenty-Fourth Lunar and Planetary Science Conference. Part 3: N-Z 1993 p 1335-1336 (For primary document see N94-20636 05-91)
Avail: CASI HC A01/MF A06

The determination of the shape and size of terrestrial impact craters is problematic, yet is critical to understanding cratering mechanics and for scaling bolide mass, volume, and impact velocity with crater size and target response. The problem is particularly difficult in older geological terrains (e.g. Precambrian) which are more likely to have suffered post-impact deformation and hence distortion of the original structure and/or where weathering may have partly removed or obscured its original shape. Traditionally, a number of features are used to assist us in determining the shape and size of an impact structure. These include the following: (1) the occurrence of faults, especially those disposed concentrically relative to the crater--the outermost ring faults being interpreted as indicating a viable minimum diameter; and (2) the development of so-called breccias, some of which are also associated with faults (e.g. the Sudbury Breccia developed within the target rocks of the Sudbury Structure of Onta rio, Canada). 'Breccia' is not a satisfactory term because a number of breccia-types exist at impact sites (e.g. fall-back breccias and in-situ brecciated target material). Of relevance to crater diameter determination is the recognition of discrete zones and fault- and shock-related pseudotachylyte. Pseudotachylyte is a rock type comprising a fine-grained, usually dark matrix containing clasts of minerals and/or rock derived from the country rock target material. It origin is normally attributed to high-speed slip (including vibration) along a slip surface (i.e. fault) or to the passage of a shock wave through the host material. The clasts can occur as angular fragments (i.e. like a breccia), but are more commonly developed as rounded to sub-rounded fragments. Significantly, the scale of these pseudotachylytes can range from sub-millimeter thick veinlets to dyke-like bodies up to 1 km or more thick. It is the latter, larger occurrence which has been referred to as 'breccia.' The smaller-sized occurrence is generally not recognized in the field, nor is it traditionally associated with its larger counterpart. Author (revised)

N94-20784*# Lunar and Planetary Inst., Houston, TX.
CONTRIBUTIONS OF THE CLEMENTINE MISSION TO OUR UNDERSTANDING OF THE PROCESSES AND HISTORY OF THE MOON Abstract Only
Paul D. Spudis and Paul G. Lucey (Hawaii Univ., Honolulu.) *In its* Twenty-Fourth Lunar and Planetary Science Conference. Part 3: N-Z 1993 p 1337-1338 (For primary document see N94-20636 05-91)
Avail: CASI HC A01/MF A06

The Clementine mission will provide us with an abundance of information about lunar surface morphology, topography, and composition, and it will permit us to infer the history of the Moon and the processes that have shaped that history. This information can be used to address fundamental questions in lunar science and allow us to make significant advances towards deciphering the complex story of the Moon. The Clementine mission will also permit a first-order global assessment of the resources of the Moon and provide a strategic base of knowledge upon which future robotic and human missions to the Moon can build. Author (revised)

N94-20785*# Lunar and Planetary Inst., Houston, TX.
IMPACT BASINS ON VENUS AND SOME INTERPLANETARY COMPARISONS Abstract Only
Paul D. Spudis and Virgil L. Sharpton *In its* Twenty-Fourth Lunar and Planetary Science Conference. Part 3: N-Z 1993 p 1339-1340 (For primary document see N94-20636 05-91)
Avail: CASI HC A01/MF A06

Impact is one of the many processes that have shaped the surface of Venus. The largest impact craters, basins, are important features affecting the evolution of the terrestrial planets. Because Venus has an atmosphere, a gravity similar to Earth's, and a surface target with a high geothermal gradient, venusian basins provide an important comparative set of data to test our ideas about basin-forming impacts and their geological effects on the evolution of the crusts of the terrestrial planets. Author (revised)

N94-20786*# Lunar and Planetary Inst., Houston, TX.
GEOLOGY AND DEPOSITS OF THE SERENITATIS BASIN Abstract Only
Paul D. Spudis, B. Ray Hawke (Hawaii Univ., Honolulu.), and Paul G. Lucey (Hawaii Univ., Honolulu.) *In its* Twenty-Fourth Lunar and Planetary Science Conference. Part 3: N-Z 1993 p 1341-1342 (For primary document see N94-20636 05-91)
Avail: CASI HC A01/MF A06

The Serenitatis basin is prominent on the near side of the Moon, just east of Mare Imbrium. Originally thought to be one of the oldest lunar basins, re-interpretation of both geological relations and Apollo 17 isotopic data suggest instead that Serenitatis is one of the youngest basins, having formed in the Nectarian Period about 3.87 Ga ago. As part of our continuing effort to understand the geology of multi-ring basins on the Moon and to use basins as probes of the deep lunar crust, we here report results for the Serenitatis basin. Our examination of Serenitatis was stimulated in part by a new effort to re-examine the geology of the Apollo 17 landing site. Author (revised)

N94-20787*# Cornell Univ., Ithaca, NY. Dept. of Astronomy.
EARTH-BASED MEASUREMENT OF LUNAR TOPOGRAPHY USING DELAYED RADAR INTERFEROMETRY Abstract Only
N. J. S. Stacy and D. B. Campbell *In* Lunar and Planetary Inst., Twenty-Fourth Lunar and Planetary Science Conference. Part 3: N-Z 1993 p 1343-1344 (For primary document see N94-20636 05-91)
Avail: CASI HC A01/MF A06

Radar interferometry has been applied to radar mapping of the surface of Venus to resolve the ambiguity in the backscatter from the areas with

the same delay-Doppler coordinates. For observations of the Moon these points are usually isolated by the small extent of the area illuminated by the radar beam so that interferometric techniques can be used to determine a third dimension to the location of the radar backscatter. Recent observations of Sinus Iridum (41.5 deg N, 31.0 deg W) using the Arecibo Observatory S-Band radar system (12.6 cm wavelength) in Apr. and Aug. 1992 have yielded a pair of images viewed with a very small 0.0420 deg difference in incidence angle. These images can be used as a delay interferometric pair and have been correlated to generate phase fringes that are related to topography. The spatial resolution of the images are 18 m in delay and 33 m in cross range (Doppler). The anticipated topographic resolution once the phase fringes have been unwrapped is approximately +/- 10 m. Author (revised)

N94-20788*# Chicago Univ., IL. Dept. of Geophysical Sciences.
Fe/Mn IN OLIVINE OF CARBONACEOUS METEORITES Abstract Only **c90**

Ian M. Steele *In* Lunar and Planetary Inst., Twenty-Fourth Lunar and Planetary Science Conference. Part 3: N-Z 1993 p 1345-1346 (For primary document see N94-20636 05-91)
Avail: CASI HC A01/MF A06

Olivines in primitive meteorites show a range of Fe/Mn both within one grain and among grains suggesting that they have recorded changing conditions during or after growth. Because olivine should be an early forming phase, Fe/Mn is used here to infer these earliest conditions. Initial Fe/Mn in cores of isolated, euhedral forsterite in both C2 and C3 meteorites ranges from 25 to 35 but differs at grain edge. Murchison (C2) forsterites show Fe/Mn approaching 1.0 at the grain edge while Ornans Fe/Mn is near 60 at grain edge. These values are lower than the matrix Fe/Mn for both meteorites and the distinct difference in zoning profile indicates different processes operating during and after grain growth. The Fe/Mn of bulk samples from a particular source such as the Moon is nearly constant. Individual samples show variation suggesting that there is some fractionation of Mn from Fe. Minerals have their individual ranges of Fe/Mn which has been used to recognize different types of olivine within one meteorite. Extreme values of Fe/Mn below 1.0 occur in forsterite from some IDP's, UOC matrix, and C1 meteorites. There are apparently no detailed studies of Fe/Mn variation within single olivine grains. Forsterite grains in C2 and C3 carbonaceous chondrites show complex zoning, and the nearly pure forsterites (Fo greater than approximately 99.5) have high levels of some minor elements including Ti, Al, V, and Sc. There is disagreement on the original source of these grains and both chondrule and vapor growth have been proposed. In addition, there is clear evidence that diffusion has affected the outer margins but in some cases the whole grain. Within the cores, the FeO range is limited, and if growing under constant conditions, the Fe/Mn should be near constant as there is little fractionation of Mn from Fe by forsterite. Additionally, there are apparently no co-crystallizing phases as evidenced by a lack of common inclusions in the forsterites. These observations are now followed by analyses of isolated olivine grains in C2 and C3 meteorites. Author (revised)

N94-20789*# Wyoming Univ., Laramie. Dept. of Geology/Geophysics.
TWO-POLARITY MAGNETIZATION IN THE MANSON IMPACT BRECCIA Abstract Only **c46**

M. B. Steiner and E. M. Shoemaker (Geological Survey, Flagstaff, AZ.) *In* Lunar and Planetary Inst., Twenty-Fourth Lunar and Planetary Science Conference. Part 3: N-Z 1993 p 1347-1348 (For primary document see N94-20636 05-91)
Avail: CASI HC A01/MF A06

A preliminary paleomagnetic study of the impact breccia matrix and clasts has produced surprising results--nearly antipodal normal and reversed polarity magnetic vectors are observed in different portions of the core. Near-antipodal magnetizations within a segment of matrix and within individual samples rule out core inversion as the explanation of the dual polarity. In both the dense and the sandy matrix breccias, the magnetizations of clasts and matrix within the same core segment are identical; this negative 'conglomerate test' indicates that magnetization originated after impact. Paleomagnetic study of the Manson Impact Structure is an attempt to refine the Ar-40/Ar-39 age (65.7 +/- 1 m.y.) that suggests Manson to be a Cretaceous-Tertiary boundary impact. Refinement is possible because the boundary occurs within a reversed polarity interval (29R) of only 0.5 m.y. duration. The two breccia types in the Manson structure were both examined: one of a very dense matrix and apparently partially melted, and the breccia stratigraphically below it of granular or 'sandy' chloritic matrix. Samples were taken from the matrixes and a wide variety of clast compositions, including granite, diabase, gneiss, amphibolite, and melted granite. Currently, measurements have been made on 22 samples, using 30-35 steps of either alternating field (AF) or thermal demagnetization. Author (revised)

N94-20790*# Muenster Univ. (Germany). Inst. of Physikalisches.
MULTIELEMENT ANALYSIS OF INTERPLANETARY DUST PARTICLES USING TOF-SIMS Abstract Only **c90**

T. Stephan, W. Kloeck, E. K. Jessberger (Max-Planck-Inst. fuer Kernphysik, Heidelberg, Germany.), H. Rulle, and J. Zehnpfenning *In* Lunar and Planetary Inst., Twenty-Fourth Lunar and Planetary Science Conference. Part 3: N-Z 1993 p 1349-1350 (For primary document see N94-20636 05-91)
Avail: CASI HC A01/MF A06

Sections of three stratospheric particles (U2015G1, W7029*A27, and L2005P9) were analyzed with TOF-SIMS (Time Of Flight-Secondary Ion Mass Spectrometry) continuing our efforts to investigate the element distribution in interplanetary dust particles (IDP's) with high lateral resolution (approximately 0.2 micron), to examine possible atmospheric contamination effects, and to further explore the abilities of this technique for element analysis of small samples. The samples, previously investigated with SXRF (synchrotron X-ray fluorescence analysis), are highly enriched in Br (Br/Fe: 59 x CI, 9.2 x CI, and 116 x CI, respectively). U2015G1 is the IDP with the by far highest Zn/Fe-ratio (81 x CI) ever reported in chondritic particles. Author (revised)

N94-20791*# Lunar and Planetary Inst., Houston, TX.
MAGNETICALLY CONTROLLED SOLAR NEBULA Abstract Only **c92**

T. F. Stepinski and M. Reyes-Ruiz (Rice Univ., Houston, TX.) *In its* Twenty-Fourth Lunar and Planetary Science Conference. Part 3: N-Z 1993 p 1351-1352 (For primary document see N94-20636 05-91)
Avail: CASI HC A01/MF A06

It is widely believed that a primordial solar nebula, the precursor of the Sun and its planetary system, could be best described in terms of an accretion disk. Such an accretion disk is though to be turbulent, and it is usually imagined that turbulent viscosity alone provides the torque responsible for the structure and the evolution of the nebula. However, it was found that an MHD dynamo operating in a turbulent nebula can contemporaneously produce magnetic fields capable of significantly altering or even dominating the total torque. Thus, it seems that no model of a viscous solar nebula is complete without taking magnetic fields into consideration. It was demonstrated that there are usually two distinct regions of nebular disk where a dynamo can operate: the inner region, where the magnetic field coupled to gas due to relatively high thermal ionization; and the outer region, where this coupling is achieved due to nonthermal ionization. Most models also show the existence of an intermediate region, 'the magnetic gap,' where neither thermal nor nonthermal sources can produce enough ionization to provide the necessary coupling between the magnetic field and the gas. The location and width of the gap change substantially from one model to another. At present, we can only estimate the strength of a generated magnetic field. It seems that a large-scale magnetic field is likely to be in the equipartition with the turbulent kinetic energy; however, the intense magnetic fluctuations may greatly exceed this equipartition strength on short time and length scales. To show how a dynamo-generated magnetic field changes the structure of a viscous nebula, we consider four nebula models extensively. Author (revised)

N94-20792*# California Inst. of Tech., Pasadena.
EXPECTATIONS FOR THE MARTIAN CORE MAGNETIC FIELD Abstract Only

D. J. Stevenson *In* Lunar and Planetary Inst., Twenty-Fourth Lunar and Planetary Science Conference. Part 3: N-Z 1993 p 1353-1354 (For primary document see N94-20636 05-91)
Avail: CASI HC A01/MF A06

In the traditional view of planetary magnetism, a planet either has a core dynamo (Earth, Jupiter, Saturn, Uranus, Neptune, maybe Mercury) or does not (Mars, Venus, Moon...) I argue that this view is simplistic in two respects. First, mantle convection in terrestrial planets is invariably ata high enough Rayleigh number that it is time variable; this leads to the

intermittent arrival of mantle 'cold fingers' at the core-mantle boundary promoting at least local core convection and dynamo action even when the planetary core is stably stratified on average. Thus, I predict an intermittent dynamo regime in addition to the simple dynamo-on (Earth) and dynamo-off regimes. Second, the mantle convection-driven horizontal temperature gradients just below the core-mantle boundary can lead to unstable flows that will convert thermoelectric or electrochemical toroidal fields into externally detectable poloidal fields, even when a dynamo is not possible. It is likely that Mars possesses an interesting core magnetic field of the latter kind, complex but with a dipole that might be approximately aligned with the rotation axis and a surface field of a few to tens of gammas. Author (revised)

N94-20793*# California Inst. of Tech., Pasadena.
VOLATILE LOSS FROM ACCRETING ICY PROTOPLANETS Abstract Only **c90**
D. J. Stevenson *In* Lunar and Planetary Inst., Twenty-Fourth Lunar and Planetary Science Conference. Part 3: N-Z 1993 p 1355-1356 (For primary document see N94-20636 05-91)
Avail: CASI HC A01/MF A06

A large self-gravitating body does not easily lose significant mass because the escape velocity is much larger than the sound speed of atmosphere-forming species under ambient thermal conditions. The most significant exceptions to this are giant impacts or impact jetting by fast-moving projectiles. A very small object (e.g. a comet) also does not easily lose significant volatile mass upon formation because the energy release associated with its accretion is so small. (It can however lose a great deal of mass if it is subsequently moved closer to the Sun.) I argue that there is an intermediate mass range (corresponding to bodies with radii of approximately 300-800 km) for which the ambient steady-state mass loss is a maximum. By ambient, I mean those conditions pertaining to the formation region of the body. By steady state, I mean to exclude infrequent traumas (giant impacts). The existence of a preferred intermediate mass arises through the competition of growing gravitational containment and growing energy release by accretion; it corresponds typically to GM/(Rc(sub s)(exp 2)) approximately equals 2 to 4, where M is the protoplanet mass of radius R, and c(sub s) is the sound speed. Several factors determine the amount of volatile loss is this vulnerable zone during accretion but in general the loss is a substantial fraction of the volatiles, sometimes approaching 100 percent. The principal implication is that bodies larger than a few hundred kilometers in radius will not have a 'primitive' (i.e. cometary) composition. This is relevant for understanding Triton, Pluto, Charon, and perhaps Chiron. Author (revised)

N94-20794*# California Inst. of Tech., Pasadena. Div. of Geological and Planetary Sciences.
FINE RESOLUTION CHRONOLOGY BASED ON INITIAL Sr-87/Sr-86 Abstract Only **c25**
B. W. Stewart, D. A. Papanastassiou, R. C. Capo, and G. J. Wasserburg *In* Lunar and Planetary Inst., Twenty-Fourth Lunar and Planetary Science Conference. Part 3: N-Z 1993 p 1357-1358 (For primary document see N94-20636 05-91)
(Grant NAG9-43)
(Contrib-5230(794)) Avail: CASI HC A01/MF A06

It has been recognized that small variations in initial Sr-87/Sr-86 (Sr(sub I)), can provide a fine scale relative chronology for the chemical fractionation of materials with low Rb/Sr from parent reservoirs with high Rb/Sr. Similarly, Sr(sub I), as determined for low Rb/Sr phases in meteorites, may permit a fine resolution chronology of the recrystallization or metamorphism of planetary materials. For the establishment of a primitive Sr-87/Sr-86 chronology, it is important to search for samples with extremely low Rb/Sr for which the measured Sr-87/Sr-86 is below BABI, in which case the primitive nature of the Sr can be directly established. Using the measured Rb/Sr to calculate an initial Sr-87/Sr-86 can introduce substantial uncertainty if the Rb-Sr are disturbed. We report Sr-87/Sr-86 in plagioclase from silicate pebbles from the Vaca Muerta mesosiderite on which we have reported Sm-147-Nd-143 and Ne-142 correlations. For the purpose of cross-calibration with our previous work we have performed extensive new measurements on Angra dos Reis and on anorthite from Moore County, which have very low Rb/Sr and primitive Sr-87/Sr-86. Author (revised)

N94-20795*# California Inst. of Tech., Pasadena. Div. of Geological and Planetary Sciences.
THE Sm-Nd SYSTEMATICS OF SILICATE INCLUSIONS IN IRON METEORITES: RESULTS FROM CADDO (IAB) Abstract Only **c90**
Brian W. Stewart, D. A. Papanastassiou, and G. J. Wasserburg *In* Lunar and Planetary Inst., Twenty-Fourth Lunar and Planetary Science Conference. Part 3: N-Z 1993 p 1359-1360 (For primary document see N94-20636 05-91)
(Grant NAG9-43)
(Contrib-5241(804)) Avail: CASI HC A01/MF A06

The timing of events leading to the formation of silicate-rich and metal-rich regions in planetesimals remains an important problem in the study of planetary formation and differentiation in the early solar system. The IAB irons are especially important as they are considered to represent a magmatic differentiation series. Iron meteorites present a particular challenge for chronological studies, due to the relative paucity of phases serving as hosts for radioactive parent-daughter nuclides. Recent work using the Re-Os system, following on the pioneering work by Herr et al. and Luck and Allegre, appears promising, but investigators up to now have concentrated on whole rock isochrons. Silicate clasts enclosed within iron meteorites can provide information about the chronology and thermal history of irons. Extensive work on Rb-Sr, K-Ar, and I-Xe has been reported on silicate inclusions in iron meteorites. We report the initial results from our Sm-Nd study of an inclusion with the Caddo IAB iron, the first Sm-Nd isotopic study of a silicate clast embedded within an iron meteorite. Our results include measurements of the standard long-lived Sm-147/Nd-143 (tau = 152 AE) system, as well as the shorter-lived SM-146/Nd-142 (tau = 0.149 AE) system, which has been shown to be very useful in deciphering the history of the early solar system. The Caddo silicate clast was described by Palme et al., who kindly provided us with a major part of the inclusion. The inclusion is coarse-grained consisting predominantly of olivine, clinopyroxene, and plagioclase, with lesser amounts of orthopyroxene, Fe-Ni metal, sulfide, and phosphate. The relatively large grain size (up to 3 mm) and 120 degree grain boundaries suggest extensive metamorphism at high temperatures. Based on study of a thin section, there is evidence for metal invading along grain boundaries in some regions of the inclusion, suggesting that the Fe-Ni metal was molten when the silicate clast was incorporated. Metamorphic recrystallization may have occurred during this event. Author (revised)

N94-20796*# Jet Propulsion Lab., California Inst. of Tech., Pasadena.
PARGA AND HECATE CHASMATA, VENUS: STRUCTURE, VOLCANISM AND MODELS OF FORMATION Abstract Only
Ellen R. Stofan, Victoria E. Hamilton (Occidental Coll., Los Angeles, CA.), and Kristen Cotugno (Massachusetts Univ., Amherst.) *In* Lunar and Planetary Inst., Twenty-Fourth Lunar and Planetary Science Conference. Part 3: N-Z 1993 p 1361-1362 (For primary document see N94-20636 05-91)
Avail: CASI HC A01/MF A06

Linear zones of deformation in the equatorial zone of Venus characterized by extension and volcanism have previously been identified in Pioneer Venus and Arecibo data. Two of these zones, Parga and Hecate Chasmata, are seen in Magellan data to be characterized by systems of fractures along which lie numerous coronae and corona-like features. The relationship between tectonic deformation, corona formation, and volcanism in Parga and Hecate Chasmata is examined using Magellan image and altimetry data. We examine several hypotheses for the origin of these zones, including extension and upwelling and delamination or subduction. In a companion abstract, we examine a section of Hecate Chasma in detail.
Author (revised)

N94-20797*# University of Western Ontario, London. Dept. of Geography.
LINEAR STRUCTURES ON THE SMALL INNER SATELLITES OF SATURN Abstract Only
Philip J. Stooke *In* Lunar and Planetary Inst., Twenty-Fourth Lunar and Planetary Science Conference. Part 3: N-Z 1993 p 1363-1364 (For primary document see N94-20636 05-91)
Avail: CASI HC A01/MF A06

Shape modelling methods developed for non-spherical worlds were applied to four satellites of Saturn: Prometheus, Pandora, Janus, and Epimetheus. This results in the first detailed shaded relief maps of their

surfaces. Ridges and valleys are described with their implications for satellite history and asteroid 951 Gaspra. They probably result from fracturing during break-up of parent bodies and/or later large impacts. Prometheus and perhaps Gaspra may be coated with debris from parent body fragmentation as well as more recent regolith. These four satellites are covered by relatively few useful images, so the shapes are imperfectly known and positions of features on maps may be wrong by up to a few tens of degrees in some areas (worst where a feature is seen only near a limb). Nevertheless, these shape models are more useful than the previous triaxial ellipsoid models. Author (revised)

N94-20798*# National Museum of Natural History, Paris (France).
THE AGE OF THE PRETORIA SALTPAN IMPACT CRATER, SOUTH AFRICA Abstract Only **c46**
Dieter Storzer, Christian Koeberl (Wien Univ., Austria.), and Wolf Uwe Reimold (Witwatersrand Univ., Johannesburg, South Africa.) *In* Lunar and Planetary Inst., Twenty-Fourth Lunar and Planetary Science Conference. Part 3: N-Z 1993 p 1365-1366 (For primary document see N94-20636 05-91)
Avail: CASI HC A01/MF A06

The Pretoria Saltpan impact crater, situated about 40 km NNW of Pretoria, South Africa, has a diameter of about 1.13 km. The structure was formed in 2.05 Ga Nebo granite of the Bushveld Complex. The impact origin of the crater was recently established by the discovery of characteristic shock-metamorphic features in breccias found in drill cores at depths greater than 90 m. Impact glass fragments were recovered by standard magnetic separation techniques and handpicking from the melt breccias. As no reliable crater age was known so far, several hundred sub-millimeter-sized glass fragments were studied for fission tracks. The results show that the Saltpan impact crater has an age of 220 +/- 52 ka. This is in agreement with field geological observations. Author (revised)

N94-20799*# Massachusetts Inst. of Tech., Cambridge. Dept. of Earth, Atmospheric and Planetary Sciences.
THE ROLE OF CO2 IN WEATHERING REACTIONS AND THE PRESENCE OF S2 ON VENUS: IMPLICATIONS FOR THE PYRITE STABILITY FIELD Abstract Only
DArcy W. Straub *In* Lunar and Planetary Inst., Twenty-Fourth Lunar and Planetary Science Conference. Part 3: N-Z 1993 p 1369-1370 (For primary document see N94-20636 05-91)
(Grant NAGw-2220)
Avail: CASI HC A01/MF A06

The stability of pyrite has become the focal point of study, since regions of low radio thermal emissivity were detected during the Pioneer Venus and Magellan radar mapping missions of Venus. Thermodynamic calculations and experimental studies have been performed assuming CO2 is a major contributor to the weathering of sulfides, as CO2 is the major gas species in the Venusian atmosphere. The purpose of the present study, however, is to demonstrate that CO2 is a non-reactive gas and that a minor species, S2, is the most important gas in determining whether pyrite is stable in the high radar reflectivity regions. Author (revised)

N94-20800*# Massachusetts Inst. of Tech., Cambridge. Dept. of Earth, Atmospheric and Planetary Sciences.
THE STABILITY OF OXYAMPHIBOLES: EXISTENCE OF FERRIC-BEARING MINERALS UNDER THE REDUCING CONDITIONS ON THE SURFACE OF VENUS Abstract Only
DArcy W. Straub and Roger G. Burns *In* Lunar and Planetary Inst., Twenty-Fourth Lunar and Planetary Science Conference. Part 3: N-Z 1993 p 1369-1370 (For primary document see N94-20636 05-91)
(Grant NAGw-2220)
Avail: CASI HC A01/MF A06

An enigma of Venusian mineralogy is the suggestion that Fe(3+)-bearing minerals exist under the reducing conditions of the Venusian atmosphere. Analysis of the spectrophotometric data from the Venera 13 and 14 missions, combined with the laboratory reflectance spectral measurements of oxidized basalts at elevated temperatures, led to the suggestion that metastable hematite might exist on Venus. Heating experiments at 475 C when f(sub O2) approximately 10(exp -24) demonstrated that the hematite to magnetite conversion is rapid indicating metastable hematite is not present on Venus. In addition to hematite, several other ferric oxide and silicate minerals have been proposed to occur on Venus, including laihunite or ferrifayalite, Fe(3+)-bearing tephroite, oxyamphiboles, and oxybiotites. Heating experiments performed on these Fe(3+)-bearing minerals under temperature-f(sub O2) conditions existing on Venus suggest that only oxyamphiboles and oxybiotites may be stable on the surface of Venus. Author (revised)

N94-20801*# Arizona Univ., Tucson. Dept. of Planetary Sciences.
PARABOLIC FEATURES AND THE EROSION RATE ON VENUS Abstract Only
Robert G. Strom *In* Lunar and Planetary Inst., Twenty-Fourth Lunar and Planetary Science Conference. Part 3: N-Z 1993 p 1371-1372 (For primary document see N94-20636 05-91)
Avail: CASI HC A01/MF A06

The impact cratering record on Venus consists of 919 craters covering 98 percent of the surface. These craters are remarkably well preserved, and most show pristine structures including fresh ejecta blankets. Only 35 craters (3.8 percent) have had their ejecta blankets embayed by lava and most of these occur in the Atla-Beta Regio region; an area thought to be recently active. parabolic features are associated with 66 of the 919 craters. These craters range in size from 6 to 105 km diameter. The parabolic features are thought to be the result of the deposition of fine-grained ejecta by winds in the dense venusian atmosphere. The deposits cover about 9 percent of the surface and none appear to be embayed by younger volcanic materials. However, there appears to be a paucity of these deposits in the Atla-Beta Regio region, and this may be due to the more recent volcanism in this area of Venus. Since parabolic features are probably fine-grain, wind-deposited ejecta, then all impact craters on Venus probably had these deposits at some time in the past. The older deposits have probably been either eroded or buried by eolian processes. Therefore, the present population of these features is probably associated with the most recent impact craters on the planet. Furthermore, the size/frequency distribution of craters with parabolic features is virtually identical to that of the total crater population. This suggests that there has been little loss of small parabolic features compared to large ones, otherwise there should be a significant and systematic paucity of craters with parabolic features with decreasing size compared to the total crater population. Whatever is erasing the parabolic features apparently does so uniformly regardless of the areal extent of the deposit. The lifetime of parabolic features and the eolian erosion rate on Venus can be estimated from the average age of the surface and the present population of parabolic features. Author (revised)

N94-20802*# Arizona Univ., Tucson. Lunar and Planetary Lab.
TRITON'S CRATERING RECORD AND ITS TIME OF CAPTURE Abstract Only
R. G. Strom and S. K. Croft *In* Lunar and Planetary Inst., Twenty-Fourth Lunar and Planetary Science Conference. Part 3: N-Z 1993 p 1373-1374 (For primary document see N94-20636 05-91)
Avail: CASI HC A01/MF A06

Recent impact crater counts on the Voyager 2 high resolution images of Triton have resulted in a more accurate crater size/frequency distribution down to about 3 km diameter. These counts reveal a size/frequency distribution characterized by a differential -4 slope. This is consistent with the observation that there are no craters larger than 27 km diameter on the 20 percent of Triton viewed at resolutions capable of detecting them. A -4 slope is deficient in large craters and at the very low crater density on Triton no craters larger than about 30 km are expected on just 20 percent of the satellite. The Triton size distribution is significantly different from the differential -3 slope of the fresh crater population on Miranda, but both show leading/trailing asymmetries. Since Miranda is in prograde orbit this crater population is probably due to objects in heliocentric orbit, i.e., comets. If this crater population is due to comets, then the significantly different crater population on Triton is probably due to some other population of impacting objects. The most likely origin of these objects is planetesimals in planetocentric orbits. Because Triton is in retrograde orbit, objects in prograde planetocentric orbits will also produce a leading/trailing asymmetry. If the Triton craters are largely the result of objects in planetocentric orbit, then where are the comet craters that should be there if they have a differential -3 distribution function as inferred from the Miranda fresh crater population? The most likely answer is that they are there, but at such a low density that they can not be distinguished from the planetocentric population. An upper bound on this density can be estimated by determining

the density of a crater population with a differential -3 slope where no craters larger than 27 km would be expected on the 20 percent of Triton viewed by Voyager at resolutions sufficient to detect them. This density is at the density of the largest crater. At this density the number of craters in size bins greater than 27 km is less than 1 for a -3 distribution function. The observed size distribution, the upper limit of the hypothetical comet crater size distribution, and the difference between the observed and the hypothetical comet crater populations is shown. Author (revised)

N94-20803*# Brown Univ., Providence, RI. Dept. of Geological Sciences.
ARE PLINIAN TYPE ERUPTIONS POSSIBLE ON VENUS? Abstract Only
Seiji Sugita and Takafumi Matsui (Tokyo Univ., Japan.) *In* Lunar and Planetary Inst., Twenty-Fourth Lunar and Planetary Science Conference. Part 3: N-Z 1993 p 1375-1376 (For primary document see N94-20636 05-91)
Avail: CASI HC A01/MF A06

Calculations of dynamics of eruption plumes in the Venusian atmosphere reveal the following results: (1) conditions for a convective eruption column are very limited on Venus with required magma temperatures higher than 1100 K; otherwise pyroclastic flows form; (2) once a convective eruption column is established, it may extend as high as about the tropopause (approximately 60 km); and (3) critical eruption velocities for a convective eruption column as a function of temperature and gas content of magma may provide a useful tool for estimating interior condition of Venus, including its volatile inventory. Volcanism is a major process to transport volatile from mantle of a planet to its surface (degassing) as well as heat and mass, all of which affect planetary evolution. For example, after completion of planetary accretion, volcanism is the dominant continuous degassing process for all the terrestrial planets. Explosive volcanism is a very important process for mantle degassing due to its high magma gas content. Consequently, eruption styles and the controlling physical processes need to be understood. Recent satellite and terrestrial ground-based observations suggest existence of explosive volcanism on Venus even though explosive volcanism is very difficult to occur on Venus due to its high atmospheric pressure. The purpose is to investigate dynamics of explosive eruption on Venus and the relation between eruption conditions such as gas content and temperature of magma and eruption velocity, and eruption styles such as Plinian type and pyroclastic flow type. Author (revised)

N94-20804*# Tokyo Univ. (Japan). Dept. of Earth and Planetary Physics.
IMPLANTATION OF NITROGEN: EFFECTS OF HYDROGEN AND IMPLANTATION ENERGY Abstract Only **c25**
Naoji Sugiura, Tsuneji Futagami (Japan Atomic Energy Research Inst., Tokyo.), and Siro Nagai (Japan Atomic Energy Research Inst., Tokyo.) *In* Lunar and Planetary Inst., Twenty-Fourth Lunar and Planetary Science Conference. Part 3: N-Z 1993 p 1377-1378 (For primary document see N94-20636 05-91)
Avail: CASI HC A01/MF A06

To solve the question on solar nitrogen in lunar soils, i.e. variation in isotopic composition and apparently high retentivity compared with rare gases, nitrogen implantation experiments were conducted. At the Meteoritical Society Meeting in Copenhagen, the results of stepped combustion of implanted nitrogen in ilmenite and olivine were presented. The degassing behavior of nitrogen (and also Ar) was quite different from that observed in the case of lunar soils. Extraction temperatures are higher (greater than 1100 C for ilmenite and 1500 C for olivine) than that for lunar soils. Both nitrogen and Ar seem to be retained at the same efficiency. Therefore, additional experiments were conducted to make degassing behavior of nitrogen more close to that observed in the case of lunar soils.
Author (revised)

N94-20805*# Brown Univ., Providence, RI. Dept. of Geological Sciences.
DETERMINING THE COMPOSITION OF OLIVINE ON ASTEROIDAL SURFACES Abstract Only **c25**
Jessica M. Sunshine and Carle M. Pieters *In* Lunar and Planetary Inst., Twenty-Fourth Lunar and Planetary Science Conference. Part 3: N-Z 1993 p 1379-1380 (For primary document see N94-20636 05-91)
(Grant NAGw-28)
Avail: CASI HC A01/MF A06

Olivine was remotely identified as a major component on many S- and A-type asteroids based on qualitative analyses of broad absorption features near 1.0 micron in their telescopic reflectance spectra. Laboratory studies showed that this diagnostic olivine absorption feature is composed of three individual absorption bands resulting from electronic transitions of Fe(+2) in distorted M1 and M2 sites. Both the overall absorption feature and each of the individual absorption bands are also known to vary systematically as a function of olivine composition. Thus, it should be possible to remotely determine the composition of olivine present on the surfaces of the various olivine-rich asteroids. However, extrapolation of laboratory studies to compositional interpretation of asteroid spectra is complicated by several factors: observational noise; lower spectral resolution; compositional heterogeneities (including the presence of other phases such as pyroxenes and/or metal); and the effects of alteration processes. In order to address such complex problems, a quantitative approach to spectral analysis, the modified Gaussian model (MGM) was developed by Sunshine et al., which deconvolves spectra into their constituent absorption bands. The MGM, a refinement of the Gaussian model, more accurately adheres to the physical processes involved in electronic transition absorptions. Under the MGM, each spectrum is modeled in log reflectance and energy as a sum of absorption bands superimposed onto a baseline or continuum. Each absorption band is described by three model parameters (center, width, and strength) which can be interpreted and used to infer composition. One of the strengths of the MGM is that it allows compositional information to be extracted directly from measured spectra and is therefore complementary to other approaches to modeling asteroid spectra which require the use of meteorites and/or terrestrial samples as spectral analogs. A quantitative understanding of the properties of olivine absorptions was established by using the MGM to analyze a laboratory suite of spectra spanning a full range of olivine compositions. Author (revised)

N94-20806*# Jet Propulsion Lab., California Inst. of Tech., Pasadena.
DISCOVERY VENERA SURFACE: ATMOSPHERE GEOCHEMISTRY EXPERIMENTS MISSION CONCEPT Abstract Only
Yuri A. Surkov (Academy of Sciences, USSR, Moscow.), James W. Head (Brown Univ., Providence, RI.), Roald Kremnev (Babakin Engineering and Research Center, Moscow, Russia.), and K. T. Nock *In* Lunar and Planetary Inst., Twenty-Fourth Lunar and Planetary Science Conference. Part 3: N-Z 1993 p 1381-1382 (For primary document see N94-20636 05-91)
Avail: CASI HC A01/MF A06

The phenomenal increase in our understanding of Venus provided by the Magellan Mission has raised a series of focused, fundamental scientific questions about the geochemistry of the surface of Venus, the nature of the lower atmosphere, and the relationship of the lower atmosphere and surface. First, surface geochemical measurements from the Venera/Vega spacecraft showed that widely spaced regions of the venusian plains are made of basalts; thus basalts are significant and may be the only component of the venusian crust. But we lack information on the composition of several key elements of Venus geology: (1) Tessera terrain (which may be outcrops of continental-like non-basaltic crustal material) and steep-sided domes/festoons are promising candidates for non-basaltic geochemically evolved material. The composition of the lower part of the Venusian crust is unknown: however, ejecta from large venusian craters provides us with the possibility of sampling this material on the surface; (2) bulk chemistry (structure and dynamics) of the venusian atmosphere are known. The altitude profiles of water vapor content and minor admixtures relevant to redox conditions in the lower atmosphere (less than 20 km altitude) remain uncertain. Lack of that knowledge means that we do not understand the fine chemical structure of the main mass of the Venusian atmosphere; and (3) thermodynamic models predict that igneous materials on the surface of Venus should react with gases of the venusian atmosphere. But because the water vapor content and redox conditions in the lower atmosphere are not well known, we do not understand the nature of venusian weathering: oxidation, sulfatization, carbonatization, and hydration. The answers to these questions are critical to the understanding of Venus, the most Earth-like of the terrestrial planets. Author (revised)

N94-20807*# Chicago Univ., IL. Dept. of Geophysical Sciences.
THE X RAY MICROPROBE DETERMINATION OF CHROMIUM OXIDATION STATE IN OLIVINE FROM LUNAR BASALT AND KIMBERLITIC DIAMONDS Abstract Only **c25**

S. R. Sutton, S. Bajt, M. L. Rivers, and J. V. Smith *In* Lunar and Planetary Inst., Twenty-Fourth Lunar and Planetary Science Conference. Part 3: N-Z 1993 p 1383-1384 (For primary document see N94-20636 05-91)
(Contract NAG9-106; DE-AC02-76CH-00016; NSF EAR-89-15699)
Avail: CASI HC A01/MF A06

The synchrotron x-ray microprobe is being used to obtain oxidation state information on planetary materials with high spatial resolution. Initial results on chromium in olivine from various sources including laboratory experiments, lunar basalt, and kimberlitic diamonds are reported. The lunar olivine was dominated by Cr(2+) whereas the diamond inclusions had Cr(2+/Cr(3+) ratios up to about 0.3. The simpliest interpretation is that the terrestrial olivine crystallized in a more oxidizing environment than the lunar olivine. Author (revised)

N94-20808*# Chicago Univ., IL. Dept. of Geophysical Sciences.
MICROANALYSIS OF IRON OXIDATION STATE IN IRON OXIDES USING X RAY ABSORPTION NEAR EDGE STRUCTURE (XANES) Abstract Only **c25**
S. R. Sutton, J. Delaney (Rutgers Univ., New Brunswick, NJ.), S. Bajt, M. L. Rivers, and J. V. Smith *In* Lunar and Planetary Inst., Twenty-Fourth Lunar and Planetary Science Conference. Part 3: N-Z 1993 p 1385-1386 (For primary document see N94-20636 05-91)
(Contracts NAG9-106; NAG9-104; DE-FG02-92ER-14244; DE-AC02-76CH-00016; NSF EAR-89-15699)
Avail: CASI HC A01/MF A06

An exploratory application of x ray absorption near edge structure (XANES) analysis using the synchrotron x ray microprobe was undertaken to obtain Fe XANES spectra on individual sub-millimeter grains in conventional polished sections. The experiments concentrated on determinations of Fe valence in a suite of iron oxide minerals for which independent estimates of the iron speciation could be made by electron microprobe analysis and x ray diffraction. Author

N94-20809*# California Inst. of Tech., Pasadena. Div. of Geological and Planetary Sciences.
SPH MODELLING OF ENERGY PARTITIONING DURING IMPACTS ON VENUS Abstract Only
T. Takata and T. J. Ahrens *In* Lunar and Planetary Inst., Twenty-Fourth Lunar and Planetary Science Conference. Part 3: N-Z 1993 p 1387-1388 (For primary document see N94-20636 05-91)
Avail: CASI HC A01/MF A06

Impact cratering of the Venusian planetary surface by meteorites was investigated numerically using the Smoothed Particle Hydrodynamics (SPH) method. Venus presently has a dense atmosphere. Vigorous transfer of energy between impacting meteorites, the planetary surface, and the atmosphere is expected during impact events. The investigation concentrated on the effects of the atmosphere on energy partitioning and the flow of ejecta and gas. The SPH method is particularly suitable for studying complex motion, especially because of its ability to be extended to three dimensions. In our simulations, particles representing impactors and targets are initially set to a uniform density, and those of atmosphere are set to be in hydrostatic equilibrium. Target, impactor, and atmosphere are represented by 9800, 80, and 4200 particles, respectively. A Tillotson equation of state for granite is assumed for the target and impactor, and an ideal gas with constant specific heat ratio is used for the atmosphere. Two dimensional axisymmetric geometry was assumed and normal impacts of 10km diameter projectiles with velocities of 5, 10, 20, and 40 km/s, both with and without an atmosphere present were modeled. Author (revised)

N94-20810*# Tokyo Univ. (Japan). Mineralogical Inst.
HYDROTHERMAL ALTERATION EXPERIMENTS OF OLIVINE WITH VARYING Fe CONTENTS: AN ATTEMPT TO SIMULATE AQUEOUS ALTERATION OF THE CARBONACEOUS CHONDRITES Abstract Only **c25**
Koichi Takatori, Kazushige Tomeoka (Kobe Univ., Japan.), Katsuhiro Tsukimura (Geological Survey of Japan, Tsukuba.), and Hiroshi Takeda *In* Lunar and Planetary Inst., Twenty-Fourth Lunar and Planetary Science Conference. Part 3: N-Z 1993 p 1389-1390 (For primary document see N94-20636 05-91)
Avail: CASI HC A01/MF A06

Hydrothermal alteration experiments of olivine powder with several Fe/Mg ratios were carried out under acidic and neutral conditions, and transition electron microscopy (TEM) observations were made on the run products. Well-developed tubular crystals of serpentine (chrysotile) were synthesized from Fo100 under both acidic and neutral conditions, and from Fo92 and Fo80 under acidic condition. Abundance and size of chrysotile apparenlty dependent on the Fe contents of olivine, i.e. with increasing Fe contents, less and smaller chrysotile was formed. Acidity of the solution plays an important role for the formation of chrysotile. Platy and fibrous crystals of phyllosilicate, probably serpentine, were obtained from Fo50 and Fo20 treated under acidic condition, which are most similar to the phyllosilicates in the CI and CM chondrites. Framboidal aggregates of Fe-rich grains (presumably Fe-hydroxide) were formed from Fa100 and Fo20, but no phyllosilicate was formed from Fa100. Author

N94-20811*# Tokyo Univ. (Japan). Mineralogical Inst.
MINERALOGY AND COOLING HISTORY OF MAGNESIAN LUNAR GRANULITE 67415 Abstract Only
Hiroshi Takeda and Masamichi Miyamoto *In* Lunar and Planetary Inst., Twenty-Fourth Lunar and Planetary Science Conference. Part 3: N-Z 1993 p 1391-1392 (For primary document see N94-20636 05-91)
Avail: CASI HC A01/MF A06

Apollo granulite 67415 was investigated by mineralogical techniques to gain better understanding of cooling histories of lunar granulities. Cooling rates were estimated from chemical zoning of olivines in magnesian granulitic clasts by computer simulation of diffusion processes. The cooling rate of 10 deg C/yr obtained is compatible with a model of the granulite formation, in which the impact deposit was cooled from high temperature or annealed, at the depth of about 25 m beneath the surface. Author

N94-20812*# Tokyo Univ. (Japan). Mineralogical Inst.
TI-BEARING OXIDE MINERALS IN LUNAR METEORITE Y793169 WITH THE VLT AFFINITY Abstract Only **c90**
Hiroshi Takeda, Tomoko Arai, and Kazuto Saiki *In* Lunar and Planetary Inst., Twenty-Fourth Lunar and Planetary Science Conference. Part 3: N-Z 1993 p 1393-1394 (For primary document see N94-20636 05-91)
Avail: CASI HC A01/MF A06

Lunar meteorite, Yamato 793169 previously classified as a VLT mare basalt contains considerable amounts of Ti-bearing oxides in the mesostasis area (2 vol. percent). Mineralogical study of these oxides revealed that they are isolated grains of ilmenite, ulvospinel and chromite, which are formed at the last stage of crystallization. Ti/(Ti+Al+Cr) and Cr/(Cr+Al) versus Fe/(Mg+Fe) variations of these phases are not in the same trends as in the low Ti pigeonite basalts of Apollo 12 and 15 in spite of its higher TiO2 contents. Among four lunar meteorites proposed to be samples of mare regions of the Moon, EET87521 and Y793274 are breccias rich in lunar mare components, but Y793169 and A881757 are crystalline rocks composed of Fe-rich pigeonite and plagioclase with affinity to the VLT basalts, despite their higher bulk TiO2 contents than the limit for VLT. Polished think sections (PTS) Y793169,51-3 and A881757,51-4 (Asuka-31) supplied by the National Institute of Polar Research (NIPR) were investigated. Both samples were allocated as parts of two consortium studies. Mineral chemistries and textures were examined by an electron probe micro-analyzer (EPMA) and scanning electron microscope (SEM), JEOL 840A with X-ray chemical map analysis (CMA) utilities. Modal abundances of minerals in Y793169 were obtained from colored backscattered electron (BSE) image of SEM for a particular mineral by a computer and by point analysis for minerals with a similar BSE intensity. Author (revised)

N94-20813*# National Aeronautics and Space Administration. Lyndon B. Johnson Space Center, Houston, TX.
A NEW ANTARCTIC METEORITE WITH CHROMITE, ORTHOPYROXENE AND METAL WITH REFERENCE TO A FORMATION MODEL OF S ASTEROIDS Abstract Only **c90**
Hiroshi Takeda (Tokyo Univ., Japan.), Kazuto Saiki (Tokyo Univ., Japan.), Mayumi Otsuki (Tokyo Univ., Japan.), and Takahiro Hiroi *In* Lunar and Planetary Inst., Twenty-Fourth Lunar and Planetary Science Conference. Part 3: N-Z 1993 p 1395-1396 (For primary document see N94-20636 05-91)
Avail: CASI HC A01/MF A06

Mineralogy of a unique meteorite from Antarctica, EET84302 and the related primitive achondrites, was studied to gain better understanding on relationship between S asteroids and this meteorite group. EET84302

consists of metal-rich (M) region with metal filling interstices of silicate grains of orthopyroxene (Opx), olivine Fa8, plagioclase An24, and augite (Aug), chromite-rich (C) region with major chromite and Opx, and silicate-rich (S) region with mainly Opx. This is the first example of chromite-rich achondrite. Distribution of three areas (C, M, S) are in line with a proposed model of primitive achondrites and S asteroids. Since reflectance spectra of some members of primitive achondrites combined with those of iron meteorites, resemble those of the S asteroids, there is an expectation that S asteroids are modified products of chondrites. The trends of the variations in their mineral assemblages are in line with those of the S asteroids. Hiroi proposed a stony-iron model of S asteroids, which assumes that a few domains of various primitive achondrites are embedded in iron matrix. Polished thin sections (PTS) of EET84302,19 and ALH81187,16 were supplied from Meteorite Working Group (MWG). A previously studied PTS of EET84302 was similar in both texture and mineralogy to silicate inclusions in some iron meteorites. PTS EET84302,19 was studied by electron probe microanalyzer (EPMA) and scanning electron microscope (SEM). The reflectance spectra of EET84302 showed a weathering problem and was not used to match with those of S asteroids. Author (revised)

N94-20814*# Geological Survey, Flagstaff, AZ.
EXTENSIONAL HISTORY OF MARS' THARSIS REGION Abstract Only
Kenneth L. Tanaka and D. John Chadwick *In* Lunar and Planetary Inst., Twenty-Fourth Lunar and Planetary Science Conference. Part 3: N-Z 1993 p 1397-1398 (For primary document see N94-20636 05-91)
Avail: CASI HC A01/MF A06

Graben structures in the outer part of Mars' Tharsis region follow calculated stress patterns that are based on Tharsis topographic and gravity anomalies and flexural response of the lithosphere. However, Tharsis extension is not evenly distributed - most extension is concentrated in the Alba, Tempe, Valles Marineris, and Syria-Thaumasia volcanotectonic provinces. Preliminary results suggest that the overall extension of Tharsis produced by loading is about 8 km (based on the assumption that the Sirenum province exemplifies the overall extension of Tharsis), whereas the total circumferential extension of the Tharsis region estimated thus far is about 33 km (an estimate was not made for the Syria-Thaumasia province, and evidence in some other areas may be buried). It is concluded that local tectonism, possibly caused by intrusion and passive and active rifting, produced most of the extension in the Tharsis region. Author (revised)

N94-20815*# Geological Survey, Flagstaff, AZ.
COMPLEX STRUCTURE OF THE THAUMASIA REGION OF MARS Abstract Only
Kenneth L. Tanaka and James M. Dohm *In* Lunar and Planetary Inst., Twenty-Fourth Lunar and Planetary Science Conference. Part 3: N-Z 1993 p 1399-1400 (For primary document see N94-20636 05-91)
Avail: CASI HC A01/MF A06

The Thaumasia region was the first center of Tharsis tectonism, and it is the most complex and poorly understood. Therefore, a geologic map of the entire Thaumasia region (lat 15 deg to 50 deg S, long 50 deg to 115 deg), at 1:5,000,000 scale is being compiled. This region is mostly made up of the Thaumasia plateau, the highlands are fractured by Thaumasia, southern Claritas, Coracis, Melas, and Nectaris Fossae. Preliminary structural analysis of the most complexly faulted area in the region (the central part, at lat 30 deg to 45 deg S, long 80 deg to 100 deg) indicates that, unlike other regions of Mars, Thaumasia has undergone extensive deformation by both small- and large-scale extensional and compressional structures. These results indicate that the early (Noachian) style of tectonism commonly involved lithospheric-scale deformation, in contrast to most younger tectonism (which mainly affected the upper parts of the crust above mechanical discontinuities); this difference may be due to a weaker (and thus more readily deformable) early lithosphere in this region.
Author (revised)

N94-20816*# Geological Survey, Flagstaff, AZ.
LARGE, ANCIENT, COMPRESSIONAL STRUCTURES ON MARS Abstract Only
Kenneth L. Tanaka and Richard A. Schultz (Nevada Univ., Reno.) *In* Lunar and Planetary Inst., Twenty-Fourth Lunar and Planetary Science Conference. Part 3: N-Z 1993 p 1401-1402 (For primary document see N94-20636 05-91)
Avail: CASI HC A01/MF A06

Our search for large compressional structures similar to the Coprates rise reveals that the rise is part of a group of about three dozen structures (the 'Thaumasia fold belt') that encircles the southern part of the Tharsis region. Similar structures are scattered over Mars. All appear to be Noachian or Early Hesperian in age, suggesting that lithospheric-scale buckling was a common form of early Martian compressional deformation.
Author (revised)

N94-20817*# Baylor Univ., Waco, TX. Dept. of Physics.
DETERMINATION OF PARAMETERS FOR HYPERVELOCITY DUST GRAINS ENCOUNTERED IN NEAR-EARTH SPACE Abstract Only **c90**
William G. Tanner, Carl R. Maag (Science Applications International Corp., Glendora, CA.), W. Merle Alexander, and Patricia Sappenfield *In* Lunar and Planetary Inst., Twenty-Fourth Lunar and Planetary Science Conference. Part 3: N-Z 1993 p 1403-1404 (For primary document see N94-20636 05-91)
Avail: CASI HC A01/MF A06

Primarily interest was in the determination of the population of micrometeoroids and space debris and interpretation of the hole size in a thin film or in a micropore foam returned from space with theoretical calculations describing the event. In order to augment the significance of the theoretical calculations of the impact event, an experiment designed to analyze the charge production due to hypervelocity impacts on thin films also produced data which described the penetration properties of micron and sub-micron sized projectiles. The thin film penetration sites in the 500 A and 1000 A aluminum films were counted and a size distribution function was derived. In the case of the very smallest dust grains, there were no independent measurements of velocities like that which existed for the larger dust grains (d(sub p) is less than or equal to 1 micron). The primary task then became to assess the relationship between the penetration hole and the particle diameter of the projectile which made the hole. The most promising means to assess the measure of the diameters of impacting grains came in the form of comparing cratering mechanics to penetration mechanics. Future experimentation will produce measurements of the cratering as opposed to the penetrating event. Particles encountered by surfaces while being flown in space will degrade that surface in a systematic manner even when the impact is with small hypervelocity particles, d(sub p) is less than or equal to 10 microns. Though not to a degree which would precipitate a catastrophic failure of a system, the degradation of the materials comprising the interconnected system will occur. It is the degradation of the optical system and the subsequent embrittlement of other materials that can lead to degradation if not to failure. It is to this end that research was conducted to compare the primary consequences for experiments which will be flown to those which have been returned.
Author (revised)

N94-20818*# Hawaii Univ., Honolulu. Dept. of Geology and Geophysics.
TUMULI AND TUBES: TEACHING SCIENTIFIC TECHNIQUES Abstract Only **c80**
Michelle J. Tatsumura, G. J. Taylor, and P. J. Mouginis-Mark *In* Lunar and Planetary Inst., Twenty-Fourth Lunar and Planetary Science Conference. Part 3: N-Z 1993 p 1405-1406 (For primary document see N94-20636 05-91)
(Grant NAGw-2955)
Avail: CASI HC A01/MF A06

Planetary and space science is the best way to teach basic chemistry, physics, and math. Einstein once said that 'man is drawn to the mysterious and it is from that that we achieve true art and science.' Planets and the processes that shape them are especially mysterious and fascinating to students, young and old, and because of this planetary geology kindles interest that draws them further into the world of science. At the very least, they are engaged enough to learn how science works, a key ingredient in scientific literacy. A project involving field measurements on Kilauea volcano, Hawaii, by a Geology 101 honors class is described. Hawaii is blessed with spectacular, active, accessible, and relatively safe basaltic eruptions. The study of volcanoes, the landforms they produce, and the processes that operate on and in volcanoes, combined with the study of volcanoes on the other planets, is an excellent way to link aspects of Hawaiian geology to the planets. During the past year we have taken advantage of our setting to organize a NASA field workshop for junior investigators and senior graduate students, made field trips and planetary

volcanism the centerpieces of our annual Summer Workshop for Teachers, and led a field trip around Kilauea Volcano during the Challenger Center Faculty Development conference, held on the island of Hawaii last summer. An activity for the honors Geology 101 class (all undergraduates) at the University of Hawaii is presently being planned. Our goal is to give them some hands on experience working on a field project and applying what they have learned to planetary volcanoes. The work will include qualitative observations and quantitative measurements on volcanic lava flows. Follow-up activities will involve data analysis. The trip requires planning (at least 3 months before hand) everything from accommodations and insurance to the actual activities we will be doing. Our goal is to stimulate interest and awareness in the students' surroundings, in this case, volcanoes, and to include planetary applications and how studies of terrestrial geology greatly aids studies of the other planets. Two studies are planned both of which are active research projects being conducted by the authors. These projects, tumuli in pahoehoe flow fileds and lava tube cross-secational areas, are described. Author (revised)

N94-20819*# National Aeronautics and Space Administration. Lyndon B. Johnson Space Center, Houston, TX.

SPARKING YOUNG MINDS WITH MOON ROCKS AND METEORITES Abstract Only **c80**

G. Jeffrey Taylor (Hawaii Univ., Honolulu.) and Marilyn M. Lindstrom *In* Lunar and Planetary Inst., Twenty-Fourth Lunar and Planetary Science Conference. Part 3: N-Z 1993 p 1407 (For primary document see N94-20636 05-91)

Avail: CASI HC A01/MF A06

What could be more exciting than seeing pieces of other worlds? The Apollo program left a legacy of astounding accomplishments and precious samples. Part of the thrill of those lunar missions is brought to schools by the lunar sample educational disks, which contain artifacts of six piloted trips to the Moon. Johnson Space Center (JSC) is preparing 100 new educational disks containing pieces of meteorites collected in Antarctica. These represent chunks of several different asteroids, that were collected in one of the most remote, forbidding environments on Earth. These pieces of the Moon and asteroids represent the products of basic planetary processes (solar nebular processes, initial differentiation, volcanism, and impact), and, in turn, these processes are controlled by basic physical and chemical processes (energy, energy transfer, melting, buoyancy, etc.). Thus, the lunar and meteorite sample disks have enormous educational potential. New educational materials are being developed to accompany the disks. Present materials are not as effective as they could be, especially in relating samples to processes and to other types of data such as spectral studies and photogeology. Furthermore, the materials are out of date. New background materials will be produced for teachers, assembling slide sets with extensive captions, and devising numerous hands-on classroom activities to do while the disks are at a school and before and after they arrive. The classroom activities will be developed by teams of experienced teachers working with lunar and meteorite experts. Author (revised)

N94-20820*# National Aeronautics and Space Administration. Lyndon B. Johnson Space Center, Houston, TX.

EVALUATION OF LUNAR ROCKS AND SOILS FOR RESOURCE UTILIZATION: DETAILED IMAGE ANALYSIS OF RAW MATERIALS AND BENEFICIATED PRODUCTS Abstract Only

Lawrence A. Taylor (Tennessee Univ., Knoxville.), John G. Chambers (Tennessee Univ., Knoxville.), Allan Patchen (Tennessee Univ., Knoxville.), Eric A. Jerde (Tennessee Univ., Knoxville.), David S. McKay, John Graf, and Robin R. Oder (Exportech Co., Inc., New Kensington, PA.) *In* Lunar and Planetary Inst., Twenty-Fourth Lunar and Planetary Science Conference. Part 3: N-Z 1993 p 1409-1410 (For primary document see N94-20636 05-91)

Avail: CASI HC A01/MF A06

The rocks and soils of the Moon will be the raw materials for fuels and construction needs at a lunar base. This includes sources of materials for the generation of hydrogen, oxygen, metals, and other potential construction materials. For most of the bulk material needs, the regolith, and its less than 1 cm fraction, the soil, will suffice. But for specific mineral resources, it may be necessary to concentrate minerals from rocks or soils, and it is not always obvious which is the more appropriate feedstock. Besides an appreciation of site geology, the mineralogy and petrography of local rocks and soils is important for consideration of the resources which can provide feedstocks of ilmenite, glass, agglutinates, anorthite, etc. In such studies, it is very time-consuming and practically impossible to correlate particle counts (the traditional method of characterizing lunar soil petrography) with accurate modal analyses and with mineral associations in multi-mineralic grains. But x ray digital imaging, using x rays characteristic of each element, makes all this possible and much more (e.g., size and shape analysis). An application of beneficiation image analysis, in use in our lab (Oxford Instr. EDS and Cameca SX-50 EMP), was demonstrated to study mineral liberation from lunar rocks and soils. Results of x ray image analysis are presented. Author (revised)

N94-20821*# Tennessee Univ., Knoxville. Dept. of Geological Sciences.

PRODUCTION OF O2 ON THE MOON: A LAB-TOP DEMONSTRATION OF ILMENITE REDUCTION WITH HYDROGEN Abstract Only

Lawrence A. Taylor, Eric A. Jerde, David S. McKay, Michael A. Gibson (Carbotek, Inc., Houston, TX.), Christian W. Knudsen (Carbotek, Inc., Houston, TX.), and Hiroshi Kanamori (Shimizu Corp., Japan.) *In* Lunar and Planetary Inst., Twenty-Fourth Lunar and Planetary Science Conference. Part 3: N-Z 1993 p 1411-1412 (For primary document see N94-20636 05-91)

Avail: CASI HC A01/MF A06

Estimates of the costs of transporting materials from Earth to the Moon are around $25,000 per pound. Therefore, it is imperative that we learn to utilize the resources on the Moon to partially offset these 'astronomical' expenses. The production of oxygen on the Moon utilizing indigenous materials is crucial to the establishment and development of an autonomous lunar colony. Besides obvious biologic needs, this lunar liquid oxygen (LLOX) could result in tremendous cost savings on fuel for effective transportation systems, particularly with its export to low-Earth orbit. Over 20 different process concepts were proposed and evaluated for the production of oxygen from lunar materials. Simplicity, low energy, easily attainable feedstock, and low resupply mass are the keywords for the process(es) which will ultimately be selected for the initial production of oxygen on the Moon. One of these schemes, which has received considerable study to date, is the hydrogen reduction of ilmenite. In fact, Carbotek, Inc. (Houston, TX) patented an ilmenite, hydrogen-reduction technique involving a three-stage, fluidized-bed process for the production of LLOX. A lab-top demonstration unit of the basic concepts of this oxygen generation process that was constructed by our group at the University of Tennessee is explained. It utilizes many of the principles which must be addressed in designing an effective production plant for operation on the Moon. Author (revised)

N94-20822*# Australian National Univ., Canberra. Dept. of Nuclear Physics.

THE Mg-SUITE AND THE HIGHLAND CRUST: AN UNSOLVED ENIGMA Abstract Only

Stuart Ross Taylor, Marc D. Norman (Hawaii Univ., Honolulu.), and Tezer M. Esat *In* Lunar and Planetary Inst., Twenty-Fourth Lunar and Planetary Science Conference. Part 3: N-Z 1993 p 1413-1414 (For primary document see N94-20636 05-91)

Avail: CASI HC A01/MF A06

Most of the rocks returned from the highlands are polymict breccias, pulverized by the massive bombardment. However, some monomict breccias with low siderophile element contents are considered to be 'pristine' rocks that represent the original igneous components making up the highland crust. Three principal pristine constituents make up the lunar highland crust: ferroan anorthosites, the Mg-suite, and KREEP. A discussion of these three constituents is presented. Author (revised)

N94-20823*# Belorussian State Univ., Minsk (Belarus).

THE SAND BAG MODEL OF THE DISPERSION OF THE COSMIC BODY IN THE ATMOSPHERE Abstract Only **c90**

A. V. Teterev and I. V. Nemchinov (Academy of Sciences, USSR, Moscow.) *In* Lunar and Planetary Inst., Twenty-Fourth Lunar and Planetary Science Conference. Part 3: N-Z 1993 p 1415-1416 (For primary document see N94-20636 05-91)

Avail: CASI HC A01/MF A06

The strength of the extraterrestrial bodies depends on their structure, composition, dimensions, and the history of this body. The fragmentation of the body due to aerodynamic stresses begins at sufficiently large heights above the surface of the Earth. The process of fragmentation and dispersion

of the fragments usually is studied by the hydrodynamic or even gasdynamic models. If the fragmentation process begins due to the initial cracks and faults of the body, or this body consists of large boulders glued by ice, the strength of these boulders after fragmentation remains higher than the aerodynamic stresses exerted at the remaining part of the body. It is supposed that fragmentation occurs at initial moment t = 0 at some height z(sub o) above the surface of the air, these fragments remain solid. The possibility of further fragmentation during the remaining part of the trajectory is not taken into account. If the number of these parts is large enough and their size is small in comparison to the initial radius of the body than we can use the sand bag model proposed in qualitative form.

Author (revised)

N94-20824*# Belorussian State Univ., Minsk (Belarus).

ATMOSPHERIC BREAKUP OF A SMALL COMET IN THE EARTH'S ATMOSPHERE Abstract Only **c90**

A. V. Teterev, N. I. Misychenko, L. V. Rudak, G. S. Romanov (Institute of Heat and Mass Transfer, Minsk, Belarus.), A. S. Smetannikov (Institute of Heat and Mass Transfer, Minsk, Belarus.), and I. V. Nemchinov (Academy of Sciences, USSR, Moscow.) *In* Lunar and Planetary Inst., Twenty-Fourth Lunar and Planetary Science Conference. Part 3: N-Z 1993 p 1417-1418 (For primary document see N94-20636 05-91)

Avail: CASI HC A01/MF A06

The aerodynamic stresses can lead to the deformation and even to destruction of the meteoroids during their flight through the atmosphere. The pressure at the blunt nose of the cosmic body moving at very high speed through the dense layers of the atmosphere may be much larger than the tensile or the compressive strength of the body. So the usage of the hydrodynamics theory is validated. The estimates show that the transverse velocity of the substance of the body U is of the order of (rho(sub a)/rho(sub o))(sup 1/2)V where V is the velocity of the body and rho(sub o) is its density, rho(sub a) is the density of the atmosphere. The separation of the fragments is larger than the diameter of the body D if D is less than D(sub c) = 2H(square root of rho(sub a)/rho(sub o)), where H is the characteristic scale of the atmosphere. For an icy body one obtains U = 1/30(V) and critical diameter D(sub C) = 500 m. The process of the disintegration of the body is still not fully understood and so one can use the numerical simulation to investigate it. Such simulations where conducted for the Venusian atmosphere and the gaseous equation of state of the body was used. For the Earth atmosphere for the velocity V = 50 km/s the pressure at the blunt nose of the body is 25 kbar, and is of the order of bulk modulus of compressibility of the water or ice. The realistic EOS of water in tabular form was used. It was assumed that the initial shape of the body was spherical and the initial diameter D(sub o) of the body is 200 m and so it is smaller than the critical diameter D(sub C). The initial kinetic energy of the icy body is equivalent to the energy of the explosion 1200 Mt of TNT. The results of the simulation of the deformation of the body during its vertical flight through the atmosphere and during its impact into the ocean are presented.

Author (revised)

N94-20825*# Houston Univ., TX. Dept. of Geosciences.

ORIGINAL SIZE OF THE VREDEFORT STRUCTURE, SOUTH AFRICA Abstract Only **c46**

A. M. Therriault, A. M. Reid, and W. U. Reimold (Witwatersrand Univ., Johannesburg, South Africa.) *In* Lunar and Planetary Inst., Twenty-Fourth Lunar and Planetary Science Conference. Part 3: N-Z 1993 p 1419-1420 (For primary document see N94-20636 05-91)

Avail: CASI HC A01/MF A06

The Vredefort structure is located approximately 120 km southwest of Johannesburg, South Africa, and is deeply eroded. Controversies remain on the origin of this structure with the most popular hypotheses being: (1) by impact cratering about 2.0 Ga; (2) as a cryptoexplosion structure about 2.0 Ga; and (3) by purely tectonic processes starting at about 3.0 Ga and ending with the Vredefort event at 2.0 Ga. In view of recent work in which the granophyre dikes are interpreted as the erosional remants of a more extensive impact melt sheet, injected downward into the underlying country rocks, the impact origin hypothesis for Vredefort is adopted. In order to estimate the original dimensions of the Vredefort impact structure, it is assumed that the structure was initially circular, that its predeformation center corresponds to the center of the granitic core, and that the pre-Vredefort geology of the area prior to approximately 2.0 Ga ago is as suggested by Fletcher and Reimold. The spatial relationship between shock metamorphic effects, the shock pressures they record, and the morphological features of the crater were established for a number of large terrestrial craters. The principles of crater formation at large complex impact structures comparable in size to Vredefort were also established, although many details remain unresolved. An important conclusion is that the transient crater, which is formed directly by excavation and displacement by the shock-induced cratering flow-field (i.e., the particle velocity flow field existing in the region of the transient crater but behind the initial outgoing shock front), is highly modified during the late stage processes. The original transient crater diameter lies well within the final rim of the crater, which is established by structural movements during late-stage cavity modification.

Author (revised)

N94-20826*# Houston Univ., TX. Dept. of Geosciences.

ORIGIN OF THE VREDEFORT STRUCTURE, SOUTH AFRICA: IMPACT MODEL Abstract Only **c46**

A. M. Therriault, A. M. Reid (McMaster Univ., Hamilton, Ontario.), and W. U. Reimold (Witwatersrand Univ., Johannesburg, South Africa.) *In* Lunar and Planetary Inst., Twenty-Fourth Lunar and Planetary Science Conference. Part 3: N-Z 1993 p 1421-1422 (For primary document see N94-20636 05-91)

Avail: CASI HC A01/MF A06

A model is presented for the evolution of the Vredefort structure, based on reasoned constraints on the original size of the Vredefort structure from observational data and comparison with other terrestrial impact craters. The models for complex craters (ring and multi-ring basins) of Croft, Grieve, and co-workers, and Schultz and co-workers, were used to reconstruct the Vredefort impact event, using a final crater diameter of 300 km, as estimated by Therriault. The sequence of events (stages 2-5) is illustrated diagramatically. The stages are: initial penetration, excavation and compression, dynamic rebound and uplift, maximum radial growth and collapse, and final crater form.

Author (revised)

N94-20827*# Cologne Univ. (Germany).

SYNOPTIC OBSERVATIONS OF NEAR SURFACE PROCESSES OF AN INSOLATED ICE-DUST BODY UNDER SPACE CONDITIONS: THE CASE OF KOSI 9 AND 10 Abstract Only **c90**

K. Thiel, G. Koelzer, E. Lorenz (Deutsche Forschungsanstalt fuer Luft- und Raumfahrt, Berlin, Germany.), H. Kochan (Deutsche Forschungsanstalt fuer Luft- und Raumfahrt, Cologne, Germany.), J. Gebhard (Max-Planck-Inst. fuer Kernphysik, Heidelberg, Germany.), and E. Gruen (Max-Planck-Inst. fuer Kernphysik, Heidelberg, Germany.) *In* Lunar and Planetary Inst., Twenty-Fourth Lunar and Planetary Science Conference. Part 3: N-Z 1993 p 1423-1424 (For primary document see N94-20636 05-91)

Avail: CASI HC A01/MF A06

The recent experiments of the Comet Simulation Project, KOSI 9 and KOSI 10, for the first time yielded synoptic results of physically correlated phenomena near the surface of insolated porous ice dust mixtures (90% H2O, 10% olivine, 0.1% fine dispersed carbon, sample mean density 0.40 +/- 0.001 g/cm(sup 3)) under space conditions. Correlations were observed e.g. between (1) grain size of emitted dust and dust mantle formation; (2) surface avalanches and local surface temperature; and (3) lateral variations of the surface temperature and the thickness of the dust mantle at the end of the experiment. The dynamic surface processes and the observed structural parameters of the dust mantle and the emitted mineral residues are discussed in view of real comets.

Author (revised)

N94-20828*# National Aeronautics and Space Administration. Lyndon B. Johnson Space Center, Houston, TX.

COMETARY INTERPLANETARY DUST PARTICLES? AN UPDATE ON CARBON IN ANHYDROUS IDPS Abstract Only **c90**

K. L. Thomas (Lockheed Engineering and Sciences Co., Houston, TX.), L. P. Keller, G. E. Blanford (Houston Univ., TX.), and D. S. McKay *In* Lunar and Planetary Inst., Twenty-Fourth Lunar and Planetary Science Conference. Part 3: N-Z 1993 p 1425-1426 (For primary document see N94-20636 05-91)

Avail: CASI HC A01/MF A06

Chondritic anhydrous interplanetary dust particles (IDP's) are widely considered to be the most pristine samples available for the study of the early solar system because of their primitive mineralogy, chemistry, and isotopic characteristics. Previously, anhydrous IDP's were analyzed quantitatively for light elements and found that these particles have

significantly higher bulk carbon abundances than known chondritic meteorites. A relationship between carbon abundance and silicate mineralogy was also identified which, in general, shows that particles dominated by pyroxenes have a higher carbon abundance than those dominated by olivines. Particles containing equal amounts of olivine and pyroxene show a range of carbon contents and can be grouped with either the pyroxene- or olivine-dominated particles based on their carbon abundance. It was suggested that high carbon pyroxene-rich IDP's are derived from cometary sources. Bulk compositions and mineralogy of our additional IDP's were determined; one particle has the highest carbon abundance reported in IDP's or any other chondritic material, with the possible exception of the carbon-rich Halley particles. Author (revised)

N94-20829*# Jet Propulsion Lab., California Inst. of Tech., Pasadena.
MAGELLAN MISSION Abstract Only Progress Report c12
Thomas W. Thompson *In* Lunar and Planetary Inst., Twenty-Fourth Lunar and Planetary Science Conference. Part 3: N-Z 1993 p 1427-1428 (For primary document see N94-20636 05-91)
Avail: CASI HC A01/MF A06

The Magellan spacecraft was launched from Cape Kennedy on 4 May 1989 and was inserted into orbit around Venus on 10 Aug. 1990. The Magellan spacecraft carries a radar instrument that makes synthetic aperture radar (SAR) images of the surface, measures the altitude of the Venusian surface directly below the spacecraft, and obtains radiometric observations of the surface. Radar and radiometric observations of the Venusian surface commenced on 15 Sep. 1990 and continued until 15 Sep. 1992. Gravity observations began on 24 Sep. 1992 and will continue until late May 1993. The radar observations produced SAR images and surface topography for 99 percent of the surface. These radar observations support the objective of improving the knowledge of the geological history of Venus by analysis of surface morphology and the processes that control them. The gravity observations that are being conducted now support the Magellan objective of improving the knowledge of the geophysics of Venus, principally its density distribution and dynamics. Also, Magellan generated more digital planetary image data than all previous planetary missions.
Author (revised)

N94-20830*# Open Univ., Milton (England). Dept. of Earth Sciences.
DISCHARGE RATES IN MA'ADIM VALLIS, MARS Abstract Only
G. D. Thornhill, D. A. Rothery, J. B. Murray, T. Day (University Coll., London, England.), A. C. Cook (University Coll., London, England.), J-P. Muller (University Coll., London, England.), and J. C. Iliffe (University Coll., London, England.) *In* Lunar and Planetary Inst., Twenty-Fourth Lunar and Planetary Science Conference. Part 3: N-Z 1993 p 1429-1430 (For primary document see N94-20636 05-91)
Avail: CASI HC A01/MF A06

A digital elevation model (DEM) of a small part of the Martian channel Ma'adim Vallis was produced using the Frankot and Chellappa shape-from-shading algorithm. Software developed by the Dept. of Photogrammetry and Surveying at University College London uses this technique to extract slope information from the grey levels of image pixels. This technique was applied to a Viking Orbiter image of part of Ma'adim Vallis, and measurements of the channel depth and bed-slope of a channel incised into the floor of Ma'adim Vallis were made. These results were used to calculate order of magnitude estimates for discharge rates through the channel. The maximum values calculated are three orders of magnitude less than those for N. Kasei Vallis and are similar to values cited for the Missoula floods. However, when more realistic values of the water depth are used, discharge rates comparable with those for the Mississippi River result. Author (revised)

N94-20831*# Brown Univ., Providence, RI. Dept. of Geological Sciences.
OBJECTIVE DETERMINATION OF IMAGE END-MEMBERS IN SPECTRAL MIXTURE ANALYSIS Abstract Only c25
Stefanie Tompkins, John F. Mustard, Carle M. Pieters, and Donald W. Forsyth *In* Lunar and Planetary Inst., Twenty-Fourth Lunar and Planetary Science Conference. Part 3: N-Z 1993 p 1431-1432 (For primary document see N94-20636 05-91)
Avail: CASI HC A01/MF A06

Spectral mixture analysis was shown to be a powerful, multifaceted tool for analysis of multi- and hyper-spectral data. The essence of the first phase of the approach is to determine a set of image end-members that best account for the spectral variance in an image cube within a constrained, linear least squares mixing model. The selection of the image end-member is usually achieved using a priori knowledge and successive trial and error solutions to refine the total number and physical location of the end-members. However, in many situations a more objective method of determining these essential components is desired. The problem of image end-member determination was approached objectively by using the inherent variance of the data. Unlike purely statistical methods such as factor analysis, this approach derives solutions that conform to a physically realistic model. Author (revised)

N94-20832*# Brown Univ., Providence, RI. Dept. of Geological Sciences.
DISTRIBUTION AND GEOLOGIC HISTORY OF MATERIALS EXCAVATED BY THE LUNAR CRATER BULLIALDUS Abstract Only
Stefanie Tompkins, Carle M. Pieters, and John F. Mustard *In* Lunar and Planetary Inst., Twenty-Fourth Lunar and Planetary Science Conference. Part 3: N-Z 1993 p 1433-1434 (For primary document see N94-20636 05-91)
Avail: CASI HC A01/MF A06

The crater Bullialdus is a 61 km, Eratosthenian-age impact crater located on the western edge of Mare Nubium. Previous analysis of the spatial distribution of materials in the area using nine telescopic near-infrared spectra suggested a possible three-layer structure prior to the impact event: two shallow gabbroic layers and one deeper noritic layer (from a potential depth of 5.5 km). The initial interpretation of this stratigraphy was that Bullialdus may have tapped a layered mafic pluton, such as have been invoked to explain the existence of Mg-suite rocks. High-spatial resolution CCD images of Bullialdus were analyzed to better map the spatial distribution of the observed lithologies, and to assess the plausibility of the pluton interpretation. Author (revised)

N94-20833*# Arizona Univ., Tucson.
CORE FORMATION BY GIANT IMPACTS: CONDITIONS FOR INTACT MELT REGION FORMATION Abstract Only c46
W. B. Tonks and H. J. Melosh *In* Lunar and Planetary Inst., Twenty-Fourth Lunar and Planetary Science Conference. Part 3: N-Z 1993 p 1435-1436 (For primary document see N94-20636 05-91)
Avail: CASI HC A01/MF A06

Among the many effects of high-speed, giant impacts is widescale melting that can potentially trigger catastrophic core formation. If the projectile is sufficiently large, the melt pools to form an intact melt region. The dense phase then segregates from the melt, forming a density anomoly at the melt region's base. If the anomoly produces a differential stress larger than a certain minimum, it overcomes the mantle's long-term elastic strength and rapidly forms a core. It was previously shown that giant impacts effectively trigger core formation in silicate bodies by the time they grow to the mass of Mercury and in icy bodies by the time they grow larger than Triton. In order for this process to be viable, an intact melt region must be formed. Conditions under which this occurs is examined in more detail than previously published. Author (revised)

N94-20834*# Geological Survey, Denver, CO.
THE U-Th-Pb, Sm-Nd, AND Ar-Ar ISOTOPIC SYSTEMATICS OF LUNAR METEORITE YAMATO-793169 Abstract Only c90
Noriko Torigoye, Keji Misawa, G. Brent Dalrymple (Geological Survey, Menlo Park, CA.), and Mitsunobu Tatsumoto *In* Lunar and Planetary Inst., Twenty-Fourth Lunar and Planetary Science Conference. Part 3: N-Z 1993 p 1437-1438 (For primary document see N94-20636 05-91)
Avail: CASI HC A01/MF A06

U-Th-Pb, Sm-Nd, and (Ar-40)-(Ar-39) isotopic studies were performed on Yamato (Y)-793169, an unbrecciated diabasic lunar meteorite whose chemical composition is close to low Ti(LT) and very low-Ti (VLT) mare basalts. The isotopic data indicate that the meteorite was formed earlier than 3.9 Ga from a source with low U/Pb and high Sm/Nd and was distributed by a thermal event at 751 Ma. due to the small sample size (104 mg), a plagioclase crystal and glass grains were handpicked for Ar analysis, leaving four fractions for the U-Th-Pb and Sm-Nd studies; a fine-grained fraction (less than 63 microns; Fine) and three medium-grained fractions (63-150 microns). Medium-grained fractions were divided by density; a heavy fraction (rho greater than 3.3) consisting mainly of pyroxene (PX1),

a lighter fraction (rho less than 2.8) consisting of plagioclase (PL), and a middle density fraction (predominantly pyroxene; PX2). The fractions were washed with acetone and alcohol, and then leached in 0.01 HBr and 0.1N HBr in order to remove any terrestrial Pb contamination. Analysis of the HBr leaches revealed that this meteorite was heavily contaminated with terrestrial Pb during its residence in Antarctic ice. Author (revised)

N94-20835*# Oulu Univ. (Finland). Dept. of Astronomy.
COMPLEX RIDGED TERRAIN-RELATED RIDGE BELTS ON VENUS: GLOBAL DISTRIBUTION AND CLASSIFICATION Abstract Only
T. Toermaenen *In* Lunar and Planetary Inst., Twenty-Fourth Lunar and Planetary Science Conference. Part 3: N-Z 1993 p 1439-1440 (For primary document see N94-20636 05-91)
Avail: CASI HC A01/MF A06

Fifty-six features were identified in a global survey of complex ridged terrain (CRT)-related ridge belts. Nonrandom aerial distribution was observed with all of the CRT-related ridge belts located to the north of 20 deg S and increasing in number towards the north. In the equatorial highlands the only concentration of CRT-related ridge belts occurs along N and NE Ovda Regio and western Thetis Regio. Major areas of CRT devoid of related ridge belts (Beta, Phoebe, Alpha Regiones, and northern Lada Terra) are regions dominated by rifting, fractures, coronae, and volcanic features. A noticeable concentration of ridge belts is located within a region 20 deg S - 80 deg N, 0 deg - 150 deg E. Three classes of CRT-related ridge belts were defined: (1) ridge belts directly in contact with CRT margins, (2) ridge belts located apart from the CRT boundary, but whose shape and strike are affected by CRT, and (3) ridge belts terminating against a margin of CRT. There does not appear to be any relation between ridge belt class and type of CRT margin. Some of the class 2 and 3 belts of the 20 deg S - 80 deg N, 0 deg - 150 deg E region seem to be continuations of adjacent elongated blocks of CRT and could reflect the hypothesized basement of tessera-like material. Majority of class 1 and 2 ridge belts within this region parallel N of NE boundaries of large CRT plateaus of arc-like arrangements of tesserae. These relationships show that this region was dominated by compressional stresses oriented perpendicular to the CRT boundaries, in N-S/NE-SW direction. Author (revised)

N94-20836*# Lockheed Engineering and Sciences Co., Houston, TX.
THE PARENT MAGMA OF THE NAKHLA (SNC) METEORITE: RECONCILIATION OF COMPOSITION ESTIMATES FROM MAGMATIC INCLUSIONS AND ELEMENT PARTITIONING Abstract Only **c90**
A. H. Treiman *In* Lunar and Planetary Inst., Twenty-Fourth Lunar and Planetary Science Conference. Part 3: N-Z 1993 p 1441-1442 (For primary document see N94-20636 05-91)
Avail: CASI HC A01/MF A06

The composition of the parent magma of the Nakhla meteorite was difficult to determine, because it is accumulate rock, enriched in olivine and augite relative to a basalt magma. A parent magma composition is estimated from electron microprobe area analyses of magmatic inclusions in olivine. This composition is consistent with an independent estimate based on the same inclusions, and with chemical equilibria with the cores of Nakhla's augites. This composition reconciles most of the previous estimates of Nakhla's magma composition, and obviates the need for complex magmatic processes. Inconsistency between this composition and those calculated previously suggests that magma flowed through and crystallized into Nakhla as it cooled. Author (revised)

N94-20837*# Jet Propulsion Lab., California Inst. of Tech., Pasadena.
INTACT CAPTURE OF HYPERVELOCITY PARTICLES ON SHUTTLE Abstract Only **c90**
P. Tsou, D. E. Brownlee (Washington Univ., Seattle.), and A. L. Albee (California Inst. of Tech., Pasadena.) *In* Lunar and Planetary Inst., Twenty-Fourth Lunar and Planetary Science Conference. Part 3: N-Z 1993 p 1443-1444 (For primary document see N94-20636 05-91)
Avail: CASI HC A01/MF A06

The capability for capturing micrometeoroid analogs intact through laboratory simulations in passive underdense media offers a valuable tool for cosmic dust research. However, no amount of laboratory simulations can replace actual space experiments due to the technical inability to launch high fidelity analogs of micrometeoroids in ground laboratories and then reliably simulating high hypervelocities (greater than 7 km/s). Fluffy composite micrometeoroid analogs tend to break up and have not survived laboratory launches at beyond 4 km/s, however, a new technique of launching cluster analogs was developed for the two-stage light-gas gun at NASA Ames Vertical Gun Range. Plasma drag or electrostatic accelerators may be able to achieve higher speeds than two-stage light-gas guns but only with very limited projectile compositions and may result in severe projectile deformation. Consequently, a space demonstration of intact capture was sought since 1983. Initial results from our STS-47 flight, which carried the first Shuttle Sample Return Experiment (SRE) with silica aerogel capture media, are reported. Author (revised)

N94-20838*# Arizona Univ., Tucson. Dept. of Geosciences.
PHOTOGEOLOGICAL ANALYSIS OF EUROPAN TECTONIC FEATURES Abstract Only
B. R. Tufts *In* Lunar and Planetary Inst., Twenty-Fourth Lunar and Planetary Science Conference. Part 3: N-Z 1993 p 1445-1446 (For primary document see N94-20636 05-91)
Avail: CASI HC A01/MF A06

Preliminary photogeological analyses of the Pelorus Linea and Sidon Flexus regions of Europa were conducted to explore the proposal by Schenk that lateral motion of crustal blocks has occurred in a 'rift zone' including possible strike-slip, tension fracturing, and geometric plate rotation about an Euler pole. These analyses revealed features interpreted as tensional structures and block rotation in a strike-slip regime consistent with the Schenk hypotheses and implied the presence of at least two stages of crustal deformation consistent with a chronology developed by Lucchitta. Confirmation of regional scale Euler pole rotation was ambiguous, however. Up to 80 kilometers of possible extension was identified in the rift zone; to accommodate this, 'cryosubduction' is speculatively proposed as a mechanism for recycling Europan 'ice lithosphere'. The cumulative width of wedge-shaped bands included in the rift zone was measured and plotted versus distance from the inferred rotation pole. Three sharp decreases in the total width were noted. These occur roughly where certain triple bands cross the rift zone suggesting that the bands are structural features that predate and influence the zone. While the curve hints at one or more sinusoidal relationships consistent with rotation geometry, given the low photographic resolution and the preliminary nature of this examination the question of whether the observations represent coherent regional rotation modified by crosscutting structures or instead imply independent local rotations separated by these structures is unanswered by this analysis. Author (revised)

N94-20839*# Cornell Univ., Ithaca, NY. Dept. of Geological Sciences.
IS THERE UNIFORMITARIAN OR CATASTROPHIC TECTONICS ON VENUS? Abstract Only
Donald L. Turcotte *In* Lunar and Planetary Inst., Twenty-Fourth Lunar and Planetary Science Conference. Part 3: N-Z 1993 p 1447-1448 (For primary document see N94-20636 05-91)
Avail: CASI HC A01/MF A06

The distribution and modification of craters on Venus favors a near global, volcanic resurfacing event about 500 Myrs ago. Such an event indicates that the tectonic evolution of Venus was catastrophic rather than uniformitarian. The creation of a global, single-plate lithosphere on Venus about 500 Myrs ago can explain a variety of tectonic features on Venus that are not consistent with the thin lithosphere required by a uniformitarian hypothesis. A lithosphere on Venus that has thickened for 500 Myrs has a present thickness of about 300 km whereas steady-state heat loss from Venus requires a mean lithospheric thickness near 40 km. A thick lithosphere on Venus can support the high plateaus (elevations of 3-4 km) and mountain belts (up to 9 km) using the same isostatic compensation concepts applicable to the earth. If a thick lithosphere is thinned by a mantle plume, elevation is caused by thermal isostasy. The elevation due to the thinning of a 300 km thick lithosphere is about 3 km. Thus the domal elevation of Beta Regio can be explained by the same mechanism responsible for the elevation of the Hawaiian Swell. While the broad highland plateaus on Venus may be associated with thermal isostasy, the mountain belts in Ishtar Terra clearly cannot be. The high topography of Freyja Montes is almost certainly associated with underthrusting and the likely compensation mechanism is Airy isostasy associated with a thickened crust. With a density contrast delta, of 500 kg m(exp -3) an elevation of 9 km requires a crustal thickening of about 70 km. With a thick lithosphere there is no difficulty in supporting such a thick crust. Author (revised)

N94-20840*# Arizona State Univ., Tempe. Dept. of Geology.
IMPACT-INDUCED DEVOLATILIZATION OF CaSO4 ANHYDRITE AND IMPLICATIONS FOR K-T EXTINCTIONS: PRELIMINARY RESULTS Abstract Only **c90**

James A. Tyburczy and Thomas J. Ahrens (California Inst. of Tech., Pasadena.) *In* Lunar and Planetary Inst., Twenty-Fourth Lunar and Planetary Science Conference. Part 3: N-Z 1993 p 1449-1450 (For primary document see N94-20636 05-91)
Avail: CASI HC A01/MF A06

The recent suggestions that the target area for the K-T bolide may have been a sulfate-rich evaporite and that the resulting sulfuric acid-rich aerosol was responsible for the subsequent cooling of the Earth and the resulting biological extinctions has prompted us to experimentally examine the impact-induced devolatization of the sulfate minerals anhydrite (CaSO4) and gypsum (CaSO4(2H2O)). Preliminary results for anhydrite are reported. Up to 42 GPa peak shock pressure, little or no devolatilization occurs, consistent with chemical thermodynamic calculations. Calculation of the influence of the partial pressure of the gas species on impact-induced devolatilization suggests that an even greater amount of sulfur than that proposed by Brett could have been released to the atmosphere by an impact into a sulfate-rich layer. Solid recovery, impact-induced devolatilization experiments were performed on the Caltech 20mm gun using vented, stainless steel sample assemblies. Author (revised)

N94-20841*# European Space Research Organization, Noordwikj (Netherlands). Dept. of Space Science.
MEASUREMENTS OF THE DIELECTRIC PROPERTIES OF SIMULATED COMET MATERIAL AS PART OF THE KOSI 10 EXPERIMENT Abstract Only **c90**

S. Ulamec, H. Svedhem, and H. Kochan (Deutsche Forschungsanstalt fuer Luft- und Raumfahrt, Cologne, Germany.) *In* Lunar and Planetary Inst., Twenty-Fourth Lunar and Planetary Science Conference. Part 3: N-Z 1993 p 1451-1452 (For primary document see N94-20636 05-91)
Avail: CASI HC A01/MF A06

The dielectric constant epsilon of the snow-mineral used for the comet simulation in the German KOSI 10 experiment was measured in the radio frequency range from 2 to 4 GHz. The traditional microwave bridge method was used, but instead of using a waveguide that contains the sample material small lambda/4 antennas were used as sensors. A change in the dielectric properties indicates a change in density and/or composition, respectively. The method is presented as an analytical tool for measuring such density or composition changes during alteration snow-dust materials. The KOSI (determined from the German: Kometen Simulation) experiments, performed in the Space simulator of the DLR/Institut for Raumsimulation, during the last years revealed many processes that presumably take place on comets. So far, modifications of the internal structure could be identified only during the post-experiment inspection via hardness tests. It was the aim of the KOSI 10 and KOSI 10a experiments to emphasize on a synoptic detection of events like particle emission or crust formation. The composition of the KOSI 10 sample material was an ice-mineral mixture with about 10 percent mineral (olivine) content. An excellent method to investigate the change of the density of the probe material during its exposure to the artificial sun in situ is to do it via the measurement of the dielectric constant. The traditional method to determine epsilon, by using a microwave-bridge to measure the transmission and the reflection factor of the sample material for electromagnetic waves in the radio frequency range, was modified, since the commonly used practice to fill the sample material into a waveguide was not compatible with the need for in situ measurements during the simulation experiment. Author (revised)

N94-20842*# Kansas State Univ., Manhattan. Dept. of Geology.
GEOLOGY OF GALILEO REGIO QUADRANGLE, GANYMEDE Abstract Only

James R. Underwood, Jr., Ruggero Casacchia (Instituto de Astrofisica de Andalucia, Granada, Spain.), Reparto diPlanetologia (Viale Univ., Rome, Italy.), Alex Woronow (Houston Univ., TX.), and Michael J. Teeling (Groundwater Technology, Inc., Checktowaga, NY.) *In* Lunar and Planetary Inst., Twenty-Fourth Lunar and Planetary Science Conference. Part 3: N-Z 1993 p 1453-1454 (For primary document see N94-20636 05-91)
Avail: CASI HC A01/MF A06

Galileo Regio quadrangle, including most of Galileo Regio, contains two basic geologic units: older dark, furrowed, and heavily cratered material and younger light, grooved, relatively less-cratered material. Dark material dominates, the light material occurring to the W and SW in about five percent of the quadrangle. Dominant structural features, of uncertain origin, are the NW-trending arcuate furrows and associated orthogonal and oblique furrows in the dark material; grooves in the light material are not as well-ordered nor as intensely developed as elsewhere on Ganymede. Fifteen palimpsests, located partly or totally in the quadrangle and representing the period when the crust became sufficiently strong to record impact events, are subdivided into three relative-age classes, as are the numerous impact craters, some of which are dome, moat, and rampart-like. Galileo Regio is believed to have formed when, because of cooling, differentiation, and expansion, the thin, weak, icy lithosphere broke into blocks and light material filled the space between, or overspread those blocks that subsided, or both. Grooves formed in most of the light material and both light and dark material were cratered by impact, the most recent of which created bright-ray craters, the youngest features visible in the quadrangle. Author

N94-20843*# Universidad Nacional Autonoma de Mexico, Coyoacan. Inst. de Geofisica.
REVERSE POLARITY MAGNETIZED MELT ROCKS FROM THE CHICXULUB IMPACT STRUCTURE, YUCATAN PENINSULA, MEXICO Abstract Only **c46**

Jaime Urrutia-Fucugauchi, Luis E. Marin, Virgil L. Sharpton (Lunar and Planetary Inst., Houston, TX.), and Juan Manuel Quezada (Gerencia de Exploracion, Petroleos Mexicanos, Mexico City.) *In* Lunar and Planetary Inst., Twenty-Fourth Lunar and Planetary Science Conference. Part 3: N-Z 1993 p 1455-1456 (For primary document see N94-20636 05-91)
Avail: CASI HC A01/MF A06

Further paleomagnetic data for core samples of melt rock recovered in the Petroleos Mexicanos (PEMEX) exploratory wells within the Chicxulub structure, northern Yucatan peninsula, Mexico are reported. A previous report by Sharpton showed that the rocks studied contain high iridium levels and shocked breccia clasts, and an Ar-40/Ar-39 age of 65.2 plus or minus 0.4 Ma. The geomagnetic polarity determined for two samples is reverse (R) and was correlated with chron 29R that includes the K/T boundary. Our present analysis is based on two samples from each of three clasts of the melt rock from PEMEX well Y6-N17 (1295 to 1299 m b.s.l.). This study concentrates on the vectorial nature and stability of the remanence (NRM), the magnetic mineralogy and remanence carriers (i.e., the reliability and origin of the record), and on the implications (correlation with expected paleolatitude and polarity). The relative orientation of the drill core samples with respect to the horizontal is known. Samples were stable under alternating field (AF) and thermal treatments, and after removal of a small component they exhibited single-vectorial behavior. The characteristic remanence inclinations show small dispersion and a mean value (-43 deg) in close agreement with the expected inclination and paleolatitude (derived from the North American apparent polar wander path). Isothermal remenence (IRM) acquisition experiments, Lowrie-Fuller tests, coercivity and unblocking temperature spectra of NRM and saturation IRM, susceptibility and Q-coefficient analyses, and the single-component nature indicate a dominant mineralogy of iron-rich titanomagnetites with single or pseduo-single domain states. The stable characteristic magnetization may be interpreted as a result of shock heating of the rock at the time of formation of the inpact structure and its polarity, age, and paleolatitude are consistent with a time about the K/T boundary. Author (revised)

N94-20844*# Academy of Sciences (USSR), Moscow. Inst. of Geochemistry and Analytical Chemistry.
ON MODELLING NUCLEAR REACTIONS IN METEORITES Abstract Only **c90**

G. K. Ustinova and A. K. Lavrukhina *In* Lunar and Planetary Inst., Twenty-Fourth Lunar and Planetary Science Conference. Part 3: N-Z 1993 p 1457-1458 (For primary document see N94-20636 05-91)
Avail: CASI HC A01/MF A06

An original method of experimental modeling depth distribution of radionuclides in sphere thick targets irradiated by protons in 4(pi)-geometry on JINR (Dubna) synchrocyclotron is described. Some results are presented. Author (revised)

N94-20845*# Jet Propulsion Lab., California Inst. of Tech., Pasadena.
IMPS ALBEDO AND DIAMETER FOR ASTEROID 243 IDA Abstract Only **c90**

G. J. Veeder and E. F. Tedesco (Mission Research Corp., Santa Barbara, CA.) *In* Lunar and Planetary Inst., Twenty-Fourth Lunar and Planetary Science Conference. Part 3: N-Z 1993 p 1459-1460 (For primary document see N94-20636 05-91)
Avail: CASI HC A01/MF A06

243 Ida is the second asteroid target of the Galileo mission. The Infrared Astronomical Satellite (IRAS) detected Ida several times during its 1983 sky survey. The IRAS Minor Planet Survey (IMPS) yields a total of 13 usable observations during 6 sightings of Ida. These data result in a geometric visual albedo of 0.24 and a mean diameter of 28 km for Ida. The IMPS catalog updates and extends the IRAS Asteroid and Comet Survey through asteroid number 4679. File versions of IMPS final products will be available from the National Space Science Data Center (NSSDC). The input for IMPS processing includes updated visual absolute magnitudes and orbital elements for each asteroid. H and G are 9.94 and 0.15 for Ida. IMPS also includes a correction for low flux densities (less than approximately 1 Jansky). In the case of Ida, 3 observations at 12 microns, 6 at 25 microns, and 4 at 60 microns were considered acceptable for analysis. Most of these do have flux densities less than 1 Jansky with a value of approximately 5 for their estimated SNR. The 25 microns observations as plotted in the figure are consistent with the variation expected for the cross section of Ida with rotation. Ida is a main belt asteroid with an S taxonomic classification. The spectra of S asteroids tend to be dominated by pyroxene with visual albedos from 0.1 to 0.3. The IMPS average albedo of 0.24 (plus or minus 0.07) for 243 Ida is in the upper range observed for S asteroids. Author (revised)

N94-20846*# Open Univ., Milton (England).
ARE THE C DELTA LIGHT NITROGEN AND NOBLE GASES LOCATED IN THE SAME CARRIER? Abstract Only **c90**
A. B. Verchovsky, S. S. Russell, C. T. Pillinger, A. V. Fisenko (Academy of Sciences, USSR, Moscow.), and Yuri A. Shukolyukov (Academy of Sciences, USSR, Moscow.) *In* Lunar and Planetary Inst., Twenty-Fourth Lunar and Planetary Science Conference. Part 3: N-Z 1993 p 1461-1462 (For primary document see N94-20636 05-91)
Avail: CASI HC A01/MF A06

Light nitrogen and the HL family noble gas components of C(sub delta) appear to be separable by high resolution pyrolysis experiments. Thus C(sub delta) is not a homogeneous material and probably consists of debris of many stars. The question of whether the N and Xe(HL) actually reside in different carriers continues to be addressed. It is well known that C(sub delta) which was identified as nanometer sized diamonds contains isotopically anamalous elements, in particular noble gases including Xe(HL) and its family and light nitrogen (delta(N-15) down to -350 percent). Before the true nature of C(sub delta) was recognized, it was easy to suppose that the Xe(HL) and light nitrogen were located in the same carrier. However, recognition that light nitrogen in diamond from different samples varies by greater than a factor of six compared to Xe(HL) fluctuations of ca. 20 percent makes such an assumption questionable. On the basis of simple arithmetic logic, the Xe and nitrogen cannot be absolutely co-located. The average diamond grain consists of only about 1000-2000 atoms of carbon; one grain among a few x 10(exp 6) contains an atom of Xe(HL) while 5-30 atoms of light nitrogen are the typical number which need to be in every diamond grain to account for observed concentrations. If some grains are devoid of N, the others have to have a higher N concentration. Even if we were able to analyze an individual grain of the diamond for noble gases and nitrogen, we would be faced with the monumental task of locating the one amongst 10(exp 6) identical grains containing the Xe atom to examine its nitrogen content. The problem can be simplified to some extent if instead of Xe, He which is 10(exp 4) times more abundant is assumed to be a member of the HL family. Attempts to fractionate the separate carriers might be attempted using He and N as guiding indicators but even experiments of this nature are for the future. Faced with apparently insoluble problems, we have returned to an investigation we last used in our original efforts to find isotopically light nitrogen, that is to compare release patterns of the different components during stepped pyrolysis and combustion. Author (revised)

N94-20847*# Arizona Univ., Tucson. Lunar and Planetary Lab.
NUMERICAL MODELING OF IMPACT EROSION OF ATMOSPHERES: PRELIMINARY RESULTS Abstract Only
A. M. Vickery *In* Lunar and Planetary Inst., Twenty-Fourth Lunar and Planetary Science Conference. Part 3: N-Z 1993 p 1463-1464 (For primary document see N94-20636 05-91)
Avail: CASI HC A01/MF A06

It is clear from the great diversity of atmospheres among the terrestrial planets that their formation and evolution must have depended on a balance among a number of different processes. One of these processes is atmospheric erosion by impacts, which may have been particularly effective on Mars. The reason is that geomorphic evidence on Mars suggests that this planet had, early in its history, dense enough atmosphere to sustain active precipitation over geologically significant periods of time. Analytic calculations indicate that neither the projectile entering the atmosphere nor the main crater ejecta can cause the lose of significant amounts of atmosphere. The vapor plume that is formed, however, expands rapidly as its internal energy is converted into kinetic energy, and may blow off the overlying atmosphere. A model of this part of the impact/atmosphere interaction predicts Mars could have lost a substantial early atmosphere by impact erosion alone. Although our more detailed calculations, which took into account the anisotropy of the atmosphere with respect to zenith angle, show that the process isn't quite as effective, they still indicate the probability of substantial atmospheric loss from Mars. The first results from 2-D hydrocode runs are discussed. These include two runs which make most of the same simplifying approximations as the analytic models, in order to compare the analytic and numerical results directly, and one run (as yet incomplete) that models the full impact. Author (revised)

N94-20848*# National Aeronautics and Space Administration. Lyndon B. Johnson Space Center, Houston, TX.
COMPARISON OF VISIBLE AND NEAR-INFRARED REFLECTANCE SPECTRA OF CM2 CARBONACEOUS CHONDRITES AND PRIMITIVE ASTEROIDS Abstract Only **c90**
F. Vilas, T. Hiroi, and M. E. Zolensky *In* Lunar and Planetary Inst., Twenty-Fourth Lunar and Planetary Science Conference. Part 3: N-Z 1993 p 1465-1466 (For primary document see N94-20636 05-91)
Avail: CASI HC A01/MF A06

Spectra of primitive asteroids (defined as C, P, and D classes and associated subclasses) were compared to the limited number of spectra of CM2 carbonaceous chondrites. An absorption feature located at 0.7 microns attributed to an Fe(+2) - Fe(+3) charge transfer absorption in iron oxides in phyllosilicates is apparent in some of the CM2 carbonaceous chondrite spectra and many of the asteroid spectra. Sawyer found a correlation between the area of the 0.7 micron feature and the mean semimajor axis of the asteroids. Spectra of a larger sample of carbonaceous chondrites, including 7 CM2 chondrites, covering a spectral interval of 0.30-2.5 microns were recently obtained using the Relab instrument at Brown University. These spectra were compared with spectrophotometric asteroid observations in a separate abstract. Those spectra of CM2 chondrites were isolated into the UV, visible and near-infrared spectral regions in order to compare them with high-quality narrowband reflectance spectra. Author (revised)

N94-20849*# Academy of Sciences (USSR), Moscow. Inst. of Physics of the Earth.
RECONDENSATION IN THE EARLY SOLAR SYSTEM: PHYSICAL CONDITIONS AND SOURCE MATERIAL Abstract Only **c90**
A. V. Vityazev, V. A. Dorofeyeva, and A. B. Makalkin *In* Lunar and Planetary Inst., Twenty-Fourth Lunar and Planetary Science Conference. Part 3: N-Z 1993 p 1467-1468 (For primary document see N94-20636 05-91)
Avail: CASI HC A01/MF A06

Many physical processes in the solar nebula led to fractionation of the gaseous phase of the preplanetary material. Some of these processes are listed with corresponding type of fractionation in terms of Rock/Ice/Gas. Recondensation from fractionated gas phase yields different compositions of condensates. In some detail, one type of fractionation is considered: impact heating with evaporation and subsequent recondensation of material during intercollisions of planetesimals. For thermodynamical simulation of recondensation in such a process one needs (1) P-T parameters and (2) some initial source material to be heated, evaporated, and recondensed. These two problems are addressed. Author (revised)

N94-20850*# Science Applications International Corp., Washington, DC.
THE CLEMENTINE MISSION SCIENCE RETURN AT THE MOON AND GEOGRAPHOS Abstract Only **c12**

R. W. VorderBruegge, M. E. Davies (RAND Corp., Santa Monica, CA.), D. M. Horan (Naval Research Lab., Washington, DC.), P. G. Lucey (Hawaii Univ., Honolulu.), C. M. Pieters (Brown Univ., Providence, RI.), A. S. McEwen (Geological Survey, Flagstaff, AZ.), S. Nozette (Strategic Defense Initiative Organization, Washington, DC.), E. M. Shoemaker (Geological Survey, Flagstaff, AZ.), S. W. Squyres (Cornell Univ., Buffalo, NY.), and P. C. Thomas (Cornell Univ., Buffalo, NY.) *In* Lunar and Planetary Inst., Twenty-Fourth Lunar and Planetary Science Conference. Part 3: N-Z 1993 p 1469-1470 (For primary document see N94-20636 05-91)
Avail: CASI HC A01/MF A06

The Clementine Mission is being built and flown by the Naval Research Laboratory under the sponsorship of the Strategic Defense Initiative Organization of the United States Department of Defense in joint-cooperation with NASA, and will explore the Moon and the near-Earth asteroid (NEA) 1620 Geographos with lightweight sensors developed by the Lawrence Livermore National Laboratory. A NASA Science Team for this mission will be selected by way of a NRA in April 1993. The instrument suite includes imaging cameras that cover a spectral range from the near-ultraviolet to the mid-infrared, a laser ranger, and, potentially, a charged particle telescope. To be launched in early 1994, Clementine will be in lunar orbit from February through May 1994, at which time it will depart the Moon for a flyby of 1620 Geographos in August 1994. This mission represents an outstanding opportunity for scientists interested in the Moon and asteroids. It is anticipated that the data returned from this mission will permit: an assessment of global lunar crustal heterogeneity and a resolution of less than 1 km; an assessment of the lithologic heterogeneity of Geographos at a scale of 100 m or better; and an assessment of surface processes on Geographos on the order of 10 m. The basic mission of Clementine and some of the key scientific questions that will be addressed are described. Additional material on the Clementine mission, its data handling and processing, and its instrument suite is presented elsewhere.

Author (revised)

N94-20851*# Battelle Northwest Labs., Richland, WA.
ALUMINUM-26 ACTIVITIES IN METEORITES Abstract Only **c25**

J. F. Wacker *In* Lunar and Planetary Inst., Twenty-Fourth Lunar and Planetary Science Conference. Part 3: N-Z 1993 p 1471-1472 (For primary document see N94-20636 05-91)
Avail: CASI HC A01/MF A06

Al-26 activities for 686 Antarctic meteorites and 46 non-Antarctic meteorites are reported. The data set includes new results for 253 Antarctic and 5 non-Antarctic meteorites. Most of the Antarctic specimens were collected from the Allan Hills region, but specimens from other regions were measured as well. The non-Antarctic specimens include freshly fallen meteorites, in which short-lived radionuclides (e.g., Na-22, Mn-54, Co-57, etc.) were also measured. The data were analyzed for terrestrial age distributions, identification of samples with unusual activities, pairing of specimens, and comparisons of Antarctic and non-Antarctic activity distributions.

Author (revised)

N94-20852*# Washington Univ., Saint Louis, MO. Dept. of Earth and Planetary Sciences.
RARE EARTH ELEMENTS IN INDIVIDUAL MINERALS IN SHERGOTTITES Abstract Only **c25**

Meenakshi Wadhwa and Ghislaine Crozaz *In* Lunar and Planetary Inst., Twenty-Fourth Lunar and Planetary Science Conference. Part 3: N-Z 1993 p 1473-1474 (For primary document see N94-20636 05-91)
Avail: CASI HC A01/MF A06

Shergottites (i.e., Shergotty, Zagami, EETA79001, ALHA77005, and LEW88516) are an important set of achondrites because they comprise the majority of the SNC group of meteorites (nine, in total, known to us), which are likely to be samples of the planet Mars. Study of these meteorites may therefore provide valuable information about petrogenetic processes on a large planetary body other than Earth. Rare earth element (REE) distributions between various mineral phases were found to be useful in geochemically modeling the petrogenesis of various rock types (terrestrial and meteoritic). However, with the exception of a few ion microprobe studies and analyses of mineral separates, there has previously not been any comprehensive effort to characterize and directly compare REE in individual minerals in each of the five known shergottites. Ion microprobe analyses were made on thin sections of each of the shergottites. Minerals analyzed were pyroxenes (pigeonite and augite), maskelynite, and whitlockite. The REE concentrations in each mineral type in each shergottite is given.

Author (revised)

N94-20853*# Massachusetts Inst. of Tech., Cambridge. Dept. of Earth, Atmospheric and Planetary Sciences.
ORIGIN OF HIGH-Ti LUNAR ULTRAMAFIC GLASSES Abstract Only **c25**

T. P. Wagner and T. L. Grove *In* Lunar and Planetary Inst., Twenty-Fourth Lunar and Planetary Science Conference. Part 3: N-Z 1993 p 1475-1476 (For primary document see N94-20636 05-91)
Avail: CASI HC A01/MF A06

A series of high pressure melting experiments were performed on a synthetic analog of the Apollo 14 Black Glass. At 15 kb and 1400 C, olivine is the liquidus phase. At 25 kb and 1450 C, orthopyroxene and Cr-spinel crystallize. A multiple saturation point with olivine + orthopyroxene + spinel on the liquidus occurs at 20 kb and 1440 C. It was proposed that the high-Ti ultramafic glass evolved from a low-Ti Green Glass generated deep in the lunar interior that assimilated shallow-level, late stage cumulates of magma ocean differentiation. Heat for assimilation is provided by superheat of the low-Ti magma and melts high-Ca pyroxene and ilmenite cumulates at a depth of 100 km. This model is a variant of that proposed by Hubbard and Minear and rejected by Ringwood and Kesson.

Author (revised)

N94-20854*# Maryland Univ., College Park. Dept. of Geology.
RHENIUM-OSMIUM ISOTOPE SYSTEMATICS OF ORDINARY CHONDRITES AND IRON METEORITES Abstract Only **c90**

R. J. Walker, J. W. Morgan (Geological Survey, Reston, VA.), M. F. Horan (Geological Survey, Reston, VA.), and J. N. Grossman (Geological Survey, Reston, VA.) *In* Lunar and Planetary Inst., Twenty-Fourth Lunar and Planetary Science Conference. Part 3: N-Z 1993 p 1477-1478 (For primary document see N94-20636 05-91)
Avail: CASI HC A01/MF A06

Using negative thermal ionization mass spectrometry, Re and Os abundances were determined by isotope dilution and Os-187/Os-186 measured in 11 ordinary chondrites, and also in 1 IIB and 3 IIIB irons. In addition, Os-186/Os-188 and Os-189/Os-188 ratios were precisely determined for 3 unspiked ordinary chondrites as a means of constraining the intensity of any neutron irradiation these meteorites may have experienced.

Author (revised)

N94-20855*# Chicago Univ., IL. Dept. of the Geophysical Sciences.
DIFFUSION-CONTROLLED MAGNESIUM ISOTOPIC FRACTIONATION OF A SINGLE CRYSTAL FORSTERITE EVAPORATED FROM THE SOLID STATE Abstract Only **c25**

Jianhua Wang, Andrew M. Davis, Akihiko Hashimoto (Harvard-Smithsonian Center for Astrophysics, Cambridge, MA.), and Robert N. Clayton *In* Lunar and Planetary Inst., Twenty-Fourth Lunar and Planetary Science Conference. Part 3: N-Z 1993 p 1479-1480 (For primary document see N94-20636 05-91)
Avail: CASI HC A01/MF A06

Though the origin of calcium- and aluminum-rich inclusions (CAI's) in carbonaceous chondrites is till a disputed issue, evaporation is no doubt one of the most important processes for the formation of CAI's in the early solar nebula. The mechanism for production of large isotopic mass fractionation effects in magnesium, silicon, oxygen, and chromium in CAI's can be better understood by examining isotopic fractionation during the evaporation of minerals. New evaporation experiments were performed on single-crystal forsterite. The magnesium isotopic distribution near the evaporating surfaces of the residues using a modified AEI IM-20 ion microprobe to obtain rastered beam depth profiles was measured. A theoretical model was used to explain the profiles and allowed determination of the diffusion coefficient of Mg(++) in forsterite at higher temperatures than previous measurements. The gas/solid isotopic fractionation factor for magnesium for evaporation from solid forsterite was also determined and found to be nearly the same as that for evaporation of liquid Mg2SiO4.

Author (revised)

N94-20856*# California Univ., Los Angeles. Inst. of Geophysics and Planetary Physics.

LIMITS ON DIFFERENTIATION OF MELT SHEETS FROM BASIN-SCALE LUNAR IMPACTS Abstract Only

Paul H. Warren *In* Lunar and Planetary Inst., Twenty-Fourth Lunar and Planetary Science Conference. Part 3: N-Z 1993 p 1481-1482 (For primary document see N94-20636 05-91)

Avail: CASI HC A01/MF A06

In the literature on cratering, one frequently finds allusions to the 'sheet' of impact melt that supposedly forms in the aftermath of any large impact. The presumption seems to be that either (1) most of the impact melt is formed virtually at the surface, or else (2) most of the melt inevitably collects into a near-surface, roughly sill-shaped 'sheet,' soon after the impact. However, in basin-scale impacts on the mature Moon, neither of these scenarios appears likely. Differentiation of impact melts on the Moon is hampered by similarity in density vs. the porous lunar crust, and by the adverse melt/'displaced' matter ratio that results from the lunar g.

Author (revised)

N94-20857*# National Aeronautics and Space Administration. Lyndon B. Johnson Space Center, Houston, TX.

CONSORTIUM STUDY OF LUNAR METEORITES YAMATO-793169 AND ASUKA-881757: GEOCHEMICAL EVIDENCE OF MUTUAL SIMILARITY, AND DISSIMILARITY VERSUS OTHER MARE BASALTS Abstract Only c90

Paul H. Warren (California Univ., Los Angeles.) and Marilyn M. Lindstrom *In* Lunar and Planetary Inst., Twenty-Fourth Lunar and Planetary Science Conference. Part 3: N-Z 1993 p 1483-1484 (For primary document see N94-20636 05-91)

Avail: CASI HC A01/MF A06

Compositions of bulk powders and separated minerals from two meteorites derived from the mare lava plains of the Earth's Moon, Yamato-793169 and Asuka-881757, indicate a remarkable degree of similarity to one another, and clearly favor lunar origin. However, these meteorites are unlike any previously studied lunar rock. In both cases, the bulk-rock TiO2 content is slightly greater than the level separating VLT from low-Ti mare basalt, yet the Sc content is much higher than previously observed except among high-Ti mare basalts. Conceivably, the Sc enrichment in A881757 reflects origin of this rock as a cumulate from a mare magma of 'normal' Sc content, but this seems unlikely. Mineral-separate data suggest that most of the Sc is in pyroxene, and a variety of evidence weighs against the cumulus hypothesis as a major cause for the high Sc. The remarkable similarity between Y793169 and A881757 suggests the possibility that they were derived from a single source crater on the Moon.

Author (revised)

N94-20858*# National Aeronautics and Space Administration. Goddard Space Flight Center, Greenbelt, MD.

MAGNETIC RECORD IN CHONDRITE METEORITES Abstract Only c90

P. J. Wasilewski, J. L. Faris, and M. V. OBryan *In* Lunar and Planetary Inst., Twenty-Fourth Lunar and Planetary Science Conference. Part 3: N-Z 1993 p 1485-1486 (For primary document see N94-20636 05-91)

Avail: CASI HC A01/MF A06

What we know about the magnetic record in chondrite meteorites based on new data and previously published results is summarized. Strips from thin slabs of chondrite meteorites were cut into near cubical subsamples (several mm on edge) numbering approximately 60 to approximately 120 per meteorite. A common orientation was assigned to each subsample from a given meteorite in order to ensure that we could discover the vector makeup of the bulk meteorite. The new data set includes: Shaw (L7), Roy (L5/6), Claytonville (L5), Plainview (H5), Etter (H5), Leoville (C3V), and Allende (C3V). In addition to these new results, literature data of sufficient detail, e.g. Bjurbole (L4), ALH769 (L6), Abee (E4), Allende (C3V), and Olivenza (L5), is considered.

Author (revised)

N94-20859*# California Inst. of Tech., Pasadena. Div. of Geological and Planetary Sciences.

AGB STARS AS A SOURCE OF SHORT-LIVED RADIOACTIVE NUCLEI IN THE SOLAR NEBULA Abstract Only c92

G. J. Wasserburg, R. Gallino (Turin Univ., Italy.), M. Busso (Turin Univ., Italy.), and C. M. Raiteri (Turin Univ., Italy.) *In* Lunar and Planetary Inst., Twenty-Fourth Lunar and Planetary Science Conference. Part 3: N-Z 1993 p 1487-1488 (For primary document see N94-20636 05-91)

Avail: CASI HC A01/MF A06

The purpose is to estimate the possible contribution of some short-lived nuclei to the early solar nebula from asymptotic giant branch (AGB) sources. Low mass (1 to 3 solar mass) AGB stars appear to provide a site for synthesis of the main s process component for solar system material with an exponential distribution of neutron irradiations varies as exp(-tau/tau(sub 0)) (where tau is the time integrated neutron flux with a mean neutron exposure tau(sub 0)) for solar abundances with tau(sub 0) = 0.28 mb(sup -1). Previous workers estimated the synthesis of key short-lived nuclei which might be produced in AGB stars. While these calculations exhibit the basic characteristics of nuclei production by neutron exposure, there is need for a self-consistent calculation that follows AGB evolution and takes into account the net production from a star and dilution with the cloud medium. Many of the general approaches and the conclusions arrived at were presented earlier by Cameron. The production of nuclei for a star of 1.5 solar mass during the thermal pulsing of the AGB phase was evaluated. Calculations were done for a series of thermal pulses with tau(sub 0) = 0.12 and 0.28 mb(sup -1). These pulses involve s nucleosynthesis in the burning shell at the base of the He zone followed by the ignition of the H burning shell at the top of the He zone. After about 10-15 cycles the abundances of the various nuclei in the He zone become constant. Computations of the abundances of all nuclei in the He zone were made following Gallino. The mass of the solar nebula was considered to consist of some initial material of approximately solar composition plus some contributions from AGB stars. The ratios of the masses required from the AGB He burning zone to the ISM necessary to produce the observed value of Pd-107/Pd-108 in the early solar system were calculated and this dilution factor was applied to all other relevant nuclei. Author (revised)

N94-20860*# California Univ., Los Angeles. Inst. of Geophysics and Planetary Physics.

MULTIPLICITY OF CHONDRULE HEATING EVENTS AND THE COARSENING OF CHONDRULE TEXTURES Abstract Only c90

John T. Wasson *In* Lunar and Planetary Inst., Twenty-Fourth Lunar and Planetary Science Conference. Part 3: N-Z 1993 p 1489-1490 (For primary document see N94-20636 05-91)

Avail: CASI HC A01/MF A06

Our studies of compound chondrules show that most chondrules experienced at least two thermal events that produced appreciable amounts of melt. I suggest that chondrules were subjected to a hierarchy of brief heating events, the number increasing exponentially with decreasing intensity, and that some of intermediate intensity deposited enough heat to partially melt mesostasis glass and promote the growth of mafic mineral grains. This scenario can account for textures that require improbably low monotonic cooling rates in laboratory simulations, and also for the rarity of glassy chondrule textures despite the ease with which these are produced in the laboratory.

Author (revised)

N94-20861*# National Aeronautics and Space Administration. Lyndon B. Johnson Space Center, Houston, TX.

EQUILIBRIUM AND FRACTIONAL CRYSTALLIZATION OF A PRIMITIVE SHERGOTTITE COMPOSITION Abstract Only c90

L. E. Wasylenki (California Inst. of Tech., Pasadena.), J. H. Jones, L. Le (Lockheed Engineering and Sciences Co., Houston, TX.), and A. J. G. Jurewicz (Lockheed Engineering and Sciences Co., Houston, TX.) *In* Lunar and Planetary Inst., Twenty-Fourth Lunar and Planetary Science Conference. Part 3: N-Z 1993 p 1491-1492 (For primary document see N94-20636 05-91)

Avail: CASI HC A01/MF A06

The shergottites are a subset of the Shergottites Nakhlites Chassignites (SNC) meteorites, which are believed to have come from Mars. Petrologic studies of these basaltic meteorites suggest that the most primitive shergottite composition is the groundmass of EETA79001 (a lithology). This inference is based on (1) its high Mg relative to the other shergottites; (2) it normative olivine; and (3) its lack of the cumulate crystals found in most other SNC meteorites. However, the relationship between this primitive composition and the compositions of the other, more evolved shergottites cannot be discovered through petrologic investigations alone. Therefore, liquidus phase relations were experimentally determined for a synthetic EETA79001A groundmass composition at 1 bar and QFM in order to find

whether the bulk compositions of other shergottites could be derived by simple equilibrium or fractional crystallization of the EETA79001A groundmass composition. Author (revised)

N94-20862*# California Inst. of Tech., Pasadena. Div. of Geological and Planetary Sciences.

HIGH D/H RATIOS OF WATER IN MAGMATIC AMPHIBOLES IN CHASSIGNY: POSSIBLE CONSTRAINTS ON THE ISOTOPIC COMPOSITION OF MAGMATIC WATER ON MARS Abstract Only

L. L. Watson, I. D. Hutcheon, S. Epstein, and E. M. Stolper *In* Lunar and Planetary Inst., Twenty-Fourth Lunar and Planetary Science Conference. Part 3: N-Z 1993 p 1493-1494 (For primary document see N94-20636 05-91)

Avail: CASI HC A01/MF A06

The D/H ratios of kaersutitic amphiboles contained in magmatic inclusions in the Shergottites Nakhlites Chassignites (SNC) meteorite Chassigny using the ion microprobe were measured. A lower limit on the delta(D(sub SMOW)) of the amphiboles is +1420 +/- 47 percent. Assuming Chassigny comes from Mars and the amphiboles have not been subject to alteration after their crystallization, this result implies either that recycling of D-enriched Martian atmosphere-derived waters into the planetary interior has taken place, or that the primordial hydrogen isotopic composition of the interior of Mars differs significantly from that of the Earth (delta(D(sub SMOW)) approximately 0 percent). In addition, the measurements indicate that the amphiboles contain less than 0.3 wt. percent water. This is much lower than published estimates, and indicates a less-hydrous Chassigny parent magma than previously suggested. Author (revised)

N94-20863*# Smithsonian Institution, Washington, DC. Center for Earth and Planetary Studies.

ARCUATE AND CIRCULAR STRUCTURES IN THE THARSIS REGION: EVIDENCE OF CORONAE ON MARS Abstract Only

T. R. Watters, J. R. Zimbelman, and D. H. Scott (Geological Survey, Flagstaff, AZ.) *In* Lunar and Planetary Inst., Twenty-Fourth Lunar and Planetary Science Conference. Part 3: N-Z 1993 p 1495-1496 (For primary document see N94-20636 05-91)

Avail: CASI HC A01/MF A06

Arcuate and circular structures are evident in the Tharsis region of Mars. They involve concentric graben and fracture systems and are often associated with volcanic centers. The most prominent example is Alba Patera, a low relief volcanotectonic center. It is surrounded by a graben system comprised of the Alba and Tantalus Fossae and part of the Ceranius Fossae system that are thought to have formed during the Early Amazonian. The graben concentric to Alba Patera form an annulus that is 600 km in diameter. The similarity between Alba Patera and coronae on Venus was observed prior to the Magellan mission. Magellan imagery of Venusian coronae has revealed a number of striking similarities between these structures, Alba Patera, and the other circular structures on Mars. Coronae on Venus are circular to ovoidal volcanotectonic features that range in diameter from 60 to over 1000 km. Concentric graben form partial to complete tectonic annuli. More regionally extensive graben systems are deflected toward, and in many cases merge with, the concentric graben. Volcanic flows and domes dominate the surface enclosed within the concentric graben. However, distinctive differences exist between coronae on Venus and the structures on Mars. Circular structures on Mars lack radial graben crosscut by concentric graben. There is also no evidence of the complex topography associated with coronae on Venus. The differences between coronae on Venus and the suspected coronae on Mars may be largely due to the difference in the thickness of the elastic lithosphere on the two planets. The topographic expression of the interaction between the diapir and the lithosphere would be expected to be greatly subdued on Mars because of the large difference in lithospheric thickness. The lack of circular structures with diameters below 200 km suggests a lower limit to the size that coronae could form on Mars. Derived from text

N94-20864*# POD Associates, Inc., Albuquerque, NM.

A FRESH LOOK AT CRATER SCALING LAWS FOR NORMAL AND OBLIQUE HYPERVELOCITY IMPACTS Abstract Only **c18**

A. J. Watts, D. R. Atkinson, S. R. Rieco, J. B. Brandvold, S. L. Lapin, and C. R. Coombs *In* Lunar and Planetary Inst., Twenty-Fourth Lunar and Planetary Science Conference. Part 3: N-Z 1993 p 1497-1498 (For primary document see N94-20636 05-91)

Avail: CASI HC A01/MF A06

With the concomitant increase in the amount of man-made debris and an ever increasing use of space satellites, the issue of accidental collisions with particles becomes more severe. While the natural micrometeoroid population is unavoidable and assumed constant, continued launches increase the debris population at a steady rate. Debris currently includes items ranging in size from microns to meters which originated from spent satellites and rocket cases. To understand and model these environments, impact damage in the form of craters and perforations must be analyzed. Returned spacecraft materials such as those from LDEF and Solar Max have provided such a testbed. From these space-aged samples various impact parameters (i.e., particle size, particle and target material, particle shape, relative impact speed, etc.) may be determined. These types of analyses require the use of generic analytic scaling laws which can adequately describe the impact effects. Currently, most existing analytic scaling laws are little more than curve-fits to limited data and are not based on physics, and thus are not generically applicable over a wide range of impact parameters. During this study, a series of physics-based scaling laws for normal and oblique crater and perforation formation has been generated into two types of materials: aluminum and Teflon. Derived from text

N94-20865*# Arizona Univ., Tucson. Planetary Science Inst.

COAGULATION OF GRAINS IN STATIC AND COLLAPSING PROTOSTELLAR CLOUDS Abstract Only **c90**

S. J. Weidenschilling and T. V. Ruzmaikina (Academy of Sciences, USSR, Moscow.) *In* Lunar and Planetary Inst., Twenty-Fourth Lunar and Planetary Science Conference. Part 3: N-Z 1993 p 1499-1500 (For primary document see N94-20636 05-91)

(Contract NASw-4616)

Avail: CASI HC A01/MF A06

The wavelength dependence of extinction in the diffuse interstellar medium implies that it is produced by particles of dominant size of approximately 10(exp -5) cm. There is some indication that in the cores of dense molecular clouds, sub-micron grains can coagulate to form larger particles; this process is probably driven by turbulence. The most primitive meteorites (carbonaceous chondrites) are composed of particles with a bimodal size distribution with peaks near 1 micron (matrix) and 1 mm (chondrules). Models for chondrule formation that involve processing of presolar material by chemical reactions or through an accretion shock during infall assume that aggregates of the requisite mass could form before or during collapse. The effectiveness of coagulation during collapse has been disputed; it appears to depend on specific assumptions. The first results of detailed numerical modeling of spatial and temporal variations of particle sizes in presolar clouds, both static and collapsing, is reported in this article. Derived from text

N94-20866*# American Museum of Natural History, New York, NY. Dept. of Mineral Sciences.

THE FORMATION OF FeO-RICH PYROXENE AND ENSTATITE IN UNEQUILIBRATED ENSTATITE CHONDRITES: A PETROLOGIC-TRACE ELEMENT (SIMS) STUDY Abstract Only **c90**

M. K. Weisberg, M. Prinz, R. A. Fogel, and N. Shimizu (Woods Hole Oceanographic Inst., MA.) *In* Lunar and Planetary Inst., Twenty-Fourth Lunar and Planetary Science Conference. Part 3: N-Z 1993 p 1501-1502 (For primary document see N94-20636 05-91)

Avail: CASI HC A01/MF A06

Enstatite (En) chondrites record the most reducing conditions known in the early solar system. Their oxidation state may be the result of condensation in a nebular region having an enhanced C/O ratio, reduction of more oxidized materials in a reducing nebula, reduction during metamorphic reheating in a parent body, or a combination of these events. The presence of more oxidized Fe-rich silicates, two types of En (distinguished by red and blue CL), and the juxtaposition of FeO-rich pyroxenes (Fe-pyx) surrounded by blue En (enstatite) in the UEC's (unequilibrated enstatite chondrites) is intriguing and led to the examination of the question of enstatite chondrite formation. Previously, data was presented on the petrologic-geochemical characteristics of the Fe-pyx and coexisting red and blue En. Here minor and trace element abundances (determined by ion probe-SIMS) on these three types of pyroxenes are

reported on in the following meteorites: Kota Kota and LEW87223 (EH3), MAC88136 (EL3), St. Marks (EH4), and Hvittis (EL6). More data are currently being collected. Derived from text

N94-20867*# Jet Propulsion Lab., California Inst. of Tech., Pasadena.
GEOLOGY AND RADIOPHYSICAL PROPERTIES OF THE VENERA AND VEGA LANDING SITES Abstract Only
C. M. Weitz and A. T. Basilevsky (Brown Univ., Providence, RI.) *In* Lunar and Planetary Inst., Twenty-Fourth Lunar and Planetary Science Conference. Part 3: N-Z 1993 p 1503-1504 (For primary document see N94-20636 05-91)
Avail: CASI HC A01/MF A06

Geologic maps for all seven Venera and Vega landing sites have been produced. Because the radius of error for each landing site is 150 km, the entire landing circle has been mapped centered about the estimated landing point. Correlations were found between the Magellan imagery and the lander TV panoramas and geochemical measurements made at the landing site. Radiophysical properties, including backscatter cross-sections, altimetry, emissivity, and rms slopes, were determined for each landing circle. After mapping the geology of the landing circles, the regional geology of the seven sites was mapped and the geologic history of theses large regions was determined. Derived from text

N94-20868*# Arizona State Univ., Tempe. Dept. of Geology.
A STUDY OF CARBONATES, SULFATES, AND PHOSPHATES USING THERMAL EMISSION SPECTROSCOPY Abstract Only c25
M. L. Wenrich and P. R. Christensen *In* Lunar and Planetary Inst., Twenty-Fourth Lunar and Planetary Science Conference. Part 3: N-Z 1993 p 1505-1506 (For primary document see N94-20636 05-91)
Avail: CASI HC A01/MF A06

Thermal emission spectroscopy is useful for identifying mineralogies including carbonates, sulfates, and phosphates. Each of these groups of minerals has a distinct emissivity profile that allows for general identification (e.g., carbonate). Laboratory data are being collected that suggest the potential for determining specific composition of these minerals (e.g., calcite, magnesite). Previous studies of Mars suggest that the above groups of minerals should be present. On Mars fine-grained mineralogies are likely to be intimately mixed due to aeolian activity. Mixtures of calcite with palagonite will be studied to determine the volume percent requirement for salt identification and to understand the complexities of fine-grained mixtures observed by thermal emission. Further work with mixtures will include sulfate and phosphate mineralogies. Derived from text

N94-20869*# National Aeronautics and Space Administration. Lyndon B. Johnson Space Center, Houston, TX.
WEATHERING FEATURES AND SECONDARY MINERALS IN ANTARCTIC SHERGOTTITES ALHA77005 AND LEW88516 Abstract Only c90
Susan J. Wentworth (Lockheed Engineering and Sciences Co., Houston, TX.) and James L. Gooding *In* Lunar and Planetary Inst., Twenty-Fourth Lunar and Planetary Science Conference. Part 3: N-Z 1993 p 1507-1508 (For primary document see N94-20636 05-91)
Avail: CASI HC A01/MF A06

Previous work has shown that all three sub-groups of the shergottite, nakhlite, and chassignite (SNC) clan of meteorites contain aqueous precipitates of probable pre-terrestrial origin. In the context of secondary minerals, the most thoroughly studied shergottite has been Elephant Moraine, Antarctica A79001 (EETA79001). The recognition of LEW88516 as the latest SNC specimen, and its close similarity with ALHA77005, invite a comparative study of the latter two meteorites, and with EETA79001, from the perspective of aqueous alteration. The fusion crusts of the two meteorites are quite similar except that ALHA77005 is more vesicular (possibly indicating a higher indigenous volatile content). Secondary aluminosilicates (and salts on LEW88516) of definite Antarctic origin partially fill vesicles and fractures on both fusion crusts. Interior samples of the two meteorites are grossly similar in that traces of secondary minerals are present in both. Derived from text

N94-20870*# National Aeronautics and Space Administration. Lyndon B. Johnson Space Center, Houston, TX.
PETROLOGY AND GEOCHEMISTRY OF VLT GLASSES FROM DOUBLE DRIVE TUBE 79001/2 Abstract Only c25
Susan J. Wentworth (Lockheed Engineering and Sciences Co., Houston, TX.), D. J. Lindstrom, R. R. Martinez (Lockheed Engineering and Sciences Co., Houston, TX.), and D. S. McKay *In* Lunar and Planetary Inst., Twenty-Fourth Lunar and Planetary Science Conference. Part 3: N-Z 1993 p 1509-1510 (For primary document see N94-20636 05-91)
Avail: CASI HC A01/MF A06

As a part of more general studies of soils from Apollo 17 double drive tube 79001/2, glasses from the 79001/2 core are being analyzed by a multidisciplinary approach including SEM/EDS and INAA. Efforts are currently focused on VLT (very low-Ti; TiO_2 less than 1 wt%) mare glasses, which are common in 79001/2 and have also been found in other Apollo 17 soils. One of the primary objectives is to determine whether any or all of the Apollo 17 VLT glasses represent pristine volcanic compositions. In addition, the range of VLT glass compositions and possible relationships between the glasses and VLT lithic samples, for which some geochemical data have been obtained previously, is being defined. Derived from text

N94-20871*# Carnegie Institution of Washington, DC.
VARIETY IN PLANETARY SYSTEMS Abstract Only c90
George W. Wetherill *In* Lunar and Planetary Inst., Twenty-Fourth Lunar and Planetary Science Conference. Part 3: N-Z 1993 p 1511-1512 (For primary document see N94-20636 05-91)
Avail: CASI HC A01/MF A06

Observation of circumstellar disks, regular satellite systems of outer planets, and planet-size objects orbiting pulsars support the supposition that formation of planetary systems is a robust, rather than a fragile, byproduct of the formation and evolution of stars. The extent to which these systems may be expected to resemble one another and our Solar System, either in overall structure or in detail remains uncertain. When the full range of possible stellar masses, disk masses, and initial specific angular momenta are considered, the possible variety of planetary configurations is very large. Numerical modeling indicates a difference between the formation of small, inner, terrestrial planets and the outer planets. Derived from text

N94-20872*# North Dakota Univ., Grand Forks. Dept. of Space Studies.
ELEVATION AND IGNEOUS CRATER MODIFICATION ON VENUS: IMPLICATIONS FOR MAGMATIC VOLATILE CONTENT Abstract Only
R. W. Wichman *In* Lunar and Planetary Inst., Twenty-Fourth Lunar and Planetary Science Conference. Part 3: N-Z 1993 p 1513-1514 (For primary document see N94-20636 05-91)
Avail: CASI HC A01/MF A06

Although most impact craters on Venus preserve nearly pristine crater rim and ejecta features, a small number of craters have been identified showing clear evidence of either igneous intrusion emplacement (floor-fracturing) beneath the crater floor or of volcanically embayed exterior ejecta deposits. Since the volcanically embayed craters consistently occur at higher elevations than the identified floor-fractured craters, this report proposes that igneous crater modification on Venus is elevation dependent. This report describes how regional variations in magmatic neutral buoyancy could produce such elevation dependent crater modification and considers the implications for typical magmatic volatile contents on Venus. Derived from text

N94-20873*# North Dakota Univ., Grand Forks. Dept. of Space Studies.
LARGE FLOOR-FRACTURED CRATERS AND ISOSTATIC CRATER MODIFICATION: IMPLICATIONS FOR LITHOSPHERIC THICKNESS ON VENUS Abstract Only
R. W. Wichman and P. H. Schultz (Brown Univ., Providence, RI.) *In* Lunar and Planetary Inst., Twenty-Fourth Lunar and Planetary Science Conference. Part 3: N-Z 1993 p 1515-1516 (For primary document see N94-20636 05-91)
Avail: CASI HC A01/MF A06

Several of the largest craters on Venus, including Mead, Meitner and Isabella, exhibit well-developed floor fracture patterns combining a central set of radial features with a peripheral set of concentric fractures. This pattern strongly resembles the fracture patterns observed in the largest floor-fractured craters on the Moon (e.g. Humboldt, Gauss, Petavius). Although most lunar floor-fractured craters apparently reflect crater modification by igneous intrusions and volcanism, we propose that the

fractures in these larger craters represent domical flexure events in response to post-impact isostatic uplift. Since the extent of uplift and surface failure in this model depends on both the size of the basin cavity and the local lithospheric thickness, this interpretation also provides a means for constraining lithospheric thicknesses on Venus. Based on the apparent onset diameter of isostatic crater modification, we derive lithospheric thickness estimates for the Moon of approximately 80 - 100 km, and for Venus of approximately 50 - 70 km. Derived from text

N94-20874*# National Aeronautics and Space Administration. Lyndon B. Johnson Space Center, Houston, TX.

DEGRADATION SEQUENCE OF YOUNG LUNAR CRATERS FROM ORBITAL INFRARED SURVEY Abstract Only

M. A. Wieczorek (State Univ. of New York, Buffalo.) and W. W. Mendell *In* Lunar and Planetary Inst., Twenty-Fourth Lunar and Planetary Science Conference. Part 3: N-Z 1993 p 1517-1518 (For primary document see N94-20636 05-91)

Avail: CASI HC A01/MF A06

Using new software, nighttime thermal maps of the lunar surface have been generated from data obtained by the Apollo 17 Infrared Scanning Radiometer (ISR) in lunar orbit. Most of the thermal anomalies observed in the maps correspond to fresh lunar craters because blocks on the lunar surface maintain a thermal contrast relative to surrounding soil during the lunar night. Craters of Erastosthenian age and older - relatively young by lunar standards - have developed soil covers that make them almost indistinguishable from their surroundings in the thermal data. Thermal images of Copernican age craters show various stages of a degradation process, allowing the craters to be ranked by age. The ISR data should yield insights into lunar surface evolution as well as a more detailed understanding of the bombardment history after formation of the great mare basins.

Derived from text

N94-20875*# Eidgenoessische Technische Hochschule, Zurich (Switzerland).

A LONG-TERM CHANGE OF THE AR/KR/XE FRACTIONATION IN THE SOLAR CORPUSCULAR RADIATION Abstract Only c92

R. Wieler, H. Baur, and P. Signer *In* Lunar and Planetary Inst., Twenty-Fourth Lunar and Planetary Science Conference. Part 3: N-Z 1993 p 1519-1520 Sponsored in part by the Swiss NSF (For primary document see N94-20636 05-91)

Avail: CASI HC A01/MF A06

Solar noble gases in an ilmenite separate from breccia 79035 (antiquity greater than 1 Ga) were analyzed by closed system stepped etching (CSSE). All five gases show the familiar two-component structure: first solar-wind (SW) gases are released, followed by gases from solar energetic particles (SEP). Element patterns in 79035 are similar to those of 71501 ilmenite. SW-He-Ne were partly lost, but SEP-He-Ne-Ar are retained (nearly) unfractionated. Constant Ar/Kr/Xe ratios indicate that ilmenites contain an unfractionated sample of the heavy SW-SEP noble gases. Ar/Kr/Xe ratios in the solar corpuscular radiation are, however, different from 'solar system' values, whereby the Kr/Xe difference in 79035 is about twice as large as in 71501. We propose that Xe is less fractionated than Kr and Ar, though its first ionization potential (FIP) is higher than the 'cutoff' at approximately 11.5 eV, above which all elements in SEP are usually assumed to be depleted by a roughly constant factor. SW-Ne may be isotopically slightly heavier in the ancient SW trapped by 79035, as proposed earlier. In this work we extend our previous CSSE studies of solar noble gases including Kr and Xe to a lunar sample irradiated at least 1 Ga ago (breccia 79035, ilmenite separate, 42-64 microns). This sample was particularly gently etched in the first steps. Surprisingly, the first three steps, each releasing less than or equal to 0.5% of the total 36-Ar, showed an SEP-like trapped component plus relatively large concentrations of cosmogenic gases. Steps 4ff contain much less cosmogenic and more solar gas with a SW-like isotope pattern. Thus, a very minor easily etchable phase that has completely lost its SW-gases must be responsible for steps 1-3. We will not discuss these steps here and refer to the actual step 4 as the 'initial' etching step. Derived from text

N94-20876*# Arizona State Univ., Tempe. Dept. of Geology.

MULTISPECTRAL STUDIES OF SELECTED CRATER- AND BASIN-FILLING LUNAR MARIA FROM GALILEO EARTH-MOON ENCOUNTER 1 Abstract Only

D. A. Williams, R. Greeley, G. Neukum (Deutsche Forschungs- und Versuchsanstalt fuer Luft- und Raumfahrt, Berlin, Germany.), and R. Wagner (Deutsche Forschungs- und Versuchsanstalt fuer Luft- und Raumfahrt, Berlin, Germany.) *In* Lunar and Planetary Inst., Twenty-Fourth Lunar and Planetary Science Conference. Part 3: N-Z 1993 p 1521-1522 (For primary document see N94-20636 05-91)

Avail: CASI HC A01/MF A06

New visible and near-infrared multispectral data of the Moon were obtained by the Galileo spacecraft in December, 1990. These data were calibrated with Earth-based spectral observations of the nearside to compare compositional information to previously uncharacterized mare basalts filling craters and basins on the western near side and eastern far side. A Galileo-based spectral classification scheme, modified from the Earth-based scheme developed by Pieters, designates the different spectral classifications of mare basalt observed using the 0.41/0.56 micron reflectance ratio (titanium content), 0.56 micron reflectance values (albedo), and 0.76/0.99 micron reflectance ratio (absorption due to Fe(2+) in mafic minerals and glass). In addition, age determinations from crater counts and results of a linear spectral mixing model were used to assess the volcanic histories of specific regions of interest. These interpreted histories were related to models of mare basalt petrogenesis in an attempt to better understand the evolution of lunar volcanism. Derived from text

N94-20877*# Carnegie Institution of Washington, DC.

EQUILIBRIUM MODELS OF MASS DISTRIBUTION AND COLLISIONAL LIFETIMES OF ASTEROIDS Abstract Only c90

David R. Williams and George Wetherill *In* Lunar and Planetary Inst., Twenty-Fourth Lunar and Planetary Science Conference. Part 3: N-Z 1993 p 1523-1524 (For primary document see N94-20636 05-91)

Avail: CASI HC A01/MF A06

An understanding of the steady state distribution expected in the present day asteroid belt is important to our understanding of the collisional evolution of the asteroids and their physical properties. We have extended earlier work to show that, in the absence of gravity, a simple power law distribution as a function of mass with constant exponent will give an equilibrium distribution of asteroids for all bodies much smaller than the largest asteroids. This result holds for realistic fragmentation mechanisms and is independent of the physical properties of the asteroids. Inclusion of the effects of gravity on disruption and fragmentation of asteroids precludes an analytic solution to this problem, and rules out a simple power law distribution. We are currently calculating numerical solutions in order to determine the expected steady state mass distribution in the asteroid belt.

Derived from text

N94-20878*# Brown Univ., Providence, RI. Dept. of Geological Sciences.

FORMATION OF PERCHED LAVA PONDS ON BASALTIC VOLCANOES: INTERACTION BETWEEN COOLING RATE AND FLOW GEOMETRY ALLOWS ESTIMATION OF LAVA EFFUSION RATES Abstract Only c46

L. Wilson and E. A. Parfitt *In* Lunar and Planetary Inst., Twenty-Fourth Lunar and Planetary Science Conference. Part 3: N-Z 1993 p 1525-1526 (For primary document see N94-20636 05-91)

Avail: CASI HC A01/MF A06

Perched lava ponds are infrequent but distinctive topographic features formed during some basaltic eruptions. Two such ponds, each approximately 150 m in diameter, formed during the 1968 eruption at Napau Crater and the 1974 eruption of Mauna Ulu, both on Kilauea Volcano, Hawaii. Each one formed where a channelized, high volume flux lava flow encountered a sharp reduction of slope: the flow spread out radially and stalled, forming a well-defined terminal levee enclosing a nearly circular lava pond. We describe a model of how cooling limits the motion of lava spreading radially into a pond and compare this with the case of a channelized flow. The difference in geometry has a major effect, such that the size of a pond is a good indicator of the volume flux of the lava forming it. Lateral spreading on distal shallow slopes is a major factor limiting the lengths of lava flows.

Derived from text

N94-20879*# Lancaster Univ. (England). Environmental Science Div.

A CLASSIFICATION SCHEME FOR THE MORPHOLOGY OF LAVA FLOW FIELDS Abstract Only c46

L. Wilson, H. Pinkerton, James W. Head (Brown Univ., Providence, RI.),

and K. Magee Roberts (Brown Univ., Providence, RI.) *In* Lunar and Planetary Inst., Twenty-Fourth Lunar and Planetary Science Conference. Part 3: N-Z 1993 p 1527-1528 (For primary document see N94-20636 05-91)
Avail: CASI HC A01/MF A06

Analysis of the processes controlling the advance of lava flows shows that, if no other factors intervene, thermal constraints will act to limit the maximum length of a flow being fed at a given volume or mass effusion rate from a vent. These constraints can be characterized through the Gratz number, which takes on a large value at the vent and decreases down flow. Early application of this principle showed that, despite the many subtleties of modes of heat loss from flows, motion apparently ceases when the Gratz number has decreased to a value close to 300. Recent analyses of flow units from the 1983-86 Pu'u 'O'o eruption of Kilauea and of other, more silicic lava flow units confirm this finding.
Derived from text

N94-20880*# National Aeronautics and Space Administration. Lyndon B. Johnson Space Center, Houston, TX.
CERN-DERIVED ANALYSIS OF LUNAR RADIATION BACKGROUNDS Abstract Only **c89**
Thomas L. Wilson and Robert Svoboda (Louisiana State Univ., Baton Rouge.) *In* Lunar and Planetary Inst., Twenty-Fourth Lunar and Planetary Science Conference. Part 3: N-Z 1993 p 1529-1530 (For primary document see N94-20636 05-91)
Avail: CASI HC A01/MF A06

The Moon produces radiation which background-limits scientific experiments there. Early analyses of these backgrounds have either failed to take into consideration the effect of charm in particle physics (because they pre-dated its discovery), or have used branching ratios which are no longer strictly valid (due to new accelerator data). We are presently investigating an analytical program for deriving muon and neutrino spectra generated by the Moon, converting an existing CERN computer program known as GEANT which does the same for the Earth. In so doing, this will (1) determine an accurate prompt neutrino spectrum produced by the lunar surface; (2) determine the lunar subsurface particle flux; (3) determine the consequence of charm production physics upon the lunar background radiation environment; and (4) provide an analytical tool for the NASA astrophysics community with which to begin an assessment of the Moon as a scientific laboratory versus its particle radiation environment. This will be done on a recurring basis with the latest experimental results of the particle data groups at Earth-based high-energy accelerators, in particular with the latest branching ratios for charmed meson decay. This will be accomplished for the first time as a full 3-dimensional simulation.
Derived from text

N94-20881*# Purdue Univ., West Lafayette, IN. Dept. of Chemistry.
MULTIVARIATE STATISTICAL ANALYSIS: PRINCIPLES AND APPLICATIONS TO COORBITAL STREAMS OF METEORITE FALLS Abstract Only **c65**
S. F. Wolf and M. E. Lipschutz *In* Lunar and Planetary Inst., Twenty-Fourth Lunar and Planetary Science Conference. Part 3: N-Z 1993 p 1531-1532 (For primary document see N94-20636 05-91)
Avail: CASI HC A01/MF A06

Multivariate statistical analysis techniques (linear discriminant analysis and logistic regression) can provide powerful discrimination tools which are generally unfamiliar to the planetary science community. Fall parameters were used to identify a group of 17 H chondrites (Cluster 1) that were part of a coorbital stream which intersected Earth's orbit in May, from 1855 - 1895, and can be distinguished from all other H chondrite falls. Using multivariate statistical techniques, it was demonstrated that a totally different criterion, labile trace element contents - hence thermal histories - or 13 Cluster 1 meteorites are distinguishable from those of 45 non-Cluster 1 H chondrites. Here, we focus upon the principles of multivariate statistical techniques and illustrate their application using non-meteoritic and meteoritic examples.
Derived from text

N94-20882*# Houston Univ., TX. Dept. of Geosciences.
CHARACTERIZATION OF THE MARQUEZ DOME BURIED IMPACT CRATER USING GRAVITY AND MAGNETIC DATA Abstract Only **c46**
A. M. Wong, A. M. Reid, S. A. Hall, and V. L. Sharpton (Lunar and Planetary Inst., Houston, TX.) *In* Lunar and Planetary Inst., Twenty-Fourth Lunar and Planetary Science Conference. Part 3: N-Z 1993 p 1533-1534 (For primary document see N94-20636 05-91)
Avail: CASI HC A01/MF A06

The buried impact crater, Marquez Dome, located in Leon County in east central Texas, is an approximately 15 km diameter structure whose central uplift is now partially exposed due to headward erosion of the post-impact cover. The central uplift is approximately 3 km in diameter and the rocks within it have been uplifted more than 1200 m above their regional level. The crater rim remains buried and previous attempts to determine its location have had to rely on seismic reflection data and geologic well logs. These attempts have been somewhat successful in mapping the extent of the disturbed zone around Marquez Dome, but more limited in their ability to image the shallow buried rim. In an attempt to define accurately the whole Marquez Dome structure and assist in the selection of drilling sites, a geophysical investigation involving gravity and magnetic data over the central uplift and the surrounding area has been undertaken.
Derived from text

N94-20883*# North Dakota Univ., Grand Forks. Space Studies.
MORPHOLOGIC CLASSES OF IMPACT BASINS ON VENUS Abstract Only
Charles A. Wood and Wesley Tam *In* Lunar and Planetary Inst., Twenty-Fourth Lunar and Planetary Science Conference. Part 3: N-Z 1993 p 1535-1536 (For primary document see N94-20636 05-91)
Avail: CASI HC A01/MF A06

An independent survey of 60% of Venus has resulted in the detection of 35 impact basins and associated transitional rings. Contrary to previous studies central peak basins have been identified, as well as peak ring basins. But no unambiguous multi-ring basins have been detected. A new class of crateriform - expanded peak structure - has been noticed, which is transitional in diameter, but apparently not in structure, between central peak and peak ring basins.
Derived from text

N94-20884*# California State Univ., Fullerton.
LREE VARIABILITY IN CM MATRICES: ANOTHER LOOK AT METEORITE COMPACTION AGES Abstract Only **c90**
Dorothy S. Woolum, Karen Poelstra, C. Alexander (Washington Univ., Saint Louis, MO.), and T. Ireland (Australian National Univ., Canberra.) *In* Lunar and Planetary Inst., Twenty-Fourth Lunar and Planetary Science Conference. Part 3: N-Z 1993 p 1537-1538 (For primary document see N94-20636 05-91)
Avail: CASI HC A01/MF A06

Recent Neon-21 analyses indicate that individual grains in some CM meteorites show the effects of enhanced exposures to energetic particles beyond that which can be attributed to conventional cosmic ray exposure. The exposures clearly occurred prior to the final compaction of the CM meteorites. These exposures were of such a magnitude that they require that we either have to revise our understanding of regolith dynamics and the time scales involved in the regolith activity of meteorite parent bodies, or must invoke an exposure of the irradiated grains to an enhanced energetic particle environment, an environment which would most likely be produced by an early active sun. Constraints on the compaction ages of the meteorites which exhibit the large precompaction exposures could play a critical role in resolving this issue.
Derived from text

N94-20885*# Open Univ., Milton (England). Dept. of Earth Sciences.
THE CARBON COMPONENTS IN SNC METEORITES OF FELDSPATHIC HARZBURGITE COMPOSITION Abstract Only **c90**
I. P. Wright, C. Douglas, and C. T. Pillinger *In* Lunar and Planetary Inst., Twenty-Fourth Lunar and Planetary Science Conference. Part 3: N-Z 1993 p 1539-1540 (For primary document see N94-20636 05-91)
Avail: CASI HC A01/MF A06

Two meteorites collected in Antarctica, ALH A77005 and LEW 88516, have characteristics which link them to the shergottite group of SNC meteorites. Essentially, ALH A77005 and LEW 88516 are feldspathic harzburgites, being comprised of roughly equal quantities of olivine and pyroxene, with an additional few percent of feldspar which has subsequently been converted to maskelynite by shock. The meteorites represent samples of a cumulate rock which is itself composed of two different lithologies: in one, large pyroxenes poikilitically enclose olivine crystals, while the other consists of interstitial areas made up of pyroxene, olivine, maskelynite, whitlockite, troilite, ilmenite and chlorapatite. It has been proposed that

meteorites such as ALH A77005 (and LEW 88516) are relict samples of the source peridotite from which the other shergottites formed. As such it should be informative to study in detail the carbon components present within these samples, in order to make comparisons with data from other shergottites. Although not plutonic in origin, and therefore not sampling a truly deep source, analyses of ALH A77005 and LEW 88516 should assist with attempts to define the bulk carbon isotopic composition of Mars. This has been assessed previously through analyses of carbon of presumed magmatic origin in other SNC meteorites, but the carbon isotopic compositions obtained seem to be at variance with what might be expected. It is important to constrain the carbon isotopic composition of Mars as well as possible so that models of atmospheric evolution, based on carbon isotopic data, can yield the most reliable results. Author

N94-20886*# Open Univ., Milton (England). Dept. of Earth Sciences.
FURTHER CARBON ISOTOPE MEASUREMENTS OF LEW 88516 Abstract Only **c90**
I. P. Wright, C. Douglas, and C. T. Pillinger *In* Lunar and Planetary Inst., Twenty-Fourth Lunar and Planetary Science Conference. Part 3: N-Z 1993 p 1541-1542 (For primary document see N94-20636 05-91)
Avail: CASI HC A01/MF A06

Douglas et al. have previously analyzed the carbon content and isotopic composition of a crushed sample (sub-sample 13) of the shergottite, LEW 88516. The powder, which was from a relatively large portion of the meteorite in order to obtain a representative sample, was distributed amongst the scientific community. However, it is probable that the preparation procedure was not optimized for the purposes of carbon measurements. Indeed, it was found that LEW 88516,13 contained over 1200 ppm carbon, a concentration which is greater than that present in any other SNC meteorite. That a close relative, ALH A77005, contains only 141 ppm carbon seems to implicate the preparation procedure as being responsible for the apparently high carbon content of LEW 88516. However, it may also be the nature of the fine powder which has resulted in contamination. The observation of high carbon content in LEW 88516,13 highlights the extreme difficulty of trying to obtain representative samples of whole meteorites for this kind of investigation. Presented herein are some further measurements of LEW 88516 which should serve to clarify some of the issues raised by the previous investigation. Author

N94-20887*# Chinese Academy of Geological Sciences, Beijing. Inst. of Mineral Deposits.
SHOCK ATTENUATION AT THE SLATE ISLANDS REVISITED Abstract Only **c46**
S. Wu, P. B. Robertson (Geological Survey of Canada, Ottawa, Ontario.), and R. A. F. Grieve (Geological Survey of Canada, Ottawa, Ontario.) *In* Lunar and Planetary Inst., Twenty-Fourth Lunar and Planetary Science Conference. Part 3: N-Z 1993 p 1543-1544 (For primary document see N94-20636 05-91)
Avail: CASI HC A01/MF A06

This study of a more extensive suite of Slate Islands samples confirms previous interpretations. It indicates clearly that recorded shock pressures, as determined by planar deformation feature orientations, increased towards the center. The 'shock center' is very close (considering the structural movements during cavity modification) to that from an independent determination from shatter cone orientations. Shock metamorphism at a higher level in breccia clasts than in the adjacent country rocks is evidence that the shock event preceded the formation of the breccia dikes. These observations, which are consistent with those at other impact structures, are all contrary to the interpretation by Sage that breccia dike formation by diatreme action was the source of the shock event. There is no plausible reason to consider the Slate Islands as anything but the emergent portion of the central uplift of a complex impact crater. It cannot be cited as an example of endogenic shock in arguments regarding evidence of impact in the terrestrial stratigraphic record. Author

N94-20888*# Arizona State Univ., Tempe. Dept. of Geology.
CONVEX SET AND LINEAR MIXING MODEL Abstract Only **c43**
P. Xu and R. Greeley *In* Lunar and Planetary Inst., Twenty-Fourth Lunar and Planetary Science Conference. Part 3: N-Z 1993 p 1545-1546 (For primary document see N94-20636 05-91)
Avail: CASI HC A01/MF A06

A major goal of optical remote sensing is to determine surface compositions of the earth and other planetary objects. For assessment of composition, single pixels in multi-spectral images usually record a mixture of the signals from various materials within the corresponding surface area. In this report, we introduce a closed and bounded convex set as a mathematical model for linear mixing. This model has a clear geometric implication because the closed and bounded convex set is a natural generalization of a triangle in n-space. The endmembers are extreme points of the convex set. Every point in the convex closure of the endmembers is a linear mixture of those endmembers, which is exactly how linear mixing is defined. With this model, some general criteria for selecting endmembers could be described. This model can lead to a better understanding of linear mixing models. Author

N94-20889*# Rutgers Univ., New Brunswick, NJ. Dept. of Chemistry.
STABLE Ni ISOTOPES AND Be-10 AND Al-26 IN METALLIC SPHEROIDS FROM METEOR CRATER, ARIZONA Abstract Only **c46**
S. Xue, G. F. Herzog, G. S. Hall, J. Klein (Pennsylvania Univ., Philadelphia.), R. Middleton (Pennsylvania Univ., Philadelphia.), and D. Juenemann (Pennsylvania Univ., Philadelphia.) *In* Lunar and Planetary Inst., Twenty-Fourth Lunar and Planetary Science Conference. Part 3: N-Z 1993 p 1547-1548 (For primary document see N94-20636 05-91)
Avail: CASI HC A01/MF A06

The Canyon Diablo spheroids, which are found around Meteor Crater, Arizona, are nickel-enriched objects with diameters from less than 0.1 to several mm. Previous studies have suggested that the enrichment of nickel resulted either from shock-melting of S-rich areas followed by solidification of the liquids under strongly non-equilibrium conditions at rapid cooling rates during flight outward from the crater or from the selective oxidation of iron. Isotopic studies are an effective tool for constraining the degree of open-system evaporation experienced by a system. The purpose of this study was to see whether Ni isotopes had been fractionated by volatilization during spheroid formation. In addition, the cosmogenic nuclides Be-10 and Al-26 were measured to try to estimate the depths in the parent meteorite from which the spheroids came. Author

N94-20890*# Tokyo Univ. (Japan). Inst. for Cosmic Ray Research.
GEOMETRICAL ANALYSIS OF THE MICROCRATERS FOUND ON LDEF SAMPLES Abstract Only **c18**
Kazuo Yamakoshi, Hideo Ohashi, Motosaku Noma (Yamagata Univ., Japan.), Hirohisa Sakurai (Yamagata Univ., Japan.), Kazuo Nakashima (Yamagata Univ., Japan.), Kenichi Nogami (Dokkyo Univ., Tochigi, Japan.), and Rie Omori (Dokkyo Univ., Tochigi, Japan.) *In* Lunar and Planetary Inst., Twenty-Fourth Lunar and Planetary Science Conference. Part 3: N-Z 1993 p 1549-1550 (For primary document see N94-20636 05-91)
Avail: CASI HC A01/MF A06

Diameters (D) and depths (T) of microcraters found on LDEF samples were measured and their origins were deduced by the (D/T) ratios, which distinguish projectile materials. From the results, one iron and several stony projectiles could be recognized. Author (revised)

N94-20891*# Tokyo Univ. (Japan). Electro-Communications.
ANTIPODAL FRAGMENT VELOCITIES FOR POROUS AND WEAK TARGETS AT CATASTROPHIC IMPACTS Abstract Only **c39**
M. Yanagisawa and T. Itoi *In* Lunar and Planetary Inst., Twenty-Fourth Lunar and Planetary Science Conference. Part 3: N-Z 1993 p 1551-1552 Sponsored in part by ISAS (For primary document see N94-20636 05-91)
Avail: CASI HC A01/MF A06

Mortar, porous alumina, and sand targets, which were spherical in shape and from 11 to 15 cm in diameter, were impacted normally by plastic (polycarbonate) projectiles of nearly 1 g in mass at velocities about 6 km/s. Fragment velocity at the antipole of impact site (antipodal velocity, V(sub a)), for each experiment, was obtained from two Flash X-ray images recorded prior to and at predetermined delayed time after impact event. It has been revealed that the velocities for the same E/M(sub t) (impact energy divided by target mass) depend strongly on target material, and differ about an order of magnitude between the sand and basalt.
Author (revised)

N94-20893*# National Aeronautics and Space Administration. Lyndon B. Johnson Space Center, Houston, TX.
CONSORTIUM REPORTS ON LUNAR METEORITES YAMATO 793169 AND ASUKA 881757, A NEW TYPE OF MARE BASALT Abstract Only **c90**

Keizo Yanai (National Inst. of Polar Research, Tokyo, Japan.), Hiroshi Takeda (Tokyo Univ., Japan.), M. M. Lindstrom, M. Tatsumoto (Geological Survey, Denver, CO.), N. Torigoe (Geological Survey, Denver, CO.), K. Misawa (National Inst. of Polar Research, Tokyo, Japan.), P. H. Warren (California Univ., Los Angeles.), G. W. Kallemeyn (California Univ., Los Angeles.), C. Koeberl (Wien Univ., Austria.), and H. Kojima (National Inst. of Polar Research, Tokyo, Japan.) et al *In* Lunar and Planetary Inst., Twenty-Fourth Lunar and Planetary Science Conference. Part 3: N-Z 1993 p 1555-1556 (For primary document see N94-20636 05-91)
Avail: CASI HC A01/MF A06

Consortium studies on lunar meteorites Yamato 793169 and Asuka 881757 (formerly Asuka-31) were performed to characterize these new samples from unknown locations in the lunar mare. Both meteorites are coarse-grained mare rocks having low Mg/Fe ratios (bulk mg'=30-35) and low TiO2 (1.5-2.5 percent in homogenized bulk samples). They are intermediate between VLT and low-Ti mare basalts. Although these meteorites are not identical to each other, their mineral and bulk compositions, isotopic systematics, and crystallization ages are remarkably similar and distinct from those of all other mare basalts. They appear to represent a new type of low-Ti mare basalt that crystallized at about 3.9Ga. These meteorites are inconsistent with the canonical correlation between the TiO2 contents and ages of mare basalts and suggest that our knowledge of lunar volcanism is far from complete. Author

N94-20894*# Lehigh Univ., Bethlehem, PA. Dept. of Materials Science and Engineering.
PRELIMINARY AEM STUDY OF THE MICROSTRUCTURE AND COMPOSITION OF METAL PARTICLES IN ORDINARY CHONDRITES Abstract Only **c90**

C. W. Yang, D. B. Williams, and J. I. Goldstein *In* Lunar and Planetary Inst., Twenty-Fourth Lunar and Planetary Science Conference. Part 3: N-Z 1993 p 1557-1558 (For primary document see N94-20636 05-91)
Avail: CASI HC A01/MF A06

The purpose of this study is to examine the microstructure and composition of the metal particles in ordinary chondrites using analytical electron microscopy (AEM) techniques. Since the phases produced within the metal particles are very fine, the application of various AEM techniques for structural and chemical characterization is critical. However, thin specimen preparation for AEM study has proven very difficult because of the matrix silicate which is present. This is the first AEM study of the metal particles in chondrites. A type 6 chondrite, Saint Severin (LL6), was selected for examination because the metal phases have been reheated into the single phase taenite region (greater than 700 C), and cooled slowly to lower temperatures. A combination of electron optical instruments was employed including a field emission gun (FEG) JEOL 840F high resolution scanning electron microscope (HRSEM), a JEOL 6300F FEG-HRSEM, a Philips 400T AEM, and a JEOL 733 electron probe microanalyzer (EPMA). Author

N94-20895*# European Space Research Lab., Noordwijk (Netherlands). Space Science Dept.
MICROMETEORITE PRE-SOLAR DIAMONDS FROM GREENLAND CRYOCONITE? Abstract Only **c90**

P. D. Yates *In* Lunar and Planetary Inst., Twenty-Fourth Lunar and Planetary Science Conference. Part 3: N-Z 1993 p 1559-1560 (For primary document see N94-20636 05-91)
Avail: CASI HC A01/MF A06

An acid-resistant residue prepared from Greenland cryoconite has been investigated to determine whether the micrometeorite component within the cryoconite contains pre-solar material analogous to that found in primitive chondritic meteorites. The residue has been analyzed for carbon content and stable isotopic comparison, by electron probe micro-analysis (EPMA) for major element chemistry and then by a combination of X-ray diffraction (XRD) and transmission electron microscopy (TEM) to elucidate the structure of any constituent mineral phases. The cryoconite sample, which was collected ca. 25 km inland of the ice margin at the latitude of Sondre Stromfjord on the west coast of Greenland, was processed following procedures used on bulk meteorite samples for the isolation of pre-solar dust components. Author (revised)

N94-20896*# Jet Propulsion Lab., California Inst. of Tech., Pasadena.
THE CONNECTION BETWEEN VENUS' FREE OBLIQUITY AND ITS CMB OBLATENESS Abstract Only

C. F. Yoder *In* Lunar and Planetary Inst., Twenty-Fourth Lunar and Planetary Science Conference. Part 3: N-Z 1993 p 1561-1562 (For primary document see N94-20636 05-91)
Avail: CASI HC A01/MF A06

The most striking feature of Venus rotational state is its slow retrograde rotation which is apparently maintained by a balance between solid tidal friction and thermal tidal torques. Solid tides tend to drive the spin toward synchronous rotation while thermal tides drive it away. A balance is achieved at a specific rate because of the inverse frequency dependence of the thermal tide to the semi-diurnal heating. Atmospheric models have been constructed to estimate the thermal tidal torque based on ground heating. The solid friction dissipation factor Q approximately equal to 50 can be deduced assuming rotation has achieved steady state. The most perplexing feature of Venus orientation is its non-zero free obliquity epsilon approximately equal to 1.5 deg relative to its orbit. Although solid tides and perhaps atmospheric tides tend to increase the free obliquity on a time 1/K(sub t) approximately equal to 1 x 10(exp 8) yr, viscous friction (CMF) at a core-mantle boundary (CMB) resulting from the differential angular orientation Delta-epsilon of the core and mantle spin axes should have damped the free obliquity on a time scale as short as 10(exp 6) yr. One means of achieving a balance similar to that controlling rotation is to introduce a comparatively large CMB ellipticity e(sub c) to reduce Delta-epsilon such that there is a balance between solid-thermal tides and CMF. The balance depends not so much on the potential frequency dependence on the tides as on the quadratic dependence of CMF on Delta-epsilon if the layer is turbulent. Author

N94-20897*# Chicago Univ., IL. Dept. of the Geophysical Sciences.
TRACE ELEMENT COMPOSITIONS OF SPINEL-RICH REFRACTORY INCLUSIONS FROM THE MURCHISON METEORITE Abstract Only **c90**

S. Yoneda, P. J. Sylvester, S. B. Simon, L. Grossman, and A. Hsu (Illinois Mathematics and Science Academy, Aurora.) *In* Lunar and Planetary Inst., Twenty-Fourth Lunar and Planetary Science Conference. Part 3: N-Z 1993 p 1563-1564 (For primary document see N94-20636 05-91)
Avail: CASI HC A01/MF A06

Three spinel-rich, perovskite-bearing, pyroxene-rimmed, hibonite-free inclusions from the Murchison C2 chondrite have volatility controlled, modified group II REE patterns. Two have high Eu/Yb ratios, two have small positive Ce anomalies and one has high refractory siderophiles for a group II inclusion. Two additional spinel-rich inclusions have subchondritic Ce/La ratios and negative Eu and Yb anomalies, the Eu anomalies being larger than the Yb ones. One of these inclusions is enriched in La relative to all HREE and the other is enriched in HREE relative to all LREE except La, possibly suggesting the presence of an ultrarefractory component in the latter. One hibonite-rich inclusion has a group III REE pattern with a negative Ce anomaly. A calcium dialuminate-bearing inclusion known to have crystallized from a melt at 2100-1800K has a modified group II REE pattern, rather than a pattern which would be predicted from the evaporation expected from such a droplet, e.g., a group III or ultrarefractory pattern. Volatile element contents of these inclusions are among the lowest found in any refractory inclusions. Author

N94-20898*# Tsukuba Univ. (Japan). Inst. of Geoscience.
INTER- AND INTRA-CRYSTALLINE OXYGEN ISOTOPE DISTRIBUTION OF FASSAITES IN ALLENDE CAI Abstract Only **c90**

Hisayoshi Yurimoto, Hiroshi Nagasawa (Gakushuin Univ., Tokyo, Japan.), and Yoshiharu Mori (National Lab. for High Energy Physics, Ibaraki, Japan.) *In* Lunar and Planetary Inst., Twenty-Fourth Lunar and Planetary Science Conference. Part 3: N-Z 1993 p 1565-1566 (For primary document see N94-20636 05-91)
Avail: CASI HC A01/MF A06

Calcium, aluminum-rich inclusions (CAI's) from carbonaceous chondrite are believed to be among the first solids to have formed in the early solar system and thus to preserve a record of conditions and processes that prevailed early in the solar nebula. We have measured inter- and intra-crystalline oxygen isotope distribution of fassaite in Type B1 CAI of Allende

meteorite. Secondary ion mass spectrometry (SIMS) using negative Au primary ion was applied to in situ oxygen isotope ratio analysis on a polished thin section of the CAI. Present data indicate that O isotope composition is homogeneous inside of fassaite grains as well as among grains in the HN3-1 CAI, and that the delta(exp 18) O value (-24.14 percent relative to SMOW) determined previously could be applied to most fassaite grains. The results suggest that most fassaite grains are preexisting solids like spinel grains. Author

N94-20899*# Lehigh Univ., Bethlehem, PA. Dept. of Earth and Environmental Sciences.
AGE AND THERMOCHRONOLOGY OF K-FELDSPARS FROM THE MANSON IMPACT STRUCTURE Abstract Only **c46**
P. K. Zeitler and M. J. Kunk (Geological Survey, Reston, VA.) *In* Lunar and Planetary Inst., Twenty-Fourth Lunar and Planetary Science Conference. Part 3: N-Z 1993 p 1567-1568 (For primary document see N94-20636 05-91)
Avail: CASI HC A01/MF A06

As a contribution to the effort to obtain a precise age for the Manson Impact Structure, we are approaching the problem from a thermo chronological perspective, with the goal of extracting an age from Ar-40/Ar-39 age-spectrum analysis of partially overprinted K-feldspars taken from granitoid clasts. We find that shocked feldspars from Manson generally show a strong overprint in their age spectra, with more than 50 percent of each spectrum being reset. The reset portions of the age spectra correspond to gas lost from very small diffusion domains, and a characteristic of the Manson samples is the very large range in apparent diffusion dimensions that they display, with the smallest domains being some 400 times smaller than the largest domains. It is also noteworthy that the small domains comprise a substantial portion of the volume of the feldspars (50 percent or more). These observations are consistent with the extreme shock experienced by these samples. In detail, the spectra we have measured to date are saddle-shaped and show minimum ages of between 67 and 72 Ma, which we interpret to be maximum estimates for the age of the impact. In the case of one sample (M1-678.3; K-feldspar from a large syenite block located well below the apparent melt-matrix breccia in the M1 borehole), isotope correlation analysis suggests the presence of a non-atmospheric trapped Ar component (Ar-40/Ar-36 of 660 plus or minus 40), and an age of about 65.3 plus or minus 0.5 Ma (2 sigma). Our interpretation of our results is that the shock of impact greatly reduced the diffusion-domain sizes of our samples, making them susceptible to significant Ar loss during heating associated with impact. It appears that while our feldspars were partially open to Ar loss, they equilibrated with a non-atmospheric Ar component, probably related to impact-related degassing of old basement around the impact site. Author

N94-20900*# National Aeronautics and Space Administration. Ames Research Center, Moffett Field, CA.
SPECTRAL ANALYSIS OF CHEMISORBED CO2 ON MARS ANALOG MATERIALS Abstract Only
A. P. Zent and T. L. Roush *In* Lunar and Planetary Inst., Twenty-Fourth Lunar and Planetary Science Conference. Part 3: N-Z 1993 p 1569-1570 (For primary document see N94-20636 05-91)
Avail: CASI HC A01/MF A06

The goal of this work is to estimate the mass of CO2 that may have been removed to a quasi-stable reservoir on the Martian surface by chemisorption and to estimate the spectral effects of chemisorbed CO2 in remotely-sensed Martian spectra. Our approach is to characterize the conditions most favorable for the formation of carbonate on common terrestrial oxide minerals and to search for infrared spectral bands that result from chemisorption of CO2 molecules onto oxide and other Mars analog materials. Author

N94-20901*# Arkansas Univ., Fayetteville. Cosmochemistry Group.
LEWIS CLIFF 87057: A NEW METAL-RICH E3 CHONDRITE WITH SIMILARITIES TO MT. EGERTON, SHALLOWATER AND HAPPY CANYON Abstract Only **c90**
Y. Zhang, P. H. Benoit, and D. W. G. Sears *In* Lunar and Planetary Inst., Twenty-Fourth Lunar and Planetary Science Conference. Part 3: N-Z 1993 p 1571-1572 (For primary document see N94-20636 05-91)
(Grant NAG9-81)
Avail: CASI HC A01/MF A06

The Antarctic meteorites LEW87057, LEW87220, LEW87223, LEW87234, LEW87237, and LEW87285 were described as paired E3 chondrites by Brian Mason (Antarctic Meteorite Newsletters, 12(1) and 15(1,2)). LEW87223 is texturally unusual, containing abundant chondrules and jagged troilite grains which are enclosed in metal. Our INAA data show that the siderophile element abundance in two splits of LEW87223 are higher than the EH range, while chalcophile elements (Cr excepted) are highly depleted. Mineral compositions are unlike those normally found in EH or EL chondrites or aubites, and in some respects resemble those of several anomalous enstatite meteorites such as Shallowater, Mt. Egerton, and Happy Canyon. The bulk and mineral compositions are consistent with the addition of EL chondrite metal to an EL3 chondrite with the removal of sulfides other than troilite which is now Cr-rich. We suggest that this meteorite is an EL3 chondrite into which metal was introduced and sulfides redistributed during an event involving impact melting and brecciation. Author

N94-20902*# Chicago Univ., IL. Dept. of Geophysical Sciences.
CHEMICAL ZONING AND DIFFUSION OF Ca, Al, Mn, AND Cr IN OLIVINE OF SPRINGWATER PALLASITE Abstract Only **c90**
Y. Zhou and Ian M. Steele *In* Lunar and Planetary Inst., Twenty-Fourth Lunar and Planetary Science Conference. Part 3: N-Z 1993 p 1573-1574 (For primary document see N94-20636 05-91)
Avail: CASI HC A01/MF A06

The pallasites, consisting mainly of Fe-Ni metal and olivine, are thought to represent the interior of a planetary body which slowly cooled from high temperature. Although the olivines are nearly homogeneous, ion microprobe studies revealed variations of Ca, Ti, Co, Cr, and Ni near grain edges. These variations were thought to represent diffusion in response to falling temperature of the parent body. Pallasite cooling rates have been estimated based on kamacite taenite textures but results differ by x100. In principle elemental profiles in olivine can allow estimates of cooling rate if diffusion coefficients are known; in addition, given a cooling rate, diffusion coefficients could be derived. Data are presented which show that apparent diffusion profiles can be measured for Al, Ca, Cr, and Mn which qualitatively agree with expected diffusion rates and have the potential of providing independent estimates of pallasite cooling rates. Author

N94-20903*# Smithsonian Institution, Washington, DC.
COMPARISON OF FLANK MODIFICATION ON ASCRAEUS AND ARSIA MONTES VOLCANOES, MARS Abstract Only
James R. Zimbelman *In* Lunar and Planetary Inst., Twenty-Fourth Lunar and Planetary Science Conference. Part 3: N-Z 1993 p 1575 (For primary document see N94-20636 05-91)
Avail: CASI HC A01/MF A06

Geologic mapping of the Tharsis Montes on Mars is in progress as part of the Mars Geologic Mapping Program of NASA. Mapping of the southern flanks of Ascraeus Mons at 1:500,000 scale was undertaken first followed by detailed mapping of Arsia Mons; mapping of Pavonis Mons will begin later this year. Results indicate that each of the Tharsis volcanoes displays unique variations on the general 'theme' of a martian shield volcano. Here we concentrate on the flank characteristics on Ascraeus Mons and Arsia Mons, the northernmost and southernmost of the Tharsis Montes, as illustrative of the most prominent trends. Author (revised)

N94-20904*# Smithsonian Institution, Washington, DC.
NUMERICAL SIMULATION OF LAVA FLOWS: APPLICATIONS TO THE TERRESTRIAL PLANETS Abstract Only **c46**
James R. Zimbelman, Bruce A. Campbell, Juliana Kousoum (Thomas Jefferson High School, Falls Church, VA.), and Derrick J. Lampkin (Ohio State Univ., Columbus.) *In* Lunar and Planetary Inst., Twenty-Fourth Lunar and Planetary Science Conference. Part 3: N-Z 1993 p 1577-1578 (For primary document see N94-20636 05-91)
Avail: CASI HC A01/MF A06

Lava flows are the visible expression of the extrusion of volcanic materials on a variety of planetary surfaces. A computer program described by Ishihara et al. appears to be well suited for application to different environments, and we have undertaken tests to evaluate their approach. Our results are somewhat mixed; the program does reproduce reasonable lava flow behavior in many situations, but we have encountered some conditions common to planetary environments for which the current program is inadequate. Here we present our initial efforts to identify the 'parameter space' for reasonable numerical simulations of lava flows. Author

N94-20905*# Max-Planck-Inst. fuer Chemie, Mainz (Germany).
CHEMICAL COMPOSITION OF NEW ACAPULCOITES AND LODRANITES Abstract Only **c90**
J. Zipfel and H. Palme *In* Lunar and Planetary Inst., Twenty-Fourth Lunar and Planetary Science Conference. Part 3: N-Z 1993 p 1579-1580 (For primary document see N94-20636 05-91)
Avail: CASI HC A01/MF A06

The bulk compositions of two Antarctic Lodranites, MAC 88177 and FRO 90011, and two Acapulcoites, ALH 81261 and Monument Draw, were determined with instrumental neutron activation analysis. Acapulcoites have essentially chondritic major and trace element abundances but achondritic texture. They consist of entirely recrystallized, fine grained mineral assemblages. Chondrules are extremely rare; one relict radiating pyroxene chondrule was described in Monument Draw (MD). The coarse grained Lodranites also have achondritic textures, but they are different compositionally with depletions in Al, Na, and incompatible elements probably a result of separation of partial, feldspar-rich melt. MAC 88177 is significantly more depleted in incompatible elements than FRO 90011 suggesting a higher degree of partial melting for the MAC-Lodranite. The chemical data support a genetic relationship between Lodranites and Acapulcoites inferred earlier from oxygen isotopes, petrology, and mineral composition. Author

N94-20906*# National Aeronautics and Space Administration. Lyndon B. Johnson Space Center, Houston, TX.
DIFFUSE REFLECTANCE SPECTRA OF ORTHOPYROXENE, OLIVINE, AND PLAGIOCLASE AS A FUNCTION OF COMPOSITION AND STRUCTURE Abstract Only **c90**
M. E. Zolensky, L. Le (Lockheed Engineering and Sciences Co., Houston, TX.), C. Galindo (Lockheed Engineering and Sciences Co., Houston, TX.), R. Morris, V. Lauer (Lockheed Engineering and Sciences Co., Houston, TX.), and F. Vilas *In* Lunar and Planetary Inst., Twenty-Fourth Lunar and Planetary Science Conference. Part 3: N-Z 1993 p 1581-1582 (For primary document see N94-20636 05-91)
Avail: CASI HC A01/MF A06

Although many similarities exist between meteorite spectra and 'primitive' asteroids, there are unexplained discrepancies. These discrepancies do not appear to arise from grain size effects. Assuming that primitive meteorites did in fact originate from the 'primitive' asteroids, we believe that there are two testable explanations for the observed spectral discrepancies: compositional or structural differences. We have begun to synthesize and collect reflectance and Mossbauer spectra of pertinent materials, beginning with olivine, pyroxene, and plagioclase (all found in primitive meteorites), and to assess the possible effects composition may have on spectral features. Our study focuses on the combination of composition and structural effects. Author

N94-20907*# National Aeronautics and Space Administration. Lyndon B. Johnson Space Center, Houston, TX.
MINERALOGY OF DARK CLASTS IN PRIMITIVE VERSUS DIFFERENTIATED METEORITES Abstract Only **c90**
M. E. Zolensky, M. K. Weisberg (American Museum of Natural History, New York, NY.), R. A. Barrett (Lockheed Engineering and Sciences Co., Houston, TX.), and M. Prinz (American Museum of Natural History, New York, NY.) *In* Lunar and Planetary Inst., Twenty-Fourth Lunar and Planetary Science Conference. Part 3: N-Z 1993 p 1583-1584 (For primary document see N94-20636 05-91)
Avail: CASI HC A01/MF A06

The presence of dark lithic clasts within meteorites can provide information concerning asteroidal regolith processes, the extent of interactions between asteroids, and the relationship between meteorite types, micrometeorites, and interplanetary dust particles. Accordingly, we have been seeking and characterizing dark clasts found within carbonaceous chondrites, unequilibrated ordinary chondrites, howardites, and eucrites. We find that unequilibrated chondrites in this study contain fine-grained, anhydrous unequilibrated inclusions, while the howardites often contain inclusions from geochemically processed, hydrous asteroids (type 1 and 2 carbonaceous chondrites). Eucrites and howardities contain unusual clasts, not easily classified. Author

N94-20908*# Academy of Sciences (USSR), Moscow. Inst. of Geochemistry and Analytical Chemistry.
K, U, AND Th BEHAVIOR IN MARTIAN ENVIRONMENTAL CONDITIONS Abstract Only
M. Yu. Zolotov, T. V. Krot, and L. V. Moroz *In* Lunar and Planetary Inst., Twenty-Fourth Lunar and Planetary Science Conference. Part 3: N-Z 1993 p 1585-1586 Sponsored in part by Max-Planck-Inst. fuer Chemie (For primary document see N94-20636 05-91)
Avail: CASI HC A01/MF A06

The possibility of K, U, and Th content determination from orbit and in situ allows consideration of those elements as geochemical indicators in the planetary studies. In the case of Mars the unambiguous interpretations of such data in terms of igneous rocks are remarkably constrained by the widespread rock alteration and the existence of exogenic deposits. Besides, the terrestrial experience indicates that K, U, and Th contents could be used as indicators of environmental geochemical processes. Thus the determination of K, U, and Th contents in the Martian surface materials could provide the indirect data on the conditions of some exogenic geological processes. The speculations on the K, U, and Th behavior in the Martian environments show that aeolian and aqueous processes leads to the preferential accumulation of K, U, and Th in fine dust material. The separation of K, U, and Th on Mars is smaller in scale to that on Earth. Author

N94-20909*# National Aeronautics and Space Administration. Lyndon B. Johnson Space Center, Houston, TX.
ON DUST EMISSIONS FROM THE JOVIAN SYSTEM Abstract Only
H. A. Zook, E. Gruen (Max-Planck-Inst. fuer Kernphysik, Heidelberg, Germany.), M. Baguhl (Max-Planck-Inst. fuer Kernphysik, Heidelberg, Germany.), A. Balogh (Imperial Coll. of Science and Technology, London, England.), S. J. Bame (Los Alamos National Lab., NM.), H. Fechtig (Max-Planck-Inst. fuer Kernphysik, Heidelberg, Germany.), R. Forsyth (Imperial Coll. of Science and Technology, London, England.), M. S. Hanner (Jet Propulsion Lab., California Inst. of Tech., Pasadena.), M. Horanyi (Colorado Univ., Boulder.), and J. Kissel (Max-Planck-Inst. fuer Kernphysik, Heidelberg, Germany.) et al *In* Lunar and Planetary Inst., Twenty-Fourth Lunar and Planetary Science Conference. Part 3: N-Z 1993 p 1587-1588 (For primary document see N94-20636 05-91)
Avail: CASI HC A01/MF A06

As described by Gruen et al., the dust impact detector on the Ulysses spacecraft detected a totally unexpected series of dust streams in the outer solar system near the orbit of Jupiter. Five considerations lead us to believe that the dust streams emanate from the jovian system itself: the dust streams only occur within about 1 AU of the jovian system, with the strongest stream being the one closest to Jupiter (about 550 R(sub J) away); the direction from which they arrive is never far from the line-of-sight direction to Jupiter; the time period between streams is about 28 (+/- 3) days; the impact velocities are very high--mostly around 40 km/s; and we can think of no cometary, asteroidal, or interstellar source that could give rise to the above four phenomena (such streams have never before been detected). Author

N94-20910*# Johns Hopkins Univ., Baltimore, MD. Dept. of Earth and Planetary Sciences.
WRINKLE RIDGES, REVERSE FAULTING, AND THE DEPTH PENETRATION OF LITHOSPHERIC STRESS IN LUNAE PLANUM, MARS Abstract Only
M. T. Zuber *In* Lunar and Planetary Inst., Twenty-Fourth Lunar and Planetary Science Conference. Part 3: N-Z 1993 p 1589-1590 (For primary document see N94-20636 05-91)
Avail: CASI HC A01/MF A06

Tectonic features on a planetary surface are commonly used as constraints on models to determine the state of stress at the time the features formed. Quantitative global stress models applied to understand the formation of the Tharsis province on Mars constrained by observed tectonics have calculated stresses at the surface of a thin elastic shell and have neglected the role of vertical structure in influencing the predicted pattern of surface deformation. Wrinkle ridges in the Lunae Planum region of Mars form a conentric pattern of regularly spaced features in the eastern and southeastern part of Tharsis; they are formed due to compressional stresses related to the response of the Martian lithosphere to the Tharsis bulge. As observed in the exposures of valley walls in areas such as the Kasei Valles, the surface plains unit is underlain by an unconsolidated

impact-generated megaregolith that grades with depth into structurally competent lithospheric basement. The ridges have alternatively been hypothesized to reflect deformation restricted to the surface plains unit ('thin skinned deformation') and deformation that includes the surface unit, megaregolith and basement lithosphere ('thick skinned deformation'). We have adopted a finite element approach to quantify the nature of deformation associated with the development of wrinkle ridges in a vertically stratified elastic lithosphere. We used the program TECTON, which contains a slippery node capability that allowed us to explicitly take into account the presence of reverse faults believed to be associated with the ridges. In this study we focused on the strain field in the vicinity of a single ridge when slip occurs along the fault. We considered two initial model geometries. In the first, the reverse fault was assumed to be in the surface plains unit, and in the second the initial fault was located in lithospheric basement, immediately beneath the weak megaregolith. We are interested in the conditions underwhich strain in the surface layer and basement either penetrates or fails to penetrate through the megaregolith. We thus address the conditions required for an initial basement fault to propagate through the megaregolith to the surface, as well as the effect of the megareolith on the strain tensor in the vicinity of a fault that nucleates in the surface plains unit. Author (revised)

N94-20911*# National Aeronautics and Space Administration. Goddard Space Flight Center, Greenbelt, MD.

POSSIBLE FLEXURAL SIGNATURES AROUND OLYMPUS AND ASCRAEUS MONTES, MARS Abstract Only

M. T. Zuber (Johns Hopkins Univ., Baltimore, MD.), B. G. Bills, H. V. Frey, W. S. Kiefer, R. S. Nerem, and J. H. Roark *In* Lunar and Planetary Inst., Twenty-Fourth Lunar and Planetary Science Conference. Part 3: N-Z 1993 p 1591-1592 (For primary document see N94-20636 05-91)
Avail: CASI HC A01/MF A06

The effective elastic thickness (h) of the lithosphere provides a measure of the thermal and mechanical state of a planet's shallow interior. An estimate of h in the vicinity of a feature that constitutes a load on a planetary surface can be determined from the flexural response of the lithosphere to the load. This approach has been applied to Mars by calculating radial stresses associated with lithospheric flexure associated with surface loads, and comparing the results to the positions of circumferential graben surrounding the major Martian shield volcanoes and mascon basins. However, many prominent surface loads on Mars, most notably the Olympus Mons volcano, do not exhibit flexural graben. In these instances application of the above method can provide only a lower limit of effective elastic thickness. An alternative method of determining h is to calculate the vertical displacements associated with the flexural loading and to compare the amplitude and shape of the flexural profile to observed topography. This method has not been applied to flexural problems on Mars because of the poor resolution of Martian topographic data. However, previous analyses have shown that the lithosphere around major volcanic shields should exhibit vertical deflections of order 1 km over horizontal baselines of order 100 km. We were thus motivated to search for the presence of flexural troughs in the existing Mars topography data. Author

N94-21659*# Lunar and Planetary Inst., Houston, TX. Mars Surface and Atmosphere Through Time Study Group.

WORKSHOP ON EARLY MARS: HOW WARM AND HOW WET?, PART 1 Abstracts Only

S. Squyres, ed. (Cornell Univ., Ithaca, NY.) and J. Kasting, ed. (Pennsylvania State Univ., University Park.) 1993 29 p Workshop held in Breckenridge, CO, 26-28 Jul. 1993
(Contract NASw-4574)
(NASA-CR-193553; NAS 1.26:193553; LPI-TR-93-03-Pt-1) Avail: CASI HC A03/MF A01

This volume contains papers that have been accepted for presentation at the Workshop on Early Mars: How Warm and How Wet?, 26-28 Jul. 1993, in Breckenridge, CO. The following topics are covered: the Martian water cycle; Martian paleoclimatology; CO2/CH4 atmosphere on early Mars; Noechian hydrology; early Martian environment; Martian weathering; nitrogen isotope ratios; CO2 evolution on Mars; and climate change. For individual titles, see N94-21660 through N94-21683.

N94-21660*# Arizona Univ., Tucson. Lunar and Planetary Lab.

EVOLUTION OF THE GLOBAL WATER CYCLE ON MARS: THE GEOLOGICAL EVIDENCE Abstract Only

V. R. Baker and V. C. Gulick *In* Lunar and Planetary Inst., Workshop on Early Mars: How Warm and How Wet?, Part 1 1993 p 1-2 (For primary document see N94-21659 05-91)
Avail: CASI HC A01/MF A01

The geological evidence for active water cycling early in the history of Mars (Noachian geological system or heavy bombardment) consists almost exclusively of fluvial valley networks in the heavily cratered uplands of the planet. It is commonly assumed that these landforms required explanation by atmospheric processes operating above the freezing point of water and at high pressure to allow rainfall and liquid surface runoff. However, it has also been documented that nearly all valley networks probably formed by subsurface outflow and sapping erosion involving groundwater outflow prior to surface-water flow. The prolonged ground-water flow also requires extensive water cycling to maintain hydraulic gradients, but is this done via rainfall recharge, as in terrestrial environments? Author (revised)

N94-21661*# Dartmouth Coll., Hanover, NH. Surficial Processes Lab.

ANCIENT MARTIAN VALLEY GENESIS AND PALEOCLIMATIC INFERENCE: THE PRESENT AS A KEY TO THE PAST Abstract Only

G. R. Brakenridge *In* Lunar and Planetary Inst., Workshop on Early Mars: How Warm and How Wet?, Part 1 1993 p 2-3 (For primary document see N94-21659 05-91)
Avail: CASI HC A01/MF A01

I offer here the speculative genetic hypothesis that the flat-floored landforms represent episodically active, sediment-laden valley glaciers formed by localized geothermal melting of abundant interstitial ice (permafrost) in a fine-grained sedimentary terrain. Geothermal melting may also localize spring heads for the narrow deep, high-gradient valleys, or the collapse process itself may result in the generation of decanted, relatively sediment-poor overland water flows (some local evidence of fluid overtopping of the localized depressions exists). Whatever the generic mechanisms for the suite of valley landforms, perhaps the most interesting observation is simply their youth. In aggregate, the morphologies are similar to the ancient valley systems cited as evidence for a previously much denser atmosphere on Mars. Author

N94-21662*# Pennsylvania State Univ., University Park. Dept. of Geosciences.

A CARBON DIOXIDE/METHANE GREENHOUSE ATMOSPHERE ON EARLY MARS Abstract Only

L. L. Brown and J. F. Kasting *In* Lunar and Planetary Inst., Workshop on Early Mars: How Warm and How Wet?, Part 1 1993 p 3 (For primary document see N94-21659 05-91)
Avail: CASI HC A01/MF A01

One explanation for the formation of fluvial surface features on early Mars is that the global average surface temperature was maintained at or above the freezing point of water by the greenhouse warming of a dense CO2 atmosphere; however, Kasting has shown that CO2 alone is insufficient because the formation of CO2 clouds reduces the magnitude of the greenhouse effect. It is possible that other gases, such as NH3 and CH4, were present in the early atmosphere of Mars and contributed to the greenhouse effect. Kasting et al. investigated the effect of NH3 in a CO2 atmosphere and calculated that an NH3 mixing ratio of approximately 5 x 10 (exp -4) by volume, combined with a CO2 partial pressure of 4-5 bar, could generate a global average surface temperature of 273 K near 3.8 b.y. ago when the fluvial features are believed to have formed. Atmospheric NH3 is photochemically converted to N2 by ultraviolet radiation at wavelengths shortward of 230 nm; maintenance of sufficient NH3 concentrations would therefore require a source of NH3 to balance the photolytic destruction. We have used a one-dimensional photochemical model to estimate the magnitude of the NH3 source required to maintain a given NH3 concentration in a dense CO2 atmosphere. We calculate that an NH3 mixing ratio of 10(exp -4) requires a flux of NH3 on the order of 10(exp 12) molecules /cm-s. This figure is several orders of magnitude greater than estimates of the NH3 flux on early Mars; thus it appears that NH3 with CO2 is not enough to keep early Mars warm. Author (revised)

N94-21663*# Massachusetts Inst. of Tech., Cambridge. Dept. of Earth, Atmospheric and Planetary Sciences.

OXIDATION OF DISSOLVED IRON UNDER WARMER, WETTER CONDITIONS ON MARS: TRANSITIONS TO PRESENT-DAY ARID ENVIRONMENTS Abstract Only

R. G. Burns *In* Lunar and Planetary Inst., Workshop on Early Mars: How Warm and How Wet?, Part 1 1993 p 3-4 (For primary document see N94-21659 05-91)

(Grant NAGw-2220)

Avail: CASI HC A01/MF A01

The copious deposits of ferric-iron assemblages littering the surface of bright regions of Mars indicate that efficient oxidative weathering reactions have taken place during the evolution of the planet. Because the kinetics of atmosphere-surface (gas-solid) reactions are considerably slower than chemical weathering reactions involving an aqueous medium, most of the oxidation products now present in the martian regolith probably formed when groundwater flowed near the surface. This paper examines how chemical weathering reactions were effected by climatic variations when warm, wet environments became arid on Mars. Analogies are drawn with hydrogeochemical and weathering environments on the Australian continent where present-day oxidation of iron is occurring in acidic ground water under arid conditions. Author

N94-21664*# Observatoire de Paris-Meudon (France). Lab. de Physique du Systeme Solaire.

MARS: NOACHIAN HYDROLOGY BY ITS STATISTICS AND TOPOLOGY Abstract Only

N. A. Cabrol and E. A. Grin *In* Lunar and Planetary Inst., Workshop on Early Mars: How Warm and How Wet?, Part 1 1993 p 4-6 (For primary document see N94-21659 05-91)

Avail: CASI HC A01/MF A01

Discrimination between fluvial features generated by surface drainage and subsurface aquifer discharges will provide clues to the understanding of early Mars' climatic history. Our approach is to define the process of formation of the oldest fluvial valleys by statistical and topological analyses. Formation of fluvial valley systems reached its highest statistical concentration during the Noachian Period. Nevertheless, they are a scarce phenomenom in Martian history, localized on the craterized upland, and subject to latitudinal distribution. They occur sparsely on Noachian geological units with a weak distribution density, and appear in reduced isolated surface (around 5 x 10(exp 3)(sq km)), filled by short streams (100-300 km length). Topological analysis of the internal organization of 71 surveyed Noachian fluvial valley networks also provides information on the mechanisms of formation. Author

N94-21665*# Lunar and Planetary Inst., Houston, TX.

THE EVOLUTION OF THE EARLY MARTIAN CLIMATE AND THE INITIAL EMPLACEMENT OF CRUSTAL H2O Abstract Only

S. M. Clifford *In its* Workshop on Early Mars: How Warm and How Wet?, Part 1 1993 p 6-7 (For primary document see N94-21659 05-91)

Avail: CASI HC A01/MF A01

Given the geomorphic evidence for the widespread occurrence of water and ice in the early Martian crust, and the difficulty involved in accounting for this distribution given the present climate, it has been suggested that the planet's early climate was originally more Earth-like, permitting the global emplacement of crustal H2O by direct precipitation as snow or rain. The resemblance of the Martian valley networks to terrestrial runoff channels and their almost exclusive occurrence in the planet's ancient (approximately 4-b.y.-old) heavily cratered terrain are often cited as evidence of just such a period. An alternative school of thought suggests that the early climate did not differ substantially from that of today. Advocates of this view find no compelling reason to invoke a warmer, wetter period to explain the origin of the valley networks. Rather, they cite evidence that the primary mechanism of valley formation was groundwater sapping, a process that does not require that surface water exists in equilibrium with the atmosphere. However, while sapping may successfully explain the origin of the small valleys, it fails to address how the crust was initially charged with ice as the climate evolved towards its present state. Therefore, given the uncertainty regarding the environmental conditions that prevailed on early Mars, the initial emplacement of ground ice is considered here from two perspectives: (1) the early climate started warm and wet, but gradually cooled with time, and (2) the early climate never differed substantially from that of today. Author

N94-21666*# Lunar and Planetary Inst., Houston, TX.

THE HYDROLOGIC RESPONSE OF MARS TO THE ONSET OF A COLDER CLIMATE AND TO THE THERMAL EVOLUTION OF ITS EARLY CRUST Abstract Only

S. M. Clifford *In its* Workshop on Early Mars: How Warm and How Wet?, Part 1 1993 p 7-9 (For primary document see N94-21659 05-91)

Avail: CASI HC A01/MF A01

Morphologic similarities between the Martian valley networks and terrestrial runoff channel have been cited as evidence that the early Martian climate was originally more Earth-like, with temperatures and pressures high enough to permit the precipitation of H2O as snow or rain. Although unambiguous evidence that Mars once possessed a warmer, wetter climate is lacking, a study of the transition from such conditions to the present climate can benefit our understanding of both the early development of the cryosphere and the various ways in which the current subsurface hydrology of Mars is likely to differ from that of the Earth. Viewed from this perspective, the early hydrologic evolution of Mars is essentially identical to considering the hydrologic response of the Earth to the onset of a global subfreezing climate. Author

N94-21667*# National Air and Space Museum, Washington, DC. Center for Earth and Planetary Studies.

THE EARLY MARTIAN ENVIRONMENT: CLUES FROM THE CRATERED HIGHLANDS AND THE PRECAMBRIAN EARTH Abstract Only

R. A. Craddock and T. A. Maxwell *In* Lunar and Planetary Inst., Workshop on Early Mars: How Warm and How Wet?, Part 1 1993 p 9-10 (For primary document see N94-21659 05-91)

Avail: CASI HC A01/MF A01

There is abundant geomorphic evidence to suggest that Mars once had a much denser and warmer atmosphere than present today. Outflow channel, ancient valley networks, and degraded impact craters in the highlands all suggest that ancient Martian atmospheric conditions supported liquid water on the surface. The pressure, composition, and duration of this atmosphere is largely unknown. However, we have attempted to place some constraints on the nature of the early Martian atmosphere by analyzing morphologic variations of highland impact crater populations, synthesizing results of other investigators, and incorporating what is know about the geologic history of the early Earth. This is important for understanding the climatic evolution of Mars, the relative abundance of martian volatiles, and the nature of highland surface materials. Author

N94-21668*# National Aeronautics and Space Administration. Ames Research Center, Moffett Field, CA.

AN ATTEMPT TO COMPREHEND MARTIAN WEATHERING CONDITIONS THROUGH THE ANALYSIS OF TERRESTRIAL PALAGONITE SAMPLES Abstract Only

C. Douglas (Open Univ., Milton, England.), I. P. Wright (Open Univ., Milton, England.), J. B. Bell, R. V. Morris (National Aeronautics and Space Administration. Lyndon B. Johnson Space Center, Houston, TX.), D. C. Golden (National Aeronautics and Space Administration. Lyndon B. Johnson Space Center, Houston, TX.), and C. T. Pillinger *In* Lunar and Planetary Inst., Workshop on Early Mars: How Warm and How Wet?, Part 1 1993 p 10-11 (For primary document see N94-21659 05-91)

Avail: CASI HC A01/MF A01

Spectroscopic observations of the Martian surface in the invisible to near infrared (0.4-1.0 micron), coupled with measurements made by Viking, have shown that the surface is composed of a mixture of fine-grained weathered and nonweathered minerals. The majority of the weathered components are thought to be materials like smectite clays, scapolite, or palagonite. Until materials are returned for analysis there are two possible ways of proceeding with an investigation of Martian surface processes: (1) the study of weathering products in meteorites that have a Martian origin (SNC's), and (2) the analysis of certain terrestrial weathering products as analogs to the material found in SNC's, or predicted to be present on the Martian surface. We describe some preliminary measurements of the carbon chemistry of terrestrial palagonite samples that exhibit spectroscopic

similarities with the Martian surface. The data should aid the understanding of weathering in SNC's and comparisons between terrestrial palagonites and the Martian surface. Author

N94-21669*# State Univ. of New York, Stony Brook. Inst. for Terrestrial and Planetary Atmospheres.

REQUIREMENTS FOR THE EARLY ATMOSPHERE OF MARS FROM NITROGEN ISOTOPE RATIOS Abstract Only

J. L. Fox *In* Lunar and Planetary Inst., Workshop on Early Mars: How Warm and How Wet?, Part 1 1993 p 11-12 (For primary document see N94-21659 05-91)

Avail: CASI HC A01/MF A01

The N escape models of Fox and Dalgarno and Fox required the presence of a dense, early CO2 atmosphere to inhibit fractionation of the N isotopes N-15 and N-14. The computed photochemical escape fluxes are so large at the present that the isotope ratio measured by Viking (about 1.62x terrestrial) can be produced in about 1.5 b.y. This model was refined in several ways. It was updated to incorporate the variation of the escape fluxes with increases in the solar fluxes at earlier times according to the model of Zahnle and Walker. As expected, this exacerbates the problem with overfractionation, but not greatly. Most of the escape and fractionation of the N occurs in the last 1.5 b.y., when the solar flux was only slightly different from the present. The dense early atmosphere must persist only a bit longer in order to reproduce the measured isotope ratio. The model was also modified to take into account changes in the O mixing ratio with time in the past, assuming that the O abundance is proportional to the square root of the solar flux. Although the production rate of O from photodissociation of CO2 scales as the solar flux, the strength of the winds and other mixing processes also increases with the solar flux, resulting in possibly more effective transport of O to the lower atmosphere where it is destroyed by catalytic and three-body recombination mechanisms. Author (revised)

N94-21670*# Arizona Univ., Tucson. Lunar and Planetary Lab.

FLUVIAL VALLEYS IN THE HEAVILY CRATERED TERRAINS OF MARS: EVIDENCE FOR PALEOCLIMATIC CHANGE? Abstract Only

V. C. Gulick and V. R. Baker *In* Lunar and Planetary Inst., Workshop on Early Mars: How Warm and How Wet?, Part 1 1993 p 12-13 (For primary document see N94-21659 05-91)

Avail: CASI HC A01/MF A01

Whether the formation of the Martian valley networks provides unequivocal evidence for drastically different climatic conditions remains debatable. Recent theoretical climate modeling precludes the existence of a temperate climate early in Mars' geological history. An alternative hypothesis suggests that Mars had a globally higher heat flow early in its geological history, bringing water tables to within 350 m of the surface. While a globally higher heat flow would initiate ground water circulation at depth, the valley networks probably required water tables to be even closer to the surface. Additionally, it was previously reported that the clustered distribution of the valley networks within terrain types, particularly in the heavily cratered highlands, suggests regional hydrological processes were important. The case for localized hydrothermal systems is summarized and estimates of both erosion volumes and of the implied water volumes for several Martian valley systems are presented. Author (revised)

N94-21671*# National Aeronautics and Space Administration. Ames Research Center, Moffett Field, CA.

A MODEL FOR THE EVOLUTION OF CO2 ON MARS Abstract Only

R. M. Haberle, D. Tyler (San Jose State Univ., CA.), C. P. McKay, and W. L. Davis *In* Lunar and Planetary Inst., Workshop on Early Mars: How Warm and How Wet?, Part 1 1993 p 13-14 (For primary document see N94-21659 05-91)

Avail: CASI HC A01/MF A01

There are several lines of evidence that suggest early Mars was warmer and wetter than it is at present. Perhaps the most convincing of these are the valley networks and degraded craters that characterize much of the ancient terrains. In both cases, fluvial activity associated with liquid water is believed to be involved. Thus, Mars appears to have had a warmer climate early in its history than it does today. How much warmer is not clear, but a common perception has been that global mean surface temperatures must have been near freezing - almost 55 K warmer than at present. The most plausible way to increase surface temperatures is through the greenhouse effect, and the most plausible greenhouse gas is CO2. Pollack et al. estimate that in the presence of the faint young Sun, the early Martian atmosphere would have to contain almost 5 bar of CO2 to raise the mean surface temperature up to the freezing level; only 1 bar would be required if the fluvial features were formed near the calculations now appear to be wrong since Kasting showed that CO2 will condense in the atmosphere at these pressures and that this greatly reduces the greenhouse effect of a pure CO2 atmosphere. He suggested that alternative greenhouse gases such as CH4 or NH3, are required. The early Mars dilemma is approached from a slightly different point of view. In particular, a model for the evolution of CO2 on Mars that draws upon published processes that affect such evolution was constructed. Thus, the model accounts for the variation of solar luminosity with time, the greenhouse effect, regolith uptake, polar cap formation, escape, and weathering. Author (revised)

N94-21672*# Colorado Univ., Boulder. Lab. for Atmospheric and Space Physics.

MARS ATMOSPHERE LOSS AND ISOTOPIC FRACTIONATION BY SOLAR-WIND-INDUCED SPUTTERING AND PHOTOCHEMICAL ESCAPE Abstract Only

B. M. Jakosky, R. O. Pepin (Minnesota Univ., Minneapolis.), R. E. Johnson (Virginia Univ., Charlottesville.), and J. L. Fox (State Univ. of New York, Stony Brook.) *In* Lunar and Planetary Inst., Workshop on Early Mars: How Warm and How Wet?, Part 1 1993 p 14-15 (For primary document see N94-21659 05-91)

Avail: CASI HC A01/MF A01

The effects of loss of Mars atmospheric constituents by solar-wind-induced sputtering and by photochemical escape during the last 3.8 b.y. were examined. Sputtering is capable of efficiently removing all species from the upper atmosphere, including the light noble gases; N also is removed by photochemical processes. Due to the diffusive separation by mass above the homopause, removal from the top of the atmosphere will fractionate the isotopes of each species, with the lighter mass being preferentially lost. For C and O, this allows us to determine the size of nonatmospheric reservoirs that mix with the atmosphere; these reserviors can be accounted for by exchange with CO2 adsorbed in the regolith and with H2O in the polar ice deposits. Both simple analytical models and time-dependent models of the loss of volatiles from and supply to the Martian atmosphere were constructed. Both Ar and Ne require continued replenishment from outgassing over geologic time. Author (revised)

N94-21673*# Pennsylvania State Univ., University Park. Dept. of Geosciences.

POSSIBLE SOLUTIONS TO THE PROBLEM OF CHANNEL FORMATION ON EARLY MARS Abstract Only

J. F. Kasting *In* Lunar and Planetary Inst., Workshop on Early Mars: How Warm and How Wet?, Part 1 1993 p 15 (For primary document see N94-21659 05-91)

Avail: CASI HC A01/MF A01

A warm climate on early Mars would provide a natural, although not unique, explanation for the presence of fluvial networks on the ancient, heavily cratered terrains. Explaining how the climate could have been kept warm, however, is not easy. The idea that the global average surface temperature, T(sub s), could have been kept warm by a dense, CO2 atmosphere supplied by volcanism or impacts is no longer viable. It was shown that CO2 cloud formation should have kept T(sub s) well below freezing until approximately 2 b.y. ago, when the Sun had brightened to at least 86 percent of its present value. Warm equatorial regions on an otherwise cold planet seem unlikely because atmospheric CO2 would probably condense out at the poles. Warming by impact-produced dust in the atmosphere seems unlikely because the amount of warming expected for silicate dust particles is relatively small. Greenhouse warming by high altitude CO2 ice clouds seems unlikely because such are poor absorbers of infrared radiation at most wavelengths. Warming by atmospheric NH3 seems unlikely because NH3 is readily photodissociated and because N may have been in short supply as consequence of impact erosion and the high solubility of NH3. A brighter, mass-losing young Sun seems unlikely because stellar winds of the required strength were not observed on other solar-type stars. In short, most of the explanations for a warm Martian paleoclimate that were proposed in the past seem unlikely. One possibility that seems feasible from radiative/photochemical standpoint is that CH4

and associated hydrocarbon gases and particles contributed substantially to the greenhouse effect on early Mars. Methane is photochemically more stable than NH3 and the gases and particles that can be formed from it are all good absorbers of infrared radiation. The idea of a CH4-rich Martian paleoatmosphere was suggested a long time ago but has fallen out of favor because of perceived difficulties in maintaining a CH4-rich atmosphere. In particular, it is not obvious where the CH4 might come from, since volcanic gases (on Earth, at least) contain very little CH4. This difficulty could be largely overcome if early Mars was inhabited by microorganisms. Then, methanogenic bacteria living in sediments could presumably have supplied CH4 to the atmosphere in copious quantities. Author (revised)

N94-21674*# Tokyo Univ. (Japan). Dept. of Earth and Planetary Physics.

CORE FORMATION, WET EARLY MANTLE, AND H2O DEGASSING ON EARLY MARS Abstract Only

K. Kuramoto and T. Matsui *In* Lunar and Planetary Inst., Workshop on Early Mars: How Warm and How Wet?, Part 1 1993 p 15-17 (For primary document see N94-21659 05-91)

Avail: CASI HC A01/MF A01

Geophysical and geochemical observations strongly suggest a 'hot origin of Mars,' i.e., the early formation of both the core and the crust-mantle system either during or just after planetary accretion. To consider the behavior of H2O in the planetary interior it is specifically important to determine by what mechanism the planet is heated enough to cause melting. For Mars, the main heat source is probably accretional heating. Because Mars is small, the accretion energy needs to be effectively retained in its interior. Therefore, the three candidates of heat retention mechanism are discussed first: (1) the blanketing effect of the primordial H2-He atmosphere; (2) the blanketing effect of the impact-induced H2O-CO2 atmosphere; and (3) the higher deposition efficiency of impact energy due to larger impacts. It was concluded that (3) the is the most plausible mechanism for Mars. Then, its possible consequence on how wet the early martian mantle was is discussed. Author (revised)

N94-21675*# Cornell Univ., Ithaca, NY.

BRINY LAKES ON EARLY MARS? TERRESTRIAL INTRACRATER PLAYAS AND MARTIAN CANDIDATES Abstract Only

P. Lee *In* Lunar and Planetary Inst., Workshop on Early Mars: How Warm and How Wet?, Part 1 1993 p 17 (For primary document see N94-21659 05-91)

Avail: CASI HC A01/MF A01

Recently, salt-rich aqueous solutions have been invoked in the preterrestrial alteration of the Nakhla and Lafayette SNC meteorites. The findings substantiate the long-standing suspicion that salts are abundant on Mars and, more importantly, that brines have played a significant role in Martian hydrogeological history. Adding to the growing body of evidence, I report here on the identification of several unusual intracrater high-albedo features in the ancient cratered highlands of Mars, which I interpret as possible saline playas, or salt pans. Author

N94-21676*# National Air and Space Museum, Washington, DC. Center for Earth and Planetary Studies.

EARLY MARS: A REGIONAL ASSESSMENT OF DENUDATION CHRONOLOGY Abstract Only

T. A. Maxwell and R. A. Craddock *In* Lunar and Planetary Inst., Workshop on Early Mars: How Warm and How Wet?, Part 1 1993 p 18 (For primary document see N94-21659 05-91)

Avail: CASI HC A01/MF A01

Within the oldest highland units on Mars, the record of crater degradation indicates that fluvial resurfacing was responsible for modifying the Noachian through middle-Hesperian crater population. Based on crater frequency in the Noachian cratered terrain, age/elevation relations suggest that the highest exposures of Noachian dissected and plateau units became stabilized first, followed by successively lower units. In addition, studies of drainage networks indicate that the frequency of Noachian channels is greatest at high elevations. Together, these observations provide strong evidence of atmospheric involvement in volatile recycling. The long time period of crater modification also suggests that dendritic highland drainage was not simply the result of sapping by release of juvenile water, because the varied geologic units as well as the elevation dependence of stability ages makes it unlikely that subsurface recycling could provide a continuous supply of water for channel formation by sapping. While such geomorphic constraints on volatile history have been established by crater counts and stratigraphic relations using the 1:2M photomosaic series, photogeologic age relationships at the detailed level are needed to establish a specific chronology of erosion and sedimentation. Age relations for discrete erosional slopes and depositional basins will help refine ages of fluvial degradation, assess effectiveness of aeolian processes, and provide a regional chronology of fluvial events. Author

N94-21677*# National Aeronautics and Space Administration. Ames Research Center, Moffett Field, CA.

EARLY MARS WAS WET BUT NOT WARM: EROSION, FLUVIAL FEATURES, LIQUID WATER HABITATS, AND LIFE BELOW FREEZING Abstract Only

C. P. McKay and W. L. Davis *In* Lunar and Planetary Inst., Workshop on Early Mars: How Warm and How Wet?, Part 1 1993 p 18 (For primary document see N94-21659 05-91)

Avail: CASI HC A01/MF A01

There is considerable evidence that Mars had liquid water early in its history and possibly at recurrent interval. It has generally been assumed that this implied that the climate was warmer as a result of a thicker CO2 atmosphere than at the present. However, recent models suggest that Mars may have had a thick atmosphere but may not have experienced mean annual temperatures above freezing. In this paper we report on models of liquid water formation and maintenance under temperatures well below freezing. Our studies are based on work in the north and south polar regions of Earth. Our results suggest that early Mars did have a thick atmosphere but precipitation and hence erosion was rare. Transient liquid water, formed under temperature extremes and maintained under thick ice covers, could account for the observed fluvial features. The main difference between the present climate and the early climate was that the total surface pressure was well above the triple point of water. Author

N94-21678*# Tennessee Univ., Knoxville. Dept. of Geological Sciences.

WET INSIDE AND OUT? CONSTRAINTS ON WATER IN THE MARTIAN MANTLE AND ON OUTGASSED WATER, BASED ON MELT INCLUSIONS IN SNC METEORITES Abstract Only

H. Y. McSween, Jr. and R. P. Harvey *In* Lunar and Planetary Inst., Workshop on Early Mars: How Warm and How Wet?, Part 1 1993 p 18-19 (For primary document see N94-21659 05-91)

Avail: CASI HC A01/MF A01

Constraints on the volatile inventory and outgassing history of Mars are critical to understanding the origin of ancient valley systems and paleoclimates. Planetary accretion models for Mars allow either a volatile-rich or volatile-poor mantle, depending on whether the accreted materials were fully oxidized or whether accretion was homogeneous so that water was lost through reaction with metallic iron. The amount of water that has been outgassed from the interior is likewise a contentious subject, and estimates of globally distributed water based on various geochemical and geological measurements vary from a few meters to more than a thousand meters. New data on SNC meteorites, which are thought to be Martian igneous rocks, provide constraints on both mantle and outgassed water. Author

N94-21679*# California Inst. of Tech., Pasadena. Div. of Geological and Planetary Sciences.

THE YOUNG SUN AND PHOTOCHEMISTRY OF THE PRIMITIVE MARTIAN ATMOSPHERE Abstract Only

H. Nair, M. F. Gerstell, and Y. L. Yung *In* Lunar and Planetary Inst., Workshop on Early Mars: How Warm and How Wet?, Part 1 1993 p 19 (For primary document see N94-21659 05-91)

Avail: CASI HC A01/MF A01

We will investigate the climatology of an atmosphere where CO2 is a minor constituent but still the key radiative species. The thermal structure of the dust-free atmosphere is estimated by employing a simple radiative-convective model similar to that used by Gierasch and Goody. Radiative heating rates are computed using the Caltech/JPL one-dimensional photochemical model. Thermal cooling rates for a Martian atmosphere containing O2, O3, H2O, N2O, CO, and CO2 are calculated using FASCODE and k-distribution methods. The effects due to pressure broadening of the infrared absorption lines of CO2 by CO and O2, as well as the radiative

effects of increased ozone densities in the atmosphere, will be examined.
Derived from text

N94-21680*# Minnesota Univ., Minneapolis. School of Physics and Astronomy.
EVOLUTION OF THE MARTIAN ATMOSPHERE Abstract Only
R. O. Pepin *In* Lunar and Planetary Inst., Workshop on Early Mars: How Warm and How Wet?, Part 1 1993 p 20 (For primary document see N94-21659 05-91)
Avail: CASI HC A01/MF A01

Evolution of Mars' noble gases through two stages of hydrodynamic escape early in planetary history has been proposed previously by the author. In the first evolutionary stage of this earlier model, beginning at a solar age of approximately 50 m.y., fractionating escape of a H2-rich primordial atmosphere containing CO2, N2, and the noble gases in roughly the proportions found in primitive carbonaceous (CI) chondrites is driven by intense extreme-ultraviolet (EUV) leads to a long (approximately 80 m.y.) period of quiescence, followed by an abrupt degassing of remnant H2, CO2, and N2 from the mantle and of solar-composition noble gases lighter than Xe from the planet's volatile-rich accretional core. Degassed H refuels hydrodynamic loss in a waning but still potent solar EUV flux. Atmospheric Xe, Kr, and Ar remaining at the end of this second escape stage, approximately 4.2 G.y. ago, have evolved to their present-day abundances and compositions. Residual Ne continues to be modified by accretion of solar wind gases throughout the later history of the planet. This model does not address a number of processes that now appear germane to Martian atmospheric history. One, gas loss and fractionation by sputtering, has recently been shown to be relevant. Another, atmospheric erosion, appears increasingly important. In the absence then of a plausible mechanism, the model did not consider the possibility of isotopic evolution of noble gases heavier than Ne after the termination of hydrodynamic escape. Subsequent non-thermal loss of N was assumed, in an unspecified way, to account for the elevation of N from the model value of approximately 250 percent at the end of the second escape stage to approximately 620 percent today. Only qualitative attention was paid to the eroding effects of impact on abundances of all atmophilic species prior to the end of heavy bombardment approximately 3.8 G.y. ago. No attempt was made to include precipitation and recycling of carbonates in tracking the pressure and isotopic history of CO2. Derived from text

N94-21681*# Oklahoma Univ., Norman. School of Meteorology.
EARLY MARS: THE INEXTRICABLE LINK BETWEEN INTERNAL AND EXTERNAL INFLUENCES ON VALLEY NETWORK FORMATION Abstract Only
S. E. Postawko and F. P. Fanale (Hawaii Univ., Honolulu.) *In* Lunar and Planetary Inst., Workshop on Early Mars: How Warm and How Wet?, Part 1 1993 p 20-22 (For primary document see N94-21659 05-91)
Avail: CASI HC A01/MF A01

The conditions under which the valley networks on the ancient cratered terrain on Mars formed are still highly debated within the scientific community. While liquid water was almost certainly involved, the exact mechanism of formation is uncertain. The networks most resemble terrestrial sapping channels, although some systems exhibit a runoff-dominated morphology. The major question in the formation of these networks is what, if anything, do they imply about early Martian climate? There are typically two major theories advanced to explain the presence of these networks. The first is that higher internal regolith temperatures, associated with a much higher heat flow 3.8 b.y. ago, would cause ground water to be closer to the surface than at present. Just how close to the surface ground water would have to exist in order to form these valley networks has recently been questioned. The second major theory is that early Mars had a much thicker atmosphere than at present, and an enhanced atmospheric greenhouse may have increased surface temperatures to near the freezing point of water. While recent calculations indicate that CO2 alone could not have produced the needed warming, the presence of other greenhouse gases may have contributed to surface warming. Derived from text

N94-21682*# Arizona State Univ., Tempe. Dept. of Geography.
THE MARTIAN VALLEY NETWORKS: ORIGIN BY NIVEO-FLUVIAL PROCESSES Abstract Only
J. W. Rice, Jr. *In* Lunar and Planetary Inst., Workshop on Early Mars: How Warm and How Wet?, Part 1 1993 p 22-23 (For primary document see N94-21659 05-91)
Avail: CASI HC A01/MF A01

The valley networks may hold the key to unlocking the paleoclimatic history of Mars. These enigmatic landforms may be regarded as the Martian equivalent of the Rosetta Stone. Therefore, a more thorough understanding of their origin and evolution is required. However, there is still no consensus among investigators regarding the formation (runoff vs. sapping) of these features. Recent climatic modeling precludes warm (0 degrees C) globally averaged surface temperatures prior to 2 b.y. when solar luminosity was 25-30 percent less than present levels. This paper advocates snowmelt as the dominant process responsible for the formation of the dendritic valley networks. Evidence for Martian snowfall and subsequent melt has been discussed in previous studies. Derived from text

N94-21683*# National Aeronautics and Space Administration. Ames Research Center, Moffett Field, CA.
MARS AND THE EARLY SUN Abstract Only
D. P. Whitmire (University of Southwestern Louisiana, Lafayette.), L. R. Doyle, R. T. Reynolds, and P. G. Whitman (University of Southwestern Louisiana, Lafayette.) *In* Lunar and Planetary Inst., Workshop on Early Mars: How Warm and How Wet?, Part 1 1993 p 23 Sponsored in part by Louisiana Educational Quality Support Fund (For primary document see N94-21659 05-91)
Avail: CASI HC A01/MF A01

Global mean temperatures near 273 K on early Mars are difficult to explain in the context of standards solar evolution models. Even assuming maximum CO2 greenhouse warming, the required flux is approximately 15 percent too low. Here we consider two astrophysical models that could increase the flux by this amount. The first model is a nonstandard solar model in which the early Sun had a mass somewhat greater than today's mass (1.02-1.06 solar mass). The second model is based on a standard evolutionary solar model, but the ecliptic flux is increased due to focusing by an (expected) heavily spotted early Sun. Derived from text

N94-21883*# National Aeronautics and Space Administration. Lyndon B. Johnson Space Center, Houston, TX.
MARS EXPLORATION STUDY WORKSHOP 2
Michael B. Duke and Nancy Ann Budden Nov. 1993 98 p Workshop held at Moffett Field, CA, 24-25 May 1993
(NASA-CP-3243; S-750; NAS 1.55:3243) Avail: CASI HC A05/MF A02

A year-long NASA-wide study effort has led to the development of an innovative strategy for the human exploration of Mars. The latest Mars Exploration Study Workshop 2 advanced a design reference mission (DRM) that significantly reduces the perceived high costs, complex infrastructure, and long schedules associated with previous Mars scenarios. This surface-oriented philosophy emphasizes the development of high-leveraging surface technologies in lieu of concentrating exclusively on space transportation technologies and development strategies. As a result of the DRM's balanced approach to mission and crew risk, element commonality, and technology development, human missions to Mars can be accomplished without the need for complex assembly operations in low-Earth orbit. This report, which summarizes the Mars Exploration Study Workshop held at the Ames Research Center on May 24-25, 1993, provides an overview of the status of the Mars Exploration Study, material presented at the workshop, and discussions of open items being addressed by the study team. The workshop assembled three teams of experts to discuss cost, dual-use technology, and international involvement, and to generate a working group white paper addressing these issues. The three position papers which were generated are included in section three of this publication.
Author (revised)

N94-22635# Cambridge Univ. (England).
NONTHERMAL PLANETARY RADIO EMISSIONS: THEORIES AND OBSERVATIONS
Abraham C.-L. Chian (Instituto de Pesquisas Espaciais, Sao Jose dos Campos, Brazil.) *In* ESA, Fourth International Toki Conference on Plasma Physics and Controlled Nuclear Fusion May 1993 p 101-104 Sponsored by Commission of the European Communities and CNPq (For primary document see N94-22624 05-75)
Copyright Avail: CASI HC A01/MF A03

92 SOLAR PHYSICS

Includes solar activity, solar flares, solar radiation and sunspots. For related information see *93 Space Radiation.*

N94-21150 Bern Univ. (Switzerland). Solar Observations Div.
BERNE (SWITZERLAND) SOLAR OBSERVATIONS: DATA FOR APRIL 1991 - AUGUST 1992
1992 75 p Limited Reproducibility: More than 20% of this document may be affected by microfiche quality
(Rept-59; ETN-93-93881) Avail: CASI HC A04

Specifications for the solar radio observatory and the optical solar flare observations are listed. Statistics on outstanding events, giving the dates, frequencies, type, duration, peak, and flux levels, are presented. Graphs are included. ESA

N94-21196# Kansas Univ. Center for Research, Inc., Lawrence.
SOLAR PROTON EVENTS FROM A 180 YEAR DEPTH PROFILE OF NITRATE CONCENTRATIONS FROM THE CENTRAL GREENLAND ICE SHEET Annual Report, 1 Nov. 1992 - 31 Oct. 1993
Gisela A. Dreschhoff and Edward J. Zeller 1 Nov. 1993 32 p
(Grant AF-AFOSR-0065-88)
(AD-A272888; AFOSR-93-0834TR) Avail: CASI HC A03/MF A01

Operations have been concentrated on the micro-resolution analysis of the 120 meter ice core that was collected in Greenland in June, 1992. Thus far, 64 meters of the ice core have been sampled and a total of over 4000 individual samples have been analyzed for both nitrate and electrical conductivity. It has been possible to identify a number of specific anomalies in both the nitrate and the electrical conductivity records. Strong nitrate anomalies related to known solar flares have been identified, and it will become possible to delineate a signal of solar activity well beyond the known geophysical records. It has also been observed that periods of known low solar activity also correlate with lower than normal nitrate concentration and yearly nitrate flux. A new automatic ice core melting apparatus has been designed and built that will permit sampling the remaining ice cores at a higher resolution than was previously possible. This is a significant advantage because deeper ice cores are more compacted and the higher sampling frequency will maintain nearly the same time resolution as that obtained nearer the surface. DTIC

N94-21522# Smithsonian Astrophysical Observatory, Cambridge, MA.
HIGH RESOLUTION STUDIES OF THE STRUCTURE OF THE SOLAR ATMOSPHERE Annual Report, 1 Jul. 1992 - 30 Jun. 1993
Shadia R. Habbal 4 Aug. 1993 13 p
(Grant AF-AFOSR-0244-91)
(AD-A273084; AFOSR-93-0833TR) Avail: CASI HC A03/MF A01

During this second year we pursued the analysis, image enhancement, and processing of an extensive set of the EUV/Skylab data for the search of empirical characteristics of coronal heating in different scale magnetic regions on the Sun. Student involvement in our research projects included Martina Arndt, Gretchen McPhee and Jennifer Yeh. During this funding period we published three papers in refereed journals, one in a conference proceedings, submitted three papers to refereed journals, and have several manuscripts under preparation. We have also made two conference presentations and given three invited talks. Our future projects are continuations of our ongoing long term projects and include the following: (1) The comparison of the temperature in coronal holes and the quiet sun--the implication for solar wind models; (2) The energy spectrum of the variability of the emission in active regions, the quiet sun, and coronal holes; (3) Studies of the fine scale structure in the quiet sun and active regions; and (4) Modeling the radio emission in the presence of structure in the quiet sun and active regions. DTIC

N94-21815*# Alabama Univ., Huntsville. Center for Space Plasma and Aeronomic Research.
DEVELOPMENT, REFINEMENT, AND TESTING OF A SHORT TERM SOLAR FLARE PREDICTION ALGORITHM Semiannual Progress Report, Aug. 1992 - Feb. 1993
Jesse B. Smith, Jr. 1993 16 p
(Grant NAG8-888)
(NASA-CR-194726; NAS 1.26:194726) Avail: CASI HC A03/MF A01

Progress toward performance of the tasks and accomplishing the goals set forth in the two year Research Grant included primarily analysis of digital data sets and determination of methodology associated with the analysis of the very large, unique, and complex collection of digital solar magnetic field data. The treatment of each magnetogram as a unique set of data requiring special treatment was found to be necessary. It is determined that a person familiar with the data, the analysis system, and logical, coherent outcome of the analysis must conduct each analysis, and interact with the analysis program(s) significantly sometimes many iterations for successful calibration and analysis of the data set. With this interaction, the data sets yield valuable, coherent analyses. During this period, it was also decided that only data sets taken inside heliographic longitudes (Central Meridian Distance) East and West 30 degrees (within 30 degrees of the Central Meridian of the Sun). If the total data set is then found to be numerically inadequate for the final analysis, 30 - 45 degrees Central Meridian Distance data will then be analyzed. The Optical Data storage system (MSFC observatory) was found appropriate for use both in intermediate storage of the data (preliminary to analysis), and for storage of the analyzed data sets for later parametric extraction. Author (revised)

N94-21832*# Alabama Univ., Huntsville. Center for Space Plasma and Aeronomic Research.
DEVELOPMENT, REFINEMENT, AND TESTING OF A SHORT TERM SOLAR FLARE PREDICTION ALGORITHM Semiannual Progress Report, 1 Feb. - 1 Aug. 1993
Jesse B. Smith, Jr. 1993 8 p
(Grant NAG8-888)
(NASA-CR-194727; NAS 1.26:194727) Avail: CASI HC A02/MF A01

During the period included in this report, the expenditure of time and effort, and progress toward performance of the tasks and accomplishing the goals set forth in the two year research grant proposal, consisted primarily of calibration and analysis of selected data sets. The heliographic limits of 30 degrees from central meridian were continued. As previously reported, all analyses are interactive and are performed by the Principal Investigator. It should also be noted that the analysis time involved by the Principal Investigator during this reporting period was limited, partially due to illness and partially resulting from other uncontrollable factors. The calibration technique (as developed by MSFC solar scientists), incorporates sets of constants which vary according to the wave length of the observation data set. One input constant is then varied interactively to correct for observing conditions, etc., to result in a maximum magnetic field strength (in the calibrated data), based on a separate analysis. There is some insecurity in the methodology and the selection of variables to yield the most self-consistent results for variable maximum field strengths and for variable observing/atmospheric conditions. Several data sets were analyzed using differing constant sets, and separate analyses to differing maximum field strength - toward standardizing methodology and technique for the most self-consistent results for the large number of cases. It may be necessary to recalibrate some of the analyses, but the sc analyses are retained on the optical disks and can still be used with recalibration where necessary. Only the extracted parameters will be changed.
Derived from text

N94-21877*# Science Applications International Corp., San Diego, CA.
DETERMINATION OF CORONAL MAGNETIC FIELDS FROM VECTOR MAGNETOGRAMS Progress Report No. 2, 1 Jan. - 31 Dec. 1993
Zoran Mikic 16 Dec. 1993 103 p Original contains color illustrations
(Contract NASw-4728; NAG5-1492; NSF ATM-92-96165)
(NASA-CR-194744; NAS 1.26:194744; SAIC-93/1224:APPAT-158) Avail: CASI HC A06/MF A02; 2 functional color pages

This report covers technical progress during the second year of the contract entitled 'Determination of Coronal Magnetic Fields from Vector Magnetograms,' NASW-4728, between NASA and Science Applications International Corporation, and covers the period January 1, 1993 to December 31, 1993. Under this contract SAIC has conducted research into the determination of coronal magnetic fields from vector magnetograms, including the development and application of algorithms to determine force-free coronal fields above selected observations of active regions. The contract began on June 30, 1992 and has a completion date of December 31, 1994. This contract is a continuation of work started in a previous contract, NASW-4571, which covered the period November 15, 1990 to December 14, 1991. During this second year we have concentrated

on studying additional active regions and in using the estimated coronal magnetic fields to compare to coronal features inferred from observations.
Derived from text

N94-20712*# National Aeronautics and Space Administration. Lyndon B. Johnson Space Center, Houston, TX.
SCR NEON AND ARGON IN KAPOETA FELDSPAR: EVIDENCE FOR AN ACTIVE ANCIENT SUN Abstract Only
M. N. Rao, D. H. Garrison, and D. D. Bogard *In* Lunar and Planetary Inst., Twenty-Fourth Lunar and Planetary Science Conference. Part 3: N-Z 1993 p 1193-1194 (For primary document see N94-20636 05-91)
Avail: CASI HC A01/MF A06

N94-20728*# Arizona Univ., Tucson. Lunar and Planetary Lab.
FORMATION OF THE LOW-MASS SOLAR NEBULA
T. V. Ruzmaikina, I. V. Khatuncev (Academy of Sciences, USSR, Moscow.), and T. V. Konkina (Academy of Sciences, USSR, Moscow.) *In* Lunar and Planetary Inst., Twenty-Fourth Lunar and Planetary Science Conference. Part 3: N-Z 1993 p 1225-1226 (For primary document see N94-20636 05-91)
Avail: CASI HC A01/MF A06

N94-20751*# Arizona Univ., Tucson. Dept. of Planetary Science.
DIFFUSIVE REDISTRIBUTION OF WATER VAPOR IN THE SOLAR NEBULA REVISITED Abstract Only
William D. Sears *In* Lunar and Planetary Inst., Twenty-Fourth Lunar and Planetary Science Conference. Part 3: N-Z 1993 p 1271-1272 (For primary document see N94-20636 05-91)
Avail: CASI HC A01/MF A06

N94-20791*# Lunar and Planetary Inst., Houston, TX.
MAGNETICALLY CONTROLLED SOLAR NEBULA Abstract Only
T. F. Stepinski and M. Reyes-Ruiz (Rice Univ., Houston, TX.) *In its* Twenty-Fourth Lunar and Planetary Science Conference. Part 3: N-Z 1993 p 1351-1352 (For primary document see N94-20636 05-91)
Avail: CASI HC A01/MF A06

N94-20859*# California Inst. of Tech., Pasadena. Div. of Geological and Planetary Sciences.
AGB STARS AS A SOURCE OF SHORT-LIVED RADIOACTIVE NUCLEI IN THE SOLAR NEBULA Abstract Only
G. J. Wasserburg, R. Gallino (Turin Univ., Italy.), M. Busso (Turin Univ., Italy.), and C. M. Raiteri (Turin Univ., Italy.) *In* Lunar and Planetary Inst., Twenty-Fourth Lunar and Planetary Science Conference. Part 3: N-Z 1993 p 1487-1488 (For primary document see N94-20636 05-91)
Avail: CASI HC A01/MF A06

N94-20875*# Eidgenoessische Technische Hochschule, Zurich (Switzerland).
A LONG-TERM CHANGE OF THE AR/KR/XE FRACTIONATION IN THE SOLAR CORPUSCULAR RADIATION Abstract Only
R. Wieler, H. Baur, and P. Signer *In* Lunar and Planetary Inst., Twenty-Fourth Lunar and Planetary Science Conference. Part 3: N-Z 1993 p 1519-1520 Sponsored in part by the Swiss NSF (For primary document see N94-20636 05-91)
Avail: CASI HC A01/MF A06

N94-21085*# Johns Hopkins Univ., Laurel, MD. Applied Physics Lab.
COMPARISON OF SINGLE EVENT UPSET RATES FOR MICROELECTRONIC MEMORY DEVICES DURING INTERPLANETARY SOLAR PARTICLE EVENTS
P. L. McKerracher, J. D. Kinnison, and R. H. Maurer *In* New Mexico Univ., The Fifth NASA Symposium on VLSI Design 1993 13 p (For primary document see N94-21079 05-33)
Avail: CASI HC A03/MF A06

N94-22632# Tokyo Univ., Mitake (Japan). Inst. of Astronomy.
HIGHLIGHTS OF YOHKOH RESULTS
Saku Tsuneta *In* ESA, Fourth International Toki Conference on Plasma Physics and Controlled Nuclear Fusion May 1993 p 75-8 (For primary document see N94-22624 05-75)
Copyright Avail: CASI HC A02/MF A03

N94-22633# Nobeyema Solar Radio Observatory (Japan).
PRELIMINARY RESULTS OF OBSERVATIONS OF SOLAR FLARES WITH NOBEYAMA RADIOHELIOGRAPH
Hiroshi Nakajima, S. Enome, K. Shibasaki, M. Nishio, T. Takano, Y. Hanaoka, C. Torii, H. Sekiguchi, T. Bushimata, and S. Kawashima et al *In* ESA, Fourth International Toki Conference on Plasma Physics and Controlled Nuclear Fusion May 1993 p 85-8 (For primary document see N94-22624 05-75)
Copyright Avail: CASI HC A01/MF A03

N94-22634# Sydney Univ. (Australia). Research Center for Theoretical Astrophysics.
RADIATION FROM SOLAR FLARES
Don B. Melrose *In* ESA, Fourth International Toki Conference on Plasma Physics and Controlled Nuclear Fusion May 1993 p 91-9 (For primary document see N94-22624 05-75)
Copyright Avail: CASI HC A02/MF A03

N94-22647# Osaka City Univ. (Japan). Dept. of Electrical Engineering.
LABORATORY RELATIONS BETWEEN THE SOLAR WIND DYNAMIC PRESSURE AND THE MAGNETOSPHERIC STRUCTURES OF THE EARTH AND COMETS
Shigeyuki Minami, T. Saito (Tohoku Univ., Sendai, Japan.), H. U. Rahman (California Univ., Riverside.), and R. S. White (California Univ., Riverside.) *In* ESA, Fourth International Toki Conference on Plasma Physics and Controlled Nuclear Fusion May 1993 p 171-176 (For primary document see N94-22624 05-75)
Copyright Avail: CASI HC A02/MF A03

N94-22648# Osaka City Univ. (Japan). Dept. of Electrical Engineering.
LABORATORY STRUCTURE OF THE HELIOPAUSE
Shigeyuki Minami *In* ESA, Fourth International Toki Conference on Plasma Physics and Controlled Nuclear Fusion May 1993 p 177-179 (For primary document see N94-22624 05-75)
Copyright Avail: CASI HC A01/MF A03

N94-22652# Sydney Univ. (Australia). Research Center for Theoretical Astrophysics.
ENERGY RELEASE AT ALFVENIC FRONTS IN SOLAR FLARES
Jennifer Nicholls *In* ESA, Fourth International Toki Conference on Plasma Physics and Controlled Nuclear Fusion May 1993 p 195-197 (For primary document see N94-22624 05-75)
Copyright Avail: CASI HC A01/MF A03

N94-22653# National Inst. for Fusion Science, Nagoya (Japan).
NON-EQUILIBRIUM IONIZATION IN AN M CLASS SOLAR FLARE
Takako Kato, Kuniaki Masai, K. Sakimoto (Tokyo Univ., Sagamihara, Japan.), Y. Itikawa (Tokyo Univ., Sagamihara, Japan.), and T. Watanabe (Tokyo Astronomical Observatory, Mitaka, Japan.) et al *In* ESA, Fourth International Toki Conference on Plasma Physics and Controlled Nuclear Fusion May 1993 p 199-202 (For primary document see N94-22624 05-75)
Copyright Avail: CASI HC A01/MF A03

N94-22654# Graduate Univ. for Advanced Studies (Japan). Dept. of Astronomical Science.
NUMERICAL SIMULATION OF MAGNETIC RECONNECTION ASSOCIATED WITH EMERGING FLUX IN THE SOLAR ATMOSPHERE
Takaaki Yokoyama and Kazumari Shibata (Tokyo Astronomical Observatory, Mitaka, Japan.) *In* ESA, Fourth International Toki Conference on Plasma Physics and Controlled Nuclear Fusion May 1993 p 203-206 (For primary document see N94-22624 05-75)
Copyright Avail: CASI HC A01/MF A03

N94-22655# Tokyo Astronomical Observatory, Mitaka (Japan).
X RAY JETS IN THE SOLAR CORONA: OBSERVATIONS WITH YOHKOH SOFT X RAY TELESCOPE
Kazunari Shibata, Y. Ishido, L. Acton, K. Strong, T. Hirayama, Yutaka Uchida, A. McAllister, R. Matsumoto, Saku Tsuneta, and T. Shimizu et al *In* ESA, Fourth International Toki Conference on Plasma Physics and Controlled Nuclear Fusion May 1993 p 207-210 (For primary document see N94-22624 05-75)
Copyright Avail: CASI HC A01/MF A03

N94-22657# Onagawa Magnetic Observatory (Japan). Astrogeophysics Inst.
LARGE-SCALE STRUCTURE OF THE SOLAR PLASMA CORONA: AN ANALYSIS OF YOHKOH SXT IMAGES
T. Saito, Shigeyuki Minami (Osaka City Univ., Japan.), Y. Kozuka (Nagoya Univ., Toyokawa, Japan.), T. Takahashi, H. Hudson (Hawaii Univ., Honolulu.), Saku Tsuneta (Tokyo Univ., Mitake, Japan.), and T. Watanabe (Nagoya Univ., Toyokawa, Japan.) *In* ESA, Fourth International Toki Conference on Plasma Physics and Controlled Nuclear Fusion May 1993 p 215-218 (For primary document see N94-22624 05-75)
Copyright Avail: CASI HC A01/MF A03

N94-22658# Hiroshima Univ. (Japan). Dept. of Materials Science.
MHD RELAXATION IN MAGNETIC LOOPS
Yoshio Suzuki, Kanya Kusano, Hiroko Kubo, Tetsuya Sato (National Inst. for Fusion Science, Nagoya, Japan.), and Kyoji Nishikawa *In* ESA, Fourth International Toki Conference on Plasma Physics and Controlled Nuclear Fusion May 1993 p 219-221 (For primary document see N94-22624 05-75)
Copyright Avail: CASI HC A01/MF A03

N94-22659# Academy of Sciences, Potsdam (German D.R.). Astrophysical Inst.
PARTICLE ACCELERATION IN A FILAMENTARY CURRENT SHEET MODEL
Bernhard Kliem *In* ESA, Fourth International Toki Conference on Plasma Physics and Controlled Nuclear Fusion May 1993 p 223-228 (For primary document see N94-22624 05-75)
(Contract DARA-50-QL-9208-5)
Copyright Avail: CASI HC A02/MF A03

N94-22660*# Iowa Univ., Iowa City.
CURRENT LOOP COALESCENCE STUDIED BY 3-D ELECTROMAGNETIC PARTICLE CODE
Ken-Ichi Nishikawa, Jun-Ichi Sakai (Toyama Univ., Japan.), Shinji Koide (Toyama Univ., Japan.), O. Buneman (Stanford Univ., CA.), and T. Neubert (Michigan Univ., Ann Arbor.) *In* ESA, Fourth International Toki Conference on Plasma Physics and Controlled Nuclear Fusion May 1993 p 229-232 (For primary document see N94-22624 05-75)
(Contract NAS8-38772; NAGw-2350; NSF ATM-91-06639; NSF ATM-91-21116; ASR-ME-03640247)
Copyright Avail: CASI HC A01/MF A03

N94-22661# Toyama Univ. (Japan). Plasma Astrophysics and Fusion Science Lab.
PROMPT HIGH-ENERGY PARTICLE ACCELERATION DURING TWO CURRENT LOOPS COLLISION
Jie Zhao, Bidzina Chargeishvili, and Jun-Ichi Sakai *In* ESA, Fourth International Toki Conference on Plasma Physics and Controlled Nuclear Fusion May 1993 p 233-236 (For primary document see N94-22624 05-75)
(Grant ASR-ME-03640247)
Copyright Avail: CASI HC A01/MF A03

N94-22662# Toyama Univ. (Japan). Plasma Astrophysics and Fusion Science Lab.
FORMATION OF FAST MAGNETOSONIC SHOCK WAVES DURING TWO CURRENT LOOPS COLLISION IN SOLAR FLARE
Shinji Koide and Jun-Ichi Sakai *In* ESA, Fourth International Toki Conference on Plasma Physics and Controlled Nuclear Fusion May 1993 p 237-240 Sponsored in part by YKK Foundation (For primary document see N94-22624 05-75)
(Grant ASR-ME-03640247)
Copyright Avail: CASI HC A01/MF A03

N94-22663# Toyama Univ. (Japan). Plasma Astrophysics and Fusion Science Lab.
DYNAMICS OF PHYSICAL STATE DURING TWO CURRENT LOOPS COLLISION
Bidzina Chargeishvili (Abastumani Astrophysical Observatory, Georgia, USSR.), Jie Zhao, and Jun-Ichi Sakai *In* ESA, Fourth International Toki Conference on Plasma Physics and Controlled Nuclear Fusion May 1993 p 241-244 (For primary document see N94-22624 05-75)
(Grant ASR-ME-03640247)
Copyright Avail: CASI HC A01/MF A03

N94-22670# Nagoya Univ. (Japan). Plasma Science Center.
MEAN ELEMENTAL COMPOSITION AND He-3 ENRICHMENTS IN SOLAR ENERGETIC PARTICLES
M. Toida, T. X. Zhang, and Yukiharu Ohsawa *In* ESA, Fourth International Toki Conference on Plasma Physics and Controlled Nuclear Fusion May 1993 p 269-273 (For primary document see N94-22624 05-75)
Copyright Avail: CASI HC A01/MF A03

N94-22671# Hawaii Univ., Honolulu. Inst. of Astronomy.
ENHANCED ABSORPTION OF p-MODES ON SUNSPOT AND PLAGE REGIONS
Barry J. LaBonte and Margarita Ryutova (Institute of Nuclear Physics, Novosibirsk, USSR.) *In* ESA, Fourth International Toki Conference on Plasma Physics and Controlled Nuclear Fusion May 1993 p 275-278 (For primary document see N94-22624 05-75)
Copyright Avail: CASI HC A01/MF A03

N94-22672# Kanagawa Univ., Yokahama (Japan). Inst. of Physics.
ACCELERATION OF SOLAR-FLARE PARTICLES AS VIEWED FROM THEIR CHEMICAL COMPOSITION
Kunitomo Sakurai *In* ESA, Fourth International Toki Conference on Plasma Physics and Controlled Nuclear Fusion May 1993 p 279-280 (For primary document see N94-22624 05-75)
Copyright Avail: CASI HC A01/MF A03

N94-22674*# Stanford Univ., CA.
SOLAR WIND-MAGNETOSPHERE INTERACTION AS SIMULATED BY A 3D, EM PARTICLE CODE
O. Buneman, Ken-Ichi Nishikawa (Iowa Univ., Iowa City.), and T. Neubert (Michigan Univ., Ann Arbor.) *In* ESA, Fourth International Toki Conference on Plasma Physics and Controlled Nuclear Fusion May 1993 p 285-288 (For primary document see N94-22624 05-75)
(Contract NAS8-38772; NAGw-2350; NSF ATM-91-06639; NSF ATM-91-21116)
Copyright Avail: CASI HC A01/MF A03

93 SPACE RADIATION

Includes cosmic radiation; and inner and outer earth's radiation belts.

For biological effects of radiation see *52 Aerospace Medicine*. For theory see *73 Nuclear and High-Energy Physics*.

N94-20602*# Max-Planck-Inst. fuer Physik und Astrophysik, Garching (Germany). Inst. fuer Extrateterrestriche Physik.
[OPTICAL AND GAMMA RAY SPACE OBSERVATIONS]
Nov. 1992 12 p Presented at the Compton Symposium, Saint Louis, MO, Oct. 1992
(NASA-TM-109389; NAS 1.15:109389; MPE-Preprint-235) Copyright Avail: CASI HC A03/MF A01

Results of the first year of data acquired from several Earth observatories concerning the optical counterparts gamma ray bursts (GRB) are presented. From the present statistics, it seems to be obvious that typical GRB's have optical emission at the time of the burst at a level at least below 1/(F(sub gamma)/F(sub opt)) approximately equal to 1/0.5 and optical emission a few hours after the burst is lower by a factor of 10 to 200 than the simultaneous emission. Given the fact that GRB spectra are rather broad over the observed energy range of say 20 keV up to 100 MeV, the observations indicate that the broad spectral shape may not continue into the optical range. After the confirmation of the isotropic distribution of GRB's by the BATSE experiment the interpretation now tends to put the sources at cosmological distances. For individual titles, see N94-20603 through N94-20604.

N94-20603*# National Aeronautics and Space Administration. Marshall Space Flight Center, Huntsville, AL.
SIMULTANEOUS OPTICAL/GAMMA RAY OBSERVATIONS OF GRB'S

C. Kouveliotou, G. J. Fishman, C. A. Meegan, W. S. Paciesas, R. B. Wilson, J. Greiner (Max-Planck-Inst. fuer Physik und Astrophysik, Garching, Germany.), W. Wenzel (Sternwarte der Deutschen Akademie der Wissenschaften, Sonneberg, German D.R.), R. Hudec (Ceskoslovenska Akademie Ved, Ondrejov.), P. Pravec (Ceskoslovenska Akademie Ved, Ondrejov.), and T. Rezek (Ceskoslovenska Akademie Ved, Ondrejov.) *et al* *In* Max-Planck-Inst. fuer Physik und Astrophysik, Optical and Gamma Ray Space Observations Nov. 1992 p 1-5 (For primary document see N94-20602 05-93)
(Contracts DARA-50-OR-9104-3; DESY-PH-05-5S414(4))
Copyright Avail: CASI HC A01/MF A01

The photographic sky patrols of the Observatories Sonneberg (FRG), Ondrejov (CSFR), Odessa (Ukraine) are used to look for patrol plates which were exposed simultaneously with a gamma-ray burst (GRB) detected by gamma ray observations. The results for the first year of data are presented. For several GRB plates which contain the GRB location, and the exposure time of which contains the time of the GRB are presented. The results of the research for optical flashes on these simultaneous plates are discussed. ESA

N94-20604*# Max-Planck-Inst. fuer Physik und Astrophysik, Garching (Germany). Inst. fuer Extraterrestrische Physik.
GAMMA RAY BURSTS FROM COLLISIONS OF PRIMORDIAL SMALL MASS BLACK HOLES WITH COMETS
K. F. Bickert and J. Greiner *In its* Optical and Gamma Ray Space Observations Nov. 1992 p 6-10 (For primary document see N94-20602 05-93)
Copyright Avail: CASI HC A01/MF A01

Recent results of BATSE (a collaborative project on independent sky surveys of gamm ray bursts and optical sky patrols) reinforce the isotropic distribution of gamm-ray bursts. Alternatively to cosmological models, collisions between small mas primordial black holes and comets in the Oort cloud are proposed. Assuming typical Oort cloud densities and velocities for comets and primordial black holes, many of the observed properties of gamma-ray bursts can be explained. ESA

N94-21056 Karlsruhe Univ. (Germany). Fakultaet fuer Physik.
EVALUATION OF THE CHEMICAL COMPOSITION OF COSMIC RADIATION IN ENERGY AREA OF 10(EXP 15) eV Ph.D. Thesis [BESTIMMUNG DER CHEMISCHEN ZUSAMMENSETZUNG DER KOSMISCHEN STRAHLUNG IM ENERGIEBEREICH VON E(SUB)0 OF 10(EXP 15) EV]
Peter Gabriel 1992 127 p In GERMAN Limited Reproducibility: More than 20% of this document may be affected by microfiche quality
(ETN-93-93682) Avail: CASI HC A07

The electromagnetic components of a hadronic shower are investigated with focus on pions and iron kernels. A Monte Carlo simulation program was developed: CORSIKA (German acronym for cosmic ray simulations for cascade) is based on the simulation of strong interaction by high energies with an algorithm written from the dual parton model; the strong interaction by least energies was described by the isobar model and the electromagnetic part can be simulated with Nishimura-Kamata-Greisen formula. Simulation calculations allow lateral distribution and energy and number spectra of electrons, photons, hadrons and muons to be obtained. The dependence of shower parameters on primary energy was established. Results are found to agree with experimental data from magnetic spectrometry and scintillation counting measurements. Methods for primary particle identificiation, such as the covariance method and principal components analysis are proposed. ESA

N94-21781*# Washington Univ., Saint Louis, MO. Dept. of Physics.
RADIO AND OPTICAL EMISSION: SPECTRAL SHAPES AND BREAKS IN GRB
J. I. Katz 1994 4 p
(Grant NAGw-2918)
(NASA-CR-194763; NAS 1.26:194763) Avail: CASI HC A01/MF A01

Relativistic blast wave models of Gamma Ray Bursts (GRB) predict the spectrum of the emitted synchrotron radiation. The electrons in the shocked region are heated to a Wien distribution whose 'temperature' is 1/3 of the mean electron energy. This energy determines a characteristic (break) frequency of synchrotron radiation. At much lower frequencies, a spectrum F(sub nu) varies as nu(sup 1/3) is predicted independently of the details of the emitting region. This is consistent with the observed soft x ray emission of GRB. It implies low visible and radio intensities, unless there are collective emission processes. Author (revised)

N94-21782*# Washington Univ., Saint Louis, MO. Dept. of Physics.
RELATIVISTIC SHOCK SPECTRA: A PREDICTION
J. I. Katz 1994 9 p
(Grant NAGw-2918)
(NASA-CR-194764; NAS 1.26:194764) Avail: CASI HC A02/MF A01

I argue that particles heated by relativistic shocks should assume an equilibrium energy distribution. This leads to a synchrotron spectrum F(sub nu) varies as nu(sup 1/3) up to approximately the critical frequency nu(sub 0) of an electron with the mean electron energy. Application to gamma ray bursts (GRB's) implies that a burst with 10(exp -5) erg/(sq cm s) of soft gamma-rays and h(nu(sub 0)) = 300 KeV should be about 18th magnitude in visible light and a few micro-Jy at 1 GHz (less if self-absorbed).
Author (revised)

N94-22397# Lawrence Livermore National Lab., CA.
RADIO GALAXIES AND THEIR ENVIRONMENT
W. vanBreugel 24 Feb. 1993 12 p Presented at the Jets in Extragalactic Radio Sources, Germany, 22-28 Sep. 1991
(Contract W-7405-eng-48)
(DE93-040851; UCRL-JC-114095; CONF-9109510-1) Avail: CASI HC A03/MF A01

The relationships between radio galaxies and their environment are varied, complex, and evolve with cosmic epoch. Basic questions are what role the environment plays in triggering and fuelling (radio) galaxy activity, what the effects of this activity are on its environment, and how radio galaxies and environment evolve. Clearly, this could be the topic of a workshop all in itself and the scope of this review will necessarily be limited. A review of the connections between environment and galaxy activity in general has been given by Heckman. First, I will briefly summarize the relationships between parent galaxy and cluster environments, and radio galaxies. A more detailed discussion of various aspects of this will be given elsewhere by F. Owen, J.0. Burns and R. Perley. I will then discuss the current status of investigations of extended emission-line regions in radio galaxies, again referring elsewhere in this volume for more detailed discussions of some particular aspects (kinematics and ionization mechanisms by K. Meisenheimer; polarization and spectral index lobe asymmetries by G. Pooley). I will conclude with a brief discussion of the current status of observations of high redshift radio galaxies. DOE

N94-20713*# Los Alamos National Lab., NM.
COSMOGENIC-RADIONUCLIDE PROFILES IN KNYAHINYA: NEW MEASUREMENTS AND MODELS Abstract Only
R. C. Reedy, J. Masarik, K. Nishiizumi (California Univ., La Jolla.), J. R. Arnold (California Univ., La Jolla.), R. C. Finkel (Lawrence Livermore National Lab., CA.), M. W. Caffee (Lawrence Livermore National Lab., CA.), J. Southon (Lawrence Livermore National Lab., CA.), A. J. T. Jull (Arizona Univ., Tucson.), and D. J. Donahue (Arizona Univ., Tucson.) *In* Lunar and Planetary Inst., Twenty-Fourth Lunar and Planetary Science Conference. Part 3: N-Z 1993 p 1195-1196 (For primary document see N94-20636 05-91)
Avail: CASI HC A01/MF A06

N94-22646*# Pennsylvania State Univ., University Park.
RELATIVISTICALLY EXPANDING PAIR PLASMAS AS BURSTING SOURCES OF COSMIC GAMMA RAYS
Peter Meszaros and M. J. Rees (Cambridge Univ., England.) *In* ESA, Fourth International Toki Conference on Plasma Physics and Controlled Nuclear Fusion May 1993 p 165-168 (For primary document see N94-22624 05-75)
(Grant NAGw-1522)
Copyright Avail: CASI HC A01/MF A03

N94-22649# Instituto de Pesquisas Espaciais, Sao Jose dos Campos (Brazil).
THEORY OF LEAKED AURORAL KILOMETRIC RADIATION
Maria Virginia Alves, Sergio R. Lopes, and Abraham C.-L. Chian (Cambridge Univ., England.) *In* ESA, Fourth International Toki Conference on Plasma Physics and Controlled Nuclear Fusion May 1993 p 181-183 Sponsored

by FAPESP; CNPq; and Commission of the European Communities (For primary document see N94-22624 05-75)
Copyright Avail: CASI HC A01/MF A03

N94-22656# Rikkyo Univ., Tokyo (Japan). Dept. of Physics.
YOHKOH GAMMA RAY SPECTRAL OBSERVATIONS (YGSO)
M. Yoshimori *In* ESA, Fourth International Toki Conference on Plasma Physics and Controlled Nuclear Fusion May 1993 p 211-214 (For primary document see N94-22624 05-75)
Copyright Avail: CASI HC A01/MF A03

N94-22675# Academy of Sciences (USSR), Moscow. Inst. of Physics.
GAMMA RAY BURST AS A RESULT OF THE EXPLOSIVE INSTABILITY IN THE MAGNETOSPHERE OF OLD NEUTRON STAR
Y. N. Istomin and D. V. Mosyagin *In* ESA, Fourth International Toki Conference on Plasma Physics and Controlled Nuclear Fusion May 1993 p 291-295 (For primary document see N94-22624 05-75)
Copyright Avail: CASI HC A01/MF A03

N94-22676# Osaka Univ., Toyonaka (Japan). Dept. of Earth and Space Science.
PROPERTIES OF X RAY EMISSION FROM X RAY NOVAE
Shunji Kitamoto *In* ESA, Fourth International Toki Conference on Plasma Physics and Controlled Nuclear Fusion May 1993 p 297-299 (For primary document see N94-22624 05-75)
Copyright Avail: CASI HC A01/MF A03

N94-22677# Sydney Univ. (Australia). Research Center for Theoretical Astrophysics.
ELECTRON ACCELERATION IN AND RADIO EMISSION FROM SN1987A
Lewis Ball and J. G. Kirk (Max-Planck-Inst. fuer Kernphysik, Heidelberg, Germany.) *In* ESA, Fourth International Toki Conference on Plasma Physics and Controlled Nuclear Fusion May 1993 p 301-303 (For primary document see N94-22624 05-75)
Copyright Avail: CASI HC A01/MF A03

N94-22678# Ecole Polytechnique, Palaiseau (France). Centre de Physique Theorique.
LANGMUIR MICROSTRUCTURES AND PULSAR RADIO EMISSION
Estelle Asseo *In* ESA, Fourth International Toki Conference on Plasma Physics and Controlled Nuclear Fusion May 1993 p 305-308 (For primary document see N94-22624 05-75)
Copyright Avail: CASI HC A01/MF A03

N94-22679# Institute of Physical and Chemical Research, Saitama (Japan).
STRUCTURE OF ACCRETION PLASMAS OF X RAY BINARY PULSARS IN MHD TURBULENCE
Masahiro Hoshino and Toshiaki Takeshima *In* ESA, Fourth International Toki Conference on Plasma Physics and Controlled Nuclear Fusion May 1993 p 309-312 (For primary document see N94-22624 05-75)
Copyright Avail: CASI HC A01/MF A03

N94-22680# Moscow Physical-Engineering Inst. (Russia).
VHE GAMMA RAY GENERATION BY RADIO PULSARS
Sergeii Vladimirovic Bogovalov (Institute of Physical and Chemical Research, Saitama, Japan.) and Y. D. Kotov *In* ESA, Fourth International Toki Conference on Plasma Physics and Controlled Nuclear Fusion May 1993 p 313-316 (For primary document see N94-22624 05-75)
Copyright Avail: CASI HC A01/MF A03

N94-22685# Sao Paulo Univ. (Brazil). Inst. Astronomico e Geofisico.
THREE-DIMENSIONAL SIMULATIONS OF COSMIC JETS EMPLOYING THE SMOOTHED PARTICLE HYDRODYNAMICS TECHNIQUE
Elisabete M. deGouveiaDalPino (Harvard-Smithsonian Center for Astrophysics, Cambridge, MA.) and Willy Benz (Arizona Univ., Tucson.) *In* ESA, Fourth International Toki Conference on Plasma Physics and Controlled Nuclear Fusion May 1993 p 333-336 (For primary document see N94-22624 05-75)
Copyright Avail: CASI HC A01/MF A03

N94-22686# National Inst. for Fusion Science, Nagoya (Japan).
HELICAL KINK INSTABILITY OF JETS FROM YOUNG STELLAR OBJECTS
Yasushi Todo *In* ESA, Fourth International Toki Conference on Plasma Physics and Controlled Nuclear Fusion May 1993 p 337-340 (For primary document see N94-22624 05-75)
Copyright Avail: CASI HC A01/MF A03

99 GENERAL

N94-20150# Wichita State Univ., KS. National Inst. for Aviation Research.
[ACTIVITIES OF NATIONAL INST. FOR AVIATION RESEARCH]
1993 72 p Sponsored by Kansas Technology Enterprise Corp.
(NIAR-93-16) Avail: CASI HC A04/MF A01

In response to a letter from Dr. Bill Brundage, KTEC president, dated August 2, 1993, the NIAR prepared information regarding the economic benefits the state has received for its six year investment of $3,402,500 through fiscal year 1993 in the National Institute for Aviation Research. Following is the summary of measurable outcomes: Established a research, technical assistance and education center operating as the primary channel for state research and development support to the aviation industry which accounts for 11.3 percent of the state's total employee earnings; Generated $23,529,000 from non-state sources producing a return on the KTEC investment of 7.9 : 1; Constructed a research facility of 74,000 gross sq ft with laboratories and equipment valued at $17,000,000. This is a return on the KTEC $475,000 equipment investment of 42.5 : 1; Established a Manufacturing Technology Center (MAMTC) Regional Office in Wichita with KTEC and NIST funding, which has provided assistance to 168 aviation support and non-aviation manufacturing firms with a combined employment of more than 18,400 Kansas; Received industry contracts valued at $2,902,000; Received federal grants/contracts valued at $13,727,000; Provided assistantships for 257 students in engineering and science. Alumni data suggest that 50 percent of engineering graduates remain in Kansas; Conducted 320 technology transfer workshops with a total of 9,450 attendees; Published 348 technical papers; Created and saved a total of 649 jobs (84 new jobs within the NIAR - 124 new jobs reported by NIAR/MAMTC clients - 251 jobs saved reported by NIAR/MAMTC clients - 190 indirect jobs created according to CEBDR estimate); and Provided substantial technical assistance to Boeing, Beech, Cessna and Learjet, which have combined employment of 31,000 Kansans, on seven new airplane models. The total sales potential of these projects manufactured by the Kansas Aviation Industry exceeds $10 billion. Derived from text

N94-20342# Japan Broadcasting Corp., Tokyo. Science and Technical Research Labs.
NHK SCIENCE AND TECHNICAL RESEARCH LABORATORIES Annual Report, 1992
18 Jun. 1993 40 p Original contains color illustrations
Avail: CASI HC A03/MF A01

NHK (Japan Broadcasting Corporation), founded under the Broadcast Law of Japan, is a public broadcasting enterprise whose operations are supported by reception fees paid by viewers throughout Japan. In 1992, the World Administrative Radio Conference (WARC) made an international allocation of frequency bands for broadband HDTV satellite broadcasts in the 21 GHz band and digital audio satellite broadcasts in the 2.5 GHz band for mobile receivers. In Japan, government-level studies have begun to decide how the eight satellite broadcasting channels assigned to this country should be utilized in the future. These moves will help to establish the framework for the development of future broadcasting systems including digital broadcasting and have close connection to the R&D activities of the laboratories. During 1992, the laboratories conducted active R&D on digital broadcasts which provide diverse and flexible services, and 3D TV broadcasts, as well as infrastructural technologies which will contribute to the realization of next-generation broadcasting. The laboratories also conducted R&D to promote further penetration of DBS services which have been available in Japan since 1984, to expand Hi-Vision (HDTV) broadcasting which NHK started in 1989, and to enhance existing broadcast activities. Derived from text

N94-20543# Deutsche Forschungsanstalt fuer Luft- und Raumfahrt, Munich (Germany). Abt. Bibliothekswesen.

DOCUMENTS ON THE HISTORY OF AERONAUTICAL AND SPACE RESEARCH IN GERMANY, 1900 - 1970 [DOKUMENTE ZUR GESCHICHTE DER LUFT- UND RAUMFAHRTFORSCHUNG IN DEUTSCHLAND 1900 - 1970]

Helmuth Trischler, ed. (Deutsches Museum, Munich, Germany.) Dec. 1992 435 p In GERMAN

(DLR-Mitt-92-08; ETN-93-94864) Avail: CASI HC A19/MF A04

The accompanying edition of sources to a reference book on air and aerospace research in Germany, 1900-1970, political history of science, is presented. 148 unpublished documents on the history of aeronautical and space research in its political context are contained. The main emphasis is put on the era of the 'Third Reich' and the Federal Republic of Germany. More than half of the documents deal with the years after World War Two. ESA

N94-21858# Lawrence Livermore National Lab., CA.

CHEMISTRY AND MATERIALS SCIENCE

Jul. 1993 101 p

(Contract W-7405-eng-48)

(DE94-001449; UCID-20622-93-1) Avail: CASI HC A06/MF A02

The major thrust areas of the weapons-supporting research are growth, structure, and reactivity of surfaces and thin films; uranium research; physics and processing of metals; and energetic materials. The laboratory-directed R and D includes the director's initiatives and individual projects and the transactinium institute studies. DOE

SUBJECT INDEX

Typical Subject Index Listing

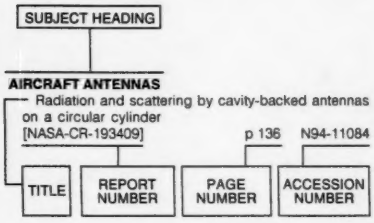

The subject heading is a key to the subject content of the document. Titles, report numbers, and accession numbers of pertinent documents are provided under each subject heading. When the title is insufficiently descriptive of the document content, a title extension is added, separated from the title by three hyphens. The report number helps to indicate the type of document cited (e.g., NASA report, NASA translation, NASA contractor report). The accession number is the number by which the document abstracts are arranged in this journal and by which the document is sold or requested. The page number helps you locate the citation in the abstract section. The titles, with title extensions if present, are arranged under each subject heading in ascending accession number order. The subject headings have been selected from the latest revision of the *NASA Thesaurus*.

A

A STARS
What is normal among the A-type stars?
[ISBN-0-315-83947-3] p 2081 N94-22592
ABLATION
The effects of area postrema lesions and selective vagotomy on motion-induced conditioned taste aversion p 1888 N94-21910
ABORTED MISSIONS
A simulation model for probabilistic analysis of Space Shuttle abort modes
[NASA-TM-108432] p 1656 N94-21859
ABRASION RESISTANCE
The use of screening tests in spacecraft lubricant evaluation
[AD-A272943] p 1705 N94-21225
ABSORBENTS
High temperature size selective membranes
[DE93-019865] p 1709 N94-21982
ABSORPTION COOLING
Heat transfer additives for absorption cooling system fluids
[PB93-202521] p 1714 N94-21426
ABSORPTION CROSS SECTIONS
Documentation for PCDIST, a FORTRAN subroutine to calculate Pollack-Cuzzi scattering
[AD-A273070] p 1988 N94-21491
ABSORPTION SPECTRA
Innovative acoustic technique for studying new materials and new developments in solid state physics
[AD-A270540] p 2013 N94-19933
Optical effects of space weathering on lunar soils and the role of the finest fraction p 2101 N94-20687
Determining the composition of olivine on asteroidal surfaces p 1686 N94-20805
Comparison of visible and near-infrared reflectance spectra of CM2 carbonaceous chondrites and primitive asteroids p 2085 N94-20848
Optical properties of chromium and neodymium in zirconium - barium - lanthanum - aluminum fluoride glass
[AD-A271609] p 1987 N94-21236
Infrared absorption spectroscopy of the weakly bonded CO-Cl2 complex
[AD-A271757] p 2027 N94-21304
RADCAL: A narrow-band model for radiation calculations in a combustion environment
[PB93-200889] p 1682 N94-21448
VVNRS: Variable phenomena in VV Cephei
[NASA-CR-194731] p 2056 N94-21835
Low temperature absorption spectra and ground state electronic structure of tetrakis(2,6-di-tert-butylphenoxide)uranium(IV)
[DE94-000774] p 2035 N94-22387
Infrared FEL photochemistry: Multiple-photon dissociation of freon gas
[DE94-000817] p 1820 N94-22585
ABSORPTION SPECTROSCOPY
Examinations of a thallium atomic vapor filter for a Raman temperature lidar
[GKSS-92/E/13] p 1857 N94-21044
Infrared absorption spectroscopy of the weakly bonded CO-Cl2 complex
[AD-A271757] p 2027 N94-21304
ABSORPTIVITY
RADCAL: A narrow-band model for radiation calculations in a combustion environment
[PB93-200889] p 1682 N94-21448
Cirrus microphysics observations made during FIRE 2: Small particles, high concentrations, and probe comparisons p 1871 N94-22294
ABSTRACTS
Progress In Electromagnetics Research Symposium (PIERS)
[NASA-CR-194629] p 1718 N94-20403
Intelligent text retrieval in the NASA astrophysics data system p 2048 N94-22499
ABUNDANCE
Core formation in the Moon: The mystery of the excess depletion of Mo, W and P p 2095 N94-20651
Volatility in the lunar crust: Trace element analyses of lunar minerals by PIXE proton microprobe p 2097 N94-20661
Abundance and composition of solar KR in the H3-H6 chondrite ACFER111 p 1684 N94-20676
Iridium in sediments containing large abundances of Australasian microtektites from DSDP hole 758B in the Eastern Indian Ocean and from DSDP hole 769A in the Sulu Sea p 2083 N94-20741
Cometary interplanetary dust particles? An update on carbon in anhydrous IDPS p 2084 N94-20828
Rhenium-osmium isotope systematics of ordinary chondrites and iron meteorites p 2085 N94-20854
The atomic weight and isotopic composition of boron and their variation in nature
[DE93-019046] p 1682 N94-21631
What is normal among the A-type stars?
[ISBN-0-315-83947-3] p 2081 N94-22592
ACCELERATION (PHYSICS)
Vector gravimetry by a combination of inertial and GPS satellite measurements
[ISBN-0-315-61980-5] p 1861 N94-22424
ACCELERATION STRESSES (PHYSIOLOGY)
System test results of the Advanced Technology Anti-G Suit (ATAGS)
[AD-A271535] p 1896 N94-20914
ACCELERATION TOLERANCE
System test results of the Advanced Technology Anti-G Suit (ATAGS)
[AD-A271535] p 1896 N94-20914
ACCELEROMETERS
Silicon micromachined threshold accelerometers p 1778 N94-22151
ACCEPTOR MATERIALS
Implantation of carbon in GaAs and compensating native defects
[DE93-040122] p 2030 N94-21763
Hydrogen in compound semiconductors
[DE93-040300] p 2031 N94-21922
ACCESS CONTROL
A semi-Markov model of a home network access protocol
[MEMO-INF-92-71] p 1909 N94-21045
ACCIDENT PREVENTION
Evaluation of head injury criteria
[NIAR-93-2] p 1890 N94-20190
ACCRETION DISKS
Magnetically controlled solar nebula p 2120 N94-20791
VVNRS: Variable phenomena in VV Cephei
[NASA-CR-194731] p 2056 N94-21835
Accretion disks in bright x ray binaries p 2002 N94-22639
Vertical structure of accretion disks p 2002 N94-22645
Hydrodynamical winds from an accretion disk p 2008 N94-22663
MHD flows from compact objects: Effects on magnetic field configurations p 2008 N94-22684
Pair plasmas in the galactic center region and in Nova Muscae p 2009 N94-22691
Spiral Alfven instability in accretion disks p 2010 N94-22698
ACCUMULATORS
The aerogel mesh contamination collector
[AD-A270537] p 1651 N94-20011
Charge collectors for the omega upgrade
[DE93-019684] p 1972 N94-20264
Wide-bandwidth high-resolution search for extraterrestrial intelligence
[NASA-CR-194724] p 1897 N94-20336
Low-latency digital frequency synthesizer using the residue number system p 1759 N94-21121
ACCURACY
Techniques for reducing error in the calorimetric measurement of low wattage items
[DE93-018472] p 1807 N94-20114
Calorimeter measurements of low wattage items
[DE93-018473] p 1807 N94-20115
Using the USCCS for sub microsecond spacecraft clock calibration p 1813 N94-21346
Order of accuracy of QUICK and related convection-diffusion schemes
[NASA-TM-106402] p 1959 N94-21588
Accuracy requirements — for monitoring of climate changes p 1869 N94-21642
Satellite orbit and data sampling requirements p 1870 N94-21648
Accuracy assessment for grid adaptation p 1920 N94-22368
Utilization of lasers for air data measurements p 1640 N94-22603
ACETIC ACID
Water-enhanced solvation of organics
[DE93-040297] p 1683 N94-21947
ACETONITRILE
Evaluation of pre-extraction analytical holding times for nitroaromatic and nitramine explosives in water
[AD-A271547] p 1712 N94-20927
ACETYLENE
Simulated space environmental effects on some experimental high performance polymers p 1662 N94-21385
ACHONDRITES
REE and other trace lithophiles in MAC88177, LEW88280 and LEW88763 p 2082 N94-20639
The Erevan howardite: Petrology of glassy clasts and mineral chemistry p 1684 N94-20640
Carbonaceous xenoliths from the Erevan howardite p 1684 N94-20642
Orthopyroxenes as recorders of diogenite petrogenesis: Major and minor element systematics p 1684 N94-20670
Lamellar olivine in the Divnoe achondrite: Evidence for high-pressure exsolution? p 1685 N94-20679
Opaque-rich lithology in the Divnoe achondrite: Petrology and origin p 2082 N94-20680
Post-igneous redistribution of components in eucrites p 1685 N94-20684
Orthopyroxenes as recorders of diogenite petrogenesis: Trace element systematics p 1686 N94-20760

A new Antarctic meteorite with chromite, orthopyroxene and metal with reference to a formation model of S asteroids p 2084 N94-20813
Chemical composition of new Acapulcoites and Lodranites p 2086 N94-20905
Mineralogy of dark clasts in primitive versus differentiated meteorites p 2087 N94-20907

ACID RAIN
Tropospheric chemistry of natural hydrocarbons, aldehydes, and peroxy radicals: Their connections to sulfuric acid production and climate effects
[DE93-019525] p 1855 N94-20220

ACOUSTIC ATTENUATION
Acoustic microscopy and nonlinear effects in pressurized superfluid helium
[AD-A270598] p 1967 N94-19949
Airborne surface backscattering strength measurements in the western Atlantic Ocean
[AD-A271737] p 1883 N94-21358

ACOUSTIC COUPLING
Acoustic microscopy and nonlinear effects in pressurized superfluid helium
[AD-A270598] p 1967 N94-19949

ACOUSTIC EMISSION
Fundamental studies of stress distributions and stress relaxation in oxide scales on high temperature alloys
[DE94-001444] p 1693 N94-21854
Three dimensional ultrasonic imaging
[DE93-040549] p 1968 N94-22003

ACOUSTIC EXCITATION
Development of phased twin flip-flop jets
[NASA-TM-106404] p 1637 N94-20563

ACOUSTIC FREQUENCIES
Computation of the sound generated by isotropic turbulence
[NASA-CR-191543] p 1804 N94-21880

ACOUSTIC INSTABILITY
Investigation of flame driving and flow turning in axial solid rocket instabilities
[AD-A271066] p 1667 N94-20015

ACOUSTIC MICROSCOPES
Acoustic microscopy and nonlinear effects in pressurized superfluid helium
[AD-A270598] p 1967 N94-19949

ACOUSTIC PROPAGATION
A survey of the impact on acoustic propagation of warm core ocean eddys
[AD-A272188] p 1883 N94-20925
Acoustic monitoring of global ocean variability
[AD-A271998] p 1883 N94-21366

ACOUSTIC PROPERTIES
Nonlinear acoustics: Periodic waveguide, finite-amplitude propagation in a medium having a distribution of relaxation processes, and production of an isolated negative pulse in water
[AD-A270530] p 1967 N94-19894
Segment-based acoustic models for continuous speech recognition
[AD-A271483] p 1736 N94-20547
Airborne surface backscattering strength measurements in the western Atlantic Ocean
[AD-A271737] p 1883 N94-21358

ACOUSTIC SCATTERING
Approximation to sound radiation and scattering by simply supported layered cylinder
[AD-A272964] p 1967 N94-21306
Airborne surface backscattering strength measurements in the western Atlantic Ocean
[AD-A271737] p 1883 N94-21358

ACOUSTIC SIMULATION
Computation of the sound generated by isotropic turbulence
[NASA-CR-191543] p 1804 N94-21880

ACOUSTIC VELOCITY
Volatile loss from accreting icy protoplanets p 2084 N94-20793
A survey of the impact on acoustic propagation of warm core ocean eddys
[AD-A272188] p 1883 N94-20925
Airborne surface backscattering strength measurements in the western Atlantic Ocean
[AD-A271737] p 1883 N94-21358
Speed of sound data and related models for mixtures of natural gas constituents
[PB93-200822] p 1968 N94-21447

ACOUSTICS
Innovative acoustic technique for studying new materials and new developments in solid state physics
[AD-A270540] p 2013 N94-19933
Mathematical model and analysis of the Tactical Unmanned Ground Vehicle (TUGV) using computer simulation
[AD-A272258] p 1824 N94-20576
Approximation to sound radiation and scattering by simply supported layered cylinder
[AD-A272964] p 1967 N94-21306
U.S. Tag for ISO/TC 43, acoustics, IEC/TC 29 electroacoustics, and ISO/TC 108/SC4 human exposure to mechanical vibration and shock: Minutes of the accredited standards committee on bioacoustics, S3
[AD-A273014] p 1897 N94-21309
Surface acoustic wave sensing of VOC's in harsh chemical environments
[DE93-040721] p 1968 N94-21751
The relative noise levels of parallel axis gear sets with various contact ratios and gear tooth forms
[NASA-TM-106431] p 1826 N94-21756
Acoustic, fiber optic, and silicon microelectronic microsensors research and development activities at Sandia National Laboratories
[DE93-019075] p 1770 N94-22040

ACOUSTO-OPTICS
Optical signal processing
[AD-A271036] p 1983 N94-20013

ACRYLATES
The 13C-NMR spectra of poly (4-((2-(acryloyloxy) ethyl) ethyl amino)- 4-nitroazobenzene-co-methyl methacrylate)
[AD-A273016] p 1705 N94-21238
Optically induced birefringence in copolymers and blends containing azobenzene groups
[AD-A273065] p 1706 N94-21523
Swelling equilibria for cationic 2-hydroxyethyl methacrylate (HEMA)-based hydrogels
[DE94-000728] p 1707 N94-21856

ACTINIDE SERIES
Crystallographic phase transitions in actinide metals as a function of pressure
[DE93-040138] p 2011 N94-19827
Static ultra-high pressure study of lanthanide and actinide metals using a diamond-anvil cell
[DE94-000369] p 1693 N94-21656
Theoretical studies of structural phase transitions in actinide metals
[DE94-000796] p 1696 N94-22388

ACTIVATION ENERGY
Integral equation calculation of solvent activation free energies for electron and proton transfer reactions
[AD-A272665] p 1681 N94-21216

ACTIVE CONTROL
Improvement of helicopter attitude stability by active control of the conventional swash plate
[NASA-CR-194786] p 1650 N94-20524
Actively controlled shaft seals for aerospace applications
[NASA-CR-194759] p 1823 N94-20538
Prediction and control of vortex-dominated and vortex-wake flows
[NASA-CR-194722] p 1637 N94-21054
Distributed intelligent control and status networking p 1932 N94-21335
Active control of wake/blade-row interaction noise through the use of blade surface actuators
[NASA-CR-4556] p 1968 N94-21608
Proceedings of the IMOG (Interagency Manufacturing Operations Group) Numerical Systems Group
[DE94-001009] p 1917 N94-21851
Active damping of oscillations in a long compliant manipulator link
[DE93-018878] p 1826 N94-22038

ACTIVE GALACTIC NUCLEI
Jets associated with active galactic nuclei p 2000 N94-22631
Pair plasmas in the central engine of active galactic nuclei p 2002 N94-22641
Vertical structure of accretion disks p 2002 N94-22645
Time variation of MHD accretion onto a black hole p 2009 N94-22692

ACTIVE SATELLITES
FITS data conversion efforts at the Compton Observatory Science Support Center p 1926 N94-22488

ACTIVITY (BIOLOGY)
Cosmos 2229
[NASA-CR-194734] p 1895 N94-20338

ACTS
Mobile antenna development at JPL p 1731 N94-20457

ACTUATION
Quantification of uncertainties in the performance of smart composite structures
[NASA-TM-106335] p 1830 N94-20171

ACTUATORS
Development and operation of the F/A-18 model control surface actuators
[AD-A271330] p 1645 N94-19914
Feedback controlled optics with wavefront compensation
[NASA-CASE-NPO-18194-1-CU] p 1985 N94-20305
Climbing robot --- caterpillar design
[NASA-CASE-GSC-13442-1] p 1823 N94-20494
Actively controlled shaft seals for aerospace applications
[NASA-CR-194759] p 1823 N94-20538
Torsion spring powered missile wing deployment system
[CA-PATENT-1,306,384] p 1645 N94-21051
Long range fast tool servo
[AD-A271614] p 1761 N94-21257
Active control of wake/blade-row interaction noise through the use of blade surface actuators
[NASA-CR-4556] p 1968 N94-21608
Micromachined actuator and sensor capabilities at the Microelectronics Development Laboratory
[DE93-019417] p 1769 N94-21918
Shape memory metals
[DE94-001373] p 1695 N94-21976

ADA (PROGRAMMING LANGUAGE)
A comprehensive software engineering educational experience
[AD-A270583] p 1905 N94-20109
The why, what, and how of Ada software development p 1779 N94-22157

ADAPTATION
Local uniform grid refinement and brine transport in porous media with inhomogeneities
[CWI-NM-R9224] p 1803 N94-21609

ADAPTERS
Disengagable adapter for an optical fiber connector
[AD-D015959] p 1822 N94-20356

ADAPTIVE CONTROL
Telerobotic control of a mobile coordinated robotic server, executive summary
[NASA-CR-194685] p 1821 N94-20044
Self-organization via active exploration in robotic applications. Phase 2: Hybrid hardware prototype
[NASA-CR-194723] p 1939 N94-20212
Optimization and control of a small angle ion source using an adaptive neural network controller
[DE93-040063] p 1946 N94-21845
On the estimation algorithm used in adaptive performance optimization of turbofan engines
[NASA-TM-4551] p 1649 N94-21879
An adaptive control to enable a robot to follow Cartesian trajectories p 1790 N94-22229
A robust adaptive control design for flexible joint manipulators p 1790 N94-22230

ADAPTIVE FILTERS
Sub-band adaptive noise cancelling p 1774 N94-22125
Timing recovery in the channel processor of a digital group demodulator p 1780 N94-22169
Applications of a two-dimensional nonlinear filters to image restoration p 1789 N94-22225
Adaptive filtering of Echelle spectra of distant Quasars p 2072 N94-22520

ADAPTIVE OPTICS
Long-range laser imaging
[AD-A273020] p 1817 N94-21253
Laser guide star adaptive optics: Present and future
[DE93-018642] p 1989 N94-21619
HST image restoration: A comparison of pre- and post-servicing mission results p 1925 N94-22478

ADDING CIRCUITS
Low-latency digital frequency synthesizer using the residue number system p 1759 N94-21121
Evaluation of floating-point sum or difference of products in carry-save domain p 1764 N94-21705
On fast carry select adders p 1767 N94-21728
Formal verification of an ALU p 1772 N94-22114

ADDITIVES
Thrust expansion engine
[AD-D015896] p 1669 N94-20121
The use of screening tests in spacecraft lubricant evaluation
[AD-A272943] p 1705 N94-21225
Optical properties of chromium and neodymium in zirconium - barium - lanthanum - aluminum fluoride glass
[AD-A271609] p 1987 N94-21236
Investigation of the effect of various oxide and fluoride additives on the microstructure, electronic properties, and phase shifting ability of Ba(1-x)Sr(x)TiO3
[AD-A271756] p 2027 N94-21303
Heat transfer additives for absorption cooling system fluids
[PB93-202521] p 1714 N94-21426
Refractive index behaviour of phosphorus-doped planar silica waveguides, appendix 7 p 1989 N94-21601
Research and development of alternative components at Argonne National Laboratory for molten carbonate fuel cells
[DE93-019536] p 1847 N94-21650
Ni3Al aluminide alloys
[DE94-000493] p 1694 N94-21933
Alloying effects on mechanical and metallurgical properties of NiAl
[DE93-040814] p 1694 N94-21948

Thin-film fabrication of Pb-doped BiSrCaCuO superconductor p 1781 N94-22176

ADDUCTS

Fullerene derivatives and fullerene superconductors [DE93-019568] p 2031 N94-21871

ADHESION

Microscopic modeling of tribological and interfacial phenomena [AD-A271864] p 1823 N94-20464

Interleaved bismaleimide composites [AD-A272233] p 1674 N94-20574

ADHESIVE BONDING

Durability predictions for adhesively bonded joints in humid environments [AD-A271177] p 1830 N94-20001

Adhesive bonded joint with improved cyclic fatigue life for alumina-ceramic cylinders and hemispheres: Fourth generation housings [AD-A273061] p 1831 N94-21310

ADHESIVES

Characterization studies of lower and non-TDI polyurethane encapsulants [DE93-041129] p 1698 N94-19857

Durability predictions for adhesively bonded joints in humid environments [AD-A271177] p 1830 N94-20001

Adhesive electroless metallization of fluoropolymeric substrates [AD-A271858] p 1703 N94-20526

Adhesive bonded joint with improved cyclic fatigue life for alumina-ceramic cylinders and hemispheres: Fourth generation housings [AD-A273061] p 1831 N94-21310

ADJOINTS

Shape optimization governed by the Euler equations using an adjoint method [NASA-CR-191555] p 1950 N94-20092

ADSORPTION

Common Themes and Mechanisms of Epitaxial Growth, volume 312 — Materials Research Society symposium proceedings [AD-A270513] p 2013 N94-19967

A Green function method for calculation of atomic and electronic properties of isolated adsorbate atoms [ETN-93-95055] p 2014 N94-20018

Collisions of molecules with clusters: A quasiclassical study [DE93-018614] p 1971 N94-20050

Photoelectron spectroscopy at model boundary surfaces of energy converter semiconductors/electrolyte contacts: Adsorption, coadsorption, and triadsorption of Br2, Na, and H2O on Van der Waals surfaces of metal chalocogenide semiconductors [ETN-93-95063] p 2015 N94-20152

The metallic bond for monolayer transition metal layers on transition metal surfaces [DE93-019060] p 1691 N94-20313

Surface electrochemistry of metals [AD-A272913] p 1691 N94-21245

Dynamics of adsorbed, swollen block copolymers [AD-A272013] p 1706 N94-21460

Sulfur-bonded thiophenes in organometallic rhenium complexes and adsorption of isocyanides on gold [DE93-041126] p 1694 N94-21937

Quantitative analysis of scanning tunneling microscopy images for surface structure determination: Sulfur on Re(0001) [DE93-019235] p 2034 N94-22041

ADVANCED TEST REACTORS

Hydrogen pickup and redistribution in alpha-annealed zircaloy-4 [DE93-018050] p 1689 N94-20182

ADVANCED VERY HIGH RESOLUTION RADIOMETER

Global and regional comparative performance of linear and nonlinear satellite multichannel sea surface temperature algorithms [AD-A270475] p 1837 N94-20028

Automatic AVHRR image navigation software [NASA-CR-194602] p 1643 N94-20148

Linear mixing model applied to AVHRR LAC data p 1838 N94-20958

Using NDVI/AVHRR data for crop monitoring and forecasting in South Italy p 1841 N94-20970

Comparison of satellite-derived velocity fields in the coastal transition zone [AD-A272565] p 1883 N94-21360

Cloud properties from the analysis of AVHRR observations for FIRE 2 p 1872 N94-22300

Remote sensing of multilevel clouds during FIRE IFO 2 p 1844 N94-22303

Atmospheric parameterization schemes for satellite cloud property retrieval during FIRE IFO 2 p 1874 N94-22312

ADVECTION

Predicting lightning events in the KSC area: A feasibility study using single station data [AD-A271440] p 1864 N94-20088

Modeling the minimum energy state of the Earth's magnetotail [AD-A267984] p 1856 N94-20485

Multigrid schemes for viscous hypersonic flows p 1641 N94-21473

AERIAL PHOTOGRAPHY

Mapping of taiga forest units using AIRSAR data and/or optical data, and retrieval of forest parameters p 1729 N94-20452

Experiments in knowledge refinement for a large rule-based system [AD-A272055] p 1809 N94-21445

An approach to the estimation of ground structure and aircraft motion from aerial image sequences p 1789 N94-22226

AEROACOUSTICS

Evaluation of a nonlinear method for the enhancement of tonal signal detection [NASA-CR-191562] p 1968 N94-21741

Computation of the sound generated by isotropic turbulence [NASA-CR-191543] p 1804 N94-21880

Instability modes excited by natural screech tones in a supersonic rectangular jet [NASA-TM-106409] p 1638 N94-22274

AEROASSIST

Effects of thrust vector control on the performance of the aerobang orbital plane change maneuver [AD-A272532] p 1646 N94-21418

AEROBRAKING

Entry velocities at Mars and Earth for short transit times [AD-A272591] p 1665 N94-21420

AERODYNAMIC BALANCE

Experimental study on interference aerodynamics of close-coupled canard configuration [AD-A267760] p 1636 N94-19963

AERODYNAMIC BRAKES

Tetrahedral lander [NASA-CASE-MSC-22062-1] p 1658 N94-20590

AERODYNAMIC DRAG

An experimental investigation of the drag mechanisms of a helicopter rotor in hovering flight [AD-A270201] p 1636 N94-20486

Pressure versus drag effects on crater size p 1862 N94-20742

Nonlinear aerodynamics and the design of wing tips [NASA-CR-194732] p 1638 N94-21833

AERODYNAMIC HEATING

Space Station trash removal system [NASA-CASE-MSC-21723-1] p 1657 N94-20367

Micrometeorite dynamic pyrometamorphism: Nonstoichiometric clinoenstatite (CLEN) p 2083 N94-20715

Effects of thrust vector control on the performance of the aerobang orbital plane change maneuver [AD-A272532] p 1646 N94-21418

AERODYNAMIC INTERFERENCE

Experimental study on interference aerodynamics of close-coupled canard configuration [AD-A267760] p 1636 N94-19963

AERODYNAMIC NOISE

Instability modes excited by natural screech tones in a supersonic rectangular jet [NASA-TM-106409] p 1638 N94-22274

AERODYNAMIC STABILITY

AIAA Techfest 29 proceedings [NIAR-93-1] p 1635 N94-20191

Modelling stalled airfoils [ISBN-0-315-59525-6] p 1639 N94-22382

AERODYNAMIC STALLING

A theoretical investigation of unsteady separation phenomena related to dynamic stall [AD-A271865] p 1636 N94-20465

AERODYNAMICS

Proceedings of the Twentieth Annual Technologyfest p 1645 N94-20188

AIAA Techfest 29 proceedings [NIAR-93-1] p 1635 N94-20191

Aeronautical engineering: A continuing bibliography with indexes (supplement 294) [NASA-SP-7037(294)] p 1635 N94-20267

Survey of lift-fan aerodynamic technology [NASA-CR-177615] p 1646 N94-21592

Nonlinear aerodynamics and the design of wing tips [NASA-CR-194732] p 1638 N94-21833

Instability modes excited by natural screech tones in a supersonic rectangular jet [NASA-TM-106409] p 1638 N94-22274

Measurement of the influence of deicing liquids on aircraft aerodynamics p 1640 N94-22602

AEROGELS

The aerogel mesh contamination collector [AD-A270537] p 1651 N94-20011

Intact capture of hypervelocity particles on Shuttle p 2085 N94-20837

Effects of aqueous solution compositions on Aerocapacitor energy density [DE94-000385] p 1768 N94-21753

AERONAUTICAL ENGINEERING

Proceedings of the Twentieth Annual Technologyfest p 1645 N94-20188

Aeronautical engineering: A continuing bibliography with indexes (supplement 294) [NASA-SP-7037(294)] p 1635 N94-20267

Documents on the history of aeronautical and space research in Germany, 1900 - 1970 [DLR-MITT-92-08] p 2152 N94-20543

AEROSOLS

Parameters affecting hydrogen chloride measurements [AD-A271326] p 1851 N94-20025

Tropospheric chemistry of natural hydrocarbons, aldehydes, and peroxy radicals: Their connections to sulfuric acid production and climate effects [DE93-019525] p 1855 N94-20220

Global blackout following the K/T Chicxulub impact: Results of impact and atmospheric modeling p 1854 N94-20696

Sunphotometer network for monitoring aerosol properties in the Brazilian Amazon p 1839 N94-20961

Obtaining surface optical properties from space-based lidar systems [AD-A272831] p 1987 N94-21172

NOVAM evaluation utilizing electro-optics and meteorological data from KEY-90 [AD-A271722] p 1868 N94-21356

Documentation for PCDIST, a FORTRAN subroutine to calculate Pollack-Cuzzi scattering [AD-A273070] p 1988 N94-21491

Stratospheric Aerosol and Gas Experiment (SAGE 3) p 1869 N94-21644

Earth observing scanning polarimeter p 1844 N94-21645

Global emissions and models of photochemically active compounds [DE93-040490] p 1852 N94-21969

CO2 lidar observations of Mount Pinatubo debris: FIRE 2 and longer-term measurements p 1876 N94-22323

Examination of the observed synoptic scale cirrus cloud environment: The December 3-6 FIRE cirrus case study p 1877 N94-22325

The 5-6 December 1991 FIRE IFO 2 jet stream cirrus case study: The influence of volcanic aerosols p 1877 N94-22326

Three dimensional modeling of cirrus during the 1991 FIRE IFO 2: Detailed process study p 1877 N94-22327

Development of advanced cloud parameterizations to examine air quality, cloud properties, and cloud-radiation feedback in mesoscale models [DE93-041164] p 1853 N94-22384

AEROSPACE ENGINEERING

Actively controlled shaft seals for aerospace applications [NASA-CR-194759] p 1823 N94-20538

Documents on the history of aeronautical and space research in Germany, 1900 - 1970 [DLR-MITT-92-08] p 2152 N94-20543

NASA patent abstracts bibliography: A continuing bibliography. Section 1: Abstracts (supplement 44) [NASA-SP-7039(44)-SECT-1] p 2043 N94-21254

Spinoff, 1992 [NASA-NP-201] p 2054 N94-21739

The 1992 Seals Flow Code Development Workshop [NASA-CP-10124] p 1654 N94-21790

Cognitive engineering in aerospace applications [NASA-CR-194782] p 1647 N94-21819

NASA Propulsion Engineering Research Center, volume 1 [NASA-CR-194721-VOL-1] p 1671 N94-22428

AEROSPACE ENVIRONMENTS

Synoptic observations of near surface processes of an insolated ice-dust body under space conditions: The case of KOSI 9 and 10 p 2084 N94-20827

Residual atmosphere in the FRECOPA experiment and degassing of materials p 1660 N94-21374

Some results of the oxidation investigation of copper and silver samples flown on LDEF p 1660 N94-21375

Aragatz project samples experiment/MAPOL (polymer materials) experiment: Postflight expert evaluation p 1660 N94-21376

Thermal stress analysis of composites in the space environment p 1661 N94-21379

Columbus PMP Critical Technologies Program: Approach for materials life time prediction p 1664 N94-21402

Spaceflight Radiation Health program at the Lyndon B. Johnson Space Center
[NASA-TM-104782] p 1893 N94-21863

AEROSPACE INDUSTRY
Aerospace: Facts and figures, 1992-1993
[AD-A272571] p 1635 N94-21419

AEROSPACE MEDICINE
Aerospace medicine and biology: A continuing bibliography with indexes (supplement 383)
[NASA-SP-7011(383)] p 1892 N94-21288

AEROSPACE PLANES
R and D to HOPE airframe p 1665 N94-21406
Thrust augmentation options for the Beta 2 two-stage-to-orbit vehicle
[NASA-TM-106448] p 1648 N94-21563
Spaceplane flight simulation: Project definition
[PB93-211399] p 1651 N94-22094

AEROSPACE SCIENCES
Electronic publishing and intelligent information retrieval p 2047 N94-22479

AEROSPACE SYSTEMS
Telerobotic control of a mobile coordinated robotic server, executive summary
[NASA-CR-194685] p 1821 N94-20044

AEROSPACE TECHNOLOGY TRANSFER
Index to 1992 NASA Tech Briefs, volume 16, numbers 1-12
[NASA-TM-109377] p 2053 N94-21736
Index to 1991 NASA Tech Briefs, volume 15, numbers 1-12
[NASA-TM-109376] p 2053 N94-21737
Cumulative index to NASA Tech Briefs, 1986-1990, volumes 10-14
[NASA-TM-109378] p 2054 N94-21738
Spinoff, 1992
[NASA-NP-201] p 2054 N94-21739

AEROTHERMODYNAMICS
Boost-phase discrimination research
[NASA-TM-109347] p 1666 N94-19818
Two dimensional simulation of the electric arc behavior in a cut-off device
[ECL-92-41] p 1751 N94-20595
Flow interaction experiment. Volume 1: Aerothermal modeling, phase 1
[NASA-CR-189192-VOL-1] p 1648 N94-21582
Flow interaction experiment. Volume 2: Aerothermalmodeling, phase 2
[NASA-CR-189192-VOL-2] p 1648 N94-21583

AFFERENT NERVOUS SYSTEMS
Effect of copper sulphate on the rate of afferent discharge in the gastric branch of the vagus nerve in the rat p 1887 N94-21907

AGGLOMERATION
Development of a technique to determine the morphology and dynamics of agglomerates in chemically reacting flows
[AD-A271160] p 1678 N94-20000
Unstructured multigrid through agglomeration p 1958 N94-21484

AGGREGATES
Strength and deformation properties of basaltic lava flows on planetary surfaces p 1862 N94-20747

AGING (MATERIALS)
A novel method for characterizing the electrical Priorities of lead Zirconate Titanate (PZT) ferroelectric films and memory devices
[AD-A270463] p 2013 N94-19966

AGING (METALLURGY)
Evaluation of a diffusion/trapping model for hydrogen ingress in high-strength alloys
[AD-A271328] p 1689 N94-20027
Microscopic evaluation of low-temperature embrittlement in type 308 stainless steel welds
[DE93-040266] p 1690 N94-20282

AGRICULTURE
Health effects of global warming: Problems in assessment
[DE93-040323] p 1850 N94-19930
A general rough-surface inversion algorithm: Theory and application to SAR data p 1719 N94-20407
Direction angle sensitivity of agricultural field backscatter with AIRSAR data p 1724 N94-20430
Rapid estimates of crop production using remote sensing: European experience p 1840 N94-20969
Multicriteria optimisation problem in the agricultural modelling p 1844 N94-22073

AGROCLIMATOLOGY
Drought early warning system for crop production p 1840 N94-20966

AGROMETEOROLOGY
Drought early warning system for crop production p 1840 N94-20966

AIR BREATHING BOOSTERS
Thrust augmentation options for the Beta 2 two-stage-to-orbit vehicle
[NASA-TM-106448] p 1648 N94-21563

AIR BREATHING ENGINES
Navy GTE seal development activity p 1655 N94-21794

AIR CONDITIONING
EHD enhancement of pool and in-tube boiling of alternate refrigerants
[DE94-000787] p 1798 N94-20101

AIR CONDITIONING EQUIPMENT
Physiological efficacy of a lightweight ambient air cooling unit for various applications
[AD-A272952] p 1896 N94-21247

AIR COOLING
Wind chill: The temperature feeling caused by the wind velocity
[KNMI-TR-103A] p 1890 N94-20238
Physiological efficacy of a lightweight ambient air cooling unit for various applications
[AD-A272952] p 1896 N94-21247

AIR DATA SYSTEMS
Handbook. Volume 2: Digital systems validation. Chapter 18: Avionic data bus integration technology
[DOT/FAA/CT-88/10-VOL-2] p 1647 N94-20343

AIR FLOW
Principles and applications of oil film interferometry for measuring wall friction fields in air flows
[ETN-93-95062] p 1798 N94-20147
An analysis of pool surface deformation due to a plunging liquid jet
[AD-A272970] p 1802 N94-21261
Performance calculations and research direction for a water enhanced regenerative gas turbine cycle
[DE93-019866] p 1826 N94-21983

AIR LAND INTERACTIONS
Simulated retrieval of land surface parameters using multichannel satellite microwave radiometry p 1727 N94-20443
MSATT Workshop on Innovative Instrumentation for the In Situ Study of Atmosphere-Surface Interactions on Mars
[NASA-CR-194584] p 1811 N94-22430

AIR POLLUTION
Alternative refrigerants and refrigeration cycles for domestic refrigerators
[DE93-040481] p 1714 N94-20099
Tropospheric chemistry of natural hydrocarbons, aldehydes, and peroxy radicals: Their connections to sulfuric acid production and climate effects
[DE93-019525] p 1855 N94-20220
Analysis of wind observation from towers in the period 1977-1991
[KNMI-TR-148] p 1865 N94-20239
EDMS microcomputer pollution model for civilian airports and Air Forces bases: User's guide, supplement A
[AD-A271596] p 1851 N94-20948
Role of surface characteristics in urban meteorology and air quality
[DE93-040929] p 1851 N94-21740
Global emissions and models of photochemically active compounds
[DE93-040490] p 1852 N94-21969
The use of lidar for the evaluation of traffic-related urban pollution
[DE94-000704] p 1852 N94-22017
Survey on evaluation of energy technology contributing to preservation of the global environment. 2
[DE94-714884] p 1853 N94-22051
An economic analysis of transboundary air pollution between Finland and the Soviet Union
[ETLA-DISCUSSION-PAPER-335] p 1854 N94-22072
Development of advanced cloud parameterizations to examine air quality, cloud properties, and cloud-radiation feedback in mesoscale models
[DE93-041164] p 1853 N94-22384
Environmental protection using social costing
[DE94-000492] p 1853 N94-22569

AIR QUALITY
Advanced batteries for electric vehicle applications: Nontechnical summary
[DE93-019007] p 1748 N94-19885
EDMS microcomputer pollution model for civilian airports and Air Forces bases: User's guide, supplement A
[AD-A271596] p 1851 N94-20948
Role of surface characteristics in urban meteorology and air quality
[DE93-040929] p 1851 N94-21740
The use of lidar for the evaluation of traffic-related urban pollution
[DE94-000704] p 1852 N94-22017
Development of advanced cloud parameterizations to examine air quality, cloud properties, and cloud-radiation feedback in mesoscale models
[DE93-041164] p 1853 N94-22384
Passive Cryogenic Sampler
[DE94-000918] p 1811 N94-22392

AIR SAMPLING
Atmospheric sampling glow discharge ionization and triple quadrupole tandem mass spectrometry for explosives vapor detection
[DE93-040593] p 1852 N94-22004
Passive Cryogenic Sampler
[DE94-000918] p 1811 N94-22392

AIR TRAFFIC CONTROL
ATC/pilot voice communications: A survey of the literature
[DOT/FAA/AM-93/20] p 1738 N94-21201
Next Generation Weather Radar (NEXRAD) Principal User Processor (PUP) Operational Test and Evaluation (OT/E)
[AD-A273075] p 1868 N94-21519
Development and evaluation of a profile negotiation process for integrating aircraft and air traffic control automation
[NASA-TM-4360] p 1643 N94-21606
Techniques used for the analysis of oculometer eye-scanning data obtained from an air traffic control display
[NASA-CR-191559] p 1643 N94-21629
Parallel runway requirement analysis study. Volume 1: The analysis
[NASA-CR-191549-VOL-1] p 1644 N94-22277
Parallel runway requirement analysis study. Volume 2: Simulation manual
[NASA-CR-191549-VOL-2] p 1644 N94-22278

AIR TRAFFIC CONTROLLERS (PERSONNEL)
Research, Development, Training, and Evaluation (RDTE) support delivery order 1: Computational cognitive models
[AD-A271837] p 1894 N94-20610

AIR TRANSPORTATION
Aerospace: Facts and figures, 1992-1993
[AD-A272571] p 1635 N94-21419
Air transport of samples containing chemical warfare agents
[FFI-93/6005] p 1851 N94-21455
Public-sector aviation issues: Graduate research award papers, 1991-1992
[PB93-206258] p 1642 N94-22055

AIR WATER INTERACTIONS
The marine light-mixed layer experiment cruise and data report: R/V endeavor cruise EN-224, mooring deployment, 27 April-1 May 1991: Cruise EN-227, mooring recovery, 5-23 September 1991
[AD-A271175] p 1864 N94-20186
ERS-1 and Seasat scatterometer measurements of ocean winds: Model functions and the directional distribution of short waves p 1720 N94-20412
Ku-band ocean radar backscatter observations during SWADE p 1720 N94-20413
Comparison of remote sensing measurements with a two-scale polarimetric emission and scattering model for sea surfaces p 1721 N94-20415
Four-dimensional remote sensing of the marine boundary layer with a digital beamforming radar wind profiler
[AD-A270627] p 1882 N94-20564
NOVAM evaluation utilizing electro-optics and meteorological data from KEY-90
[AD-A271722] p 1868 N94-21356

AIRBORNE EQUIPMENT
Description and availability of airborne Doppler radar data p 1722 N94-20419
Advances in spaceborne radar remote sensing p 1723 N94-20424
Optical properties of cirrus derived from airborne measurements during FIRE IFO 2 p 1872 N94-22297
Intercomparison of MAS, AVIRIS, and HIS data from FIRE cirrus 2 p 1872 N94-22298

AIRBORNE RADAR
All-weather precision landing system for aircraft in remote areas
[AD-D015924] p 1643 N94-20197
Description and availability of airborne Doppler radar data p 1722 N94-20419
Two microstrip arrays for interferometric SAR applications p 1722 N94-20421
Advances in spaceborne radar remote sensing p 1723 N94-20424
On evaluating the accuracy of SAR sea-ice classification using multifrequency polarimetric AIRSAR data p 1724 N94-20428
Direction angle sensitivity of agricultural field backscatter with AIRSAR data p 1724 N94-20430
Radar backscattering from snow facies of the Greenland ice sheet: Results from the AIRSAR 1991 campaign p 1725 N94-20434

AIRBORNE SURVEILLANCE RADAR
Target angular motion and its effects on simulated SSAR ship images p 1745 N94-22161

AIRBORNE/SPACEBORNE COMPUTERS
Mongoose: Creation of a Rad-Hard MIPS R3000
p 1754 N94-21090
A simple modern correctness condition for a space-based high-performance multiprocessor
p 1766 N94-21718
Low energy CMOS for space applications
p 1768 N94-21735
Experiences in airborne computing at NRC for geophysical exploration applications
p 1783 N94-22185
Space Generic Open Avionics Architecture (SGOAA) standard specification
[NASA-CR-188269] p 1666 N94-22275
Towards the formal verification of the requirements and design of a processor interface unit: HOL listings
[NASA-CR-191466] p 1937 N94-22414
Second Annual Conference on Astronomical Data Analysis Software and Systems. Abstracts
[NASA-TM-108245] p 2057 N94-22438
IRAF and STSDAS under the new ALPHA architecture
p 2049 N94-22553
AIRCRAFT ACCIDENTS
Ground proximity warning system voice warning unit requirements study
[AD-A270541] p 1641 N94-19876
Aviation safety research at the National Institute for Aviation Research, Wichita State University
[NIAR-93-4] p 1641 N94-20189
Aviation safety research. Volume 1: Literature review of sources of aviation accident and incident data and selected factors contributing to accidents
[PB93-202685] p 1641 N94-21428
Aircraft cabin water spray disbenefits study
[NASA-CR-194750] p 1642 N94-21818
AIRCRAFT ANTENNAS
Mobile terminal antennas for helicopters
p 1731 N94-20458
Improvements in antenna coupling path algorithms for aircraft EMC analysis p 1745 N94-22126
AIRCRAFT APPROACH SPACING
Parallel runway requirement analysis study. Volume 1: The analysis
[NASA-CR-191549-VOL-1] p 1644 N94-22277
Parallel runway requirement analysis study. Volume 2: Simulation manual
[NASA-CR-191549-VOL-2] p 1644 N94-22278
AIRCRAFT COMPARTMENTS
Aviation safety research at the National Institute for Aviation Research, Wichita State University
[NIAR-93-4] p 1641 N94-20189
Aircraft cabin water spray disbenefits study
[NASA-CR-194750] p 1642 N94-21818
AIRCRAFT CONFIGURATIONS
AIAA Techfest 29 proceedings
[NIAR-93-1] p 1635 N94-20191
Apparatus and method for improving spin recovery on aircraft
[NASA-CASE-LAR-14747-1] p 1650 N94-20556
AIRCRAFT CONSTRUCTION MATERIALS
Strengthening and toughening in refractory metal alloys
[DE93-019942] p 1695 N94-21986
AIRCRAFT CONTROL
Handbook. Volume 3: Digital systems validation book plan
[DOT/FAA/CT-93/16-VOL-3] p 1647 N94-20053
Handbook. Volume 2: Digital systems validation. Chapter 18: Avionic data bus integration technology
[DOT/FAA/CT-88/10-VOL-2] p 1647 N94-20343
Control vane guidance for a ducted-fan unmanned air vehicle
[AD-A271957] p 1645 N94-20561
A comparative robustness evaluation of feedforward neurofilters
[NASA-TM-106440] p 1650 N94-21742
AIRCRAFT DESIGN
Apparatus and method for improving spin recovery on aircraft
[NASA-CASE-LAR-14747-1] p 1650 N94-20556
Optimization and performance analysis of a supersonic conical-flow waverider for a deck-launched intercept mission
[AD-A272498] p 1648 N94-21433
Low-cost Unmanned Air Vehicle (UAV) for oceanographic research
[AD-A273103] p 1646 N94-21507
AIRCRAFT ENGINES
Navy GTE seal development activity
p 1655 N94-21794
AIRCRAFT EQUIPMENT
Windshear detection for aircraft using temperature lapse rate
[CA-PATENT-1,295,736] p 1641 N94-21030
AIRCRAFT GUIDANCE
Optimal flight guidance for aircraft in windshear
[CA-PATENT-1,307,573] p 1650 N94-21050
Public-sector aviation issues: Graduate research award papers, 1991-1992
[PB93-206258] p 1642 N94-22055
AIRCRAFT HYDRAULIC SYSTEMS
The optohydraulic servovalve: A novel device for the precise optical control of hydraulic pressure
[ISBN-0-315-83580-X] p 1827 N94-22577
AIRCRAFT ICING
Users manual for the NASA Lewis three-dimensional ice accretion code (LEWICE 3D)
[NASA-TM-105974] p 1642 N94-21590
AIRCRAFT INDUSTRY
Activities of National Inst. for Aviation Research
[NIAR-93-16] p 2151 N94-20150
AIRCRAFT LANDING
All-weather precision landing system for aircraft in remote areas
[AD-D015924] p 1643 N94-20197
Public-sector aviation issues: Graduate research award papers, 1991-1992
[PB93-206258] p 1642 N94-22055
AIRCRAFT MAINTENANCE
The 1992 USAF structural integrity program conference
[AD-A272876] p 1635 N94-21194
AIRCRAFT MODELS
Development and operation of the F/A-18 model control surface actuators
[AD-A271330] p 1645 N94-19914
Activities of National Inst. for Aviation Research
[NIAR-93-16] p 2151 N94-20150
Improved ceramic slip casting technique --- application to aircraft model fabrication
[NASA-CASE-LAR-14471-1] p 1702 N94-20377
AIRCRAFT NOISE
Rotorcraft noise: Status and recent developments
[NASA-CR-194761] p 1967 N94-20523
The relative noise levels of parallel axis gear sets with various contact ratios and gear tooth forms
[NASA-TM-106431] p 1826 N94-21756
Aircraft noise effects on cultural resources: Recommendation and rationale for further research
[PB93-205326] p 1968 N94-22053
Aircraft noise effects on cultural resources: Annotated bibliography
[PB93-205334] p 1969 N94-22054
AIRCRAFT PERFORMANCE
Apparatus and method for improving spin recovery on aircraft
[NASA-CASE-LAR-14747-1] p 1650 N94-20556
AIRCRAFT PRODUCTION
Aerospace: Facts and figures, 1992-1993
[AD-A272571] p 1635 N94-21419
AIRCRAFT SAFETY
Aviation safety research at the National Institute for Aviation Research, Wichita State University
[NIAR-93-4] p 1641 N94-20189
Army aircraft fire-detection systems operation and reliability
[AD-A271327] p 1641 N94-20912
A proposed methodology for combustion toxicology testing of combined halon replacement agent/jet fuel interaction
[AD-A272695] p 1681 N94-21165
ATC/pilot voice communications: A survey of the literature
[DOT/FAA/AM-93/20] p 1738 N94-21201
Aviation safety research. Volume 1: Literature review of sources of aviation accident and incident data and selected factors contributing to accidents
[PB93-202885] p 1641 N94-21428
Aircraft cabin water spray disbenefits study
[NASA-CR-194750] p 1642 N94-21818
Public-sector aviation issues: Graduate research award papers, 1991-1992
[PB93-206258] p 1642 N94-22055
Parallel runway requirement analysis study. Volume 1: The analysis
[NASA-CR-191549-VOL-1] p 1644 N94-22277
AIRCRAFT SPIN
Apparatus and method for improving spin recovery on aircraft
[NASA-CASE-LAR-14747-1] p 1650 N94-20556
AIRCRAFT STRUCTURES
The 1992 USAF structural integrity program conference
[AD-A272876] p 1635 N94-21194
AIRCRAFT SURVIVABILITY
Long-range laser imaging
[AD-A273020] p 1817 N94-21253
AIRFOIL OSCILLATIONS
AIAA Techfest 29 proceedings
[NIAR-93-1] p 1635 N94-20191
AIRFOILS
A theoretical investigation of unsteady separation phenomena related to dynamic stall
[AD-A271865] p 1636 N94-20485
Robust unstructured grid generation with VGRID
p 1919 N94-22359
Development of a gridless CFD method
p 1919 N94-22361
Modelling stalled airfoils
[ISBN-0-315-59525-6] p 1639 N94-22382
Transonic flow calculations: Integral method
[ISBN-0-315-83538-9] p 1639 N94-22586
AIRFRAMES
AIAA Techfest 29 proceedings
[NIAR-93-1] p 1635 N94-20191
AIRLINE OPERATIONS
Public-sector aviation issues: Graduate research award papers, 1991-1992
[PB93-206258] p 1642 N94-22055
Demonstrating damage tolerance of composite airframes p 1647 N94-22623
AIRPORT PLANNING
Public-sector aviation issues: Graduate research award papers, 1991-1992
[PB93-206258] p 1642 N94-22055
A study of parallel pier finger airport terminal configuration
[ISBN-0-315-83128-6] p 1652 N94-22425
AIRPORTS
EDMS microcomputer pollution model for civilian airports and Air Forces bases: User's guide, supplement A
[AD-A271596] p 1851 N94-20948
Notes on Antarctic aviation
[AD-A273018] p 1651 N94-21239
Observations of multi-layered clouds using K-band radar p 1874 N94-22311
Passenger terminal level of service measurement: A utility theoretic approach
[ISBN-0-315-59037-8] p 1651 N94-22418
An airport economic impact study procedure for Atlantic Canada
[ISBN-0-315-59445-4] p 1651 N94-22419
Passenger terminal simulation model
[ISBN-0-315-61113-8] p 1652 N94-22423
A study of parallel pier finger airport terminal configuration
[ISBN-0-315-83128-6] p 1652 N94-22425
ALANINE
Development of bioelastic material for aspects of wound repair
[AD-A267832] p 1673 N94-20208
ALBEDO
The 3-D Moons: The Voyager stereo atlas of the outer solar system p 2111 N94-20740
IMPS albedo and diameter for Asteroid 243 Ida
p 2085 N94-20845
Multispectral studies of selected crater- and basin-filling lunar Maria from Galileo Earth-Moon encounter 1
p 2136 N94-20876
Are tropical cirrus brighter than mid-latitude cirrus?
p 1881 N94-22343
ALCOHOLS
Investigation on the chemically fixing technique of carbon dioxide utilizing solar energy
[DE94-714886] p 1849 N94-22043
ALDEHYDES
Tropospheric chemistry of natural hydrocarbons, aldehydes, and peroxy radicals: Their connections to sulfuric acid production and climate effects
[DE93-019525] p 1855 N94-20220
ALGEBRA
Representation and recognition with algebraic invariants and geometric constraint models
[AD-A271395] p 1949 N94-19838
Numerical solution of differential-algebraic equations with ill-conditioned constraints
[AD-A270934] p 1949 N94-19898
Partition algebraic design of asynchronous sequential circuits p 1759 N94-21125
On semisimple cocommutative bialgebras
[CWI-AM-R9210] p 1954 N94-21158
Classical and generalized solutions of time-dependent linear differential algebraic equations
[AD-A272834] p 1954 N94-21173
Toward a new method of decoding algebraic codes using Groebner bases
[AD-A273089] p 1959 N94-21524
A mechanized process algebra for verification of device synchronization protocols p 1766 N94-21716
The accuracy-through-order and the equivalence properties in the algebraic approximant
[DE93-040188] p 1960 N94-21946
The design of linear algebra libraries for high performance computers
[DE93-040458] p 1960 N94-21957

Vanishing theorem on arithmetic surfaces
[PB93-215481] p 1961 N94-22263
Non commutative geometry and physics
[PB93-215499] p 1961 N94-22264
Modular interval spaces
[PB93-220663] p 1961 N94-22266

ALGORITHMS
A distributed reinforcement learning scheme for network routing
[AD-A270600] p 1938 N94-19845
Method to evaluate steering and alignment algorithms for controlling emittance growth
[DE93-041004] p 1978 N94-19856
A comparison of data-parallel algorithms for connected components
[AD-A270551] p 1902 N94-19918
Set based analysis of ML programs
[AD-A270597] p 1902 N94-19948
Segmented operations for sparse matrix computation on vector multiprocessors
[AD-A270601] p 1928 N94-19950
Global combine on mesh architectures with wormhole routing
[DE93-018792] p 1903 N94-19959
Program derivation in acyclic graphs and related problems
[PB93-191765] p 1903 N94-19994
Stochastic optimization by simulation: Convergence proofs for the G1/G/1 queue in steady-state
[AD-A271141] p 1962 N94-19999
Global and regional comparative performance of linear and nonlinear satellite multichannel sea surface temperature algorithms
[AD-A270475] p 1637 N94-20028
A weighted least-squares lump correction algorithm for transmission-corrected gamma ray nondestructive assay
[DE93-018474] p 1904 N94-20049
On multiflow problems
[RR-889-M] p 1950 N94-20125
Determining the distance to the perfect matching polytope of a bipartite graph
[RR-895-M] p 1950 N94-20161
Fast scalar algorithms for multivariate partial correlations and their empirical counterparts
[RR-903-M] p 1905 N94-20201
Determination of the optimal stochastic upper bound of a Markovian generator
[RR-906-I] p 1963 N94-20202
New algorithm of ground track processing in high-frequency skywave over-the-horizon-B radar
[AD-A267821] p 1717 N94-20207
Representation of spoken words in a self-organizing neural net p 1940 N94-20243
Modeling the human mental lexicon with self-organizing feature maps p 1743 N94-20244
Teleoperation with virtual force feedback
[DE93-019406] p 1942 N94-20293
Atmospheric infrared sounder
[NASA-CR-194814] p 1856 N94-20362
Neural network for processing both spatial and temporal data with time based back-propagation
[NASA-CASE-MSC-21874-1] p 1942 N94-20366
A general rough-surface inversion algorithm: Theory and application to SAR data p 1719 N94-20407
Modifications to the three-component classification algorithm for SAR data p 1719 N94-20410
Time-domain analysis of planar microstrip devices using a generalized Yee-algorithm based on unstructured grids p 1724 N94-20431
Topographic slope from the SAR interferometric phase gradient p 1731 N94-20459
Graph minors: Structure theory and algorithms
[AD-A271851] p 1952 N94-20613
Reduction of network cost and wiring in Ranade's butterfly routing
[CWI-CS-R9243] p 1930 N94-21023
Optimal sorting in linear arrays with minimum global control
[CWI-CS-R9244] p 1908 N94-21024
Efficient comparison based string matching
[CWI-CS-R9249] p 1909 N94-21028
Tight comparison bounds for the string prefix-matching problem
[CWI-CS-R9250] p 1952 N94-21029
MGD1M: A parallel multigrid code with a fast vectorized ILU-relaxation
[CWI-NM-R9222] p 1930 N94-21077
An adaptive, lossless data compression algorithm and VLSI implementations p 1753 N94-21080
Practical issues in implementing roving spares in VLSI systolic arrays p 1758 N94-21114
A novel VLSI processor architecture for supercomputing arrays p 1758 N94-21115
Synthesis algorithm of VLSI multipliers for ASIC p 1758 N94-21116
Experiments on technology mapping using different cell libraries p 1758 N94-21118
A unified approach to VLSI layout automation and algorithm mapping on processor arrays p 1759 N94-21127
The Robinson-Schensted and Schuetzenberger algorithms. Part 1: New combinatorial proofs
[CWI-AM-R9208-PT-1] p 1911 N94-21156
The Robinson-Schensted and Schuetzenberger algorithms. Part 2: Geometric interpretations
[CWI-AM-R9209-PT-2] p 1911 N94-21157
Classification in feature-based default inheritance hierarchies
[TR-473] p 1911 N94-21180
Fault tolerant real-time systems
[AD-A272878] p 1899 N94-21195
Fast mutual exclusion, even with contention
[AD-A272947] p 1912 N94-21227
Selectivity: Reductions, nondeterminism, and function classes
[TR-469] p 1912 N94-21273
Using the USCCS for sub microsecond spacecraft clock calibration p 1813 N94-21346
An efficient numerical method for three-dimensional hypersonic flow
[AD-A272506] p 1637 N94-21411
Conversion and maintenance of Co-oP for Windows
[AD-A272513] p 1914 N94-21414
Mapping robust parallel multigrid algorithms to scalable memory architectures p 1922 N94-21483
Uniform self-stabilizing leader election. Part 1: Complete graph protocols
[CWI-CS-R9308-PT-1] p 1935 N94-21549
Comparing quasi-Newton methods for solving sparse interface problems
[CWI-NM-R9303] p 1959 N94-21576
A data distributed, parallel algorithm for ray-traced volume rendering
[DE93-040150] p 1935 N94-21622
Design of a new squaring function for the Viterbi algorithm p 1764 N94-21699
Heuristic-based scheduling algorithm for high level synthesis p 1764 N94-21704
A statistical-based scheduling algorithm in automated data path synthesis p 1764 N94-21706
Reduction of blocking effects for the JPEG baseline image compression standard p 1765 N94-21714
A VLSI implementation of DCT using pass transistor technology p 1767 N94-21725
A DRAM compiler algorithm for high performance VLSI embedded memories p 1767 N94-21729
A set-associative, fault-tolerant cache design p 1768 N94-21731
Development, refinement, and testing of a short term solar flare prediction algorithm
[NASA-CR-194727] p 2147 N94-21832
Imaging vector fields using line integral convolution
[DE93-019922] p 1917 N94-21841
Reentry vehicle adaptive telemetry
[DE94-001168] p 1656 N94-21852
The design of linear algebra libraries for high performance computers
[DE93-040458] p 1960 N94-21967
The combinatorial algorithms for large scale discrete optimization problems p 1923 N94-22079
Algorithms for Markov decision chains with partial information
[PB93-220085] p 1918 N94-22098
VLSI architectures for the new (T,L) algorithm p 1745 N94-22110
An in-place and in-order algorithm for the discrete cosine transform p 1771 N94-22111
A one-shot access scheme for a multicast switch p 1773 N94-22120
Improvements on the design of optimum SAW filters with the Remez Exchange Algorithm p 1773 N94-22123
Software implementation of an adaptive digital automatic level control p 1773 N94-22124
Cascaded recursive artificial neural networks p 1780 N94-22167
The Schur Berlekamp-Massey algorithm is parallelizable p 1784 N94-22191
Image convolution using the Myrias SPS-2 parallel computer p 1786 N94-22207
Asynchronous detection of SSB-SC data signals p 1747 N94-22217
An algorithm for the interference detection among polygonal surfaces p 1791 N94-22239
Extended range modified gradient technique for profile inversion (extended version of report Et/Em-1992-8)
[PB93-215242] p 1742 N94-22346
Development of a gridless CFD method p 1919 N94-22361
An advancing-front Delaunay-triangulation algorithm designed for robustness p 1920 N94-22362
Distributed input/output processing in data-driven multiprocessors
[DE94-000323] p 1937 N94-22378
How is WFPC flat field made p 1926 N94-22484
SkICAT: A cataloging and analysis tool for wide field imaging surveys p 2049 N94-22546
Tests of a simple data merging algorithm for the GONG project p 1927 N94-22549

ALIGNMENT
Method to evaluate steering and alignment algorithms for controlling emittance growth
[DE93-041004] p 1978 N94-19856
Evaluation of a scanning Hartmann device for single point turning applications
[DE93-019204] p 1821 N94-19891
Robust and efficient 3D recognition by alignment
[AD-A270839] p 1904 N94-20041
Multibunch beam break-up in detuned structures
[DE93-041056] p 1981 N94-21686
The preservation of low emittance flat beams
[DE93-040964] p 1981 N94-21773
Survey and alignment analysis for the ALS storage ring using computer spreadsheets
[DE93-019254] p 1917 N94-21917

ALIPHATIC HYDROCARBONS
Direct aromatization of methane
[DE93-040631] p 1678 N94-19890
Electron reactions in nonpolar liquids: Pressure effects
[DE93-040328] p 1970 N94-19931

ALKALIES
Geochronology and petrogenesis of the western highlands alkali suite: Radiogenic isotopic evidence from Apollo 14 p 2118 N94-20778

ALKALINE EARTH METALS
Self diffusion of alkaline-Earth in Ca-Mg-aluminosilicate melts: Experimental improvements on the determination of the self-diffusion coefficients p 1684 N94-20669

ALKANES
Microscopic modeling of tribological and interfacial phenomena
[AD-A271864] p 1823 N94-20464

ALKYL COMPOUNDS
Volatile CVD precursors based on copper alkoxides and mixed group 2A-copper alkoxides
[AD-D015930] p 1701 N94-20349

ALKYLIDENE
Rotational isomers of Mo(VI) alkylidene complexes and Cis/trans polymer structure: Investigations in ring-opening metathesis polymerization
[AD-A272647] p 1704 N94-21184

ALL-WEATHER LANDING SYSTEMS
All-weather precision landing system for aircraft in remote areas
[AD-D015924] p 1643 N94-20197

ALLENDE METEORITE
Inter- and intra-crystalline oxygen isotope distribution of fassaites in Allende CAI p 2086 N94-20898

ALLOYING
Metastable bcc phase formation in the Nb-Cr system
[DE93-018376] p 2012 N94-19926
High performance heavy alloys by alloying and process control
[AD-A271129] p 1689 N94-20019
Production of NiAl and TiAl intermetallics by mechanical alloying
[VTT-JULK-760] p 1691 N94-20530
Alloying effects on mechanical and metallurgical properties of NiAl
[DE93-040814] p 1694 N94-21948
Alloying studies in U(1-x)Th(x)Pd2Al3 (0 (le) x (le) 1)
[DE94-000807] p 2036 N94-22584

ALOHA SYSTEM
Comparison of theoretical and simulated performance results for sloppy-slotted Aloha signaling p 1746 N94-22204

ALPHA PARTICLES
Radial diffusion of toroidally trapped particles induced by lower hybrid and fast waves
[IPPCZ-327] p 1996 N94-21593

ALTERNATING CURRENT
Operational Requirements Document (ORD) for the Alternating Current/Direct Current (AC/DC) clamp-on ammeter, mE-563
[AD-A271808] p 1751 N94-20555
Surveys on specific patterns of facility intallation of photovoltaic power generating technologies for international cooperation
[DE94-714901] p 1850 N94-22092

ALTIMETERS
Comparative hypsometric analysis of both Earth and Venus topographic distributions p 2108 N94-20722

ALTIMETRY
Magellan at Venus: Summary of science findings p 2110 N94-20734

ALTITUDE
Worldwide frequency of temperatures at selected altitudes
[AD-A271111] p 1864 N94-19908
ALTITUDE CONTROL
Perception/action: An holistic approach 2
[AD-A271822] p 1891 N94-20627
ALUMINIDES
Fundamentals of mechanical behavior in structural intermetallics: A synthesis of atomistic and continuum modeling
[DE93-019166] p 1690 N94-20232
Applicability and performance benefits of XD (Tradename) titanium aluminides to expendable gas turbine engines
[AD-A272998] p 1648 N94-21268
Evaluation of the fabricability of advanced iron aluminide-clad austenitic stainless steel tubing
[DE93-040598] p 1693 N94-21771
Ni3Al aluminide alloys
[DE94-000493] p 1694 N94-21933
Investigation of moisture-induced embrittlement of iron aluminides
[DE93-040841] p 1695 N94-21949
Miniaturized disk-bend testing, nano-indentation, and the microstructure of ion-irradiated titanium aluminides
[DE93-040600] p 1697 N94-22559
ALUMINUM
Chemical zoning and diffusion of Ca, Al, Mn, and Cr in olivine of springwater pallasite p 2086 N94-20902
Experimental study of void formation during aluminum solidification in reduced gravity
[NASA-TM-106190] p 1692 N94-21604
Evaluation of non-chromium-containing deoxidizers for aluminum
[DE94-001377] p 1695 N94-21978
Gamma ray spectrometry of LDEF samples: Results of 1992 analyses
[DE94-001177] p 1684 N94-22046
ALUMINUM ALLOYS
Investigation of austenitic alloys for advanced heat recovery and hot gas cleanup systems
[DE93-017863] p 1687 N94-19802
On the experimental determination of low order structure factors in TiAl by energy filtered convergent beam electron diffraction
[DE93-019521] p 1687 N94-19806
Innovative acoustic technique for studying new materials and new developments in solid state physics
[AD-A270540] p 2013 N94-19933
The use of backscattered electron imaging mode to assess the effect of fine dispersions on development of superplastic microstructure in Al-Mg alloys
[AD-A272426] p 1691 N94-21258
Results of the second Round Robin on opening-load measurement conducted by ASTM Task Group E24.04.04 on crack closure measurement and analysis
[NASA-TM-109032] p 1832 N94-21624
Powdered aluminum and oxygen rocket propellants: Subscale combustion experiments
[NASA-TM-106439] p 1713 N94-21760
Evaluation of the fabricability of advanced iron aluminide-clad austenitic stainless steel tubing
[DE93-040598] p 1693 N94-21771
Alloying effects on mechanical and metallurgical properties of NiAl
[DE93-040814] p 1694 N94-21948
First principles calculations for analysis martensitic transformations
[DE94-000666] p 1695 N94-21964
Transferable tight-binding parameters: An application to Ni and Ni-Al alloys
[DE94-001044] p 1695 N94-22023
Surface modification of Ti3Al for improved oxidation resistance
[DE93-018297] p 1696 N94-22034
ALUMINUM ARSENIDES
High efficiency epitaxial optical reflector solar cells
[DE93-017115] p 1845 N94-19805
Temperature dependence of optical properties of AlAs, studied by in-situ spectroscopic ellipsometry
p 2023 N94-20999
Synthesis and properties of mismatched heterojunction/substrate interfaces
[AD-A272904] p 1760 N94-21229
ALUMINUM COATINGS
Evaluation of non-chromium-containing deoxidizers for aluminum
[DE94-001377] p 1695 N94-21978
ALUMINUM GALLIUM ARSENIDES
Variable angle of incidence spectroscopic ellipsometric study of semiconductor multilayer structures
p 2020 N94-20982
Ellipsometric measurements of molecular-beam-epitaxy-grown semiconductor multilayer thicknesses: A comparative study p 1710 N94-20983
Comparative thickness measurements of heterojunction layers by ellipsometric, RBS, and XTEM analysis
p 1710 N94-20984
Characterization of multilayer GaAs/AlGaAs transistor structures by variable angle spectroscopic ellipsometry
p 1796 N94-20985
Variable angle of incidence spectroscopic ellipsometric measurement of the Franz-Keldysh effect in MODFET structures p 2021 N94-20987
Ellipsometric analysis of built-in electric fields in semiconductor heterostructures p 1796 N94-20988
Optical measurement of built-in and applied electric fields in Al(x)Ga(1-x)As/GaAs heterostructures
p 1796 N94-20989
In-situ spectroscopic ellipsometry for real time semiconductor growth monitor p 2024 N94-21003
Real-time analysis of in-situ spectroscopic ellipsometric data during MBE growth of III-V semiconductors
p 2024 N94-21004
Dephasing processes in III-V semiconductors
[AD-A271677] p 2028 N94-21362
ALUMINUM ISOTOPES
Aluminum-26 activities in meteorites
p 1686 N94-20851
ALUMINUM OXIDES
Dynamic, multiaxial impact response of confined and unconfined ceramic rods
[DE93-040057] p 1829 N94-19824
Sol-spray preparation, particulate characteristics, and sintering of alumina powders
[DE93-018577] p 1690 N94-20183
Guanidine based vehicle/binders for use with oxides, metals, and ceramics
[NASA-CASE-LEW-15314-1] p 1700 N94-20195
Identification of an interstellar oxide grain from the Murchison meteorite by ion imaging
p 2082 N94-20659
Alumoxanes: Rationalization of black box materials
[AD-A272805] p 1704 N94-21170
Properties of E-beam interactive oxide films for nanometer scale structures
[AD-A272848] p 1675 N94-21191
On one numerical approach to Stefan problem
[IPPCZ-330] p 1996 N94-21572
Fabrication of whisker-toughened alumina tubes
[DE94-001012] p 1677 N94-22022
Interface science of controlled metal/metal and metal/ceramic interfaces prepared using ultrahigh vacuum diffusion bonding
[DE94-001066] p 1696 N94-22025
Surface modification of Ti3Al for improved oxidation resistance
[DE93-018297] p 1696 N94-22034
ALUMINUM SILICATES
Self diffusion of alkaline-Earth in Ca-Mg-aluminosilicate melts: Experimental improvements on the determination of the self-diffusion coefficients p 1684 N94-20669
ALUMINUM 26
Stable Ni isotopes and Be-10 and Al-26 in metallic spheroids from Meteor Crater, Arizona
p 1863 N94-20889
ALUMINUM-LITHIUM ALLOYS
Weldalite (tm) 049 (Al 2095-T8): Anisotropy effects at cryogenic conditions
[AD-A272658] p 1691 N94-21188
The mechanical property data base from an Air Force/industry cooperative test program on advanced aluminum alloys: 2091 sheet, plate, and 8090 extrusion
[AD-A273091] p 1692 N94-21525
AMAZON REGION (SOUTH AMERICA)
The use of satellite images in Amazonian archaeology: A case study in the Upper Rio Negro Basin
p 1838 N94-20954
The 7th Brazilian Remote Sensing Symposium, volume 2 p 1838 N94-20956
The 7th Brazilian Remote Sensing Symposium, volume 3 p 1839 N94-20960
Sunphotometer network for monitoring aerosol properties in the Brazilian Amazon p 1839 N94-20961
AMBIGUITY
Representation of idioms in connectionist models
p 1940 N94-20247
Procedural dynamic semantics, verb-phrase ellipsis, and presupposition
[CWI-CS-R9311] p 1914 N94-21495
AMIDES
Femtosecond Raman-induced Kerr effect study of polar solvent dynamics: Amides
[DE93-017563] p 1678 N94-19924
High resolution infrared spectroscopy of formamide and deuterated formamide in a molecular beam
[AD-A271986] p 1973 N94-20618
Theoretical studies of the structures and electronic properties of U(NH2)(sub 3) and Np(NH2)(sub 3)
[DE94-000768] p 2031 N94-21857
AMINES
Physical chemistry of energetic nitrogen compounds
[AD-A271819] p 1712 N94-20625
Stress-induced cracking of fluorocarbon rubber MTL-0002 after exposure to DS-2
[AD-A271753] p 1705 N94-21302
AMINO ACIDS
Development of bioelastic material for aspects of wound repair
[AD-A272000] p 1892 N94-21503
AMMETERS
Operational Requirements Document (ORD) for the Alternating Current/Direct Current (AC/DC) clamp-on ammeter, mE-563
[AD-A271808] p 1751 N94-20555
A new innovative instrument for space plasma instrumentation
[NASA-CR-194736] p 1666 N94-21780
AMMONIUM COMPOUNDS
Chemistry of the burning surface
[AD-A272725] p 1681 N94-21181
AMMONIUM NITRATES
Monopropellant aqueous hydroxyl ammonium nitrate/fuel
[AD-D015922] p 1712 N94-20061
Growth and morphology of crystals: Theory and observations
[PB93-221166] p 2035 N94-22273
AMORPHOUS MATERIALS
Research on defects and transport in amorphous-silicon-based semiconductors
[DE93-017117] p 2013 N94-19939
Microscopic origins of metastable effects in a-Si:H and deep defect characterization in a-Si,Ge:H alloys
[DE93-018205] p 1688 N94-19985
Characterization of amorphous material in shocked quartz by NMR spectroscopy
[DE93-019069] p 1679 N94-20307
C/O atomic ratios in micrometer-size crushed grains from Antarctic micrometeorites and two carbonaceous meteorites* p 2082 N94-20678
InP MIS structures with diamondlike amorphous carbon films deposited by ion-beam sputtering and from plasma
p 1710 N94-20979
Interfacial properties of diamondlike amorphous carbon films on InP: Metal-insulator-semiconductor structures
p 1710 N94-20980
High temperature stability of amorphous Ta(x)Cu(1-x) diffusion barriers on GaAs p 2022 N94-20990
Amorphous Ta-rich Ta-Cu films as diffusion barriers between Au and GaAs p 1710 N94-20991
Alumoxanes: Rationalization of black box materials
[AD-A272805] p 1704 N94-21170
Fabrication of amorphous diamond films
[DE94-000404] p 2032 N94-21960
AMORPHOUS SILICON
Growth mechanisms and characterization of hydrogenated amorphous-silicon-alloy films
[DE93-018202] p 1699 N94-20047
Development of a numerical simulation model for a-Si:H solar cells and application to the analysis of experimentally obtained spectral characteristics
[ETN-93-95061] p 1846 N94-20151
Characterization of amorphous material in shocked quartz by NMR spectroscopy
[DE93-019069] p 1679 N94-20307
Fundamental studies of defect generation in amorphous silicon alloys grown by remote plasma-enhanced chemical-vapor deposition
[DE93-017083] p 2029 N94-21615
Stable, high-efficiency amorphous-silicon solar cells with low hydrogen content
[DE93-018214] p 1848 N94-21826
Annual Report, Materials Science Branch, FY 1992
[DE94-000204] p 1849 N94-22015
Research on stable, high-efficiency amorphous silicon multijunction modules
[DE93-018220] p 1850 N94-22257
AMPHIBOLES
The stability of oxyamphiboles: Existence of Ferric-bearing minerals under the reducing conditions on the surface of Venus p 2122 N94-20800
High D/H ratios of water in magmatic amphiboles in Chassigny: Possible constraints on the isotopic composition of magmatic water on Mars
p 2134 N94-20662
AMPLIFICATION
Optically controlled current filamentation in GaAs photoconductive semiconductor switches
[DE93-019427] p 2016 N94-20296
AMPLIFIERS
Y-Ba-Cu-O superconducting/GaAs semiconducting hybrid circuits for microwave applications
p 1735 N94-20514

AMPOULES
Growth of zinc selenide single crystals by physical vapor transport in microgravity
[NASA-CR-194679] p 2017 N94-20346
ANALOG CIRCUITS
Fault detection in digital and analog circuits using an i(DD) temporal analysis technique p 1757 N94-21106
ANALOG DATA
VLSI mixed signal processing system p 1744 N94-21100
An optically-assisted 3-D cellular array machine
[AD-A272683] p 1987 N94-21163
ANALOG TO DIGITAL CONVERTERS
A SCSI-bus data acquisition system for nuclear spectroscopy experiments
[USIP-92-03] p 2042 N94-20193
Rotary encoding device using polygonal mirror with diffraction gratings on each facet
[NASA-CASE-GSC-13543-1] p 1985 N94-20240
Control vane guidance for a ducted-fan unmanned air vehicle
[AD-A271957] p 1645 N94-20561
Proton radiation testing of an 18 bit A/D converter p 1755 N94-21096
Adaptive analog video signal conditioner p 1744 N94-21099
Analog/digital pH meter system I.C. p 1764 N94-21701
An 18 bit 50 kHz ADC for low earth orbit p 1764 N94-21702
A high speed CMOS A/D converter p 1767 N94-21726
Surface acquisition through virtual milling p 1920 N94-22372
ANALOGIES
Characterization of Minnesota lunar simulant for plant growth p 1897 N94-20665
Low Reynolds-number turbulent boundary layers
[AD-A272011] p 1803 N94-21459
ANALYSIS OF VARIANCE
A retrieval error analysis technique for passive infrared atmospheric sounders
[AD-A272618] p 1867 N94-21212
ANGIOGRAPHY
Coronary angiography outcomes of US Army aircrew with the finding of coronary artery calcifications: Aviation epidemiology data register
[AD-A271968] p 1891 N94-20615
Center for X-Ray Optics, 1992
[DE94-000726] p 1990 N94-21868
ANGLE OF ATTACK
Effects of thrust vector control on the performance of the aerobang orbital plane change maneuver
[AD-A272532] p 1646 N94-21418
ANGLES (GEOMETRY)
Multiple-wavelength angle-of-incidence ellipsometry: Application to silicon nitride-gallium arsenide structures p 2019 N94-20974
Thin film compositional analysis using null or fixed wavelength ellipsometry p 1709 N94-20976
Variable wavelength, variable angle ellipsometry including a sensitivities correlation test p 1710 N94-20978
Variable angle of incidence spectroscopic ellipsometric study of semiconductor multilayer structures p 2020 N94-20982
Ellipsometric analysis of built-in electric fields in semiconductor heterostructures p 1796 N94-20988
Superlattice optical properties measured by variable angle spectroscopic ellipsometry p 2022 N94-20993
GaAs/AlGaAs superlattice characterization by variable angle spectroscopic ellipsometry p 2022 N94-20994
Micro-ellipsometric measurements of strained layer structures p 2025 N94-21008
Fundamentals and applications of variable angle spectroscopic ellipsometry p 1687 N94-21011
ANGULAR DISTRIBUTION
Angular distributions of high-order ATI
[DE93-019125] p 1972 N94-20230
Direct images of thermal disorder in the Cl-Si and H-O-Si chemisorption bond on Si(100)
[AD-A272386] p 1680 N94-21145
ANGULAR MOMENTUM
Physical chemistry of energetic nitrogen compounds
[AD-A271819] p 1712 N94-20625
Formation of the low-mass solar nebula p 2109 N94-20728
Variety in planetary systems p 2086 N94-20871
ANGULAR VELOCITY
The angular velocity spread of REB induced by magnetic field discontinuity
[IPPCZ-331] p 1996 N94-21573
ANIMALS
Health effects of global warming: Problems in assessment
[DE93-040323] p 1850 N94-19930
Self-Motion Perception and Motion Sickness
[NASA-CR-194276] p 1885 N94-21897
Current status: Animal models of nausea p 1889 N94-21915
ANIMATION
Visualizing the universe, part 2 p 2063 N94-22472
ANISOTROPIC FLUIDS
Liquid crystal displays p 1752 N94-20634
ANISOTROPY
Innovative acoustic technique for studying new materials and new developments in solid state physics
[AD-A270540] p 2013 N94-19933
A theoretical and numerical study of polarimetric scattering and emission from random rough surfaces with anisotropic directional spectrum p 1730 N94-20454
Method for anisotropic etching in the manufacture of semiconductor devices
[NASA-CASE-MSC-21631-1] p 1993 N94-20491
Weldalite (tm) 049 (Al 2095-T8): Anisotropy effects at cryogenic conditions
[AD-A272658] p 1691 N94-21188
Mapping robust parallel multigrid algorithms to scalable memory architectures p 1922 N94-21483
Using the rule of mixtures to examine the hardness of Cu/Cu-Zr multilayers
[DE94-001068] p 1697 N94-22402
ANNEALING
Development of high-efficiency CdTe solar cells
[DE93-018206] p 1845 N94-19925
Hydrogen pickup and redistribution in alpha-annealed zircaloy-4
[DE93-018050] p 1689 N94-20182
Surface states at the GaAs-germanium nitride interface p 1709 N94-20973
High temperature stability of amorphous Ta(x)Cu(1-x) diffusion barriers on GaAs p 2022 N94-20990
Amorphous Ta-rich Ta-Cu films as diffusion barriers between Au and GaAs p 1710 N94-20991
Tensile and shear fracture behavior of fiber reinforced plastics at 77K irradiated by various radiation sources
[DE93-040280] p 1706 N94-21542
Refractive index behaviour of phosphorus-doped planar silica waveguides, appendix 7 p 1989 N94-21601
Disks of YBa2Cu3O7 shocked to 10 GPa pressures
[DE94-000464] p 2031 N94-21931
The effect of microstructural evolution on superplasticity in Ni3Si(V, Mo)
[DE93-041320] p 1694 N94-21943
Microtextural characterization of annealed and deformed copper
[DE93-040144] p 1695 N94-21990
Interface science of controlled metal/metal and metal/ceramic interfaces prepared using ultrahigh vacuum diffusion bonding
[DE94-001066] p 1696 N94-22025
Thin-film fabrication of Pb-doped BiSrCaCuO superconductor p 1781 N94-22176
Melt-spin processing of high (Tc) oxide superconductors
[DE94-000896] p 2036 N94-22582
ANNIHILATION REACTIONS
IR materials producibility
[AD-A273031] p 1987 N94-21321
ANNUAL VARIATIONS
Studies of Greenland using the SEASAT scatterometer p 1725 N94-20433
Satellite validation of GCM-simulated annual cycle of the Earth radiation budget and cloud forcing p 1860 N94-22287
The seasonal variation of the cloud radiative forcing: Comparison of ECHAM model simulations with ERBE data p 1860 N94-22288
Use of satellite data for validation of the ECHAM models p 1861 N94-22289
ANNULAR FLOW
Measurement and prediction of the flow through an annular turbine cascade
[AD-A272530] p 1803 N94-21417
ANNULI
Arcuate and circular structures in the Tharsis region: Evidence of coronae on Mars p 2134 N94-20863
ANODES
Evaluation of a diffusion/trapping model for hydrogen ingress in high-strength alloys
[AD-A271328] p 1689 N94-20027
Research and development of alternative components at Argonne National Laboratory for molten carbonate fuel cells
[DE93-019536] p 1847 N94-21650
ANODIC COATINGS
A comparison of sulfuric acid/boric acid anodize and chromic acid anodize processes
[AD-A271933] p 1703 N94-20614
ANODIZING
A comparison of sulfuric acid/boric acid anodize and chromic acid anodize processes
[AD-A271933] p 1703 N94-20614
Evaluation of non-chromium-containing deoxidizers for aluminum
[DE94-001377] p 1695 N94-21978
ANOMALIES
The Coulomb anomaly in strongly disordered films
[AD-A271095] p 2012 N94-19849
ANORTHOSITE
Fragments of ancient lunar crust: Ferroan noritic anorthosites from the descartes region of the Moon p 2096 N94-20660
Spectral reflectance studies of the Humorum Basin region p 2101 N94-20682
U-Pb isotopic ages and characteristics of ancient (greater than 4.0 Ga) lunar highland rocks p 2104 N94-20700
U-Pb isotopic systematics of ferroan anorthosite 60025 p 1685 N94-20702
Magnesian anorthosites from the western highlands of the Moon: Isotope geochemistry and petrogenesis p 2118 N94-20779
The Mg-suite and the highland crust: An unsolved enigma p 2126 N94-20822
ANTARCTIC REGIONS
C-band radar backscatter of sea ice in the Weddell Sea, Antarctica during the austral winter of 1992 p 1725 N94-20435
Aluminum-26 activities in meteorites p 1686 N94-20851
Notes on Antarctic aviation
[AD-A273018] p 1651 N94-21239
ANTENNA ARRAYS
Wide-bandwidth high-resolution search for extraterrestrial intelligence
[NASA-CR-194724] p 1897 N94-20336
Two microstrip arrays for interferometric SAR applications p 1722 N94-20421
Optical beam forming techniques for phased array antennas p 1727 N94-20442
Mobile antenna development at JPL p 1731 N94-20457
Mobile terminal antennas for helicopters p 1731 N94-20458
Four-channel HF receiving antenna array simulator
[AD-A271876] p 1732 N94-20471
Use of the Weiss-Weinstein bound to compare the direction-finding performance of sparse arrays
[AD-A272582] p 1738 N94-21210
Investigation of the effect of various oxide and fluoride additives on the microstructure, electronic properties, and phase shifting ability of Ba(1-x)Sr(x)TiO3
[AD-A271756] p 2027 N94-21303
Analysis of the TDRS multiple access system for possible use as an attitude control system sensor p 1666 N94-21338
Array Simulations Platform (ASP) predicts NASA Data Link Module (NDLM) performance p 1744 N94-21348
Linearly tapered slot antenna circular array for mobile communications
[NASA-TM-106441] p 1769 N94-21808
Radiation and scattering from printed antennas on cylindrically conformal platforms
[NASA-CR-194703] p 1741 N94-21885
Scattering by cavity-backed antennas on a circular cylinder p 1741 N94-21886
Radiation by cavity-backed antennas on a circular cylinder p 1741 N94-21887
User manual for EXCALIBUR: A FE-BI numerical laboratory for cavity-backed antennas in a circular cylinder, version 1.2 p 1741 N94-21888
Adaptive synthesis of a ray diagram for an antenna array p 1745 N94-22160
ANTENNA COMPONENTS
Recent activities in printed Antennas at LeRC p 1722 N94-20422
ANTENNA COUPLERS
Aperture coupling of circular cylindrical dielectric resonator antenna
[ISBN-0-315-60632-0] p 1743 N94-22409
ANTENNA DESIGN
Recent activities in printed Antennas at LeRC p 1722 N94-20422
Multi-band reflector antenna with double-ring element frequency selective subreflector p 1728 N94-20447
Mobile antenna development at JPL p 1731 N94-20457
Mobile terminal antennas for helicopters p 1731 N94-20458
Linearly tapered slot antenna with dielectric superstrate p 1734 N94-20505

Mathcad computer applications predicting antenna parameters from antenna physical dimensions and ground characteristics
[AD-A272987] p 1740 N94-21264
Radiation by cavity-backed antennas on a circular cylinder p 1741 N94-21887
User manual for EXCALIBUR: A FE-BI numerical laboratory for cavity-backed antennas in a circular cylinder, version 1.2 p 1741 N94-21888
Adaptive synthesis of a ray diagram for an antenna array p 1745 N94-22160
Aperture coupling of circular cylindrical dielectric resonator antenna
[ISBN-0-315-60632-0] p 1743 N94-22409
Initial operation of a large-scale plasma source ion implantation experiment
[DE94-000805] p 2036 N94-22583

ANTENNA FEEDS
Slot-coupled patch antenna with coplanar waveguide feed p 1734 N94-20506

ANTENNA RADIATION PATTERNS
Probe compensation in cylindrical near-field scanning: A novel simulation methodology p 1718 N94-20404
Recent activities in printed Antennas at LeRC p 1722 N94-20422
Multi-band reflector antenna with double-ring element frequency selective subreflector p 1728 N94-20447
Linearly tapered slot antenna with dielectric superstrate p 1734 N94-20505
A 10 GHz Y-Ba-Cu-O/GaAs hybrid oscillator proximity coupled to a circular microstrip patch antenna p 1736 N94-20517
Mathcad computer applications predicting antenna parameters from antenna physical dimensions and ground characteristics
[AD-A272987] p 1740 N94-21264
Array Simulations Platform (ASP) predicts NASA Data Link Module (NDLM) performance p 1744 N94-21348
Adaptive synthesis of a ray diagram for an antenna array p 1745 N94-22160
Numerical method for computing the electric field produced by a microwave beam in a stratified medium p 1746 N94-22197
Applications of planar near-field measurements to electromagnetic radiation and interference problems p 1747 N94-22252
Aperture coupling of circular cylindrical dielectric resonator antenna
[ISBN-0-315-60632-0] p 1743 N94-22409

ANTICYCLONES
The life cycles of intense cyclonic and anticyclonic circulation systems observed over oceans
[NASA-CR-194760] p 1865 N94-20353

ANTIEMETICS AND ANTINAUSEANTS
Susceptibility of the squirrel monkey to different motion conditions p 1885 N94-21899

ANTIFERROMAGNETISM
Spin-polaron theory of high-(Tc) superconductivity. 1: Spin polarons and high (Tc) pairing
[DE93-019196] p 2014 N94-20002
Magnetic instability of Kondo insulators
[DE93-040064] p 1768 N94-21762
Local structure in oxygen-doped La2CuO(4+delta)
[DE93-040248] p 2030 N94-21768
Photo- and thermal-induced antiferromagnetic interlayer coupling in Fe/(Fe-Si) superlattices
[DE93-040822] p 2031 N94-21930
Orientationally independent antiferromagnetic coupling in epitaxial Fe/Cr (211) and (100) superlattices
[DE94-001270] p 2035 N94-22564

ANTIGRAVITY
System test results of the Advanced Technology Anti-G Suit (ATAGS)
[AD-A271535] p 1896 N94-20914

ANTIICING ADDITIVES
Compatibility and efficacy of biocides qualified under military specification MIL-S-53021
[AD-A271496] p 1712 N94-20551

ANTIMONY COMPOUNDS
Theory of energy-assisted epitaxy; theory of ordered semiconductor alloys: In(1-x)Tl(x)Sb as a long-wave infrared material
[AD-A271007] p 2012 N94-19835

ANTIPROTONS
A study of events with the highest total transverse energy in CDF
[DE93-019904] p 1978 N94-19972
The cross section for the production of b(bar-b) pairs in p(bar p) collisions at the square root of s equals 1.8 TeV
[DE93-019900] p 1972 N94-20225

ANVIL CLOUDS
Are tropical cirrus brighter than mid-latitude cirrus? p 1881 N94-22343

APERTURES
Evaluation of a single stage of the LADS filter
[AD-A271101] p 1814 N94-19851
A summary of studies of particle stability at RHIC
[DE93-040173] p 1970 N94-19868
Aperture determination of RHIC92 from randomly generated initial coordinates
[DE93-040174] p 1978 N94-19945
Study of possible energy upgrade for the ALS and modeling of the real lattice for the diagnosis of lattice problems
[DE93-040286] p 2016 N94-20323
Probe compensation in cylindrical near-field scanning: A novel simulation methodology p 1718 N94-20404
A compact, portable EHF/SHF antenna for advanced SCAMP
[AD-A272614] p 1739 N94-21211
Stability of beam in the Fermilab Main Injector
[DE94-000619] p 1982 N94-21934
Formulation for numerical solution of radiation and transmission from arbitrary apertures p 1745 N94-22140

APL (PROGRAMMING LANGUAGE)
APL-technology of computer simulation p 1923 N94-22077

APOLLO ASTEROIDS
Clementine: An inexpensive mission to the Moon and Geographos p 1652 N94-20765

APPLICATION SPECIFIC INTEGRATED CIRCUITS
Quartz/fused silica chip carriers
[NASA-CR-194154] p 2016 N94-20340
An ASIC memory buffer controller for a high speed disk system p 1754 N94-21089
Mongoose: Creation of a Rad-Hard MIPS R3000 p 1754 N94-21090
Synthesis algorithm of VLSI multipliers for ASIC p 1758 N94-21116
Automated synthesis and verification of configurable DRAM blocks for ASIC's p 1759 N94-21123
Automated radiation hard ASIC design tool p 1759 N94-21126
A DRAM compiler algorithm for high performance VLSI embedded memories p 1767 N94-21729

APPLICATIONS PROGRAMS (COMPUTERS)
Development and operation of the F/A-18 model control surface actuators
[AD-A271330] p 1645 N94-19914
An introduction to GUGA in the COLUMBUS Program System
[DE93-018994] p 1902 N94-19928
CTH: A software family for multi-dimensional shock physics analysis
[DE93-019428] p 1904 N94-20052
Design and implementation of a prototype PC based graphical and interactive MILSATCOM requirements database system
[AD-A272960] p 1658 N94-21251
The Test Analysis Retrieval System (TARS): Meeting the challenges of the network's test processes p 1933 N94-21337
The Automated Conflict Resolution System (ACRS) p 1744 N94-21341
Use of computers in the instruction of integral calculus
[AD-A272500] p 1913 N94-21409
Compatibility evaluation and research on the Computerized Adaptive Screening Test (CAST): User and programmer's guide
[AD-A273112] p 1894 N94-21510
Users manual for the NASA Lewis three-dimensional ice accretion code (LEWICE 3D)
[NASA-TM-105974] p 1642 N94-21590
Development of BEM for ceramic composites
[NASA-CR-194718] p 1676 N94-21777
User's guide for the casting process simulator software CaPS-2D, version 1.0
[DE93-040398] p 1917 N94-21923
The Soviet software market: Current state and aspects of development p 1923 N94-22066
Application development in a PC/LAN environment p 1923 N94-22067
Three original programmes for managers p 1923 N94-22083
Reverse automatic differentiation of modular FORTRAN programs
[DE94-000336] p 1918 N94-22088
Radio wave propagation studies along an Earth-space satellite link
[ISBN-0-315-60627-4] p 1742 N94-22408
A feasibility study of a parallax-based passive missile approach warning system
[ISBN-0-315-60640-1] p 1743 N94-22410
Passenger terminal simulation model
[ISBN-0-315-61113-8] p 1652 N94-22423
An object-oriented data reduction system in Fortran p 2046 N94-22447
Database activity in the Italian Astronet: DIRA 2 p 2047 N94-22452
PROS: An IRAF based system for analysis of x ray data p 1925 N94-22461
Programmability in AIPS++ p 1926 N94-22482
ASpect: A new spectrum and line analysis package for IRAF p 1926 N94-22485
The HEASARC graphical user interface p 1926 N94-22487
The application of artificial intelligence to astronomical scheduling problems p 1949 N94-22492
HST PSF simulation using Tiny Tim p 1926 N94-22498
The Keck Task Library (KTL) p 2048 N94-22504
SKYMAP: Exploring the Universe in software p 1927 N94-22511
IRAF in the nineties p 2048 N94-22535
DECONV-TOOL: An IDL based deconvolution software package p 1927 N94-22542
MOSAIC: Software for creating mosaics from collections of images p 1927 N94-22543
ROSAT data analysis with EXSAS p 2080 N94-22555

APPROACH
Parallel runway requirement analysis study. Volume 2: Simulation manual
[NASA-CR-191549-VOL-2] p 1644 N94-22278

APPROACH CONTROL
Parallel runway requirement analysis study. Volume 1: The analysis
[NASA-CR-191549-VOL-1] p 1644 N94-22277

APPROACH INDICATORS
Techniques used for the analysis of oculometer eye-scanning data obtained from an air traffic control display
[NASA-CR-191559] p 1643 N94-21629
Application of scattering by arrays of cylinders to MLS signal propagation error estimation p 1644 N94-22135

APPROXIMATION
Stochastic optimization by simulation: Numerical experiments with M/M/1 queue in steady-state
[AD-A271143] p 1949 N94-19854
Approximate methods for N-component solute transport and ion-exchange
[CWI-NM-R9223] p 1910 N94-21078
Fast fourier transforms for nonequispaced data
[AD-A272687] p 1954 N94-21164
Measure fields for function approximation
[AD-A272660] p 1964 N94-21215
Design of a new squaring function for the Viterbi algorithm p 1764 N94-21699
Interface reflection of spherical acoustic waves in the first- and second-order rational parabolic approximations and their artifacts
[PB93-215424] p 1969 N94-22261
Extinction efficiencies from DDA calculations solved for finite circular cylinders and disks p 1880 N94-22340

APTITUDE
Extracting information from wrong answers in computerized adaptive testing
[AD-A272832] p 1894 N94-21434

AQUEOUS SOLUTIONS
Monopropellant aqueous hydroxyl ammonium nitrate/fuel
[AD-D015922] p 1712 N94-20061
Briny lakes on early Mars? Terrestrial intracrater playas and Martian candidates p 2145 N94-21675
Swelling equilibria for cationic 2-hydroxyethyl methacrylate (HEMA)-based hydrogels
[DE94-000728] p 1707 N94-21856

AQUIFERS
High-resolution numerical methods for compressible multi-phase flow in hierarchical porous media
[DE94-000740] p 1799 N94-20351

ARAMID FIBER COMPOSITES
Aragatz project samples experiment/MAPOL (polymer materials) experiment: Postflight expert evaluation p 1660 N94-21378

ARC DISCHARGES
Two dimensional simulation of the electric arc behavior in a cut-off device
[ECL-92-41] p 1751 N94-20595

ARC JET ENGINES
Performance potential of plasma thrusters: Arcjet and Hall thruster modeling
[AD-A271085] p 1667 N94-19847

ARC LAMPS
Miniature color display, phase 4
[AD-A272920] p 1760 N94-21221

ARCHAEOLOGY
The 7th Brazilian Remote Sensing Symposium, volume 1 p 1838 N94-20953
The use of satellite images in Amazonian archaeology: A case study in the Upper Rio Negro Basin p 1838 N94-20954

ARCHITECTURE (COMPUTERS)
Global combine on mesh architectures with wormhole routing
[DE93-018792] p 1903 N94-19959
A software architecture for the construction and management of real-time virtual worlds
[AD-A271465] p 1904 N94-20091
A modular design for connectionist parsing
p 1941 N94-20252
M-dimensional computer memory with M-1 dimensional hyperplane access
[AD-D015960] p 1898 N94-20357
Electronic neural network for solving traveling salesman and similar global optimization problems
[NASA-CASE-NPO-17807-2-CU] p 1942 N94-20360
Algorithm/architecture study for artificial neural nets
[AD-A271820] p 1943 N94-20626
Measuring the effects of thread placement on the Kendall Square KSR1
[DE93-040655] p 1908 N94-20932
Analysis and evaluation of configuring of graphical systems on multiprocessor architectures
[ETN-93-93618] p 1930 N94-21018
Reduction of network cost and wiring in Ranade's butterfly routing
[CWI-CS-R9243] p 1930 N94-21023
The Fifth NASA Symposium on VLSI Design
[NASA-CR-194644] p 1753 N94-21079
An ASIC memory buffer controller for a high speed disk system p 1754 N94-21089
High performance MPEG-audio decoder IC
p 1744 N94-21092
Multiple-fold clustered processor mesh array
p 1757 N94-21113
A novel VLSI processor architecture for supercomputing arrays p 1758 N94-21115
A fixed/variable bit-rate data compression architecture
p 1759 N94-21128
Scheduling for locality in shared-memory multiprocessors
[AD-A272948] p 1930 N94-21228
Decoupled computer architectures for very high-speed technologies
[AD-A271646] p 1900 N94-21301
Using manufacturing message specification for monitor and control at Venus p 1932 N94-21333
MAYGEN: A symbolic debugger generation system
[AD-A272512] p 1913 N94-21413
Analysis of multigrid methods on massively parallel computers: Architectural implications
p 1938 N94-21468
The 1992 4th NASA SERC Symposium on VLSI Design
[NASA-CR-194591] p 1763 N94-21694
A 20 MHz CMOS reorder buffer for a superscalar microprocessor p 1764 N94-21700
Instruction set commutivity p 1766 N94-21719
On fast carry select adders p 1767 N94-21726
A novel cache mechanism p 1767 N94-21730
A 1 GHz sample rate, 256-channel, 1-bit quantization, CMOS, digital correlator chip p 1768 N94-21732
A real time correlator architecture using distributed arithmetic principles p 1768 N94-21734
Simulated behaviour of large scale SCI rings and tori
[DE93-040149] p 1935 N94-21745
Physics Detector Simulation Facility (PDSF) architecture/utilization
[DE93-019744] p 1936 N94-21919
Robotic concepts for operation in barren terrain
[DE93-040539] p 1946 N94-21925
System architectures for banking applications
p 2046 N94-22057
VLSI architectures for the new (T,L) algorithm
p 1745 N94-22110
Addition of decimal numbers in optical computing architecture by Walsh coded digits p 1773 N94-22122
A pyramid neural network architecture for stereo fusion p 1785 N94-22201
Acceleration of backpropagation learning using a parallel DSP machine p 1786 N94-22206
Image convolution using the Myrias SPS-2 parallel computer p 1786 N94-22207
Architectures of the free space optical interconnects
p 1789 N94-22220
Space Generic Open Avionics Architecture (SGOAA) standard specification
[NASA-CR-188269] p 1666 N94-22275
A comparison of IDEF1X and NIAM ISDM
[DE93-040899] p 1921 N94-22363
A neural network prototyping package within IRAF
p 1949 N94-22451
VETA x ray data acquisition and control system
p 2047 N94-22455
Integrating a local database into the StarView distributed user interface p 2048 N94-22530
IRAF and STSDAS under the new ALPHA architecture
p 2049 N94-22553
ARGON
Absolute total and one and two electron transfer cross sections for Ar(8+) on Ar as a function of energy
[DE93-040283] p 1970 N94-19870
Energy gain spectroscopic study of Ar(q+)-Ar collisions at 40 qeV
[DE93-040284] p 1970 N94-19871
Thermal information regarding the cooldown and operation of liquid argon calorimeters
[DE93-019391] p 1807 N94-19987
Detailed structure study of an H2/N2O/Ar flame employing molecular beam mass spectrometry, laser spectroscopy, and modeling
[AD-A270720] p 1679 N94-20111
Low-energy ion implantation: Large mass fractionation of argon p 1685 N94-20697
Electron emissions in low energy Ar(q+)-Ar collisions
[DE93-040285] p 1974 N94-21543
ARGON ISOTOPES
SCR neon and argon in Kapoeta feldspar: Evidence for an active ancient Sun p 2105 N94-20712
Age and thermochronology of K-feldspars from the Manson Impact Structure p 1863 N94-20899
ARGON PLASMA
Impact of copper vapour contamination on argon arcs
p 1994 N94-21053
Opacity measurements in shock-generated argon plasmas
[DE94-001057] p 1998 N94-22399
ARIANE LAUNCH VEHICLE
Turbine design p 1668 N94-20075
The Vulcain cryogenic engine p 1668 N94-20077
ARID LANDS
The 7th Brazilian Remote Sensing Symposium, volume 1 p 1838 N94-20953
Application of SPOT to GIS/LIS in land capability evaluation for regional planning of JAICO semi-arid region of Piaui, Brazil p 1838 N94-20955
Oxidation of dissolved iron under warmer, wetter conditions on Mars: Transitions to present-day arid environments p 2143 N94-21663
ARITHMETIC
Correctness properties for iterated hardware structures p 1759 N94-21124
Arithmetic in large GF(2(exp n)) p 1760 N94-21131
A package for long integer arithmetic on the Cray Y-MP
[CWI-NM-R9227] p 1916 N94-21612
A novel cache mechanism p 1767 N94-21730
A real time correlator architecture using distributed arithmetic principles p 1768 N94-21734
On the discovery of approximate arithmetic relations by backpropegation networks p 1782 N94-22181
Vanishing theorem on arithmetic surfaces
[PB93-215481] p 1961 N94-22263
ARITHMETIC AND LOGIC UNITS
Formal verification of an ALU p 1772 N94-22114
ARMED FORCES (UNITED STATES)
Compatibility evaluation and research on the Computerized Adaptive Screening Test (CAST): User and programmer's guide
[AD-A273112] p 1894 N94-21510
ARMOR
Hypervelocity impact
[AD-A272957] p 1831 N94-21249
An assessment of the cost of microwave sintering ceramic tiles for armor applications
[DE94-000978] p 1693 N94-21350
Dynamic properties of ceramic materials
[DE94-000654] p 1708 N94-21963
AROMATIC COMPOUNDS
High melting amino aromatic nitrate esters
[AD-D015929] p 1711 N94-19801
Direct aromatization of methane
[DE93-040631] p 1678 N94-19890
Recent developments in aromatic azo polymers research
[AD-A272966] p 1705 N94-21259
ARRAYS
Metal-glass composite field-emitting arrays
[AD-D015942] p 1673 N94-20064
A unified approach to VLSI layout automation and algorithm mapping on processor arrays
p 1759 N94-21127
A cost-effective methodology for the design of massively-parallel VLSI functional units
p 1760 N94-21132
A software environment for the exploitation of the MAR image sensor p 1785 N94-22200
ARTERIES
Coronary angiography outcomes of US Army aircrew with the finding of coronary artery calcifications: Aviation epidemiology data register
[AD-A271968] p 1891 N94-20615
Review of using cardiac fluoroscopy in symptomatic and asymptomatic patients
[AD-A271690] p 1891 N94-20928
ARTICULATION (SPEECH)
Recognizing hesitation phenomena in continuous, spontaneous speech p 1746 N94-22210
ARTIFICIAL INTELLIGENCE
Building brains for bodies
[AD-A270531] p 1939 N94-19875
Handbook. Volume 3: Digital systems validation book plan
[DOT/FAA/CT-93/16-VOL-3] p 1647 N94-20053
Self-organization via active exploration in robotic applications. Phase 2: Hybrid hardware prototype
[NASA-CR-194723] p 1939 N94-20212
Connectionism and Natural Language Processing
[MEMO-INF-92-64] p 1940 N94-20242
Speech synthesis with artificial neural networks
p 1743 N94-20245
Believing in the basis of the evidence
[TR-438] p 2039 N94-20364
The Seventh International Symposium on Methodologies for Intelligent Systems (Poster Session)
[AD-A272125] p 1942 N94-20573
Research, Development, Training, and Evaluation (RDTE) support delivery order 1: Computational cognitive models
[AD-A271837] p 1894 N94-20610
Simulating a user's preferences: Towards automated artificial evolution for computer generated images
[AD-A272058] p 1942 N94-20621
Causal reconstruction
[AD-A271692] p 1908 N94-20929
AIDA: A graphical interactive system, adapted to the user
[ETN-93-93792] p 1908 N94-21020
Lecture notes in artificial intelligence 689: The 7th International Symposium on Methodologies for Intelligent Symposium (ISMIS 1993)
[AD-A271768] p 1944 N94-21162
Computing with Bayesian multi-networks
[AD-A273106] p 1914 N94-21501
Reentry vehicle adaptive telemetry
[DE94-001168] p 1656 N94-21852
Controlling multisupplier operations by intelligent EDI
p 1744 N94-22076
Manufacturing and information technology
p 2046 N94-22082
Canadian Conference on Electrical and Computer Engineering, volumes 1 and 2
[ISBN-0-9694170-2-0] p 1770 N94-22101
Language as primary dimension of distributed AI systems activity p 1776 N94-22141
Cascaded recursive artificial neural networks
p 1780 N94-22167
The application of artificial intelligence to astronomical scheduling problems p 1949 N94-22492
ARTIFICIAL SATELLITES
The NRL LACE program
[AD-A270861] p 1657 N94-19896
ASBESTOS
Asbestos characterization using scanning electron microscopy/light element x ray spectrometry
[AD-A271611] p 1681 N94-21241
ASPECT RATIO
Intensity and polarization of light scattered by size distributions of randomly oriented nonspherical particles
p 1721 N94-20416
ASSAYING
A weighted least-squares lump correction algorithm for transmission-corrected gamma ray nondestructive assay
[DE93-018474] p 1904 N94-20049
ASSESSMENTS
Manual of DRANC (release 1.1): A computer program for the Dutch risk assessment of new chemical substances
[PB93-194827] p 1851 N94-19998
ASSOCIATIVE PROCESSING (COMPUTERS)
Connectionism and Natural Language Processing
[MEMO-INF-92-64] p 1940 N94-20242
Generalization performance of backpropagation learning on a syllabification task p 1940 N94-20246
Representation of idioms in connectionist models
p 1940 N94-20247
A connectionist representation for phrase structures
p 1941 N94-20249
Hopfield models as neural-network acceptors
p 1941 N94-20250
A modular design for connectionist parsing
p 1941 N94-20252
An exploration of clause boundary effects in SRN representations p 1937 N94-20253
ASTEROID BELTS
IMPS albedo and diameter for Asteroid 243 Ida
p 2085 N94-20845

Equilibrium models of mass distribution and collisional lifetimes of asteroids p 2086 N94-20877

ASTEROIDS

Determination of cosmic bodies size-velocity distribution by observation of current impacts on Mars p 2082 N94-20648

Asteroid collisions: Target size effects and resultant velocity distributions p 2083 N94-20729

Diffusive redistribution of water vapor in the solar nebula revisited p 2113 N94-20751

Research program on the Manson impact structure, Iowa p 1862 N94-20766

Linear structures on the small inner satellites of Saturn p 2121 N94-20797

Determining the composition of olivine on asteroidal surfaces p 1686 N94-20805

A new Antarctic meteorite with chromite, orthopyroxene and metal with reference to a formation model of S asteroids p 2084 N94-20813

IMPS albedo and diameter for Asteroid 243 Ida p 2085 N94-20845

Comparison of visible and near-infrared reflectance spectra of CM2 carbonaceous chondrites and primitive asteroids p 2085 N94-20848

The Clementine Mission science return at the Moon and Geographos p 1652 N94-20850

Equilibrium models of mass distribution and collisional lifetimes of asteroids p 2086 N94-20877

ASTROMETRY

Database activity in the Italian Astronet: DIRA 2 p 2047 N94-22452

ASTRONAUTS

Space Shuttle Mission STS-61: Hubble Space Telescope servicing mission-01 [NASA-TM-109344] p 1653 N94-20192

ASTRONOMICAL CATALOGS

IMPS albedo and diameter for Asteroid 243 Ida p 2085 N94-20845

Development and operations of the Astrophysics Data System [NASA-CR-194691] p 2043 N94-21270

Archiving data from ground-based telescopes p 2046 N94-22442

The cool-star spectral catalog: A uniform collection of IUE SWP-LOs p 2046 N94-22446

Database activity in the Italian Astronet: DIRA 2 p 2047 N94-22452

PHOTCAL: The IRAF photometric calibration package p 1925 N94-22465

SKYMAP: Exploring the Universe in software p 1927 N94-22511

The EXOSAT database and archive p 2048 N94-22521

Guide star catalogue data retrieval software 2 p 1927 N94-22533

Recommendations for a service framework to access astronomical archives p 2049 N94-22537

StarView: The object oriented design of the ST DADS user interface p 2049 N94-22548

Miyun 232 MHz survey 1: Fields centered at: alpha:00(h)41(m), delta:41 deg 12 min and alpha: 07(h)00(m),delta:35 deg 00 min p 2080 N94-22554

ASTRONOMICAL MAPS

CCD surface photometry of galaxies p 2058 N94-22445

Data indexing techniques for the EUVE all-sky survey p 2048 N94-22503

SKYMAP: Exploring the Universe in software p 1927 N94-22511

ASTRONOMICAL MODELS

Variety in planetary systems p 2086 N94-20871

New production mechanisms for unstable nuclei in stars, supernovae, and the big bang [DE93-018627] p 2081 N94-21618

CCD surface photometry of galaxies p 2058 N94-22445

C++, objected-oriented programming, and astronomical data models p 2063 N94-22473

Helical kink instability of jets from young stellar objects p 2008 N94-22686

Fragmentation of magnetized filamentary interstellar clouds p 2008 N94-22687

Gravitational instability of magnetized filamentary clouds. 2: Rotation p 2009 N94-22689

Magnetic fields in spiral galaxies p 2010 N94-22697

ASTRONOMICAL OBSERVATORIES

Second Annual Conference on Astronomical Data Analysis Software and Systems. Abstracts [NASA-TM-108245] p 2057 N94-22438

A neural network prototyping package within IRAF p 1949 N94-22451

The ADAM environment and transputers p 1926 N94-22494

CCD data acquisition systems at Lick and Keck Observatories p 2047 N94-22495

The spectral world coordinate systems in IRAF/NOAO p 2049 N94-22539

SPECFOCUS: An IRAF task: for focusing spectrographs p 1965 N94-22540

Solar full-disk magnetic field image receiving system and observation software p 2079 N94-22552

IRAF and STSDAS under the new ALPHA architecture p 2049 N94-22553

ROSAT data analysis with EXSAS p 2080 N94-22555

ASTRONOMICAL PHOTOGRAPHY

How is WFPC flat field made p 1926 N94-22484

Efficient transfer of images over networks p 1748 N94-22517

SkiCAT: A cataloging and analysis tool for wide field imaging surveys p 2049 N94-22546

ASTRONOMICAL PHOTOMETRY

Wavelength dependence of limb-darkening of Mars from visible and near-IR telescopic spectral imaging p 2101 N94-20685

Compositional diversity of the lunar North Pole: Preliminary analyses of Galileo SSI data p 2101 N94-20686

Surface photometry of the shell galaxy NGC 2865 [ISBN-0-315-60441-7] p 2056 N94-22412

How to handle 6GBytes a night and not get swamped p 2058 N94-22444

CCD surface photometry of galaxies p 2058 N94-22445

How is WFPC flat field made p 1926 N94-22484

ASTRONOMICAL POLARIMETRY

Solar imaging vector magnetograph [NASA-CR-194729] p 1810 N94-21876

ASTRONOMICAL SPECTROSCOPY

Goniospectrometric properties of a white standard p 1684 N94-20684

Detectability of crystalline ferric and ferrous minerals on Mars p 2110 N94-20730

Deep near-infrared survey of the Southern Sky (DENIS) p 2062 N94-22467

The extreme ultraviolet explorer archive p 2047 N94-22468

ASTRONOMY

Multi Wave Link: An interactive database for co-ordination of multiwavelength programs [NASA-CR-194778] p 2043 N94-21055

Laser guide star adaptive optics: Present and future [DE93-018642] p 1989 N94-21619

Second Annual Conference on Astronomical Data Analysis Software and Systems. Abstracts [NASA-TM-108245] p 2057 N94-22438

Scientific computing in the 1990ies: An astronomical perspective p 2057 N94-22440

Multifrequency data analysis software on STARLINK p 1925 N94-22443

GUIs in the MIDAS environment p 2047 N94-22449

Database activity in the Italian Astronet: DIRA 2 p 2047 N94-22452

Seeing the forest for the trees: Networked workstations as a parallel processing computer p 1938 N94-22454

Experiments with recursive estimation in astronomical image processing p 2047 N94-22457

An IDL-based analysis package for COBE and other skycube-formatted astronomical data p 1925 N94-22471

Electronic publishing and intelligent information retrieval p 2047 N94-22479

Intelligent text retrieval in the NASA astrophysics data system p 2048 N94-22499

Evaluation of RDBMS packages for use in astronomy p 2048 N94-22514

NASA's astrophysics archives at the National Space Science Data Center p 2049 N94-22541

MOSAIC: Software for creating mosaics from collections of images p 1927 N94-22543

STELAR: An experiment in the electronic distribution of astronomical literature p 2049 N94-22544

The STARLINK software collection p 1927 N94-22545

Pair plasmas in the galactic center region and in Nova Muscae p 2009 N94-22691

ASTROPHYSICS

High energy physics program at Texas A/M University [DE93-041089] p 1980 N94-20933

Development and operations of the Astrophysics Data System [NASA-CR-194691] p 2043 N94-21270

Advanced far infrared detectors [DE93-040289] p 1968 N94-21526

Symmetry-dictated trucation: Solutions of the spherical shell model for heavy nuclei [DE94-000482] p 1976 N94-21961

The cool-star spectral catalog: A uniform collection of IUE SWP-LOs p 2046 N94-22446

NASA's astrophysics archives at the National Space Science Data Center p 2049 N94-22541

Fourth International Toki Conference on Plasma Physics and Controlled Nuclear Fusion [ESA-SP-351] p 2000 N94-22624

Thermal properties and radiation processes in astrophysical plasmas p 2002 N94-22640

ASYMMETRY

The lepton charge asymmetry in the decay of W bosons produced in p(bar p) collisions at (radical)s = 1.8 TeV [DE93-019903] p 1976 N94-21847

Likelihood analysis of parity violation in the compound nucleus [DE94-000671] p 1977 N94-22572

ASYMPTOTES

Asymptotic behavior of Fourier transform of surface measures on convex and radial hypersurfaces [ETN-93-93790] p 1952 N94-21019

ASYMPTOTIC GIANT BRANCH STARS

Molecular equilibria and condensation sequences in carbon rich gases p 2083 N94-20756

AGB stars as a source of short-lived radioactive nuclei in the solar nebula p 2133 N94-20859

ASYMPTOTIC METHODS

Asymptotic analysis: Basic concepts and definitions [DE94-001000] p 1961 N94-22393

Orthogonalization method for determination of boundary layer receptivity coefficients [ISBN-0-315-83426-9] p 1805 N94-22580

ASYMPTOTIC PROPERTIES

Large deviations behavior of counting processes and their inverses [AD-A271142] p 1939 N94-19909

Asymptotics of the GLRT for the disorder problem in diffusion processes [INRIA-RR-1735] p 1951 N94-20227

On estimation and testing in Poisson regression models with over-dispersion [MEMO-1083] p 1963 N94-21076

Universality in blow-up for non linear heat equations [PB93-215465] p 2038 N94-22095

Asymptotic analysis: Basic concepts and definitions [DE94-001000] p 1961 N94-22393

ASYMPTOTIC SERIES

Transient acoustic wave modeling: Higher-order WKBJ asymptotics and symbolical manipulation (revised) [PB93-215432] p 1969 N94-22262

Asymptotic analysis. Working Note No. 2, approximation of integrals [DE94-000433] p 1961 N94-22381

Asymptotic analysis: Basic concepts and definitions [DE94-001000] p 1961 N94-22393

ATLANTIC OCEAN

On the sources of North Atlantic deep water [AD-A270854] p 1881 N94-19895

The marine light-mixed layer experiment cruise and data report: R/V endeavor cruise EN-224, mooring deployment, 27 April-1 May 1991: Cruise EN-227, mooring recovery, 5-23 September 1991 [AD-A271175] p 1864 N94-20186

Processing of climatological data for model initialization [AD-A271878] p 1865 N94-20487

ATMOSPHERIC & OCEANOGRAPHIC INFORM SYS

Offshore decision support system: ERS-1 pilot project WAVEWATCH [BCRS-92-09] p 1865 N94-20532

ATMOSPHERIC ATTENUATION

Obtaining surface optical properties from space-based lidar systems [AD-A272831] p 1987 N94-21172

ATMOSPHERIC BOUNDARY LAYER

Refractive index structure in the lower atmosphere [AD-A270935] p 1854 N94-19899

Four-dimensional remote sensing of the marine boundary layer with a digital beamforming radar wind profiler [AD-A270627] p 1882 N94-20564

Models of refraction in the marine atmosphere surface layer [AD-A271724] p 1858 N94-21357

Marine boundary layer model evaluation by using a height gain measurement technique in the interference region p 1777 N94-22145

Breaking Kelvin-Helmholtz waves and cloud-top entrainment as revealed by K-band Doppler radar p 1874 N94-22310

Cloud boundaries during FIRE 2 p 1876 N94-22318

ATMOSPHERIC CHEMISTRY

Parameters affecting hydrogen chloride measurements [AD-A271326] p 1851 N94-20025

Laboratory studies of low temperature rate coefficients: The atmospheric chemistry of the outer planets [NASA-CR-193485] p 1972 N94-20130

Tropospheric chemistry of natural hydrocarbons, aldehydes, and peroxy radicals: Their connections to sulfuric acid production and climate effects [DE93-019525] p 1855 N94-20220

Research in progress: FY 1992
[DE94-000410] p 1836 N94-20936
Evolution of the Martian atmosphere
p 2146 N94-21680
Global emissions and models of photochemically active compounds
[DE93-040490] p 1852 N94-21969
Development of advanced cloud parameterizations to examine air quality, cloud properties, and cloud-radiation feedback in mesoscale models
[DE93-041164] p 1853 N94-22384
Mass spectrometer-pyrolysis experiment for atmospheric and soil sample analysis on the surface of Mars p 1812 N94-22435

ATMOSPHERIC CIRCULATION
Meso-Beta scale numerical simulation studies of terrain-induced jet streak mass/momentum perturbations
[NASA-CR-194627] p 1864 N94-20138
Dynamics Explorer 2: Continued FPI and NACS instrument data analysis and associated scientific activity at the University of Michigan
[NASA-CR-194689] p 1857 N94-20173
Modeling of interactions between biosphere and atmosphere on the global scale
[NASA-CR-193423] p 1837 N94-20205
The life cycles of intense cyclonic and anticyclonic circulation systems observed over oceans
[NASA-CR-194760] p 1865 N94-20353
Incorporation and comparative evaluation of a non-convective cloud parameterization scheme in the Naval Research Laboratory west coast mesoscale weather prediction model
[AD-A272417] p 1867 N94-21146
Analysis of a sandstorm weather process-translation
[AD-A272959] p 1867 N94-21250
Large-scale circulation regimes and tropical cyclone characteristics over the western pacific ocean
[AD-A273004] p 1867 N94-21307
Comparison of cloud microphysical parameters derived from surface and satellite measurements during FIRE phase 2 p 1873 N94-22306
Vertical velocity in cirrus case obtained from wind profiler p 1878 N94-22330
Dynamical characteristics of cirrus clouds from aircraft and radar measurements p 1878 N94-22332

ATMOSPHERIC COMPOSITION
Collisional processes involving atmospheric gases
[AD-A270729] p 1854 N94-19954
Remote sounding of tropospheric minor constituents
[NASA-CR-194265] p 1855 N94-20132
Tropospheric chemistry of natural hydrocarbons, aldehydes, and peroxy radicals: Their connections to sulfuric acid production and climate effects
[DE93-019525] p 1855 N94-20220
Derivation of the midinfrared (5.0-25.0 micron) optical constants of hydrous carbonate and sulfate
p 2108 N94-20723
Stratospheric Aerosol and Gas Experiment (SAGE 3)
p 1869 N94-21644
The early Martian environment: Clues from the cratered highlands and the Precambrian Earth
p 2143 N94-21667
Mars atmosphere loss and isotopic fractionation by solar-wind-induced sputtering and photochemical escape
p 2144 N94-21672
Possible solutions to the problem of channel formation on early Mars p 2144 N94-21673
Evolution of the Martian atmosphere
p 2146 N94-21680
Studies in remotely sensed geophysical parameter retrieval and analysis
[NASA-CR-194768] p 1842 N94-22374
Determination of Martian soil mineralogy and water content using the Thermal Analyzer for Planetary Soils (TAPS) p 1812 N94-22433
Mass spectrometer-pyrolysis experiment for atmospheric and soil sample analysis on the surface of Mars p 1812 N94-22435

ATMOSPHERIC CORRECTION
Global and regional comparative performance of linear and nonlinear satellite multichannel sea surface temperature algorithms
[AD-A270475] p 1837 N94-20028
Laser guide star adaptive optics: Present and future
[DE93-018642] p 1989 N94-21619
Comparisons of downwelling radiation to model predictions based on groundbased measurements during FIRE 1991 p 1876 N94-22320

ATMOSPHERIC EFFECTS
Dynamics of large scale impacts on Venus and Earth
p 2098 N94-20666
Pressure versus drag effects on crater size
p 1862 N94-20742
Searching for ancient Venus p 2111 N94-20743
A study of carbonates, sulfates, and phosphates using thermal emission spectroscopy p 1686 N94-20868
Measurement of evapotranspiration with combined reflective and thermal infrared radiance observations
[NASA-CR-194802] p 1837 N94-20951
Standard atmospheres for engagement modeling
[AD-A272447] p 1858 N94-21207

ATMOSPHERIC ELECTRICITY
Predicting lightning events in the KSC area: A feasibility study using single station data
[AD-A271440] p 1864 N94-20088

ATMOSPHERIC ENTRY
Micrometeorite dynamic pyrometamorphism: Nonstoichiometric clinoenstatite (CLEN)
p 2083 N94-20715
Micrometeorite dynamic pyrometamorphism: Observation of a thermal gradient in iron-nickel sulfide
p 2083 N94-20716
Effects of thrust vector control on the performance of the aerobang orbital plane change maneuver
[AD-A272532] p 1646 N94-21418
Entry velocities at Mars and Earth for short transit times
[AD-A272591] p 1865 N94-21420

ATMOSPHERIC ENTRY SIMULATION
High temperature simulation chambers. Physico-chemical and thermal effect of atmospheric reentry on ceramic materials p 1653 N94-21404
A method of measuring the thermoradiative properties of ceramic materials in a space environment
p 1665 N94-21405
Material properties and behavior during simulated atmospheric reentry p 1665 N94-21408

ATMOSPHERIC GENERAL CIRCULATION MODELS
Study of regional climate change
[DE93-018926] p 1850 N94-19941
Modeling of interactions between biosphere and atmosphere on the global scale
[NASA-CR-193423] p 1837 N94-20205
The CSIRO 9-level atmospheric general circulation model
[CSIRO-TP-26] p 1855 N94-20256
Orbit and sampling requirements: TRMM experience
p 1870 N94-21647
Proceedings of the Workshop on New Generation of Radiation Budget Measurements From Space and Their Use in Climate Modelling and Diagnostic Studies
[MPIM-90] p 1860 N94-22283
Satellite validation of GCM-simulated annual cycle of the Earth radiation budget and cloud forcing
p 1860 N94-22287
The seasonal variation of the cloud radiative forcing: Comparison of ECHAM model simulations with ERBE data p 1860 N94-22288
Use of satellite data for validation of the ECHAM models p 1861 N94-22289
Simulation of clear-sky outgoing longwave radiation over the oceans using operational analysis
p 1861 N94-22290
Use of satellite data for validation of operational forecast models and operational analyses p 1861 N94-22291
Analysis of the tropospheric water distribution during FIRE 2 p 1876 N94-22324
Three dimensional modeling of cirrus during the 1991 FIRE IFO 2: Detailed process study
p 1877 N94-22327
Cirrus cloud development in a mobile upper tropospheric trough: The November 26th FIRE cirrus case study
p 1878 N94-22329

ATMOSPHERIC HEATING
Spatial and temporal variations of satellite microwave measurements of latent heat release in tropic cyclones due to environmental forcing obtained from a numerical model
[AD-A267947] p 1865 N94-20482
A carbon dioxide/methane greenhouse atmosphere on early Mars p 2142 N94-21662
Possible solutions to the problem of channel formation on early Mars p 2144 N94-21673

ATMOSPHERIC LASERS
The NRL LACE program
[AD-A270861] p 1657 N94-19896

ATMOSPHERIC MODELS
Clouds: Their prediction and simulation
[AD-A271161] p 1864 N94-19900
Worldwide frequency of temperatures at selected altitudes
[AD-A271111] p 1864 N94-19908
Sporadic-E observations during LoVHF transionospheric direction finder measurements
[AD-A270619] p 1716 N94-19951
Intrusion of stratospheric ozone in the troposphere through tropopause folding and cold air droplets
[REPT-87] p 1851 N94-20154
Scientific development of a massively parallel ocean climate model
[DE93-019446] p 1855 N94-20219
Spatial and temporal variations of satellite microwave measurements of latent heat release in tropic cyclones due to environmental forcing obtained from a numerical model
[AD-A267947] p 1865 N94-20482
Processing of climatological data for model initialization
[AD-A271878] p 1865 N94-20487
Global blackout following the K/T Chicxulub impact: Results of impact and atmospheric modeling
p 1854 N94-20698
Incorporation and comparative evaluation of a non-convective cloud parameterization scheme in the Naval Research Laboratory west coast mesoscale weather prediction model
[AD-A272417] p 1867 N94-21146
Standard atmospheres for engagement modeling
[AD-A272447] p 1858 N94-21207
NOVAM evaluation utilizing electro-optics and meteorological data from KEY-90
[AD-A271722] p 1868 N94-21356
Models of refraction in the marine atmosphere surface layer
[AD-A271724] p 1858 N94-21357
Development and tests of a cloud physics parameterization for real-time aviation and public numerical weather forecasting
[PB93-202711] p 1868 N94-21427
Climate forcings and feedbacks p 1869 N94-21641
Fluvial valleys in the heavily cratered terrains of Mars: Evidence for paleoclimatic change?
p 2144 N94-21670
Evolution of the Martian atmosphere
p 2146 N94-21680
Empirical wind model for the middle and lower atmosphere. Part 2: Local time variations
[NASA-TM-104592] p 1870 N94-21862
Global emissions and models of photochemically active compounds
[DE93-040490] p 1852 N94-21969
Marine boundary layer model evaluation by using a height gain measurement technique in the interference region p 1777 N94-22145
Comparison of cloud microphysical parameters derived from surface and satellite measurements during FIRE phase 2 p 1873 N94-22306
Spectral variation of scattering and absorption by cirrus p 1876 N94-22321
Mesoscale simulations of the November 25-26 and December 5-6 cirrus cases using the RAMS model
p 1878 N94-22331
Importance of aggregation and small ice crystals in cirrus clouds, based on observations and an ice particle growth model p 1879 N94-22336
Calibration of radiation codes in climate models: Comparison of calculations with observations from the SPECtral Radiation Experiment (SPECTRE)
p 1879 N94-22337
Investigation of the effects of the macrophysical and microphysical properties of cirrus clouds on the retrieval of optical properties: Results for FIRE 2
p 1880 N94-22339
Extinction efficiencies from DDA calculations solved for finite circular cylinders and disks p 1880 N94-22340
Remote sensing estimates of cirrus particle size for tropical and midlatitude cirrus: Hexagonal crystals and ice spheres p 1880 N94-22342
Development of advanced cloud parameterizations to examine air quality, cloud properties, and cloud-radiation feedback in mesoscale models
[DE93-041164] p 1853 N94-22384

ATMOSPHERIC MOISTURE
Predicting lightning events in the KSC area: A feasibility study using single station data
[AD-A271440] p 1864 N94-20088
Atmospheric moisture collection device
[AD-D015935] p 1865 N94-20332
Atmospheric infrared sounder
[NASA-CR-194814] p 1856 N94-20362
Stratospheric Aerosol and Gas Experiment (SAGE 3)
p 1869 N94-21644
A documentation of icing relevant cloud physical parameters on horizontal soundings of stratiform clouds (continuation)
[DLR-MITT-92-10] p 1871 N94-22280
Microphysical properties of the November 26 cirrus cloud retrieved by Doppler radar/IR radiometer technique
p 1873 N94-22304
Comparison of cloud microphysical parameters derived from surface and satellite measurements during FIRE phase 2 p 1873 N94-22306
Observations of multi-layered clouds using K-band radar p 1874 N94-22311
Analysis of the GOES 6.7 micrometer channel observations during FIRE 2 p 1875 N94-22316

Analysis of the tropospheric water distribution during FIRE 2 p 1876 N94-22324
Three dimensional modeling of cirrus during the 1991 FIRE IFO 2: Detailed process study p 1877 N94-22327
Estimation of cirrus cloud particle fallspeeds from vertically pointing Doppler radar p 1879 N94-22333
A comparison of small and larger mesoscale latent heat and radiative fluxes: December 6 case study p 1879 N94-22335

ATMOSPHERIC PHYSICS
Convergence of the hermite wavelet expansion [AD-A271435] p 1854 N94-19841
Collisional processes involving atmospheric gases [AD-A270729] p 1854 N94-19954
Remote sounding of tropospheric minor constituents [NASA-CR-194265] p 1855 N94-20132
Accuracy requirements --- for monitoring of climate changes p 1869 N94-21642
Multiorder etalon sounder (MOES) development and test for balloon experiment [NASA-CR-194730] p 1859 N94-22026
Meteorological analysis of the December 4-6 FIRE cirrus-2 case p 1875 N94-22314
CO2 lidar observations of Mount Pinatubo debris: FIRE 2 and longer-term measurements p 1876 N94-22323

ATMOSPHERIC PRESSURE
Pressure versus drag effects on crater size p 1862 N94-20742
Are Plinian type eruptions possible on Venus? p 2123 N94-20803
Alumoxanes: Rationalization of black box materials [AD-A272805] p 1704 N94-21170

ATMOSPHERIC RADIATION
The analysis of global cloud and radiation data for the study of cloud-climate interactions [NASA-CR-193388] p 1865 N94-20535
Effects of hydrodynamics and thermal radiation in the atmosphere after comet impacts p 1862 N94-20649

ATMOSPHERIC REFRACTION
Refractive index structure in the lower atmosphere [AD-A270935] p 1854 N94-19899
Sporadic-E observations during LoVHF transionospheric direction finder measurements [AD-A270619] p 1716 N94-19951
Models of refraction in the marine atmosphere surface layer [AD-A271724] p 1858 N94-21357

ATMOSPHERIC SCATTERING
Refractive index structure in the lower atmosphere [AD-A270935] p 1854 N94-19899
Low-power millimeter-wave radar observations of the atmosphere [NASA-CR-194738] p 1858 N94-21811
Spectral variation of scattering and absorption by cirrus p 1876 N94-22321

ATMOSPHERIC SOUNDING
Atmospheric infrared sounder [NASA-CR-194814] p 1856 N94-20362
Spatial and temporal variations of satellite microwave measurements of latent heat release in tropic cyclones due to environmental forcing obtained from a numerical model [AD-A267947] p 1865 N94-20482
A retrieval error analysis technique for passive infrared atmospheric sounders [AD-A272618] p 1867 N94-21212
Validation of the design of a high resolution all-reflection Michelson interferometer for atmospheric spectroscopy [AD-A272505] p 1987 N94-21410
Multiorder etalon sounder (MOES) development and test for balloon experiment [NASA-CR-194730] p 1859 N94-22026
A documentation of icing relevant cloud physical parameters on horizontal soundings of stratiform clouds (continuation) [DLR-MITT-92-10] p 1871 N94-22280
Intercomparison of MAS, AVIRIS, and HIS data from FIRE cirrus 2 p 1872 N94-22298
Remote sensing of multilevel clouds during FIRE IFO 2 p 1844 N94-22303
Lidar and radar derived cirrus microphysical properties for the 26 November 1991 case study p 1873 N94-22305
Comparison of cloud microphysical parameters derived from surface and satellite measurements during FIRE phase 2 p 1873 N94-22306
CIMSS FIRE research activities p 1873 N94-22307
Progress in interpreting CO2 lidar signatures to obtain cirrus microphysical and optical properties p 1874 N94-22308
A numerical technique for the calculation of cloud optical extinction from lidar p 1874 N94-22309
Atmospheric parameterization schemes for satellite cloud property retrieval during FIRE IFO 2 p 1874 N94-22312
SSH-2 measurements of cirrus at 18-28 micrometers from the King Air during FIRE 2 p 1880 N94-22338
An overview of the radiation component of the NASA TOGA-COARE experiment p 1881 N94-22344
Temperature/pressure and water vapor sounding with microwave spectroscopy p 1812 N94-22436

ATMOSPHERIC TEMPERATURE
Worldwide frequency of temperatures at selected altitudes [AD-A271111] p 1864 N94-19908
Atmospheric infrared sounder [NASA-CR-194814] p 1856 N94-20362
Atmospheric parameterization schemes for satellite cloud property retrieval during FIRE IFO 2 p 1874 N94-22312

ATMOSPHERIC TIDES
Interactions of free modes, tides, and gravity waves in the middle atmosphere [REPT-84] p 1855 N94-20155

ATMOSPHERIC TURBULENCE
Coherent lidar design and performance verification [NASA-CR-193813] p 1816 N94-20341
Measurement of mesospheric turbulence in the framework of the metal campaign and development of a sensor for static pressure free measurements of neutral and electron density [BONN-IR-92-45] p 1857 N94-21149
Long-range laser imaging [AD-A273020] p 1817 N94-21253
Areally averaged estimates of surface heat flux from ARM field studies [DE93-018569] p 1859 N94-22036

ATOM CONCENTRATION
Energy storage and conversion in solid hydrogen [AD-A271439] p 1845 N94-20086
Laser diagnostics of RF hydrogen plasma reactors: Application to the processing of III-V materials [AD-A272659] p 1994 N94-21214

ATOMIC COLLISIONS
Absolute total and one and two electron transfer cross sections for Ar(8+) on Ar as a function of energy [DE93-040283] p 1970 N94-19870
Interactions of slow H, H2, and H3 with thin foils [DE93-040263] p 1976 N94-21995

ATOMIC EXCITATIONS
Angular distributions of high-order ATI [DE93-019125] p 1972 N94-20230
Optical luminescence spectroscopy as a probe of the surface mineralogy of Mars p 1813 N94-22437

ATOMIC INTERACTIONS
Measurements of atomic interactions and frequency stability with a cryogenic hydrogen maser [AD-A271132] p 1814 N94-19853
Collisions of molecules with clusters: A quasiclassical study [DE93-018614] p 1971 N94-20050

ATOMIC PHYSICS
Uncertainty limited atomic position measurement using optical fields [AD-A271013] p 1970 N94-19822
Observation of x ray absorption magnetic circular dichroism in well-characterized iron-cobalt-platinum multilayers [DE94-000303] p 1694 N94-21944

ATOMIC RECOMBINATION
Energy storage and conversion in solid hydrogen [AD-A271439] p 1845 N94-20086

ATOMIC STRUCTURE
A Green function method for calculation of atomic and electronic properties of isolated adsorbate atoms [ETN-93-95055] p 2014 N94-20018
The metallic bond for monolayer transition metal layers on transition metal surfaces [DE93-019060] p 1691 N94-20313
In-situ electrochemical surface science [AD-A265942] p 1680 N94-20330
Molecular and atomic arrays in nano- and mesoporous materials synthesis [AD-A271500] p 2017 N94-20544
Scanning tunneling microscopy investigations of metal dichalcogenide materials [AD-A272910] p 2027 N94-21242
IR materials producibility [AD-A273031] p 1987 N94-21321
Structure and morphology of Pd overlayers on epitaxial SnO2 films studies with the atomic force microscope [AD-A271827] p 2028 N94-21458
Local structure and superconductivity in La(2-x)Ba(x)CuO4 for x=0.125 and x=0.15 [DE93-040193] p 2029 N94-21555
Electron emission from nanometer-size metallic clusters: Electronic states and structural stability of supported Au clusters [DE93-040184] p 1975 N94-21766
Theoretical studies of the structures and electronic properties of U(NH2)(sub 3) and Np(NH2)(sub 3) [DE94-000768] p 2031 N94-21857
Observation of x ray absorption magnetic circular dichroism in well-characterized iron-cobalt-platinum multilayers [DE94-000303] p 1694 N94-21944
First principles calculations for analysis martensitic transformations [DE94-000666] p 1695 N94-21984
Transferable tight-binding parameters: An application to Ni and Ni-Al alloys [DE94-001044] p 1695 N94-22023
Theoretical research program to study chemical reactions in AOTV bow shock tubes [NASA-CR-194710] p 1804 N94-22027
Low temperature absorption spectra and ground state electronic structure of tetrakis(2,6-di-tert-butylphenoxide)uranium(IV) [DE94-000774] p 2035 N94-22387
Theoretical studies of structural phase transitions in actinide metals [DE94-000796] p 1696 N94-22388
Positron annihilation study of Sr Doping in La(2-x)Sr(x)CuO4 [DE94-000307] p 2036 N94-22594

ATOMIC WEIGHTS
The atomic weight and isotopic composition of boron and their variation in nature [DE93-019046] p 1682 N94-21631

ATOMIZERS
Cold starting an alcohol-fueled engine with ultrasonic fuel atomization [PB93-206597] p 1826 N94-22093

ATOMS
C/O atomic ratios in micrometer-size crushed grains from Antarctic micrometeorites and two carbonaceous meteorites p 2082 N94-20678
Direct detection of atomic ions from molecular photofragmentation during nonresonant multiphoton ionization of sputtered species [DE93-040886] p 1976 N94-21951

ATROPINE
Physiological correlates of stress-induced decrements in human perceptual performance [DOT/FAA/AM-93/19] p 1893 N94-20081

ATTENTION
Toward a neurobiological theory of visual attention [AD-A270724] p 1890 N94-20112

ATTENUATION COEFFICIENTS
Quantitative evaluation of material composition of composites using x ray energy-dispersive NDE technique [DE93-041157] p 1672 N94-19888
Variable wavelength, variable angle ellipsometry including a sensitivities correlation test p 1710 N94-20978
Superlattice optical properties measured by variable angle spectroscopic ellipsometry p 2022 N94-20993
The optical constants and spectral specular reflectivity of Highly Oriented Pyrolytic Graphite (HOPG) [DE93-040546] p 1709 N94-21970
A numerical technique for the calculation of cloud optical extinction from lidar p 1874 N94-22309

ATTENUATORS
Manual design technique for broadband passive thin-film attenuators using the Smith chart p 1782 N94-22178

ATTITUDE (INCLINATION)
Automatic AVHRR image navigation software [NASA-CR-194602] p 1643 N94-20148
Analysis of the TDRS multiple access system for possible use as an attitude control system sensor p 1666 N94-21338

ATTITUDE CONTROL
Pointing control design for autonomous space vehicle applications [DE93-019943] p 1657 N94-19863
Analysis of the TDRS multiple access system for possible use as an attitude control system sensor p 1666 N94-21338

ATTITUDE INDICATORS
Multisensor pinhole yawsonde [AD-A271715] p 1808 N94-20930

ATTITUDE STABILITY
Improvement of helicopter attitude stability by active control of the conventional swash plate [NASA-CR-194786] p 1650 N94-20524

AUDIO DATA
High performance MPEG-audio decoder IC p 1744 N94-21092
The Amsterdam hypermedia model: Extending hypertext to support real multimedia [CWI-CS-R9306] p 2045 N94-21536

AUDIO FREQUENCIES
Sub-band adaptive noise cancelling p 1774 N94-22125

AUDIO SIGNALS
Detection of emetic activity in the cat by monitoring venous pressure and audio signals
p 1886 N94-21903
AUDITORY DEFECTS
Journal of rehabilitation research and development, volume 30, number 1, 1993
[AD-A272956] p 1893 N94-21613
AUDITORY PERCEPTION
Segmentation and frequency domain ML pitch estimation of speech signals p 1747 N94-22212
AUGER EFFECT
Segregation of Si to the surface of Fe-29Ni-17Co alloy
[DE93-040053] p 1687 N94-19864
Electron emissions in low energy Ar(q+)-Ar collisions
[DE93-040285] p 1974 N94-21543
AUGER SPECTROSCOPY
Observation of x ray absorption magnetic circular dichroism in well-characterized iron-cobalt-platinum multilayers
[DE94-000303] p 1694 N94-21944
AUGMENTATION
Enhanced software for the GT1022 automated gaging system
[DE94-001374] p 1918 N94-21977
AURORAL IONIZATION
Theory of leaked auroral kilometric radiation
p 2003 N94-22649
AURORAL ZONES
The effects of magnetic storm phases on F-layer irregularities from auroral to equatorial latitudes
[AD-A272685] p 1857 N94-21189
Studies of electromagnetic ion cyclotron waves using AMPTE/CCE and Dynamics Explorer
[NASA-CR-194711] p 1982 N94-21878
AURORAS
Implications of Viking dayside auroral measurements
[ISBN-0-315-83273-8] p 1861 N94-22575
AUSTENITIC STAINLESS STEELS
Investigation of austenitic alloys for advanced heat recovery and hot gas cleanup systems
[DE93-017863] p 1687 N94-19802
Rapid heating tensile testing update: 304L stainless steel
[DE93-018770] p 1688 N94-19942
Evaluation of the fabricability of advanced iron aluminide-clad austenitic stainless steel tubing
[DE93-040598] p 1693 N94-21771
Proceedings of the Seventh Annual Conference on Fossil Energy Materials
[DE94-001091] p 1848 N94-21823
AUTOCORRELATION
Particle dispersion in turbulent sprays
[AD-A271314] p 1796 N94-19913
Partial empirical autocorrelation of a vectorial chronological series
[RR-896-M] p 1963 N94-20162
Fast scalar algorithms for multivariate partial correlations and their empirical counterparts
[RR-903-M] p 1905 N94-20201
Applications of correlator chips in radio science
p 1763 N94-21695
Experiments with recursive estimation in astronomical image processing p 2047 N94-22457
SPECFOCUS: An IRAF task for focusing spectrographs p 1965 N94-22540
DECONV-TOOL: An IDL based deconvolution software package p 1927 N94-22542
AUTOMATA THEORY
Closure properties of stochastic languages
[TR-441] p 1907 N94-20521
Space-efficient deterministic simulation of probabilistic automata
[TR-463] p 1900 N94-21281
Computerized simulations with cellular automates for cloud formation
[GKSS-92/E/22] p 1867 N94-21312
Manufacturing and information technology
p 2046 N94-22082
AUTOMATIC CONTROL
Pointing control design for autonomous space vehicle applications
[DE93-019943] p 1657 N94-19863
Aviation safety research at the National Institute for Aviation Research, Wichita State University
[NIAR-93-4] p 1641 N94-20189
Massachusetts Institute of Technology Lincoln Laboratory Journal volume 6, number 1, Spring 1993
[AD-A272273] p 1737 N94-20944
Internal camera calibration using rotation and geometric shapes
[AD-A272718] p 1808 N94-21167
Intelligent processing of ferroelectric thin films
[AD-A272518] p 1705 N94-21416
The Milling assistant, case-based Reasoning, and machining strategy: A report on the development of automated numerical control programming systems at New Mexico State University
[DE93-041101] p 2029 N94-21690
Cognitive engineering in aerospace applications
[NASA-CR-194782] p 1647 N94-21819
Automating the control of robotic systems in unstructured environments
[DE93-040753] p 1946 N94-21929
AUTOMATIC GAIN CONTROL
Software implementation of an adaptive digital automatic level control p 1773 N94-22124
AUTOMATIC PILOTS
Low-cost Unmanned Air Vehicle (UAV) for oceanographic research
[AD-A273103] p 1646 N94-21507
AUTOMATIC TEST EQUIPMENT
Design and test of field programmable gate arrays in space applications p 1765 N94-21710
AUTOMATION
A unified approach to VLSI layout automation and algorithm mapping on processor arrays
p 1759 N94-21127
AUTOMOBILE ENGINES
Cold starting an alcohol-fueled engine with ultrasonic fuel atomization
[PB93-206597] p 1826 N94-22093
AUTOMOBILE FUELS
Technology to prevent greenhouse effect gases
[DE94-707420] p 1851 N94-20116
Cold starting an alcohol-fueled engine with ultrasonic fuel atomization
[PB93-206597] p 1826 N94-22093
AUTOMOBILES
Some evidence on determinants of fuel economy as a function of driving cycle and test type
[DE93-019511] p 1825 N94-21637
Traffic noise in a roundabout way
p 1966 N94-21799
Ceramic Technology Project
[DE94-001011] p 1707 N94-21822
AUTONOMOUS NAVIGATION
A software architecture for a small autonomous underwater vehicle navigation system
[AD-A272322] p 1643 N94-21037
AUTOREGRESSIVE PROCESSES
Partial empirical autocorrelation of a vectorial chronological series
[RR-896-M] p 1963 N94-20162
AVALANCHE DIODES
Improvement of the performance of IMPATT oscillators through appropriate modification of resonant-cap activity
p 1782 N94-22179
AVIONICS
Rotorcraft low altitude IFR benefit/cost analysis: Conclusions and recommendations
[DOT/FAA/RD-93/22] p 1642 N94-20051
Handbook. Volume 3: Digital systems validation book plan
[DOT/FAA/CT-93/16-VOL-3] p 1647 N94-20053
Handbook. Volume 2: Digital systems validation. Chapter 18: Avionic data bus integration technology
[DOT/FAA/CT-88/10-VOL-2] p 1647 N94-20343
Space Generic Open Avionics Architecture (SGOAA) standard specification
[NASA-CR-188269] p 1666 N94-22275
Towards the formal verification of the requirements and design of a processor interface unit: HOL listings
[NASA-CR-191466] p 1937 N94-22414
AXIAL FLOW
Particle dispersion in turbulent sprays
[AD-A271314] p 1796 N94-19913
AIAA Techfest 29 proceedings
[NIAR-93-1] p 1635 N94-20191
The effect of transverse curvature on the fluctuating wall pressure and structure of boundary layer turbulence
[AD-A271868] p 1800 N94-20486
AXIAL LOADS
A benchmark study of 2D and 3D finite element calculations simulating dynamic pulse buckling tests of cylindrical shells under axial impact
[DE93-018859] p 1829 N94-19940
Biaxial flexural testing of a carbon fiber reinforced epoxy composite
[AD-A271956] p 1674 N94-20577
Improvements to a method for the geometrically nonlinear analysis of compressively loaded stiffened composite panels
[NASA-CR-194715] p 1832 N94-21814
AXIAL STRAIN
Biaxial flexural testing of a carbon fiber reinforced epoxy composite
[AD-A271956] p 1674 N94-20577
AXONS
The role of axon-Schwann cell interactions in nervous system ionic homeostasis
[AD-A270936] p 1890 N94-20045
Theoretical and numerical examinations of nonlinear parameter dependent advanced differential difference equations
[ETN-93-93681] p 1952 N94-21042
AZIMUTH
Comparison of remote sensing measurements with a two-scale polarimetric emission and scattering model for sea surfaces p 1721 N94-20415
A motion extraction method for synthetic aperture radars
[DLR-FB-92-31] p 1742 N94-22279
AZO COMPOUNDS
Efficiency of reversible optical storage in azo polymers
[AD-A272923] p 1705 N94-21223
The 13C-NMR spectra of poly (4-((2-(acryloyloxy) ethyl) ethyl amino)- 4-nitroazobenzene-co-methyl methacrylate)
[AD-A273016] p 1705 N94-21238
Recent developments in aromatic azo polymers research
[AD-A272966] p 1705 N94-21259
Azo polymers for optical storage 3: Effect of film thickness on net phase retardation and writing speed
[AD-A272994] p 1705 N94-21267
Optically induced birefringence in copolymers and blends containing azobenzene groups
[AD-A273085] p 1706 N94-21523

B

B STARS
Circumstellar environments of Be stars at infra-red and radio wavelengths
[ISBN-0-315-83135-9] p 2081 N94-22426
BACKGROUND NOISE
Evaluation of a nonlinear method for the enhancement of tonal signal detection
[NASA-CR-191562] p 1968 N94-21741
BACKGROUND RADIATION
The NRL LACE program
[AD-A270861] p 1657 N94-19896
A deep x ray survey in the Lockman hole and the soft x ray log N - log S
[NASA-CR-194698] p 2054 N94-20174
CERN-derived analysis of lunar radiation backgrounds
p 2080 N94-20880
Visualizing the universe, part 1 p 2064 N94-22476
BACKSCATTERING
Radar backscatter measurements from simulated sea ice during CRRELEX 1990
[AD-A271034] p 1715 N94-19823
An assessment of COMSCAN, a Compton backscatter imaging camera, for the one-sided non-destructive inspection of aerospace components
[AD-A271331] p 1806 N94-19837
Study of electromagnetic wave scattering from characterized rough surfaces
[AD-A270931] p 1716 N94-19934
Time-of-flight heavy ion backscattering spectrometry
[DE93-019067] p 1973 N94-20306
Coherent lidar design and performance verification
[NASA-CR-193813] p 1816 N94-20341
A general rough-surface inversion algorithm: Theory and application to SAR data p 1719 N94-20407
Variable-permittivity linear inverse problem for the H(sub z)-polarized case p 1719 N94-20408
Relating ground truth collection to model sensitivity
p 1719 N94-20409
Determination of noise equivalent sigma(0) using highly correlated repeat-pass SAR images
p 1720 N94-20411
ERS-1 and Seasat scatterometer measurements of ocean winds: Model functions and the directional distribution of short waves p 1720 N94-20412
Ku-band ocean radar backscatter observations during SWADE p 1720 N94-20413
Analysis of Ku-band cross section at low incidence angles p 1720 N94-20414
Polarimetric backscattering from sea ice
p 1723 N94-20426
Direction angle sensitivity of agricultural field backscatter with AIRSAR data p 1724 N94-20430
Retrieval of ice thickness from polarimetric SAR data
p 1724 N94-20432
Studies of Greenland using the SEASAT scatterometer p 1725 N94-20433
Radar backscattering from snow facies of the Greenland ice sheet: Results from the AIRSAR 1991 campaign
p 1725 N94-20434
C-band radar backscatter of sea ice in the Weddell Sea, Antarctica during the austral winter of 1992
p 1725 N94-20435

Near grazing scattering from non-Gaussian ocean surfaces p 1726 N94-20438
Second order distorted born approximation for backscattering from a layer of discrete random medium p 1728 N94-20448
Symmetry in polarimetric remote sensing p 1729 N94-20449
Application of neural network to remote sensing of soil moisture using theoretical polarimetric backscattering coefficients p 1730 N94-20455
Use of microwave polarimetry to enhance SAR images of the ocean surface
[AD-A271911] p 1882 N94-20489
The coherent backscattering opposition effect p 1991 N94-20646
Magellan vertical polarization radar observations p 1744 N94-20691
Combined backscatter Moessbauer spectrometer/x ray fluorescence analyzer (BaMS/XRF) for extraterrestrial surfaces p 1686 N94-20761
Scattering by Venus' surface p 2117 N94-20771
Earth-based measurement of lunar topography using delayed radar interferometry p 2119 N94-20787
Amorphous Ta-rich Ta-Cu films as diffusion barriers between Au and GaAs p 1710 N94-20991
Obtaining surface optical properties from space-based lidar systems
[AD-A272831] p 1987 N94-21172
The use of backscattered electron imaging mode to assess the effect of fine dispersions on development of superplastic microstructure in Al-Mg alloys
[AD-A272426] p 1691 N94-21258
Airborne surface backscattering strength measurements in the western Atlantic Ocean
[AD-A271737] p 1883 N94-21358
Cirrus properties deduced from CO2 lidar observations of zenith-enhanced backscatter from oriented crystals p 1871 N94-22295
CO2 lidar observations of Mount Pinatubo debris: FIRE 2 and longer-term measurements p 1876 N94-22323
A Backscatter Moessbauer Spectrometer (BaMS) for use on Mars p 1811 N94-22431

BACKWARD FACING STEPS
On the prediction of multigrid efficiency through local mode analysis p 1959 N94-21486

BALANCING
Analysis and design of weight balancing system for laser velocimetry traverse
[AD-A271171] p 1816 N94-20546

BALL BEARINGS
Detailed study of oxidation/wear mechanism in lox turbopump bearings
[NASA-TM-108434] p 1825 N94-21580

BALLISTIC MISSILES
Standard atmospheres for engagement modeling
[AD-A272447] p 1858 N94-21207
High-velocity interceptors for boost-phase intercepts
[DE94-001077] p 1965 N94-22403

BALLOON FLIGHT
Balloon exploration of the northern plains of Mars near and north of the Viking 2 landing site p 2092 N94-20401

BALLOON SOUNDING
Multiorder etalon sounder (MOES) development and test for balloon experiment
[NASA-CR-194730] p 1859 N94-22026

BALLOON-BORNE INSTRUMENTS
Concept report: Experimental vector magnetograph (EXVM) operational configuration balloon flight assembly
[NASA-CR-194702] p 1638 N94-21776
A High Resolution Liquid Xenon Imaging Telescope for 0.3-10 MeV Gamma Ray Astrophysics: Construction and Initial Balloon Flights
[NASA-CR-194709] p 2056 N94-22281

BALLOONING MODES
Continuum damping of ideal toroidal Alfven eigenmodes
[DE94-001233] p 1998 N94-22560

BANACH SPACE
Modular interval spaces
[PB93-220663] p 1961 N94-22266

BAND STRUCTURE OF SOLIDS
Photoelectron spectroscopy at model boundary surfaces of energy converter semiconductors/electrolyte contacts: Adsorption, coadsorption, and triadsorption of Br2, Na, and H2O on Van der Waals surfaces of metal chalocogenide semiconductors
[ETN-93-95063] p 2015 N94-20152
The x ray microprobe determination of chromium oxidation state in olivine from lunar basalt and kimberlitic diamonds p 1686 N94-20807
Solid-state dynamics and quantum transport in novel semiconductor nanostructures
[AD-A272955] p 2027 N94-21248

BANDPASS FILTERS
Y-Ba-Cu-O superconducting/GaAs semiconducting hybrid circuits for microwave applications p 1735 N94-20514
UVPI imaging from the LACE satellite: The Starbird rocket plume
[AD-A271981] p 1658 N94-20617
Examinations of a thallium atomic vapor filter for a Raman temperature lidar
[GKSS-92/E/13] p 1857 N94-21044

BANDWIDTH
Wide-bandwidth high-resolution search for extraterrestrial intelligence
[NASA-CR-194724] p 1897 N94-20336
Delivery of very high bandwidth with ATM switches and SONET
[DE93-019432] p 1899 N94-20476
Bandwidth enhancement of dielectric resonator antennas p 1734 N94-20507
On-board closed-loop congestion control for satellite based packet switching networks
[NASA-TM-106446] p 1656 N94-21581
Simulated behaviour of large scale SCI rings and tori
[DE93-040149] p 1935 N94-21745
Reentry vehicle adaptive telemetry
[DE94-001168] p 1656 N94-21852
Evaluation of DEC's GIGAswitch for distributed parallel computing
[DE94-001356] p 1936 N94-21853

BARIUM
Electron quantum yields from a barium photocathode illuminated with polarized light
[DE93-019232] p 1980 N94-20475

BARIUM COMPOUNDS
Techniques for the flux growth of optical materials: Growth of beta-barium borate
[AD-A272717] p 2028 N94-21505

BARIUM OXIDES
Local structure and superconductivity in La(2-x)Ba(x)CuO4 for x=0.125 and x=0.15
[DE93-040193] p 2029 N94-21555
Disks of YBa2Cu3O7 shocked to 10 GPa pressures
[DE94-000464] p 2031 N94-21931

BARIUM TITANATES
Investigation of the effect of various oxide and fluoride additives on the microstructure, electronic properties, and phase shifting ability of Ba(1-x)Sr(x)TiO3
[AD-A271756] p 2027 N94-21303
Optical processing in photorefractive media p 1789 N94-22222

BARRIER LAYERS
Measurement of superlattice optical properties by variable angle spectroscopic ellipsometry p 2022 N94-20992

BARYONS
High-energy astrophysics: A theoretical analysis of thermal radiation from neutron stars
[NASA-CR-194808] p 2055 N94-20952
New production mechanisms for unstable nuclei in stars, supernovae, and the big bang
[DE93-018627] p 2081 N94-21618
A relativistic constituent quark model
[DE93-041085] p 1946 N94-21689
Searching for high baryon density at the AGS with ARC
[DE93-041155] p 1975 N94-21693

BASALT
Petrogenesis of Apollo 12 mare basalts. Part 1: Multiple melts and fractional crystallization to explain olivine and ilmenite basalt compositions p 1684 N94-20644
Petrogenesis of Apollo 12 mare basalts. Part 2: An open system model to explain the pigeonite basalt compositions p 1684 N94-20645
Spectral reflectance studies of the Humorum Basin region p 2101 N94-20682
Euhedral metallic-Fe-Ni grains in extraterrestrial samples p 1697 N94-20724
Strength and deformation properties of basaltic lava flows on planetary surfaces p 1862 N94-20747
Lunar basalt meteorite EET 87521: Petrology of the clast population p 2083 N94-20752
Basaltic magmatism on the Moon. A perspective from volcanic picritic glasses p 2114 N94-20758
FE-60 and the evolution of eucrites p 2083 N94-20768
Chronology and genesis of high-Ti mare volcanism: Melting of cogenetic depleted and enriched reservoirs p 2118 N94-20777
Geology and deposits of the Serenitatis basin p 2119 N94-20786
The U-Th-Pb, Sm-Nd, and Ar-Ar isotopic systematics of lunar meteorite Yamato-793169 p 2084 N94-20834
Consortium study of lunar meteorites Yamato-793169 and Asuka-881757: Geochemical evidence of mutual similarity, and dissimilarity versus other mare basalts p 2085 N94-20857
Multispectral studies of selected crater- and basin-filling lunar Maria from Galileo Earth-Moon encounter 1 p 2136 N94-20876
Formation of perched lava ponds on basaltic volcanoes: Interaction between cooling rate and flow geometry allows estimation of lava effusion rates p 1863 N94-20878
Consortium reports on lunar meteorites Yamato 793169 and Asuka 881757, a new type of mare basalt p 2086 N94-20893

BATCH PROCESSING
Physics Detector Simulation Facility. Phase 2: System software description
[DE93-019745] p 1928 N94-19812

BATHYMETERS
Inversion of gravity and bathymetry in oceanic regions for long-wavelength variations in upper mantle temperature and composition
[NASA-CR-192272] p 1882 N94-20131

BAYES THEOREM
On evaluating the accuracy of SAR sea-ice classification using multifrequency polarimetric AIRSAR data p 1724 N94-20428
The Seventh International Symposium on Methodologies for Intelligent Systems (Poster Session)
[AD-A272125] p 1942 N94-20573
Computing with Bayesian multi-networks
[AD-A273106] p 1914 N94-21501
Extracting galactic structure parameters from multivariated density estimation p 1964 N94-22458
Mobile robot perception in unknown and unstructured dynamic voxel environments
[ISBN-0-315-83951-1] p 1947 N94-22591

BCH CODES
Arithmetic in large GF(2(exp n)) p 1760 N94-21131
Toward a new method of decoding algebraic codes using Groebner bases
[AD-A273089] p 1959 N94-21524
The Schur Berlekamp-Massey algorithm is parallelizable p 1784 N94-22191

BCS THEORY
Microwave properties and characterization of co-evaporated BSCCO thin films p 1709 N94-20518

BEACON SATELLITES
Radio wave propagation studies along an Earth-space satellite link
[ISBN-0-315-60627-4] p 1742 N94-22408

BEAM CURRENTS
Observation of reflected waves on the SABRE positive polarity inductive adder MITL
[DE93-019413] p 1980 N94-20295
Optimization and control of a small angle ion source using an adaptive neural network controller
[DE93-040063] p 1946 N94-21845

BEAM INJECTION
Study of transverse coupled bunch instabilities by using non-linear Taylor maps for the Advanced Light Source (ALS)
[DE93-040267] p 1979 N94-19989
Fast ion behavior during neutral beam injection in ATF
[DE93-040267] p 1992 N94-20056
Bundle profile monitor for AmPS
[DIGEL-1992-8] p 1979 N94-20123
Heavy ion fusion injector experiments
[DE93-019188] p 1993 N94-20234
Emittance measurement and modeling of the ALS 50 MeV LINAC to booster line
[DE93-040116] p 1979 N94-20273
Performance of the high brightness linac for the Advanced Free Electron Laser Initiative at Los Alamos
[DE93-040141] p 1816 N94-20277
High current injector for heavy ion fusion
[DE93-019241] p 1979 N94-20289
Study of possible energy upgrade for the ALS and modeling of the real lattice for the diagnosis of lattice problems
[DE93-040286] p 2016 N94-20323
Multibunch beam break-up in detuned structures
[DE93-041056] p 1991 N94-21686
Stability of beam in the Fermilab Main Injector
[DE94-000619] p 1982 N94-21934
Plasma heating in toroidal systems p 2000 N94-22629

BEAM SPLITTERS
Optical beam forming techniques for phased array antennas p 1727 N94-20442
Dual-beam multiple wavelength light transmittance measurement for particle sizing in rocket motor plumes
[AD-A272491] p 1670 N94-21208
An integrated-optic polarization splitter on silicon substrate, appendix 4 p 1989 N94-21598

BEAMFORMING
Method to evaluate steering and alignment algorithms for controlling emittance growth
[DE93-041004] p 1978 N94-19856
Optical beam forming techniques for phased array antennas p 1727 N94-20442

Four-channel HF receiving antenna array simulator
[AD-A271876] p 1732 N94-20471

BEAMS (RADIATION)
Method to evaluate steering and alignment algorithms for controlling emittance growth
[DE93-041004] p 1978 N94-19856
Determination of structure factors of copper by convergent beam electron diffraction
[DE93-019520] p 2019 N94-20941
The preservation of low emittance flat beams
[DE93-040964] p 1981 N94-21773
Numerical method for computing the electric field produced by a microwave beam in a stratified medium
p 1746 N94-22197

BEARINGS
Frequency and temperature dependence of high damping elastomers
[DE93-019539] p 1697 N94-19809

BEAT FREQUENCIES
Fermiology and De Haas-Van Alphen effect of beta-(ET)2IBr2
[DE93-019523] p 2011 N94-19807

BEDROCK
Cryoplanation terraces of interior and western Alaska
p 2091 N94-20396

BEHAVIOR
Current status: Animal models of nausea
p 1889 N94-21915

BENDING
Automatic locking orthotic knee device
[NASA-CASE-MFS-28633-1] p 1896 N94-20493

BENDING VIBRATION
Interactive simulation package for coupled bending and torsional vibrations in flexible robot arms
[MEMO-1089] p 1944 N94-21140

BERNOULLI THEOREM
Acoustic radiation damping of flat rectangular plates subjected to subsonic flows
[NASA-TM-109382] p 1967 N94-20211

BERYLLIUM ALLOYS
Properties and potential of high-temperature niobium beryllides
[DE93-019169] p 1690 N94-20233
High current density contacts for photoconductive semiconductor switches
[DE93-018837] p 1750 N94-20312

BERYLLIUM COMPOUNDS
Properties and potential of high-temperature niobium beryllides
[DE93-019169] p 1690 N94-20233

BERYLLIUM 10
Stable Ni isotopes and Be-10 and Al-26 in metallic spheroids from Meteor Crater, Arizona
p 1863 N94-20889

BETATRONS
Engineering design, fabrication, installation, operation, and maintenance services in support of research on laser plasma physics
[AD-A272249] p 1994 N94-20943
The preservation of low emittance flat beams
[DE93-040964] p 1981 N94-21773

BETHE-SALPETER EQUATION
Second order distorted born approximation for backscattering from a layer of discrete random medium
p 1728 N94-20448

BIBLIOGRAPHIES
Aeronautical engineering: A continuing bibliography with indexes (supplement 294)
[NASA-SP-7037(294)] p 1635 N94-20267
NASA patent abstracts bibliography: A continuing bibliography. Section 1: Abstracts (supplement 44)
[NASA-SP-7039(44)-SECT-1] p 2043 N94-21254
Index to 1992 NASA Tech Briefs, volume 16, numbers 1-12
[NASA-TM-109377] p 2053 N94-21736
Index to 1991 NASA Tech Briefs, volume 15, numbers 1-12
[NASA-TM-109376] p 2053 N94-21737
Cumulative index to NASA Tech Briefs, 1986-1990, volumes 10-14
[NASA-TM-109378] p 2054 N94-21738
Aircraft noise effects on cultural resources: Annotated bibliography
[PB93-205334] p 1969 N94-22054
SIMBAD quality-control p 2048 N94-22502

BICRYSTALS
Interface science of controlled metal/metal and metal/ceramic interfaces prepared using ultrahigh vacuum diffusion bonding
[DE94-001066] p 1696 N94-22025

BIDIRECTIONAL REFLECTANCE
Goniospectrometric properties of a white standard
p 1684 N94-20864
Optical effects of space weathering on lunar soils and the role of the finest fraction p 2101 N94-20687
The roughness of the Martian surface: A scale dependent model p 2115 N94-20762
Bi-directional reflectance and other radiation parameters of cirrus from ER-2 observations p 1871 N94-22296

BIMETALS
Evaluation of the fabricability of advanced iron aluminide-clad austenitic stainless steel tubing
[DE93-040598] p 1693 N94-21771

BINARY ALLOYS
First principles calculations for analysis martensitic transformations
[DE94-000666] p 1695 N94-21964

BINARY CODES
Toward a new method of decoding algebraic codes using Groebner bases
[AD-A273089] p 1959 N94-21524
Coded 64QAM using a binary convolutional code
p 1747 N94-22223
Some best rate 1/p and rate (p-1)/p systematic quasi-cyclic codes over GF(3) and GF(4)
p 1792 N94-22243

BINARY DATA
On a proposed symbolic dynamics for the Henon map
[AD-A272514] p 1955 N94-21359
Toward a new method of decoding algebraic codes using Groebner bases
[AD-A273089] p 1959 N94-21524
Interference reduction using neural networks
p 1783 N94-22186

BINARY DIGITS
A cost-effective methodology for the design of massively-parallel VLSI functional units
p 1760 N94-21132

BINARY MIXTURES
Lateral distribution of lipids in membranes at high pressure
[AD-A271183] p 1700 N94-20299
Speed of sound data and related models for mixtures of natural gas constituents
[PB93-200822] p 1968 N94-21447

BINARY PHASE SHIFT KEYING
Digital receiver for on-board FM/FSK-FM/BPSK demodulation p 1744 N94-21091

BINARY STARS
VVNRS: Variable phenomena in VV Cephei
[NASA-CR-194731] p 2056 N94-21835

BINDERS (MATERIALS)
Guanidine based vehicle/binders for use with oxides, metals, and ceramics
[NASA-CASE-LEW-15314-1] p 1700 N94-20195

BIOACOUSTICS
U.S. Tag for ISO/TC 43, acoustics, IEC/TC 29 electroacoustics, and ISO/TC 108/SC4 human exposure to mechanical vibration and shock: Minutes of the accredited standards committee on bioacoustics, S3
[AD-A273014] p 1897 N94-21309

BIOCHEMISTRY
Enhancement of wound healing by biosynthetic growth factor
[AD-A272517] p 1892 N94-21415

BIODEGRADATION
Evaluation of pre-extraction analytical holding times for nitroaromatic and nitramine explosives in water
[AD-A271547] p 1712 N94-20927

BIODYNAMICS
Aviation safety research at the National Institute for Aviation Research, Wichita State University
[NIAR-93-4] p 1641 N94-20189

BIOELECTRIC POTENTIAL
Studies of neural and cognitive function in subjects exposed to the marine-air interface, phases 1 and 2
[AD-A272282] p 1891 N94-20624

BIOGRAPHY
Mathematician Wang Ju
[AD-A267882] p 1912 N94-21255

BIOLOGICAL EFFECTS
Technology to prevent greenhouse effect gases
[DE94-707421] p 1850 N94-19976
Extra-corporeal blood access, sensing, and radiation methods and apparatuses
[NASA-CASE-MSC-21775-1] p 1890 N94-20372
Compatibility and efficacy of biocides qualified under military specification MIL-S-53021
[AD-A271496] p 1712 N94-20551
Aerospace medicine and biology: A continuing bibliography with indexes (supplement 383)
[NASA-SP-7011(383)] p 1892 N94-21288
ELF communications system ecological monitoring program
[AD-A272507] p 1740 N94-21412
Modeling the response of ecosystems to CO2 and climate change
[DE94-000748] p 1852 N94-21787
Spaceflight Radiation Health program at the Lyndon B. Johnson Space Center
[NASA-TM-104782] p 1893 N94-21863

BIOLOGICAL EVOLUTION
Derivation of the midinfrared (5.0-25.0 micron) optical constants of hydrous carbonate and sulfate
p 2108 N94-20723
Fourier calculus on evolutionary trees
[CWI-BS-R9234] p 1954 N94-21231

BIOLOGICAL MODELS (MATHEMATICS)
Theoretical and numerical examinations of nonlinear parameter dependent advanced differential difference equations
[ETN-93-93681] p 1952 N94-21042
Modeling the response of ecosystems to CO2 and climate change
[DE94-000748] p 1852 N94-21787

BIOMASS
Biofuels: Project summaries
[DE93-010003] p 1712 N94-19984
First Biomass Conference of the Americas: Energy, Environment, Agriculture, and Industry, volume 2
[DE94-000435] p 1847 N94-21562

BIOMASS ENERGY PRODUCTION
First Biomass Conference of the Americas: Energy, Environment, Agriculture, and Industry, volume 2
[DE94-000435] p 1847 N94-21562
Current situation of development of petroleum substituting energies (USA)
[DE94-707492] p 1848 N94-22013
Current situation of development of petroleum substituting energies (Canada)
[DE94-707493] p 1849 N94-22014

BIOMEDICAL DATA
Development of bioelastic material for aspects of wound repair
[AD-A272000] p 1892 N94-21503

BIONICS
Application of molecular modeling to biological processing
[AD-A272612] p 1974 N94-21185

BIOPHYSICS
Lateral distribution of lipids in membranes at high pressure
[AD-A271183] p 1700 N94-20299

BIOREACTORS
Survey on chemical engineering technologies for the global environmental protection
[DE94-714887] p 1852 N94-22044

BIOSPHERE
Modeling of interactions between biosphere and atmosphere on the global scale
[NASA-CR-193423] p 1837 N94-20205
Global blackout following the K/T Chicxulub impact: Results of impact and atmospheric modeling
p 1854 N94-20698
Monitoring issues from a modeling perspective
p 1868 N94-21640

BIOTECHNOLOGY
Biotechnology and composite materials
[AD-A264278] p 1673 N94-20327
Research in progress: FY 1992
[DE94-000410] p 1836 N94-20936
The laser and its applications on environment and biotechnology research
[DE94-000376] p 1820 N94-21957

BIPOLAR TRANSISTORS
A breakdown model for the bipolar transistor to be used with circuit simulators
[DE93-019422] p 1750 N94-20218
A contribution to development and parameter extraction of SPICE compatible macromodels for discrete bipolar transistors
[HMI-B-499] p 1753 N94-21021
Bridging faults in BiCMOS circuits
p 1756 N94-21105
Design and implementation of GaAs HBT circuits with ACME p 1758 N94-21117
Heterojunction bipolar transistor technology for data acquisition and communication p 1763 N94-21697
Behavior of faulty double BJT BiCMOS logic gates
p 1767 N94-21727

BIPOLARITY
Behavior of faulty double BJT BiCMOS logic gates
p 1767 N94-21727

BIREFRINGENCE
Recent developments in aromatic azo polymers research
[AD-A272966] p 1705 N94-21259
Azo polymers for optical storage 3: Effect of film thickness on net phase retardation and writing speed
[AD-A272994] p 1705 N94-21267
Optically induced birefringence in copolymers and blends containing azobenzene groups
[AD-A273085] p 1706 N94-21523
Birefringence control and dispersion characteristics of silicon oxynitride optical waveguides, appendix 6
p 1989 N94-21600

BIREFRINGENT FILTERS
Evaluation of a single stage of the LADS filter
[AD-A271101] p 1814 N94-19851
BISMALEIMIDE
Interleaved bismaleimide composites
[AD-A272233] p 1674 N94-20574
Tensile and shear fracture behavior of fiber reinforced plastics at 77K irradiated by various radiation sources
[DE93-040280] p 1706 N94-21542
Tensile strength of fiber reinforced plastics at 77K irradiated by various radiation sources
[DE93-040826] p 1709 N94-22008
BISMUTH
Application of an electrochemical quartz crystal microbalance to the study of electrocatalytic films
[DE93-041124] p 2029 N94-21691
BIT ERROR RATE
Advanced coding and modulation schemes for TDRSS
p 1744 N94-21350
QPPM receiver for free-space laser communications
[NASA-TM-106424] p 1741 N94-21567
Design of a new squaring function for the Viterbi algorithm p 1764 N94-21699
Adaptive decoding of convolutional codes
p 1793 N94-22246
Bidirectional algorithms for the decoding of convolutional codes over memoryless channels p 1793 N94-22247
BIT SYNCHRONIZATION
A low cost alternative to high performance PCM bit synchronizers p 1813 N94-21347
BITS
A cost-effective methodology for the design of massively-parallel VLSI functional units
p 1760 N94-21132
BLACK BODY RADIATION
Fluorescent microthermographic imaging
[DE93-040332] p 1810 N94-22000
BLACK HOLES (ASTRONOMY)
Gamma ray bursts from collisions of primordial small mass black holes with comets p 2150 N94-20604
Accretion disks in bright x ray binaries
p 2002 N94-22639
General relativistic winds in a black hole magnetosphere p 2002 N94-22644
Properties of x ray emission from x ray novae
p 2007 N94-22676
Time variations of x rays from black hole candidates: Canonical time variations in high and low intensity states
p 2009 N94-22690
Pair plasmas in the galactic center region and in Nova Muscae p 2009 N94-22691
Time variation of MHD accretion onto a black hole
p 2009 N94-22692
Accretion of a hot plasma onto the central black hole: Fokker-Planck formulation p 2009 N94-22693
Shock formation in magnetohydrodynamical accretion onto a black hole p 2010 N94-22699
BLADE-VORTEX INTERACTION
The fluid mechanics of vortex cutting by a blade
[AD-A270932] p 1636 N94-20043
Rotorcraft noise: Status and recent developments
[NASA-CR-194761] p 1967 N94-20523
BLOCK COPOLYMERS
Dynamics of adsorbed, swollen block copolymers
[AD-A272013] p 1706 N94-21460
BLOCK DIAGRAMS
Development and testing of a reliability performance index for modular robotic systems
[AD-A271901] p 1942 N94-20488
BLOCKING
Throughput and blocking in circuit-switched interconnection networks p 1784 N94-22189
Throughput, blocking, and interference in packet radio networks p 1746 N94-22190
BLOOD
Physiologically based pharmacokinetic modelling of percutaneously absorbed dibromomethane utilizing multiple dermal sub-compartments
[AD-A271106] p 1889 N94-19981
Extra-corporeal blood access, sensing, and radiation methods and apparatuses
[NASA-CASE-MSC-21775-1] p 1890 N94-20372
BLOOD PRESSURE
Detection of emetic activity in the cat by monitoring venous pressure and audio signals
p 1886 N94-21903
BLUNT BODIES
Atmospheric breakup of a small comet in the Earth's atmosphere p 2084 N94-20824
BODY CENTERED CUBIC LATTICES
Crystallographic phase transitions in actinide metals as a function of pressure
[DE93-040138] p 2011 N94-19827
Metastable bcc phase formation in the Nb-Cr system
[DE93-018376] p 2012 N94-19926
Neutron and PIMC determination of the longitudinal momentum distribution of HCP, BCC and normal liquid He-4
[DE93-019009] p 1972 N94-20187
Transmission electron microscopy study of thick copper-304 stainless steel multilayers
[DE94-001045] p 1696 N94-22394
First-principles pressure-temperature phase diagrams in metals
[DE94-001056] p 1696 N94-22398
BODY TEMPERATURE
Wind chill: The temperature feeling caused by the wind velocity
[KNMI-TR-103A] p 1890 N94-20238
Studies of neural and cognitive function in subjects exposed to the marine-air interface, phases 1 and 2
[AD-A272282] p 1891 N94-20624
BOEING 737 AIRCRAFT
Measurement of the influence of deicing liquids on aircraft aerodynamics p 1640 N94-22602
BOILING
Thermal information regarding the cooldown and operation of liquid argon calorimeters
[DE93-019391] p 1807 N94-19987
EHD enhancement of pool and in-tube boiling of alternate refrigerants
[DE94-000787] p 1798 N94-20101
BOLIDES
Dynamics of large scale impacts on Venus and Earth
p 2098 N94-20666
Delimitation of terrestrial impact craters by way of pseudotachylytic rock distribution p 1863 N94-20783
Impact-induced devolatilization of CaSO4 anhydrite and implications for K-T extinctions: Preliminary results
p 2085 N94-20840
BOLOMETERS
Advanced far infrared detectors
[DE93-040289] p 1988 N94-21528
BOLTS
Mold bolt and means for achieving close tolerances between bolts and bolt holes
[NASA-CASE-MFS-28720-1] p 1823 N94-20379
BOLTZMANN TRANSPORT EQUATION
Kinetic theory of runaway air-breakdown
[DE93-040731] p 1750 N94-20325
IR materials producibility
[AD-A273031] p 1987 N94-21321
BOMBARDMENT
Neutral copper cluster sputtering yields: Ne(+), Ar(+) and Xe(+) bombardment
[DE93-019010] p 1690 N94-20288
BONDED JOINTS
Durability predictions for adhesively bonded joints in humid environments
[AD-A271177] p 1830 N94-20001
Adhesive bonded joint with improved cyclic fatigue life for alumina-ceramic cylinders and hemispheres: Fourth generation housings
[AD-A273061] p 1831 N94-21310
BONDING
ALE project
[AD-A271080] p 2014 N94-19980
Automated HMC assembly
[DE93-040641] p 1749 N94-20005
A process for preparing an assembly of an article and a soluble polyimide which resists dimensional change, delamination, and debonding when exposed to changes in temperature
[NASA-CASE-LAR-14763-1] p 1702 N94-20373
Interface science of controlled metal/metal and metal/ceramic interfaces prepared using ultrahigh vacuum diffusion bonding
[DE94-001066] p 1696 N94-22025
BONES
A geometrical process for three dimensional osteotomy planning
[ETN-93-93602] p 1892 N94-21134
BOOLEAN ALGEBRA
System for solving Boolean equations using optical lookup tables
[AD-D015962] p 1951 N94-20358
Advice from nonadaptive queries to NP
[TR-470] p 1911 N94-21200
A new class of multi-function two-rail totally self-checking basic building blocks p 1788 N94-22215
Spatial region filtering in IRAF/PROS
p 1927 N94-22524
BORATES
Techniques for the flux growth of optical materials: Growth of beta-barium borate
[AD-A272717] p 2028 N94-21505
Interfacial reactions between titanium and borate glass
[DE93-012847] p 1683 N94-22031
BORIC ACIDS
A comparison of sulfuric acid/boric acid anodize and chromic acid anodize processes
[AD-A271933] p 1703 N94-20614
BORN APPROXIMATION
Second order distorted born approximation for backscattering from a layer of discrete random medium
p 1728 N94-20448
Application of the target decomposition theorem to a polarimetric random media model p 1730 N94-20453
BORON CARBIDES
Hydrodynamic compressibility of high-strength ceramics
[DE93-019424] p 1698 N94-19903
BORON ISOTOPES
The atomic weight and isotopic composition of boron and their variation in nature
[DE93-019046] p 1682 N94-21631
BORON OXIDES
Model for liquid boron oxide droplet gasification in H/O/C/F combustion environments
[AD-A272911] p 1682 N94-21243
BOSONS
A search for new gauge bosons in (bar p)p collisions at square root of s equals 1.8 TeV in the dielectron decay mode
[DE93-019901] p 1969 N94-19813
F-spin concept and g-bosons in the interceding boson model
[ETN-93-93607] p 1973 N94-21136
The lepton charge asymmetry in the decay of W bosons produced in p(bar p) collisions at (radical)s = 1.8 TeV
[DE93-019903] p 1976 N94-21847
BOUNDARIES
Generalization performance of backpropagation learning on a syllabification task p 1940 N94-20246
BOUNDARY CONDITIONS
The best of GYMNOS: A users guide
[DE93-041275] p 1992 N94-19991
A new conformal absorbing boundary condition for finite element meshes and parallelization of FEMATS
[NASA-CR-194740] p 1950 N94-20034
Meso-Beta scale numerical simulation studies of terrain-induced jet streak mass/momentum perturbations
[NASA-CR-194627] p 1864 N94-20138
Polarimetric thermal emission from rough surfaces
p 1727 N94-20441
An integro-algebraic equation for high frequency wake fields in a tube with smoothly varying radius
[DE93-040940] p 1741 N94-21684
Microscopic and macroscopic dynamics
[DE93-019576] p 1937 N94-22042
BOUNDARY ELEMENT METHOD
Development of BEM for ceramic composites
[NASA-CR-194718] p 1676 N94-21777
BOUNDARY INTEGRAL METHOD
Scattering by cavity-backed antennas on a circular cylinder p 1741 N94-21886
Radiation by cavity-backed antennas on a circular cylinder p 1741 N94-21887
User manual for EXCALIBUR: A FE-BI numerical laboratory for cavity-backed antennas in a circular cylinder, version 1.2 p 1741 N94-21888
BOUNDARY LAYER FLOW
Experimental and computational results from a large low-speed centrifugal impeller
[NASA-TM-106421] p 1636 N94-20136
A theoretical investigation of unsteady separation phenomena related to dynamic stall
[AD-A271865] p 1636 N94-20465
The effect of transverse curvature on the fluctuating wall pressure and structure of boundary layer turbulence
[AD-A271868] p 1800 N94-20466
Orthogonalization method for determination of boundary layer receptivity coefficients
[ISBN-0-315-83426-9] p 1805 N94-22580
BOUNDARY LAYER SEPARATION
Fluid dynamic mechanisms and interactions within separated flows
[AD-A271037] p 1797 N94-19978
A theoretical investigation of unsteady separation phenomena related to dynamic stall
[AD-A271865] p 1636 N94-20465
Computational and analytical methods in nonlinear fluid dynamics
[AD-A272722] p 1802 N94-21169
BOUNDARY LAYER STABILITY
Some practical turbulence modeling options for Reynolds-averaged full Navier-Stokes calculations of three-dimensional flows
[NASA-TM-106399] p 1637 N94-20534
Orthogonalization method for determination of boundary layer receptivity coefficients
[ISBN-0-315-83426-9] p 1805 N94-22580

BOUNDARY LAYER TRANSITION
Numerical investigation of laminar-turbulent transition in two- and three-dimensional boundary layers
[DLR-FB-92-36] p 1800 N94-20533
Low Reynolds-number turbulent boundary layers
[AD-A272011] p 1803 N94-21459
Flow transition with 2-D roughness elements in a 3-D channel p 1806 N94-21466
Orthogonalization method for determination of boundary layer receptivity coefficients
[ISBN-0-315-83426-9] p 1805 N94-22580
Surface hot film measurements at ATTAS laminar glove p 1639 N94-22598
Testing of a multisensor hot film technique in wind tunnel and free flight p 1639 N94-22599
Free flight experiment with a laminar wing glove p 1639 N94-22600

BOUNDARY LAYERS
Experimental study of a shock accelerated thin gas layer
[DE93-018354] p 1799 N94-20286
Response of the topography and gravity field on Venus to mantle upwelling beneath a chemical boundary layer p 2117 N94-20775
Physics of magnetospheric boundary layers
[NASA-CR-194725] p 1858 N94-21836
Riblet boundary layer measurements of an A-310 fuselage with Pitot combs p 1640 N94-22605

BOUNDARY VALUE PROBLEMS
Analytical evaluation of a surface integral expressing the coupling between interior and exterior volumes in a FE-IE approach p 1722 N94-20423
Stoermer-Cowell and related methods for the numerical solution of second order periodic initial value problems for ODE's 2: Numerical characteristics of the methods
[MEMO-1082] p 1953 N94-21075
Adaptive grids for quasilinear parabolic systems in one space dimension
[ETN-93-93611] p 1954 N94-21137
Some experiences of solving 1-D semiconductor device equations on a matrix coprocessor by a domain decomposition method
[CWI-NM-R9304] p 1935 N94-21492
Butcher-Kuntzmann methods for nonstiff problems on parallel computers
[CWI-NM-R9305] p 1935 N94-21493
Hybrid finite element/waveguide mode analysis of passive RF devices
[AD-A273074] p 1740 N94-21518
Comparing quasi-Newton methods for solving sparse interface problems
[CWI-NM-R9303] p 1959 N94-21576
Universality in blow-up for non linear heat equations
[PB93-215465] p 2038 N94-22095
Hypersingular integrals at a corner
[DE94-000340] p 1961 N94-22379
Asymptotic analysis: Basic concepts and definitions
[DE94-001000] p 1961 N94-22393

BOW WAVES
Physics of magnetospheric boundary layers
[NASA-CR-194725] p 1858 N94-21836
Theoretical research program to study chemical reactions in AOTV bow shock tubes
[NASA-CR-194710] p 1804 N94-22027

BRAGG ANGLE
Modifications to the three-component classification algorithm for SAR data p 1719 N94-20410
Direction angle sensitivity of agricultural field backscatter with AIRSAR data p 1724 N94-20430
Rough surface scattering from moving ocean surfaces as an indicator of scattering mechanisms p 1726 N94-20439

BRAIN
Cognition and the brain: A continuation of the university research initiative at New York University
[AD-A271872] p 1894 N94-20467

BRAKES (FOR ARRESTING MOTION)
In-vacuo slip testing of materials for SSRMS friction brakes p 1661 N94-21381

BRANCHING (MATHEMATICS)
Back and forth bisimulations on prime event structures
[RR-888-I-IMAG-124-LIFIA] p 1929 N94-20124
SLD results from the study of polarized Z(sup 0) produced at the SLC
[DE93-041020] p 1982 N94-21952

BRAYTON CYCLE
Brayton power conversion system parametric design modelling for nuclear electric propulsion
[NASA-CR-191135] p 1671 N94-21874

BRAZING
Segregation of Si to the surface of Fe-29Ni-17Co alloy
[DE93-040053] p 1687 N94-19864

BRECCIA
The Erevan howardite: Petrology of glassy clasts and mineral chemistry p 1684 N94-20640
Carbonaceous xenoliths from the Erevan howardite p 1684 N94-20642
Fragments of ancient lunar crust: Ferroan noritic anorthosites from the descartes region of the Moon p 2096 N94-20660
Abundance and composition of solar KR in the H3-H6 chondrite ACFER111 p 1684 N94-20676
Post-igneous redistribution of components in eucrites p 1685 N94-20684
Kalkkop crater, Eastern Cape: A new impact crater in South Africa p 1862 N94-20714
Post-metamorphic brecciation in type 3 ordinary chondrites p 2083 N94-20749
Lunar basalt meteorite EET 87521: Petrology of the clast population p 2083 N94-20752
Petrography of shock features in the 1953 Manson 2-A drill core p 1862 N94-20767
Magnesian anorthosites from the western highlands of the Moon: Isotope geochemistry and petrogenesis p 2118 N94-20779
Delimitation of terrestrial impact craters by way of pseudotachylytic rock distribution p 1863 N94-20783
Two-polarity magnetization in the Manson impact breccia p 1863 N94-20789
The Sm-Nd systematics of silicate inclusions in iron meteorites: Results from Caddo (IAB)
[CONTRIB-5241(804)] p 2084 N94-20795
The age of the Pretoria Saltpan impact crater, South Africa p 1863 N94-20798
A long-term change of the AR/KR/XE fractionation in the solar corpuscular radiation p 2136 N94-20875
Regolith breccia consisting of H and LL chondrite mixture p 2080 N94-20892
Mineralogy of dark clasts in primitive versus differentiated meteorites p 2087 N94-20907

BREWSTER ANGLE
The Brewster angle effect in SAR polarimetry p 1731 N94-20456

BRIDGMAN METHOD
Characterization of convection related defects in II-VI compound semiconductors
[NASA-CR-194704] p 2030 N94-21778

BRIGHTNESS
Performance of the high brightness linac for the Advanced Free Electron Laser Initiative at Los Alamos
[DE93-040141] p 1816 N94-20277
Detection of x ray sources in PROS p 2062 N94-22466

BRIGHTNESS DISTRIBUTION
An x ray archive on your desk: The Einstein CD-ROM's p 2048 N94-22519

BRIGHTNESS TEMPERATURE
Comparison of remote sensing measurements with a two-scale polarimetric emission and scattering model for sea surfaces p 1721 N94-20415
Ground-based passive remote sensing during FIRE IFO 2 p 1844 N94-22319
Surface-induced brightness temperature variations and their effects on detecting thin cirrus clouds using IR emission channels in the 8-12 micrometer region p 1880 N94-22341

BRILLOUIN EFFECT
Parametric instabilities in picosecond time scales
[DE94-000384] p 1966 N94-21958

BRILLOUIN ZONES
Phonons and metastability in compressed nitrogen
[DE93-019913] p 2016 N94-20318
Non commutative geometry and physics
[PB93-215499] p 1961 N94-22264

BRINES
Polarimetric backscattering from sea ice p 1723 N94-20426
Briny lakes on early Mars? Terrestrial intracrater playas and Martian candidates p 2145 N94-21675

BRITTLE MATERIALS
A thermodynamic theory of dynamic fragmentation
[DE93-019066] p 1833 N94-21916

BRITTLENESS
Interleaved bismaleimide composites
[AD-A272233] p 1674 N94-20574
Ductile-brittle transition behavior of tungsten under shock loading conditions
[DE93-019945] p 1693 N94-21843
Ni3Al aluminide alloys
[DE94-000493] p 1694 N94-21933

BROADBAND
Recent activities in printed Antennas at LeRC p 1722 N94-20422
Simulations of spectral broadening by cross-phase modulation (XPM) with chaotic light pulses
[DE93-019623] p 1819 N94-21872
Effect of bandwidth on beam smoothing and frequency conversion at the third harmonic of the Nova laser
[DE93-019917] p 1819 N94-21920
Wideband source location in two-dimensional array processing p 1747 N94-22250

BROADCASTING
NHK Science and Technical Research Laboratories p 2151 N94-20342
Spread spectrum random access networks
[AD-A272280] p 1737 N94-20585

BROKEN SYMMETRY
Summary of the Hadronic Weak Interaction session
[DE94-000592] p 1975 N94-21775
The lepton charge asymmetry in the decay of W bosons produced in p(bar p) collisions at (radical)s = 1.8 TeV
[DE93-019903] p 1976 N94-21847
Theoretical phase diagrams for solid H(sub 2)
[DE94-001049] p 1684 N94-22395
Likelihood analysis of parity violation in the compound nucleus
[DE94-000671] p 1977 N94-22572

BROMIDES
Fermiology and De Haas-Van Alphen effect of beta-(ET)2IBr2
[DE93-019523] p 2011 N94-19807
Heat transfer additives for absorption cooling system fluids
[PB93-202521] p 1714 N94-21426

BROMINE
Photoelectron spectroscopy at model boundary surfaces of energy converter semiconductors/electrolyte contacts: Adsorption, coadsorption, and triadsorption of Br2, Na, and H2O on Van der Waals surfaces of metal chalocogenide semiconductors
[ETN-93-95063] p 2015 N94-20152

BROMINE COMPOUNDS
Laser driven hydrodynamic instability experiments
[DE93-040550] p 1818 N94-21547

BRUSH SEALS
The 1992 Seals Flow Code Development Workshop
[NASA-CP-10124] p 1654 N94-21790
Brush seal bristle flexure and hard-rub characteristics p 1654 N94-21791
Integrity testing of brush seal in a T-700 engine p 1654 N94-21792
Air Force brush seal programs p 1655 N94-21793
Compliant seal development p 1655 N94-21795
Modeling bristle lift-off in idealized brush seal configurations p 1655 N94-21797

BSCCO SUPERCONDUCTORS
Machinable oxide ceramic
[AD-D015927] p 1699 N94-20017
Microwave properties and characterization of co-evaporated BSCCO thin films p 1709 N94-20518
The incongruent melting and melt textured solidification process of Bi2Sr2CaCu3O8
[DE93-041123] p 2032 N94-21936
High oxygen pressure synthesis of new copper oxide superconductors
[DE93-040278] p 2033 N94-21998
Thin-film fabrication of Pb-doped BiSrCaCuO superconductor p 1781 N94-22176

BUCKLING
A benchmark study of 2D and 3D finite element calculations simulating dynamic pulse buckling tests of cylindrical shells under axial impact
[DE93-018859] p 1829 N94-19940
Probabilistic assessment of composite structures
[NASA-TM-106368] p 1832 N94-21757
Improvements to a method for the geometrically nonlinear analysis of compressively loaded stiffened composite panels
[NASA-CR-194715] p 1832 N94-21814

BUFFER STORAGE
A 20 MHz CMOS reorder buffer for a superscalar microprocessor p 1764 N94-21700
A shared buffer memory switch with maximum queue and minimum allocation p 1773 N94-22119
Buffer allocation in an ATM switch with output buffer and speed constraints p 1746 N94-22203
A self-defining hierarchical data system p 2046 N94-22448

BUILDINGS
Building integrated photovoltaic systems analysis
[DE93-018208] p 1846 N94-21298
The energy performance of prototype holographic glazings
[DE93-040451] p 1809 N94-21545
Aircraft noise effects on cultural resources: Recommendation and rationale for further research
[PB93-205326] p 1968 N94-22053
Aircraft noise effects on cultural resources: Annotated bibliography
[PB93-205334] p 1969 N94-22054

BUMPERS
PVDF gauge characterization of hypervelocity-impact-generated debris clouds
[DE93-018831] p 1829 N94-19943

BUNCHING
Persistent wakefields associated with waveguide damping of higher order modes
[DE93-040973] p 1715 N94-19874
Study of transverse coupled bunch instabilities by using non-linear Taylor maps for the Advanced Light Source (ALS)
[DE93-040287] p 1979 N94-19989
Multibunch beam break-up in detuned structures
[DE93-041056] p 1981 N94-21686
Simulation and compensation of multibunch energy variation in NLC
[DE93-041057] p 1981 N94-21687
Generation of harmonic radiation using the multi-cavity free-electron laser
[DE94-001261] p 1820 N94-21975
BUNDLES
Semi-stability and heights of cycles
[PB93-215507] p 1961 N94-22377
BUOYANCY
Mixing of a chemically buoyant layer at the top of a thermally convecting fluid: Implications for mantle dynamics with application to Venus
p 2099 N94-20675
Combustion in turbulent jets and buoyant flames
[PB93-202372] p 1682 N94-21452
BURN-IN
Design and test of field programmable gate arrays in space applications p 1765 N94-21710
BURNING RATE
Ageing studies on a composite propellant containing a new organo-copper burn rate catalyst
[AD-A271060] p 1711 N94-19906
Investigation of flame driving and flow turning in axial solid rocket instabilities
[AD-A271066] p 1667 N94-20015
BURNS (INJURIES)
Non-ionic surfactants in the treatment of third degree burns
[AD-A271582] p 1891 N94-21035
BUS CONDUCTORS
A SCSI-bus data acquisition system for nuclear spectroscopy experiments
[USIP-92-03] p 2042 N94-20193
BUTANES
Computer simulation of molecular response at a shock front
[DE94-001050] p 1977 N94-22396
BYPASSES
A comprehensive theoretical and experimental study of coplanar waveguide shunt stubs p 1733 N94-20500
A comparative study between shielded and open coplanar waveguide discontinuities
p 1733 N94-20501
A theoretical and experimental study of coplanar waveguide shunt stubs p 1733 N94-20502

C

C (PROGRAMMING LANGUAGE)
Efficient and correct translation of strict applicative programming languages
[ETN-93-95056] p 1903 N94-20020
A self-defining hierarchical data system
p 2046 N94-22448
Writing instrument interfaces with xf/tktcl
p 1925 N94-22480
C BAND
Mapping of taiga forest units using AIRSAR data and/or optical data, and retrieval of forest parameters
p 1729 N94-20452
C++ (PROGRAMMING LANGUAGE)
An evaluation of integration of the trace assertion method with the box structure method for coding in C++
[DE93-040480] p 1918 N94-21924
A structured data transfer protocol
p 2047 N94-22450
On AIPS++, a new astronomical information processing system p 2047 N94-22463
C++, objected-oriented programming, and astronomical data models p 2063 N94-22473
CABLES (ROPES)
Counter-balanced, multiple cable construction crane
[NASA-CASE-LAR-14565-1-CU] p 1822 N94-20369
CADMIUM
Lightweight battery electrode and method of making it
[AD-D015895] p 1749 N94-20120
CADMIUM SULFIDES
Development of high-efficiency CdTe solar cells
[DE93-018206] p 1845 N94-19925
Research on polycrystalline thin-film submodules based on CuInSe2 materials
[DE93-018223] p 2029 N94-21617
CADMIUM TELLURIDES
Development of high-efficiency CdTe solar cells
[DE93-018206] p 1845 N94-19925
Fabrication of stable large-area thin-film CdTe photovoltaic modules
[DE93-018204] p 1845 N94-20095
Thin-film CdTe and CuInSe2 photovoltaic technologies
[DE93-018217] p 1848 N94-21827
Hydrogen in compound semiconductors
[DE93-040300] p 2031 N94-21922
CALCIFICATION
Review of using cardiac fluoroscopy in symptomatic and asymptomatic patients
[AD-A271690] p 1891 N94-20928
CALCIUM
Chemical zoning and diffusion of Ca, Al, Mn, and Cr in olivine of springwater pallasite p 2086 N94-20902
CALCIUM OXIDES
A calcium oxide sorbent process for bulk separation of carbon dioxide
[DE93-019288] p 1847 N94-21540
Synthesis and characterization of charge-substituted garnets YCaLnGa5O12 (Ln = Ce, Pr, Tb)
[DE93-040227] p 2033 N94-21992
CALCIUM PHOSPHATES
Effect of powder characteristics on gas-pressure sintering of Si3N4 with rare earth additives
[DE94-000330] p 1894 N94-21945
CALCULUS
Are types needed for natural language?
[PB93-191831] p 1949 N94-19997
Set theory and nominalisation, part 1
[PB93-191807-PT-1] p 1962 N94-20007
Fourier calculus on evolutionary trees
[CWI-BS-R9234] p 1954 N94-21231
CALDERAS
Calderas produced by hydromagmatic eruptions through permafrost in northwest Alaska p 2089 N94-20385
Formation and evolution of radial fracture systems on Venus p 2099 N94-20672
Geology of Biblis Patera, Ulysses Patera, and Jovis Tholus, Mars p 2103 N94-20693
CALIBRATING
Focus history of the Hubble Space Telescope: Launch to May 1993
[NASA-CR-194179] p 2055 N94-20204
Radar backscattering from snow facies of the Greenland ice sheet: Results from the AIRSAR 1991 campaign
p 1725 N94-20434
Internal camera calibration using rotation and geometric shapes
[AD-A272718] p 1808 N94-21167
Using the USCCS for sub microsecond spacecraft clock calibration p 1813 N94-21346
Calibration of a calorimeter for measuring the performance of thermal control surfaces
p 1660 N94-21378
An 18 bit 50 kHz ADC for low earth orbit
p 1764 N94-21702
Application guide for universal source encoding for space
[NASA-TP-3441] p 1741 N94-21783
Development, refinement, and testing of a short term solar flare prediction algorithm
[NASA-CR-194727] p 2147 N94-21832
Calibration of radiation codes in climate models: Comparison of calculations with observations from the SPECtral Radiation Experiment (SPECTRE)
p 1879 N94-22337
SSH-2 measurements of cirrus at 18-28 micrometers from the King Air during FIRE 2 p 1880 N94-22338
PHOTCAL: The IRAF photometric calibration package
p 1925 N94-22465
The spectral world coordinate systems in IRAF/NOAO
p 2049 N94-22539
CALORIMETERS
Thermal information regarding the cooldown and operation of liquid argon calorimeters
[DE93-019391] p 1807 N94-19987
A conceptual design for the STAR endcap electromagnetic calorimeter
[DE93-040801] p 1807 N94-19990
Techniques for reducing error in the calorimetric measurement of low wattage items
[DE93-018472] p 1807 N94-20114
Calorimeter measurements of low wattage items
[DE93-018473] p 1807 N94-20115
Calibration of a calorimeter for measuring the performance of thermal control surfaces
p 1660 N94-21378
CAMERAS
An assessment of COMSCAN, a Compton backscatter imaging camera, for the one-sided non-destructive inspection of aerospace components
[AD-A271331] p 1806 N94-19837
Head-centered orientation strategies in animate vision
[TR-442] p 1894 N94-20520
The High Resolution Stereo Camera (HRSC) for the Lunar Scout 1 Mission p 1813 N94-20650
Compositional diversity of the lunar North Pole: Preliminary analyses of Galileo SSI data
p 2101 N94-20686
Internal camera calibration using rotation and geometric shapes
[AD-A272718] p 1808 N94-21167
Restoration of HST images with missing data
p 2057 N94-22439
Writing instrument interfaces with xf/tktcl
p 1925 N94-22480
The University of Hawaii Institute for Astronomy CCD camera control system p 1828 N94-22489
Deconvolution of Hubble Space Telescope images using simulated point spread functions p 2048 N94-22497
HST PSF simulation using Tiny Tim
p 1926 N94-22498
Wilbur: A low-cost CCD camera system for MDM Observatory p 1814 N94-22510
CANADA
Current situation of development of petroleum substituting energies (Canada)
[DE94-707493] p 1849 N94-22014
CANALS
Early Mars: The inextricable link between internal and external influences on valley network formation
p 2146 N94-21681
The Martian valley networks: Origin by niveo-fluvial processes p 2146 N94-21682
CANARD CONFIGURATIONS
Experimental study on interference aerodynamics of close-coupled canard configuration
[AD-A267760] p 1636 N94-19963
CANCELLATION
System and method for cancelling expansion waves in a wave rotor
[NASA-CASE-LEW-15218-1] p 1801 N94-20588
CANOPIES (VEGETATION)
Second order distorted born approximation for backscattering from a layer of discrete random medium
p 1728 N94-20448
Relationship of attenuation in a vegetation canopy to physical parameters of the canopy p 1729 N94-20450
Application of the target decomposition theorem to a polarimetric random media model p 1730 N94-20453
Evaluation of C-band SAR data from SAREX 1992: Tapajos study site p 1839 N94-20964
CANYONS
Mars: New evidence for origin of some Valles Marineris layered deposits p 2112 N94-20748
CAPACITANCE
Microscopic origins of metastable effects in a-Si:H and deep defect characterization in a-Si,Ge:H alloys
[DE93-018205] p 1688 N94-19985
Surface states at the GaAs-germanium nitride interface p 1709 N94-20973
InP MIS structures with diamondlike amorphous carbon films deposited by ion-beam sputtering and from plasma
p 1710 N94-20979
Use of switched capacitor filters to implement the discrete wavelet transform p 1755 N94-21097
Fully-depleted silicon-on-sapphire and its application to advanced VLSI design p 1765 N94-21709
Effects of aqueous solution compositions on Aerocapacitor energy density
[DE94-000385] p 1768 N94-21753
Verification of frequency scaling laws for capacitive rf discharges using two-dimensional simulations
[DE94-001306] p 1999 N94-22595
CAPACITORS
Preparation and properties of sol-gel derived PZT thin films for decoupling capacitor applications
[DE93-018853] p 2013 N94-19961
Flexible heating head for induction heating
[NASA-CASE-LAR-14418-15-B] p 1718 N94-20388
INPIStron switched pulsed power for dense plasma pinches p 1995 N94-21294
An 18 bit 50 kHz ADC for low earth orbit
p 1764 N94-21702
Effects of aqueous solution compositions on Aerocapacitor energy density
[DE94-000385] p 1768 N94-21753
An adaptive method for group delay compensation using switched capacitor filters p 1793 N94-22248
CAPILLARY FLOW
Thermocapillary and arc phenomena in stainless steel welds
[DE94-000518] p 1821 N94-19859
Surface path lines in plane Stokes flow driven by capillarity
[DE93-041277] p 1803 N94-21651

CARBON
C/O atomic ratios in micrometer-size crushed grains from Antarctic micrometeorites and two carbonaceous meteorites p 2082 N94-20678
C-O volatiles in Apollo 15 and Apollo 17 picritic glasses p 1685 N94-20727
C2, CN and dust in Comet Wilson (1987VII) p 2083 N94-20746
Molecular equilibria and condensation sequences in carbon rich gases p 2083 N94-20756
Cometary interplanetary dust particles? An update on carbon in anhydrous IDPS p 2084 N94-20828
The carbon components in SNC meteorites of feldspathic harzburgite composition p 2086 N94-20885
Further carbon isotope measurements of LEW 88516 p 2086 N94-20886
InP MIS structures with diamondlike amorphous carbon films deposited by ion-beam sputtering and from plasma p 1710 N94-20979
Interfacial properties of diamondlike amorphous carbon films on InP: Metal-insulator-semiconductor structures p 1710 N94-20980
Thin-film hermeticity: A quantitative analysis of diamondlike carbon using variable angle spectroscopic ellipsometry p 1710 N94-20981
Effects of aqueous solution compositions on Aerocapacitor energy density [DE94-000385] p 1768 N94-21753
Implantation of carbon in GaAs and compensating native defects [DE93-040122] p 2030 N94-21763
High temperature size selective membranes [DE93-019865] p 1709 N94-21982
Research on stable, high-efficiency amorphous silicon multijunction modules [DE93-018220] p 1850 N94-22257

CARBON CYCLE
Modeling the response of ecosystems to CO2 and climate change [DE94-000748] p 1852 N94-21787

CARBON DIOXIDE
Unlike-pair interactions at high pressure and high temperature [DE93-019948] p 1796 N94-19916
Technology to prevent greenhouse effect gases [DE94-707421] p 1850 N94-19976
Technology to prevent greenhouse effect gases [DE94-707420] p 1851 N94-20116
The role of CO2 in weathering reactions and the presence of S2 on Venus: Implications for the pyrite stability field p 2122 N94-20799
Spectral analysis of chemisorbed CO2 on Mars analog materials p 2140 N94-20900
One- and multi-component theories of mixtures [DE93-040543] p 1966 N94-21511
A calcium oxide sorbent process for bulk separation of carbon dioxide [DE93-019288] p 1847 N94-21540
A carbon dioxide/methane greenhouse atmosphere on early Mars p 2142 N94-21662
A model for the evolution of CO2 on Mars p 2144 N94-21671
The young Sun and photochemistry of the primitive Martian atmosphere p 2145 N94-21679
Early Mars: The inextricable link between internal and external influences on valley network formation p 2146 N94-21681
Modeling the response of ecosystems to CO2 and climate change [DE94-000748] p 1852 N94-21787
Plasma-chemical conversion of hydrogen sulfide into hydrogen and sulfur [DE93-041167] p 1682 N94-21789
Investigation on the chemically fixing technique of carbon dioxide utilizing solar energy [DE94-714886] p 1849 N94-22043
Survey on chemical engineering technologies for the global environmental protection [DE94-714887] p 1852 N94-22044
Investigations on trends in global environment adaptive industrial technologies [DE94-714888] p 1853 N94-22258
Atmospheric parameterization schemes for satellite cloud property retrieval during FIRE IFO 2 p 1874 N94-22312

CARBON DIOXIDE CONCENTRATION
Derivation of the midinfrared (5.0-25.0 micron) optical constants of hydrous carbonate and sulfate p 2108 N94-20723
Modeling the response of ecosystems to CO2 and climate change [DE94-000748] p 1852 N94-21787

CARBON DIOXIDE LASERS
Rotational spectrum of a dark state in 2-fluoroethanol using microwave/radiofrequency-infrared multiple resonance [AD-A272101] p 1817 N94-20583
Compact lightweight CO2 laser for SDIO application [AD-A273010] p 1817 N94-21284

CARBON FIBER REINFORCED PLASTICS
Thermal stability relationships between PMR-15 resin and its composites [NASA-TM-106285] p 1675 N94-21488
Creep damage of carbon fiber reinforced PEEK [ISBN-0-315-58962-0] p 1677 N94-22420

CARBON FIBERS
Intercalated hybrid graphite fiber composite [NASA-CASE-LEW-15241-1] p 1673 N94-20539
Biaxial flexural testing of a carbon fiber reinforced epoxy composite [AD-A271956] p 1674 N94-20577

CARBON ISOTOPES
A carbon and nitrogen isotope study of carbonaceous vein material in ureilite meteorites p 2083 N94-20726
Micrometeorite pre-solar diamonds from Greenland cryoconite? p 2086 N94-20895

CARBON MONOXIDE
Unlike-pair interactions at high pressure and high temperature [DE93-019948] p 1796 N94-19916
Ab initio potential energy surface for the H + OCS reaction [AD-A270577] p 1698 N94-19947
Catalytic hydrogenation of carbon monoxide [DE94-000881] p 1678 N94-20103
Theoretical investigations of metastability and energy storage in molecular systems [AD-A271849] p 1973 N94-20612
Infrared absorption spectroscopy of the weakly bonded CO-Cl2 complex [AD-A271757] p 2027 N94-21304

CARBON 13
The carbon components in SNC meteorites of feldspathic harzburgite composition p 2086 N94-20885
Further carbon isotope measurements of LEW 88516 p 2086 N94-20886
The 13C-NMR spectra of poly (4-((2-(acryloyloxy) ethyl) ethyl amino)- 4-nitroazobenzene-co-methyl methacrylate) [AD-A273016] p 1705 N94-21238

CARBON-CARBON COMPOSITES
Performance of carbon-based hot frit substrates [DE94-000509] p 1676 N94-21754
Compilation of reinforced carbon-carbon transatlantic abort landing arc jet test results [NASA-TM-104778] p 1676 N94-21834

CARBON-PHENOLIC COMPOSITES
Modeling of outgassing and matrix decomposition in carbon-phenolic composites [NASA-CR-194741] p 1676 N94-21743

CARBONACEOUS CHONDRITES
The Erevan howardite: Petrology of glassy clasts and mineral chemistry p 1684 N94-20640
Igneous rock from Severnyi Kolchim (H3) chondrite: Nebular origin p 2082 N94-20643
Exposure ages of carbonaceous chondrites, 1 p 2082 N94-20658
The Sm-(146,147)-Nd-(142,143) formation interval for the lunar mantle and implications for lunar evolution p 2097 N94-20663
Oxygen isotopic relationships between the LEW85332 carbonaceous chondrite and CR chondrites p 2083 N94-20708
Euhedral metallic-Fe-Ni grains in extraterrestrial samples p 1697 N94-20724
Fe/Mn in olivine of carbonaceous meteorites p 2084 N94-20788
Hydrothermal alteration experiments of olivine with varying Fe contents: An attempt to simulate aqueous alteration of the carbonaceous chondrites p 1686 N94-20810
Comparison of visible and near-infrared reflectance spectra of CM2 carbonaceous chondrites and primitive asteroids p 2085 N94-20848
Diffusion-controlled magnesium isotopic fractionation of a single crystal forsterite evaporated from the solid state p 1686 N94-20855

CARBONACEOUS MATERIALS
A carbon and nitrogen isotope study of carbonaceous vein material in ureilite meteorites p 2083 N94-20726

CARBONACEOUS METEORITES
Carbonaceous xenoliths from the Erevan howardite p 1684 N94-20642
C/O atomic ratios in micrometer-size crushed grains from Antarctic micrometeorites and two carbonaceous meteorites p 2082 N94-20678

CARBONATES
A study of carbonates, sulfates, and phosphates using thermal emission spectroscopy p 1686 N94-20868
Spectral analysis of chemisorbed CO2 on Mars analog materials p 2140 N94-20900
Molten carbonate fuel cell networks: Principles, analysis, and performance [DE93-019872] p 1846 N94-21527
A calcium oxide sorbent process for bulk separation of carbon dioxide [DE93-019288] p 1847 N94-21540
Research and development of alternative components at Argonne National Laboratory for molten carbonate fuel cells [DE93-019536] p 1847 N94-21650

CARBONIZATION
A calcium oxide sorbent process for bulk separation of carbon dioxide [DE93-019288] p 1847 N94-21540

CARBONYL COMPOUNDS
Lightweight battery electrode and method of making it [AD-D015895] p 1749 N94-20120

CARBOXYLIC ACIDS
Column chromatographic separation of Y(3+) from Sr(2+) by polymeric ionizable crown ether resins [DE94-000935] p 1683 N94-22021

CARDIOVASCULAR SYSTEM
Coronary angiography outcomes of US Army aircrew with the finding of coronary artery calcifications: Aviation epidemiology data register [AD-A271968] p 1891 N94-20615

CARRIER MOBILITY
Dephasing processes in III-V semiconductors [AD-A271677] p 2028 N94-21362

CARRIER TRANSPORT (SOLID STATE)
Are the C delta light nitrogen and noble gases located in the same carrier? p 2085 N94-20846
Solid-state dynamics and quantum transport in novel semiconductor nanostructures [AD-A272955] p 2027 N94-21248

CARTESIAN COORDINATES
Characteristic based methods for the time-domain Maxwell equations [AD-A272973] p 1802 N94-21263
An adaptive control to enable a robot to follow Cartesian trajectories p 1790 N94-22229
The 3D Euler solutions using automated Cartesian grid generation p 1920 N94-22367

CASCADE CONTROL
Cascaded recursive artificial neural networks p 1780 N94-22167

CASCADE FLOW
Measurement and prediction of the flow through an annular turbine cascade [AD-A272530] p 1803 N94-21417

CASES (CONTAINERS)
Characterization and modelling of extremely high frequency enclosures p 1782 N94-22177

CASSEGRAIN ANTENNAS
Performance of a simple circular polarization selective surface p 1746 N94-22198

CASTING
Machinable oxide ceramic [AD-D015927] p 1699 N94-20017
Fabrication of porous ceramics by freeze-casting/freeze-drying [PB93-202513] p 1705 N94-21425
Materials Science and Engineering [DE93-040497] p 1675 N94-21530
User's guide for the casting process simulator software CaPS-2D, version 1.0 [DE93-040398] p 1917 N94-21923

CATACLYSMIC VARIABLES
The x ray halo of AM Her [NASA-CR-189310] p 2054 N94-20142
Studies of an x ray selected sample of cataclysmic variables [NASA-CR-194773] p 2055 N94-20344

CATALYSIS
Catalytic hydrogenation of carbon monoxide [DE94-000881] p 1678 N94-20103
Surface science and modeling studies of endothermic fuels catalysis [AD-A272850] p 1712 N94-21192

CATALYSTS
Ageing studies on a composite propellant containing a new organo-copper burn rate catalyst [AD-A271060] p 1711 N94-19906
Fuel processing requirements and techniques for fuel cell propulsion power [DE93-019516] p 1750 N94-20257
Transient studies of low temperature catalysts for methane conversion [DE93-041232] p 1680 N94-20934

Polymerization of enantiomerically pure 2,3-dicarboalkoxy norbornadienes and 5,6-disubstituted norbornenes by well-characterized molybdenum ROMP catalysts
[AD-A272649] p 1704 N94-21186
Surface science and modeling studies of endothermic fuels catalysis
[AD-A272850] p 1712 N94-21192
Synthesis and catalytic properties of metal and semiconductor nanoclusters
[DE93-019418] p 2028 N94-21541
Investigation on the chemically fixing technique of carbon dioxide utilizing solar energy
[DE94-714886] p 1849 N94-22043

CATHETERIZATION
Detection of emetic activity in the cat by monitoring venous pressure and audio signals
p 1886 N94-21903

CATHODES
Evaluation of externally heated pulsed MPD thruster cathodes
[NASA-CR-191090] p 1670 N94-21565
Research and development of alternative components at Argonne National Laboratory for molten carbonate fuel cells
[DE93-019536] p 1847 N94-21650
Cathode materials for the molten carbonate fuel cell
[DE93-019515] p 1848 N94-21870

CATHODOLUMINESCENCE
Photoluminescence spectroscopy of zinc germanium diphosphide (ZnGeP2)
[AD-A270705] p 1678 N94-19953
Cathodoluminescence observations of in situ aqueous destruction of chondrules in the Murchison CM chondrite
p 2083 N94-20750

CATS
Changes in plasma vasopressin during motion sickness in cats p 1885 N94-21898
Detection of emetic activity in the cat by monitoring venous pressure and audio signals
p 1886 N94-21903
Area postrema ablations in cats: Evidence for separate neural routes for motion- and xylazine-induced CTA and emesis p 1887 N94-21906
Conditioned taste aversion and motion sickness in cats and squirrel monkeys p 1888 N94-21914

CAUCHY PROBLEM
Approximate methods for N-component solute transport and ion-exchange
[CWI-NM-R9223] p 1910 N94-21078

CAVITATION FLOW
Cavitation modelling p 1668 N94-20079
The effect of microstructural evolution on superplasticity in Ni3Si(V, Mo)
[DE93-041320] p 1694 N94-21943

CAVITIES
Measurement and computation of the higher order modes of the ALS 500 MHz accelerating cavities
[DE93-019256] p 1980 N94-20292
Speed of sound data and related models for mixtures of natural gas constituents
[PB93-200822] p 1968 N94-21447
Generation of harmonic radiation using the multi-cavity free-electron laser
[DE94-001261] p 1820 N94-21975

CAVITY RESONATORS
Tunable laser frequency stabilizing system
[AD-D015904] p 1815 N94-20055
Study of coupled-bunch collective effects in the PEP-2 B-Factory
[DE93-040117] p 1979 N94-20274
Measurement and computation of the higher order modes of the ALS 500 MHz accelerating cavities
[DE93-019256] p 1980 N94-20292
Three point lead screw positioning apparatus for a cavity tuning plate
[NASA-CASE-LEW-15216-1] p 1822 N94-20375
A comprehensive theoretical and experimental study of coplanar waveguide shunt stubs p 1733 N94-20500
Microwave properties and characterization of co-evaporated BSCCO thin films p 1709 N94-20518
An 85 GHz quasioptical gyroklystron experiment
[AD-A272020] p 1752 N94-20931
Simulation of traveling-wave output structures for high power RF tubes
[DE93-041005] p 1763 N94-21685
Improvement of the performance of IMPATT oscillators through appropriate modification of resonant-cap activity
p 1782 N94-22179
Aperture coupling of circular cylindrical dielectric resonator antenna
[ISBN-0-315-60632-0] p 1743 N94-22409

CCD STAR TRACKER
Wilbur: A low-cost CCD camera system for MDM Observatory p 1814 N94-22510

CD-ROM
Publication of science data on CD-ROM: A guide and example
[NASA-CR-4560] p 1842 N94-21585
The digital archive of the International Halley Watch
p 2047 N94-22496
An x ray archive on your desk: The Einstein CD-ROM's p 2048 N94-22519
UIT support observations archive
p 2048 N94-22534

CELESTIAL MECHANICS
A new procedure for orbit determination based on three lines of sight: Angles only
[AD-A272937] p 1652 N94-21224

CEMENTS
Some experiments on using backscattered electron and energy dispersive x ray imaging in determination of portland cement clinker phase composition p 1708 N94-21893
A quantitative S.E.M. image analysis of cement paste microstructure p 1708 N94-21894

CENTRAL NERVOUS SYSTEM
Reassessment of area postrema's role in motion sickness and conditioned taste aversion
p 1886 N94-21901

CENTRAL PROCESSING UNITS
Mongoose: Creation of a Rad-Hard MIPS R3000
p 1754 N94-21090
Practical issues in implementing roving spares in VLSI systolic arrays p 1758 N94-21114
Seeing the forest for the trees: Networked workstations as a parallel processing computer p 1938 N94-22454

CENTRIFUGAL COMPRESSORS
Experimental and computational results from a large low-speed centrifugal impeller
[NASA-TM-106421] p 1636 N94-20136

CENTRIFUGAL FORCE
A vibration model for centrifugal contactors
[DE93-040645] p 1833 N94-21927

CENTROIDS
A formulation of quantum statistical mechanics based on the Feynman path centroid density 2 dynamical properties
[AD-A272698] p 2037 N94-21166
A formulation of quantum statistical mechanics based on the Feynman path centroid density 1: Equilibrium properties
[AD-A272809] p 2037 N94-21171

CEPHEID VARIABLES
VVNRS: Variable phenomena in VV Cephei
[NASA-CR-194731] p 2056 N94-21835

CERAMIC BONDING
Interface science of controlled metal/metal and metal/ceramic interfaces prepared using ultrahigh vacuum diffusion bonding
[DE94-001066] p 1696 N94-22025

CERAMIC FIBERS
Analysis of thermal mechanical fatigue in titanium matrix composites p 1835 N94-22618

CERAMIC MATRIX COMPOSITES
Integrity and testing concerns of thermostructural materials p 1661 N94-21384
Thermostructural material composites for space applications p 1664 N94-21398

CERAMICS
Dynamic, multiaxial impact response of confined and unconfined ceramic rods
[DE93-040057] p 1829 N94-19824
Hydrodynamic compressibility of high-strength ceramics
[DE93-019424] p 1698 N94-19903
Preparation and properties of sol-gel derived PZT thin films for decoupling capacitor applications
[DE93-018853] p 2013 N94-19961
Machinable oxide ceramic
[AD-D015927] p 1699 N94-20017
Polymer gels as precursors to high-performance materials
[AD-A270937] p 1699 N94-20046
Silver lined ceramic vessel
[AD-D015917] p 1700 N94-20057
Guanidine based vehicle/binders for use with oxides, metals, and ceramics
[NASA-CASE-LEW-15314-1] p 1700 N94-20195
Improved ceramic slip casting technique --- application to aircraft model fabrication
[NASA-CASE-LAR-14471-1] p 1702 N94-20377
Mold bolt and means for achieving close tolerances between bolts and bolt holes
[NASA-CASE-MFS-28720-1] p 1823 N94-20379
Development of improved processing and evaluation methods for high reliability structural ceramics for advanced heat engine applications, phase 1
[DE93-040528] p 1702 N94-20481
Sintering silicon nitride
[NASA-CASE-LEW-15489-1] p 1703 N94-20529
Development of fundamental understanding of friction and wear mechanisms by atomic-scale tribological studies of ceramic materials and multilayered thin films
[AD-A271485] p 1703 N94-20548
Direct imaging of the surface microstructure of dielectric materials using an atomic force microscope
[AD-A272251] p 2018 N94-20575
Microstructural modeling and toughening of Si3N4 ceramics for high temperature engine applications
[AD-A272897] p 1704 N94-21197
Investigation of the effect of various oxide and fluoride additives on the microstructure, electronic properties, and phase shifting ability of Ba(1-x)Sr(x)TiO3
[AD-A271756] p 2027 N94-21303
Adhesive bonded joint with improved cyclic fatigue life for alumina-ceramic cylinders and hemispheres: Fourth generation housings
[AD-A273061] p 1831 N94-21310
In-vacuo slip testing of materials for SSRMS friction brakes p 1661 N94-21381
High temperature simulation chambers. Physico-chemical and thermal effect of atmospheric reentry on ceramic materials p 1653 N94-21404
A method of measuring the thermoradiative properties of ceramic materials in a space environment
p 1665 N94-21405
Intelligent processing of ferroelectric thin films
[AD-A272518] p 1705 N94-21416
Utilization of metals to improve the lubrication of ceramic load-bearing devices
[PB93-202448] p 1825 N94-21424
Fabrication of porous ceramics by freeze-casting/freeze-drying
[PB93-202513] p 1705 N94-21425
Lubricated wear of steel-ceramic and ceramic-ceramic systems
[PB93-202356] p 1825 N94-21450
Vapor-delivered lubrication of steel-steel and steel-ceramic systems
[PB93-202364] p 1825 N94-21451
Review of corrosion behavior of ceramic heat exchanger materals: Corrosion characteristics of silicon carbide and silicon nitride
[DE93-041307] p 1706 N94-21516
Issues related to mechanical properties of neutron-irradiated ceramics
[DE93-040262] p 1707 N94-21560
Electron holography applied to the study of ceramic materials
[DE94-000329] p 1707 N94-21653
Ceramic Technology Project
[DE94-001011] p 1707 N94-21822
Proceedings of the Seventh Annual Conference on Fossil Energy Materials
[DE94-001091] p 1848 N94-21823
An assessment of the cost of microwave sintering ceramic tiles for armor applications
[DE94-000978] p 1693 N94-21850
Dynamic properties of ceramic materials
[DE94-000654] p 1708 N94-21963
Time-dependent reliability analysis of ceramic engine components p 1828 N94-22619

CEREBRAL CORTEX
Toward a neurobiological theory of visual attention
[AD-A270724] p 1890 N94-20112

CERENKOV COUNTERS
A Monte Carlo study of the Sudbury Neutrino Observatory small test detector experiment
[ISBN-0-315-59056-4] p 1977 N94-22416

CERIUM
Magnetism in CeRu2Ge2 and CeRh2Ge2 and its pressure dependence
[DE93-040061] p 2032 N94-21987

CERIUM OXIDES
Synthesis and characterization of charge-substituted garnets YCaLnGa5O12 (Ln = Ce, Pr, Tb)
[DE93-040227] p 2033 N94-21992

CERMETS
In-vacuo slip testing of materials for SSRMS friction brakes p 1661 N94-21381
Dynamic properties of ceramic materials
[DE94-000654] p 1708 N94-21963

CESIUM ALLOYS
Magnetic instability of Kondo insulators
[DE93-040064] p 1768 N94-21762

CESIUM IODIDES
Csl and some new photocathodes
[DE93-019387] p 1750 N94-20314

CHALCOGENIDES
Photoelectron spectroscopy at model boundary surfaces of energy converter semiconductors/electrolyte contacts: Adsorption, coadsorption, and triadsorption of Br2, Na, and H2O on Van der Waals surfaces of metal chalocogenide semiconductors
[ETN-93-95063] p 2015 N94-20152

CHANGE DETECTION
Application of change detection to dynamic contact sensing
[AD-A270523] p 1939 N94-20105
Asymptotics of the GLRT for the disorder problem in diffusion processes
[INRIA-RR-1735] p 1951 N94-20227
The 7th Brazilian Remote Sensing Symposium, volume 2 p 1838 N94-20956
Change detection on land use and rainforest cover at Paragominas region, Brazilian Amazon p 1838 N94-20957

CHANNEL CAPACITY
Comparison of theoretical and simulated performance results for sloppy-slotted Aloha signaling p 1746 N94-22204
ARQ on fading channels p 1747 N94-22242

CHANNEL FLOW
Seismic-triggering history of the catastrophic outflows in the Chryse region of Mars p 2091 N94-20399
Discharge rates in Ma'adim Vallis, Mars p 2128 N94-20830
An analysis of pressure driven cross-flow through a long slot connecting two parallel channels
[DE93-040181] p 1804 N94-21765

CHANNELS (DATA TRANSMISSION)
Handbook. Volume 2: Digital systems validation. Chapter 18: Avionic data bus integration technology
[DOT/FAA/CT-88/10-VOL-2] p 1647 N94-20343
Characteristics of 0.8- and 0.2-microns gate length In(x)Ga(1-x) As/In(0.52)Al(0.48)As/InP (0.53 less than or equal to x less than or equal to 0.70) modulation-doped field-effect transistors at cryogenic temperatures p 1733 N94-20499
A simplified token bus protocol specified using LOTOS
[TR-92-15] p 1910 N94-21062
A consideration of the integration of terrestrial and satellite mobile systems p 1746 N94-22172
Specification and formal verification of the safety criterion in the alternating bit protocol p 1784 N94-22193
Trellis coded multi-orthogonal modulation p 1747 N94-22231

CHAOS
Convergence of the hermite wavelet expansion
[AD-A271435] p 1854 N94-19841
Research, Development, Training, and Evaluation (RDTE) support delivery order 1: Computational cognitive models
[AD-A271837] p 1894 N94-20610
On a proposed symbolic dynamics for the Henon map
[AD-A272514] p 1955 N94-21359

CHARACTER RECOGNITION
Three original programmes for managers p 1923 N94-22083

CHARACTERIZATION
CMOS gate array characterization procedures
[AD-A269943] p 2014 N94-20029
Birefringence control and dispersion characteristics of silicon oxynitride optical waveguides, appendix 6 p 1989 N94-21600

CHARGE CARRIERS
Optical amplification and threshold behavior on InGaAs/InGaAsP multiquantum well structures
[ETN-93-94181] p 2026 N94-21151

CHARGE COUPLED DEVICES
Multiport solid-state imager characterization at variable pixel rates
[DE93-018366] p 1808 N94-20287
Development and characterization of a time-, position- and energy-resolved x ray diagnostic for PBFA 2 target experiments
[DE93-019429] p 1808 N94-20297
UVPI imaging from the LACE satellite: The Starbird rocket plume
[AD-A271981] p 1658 N94-20617
Identification of an interstellar oxide grain from the Murchison meteorite by ion imaging p 2082 N94-20659
An 18 bit 50 kHz ADC for low earth orbit p 1764 N94-21702
Charge integrating optical position sensor p 1778 N94-22152
Restoration of HST images with missing data p 2057 N94-22439
CCD surface photometry of galaxies p 2058 N94-22445
Visualizing the universe, part 2 p 2063 N94-22472
The University of Hawaii Institute for Astronomy CCD camera control system p 1826 N94-22489
CCD data acquisition systems at Lick and Keck Observatories p 2047 N94-22495
Wilbur: A low-cost CCD camera system for MDM Observatory p 1814 N94-22510
Solar full-disk magnetic field image receiving system and observation software p 2079 N94-22552

CHARGE DISTRIBUTION
Interactions of slow H, H2, and H3 with thin foils
[DE93-040263] p 1976 N94-21995

CHARGE EXCHANGE
Testing double ionization mechanisms with highly-charged ions
[DE93-018750] p 1970 N94-19958

CHARGE TRANSFER
Integral equation calculation of solvent activation free energies for electron and proton transfer reactions
[AD-A272665] p 1681 N94-21216

CHARGED PARTICLES
Surface science at the solid liquid interface
[AD-A271422] p 1678 N94-19839
Absolute total and one and two electron transfer cross sections for Ar(8+) on Ar as a function of energy
[DE93-040283] p 1970 N94-19870
Energy gain spectroscopic study of Ar(q+)-Ar collisions at 40 qeV
[DE93-040284] p 1970 N94-19871
Persistent wakefields associated with waveguide damping of higher order modes
[DE93-040973] p 1715 N94-19874
Tactical laser weapons and other directed-energy weapons
[AD-A267961] p 1816 N94-20484
Theoretical and numerical studies in magnetic fusion
[DE94-000536] p 1993 N94-20937
Electrostatic charging and secondary effects in materials submitted to radiation in space p 1661 N94-21383
Detailed analysis case studies of trapped plasmas at the Earth's magnetic equator
[AD-A272497] p 1858 N94-21432
Production, collection and utilization of very long-lived heavy charged leptons
[DE93-040867] p 1977 N94-22009

CHARM (PARTICLE PHYSICS)
Measurement of the strange quark distribution function in W(+) charm quark events
[DE93-018267] p 1973 N94-20474
CERN-derived analysis of lunar radiation backgrounds p 2080 N94-20880
Recent Fermilab results on hadroproduction of heavy flavors
[DE94-000595] p 1976 N94-21867

CHARPY IMPACT TEST
Microscopic evaluation of low-temperature embrittlement in type 308 stainless steel welds
[DE93-040266] p 1690 N94-20282

CHASSIGNITES
High D/H ratios of water in magmatic amphiboles in Chassigny: Possible constraints on the isotopic composition of magmatic water on Mars p 2134 N94-20862
An attempt to comprehend Martian weathering conditions through the analysis of terrestrial palagonite samples p 2143 N94-21668

CHEMICAL ANALYSIS
Wavelength dispersive analysis with the synchrotron x ray fluorescence microprobe p 1685 N94-20717
The chondrite Mihonoseki: New observed fall p 2083 N94-20764
Evaluation of pre-extraction analytical holding times for nitroaromatic and nitramine explosives in water
[AD-A271547] p 1712 N94-20927
Structural and chemical analysis of a silicon nitride film on GaAs by null ellipsometry p 1709 N94-20975
Orbital debris and micrometeoroids: LDEF and Mir data p 1659 N94-21368
Atomic oxygen interaction with spacecraft materials: Relationship between orbital and ground-based testing for materials certification p 1663 N94-21393
Improvement of the stability of the process for synthesizing chemically prepared varistor powder
[DE94-000345] p 1763 N94-21654

CHEMICAL BONDS
Synthesis and structural characterization of new light molecular weight inorganic oxidizers and relative derivatives, volume 1
[AD-A271437] p 2012 N94-19842
Polyimides containing amide and perfluoroisopropylidene connecting groups
[NASA-CASE-LAR-14608-1] p 1702 N94-20374
Infrared absorption spectroscopy of the weakly bonded CO-Cl2 complex
[AD-A271757] p 2027 N94-21304

CHEMICAL CLEANING
Spectroscopic ellipsometric characterization of Si/Si(1-x)Ge(x) strained-layer superlattices p 2025 N94-21009

CHEMICAL COMPOSITION
Chemical equilibrium in high pressure molecular fluid mixtures
[DE93-040160] p 1796 N94-19829
Near atomic resolution microanalysis of interfaces by analytical electron microscopy
[DE93-019437] p 1687 N94-19904
Unlike-pair interactions at high pressure and high temperature
[DE93-019948] p 1796 N94-19916
Polybenzoxazole via aromatic nucleophilic displacement
[NASA-CASE-LAR-14606-1-CU] p 1672 N94-20540
Zinc and titanium smoke: Chemical composition and physical characteristics
[FOA-C-40277-4.9] p 1680 N94-20552
Helium in interplanetary dust particles p 2082 N94-20653
Impact glasses from the ultrafine fraction of lunar soils p 2097 N94-20662
Self diffusion of alkaline-Earth in Ca-Mg-aluminosilicate melts: Experimental improvements on the determination of the self-diffusion coefficients p 1684 N94-20669
Micrometeorite dynamic pyrometamorphism: Observation of a thermal gradient in iron-nickel sulfide p 2083 N94-20716
Further analyses of Rio Cuarto impact glass p 1685 N94-20745
Combined backscatter Moessbauer spectrometer/x ray fluorescence analyzer (BaMS/XRF) for extraterrestrial surfaces p 1686 N94-20761
The U-Th-Pb, Sm-Nd, and Ar-Ar isotopic systematics of lunar meteorite Yamato-793169 p 2084 N94-20834
Petrology and geochemistry of VLT glasses from double drive tube 79001/2 p 1687 N94-20870
The carbon components in SNC meteorites of feldspathic harzburgite composition p 2086 N94-20885
Further carbon isotope measurements of LEW 88516 p 2086 N94-20886
Stable Ni isotopes and Be-10 and Al-26 in metallic spheroids from Meteor Crater, Arizona p 1863 N94-20889
Regolith breccia consisting of H and LL chondrite mixture p 2080 N94-20892
Consortium reports on lunar meteorites Yamato 793169 and Asuka 881757, a new type of mare basalt p 2086 N94-20893
Preliminary AEM study of the microstructure and composition of metal particles in ordinary chondrites p 2086 N94-20894
Micrometeorite pre-solar diamonds from Greenland cryoconite? p 2086 N94-20895
Age and thermochronology of K-feldspars from the Manson Impact Structure p 1863 N94-20899
Chemical composition of new Acapulcoites and Lodranites p 2086 N94-20905
Thin film compositional analysis using null or fixed wavelength ellipsometry p 1709 N94-20976
Analysis of a sandstorm weather process-translation
[AD-A272959] p 1867 N94-21250
Effects of aqueous solution compositions on Aerocapacitor energy density
[DE94-000385] p 1768 N94-21753
Acceleration of solar-flare particles as viewed from their chemical composition p 2006 N94-22672

CHEMICAL ENGINEERING
A project on parameter identification in reaction kinetics
[CWI-NM-R9301] p 1682 N94-21574
Survey on chemical engineering technologies for the global environmental protection
[DE94-714887] p 1852 N94-22044
Investigations on trends in global environment adaptive industrial technologies
[DE94-714868] p 1853 N94-22258

CHEMICAL EQUILIBRIUM
Chemical equilibrium in high pressure molecular fluid mixtures
[DE93-040160] p 1796 N94-19829
Molecular equilibria and condensation sequences in carbon rich gases p 2083 N94-20756

CHEMICAL EXPLOSIONS
Unlike-pair interactions at high pressure and high temperature
[DE93-019948] p 1796 N94-19916
Atmospheric sampling glow discharge ionization and triple quadrupole tandem mass spectrometry for explosives vapor detection
[DE93-040593] p 1852 N94-22004
Computer simulation of molecular response at a shock front
[DE94-001050] p 1977 N94-22396

CHEMICAL FRACTIONATION
Fine resolution chronology based on initial Sr-87/Sr-86
[CONTRIB-5230(794)] p 1686 N94-20794
A long-term change of the AR/KR/XE fractionation in the solar corpuscular radiation p 2136 N94-20875

CHEMICAL LASERS
A theory for optical wavelength control in short pulse free electron laser oscillators
[AD-A271706] p 1817 N94-21353
CHEMICAL MACHINING
Focused-ion-beam material removal rates
[AD-A270852] p 1713 N94-19834
CHEMICAL PROPERTIES
The metallic bond for monolayer transition metal layers on transition metal surfaces
[DE93-019060] p 1691 N94-20313
First discovery of the organic materials in deep-sea iron cosmic spherule p 1685 N94-20677
CHEMICAL REACTIONS
Chemical equilibrium in high pressure molecular fluid mixtures
[DE93-040160] p 1796 N94-19829
Unlike-pair interactions at high pressure and high temperature
[DE93-019948] p 1796 N94-19916
ALE project
[AD-A271080] p 2014 N94-19980
Computed potential energy surfaces for chemical reactions
[NASA-CR-194600] p 1679 N94-20169
On demand, non-halon, fire extinguishing systems
[AD-D015957] p 1714 N94-20355
Polybenzoxazole via aromatic nucleophilic displacement
[NASA-CASE-LAR-14606-1-CU] p 1672 N94-20540
Physical chemistry of energetic nitrogen compounds
[AD-A271819] p 1712 N94-20625
Chemical reaction fouling model for single-phase heat transfer
[DE93-019556] p 1802 N94-20942
A proposed methodology for combustion toxicology testing of combined halon replacement agent/jet fuel interaction
[AD-A272695] p 1681 N94-21165
Chemistry of the burning surface
[AD-A272725] p 1681 N94-21181
Strength and toughness improvement of silicide intermetallics by nanophase and microphase reinforcements
[AD-A272914] p 1692 N94-21320
Atomic oxygen interaction with spacecraft materials: Relationship between orbital and ground-based testing for materials certification p 1663 N94-21393
Oxidation of dissolved iron under warmer, wetter conditions on Mars: Transitions to present-day arid environments p 2143 N94-21663
Femtosecond dynamics in hydrogen-bonded solvents
[DE93-019937] p 1683 N94-21842
Theoretical research program to study chemical reactions in AOTV bow shock tubes
[NASA-CR-194710] p 1804 N94-22027
Interfacial reactions between titanium and borate glass
[DE93-012847] p 1683 N94-22031
Characteristics of shock-compressed configuration of Ti and Si powder mixtures
[DE93-018857] p 1713 N94-22033
Development of advanced cloud parameterizations to examine air quality, cloud properties, and cloud-radiation feedback in mesoscale models
[DE93-041164] p 1853 N94-22384
CHEMICAL REACTORS
Direct aromatization of methane
[DE93-040631] p 1678 N94-19890
CHEMICAL TESTS
Materials evaluation at ESA/ESTEC
p 1662 N94-21386
CHEMICAL WARFARE
Air transport of samples containing chemical warfare agents
[FFI-93/6005] p 1851 N94-21455
CHEMILUMINESCENCE
Optical fibers and Fluorosensors having improved power efficiency and methods of producing same
[NASA-CASE-LAR-14525-1-CU] p 1986 N94-20378
CHEMISORPTION
Adhesive electroless metallization of fluoropolymeric substrates
[AD-A271858] p 1703 N94-20526
Spectral analysis of chemisorbed CO2 on Mars analog materials p 2140 N94-20900
Direct images of thermal disorder in the Cl-Si and H-O-Si chemisorption bond on Si(100)
[AD-A272386] p 1680 N94-21145
CHEMOTHERAPY
Numerical modeling for an electric-field hyperthermia applicator p 1729 N94-20451
CHIPS (ELECTRONICS)
Materials processing and manufacturing technologies for Diamond Substrate MultiChip Modules (DSMCM)
[AD-A271011] p 2011 N94-19821
CMOS gate array characterization procedures
[AD-A269943] p 2014 N94-20029
Efficient chip signature checking for diagnosing boundary scan systems
[RR-901-I] p 1749 N94-20166
Single-event upset testing of the performance semiconductor 1750A CMOS/SOS chip set
[AD-A271158] p 2015 N94-20184
Quartz/fused silica chip carriers
[NASA-CR-194154] p 2016 N94-20340
High accuracy die mechanical stress measurement with the ATC04 Assembly Test Chip
[DE93-019435] p 1830 N94-20477
Cratering evaluations and results
[DE93-040347] p 1691 N94-20478
An adaptive, lossless data compression algorithm and VLSI implementations p 1753 N94-21080
Test results for SEU and SEL immune memory circuits p 1754 N94-21087
Space qualified high speed Reed Solomon encoder p 1754 N94-21088
Mixed voltage VLSI design p 1756 N94-21104
Materials processing and manufacturing technologies for diamond substrate multichip modules
[AD-A271484] p 2027 N94-21319
The 1992 4th NASA SERC Symposium on VLSI Design
[NASA-CR-194591] p 1763 N94-21694
Applications of correlator chips in radio science p 1763 N94-21695
An 18 bit 50 kHz ADC for low earth orbit p 1764 N94-21702
On the decomposition of synchronous state mechines using sequence invariant state machines p 1764 N94-21703
Schematic driven layout of Reed Solomon encoders p 1766 N94-21722
A 1 GHz sample rate, 256-channel, 1-bit quantization, CMOS, digital correlator chip p 1768 N94-21732
Low power, CMOS digital autocorrelator spectrometer for spaceborne applications p 1666 N94-21733
The distributed CAD system for LSI/VLSI design p 1923 N94-22068
VLSI design of a parallel video output interface p 1778 N94-22153
Architectures of the free space optical interconnects p 1789 N94-22220
Towards the formal verification of the requirements and design of a processor interface unit: HOL listings
[NASA-CR-191466] p 1937 N94-22414
The VLBA correlator: Real-time in the distributed era p 2049 N94-22547
IRAF and STSDAS under the new ALPHA architecture p 2049 N94-22553
CHIPS (MEMORY DEVICES)
A DRAM compiler algorithm for high performance VLSI embedded memories p 1767 N94-21729
A novel cache mechanism p 1767 N94-21730
A set-associative, fault-tolerant cache design p 1768 N94-21731
CHIRAL DYNAMICS
Lattice gauge theory: Present status
[DE93-041154] p 2038 N94-21692
CHLORINE
Optical diagnostic instrument for monitoring etch uniformity during plasma etching of polysilicon in a chlorine-helium plasma
[DE93-019582] p 1993 N94-20261
Direct images of thermal disorder in the Cl-Si and H-O-Si chemisorption bond on Si(100)
[AD-A272386] p 1680 N94-21145
Infrared absorption spectroscopy of the weakly bonded CO-Cl2 complex
[AD-A271757] p 2027 N94-21304
CHLOROFLUOROCARBONS
Alternative refrigerants and refrigeration cycles for domestic refrigerators
[DE93-040481] p 1714 N94-20099
CHOLESKY FACTORIZATION
Fast scalar algorithms for multivariate partial correlations and their empirical counterparts
[RR-903-M] p 1905 N94-20201
The design of linear algebra libraries for high performance computers
[DE93-040458] p 1960 N94-21967
CHONDRITES
Evaporation in equilibrium, in vacuum, and in hydrogen gas p 1684 N94-20638
Carbonaceous xenoliths from the Erevan howardite p 1684 N94-20642
Igneous rock from Severnyi Kolchim (H3) chondrite: Nebular origin p 2082 N94-20643
The Sm-(146,147)-Nd-(142,143) formation interval for the lunar mantle and implications for lunar evolution p 2097 N94-20663
Abundance and composition of solar KR in the H3-H6 chondrite ACFER111 p 1684 N94-20676
Elevated initial Sr-87/Sr-86 in ordinary chondrite metal p 1685 N94-20695
Oxygen isotopic relationships between the LEW85332 carbonaceous chondrite and CR chondrites p 2083 N94-20708
Cosmogenic-radionuclide profiles in Knyahinya: New measurements and models p 2106 N94-20713
Post-metamorphic brecciation in type 3 ordinary chondrites p 2083 N94-20749
Cathodoluminescence observations of in situ aqueous destruction of chondrules in the Murchison CM chondrite p 2083 N94-20750
Orthopyroxenes as recorders of diogenite petrogenesis: Trace element systematics p 1686 N94-20760
The chondrite Mihonoseki: New observed fall p 2083 N94-20764
Size distributions and aerodynamic equivalence of metal chondrules and silicate chondrules in Acfer 059 p 2084 N94-20773
Multielement analysis of interplanetary dust particles using TOF-SIMS p 2084 N94-20790
A new Antarctic meteorite with chromite, orthopyroxene and metal with reference to a formation model of S asteroids p 2084 N94-20813
Rhenium-osmium isotope systematics of ordinary chondrites and iron meteorites p 2085 N94-20854
Magnetic record in chondrite meteorites p 2085 N94-20858
The formation of FeO-rich pyroxene and enstatite in unequilibrated enstatite chondrites: A petrologic-trace element (SIMS) study p 2086 N94-20866
Multivariate statistical analysis: Principles and applications to coorbital streams of meteorite falls p 1964 N94-20881
Regolith breccia consisting of H and LL chondrite mixture p 2080 N94-20892
Preliminary AEM study of the microstructure and composition of metal particles in ordinary chondrites p 2086 N94-20894
Lewis Cliff 87057: A new metal-rich E3 chondrite with similarities to Mt. Egerton, Shallowater and Happy Canyon p 2086 N94-20901
Mineralogy of dark clasts in primitive versus differentiated meteorites p 2087 N94-20907
CHONDRULE
Igneous rock from Severnyi Kolchim (H3) chondrite: Nebular origin p 2082 N94-20643
Oxygen isotopic relationships between the LEW85332 carbonaceous chondrite and CR chondrites p 2083 N94-20708
Euhedral metallic-Fe-Ni grains in extraterrestrial samples p 1697 N94-20724
Post-metamorphic brecciation in type 3 ordinary chondrites p 2083 N94-20749
Cathodoluminescence observations of in situ aqueous destruction of chondrules in the Murchison CM chondrite p 2083 N94-20750
Size distributions and aerodynamic equivalence of metal chondrules and silicate chondrules in Acfer 059 p 2084 N94-20773
Multiplicity of chondrule heating events and the coarsening of chondrule textures p 2085 N94-20860
The formation of FeO-rich pyroxene and enstatite in unequilibrated enstatite chondrites: A petrologic-trace element (SIMS) study p 2086 N94-20866
CHROMATES
Evaluation of non-chromium-containing deoxidizers for aluminum
[DE94-001377] p 1695 N94-21978
CHROMATOGRAPHY
Hydrogen isotope separation experience at the Savannah River Site
[DE93-019832] p 1679 N94-20266
Column chromatographic separation of Y(3+) from Sr(2+) by polymeric ionizable crown ether resins
[DE94-000935] p 1683 N94-22021
CHROMIC ACID
A comparison of sulfuric acid/boric acid anodize and chromic acid anodize processes
[AD-A271933] p 1703 N94-20614
CHROMITES
Ageing studies on a composite propellant containing a new organo-copper burn rate catalyst
[AD-A271060] p 1711 N94-19906
CHROMIUM
Chemical zoning and diffusion of Ca, Al, Mn, and Cr in olivine of springwater pallasite p 2086 N94-20902
Optical properties of chromium and neodymium in zirconium - barium - lanthanum - aluminum fluoride glass
[AD-A271609] p 1987 N94-21236
Shattering the myth of the resonantly photo-pumped neon-like titanium laser
[DE93-019624] p 1819 N94-21873

Evaluation of non-chromium-containing deoxidizers for aluminum
[DE94-001377] p 1695 N94-21978
Orientationally independent antiferromagnetic coupling in epitaxial Fe/Cr (211) and (100) superlattices
[DE94-001270] p 2035 N94-22584

CHROMIUM ALLOYS
Investigation of austenitic alloys for advanced heat recovery and hot gas cleanup systems
[DE93-017863] p 1687 N94-19802
Metastable bcc phase formation in the Nb-Cr system
[DE93-018376] p 2012 N94-19926
Investigation of moisture-induced embrittlement of iron aluminides
[DE93-040841] p 1695 N94-21949
Microstructural evolution of neutron-irradiated Fe-Cr-Ni ternary alloys at high helium generation rates
[DE93-018786] p 1696 N94-22037

CHRONOLOGY
Chronology of lunar granite 12033,576: Resetting of Rb-Sr and K-Ca isochrons p 2115 N94-20763
Chronology and genesis of high-Ti mare volcanism: Melting of cogenetic depleted and enriched reservoirs p 2118 N94-20777
Fine resolution chronology based on initial Sr-87/Sr-86
[CONTRIB-5230(794)] p 1686 N94-20794
The Sm-Nd systematics of silicate inclusions in iron meteorites: Results from Caddo (IAB)
[CONTRIB-5241(804)] p 2084 N94-20795
Aluminum-26 activities in meteorites p 1686 N94-20851
Consortium reports on lunar meteorites Yamato 793169 and Asuka 881757, a new type of mare basalt p 2086 N94-20893

CINETHEODOLITES
Trajectory computations for an improved cinetheodolite tracking system p 1791 N94-22236

CIRCLES (GEOMETRY)
Higher order Bezier circles
[NASA-CR-177633] p 1897 N94-21784

CIRCUIT BOARDS
Solder technology in the manufacturing of electronic products
[DE93-018842] p 1699 N94-19960
Wide-bandwidth high-resolution search for extraterrestrial intelligence
[NASA-CR-194724] p 1897 N94-20336

CIRCUIT RELIABILITY
VLSI design for reliability-current density
[AD-A270719] p 1749 N94-20110
Correct CMOS IC defect models for quality testing p 1755 N94-21093

CIRCUITS
CMOS gate array characterization procedures
[AD-A269943] p 2014 N94-20029
Wire assembly for electrically conductive circuits
[AD-D015966] p 1761 N94-21275
Variable-field permanent magnet dipole
[DE94-000800] p 1820 N94-22020

CIRCULAR CYLINDERS
Extinction efficiencies from DDA calculations solved for finite circular cylinders and disks p 1880 N94-22340

CIRCULAR ORBITS
Venus gravity: New Magellan low altitude data p 2117 N94-20772

CIRCULAR POLARIZATION
Circular polarizing mirrors for high power lasers
[AD-A267820] p 1815 N94-19965
Magnetic circular dichroism in x ray absorption and core-level photoemission
[DE93-019381] p 1688 N94-19986
The coherent backscattering opposition effect p 1991 N94-20646
Performance of a simple circular polarization selective surface p 1746 N94-22198

CIRCULATION
Liquid-phase circulation and mixing in multicomponent droplets vaporizing in a laminar convective environment
[AD-A272851] p 1802 N94-21193

CIRCULATION DISTRIBUTION
Liquid-phase circulation and mixing in multicomponent droplets vaporizing in a laminar convective environment
[AD-A272851] p 1802 N94-21193
Large-scale circulation regimes and tropical cyclone characteristics over the western pacific ocean
[AD-A273004] p 1867 N94-21307

CIRROSTRATUS CLOUDS
Remote sensing of multilevel clouds during FIRE IFO 2 p 1844 N94-22303

CIRRUS CLOUDS
Holographic measurements of ice crystals in cirrus clouds during International Cirrus Experiment ICE
[GKSS-92/E/14] p 1866 N94-21052
The FIRE Cirrus Science Results 1993
[NASA-CP-3238] p 1871 N94-22292
Cirrus microphysics observations made during FIRE 2: Small particles, high concentrations, and probe comparisons p 1871 N94-22294
Cirrus properties deduced from CO2 lidar observations of zenith-enhanced backscatter from oriented crystals p 1871 N94-22295
Bi-directional reflectance and other radiation parameters of cirrus from ER-2 observations p 1871 N94-22296
Intercomparison of MAS, AVIRIS, and HIS data from FIRE cirrus 2 p 1872 N94-22298
Comparison of radiation and cloud parameters derived from satellite and aircraft measurements during FIRE 2 cirrus IFO p 1872 N94-22299
Microphysical properties of the November 26 cirrus cloud retrieved by Doppler radar/IR radiometer technique p 1873 N94-22304
Lidar and radar derived cirrus microphysical properties for the 26 November 1991 case study p 1873 N94-22305
CIMSS FIRE research activities p 1873 N94-22307
Meteorological analysis of the December 4-6 FIRE cirrus-2 case p 1875 N94-22314
Cirrus cloud retrievals from HIS observations during FIRE 2 p 1875 N94-22315
Analysis of the GOES 6.7 micrometer channel observations during FIRE 2 p 1875 N94-22316
Ground-based passive remote sensing during FIRE IFO 2 p 1844 N94-22319
Comparisons of downwelling radiation to model predictions based on groundbased measurements during FIRE 1991 p 1876 N94-22320
Spectral variation of scattering and absorption by cirrus p 1876 N94-22321
Spectral emissivity of cirrus clouds p 1876 N94-22322
Examination of the observed synoptic scale cirrus cloud environment: The December 3-6 FIRE cirrus case study p 1877 N94-22325
The 5-6 December 1991 FIRE IFO 2 jet stream cirrus case study: The influence of volcanic aerosols p 1877 N94-22326
Three dimensional modeling of cirrus during the 1991 FIRE IFO 2: Detailed process study p 1877 N94-22327
Meteorological analysis of the November 25 FIRE cirrus-2 case: A well-defined ridge-crest cirrus system over Oklahoma p 1877 N94-22328
Cirrus cloud development in a mobile upper tropospheric trough: The November 26th FIRE cirrus case study p 1878 N94-22329
Vertical velocity in cirrus case obtained from wind profiler p 1878 N94-22330
Mesoscale simulations of the November 25-26 and December 5-6 cirrus cases using the RAMS model p 1878 N94-22331
Dynamical characteristics of cirrus clouds from aircraft and radar measurements p 1878 N94-22332
Estimation of cirrus cloud particle fallspeeds from vertically pointing Doppler radar p 1879 N94-22333
Normalized vertical ice mass flux profiles from vertically pointing 8-mm-wavelength Doppler radar p 1879 N94-22334
Importance of aggregation and small ice crystals in cirrus clouds, based on observations and an ice particle growth model p 1879 N94-22336
SSH-2 measurements of cirrus at 18-28 micrometers from the King Air during FIRE 2 p 1880 N94-22338
Investigation of the effects of the macrophysical and microphysical properties of cirrus clouds on the retrieval of optical properties: Results for FIRE 2 p 1880 N94-22339
Extinction efficiencies from DDA calculations solved for finite circular cylinders and disks p 1880 N94-22340
Surface-induced brightness temperature variations and their effects on detecting thin cirrus clouds using IR emission channels in the 8-12 micrometer region p 1880 N94-22341
Remote sensing estimates of cirrus particle size for tropical and midlatitude cirrus: Hexagonal crystals and ice spheres p 1880 N94-22342
Are tropical cirrus brighter than mid-latitude cirrus? p 1881 N94-22343
An overview of the radiation component of the NASA TOGA-COARE experiment p 1881 N94-22344

CIRRUS SHIELDS
Spectral emissivity of cirrus clouds p 1876 N94-22322

CITIES
Role of surface characteristics in urban meteorology and air quality
[DE93-040929] p 1851 N94-21740
Urban applications of satellite remote sensing and GIS analysis
[PB93-202174] p 1842 N94-21855
The use of lidar for the evaluation of traffic-related urban pollution
[DE94-000704] p 1852 N94-22017

CITRIC ACID
Water-enhanced solvation of organics
[DE93-040297] p 1683 N94-21947

CLADDING
Optical fibers and Fluorosensors having improved power efficiency and methods of producing same
[NASA-CASE-LAR-14525-1-CU] p 1986 N94-20378
Evaluation of the fabricability of advanced iron aluminide-clad austenitic stainless steel tubing
[DE93-040598] p 1693 N94-21771

CLASSICAL MECHANICS
On the correspondence limit of relativistic quantum mechanics
[DE93-040939] p 2038 N94-21971

CLASSIFICATIONS
Modifications to the three-component classification algorithm for SAR data p 1719 N94-20410
Classification of simple vegetation types using POLSAR image data p 1722 N94-20420
Post-metamorphic brecciation in type 3 ordinary chondrites p 2083 N94-20749
A classification scheme for the morphology of lava flow fields p 1863 N94-20879
Application of SPOT to GIS/LIS in land capability evaluation for regional planning of JAICO semi-arid region of Piaui, Brazil p 1838 N94-20955
Classification in feature-based default inheritance hierarchies
[TR-473] p 1911 N94-21180
Some extensions of the k-means algorithm for image segmentation and pattern classification
[AD-A271691] p 1913 N94-21364
Automated cloud classification with a fuzzy logic expert system p 1875 N94-22313

CLASSIFIERS
Classification of simple vegetation types using POLSAR image data p 1722 N94-20420

CLASSIFYING
Optimal sorting in linear arrays with minimum global control
[CWI-CS-R9244] p 1908 N94-21024
Sorting network for the partial selection problem p 1773 N94-22121

CLAYS
An attempt to comprehend Martian weathering conditions through the analysis of terrestrial palagonite samples p 2143 N94-21668

CLEANERS
Evaluation of non-chromium-containing deoxidizers for aluminum
[DE94-001377] p 1695 N94-21978

CLEANING
A calcium oxide sorbent process for bulk separation of carbon dioxide
[DE93-019288] p 1847 N94-21540
Evaluation of non-chromium-containing deoxidizers for aluminum
[DE94-001377] p 1695 N94-21978
Experiments with a fluid deicing system for cleaning laminar wings p 1640 N94-22601

CLIMATE
Scientific development of a massively parallel ocean climate model
[DE93-019446] p 1855 N94-20219
Tropospheric chemistry of natural hydrocarbons, aldehydes, and peroxy radicals: Their connections to sulfuric acid production and climate effects
[DE93-019525] p 1855 N94-20220
A wet-geology and cold-climate Mars model: Punctuation of a slow dynamic approach to equilibrium p 2090 N94-20389
Climate forcings and feedbacks p 1869 N94-21641
Mars: Noachian hydrology by its statistics and topology p 2143 N94-21664
The evolution of the early Martian climate and the initial emplacement of crustal H2O p 2143 N94-21665
The hydrologic response of Mars to the onset of a colder climate and to the thermal evolution of its early crust p 2143 N94-21666
The early Martian environment: Clues from the cratered highlands and the Precambrian Earth p 2143 N94-21667
A model for the evolution of CO2 on Mars p 2144 N94-21671
Possible solutions to the problem of channel formation on early Mars p 2144 N94-21673
CIMSS FIRE research activities p 1873 N94-22307
Analysis of the tropospheric water distribution during FIRE 2 p 1876 N94-22324

CLIMATE CHANGE
Health effects of global warming: Problems in assessment
[DE93-040323] p 1850 N94-19930

Study of regional climate change
[DE93-018926] p 1850 N94-19941
The CSIRO 9-level atmospheric general circulation model
[CSIRO-TP-26] p 1855 N94-20256
Soil temperatures
[KNMI-WR-92-05] p 1865 N94-20309
The fate of water deposited in the low-lying northern plains p 2089 N94-20387
Global blackout following the K/T Chicxulub impact: Results of impact and atmospheric modeling p 1854 N94-20698
Schools of the Pacific rainfall climate experiment p 1881 N94-20699
Research in progress: FY 1992
[DE94-000410] p 1836 N94-20936
Sunphotometer network for monitoring aerosol properties in the Brazilian Amazon p 1839 N94-20961
Long-Term Monitoring of Global Climate Forcings and Feedbacks
[NASA-CP-3234] p 1868 N94-21639
Monitoring issues from a modeling perspective p 1868 N94-21640
Climate forcings and feedbacks p 1869 N94-21641
Accuracy requirements — for monitoring of climate changes p 1869 N94-21642
Climsat rationale p 1869 N94-21643
Satellite orbit and data sampling requirements p 1870 N94-21648
The hydrologic response of Mars to the onset of a colder climate and to the thermal evolution of its early crust p 2143 N94-21666
Role of surface characteristics in urban meteorology and air quality
[DE93-040929] p 1851 N94-21740
Modeling the response of ecosystems to CO2 and climate change
[DE94-000748] p 1852 N94-21787
Survey on evaluation of energy technology contributing to preservation of the global environment. 2
[DE94-714884] p 1853 N94-22051

CLIMATOLOGY
Worldwide frequency of temperatures at selected altitudes
[AD-A271111] p 1864 N94-19908
Study of regional climate change
[DE93-018926] p 1850 N94-19941
Scientific development of a massively parallel ocean climate model
[DE93-019446] p 1855 N94-20219
Observed climatic activity pertaining to the evolution of the northern plains p 2090 N94-20392
Processing of climatological data for model initialization
[AD-A271878] p 1865 N94-20487
The analysis of global cloud and radiation data for the study of cloud-climate interactions
[NASA-CR-193388] p 1865 N94-20535
Optical climatology of the Northeast Pacific Ocean
[AD-A271671] p 1866 N94-20559
Schools of the Pacific rainfall climate experiment p 1881 N94-20699
Research in progress: FY 1992
[DE94-000410] p 1836 N94-20936
Large-scale circulation regimes and tropical cyclone characteristics over the western pacific ocean
[AD-A273004] p 1867 N94-21307
Acoustic monitoring of global ocean variability
[AD-A271998] p 1883 N94-21366
A synoptic-scale overview of the TOGA COARE intensive observing period November 1992 to February 1993 based on analyses from US operational global data assimilation systems
[NASA-TM-104593] p 1868 N94-21605
Long-Term Monitoring of Global Climate Forcings and Feedbacks
[NASA-CP-3234] p 1868 N94-21639
Monitoring issues from a modeling perspective p 1868 N94-21640
Climate forcings and feedbacks p 1869 N94-21641
Accuracy requirements — for monitoring of climate changes p 1869 N94-21642
Climsat rationale p 1869 N94-21643
Michelson Interferometer (MINT) p 1813 N94-21646
Satellite orbit and data sampling requirements p 1870 N94-21648
The evolution of the early Martian climate and the initial emplacement of crustal H2O p 2143 N94-21665
The hydrologic response of Mars to the onset of a colder climate and to the thermal evolution of its early crust p 2143 N94-21666
Fluvial valleys in the heavily cratered terrains of Mars: Evidence for paleoclimatic change? p 2144 N94-21670
The young Sun and photochemistry of the primitive Martian atmosphere p 2145 N94-21679
Proceedings of the Workshop on New Generation of Radiation Budget Measurements From Space and Their Use in Climate Modelling and Diagnostic Studies
[MPIM-90] p 1860 N94-22283
Satellite measurements of radiation budget parameters p 1860 N94-22284
The use of ERBE data for climate studies p 1860 N94-22286
Satellite validation of GCM-simulated annual cycle of the Earth radiation budget and cloud forcing p 1860 N94-22287
The seasonal variation of the cloud radiative forcing: Comparison of ECHAM model simulations with ERBE data p 1860 N94-22288
Use of satellite data for validation of the ECHAM models p 1861 N94-22289
Use of satellite data for validation of operational forecast models and operational analyses p 1861 N94-22291
The FIRE Cirrus Science Results 1993
[NASA-CP-3238] p 1871 N94-22292
Overview of microphysical and state parameter measurements from FIRE 2 p 1871 N94-22293
Development of methods for inferring cloud thickness and cloud-base height from satellite radiance data p 1872 N94-22301
Cloud fields derived from satellite and surface data during FIRE cirrus phase 2 p 1872 N94-22302
Remote sensing of multilevel clouds during FIRE IFO 2 p 1844 N94-22303
Comparison of cloud microphysical parameters derived from surface and satellite measurements during FIRE phase 2 p 1873 N94-22306
CIMSS FIRE research activities p 1873 N94-22307
Progress in interpreting CO2 lidar signatures to obtain cirrus microphysical and optical properties p 1874 N94-22308
Atmospheric parameterization schemes for satellite cloud property retrieval during FIRE IFO 2 p 1874 N94-22312
Mesoscale simulations of the November 25-26 and December 5-6 cirrus cases using the RAMS model p 1878 N94-22331
Estimation of cirrus cloud particle fallspeeds from vertically pointing Doppler radar p 1879 N94-22333
Calibration of radiation codes in climate models: Comparison of calculations with observations from the SPECtral Radiation Experiment (SPECTRE) p 1879 N94-22337
SSH-2 measurements of cirrus at 18-26 micrometers from the King Air during FIRE 2 p 1880 N94-22338
Studies in remotely sensed geophysical parameter retrieval and analysis
[NASA-CR-194768] p 1842 N94-22374

CLINICAL MEDICINE
A concept for implementing hypermedia technology in computer aided workplaces in medicine
[ETN-93-95057] p 1889 N94-20022
Calculation and optimization of electromagnetic fields in a patient by local hyperthermia utilization
[ETN-93-95059] p 1889 N94-20024
Review of using cardiac fluoroscopy in symptomatic and asymptomatic patients
[AD-A271690] p 1891 N94-20928
Non-ionic surfactants in the treatment of third degree burns
[AD-A271582] p 1891 N94-21035

CLOCKS
The One-Day Workshop on Batteries, Stepping Motors, and Electronic Clock Displays
[ETN-93-94632] p 1752 N94-20628
Silver oxide batteries: Recent improvements and developments p 1752 N94-20629
Lithium batteries: Future batteries p 1752 N94-20630
Reliable interface design for combining asynchronous and synchronous circuits p 1758 N94-21119
Using the USCCS for sub microsecond spacecraft clock calibration p 1813 N94-21346
A low cost alternative to high performance PCM bit synchronizers p 1813 N94-21347

CLOSED CYCLES
Brayton power conversion system parametric design modelling for nuclear electric propulsion
[NASA-CR-191135] p 1671 N94-21874

CLOSED ECOLOGICAL SYSTEMS
Quinoa: An emerging new crop with potential for CELSS
[NASA-TP-3422] p 1895 N94-20137

CLOUD COVER
An analysis of cloud-cover reporting in the 1977 surface observation database
[AD-A271102] p 1864 N94-19852
The analysis of global cloud and radiation data for the study of cloud-climate interactions
[NASA-CR-193388] p 1865 N94-20535
Overview of microphysical and state parameter measurements from FIRE 2 p 1871 N94-22293
Comparison of radiation and cloud parameters derived from satellite and aircraft measurements during FIRE 2 cirrus IFO p 1872 N94-22299
Cloud properties from the analysis of AVHRR observations for FIRE 2 p 1872 N94-22300
Cloud fields derived from satellite and surface data during FIRE cirrus phase 2 p 1872 N94-22302
Remote sensing of multilevel clouds during FIRE IFO 2 p 1844 N94-22303
Observations of multi-layered clouds using K-band radar p 1874 N94-22311
Automated cloud classification with a fuzzy logic expert system p 1875 N94-22313
Comparison of cloud boundaries measured with 8.6 mm radar and 10.6 micrometer lidar p 1875 N94-22317
Cloud boundaries during FIRE 2 p 1876 N94-22318
Cirrus cloud development in a mobile upper tropospheric trough: The November 26th FIRE cirrus case study p 1878 N94-22329

CLOUD GLACIATION
Importance of aggregation and small ice crystals in cirrus clouds, based on observations and an ice particle growth model p 1879 N94-22336

CLOUD HEIGHT INDICATORS
Development of methods for inferring cloud thickness and cloud-base height from satellite radiance data p 1872 N94-22301
Remote sensing of multilevel clouds during FIRE IFO 2 p 1844 N94-22303
Comparison of cloud boundaries measured with 8.6 mm radar and 10.6 micrometer lidar p 1875 N94-22317
Cloud boundaries during FIRE 2 p 1876 N94-22318

CLOUD PHYSICS
Clouds: Their prediction and simulation
[AD-A271161] p 1864 N94-19900
The analysis of global cloud and radiation data for the study of cloud-climate interactions
[NASA-CR-193388] p 1865 N94-20535
Computerized simulations with cellular automates for cloud formation
[GKSS-92/E/22] p 1867 N94-21312
Cirrus microphysics observations made during FIRE 2: Small particles, high concentrations, and probe comparisons p 1871 N94-22294
Bi-directional reflectance and other radiation parameters of cirrus from ER-2 observations p 1871 N94-22296
Cloud properties from the analysis of AVHRR observations for FIRE 2 p 1872 N94-22300
Cloud fields derived from satellite and surface data during FIRE cirrus phase 2 p 1872 N94-22302
Microphysical properties of the November 26 cirrus cloud retrieved by Doppler radar/IR radiometer technique p 1873 N94-22304
Lidar and radar derived cirrus microphysical properties for the 26 November 1991 case study p 1873 N94-22305
Comparison of cloud microphysical parameters derived from surface and satellite measurements during FIRE phase 2 p 1873 N94-22306
CIMSS FIRE research activities p 1873 N94-22307
Progress in interpreting CO2 lidar signatures to obtain cirrus microphysical and optical properties p 1874 N94-22308
A numerical technique for the calculation of cloud optical extinction from lidar p 1874 N94-22309
Atmospheric parameterization schemes for satellite cloud property retrieval during FIRE IFO 2 p 1874 N94-22312
Cirrus cloud retrievals from HIS observations during FIRE 2 p 1875 N94-22315
Comparison of cloud boundaries measured with 8.6 mm radar and 10.6 micrometer lidar p 1875 N94-22317
Spectral variation of scattering and absorption by cirrus p 1876 N94-22321
Spectral emissivity of cirrus clouds p 1876 N94-22322
Three dimensional modeling of cirrus during the 1991 FIRE IFO 2: Detailed process study p 1877 N94-22327
Normalized vertical ice mass flux profiles from vertically pointing 8-mm-wavelength Doppler radar p 1879 N94-22334
Importance of aggregation and small ice crystals in cirrus clouds, based on observations and an ice particle growth model p 1879 N94-22336
Investigation of the effects of the macrophysical and microphysical properties of cirrus clouds on the retrieval of optical properties: Results for FIRE 2 p 1880 N94-22339

Remote sensing estimates of cirrus particle size for tropical and midlatitude cirrus: Hexagonal crystals and ice spheres p 1880 N94-22342
Are tropical cirrus brighter than mid-latitude cirrus? p 1881 N94-22343
Development of advanced cloud parameterizations to examine air quality, cloud properties, and cloud-radiation feedback in mesoscale models
[DE93-041164] p 1853 N94-22384

CLOUD SEEDING
The 5-6 December 1991 FIRE IFO 2 jet stream cirrus case study: The influence of volcanic aerosols p 1877 N94-22326

CLOUDS (METEOROLOGY)
Intrusion of stratospheric ozone in the troposphere through tropopause folding and cold air droplets
[REPT-87] p 1851 N94-20154
Computerized simulations with cellular automates for cloud formation
[GKSS-92/E/22] p 1867 N94-21312
Low-power millimeter-wave radar observations of the atmosphere
[NASA-CR-194738] p 1858 N94-21811
A documentation of icing relevant cloud physical parameters on horizontal soundings of stratiform clouds (continuation)
[DLR-MITT-92-10] p 1871 N94-22280
The use of ERBE data for climate studies p 1860 N94-22286
Satellite validation of GCM-simulated annual cycle of the Earth radiation budget and cloud forcing p 1860 N94-22287
The seasonal variation of the cloud radiative forcing: Comparison of ECHAM model simulations with ERBE data p 1860 N94-22288
Overview of microphysical and state parameter measurements from FIRE 2 p 1871 N94-22293
Cloud properties from the analysis of AVHRR observations for FIRE 2 p 1872 N94-22300
Development of methods for inferring cloud thickness and cloud-base height from satellite radiance data p 1872 N94-22301
Cloud fields derived from satellite and surface data during FIRE cirrus phase 2 p 1872 N94-22302
Remote sensing of multilevel clouds during FIRE IFO 2 p 1844 N94-22303
Comparison of cloud microphysical parameters derived from surface and satellite measurements during FIRE phase 2 p 1873 N94-22306
A numerical technique for the calculation of cloud optical extinction from lidar p 1874 N94-22309
Automated cloud classification with a fuzzy logic expert system p 1875 N94-22313
Analysis of the tropospheric water distribution during FIRE 2 p 1876 N94-22324

CLUSTER ANALYSIS
On evaluating the accuracy of SAR sea-ice classification using multifrequency polarimetric AIRSAR data p 1724 N94-20428
Large-scale circulation regimes and tropical cyclone characteristics over the western pacific ocean
[AD-A273004] p 1867 N94-21307
Detecting topographical regions in digital terrain maps
[AD-A272889] p 1841 N94-21453
Extracting galactic structure parameters from multivariated density estimation p 1964 N94-22458

CLUSTERS
Neutral copper cluster sputtering yields: Ne(+), Ar(+) and Xe(+) bombardment
[DE93-019010] p 1690 N94-20288

CLUTTER
State-space models for multichannel detection
[AD-A270608] p 1715 N94-19816

CMOS
CMOS gate array characterization procedures
[AD-A269943] p 2014 N94-20029
VLSI design for reliability-current density
[AD-A270719] p 1749 N94-20110
Single-event upset testing of the performance semiconductor 1750A CMOS/SOS chip set
[AD-A271158] p 2015 N94-20184
Rad-hard computer elements for space applications p 1753 N94-21082
Design of CMOS logic gates for TID radiation p 1754 N94-21083
Test results for SEU and SEL immune memory circuits p 1754 N94-21087
Correct CMOS IC defect models for quality testing p 1755 N94-21093
Power optimization in logic isomers p 1756 N94-21101
Delay analysis of combinations of pass transistors and classical logic gates p 1756 N94-21103
Bridging faults in BiCMOS circuits p 1756 N94-21105
A CAM-based LZ data compression IC p 1759 N94-21129
VLSI design for reliability-hot carrier effects
[AD-A271586] p 1761 N94-21256
The 1992 4th NASA SERC Symposium on VLSI Design
[NASA-CR-194591] p 1763 N94-21694
A 20 MHz CMOS reorder buffer for a superscalar microprocessor p 1764 N94-21700
Defect-sensitivity analysis of an SEU immune CMOS logic family p 1765 N94-21711
Detection of feed-through faults in CMOS storage elements p 1766 N94-21721
Bit-systolic arithmetic arrays using dynamic differential gallium arsenide circuits p 1767 N94-21724
A VLSI implementation of DCT using pass transistor technology p 1767 N94-21725
A high speed CMOS A/D converter p 1767 N94-21726
Behavior of faulty double BJT BiCMOS logic gates p 1767 N94-21727
A 1 GHz sample rate, 256-channel, 1-bit quantization, CMOS, digital correlator chip p 1768 N94-21732
Low power, CMOS digital autocorrelator spectrometer for spaceborne applications p 1666 N94-21733
Low energy CMOS for space applications p 1768 N94-21735
Micromachined actuator and sensor capabilities at the Microelectronics Development Laboratory
[DE93-019417] p 1769 N94-21918

COAGULATION
Coagulation of grains in static and collapsing protostellar clouds p 2085 N94-20865

COAL
Current situation in developing petroleum substituting energy (the United Kingdom)
[DE94-714897] p 1713 N94-22091
Environmental protection using social costing
[DE94-000492] p 1853 N94-22569

COAL DERIVED GASES
A calcium oxide sorbent process for bulk separation of carbon dioxide
[DE93-019288] p 1847 N94-21540

COAL GASIFICATION
Surface modification for corrosion resistance
[DE93-017419] p 1693 N94-21825
Development of an electrochemical hydrogen separator
[DE93-019877] p 1683 N94-21984
Survey on chemical engineering technologies for the global environmental protection
[DE94-714887] p 1852 N94-22044

COALESCING
Head-on collision of drops: A numerical investigation
[NASA-TM-106394] p 1798 N94-20167

COASTAL PLAINS
Post-Palbozoic crustal responses to the contemporary stress field in the eastern United States
[DE93-040604] p 1859 N94-22006

COASTAL WATER
Distribution of turbidity in Australian tropical waters
[AD-A271059] p 1881 N94-19905

COASTS
Comparison of satellite-derived velocity fields in the coastal transition zone
[AD-A272565] p 1883 N94-21360

COATING
Metal-glass composite field-emitting arrays
[AD-D015942] p 1673 N94-20064
Surface modification for corrosion resistance
[DE93-017419] p 1693 N94-21825
Techniques for producing free-standing thin films on frames
[DE93-041144] p 1708 N94-21954

COATINGS
Substrate recovery of Mo-Si multilayer coated optics
[DE93-019610] p 1698 N94-19810
Plasma chemical vapor deposition of halide glasses
[AD-D015933] p 1701 N94-20331
X ray characterization of a three-element condenser system for soft x ray projection lithography
[DE93-019916] p 1990 N94-21985

COBALT
Observation of x ray absorption magnetic circular dichroism in well-characterized iron-cobalt-platinum multilayers
[DE94-000303] p 1694 N94-21944

COBALT OXIDES
Cathode materials for the molten carbonate fuel cell
[DE93-019515] p 1848 N94-21870

COCKPITS
Intervention strategies for the management of human error
[NASA-CR-4547] p 1642 N94-22373

CODE DIVISION MULTIPLE ACCESS
Spread spectrum random access networks
[AD-A272280] p 1737 N94-20585
Capacity comparison between direct sequence PSK and MFSK spread spectrum systems in CDMA applications p 1747 N94-22224

CODERS
Space qualified high speed Reed Solomon encoder p 1754 N94-21088
Schematic driven layout of Reed Solomon encoders p 1766 N94-21722
Encoding and decoding quasi-spherical signal sets p 1747 N94-22233

CODING
Optical encoding of imaging data
[AD-D015915] p 1984 N94-20056
Low bit rate coding of Earth science images
[NASA-CR-193729] p 2041 N94-20158
Rotary encoding device using polygonal mirror with diffraction gratings on each facet
[NASA-CASE-GSC-13543-1] p 1985 N94-20240
A fixed/variable bit-rate data compression architecture p 1759 N94-21128
Behavioral model simulation studies of an image compressor p 1760 N94-21133
The Composite Analytic and Simulation Package or RFI (CASPR) on a coded channel p 1744 N94-21339
Reduction of blocking effects for the JPEG baseline image compression standard p 1765 N94-21714
A mean field neural network for hierarchical module placement p 1766 N94-21720
Directional coding of morphological pyramidal representations p 1771 N94-22106
Formal methods in the design of critical software systems p 1779 N94-22158
Coding of color quantized images p 1781 N94-22173
Hierarchical multirate vector quantization for image coding p 1781 N94-22174
A framework of connectionist network toward speech waveform coding p 1746 N94-22211

COEFFICIENTS
A real time correlator architecture using distributed arithmetic principles p 1768 N94-21734
Temperature and Doppler coefficients of various space nuclear reactors
[DE94-001388] p 1671 N94-21979

COGNITION
Building brains for bodies
[AD-A270531] p 1939 N94-19875
Incongruity, incongruity resolution, and mental states: The measure and modification of situational awareness and control
[NASA-CR-194568] p 1893 N94-20188
Cognition and the brain: A continuation of the university research initiative at New York University
[AD-A271872] p 1894 N94-20467
Research, Development, Training, and Evaluation (RDTE) support delivery order 1: Computational cognitive models
[AD-A271837] p 1894 N94-20610
Cognitive engineering in aerospace applications
[NASA-CR-194782] p 1647 N94-21819

COGNITIVE PSYCHOLOGY
Research, Development, Training, and Evaluation (RDTE) support delivery order 1: Computational cognitive models
[AD-A271837] p 1894 N94-20610

COHERENT LIGHT
Optical processing in photorefractive media p 1789 N94-22222

COHERENT RADAR
Direction angle sensitivity of agricultural field backscatter with AIRSAR data p 1724 N94-20430

COHERENT RADIATION
Monte Carlo calculation of multi-electron effects on synchrotron radiation
[DE94-001259] p 1982 N94-21974

COHERENT SCATTERING
The coherent backscattering opposition effect p 1991 N94-20646

COLD GAS
Optical metrology of magnetically trapped hydrogen
[AD-A272110] p 1680 N94-20584

COLD PLASMAS
Laser diagnostics of RF hydrogen plasma reactors: Application to the processing of III-V materials
[AD-A272659] p 1994 N94-21214

COLD TOLERANCE
Studies of neural and cognitive function in subjects exposed to the marine-air interface, phases 1 and 2
[AD-A272282] p 1891 N94-20624

COLD WORKING
Microstructural evolution of neutron-irradiated Fe-Cr-Ni ternary alloys at high helium generation rates
[DE93-018786] p 1696 N94-22037

COLLAPSE
Computing solutions uniquely collapses the polynomial hierarchy
[TR-467] p 1954 N94-21314
COLLECTION
The aerogel mesh contamination collector
[AD-A270537] p 1651 N94-20011
COLLIMATION
Focus history of the Hubble Space Telescope: Launch to May 1993
[NASA-CR-194179] p 2055 N94-20204
COLLISION AVOIDANCE
Ground proximity warning system voice warning unit requirements study
[AD-A270541] p 1641 N94-19876
An algorithm for the interference detection among polygonal surfaces p 1791 N94-22239
Strategy for motion of a moving body of quasi-polygonal form within a polygonal space p 1792 N94-22240
Analytical representation of working articulation space of a plane manipulator in an encumbered environment p 1792 N94-22241
Parallel runway requirement analysis study. Volume 1: The analysis
[NASA-CR-191549-VOL-1] p 1644 N94-22277
COLLISIONAL PLASMAS
Prompt high-energy particle acceleration during two current loops collision p 2005 N94-22661
Formation of fast magnetosonic shock waves during two current loops collision in solar flare p 2005 N94-22662
Dynamics of physical state during two current loops collision p 2005 N94-22663
COLLISIONLESS PLASMAS
Consequences of chaotic particle motion for the stability of space plasma current sheets p 2001 N94-22636
COLLISIONS
Energy gain spectroscopic study of Ar(q+)-Ar collisions at 40 qeV
[DE93-040284] p 1970 N94-19871
Head-on collision of drops: A numerical investigation
[NASA-TM-106394] p 1798 N94-20167
Determination of cosmic bodies size-velocity distribution by observation of current impacts on Mars p 2082 N94-20648
Asteroid collisions: Target size effects and resultant velocity distributions p 2083 N94-20729
Equilibrium models of mass distribution and collisional lifetimes of asteroids p 2086 N94-20877
Antipodal fragment velocities for porous and weak targets at catastrophic impacts p 1836 N94-20891
Electron emissions in low energy Ar(q+)-Ar collisions
[DE93-040285] p 1974 N94-21543
Measurement of the inclusive jet cross section in p(bar-p) collisions at CDF
[DE94-000581] p 1982 N94-21866
COLLOIDS
Formation of colloidal Ag precipitates in fused silica by MeV ion implantation
[DE93-040268] p 2012 N94-19869
COLOR
Miniature color display, phase 4
[AD-A272920] p 1760 N94-21221
Dynamics of surface thermal expansion and diffusivity using two-color reflection transient gratings
[DE93-040547] p 1990 N94-22002
COLOR CODING
Coding of color quantized images p 1781 N94-22173
COLOR TELEVISION
Initial laboratory evaluation of color video cameras, phase 2
[DE93-040201] p 1809 N94-21556
COLUMBUS SPACE STATION
Columbus: Materials for 30 years habitability in space p 1662 N94-21387
COMBINATORIAL ANALYSIS
Eliminating amortization: On data structures with guaranteed response time
[TR-439] p 2049 N94-20098
On multiflow problems
[RR-889-M] p 1950 N94-20125
Applying the INN model to the MaxClique
[DE93-040137] p 1906 N94-20276
The combinatorics of reconstructing evolutionary trees
[CWI-BS-R9233] p 1963 N94-21022
On Update Last schemes
[CWI-CS-R9247] p 1952 N94-21027
The Robinson-Schensted and Schuetzenberger algorithms. Part 1: New combinatorial proofs
[CWI-AM-R9208-PT-1] p 1911 N94-21156
A mean field neural network for hierarchical module placement p 1766 N94-21720
The combinatorial algorithms for large scale discrete optimization problems p 1923 N94-22079
Some best rate 1/p and rate (p-1)/p systematic quasi-cyclic codes over GF(3) and GF(4) p 1792 N94-22243
COMBINED CYCLE POWER GENERATION
Investigation of austenitic alloys for advanced heat recovery and hot gas cleanup systems
[DE93-017863] p 1687 N94-19802
COMBUSTIBLE FLOW
Initiation and modification of reaction by energy addition: Kinetic and transport phenomena
[AD-A271315] p 1797 N94-19936
Liquid rocket propulsion. Theory p 1667 N94-20069
Reaction zone models for vortex simulation of turbulent combustion
[AD-A272723] p 1681 N94-21213
COMBUSTION
A database of selected transport coefficients for combustion studies
[DE93-041278] p 1678 N94-19889
Detailed structure study of an H2/N2O/Ar flame employing molecular beam mass spectrometry, laser spectroscopy, and modeling
[AD-A270720] p 1679 N94-20111
Numerical methods for singularly perturbed differential equations with applications
[AD-A272112] p 1952 N94-20568
Toxicity of thermal degradation in a manned space environment p 1664 N94-21403
COMBUSTION CHAMBERS
Initiation and modification of reaction by energy addition: Kinetic and transport phenomena
[AD-A271315] p 1797 N94-19936
Experimental investigation of nozzle/plume aerodynamics at hypersonic speeds
[NASA-CR-194628] p 1636 N94-20014
Method of fabricating a rocket engine combustion chamber
[NASA-CASE-MFS-28569-1] p 1703 N94-20541
Heat regenerative external combustion engine
[AD-D015965] p 1824 N94-21274
Combustion in turbulent jets and buoyant flames
[PB93-202372] p 1682 N94-21452
Flow interaction experiment. Volume 1: Aerothermal modeling, phase 1
[NASA-CR-189192-VOL-1] p 1648 N94-21582
Flow interaction experiment. Volume 2: Aerothermalmodeling, phase 2
[NASA-CR-189192-VOL-2] p 1648 N94-21583
Comparison of mixing calculations for reacting and non-reacting flows in a cylindrical duct
[NASA-TM-106435] p 1649 N94-21758
COMBUSTION CHEMISTRY
Development of a technique to determine the morphology and dynamics of agglomerates in chemically reacting flows
[AD-A271160] p 1678 N94-20000
Liquid rocket propulsion. Theory p 1667 N94-20069
Model for liquid boron oxide droplet gasification in H/O/C/F combustion environments
[AD-A272911] p 1682 N94-21243
Theoretical research program to study chemical reactions in AOTV bow shock tubes
[NASA-CR-194710] p 1804 N94-22027
COMBUSTION EFFICIENCY
Cryogenic propellant rocket engine problems p 1668 N94-20076
COMBUSTION PHYSICS
RADCAL: A narrow-band model for radiation calculations in a combustion environment
[PB93-200889] p 1682 N94-21448
Combustion in turbulent jets and buoyant flames
[PB93-202372] p 1682 N94-21452
COMBUSTION PRODUCTS
Unlike-pair interactions at high pressure and high temperature
[DE93-019948] p 1796 N94-19916
Cryogenic propellant rocket engine problems p 1668 N94-20076
RADCAL: A narrow-band model for radiation calculations in a combustion environment
[PB93-200889] p 1682 N94-21448
Global emissions and models of photochemically active compounds
[DE93-040490] p 1852 N94-21969
Survey on chemical engineering technologies for the global environmental protection
[DE94-714887] p 1852 N94-22044
Cold starting an alcohol-fueled engine with ultrasonic fuel atomization
[PB93-206597] p 1826 N94-22093
Investigations on trends in global environment adaptive industrial technologies
[DE94-714888] p 1853 N94-22258
COMBUSTION STABILITY
Investigation of flame driving and flow turning in axial solid rocket instabilities
[AD-A271066] p 1667 N94-20015
COMET TAILS
Laboratory relations between the solar wind dynamic pressure and the magnetospheric structures of the Earth and comets p 2003 N94-22647
COMETARY ATMOSPHERES
C2, CN and dust in Comet Wilson (1987VII) p 2083 N94-20746
Atmospheric breakup of a small comet in the Earth's atmosphere p 2084 N94-20824
COMETS
Gamma ray bursts from collisions of primordial small mass black holes with comets p 2150 N94-20604
Effects of hydrodynamics and thermal radiation in the atmosphere after comet impacts p 1862 N94-20649
First discovery of the organic materials in deep-sea iron cosmic spherule p 1685 N94-20677
C2, CN and dust in Comet Wilson (1987VII) p 2083 N94-20746
Research program on the Manson impact structure, Iowa p 1862 N94-20766
Volatile loss from accreting icy protoplanets p 2084 N94-20793
Triton's cratering record and its time of capture p 2122 N94-20802
Synoptic observations of near surface processes of an insolated ice-dust body under space conditions: The case of KOSI 9 and 10 p 2084 N94-20827
Cometary interplanetary dust particles? An update on carbon in anhydrous IDPS p 2084 N94-20828
Measurements of the dielectric properties of simulated comet material as part of the KOSI 10 experiment p 2085 N94-20841
COMMAND AND CONTROL
Network command processing system overview p 1935 N94-21351
Data link development for the archytas vertical takeoff and landing transitional flight unmanned aerial vehicle
[AD-A272499] p 1646 N94-21548
High-velocity interceptors for boost-phase intercepts
[DE94-001077] p 1965 N94-22403
COMMAND LANGUAGES
The NSO FTS database program and archive (FTSDBM) p 1926 N94-22506
GammaCore: The Compton Observatory research environment p 2048 N94-22509
XPI: The Xanadu Parameter Interface p 1927 N94-22513
COMMERCE
Information sciences and business enterprises p 2046 N94-22059
The Soviet software market: Current state and aspects of development p 1923 N94-22066
Experiences of the bank of Finland's econometric simulation model p 2053 N94-22086
COMMERCIAL AIRCRAFT
Radiometry in commercial aircraft
[GSF-41/91] p 1892 N94-21141
Aviation safety research. Volume 1: Literature review of sources of aviation accident and incident data and selected factors contributing to accidents
[PB93-202885] p 1641 N94-21428
Utilization of lasers for air data measurements p 1640 N94-22603
Riblet boundary layer measurements of an A-310 fuselage with Pitot combs p 1640 N94-22605
Recent ONERA contributions to the development of flight test measurement techniques p 1641 N94-22607
Demonstrating damage tolerance of composite airframes p 1647 N94-22623
COMMUNICATING
Controlling multisupplier operations by intelligent EDI p 1744 N94-22076
COMMUNICATION
The communication complexity of set intersection problems
[MEMO-1077] p 1738 N94-21073
A response to Cheriton and Skeen's criticism of casual and totally ordered communication
[AD-A271486] p 1912 N94-21300
COMMUNICATION CABLES
Delivery of very high bandwidth with ATM switches and SONET
[DE93-019432] p 1899 N94-20476
COMMUNICATION EQUIPMENT
Satellite Communication Hardware Emulation System (SCHES) p 1744 N94-21344
COMMUNICATION NETWORKS
Ground wave emergency network. Final operational capability. Environmental assessment for south central Montana relay node, site no. RN8C925MT
[AD-A267795] p 1716 N94-19964

Label-connected graphs: An overview
[RR-898-M] p 1950 N94-20163
Design considerations for a fiber optic communications network for power systems
[DE93-018404] p 1984 N94-20179
A semi-Markov model of a home network access protocol
[MEMO-INF-92-71] p 1909 N94-21045
On the optimality of FCFS for networks of multi-server queues
[CWI-BS-R9235] p 1944 N94-21160
The NCC project: A quality management perspective p 1828 N94-21324
Software metrics: The key to quality software on the NCC project p 1922 N94-21326
Problem reporting management system performance simulation p 1931 N94-21328
Mission Operations Support Area (MOSA) for ground network support p 1932 N94-21331
Space network scheduling benchmark: A proof-of-concept process for technology transfer p 1932 N94-21332
Using manufacturing message specification for monitor and control at Venus p 1932 N94-21333
Predicting scheduling success p 1932 N94-21334
Generating and evaluating alternate schedules p 1933 N94-21336
The three-dimensional Event-Driven Graphics Environment (3D-EDGE) p 1922 N94-21342
Developing a space network interface simulator: The NTS approach p 1933 N94-21343
Satellite Communication Hardware Emulation System (SCHES) p 1744 N94-21344
Conversion of the proprietary ROLM (tm) inter-node link from multimode to singlemode operation p 1744 N94-21349
Telecommunications services for multimedia data exchange support
[AD-A271704] p 1740 N94-21352
PEGASUS, electronic bulletin board system user's guide
[AD-A271679] p 2044 N94-21363
On-board closed-loop congestion control for satellite based packet switching networks
[NASA-TM-106446] p 1656 N94-21581
IAS telecommunication infrastructure and value added network services provided by IASNET p 1744 N94-22069
Controlling multisupplier operations by intelligent EDI p 1744 N94-22076
TDMA satellite communication systems for ISDN services p 1746 N94-22171
A consideration of the integration of terrestrial and satellite mobile systems p 1746 N94-22172
Throughput and blocking in circuit-switched interconnection networks p 1784 N94-22189
Modeling and analysis of secure communication protocols using Petri net formalism p 1784 N94-22194
Neural networks for optimum routing in packet-switched communications networks p 1746 N94-22205
Recommendations for a service framework to access astronomical archives p 2049 N94-22537
STELAR: An experiment in the electronic distribution of astronomical literature p 2049 N94-22544

COMMUNICATION SATELLITES
NHK Science and Technical Research Laboratories p 2151 N94-20342
Multi-band reflector antenna with double-ring element frequency selective subreflector p 1728 N94-20447
A compact, portable EHF/SHF antenna for advanced SCAMP
[AD-A272614] p 1739 N94-21211
Downlink acquisition and tracking procedures for the ASCAMP satellite communications terminal
[AD-A272912] p 1739 N94-21244
A laboratory system for the investigation of rain fade compensation techniques for Ka-band satellites
[NASA-CR-191200] p 1762 N94-21566
Visibility considerations in frequency sharing with low Earth orbit satellites p 1746 N94-22187
Inclined orbits and interference to stationary service and to stationary service by satellite p 1653 N94-22188

COMMUNICATION THEORY
Specification and generation of Markov reward models
[MEMO-INF-92-60] p 1963 N94-21058

COMPANION STARS
Studies of an x ray selected sample of cataclysmic variables
[NASA-CR-194773] p 2055 N94-20344

COMPARATOR CIRCUITS
A high speed CMOS A/D converter p 1767 N94-21726

COMPARISON
Efficient comparison based string matching
[CWI-CS-R9249] p 1909 N94-21028
Tight comparison bounds for the string prefix-matching problem
[CWI-CS-R9250] p 1952 N94-21029
Simulated real-time intercomparison of hydrological models
[WMO-779] p 1867 N94-21070
Simulation of clear-sky outgoing longwave radiation over the oceans using operational analysis p 1861 N94-22290

COMPATIBILITY
Use of open systems for control, analysis, and data acquisition of the DIII-D tokamak
[DE94-001101] p 1998 N94-22089

COMPILERS
A parallelizing compiler based on partial evaluation
[AD-A270838] p 1898 N94-19832
Exploiting the parallelism exposed by partial evaluation
[AD-A270678] p 1928 N94-19877
Set based analysis of ML programs
[AD-A270597] p 1902 N94-19948
Standard ML signatures for a protocol stack
[AD-A272060] p 1908 N94-20622
Automated synthesis and verification of configurable DRAM blocks for ASIC's p 1759 N94-21123
Automated radiation hard ASIC design tool p 1759 N94-21126
A DRAM compiler algorithm for high performance VLSI embedded memories p 1767 N94-21729
Fortran for the nineties p 1926 N94-22481

COMPLETENESS
A declarative approach for first-order built-in's of PROLOG
[CWI-CS-R9246] p 1909 N94-21026

COMPLEX COMPOUNDS
Hydrogen in compound semiconductors
[DE93-040300] p 2031 N94-21922

COMPLEX NUMBERS
Method for design rotation
[AD-A272440] p 1911 N94-21204

COMPLEX SYSTEMS
A complex systems approach to computational molecular biology
[DE93-040062] p 1884 N94-19866
Interval timed coloured petri nets and their analysis
[PB93-191732] p 1903 N94-19992
Feedback controlled optics with wavefront compensation
[NASA-CASE-NPO-18194-1-CU] p 1985 N94-20305
Experiments in knowledge refinement for a large rule-based system
[AD-A272055] p 1809 N94-21445

COMPLEX VARIABLES
Column reduced rational matrix functions with given null-pole data in the complex plane
[PB93-220531] p 1960 N94-22099

COMPLEXITY
Efficient comparison based string matching
[CWI-CS-R9249] p 1909 N94-21028
The communication complexity of set intersection problems
[MEMO-1077] p 1738 N94-21073
On the topological size of p-m-complete degrees
[TR-459] p 1965 N94-21286

COMPONENT RELIABILITY
Modeling failure and reliability in new-generation devices
[AD-A271150] p 1748 N94-19910

COMPOSITE FUNCTIONS
Scattering by Venus' surface p 2117 N94-20771

COMPOSITE MATERIALS
Quantitative evaluation of material composition of composites using x ray energy-dispersive NDE technique
[DE93-041157] p 1672 N94-19688
The Seventh International Conference on Composite Structures, volume 25, numbers 1-4
[AD-A269961] p 1672 N94-20031
Biotechnology and composite materials
[AD-A264278] p 1673 N94-20327
Electrochemical synthesis of ultrathin film composite membranes
[AD-A272721] p 1681 N94-21168
Composite materials with improved properties in compression
[AD-A272837] p 1675 N94-21176
A study of the induction heating of organic composites
[AD-A272657] p 1675 N94-21187
Materials Science and Engineering
[DE93-040497] p 1675 N94-21530
Millimeter-wave imaging of composite materials
[DE93-041160] p 1677 N94-21940
The effect of delamination on the dynamic response of composite laminates as measured by embedded fiber optic Michelson sensor
[ISBN-0-315-83534-6] p 1677 N94-22587
Life prediction systems for critical rotating components p 1835 N94-22615
NASA Langley developments in response calculations needed for failure and life prediction p 1836 N94-22621

COMPOSITE PROPELLANTS
Ageing studies on a composite propellant containing a new organo-copper burn rate catalyst
[AD-A271060] p 1711 N94-19906

COMPOSITE STRUCTURES
Structural crashworthiness and failure
[AD-A270429] p 1828 N94-19815
The Seventh International Conference on Composite Structures, volume 25, numbers 1-4
[AD-A269961] p 1672 N94-20031
Compression strength of composite primary structural components
[NASA-CR-194561] p 1830 N94-20159
Quantification of uncertainties in the performance of smart composite structures
[NASA-TM-106335] p 1830 N94-20171
Aviation safety research at the National Institute for Aviation Research, Wichita State University
[NIAR-93-4] p 1641 N94-20189
Biotechnology and composite materials
[AD-A264278] p 1673 N94-20327
Interleaved bismaleimide composites
[AD-A272233] p 1674 N94-20574
Electrochemical synthesis of ultrathin film composite membranes
[AD-A272721] p 1681 N94-21168
A study of the structural stability of an unbalanced sandwich composite configuration
[AD-A272496] p 1675 N94-21431
Materials Science and Engineering
[DE93-040497] p 1675 N94-21530
Probabilistic assessment of composite structures
[NASA-TM-106368] p 1832 N94-21757
Development of BEM for ceramic composites
[NASA-CR-194718] p 1676 N94-21777
Computational Methods for Failure Analysis and Life Prediction
[NASA-CP-3230] p 1833 N94-22608
Nonlinear and progressive failure aspects of transport composite fuselage damage tolerance p 1834 N94-22609
An overview of computational simulation methods for composite structures failure and life analysis p 1835 N94-22617
Demonstrating damage tolerance of composite airframes p 1647 N94-22623

COMPOSITION (PROPERTY)
Contributions of the Clementine mission to our understanding of the processes and history of the Moon p 2119 N94-20784
Some experiments on using backscattered electron and energy dispersive x ray imaging in determination of portland cement clinker phase composition p 1708 N94-21893

COMPRESSED GAS
Phonons and metastability in compressed nitrogen
[DE93-019913] p 2016 N94-20318

COMPRESSIBILITY
Hydrodynamic compressibility of high-strength ceramics
[DE93-019424] p 1698 N94-19903
Shock response of porous Al-2 + Fe2O3 powder mixtures
[DE93-018851] p 1688 N94-19944
A comparison of two incompressible Navier-Stokes algorithms for unsteady internal flow
[NASA-TM-108794] p 1798 N94-20104
The effects of processing and constituent materials on compressive strength of thick composite laminates
[AD-A271912] p 1673 N94-20490
Two-dimensional finite element analysis of porous media at multikilobar stress levels
[AD-A271540] p 1831 N94-20916

COMPRESSIBILITY EFFECTS
Turbulence modeling for high speed compressible flows
[NASA-CR-194547] p 1799 N94-20210

COMPRESSIBLE BOUNDARY LAYER
Linear and nonlinear PSE for compressible boundary layers
[NASA-CR-191537] p 1797 N94-20033

COMPRESSIBLE FLOW
Turbulence modeling for high speed compressible flows
[NASA-CR-194547] p 1799 N94-20210
High-resolution numerical methods for compressible multi-phase flow in hierarchical porous media
[DE94-000740] p 1799 N94-20351
Some practical turbulence modeling options for Reynolds-averaged full Navier-Stokes calculations of three-dimensional flows
[NASA-TM-106399] p 1637 N94-20534

Numerical methods for singularly perturbed differential equations with applications
[AD-A272112] p 1952 N94-20568
A study of the compressible flow through a diffusing S-duct
[NASA-TM-106411] p 1638 N94-21591
F2D users manual: A two-dimensional compressible gas flow code
[DE94-000653] p 1805 N94-22386

COMPRESSIBLE FLUIDS
Numerical methods for singularly perturbed differential equations with applications
[AD-A272112] p 1952 N94-20568
Two-dimensional finite element analysis of porous media at multikilobar stress levels
[AD-A271540] p 1831 N94-20916

COMPRESSION LOADS
Time-resolved shock compression of porous rutile: Wave dispersion in porous solids
[DE93-018848] p 1829 N94-19927
Disks of YBa2Cu3O7 shocked to 10 GPa pressures
[DE94-000464] p 2031 N94-21931

COMPRESSION RATIO
A comparison of some of the most current methods of image compression
[AD-A271841] p 1907 N94-20525

COMPRESSION TESTS
Hydrodynamic compressibility of high-strength ceramics
[DE93-019424] p 1698 N94-19903
Deformation of an alumina-zirconia-silicon carbide-whisker reinforced composite
[DE93-040244] p 1676 N94-21559

COMPRESSIVE STRENGTH
Compression strength of composite primary structural components
[NASA-CR-194561] p 1830 N94-20159
Properties and potential of high-temperature niobium beryllides
[DE93-019169] p 1690 N94-20233
The effects of processing and constituent materials on compressive strength of thick composite laminates
[AD-A271912] p 1673 N94-20490
Strength and deformation properties of basaltic lava flows on planetary surfaces p 1862 N94-20747
Composite materials with improved properties in compression
[AD-A272837] p 1675 N94-21176

COMPRESSOR ROTORS
Applicability and performance benefits of XD (Tradename) titanium aluminides to expendable gas turbine engines
[AD-A272998] p 1648 N94-21268

COMPRESSORS
Navy GTE seal development activity
p 1655 N94-21794
Performance calculations and research direction for a water enhanced regenerative gas turbine cycle
[DE93-019866] p 1826 N94-21983

COMPTON EFFECT
An assessment of COMSCAN, a Compton backscatter imaging camera, for the one-sided non-destructive inspection of aerospace components
[AD-A271331] p 1806 N94-19837
New relativistic S-matrix results for scattering -- beyond the usual anomalous factors/beyond impulse approximation
[DE93-019148] p 1971 N94-20096
Photoabsorption and Compton scattering in ionization of helium at high photon energies
[DE94-000380] p 1974 N94-21658
Single and double ionization of helium by high-energy photon impact
[DE94-000381] p 1975 N94-21785
The polarization sensitivity of the liquid xenon imaging telescope p 2056 N94-22282
The effect of Compton scattering on the double to single ionization ratio in helium
[DE94-000884] p 1827 N94-22390
Compton Gamma Ray Observatory highlights of the sky survey p 2002 N94-22642

COMPUTATION
A declarative approach for first-order built-in's of PROLOG
[CWI-CS-R9246] p 1909 N94-21026
An NP set with no co-DP sparse subset
[TR-475] p 1954 N94-21199
Advice from nonadaptive queries to NP
[TR-470] p 1911 N94-21200
Threshold computation and cryptographic security
[TR-461] p 1912 N94-21285
Promises and fault-tolerant database access
[TR-447] p 2043 N94-21287
On the closure properties of #P in the context of PF of #P
[TR-445] p 1955 N94-21456
Mathematical theory of thermodynamics of computation
[CWI-CS-R9251] p 2038 N94-21533
Using parallel banded linear system solvers in generalized eigenvalue problems
[NASA-CR-191540] p 1915 N94-21584
A Hopfield neural net for discrete Fourier transform calculation p 1783 N94-22184

COMPUTATIONAL CHEMISTRY
Boost-phase discrimination research
[NASA-TM-109347] p 1666 N94-19818
Application of molecular modeling to biological processing
[AD-A272612] p 1974 N94-21185

COMPUTATIONAL FLUID DYNAMICS
Boost-phase discrimination research
[NASA-TM-109347] p 1666 N94-19818
Experimental investigation of nozzle/plume aerodynamics at hypersonic speeds
[NASA-CR-194628] p 1636 N94-20014
Future technical directions p 1668 N94-20072
Distributed loss model: Application to a spatial turbopump inducer p 1668 N94-20078
Cavitation modelling p 1668 N94-20079
Three dimensional unsteady flow calculations in radial components p 1669 N94-20080
Shape optimization governed by the Euler equations using an adjoint method
[NASA-CR-191555] p 1950 N94-20092
Head-on collision of drops: A numerical investigation
[NASA-TM-106394] p 1798 N94-20167
Turbulence modeling for high speed compressible flows
[NASA-CR-194547] p 1799 N94-20210
Prediction and control of vortex-dominated and vortex-wake flows
[NASA-CR-194722] p 1637 N94-21054
Computational and analytical methods in nonlinear fluid dynamics
[AD-A272722] p 1802 N94-21169
Reaction zone models for vortex simulation of turbulent combustion
[AD-A272723] p 1681 N94-21213
An efficient numerical method for three-dimensional hypersonic flow
[AD-A272506] p 1637 N94-21411
Measurement and prediction of the flow through an annular turbine cascade
[AD-A272530] p 1803 N94-21417
The Sixth Copper Mountain Conference on Multigrid Methods, part 2
[NASA-CP-3224-PT-2] p 1955 N94-21464
Looking for O(N) Navier-Stokes solutions on non-structured meshes p 1806 N94-21471
Superpatch
[NASA-CR-177627] p 1914 N94-21489
Mathematical theory of thermodynamics of computation
[CWI-CS-R9251] p 2038 N94-21533
Flow interaction experiment. Volume 1: Aerothermal modeling, phase 1
[NASA-CR-189192-VOL-1] p 1648 N94-21582
Flow interaction experiment. Volume 2: Aerothermalmodeling, phase 2
[NASA-CR-189192-VOL-2] p 1648 N94-21583
Order of accuracy of QUICK and related convection-diffusion schemes
[NASA-TM-106402] p 1959 N94-21588
A study of the compressible flow through a diffusing S-duct
[NASA-TM-106411] p 1638 N94-21591
Comparison of mixing calculations for reacting and non-reacting flows in a cylindrical duct
[NASA-TM-106435] p 1649 N94-21758
The 1992 Seals Flow Code Development Workshop
[NASA-CP-10124] p 1654 N94-21790
Computation of the sound generated by isotropic turbulence
[NASA-CR-191543] p 1804 N94-21880
Unstructured Grid Generation Techniques and Software
[NASA-CP-10119] p 1918 N94-22350
Unstructured grid research and use at NASA Lewis Research Center p 1919 N94-22353
Johnson Space Center CFD grid generation requirements p 1919 N94-22355
The 3-D unstructured mesh generation using local transformations p 1919 N94-22356
Status of VGRID/USM3D aero analysis system p 1919 N94-22357
Unstructured low-Mach number viscous flow solver p 1919 N94-22358
Three-dimensional unstructured grid method applied to turbomachinery p 1919 N94-22360
Development of a gridless CFD method p 1919 N94-22361
An advancing-front Delaunay-triangulation algorithm designed for robustness p 1920 N94-22362
The 3D Euler solutions using automated Cartesian grid generation p 1920 N94-22367
Time-dependent grid adaptation for meshes of triangles and tetrahedra p 1920 N94-22369
NASA data exchange standards for computational fluid dynamics p 1920 N94-22371
F2D users manual: A two-dimensional compressible gas flow code
[DE94-000653] p 1805 N94-22386

COMPUTATIONAL GEOMETRY
Eliminating amortization: On data structures with guaranteed response time
[TR-439] p 2049 N94-20098
Achieving high data reduction with integral cubic B-splines
[NASA-CR-177628] p 1966 N94-21881
An advancing-front Delaunay-triangulation algorithm designed for robustness p 1920 N94-22362
Dynamic mesh adaption for triangular and tetrahedral grids p 1920 N94-22363
Computational geometry issues p 1920 N94-22370
Surface acquisition through virtual milling p 1920 N94-22372

COMPUTATIONAL GRIDS
Finite element mesh generation and analysis of solder joints for fatigue life predictions
[AD-A271329] p 1829 N94-19937
A new conformal absorbing boundary condition for finite element meshes and parallelization of FEMATS
[NASA-CR-194740] p 1950 N94-20034
A comparative study of an ABC and an artificial absorber for truncating finite element meshes
[NASA-CR-194275] p 1716 N94-20160
Time-domain analysis of planar microstrip devices using a generalized Yee-algorithm based on unstructured grids p 1724 N94-20431
Multigrid approach to solving the long transportation problem on a regular grid in cost space
[AD-A272323] p 1909 N94-21038
Approximate methods for N-component solute transport and ion-exchange
[CWI-NM-R9223] p 1910 N94-21078
Adaptive grids for quasilinear parabolic systems in one space dimension
[ETN-93-93611] p 1954 N94-21137
Numerical modeling of a propegating crack
[AD-A272604] p 1832 N94-21421
The block adaptive multigrid method applied to the solution of the Euler equations p 1641 N94-21472
A multigrid method for steady Euler equations on unstructured adaptive grids p 1957 N94-21476
Two-level Schwartz methods for nonconforming finite elements and discontinuous coefficients p 1957 N94-21477
Multigrid solution of the Navier-Stokes equations on highly stretched grids with defect correction p 1806 N94-21481
Superpatch
[NASA-CR-177627] p 1914 N94-21489
Direct simulation of shock-induced mixing layer
[DE93-040498] p 1803 N94-21531
Local uniform grid refinement and brine transport in porous media with inhomogeneities
[CWI-NM-R9224] p 1803 N94-21609
RHALE: A 3-D MMALE code for unstructured grids
[DE93-019405] p 1916 N94-21635
User's guide for the casting process simulator software CaPS-2D, version 1.0
[DE93-040398] p 1917 N94-21923
A moving finite element model of the tokamak scrapeoff layer
[DE94-000673] p 1997 N94-21965
Software systems used for unstructured grid generation at NASA Langley p 1918 N94-22351
NASA-Ames Research Center unstructured technology development p 1919 N94-22352
Unstructured grid research and use at NASA Lewis Research Center p 1919 N94-22353
Robust unstructured grid generation with VGRID p 1919 N94-22359
Three-dimensional unstructured grid method applied to turbomachinery p 1919 N94-22360
An advancing-front Delaunay-triangulation algorithm designed for robustness p 1920 N94-22362
Dynamic mesh adaption for triangular and tetrahedral grids p 1920 N94-22363
Cartesian-cell based grid generation and adaptive mesh refinement p 1920 N94-22364
The 2D and 3D hypersonic flows with unstructured meshes p 1920 N94-22365
Unstructured surface grid generation p 1920 N94-22366
The 3D Euler solutions using automated Cartesian grid generation p 1920 N94-22367

Accuracy assessment for grid adaptation
p 1920 N94-22368
Time-dependent grid adaptation for meshes of triangles and tetrahedra p 1920 N94-22369
Computational geometry issues p 1920 N94-22370
NASA data exchange standards for computational fluid dynamics p 1920 N94-22371

COMPUTER AIDED DESIGN
Handbook. Volume 3: Digital systems validation book plan
[DOT/FAA/CT-93/16-VOL-3] p 1647 N94-20053
VLSI design for reliability-current density
[AD-A270719] p 1749 N94-20110
PREVAIL-DM: A framework-based environment for formal hardware verification
[RR-899] p 1905 N94-20164
A proposal for reverse engineering CASE tools to support new software development
[DE93-040207] p 1906 N94-20281
Design structuring and allocation optimization (Destination) prototype level 1 user's manual
[AD-A272115] p 1929 N94-20571
The flow of gas across the piston-segments-cylinder interface
[ECL-92-40] p 1824 N94-20594
The electronics technology policy of the NLR Informatics Division: The NLR electronics CAE infrastructure
[NLR-TP-91001-U] p 1753 N94-21067
Design and implementation of GaAs HBT circuits with ACME p 1758 N94-21117
An investigation into the state of the practice of CASE tool integration
[AD-A272441] p 1912 N94-21205
VLSI design for reliability-hot carrier effects
[AD-A271586] p 1761 N94-21256
Hybrid finite element/waveguide mode analysis of passive RF devices
[AD-A273074] p 1740 N94-21518
Model-based automatic generation of grasping regions
[NASA-TM-104785] p 1946 N94-21550
Computer-Aided Test Equipment Graphics System (CATEGS)
[DE94-000383] p 1915 N94-21561
Advanced failure analysis laboratory equipment networking
[DE93-019070] p 1916 N94-21633
The Milling assistant, case-based Reasoning, and machining strategy: A report on the development of automated numerical control programming systems at New Mexico State University
[DE93-041101] p 2029 N94-21690
HDL to verification logic translator
p 1766 N94-21717
Higher order Bezier circles
[NASA-CR-177633] p 1897 N94-21784
Proceedings of the IMOG (Interagency Manufacturing Operations Group) Numerical Systems Group
[DE94-001009] p 1917 N94-21851
User's guide for the casting process simulator software CaPS-2D, version 1.0
[DE93-040398] p 1917 N94-21923
Information sciences and business enterprises
p 2046 N94-22059
Computer-aided design system for objects location and reservoir with dispersed resource evolution investigation
p 1923 N94-22064
The distributed CAD system for LSI/VLSI design
p 1923 N94-22068
NASA data exchange standards for computational fluid dynamics p 1920 N94-22371

COMPUTER AIDED MANUFACTURING
Feature-based tolerancing for intelligent inspection process definition
[DE93-017984] p 1906 N94-20311
Graphical interactive planning of robotic applications with support of integrated simulation
[ETN-93-93793] p 1944 N94-21057
Advanced failure analysis laboratory equipment networking
[DE93-019070] p 1916 N94-21633
The Milling assistant, case-based Reasoning, and machining strategy: A report on the development of automated numerical control programming systems at New Mexico State University
[DE93-041101] p 2029 N94-21690
Proceedings of the IMOG (Interagency Manufacturing Operations Group) Numerical Systems Group
[DE94-001009] p 1917 N94-21851
Information sciences and business enterprises
p 2046 N94-22059
Manufacturing and information technology
p 2046 N94-22082

COMPUTER AIDED MAPPING
Application of SPOT to GIS/LIS in land capability evaluation for regional planning of JAICO semi-arid region of Piaui, Brazil p 1838 N94-20955

COMPUTER AIDED TOMOGRAPHY
Three-dimensional dynamic thermal imaging of structural flaws by dual-band infrared computed tomography
[DE93-019575] p 1908 N94-20316
A geometrical process for three dimensional osteotomy planning
[ETN-93-93602] p 1892 N94-21134
Optimal resolution in maximum entropy image reconstruction from projections with multigrid acceleration p 1955 N94-21465

COMPUTER ASSISTED INSTRUCTION
Weather tutor 1: Stability basics
[AD-A270758] p 1866 N94-20565
A graphical user-interface development tool for intelligent computer-assisted instruction systems
[AD-A272988] p 1912 N94-21265
Use of computers in the instruction of integral calculus
[AD-A272500] p 1913 N94-21409
The effects of instructional sets on reactions to and performance on an intelligent tutoring system
[NASA-CR-194739] p 1895 N94-21810

COMPUTER COMPONENTS
Rad-hard computer elements for space applications
p 1753 N94-21082
Crystal ball gazing p 1925 N94-22477

COMPUTER DESIGN
Multiple-fold clustered processor mesh array
p 1757 N94-21113
A novel visual hardware behavioral language
p 1765 N94-21715

COMPUTER GRAPHICS
A software architecture for the construction and management of real-time virtual worlds
[AD-A271465] p 1904 N94-20091
A full-color, high-resolution laser projector for a flight simulator visual display
[AD-A270578] p 1651 N94-20108
Weather tutor 1: Stability basics
[AD-A270758] p 1866 N94-20565
Simulating a user's preferences: Towards automated artificial evolution for computer generated images
[AD-A272058] p 1942 N94-20621
Analysis and evaluation of configuring of graphical systems on multiprocessor architectures
[ETN-93-93618] p 1930 N94-21018
AIDA: A graphical interactive system, adapted to the user
[ETN-93-93792] p 1908 N94-21020
Graphical interactive planning of robotic applications with support of integrated simulation
[ETN-93-93793] p 1944 N94-21057
A graphical user-interface development tool for intelligent computer-assisted instruction systems
[AD-A272988] p 1912 N94-21265
The three-dimensional Event-Driven Graphics Environment (3D-EDGE) p 1922 N94-21342
Simulation of tripod gaits for a hexapod underwater walking machine
[AD-A271719] p 1945 N94-21355
Computer-Aided Test Equipment Graphics System (CATEGS)
[DE94-000383] p 1915 N94-21561
Visualization on massively parallel computers using CM/AVS
[DE93-040151] p 1936 N94-21746
Geometric optimization
[DE93-040152] p 1917 N94-21764
Imaging vector fields using line integral convolution
[DE93-019922] p 1917 N94-21841
Post-experimental plots for high speed data acquisition program
[DE94-000956] p 1918 N94-22011
Unstructured grid research and use at NASA Lewis Research Center p 1919 N94-22353
Grid generation requirements at Marshall Space Flight Center p 1919 N94-22354
Status of VGRID/USM3D aero analysis system
p 1919 N94-22357
PROS: An IRAF based system for analysis of x ray data p 1925 N94-22461
Enhancements to IRAF/STSDAS graphics
p 1925 N94-22470
An IDL-based analysis package for COBE and other skycube-formatted astronomical data
p 1925 N94-22471
SKYMAP: Exploring the Universe in software
p 1927 N94-22511

COMPUTER INFORMATION SECURITY
Distributed Virtual System (DIVIRS) project
[NASA-CR-194360] p 1905 N94-20228
Threshold computation and cryptographic security
[TR-443] p 1907 N94-20536
Security management of electronic data interchange
[AD-A272962] p 1899 N94-21252
Threshold computation and cryptographic security
[TR-461] p 1912 N94-21285
Security evaluation of Unix networks
[AD-A273076] p 1945 N94-21520
Electronic resources for security related information: Reference document
[DE93-040488] p 2044 N94-21529
Formal methods in the design of critical software systems p 1779 N94-22158
Modeling and analysis of secure communication protocols using Petri net formalism
p 1784 N94-22194

COMPUTER NETWORKS
SISSY: An example of a multi-threaded, networked, object-oriented databased application
[DE93-019742] p 2041 N94-19811
Physics Detector Simulation Facility. Phase 2: System software description
[DE93-019745] p 1928 N94-19812
TCP performance analysis for wide area networks
[DE94-000449] p 1928 N94-19858
Robust, high-speed network design for large-scale multiprocessing
[AD-A271003] p 1716 N94-19977
Two-dimensional particle-in-cell simulation on transputer arrays
[DE93-017977] p 1972 N94-20181
Center for neural engineering
[AD-A271164] p 1890 N94-20185
Distributed Virtual System (DIVIRS) project
[NASA-CR-194360] p 1905 N94-20228
Research in image management and access
[NASA-CR-194797] p 1907 N94-20376
Delivery of very high bandwidth with ATM switches and SONET
[DE93-019432] p 1899 N94-20476
Standard ML signatures for a protocol stack
[AD-A272060] p 1908 N94-20622
Reduction of network cost and wiring in Ranade's butterfly routing
[CWI-CS-R9243] p 1930 N94-21023
Multi Wave Link: An interactive database for co-ordination of multiwavelength programs
[NASA-CR-194778] p 2043 N94-21055
On the optimality of FCFS for networks of multi-server queues
[CWI-BS-R9235] p 1944 N94-21160
Optimization of static traffic allocation policies
[CWI-BS-R9302] p 1930 N94-21161
The effects of block size on the performance of coherent caches in shared-memory multiprocessors
[AD-A272838] p 1899 N94-21177
Scheduling for locality in shared-memory multiprocessors
[AD-A272948] p 1930 N94-21228
Government Open Systems Interconnection Profile (GOSIP) transition strategy
[AD-A273005] p 1740 N94-21308
Networks Technology Conference
[NASA-CP-3241] p 1931 N94-21323
Security evaluation of Unix networks
[AD-A273076] p 1945 N94-21520
Electronic resources for security related information: Reference document
[DE93-040488] p 2044 N94-21529
Advanced failure analysis laboratory equipment networking
[DE93-019070] p 1916 N94-21633
Simulated behaviour of large scale SCI rings and tori
[DE93-040149] p 1935 N94-21745
Evaluation of DEC's GIGAswitch for distributed parallel computing
[DE94-001356] p 1936 N94-21853
Physics Detector Simulation Facility (PDSF) architecture/utilization
[DE93-019744] p 1936 N94-21919
Efficient communication primitives on mesh architectures with hardware routing
[DE93-018791] p 1936 N94-22032
Industry standards: Key to distributed computing
p 1938 N94-22070
Databases in distributed systems
p 2046 N94-22080
Investigation on construction of the database system for research and development of the global environment industry technology
[DE94-714890] p 1853 N94-22090
Introduction to the LaRC central scientific computing complex
[NASA-TM-104092-REV-1] p 1900 N94-22100
Distributed processing using Oracle7 and SQL*Net v2: An implementation story
[DE94-000494] p 1937 N94-22267
Everything you might want to know about the Internet but are afraid to ask!
[DE93-041118] p 2046 N94-22413
Scientific computing in the 1990ies: An astronomical perspective p 2057 N94-22440

Seeing the forest for the trees: Networked workstations as a parallel processing computer p 1938 N94-22454
A distributed clients/distributed servers model for STARCAT p 2047 N94-22469
Crystal ball gazing p 1925 N94-22477
Quality control of EUVE databases p 2047 N94-22490

COMPUTER PROGRAM INTEGRITY
Development and operations of the Astrophysics Data System
[NASA-CR-194691] p 2043 N94-21270

COMPUTER PROGRAMMING
Development and operation of the F/A-18 model control surface actuators
[AD-A271330] p 1645 N94-19914
System at the cross-roads of functional and logic programming
[PB93-191823] p 1928 N94-20009
An expert system executive for automated assembly of large space truss structures
[NASA-TM-4487] p 1939 N94-20089
A proposal for reverse engineering CASE tools to support new software development
[DE93-040207] p 1906 N94-20281
Four-channel HF receiving antenna array simulator
[AD-A271876] p 1732 N94-20471
A simplified token bus protocol specified using LOTOS
[TR-92-15] p 1910 N94-21062
Mathematician Wang Ju
[AD-A267882] p 1912 N94-21255
A response to Cheriton and Skeen's criticism of casual and totally ordered communication
[AD-A271486] p 1912 N94-21300
Computing solutions uniquely collapses the polynomial hierarchy
[TR-467] p 1954 N94-21314
The term processor Kimwitu manual and cookbook
[MEMO-INF-92-67] p 1914 N94-21454
Information Technology and Economic Modelling
[VTT-SYMP-135] p 2049 N94-22056
Soviet society informatization: The USSR state program p 2046 N94-22058
Information sciences and business enterprises p 2046 N94-22059
Industry standards: Key to distributed computing p 1938 N94-22070
Formal methods in the design of critical software systems p 1779 N94-22158
SPPTOOLS: Programming tools for the IRAF SPP language p 1925 N94-22474
Writing instrument interfaces with xf/tktcl p 1925 N94-22480
Fortran for the nineties p 1926 N94-22481
The Keck Task Library (KTL) p 2048 N94-22504
Development of the FITS tools package for multiple software environments p 1927 N94-22516

COMPUTER PROGRAMS
Set based analysis of ML programs
[AD-A270597] p 1902 N94-19948
Manual of DRANC (release 1.1): A computer program for the Dutch risk assessment of new chemical substances
[PB93-194827] p 1851 N94-19998
System at the cross-roads of functional and logic programming
[PB93-191823] p 1928 N94-20009
Absorption heat pump for space applications
[NASA-CR-194693] p 1845 N94-20066
A software architecture for the construction and management of real-time virtual worlds
[AD-A271465] p 1904 N94-20091
Qualifying codes under software quality assurance: Two examples as guidelines for codes that are existing or under development
[DE93-040452] p 1904 N94-20097
Object-oriented DFD models to present the functional and behavioral views
[DE93-040206] p 1906 N94-20280
A proposal for reverse engineering CASE tools to support new software development
[DE93-040207] p 1906 N94-20281
HERMES, a report generator for research on information processing in command posts: The effect of missing information
[IZF-1992-A-28] p 2042 N94-20310
Design structuring and allocation optimization (Destination) prototype level 1 user's manual
[AD-A272115] p 1929 N94-20571
Probability of detection calculations using MATLAB
[AD-A271958] p 1736 N94-20578
A parametric representation of a thunderstorm cell
[AD-A271983] p 1866 N94-20579
CERN-derived analysis of lunar radiation backgrounds p 2080 N94-20880
Test and evaluation: DOD has been slow in improving testing of software-intensive systems
[AD-A271541] p 1908 N94-20917
Imaging radar studies of atmospheric winds and waves
[AD-A271672] p 1866 N94-20918
Proving run-time properties of general programs w.r.t. constructive negation
[CWI-CS-R9245] p 1909 N94-21025
A declarative approach for first-order built-in's of PROLOG
[CWI-CS-R9246] p 1909 N94-21026
A software architecture for a small autonomous underwater vehicle navigation system
[AD-A272322] p 1643 N94-21037
GWB: Manual for the Grammar WorkBench version 1.5
[TR-92-14] p 1909 N94-21061
The readiness growth model: A quantitative analysis of software risk
[AD-A272383] p 1910 N94-21144
Mathcad computer applications predicting antenna parameters from antenna physical dimensions and ground characteristics
[AD-A272987] p 1740 N94-21264
Development and operations of the Astrophysics Data System
[NASA-CR-194691] p 2043 N94-21270
Network command processing system overview p 1935 N94-21351
Integration opportunities for computer models, methods, and GIS used in Corps planning studies
[AD-A271714] p 2044 N94-21354
On a proposed symbolic dynamics for the Henon map
[AD-A272514] p 1955 N94-21359
The term processor Kimwitu manual and cookbook
[MEMO-INF-92-67] p 1914 N94-21454
MGGHAT: Elliptic PDE software with adaptive refinement, multigrid and high order finite elements p 1956 N94-21470
CMIFed: A presentation environment for porta ble hypermedia documents
[CWI-CS-R9305] p 2044 N94-21494
The Amsterdam hypermedia model: Extending hypertext to support real multimedia
[CWI-CS-R9306] p 2045 N94-21536
Computer-Aided Test Equipment Graphics System (CATEGS)
[DE94-000383] p 1915 N94-21561
A package for long integer arithmetic on the Cray Y-MP
[CWI-NM-R9227] p 1916 N94-21612
The 1992 Seals Flow Code Development Workshop
[NASA-CP-10124] p 1654 N94-21790
An evaluation of integration of the trace assertion method with the box structure method for coding in C++
[DE93-040480] p 1918 N94-21924
AJKA: An econometric macromodel for Finland p 2050 N94-22061
APL-technology of computer simulation p 1923 N94-22077
Method and software for decision making in public problems p 1923 N94-22087
Canadian Conference on Electrical and Computer Engineering, volumes 1 and 2
[ISBN-0-9694170-2-0] p 1770 N94-22101
Tests of logic spaces: A new strategy for certifying the accuracy of programs p 1772 N94-22116
Modeling software systems for data flow testing p 1772 N94-22117
The conformance testing methodology to CTRON (communication and central TRON) extended OS p 1772 N94-22118
Unstructured Grid Generation Techniques and Software
[NASA-CP-10119] p 1918 N94-22350
F2D users manual: A two-dimensional compressible gas flow code
[DE94-000653] p 1805 N94-22386
Towards the formal verification of the requirements and design of a processor interface unit: HOL listings
[NASA-CR-191466] p 1937 N94-22414
Second Annual Conference on Astronomical Data Analysis Software and Systems. Abstracts
[NASA-TM-108245] p 2057 N94-22438
Multifrequency data analysis software on STARLINK p 1925 N94-22443
A self-defining hierarchical data system p 2046 N94-22448
A structured data transfer protocol p 2047 N94-22450
The ALEXIS data processing package: An IDL based system p 2047 N94-22453
New IRAF stellar photometry software p 1925 N94-22464
Enhancements to IRAF/STSDAS graphics p 1925 N94-22470
CCD data acquisition systems at Lick and Keck Observatories p 2047 N94-22495
AXAF user interfaces for heterogeneous analysis environments p 1926 N94-22507
Khoros software specification format and interoperability p 1927 N94-22523
The STARLINK software collection p 1927 N94-22545
Solar full-disk magnetic field image receiving system and observation software p 2079 N94-22552
Parallel functional programming in SISAL: Fictions, facts, and future
[DE93-040486] p 1937 N94-22558
Time-dependent reliability analysis of ceramic engine components p 1828 N94-22619

COMPUTER STORAGE DEVICES
A novel method for characterizing the electrical Priorities of lead Zirconate Titanate (PZT) ferroelectric films and memory devices
[AD-A270463] p 2013 N94-19966
Single-event upset testing of the performance semiconductor 1750A CMOS/SOS chip set
[AD-A271158] p 2015 N94-20184
Comparison of single event upset rates for microelectronic memory devices during interplanetary solar particle events p 1754 N94-21085

COMPUTER SYSTEMS DESIGN
Fast mutual exclusion, even with contention
[AD-A272947] p 1912 N94-21227
Software coherence in multiprocessor memory systems
[NASA-CR-194696] p 1931 N94-21272
Termination and confluence of rule execution
[CWI-CS-R9309] p 1916 N94-21587
A 20 MHz CMOS reorder buffer for a superscalar microprocessor p 1764 N94-21700
Micro-rollback and self-recovery synthesis p 1765 N94-21707
Application development in a PC/LAN environment p 1923 N94-22067
Use of open systems for control, analysis, and data acquisition of the DIII-D tokamak
[DE94-001101] p 1998 N94-22089
Canadian Conference on Electrical and Computer Engineering, volumes 1 and 2
[ISBN-0-9694170-2-0] p 1770 N94-22101
System level modelling using Petri nets and VHDL p 1772 N94-22113
Fault tolerance for real-time multiprocessor operating systems p 1788 N94-22216
On AIPS++, a new astronomical information processing system p 2047 N94-22463
Crystal ball gazing p 1925 N94-22477
Khoros software specification format and interoperability p 1927 N94-22523

COMPUTER SYSTEMS PERFORMANCE
TCP performance analysis for wide area networks
[DE94-000449] p 1928 N94-19858
Global combine on mesh architectures with wormhole routing
[DE93-018792] p 1903 N94-19959
Specification and generation of Markov reward models
[MEMO-INF-92-60] p 1963 N94-21058
Avoiding and tolerating latency in large-scale next-generation shared-memory multiprocessors p 1753 N94-21081
The effects of block size on the performance of coherent caches in shared-memory multiprocessors
[AD-A272838] p 1899 N94-21177
Real-time fault tolerant computer systems
[AD-A272909] p 1899 N94-21230
Uniform self-stabilizing leader election. Part 1: Complete graph protocols
[CWI-CS-R9308-PT-1] p 1935 N94-21549
Efficient communication primitives on mesh architectures with hardware routing
[DE93-018791] p 1936 N94-22032
Introduction to the LaRC central scientific computing complex
[NASA-TM-104092-REV-1] p 1900 N94-22100
Scientific computing in the 1990ies: An astronomical perspective p 2057 N94-22440

COMPUTER SYSTEMS PROGRAMS
Physics Detector Simulation Facility. Phase 2: System software description
[DE93-019745] p 1928 N94-19812
NAVSPASUR sensor system digital signal processing receiver. Volume 2: Function and capabilities of hardware and software components
[AD-A272900] p 1739 N94-21218
The NCC project: A quality management perspective p 1828 N94-21324
Developing a space network interface simulator: The NTS approach p 1933 N94-21343

COMPUTER SYSTEMS SIMULATION
APL-technology of computer simulation
p 1923 N94-22077
Formal verification of an ALU
p 1772 N94-22114
COMPUTER TECHNIQUES
A concept for implementing hypermedia technology in computer aided workplaces in medicine
[ETN-93-95057] p 1889 N94-20022
Time-domain analysis of planar microstrip devices using a generalized Yee-algorithm based on unstructured grids
p 1724 N94-20431
Mathcad computer applications predicting antenna parameters from antenna physical dimensions and ground characteristics
[AD-A272987] p 1740 N94-21264
Implementing Electronic Data Interchange (EDI) with small business suppliers in the pre-award acquisition process
[AD-A271767] p 1945 N94-21305
Extracting information from wrong answers in computerized adaptive testing
[AD-A272832] p 1894 N94-21434
Compatibility evaluation and research on the Computerized Adaptive Screening Test (CAST): User and programmer's guide
[AD-A273112] p 1894 N94-21510
Structured multimedia authoring
[CWI-CS-R9304] p 2044 N94-21535
An expert system of econometric analysis
p 2052 N94-22081
Surface acquisition through virtual milling
p 1920 N94-22372
Scientific computing in the 1990ies: An astronomical perspective
p 2057 N94-22440
The Keck keyword layer
p 1925 N94-22460
A high temperature fatigue life prediction computer code based on the total strain version of StrainRange Partitioning (SRP)
p 1835 N94-22620
COMPUTER VISION
Recognizing 3-D objects using 2-D images
[AD-A271005] p 1983 N94-19819
Robust photo-topography by fusing shape-from-shading and stereo
[NASA-CR-194697] p 1806 N94-19920
On geometric and algebraic aspects of 3D affine and projective structures from perspective 2D views
[AD-A270520] p 1983 N94-19968
Robust and efficient 3D recognition by alignment
[AD-A270839] p 1904 N94-20041
Statistical object recognition
[AD-A270887] p 1962 N94-20113
Head-centered orientation strategies in animate vision
[TR-442] p 1894 N94-20520
Visual tracking
[AD-A271686] p 1943 N94-20920
Recognition by prototypes
[AD-A271687] p 1943 N94-20921
Graphical interactive planning of robotic applications with support of integrated simulation
[ETN-93-93793] p 1944 N94-21057
Nature's crucible: Manufacturing optical nonlinearities for high resolution, high sensitivity encoding in the compound eye of the fly, Musca domestica
p 1755 N94-21095
Adaptive analog video signal conditioner
p 1744 N94-21099
Internal camera calibration using rotation and geometric shapes
[AD-A272718] p 1808 N94-21167
Goal-oriented dynamic vision
[TR-466] p 1945 N94-21315
Experiments in knowledge refinement for a large rule-based system
[AD-A272055] p 1809 N94-21445
A 3-D vision method for estimating workspace occupancy of a power-line maintenance robot
p 1770 N94-22105
Optimal object modelling for an active-vision system
p 1771 N94-22107
Segmentation and fitting by residual consensus
p 1771 N94-22109
Sensor integration and data fusion for object localization in robotic workcells
p 1774 N94-22130
Ultrasonic sensor vision in robotics
p 1775 N94-22131
Segmenting the optical flow due to the motion of several rigid objects
p 1777 N94-22147
A neural network for multiresolution edge detection
p 1779 N94-22163
A software environment for the exploitation of the MAR image sensor
p 1785 N94-22200
A pyramid neural network architecture for stereo fusion
p 1785 N94-22201
An approach to the estimation of ground structure and aircraft motion from aerial image sequences
p 1789 N94-22226
Memory based vision: A new concept
p 1790 N94-22228
An insensitive algorithm for template matching with correlation
p 1793 N94-22249
Mobile robot perception in unknown and unstructured dynamic voxel environments
[ISBN-0-315-83951-1] p 1947 N94-22591
COMPUTERIZED SIMULATION
Simulating supersymmetry with ISAJET 7.0/ISASUSY 1.0
[DE93-018266] p 1969 N94-19804
State-space models for multichannel detection
[AD-A270608] p 1715 N94-19816
Some topics in regenerative steady-state simulation
[AD-A271145] p 1902 N94-19855
Pointing control design for autonomous space vehicle applications
[DE93-019943] p 1657 N94-19863
Longitudinal beam dynamics for heavy ion fusion using WARPrz
[DE93-019154] p 1992 N94-19915
A benchmark study of 2D and 3D finite element calculations simulating dynamic pulse buckling tests of cylindrical shells under axial impact
[DE93-018859] p 1829 N94-19940
The best of GYMNOS: A users guide
[DE93-041275] p 1992 N94-19991
CTH: A software family for multi-dimensional shock physics analysis
[DE93-019428] p 1904 N94-20052
A software architecture for the construction and management of real-time virtual worlds
[AD-A271465] p 1904 N94-20091
Qualifying codes under software quality assurance: Two examples as guidelines for codes that are existing or under development
[DE93-040452] p 1904 N94-20097
Toward a neurobiological theory of visual attention
[AD-A270724] p 1890 N94-20112
Development of a numerical simulation model for a-Si:H solar cells and application to the analysis of experimentally obtained spectral characteristics
[ETN-93-95061] p 1846 N94-20151
Multi-disciplinary coupling effects for integrated design of propulsion systems
[NASA-TM-106349] p 1830 N94-20170
Two-dimensional particle-in-cell simulation on transputer arrays
[DE93-017977] p 1972 N94-20181
High resolution signal processing
[AD-A271181] p 1717 N94-20215
A breakdown model for the bipolar transistor to be used with circuit simulators
[DE93-019422] p 1750 N94-20218
Computational model of a magnetic modulator for copper lasers
[DE93-019603] p 1815 N94-20223
Fast data parallel polygon rendering
[DE93-040157] p 1929 N94-20279
The GEM Silicon Tracking System
[DE93-040133] p 2016 N94-20322
Embedded microclusters in zeolites and cluster beam sputtering: Simulation on parallel computers
[DE94-000741] p 1701 N94-20352
An investigation into the integration of meter-level range and millimeter-level phase data using a multimode stimulation for optimal filter estimation software package
[AD-A267955] p 1751 N94-20483
Time warp operating system version 2.7 internals manual
[NASA-CR-194798] p 1899 N94-20549
Numerical simulations of hypervelocity impact experiments involving single Whipple bumper shields
[AD-A272123] p 1831 N94-20572
Mathematical model and analysis of the Tactical Unmanned Ground Vehicle (TUGV) using computer simulation
[AD-A272258] p 1824 N94-20576
A parametric representation of a thunderstorm cell
[AD-A271983] p 1866 N94-20579
Spread spectrum random access networks
[AD-A272280] p 1737 N94-20585
Modeling of particle dispersion in a stationary isotropic homogeneous turbulence by large scale numerical simulation
[ETN-93-94604] p 1801 N94-20601
Research, Development, Training, and Evaluation (RDTE) support delivery order 1: Computational cognitive models
[AD-A271837] p 1894 N94-20610
Asteroid collisions: Target size effects and resultant velocity distributions
p 2083 N94-20729
Mineralogy and cooling history of magnesian lunar granulite 67415
p 2124 N94-20811
The sand bag model of the dispersion of the cosmic body in the atmosphere
p 2084 N94-20823
Numerical simulation of lava flows: Applications to the terrestrial planets
p 1863 N94-20904
Formulation of a next-generation interior ballistic code
[AD-A271539] p 1801 N94-20915
A contribution to development and parameter extraction of SPICE compatible macromodels for discrete bipolar transistors
[HMI-B-499] p 1753 N94-21021
Graphical interactive planning of robotic applications with support of integrated simulation
[ETN-93-93793] p 1944 N94-21057
A geometrical process for three dimensional osteotomy planning
[ETN-93-93602] p 1892 N94-21134
A formulation of quantum statistical mechanics based on the Feynman path centroid density 2 dynamical properties
[AD-A272698] p 2037 N94-21166
Power conditioning system modelling for nuclear electric propulsion
[NASA-CR-191136] p 1846 N94-21179
Standard atmospheres for engagement modeling
[AD-A272447] p 1858 N94-21207
A graphical user-interface development tool for intelligent computer-assisted instruction systems
[AD-A272988] p 1912 N94-21265
Analysis of a diesel-electric hybrid urban bus system
[DE93-019514] p 1825 N94-21297
Computerized simulations with cellular automates for cloud formation
[GKSS-92/E/22] p 1867 N94-21312
The Composite Analytic and Simulation Package or RFI (CASPR) on a coded channel
p 1744 N94-21339
The three-dimensional Event-Driven Graphics Environment (3D-EDGE)
p 1922 N94-21342
Satellite Communication Hardware Emulation System (SCHES)
p 1744 N94-21344
Array Simulations Platform (ASP) predicts NASA Data Link Module (NDLM) performance
p 1744 N94-21348
Simulation of tripod gaits for a hexapod underwater walking machine
[AD-A271719] p 1945 N94-21355
Electrostatic charging and secondary effects in materials submitted to radiation in space
p 1661 N94-21383
Development and tests of a cloud physics parameterization for real-time aviation and public numerical weather forecasting
[PB93-202711] p 1868 N94-21427
Simulation studies of space-charge-dominated beam transport in large aperture ratio quadrupoles
[DE93-019238] p 1981 N94-21440
One- and multi-component theories of mixtures
[DE93-040543] p 1966 N94-21511
Direct simulation of shock-induced mixing layer
[DE93-040498] p 1803 N94-21531
The energy performance of prototype holographic glazings
[DE93-040451] p 1809 N94-21545
Development and evaluation of a profile negotiation process for integrating aircraft and air traffic control automation
[NASA-TM-4360] p 1643 N94-21606
RHALE: A 3-D MMALE code for unstructured grids
[DE93-019405] p 1916 N94-21635
Simulation of traveling-wave output structures for high power RF tubes
[DE93-041005] p 1763 N94-21685
Probabilistic assessment of composite structures
[NASA-TM-106368] p 1832 N94-21757
Stochastic simulation for imaging spatial uncertainty: Comparison and evaluation of available algorithms
[DE93-040058] p 1916 N94-21761
Performance assessment of low pressure nuclear thermal propulsion
[NASA-TM-108433] p 1671 N94-21860
Simulations of diffusion-reaction equations with implications to turbulent combustion modeling
[NASA-CR-191536] p 1804 N94-21861
User's guide for the casting process simulator software CaPS-2D, version 1.0
[DE93-040398] p 1917 N94-21923
An evaluation of integration of the trace assertion method with the box structure method for coding in C++
[DE93-040480] p 1918 N94-21924
A moving finite element model of the tokamak scrapeoff layer
[DE94-000673] p 1997 N94-21965
Transferable tight-binding parameters: An application to Ni and Ni-Al alloys
[DE94-001044] p 1695 N94-22023
Parallel runway requirement analysis study. Volume 1: The analysis
[NASA-CR-191549-VOL-1] p 1644 N94-22277

Parallel runway requirement analysis study. Volume 2: Simulation manual
[NASA-CR-191549-VOL-2] p 1644 N94-22278
Simulation of clear-sky outgoing longwave radiation over the oceans using operational analysis
p 1861 N94-22290
Calibration of radiation codes in climate models: Comparison of calculations with observations from the SPECtral Radiation Experiment (SPECTRE)
p 1879 N94-22337
Simulating the Euclidean time Schroedinger equations using an INTEL iPSC/860 hypercube: Application to the t-J model of high-T(sub c) superconductivity
[DE94-000489] p 2035 N94-22385
Computer simulation of molecular response at a shock front
[DE94-001050] p 1977 N94-22396
Smoothed-particle hydrodynamics and nonequilibrium molecular dynamics
[DE94-001059] p 1977 N94-22400
HST PSF simulation using Tiny Tim
p 1926 N94-22498
Verification of frequency scaling laws for capacitive rf discharges using two-dimensional simulations
[DE94-001306] p 1999 N94-22595
An overview of computational simulation methods for composite structures failure and life analysis
p 1835 N94-22617
Laboratory structure of the heliopause
p 2003 N94-22648
The onset and spectra of a magnetized Langmuir turbulence p 2006 N94-22673
Solar wind-magnetosphere interaction as simulated by a 3D, EM particle code p 2007 N94-22674
Hydrodynamical winds from an accretion disk
p 2008 N94-22683

COMPUTERS
Information Technology and Economic Modelling
[VTT-SYMP-135] p 2049 N94-22056
Introduction to the LaRC central scientific computing complex
[NASA-TM-104092-REV-1] p 1900 N94-22100
Canadian Conference on Electrical and Computer Engineering, volumes 1 and 2
[ISBN-0-9694170-2-0] p 1770 N94-22101

CONCENTRATION (COMPOSITION)
A long-term change of the AR/KR/XE fractionation in the solar corpuscular radiation p 2136 N94-20875

CONCENTRATORS
An improved patch for radiative coolers
[NASA-CASE-GSC-13503-1] p 1822 N94-20127

CONCRETES
Preparation of concrete specimens for microstructural image analysis studies p 1707 N94-21891
Optical air pore analysis p 1708 N94-21892
Determination of pore structure of concrete from thin sections by image analysis p 1708 N94-21895

CONCURRENT PROCESSING
Interval timed coloured petri nets and their analysis
[PB93-191732] p 1903 N94-19992
Total order assumption
[PB93-191740] p 1903 N94-19993
Bottom-up abstract interpretation of logic programs
[PB93-191773] p 1928 N94-19995
Multi-CPU plasma fluid turbulence calculations on a CRAY Y-MP C90
[DE93-015425] p 1801 N94-20562
MINIFOLD: A kernel for a MANIFOLD-like coordination language
[CWI-CS-R9252] p 1915 N94-21534

CONDENSATES
Atmospheric moisture collection device
[AD-D015935] p 1865 N94-20332
Molecular equilibria and condensation sequences in carbon rich gases p 2083 N94-20756

CONDENSATION NUCLEI
Shock induced condensation in fluids of high molar specific heat: Shock structure and relaxation
[MPIS-106/1993] p 1798 N94-20145

CONDENSING
Outgassing data for selecting spacecraft materials
[NASA-RP-1124-REV-3] p 1676 N94-21889

CONDITIONING (LEARNING)
Conditioned taste aversion induced by motion is prevented by selective vagotomy in the rat
p 1887 N94-21908
Investigating motion sickness using the conditioned taste aversion paradigm p 1888 N94-21913
Conditioned taste aversion and motion sickness in cats and squirrel monkeys p 1888 N94-21914
Current status: Animal models of nausea
p 1889 N94-21915

CONDUCTING FLUIDS
Electrode array electromagnetic velocimeter
[AD-D015950] p 1806 N94-19882

CONDUCTION BANDS
Photoluminescence spectroscopy of zinc germanium diphosphide (ZnGeP2)
[AD-A270705] p 1678 N94-19953

CONDUCTORS
Time-domain analysis of planar microstrip devices using a generalized Yee-algorithm based on unstructured grids
p 1724 N94-20431
Magnetic force microscopy/current contrast imaging: A new technique for internal current probing of IC's
[DE93-040754] p 1761 N94-21532

CONES (VOLCANOES)
Venus pancake dome formation: Morphologic effects of a cooling-induced variable viscosity during emplacement p 2110 N94-20732

CONFERENCES
Surface science at the solid liquid interface
[AD-A271422] p 1678 N94-19839
Proceedings of the 8th International Symposium on Applications of Ferroelectrics
[AD-A270679] p 1749 N94-20012
The Seventh International Conference on Composite Structures, volume 25, numbers 1-4
[AD-A269961] p 1672 N94-20031
Proceedings of the 15th Annual Seismic Research Symposium
[AD-A271458] p 1855 N94-20090
Proceedings of the Twentieth Annual Technologyfest
p 1645 N94-20188
AIAA Techfest 29 proceedings
[NIAR-93-1] p 1635 N94-20191
Biotechnology and composite materials
[AD-A264278] p 1673 N94-20327
Progress In Electromagnetics Research Symposium (PIERS)
[NASA-CR-194629] p 1718 N94-20403
The Seventh International Symposium on Methodologies for Intelligent Systems (Poster Session)
[AD-A272125] p 1942 N94-20573
Twenty-Fourth Lunar and Planetary Science Conference. Part 3: N-Z
[NASA-CR-193149] p 2092 N94-20636
The Fifth NASA Symposium on VLSI Design
[NASA-CR-194644] p 1753 N94-21079
Lecture notes in artificial intelligence 689: The 7th International Symposium on Methodologies for Intelligent Symposium (ISMIS 1993)
[AD-A271768] p 1944 N94-21162
The 1992 USAF structural integrity program conference
[AD-A272876] p 1635 N94-21194
Hypervelocity impact
[AD-A272957] p 1831 N94-21249
Networks Technology Conference
[NASA-CP-3241] p 1931 N94-21323
The Sixth Copper Mountain Conference on Multigrid Methods, part 2
[NASA-CP-3224-PT-2] p 1955 N94-21464
The 13th International Conference on Magnetically Levitated Systems and Linear Drives MAGLEV 1993
[DE93-040381] p 1825 N94-21544
First Biomass Conference of the Americas: Energy, Environment, Agriculture, and Industry, volume 2
[DE94-000435] p 1847 N94-21562
The 1992 4th NASA SERC Symposium on VLSI Design
[NASA-CR-194591] p 1763 N94-21694
The 1992 Seals Flow Code Development Workshop
[NASA-CP-10124] p 1654 N94-21790
Proceedings of the Seventh Annual Conference on Fossil Energy Materials
[DE94-001091] p 1848 N94-21823
Proceedings of the IMOG (Interagency Manufacturing Operations Group) Numerical Systems Group
[DE94-001009] p 1917 N94-21851
Canadian Conference on Electrical and Computer Engineering, volumes 1 and 2
[ISBN-0-9694170-2-0] p 1770 N94-22101
Proceedings of the Workshop on New Generation of Radiation Budget Measurements From Space and Their Use in Climate Modelling and Diagnostic Studies
[MPIM-90] p 1860 N94-22283
The FIRE Cirrus Science Results 1993
[NASA-CP-3238] p 1871 N94-22292
Unstructured Grid Generation Techniques and Software
[NASA-CP-10119] p 1918 N94-22350
Second Annual Conference on Astronomical Data Analysis Software and Systems. Abstracts
[NASA-TM-108245] p 2057 N94-22438
Electronic publishing and intelligent information retrieval p 2047 N94-22479
Computational Methods for Failure Analysis and Life Prediction
[NASA-CP-3230] p 1833 N94-22608
Fourth International Toki Conference on Plasma Physics and Controlled Nuclear Fusion
[ESA-SP-351] p 2000 N94-22624

CONFIDENCE
Believing in the basis of the evidence
[TR-438] p 2039 N94-20364

CONFIDENCE LIMITS
A search for new gauge bosons in (bar p)p collisions at square root of s equals 1.8 TeV in the dielectron decay mode
[DE93-019901] p 1969 N94-19813

CONFIGURATION INTERACTION
An introduction to GUGA in the COLUMBUS Program System
[DE93-018994] p 1902 N94-19928

CONFIGURATION MANAGEMENT
NCCDS configuration management process improvement p 1931 N94-21327

CONFINEMENT
Longitudinal beam dynamics for heavy ion fusion using WARPrz
[DE93-019154] p 1992 N94-19915
Enhanced confinement regimes and control technology in the DIII-D tokamak
[DE93-019004] p 1998 N94-22039
Physics of transport phenomena in magnetic confinement plasmas p 2000 N94-22628

CONFORMAL MAPPING
Surface path lines in plane Stokes flow driven by capillarity
[DE93-041277] p 1803 N94-21651

CONGRUENCES
Instruction set commutivity p 1766 N94-21719

CONICAL SCANNING
Conically scanned holographic lidar telescope
[NASA-CASE-GSC-13462-1] p 1986 N94-20591

CONJUGATE GRADIENT METHOD
Layout optimization with algebraic multigrid methods
p 1957 N94-21474
The multigrid preconditioned conjugate gradient method p 1958 N94-21482
Extended range modified gradient technique for profile inversion (extended version of report Et/Em-1992-8)
[PB93-215242] p 1742 N94-22346

CONJUGATES
The Robinson-Schensted and Schuetzenberger algorithms. Part 2: Geometric interpretations
[CWI-AM-R9209-PT-2] p 1911 N94-21157

CONNECTORS
Disengagable adapter for an optical fiber connector
[AD-D015959] p 1822 N94-20356

CONSERVATION EQUATIONS
CTH: A software family for multi-dimensional shock physics analysis
[DE93-019428] p 1904 N94-20052

CONSERVATION LAWS
Problems related to conservation laws: Phase transitions and viscoelasticity
[AD-A271429] p 1698 N94-19840
Numerical methods for singularly perturbed differential equations with applications
[AD-A272112] p 1952 N94-20568
Symmetries and conservation laws of the system: $u(x)=vw(x)$, $v(y)=uw(y)$, $uv+w(xx)+w(yy)=0$
[MEMO-1084] p 1953 N94-21046

CONSISTENCY
On estimation and testing in Poisson regression models with over-dispersion
[MEMO-1083] p 1963 N94-21076

CONSTITUTIVE EQUATIONS
Modeling of failure and response to laminated composites subjected to in-plane loads
p 1834 N94-22612

CONSTRAINTS
Evaluation of head injury criteria
[NIAR-93-2] p 1890 N94-20190
Buffer allocation in an ATM switch with output buffer and speed constraints p 1746 N94-22203

CONSTRUCTION
Counter-balanced, multiple cable construction crane
[NASA-CASE-LAR-14565-1-CU] p 1822 N94-20369

CONSTRUCTION MATERIALS
Biotechnology and composite materials
[AD-A264278] p 1673 N94-20327
Production of NiAl and TiAl intermetallics by mechanical alloying
[VTT-JULK-760] p 1691 N94-20530
Symposium on Microscopy and Image Analysis of Building Materials
[VTT-SYMP-136] p 1707 N94-21890

CONSUMPTION
Analysis of consumer demand structure by means of economic indexes p 2052 N94-22074

CONTACT RESISTANCE
A finite element formulation and adaptive solution approach for large-scale thermomechanical problems with complex contact conditions
[DE93-019605] p 1960 N94-21996
CONTACTORS
A vibration model for centrifugal contactors
[DE93-040645] p 1833 N94-21927
CONTAMINANTS
The aerogel mesh contamination collector
[AD-A270537] p 1651 N94-20011
Spiral fluid separator
[NASA-CASE-MFS-28658-1] p 1800 N94-20361
CONTAMINATION
The aerogel mesh contamination collector
[AD-A270537] p 1651 N94-20011
New technique for oil backstreaming contamination measurements p 1652 N94-20511
Further carbon isotope measurements of LEW 88516 p 2086 N94-20886
Long Duration Exposure Facility (LDEF) contamination study
[AD-A272419] p 1658 N94-21147
Melt-spin processing of high (Tc) oxide superconductors
[DE94-000696] p 2036 N94-22582
CONTEXT FREE LANGUAGES
Hopfield models as neural-network acceptors p 1941 N94-20250
A single layer higher order neural net and its application to grammar recognition p 1941 N94-20251
CONTINUITY EQUATION
Acoustic radiation damping of flat rectangular plates subjected to subsonic flows
[NASA-TM-109362] p 1967 N94-20211
A parametric study of heat transfer within a planar thermosyphon
[DE93-019546] p 1799 N94-20258
F2D users manual: A two-dimensional compressible gas flow code
[DE94-000653] p 1805 N94-22386
CONTINUOUS RADIATION
Design aspects and parametric characterisation of a neutral rare gas laser
[AD-A271100] p 1814 N94-19850
CONTINUOUS WAVE RADAR
C-band radar backscatter of sea ice in the Weddell Sea, Antarctica during the austral winter of 1992 p 1725 N94-20435
CONTINUUM MECHANICS
Dynamical systems and nonlinear partial differential equations
[AD-A271514] p 1951 N94-20545
Microscopic and macroscopic dynamics
[DE93-019576] p 1937 N94-22042
Smoothed-particle hydrodynamics and nonequilibrium molecular dynamics
[DE94-001059] p 1977 N94-22400
CONTINUUM MODELING
Fundamentals of mechanical behavior in structural intermetallics: A synthesis of atomistic and continuum modeling
[DE93-019166] p 1690 N94-20232
CONTOURS
Characterization of the Marquez Dome buried impact crater using gravity and magnetic data p 1863 N94-20882
CONTRACT MANAGEMENT
NASA property: Improving management of government equipment provided to contractors. Report to the Chairman, Subcommittee on Investigations and Oversight, Committee on Science, Space, and Technology, House of Representatives
[GAO/NSIAD-93-191] p 2039 N94-20206
NASA procurement: Planning for pilot test of new procurement procedures is adequate. Report to the Chairman, Committee on Governmental Affairs, US Senate
[GAO/NSIAD-94-67] p 2039 N94-20236
A guide to resolving disputes over contractor delay entitlements
[AD-A272022] p 2039 N94-21444
Summary data on all NASA procurement actions
[NASA-TM-109392] p 2040 N94-21638
CONTRACT NEGOTIATION
Implementing Electronic Data Interchange (EDI) with small business suppliers in the pre-award acquisition process
[AD-A271767] p 1945 N94-21305
CONTRACTION
Thermal behavior of natural zeolites
[DE93-040091] p 1699 N94-19975
CONTRACTORS
NASA property: Improving management of government equipment provided to contractors. Report to the Chairman, Subcommittee on Investigations and Oversight, Committee on Science, Space, and Technology, House of Representatives
[GAO/NSIAD-93-191] p 2039 N94-20206
A guide to resolving disputes over contractor delay entitlements
[AD-A272022] p 2039 N94-21444
CONTRACTS
NASA procurement report, FY 1992
[NASA-TM-109390] p 2040 N94-21623
Summary data on all NASA procurement actions
[NASA-TM-109392] p 2040 N94-21638
CONTROL BOARDS
Wide-bandwidth high-resolution search for extraterrestrial intelligence
[NASA-CR-194724] p 1897 N94-20336
CONTROL EQUIPMENT
Proceedings of the Twentieth Annual Technologyfest p 1645 N94-20188
Optimal flight guidance for aircraft in windshear
[CA-PATENT-1,307,573] p 1650 N94-21050
CONTROL STICKS
FSR based force torque transducer design
[AD-A271337] p 1650 N94-19879
CONTROL SURFACES
Development and operation of the F/A-18 model control surface actuators
[AD-A271330] p 1645 N94-19914
Active control of wake/blade-row interaction noise through the use of blade surface actuators
[NASA-CR-4556] p 1968 N94-21608
CONTROL SYSTEMS DESIGN
Pointing control design for autonomous space vehicle applications
[DE93-019943] p 1657 N94-19863
FSR based force torque transducer design
[AD-A271337] p 1650 N94-19879
Design of a state-space controller for an advanced gas turbine engine
[AD-A270859] p 1647 N94-20042
Telerobotic control of a mobile coordinated robotic server, executive summary
[NASA-CR-194685] p 1821 N94-20044
Control and readout of the extraction septum of AmPS
[DIGEL-1993-2] p 1979 N94-20117
Proceedings of the Twentieth Annual Technologyfest p 1645 N94-20188
Reconfigurable fuzzy cell
[NASA-CASE-MSC-21613-1] p 1907 N94-20492
Diagnostics and methods for real-time laser microchemistry
[AD-A270871] p 1680 N94-20566
An application of the Cerebellar Model Articulation Controller for a switched reluctance rotor position estimator
[AD-A271769] p 1943 N94-20926
Power supply and controller for the Sextupole magnet of AmPS
[DIGEL-1992-3] p 1753 N94-21064
Design, fabrication and test of a vertical attitude takeoff and landing unmanned air vehicle
[AD-A273003] p 1646 N94-21283
High dimension action spaces in robot skill learning
[TR-458] p 1945 N94-21317
A new eddy current model for magnetic bearing control system design p 1763 N94-21698
On the estimation algorithm used in adaptive performance optimization of turbofan engines
[NASA-TM-4551] p 1649 N94-21879
Public-sector aviation issues: Graduate research award papers, 1991-1992
[PB93-206258] p 1642 N94-22055
A robust adaptive control design for flexible joint manipulators p 1790 N94-22230
Fuzzy and neural control
[NASA-TM-108753] p 1947 N94-22270
VETA x ray data acquisition and control system p 2047 N94-22455
Wilbur: A low-cost CCD camera system for MDM Observatory p 1814 N94-22510
CONTROL THEORY
Design of a state-space controller for an advanced gas turbine engine
[AD-A270859] p 1647 N94-20042
Routing of freeway traffic: A discrete-time state space model and routing problems
[CWI-BS-R9232] p 1944 N94-21033
Replica control algorithms in distributed databases
[AD-A271571] p 1909 N94-21034
Linear programming for standard and nonstandard Markovian control problems. A survey
[PB93-191948] p 1963 N94-21066
A new eddy current model for magnetic bearing control system design p 1763 N94-21698
CONTROL VALVES
A novel scheme to handle highly pulsed loads with a standard helium refrigerator
[DE93-019617] p 1799 N94-20263
High-temperature, high-pressure oxygen metering valve
[NASA-CASE-MSC-21823-1] p 1824 N94-20589
The optohydraulic servovalve: A novel device for the precise optical control of hydraulic pressure
[ISBN-0-315-83580-X] p 1827 N94-22577
CONTROLLED ATMOSPHERES
Quinoa: An emerging new crop with potential for CELSS
[NASA-TP-3422] p 1895 N94-20137
CONTROLLERS
Design of a state-space controller for an advanced gas turbine engine
[AD-A270859] p 1647 N94-20042
Robot skill learning and the effects of basis function choice
[TR-437] p 1939 N94-20135
Reconfigurable fuzzy cell
[NASA-CASE-MSC-21613-1] p 1907 N94-20492
Analysis and design of weight balancing system for laser velocimetry traverse
[AD-A271171] p 1816 N94-20546
An application of the Cerebellar Model Articulation Controller for a switched reluctance rotor position estimator
[AD-A271769] p 1943 N94-20926
An ASIC memory buffer controller for a high speed disk system p 1754 N94-21089
Acceleration-augmented LQG control of an active magnetic bearing p 1757 N94-21112
Development and evaluation of a profile negotiation process for integrating aircraft and air traffic control automation
[NASA-TM-4360] p 1643 N94-21606
A new eddy current model for magnetic bearing control system design p 1763 N94-21698
On the decomposition of synchronous state machines using sequence invariant state machines p 1764 N94-21703
Optimization and control of a small angle ion source using an adaptive neural network controller
[DE93-040063] p 1946 N94-21845
Proceedings of the IMOG (Interagency Manufacturing Operations Group) Numerical Systems Group
[DE94-001009] p 1917 N94-21851
A software environment for the exploitation of the MAR image sensor p 1785 N94-22200
Fuzzy and neural control
[NASA-TM-108753] p 1947 N94-22270
VETA x ray data acquisition and control system p 2047 N94-22455
The University of Hawaii Institute for Astronomy CCD camera control system p 1828 N94-22489
CCD data acquisition systems at Lick and Keck Observatories p 2047 N94-22495
CONVECTION
Thermocapillary and arc phenomena in stainless steel welds
[DE94-000518] p 1821 N94-19859
A parametric representation of a thunderstorm cell
[AD-A271983] p 1866 N94-20579
Expectations for the Martian core magnetic field p 2120 N94-20792
Liquid-phase circulation and mixing in multicomponent droplets vaporizing in a laminar convective environment
[AD-A272851] p 1802 N94-21193
Characterization of convection related defects in II-VI compound semiconductors
[NASA-CR-194704] p 2030 N94-21778
Breaking Kelvin-Helmholtz waves and cloud-top entrainment as revealed by K-band Doppler radar p 1874 N94-22310
CONVECTION-DIFFUSION EQUATION
Order of accuracy of QUICK and related convection-diffusion schemes
[NASA-TM-106402] p 1959 N94-21588
CONVECTIVE FLOW
Mixing of a chemically buoyant layer at the top of a thermally convecting fluid: Implications for mantle dynamics with application to Venus p 2099 N94-20675
CONVECTIVE HEAT TRANSFER
Thermal information regarding the cooldown and operation of liquid argon calorimeters
[DE93-019391] p 1807 N94-19987
Mixing of a chemically buoyant layer at the top of a thermally convecting fluid: Implications for mantle dynamics with application to Venus p 2099 N94-20675

CONVENTIONS
Development of a naming convention and data ma nagement system
[NASA-CR-193860] p 2042 N94-20268
Asymptotic analysis. Working Note No. 2, approximation of integrals
[DE94-000433] p 1961 N94-22381
CONVERGENCE
Convergence of the hermite wavelet expansion
[AD-A271435] p 1854 N94-19841
Stochastic optimization by simulation: Numerical experiments with M/M/1 queue in steady-state
[AD-A271143] p 1949 N94-19854
Large deviations behavior of counting processes and their inverses
[AD-A271142] p 1939 N94-19909
Stochastic optimization by simulation: Convergence proofs for the G1/G/1 queue in steady-state
[AD-A271141] p 1962 N94-19999
A general rough-surface inversion algorithm: Theory and application to SAR data p 1719 N94-20407
Determination of structure factors of copper by convergent beam electron diffraction
[DE93-019520] p 2019 N94-20941
An automatic multigrid method for the solution of sparse linear systems p 1957 N94-21478
Sub-band adaptive noise cancelling p 1774 N94-22125
Development of a gridless CFD method p 1919 N94-22361
Accuracy assessment for grid adaptation p 1920 N94-22368
CONVERGENT NOZZLES
Instability modes excited by natural screech tones in a supersonic rectangular jet
[NASA-TM-106409] p 1638 N94-22274
CONVEXITY
Convex set and linear mixing model p 1844 N94-20888
CONVOLUTION INTEGRALS
The Composite Analytic and Simulation Package or RFI (CASPR) on a coded channel p 1744 N94-21339
Imaging vector fields using line integral convolution
[DE93-019922] p 1917 N94-21841
VLSI design of a bit serial parallel processing 4 extender chip for M-path convolutional decoding p 1775 N94-22132
Image convolution using the Myrias SPS-2 parallel computer p 1786 N94-22207
Parallelizing a maximum entropy image deconvolution algorithm p 1787 N94-22208
Coded 64QAM using a binary convolutional code p 1747 N94-22223
Deconvolution of Hubble Space Telescope images using simulated point spread functions p 2048 N94-22497
COOL STARS
The cool-star spectral catalog: A uniform collection of IUE SWP-LOs p 2046 N94-22446
COOLANTS
Cooling apparatus and couplings therefor
[NASA-CASE-ARC-11921-1] p 1800 N94-20371
Heat exchanger with oscillating flow
[NASA-CASE-LAR-14033-2] p 1800 N94-20495
Temperature and Doppler coefficients of various space nuclear reactors
[DE94-001388] p 1671 N94-21979
COOLING
Venus pancake dome formation: Morphologic effects of a cooling-induced variable viscosity during emplacement p 2110 N94-20732
Preliminary estimation of tagamite cooling conditions (Puchezh-Katunki Astrobleme, Russia) p 2083 N94-20735
Mineralogy and cooling history of magnesian lunar granulite 67415 p 2124 N94-20811
High-energy astrophysics: A theoretical analysis of thermal radiation from neutron stars
[NASA-CR-194808] p 2055 N94-20952
The energy performance of prototype holographic glazings
[DE93-040451] p 1809 N94-21545
COOLING FLOWS (ASTROPHYSICS)
Magnetic reconnection in emission nebulae in clusters of galaxies p 2010 N94-22700
COOLING SYSTEMS
A tutorial on the aero/thermodynamical design of liquid-propellant rocket engine nozzles p 1668 N94-20074
Cooling apparatus and couplings therefor
[NASA-CASE-ARC-11921-1] p 1800 N94-20371
Cold-start minidiesel engine development
[AD-A271064] p 1823 N94-20567
Physiological efficacy of a lightweight ambient air cooling unit for various applications
[AD-A272952] p 1896 N94-21247
Heat transfer additives for absorption cooling system fluids
[PB93-202521] p 1714 N94-21426
COORDINATE TRANSFORMATIONS
New algorithm of ground track processing in high-frequency skywave over-the-horizon-B radar
[AD-A267821] p 1717 N94-20207
Registering and resampling images in STSDAS p 1927 N94-22550
COORDINATES
Processing of climatological data for model initialization
[AD-A271878] p 1865 N94-20487
Guide star catalogue data retrieval software 2 p 1927 N94-22533
The spectral world coordinate systems in IRAF/NOAO p 2049 N94-22539
COORDINATION
Structural modeling: An application framework and development process for flight simulators
[AD-A271348] p 1650 N94-19880
COPOLYMERIZATION
Swelling equilibria for cationic 2-hydroxyethyl methacrylate (HEMA)-based hydrogels
[DE94-000728] p 1707 N94-21856
COPOLYMERS
Optically induced rotation diffusion in polymer liquid crystals: Phenomenological theory and experimental verification
[ETN-93-95068] p 2014 N94-20026
Spatial organization of polymer chains in a crystallizable diblock polyethylene and polystyrene
[AD-A271862] p 1702 N94-20463
Mechanical properties and reliability of semi-crystalline polymers
[AD-A271591] p 1704 N94-20946
The 13C-NMR spectra of poly (4-((2-(acryloyloxy) ethyl) ethyl amino)- 4-nitroazobenzene-co-methyl methacrylate)
[AD-A273016] p 1705 N94-21238
Optically induced birefringence in copolymers and blends containing azobenzene groups
[AD-A273085] p 1706 N94-21523
COPPER
Ageing studies on a composite propellant containing a new organo-copper burn rate catalyst
[AD-A271060] p 1711 N94-19906
Computational model of a magnetic modulator for copper lasers
[DE93-019603] p 1815 N94-20223
Neutral copper cluster sputtering yields: Ne(+), Ar(+) and Xe(+) bombardment
[DE93-019010] p 1690 N94-20288
Determination of structure factors of copper by convergent beam electron diffraction
[DE93-019520] p 2019 N94-20941
Impact of copper vapour contamination on argon arcs p 1994 N94-21053
Growth, characterization and device development in monocrystalline diamond films
[AD-A272715] p 2026 N94-21190
Some results of the oxidation investigation of copper and silver samples flown on LDEF p 1660 N94-21375
Local structure in oxygen-doped La2CuO(4+delta)
[DE93-040248] p 2030 N94-21768
High-power copper vapor lasers and their application to precision drilling and cutting
[DE93-019951] p 1819 N94-21844
Effect of copper sulphate on the rate of afferent discharge in the gastric branch of the vagus nerve in the rat p 1887 N94-21907
Experimental studies of gastric dysfunction in motion sickness: The effect of gastric and vestibular stimulation on the vagal and splanchnic gastric efferents p 1888 N94-21911
Microtextural characterization of annealed and deformed copper
[DE93-040144] p 1695 N94-21990
Interface science of controlled metal/metal and metal/ceramic interfaces prepared using ultrahigh vacuum diffusion bonding
[DE94-001066] p 1696 N94-22025
COPPER ALLOYS
Method of fabricating a rocket engine combustion chamber
[NASA-CASE-MFS-28569-1] p 1703 N94-20541
Molecular dynamics modeling of the mechanical behavior of metallic multilayers
[DE93-019947] p 1694 N94-21921
Using the rule of mixtures to examine the hardness of Cu/Cu-Zr multilayers
[DE94-001068] p 1697 N94-22402
COPPER COMPOUNDS
Volatile CVD precursors based on copper alkoxides and mixed group 2A-copper alkoxides
[AD-D015930] p 1701 N94-20349
High temperature stability of amorphous Ta(x)Cu(1-x) diffusion barriers on GaAs p 2022 N94-20990
COPPER OXIDES
Local structure and superconductivity in La(2-x)Ba(x)CuO4 for x=0.125 and x=0.15
[DE93-040193] p 2029 N94-21555
Disks of YBa2Cu3O7 shocked to 10 GPa pressures
[DE94-000464] p 2031 N94-21931
High oxygen pressure synthesis of new copper oxide superconductors
[DE93-040278] p 2033 N94-21998
NMR studies of oxygen-doped La2CuO(4+delta)
[DE93-040756] p 2034 N94-22007
COPPER SELENIDES
Advanced processing technology for high-efficiency thin-film CuInSe2 solar cells
[DE93-010045] p 1847 N94-21614
Research on polycrystalline thin-film submodules based on CuInSe2 materials
[DE93-018223] p 2029 N94-21617
Thin-film CdTe and CuInSe2 photovoltaic technologies
[DE93-018217] p 1848 N94-21827
CORE SAMPLING
The age of the Pretoria Saltpan impact crater, South Africa p 1863 N94-20798
Solar proton events from a 180 year depth profile of nitrate concentrations from the central Greenland ice sheet
[AD-A272888] p 2147 N94-21196
CORNEA
Ocular damage induced by ultrashort laser pulses
[AD-A271859] p 1890 N94-20462
CORNERS
Hypersingular integrals at a corner
[DE94-000340] p 1961 N94-22379
CORONAL HOLES
High resolution studies of the structure of the solar atmosphere
[AD-A273084] p 2147 N94-21522
CORONAL LOOPS
MHD relaxation in magnetic loops p 2004 N94-22658
CORONARY ARTERY DISEASE
Coronary angiography outcomes of US Army aircrew with the finding of coronary artery calcifications: Aviation epidemiology data register
[AD-A271988] p 1891 N94-20615
Review of using cardiac fluoroscopy in symptomatic and asymptomatic patients
[AD-A271690] p 1891 N94-20928
CORONARY CIRCULATION
Coronary angiography outcomes of US Army aircrew with the finding of coronary artery calcifications: Aviation epidemiology data register
[AD-A271988] p 1891 N94-20615
CORONAS
Parga and Hecate Chasmata, Venus: Structure, volcanism and models of formation p 2121 N94-20786
CORRECTION
Automatic AVHRR image navigation software
[NASA-CR-194602] p 1643 N94-20148
CORRELATION COEFFICIENTS
Fast scalar algorithms for multivariate partial correlations and their empirical counterparts
[RR-903-M] p 1905 N94-20201
Results of the second Round Robin on opening-load measurement conducted by ASTM Task Group E24.04.04 on crack closure measurement and analysis
[NASA-TM-109032] p 1832 N94-21624
CORRELATORS
Applications of correlator chips in radio science p 1763 N94-21695
NASA SERC digital correlator projects p 1765 N94-21706
A 1 GHz sample rate, 256-channel, 1-bit quantization, CMOS, digital correlator chip p 1768 N94-21732
Low power, CMOS digital autocorrelator spectrometer for spaceborne applications p 1666 N94-21733
A real time correlator architecture using distributed arithmetic principles p 1768 N94-21734
The VLBA correlator: Real-time in the distributed era p 2049 N94-22547
CORROSION
Review of corrosion behavior of ceramic heat exchanger materals: Corrosion characteristics of silicon carbide and silicon nitride
[DE93-041307] p 1706 N94-21516
Laser Raman and x ray scattering studies of corrosion films on metals
[DE93-040243] p 1692 N94-21558
CORROSION PREVENTION
Corrosion inhibition in high temperature environment
[AD-D015910] p 1698 N94-19830

A comparison of sulfuric acid/boric acid anodize and chromic acid anodize processes
[AD-A271933] p 1703 N94-20614
Oxidation resistant protective coating system for gas turbine components and process for penetration thereof
[CA-PATENT-1,294,155] p 1704 N94-21143
Surface modification of TI3AI for improved oxidation resistance
[DE93-018297] p 1696 N94-22034

CORROSION RESISTANCE
Corrosion inhibition in high temperature environment
[AD-D015910] p 1698 N94-19830
Evaluation of a diffusion/trapping model for hydrogen ingress in high-strength alloys
[AD-A271328] p 1689 N94-20027
A comparison of sulfuric acid/boric acid anodize and chromic acid anodize processes
[AD-A271933] p 1703 N94-20614
Review of corrosion behavior of ceramic heat exchanger materals: Corrosion characteristics of silicon carbide and silicon nitride
[DE93-041307] p 1706 N94-21516
Surface modification for corrosion resistance
[DE93-017419] p 1693 N94-21825

COSINE SERIES
Operational equations for the five-point rectangle
[DE94-000366] p 1959 N94-21655
An in-place and in-order algorithm for the discrete cosine transform p 1771 N94-22111

COSMIC BACKGROUND EXPLORER SATELLITE
An IDL-based analysis package for COBE and other skycube-formatted astronomical data
p 1925 N94-22471
Visualizing the universe, part 1 p 2064 N94-22476

COSMIC DUST
A study of Saturn's E-ring particles using the Voyager 1 plasma wave instrument
[NASA-CR-194694] p 2088 N94-20048
The x ray halo of AM Her
[NASA-CR-189310] p 2054 N94-20142
Identification of an interstellar oxide grain from the Murchison meteorite by ion imaging
p 2082 N94-20659
First discovery of the organic materials in deep-sea iron cosmic spherule p 1685 N94-20677
Molecular equilibria and condensation sequences in carbon rich gases p 2083 N94-20756
Intact capture of hypervelocity particles on Shuttle
p 2085 N94-20837
The x ray halo of Cen X-3
[NASA-CR-189309] p 2055 N94-21295
Dust content of a hydrogen rich, low surface brightness galaxy and the luminosity history of 3C273
[NASA-CR-194705] p 2056 N94-21779

COSMIC PLASMA
MHD flows from compact objects: Effects on magnetic field configurations p 2008 N94-22684
Three-dimensional simulations of cosmic jets employing the smoothed particle hydrodynamics technique
p 2008 N94-22685

COSMIC RAY SHOWERS
Evaluation of the chemical composition of cosmic radiation in energy area of 10(exp 15) eV
[ETN-93-93682] p 2150 N94-21056

COSMIC RAYS
Single-event upset testing of the performance semiconductor 1750A CMOS/SOS chip set
[AD-A271158] p 2015 N94-20184
Gamma ray spectrometry of LDEF samples: Results of 1992 analyses
[DE94-001177] p 1684 N94-22046

COST ANALYSIS
Rotorcraft low altitude IFR benefit/cost analysis: Conclusions and recommendations
[DOT/FAA/RD-93/22] p 1642 N94-20051
Activities of National Inst. for Aviation Research
[NIAR-93-16] p 2151 N94-20150
Analysis of cost: CVD diamond deposition
[AD-A271980] p 2018 N94-20616
Multigrid approach to solving the long transportation problem on a regular grid in cost space
[AD-A272323] p 1909 N94-21038
On the selection of indices in relational databases
[MEMO-INF-92-72] p 2043 N94-21071
An assessment of the cost of microwave sintering ceramic tiles for armor applications
[DE94-000978] p 1693 N94-21850

COST EFFECTIVENESS
Turbine design p 1668 N94-20075
A full-color, high-resolution laser projector for a flight simulator visual display
[AD-A270578] p 1651 N94-20108
The manager's guide to NASA graphics standards
[NHB-1430.2] p 2042 N94-20308
Parallel runway requirement analysis study. Volume 1: The analysis
[NASA-CR-191549-VOL-1] p 1644 N94-22277

COST ESTIMATES
A conceptual design for the STAR endcap electromagnetic calorimeter
[DE93-040801] p 1807 N94-19990
An assessment of the cost of microwave sintering ceramic tiles for armor applications
[DE94-000978] p 1693 N94-21850
Environmental protection using social costing
[DE94-000492] p 1853 N94-22569

COSTS
Analysis of cost: CVD diamond deposition
[AD-A271980] p 2018 N94-20616
Japanese space program p 1652 N94-21407

COUETTE FLOW
Turbulization of free shear flows: 3D perturbations
p 2000 N94-22626

COULOMB COLLISIONS
Accretion of a hot plasma onto the central black hole: Fokker-Planck formulation p 2009 N94-22693

COUNTER ROTATION
Direct simulation of shock-induced mixing layer
[DE93-040498] p 1803 N94-21531

COUNTERS
A lower bound on wait-free counting
[CWI-CS-R9307] p 1915 N94-21537

COUNTING
Large deviations behavior of counting processes and their inverses
[AD-A271142] p 1939 N94-19909
A lower bound on wait-free counting
[CWI-CS-R9307] p 1915 N94-21537

COUNTING CIRCUITS
A lower bound on wait-free counting
[CWI-CS-R9307] p 1915 N94-21537

COUPLED MODES
High resolution infrared spectroscopy of cyclobutane: A study of vibrational mode coupling involving large amplitude, low frequency modes
[AD-A271987] p 1973 N94-20619
Laser driven hydrodynamic instability experiments
[DE93-040550] p 1818 N94-21547

COUPLERS
Shaft mount for data coupler system
[NASA-CASE-LAR-13805-1] p 1822 N94-20365

COUPLING
Multi-disciplinary coupling effects for integrated design of propulsion systems
[NASA-TM-106349] p 1830 N94-20170
High resolution infrared spectroscopy of formamide and deuterated formamide in a molecular beam
[AD-A271986] p 1973 N94-20618
Photo- and thermal-induced antiferromagnetic interlayer coupling in Fe/(Fe-Si) superlattices
[DE93-040822] p 2031 N94-21930
Orientationally independent antiferromagnetic coupling in epitaxial Fe/Cr (211) and (100) superlattices
[DE94-001270] p 2035 N94-22564

COUPLING CIRCUITS
Analysis of microstrip dipoles and slots transversely coupled to a microstrip line using the FDTD method
p 1718 N94-20405

COUPLING COEFFICIENTS
Formulation for numerical solution of radiation and transmission from arbitrary apertures
p 1745 N94-22140
Orthogonalization method for determination of boundary layer receptivity coefficients
[ISBN-0-315-83426-9] p 1805 N94-22580

COUPLINGS
Cooling apparatus and couplings therefor
[NASA-CASE-ARC-11921-1] p 1800 N94-20371

COVALENT BONDS
Composite materials with improved properties in compression
[AD-A272837] p 1675 N94-21176

COVARIANCE
Stochastic simulation for imaging spatial uncertainty: Comparison and evaluation of available algorithms
[DE93-040058] p 1916 N94-21761
Canonically covariant formulation of Landau's Newtonian superfluid dynamics
[PB93-221034] p 1805 N94-22272

COVERINGS
Development of bioelastic material for aspects of wound repair
[AD-A267832] p 1673 N94-20208

CRACK CLOSURE
Results of the second Round Robin on opening-load measurement conducted by ASTM Task Group E24.04.04 on crack closure measurement and analysis
[NASA-TM-109032] p 1832 N94-21624

CRACK INITIATION
Brief summary of the evolution of high-temperature creep-fatigue life prediction models for crack initiation
p 1834 N94-22613

CRACK PROPAGATION
Asteroid collisions: Target size effects and resultant velocity distributions p 2083 N94-20729
Weldalite (tm) 049 (Al 2095-T8): Anisotropy effects at cryogenic conditions
[AD-A272658] p 1691 N94-21188
Numerical modeling of a propagating crack
[AD-A272604] p 1832 N94-21421
The mechanical property data base from an Air Force/industry cooperative test program on advanced aluminum alloys: 2091 sheet, plate, and 8090 extrusion
[AD-A273091] p 1692 N94-21525
Results of the second Round Robin on opening-load measurement conducted by ASTM Task Group E24.04.04 on crack closure measurement and analysis
[NASA-TM-109032] p 1832 N94-21624
Investigation of moisture-induced embrittlement of iron aluminides
[DE93-040841] p 1695 N94-21949
Nonlinear and progressive failure aspects of transport composite fuselage damage tolerance
p 1834 N94-22609
Projections on structures and material strength in the computational context p 1834 N94-22610
A thermodynamic analysis of propagating subcritical cracks with cohesive zones p 1834 N94-22611
Life prediction systems for critical rotating components
p 1835 N94-22615
Demonstrating damage tolerance of composite airframes p 1647 N94-22623

CRACK TIPS
Numerical modeling of a propagating crack
[AD-A272604] p 1832 N94-21421
Projections on structures and material strength in the computational context p 1834 N94-22610
A thermodynamic analysis of propagating subcritical cracks with cohesive zones p 1834 N94-22611

CRACKING (FRACTURING)
Investigation of cracking and erratic behavior of the uranium-titanium alloy
[DE93-018591] p 1688 N94-19957
Cratering evaluations and results
[DE93-040347] p 1691 N94-20478
Weldalite (tm) 049 (Al 2095-T8): Anisotropy effects at cryogenic conditions
[AD-A272658] p 1691 N94-21188
Stress-induced cracking of fluorocarbon rubber MTL-0002 after exposure to DS-2
[AD-A271753] p 1705 N94-21302
Numerical modeling of a propagating crack
[AD-A272604] p 1832 N94-21421
Damage states around fastener holes in thick graphite/epoxy composite laminates
[AD-A272613] p 1675 N94-21504

CRACKS
Results of the second Round Robin on opening-load measurement conducted by ASTM Task Group E24.04.04 on crack closure measurement and analysis
[NASA-TM-109032] p 1832 N94-21624
A thermodynamic theory of dynamic fragmentation
[DE93-019066] p 1833 N94-21916

CRANES
Counter-balanced, multiple cable construction crane
[NASA-CASE-LAR-14565-1-CU] p 1822 N94-20369

CRASHWORTHINESS
Structural crashworthiness and failure
[AD-A270429] p 1828 N94-19815

CRATERING
Cratering evaluations and results
[DE93-040347] p 1691 N94-20478
Determination of cosmic bodies size-velocity distribution by observation of current impacts on Mars
p 2082 N94-20648
Searching for ancient Venus p 2111 N94-20743
SPH modelling of energy partitioning during impacts on Venus p 2124 N94-20809
Determination of parameters for hypervelocity dust grains encountered in near-Earth space
p 2084 N94-20817
Original size of the Vredefort structure, South Africa
p 1863 N94-20825
Limits on differentiation of melt sheets from basin-scale lunar impacts p 2133 N94-20856
A fresh look at crater scaling laws for normal and oblique hypervelocity impacts p 1666 N94-20864
Shock attenuation at the Slate Islands revisited
p 1863 N94-20887

CRATERS
Calderas produced by hydromagmatic eruptions through permafrost in northwest Alaska p 2089 N94-20385
Gravity investigation of the Manson impact structure, Iowa p 2082 N94-20694

Pressure versus drag effects on crater size
p 1862 N94-20742
Impactor control of central peak and peak-ring formation p 1862 N94-20744
Linear structures on the small inner satellites of Saturn p 2121 N94-20797
Characterization of the Marquez Dome buried impact crater using gravity and magnetic data
p 1863 N94-20882

CRATONS
Primary differentiation in the early Earth: Nd and Sr isotopic evidence from diamondiferous eclogites for both old depleted and old enriched mantle, Yakutia, Siberia
p 1862 N94-20776

CRAY COMPUTERS
Segmented operations for sparse matrix computation on vector multiprocessors
[AD-A270601] p 1928 N94-19950
Two-dimensional particle-in-cell simulation on transputer arrays
[DE93-017977] p 1972 N94-20181
Multi-CPU plasma fluid turbulence calculations on a CRAY Y-MP C90
[DE93-015425] p 1801 N94-20562
Some experiences of solving 1-D semiconductor device equations on a matrix coprocessor by a domain decomposition method
[CWI-NM-R9304] p 1935 N94-21492

CREEP ANALYSIS
Development of BEM for ceramic composites
[NASA-CR-194718] p 1676 N94-21777

CREEP PROPERTIES
Investigation of austenitic alloys for advanced heat recovery and hot gas cleanup systems
[DE93-017863] p 1687 N94-19802
Finite element mesh generation and analysis of solder joints for fatigue life predictions
[AD-A271329] p 1829 N94-19937
Durability predictions for adhesively bonded joints in humid environments
[AD-A271177] p 1830 N94-20001
Effects of processing history on the creep strength of Nb-1Zr
[DE93-015905] p 1689 N94-20093
Alloying effects on mechanical and metallurgical properties of NiAl
[DE93-040814] p 1694 N94-21948
Creep damage of carbon fiber reinforced PEEK
[ISBN-0-315-58962-0] p 1677 N94-22420
Brief summary of the evolution of high-temperature creep-fatigue life prediction models for crack initiation
p 1834 N94-22613

CREEP RUPTURE STRENGTH
Creep damage of carbon fiber reinforced PEEK
[ISBN-0-315-58962-0] p 1677 N94-22420

CREEP STRENGTH
Effects of processing history on the creep strength of Nb-1Zr
[DE93-015905] p 1689 N94-20093

CREEP TESTS
Creep damage of carbon fiber reinforced PEEK
[ISBN-0-315-58962-0] p 1677 N94-22420

CRETACEOUS PERIOD
Research program on the Manson impact structure, Iowa p 1862 N94-20766

CRETACEOUS-TERTIARY BOUNDARY
The Koshak section: Evidence for element fractionation and an oxidation event at the K/T boundary
p 1862 N94-20641
Modelling the gravity and magnetic field anomalies of the Chicxulub crater p 1862 N94-20668
Global blackout following the K/T Chicxulub impact: Results of impact and atmospheric modeling
p 1854 N94-20698
U-Pb provenance ages of shocked zircons from the K-T boundary, Raton Basin, Colorado p 1685 N94-20701
Research program on the Manson impact structure, Iowa p 1862 N94-20766
Two-polarity magnetization in the Manson impact breccia p 1863 N94-20789

CRITICAL FREQUENCIES
Sporadic-E observations during LoVHF transionospheric direction finder measurements
[AD-A270619] p 1716 N94-19951

CRITICAL LOADING
Crystal orientation dependence of elastic precursor strength in pentaerythritol tetranitrate
[DE93-018340] p 2034 N94-22035

CRITICAL TEMPERATURE
Thermal expansion of electronic highly correlated materials
[ETN-93-93605] p 2026 N94-21135
Spin-polaron theory of high-T(c) superconductivity. 3: Gap function and critical temperature
[DE93-019198] p 2030 N94-21831

CROP GROWTH
Quinoa: An emerging new crop with potential for CELSS
[NASA-TP-3422] p 1895 N94-20137
The 7th Brazilian Remote Sensing Symposium, volume4 p 1840 N94-20965

CROSS CORRELATION
Optoelectronic associative memory
[NASA-CASE-NPO-18278-1-CU] p 1985 N94-20303
Using crosscorrelation techniques to determine the impulse response of linear systems
p 1759 N94-21122
The IRAF radial velocity analysis package
p 1925 N94-22475
SPECFOCUS: An IRAF task for focusing spectrographs p 1965 N94-22540
Registering and resampling images in STSDAS
p 1927 N94-22550

CROSS FLOW
An analysis of pressure driven cross-flow through a long slot connecting two parallel channels
[DE93-040181] p 1804 N94-21765

CROSS POLARIZATION
Radar backscatter measurements from simulated sea ice during CRRELEX 1990
[AD-A271034] p 1715 N94-19823
Multiple scattering effects on the Linear Depolarization Ratio (LDR) measured during CaPE by a Ka-band air-borne radar p 1728 N94-20446

CROSS SECTIONS
Absolute total and one and two electron transfer cross sections for Ar(8+) on Ar as a function of energy
[DE93-040283] p 1970 N94-19870

CROSSLINKING
Polyimide-based electrooptic materials
[DE93-019416] p 1706 N94-21526

CRUDE OIL
Biofuels: Project summaries
[DE93-010003] p 1712 N94-19984
High-resolution numerical methods for compressible multi-phase flow in hierarchical porous media
[DE94-000740] p 1799 N94-20351
Plasma-chemical conversion of hydrogen sulfide into hydrogen and sulfur
[DE93-041167] p 1682 N94-21789
Current situation in developing petroleum substituting energy (the United Kingdom)
[DE94-714897] p 1713 N94-22091
Environmental protection using social costing
[DE94-000492] p 1853 N94-22569

CRUSTAL FRACTURES
Ridge belt-related scarps and troughs: Compressional crustal bending on Venus p 2106 N94-20711
Geoid, topography, and convection-driven crustal deformation on Venus p 2116 N94-20769
Photogeological analysis of Europan tectonic features
p 2129 N94-20838
Arcuate and circular structures in the Tharsis region: Evidence of coronae on Mars p 2134 N94-20863
Large floor-fractured craters and isostatic crater modification: Implications for lithospheric thickness on Venus p 2135 N94-20873

CRUSTS
Diapirs and cantaloupes: Layering and overturn of Triton's crust p 2111 N94-20738

CRYOGENIC COOLING
Properties of cryogenic liquids p 1668 N94-20073
Flow and heat transfer model for a rotating cryogenic motor
[DE94-001151] p 1794 N94-22405

CRYOGENIC EQUIPMENT
Measurements of atomic interactions and frequency stability with a cryogenic hydrogen maser
[AD-A271132] p 1814 N94-19853
Acoustic microscopy and nonlinear effects in pressurized superfluid helium
[AD-A270598] p 1967 N94-19949
The Vulcain cryogenic engine p 1668 N94-20077
A novel scheme to handle highly pulsed loads with a standard helium refrigerator
[DE93-019617] p 1799 N94-20263
Detailed study of oxidation/wear mechanism in lox turbopump bearings
[NASA-TM-108434] p 1825 N94-21580
Passive Cryogenic Sampler
[DE94-000918] p 1811 N94-22392

CRYOGENIC FLUID STORAGE
Properties of cryogenic liquids p 1668 N94-20073
Pressurization and expulsion of a flightweight liquid hydrogen tank
[NASA-TM-106427] p 1799 N94-20177

CRYOGENIC FLUIDS
Spacecraft Propulsion
[VKI-LS-1993-01] p 1667 N94-20068

CRYOGENIC ROCKET PROPELLANTS
Spacecraft Propulsion
[VKI-LS-1993-01] p 1667 N94-20068
Properties of cryogenic liquids p 1668 N94-20073
Cryogenic propellant rocket engine problems
p 1668 N94-20076
The Vulcain cryogenic engine p 1668 N94-20077

CRYOGENIC TEMPERATURE
The National High Magnetic Field Laboratory, a user facility in support of research in high magnetic fields
[DE93-040145] p 1714 N94-20278

CRYOGENICS
A novel scheme to handle highly pulsed loads with a standard helium refrigerator
[DE93-019617] p 1799 N94-20263
Weldalite (tm) 049 (Al 2095-T8): Anisotropy effects at cryogenic conditions
[AD-A272658] p 1691 N94-21188
Fabrication of porous ceramics by freeze-casting/freeze-drying
[PB93-202513] p 1705 N94-21425
Stability of an uncooled segment of a high-temperature superconductor
[DE94-000476] p 2032 N94-21932
Passive Cryogenic Sampler
[DE94-000918] p 1811 N94-22392
Flow and heat transfer model for a rotating cryogenic motor
[DE94-001151] p 1794 N94-22405

CRYOSTATS
Operation of a test bed axial-gap brushless dc rotor with a superconducting stator
[DE93-019167] p 1769 N94-21830
Test results of two high temperature superconducting sample coils
[DE94-000496] p 2035 N94-22570

CRYPTOGRAPHY
Threshold computation and cryptographic security
[TR-443] p 1907 N94-20536
Threshold computation and cryptographic security
[TR-461] p 1912 N94-21285
Modeling and analysis of secure communication protocols using Petri net formalism
p 1784 N94-22194

CRYSTAL DEFECTS
General introduction to microstructural evolution under cascade damage conditions
[DE93-017443] p 2012 N94-19923
Fundamentals of mechanical behavior in structural intermetallics: A synthesis of atomistic and continuum modeling
[DE93-019166] p 1690 N94-20232
X ray analysis of alpha mercuric iodide crystal structure and processing effects
[DE93-017620] p 2027 N94-21296
IR materials producibility
[AD-A273031] p 1987 N94-21321
Defect motion as the origin of the 1/f conductance noise in solids
[EUT-92-E-259] p 2029 N94-21552
Fundamental studies of defect generation in amorphous silicon alloys grown by remote plasma-enhanced chemical-vapor deposition
[DE93-017083] p 2029 N94-21615
Implantation of carbon in GaAs and compensating native defects
[DE93-040122] p 2030 N94-21763
Surface and subsurface defect detection in Si3N4 components by laser scattering
[DE93-040829] p 1832 N94-21772
Characterization of convection related defects in II-VI compound semiconductors
[NASA-CR-194704] p 2030 N94-21778

CRYSTAL DISLOCATIONS
On the experimental determination of low order structure factors in TiAl by energy filtered convergent beam electron diffraction
[DE93-019521] p 1687 N94-19806
Examinations of composition and deformation behavior of intermetallic phases on the basis of Fe3(AlSi)
[GKSS-92/E/16] p 1692 N94-21311
Crystal structure and short-range oxygen defects in La- and Nd-modified ZrO2
[DE93-040229] p 2033 N94-21993

CRYSTAL GROWTH
Materials processing and manufacturing technologies for Diamond Substrate MultiChip Modules (DSMCM)
[AD-A271011] p 2011 N94-19821
Growth mechanisms and characterization of hydrogenated amorphous-silicon-alloy films
[DE93-018202] p 1699 N94-20047
Growth of zinc selenide single crystals by physical vapor transport in microgravity
[NASA-CR-194679] p 2017 N94-20346

Real-time analysis of in-situ spectroscopic ellipsometric data during MBE growth of III-V semiconductors
p 2024 N94-21004
Holographic measurements of ice crystals in cirrus clouds during International Cirrus Experiment ICE
[GKSS-92/E/14] p 1866 N94-21052
X ray analysis of alpha mercuric iodide crystal structure and processing effects
[DE93-017620] p 2027 N94-21296
Materials processing and manufacturing technologies for diamond substrate multichip modules
[AD-A271484] p 2027 N94-21319
Techniques for the flux growth of optical materials: Growth of beta-barium borate
[AD-A272717] p 2028 N94-21505
Characterization of convection related defects in II-VI compound semiconductors
[NASA-CR-194704] p 2030 N94-21778
Initial development of a high-pressure crystal growth facility: Center director's discretionary fund
[NASA-TM-108430] p 2030 N94-21807
Annual Report, Materials Science Branch, FY 1992
[DE94-000204] p 1849 N94-22015
Growth and morphology of crystals: Theory and observations
[PB93-221166] p 2035 N94-22273

CRYSTAL LATTICES
Synthesis and structural characterization of new light molecular weight inorganic oxidizers and relative derivatives, volume 1
[AD-A271437] p 2012 N94-19842
Fundamentals of mechanical behavior in structural intermetallics: A synthesis of atomistic and continuum modeling
[DE93-019166] p 1690 N94-20232
Phonons and metastability in compressed nitrogen
[DE93-019913] p 2016 N94-20318
Techniques for the flux growth of optical materials: Growth of beta-barium borate
[AD-A272717] p 2028 N94-21505
Static ultra-high pressure study of lanthanide and actinide metals using a diamond-anvil cell
[DE94-000369] p 1693 N94-21656
Microtextural characterization of annealed and deformed copper
[DE93-040144] p 1695 N94-21990
Synthesis and characterization of charge-substituted garnets YCaLnGa5O12 (Ln = Ce, Pr, Tb)
[DE93-040227] p 2033 N94-21992
The effect of correlated and point defects on the vortex lattice melting transition in single crystal YBa2Cu3O(7-delta)
[DE93-040277] p 2033 N94-21997
Lattice damage during ion implantation of semiconductors
[DE94-000335] p 2034 N94-22016
Theoretical studies of structural phase transitions in actinide metals
[DE94-000796] p 1696 N94-22388
Theoretical phase diagrams for solid H(sub 2)
[DE94-001049] p 1684 N94-22395
Spectroscopic studies of magnetic transitions in TbPO4
[DE94-001274] p 2035 N94-22565

CRYSTAL OSCILLATORS
Measuring liquid properties with smooth and textured-surface resonators
[DE93-019433] p 1749 N94-20054

CRYSTAL STRUCTURE
Synthesis and structural characterization of new light molecular weight inorganic oxidizers and relative derivatives, volume 1
[AD-A271437] p 2012 N94-19842
Common Themes and Mechanisms of Epitaxial Growth, volume 312 — Materials Research Society symposium proceedings
[AD-A270513] p 2013 N94-19967
Neutron-scattering studies of Yb-bearing silicate glasses
[DE93-019768] p 1700 N94-20265
Molecular and atomic arrays in nano- and mesoporous materials synthesis
[AD-A271500] p 2017 N94-20544
Microstructure evolution in the presence of constraints and implications on the properties of Mg-Li and Nb-Al constraints
[AD-A272088] p 1674 N94-20623
Inter- and intra-crystalline oxygen isotope distribution of fassaites in Allende CAI p 2086 N94-20898
Determination of structure factors of copper by convergent beam electron diffraction
[DE93-019520] p 2019 N94-20941
Measurement of superlattice optical properties by variable angle spectroscopic ellipsometry
p 2022 N94-20992
X ray analysis of alpha mercuric iodide crystal structure and processing effects
[DE93-017620] p 2027 N94-21296
Synthesis and catalytic properties of metal and semiconductor nanoclusters
[DE93-019418] p 2028 N94-21541
First principles calculations for analysis martensitic transformations
[DE94-000666] p 1695 N94-21964
Crystal structure and short-range oxygen defects in La- and Nd-modified ZrO2
[DE93-040229] p 2033 N94-21993
Growth and morphology of crystals: Theory and observations
[PB93-221166] p 2035 N94-22273
Theoretical studies of structural phase transitions in actinide metals
[DE94-000796] p 1696 N94-22388

CRYSTAL SURFACES
Oxidation-reduction induced roughening of platinum (111) surface
[DE93-017406] p 1687 N94-19922
Evaporation in equilibrium, in vacuum, and in hydrogen gas p 1684 N94-20638

CRYSTALLINITY
Complex and stereoregular nonlinear optical materials
[AD-A271067] p 1983 N94-19848
Petrography of shock features in the 1953 Manson 2-A drill core p 1862 N94-20767
Mechanical properties and reliability of semi-crystalline polymers
[AD-A271591] p 1704 N94-20946

CRYSTALLIZATION
Method for controlling protein crystallization
[NASA-CASE-MFS-28688-1] p 2017 N94-20528
Evaporation of a sodium tellurite melt in the jamic low gravity drop shaft p 1713 N94-20605
Petrogenesis of Apollo 12 mare basalts. Part 1: Multiple melts and fractional crystallization to explain olivine and ilmenite basalt compositions p 1684 N94-20644
Fragments of ancient lunar crust: Ferroan noritic anorthosites from the descartes region of the Moon
p 2096 N94-20660
A comparison of calculated and measured rheological properties of crystallising lavas in the field and in the laboratory p 1862 N94-20690
Preliminary estimation of tagamite cooling conditions (Puchezh-Katunki Astrobleme, Russia)
p 2083 N94-20735
Origin of the Apollo 15 very low Ti green glass. A perspective from the compositional diversity in the very low Ti glasses p 1685 N94-20759
Orthopyroxenes as recorders of diogenite petrogenesis: Trace element systematics p 1686 N94-20760
Ti-bearing oxide minerals in lunar meteorite Y793169 with the VLT affinity p 2084 N94-20812
Equilibrium and fractional crystallization of a primitive Shergottite composition p 2085 N94-20861
Mechanical properties and reliability of semi-crystalline polymers
[AD-A271591] p 1704 N94-20946

CRYSTALLOGRAPHY
High resolution electron crystallography of protein molecules
[DE93-040114] p 1884 N94-19826
Crystallographic phase transitions in actinide metals as a function of pressure
[DE93-040138] p 2011 N94-19827
Synthesis and structural characterization of new light molecular weight inorganic oxidizers and relative derivatives, volume 1
[AD-A271437] p 2012 N94-19842
Thermal expansion of electronic highly correlated materials
[ETN-93-93605] p 2026 N94-21135
Static ultra-high pressure study of lanthanide and actinide metals using a diamond-anvil cell
[DE94-000369] p 1693 N94-21656
Synthesis and characterization of charge-substituted garnets YCaLnGa5O12 (Ln = Ce, Pr, Tb)
[DE93-040227] p 2033 N94-21992
Crystal structure and short-range oxygen defects in La- and Nd-modified ZrO2
[DE93-040229] p 2033 N94-21993
Growth and morphology of crystals: Theory and observations
[PB93-221166] p 2035 N94-22273
Transmission electron microscopy study of thick copper-304 stainless steel multilayers
[DE94-001045] p 1696 N94-22394

CRYSTALS
Modeling failure and reliability in new-generation devices
[AD-A271150] p 1748 N94-19910
Synchrotron x ray diffraction analysis of photorefractive crystals and their gratings
[AD-A271176] p 2015 N94-20213
Optics survivability support, volume 1
[DE93-019616] p 1985 N94-20262
Spatial organization of polymer chains in a crystallizable diblock polyethylene and polystyrene
[AD-A271862] p 1702 N94-20463
First principles calculations for analysis martensitic transformations
[DE94-000666] p 1695 N94-21964
Crystal orientation dependence of elastic precursor strength in pentaerythritol tetranitrate
[DE93-018340] p 2034 N94-22035
Growth and morphology of crystals: Theory and observations
[PB93-221166] p 2035 N94-22273
Cirrus microphysics observations made during FIRE 2: Small particles, high concentrations, and probe comparisons p 1871 N94-22294
Cirrus properties deduced from CO2 lidar observations of zenith-enhanced backscatter from oriented crystals
p 1871 N94-22295
Theoretical studies of structural phase transitions in actinide metals
[DE94-000796] p 1696 N94-22388

CUBIC EQUATIONS
Achieving high data reduction with integral cubic B-splines
[NASA-CR-177628] p 1966 N94-21881

CULTURAL RESOURCES
Aircraft noise effects on cultural resources: Recommendation and rationale for further research
[PB93-205326] p 1968 N94-22053
Aircraft noise effects on cultural resources: Annotated bibliography
[PB93-205334] p 1969 N94-22054

CUMULATIVE DAMAGE
Damage states around fastener holes in thick graphite/epoxy composite laminates
[AD-A272613] p 1675 N94-21504

CUMULUS CLOUDS
Clouds: Their prediction and simulation
[AD-A271161] p 1864 N94-19900
Breaking Kelvin-Helmholtz waves and cloud-top entrainment as revealed by K-band Doppler radar
p 1874 N94-22310

CURING
Phthalonitrile prepolymer as high temperature sizing material for composite fibers
[AD-D015912] p 1672 N94-20010
Stress-induced cracking of fluorocarbon rubber MTL-0002 after exposure to DS-2
[AD-A271753] p 1705 N94-21302

CURRENT DENSITY
First results on InGaAsP separate confinement heterostructure diode lasers
[AD-A270849] p 1815 N94-19878
Superconducting property measurements in tape geometry
[DE93-018943] p 2014 N94-19970
VLSI design for reliability-current density
[AD-A270719] p 1749 N94-20110
High current density contacts for photoconductive semiconductor switches
[DE93-018837] p 1750 N94-20312
CsI and some new photocathodes
[DE93-019387] p 1750 N94-20314
Beta-limiting instabilities in D3-D discharges with large bootstrap current
[DE93-015476] p 1993 N94-20326
Microwave properties and characterization of co-evaporated BSCCO thin films p 1709 N94-20518
Field emitter array RF amplifier development project, phase 1, option 1
[AD-A272567] p 1740 N94-21361
A new innovative instrument for space plasma instrumentation
[NASA-CR-194736] p 1666 N94-21780
Initial operation of a large-scale plasma source ion implantation experiment
[DE94-000805] p 2036 N94-22583

CURVATURE
The effect of transverse curvature on the fluctuating wall pressure and structure of boundary layer turbulence
[AD-A271868] p 1800 N94-20466

CURVE FITTING
A database of selected transport coefficients for combustion studies
[DE93-041278] p 1678 N94-19889
Measure fields for function approximation
[AD-A272660] p 1964 N94-21215
Achieving high data reduction with integral cubic B-splines
[NASA-CR-177628] p 1966 N94-21881

Segmentation and fitting by residual consensus
p 1771 N94-22109
Interactive Spectral Analysis and Computation (ISAAC)
p 1926 N94-22505

CURVES (GEOMETRY)
Affine and non-affine blossoms
[RR-913-M] p 1950 N94-20200

CUTTING
High-power copper vapor lasers and their application to precision drilling and cutting
[DE93-019951] p 1819 N94-21844

CYANIDES
C2, CN and dust in Comet Wilson (1987VII)
p 2083 N94-20746
Sulfur-bonded thiophenes in organometallic rhenium complexes and adsorption of isocyanides on gold
[DE93-041126] p 1694 N94-21937

CYCLES
Long cycles in graphs containing a 2-factor with many odd components
[MEMO-1086] p 1953 N94-21048
Degree sums, k-factors and Hamiltonian cycles in graphs
[MEMO-1078] p 1953 N94-21074
Semi-stability and heights of cycles
[PB93-215507] p 1961 N94-22377

CYCLIC COMPOUNDS
Fullerene derivatives and fullerene superconductors
[DE93-019568] p 2031 N94-21871

CYCLIC LOADS
Biaxial flexural testing of a carbon fiber reinforced epoxy composite
[AD-A271956] p 1674 N94-20577
Life assessment of structural components using inelastic finite element analyses p 1834 N94-22614
Time-dependent reliability analysis of ceramic engine components p 1828 N94-22619

CYCLOBUTANE
High resolution infrared spectroscopy of cyclobutane: A study of vibrational mode coupling involving large amplitude, low frequency modes
[AD-A271987] p 1973 N94-20619

CYCLOHEXANE
Surface science and modeling studies of endothermic fuels catalysis
[AD-A272850] p 1712 N94-21192

CYCLONES
The life cycles of intense cyclonic and anticyclonic circulation systems observed over oceans
[NASA-CR-194760] p 1865 N94-20353
Spatial and temporal variations of satellite microwave measurements of latent heat release in tropic cyclones due to environmental forcing obtained from a numerical model
[AD-A267947] p 1865 N94-20482
Large-scale circulation regimes and tropical cyclone characteristics over the western pacific ocean
[AD-A273004] p 1867 N94-21307
A synoptic-scale overview of the TOGA COARE intensive observing period November 1992 to February 1993 based on analyses from US operational global data assimilation systems
[NASA-TM-104593] p 1868 N94-21605

CYCLOTRON FREQUENCY
Fusion plasma theory grant. Task 3: Auxiliary radiofrequency heating of tokamaks
[DE94-000779] p 1994 N94-20940

CYCLOTRON RADIATION
Particle behavior in an ECR plasma etch tool
[DE93-040343] p 1996 N94-21769

CYCLOTRON RESONANCE
Particle behavior in an ECR plasma etch tool
[DE93-040343] p 1996 N94-21769

CYCLOTRON RESONANCE DEVICES
An 85 GHz quasioptical gyroklystron experiment
[AD-A272020] p 1752 N94-20931

CYLINDRICAL ANTENNAS
Radiation and scattering from printed antennas on cylindrically conformal platforms
[NASA-CR-194703] p 1741 N94-21885
Scattering by cavity-backed antennas on a circular cylinder p 1741 N94-21886
Radiation by cavity-backed antennas on a circular cylinder p 1741 N94-21887
User manual for EXCALIBUR: A FE-BI numerical laboratory for cavity-backed antennas in a circular cylinder, version 1.2 p 1741 N94-21888
Aperture coupling of circular cylindrical dielectric resonator antenna
[ISBN-0-315-60632-0] p 1743 N94-22409

CYLINDRICAL BODIES
Probe compensation in cylindrical near-field scanning: A novel simulation methodology p 1718 N94-20404
The effect of transverse curvature on the fluctuating wall pressure and structure of boundary layer turbulence
[AD-A271868] p 1800 N94-20466
Approximation to sound radiation and scattering by simply supported layered cylinder
[AD-A272964] p 1967 N94-21306
Speed of sound data and related models for mixtures of natural gas constituents
[PB93-200822] p 1968 N94-21447
Improved approximate formulas for flux from cylindrical and rectangular sources
[DE93-011390] p 1742 N94-22268

CYLINDRICAL CHAMBERS
Initial operation of a large-scale plasma source ion implantation experiment
[DE94-000805] p 2036 N94-22583

CYLINDRICAL COORDINATES
A moving finite element model of the tokamak scrapeoff layer
[DE94-000673] p 1997 N94-21965

CYLINDRICAL SHELLS
A benchmark study of 2D and 3D finite element calculations simulating dynamic pulse buckling tests of cylindrical shells under axial impact
[DE93-018859] p 1829 N94-19940
Compression strength of composite primary structural components
[NASA-CR-194561] p 1830 N94-20159
Approximation to sound radiation and scattering by simply supported layered cylinder
[AD-A272964] p 1967 N94-21306
Adhesive bonded joint with improved cyclic fatigue life for alumina-ceramic cylinders and hemispheres: Fourth generation housings
[AD-A273061] p 1831 N94-21310
Probabilistic assessment of composite structures
[NASA-TM-106368] p 1832 N94-21757

CYLINDRICAL WAVES
Probe compensation in cylindrical near-field scanning: A novel simulation methodology p 1718 N94-20404

D

D REGION
Imaging radar studies of atmospheric winds and waves
[AD-A271672] p 1866 N94-20918
High Frequency (HF) and meteor burst communications in a polar environment
[AD-A271604] p 1737 N94-20949

DAMAGE
Cratering evaluations and results
[DE93-040347] p 1691 N94-20478
Lattice damage during ion irnplantation of semiconductors
[DE94-000335] p 2034 N94-22016
Demonstrating damage tolerance of composite airframes p 1647 N94-22623

DAMAGE ASSESSMENT
The Seventh International Conference on Composite Structures, volume 25, numbers 1-4
[AD-A269961] p 1672 N94-20031
Numerical simulations of hypervelocity impact experiments involving single Whipple bumper shields
[AD-A272123] p 1831 N94-20572
Asteroid collisions: Target size effects and resultant velocity distributions p 2083 N94-20729
Variable angle spectroscopic ellipsometric characterization of surface damage in chemical-mechanical polished GaAs p 1710 N94-20986
Flight and laboratory testing of materials in low Earth orbit p 1659 N94-21389
Measured space environmental effects to LDEF during retrieval p 1659 N94-21372
Thermostructural material composites for space applications p 1664 N94-21398
Damage states around fastener holes in thick graphite/epoxy composite laminates
[AD-A272613] p 1675 N94-21504
Debris/ice/TPS assessment and integrated photographic analysis for Shuttle Mission STS-51
[NASA-TM-109189] p 1656 N94-21884
Aircraft noise effects on cultural resources: Recommendation and rationale for further research
[PB93-205326] p 1968 N94-22053
Aircraft noise effects on cultural resources: Annotated bibliography
[PB93-205334] p 1969 N94-22054

DAMPING
Frequency and temperature dependence of high damping elastomers
[DE93-019539] p 1697 N94-19809
Persistent wakefields associated with waveguide damping of higher order modes
[DE93-040973] p 1715 N94-19874
Acoustic radiation damping of flat rectangular plates subjected to subsonic flows
[NASA-TM-109382] p 1967 N94-20211
Measurement and computation of the higher order modes of the ALS 500 MHz accelerating cavities
[DE93-019256] p 1980 N94-20292
Teleoperation with virtual force feedback
[DE93-019406] p 1942 N94-20293
Active damping of oscillations in a long compliant manipulator link
[DE93-018878] p 1826 N94-22038
Continuum damping of ideal toroidal Alfven eigenmodes
[DE94-001233] p 1998 N94-22560

DARK MATTER
The distribution of dark matter in the A2256 cluster
[NASA-CR-194699] p 2055 N94-21579
How to handle 6GBytes a night and not get swamped p 2058 N94-22444
Dark matter: Neutron star halo and the nature of gamma-bursts p 2002 N94-22643

DATA ACQUISITION
SISSY: An example of a multi-threaded, networked, object-oriented databased application
[DE93-019742] p 2041 N94-19811
Data management for support of the Oregon Transect Ecosystem Research (OTTER) project
[NASA-CR-4557] p 1905 N94-20149
A SCSI-bus data acquisition system for nuclear spectroscopy experiments
[USIP-92-03] p 2042 N94-20193
Development of a naming convention and data ma nagement system
[NASA-CR-193860] p 2042 N94-20268
The GEM Silicon Tracking System
[DE93-040133] p 2016 N94-20322
Recommendations resulting from the SPDS Community-Wide Workshop
[NASA-CR-194684] p 2042 N94-20363
Magellan at Venus: Summary of science findings p 2110 N94-20734
NAVSPASUR sensor system digital signal processing receiver. Volume 1: Hardware and software overview
[AD-A272899] p 1736 N94-21198
NAVSPASUR sensor system digital signal processing receiver. Volume 2: Function and capabilities of hardware and software components
[AD-A272900] p 1739 N94-21218
Estimating the rotation rate of mesoscale ocean rings from satellite altimetry
[AD-A272922] p 1883 N94-21222
Low-cost, dual-use platforms for environmental sensing, phase 1
[AD-A272951] p 1646 N94-21246
Software metrics: The key to quality software on the NCC project p 1922 N94-21326
Heterojunction bipolar transistor technology for data acquisition and communication p 1763 N94-21697
Geometric optimization
[DE93-040152] p 1917 N94-21764
Three dimensional ultrasonic imaging
[DE93-040549] p 1968 N94-22003
Post-experimental plots for high speed data acquisition program
[DE94-000956] p 1918 N94-22011
Use of open systems for control, analysis, and data acquisition of the DIII-D tokamak
[DE94-001101] p 1998 N94-22089
A four-band infrared data acquisition facility for signal processing development p 1791 N94-22235
Near wake measurements on a rotor model with Mie-vanes in the Delft open jet tunnel
[PB93-215382] p 1638 N94-22260
An overview of the radiation component of the NASA TOGA-COARE experiment p 1881 N94-22344
Access to D3-D data located in multiple files and multiple locations
[DE94-001104] p 2045 N94-22404
Second Annual Conference on Astronomical Data Analysis Software and Systems. Abstracts
[NASA-TM-108245] p 2057 N94-22438
VETA x ray data acquisition and control system p 2047 N94-22455
The Keck keyword layer p 1925 N94-22460
ROSAT implementation of a proposed multi-mission x ray data format p 2047 N94-22462
The ADAM environment and transputers p 1926 N94-22494
CCD data acquisition systems at Lick and Keck Observatories p 2047 N94-22495
The digital archive of the International Halley Watch p 2047 N94-22496
The ISO SWS on-line system p 1927 N94-22522
The data acquisition system for the Anglo-Australian Observatory 2-degree field project p 2048 N94-22529

NASA's astrophysics archives at the National Space Science Data Center p 2049 N94-22541
Solar full-disk magnetic field image receiving system and observation software p 2079 N94-22552
Interpretation of Ground Penetrating Radar data at the Hanford Site, Richland, Washington
[DE93-040409] p 1743 N94-22557
Measurement of the influence of deicing liquids on aircraft aerodynamics p 1640 N94-22602

DATA BASE MANAGEMENT SYSTEMS
SISSY: An example of a multi-threaded, networked, object-oriented databased application
[DE93-019742] p 2041 N94-19811
RDA-PC system user's guide
[AD-A270356] p 2041 N94-20038
Dynamics Explorer 2: Continued FPI and NACS instrument data analysis and associated scientific activity at the University of Michigan
[NASA-CR-194689] p 1657 N94-20173
Optics survivability support, volume 2
[DE93-040310] p 1985 N94-20283
Design and implementation of a prototype PC based graphical and interactive MILSATCOM requirements database system
[AD-A272960] p 1658 N94-21251
Let your fingers do the walking: The projects most invaluable tool p 1922 N94-21325
Termination and confluence of rule execution
[CWI-CS-R9309] p 1916 N94-21587
Advanced failure analysis laboratory equipment networking
[DE93-019070] p 1916 N94-21633
Proceedings of the IMOG (Interagency Manufacturing Operations Group) Numerical Systems Group
[DE94-001009] p 1917 N94-21851
Project Records Information System (PRIS): User's manual
[DE94-001548] p 2045 N94-22047
Investigation on construction of the database system for research and development of the global environment industry technology
[DE94-714890] p 1853 N94-22090
Distributed processing using Oracle7 and SQL*Net v2: An implementation story
[DE94-000494] p 1937 N94-22267
Access to D3-D data located in multiple files and multiple locations
[DE94-001104] p 2045 N94-22404
Implementation of a laboratory information management system for environmental regulatory analyses
[DE94-001198] p 2046 N94-22407
The extreme ultraviolet explorer archive p 2047 N94-22468
The NSO FTS database program and archive (FTSDBM) p 1926 N94-22506
STARBASE: Database software for the automated plate scanner p 1927 N94-22512
Evaluation of RDBMS packages for use in astronomy p 2048 N94-22514
The EXOSAT database and archive p 2048 N94-22521
SkiCAT: A cataloging and analysis tool for wide field imaging surveys p 2049 N94-22546

DATA BASES
An analysis of cloud-cover reporting in the 1977 surface observation database
[AD-A271102] p 1864 N94-19852
Development of the UTC-PAB normative database
[AD-A271319] p 1893 N94-20023
RDA-PC system user's guide
[AD-A270356] p 2041 N94-20038
Data and Analysis Center for Software
[AD-A270571] p 2041 N94-20106
Optics survivability support, volume 1
[DE93-019616] p 1985 N94-20262
Development of a naming convention and data management system
[NASA-CR-193860] p 2042 N94-20268
Optics survivability support, volume 2
[DE93-040310] p 1985 N94-20283
Recommendations resulting from the SPDS Community-Wide Workshop
[NASA-CR-194684] p 2042 N94-20363
Processing of climatological data for model initialization
[AD-A271878] p 1865 N94-20487
Threshold computation and cryptographic security
[TR-443] p 1907 N94-20536
Studying Venus using a GIS database p 2105 N94-20707
Named Venusian craters p 2109 N94-20725
Replica control algorithms in distributed databases
[AD-A271571] p 1909 N94-21034
Multi Wave Link: An interactive database for co-ordination of multiwavelength programs
[NASA-CR-194778] p 2043 N94-21055
On the selection of indices in relational databases
[MEMO-INF-92-72] p 2043 N94-21071
A conceptual database design and performance analysis of the MILSATCOM requirements database
[AD-A272672] p 1658 N94-21217
Conversion of LDEF experiment M0003 sample observation database to MS-DOS formats
[AD-A272945] p 1681 N94-21226
Design and implementation of a prototype PC based graphical and interactive MILSATCOM requirements database system
[AD-A272980] p 1658 N94-21251
Light update notification mechanism for shared data structures
[AD-D015967] p 2043 N94-21276
Threshold computation and cryptographic security
[TR-461] p 1912 N94-21285
Promises and fault-tolerant database access
[TR-447] p 2043 N94-21287
Problem reporting management system performance simulation p 1931 N94-21328
The Test Analysis Retrieval System (TARS): Meeting the challenges of the network's test processes p 1933 N94-21337
The mechanical property data base from an Air Force/industry cooperative test program on advanced aluminum alloys: 2091 sheet, plate, and 8090 extrusion
[AD-A273091] p 1692 N94-21525
Interpolative modeling of GaAs FET S-parameter data bases for use in Monte Carlo simulations p 1767 N94-21723
Databases in distributed systems p 2046 N94-22080
Investigation on construction of the database system for research and development of the global environment industry technology
[DE94-714890] p 1853 N94-22090
Survey on utilization of database for research and development of global environmental industry technology
[DE94-714891] p 1853 N94-22259
Distributed processing using Oracle7 and SQL*Net v2: An implementation story
[DE94-000494] p 1937 N94-22267
Database computing in HEP
[NASA-CR-194791] p 1921 N94-22375
Implementation of a laboratory information management system for environmental regulatory analyses
[DE94-001198] p 2046 N94-22407
Database of proposed payloads and instruments for SEI missions p 1811 N94-22432
Archiving data from ground-based telescopes p 2045 N94-22442
How to handle 6GBytes a night and not get swamped p 2058 N94-22444
Database activity in the Italian Astronet: DIRA 2 p 2047 N94-22452
The EUVE proposal database and scheduling system p 2047 N94-22459
A distributed clients/distributed servers model for STARCAT p 2047 N94-22469
An IDL-based analysis package for COBE and other skycube-formatted astronomical data p 1925 N94-22471
C++, objected-oriented programming, and astronomical data models p 2063 N94-22473
The IRAF radial velocity analysis package p 1925 N94-22475
Programmability in AIPS++ p 1926 N94-22482
The HEASARC graphical user interface p 1926 N94-22487
Quality control of EUVE databases p 2047 N94-22490
A generic archive protocol and an implementation p 2047 N94-22493
SIMBAD quality-control p 2048 N94-22502
The NSO FTS database program and archive (FTSDBM) p 1926 N94-22506
STARBASE: Database software for the automated plate scanner p 1927 N94-22512
Evaluation of RDBMS packages for use in astronomy p 2048 N94-22514
The European Southern Observatory-MIDAS table file system p 2048 N94-22518
Integrating a local database into the StarView distributed user interface p 2048 N94-22530
STELAR: An experiment in the electronic distribution of astronomical literature p 2049 N94-22544
StarView: The object oriented design of the ST DADS user interface p 2049 N94-22548

DATA COMPRESSION
Low bit rate coding of Earth science images
[NASA-CR-193729] p 2041 N94-20158
A comparison of some of the most current methods of image compression
[AD-A271841] p 1907 N94-20525
An adaptive, lossless data compression algorithm and VLSI implementations p 1753 N94-21080
High performance MPEG-audio decoder IC p 1744 N94-21092
A fixed/variable bit-rate data compression architecture p 1759 N94-21128
A CAM-based LZ data compression IC p 1759 N94-21129
Behavioral model simulation studies of an image compressor p 1760 N94-21133
Data compression by using wavelet transforms and vector quantization
[AD-A272763] p 1738 N94-21182
Reduction of blocking effects for the JPEG baseline image compression standard p 1765 N94-21714
Application guide for universal source encoding for space
[NASA-TP-3441] p 1741 N94-21783
A neural M-ary tree method for data compression p 1780 N94-22166
Coding of color quantized images p 1781 N94-22173
Hierarchical multirate vector quantization for image coding p 1781 N94-22174
Efficient transfer of images over networks p 1748 N94-22517

DATA CONVERSION ROUTINES
FITS data conversion efforts at the Compton Observatory Science Support Center p 1926 N94-22488

DATA CORRELATION
Performance evaluation of the JPL TOPSAR system: An across-track interferometric SAR system for topographic mapping p 1732 N94-20461
Specific heat of YBa2Cu3O7
[DE93-040640] p 2031 N94-21926
Sensor integration and data fusion for object localization in robotic workcells p 1774 N94-22130
STAR-1 SAR road extraction using texture analysis and mathematical morphology
[ISBN-0-315-83255-X] p 1843 N94-22429

DATA FLOW ANALYSIS
Set based analysis of ML programs
[AD-A270597] p 1902 N94-19948
Object-oriented DFD models to present the functional and behavioral views
[DE93-040206] p 1906 N94-20280
MINIFOLD: A kernel for a MANIFOLD-like coordination language
[CWI-CS-R9252] p 1915 N94-21534
Micro-rollback and self-recovery synthesis p 1765 N94-21707
Modeling software systems for data flow testing p 1772 N94-22117
A neural network approach to the maximum flow problem p 1783 N94-22183
Throughput and blocking in circuit-switched interconnection networks p 1784 N94-22189
GRO/EGRET data analysis software: An integrated system of custom and commercial software using standard interfaces p 1926 N94-22501

DATA INTEGRATION
Robust photo-topography by fusing shape-from-shading and stereo
[NASA-CR-194697] p 1806 N94-19920
GammaCore: The Compton Observatory research environment p 2048 N94-22509

DATA LINKS
Understanding Open Systems Interconnection (OSI)
[AD-A271877] p 1929 N94-20472
Satellite Communication Hardware Emulation System (SCHES) p 1744 N94-21344
A packet switched communications system for GRO p 1744 N94-21345
Array Simulations Platform (ASP) predicts NASA Data Link Module (NDLM) performance p 1744 N94-21348
Advanced coding and modulation schemes for TDRSS p 1744 N94-21350
PEGASUS, electronic bulletin board system user's guide
[AD-A271679] p 2044 N94-21363
Low-cost Unmanned Air Vehicle (UAV) for oceanographic research
[AD-A273103] p 1646 N94-21507
Data link development for the archytas vertical takeoff and landing transitional flight unmanned aerial vehicle
[AD-A272499] p 1646 N94-21548
Specification and formal verification of the safety criterion in the alternating bit protocol p 1784 N94-22193

DATA MANAGEMENT
RDA-PC system user's guide
[AD-A270356] p 2041 N94-20038
Data and Analysis Center for Software
[AD-A270571] p 2041 N94-20106

Data management for support of the Oregon Transect Ecosystem Research (OTTER) project
[NASA-CR-4557] p 1905 N94-20149
Development of a naming convention and data management system
[NASA-CR-193860] p 2042 N94-20268
On Update Last schemes
[CWI-CS-R9247] p 1952 N94-21027
The electronics technology policy of the NLR Informatics Division: The NLR electronics CAE infrastructure
[NLR-TP-91001-U] p 1753 N94-21067
Light update notification mechanism for shared data structures
[AD-D015967] p 2043 N94-21276
Distributed processing using Oracle7 and SQL*Net v2: An implementation story
[DE94-000494] p 1937 N94-22267
Data management for interdisciplinary field experiments: OTTER project support
[NASA-CR-4559] p 1842 N94-22345
Database computing in HEP
[NASA-CR-194791] p 1921 N94-22375
A proof-of-concept implementation of persistence in a hierarchical storage system
[NASA-CR-194790] p 1921 N94-22376
Access to D3-D data located in multiple files and multiple locations
[DE94-001104] p 2045 N94-22404
How to handle 6GBytes a night and not get swamped
p 2058 N94-22444
ROSAT implementation of a proposed multi-mission x ray data format p 2047 N94-22462
The extreme ultraviolet explorer archive
p 2047 N94-22468
Programmability in AIPS++ p 1926 N94-22482
The NSO FTS database program and archive (FTSDBM) p 1926 N94-22506
The European Southern Observatory-MIDAS table file system p 2048 N94-22518

DATA PROCESSING

A concept for implementing hypermedia technology in computer aided workplaces in medicine
[ETN-93-95057] p 1889 N94-20022
Explainable expert systems: A research program in information processing
[NASA-CR-193422] p 2041 N94-20133
A proposed research program in information processing
[NASA-CR-194271] p 2041 N94-20134
Two-dimensional particle-in-cell simulation on transputer arrays
[DE93-017977] p 1972 N94-20181
Connectionism and Natural Language Processing
[MEMO-INF-92-64] p 1940 N94-20242
Speech synthesis with artificial neural networks
p 1743 N94-20245
A single layer higher order neural net and its application to grammar recognition p 1941 N94-20251
Syntactic neural networks for natural language processing p 1941 N94-20254
Development of a naming convention and data management system
[NASA-CR-193860] p 2042 N94-20268
Understanding Open Systems Interconnection (OSI)
[AD-A271877] p 1929 N94-20472
Shipboard ADCP observations during RRS Charles Darwin Cruise 62
[IOS-298-1992] p 1882 N94-20531
Standard ML signatures for a protocol stack
[AD-A272060] p 1908 N94-20622
Data format standards for civilian remote sensing satellites
[PB93-192920] p 1841 N94-21446
Self assembly: An approach to terascale integration
[DE93-040104] p 1769 N94-21846
Design document and database specifications for the Naval Interactive Data Analysis System (NIDAS), version 1.0
[NASA-CR-194817] p 2045 N94-21865
Enhanced software for the GT1022 automated gaging system
[DE94-001374] p 1918 N94-21977
System architectures for banking applications
p 2046 N94-22057
Use of open systems for control, analysis, and data acquisition of the DIII-D tokamak
[DE94-001101] p 1998 N94-22089
Progress in interpreting CO2 lidar signatures to obtain cirrus microphysical and optical properties
p 1874 N94-22308
How to handle 6GBytes a night and not get swamped
p 2058 N94-22444
The ALEXIS data processing package: An IDL based system p 2047 N94-22453
PROS: An IRAF based system for analysis of x ray data p 1925 N94-22461
On AIPS++, a new astronomical information processing system p 2047 N94-22463
Deep near-infrared survey of the Southern Sky (DENIS) p 2062 N94-22467
A distributed clients/distributed servers model for STARCAT p 2047 N94-22469
An IDL-based analysis package for COBE and other skycube-formatted astronomical data
p 1925 N94-22471
GRO/EGRET data analysis software: An integrated system of custom and commercial software using standard interfaces p 1926 N94-22501
Data indexing techniques for the EUVE all-sky survey
p 2048 N94-22503
AXAF user interfaces for heterogeneous analysis environments p 1926 N94-22507
GammaCore: The Compton Observatory research environment p 2048 N94-22509
Evaluation of RDBMS packages for use in astronomy
p 2048 N94-22514
Managing an archive of weather satellite images
p 2048 N94-22525
The IRAF Fabry-Perot analysis package: Ring fitting
p 2048 N94-22527
PCIPS 2.0: Powerful multiprofile image processing implemented on PCs p 1927 N94-22532
IRAF in the nineties p 2048 N94-22535

DATA PROCESSING EQUIPMENT

A SCSI-bus data acquisition system for nuclear spectroscopy experiments
[USIP-92-03] p 2042 N94-20193
NAVSPASUR sensor system digital signal processing receiver. Volume 1: Hardware and software overview
[AD-A272899] p 1738 N94-21198
NAVSPASUR sensor system digital signal processing receiver. Volume 2: Function and capabilities of hardware and software components
[AD-A272900] p 1739 N94-21218

DATA RECORDERS

Audit report. Navy's aircraft structural life surveillance program data recorders
[AD-A270391] p 1645 N94-20040

DATA RECORDING

Efficiency of reversible optical storage in azo polymers
[AD-A272923] p 1705 N94-21223
The VLBA correlator: Real-time in the distributed era
p 2049 N94-22547

DATA REDUCTION

Study of regional climate change
[DE93-018926] p 1850 N94-19941
Imaging radar studies of atmospheric winds and waves
[AD-A271672] p 1866 N94-20918
A geometrical process for three dimensional osteotomy planning
[ETN-93-93602] p 1892 N94-21134
Results of the second Round Robin on opening-load measurement conducted by ASTM Task Group E24.04.04 on crack closure measurement and analysis
[NASA-TM-109032] p 1832 N94-21624
Development, refinement, and testing of a short term solar flare prediction algorithm
[NASA-CR-194726] p 2147 N94-21815
Achieving high data reduction with integral cubic B-splines
[NASA-CR-177628] p 1966 N94-21881
Automated analysis tools for reducing spacecraft telemetry data
[DE94-000400] p 1657 N94-21981
On the discovery of approximate arithmetic relations by backpropagation networks p 1782 N94-22181
Studies in remotely sensed geophysical parameter retrieval and analysis
[NASA-CR-194768] p 1842 N94-22374
Second Annual Conference on Astronomical Data Analysis Software and Systems. Abstracts
[NASA-TM-108245] p 2057 N94-22438
Multifrequency data analysis software on STARLINK
p 1925 N94-22443
CCD surface photometry of galaxies
p 2058 N94-22445
An object-oriented data reduction system in Fortran
p 2046 N94-22447
GUIs in the MIDAS environment p 2047 N94-22449
PROS: An IRAF based system for analysis of x ray data p 1925 N94-22461
PHOTCAL: The IRAF photometric calibration package
p 1925 N94-22465
The HEASARC graphical user interface
p 1926 N94-22487
Interactive Spectral Analysis and Computation (ISAAC)
p 1926 N94-22505
The European Southern Observatory-MIDAS table file system p 2048 N94-22518
Adaptive filtering of Echelle spectra of distant Quasars
p 2072 N94-22520
The IRAF Fabry-Perot analysis package: Ring fitting
p 2048 N94-22527
The evolution of the FIGARO data reduction system
p 2048 N94-22528
IRAF in the nineties p 2048 N94-22535
Miyun 232 MHz survey 1: Fields centered at: alpha:00(h)41(m), delta:41 deg 12 min and alpha: 07(h)00(m),delta:35 deg 00 min p 2060 N94-22554
ROSAT data analysis with EXSAS
p 2060 N94-22555

DATA RETRIEVAL

On the selection of indices in relational databases
[MEMO-INF-92-72] p 2043 N94-21071
Database computing in HEP
[NASA-CR-194791] p 1921 N94-22375
A generic archive protocol and an implementation
p 2047 N94-22493
STARBASE: Database software for the automated plate scanner p 1927 N94-22512
Guide star catalogue data retrieval software 2
p 1927 N94-22533
Recommendations for a service framework to access astronomical archives p 2049 N94-22537

DATA SAMPLING

Satellite orbit and data sampling requirements
p 1870 N94-21648
Specific heat of YBa2Cu3O7
[DE93-040640] p 2031 N94-21926
Some practicable applications of quadtree data structures/representation in astronomy
p 1927 N94-22515

DATA SIMULATION

Tests of a simple data merging algorithm for the GONG project p 1927 N94-22549

DATA SMOOTHING

A geometrical process for three dimensional osteotomy planning
[ETN-93-93602] p 1892 N94-21134
Measure fields for function approximation
[AD-A272660] p 1964 N94-21215

DATA STORAGE

M-dimensional computer memory with M-1 dimensional hyperplane access
[AD-D015960] p 1898 N94-20357
Recommendations resulting from the SPDS Community-Wide Workshop
[NASA-CR-194684] p 2042 N94-20363
A comparison of some of the most current methods of image compression
[AD-A271841] p 1907 N94-20525
An ASIC memory buffer controller for a high speed disk system p 1754 N94-21089
The effects of block size on the performance of coherent caches in shared-memory multiprocessors
[AD-A272838] p 1899 N94-21177
Mode transition matrix measuring system
[AD-D015973] p 1987 N94-21279
Publication of science data on CD-ROM: A guide and example
[NASA-CR-4560] p 1842 N94-21585
A simple modern correctness condition for a space-based high-performance multiprocessor
p 1766 N94-21718
A proof-of-concept implementation of persistence in a hierarchical storage system
[NASA-CR-194790] p 1921 N94-22376
Access to D3-D data located in multiple files and multiple locations
[DE94-001104] p 2045 N94-22404
ROSAT implementation of a proposed multi-mission x ray data format p 2047 N94-22462
The extreme ultraviolet explorer archive
p 2047 N94-22468
A generic archive protocol and an implementation
p 2047 N94-22493
The digital archive of the International Halley Watch
p 2047 N94-22496
Integrating a local database into the StarView distributed user interface p 2048 N94-22530

DATA STRUCTURES

Exploiting the parallelism exposed by partial evaluation
[AD-A270678] p 1928 N94-19677
Implementation of a portable nested data-parallel language
[AD-A270524] p 1902 N94-19932
Eliminating amortization: On data structures with guaranteed response time
[TR-439] p 2049 N94-20096
Structural similitude and design of scaled down laminated models
[NASA-CR-194687] p 1673 N94-20172
Parallel logic programming systems
[RR-891-I] p 1929 N94-20176

A conceptual database design and performance analysis of the MILSATCOM requirements database
[AD-A272672] p 1858 N94-21217
The term processor Kimwitu manual and cookbook
[MEMO-INF-92-67] p 1914 N94-21454
Databases in distributed systems
p 2046 N94-22080
Dynamic mesh adaption for triangular and tetrahedral grids p 1920 N94-22363
Surface acquisition through virtual milling
p 1920 N94-22372
A self-defining hierarchical data system
p 2046 N94-22448
A structured data transfer protocol
p 2047 N94-22450
Some practicable applications of quadtree data structures/representation in astronomy
p 1927 N94-22515
The evolution of the FIGARO data reduction system
p 2048 N94-22528

DATA SYSTEMS
The EXOSAT operational experience
[ESA-STM-248] p 1657 N94-20235
Recommendations resulting from the SPDS Community-Wide Workshop
[NASA-CR-194684] p 2042 N94-20363
Shaft mount for data coupler system
[NASA-CASE-LAR-13805-1] p 1822 N94-20365
Development and operations of the Astrophysics Data System
[NASA-CR-194691] p 2043 N94-21270
Structured multimedia authoring
[CWI-CS-R9304] p 2044 N94-21535
The 1992 4th NASA SERC Symposium on VLSI Design
[NASA-CR-194591] p 1763 N94-21694
Design document and database specifications for the Naval Interactive Data Analysis System (NIDAS), version 1.0
[NASA-CR-194817] p 2045 N94-21865
A packet based, data driven telemetry system for autonomous experimental sub-orbital spacecraft
[DE94-000399] p 1657 N94-21980
System architectures for banking applications
p 2046 N94-22057
Data management for interdisciplinary field experiments: OTTER project support
[NASA-CR-4559] p 1842 N94-22345
Access to D3-D data located in multiple files and multiple locations
[DE94-001104] p 2045 N94-22404
Multifrequency data analysis software on STARLINK
p 1925 N94-22443
An object-oriented data reduction system in Fortran
p 2046 N94-22447
A self-defining hierarchical data system
p 2046 N94-22448
On AIPS++, a new astronomical information processing system p 2047 N94-22463
C++, objected-oriented programming, and astronomical data models p 2063 N94-22473
Crystal ball gazing p 1925 N94-22477
A generic archive protocol and an implementation
p 2047 N94-22493
The ADAM environment and transputers
p 1926 N94-22494
Intelligent text retrieval in the NASA astrophysics data system p 2048 N94-22499
AXAF user interfaces for heterogeneous analysis environments p 1926 N94-22507
GammaCore: The Compton Observatory research environment p 2048 N94-22509
Recommendations for a service framework to access astronomical archives p 2049 N94-22537

DATA TRANSFER (COMPUTERS)
TCP performance analysis for wide area networks
[DE94-000449] p 1928 N94-19858
A SCSI-bus data acquisition system for nuclear spectroscopy experiments
[USIP-92-03] p 2042 N94-20193
Using electronic data interchange to report product quality
[AD-A271843] p 1828 N94-20468
Telecommunications services for multimedia data exchange support
[AD-A271704] p 1740 N94-21352
File transfer performance in LAN interconnection through a satellite channel p 1746 N94-22209
NASA data exchange standards for computational fluid dynamics p 1920 N94-22371
A structured data transfer protocol
p 2047 N94-22450
Efficient transfer of images over networks
p 1748 N94-22517
The European Southern Observatory-MIDAS table file system p 2048 N94-22518

DATA TRANSMISSION
Shaft mount for data coupler system
[NASA-CASE-LAR-13805-1] p 1822 N94-20365
Using electronic data interchange to report product quality
[AD-A271843] p 1828 N94-20468
Delivery of very high bandwidth with ATM switches and SONET
[DE93-019432] p 1899 N94-20476
A comparison of some of the most current methods of image compression
[AD-A271841] p 1907 N94-20525
Optimization of a satellite localization and message sending system
[ETN-93-94448] p 1737 N94-20592
Measuring the effects of thread placement on the Kendall Square KSR1
[DE93-040655] p 1906 N94-20932
An optically-assisted 3-D cellular array machine
[AD-A272683] p 1987 N94-21163
Security management of electronic data interchange
[AD-A272962] p 1899 N94-21252
Generating and evaluating alternate schedules
p 1933 N94-21336
A low cost alternative to high performance PCM bit synchronizers p 1813 N94-21347
Array Simulations Platform (ASP) predicts NASA Data Link Module (NDLM) performance p 1744 N94-21348
Telecommunications services for multimedia data exchange support
[AD-A271704] p 1740 N94-21352
Tandem queues with deterministic service times
[CWI-BS-R9238] p 1946 N94-21577
Design of a new squaring function for the Viterbi algorithm p 1764 N94-21699
Investigation on construction of the database system for research and development of the global environment industry technology
[DE94-714890] p 1853 N94-22090
CREIR: A multiaccess protocol for on-board processing satellite systems p 1780 N94-22168
Specification and formal verification of the safety criterion in the alternating bit protocol
p 1784 N94-22193
Coded 64QAM using a binary convolutional code
p 1747 N94-22223
Access to D3-D data located in multiple files and multiple locations
[DE94-001104] p 2045 N94-22404
Everything you might want to know about the Internet but are afraid to ask!
[DE93-041118] p 2046 N94-22413

DAYGLOW
A comparison of a simple model of EUV dayglow with Viking data
[ISBN-0-315-83258-4] p 1861 N94-22574

DAYTIME
Evaluation of a single stage of the LADS filter
[AD-A271101] p 1814 N94-19851

DEBRIS
PVDF gauge characterization of hypervelocity-impact-generated debris clouds
[DE93-018831] p 1829 N94-19943
Debris/ice/TPS assessment and integrated photographic analysis for Shuttle Mission STS-51
[NASA-TM-109189] p 1656 N94-21884
CO2 lidar observations of Mount Pinatubo debris: FIRE 2 and longer-term measurements p 1876 N94-22323

DECAY RATES
Optical properties of chromium and neodymium in zirconium - barium - lanthanum - aluminum fluoride glass
[AD-A271609] p 1987 N94-21236

DECISION MAKING
Believing in the basis of the evidence
[TR-438] p 2039 N94-20364
Neural network for processing both spatial and temporal data with time based back-propagation
[NASA-CASE-MSC-21874-1] p 1942 N94-20366
Integration opportunities for computer models, methods, and GIS used in Corps planning studies
[AD-A271714] p 2044 N94-21354
Conversion and maintenance of Co-oP for Windows
[AD-A272513] p 1914 N94-21414
Modelling decision-making by pilots
[NASA-CR-194767] p 2040 N94-21821
Information and decision structure in a Japanese type of management with respect to QCC and just-in-time systems p 2046 N94-22063
Method and software for decision making in public problems p 1923 N94-22087

DECISION THEORY
Linear programming for standard and nonstandard Markovian control problems. A survey
[PB93-191948] p 1963 N94-21066
Goal-oriented dynamic vision
[TR-466] p 1945 N94-21315
Method and software for decision making in public problems p 1923 N94-22087
Algorithms for Markov decision chains with partial information
[PB93-220085] p 1918 N94-22098
SkICAT: A cataloging and analysis tool for wide field imaging surveys p 2049 N94-22546

DECODERS
High performance MPEG-audio decoder IC
p 1744 N94-21092
VLSI design of a bit serial parallel processing 4 extender chip for M-path convolutional decoding
p 1775 N94-22132

DECODING
High-speed Viterbi decoding with overlapping code sequences p 1760 N94-21130
Arithmetic in large GF(2(exp n)) p 1760 N94-21131
Toward a new method of decoding algebraic codes using Groebner bases
[AD-A273089] p 1959 N94-21524
The Schur Berlekamp-Massey algorithm is parallelizable p 1784 N94-22191
Encoding and decoding quasi-spherical signal sets
p 1747 N94-22233
On the capacity of (T,U) permutation decoding method
p 1792 N94-22245
Adaptive decoding of convolutional codes
p 1793 N94-22246
Bidirectional algorithms for the decoding of convolutional codes over memoryless channels p 1793 N94-22247

DECOMPOSITION
Space-charge dominated beam transport in magnetic quadrupoles with large aperture ratios
[DE93-040443] p 1992 N94-20004
Signal processing in the linear statistical model
[AD-A272114] p 1736 N94-20570
Impact-induced devolatilization of CaSO4 anhydrite and implications for K-T extinctions: Preliminary results
p 2085 N94-20840
On the decomposition of synchronous state mechines using sequence invariant state machines
p 1764 N94-21703
Modeling of outgassing and matrix decomposition in carbon-phenolic composites
[NASA-CR-194741] p 1676 N94-21743
A multiresolution wavelet representation in two or more dimensions p 1925 N94-22456

DEEP SPACE NETWORK
Networks Technology Conference
[NASA-CP-3241] p 1931 N94-21323
Using manufacturing message specification for monitor and control at Venus p 1932 N94-21333
The Test Analysis Retrieval System (TARS): Meeting the challenges of the network's test processes
p 1933 N94-21337

DEEP WATER
On the sources of North Atlantic deep water
[AD-A270854] p 1881 N94-19895

DEFECTS
Research on defects and transport in amorphous-silicon-based semiconductors
[DE93-017117] p 2013 N94-19939
Solder technology in the manufacturing of electronic products
[DE93-018842] p 1699 N94-19960
Characterization and possible repair of defects in soft x ray projection lithography masks
[DE93-019147] p 1750 N94-20231
Using electronic data interchange to report product quality
[AD-A271843] p 1828 N94-20468
Process characterization and control of hand-soldered printed wiring assemblies
[DE93-041290] p 1763 N94-21652
Defect-sensitivity analysis of an SEU immune CMOS logic family p 1765 N94-21711
Behavior of faulty double BJT BiCMOS logic gates
p 1767 N94-21727
A set-associative, fault-tolerant cache design
p 1768 N94-21731
Strength, ultrasonic and metallurgical evaluation of diffusion bonds
[DE94-000665] p 1697 N94-22571

DEFENSE PROGRAM
Data and Analysis Center for Software
[AD-A270571] p 2041 N94-20106
Using electronic data interchange to report product quality
[AD-A271843] p 1828 N94-20468
Clementine: An inexpensive mission to the Moon and Geographos p 1652 N94-20765
Listing of approved recurring information requirements
[AD-A271673] p 2042 N94-20919

Implementing Electronic Data Interchange (EDI) with small business suppliers in the pre-award acquisition process
[AD-A271767] p 1945 N94-21305

DEFLECTION
Thermal characterization of thin films by photothermally induced laser beam deflection p 1710 N94-21007
The preservation of low emittance flat beams
[DE93-040964] p 1981 N94-21773

DEFORMATION
Durability predictions for adhesively bonded joints in humid environments
[AD-A271177] p 1830 N94-20001
Effects of processing history on the creep strength of Nb-1Zr
[DE93-015905] p 1689 N94-20093
Some deformation trends and topographic characteristics of tesserae on Venus
p 2105 N94-20706
Strength and deformation properties of basaltic lava flows on planetary surfaces p 1862 N94-20747
A tectonic resurfacing model for Venus
p 2118 N94-20781
Parga and Hecate Chasmata, Venus: Structure, volcanism and models of formation
p 2121 N94-20796
Atmospheric breakup of a small comet in the Earth's atmosphere p 2084 N94-20824
Adaptation of model parameters of a rail model at measured rail compliances
[ILR-MITT-274(1992)] p 1831 N94-21153
Experimental and numerical studies of high-velocity impact fragmentation
[DE93-040205] p 1832 N94-21557
Deformation of an alumina-zirconia-silicon carbide-whisker reinforced composite
[DE93-040244] p 1676 N94-21559
Microtextural characterization of annealed and deformed copper
[DE93-040144] p 1695 N94-21990
A finite element formulation and adaptive solution approach for large-scale thermomechanical problems with complex contact conditions
[DE93-019605] p 1960 N94-21996

DEGASSING
Are Plinian type eruptions possible on Venus?
p 2123 N94-20803
Residual atmosphere in the FRECOPA experiment and degassing of materials p 1660 N94-21374
Core formation, wet early mantle, and H2O degassing on early Mars p 2145 N94-21674
Evolution of the Martian atmosphere
p 2146 N94-21680

DEGRADATION
Degradation sequence of young lunar craters from orbital infrared survey p 2136 N94-20874
Evaluation of radiation effects in re-oxidized nitrided oxide devices by hot carrier stressing at 77 K
p 1754 N94-21084
Conversion of LDEF experiment M0003 sample observation database to MS-DOS formats
[AD-A272945] p 1681 N94-21226
Fifth International Symposium on Materials in a Space Environment
[ISBN-2-85-428293-0] p 1659 N94-21367
German space experiments on Spacelab D-2 and Eureca-1 to investigate atomic oxygen interaction with materials p 1662 N94-21390
Early Mars: A regional assessment of denudation chronology p 2145 N94-21676

DEGREES OF FREEDOM
Collisions of molecules with clusters: A quasiclassical study
[DE93-018614] p 1971 N94-20050

DEHYDRATION
Thermal behavior of natural zeolites
[DE93-040091] p 1699 N94-19975

DEHYDROGENATION
Surface science and modeling studies of endothermic fuels catalysis
[AD-A272850] p 1712 N94-21192
Investigations on trends in global environment adaptive industrial technologies
[DE94-714888] p 1853 N94-22258

DEICERS
Radome having integral heating and impedance matching elements
[CA-PATENT-APPL-SN-2,026,85] p 1738 N94-21049
Measurement of the influence of deicing liquids on aircraft aerodynamics p 1640 N94-22602

DEICING
Measurement Technology for Flight Tests
[ILR-MITT-256(1991)] p 1639 N94-22597
Experiments with a fluid deicing system for cleaning laminar wings p 1640 N94-22601
Measurement of the influence of deicing liquids on aircraft aerodynamics p 1640 N94-22602

DELAMINATING
Compression strength of composite primary structural components
[NASA-CR-194561] p 1830 N94-20159
A process for preparing an assembly of an article and a soluble polyimide which resists dimensional change, delamination, and debonding when exposed to changes in temperature
[NASA-CASE-LAR-14763-1] p 1702 N94-20373
Interleaved bismaleimide composites
[AD-A272233] p 1674 N94-20574
Biaxial flexural testing of a carbon fiber reinforced epoxy composite
[AD-A271956] p 1674 N94-20577
Damage states around fastener holes in thick graphite/epoxy composite laminates
[AD-A272613] p 1675 N94-21504
The effect of delamination on the dynamic response of composite laminates as measured by embedded fiber optic Michelson sensor
[ISBN-0-315-83534-6] p 1677 N94-22587
An embedded fibre optic for damage growth monitoring in Kevlar composites
[ISBN-0-315-83501-X] p 1677 N94-22589
Delamination, durability, and damage tolerance of laminated composite materials p 1678 N94-22622

DELAY
The correlated M/G/1 queue
[CWI-BS-R9303] p 1943 N94-21032
Computation of signal delays in RC networks
p 1744 N94-21102
Optimization of static traffic allocation policies
[CWI-BS-R9302] p 1930 N94-21161
Optimization of fixed time polling schemes
[CWI-BS-R9237] p 1945 N94-21233
Optimal repairman assignment in two maintenance models which are equivalent to routing models with early decisions
[CWI-BS-R9301] p 1930 N94-21234

DELAY CIRCUITS
Computation of signal delays in RC networks
p 1744 N94-21102
Delay analysis of combinations of pass transistors and classical logic gates p 1756 N94-21103
An adaptive method for group delay compensation using switched capacitor filters p 1793 N94-22248

DEMAGNETIZATION
Magnetic record in chondrite meteorites
p 2085 N94-20858

DEMAND (ECONOMICS)
Analysis of consumer demand structure by means of economic indexes p 2052 N94-22074

DEMODULATION
Digital receiver for on-board FM/FSK-FM/BPSK demodulation p 1744 N94-21091
A digital demodulation scheme for use in a high dynamic range radar system p 1745 N94-22144
The influence of lowpass filtering and the effects of fading on the group demodulation of QPSK signals
p 1746 N94-22170
Demodulation of a fiber Fabry-Perot strain rosette using white light interferometry
[ISBN-0-315-83427-7] p 1990 N94-22579

DEMODULATORS
Digital receiver for on-board FM/FSK-FM/BPSK demodulation p 1744 N94-21091
Timing recovery in the channel processor of a digital group demodulator p 1780 N94-22169

DEMULTIPLEXING
Wide passband wavelength multi/demultiplexer at 1.3/1.55 micrometers based on etched Fresnel mirror, appendix 8 p 1989 N94-21602

DENDRITIC CRYSTALS
Microstructure evolution in the presence of constraints and implications on the properties of Mg-Li and Nb-Al constraints
[AD-A272088] p 1674 N94-20623

DENMARK
Magnetic results 1991: Brorfelde, Godhavn, Thule and Narsarsuaq
[DATA-REPT-92-3] p 1856 N94-20609

DENSE PLASMAS
Opacity measurements in shock-generated argon plasmas
[DE94-001057] p 1998 N94-22399
Physical properties of dense astrophysical plasmas
p 2001 N94-22637
Neutrino emission processes in dense high-temperature plasmas p 2001 N94-22638
Thermal properties and radiation processes in astrophysical plasmas p 2002 N94-22640
Pair plasmas in the central engine of active galactic nuclei p 2002 N94-22641
Pair plasmas in the galactic center region and in Nova Muscae p 2009 N94-22691

DENSIFICATION
Polymer gels as precursors to high-performance materials
[AD-A270937] p 1699 N94-20046
Effect of powder characteristics on gas-pressure sintering of Si3N4 with rare earth additives
[DE94-000330] p 1694 N94-21945

DENSITY (MASS/VOLUME)
Quantitative evaluation of material composition of composites using x ray energy-dispersive NDE technique
[DE93-041157] p 1672 N94-19888
Measuring liquid properties with smooth and textured-surface resonators
[DE93-019433] p 1749 N94-20054

DENSITY DISTRIBUTION
On the experimental determination of low order structure factors in TiAl by energy filtered convergent beam electron diffraction
[DE93-019521] p 1687 N94-19806
Impact of copper vapour contamination on argon arcs
p 1994 N94-21053
Accretion of a hot plasma onto the central black hole: Fokker-Planck formulation p 2009 N94-22693

DENSITY MEASUREMENT
Wavefront sensors for optical diagnostics in fluid mechanics: Application to heated flow, turbulence, and droplet evaporation
[DE93-040060] p 1797 N94-19974
Measuring liquid properties with smooth and textured-surface resonators
[DE93-019433] p 1749 N94-20054

DEPLOYMENT
Self-deploying photovoltaic power system
[NASA-CASE-LEW-15308-1] p 1846 N94-20196

DEPOLARIZATION
Multiple scattering effects on the Linear Depolarization Ratio (LDR) measured during CaPE by a Ka-band air-borne radar p 1728 N94-20446
Radio wave propagation studies along an Earth-space satellite link
[ISBN-0-315-60627-4] p 1742 N94-22408

DEPOLYMERIZATION
Chain propagation/step propagation polymerization chemistry. The preparation of solvent resistant well phase-separated thermoplastic elastomers
[AD-A271128] p 1699 N94-20016

DEPOSITION
Geomorphic evidence for an eolian contribution to the formation of the Martian northern plains
p 2092 N94-20402
Surface states at the GaAs-germanium nitride interface p 1709 N94-20973
Properties of E-beam interactive oxide films for nanometer scale structures
[AD-A272848] p 1675 N94-21191
Single crystal diamond films
[AD-A266759] p 2028 N94-21517

DEPOSITS
Adhesive electroless metallization of fluoropolymeric substrates
[AD-A271858] p 1703 N94-20526
Mars: New evidence for origin of some Valles Marineris layered deposits p 2112 N94-20748
Geology and deposits of the Serenitatis basin
p 2119 N94-20786
Oxidation of dissolved iron under warmer, wetter conditions on Mars: Transitions to present-day arid environments p 2143 N94-21663

DEPTH
Oceanic in situ Fraunhofer-line characteristics: Fraunhofer-line underwater experiment (FLUX)
[AD-A270659] p 1881 N94-19952
Impactor control of central peak and peak-ring formation p 1862 N94-20744
Geometrical analysis of the microcraters found on LDEF samples p 1666 N94-20890
A quantitative model for interpreting nanometer scale hardness measurements of thin films
[DE93-040601] p 2034 N94-22005

DEPTH MEASUREMENT
Evaluation of a single stage of the LADS filter
[AD-A271101] p 1814 N94-19851
High power, electron-beam induced switching in diamond
[DE93-040535] p 1768 N94-21770

DERIVATION
Development of a gridless CFD method
p 1919 N94-22361

DESERTS
Areally averaged estimates of surface heat flux from ARM field studies
[DE93-018569] p 1859 N94-22036

DESICCANTS
Atmospheric moisture collection device
[AD-D015935] p 1865 N94-20332
DESIGN ANALYSIS
Turbine design p 1668 N94-20075
Total systems design analysis of high performance structures
[NASA-TP-3432] p 1653 N94-20141
A design optimization procedure for epicyclic gears
[MATHS-REPT-A-188] p 1822 N94-20146
The GEM Silicon Tracking System
[DE93-040133] p 2016 N94-20322
Coherent lidar design and performance verification
[NASA-CR-193813] p 1816 N94-20341
Design structuring and allocation optimization (Destination) prototype level 1 user's manual
[AD-A272115] p 1929 N94-20571
Validation of the design of a high resolution all-reflection Michelson interferometer for atmospheric spectroscopy
[AD-A272505] p 1987 N94-21410
Dynamics of face seals for high speed turbomachinery p 1655 N94-21796
Improvements on the design of optimum SAW filters with the Remez Exchange Algorithm p 1773 N94-22123
Manual design technique for broadband passive thin-film attenuators using the Smith chart p 1782 N94-22178
The logistic model: The integration of business process redesign and information systems development based on logistic principles
[MEMO-INF-92-70] p 2045 N94-22276
Towards the formal verification of the requirements and design of a processor interface unit: HOL listings
[NASA-CR-191466] p 1937 N94-22414
A study of parallel pier finger airport terminal configuration
[ISBN-0-315-83126-6] p 1652 N94-22425
DESORPTION
Focus history of the Hubble Space Telescope: Launch to May 1993
[NASA-CR-194179] p 2055 N94-20204
DETECTION
Resistive gate magnetic field sensor
[AD-D015923] p 1749 N94-20199
Direct photon results from CDF
[DE93-019908] p 1980 N94-20317
Detection of feed-through faults in CMOS storage elements p 1766 N94-21721
Atmospheric sampling glow discharge ionization and triple quadrupole tandem mass spectrometry for explosives vapor detection
[DE93-040593] p 1852 N94-22004
DETONATION WAVES
Initiation and modification of reaction by energy addition: Kinetic and transport phenomena
[AD-A271315] p 1797 N94-19936
DETONATORS
SPICE macromodel for a 1-megawatt power MOSFET switch
[DE93-019415] p 1748 N94-19844
Digital wireless control system
[DE93-040211] p 1714 N94-19946
DEUTERIUM
Encounters of H and D atoms with O2 in water: Relative diffusion and reaction rates
[DE93-016587] p 1970 N94-19956
Collisions of molecules with clusters: A quasiclassical study
[DE93-018614] p 1971 N94-20050
High D/H ratios of water in magmatic amphiboles in Chassigny: Possible constraints on the isotopic composition of magmatic water on Mars p 2134 N94-20862
Studies of the deuteron at high energy and momentum transfer
[DE93-041162] p 1976 N94-21941
DEUTERIUM COMPOUNDS
High resolution infrared spectroscopy of formamide and deuterated formamide in a molecular beam
[AD-A271986] p 1973 N94-20618
Dynamics of adsorbed, swollen block copolymers
[AD-A272013] p 1706 N94-21460
DEUTERONS
Studies of the deuteron at high energy and momentum transfer
[DE93-041162] p 1976 N94-21941
DEVELOPING NATIONS
Urban applications of satellite remote sensing and GIS analysis
[PB93-202174] p 1842 N94-21855
DIAGNOSIS
A concept for implementing hypermedia technology in computer aided workplaces in medicine
[ETN-93-95057] p 1889 N94-20022
Diagnostics and methods for real-time laser microchemistry
[AD-A270871] p 1680 N94-20566
DIAMETERS
Impactor control of central peak and peak-ring formation p 1862 N94-20744
Geometrical analysis of the microcraters found on LDEF samples p 1666 N94-20890
DIAMOND FILMS
Thermal diffusivity measurements by photothermal laser beam deflection (PTD): Data analysis using the Levenberg-Marquardt algorithm p 1820 N94-21006
Growth, characterization and device development in monocrystalline diamond films
[AD-A272715] p 2026 N94-21190
Materials processing and manufacturing technologies for diamond substrate multichip modules
[AD-A271484] p 2027 N94-21319
Growth, characterization and device development in monocrystalline diamond films
[AD-A273097] p 2028 N94-21506
Single crystal diamond films
[AD-A266759] p 2028 N94-21517
Fabrication of amorphous diamond films
[DE94-000404] p 2032 N94-21960
DIAMONDS
Materials processing and manufacturing technologies for Diamond Substrate MultiChip Modules (DSMCM)
[AD-A271011] p 2011 N94-19821
Analysis of cost: CVD diamond deposition
[AD-A271980] p 2018 N94-20616
A carbon and nitrogen isotope study of carbonaceous vein material in ureilite meteorites p 2083 N94-20726
Are the C delta light nitrogen and noble gases located in the same carrier? p 2085 N94-20846
High power, electron-beam induced switching in diamond
[DE93-040535] p 1768 N94-21770
Fabrication of amorphous diamond films
[DE94-000404] p 2032 N94-21960
Shock temperature measurements of iron to 350 GPa
[DE94-001058] p 1695 N94-22024
DIAPHRAGMS (MECHANICS)
Bladder operated robotic joint
[NASA-CASE-MFS-28682-1] p 1701 N94-20359
DIATOMIC GASES
Polymeric nitrogen
[DE93-040544] p 1706 N94-21512
DIATOMIC MOLECULES
Theoretical investigations of metastability and energy storage in molecular systems
[AD-A271849] p 1973 N94-20612
Establishing the basis for validated predictions of highly non-equilibrium flows (with 9 attachments)
[AD-A272918] p 1802 N94-21220
Polymeric nitrogen
[DE93-040544] p 1706 N94-21512
Non-adiabatic effects in low-energy electron-molecule scattering
[DE93-040485] p 1976 N94-21968
DICHROISM
Magnetic circular dichroism in x ray absorption and core-level photoemission
[DE93-019381] p 1688 N94-19986
Recent developments in aromatic azo polymers research
[AD-A272966] p 1705 N94-21259
Azo polymers for optical storage 3: Effect of film thickness on net phase retardation and writing speed
[AD-A272994] p 1705 N94-21267
Observation of x ray absorption magnetic circular dichroism in well-characterized iron-cobalt-platinum multilayers
[DE94-000303] p 1694 N94-21944
DICTIONARIES
A computational theory of lexical relatedness
[TR-421] p 1904 N94-20067
DIELECTRIC PROPERTIES
Numerical modeling of fringing fields and their use for complex permittivity measurements at high frequencies
[AD-A270478] p 1966 N94-19917
Preparation and properties of sol-gel derived PZT thin films for decoupling capacitor applications
[DE93-018853] p 2013 N94-19961
Sol-spray preparation, particulate characteristics, and sintering of alumina powders
[DE93-018577] p 1690 N94-20183
Measurements of the dielectric properties of simulated comet material as part of the KOSI 10 experiment p 2085 N94-20841
Characterization of an asymmetric triangular multiple quantum well, by variable angle spectroscopic ellipsometry p 2022 N94-20995
Temperature dependence of optical properties of AlAs, studied by in-situ spectroscopic ellipsometry p 2023 N94-20999
Dielectric function of InGaAs in the visible p 2023 N94-21000
Study of concentration-dependent dielectric properties of n-type GaAs using variable angle spectroscopic ellipsometry p 2024 N94-21002
Spectroscopic ellipsometric characterization of Si/Si(1-x)Ge(x) strained-layer superlattices p 2025 N94-21009
In-situ and ex-situ ellipsometric characterization for semiconductor technology p 2026 N94-21013
Millimeter-wave imaging of composite materials
[DE93-041160] p 1677 N94-21940
DIELECTRICS
Numerical modeling of fringing fields and their use for complex permittivity measurements at high frequencies
[AD-A270478] p 1966 N94-19917
Development of a technique to determine the morphology and dynamics of agglomerates in chemically reacting flows
[AD-A271160] p 1678 N94-20000
EHD enhancement of pool and in-tube boiling of alternate refrigerants
[DE94-000787] p 1798 N94-20101
FD-TD modeling of 2-D dielectric waveguides for propagation and scattering of femtosecond optical solitons p 1719 N94-20406
Linearly tapered slot antenna with dielectric superstrate p 1734 N94-20505
Bandwidth enhancement of dielectric resonator antennas p 1734 N94-20507
Direct imaging of the surface microstructure of dielectric materials using an atomic force microscope
[AD-A272251] p 2018 N94-20575
Interfacial properties of diamondlike amorphous carbon films on InP: Metal-insulator-semiconductor structures p 1710 N94-20980
A new matrix formulation of classical electrodynamics. Part 3: Wave propagation through a multilayer dielectric medium with planar boundaries
[AD-A271610] p 1739 N94-21240
Fully-depleted silicon-on-sapphire and its application to advanced VLSI design p 1765 N94-21709
Millimeter-wave imaging of composite materials
[DE93-041160] p 1677 N94-21940
Time-laplace-transform-domain analysis of wave propagation in planar waveguides
[PB93-215226] p 1960 N94-22096
Study of TE(1-delta) mode in open dielectric resonators by a finite difference time domain method p 1747 N94-22253
Modelling short bent, graded index dielectric slab waveguides
[PB93-215283] p 1742 N94-22349
DIESEL ENGINES
Analysis of a diesel-electric hybrid urban bus system
[DE93-019514] p 1825 N94-21297
Utilization of metals to improve the lubrication of ceramic load-bearing devices
[PB93-202448] p 1825 N94-21424
Ceramic Technology Project
[DE94-001011] p 1707 N94-21822
Experimental evaluation of oxygen-enriched air and emulsified fuels in a six-cylinder diesel engine
[DE94-000907] p 1811 N94-22391
DIESEL FUELS
Experimental evaluation of oxygen-enriched air and emulsified fuels in a six-cylinder diesel engine
[DE94-000907] p 1811 N94-22391
DIFFERENCE EQUATIONS
Theoretical and numerical examinations of nonlinear parameter dependent advanced differential difference equations
[ETN-93-93681] p 1952 N94-21042
Adaptive grids for quasilinear parabolic systems in one space dimension
[ETN-93-93611] p 1954 N94-21137
F2D users manual: A two-dimensional compressible gas flow code
[DE94-000653] p 1805 N94-22386
DIFFERENTIAL CALCULUS
Explicit results on gl(lambda) and sl(lambda)
[MEMO-1075] p 1953 N94-21072
Non commutative geometry and physics
[PB93-215499] p 1961 N94-22264
DIFFERENTIAL EQUATIONS
Dynamics of vortices in superconductors
[DE93-019535] p 2011 N94-19808
Numerical solution of differential-algebraic equations with ill-conditioned constraints
[AD-A270934] p 1949 N94-19898
Asymptotics of the GLRT for the disorder problem in diffusion processes
[INRIA-RR-1735] p 1951 N94-20227
Numerical methods for singularly perturbed differential equations with applications
[AD-A272112] p 1952 N94-20568

Theoretical and numerical examinations of nonlinear parameter dependent advanced differential difference equations
[ETN-93-93681] p 1952 N94-21042
Stoermer-Cowell and related methods for the numerical solution of second order periodic initial value problems for ODE's 2: Numerical characteristics of the methods
[MEMO-1082] p 1953 N94-21075
Classical and generalized solutions of time-dependent linear differential algebraic equations
[AD-A272834] p 1954 N94-21173
Finite difference methods for time-dependent, linear differential algebraic equations
[AD-A272835] p 1954 N94-21174
Derivation of a model of the exciter of a brushless synchronous machine
[EUT-92-E-258] p 1761 N94-21538
A project on parameter identification in reaction kinetics
[CWI-NM-R9301] p 1682 N94-21574
Surface path lines in plane Stokes flow driven by capillarity
[DE93-041277] p 1803 N94-21651

DIFFERENTIAL GEOMETRY
Detecting topographical regions in digital terrain maps
[AD-A272889] p 1841 N94-21453

DIFFERENTIAL INTERFEROMETRY
Demodulation of a fiber Fabry-Perot strain rosette using white light interferometry
[ISBN-0-315-83427-7] p 1990 N94-22579

DIFFERENTIAL PRESSURE
System test results of the Advanced Technology Anti-G Suit (ATAGS)
[AD-A271535] p 1896 N94-20914

DIFFERENTIAL PULSE CODE MODULATION
A fixed/variable bit-rate data compression architecture p 1759 N94-21128

DIFFRACTION
Variable-permittivity linear inverse problem for the H(sub z)-polarized case p 1719 N94-20408
Calculation of a diffracted electric field with the aid of the Method of Equivalent Currents (MEC) p 1745 N94-22127

DIFFRACTION PATTERNS
Determination of structure factors of copper by convergent beam electron diffraction
[DE93-019520] p 2019 N94-20941

DIFFUSE RADIATION
Diffuse reflectance spectra of orthopyroxene, olivine, and plagioclase as a function of composition and structure p 2087 N94-20906
Sulfur-bonded thiophenes in organometallic rhenium complexes and adsorption of isocyanides on gold
[DE93-041126] p 1694 N94-21937

DIFFUSION
Femtosecond Raman-induced Kerr effect study of polar solvent dynamics: Amides
[DE93-017563] p 1678 N94-19924
Technology to prevent greenhouse effect gases
[DE94-707421] p 1850 N94-19976
The use of x ray techniques in the in situ study of corrosion
[DE93-019845] p 1690 N94-20301
Tambo Quemado: Extraordinary concentrations of REE and refractory trace elements caused by artificial heating p 1684 N94-20667
Self diffusion of alkaline-Earth in Ca-Mg-aluminosilicate melts: Experimental improvements on the determination of the self-diffusion coefficients p 1684 N94-20669
Chronology of lunar granite 12033,576: Resetting of Rb-Sr and K-Ca isochrons p 2115 N94-20763
Chemical zoning and diffusion of Ca, Al, Mn, and Cr in olivine of springwater pallasite p 2086 N94-20902
High temperature stability of amorphous Ta(x)Cu(1-x) diffusion barriers on GaAs p 2022 N94-20990
Amorphous Ta-rich Ta-Cu films as diffusion barriers between Au and GaAs p 1710 N94-20991
Multilevel methods for transport equations in diffusive regimes p 1955 N94-21467
A note on singularities caused by the hydrodynamic dispersion tensor
[CWI-NM-R9302] p 1803 N94-21575

DIFFUSION FLAMES
Combustion in turbulent jets and buoyant flames
[PB93-202372] p 1682 N94-21452

DIFFUSION PUMPS
New technique for oil backstreaming contamination measurements p 1652 N94-20511

DIFFUSION WELDING
Interface science of controlled metal/metal and metal/ceramic interfaces prepared using ultrahigh vacuum diffusion bonding
[DE94-001066] p 1896 N94-22025
Strength, ultrasonic and metallurgical evaluation of diffusion bonds
[DE94-000665] p 1697 N94-22571

DIFFUSIVITY
Diffusive redistribution of water vapor in the solar nebula revisited p 2113 N94-20751
Multilevel methods for transport equations in diffusive regimes p 1955 N94-21467
Femtosecond dynamics in hydrogen-bonded solvents
[DE93-019937] p 1683 N94-21842

DIGITAL COMPUTERS
System for solving Boolean equations using optical lookup tables
[AD-D015962] p 1951 N94-20358

DIGITAL DATA
Handbook. Volume 2: Digital systems validation. Chapter 18: Avionic data bus integration technology
[DOT/FAA/CT-88/10-VOL-2] p 1647 N94-20343
Local topography of Mars and its relationship to surface weathering processes p 2111 N94-20737
High performance MPEG-audio decoder IC p 1744 N94-21092
VLSI mixed signal processing system p 1744 N94-21100
Reduction of blocking effects for the JPEG baseline image compression standard p 1765 N94-21714

DIGITAL ELECTRONICS
Handbook. Volume 3: Digital systems validation book plan
[DOT/FAA/CT-93/16-VOL-3] p 1647 N94-20053
VLSI design for reliability-current density
[AD-A270719] p 1749 N94-20110
Fault detection in digital and analog circuits using an i(DD) temporal analysis technique p 1757 N94-21106
Faulty behavior of asynchronous storage elements p 1757 N94-21108
Detection of CMOS bridging faults using minimal stuck-at fault test sets p 1757 N94-21110
QPPM receiver for free-space laser communications
[NASA-TM-106424] p 1741 N94-21567
Dimension scaling effects on the yield sensitivity of HEMT digital circuits p 1765 N94-21712
Real-time step frequency radar
[ISBN-0-315-83588-5] p 1743 N94-22576

DIGITAL FILTERS
Neural network for processing both spatial and temporal data with time based back-propagation
[NASA-CASE-MSC-21874-1] p 1942 N94-20366
Use of switched capacitor filters to implement the discrete wavelet transform p 1755 N94-21097
Applications of correlator chips in radio science p 1763 N94-21695
Heuristic-based scheduling algorithm for high level synthesis p 1764 N94-21704
Evaluation of floating-point sum or difference of products in carry-save domain p 1764 N94-21705
Micro-rollback and self-recovery synthesis p 1765 N94-21707
A real time correlator architecture using distributed arithmetic principles p 1768 N94-21734
Intersymbol interference effects in digital matched filters p 1788 N94-22218
On coefficient quantization and computational roundoff effects in frequency interpolation filter banks p 1793 N94-22251

DIGITAL RADAR SYSTEMS
Four-dimensional remote sensing of the marine boundary layer with a digital beamforming radar wind profiler
[AD-A270627] p 1882 N94-20564
A digital demodulation scheme for use in a high dynamic range radar system p 1745 N94-22144
Real-time step frequency radar
[ISBN-0-315-83588-5] p 1743 N94-22576

DIGITAL SIMULATION
Delay analysis of combinations of pass transistors and classical logic gates p 1756 N94-21103
Modeling of glass fabrication p 1711 N94-21800
Impact of partitioning on parallel discrete event simulation of logic circuits p 1772 N94-22115

DIGITAL SYSTEMS
A pipelined superconducting digital processor
[DE93-040852] p 1898 N94-19886
Model checking, abstraction, and compositional verification
[AD-A270552] p 1902 N94-19919
Digital wireless control system
[DE93-040211] p 1714 N94-19946
Handbook. Volume 3: Digital systems validation book plan
[DOT/FAA/CT-93/16-VOL-3] p 1647 N94-20053
A methodology for formal hardware verification, with application to microprocessors
[AD-A270550] p 1898 N94-20085
Handbook. Volume 2: Digital systems validation. Chapter 18: Avionic data bus integration technology
[DOT/FAA/CT-88/10-VOL-2] p 1647 N94-20343
Reconfigurable fuzzy cell
[NASA-CASE-MSC-21613-1] p 1907 N94-20492
Diagnostics and methods for real-time laser microchemistry
[AD-A270871] p 1680 N94-20566
Digital receiver for on-board FM/FSK-FM/BPSK demodulation p 1744 N94-21091
Testing self-timed circuits using scan paths p 1757 N94-21109
The 1992 4th NASA SERC Symposium on VLSI Design
[NASA-CR-194591] p 1763 N94-21694
On the decomposition of synchronous state machines using sequence invariant state machines p 1764 N94-21703
NASA SERC digital correlator projects p 1765 N94-21708
Particle image velocimetry
[DE93-040657] p 1804 N94-21748
The VLBA correlator: Real-time in the distributed era p 2049 N94-22547

DIGITAL TECHNIQUES
VLSI mixed signal processing system p 1744 N94-21100
An optically-assisted 3-D cellular array machine
[AD-A272683] p 1987 N94-21163
Security management of electronic data interchange
[AD-A272962] p 1899 N94-21252
Journal of rehabilitation research and development, volume 30, number 1, 1993
[AD-A272956] p 1893 N94-21613
Determination of pore structure of concrete from thin sections by image analysis p 1708 N94-21895
Hierarchical multirate vector quantization for image coding p 1781 N94-22174
Quadrature biorthogonal modulation p 1747 N94-22232
SkICAT: A cataloging and analysis tool for wide field imaging surveys p 2049 N94-22546

DIGITAL TELEVISION
NHK Science and Technical Research Laboratories p 2151 N94-20342

DIHEDRAL ANGLE
Modifications to the three-component classification algorithm for SAR data p 1719 N94-20410
Polymeric nitrogen
[DE93-040544] p 1706 N94-21512

DIMENSIONAL MEASUREMENT
Feature-based tolerancing for intelligent inspection process definition
[DE93-017984] p 1906 N94-20311
Comparative thickness measurements of heterojunction layers by ellipsometric, RBS, and XTEM analysis p 1710 N94-20984

DIMENSIONAL STABILITY
A process for preparing an assembly of an article and a soluble polyimide which resists dimensional change, delamination, and debonding when exposed to changes in temperature
[NASA-CASE-LAR-14763-1] p 1702 N94-20373

DIMERS
Photochemically induced transformations of transition complexes
[AD-A271112] p 2014 N94-19982
Direct detection of atomic ions from molecular photofragmentation during nonresonant multiphoton ionization of sputtered species
[DE93-040886] p 1976 N94-21951

DINING PHILOSOPHERS PROBLEM
System level modelling using Petri nets and VHDL p 1772 N94-22113

DIODES
First results on InGaAsP separate confinement heterostructure diode lasers
[AD-A270849] p 1815 N94-19878
High current injector for heavy ion fusion
[DE93-019241] p 1979 N94-20289

DIPHENYL COMPOUNDS
Polybenzoxazole via aromatic nucleophilic displacement
[NASA-CASE-LAR-14606-1-CU] p 1672 N94-20540

DIPOLE ANTENNAS
Analysis of microstrip dipoles and slots transversely coupled to a microstrip line using the FDTD method p 1718 N94-20405
A 10 GHz Y-Ba-Cu-O/GaAs hybrid oscillator proximity coupled to a circular microstrip patch antenna p 1736 N94-20517

DIPOLE MOMENTS
Cognition and the brain: A continuation of the university research initiative at New York University
[AD-A271872] p 1894 N94-20467

DIRAC EQUATION
The quantum structure of matter grand challenge project: Large-scale 3-D solutions in relativistic quantum dynamics
[DE94-000328] p 1960 N94-21955

DIRECT CURRENT
Operational Requirements Document (ORD) for the Alternating Current/Direct Current (AC/DC) clamp-on ammeter, mE-563
[AD-A271808] p 1751 N94-20555
A dc Penning surface-plasma source
[DE93-040126] p 1997 N94-21989
DIRECTION FINDING
Use of the Weiss-Weinstein bound to compare the direction-finding performance of sparse arrays
[AD-A272582] p 1738 N94-21210
DIRECTIONAL ANTENNAS
Mobile antenna development at JPL
p 1731 N94-20457
DIRECTIONAL SOLIDIFICATION (CRYSTALS)
Experimental study of void formation during aluminum solidification in reduced gravity
[NASA-TM-106190] p 1692 N94-21604
DIRECTORIES
PHOTCAL: The IRAF photometric calibration package
p 1925 N94-22465
DISCHARGE COEFFICIENT
Battery tests p 1752 N94-20631
DISCONTINUITY
A comparative study between shielded and open coplanar waveguide discontinuities
p 1733 N94-20501
DISCRETE FUNCTIONS
Multilevel methods for transport equations in diffusive regimes p 1955 N94-21467
An in-place and in-order algorithm for the discrete cosine transform p 1771 N94-22111
DISCRIMINANT ANALYSIS (STATISTICS)
Multivariate statistical analysis: Principles and applications to coorbital streams of meteorite falls
p 1964 N94-20881
Measure fields for function approximation
[AD-A272660] p 1964 N94-21215
Extracting galactic structure parameters from multivariated density estimation p 1964 N94-22458
DISEASES
Health effects of global warming: Problems in assessment
[DE93-040323] p 1850 N94-19930
DISILICIDES
Strength and toughness improvement of silicide intermetallics by nanophase and microphase reinforcements
[AD-A272914] p 1692 N94-21320
DISKS (SHAPES)
Extinction efficiencies from DDA calculations solved for finite circular cylinders and disks p 1880 N94-22340
DISLOCATIONS (MATERIALS)
Ductile-brittle transition behavior of tungsten under shock loading conditions
[DE93-019945] p 1693 N94-21843
DISPERSING
The use of x ray techniques in the in situ study of corrosion
[DE93-019645] p 1690 N94-20301
DISPLACEMENT
Interferometric detection of freeze-thaw displacements of Alaskan permafrost using ERS-1 data
p 1732 N94-20460
Polybenzoxazole via aromatic nucleophilic displacement
[NASA-CASE-LAR-14606-1-CU] p 1672 N94-20540
DISPLAY DEVICES
A full-color, high-resolution laser projector for a flight simulator visual display
[AD-A270578] p 1651 N94-20108
System for solving Boolean equations using optical lookup tables
[AD-D015962] p 1951 N94-20358
Liquid crystal displays p 1752 N94-20634
LCD display tests p 1752 N94-20635
Silicon microelectronic field-emissive devices for advanced display technology
[DE94-000397] p 1794 N94-22380
An object-oriented approach for supporting both X and terminal interfaces p 1926 N94-22491
STARBASE: Database software for the automated plate scanner p 1927 N94-22512
DISSOCIATION
Collisions of molecules with clusters: A quasiclassical study
[DE93-018614] p 1971 N94-20050
One- and multi-component theories of mixtures
[DE93-040543] p 1966 N94-21511
DISSOLVING
The use of x ray techniques in the in situ study of corrosion
[DE93-019645] p 1690 N94-20301
DISTANCE
Determining the distance to the perfect matching polytope of a bipartite graph
[RR-895-M] p 1950 N94-20161
DISTANCE MEASURING EQUIPMENT
Testing of DME/P equipment performance for complex MLS procedures p 1644 N94-22136
DISTORTION
Second order distorted born approximation for backscattering from a layer of discrete random medium
p 1728 N94-20448
Detector noise statistics in the non-linear regime
p 1748 N94-22526
DISTRIBUTED PARAMETER SYSTEMS
Interactive simulation package for coupled bending and torsional vibrations in flexible robot arms
[MEMO-1089] p 1944 N94-21140
Distributed intelligent control and status networking
p 1932 N94-21335
Proceedings of the IMOG (Interagency Manufacturing Operations Group) Numerical Systems Group
[DE94-001009] p 1917 N94-21851
Language as primary dimension of distributed AI systems activity p 1776 N94-22141
DISTRIBUTED PROCESSING
Physics Detector Simulation Facility. Phase 2: System software description
[DE93-019745] p 1928 N94-19812
Distributed Virtual System (DIVIRS) project
[NASA-CR-194360] p 1905 N94-20228
DISCERN: A distributed neural network model of script processing and memory p 1941 N94-20255
On Update Last schemes
[CWI-CS-R9247] p 1952 N94-21027
Practical issues in implementing roving spares in VLSI systolic arrays p 1758 N94-21114
Optimization of static traffic allocation policies
[CWI-BS-R9302] p 1930 N94-21161
Distributed intelligent control and status networking
p 1932 N94-21335
Uniform self-stabilizing leader election. Part 1: Complete graph protocols
[CWI-CS-R9308-PT-1] p 1935 N94-21549
A data distributed, parallel algorithm for ray-traced volume rendering
[DE93-040150] p 1935 N94-21622
Simulated behaviour of large scale SCI rings and tori
[DE93-040149] p 1935 N94-21745
The design of linear algebra libraries for high performance computers
[DE93-040458] p 1960 N94-21967
Efficient communication primitives on mesh architectures with hardware routing
[DE93-018791] p 1936 N94-22032
The distributed CAD system for LSI/VLSI design
p 1923 N94-22068
Industry standards: Key to distributed computing
p 1938 N94-22070
Databases in distributed systems
p 2046 N94-22080
Experiences in airborne computing at NRC for geophysical exploration applications
p 1783 N94-22185
Distributed processing using Oracle7 and SQL*Net v2: An implementation story
[DE94-000494] p 1937 N94-22267
Distributed input/output processing in data-driven multiprocessors
[DE94-000323] p 1937 N94-22378
Access to D3-D data located in multiple files and multiple locations
[DE94-001104] p 2045 N94-22404
A self-defining hierarchical data system
p 2046 N94-22448
DISTRIBUTION FUNCTIONS
Direct photon results from CDF
[DE93-019908] p 1980 N94-20317
Measurement of the strange quark distribution function in W(+) charm quark events
[DE93-018267] p 1973 N94-20474
Triton's cratering record and its time of capture
p 2122 N94-20802
Equilibrium models of mass distribution and collisional lifetimes of asteroids p 2086 N94-20877
Measure fields for function approximation
[AD-A272660] p 1964 N94-21215
Stochastic simulation for imaging spatial uncertainty: Comparison and evaluation of available algorithms
[DE93-040058] p 1916 N94-21761
DISTURBING FUNCTIONS
Turbulization of free shear flows: 3D perturbations
p 2000 N94-22626
DIURNAL VARIATIONS
Tests of a simple data merging algorithm for the GONG project p 1927 N94-22549
DIVERGENCE
Alloying studies in U(1-x)Th(x)Pd2Al3 (0 (le) x (le) 1)
[DE94-000807] p 2036 N94-22584
DIVERTERS
Transient thermal analysis of cryocondensation pump for JET
[DE93-040372] p 1992 N94-20003
Neoclassical kinetic theory near an X-point: Plateau regime
[DE93-019825] p 1951 N94-20224
Theoretical and numerical studies in magnetic fusion
[DE94-000536] p 1993 N94-20937
Enhanced confinement regimes and control technology in the DIII-D tokamak
[DE93-019004] p 1998 N94-22039
The TST: A small steady-state tokamak for integrated divertor testing
[DE94-001016] p 1998 N94-22045
DOCUMENT STORAGE
Project Records Information System (PRIS): User's manual
[DE94-001548] p 2045 N94-22047
DOCUMENTS
The manager's guide to NASA graphics standards
[NHB-1430.2] p 2042 N94-20308
Electronic publishing and intelligent information retrieval p 2047 N94-22479
DOLOMITE (MINERAL)
A calcium oxide sorbent process for bulk separation of carbon dioxide
[DE93-019288] p 1847 N94-21540
DOMES (STRUCTURAL FORMS)
Characterization of the Marquez Dome buried impact crater using gravity and magnetic data
p 1863 N94-20882
DONOR MATERIALS
Hydrogen in compound semiconductors
[DE93-040300] p 2031 N94-21922
DOPED CRYSTALS
Resonantly pumped, erbium-doped, GSGG, 2.8 micron, solid state laser with energy recycling and high slope efficiency
[AD-D015920] p 1815 N94-20060
Variable angle of incidence spectroscopic ellipsometric measurement of the Franz-Keldysh effect in MODFET structures p 2021 N94-20987
Ellipsometric analysis of built-in electric fields in semiconductor heterostructures p 1796 N94-20988
Optical measurement of built-in and applied electric fields in Al(x)Ga(1-x)As/GaAs heterostructures
p 1796 N94-20989
Study of InGaAs-based modulation doped field effect transistor structures using variable-angle spectroscopic ellipsometry p 1796 N94-21001
Study of concentration-dependent dielectric properties of n-type GaAs using variable angle spectroscopic ellipsometry p 2024 N94-21002
Single crystal diamond films
[AD-A266759] p 2028 N94-21517
Application of an electrochemical quartz crystal microbalance to the study of electrocatalytic films
[DE93-041124] p 2029 N94-21691
Semiconductor isotope engineering
[DE93-040119] p 2030 N94-21744
Local structure in oxygen-doped La2CuO(4+delta)
[DE93-040248] p 2030 N94-21768
The n-p(p(+))-n Al(yGa)(1-y) As-GaAs-In(x)Ga(1-x) as quantum well laser with p(+)-n(+)GaAs-InGaAs tunnel contact on n GaAs
[AD-A271292] p 2030 N94-21805
Cathode materials for the molten carbonate fuel cell
[DE93-019515] p 1848 N94-21870
Fullerene derivatives and fullerene superconductors
[DE93-019568] p 2031 N94-21871
Crystal structure and short-range oxygen defects in La- and Nd-modified ZrO2
[DE93-040229] p 2033 N94-21993
High oxygen pressure synthesis of new copper oxide superconductors
[DE93-040278] p 2033 N94-21998
NMR studies of oxygen-doped La2CuO(4+delta)
[DE93-040756] p 2034 N94-22007
Positron annihilation study of Sr Doping in La(2-x)Sr(x)CuO4
[DE94-000307] p 2036 N94-22594
DOPPLER EFFECT
A general purpose ionospheric ray tracing procedure
[AD-A271058] p 1854 N94-19860
Coherent lidar design and performance verification
[NASA-CR-193813] p 1816 N94-20341
Utilization of lasers for air data measurements
p 1640 N94-22603
DOPPLER RADAR
Target motion detecting impulse Doppler radar system
[AD-D015898] p 1717 N94-20198

Coherent lidar design and performance verification [NASA-CR-193813] p 1816 N94-20341
Integrated display of multi-sensor geophysical and electromagnetic flight data p 1721 N94-20418
Rough surface scattering from moving ocean surfaces as an indicator of scattering mechanisms p 1726 N94-20439
GMM-1: A 50 degree and order gravitational field model for Mars p 2117 N94-20774
Microphysical properties of the November 26 cirrus cloud retrieved by Doppler radar/IR radiometer technique p 1873 N94-22304
Breaking Kelvin-Helmholtz waves and cloud-top entrainment as revealed by K-band Doppler radar p 1874 N94-22310
Observations of multi-layered clouds using K-band radar p 1874 N94-22311
CO2 lidar observations of Mount Pinatubo debris: FIRE 2 and longer-term measurements p 1876 N94-22323
Estimation of cirrus cloud particle fallspeeds from vertically pointing Doppler radar p 1879 N94-22333
Normalized vertical ice mass flux profiles from vertically pointing 8-mm-wavelength Doppler radar p 1879 N94-22334

DOSAGE
Non-ionic surfactants in the treatment of third degree burns [AD-A271582] p 1891 N94-21035

DOSIMETERS
Radiometry in commercial aircraft [GSF-41/91] p 1892 N94-21141

DOUBLE CUSPS
Affine and non-affine blossoms [RR-913-M] p 1950 N94-20200

DOWNLINKING
Downlink acquisition and tracking procedures for the ASCAMP satellite communications terminal [AD-A272912] p 1739 N94-21244

DOWNWASH
Rotorwash wind sensor evaluation [AD-A268987] p 1807 N94-20203

DRAINAGE
Geologic mapping of Harmakhis and Reull Valles region, Mars: Evidence for multiple resurfacing and drainage events p 1844 N94-20705
Mars: Noachian hydrology by its statistics and topology p 2143 N94-21664

DRAINAGE PATTERNS
Early Mars: A regional assessment of denudation chronology p 2145 N94-21676

DRIFT RATE
Interfacial properties of diamondlike amorphous carbon films on InP: Metal-insulator-semiconductor structures p 1710 N94-20980

DRILLING
Petrography of shock features in the 1953 Manson 2-A drill core p 1862 N94-20767
High-power copper vapor lasers and their application to precision drilling and cutting [DE93-019951] p 1819 N94-21844

DROP SIZE
A laboratory system for the investigation of rain fade compensation techniques for Ka-band satellites [NASA-CR-191200] p 1762 N94-21566

DROP TOWERS
Evaporation of a sodium tellurite melt in the jamic low gravity drop shaft p 1713 N94-20605

DROPS (LIQUIDS)
Particle dispersion in turbulent sprays [AD-A271314] p 1796 N94-19913
Wavefront sensors for optical diagnostics in fluid mechanics: Application to heated flow, turbulence, and droplet evaporation [DE93-040060] p 1797 N94-19974
Shock induced condensation in fluids of high molar specific heat: Shock structure and relaxation [MPIS-106/1993] p 1798 N94-20145
Head-on collision of drops: A numerical investigation [NASA-TM-106394] p 1798 N94-20167
Size distributions and aerodynamic equivalence of metal chondrules and silicate chondrules in Acfer 059 p 2084 N94-20773
Liquid-phase circulation and mixing in multicomponent droplets vaporizing in a laminar convective environment [AD-A272851] p 1802 N94-21193

DROUGHT
Health effects of global warming: Problems in assessment [DE93-040323] p 1850 N94-19930
The 7th Brazilian Remote Sensing Symposium, volume4 p 1840 N94-20965
Drought early warning system for crop production p 1840 N94-20966

DUCTED FLOW
A study of the compressible flow through a diffusing S-duct [NASA-TM-106411] p 1638 N94-21591
Comparison of mixing calculations for reacting and non-reacting flows in a cylindrical duct [NASA-TM-106435] p 1649 N94-21758

DUCTILITY
Structural crashworthiness and failure [AD-A270429] p 1828 N94-19815
Investigation of cracking and erratic behavior of the uranium-titanium alloy [DE93-018591] p 1688 N94-19957
Ductile-brittle transition behavior of tungsten under shock loading conditions [DE93-019945] p 1693 N94-21843
Ni3Al aluminide alloys [DE94-000493] p 1694 N94-21933
Alloying effects on mechanical and metallurgical properties of NiAl [DE93-040814] p 1694 N94-21948

DUMMIES
Evaluation of head injury criteria [NIAR-93-2] p 1890 N94-20190

DURABILITY
Durability predictions for adhesively bonded joints in humid environments [AD-A271177] p 1830 N94-20001
Study of space factors effect on materials for spacecraft external surfaces in NPO Energia programs p 1664 N94-21401
Review of corrosion behavior of ceramic heat exchanger materals: Corrosion characteristics of silicon carbide and silicon nitride [DE93-041307] p 1706 N94-21516
Delamination, durability, and damage tolerance of laminated composite materials p 1678 N94-22622

DUST
Cathodoluminescence observations of in situ aqueous destruction of chondrules in the Murchison CM chondrite p 2083 N94-20750
Analysis of a sandstorm weather process-translation [AD-A272959] p 1867 N94-21250

DUST STORMS
Analysis of a sandstorm weather process-translation [AD-A272959] p 1867 N94-21250

DWARF GALAXIES
Dust content of a hydrogen rich, low surface brightness galaxy and the luminosity history of 3C273 [NASA-CR-194705] p 2056 N94-21779

DYE LASERS
Ocular damage induced by ultrashort laser pulses [AD-A271859] p 1890 N94-20462
Examinations of a thallium atomic vapor filter for a Raman temperature lidar [GKSS-92/E/13] p 1857 N94-21044

DYES
Green Sheet project: Dye sheet evolution [AD-A272019] p 1883 N94-21443

DYNAMIC CHARACTERISTICS
Interval timed coloured petri nets and their analysis [PB93-191732] p 1903 N94-19992
Design of a controllable pitch underwater thruster system [AD-A271140] p 1821 N94-20021
Specialized data analysis for the Space Shuttle Main Engine and diagnostic evaluation of advanced propulsion system components [NASA-CR-194720] p 1656 N94-21813
Dynamic properties of ceramic materials [DE94-000654] p 1708 N94-21963

DYNAMIC CONTROL
Replica control algorithms in distributed databases [AD-A271571] p 1909 N94-21034
COCOLOG: A conditional observer and controller logic for finite machines [INRIA-RR-1714] p 1910 N94-21063

DYNAMIC LOADS
Acceleration-augmented LQG control of an active magnetic bearing p 1757 N94-21112
Dynamic properties of ceramic materials [DE94-000654] p 1708 N94-21963
Time-dependent reliability analysis of ceramic engine components p 1828 N94-22619

DYNAMIC MODELS
Interval timed coloured petri nets and their analysis [PB93-191732] p 1903 N94-19992
Dynamics Explorer 2: Continued FPI and NACS instrument data analysis and associated scientific activity at the University of Michigan [NASA-CR-194689] p 1657 N94-20173
Interactive simulation package for coupled bending and torsional vibrations in flexible robot arms [MEMO-1089] p 1944 N94-21140
Paired comparison models with time-varying parameters [AD-A272016] p 1964 N94-21442
Derivation of a model of the exciter of a brushless synchronous machine [EUT-92-E-258] p 1761 N94-21538

DYNAMIC PROGRAMMING
Algorithm/architecture study for artificial neural nets [AD-A271820] p 1943 N94-20626
Optimal repairman assignment in two maintenance models which are equivalent to routing models with early decisions [CWI-BS-R9301] p 1930 N94-21234
Procedural dynamic semantics, verb-phrase ellipsis, and presupposition [CWI-CS-R9311] p 1914 N94-21495

DYNAMIC RESPONSE
Frequency and temperature dependence of high damping elastomers [DE93-019539] p 1697 N94-19809
Structural crashworthiness and failure [AD-A270429] p 1828 N94-19815
Design of a controllable pitch underwater thruster system [AD-A271140] p 1821 N94-20021
Using crosscorrelation techniques to determine the impulse response of linear systems p 1759 N94-21122
Dynamic response of multiphase porous media [AD-A272915] p 1831 N94-21219
Dynamic properties of ceramic materials [DE94-000654] p 1708 N94-21963
Computer simulation of molecular response at a shock front [DE94-001050] p 1977 N94-22396
Response statistics of shell structures with geometrical and material nonlinearities, volume 1 [ISBN-0-315-84006-4] p 1833 N94-22590

DYNAMIC STABILITY
Problems related to conservation laws: Phase transitions and viscoelasticity [AD-A271429] p 1698 N94-19840
Stability limits and dynamics of nonaxisymmetric liquid bridges [NASA-CR-194706] p 1797 N94-20037
Robot link and contact surface dynamic interaction: An experimental study of contact instability [ISBN-0-315-83439-0] p 1827 N94-22578

DYNAMIC STRUCTURAL ANALYSIS
Interactive simulation package for coupled bending and torsional vibrations in flexible robot arms [MEMO-1089] p 1944 N94-21140
Modal combination in response spectrum modal dynamic analysis [DE94-000339] p 1833 N94-21956
Robot link and contact surface dynamic interaction: An experimental study of contact instability [ISBN-0-315-83439-0] p 1827 N94-22578
System identification of the Daisy large space structure emulator [ISBN-0-315-83533-8] p 1653 N94-22588
Response statistics of shell structures with geometrical and material nonlinearities, volume 1 [ISBN-0-315-84006-4] p 1833 N94-22590

DYNAMIC TESTS
Solar simulator for solar dynamic space power system testing [NASA-TM-106393] p 1984 N94-20140

DYNAMICAL SYSTEMS
Literature review of the errors-in-variables approach to the problem of system identification [AD-A271098] p 1949 N94-19907
Dynamical systems and nonlinear partial differential equations [AD-A271514] p 1951 N94-20545

DYNAMO THEORY
Modeling of the coupled magnetospheric and neutral wind dynamos [NASA-CR-194728] p 1856 N94-20537
Magnetically controlled solar nebula p 2120 N94-20791
Expectations for the Martian core magnetic field p 2120 N94-20792
Dynamo driven by weak plasma turbulence: The effect of differential rotation p 2005 N94-22665
Double diffusion convection in a rotating spherical shell p 2006 N94-22666
Generation and maintenance of bisymmetric spiral magnetic fields in disk galaxies in differential rotation p 2010 N94-22695
Magnetic fields in spiral galaxies p 2010 N94-22697

E

E REGION
Imaging radar studies of atmospheric winds and waves
[AD-A271672] p 1866 N94-20918
High Frequency (HF) and meteor burst communications in a polar environment
[AD-A271604] p 1737 N94-20949
EARLY WARNING SYSTEMS
Drought early warning system for crop production
p 1840 N94-20966
EARTH (PLANET)
Dynamics of large scale impacts on Venus and Earth
p 2098 N94-20666
EARTH ATMOSPHERE
Remote sounding of tropospheric minor constituents
[NASA-CR-194265] p 1855 N94-20132
Atmospheric infrared sounder
[NASA-CR-194814] p 1856 N94-20362
Atmospheric breakup of a small comet in the Earth's atmosphere p 2084 N94-20824
EARTH CORE
Iridium in sediments containing large abundances of Australasian microtektites from DSDP hole 758B in the Eastern Indian Ocean and from DSDP hole 769A in the Sulu Sea p 2083 N94-20741
Shock temperature measurements of iron to 350 GPa
[DE94-001058] p 1695 N94-22024
EARTH CRUST
Analysis of the effects of eurasian crustal and upper mantel structure on regional phases using broadband seismic data
[AD-A272446] p 1858 N94-21206
Post-Palbozoic crustal responses to the contemporary stress field in the eastern United States
[DE93-040604] p 1859 N94-22006
EARTH GRAVITATION
Inversion of gravity and bathymetry in oceanic regions for long-wavelength variations in upper mantle temperature and composition
[NASA-CR-192272] p 1882 N94-20131
EARTH IONOSPHERE
Ionospheric tomography using the FORTE satellite
[DE93-018545] p 1854 N94-19955
Detection of traveling ionospheric disturbances induced by atmospheric gravity waves using the global positioning system p 1723 N94-20425
Measurement of mesospheric turbulence in the framework of the metal campaign and development of a sensor for static pressure free measurements of neutral and electron density
[BONN-IR-92-45] p 1857 N94-21149
Physics of magnetospheric boundary layers
[NASA-CR-194725] p 1858 N94-21836
Studies of electromagnetic ion cyclotron waves using AMPTE/CCE and Dynamics Explorer
[NASA-CR-194711] p 1982 N94-21878
EARTH MAGNETOSPHERE
Modeling of the coupled magnetospheric and neutral wind dynamos
[NASA-CR-194728] p 1856 N94-20537
Physics of magnetospheric boundary layers
[NASA-CR-194725] p 1858 N94-21836
Implications of Viking dayside auroral measurements
[ISBN-0-315-83273-8] p 1861 N94-22575
EARTH MANTLE
Inversion of gravity and bathymetry in oceanic regions for long-wavelength variations in upper mantle temperature and composition
[NASA-CR-192272] p 1882 N94-20131
Mixing of a chemically buoyant layer at the top of a thermally convecting fluid: Implications for mantle dynamics with application to Venus
p 2099 N94-20675
Analysis of the effects of eurasian crustal and upper mantel structure on regional phases using broadband seismic data
[AD-A272446] p 1858 N94-21206
Shock temperature measurements of iron to 350 GPa
[DE94-001058] p 1695 N94-22024
EARTH OBSERVATIONS (FROM SPACE)
Application of the target decomposition theorem to a polarimetric random media model p 1730 N94-20453
Data format standards for civilian remote sensing satellites
[PB93-192920] p 1841 N94-21446
EARTH OBSERVING SYSTEM (EOS)
Earth observing scanning polarimeter
p 1844 N94-21645
EARTH ORBITAL ENVIRONMENTS
Fifth International Symposium on Materials in a Space Environment
[ISBN-2-85-428293-0] p 1659 N94-21367
Flight and laboratory testing of materials in low Earth orbit p 1659 N94-21369
Complex-2: Low Earth orbital environment simulation facility for materials durability evaluation
p 1653 N94-21370
Results of the post flight analyses on system materials for the LDEF-FRECOPA experiment
p 1659 N94-21371
Measured space environmental effects to LDEF during retrieval p 1659 N94-21372
Space environmental effects on polymer matrix composites: The UTIAS/LDEF experiment
p 1660 N94-21373
The implications of the LDEF results on Space Station Freedom power system materials p 1660 N94-21377
Durability of thermal control and environmental protective materials for the SSRMS in simulated LEO environment p 1663 N94-21392
Atomic oxygen interaction with spacecraft materials: Relationship between orbital and ground-based testing for materials certification p 1663 N94-21393
Study of space factors effect on materials for spacecraft external surfaces in NPO Energia programs
p 1664 N94-21401
Evaluation of electroconductivity of two surface paints for spacecraft
[AD-A273063] p 1706 N94-21437
Single event phenomena: Testing and prediction
p 1763 N94-21696
An 18 bit 50 kHz ADC for low earth orbit
p 1764 N94-21702
EARTH PLANETARY STRUCTURE
Origin of the Vredefort structure, South Africa: Impact model p 1863 N94-20826
EARTH RADIATION BUDGET
Climate forcings and feedbacks p 1869 N94-21641
Proceedings of the Workshop on New Generation of Radiation Budget Measurements From Space and Their Use in Climate Modelling and Diagnostic Studies
[MPIM-90] p 1860 N94-22283
Satellite measurements of radiation budget parameters p 1860 N94-22284
ScaRaB and its subsystems p 1860 N94-22285
The use of ERBE data for climate studies
p 1860 N94-22286
Satellite validation of GCM-simulated annual cycle of the Earth radiation budget and cloud forcing
p 1860 N94-22287
The seasonal variation of the cloud radiative forcing: Comparison of ECHAM model simulations with ERBE data p 1860 N94-22288
Simulation of clear-sky outgoing longwave radiation over the oceans using operational analysis
p 1861 N94-22290
EARTH RADIATION BUDGET EXPERIMENT
The seasonal variation of the cloud radiative forcing: Comparison of ECHAM model simulations with ERBE data p 1860 N94-22288
EARTH RESOURCES
Application of SPOT to GIS/LIS in land capability evaluation for regional planning of JAICO semi-arid region of Piaui, Brazil p 1838 N94-20955
The development of remote sensing in Brazil and Canada: Comparative case studies
p 1840 N94-20968
EARTH ROTATION
Estimability of polar motion using range observations to satellites
[PB93-219319] p 1842 N94-22265
EARTH SCIENCES
The Board on Earth sciences and resources
[DE94-000745] p 1859 N94-22018
Data management for interdisciplinary field experiments: OTTER project support
[NASA-CR-4559] p 1842 N94-22345
EARTH SURFACE
Cryoplanation terraces of interior and western Alaska
p 2091 N94-20396
Simulsted retrieval of land surface parameters using multichannel satellite microwave radiometry
p 1727 N94-20443
A theoretical and numerical study of polarimetric scattering and emission from random rough surfaces with anisotropic directional spectrum p 1730 N94-20454
Interferometric detection of freeze-thaw displacements of Alaskan permafrost using ERS-1 data
p 1732 N94-20460
Areally averaged estimates of surface heat flux from ARM field studies
[DE93-018569] p 1859 N94-22036
EARTH TERMINALS
Downlink acquisition and tracking procedures for the ASCAMP satellite communications terminal
[AD-A272912] p 1739 N94-21244
EARTH-MARS TRAJECTORIES
Entry velocities at Mars and Earth for short transit times
[AD-A272591] p 1665 N94-21420
EARTHQUAKES
Detection of traveling ionospheric disturbances induced by atmospheric gravity waves using the global positioning system p 1723 N94-20425
Post-Palbozoic crustal responses to the contemporary stress field in the eastern United States
[DE93-040604] p 1859 N94-22006
The Board on Earth sciences and resources
[DE94-000745] p 1859 N94-22018
ECOLOGY
ELF communications system ecological monitoring program
[AD-A272507] p 1740 N94-21412
ECONOMIC ANALYSIS
Wind energy: Program overview, FY 1992
[DE93-000056] p 1845 N94-19921
Technology to prevent greenhouse effect gases
[DE94-707420] p 1851 N94-20116
Low-cost, dual-use platforms for environmental sensing, phase 1
[AD-A272951] p 1646 N94-21246
Information Technology and Economic Modelling
[VTT-SYMP-135] p 2049 N94-22056
Mathematical modelling of economic systems
p 2050 N94-22060
AJKA: An econometric macromodel for Finland
p 2050 N94-22061
Macromodel of centrally planned economy
p 2050 N94-22062
The Soviet software market: Current state and aspects of development p 1923 N94-22066
Models of transient processes in centrally planned economy p 2051 N94-22071
An economic analysis of transboundary air pollution between Finland and the Soviet Union
[ETLA-DISCUSSION-PAPER-335] p 1854 N94-22072
An expert system of econometric analysis
p 2052 N94-22081
Use of economic models in Finnish economic policy
p 2053 N94-22085
Experiences of the bank of Finland's econometric simulation model p 2053 N94-22086
ECONOMIC DEVELOPMENT
Technology to prevent greenhouse effect gases
[DE94-707420] p 1851 N94-20116
Soviet society informatization: The USSR state program p 2046 N94-22058
Models of transient processes in centrally planned economy p 2051 N94-22071
ECONOMIC FACTORS
Rotorcraft low altitude IFR benefit/cost analysis: Conclusions and recommendations
[DOT/FAA/RD-93/22] p 1642 N94-20051
Activities of National Inst. for Aviation Research
[NIAR-93-16] p 2151 N94-20150
ECONOMIC IMPACT
Biofuels: Project summaries
[DE93-010003] p 1712 N94-19984
An airport economic impact study procedure for Atlantic Canada
[ISBN-0-315-59445-4] p 1651 N94-22419
ECONOMICS
Information Technology and Economic Modelling
[VTT-SYMP-135] p 2049 N94-22056
Mathematical modelling of economic systems
p 2050 N94-22060
AJKA: An econometric macromodel for Finland
p 2050 N94-22061
Microdynamic model of reproduction: Taxation and currency issue as regulators of economy
p 2053 N94-22084
Use of economic models in Finnish economic policy
p 2053 N94-22085
Experiences of the bank of Finland's econometric simulation model p 2053 N94-22086
ECONOMY
The Soviet software market: Current state and aspects of development p 1923 N94-22066
Models of transient processes in centrally planned economy p 2051 N94-22071
Microdynamic model of reproduction: Taxation and currency issue as regulators of economy
p 2053 N94-22084
ECOSYSTEMS
Technology to prevent greenhouse effect gases
[DE94-707421] p 1850 N94-19976
Data management for support of the Oregon Transect Ecosystem Research (OTTER) project
[NASA-CR-4557] p 1905 N94-20149
Analysis of hyper-spectral AVIRIS image data over a mixed-conifer forest in Maine p 1838 N94-20959

Modeling the response of ecosystems to CO2 and climate change
[DE94-000748] p 1852 N94-21787

EDDY CURRENTS
A new eddy current model for magnetic bearing control system design p 1763 N94-21698
Demonstrating damage tolerance of composite airframes p 1647 N94-22623

EDGE DETECTION
Image detection using edge extraction algorithms
[AD-A272439] p 1911 N94-21203
Elliptical-shape parameter estimation from a set of normal lines p 1777 N94-22148
A neural network for multiresolution edge detection p 1779 N94-22163

EDITING
An assessment of the statistical and editorial output of text analysis programs
[AD-A272185] p 2042 N94-20924
CMIFed: A presentation environment for porta ble hypermedia documents
[CWI-CS-R9305] p 2044 N94-21494
New IRAF stellar photometry software p 1925 N94-22464

EDITING ROUTINES (COMPUTERS)
An assessment of the statistical and editorial output of text analysis programs
[AD-A272185] p 2042 N94-20924
CMIFed: A presentation environment for porta ble hypermedia documents
[CWI-CS-R9305] p 2044 N94-21494

EDUCATION
Mathematics B for the study direction VWO: A reconnaissance
[REPT-92-80] p 1950 N94-20032
A comprehensive software engineering educational experience
[AD-A270583] p 1905 N94-20109
NASA's Education Program
[NASA-EP-297] p 2038 N94-20129
Rockets: Physical science teacher's guide with activities
[NASA-EP-291] p 1669 N94-20226
Schools of the Pacific rainfall climate experiment p 1881 N94-20699
Tumuli and tubes: Teaching scientific techniques p 2039 N94-20818
Sparking young minds with Moon rocks and meteorites p 2039 N94-20819
A practical software engineering curriculum: A pilot study
[AD-A272781] p 1911 N94-21183
Use of computers in the instruction of integral calculus
[AD-A272500] p 1913 N94-21409
Extracting information from wrong answers in computerized adaptive testing
[AD-A272832] p 1894 N94-21434
NASA Propulsion Engineering Research Center, volume 1
[NASA-CR-194721-VOL-1] p 1671 N94-22428

EFFUSIVES
Elevation and igneous crater modification on Venus: Implications for magmatic volatile content p 2135 N94-20872

EIGENVALUES
Parallel band reduction and tridiagonalization
[DE93-019566] p 1951 N94-20221
Numerical ranges and stability estimates
[TW-92-10] p 1953 N94-21060
The multigrid preconditioned conjugate gradient method p 1958 N94-21482
Using parallel banded linear system solvers in generalized eigenvalue problems
[NASA-CR-191540] p 1915 N94-21584
A sharp upper bound for departure from normality
[DE93-040457] p 1960 N94-21966

EJECTA
Morphologic and morphometric studies of impact craters in the northern plains of Mars p 2089 N94-20384
The Manson impact crater: Estimation of the energy of formation, possible size of the impacting asteroid or comet, and ejecta volume and mass p 2083 N94-20721
Parabolic features and the erosion rate on Venus p 2122 N94-20801
Stable Ni isotopes and Be-10 and Al-26 in metallic spheroids from Meteor Crater, Arizona p 1863 N94-20889
Antipodal fragment velocities for porous and weak targets at catastrophic impacts p 1836 N94-20891

ELASTIC BODIES
Research in lightweight elastic robotic arms
[AD-A270846] p 1821 N94-19833

ELASTIC DEFORMATION
Graphite/polyurethane flexible composites: Mechanical and vibration damping properties
[AD-A271608] p 1674 N94-20950

ELASTIC PROPERTIES
Research in lightweight elastic robotic arms
[AD-A270846] p 1821 N94-19833
Innovative acoustic technique for studying new materials and new developments in solid state physics
[AD-A270540] p 2013 N94-19933
CTH: A software family for multi-dimensional shock physics analysis
[DE93-019428] p 1904 N94-20052
Compliant seal development p 1655 N94-21795
Crystal orientation dependence of elastic precursor strength in pentaerythritol tetranitrate
[DE93-018340] p 2034 N94-22035

ELASTIC SCATTERING
Examinations of a thallium atomic vapor filter for a Raman temperature lidar
[GKSS-92/E/13] p 1857 N94-21044
Parton-parton elastic scattering and rapidity gaps at Tevatron energies
[DE93-041024] p 1974 N94-21515
Studies of the deuteron at high energy and momentum transfer
[DE93-041162] p 1976 N94-21941
Non-adiabatic effects in low-energy electron-molecule scattering
[DE93-040485] p 1976 N94-21968

ELASTIC WAVES
System and method for cancelling expansion waves in a wave rotor
[NASA-CASE-LEW-15218-1] p 1801 N94-20588

ELASTIN
Development of bioelastic material for aspects of wound repair
[AD-A272000] p 1892 N94-21503

ELASTOMERS
Frequency and temperature dependence of high damping elastomers
[DE93-019539] p 1697 N94-19809
Chain propagation/step propagation polymerization chemistry. The preparation of solvent resistant well phase-separated thermoplastic elastomers
[AD-A271128] p 1699 N94-20016

ELASTOPLASTICITY
The p-version of the finite element method in incremental elasto-plastic analysis
[NASA-CR-194707] p 1830 N94-20036

ELASTOSTATICS
Development of BEM for ceramic composites
[NASA-CR-194718] p 1676 N94-21777

ELECTRIC ARCS
Two dimensional simulation of the electric arc behavior in a cut-off device
[ECL-92-41] p 1751 N94-20595

ELECTRIC BATTERIES
Current status of environmental, health, and safety issues of nickel metal-hydride batteries for electric vehicles
[DE93-017079] p 1748 N94-19902
Development of the UTC-PAB normative database
[AD-A271319] p 1893 N94-20023
Lightweight battery electrode and method of making it
[AD-D015895] p 1749 N94-20120
Power standard
[ESA-PSS-02-10-VOL-1-ISSUE-] p 1669 N94-20241
Analysis of a diesel-electric hybrid urban bus system
[DE93-019514] p 1825 N94-21297

ELECTRIC BRIDGES
A comprehensive theoretical and experimental study of coplanar waveguide shunt stubs p 1733 N94-20500
A theoretical and experimental study of coplanar waveguide shunt stubs p 1733 N94-20502

ELECTRIC CONDUCTORS
Operational Requirements Document (ORD) for the Alternating Current/Direct Current (AC/DC) clamp-on ammeter, mE-563
[AD-A271808] p 1751 N94-20555

ELECTRIC CONNECTORS
Spline screw payload fastening system
[NASA-CASE-GSC-13454-1] p 1821 N94-20126

ELECTRIC CONTACTS
High current density contacts for photoconductive semiconductor switches
[DE93-018837] p 1750 N94-20312

ELECTRIC CURRENT
Superconducting property measurements in tape geometry
[DE93-018943] p 2014 N94-19970
Microscopic origins of metastable effects in a-Si:H and deep defect characterization in a-Si,Ge:H alloys
[DE93-018205] p 1688 N94-19985
Modeling of the coupled magnetospheric and neutral wind dynamos
[NASA-CR-194728] p 1856 N94-20537
Correct CMOS IC defect models for quality testing p 1755 N94-21093

ELECTRIC DISCHARGES
An improved patch for radiative coolers
[NASA-CASE-GSC-13503-1] p 1822 N94-20127
Kinetic theory of runaway air-breakdown
[DE93-040731] p 1750 N94-20325
Research on plasma-puff initiation of high Coulomb transfer switches
[NASA-CR-194371] p 1994 N94-21289
INPIStron switched pulsed power for dense plasma pinches p 1995 N94-21294

ELECTRIC EQUIPMENT TESTS
Lavet type stepping motors and associated controls p 1752 N94-20632
Test device for Lavet motors p 1752 N94-20633

ELECTRIC FIELDS
A novel method for characterizing the electrical Priorities of lead Zirconate Titanate (PZT) ferroelectric films and memory devices
[AD-A270463] p 2013 N94-19966
Calculation and optimization of electromagnetic fields in a patient by local hyperthermia utilization
[ETN-93-95059] p 1889 N94-20024
Metal-glass composite field-emitting arrays
[AD-D015942] p 1673 N94-20064
CsI and some new photocathodes
[DE93-019387] p 1750 N94-20314
Light scattering studies of an electrorheological fluid
[DE93-019419] p 1700 N94-20315
Layered thin-edged field-emitter device
[AD-D015932] p 1751 N94-20350
Statistical fluctuations in lasers
[DE94-000710] p 1817 N94-20939
Ellipsometric analysis of built-in electric fields in semiconductor heterostructures p 1796 N94-20988
Optical measurement of built-in and applied electric fields in Al(x)Ga(1-x)As/GaAs heterostructures p 1796 N94-20989
The sea breeze convergence zone and its relationship to fair weather electricity in east central Florida
[AD-A268511] p 1868 N94-21502
Hybrid finite element/waveguide mode analysis of passive RF devices
[AD-A273074] p 1740 N94-21518
Simulation and compensation of multibunch energy variation in NLC
[DE93-041057] p 1981 N94-21687
Electron emission from nanometer-size metallic clusters: Electronic states and structural stability of supported Au clusters
[DE93-040184] p 1975 N94-21766
Studies of electromagnetic ion cyclotron waves using AMPTE/CCE and Dynamics Explorer
[NASA-CR-194711] p 1982 N94-21878
Calculation of a diffracted electric field with the aid of the Method of Equivalent Currents (MEC) p 1745 N94-22127
Numerical method for computing the electric field produced by a microwave beam in a stratified medium p 1746 N94-22197

ELECTRIC FILTERS
An adaptive method for group delay compensation using switched capacitor filters p 1793 N94-22248

ELECTRIC GENERATORS
Building integrated photovoltaic systems analysis
[DE93-018208] p 1846 N94-21298
Derivation of a model of the exciter of a brushless synchronous machine
[EUT-92-E-258] p 1761 N94-21538
Environmental protection using social costing
[DE94-000492] p 1853 N94-22569

ELECTRIC MOTOR VEHICLES
Advanced batteries for electric vehicle applications: Nontechnical summary
[DE93-019007] p 1748 N94-19885
Evaluation of externally heated pulsed MPD thruster cathodes
[NASA-CR-191090] p 1670 N94-21565
Electromechanical battery research and development at the Lawrence Livermore National Laboratory
[DE93-019159] p 1762 N94-21620
Electromechanical battery research and development at the Lawrence Livermore National Laboratory
[DE94-000391] p 1762 N94-21621

ELECTRIC MOTORS
Operation of a test bed axial-gap brushless dc rotor with a superconducting stator
[DE93-019167] p 1769 N94-21830
A vibration model for centrifugal contactors
[DE93-040645] p 1833 N94-21927

Flow and heat transfer model for a rotating cryogenic motor
[DE94-001151] p 1794 N94-22405

ELECTRIC NETWORKS
High resolution signal processing
[AD-A271181] p 1717 N94-20215

ELECTRIC POTENTIAL
Surface states at the GaAs-germanium nitride interface p 1709 N94-20973
The sea breeze convergence zone and its relationship to fair weather electricity in east central Florida
[AD-A268511] p 1868 N94-21502
Results from long conduction time plasma opening switch experiments at Sandia National Laboratories
[DE93-019063] p 1762 N94-21632
Localization of pellicle-induced open contacts using charge-induced voltage alteration
[DE93-019407] p 1762 N94-21636
Analog/digital pH meter system I.C.
p 1764 N94-21701
Low energy CMOS for space applications
p 1768 N94-21735
Initial operation of a large-scale plasma source ion implantation experiment
[DE94-000805] p 2036 N94-22583

ELECTRIC POWER
Technology to prevent greenhouse effect gases
[DE94-707420] p 1851 N94-20116

ELECTRIC POWER SUPPLIES
System performance predictions for Space Station Freedom's electric power system
[NASA-TM-106396] p 1667 N94-20062
Self-deploying photovoltaic power system
[NASA-CASE-LEW-15308-1] p 1846 N94-20196
Power supply and controller for the Sextupole magnet of AmPS
[DIGEL-1992-3] p 1753 N94-21064

ELECTRIC PROPULSION
Performance potential of plasma thrusters: Arcjet and Hall thruster modeling
[AD-A271085] p 1667 N94-19847

ELECTRIC SWITCHES
Research on plasma-puff initiation of high Coulomb transfer switches
[NASA-CR-194371] p 1994 N94-21289
Plasma-puff initiation of high Coulomb transfer switches p 1994 N94-21290
Characteristics of plasma-puff trigger for a inverse-pinch plasma switch p 1995 N94-21291
Characteristics of switching plasma in an inverse-pinch switch p 1995 N94-21292
Comparative study of INPIStron and spark gap p 1995 N94-21293
INPIStron switched pulsed power for dense plasma pinches p 1995 N94-21294
High power, electron-beam induced switching in diamond
[DE93-040535] p 1768 N94-21770

ELECTRICAL ENGINEERING
Progress In Electromagnetics Research Symposium (PIERS)
[NASA-CR-194629] p 1718 N94-20403
Computer-Aided Test Equipment Graphics System (CATEGS)
[DE94-000383] p 1915 N94-21561
Canadian Conference on Electrical and Computer Engineering, volumes 1 and 2
[ISBN-0-9694170-2-0] p 1770 N94-22101

ELECTRICAL FAULTS
VLSI design for reliability-current density
[AD-A270719] p 1749 N94-20110
Correct CMOS IC defect models for quality testing p 1755 N94-21093
Faulty behavior of asynchronous storage elements p 1757 N94-21108
Detection of CMOS bridging faults using minimal stuck-at fault test sets p 1757 N94-21110

ELECTRICAL IMPEDANCE
Numerical modeling of fringing fields and their use for complex permittivity measurements at high frequencies
[AD-A270478] p 1966 N94-19917
Microscopic origins of metastable effects in a-Si:H and deep defect characterization in a-Si,Ge:H alloys
[DE93-016205] p 1688 N94-19985
Manual design technique for broadband passive thin-film attenuators using the Smith chart p 1782 N94-22178

ELECTRICAL MEASUREMENT
Numerical modeling of fringing fields and their use for complex permittivity measurements at high frequencies
[AD-A270478] p 1966 N94-19917
Superconducting property measurements in tape geometry
[DE93-016943] p 2014 N94-19970
Optical measurement of built-in and applied electric fields in Al(x)Ga(1-x)As/GaAs heterostructures p 1796 N94-20989
Amorphous Ta-rich Ta-Cu films as diffusion barriers between Au and GaAs p 1710 N94-20991
A new innovative instrument for space plasma instrumentation
[NASA-CR-194736] p 1668 N94-21780
Test results of two high temperature superconducting sample coils
[DE94-000496] p 2035 N94-22570

ELECTRICAL PROPERTIES
Characterization studies of lower and non-TDI polyurethane encapsulants
[DE93-041129] p 1696 N94-19857
Frequency dependent electrical properties of minerals and partial-melts
[DE93-019918] p 2012 N94-19861
Investigation of heterojunctions and multiple quantum well structures using crystalline organic semiconductors
[AD-A272113] p 2018 N94-20569
Surface treatment of InP and contribution to the optimization of the InP(p)/InP(p) regrown interfaces grown by GSMBE
[ECL-92-48] p 2018 N94-20598
Synthesis and properties of mismatched heterojunction/substrate interfaces
[AD-A272904] p 1760 N94-21229
Solid-state dynamics and quantum transport in novel semiconductor nanostructures
[AD-A272955] p 2027 N94-21248
Semiconductors A(III)B(VI): Translation
[AD-A273064] p 2028 N94-21438
Research and development of alternative components at Argonne National Laboratory for molten carbonate fuel cells
[DE93-019536] p 1847 N94-21650
Implantation of carbon in GaAs and compensating native defects
[DE93-040122] p 2030 N94-21763
Non-linear analysis of the electrical properties of the active circuits of high-frequency oscillators p 1785 N94-22195

ELECTRICAL RESISTANCE
Magnetism in CeRu2Ge2 and CeRh2Ge2 and its pressure dependence
[DE93-040061] p 2032 N94-21987
Thin-film fabrication of Pb-doped BiSrCaCuO superconductor p 1781 N94-22176

ELECTRICAL RESISTIVITY
Non-Fermi-liquid and multichannel Kondo phenomena in Y(1-x)U(x)Pd3 and related alloys
[DE93-040135] p 2015 N94-20275
Non-fermi liquid and spin-glass behavior of the Sc(1-x)U(x)Pd3 system
[DE93-040134] p 2016 N94-20335
Fabrication and evaluation of superconducting and semiconducting materials
[AD-A271645] p 2018 N94-20558
High temperature stability of amorphous Ta(x)Cu(1-x) diffusion barriers on GaAs p 2022 N94-20990
Solar proton events from a 180 year depth profile of nitrate concentrations from the central Greenland ice sheet
[AD-A272888] p 2147 N94-21196
Wire assembly for electrically conductive circuits
[AD-D015966] p 1761 N94-21275
Evaluation of electroconductivity of two surface paints for spacecraft
[AD-A273063] p 1706 N94-21437
Defect motion as the origin of the 1/f conductance noise in solids
[EUT-92-E-259] p 2029 N94-21552
Cathode materials for the molten carbonate fuel cell
[DE93-019515] p 1848 N94-21870
Iterative electromagnetic Born inversion applied to earth conductivity imaging
[DE93-040668] p 1859 N94-21928
Alloying studies in U(1-x)Th(x)Pd2Al3 (0 (le) x (le) 1)
[DE94-000807] p 2036 N94-22584

ELECTRICITY
Environmental protection using social costing
[DE94-000492] p 1853 N94-22569

ELECTRO-OPTICS
Proceedings of the 8th International Symposium on Applications of Ferroelectrics
[AD-A270679] p 1749 N94-20012
Synchrotron x ray diffraction analysis of photorefractive crystals and their gratings
[AD-A271176] p 2015 N94-20213
Photonic electromagnetic field sensor apparatus
[AD-D015939] p 1718 N94-20334
System for solving Boolean equations using optical lookup tables
[AD-D015962] p 1951 N94-20358
Transport in microstructures in the microwave and millimeter-wave regime
[AD-A271875] p 2017 N94-20470
High Speed/High Frequency Optoelectronics
[AD-A271985] p 1751 N94-20580
Recent developments in aromatic azo polymers research
[AD-A272966] p 1705 N94-21259
NOVAM evaluation utilizing electro-optics and meteorological data from KEY-90
[AD-A271722] p 1868 N94-21356
Intelligent processing of ferroelectric thin films
[AD-A272518] p 1705 N94-21416
Photonics and nonlinear optics with molecular materials and polymers
[AD-A271747] p 1988 N94-21457
Polyimide-based electrooptic materials
[DE93-019416] p 1706 N94-21526
Optical integrated structures and circuits on silicon
[VTT-PUBS-106] p 1988 N94-21594
Architectures of the free space optical interconnects p 1789 N94-22220

ELECTROACOUSTICS
U.S. Tag for ISO/TC 43, acoustics, IEC/TC 29 electroacoustics, and ISO/TC 108/SC4 human exposure to mechanical vibration and shock: Minutes of the accredited standards committee on bioacoustics, S3
[AD-A273014] p 1897 N94-21309

ELECTROCATALYSTS
Application of an electrochemical quartz crystal microbalance to the study of electrocatalytic films
[DE93-041124] p 2029 N94-21691

ELECTROCHEMICAL CELLS
The One-Day Workshop on Batteries, Stepping Motors, and Electronic Clock Displays
[ETN-93-94632] p 1752 N94-20628
Silver oxide batteries: Recent improvements and developments p 1752 N94-20629
Battery tests p 1752 N94-20631

ELECTROCHEMICAL CORROSION
The use of x ray techniques in the in situ study of corrosion
[DE93-019845] p 1690 N94-20301
In-situ electrochemical surface science
[AD-A265942] p 1680 N94-20330

ELECTROCHEMICAL OXIDATION
Development of an electrochemical hydrogen separator
[DE93-019877] p 1683 N94-21984

ELECTROCHEMISTRY
In-situ electrochemical surface science
[AD-A265942] p 1680 N94-20330
Electrochemical synthesis of ultrathin film composite membranes
[AD-A272721] p 1681 N94-21168
Laser Raman and x ray scattering studies of corrosion films on metals
[DE93-040243] p 1692 N94-21558
The electrochemical performance of thin-electrolyte solid oxide fuel cells
[DE93-041184] p 1848 N94-21942
Development of an electrochemical hydrogen separator
[DE93-019877] p 1683 N94-21984

ELECTRODE MATERIALS
High-power gas switch with hydride electrodes
[AD-D015956] p 1751 N94-20354
Research and development of alternative components at Argonne National Laboratory for molten carbonate fuel cells
[DE93-019536] p 1847 N94-21650
Effects of aqueous solution compositions on Aerocapacitor energy density
[DE94-000385] p 1768 N94-21753
Cathode materials for the molten carbonate fuel cell
[DE93-019515] p 1848 N94-21870

ELECTRODEPOSITION
Surface electrochemistry of metals
[AD-A272913] p 1691 N94-21245
Application of an electrochemical quartz crystal microbalance to the study of electrocatalytic films
[DE93-041124] p 2029 N94-21691
Surface modification for corrosion resistance
[DE93-017419] p 1693 N94-21825

ELECTRODES
Electrode array electromagnetic velocimeter
[AD-D015950] p 1806 N94-19882
Process to fabricate thick coplanar microwave electrode structures
[AD-D015913] p 1748 N94-19892
Lightweight battery electrode and method of making it
[AD-D015895] p 1749 N94-20120
Layered thin-edged field-emitter device
[AD-D015932] p 1751 N94-20350
High-power gas switch with hydride electrodes
[AD-D015956] p 1751 N94-20354
Laser Raman and x ray scattering studies of corrosion films on metals
[DE93-040243] p 1692 N94-21558

Investigation on the chemically fixing technique of carbon dioxide utilizing solar energy
[DE94-714886] p 1849 N94-22043

ELECTRODYNAMICS

Measurement and computation of the higher order modes of the ALS 500 MHz accelerating cavities
[DE93-019256] p 1980 N94-20292
A new matrix formulation of classical electrodynamics. Part 3: Wave propagation through a multilayer dielectric medium with planar boundaries
[AD-A271610] p 1739 N94-21240
Data analysis support for the SPREE instruments on the TSS-1 shuttle flight
[AD-A272445] p 1654 N94-21429

ELECTROENCEPHALOGRAPHY

Cognition and the brain: A continuation of the university research initiative at New York University
[AD-A271872] p 1894 N94-20467
Localization from near-source quasi-static electromagnetic fields
[DE93-040390] p 1732 N94-20479

ELECTROHYDRODYNAMICS

Absorption heat pump for space applications
[NASA-CR-194693] p 1845 N94-20066
EHD enhancement of pool and in-tube boiling of alternate refrigerants
[DE94-000787] p 1798 N94-20101

ELECTROLESS DEPOSITION

Adhesive electroless metallization of fluoropolymeric substrates
[AD-A271858] p 1703 N94-20526

ELECTROLYTES

Surface science at the solid liquid interface
[AD-A271422] p 1678 N94-19839
Photoelectron spectroscopy at model boundary surfaces of energy converter semiconductors/electrolyte contacts: Adsorption, coadsorption, and triadsorption of Br2, Na, and H2O on Van der Waals surfaces of metal chalocogenide semiconductors
[ETN-93-95063] p 2015 N94-20152
Research and development of alternative components at Argonne National Laboratory for molten carbonate fuel cells
[DE93-019536] p 1847 N94-21650
Effects of aqueous solution compositions on Aerocapacitor energy density
[DE94-000385] p 1768 N94-21753
The electrochemical performance of thin-electrolyte solid oxide fuel cells
[DE93-041184] p 1848 N94-21942

ELECTROLYTIC CELLS

Modeling of polymer electrolyte fuel cell systems
[DE93-041187] p 1847 N94-21774
The electrochemical performance of thin-electrolyte solid oxide fuel cells
[DE93-041184] p 1848 N94-21942
Investigation on the chemically fixing technique of carbon dioxide utilizing solar energy
[DE94-714886] p 1849 N94-22043
Survey on chemical engineering technologies for the global environmental protection
[DE94-714887] p 1852 N94-22044

ELECTROMAGNETIC ABSORPTION

High efficiency epitaxial optical reflector solar cells
[DE93-017115] p 1845 N94-19805
Optically induced rotation diffusion in polymer liquid crystals: Phenomenological theory and experimental verification
[ETN-93-95068] p 2014 N94-20026
Optical and transport properties of metallic and semiconductor nanostructures
[AD-A271716] p 2018 N94-20554
Optical metrology of magnetically trapped hydrogen
[AD-A272110] p 1680 N94-20584
Forecasting technique of variations of the optical absorptivity of thermal control coatings under different simultaneous radiations p 1664 N94-21399
Photonics and nonlinear optics with molecular materials and polymers
[AD-A271747] p 1988 N94-21457
The use of ERBE data for climate studies
p 1860 N94-22286
Low temperature absorption spectra and ground state electronic structure of tetrakis(2,6-di-tert-butylphenoxide)uranium(IV)
[DE94-000774] p 2035 N94-22387

ELECTROMAGNETIC COMPATIBILITY

SLAC measurement of the neutron spin structure function
[DE93-040998] p 1975 N94-21788
Improvements in antenna coupling path algorithms for aircraft EMC analysis p 1745 N94-22126

ELECTROMAGNETIC COUPLING

The preservation of low emittance flat beams
[DE93-040964] p 1981 N94-21773
Linearly tapered slot antenna circular array for mobile communications
[NASA-TM-106441] p 1769 N94-21808
Full wave numerical model of arbitrarily-shaped proximity coupled microstrip antennas p 1745 N94-22137

ELECTROMAGNETIC FIELDS

Characterization of electromagnetic fields in an extended chamber at the Short Pulse Experimental Electron Device (SPEED) simulator
[AD-A265955] p 1717 N94-20329
Photonic electromagnetic field sensor apparatus
[AD-D015938] p 1717 N94-20333
Photonic electromagnetic field sensor apparatus
[AD-D015939] p 1718 N94-20334
FD-TD modeling of 2-D dielectric waveguides for propagation and scattering of femtosecond optical solitons p 1719 N94-20406
An efficient formulation of the coupled finite element-integral equation technique for solving large 3D scattering problems p 1725 N94-20436
Localization from near-source quasi-static electromagnetic fields
[DE93-040390] p 1732 N94-20479
VLF Harold E. Holt RADHAZ measurements
[AD-A272018] p 1737 N94-20620
A new matrix formulation of classical electrodynamics. Part 3: Wave propagation through a multilayer dielectric medium with planar boundaries
[AD-A271610] p 1739 N94-21240
ELF communications system ecological monitoring program
[AD-A272507] p 1740 N94-21412
Hybrid finite element/waveguide mode analysis of passive RF devices
[AD-A273074] p 1740 N94-21518
An integro-algebraic equation for high frequency wake fields in a tube with smoothly varying radius
[DE93-040940] p 1741 N94-21684
Performance of a simple circular polarization selective surface p 1746 N94-22198
Electromagnetic interference and shielding: An introduction (revised version of 1991-23)
[PB93-215275] p 1742 N94-22348
Prompt high-energy particle acceleration during two current loops collision p 2005 N94-22661
Dynamics of physical state during two current loops collision p 2005 N94-22663
Time variation of MHD accretion onto a black hole
p 2009 N94-22692

ELECTROMAGNETIC INTERACTIONS

A Monte Carlo study of the Sudbury Neutrino Observatory small test detector experiment
[ISBN-0-315-59056-4] p 1977 N94-22416

ELECTROMAGNETIC INTERFERENCE

Improvements in antenna coupling path algorithms for aircraft EMC analysis p 1745 N94-22126
Characterization and modelling of extremely high frequency enclosures p 1782 N94-22177
FM interference in radio navigation receivers
p 1645 N94-22219
Applications of planar near-field measurements to electromagnetic radiation and interference problems
p 1747 N94-22252
Electromagnetic interference and shielding: An introduction (revised version of 1991-23)
[PB93-215275] p 1742 N94-22348

ELECTROMAGNETIC MEASUREMENT

Integrated display of multi-sensor geophysical and electromagnetic flight data p 1721 N94-20418
Localization from near-source quasi-static electromagnetic fields
[DE93-040390] p 1732 N94-20479
Iterative electromagnetic Born inversion applied to earth conductivity imaging
[DE93-040668] p 1859 N94-21928

ELECTROMAGNETIC NOISE

Literature review of the errors-in-variables approach to the problem of system identification
[AD-A271098] p 1949 N94-19907
Proton radiation testing of an 18 bit A/D converter
p 1755 N94-21096

ELECTROMAGNETIC PROPERTIES

Electrode array electromagnetic velocimeter
[AD-D015950] p 1806 N94-19882
High temperature superconducting planar circuit structure for high frequency applications
[AD-A273083] p 2028 N94-21521

ELECTROMAGNETIC PULSES

Measurement and correction of magnetic fields in pulsed slotted-tube microwigglers
[DE93-040100] p 1815 N94-20272
Ultrafast gas switching experiments
[DE93-019071] p 1762 N94-21634
A broadband V-antenna for pulsed field measurements: Experimental results p 1745 N94-22139
Continuous-time discretized-space approach to modeling short-pulse propagation and scattering
[PB93-215259] p 1742 N94-22347

ELECTROMAGNETIC RADIATION

Near grazing scattering from non-Gaussian ocean surfaces p 1726 N94-20438
A comparative study between shielded and open coplanar waveguide discontinuities
p 1733 N94-20501
Modeling of coaxial-fed microstrip patch antenna by finite difference time domain method p 1745 N94-22138
Langmuir microstructures and pulsar radio emission
p 2007 N94-22678

ELECTROMAGNETIC SCATTERING

Study of electromagnetic wave scattering from characterized rough surfaces
[AD-A270931] p 1716 N94-19934
Analytical evaluation of a surface integral expressing the coupling between interior and exterior volumes in a FE-IE approach p 1722 N94-20423
Polarimetric backscattering from sea ice
p 1723 N94-20426
An efficient formulation of the coupled finite element-integral equation technique for solving large 3D scattering problems p 1725 N94-20436
Near grazing scattering from non-Gaussian ocean surfaces p 1726 N94-20438
Extinction efficiencies from DDA calculations solved for finite circular cylinders and disks p 1880 N94-22340
Extended range modified gradient technique for profile inversion (extended version of report Et/Em-1992-8)
[PB93-215242] p 1742 N94-22346
Continuous-time discretized-space approach to modeling short-pulse propagation and scattering
[PB93-215259] p 1742 N94-22347

ELECTROMAGNETIC SHIELDING

Characterization of electromagnetic fields in an extended chamber at the Short Pulse Experimental Electron Device (SPEED) simulator
[AD-A265955] p 1717 N94-20329
Electromagnetic interference and shielding: An introduction (revised version of 1991-23)
[PB93-215275] p 1742 N94-22348

ELECTROMAGNETIC WAVE TRANSMISSION

Photonic electromagnetic field sensor apparatus
[AD-D015938] p 1717 N94-20333
A new matrix formulation of classical electrodynamics. Part 3: Wave propagation through a multilayer dielectric medium with planar boundaries
[AD-A271610] p 1739 N94-21240
Time-laplace-transform-domain analysis of wave propagation in planar waveguides
[PB93-215226] p 1980 N94-22096
Continuous-time discretized-space approach to modeling short-pulse propagation and scattering
[PB93-215259] p 1742 N94-22347
Electromagnetic interference and shielding: An introduction (revised version of 1991-23)
[PB93-215275] p 1742 N94-22348

ELECTROMAGNETISM

Progress In Electromagnetics Research Symposium (PIERS)
[NASA-CR-194629] p 1718 N94-20403
Electromagnetic interference and shielding: An introduction (revised version of 1991-23)
[PB93-215275] p 1742 N94-22348

ELECTROMAGNETS

Power supply and controller for the Sextupole magnet of AmPS
[DIGEL-1992-3] p 1753 N94-21064

ELECTROMECHANICAL DEVICES

Electromechanical battery research and development at the Lawrence Livermore National Laboratory
[DE93-019159] p 1762 N94-21620
Electromechanical battery research and development at the Lawrence Livermore National Laboratory
[DE94-000391] p 1762 N94-21621

ELECTROMECHANICS

Electromechanical battery research and development at the Lawrence Livermore National Laboratory
[DE94-000391] p 1762 N94-21621

ELECTROMIGRATION

VLSI design for reliability-current density
[AD-A270719] p 1749 N94-20110

ELECTROMOTIVE FORCES

Data analysis support for the SPREE instruments on the TSS-1 shuttle flight
[AD-A272445] p 1654 N94-21429

ELECTROMYOGRAPHY

Cosmos 2229
[NASA-CR-194734] p 1895 N94-20338

ELECTRON ACCELERATION

Electron acceleration in and radio emission from SN1987A p 2007 N94-22677

ELECTRON ACCELERATORS
Jet shapes in hadron and electron colliders
[DE93-019386] p 1979 N94-20216
Demonstration of ultraviolet lasing with a low energy electron beam
[DE93-040192] p 1818 N94-21554
ELECTRON ATTACHMENT
Electron reactions in nonpolar liquids: Pressure effects
[DE93-040328] p 1970 N94-19931
ELECTRON AVALANCHE
SPICE macromodel for a 1-megawatt power MOSFET switch
[DE93-019415] p 1748 N94-19844
ELECTRON BEAM WELDING
Thermocapillary and arc phenomena in stainless steel welds
[DE94-000518] p 1821 N94-19859
ELECTRON BEAMS
Initial performance of Los Alamos advanced free electron laser
[DE93-040158] p 1814 N94-19828
Laser amplifier developments at Mercury
[DE93-040103] p 1814 N94-19867
Absolute total and one and two electron transfer cross sections for Ar(8+) on Ar as a function of energy
[DE93-040283] p 1970 N94-19870
A field-based technique for the longitudinal profiling of ultrarelativistic electron or positron bunches down to lengths of less than or equal to 10 microns
[DE93-040954] p 1978 N94-19873
Near atomic resolution microanalysis of interfaces by analytical electron microscopy
[DE93-019437] p 1687 N94-19904
Bundle profile monitor for AmPS
[DIGEL-1992-8] p 1979 N94-20123
Performance of the high brightness linac for the Advanced Free Electron Laser Initiative at Los Alamos
[DE93-040141] p 1816 N94-20277
The modification of polymer surfaces and the fabrication of submicron-scale functionalized structures by deep-UV and electron beam lithography
[AD-A265956] p 1700 N94-20328
Characterization of electromagnetic fields in an extended chamber at the Short Pulse Experimental Electron Device (SPEED) simulator
[AD-A265955] p 1717 N94-20329
Electron quantum yields from a barium photocathode illuminated with polarized light
[DE93-019232] p 1980 N94-20475
An 85 GHz quasioptical gyroklystron experiment
[AD-A272020] p 1752 N94-20931
Properties of E-beam interactive oxide films for nanometer scale structures
[AD-A272848] p 1675 N94-21191
Simulated space environmental effects on some experimental high performance polymers
p 1662 N94-21385
Demonstration of ultraviolet lasing with a low energy electron beam
[DE93-040192] p 1818 N94-21554
High power, electron-beam induced switching in diamond
[DE93-040535] p 1768 N94-21770
SLAC measurement of the neutron spin structure function
[DE93-040998] p 1975 N94-21788
Monte Carlo calculation of multi-electron effects on synchrotron radiation
[DE94-001259] p 1982 N94-21974
ELECTRON BUNCHING
A field-based technique for the longitudinal profiling of ultrarelativistic electron or positron bunches down to lengths of less than or equal to 10 microns
[DE93-040954] p 1978 N94-19873
Study of coupled-bunch collective effects in the PEP-2 B-Factory
[DE93-040117] p 1979 N94-20274
An 85 GHz quasioptical gyroklystron experiment
[AD-A272020] p 1752 N94-20931
Monte Carlo calculation of multi-electron effects on synchrotron radiation
[DE94-001259] p 1982 N94-21974
ELECTRON CAPTURE
Energy gain spectroscopic study of Ar(q+)-Ar collisions at 40 qeV
[DE93-040284] p 1970 N94-19871
ELECTRON COUNTERS
A search for new gauge bosons in (bar p)p collisions at square root of s equals 1.8 TeV in the dielectron decay mode
[DE93-019901] p 1969 N94-19813
ELECTRON DENSITY (CONCENTRATION)
On the experimental determination of low order structure factors in TiAl by energy filtered convergent beam electron diffraction
[DE93-019521] p 1687 N94-19806
Ionospheric tomography using the FORTE satellite
[DE93-018545] p 1854 N94-19955
Spectral characterization of lithographic sources
[DE93-019941] p 1997 N94-21848
ELECTRON DIFFRACTION
On the experimental determination of low order structure factors in TiAl by energy filtered convergent beam electron diffraction
[DE93-019521] p 1687 N94-19806
Facilities for in situ ion beam studies in transmission electron microscopes
[DE93-019567] p 1979 N94-20222
Determination of structure factors of copper by convergent beam electron diffraction
[DE93-019520] p 2019 N94-20941
Diffraction and holography of photoelectrons and fluorescent x rays
[DE93-019240] p 1808 N94-21441
Synthesis and catalytic properties of metal and semiconductor nanoclusters
[DE93-019418] p 2028 N94-21541
ELECTRON DISTRIBUTION
Kinetic theory of runaway air-breakdown
[DE93-040731] p 1750 N94-20325
Detailed analysis case studies of trapped plasmas at the Earth's magnetic equator
[AD-A272497] p 1858 N94-21432
Studies of electromagnetic ion cyclotron waves using AMPTE/CCE and Dynamics Explorer
[NASA-CR-194711] p 1982 N94-21878
ELECTRON EMISSION
Research on defects and transport in amorphous-silicon-based semiconductors
[DE93-017117] p 2013 N94-19939
Study of mechanisms for long wavelength Schottky-barrier infrared detectors
[AD-A270538] p 1971 N94-20083
Electron emissions in low energy Ar(q+)-Ar collisions
[DE93-040285] p 1974 N94-21543
Electron emission from nanometer-size metallic clusters: Electronic states and structural stability of supported Au clusters
[DE93-040184] p 1975 N94-21766
Magnetic insulation of secondary electrons in plasma source ion implantation
[DE93-040106] p 1997 N94-21988
ELECTRON ENERGY
Electron reactions in nonpolar liquids: Pressure effects
[DE93-040328] p 1970 N94-19931
Angular distributions of high-order ATI
[DE93-019125] p 1972 N94-20230
In-situ electrochemical surface science
[AD-A265942] p 1680 N94-20330
Electron emissions in low energy Ar(q+)-Ar collisions
[DE93-040285] p 1974 N94-21543
Spectral characterization of lithographic sources
[DE93-019941] p 1997 N94-21848
Studies of electromagnetic ion cyclotron waves using AMPTE/CCE and Dynamics Explorer
[NASA-CR-194711] p 1982 N94-21878
Inelastic electron scattering from surfaces
[DE94-001738] p 1977 N94-22049
Fluid simulations of Delta T(sub e)-driven turbulence and transport in boundary plasmas
[DE94-001304] p 1999 N94-22566
Electron temperature gradient driven instability in the tokamak boundary plasma
[DE94-001307] p 1999 N94-22596
ELECTRON FLUX DENSITY
Photoelectron holography of platinum (111)
[DE93-040856] p 1810 N94-21950
ELECTRON GAS
Synthesis and properties of mismatched heterojunction/substrate interfaces
[AD-A272904] p 1760 N94-21229
ELECTRON IMPACT
Collisional processes involving atmospheric gases
[AD-A270729] p 1854 N94-19954
ELECTRON IRRADIATION
Tensile and shear fracture behavior of fiber reinforced plastics at 77K irradiated by various radiation sources
[DE93-040280] p 1706 N94-21542
ELECTRON MICROSCOPES
Study of mechanisms for long wavelength Schottky-barrier infrared detectors
[AD-A270538] p 1971 N94-20083
Facilities for in situ ion beam studies in transmission electron microscopes
[DE93-019567] p 1979 N94-20222
Electron holography applied to the study of ceramic materials
[DE94-000329] p 1707 N94-21653
ELECTRON MICROSCOPY
Near atomic resolution microanalysis of interfaces by analytical electron microscopy
[DE93-019437] p 1687 N94-19904
Preliminary AEM study of the microstructure and composition of metal particles in ordinary chondrites
p 2086 N94-20894
ELECTRON MOBILITY
Electron reactions in nonpolar liquids: Pressure effects
[DE93-040328] p 1970 N94-19931
Research on defects and transport in amorphous-silicon-based semiconductors
[DE93-017117] p 2013 N94-19939
Defect motion as the origin of the 1/f conductance noise in solids
[EUT-92-E-259] p 2029 N94-21552
ELECTRON ORBITALS
Rotational isomers of Mo(VI) alkylidene complexes and Cis/trans polymer structure: Investigations in ring-opening metathesis polymerization
[AD-A272647] p 1704 N94-21184
ELECTRON PLASMA
Spectral characterization of lithographic sources
[DE93-019941] p 1997 N94-21848
A unified Monte Carlo interpretation of particle simulations and applications to nonneutral plasmas
[DE94-001231] p 1997 N94-21973
ELECTRON PROBES
Microscopic origins of metastable effects in a-Si:H and deep defect characterization in a-Si,Ge:H alloys
[DE93-018205] p 1688 N94-19985
ELECTRON RADIATION
Monte Carlo calculation of multi-electron effects on synchrotron radiation
[DE94-001259] p 1982 N94-21974
ELECTRON SCATTERING
Near atomic resolution microanalysis of interfaces by analytical electron microscopy
[DE93-019437] p 1687 N94-19904
Electron reactions in nonpolar liquids: Pressure effects
[DE93-040328] p 1970 N94-19931
New relativistic S-matrix results for scattering -- beyond the usual anomalous factors/beyond impulse approximation
[DE93-019148] p 1971 N94-20096
The angular velocity spread of REB induced by magnetic field discontinuity
[IPPCZ-331] p 1996 N94-21573
Non-adiabatic effects in low-energy electron-molecule scattering
[DE93-040485] p 1976 N94-21968
Inelastic electron scattering from surfaces
[DE94-001738] p 1977 N94-22049
The effect of Compton scattering on the double to single ionization ratio in helium
[DE94-000884] p 1827 N94-22390
ELECTRON SOURCES
Performance of the high brightness linac for the Advanced Free Electron Laser Initiative at Los Alamos
[DE93-040141] p 1816 N94-20277
Electron quantum yields from a barium photocathode illuminated with polarized light
[DE93-019232] p 1980 N94-20475
ELECTRON SPECTROSCOPY
Energy gain spectroscopic study of Ar(q+)-Ar collisions at 40 qeV
[DE93-040284] p 1970 N94-19871
Observation of x ray absorption magnetic circular dichroism in well-characterized iron-cobalt-platinum multilayers
[DE94-000303] p 1694 N94-21944
Inelastic electron scattering from surfaces
[DE94-001738] p 1977 N94-22049
ELECTRON STATES
The Coulomb anomaly in strongly disordered films
[AD-A271095] p 2012 N94-19849
Collisional processes involving atmospheric gases
[AD-A270729] p 1854 N94-19954
Rotational spectrum of a dark state in 2-fluoroethanol using microwave/radiofrequency-infrared multiple resonance
[AD-A272101] p 1817 N94-20583
Optical amplification and threshold behavior on InGaAs/InGaAsP multiquantum well structures
[ETN-93-94181] p 2026 N94-21151
Electron emission from nanometer-size metallic clusters: Electronic states and structural stability of supported Au clusters
[DE93-040184] p 1975 N94-21766
Ionization of H2(+) in intense laser fields
[DE93-019160] p 1818 N94-21829
Theoretical studies of the structures and electronic properties of U(NH2)(sub 3) and Np(NH2)(sub 3)
[DE94-000768] p 2031 N94-21857
ELECTRON TRAJECTORIES
Magnetic insulation of secondary electrons in plasma source ion implantation
[DE93-040106] p 1997 N94-21988

ELECTRON TRANSFER
The proximity effect in ultrathin granular Pb films
[AD-A271094] p 2012 N94-19848
Absolute total and one and two electron transfer cross sections for Ar(8+) on Ar as a function of energy
[DE93-040283] p 1970 N94-19870
Modeling failure and reliability in new-generation devices
[AD-A271150] p 1748 N94-19910
Study of mechanisms for long wavelength Schottky-barrier infrared detectors
[AD-A270538] p 1971 N94-20083
Transport in microstructures in the microwave and millimeter-wave regime
[AD-A271875] p 2017 N94-20470
Ionospheric photoelectrons measured at geosynchronous orbit
[AD-A272431] p 1857 N94-21202
Integral equation calculation of solvent activation free energies for electron and proton transfer reactions
[AD-A272665] p 1681 N94-21216
Infrared absorption spectroscopy of the weakly bonded CO-Cl2 complex
[AD-A271757] p 2027 N94-21304
Data analysis support for the SPREE instruments on the TSS-1 shuttle flight
[AD-A272445] p 1654 N94-21429
Photochemical approaches to conversion of light to electricity or fuel
[DE94-001650] p 1849 N94-22048
ELECTRON TRANSITIONS
Collisional processes involving atmospheric gases
[AD-A270729] p 1854 N94-19954
Determining the composition of olivine on asteroidal surfaces p 1686 N94-20805
Electron emissions in low energy Ar(q+)-Ar collisions
[DE93-040285] p 1974 N94-21543
Local structure and superconductivity in La(2-x)Ba(x)CuO4 for x=0.125 and x=0.15
[DE93-040193] p 2029 N94-21555
ELECTRON TUNNELING
The Coulomb anomaly in strongly disordered films
[AD-A271095] p 2012 N94-19849
Growth mechanisms and characterization of hydrogenated amorphous-silicon-alloy films
[DE93-018202] p 1699 N94-20047
Study of mechanisms for long wavelength Schottky-barrier infrared detectors
[AD-A270538] p 1971 N94-20083
Energy-resolving x ray detectors with charge amplification due to multiple quasiparticle tunneling
[DE93-019506] p 2031 N94-21869
ELECTRON-POSITRON PAIRS
Study of coupled-bunch collective effects in the PEP-2 B-Factory
[DE93-040117] p 1979 N94-20274
ELECTRON-POSITRON PLASMAS
Gamma ray burst as a result of the explosive instability in the magnetosphere of old neutron star p 2007 N94-22675
ELECTRONIC BULLETIN BOARDS
PEGASUS, electronic bulletin board system user's guide
[AD-A271679] p 2044 N94-21363
ELECTRONIC EQUIPMENT
Control vane guidance for a ducted-fan unmanned air vehicle
[AD-A271957] p 1645 N94-20561
The electronics technology policy of the NLR Informatics Division: The NLR electronics CAE infrastructure
[NLR-TP-91001-U] p 1753 N94-21067
The 1992 4th NASA SERC Symposium on VLSI Design
[NASA-CR-194591] p 1763 N94-21694
Electronic locking system p 1796 N94-21801
ELECTRONIC EQUIPMENT TESTS
An x-band peeled HEMT amplifier p 1732 N94-20498
Proton radiation testing of an 18 bit A/D converter p 1755 N94-21096
Non-destructive semiconductor wafer probing system using laser pulses to generate and detect millimeter-wave signals
[CA-PATENT-APPL-SN-2,020,73] p 1760 N94-21178
ELECTRONIC FILTERS
An investigation into the integration of meter-level range and millimeter-level phase data using a multimode stimulation for optimal filter estimation software package
[AD-A267955] p 1751 N94-20483
ELECTRONIC MAIL
Multi Wave Link: An interactive database for co-ordination of multiwavelength programs
[NASA-CR-194778] p 2043 N94-21055
PEGASUS, electronic bulletin board system user's guide
[AD-A271679] p 2044 N94-21363
Controlling multisupplier operations by intelligent EDI p 1744 N94-22076
ELECTRONIC PACKAGING
Quartz/fused silica chip carriers
[NASA-CR-194154] p 2016 N94-20340
A simple modern correctness condition for a space-based high-performance multiprocessor p 1786 N94-21718
Characterization and modelling of extremely high frequency enclosures p 1782 N94-22177
ELECTRONIC WARFARE
Operational test and evaluation of electronic combat systems
[AD-A273093] p 1647 N94-21500
ELECTRONS
Electron reactions in nonpolar liquids: Pressure effects
[DE93-040328] p 1970 N94-19931
Evaluation of the chemical composition of cosmic radiation in energy area of 10(exp 15) eV
[ETN-93-93682] p 2150 N94-21056
Electron emissions in low energy Ar(q+)-Ar collisions
[DE93-040285] p 1974 N94-21543
Electron emission from nanometer-size metallic clusters: Electronic states and structural stability of supported Au clusters
[DE93-040184] p 1975 N94-21766
SLAC measurement of the neutron spin structure function
[DE93-040998] p 1975 N94-21788
Energy-resolving x ray detectors with charge amplification due to multiple quasiparticle tunneling
[DE93-019506] p 2031 N94-21869
ELECTRORHEOLOGICAL FLUIDS
Light scattering studies of an electrorheological fluid
[DE93-019419] p 1700 N94-20315
ELECTROSTATIC CHARGE
An improved patch for radiative coolers
[NASA-CASE-GSC-13503-1] p 1822 N94-20127
Electrostatic charging and secondary effects in materials submitted to radiation in space p 1661 N94-21383
ELECTROSTATICS
EHD enhancement of pool and in-tube boiling of alternate refrigerants
[DE94-000787] p 1798 N94-20101
High current injector for heavy ion fusion
[DE93-019241] p 1979 N94-20289
Theoretical studies of structural phase transitions in actinide metals
[DE94-000796] p 1696 N94-22388
ELEMENTARY EXCITATIONS
Energy-resolving x ray detectors with charge amplification due to multiple quasiparticle tunneling
[DE93-019506] p 2031 N94-21869
ELEMENTARY PARTICLE INTERACTIONS
The cross section for the production of b(bar-b) pairs in p(bar p) collisions at the square root of s equals 1.8 TeV
[DE93-019900] p 1972 N94-20225
Measurement of the strange quark distribution function in W(+) charm quark events
[DE93-018267] p 1973 N94-20474
Hadronic molecules and scattering amplitudes from the nonrelativistic quark model
[DE94-000377] p 1974 N94-21657
Measurement of the inclusive jet cross section in p(bar-p) collisions at CDF
[DE94-000581] p 1982 N94-21866
ELEVATION
Topographic mapping using a monopulse SAR system p 1721 N94-20417
Distribution of small volcanic cones on the surface of Venus by size and elevation: Implications for differential deposition of volcanic features p 2110 N94-20731
Discharge rates in Ma'adim Vallis, Mars p 2128 N94-20830
Elevation and igneous crater modification on Venus: Implications for magmatic volatile content p 2135 N94-20872
ELEVATION ANGLE
Topographic mapping using a monopulse SAR system p 1721 N94-20417
ELLIPSOIDS
Linear structures on the small inner satellites of Saturn p 2121 N94-20797
Elliptical-shape parameter estimation from a set of normal lines p 1777 N94-22148
ELLIPSOMETERS
Thin film compositional analysis using null or fixed wavelength ellipsometry p 1709 N94-20976
Applications of variable angle spectroscopic ellipsometry in semiconductor technology p 2025 N94-21010
ELLIPSOMETRY
Spectroscopic ellipsometry studies of HF treated Si (100) surfaces p 1734 N94-20508
Ellipsometric study of Si(0.5)Ge(0.5)/Si strained-layer superlattices p 1734 N94-20509
Spectroscopic ellipsometric characterization of Si/Si(1-x)Ge(x) strained-layer superlattices p 1734 N94-20510
New technique for oil backstreaming contamination measurements p 1652 N94-20511
Materials, Structures, and Devices for High-Speed Electronics
[NASA-CR-193177] p 2019 N94-20971
Ellipsometric studies of sputtered silicon nitride on n-GaAs p 1709 N94-20972
Multiple-wavelength angle-of-incidence ellipsometry: Application to silicon nitride-gallium arsenide structures p 2019 N94-20974
Structural and chemical analysis of a silicon nitride film on GaAs by null ellipsometry p 1709 N94-20975
Thin film compositional analysis using null or fixed wavelength ellipsometry p 1709 N94-20976
Analytic solutions for optimized ellipsometric measurements of interfaces and surface layers in thin film structures p 2019 N94-20977
Variable wavelength, variable angle ellipsometry including a sensitivities correlation test p 1710 N94-20978
Thin-film hermeticity: A quantitative analysis of diamondlike carbon using variable angle spectroscopic ellipsometry p 1710 N94-20981
Variable angle of incidence spectroscopic ellipsometric study of semiconductor multilayer structures p 2020 N94-20982
Ellipsometric measurements of molecular-beam-epitaxy-grown semiconductor multilayer thicknesses: A comparative study p 1710 N94-20983
Comparative thickness measurements of heterojunction layers by ellipsometric, RBS, and XTEM analysis p 1710 N94-20984
Characterization of multilayer GaAs/AlGaAs transistor structures by variable angle spectroscopic ellipsometry p 1796 N94-20985
Variable angle spectroscopic ellipsometric characterization of surface damage in chemical-mechanical polished GaAs p 1710 N94-20986
Variable angle of incidence spectroscopic ellipsometric measurement of the Franz-Keldysh effect in MODFET structures p 2021 N94-20987
Ellipsometric analysis of built-in electric fields in semiconductor heterostructures p 1796 N94-20988
Optical measurement of built-in and applied electric fields in Al(x)Ga(1-x)As/GaAs heterostructures p 1796 N94-20989
Measurement of superlattice optical properties by variable angle spectroscopic ellipsometry p 2022 N94-20992
Superlattice optical properties measured by variable angle spectroscopic ellipsometry p 2022 N94-20993
GaAs/AlGaAs superlattice characterization by variable angle spectroscopic ellipsometry p 2022 N94-20994
Characterization of an asymmetric triangular multiple quantum well, by variable angle spectroscopic ellipsometry p 2022 N94-20995
GaAs(100) surface modifications at elevated temperatures, studied by in-situ spectroscopic ellipsometry p 2023 N94-20997
Ellipsometric study of GaAs(100) surface changes induced at elevated temperatures p 2023 N94-20998
Temperature dependence of optical properties of AlAs, studied by in-situ spectroscopic ellipsometry p 2023 N94-20999
Dielectric function of InGaAs in the visible p 2023 N94-21000
Study of InGaAs-based modulation doped field effect transistor structures using variable-angle spectroscopic ellipsometry p 1796 N94-21001
Study of concentration-dependent dielectric properties of n-type GaAs using variable angle spectroscopic ellipsometry p 2024 N94-21002
In-situ spectroscopic ellipsometry for real time semiconductor growth monitor p 2024 N94-21003
Real-time analysis of in-situ spectroscopic ellipsometric data during MBE growth of III-V semiconductors p 2024 N94-21004
In-situ spectroscopic ellipsometry in molecular beam epitaxy p 2024 N94-21005
Micro-ellipsometric measurements of strained layer structures p 2025 N94-21008
Spectroscopic ellipsometric characterization of Si/Si(1-x)Ge(x) strained-layer superlattices p 2025 N94-21009
Applications of variable angle spectroscopic ellipsometry in semiconductor technology p 2025 N94-21010
Fundamentals and applications of variable angle spectroscopic ellipsometry p 1687 N94-21011
Non-destructive evaluation in manufacturing using spectroscopic ellipsometry p 1828 N94-21012
In-situ and ex-situ ellipsometric characterization for semiconductor technology p 2026 N94-21013

VASE (variable angle spectroscopic ellipsometry) p 1687 N94-21014
The optical constants and spectral specular reflectivity of Highly Oriented Pyrolytic Graphite (HOPG) [DE93-040546] p 1709 N94-21970
ELLIPTIC DIFFERENTIAL EQUATIONS
MGGHAT: Elliptic PDE software with adaptive refinement, multigrid and high order finite elements p 1956 N94-21470
Two-level Schwartz methods for nonconforming finite elements and discontinuous coefficients p 1957 N94-21477
A multigrid algorithm for the cell-centered finite difference scheme p 1957 N94-21479
ELLIPTIC FUNCTIONS
MGD1M: A parallel multigrid code with a fast vectorized ILU-relaxation [CWI-NM-R9222] p 1930 N94-21077
Numerical multigrid software (MGD5M): A parallel multigrid code with a twisted ILLU-relaxation [CWI-NM-R9226] p 1916 N94-21611
ELLIPTICAL GALAXIES
Surface photometry of the shell galaxy NGC 2865 [ISBN-0-315-60441-7] p 2056 N94-22412
Visualizing the universe, part 2 p 2063 N94-22472
ELLIPTICITY
The connection between Venus' free obliquity and its CMB oblateness p 2139 N94-20896
EMBEDDED COMPUTER SYSTEMS
The University of Hawaii Institute for Astronomy CCD camera control system p 1828 N94-22489
EMBEDDING
Embedded microclusters in zeolites and cluster beam sputtering: Simulation on parallel computers [DE94-000741] p 1701 N94-20352
Writing instrument interfaces with xf/tktcl p 1925 N94-22480
EMBRITTLEMENT
Rapid heating tensile testing update: 304L stainless steel [DE93-018770] p 1688 N94-19942
Microscopic evaluation of low-temperature embrittlement in type 308 stainless steel welds [DE93-040266] p 1690 N94-20282
EMISSION
On dust emissions from the jovian system p 2141 N94-20909
EMISSION SPECTRA
Derivation of the midinfrared (5.0-25.0 micron) optical constants of hydrous carbonate and sulfate p 2108 N94-20723
A study of carbonates, sulfates, and phosphates using thermal emission spectroscopy p 1686 N94-20868
Spatial distribution of near infrared line radiation in galactic nuclei measured with Fabry-Perot spectrometer FAST [MPE-239] p 2081 N94-21138
Comparative study of INPIStron and spark gap p 1995 N94-21293
Spectral characterization of lithographic sources [DE93-019941] p 1997 N94-21848
Temperature dependence of CsI(Tl) gamma ray excited scintillation characteristics [DE94-000836] p 2034 N94-22028
Radio galaxies and their environment [DE93-040851] p 2150 N94-22397
The cool-star spectral catalog: A uniform collection of IUE SWP-LOs p 2046 N94-22446
The ALEXIS data processing package: An IDL based system p 2047 N94-22453
Magnetic reconnection in emission nebulae in clusters of galaxies p 2010 N94-22700
EMISSIVITY
Polarimetric thermal emission from periodic water surfaces p 1728 N94-20445
Relationship of attenuation in a vegetation canopy to physical parameters of the canopy p 1729 N94-20450
Subduction on the margins of coronae on Venus: Evidence from radiothermal emissivity measurements p 2107 N94-20718
Thermal infrared remote sensing and Kirchhoff's law: 1. Laboratory measurements p 1685 N94-20733
The role of CO2 in weathering reactions and the presence of S2 on Venus: Implications for the pyrite stability field p 2122 N94-20799
Cloud properties from the analysis of AVHRR observations for FIRE 2 p 1872 N94-22300
Surface-induced brightness temperature variations and their effects on detecting thin cirrus clouds using IR emission channels in the 8-12 micrometer region p 1880 N94-22341
EMITTANCE
Initial performance of Los Alamos advanced free electron laser [DE93-040158] p 1814 N94-19828
Aperture determination of RHIC92 from randomly generated initial coordinates [DE93-040174] p 1978 N94-19945
Emittance measurement and modeling of the ALS 50 MeV LINAC to booster line [DE93-040116] p 1979 N94-20273
Performance of the high brightness linac for the Advanced Free Electron Laser Initiative at Los Alamos [DE93-040141] p 1816 N94-20277
Demonstration of ultraviolet lasing with a low energy electron beam [DE93-040192] p 1818 N94-21554
The preservation of low emittance flat beams [DE93-040964] p 1981 N94-21773
Detector noise statistics in the non-linear regime p 1748 N94-22526
EMITTERS
Layered thin-edged field-emitter device [AD-D015932] p 1751 N94-20350
Field emitter array RF amplifier development project, phase 1, option 1 [AD-A272567] p 1740 N94-21361
Silicon microelectronic field-emissive devices for advanced display technology [DE94-000397] p 1794 N94-22380
EMOTIONS
Female security as a general mobility condition [ISBN-3-79-831536-1] p 2039 N94-20153
ENCAPSULATING
Characterization studies of lower and non-TDI polyurethane encapsulants [DE93-041129] p 1698 N94-19857
END EFFECTORS
Spline screw payload fastening system [NASA-CASE-GSC-13454-1] p 1821 N94-20126
Bladder operated robotic joint [NASA-CASE-MFS-28682-1] p 1701 N94-20359
Counter-balanced, multiple cable construction crane [NASA-CASE-LAR-14565-1-CU] p 1822 N94-20369
Model-based automatic generation of grasping regions [NASA-TM-104785] p 1946 N94-21550
END-TO-END DATA SYSTEMS
PROS: An IRAF based system for analysis of x ray data p 1925 N94-22461
ENDOTHERMIC FUELS
Surface science and modeling studies of endothermic fuels catalysis [AD-A272650] p 1712 N94-21192
ENDOTHERMIC REACTIONS
Micrometeorite dynamic pyrometamorphism: Observation of a thermal gradient in iron-nickel sulfide p 2083 N94-20716
Surface science and modeling studies of endothermic fuels catalysis [AD-A272850] p 1712 N94-21192
ENERGETIC PARTICLES
Fast ion behavior during neutral beam injection in ATF [DE93-040267] p 1992 N94-20058
ENERGY ABSORPTION
Magnetic circular dichroism in x ray absorption and core-level photoemission [DE93-019381] p 1688 N94-19986
Fluid absorption solar energy receiver [NASA-CR-194688] p 1846 N94-20229
Ocular damage induced by ultrashort laser pulses [AD-A271859] p 1890 N94-20462
Infrared FEL photochemistry: Multiple-photon dissociation of freon gas [DE94-000817] p 1820 N94-22585
ENERGY BUDGETS
Measurement of evapotranspiration with combined reflective and thermal infrared radiance observations [NASA-CR-194802] p 1837 N94-20951
Role of surface characteristics in urban meteorology and air quality [DE93-040929] p 1851 N94-21740
ENERGY CONSERVATION
Biofuels: Project summaries [DE93-010003] p 1712 N94-19984
Alternative refrigerants and refrigeration cycles for domestic refrigerators [DE93-040481] p 1714 N94-20099
Technology to prevent greenhouse effect gases [DE94-707420] p 1851 N94-20116
The energy performance of prototype holographic glazings [DE93-040451] p 1809 N94-21545
Advanced Energy Projects, FY 1993 [DE94-000539] p 1847 N94-21755
The FY1992 survey on multi-purpose dam and energy utilization system by the wind power generation eration [DE94-707408] p 1848 N94-22012
Present status of developing petroleum-substituting energy (EC) [DE94-707494] p 1849 N94-22030
Study on possibility of developing energy integration technology [DE94-714903] p 1849 N94-22052
Current situation in developing petroleum substituting energy (the United Kingdom) [DE94-714897] p 1713 N94-22091
ENERGY CONSUMPTION
Survey on chemical engineering technologies for the global environmental protection [DE94-714887] p 1852 N94-22044
Silicon microelectronic field-emissive devices for advanced display technology [DE94-000397] p 1794 N94-22380
ENERGY CONVERSION
Technology to prevent greenhouse effect gases [DE94-707420] p 1851 N94-20116
In-situ electrochemical surface science [AD-A265942] p 1680 N94-20330
Advanced Energy Projects, FY 1993 [DE94-000539] p 1847 N94-21755
Current situation of development of petroleum substituting energies (USA) [DE94-707492] p 1848 N94-22013
Study on possibility of developing energy integration technology [DE94-714903] p 1849 N94-22052
ENERGY CONVERSION EFFICIENCY
Development of high-efficiency CdTe solar cells [DE93-018206] p 1845 N94-19925
Generation of intense ultrashort x ray pulses [DE93-019607] p 1817 N94-21299
Effects of stimulated Raman scattering on light beam properties during high-power laser beam long-path propagation [AD-A273109] p 1818 N94-21509
Electromechanical battery research and development at the Lawrence Livermore National Laboratory [DE93-019159] p 1762 N94-21620
Thin-film CdTe and CuInSe2 photovoltaic technologies [DE93-018217] p 1848 N94-21827
Investigation on the chemically fixing technique of carbon dioxide utilizing solar energy [DE94-714886] p 1849 N94-22043
ENERGY DISSIPATION
Fluid absorption solar energy receiver [NASA-CR-194688] p 1846 N94-20229
Mixed voltage VLSI design p 1756 N94-21104
A thermodynamic analysis of propagating subcritical cracks with cohesive zones p 1834 N94-22611
ENERGY DISTRIBUTION
Ab initio potential energy surface for the H + OCS reaction [AD-A270577] p 1698 N94-19947
ENERGY GAPS (SOLID STATE)
Variable angle of incidence spectroscopic ellipsometric measurement of the Franz-Keldysh effect in MODFET structures p 2021 N94-20987
Spin-polaron theory of high-T(c) superconductivity. 3: Gap function and critical temperature [DE93-019198] p 2030 N94-21831
ENERGY LEVELS
Electron reactions in nonpolar liquids: Pressure effects [DE93-040328] p 1970 N94-19931
Microscopic origins of metastable effects in a-Si:H and deep defect characterization in a-Si,Ge:H alloys [DE93-018205] p 1688 N94-19985
ENERGY OF FORMATION
The Manson impact crater: Estimation of the energy of formation, possible size of the impacting asteroid or comet, and ejecta volume and mass p 2083 N94-20721
ENERGY POLICY
Biofuels: Project summaries [DE93-010003] p 1712 N94-19984
Technology to prevent greenhouse effect gases [DE94-707420] p 1851 N94-20116
Research in progress: FY 1992 [DE94-000410] p 1836 N94-20936
Present status of developing petroleum-substituting energy (EC) [DE94-707494] p 1849 N94-22030
Current situation in developing petroleum substituting energy (the United Kingdom) [DE94-714897] p 1713 N94-22091
ENERGY SOURCES
Biofuels: Project summaries [DE93-010003] p 1712 N94-19984
ENERGY SPECTRA
Energy gain spectroscopic study of Ar(q+)-Ar collisions at 40 qeV [DE93-040284] p 1970 N94-19871
Fast ion behavior during neutral beam injection in ATF [DE93-040267] p 1992 N94-20058

Characterization of electromagnetic fields in an extended chamber at the Short Pulse Experimental Electron Device (SPEED) simulator
[AD-A265955] p 1717 N94-20329
CERN-derived analysis of lunar radiation backgrounds
p 2080 N94-20880
Evaluation of the chemical composition of cosmic radiation in energy area of 10(exp 15) eV
[ETN-93-93682] p 2150 N94-21056
Comparison of higher order moment spectrum estimation techniques
[AD-A272967] p 1967 N94-21260
Semiconductors A(III)B(VI): Translation
[AD-A273064] p 2028 N94-21438
Electron emissions in low energy Ar(q+)-Ar collisions
[DE93-040285] p 1974 N94-21543
Electron emission from nanometer-size metallic clusters: Electronic states and structural stability of supported Au clusters
[DE93-040184] p 1975 N94-21786

ENERGY STORAGE
Statement of David E. Baldwin, Associate Director for Energy, Lawrence Livermore National Laboratory and John C. Crawford, Vice President, Sandia National Laboratories, California, to the Subcommittee on Research and Development of the Committee on Environment and Public Works, US Senate, Washington, DC, 22 March 1993
[DE93-017991] p 1844 N94-19803
Energy storage and conversion in solid hydrogen
[AD-A271439] p 1845 N94-20086
Theoretical investigations of metastability and energy storage in molecular systems
[AD-A271849] p 1973 N94-20612
Electromechanical battery research and development at the Lawrence Livermore National Laboratory
[DE93-019159] p 1762 N94-21620
Electromechanical battery research and development at the Lawrence Livermore National Laboratory
[DE94-000391] p 1762 N94-21621
Advanced Energy Projects, FY 1993
[DE94-000539] p 1847 N94-21755
Study on possibility of developing energy integration technology
[DE94-714903] p 1849 N94-22052

ENERGY TECHNOLOGY
Statement of David E. Baldwin, Associate Director for Energy, Lawrence Livermore National Laboratory and John C. Crawford, Vice President, Sandia National Laboratories, California, to the Subcommittee on Research and Development of the Committee on Environment and Public Works, US Senate, Washington, DC, 22 March 1993
[DE93-017991] p 1844 N94-19803
Research in progress: FY 1992
[DE94-000410] p 1836 N94-20936
First Biomass Conference of the Americas: Energy, Environment, Agriculture, and Industry, volume 2
[DE94-000435] p 1847 N94-21562
Proceedings of the 1993 DOE/NREL Hydrogen Program Review
[DE93-018207] p 1847 N94-21616
Advanced Energy Projects, FY 1993
[DE94-000539] p 1847 N94-21755
Proceedings of the Seventh Annual Conference on Fossil Energy Materials
[DE94-001091] p 1848 N94-21823
Current situation of development of petroleum substituting energies (Canada)
[DE94-707493] p 1849 N94-22014
Survey on evaluation of energy technology contributing to preservation of the global environment. 2
[DE94-714884] p 1853 N94-22051
Study on possibility of developing energy integration technology
[DE94-714903] p 1849 N94-22052
Investigations on trends in global environment adaptive industrial technologies
[DE94-714888] p 1853 N94-22258
Environmental protection using social costing
[DE94-000492] p 1853 N94-22569

ENERGY TRANSFER
Modeling failure and reliability in new-generation devices
[AD-A271150] p 1748 N94-19910
Physical chemistry of energetic nitrogen compounds
[AD-A271819] p 1712 N94-20625
Measurement of evapotranspiration with combined reflective and thermal infrared radiance observations
[NASA-CR-194802] p 1837 N94-20951
Establishing the basis for validated predictions of highly non-equilibrium flows (with 9 attachments)
[AD-A272918] p 1802 N94-21220
Studies of the deuteron at high energy and momentum transfer
[DE93-041162] p 1976 N94-21941
Energy release at Alfvenic fronts in solar flares
p 2003 N94-22652

ENGINE DESIGN
Design of a state-space controller for an advanced gas turbine engine
[AD-A270859] p 1647 N94-20042
Cold-start minidiesel engine development
[AD-A271064] p 1823 N94-20567
Advanced transportation system studies, technical area 3. Alternate propulsion subsystem concepts: J-2S restart study
[NASA-CR-193874] p 1670 N94-21271
The 1992 Seals Flow Code Development Workshop
[NASA-CP-10124] p 1654 N94-21790
Navy GTE seal development activity
p 1655 N94-21794
Modeling bristle lift-off in idealized brush seal configurations p 1655 N94-21797
Specialized data analysis for the Space Shuttle Main Engine and diagnostic evaluation of advanced propulsion system components
[NASA-CR-194720] p 1656 N94-21813

ENGINE PARTS
Development of improved processing and evaluation methods for high reliability structural ceramics for advanced heat engine applications, phase 1
[DE93-040528] p 1702 N94-20481
The flow of gas across the piston-segments-cylinder interface
[ECL-92-40] p 1824 N94-20594
The 1992 Seals Flow Code Development Workshop
[NASA-CP-10124] p 1654 N94-21790
Brush seal bristle flexure and hard-rub characteristics
p 1654 N94-21791
Compliant seal development p 1655 N94-21795
Ceramic Technology Project
[DE94-001011] p 1707 N94-21822
Time-dependent reliability analysis of ceramic engine components p 1828 N94-22619

ENGINE TESTS
Powdered aluminum and oxygen rocket propellants: Subscale combustion experiments
[NASA-TM-106439] p 1713 N94-21760
Air Force brush seal programs p 1655 N94-21793

ENGINEERS
Improved approximate formulas for flux from cylindrical and rectangular sources
[DE93-011390] p 1742 N94-22268

ENGINES
Thrust expansion engine
[AD-D015896] p 1669 N94-20121

ENSTATITE
Micrometeorite dynamic pyrometamorphism: Nonstoichiometric clinoenstatite (CLEN)
p 2083 N94-20715
The formation of FeO-rich pyroxene and enstatite in unequilibrated enstatite chondrites: A petrologic-trace element (SIMS) study p 2086 N94-20866

ENTHALPY
On one numerical approach to Stefan problem
[IPPCZ-330] p 1996 N94-21572

ENTRAINMENT
An analysis of pool surface deformation due to a plunging liquid jet
[AD-A272970] p 1802 N94-21261
Breaking Kelvin-Helmholtz waves and cloud-top entrainment as revealed by K-band Doppler radar
p 1874 N94-22310

ENTROPY
Image detection using edge extraction algorithms
[AD-A272439] p 1911 N94-21203
A thermodynamic theory of dynamic fragmentation
[DE93-019066] p 1833 N94-21916
DECONV-TOOL: An IDL based deconvolution software package p 1927 N94-22542
The relaxed state and entropy production due to the electric resistivity and viscosity of plasma
p 2010 N94-22696

ENVIRONMENT EFFECTS
Health effects of global warming: Problems in assessment
[DE93-040323] p 1850 N94-19930
Technology to prevent greenhouse effect gases
[DE94-707421] p 1850 N94-19976
ELF communications system ecological monitoring program
[AD-A272507] p 1740 N94-21412
First Biomass Conference of the Americas: Energy, Environment, Agriculture, and Industry, volume 2
[DE94-000435] p 1847 N94-21562
Modeling the response of ecosystems to CO2 and climate change
[DE94-000748] p 1852 N94-21787

ENVIRONMENT MANAGEMENT
EDMS microcomputer pollution model for civilian airports and Air Forces bases: User's guide, supplement A
[AD-A271596] p 1851 N94-20948
Present status of developing petroleum-substituting energy (EC)
[DE94-707494] p 1849 N94-22030
Current situation in developing petroleum substituting energy (the United Kingdom)
[DE94-714897] p 1713 N94-22091
Implementation of a laboratory information management system for environmental regulatory analyses
[DE94-001198] p 2046 N94-22407

ENVIRONMENT MODELS
EDMS microcomputer pollution model for civilian airports and Air Forces bases: User's guide, supplement A
[AD-A271596] p 1851 N94-20948

ENVIRONMENT PROTECTION
Current status of environmental, health, and safety issues of nickel metal-hydride batteries for electric vehicles
[DE93-017079] p 1748 N94-19902
Parameters affecting hydrogen chloride measurements
[AD-A271326] p 1851 N94-20025
Alternative refrigerants and refrigeration cycles for domestic refrigerators
[DE93-040481] p 1714 N94-20099
Technology to prevent greenhouse effect gases
[DE94-707420] p 1851 N94-20116
Durability of thermal control and environmental protective materials for the SSRMS in simulated LEO environment p 1663 N94-21392
Present status of developing petroleum-substituting energy (EC)
[DE94-707494] p 1849 N94-22030
Survey on chemical engineering technologies for the global environmental protection
[DE94-714887] p 1852 N94-22044
Environmental protection using social costing
[DE94-000492] p 1853 N94-22569

ENVIRONMENT SIMULATION
Apparatus and method for measuring subject work rate on an exercise device
[NASA-CASE-MSC-21752-1] p 1895 N94-20194

ENVIRONMENT SIMULATORS
Complex-2: Low Earth orbital environment simulation facility for materials durability evaluation
p 1653 N94-21370

ENVIRONMENTAL ENGINEERING
Investigation on construction of the database system for research and development of the global environment industry technology
[DE94-714890] p 1853 N94-22090
Survey on utilization of database for research and development of global environmental industry technology
[DE94-714891] p 1853 N94-22259

ENVIRONMENTAL MONITORING
Research in progress: FY 1992
[DE94-000410] p 1836 N94-20936
The 7th Brazilian Remote Sensing Symposium, volume4 p 1840 N94-20965
SIMA: An integrated environmental monitoring system
p 1840 N94-20967
Low-cost, dual-use platforms for environmental sensing, phase 1
[AD-A272951] p 1646 N94-21246
Long-Term Monitoring of Global Climate Forcings and Feedbacks
[NASA-CP-3234] p 1868 N94-21639
Monitoring issues from a modeling perspective
p 1868 N94-21640
Climate forcings and feedbacks p 1869 N94-21641
Accuracy requirements --- for monitoring of climate changes p 1869 N94-21642
Climsat rationale p 1869 N94-21643
Michelson Interferometer (MINT)
p 1813 N94-21646
Orbit and sampling requirements: TRMM experience
p 1870 N94-21647
Satellite orbit and data sampling requirements
p 1870 N94-21648
Implementation of a laboratory information management system for environmental regulatory analyses
[DE94-001198] p 2046 N94-22407

ENVIRONMENTAL QUALITY
Technology to prevent greenhouse effect gases
[DE94-707420] p 1851 N94-20116
SIMA: An integrated environmental monitoring system
p 1840 N94-20967

ENVIRONMENTAL SURVEYS
Ground wave emergency network. Final operational capability. Environmental assessment for south central Montana relay node, site no. RN8C925MT
[AD-A267795] p 1716 N94-19964
Interpretation of Ground Penetrating Radar data at the Hanford Site, Richland, Washington
[DE93-040409] p 1743 N94-22557

ENVIRONMENTAL TESTS
Proton radiation testing of an 18 bit A/D converter p 1755 N94-21096
Fifth International Symposium on Materials in a Space Environment
[ISBN-2-85-428293-0] p 1659 N94-21367
Complex-2: Low Earth orbital environment simulation facility for materials durability evaluation p 1653 N94-21370
Space environmental effects on polymer matrix composites: The UTIAS/LDEF experiment p 1660 N94-21373
Aragatz project samples experiment/MAPOL (polymer materials) experiment: Postflight expert evaluation p 1660 N94-21376
The implications of the LDEF results on Space Station Freedom power system materials p 1660 N94-21377
Effect of geostationary environment constituents on secondary electron emission rates p 1661 N94-21382
Simulated space environmental effects on some experimental high performance polymers p 1662 N94-21385
Fast oxygen atom studies related to low Earth orbit activities p 1663 N94-21395

ENZYMES
Immunocytochemical localization of glutamic acid decarboxylase (GAD) and substance P in neural areas mediating motion-induced emesis: Effects of vagal stimulation on GAD immunoreactivity p 1887 N94-21909

EPIDERMIS
Physiologically based pharmacokinetic modelling of percutaneously absorbed dibromomethane utilizing multiple dermal sub-compartments
[AD-A271106] p 1889 N94-19981

EPITAXY
High efficiency epitaxial optical reflector solar cells
[DE93-017115] p 1845 N94-19805
Theory of energy-assisted epitaxy; theory of ordered semiconductor alloys: In(1-x)Ti(x)Sb as a long-wave infrared material
[AD-A271007] p 2012 N94-19835
Common Themes and Mechanisms of Epitaxial Growth, volume 312 — Materials Research Society symposium proceedings
[AD-A270513] p 2013 N94-19967
ALE project
[AD-A271080] p 2014 N94-19980
Process for the homoepitaxial growth of single-crystal silicon carbide films on silicon carbide wafers
[NASA-CASE-LEW-15223-1] p 2017 N94-20381
Transport in microstructures in the microwave and millimeter-wave regime
[AD-A271875] p 2017 N94-20470
Investigation of heterojunctions and multiple quantum well structures using crystalline organic semiconductors
[AD-A272113] p 2018 N94-20569
Direct imaging of the surface microstructure of dielectric materials using an atomic force microscope
[AD-A272251] p 2018 N94-20575
Growth, characterization and device development in monocrystalline diamond films
[AD-A272715] p 2026 N94-21190
Structure and morphology of Pd overlayers on epitaxial SnO2 films studies with the atomic force microscope
[AD-A271827] p 2028 N94-21458
Growth, characterization and device development in monocrystalline diamond films
[AD-A273097] p 2028 N94-21506
Transmission electron microscopy study of thick copper-304 stainless steel multilayers
[DE94-001045] p 1696 N94-22394

EPOXY MATRIX COMPOSITES
Biaxial flexural testing of a carbon fiber reinforced epoxy composite
[AD-A271956] p 1674 N94-20577
Fiber reinforced thermosetting resin composition with coated fibers for improved toughness
[CA-PATENT-1,306,320] p 1674 N94-21040

EPOXY RESINS
Biaxial flexural testing of a carbon fiber reinforced epoxy composite
[AD-A271956] p 1674 N94-20577
Thermal stability relationships between PMR-15 resin and its composites
[NASA-TM-106285] p 1675 N94-21488
Tensile and shear fracture behavior of fiber reinforced plastics at 77K irradiated by various radiation sources
[DE93-040280] p 1706 N94-21542
Tensile strength of fiber reinforced plastics at 77K irradiated by various radiation sources
[DE93-040826] p 1709 N94-22008

EQUATIONS OF MOTION
Rockets: Physical science teacher's guide with activities
[NASA-EP-291] p 1669 N94-20226
Microscopic and macroscopic dynamics
[DE93-019576] p 1937 N94-22042

EQUATIONS OF STATE
Further examinations on the thermodynamic stability of the Mie-Grueneisen equation of state
[AD-A270526] p 2037 N94-19631
An equation of state for shock in homogeneous materials and comparison to shock data
[AD-A271436] p 1829 N94-19881
CTH: A software family for multi-dimensional shock physics analysis
[DE93-019428] p 1904 N94-20052
SPH modelling of energy partitioning during impacts on Venus p 2124 N94-20809
Multilevel methods for transport equations in diffusive regimes p 1955 N94-21467
Shock compression of low-density foams
[DE93-040545] p 1707 N94-21546

EQUATORIAL REGIONS
Volcanic rises on Venus: Geology, formation, and sequence of evolution p 2113 N94-20755
The effects of magnetic storm phases on F-layer irregularities from auroral to equatorial latitudes
[AD-A272685] p 1857 N94-21189

EQUILIBRIUM FLOW
Cavitation modelling p 1668 N94-20079

EQUIVALENCE
The accuracy-through-order and the equivalence properties in the algebraic approximant
[DE93-040188] p 1960 N94-21946

EQUIVALENT CIRCUITS
A comprehensive theoretical and experimental study of coplanar waveguide shunt stubs p 1733 N94-20500
A theoretical and experimental study of coplanar waveguide shunt stubs p 1733 N94-20502

ERBIUM
Resonantly pumped, erbium-doped, GSGG, 2.8 micron, solid state laser with energy recycling and high slope efficiency
[AD-D015920] p 1815 N94-20060

EROSION
On magnetodynamic effects initiated by a high-speed impact of a large cosmic body upon the Earth's surface p 2082 N94-20647
Geologic mapping of Harmakhis and Reull Valles region, Mars: Evidence for multiple resurfacing and drainage events p 1844 N94-20705
Mars: New evidence for origin of some Valles Marineris layered deposits p 2112 N94-20748
Parabolic features and the erosion rate on Venus p 2122 N94-20801
Numerical modeling of impact erosion of atmospheres: Preliminary results p 2131 N94-20847
Early Mars: A regional assessment of denudation chronology p 2145 N94-21676
Performance of carbon-based hot frit substrates
[DE94-000509] p 1676 N94-21754

ERROR ANALYSIS
Comparison of a distributed Kalman filter versus a centralized Kalman filter with fault detection considerations
[AD-A270713] p 1903 N94-19969
Some VTOL head-up display drive-law problems and solutions
[NASA-TM-104027] p 1635 N94-20035
Techniques for reducing error in the calorimetric measurement of low wattage items
[DE93-018472] p 1807 N94-20114
Threshold computation and cryptographic security
[TR-443] p 1907 N94-20536
A retrieval error analysis technique for passive infrared atmospheric sounders
[AD-A272618] p 1867 N94-21212
Two visually meaningful correlation measures for comparing calculated and measured response histories
[AD-A273044] p 1964 N94-21322
Links between N-modular redundancy and the theory of error-correcting codes p 1765 N94-21713
A methodology for quantifying uncertainty in models
[DE93-040154] p 1916 N94-21747
Stochastic simulation for imaging spatial uncertainty: Comparison and evaluation of available algorithms
[DE93-040058] p 1916 N94-21761
Application guide for universal source encoding for space
[NASA-TP-3441] p 1741 N94-21783
MLS signal-in-space category 3 landing hazard analysis p 1644 N94-22134
Application of scattering by arrays of cylinders to MLS signal propagation error estimation p 1644 N94-22135

ERROR CORRECTING CODES
Links between N-modular redundancy and the theory of error-correcting codes p 1765 N94-21713
VLSI design of a bit serial parallel processing 4 extender chip for M-path convolutional decoding p 1775 N94-22132
The Schur Berlekamp-Massey algorithm is parallelizable p 1784 N94-22191
Some best rate 1/p and rate (p-1)/p systematic quasi-cyclic codes over GF(3) and GF(4) p 1792 N94-22243
On the capacity of (T,U) permutation decoding method p 1792 N94-22245

ERROR CORRECTING DEVICES
Micro-rollback and self-recovery synthesis p 1765 N94-21707
A new class of multi-function two-rail totally self-checking basic building blocks p 1788 N94-22215

ERROR DETECTION CODES
Space qualified high speed Reed Solomon encoder p 1754 N94-21088
The Schur Berlekamp-Massey algorithm is parallelizable p 1784 N94-22191
ARQ on fading channels p 1747 N94-22242

ERROR SIGNALS
Tunable laser frequency stabilizing system
[AD-D015904] p 1815 N94-20055
Silicon retina for optical tracking systems p 1755 N94-21098

ERRORS
Literature review of the errors-in-variables approach to the problem of system identification
[AD-A271098] p 1949 N94-19907
Feedback controlled optics with wavefront compensation
[NASA-CASE-NPO-18194-1-CU] p 1985 N94-20305
Snow cover measurements and areal assessment of precipitation and soil moisture
[WMO-749] p 1841 N94-21068
Two visually meaningful correlation measures for comparing calculated and measured response histories
[AD-A273044] p 1964 N94-21322
Toward a new method of decoding algebraic codes using Groebner bases
[AD-A273089] p 1959 N94-21524
Schematic driven layout of Reed Solomon encoders p 1766 N94-21722
Influence of geoid model uncertainty on the determination of ocean circulation with satellite altimetry
[PB93-219301] p 1842 N94-22097
Time-dependent grid adaptation for meshes of triangles and tetrahedra p 1920 N94-22369
Intervention strategies for the management of human error
[NASA-CR-4547] p 1642 N94-22373
HST PSF simulation using Tiny Tim p 1926 N94-22498

ERS-1 (ESA SATELLITE)
Offshore decision support system: ERS-1 pilot project WAVEWATCH
[BCRS-92-09] p 1865 N94-20532

ESCAPE VELOCITY
Volatile loss from accreting icy protoplanets p 2084 N94-20793
Variety in planetary systems p 2086 N94-20871

ESCARPMENTS
Cryoplanation terraces of interior and western Alaska p 2091 N94-20396
Geologic mapping of Harmakhis and Reull Valles region, Mars: Evidence for multiple resurfacing and drainage events p 1844 N94-20705
Ridge belt-related scarps and troughs: Compressional crustal bending on Venus p 2106 N94-20711
Comparison of flank modification on Ascraeus and Arsia Montes volcanoes, Mars p 2140 N94-20903

ESTIMATES
Parameter estimation with cost function of second order in output-error-problem
[DLR-FB-92-38] p 1964 N94-21139
Experiments with recursive estimation in astronomical image processing p 2047 N94-22457

ESTIMATING
An investigation into the integration of meter-level range and millimeter-level phase data using a multimode stimulation for optimal filter estimation software package
[AD-A267955] p 1751 N94-20483
The Manson impact crater: Estimation of the energy of formation, possible size of the impacting asteroid or comet, and ejecta volume and mass p 2083 N94-20721
On estimation and testing in Poisson regression models with over-dispersion
[MEMO-1083] p 1963 N94-21076
Estimability of polar motion using range observations to satellites
[PB93-219319] p 1842 N94-22265

ETALONS
Multiorder etalon sounder (MOES) development and test for balloon experiment
[NASA-CR-194730] p 1859 N94-22026
ETCHING
Substrate recovery of Mo-Si multilayer coated optics
[DE93-019610] p 1698 N94-19810
Process for the homoepitaxial growth of single-crystal silicon carbide films on silicon carbide wafers
[NASA-CASE-LEW-15223-1] p 2017 N94-20381
Method for anisotropic etching in the manufacture of semiconductor devices
[NASA-CASE-MSC-21631-1] p 1993 N94-20491
A long-term change of the AR/KR/XE fractionation in the solar corpuscular radiation p 2136 N94-20875
Particle behavior in an ECR plasma etch tool
[DE93-040343] p 1996 N94-21769
Micromachined actuator and sensor capabilities at the Microelectronics Development Laboratory
[DE93-019417] p 1769 N94-21918
ETHERS
Column chromatographic separation of Y(3+) from Sr(2+) by polymeric ionizable crown ether resins
[DE94-000935] p 1683 N94-22021
ETHYL ALCOHOL
Fuel processing requirements and techniques for fuel cell propulsion power
[DE93-019516] p 1750 N94-20257
Water-enhanced solvation of organics
[DE93-040297] p 1683 N94-21947
ETHYL COMPOUNDS
The 13C-NMR spectra of poly (4-((2-(acryloyloxy) ethyl) ethyl amino)- 4-nitroazobenzene-co-methyl methacrylate)
[AD-A273016] p 1705 N94-21238
Stress-induced cracking of fluorocarbon rubber MTL-0002 after exposure to DS-2
[AD-A271753] p 1705 N94-21302
ETHYLENE
Investigation on the chemically fixing technique of carbon dioxide utilizing solar energy
[DE94-714886] p 1849 N94-22043
EUCLIDEAN GEOMETRY
Representation and recognition with algebraic invariants and geometric constraint models
[AD-A271395] p 1949 N94-19838
Determining the distance to the perfect matching polytope of a bipartite graph
[RR-895-M] p 1950 N94-20161
Simulating the Euclidean time Schroedinger equations using an INTEL iPSC/860 hypercube: Application to the t-J model of high-T(sub c) superconductivity
[DE94-000489] p 2035 N94-22385
EULER EQUATIONS OF MOTION
Distributed loss model: Application to a spatial turbopump inducer p 1668 N94-20078
Three dimensional unsteady flow calculations in radial components p 1669 N94-20080
Shape optimization governed by the Euler equations using an adjoint method
[NASA-CR-191555] p 1950 N94-20092
Looking for O(N) Navier-Stokes solutions on non-structured meshes p 1806 N94-21471
The block adaptive multigrid method applied to the solution of the Euler equations p 1641 N94-21472
A multigrid method for steady Euler equations on unstructured adaptive grids p 1957 N94-21476
Unstructured multigrid through agglomeration p 1958 N94-21484
Multigrid properties of upwind-biased data reconstructions p 1806 N94-21485
EUROPA
Photogeological analysis of Europan tectonic features p 2129 N94-20838
EUROPE
Rapid estimates of crop production using remote sensing: European experience p 1840 N94-20969
Present status of developing petroleum-substituting energy (EC)
[DE94-707494] p 1849 N94-22030
EUROPEAN SPACE AGENCY
Power standard
[ESA-PSS-02-10-VOL-1-ISSUE-] p 1669 N94-20241
EVALUATION
Evaluation of plasma-deposited protective coatings for spacecraft applications p 1663 N94-21394
EVAPORATION
Method for controlling protein crystallization
[NASA-CASE-MFS-28688-1] p 2017 N94-20528
Evaporation in equilibrium, in vacuum, and in hydrogen gas p 1684 N94-20638
Diffusion-controlled magnesium isotopic fractionation of a single crystal forsterite evaporated from the solid state p 1686 N94-20855
Liquid-phase circulation and mixing in multicomponent droplets vaporizing in a laminar convective environment
[AD-A272851] p 1802 N94-21193
Modeling of outgassing and matrix decomposition in carbon-phenolic composites
[NASA-CR-194741] p 1676 N94-21743
EVAPORATION RATE
Liquid-phase circulation and mixing in multicomponent droplets vaporizing in a laminar convective environment
[AD-A272851] p 1802 N94-21193
EVAPOTRANSPIRATION
Measurement of evapotranspiration with combined reflective and thermal infrared radiance observations
[NASA-CR-194802] p 1837 N94-20951
EXCIMER LASERS
Laser amplifier developments at Mercury
[DE93-040103] p 1814 N94-19867
EXCIMERS
Lateral distribution of lipids in membranes at high pressure
[AD-A271183] p 1700 N94-20299
EXCITATION
Optical fiber sensor having an active core
[NASA-CASE-LAR-14607-1-SB] p 1986 N94-20586
Derivation of a model of the exciter of a brushless synchronous machine
[EUT-92-E-258] p 1761 N94-21538
Electron emissions in low energy Ar(q+)-Ar collisions
[DE93-040285] p 1974 N94-21543
EXCITONS
Effect of exciton localization and delocalization on magnetic-field-dependent photoluminescence linewidths in semiconductors
[DE93-018860] p 1748 N94-19884
Investigation of heterojunctions and multiple quantum well structures using crystalline organic semiconductors
[AD-A272113] p 2018 N94-20569
GaAs/AlGaAs superlattice characterization by variable angle spectroscopic ellipsometry p 2022 N94-20994
Dephasing processes in III-V semiconductors
[AD-A271677] p 2028 N94-21362
EXCLUSION
Fast mutual exclusion, even with contention
[AD-A272947] p 1912 N94-21227
EXERCISE PHYSIOLOGY
Maximum team lifting capacity as a function of team size
[AD-A271642] p 1892 N94-21036
EXHAUST EMISSION
Advanced Turbine Systems (ATS). Phase 1: System scoping and feasibility studies
[DE93-041130] p 1826 N94-21938
Survey on evaluation of energy technology contributing to preservation of the global environment. 2
[DE94-714884] p 1853 N94-22051
Experimental evaluation of oxygen-enriched air and emulsified fuels in a six-cylinder diesel engine
[DE94-000907] p 1811 N94-22391
EXHAUST GASES
Dual-beam multiple wavelength light transmittance measurement for particle sizing in rocket motor plumes
[AD-A272491] p 1670 N94-21208
Survey on evaluation of energy technology contributing to preservation of the global environment. 2
[DE94-714884] p 1853 N94-22051
EXHAUST VELOCITY
Powdered aluminum and oxygen rocket propellants: Subscale combustion experiments
[NASA-TM-106439] p 1713 N94-21760
EXOBIOLOGY
Aerospace medicine and biology: A continuing bibliography with indexes (supplement 383)
[NASA-SP-7011(383)] p 1892 N94-21288
EXOSAT SATELLITE
The EXOSAT operational experience
[ESA-STM-248] p 1657 N94-20235
The EXOSAT database and archive p 2048 N94-22521
EXOTHERMIC REACTIONS
Shock wave interactions with exothermic mixtures
[AD-A271149] p 1829 N94-19836
Chemistry of the burning surface
[AD-A272725] p 1681 N94-21181
EXPERIMENT DESIGN
German space experiments on Spacelab D-2 and Eureca-1 to investigate atomic oxygen interaction with materials p 1662 N94-21390
EXPERT SYSTEMS
An expert system executive for automated assembly of large space truss structures
[NASA-TM-4487] p 1939 N94-20089
Explainable expert systems: A research program in information processing
[NASA-CR-193422] p 2041 N94-20133
An expert system shell for inferring vegetation characteristics
[NASA-CR-189318] p 1837 N94-20284
The Seventh International Symposium on Methodologies for Intelligent Systems (Poster Session)
[AD-A272125] p 1942 N94-20573
Design of a computer assisted tool for object oriented acquisition, modeling and simulation of knowledge structure
[ETN-93-94183] p 1910 N94-21152
Lecture notes in artificial intelligence 689: The 7th International Symposium on Methodologies for Intelligent Symposium (ISMIS 1993)
[AD-A271768] p 1944 N94-21162
Intelligent processing of ferroelectric thin films
[AD-A272518] p 1705 N94-21416
Experiments in knowledge refinement for a large rule-based system
[AD-A272055] p 1809 N94-21445
Reducing the cognitive workload: Trouble managing power systems
[NASA-TM-106413] p 1714 N94-21564
Design and implementation of a status at a glance user interface for a power distribution expert system
[NASA-TM-106412] p 1715 N94-21589
The program system for the diagnostics of strains and fracture prediction of solids p 1836 N94-22065
An expert system of econometric analysis p 2052 N94-22081
EXPLORER 2 SATELLITE
Dynamics Explorer 2: Continued FPI and NACS instrument data analysis and associated scientific activity at the University of Michigan
[NASA-CR-194689] p 1657 N94-20173
EXPLOSIONS
Effects of hydrodynamics and thermal radiation in the atmosphere after comet impacts p 1862 N94-20649
EXPOSURE
Studies of neural and cognitive function in subjects exposed to the marine-air interface, phases 1 and 2
[AD-A272282] p 1891 N94-20624
Development and demonstration of a personal monitoring system for exposure to hydrogen fluoride
[DE93-041273] p 1891 N94-20935
U.S. Tag for ISO/TC 43, acoustics, IEC/TC 29 electroacoustics, and ISO/TC 108/SC4 human exposure to mechanical vibration and shock: Minutes of the accredited standards committee on bioacoustics, S3
[AD-A273014] p 1897 N94-21309
EXPULSION
Pressurization and expulsion of a flightweight liquid hydrogen tank
[NASA-TM-106427] p 1799 N94-20177
EXTERNAL COMBUSTION ENGINES
Heat regenerative external combustion engine
[AD-D015965] p 1824 N94-21274
EXTRACTION
Control and readout of the extraction septum of AmPS
[DIGEL-1993-2] p 1979 N94-20117
Observation of reflected waves on the SABRE positive polarity inductive adder MITL
[DE93-019413] p 1980 N94-20295
One- and multi-component theories of mixtures
[DE93-040543] p 1966 N94-21511
EXTRATERRESTRIAL ENVIRONMENTS
Evaluation of plasma-deposited protective coatings for spacecraft applications p 1663 N94-21394
EXTRATERRESTRIAL MATTER
The sand bag model of the dispersion of the cosmic body in the atmosphere p 2084 N94-20823
EXTRATERRESTRIAL RADIATION
Spaceflight Radiation Health program at the Lyndon B. Johnson Space Center
[NASA-TM-104782] p 1893 N94-21863
Jets associated with active galactic nuclei p 2000 N94-22631
EXTRAVEHICULAR ACTIVITY
Loads produced by a suited subject performing tool tasks without the use of foot restraints
[NASA-TP-3424] p 1896 N94-20606
EVA tools and equipment reference book
[NASA-TM-109350] p 1897 N94-21812
EXTREME ULTRAVIOLET EXPLORER SATELLITE
The EUVE proposal database and scheduling system p 2047 N94-22459
The extreme ultraviolet explorer archive p 2047 N94-22468
Quality control of EUVE databases p 2047 N94-22490
EXTREME ULTRAVIOLET RADIATION
X ray, extreme and far ultraviolet optical thin films for space applications
[NASA-CR-194635] p 1984 N94-20128
ROSAT data analysis with EXSAS p 2080 N94-22555
A comparison of a simple model of EUV dayglow with Viking data
[ISBN-0-315-83258-4] p 1861 N94-22574

EXTREMELY HIGH FREQUENCIES
Mobile antenna development at JPL
p 1731 N94-20457
A compact, portable EHF/SHF antenna for advanced SCAMP
[AD-A272614] p 1739 N94-21211
Characterization and modelling of extremely high frequency enclosures p 1782 N94-22177

EXTREMELY LOW RADIO FREQUENCIES
ELF communications system ecological monitoring program
[AD-A272507] p 1740 N94-21412

EXTRUDING
The mechanical property data base from an Air Force/industry cooperative test program on advanced aluminum alloys: 2091 sheet, plate, and 8090 extrusion
[AD-A273091] p 1692 N94-21525
Evaluation of the fabricability of advanced iron aluminide-clad austenitic stainless steel tubing
[DE93-040598] p 1693 N94-21771
Alloying effects on mechanical and metallurgical properties of NiAl
[DE93-040814] p 1694 N94-21948

EYE (ANATOMY)
Analysis of health status from preliminary physical examination of flight academy applicants
[AD-A267759] p 1889 N94-19962
Ocular damage induced by ultrashort laser pulses
[AD-A271859] p 1890 N94-20462

EYE MOVEMENTS
Techniques used for the analysis of oculometer eye-scanning data obtained from an air traffic control display
[NASA-CR-191559] p 1643 N94-21629

F

F REGION
The effects of magnetic storm phases on F-layer irregularities from auroral to equatorial latitudes
[AD-A272685] p 1857 N94-21189

F-18 AIRCRAFT
Development and operation of the F/A-18 model control surface actuators
[AD-A271330] p 1645 N94-19914

FABRICATION
Process to fabricate thick coplanar microwave electrode structures
[AD-D015913] p 1748 N94-19892
Fabrication of stable large-area thin-film CdTe photovoltaic modules
[DE93-018204] p 1845 N94-20095
Improved ceramic slip casting technique --- application to aircraft model fabrication
[NASA-CASE-LAR-14471-1] p 1702 N94-20377
Mold bolt and means for achieving close tolerances between bolts and bolt holes
[NASA-CASE-MFS-28720-1] p 1823 N94-20379
Engineering design, fabrication, installation, operation, and maintenance services in support of research on laser plasma physics
[AD-A272249] p 1994 N94-20943
Long range fast tool servo
[AD-A271614] p 1761 N94-21257
Design, fabrication and test of a vertical attitude takeoff and landing unmanned air vehicle
[AD-A273003] p 1646 N94-21283
Thermostructural material composites for space applications p 1664 N94-21398
Intelligent processing of ferroelectric thin films
[AD-A272518] p 1705 N94-21416
Fabrication of porous ceramics by freeze-casting/freeze-drying
[PB93-202513] p 1705 N94-21425
Materials Science and Engineering
[DE93-040497] p 1675 N94-21530
A novel semiconductor process for optoelectronic applications on silicon substrate p 1988 N94-21595
Advanced processing technology for high-efficiency thin-film CuInSe2 solar cells
[DE93-010045] p 1647 N94-21614
Research on polycrystalline thin-film submodules based on CuInSe2 materials
[DE93-018223] p 2029 N94-21617
Fabrication of amorphous diamond films
[DE94-000404] p 2032 N94-21960
High temperature size selective membranes
[DE93-019865] p 1709 N94-21982
Variable-field permanent magnet dipole
[DE94-000800] p 1820 N94-22020
Fabrication of whisker-toughened alumina tubes
[DE94-001012] p 1677 N94-22022
Silicon micromachined threshold accelerometers
p 1778 N94-22151

FABRY-PEROT INTERFEROMETERS
Remote sounding of tropospheric minor constituents
[NASA-CR-194265] p 1855 N94-20132
Multiorder etalon sounder (MOES) development and test for balloon experiment
[NASA-CR-194730] p 1859 N94-22026
Demodulation of a fiber Fabry-Perot strain rosette using white light interferometry
[ISBN-0-315-83427-7] p 1990 N94-22579
Phase demodulation of interferometric fiber-optic sensors
[ISBN-0-315-83425-0] p 1991 N94-22581

FABRY-PEROT SPECTROMETERS
Spatial distribution of near infrared line radiation in galactic nuclei measured with Fabry-Perot spectrometer FAST
[MPE-239] p 2081 N94-21138

FACE CENTERED CUBIC LATTICES
Crystallographic phase transitions in actinide metals as a function of pressure
[DE93-040138] p 2011 N94-19827
Stability of the face-centered-cubic phase of heavy rare gas solids
[DE93-019949] p 1679 N94-20319
Molecular dynamics modeling of the mechanical behavior of metallic multilayers
[DE93-019947] p 1694 N94-21921
Transmission electron microscopy study of thick copper-304 stainless steel multilayers
[DE94-001045] p 1696 N94-22394

FACTOR ANALYSIS
Factor analysis as a tool for spectral line component separation 21cm emission in the direction of L1780
p 1965 N94-22536

FACTORIZATION
On the numerical stability of quasi-definite systems
[DE93-019404] p 1950 N94-20217

FAILURE
Modeling failure and reliability in new-generation devices
[AD-A271150] p 1748 N94-19910

FAILURE ANALYSIS
The Seventh International Conference on Composite Structures, volume 25, numbers 1-4
[AD-A269961] p 1672 N94-20031
Efficient chip signature checking for diagnosing boundary scan systems
[RR-901-I] p 1749 N94-20166
High current density contacts for photoconductive semiconductor switches
[DE93-018837] p 1750 N94-20312
Interleaved bismaleimide composites
[AD-A272233] p 1674 N94-20574
Biaxial flexural testing of a carbon fiber reinforced epoxy composite
[AD-A271956] p 1674 N94-20577
Advanced failure analysis laboratory equipment networking
[DE93-019070] p 1916 N94-21633
Localization of pellicle-induced open contacts using charge-induced voltage alteration
[DE93-019407] p 1762 N94-21636
Micro-rollback and self-recovery synthesis
p 1765 N94-21707
Design and test of field programmable gate arrays in space applications p 1765 N94-21710
Brush seal bristle flexure and hard-rub characteristics
p 1654 N94-21791
The effect of microstructural evolution on superplasticity in Ni3Si(V, Mo)
[DE93-041320] p 1694 N94-21943
A robust quality control system for GPS navigation and kinematic positioning
[ISBN-0-315-83148-0] p 1644 N94-22427
Computational Methods for Failure Analysis and Life Prediction
[NASA-CP-3230] p 1833 N94-22608
Nonlinear and progressive failure aspects of transport composite fuselage damage tolerance
p 1834 N94-22609
Modeling of failure and response to laminated composites subjected to in-plane loads
p 1834 N94-22612
An overview of computational simulation methods for composite structures failure and life analysis
p 1835 N94-22617
NASA Langley developments in response calculations needed for failure and life prediction
p 1836 N94-22621
Delamination, durability, and damage tolerance of laminated composite materials p 1678 N94-22622

FAILURE MODES
A process for preparing an assembly of an article and a soluble polyimide which resists dimensional change, delamination, and debonding when exposed to changes in temperature
[NASA-CASE-LAR-14763-1] p 1702 N94-20373
A study of the structural stability of an unbalanced sandwich composite configuration
[AD-A272496] p 1675 N94-21431
Magnetic force microscopy/current contrast imaging: A new technique for internal current probing of IC's
[DE93-040754] p 1761 N94-21532
Modeling of failure and response to laminated composites subjected to in-plane loads
p 1834 N94-22612
Recent advances in computational structural reliability analysis methods p 1828 N94-22616

FAINT OBJECT CAMERA
Restoration of HST images with missing data
p 2057 N94-22439

FALSE ALARMS
Asymptotics of the GLRT for the disorder problem in diffusion processes
[INRIA-RR-1735] p 1951 N94-20227
Army aircraft fire-detection systems operation and reliability
[AD-A271327] p 1641 N94-20912
CFAR processing for airborne pulse-Doppler radars
p 1745 N94-22142

FAR FIELDS
Radiation of plasma wave wings through an electrodynamic tether satellite system with any sharp angle geometry
[REPT-85] p 1993 N94-20156
Variable-permittivity linear inverse problem for the H(sub z)-polarized case p 1719 N94-20408
An efficient formulation of the coupled finite element-integral equation technique for solving large 3D scattering problems p 1725 N94-20436

FAR INFRARED RADIATION
Advanced far infrared detectors
[DE93-040289] p 1988 N94-21528

FAR ULTRAVIOLET RADIATION
X ray, extreme and far ultraviolet optical thin films for space applications
[NASA-CR-194635] p 1984 N94-20128
National Synchrotron Light Source user's manual: Guide to the VUV and x ray beamlines
[DE93-019564] p 2015 N94-20260

FARADAY EFFECT
A new innovative instrument for space plasma instrumentation
[NASA-CR-194736] p 1666 N94-21780

FARM CROPS
Drought early warning system for crop production
p 1840 N94-20966
Rapid estimates of crop production using remote sensing: European experience p 1840 N94-20969
Using NDVI/AVHRR data for crop monitoring and forecasting in South Italy p 1841 N94-20970

FAST FOURIER TRANSFORMATIONS
SIMBAT theoretical manual
[AD-A271063] p 1882 N94-19979
A comparative study of an ABC and an artificial absorber for truncating finite element meshes
[NASA-CR-194275] p 1716 N94-20160
Wide-bandwidth high-resolution search for extraterrestrial intelligence
[NASA-CR-194724] p 1897 N94-20336
Fast fourier transforms for nonequispaced data
[AD-A272687] p 1954 N94-21164
Continuous-time discretized-space approach to modeling short-pulse propagation and scattering
[PB93-215259] p 1742 N94-22347

FASTENERS
Self locking set screw
[AD-D015969] p 1824 N94-21277
Damage states around fastener holes in thick graphite/epoxy composite laminates
[AD-A272613] p 1675 N94-21504

FATIGUE (MATERIALS)
Aviation safety research at the National Institute for Aviation Research, Wichita State University
[NIAR-93-4] p 1641 N94-20189
Weldalite (tm) 049 (Al 2095-T8): Anisotropy effects at cryogenic conditions
[AD-A272658] p 1691 N94-21188
The 1992 USAF structural integrity program conference
[AD-A272876] p 1635 N94-21194
Applicability and performance benefits of XD (Tradename) titanium aluminides to expendable gas turbine engines
[AD-A272998] p 1648 N94-21268

The mechanical property data base from an Air Force/industry cooperative test program on advanced aluminum alloys: 2091 sheet, plate, and 8090 extrusion
[AD-A273091] p 1692 N94-21525
Benefits of thread rolling process to the stress corrosion cracking and fatigue resistance of high strength fasteners
[DE93-040438] p 1833 N94-22001

FATIGUE LIFE
Finite element mesh generation and analysis of solder joints for fatigue life predictions
[AD-A271329] p 1829 N94-19937
Biaxial flexural testing of a carbon fiber reinforced epoxy composite
[AD-A271956] p 1674 N94-20577
The 1992 USAF structural integrity program conference
[AD-A272876] p 1635 N94-21194
Adhesive bonded joint with improved cyclic fatigue life for alumina-ceramic cylinders and hemispheres: Fourth generation housings
[AD-A273061] p 1831 N94-21310
Columbus PMP Critical Technologies Program: Approach for materials life time prediction
p 1664 N94-21402
Brief summary of the evolution of high-temperature creep-fatigue life prediction models for crack initiation
p 1834 N94-22613
A high temperature fatigue life prediction computer code based on the total strain version of StrainRange Partitioning (SRP) p 1835 N94-22620

FATIGUE TESTS
Biaxial flexural testing of a carbon fiber reinforced epoxy composite
[AD-A271956] p 1674 N94-20577
Damage states around fastener holes in thick graphite/epoxy composite laminates
[AD-A272613] p 1675 N94-21504

FAULT DETECTION
Comparison of a distributed Kalman filter versus a centralized Kalman filter with fault detection considerations
[AD-A270713] p 1903 N94-19969
Correct CMOS IC defect models for quality testing
p 1755 N94-21093
Fault detection in digital and analog circuits using an i(DD) temporal analysis technique p 1757 N94-21106
Test pattern generation for ILA sequential circuits
p 1757 N94-21107
Detection of CMOS bridging faults using minimal stuck-at fault test sets p 1757 N94-21110
Model-based reasoning for power system management using KATE and the SSM/PMAD
[NASA-CR-194716] p 1671 N94-21882
A robust quality control system for GPS navigation and kinematic positioning
[ISBN-0-315-83148-0] p 1644 N94-22427

FAULT TOLERANCE
Robust, high-speed network design for large-scale multiprocessing
[AD-A271003] p 1716 N94-19977
Lightweight recoverable virtual memory
[AD-A270576] p 1898 N94-20107
Design considerations for a fiber optic communications network for power systems
[DE93-018404] p 1984 N94-20179
Self-organization via active exploration in robotic applications. Phase 2: Hybrid hardware prototype
[NASA-CR-194723] p 1939 N94-20212
Design methods for fault-tolerant finite state machines
p 1758 N94-21120
Fault tolerant real-time systems
[AD-A272878] p 1899 N94-21195
Real-time fault tolerant computer systems
[AD-A272909] p 1899 N94-21230
Promises and fault-tolerant database access
[TR-447] p 2043 N94-21287
Links between N-modular redundancy and the theory of error-correcting codes p 1765 N94-21713
Model-based reasoning for power system management using KATE and the SSM/PMAD
[NASA-CR-194716] p 1671 N94-21882
A new class of multi-function two-rail totally self-checking basic building blocks p 1788 N94-22215
Fault tolerance for real-time multiprocessor operating systems p 1788 N94-22216
Intervention strategies for the management of human error
[NASA-CR-4547] p 1642 N94-22373
Towards the formal verification of the requirements and design of a processor interface unit: HOL listings
[NASA-CR-191466] p 1937 N94-22414

FEASIBILITY ANALYSIS
Performance evaluation of video on ethernet
[DE93-040696] p 1936 N94-21749
Advanced Turbine Systems (ATS). Phase 1: System scoping and feasibility studies
[DE93-041130] p 1826 N94-21938

FEDERAL BUDGETS
The future of remote sensing from space: Civilian satellite systems and applications
[OTA-ISC-558] p 1837 N94-20209
NASA procurement report, FY 1992
[NASA-TM-109390] p 2040 N94-21623

FEEDBACK
Measurement and computation of the higher order modes of the ALS 500 MHz accelerating cavities
[DE93-019256] p 1980 N94-20292
Teleoperation with virtual force feedback
[DE93-019406] p 1942 N94-20293
Accuracy requirements — for monitoring of climate changes p 1869 N94-21642
Climsat rationale p 1869 N94-21643
A software environment for the exploitation of the MAR image sensor p 1785 N94-22200
General asymmetric neural networks and structure design by genetic algorithms: A learning rule for temporal patterns
[DE94-001254] p 1947 N94-22563

FEEDBACK CONTROL
Feedback controlled optics with wavefront compensation
[NASA-CASE-NPO-18194-1-CU] p 1985 N94-20305
Actively controlled shaft seals for aerospace applications
[NASA-CR-194759] p 1823 N94-20538
Diagnostics and methods for real-time laser microchemistry
[AD-A270871] p 1680 N94-20566
On-board closed-loop congestion control for satellite based packet switching networks
[NASA-TM-106446] p 1656 N94-21581

FEEDFORWARD CONTROL
A comparative robustness evaluation of feedforward neurofilters
[NASA-TM-106440] p 1650 N94-21742

FELDSPARS
Post-igneous redistribution of components in eucrites
p 1685 N94-20684
SCR neon and argon in Kapoeta feldspar: Evidence for an active ancient Sun p 2106 N94-20712
Age and thermochronology of K-feldspars from the Manson impact Structure p 1863 N94-20899
Diffuse reflectance spectra of orthopyroxene, olivine, and plagioclase as a function of composition and structure p 2087 N94-20906

FELSITE
Chronology of lunar granite 12033,576: Resetting of Rb-Sr and K-Ca isochrons p 2115 N94-20763

FEMALES
Female security as a general mobility condition
[ISBN-3-79-831536-1] p 2039 N94-20153

FERMI SURFACES
Fermiology and De Haas-Van Alphen effect of beta-(ET)2IBr2
[DE93-019523] p 2011 N94-19807
Spin dynamics and implications for superconductivity: Some problems with the d-wave scenario
[DE94-001183] p 2032 N94-21972
Positron annihilation study of Sr Doping in La(2-x)Sr(x)CuO4
[DE94-000307] p 2036 N94-22594

FERMIONS
Temperature dependence of 4f PES features and hole occupancy in ytterbium heavy fermions
[DE93-040131] p 1691 N94-20321
F-spin concept and g-bosons in the interceding boson model
[ETN-93-93607] p 1973 N94-21136
Photoemission and the electronic properties of heavy fermions: Limitations of the Kondo model
[DE93-040191] p 1974 N94-21553
Simulating the Euclidean time Schroedinger equations using an INTEL iPSC/860 hypercube: Application to the t-J model of high-T(sub c) superconductivity
[DE94-000489] p 2035 N94-22385

FERROELECTRICITY
A novel method for characterizing the electrical Priorities of lead Zirconate Titanate (PZT) ferroelectric films and memory devices
[AD-A270463] p 2013 N94-19966
Proceedings of the 8th International Symposium on Applications of Ferroelectrics
[AD-A270679] p 1749 N94-20012
Synchrotron x ray diffraction analysis of photorefractive crystals and their gratings
[AD-A271176] p 2015 N94-20213
Intelligent processing of ferroelectric thin films
[AD-A272518] p 1705 N94-21416

FERROMAGNETISM
A microscopic theory of quantum optics and new photon-locked bistable states
[AD-A271250] p 1983 N94-19901

FEYNMAN DIAGRAMS
A formulation of quantum statistical mechanics based on the Feynman path centroid density 1: Equilibrium properties
[AD-A272809] p 2037 N94-21171

FIBER COMPOSITES
The Seventh International Conference on Composite Structures, volume 25, numbers 1-4
[AD-A269961] p 1672 N94-20031
Strengthening of NiAl matrix composites
[AD-A271491] p 1674 N94-20550
Biaxial flexural testing of a carbon fiber reinforced epoxy composite
[AD-A271956] p 1674 N94-20577
Fiber reinforced thermosetting resin composition with coated fibers for improved toughness
[CA-PATENT-1,306,320] p 1674 N94-21040
Probabilistic assessment of composite structures
[NASA-TM-106368] p 1832 N94-21757
Development of BEM for ceramic composites
[NASA-CR-194718] p 1676 N94-21777
An embedded fibre optic for damage growth monitoring in Kevlar composites
[ISBN-0-315-83501-X] p 1677 N94-22586

FIBER OPTICS
Optical signal processing
[AD-A271036] p 1983 N94-20013
Fiber optic Michelson sensor and arrays with passive elimination of polarization fading and source feedback isolation
[AD-D015944] p 1984 N94-20065
Thermal dilation fiber optical flow sensor
[AD-D015926] p 1797 N94-20094
Design considerations for a fiber optic communications network for power systems
[DE93-018404] p 1984 N94-20179
Optically controlled current filamentation in GaAs photoconductive semiconductor switches
[DE93-019427] p 2016 N94-20296
Development and characterization of a time-, position- and energy-resolved x ray diagnostic for PBFA 2 target experiments
[DE93-019429] p 1808 N94-20297
Plasma chemical vapor deposition of halide glasses
[AD-D015933] p 1701 N94-20331
Wide-angle imaging system with fiberoptic components providing angle-dependent virtual material stops
[NASA-CASE-NPO-18146-1-CU] p 1986 N94-20345
Disengagable adapter for an optical fiber connector
[AD-D015959] p 1822 N94-20356
Understanding Open Systems Interconnection (OSI)
[AD-A271877] p 1929 N94-20472
Novel N x N integrated channel waveguide optical crossbars for large scale high speed non-blocking data switching
[AD-A272065] p 1986 N94-20922
Mode transition matrix measuring system
[AD-D015973] p 1987 N94-21279
Conversion of the proprietary ROLM (tm) inter-node link from multimode to singlemode operation
p 1744 N94-21349
Materials Science and Engineering
[DE93-040497] p 1675 N94-21530
Fibre pigtailed silicon based low cost passive optical components, appendix 5 p 1989 N94-21599
Acoustic, fiber optic, and silicon microelectronic microsensors research and development activities at Sandia National Laboratories
[DE93-019075] p 1770 N94-22040
The effect of delamination on the dynamic response of composite laminates as measured by embedded fiber optic Michelson sensor
[ISBN-0-315-83534-6] p 1677 N94-22587

FIBERS
Phthalonitrile prepolymer as high temperature sizing material for composite fibers
[AD-D015912] p 1672 N94-20010

FIELD EFFECT TRANSISTORS
SPICE macromodel for a 1-megawatt power MOSFET switch
[DE93-019415] p 1748 N94-19844
Modeling failure and reliability in new-generation devices
[AD-A271150] p 1748 N94-19910
Resistive gate magnetic field sensor
[AD-D015923] p 1749 N94-20199
Study of InGaAs-based modulation doped field effect transistor structures using variable-angle spectroscopic ellipsometry p 1796 N94-21001
Design of CMOS logic gates for TID radiation
p 1754 N94-21083

Complementary heterojunction FET technology for space application p 1755 N94-21094
Growth, characterization and device development in monocrystalline diamond films
[AD-A273097] p 2028 N94-21506
Interpolative modeling of GaAs FET S-parameter data bases for use in Monte Carlo simulations p 1767 N94-21723
Bit-systolic arithmetic arrays using dynamic differential gallium arsenide circuits p 1767 N94-21724
A FET-switched induction accelerator cell
[DE93-019604] p 1769 N94-21838

FIELD EMISSION
Metal-glass composite field-emitting arrays
[AD-D015942] p 1673 N94-20064
Silicon microelectronic field-emissive devices for advanced display technology
[DE94-000397] p 1794 N94-22380

FIELD OF VIEW
The data acquisition system for the Anglo-Australian Observatory 2-degree field project p 2048 N94-22529
UIT support observations archive p 2048 N94-22534

FIELD STRENGTH
Photonic electromagnetic field sensor apparatus
[AD-D015939] p 1718 N94-20334
Variable-field permanent magnet dipole
[DE94-000800] p 1820 N94-22020

FIELD THEORY (PHYSICS)
Relativistic calculations of the superheavy nucleus (sup 298)114
[KVI-969] p 1971 N94-20119

FIGURE OF MERIT
Optimization and control of a small angle ion source using an adaptive neural network controller
[DE93-040063] p 1946 N94-21845

FILAMENT WINDING
The effects of processing and constituent materials on compressive strength of thick composite laminates
[AD-A271912] p 1673 N94-20490

FILE MAINTENANCE (COMPUTERS)
A proof-of-concept implementation of persistence in a hierarchical storage system
[NASA-CR-194790] p 1921 N94-22376
ROSAT implementation of a proposed multi-mission x ray data format p 2047 N94-22462

FILLERS
Thermally activated retainer means utilizing shape memory alloy
[NASA-CASE-MSC-21793-1] p 1654 N94-20304
Mold bolt and means for achieving close tolerances between bolts and bolt holes
[NASA-CASE-MFS-28720-1] p 1823 N94-20379

FILM THICKNESS
Particles on surfaces of laser ablated Y1Ba2Cu3O(7-delta) films
[DE93-040269] p 2013 N94-19929
Structural and chemical analysis of a silicon nitride film on GaAs by null ellipsometry p 1709 N94-20975
Variable wavelength, variable angle ellipsometry including a sensitivities correlation test p 1710 N94-20978
Applications of variable angle spectroscopic ellipsometry in semiconductor technology p 2025 N94-21010
Non-destructive evaluation in manufacturing using spectroscopic ellipsometry p 1828 N94-21012
In-situ and ex-situ ellipsometric characterization for semiconductor technology p 2026 N94-21013
VASE (variable angle spectroscopic ellipsometry) p 1687 N94-21014
Properties of E-beam interactive oxide films for nanometer scale structures
[AD-A272848] p 1675 N94-21191
Azo polymers for optical storage 3: Effect of film thickness on net phase retardation and writing speed
[AD-A272994] p 1705 N94-21267
A quantitative model for interpreting nanometer scale hardness measurements of thin films
[DE93-040601] p 2034 N94-22005

FILMS
Image processing as a tool in flight testing evaluation p 1640 N94-22606

FILTRATION
Fabrication of porous ceramics by freeze-casting/freeze-drying
[PB93-202513] p 1705 N94-21425

FINANCE
System architectures for banking applications p 2046 N94-22057

FINANCIAL MANAGEMENT
Aerospace: Facts and figures, 1992-1993
[AD-A272571] p 1635 N94-21419

FINE STRUCTURE
Magnetic circular dichroism in x ray absorption and core-level photoemission
[DE93-019381] p 1688 N94-19986
High resolution studies of the structure of the solar atmosphere
[AD-A273084] p 2147 N94-21522

FINITE DIFFERENCE THEORY
A Kirchhoff approach to seismic modeling and prestack depth migration
[AD-A271010] p 1854 N94-19820
Stochastic differential equations and numerical simulation for pedestrians
[DE93-040651] p 1949 N94-20006
On the spline-based wavelet differentiation matrix
[NASA-CR-191557] p 1950 N94-20087
A comparison of two incompressible Navier-Stokes algorithms for unsteady internal flow
[NASA-TM-108794] p 1798 N94-20104
Development of a numerical simulation model for a-Si:H solar cells and application to the analysis of experimentally obtained spectral characteristics
[ETN-93-95061] p 1846 N94-20151
Head-on collision of drops: A numerical investigation
[NASA-TM-106394] p 1798 N94-20167
Analysis of microstrip dipoles and slots transversely coupled to a microstrip line using the FDTD method p 1718 N94-20405
FD-TD modeling of 2-D dielectric waveguides for propagation and scattering of femtosecond optical solitons p 1719 N94-20406
Interactive simulation package for coupled bending and torsional vibrations in flexible robot arms
[MEMO-1089] p 1944 N94-21140
Finite difference methods for time-dependent, linear differential algebraic equations
[AD-A272635] p 1954 N94-21174
A multigrid algorithm for the cell-centered finite difference scheme p 1957 N94-21479
High temperature superconducting planar circuit structure for high frequency applications
[AD-A273083] p 2028 N94-21521
On one numerical approach to Stefan problem
[IPPCZ-330] p 1996 N94-21572
Order of accuracy of QUICK and related convection-diffusion schemes
[NASA-TM-106402] p 1959 N94-21588
Study of TE(1-delta) mode in open dielectric resonators by a finite difference time domain method p 1747 N94-22253
On the relationship between spectral domain approach and method of lines p 1794 N94-22254
F2D users manual: A two-dimensional compressible gas flow code
[DE94-000653] p 1805 N94-22386

FINITE ELEMENT METHOD
Finite element mesh generation and analysis of solder joints for fatigue life predictions
[AD-A271329] p 1829 N94-19937
A benchmark study of 2D and 3D finite element calculations simulating dynamic pulse buckling tests of cylindrical shells under axial impact
[DE93-018859] p 1829 N94-19940
A new conformal absorbing boundary condition for finite element meshes and parallelization of FEMATS
[NASA-CR-194740] p 1950 N94-20034
The p-version of the finite element method in incremental elasto-plastic analysis
[NASA-CR-194707] p 1830 N94-20036
A comparative study of an ABC and an artificial absorber for truncating finite element meshes
[NASA-CR-194275] p 1716 N94-20160
Analytical evaluation of a surface integral expressing the coupling between interior and exterior volumes in a FE-IE approach p 1722 N94-20423
An efficient formulation of the coupled finite element-integral equation technique for solving large 3D scattering problems p 1725 N94-20436
Massively parallel computation of RCS with finite elements p 1726 N94-20437
Numerical methods for singularly perturbed differential equations with applications
[AD-A272112] p 1952 N94-20568
Finite element numerical simulation of three dimensional turbulent flows with dispersion: Eulerian and Lagrangian approaches
[ECL-92-42] p 1801 N94-20597
Wrinkle ridges, reverse faulting, and the depth penetration of lithospheric stress in lunae planum, Mars p 2141 N94-20910
Two-dimensional finite element analysis of porous media at multikilobar stress levels
[AD-A271540] p 1831 N94-20916
Thermal stress analysis of composites in the space environment p 1661 N94-21379
Numerical modeling of a propagating crack
[AD-A272604] p 1832 N94-21421
MGGHAT: Elliptic PDE software with adaptive refinement, multigrid and high order finite elements p 1956 N94-21470
Two-level Schwartz methods for nonconforming finite elements and discontinuous coefficients p 1957 N94-21477
Coupling of smooth particle hydrodynamics with PRONTO
[DE93-019080] p 1915 N94-21539
Radiation and scattering from printed antennas on cylindrically conformal platforms
[NASA-CR-194703] p 1741 N94-21885
Scattering by cavity-backed antennas on a circular cylinder p 1741 N94-21886
Radiation by cavity-backed antennas on a circular cylinder p 1741 N94-21887
User manual for EXCALIBUR: A FE-BI numerical laboratory for cavity-backed antennas in a circular cylinder, version 1.2 p 1741 N94-21888
Modal combination in response spectrum modal dynamic analysis
[DE94-000339] p 1833 N94-21956
A moving finite element model of the tokamak scrapeoff layer
[DE94-000673] p 1997 N94-21965
A finite element formulation and adaptive solution approach for large-scale thermomechanical problems with complex contact conditions
[DE93-019605] p 1960 N94-21996
Mixed finite element and finite volume methods
[ISBN-0-315-63035-3] p 1805 N94-22417
Coupling of smooth particle hydrodynamics with the finite element method
[DE93-019081] p 1805 N94-22556
Response statistics of shell structures with geometrical and material nonlinearities, volume 1
[ISBN-0-315-84006-4] p 1833 N94-22590
Life assessment of structural components using inelastic finite element analyses p 1834 N94-22614
NASA Langley developments in response calculations needed for failure and life prediction p 1836 N94-22621

FINITE VOLUME METHOD
A comparison of two incompressible Navier-Stokes algorithms for unsteady internal flow
[NASA-TM-108794] p 1798 N94-20104
Approximate methods for N-component solute transport and ion-exchange
[CWI-NM-R9223] p 1910 N94-21078
Unstructured multigrid through agglomeration p 1958 N94-21484
Order of accuracy of QUICK and related convection-diffusion schemes
[NASA-TM-106402] p 1959 N94-21588
User's guide for the casting process simulator software CaPS-2D, version 1.0
[DE93-040398] p 1917 N94-21923
Mixed finite element and finite volume methods
[ISBN-0-315-63035-3] p 1805 N94-22417

FINNED BODIES
Thermal information regarding the cooldown and operation of liquid argon calorimeters
[DE93-019391] p 1807 N94-19987

FIR FILTERS
Timing recovery in the channel processor of a digital group demodulator p 1780 N94-22169

FIRE (CLIMATOLOGY)
Overview of microphysical and state parameter measurements from FIRE 2 p 1871 N94-22293
Cirrus microphysics observations made during FIRE 2: Small particles, high concentrations, and probe comparisons p 1871 N94-22294
Optical properties of cirrus derived from airborne measurements during FIRE IFO 2 p 1872 N94-22297
Intercomparison of MAS, AVIRIS, and HIS data from FIRE cirrus 2 p 1872 N94-22298
Comparison of radiation and cloud parameters derived from satellite and aircraft measurements during FIRE 2 cirrus IFO p 1872 N94-22299
Cloud properties from the analysis of AVHRR observations for FIRE 2 p 1872 N94-22300
Development of methods for inferring cloud thickness and cloud-base height from satellite radiance data p 1872 N94-22301
Meteorological analysis of the December 4-6 FIRE cirrus-2 case p 1875 N94-22314
Cirrus cloud retrievals from HIS observations during FIRE 2 p 1875 N94-22315
Analysis of the GOES 6.7 micrometer channel observations during FIRE 2 p 1875 N94-22316
Cloud boundaries during FIRE 2 p 1876 N94-22318
Ground-based passive remote sensing during FIRE IFO 2 p 1844 N94-22319
Comparisons of downwelling radiation to model predictions based on groundbased measurements during FIRE 1991 p 1876 N94-22320

FIRE CONTROL
Digital wireless control system
[DE93-040211] p 1714 N94-19946

FIRE EXTINGUISHERS
On demand, non-halon, fire extinguishing systems
[AD-D015957] p 1714 N94-20355
A proposed methodology for combustion toxicology testing of combined halon replacement agent/jet fuel interaction
[AD-A272695] p 1681 N94-21165
FIRE FIGHTING
Expanded polystyrene protective barricade full-scale fire exposure test
[AD-A271450] p 1698 N94-19938
On demand, non-halon, fire extinguishing systems
[AD-D015957] p 1714 N94-20355
Aircraft cabin water spray disbenefits study
[NASA-CR-194750] p 1642 N94-21818
FIRE PREVENTION
Army aircraft fire-detection systems operation and reliability
[AD-A271327] p 1641 N94-20912
FIRES
Expanded polystyrene protective barricade full-scale fire exposure test
[AD-A271450] p 1698 N94-19938
A proposed methodology for combustion toxicology testing of combined halon replacement agent/jet fuel interaction
[AD-A272695] p 1681 N94-21165
FITTING
The IRAF Fabry-Perot analysis package: Ring fitting
p 2048 N94-22527
FIXED WINGS
Torsion spring powered missile wing deployment system
[CA-PATENT-1,306,384] p 1645 N94-21051
FLAME PROPAGATION
Investigation of flame driving and flow turning in axial solid rocket instabilities
[AD-A271066] p 1667 N94-20015
Reaction zone models for vortex simulation of turbulent combustion
[AD-A272723] p 1681 N94-21213
FLAME RETARDANTS
Expanded polystyrene protective barricade full-scale fire exposure test
[AD-A271450] p 1698 N94-19938
FLAMES
Development of a technique to determine the morphology and dynamics of agglomerates in chemically reacting flows
[AD-A271160] p 1678 N94-20000
FLAMMABILITY
Expanded polystyrene protective barricade full-scale fire exposure test
[AD-A271450] p 1698 N94-19938
Materials evaluation at ESA/ESTEC
p 1662 N94-21386
Toxicity of thermal degradation in a manned space environment p 1664 N94-21403
FLANGES
Compression strength of composite primary structural components
[NASA-CR-194561] p 1830 N94-20159
FLASHOVER
Research on plasma-puff initiation of high Coulomb transfer switches
[NASA-CR-194371] p 1994 N94-21289
Plasma-puff initiation of high Coulomb transfer switches p 1994 N94-21290
Characteristics of plasma-puff trigger for a inverse-pinch plasma switch p 1995 N94-21291
FLAT PLATES
Acoustic radiation damping of flat rectangular plates subjected to subsonic flows
[NASA-TM-109382] p 1967 N94-20211
The effect of transverse curvature on the fluctuating wall pressure and structure of boundary layer turbulence
[AD-A271868] p 1800 N94-20466
FLAT SURFACES
Cirrus properties deduced from CO2 lidar observations of zenith-enhanced backscatter from oriented crystals
p 1871 N94-22295
FLEXIBLE BODIES
Flexible heating head for induction heating
[NASA-CASE-LAR-14418-15-B] p 1718 N94-20368
Active damping of oscillations in a long compliant manipulator link
[DE93-018878] p 1826 N94-22038
A robust adaptive control design for flexible joint manipulators p 1790 N94-22230
Optimal control of the tip of a flexible arm
p 1794 N94-22256
Dynamic analyses of flexible robotic manipulators
[ISBN-0-315-59251-6] p 1827 N94-22421
Robot link and contact surface dynamic interaction: An experimental study of contact instability
[ISBN-0-315-83439-0] p 1827 N94-22578
FLIGHT ALTITUDE
Radiometry in commercial aircraft
[GSF-41/91] p 1892 N94-21141
FLIGHT CONTROL
Ground proximity warning system voice warning unit requirements study
[AD-A270541] p 1641 N94-19876
AIAA Techfest 29 proceedings
[NIAR-93-1] p 1635 N94-20191
Control vane guidance for a ducted-fan unmanned air vehicle
[AD-A271957] p 1645 N94-20561
Perception/action: An holistic approach 2
[AD-A271822] p 1891 N94-20627
Optimal flight guidance for aircraft in windshear
[CA-PATENT-1,307,573] p 1650 N94-21050
FLIGHT CREWS
Coronary angiography outcomes of US Army aircrew with the finding of coronary artery calcifications: Aviation epidemiology data register
[AD-A271968] p 1891 N94-20615
Radiometry in commercial aircraft
[GSF-41/91] p 1892 N94-21141
In-flight measurement of aircrew breathing in Navy aircraft
[AD-A271811] p 1896 N94-21154
Long-range laser imaging
[AD-A273020] p 1817 N94-21253
Strength capabilities and load requirements while performing torquing tasks in zero gravity
[NASA-TP-3433] p 1897 N94-21627
FLIGHT HAZARDS
Integrated display of multi-sensor geophysical and electromagnetic flight data p 1721 N94-20418
MLS signal-in-space category 3 landing hazard analysis p 1644 N94-22134
FLIGHT MANAGEMENT SYSTEMS
Incongruity, incongruity resolution, and mental states: The measure and modification of situational awareness and control
[NASA-CR-194568] p 1893 N94-20168
Development and evaluation of a profile negotiation process for integrating aircraft and air traffic control automation
[NASA-TM-4360] p 1643 N94-21606
FLIGHT OPERATIONS
Aircraft noise effects on cultural resources: Recommendation and rationale for further research
[PB93-205326] p 1968 N94-22053
FLIGHT PATHS
Optimal flight guidance for aircraft in windshear
[CA-PATENT-1,307,573] p 1650 N94-21050
Radiometry in commercial aircraft
[GSF-41/91] p 1892 N94-21141
Parallel runway requirement analysis study. Volume 2: Simulation manual
[NASA-CR-191549-VOL-2] p 1644 N94-22278
FLIGHT SAFETY
Integrated display of multi-sensor geophysical and electromagnetic flight data p 1721 N94-20418
Description and availability of airborne Doppler radar data p 1722 N94-20419
ATC/pilot voice communications: A survey of the literature
[DOT/FAA/AM-93/20] p 1738 N94-21201
Intervention strategies for the management of human error
[NASA-CR-4547] p 1642 N94-22373
Delamination, durability, and damage tolerance of laminated composite materials p 1678 N94-22622
FLIGHT SIMULATION
Some VTOL head-up display drive-law problems and solutions
[NASA-TM-104027] p 1635 N94-20035
AIAA Techfest 29 proceedings
[NIAR-93-1] p 1635 N94-20191
A simulation model for probabilistic analysis of Space Shuttle abort modes
[NASA-TM-108432] p 1656 N94-21859
Spaceplane flight simulation: Project definition
[PB93-211399] p 1651 N94-22094
FLIGHT SIMULATORS
Structural modeling: An application framework and development process for flight simulators
[AD-A271348] p 1650 N94-19880
A full-color, high-resolution laser projector for a flight simulator visual display
[AD-A270578] p 1651 N94-20108
FLIGHT TEST INSTRUMENTS
The modern rotor aerodynamic limits survey: A report and data survey
[NASA-TM-4446] p 1635 N94-21490
FLIGHT TESTS
Flight and laboratory testing of materials in low Earth orbit p 1659 N94-21369
Results of the post flight analyses on system materials for the LDEF-FRECOPA experiment
p 1659 N94-21371
The modern rotor aerodynamic limits survey: A report and data survey
[NASA-TM-4446] p 1635 N94-21490
Low-cost Unmanned Air Vehicle (UAV) for oceanographic research
[AD-A273103] p 1646 N94-21507
A flight test system design for the microwave landing system p 1645 N94-22156
Measurement Technology for Flight Tests
[ILR-MITT-256(1991)] p 1639 N94-22597
Testing of a multisensor hot film technique in wind tunnel and free flight p 1639 N94-22599
Free flight experiment with a laminar wing glove
p 1639 N94-22600
Measurement of the influence of deicing liquids on aircraft aerodynamics p 1640 N94-22602
Utilization of lasers for air data measurements
p 1640 N94-22603
Hot wire anemometry: A versatile instrumentation used for predevelopment studies and flight testing of the Do-328 aircraft p 1640 N94-22604
Image processing as a tool in flight testing evaluation
p 1640 N94-22606
Recent ONERA contributions to the development of flight test measurement techniques
p 1641 N94-22607
FLIP-FLOPS
Reliable interface design for combining asynchronous and synchronous circuits p 1758 N94-21119
FLOATING POINT ARITHMETIC
Evaluation of floating-point sum or difference of products in carry-save domain p 1764 N94-21705
Reverse automatic differentiation of modular FORTRAN programs
[DE94-000336] p 1918 N94-22088
FLOODS
Constraints on the rate of discharge and duration of the Mangala Valles flood p 2099 N94-20674
FLOW CHARACTERISTICS
Comparison of mixing calculations for reacting and non-reacting flows in a cylindrical duct
[NASA-TM-106435] p 1649 N94-21758
FLOW DISTRIBUTION
Fluid dynamic mechanisms and interactions within separated flows
[AD-A271037] p 1797 N94-19978
Three dimensional unsteady flow calculations in radial components p 1669 N94-20080
Experimental and computational results from a large low-speed centrifugal impeller
[NASA-TM-106421] p 1636 N94-20136
Perception/action: An holistic approach 2
[AD-A271822] p 1891 N94-20627
A classification scheme for the morphology of lava flow fields p 1863 N94-20879
Liquid-phase circulation and mixing in multicomponent droplets vaporizing in a laminar convective environment
[AD-A272851] p 1802 N94-21193
Measurement and prediction of the flow through an annular turbine cascade
[AD-A272530] p 1803 N94-21417
Flow interaction experiment. Volume 1: Aerothermal modeling, phase 1
[NASA-CR-189192-VOL-1] p 1648 N94-21582
Flow interaction experiment. Volume 2: Aerothermalmodeling, phase 2
[NASA-CR-189192-VOL-2] p 1648 N94-21583
A study of the compressible flow through a diffusing S-duct
[NASA-TM-106411] p 1638 N94-21591
Particle image velocimetry
[DE93-040657] p 1804 N94-21748
Comparison of mixing calculations for reacting and non-reacting flows in a cylindrical duct
[NASA-TM-106435] p 1649 N94-21758
Instability modes excited by natural screech tones in a supersonic rectangular jet
[NASA-TM-106409] p 1638 N94-22274
Johnson Space Center CFD grid generation requirements p 1919 N94-22355
Flow and heat transfer model for a rotating cryogenic motor
[DE94-001151] p 1794 N94-22405
Recent ONERA contributions to the development of flight test measurement techniques
p 1641 N94-22607
FLOW EQUATIONS
Formation of perched lava ponds on basaltic volcanoes: Interaction between cooling rate and flow geometry allows estimation of lava effusion rates p 1863 N94-20878
A semi-Lagrangian approach to the shallow water equation p 1806 N94-21480

NASA-Ames Research Center unstructured technology development p 1919 N94-22352
FLOW GEOMETRY
Formation of perched lava ponds on basaltic volcanoes: Interaction between cooling rate and flow geometry allows estimation of lava effusion rates p 1863 N94-20878
A classification scheme for the morphology of lava flow fields p 1863 N94-20879
Unstructured grid research and use at NASA Lewis Research Center p 1919 N94-22353
FLOW MEASUREMENT
Experimental investigation of nozzle/plume aerodynamics at hypersonic speeds
[NASA-CR-194626] p 1636 N94-20014
Thermal dilation fiber optical flow sensor
[AD-D015926] p 1797 N94-20094
Rotorwash wind sensor evaluation
[AD-A268987] p 1807 N94-20203
An experimental investigation of the drag mechanisms of a helicopter rotor in hovering flight
[AD-A270201] p 1636 N94-20486
Speed of sound data and related models for mixtures of natural gas constituents
[PB93-200822] p 1968 N94-21447
Particle image velocimetry
[DE93-040657] p 1804 N94-21748
FLOW STABILITY
Experimental study of a shock accelerated thin gas layer
[DE93-018354] p 1799 N94-20286
Numerical investigation of laminar-turbulent transition in two- and three-dimensional boundary layers
[DLR-FB-92-36] p 1800 N94-20533
Time-accurate Navier-Stokes calculations with multigrid acceleration p 1956 N94-21469
Laser driven hydrodynamic instability experiments
[DE93-040550] p 1818 N94-21547
Instability modes excited by natural screech tones in a supersonic rectangular jet
[NASA-TM-106409] p 1638 N94-22274
FLOW VELOCITY
Design of a state-space controller for an advanced gas turbine engine
[AD-A270659] p 1647 N94-20042
Absorption heat pump for space applications
[NASA-CR-194693] p 1845 N94-20066
Thermal dilation fiber optical flow sensor
[AD-D015926] p 1797 N94-20094
Experimental and computational results from a large low-speed centrifugal impeller
[NASA-TM-106421] p 1636 N94-20136
An experimental investigation of the drag mechanisms of a helicopter rotor in hovering flight
[AD-A270201] p 1636 N94-20486
Perception/action: An holistic approach 2
[AD-A271822] p 1891 N94-20627
Formation of perched lava ponds on basaltic volcanoes: Interaction between cooling rate and flow geometry allows estimation of lava effusion rates p 1863 N94-20878
Testing of a multisensor hot film technique in wind tunnel and free flight p 1639 N94-22599
FLOW VISUALIZATION
Principles and applications of oil film interferometry for measuring wall friction fields in air flows
[ETN-93-95062] p 1798 N94-20147
Formulation of a next-generation interior ballistic code
[AD-A271539] p 1801 N94-20915
Description and assessment of a new Optical Pressure Measurement System (OPMS) demonstrated in the high speed wind tunnel in Goettingen (Germany)
[DLR-FB-92-24] p 1651 N94-21280
Particle image velocimetry
[DE93-040657] p 1804 N94-21748
Measurement of thermal-hydraulic parameters in two-phase flow using flow visualization image analysis
[DE93-006255] p 1805 N94-22269
NASA-Ames Research Center unstructured technology development p 1919 N94-22352
Unstructured grid research and use at NASA Lewis Research Center p 1919 N94-22353
Grid generation requirements at Marshall Space Flight Center p 1919 N94-22354
FLUENCE
Combination of on ground experiments and analysis software for the evaluation of material degradation in space (SILEX project) p 1662 N94-21389
German space experiments on Spacelab D-2 and Eureca-1 to investigate atomic oxygen interaction with materials p 1662 N94-21390
The International Telecommunications Satellite (INTELSAT) Solar Array Coupon (ISAC) atomic oxgyen flight experiment: Techniques, results and summary p 1662 N94-21391
FLUID DYNAMICS
Pressurization and expulsion of a flightweight liquid hydrogen tank
[NASA-TM-106427] p 1799 N94-20177
A comparison of calculated and measured rheological properties of crystallising lavas in the field and in the laboratory p 1862 N94-20690
Investigation of the physics of the turbulent boundary layer focusing on vortex structures
[AD-A272879] p 1802 N94-21155
Computational and analytical methods in nonlinear fluid dynamics
[AD-A272722] p 1802 N94-21169
An analysis of pressure driven cross-flow through a long slot connecting two parallel channels
[DE93-040181] p 1804 N94-21765
FLUID FILMS
Principles and applications of oil film interferometry for measuring wall friction fields in air flows
[ETN-93-95062] p 1798 N94-20147
Compliant seal development p 1655 N94-21795
FLUID FLOW
Hydrostatic/nonhydrostatic comparison with the MERCURE code on orographic flows
[ETN-93-94603] p 1866 N94-20600
Thermal and rheological controls on magma migration in dikes: Examples from the east rift zone of Kilauea volcano, Hawaii p 1862 N94-20673
A comparison of calculated and measured rheological properties of crystallising lavas in the field and in the laboratory p 1862 N94-20690
Formation of perched lava ponds on basaltic volcanoes: Interaction between cooling rate and flow geometry allows estimation of lava effusion rates p 1863 N94-20878
A classification scheme for the morphology of lava flow fields p 1863 N94-20879
Numerical simulation of lava flows: Applications to the terrestrial planets p 1863 N94-20904
Chemical reaction fouling model for single-phase heat transfer
[DE93-019556] p 1802 N94-20942
Dynamic response of multiphase porous media
[AD-A272915] p 1831 N94-21219
A note on singularities caused by the hydrodynamic dispersion tensor
[CWI-NM-R9302] p 1803 N94-21575
An analysis of pressure driven cross-flow through a long slot connecting two parallel channels
[DE93-040181] p 1804 N94-21765
Iterative electromagnetic Born inversion applied to earth conductivity imaging
[DE93-040668] p 1859 N94-21928
Microscopic and macroscopic dynamics
[DE93-019576] p 1937 N94-22042
Development of a gridless CFD method p 1919 N94-22361
FLUID INJECTION
Iterative electromagnetic Born inversion applied to earth conductivity imaging
[DE93-040668] p 1859 N94-21928
FLUID JETS
An analysis of pool surface deformation due to a plunging liquid jet
[AD-A272970] p 1802 N94-21261
FLUID MECHANICS
Wavefront sensors for optical diagnostics in fluid mechanics: Application to heated flow, turbulence, and droplet evaporation
[DE93-040060] p 1797 N94-19974
Numerical methods for singularly perturbed differential equations with applications
[AD-A272112] p 1952 N94-20568
Microscopic and macroscopic dynamics
[DE93-019576] p 1937 N94-22042
FLUID PRESSURE
Two-dimensional finite element analysis of porous media at multikilobar stress levels
[AD-A271540] p 1831 N94-20916
An analysis of pressure driven cross-flow through a long slot connecting two parallel channels
[DE93-040181] p 1804 N94-21765
FLUIDS
Spiral fluid separator
[NASA-CASE-MFS-28658-1] p 1800 N94-20361
FLUORESCENCE
Optical fibers and Fluorosensors having improved power efficiency and methods of producing same
[NASA-CASE-LAR-14525-1-CU] p 1986 N94-20378
Optical fiber sensor having an active core
[NASA-CASE-LAR-14607-1-SB] p 1986 N94-20566
Optical properties of chromium and neodymium in zirconium - barium - lanthanum - aluminum fluoride glass
[AD-A271609] p 1987 N94-21236
Diffraction and holography of photoelectrons and fluorescent x rays
[DE93-019240] p 1808 N94-21441
Fluorescent microthermographic imaging
[DE93-040332] p 1810 N94-22000
FLUORIDES
Investigation of the effect of various oxide and fluoride additives on the microstructure, electronic properties, and phase shifting ability of Ba(1-x)Sr(x)TiO3
[AD-A271756] p 2027 N94-21303
FLUORINE ORGANIC COMPOUNDS
Laser driven hydrodynamic instability experiments
[DE93-040550] p 1818 N94-21547
FLUOROCARBONS
Stress-induced cracking of fluorocarbon rubber MTL-0002 after exposure to DS-2
[AD-A271753] p 1705 N94-21302
Survey on chemical engineering technologies for the global environmental protection
[DE94-714887] p 1852 N94-22044
Investigations on trends in global environment adaptive industrial technologies
[DE94-714888] p 1853 N94-22258
FLUOROHYDROCARBONS
Electron reactions in nonpolar liquids: Pressure effects
[DE93-040328] p 1970 N94-19931
Rotational spectrum of a dark state in 2-fluoroethanol using microwave/radiofrequency-infrared multiple resonance
[AD-A272101] p 1817 N94-20583
A proposed methodology for combustion toxicology testing of combined halon replacement agent/jet fuel interaction
[AD-A272695] p 1681 N94-21165
FLUOROPOLYMERS
Adhesive electroless metallization of fluoropolymeric substrates
[AD-A271858] p 1703 N94-20526
FLUOROSCOPY
Coronary angiography outcomes of US Army aircrew with the finding of coronary artery calcifications: Aviation epidemiology data register
[AD-A271968] p 1891 N94-20615
Review of using cardiac fluoroscopy in symptomatic and asymptomatic patients
[AD-A271690] p 1891 N94-20928
FLUTTER ANALYSIS
The Seventh International Conference on Composite Structures, volume 25, numbers 1-4
[AD-A269961] p 1672 N94-20031
Blade row interaction effects on flutter and forced response
[NASA-TM-106438] p 1649 N94-21586
FLUX (RATE)
CERN-derived analysis of lunar radiation backgrounds p 2080 N94-20880
Improved approximate formulas for flux from cylindrical and rectangular sources
[DE93-011390] p 1742 N94-22268
FLUX DENSITY
IMPS albedo and diameter for Asteroid 243 Ida p 2085 N94-20845
Orbital debris and micrometeoroids: LDEF and Mir data p 1659 N94-21368
Effects of aqueous solution compositions on Aerocapacitor energy density
[DE94-000385] p 1768 N94-21753
Satellite measurements of radiation budget parameters p 1860 N94-22284
FLUX PINNING
The effect of correlated and point defects on the vortex lattice melting transition in single crystal YBa2Cu3O(7-delta)
[DE93-040277] p 2033 N94-21997
FLYBY MISSIONS
Contributions of the Clementine mission to our understanding of the processes and history of the Moon p 2119 N94-20784
The Clementine Mission science return at the Moon and Geographos p 1652 N94-20850
FLYWHEELS
Electromechanical battery research and development at the Lawrence Livermore National Laboratory
[DE93-019159] p 1762 N94-21620
Electromechanical battery research and development at the Lawrence Livermore National Laboratory
[DE94-000391] p 1762 N94-21621
FM/PM (MODULATION)
Trellis coded multi-orthogonal modulation p 1747 N94-22231
Quadrature biorthogonal modulation p 1747 N94-22232
FOAMS
Structural crashworthiness and failure
[AD-A270429] p 1828 N94-19815
Expanded polystyrene protective barricade full-scale fire exposure test
[AD-A271450] p 1698 N94-19938

Shock compression of low-density foams
[DE93-040545] p 1707 N94-21546
FOCAL PLANE DEVICES
Multiport solid-state imager characterization at variable pixel rates
[DE93-018366] p 1808 N94-20287
Silicon retina for optical tracking systems
p 1755 N94-21098
ROSAT data analysis with EXSAS
p 2080 N94-22555
FOCI
Focus history of the Hubble Space Telescope: Launch to May 1993
[NASA-CR-194179] p 2055 N94-20204
FOCUSING
Focus history of the Hubble Space Telescope: Launch to May 1993
[NASA-CR-194179] p 2055 N94-20204
Micro-ellipsometric measurements of strained layer structures p 2025 N94-21008
Plasma lens experiments at the Final Focus Test Beam
[DE93-041081] p 1981 N94-21688
SPECFOCUS: An IRAF task for focusing spectrographs p 1965 N94-22540
FOILS (MATERIALS)
Interactions of slow H, H2, and H3 with thin foils
[DE93-040263] p 1976 N94-21995
FOKKER-PLANCK EQUATION
Accretion of a hot plasma onto the central black hole: Fokker-Planck formulation p 2009 N94-22693
FOLDING STRUCTURES
Torsion spring powered missile wing deployment system
[CA-PATENT-1,306,384] p 1645 N94-21051
FOLDS (GEOLOGY)
Diapirs and cantaloupes: Layering and overturn of Triton's crust p 2111 N94-20738
FORCE DISTRIBUTION
Control of multiple robot manipulators with optimal force distribution p 1794 N94-22255
FORCE-FREE MAGNETIC FIELDS
Determination of coronal magnetic fields from vector magnetograms
[NASA-CR-194744] p 2147 N94-21877
FORECASTING
Using NDVI/AVHRR data for crop monitoring and forecasting in South Italy p 1841 N94-20970
An evaluation of artificial neural network modeling for manpower analysis
[AD-A273001] p 1945 N94-21269
FOREST MANAGEMENT
Data management for support of the Oregon Transect Ecosystem Research (OTTER) project
[NASA-CR-4557] p 1905 N94-20149
FORESTS
Relating ground truth collection to model sensitivity
p 1719 N94-20409
Application of Cloude's target decomposition theorem to polarimetric imaging radar data p 1724 N94-20429
Mapping of taiga forest units using AIRSAR data and/or optical data, and retrieval of forest parameters
p 1729 N94-20452
Analysis of hyper-spectral AVIRIS image data over a mixed-conifer forest in Maine p 1838 N94-20959
FORM FACTORS
Qualitative and quantitative aspects of the QCD theory of elastic form factors
[DE93-040864] p 2038 N94-21513
A relativistic constituent quark model
[DE93-041085] p 1946 N94-21689
FORMALISM
Application of the reactive flux formalism to study water hydrogen bond dynamics
[AD-A271824] p 1680 N94-20560
GWB: Manual for the Grammar WorkBench version 1.5
[TR-92-14] p 1909 N94-21061
Likelihood analysis of parity violation in the compound nucleus
[DE94-000671] p 1977 N94-22572
FORMAT
Conversion of LDEF experiment M0003 sample observation database to MS-DOS formats
[AD-A272945] p 1681 N94-21226
Data format standards for civilian remote sensing satellites
[PB93-192920] p 1841 N94-21446
ROSAT implementation of a proposed multi-mission x ray data format p 2047 N94-22462
FITS data conversion efforts at the Compton Observatory Science Support Center
p 1926 N94-22488
FORSTERITE
Fe/Mn in olivine of carbonaceous meteorites
p 2084 N94-20788
Diffusion-controlled magnesium isotopic fractionation of a single crystal forsterite evaporated from the solid state
p 1686 N94-20855
FORTRAN
Documentation for PCDIST, a FORTRAN subroutine to calculate Poliack-Cuzzi scattering
[AD-A273070] p 1988 N94-21491
Reverse automatic differentiation of modular FORTRAN programs
[DE94-000336] p 1918 N94-22088
An object-oriented data reduction system in Fortran
p 2046 N94-22447
A self-defining hierarchical data system
p 2046 N94-22448
Fortran for the nineties p 1926 N94-22481
FOSSIL FUELS
Proceedings of the Seventh Annual Conference on Fossil Energy Materials
[DE94-001091] p 1848 N94-21823
Global emissions and models of photochemically active compounds
[DE93-040490] p 1852 N94-21989
FOULING
Chemical reaction fouling model for single-phase heat transfer
[DE93-019556] p 1802 N94-20942
FOUR-WAVE MIXING
Center for the integration of optical computing
[AD-A271874] p 1899 N94-20469
Statistical fluctuations in lasers
[DE94-000710] p 1817 N94-20939
Photonics and nonlinear optics with molecular materials and polymers
[AD-A271747] p 1988 N94-21457
FOURIER ANALYSIS
High resolution signal processing
[AD-A271181] p 1717 N94-20215
Fast fourier transforms for nonequispaced data
[AD-A272687] p 1954 N94-21164
Fourier calculus on evolutionary trees
[CWI-BS-R9234] p 1954 N94-21231
Flow transition with 2-D roughness elements in a 3-D channel p 1806 N94-21466
Multigrid schemes for viscous hypersonic flows
p 1641 N94-21473
Optimal convolution SOR acceleration of waveform relaxation with application to semiconductor device simulation p 1922 N94-21475
FOURIER SERIES
Rational trigonometric approximations using Fourier series partial sums
[NASA-CR-191535] p 1959 N94-21568
FOURIER TRANSFORMATION
High resolution signal processing
[AD-A271181] p 1717 N94-20215
Analysis of microstrip dipoles and slots transversely coupled to a microstrip line using the FDTD method
p 1718 N94-20405
Asymptotic behavior of Fourier transform of surface measures on convex and radial hypersurfaces
[ETN-93-93790] p 1952 N94-21019
Fast fourier transforms for nonequispaced data
[AD-A272687] p 1954 N94-21164
Femtosecond dynamics in hydrogen-bonded solvents
[DE93-019937] p 1683 N94-21842
A Hopfield neural net for discrete Fourier transform calculation p 1783 N94-22184
Transient acoustic wave modeling: Higher-order WKBJ asymptotics and symbolical manipulation (revised)
[PB93-215432] p 1969 N94-22262
Verification of the PROS timing analysis package
p 1926 N94-22508
FRACTALS
A comparison of some of the most current methods of image compression
[AD-A271841] p 1907 N94-20525
Computerized simulations with cellular automates for cloud formation
[GKSS-92/E/22] p 1867 N94-21312
FRACTIONATION
Evaporation in equilibrium, in vacuum, and in hydrogen gas p 1684 N94-20636
The Koshak section: Evidence for element fractionation and an oxidation event at the K/T boundary
p 1862 N94-20641
Low-energy ion implantation: Large mass fractionation of argon p 1685 N94-20697
FE-60 and the evolution of eucrites
p 2083 N94-20768
Fe/Mn in olivine of carbonaceous meteorites
p 2084 N94-20788
Recondensation in the early solar system: Physical conditions and source material p 2085 N94-20849
Diffusion-controlled magnesium isotopic fractionation of a single crystal forsterite evaporated from the solid state
p 1686 N94-20855
Stable Ni isotopes and Be-10 and Al-26 in metallic spheroids from Meteor Crater, Arizona
p 1863 N94-20889
Requirements for the early atmosphere of Mars from nitrogen isotope ratios p 2144 N94-21669
Mars atmosphere loss and isotopic fractionation by solar-wind-induced sputtering and photochemical escape
p 2144 N94-21672
FRACTURE MECHANICS
Innovative acoustic technique for studying new materials and new developments in solid state physics
[AD-A270540] p 2013 N94-19933
Interleaved bismaleimide composites
[AD-A272233] p 1674 N94-20574
The 1992 USAF structural integrity program conference
[AD-A272878] p 1635 N94-21194
Numerical modeling of a propagating crack
[AD-A272604] p 1832 N94-21421
Tensile and shear fracture behavior of fiber reinforced plastics at 77K irradiated by various radiation sources
[DE93-040280] p 1706 N94-21542
Ni3Al aluminide alloys
[DE94-000493] p 1694 N94-21933
The program system for the diagnostics of strains and fracture prediction of solids p 1836 N94-22065
Nonlinear and progressive failure aspects of transport composite fuselage damage tolerance
p 1834 N94-22609
Projections on structures and material strength in the computational context p 1834 N94-22610
A thermodynamic analysis of propagating subcritical cracks with cohesive zones p 1834 N94-22611
Modeling of failure and response to laminated composites subjected to in-plane loads
p 1834 N94-22612
FRACTURE STRENGTH
Investigation of austenitic alloys for advanced heat recovery and hot gas cleanup systems
[DE93-017863] p 1687 N94-19802
Properties and potential of high-temperature niobium beryllides
[DE93-019169] p 1690 N94-20233
Composite materials with improved properties in compression
[AD-A272837] p 1675 N94-21176
Weldalite (tm) 049 (Al 2095-T8): Anisotropy effects at cryogenic conditions
[AD-A272658] p 1691 N94-21188
Microstructural modeling and toughening of Si3N4 ceramics for high temperature engine applications
[AD-A272897] p 1704 N94-21197
Strength and toughness improvement of silicide intermetallics by nanophase and microphase reinforcements
[AD-A272914] p 1692 N94-21320
Review of corrosion behavior of ceramic heat exchanger materals: Corrosion characteristics of silicon carbide and silicon nitride
[DE93-041307] p 1706 N94-21516
The mechanical property data base from an Air Force/industry cooperative test program on advanced aluminum alloys: 2091 sheet, plate, and 8090 extrusion
[AD-A273091] p 1692 N94-21525
Fundamental studies of stress distributions and stress relaxation in oxide scales on high temperature alloys
[DE94-001444] p 1693 N94-21854
Effect of powder characteristics on gas-pressure sintering of Si3N4 with rare earth additives
[DE94-000330] p 1694 N94-21945
Dynamic properties of ceramic materials
[DE94-000654] p 1706 N94-21963
Benefits of thread rolling process to the stress corrosion cracking and fatigue resistance of high strength fasteners
[DE93-040438] p 1833 N94-22001
Miniaturized disk-bend testing, nano-indentation, and the microstructure of ion-irradiated titanium aluminides
[DE93-040600] p 1697 N94-22559
FRACTURES (MATERIALS)
Coupling of smooth particle hydrodynamics with PRONTO
[DE93-019080] p 1915 N94-21539
Investigation of moisture-induced embrittlement of iron aluminides
[DE93-040841] p 1695 N94-21949
FRACTURING
Strength and deformation properties of basaltic lava flows on planetary surfaces p 1862 N94-20747
Linear structures on the small inner satellites of Saturn p 2121 N94-20797
Coupling of smooth particle hydrodynamics with PRONTO
[DE93-019080] p 1915 N94-21539

Experimental and numerical studies of high-velocity impact fragmentation
[DE93-040205] p 1832 N94-21557
Ductile-brittle transition behavior of tungsten under shock loading conditions
[DE93-019945] p 1693 N94-21843
Fundamental studies of stress distributions and stress relaxation in oxide scales on high temperature alloys
[DE94-001444] p 1693 N94-21854
An overview of computational simulation methods for composite structures failure and life analysis
p 1835 N94-22617

FRAGMENTATION
The sand bag model of the dispersion of the cosmic body in the atmosphere p 2084 N94-20823
Equilibrium models of mass distribution and collisional lifetimes of asteroids p 2086 N94-20877
Hypervelocity impact
[AD-A272957] p 1831 N94-21249
Experimental and numerical studies of high-velocity impact fragmentation
[DE93-040205] p 1832 N94-21557
A thermodynamic theory of dynamic fragmentation
[DE93-019066] p 1833 N94-21916
Fragmentation of magnetized filamentary interstellar clouds p 2008 N94-22687

FRAGMENTS
Antipodal fragment velocities for porous and weak targets at catastrophic impacts p 1836 N94-20891

FRAUNHOFER LINES
Oceanic in situ Fraunhofer-line characteristics: Fraunhofer-line underwater experiment (FLUX)
[AD-A270659] p 1881 N94-19952

FREE ATMOSPHERE
Convergence of the hermite wavelet expansion
[AD-A271435] p 1854 N94-19841

FREE ELECTRON LASERS
Initial performance of Los Alamos advanced free electron laser
[DE93-040158] p 1814 N94-19828
Measurement and correction of magnetic fields in pulsed slotted-tube microwigglers
[DE93-040100] p 1815 N94-20272
Performance of the high brightness linac for the Advanced Free Electron Laser Initiative at Los Alamos
[DE93-040141] p 1816 N94-20277
A theory for optical wavelength control in short pulse free electron laser oscillators
[AD-A271706] p 1817 N94-21353
Demonstration of ultraviolet lasing with a low energy electron beam
[DE93-040192] p 1818 N94-21554
Generation of harmonic radiation using the multi-cavity free-electron laser
[DE94-001261] p 1820 N94-21975
Variable-field permanent magnet dipole
[DE94-000800] p 1820 N94-22020
Infrared FEL photochemistry: Multiple-photon dissociation of freon gas
[DE94-000817] p 1820 N94-22585

FREE ENERGY
Stability of the face-centered-cubic phase of heavy rare gas solids
[DE93-019949] p 1679 N94-20319
Integral equation calculation of solvent activation free energies for electron and proton transfer reactions
[AD-A272665] p 1681 N94-21216

FREE FALL
Melt-spin processing of high (Tc) oxide superconductors
[DE94-000696] p 2036 N94-22582

FREEZE DRYING
Fabrication of porous ceramics by freeze-casting/freeze-drying
[PB93-202513] p 1705 N94-21425

FREON
Infrared FEL photochemistry: Multiple-photon dissociation of freon gas
[DE94-000817] p 1820 N94-22585

FREQUENCIES
Worldwide frequency of temperatures at selected altitudes
[AD-A271111] p 1864 N94-19908
Longitudinal instability of an induction linac with acceleration
[DE93-019249] p 1980 N94-20290
High Speed/High Frequency Optoelectronics
[AD-A271985] p 1751 N94-20580

FREQUENCY ASSIGNMENT
Visibility considerations in frequency sharing with low Earth orbit satellites p 1746 N94-22187

FREQUENCY CONTROL
Millimeter wave imaging technology
[AD-A271257] p 1715 N94-19912

FREQUENCY DIVISION MULTIPLEXING
Multi-band reflector antenna with double-ring element frequency selective subreflector p 1728 N94-20447

FREQUENCY MEASUREMENT
Millimeter wave imaging technology
[AD-A271257] p 1715 N94-19912
Strength, ultrasonic and metallurgical evaluation of diffusion bonds
[DE94-000685] p 1697 N94-22571

FREQUENCY MODULATION
C-band radar backscatter of sea ice in the Weddell Sea, Antarctica during the austral winter of 1992
p 1725 N94-20435
High Speed/High Frequency Optoelectronics
[AD-A271985] p 1751 N94-20580
Effect of bandwidth on beam smoothing and frequency conversion at the third harmonic of the Nova laser
[DE93-019917] p 1819 N94-21920
FM interference in radio navigation receivers
p 1645 N94-22219

FREQUENCY MULTIPLIERS
Millimeter wave imaging technology
[AD-A271257] p 1715 N94-19912

FREQUENCY RANGES
Frequency and temperature dependence of high damping elastomers
[DE93-019539] p 1697 N94-19809

FREQUENCY RESPONSE
Frequency dependent electrical properties of minerals and partial-melts
[DE93-019918] p 2012 N94-19861

FREQUENCY SHIFT
Measuring liquid properties with smooth and textured-surface resonators
[DE93-019433] p 1749 N94-20054
A motion extraction method for synthetic aperture radars
[DLR-FB-92-31] p 1742 N94-22279

FREQUENCY SHIFT KEYING
Digital receiver for on-board FM/FSK-FM/BPSK demodulation p 1744 N94-21091
Capacity comparison between direct sequence PSK and MFSK spread spectrum systems in CDMA applications
p 1747 N94-22224

FREQUENCY STABILITY
Measurements of atomic interactions and frequency stability with a cryogenic hydrogen maser
[AD-A271132] p 1814 N94-19853
Tunable laser frequency stabilizing system
[AD-D015904] p 1815 N94-20055

FREQUENCY STANDARDS
Measurements of atomic interactions and frequency stability with a cryogenic hydrogen maser
[AD-A271132] p 1814 N94-19853

FREQUENCY SYNTHESIZERS
Low-latency digital frequency synthesizer using the residue number system p 1759 N94-21121

FRESNEL DIFFRACTION
Wide passband wavelength multi/demultiplexer at 1.3/1.55 micrometers based on etched Fresnel mirror, appendix B p 1989 N94-21602

FRESNEL REGION
Material optimization for hard x ray Fresnel zone plates
[DE93-019569] p 1990 N94-21837

FRICTION
Development of fundamental understanding of friction and wear mechanisms by atomic-scale tribological studies of ceramic materials and multilayered thin films
[AD-A271485] p 1703 N94-20548
The connection between Venus' free obliquity and its CMB oblateness p 2139 N94-20896
Lubricated wear of steel-ceramic and ceramic-ceramic systems
[PB93-202356] p 1825 N94-21450
Dynamics of face seals for high speed turbomachinery
p 1655 N94-21796

FRICTION FACTOR
Distributed loss model: Application to a spatial turbopump inducer p 1668 N94-20078

FUEL CELL POWER PLANTS
Molten carbonate fuel cell networks: Principles, analysis, and performance
[DE93-019872] p 1846 N94-21527
Modeling of polymer electrolyte fuel cell systems
[DE93-041187] p 1847 N94-21774

FUEL CELLS
Fuel processing requirements and techniques for fuel cell propulsion power
[DE93-019516] p 1750 N94-20257
Molten carbonate fuel cell networks: Principles, analysis, and performance
[DE93-019872] p 1846 N94-21527
A calcium oxide sorbent process for bulk separation of carbon dioxide
[DE93-019288] p 1847 N94-21540
Research and development of alternative components at Argonne National Laboratory for molten carbonate fuel cells
[DE93-019536] p 1847 N94-21650
Modeling of polymer electrolyte fuel cell systems
[DE93-041187] p 1847 N94-21774
Cathode materials for the molten carbonate fuel cell
[DE93-019515] p 1848 N94-21870
The electrochemical performance of thin-electrolyte solid oxide fuel cells
[DE93-041184] p 1848 N94-21942
Survey on chemical engineering technologies for the global environmental protection
[DE94-714887] p 1852 N94-22044

FUEL COMBUSTION
On demand, non-halon, fire extinguishing systems
[AD-D015957] p 1714 N94-20355
Global emissions and models of photochemically active compounds
[DE93-040490] p 1852 N94-21969
Investigations on trends in global environment adaptive industrial technologies
[DE94-714888] p 1853 N94-22258
Experimental evaluation of oxygen-enriched air and emulsified fuels in a six-cylinder diesel engine
[DE94-000907] p 1811 N94-22391

FUEL CONSUMPTION
Some evidence on determinants of fuel economy as a function of driving cycle and test type
[DE93-019511] p 1825 N94-21637

FUEL CONTAMINATION
Compatibility and efficacy of biocides qualified under military specification MIL-S-53021
[AD-A271496] p 1712 N94-20551

FUEL FLOW
Design of a state-space controller for an advanced gas turbine engine
[AD-A270859] p 1647 N94-20042
Some evidence on determinants of fuel economy as a function of driving cycle and test type
[DE93-019511] p 1825 N94-21637

FUEL INJECTION
Liquid fuel injection elements for rocket engines
[NASA-CASE-MFS-28547-1] p 1669 N94-20370
Experimental evaluation of oxygen-enriched air and emulsified fuels in a six-cylinder diesel engine
[DE94-000907] p 1811 N94-22391

FUEL PRODUCTION
Fuel processing requirements and techniques for fuel cell propulsion power
[DE93-019516] p 1750 N94-20257

FUEL SYSTEMS
Cold starting an alcohol-fueled engine with ultrasonic fuel atomization
[PB93-206597] p 1826 N94-22093

FUEL TANK PRESSURIZATION
Pressurization and expulsion of a flightweight liquid hydrogen tank
[NASA-TM-106427] p 1799 N94-20177

FUEL TANKS
On demand, non-halon, fire extinguishing systems
[AD-D015957] p 1714 N94-20355

FUEL TESTS
Cold starting an alcohol-fueled engine with ultrasonic fuel atomization
[PB93-206597] p 1826 N94-22093

FUEL VALVES
High-temperature, high-pressure oxygen metering valve
[NASA-CASE-MSC-21823-1] p 1824 N94-20589

FUEL-AIR RATIO
Experimental evaluation of oxygen-enriched air and emulsified fuels in a six-cylinder diesel engine
[DE94-000907] p 1811 N94-22391

FUELS
Biofuels: Project summaries
[DE93-010003] p 1712 N94-19984
Monopropellant aqueous hydroxyl ammonium nitrate/fuel
[AD-D015922] p 1712 N94-20061

FULLERENES
Fullerene derivatives and fullerene superconductors
[DE93-019568] p 2031 N94-21871

FUNCTION SPACE
Large deviations behavior of counting processes and their inverses
[AD-A271142] p 1939 N94-19909

FUNCTIONAL ANALYSIS
Functional statistical data analysis and modeling
[AD-A271520] p 1963 N94-20913
Large-scale circulation regimes and tropical cyclone characteristics over the western pacific ocean
[AD-A273004] p 1867 N94-21307

FUNCTIONAL DESIGN SPECIFICATIONS
Structural modeling: An application framework and development process for flight simulators
[AD-A271348] p 1650 N94-19880
Proceedings of the Twentieth Annual Technologyfest p 1645 N94-20188
FUNCTIONS (MATHEMATICS)
Polynomial interpolation of real functions 1: Interpolation in an interval
[AD-A272330] p 1951 N94-20527
On the closure properties of #P in the context of PF of #P
[TR-445] p 1955 N94-21456
FURNACES
Initial development of a high-pressure crystal growth facility: Center director's discretionary fund
[NASA-TM-108430] p 2030 N94-21807
Melt-spin processing of high (Tc) oxide superconductors
[DE94-000696] p 2036 N94-22582
FUSELAGES
Probabilistic assessment of composite structures
[NASA-TM-106368] p 1832 N94-21757
Nonlinear and progressive failure aspects of transport composite fuselage damage tolerance p 1834 N94-22609
Demonstrating damage tolerance of composite airframes p 1647 N94-22623
FUSION REACTORS
Multi-CPU plasma fluid turbulence calculations on a CRAY Y-MP C90
[DE93-015425] p 1801 N94-20562
FUZZY SETS
Logic oriented neural networks p 1782 N94-22182
FUZZY SYSTEMS
Telerobotic control of a mobile coordinated robotic server, executive summary
[NASA-CR-194685] p 1821 N94-20044
Reconfigurable fuzzy cell
[NASA-CASE-MSC-21613-1] p 1907 N94-20492
Reentry vehicle adaptive telemetry
[DE94-001168] p 1656 N94-21852
Fuzzy and neural control
[NASA-TM-108753] p 1947 N94-22270
Automated cloud classification with a fuzzy logic expert system p 1875 N94-22313

G

GALACTIC CLUSTERS
X ray archeology in the Coma cluster
[NASA-CR-194799] p 2054 N94-20175
Radio galaxies and their environment
[DE93-040851] p 2150 N94-22397
Magnetic reconnection in emission nebulae in clusters of galaxies p 2010 N94-22700
GALACTIC EVOLUTION
Dust content of a hydrogen rich, low surface brightness galaxy and the luminosity history of 3C273
[NASA-CR-194705] p 2056 N94-21779
Magnetic superbubbles in the galactic disk and halo p 2009 N94-22694
GALACTIC HALOS
The x ray halo of Cen X-3
[NASA-CR-189309] p 2055 N94-21295
How to handle 6GBytes a night and not get swamped p 2058 N94-22444
GALACTIC MASS
Magnetic superbubbles in the galactic disk and halo p 2009 N94-22694
GALACTIC NUCLEI
Spatial distribution of near infrared line radiation in galactic nuclei measured with Fabry-Perot spectrometer FAST
[MPE-239] p 2081 N94-21136
Pair plasmas in the galactic center region and in Nova Muscae p 2009 N94-22691
GALACTIC RADIATION
Radio galaxies and their environment
[DE93-040851] p 2150 N94-22397
GALACTIC ROTATION
Generation and maintenance of bisymmetric spiral magnetic fields in disk galaxies in differential rotation p 2010 N94-22695
GALACTIC STRUCTURE
X ray archeology in the Coma cluster
[NASA-CR-194799] p 2054 N94-20175
Extracting galactic structure parameters from multivariated density estimation p 1964 N94-22458
GALAXIES
CCD surface photometry of galaxies p 2058 N94-22445
Visualizing the universe, part 1 p 2064 N94-22476
GALERKIN METHOD
Numerical methods for singularly perturbed differential equations with applications
[AD-A272112] p 1952 N94-20568
MGGHAT: Elliptic PDE software with adaptive refinement, multigrid and high order finite elements p 1956 N94-21470
Numerical study of a multigrid method with four smoothing methods for the incompressible Navier-Stokes equations in general coordinates p 1806 N94-21487
Hybrid finite element/waveguide mode analysis of passive RF devices
[AD-A273074] p 1740 N94-21518
GALILEO PROJECT
Compositional diversity of the lunar North Pole: Preliminary analyses of Galileo SSI data p 2101 N94-20686
GALLIUM ARSENIDE LASERS
First results on InGaAsP separate confinement heterostructure diode lasers
[AD-A270849] p 1815 N94-19878
AlGaAs laser diode FM spectrum: Phased array antenna application p 1746 N94-22196
GALLIUM ARSENIDES
High efficiency epitaxial optical reflector solar cells
[DE93-017115] p 1845 N94-19805
Modeling failure and reliability in new-generation devices
[AD-A271150] p 1748 N94-19910
High current density contacts for photoconductive semiconductor switches
[DE93-018837] p 1750 N94-20312
An x-band peeled HEMT amplifier p 1732 N94-20498
High Speed/High Frequency Optoelectronics
[AD-A271985] p 1751 N94-20580
Ellipsometric studies of sputtered silicon nitride on n-GaAs p 1709 N94-20972
Multiple-wavelength angle-of-incidence ellipsometry: Application to silicon nitride-gallium arsenide structures p 2019 N94-20974
Structural and chemical analysis of a silicon nitride film on GaAs by null ellipsometry p 1709 N94-20975
Ellipsometric measurements of molecular-beam-epitaxy-grown semiconductor multilayer thicknesses: A comparative study p 1710 N94-20983
Comparative thickness measurements of heterojunction layers by ellipsometric, RBS, and XTEM analysis p 1710 N94-20984
Characterization of multilayer GaAs/AlGaAs transistor structures by variable angle spectroscopic ellipsometry p 1796 N94-20985
Variable angle spectroscopic ellipsometric characterization of surface damage in chemical-mechanical polished GaAs p 1710 N94-20986
High temperature stability of amorphous Ta(x)Cu(1-x) diffusion barriers on GaAs p 2022 N94-20990
Polarized-light reflection mode p-i-n modulators with GaAs/AlGaAs multiple quantum well active layers: Design and simulation p 2023 N94-20996
GaAs(100) surface modifications at elevated temperatures, studied by in-situ spectroscopic ellipsometry p 2023 N94-20997
Ellipsometric study of GaAs(100) surface changes induced at elevated temperatures p 2023 N94-20998
Temperature dependence of optical properties of AlAs, studied by in-situ spectroscopic ellipsometry p 2023 N94-20999
Study of concentration-dependent dielectric properties of n-type GaAs using variable angle spectroscopic ellipsometry p 2024 N94-21002
In-situ spectroscopic ellipsometry for real time semiconductor growth monitor p 2024 N94-21003
Real-time analysis of in-situ spectroscopic ellipsometric data during MBE growth of III-V semiconductors p 2024 N94-21004
Design and implementation of GaAs HBT circuits with ACME p 1758 N94-21117
Synthesis and properties of mismatched heterojunction/substrate interfaces
[AD-A272904] p 1760 N94-21229
Decoupled computer architectures for very high-speed technologies
[AD-A271646] p 1900 N94-21301
Dephasing processes in III-V semiconductors
[AD-A271677] p 2028 N94-21362
Analysis of semi-insulating bulk GaAs using glow discharge mass spectrometry
[AD-A273032] p 1682 N94-21435
Bit-systolic arithmetic arrays using dynamic differential gallium arsenide circuits p 1767 N94-21724
Implantation of carbon in GaAs and compensating native defects
[DE93-040122] p 2030 N94-21763
Hydrogen in compound semiconductors
[DE93-040300] p 2031 N94-21922
SLD results from the study of polarized Z(sup 0) produced at the SLC
[DE93-041020] p 1982 N94-21952
Dynamics of surface thermal expansion and diffusivity using two-color reflection transient gratings
[DE93-040547] p 1990 N94-22002
GALLIUM OXIDES
Synthesis and characterization of charge-substituted garnets YCaLnGa5O12 (Ln = Ce, Pr, Tb)
[DE93-040227] p 2033 N94-21992
GALLIUM PHOSPHIDES
Photoconductive Semiconductor Switches for pulsed power applications
[DE93-019411] p 1750 N94-20294
Hydrogen in compound semiconductors
[DE93-040300] p 2031 N94-21922
GAME THEORY
Explanation closure, action closure, and the Sandewall test suite for reasoning about change
[TR-440] p 1907 N94-20522
The Seventh International Symposium on Methodologies for Intelligent Systems (Poster Session)
[AD-A272125] p 1942 N94-20573
On the core-structure of minimum cost spanning tree games
[MEMO-1085] p 1953 N94-21047
Linear programming for standard and nonstandard Markovian control problems. A survey
[PB93-191948] p 1963 N94-21066
The communication complexity of set intersection problems
[MEMO-1077] p 1738 N94-21073
A model of negotiation in an extensive form game p 1965 N94-22075
GAMMA RAY ASTRONOMY
A High Resolution Liquid Xenon Imaging Telescope for 0.3-10 MeV Gamma Ray Astrophysics: Construction and Initial Balloon Flights
[NASA-CR-194709] p 2056 N94-22281
GAMMA RAY BURSTS
Optical and Gamma Ray Space Observations
[NASA-TM-109389] p 2149 N94-20602
Simultaneous optical/gamma ray observations of GRB's p 2149 N94-20603
Gamma ray bursts from collisions of primordial small mass black holes with comets p 2150 N94-20604
Radio and optical emission: Spectral shapes and breaks in GRB
[NASA-CR-194763] p 2150 N94-21781
Relativistic shock spectra: A prediction
[NASA-CR-194764] p 2150 N94-21782
Compton Gamma Ray Observatory highlights of the sky survey p 2002 N94-22642
Dark matter: Neutron star halo and the nature of gamma-bursts p 2002 N94-22643
Relativistically expanding pair plasmas as bursting sources of cosmic gamma rays p 2003 N94-22646
Yohkoh Gamma ray Spectral Observations (YGSO) p 2004 N94-22656
Gamma ray burst as a result of the explosive instability in the magnetosphere of old neutron star p 2007 N94-22675
VHE gamma ray generation by radio pulsars p 2007 N94-22680
GAMMA RAY OBSERVATORY
Simultaneous optical/gamma ray observations of GRB's p 2149 N94-20603
A packet switched communications system for GRO p 1744 N94-21345
FITS data conversion efforts at the Compton Observatory Science Support Center p 1926 N94-22488
Compton Gamma Ray Observatory highlights of the sky survey p 2002 N94-22642
GAMMA RAY SPECTRA
Temperature dependence of CsI(Tl) gamma ray excited scintillation characteristics
[DE94-000836] p 2034 N94-22028
Yohkoh Gamma ray Spectral Observations (YGSO) p 2004 N94-22656
VHE gamma ray generation by radio pulsars p 2007 N94-22680
GAMMA RAY TELESCOPES
A High Resolution Liquid Xenon Imaging Telescope for 0.3-10 MeV Gamma Ray Astrophysics: Construction and Initial Balloon Flights
[NASA-CR-194709] p 2056 N94-22281
The polarization sensitivity of the liquid xenon imaging telescope p 2056 N94-22282
GAMMA RAYS
A weighted least-squares lump correction algorithm for transmission-corrected gamma ray nondestructive assay
[DE93-018474] p 1904 N94-20049

Simultaneous optical/gamma ray observations of GRB's p 2149 N94-20603
Gamma ray bursts from collisions of primordial small mass black holes with comets p 2150 N94-20604
Tensile and shear fracture behavior of fiber reinforced plastics at 77K irradiated by various radiation sources [DE93-040260] p 1706 N94-21542
A High Resolution Liquid Xenon Imaging Telescope for 0.3-10 MeV Gamma Ray Astrophysics: Construction and Initial Balloon Flights [NASA-CR-194709] p 2056 N94-22281
The polarization sensitivity of the liquid xenon imaging telescope p 2056 N94-22282
ASpect: A new spectrum and line analysis package for IRAF p 1926 N94-22485

GANYMEDE
Geology of Galileo Regio quadrangle, Ganymede p 2130 N94-20642

GAPS
Thermally activated retainer means utilizing shape memory alloy [NASA-CASE-MSC-21793-1] p 1654 N94-20304

GARNETS
Primary differentiation in the early Earth: Nd and Sr isotopic evidence from diamondiferous eclogites for both old depleted and old enriched mantle, Yakutia, Siberia p 1862 N94-20776
Synthesis and characterization of charge-substituted garnets YCaLnGa5O12 (Ln = Ce, Pr, Tb) [DE93-040227] p 2033 N94-21992

GAS ANALYSIS
Outgassing rate of Reemay Spunbonded Polyester and DuPont Double Aluminized Mylar [DE93-040015] p 1699 N94-19973
Dating native gold by noble gas analyses p 1684 N94-20652
The chondrite Mihonoseki: New observed fall p 2083 N94-20764
Materials processing and manufacturing technologies for diamond substrate multichip modules [AD-A271484] p 2027 N94-21319
Instantaneous velocity field imaging instrument for supersonic reacting flows [NASA-CR-191162] p 1809 N94-21607
The laser and its applications on environment and biotechnology research [DE94-000376] p 1820 N94-21957
Atmospheric sampling glow discharge ionization and triple quadrupole tandem mass spectrometry for explosives vapor detection [DE93-040593] p 1852 N94-22004
Passive Cryogenic Sampler [DE94-000918] p 1811 N94-22392

GAS COMPOSITION
A long-term change of the AR/KR/XE fractionation in the solar corpuscular radiation p 2136 N94-20875
A calcium oxide sorbent process for bulk separation of carbon dioxide [DE93-019288] p 1847 N94-21540

GAS DETECTORS
Outgassing rate of Reemay Spunbonded Polyester and DuPont Double Aluminized Mylar [DE93-040015] p 1699 N94-19973
Development and demonstration of a personal monitoring system for exposure to hydrogen fluoride [DE93-041273] p 1891 N94-20935
Surface acoustic wave sensing of VOC's in harsh chemical environments [DE93-040721] p 1968 N94-21751

GAS DISCHARGES
Evaluation of externally heated pulsed MPD thruster cathodes [NASA-CR-191090] p 1670 N94-21565

GAS DISSOCIATION
Unlike-pair interactions at high pressure and high temperature [DE93-019948] p 1796 N94-19916
Ultrafast gas switching experiments [DE93-019071] p 1782 N94-21634
Performance assessment of low pressure nuclear thermal propulsion [NASA-TM-106433] p 1671 N94-21860
Infrared FEL photochemistry: Multiple-photon dissociation of freon gas [DE94-000817] p 1820 N94-22585

GAS DYNAMICS
The sand bag model of the dispersion of the cosmic body in the atmosphere p 2084 N94-20823
Computational and analytical methods in nonlinear fluid dynamics [AD-A272722] p 1802 N94-21169
Establishing the basis for validated predictions of highly non-equilibrium flows (with 9 attachments) [AD-A272918] p 1802 N94-21220
An analysis of pool surface deformation due to a plunging liquid jet [AD-A272970] p 1802 N94-21261
Dynamics of face seals for high speed turbomachinery p 1655 N94-21796

GAS EVOLUTION
Evolution of the Martian atmosphere p 2146 N94-21680

GAS EXPANSION
On magnetodynamic effects initiated by a high-speed impact of a large cosmic body upon the Earth's surface p 2082 N94-20647

GAS FLOW
The flow of gas across the piston-segments-cylinder interface [ECL-92-40] p 1824 N94-20594
Establishing the basis for validated predictions of highly non-equilibrium flows (with 9 attachments) [AD-A272918] p 1802 N94-21220
Compliant seal development p 1655 N94-21795
F2D users manual: A two-dimensional compressible gas flow code [DE94-000653] p 1805 N94-22386

GAS GIANT PLANETS
Laboratory studies of low temperature rate coefficients: The atmospheric chemistry of the outer planets [NASA-CR-193485] p 1972 N94-20130

GAS INJECTION
Thrust expansion engine [AD-D015896] p 1669 N94-20121

GAS IONIZATION
Photoabsorption and Compton scattering in ionization of helium at high photon energies [DE94-000380] p 1974 N94-21658
Plasma lens experiments at the Final Focus Test Beam [DE93-041081] p 1981 N94-21688

GAS JETS
A high-intensity He-jet production source for radioactive beams [DE93-040247] p 1981 N94-21767

GAS LASERS
Design aspects and parametric characterisation of a neutral rare gas laser [AD-A271100] p 1814 N94-19850

GAS MIXTURES
Speed of sound data and related models for mixtures of natural gas constituents [PB93-200822] p 1968 N94-21447

GAS PRESSURE
Research on plasma-puff initiation of high Coulomb transfer switches [NASA-CR-194371] p 1994 N94-21289
Plasma-puff initiation of high Coulomb transfer switches p 1994 N94-21290
Characteristics of plasma-puff trigger for a inverse-pinch plasma switch p 1995 N94-21291
Stability curves for a thermoacoustic prime mover [AD-A272607] p 1968 N94-21422
Effect of powder characteristics on gas-pressure sintering of Si3N4 with rare earth additives [DE94-000330] p 1694 N94-21945

GAS TEMPERATURE
Fluid absorption solar energy receiver [NASA-CR-194688] p 1846 N94-20229
Are Plinian type eruptions possible on Venus? p 2123 N94-20803

GAS TRANSPORT
Parameters affecting hydrogen chloride measurements [AD-A271326] p 1851 N94-20025

GAS TUNGSTEN ARC WELDING
Thermocapillary and arc phenomena in stainless steel welds [DE94-000518] p 1821 N94-19859
Microscopic evaluation of low-temperature embrittlement in type 308 stainless steel welds [DE93-040266] p 1690 N94-20282

GAS TURBINE ENGINES
Design of a state-space controller for an advanced gas turbine engine [AD-A270859] p 1647 N94-20042
Applicability and performance benefits of XD (Tradename) titanium aluminides to expendable gas turbine engines [AD-A272998] p 1648 N94-21268
Thrust augmentation options for the Beta 2 two-stage-to-orbit vehicle [NASA-TM-106448] p 1648 N94-21563
The 1992 Seals Flow Code Development Workshop [NASA-CP-10124] p 1654 N94-21790
Brush seal bristle flexure and hard-rub characteristics p 1654 N94-21791
Air Force brush seal programs p 1655 N94-21793
Navy GTE seal development activity p 1655 N94-21794
Compliant seal development p 1655 N94-21795
Ceramic Technology Project [DE94-001011] p 1707 N94-21822
Advanced Turbine Systems (ATS). Phase 1: System scoping and feasibility studies [DE93-041130] p 1826 N94-21938
Life prediction systems for critical rotating components p 1835 N94-22615

GAS TURBINES
Flow interaction experiment. Volume 1: Aerothermal modeling, phase 1 [NASA-CR-189192-VOL-1] p 1648 N94-21582
Flow interaction experiment. Volume 2: Aerothermalmodeling, phase 2 [NASA-CR-189192-VOL-2] p 1648 N94-21583
Comparison of mixing calculations for reacting and non-reacting flows in a cylindrical duct [NASA-TM-106435] p 1649 N94-21758
Advanced Turbine Systems (ATS). Phase 1: System scoping and feasibility studies [DE93-041130] p 1826 N94-21938
Performance calculations and research direction for a water enhanced regenerative gas turbine cycle [DE93-019866] p 1826 N94-21983

GAS-SOLID INTERACTIONS
Model for liquid boron oxide droplet gasification in H/O/C/F combustion environments [AD-A272911] p 1682 N94-21243
Oxidation of dissolved iron under warmer, wetter conditions on Mars: Transitions to present-day arid environments p 2143 N94-21663

GASEOUS DIFFUSION
A database of selected transport coefficients for combustion studies [DE93-041278] p 1678 N94-19889
Encounters of H and D atoms with O2 in water: Relative diffusion and reaction rates [DE93-018587] p 1970 N94-19956

GASEOUS FUELS
Biofuels: Project summaries [DE93-010003] p 1712 N94-19984

GASIFICATION
Model for liquid boron oxide droplet gasification in H/O/C/F combustion environments [AD-A272911] p 1682 N94-21243

GASTROINTESTINAL SYSTEM
Effect of copper sulphate on the rate of afferent discharge in the gastric branch of the vagus nerve in the rat p 1887 N94-21907
Conditioned taste aversion induced by motion is prevented by selective vagotomy in the rat p 1887 N94-21908

GATES (CIRCUITS)
CMOS gate array characterization procedures [AD-A269943] p 2014 N94-20029
Resistive gate magnetic field sensor [AD-D015923] p 1749 N94-20199
Characteristics of 0.8- and 0.2-microns gate length In(x)Ga(1-x) As/In(0.52)Al(0.48)As/InP (0.53 less than or equal to x less than or equal to 0.70) modulation-doped field-effect transistors at cryogenic temperatures p 1733 N94-20499
Design of CMOS logic gates for TID radiation p 1754 N94-21083
Mixed voltage VLSI design p 1756 N94-21104
Test pattern generation for ILA sequential circuits p 1757 N94-21107
VLSI design for reliability-hot carrier effects [AD-A271586] p 1761 N94-21256
Design and test of field programmable gate arrays in space applications p 1765 N94-21710
Defect-sensitivity analysis of an SEU immune CMOS logic family p 1765 N94-21711
Dimension scaling effects on the yield sensitivity of HEMT digital circuits p 1765 N94-21712
A high speed CMOS A/D converter p 1767 N94-21726
Behavior of faulty double BJT BiCMOS logic gates p 1767 N94-21727
On fast carry select adders p 1767 N94-21728

GAUGE INVARIANCE
On the twisted N=2 superconformal structure in 2d gravity coupled to matter [DE93-628627] p 2037 N94-20178

GAUGE THEORY
On the twisted N=2 superconformal structure in 2d gravity coupled to matter [DE93-628627] p 2037 N94-20178
Lattice gauge theory: Present status [DE93-041154] p 2038 N94-21692

GAUSSIAN ELIMINATION
On the numerical stability of quasi-definite systems [DE93-019404] p 1950 N94-20217

GEAR TEETH
The relative noise levels of parallel axis gear sets with various contact ratios and gear tooth forms [NASA-TM-106431] p 1826 N94-21756

GEARS
A design optimization procedure for epicyclic gears
[MATHS-REPT-A-188] p 1822 N94-20146
The relative noise levels of parallel axis gear sets with various contact ratios and gear tooth forms
[NASA-TM-106431] p 1826 N94-21756
GELATION
Polymer gels as precursors to high-performance materials
[AD-A270937] p 1699 N94-20046
GELS
Polymer gels as precursors to high-performance materials
[AD-A270937] p 1699 N94-20046
Shock compression of low-density foams
[DE93-040545] p 1707 N94-21546
Swelling equilibria for cationic 2-hydroxyethyl methacrylate (HEMA)-based hydrogels
[DE94-000728] p 1707 N94-21856
GENERAL AVIATION AIRCRAFT
Aviation safety research. Volume 1: Literature review of sources of aviation accident and incident data and selected factors contributing to accidents
[PB93-202885] p 1641 N94-21428
GENETIC ALGORITHMS
General asymmetric neural networks and structure design by genetic algorithms: A learning rule for temporal patterns
[DE94-001254] p 1947 N94-22563
GENETICS
Statistical analysis of a reciprocal translocations data base
[RR-900-I] p 1963 N94-20165
GEOCHEMISTRY
The Koshak section: Evidence for element fractionation and an oxidation event at the K/T boundary p 1862 N94-20641
Core formation in the Moon: The mystery of the excess depletion of Mo, W and P p 2095 N94-20651
Detectability of crystalline ferric and ferrous minerals on Mars p 2110 N94-20730
Primary differentiation in the early Earth: Nd and Sr isotopic evidence from diamondiferous eclogites for both old depleted and old enriched mantle, Yakutia, Siberia p 1862 N94-20776
Magnesian anorthosites from the western highlands of the Moon: Isotope geochemistry and petrogenesis p 2118 N94-20779
Discovery Venera surface: Atmosphere geochemistry experiments mission concept p 2123 N94-20806
Consortium study of lunar meteorites Yamato-793169 and Asuka-881757: Geochemical evidence of mutual similarity, and dissimilarity versus other mare basalts p 2085 N94-20857
Petrology and geochemistry of VLT glasses from double drive tube 79001/2 p 1687 N94-20870
K, U, and Th behavior in Martian environmental conditions p 2141 N94-20908
Core formation, wet early mantle, and H2O degassing on early Mars p 2145 N94-21674
GEOCHRONOLOGY
Twenty-Fourth Lunar and Planetary Science Conference. Part 3: N-Z
[NASA-CR-193149] p 2092 N94-20636
Dating native gold by noble gas analyses p 1684 N94-20652
Geologic mapping of Northern Atla Regio on Venus: Preliminary data p 2095 N94-20654
Modelling the gravity and magnetic field anomalies of the Chicxulub crater p 1862 N94-20668
Structural evidence for reorientation of Miranda about a paleo-pole p 2098 N94-20671
U-Pb provenance ages of shocked zircons from the K-T boundary, Raton Basin, Colorado p 1685 N94-20701
Geochronology and petrogenesis of the western highlands alkali suite: Radiogenic isotopic evidence from Apollo 14 p 2118 N94-20778
The age of the Pretoria Saltpan impact crater, South Africa p 1863 N94-20798
Age and thermochronology of K-feldspars from the Manson Impact Structure p 1863 N94-20899
The early Martian environment: Clues from the cratered highlands and the Precambrian Earth p 2143 N94-21667
Early Mars: A regional assessment of denudation chronology p 2145 N94-21676
GEODESY
Estimability of polar motion using range observations to satellites
[PB93-219319] p 1842 N94-22265
GEODYNAMICS
Dynamics of large scale impacts on Venus and Earth p 2098 N94-20666
Estimability of polar motion using range observations to satellites
[PB93-219319] p 1842 N94-22265
GEOGRAPHIC INFORMATION SYSTEMS
Studying Venus using a GIS database p 2105 N94-20707
Drought early warning system for crop production p 1840 N94-20966
Integration opportunities for computer models, methods, and GIS used in Corps planning studies
[AD-A271714] p 2044 N94-21354
Urban applications of satellite remote sensing and GIS analysis
[PB93-202174] p 1842 N94-21855
Computer-aided design system for objects location and reservoir with dispersed resource evolution investigation p 1923 N94-22064
GEOIDS
Geoid, topography, and convection-driven crustal deformation on Venus p 2116 N94-20769
Influence of geoid model uncertainty on the determination of ocean circulation with satellite altimetry
[PB93-219301] p 1842 N94-22097
GEOLOGICAL FAULTS
Beta Regio rift system on Venus: Geologic interpretation of Magellan images p 2095 N94-20655
Beta Regio - Phoebe Regio on Venus: Geologic mapping with the Magellan data p 2096 N94-20656
Formation and evolution of radial fracture systems on Venus p 2099 N94-20672
Thermal and rheological controls on magma migration in dikes: Examples from the east rift zone of Kilauea volcano, Hawaii p 1862 N94-20673
Constraints on the rate of discharge and duration of the Mangala Valles flood p 2099 N94-20674
Chocolate tablet aspects of cytherean Meshkenet Tessera p 2106 N94-20710
Ridge belt-related scarps and troughs: Compressional crustal bending on Venus p 2106 N94-20711
Rifting at Devana Chasma, Venus: Structure and estimation of the effective thickness of the elastic lithosphere p 2113 N94-20754
Extensional history of Mars' Tharsis Region p 2125 N94-20814
Complex structure of the Thaumasia region of Mars p 2125 N94-20815
Arcuate and circular structures in the Tharsis region: Evidence of coronae on Mars p 2134 N94-20863
Wrinkle ridges, reverse faulting, and the depth penetration of lithospheric stress in lunae planum, Mars p 2141 N94-20910
On the origin and evolution of circular forms observed in remote sensing images of the Rio de Janeiro State, Brazil p 1839 N94-20963
GEOLOGICAL SURVEYS
Evidence for an ice sheet/frozen lake in Utopia Planitia, Mars p 2089 N94-20388
Geologic mapping of Northern Atla Regio on Venus: Preliminary data p 2095 N94-20654
Beta Regio - Phoebe Regio on Venus: Geologic mapping with the Magellan data p 2096 N94-20656
Formation and evolution of radial fracture systems on Venus p 2099 N94-20672
Constraints on the rate of discharge and duration of the Mangala Valles flood p 2099 N94-20674
Kalkkop crater, Eastern Cape: A new impact crater in South Africa p 1862 N94-20714
Discharge rates in Ma'adim Vallis, Mars p 2128 N94-20830
Complex ridged terrain-related ridge belts on Venus: Global distribution and classification p 2129 N94-20835
Experiences in airborne computing at NRC for geophysical exploration applications p 1783 N94-22185
Interpretation of Ground Penetrating Radar data at the Hanford Site, Richland, Washington
[DE93-040409] p 1743 N94-22557
GEOLOGY
Cryoplanation terraces of interior and western Alaska p 2091 N94-20396
Delimitation of terrestrial impact craters by way of pseudotachylytic rock distribution p 1863 N94-20783
Tumuli and tubes: Teaching scientific techniques p 2039 N94-20818
Geology and radiophysical properties of the Venera and Vega landing sites p 2135 N94-20867
GEOMAGNETIC TAIL
Modeling the minimum energy state of the Earth's magnetotail
[AD-A267984] p 1856 N94-20485
GEOMAGNETISM
A general purpose ionospheric ray tracing procedure
[AD-A271058] p 1854 N94-19860
Narsarsuaq Geophysical Observatory: Magnetic results, 1985 - 1990
[DATA-REPT-93-1] p 1856 N94-20607
Magnetic results 1991: Brorfelde, Godhavn, Thule and Narsarsuaq
[DATA-REPT-92-3] p 1856 N94-20608
Thule Geophysical Observatory: Magnetic results 1985 - 1990
[DATA-REPT-92-4] p 1857 N94-20609
On magnetodynamic effects initiated by a high-speed impact of a large cosmic body upon the Earth's surface p 2082 N94-20647
Structural evidence for reorientation of Miranda about a paleo-pole p 2098 N94-20671
Reverse polarity magnetized melt rocks from the Chicxulub impact structure, Yucatan Peninsula, Mexico p 1863 N94-20843
Physics of magnetospheric boundary layers
[NASA-CR-194725] p 1858 N94-21836
GEOMETRICAL OPTICS
RCS Analysis of Plate Geometries, parts 1 and 2
[NASA-CR-194173] p 1717 N94-20269
GEOMETRICAL THEORY OF DIFFRACTION
High resolution electron crystallography of protein molecules
[DE93-040114] p 1884 N94-19826
An extended UTD analysis for the scattering and diffraction from cubic polynomial strips
[NASA-CR-194581] p 1716 N94-20139
RCS Analysis of Plate Geometries, parts 1 and 2
[NASA-CR-194173] p 1717 N94-20269
High-frequency techniques for RCS prediction of plate geometries p 1717 N94-20270
GEOMETRY
Geometric optimization
[DE93-040152] p 1917 N94-21764
Non commutative geometry and physics
[PB93-215499] p 1961 N94-22264
GEOMORPHOLOGY
Hydrological consequences of ponded water on Mars p 2089 N94-20383
Evidence for an ice sheet/frozen lake in Utopia Planitia, Mars p 2089 N94-20388
Geomorphic evidence for an eolian contribution to the formation of the Martian northern plains p 2092 N94-20402
Geologic mapping of Northern Atla Regio on Venus: Preliminary data p 2095 N94-20654
Largest impact features on Venus: Non-preserved or non-recognizable? p 2096 N94-20657
Venus pancake dome formation: Morphologic effects of a cooling-induced variable viscosity during emplacement p 2110 N94-20732
Chicxulub impact basin: Gravity characteristics and implications for basin morphology and deep structure p 1862 N94-20757
Numerical modeling of impact erosion of atmospheres: Preliminary results p 2131 N94-20847
Arcuate and circular structures in the Tharsis region: Evidence of coronae on Mars p 2134 N94-20863
Degradation sequence of young lunar craters from orbital infrared survey p 2136 N94-20874
On the origin and evolution of circular forms observed in remote sensing images of the Rio de Janeiro State, Brazil p 1839 N94-20963
The evolution of the early Martian climate and the initial emplacement of crustal H2O p 2143 N94-21665
The early Martian environment: Clues from the cratered highlands and the Precambrian Earth p 2143 N94-21667
GEOPHYSICAL OBSERVATORIES
Narsarsuaq Geophysical Observatory: Magnetic results, 1985 - 1990
[DATA-REPT-93-1] p 1856 N94-20607
Magnetic results 1991: Brorfelde, Godhavn, Thule and Narsarsuaq
[DATA-REPT-92-3] p 1856 N94-20608
Thule Geophysical Observatory: Magnetic results 1985 - 1990
[DATA-REPT-92-4] p 1857 N94-20609
GEOPHYSICS
Inversion of gravity and bathymetry in oceanic regions for long-wavelength variations in upper mantle temperature and composition
[NASA-CR-192272] p 1882 N94-20131
Progress In Electromagnetics Research Symposium (PIERS)
[NASA-CR-194629] p 1718 N94-20403
Integrated display of multi-sensor geophysical and electromagnetic flight data p 1721 N94-20418
Modelling the gravity and magnetic field anomalies of the Chicxulub crater p 1862 N94-20668
Comparative hypsometric analysis of both Earth and Venus topographic distributions p 2108 N94-20722
A tectonic resurfacing model for Venus p 2118 N94-20781
Shock temperature measurements of iron to 350 GPa
[DE94-001058] p 1695 N94-22024

GEOSYNCHRONOUS ORBITS
Inclined orbits and interference to stationary service and to stationary service by satellite p 1653 N94-22188
GERMANIUM
Photoluminescence spectroscopy of zinc germanium diphosphide (ZnGeP2)
[AD-A270705] p 1678 N94-19953
Monocrystalline germanium film on sapphire
[AD-D015925] p 2017 N94-20348
Spectroscopic ellipsometric characterization of Si/Si(1-x)Ge(x) strained-layer superlattices p 2025 N94-21009
GERMANIUM ALLOYS
High current density contacts for photoconductive semiconductor switches
[DE93-018837] p 1750 N94-20312
Stable, high-efficiency amorphous-silicon solar cells with low hydrogen content
[DE93-018214] p 1848 N94-21826
Magnetism in CeRu2Ge2 and CeRh2Ge2 and its pressure dependence
[DE93-040061] p 2032 N94-21987
GERMANIUM COMPOUNDS
Surface states at the GaAs-germanium nitride interface p 1709 N94-20973
GERMANIUM ISOTOPES
Semiconductor isotope engineering
[DE93-040119] p 2030 N94-21744
GERMANY
Documents on the history of aeronautical and space research in Germany, 1900 - 1970
[DLR-MITT-92-08] p 2152 N94-20543
GIBBS FREE ENERGY
A Green function method for calculation of atomic and electronic properties of isolated adsorbate atoms
[ETN-93-95055] p 2014 N94-20018
GIMBALS
Apparatus for simulating an exoatmospheric structure
[NASA-CASE-MSC-21975-1] p 1653 N94-20339
GLACIAL DRIFT
Ice in the northern plains: Relic of a frozen ocean? p 2090 N94-20391
GLACIERS
Workshop on the Martian Northern Plains: Sedimentological, Periglacial, and Paleoclimatic Evolution
[NASA-CR-194831] p 2088 N94-20382
Milankovitch insulation forcing and cyclic formation of large-scale glacial, fluvial, and eolian landforms in central Alaska p 2089 N94-20386
A wet-geology and cold-climate Mars model: Punctuation of a slow dynamic approach to equilibrium p 2090 N94-20389
Studies of Greenland using the SEASAT scatterometer p 1725 N94-20433
Radar backscattering from snow facies of the Greenland ice sheet: Results from the AIRSAR 1991 campaign p 1725 N94-20434
Ancient Martian valley genesis and paleoclimatic inference: The present as a key to the past p 2142 N94-21661
GLASS
Metal-glass composite field-emitting arrays
[AD-D015942] p 1673 N94-20064
Optics survivability support, volume 1
[DE93-019616] p 1985 N94-20262
Neutron-scattering studies of Yb-bearing silicate glasses
[DE93-019768] p 1700 N94-20265
Optics survivability support, volume 2
[DE93-040310] p 1985 N94-20263
Plasma chemical vapor deposition of halide glasses
[AD-D015933] p 1701 N94-20331
Kinetics of phase transformations in glass forming systems
[NASA-CR-194270] p 1701 N94-20347
Sintering silicon nitride
[NASA-CASE-LEW-15489-1] p 1703 N94-20529
The Erevan howardite: Petrology of glassy clasts and mineral chemistry p 1684 N94-20640
Impact glasses from the ultrafine fraction of lunar soils p 2097 N94-20662
Self diffusion of alkaline-Earth in Ca-Mg-aluminosilicate melts: Experimental improvements on the determination of the self-diffusion coefficients p 1684 N94-20669
Post-igneous redistribution of components in eucrites p 1685 N94-20684
C-O volatiles in Apollo 15 and Apollo 17 picritic glasses p 1685 N94-20727
Further analyses of Rio Cuarto impact glass p 1685 N94-20745
Magnetic properties and Moessbauer analyses of glass from the K-T boundary, Beloc, Haiti p 1685 N94-20753
Basaltic magmatism on the Moon. A perspective from volcanic picritic glasses p 2114 N94-20758
Origin of the Apollo 15 very low Ti green glass. A perspective from the compositional diversity in the very low Ti glasses p 1685 N94-20759
The age of the Pretoria Saltpan impact crater, South Africa p 1863 N94-20798
Origin of high-Ti lunar ultramafic glasses p 1686 N94-20853
Petrology and geochemistry of VLT glasses from double drive tube 79001/2 p 1687 N94-20870
Optical properties of chromium and neodymium in zirconium - barium - lanthanum - aluminum fluoride glass
[AD-A271609] p 1987 N94-21236
The energy performance of prototype holographic glazings
[DE93-040451] p 1809 N94-21545
Activities Report of the Institute of Applied Physics
[ETN-93-93749] p 1966 N94-21798
Modeling of glass fabrication p 1711 N94-21800
GLAZES
Microstructural stability of wrought, laser and electron beam glazed NARloy-Z alloy at elevated temperatures
[NASA-TM-108431] p 1689 N94-20100
GLIDE PATHS
All-weather precision landing system for aircraft in remote areas
[AD-D015924] p 1643 N94-20197
GLOBAL POSITIONING SYSTEM
Detection of traveling ionospheric disturbances induced by atmospheric gravity waves using the global positioning system p 1723 N94-20425
An investigation into the integration of meter-level range and millimeter-level phase data using a multimode stimulation for optimal filter estimation software package
[AD-A267955] p 1751 N94-20483
A software architecture for a small autonomous underwater vehicle navigation system
[AD-A272322] p 1643 N94-21037
Vector gravimetry by a combination of inertial and GPS satellite measurements
[ISBN-0-315-61980-5] p 1861 N94-22424
A robust quality control system for GPS navigation and kinematic positioning
[ISBN-0-315-83148-0] p 1644 N94-22427
GLOBAL WARMING
Health effects of global warming: Problems in assessment
[DE93-040323] p 1850 N94-19930
Climate forcings and feedbacks p 1869 N94-21641
Accuracy requirements — for monitoring of climate changes p 1869 N94-21642
GLOW DISCHARGES
Microscopic origins of metastable effects in a-Si:H and deep defect characterization in a-Si,Ge:H alloys
[DE93-018205] p 1688 N94-19985
Growth mechanisms and characterization of hydrogenated amorphous-silicon-alloy films
[DE93-018202] p 1699 N94-20047
Laser diagnostics of RF hydrogen plasma reactors: Application to the processing of III-V materials
[AD-A272659] p 1994 N94-21214
Analysis of semi-insulating bulk GaAs using glow discharge mass spectrometry
[AD-A273032] p 1682 N94-21435
Atmospheric sampling glow discharge ionization and triple quadrupole tandem mass spectrometry for explosives vapor detection
[DE93-040593] p 1852 N94-22004
GLUONS
A conceptual design for the STAR endcap electromagnetic calorimeter
[DE93-040801] p 1807 N94-19990
Jet shapes in hadron and electron colliders
[DE93-019386] p 1979 N94-20216
B production at D0
[DE93-019250] p 1972 N94-20291
New perspectives in quantum chromodynamics
[DE93-041021] p 2038 N94-21935
Time evolution of the quark-gluon plasma
[DE94-000804] p 1998 N94-22389
GLUTAMIC ACID
Immunocytochemical localization of glutamic acid decarboxylase (GAD) and substance P in neural areas mediating motion-induced emesis: Effects of vagal stimulation on GAD immunoreactivity p 1887 N94-21909
GLYCOLS
Water-enhanced solvation of organics
[DE93-040297] p 1683 N94-21947
Column chromatographic separation of Y(3+) from Sr(2+) by polymeric ionizable crown ether resins
[DE94-000935] p 1683 N94-22021
GOES SATELLITES
Comparison of radiation and cloud parameters derived from satellite and aircraft measurements during FIRE 2 cirrus IFO p 1872 N94-22299
GOGGLES
Night vision goggle model F4949 preflight adjustment/assessment procedures
[AD-A271079] p 1895 N94-19935
GOLD
Automated HMC assembly
[DE93-040641] p 1749 N94-20005
Dating native gold by noble gas analyses p 1684 N94-20652
Application of an electrochemical quartz crystal microbalance to the study of electrocatalytic films
[DE93-041124] p 2029 N94-21691
Electron emission from nanometer-size metallic clusters: Electronic states and structural stability of supported Au clusters
[DE93-040184] p 1975 N94-21766
Sulfur-bonded thiophenes in organometallic rhenium complexes and adsorption of isocyanides on gold
[DE93-041126] p 1694 N94-21937
GOLD ALLOYS
High current density contacts for photoconductive semiconductor switches
[DE93-018837] p 1750 N94-20312
GOLD ISOTOPES
Searching for high baryon density at the AGS with ARC
[DE93-041155] p 1975 N94-21693
GOODNESS OF FIT
Extracting information from wrong answers in computerized adaptive testing
[AD-A272832] p 1894 N94-21434
GOVERNMENT PROCUREMENT
NASA procurement: Planning for pilot test of new procurement procedures is adequate. Report to the Chairman, Committee on Governmental Affairs, US Senate
[GAO/NSIAD-94-67] p 2039 N94-20236
Implementing Electronic Data Interchange (EDI) with small business suppliers in the pre-award acquisition process
[AD-A271767] p 1945 N94-21305
NASA procurement report, FY 1992
[NASA-TM-109390] p 2040 N94-21623
Summary data on all NASA procurement actions
[NASA-TM-109392] p 2040 N94-21638
GOVERNMENT/INDUSTRY RELATIONS
Statement of David E. Baldwin, Associate Director for Energy, Lawrence Livermore National Laboratory and John C. Crawford, Vice President, Sandia National Laboratories, California, to the Subcommittee on Research and Development of the Committee on Environment and Public Works, US Senate, Washington, DC, 22 March 1993
[DE93-017991] p 1844 N94-19803
Microdynamic model of reproduction: Taxation and currency issue as regulators of economy p 2053 N94-22084
GRADIENTS
Chicxulub impact basin: Gravity characteristics and implications for basin morphology and deep structure p 1862 N94-20757
GRAIN BOUNDARIES
Near atomic resolution microanalysis of interfaces by analytical electron microscopy
[DE93-019437] p 1687 N94-19904
Evaluation of a diffusion/trapping model for hydrogen ingress in high-strength alloys
[AD-A271328] p 1689 N94-20027
Microstructural stability of wrought, laser and electron beam glazed NARloy-Z alloy at elevated temperatures
[NASA-TM-108431] p 1689 N94-20100
Examinations of composition and deformation behavior of intermetallic phases on the basis of Fe3(AlSi)
[GKSS-92/E/16] p 1692 N94-21311
Electron holography applied to the study of ceramic materials
[DE94-000329] p 1707 N94-21653
Microtextural characterization of annealed and deformed copper
[DE93-040144] p 1695 N94-21990
Temperature-dependent ion beam mixing
[DE93-040281] p 2033 N94-21999
GRAIN SIZE
Effects of processing history on the creep strength of Nb-1Zr
[DE93-015905] p 1689 N94-20093
Identification of an interstellar oxide grain from the Murchison meteorite by ion imaging p 2082 N94-20659
Lamellar olivine in the Divnoe achondrite: Evidence for high-pressure exsolution? p 1685 N94-20679
Optical effects of space weathering on lunar soils and the role of the finest fraction p 2101 N94-20687
Visible-infrared properties of controlled laboratory soils p 1685 N94-20689
Thermal conductivity measurements of particulate materials under Martian conditions p 1685 N94-20703

The Sm-Nd systematics of silicate inclusions in iron meteorites: Results from Caddo (IAB)
[CONTRIB-5241(804)] p 2084 N94-20795
Coagulation of grains in static and collapsing protostellar clouds p 2085 N94-20865
Microstructural modeling and toughening of Si3N4 ceramics for high temperature engine applications
[AD-A272897] p 1704 N94-21197

GRAMMARS
Program derivation in acyclic graphs and related problems
[PB93-191765] p 1903 N94-19994
Bottom-up abstract interpretation of logic programs
[PB93-191773] p 1928 N94-19995
Representation of idioms in connectionist models p 1940 N94-20247
A single layer higher order neural net and its application to grammar recognition p 1941 N94-20251
Syntactic neural networks for natural language processing p 1941 N94-20254
GWB: Manual for the Grammar WorkBench version 1.5
[TR-92-14] p 1909 N94-21061

GRANITE
Chronology of lunar granite 12033,576: Resetting of Rb-Sr and K-Ca isochrons p 2115 N94-20763
The age of the Pretoria Saltpan impact crater, South Africa p 1863 N94-20798

GRANTS
Summary data on all NASA procurement actions
[NASA-TM-109392] p 2040 N94-21638

GRANULAR MATERIALS
The Coulomb anomaly in strongly disordered films
[AD-A271095] p 2012 N94-19849
Multiplicity of chondrule heating events and the coarsening of chondrule textures p 2085 N94-20860
Dynamic response of multiphase porous media
[AD-A272915] p 1831 N94-21219

GRAPH THEORY
Program derivation in acyclic graphs and related problems
[PB93-191765] p 1903 N94-19994
On multiflow problems
[RR-889-M] p 1950 N94-20125
Determining the distance to the perfect matching polytope of a bipartite graph
[RR-895-M] p 1950 N94-20161
Label-connected graphs: An overview
[RR-898-M] p 1950 N94-20163
Totally strong and strong graphs
[RR-902-I] p 1951 N94-20237
Applying the INN model to the MaxClique
[DE93-040137] p 1906 N94-20276
Half-integral flows in a planar graph with four holes
[RR-894-M] p 1951 N94-20302
Graph minors: Structure theory and algorithms
[AD-A271851] p 1952 N94-20613
Long cycles in graphs containing a 2-factor with many odd components
[MEMO-1086] p 1953 N94-21048
Degree sums, k-factors and Hamiltonian cycles in graphs
[MEMO-1078] p 1953 N94-21074
Modular interval spaces
[PB93-220663] p 1961 N94-22266

GRAPHIC ARTS
The manager's guide to NASA graphics standards
[NHB-1430.2] p 2042 N94-20308

GRAPHICAL USER INTERFACE
Advanced software development workstation: Knowledge base methodology: Methodology for first Engineering Script Language (ESL) knowledge base
[NASA-CR-193643] p 1930 N94-21065
A graphical user-interface development tool for intelligent computer-assisted instruction systems
[AD-A272988] p 1912 N94-21265
Military satellite communications decision support system requirements analysis and user interface design
[AD-A273047] p 1740 N94-21436
Design and implementation of a status at a glance user interface for a power distribution expert system
[NASA-TM-106412] p 1715 N94-21589
Design document and database specifications for the Naval Interactive Data Analysis System (NIDAS), version 1.0
[NASA-CR-194817] p 2045 N94-21865
Application development in a PC/LAN environment p 1923 N94-22067
Software systems used for unstructured grid generation at NASA Langley p 1918 N94-22351
An object-oriented data reduction system in Fortran p 2046 N94-22447
GUIs in the MIDAS environment p 2047 N94-22449
Writing instrument interfaces with xf/tktcl p 1925 N94-22480
ASpect: A new spectrum and line analysis package for IRAF p 1926 N94-22485
The HEASARC graphical user interface p 1926 N94-22487
The University of Hawaii Institute for Astronomy CCD camera control system p 1828 N94-22489
An object-oriented approach for supporting both X and terminal interfaces p 1926 N94-22491
AXAF user interfaces for heterogeneous analysis environments p 1926 N94-22507
STARBASE: Database software for the automated plate scanner p 1927 N94-22512
XPI: The Xanadu Parameter Interface p 1927 N94-22513
PCIPS 2.0: Powerful multiprofile image processing implemented on PCs p 1927 N94-22532
SPECFOCUS: An IRAF task for focusing spectrographs p 1965 N94-22540

GRAPHITE
Lightweight battery electrode and method of making it
[AD-D015895] p 1749 N94-20120
Intercalated hybrid graphite fiber composite
[NASA-CASE-LEW-15241-1] p 1673 N94-20539
Graphite/polyurethane flexible composites: Mechanical and vibration damping properties
[AD-A271608] p 1674 N94-20950
Performance of carbon-based hot frit substrates
[DE94-000509] p 1676 N94-21754

GRAPHITE-EPOXY COMPOSITES
Thermal stability relationships between PMR-15 resin and its composites
[NASA-TM-106285] p 1675 N94-21486
Damage states around fastener holes in thick graphite/epoxy composite laminates
[AD-A272613] p 1675 N94-21504

GRAPHITE-POLYIMIDE COMPOSITES
R and D to HOPE airframe p 1665 N94-21406

GRAPHS (CHARTS)
Degree sums, k-factors and Hamiltonian cycles in graphs
[MEMO-1078] p 1953 N94-21074
Mathcad computer applications predicting antenna parameters from antenna physical dimensions and ground characteristics
[AD-A272987] p 1740 N94-21264

GRATINGS (SPECTRA)
Synchrotron x ray diffraction analysis of photorefractive crystals and their gratings
[AD-A271176] p 2015 N94-20213
Dynamics of surface thermal expansion and diffusivity using two-color reflection transient gratings
[DE93-040547] p 1990 N94-22002

GRAVIMETRY
Vector gravimetry by a combination of inertial and GPS satellite measurements
[ISBN-0-315-61980-5] p 1861 N94-22424

GRAVITATION
On the twisted N=2 superconformal structure in 2d gravity coupled to matter
[DE93-628627] p 2037 N94-20178
Venus gravity: New Magellan low altitude data p 2117 N94-20772

GRAVITATION THEORY
On the twisted N=2 superconformal structure in 2d gravity coupled to matter
[DE93-628627] p 2037 N94-20178

GRAVITATIONAL COLLAPSE
Coagulation of grains in static and collapsing protostellar clouds p 2085 N94-20865
New production mechanisms for unstable nuclei in stars, supernovae, and the big bang
[DE93-018627] p 2081 N94-21618

GRAVITATIONAL EFFECTS
Equilibrium models of mass distribution and collisional lifetimes of asteroids p 2088 N94-20877
System test results of the Advanced Technology Anti-G Suit (ATAGS)
[AD-A271535] p 1896 N94-20914

GRAVITATIONAL FIELDS
Gravity investigation of the Manson impact structure, Iowa p 2082 N94-20694
Geoid, topography, and convection-driven crustal deformation on Venus p 2116 N94-20769
GMM-1: A 50 degree and order gravitational field model for Mars p 2117 N94-20774
Response of the topography and gravity field on Venus to mantle upwelling beneath a chemical boundary layer p 2117 N94-20775
Vector gravimetry by a combination of inertial and GPS satellite measurements
[ISBN-0-315-61980-5] p 1861 N94-22424

GRAVITATIONAL WAVES
Interactions of free modes, tides, and gravity waves in the middle atmosphere
[REPT-84] p 1855 N94-20155

GRAVITY ANOMALIES
Modelling the gravity and magnetic field anomalies of the Chicxulub crater p 1862 N94-20668
Gravity investigation of the Manson impact structure, Iowa p 2082 N94-20694
Chicxulub impact basin: Gravity characteristics and implications for basin morphology and deep structure p 1862 N94-20757
Is there uniformitarian or catastrophic tectonics on Venus? p 2129 N94-20839
Characterization of the Marquez Dome buried impact crater using gravity and magnetic data p 1863 N94-20862
Possible flexural signatures around Olympus and Ascraeus Montes, Mars p 2142 N94-20911
Vector gravimetry by a combination of inertial and GPS satellite measurements
[ISBN-0-315-61980-5] p 1861 N94-22424

GRAVITY WAVES
Meso-Beta scale numerical simulation studies of terrain-induced jet streak mass/momentum perturbations
[NASA-CR-194627] p 1864 N94-20138
Detection of traveling ionospheric disturbances induced by atmospheric gravity waves using the global positioning system p 1723 N94-20425
Breaking Kelvin-Helmholtz waves and cloud-top entrainment as revealed by K-band Doppler radar p 1874 N94-22310

GRAZING INCIDENCE
Near grazing scattering from non-Gaussian ocean surfaces p 1726 N94-20438
Variable angle of incidence spectroscopic ellipsometric measurement of the Franz-Keldysh effect in MODFET structures p 2021 N94-20987

GREEN'S FUNCTIONS
A Green function method for calculation of atomic and electronic properties of isolated adsorbate atoms
[ETN-93-95055] p 2014 N94-20018
Shielding from space radiations
[NASA-CR-194683] p 1895 N94-20063
Multigrid properties of upwind-biased data reconstructions p 1806 N94-21485
Scattering by cavity-backed antennas on a circular cylinder p 1741 N94-21886
Interface reflection of spherical acoustic waves in the first- and second-order rational parabolic approximations and their artifacts
[PB93-215424] p 1969 N94-22261
Transient acoustic wave modeling: Higher-order WKBJ asymptotics and symbolical manipulation (revised)
[PB93-215432] p 1969 N94-22262

GREENHOUSE EFFECT
Health effects of global warming: Problems in assessment
[DE93-040323] p 1850 N94-19930
Technology to prevent greenhouse effect gases
[DE94-707421] p 1850 N94-19976
Technology to prevent greenhouse effect gases
[DE94-707420] p 1851 N94-20116
Tropospheric chemistry of natural hydrocarbons, aldehydes, and peroxy radicals: Their connections to sulfuric acid production and climate effects
[DE93-019525] p 1855 N94-20220
Research in progress: FY 1992
[DE94-000410] p 1836 N94-20936
Accuracy requirements --- for monitoring of climate changes p 1869 N94-21642
A carbon dioxide/methane greenhouse atmosphere on early Mars p 2142 N94-21662
A model for the evolution of CO2 on Mars p 2144 N94-21671
Early Mars: The inextricable link between internal and external influences on valley network formation p 2146 N94-21681
Survey on chemical engineering technologies for the global environmental protection
[DE94-714887] p 1852 N94-22044
Survey on evaluation of energy technology contributing to preservation of the global environment. 2
[DE94-714884] p 1853 N94-22051
Investigations on trends in global environment adaptive industrial technologies
[DE94-714888] p 1853 N94-22258

GREENLAND
Studies of Greenland using the SEASAT scatterometer p 1725 N94-20433
Radar backscattering from snow facies of the Greenland ice sheet: Results from the AIRSAR 1991 campaign p 1725 N94-20434
Narsarsuaq Geophysical Observatory: Magnetic results, 1985 - 1990
[DATA-REPT-93-1] p 1856 N94-20607
Magnetic results 1991: Brorfelde, Godhavn, Thule and Narsarsuaq
[DATA-REPT-92-3] p 1856 N94-20608

Thule Geophysical Observatory: Magnetic results 1985 - 1990
[DATA-REPT-92-4] p 1857 N94-20609

GRID GENERATION (MATHEMATICS)
Finite element mesh generation and analysis of solder joints for fatigue life predictions
[AD-A271329] p 1829 N94-19937
A comparative study of an ABC and an artificial absorber for truncating finite element meshes
[NASA-CR-194275] p 1716 N94-20160
Time-domain analysis of planar microstrip devices using a generalized Yee-algorithm based on unstructured grids p 1724 N94-20431
Massively parallel computation of RCS with finite elements p 1728 N94-20437
Numerical methods for singularly perturbed differential equations with applications
[AD-A272112] p 1952 N94-20568
Adaptive grids for quasilinear parabolic systems in one space dimension
[ETN-93-93611] p 1954 N94-21137
Flow transition with 2-D roughness elements in a 3-D channel p 1806 N94-21466
A multigrid method for steady Euler equations on unstructured adaptive grids p 1957 N94-21476
Two-level Schwartz methods for nonconforming finite elements and discontinuous coefficients p 1957 N94-21477
Unstructured multigrid through agglomeration p 1958 N94-21484
Multigrid properties of upwind-biased data reconstructions p 1806 N94-21485
Superpatch
[NASA-CR-177627] p 1914 N94-21489
Direct simulation of shock-induced mixing layer
[DE93-040498] p 1803 N94-21531
RHALE: A 3-D MMALE code for unstructured grids
[DE93-019405] p 1916 N94-21635
User's guide for the casting process simulator software CaPS-2D, version 1.0
[DE93-040398] p 1917 N94-21923
Unstructured Grid Generation Techniques and Software
[NASA-CP-10119] p 1918 N94-22350
Software systems used for unstructured grid generation at NASA Langley p 1918 N94-22351
NASA-Ames Research Center unstructured technology development p 1919 N94-22352
Unstructured grid research and use at NASA Lewis Research Center p 1919 N94-22353
Grid generation requirements at Marshall Space Flight Center p 1919 N94-22354
Johnson Space Center CFD grid generation requirements p 1919 N94-22355
The 3-D unstructured mesh generation using local transformations p 1919 N94-22356
Status of VGRID/USM3D aero analysis system p 1919 N94-22357
Unstructured low-Mach number viscous flow solver p 1919 N94-22358
Robust unstructured grid generation with VGRID p 1919 N94-22359
Three-dimensional unstructured grid method applied to turbomachinery p 1919 N94-22360
Dynamic mesh adaption for triangular and tetrahedral grids p 1920 N94-22363
Cartesian-cell based grid generation and adaptive mesh refinement p 1920 N94-22364
The 2D and 3D hypersonic flows with unstructured meshes p 1920 N94-22365
Unstructured surface grid generation p 1920 N94-22366
The 3D Euler solutions using automated Cartesian grid generation p 1920 N94-22367
Accuracy assessment for grid adaptation p 1920 N94-22368
Time-dependent grid adaptation for meshes of triangles and tetrahedra p 1920 N94-22369
Computational geometry issues p 1920 N94-22370
NASA Langley developments in response calculations needed for failure and life prediction p 1836 N94-22621

GROUND BASED CONTROL
Automatic AVHRR image navigation software
[NASA-CR-194602] p 1643 N94-20148
Control vane guidance for a ducted-fan unmanned air vehicle
[AD-A271957] p 1645 N94-20561
Next Generation Weather Radar (NEXRAD) Principal User Processor (PUP) Operational Test and Evaluation (OT/E)
[AD-A273075] p 1868 N94-21519

GROUND EFFECT (COMMUNICATIONS)
Breaking Kelvin-Helmholtz waves and cloud-top entrainment as revealed by K-band Doppler radar p 1874 N94-22310

GROUND HANDLING
A study of parallel pier finger airport terminal configuration
[ISBN-0-315-83128-6] p 1652 N94-22425

GROUND STATE
High resolution infrared spectroscopy of cyclobutane: A study of vibrational mode coupling involving large amplitude, low frequency modes
[AD-A271987] p 1973 N94-20619
Proof of stability of the hydrogen molecule
[PB93-221026] p 1977 N94-22271
Low temperature absorption spectra and ground state electronic structure of tetrakis(2,6-di-tert-butylphenoxide)uranium(IV)
[DE94-000774] p 2035 N94-22387

GROUND STATIONS
Enhanced networks operations using the X Window System p 1932 N94-21329
The automated ground network system p 1932 N94-21330
Mission Operations Support Area (MOSA) for ground network support p 1932 N94-21331
Network command processing system overview p 1935 N94-21351
On-board closed-loop congestion control for satellite based packet switching networks
[NASA-TM-106446] p 1656 N94-21581
Tests of a simple data merging algorithm for the GONG project p 1927 N94-22549

GROUND TESTS
Combination of on ground experiments and analysis software for the evaluation of material degradation in space (SILEX project) p 1662 N94-21389
The International Telecommunications Satellite (INTELSAT) Solar Array Coupon (ISAC) atomic oxygen flight experiment: Techniques, results and summary p 1662 N94-21391
Atomic oxygen interaction with spacecraft materials: Relationship between orbital and ground-based testing for materials certification p 1663 N94-21393
Interpretation of Ground Penetrating Radar data at the Hanford Site, Richland, Washington
[DE93-040409] p 1743 N94-22557

GROUND TRACKS
New algorithm of ground track processing in high-frequency skywave over-the-horizon-B radar
[AD-A267821] p 1717 N94-20207

GROUND TRUTH
A general rough-surface inversion algorithm: Theory and application to SAR data p 1719 N94-20407
Relating ground truth collection to model sensitivity p 1719 N94-20409
Predicting LANDSAT MSS endmember signatures from corresponding higher resolution TM fraction images p 1839 N94-20962

GROUND WATER
Calderas produced by hydromagmatic eruptions through permafrost in northwest Alaska p 2089 N94-20385
Possible occurrence and origin of massive ice in Utopia Planitia p 2090 N94-20390
The distribution of ground ice on Mars p 2090 N94-20394
Seismic-triggering history of the catastrophic outflows in the Chryse region of Mars p 2091 N94-20399
Remote sensing for hydrology progress and prospects
[WMO-773] p 1841 N94-21069
Oxidation of dissolved iron under warmer, wetter conditions on Mars: Transitions to present-day arid environments p 2143 N94-21663
The evolution of the early Martian climate and the initial emplacement of crustal H2O p 2143 N94-21665
Fluvial valleys in the heavily cratered terrains of Mars: Evidence for paleoclimatic change? p 2144 N94-21670
Early Mars: The inextricable link between internal and external influences on valley network formation p 2146 N94-21681
The Martian valley networks: Origin by niveo-fluvial processes p 2146 N94-21682

GROUND WIND
Analysis of wind observation from towers in the period 1977-1991
[KNMI-TR-148] p 1865 N94-20239
Ku-band ocean radar backscatter observations during SWADE p 1720 N94-20413
A synoptic-scale overview of the TOGA COARE intensive observing period November 1992 to February 1993 based on analyses from US operational global data assimilation systems
[NASA-TM-104593] p 1868 N94-21605

GROUND-AIR-GROUND COMMUNICATION
A laboratory system for the investigation of rain fade compensation techniques for Ka-band satellites
[NASA-CR-191200] p 1762 N94-21566

GROUP DYNAMICS
Conversion and maintenance of Co-oP for Windows
[AD-A272513] p 1914 N94-21414

GROUP THEORY
F-spin concept and g-bosons in the interceding boson model
[ETN-93-93607] p 1973 N94-21136
The Robinson-Schensted and Schuetzenberger algorithms. Part 1: New combinatorial proofs
[CWI-AM-R9208-PT-1] p 1911 N94-21156
The Robinson-Schensted and Schuetzenberger algorithms. Part 2: Geometric interpretations
[CWI-AM-R9209-PT-2] p 1911 N94-21157
On semisimple cocommutative bialgebras
[CWI-AM-R9210] p 1954 N94-21158

GRUNEISEN CONSTANT
An equation of state for shock in homogeneous materials and comparison to shock data
[AD-A271436] p 1829 N94-19881

GUANIDINES
Guanidine based vehicle/binders for use with oxides, metals, and ceramics
[NASA-CASE-LEW-15314-1] p 1700 N94-20195

GUIDANCE (MOTION)
Strategy for motion of a moving body of quasi-polygonal form within a polygonal space p 1792 N94-22240

GUIDE VANES
Control vane guidance for a ducted-fan unmanned air vehicle
[AD-A271957] p 1645 N94-20561
Active control of wake/blade-row interaction noise through the use of blade surface actuators
[NASA-CR-4556] p 1968 N94-21608

GULF OF MEXICO
Research program on the Manson impact structure, Iowa p 1862 N94-20766
Green Sheet project: Dye sheet evolution
[AD-A272019] p 1883 N94-21443

GULF STREAM
Ku-band ocean radar backscatter observations during SWADE p 1720 N94-20413

GYPSUM
Impact-induced devolatilization of CaSO4 anhydrite and implications for K-T extinctions: Preliminary results p 2085 N94-20840

H

H ALPHA LINE
Berne (Switzerland) solar observations: Data for April 1991 - August 1992
[REPT-59] p 2147 N94-21150

HABITABILITY
Columbus: Materials for 30 years habitability in space p 1662 N94-21387

HADRONS
The two-jet differential cross-section at CDF
[DE93-019905] p 1978 N94-19983
Jet shapes in hadron and electron colliders
[DE93-019386] p 1979 N94-20216
Energy and luminosity limits of hadron supercolliders
[DE93-019248] p 1980 N94-20300
Qualitative and quantitative aspects of the QCD theory of elastic form factors
[DE93-040864] p 2038 N94-21513
Hadronic molecules and scattering amplitudes from the nonrelativistic quark model
[DE94-000377] p 1974 N94-21657
Summary of the Hadronic Weak Interaction session
[DE94-000592] p 1975 N94-21775
New perspectives in quantum chromodynamics
[DE93-041021] p 2038 N94-21935

HALIDES
Plasma chemical vapor deposition of halide glasses
[AD-D015933] p 1701 N94-20331

HALL EFFECT
Performance potential of plasma thrusters: Arcjet and Hall thruster modeling
[AD-A271085] p 1667 N94-19847
Implantation of carbon in GaAs and compensating native defects
[DE93-040122] p 2030 N94-21763

HALLEY'S COMET
The digital archive of the International Halley Watch p 2047 N94-22496

HALOGENS
Plasma chemical vapor deposition of halide glasses
[AD-D015933] p 1701 N94-20331

HALOS
The x ray halo of AM Her
[NASA-CR-189310] p 2054 N94-20142

HAMILTONIAN FUNCTIONS
A microscopic theory of quantum optics and new photon-locked bistable states
[AD-A271250] p 1983 N94-19901

Long cycles in graphs containing a 2-factor with many odd components
[MEMO-1086] p 1953 N94-21048
Degree sums, k-factors and Hamiltonian cycles in graphs
[MEMO-1078] p 1953 N94-21074
F-spin concept and g-bosons in the interceding boson model
[ETN-93-93607] p 1973 N94-21136

HANDBOOKS
Handbook. Volume 3: Digital systems validation book plan
[DOT/FAA/CT-93/16-VOL-3] p 1647 N94-20053
Handbook. Volume 2: Digital systems validation. Chapter 18: Avionic data bus integration technology
[DOT/FAA/CT-88/10-VOL-2] p 1647 N94-20343
Technical manual PCDU MT 254
[FFI-92/7020] p 1751 N94-20553

HARDENING (MATERIALS)
Rad-hard computer elements for space applications p 1753 N94-21082

HARDNESS
Properties and potential of high-temperature niobium beryllides
[DE93-019169] p 1690 N94-20233
Automated radiation hard ASIC design tool p 1759 N94-21126
A quantitative model for interpreting nanometer scale hardness measurements of thin films
[DE93-040601] p 2034 N94-22005
Using the rule of mixtures to examine the hardness of Cu/Cu-Zr multilayers
[DE94-001068] p 1697 N94-22402

HARDNESS TESTS
Using the rule of mixtures to examine the hardness of Cu/Cu-Zr multilayers
[DE94-001068] p 1697 N94-22402

HARDWARE
Handbook. Volume 3: Digital systems validation book plan
[DOT/FAA/CT-93/16-VOL-3] p 1647 N94-20053
PREVAIL-DM: A framework-based environment for formal hardware verification
[RR-899] p 1905 N94-20164
A SCSI-bus data acquisition system for nuclear spectroscopy experiments
[USIP-92-03] p 2042 N94-20193
Technical manual PCDU MT 254
[FFI-92/7020] p 1751 N94-20553
Correctness properties for iterated hardware structures p 1759 N94-21124

HARDWARE DESCRIPTION LANGUAGES
A statistical-based scheduling algorithm in automated data path synthesis p 1764 N94-21706
A novel visual hardware behavioral language p 1765 N94-21715
System level modelling using Petri nets and VHDL p 1772 N94-22113

HARMONIC EXCITATION
Adaptation of model parameters of a rail model at measured rail compliances
[ILR-MITT-274(1992)] p 1831 N94-21153

HARMONIC GENERATIONS
Acoustic microscopy and nonlinear effects in pressurized superfluid helium
[AD-A270598] p 1967 N94-19949
Photonics and nonlinear optics with molecular materials and polymers
[AD-A271747] p 1988 N94-21457
Effect of bandwidth on beam smoothing and frequency conversion at the third harmonic of the Nova laser
[DE93-019917] p 1819 N94-21920
Generation of harmonic radiation using the multi-cavity free-electron laser
[DE94-001261] p 1820 N94-21975

HARMONIC RADIATION
Generation of harmonic radiation using the multi-cavity free-electron laser
[DE94-001261] p 1820 N94-21975

HAZARDS
The roughness of the Martian surface: A scale dependent model p 2115 N94-20762

HEAD (ANATOMY)
Evaluation of head injury criteria
[NIAR-93-2] p 1890 N94-20190

HEAD-UP DISPLAYS
Some VTOL head-up display drive-law problems and solutions
[NASA-TM-104027] p 1635 N94-20035
Image processing as a tool in flight testing evaluation p 1640 N94-22606

HEALTH
Current status of environmental, health, and safety issues of nickel metal-hydride batteries for electric vehicles
[DE93-017079] p 1748 N94-19902
Analysis of health status from preliminary physical examination of flight academy applicants
[AD-A267759] p 1889 N94-19962
Research in progress: FY 1992
[DE94-000410] p 1836 N94-20936
Journal of rehabilitation research and development, volume 30, number 1, 1993
[AD-A272956] p 1893 N94-21613
Self-Motion Perception and Motion Sickness
[NASA-CR-194276] p 1885 N94-21897

HEART
Review of using cardiac fluoroscopy in symptomatic and asymptomatic patients
[AD-A271690] p 1891 N94-20928

HEAT ACCLIMATIZATION
Human responses to exercise-heat stress
[AD-A272581] p 1892 N94-21209

HEAT ENGINES
Development of improved processing and evaluation methods for high reliability structural ceramics for advanced heat engine applications, phase 1
[DE93-040526] p 1702 N94-20481
Heat regenerative external combustion engine
[AD-D015965] p 1824 N94-21274
Ceramic Technology Project
[DE94-001011] p 1707 N94-21822

HEAT EXCHANGERS
Thermal information regarding the cooldown and operation of liquid argon calorimeters
[DE93-019391] p 1807 N94-19987
A novel scheme to handle highly pulsed loads with a standard helium refrigerator
[DE93-019617] p 1799 N94-20263
Heat exchanger with oscillating flow
[NASA-CASE-LAR-14033-2] p 1800 N94-20495
Review of corrosion behavior of ceramic heat exchanger materials: Corrosion characteristics of silicon carbide and silicon nitride
[DE93-041307] p 1706 N94-21516
Preliminary SP-100/Stirling heat exchanger designs
[NASA-TM-106444] p 1670 N94-21809
Fabrication of whisker-toughened alumina tubes
[DE94-001012] p 1677 N94-22022

HEAT FLUX
On the sources of North Atlantic deep water
[AD-A270854] p 1881 N94-19895
Heat exchanger with oscillating flow
[NASA-CASE-LAR-14033-2] p 1800 N94-20495
Low Reynolds-number turbulent boundary layers
[AD-A272011] p 1803 N94-21459
Areally averaged estimates of surface heat flux from ARM field studies
[DE93-018569] p 1859 N94-22036
A comparison of small and larger mesoscale latent heat and radiative fluxes: December 6 case study p 1879 N94-22335

HEAT MEASUREMENT
Techniques for reducing error in the calorimetric measurement of low wattage items
[DE93-018472] p 1807 N94-20114
Calorimeter measurements of low wattage items
[DE93-018473] p 1807 N94-20115

HEAT OF COMBUSTION
Combustion in turbulent jets and buoyant flames
[PB93-202372] p 1682 N94-21452

HEAT PIPES
Preliminary SP-100/Stirling heat exchanger designs
[NASA-TM-106444] p 1670 N94-21809
Rewetting of monogroove heat pipe in Space Station radiators
[NASA-CR-194781] p 1804 N94-21820

HEAT PUMPS
Absorption heat pump for space applications
[NASA-CR-194693] p 1845 N94-20066
The FY1992 survey on commercialization of Stirling engine utilization equipment
[DE94-707416] p 1849 N94-22029

HEAT RESISTANT ALLOYS
Investigation of austenitic alloys for advanced heat recovery and hot gas cleanup systems
[DE93-017863] p 1687 N94-19802
Fundamental studies of stress distributions and stress relaxation in oxide scales on high temperature alloys
[DE94-001444] p 1693 N94-21854

HEAT SINKS
Cooling apparatus and couplings therefor
[NASA-CASE-ARC-11921-1] p 1800 N94-20371
Analysis of cost: CVD diamond deposition
[AD-A271980] p 2018 N94-20616

HEAT SOURCES
Core formation, wet early mantle, and H2O degassing on early Mars p 2145 N94-21674

HEAT STORAGE
Fluid absorption solar energy receiver
[NASA-CR-194688] p 1846 N94-20229

HEAT TOLERANCE
Human responses to exercise-heat stress
[AD-A272581] p 1892 N94-21209
Physiological efficacy of a lightweight ambient air cooling unit for various applications
[AD-A272952] p 1896 N94-21247

HEAT TRANSFER
Parametric variations of ion transport in TFTR
[DE93-012653] p 1991 N94-19883
High performance heavy alloys by alloying and process control
[AD-A271129] p 1689 N94-20019
EHD enhancement of pool and in-tube boiling of alternate refrigerants
[DE94-000787] p 1798 N94-20101
Pressurization and expulsion of a flightweight liquid hydrogen tank
[NASA-TM-106427] p 1799 N94-20177
Fluid absorption solar energy receiver
[NASA-CR-194688] p 1846 N94-20229
A parametric study of heat transfer within a planar thermosyphon
[DE93-019546] p 1799 N94-20256
Spatial and temporal variations of satellite microwave measurements of latent heat release in tropic cyclones due to environmental forcing obtained from a numerical model
[AD-A267947] p 1865 N94-20482
Heat exchanger with oscillating flow
[NASA-CASE-LAR-14033-2] p 1800 N94-20495
Heat transfer additives for absorption cooling system fluids
[PB93-202521] p 1714 N94-21426
Combustion in turbulent jets and buoyant flames
[PB93-202372] p 1682 N94-21452
Molten carbonate fuel cell networks: Principles, analysis, and performance
[DE93-019872] p 1846 N94-21527
On one numerical approach to Stefan problem
[IPPCZ-330] p 1996 N94-21572
Flow and heat transfer model for a rotating cryogenic motor
[DE94-001151] p 1794 N94-22405

HEAT TRANSMISSION
Three-dimensional dynamic thermal imaging of structural flaws by dual-band infrared computed tomography
[DE93-019575] p 1906 N94-20316
A finite element formulation and adaptive solution approach for large-scale thermomechanical problems with complex contact conditions
[DE93-019605] p 1960 N94-21996
Dynamics of surface thermal expansion and diffusivity using two-color reflection transient gratings
[DE93-040547] p 1990 N94-22002
Flow and heat transfer model for a rotating cryogenic motor
[DE94-001151] p 1794 N94-22405

HEAT TREATMENT
GaAs(100) surface modifications at elevated temperatures, studied by in-situ spectroscopic ellipsometry p 2023 N94-20997
Microstructural modeling and toughening of Si3N4 ceramics for high temperature engine applications
[AD-A272897] p 1704 N94-21197
Applicability and performance benefits of XD (Tradename) titanium aluminides to expendable gas turbine engines
[AD-A272998] p 1648 N94-21266
Specific heat of YBa2Cu3O7
[DE93-040640] p 2031 N94-21926

HEATING
Thermal behavior of natural zeolites
[DE93-040091] p 1699 N94-19975
Tambo Quemado: Extraordinary concentrations of REE and refractory trace elements caused by artificial heating p 1684 N94-20667
Multiplicity of chondrule heating events and the coarsening of chondrule textures p 2085 N94-20860
The energy performance of prototype holographic glazings
[DE93-040451] p 1809 N94-21545

HEATING EQUIPMENT
Numerical modeling for an electric-field hyperthermia applicator p 1729 N94-20451

HEAVY IONS
Longitudinal beam dynamics for heavy ion fusion using WARPrz
[DE93-019154] p 1992 N94-19915
Space-charge dominated beam transport in magnetic quadrupoles with large aperture ratios
[DE93-040443] p 1992 N94-20004
Shielding from space radiations
[NASA-CR-194683] p 1895 N94-20063
High current injector for heavy ion fusion
[DE93-019241] p 1979 N94-20289

Time-of-flight heavy ion backscattering spectrometry
[DE93-019067] p 1973 N94-20306
Comparison of single event upset rates for microelectronic memory devices during interplanetary solar particle events p 1754 N94-21085
STRV RADMON: An integrated high-energy particle detector p 1666 N94-21086
Low emittance 0.8A K(+) ion source for the LBL Induction Linac System Experiment (ILSE)
[DE93-019237] p 1981 N94-21439
Simulation studies of space-charge-dominated beam transport in large aperture ratio quadrupoles
[DE93-019238] p 1981 N94-21440
Searching for high baryon density at the AGS with ARC
[DE93-041155] p 1975 N94-21693
Implantation of carbon in GaAs and compensating native defects
[DE93-040122] p 2030 N94-21763
Low p(sub T) phenomena observed in high energy nuclear collisions
[DE94-000825] p 1982 N94-21849
Time evolution of the quark-gluon plasma
[DE94-000804] p 1998 N94-22389

HEAVY NUCLEI
Relativistic calculations of the superheavy nucleus (sup 298)114
[KVI-969] p 1971 N94-20119
New perspectives in quantum chromodynamics
[DE93-041021] p 2038 N94-21935
Symmetry-dictated trucation: Solutions of the spherical shell model for heavy nuclei
[DE94-000482] p 1976 N94-21961

HEIGHT
Ocean wave height transformation model using surface roller theory
[AD-A272610] p 1883 N94-21423
Semi-stability and heights of cycles
[PB93-215507] p 1961 N94-22377

HEISENBERG THEORY
A microscopic theory of quantum optics and new photon-locked bistable states
[AD-A271250] p 1983 N94-19901

HELICAL ANTENNAS
Mobile terminal antennas for helicopters
p 1731 N94-20458

HELICAL FLOW
Gravitational instability of magnetized filamentary clouds. 1: Helical magnetic fields p 2008 N94-22688

HELICOPTER CONTROL
Improvement of helicopter attitude stability by active control of the conventional swash plate
[NASA-CR-194786] p 1650 N94-20524

HELICOPTER PERFORMANCE
Rotorcraft low altitude IFR benefit/cost analysis: Conclusions and recommendations
[DOT/FAA/RD-93/22] p 1642 N94-20051

HELICOPTER WAKES
Rotorwash wind sensor evaluation
[AD-A268987] p 1807 N94-20203

HELICOPTERS
Mobile terminal antennas for helicopters
p 1731 N94-20458
The relative noise levels of parallel axis gear sets with various contact ratios and gear tooth forms
[NASA-TM-106431] p 1826 N94-21756
Aircraft noise effects on cultural resources: Recommendation and rationale for further research
[PB93-205326] p 1968 N94-22053
Aircraft noise effects on cultural resources: Annotated bibliography
[PB93-205334] p 1969 N94-22054

HELIOSEISMOLOGY
Solar simulator for solar dynamic space power system testing
[NASA-TM-106393] p 1984 N94-20140
Tests of a simple data merging algorithm for the GONG project p 1927 N94-22549

HELIOSPHERE
Laboratory structure of the heliopause
p 2003 N94-22648
Large-scale structure of the solar plasma corona: An analysis of Yohkoh SXT images p 2004 N94-22657

HELIUM
Testing double ionization mechanisms with highly-charged ions
[DE93-018750] p 1970 N94-19958
A novel scheme to handle highly pulsed loads with a standard helium refrigerator
[DE93-019617] p 1799 N94-20263
Helium in interplanetary dust particles
p 2082 N94-20653
Stability curves for a thermoacoustic prime mover
[AD-A272607] p 1968 N94-21422
A high-intensity He-jet production source for radioactive beams
[DE93-040247] p 1981 N94-21767
The FY1992 survey on commercialization of Stirling engine utilization equipment
[DE94-707416] p 1849 N94-22029
The effect of Compton scattering on the double to single ionization ratio in helium
[DE94-000884] p 1827 N94-22390

HELIUM FILM
Optical metrology of magnetically trapped hydrogen
[AD-A272110] p 1680 N94-20584

HELIUM IONS
Photoabsorption and Compton scattering in ionization of helium at high photon energies
[DE94-000380] p 1974 N94-21658
Single and double ionization of helium by high-energy photon impact
[DE94-000381] p 1975 N94-21785

HELIUM ISOTOPES
Rapid heating tensile testing update: 304L stainless steel
[DE93-018770] p 1688 N94-19942
Neutron and PIMC determination of the longitudinal momentum distribution of HCP, BCC and normal liquid He-4
[DE93-019009] p 1972 N94-20187
SLAC measurement of the neutron spin structure function
[DE93-040998] p 1975 N94-21788
Mean elemental composition and He-3 enrichments in solar energetic particles p 2006 N94-22670

HELIUM PLASMA
Optical diagnostic instrument for monitoring etch uniformity during plasma etching of polysilicon in a chlorine-helium plasma
[DE93-019582] p 1993 N94-20261

HELIUM-NEON LASERS
Micro-ellipsometric measurements of strained layer structures p 2025 N94-21008

HELMET MOUNTED DISPLAYS
Miniature color display, phase 4
[AD-A272920] p 1760 N94-21221

HEMATITE
The stability of oxyamphiboles: Existence of Ferric-bearing minerals under the reducing conditions on the surface of Venus p 2122 N94-20800

HEMORRHAGES
Ocular damage induced by ultrashort laser pulses
[AD-A271859] p 1890 N94-20462

HERBIG-HARO OBJECTS
Three-dimensional simulations of cosmic jets employing the smoothed particle hydrodynamics technique
p 2008 N94-22685
Helical kink instability of jets from young stellar objects p 2008 N94-22686

HERMES MANNED SPACEPLANE
Meteoroids and debris impact risk assessment on Columbus and Hermes using a realistic geometrical analysis tool p 1662 N94-21388

HERMITIAN POLYNOMIAL
A sharp upper bound for departure from normality
[DE93-040457] p 1960 N94-21966

HETEROCYCLIC COMPOUNDS
Catalytic hydrogenation of carbon monoxide
[DE94-000881] p 1678 N94-20103
Polybenzoxazole via aromatic nucleophilic displacement
[NASA-CASE-LAR-14606-1-CU] p 1672 N94-20540

HETEROJUNCTION DEVICES
High efficiency epitaxial optical reflector solar cells
[DE93-017115] p 1845 N94-19805
Investigation of quantum effects in heterostructures
[AD-A270938] p 2011 N94-19817
Design and implementation of GaAs HBT circuits with ACME p 1758 N94-21117
Advanced processing technology for high-efficiency thin-film CuInSe2 solar cells
[DE93-010045] p 1847 N94-21614
Heterojunction bipolar transistor technology for data acquisition and communication p 1763 N94-21697

HETEROJUNCTIONS
Investigation of heterojunctions and multiple quantum well structures using crystalline organic semiconductors
[AD-A272113] p 2018 N94-20569
Ellipsometric measurements of molecular-beam-epitaxy-grown semiconductor multilayer thicknesses: A comparative study p 1710 N94-20983
Comparative thickness measurements of heterojunction layers by ellipsometric, RBS, and XTEM analysis
p 1710 N94-20984
Variable angle of incidence spectroscopic ellipsometric measurement of the Franz-Keldysh effect in MODFET structures p 2021 N94-20987
In-situ spectroscopic ellipsometry in molecular beam epitaxy p 2024 N94-21005
Complementary heterojunction FET technology for space application p 1755 N94-21094
Synthesis and properties of mismatched heterojunction/substrate interfaces
[AD-A272904] p 1760 N94-21229
Solid-state dynamics and quantum transport in novel semiconductor nanostructures
[AD-A272955] p 2027 N94-21248
Heterojunction bipolar transistor technology for data acquisition and communication p 1763 N94-21697

HEURISTIC METHODS
Program derivation in acyclic graphs and related problems
[PB93-191765] p 1903 N94-19994
Retrieval of ice thickness from polarimetric SAR data
p 1724 N94-20432
On the selection of indices in relational databases
[MEMO-INF-92-72] p 2043 N94-21071
Heuristic-based scheduling algorithm for high level synthesis p 1764 N94-21704
A statistical-based scheduling algorithm in automated data path synthesis p 1764 N94-21706
Fuzzy and neural control
[NASA-TM-108753] p 1947 N94-22270

HIERARCHIES
Nominalization, prediction and type containment
[PB93-191799] p 1898 N94-20082
Classification in feature-based default inheritance hierarchies
[TR-473] p 1911 N94-21180
Computing solutions uniquely collapses the polynomial hierarchy
[TR-467] p 1954 N94-21314
On the closure properties of #P in the context of PF of #P
[TR-445] p 1955 N94-21456
A proof-of-concept implementation of persistence in a hierarchical storage system
[NASA-CR-194790] p 1921 N94-22376
A self-defining hierarchical data system
p 2046 N94-22448
Some practicable applications of quadtree data structures/representation in astronomy
p 1927 N94-22515

HIGH ALTITUDE BREATHING
In-flight measurement of aircrew breathing in Navy aircraft
[AD-A271811] p 1896 N94-21154

HIGH CURRENT
SPICE macromodel for a 1-megawatt power MOSFET switch
[DE93-019415] p 1748 N94-19844
High current injector for heavy ion fusion
[DE93-019241] p 1979 N94-20289
High current density contacts for photoconductive semiconductor switches
[DE93-018837] p 1750 N94-20312
Demonstration of ultraviolet lasing with a low energy electron beam
[DE93-040192] p 1818 N94-21554

HIGH DEFINITION TELEVISION
NHK Science and Technical Research Laboratories
p 2151 N94-20342

HIGH ELECTRON MOBILITY TRANSISTORS
An x-band peaked HEMT amplifier
p 1732 N94-20498
Dimension scaling effects on the yield sensitivity of HEMT digital circuits p 1765 N94-21712

HIGH ENERGY INTERACTIONS
Top search at the TEVATRON
[DE93-019392] p 1978 N94-19988
Energy and luminosity limits of hadron supercolliders
[DE93-019248] p 1980 N94-20300
High energy physics program at Texas A/M University
[DE93-041089] p 1980 N94-20933
Theoretical particle physics
[DE94-000538] p 1973 N94-20938
Photoabsorption and Compton scattering in ionization of helium at high photon energies
[DE94-000380] p 1974 N94-21658
Low p(sub T) phenomena observed in high energy nuclear collisions
[DE94-000825] p 1982 N94-21849

HIGH FREQUENCIES
New algorithm of ground track processing in high-frequency skywave over-the-horizon-B radar
[AD-A267821] p 1717 N94-20207
High Speed/High Frequency Optoelectronics
[AD-A271985] p 1751 N94-20580
High Frequency (HF) and meteor burst communications in a polar environment
[AD-A271604] p 1737 N94-20949
An integro-algebraic equation for high frequency wake fields in a tube with smoothly varying radius
[DE93-040940] p 1741 N94-21684

HIGH LEVEL LANGUAGES
Explainable expert systems: A research program in information processing
[NASA-CR-193422] p 2041 N94-20133
MAYGEN: A symbolic debugger generation system
[AD-A272512] p 1913 N94-21413
HIGH POWER LASERS
Circular polarizing mirrors for high power lasers
[AD-A267820] p 1815 N94-19965
High-power copper vapor lasers and their application to precision drilling and cutting
[DE93-019951] p 1819 N94-21844
Simulations of spectral broadening by cross-phase modulation (XPM) with chaotic light pulses
[DE93-019623] p 1819 N94-21872
Phase screens for the control of the focal irradiance of the Nova laser
[DE94-001067] p 1820 N94-22401
HIGH PRESSURE
Chemical equilibrium in high pressure molecular fluid mixtures
[DE93-040160] p 1796 N94-19829
Unlike-pair interactions at high pressure and high temperature
[DE93-019948] p 1796 N94-19916
Electron reactions in nonpolar liquids: Pressure effects
[DE93-040328] p 1970 N94-19931
Shock response of porous Al-2 + Fe2O3 powder mixtures
[DE93-018851] p 1688 N94-19944
Lateral distribution of lipids in membranes at high pressure
[AD-A271183] p 1700 N94-20299
High-temperature, high-pressure oxygen metering valve
[NASA-CASE-MSC-21823-1] p 1824 N94-20589
Lamellar olivine in the Divnoe achondrite: Evidence for high-pressure exsolution? p 1685 N94-20679
Static ultra-high pressure study of lanthanide and actinide metals using a diamond-anvil cell
[DE94-000369] p 1693 N94-21656
Disks of YBa2Cu3O7 shocked to 10 GPa pressures
[DE94-000464] p 2031 N94-21931
High oxygen pressure synthesis of new copper oxide superconductors
[DE93-040278] p 2033 N94-21998
The FY1992 survey on commercialization of Stirling engine utilization equipment
[DE94-707416] p 1849 N94-22029
HIGH PRESSURE OXYGEN
Detailed study of oxidation/wear mechanism in lox turbopump bearings
[NASA-TM-108434] p 1825 N94-21580
HIGH RESOLUTION
Near atomic resolution microanalysis of interfaces by analytical electron microscopy
[DE93-019437] p 1687 N94-19904
A full-color, high-resolution laser projector for a flight simulator visual display
[AD-A270578] p 1651 N94-20108
High resolution signal processing
[AD-A271181] p 1717 N94-20215
Ultrafast scanning microscopy
[DE93-040121] p 1985 N94-20320
Wide-bandwidth high-resolution search for extraterrestrial intelligence
[NASA-CR-194724] p 1897 N94-20336
The High Resolution Stereo Camera (HRSC) for the Lunar Scout 1 Mission p 1813 N94-20650
Constraints on the rate of discharge and duration of the Mangala Valles flood p 2099 N94-20674
MinMap: An imaging spectrometer for high resolution compositional mapping of the Moon p 1813 N94-20688
Preliminary results from Mariner 10: High resolution images of the Moon p 2107 N94-20719
Predicting LANDSAT MSS endmember signatures from corresponding higher resolution TM fraction images p 1839 N94-20962
Nature's crucible: Manufacturing optical nonlinearities for high resolution, high sensitivity encoding in the compound eye of the fly, Musca domestica p 1755 N94-21095
Validation of the design of a high resolution all-reflection Michelson interferometer for atmospheric spectroscopy
[AD-A272505] p 1987 N94-21410
High resolution studies of the structure of the solar atmosphere
[AD-A273084] p 2147 N94-21522
HIGH REYNOLDS NUMBER
Low Reynolds-number turbulent boundary layers
[AD-A272011] p 1803 N94-21459
HIGH SPEED
Experimental evaluation of oxygen-enriched air and emulsified fuels in a six-cylinder diesel engine
[DE94-000907] p 1811 N94-22391
HIGH SPEED PHOTOGRAPHY
Multiport solid-state imager characterization at variable pixel rates
[DE93-018366] p 1808 N94-20287
HIGH STRENGTH ALLOYS
Evaluation of a diffusion/trapping model for hydrogen ingress in high-strength alloys
[AD-A271328] p 1689 N94-20027
HIGH STRENGTH STEELS
Experimental and numerical studies of high-velocity impact fragmentation
[DE93-040205] p 1832 N94-21557
HIGH TEMPERATURE
Unlike-pair interactions at high pressure and high temperature
[DE93-019948] p 1796 N94-19916
Effects of processing history on the creep strength of Nb-1Zr
[DE93-015905] p 1689 N94-20093
Microstructural stability of wrought, laser and electron beam glazed NARloy-Z alloy at elevated temperatures
[NASA-TM-108431] p 1689 N94-20100
Strengthening of NiAl matrix composites
[AD-A271491] p 1674 N94-20550
Tambo Quemado: Extraordinary concentrations of REE and refractory trace elements caused by artificial heating p 1684 N94-20667
High temperature stability of amorphous Ta(x)Cu(1-x) diffusion barriers on GaAs p 2022 N94-20990
Ellipsometric study of GaAs(100) surface changes induced at elevated temperatures p 2023 N94-20998
Microstructural modeling and toughening of Si3N4 ceramics for high temperature engine applications
[AD-A272897] p 1704 N94-21197
Performance of carbon-based hot frit substrates
[DE94-000509] p 1676 N94-21754
Ceramic Technology Project
[DE94-001011] p 1707 N94-21822
High temperature size selective membranes
[DE93-019865] p 1709 N94-21982
Strengthening and toughening in refractory metal alloys
[DE93-019942] p 1695 N94-21986
Projections on structures and material strength in the computational context p 1834 N94-22610
HIGH TEMPERATURE ENVIRONMENTS
Corrosion inhibition in high temperature environment
[AD-D015910] p 1698 N94-19830
Cold-start minidiesel engine development
[AD-A271064] p 1823 N94-20567
Model for liquid boron oxide droplet gasification in H/O/C/F combustion environments
[AD-A272911] p 1682 N94-21243
Utilization of metals to improve the lubrication of ceramic load-bearing devices
[PB93-202448] p 1825 N94-21424
Fundamental studies of stress distributions and stress relaxation in oxide scales on high temperature alloys
[DE94-001444] p 1693 N94-21854
Benefits of thread rolling process to the stress corrosion cracking and fatigue resistance of high strength fasteners
[DE93-040438] p 1833 N94-22001
Brief summary of the evolution of high-temperature creep-fatigue life prediction models for crack initiation p 1834 N94-22613
HIGH TEMPERATURE GASES
High-temperature, high-pressure oxygen metering valve
[NASA-CASE-MSC-21823-1] p 1824 N94-20589
A calcium oxide sorbent process for bulk separation of carbon dioxide
[DE93-019288] p 1847 N94-21540
HIGH TEMPERATURE LUBRICANTS
Lubricated wear of steel-ceramic and ceramic-ceramic systems
[PB93-202356] p 1825 N94-21450
Vapor-delivered lubrication of steel-steel and steel-ceramic systems
[PB93-202364] p 1825 N94-21451
HIGH TEMPERATURE PLASMAS
Kinetic resonance damping rate of the toroidal ion temperature gradient mode
[DE94-001234] p 1998 N94-22561
Neutrino emission processes in dense high-temperature plasmas p 2001 N94-22638
Accretion of a hot plasma onto the central black hole: Fokker-Planck formulation p 2009 N94-22693
HIGH TEMPERATURE SUPERCONDUCTORS
Superconductivity Technology Program for Electric Power Systems: Proceedings
[DE93-040074] p 2011 N94-19825
Superconducting property measurements in tape geometry
[DE93-018943] p 2014 N94-19970
Spin-polaron theory of high-(Tc) superconductivity. 1: Spin polarons and high (Tc) pairing
[DE93-019196] p 2014 N94-20002
Non-Fermi-liquid and multichannel Kondo phenomena in Y(1-x)U(x)Pd3 and related alloys
[DE93-040135] p 2015 N94-20275
Space applications of superconducting microwave electronics at NASA Lewis Research Center p 1671 N94-20513
TlCaBaCuO high Tc superconducting microstrip ring resonators designed for 12 GHz p 1735 N94-20516
Thermal expansion of electronic highly correlated materials
[ETN-93-93605] p 2026 N94-21135
High temperature superconducting planar circuit structure for high frequency applications
[AD-A273083] p 2026 N94-21521
Photoemission and the electronic properties of heavy fermions: Limitations of the Kondo model
[DE93-040191] p 1974 N94-21553
Local structure and superconductivity in La(2-x)Ba(x)CuO4 for x=0.125 and x=0.15
[DE93-040193] p 2029 N94-21555
Local structure in oxygen-doped La2CuO(4+delta)
[DE93-040248] p 2030 N94-21788
Spin-polaron theory of high-T(c) superconductivity. 3: Gap function and critical temperature
[DE93-019198] p 2030 N94-21831
Disks of YBa2Cu3O7 shocked to 10 GPa pressures
[DE94-000464] p 2031 N94-21931
Stability of an uncooled segment of a high-temperature superconductor
[DE94-000476] p 2032 N94-21932
The effect of correlated and point defects on the vortex lattice melting transition in single crystal YBa2Cu3O(7-delta)
[DE93-040277] p 2033 N94-21997
NMR studies of oxygen-doped La2CuO(4+delta)
[DE93-040756] p 2034 N94-22007
Simulating the Euclidean time Schroedinger equations using an INTEL iPSC/860 hypercube: Application to the t-J model of high-T(sub c) superconductivity
[DE94-000489] p 2035 N94-22385
Flow and heat transfer model for a rotating cryogenic motor
[DE94-001151] p 1794 N94-22405
Test results of two high temperature superconducting sample coils
[DE94-000496] p 2035 N94-22570
Positron annihilation study of Sr Doping in La(2-x)Sr(x)CuO4
[DE94-000307] p 2036 N94-22594
HIGH TEMPERATURE TESTS
Rapid heating tensile testing update: 304L stainless steel
[DE93-018770] p 1688 N94-19942
Integrity and testing concerns of thermostructural materials p 1681 N94-21384
Compilation of reinforced carbon-carbon transatlantic abort landing arc jet test results
[NASA-TM-104778] p 1676 N94-21834
HIGH VOLTAGES
SPICE macromodel for a 1-megawatt power MOSFET switch
[DE93-019415] p 1748 N94-19844
Characteristics of switching plasma in an inverse-pinch switch p 1995 N94-21292
High power, electron-beam induced switching in diamond
[DE93-040535] p 1768 N94-21770
Initial operation of a large-scale plasma source ion implantation experiment
[DE94-000805] p 2036 N94-22583
HIGHLANDS
Crater destruction on the Venusian highlands by tectonic processes p 2103 N94-20696
U-Pb isotopic ages and characteristics of ancient (greater than 4.0 Ga) lunar highland rocks p 2104 N94-20700
Some deformation trends and topographic characteristics of tesserae on Venus p 2105 N94-20706
Volcanic rises on Venus: Geology, formation, and sequence of evolution p 2113 N94-20755
The Mg-suite and the highland crust: An unsolved enigma p 2126 N94-20822
Briny lakes on early Mars? Terrestrial intracrater playas and Martian candidates p 2145 N94-21675
Early Mars: A regional assessment of denudation chronology p 2145 N94-21676
HILBERT SPACE
Totally strong and strong graphs
[RR-902-I] p 1951 N94-20237
Hilbert 90 for polynomial matrices
[CWI-AM-R9211] p 1954 N94-21159

HILL METHOD
Estimability of polar motion using range observations to satellites
[PB93-219319] p 1842 N94-22265
HISTOGRAMS
Dimension scaling effects on the yield sensitivity of HEMT digital circuits p 1765 N94-21712
Scale-space filtering and threshold hierarchy for image segmentation p 1777 N94-22149
HISTOLOGY
Non-ionic surfactants in the treatment of third degree burns
[AD-A271582] p 1891 N94-21035
HISTORIES
Documents on the history of aeronautical and space research in Germany, 1900 - 1970
[DLR-MITT-92-08] p 2152 N94-20543
Asymptotic analysis. Working Note No. 2, approximation of integrals
[DE94-000433] p 1961 N94-22381
HMX
Evaluation of pre-extraction analytical holding times for nitroaromatic and nitramine explosives in water
[AD-A271547] p 1712 N94-20927
Chemistry of the burning surface
[AD-A272725] p 1681 N94-21181
HOLES (ELECTRON DEFICIENCIES)
Study of mechanisms for long wavelength Schottky-barrier infrared detectors
[AD-A270538] p 1971 N94-20083
Measurement of superlattice optical properties by variable angle spectroscopic ellipsometry p 2022 N94-20992
Superlattice optical properties measured by variable angle spectroscopic ellipsometry p 2022 N94-20993
GaAs/AlGaAs superlattice characterization by variable angle spectroscopic ellipsometry p 2022 N94-20994
HOLES (MECHANICS)
Mold bolt and means for achieving close tolerances between bolts and bolt holes
[NASA-CASE-MFS-28720-1] p 1623 N94-20379
Damage states around fastener holes in thick graphite/epoxy composite laminates
[AD-A272613] p 1675 N94-21504
HOLOGRAPHY
Conically scanned holographic lidar telescope
[NASA-CASE-GSC-13462-1] p 1986 N94-20591
Holographic measurements of ice crystals in cirrus clouds during International Cirrus Experiment ICE
[GKSS-92/E/14] p 1866 N94-21052
Diffraction and holography of photoelectrons and fluorescent x rays
[DE93-019240] p 1808 N94-21441
The energy performance of prototype holographic glazings
[DE93-040451] p 1809 N94-21545
High resolution, three dimensional soft x ray imaging
[DE93-018667] p 1989 N94-21630
Electron holography applied to the study of ceramic materials
[DE94-000329] p 1707 N94-21653
Photoelectron holography of platinum (111)
[DE93-040856] p 1810 N94-21950
Optical processing in photorefractive media p 1789 N94-22222
Holographic optical elements correcting the off-axis aberrations of a parabolic mirror
[ISBN-0-315-57581-6] p 1990 N94-22411
HOMEOSTASIS
The role of axon-Schwann cell interactions in nervous system ionic homeostasis
[AD-A270936] p 1890 N94-20045
HOMOGENEITY
Applications of variable angle spectroscopic ellipsometry in semiconductor technology p 2025 N94-21010
HOMOGENEOUS TURBULENCE
Modeling of particle dispersion in a stationary isotropic homogeneous turbulence by large scale numerical simulation
[ETN-93-94604] p 1801 N94-20601
New results on the realizability of Reynolds stress turbulence closures
[NASA-CR-191548] p 1804 N94-21875
HOMOLOGY
Hilbert 90 for polynomial matrices
[CWI-AM-R9211] p 1954 N94-21159
HORIZONTAL FLIGHT
Rotorcraft noise: Status and recent developments
[NASA-CR-194761] p 1967 N94-20523
HORIZONTAL TAIL SURFACES
Apparatus and method for improving spin recovery on aircraft
[NASA-CASE-LAR-14747-1] p 1650 N94-20556
HORMONES
Changes in plasma vasopressin during motion sickness in cats p 1885 N94-21868
HORN ANTENNAS
Applications of planar near-field measurements to electromagnetic radiation and interference problems p 1747 N94-22252
HORSEPOWER
Advanced Turbine Systems (ATS). Phase 1: System scoping and feasibility studies
[DE93-041130] p 1826 N94-21938
HORSESHOE VORTICES
Direct simulation of shock-induced mixing layer
[DE93-040498] p 1803 N94-21531
HOT ELECTRONS
Modeling failure and reliability in new-generation devices
[AD-A271150] p 1748 N94-19910
HOT ISOSTATIC PRESSING
Microstructural modeling and toughening of Si3N4 ceramics for high temperature engine applications
[AD-A272897] p 1704 N94-21197
Strength and toughness improvement of silicide intermetallics by nanophase and microphase reinforcements
[AD-A272914] p 1692 N94-21320
HOT STARS
Radiation driven winds of hot stars: Some remarks on stationary models and spectrum synthesis in time-dependent simulations
[NASA-CR-194691] p 2081 N94-21578
HOT-FILM ANEMOMETERS
Measurement Technology for Flight Tests
[ILR-MITT-256(1991)] p 1639 N94-22597
Surface hot film measurements at ATTAS laminar glove p 1639 N94-22598
Testing of a multisensor hot film technique in wind tunnel and free flight p 1639 N94-22599
HOT-WIRE ANEMOMETERS
Near wake measurements on a rotor model with Mie-vanes in the Delft open jet tunnel
[PB93-215362] p 1638 N94-22260
Hot wire anemometry: A versatile instrumentation used for predevelopment studies and flight testing of the Do-328 aircraft p 1640 N94-22604
HOUSINGS
Cooling apparatus and couplings therefor
[NASA-CASE-ARC-11921-1] p 1800 N94-20371
Characterization and modelling of extremely high frequency enclosures p 1782 N94-22177
HOVERING
An experimental investigation of the drag mechanisms of a helicopter rotor in hovering flight
[AD-A270201] p 1636 N94-20486
Rotorcraft noise: Status and recent developments
[NASA-CR-194761] p 1967 N94-20523
HUBBLE SPACE TELESCOPE
Space Shuttle Mission STS-61: Hubble Space Telescope servicing mission-01
[NASA-TM-109344] p 1653 N94-20192
Focus history of the Hubble Space Telescope: Launch to May 1993
[NASA-CR-194179] p 2055 N94-20204
Restoration of HST images with missing data p 2057 N94-22439
HST image restoration: A comparison of pre- and post-servicing mission results p 1925 N94-22478
SPIKE: Application for ASTRO-D mission planning p 1926 N94-22486
The application of artificial intelligence to astronomical scheduling problems p 1949 N94-22492
Deconvolution of Hubble Space Telescope images using simulated point spread functions p 2048 N94-22497
HST PSF simulation using Tiny Tim p 1926 N94-22498
StarView: The object oriented design of the ST DADS user interface p 2049 N94-22548
HUGONIOT EQUATION OF STATE
Shock temperature measurements of iron to 350 GPa
[DE94-001058] p 1695 N94-22024
HUMAN BEHAVIOR
Female security as a general mobility condition
[ISBN-3-79-831536-1] p 2039 N94-20153
HUMAN FACTORS ENGINEERING
Aviation safety research at the National Institute for Aviation Research, Wichita State University
[NIAR-93-4] p 1641 N94-20189
AIDA: A graphical interactive system, adapted to the user
[ETN-93-93792] p 1908 N94-21020
Columbus: Materials for 30 years habitability in space p 1662 N94-21387
Design and implementation of a status at a glance user interface for a power distribution expert system
[NASA-TM-106412] p 1715 N94-21589
Cognitive engineering in aerospace applications
[NASA-CR-194782] p 1647 N94-21819
Intervention strategies for the management of human error
[NASA-CR-4547] p 1642 N94-22373
HUMAN PERFORMANCE
Development of the UTC-PAB normative database
[AD-A271319] p 1893 N94-20023
Physiological correlates of stress-induced decrements in human perceptual performance
[DOT/FAA/AM-93/19] p 1893 N94-20061
Loads produced by a suited subject performing tool tasks without the use of foot restraints
[NASA-TP-3424] p 1896 N94-20606
Research, Development, Training, and Evaluation (RDTE) support delivery order 1: Computational cognitive models
[AD-A271837] p 1894 N94-20610
Maximum team lifting capacity as a function of team size
[AD-A271642] p 1892 N94-21036
Psychometric developments related to tests and selection
[AD-A272971] p 1894 N94-21262
Strength capabilities and load requirements while performing torquing tasks in zero gravity
[NASA-TP-3433] p 1897 N94-21627
The effects of instructional sets on reactions to and performance on an intelligent tutoring system
[NASA-CR-194739] p 1895 N94-21810
Intervention strategies for the management of human error
[NASA-CR-4547] p 1642 N94-22373
HUMAN TOLERANCES
Evaluation of head injury criteria
[NIAR-93-2] p 1890 N94-20190
HUMAN-COMPUTER INTERFACE
CMIFed: A presentation environment for porta ble hypermedia documents
[CWI-CS-R9305] p 2044 N94-21494
Structured multimedia authoring
[CWI-CS-R9304] p 2044 N94-21535
Design and implementation of a status at a glance user interface for a power distribution expert system
[NASA-TM-106412] p 1715 N94-21589
Modelling decision-making by pilots
[NASA-CR-194767] p 2040 N94-21821
Application development in a PC/LAN environment p 1923 N94-22067
Integrating a local database into the StarView distributed user interface p 2048 N94-22530
HUMIDITY
Durability predictions for adhesively bonded joints in humid environments
[AD-A271177] p 1830 N94-20001
Incorporation and comparative evaluation of a non-convective cloud parameterization scheme in the Naval Research Laboratory west coast mesoscale weather prediction model
[AD-A272417] p 1867 N94-21146
Analysis of the GOES 6.7 micrometer channel observations during FIRE 2 p 1875 N94-22316
HUMIDITY MEASUREMENT
Overview of microphysical and state parameter measurements from FIRE 2 p 1871 N94-22293
Analysis of the tropospheric water distribution during FIRE 2 p 1876 N94-22324
HYBRID CIRCUITS
Y-Ba-Cu-O superconducting/GaAs semiconducting hybrid circuits for microwave applications p 1735 N94-20514
MHMIC: Technology for the integration of microwave sub-assemblies p 1785 N94-22199
HYBRID COMPOSITES
Polymer gels as precursors to high-performance materials
[AD-A270937] p 1699 N94-20046
Quantification of uncertainties in the performance of smart composite structures
[NASA-TM-106335] p 1830 N94-20171
HYBRID PROPULSION
Analysis of a diesel-electric hybrid urban bus system
[DE93-019514] p 1825 N94-21297
HYDRATES
Technology to prevent greenhouse effect gases
[DE94-707421] p 1850 N94-19976
HYDRATION
Thermal behavior of natural zeolites
[DE93-040091] p 1699 N94-19975
Application of an electrochemical quartz crystal microbalance to the study of electrocatalytic films
[DE93-041124] p 2029 N94-21691
A quantitative S.E.M. image analysis of cement paste microstructure p 1708 N94-21894
HYDRAULIC EQUIPMENT
Long range fast tool servo
[AD-A271614] p 1761 N94-21257

HYDRAZINES
N,N'-bis(4,4,4-trinitro butyryl) hydrazine
[AD-D015897] p 1712 N94-20122
HYDROCARBON COMBUSTION
Theoretical research program to study chemical reactions in AOTV bow shock tubes
[NASA-CR-194710] p 1804 N94-22027
HYDROCARBON FUELS
On demand, non-halon, fire extinguishing systems
[AD-D015957] p 1714 N94-20355
First Biomass Conference of the Americas: Energy, Environment, Agriculture, and Industry, volume 2
[DE94-000435] p 1847 N94-21562
HYDROCARBONS
Electron reactions in nonpolar liquids: Pressure effects
[DE93-040328] p 1970 N94-19931
Tropospheric chemistry of natural hydrocarbons, aldehydes, and peroxy radicals: Their connections to sulfuric acid production and climate effects
[DE93-019525] p 1855 N94-20220
HYDROCHLORIC ACID
Parameters affecting hydrogen chloride measurements
[AD-A271326] p 1851 N94-20025
HYDRODYNAMICS
Hydrodynamic compressibility of high-strength ceramics
[DE93-019424] p 1698 N94-19903
Development and characterization of a time-, position- and energy-resolved x ray diagnostic for PBFA 2 target experiments
[DE93-019429] p 1808 N94-20297
Numerical simulations of hypervelocity impact experiments involving single Whipple bumper shields
[AD-A272123] p 1831 N94-20572
Effects of hydrodynamics and thermal radiation in the atmosphere after comet impacts p 1862 N94-20649
Asteroid collisions: Target size effects and resultant velocity distributions p 2083 N94-20729
SPH modelling of energy partitioning during impacts on Venus p 2124 N94-20809
The sand bag model of the dispersion of the cosmic body in the atmosphere p 2084 N94-20823
Atmospheric breakup of a small comet in the Earth's atmosphere p 2084 N94-20824
Coupling of smooth particle hydrodynamics with PRONTO
[DE93-019080] p 1915 N94-21539
Laser driven hydrodynamic instability experiments
[DE93-040550] p 1818 N94-21547
A note on singularities caused by the hydrodynamic dispersion tensor
[CWI-NM-R9302] p 1803 N94-21575
RHALE: A 3-D MMALE code for unstructured grids
[DE93-019405] p 1916 N94-21635
Canonically covariant formulation of Landau's Newtonian superfluid dynamics
[PB93-221034] p 1805 N94-22272
Smoothed-particle hydrodynamics and nonequilibrium molecular dynamics
[DE94-001059] p 1977 N94-22400
Coupling of smooth particle hydrodynamics with the finite element method
[DE93-019081] p 1905 N94-22556
Hydrodynamical winds from an accretion disk p 2008 N94-22683
HYDROELECTRIC POWER STATIONS
Current situation of development of petroleum substituting energies (USA)
[DE94-707492] p 1848 N94-22013
HYDROFLUORIC ACID
Spectroscopic ellipsometry studies of HF treated Si (100) surfaces p 1734 N94-20508
Development and demonstration of a personal monitoring system for exposure to hydrogen fluoride
[DE93-041273] p 1891 N94-20935
HYDROGEN
Encounters of H and D atoms with O2 in water: Relative diffusion and reaction rates
[DE93-018587] p 1970 N94-19956
Evaluation of a diffusion/trapping model for hydrogen ingress in high-strength alloys
[AD-A271328] p 1689 N94-20027
Energy storage and conversion in solid hydrogen
[AD-A271439] p 1845 N94-20086
Detailed structure study of an H2/N2O/Ar flame employing molecular beam mass spectrometry, laser spectroscopy, and modeling
[AD-A270720] p 1679 N94-20111
Hydrogen pickup and redistribution in alpha-annealed zircaloy-4
[DE93-018050] p 1689 N94-20182
Optical metrology of magnetically trapped hydrogen
[AD-A272110] p 1680 N94-20584
Evaporation in equilibrium, in vacuum, and in hydrogen gas p 1684 N94-20638
High D/H ratios of water in magmatic amphiboles in Chassigny: Possible constraints on the isotopic composition of magmatic water on Mars p 2134 N94-20862
Performance of carbon-based hot frit substrates
[DE94-000509] p 1676 N94-21754
Performance assessment of low pressure nuclear thermal propulsion
[NASA-TM-108433] p 1671 N94-21860
Hydrogen in compound semiconductors
[DE93-040300] p 2031 N94-21922
Development of an electrochemical hydrogen separator
[DE93-019877] p 1683 N94-21984
Proof of stability of the hydrogen molecule
[PB93-221026] p 1977 N94-22271
HYDROGEN ATOMS
Energy storage and conversion in solid hydrogen
[AD-A271439] p 1845 N94-20086
Laser diagnostics of RF hydrogen plasma reactors: Application to the processing of III-V materials
[AD-A272659] p 1994 N94-21214
HYDROGEN BONDS
Application of the reactive flux formalism to study water hydrogen bond dynamics
[AD-A271824] p 1680 N94-20560
Femtosecond dynamics in hydrogen-bonded solvents
[DE93-019937] p 1683 N94-21842
HYDROGEN CLOUDS
Dust content of a hydrogen rich, low surface brightness galaxy and the luminosity history of 3C273
[NASA-CR-194705] p 2056 N94-21779
HYDROGEN COMPOUNDS
Hydrogen in compound semiconductors
[DE93-040300] p 2031 N94-21922
HYDROGEN EMBRITTLEMENT
Evaluation of a diffusion/trapping model for hydrogen ingress in high-strength alloys
[AD-A271328] p 1689 N94-20027
Hydrogen pickup and redistribution in alpha-annealed zircaloy-4
[DE93-018050] p 1689 N94-20182
Investigation of moisture-induced embrittlement of iron aluminides
[DE93-040841] p 1695 N94-21949
HYDROGEN FUELS
Statement of David E. Baldwin, Associate Director for Energy, Lawrence Livermore National Laboratory and John C. Crawford, Vice President, Sandia National Laboratories, California, to the Subcommittee on Research and Development of the Committee on Environment and Public Works, US Senate, Washington, DC, 22 March 1993
[DE93-017991] p 1844 N94-19803
Fuel processing requirements and techniques for fuel cell propulsion power
[DE93-019516] p 1750 N94-20257
HYDROGEN IONS
Ionization of H2(+) in intense laser fields
[DE93-019160] p 1818 N94-21829
A dc Penning surface-plasma source
[DE93-040126] p 1997 N94-21989
Interactions of slow H, H2, and H3 with thin foils
[DE93-040263] p 1976 N94-21995
HYDROGEN ISOTOPES
Hydrogen isotope separation experience at the Savannah River Site
[DE93-019832] p 1679 N94-20266
HYDROGEN MASERS
Measurements of atomic interactions and frequency stability with a cryogenic hydrogen maser
[AD-A271132] p 1814 N94-19853
HYDROGEN OXYGEN ENGINES
Turbine design p 1668 N94-20075
The Vulcain cryogenic engine p 1668 N94-20077
HYDROGEN PEROXIDE
Tropospheric chemistry of natural hydrocarbons, aldehydes, and peroxy radicals: Their connections to sulfuric acid production and climate effects
[DE93-019525] p 1855 N94-20220
HYDROGEN PLASMA
Laser diagnostics of RF hydrogen plasma reactors: Application to the processing of III-V materials
[AD-A272659] p 1994 N94-21214
HYDROGEN PRODUCTION
Statement of David E. Baldwin, Associate Director for Energy, Lawrence Livermore National Laboratory and John C. Crawford, Vice President, Sandia National Laboratories, California, to the Subcommittee on Research and Development of the Committee on Environment and Public Works, US Senate, Washington, DC, 22 March 1993
[DE93-017991] p 1844 N94-19803
A calcium oxide sorbent process for bulk separation of carbon dioxide
[DE93-019288] p 1847 N94-21540
Proceedings of the 1993 DOE/NREL Hydrogen Program Review
[DE93-018207] p 1847 N94-21616
Plasma-chemical conversion of hydrogen sulfide into hydrogen and sulfur
[DE93-041167] p 1682 N94-21789
HYDROGEN RECOMBINATIONS
Energy storage and conversion in solid hydrogen
[AD-A271439] p 1845 N94-20086
Performance assessment of low pressure nuclear thermal propulsion
[NASA-TM-108433] p 1671 N94-21860
HYDROGEN SULFIDE
Plasma-chemical conversion of hydrogen sulfide into hydrogen and sulfur
[DE93-041167] p 1682 N94-21789
HYDROGEN-BASED ENERGY
Statement of David E. Baldwin, Associate Director for Energy, Lawrence Livermore National Laboratory and John C. Crawford, Vice President, Sandia National Laboratories, California, to the Subcommittee on Research and Development of the Committee on Environment and Public Works, US Senate, Washington, DC, 22 March 1993
[DE93-017991] p 1844 N94-19803
Proceedings of the 1993 DOE/NREL Hydrogen Program Review
[DE93-018207] p 1847 N94-21616
HYDROGENATION
Catalytic hydrogenation of carbon monoxide
[DE94-000881] p 1678 N94-20103
Synthesis and catalytic properties of metal and semiconductor nanoclusters
[DE93-019418] p 2028 N94-21541
Investigations on trends in global environment adaptive industrial technologies
[DE94-714888] p 1853 N94-22258
HYDROLOGICAL CYCLE
A wet-geology and cold-climate Mars model: Punctuation of a slow dynamic approach to equilibrium p 2090 N94-20389
A marine sedimentary model for the evolution of the northern plains p 2091 N94-20395
Workshop on Early Mars: How Warm and How Wet?, part 1
[NASA-CR-193553] p 2142 N94-21659
Evolution of the global water cycle on Mars: The geological evidence p 2142 N94-21660
HYDROLOGY
Remote sensing for hydrology progress and prospects
[WMO-773] p 1841 N94-21069
Simulated real-time intercomparison of hydrological models
[WMO-779] p 1867 N94-21070
Workshop on Early Mars: How Warm and How Wet?, part 1
[NASA-CR-193553] p 2142 N94-21659
Mars: Noachian hydrology by its statistics and topology p 2143 N94-21664
The hydrologic response of Mars to the onset of a colder climate and to the thermal evolution of its early crust p 2143 N94-21666
HYDROLOGY MODELS
Hydrological consequences of ponded water on Mars p 2089 N94-20383
Remote sensing for hydrology progress and prospects
[WMO-773] p 1841 N94-21069
Simulated real-time intercomparison of hydrological models
[WMO-779] p 1867 N94-21070
HYDROMETEOROLOGY
Radio wave propagation studies along an Earth-space satellite link
[ISBN-0-315-60627-4] p 1742 N94-22408
HYDRONIUM IONS
Electronically metastable molecules of high symmetry
[AD-A272015] p 1974 N94-21461
HYDROPYROLYSIS
Synthesis and catalytic properties of metal and semiconductor nanoclusters
[DE93-019418] p 2028 N94-21541
HYDROSTATIC PRESSURE
Durability predictions for adhesively bonded joints in humid environments
[AD-A271177] p 1830 N94-20001
Hydrostatic/nonhydrostatic comparison with the MERCURE code on orographic flows
[ETN-93-94603] p 1866 N94-20600
HYDROTHERMAL SYSTEMS
Fluvial valleys in the heavily cratered terrains of Mars: Evidence for paleoclimatic change? p 2144 N94-21670
HYGROMETERS
Overview of microphysical and state parameter measurements from FIRE 2 p 1871 N94-22293

A comparison of small and larger mesoscale latent heat and radiative fluxes: December 6 case study p 1879 N94-22335

HYGROSCOPICITY
Development of advanced cloud parameterizations to examine air quality, cloud properties, and cloud-radiation feedback in mesoscale models [DE93-041164] p 1853 N94-22384

HYPERBOLIC FUNCTIONS
Approximate methods for N-component solute transport and ion-exchange [CWI-NM-R9223] p 1910 N94-21078

HYPERCUBE MULTIPROCESSORS
The quantum structure of matter grand challenge project: Large-scale 3-D solutions in relativistic quantum dynamics [DE94-000328] p 1960 N94-21955
Simulating the Euclidean time Schroedinger equations using an INTEL iPSC/860 hypercube: Application to the t-J model of high-T(sub c) superconductivity [DE94-000489] p 2035 N94-22385

HYPERGEOMETRIC FUNCTIONS
Asymptotic behavior of Fourier transform of surface measures on convex and radial hypersurfaces [ETN-93-93790] p 1952 N94-21019

HYPERPLANES
M-dimensional computer memory with M-1 dimensional hyperplane access [AD-D015960] p 1898 N94-20357

HYPERSONIC AIRCRAFT
Optimization and performance analysis of a supersonic conical-flow waverider for a deck-launched intercept mission [AD-A272498] p 1648 N94-21433

HYPERSONIC FLOW
Experimental investigation of nozzle/plume aerodynamics at hypersonic speeds [NASA-CR-194628] p 1636 N94-20014
Establishing the basis for validated predictions of highly non-equilibrium flows (with 9 attachments) [AD-A272918] p 1802 N94-21220
An efficient numerical method for three-dimensional hypersonic flow [AD-A272506] p 1637 N94-21411
Multigrid schemes for viscous hypersonic flows p 1641 N94-21473
The 2D and 3D hypersonic flows with unstructured meshes p 1920 N94-22365

HYPERSONIC SPEED
Optimization and performance analysis of a supersonic conical-flow waverider for a deck-launched intercept mission [AD-A272498] p 1648 N94-21433
Thrust augmentation options for the Beta 2 two-stage-to-orbit vehicle [NASA-TM-106448] p 1648 N94-21563

HYPERSONICS
On magnetodynamic effects initiated by a high-speed impact of a large cosmic body upon the Earth's surface p 2082 N94-20647
An efficient numerical method for three-dimensional hypersonic flow [AD-A272506] p 1637 N94-21411

HYPERTHERMIA
Calculation and optimization of electromagnetic fields in a patient by local hyperthermia utilization [ETN-93-95059] p 1889 N94-20024
Numerical modeling for an electric-field hyperthermia applicator p 1729 N94-20451

HYPERVELOCITY IMPACT
An equation of state for shock in homogeneous materials and comparison to shock data [AD-A271436] p 1829 N94-19881
PVDF gauge characterization of hypervelocity-impact-generated debris clouds [DE93-018831] p 1829 N94-19943
Numerical simulations of hypervelocity impact experiments involving single Whipple bumper shields [AD-A272123] p 1831 N94-20572
On magnetodynamic effects initiated by a high-speed impact of a large cosmic body upon the Earth's surface p 2082 N94-20647
Impact glasses from the ultrafine fraction of lunar soils p 2097 N94-20662
Impactor control of central peak and peak-ring formation p 1862 N94-20744
Further analyses of Rio Cuarto impact glass p 1685 N94-20745
Determination of parameters for hypervelocity dust grains encountered in near-Earth space p 2084 N94-20817
Antipodal fragment velocities for porous and weak targets at catastrophic impacts p 1836 N94-20891
Hypervelocity impact [AD-A272957] p 1831 N94-21249
Meteoroids and debris impact risk assessment on Columbus and Hermes using a realistic geometrical analysis tool p 1662 N94-21388
Hypervelocity impact studies at CEG: Experimental and numerical capabilities p 1664 N94-21397

HYPERVELOCITY PROJECTILES
Impactor control of central peak and peak-ring formation p 1862 N94-20744
Determination of parameters for hypervelocity dust grains encountered in near-Earth space p 2084 N94-20817
Core formation by giant impacts: Conditions for intact melt region formation p 1863 N94-20833
Intact capture of hypervelocity particles on Shuttle p 2085 N94-20837
Hypervelocity impact [AD-A272957] p 1831 N94-21249
Experimental and numerical studies of high-velocity impact fragmentation [DE93-040205] p 1832 N94-21557

HYPSOGRAPHY
Comparative hypsometric analysis of both Earth and Venus topographic distributions p 2108 N94-20722

HYSTERESIS
Relaxation of hysteresis loop in a single crystal of YBa2Cu4O8 [DE93-019519] p 2029 N94-21649
Disks of YBa2Cu3O7 shocked to 10 GPa pressures [DE94-000464] p 2031 N94-21931

I

IBM PERSONAL COMPUTERS
An expert system of econometric analysis p 2052 N94-22081

ICE
Calderas produced by hydromagmatic eruptions through permafrost in northwest Alaska p 2089 N94-20385
Ice in the northern plains: Relic of a frozen ocean? p 2090 N94-20391
The thumbprint terrain: What will Mars Observer tell us? p 2091 N94-20397
Volatile loss from accreting icy protoplanets p 2084 N94-20793
Solar proton events from a 180 year depth profile of nitrate concentrations from the central Greenland ice sheet [AD-A272888] p 2147 N94-21196
The evolution of the early Martian climate and the initial emplacement of crustal H2O p 2143 N94-21665
Cirrus microphysics observations made during FIRE 2: Small particles, high concentrations, and probe comparisons p 1871 N94-22294
Spectral variation of scattering and absorption by cirrus p 1876 N94-22321
Mesoscale simulations of the November 25-26 and December 5-6 cirrus cases using the RAMS model p 1878 N94-22331
Estimation of cirrus cloud particle fallspeeds from vertically pointing Doppler radar p 1879 N94-22333
Normalized vertical ice mass flux profiles from vertically pointing 8-mm-wavelength Doppler radar p 1879 N94-22334

ICE CLOUDS
Cirrus properties deduced from CO2 lidar observations of zenith-enhanced backscatter from oriented crystals p 1871 N94-22295
Microphysical properties of the November 26 cirrus cloud retrieved by Doppler radar/IR radiometer technique p 1873 N94-22304
Comparison of cloud microphysical parameters derived from surface and satellite measurements during FIRE phase 2 p 1873 N94-22306
Progress in interpreting CO2 lidar signatures to obtain cirrus microphysical and optical properties p 1874 N94-22308
Importance of aggregation and small ice crystals in cirrus clouds, based on observations and an ice particle growth model p 1879 N94-22336
SSH-2 measurements of cirrus at 18-28 micrometers from the King Air during FIRE 2 p 1880 N94-22338
Remote sensing estimates of cirrus particle size for tropical and midlatitude cirrus: Hexagonal crystals and ice spheres p 1880 N94-22342
Are tropical cirrus brighter than mid-latitude cirrus? p 1881 N94-22343

ICE ENVIRONMENTS
A wet-geology and cold-climate Mars model: Punctuation of a slow dynamic approach to equilibrium p 2090 N94-20389
Early Mars was wet but not warm: Erosion, fluvial features, liquid water habitats, and life below freezing p 2145 N94-21677

ICE FORMATION
Debris/ice/TPS assessment and integrated photographic analysis for Shuttle Mission STS-51 [NASA-TM-109189] p 1656 N94-21884

ICE MAPPING
Polarimetric backscattering from sea ice p 1723 N94-20426
Observation of pressure ridges in SAR images of sea ice: Scattering theory and comparison with observations p 1723 N94-20427
On evaluating the accuracy of SAR sea-ice classification using multifrequency polarimetric AIRSAR data p 1724 N94-20428
C-band radar backscatter of sea ice in the Weddell Sea, Antarctica during the austral winter of 1992 p 1725 N94-20435

ICE NUCLEI
Holographic measurements of ice crystals in cirrus clouds during International Cirrus Experiment ICE [GKSS-92/E/14] p 1866 N94-21052
Remote sensing estimates of cirrus particle size for tropical and midlatitude cirrus: Hexagonal crystals and ice spheres p 1880 N94-22342
Are tropical cirrus brighter than mid-latitude cirrus? p 1881 N94-22343

ICE REPORTING
Observation of pressure ridges in SAR images of sea ice: Scattering theory and comparison with observations p 1723 N94-20427
Radar backscattering from snow facies of the Greenland ice sheet: Results from the AIRSAR 1991 campaign p 1725 N94-20434

ICY SATELLITES
The 3-D Moons: The Voyager stereo atlas of the outer solar system p 2111 N94-20740

IDENTIFYING
Experiments in knowledge refinement for a large rule-based system [AD-A272055] p 1809 N94-21445

IDENTITIES
Vanishing theorem on arithmetic surfaces [PB93-215481] p 1961 N94-22263

IGNEOUS ROCKS
The Erevan howardite: Petrology of glassy clasts and mineral chemistry p 1684 N94-20640
Carbonaceous xenoliths from the Erevan howardite p 1684 N94-20642
Igneous rock from Severnyi Kolchim (H3) chondrite: Nebular origin p 2082 N94-20643
Venus magmatic and tectonic evolution p 2101 N94-20683
Post-igneous redistribution of components in eucrites p 1685 N94-20684

IGNITION
A spheromak ignition experiment reusing Mirror Fusion Test Facility (MFTF) equipment [DE94-001856] p 2034 N94-22050

ILLUMINATING
The energy performance of prototype holographic glazings [DE93-040451] p 1809 N94-21545

ILMENITE
Petrogenesis of Apollo 12 mare basalts. Part 1: Multiple melts and fractional crystallization to explain olivine and ilmenite basalt compositions p 1684 N94-20644
Abundance and composition of solar KR in the H3-H6 chondrite ACFER111 p 1684 N94-20676
Production of O2 on the Moon: A lab-top demonstration of ilmenite reduction with hydrogen p 2126 N94-20821
A Backscatter Moessbauer Spectrometer (BaMS) for use on Mars p 1811 N94-22431

IMAGE ANALYSIS
Recognizing 3-D objects using 2-D images [AD-A271005] p 1983 N94-19819
Statistical object recognition [AD-A270887] p 1962 N94-20113
Evaluation of lunar rocks and soils for resource utilization: Detailed image analysis of raw materials and beneficiated products p 2126 N94-20820
Objective determination of image end-members in spectral mixture analysis p 1686 N94-20831
Rapid estimates of crop production using remote sensing: European experience p 1840 N94-20969
Holographic measurements of ice crystals in cirrus clouds during International Cirrus Experiment ICE [GKSS-92/E/14] p 1866 N94-21052
Determining the 3-D structure and motion of objects using a scanning laser range sensor [NASA-CR-194745] p 1818 N94-21817
Symposium on Microscopy and Image Analysis of Building Materials [VTT-SYMP-136] p 1707 N94-21890
Preparation of concrete specimens for microstructural image analysis studies p 1707 N94-21891
Optical air pore analysis p 1708 N94-21892

A quantitative S.E.M. image analysis of cement paste microstructure p 1708 N94-21894
Determination of pore structure of concrete from thin sections by image analysis p 1708 N94-21895
Microstructure in mortar: A summary of a new project of research p 1708 N94-21896
Quantitative analysis of scanning tunneling microscopy images for surface structure determination: Sulfur on Re(0001)
[DE93-019235] p 2034 N94-22041
A 3-D vision method for estimating workspace occupancy of a power-line maintenance robot p 1770 N94-22105
Directional coding of morphological pyramidal representations p 1771 N94-22106
Optimal object modelling for an active-vision system p 1771 N94-22107
Hierarchical surface triangulation of range data p 1771 N94-22108
Segmenting the optical flow due to the motion of several rigid objects p 1777 N94-22147
Elliptical-shape parameter estimation from a set of normal lines p 1777 N94-22148
An insensitive algorithm for template matching with correlation p 1793 N94-22249
Measurement of thermal-hydraulic parameters in two-phase flow using flow visualization image analysis
[DE93-006255] p 1805 N94-22269
STAR-1 SAR road extraction using texture analysis and mathematical morphology
[ISBN-0-315-83255-X] p 1843 N94-22429
GUIs in the MIDAS environment p 2047 N94-22449
An IDL-based analysis package for COBE and other skycube-formatted astronomical data p 1925 N94-22471
SkICAT: A cataloging and analysis tool for wide field imaging surveys p 2049 N94-22546

IMAGE CLASSIFICATION
Recognition by prototypes
[AD-A271687] p 1943 N94-20921
Goal-oriented dynamic vision
[TR-466] p 1945 N94-21315
Improvement in invariant pattern recognition with neural networks and Fourier-Mellin filters p 1780 N94-22164
A modified moment invariants technique for classification of noisy objects p 1780 N94-22165
Automated cloud classification with a fuzzy logic expert system p 1875 N94-22313
STARBASE: Database software for the automated plate scanner p 1927 N94-22512

IMAGE CONTRAST
Why stereo vision is not always about 3D reconstruction
[AD-A270522] p 1939 N94-19893
Millimeter-wave imaging of composite materials
[DE93-041160] p 1677 N94-21940

IMAGE ENHANCEMENT
High resolution studies of the structure of the solar atmosphere
[AD-A273084] p 2147 N94-21522
Particle image velocimetry
[DE93-040657] p 1804 N94-21748
Experiments with recursive estimation in astronomical image processing p 2047 N94-22457

IMAGE FILTERS
Improvement in invariant pattern recognition with neural networks and Fourier-Mellin filters p 1780 N94-22164

IMAGE INTENSIFIERS
UVPI imaging from the LACE satellite: The Starbird rocket plume
[AD-A271981] p 1658 N94-20617

IMAGE MOTION COMPENSATION
Visual tracking
[AD-A271686] p 1943 N94-20920
Determining the 3-D structure and motion of objects using a scanning laser range sensor
[NASA-CR-194745] p 1818 N94-21817
A motion extraction method for synthetic aperture radars
[DLR-FB-92-31] p 1742 N94-22279

IMAGE PROCESSING
Metrics for specifying and/or testing neural networks statement of government interest
[AD-D015946] p 1938 N94-19843
Robust photo-topography by fusing shape-from-shading and stereo
[NASA-CR-194697] p 1808 N94-19920
Robust and efficient 3D recognition by alignment
[AD-A270839] p 1904 N94-20041
Low bit rate coding of Earth science images
[NASA-CR-193729] p 2041 N94-20158
Optoelectronic associative memory
[NASA-CASE-NPO-18278-1-CU] p 1985 N94-20303
A comparison of some of the most current methods of image compression
[AD-A271841] p 1907 N94-20525
Simulating a user's preferences: Towards automated artificial evolution for computer generated images
[AD-A272058] p 1942 N94-20621
Identification of an interstellar oxide grain from the Murchison meteorite by ion imaging p 2082 N94-20659
Visual tracking
[AD-A271686] p 1943 N94-20920
Recognition by prototypes
[AD-A271687] p 1943 N94-20921
Nature's crucible: Manufacturing optical nonlinearities for high resolution, high sensitivity encoding in the compound eye of the fly, Musca domestica p 1755 N94-21095
Adaptive analog video signal conditioner p 1744 N94-21099
Multiple-fold clustered processor mesh array p 1757 N94-21113
An optically-assisted 3-D cellular array machine
[AD-A272683] p 1987 N94-21163
Internal camera calibration using rotation and geometric shapes
[AD-A272718] p 1808 N94-21167
Image detection using edge extraction algorithms
[AD-A272439] p 1911 N94-21203
Some extensions of the k-means algorithm for image segmentation and pattern classification
[AD-A271691] p 1913 N94-21364
Data and model-driven selection using parallel-line groups
[AD-A271702] p 1913 N94-21365
Magnetic force microscopy/current contrast imaging: A new technique for internal current probing of IC's
[DE93-040754] p 1761 N94-21532
A data distributed, parallel algorithm for ray-traced volume rendering
[DE93-040150] p 1935 N94-21622
Reduction of blocking effects for the JPEG baseline image compression standard p 1765 N94-21714
Visualization on massively parallel computers using CM/AVS
[DE93-040151] p 1936 N94-21746
Particle image velocimetry
[DE93-040657] p 1804 N94-21748
Performance evaluation of video on ethernet
[DE93-040696] p 1936 N94-21749
Stochastic simulation for imaging spatial uncertainty: Comparison and evaluation of available algorithms
[DE93-040058] p 1916 N94-21761
Geometric optimization
[DE93-040152] p 1917 N94-21764
Imaging vector fields using line integral convolution
[DE93-019922] p 1917 N94-21841
Three dimensional ultrasonic imaging
[DE93-040549] p 1968 N94-22003
A 3-D vision method for estimating workspace occupancy of a power-line maintenance robot p 1770 N94-22105
Directional coding of morphological pyramidal representations p 1771 N94-22106
Segmentation and fitting by residual consensus p 1771 N94-22109
The local measurement and global interpretation of 3D motion field generated by several moving objects from range image sequences p 1777 N94-22146
Scale-space filtering and threshold hierarchy for image segmentation p 1777 N94-22149
New algorithm for the detection of the orientation of a planar Lambertian surface in 3D p 1777 N94-22150
VLSI design of a parallel video output interface p 1778 N94-22153
Coding of color quantized images p 1781 N94-22173
Hierarchical multirate vector quantization for image coding p 1781 N94-22174
Image convolution using the Myrias SPS-2 parallel computer p 1786 N94-22207
Parallelizing a maximum entropy image deconvolution algorithm p 1787 N94-22208
Optical processing in photorefractive media p 1789 N94-22222
A real-time infrared image processing testbed p 1790 N94-22227
Memory based vision: A new concept p 1790 N94-22228
Automated investigation of quasars at a galactic latitude of -45 deg
[ISBN-0-315-57576-X] p 2056 N94-22415
Second Annual Conference on Astronomical Data Analysis Software and Systems. Abstracts
[NASA-TM-108245] p 2057 N94-22438
A low-cost vector processor boosting compute-intensive image processing operations p 1925 N94-22441
Multifrequency data analysis software on STARLINK p 1925 N94-22443
CCD surface photometry of galaxies p 2058 N94-22445
GUIs in the MIDAS environment p 2047 N94-22449
A neural network prototyping package within IRAF p 1949 N94-22451
Experiments with recursive estimation in astronomical image processing p 2047 N94-22457
PROS: An IRAF based system for analysis of x ray data p 1925 N94-22461
PHOTCAL: The IRAF photometric calibration package p 1925 N94-22465
Deep near-infrared survey of the Southern Sky (DENIS) p 2062 N94-22467
Enhancements to IRAF/STSDAS graphics p 1925 N94-22470
An IDL-based analysis package for COBE and other skycube-formatted astronomical data p 1925 N94-22471
Programmability in AIPS++ p 1926 N94-22482
Telescope image modelling software in STSDAS p 1926 N94-22483
How is WFPC flat field made p 1926 N94-22484
Deconvolution of Hubble Space Telescope images using simulated point spread functions p 2048 N94-22497
The IDL astronomy user's library p 2048 N94-22500
SKYMAP: Exploring the Universe in software p 1927 N94-22511
Some practicable applications of quadtree data structures/representation in astronomy p 1927 N94-22515
A new programming metaphor for image processing procedures p 1927 N94-22531
PCIPS 2.0: Powerful multiprofile image processing implemented on PCs p 1927 N94-22532
The spectral world coordinate systems in IRAF/NOAO p 2049 N94-22539
MOSAIC: Software for creating mosaics from collections of images p 1927 N94-22543
Registering and resampling images in STSDAS p 1927 N94-22550
First MEM task IRMEO in IRAF p 1928 N94-22551
Image processing as a tool in flight testing evaluation p 1640 N94-22606

IMAGE RECONSTRUCTION
Optimal resolution in maximum entropy image reconstruction from projections with multigrid acceleration p 1955 N94-21465
Hierarchical surface triangulation of range data p 1771 N94-22108
A software environment for the exploitation of the MAR image sensor p 1785 N94-22200
Applications of a two-dimensional nonlinear filters to image restoration p 1789 N94-22225
Memory based vision: A new concept p 1790 N94-22228
Surface acquisition through virtual milling p 1920 N94-22372
STAR-1 SAR road extraction using texture analysis and mathematical morphology
[ISBN-0-315-83255-X] p 1843 N94-22429
Restoration of HST images with missing data p 2057 N94-22439
Efficient transfer of images over networks p 1748 N94-22517
First MEM task IRMEO in IRAF p 1928 N94-22551

IMAGE RESOLUTION
Why stereo vision is not always about 3D reconstruction
[AD-A270522] p 1939 N94-19893
Nature's crucible: Manufacturing optical nonlinearities for high resolution, high sensitivity encoding in the compound eye of the fly, Musca domestica p 1755 N94-21095
Data compression by using wavelet transforms and vector quantization
[AD-A272763] p 1738 N94-21182
A neural network for multiresolution edge detection p 1779 N94-22163
Remote sensing of multilevel clouds during FIRE IFO 2 p 1844 N94-22303
A multiresolution wavelet representation in two or more dimensions p 1925 N94-22456
Enhancements to IRAF/STSDAS graphics p 1925 N94-22470
An IDL-based analysis package for COBE and other skycube-formatted astronomical data p 1925 N94-22471
HST image restoration: A comparison of pre- and post-servicing mission results p 1925 N94-22478

IMAGE ROTATION
Registering and resampling images in STSDAS p 1927 N94-22550

IMAGERY
The digital archive of the International Halley Watch p 2047 N94-22496

IMAGES
Optical encoding of imaging data
[AD-D015915] p 1984 N94-20056
Hierarchical multirate vector quantization for image coding p 1781 N94-22174
Tests of a simple data merging algorithm for the GONG project p 1927 N94-22549
IMAGING RADAR
Application of Cloude's target decomposition theorem to polarimetric imaging radar data p 1724 N94-20429
Imaging radar studies of atmospheric winds and waves
[AD-A271672] p 1866 N94-20918
IMAGING SPECTROMETERS
MinMap: An imaging spectrometer for high resolution compositional mapping of the Moon p 1813 N94-20686
Intercomparison of MAS, AVIRIS, and HIS data from FIRE cirrus 2 p 1872 N94-22298
IMAGING TECHNIQUES
Uncertainty limited atomic position measurement using optical fields
[AD-A271013] p 1970 N94-19822
An assessment of COMSCAN, a Compton backscatter imaging camera, for the one-sided non-destructive inspection of aerospace components
[AD-A271331] p 1906 N94-19837
The NRL LACE program
[AD-A270861] p 1657 N94-19896
Proceedings of the 8th International Symposium on Applications of Ferroelectrics
[AD-A270679] p 1749 N94-20012
Optical encoding of imaging data
[AD-D015915] p 1984 N94-20056
X ray, extreme and far ultraviolet optical thin films for space applications
[NASA-CR-194635] p 1984 N94-20128
Automatic AVHRR image navigation software
[NASA-CR-194602] p 1643 N94-20148
Synchrotron x ray diffraction analysis of photorefractive crystals and their gratings
[AD-A271176] p 2015 N94-20213
Optical diagnostic instrument for monitoring etch uniformity during plasma etching of polysilicon in a chlorine-helium plasma
[DE93-019582] p 1993 N94-20261
The National High Magnetic Field Laboratory, a user facility in support of research in high magnetic fields
[DE93-040145] p 1714 N94-20278
Three-dimensional dynamic thermal imaging of structural flaws by dual-band infrared computed tomography
[DE93-019575] p 1906 N94-20316
Ultrafast scanning microscopy
[DE93-040121] p 1985 N94-20320
Wide-angle imaging system with fiberoptic components providing angle-dependent virtual material stops
[NASA-CASE-NPO-18146-1-CU] p 1986 N94-20345
Cognition and the brain: A continuation of the university research initiative at New York University
[AD-A271872] p 1894 N94-20467
Direct imaging of the surface microstructure of dielectric materials using an atomic force microscope
[AD-A272251] p 2018 N94-20575
UVPI imaging from the LACE satellite: The Starbird rocket plume
[AD-A271981] p 1658 N94-20617
The High Resolution Stereo Camera (HRSC) for the Lunar Scout 1 Mission p 1813 N94-20650
Identification of an interstellar oxide grain from the Murchison meteorite by ion imaging p 2082 N94-20659
Wavelength dependence of limb-darkening of Mars from visible and near-IR telescopic spectral imaging p 2101 N94-20685
The 3-D Moons: The Voyager stereo atlas of the outer solar system p 2111 N94-20740
The Clementine Mission science return at the Moon and Geographos p 1652 N94-20850
Information extraction for multispectral images using radiation interaction models
[BCRS-90-22] p 1841 N94-21015
Image detection using edge extraction algorithms
[AD-A272439] p 1911 N94-21203
Long-range laser imaging
[AD-A273020] p 1817 N94-21253
Some extensions of the k-means algorithm for image segmentation and pattern classification
[AD-A271691] p 1913 N94-21364
Data and model-driven selection using parallel-line groups
[AD-A271702] p 1913 N94-21365
Magnetic force microscopy/current contrast imaging: A new technique for internal current probing of IC's
[DE93-040754] p 1761 N94-21532
Instantaneous velocity field imaging instrument for supersonic reacting flows
[NASA-CR-191162] p 1809 N94-21607
A data distributed, parallel algorithm for ray-traced volume rendering
[DE93-040150] p 1935 N94-21622
High resolution, three dimensional soft x ray imaging
[DE93-018667] p 1989 N94-21630
Electron holography applied to the study of ceramic materials
[DE94-000329] p 1707 N94-21653
Stochastic simulation for imaging spatial uncertainty: Comparison and evaluation of available algorithms
[DE93-040058] p 1916 N94-21761
Imaging vector fields using line integral convolution
[DE93-019922] p 1917 N94-21841
Some experiments on using backscattered electron and energy dispersive x ray imaging in determination of portland cement clinker phase composition p 1708 N94-21893
Iterative electromagnetic Born inversion applied to earth conductivity imaging
[DE93-040668] p 1859 N94-21928
Millimeter-wave imaging of composite materials
[DE93-041160] p 1677 N94-21940
Three dimensional ultrasonic imaging
[DE93-040549] p 1968 N94-22003
Inelastic electron scattering from surfaces
[DE94-001738] p 1977 N94-22049
Surface acquisition through virtual milling p 1920 N94-22372
Transmission electron microscopy study of thick copper-304 stainless steel multilayers
[DE94-001045] p 1696 N94-22394
Experiments with recursive estimation in astronomical image processing p 2047 N94-22457
New IRAF stellar photometry software p 1925 N94-22464
How is WFPC flat field made p 1926 N94-22484
SPIKE: Application for ASTRO-D mission planning p 1926 N94-22486
HST PSF simulation using Tiny Tim p 1926 N94-22498
An x ray archive on your desk: The Einstein CD-ROM's p 2048 N94-22519
UIT support observations archive p 2048 N94-22534
SkICAT: A cataloging and analysis tool for wide field imaging surveys p 2049 N94-22546
Solar full-disk magnetic field image receiving system and observation software p 2079 N94-22552
IMPACT
Impact-induced devolatilization of CaSO4 anhydrite and implications for K-T extinctions: Preliminary results p 2085 N94-20840
IMPACT DAMAGE
On magnetodynamic effects initiated by a high-speed impact of a large cosmic body upon the Earth's surface p 2082 N94-20647
Determination of cosmic bodies size-velocity distribution by observation of current impacts on Mars p 2082 N94-20648
Effects of hydrodynamics and thermal radiation in the atmosphere after comet impacts p 1862 N94-20649
Largest impact features on Venus: Non-preserved or non-recognizable? p 2096 N94-20657
Dynamics of large scale impacts on Venus and Earth p 2098 N94-20666
Kalkkop crater, Eastern Cape: A new impact crater in South Africa p 1862 N94-20714
Asteroid collisions: Target size effects and resultant velocity distributions p 2083 N94-20729
Numerical modeling of impact erosion of atmospheres: Preliminary results p 2131 N94-20847
Morphologic classes of impact basins on Venus p 2137 N94-20883
Orbital debris and micrometeoroids: LDEF and Mir data p 1659 N94-21368
Measured space environmental effects to LDEF during retrieval p 1659 N94-21372
The implications of the LDEF results on Space Station Freedom power system materials p 1660 N94-21377
An attempt to comprehend Martian weathering conditions through the analysis of terrestrial palagonite samples p 2143 N94-21668
IMPACT LOADS
Shock wave interactions with exothermic mixtures
[AD-A271149] p 1829 N94-19836
A benchmark study of 2D and 3D finite element calculations simulating dynamic pulse buckling tests of cylindrical shells under axial impact
[DE93-018859] p 1829 N94-19940
Shock response of porous Al-2 + Fe2O3 powder mixtures
[DE93-018851] p 1688 N94-19944
Numerical simulations of hypervelocity impact experiments involving single Whipple bumper shields
[AD-A272123] p 1831 N94-20572
Shock attenuation at the Slate Islands revisited p 1863 N94-20887
Disks of YBa2Cu3O7 shocked to 10 GPa pressures
[DE94-000464] p 2031 N94-21931
IMPACT MELTS
Largest impact features on Venus: Non-preserved or non-recognizable? p 2096 N94-20657
Impact glasses from the ultrafine fraction of lunar soils p 2097 N94-20662
Modelling the gravity and magnetic field anomalies of the Chicxulub crater p 1862 N94-20668
Self diffusion of alkaline-Earth in Ca-Mg-aluminosilicate melts: Experimental improvements on the determination of the self-diffusion coefficients p 1684 N94-20669
Preliminary estimation of tagamite cooling conditions (Puchezh-Katunki Astrobleme, Russia) p 2083 N94-20735
Original size of the Vredefort structure, South Africa p 1863 N94-20825
Core formation by giant impacts: Conditions for intact melt region formation p 1863 N94-20833
Reverse polarity magnetized melt rocks from the Chicxulub impact structure, Yucatan Peninsula, Mexico p 1863 N94-20843
Limits on differentiation of melt sheets from basin-scale lunar impacts p 2133 N94-20856
IMPACT STRENGTH
Dynamic properties of ceramic materials
[DE94-000654] p 1708 N94-21963
IMPACT TESTS
Dynamic, multiaxial impact response of confined and unconfined ceramic rods
[DE93-040057] p 1829 N94-19824
Shock wave interactions with exothermic mixtures
[AD-A271149] p 1829 N94-19836
A benchmark study of 2D and 3D finite element calculations simulating dynamic pulse buckling tests of cylindrical shells under axial impact
[DE93-018859] p 1829 N94-19940
Impactor control of central peak and peak-ring formation p 1862 N94-20744
A fresh look at crater scaling laws for normal and oblique hypervelocity impacts p 1666 N94-20864
Combination of on ground experiments and analysis software for the evaluation of material degradation in space (SILEX project) p 1662 N94-21389
Hypervelocity impact studies at CEG: Experimental and numerical capabilities p 1664 N94-21397
Experimental and numerical studies of high-velocity impact fragmentation
[DE93-040205] p 1832 N94-21557
Dynamic properties of ceramic materials
[DE94-000654] p 1708 N94-21963
IMPACT TOLERANCES
A fresh look at crater scaling laws for normal and oblique hypervelocity impacts p 1666 N94-20864
IMPACTORS
Searching for ancient Venus p 2111 N94-20743
IMPEDANCE
Observation of reflected waves on the SABRE positive polarity inductive adder MITL
[DE93-019413] p 1980 N94-20295
IMPELLERS
Three dimensional unsteady flow calculations in radial components p 1669 N94-20080
Experimental and computational results from a large low-speed centrifugal impeller
[NASA-TM-106421] p 1636 N94-20136
IMPLANTATION
Implantation of nitrogen: Effects of hydrogen and implantation energy p 1686 N94-20804
Implantation of carbon in GaAs and compensating native defects
[DE93-040122] p 2030 N94-21763
Initial operation of a large-scale plasma source ion implantation experiment
[DE94-000805] p 2036 N94-22583
IMPLOSIONS
Laser driven hydrodynamic instability experiments
[DE93-040550] p 1818 N94-21547
IMPULSES
Using crosscorrelation techniques to determine the impulse response of linear systems p 1759 N94-21122
IMPURITIES
Segregation of Si to the surface of Fe-29Ni-17Co alloy
[DE93-040053] p 1687 N94-19864
Transient thermal analysis of cryocondensation pump for JET
[DE93-040372] p 1992 N94-20003
Semiconductor isotope engineering
[DE93-040119] p 2030 N94-21744

Plasma-chemical conversion of hydrogen sulfide into hydrogen and sulfur
[DE93-041167] p 1682 N94-21789
On Plasma Edge Spectroscopy and Spectroscopic Studies of Impurity Densities and Impurity Transport
[IPF-92-2] p 1996 N94-21802
Plasma edge spectroscopy p 1996 N94-21803
Spectroscopic studies of impurity densities and impurity transport p 1997 N94-21804

IN SITU MEASUREMENT
Optical diagnostic instrument for monitoring etch uniformity during plasma etching of polysilicon in a chlorine-helium plasma
[DE93-019582] p 1993 N94-20261
Comparison of satellite-derived velocity fields in the coastal transition zone
[AD-A272565] p 1883 N94-21360
In situ identification of the Martian surface material and its interaction with the Martian atmosphere using DTA/GC p 1812 N94-22434

IN-FLIGHT MONITORING
In-flight measurement of aircrew breathing in Navy aircraft
[AD-A271811] p 1896 N94-21154

INCIDENCE
Topographic mapping using a monopulse SAR system p 1721 N94-20417
Multiple-wavelength angle-of-incidence ellipsometry: Application to silicon nitride-gallium arsenide structures p 2019 N94-20974
Thin film compositional analysis using null or fixed wavelength ellipsometry p 1709 N94-20976
Variable wavelength, variable angle ellipsometry including a sensitivities correlation test p 1710 N94-20978
Variable angle of incidence spectroscopic ellipsometric study of semiconductor multilayer structures p 2020 N94-20982
Ellipsometric analysis of built-in electric fields in semiconductor heterostructures p 1796 N94-20988
Superlattice optical properties measured by variable angle spectroscopic ellipsometry p 2022 N94-20993
GaAs/AlGaAs superlattice characterization by variable angle spectroscopic ellipsometry p 2022 N94-20994
Micro-ellipsometric measurements of strained layer structures p 2025 N94-21008
Fundamentals and applications of variable angle spectroscopic ellipsometry p 1687 N94-21011
In-situ and ex-situ ellipsometric characterization for semiconductor technology p 2026 N94-21013
VASE (variable angle spectroscopic ellipsometry) p 1687 N94-21014

INCLUSIONS
Petrography and origin of refractory inclusions from the Murray and Murchison C2 chondrites p 2084 N94-20770
Primary differentiation in the early Earth: Nd and Sr isotopic evidence from diamondiferous eclogites for both old depleted and old enriched mantle, Yakutia, Siberia p 1662 N94-20776
Fe/Mn in olivine of carbonaceous meteorites p 2084 N94-20788
The Sm-Nd systematics of silicate inclusions in iron meteorites: Results from Caddo (IAB)
[CONTRIB-5241(804)] p 2084 N94-20795
Diffusion-controlled magnesium isotopic fractionation of a single crystal forsterite evaporated from the solid state p 1686 N94-20855
Trace element compositions of spinel-rich refractory inclusions from the Murchison meteorite p 2086 N94-20897
Inter- and intra-crystalline oxygen isotope distribution of fassaites in Allende CAI p 2086 N94-20898
Mineralogy of dark clasts in primitive versus differentiated meteorites p 2087 N94-20907
Surface and subsurface defect detection in Si3N4 components by laser scattering
[DE93-040829] p 1832 N94-21772

INCOMPRESSIBLE FLOW
A comparison of two incompressible Navier-Stokes algorithms for unsteady internal flow
[NASA-TM-108794] p 1798 N94-20104
Multigrid solution of the Navier-Stokes equations on highly stretched grids with defect correction p 1806 N94-21481
Modelling stalled airfoils
[ISBN-0-315-59525-6] p 1639 N94-22382

INDENE
Chemical reaction fouling model for single-phase heat transfer
[DE93-019556] p 1802 N94-20942

INDEPENDENT VARIABLES
Longitudinal instability of an induction linac with acceleration
[DE93-019249] p 1980 N94-20290

INDEXES (DOCUMENTATION)
Aeronautical engineering: A continuing bibliography with indexes (supplement 294)
[NASA-SP-7037(294)] p 1635 N94-20267
On the selection of indices in relational databases
[MEMO-INF-92-72] p 2043 N94-21071
Index to 1992 NASA Tech Briefs, volume 16, numbers 1-12
[NASA-TM-109377] p 2053 N94-21736
Index to 1991 NASA Tech Briefs, volume 15, numbers 1-12
[NASA-TM-109376] p 2053 N94-21737
Cumulative index to NASA Tech Briefs, 1986-1990, volumes 10-14
[NASA-TM-109378] p 2054 N94-21738
Data indexing techniques for the EUVE all-sky survey p 2048 N94-22503

INDEXES (RATIOS)
Analysis of consumer demand structure by means of economic indexes p 2052 N94-22074

INDIUM ALLOYS
Thin-film CdTe and CuInSe2 photovoltaic technologies
[DE93-018217] p 1848 N94-21827

INDIUM ARSENIDES
High Speed/High Frequency Optoelectronics
[AD-A271985] p 1751 N94-20580
Synthesis and properties of mismatched heterojunction/substrate interfaces
[AD-A272904] p 1760 N94-21229

INDIUM COMPOUNDS
Theory of energy-assisted epitaxy; theory of ordered semiconductor alloys: In(1-x)Tl(x)Sb as a long-wave infrared material
[AD-A271007] p 2012 N94-19835
Advanced processing technology for high-efficiency thin-film CuInSe2 solar cells
[DE93-010045] p 1847 N94-21614
Research on polycrystalline thin-film submodules based on CuInSe2 materials
[DE93-018223] p 2029 N94-21617

INDIUM GALLIUM ARSENIDES
Characteristics of 0.8- and 0.2-microns gate length In(x)Ga(1-x) As/In(0.52)Al(0.48)As/InP (0.53 less than or equal to x less than or equal to 0.70) modulation-doped field-effect transistors at cryogenic temperatures p 1733 N94-20499
Dielectric function of InGaAs in the visible p 2023 N94-21000
Study of InGaAs-based modulation doped field effect transistor structures using variable-angle spectroscopic ellipsometry p 1796 N94-21001

INDIUM PHOSPHIDES
First results on InGaAsP separate confinement heterostructure diode lasers
[AD-A270849] p 1815 N94-19878
Study of the utilization of thin oxides in indium phosphides for the realisation of electron components
[ECL-92-38] p 2018 N94-20593
Surface treatment of InP and contribution to the optimization of the InP(p)/InP(p) regrown interfaces grown by GSMBE
[ECL-92-48] p 2018 N94-20598

INDOOR AIR POLLUTION
Long Duration Exposure Facility (LDEF) contamination study
[AD-A272419] p 1658 N94-21147

INDUCTION HEATING
Flexible heating head for induction heating
[NASA-CASE-LAR-14418-15-B] p 1718 N94-20368
A study of the induction heating of organic composites
[AD-A272657] p 1675 N94-21187

INDUSTRIAL PLANTS
Survey on chemical engineering technologies for the global environmental protection
[DE94-714887] p 1852 N94-22044

INDUSTRIAL WASTES
Plasma-chemical conversion of hydrogen sulfide into hydrogen and sulfur
[DE93-041167] p 1682 N94-21789

INDUSTRIES
Wind energy: Program overview, FY 1992
[DE93-000056] p 1845 N94-19921
Self assembly: An approach to terascale integration
[DE93-040104] p 1769 N94-21846
Industry standards: Key to distributed computing p 1938 N94-22070
Investigation on construction of the database system for research and development of the global environment industry technology
[DE94-714890] p 1853 N94-22090
Survey on utilization of database for research and development of global environmental industry technology
[DE94-714891] p 1853 N94-22259

INELASTIC SCATTERING
Examination of low level magnetic dipole intensities in the transition nuclei Sm-148, Sm-150, Sm-152 and Sm-154, with inelastic photon scattering at S-DALINAC
[ETN-93-95069] p 1971 N94-20030
Study of mechanisms for long wavelength Schottky-barrier infrared detectors
[AD-A270538] p 1971 N94-20083
Neutron and PIMC determination of the longitudinal momentum distribution of HCP, BCC and normal liquid He-4
[DE93-019009] p 1972 N94-20187
Neutron-scattering studies of Yb-bearing silicate glasses
[DE93-019768] p 1700 N94-20265
Measurement of the strange quark distribution function in W(+) charm quark events
[DE93-018267] p 1973 N94-20474
SLAC measurement of the neutron spin structure function
[DE93-040998] p 1975 N94-21788
Toward a QCD analysis of jet rates in deep-inelastic Muon-Proton scattering
[DE94-000618] p 1976 N94-21962
Non-adiabatic effects in low-energy electron-molecule scattering
[DE93-040485] p 1976 N94-21968
Inelastic electron scattering from surfaces
[DE94-001738] p 1977 N94-22049
Inelastic neutron scattering of (gamma)-iron, and the determination of the elastic constants by lattice dynamics
[DE94-000694] p 1978 N94-22573

INEQUALITIES
Vanishing theorem on arithmetic surfaces
[PB93-215481] p 1961 N94-22263

INERTIAL CONFINEMENT FUSION
Parametric instabilities in picosecond time scales
[DE94-000384] p 1966 N94-21958
Phase screens for the control of the focal irradiance of the Nova laser
[DE94-001067] p 1820 N94-22401

INERTIAL NAVIGATION
Automatic AVHRR image navigation software
[NASA-CR-194602] p 1643 N94-20148
A software architecture for a small autonomous underwater vehicle navigation system
[AD-A272322] p 1643 N94-21037
Vector gravimetry by a combination of inertial and GPS satellite measurements
[ISBN-0-315-61980-5] p 1861 N94-22424

INFLATABLE STRUCTURES
Tetrahedral lander
[NASA-CASE-MSC-22082-1] p 1658 N94-20590
System test results of the Advanced Technology Anti-G Suit (ATAGS)
[AD-A271535] p 1896 N94-20914

INFORMATION DISSEMINATION
Label-connected graphs: An overview
[RR-898-M] p 1950 N94-20163
Listing of approved recurring information requirements
[AD-A271673] p 2042 N94-20919
Assessment of the organizational structure and services of DOE National Laboratory Libraries
[DE93-040697] p 2045 N94-21750
Implementation of a laboratory information management system for environmental regulatory analyses
[DE94-001198] p 2046 N94-22407
Everything you might want to know about the Internet but are afraid to ask!
[DE93-041118] p 2046 N94-22413
The extreme ultraviolet explorer archive p 2047 N94-22468
A distributed clients/distributed servers model for STARCAT p 2047 N94-22469
STELAR: An experiment in the electronic distribution of astronomical literature p 2049 N94-22544
The STARLINK software collection p 1927 N94-22545

INFORMATION MANAGEMENT
Distributed Virtual System (DIVIRS) project
[NASA-CR-194360] p 1905 N94-20228
HERMES, a report generator for research on information processing in command posts: The effect of missing information
[IZF-1992-A-28] p 2042 N94-20310
Security management of electronic data interchange
[AD-A272962] p 1899 N94-21252
Urban applications of satellite remote sensing and GIS analysis
[PB93-202174] p 1842 N94-21855
Implementation of a laboratory information management system for environmental regulatory analyses
[DE94-001198] p 2046 N94-22407
The extreme ultraviolet explorer archive p 2047 N94-22468

A distributed clients/distributed servers model for STARCAT p 2047 N94-22469
SIMBAD quality-control p 2048 N94-22502
Data indexing techniques for the EUVE all-sky survey p 2048 N94-22503
The NSO FTS database program and archive (FTSDBM) p 1926 N94-22506

INFORMATION PROCESSING (BIOLOGY)
Physiological correlates of stress-induced decrements in human perceptual performance
[DOT/FAA/AM-93/19] p 1893 N94-20081
Toward a neurobiological theory of visual attention
[AD-A270724] p 1890 N94-20112
Incongruity, incongruity resolution, and mental states: The measure and modification of situational awareness and control
[NASA-CR-194568] p 1893 N94-20168
Research, Development, Training, and Evaluation (RDTE) support delivery order 1: Computational cognitive models
[AD-A271837] p 1894 N94-20610
Nature's crucible: Manufacturing optical nonlinearities for high resolution, high sensitivity encoding in the compound eye of the fly, Musca domestica p 1755 N94-21095

INFORMATION RETRIEVAL
Research in image management and access
[NASA-CR-194797] p 1907 N94-20376
Information extraction for multispectral images using radiation interaction models
[BCRS-90-22] p 1841 N94-21015
A conceptual database design and performance analysis of the MILSATCOM requirements database
[AD-A272672] p 1658 N94-21217
Extracting information from wrong answers in computerized adaptive testing
[AD-A272832] p 1894 N94-21434
Project Records Information System (PRIS): User's manual
[DE94-001548] p 2045 N94-22047
The Keck keyword layer p 1925 N94-22460
Electronic publishing and intelligent information retrieval p 2047 N94-22479
Intelligent text retrieval in the NASA astrophysics data system p 2048 N94-22499
SIMBAD quality-control p 2048 N94-22502
StarView: The object oriented design of the ST DADS user interface p 2049 N94-22548

INFORMATION SYSTEMS
Data and Analysis Center for Software
[AD-A270571] p 2041 N94-20106
A proposed research program in information processing
[NASA-CR-194271] p 2041 N94-20134
Distributed Virtual System (DIVIRS) project
[NASA-CR-194360] p 1905 N94-20228
HERMES, a report generator for research on information processing in command posts: The effect of missing information
[IZF-1992-A-28] p 2042 N94-20310
Multi Wave Link: An interactive database for co-ordination of multiwavelength programs
[NASA-CR-194778] p 2043 N94-21055
The electronics technology policy of the NLR Informatics Division: The NLR electronics CAE infrastructure
[NLR-TP-91001-U] p 1753 N94-21067
Government Open Systems Interconnection Profile (GOSIP) transition strategy
[AD-A273005] p 1740 N94-21308
PEGASUS, electronic bulletin board system user's guide
[AD-A271679] p 2044 N94-21363
CMIFed: A presentation environment for porta ble hypermedia documents
[CWI-CS-R9305] p 2044 N94-21494
Electronic resources for security related information: Reference document
[DE93-040488] p 2044 N94-21529
Assessment of the organizational structure and services of DOE National Laboratory Libraries
[DE93-040697] p 2045 N94-21750
Project Records Information System (PRIS): User's manual
[DE94-001548] p 2045 N94-22047
Information Technology and Economic Modelling
[VTT-SYMP-135] p 2049 N94-22056
Soviet society informatization: The USSR state program p 2046 N94-22058
Information sciences and business enterprises p 2046 N94-22059
Information and decision structure in a Japanese type of management with respect to QCC and just-in-time systems p 2046 N94-22063
Manufacturing and information technology p 2046 N94-22082
Survey on utilization of database for research and development of global environmental industry technology
[DE94-714891] p 1853 N94-22259
The logistic model: The integration of business process redesign and information systems development based on logistic principles
[MEMO-INF-92-70] p 2045 N94-22276
A comparison of IDEF1X and NIAM ISDM
[DE93-040899] p 1921 N94-22383
Everything you might want to know about the Internet but are afraid to ask!
[DE93-041118] p 2046 N94-22413
Archiving data from ground-based telescopes p 2046 N94-22442
Electronic publishing and intelligent information retrieval p 2047 N94-22479
Programmability in AIPS++ p 1926 N94-22482
Intelligent text retrieval in the NASA astrophysics data system p 2048 N94-22499
SIMBAD quality-control p 2048 N94-22502
NASA's astrophysics archives at the National Space Science Data Center p 2049 N94-22541
STELAR: An experiment in the electronic distribution of astronomical literature p 2049 N94-22544
The STARLINK software collection p 1927 N94-22545

INFORMATION THEORY
A complex systems approach to computational molecular biology
[DE93-040062] p 1884 N94-19866
The communication complexity of set intersection problems
[MEMO-1077] p 1738 N94-21073
Reasoning about update logic
[CWI-CS-R9312] p 1914 N94-21496

INFORMATION TRANSFER
Data and Analysis Center for Software
[AD-A270571] p 2041 N94-20106
Security management of electronic data interchange
[AD-A272962] p 1899 N94-21252
Implementing Electronic Data Interchange (EDI) with small business suppliers in the pre-award acquisition process
[AD-A271767] p 1945 N94-21305
Government Open Systems Interconnection Profile (GOSIP) transition strategy
[AD-A273005] p 1740 N94-21308
Survey on utilization of database for research and development of global environmental industry technology
[DE94-714891] p 1853 N94-22259
NASA data exchange standards for computational fluid dynamics p 1920 N94-22371

INFRARED ABSORPTION
Infrared absorption spectroscopy of the weakly bonded CO-Cl2 complex
[AD-A271757] p 2027 N94-21304

INFRARED ASTRONOMY
Circumstellar environments of Be stars at infra-red and radio wavelengths
[ISBN-0-315-83135-9] p 2081 N94-22426
A neural network prototyping package within IRAF p 1949 N94-22451
The spectral world coordinate systems in IRAF/NOAO p 2049 N94-22539
SPECFOCUS: An IRAF task for focusing spectrographs p 1965 N94-22540

INFRARED DETECTORS
Theory of energy-assisted epitaxy; theory of ordered semiconductor alloys: In(1-x)Tl(x)Sb as a long-wave infrared material
[AD-A271007] p 2012 N94-19835
Study of mechanisms for long wavelength Schottky-barrier infrared detectors
[AD-A270538] p 1971 N94-20083
Integrated display of multi-sensor geophysical and electromagnetic flight data p 1721 N94-20418
Models of refraction in the marine atmosphere surface layer
[AD-A271724] p 1858 N94-21357
Advanced far infrared detectors
[DE93-040289] p 1988 N94-21528
Optical properties of cirrus derived from airborne measurements during FIRE IFO 2 p 1872 N94-22297

INFRARED IMAGERY
Three-dimensional dynamic thermal imaging of structural flaws by dual-band infrared computed tomography
[DE93-019575] p 1906 N94-20316
The quantum efficiency of HgCdTe photodiodes in relation to the direction of illumination and to their geometry p 1735 N94-20512
The 7th Brazilian Remote Sensing Symposium, volume 2 p 1838 N94-20956
Analysis of hyper-spectral AVIRIS image data over a mixed-conifer forest in Maine p 1838 N94-20959
A real-time infrared image processing testbed p 1790 N94-22227
A four-band infrared data acquisition facility for signal processing development p 1791 N94-22235
Deep near-infrared survey of the Southern Sky (DENIS) p 2062 N94-22467

INFRARED INSTRUMENTS
Atmospheric infrared sounder
[NASA-CR-194814] p 1856 N94-20362
A retrieval error analysis technique for passive infrared atmospheric sounders
[AD-A272618] p 1867 N94-21212
Fluorescent microthermographic imaging
[DE93-040332] p 1810 N94-22000

INFRARED PHOTOMETRY
Wavelength dependence of limb-darkening of Mars from visible and near-IR telescopic spectral imaging p 2101 N94-20685
Circumstellar environments of Be stars at infra-red and radio wavelengths
[ISBN-0-315-83135-9] p 2081 N94-22426

INFRARED RADAR
Cirrus properties deduced from CO2 lidar observations of zenith-enhanced backscatter from oriented crystals p 1871 N94-22295
Progress in interpreting CO2 lidar signatures to obtain cirrus microphysical and optical properties p 1874 N94-22308

INFRARED RADIATION
Innovative acoustic technique for studying new materials and new developments in solid state physics
[AD-A270540] p 2013 N94-19933
Visible-infrared properties of controlled laboratory soils p 1685 N94-20689
Derivation of the midinfrared (5.0-25.0 micron) optical constants of hydrous carbonate and sulfate p 2108 N94-20723
Thermal infrared remote sensing and Kirchhoff's law: 1. Laboratory measurements p 1685 N94-20733
Comparisons of downwelling radiation to model predictions based on groundbased measurements during FIRE 1991 p 1876 N94-22320
Calibration of radiation codes in climate models: Comparison of calculations with observations from the SPECtral Radiation Experiment (SPECTRE) p 1879 N94-22337
Infrared FEL photochemistry: Multiple-photon dissociation of freon gas
[DE94-000817] p 1820 N94-22585

INFRARED RADIOMETERS
Remote sensing of multilevel clouds during FIRE IFO 2 p 1844 N94-22303
Microphysical properties of the November 26 cirrus cloud retrieved by Doppler radar/IR radiometer technique p 1873 N94-22304
Observations of multi-layered clouds using K-band radar p 1874 N94-22311
SSH-2 measurements of cirrus at 18-28 micrometers from the King Air during FIRE 2 p 1880 N94-22338

INFRARED SCANNERS
A four-band infrared data acquisition facility for signal processing development p 1791 N94-22235
Signal processing and target discrimination algorithms for a rosette scan tracker p 1747 N94-22237

INFRARED SIGNATURES
Optical properties of cirrus derived from airborne measurements during FIRE IFO 2 p 1872 N94-22297

INFRARED SPACE OBSERVATORY (ISO)
The ISO SWS on-line system p 1927 N94-22522

INFRARED SPECTRA
Phonons and metastability in compressed nitrogen
[DE93-019913] p 2016 N94-20318
Rotational spectrum of a dark state in 2-fluoroethanol using microwave/radiofrequency-infrared multiple resonance
[AD-A272101] p 1817 N94-20583
High resolution infrared spectroscopy of formamide and deuterated formamide in a molecular beam
[AD-A271986] p 1973 N94-20618
Wavelength dependence of limb-darkening of Mars from visible and near-IR telescopic spectral imaging p 2101 N94-20685
Visible-infrared properties of controlled laboratory soils p 1685 N94-20689
Derivation of the midinfrared (5.0-25.0 micron) optical constants of hydrous carbonate and sulfate p 2108 N94-20723
C-O volatiles in Apollo 15 and Apollo 17 picritic glasses p 1685 N94-20727
A retrieval error analysis technique for passive infrared atmospheric sounders
[AD-A272618] p 1867 N94-21212
Michelson Interferometer (MINT) p 1813 N94-21646

Calibration of radiation codes in climate models: Comparison of calculations with observations from the SPECtral Radiation Experiment (SPECTRE)
p 1879 N94-22337
The spectral world coordinate systems in IRAF/NOAO
p 2049 N94-22539
SPECFOCUS: An IRAF task for focusing spectrographs
p 1965 N94-22540

INFRARED SPECTROMETERS
Intercomparison of MAS, AVIRIS, and HIS data from FIRE cirrus 2
p 1872 N94-22298
The ISO SWS on-line system
p 1927 N94-22522

INFRARED SPECTROSCOPY
High resolution infrared spectroscopy of formamide and deuterated formamide in a molecular beam
[AD-A271986]
p 1973 N94-20618
High resolution infrared spectroscopy of cyclobutane: A study of vibrational mode coupling involving large amplitude, low frequency modes
[AD-A271987]
p 1973 N94-20619
Chemistry of the burning surface
[AD-A272725]
p 1681 N94-21181
Infrared absorption spectroscopy of the weakly bonded CO-Cl2 complex
[AD-A271757]
p 2027 N94-21304
Deep near-infrared survey of the Southern Sky (DENIS)
p 2062 N94-22467

INFRARED TRACKING
A real-time infrared image processing testbed
p 1790 N94-22227
Signal processing and target discrimination algorithms for a rosette scan tracker
p 1747 N94-22237

INHIBITORS
Enhancement of wound healing by biosynthetic growth factor
[AD-A272517]
p 1892 N94-21415

INHOMOGENEITY
Chemical zoning and diffusion of Ca, Al, Mn, and Cr in olivine of springwater pallasite
p 2086 N94-20902

INITIATION
Digital wireless control system
[DE93-040211]
p 1714 N94-19946

INITIATORS (EXPLOSIVES)
N,N'-bis(4,4,4-trinitro butyryl) hydrazine
[AD-D015897]
p 1712 N94-20122

INJECTORS
Heavy ion fusion injector experiments
[DE93-019188]
p 1993 N94-20234
High current injector for heavy ion fusion
[DE93-019241]
p 1979 N94-20289
Liquid fuel injection elements for rocket engines
[NASA-CASE-MFS-28547-1]
p 1669 N94-20370
Cold starting an alcohol-fueled engine with ultrasonic fuel atomization
[PB93-206597]
p 1826 N94-22093

INJURIES
Evaluation of head injury criteria
[NIAR-93-2]
p 1890 N94-20190

INLET FLOW
Design of a state-space controller for an advanced gas turbine engine
[AD-A270859]
p 1647 N94-20042

INLET TEMPERATURE
Design of a state-space controller for an advanced gas turbine engine
[AD-A270859]
p 1647 N94-20042

INPUT/OUTPUT ROUTINES
Database computing in HEP
[NASA-CR-194791]
p 1921 N94-22375
Distributed input/output processing in data-driven multiprocessors
[DE94-000323]
p 1937 N94-22378
Development of the FITS tools package for multiple software environments
p 1927 N94-22516

INSOLATION
Surveys on specific patterns of facility intallation of photovoltaic power generating technologies for international cooperation
[DE94-714901]
p 1850 N94-22092

INSPECTION
Demonstrating damage tolerance of composite airframes
p 1647 N94-22623

INSTALLING
Engineering design, fabrication, installation, operation, and maintenance services in support of research on laser plasma physics
[AD-A272249]
p 1994 N94-20943

INSTRUCTION SETS (COMPUTERS)
A set-associative, fault-tolerant cache design
p 1768 N94-21731

INSTRUMENT ERRORS
Techniques for reducing error in the calorimetric measurement of low wattage items
[DE93-018472]
p 1807 N94-20114
Calorimeter measurements of low wattage items
[DE93-018473]
p 1807 N94-20115
Parameter estimation with cost function of second order in output-error-problem
[DLR-FB-92-38]
p 1964 N94-21139
Description and assessment of a new Optical Pressure Measurement System (OPMS) demonstrated in the high speed wind tunnel in Goettingen (Germany)
[DLR-FB-92-24]
p 1651 N94-21280
Mirror velocity sampling errors in a Michelson interferometer
[AD-A273105]
p 1809 N94-21508
Orbit and sampling requirements: TRMM experience
p 1870 N94-21647
MLS pointing angle error sources and effects
p 1644 N94-22154

INSTRUMENT FLIGHT RULES
Rotorcraft low altitude IFR benefit/cost analysis: Conclusions and recommendations
[DOT/FAA/RD-93/22]
p 1642 N94-20051
Parallel runway requirement analysis study. Volume 2: Simulation manual
[NASA-CR-191549-VOL-2]
p 1644 N94-22278

INSTRUMENT LANDING SYSTEMS
Public-sector aviation issues: Graduate research award papers, 1991-1992
[PB93-206258]
p 1642 N94-22055
FM interference in radio navigation receivers
p 1645 N94-22219

INSTRUMENT ORIENTATION
Analysis and dosign of weight balancing system for laser velocimetry traverse
[AD-A271171]
p 1816 N94-20546
An application of the Cerebellar Model Articulation Controller for a switched reluctance rotor position estimator
[AD-A271769]
p 1943 N94-20926

INSTRUMENT PACKAGES
Database of proposed payloads and instruments for SEI missions
p 1811 N94-22432

INSULATION
Milankovitch insulation forcing and cyclic formation of large-scale glacial, fluvial, and eolian landforms in central Alaska
p 2089 N94-20386
Asbestos characterization using scanning electron microscopy/light element x ray spectrometry
[AD-A271611]
p 1681 N94-21241

INSULATORS
The proximity effect in ultrathin granular Pb films
[AD-A271094]
p 2012 N94-19848
Magnetic instability of Kondo insulators
[DE93-040064]
p 1768 N94-21762

INTAKE SYSTEMS
Cold starting an alcohol-fueled engine with ultrasonic fuel atomization
[PB93-206597]
p 1826 N94-22093

INTEGERS
A package for long integer arithmetic on the Cray Y-MP
[CWI-NM-R9227]
p 1916 N94-21612

INTEGRAL CALCULUS
Use of computers in the instruction of integral calculus
[AD-A272500]
p 1913 N94-21409
Asymptotic analysis. Working Note No. 2, approximation of integrals
[DE94-000433]
p 1961 N94-22381

INTEGRAL EQUATIONS
A Kirchhoff approach to seismic modeling and prestack depth migration
[AD-A271010]
p 1854 N94-19820
Analytical evaluation of a surface integral expressing the coupling between interior and exterior volumes in a FE-IE approach
p 1722 N94-20423
An efficient formulation of the coupled finite element-integral equation technique for solving large 3D scattering problems
p 1725 N94-20436
Integral equation calculation of solvent activation free energies for electron and proton transfer reactions
[AD-A272665]
p 1681 N94-21216
An integro-algebraic equation for high frequency wake fields in a tube with smoothly varying radius
[DE93-040940]
p 1741 N94-21684
Continuous-time discretized-space approach to modeling short-pulse propagation and scattering
[PB93-215259]
p 1742 N94-22347
Modelling short bent, graded index dielectric slab waveguides
[PB93-215283]
p 1742 N94-22349

INTEGRALS
Use of computers in the instruction of integral calculus
[AD-A272500]
p 1913 N94-21409
Asymptotic analysis. Working Note No. 2, approximation of integrals
[DE94-000433]
p 1961 N94-22381

INTEGRATED CIRCUITS
Preparation and properties of sol-gel derived PZT thin films for decoupling capacitor applications
[DE93-018853]
p 2013 N94-19961
Automated HMC assembly
[DE93-040641]
p 1749 N94-20005
A methodology for formal hardware verification, with application to microprocessors
[AD-A270550]
p 1898 N94-20085
Single-event upset testing of the performance semiconductor 1750A CMOS/SOS chip set
[AD-A271158]
p 2015 N94-20184
Interinjection-locked quasioptical power combiners and phased arrays
[AD-A271178]
p 2015 N94-20214
High resolution signal processing
[AD-A271181]
p 1717 N94-20215
A breakdown model for the bipolar transistor to be used with circuit simulators
[DE93-019422]
p 1750 N94-20218
Recent activities in printed Antennas at LeRC
p 1722 N94-20422
Cratering evaluations and results
[DE93-040347]
p 1691 N94-20478
Solid State Technology Branch of NASA Lewis Research Center: Fifth Annual Digest
[NASA-TM-106303]
p 1732 N94-20497
An x-band peeled HEMT amplifier
p 1732 N94-20498
Coplanar waveguide radial line stub
p 1733 N94-20503
Correct CMOS IC defect models for quality testing
p 1755 N94-21093
Fault detection in digital and analog circuits using an i(DD) temporal analysis technique
p 1757 N94-21106
Experiments on technology mapping using different cell libraries
p 1758 N94-21118
A CAM-based LZ data compression IC
p 1759 N94-21129
Decoupled computer architectures for very high-speed technologies
[AD-A271646]
p 1900 N94-21301
Layout optimization with algebraic multigrid methods
p 1957 N94-21474
Magnetic force microscopy/current contrast imaging: A new technique for internal current probing of IC's
[DE93-040754]
p 1761 N94-21532
Optical integrated structures and circuits on silicon
[VTT-PUBS-106]
p 1988 N94-21594
A novel semiconductor process for optoelectronic applications on silicon substrate
p 1988 N94-21595
Advanced failure analysis laboratory equipment networking
[DE93-019070]
p 1916 N94-21633
Localization of pellicle-induced open contacts using charge-induced voltage alteration
[DE93-019407]
p 1762 N94-21636
Heterojunction bipolar transistor technology for data acquisition and communication
p 1763 N94-21697
Design and test of field programmable gate arrays in space applications
p 1765 N94-21710
A high speed CMOS A/D converter
p 1767 N94-21726
A novel cache mechanism
p 1767 N94-21730
A set-associative, fault-tolerant cache design
p 1768 N94-21731
Spectral characterization of lithographic sources
[DE93-019941]
p 1997 N94-21848
Fluorescent microthermographic imaging
[DE93-040332]
p 1810 N94-22000
Characterization and modelling of extremely high frequency enclosures
p 1782 N94-22177
MHMIC: Technology for the integration of microwave sub-assemblies
p 1785 N94-22199

INTEGRATED LIBRARY SYSTEMS
Research in image management and access
[NASA-CR-194797]
p 1907 N94-20376

INTEGRATED OPTICS
Optical integrated structures and circuits on silicon
[VTT-PUBS-106]
p 1988 N94-21594
A novel semiconductor process for optoelectronic applications on silicon substrate
p 1988 N94-21595
Integrated optical coupling element on silicon substrate, appendix 2
p 1988 N94-21596
Bidirectional method for optical channel waveguide attenuation measurement by detectors integrated on the wafer, appendix 3
p 1988 N94-21597
An integrated-optic polarization splitter on silicon substrate, appendix 4
p 1989 N94-21598
Fibre pigtailed silicon based low cost passive optical components, appendix 5
p 1989 N94-21599
Wide passband wavelength multi/demultiplexer at 1.3/1.55 micrometers based on etched Fresnel mirror, appendix 8
p 1989 N94-21602
Architectures of the free space optical interconnects
p 1789 N94-22220

INTELLIGENCE TESTS
Compatibility evaluation and research on the Computerized Adaptive Screening Test (CAST): User and programmer's guide
[AD-A273112] p 1894 N94-21510
INTERATOMIC FORCES
First-principles pressure-temperature phase diagrams in metals
[DE94-001056] p 1696 N94-22398
INTERCEPTION
High-velocity interceptors for boost-phase intercepts
[DE94-001077] p 1965 N94-22403
INTERCONTINENTAL BALLISTIC MISSILES
Mathematician Wang Ju
[AD-A267882] p 1912 N94-21255
INTERFACES
Near atomic resolution microanalysis of interfaces by analytical electron microscopy
[DE93-019437] p 1687 N94-19904
Comparing quasi-Newton methods for solving sparse interface problems
[CWI-NM-R9303] p 1959 N94-21576
The conformance testing methodology to CTRON (communication and central TRON) extended OS
p 1772 N94-22118
VLSI design of a parallel video output interface
p 1778 N94-22153
INTERFACIAL ENERGY
Thermal stability relationships between PMR-15 resin and its composites
[NASA-TM-106285] p 1675 N94-21488
INTERFACIAL TENSION
Surface path lines in plane Stokes flow driven by capillarity
[DE93-041277] p 1803 N94-21651
Interfacial reactions between titanium and borate glass
[DE93-012847] p 1683 N94-22031
INTERFERENCE LIFT
Experimental study on interference aerodynamics of close-coupled canard configuration
[AD-A267760] p 1636 N94-19963
INTERFEROMETERS
Analysis of the TDRS multiple access system for possible use as an attitude control system sensor
p 1666 N94-21338
Intercomparison of MAS, AVIRIS, and HIS data from FIRE cirrus 2 p 1872 N94-22296
CIMSS FIRE research activities p 1873 N94-22307
INTERFEROMETRY
Spatial patterns in semiconductor lasers
[DE93-040056] p 1814 N94-19865
Principles and applications of oil film interferometry for measuring wall friction fields in air flows
[ETN-93-95062] p 1798 N94-20147
Two microstrip arrays for interferometric SAR applications p 1722 N94-20421
Advances in spaceborne radar remote sensing
p 1723 N94-20424
Topographic slope from the SAR interferometric phase gradient p 1731 N94-20459
Interferometric detection of freeze-thaw displacements of Alaskan permafrost using ERS-1 data
p 1732 N94-20460
Performance evaluation of the JPL TOPSAR system: An across-track interferometric SAR system for topographic mapping p 1732 N94-20461
Earth-based measurement of lunar topography using delayed radar interferometry p 2119 N94-20787
Mirror velocity sampling errors in a Michelson interferometer
[AD-A273105] p 1809 N94-21508
INTERIOR BALLISTICS
Formulation of a next-generation interior ballistic code
[AD-A271539] p 1801 N94-20915
INTERLAMINAR STRESS
Compression strength of composite primary structural components
[NASA-CR-194561] p 1830 N94-20159
INTERLAYERS
Growth, characterization and device development in monocrystalline diamond films
[AD-A272715] p 2026 N94-21190
Synthesis and properties of mismatched heterojunction/substrate interfaces
[AD-A272904] p 1760 N94-21229
Orientationally independent antiferromagnetic coupling in epitaxial Fe/Cr (211) and (100) superlattices
[DE94-001270] p 2035 N94-22564
INTERMETALLICS
Fundamentals of mechanical behavior in structural intermetallics: A synthesis of atomistic and continuum modeling
[DE93-019166] p 1690 N94-20232
Properties and potential of high-temperature niobium beryllides
[DE93-019169] p 1690 N94-20233
Production of NiAl and TiAl intermetallics by mechanical alloying
[VTT-JULK-760] p 1691 N94-20530
Strengthening of NiAl matrix composites
[AD-A271491] p 1674 N94-20550
Microstructure evolution in the presence of constraints and implications on the properties of Mg-Li and Nb-Al constraints
[AD-A272088] p 1674 N94-20623
Surface science and modeling studies of endothermic fuels catalysis
[AD-A272850] p 1712 N94-21192
Examinations of composition and deformation behavior of intermetallic phases on the basis of Fe3(AlSi)
[GKSS-92/E/16] p 1692 N94-21311
Strength and toughness improvement of silicide intermetallics by nanophase and microphase reinforcements
[AD-A272914] p 1692 N94-21320
Proceedings of the Seventh Annual Conference on Fossil Energy Materials
[DE94-001091] p 1848 N94-21823
Ni3Al aluminide alloys
[DE94-000493] p 1694 N94-21933
The effect of microstructural evolution on superplasticity in Ni3Si(V, Mo)
[DE93-041320] p 1694 N94-21943
Characteristics of shock-compressed configuration of Ti and Si powder mixtures
[DE93-018857] p 1713 N94-22033
Alloying studies in U(1-x)Th(x)Pd2Al3 (0 (le) x (le) 1)
[DE94-000807] p 2036 N94-22584
INTERNAL COMBUSTION ENGINES
Vapor-delivered lubrication of steel-steel and steel-ceramic systems
[PB93-202364] p 1825 N94-21451
INTERNAL ENERGY
Electronically metastable molecules of high symmetry
[AD-A272015] p 1974 N94-21461
INTERNATIONAL COOPERATION
An economic analysis of transboundary air pollution between Finland and the Soviet Union
[ETLA-DISCUSSION-PAPER-335] p 1854 N94-22072
Surveys on specific patterns of facility intallation of photovoltaic power generating technologies for international cooperation
[DE94-714901] p 1850 N94-22092
Fortran for the nineties p 1926 N94-22481
INTERNATIONAL RELATIONS
The future of remote sensing from space: Civilian satellite systems and applications
[OTA-ISC-558] p 1837 N94-20209
INTERNATIONAL TRADE
Aerospace: Facts and figures, 1992-1993
[AD-A272571] p 1635 N94-21419
INTERNETS
Survey on utilization of database for research and development of global environmental industry technology
[DE94-714891] p 1853 N94-22259
INTERPLANETARY DUST
Helium in interplanetary dust particles
p 2082 N94-20653
Micrometeorite dynamic pyrometamorphism: Observation of a thermal gradient in iron-nickel sulfide
p 2083 N94-20716
Euhedral metallic-Fe-Ni grains in extraterrestrial samples p 1697 N94-20724
Multielement analysis of interplanetary dust particles using TOF-SIMS p 2084 N94-20790
Determination of parameters for hypervelocity dust grains encountered in near-Earth space
p 2084 N94-20817
Cometary interplanetary dust particles? An update on carbon in anhydrous IDPS p 2084 N94-20828
Micrometeorite pre-solar diamonds from Greenland cryoconite? p 2086 N94-20895
On dust emissions from the jovian system
p 2141 N94-20909
INTERPLANETARY MAGNETIC FIELDS
Magnetic fields in spiral galaxies
p 2010 N94-22697
Magnetic reconnection in emission nebulae in clusters of galaxies p 2010 N94-22700
INTERPLANETARY MEDIUM
Compressible MHD turbulence in the interplanetary medium p 2003 N94-22650
INTERPOLATION
Polynomial interpolation of real functions 1: Interpolation in an interval
[AD-A272330] p 1951 N94-20527
Theoretical and numerical examinations of nonlinear parameter dependent advanced differential difference equations
[ETN-93-93681] p 1952 N94-21042
A geometrical process for three dimensional osteotomy planning
[ETN-93-93602] p 1892 N94-21134
Fast fourier transforms for nonequispaced data
[AD-A272687] p 1954 N94-21164
Operational equations for the five-point rectangle
[DE94-000366] p 1959 N94-21655
On coefficient quantization and computational roundoff effects in frequency interpolation filter banks
p 1793 N94-22251
INTERPROCESSOR COMMUNICATION
Exploiting the parallelism exposed by partial evaluation
[AD-A270678] p 1928 N94-19877
Global combine on mesh architectures with wormhole routing
[DE93-018792] p 1903 N94-19959
Robust, high-speed network design for large-scale multiprocessing
[AD-A271003] p 1716 N94-19977
Multilist scheduling: A new parallel programming model
[AD-A270549] p 1929 N94-20084
Standard ML signatures for a protocol stack
[AD-A272060] p 1908 N94-20622
Using manufacturing message specification for monitor and control at Venus p 1932 N94-21333
Analysis of multigrid methods on massively parallel computers: Architectural implications
p 1938 N94-21468
Uniform self-stabilizing leader election. Part 1: Complete graph protocols
[CWI-CS-R9308-PT-1] p 1935 N94-21549
A simple modern correctness condition for a space-based high-performance multiprocessor
p 1766 N94-21718
Using stream interleaving to eliminate the need for interlocks in deeply pipelined processors
p 1781 N94-22175
Integration of parallel processing structures using a matrix approach p 1784 N94-22192
Survey on utilization of database for research and development of global environmental industry technology
[DE94-714891] p 1853 N94-22259
A self-defining hierarchical data system
p 2046 N94-22448
INTERSTELLAR CHEMISTRY
Evaporation in equilibrium, in vacuum, and in hydrogen gas p 1684 N94-20638
INTERSTELLAR EXTINCTION
Coagulation of grains in static and collapsing protostellar clouds p 2085 N94-20865
INTERSTELLAR GAS
Fragmentation of magnetized filamentary interstellar clouds p 2008 N94-22687
Gravitational instability of magnetized filamentary clouds. 1: Helical magnetic fields p 2008 N94-22688
Gravitational instability of magnetized filamentary clouds. 2: Rotation p 2009 N94-22689
INTERSTELLAR MAGNETIC FIELDS
Helical kink instability of jets from young stellar objects p 2008 N94-22686
Fragmentation of magnetized filamentary interstellar clouds p 2008 N94-22687
Generation and maintenance of bisymmetric spiral magnetic fields in disk galaxies in differential rotation
p 2010 N94-22695
INTERSTELLAR MASERS
Consequences of plasma-maser in plasma astrophysics p 2006 N94-22669
INTERSTELLAR MATTER
The x ray halo of AM Her
[NASA-CR-189310] p 2054 N94-20142
Evaporation in equilibrium, in vacuum, and in hydrogen gas p 1684 N94-20638
Identification of an interstellar oxide grain from the Murchison meteorite by ion imaging
p 2082 N94-20659
Molecular equilibria and condensation sequences in carbon rich gases p 2083 N94-20756
Coagulation of grains in static and collapsing protostellar clouds p 2085 N94-20865
The x ray halo of Cen X-3
[NASA-CR-189309] p 2055 N94-21295
Non-linear thermal instability of optical thin molecular structures p 2006 N94-22667
Magnetic superbubbles in the galactic disk and halo
p 2009 N94-22694
INTERSTITIALS
Temperature-dependent ion beam mixing
[DE93-040281] p 2033 N94-21999

INTERSYMBOLIC INTERFERENCE
Interference reduction using neural networks
p 1783 N94-22186
Intersymbol interference effects in digital matched filters
p 1788 N94-22218
INVARIANCE
Representation and recognition with algebraic invariants and geometric constraint models
[AD-A271395] p 1949 N94-19838
Restoring locality with faster-than-light velocities
[DE93-040926] p 2038 N94-22010
A multiresolution wavelet representation in two or more dimensions
p 1925 N94-22456
INVENTIONS
The official gazette of the United States Patent and Trademark Office, vol. 1145, no. 4
[PB93-202240] p 2044 N94-21449
INVENTORIES
Recommendations resulting from the SPDS Community-Wide Workshop
[NASA-CR-194684] p 2042 N94-20363
Venus' impact-crater database: Update to approximately 98 percent of the planet's surface
p 2110 N94-20736
INVENTORY MANAGEMENT
NASA property: Improving management of government equipment provided to contractors. Report to the Chairman, Subcommittee on Investigations and Oversight, Committee on Science, Space, and Technology, House of Representatives
[GAO/NSIAD-93-191] p 2039 N94-20206
Data management for interdisciplinary field experiments: OTTER project support
[NASA-CR-4559] p 1842 N94-22345
INVERSE KINEMATICS
Dynamic analyses of flexible robotic manipulators
[ISBN-0-315-59251-6] p 1827 N94-22421
INVERSE SCATTERING
Extended range modified gradient technique for profile inversion (extended version of report Et/Em-1992-8)
[PB93-215242] p 1742 N94-22346
INVERSIONS
Inversion of gravity and bathymetry in oceanic regions for long-wavelength variations in upper mantle temperature and composition
[NASA-CR-192272] p 1882 N94-20131
High resolution signal processing
[AD-A271181] p 1717 N94-20215
Photopumped x ray laser research on Saturn
[DE93-019430] p 1816 N94-20298
A general rough-surface inversion algorithm: Theory and application to SAR data
p 1719 N94-20407
An inverse DWT for nonorthogonal wavelets
[AD-A272064] p 1737 N94-20582
Two-polarity magnetization in the Manson impact breccia
p 1863 N94-20789
INVERTERS
Surveys on specific patterns of facility intallation of photovoltaic power generating technologies for international cooperation
[DE94-714901] p 1850 N94-22092
INVISCID FLOW
Long-range laser imaging
[AD-A273020] p 1817 N94-21253
IODIDES
X ray analysis of alpha mercuric iodide crystal structure and processing effects
[DE93-017620] p 2027 N94-21296
IODINE
Establishing the basis for validated predictions of highly non-equilibrium flows (with 9 attachments)
[AD-A272918] p 1802 N94-21220
IODINE COMPOUNDS
Fermiology and De Haas-Van Alphen effect of beta-(ET)2IBr2
[DE93-019523] p 2011 N94-19807
ION ACCELERATORS
Facilities for in situ ion beam studies in transmission electron microscopes
[DE93-019567] p 1979 N94-20222
ION ATOM INTERACTIONS
Testing double ionization mechanisms with highly-charged ions
[DE93-018750] p 1970 N94-19958
Interactions of slow H, H2, and H3 with thin foils
[DE93-040263] p 1976 N94-21995
ION BEAMS
Focused-ion-beam material removal rates
[AD-A270852] p 1713 N94-19834
Longitudinal beam dynamics for heavy ion fusion using WARPrz
[DE93-019154] p 1992 N94-19915
Two-dimensional particle-in-cell simulation on transputer arrays
[DE93-017977] p 1972 N94-20181
Facilities for in situ ion beam studies in transmission electron microscopes
[DE93-019567] p 1979 N94-20222
High current injector for heavy ion fusion
[DE93-019241] p 1979 N94-20289
Observation of reflected waves on the SABRE positive polarity inductive adder MITL
[DE93-019413] p 1980 N94-20295
Development and characterization of a time-, position- and energy-resolved x ray diagnostic for PBFA 2 target experiments
[DE93-019429] p 1808 N94-20297
InP MIS structures with diamondlike amorphous carbon films deposited by ion-beam sputtering and from plasma
p 1710 N94-20979
A dc Penning surface-plasma source
[DE93-040126] p 1997 N94-21989
Temperature-dependent ion beam mixing
[DE93-040281] p 2033 N94-21999
ION CURRENTS
Charge collectors for the omega upgrade
[DE93-019684] p 1972 N94-20264
Low emittance 0.8A K(+) ion source for the LBL Induction Linac System Experiment (ILSE)
[DE93-019237] p 1981 N94-21439
ION CYCLOTRON RADIATION
Fusion plasma theory grant. Task 3: Auxiliary radiofrequency heating of tokamaks
[DE94-000779] p 1994 N94-20940
Studies of electromagnetic ion cyclotron waves using AMPTE/CCE and Dynamics Explorer
[NASA-CR-194711] p 1982 N94-21878
ION DENSITY (CONCENTRATION)
High energy ionization in liquids: The free ion yield
[DE93-040329] p 1973 N94-20324
ION DISTRIBUTION
Direct images of thermal disorder in the Cl-Si and H-O-Si chemisorption bond on Si(100)
[AD-A272386] p 1680 N94-21145
Detailed analysis case studies of trapped plasmas at the Earth's magnetic equator
[AD-A272497] p 1858 N94-21432
ION ENGINES
Segmented ion thruster
[NASA-CASE-NPO-18192-1-CU] p 1669 N94-20496
SPACE-R Thermionic Space Nuclear Power System: Design and Technology Demonstration Program
[DE93-013969] p 1670 N94-21824
ION EXCHANGING
Approximate methods for N-component solute transport and ion-exchange
[CWI-NM-R9223] p 1910 N94-21078
ION IMPLANTATION
Formation of colloidal Ag precipitates in fused silica by MeV ion implantation
[DE93-040268] p 2012 N94-19869
Low-energy ion implantation: Large mass fractionation of argon
p 1685 N94-20697
Implantation of carbon in GaAs and compensating native defects
[DE93-040122] p 2030 N94-21763
Surface modification for corrosion resistance
[DE93-017419] p 1693 N94-21825
Magnetic insulation of secondary electrons in plasma source ion implantation
[DE93-040106] p 1997 N94-21988
Lattice damage during ion implantation of semiconductors
[DE94-000335] p 2034 N94-22016
Initial operation of a large-scale plasma source ion implantation experiment
[DE94-000805] p 2036 N94-22583
ION IRRADIATION
Facilities for in situ ion beam studies in transmission electron microscopes
[DE93-019567] p 1979 N94-20222
Neutral copper cluster sputtering yields: Ne(+), Ar(+) and Xe(+) bombardment
[DE93-019010] p 1690 N94-20288
Miniaturized disk-bend testing, nano-indentation, and the microstructure of ion-irradiated titanium aluminides
[DE93-040600] p 1697 N94-22559
ION MICROSCOPES
Atom probe field ion microscopy characterizations of VVER steels
[DE93-017864] p 1689 N94-20180
ION MOTION
Parametric variations of ion transport in TFTR
[DE93-012653] p 1991 N94-19883
Fast ion behavior during neutral beam injection in ATF
[DE93-040267] p 1992 N94-20058
High energy ionization in liquids: The free ion yield
[DE93-040329] p 1973 N94-20324
ION PROBES
Hydrogen pickup and redistribution in alpha-annealed zircaloy-4
[DE93-018050] p 1689 N94-20182
Identification of an interstellar oxide grain from the Murchison meteorite by ion imaging
p 2082 N94-20659
ION PROPULSION
Segmented ion thruster
[NASA-CASE-NPO-18192-1-CU] p 1669 N94-20496
ION SCATTERING
Time-of-flight heavy ion backscattering spectrometry
[DE93-019067] p 1973 N94-20306
Accretion of a hot plasma onto the central black hole: Fokker-Planck formulation
p 2009 N94-22693
ION SOURCES
Absolute total and one and two electron transfer cross sections for Ar(8+) on Ar as a function of energy
[DE93-040283] p 1970 N94-19870
Low emittance 0.8A K(+) ion source for the LBL Induction Linac System Experiment (ILSE)
[DE93-019237] p 1981 N94-21439
Simulation studies of space-charge-dominated beam transport in large aperture ratio quadrupoles
[DE93-019236] p 1981 N94-21440
Optimization and control of a small angle ion source using an adaptive neural network controller
[DE93-040063] p 1946 N94-21845
A dc Penning surface-plasma source
[DE93-040126] p 1997 N94-21989
ION TEMPERATURE
Parametric variations of ion transport in TFTR
[DE93-012653] p 1991 N94-19883
Kinetic resonance damping rate of the toroidal ion temperature gradient mode
[DE94-001234] p 1998 N94-22561
IONIC COLLISIONS
Absolute total and one and two electron transfer cross sections for Ar(8+) on Ar as a function of energy
[DE93-040283] p 1970 N94-19870
Testing double ionization mechanisms with highly-charged ions
[DE93-018750] p 1970 N94-19958
Interactions of slow H, H2, and H3 with thin foils
[DE93-040263] p 1976 N94-21995
IONIC MOBILITY
Implantation of carbon in GaAs and compensating native defects
[DE93-040122] p 2030 N94-21763
Local structure in oxygen-doped La2CuO(4+delta)
[DE93-040248] p 2030 N94-21768
IONIZATION
Testing double ionization mechanisms with highly-charged ions
[DE93-018750] p 1970 N94-19958
High energy ionization in liquids: The free ion yield
[DE93-040329] p 1973 N94-20324
On magnetodynamic effects initiated by a high-speed impact of a large cosmic body upon the Earth's surface
p 2082 N94-20647
Spectral characterization of lithographic sources
[DE93-019941] p 1997 N94-21848
Atmospheric sampling glow discharge ionization and triple quadrupole tandem mass spectrometry for explosives vapor detection
[DE93-040593] p 1852 N94-22004
The effect of Compton scattering on the double to single ionization ratio in helium
[DE94-000884] p 1827 N94-22390
Non-equilibrium ionization in an M class solar flare
p 2004 N94-22653
IONIZATION CHAMBERS
Segmented ion thruster
[NASA-CASE-NPO-18192-1-CU] p 1669 N94-20496
A High Resolution Liquid Xenon Imaging Telescope for 0.3-10 MeV Gamma Ray Astrophysics: Construction and Initial Balloon Flights
[NASA-CR-194709] p 2056 N94-22281
IONIZATION CROSS SECTIONS
The effect of Compton scattering on the double to single ionization ratio in helium
[DE94-000884] p 1827 N94-22390
IONIZATION GAGES
Measurement of mesospheric turbulence in the framework of the metal campaign and development of a sensor for static pressure free measurements of neutral and electron density
[BONN-IR-92-45] p 1857 N94-21149
IONIZING RADIATION
Design of CMOS logic gates for TID radiation
p 1754 N94-21083
Improved approximate formulas for flux from cylindrical and rectangular sources
[DE93-011390] p 1742 N94-22268

IONOSPHERIC CONDUCTIVITY
Sporadic-E observations during LoVHF transionospheric direction finder measurements
[AD-A270619] p 1716 N94-19951
IONOSPHERIC CURRENTS
Radiation of plasma wave wings through an electrodynamic tether satellite system with any sharp angle geometry
[REPT-85] p 1993 N94-20156
IONOSPHERIC PROPAGATION
A general purpose ionospheric ray tracing procedure
[AD-A271058] p 1854 N94-19860
Sporadic-E observations during LoVHF transionospheric direction finder measurements
[AD-A270619] p 1716 N94-19951
IONS
Absolute total and one and two electron transfer cross sections for Ar(8+) on Ar as a function of energy
[DE93-040283] p 1970 N94-19870
Energy gain spectroscopic study of Ar(q+)-Ar collisions at 40 qeV
[DE93-040284] p 1970 N94-19871
Charge collectors for the omega upgrade
[DE93-019684] p 1972 N94-20264
Neutron-scattering studies of Yb-bearing silicate glasses
[DE93-019768] p 1700 N94-20265
Integral equation calculation of solvent activation free energies for electron and proton transfer reactions
[AD-A272665] p 1681 N94-21216
Electron emissions in low energy Ar(q+)-Ar collisions
[DE93-040285] p 1974 N94-21543
Radial diffusion of toroidally trapped particles induced by lower hybrid and fast waves
[IPPCZ-327] p 1996 N94-21593
Column chromatographic separation of Y(3+) from Sr(2+) by polymeric ionizable crown ether resins
[DE94-000935] p 1683 N94-22021
Alloying studies in U(1-x)Th(x)Pd2Al3 (0 (le) x (le) 1)
[DE94-000807] p 2036 N94-22584
IOWA
Research program on the Manson impact structure, Iowa p 1862 N94-20766
Petrography of shock features in the 1953 Manson 2-A drill core p 1862 N94-20767
IRIDIUM
Iridium in sediments containing large abundances of Australasian microtektites from DSDP hole 758B in the Eastern Indian Ocean and from DSDP hole 769A in the Sulu Sea p 2083 N94-20741
IRON
First discovery of the organic materials in deep-sea iron cosmic spherule p 1685 N94-20677
Integral equation calculation of solvent activation free energies for electron and proton transfer reactions
[AD-A272665] p 1681 N94-21216
Oxidation of dissolved iron under warmer, wetter conditions on Mars: Transitions to present-day arid environments p 2143 N94-21663
Shattering the myth of the resonantly photo-pumped neon-like titanium laser
[DE93-019624] p 1819 N94-21873
Photo- and thermal-induced antiferromagnetic interlayer coupling in Fe/(Fe-Si) superlattices
[DE93-040822] p 2031 N94-21930
Observation of x ray absorption magnetic circular dichroism in well-characterized iron-cobalt-platinum multilayers
[DE94-000303] p 1694 N94-21944
Shock temperature measurements of iron to 350 GPa
[DE94-001058] p 1695 N94-22024
Orientationally independent antiferromagnetic coupling in epitaxial Fe/Cr (211) and (100) superlattices
[DE94-001270] p 2035 N94-22564
IRON ALLOYS
Segregation of Si to the surface of Fe-29Ni-17Co alloy
[DE93-040053] p 1687 N94-19864
Examinations of composition and deformation behavior of intermetallic phases on the basis of Fe3(AlSi)
[GKSS-92/E/16] p 1692 N94-21311
Investigation of moisture-induced embrittlement of iron aluminides
[DE93-040841] p 1695 N94-21949
Microstructural evolution of neutron-irradiated Fe-Cr-Ni ternary alloys at high helium generation rates
[DE93-018788] p 1696 N94-22037
IRON COMPOUNDS
Detectability of crystalline ferric and ferrous minerals on Mars p 2110 N94-20730
Fe/Mn in olivine of carbonaceous meteorites p 2084 N94-20788
Microanalysis of iron oxidation state in iron oxides using X Ray Absorption Near Edge Structure (XANES) p 1686 N94-20808
IRON ISOTOPES
Shielding from space radiations
[NASA-CR-194683] p 1895 N94-20063
FE-60 and the evolution of eucrites p 2083 N94-20768
IRON METEORITES
Tambo Quemado: Extraordinary concentrations of REE and refractory trace elements caused by artificial heating p 1684 N94-20667
Chaunskij: The most highly metamorphosed, shock-modified and metal-rich mesosiderite p 2082 N94-20681
Magnetic properties and Mcessbauer analyses of glass from the K-T boundary, Beloc, Haiti p 1685 N94-20753
The Sm-Nd systematics of silicate inclusions in iron meteorites: Results from Caddo (IAB)
[CONTRIB-5241(804)] p 2084 N94-20795
A new Antarctic meteorite with chromite, orthopyroxene and metal with reference to a formation model of S asteroids p 2084 N94-20813
Rhenium-osmium isotope systematics of ordinary chondrites and iron meteorites p 2085 N94-20854
The formation of FeO-rich pyroxene and enstatite in unequilibrated enstatite chondrites: A petrologic-trace element (SIMS) study p 2086 N94-20866
IRON OXIDES
Cathode materials for the molten carbonate fuel cell
[DE93-019515] p 1848 N94-21870
IRRADIANCE
Phase screens for the control of the focal irradiance of the Nova laser
[DE94-001067] p 1820 N94-22401
IRRADIATION
General introduction to microstructural evolution under cascade damage conditions
[DE93-017443] p 2012 N94-19923
Extra-corporeal blood access, sensing, and radiation methods and apparatuses
[NASA-CASE-MSC-21775-1] p 1890 N94-20372
LREE variability in CM matrices: Another look at meteorite compaction ages p 2086 N94-20884
Evaluation of radiation effects in re-oxidized nitrided oxide devices by hot carrier stressing at 77 K p 1754 N94-21084
Tensile strength of fiber reinforced plastics at 77K irradiated by various radiation sources
[DE93-040826] p 1709 N94-22008
IRREGULARITIES
The effects of magnetic storm phases on F-layer irregularities from auroral to equatorial latitudes
[AD-A272685] p 1857 N94-21189
IRRIGATION
The FY1992 survey on multi-purpose dam and energy utilization system by the wind power generation eration
[DE94-707408] p 1848 N94-22012
Areally averaged estimates of surface heat flux from ARM field studies
[DE93-018569] p 1859 N94-22036
ISCCP PROJECT
The FIRE Cirrus Science Results 1993
[NASA-CP-3238] p 1871 N94-22292
Cloud fields derived from satellite and surface data during FIRE cirrus phase 2 p 1872 N94-22302
SSH-2 measurements of cirrus at 18-28 micrometers from the King Air during FIRE 2 p 1880 N94-22338
An overview of the radiation component of the NASA TOGA-COARE experiment p 1881 N94-22344
ISING MODEL
Study of (+-)J Ising spin glasses via multicanonical ensemble
[DE93-018269] p 2016 N94-20285
ISOCHORIC PROCESSES
Neutron and PIMC determination of the longitudinal momentum distribution of HCP, BCC and normal liquid He-4
[DE93-019009] p 1972 N94-20187
ISOELECTRONIC SEQUENCE
Magnetic instability of Kondo insulators
[DE93-040064] p 1768 N94-21762
ISOLATION
Comparison of a distributed Kalman filter versus a centralized Kalman filter with fault detection considerations
[AD-A270713] p 1903 N94-19989
ISOMERIZATION
Optically induced rotation diffusion in polymer liquid crystals: Phenomenological theory and experimental verification
[ETN-93-95068] p 2014 N94-20026
Recent developments in aromatic azo polymers research
[AD-A272966] p 1705 N94-21259
ISOMERS
Rotational isomers of Mo(VI) alkylidene complexes and Cis/trans polymer structure: Investigations in ring-opening metathesis polymerization
[AD-A272647] p 1704 N94-21184
ISOPROPYL COMPOUNDS
Polyimides containing amide and perfluoroisopropylidene connecting groups
[NASA-CASE-LAR-14608-1] p 1702 N94-20374
ISOTHERMAL PROCESSES
Applicability and performance benefits of XD (Tradename) titanium aluminides to expendable gas turbine engines
[AD-A272998] p 1648 N94-21268
ISOTOPE EFFECT
Semiconductor isotope engineering
[DE93-040119] p 2030 N94-21744
ISOTOPE SEPARATION
Computational model of a magnetic modulator for copper lasers
[DE93-019603] p 1815 N94-20223
Hydrogen isotope separation experience at the Savannah River Site
[DE93-019832] p 1679 N94-20266
High-power copper vapor lasers and their application to precision drilling and cutting
[DE93-019951] p 1819 N94-21844
ISOTOPES
Milankovitch insulation forcing and cyclic formation of large-scale glacial, fluvial, and eolian landforms in central Alaska p 2089 N94-20386
Helium in interplanetary dust particles p 2082 N94-20653
Cosmogenic-radionuclide profiles in Knyahinya: New measurements and models p 2106 N94-20713
Kalkkop crater, Eastern Cape: A new impact crater in South Africa p 1862 N94-20714
Primary differentiation in the early Earth: Nd and Sr isotopic evidence from diamondiferous eclogites for both old depleted and old enriched mantle, Yakutia, Siberia p 1862 N94-20776
The U-Th-Pb, Sm-Nd, and Ar-Ar isotopic systematics of lunar meteorite Yamato-793169 p 2084 N94-20834
Consortium reports on lunar meteorites Yamato 793169 and Asuka 881757, a new type of mare basalt p 2086 N94-20893
Mars atmosphere loss and isotopic fractionation by solar-wind-induced sputtering and photochemical escape p 2144 N94-21672
Semiconductor isotope engineering
[DE93-040119] p 2030 N94-21744
ISOTOPIC LABELING
Geochronology and petrogenesis of the western highlands alkali suite: Radiogenic isotopic evidence from Apollo 14 p 2118 N94-20778
The Sm-Nd systematics of silicate inclusions in iron meteorites: Results from Caddo (IAB)
{CONTRIB-5241(804)} p 2084 N94-20795
ISOTROPIC MEDIA
Acoustic radiation damping of flat rectangular plates subjected to subsonic flows
[NASA-TM-109382] p 1967 N94-20211
ISOTROPIC TURBULENCE
Modeling of particle dispersion in a stationary isotropic homogeneous turbulence by large scale numerical simulation
[ETN-93-94604] p 1801 N94-20601
Computation of the sound generated by isotropic turbulence
[NASA-CR-191543] p 1804 N94-21880
ITALY
Using NDVI/AVHRR data for crop monitoring and forecasting in South Italy p 1841 N94-20970
ITERATION
Stochastic optimization by simulation: Convergence proofs for the G1/G/1 queue in steady-state
[AD-A271141] p 1962 N94-19999
Correctness properties for iterated hardware structures p 1759 N94-21124
Optimal convolution SOR acceleration of waveform relaxation with application to semiconductor device simulation p 1922 N94-21475
Butcher-Kuntzmann methods for nonstiff problems on parallel computers
[CWI-NM-R9305] p 1935 N94-21493
ITERATIVE SOLUTION
Set theory and nominalisation, part 1
[PB93-191807-PT-1] p 1962 N94-20007
A multi-level solution algorithm for steady-state Markov chains
[NASA-CR-191558] p 1914 N94-21462
Using parallel banded linear system solvers in generalized eigenvalue problems
[NASA-CR-191540] p 1915 N94-21584

Extended range modified gradient technique for profile inversion (extended version of report Et/Em-1992-8)
[PB93-215242] p 1742 N94-22346

IUE
The cool-star spectral catalog: A uniform collection of IUE SWP-LOs p 2046 N94-22446

J

J-2 ENGINE
Advanced transportation system studies, technical area 3. Alternate propulsion subsystem concepts: J-2S restart study
[NASA-CR-193874] p 1670 N94-21271

JAMMERS
The application of sample vector selection to adaptive nulling: Performance comparison for techniques combining Gram-Schmidt orthogonalization with averaging
p 1747 N94-22234

JAPAN
The chondrite Mihonoseki: New observed fall
p 2083 N94-20764

JAPANESE SPACE PROGRAM
Japanese space program p 1652 N94-21407

JAPANESE SPACECRAFT
Japanese space program p 1652 N94-21407
SPIKE: Application for ASTRO-D mission planning
p 1926 N94-22486

JET ENGINE FUELS
A proposed methodology for combustion toxicology testing of combined halon replacement agent/jet fuel interaction
[AD-A272695] p 1681 N94-21165

JET FLOW
Development of phased twin flip-flop jets
[NASA-TM-106404] p 1637 N94-20563
Combustion in turbulent jets and buoyant flames
[PB93-202372] p 1682 N94-21452
Flow interaction experiment. Volume 1: Aerothermal modeling, phase 1
[NASA-CR-189192-VOL-1] p 1648 N94-21582
Flow interaction experiment. Volume 2: Aerothermalmodeling, phase 2
[NASA-CR-189192-VOL-2] p 1648 N94-21583

JET MIXING FLOW
Finite element numerical simulation of three dimensional turbulent flows with dispersion: Eulerian and Lagrangian approaches
[ECL-92-42] p 1801 N94-20597
Flow interaction experiment. Volume 1: Aerothermal modeling, phase 1
[NASA-CR-189192-VOL-1] p 1648 N94-21582
Flow interaction experiment. Volume 2: Aerothermalmodeling, phase 2
[NASA-CR-189192-VOL-2] p 1648 N94-21583
Comparison of mixing calculations for reacting and non-reacting flows in a cylindrical duct
[NASA-TM-106435] p 1649 N94-21758

JET STREAMS (METEOROLOGY)
Meso-Beta scale numerical simulation studies of terrain-induced jet streak mass/momentum perturbations
[NASA-CR-194627] p 1864 N94-20138
Examination of the observed synoptic scale cirrus cloud environment: The December 3-6 FIRE cirrus case study
p 1877 N94-22325
The 5-6 December 1991 FIRE IFO 2 jet stream cirrus case study: The influence of volcanic aerosols
p 1877 N94-22326

JETS
Toward a QCD analysis of jet rates in deep-inelastic Muon-Proton scattering
[DE94-000618] p 1976 N94-21962

JOINT EUROPEAN TORUS
Transient thermal analysis of cryocondensation pump for JET
[DE93-040372] p 1992 N94-20003

JOINTS (ANATOMY)
Automatic locking orthotic knee device
[NASA-CASE-MFS-28633-1] p 1896 N94-20493

JOINTS (JUNCTIONS)
Bladder operated robotic joint
[NASA-CASE-MFS-28682-1] p 1701 N94-20359
Interleaved bismaleimide composites
[AD-A272233] p 1674 N94-20574
Strength, ultrasonic and metallurgical evaluation of diffusion bonds
[DE94-000665] p 1697 N94-22571

JOSEPHSON JUNCTIONS
A pipelined superconducting digital processor
[DE93-040852] p 1898 N94-19886

JP-8 JET FUEL
A proposed methodology for combustion toxicology testing of combined halon replacement agent/jet fuel interaction
[AD-A272695] p 1681 N94-21165

JUNCTION TRANSISTORS
A breakdown model for the bipolar transistor to be used with circuit simulators
[DE93-019422] p 1750 N94-20218
A contribution to development and parameter extraction of SPICE compatible macromodels for discrete bipolar transistors
[HMI-B-499] p 1753 N94-21021
Behavior of faulty double BJT BiCMOS logic gates
p 1767 N94-21727

JUPITER (PLANET)
Diffusive redistribution of water vapor in the solar nebula revisited p 2113 N94-20751
On dust emissions from the jovian system
p 2141 N94-20909

K

K-EPSILON TURBULENCE MODEL
Finite element numerical simulation of three dimensional turbulent flows with dispersion: Eulerian and Lagrangian approaches
[ECL-92-42] p 1801 N94-20597

KALMAN FILTERS
Comparison of a distributed Kalman filter versus a centralized Kalman filter with fault detection considerations
[AD-A270713] p 1903 N94-19969
Paired comparison models with time-varying parameters
[AD-A272016] p 1964 N94-21442
Experiments with recursive estimation in astronomical image processing p 2047 N94-22457

KAPOETA ACHONDRITE
SCR neon and argon in Kapoeta feldspar: Evidence for an active ancient Sun p 2106 N94-20712

KAPTON (TRADEMARK)
Interleaved bismaleimide composites
[AD-A272233] p 1674 N94-20574

KELVIN-HELMHOLTZ INSTABILITY
Shear flow generation by Reynolds stress and suppression of resistive g-modes
[DE93-040911] p 1995 N94-21514
Breaking Kelvin-Helmholtz waves and cloud-top entrainment as revealed by K-band Doppler radar
p 1874 N94-22310
Implications of Viking dayside auroral measurements
[ISBN-0-315-83273-8] p 1861 N94-22575
Tangential stress due to Kelvin-Helmholtz instability at the magnetospheric boundary p 2003 N94-22651
Three-dimensional simulations of cosmic jets employing the smoothed particle hydrodynamics technique
p 2008 N94-22685

KEROSENE
Compatibility and efficacy of biocides qualified under military specification MIL-S-53021
[AD-A271496] p 1712 N94-20551
Chemical reaction fouling model for single-phase heat transfer
[DE93-019556] p 1802 N94-20942

KETONES
Catalytic hydrogenation of carbon monoxide
[DE94-000681] p 1678 N94-20103

KEVLAR (TRADEMARK)
Millimeter-wave imaging of composite materials
[DE93-041160] p 1677 N94-21940
An embedded fibre optic for damage growth monitoring in Kevlar composites
[ISBN-0-315-83501-X] p 1677 N94-22589

KINEMATIC EQUATIONS
Dynamic analyses of flexible robotic manipulators
[ISBN-0-315-59251-6] p 1827 N94-22421

KINEMATICS
Development and testing of a reliability performance index for modular robotic systems
[AD-A271901] p 1942 N94-20488
Smoothed-particle hydrodynamics and nonequilibrium molecular dynamics
[DE94-001059] p 1977 N94-22400
Vector gravimetry by a combination of inertial and GPS satellite measurements
[ISBN-0-315-61980-5] p 1861 N94-22424
A robust quality control system for GPS navigation and kinematic positioning
[ISBN-0-315-83148-0] p 1644 N94-22427

KINETIC ENERGY
On magnetodynamic effects initiated by a high-speed impact of a large cosmic body upon the Earth's surface
p 2082 N94-20647
Micrometeorite dynamic pyrometamorphism: Nonstoichiometric clinoenstatite (CLEN)
p 2083 N94-20715
Magnetically controlled solar nebula
p 2120 N94-20791
Computer simulation of molecular response at a shock front
[DE94-001050] p 1977 N94-22396

KINETIC EQUATIONS
Neoclassical kinetic theory near an X-point: Plateau regime
[DE93-019825] p 1951 N94-20224
Theoretical and numerical studies in magnetic fusion
[DE94-000536] p 1993 N94-20937
A two-dimensional kinetic model of the scrape-off layer
[DE94-001235] p 1999 N94-22562

KINETIC THEORY
Neoclassical kinetic theory near an X-point: Plateau regime
[DE93-019825] p 1951 N94-20224
Kinetic theory of runaway air-breakdown
[DE93-040731] p 1750 N94-20325
Theoretical and numerical studies in magnetic fusion
[DE94-000536] p 1993 N94-20937

KINETICS
Kinetics of phase transformations in glass forming systems
[NASA-CR-194270] p 1701 N94-20347

KINOFORM
Phase screens for the control of the focal irradiance of the Nova laser
[DE94-001067] p 1820 N94-22401

KIRCHHOFF LAW OF RADIATION
Thermal infrared remote sensing and Kirchhoff's law: 1. Laboratory measurements p 1685 N94-20733

KLYSTRONS
An 85 GHz quasioptical gyroklystron experiment
[AD-A272020] p 1752 N94-20931
Simulation of traveling-wave output structures for high power RF tubes
[DE93-041005] p 1763 N94-21685

KNEE (ANATOMY)
Automatic locking orthotic knee device
[NASA-CASE-MFS-28633-1] p 1896 N94-20493

KNOWLEDGE BASED SYSTEMS
Building brains for bodies
[AD-A270531] p 1939 N94-19875
An expert system shell for inferring vegetation characteristics
[NASA-CR-189318] p 1837 N94-20284
The Seventh International Symposium on Methodologies for Intelligent Systems (Poster Session)
[AD-A272125] p 1942 N94-20573
The Milling assistant, case-based Reasoning, and machining strategy: A report on the development of automated numerical control programming systems at New Mexico State University
[DE93-041101] p 2029 N94-21690
Model-based reasoning for power system management using KATE and the SSM/PMAD
[NASA-CR-194716] p 1671 N94-21882

KNOWLEDGE BASES (ARTIFICIAL INTELLIGENCE)
Advanced software development workstation: Knowledge base methodology: Methodology for first Engineering Script Language (ESL) knowledge base
[NASA-CR-193643] p 1930 N94-21065
Computing with Bayesian multi-networks
[AD-A273106] p 1914 N94-21501

KNOWLEDGE REPRESENTATION
Building brains for bodies
[AD-A270531] p 1939 N94-19875
A computational theory of lexical relatedness
[TR-421] p 1904 N94-20067
Causal reconstruction
[AD-A271692] p 1908 N94-20929
Design of a computer assisted tool for object oriented acquisition, modeling and simulation of knowledge structure
[ETN-93-94183] p 1910 N94-21152
Experiments in knowledge refinement for a large rule-based system
[AD-A272055] p 1809 N94-21445
Reasoning about update logic
[CWI-CS-R9312] p 1914 N94-21496
Computing with Bayesian multi-networks
[AD-A273106] p 1914 N94-21501
Changing preferences
[CWI-CS-R9310] p 1915 N94-21551

KNUDSEN FLOW
Shock induced condensation in fluids of high molar specific heat: Shock structure and relaxation
[MPIS-106/1993] p 1798 N94-20145

KOLMOGOROV THEORY
Mathematical theory of thermodynamics of computation
[CWI-CS-R9251] p 2038 N94-21533

KONDO EFFECT
Non-Fermi-liquid and multichannel Kondo phenomena in Y(1-x)U(x)Pd3 and related alloys
[DE93-040135] p 2015 N94-20275

Temperature dependence of 4f PES features and hole occupancy in ytterbium heavy fermions
[DE93-040131] p 1691 N94-20321
Non-fermi liquid and spin-glass behavior of the Sc(1-x)U(x)Pd3 system
[DE93-040134] p 2016 N94-20335
Thermal expansion of electronic highly correlated materials
[ETN-93-93605] p 2026 N94-21135
Photoemission and the electronic properties of heavy fermions: Limitations of the Kondo model
[DE93-040191] p 1974 N94-21553
Magnetic instability of Kondo insulators
[DE93-040064] p 1768 N94-21762
Alloying studies in U(1-x)Th(x)Pd2Al3 (0 (le) x (le) 1)
[DE94-000807] p 2036 N94-22584

KOVAR (TRADEMARK)
Segregation of Si to the surface of Fe-29Ni-17Co alloy
[DE93-040053] p 1687 N94-19864

KREEP
The Mg-suite and the highland crust: An unsolved enigma p 2126 N94-20822

KRYPTON FLUORIDE LASERS
Laser amplifier developments at Mercury
[DE93-040103] p 1814 N94-19867

L

LABORATORY EQUIPMENT
The National High Magnetic Field Laboratory, a user facility in support of research in high magnetic fields
[DE93-040145] p 1714 N94-20278
Advanced failure analysis laboratory equipment networking
[DE93-019070] p 1916 N94-21633

LABYRINTH SEALS
Navy GTE seal development activity p 1655 N94-21794
Compliant seal development p 1655 N94-21795

LAGRANGE MULTIPLIERS
Shape optimization governed by the Euler equations using an adjoint method
[NASA-CR-191555] p 1950 N94-20092

LAGRANGIAN FUNCTION
Effect of limiter end loss in finite Larmor radius theory
[DE93-040913] p 1992 N94-19887
Coupling of smooth particle hydrodynamics with PRONTO
[DE93-019080] p 1915 N94-21539
RHALE: A 3-D MMALE code for unstructured grids
[DE93-019405] p 1916 N94-21635
Microscopic and macroscopic dynamics
[DE93-019576] p 1937 N94-22042
Coupling of smooth particle hydrodynamics with the finite element method
[DE93-019081] p 1805 N94-22556

LAKES
Chromaticity analysis of LANDSAT multispectral scanner and thematic mapper imagery of Chilko Lake, British Columbia, using a theoretical optical water quality model
[ISBN-0-315-63832-X] p 1843 N94-22422

LAMBERT SURFACE
Goniospectrometric properties of a white standard p 1684 N94-20664
New algorithm for the detection of the orientation of a planar Lambertian surface in 3D p 1777 N94-22150

LAMINAR FLOW
Detailed structure study of an H2/N2O/Ar flame employing molecular beam mass spectrometry, laser spectroscopy, and modeling
[AD-A270720] p 1679 N94-20111
Surface hot film measurements at ATTAS laminar glove p 1639 N94-22596
Recent ONERA contributions to the development of flight test measurement techniques p 1641 N94-22607

LAMINAR FLOW AIRFOILS
Measurement Technology for Flight Tests
[ILR-MITT-256(1991)] p 1639 N94-22597
Surface hot film measurements at ATTAS laminar glove p 1639 N94-22598
Testing of a multisensor hot film technique in wind tunnel and free flight p 1639 N94-22599
Free flight experiment with a laminar wing glove p 1639 N94-22600
Experiments with a fluid deicing system for cleaning laminar wings p 1640 N94-22601

LAMINATES
Quantification of uncertainties in the performance of smart composite structures
[NASA-TM-106335] p 1830 N94-20171
Structural similitude and design of scaled down laminated models
[NASA-CR-194687] p 1673 N94-20172
Layered thin-edged field-emitter device
[AD-D015932] p 1751 N94-20350
The effects of processing and constituent materials on compressive strength of thick composite laminates
[AD-A271912] p 1673 N94-20490
Intercalated hybrid graphite fiber composite
[NASA-CASE-LEW-15241-1] p 1673 N94-20539
Characterization of multilayer GaAs/AlGaAs transistor structures by variable angle spectroscopic ellipsometry p 1796 N94-20985
A new matrix formulation of classical electrodynamics. Part 3: Wave propagation through a multilayer dielectric medium with planar boundaries
[AD-A271610] p 1739 N94-21240
Approximation to sound radiation and scattering by simply supported layered cylinder
[AD-A272964] p 1967 N94-21306
Damage states around fastener holes in thick graphite/epoxy composite laminates
[AD-A272613] p 1675 N94-21504
Materials Science and Engineering
[DE93-040497] p 1675 N94-21530
Modeling of failure and response to laminated composites subjected to in-plane loads p 1834 N94-22612
Delamination, durability, and damage tolerance of laminated composite materials p 1678 N94-22622

LAND ICE
The distribution of ground ice on Mars p 2090 N94-20394

LAND USE
Application of SPOT to GIS/LIS in land capability evaluation for regional planning of JAICO semi-arid region of Piaui, Brazil p 1838 N94-20955
The 7th Brazilian Remote Sensing Symposium, volume 2 p 1838 N94-20956
Change detection on land use and rainforest cover at Paragominas region, Brazilian Amazon p 1838 N94-20957
Remote sensing for hydrology progress and prospects
[WMO-773] p 1841 N94-21069
Urban applications of satellite remote sensing and GIS analysis
[PB93-202174] p 1842 N94-21855

LANDAU DAMPING
Kinetic resonance damping rate of the toroidal ion temperature gradient mode
[DE94-001234] p 1998 N94-22561

LANDAU FACTOR
On the nonlinear instability of thermal structures p 2006 N94-22668

LANDAU-GINZBURG EQUATIONS
Dynamics of vortices in superconductors
[DE93-019535] p 2011 N94-19808

LANDFORMS
The distribution of ground ice on Mars p 2090 N94-20394
The thumbprint terrain: What will Mars Observer tell us? p 2091 N94-20397
Local topography of Mars and its relationship to surface weathering processes p 2111 N94-20737
A carbon dioxide/methane greenhouse atmosphere on early Mars p 2142 N94-21662

LANDING GEAR
Tetrahedral lander
[NASA-CASE-MSC-22082-1] p 1658 N94-20590

LANDING LOADS
Tetrahedral lander
[NASA-CASE-MSC-22082-1] p 1658 N94-20590

LANDING SITES
The roughness of the Martian surface: A scale dependent model p 2115 N94-20762
Geology and radiophysical properties of the Venera and Vega landing sites p 2135 N94-20867
Notes on Antarctic aviation
[AD-A273018] p 1651 N94-21239

LANDSAT SATELLITES
The development of remote sensing in Brazil and Canada: Comparative case studies p 1840 N94-20968
Comparison of radiation and cloud parameters derived from satellite and aircraft measurements during FIRE 2 cirrus IFO p 1872 N94-22299

LANGEVIN FORMULA
Stochastic differential equations and numerical simulation for pedestrians
[DE93-040651] p 1949 N94-20006

LANGUAGES
Beta(sub k)-complete problems and greediness
[TR-455] p 1913 N94-21318
Language as primary dimension of distributed AI systems activity p 1776 N94-22141

LANTHANUM ALLOYS
Intelligent processing of ferroelectric thin films
[AD-A272518] p 1705 N94-21416

LANTHANUM ISOTOPES
NMR studies of oxygen-doped La2CuO(4+delta)
[DE93-040756] p 2034 N94-22007

LANTHANUM OXIDES
Local structure and superconductivity in La(2-x)Ba(x)CuO4 for x=0.125 and x=0.15
[DE93-040193] p 2029 N94-21555
Crystal structure and short-range oxygen defects in La- and Nd-modified ZrO2
[DE93-040229] p 2033 N94-21993
NMR studies of oxygen-doped La2CuO(4+delta)
[DE93-040756] p 2034 N94-22007

LAPLACE TRANSFORMATION
Time-laplace-transform-domain analysis of wave propagation in planar waveguides
[PB93-215226] p 1960 N94-22096
Transient acoustic wave modeling: Higher-order WKBJ asymptotics and symbolical manipulation (revised)
[PB93-215432] p 1969 N94-22262
Continuous-time discretized-space approach to modeling short-pulse propagation and scattering
[PB93-215259] p 1742 N94-22347

LAPSE RATE
Windshear detection for aircraft using temperature lapse rate
[CA-PATENT-1,295,736] p 1641 N94-21030

LARGE SCALE INTEGRATION
Self assembly: An approach to terascale integration
[DE93-040104] p 1769 N94-21846
The distributed CAD system for LSI/VLSI design p 1923 N94-22068

LARGE SPACE STRUCTURES
An expert system executive for automated assembly of large space truss structures
[NASA-TM-4487] p 1939 N94-20089
Phase demodulation of interferometric fiber-optic sensors
[ISBN-0-315-83425-0] p 1991 N94-22581
System identification of the Daisy large space structure emulator
[ISBN-0-315-83533-8] p 1653 N94-22588

LARMOR RADIUS
Finite Larmor radius flute mode theory with end loss
[DE93-040914] p 1991 N94-19872
Effect of limiter end loss in finite Larmor radius theory
[DE93-040913] p 1992 N94-19887

LASER ABLATION
Particles on surfaces of laser ablated Y1Ba2Cu3O(7-delta) films
[DE93-040269] p 2013 N94-19929
Charge collectors for the omega upgrade
[DE93-019684] p 1972 N94-20264
Stability analysis of unsteady ablation fronts
[DE93-019689] p 1819 N94-21839

LASER ANEMOMETERS
Utilization of lasers for air data measurements p 1640 N94-22603

LASER APPLICATIONS
Laser amplifier developments at Mercury
[DE93-040103] p 1814 N94-19867
Initiation and modification of reaction by energy addition: Kinetic and transport phenomena
[AD-A271315] p 1797 N94-19936
PVDF gauge characterization of hypervelocity-impact-generated debris clouds
[DE93-018831] p 1829 N94-19943
Photoconductive Semiconductor Switches for pulsed power applications
[DE93-019411] p 1750 N94-20294
Coherent lidar design and performance verification
[NASA-CR-193813] p 1816 N94-20341
Engineering design, fabrication, installation, operation, and maintenance services in support of research on laser plasma physics
[AD-A272249] p 1994 N94-20943
Obtaining surface optical properties from space-based lidar systems
[AD-A272831] p 1987 N94-21172
Non-destructive semiconductor wafer probing system using laser pulses to generate and detect millimeter-wave signals
[CA-PATENT-APPL-SN-2,020,73] p 1760 N94-21178
Long-range laser imaging
[AD-A273020] p 1817 N94-21253
Compact lightweight CO2 laser for SDIO application
[AD-A273010] p 1817 N94-21264
Techniques for the flux growth of optical materials: Growth of beta-barium borate
[AD-A272717] p 2028 N94-21505
Laser driven hydrodynamic instability experiments
[DE93-040550] p 1818 N94-21547
Surface and subsurface defect detection in Si3N4 components by laser scattering
[DE93-040829] p 1832 N94-21772

The laser and its applications on environment and biotechnology research
[DE94-000376] p 1820 N94-21957
Surface acquisition through virtual milling p 1920 N94-22372

LASER ARRAYS
Statistical fluctuations in lasers
[DE94-000710] p 1817 N94-20939

LASER BEAMS
The NRL LACE program
[AD-A270861] p 1657 N94-19896
Optically controlled current filamentation in GaAs photoconductive semiconductor switches
[DE93-019427] p 2016 N94-20296
Laser propagation in underdense plasmas: Scaling arguments
[DE93-040439] p 1816 N94-20480
Optical metrology of magnetically trapped hydrogen
[AD-A272110] p 1680 N94-20584
Statistical fluctuations in lasers
[DE94-000710] p 1817 N94-20939
Thermal diffusivity measurements by photothermal laser beam deflection (PTD): Data analysis using the Levenberg-Marquardt algorithm p 1820 N94-21006
Thermal characterization of thin films by photothermally induced laser beam deflection p 1710 N94-21007
Micro-ellipsometric measurements of strained layer structures p 2025 N94-21008
Effects of stimulated Raman scattering on light beam properties during high-power laser beam long-path propagation
[AD-A273109] p 1818 N94-21509
Plasma lens experiments at the Final Focus Test Beam
[DE93-041081] p 1981 N94-21688
Surface and subsurface defect detection in Si3N4 components by laser scattering
[DE93-040829] p 1832 N94-21772
Ionization of H2(+) in intense laser fields
[DE93-019160] p 1818 N94-21829
Parametric instabilities in picosecond time scales
[DE94-000384] p 1966 N94-21958
The optical constants and spectral specular reflectivity of Highly Oriented Pyrolytic Graphite (HOPG)
[DE93-040546] p 1709 N94-21970
Phase screens for the control of the focal irradiance of the Nova laser
[DE94-001067] p 1820 N94-22401

LASER CAVITIES
Initial performance of Los Alamos advanced free electron laser
[DE93-040158] p 1814 N94-19828
Tunable laser frequency stabilizing system
[AD-D015904] p 1815 N94-20055
Compact lightweight CO2 laser for SDIO application
[AD-A273010] p 1817 N94-21284
The n-p(p(+))-n Al(yGa)(1-y) As-GaAs-In(x)Ga(1-x) as quantum well laser with p(+)-n(+)GaAs-InGaAs tunnel contact on n GaAs
[AD-A271292] p 2030 N94-21805

LASER DAMAGE
Ocular damage induced by ultrashort laser pulses
[AD-A271859] p 1890 N94-20462

LASER DOPPLER VELOCIMETERS
Fluid dynamic mechanisms and interactions within separated flows
[AD-A271037] p 1797 N94-19978
An experimental investigation of the drag mechanisms of a helicopter rotor in hovering flight
[AD-A270201] p 1636 N94-20486
Two-point laser Doppler velocimetry measurements of length-turbulent scales
[ECL-92-12] p 1801 N94-20542
Analysis and design of weight balancing system for laser velocimetry traverse
[AD-A271171] p 1816 N94-20546
Low-altitude cross-wind velocity measurements using pulsed visible fringe-type laser anemometry
[ISL-CO-216/92] p 1866 N94-20557
Measurement and prediction of the flow through an annular turbine cascade
[AD-A272530] p 1803 N94-21417

LASER GUIDANCE
Laser guide star adaptive optics: Present and future
[DE93-018642] p 1989 N94-21619

LASER INDUCED FLUORESCENCE
Experimental study of a shock accelerated thin gas layer
[DE93-018354] p 1799 N94-20286
Laser diagnostics of RF hydrogen plasma reactors: Application to the processing of III-V materials
[AD-A272659] p 1994 N94-21214
Instantaneous velocity field imaging instrument for supersonic reacting flows
[NASA-CR-191162] p 1809 N94-21607

LASER MATERIALS
Optics survivability support, volume 1
[DE93-019616] p 1985 N94-20262

LASER MODE LOCKING
High Speed/High Frequency Optoelectronics
[AD-A271985] p 1751 N94-20580

LASER OUTPUTS
Suppression of relaxation oscillations in flashpumped, two-micron tunable solid state lasers
[AD-D015928] p 1814 N94-19800
Initial performance of Los Alamos advanced free electron laser
[DE93-040158] p 1814 N94-19828
Tunable laser frequency stabilizing system
[AD-D015904] p 1815 N94-20055
Resonantly pumped, erbium-doped, GSGG, 2.8 micron, solid state laser with energy recycling and high slope efficiency
[AD-D015920] p 1815 N94-20060
Compact lightweight CO2 laser for SDIO application
[AD-A273010] p 1817 N94-21284
Conversion of the proprietary ROLM (tm) inter-node link from multimode to singlemode operation p 1744 N94-21349
Simulations of spectral broadening by cross-phase modulation (XPM) with chaotic light pulses
[DE93-019623] p 1819 N94-21872
Shattering the myth of the resonantly photo-pumped neon-like titanium laser
[DE93-019624] p 1819 N94-21873
Effect of bandwidth on beam smoothing and frequency conversion at the third harmonic of the Nova laser
[DE93-019917] p 1819 N94-21920
Parametric instabilities in picosecond time scales
[DE94-000384] p 1966 N94-21958

LASER PLASMA INTERACTIONS
Laser propagation in underdense plasmas: Scaling arguments
[DE93-040439] p 1816 N94-20480
Spectral characterization of lithographic sources
[DE93-019941] p 1997 N94-21848

LASER PLASMAS
Charge collectors for the omega upgrade
[DE93-019684] p 1972 N94-20264
Engineering design, fabrication, installation, operation, and maintenance services in support of research on laser plasma physics
[AD-A272249] p 1994 N94-20943

LASER POWER BEAMING
Power transmission by laser beam from lunar-synchronous satellite
[NASA-TM-4496] p 1669 N94-20102
Method for remotely powering a device such as a lunar rover
[NASA-CASE-LAR-14789-1] p 1824 N94-20587

LASER PUMPING
Suppression of relaxation oscillations in flashpumped, two-micron tunable solid state lasers
[AD-D015928] p 1814 N94-19800
Resonantly pumped, erbium-doped, GSGG, 2.8 micron, solid state laser with energy recycling and high slope efficiency
[AD-D015920] p 1815 N94-20060

LASER RANGE FINDERS
Development of a lidar for integration with the Naval Postgraduate School Infrared Search and Target Designation (NPS-IRSTD) system
[AD-A271847] p 1817 N94-20611
Determining the 3-D structure and motion of objects using a scanning laser range sensor
[NASA-CR-194745] p 1818 N94-21817
Two-dimensional perception based on a laser rangefinder p 1786 N94-22202

LASER SPECTROSCOPY
Detailed structure study of an H2/N2O/Ar flame employing molecular beam mass spectrometry, laser spectroscopy, and modeling
[AD-A270720] p 1679 N94-20111
Optical metrology of magnetically trapped hydrogen
[AD-A272110] p 1680 N94-20584
Laser Raman and x ray scattering studies of corrosion films on metals
[DE93-040243] p 1692 N94-21558

LASER STABILITY
Parametric instabilities in picosecond time scales
[DE94-000384] p 1966 N94-21958

LASER TARGET DESIGNATORS
Long-range laser imaging
[AD-A273020] p 1817 N94-21253

LASER TARGET INTERACTIONS
Stability analysis of unsteady ablation fronts
[DE93-019689] p 1819 N94-21839

LASER TARGETS
Photopumped x ray laser research on Saturn
[DE93-019430] p 1816 N94-20298
Long-range laser imaging
[AD-A273020] p 1817 N94-21253
Stability analysis of unsteady ablation fronts
[DE93-019689] p 1819 N94-21839
Shattering the myth of the resonantly photo-pumped neon-like titanium laser
[DE93-019624] p 1819 N94-21873

LASER WEAPONS
Tactical laser weapons and other directed-energy weapons
[AD-A267961] p 1816 N94-20484

LASERS
Diagnostics and methods for real-time laser microchemistry
[AD-A270871] p 1680 N94-20566

LASING
Photopumped x ray laser research on Saturn
[DE93-019430] p 1816 N94-20298
Generation of intense ultrashort x ray pulses
[DE93-019607] p 1817 N94-21299
Shattering the myth of the resonantly photo-pumped neon-like titanium laser
[DE93-019624] p 1819 N94-21873

LATCH-UP
Test results for SEU and SEL immune memory circuits p 1754 N94-21087
Proton radiation testing of an 18 bit A/D converter p 1755 N94-21096
Single event phenomena: Testing and prediction p 1763 N94-21696

LATE STARS
The cool-star spectral catalog: A uniform collection of IUE SWP-LOs p 2046 N94-22446

LATENT HEAT
Spatial and temporal variations of satellite microwave measurements of latent heat release in tropic cyclones due to environmental forcing obtained from a numerical model
[AD-A267947] p 1865 N94-20482
A comparison of small and larger mesoscale latent heat and radiative fluxes: December 6 case study p 1879 N94-22335

LATITUDE
Radiometry in commercial aircraft
[GSF-41/91] p 1892 N94-21141

LATTICE PARAMETERS
Metastable bcc phase formation in the Nb-Cr system
[DE93-018376] p 2012 N94-19926
Fundamentals of mechanical behavior in structural intermetallics: A synthesis of atomistic and continuum modeling
[DE93-019166] p 1690 N94-20232
Non-Fermi-liquid and multichannel Kondo phenomena in Y(1-x)U(x)Pd3 and related alloys
[DE93-040135] p 2015 N94-20275
Lattice gauge theory: Present status
[DE93-041154] p 2038 N94-21692

LATTICE VIBRATIONS
Inelastic neutron scattering of (gamma)-iron, and the determination of the elastic constants by lattice dynamics
[DE94-000694] p 1978 N94-22573

LATTICES (MATHEMATICS)
Lattice gauge theory: Present status
[DE93-041154] p 2038 N94-21692

LAUNCH VEHICLES
Total systems design analysis of high performance structures
[NASA-TP-3432] p 1653 N94-20141
Japanese space program p 1652 N94-21407
Options for thrust augmentation for the Beta 2 two-stage-to-orbit launch vehicle
[NASA-TM-106418] p 1649 N94-21759
Specialized data analysis for the Space Shuttle Main Engine and diagnostic evaluation of advanced propulsion system components
[NASA-CR-194720] p 1656 N94-21813
Spaceplane flight simulation: Project definition
[PB93-211399] p 1651 N94-22094

LAVA
Formation and evolution of radial fracture systems on Venus p 2099 N94-20672
A comparison of calculated and measured rheological properties of crystallising lavas in the field and in the laboratory p 1862 N94-20690
Parabolic features and the erosion rate on Venus p 2122 N94-20801
Tumuli and tubes: Teaching scientific techniques p 2039 N94-20818
Formation of perched lava ponds on basaltic volcanoes: Interaction between cooling rate and flow geometry allows estimation of lava effusion rates p 1863 N94-20878
A classification scheme for the morphology of lava flow fields p 1863 N94-20879
Numerical simulation of lava flows: Applications to the terrestrial planets p 1863 N94-20904

LAYOUTS
Engineering design, fabrication, installation, operation, and maintenance services in support of research on laser plasma physics
[AD-A272249] p 1994 N94-20943
A unified approach to VLSI layout automation and algorithm mapping on processor arrays p 1759 N94-21127
Layout optimization with algebraic multigrid methods p 1957 N94-21474
Schematic driven layout of Reed Solomon encoders p 1766 N94-21722

LEACHING
Elemental depletions in Antarctic micrometeorites and Arctic cosmic spherules: Comparison and relationships p 2082 N94-20704

LEAD (METAL)
The proximity effect in ultrathin granular Pb films
[AD-A271094] p 2012 N94-19848
Thin-film fabrication of Pb-doped BiSrCaCuO superconductor p 1781 N94-22176

LEAD ACID BATTERIES
Advanced batteries for electric vehicle applications: Nontechnical summary
[DE93-019007] p 1748 N94-19885

LEAD COMPOUNDS
Preparation and properties of sol-gel derived PZT thin films for decoupling capacitor applications
[DE93-018853] p 2013 N94-19961
MOCVD growth and structure of PbTiO3 thin films
[DE93-040230] p 2033 N94-21994

LEAD ISOTOPES
U-Pb isotopic ages and characteristics of ancient (greater than 4.0 Ga) lunar highland rocks p 2104 N94-20700
U-Pb provenance ages of shocked zircons from the K-T boundary, Raton Basin, Colorado p 1685 N94-20701
U-Pb isotopic systematics of ferroan anorthosite 60025 p 1685 N94-20702

LEAD TITANATES
The multicomponent lineshape of the anharmonic A(1)(TO) phonon in PbTiO3
[DE93-018995] p 1970 N94-19971

LEAD ZIRCONATE TITANATES
A novel method for characterizing the electrical Priorities of lead Zirconate Titanate (PZT) ferroelectric films and memory devices
[AD-A270463] p 2013 N94-19966
Long range fast tool servo
[AD-A271614] p 1761 N94-21257
Intelligent processing of ferroelectric thin films
[AD-A272518] p 1705 N94-21416

LEADING EDGES
Compilation of reinforced carbon-carbon transatlantic abort landing arc jet test results
[NASA-TM-104778] p 1676 N94-21834

LEAKAGE
Brush seal bristle flexure and hard-rub characteristics p 1654 N94-21791
Compliant seal development p 1655 N94-21795

LEARNING
High dimension action spaces in robot skill learning
[TR-458] p 1945 N94-21317

LEARNING THEORY
The effects of instructional sets on reactions to and performance on an intelligent tutoring system
[NASA-CR-194739] p 1895 N94-21810

LEAST SQUARES METHOD
Literature review of the errors-in-variables approach to the problem of system identification
[AD-A271098] p 1949 N94-19907
A weighted least-squares lump correction algorithm for transmission-corrected gamma ray nondestructive assay
[DE93-018474] p 1904 N94-20049
Signal processing in the linear statistical model
[AD-A272114] p 1736 N94-20570
Predicting LANDSAT MSS endmember signatures from corresponding higher resolution TM fraction images p 1839 N94-20962
Development of a gridless CFD method p 1919 N94-22361
Extracting galactic structure parameters from multivariated density estimation p 1964 N94-22458
Interactive Spectral Analysis and Computation (ISAAC) p 1926 N94-22505

LEGAL LIABILITY
A guide to resolving disputes over contractor delay entitlements
[AD-A272022] p 2039 N94-21444

LENNARD-JONES POTENTIAL
A database of selected transport coefficients for combustion studies
[DE93-041278] p 1678 N94-19689

LENSES
System for solving Boolean equations using optical lookup tables
[AD-D015962] p 1951 N94-20358
Ocular damage induced by ultrashort laser pulses
[AD-A271859] p 1890 N94-20462
Plasma lens experiments at the Final Focus Test Beam
[DE93-041081] p 1981 N94-21688

LEPTONS
Top search at the TEVATRON
[DE93-019392] p 1978 N94-19988
Recent results on top, bottom and exotic physics at the Tevatron
[DE94-000578] p 1975 N94-21786
The lepton charge asymmetry in the decay of W bosons produced in p(bar p) collisions at (radical)s = 1.8 TeV
[DE93-019903] p 1976 N94-21847
Production, collection and utilization of very long-lived heavy charged leptons
[DE93-040867] p 1977 N94-22009

LESIONS
Ocular damage induced by ultrashort laser pulses
[AD-A271859] p 1890 N94-20462
Area postrema ablations in cats: Evidence for separate neural routes for motion- and xylazine-induced CTA and emesis p 1887 N94-21906

LETHALITY
Current directions in the vulnerability/lethality process structure
[AD-A272836] p 1964 N94-21175

LEWIS BASE
Synthesis and structural characterization of new light molecular weight inorganic oxidizers and relative derivatives, volume 1
[AD-A271437] p 2012 N94-19842
Volatile CVD precursors based on copper alkoxides and mixed group 2A-copper alkoxides
[AD-D015930] p 1701 N94-20349

LIBRARIES
Research in image management and access
[NASA-CR-194797] p 1907 N94-20376
Experiments on technology mapping using different cell libraries p 1758 N94-21118
The three-dimensional Event-Driven Graphics Environment (3D-EDGE) p 1922 N94-21342
Assessment of the organizational structure and services of DOE National Laboratory Libraries
[DE93-040697] p 2045 N94-21750

LIE GROUPS
Explicit results on gl(lambda) and sl(lambda)
[MEMO-1075] p 1953 N94-21072

LIFE (DURABILITY)
Measurement of the B(+) and B(0) lifetimes
[DE93-019906] p 1969 N94-19814
Computational Methods for Failure Analysis and Life Prediction
[NASA-CP-3230] p 1833 N94-22608
Nonlinear and progressive failure aspects of transport composite fuselage damage tolerance p 1834 N94-22609
NASA Langley developments in response calculations needed for failure and life prediction p 1836 N94-22621

LIFE CYCLE COSTS
The automated ground network system p 1932 N94-21330

LIFE SCIENCES
Aerospace medicine and biology: A continuing bibliography with indexes (supplement 383)
[NASA-SP-7011(383)] p 1892 N94-21288

LIFE SUPPORT SYSTEMS
Quinoa: An emerging new crop with potential for CELSS
[NASA-TP-3422] p 1895 N94-20137
Characterization of Minnesota lunar simulant for plant growth p 1897 N94-20665
Aerospace medicine and biology: A continuing bibliography with indexes (supplement 383)
[NASA-SP-7011(383)] p 1892 N94-21288

LIFT
Nonlinear aerodynamics and the design of wing tips
[NASA-CR-194732] p 1638 N94-21833

LIFT DRAG RATIO
Optimization and performance analysis of a supersonic conical-flow waverider for a deck-launched intercept mission
[AD-A272498] p 1648 N94-21433

LIFT FANS
Survey of lift-fan aerodynamic technology
[NASA-CR-177615] p 1646 N94-21592

LIFTING BODIES
Users manual for the NASA Lewis three-dimensional ice accretion code (LEWICE 3D)
[NASA-TM-105974] p 1642 N94-21590

LIGANDS
Synthesis and structural characterization of new light molecular weight inorganic oxidizers and relative derivatives, volume 1
[AD-A271437] p 2012 N94-19842
Catalytic hydrogenation of carbon monoxide
[DE94-000881] p 1678 N94-20103
Low temperature absorption spectra and ground state electronic structure of tetrakis(2,6-di-tert-butylphenoxide)uranium(IV)
[DE94-000774] p 2035 N94-22367

LIGHT (VISIBLE RADIATION)
Optical and Gamma Ray Space Observations
[NASA-TM-109389] p 2149 N94-20602
Simultaneous optical/gamma ray observations of GRB's p 2149 N94-20603

LIGHT AMPLIFIERS
Laser amplifier developments at Mercury
[DE93-040103] p 1814 N94-19867
Compact lightweight CO2 laser for SDIO application
[AD-A273010] p 1817 N94-21284

LIGHT BEAMS
Rotary encoding device using polygonal mirror with diffraction gratings on each facet
[NASA-CASE-GSC-13543-1] p 1985 N94-20240
Study of possible energy upgrade for the ALS and modeling of the real lattice for the diagnosis of lattice problems
[DE93-040286] p 2016 N94-20323
System for solving Boolean equations using optical lookup tables
[AD-D015962] p 1951 N94-20358
Optical beam forming techniques for phased array antennas p 1727 N94-20442
Effects of stimulated Raman scattering on light beam properties during high-power laser beam long-path propagation
[AD-A273109] p 1818 N94-21509
Particle image velocimetry
[DE93-040657] p 1804 N94-21748
Parametric instabilities in picosecond time scales
[DE94-000384] p 1966 N94-21958

LIGHT ELEMENTS
Cometary interplanetary dust particles? An update on carbon in anhydrous IDPS p 2084 N94-20828
Asbestos characterization using scanning electron microscopy/light element x ray spectrometry
[AD-A271611] p 1681 N94-21241

LIGHT EMISSION
Collisional processes involving atmospheric gases
[AD-A270729] p 1854 N94-19954
Radio and optical emission: Spectral shapes and breaks in GRB
[NASA-CR-194763] p 2150 N94-21781

LIGHT GAS GUNS
Intact capture of hypervelocity particles on Shuttle p 2085 N94-20837
Shock compression of low-density foams
[DE93-040545] p 1707 N94-21546

LIGHT IONS
Development and characterization of a time-, position- and energy-resolved x ray diagnostic for PBFA 2 target experiments
[DE93-019429] p 1808 N94-20297

LIGHT MODULATION
Optoelectronic associative memory
[NASA-CASE-NPO-18278-1-CU] p 1985 N94-20303
System for solving Boolean equations using optical lookup tables
[AD-D015962] p 1951 N94-20358
Optical beam forming techniques for phased array antennas p 1727 N94-20442
Center for the integration of optical computing
[AD-A271874] p 1899 N94-20469
Ellipsometric analysis of built-in electric fields in semiconductor heterostructures p 1796 N94-20988
Polarized-light reflection mode p-i-n modulators with GaAs/AlGaAs multiple quantum well active layers: Design and simulation p 2023 N94-20996
Simulations of spectral broadening by cross-phase modulation (XPM) with chaotic light pulses
[DE93-019623] p 1819 N94-21872
Effect of bandwidth on beam smoothing and frequency conversion at the third harmonic of the Nova laser
[DE93-019917] p 1819 N94-21920

LIGHT SCATTERING
Study of electromagnetic wave scattering from characterized rough surfaces
[AD-A270931] p 1716 N94-19934
Oceanic in situ Fraunhofer-line characteristics: Fraunhofer-line underwater experiment (FLUX)
[AD-A270659] p 1881 N94-19952
Development of a technique to determine the morphology and dynamics of agglomerates in chemically reacting flows
[AD-A271160] p 1678 N94-20000

Light scattering studies of an electrorheological fluid
[DE93-019419] p 1700 N94-20315
Intensity and polarization of light scattered by size distributions of randomly oriented nonspherical particles
p 1721 N94-20416
Obtaining surface optical properties from space-based lidar systems
[AD-A272831] p 1987 N94-21172
Documentation for PCDIST, a FORTRAN subroutine to calculate Pollack-Cuzzi scattering
[AD-A273070] p 1988 N94-21491
Surface and subsurface defect detection in SI3N4 components by laser scattering
[DE93-040829] p 1832 N94-21772

LIGHT SOURCES
Robust photo-topography by fusing shape-from-shading and stereo
[NASA-CR-194697] p 1806 N94-19920
ALE project
[AD-A271080] p 2014 N94-19980
Study of transverse coupled bunch instabilities by using non-linear Taylor maps for the Advanced Light Source (ALS)
[DE93-040287] p 1979 N94-19989
Emittance measurement and modeling of the ALS 50 MeV LINAC to booster line
[DE93-040116] p 1979 N94-20273
Measurement and computation of the higher order modes of the ALS 500 MHz accelerating cavities
[DE93-019256] p 1980 N94-20292
Study of possible energy upgrade for the ALS and modeling of the real lattice for the diagnosis of lattice problems
[DE93-040286] p 2016 N94-20323
System for solving Boolean equations using optical lookup tables
[AD-D015962] p 1951 N94-20358
Survey and alignment analysis for the ALS storage ring using computer spreadsheets
[DE93-019254] p 1917 N94-21917

LIGHT TRANSMISSION
Photonic electromagnetic field sensor apparatus
[AD-D015939] p 1718 N94-20334
Optical and transport properties of metallic and semiconductor nanostructures
[AD-A271716] p 2018 N94-20554
X ray reflection masks: Manufacturing, characterization and first tests
[BONN-IR-92-31] p 1986 N94-21043
Photonics and nonlinear optics with molecular materials and polymers
[AD-A271747] p 1988 N94-21457
Effects of stimulated Raman scattering on light beam properties during high-power laser beam long-path propagation
[AD-A273109] p 1818 N94-21509
OTDR strain gauge for smart skins
[DE93-041043] p 1810 N94-21953

LIGHT VALVES
A full-color, high-resolution laser projector for a flight simulator visual display
[AD-A270578] p 1651 N94-20108

LIGHTHILL GAS MODEL
Computation of the sound generated by isotropic turbulence
[NASA-CR-191543] p 1804 N94-21880

LIGHTNING
Predicting lightning events in the KSC area: A feasibility study using single station data
[AD-A271440] p 1864 N94-20088

LIKELIHOOD RATIO
Stochastic optimization by simulation: Convergence proofs for the G1/G/1 queue in steady-state
[AD-A271141] p 1962 N94-19999
Asymptotics of the GLRT for the disorder problem in diffusion processes
[INRIA-RR-1735] p 1951 N94-20227

LIMB DARKENING
Wavelength dependence of limb-darkening of Mars from visible and near-IR telescopic spectral imaging
p 2101 N94-20685

LIMITERS (FUSION REACTORS)
A two-dimensional kinetic model of the scrape-off layer
[DE94-001235] p 1999 N94-22562

LINE OF SIGHT
Sporadic-E observations during LoVHF transionospheric direction finder measurements
[AD-A270619] p 1716 N94-19951
A new procedure for orbit determination based on three lines of sight: Angles only
[AD-A272937] p 1652 N94-21224

LINE SHAPE
Photoemission and the electronic properties of heavy fermions: Limitations of the Kondo model
[DE93-040191] p 1974 N94-21553

LINE SPECTRA
Interactive Spectral Analysis and Computation (ISAAC)
p 1926 N94-22505
Adaptive filtering of Echelle spectra of distant Quasars
p 2072 N94-22520
Factor analysis as a tool for spectral line component separation 21cm emission in the direction of L1780
p 1965 N94-22536

LINEAR ACCELERATORS
Method to evaluate steering and alignment algorithms for controlling emittance growth
[DE93-041004] p 1978 N94-19856
Emittance measurement and modeling of the ALS 50 MeV LINAC to booster line
[DE93-040116] p 1979 N94-20273
Performance of the high brightness linac for the Advanced Free Electron Laser Initiative at Los Alamos
[DE93-040141] p 1816 N94-20277
Longitudinal instability of an induction linac with acceleration
[DE93-019249] p 1980 N94-20290
Low emittance 0.8A K(+) ion source for the LBL Induction Linac System Experiment (ILSE)
[DE93-019237] p 1981 N94-21439
Demonstration of ultraviolet lasing with a low energy electron beam
[DE93-040192] p 1818 N94-21554
A high-intensity He-jet production source for radioactive beams
[DE93-040247] p 1981 N94-21767
The preservation of low emittance flat beams
[DE93-040964] p 1981 N94-21773
A FET-switched induction accelerator cell
[DE93-019604] p 1769 N94-21838

LINEAR AMPLIFIERS
Quantum noise studies with superconducting tunnel junction mixers
[AD-A270897] p 2012 N94-19897

LINEAR ARRAYS
Rotary encoding device using polygonal mirror with diffraction gratings on each facet
[NASA-CASE-GSC-13543-1] p 1985 N94-20240
Probe compensation in cylindrical near-field scanning: A novel simulation methodology p 1718 N94-20404
Analysis of microstrip dipoles and slots transversely coupled to a microstrip line using the FDTD method
p 1718 N94-20405
Optimal sorting in linear arrays with minimum global control
[CWI-CS-R9244] p 1908 N94-21024

LINEAR CIRCUITS
Using crosscorrelation techniques to determine the impulse response of linear systems
p 1759 N94-21122

LINEAR EQUATIONS
On the numerical stability of quasi-definite systems
[DE93-019404] p 1950 N94-20217
Classical and generalized solutions of time-dependent linear differential algebraic equations
[AD-A272834] p 1954 N94-21173
Finite difference methods for time-dependent, linear differential algebraic equations
[AD-A272835] p 1954 N94-21174
A retrieval error analysis technique for passive infrared atmospheric sounders
[AD-A272618] p 1867 N94-21212
Derivation of a model of the exciter of a brushless synchronous machine
[EUT-92-E-258] p 1761 N94-21538
Universality in blow-up for non linear heat equations
[PB93-215465] p 2038 N94-22095

LINEAR FILTERS
A comparative robustness evaluation of feedforward neurofilters
[NASA-TM-106440] p 1650 N94-21742
Imaging vector fields using line integral convolution
[DE93-019922] p 1917 N94-21841
An adaptive method for group delay compensation using switched capacitor filters p 1793 N94-22248

LINEAR OPERATORS
Parameter estimation with cost function of second order in output-error-problem
[DLR-FB-92-38] p 1964 N94-21139

LINEAR POLARIZATION
Intensity and polarization of light scattered by size distributions of randomly oriented nonspherical particles
p 1721 N94-20416
The Brewster angle effect in SAR polarimetry
p 1731 N94-20456
The coherent backscattering opposition effect
p 1991 N94-20846
Magellan vertical polarization radar observations
p 1744 N94-20691
SLD results from the study of polarized Z(sup 0) produced at the SLC
[DE93-041020] p 1982 N94-21952

LINEAR PROGRAMMING
Optimal sorting in linear arrays with minimum global control
[CWI-CS-R9244] p 1908 N94-21024
Multigrid approach to solving the long transportation problem on a regular grid in cost space
[AD-A272323] p 1909 N94-21038
Linear programming for standard and nonstandard Markovian control problems. A survey
[PB93-191948] p 1963 N94-21066
A neural network approach to the maximum flow problem p 1783 N94-22183
Algorithmic advances in stochastic programming
[DE94-001160] p 1921 N94-22406

LINEAR QUADRATIC GAUSSIAN CONTROL
Acceleration-augmented LQG control of an active magnetic bearing p 1757 N94-21112
A new eddy current model for magnetic bearing control system design p 1763 N94-21698

LINEAR SYSTEMS
Convex set and linear mixing model
p 1844 N94-20888
Using crosscorrelation techniques to determine the impulse response of linear systems
p 1759 N94-21122
An automatic multigrid method for the solution of sparse linear systems p 1957 N94-21478
Hybrid finite element/waveguide mode analysis of passive RF devices
[AD-A273074] p 1740 N94-21518
Using parallel banded linear system solvers in generalized eigenvalue problems
[NASA-CR-191540] p 1915 N94-21584

LINEAR TRANSFORMATIONS
On geometric and algebraic aspects of 3D affine and projective structures from perspective 2D views
[AD-A270520] p 1963 N94-19968

LINEAR VIBRATION
Acoustic radiation damping of flat rectangular plates subjected to subsonic flows
[NASA-TM-109382] p 1967 N94-20211

LINGUISTICS
Connectionism and Natural Language Processing
[MEMO-INF-92-64] p 1940 N94-20242
Representation of idioms in connectionist models
p 1940 N94-20247
Neural data oriented parsing p 1940 N94-20248
Hopfield models as neural-network acceptors
p 1941 N94-20250
Recognizing hesitation phenomena in continuous, spontaneous speech p 1746 N94-22210

LINKAGES
A robust adaptive control design for flexible joint manipulators p 1790 N94-22230
Robot link and contact surface dynamic interaction: An experimental study of contact instability
[ISBN-0-315-83439-0] p 1827 N94-22578

LIOUVILLE THEOREM
On the twisted N=2 superconformal structure in 2d gravity coupled to matter
[DE93-628627] p 2037 N94-20178

LIPIDS
Lateral distribution of lipids in membranes at high pressure
[AD-A271183] p 1700 N94-20299

LIQUEFIED GASES
Thermal information regarding the cooldown and operation of liquid argon calorimeters
[DE93-019391] p 1807 N94-19987
A High Resolution Liquid Xenon Imaging Telescope for 0.3-10 MeV Gamma Ray Astrophysics: Construction and Initial Balloon Flights
[NASA-CR-194709] p 2056 N94-22281
The polarization sensitivity of the liquid xenon imaging telescope p 2056 N94-22282

LIQUID BRIDGES
Stability limits and dynamics of nonaxisymmetric liquid bridges
[NASA-CR-194706] p 1797 N94-20037

LIQUID COOLING
Cold-start minidiesel engine development
[AD-A271064] p 1823 N94-20567
A dc Penning surface-plasma source
[DE93-040126] p 1997 N94-21989

LIQUID CRYSTALS
Complex and stereoregular nonlinear optical materials
[AD-A271067] p 1983 N94-19846
Optically induced rotation diffusion in polymer liquid crystals: Phenomenological theory and experimental verification
[ETN-93-95068] p 2014 N94-20026
A full-color, high-resolution laser projector for a flight simulator visual display
[AD-A270578] p 1651 N94-20108

Molecular and atomic arrays in nano- and mesoporous materials synthesis
[AD-A271500] p 2017 N94-20544
Liquid crystal displays p 1752 N94-20634
LCD display tests p 1752 N94-20635
Miniature color display, phase 4
[AD-A272920] p 1760 N94-21221
Recent developments in aromatic azo polymers research
[AD-A272966] p 1705 N94-21259
Fluorescent microthermographic imaging
[DE93-040332] p 1810 N94-22000

LIQUID FUELS
Liquid rocket propulsion. Theory p 1667 N94-20069
Cryogenic propellant rocket engine problems p 1668 N94-20076

LIQUID HELIUM
Acoustic microscopy and nonlinear effects in pressurized superfluid helium
[AD-A270598] p 1967 N94-19949
Neutron and PIMC determination of the longitudinal momentum distribution of HCP, BCC and normal liquid He-4
[DE93-019009] p 1972 N94-20187

LIQUID OXYGEN
Actively controlled shaft seals for aerospace applications
[NASA-CR-194759] p 1823 N94-20538
Production of O2 on the Moon: A lab-top demonstration of ilmenite reduction with hydrogen p 2126 N94-20821
Detailed study of oxidation/wear mechanism in lox turbopump bearings
[NASA-TM-108434] p 1825 N94-21580

LIQUID PHASE SINTERING
High performance heavy alloys by alloying and process control
[AD-A271129] p 1689 N94-20019

LIQUID PHASES
Neutron and PIMC determination of the longitudinal momentum distribution of HCP, BCC and normal liquid He-4
[DE93-019009] p 1972 N94-20187

LIQUID PROPELLANT ROCKET ENGINES
A tutorial on the aero/thermodynamical design of liquid-propellant rocket engine nozzles p 1668 N94-20074
Liquid fuel injection elements for rocket engines
[NASA-CASE-MFS-28547-1] p 1669 N94-20370
Method of fabricating a rocket engine combustion chamber
[NASA-CASE-MFS-28569-1] p 1703 N94-20541
Advanced transportation system studies, technical area 3. Alternate propulsion subsystem concepts: J-2S restart study
[NASA-CR-193874] p 1670 N94-21271
NASA Propulsion Engineering Research Center, volume 1
[NASA-CR-194721-VOL-1] p 1671 N94-22428

LIQUID ROCKET PROPELLANTS
Liquid rocket propulsion. Theory p 1667 N94-20069
Cryogenic propellant rocket engine problems p 1668 N94-20076
The Vulcain cryogenic engine p 1668 N94-20077

LIQUID-SOLID INTERFACES
Surface science at the solid liquid interface
[AD-A271422] p 1678 N94-19839
Surface electrochemistry of metals
[AD-A272913] p 1691 N94-21245

LIQUID-VAPOR INTERFACES
Pressurization and expulsion of a flightweight liquid hydrogen tank
[NASA-TM-106427] p 1799 N94-20177
Experimental study of void formation during aluminum solidification in reduced gravity
[NASA-TM-106190] p 1692 N94-21604

LIQUIDS
Femtosecond Raman-induced Kerr effect study of polar solvent dynamics: Amides
[DE93-017563] p 1678 N94-19924
Electron reactions in nonpolar liquids: Pressure effects
[DE93-040328] p 1970 N94-19931
Measuring liquid properties with smooth and textured-surface resonators
[DE93-019433] p 1749 N94-20054

LIQUIDUS
Origin of high-Ti lunar ultramafic glasses p 1666 N94-20853

LISP (PROGRAMMING LANGUAGE)
A proposed research program in information processing
[NASA-CR-194271] p 2041 N94-20134

LITHIUM
Transient studies of low temperature catalysts for methane conversion
[DE93-041232] p 1680 N94-20934
Heat transfer additives for absorption cooling system fluids
[PB93-202521] p 1714 N94-21426
Preliminary SP-100/Stirling heat exchanger designs
[NASA-TM-106444] p 1670 N94-21809

LITHIUM OXIDES
Cathode materials for the molten carbonate fuel cell
[DE93-019515] p 1848 N94-21870

LITHIUM SULFUR BATTERIES
Lithium batteries: Future batteries p 1752 N94-20630

LITHOGRAPHY
Uncertainty limited atomic position measurement using optical fields
[AD-A271013] p 1970 N94-19822
Characterization and possible repair of defects in soft x ray projection lithography masks
[DE93-019147] p 1750 N94-20231
The modification of polymer surfaces and the fabrication of submicron-scale functionalized structures by deep-UV and electron beam lithography
[AD-A265956] p 1700 N94-20328
Spectral characterization of lithographic sources
[DE93-019941] p 1997 N94-21848
Center for X-Ray Optics, 1992
[DE94-000726] p 1990 N94-21868

LITHOLOGY
Twenty-Fourth Lunar and Planetary Science Conference. Part 3: N-Z
[NASA-CR-193149] p 2092 N94-20636
The Erevan howardite: Petrology of glassy clasts and mineral chemistry p 1684 N94-20640
Modelling the gravity and magnetic field anomalies of the Chicxulub crater p 1862 N94-20668
Opaque-rich lithology in the Divnoe achondrite: Petrology and origin p 2082 N94-20680
Chaunskij: The most highly metamorphosed, shock-modified and metal-rich mesosiderite p 2082 N94-20681
Spectral reflectance studies of the Humorum Basin region p 2101 N94-20682
Petrography of shock features in the 1953 Manson 2-A drill core p 1862 N94-20767
Distribution and geologic history of materials excavated by the lunar crater Bullialdus p 2128 N94-20832
Equilibrium and fractional crystallization of a primitive Shergottite composition p 2085 N94-20861

LITHOSPHERE
Beta Regio rift system on Venus: Geologic interpretation of Magellan images p 2095 N94-20655
Venus magmatic and tectonic evolution p 2101 N94-20683
Rifting at Devana Chasma, Venus: Structure and estimation of the effective thickness of the elastic lithosphere p 2113 N94-20754
Geoid, topography, and convection-driven crustal deformation on Venus p 2116 N94-20769
A tectonic resurfacing model for Venus p 2118 N94-20781
Arcuate and circular structures in the Tharsis region: Evidence of coronae on Mars p 2134 N94-20863
Large floor-fractured craters and isostatic crater modification: Implications for lithospheric thickness on Venus p 2135 N94-20873

LOAD TESTS
Biaxial flexural testing of a carbon fiber reinforced epoxy composite
[AD-A271956] p 1674 N94-20577

LOADS (FORCES)
Automatic locking orthotic knee device
[NASA-CASE-MFS-28633-1] p 1896 N94-20493
Loads produced by a suited subject performing tool tasks without the use of foot restraints
[NASA-TP-3424] p 1896 N94-20606
Possible flexural signatures around Olympus and Ascraeus Montes, Mars p 2142 N94-20911
Maximum team lifting capacity as a function of team size
[AD-A271642] p 1892 N94-21036
Results of the second Round Robin on opening-load measurement conducted by ASTM Task Group E24.04.04 on crack closure measurement and analysis
[NASA-TM-109032] p 1832 N94-21624
Strength capabilities and load requirements while performing torquing tasks in zero gravity
[NASA-TP-3433] p 1897 N94-21627
Analysis of thermal mechanical fatigue in titanium matrix composites p 1835 N94-22618

LOCAL AREA NETWORKS
A distributed reinforcement learning scheme for network routing
[AD-A270600] p 1938 N94-19845
Understanding Open Systems Interconnection (OSI)
[AD-A271877] p 1929 N94-20472
Using manufacturing message specification for monitor and control at Venus p 1932 N94-21333
Distributed intelligent control and status networking p 1932 N94-21335
The Test Analysis Retrieval System (TARS): Meeting the challenges of the network's test processes p 1933 N94-21337
Performance evaluation of video on ethernet
[DE93-040696] p 1936 N94-21749
Evaluation of DEC's GIGAswitch for distributed parallel computing
[DE94-001356] p 1936 N94-21853
Application development in a PC/LAN environment p 1923 N94-22067
File transfer performance in LAN interconnection through a satellite channel p 1746 N94-22209

LOCKING
Automatic locking orthotic knee device
[NASA-CASE-MFS-28633-1] p 1896 N94-20493
Self locking set screw
[AD-D015969] p 1824 N94-21277

LOCKS (FASTENERS)
Activities Report of the Institute of Applied Physics
[ETN-93-93749] p 1966 N94-21798
Electronic locking system p 1796 N94-21801

LOCOMOTION
Apparatus and method for measuring subject work rate on an exercise device
[NASA-CASE-MSC-21752-1] p 1895 N94-20194
Perception/action: An holistic approach 2
[AD-A271822] p 1891 N94-20627

LOCOMOTIVES
Adaptation of model parameters of a rail model at measured rail compliances
[ILR-MITT-274(1992)] p 1831 N94-21153

LOGARITHMS
Vanishing theorem on arithmetic surfaces
[PB93-215481] p 1961 N94-22263

LOGIC CIRCUITS
Reconfigurable fuzzy cell
[NASA-CASE-MSC-21613-1] p 1907 N94-20492
Design of CMOS logic gates for TID radiation p 1754 N94-21083
Complementary heterojunction FET technology for space application p 1755 N94-21094
Bridging faults in BiCMOS circuits p 1756 N94-21105
Fault detection in digital and analog circuits using an i(DD) temporal analysis technique p 1757 N94-21106
Faulty behavior of asynchronous storage elements p 1757 N94-21108
Detection of CMOS bridging faults using minimal stuck-at fault test sets p 1757 N94-21110
Practical issues in implementing roving spares in VLSI systolic arrays p 1758 N94-21114
Experiments on technology mapping using different cell libraries p 1758 N94-21118
Low-latency digital frequency synthesizer using the residue number system p 1759 N94-21121
Correctness properties for iterated hardware structures p 1759 N94-21124
Partition algebraic design of asynchronous sequential circuits p 1759 N94-21125
Defect-sensitivity analysis of an SEU immune CMOS logic family p 1765 N94-21711
Dimension scaling effects on the yield sensitivity of HEMT digital circuits p 1765 N94-21712
Detection of feed-through faults in CMOS storage elements p 1766 N94-21721
Bit-systolic arithmetic arrays using dynamic differential gallium arsenide circuits p 1767 N94-21724
A VLSI implementation of DCT using pass transistor technology p 1767 N94-21725
On fast carry select adders p 1767 N94-21728
A 1 GHz sample rate, 256-channel, 1-bit quantization, CMOS, digital correlator chip p 1768 N94-21732
Formal hardware verification in Maple p 1771 N94-22112
Impact of partitioning on parallel discrete event simulation of logic circuits p 1772 N94-22115
Logic oriented neural networks p 1782 N94-22182
A Hopfield neural net for discrete Fourier transform calculation p 1783 N94-22184
A new class of multi-function two-rail totally self-checking basic building blocks p 1788 N94-22215
Fuzzy and neural control
[NASA-TM-108753] p 1947 N94-22270

LOGIC DESIGN
Power optimization in logic isomers p 1756 N94-21101
Test pattern generation for ILA sequential circuits p 1757 N94-21107
Partition algebraic design of asynchronous sequential circuits p 1759 N94-21125
High-speed Viterbi decoding with overlapping code sequences p 1760 N94-21130
Behavioral model simulation studies of an image compressor p 1760 N94-21133

HDL to verification logic translator
p 1766 N94-21717
Detection of feed-through faults in CMOS storage elements p 1766 N94-21721
Formal hardware verification in Maple
p 1771 N94-22112
Towards the formal verification of the requirements and design of a processor interface unit: HOL listings
[NASA-CR-191466] p 1937 N94-22414

LOGIC PROGRAMMING
Bottom-up abstract interpretation of logic programs
[PB93-191773] p 1928 N94-19995
Programming logic for F omega
[PB93-191781] p 1928 N94-19996
System at the cross-roads of functional and logic programming
[PB93-191823] p 1928 N94-20009
Parallel logic programming systems
[RR-691-I] p 1929 N94-20176
A declarative approach for first-order built-in's of PROLOG
[CWI-CS-R9246] p 1909 N94-21026
COCOLOG: A conditional observer and controller logic for finite machines
[INRIA-RR-1714] p 1910 N94-21063
Correctness properties for iterated hardware structures p 1759 N94-21124
Reasoning about update logic
[CWI-CS-R9312] p 1914 N94-21496
Changing preferences
[CWI-CS-R9310] p 1915 N94-21551
Termination and confluence of rule execution
[CWI-CS-R9309] p 1916 N94-21587

LOGISTICS
Planning process software: A user guide for the DMCA
[AD-A271252] p 1902 N94-19911
The logistic model: The integration of business process redesign and information systems development based on logistic principles
[MEMO-INF-92-70] p 2045 N94-22276

LOGISTICS MANAGEMENT
Multigrid approach to solving the long transportation problem on a regular grid in cost space
[AD-A272323] p 1909 N94-21038

LONG DURATION EXPOSURE FACILITY
Long Duration Exposure Facility (LDEF) contamination study
[AD-A272419] p 1658 N94-21147
Conversion of LDEF experiment M0003 sample observation database to MS-DOS formats
[AD-A272945] p 1681 N94-21226
Results of the post flight analyses on system materials for the LDEF-FRECOPA experiment
p 1659 N94-21371
Measured space environmental effects to LDEF during retrieval p 1659 N94-21372
Space environmental effects on polymer matrix composites: The UTIAS/LDEF experiment
p 1660 N94-21373
Some results of the oxidation investigation of copper and silver samples flown on LDEF p 1660 N94-21375
The implications of the LDEF results on Space Station Freedom power system materials p 1660 N94-21377
Gamma ray spectrometry of LDEF samples: Results of 1992 analyses
[DE94-001177] p 1684 N94-22046

LONG WAVE RADIATION
Simulation of clear-sky outgoing longwave radiation over the oceans using operational analysis
p 1861 N94-22290

LONGITUDE
Venus gravity: New Magellan low altitude data
p 2117 N94-20772

LONGITUDINAL STABILITY
Longitudinal beam dynamics for heavy ion fusion using WARPrz
[DE93-019154] p 1992 N94-19915

LORENTZ FORCE
Electrode array electromagnetic velocimeter
[AD-D015950] p 1806 N94-19882
Modeling the minimum energy state of the Earth's magnetotail
[AD-A267984] p 1856 N94-20485

LORENTZ GAS
Theoretical and numerical studies in magnetic fusion
[DE94-000536] p 1993 N94-20937

LOSSES
Volatile loss from accreting icy protoplanets
p 2084 N94-20793
Outgassing data for selecting spacecraft materials
[NASA-RP-1124-REV-3] p 1676 N94-21889

LOW ALTITUDE
Low-cost, dual-use platforms for environmental sensing, phase 1
[AD-A272951] p 1646 N94-21246

LOW COST
Clementine: An inexpensive mission to the Moon and Geographos p 1652 N94-20765
A low cost alternative to high performance PCM bit synchronizers p 1813 N94-21347
Silicon microelectronic field-emissive devices for advanced display technology
[DE94-000397] p 1794 N94-22380
A low-cost vector processor boosting compute-intensive image processing operations p 1925 N94-22441
Wilbur: A low-cost CCD camera system for MDM Observatory p 1814 N94-22510

LOW DENSITY MATERIALS
Shock compression of low-density foams
[DE93-040545] p 1707 N94-21546

LOW FREQUENCIES
High resolution infrared spectroscopy of cyclobutane: A study of vibrational mode coupling involving large amplitude, low frequency modes
[AD-A271987] p 1973 N94-20619

LOW MOLECULAR WEIGHTS
Chain propagation/step propagation polymerization chemistry. The preparation of solvent resistant well phase-separated thermoplastic elastomers
[AD-A271128] p 1699 N94-20016

LOW NOISE
A unified Monte Carlo interpretation of particle simulations and applications to nonneutral plasmas
[DE94-001231] p 1997 N94-21973

LOW PASS FILTERS
The influence of lowpass filtering and the effects of fading on the group demodulation of QPSK signals
p 1746 N94-22170

LOW SPEED
Experimental and computational results from a large low-speed centrifugal impeller
[NASA-TM-106421] p 1636 N94-20136

LOW SPEED WIND TUNNELS
Hot wire anemometry: A versatile instrumentation used for predevelopment studies and flight testing of the Do-328 aircraft p 1640 N94-22604

LOW TEMPERATURE
N,N'-bis(4,4,4-trinitro butyryl) hydrazine
[AD-D015897] p 1712 N94-20122
Transient studies of low temperature catalysts for methane conversion
[DE93-041232] p 1680 N94-20934
Cold starting an alcohol-fueled engine with ultrasonic fuel atomization
[PB93-206597] p 1826 N94-22093
A comparison of small and larger mesoscale latent heat and radiative fluxes: December 6 case study
p 1879 N94-22335
Low temperature absorption spectra and ground state electronic structure of tetrakis(2,6-di-tert-butylphenoxide)uranium(IV)
[DE94-000774] p 2035 N94-22387
Spectroscopic studies of magnetic transitions in TbPO4
[DE94-001274] p 2035 N94-22565

LOW THRUST
Design of a controllable pitch underwater thruster system
[AD-A271140] p 1821 N94-20021

LOWER ATMOSPHERE
Refractive index structure in the lower atmosphere
[AD-A270935] p 1854 N94-19899
Empirical wind model for the middle and lower atmosphere. Part 2: Local time variations
[NASA-TM-104592] p 1870 N94-21862

LUBRICANT TESTS
The use of screening tests in spacecraft lubricant evaluation
[AD-A272943] p 1705 N94-21225

LUBRICANTS
Microscopic modeling of tribological and interfacial phenomena
[AD-A271864] p 1823 N94-20464
The use of screening tests in spacecraft lubricant evaluation
[AD-A272943] p 1705 N94-21225
Scanning tunneling microscopy investigations of metal dichalcogenide materials
[AD-A272910] p 2027 N94-21242
Utilization of metals to improve the lubrication of ceramic load-bearing devices
[PB93-202448] p 1825 N94-21424
Integrity testing of brush seal in a T-700 engine
p 1654 N94-21792
Navy GTE seal development activity
p 1655 N94-21794
Dynamics of face seals for high speed turbomachinery
p 1655 N94-21796

LUBRICATING OILS
Vapor-delivered lubrication of steel-steel and steel-ceramic systems
[PB93-202364] p 1825 N94-21451

LUBRICATION
Microscopic modeling of tribological and interfacial phenomena
[AD-A271864] p 1823 N94-20464
Utilization of metals to improve the lubrication of ceramic load-bearing devices
[PB93-202448] p 1825 N94-21424
Lubricated wear of steel-ceramic and ceramic-ceramic systems
[PB93-202356] p 1825 N94-21450
Vapor-delivered lubrication of steel-steel and steel-ceramic systems
[PB93-202364] p 1825 N94-21451
Navy GTE seal development activity
p 1655 N94-21794
Dynamics of face seals for high speed turbomachinery
p 1655 N94-21796

LUMINESCENCE
Optical luminescence spectroscopy as a probe of the surface mineralogy of Mars p 1813 N94-22437

LUMINOSITY
Energy and luminosity limits of hadron supercolliders
[DE93-019248] p 1980 N94-20300
The preservation of low emittance flat beams
[DE93-040964] p 1981 N94-21773
Silicon microelectronic field-emissive devices for advanced display technology
[DE94-000397] p 1794 N94-22380

LUMINOUS INTENSITY
Optical switching devices
[AD-D015918] p 1984 N94-20059
Intensity and polarization of light scattered by size distributions of randomly oriented nonspherical particles
p 1721 N94-20416

LUMPING
A weighted least-squares lump correction algorithm for transmission-corrected gamma ray nondestructive assay
[DE93-018474] p 1904 N94-20049

LUNAR BASES
Characterization of Minnesota lunar simulant for plant growth p 1897 N94-20665

LUNAR COMPOSITION
Core formation in the Moon: The mystery of the excess depletion of Mo, W and P p 2095 N94-20651
Fragments of ancient lunar crust: Ferroan noritic anorthosites from the descartes region of the Moon
p 2096 N94-20660
Volatility in the lunar crust: Trace element analyses of lunar minerals by PIXE proton microprobe
p 2097 N94-20661
Impact glasses from the ultrafine fraction of lunar soils
p 2097 N94-20662
The Sm-(146,147)-Nd-(142,143) formation interval for the lunar mantle and implications for lunar evolution
p 2097 N94-20663
MinMap: An imaging spectrometer for high resolution compositional mapping of the Moon
p 1813 N94-20688
Chronology and genesis of high-Ti mare volcanism: Melting of cogenetic depleted and enriched reservoirs
p 2118 N94-20777
Implantation of nitrogen: Effects of hydrogen and implantation energy p 1686 N94-20804
Mineralogy and cooling history of magnesian lunar granulite 67415 p 2124 N94-20811
Ti-bearing oxide minerals in lunar meteorite Y793169 with the VLT affinity p 2084 N94-20812
Distribution and geologic history of materials excavated by the lunar crater Bullialdus p 2128 N94-20832
Origin of high-Ti lunar ultramafic glasses
p 1686 N94-20853
Petrology and geochemistry of VLT glasses from double drive tube 79001/2 p 1687 N94-20870
Multispectral studies of selected crater- and basin-filling lunar Maria from Galileo Earth-Moon encounter 1
p 2136 N94-20876

LUNAR CORE
Petrology and geochemistry of VLT glasses from double drive tube 79001/2 p 1687 N94-20870

LUNAR CRATERS
Spectral reflectance studies of the Humorum Basin region p 2101 N94-20682
Compositional diversity of the lunar North Pole: Preliminary analyses of Galileo SSI data
p 2101 N94-20686
Chronology of lunar granite 12033,576: Resetting of Rb-Sr and K-Ca isochrons p 2115 N94-20763
Distribution and geologic history of materials excavated by the lunar crater Bullialdus p 2128 N94-20832

Consortium study of lunar meteorites Yamato-793169 and Asuka-881757: Geochemical evidence of mutual similarity, and dissimilarity versus other mare basalts p 2085 N94-20857
Large floor-fractured craters and isostatic crater modification: Implications for lithospheric thickness on Venus p 2135 N94-20873
Degradation sequence of young lunar craters from orbital infrared survey p 2136 N94-20874
Multispectral studies of selected crater- and basin-filling lunar Maria from Galileo Earth-Moon encounter 1 p 2136 N94-20876

LUNAR CRUST
Petrogenesis of Apollo 12 mare basalts. Part 2: An open system model to explain the pigeonite basalt compositions p 1684 N94-20645
Fragments of ancient lunar crust: Ferroan noritic anorthosites from the descartes region of the Moon p 2096 N94-20660
Volatility in the lunar crust: Trace element analyses of lunar minerals by PIXE proton microprobe p 2097 N94-20661
Compositional diversity of the lunar North Pole: Preliminary analyses of Galileo SSI data p 2101 N94-20686
Geology and deposits of the Serenitatis basin p 2119 N94-20786
The Mg-suite and the highland crust: An unsolved enigma p 2126 N94-20822
The Clementine Mission science return at the Moon and Geographos p 1652 N94-20850
Limits on differentiation of melt sheets from basin-scale lunar impacts p 2133 N94-20856

LUNAR EVOLUTION
The Sm-(146,147)-Nd-(142,143) formation interval for the lunar mantle and implications for lunar evolution p 2097 N94-20663
Degradation sequence of young lunar craters from orbital infrared survey p 2136 N94-20874
Multispectral studies of selected crater- and basin-filling lunar Maria from Galileo Earth-Moon encounter 1 p 2136 N94-20876

LUNAR EXPLORATION
The High Resolution Stereo Camera (HRSC) for the Lunar Scout 1 Mission p 1813 N94-20650
Clementine: An inexpensive mission to the Moon and Geographos p 1652 N94-20765
Powdered aluminum and oxygen rocket propellants: Subscale combustion experiments [NASA-TM-106439] p 1713 N94-21760

LUNAR GEOLOGY
Twenty-Fourth Lunar and Planetary Science Conference. Part 3: N-Z [NASA-CR-193149] p 2092 N94-20636
Petrogenesis of Apollo 12 mare basalts. Part 1: Multiple melts and fractional crystallization to explain olivine and ilmenite basalt compositions p 1684 N94-20644
Petrogenesis of Apollo 12 mare basalts. Part 2: An open system model to explain the pigeonite basalt compositions p 1684 N94-20645
Core formation in the Moon: The mystery of the excess depletion of Mo, W and P p 2095 N94-20651
Fragments of ancient lunar crust: Ferroan noritic anorthosites from the descartes region of the Moon p 2096 N94-20660
Volatility in the lunar crust: Trace element analyses of lunar minerals by PIXE proton microprobe p 2097 N94-20661
Impact glasses from the ultrafine fraction of lunar soils p 2097 N94-20662
The Sm-(146,147)-Nd-(142,143) formation interval for the lunar mantle and implications for lunar evolution p 2097 N94-20663
Spectral reflectance studies of the Humorum Basin region p 2101 N94-20682
U-Pb isotopic ages and characteristics of ancient (greater than 4.0 Ga) lunar highland rocks p 2104 N94-20700
U-Pb isotopic systematics of ferroan anorthosite 60025 p 1685 N94-20702
C-O volatiles in Apollo 15 and Apollo 17 picritic glasses p 1685 N94-20727
Basaltic magmatism on the Moon. A perspective from volcanic picritic glasses p 2114 N94-20758
Origin of the Apollo 15 very low Ti green glass. A perspective from the compositional diversity in the very low Ti glasses p 1685 N94-20759
Combined backscatter Moessbauer spectrometer/x ray fluorescence analyzer (BaMS/XRF) for extraterrestrial surfaces p 1686 N94-20761
Geochronology and petrogenesis of the western highlands alkali suite: Radiogenic isotopic evidence from Apollo 14 p 2118 N94-20778
Magnesian anorthosites from the western highlands of the Moon: Isotope geochemistry and petrogenesis p 2118 N94-20779
Geology and deposits of the Serenitatis basin p 2119 N94-20786
Mineralogy and cooling history of magnesian lunar granulite 67415 p 2124 N94-20811
Sparking young minds with Moon rocks and meteorites p 2039 N94-20819
Evaluation of lunar rocks and soils for resource utilization: Detailed image analysis of raw materials and beneficiated products p 2126 N94-20820
The Mg-suite and the highland crust: An unsolved enigma p 2126 N94-20822
Distribution and geologic history of materials excavated by the lunar crater Bullialdus p 2128 N94-20832
Limits on differentiation of melt sheets from basin-scale lunar impacts p 2133 N94-20856

LUNAR GRAVITATION
Compositional diversity of the lunar North Pole: Preliminary analyses of Galileo SSI data p 2101 N94-20686

LUNAR MANTLE
The Sm-(146,147)-Nd-(142,143) formation interval for the lunar mantle and implications for lunar evolution p 2097 N94-20663
C-O volatiles in Apollo 15 and Apollo 17 picritic glasses p 1685 N94-20727

LUNAR MAPS
MinMap: An imaging spectrometer for high resolution compositional mapping of the Moon p 1813 N94-20688

LUNAR MARIA
Petrogenesis of Apollo 12 mare basalts. Part 1: Multiple melts and fractional crystallization to explain olivine and ilmenite basalt compositions p 1684 N94-20644
Petrogenesis of Apollo 12 mare basalts. Part 2: An open system model to explain the pigeonite basalt compositions p 1684 N94-20645
Spectral reflectance studies of the Humorum Basin region p 2101 N94-20682
Compositional diversity of the lunar North Pole: Preliminary analyses of Galileo SSI data p 2101 N94-20686
C-O volatiles in Apollo 15 and Apollo 17 picritic glasses p 1685 N94-20727
Lunar basalt meteorite EET 87521: Petrology of the clast population p 2083 N94-20752
Basaltic magmatism on the Moon. A perspective from volcanic picritic glasses p 2114 N94-20758
Chronology of lunar granite 12033,576: Resetting of Rb-Sr and K-Ca isochrons p 2115 N94-20763
Chronology and genesis of high-Ti mare volcanism: Melting of cogenetic depleted and enriched reservoirs p 2118 N94-20777
Geology and deposits of the Serenitatis basin p 2119 N94-20786
Ti-bearing oxide minerals in lunar meteorite Y793169 with the VLT affinity p 2084 N94-20812
The U-Th-Pb, Sm-Nd, and Ar-Ar isotopic systematics of lunar meteorite Yamato-793169 p 2084 N94-20834
Consortium study of lunar meteorites Yamato-793169 and Asuka-881757: Geochemical evidence of mutual similarity, and dissimilarity versus other mare basalts p 2085 N94-20857
Multispectral studies of selected crater- and basin-filling lunar Maria from Galileo Earth-Moon encounter 1 p 2136 N94-20876
Consortium reports on lunar meteorites Yamato 793169 and Asuka 881757, a new type of mare basalt p 2086 N94-20893

LUNAR ORBITS
Degradation sequence of young lunar craters from orbital infrared survey p 2136 N94-20874

LUNAR PHOTOGRAPHS
Compositional diversity of the lunar North Pole: Preliminary analyses of Galileo SSI data p 2101 N94-20686

LUNAR PHOTOGRAPHY
Preliminary results from Mariner 10: High resolution images of the Moon p 2107 N94-20719

LUNAR PROGRAMS
MinMap: An imaging spectrometer for high resolution compositional mapping of the Moon p 1813 N94-20688

LUNAR RADIATION
CERN-derived analysis of lunar radiation backgrounds p 2080 N94-20880

LUNAR RESOURCES
Production of O2 on the Moon: A lab-top demonstration of ilmenite reduction with hydrogen p 2126 N94-20821
Powdered aluminum and oxygen rocket propellants: Subscale combustion experiments [NASA-TM-106439] p 1713 N94-21760

LUNAR ROCKS
Fragments of ancient lunar crust: Ferroan noritic anorthosites from the descartes region of the Moon p 2096 N94-20660
Volatility in the lunar crust: Trace element analyses of lunar minerals by PIXE proton microprobe p 2097 N94-20661
The Sm-(146,147)-Nd-(142,143) formation interval for the lunar mantle and implications for lunar evolution p 2097 N94-20663
Characterization of Minnesota lunar simulant for plant growth p 1897 N94-20665
Optical effects of space weathering on lunar soils and the role of the finest fraction p 2101 N94-20687
U-Pb isotopic ages and characteristics of ancient (greater than 4.0 Ga) lunar highland rocks p 2104 N94-20700
U-Pb isotopic systematics of ferroan anorthosite 60025 p 1685 N94-20702
Euhedral metallic-Fe-Ni grains in extraterrestrial samples p 1697 N94-20724
Basaltic magmatism on the Moon. A perspective from volcanic picritic glasses p 2114 N94-20758
Geochronology and petrogenesis of the western highlands alkali suite: Radiogenic isotopic evidence from Apollo 14 p 2118 N94-20778
Geology and deposits of the Serenitatis basin p 2119 N94-20786
Sparking young minds with Moon rocks and meteorites p 2039 N94-20819
A long-term change of the AR/KR/XE fractionation in the solar corpuscular radiation p 2136 N94-20875

LUNAR ROVING VEHICLES
Power transmission by laser beam from lunar-synchronous satellite [NASA-TM-4496] p 1669 N94-20102
Method for remotely powering a device such as a lunar rover [NASA-CASE-LAR-14789-1] p 1824 N94-20587

LUNAR SOIL
Fragments of ancient lunar crust: Ferroan noritic anorthosites from the descartes region of the Moon p 2096 N94-20660
Impact glasses from the ultrafine fraction of lunar soils p 2097 N94-20662
The Sm-(146,147)-Nd-(142,143) formation interval for the lunar mantle and implications for lunar evolution p 2097 N94-20663
Characterization of Minnesota lunar simulant for plant growth p 1897 N94-20665
Compositional diversity of the lunar North Pole: Preliminary analyses of Galileo SSI data p 2101 N94-20686
Optical effects of space weathering on lunar soils and the role of the finest fraction p 2101 N94-20687
Implantation of nitrogen: Effects of hydrogen and implantation energy p 1686 N94-20804
Petrology and geochemistry of VLT glasses from double drive tube 79001/2 p 1687 N94-20870
Degradation sequence of young lunar craters from orbital infrared survey p 2136 N94-20874

LUNAR SPACECRAFT
The High Resolution Stereo Camera (HRSC) for the Lunar Scout 1 Mission p 1813 N94-20650

LUNAR SURFACE
Impact glasses from the ultrafine fraction of lunar soils p 2097 N94-20662
Optical effects of space weathering on lunar soils and the role of the finest fraction p 2101 N94-20687
Preliminary results from Mariner 10: High resolution images of the Moon p 2107 N94-20719
Basaltic magmatism on the Moon. A perspective from volcanic picritic glasses p 2114 N94-20758
Chronology and genesis of high-Ti mare volcanism: Melting of cogenetic depleted and enriched reservoirs p 2118 N94-20777
Contributions of the Clementine mission to our understanding of the processes and history of the Moon p 2119 N94-20784
Earth-based measurement of lunar topography using delayed radar interferometry p 2119 N94-20787
Degradation sequence of young lunar craters from orbital infrared survey p 2136 N94-20874
CERN-derived analysis of lunar radiation backgrounds p 2080 N94-20880

LUNAR TOPOGRAPHY
Earth-based measurement of lunar topography using delayed radar interferometry p 2119 N94-20787

LYSINE
Quinoa: An emerging new crop with potential for CELSS [NASA-TP-3422] p 1895 N94-20137

M

MACH NUMBER
Linear and nonlinear PSE for compressible boundary layers [NASA-CR-191537] p 1797 N94-20033

Acoustic radiation damping of flat rectangular plates subjected to subsonic flows
[NASA-TM-109382] p 1967 N94-20211

MACH-ZEHNDER INTERFEROMETERS
Balanced arrow Mach-Zehnder interferometer
p 1789 N94-22221

MACHINE LEARNING
Building brains for bodies
[AD-A270531] p 1939 N94-19875
Robot skill learning and the effects of basis function choice
[TR-437] p 1939 N94-20135
The Seventh International Symposium on Methodologies for Intelligent Systems (Poster Session)
[AD-A272125] p 1942 N94-20573
Design of a computer assisted tool for object oriented acquisition, modeling and simulation of knowledge structure
[ETN-93-94183] p 1910 N94-21152
High dimension action spaces in robot skill learning
[TR-458] p 1945 N94-21317
A neural M-ary tree method for data compression
p 1780 N94-22166
Cascaded recursive artificial neural networks
p 1780 N94-22167
Logic oriented neural networks p 1782 N94-22182
A framework of connectionist network toward speech waveform coding p 1746 N94-22211
Speaker-independent isolated-digit recognition using neural networks and hidden Markov model
p 1747 N94-22213
Fuzzy and neural control
[NASA-TM-108753] p 1947 N94-22270
SkiCAT: A cataloging and analysis tool for wide field imaging surveys p 2049 N94-22546
General asymmetric neural networks and structure design by genetic algorithms: A learning rule for temporal patterns
[DE94-001254] p 1947 N94-22563

MACHINE TOOLS
The Milling assistant, case-based Reasoning, and machining strategy: A report on the development of automated numerical control programming systems at New Mexico State University
[DE93-041101] p 2029 N94-21690

MACHINE-INDEPENDENT PROGRAMS
SPPTOOLS: Programming tools for the IRAF SPP language p 1925 N94-22474
Development of the FITS tools package for multiple software environments p 1927 N94-22516

MACHINING
Evaluation of a scanning Hartmann device for single point turning applications
[DE93-019204] p 1821 N94-19891
High-power copper vapor lasers and their application to precision drilling and cutting
[DE93-019951] p 1819 N94-21844

MACROMOLECULES
Application of molecular modeling to biological processing
[AD-A272612] p 1974 N94-21185

MAGELLAN PROJECT (NASA)
Magellan vertical polarization radar observations
p 1744 N94-20691
Magellan at Venus: Summary of science findings
p 2110 N94-20734
Response of the topography and gravity field on Venus to mantle upwelling beneath a chemical boundary layer
p 2117 N94-20775
Magellan Mission p 1652 N94-20829

MAGELLAN SPACECRAFT (NASA)
Magellan vertical polarization radar observations
p 1744 N94-20691
Venus gravity: New Magellan low altitude data
p 2117 N94-20772
Magellan Mission p 1652 N94-20829

MAGELLANIC CLOUDS
How to handle 6GBytes a night and not get swamped
p 2058 N94-22444

MAGMA
Calderas produced by hydromagmatic eruptions through permafrost in northwest Alaska p 2089 N94-20385
Volatility in the lunar crust: Trace element analyses of lunar minerals by PIXE proton microprobe
p 2097 N94-20661
Thermal and rheological controls on magma migration in dikes: Examples from the east rift zone of Kilauea volcano, Hawaii p 1862 N94-20673
Venus magmatic and tectonic evolution
p 2101 N94-20683
Venus pancake dome formation: Morphologic effects of a cooling-induced variable viscosity during emplacement p 2110 N94-20732
Basaltic magmatism on the Moon. A perspective from volcanic picritic glasses p 2114 N94-20758
Origin of the Apollo 15 very low Ti green glass. A perspective from the compositional diversity in the very low Ti glasses p 1685 N94-20759
Orthopyroxenes as recorders of diogenite petrogenesis: Trace element systematics p 1686 N94-20760
FE-60 and the evolution of eucrites
p 2083 N94-20788
Chronology and genesis of high-Ti mare volcanism: Melting of cogenetic depleted and enriched reservoirs
p 2118 N94-20777
Geochronology and petrogenesis of the western highlands alkali suite: Radiogenic isotopic evidence from Apollo 14 p 2118 N94-20778
Magnesian anorthosites from the western highlands of the Moon: Isotope geochemistry and petrogenesis
p 2118 N94-20779
Differentiation of magma oceans and the thickness of the depleted layer on Venus p 2118 N94-20780
The parent magma of the Nakhla (SNC) meteorite: Reconciliation of composition estimates from magmatic inclusions and element partitioning
p 2085 N94-20836
Elevation and igneous crater modification on Venus: Implications for magmatic volatile content
p 2135 N94-20872

MAGNESIUM ALLOYS
The use of backscattered electron imaging mode to assess the effect of fine dispersions on development of superplastic microstructure in Al-Mg alloys
[AD-A272426] p 1691 N94-21258

MAGNESIUM COMPOUNDS
The Mg-suite and the highland crust: An unsolved enigma p 2126 N94-20822

MAGNESIUM ISOTOPES
Diffusion-controlled magnesium isotopic fractionation of a single crystal forsterite evaporated from the solid state
p 1686 N94-20855

MAGNESIUM OXIDES
Properties of E-beam interactive oxide films for nanometer scale structures
[AD-A272848] p 1675 N94-21191
MOCVD growth and structure of PbTiO3 thin films
[DE93-040230] p 2033 N94-21994
Orientationally independent antiferromagnetic coupling in epitaxial Fe/Cr (211) and (100) superlattices
[DE94-001270] p 2035 N94-22564

MAGNET COILS
Stability of an uncooled segment of a high-temperature superconductor
[DE94-000476] p 2032 N94-21932

MAGNETIC ANOMALIES
Fabrication and evaluation of superconducting and semiconducting materials
[AD-A271645] p 2018 N94-20558
Modelling the gravity and magnetic field anomalies of the Chicxulub crater p 1862 N94-20668
Characterization of the Marquez Dome buried impact crater using gravity and magnetic data
p 1863 N94-20882

MAGNETIC BEARINGS
Acceleration-augmented LQG control of an active magnetic bearing p 1757 N94-21112
A new eddy current model for magnetic bearing control system design p 1763 N94-21698

MAGNETIC CLOUDS
Fragmentation of magnetized filamentary interstellar clouds p 2008 N94-22687
Gravitational instability of magnetized filamentary clouds. 1: Helical magnetic fields p 2008 N94-22688

MAGNETIC COMPRESSION
Compact lightweight CO2 laser for SDIO application
[AD-A273010] p 1817 N94-21284
Physics of transport phenomena in magnetic confinement plasmas p 2000 N94-22628

MAGNETIC CONTROL
Optical metrology of magnetically trapped hydrogen
[AD-A272110] p 1680 N94-20584
Fusion Plasma Theory. Task 1: Magnetic confinement fusion plasma theory
[DE94-000778] p 1998 N94-22019

MAGNETIC CORES
Expectations for the Martian core magnetic field
p 2120 N94-20792

MAGNETIC DIFFUSION
Magnetic fields in spiral galaxies
p 2010 N94-22697

MAGNETIC DIPOLES
Examination of low level magnetic dipole intensities in the transition nuclei Sm-148, Sm-150, Sm-152 and Sm-154, with inelastic photon scattering at S-DALINAC
[ETN-93-95069] p 1971 N94-20030
Iterative electromagnetic Born inversion applied to earth conductivity imaging
[DE93-040668] p 1859 N94-21928
Stability of beam in the Fermilab Main Injector
[DE94-000619] p 1982 N94-21934
Variable-field permanent magnet dipole
[DE94-000800] p 1820 N94-22020

MAGNETIC DISTURBANCES
Preliminary results of observations of solar flares with Nobeyama Radioheliograph p 2001 N94-22633

MAGNETIC EFFECTS
A general purpose ionospheric ray tracing procedure
[AD-A271058] p 1854 N94-19660
Study of possible energy upgrade for the ALS and modeling of the real lattice for the diagnosis of lattice problems
[DE93-040286] p 2016 N94-20323
Characterization of convection related defects in II-VI compound semiconductors
[NASA-CR-194704] p 2030 N94-21778
Effects of magnetic field perturbations in the ATF torsatron
[DE94-000474] p 1999 N94-22568

MAGNETIC FIELD CONFIGURATIONS
Magnetically controlled solar nebula
p 2120 N94-20791
Temperature dependence of magnetic order in single-crystalline UPdSn
[DE93-040153] p 2033 N94-21991
Initial operation of a large-scale plasma source ion implantation experiment
[DE94-000805] p 2036 N94-22583
Numerical simulation of magnetic reconnection associated with emerging flux in the solar atmosphere
p 2004 N94-22654
MHD relaxation in magnetic loops
p 2004 N94-22656
Particle acceleration in a filamentary current sheet model p 2004 N94-22659
Dynamics of physical state during two current loops collision p 2005 N94-22663
Enhanced absorption of p-modes on sunspot and plage regions p 2006 N94-22671
Gamma ray burst as a result of the explosive instability in the magnetosphere of old neutron star
p 2007 N94-22675
Asymptotic structure of magnetically driven MHD wind
p 2008 N94-22682
MHD flows from compact objects: Effects on magnetic field configurations p 2008 N94-22684
Gravitational instability of magnetized filamentary clouds. 1: Helical magnetic fields p 2008 N94-22688
Gravitational instability of magnetized filamentary clouds. 2: Rotation p 2009 N94-22689
Magnetic superbubbles in the galactic disk and halo
p 2009 N94-22694
Generation and maintenance of bisymmetric spiral magnetic fields in disk galaxies in differential rotation
p 2010 N94-22695
The relaxed state and entropy production due to the electric resistivity and viscosity of plasma
p 2010 N94-22696
Magnetic fields in spiral galaxies
p 2010 N94-22697

MAGNETIC FIELD RECONNECTION
Driven reconnection and self-organization
p 2000 N94-22625
Numerical simulation of magnetic reconnection associated with emerging flux in the solar atmosphere
p 2004 N94-22654
Magnetic reconnection in emission nebulae in clusters of galaxies p 2010 N94-22700

MAGNETIC FIELDS
Effect of exciton localization and delocalization on magnetic-field-dependent photoluminescence linewidths in semiconductors
[DE93-018860] p 1748 N94-19864
Space-charge dominated beam transport in magnetic quadrupoles with large aperture ratios
[DE93-040443] p 1992 N94-20004
Resistive gate magnetic field sensor
[AD-D015923] p 1749 N94-20199
Neoclassical kinetic theory near an X-point: Plateau regime
[DE93-019825] p 1951 N94-20224
Measurement and correction of magnetic fields in pulsed slotted-tube microwigglers
[DE93-040100] p 1815 N94-20272
The National High Magnetic Field Laboratory, a user facility in support of research in high magnetic fields
[DE93-040145] p 1714 N94-20278
Longitudinal instability of an induction linac with acceleration
[DE93-019249] p 1980 N94-20290
A study of the induction heating of organic composites
[AD-A272657] p 1675 N94-21187
Ionospheric photoelectrons measured at geosynchronous orbit
[AD-A272431] p 1857 N94-21202

The angular velocity spread of REB induced by magnetic field discontinuity
[IPPCZ-331] p 1996 N94-21573
Results from long conduction time plasma opening switch experiments at Sandia National Laboratories
[DE93-019063] p 1762 N94-21632
Relaxation of hysteresis loop in a single crystal of YBa2Cu4O8
[DE93-019519] p 2029 N94-21649
On the stability of shear-Alfven vortices
[DE93-040912] p 1996 N94-21752
Studies of electromagnetic ion cyclotron waves using AMPTE/CCE and Dynamics Explorer
[NASA-CR-194711] p 1982 N94-21878
Iterative electromagnetic Born inversion applied to earth conductivity imaging
[DE93-040668] p 1859 N94-21928
A moving finite element model of the tokamak scrapeoff layer
[DE94-000673] p 1997 N94-21965
Magnetic insulation of secondary electrons in plasma source ion implantation
[DE93-040106] p 1997 N94-21988
Variable-field permanent magnet dipole
[DE94-000800] p 1820 N94-22020
Effects of magnetic field perturbations in the ATF torsatron
[DE94-000474] p 1999 N94-22568
Test results of two high temperature superconducting sample coils
[DE94-000496] p 2035 N94-22570

MAGNETIC FILMS
Magnetic circular dichroism in x ray absorption and core-level photoemission
[DE93-019381] p 1688 N94-19986

MAGNETIC FLUX
Development, refinement, and testing of a short term solar flare prediction algorithm
[NASA-CR-194727] p 2147 N94-21832
The effect of correlated and point defects on the vortex lattice melting transition in single crystal YBa2Cu3O(7-delta)
[DE93-040277] p 2033 N94-21997

MAGNETIC LEVITATION VEHICLES
The 13th International Conference on Magnetically Levitated Systems and Linear Drives MAGLEV 1993
[DE93-040381] p 1825 N94-21544

MAGNETIC MEASUREMENT
Resistive gate magnetic field sensor
[AD-D015923] p 1749 N94-20199
Measurement and correction of magnetic fields in pulsed slotted-tube microwigglers
[DE93-040100] p 1815 N94-20272
Narsarsuaq Geophysical Observatory: Magnetic results, 1985 - 1990
[DATA-REPT-93-1] p 1856 N94-20607
Thule Geophysical Observatory: Magnetic results 1985 - 1990
[DATA-REPT-92-4] p 1857 N94-20609
Magnetic properties and Moessbauer analyses of glass from the K-T boundary, Beloc, Haiti
p 1685 N94-20753
Concept report: Experimental vector magnetograph (EXVM) operational configuration balloon flight assembly
[NASA-CR-194702] p 1638 N94-21776

MAGNETIC MOMENTS
A relativistic constituent quark model
[DE93-041085] p 1946 N94-21689

MAGNETIC PERMEABILITY
Non-Fermi-liquid and multichannel Kondo phenomena in Y(1-x)U(x)Pd3 and related alloys
[DE93-040135] p 2015 N94-20275
Non-fermi liquid and spin-glass behavior of the Sc(1-x)U(x)Pd3 system
[DE93-040134] p 2016 N94-20335
Fabrication and evaluation of superconducting and semiconducting materials
[AD-A271645] p 2018 N94-20558
Alloying studies in U(1-x)Th(x)Pd2Al3 (0 (le) x (le) 1)
[DE94-000807] p 2036 N94-22584

MAGNETIC POLES
Structural evidence for reorientation of Miranda about a paleo-pole p 2098 N94-20671
Compositional diversity of the lunar North Pole: Preliminary analyses of Galileo SSI data
p 2101 N94-20686

MAGNETIC PROPERTIES
Optical metrology of magnetically trapped hydrogen
[AD-A272110] p 1680 N94-20584
Magnetic properties and Moessbauer analyses of glass from the K-T boundary, Beloc, Haiti
p 1685 N94-20753
Magnetic record in chondrite meteorites
p 2085 N94-20858
Magnetic force microscopy/current contrast imaging: A new technique for internal current probing of IC's
[DE93-040754] p 1761 N94-21532
Magnetic instability of Kondo insulators
[DE93-040064] p 1768 N94-21762
Magnetism in CeRu2Ge2 and CeRh2Ge2 and its pressure dependence
[DE93-040061] p 2032 N94-21987
Temperature dependence of magnetic order in single-crystalline UPdSn
[DE93-040153] p 2033 N94-21991
Orientationally independent antiferromagnetic coupling in epitaxial Fe/Cr (211) and (100) superlattices
[DE94-001270] p 2035 N94-22564
Spectroscopic studies of magnetic transitions in TbPO4
[DE94-001274] p 2035 N94-22565
Inelastic neutron scattering of (gamma)-iron, and the determination of the elastic constants by lattice dynamics
[DE94-000694] p 1978 N94-22573

MAGNETIC RELAXATION
Relaxation of hysteresis loop in a single crystal of YBa2Cu4O8
[DE93-019519] p 2029 N94-21649

MAGNETIC RESONANCE
The National High Magnetic Field Laboratory, a user facility in support of research in high magnetic fields
[DE93-040145] p 1714 N94-20278
Fabrication and evaluation of superconducting and semiconducting materials
[AD-A271645] p 2018 N94-20558

MAGNETIC SHIELDING
Fabrication and evaluation of superconducting and semiconducting materials
[AD-A271645] p 2018 N94-20558

MAGNETIC SIGNATURES
Development, refinement, and testing of a short term solar flare prediction algorithm
[NASA-CR-194726] p 2147 N94-21815
Solar imaging vector magnetograph
[NASA-CR-194729] p 1810 N94-21876
Determination of coronal magnetic fields from vector magnetograms
[NASA-CR-194744] p 2147 N94-21877

MAGNETIC STORMS
Dynamics Explorer 2: Continued FPI and NACS instrument data analysis and associated scientific activity at the University of Michigan
[NASA-CR-194689] p 1657 N94-20173
The effects of magnetic storm phases on F-layer irregularities from auroral to equatorial latitudes
[AD-A272685] p 1857 N94-21189

MAGNETIC SUSPENSION
The 13th International Conference on Magnetically Levitated Systems and Linear Drives MAGLEV 1993
[DE93-040381] p 1825 N94-21544

MAGNETIZATION
Fermiology and De Haas-Van Alphen effect of beta-(ET)2IBr2
[DE93-019523] p 2011 N94-19807
Two-polarity magnetization in the Manson impact breccia p 1863 N94-20789
Observation of x ray absorption magnetic circular dichroism in well-characterized iron-cobalt-platinum multilayers
[DE94-000303] p 1694 N94-21944

MAGNETOHYDRODYNAMIC FLOW
On magnetodynamic effects initiated by a high-speed impact of a large cosmic body upon the Earth's surface
p 2082 N94-20647
Driven reconnection and self-organization
p 2000 N94-22625
Turbulization of free shear flows: 3D perturbations
p 2000 N94-22626
Laboratory structure of the heliopause
p 2003 N94-22648
Prompt high-energy particle acceleration during two current loops collision p 2005 N94-22661
Plasma structure in a plasma flow along a magnetic mirror field p 2005 N94-22664
Mean elemental composition and He-3 enrichments in solar energetic particles p 2006 N94-22670
MHD flows from compact objects: Effects on magnetic field configurations p 2008 N94-22684
Three-dimensional simulations of cosmic jets employing the smoothed particle hydrodynamics technique
p 2008 N94-22685
Time variation of MHD accretion onto a black hole
p 2009 N94-22692
Magnetic fields in spiral galaxies
p 2010 N94-22697
Shock formation in magnetohydrodynamical accretion onto a black hole p 2010 N94-22699
Magnetohydrodynamic phenomena in star-forming processes and their environment p 2010 N94-22701

MAGNETOHYDRODYNAMIC STABILITY
Finite Larmor radius flute mode theory with end loss
[DE93-040914] p 1991 N94-19872
Effect of limiter end loss in finite Larmor radius theory
[DE93-040913] p 1992 N94-19887
Beta-limiting instabilities in D3-D discharges with large bootstrap current
[DE93-015476] p 1993 N94-20326
Two-dimensional nonlinear Schrodinger equations and their properties
[AD-A272184] p 1952 N94-20923
Three-wave resonant interaction in a thin layer
[AD-A272331] p 1994 N94-21039
Shear flow generation by Reynolds stress and suppression of resistive g-modes
[DE93-040911] p 1995 N94-21514
On the stability of shear-Alfven vortices
[DE93-040912] p 1996 N94-21752
Continuum damping of ideal toroidal Alfven eigenmodes
[DE94-001233] p 1998 N94-22560
Kinetic resonance damping rate of the toroidal ion temperature gradient mode
[DE94-001234] p 1998 N94-22561
Fluid simulations of Delta T(sub e)-driven turbulence and transport in boundary plasmas
[DE94-001304] p 1999 N94-22566
Driven reconnection and self-organization
p 2000 N94-22625
MHD instabilities of fusion oriented plasmas
p 2000 N94-22627
Consequences of chaotic particle motion for the stability of space plasma current sheets p 2001 N94-22636
Tangential stress due to Kelvin-Helmholtz instability at the magnetospheric boundary p 2003 N94-22651
Non-linear thermal instability of optical thin molecular structures p 2006 N94-22667
On the nonlinear instability of thermal structures
p 2006 N94-22668
Consequences of plasma-maser in plasma astrophysics p 2006 N94-22669
The onset and spectra of a magnetized Langmuir turbulence p 2006 N94-22673
Langmuir microstructures and pulsar radio emission
p 2007 N94-22678
Helical kink instability of jets from young stellar objects p 2008 N94-22686
Fragmentation of magnetized filamentary interstellar clouds p 2008 N94-22687
Gravitational instability of magnetized filamentary clouds. 1: Helical magnetic fields p 2008 N94-22688
Gravitational instability of magnetized filamentary clouds. 2: Rotation p 2009 N94-22689
Spiral Alfven instability in accretion disks
p 2010 N94-22698

MAGNETOHYDRODYNAMIC TURBULENCE
Compressible MHD turbulence in the interplanetary medium p 2003 N94-22650
Structure of accretion plasmas of x ray binary pulsars in MHD turbulence p 2007 N94-22679
Spiral Alfven instability in accretion disks
p 2010 N94-22698

MAGNETOHYDRODYNAMIC WAVES
On the stability of shear-Alfven vortices
[DE93-040912] p 1996 N94-21752
Continuum damping of ideal toroidal Alfven eigenmodes
[DE94-001233] p 1998 N94-22560
MHD instabilities of fusion oriented plasmas
p 2000 N94-22627
Theory of leaked auroral kilometric radiation
p 2003 N94-22649
Compressible MHD turbulence in the interplanetary medium p 2003 N94-22650
Energy release at Alfvenic fronts in solar flares
p 2003 N94-22652
Dynamo driven by weak plasma turbulence: The effect of differential rotation p 2005 N94-22665
The onset and spectra of a magnetized Langmuir turbulence p 2006 N94-22673
Langmuir microstructures and pulsar radio emission
p 2007 N94-22678
Magnetic superbubbles in the galactic disk and halo
p 2009 N94-22694
Spiral Alfven instability in accretion disks
p 2010 N94-22698
Shock formation in magnetohydrodynamical accretion onto a black hole p 2010 N94-22699

MAGNETOHYDRODYNAMICS
Magnetically controlled solar nebula
p 2120 N94-20791
On the stability of shear-Alfven vortices
[DE93-040912] p 1996 N94-21752
Physics of magnetospheric boundary layers
[NASA-CR-194725] p 1858 N94-21836

A spheromak ignition experiment reusing Mirror Fusion Test Facility (MFTF) equipment
[DE94-001856] p 2034 N94-22050
Compressible MHD turbulence in the interplanetary medium p 2003 N94-22650
MHD relaxation in magnetic loops p 2004 N94-22658
Formation of fast magnetosonic shock waves during two current loops collision in solar flare p 2005 N94-22662
Helical kink instability of jets from young stellar objects p 2008 N94-22686
Time variation of MHD accretion onto a black hole p 2009 N94-22692
Accretion of a hot plasma onto the central black hole: Fokker-Planck formulation p 2009 N94-22693
Magnetic superbubbles in the galactic disk and halo p 2009 N94-22694
Generation and maintenance of bisymmetric spiral magnetic fields in disk galaxies in differential rotation p 2010 N94-22695
Magnetohydrodynamic phenomena in star-forming processes and their environment p 2010 N94-22701

MAGNETOMETERS
Solar imaging vector magnetograph
[NASA-CR-194729] p 1810 N94-21876

MAGNETOPAUSE
Laboratory relations between the solar wind dynamic pressure and the magnetospheric structures of the Earth and comets p 2003 N94-22647

MAGNETOPLASMADYNAMICS
Evaluation of externally heated pulsed MPD thruster cathodes
[NASA-CR-191090] p 1670 N94-21565

MAGNETORESISTIVITY
The effect of correlated and point defects on the vortex lattice melting transition in single crystal YBa2Cu3O(7-delta)
[DE93-040277] p 2033 N94-21997

MAGNETOSHEATH
Tangential stress due to Kelvin-Helmholtz instability at the magnetospheric boundary p 2003 N94-22651

MAGNETOSONIC RESONANCE
Formation of fast magnetosonic shock waves during two current loops collision in solar flare p 2005 N94-22662
Mean elemental composition and He-3 enrichments in solar energetic particles p 2006 N94-22670

MAGNETOSPHERE-IONOSPHERE COUPLING
Modeling of the coupled magnetospheric and neutral wind dynamos
[NASA-CR-194728] p 1856 N94-20537
Implications of Viking dayside auroral measurements
[ISBN-0-315-83273-8] p 1861 N94-22575

MAGNETOSTATICS
The best of GYMNOS: A users guide
[DE93-041275] p 1992 N94-19991

MAGNETRON SPUTTERING
Fundamental studies of defect generation in amorphous silicon alloys grown by remote plasma-enhanced chemical-vapor deposition
[DE93-017083] p 2029 N94-21615
Thin-film fabrication of Pb-doped BiSrCaCuO superconductor p 1781 N94-22176

MAGNETRONS
Observation of x ray absorption magnetic circular dichroism in well-characterized iron-cobalt-platinum multilayers
[DE94-000303] p 1694 N94-21944
Transmission electron microscopy study of thick copper-304 stainless steel multilayers
[DE94-001045] p 1696 N94-22394

MAGNETS
A summary of studies of particle stability at RHIC
[DE93-040173] p 1970 N94-19868
Survey and alignment analysis for the ALS storage ring using computer spreadsheets
[DE93-019254] p 1917 N94-21917

MAIN SEQUENCE STARS
The circumstellar environments of intermediate mass main sequence stars
[NASA-CR-189311] p 2055 N94-21498
VVNRS: Variable phenomena in VV Cephei
[NASA-CR-194731] p 2056 N94-21835

MAINTENANCE
Using electronic data interchange to report product quality
[AD-A271843] p 1828 N94-20468
Four-channel HF receiving antenna array simulator
[AD-A271876] p 1732 N94-20471
Engineering design, fabrication, installation, operation, and maintenance services in support of research on laser plasma physics
[AD-A272249] p 1994 N94-20943
N parallel queueing systems with server breakdown and repair
[CWI-BS-R9236] p 1944 N94-21232
Optimal repairman assignment in two maintenance models which are equivalent to routing models with early decisions
[CWI-BS-R9301] p 1930 N94-21234
Reducing the cognitive workload: Trouble managing power systems
[NASA-TM-106413] p 1714 N94-21564

MAMMALS
Physiologically based pharmacokinetic modelling of percutaneously absorbed dibromomethane utilizing multiple dermal sub-compartments
[AD-A271106] p 1889 N94-19981

MAN ENVIRONMENT INTERACTIONS
Global emissions and models of photochemically active compounds
[DE93-040490] p 1852 N94-21969

MAN MACHINE SYSTEMS
Research in image management and access
[NASA-CR-194797] p 1907 N94-20376
AIDA: A graphical interactive system, adapted to the user
[ETN-93-93792] p 1908 N94-21020
Aerospace medicine and biology: A continuing bibliography with indexes (supplement 383)
[NASA-SP-7011(383)] p 1892 N94-21288
Automating the control of robotic systems in unstructured environments
[DE93-040753] p 1946 N94-21929
Intervention strategies for the management of human error
[NASA-CR-4547] p 1642 N94-22373

MAN-COMPUTER INTERFACE
The Keck keyword layer p 1925 N94-22480
A distributed clients/distributed servers model for STARCAT p 2047 N94-22489
GRO/EGRET data analysis software: An integrated system of custom and commercial software using standard interfaces p 1926 N94-22501
Interactive Spectral Analysis and Computation (ISAAC) p 1926 N94-22505
GammaCore: The Compton Observatory research environment p 2048 N94-22509
XPI: The Xanadu Parameter Interface p 1927 N94-22513
Khoros software specification format and interoperability p 1927 N94-22523

MANAGEMENT ANALYSIS
Development of a naming convention and data ma nagement system
[NASA-CR-193860] p 2042 N94-20268

MANAGEMENT INFORMATION SYSTEMS
Using electronic data interchange to report product quality
[AD-A271843] p 1828 N94-20468
A conceptual database design and performance analysis of the MILSATCOM requirements database
[AD-A272672] p 1658 N94-21217
Three original programmes for managers p 1923 N94-22083

MANAGEMENT METHODS
Performance management systems: A statistical analysis
[AD-A272989] p 2043 N94-21266
An evaluation of artificial neural network modeling for manpower analysis
[AD-A273001] p 1945 N94-21269
The NCC project: A quality management perspective p 1828 N94-21324
Let your fingers do the walking: The projects most invaluable tool p 1922 N94-21325
NCCDS configuration management process improvement p 1931 N94-21327
Issues in NASA program and project management. Special Report: 1993 conference
[NASA-SP-6101(07)] p 2039 N94-21497
Issues in NASA program and project management
[NASA-SP-6101(06)] p 2040 N94-21499

MANAGEMENT PLANNING
Planning process software: A user guide for the DMCA
[AD-A271252] p 1902 N94-19911
Government Open Systems Interconnection Profile (GOSIP) transition strategy
[AD-A273005] p 1740 N94-21308
Models of transient processes in centrally planned economy p 2051 N94-22071
Three original programmes for managers p 1923 N94-22083

MANAGEMENT SYSTEMS
Data management for support of the Oregon Transect Ecosystem Research (OTTER) project
[NASA-CR-4557] p 1905 N94-20149
Development of a naming convention and data ma nagement system
[NASA-CR-193860] p 2042 N94-20268
Performance management systems: A statistical analysis
[AD-A272989] p 2043 N94-21266
Problem reporting management system performance simulation p 1931 N94-21328
Information and decision structure in a Japanese type of management with respect to QCC and just-in-time systems p 2046 N94-22063

MANGANESE
High performance heavy alloys by alloying and process control
[AD-A271129] p 1689 N94-20019
Chemical zoning and diffusion of Ca, Al, Mn, and Cr in olivine of springwater pallasite p 2066 N94-20902

MANGANESE COMPOUNDS
Fe/Mn in olivine of carbonaceous meteorites p 2084 N94-20788
Characterization of convection related defects in II-VI compound semiconductors
[NASA-CR-194704] p 2030 N94-21778

MANGANESE OXIDES
Cathode materials for the molten carbonate fuel cell
[DE93-019515] p 1848 N94-21870

MANIPULATORS
Application of change detection to dynamic contact sensing
[AD-A270523] p 1939 N94-20105
Teleoperation with virtual force feedback
[DE93-019406] p 1942 N94-20293
Development and testing of a reliability performance index for modular robotic systems
[AD-A271901] p 1942 N94-20488
Active damping of oscillations in a long compliant manipulator link
[DE93-018878] p 1826 N94-22038
A robust adaptive control design for flexible joint manipulators p 1790 N94-22230
Analytical representation of working articulation space of a plane manipulator in an encumbered environment p 1792 N94-22241
Control of multiple robot manipulators with optimal force distribution p 1794 N94-22255
Optimal control of the tip of a flexible arm p 1794 N94-22256
Dynamic analyses of flexible robotic manipulators
[ISBN-0-315-59251-6] p 1827 N94-22421
Robot link and contact surface dynamic interaction: An experimental study of contact instability
[ISBN-0-315-83439-0] p 1827 N94-22578

MANNED MARS MISSIONS
Mars exploration study workshop 2
[NASA-CP-3243] p 2146 N94-21883

MANNED SPACECRAFT
Entry velocities at Mars and Earth for short transit times
[AD-A272591] p 1665 N94-21420

MANPOWER
An evaluation of artificial neural network modeling for manpower analysis
[AD-A273001] p 1945 N94-21269

MANUALS
Publication of science data on CD-ROM: A guide and example
[NASA-CR-4560] p 1842 N94-21585
Everything you might want to know about the Internet but are afraid to ask!
[DE93-041118] p 2046 N94-22413

MANUFACTURING
Materials processing and manufacturing technologies for Diamond Substrate MultiChip Modules (DSMCM)
[AD-A271011] p 2011 N94-19821
Solder technology in the manufacturing of electronic products
[DE93-018842] p 1699 N94-19980
Using electronic data interchange to report product quality
[AD-A271843] p 1828 N94-20468
Non-destructive evaluation in manufacturing using spectroscopic ellipsometry p 1828 N94-21012
Optimization of static traffic allocation policies
[CWI-BS-R9302] p 1930 N94-21161
Materials processing and manufacturing technologies for diamond substrate multichip modules
[AD-A271484] p 2027 N94-21319
Improvement of the stability of the process for synthesizing chemically prepared varistor powder
[DE94-000345] p 1763 N94-21654
Modeling of glass fabrication p 1711 N94-21800
Proceedings of the IMOG (Interagency Manufacturing Operations Group) Numerical Systems Group
[DE94-001009] p 1917 N94-21851

MANY BODY PROBLEM
A microscopic theory of quantum optics and new photon-locked bistable states
[AD-A271250] p 1983 N94-19901
MAPPING
Topographic mapping using a monopulse SAR system p 1721 N94-20417
Performance evaluation of the JPL TOPSAR system: An across-track interferometric SAR system for topographic mapping p 1732 N94-20461
Ocean mapping using satellite radar altimetry
[ETN-93-93470] p 1841 N94-21017
Remote sensing for hydrology progress and prospects
[WMO-773] p 1841 N94-21069
MAPS
Detecting topographical regions in digital terrain maps
[AD-A272889] p 1841 N94-21453
MARINE ENVIRONMENTS
SIMA: An integrated environmental monitoring system p 1840 N94-20967
Estimating the rotation rate of mesoscale ocean rings from satellite altimetry
[AD-A272922] p 1883 N94-21222
Low-cost, dual-use platforms for environmental sensing, phase 1
[AD-A272951] p 1646 N94-21246
MARINE METEOROLOGY
The marine light-mixed layer experiment cruise and data report: R/V endeavor cruise EN-224, mooring deployment, 27 April-1 May 1991: Cruise EN-227, mooring recovery, 5-23 September 1991
[AD-A271175] p 1864 N94-20186
Scientific development of a massively parallel ocean climate model
[DE93-019446] p 1855 N94-20219
Four-dimensional remote sensing of the marine boundary layer with a digital beamforming radar wind profiler
[AD-A270627] p 1882 N94-20564
Low-cost, dual-use platforms for environmental sensing, phase 1
[AD-A272951] p 1646 N94-21246
NOVAM evaluation utilizing electro-optics and meteorological data from KEY-90
[AD-A271722] p 1868 N94-21356
Acoustic monitoring of global ocean variability
[AD-A271998] p 1883 N94-21366
MARINE TECHNOLOGY
SIMBAT theoretical manual
[AD-A271063] p 1882 N94-19979
MARINER 10 SPACE PROBE
Preliminary results from Mariner 10: High resolution images of the Moon p 2107 N94-20719
MARINER 9 SPACE PROBE
GMM-1: A 50 degree and order gravitational field model for Mars p 2117 N94-20774
MARKET RESEARCH
Wind energy: Program overview, FY 1992
[DE93-000056] p 1845 N94-19921
MARKOV CHAINS
Some topics in regenerative steady-state simulation
[AD-A271145] p 1902 N94-19855
Determination of the optimal stochastic upper bound of a Markovian generator
[RR-906-I] p 1963 N94-20202
Specification and generation of Markov reward models
[MEMO-INF-92-60] p 1963 N94-21058
Linear programming for standard and nonstandard Markovian control problems. A survey
[PB93-191948] p 1963 N94-21066
A multi-level solution algorithm for steady-state Markov chains
[NASA-CR-191558] p 1914 N94-21462
Dependability and performability analysis
[NASA-CR-191565] p 1965 N94-21463
Algorithms for Markov decision chains with partial information
[PB93-220085] p 1918 N94-22098
MARKOV PROCESSES
The effect of dissipative inhomogeneous medium on the statistics of the wave intensity p 1726 N94-20440
A semi-Markov model of a home network access protocol
[MEMO-INF-92-71] p 1909 N94-21045
Linear programming for standard and nonstandard Markovian control problems. A survey
[PB93-191948] p 1963 N94-21066
N parallel queueing systems with server breakdown and repair
[CWI-BS-R9236] p 1944 N94-21232
Throughput and blocking in circuit-switched interconnection networks p 1784 N94-22189
Speaker-independent isolated-digit recognition using neural networks and hidden Markov model p 1747 N94-22213
MARS (PLANET)
Constraints on the rate of discharge and duration of the Mangala Valles flood p 2099 N94-20674
GMM-1: A 50 degree and order gravitational field model for Mars p 2117 N94-20774
Expectations for the Martian core magnetic field p 2120 N94-20792
Workshop on Early Mars: How Warm and How Wet?, part 1
[NASA-CR-193553] p 2142 N94-21659
Ancient Martian valley genesis and paleoclimatic inference: The present as a key to the past p 2142 N94-21661
Mars: Noachian hydrology by its statistics and topology p 2143 N94-21664
The hydrologic response of Mars to the onset of a colder climate and to the thermal evolution of its early crust p 2143 N94-21666
An attempt to comprehend Martian weathering conditions through the analysis of terrestrial palagonite samples p 2143 N94-21668
Briny lakes on early Mars? Terrestrial intracrater playas and Martian candidates p 2145 N94-21675
Early Mars was wet but not warm: Erosion, fluvial features, liquid water habitats, and life below freezing p 2145 N94-21677
Wet inside and out? Constraints on water in the Martian mantle and on outgassed water, based on melt inclusions in SNC meteorites p 2145 N94-21678
MARS ATMOSPHERE
Balloon exploration of the northern plains of Mars near and north of the Viking 2 landing site p 2092 N94-20401
Workshop on Early Mars: How Warm and How Wet?, part 1
[NASA-CR-193553] p 2142 N94-21659
A carbon dioxide/methane greenhouse atmosphere on early Mars p 2142 N94-21662
The early Martian environment: Clues from the cratered highlands and the Precambrian Earth p 2143 N94-21667
Requirements for the early atmosphere of Mars from nitrogen isotope ratios p 2144 N94-21669
A model for the evolution of CO2 on Mars p 2144 N94-21671
Mars atmosphere loss and isotopic fractionation by solar-wind-induced sputtering and photochemical escape p 2144 N94-21672
Possible solutions to the problem of channel formation on early Mars p 2144 N94-21673
Early Mars was wet but not warm: Erosion, fluvial features, liquid water habitats, and life below freezing p 2145 N94-21677
The young Sun and photochemistry of the primitive Martian atmosphere p 2145 N94-21679
Evolution of the Martian atmosphere p 2146 N94-21680
MSATT Workshop on Innovative Instrumentation for the In Situ Study of Atmosphere-Surface Interactions on Mars
[NASA-CR-194584] p 1811 N94-22430
Determination of Martian soil mineralogy and water content using the Thermal Analyzer for Planetary Soils (TAPS) p 1812 N94-22433
Temperature/pressure and water vapor sounding with microwave spectroscopy p 1812 N94-22436
MARS CRATERS
Morphologic and morphometric studies of impact craters in the northern plains of Mars p 2089 N94-20384
Evidence for an ice sheet/frozen lake in Utopia Planitia, Mars p 2089 N94-20388
Ice in the northern plains: Relic of a frozen ocean? p 2090 N94-20391
A model for the origin of Martian polygonal terrain p 2090 N94-20393
Determination of cosmic bodies size-velocity distribution by observation of current impacts on Mars p 2082 N94-20648
Arcuate and circular structures in the Tharsis region: Evidence of coronae on Mars p 2134 N94-20863
Early Mars: A regional assessment of denudation chronology p 2145 N94-21676
MARS ENVIRONMENT
The fate of water deposited in the low-lying northern plains p 2089 N94-20387
K, U, and Th behavior in Martian environmental conditions p 2141 N94-20908
Workshop on Early Mars: How Warm and How Wet?, part 1
[NASA-CR-193553] p 2142 N94-21659
Mars: Noachian hydrology by its statistics and topology p 2143 N94-21664
The evolution of the early Martian climate and the initial emplacement of crustal H2O p 2143 N94-21665
The hydrologic response of Mars to the onset of a colder climate and to the thermal evolution of its early crust p 2143 N94-21666
The early Martian environment: Clues from the cratered highlands and the Precambrian Earth p 2143 N94-21667
Fluvial valleys in the heavily cratered terrains of Mars: Evidence for paleoclimatic change? p 2144 N94-21670
Possible solutions to the problem of channel formation on early Mars p 2144 N94-21673
Mars and the early Sun p 2146 N94-21683
MARS LANDING
Mars exploration study workshop 2
[NASA-CP-3243] p 2146 N94-21883
MARS OBSERVER
The thumbprint terrain: What will Mars Observer tell us? p 2091 N94-20397
MARS PHOTOGRAPHS
Geomorphic evidence for an eolian contribution to the formation of the Martian northern plains p 2092 N94-20402
MARS SURFACE
Workshop on the Martian Northern Plains: Sedimentological, Periglacial, and Paleoclimatic Evolution
[NASA-CR-194831] p 2088 N94-20382
Hydrological consequences of ponded water on Mars p 2089 N94-20383
Morphologic and morphometric studies of impact craters in the northern plains of Mars p 2089 N94-20384
Evidence for an ice sheet/frozen lake in Utopia Planitia, Mars p 2089 N94-20388
A wet-geology and cold-climate Mars model: Punctuation of a slow dynamic approach to equilibrium p 2090 N94-20389
Possible occurrence and origin of massive ice in Utopia Planitia p 2090 N94-20390
Ice in the northern plains: Relic of a frozen ocean? p 2090 N94-20391
Observed climatic activity pertaining to the evolution of the northern plains p 2090 N94-20392
A model for the origin of Martian polygonal terrain p 2090 N94-20393
The distribution of ground ice on Mars p 2090 N94-20394
A marine sedimentary model for the evolution of the northern plains p 2091 N94-20395
The thumbprint terrain: What will Mars Observer tell us? p 2091 N94-20397
Stratigraphy of the Martian northern plains p 2091 N94-20398
Seismic-triggering history of the catastrophic outflows in the Chryse region of Mars p 2091 N94-20399
A formational model for the polygonal terrains of Mars: Taking a crack at the genesis of the Martian polygons p 2091 N94-20400
Balloon exploration of the northern plains of Mars near and north of the Viking 2 landing site p 2092 N94-20401
Geomorphic evidence for an eolian contribution to the formation of the Martian northern plains p 2092 N94-20402
Determination of cosmic bodies size-velocity distribution by observation of current impacts on Mars p 2082 N94-20648
Constraints on the rate of discharge and duration of the Mangala Valles flood p 2099 N94-20674
Wavelength dependence of limb-darkening of Mars from visible and near-IR telescopic spectral imaging p 2101 N94-20685
Eruption history of the Tharsis shield volcanoes, Mars p 2102 N94-20692
Geology of Biblis Patera, Ulysses Patera, and Jovis Tholus, Mars p 2103 N94-20693
Thermal conductivity measurements of particulate materials under Martian conditions p 1685 N94-20703
Geologic mapping of Harmakhis and Reull Valles region, Mars: Evidence for multiple resurfacing and drainage events p 1844 N94-20705
Derivation of the midinfrared (5.0-25.0 micron) optical constants of hydrous carbonate and sulfate p 2108 N94-20723
Detectability of crystalline ferric and ferrous minerals on Mars p 2110 N94-20730
Local topography of Mars and its relationship to surface weathering processes p 2111 N94-20737
Mars: New evidence for origin of some Valles Marineris layered deposits p 2112 N94-20748
The roughness of the Martian surface: A scale dependent model p 2115 N94-20762
Extensional history of Mars' Tharsis Region p 2125 N94-20814
Complex structure of the Thaumasia region of Mars p 2125 N94-20815

Large, ancient, compressional structures on Mars
p 2125 N94-20816
Discharge rates in Ma'adim Vallis, Mars
p 2128 N94-20830
The parent magma of the Nakhla (SNC) meteorite: Reconciliation of composition estimates from magmatic inclusions and element partitioning
p 2085 N94-20836
Arcuate and circular structures in the Tharsis region: Evidence of coronae on Mars p 2134 N94-20863
A study of carbonates, sulfates, and phosphates using thermal emission spectroscopy p 1686 N94-20868
Spectral analysis of chemisorbed CO2 on Mars analog materials p 2140 N94-20900
Comparison of flank modification on Ascraeus and Arsia Montes volcanoes, Mars p 2140 N94-20903
K, U, and Th behavior in Martian environmental conditions p 2141 N94-20908
Wrinkle ridges, reverse faulting, and the depth penetration of lithospheric stress in lunae planum, Mars
p 2141 N94-20910
Possible flexural signatures around Olympus and Ascraeus Montes, Mars p 2142 N94-20911
Workshop on Early Mars: How Warm and How Wet?, part 1
[NASA-CR-193553] p 2142 N94-21659
Evolution of the global water cycle on Mars: The geological evidence p 2142 N94-21660
Ancient Martian valley genesis and paleoclimatic inference: The present as a key to the past
p 2142 N94-21661
A carbon dioxide/methane greenhouse atmosphere on early Mars p 2142 N94-21662
Oxidation of dissolved iron under warmer, wetter conditions on Mars: Transitions to present-day arid environments p 2143 N94-21663
Mars: Noachian hydrology by its statistics and topology p 2143 N94-21664
The evolution of the early Martian climate and the initial emplacement of crustal H2O p 2143 N94-21665
The hydrologic response of Mars to the onset of a colder climate and to the thermal evolution of its early crust
p 2143 N94-21666
The early Martian environment: Clues from the cratered highlands and the Precambrian Earth
p 2143 N94-21667
An attempt to comprehend Martian weathering conditions through the analysis of terrestrial palagonite samples p 2143 N94-21668
Fluvial valleys in the heavily cratered terrains of Mars: Evidence for paleoclimatic change?
p 2144 N94-21670
Briny lakes on early Mars? Terrestrial intracrater playas and Martian candidates p 2145 N94-21675
Early Mars: A regional assessment of denudation chronology p 2145 N94-21676
Early Mars was wet but not warm: Erosion, fluvial features, liquid water habitats, and life below freezing
p 2145 N94-21677
Wet inside and out? Constraints on water in the Martian mantle and on outgassed water, based on melt inclusions in SNC meteorites p 2145 N94-21678
Early Mars: The inextricable link between internal and external influences on valley network formation
p 2146 N94-21681
The Martian valley networks: Origin by niveo-fluvial processes p 2146 N94-21682
Mars exploration study workshop 2
[NASA-CP-3243] p 2146 N94-21883
MSATT Workshop on Innovative Instrumentation for the In Situ Study of Atmosphere-Surface Interactions on Mars
[NASA-CR-194584] p 1811 N94-22430
A Backscatter Moessbauer Spectrometer (BaMS) for use on Mars p 1811 N94-22431
Determination of Martian soil mineralogy and water content using the Thermal Analyzer for Planetary Soils (TAPS) p 1812 N94-22433
In situ identification of the Martian surface material and its interaction with the Martian atmosphere using DTA/GC p 1812 N94-22434
Mass spectrometer-pyrolysis experiment for atmospheric and soil sample analysis on the surface of Mars p 1812 N94-22435
Optical luminescence spectroscopy as a probe of the surface mineralogy of Mars p 1813 N94-22437

MARS VOLCANOES

Eruption history of the Tharsis shield volcanoes, Mars
p 2102 N94-20692
Geology of Biblis Patera, Ulysses Patera, and Jovis Tholus, Mars p 2103 N94-20693
Chronology, eruption duration, and atmospheric contribution of Apollinaris Patera, Mars
p 2108 N94-20720
Arcuate and circular structures in the Tharsis region: Evidence of coronae on Mars p 2134 N94-20863
Comparison of flank modification on Ascraeus and Arsia Montes volcanoes, Mars p 2140 N94-20903
Possible flexural signatures around Olympus and Ascraeus Montes, Mars p 2142 N94-20911

MARTENSITIC TRANSFORMATION

First principles calculations for analysis martensitic transformations
[DE94-000666] p 1695 N94-21964

MASERS

Observation of pressure ridges in SAR images of sea ice: Scattering theory and comparison with observations
p 1723 N94-20427

MASKING

X ray reflection masks: Manufacturing, characterization and first tests
[BONN-IR-92-31] p 1986 N94-21043

MASKS

Characterization and possible repair of defects in soft x ray projection lithography masks
[DE93-019147] p 1750 N94-20231

MASONRY

Microstructure in mortar: A summary of a new project of research p 1708 N94-21896

MASS DISTRIBUTION

Analysis and design of weight balancing system for laser velocimetry traverse
[AD-A271171] p 1816 N94-20546
Equilibrium models of mass distribution and collisional lifetimes of asteroids p 2086 N94-20877

MASS FLOW

System and method for cancelling expansion waves in a wave rotor
[NASA-CASE-LEW-15218-1] p 1801 N94-20588
Speed of sound data and related models for mixtures of natural gas constituents
[PB93-200822] p 1966 N94-21447

MASS RATIOS

Proof of stability of the hydrogen molecule
[PB93-221026] p 1977 N94-22271

MASS SPECTRA

Measurement of the B(+) and B(0) lifetimes
[DE93-019906] p 1969 N94-19814
Search for excited quarks in p(-p) collisions at the square root of s = 1.8 TeV
[DE93-019910] p 1975 N94-21840

MASS SPECTROMETERS

The laser and its applications on environment and biotechnology research
[DE94-000376] p 1820 N94-21957
Atmospheric sampling glow discharge ionization and triple quadrupole tandem mass spectrometry for explosives vapor detection
[DE93-040593] p 1852 N94-22004

MASS SPECTROSCOPY

Detailed structure study of an H2/N2O/Ar flame employing molecular beam mass spectrometry, laser spectroscopy, and modeling
[AD-A270720] p 1679 N94-20111
Hydrogen pickup and redistribution in alpha-annealed zircaloy-4
[DE93-018050] p 1689 N94-20182
Multielement analysis of interplanetary dust particles using TOF-SIMS p 2084 N94-20790
Analysis of semi-insulating bulk GaAs using glow discharge mass spectrometry
[AD-A273032] p 1682 N94-21435
On Plasma Edge Spectroscopy and Spectroscopic Studies of Impurity Densities and Impurity Transport
[IPF-92-2] p 1996 N94-21802
Plasma edge spectroscopy p 1996 N94-21803
Spectroscopic studies of impurity densities and impurity transport p 1997 N94-21804
Atmospheric sampling glow discharge ionization and triple quadrupole tandem mass spectrometry for explosives vapor detection
[DE93-040593] p 1852 N94-22004

MASS TRANSFER

Parameters affecting hydrogen chloride measurements
[AD-A271326] p 1851 N94-20025
Pressurization and expulsion of a flightweight liquid hydrogen tank
[NASA-TM-106427] p 1799 N94-20177
Heat transfer additives for absorption cooling system fluids
[PB93-202521] p 1714 N94-21426

MASSIVE STARS

New production mechanisms for unstable nuclei in stars, supernovae, and the big bang
[DE93-018627] p 2081 N94-21618
The formation of massive stars: A 30 Mo case study
[ISBN-0-315-83944-9] p 2081 N94-22593

MASSIVELY PARALLEL PROCESSORS

Scientific development of a massively parallel ocean climate model
[DE93-019446] p 1855 N94-20219
Fast data parallel polygon rendering
[DE93-040157] p 1929 N94-20279
Massively parallel computation of RCS with finite elements p 1726 N94-20437
Multi-CPU plasma fluid turbulence calculations on a CRAY Y-MP C90
[DE93-015425] p 1801 N94-20562
Multiple-fold clustered processor mesh array
p 1757 N94-21113
A novel VLSI processor architecture for supercomputing arrays p 1758 N94-21115
Analysis of multigrid methods on massively parallel computers: Architectural implications
p 1938 N94-21468
Visualization on massively parallel computers using CM/AVS
[DE93-040151] p 1936 N94-21746
The transition to massively parallel computing within a production environment at a DOE access center
[DE93-019155] p 1936 N94-21828
Scientific computing in the 1990ies: An astronomical perspective p 2057 N94-22440

MATERIALS RECOVERY

Substrate recovery of Mo-Si multilayer coated optics
[DE93-019610] p 1698 N94-19810
Plasma-chemical conversion of hydrogen sulfide into hydrogen and sulfur
[DE93-041167] p 1682 N94-21789

MATERIALS SCIENCE

Materials Science and Engineering
[DE93-040497] p 1675 N94-21530
Chemistry and materials science
[DE94-001449] p 2152 N94-21858

MATHEMATICAL LOGIC

Are types needed for natural language?
[PB93-191831] p 1949 N94-19997
Set theory and nominalisation, part 1
[PB93-191807-PT-1] p 1962 N94-20007
Set theory and nominalisation, part 2
[PB93-191815-PT-2] p 1962 N94-20008
Back and forth bisimulations on prime event structures
[RR-888-I-IMAG-124-LIFIA] p 1929 N94-20124
Explanation closure, action closure, and the Sandewall test suite for reasoning about change
[TR-440] p 1907 N94-20522
Proving run-time properties of general programs w.r.t. constructive negation
[CWI-CS-R9245] p 1909 N94-21025
Beta(sub k)-complete problems and greediness
[TR-455] p 1913 N94-21318
Procedural dynamic semantics, verb-phrase ellipsis, and presupposition
[CWI-CS-R9311] p 1914 N94-21495
Reasoning about update logic
[CWI-CS-R9312] p 1914 N94-21496
Changing preferences
[CWI-CS-R9310] p 1915 N94-21551

MATHEMATICAL MODELS

A Kirchhoff approach to seismic modeling and prestack depth migration
[AD-A271010] p 1854 N94-19820
SPICE macromodel for a 1-megawatt power MOSFET switch
[DE93-019415] p 1748 N94-19844
Performance potential of plasma thrusters: Arcjet and Hall thruster modeling
[AD-A271085] p 1667 N94-19847
Numerical modeling of fringing fields and their use for complex permittivity measurements at high frequencies
[AD-A270478] p 1966 N94-19917
Set theory and nominalisation, part 1
[PB93-191807-PT-1] p 1962 N94-20007
Set theory and nominalisation, part 2
[PB93-191815-PT-2] p 1962 N94-20008
Absorption heat pump for space applications
[NASA-CR-194693] p 1845 N94-20066
Cavitation modelling p 1668 N94-20079
Statistical object recognition
[AD-A270887] p 1962 N94-20113
Modeling of interactions between biosphere and atmosphere on the global scale
[NASA-CR-193423] p 1837 N94-20205
A breakdown model for the bipolar transistor to be used with circuit simulators
[DE93-019422] p 1750 N94-20218
Computational model of a magnetic modulator for copper lasers
[DE93-019603] p 1815 N94-20223
The CSIRO 9-level atmospheric general circulation model
[CSIRO-TP-26] p 1855 N94-20256
RCS Analysis of Plate Geometries, parts 1 and 2
[NASA-CR-194173] p 1717 N94-20269
High-frequency techniques for RCS prediction of plate geometries p 1717 N94-20270

A physical optics/equivalent currents model for the RCS of trihedral corner reflectors p 1717 N94-20271
Applying the INN model to the MaxClique [DE93-040137] p 1906 N94-20276
Feature-based tolerancing for intelligent inspection process definition [DE93-017984] p 1906 N94-20311
The life cycles of intense cyclonic and anticyclonic circulation systems observed over oceans [NASA-CR-194760] p 1865 N94-20353
Process for the homoepitaxial growth of single-crystal silicon carbide films on silicon carbide wafers [NASA-CASE-LEW-15223-1] p 2017 N94-20381
Seismic-triggering history of the catastrophic outflows in the Chryse region of Mars p 2091 N94-20399
A formational model for the polygonal terrains of Mars: Taking a crack at the genesis of the Martian polygons p 2091 N94-20400
Time-domain analysis of planar microstrip devices using a generalized Yee-algorithm based on unstructured grids p 1724 N94-20431
Retrieval of ice thickness from polarimetric SAR data p 1724 N94-20432
Synergism of active and passive microwave data for estimating bare surface soil moisture p 1727 N94-20444
Relationship of attenuation in a vegetation canopy to physical parameters of the canopy p 1729 N94-20450
Numerical modeling for an electric-field hyperthermia applicator p 1729 N94-20451
Application of the target decomposition theorem to a polarimetric random media model p 1730 N94-20453
Modeling the minimum energy state of the Earth's magnetotail [AD-A267984] p 1856 N94-20485
Theoretical and experimental study of the winding of a thin plastic film: The role of aerodynamic effects [ECL-93-04] p 1703 N94-20599
Hydrostatic/nonhydrostatic comparison with the MERCURE code on orographic flows [ETN-93-94603] p 1866 N94-20600
A comparison of calculated and measured rheological properties of crystallising lavas in the field and in the laboratory p 1862 N94-20690
Magellan vertical polarization radar observations p 1744 N94-20691
Asteroid collisions: Target size effects and resultant velocity distributions p 2063 N94-20729
Venus pancake dome formation: Morphologic effects of a cooling-induced variable viscosity during emplacement p 2110 N94-20732
Core formation by giant impacts: Conditions for intact melt region formation p 1863 N94-20833
Numerical modeling of impact erosion of atmospheres: Preliminary results p 2131 N94-20847
Recondensation in the early solar system: Physical conditions and source material p 2085 N94-20849
Diffusion-controlled magnesium isotopic fractionation of a single crystal forsterite evaporated from the solid state p 1686 N94-20855
Convex set and linear mixing model p 1844 N94-20888
Study of concentration-dependent dielectric properties of n-type GaAs using variable angle spectroscopic ellipsometry p 2024 N94-21002
Tight comparison bounds for the string prefix-matching problem [CWI-CS-R9250] p 1952 N94-21029
The correlated M/G/1 queue [CWI-BS-R9303] p 1943 N94-21032
Routing of freeway traffic: A discrete-time state space model and routing problems [CWI-BS-R9232] p 1944 N94-21033
Specification and generation of Markov reward models [MEMO-INF-92-60] p 1963 N94-21058
Computation of signal delays in RC networks p 1744 N94-21102
Application of molecular modeling to biological processing [AD-A272612] p 1974 N94-21185
Analysis of the effects of eurasian crustal and upper mantel structure on regional phases using broadband seismic data [AD-A272446] p 1858 N94-21206
An evaluation of artificial neural network modeling for manpower analysis [AD-A273001] p 1945 N94-21269
Forecasting technique of variations of the optical absorptivity of thermal control coatings under different simultaneous radiations p 1664 N94-21399
MINIFOLD: A kernel for a MANIFOLD-like coordination language [CWI-CS-R9252] p 1915 N94-21534
Derivation of a model of the exciter of a brushless synchronous machine [EUT-92-E-258] p 1761 N94-21538
Coupling of smooth particle hydrodynamics with PRONTO [DE93-019080] p 1915 N94-21539
Defect motion as the origin of the 1/f conductance noise in solids [EUT-92-E-259] p 2029 N94-21552
Survey of lift-fan aerodynamic technology [NASA-CR-177615] p 1646 N94-21592
Local uniform grid refinement and brine transport in porous media with inhomogeneities [CWI-NM-R9224] p 1803 N94-21609
Ultrafast gas switching experiments [DE93-019071] p 1762 N94-21634
Some evidence on determinants of fuel economy as a function of driving cycle and test type [DE93-019511] p 1825 N94-21637
Monitoring issues from a modeling perspective p 1868 N94-21640
Fluvial valleys in the heavily cratered terrains of Mars: Evidence for paleoclimatic change? p 2144 N94-21670
Mars atmosphere loss and isotopic fractionation by solar-wind-induced sputtering and photochemical escape p 2144 N94-21672
A methodology for quantifying uncertainty in models [DE93-040154] p 1916 N94-21747
Stochastic simulation for imaging spatial uncertainty: Comparison and evaluation of available algorithms [DE93-040058] p 1916 N94-21761
An analysis of pressure driven cross-flow through a long slot connecting two parallel channels [DE93-040181] p 1804 N94-21765
Radio and optical emission: Spectral shapes and breaks in GRB [NASA-CR-194763] p 2150 N94-21781
Modeling bristle lift-off in idealized brush seal configurations p 1655 N94-21797
Activities Report of the Institute of Applied Physics [ETN-93-93749] p 1966 N94-21798
Edge plasma experiments on CASTOR tokamak [IPPCZ-332] p 1997 N94-21816
Simulations of diffusion-reaction equations with implications to turbulent combustion modeling [NASA-CR-191536] p 1804 N94-21861
Empirical wind model for the middle and lower atmosphere. Part 2: Local time variations [NASA-TM-104592] p 1870 N94-21862
A quantitative model for interpreting nanometer scale hardness measurements of thin films [DE93-040601] p 2034 N94-22005
Information Technology and Economic Modelling [VTT-SYMP-135] p 2049 N94-22056
Mathematical modelling of economic systems p 2050 N94-22060
AJKA: An econometric macromodel for Finland p 2050 N94-22061
Macromodel of centrally planned economy p 2050 N94-22062
Models of transient processes in centrally planned economy p 2051 N94-22071
Multicriteria optimisation problem in the agricultural modelling p 1844 N94-22073
A model of negotiation in an extensive form game p 1965 N94-22075
APL-technology of computer simulation p 1923 N94-22077
Microdynamic model of reproduction: Taxation and currency issue as regulators of economy p 2053 N94-22084
Use of economic models in Finnish economic policy p 2053 N94-22085
Experiences of the bank of Finland's econometric simulation model p 2053 N94-22086
Full wave numerical model of arbitrarily-shaped proximity coupled microstrip antennas p 1745 N94-22137
Modeling of coaxial-fed microstrip patch antenna by finite difference time domain method p 1745 N94-22138
Formulation for numerical solution of radiation and transmission from arbitrary apertures p 1745 N94-22140
Effect of errors on the phase centre and pointing angle of phased array antennas p 1746 N94-22162
A simplified method for S-parameter calculations of metal septum waveguide filters p 1782 N94-22180
Transient acoustic wave modeling: Higher-order WKBJ asymptotics and symbolical manipulation (revised) [PB93-215432] p 1969 N94-22262
The logistic model: The integration of business process redesign and information systems development based on logistic principles [MEMO-INF-92-70] p 2045 N94-22276
A thermodynamic analysis of propagating subcritical cracks with cohesive zones p 1834 N94-22611
Brief summary of the evolution of high-temperature creep-fatigue life prediction models for crack initiation p 1834 N94-22613

MATHEMATICAL PROGRAMMING
MGD1M: A parallel multigrid code with a fast vectorized ILU-relaxation [CWI-NM-R9222] p 1930 N94-21077
Parallelizing a highly vectorized multigrid code with zebra relaxation [CWI-NM-R9225] p 1935 N94-21610

MATHEMATICS
Mathematics B for the study direction VWO: A reconnaissance [REPT-92-80] p 1950 N94-20032

MATRICES (MATHEMATICS)
Segmented operations for sparse matrix computation on vector multiprocessors [AD-A270601] p 1928 N94-19950
Determination of the optimal stochastic upper bound of a Markovian generator [RR-906-I] p 1963 N94-20202
On the numerical stability of quasi-definite systems [DE93-019404] p 1950 N94-20217
Parallel band reduction and tridiagonalization [DE93-019566] p 1951 N94-20221
Numerical ranges and stability estimates [TW-92-10] p 1953 N94-21060
Method for design rotation [AD-A272440] p 1911 N94-21204
A new matrix formulation of classical electrodynamics. Part 3: Wave propagation through a multilayer dielectric medium with planar boundaries [AD-A271610] p 1739 N94-21240
Using parallel banded linear system solvers in generalized eigenvalue problems [NASA-CR-191540] p 1915 N94-21584
The quantum structure of matter grand challenge project: Large-scale 3-D solutions in relativistic quar.tum dynamics [DE94-000328] p 1960 N94-21955
A sharp upper bound for departure from normality [DE93-040457] p 1960 N94-21966
Column reduced rational matrix functions with given null-pole data in the complex plane [PB93-220531] p 1960 N94-22099
Integration of parallel processing structures using a matrix approach p 1784 N94-22192
Registering and resampling images in STSDAS p 1927 N94-22550

MATRIX MATERIALS
Composite materials with improved properties in compression [AD-A272837] p 1675 N94-21176
Thermal stability relationships between PMR-15 resin and its composites [NASA-TM-106285] p 1675 N94-21488

MAXIMA
On multiflow problems [RR-889-M] p 1950 N94-20125

MAXIMUM ENTROPY METHOD
Optimal resolution in maximum entropy image reconstruction from projections with multigrid acceleration p 1955 N94-21465
DECONV-TOOL: An IDL based deconvolution software package p 1927 N94-22542
First MEM task IRMEO in IRAF p 1928 N94-22551

MAXIMUM LIKELIHOOD ESTIMATES
Parameter estimation with cost function of second order in output-error-problem [DLR-FB-92-38] p 1964 N94-21139
DECONV-TOOL: An IDL based deconvolution software package p 1927 N94-22542

MAXWELL EQUATION
Analysis of microstrip dipoles and slots transversely coupled to a microstrip line using the FDTD method p 1718 N94-20405
FD-TD modeling of 2-D dielectric waveguides for propagation and scattering of femtosecond optical solitons p 1719 N94-20406
Time-domain analysis of planar microstrip devices using a generalized Yee-algorithm based on unstructured grids p 1724 N94-20431
Modeling the minimum energy state of the Earth's magnetotail [AD-A267984] p 1856 N94-20485
A new matrix formulation of classical electrodynamics. Part 3: Wave propagation through a multilayer dielectric medium with planar boundaries [AD-A271610] p 1739 N94-21240
Characteristic based methods for the time-domain Maxwell equations [AD-A272973] p 1802 N94-21263
Detailed analysis case studies of trapped plasmas at the Earth's magnetic equator [AD-A272497] p 1858 N94-21432

MEAN SQUARE VALUES
Likelihood analysis of parity violation in the compound nucleus [DE94-000671] p 1977 N94-22572

MEASURING INSTRUMENTS
Charge collectors for the omega upgrade
[DE93-019684] p 1972 N94-20264
Enhanced software for the GT1022 automated gaging system
[DE94-001374] p 1918 N94-21977
Acoustic, fiber optic, and silicon microelectronic microsensors research and development activities at Sandia National Laboratories
[DE93-019075] p 1770 N94-22040
Writing instrument interfaces with xf/tktcl
p 1925 N94-22480

MECHANICAL DRIVES
Experimental investigation of nozzle/plume aerodynamics at hypersonic speeds
[NASA-CR-194628] p 1636 N94-20014
Long range fast tool servo
[AD-A271614] p 1761 N94-21257

MECHANICAL ENGINEERING
Production of NiAl and TiAl intermetallics by mechanical alloying
[VTT-JULK-760] p 1691 N94-20530
Computational and analytical methods in nonlinear fluid dynamics
[AD-A272722] p 1802 N94-21169

MECHANICAL MEASUREMENT
High accuracy die mechanical stress measurement with the ATC04 Assembly Test Chip
[DE93-019435] p 1830 N94-20477

MECHANICAL PROPERTIES
Dynamic, multiaxial impact response of confined and unconfined ceramic rods
[DE93-040057] p 1829 N94-19824
Characterization studies of lower and non-TDI polyurethane encapsulants
[DE93-041129] p 1698 N94-19857
High performance heavy alloys by alloying and process control
[AD-A271129] p 1689 N94-20019
Fundamentals of mechanical behavior in structural intermetallics: A synthesis of atomistic and continuum modeling
[DE93-019166] p 1690 N94-20232
Properties and potential of high-temperature niobium beryllides
[DE93-019169] p 1690 N94-20233
Direct imaging of the surface microstructure of dielectric materials using an atomic force microscope
[AD-A272251] p 2018 N94-20575
Mechanical properties and reliability of semi-crystalline polymers
[AD-A271591] p 1704 N94-20946
Issues related to mechanical properties of neutron-irradiated ceramics
[DE93-040262] p 1707 N94-21560
Molecular dynamics modeling of the mechanical behavior of metallic multilayers
[DE93-019947] p 1694 N94-21921
Strengthening and toughening in refractory metal alloys
[DE93-019942] p 1695 N94-21986
Tensile strength of fiber reinforced plastics at 77K irradiated by various radiation sources
[DE93-040826] p 1709 N94-22008

MECHANICAL SHOCK
U.S. Tag for ISO/TC 43, acoustics, IEC/TC 29 electroacoustics, and ISO/TC 108/SC4 human exposure to mechanical vibration and shock: Minutes of the accredited standards committee on bioacoustics, S3
[AD-A273014] p 1897 N94-21309

MEDICAL ELECTRONICS
Journal of rehebilitation research and development, volume 30, number 1, 1993
[AD-A272956] p 1893 N94-21613

MEDICAL EQUIPMENT
Numerical modeling for an electric-field hyperthermia applicator p 1729 N94-20451

MELT SPINNING
Melt-spin processing of high (Tc) oxide superconductors
[DE94-000696] p 2036 N94-22582

MELTING
Orthopyroxenes as recorders of diogenite petrogenesis: Trace element systematics p 1686 N94-20760
Origin of high-Ti lunar ultramafic glasses
p 1686 N94-20853
Ancient Martian valley genesis and paleoclimatic inference: The present as a key to the past
p 2142 N94-21661
The Martian valley networks: Origin by nivео-fluvial processes p 2146 N94-21682
Modeling of glass fabrication p 1711 N94-21800
The incongruent melting and melt textured solidification process of Bi2Sr2CaCu3O8
[DE93-041123] p 2032 N94-21936
The effect of correlated and point defects on the vortex lattice melting transition in single crystal YBa2Cu3O(7-delta)
[DE93-040277] p 2033 N94-21997
Shock temperature measurements of iron to 350 GPa
[DE94-001058] p 1695 N94-22024
First-principles pressure-temperature phase diagrams in metals
[DE94-001056] p 1696 N94-22398

MELTING POINTS
High performance heavy alloys by alloying and process control
[AD-A271129] p 1689 N94-20019
The incongruent melting and melt textured solidification process of Bi2Sr2CaCu3O8
[DE93-041123] p 2032 N94-21936
Shock temperature measurements of iron to 350 GPa
[DE94-001058] p 1695 N94-22024

MELTS (CRYSTAL GROWTH)
Frequency dependent electrical properties of minerals and partial-melts
[DE93-019918] p 2012 N94-19861
Evaporation of a sodium tellurite melt in the jamic low gravity drop shaft p 1713 N94-20605
The incongruent melting and melt textured solidification process of Bi2Sr2CaCu3O8
[DE93-041123] p 2032 N94-21936

MEMBRANE STRUCTURES
Electrochemical synthesis of ultrathin film composite membranes
[AD-A272721] p 1681 N94-21168

MEMBRANES
Lateral distribution of lipids in membranes at high pressure
[AD-A271183] p 1700 N94-20299
High temperature size selective membranes
[DE93-019865] p 1709 N94-21982

MEMORY
Research, Development, Training, and Evaluation (RDTE) support delivery order 1: Computational cognitive models
[AD-A271837] p 1894 N94-20610

MEMORY (COMPUTERS)
A novel method for characterizing the electrical Priorities of lead Zirconate Titanate (PZT) ferroelectric films and memory devices
[AD-A270463] p 2013 N94-19966
A methodology for formal hardware verification, with application to microprocessors
[AD-A270550] p 1898 N94-20085
Mint tutorial and user manual
[TR-452] p 1905 N94-20143
Memory contention in scalable cache-coherent multiprocessors
[TR-448] p 1929 N94-20144
Single-event upset testing of the performance semiconductor 1750A CMOS/SOS chip set
[AD-A271158] p 2015 N94-20184
DISCERN: A distributed neural network model of script processing and memory p 1941 N94-20255
Optoelectronic associative memory
[NASA-CASE-NPO-18278-1-CU] p 1985 N94-20303
M-dimensional computer memory with M-1 dimensional hyperplane access
[AD-D015960] p 1898 N94-20357
Measuring the effects of thread placement on the Kendall Square KSR1
[DE93-040655] p 1908 N94-20932
Avoiding and tolerating latency in large-scale next-generation shared-memory multiprocessors
p 1753 N94-21081
Test results for SEU and SEL immune memory circuits
p 1754 N94-21087
An ASIC memory buffer controller for a high speed disk system p 1754 N94-21089
A CAM-based LZ data compression IC
p 1759 N94-21129
The effects of block size on the performance of coherent caches in shared-memory multiprocessors
[AD-A272638] p 1899 N94-21177
Fast mutual exclusion, even with contention
[AD-A272947] p 1912 N94-21227
Software coherence in multiprocessor memory systems
[NASA-CR-194696] p 1931 N94-21272
High dimension action spaces in robot skill learning
[TR-458] p 1945 N94-21317
A simple modern correctness condition for a space-based high-performance multiprocessor
p 1766 N94-21718
Detection of feed-through faults in CMOS storage elements p 1766 N94-21721
A novel cache mechanism p 1767 N94-21730
A set-associative, fault-tolerant cache design
p 1768 N94-21731
The quantum structure of matter grand challenge project: Large-scale 3-D solutions in relativistic quantum dynamics
[DE94-000328] p 1960 N94-21955
The design of linear algebra libraries for high performance computers
[DE93-040458] p 1960 N94-21967
Efficient communication primitives on mesh architectures with hardware routing
[DE93-018791] p 1936 N94-22032
Reverse automatic differentiation of modular FORTRAN programs
[DE94-000336] p 1918 N94-22088
Crystal ball gazing p 1925 N94-22477

MENTAL HEALTH
Incongruity, incongruity resolution, and mental states: The measure and modification of situational awareness and control
[NASA-CR-194568] p 1893 N94-20168

MENTAL PERFORMANCE
Development of the UTC-PAB normative database
[AD-A271319] p 1683 N94-20023
Incongruity, incongruity resolution, and mental states: The measure and modification of situational awareness and control
[NASA-CR-194568] p 1893 N94-20168
Cognition and the brain: A continuation of the university research initiative at New York University
[AD-A271872] p 1894 N94-20467
Compatibility evaluation and research on the Computerized Adaptive Screening Test (CAST): User and programmer's guide
[AD-A273112] p 1894 N94-21510

MERCURY CADMIUM TELLURIDES
Theory of energy-assisted epitaxy; theory of ordered semiconductor alloys: In(1-x)Tl(x)Sb as a long-wave infrared material
[AD-A271007] p 2012 N94-19835
The quantum efficiency of HgCdTe photodiodes in relation to the direction of illumination and to their geometry p 1735 N94-20512
IR materials producibility
[AD-A273031] p 1987 N94-21321

MERCURY COMPOUNDS
X ray analysis of alpha mercuric iodide crystal structure and processing effects
[DE93-017620] p 2027 N94-21296

MERCURY LAMPS
Process to fabricate thick coplanar microwave electrode structures
[AD-D015913] p 1748 N94-19892

MERCURY TELLURIDES
Characterization of convection related defects in II-VI compound semiconductors
[NASA-CR-194704] p 2030 N94-21778

MERGING ROUTINES
Tests of a simple data merging algorithm for the GONG project p 1927 N94-22549

MERIDIONAL FLOW
Empirical wind model for the middle and lower atmosphere. Part 2: Local time variations
[NASA-TM-104592] p 1870 N94-21862

MERRITT ISLAND (FL)
An in-depth analysis and modelling of the Shuttle to MILA S-band telemetry link p 1657 N94-21340

MESAS
Geologic mapping of Harmakhis and Reull Valles region, Mars: Evidence for multiple resurfacing and drainage events p 1844 N94-20705

MESOMETEOROLOGY
Clouds: Their prediction and simulation
[AD-A271161] p 1864 N94-19900
Incorporation and comparative evaluation of a non-convective cloud parameterization scheme in the Naval Research Laboratory west coast mesoscale weather prediction model
[AD-A272417] p 1867 N94-21146
Mesoscale simulations of the November 25-26 and December 5-6 cirrus cases using the RAMS model
p 1878 N94-22331
A comparison of small and larger mesoscale latent heat and radiative fluxes: December 6 case study
p 1879 N94-22335

MESONS
Measurement of the B(+) and B(0) lifetimes
[DE93-019906] p 1969 N94-19814
The cross section for the production of b(bar-b) pairs in p(bar p) collisions at the square root of s equals 1.8 TeV
[DE93-019900] p 1972 N94-20225
Recent results on top, bottom and exotic physics at the Tevatron
[DE94-000578] p 1975 N94-21786

Measurement of the B meson and b quark cross-section in (-p)p collisions at the square root of s = 1.8 TeV using the exclusive decays B(+) and B(exp 0) yields J/psiK*(exp 0)
[DE93-019907] p 1975 N94-21806

MESOSCALE PHENOMENA
Clouds: Their prediction and simulation
[AD-A271161] p 1864 N94-19900
Incorporation and comparative evaluation of a non-convective cloud parameterization scheme in the Naval Research Laboratory west coast mesoscale weather prediction model
[AD-A272417] p 1867 N94-21146
Estimating the rotation rate of mesoscale ocean rings from satellite altimetry
[AD-A272922] p 1883 N94-21222
Development and tests of a cloud physics parameterization for real-time aviation and public numerical weather forecasting
[PB93-202711] p 1868 N94-21427
Cloud fields derived from satellite and surface data during FIRE cirrus phase 2 p 1872 N94-22302
Analysis of the GOES 6.7 micrometer channel observations during FIRE 2 p 1875 N94-22316
Three dimensional modeling of cirrus during the 1991 FIRE IFO 2: Detailed process study p 1877 N94-22327
Cirrus cloud development in a mobile upper tropospheric trough: The November 26th FIRE cirrus case study p 1878 N94-22329
A comparison of small and larger mesoscale latent heat and radiative fluxes: December 6 case study p 1879 N94-22335
Development of advanced cloud parameterizations to examine air quality, cloud properties, and cloud-radiation feedback in mesoscale models
[DE93-041164] p 1853 N94-22384

MESOSPHERE
Measurement of mesospheric turbulence in the framework of the metal campaign and development of a sensor for static pressure free measurements of neutral and electron density
[BONN-IR-92-45] p 1857 N94-21149

MESSAGE PROCESSING
ATC/pilot voice communications: A survey of the literature
[DOT/FAA/AM-93/20] p 1738 N94-21201
Using manufacturing message specification for monitor and control at Venus p 1932 N94-21333
Developing a space network interface simulator: The NTS approach p 1933 N94-21343
A self-defining hierarchical data system p 2046 N94-22448
The Keck Task Library (KTL) p 2048 N94-22504

MESSAGES
Ground wave emergency network. Final operational capability. Environmental assessment for south central Montana relay node, site no. RN8C925MT
[AD-A267795] p 1716 N94-19964
The data acquisition system for the Anglo-Australian Observatory 2-degree field project p 2048 N94-22529

METAL AIR BATTERIES
Advanced batteries for electric vehicle applications: Nontechnical summary
[DE93-019007] p 1748 N94-19885

METAL BONDING
Cratering evaluations and results
[DE93-040347] p 1691 N94-20478
Transferable tight-binding parameters: An application to Ni and Ni-Al alloys
[DE94-001044] p 1695 N94-22023
Interface science of controlled metal/metal and metal/ceramic interfaces prepared using ultrahigh vacuum diffusion bonding
[DE94-001066] p 1696 N94-22025
Strength, ultrasonic and metallurgical evaluation of diffusion bonds
[DE94-000665] p 1697 N94-22571

METAL CLUSTERS
Neutral copper cluster sputtering yields: Ne(+), Ar(+) and Xe(+) bombardment
[DE93-019010] p 1690 N94-20288

METAL COATINGS
Silver lined ceramic vessel
[AD-D015917] p 1700 N94-20057
Field emitter array RF amplifier development project, phase 1, option 1
[AD-A272567] p 1740 N94-21361

METAL FATIGUE
Results of the second Round Robin on opening-load measurement conducted by ASTM Task Group E24.04.04 on crack closure measurement and analysis
[NASA-TM-109032] p 1832 N94-21624
A high temperature fatigue life prediction computer code based on the total strain version of StrainRange Partitioning (SRP) p 1835 N94-22620

METAL FILMS
The Coulomb anomaly in strongly disordered films
[AD-A271095] p 2012 N94-19849
Microscopic origins of metastable effects in a-Si:H and deep defect characterization in a-Si,Ge:H alloys
[DE93-018205] p 1688 N94-19985
Magnetic circular dichroism in x ray absorption and core-level photoemission
[DE93-019381] p 1688 N94-19986
Study of mechanisms for long wavelength Schottky-barrier infrared detectors
[AD-A270538] p 1971 N94-20083
The metallic bond for monolayer transition metal layers on transition metal surfaces
[DE93-019060] p 1691 N94-20313
High temperature stability of amorphous Ta(x)Cu(1-x) diffusion barriers on GaAs p 2022 N94-20990
Amorphous Ta-rich Ta-Cu films as diffusion barriers between Au and GaAs p 1710 N94-20991
Growth, characterization and device development in monocrystalline diamond films
[AD-A272715] p 2026 N94-21190
Shock temperature measurements of iron to 350 GPa
[DE94-001058] p 1695 N94-22024

METAL FLUORIDES
Optical properties of chromium and neodymium in zirconium - barium - lanthanum - aluminum fluoride glass
[AD-A271609] p 1987 N94-21236

METAL HYDRIDES
Current status of environmental, health, and safety issues of nickel metal-hydride batteries for electric vehicles
[DE93-017079] p 1748 N94-19902
High-power gas switch with hydride electrodes
[AD-D015956] p 1751 N94-20354

METAL IONS
Formation of colloidal Ag precipitates in fused silica by MeV ion implantation
[DE93-040268] p 2012 N94-19869
A process for preparing an assembly of an article and a soluble polyimide which resists dimensional change, delamination, and debonding when exposed to changes in temperature
[NASA-CASE-LAR-14763-1] p 1702 N94-20373
Shattering the myth of the resonantly photo-pumped neon-like titanium laser
[DE93-019624] p 1819 N94-21873
High oxygen pressure synthesis of new copper oxide superconductors
[DE93-040278] p 2033 N94-21998
Miniaturized disk-bend testing, nano-indentation, and the microstructure of ion-irradiated titanium aluminides
[DE93-040600] p 1697 N94-22559

METAL MATRIX COMPOSITES
The Seventh International Conference on Composite Structures, volume 25, numbers 1-4
[AD-A269961] p 1672 N94-20031
Metal-glass composite field-emitting arrays
[AD-D015942] p 1673 N94-20064
Strengthening of NiAl matrix composites
[AD-A271491] p 1674 N94-20550
Strength and toughness improvement of silicide intermetallics by nanophase and microphase reinforcements
[AD-A272914] p 1692 N94-21320
Analysis of thermal mechanical fatigue in titanium matrix composites p 1835 N94-22618

METAL NITRIDES
Surface states at the GaAs-germanium nitride interface p 1709 N94-20973

METAL OXIDE SEMICONDUCTORS
Modeling failure and reliability in new-generation devices
[AD-A271150] p 1748 N94-19910
Simple method to estimate MOS oxide-trap, interface-trap, and border-trap densities
[DE93-041138] p 2032 N94-21939

METAL PARTICLES
Preliminary AEM study of the microstructure and composition of metal particles in ordinary chondrites p 2086 N94-20894

METAL PLATES
Thermal information regarding the cooldown and operation of liquid argon calorimeters
[DE93-019391] p 1807 N94-19987
Numerical simulations of hypervelocity impact experiments involving single Whipple bumper shields
[AD-A272123] p 1831 N94-20572
A simplified method for S-parameter calculations of metal septum waveguide filters p 1782 N94-22180

METAL POWDER
Metastable bcc phase formation in the Nb-Cr system
[DE93-018376] p 2012 N94-19926
Shock response of porous Al-2 + Fe2O3 powder mixtures
[DE93-018851] p 1688 N94-19944
Transmission electron microscopy study of thick copper-304 stainless steel multilayers
[DE94-001045] p 1696 N94-22394

METAL PROPELLANTS
Powdered aluminum and oxygen rocket propellants: Subscale combustion experiments
[NASA-TM-106439] p 1713 N94-21760

METAL SURFACES
Segregation of Si to the surface of Fe-29Ni-17Co alloy
[DE93-040053] p 1687 N94-19864
The metallic bond for monolayer transition metal layers on transition metal surfaces
[DE93-019060] p 1691 N94-20313
In-situ electrochemical surface science
[AD-A265942] p 1680 N94-20330
Surface electrochemistry of metals
[AD-A272913] p 1691 N94-21245
Vapor-delivered lubrication of steel-steel and steel-ceramic systems
[PB93-202364] p 1825 N94-21451
Laser Raman and x ray scattering studies of corrosion films on metals
[DE93-040243] p 1692 N94-21558
Inelastic electron scattering from surfaces
[DE94-001738] p 1977 N94-22049

METAL VAPOR LASERS
Computational model of a magnetic modulator for copper lasers
[DE93-019603] p 1815 N94-20223
High-power copper vapor lasers and their application to precision drilling and cutting
[DE93-019951] p 1819 N94-21844

METAL VAPORS
Impact of copper vapour contamination on argon arcs p 1994 N94-21053

METAL-GAS SYSTEMS
Evaluation of a diffusion/trapping model for hydrogen ingress in high-strength alloys
[AD-A271328] p 1689 N94-20027

METALLIZING
Adhesive electroless metallization of fluoropolymeric substrates
[AD-A271858] p 1703 N94-20526
Diagnostics and methods for real-time laser microchemistry
[AD-A270871] p 1680 N94-20566
Direct imaging of the surface microstructure of dielectric materials using an atomic force microscope
[AD-A272251] p 2018 N94-20575

METALLOGRAPHY
Investigation of cracking and erratic behavior of the uranium-titanium alloy
[DE93-018591] p 1688 N94-19957

METALLURGY
The use of backscattered electron imaging mode to assess the effect of fine dispersions on development of superplastic microstructure in Al-Mg alloys
[AD-A272426] p 1691 N94-21258

METALORGANIC CHEMICAL VAPOR DEPOSITION
Development of high-efficiency CdTe solar cells
[DE93-018206] p 1845 N94-19925
Common Themes and Mechanisms of Epitaxial Growth, volume 312 --- Materials Research Society symposium proceedings
[AD-A270513] p 2013 N94-19967
Alumoxanes: Rationalization of black box materials
[AD-A272805] p 1704 N94-21170
The n-p(p(+))-n Al(yGa)(1-y) As-GaAs-In(x)Ga(1-x) as quantum well laser with p(+)-n(+)GaAs-InGaAs tunnel contact on n GaAs
[AD-A271292] p 2030 N94-21805
MOCVD growth and structure of PbTiO3 thin films
[DE93-040230] p 2033 N94-21994

METALS
General introduction to microstructural evolution under cascade damage conditions
[DE93-017443] p 2012 N94-19923
Lewis Cliff 87057: A new metal-rich E3 chondrite with similarities to Mt. Egerton, Shallowater and Happy Canyon p 2086 N94-20901
Utilization of metals to improve the lubrication of ceramic load-bearing devices
[PB93-202448] p 1825 N94-21424
Electron emission from nanometer-size metallic clusters: Electronic states and structural stability of supported Au clusters
[DE93-040184] p 1975 N94-21766
Theoretical studies of structural phase transitions in actinide metals
[DE94-000796] p 1696 N94-22388

METAMORPHISM (GEOLOGY)
Fragments of ancient lunar crust: Ferroan noritic anorthosites from the descartes region of the Moon p 2096 N94-20660

Orthopyroxenes as recorders of diogenite petrogenesis: Major and minor element systematics
p 1684 N94-20670
Lamellar olivine in the Divnoe achondrite: Evidence for high-pressure exsolution? p 1685 N94-20679
Chaunskij: The most highly metamorphosed, shock-modified and metal-rich mesosiderite
p 2082 N94-20681
Post-igneous redistribution of components in eucrites
p 1685 N94-20684
Micrometeorite dynamic pyrometamorphism: Nonstoichiometric clinoenstatite (CLEN)
p 2083 N94-20715
Euhedral metallic-Fe-Ni grains in extraterrestrial samples p 1697 N94-20724
Post-metamorphic brecciation in type 3 ordinary chondrites p 2083 N94-20749
Petrography of shock features in the 1953 Manson 2-A drill core p 1862 N94-20767
FE-60 and the evolution of eucrites
p 2083 N94-20768
Fine resolution chronology based on initial Sr-87/Sr-86
[CONTRIB-5230(794)] p 1686 N94-20794
Original size of the Vredefort structure, South Africa
p 1863 N94-20825
Shock attenuation at the Slate Islands revisited
p 1863 N94-20887
Chemical composition of new Acapulcoites and Lodranites p 2086 N94-20905

METASTABLE STATE

A microscopic theory of quantum optics and new photon-locked bistable states
[AD-A271250] p 1983 N94-19901
Metastable bcc phase formation in the Nb-Cr system
[DE93-018376] p 2012 N94-19926
Microscopic origins of metastable effects in a-Si:H and deep defect characterization in a-Si,Ge:H alloys
[DE93-018205] p 1688 N94-19985
Phonons and metastability in compressed nitrogen
[DE93-019913] p 2016 N94-20318
Theoretical investigations of metastability and energy storage in molecular systems
[AD-A271849] p 1973 N94-20612
The stability of oxyamphiboles: Existence of Ferric-bearing minerals under the reducing conditions on the surface of Venus p 2122 N94-20800
Reliable interface design for combining asynchronous and synchronous circuits p 1758 N94-21119
Electronically metastable molecules of high symmetry
[AD-A272015] p 1974 N94-21461
Polymeric nitrogen
[DE93-040544] p 1706 N94-21512

METATHESIS

Rotational isomers of Mo(VI) alkylidene complexes and Cis/trans polymer structure: Investigations in ring-opening metathesis polymerization
[AD-A272647] p 1704 N94-21184
Photochemical approaches to conversion of light to electricity or fuel
[DE94-001650] p 1849 N94-22048

METEORITE COLLISIONS

Impact glasses from the ultrafine fraction of lunar soils
p 2097 N94-20662
Global blackout following the K/T Chicxulub impact: Results of impact and atmospheric modeling
p 1854 N94-20698
Impact disturbance of the Venus atmosphere
p 2106 N94-20709
Euhedral metallic-Fe-Ni grains in extraterrestrial samples p 1697 N94-20724
Chicxulub impact basin: Gravity characteristics and implications for basin morphology and deep structure
p 1862 N94-20757
Chronology of lunar granite 12033,576: Resetting of Rb-Sr and K-Ca isochrons p 2115 N94-20763
Multivariate statistical analysis: Principles and applications to coorbital streams of meteorite falls
p 1964 N94-20881
LREE variability in CM matrices: Another look at meteorite compaction ages p 2086 N94-20884
Geometrical analysis of the microcraters found on LDEF samples p 1666 N94-20890

METEORITE CRATERS

Twenty-Fourth Lunar and Planetary Science Conference. Part 3: N-Z
[NASA-CR-193149] p 2092 N94-20636
Largest impact features on Venus: Non-preserved or non-recognizable? p 2096 N94-20657
Modelling the gravity and magnetic field anomalies of the Chicxulub crater p 1862 N94-20668
Structural evidence for reorientation of Miranda about a paleo-pole p 2098 N94-20671
U-Pb provenance ages of shocked zircons from the K-T boundary, Raton Basin, Colorado p 1685 N94-20701
The Manson impact crater: Estimation of the energy of formation, possible size of the impacting asteroid or comet, and ejecta volume and mass
p 2083 N94-20721
Preliminary estimation of tagamite cooling conditions (Puchezh-Katunki Astrobleme, Russia)
p 2083 N94-20735
Searching for ancient Venus p 2111 N94-20743
Chicxulub impact basin: Gravity characteristics and implications for basin morphology and deep structure
p 1862 N94-20757
Research program on the Manson impact structure, Iowa p 1862 N94-20766
A tectonic resurfacing model for Venus
p 2118 N94-20781
The missing impact craters on Venus
p 2119 N94-20782
Delimitation of terrestrial impact craters by way of pseudotachylytic rock distribution p 1863 N94-20783
Two-polarity magnetization in the Manson impact breccia p 1863 N94-20789
The age of the Pretoria Saltpan impact crater, South Africa p 1863 N94-20798
Parabolic features and the erosion rate on Venus
p 2122 N94-20801
Triton's cratering record and its time of capture
p 2122 N94-20802
Multivariate statistical analysis: Principles and applications to coorbital streams of meteorite falls
p 1964 N94-20881
Shock attenuation at the Slate Islands revisited
p 1863 N94-20887
Geometrical analysis of the microcraters found on LDEF samples p 1666 N94-20890
Age and thermochronology of K-feldspars from the Manson Impact Structure p 1863 N94-20899

METEORITES

Twenty-Fourth Lunar and Planetary Science Conference. Part 3: N-Z
[NASA-CR-193149] p 2092 N94-20636
Determination of cosmic bodies size-velocity distribution by observation of current impacts on Mars
p 2082 N94-20648
Euhedral metallic-Fe-Ni grains in extraterrestrial samples p 1697 N94-20724
Lunar basalt meteorite EET 87521: Petrology of the clast population p 2083 N94-20752
Molecular equilibria and condensation sequences in carbon rich gases p 2083 N94-20756
Fine resolution chronology based on initial Sr-87/Sr-86
[CONTRIB-5230(794)] p 1686 N94-20794
Ti-bearing oxide minerals in lunar meteorite Y793169 with the VLT affinity p 2084 N94-20812
Sparking young minds with Moon rocks and meteorites p 2039 N94-20819
The parent magma of the Nakhla (SNC) meteorite: Reconciliation of composition estimates from magmatic inclusions and element partitioning
p 2085 N94-20836
On modelling nuclear reactions in meteorites
p 2085 N94-20844
Aluminum-26 activities in meteorites
p 1686 N94-20851
LREE variability in CM matrices: Another look at meteorite compaction ages p 2086 N94-20884
Consortium reports on lunar meteorites Yamato 793169 and Asuka 881757, a new type of mare basalt
p 2086 N94-20893
Wet inside and out? Constraints on water in the Martian mantle and on outgassed water, based on melt inclusions in SNC meteorites p 2145 N94-21678

METEORITIC COMPOSITION

Twenty-Fourth Lunar and Planetary Science Conference. Part 3: N-Z
[NASA-CR-193149] p 2092 N94-20636
REE and other trace lithophiles in MAC88177, LEW88280 and LEW88763 p 2082 N94-20639
The Erevan howardite: Petrology of glassy clasts and mineral chemistry p 1684 N94-20640
Carbonaceous xenoliths from the Erevan howardite
p 1684 N94-20642
Igneous rock from Severnyi Kolchim (H3) chondrite: Nebular origin p 2082 N94-20643
Core formation in the Moon: The mystery of the excess depletion of Mo, W and P p 2095 N94-20651
Exposure ages of carbonaceous chondrites, 1
p 2082 N94-20658
Identification of an interstellar oxide grain from the Murchison meteorite by ion imaging
p 2082 N94-20659
Fragments of ancient lunar crust: Ferroan noritic anorthosites from the descartes region of the Moon
p 2096 N94-20660
Volatility in the lunar crust: Trace element analyses of lunar minerals by PIXE proton microprobe
p 2097 N94-20661
Impact glasses from the ultrafine fraction of lunar soils
p 2097 N94-20662
The Sm-(146,147)-Nd-(142,143) formation interval for the lunar mantle and implications for lunar evolution
p 2097 N94-20663
Tambo Quemado: Extraordinary concentrations of REE and refractory trace elements caused by artificial heating
p 1684 N94-20667
Modelling the gravity and magnetic field anomalies of the Chicxulub crater p 1862 N94-20668
Self diffusion of alkaline-Earth in Ca-Mg-aluminosilicate melts: Experimental improvements on the determination of the self-diffusion coefficients p 1684 N94-20669
Orthopyroxenes as recorders of diogenite petrogenesis: Major and minor element systematics
p 1684 N94-20670
Abundance and composition of solar KR in the H3-H6 chondrite ACFER111 p 1684 N94-20676
C/O atomic ratios in micrometer-size crushed grains from Antarctic micrometeorites and two carbonaceous meteorites p 2082 N94-20678
Lamellar olivine in the Divnoe achondrite: Evidence for high-pressure exsolution? p 1685 N94-20679
Opaque-rich lithology in the Divnoe achondrite: Petrology and origin p 2082 N94-20680
Chaunskij: The most highly metamorphosed, shock-modified and metal-rich mesosiderite
p 2082 N94-20681
Post-igneous redistribution of components in eucrites
p 1685 N94-20684
Elevated initial Sr-87/Sr-86 in ordinary chondrite metal
p 1685 N94-20695
Elemental depletions in Antarctic micrometeorites and Arctic cosmic spherules: Comparison and relationships
p 2082 N94-20704
Oxygen isotopic relationships between the LEW85332 carbonaceous chondrite and CR chondrites
p 2083 N94-20708
SCR neon and argon in Kapoeta feldspar: Evidence for an active ancient Sun p 2106 N94-20712
Cosmogenic-radionuclide profiles in Knyahinya: New measurements and models p 2106 N94-20713
Euhedral metallic-Fe-Ni grains in extraterrestrial samples p 1697 N94-20724
Further analyses of Rio Cuarto impact glass
p 1685 N94-20745
Post-metamorphic brecciation in type 3 ordinary chondrites p 2083 N94-20749
Cathodoluminescence observations of in situ aqueous destruction of chondrules in the Murchison CM chondrite
p 2083 N94-20750
Lunar basalt meteorite EET 87521: Petrology of the clast population p 2083 N94-20752
Orthopyroxenes as recorders of diogenite petrogenesis: Trace element systematics p 1686 N94-20760
The chondrite Mihonoseki: New observed fall
p 2083 N94-20764
FE-60 and the evolution of eucrites
p 2083 N94-20768
Size distributions and aerodynamic equivalence of metal chondrules and silicate chondrules in Acfer 059
p 2084 N94-20773
Fe/Mn in olivine of carbonaceous meteorites
p 2084 N94-20788
The Sm-Nd systematics of silicate inclusions in iron meteorites: Results from Caddo (IAB)
[CONTRIB-5241(804)] p 2084 N94-20795
Hydrothermal alteration experiments of olivine with varying Fe contents: An attempt to simulate aqueous alteration of the carbonaceous chondrites
p 1686 N94-20810
Ti-bearing oxide minerals in lunar meteorite Y793169 with the VLT affinity p 2084 N94-20812
The U-Th-Pb, Sm-Nd, and Ar-Ar isotopic systematics of lunar meteorite Yamato-793169 p 2084 N94-20834
The parent magma of the Nakhla (SNC) meteorite: Reconciliation of composition estimates from magmatic inclusions and element partitioning
p 2085 N94-20836
Rare Earth elements in individual minerals in Shergottites p 1686 N94-20852
Rhenium-osmium isotope systematics of ordinary chondrites and iron meteorites p 2085 N94-20854
Consortium study of lunar meteorites Yamato-793169 and Asuka-881757: Geochemical evidence of mutual similarity, and dissimilarity versus other mare basalts
p 2085 N94-20857
Equilibrium and fractional crystallization of a primitive Shergottite composition p 2085 N94-20861
The formation of FeO-rich pyroxene and enstatite in unequilibrated enstatite chondrites: A petrologic-trace element (SIMS) study p 2086 N94-20866

Weathering features and secondary minerals in Antarctic Shergottites ALHA77005 and LEW88516
p 2086 N94-20869
LREE variability in CM matrices: Another look at meteorite compaction ages p 2086 N94-20884
The carbon components in SNC meteorites of feldspathic harzburgite composition
p 2086 N94-20885
Further carbon isotope measurements of LEW 88516
p 2086 N94-20886
Regolith breccia consisting of H and LL chondrite mixture p 2080 N94-20892
Consortium reports on lunar meteorites Yamato 793169 and Asuka 881757, a new type of mare basalt
p 2086 N94-20893
Preliminary AEM study of the microstructure and composition of metal particles in ordinary chondrites
p 2086 N94-20894
Trace element compositions of spinel-rich refractory inclusions from the Murchison meteorite
p 2086 N94-20897
Inter- and intra-crystalline oxygen isotope distribution of fassaites in Allende CAI p 2086 N94-20898
Lewis Cliff 87057: A new metal-rich E3 chondrite with similarities to Mt. Egerton, Shallowater and Happy Canyon p 2086 N94-20901
Chemical zoning and diffusion of Ca, Al, Mn, and Cr in olivine of springwater pallasite . p 2086 N94-20902
Chemical composition of new Acapulcoites and Lodranites p 2086 N94-20905
Diffuse reflectance spectra of orthopyroxene, olivine, and plagioclase as a function of composition and structure p 2087 N94-20906
Mineralogy of dark clasts in primitive versus differentiated meteorites p 2087 N94-20907
Wet inside and out? Constraints on water in the Martian mantle and on outgassed water, based on melt inclusions in SNC meteorites p 2145 N94-21678

METEORITIC DAMAGE
On magnetodynamic effects initiated by a high-speed impact of a large cosmic body upon the Earth's surface
p 2082 N94-20647
Determination of cosmic bodies size-velocity distribution by observation of current impacts on Mars
p 2082 N94-20648
Dynamics of large scale impacts on Venus and Earth
p 2098 N94-20666
The missing impact craters on Venus
p 2119 N94-20782
A fresh look at crater scaling laws for normal and oblique hypervelocity impacts p 1666 N94-20864
Large floor-fractured craters and isostatic crater modification: Implications for lithospheric thickness on Venus p 2135 N94-20873
Multivariate statistical analysis: Principles and applications to coorbital streams of meteorite falls
p 1964 N94-20881
Geometrical analysis of the microcraters found on LDEF samples p 1666 N94-20890
Meteoroids and debris impact risk assessment on Columbus and Hermes using a realistic geometrical analysis tool p 1662 N94-21388
Combination of on ground experiments and analysis software for the evaluation of material degradation in space (SILEX project) p 1662 N94-21389
An attempt to comprehend Martian weathering conditions through the analysis of terrestrial palagonite samples p 2143 N94-21668

METEORITIC DIAMONDS
Micrometeorite pre-solar diamonds from Greenland cryoconite? p 2086 N94-20895

METEORITIC MICROSTRUCTURES
Coagulation of grains in static and collapsing protostellar clouds p 2085 N94-20865
The formation of FeO-rich pyroxene and enstatite in unequilibrated enstatite chondrites: A petrologic-trace element (SIMS) study p 2086 N94-20866
Preliminary AEM study of the microstructure and composition of metal particles in ordinary chondrites
p 2086 N94-20894
Micrometeorite pre-solar diamonds from Greenland cryoconite? p 2086 N94-20895
Diffuse reflectance spectra of orthopyroxene, olivine, and plagioclase as a function of composition and structure p 2087 N94-20906

METEOROID PROTECTION
Meteoroids and debris impact risk assessment on Columbus and Hermes using a realistic geometrical analysis tool p 1662 N94-21388

METEOROID SHOWERS
High Frequency (HF) and meteor burst communications in a polar environment
[AD-A271604] p 1737 N94-20949

METEOROIDS
Effects of hydrodynamics and thermal radiation in the atmosphere after comet impacts p 1862 N94-20649
Meteoroids and debris impact risk assessment on Columbus and Hermes using a realistic geometrical analysis tool p 1662 N94-21388

METEOROLOGICAL CHARTS
An analysis of cloud-cover reporting in the 1977 surface observation database
[AD-A271102] p 1864 N94-19852

METEOROLOGICAL PARAMETERS
The marine light-mixed layer experiment cruise and data report: R/V endeavor cruise EN-224, mooring deployment, 27 April-1 May 1991: Cruise EN-227, mooring recovery, 5-23 September 1991
[AD-A271175] p 1864 N94-20186
Simulated retrieval of land surface parameters using multichannel satellite microwave radiometry
p 1727 N94-20443
Weather tutor 1: Stability basics
[AD-A270758] p 1866 N94-20565
Mathematical model and analysis of the Tactical Unmanned Ground Vehicle (TUGV) using computer simulation
[AD-A272258] p 1824 N94-20576
A parametric representation of a thunderstorm cell
[AD-A271983] p 1866 N94-20579
Remote sensing for hydrology progress and prospects
[WMO-773] p 1841 N94-21069
NOVAM evaluation utilizing electro-optics and meteorological data from KEY-90
[AD-A271722] p 1868 N94-21356
Low-power millimeter-wave radar observations of the atmosphere
[NASA-CR-194738] p 1858 N94-21811
Design document and database specifications for the Naval Interactive Data Analysis System (NIDAS), version 1.0
[NASA-CR-194817] p 2045 N94-21865
The FIRE Cirrus Science Results 1993
[NASA-CP-3238] p 1871 N94-22292
Atmospheric parameterization schemes for satellite cloud property retrieval during FIRE IFO 2
p 1874 N94-22312
Cirrus cloud development in a mobile upper tropospheric trough: The November 26th FIRE cirrus case study
p 1878 N94-22329
Studies in remotely sensed geophysical parameter retrieval and analysis
[NASA-CR-194768] p 1842 N94-22374

METEOROLOGICAL RADAR
Description and availability of airborne Doppler radar data p 1722 N94-20419
Next Generation Weather Radar (NEXRAD) Principal User Processor (PUP) Operational Test and Evaluation (OT/E)
[AD-A273075] p 1868 N94-21519
Microphysical properties of the November 26 cirrus cloud retrieved by Doppler radar/IR radiometer technique
p 1873 N94-22304
Lidar and radar derived cirrus microphysical properties for the 26 November 1991 case study
p 1873 N94-22305
Progress in interpreting CO2 lidar signatures to obtain cirrus microphysical and optical properties
p 1874 N94-22308
Observations of multi-layered clouds using K-band radar p 1874 N94-22311

METEOROLOGICAL SATELLITES
The future of remote sensing from space: Civilian satellite systems and applications
[OTA-ISC-558] p 1837 N94-20209
Comparison of radiation and cloud parameters derived from satellite and aircraft measurements during FIRE 2 cirrus IFO p 1872 N94-22299
Managing an archive of weather satellite images
p 2048 N94-22525

METEOROLOGICAL SERVICES
Next Generation Weather Radar (NEXRAD) Principal User Processor (PUP) Operational Test and Evaluation (OT/E)
[AD-A273075] p 1868 N94-21519
Meteorological analysis of the November 25 FIRE cirrus-2 case: A well-defined ridge-crest cirrus system over Oklahoma p 1877 N94-22328

METEOROLOGY
Worldwide frequency of temperatures at selected altitudes
[AD-A271111] p 1864 N94-19908
Hydrostatic/nonhydrostatic comparison with the MERCURE code on orographic flows
[ETN-93-94603] p 1866 N94-20600
Measurement of mesospheric turbulence in the framework of the metal campaign and development of a sensor for static pressure free measurements of neutral and electron density
[BONN-IR-92-45] p 1857 N94-21149
Analysis of a sandstorm weather process-translation
[AD-A272959] p 1867 N94-21250
The early Martian environment: Clues from the cratered highlands and the Precambrian Earth
p 2143 N94-21667
Role of surface characteristics in urban meteorology and air quality
[DE93-040929] p 1851 N94-21740
Meteorological analysis of the December 4-6 FIRE cirrus-2 case p 1875 N94-22314
Meteorological analysis of the November 25 FIRE cirrus-2 case: A well-defined ridge-crest cirrus system over Oklahoma p 1877 N94-22328

METHANE
Transient studies of low temperature catalysts for methane conversion
[DE93-041232] p 1680 N94-20934
Molten carbonate fuel cell networks: Principles, analysis, and performance
[DE93-019872] p 1846 N94-21527
A carbon dioxide/methane greenhouse atmosphere on early Mars p 2142 N94-21662
Survey on chemical engineering technologies for the global environmental protection
[DE94-714887] p 1852 N94-22044
Investigations on trends in global environment adaptive industrial technologies
[DE94-714888] p 1853 N94-22258

METHOD OF CHARACTERISTICS
Characteristic based methods for the time-domain Maxwell equations
[AD-A272973] p 1802 N94-21263

METHOD OF MOMENTS
Numerical modeling of fringing fields and their use for complex permittivity measurements at high frequencies
[AD-A270478] p 1966 N94-19917
An extended UTD analysis for the scattering and diffraction from cubic polynomial strips
[NASA-CR-194581] p 1716 N94-20139
Polarimetric thermal emission from rough surfaces
p 1727 N94-20441
Comparison of higher order moment spectrum estimation techniques
[AD-A272967] p 1967 N94-21260
A modified moment invariants technique for classification of noisy objects p 1780 N94-22165
Modelling short bent, graded index dielectric slab waveguides
[PB93-215283] p 1742 N94-22349

METHYL ALCOHOL
Fuel processing requirements and techniques for fuel cell propulsion power
[DE93-019516] p 1750 N94-20257
Cold starting an alcohol-fueled engine with ultrasonic fuel atomization
[PB93-206597] p 1826 N94-22093

METHYL COMPOUNDS
Polymerization of enantiomerically pure 2,3-dicarboalkoxy norbornadienes and 5,6-disubstituted norbornenes by well-characterized molybdenum ROMP catalysts
[AD-A272649] p 1704 N94-21186
Surface science and modeling studies of endothermic fuels catalysis
[AD-A272850] p 1712 N94-21192
The 13C-NMR spectra of poly (4-((2-(acryloyloxy) ethyl) ethyl amino)- 4-nitroazobenzene-co-methyl methacrylate)
[AD-A273016] p 1705 N94-21238

METRIC SPACE
Half-integral flows in a planar graph with four holes
[RR-894-M] p 1951 N94-20302
Modular interval spaces
[PB93-220663] p 1961 N94-22266

METROLOGY
Evaluation of a scanning Hartmann device for single point turning applications
[DE93-019204] p 1821 N94-19891
Optical metrology of magnetically trapped hydrogen
[AD-A272110] p 1680 N94-20584

MICHELSON INTERFEROMETERS
Fiber optic Michelson sensor and arrays with passive elimination of polarization fading and source feedback isolation
[AD-D015944] p 1984 N94-20065
Thermal dilation fiber optical flow sensor
[AD-D015926] p 1797 N94-20094
Validation of the design of a high resolution all-reflection Michelson interferometer for atmospheric spectroscopy
[AD-A272505] p 1987 N94-21410
Mirror velocity sampling errors in a Michelson interferometer
[AD-A273105] p 1809 N94-21508
Michelson Interferometer (MINT)
p 1813 N94-21646

MICROANALYSIS
Near atomic resolution microanalysis of interfaces by analytical electron microscopy
[DE93-019437] p 1687 N94-19904

Microanalysis of iron oxidation state in iron oxides using X Ray Absorption Near Edge Structure (XANES)
p 1686 N94-20808
Micro-ellipsometric measurements of strained layer structures p 2025 N94-21008

MICROBALANCES
Atomic oxygen fluence detector for Bremsat: Scientific and technical description p 1663 N94-21396
Application of an electrochemical quartz crystal microbalance to the study of electrocatalytic films
[DE93-041124] p 2029 N94-21691

MICROCHANNELS
High power, electron-beam induced switching in diamond
[DE93-040535] p 1768 N94-21770

MICROCLIMATOLOGY
Cold-start minidiesel engine development
[AD-A271064] p 1823 N94-20567

MICROCRYSTALS
Fundamental studies of defect generation in amorphous silicon alloys grown by remote plasma-enhanced chemical-vapor deposition
[DE93-017083] p 2029 N94-21615

MICROELECTRONICS
Solder technology in the manufacturing of electronic products
[DE93-018842] p 1699 N94-19960
Automated HMC assembly
[DE93-040841] p 1749 N94-20005
The aerogel mesh contamination collector
[AD-A270537] p 1651 N94-20011
Single-event upset testing of the performance semiconductor 1750A CMOS/SOS chip set
[AD-A271158] p 2015 N94-20184
Method for anisotropic etching in the manufacture of semiconductor devices
[NASA-CASE-MSC-21631-1] p 1993 N94-20491
Materials, Structures, and Devices for High-Speed Electronics
[NASA-CR-193177] p 2019 N94-20971
X ray reflection masks: Manufacturing, characterization and first tests
[BONN-IR-92-31] p 1986 N94-21043
Comparison of single event upset rates for microelectronic memory devices during interplanetary solar particle events p 1754 N94-21085
Single event phenomena: Testing and prediction
p 1763 N94-21696
Self assembly: An approach to terascale integration
[DE93-040104] p 1769 N94-21846
Microtechnology: The key to the technical challenges of the 21st century
[DE94-000403] p 1769 N94-21959
Fluorescent microthermographic imaging
[DE93-040332] p 1810 N94-22000
Acoustic, fiber optic, and silicon microelectronic microsensors research and development activities at Sandia National Laboratories
[DE93-019075] p 1770 N94-22040
Silicon microelectronic field-emissive devices for advanced display technology
[DE94-000397] p 1794 N94-22380

MICROGRAVITY
Stability limits and dynamics of nonaxisymmetric liquid bridges
[NASA-CR-194706] p 1797 N94-20037
Growth of zinc selenide single crystals by physical vapor transport in microgravity
[NASA-CR-194679] p 2017 N94-20346
Evaporation of a sodium tellurite melt in the jamic low gravity drop shaft p 1713 N94-20605
Loads produced by a suited subject performing tool tasks without the use of foot restraints
[NASA-TP-3424] p 1896 N94-20606
Experimental study of void formation during aluminum solidification in reduced gravity
[NASA-TM-106190] p 1692 N94-21604
Strength capabilities and load requirements while performing torquing tasks in zero gravity
[NASA-TP-3433] p 1897 N94-21627
Rewetting of monogroove heat pipe in Space Station radiators
[NASA-CR-194781] p 1804 N94-21820

MICROGRAVITY APPLICATIONS
Cooling apparatus and couplings therefor
[NASA-CASE-ARC-11921-1] p 1800 N94-20371

MICROHARDNESS
Metastable bcc phase formation in the Nb-Cr system
[DE93-018376] p 2012 N94-19926

MICROMACHINING
Micromachined actuator and sensor capabilities at the Microelectronics Development Laboratory
[DE93-019417] p 1769 N94-21918

MICROMECHANICS
Biotechnology and composite materials
[AD-A264278] p 1673 N94-20327
Direct imaging of the surface microstructure of dielectric materials using an atomic force microscope
[AD-A272251] p 2018 N94-20575
Thermal stress analysis of composites in the space environment p 1661 N94-21379

MICROMETEORITES
C/O atomic ratios in micrometer-size crushed grains from Antarctic micrometeorites and two carbonaceous meteorites p 2082 N94-20678
Elemental depletions in Antarctic micrometeorites and Arctic cosmic spherules: Comparison and relationships
p 2082 N94-20704
Micrometeorite dynamic pyrometamorphism: Nonstoichiometric clinoenstatite (CLEN)
p 2083 N94-20715
Micrometeorite dynamic pyrometamorphism: Observation of a thermal gradient in iron-nickel sulfide
p 2083 N94-20716
Micrometeorite pre-solar diamonds from Greenland cryoconite? p 2086 N94-20895

MICROMETEOROIDS
Determination of parameters for hypervelocity dust grains encountered in near-Earth space
p 2084 N94-20817
Intact capture of hypervelocity particles on Shuttle
p 2085 N94-20837
A fresh look at crater scaling laws for normal and oblique hypervelocity impacts p 1666 N94-20864
Geometrical analysis of the microcraters found on LDEF samples p 1666 N94-20890
On dust emissions from the jovian system
p 2141 N94-20909
Orbital debris and micrometeoroids: LDEF and Mir data p 1659 N94-21368
Combination of on ground experiments and analysis software for the evaluation of material degradation in space (SILEX project) p 1662 N94-21389

MICROMOTORS
Lavet type stepping motors and associated controls
p 1752 N94-20632

MICROPOROSITY
High temperature size selective membranes
[DE93-019865] p 1709 N94-21982

MICROPROCESSORS
A methodology for formal hardware verification, with application to microprocessors
[AD-A270550] p 1698 N94-20085
Mongoose: Creation of a Rad-Hard MIPS R3000
p 1754 N94-21090
Network command processing system overview
p 1935 N94-21351
A 20 MHz CMOS reorder buffer for a superscalar microprocessor p 1764 N94-21700
A mechanized process algebra for verification of device synchronization protocols p 1766 N94-21716
Instruction set commutivity p 1766 N94-21719
IRAF and STSDAS under the new ALPHA architecture
p 2049 N94-22553

MICROSCOPY
Acoustic microscopy and nonlinear effects in pressurized superfluid helium
[AD-A270598] p 1967 N94-19949
Atom probe field ion microscopy characterizations of VVER steels
[DE93-017864] p 1689 N94-20180
Ultrafast scanning microscopy
[DE93-040121] p 1985 N94-20320
Variable angle spectroscopic ellipsometric characterization of surface damage in chemical-mechanical polished GaAs
p 1710 N94-20986
Structure and morphology of Pd overlayers on epitaxial SnO2 films studies with the atomic force microscope
[AD-A271827] p 2028 N94-21458
Magnetic force microscopy/current contrast imaging: A new technique for internal current probing of IC's
[DE93-040754] p 1761 N94-21532
Material optimization for hard x ray Fresnel zone plates
[DE93-019569] p 1990 N94-21837
Center for X-Ray Optics, 1992
[DE94-000726] p 1990 N94-21868

MICROSTRIP ANTENNAS
Two microstrip arrays for interferometric SAR applications p 1722 N94-20421
Bandwidth enhancement of dielectric resonator antennas p 1734 N94-20507
A 10 GHz Y-Ba-Cu-O/GaAs hybrid oscillator proximity coupled to a circular microstrip patch antenna
p 1736 N94-20517
Full wave numerical model of arbitrarily-shaped proximity coupled microstrip antennas p 1745 N94-22137
Modeling of coaxial-fed microstrip patch antenna by finite difference time domain method p 1745 N94-22138
Applications of planar near-field measurements to electromagnetic radiation and interference problems
p 1747 N94-22252

MICROSTRIP DEVICES
Time-domain analysis of planar microstrip devices using a generalized Yee-algorithm based on unstructured grids
p 1724 N94-20431
TlCaBaCuO high Tc superconducting microstrip ring resonators designed for 12 GHz p 1735 N94-20516

MICROSTRIP TRANSMISSION LINES
Analysis of microstrip dipoles and slots transversely coupled to a microstrip line using the FDTD method
p 1718 N94-20405
Linearly tapered slot antenna circular array for mobile communications
[NASA-TM-106441] p 1769 N94-21808

MICROSTRUCTURE
General introduction to microstructural evolution under cascade damage conditions
[DE93-017443] p 2012 N94-19923
Particles on surfaces of laser ablated Y1Ba2Cu3O(7-delta) films
[DE93-040269] p 2013 N94-19929
Investigation of cracking and erratic behavior of the uranium-titanium alloy
[DE93-018591] p 1686 N94-19957
Microstructural stability of wrought, laser and electron beam glazed NARloy-Z alloy at elevated temperatures
[NASA-TM-108431] p 1689 N94-20100
Atom probe field ion microscopy characterizations of VVER steels
[DE93-017864] p 1689 N94-20180
Sol-spray preparation, particulate characteristics, and sintering of alumina powders
[DE93-018577] p 1690 N94-20183
Microscopic evaluation of low-temperature embrittlement in type 308 stainless steel welds
[DE93-040266] p 1690 N94-20282
Transport in microstructures in the microwave and millimeter-wave regime
[AD-A271875] p 2017 N94-20470
The effects of processing and constituent materials on compressive strength of thick composite laminates
[AD-A271912] p 1673 N94-20490
Direct imaging of the surface microstructure of dielectric materials using an atomic force microscope
[AD-A272251] p 2018 N94-20575
Microstructure evolution in the presence of constraints and implications on the properties of Mg-Li and Nb-Al constraints
[AD-A272088] p 1674 N94-20623
Regolith breccia consisting of H and LL chondrite mixture p 2080 N94-20892
In-situ and ex-situ ellipsometric characterization for semiconductor technology p 2026 N94-21013
VASE (variable angle spectroscopic ellipsometry)
p 1687 N94-21014
Microstructural modeling and toughening of Si3N4 ceramics for high temperature engine applications
[AD-A272897] p 1704 N94-21197
The use of backscattered electron imaging mode to assess the effect of fine dispersions on development of superplastic microstructure in Al-Mg alloys
[AD-A272426] p 1691 N94-21258
Applicability and performance benefits of XD (Tradename) titanium aluminides to expendable gas turbine engines
[AD-A272998] p 1648 N94-21268
Investigation of the effect of various oxide and fluoride additives on the microstructure, electronic properties, and phase shifting ability of Ba(1-x)Sr(x)TiO3
[AD-A271756] p 2027 N94-21303
Deformation of an alumina-zirconia-silicon carbide-whisker reinforced composite
[DE93-040244] p 1676 N94-21559
High resolution, three dimensional soft x ray imaging
[DE93-018667] p 1989 N94-21630
Surface and subsurface defect detection in Si3N4 components by laser scattering
[DE93-040829] p 1832 N94-21772
Ductile-brittle transition behavior of tungsten under shock loading conditions
[DE93-019945] p 1693 N94-21843
Symposium on Microscopy and Image Analysis of Building Materials
[VTT-SYMP-136] p 1707 N94-21890
Preparation of concrete specimens for microstructural image analysis studies p 1707 N94-21891
A quantitative S.E.M. image analysis of cement paste microstructure p 1708 N94-21894
Determination of pore structure of concrete from thin sections by image analysis p 1708 N94-21895
Microstructure in mortar: A summary of a new project of research p 1708 N94-21896

The effect of microstructural evolution on superplasticity in Ni3Si(V, Mo)
[DE93-041320] p 1694 N94-21943
Dynamic properties of ceramic materials
[DE94-000654] p 1708 N94-21963
Microtextural characterization of annealed and deformed copper
[DE93-040144] p 1695 N94-21990
Benefits of thread rolling process to the stress corrosion cracking and fatigue resistance of high strength fasteners
[DE93-040438] p 1833 N94-22001
Microstructural evolution of neutron-irradiated Fe-Cr-Ni ternary alloys at high helium generation rates
[DE93-018786] p 1696 N94-22037
Quantitative analysis of scanning tunneling microscopy images for surface structure determination: Sulfur on Re(0001)
[DE93-019235] p 2034 N94-22041
Miniaturized disk-bend testing, nano-indentation, and the microstructure of ion-irradiated titanium aluminides
[DE93-040600] p 1697 N94-22559
Strength, ultrasonic and metallurgical evaluation of diffusion bonds
[DE94-000665] p 1697 N94-22571

MICROWAVE ANTENNAS
Space applications of superconducting microwave electronics at NASA Lewis Research Center p 1671 N94-20513
AlGaAs laser diode FM spectrum: Phased array antenna application p 1746 N94-22196
Numerical method for computing the electric field produced by a microwave beam in a stratified medium p 1746 N94-22197

MICROWAVE ATTENUATION
Attenuation of epsilon(sub eff) of coplanar waveguide transmission lines on silicon substrates p 1733 N94-20504

MICROWAVE CIRCUITS
Automated HMC assembly
[DE93-040641] p 1749 N94-20005
Interinjection-locked quasioptical power combiners and phased arrays
[AD-A271178] p 2015 N94-20214
Quartz/fused silica chip carriers
[NASA-CR-194154] p 2016 N94-20340
Recent activities in printed Antennas at LeRC p 1722 N94-20422
Solid State Technology Branch of NASA Lewis Research Center: Fifth Annual Digest
[NASA-TM-106303] p 1732 N94-20497
An x-band peaked HEMT amplifier p 1732 N94-20498
Coplanar waveguide radial line stub p 1733 N94-20503
Space applications of superconducting microwave electronics at NASA Lewis Research Center p 1671 N94-20513
Ten GHz YBa2Cu3O(7-delta) superconducting ring resonators on NdGaO3 substrates p 1735 N94-20515
Non-destructive semiconductor wafer probing system using laser pulses to generate and detect millimeter-wave signals
[CA-PATENT-APPL-SN-2,020,73] p 1760 N94-21178
Hybrid finite element/waveguide mode analysis of passive RF devices
[AD-A273074] p 1740 N94-21518
High temperature superconducting planar circuit structure for high frequency applications
[AD-A273083] p 2028 N94-21521
Characterization and modelling of extremely high frequency enclosures p 1782 N94-22177
Non-linear analysis of the electrical properties of the active circuits of high-frequency oscillators p 1785 N94-22195
MHMIC: Technology for the integration of microwave sub-assemblies p 1785 N94-22199

MICROWAVE COUPLING
Aperture coupling of circular cylindrical dielectric resonator antenna
[ISBN-0-315-60632-0] p 1743 N94-22409

MICROWAVE EMISSION
Radiation from solar flares p 2001 N94-22634

MICROWAVE EQUIPMENT
Automated HMC assembly
[DE93-040641] p 1749 N94-20005
Interinjection-locked quasioptical power combiners and phased arrays
[AD-A271178] p 2015 N94-20214
Three point lead screw positioning apparatus for a cavity tuning plate
[NASA-CASE-LEW-15216-1] p 1822 N94-20375
TlCaBaCuO high Tc superconducting microstrip ring resonators designed for 12 GHz p 1735 N94-20516

MICROWAVE FILTERS
Manual design technique for broadband passive thin-film attenuators using the Smith chart p 1782 N94-22178

MICROWAVE FREQUENCIES
Application of Cloude's target decomposition theorem to polarimetric imaging radar data p 1724 N94-20429
C-band radar backscatter of sea ice in the Weddell Sea, Antarctica during the austral winter of 1992 p 1725 N94-20435

MICROWAVE IMAGERY
Millimeter wave imaging technology
[AD-A271257] p 1715 N94-19912
Comparison of remote sensing measurements with a two-scale polarimetric emission and scattering model for sea surfaces p 1721 N94-20415
On evaluating the accuracy of SAR sea-ice classification using multifrequency polarimetric AIRSAR data p 1724 N94-20428
Millimeter-wave imaging of composite materials
[DE93-041160] p 1677 N94-21940

MICROWAVE LANDING SYSTEMS
MLS signal-in-space category 3 landing hazard analysis p 1644 N94-22134
Application of scattering by arrays of cylinders to MLS signal propagation error estimation p 1644 N94-22135
Testing of DME/P equipment performance for complex MLS procedures p 1644 N94-22136
MLS pointing angle error sources and effects p 1644 N94-22154
Developing software to RTCA DO-178A p 1645 N94-22155
A flight test system design for the microwave landing system p 1645 N94-22156

MICROWAVE OSCILLATORS
Interinjection-locked quasioptical power combiners and phased arrays
[AD-A271178] p 2015 N94-20214
A 10 GHz Y-Ba-Cu-O/GaAs hybrid oscillator proximity coupled to a circular microstrip patch antenna p 1736 N94-20517
Improvement of the performance of IMPATT oscillators through appropriate modification of resonant-cap activity p 1782 N94-22179
Non-linear analysis of the electrical properties of the active circuits of high-frequency oscillators p 1785 N94-22195

MICROWAVE RADIOMETERS
Atmospheric infrared sounder
[NASA-CR-194814] p 1856 N94-20362
Simulated retrieval of land surface parameters using multichannel satellite microwave radiometry p 1727 N94-20443
Polarimetric thermal emission from periodic water surfaces p 1728 N94-20445
Spatial and temporal variations of satellite microwave measurements of latent heat release in tropic cyclones due to environmental forcing obtained from a numerical model
[AD-A267947] p 1865 N94-20482

MICROWAVE RESONANCE
Improvement of the performance of IMPATT oscillators through appropriate modification of resonant-cap activity p 1782 N94-22179

MICROWAVE SCATTERING
Radar backscatter measurements from simulated sea ice during CRRELEX 1990
[AD-A271034] p 1715 N94-19823
Comparison of remote sensing measurements with a two-scale polarimetric emission and scattering model for sea surfaces p 1721 N94-20415
Use of microwave polarimetry to enhance SAR images of the ocean surface
[AD-A271911] p 1882 N94-20489
Presenting the Rain-Sea Interaction Facility
[NASA-RP-1322] p 1884 N94-21628
Application of scattering by arrays of cylinders to MLS signal propagation error estimation p 1644 N94-22135
A simplified method for S-parameter calculations of metal septum waveguide filters p 1782 N94-22180

MICROWAVE SENSORS
Synergism of active and passive microwave data for estimating bare surface soil moisture p 1727 N94-20444

MICROWAVE SPECTRA
On the relationship between spectral domain approach and method of lines p 1794 N94-22254

MICROWAVE SPECTROMETERS
Temperature/pressure and water vapor sounding with microwave spectroscopy p 1812 N94-22436

MICROWAVES
Transport in microstructures in the microwave and millimeter-wave regime
[AD-A271875] p 2017 N94-20470
Spatial and temporal variations of satellite microwave measurements of latent heat release in tropic cyclones due to environmental forcing obtained from a numerical model
[AD-A267947] p 1865 N94-20482
Use of microwave polarimetry to enhance SAR images of the ocean surface
[AD-A271911] p 1882 N94-20489
Rotational spectrum of a dark state in 2-fluoroethanol using microwave/radiofrequency-infrared multiple resonance
[AD-A272101] p 1817 N94-20583
Particle behavior in an ECR plasma etch tool
[DE93-040343] p 1996 N94-21769
Plasma-chemical conversion of hydrogen sulfide into hydrogen and sulfur
[DE93-041167] p 1682 N94-21789
An assessment of the cost of microwave sintering ceramic tiles for armor applications
[DE94-000978] p 1693 N94-21850

MIDAIR COLLISIONS
A fresh look at crater scaling laws for normal and oblique hypervelocity impacts p 1666 N94-20864

MIDDLE ATMOSPHERE
Interactions of free modes, tides, and gravity waves in the middle atmosphere
[REPT-84] p 1855 N94-20155
Empirical wind model for the middle and lower atmosphere. Part 2: Local time variations
[NASA-TM-104592] p 1870 N94-21862

MIE SCATTERING
Multiple scattering effects on the Linear Depolarization Ratio (LDR) measured during CaPE by a Ka-band air-borne radar p 1728 N94-20446
On the theory of morphology-dependent resonances: Shape resonances, width formulas, and graphical representations
[AD-A272279] p 2037 N94-20945

MILITARY AIRCRAFT
Audit report. Navy's aircraft structural life surveillance program data recorders
[AD-A270391] p 1645 N94-20040

MILITARY OPERATIONS
Planning process software: A user guide for the DMCA
[AD-A271252] p 1902 N94-19911
HERMES, a report generator for research on information processing in command posts: The effect of missing information
[IZF-1992-A-28] p 2042 N94-20310
In-flight measurement of aircrew breathing in Navy aircraft
[AD-A271811] p 1896 N94-21154

MILITARY TECHNOLOGY
Millimeter wave imaging technology
[AD-A271257] p 1715 N94-19912
Tactical laser weapons and other directed-energy weapons
[AD-A267961] p 1816 N94-20484
Documents on the history of aeronautical and space research in Germany, 1900 - 1970
[DLR-MITT-92-08] p 2152 N94-20543
Chemistry and materials science
[DE94-001449] p 2152 N94-21858
Microtechnology: The key to the technical challenges of the 21st century
[DE94-000403] p 1769 N94-21959

MILKY WAY GALAXY
Spatial distribution of near infrared line radiation in galactic nuclei measured with Fabry-Perot spectrometer FAST
[MPE-239] p 2081 N94-21138
Extracting galactic structure parameters from multivariated density estimation p 1964 N94-22458

MILLIMETER WAVES
Millimeter wave imaging technology
[AD-A271257] p 1715 N94-19912
Interinjection-locked quasioptical power combiners and phased arrays
[AD-A271178] p 2015 N94-20214
Transport in microstructures in the microwave and millimeter-wave regime
[AD-A271875] p 2017 N94-20470
An 85 GHz quasioptical gyroklystron experiment
[AD-A272020] p 1752 N94-20931
Low-power millimeter-wave radar observations of the atmosphere
[NASA-CR-194738] p 1858 N94-21811
Millimeter-wave imaging of composite materials
[DE93-041160] p 1677 N94-21940

MILLING (MACHINING)
Focused-ion-beam material removal rates
[AD-A270852] p 1713 N94-19834

MILLING MACHINES
Focused-ion-beam material removal rates
[AD-A270852] p 1713 N94-19834

MIMD (COMPUTERS)
Building brains for bodies
[AD-A270531] p 1939 N94-19875
Parallel band reduction and tridiagonalization
[DE93-019586] p 1951 N94-20221
The design of linear algebra libraries for high performance computers
[DE93-040458] p 1960 N94-21967
Parallelizing a maximum entropy image deconvolution algorithm p 1787 N94-22208

MIMO (CONTROL SYSTEMS)
Design of a state-space controller for an advanced gas turbine engine
[AD-A270859] p 1847 N94-20042
Telerobotic control of a mobile coordinated robotic server, executive summary
[NASA-CR-194685] p 1821 N94-20044

MINERAL DEPOSITS
Dating native gold by noble gas analyses p 1684 N94-20652
C/O atomic ratios in micrometer-size crushed grains from Antarctic micrometeorites and two carbonaceous meteorites p 2082 N94-20678
Mineralogy and cooling history of magnesian lunar granulite 67415 p 2124 N94-20811
A new Antarctic meteorite with chromite, orthopyroxene and metal with reference to a formation model of S asteroids p 2084 N94-20813
Evaluation of lunar rocks and soils for resource utilization: Detailed image analysis of raw materials and beneficiated products p 2126 N94-20820

MINERALOGY
The Koshak section: Evidence for element fractionation and an oxidation event at the K/T boundary p 1862 N94-20641
Petrogenesis of Apollo 12 mare basalts. Part 1: Multiple melts and fractional crystallization to explain olivine and ilmenite basalt compositions p 1684 N94-20644
Volatility in the lunar crust: Trace element analyses of lunar minerals by PIXE proton microprobe p 2097 N94-20661
Opaque-rich lithology in the Divnoe achondrite: Petrology and origin p 2082 N94-20680
Chaunskij: The most highly metamorphosed, shock-modified and metal-rich mesosiderite p 2082 N94-20681
Post-igneous redistribution of components in eucrites p 1685 N94-20684
Micrometeorite dynamic pyrometamorphism: Observation of a thermal gradient in iron-nickel sulfide p 2083 N94-20716
Derivation of the midinfrared (5.0-25.0 micron) optical constants of hydrous carbonate and sulfate p 2108 N94-20723
Detectability of crystalline ferric and ferrous minerals on Mars p 2110 N94-20730
Combined backscatter Moessbauer spectrometer/x ray fluorescence analyzer (BaMS/XRF) for extraterrestrial surfaces p 1686 N94-20761
The chondrite Mihonoseki: New observed fall p 2083 N94-20784
The stability of oxyamphiboles: Existence of Ferric-bearing minerals under the reducing conditions on the surface of Venus p 2122 N94-20800
Mineralogy and cooling history of magnesian lunar granulite 67415 p 2124 N94-20811
Ti-bearing oxide minerals in lunar meteorite Y793169 with the VLT affinity p 2084 N94-20812
A new Antarctic meteorite with chromite, orthopyroxene and metal with reference to a formation model of S asteroids p 2084 N94-20813
Evaluation of lunar rocks and soils for resource utilization: Detailed image analysis of raw materials and beneficiated products p 2126 N94-20820
Cometary interplanetary dust particles? An update on carbon in anhydrous IDPS p 2084 N94-20828
Reverse polarity magnetized melt rocks from the Chicxulub impact structure, Yucatan Peninsula, Mexico p 1863 N94-20843
Origin of high-Ti lunar ultramafic glasses p 1686 N94-20853
Multiplicity of chondrule heating events and the coarsening of chondrule textures p 2085 N94-20860
A study of carbonates, sulfates, and phosphates using thermal emission spectroscopy p 1686 N94-20868
Weathering features and secondary minerals in Antarctic Shergottites ALHA77005 and LEW88516 p 2086 N94-20869
Lewis Cliff 87057: A new metal-rich E3 chondrite with similarities to Mt. Egerton, Shallowater and Happy Canyon p 2086 N94-20901
Mineralogy of dark clasts in primitive versus differentiated meteorites p 2087 N94-20907
A Backscatter Moessbauer Spectrometer (BaMS) for use on Mars p 1811 N94-22431
Determination of Martian soil mineralogy and water content using the Thermal Analyzer for Planetary Soils (TAPS) p 1812 N94-22433
In situ identification of the Martian surface material and its interaction with the Martian atmosphere using DTA/GC p 1812 N94-22434
Optical luminescence spectroscopy as a probe of the surface mineralogy of Mars p 1813 N94-22437

MINERALS
Frequency dependent electrical properties of minerals and partial-melts
[DE93-019918] p 2012 N94-19861
Evaporation in equilibrium, in vacuum, and in hydrogen gas p 1684 N94-20638
Fragments of ancient lunar crust: Ferroan noritic anorthosites from the descartes region of the Moon p 2096 N94-20660
Volatility in the lunar crust: Trace element analyses of lunar minerals by PIXE proton microprobe p 2097 N94-20661
Characterization of Minnesota lunar simulant for plant growth p 1897 N94-20665
Abundance and composition of solar KR in the H3-H6 chondrite ACFER111 p 1684 N94-20676
Post-igneous redistribution of components in eucrites p 1685 N94-20684
U-Pb provenance ages of shocked zircons from the K-T boundary, Raton Basin, Colorado p 1685 N94-20701
Detectability of crystalline ferric and ferrous minerals on Mars p 2110 N94-20730
Research program on the Manson impact structure, Iowa p 1862 N94-20766
FE-60 and the evolution of eucrites p 2083 N94-20768
Magnesian anorthosites from the western highlands of the Moon: Isotope geochemistry and petrogenesis p 2118 N94-20779
Microanalysis of iron oxidation state in iron oxides using X Ray Absorption Near Edge Structure (XANES) p 1686 N94-20808
Regolith breccia consisting of H and LL chondrite mixture p 2080 N94-20892
Lewis Cliff 87057: A new metal-rich E3 chondrite with similarities to Mt. Egerton, Shallowater and Happy Canyon p 2086 N94-20901
An attempt to comprehend Martian weathering conditions through the analysis of terrestrial palagonite samples p 2143 N94-21668
Effect of powder characteristics on gas-pressure sintering of Si3N4 with rare earth additives
[DE94-000330] p 1694 N94-21945

MINIATURE ELECTRONIC EQUIPMENT
Miniature color display, phase 4
[AD-A272920] p 1760 N94-21221

MINIATURIZATION
Self assembly: An approach to terascale integration
[DE93-040104] p 1769 N94-21846
Microtechnology: The key to the technical challenges of the 21st century
[DE94-000403] p 1769 N94-21959

MINIMUM ENTROPY METHOD
The relaxed state and entropy production due to the electric resistivity and viscosity of plasma p 2010 N94-22696

MIRANDA
Structural evidence for reorientation of Miranda about a paleo-pole p 2098 N94-20671
Triton's cratering record and its time of capture p 2122 N94-20802

MIRRORS
Evaluation of a scanning Hartmann device for single point turning applications
[DE93-019204] p 1821 N94-19891
Circular polarizing mirrors for high power lasers
[AD-A267820] p 1815 N94-19965
Characterization and possible repair of defects in soft x ray projection lithography masks
[DE93-019147] p 1750 N94-20231
Wide-angle imaging system with fiberoptic components providing angle-dependent virtual material stops
[NASA-CASE-NPO-18146-1-CU] p 1986 N94-20345
X ray reflection masks: Manufacturing, characterization and first tests
[BONN-IR-92-31] p 1986 N94-21043
Mirror velocity sampling errors in a Michelson interferometer
[AD-A273105] p 1809 N94-21508
Generation of harmonic radiation using the multi-cavity free-electron laser
[DE94-001261] p 1820 N94-21975
X ray characterization of a three-element condenser system for soft x ray projection lithography
[DE93-019916] p 1990 N94-21985
HST PSF simulation using Tiny Tim p 1926 N94-22498

MIS (SEMICONDUCTORS)
Surface states at the GaAs-germanium nitride interface p 1709 N94-20973
InP MIS structures with diamondlike amorphous carbon films deposited by ion-beam sputtering and from plasma p 1710 N94-20979
Interfacial properties of diamondlike amorphous carbon films on InP: Metal-insulator-semiconductor structures p 1710 N94-20980

MISALIGNMENT
Stability of beam in the Fermilab Main Injector
[DE94-000619] p 1982 N94-21934

MISSILE DEFENSE
Standard atmospheres for engagement modeling
[AD-A272447] p 1858 N94-21207
High-velocity interceptors for boost-phase intercepts
[DE94-001077] p 1965 N94-22403

MISSILE DETECTION
A feasibility study of a parallax-based passive missile approach warning system
[ISBN-0-315-60640-1] p 1743 N94-22410

MISSILE SIGNATURES
Boost-phase discrimination research
[NASA-TM-109347] p 1666 N94-19818

MISSILE TRACKING
UVPI imaging from the LACE satellite: The Starbird rocket plume
[AD-A271981] p 1658 N94-20617

MISSILES
Aerospace: Facts and figures, 1992-1993
[AD-A272571] p 1635 N94-21419

MISSION PLANNING
The EXOSAT operational experience
[ESA-STM-248] p 1657 N94-20235
Clementine: An inexpensive mission to the Moon and Geographos p 1652 N94-20765
Mars exploration study workshop 2
[NASA-CP-3243] p 2146 N94-21883
SPIKE: Application for ASTRO-D mission planning p 1926 N94-22486

MIXING
Convex set and linear mixing model p 1844 N94-20888

MIXING CIRCUITS
Quantum noise studies with superconducting tunnel junction mixers
[AD-A270897] p 2012 N94-19697

MIXING LAYERS (FLUIDS)
Turbulence modeling for high speed compressible flows
[NASA-CR-194547] p 1799 N94-20210
Mixing of a chemically buoyant layer at the top of a thermally convecting fluid: Implications for mantle dynamics with application to Venus p 2099 N94-20675
Green Sheet project: Dye sheet evolution
[AD-A272019] p 1883 N94-21443
Direct simulation of shock-induced mixing layer
[DE93-040498] p 1803 N94-21531

MIXTURES
Chemical equilibrium in high pressure molecular fluid mixtures
[DE93-040160] p 1786 N94-19829
One- and multi-component theories of mixtures
[DE93-040543] p 1966 N94-21511

MOBILE COMMUNICATION SYSTEMS
Mobile antenna development at JPL p 1731 N94-20457
Mobile terminal antennas for helicopters p 1731 N94-20458
Linearly tapered slot antenna circular array for mobile communications
[NASA-TM-106441] p 1769 N94-21808
A consideration of the integration of terrestrial and satellite mobile systems p 1746 N94-22172
ARQ on fading channels p 1747 N94-22242

MODAL RESPONSE
Modal combination in response spectrum modal dynamic analysis
[DE94-000339] p 1833 N94-21956

MODELS
Rockets: Physical science teacher's guide with activities
[NASA-EP-291] p 1669 N94-20226
Current status: Animal models of nausea p 1889 N94-21915

MODERATORS
Temperature and Doppler coefficients of various space nuclear reactors
[DE94-001388] p 1671 N94-21979

MODFETS
Characteristics of 0.8- and 0.2-microns gate length In(x)Ga(1-x) As/In(0.52)Al(0.48)As/InP (0.53 less than or equal to x less than or equal to 0.70) modulation-doped field-effect transistors at cryogenic temperatures p 1733 N94-20499

Characterization of multilayer GaAs/AlGaAs transistor structures by variable angle spectroscopic ellipsometry p 1796 N94-20985
Variable angle of incidence spectroscopic ellipsometric measurement of the Franz-Keldysh effect in MODFET structures p 2021 N94-20987

MODULARITY
A modular design for connectionist parsing p 1941 N94-20252
MAYGEN: A symbolic debugger generation system [AD-A272512] p 1913 N94-21413
Modular interval spaces [PB93-220663] p 1961 N94-22266

MODULATION
Computational model of a magnetic modulator for copper lasers [DE93-019603] p 1815 N94-20223
Stability analysis of unsteady ablation fronts [DE93-019689] p 1819 N94-21839

MODULATION DOPING
Synthesis and properties of mismatched heterojunction/substrate interfaces [AD-A272904] p 1760 N94-21229

MODULATORS
Computational model of a magnetic modulator for copper lasers [DE93-019603] p 1815 N94-20223

MODULES
Research on stable, high-efficiency amorphous silicon multijunction modules [DE93-018220] p 1850 N94-22257

MODULUS OF ELASTICITY
Metastable bcc phase formation in the Nb-Cr system [DE93-018376] p 2012 N94-19926
Adaptation of model parameters of a rail model at measured rail compliances [ILR-MITT-274(1992)] p 1831 N94-21153
Results of the second Round Robin on opening-load measurement conducted by ASTM Task Group E24.04.04 on crack closure measurement and analysis [NASA-TM-109032] p 1832 N94-21624
Molecular dynamics modeling of the mechanical behavior of metallic multilayers [DE93-019947] p 1694 N94-21921
Miniaturized disk-bend testing, nano-indentation, and the microstructure of ion-irradiated titanium aluminides [DE93-040600] p 1697 N94-22559

MOISTURE
Durability predictions for adhesively bonded joints in humid environments [AD-A271177] p 1830 N94-20001
Thin-film hermeticity: A quantitative analysis of diamondlike carbon using variable angle spectroscopic ellipsometry p 1710 N94-20981

MOISTURE CONTENT
Relationship of attenuation in a vegetation canopy to physical parameters of the canopy p 1729 N94-20450
Comparison of cloud microphysical parameters derived from surface and satellite measurements during FIRE phase 2 p 1873 N94-22306
Normalized vertical ice mass flux profiles from vertically pointing 8-mm-wavelength Doppler radar p 1879 N94-22334

MOLDING MATERIALS
Machinable oxide ceramic [AD-D015927] p 1699 N94-20017
Improved ceramic slip casting technique — application to aircraft model fabrication [NASA-CASE-LAR-14471-1] p 1702 N94-20377

MOLECULAR BEAM EPITAXY
Investigation of quantum effects in heterostructures [AD-A270938] p 2011 N94-19817
Theory of energy-assisted epitaxy; theory of ordered semiconductor alloys: In(1-x)Tl(x)Sb as a long-wave infrared material [AD-A271007] p 2012 N94-19635
Common Themes and Mechanisms of Epitaxial Growth, volume 312 — Materials Research Society symposium proceedings [AD-A270513] p 2013 N94-19967
Monocrystalline germanium film on sapphire [AD-D015925] p 2017 N94-20348
Center for the integration of optical computing [AD-A271874] p 1899 N94-20469
Surface treatment of InP and contribution to the optimization of the InP(p)/InP(p) regrown interfaces grown by GSMBE [ECL-92-48] p 2018 N94-20598
Ellipsometric measurements of molecular-beam-epitaxy-grown semiconductor multilayer thicknesses: A comparative study p 1710 N94-20983
In-situ spectroscopic ellipsometry in molecular beam epitaxy p 2024 N94-21005

MOLECULAR BEAMS
Transport in microstructures in the microwave and millimeter-wave regime [AD-A271875] p 2017 N94-20470

MOLECULAR BIOLOGY
High resolution electron crystallography of protein molecules [DE93-040114] p 1884 N94-19826
A complex systems approach to computational molecular biology [DE93-040062] p 1884 N94-19866
Application of molecular modeling to biological processing [AD-A272612] p 1974 N94-21185

MOLECULAR CHAINS
Chain propagation/step propagation polymerization chemistry. The preparation of solvent resistant well phase-separated thermoplastic elastomers [AD-A271128] p 1699 N94-20016
Light scattering studies of an electrorheological fluid [DE93-019419] p 1700 N94-20315
Spatial organization of polymer chains in a crystallizable diblock polyethylene and polystyrene [AD-A271862] p 1702 N94-20463

MOLECULAR CLOUDS
Coagulation of grains in static and collapsing protostellar clouds p 2085 N94-20865
Factor analysis as a tool for spectral line component separation 21cm emission in the direction of L1780 p 1965 N94-22536
Fragmentation of magnetized filamentary interstellar clouds p 2008 N94-22687
Gravitational instability of magnetized filamentary clouds. 1: Helical magnetic fields p 2008 N94-22688
Gravitational instability of magnetized filamentary clouds. 2: Rotation p 2009 N94-22689

MOLECULAR CLUSTERS
Embedded microclusters in zeolites and cluster beam sputtering: Simulation on parallel computers [DE94-000741] p 1701 N94-20352

MOLECULAR COLLISIONS
Collisions of molecules with clusters: A quasiclassical study [DE93-018614] p 1971 N94-20050
Non-adiabatic effects in low-energy electron-molecule scattering [DE93-040485] p 1976 N94-21968

MOLECULAR DIFFUSION
A database of selected transport coefficients for combustion studies [DE93-041278] p 1678 N94-19889
Model for liquid boron oxide droplet gasification in H/O/C/F combustion environments [AD-A272911] p 1682 N94-21243
Combustion in turbulent jets and buoyant flames [PB93-202372] p 1682 N94-21452
Modeling of outgassing and matrix decomposition in carbon-phenolic composites [NASA-CR-194741] p 1676 N94-21743

MOLECULAR DYNAMICS
Embedded microclusters in zeolites and cluster beam sputtering: Simulation on parallel computers [DE94-000741] p 1701 N94-20352
Integral equation calculation of solvent activation free energies for electron and proton transfer reactions [AD-A272665] p 1681 N94-21216
Molecular dynamics modeling of the mechanical behavior of metallic multilayers [DE93-019947] p 1694 N94-21921
Transferable tight-binding parameters: An application to Ni and Ni-Al alloys [DE94-001044] p 1695 N94-22023
Microscopic and macroscopic dynamics [DE93-019576] p 1937 N94-22042
Computer simulation of molecular response at a shock front [DE94-001050] p 1977 N94-22396
Smoothed-particle hydrodynamics and nonequilibrium molecular dynamics [DE94-001059] p 1977 N94-22400

MOLECULAR ELECTRONICS
Ab initio potential energy surface for the H + OCS reaction [AD-A270577] p 1698 N94-19947

MOLECULAR INTERACTIONS
Embedded microclusters in zeolites and cluster beam sputtering: Simulation on parallel computers [DE94-000741] p 1701 N94-20352

MOLECULAR IONS
Collisional processes involving atmospheric gases [AD-A270729] p 1854 N94-19954

MOLECULAR PHYSICS
One- and multi-component theories of mixtures [DE93-040543] p 1966 N94-21511

MOLECULAR RELAXATION
Shock induced condensation in fluids of high molar specific heat: Shock structure and relaxation [MPIS-106/1993] p 1798 N94-20145

MOLECULAR ROTATION
High resolution infrared spectroscopy of cyclobutane: A study of vibrational mode coupling involving large amplitude, low frequency modes [AD-A271987] p 1973 N94-20619

MOLECULAR SPECTROSCOPY
Plasma edge spectroscopy p 1996 N94-21803

MOLECULAR STRUCTURE
Characterization studies of lower and non-TDI polyurethane encapsulants [DE93-041129] p 1698 N94-19857
Femtosecond Raman-induced Kerr effect study of polar solvent dynamics: Amides [DE93-017563] p 1678 N94-19924
Light scattering studies of an electrorheological fluid [DE93-019419] p 1700 N94-20315
High energy ionization in liquids: The free ion yield [DE93-040329] p 1973 N94-20324
In-situ electrochemical surface science [AD-A265942] p 1680 N94-20330
Molecular and atomic arrays in nano- and mesoporous materials synthesis [AD-A271500] p 2017 N94-20544
Rotational isomers of Mo(VI) alkylidene complexes and Cis/trans polymer structure: Investigations in ring-opening metathesis polymerization [AD-A272647] p 1704 N94-21184
Polymerization of enantiomerically pure 2,3-dicarboalkoxy norbornadienes and 5,6-disubstituted norbornenes by well-characterized molybdenum ROMP catalysts [AD-A272649] p 1704 N94-21186
Surface electrochemistry of metals [AD-A272913] p 1691 N94-21245
Optically induced birefringence in copolymers and blends containing azobenzene groups [AD-A273085] p 1706 N94-21523
Column chromatographic separation of Y(3+) from Sr(2+) by polymeric ionizable crown ether resins [DE94-000935] p 1683 N94-22021
Theoretical research program to study chemical reactions in AOTV bow shock tubes [NASA-CR-194710] p 1804 N94-22027
Non-linear thermal instability of optical thin molecular structures p 2006 N94-22667

MOLECULAR TRAJECTORIES
Collisions of molecules with clusters: A quasiclassical study [DE93-018614] p 1971 N94-20050

MOLECULAR WEIGHT
Synthesis and structural characterization of new light molecular weight inorganic oxidizers and relative derivatives, volume 1 [AD-A271437] p 2012 N94-19842
Polybenzoxazole via aromatic nucleophilic displacement [NASA-CASE-LAR-14606-1-CU] p 1672 N94-20540

MOLECULES
Electronically metastable molecules of high symmetry [AD-A272015] p 1974 N94-21461

MOLTEN SALT ELECTROLYTES
Molten carbonate fuel cell networks: Principles, analysis, and performance [DE93-019872] p 1846 N94-21527

MOLYBDENUM
Substrate recovery of Mo-Si multilayer coated optics [DE93-019610] p 1698 N94-19810
Core formation in the Moon: The mystery of the excess depletion of Mo, W and P p 2095 N94-20651
Rotational isomers of Mo(VI) alkylidene complexes and Cis/trans polymer structure: Investigations in ring-opening metathesis polymerization [AD-A272647] p 1704 N94-21184
Polymerization of enantiomerically pure 2,3-dicarboalkoxy norbornadienes and 5,6-disubstituted norbornenes by well-characterized molybdenum ROMP catalysts [AD-A272649] p 1704 N94-21186
Interface science of controlled metal/metal and metal/ceramic interfaces prepared using ultrahigh vacuum diffusion bonding [DE94-001066] p 1696 N94-22025

MOLYBDENUM ALLOYS
The effect of microstructural evolution on superplasticity in Ni3Si(V, Mo) [DE93-041320] p 1694 N94-21943
Alloying effects on mechanical and metallurgical properties of NiAl [DE93-040814] p 1694 N94-21948
Strengthening and toughening in refractory metal alloys [DE93-019942] p 1695 N94-21986

MOLYBDENUM COMPOUNDS
Strength and toughness improvement of silicide intermetallics by nanophase and microphase reinforcements
[AD-A272914] p 1692 N94-21320
MOLYBDENUM DISULFIDES
Scanning tunneling microscopy investigations of metal dichalcogenide materials
[AD-A272910] p 2027 N94-21242
MOMENTUM
Longitudinal beam dynamics for heavy ion fusion using WARPrz
[DE93-019154] p 1992 N94-19915
Meso-Beta scale numerical simulation studies of terrain-induced jet streak mass/momentum perturbations
[NASA-CR-194627] p 1864 N94-20138
Neutron and PIMC determination of the longitudinal momentum distribution of HCP, BCC and normal liquid He-4
[DE93-019009] p 1972 N94-20187
MOMENTUM TRANSFER
Neutron and PIMC determination of the longitudinal momentum distribution of HCP, BCC and normal liquid He-4
[DE93-019009] p 1972 N94-20187
Physical chemistry of energetic nitrogen compounds
[AD-A271819] p 1712 N94-20625
Studies of the deuteron at high energy and momentum transfer
[DE93-041162] p 1976 N94-21941
MONITORS
An embedded fibre optic for damage growth monitoring in Kevlar composites
[ISBN-0-315-83501-X] p 1677 N94-22589
MONKEYS
Susceptibility of the squirrel monkey to different motion conditions p 1885 N94-21899
Recovery of the vomiting reflex following area postrema ablation in squirrel monkeys p 1886 N94-21904
Motion sickness elicited by passive rotation in squirrel monkeys p 1887 N94-21905
Conditioned taste aversion and motion sickness in cats and squirrel monkeys p 1888 N94-21914
MONOCHROMATIC RADIATION
The coherent backscattering opposition effect p 1991 N94-20648
MONOCHROMATORS
Magnetic circular dichroism in x ray absorption and core-level photoemission
[DE93-019381] p 1688 N94-19986
MONOIDS
On semisimple cocommutative bialgebras
[CWI-AM-R9210] p 1954 N94-21158
MONOMERS
Photochemically induced transformations of transition complexes
[AD-A271112] p 2014 N94-19982
Lateral distribution of lipids in membranes at high pressure
[AD-A271183] p 1700 N94-20299
Column chromatographic separation of Y(3+) from Sr(2+) by polymeric ionizable crown ether resins
[DE94-000935] p 1683 N94-22021
MONOPOLE ANTENNAS
A broadband V-antenna for pulsed field measurements: Experimental results p 1745 N94-22139
MONOPROPELLANTS
Monopropellant aqueous hydroxyl ammonium nitrate/fuel
[AD-D015922] p 1712 N94-20061
Chemistry of the burning surface
[AD-A272725] p 1681 N94-21181
MONOPULSE ANTENNAS
Topographic mapping using a monopulse SAR system p 1721 N94-20417
MONOPULSE RADAR
Topographic mapping using a monopulse SAR system p 1721 N94-20417
MONTE CARLO METHOD
Chemical equilibrium in high pressure molecular fluid mixtures
[DE93-040160] p 1796 N94-19829
Neutron and PIMC determination of the longitudinal momentum distribution of HCP, BCC and normal liquid He-4
[DE93-019009] p 1972 N94-20187
The GEM Silicon Tracking System
[DE93-040133] p 2016 N94-20322
A theoretical and numerical study of polarimetric scattering and emission from random rough surfaces with anisotropic directional spectrum p 1730 N94-20454
One- and multi-component theories of mixtures
[DE93-040543] p 1966 N94-21511
Interpolative modeling of GaAs FET S-parameter data bases for use in Monte Carlo simulations p 1767 N94-21723
High power, electron-beam induced switching in diamond
[DE93-040535] p 1768 N94-21770
A simulation model for probabilistic analysis of Space Shuttle abort modes
[NASA-TM-108432] p 1656 N94-21859
Toward a QCD analysis of jet rates in deep-inelastic Muon-Proton scattering
[DE94-000618] p 1976 N94-21962
A unified Monte Carlo interpretation of particle simulations and applications to nonneutral plasmas
[DE94-001231] p 1997 N94-21973
Monte Carlo calculation of multi-electron effects on synchrotron radiation
[DE94-001259] p 1982 N94-21974
A High Resolution Liquid Xenon Imaging Telescope for 0.3-10 MeV Gamma Ray Astrophysics: Construction and Initial Balloon Flights
[NASA-CR-194709] p 2056 N94-22281
The polarization sensitivity of the liquid xenon imaging telescope p 2056 N94-22282
Simulating the Euclidean time Schroedinger equations using an INTEL iPSC/860 hypercube: Application to the t-J model of high-T(sub c) superconductivity
[DE94-000489] p 2035 N94-22385
Algorithmic advances in stochastic programming
[DE94-001160] p 1921 N94-22406
A Monte Carlo study of the Sudbury Neutrino Observatory small test detector experiment
[ISBN-0-315-59056-4] p 1977 N94-22416
Likelihood analysis of parity violation in the compound nucleus
[DE94-000671] p 1977 N94-22572
MOON
The Clementine Mission science return at the Moon and Geographos p 1652 N94-20850
MOORING
The marine light-mixed layer experiment cruise and data report: R/V endeavor cruise EN-224, mooring deployment, 27 April-1 May 1991: Cruise EN-227, mooring recovery, 5-23 September 1991
[AD-A271175] p 1864 N94-20186
MORPHOLOGY
Development of a technique to determine the morphology and dynamics of agglomerates in chemically reacting flows
[AD-A271160] p 1678 N94-20000
Morphologic and morphometric studies of impact craters in the northern plains of Mars p 2089 N94-20384
Response of the topography and gravity field on Venus to mantle upwelling beneath a chemical boundary layer p 2117 N94-20775
Contributions of the Clementine mission to our understanding of the processes and history of the Moon p 2119 N94-20784
A classification scheme for the morphology of lava flow fields p 1863 N94-20879
Structure and morphology of Pd overlayers on epitaxial SnO2 films studies with the atomic force microscope
[AD-A271827] p 2028 N94-21458
Growth and morphology of crystals: Theory and observations
[PB93-221166] p 2035 N94-22273
MORTALITY
Health effects of global warming: Problems in assessment
[DE93-040323] p 1850 N94-19930
MOSAICS
Cathodoluminescence observations of in situ aqueous destruction of chondrules in the Murchison CM chondrite p 2083 N94-20750
MOSSBAUER EFFECT
Fabrication and evaluation of superconducting and semiconducting materials
[AD-A271645] p 2018 N94-20558
Magnetic properties and Moessbauer analyses of glass from the K-T boundary, Beloc, Haiti p 1685 N94-20753
Combined backscatter Moessbauer spectrometer/x ray fluorescence analyzer (BaMS/XRF) for extraterrestrial surfaces p 1686 N94-20761
MOTION PERCEPTION
The local measurement and global interpretation of 3D motion field generated by several moving objects from range image sequences p 1777 N94-22146
Segmenting the optical flow due to the motion of several rigid objects p 1777 N94-22147
Mobile robot perception in unknown and unstructured dynamic voxel environments
[ISBN-0-315-83951-1] p 1947 N94-22591
MOTION SICKNESS
Self-Motion Perception and Motion Sickness
[NASA-CR-194276] p 1885 N94-21897
Changes in plasma vasopressin during motion sickness in cats p 1885 N94-21898
Susceptibility of the squirrel monkey to different motion conditions p 1885 N94-21899
Relationship of area postrema to three putative measures of motion sickness p 1885 N94-21900
Reassessment of area postrema's role in motion sickness and conditioned taste aversion p 1886 N94-21901
Gamma-aminobutyric acid (GABA) and neuropeptides in neural areas mediating motion-induced emesis p 1886 N94-21902
Motion sickness elicited by passive rotation in squirrel monkeys p 1887 N94-21905
Area postrema ablations in cats: Evidence for separate neural routes for motion- and xylazine-induced CTA and emesis p 1887 N94-21906
Immunocytochemical localization of glutamic acid decarboxylase (GAD) and substance P in neural areas mediating motion-induced emesis: Effects of vagal stimulation on GAD immunoreactivity p 1887 N94-21909
The effects of area postrema lesions and selective vagotomy on motion-induced conditioned taste aversion p 1888 N94-21910
Experimental studies of gastric dysfunction in motion sickness: The effect of gastric and vestibular stimulation on the vagal and splanchnic gastric efferents p 1888 N94-21911
Role of the area postrema in three putative measures of motion sickness in the rat p 1888 N94-21912
Investigating motion sickness using the conditioned taste aversion paradigm p 1888 N94-21913
Conditioned taste aversion and motion sickness in cats and squirrel monkeys p 1888 N94-21914
MOTION SICKNESS DRUGS
Susceptibility of the squirrel monkey to different motion conditions p 1885 N94-21899
MOTION SIMULATION
Strategy for motion of a moving body of quasi-polygonal form within a polygonal space p 1792 N94-22240
MOTOR VEHICLES
The causes of contact noise
[REPT-92-100] p 1822 N94-20157
MSAT
Mobile antenna development at JPL p 1731 N94-20457
Comparison of theoretical and simulated performance results for sloppy-slotted Aloha signaling p 1746 N94-22204
MULTICHANNEL COMMUNICATION
State-space models for multichannel detection
[AD-A270608] p 1715 N94-19816
Simulated retrieval of land surface parameters using multichannel satellite microwave radiometry p 1727 N94-20443
Four-channel HF receiving antenna array simulator
[AD-A271876] p 1732 N94-20471
Recording system using multiplexed inputs to a multichannel recorder
[AD-D015971] p 1808 N94-21278
MULTIGRID METHODS
Multigrid approach to solving the long transportation problem on a regular grid in cost space
[AD-A272323] p 1909 N94-21038
MGD1M: A parallel multigrid code with a fast vectorized ILU-relaxation
[CWI-NM-R9222] p 1930 N94-21077
A multi-level solution algorithm for steady-state Markov chains
[NASA-CR-191558] p 1914 N94-21462
The Sixth Copper Mountain Conference on Multigrid Methods, part 2
[NASA-CP-3224-PT-2] p 1955 N94-21464
Optimal resolution in maximum entropy image reconstruction from projections with multigrid acceleration p 1955 N94-21465
Multilevel methods for transport equations in diffusive regimes p 1955 N94-21467
Analysis of multigrid methods on massively parallel computers: Architectural implications p 1938 N94-21468
Time-accurate Navier-Stokes calculations with multigrid acceleration p 1956 N94-21469
Looking for O(N) Navier-Stokes solutions on non-structured meshes p 1806 N94-21471
The block adaptive multigrid method applied to the solution of the Euler equations p 1641 N94-21472
Multigrid schemes for viscous hypersonic flows p 1641 N94-21473
Layout optimization with algebraic multigrid methods p 1957 N94-21474
A multigrid method for steady Euler equations on unstructured adaptive grids p 1957 N94-21476
An automatic multigrid method for the solution of sparse linear systems p 1957 N94-21478
A multigrid algorithm for the cell-centered finite difference scheme p 1957 N94-21479

A semi-Lagrangian approach to the shallow water equation p 1806 N94-21480
Multigrid solution of the Navier-Stokes equations on highly stretched grids with defect correction p 1806 N94-21481
The multigrid preconditioned conjugate gradient method p 1958 N94-21482
Mapping robust parallel multigrid algorithms to scalable memory architectures p 1922 N94-21483
Unstructured multigrid through agglomeration p 1958 N94-21484
Multigrid properties of upwind-biased data reconstructions p 1806 N94-21485
On the prediction of multigrid efficiency through local mode analysis p 1959 N94-21486
Numerical study of a multigrid method with four smoothing methods for the incompressible Navier-Stokes equations in general coordinates p 1806 N94-21487
Parallelizing a highly vectorized multigrid code with zebra relaxation
[CWI-NM-R9225] p 1935 N94-21610
Numerical multigrid software (MGD5M): A parallel multigrid code with a twisted ILLU-relaxation
[CWI-NM-R9226] p 1916 N94-21611
The 3-D unstructured mesh generation using local transformations p 1919 N94-22356

MULTILAYER INSULATION
Outgassing rate of Reemay Spunbonded Polyester and DuPont Double Aluminized Mylar
[DE93-040015] p 1699 N94-19973

MULTIMEDIA
A concept for implementing hypermedia technology in computer aided workplaces in medicine
[ETN-93-95057] p 1889 N94-20022
Telecommunications services for multimedia data exchange support
[AD-A271704] p 1740 N94-21352
CMIFed: A presentation environment for porta ble hypermedia documents
[CWI-CS-R9305] p 2044 N94-21494
Structured multimedia authoring
[CWI-CS-R9304] p 2044 N94-21535
The Amsterdam hypermedia model: Extending hypertext to support real multimedia
[CWI-CS-R9306] p 2045 N94-21536
Publication of science data on CD-ROM: A guide and example
[NASA-CR-4560] p 1842 N94-21585

MULTIMODE RESONATORS
Stability curves for a thermoacoustic prime mover
[AD-A272607] p 1968 N94-21422

MULTIPATH TRANSMISSION
Robust, high-speed network design for large-scale multiprocessing
[AD-A271003] p 1716 N94-19977
Optical signal processing
[AD-A271036] p 1983 N94-20013

MULTIPHASE FLOW
Technology to prevent greenhouse effect gases
[DE94-707421] p 1850 N94-19976
High-resolution numerical methods for compressible multi-phase flow in hierarchical porous media
[DE94-000740] p 1799 N94-20351

MULTIPHOTON ABSORPTION
Direct detection of atomic ions from molecular photofragmentation during nonresonant multiphoton ionization of sputtered species
[DE93-040686] p 1976 N94-21951

MULTIPLE ACCESS
Analysis of the TDRS multiple access system for possible use as an attitude control system sensor p 1666 N94-21338
A one-shot access scheme for a multicast switch p 1773 N94-22120

MULTIPLEXING
Recording system using multiplexed inputs to a multichannel recorder
[AD-D015971] p 1808 N94-21278
Wide passband wavelength multi/demultiplexer at 1.3/1.55 micrometers based on etched Fresnel mirror, appendix 8 p 1989 N94-21602
Quadrature biorthogonal modulation p 1747 N94-22232

MULTIPLIERS
Complementary heterojunction FET technology for space application p 1755 N94-21094
Synthesis algorithm of VLSI multipliers for ASIC p 1758 N94-21116
Evaluation of floating-point sum or difference of products in carry-save domain p 1764 N94-21705

MULTIPOLES
A summary of studies of particle stability at RHIC
[DE93-040173] p 1970 N94-19666
Fast fourier transforms for nonequispaced data
[AD-A272687] p 1954 N94-21164

MULTIPROCESSING (COMPUTERS)
Segmented operations for sparse matrix computation on vector multiprocessors
[AD-A270601] p 1928 N94-19950
Robust, high-speed network design for large-scale multiprocessing
[AD-A271003] p 1716 N94-19977
Multilist scheduling: A new parallel programming model
[AD-A270549] p 1929 N94-20084
Memory contention in scalable cache-coherent multiprocessors
[TR-448] p 1929 N94-20144
Parallel logic programming systems
[RR-891-I] p 1929 N94-20176
Time warp operating system version 2.7 internals manual
[NASA-CR-194798] p 1899 N94-20549
Measuring the effects of thread placement on the Kendall Square KSR1
[DE93-040655] p 1908 N94-20932
Analysis and evaluation of configuring of graphical systems on multiprocessor architectures
[ETN-93-93618] p 1930 N94-21018
Avoiding and tolerating latency in large-scale next-generation shared-memory multiprocessors p 1753 N94-21081
The effects of block size on the performance of coherent caches in shared-memory multiprocessors
[AD-A272638] p 1899 N94-21177
Scheduling for locality in shared-memory multiprocessors
[AD-A272948] p 1930 N94-21228
Software coherence in multiprocessor memory systems
[NASA-CR-194696] p 1931 N94-21272
Using parallel banded linear system solvers in generalized eigenvalue problems
[NASA-CR-191540] p 1915 N94-21584
A simple modern correctness condition for a space-based high-performance multiprocessor p 1766 N94-21718
Low energy CMOS for space applications p 1768 N94-21735
Using stream interleaving to eliminate the need for interlocks in deeply pipelined processors p 1781 N94-22175
Integration of parallel processing structures using a matrix approach p 1784 N94-22192
Fault tolerance for real-time multiprocessor operating systems p 1788 N94-22216
Distributed input/output processing in data-driven multiprocessors
[DE94-000323] p 1937 N94-22378
The ADAM environment and transputers p 1926 N94-22494
A new programming metaphor for image processing procedures p 1927 N94-22531

MULTIPROGRAMMING
Scheduling for locality in shared-memory multiprocessors
[AD-A272948] p 1930 N94-21228

MULTISENSOR APPLICATIONS
Integrated display of multi-sensor geophysical and electromagnetic flight data p 1721 N94-20418
Multisensor pinhole yawsonde
[AD-A271715] p 1808 N94-20930

MULTISPECTRAL PHOTOGRAPHY
Information extraction for multispectral images using radiation interaction models
[BCRS-90-22] p 1841 N94-21015

MULTISPECTRAL RADAR
Use of microwave polarimetry to enhance SAR images of the ocean surface
[AD-A271911] p 1882 N94-20489

MULTIVARIATE STATISTICAL ANALYSIS
Fast scalar algorithms for multivariate partial correlations and their empirical counterparts
[RR-903-M] p 1905 N94-20201
Multivariate statistical analysis: Principles and applications to coorbital streams of meteorite falls p 1964 N94-20881
Method for design rotation
[AD-A272440] p 1911 N94-21204
Extracting galactic structure parameters from multivariated density estimation p 1964 N94-22458
SIMBAD quality-control p 2048 N94-22502
Factor analysis as a tool for spectral line component separation 21cm emission in the direction of L1780 p 1965 N94-22536

MUONS
Measurement of the B(+) and B(0) lifetimes
[DE93-019906] p 1969 N94-19814
B production at D0
[DE93-019250] p 1972 N94-20291
Evaluation of the chemical composition of cosmic radiation in energy area of 10(exp 15) eV
[ETN-93-93682] p 2150 N94-21056
Toward a QCD analysis of jet rates in deep-inelastic Muon-Proton scattering
[DE94-000618] p 1976 N94-21962

MURCHISON METEORITE
Identification of an interstellar oxide grain from the Murchison meteorite by ion imaging p 2082 N94-20659
Petrography and origin of refractory inclusions from the Murray and Murchison C2 chondrites p 2084 N94-20770
Trace element compositions of spinel-rich refractory inclusions from the Murchison meteorite p 2086 N94-20897

MURRAY METEORITE
Petrography and origin of refractory inclusions from the Murray and Murchison C2 chondrites p 2084 N94-20770

MUSCLES
Cosmos 2229
[NASA-CR-194734] p 1895 N94-20338

MUSCULAR FUNCTION
Cosmos 2229
[NASA-CR-194734] p 1895 N94-20338

MUSCULAR STRENGTH
Maximum team lifting capacity as a function of team size
[AD-A271642] p 1892 N94-21036
Strength capabilities and load requirements while performing torquing tasks in zero gravity
[NASA-TP-3433] p 1897 N94-21627

MYLAR (TRADEMARK)
Outgassing rate of Reemay Spunbonded Polyester and DuPont Double Aluminized Mylar
[DE93-040015] p 1699 N94-19973

N

NAKHLITES
An attempt to comprehend Martian weathering conditions through the analysis of terrestrial palagonite samples p 2143 N94-21668

NAMING
Named Venusian craters p 2109 N94-20725

NAPHTHALENE
The thermodynamic properties to 700 K of naphthalene and 2,7-dimethylnaphthalene
[DE93-000160] p 2037 N94-20473

NARROWBAND
Evaluation of a single stage of the LADS filter
[AD-A271101] p 1814 N94-19851
RADCAL: A narrow-band model for radiation calculations in a combustion environment
[PB93-200889] p 1682 N94-21448

NASA PROGRAMS
NASA's Education Program
[NASA-EP-297] p 2038 N94-20129
NASA property: Improving management of government equipment provided to contractors. Report to the Chairman, Subcommittee on Investigations and Oversight, Committee on Science, Space, and Technology, House of Representatives
[GAO/NSIAD-93-191] p 2039 N94-20206
NASA procurement: Planning for pilot test of new procurement procedures is adequate. Report to the Chairman, Committee on Governmental Affairs, US Senate
[GAO/NSIAD-94-67] p 2039 N94-20236
The manager's guide to NASA graphics standards
[NHB-1430.2] p 2042 N94-20308
NASA patent abstracts bibliography: A continuing bibliography. Section 1: Abstracts (supplement 44)
[NASA-SP-7039(44)-SECT-1] p 2043 N94-21254
Network command processing system overview p 1935 N94-21351
Issues in NASA program and project management. Special Report: 1993 conference
[NASA-SP-6101(07)] p 2039 N94-21497
Issues in NASA program and project management
[NASA-SP-6101(06)] p 2040 N94-21499
NASA procurement report, FY 1992
[NASA-TM-109390] p 2040 N94-21623
NASA procurement report, FY 1993
[NASA-TM-109393] p 2040 N94-21625
Summary data on all NASA procurement actions
[NASA-TM-109392] p 2040 N94-21638
NASA SERC digital correlator projects p 1765 N94-21708
Index to 1992 NASA Tech Briefs, volume 16, numbers 1-12
[NASA-TM-109377] p 2053 N94-21736

Index to 1991 NASA Tech Briefs, volume 15, numbers 1-12
[NASA-TM-109376] p 2053 N94-21737
Cumulative index to NASA Tech Briefs, 1986-1990, volumes 10-14
[NASA-TM-109378] p 2054 N94-21738
An overview of the radiation component of the NASA TOGA-COARE experiment p 1881 N94-22344
Johnson Space Center CFD grid generation requirements p 1919 N94-22355
NASA's astrophysics archives at the National Space Science Data Center p 2049 N94-22541

NASA SPACE PROGRAMS
The future of remote sensing from space: Civilian satellite systems and applications
[OTA-ISC-558] p 1837 N94-20209

NATIONAL PARKS
Linear mixing model applied to AVHRR LAC data p 1838 N94-20958

NATURAL GAS
Speed of sound data and related models for mixtures of natural gas constituents
[PB93-200822] p 1968 N94-21447
Vapor-delivered lubrication of steel-steel and steel-ceramic systems
[PB93-202364] p 1825 N94-21451
Combustion in turbulent jets and buoyant flames
[PB93-202372] p 1682 N94-21452
Current situation in developing petroleum substituting energy (the United Kingdom)
[DE94-714897] p 1713 N94-22091

NATURAL LANGUAGE (COMPUTERS)
Are types needed for natural language?
[PB93-191831] p 1949 N94-19997
Nominalization, prediction and type containment
[PB93-191799] p 1898 N94-20082
Connectionism and Natural Language Processing
[MEMO-INF-92-64] p 1940 N94-20242
A single layer higher order neural net and its application to grammar recognition p 1941 N94-20251
A modular design for connectionist parsing p 1941 N94-20252
Syntactic neural networks for natural language processing p 1941 N94-20254
DISCERN: A distributed neural network model of script processing and memory p 1941 N94-20255
The Seventh International Symposium on Methodologies for Intelligent Systems (Poster Session)
[AD-A272125] p 1942 N94-20573

NATURAL LANGUAGE PROCESSING
Are types needed for natural language?
[PB93-191831] p 1949 N94-19997
A computational theory of lexical relatedness
[TR-421] p 1904 N94-20067
Causal reconstruction
[AD-A271692] p 1908 N94-20929
Recognizing hesitation phenomena in continuous, spontaneous speech p 1746 N94-22210
Intelligent text retrieval in the NASA astrophysics data system p 2048 N94-22499

NAUSEA
Changes in plasma vasopressin during motion sickness in cats p 1885 N94-21898
Current status: Animal models of nausea p 1889 N94-21915

NAVIER-STOKES EQUATION
Linear and nonlinear PSE for compressible boundary layers
[NASA-CR-191537] p 1797 N94-20033
A comparison of two incompressible Navier-Stokes algorithms for unsteady internal flow
[NASA-TM-108794] p 1798 N94-20104
Head-on collision of drops: A numerical investigation
[NASA-TM-106394] p 1798 N94-20167
Some practical turbulence modeling options for Reynolds-averaged full Navier-Stokes calculations of three-dimensional flows
[NASA-TM-106399] p 1637 N94-20534
Prediction and control of vortex-dominated and vortex-wake flows
[NASA-CR-194722] p 1637 N94-21054
Computational and analytical methods in nonlinear fluid dynamics
[AD-A272722] p 1802 N94-21169
An efficient numerical method for three-dimensional hypersonic flow
[AD-A272506] p 1637 N94-21411
Time-accurate Navier-Stokes calculations with multigrid acceleration p 1956 N94-21469
Looking for O(N) Navier-Stokes solutions on non-structured meshes p 1806 N94-21471
Multigrid solution of the Navier-Stokes equations on highly stretched grids with defect correction p 1806 N94-21481
On the prediction of multigrid efficiency through local mode analysis p 1959 N94-21486
Numerical study of a multigrid method with four smoothing methods for the incompressible Navier-Stokes equations in general coordinates p 1806 N94-21487
A study of the compressible flow through a diffusing S-duct
[NASA-TM-106411] p 1638 N94-21591
Mixed finite element and finite volume methods
[ISBN-0-315-63035-3] p 1805 N94-22417

NAVIGATION AIDS
Comparison of a distributed Kalman filter versus a centralized Kalman filter with fault detection considerations
[AD-A270713] p 1903 N94-19969

NAVIGATION INSTRUMENTS
Automatic AVHRR image navigation software
[NASA-CR-194602] p 1643 N94-20148
A software architecture for a small autonomous underwater vehicle navigation system
[AD-A272322] p 1643 N94-21037

NAVY
Audit report. Navy's aircraft structural life surveillance program data recorders
[AD-A270391] p 1645 N94-20040

NEAR FIELDS
Probe compensation in cylindrical near-field scanning: A novel simulation methodology p 1718 N94-20404
Massively parallel computation of RCS with finite elements p 1726 N94-20437
Applications of planar near-field measurements to electromagnetic radiation and interference problems p 1747 N94-22252

NEAR INFRARED RADIATION
Wavelength dependence of limb-darkening of Mars from visible and near-IR telescopic spectral imaging p 2101 N94-20685
Spatial distribution of near infrared line radiation in galactic nuclei measured with Fabry-Perot spectrometer FAST
[MPE-239] p 2081 N94-21138
Deep near-infrared survey of the Southern Sky (DENIS) p 2062 N94-22467

NEAR WAKES
Near wake measurements on a rotor model with Mie-vanes in the Delft open jet tunnel
[PB93-215382] p 1638 N94-22260

NEBULAE
Formation of the low-mass solar nebula p 2109 N94-20728
Diffusive redistribution of water vapor in the solar nebula revisited p 2113 N94-20751
Magnetically controlled solar nebula p 2120 N94-20791
Magnetic reconnection in emission nebulae in clusters of galaxies p 2010 N94-22700

NEGATIVE ELECTRON AFFINITY
Growth, characterization and device development in monocrystalline diamond films
[AD-A272715] p 2026 N94-21190

NEGATIVE FEEDBACK
Temperature and Doppler coefficients of various space nuclear reactors
[DE94-001388] p 1671 N94-21979

NEGATIVE IONS
Optimization and control of a small angle ion source using an adaptive neural network controller
[DE93-040063] p 1946 N94-21845

NEGATIVE RESISTANCE CIRCUITS
Interinjection-locked quasioptical power combiners and phased arrays
[AD-A271178] p 2015 N94-20214

NEGATIVE RESISTANCE DEVICES
Interinjection-locked quasioptical power combiners and phased arrays
[AD-A271178] p 2015 N94-20214

NEODYMIUM
Optical properties of chromium and neodymium in zirconium - barium - lanthanum - aluminum fluoride glass
[AD-A271609] p 1987 N94-21236

NEODYMIUM COMPOUNDS
Crystal structure and short-range oxygen defects in La- and Nd-modified ZrO2
[DE93-040229] p 2033 N94-21993

NEODYMIUM ISOTOPES
The Sm-(146,147)-Nd-(142,143) formation interval for the lunar mantle and implications for lunar evolution p 2097 N94-20663
The Sm-Nd systematics of silicate inclusions in iron meteorites: Results from Caddo (IAB)
[CONTRIB-5241(804)] p 2084 N94-20795

NEODYMIUM LASERS
Development of a lidar for integration with the Naval Postgraduate School Infrared Search and Target Designation (NPS-IRSTD) system
[AD-A271847] p 1817 N94-20611
Simulations of spectral broadening by cross-phase modulation (XPM) with chaotic light pulses
[DE93-019623] p 1819 N94-21872
Effect of bandwidth on beam smoothing and frequency conversion at the third harmonic of the Nova laser
[DE93-019917] p 1819 N94-21920

NEON
Helium in interplanetary dust particles p 2082 N94-20653

NEON ISOTOPES
SCR neon and argon in Kapoeta feldspar: Evidence for an active ancient Sun p 2106 N94-20712

NEPHANALYSIS
An analysis of cloud-cover reporting in the 1977 surface observation database
[AD-A271102] p 1864 N94-19852

NEPTUNIUM
Crystallographic phase transitions in actinide metals as a function of pressure
[DE93-040138] p 2011 N94-19827

NEPTUNIUM COMPOUNDS
Theoretical studies of the structures and electronic properties of U(NH2)(sub 3) and Np(NH2)(sub 3)
[DE94-000768] p 2031 N94-21857

NERVES
The role of axon-Schwann cell interactions in nervous system ionic homeostasis
[AD-A270936] p 1890 N94-20045
Theoretical and numerical examinations of nonlinear parameter dependent advanced differential difference equations
[ETN-93-93681] p 1952 N94-21042
Immunocytochemical localization of glutamic acid decarboxylase (GAD) and substance P in neural areas mediating motion-induced emesis: Effects of vagal stimulation on GAD immunoreactivity p 1887 N94-21909

NERVOUS SYSTEM
The role of axon-Schwann cell interactions in nervous system ionic homeostasis
[AD-A270936] p 1890 N94-20045
The effects of area postrema lesions and selective vagotomy on motion-induced conditioned taste aversion p 1888 N94-21910

NETHERLANDS
Soil temperatures
[KNMI-WR-92-05] p 1865 N94-20309

NETWORK ANALYSIS
SPICE macromodel for a 1-megawatt power MOSFET switch
[DE93-019415] p 1748 N94-19844
High resolution signal processing
[AD-A271181] p 1717 N94-20215
An evaluation of artificial neural network modeling for manpower analysis
[AD-A273001] p 1945 N94-21269
Sorting network for the partial selection problem p 1773 N94-22121
A neural network approach to the maximum flow problem p 1783 N94-22183
Throughput and blocking in circuit-switched interconnection networks p 1784 N94-22189
Neural networks for optimum routing in packet-switched communications networks p 1746 N94-22205

NETWORK CONTROL
Physics Detector Simulation Facility. Phase 2: System software description
[DE93-019745] p 1928 N94-19812
Networks Technology Conference
[NASA-CP-3241] p 1931 N94-21323
The NCC project: A quality management perspective p 1828 N94-21324
Let your fingers do the walking: The projects most invaluable tool p 1922 N94-21325
Software metrics: The key to quality software on the NCC project p 1922 N94-21326
Enhanced networks operations using the X Window System p 1932 N94-21329
The automated ground network system p 1932 N94-21330
Mission Operations Support Area (MOSA) for ground network support p 1932 N94-21331
Space network scheduling benchmark: A proof-of-concept process for technology transfer p 1932 N94-21332
Distributed intelligent control and status networking p 1932 N94-21335
Developing a space network interface simulator: The NTS approach p 1933 N94-21343
A packet switched communications system for GRO p 1744 N94-21345
A laboratory system for the investigation of rain fade compensation techniques for Ka-band satellites
[NASA-CR-191200] p 1782 N94-21566

NETWORKS
Tests of a simple data merging algorithm for the GONG project p 1927 N94-22549

NEURAL NETS
Metrics for specifying and/or testing neural networks statement of government interest [AD-D015946] p 1938 N94-19843
A complex systems approach to computational molecular biology [DE93-040062] p 1884 N94-19866
Building brains for bodies [AD-A270531] p 1939 N94-19875
Center for neural engineering [AD-A271164] p 1890 N94-20185
Proceedings of the Twentieth Annual Technologyfest p 1645 N94-20188
Self-organization via active exploration in robotic applications. Phase 2: Hybrid hardware prototype [NASA-CR-194723] p 1939 N94-20212
Connectionism and Natural Language Processing [MEMO-INF-92-64] p 1940 N94-20242
Representation of spoken words in a self-organizing neural net p 1940 N94-20243
Modeling the human mental lexicon with self-organizing feature maps p 1743 N94-20244
Speech synthesis with artificial neural networks p 1743 N94-20245
Generalization performance of backpropagation learning on a syllabification task p 1940 N94-20246
Hopfield models as neural-network acceptors p 1941 N94-20250
A single layer higher order neural net and its application to grammar recognition p 1941 N94-20251
Syntactic neural networks for natural language processing p 1941 N94-20254
DISCERN: A distributed neural network model of script processing and memory p 1941 N94-20255
Applying the INN model to the MaxClique [DE93-040137] p 1906 N94-20276
Electronic neural network for solving traveling salesman and similar global optimization problems [NASA-CASE-NPO-17807-2-CU] p 1942 N94-20360
Neural network for processing both spatial and temporal data with time based back-propagation [NASA-CASE-MSC-21874-1] p 1942 N94-20366
Retrieval of ice thickness from polarimetric SAR data p 1724 N94-20432
Application of neural network to remote sensing of soil moisture using theoretical polarimetric backscattering coefficients p 1730 N94-20455
Center for the integration of optical computing [AD-A271874] p 1899 N94-20469
The Seventh International Symposium on Methodologies for Intelligent Systems (Poster Session) [AD-A272125] p 1942 N94-20573
Simulating a user's preferences: Towards automated artificial evolution for computer generated images [AD-A272058] p 1942 N94-20621
Algorithm/architecture study for artificial neural nets [AD-A271820] p 1943 N94-20626
An application of the Cerebellar Model Articulation Controller for a switched reluctance rotor position estimator [AD-A271769] p 1943 N94-20926
Neural network studies [AD-A271593] p 1943 N94-20947
Robust neural classifier circuits using asynchronous design p 1757 N94-21111
An evaluation of artificial neural network modeling for manpower analysis [AD-A273001] p 1945 N94-21269
Application of a back-propagation neural network to isolated-word speech recognition [AD-A272495] p 1945 N94-21430
A mean field neural network for hierarchical module placement p 1766 N94-21720
A comparative robustness evaluation of feedforward neurofilters [NASA-TM-106440] p 1650 N94-21742
Simulated behaviour of large scale SCI rings and tori [DE93-040149] p 1935 N94-21745
Optimization and control of a small angle ion source using an adaptive neural network controller [DE93-040063] p 1946 N94-21845
Estimation of AR signal patterns using competitive neural networks p 1744 N94-22102
Signal classification and noise filtering using artificial neural networks p 1744 N94-22103
Noise filtering using multilayer feedforward neural network p 1770 N94-22104
A neural network for multiresolution edge detection p 1779 N94-22163
Improvement in invariant pattern recognition with neural networks and Fourier-Mellin filters p 1780 N94-22164
A neural M-ary tree method for data compression p 1780 N94-22166
Cascaded recursive artificial neural networks p 1780 N94-22167
On the discovery of approximate arithmetic relations by backpropagation networks p 1782 N94-22181
Logic oriented neural networks p 1782 N94-22182
A neural network approach to the maximum flow problem p 1783 N94-22183
A Hopfield neural net for discrete Fourier transform calculation p 1783 N94-22184
Interference reduction using neural networks p 1783 N94-22186
A pyramid neural network architecture for stereo fusion p 1785 N94-22201
Neural networks for optimum routing in packet-switched communications networks p 1746 N94-22205
Acceleration of backpropagation learning using a parallel DSP machine p 1786 N94-22206
A framework of connectionist network toward speech waveform coding p 1746 N94-22211
Speaker-independent isolated-digit recognition using neural networks and hidden Markov model p 1747 N94-22213
Fuzzy and neural control [NASA-TM-108753] p 1947 N94-22270
A neural network prototyping package within IRAF p 1949 N94-22451
STARBASE: Database software for the automated plate scanner p 1927 N94-22512
General asymmetric neural networks and structure design by genetic algorithms: A learning rule for temporal patterns [DE94-001254] p 1947 N94-22563

NEUROLOGY
Incongruity, incongruity resolution, and mental states: The measure and modification of situational awareness and control [NASA-CR-194568] p 1893 N94-20168
Relationship of area postrema to three putative measures of motion sickness p 1885 N94-21900
The effects of area postrema lesions and selective vagotomy on motion-induced conditioned taste aversion p 1888 N94-21910
Current status: Animal models of nausea p 1889 N94-21915

NEURONS
The role of axon-Schwann cell interactions in nervous system ionic homeostasis [AD-A270936] p 1890 N94-20045
Toward a neurobiological theory of visual attention [AD-A270724] p 1890 N94-20112

NEUROPHYSIOLOGY
The role of axon-Schwann cell interactions in nervous system ionic homeostasis [AD-A270936] p 1890 N94-20045
Toward a neurobiological theory of visual attention [AD-A270724] p 1890 N94-20112
Gamma-aminobutyric acid (GABA) and neuropeptides in neural areas mediating motion-induced emesis p 1886 N94-21902

NEUROTRANSMITTERS
The role of axon-Schwann cell interactions in nervous system ionic homeostasis [AD-A270936] p 1890 N94-20045
Gamma-aminobutyric acid (GABA) and neuropeptides in neural areas mediating motion-induced emesis p 1886 N94-21902
Immunocytochemical localization of glutamic acid decarboxylase (GAD) and substance P in neural areas mediating motion-induced emesis: Effects of vagal stimulation on GAD immunoreactivity p 1887 N94-21909

NEUTRAL ATMOSPHERES
Modeling of the coupled magnetospheric and neutral wind dynamos [NASA-CR-194728] p 1856 N94-20537

NEUTRAL ATOMS
Uncertainty limited atomic position measurement using optical fields [AD-A271013] p 1970 N94-19822

NEUTRAL BEAMS
Fast ion behavior during neutral beam injection in ATF [DE93-040267] p 1992 N94-20058

NEUTRAL GASES
Design aspects and parametric characterisation of a neutral rare gas laser [AD-A271100] p 1814 N94-19850
Electronically metastable molecules of high symmetry [AD-A272015] p 1974 N94-21461

NEUTRINOS
CERN-derived analysis of lunar radiation backgrounds p 2080 N94-20880
A Monte Carlo study of the Sudbury Neutrino Observatory small test detector experiment [ISBN-0-315-59056-4] p 1977 N94-22416
Neutrino emission processes in dense high-temperature plasmas p 2001 N94-22638

NEUTRON DIFFRACTION
Neutron and PIMC determination of the longitudinal momentum distribution of HCP, BCC and normal liquid He-4 [DE93-019009] p 1972 N94-20187
Neutron-scattering studies of Yb-bearing silicate glasses [DE93-019768] p 1700 N94-20265
Non-Fermi-liquid and multichannel Kondo phenomena in Y(1-x)U(x)Pd3 and related alloys [DE93-040135] p 2015 N94-20275

NEUTRON IRRADIATION
AGB stars as a source of short-lived radioactive nuclei in the solar nebula p 2133 N94-20859
Tensile and shear fracture behavior of fiber reinforced plastics at 77K irradiated by various radiation sources [DE93-040280] p 1706 N94-21542
Issues related to mechanical properties of neutron-irradiated ceramics [DE93-040262] p 1707 N94-21560
Microstructural evolution of neutron-irradiated Fe-Cr-Ni ternary alloys at high helium generation rates [DE93-018786] p 1696 N94-22037

NEUTRON SCATTERING
Neutron and PIMC determination of the longitudinal momentum distribution of HCP, BCC and normal liquid He-4 [DE93-019009] p 1972 N94-20187
Non-Fermi-liquid and multichannel Kondo phenomena in Y(1-x)U(x)Pd3 and related alloys [DE93-040135] p 2015 N94-20275
Spectroscopic studies of magnetic transitions in TbPO4 [DE94-001274] p 2035 N94-22565
Inelastic neutron scattering of (gamma)-iron, and the determination of the elastic constants by lattice dynamics [DE94-000694] p 1978 N94-22573

NEUTRON SOURCES
Neutron and PIMC determination of the longitudinal momentum distribution of HCP, BCC and normal liquid He-4 [DE93-019009] p 1972 N94-20187

NEUTRON STARS
Dark matter: Neutron star halo and the nature of gamma-bursts p 2002 N94-22643
Relativistically expanding pair plasmas as bursting sources of cosmic gamma rays p 2003 N94-22646
Gamma ray burst as a result of the explosive instability in the magnetosphere of old neutron star p 2007 N94-22675

NEUTRONS
Neutron and PIMC determination of the longitudinal momentum distribution of HCP, BCC and normal liquid He-4 [DE93-019009] p 1972 N94-20187
SLAC measurement of the neutron spin structure function [DE93-040998] p 1975 N94-21788
Spin dynamics and implications for superconductivity: Some problems with the d-wave scenario [DE94-001183] p 2032 N94-21972

NEWTON METHODS
Comparing quasi-Newton methods for solving sparse interface problems [CWI-NM-R9303] p 1959 N94-21576
First MEM task IRMEO in IRAF p 1928 N94-22551

NEWTONIAN FLUIDS
Canonically covariant formulation of Landau's Newtonian superfluid dynamics [PB93-221034] p 1805 N94-22272

NICKEL
Collisions of molecules with clusters: A quasiclassical study [DE93-018614] p 1971 N94-20050
Lightweight battery electrode and method of making it [AD-D015895] p 1749 N94-20120
Stable Ni isotopes and Be-10 and Al-26 in metallic spheroids from Meteor Crater, Arizona p 1863 N94-20889
Preliminary AEM study of the microstructure and composition of metal particles in ordinary chondrites p 2086 N94-20894
Shattering the myth of the resonantly photo-pumped neon-like titanium laser [DE93-019624] p 1819 N94-21873
The effect of microstructural evolution on superplasticity in Ni3Si(V, Mo) [DE93-041320] p 1694 N94-21943
Transferable tight-binding parameters: An application to Ni and Ni-Al alloys [DE94-001044] p 1695 N94-22023

NICKEL ALLOYS
Segregation of Si to the surface of Fe-29Ni-17Co alloy [DE93-040053] p 1687 N94-19864

Current status of environmental, health, and safety issues of nickel metal-hydride batteries for electric vehicles
[DE93-017079] p 1748 N94-19902
Production of NiAl and TiAl intermetallics by mechanical alloying
[VTT-JULK-760] p 1691 N94-20530
Magnetic instability of Kondo insulators
[DE93-040064] p 1768 N94-21762
Molecular dynamics modeling of the mechanical behavior of metallic multilayers
[DE93-019947] p 1694 N94-21921
Ni3Al aluminide alloys
[DE94-000493] p 1694 N94-21933
Alloying effects on mechanical and metallurgical properties of NiAl
[DE93-040814] p 1694 N94-21948
First principles calculations for analysis martensitic transformations
[DE94-000666] p 1695 N94-21964
Shape memory metals
[DE94-001373] p 1695 N94-21976
Transferable tight-binding parameters: An application to Ni and Ni-Al alloys
[DE94-001044] p 1695 N94-22023
Microstructural evolution of neutron-irradiated Fe-Cr-Ni ternary alloys at high helium generation rates
[DE93-018786] p 1696 N94-22037

NICKEL CADMIUM BATTERIES
Advanced batteries for electric vehicle applications: Nontechnical summary
[DE93-019007] p 1748 N94-19885

NICKEL COATINGS
Lightweight battery electrode and method of making it
[AD-D015895] p 1749 N94-20120

NICKEL HYDROGEN BATTERIES
System performance predictions for Space Station Freedom's electric power system
[NASA-TM-106396] p 1667 N94-20062

NICKEL IRON BATTERIES
Advanced batteries for electric vehicle applications: Nontechnical summary
[DE93-019007] p 1748 N94-19885

NICKEL ISOTOPES
FE-60 and the evolution of eucrites
p 2083 N94-20768
Stable Ni isotopes and Be-10 and Al-26 in metallic spheroids from Meteor Crater, Arizona
p 1863 N94-20889

NIGHT VISION
Night vision goggle model F4949 preflight adjustment/assessment procedures
[AD-A271079] p 1895 N94-19935

NIOBIUM ALLOYS
Metastable bcc phase formation in the Nb-Cr system
[DE93-018376] p 2012 N94-19926
Effects of processing history on the creep strength of Nb-1Zr
[DE93-015905] p 1689 N94-20093
Properties and potential of high-temperature niobium beryllides
[DE93-019169] p 1690 N94-20233
Strengthening and toughening in refractory metal alloys
[DE93-019942] p 1695 N94-21986

NIOBIUM CARBIDES
Performance of carbon-based hot frit substrates
[DE94-000509] p 1676 N94-21754

NITRAMINE PROPELLANTS
Detailed structure study of an H2/N2O/Ar flame employing molecular beam mass spectrometry, laser spectroscopy, and modeling
[AD-A270720] p 1679 N94-20111
Chemistry of the burning surface
[AD-A272725] p 1681 N94-21181

NITRATE ESTERS
High melting amino aromatic nitrate esters
[AD-D015929] p 1711 N94-19801

NITRATES
Solar proton events from a 180 year depth profile of nitrate concentrations from the central Greenland ice sheet
[AD-A272888] p 2147 N94-21196

NITRIDING
Evaluation of radiation effects in re-oxidized nitrided oxide devices by hot carrier stressing at 77 K
p 1754 N94-21084

NITROBENZENES
Evaluation of pre-extraction analytical holding times for nitroaromatic and nitramine explosives in water
[AD-A271547] p 1712 N94-20927

NITROGEN
Chemical equilibrium in high pressure molecular fluid mixtures
[DE93-040160] p 1796 N94-19829
Phonons and metastability in compressed nitrogen
[DE93-019913] p 2016 N94-20318
Implantation of nitrogen: Effects of hydrogen and implantation energy p 1686 N94-20804
Are the C delta light nitrogen and noble gases located in the same carrier? p 2085 N94-20846
Polymeric nitrogen
[DE93-040544] p 1706 N94-21512

NITROGEN COMPOUNDS
Physical chemistry of energetic nitrogen compounds
[AD-A271819] p 1712 N94-20625

NITROGEN ISOTOPES
A carbon and nitrogen isotope study of carbonaceous vein material in ureilite meteorites p 2083 N94-20726
Requirements for the early atmosphere of Mars from nitrogen isotope ratios p 2144 N94-21669

NITROGEN OXIDES
Detailed structure study of an H2/N2O/Ar flame employing molecular beam mass spectrometry, laser spectroscopy, and modeling
[AD-A270720] p 1679 N94-20111
Advanced Turbine Systems (ATS). Phase 1: System scoping and feasibility studies
[DE93-041130] p 1826 N94-21938
Investigations on trends in global environment adaptive industrial technologies
[DE94-714888] p 1853 N94-22258
Experimental evaluation of oxygen-enriched air and emulsified fuels in a six-cylinder diesel engine
[DE94-000907] p 1811 N94-22391

NITROGEN PLASMA
Initial operation of a large-scale plasma source ion implantation experiment
[DE94-000805] p 2036 N94-22583

NITROMETHANE
Computer simulation of molecular response at a shock front
[DE94-001050] p 1977 N94-22396

NOISE (SOUND)
The causes of contact noise
[REPT-92-100] p 1822 N94-20157

NOISE INTENSITY
Radar backscattering from snow facies of the Greenland ice sheet: Results from the AIRSAR 1991 campaign
p 1725 N94-20434
The relative noise levels of parallel axis gear sets with various contact ratios and gear tooth forms
[NASA-TM-106431] p 1826 N94-21756

NOISE MEASUREMENT
Interinjection-locked quasioptical power combiners and phased arrays
[AD-A271178] p 2015 N94-20214
Detector noise statistics in the non-linear regime
p 1748 N94-22526

NOISE POLLUTION
Aircraft noise effects on cultural resources: Recommendation and rationale for further research
[PB93-205326] p 1968 N94-22053
Aircraft noise effects on cultural resources: Annotated bibliography
[PB93-205334] p 1969 N94-22054

NOISE PREDICTION
Activities Report of the Institute of Applied Physics
[ETN-93-93749] p 1966 N94-21798
Traffic noise in a roundabout way
p 1966 N94-21799

NOISE REDUCTION
Oceanic in situ Fraunhofer-line characteristics: Fraunhofer-line underwater experiment (FLUX)
[AD-A270659] p 1881 N94-19952
VLSI mixed signal processing system
p 1744 N94-21100
Survey of lift-fan aerodynamic technology
[NASA-CR-177615] p 1646 N94-21592
Active control of wake/blade-row interaction noise through the use of blade surface actuators
[NASA-CR-4556] p 1968 N94-21608
Journal of rehabilitation research and development, volume 30, number 1, 1993
[AD-A272956] p 1893 N94-21613
The relative noise levels of parallel axis gear sets with various contact ratios and gear tooth forms
[NASA-TM-106431] p 1826 N94-21756
Signal classification and noise filtering using artificial neural networks p 1744 N94-22103
Noise filtering using multilayer feedforward neural network p 1770 N94-22104
Sub-band adaptive noise cancelling
p 1774 N94-22125
Applications of a two-dimensional nonlinear filters to image restoration p 1789 N94-22225

NOISE SPECTRA
Study of the utilization of thin oxides in indium phosphides for the realisation of electron components
[ECL-92-38] p 2018 N94-20593
Defect motion as the origin of the 1/f conductance noise in solids
[EUT-92-E-259] p 2029 N94-21552

NOISE TEMPERATURE
Quantum noise studies with superconducting tunnel junction mixers
[AD-A270897] p 2012 N94-19897

NONADIABATIC THEORY
Consequences of chaotic particle motion for the stability of space plasma current sheets p 2001 N94-22636

NONCONDENSABLE GASES
The FY1992 survey on commercialization of Stirling engine utilization equipment
[DE94-707416] p 1849 N94-22029

NONDESTRUCTIVE TESTS
Quantitative evaluation of material composition of composites using x ray energy-dispersive NDE technique
[DE93-041157] p 1672 N94-19888
Microscopic origins of metastable effects in a-Si:H and deep defect characterization in a-Si,Ge:H alloys
[DE93-018205] p 1688 N94-19985
Three-dimensional dynamic thermal imaging of structural flaws by dual-band infrared computed tomography
[DE93-019575] p 1906 N94-20316
Development of improved processing and evaluation methods for high reliability structural ceramics for advanced heat engine applications, phase 1
[DE93-040528] p 1702 N94-20481
Spectroscopic ellipsometry studies of HF treated Si (100) surfaces p 1734 N94-20508
Ellipsometric study of Si(0.5)Ge(0.5)/Si strained-layer superlattices p 1734 N94-20509
Comparative thickness measurements of heterojunction layers by ellipsometric, RBS, and XTEM analysis
p 1710 N94-20984
Thermal diffusivity measurements by photothermal laser beam deflection (PTD): Data analysis using the Levenberg-Marquardt algorithm p 1820 N94-21006
Thermal characterization of thin films by photothermally induced laser beam deflection p 1710 N94-21007
Non-destructive evaluation in manufacturing using spectroscopic ellipsometry p 1828 N94-21012
VASE (variable angle spectroscopic ellipsometry)
p 1687 N94-21014
The 1992 USAF structural integrity program conference
[AD-A272876] p 1635 N94-21194
Damage states around fastener holes in thick graphite/epoxy composite laminates
[AD-A272613] p 1675 N94-21504
Surface and subsurface defect detection in Si3N4 components by laser scattering
[DE93-040829] p 1832 N94-21772
Millimeter-wave imaging of composite materials
[DE93-041160] p 1677 N94-21940
Three dimensional ultrasonic imaging
[DE93-040549] p 1968 N94-22003
Strength, ultrasonic and metallurgical evaluation of diffusion bonds
[DE94-000665] p 1697 N94-22571
An embedded fibre optic for damage growth monitoring in Kevlar composites
[ISBN-0-315-83501-X] p 1677 N94-22589

NONEQUILIBRIUM FLOW
Establishing the basis for validated predictions of highly non-equilibrium flows (with 9 attachments)
[AD-A272918] p 1802 N94-21220

NONINTRUSIVE MEASUREMENT
Fundamentals and applications of variable angle spectroscopic ellipsometry p 1687 N94-21011
Measurement of thermal-hydraulic parameters in two-phase flow using flow visualization image analysis
[DE93-006255] p 1805 N94-22269

NONLINEAR EQUATIONS
Dynamical systems and nonlinear partial differential equations
[AD-A271514] p 1951 N94-20545
Two-dimensional nonlinear Schrodinger equations and their properties
[AD-A272184] p 1952 N94-20923
Universality in blow-up for non linear heat equations
[PB93-215465] p 2038 N94-22095
Non-linear analysis of the electrical properties of the active circuits of high-frequency oscillators
p 1785 N94-22195
On the nonlinear instability of thermal structures
p 2006 N94-22668

NONLINEAR FILTERS
A comparative robustness evaluation of feedforward neurofilters
[NASA-TM-106440] p 1650 N94-21742
Applications of a two-dimensional nonlinear filters to image restoration p 1789 N94-22225

NONLINEAR OPTICS
Complex and stereoregular nonlinear optical materials
[AD-A271067] p 1983 N94-19846

Multidimensional solitons in fiber arrays
[DE93-019923] p 1963 N94-19862
Photoluminescence spectroscopy of zinc germanium diphosphide (ZnGeP2)
[AD-A270705] p 1678 N94-19953
Optical switching devices
[AD-D015918] p 1984 N94-20059
FD-TD modeling of 2-D dielectric waveguides for propagation and scattering of femtosecond optical solitons p 1719 N94-20406
Investigation of heterojunctions and multiple quantum well structures using crystalline organic semiconductors
[AD-A272113] p 2018 N94-20569
Statistical fluctuations in lasers
[DE94-000710] p 1817 N94-20939
Recent developments in aromatic azo polymers research
[AD-A272966] p 1705 N94-21259
Azo polymers for optical storage 3: Effect of film thickness on net phase retardation and writing speed
[AD-A272994] p 1705 N94-21267
Photonics and nonlinear optics with molecular materials and polymers
[AD-A271747] p 1988 N94-21457
Techniques for the flux growth of optical materials: Growth of beta-barium borate
[AD-A272717] p 2028 N94-21505
Optical processing in photorefractive media p 1789 N94-22222

NONLINEAR SYSTEMS
Acoustic microscopy and nonlinear effects in pressurized superfluid helium
[AD-A270598] p 1967 N94-19949
Computational and analytical methods in nonlinear fluid dynamics
[AD-A272722] p 1802 N94-21169
The block adaptive multigrid method applied to the solution of the Euler equations p 1641 N94-21472
High temperature superconducting planar circuit structure for high frequency applications
[AD-A273083] p 2028 N94-21521
Improvements to a method for the geometrically nonlinear analysis of compressively loaded stiffened composite panels
[NASA-CR-194715] p 1832 N94-21814
The spectral world coordinate systems in IRAF/NOAO p 2049 N94-22539
Response statistics of shell structures with geometrical and material nonlinearities, volume 1
[ISBN-0-315-84006-4] p 1833 N94-22590

NONLINEARITY
Nonlinear acoustics: Periodic waveguide, finite-amplitude propagation in a medium having a distribution of relaxation processes, and production of an isolated negative pulse in water
[AD-A270530] p 1967 N94-19894
Study of transverse coupled bunch instabilities by using non-linear Taylor maps for the Advanced Light Source (ALS)
[DE93-040287] p 1979 N94-19989
Design of a controllable pitch underwater thruster system
[AD-A271140] p 1821 N94-20021
Emittance measurement and modeling of the ALS 50 MeV LINAC to booster line
[DE93-040116] p 1979 N94-20273
The coherent backscattering opposition effect p 1991 N94-20646
RADCAL: A narrow-band model for radiation calculations in a combustion environment
[PB93-200889] p 1682 N94-21448
A unified Monte Carlo interpretation of particle simulations and applications to nonneutral plasmas
[DE94-001231] p 1997 N94-21973

NONNEWTONIAN FLUIDS
A comparison of calculated and measured rheological properties of crystallising lavas in the field and in the laboratory p 1862 N94-20690

NONTHERMAL RADIATION
Nonthermal planetary radio emissions: Theories and observations p 2001 N94-22635

NORMAL DENSITY FUNCTIONS
The roughness of the Martian surface: A scale dependent model p 2115 N94-20762
The missing impact craters on Venus p 2119 N94-20782
Measure fields for function approximation
[AD-A272660] p 1964 N94-21215

NORMALITY
On estimation and testing in Poisson regression models with over-dispersion
[MEMO-1083] p 1963 N94-21076
A sharp upper bound for departure from normality
[DE93-040457] p 1960 N94-21966

NORMALIZING (STATISTICS)
Set theory and nominalisation, part 2
[PB93-191815-PT-2] p 1962 N94-20008

NOSE CONES
Compilation of reinforced carbon-carbon transatlantic abort landing arc jet test results
[NASA-TM-104778] p 1676 N94-21834

NOSES (FOREBODIES)
A theoretical investigation of unsteady separation phenomena related to dynamic stall
[AD-A271865] p 1636 N94-20465

NOVA LASER SYSTEM
Effect of bandwidth on beam smoothing and frequency conversion at the third harmonic of the Nova laser
[DE93-019917] p 1819 N94-21920

NOVAE
Properties of x ray emission from x ray novae p 2007 N94-22676

NOWCASTING
Design document and database specifications for the Naval Interactive Data Analysis System (NIDAS), version 1.0
[NASA-CR-194817] p 2045 N94-21865

NOZZLE DESIGN
Experimental investigation of nozzle/plume aerodynamics at hypersonic speeds
[NASA-CR-194628] p 1636 N94-20014
A tutorial on the aero/thermodynamical design of liquid-propellant rocket engine nozzles p 1668 N94-20074
Shape optimization governed by the Euler equations using an adjoint method
[NASA-CR-191555] p 1950 N94-20092
Development of phased twin flip-flop jets
[NASA-TM-106404] p 1637 N94-20563

NOZZLE EFFICIENCY
Internal performance of a nonaxisymmetric nozzle with a rotating upper flap and a center-pivoted lower flap
[NASA-TP-3385] p 1637 N94-21569

NOZZLE GEOMETRY
A tutorial on the aero/thermodynamical design of liquid-propellant rocket engine nozzles p 1668 N94-20074
Internal performance of a nonaxisymmetric nozzle with a rotating upper flap and a center-pivoted lower flap
[NASA-TP-3385] p 1637 N94-21569

NOZZLE THRUST COEFFICIENTS
A tutorial on the aero/thermodynamical design of liquid-propellant rocket engine nozzles p 1668 N94-20074
Internal performance of a nonaxisymmetric nozzle with a rotating upper flap and a center-pivoted lower flap
[NASA-TP-3385] p 1637 N94-21569

NUCLEAR ASTROPHYSICS
New production mechanisms for unstable nuclei in stars, supernovae, and the big bang
[DE93-018627] p 2081 N94-21618

NUCLEAR BINDING ENERGY
Theoretical research program to study chemical reactions in AOTV bow shock tubes
[NASA-CR-194710] p 1804 N94-22027

NUCLEAR ELECTRIC POWER GENERATION
Technology to prevent greenhouse effect gases
[DE94-707420] p 1851 N94-20116
Current situation of development of petroleum substituting energies (USA)
[DE94-707492] p 1848 N94-22013

NUCLEAR ELECTRIC PROPULSION
Power conditioning system modelling for nuclear electric propulsion
[NASA-CR-191136] p 1846 N94-21179
NEP Early Flight program: System performance and development considerations
[NASA-TM-106415] p 1654 N94-21570
Brayton power conversion system parametric design modelling for nuclear electric propulsion
[NASA-CR-191135] p 1671 N94-21874

NUCLEAR ENGINE FOR ROCKET VEHICLES
Entry velocities at Mars and Earth for short transit times
[AD-A272591] p 1665 N94-21420

NUCLEAR EXPLOSIONS
Proceedings of the 15th Annual Seismic Research Symposium
[AD-A271458] p 1855 N94-20090
On magnetodynamic effects initiated by a high-speed impact of a large cosmic body upon the Earth's surface p 2082 N94-20647

NUCLEAR FUSION
Longitudinal beam dynamics for heavy ion fusion using WARPrz
[DE93-019154] p 1992 N94-19915
Space-charge dominated beam transport in magnetic quadrupoles with large aperture ratios
[DE93-040443] p 1992 N94-20004
AGB stars as a source of short-lived radioactive nuclei in the solar nebula p 2133 N94-20859
Theoretical and numerical studies in magnetic fusion
[DE94-000536] p 1993 N94-20937
New production mechanisms for unstable nuclei in stars, supernovae, and the big bang
[DE93-018627] p 2081 N94-21618
Fourth International Toki Conference on Plasma Physics and Controlled Nuclear Fusion
[ESA-SP-351] p 2000 N94-22624

NUCLEAR MAGNETIC RESONANCE
Synthesis and structural characterization of new light molecular weight inorganic oxidizers and relative derivatives, volume 1
[AD-A271437] p 2012 N94-19842
Examination of low level magnetic dipole intensities in the transition nuclei Sm-148, Sm-150, Sm-152 and Sm-154, with inelastic photon scattering at S-DALINAC
[ETN-93-95069] p 1971 N94-20030
Characterization of amorphous material in shocked quartz by NMR spectroscopy
[DE93-019069] p 1679 N94-20307
The 13C-NMR spectra of poly (4-((2-(acryloyloxy) ethyl) ethyl amino)- 4-nitroazobenzene-co-methyl methacrylate)
[AD-A273016] p 1705 N94-21238
Dynamics of adsorbed, swollen block copolymers
[AD-A272013] p 1706 N94-21460
Local structure in oxygen-doped La2CuO(4+delta)
[DE93-040248] p 2030 N94-21768
Spin dynamics and implications for superconductivity: Some problems with the d-wave scenario
[DE94-001183] p 2032 N94-21972
NMR studies of oxygen-doped La2CuO(4+delta)
[DE93-040756] p 2034 N94-22007

NUCLEAR PHYSICS
F-spin concept and g-bosons in the interceding boson model
[ETN-93-93607] p 1973 N94-21136
Summary of the Hadronic Weak Interaction session
[DE94-000592] p 1975 N94-21775
Likelihood analysis of parity violation in the compound nucleus
[DE94-000671] p 1977 N94-22572

NUCLEAR POWER PLANTS
Current situation of development of petroleum substituting energies (USA)
[DE94-707492] p 1848 N94-22013

NUCLEAR PROPULSION
Performance assessment of low pressure nuclear thermal propulsion
[NASA-TM-108433] p 1671 N94-21860
F2D users manual: A two-dimensional compressible gas flow code
[DE94-000653] p 1805 N94-22386

NUCLEAR REACTIONS
On modelling nuclear reactions in meteorites p 2085 N94-20844
Advanced far infrared detectors
[DE93-040289] p 1988 N94-21528
Semiconductor isotope engineering
[DE93-040119] p 2030 N94-21744

NUCLEAR REACTORS
Power transmission by laser beam from lunar-synchronous satellite
[NASA-TM-4496] p 1669 N94-20102
Method for remotely powering a device such as a lunar rover
[NASA-CASE-LAR-14789-1] p 1824 N94-20587

NUCLEAR ROCKET ENGINES
SPACE-R Thermionic Space Nuclear Power System: Design and Technology Demonstration Program
[DE93-013969] p 1670 N94-21824

NUCLEAR SPIN
F-spin concept and g-bosons in the interceding boson model
[ETN-93-93607] p 1973 N94-21136

NUCLEAR STRUCTURE
Symmetry-dictated trucation: Solutions of the spherical shell model for heavy nuclei
[DE94-000482] p 1976 N94-21961

NUCLEATION
Shock induced condensation in fluids of high molar specific heat: Shock structure and relaxation
[MPIS-106/1993] p 1798 N94-20145
Kinetics of phase transformations in glass forming systems
[NASA-CR-194270] p 1701 N94-20347
Growth, characterization and device development in monocrystalline diamond films
[AD-A273097] p 2028 N94-21506
Development of advanced cloud parameterizations to examine air quality, cloud properties, and cloud-radiation feedback in mesoscale models
[DE93-041164] p 1853 N94-22384

NUCLEI (NUCLEAR PHYSICS)
Examination of low level magnetic dipole intensities in the transition nuclei Sm-148, Sm-150, Sm-152 and Sm-154, with inelastic photon scattering at S-DALINAC
[ETN-93-95069] p 1971 N94-20030
Low p(sub T) phenomena observed in high energy nuclear collisions
[DE94-000825] p 1982 N94-21849
Likelihood analysis of parity violation in the compound nucleus
[DE94-000671] p 1977 N94-22572
NUCLEONS
A relativistic constituent quark model
[DE93-041085] p 1946 N94-21689
SLAC measurement of the neutron spin structure function
[DE93-040998] p 1975 N94-21788
NUCLIDES
Cosmogenic-radionuclide profiles in Knyahinya: New measurements and models p 2106 N94-20713
NULL HYPOTHESIS
State-space models for multichannel detection
[AD-A270608] p 1715 N94-19816
NUMBER THEORY
Semi-stability and heights of cycles
[PB93-215507] p 1961 N94-22377
NUMERICAL ANALYSIS
Numerical solution of differential-algebraic equations with ill-conditioned constraints
[AD-A270934] p 1949 N94-19898
Multi-disciplinary coupling effects for integrated design of propulsion systems
[NASA-TM-106349] p 1830 N94-20170
High-resolution numerical methods for compressible multi-phase flow in hierarchical porous media
[DE94-000740] p 1799 N94-20351
Numerical methods for singularly perturbed differential equations with applications
[AD-A272112] p 1952 N94-20568
Numerical simulation of lava flows: Applications to the terrestrial planets p 1863 N94-20904
Theoretical and numerical studies in magnetic fusion
[DE94-000536] p 1993 N94-20937
Analytic solutions for optimized ellipsometric measurements of interfaces and surface layers in thin film structures p 2019 N94-20977
Numerical ranges and stability estimates
[TW-92-10] p 1953 N94-21060
Mathcad computer applications predicting antenna parameters from antenna physical dimensions and ground characteristics
[AD-A272987] p 1740 N94-21264
Users manual for the NASA Lewis three-dimensional ice accretion code (LEWICE 3D)
[NASA-TM-105974] p 1642 N94-21590
Numerical method for computing the electric field produced by a microwave beam in a stratified medium p 1746 N94-22197
Performance of a simple circular polarization selective surface p 1746 N94-22198
NUMERICAL CONTROL
The Milling assistant, case-based Reasoning, and machining strategy: A report on the development of automated numerical control programming systems at New Mexico State University
[DE93-041101] p 2029 N94-21690
Performance evaluation of video on ethernet
[DE93-040696] p 1936 N94-21749
Proceedings of the IMOG (Interagency Manufacturing Operations Group) Numerical Systems Group
[DE94-001009] p 1917 N94-21851
Model-based reasoning for power system management using KATE and the SSM/PMAD
[NASA-CR-194716] p 1671 N94-21882
Enhanced software for the GT1022 automated gaging system
[DE94-001374] p 1918 N94-21977
Use of open systems for control, analysis, and data acquisition of the DIII-D tokamak
[DE94-001101] p 1998 N94-22089
Wilbur: A low-cost CCD camera system for MDM Observatory p 1814 N94-22510
NUMERICAL STABILITY
On the numerical stability of quasi-definite systems
[DE93-019404] p 1950 N94-20217
NUMERICAL WEATHER FORECASTING
Meso-Beta scale numerical simulation studies of terrain-induced jet streak mass/momentum perturbations
[NASA-CR-194627] p 1864 N94-20138
The CSIRO 9-level atmospheric general circulation model
[CSIRO-TP-26] p 1855 N94-20256
Development and tests of a cloud physics parameterization for real-time aviation and public numerical weather forecasting
[PB93-202711] p 1868 N94-21427
A synoptic-scale overview of the TOGA COARE intensive observing period November 1992 to February 1993 based on analyses from US operational global data assimilation systems
[NASA-TM-104593] p 1868 N94-21605
Use of satellite data for validation of operational forecast models and operational analyses p 1861 N94-22291
NUSSELT NUMBER
A parametric study of heat transfer within a planar thermosyphon
[DE93-019546] p 1799 N94-20258

O

OBJECT PROGRAMS
Structural modeling: An application framework and development process for flight simulators
[AD-A271348] p 1650 N94-19880
Mint tutorial and user manual
[TR-452] p 1905 N94-20143
OBJECT-ORIENTED PROGRAMMING
A parallelizing compiler based on partial evaluation
[AD-A270838] p 1898 N94-19832
PREVAIL-DM: A framework-based environment for formal hardware verification
[RR-899] p 1905 N94-20164
Object-oriented DFD models to present the functional and behavioral views
[DE93-040206] p 1906 N94-20280
Design of a computer assisted tool for object oriented acquisition, modeling and simulation of knowledge structure
[ETN-93-94183] p 1910 N94-21152
The Mercury user's manual
[TR-465] p 1913 N94-21316
The three-dimensional Event-Driven Graphics Environment (3D-EDGE) p 1922 N94-21342
Reducing the cognitive workload: Trouble managing power systems
[NASA-TM-106413] p 1714 N94-21564
Termination and confluence of rule execution
[CWI-CS-R9309] p 1916 N94-21587
An evaluation of integration of the trace assertion method with the box structure method for coding in C++
[DE93-040480] p 1918 N94-21924
Database computing in HEP
[NASA-CR-194791] p 1921 N94-22375
An object-oriented data reduction system in Fortran p 2046 N94-22447
A structured data transfer protocol p 2047 N94-22450
C++, objected-oriented programming, and astronomical data models p 2063 N94-22473
Programmability in AIPS++ p 1926 N94-22482
An object-oriented approach for supporting both X and terminal interfaces p 1926 N94-22491
StarView: The object oriented design of the ST DADS user interface p 2049 N94-22548
OBLATE SPHEROIDS
Intensity and polarization of light scattered by size distributions of randomly oriented nonspherical particles p 1721 N94-20416
OBLIQUENESS
The connection between Venus' free obliquity and its CMB oblateness p 2139 N94-20896
OCEAN BOTTOM
On the sources of North Atlantic deep water
[AD-A270854] p 1881 N94-19895
Seafloor characterization/Galapagos propagating rift
[AD-A272001] p 1882 N94-20581
First discovery of the organic materials in deep-sea iron cosmic spherule p 1685 N94-20677
Iridium in sediments containing large abundances of Australasian microtektites from DSDP hole 758B in the Eastern Indian Ocean and from DSDP hole 769A in the Sulu Sea p 2083 N94-20741
Green Sheet project: Dye sheet evolution
[AD-A272019] p 1883 N94-21443
OCEAN CURRENTS
Shipboard ADCP observations during RRS Charles Darwin Cruise 62
[IOS-298-1992] p 1882 N94-20531
Offshore decision support system: ERS-1 pilot project WAVEWATCH
[BCRS-92-09] p 1865 N94-20532
Ocean mapping using satellite radar altimetry
[ETN-93-93470] p 1841 N94-21017
Estimating the rotation rate of mesoscale ocean rings from satellite altimetry
[AD-A272922] p 1883 N94-21222
Comparison of satellite-derived velocity fields in the coastal transition zone
[AD-A272565] p 1883 N94-21360
Acoustic monitoring of global ocean variability
[AD-A271998] p 1883 N94-21366
Green Sheet project: Dye sheet evolution
[AD-A272019] p 1883 N94-21443
Influence of geoid model uncertainty on the determination of ocean circulation with satellite altimetry
[PB93-219301] p 1842 N94-22097
OCEAN DATA ACQUISITIONS SYSTEMS
Shipboard ADCP observations during RRS Charles Darwin Cruise 62
[IOS-298-1992] p 1882 N94-20531
OCEAN DYNAMICS
Two microstrip arrays for interferometric SAR applications p 1722 N94-20421
Optical climatology of the Northeast Pacific Ocean
[AD-A271671] p 1866 N94-20559
Ocean wave height transformation model using surface roller theory
[AD-A272610] p 1883 N94-21423
OCEAN MODELS
SIMBAT theoretical manual
[AD-A271063] p 1882 N94-19979
The CSIRO 9-level atmospheric general circulation model
[CSIRO-TP-26] p 1855 N94-20256
Processing of climatological data for model initialization
[AD-A271678] p 1865 N94-20487
Seafloor characterization/Galapagos propagating rift
[AD-A272001] p 1882 N94-20581
Estimating the rotation rate of mesoscale ocean rings from satellite altimetry
[AD-A272922] p 1883 N94-21222
Ocean wave height transformation model using surface roller theory
[AD-A272610] p 1883 N94-21423
Green Sheet project: Dye sheet evolution
[AD-A272019] p 1883 N94-21443
OCEAN SURFACE
SIMBAT theoretical manual
[AD-A271063] p 1882 N94-19979
ERS-1 and Seasat scatterometer measurements of ocean winds: Model functions and the directional distribution of short waves p 1720 N94-20412
Ku-band ocean radar backscatter observations during SWADE p 1720 N94-20413
Analysis of Ku-band cross section at low incidence angles p 1720 N94-20414
Comparison of remote sensing measurements with a two-scale polarimetric emission and scattering model for sea surfaces p 1721 N94-20415
Two microstrip arrays for interferometric SAR applications p 1722 N94-20421
Near grazing scattering from non-Gaussian ocean surfaces p 1726 N94-20436
Rough surface scattering from moving ocean surfaces as an indicator of scattering mechanisms p 1726 N94-20439
Polarimetric thermal emission from rough surfaces p 1727 N94-20441
Polarimetric thermal emission from periodic water surfaces p 1728 N94-20445
A theoretical and numerical study of polarimetric scattering and emission from random rough surfaces with anisotropic directional spectrum p 1730 N94-20454
Use of microwave polarimetry to enhance SAR images of the ocean surface
[AD-A271911] p 1882 N94-20489
Optical climatology of the Northeast Pacific Ocean
[AD-A271671] p 1866 N94-20559
Four-dimensional remote sensing of the marine boundary layer with a digital beamforming radar wind profiler
[AD-A270627] p 1882 N94-20564
Neural network studies
[AD-A271593] p 1943 N94-20947
Models of refraction in the marine atmosphere surface layer
[AD-A271724] p 1858 N94-21357
Airborne surface backscattering strength measurements in the western Atlantic Ocean
[AD-A271737] p 1883 N94-21358
Presenting the Rain-Sea Interaction Facility
[NASA-RP-1322] p 1884 N94-21628
Marine boundary layer model evaluation by using a height gain measurement technique in the interference region p 1777 N94-22145
OCEAN TEMPERATURE
On the sources of North Atlantic deep water
[AD-A270854] p 1881 N94-19895
Estimating the rotation rate of mesoscale ocean rings from satellite altimetry
[AD-A272922] p 1883 N94-21222

OCEANOGRAPHIC PARAMETERS
The marine light-mixed layer experiment cruise and data report: R/V endeavor cruise EN-224, mooring deployment, 27 April-1 May 1991: Cruise EN-227, mooring recovery, 5-23 September 1991
[AD-A271175] p 1864 N94-20186

OCEANOGRAPHY
Distribution of turbidity in Australian tropical waters
[AD-A271059] p 1881 N94-19905
The marine light-mixed layer experiment cruise and data report: R/V endeavor cruise EN-224, mooring deployment, 27 April-1 May 1991: Cruise EN-227, mooring recovery, 5-23 September 1991
[AD-A271175] p 1864 N94-20186
Progress In Electromagnetics Research Symposium (PIERS)
[NASA-CR-194629] p 1718 N94-20403
Ocean mapping using satellite radar altimetry
[ETN-93-93470] p 1841 N94-21017
Acoustic monitoring of global ocean variability
[AD-A271998] p 1883 N94-21366
Low-cost Unmanned Air Vehicle (UAV) for oceanographic research
[AD-A273103] p 1646 N94-21507
A synoptic-scale overview of the TOGA COARE intensive observing period November 1992 to February 1993 based on analyses from US operational global data assimilation systems
[NASA-TM-104593] p 1868 N94-21605
Influence of geoid model uncertainty on the determination of ocean circulation with satellite altimetry
[PB93-219301] p 1842 N94-22097

OCEANS
Technology to prevent greenhouse effect gases
[DE94-707421] p 1850 N94-19976
A survey of the impact on acoustic propagation of warm core ocean eddys
[AD-A272188] p 1883 N94-20925
Estimating the rotation rate of mesoscale ocean rings from satellite altimetry
[AD-A272922] p 1883 N94-21222
Simulation of clear-sky outgoing longwave radiation over the oceans using operational analysis
p 1861 N94-22290

OCULOMETERS
Techniques used for the analysis of oculometer eye-scanning data obtained from an air traffic control display
[NASA-CR-191559] p 1643 N94-21629

OFFSHORE ENERGY SOURCES
Computer-aided design system for objects location and reservoir with dispersed resource evolution investigation
p 1923 N94-22064

OHMIC DISSIPATION
Modeling of the coupled magnetospheric and neutral wind dynamos
[NASA-CR-194728] p 1856 N94-20537
Complementary heterojunction FET technology for space application p 1755 N94-21094
A spheromak ignition experiment reusing Mirror Fusion Test Facility (MFTF) equipment
[DE94-001856] p 2034 N94-22050

OIL RECOVERY
High-resolution numerical methods for compressible multi-phase flow in hierarchical porous media
[DE94-000740] p 1799 N94-20351

OILS
Biofuels: Project summaries
[DE93-010003] p 1712 N94-19984
EHD enhancement of pool and in-tube boiling of alternate refrigerants
[DE94-000787] p 1798 N94-20101
New technique for oil backstreaming contamination measurements p 1652 N94-20511
Navy GTE seal development activity
p 1655 N94-21794

OLIVINE
Petrogenesis of Apollo 12 mare basalts. Part 1: Multiple melts and fractional crystallization to explain olivine and ilmenite basalt compositions p 1684 N94-20644
Petrogenesis of Apollo 12 mare basalts. Part 2: An open system model to explain the pigeonite basalt compositions p 1684 N94-20645
Lamellar olivine in the Divnoe achondrite: Evidence for high-pressure exsolution? p 1685 N94-20679
Determining the composition of olivine on asteroidal surfaces p 1686 N94-20805
The x ray microprobe determination of chromium oxidation state in olivine from lunar basalt and kimberlitic diamonds p 1686 N94-20807
Hydrothermal alteration experiments of olivine with varying Fe contents: An attempt to simulate aqueous alteration of the carbonaceous chondrites
p 1686 N94-20810
Measurements of the dielectric properties of simulated comet material as part of the KOSI 10 experiment
p 2085 N94-20641
Chemical zoning and diffusion of Ca, Al, Mn, and Cr in olivine of springwater pallasite p 2086 N94-20902
Diffuse reflectance spectra of orthopyroxene, olivine, and plagioclase as a function of composition and structure p 2087 N94-20906

OMNIDIRECTIONAL ANTENNAS
Mobile antenna development at JPL
p 1731 N94-20457
Mobile terminal antennas for helicopters
p 1731 N94-20458

ON-LINE PROGRAMMING
Practical issues in implementing roving spares in VLSI systolic arrays p 1758 N94-21114

ON-LINE SYSTEMS
Recommendations resulting from the SPDS Community-Wide Workshop
[NASA-CR-194684] p 2042 N94-20363
Research in image management and access
[NASA-CR-194797] p 1907 N94-20376
Practical issues in implementing roving spares in VLSI systolic arrays p 1758 N94-21114
Data management for interdisciplinary field experiments: OTTER project support
[NASA-CR-4559] p 1842 N94-22345
ASpect: A new spectrum and line analysis package for IRAF p 1926 N94-22485
The NSO FTS database program and archive (FTSDBM) p 1926 N94-22506
The EXOSAT database and archive
p 2048 N94-22521
Recommendations for a service framework to access astronomical archives p 2049 N94-22537

ONBOARD DATA PROCESSING
On-board closed-loop congestion control for satellite based packet switching networks
[NASA-TM-106446] p 1656 N94-21581
CREIR: A multiaccess protocol for on-board processing satellite systems p 1780 N94-22168
Timing recovery in the channel processor of a digital group demodulator p 1780 N94-22169
Experiences in airborne computing at NRC for geophysical exploration applications
p 1783 N94-22185

ONE DIMENSIONAL FLOW
Formulation of a next-generation interior ballistic code
[AD-A271539] p 1801 N94-20915

OPACITY
Opacity measurements in shock-generated argon plasmas
[DE94-001057] p 1998 N94-22399
Physical properties of dense astrophysical plasmas
p 2001 N94-22637

OPEN CIRCUIT VOLTAGE
Techniques for reducing error in the calorimetric measurement of low wattage items
[DE93-018472] p 1807 N94-20114

OPERATING COSTS
Spaceplane flight simulation: Project definition
[PB93-211399] p 1651 N94-22094

OPERATING SYSTEMS (COMPUTERS)
A response to Cheriton and Skeen's criticism of casual and totally ordered communication
[AD-A271486] p 1912 N94-21300
Use of open systems for control, analysis, and data acquisition of the DIII-D tokamak
[DE94-001101] p 1998 N94-22089
Fault tolerance for real-time multiprocessor operating systems p 1788 N94-22216

OPERATIONAL AMPLIFIERS
An 18 bit 50 kHz ADC for low earth orbit
p 1764 N94-21702

OPERATIONAL PROBLEMS
Planning process software: A user guide for the DMCA
[AD-A271252] p 1902 N94-19911

OPERATIONS RESEARCH
Controlling multisupplier operations by intelligent EDI
p 1744 N94-22076

OPERATORS (MATHEMATICS)
Explicit results on gl(lambda) and sl(lambda)
[MEMO-1075] p 1953 N94-21072
On the closure properties of #P in the context of PF of #P
[TR-445] p 1955 N94-21456

OPHIUCHI CLOUDS
Pre-main sequence stars in the Chamaeleon cloud and pre-main sequence stars in the Rho Ophiuchi cloud core
[NASA-CR-194713] p 2080 N94-20337

OPTICAL BISTABILITY
System for solving Boolean equations using optical lookup tables
[AD-D015962] p 1951 N94-20358

OPTICAL COMMUNICATION
Oceanic in situ Fraunhofer-line characteristics: Fraunhofer-line underwater experiment (FLUX)
[AD-A270659] p 1881 N94-19952
Optical signal processing
[AD-A271036] p 1983 N94-20013
Design considerations for a fiber optic communications network for power systems
[DE93-018404] p 1984 N94-20179
Silicon retina for optical tracking systems
p 1755 N94-21098
QPPM receiver for free-space laser communications
[NASA-TM-106424] p 1741 N94-21567

OPTICAL COMPUTERS
Center for the integration of optical computing
[AD-A271874] p 1899 N94-20469
Addition of decimal numbers in optical computing architecture by Walsh coded digits p 1773 N94-22122

OPTICAL CONTROL
Design considerations for a fiber optic communications network for power systems
[DE93-018404] p 1984 N94-20179
A theory for optical wavelength control in short pulse free electron laser oscillators
[AD-A271706] p 1817 N94-21353

OPTICAL CORRECTION PROCEDURE
Space Shuttle Mission STS-61: Hubble Space Telescope servicing mission-01
[NASA-TM-109344] p 1653 N94-20192
Holographic optical elements correcting the off-axis aberrations of a parabolic mirror
[ISBN-0-315-57581-6] p 1990 N94-22411
HST image restoration: A comparison of pre- and post-servicing mission results p 1925 N94-22478

OPTICAL COUPLING
Effects of stimulated Raman scattering on light beam properties during high-power laser beam long-path propagation
[AD-A273109] p 1818 N94-21509
Integrated optical coupling element on silicon substrate, appendix 2 p 1988 N94-21596

OPTICAL DATA PROCESSING
Optical signal processing
[AD-A271036] p 1983 N94-20013
Optical encoding of imaging data
[AD-D015915] p 1984 N94-20056
Center for the integration of optical computing
[AD-A271874] p 1899 N94-20469
Addition of decimal numbers in optical computing architecture by Walsh coded digits p 1773 N94-22122
Optical processing in photorefractive media
p 1789 N94-22222

OPTICAL DATA STORAGE MATERIALS
Optical processing in photorefractive media
p 1789 N94-22222

OPTICAL DISKS
An ASIC memory buffer controller for a high speed disk system p 1754 N94-21089

OPTICAL EMISSION SPECTROSCOPY
Spectroscopic studies of magnetic transitions in TbPO4
[DE94-001274] p 2035 N94-22565

OPTICAL EQUIPMENT
The aerogel mesh contamination collector
[AD-A270537] p 1651 N94-20011
Feedback controlled optics with wavefront compensation
[NASA-CASE-NPO-18194-1-CU] p 1985 N94-20305
Optical metrology of magnetically trapped hydrogen
[AD-A272110] p 1680 N94-20584
Dual-beam multiple wavelength light transmittance measurement for particle sizing in rocket motor plumes
[AD-A272491] p 1670 N94-21208
QPPM receiver for free-space laser communications
[NASA-TM-106424] p 1741 N94-21567
The Keck keyword layer p 1925 N94-22460
The optohydraulic servovalve: A novel device for the precise optical control of hydraulic pressure
[ISBN-0-315-83580-X] p 1827 N94-22577

OPTICAL FIBERS
Multidimensional solitons in fiber arrays
[DE93-019923] p 1983 N94-19862
Fiber optic Michelson sensor and arrays with passive elimination of polarization fading and source feedback isolation
[AD-D015944] p 1984 N94-20085
Plasma chemical vapor deposition of halide glasses
[AD-D015933] p 1701 N94-20331
Wide-angle imaging system with fiberoptic components providing angle-dependent virtual material stops
[NASA-CASE-NPO-18146-1-CU] p 1986 N94-20345
Disengagable adapter for an optical fiber connector
[AD-D015959] p 1822 N94-20356
Optical fibers and Fluorosensors having improved power efficiency and methods of producing same
[NASA-CASE-LAR-14525-1-CU] p 1986 N94-20378

Delivery of very high bandwidth with ATM switches and SONET
[DE93-019432] p 1899 N94-20476
Optical fiber sensor having an active core
[NASA-CASE-LAR-14607-1-SB] p 1986 N94-20586
Integrated optical coupling element on silicon substrate, appendix 2 p 1988 N94-21596
Fibre pigtailed silicon based low cost passive optical components, appendix 5 p 1989 N94-21599
A new innovative instrument for space plasma instrumentation
[NASA-CR-194736] p 1666 N94-21780
Simulations of spectral broadening by cross-phase modulation (XPM) with chaotic light pulses
[DE93-019623] p 1819 N94-21872
OTDR strain gauge for smart skins
[DE93-041043] p 1810 N94-21953
The data acquisition system for the Anglo-Australian Observatory 2-degree field project p 2048 N94-22529
Demodulation of a fiber Fabry-Perot strain rosette using white light interferometry
[ISBN-0-315-83427-7] p 1990 N94-22579
Phase demodulation of interferometric fiber-optic sensors
[ISBN-0-315-83425-0] p 1991 N94-22581
An embedded fibre optic for damage growth monitoring in Kevlar composites
[ISBN-0-315-83501-X] p 1677 N94-22589

OPTICAL FLOW (IMAGE ANALYSIS)

Segmenting the optical flow due to the motion of several rigid objects p 1777 N94-22147

OPTICAL HETERODYNING

Coherent lidar design and performance verification
[NASA-CR-193813] p 1816 N94-20341

OPTICAL MATERIALS

Complex and stereoregular nonlinear optical materials
[AD-A271067] p 1983 N94-19846
Optical switching devices
[AD-D015918] p 1984 N94-20059
X ray, extreme and far ultraviolet optical thin films for space applications
[NASA-CR-194635] p 1984 N94-20128
Optics survivability support, volume 1
[DE93-019616] p 1985 N94-20262
Optics survivability support, volume 2
[DE93-040310] p 1985 N94-20283
Optical metrology of magnetically trapped hydrogen
[AD-A272110] p 1680 N94-20584
Materials, Structures, and Devices for High-Speed Electronics
[NASA-CR-193177] p 2019 N94-20971
The 13C-NMR spectra of poly (4-((2-(acryloyloxy) ethyl) ethyl amino)- 4-nitroazobenzene-co-methyl methacrylate)
[AD-A273016] p 1705 N94-21238
IR materials producibility
[AD-A273031] p 1987 N94-21321
Combination of on ground experiments and analysis software for the evaluation of material degradation in space (SILEX project) p 1662 N94-21389
Techniques for the flux growth of optical materials: Growth of beta-barium borate
[AD-A272717] p 2028 N94-21505
Polyimide-based electrooptic materials
[DE93-019416] p 1706 N94-21526

OPTICAL MEASUREMENT

Wavefront sensors for optical diagnostics in fluid mechanics: Application to heated flow, turbulence, and droplet evaporation
[DE93-040060] p 1797 N94-19974
Optical climatology of the Northeast Pacific Ocean
[AD-A271671] p 1866 N94-20559
Optical measurement of built-in and applied electric fields in Al(x)Ga(1-x)As/GaAs heterostructures p 1796 N94-20989
Measurement of superlattice optical properties by variable angle spectroscopic ellipsometry p 2022 N94-20992
Long Duration Exposure Facility (LDEF) contamination study
[AD-A272419] p 1658 N94-21147
Precision prism coupling setup applied to measure planar silica films on silicon, appendix 9 p 1989 N94-21603
OTDR strain gauge for smart skins
[DE93-041043] p 1810 N94-21953

OPTICAL MEASURING INSTRUMENTS

Pointing control design for autonomous space vehicle applications
[DE93-019943] p 1657 N94-19863
Wavefront sensors for optical diagnostics in fluid mechanics: Application to heated flow, turbulence, and droplet evaporation
[DE93-040060] p 1797 N94-19974
Thermal dilation fiber optical flow sensor
[AD-D015926] p 1797 N94-20094
Photonic electromagnetic field sensor apparatus
[AD-D015938] p 1717 N94-20333
Photonic electromagnetic field sensor apparatus
[AD-D015939] p 1718 N94-20334
Mathematical model and analysis of the Tactical Unmanned Ground Vehicle (TUGV) using computer simulation
[AD-A272258] p 1824 N94-20576
Army aircraft fire-detection systems operation and reliability
[AD-A271327] p 1641 N94-20912
Description and assessment of a new Optical Pressure Measurement System (OPMS) demonstrated in the high speed wind tunnel in Goettingen (Germany)
[DLR-FB-92-24] p 1651 N94-21280
CMU very fast range-imaging system
[AD-A272057] p 1761 N94-21282
Models of refraction in the marine atmosphere surface layer
[AD-A271724] p 1858 N94-21357
Integrated optical coupling element on silicon substrate, appendix 2 p 1988 N94-21596

OPTICAL MEMORY (DATA STORAGE)

Optoelectronic associative memory
[NASA-CASE-NPO-18278-1-CU] p 1985 N94-20303
Efficiency of reversible optical storage in azo polymers
[AD-A272923] p 1705 N94-21223
Azo polymers for optical storage 3: Effect of film thickness on net phase retardation and writing speed
[AD-A272994] p 1705 N94-21267

OPTICAL MICROSCOPES

Optical air pore analysis p 1708 N94-21892

OPTICAL PATHS

Photonic electromagnetic field sensor apparatus
[AD-D015938] p 1717 N94-20333
Photonic electromagnetic field sensor apparatus
[AD-D015939] p 1718 N94-20334
Mode transition matrix measuring system
[AD-D015973] p 1987 N94-21279

OPTICAL POLARIZATION

Optically induced rotation diffusion in polymer liquid crystals: Phenomenological theory and experimental verification
[ETN-93-95068] p 2014 N94-20026
Applications of variable angle spectroscopic ellipsometry in semiconductor technology p 2025 N94-21010
An integrated-optic polarization splitter on silicon substrate, appendix 4 p 1989 N94-21598

OPTICAL PROPERTIES

Complex and stereoregular nonlinear optical materials
[AD-A271067] p 1983 N94-19846
Innovative acoustic technique for studying new materials and new developments in solid state physics
[AD-A270540] p 2013 N94-19933
Study of electromagnetic wave scattering from characterized rough surfaces
[AD-A270931] p 1716 N94-19934
Research on defects and transport in amorphous-silicon-based semiconductors
[DE93-017117] p 2013 N94-19939
Photoluminescence spectroscopy of zinc germanium diphosphide (ZnGeP2)
[AD-A270705] p 1678 N94-19953
The marine light-mixed layer experiment cruise and data report: R/V endeavor cruise EN-224, mooring deployment, 27 April-1 May 1991: Cruise EN-227, mooring recovery, 5-23 September 1991
[AD-A271175] p 1864 N94-20186
Optical and transport properties of metallic and semiconductor nanostructures
[AD-A271716] p 2018 N94-20554
Optical climatology of the Northeast Pacific Ocean
[AD-A271671] p 1866 N94-20559
Investigation of heterojunctions and multiple quantum well structures using crystalline organic semiconductors
[AD-A272113] p 2018 N94-20569
Optical effects of space weathering on lunar soils and the role of the finest fraction p 2101 N94-20687
MinMap: An imaging spectrometer for high resolution compositional mapping of the Moon p 1813 N94-20688
Visible-infrared properties of controlled laboratory soils p 1685 N94-20689
Sunphotometer network for monitoring aerosol properties in the Brazilian Amazon p 1839 N94-20961
Superlattice optical properties measured by variable angle spectroscopic ellipsometry p 2022 N94-20993
Characterization of an asymmetric triangular multiple quantum well, by variable angle spectroscopic ellipsometry p 2022 N94-20995
Temperature dependence of optical properties of AlAs, studied by in-situ spectroscopic ellipsometry p 2023 N94-20999
In-situ and ex-situ ellipsometric characterization for semiconductor technology p 2026 N94-21013
VASE (variable angle spectroscopic ellipsometry) p 1687 N94-21014
Obtaining surface optical properties from space-based lidar systems
[AD-A272831] p 1987 N94-21172
Optical properties of chromium and neodymium in zirconium - barium - lanthanum - aluminum fluoride glass
[AD-A271609] p 1987 N94-21236
Solid-state dynamics and quantum transport in novel semiconductor nanostructures
[AD-A272955] p 2027 N94-21248
Long-range laser imaging
[AD-A273020] p 1817 N94-21253
Fundamental studies of defect generation in amorphous silicon alloys grown by remote plasma-enhanced chemical-vapor deposition
[DE93-017083] p 2029 N94-21615
Optical properties of cirrus derived from airborne measurements during FIRE IFO 2 p 1872 N94-22297
Progress in interpreting CO2 lidar signatures to obtain cirrus microphysical and optical properties p 1874 N94-22308
A numerical technique for the calculation of cloud optical extinction from lidar p 1874 N94-22309
Investigation of the effects of the macrophysical and microphysical properties of cirrus clouds on the retrieval of optical properties: Results for FIRE 2 p 1880 N94-22339

OPTICAL PUMPING

Photopumped x ray laser research on Saturn
[DE93-019430] p 1816 N94-20298
Generation of intense ultrashort x ray pulses
[DE93-019607] p 1817 N94-21299

OPTICAL RADAR

Optics survivability support, volume 1
[DE93-019616] p 1985 N94-20262
Coherent lidar design and performance verification
[NASA-CR-193813] p 1816 N94-20341
Integrated display of multi-sensor geophysical and electromagnetic flight data p 1721 N94-20418
Conically scanned holographic lidar telescope
[NASA-CASE-GSC-13462-1] p 1986 N94-20591
Development of a lidar for integration with the Naval Postgraduate School Infrared Search and Target Designation (NPS-IRSTD) system
[AD-A271847] p 1817 N94-20611
Examinations of a thallium atomic vapor filter for a Raman temperature lidar
[GKSS-92/E/13] p 1857 N94-21044
Obtaining surface optical properties from space-based lidar systems
[AD-A272831] p 1987 N94-21172
NOVAM evaluation utilizing electro-optics and meteorological data from KEY-90
[AD-A271722] p 1868 N94-21356
Green Sheet project: Dye sheet evolution
[AD-A272019] p 1883 N94-21443
The use of lidar for the evaluation of traffic-related urban pollution
[DE94-000704] p 1852 N94-22017
Cirrus properties deduced from CO2 lidar observations of zenith-enhanced backscatter from oriented crystals p 1871 N94-22295
Bi-directional reflectance and other radiation parameters of cirrus from ER-2 observations p 1871 N94-22296
Remote sensing of multilevel clouds during FIRE IFO 2 p 1844 N94-22303
Lidar and radar derived cirrus microphysical properties for the 26 November 1991 case study p 1873 N94-22305
Progress in interpreting CO2 lidar signatures to obtain cirrus microphysical and optical properties p 1874 N94-22308
A numerical technique for the calculation of cloud optical extinction from lidar p 1874 N94-22309
Observations of multi-layered clouds using K-band radar p 1874 N94-22311
Comparison of cloud boundaries measured with 8.6 mm radar and 10.6 micrometer lidar p 1875 N94-22317
CO2 lidar observations of Mount Pinatubo debris: FIRE 2 and longer-term measurements p 1876 N94-22323

OPTICAL RANGE FINDERS

The conceptual design of a short-range distance sensor p 1774 N94-22129
A feasibility study of a parallax-based passive missile approach warning system
[ISBN-0-315-60640-1] p 1743 N94-22410

OPTICAL REFLECTION

OTDR strain gauge for smart skins
[DE93-041043] p 1810 N94-21953
Chromaticity analysis of LANDSAT multispectral scanner and thematic mapper imagery of Chilko Lake, British Columbia, using a theoretical optical water quality model
[ISBN-0-315-63832-X] p 1843 N94-22422

OPTICAL RESONATORS
Novel N x N integrated channel waveguide optical crossbars for large scale high speed non-blocking data switching
[AD-A272065] p 1986 N94-20922
OPTICAL SCANNERS
Evaluation of a scanning Hartmann device for single point turning applications
[DE93-019204] p 1821 N94-19891
Conically scanned holographic lidar telescope
[NASA-CASE-GSC-13462-1] p 1986 N94-20591
Surface acquisition through virtual milling p 1920 N94-22372
OPTICAL SWITCHING
Stochastic differential equations and numerical simulation for pedestrians
[DE93-040651] p 1949 N94-20006
Optical signal processing
[AD-A271036] p 1983 N94-20013
Optical switching devices
[AD-D015918] p 1984 N94-20059
Optically controlled current filamentation in GaAs photoconductive semiconductor switches
[DE93-019427] p 2016 N94-20296
FD-TD modeling of 2-D dielectric waveguides for propagation and scattering of femtosecond optical solitons p 1719 N94-20406
Center for the integration of optical computing
[AD-A271874] p 1899 N94-20469
Novel N x N integrated channel waveguide optical crossbars for large scale high speed non-blocking data switching
[AD-A272065] p 1986 N94-20922
Non-destructive semiconductor wafer probing system using laser pulses to generate and detect millimeter-wave signals
[CA-PATENT-APPL-SN-2,020,73] p 1760 N94-21178
Mode transition matrix measuring system
[AD-D015973] p 1987 N94-21279
OPTICAL THICKNESS
Variable wavelength, variable angle ellipsometry including a sensitivities correlation test p 1710 N94-20978
Study of InGaAs-based modulation doped field effect transistor structures using variable-angle spectroscopic ellipsometry p 1796 N94-21001
Bi-directional reflectance and other radiation parameters of cirrus from ER-2 observations p 1871 N94-22296
Optical properties of cirrus derived from airborne measurements during FIRE IFO 2 p 1872 N94-22297
Development of methods for inferring cloud thickness and cloud-base height from satellite radiance data p 1872 N94-22301
A numerical technique for the calculation of cloud optical extinction from lidar p 1874 N94-22309
Ground-based passive remote sensing during FIRE IFO 2 p 1844 N94-22319
OPTICAL TRACKING
Visual tracking
[AD-A271686] p 1943 N94-20920
Silicon retina for optical tracking systems p 1755 N94-21098
OPTICAL WAVEGUIDES
Novel N x N integrated channel waveguide optical crossbars for large scale high speed non-blocking data switching
[AD-A272065] p 1986 N94-20922
Optical amplification and threshold behavior on InGaAs/InGaAsP multiquantum well structures
[ETN-93-94181] p 2026 N94-21151
Optical integrated structures and circuits on silicon
[VTT-PUBS-106] p 1988 N94-21594
A novel semiconductor process for optoelectronic applications on silicon substrate p 1988 N94-21595
Bidirectional method for optical channel waveguide attenuation measurement by detectors integrated on the wafer, appendix 3 p 1988 N94-21597
An integrated-optic polarization splitter on silicon substrate, appendix 4 p 1989 N94-21598
Fibre pigtailed silicon based low cost passive optical components, appendix 5 p 1989 N94-21599
Birefringence control and dispersion characteristics of silicon oxynitride optical waveguides, appendix 6 p 1989 N94-21600
Refractive index behaviour of phosphorus-doped planar silica waveguides, appendix 7 p 1989 N94-21601
Time-laplace-transform-domain analysis of wave propagation in planar waveguides
[PB93-215226] p 1960 N94-22096
Architectures of the free space optical interconnects p 1789 N94-22220
Balanced arrow Mach-Zehnder interferometer p 1789 N94-22221
Modelling short bent, graded index dielectric slab waveguides
[PB93-215283] p 1742 N94-22349
OPTIMAL CONTROL
Acceleration-augmented LQG control of an active magnetic bearing p 1757 N94-21112
On the estimation algorithm used in adaptive performance optimization of turbofan engines
[NASA-TM-4551] p 1649 N94-21879
Control of multiple robot manipulators with optimal force distribution p 1794 N94-22255
Optimal control of the tip of a flexible arm p 1794 N94-22256
OPTIMIZATION
A comparison of data-parallel algorithms for connected components
[AD-A270551] p 1902 N94-19918
On multiflow problems
[RR-889-M] p 1950 N94-20125
A design optimization procedure for epicyclic gears
[MATHS-REPT-A-188] p 1822 N94-20146
Determination of the optimal stochastic upper bound of a Markovian generator
[RR-906-I] p 1963 N94-20202
Applying the INN model to the MaxClique
[DE93-040137] p 1906 N94-20276
An investigation into the integration of meter-level range and millimeter-level phase data using a multimode stimulation for optimal filter estimation software package
[AD-A267955] p 1751 N94-20483
Design structuring and allocation optimization (Destination) prototype level 1 user's manual
[AD-A272115] p 1929 N94-20571
Optimization of a satellite localization and message sending system
[ETN-93-94448] p 1737 N94-20592
Routing of freeway traffic: A discrete-time state space model and routing problems
[CWI-BS-R9232] p 1944 N94-21033
On the core-structure of minimum cost spanning tree games
[MEMO-1085] p 1953 N94-21047
On the optimality of FCFS for networks of multi-server queues
[CWI-BS-R9235] p 1944 N94-21160
Optimization of static traffic allocation policies
[CWI-BS-R9302] p 1930 N94-21161
Optimization of fixed time polling schemes
[CWI-BS-R9237] p 1945 N94-21233
Optimal repairman assignment in two maintenance models which are equivalent to routing models with early decisions
[CWI-BS-R9301] p 1930 N94-21234
Selectivity: Reductions, nondeterminism, and function classes
[TR-469] p 1912 N94-21273
A mean field neural network for hierarchical module placement p 1766 N94-21720
Multicriteria optimisation problem in the agricultural modelling p 1844 N94-22073
The combinatorial algorithms for large scale discrete optimization problems p 1923 N94-22079
Improvements on the design of optimum SAW filters with the Remez Exchange Algorithm p 1773 N94-22123
Neural networks for optimum routing in packet-switched communications networks p 1746 N94-22205
Some best rate 1/p and rate (p-1)/p systematic quasi-cyclic codes over GF(3) and GF(4) p 1792 N94-22243
OPTOELECTRONIC DEVICES
Optoelectronic associative memory
[NASA-CASE-NPO-18278-1-CU] p 1985 N94-20303
System for solving Boolean equations using optical lookup tables
[AD-D015962] p 1951 N94-20358
Investigation of heterojunctions and multiple quantum well structures using crystalline organic semiconductors
[AD-A272113] p 2018 N94-20569
Surface treatment of InP and contribution to the optimization of the InP(p)/InP(p) regrown interfaces grown by GSMBE
[ECL-92-48] p 2018 N94-20598
Temperature dependence of optical properties of AlAs, studied by in-situ spectroscopic ellipsometry p 2023 N94-20999
Non-destructive semiconductor wafer probing system using laser pulses to generate and detect millimeter-wave signals
[CA-PATENT-APPL-SN-2,020,73] p 1760 N94-21178
Optical integrated structures and circuits on silicon
[VTT-PUBS-106] p 1988 N94-21594
A novel semiconductor process for optoelectronic applications on silicon substrate p 1988 N94-21595
Bidirectional method for optical channel waveguide attenuation measurement by detectors integrated on the wafer, appendix 3 p 1988 N94-21597
The conceptual design of a short-range distance sensor p 1774 N94-22129
Charge integrating optical position sensor p 1778 N94-22152
ORBIT CALCULATION
A new procedure for orbit determination based on three lines of sight: Angles only
[AD-A272937] p 1652 N94-21224
ORBIT TRANSFER VEHICLES
Evaluation of externally heated pulsed MPD thruster cathodes
[NASA-CR-191090] p 1670 N94-21565
Theoretical research program to study chemical reactions in AOTV bow shock tubes
[NASA-CR-194710] p 1804 N94-22027
ORBITAL ASSEMBLY
An expert system executive for automated assembly of large space truss structures
[NASA-TM-4487] p 1939 N94-20089
ORBITAL MANEUVERS
Effects of thrust vector control on the performance of the aerobang orbital plane change maneuver
[AD-A272532] p 1646 N94-21418
ORBITAL MECHANICS
Inclined orbits and interference to stationary service and to stationary service by satellite p 1653 N94-22188
ORBITAL POSITION ESTIMATION
Using the USCCS for sub microsecond spacecraft clock calibration p 1813 N94-21346
ORBITAL SERVICING
Spline screw payload fastening system
[NASA-CASE-GSC-13454-1] p 1821 N94-20126
ORBITAL VELOCITY
Variety in planetary systems p 2086 N94-20871
Entry velocities at Mars and Earth for short transit times
[AD-A272591] p 1665 N94-21420
ORDER-DISORDER TRANSFORMATIONS
The Coulomb anomaly in strongly disordered films
[AD-A271095] p 2012 N94-19849
Effect of exciton localization and delocalization on magnetic-field-dependent photoluminescence linewidths in semiconductors
[DE93-018860] p 1748 N94-19884
ORGANIC COMPOUNDS
Surface electrochemistry of metals
[AD-A272913] p 1691 N94-21245
Laser driven hydrodynamic instability experiments
[DE93-040550] p 1818 N94-21547
Surface acoustic wave sensing of VOC's in harsh chemical environments
[DE93-040721] p 1968 N94-21751
ORGANIC MATERIALS
First discovery of the organic materials in deep-sea iron cosmic spherule p 1685 N94-20677
A study of the induction heating of organic composites
[AD-A272657] p 1675 N94-21187
ORGANIC SEMICONDUCTORS
Investigation of heterojunctions and multiple quantum well structures using crystalline organic semiconductors
[AD-A272113] p 2018 N94-20569
ORGANIC SUPERCONDUCTORS
Fermiology and De Haas-Van Alphen effect of beta-(ET)2IBr2
[DE93-019523] p 2011 N94-19807
ORGANIZATIONS
A FET-switched induction accelerator cell
[DE93-019604] p 1769 N94-21838
ORGANOMETALLIC COMPOUNDS
Photochemically induced transformations of transition complexes
[AD-A271112] p 2014 N94-19982
Catalytic hydrogenation of carbon monoxide
[DE94-000881] p 1678 N94-20103
Sulfur-bonded thiophenes in organometallic rhenium complexes and adsorption of isocyanides on gold
[DE93-041126] p 1694 N94-21937
Low temperature absorption spectra and ground state electronic structure of tetrakis(2,6-di-tert-butylphenoxide)uranium(IV)
[DE94-000774] p 2035 N94-22387
ORGANOMETALLIC POLYMERS
A process for preparing an assembly of an article and a soluble polyimide which resists dimensional change, delamination, and debonding when exposed to changes in temperature
[NASA-CASE-LAR-14763-1] p 1702 N94-20373
ORGUEIL METEORITE
Recondensation in the early solar system: Physical conditions and source material p 2085 N94-20849
OROGRAPHY
Hydrostatic/nonhydrostatic comparison with the MERCURE code on orographic flows
[ETN-93-94603] p 1866 N94-20600
ORTHOGONAL FUNCTIONS
Orthogonal pairs and zeros of Sobolev-type orthogonal polynomials
[REPT-92-46] p 1953 N94-21059

Orthogonalization method for determination of boundary layer receptivity coefficients
[ISBN-0-315-83426-9] p 1805 N94-22580

ORTHOGONALITY
Orthogonal pairs and zeros of Sobolev-type orthogonal polynomials
[REPT-92-46] p 1953 N94-21059

ORTHOGRAPHY
Generalization performance of backpropagation learning on a syllabification task p 1940 N94-20246

OSCILLATING FLOW
Heat exchanger with oscillating flow
[NASA-CASE-LAR-14033-2] p 1800 N94-20495
Development of phased twin flip-flop jets
[NASA-TM-106404] p 1637 N94-20563

OSCILLATIONS
Suppression of relaxation oscillations in flashpumped, two-micron tunable solid state lasers
[AD-D015928] p 1814 N94-19800
A synoptic-scale overview of the TOGA COARE intensive observing period November 1992 to February 1993 based on analyses from US operational global data assimilation systems
[NASA-TM-104593] p 1868 N94-21605
Active damping of oscillations in a long compliant manipulator link
[DE93-018878] p 1826 N94-22038

OSCILLATOR STRENGTHS
Spectral characterization of lithographic sources
[DE93-019941] p 1997 N94-21848

OSCILLATORS
A theory for optical wavelength control in short pulse free electron laser oscillators
[AD-A271706] p 1817 N94-21353

OSMIUM ISOTOPES
Rhenium-osmium isotope systematics of ordinary chondrites and iron meteorites p 2085 N94-20854

OUTGASSING
Outgassing rate of Reemay Spunbonded Polyester and DuPont Double Aluminized Mylar
[DE93-040015] p 1699 N94-19973
Space environmental effects on polymer matrix composites: The UTIAS/LDEF experiment p 1660 N94-21373
Materials evaluation at ESA/ESTEC p 1662 N94-21386
Wet inside and out? Constraints on water in the Martian mantle and on outgassed water, based on melt inclusions in SNC meteorites p 2145 N94-21678
Modeling of outgassing and matrix decomposition in carbon-phenolic composites
[NASA-CR-194741] p 1676 N94-21743
Outgassing data for selecting spacecraft materials
[NASA-RP-1124-REV-3] p 1676 N94-21889

OVER-THE-HORIZON RADAR
New algorithm of ground track processing in high-frequency skywave over-the-horizon-B radar
[AD-A267821] p 1717 N94-20207

OVERVOLTAGE
Ultrafast gas switching experiments
[DE93-019071] p 1762 N94-21634

OXALIC ACID
Improvement of the stability of the process for synthesizing chemically prepared varistor powder
[DE94-000345] p 1763 N94-21654

OXIDATION
Oxidation-reduction induced roughening of platinum (111) surface
[DE93-017408] p 1687 N94-19922
Fuel processing requirements and techniques for fuel cell propulsion power
[DE93-019516] p 1750 N94-20257
Spectroscopic ellipsometric characterization of Si/Si(1-x)Ge(x) strained-layer superlattices p 1734 N94-20510
The Koshak section: Evidence for element fractionation and an oxidation event at the K/T boundary p 1862 N94-20641
The formation of FeO-rich pyroxene and enstatite in unequilibrated enstatite chondrites: A petrologic-trace element (SIMS) study p 2086 N94-20866
Transient studies of low temperature catalysts for methane conversion
[DE93-041232] p 1680 N94-20934
Chemical reaction fouling model for single-phase heat transfer
[DE93-019556] p 1802 N94-20942
Spectroscopic ellipsometric characterization of Si/Si(1-x)Ge(x) strained-layer superlattices p 2025 N94-21009
Space environmental effects on polymer matrix composites: The UTIAS/LDEF experiment p 1660 N94-21373
Some results of the oxidation investigation of copper and silver samples flown on LDEF p 1660 N94-21375
Review of corrosion behavior of ceramic heat exchanger materals: Corrosion characteristics of silicon carbide and silicon nitride
[DE93-041307] p 1706 N94-21516
Oxidation of dissolved iron under warmer, wetter conditions on Mars: Transitions to present-day arid environments p 2143 N94-21663
Application of an electrochemical quartz crystal microbalance to the study of electrocatalytic films
[DE93-041124] p 2029 N94-21691
Fundamental studies of stress distributions and stress relaxation in oxide scales on high temperature alloys
[DE94-001444] p 1693 N94-21854
High oxygen pressure synthesis of new copper oxide superconductors
[DE93-040278] p 2033 N94-21998
Surface modification of Ti3Al for improved oxidation resistance
[DE93-018297] p 1696 N94-22034
Investigations on trends in global environment adaptive industrial technologies
[DE94-714888] p 1853 N94-22258

OXIDATION RESISTANCE
Polyimides containing amide and perfluoroisopropylidene connecting groups
[NASA-CASE-LAR-14608-1] p 1702 N94-20374
Oxidation resistant protective coating system for gas turbine components and process for penetration thereof
[CA-PATENT-1,294,155] p 1704 N94-21143
Alloying effects on mechanical and metallurgical properties of NiAl
[DE93-040814] p 1694 N94-21948
Surface modification of Ti3Al for improved oxidation resistance
[DE93-018297] p 1696 N94-22034

OXIDATION-REDUCTION REACTIONS
Oxidation-reduction induced roughening of platinum (111) surface
[DE93-017408] p 1687 N94-19922
Production of O2 on the Moon: A lab-top demonstration of ilmenite reduction with hydrogen p 2126 N94-20821
Development of an electrochemical hydrogen separator
[DE93-019877] p 1683 N94-21984

OXIDE FILMS
Direct imaging of the surface microstructure of dielectric materials using an atomic force microscope
[AD-A272251] p 2018 N94-20575
Study of the utilization of thin oxides in indium phosphides for the realisation of electron components
[ECL-92-38] p 2018 N94-20593
Properties of E-beam interactive oxide films for nanometer scale structures
[AD-A272848] p 1675 N94-21191
A quantitative model for interpreting nanometer scale hardness measurements of thin films
[DE93-040601] p 2034 N94-22005

OXIDES
Identification of an interstellar oxide grain from the Murchison meteorite by ion imaging p 2082 N94-20659
Further analyses of Rio Cuarto impact glass p 1685 N94-20745
Dielectric function of InGaAs in the visible p 2023 N94-21000
Evaluation of radiation effects in re-oxidized nitrided oxide devices by hot carrier stressing at 77 K p 1754 N94-21084
Investigation of the effect of various oxide and fluoride additives on the microstructure, electronic properties, and phase shifting ability of Ba(1-x)Sr(x)TiO3
[AD-A271756] p 2027 N94-21303
Fundamental studies of stress distributions and stress relaxation in oxide scales on high temperature alloys
[DE94-001444] p 1693 N94-21854
Simple method to estimate MOS oxide-trap, interface-trap, and border-trap densities
[DE93-041138] p 2032 N94-21939
Melt-spin processing of high (Tc) oxide superconductors
[DE94-000696] p 2036 N94-22582

OXIDIZERS
Synthesis and structural characterization of new light molecular weight inorganic oxidizers and relative derivatives, volume 1
[AD-A271437] p 2012 N94-19842
Cryogenic propellant rocket engine problems p 1668 N94-20076
Dynamics of face seals for high speed turbomachinery p 1655 N94-21796

OXYGEN
Chemical equilibrium in high pressure molecular fluid mixtures
[DE93-040160] p 1796 N94-19829
Encounters of H and D atoms with O2 in water: Relative diffusion and reaction rates
[DE93-018587] p 1970 N94-19956
High-temperature, high-pressure oxygen metering valve
[NASA-CASE-MSC-21823-1] p 1824 N94-20589
C/O atomic ratios in micrometer-size crushed grains from Antarctic micrometeorites and two carbonaceous meteorites p 2082 N94-20678
C-O volatiles in Apollo 15 and Apollo 17 picritic glasses p 1685 N94-20727
Durability of thermal control and environmental protective materials for the SSRMS in simulated LEO environment p 1663 N94-21392
Fast oxygen atom studies related to low Earth orbit activities p 1663 N94-21395
Atomic oxygen fluence detector for Bremsat: Scientific and technical description p 1663 N94-21396
Powdered aluminum and oxygen rocket propellants: Subscale combustion experiments
[NASA-TM-106439] p 1713 N94-21760
Local structure in oxygen-doped La2CuO(4+delta)
[DE93-040248] p 2030 N94-21768
High oxygen pressure synthesis of new copper oxide superconductors
[DE93-040278] p 2033 N94-21998

OXYGEN ATOMS
Method for anisotropic etching in the manufacture of semiconductor devices
[NASA-CASE-MSC-21631-1] p 1993 N94-20491
Combination of on ground experiments and analysis software for the evaluation of material degradation in space (SILEX project) p 1662 N94-21389
German space experiments on Spacelab D-2 and Eureca-1 to investigate atomic oxygen interaction with materials p 1662 N94-21390
The International Telecommunications Satellite (INTELSAT) Solar Array Coupon (ISAC) atomic oxgyen flight experiment: Techniques, results and summary p 1662 N94-21391
Atomic oxygen interaction with spacecraft materials: Relationship between orbital and ground-based testing for materials certification p 1663 N94-21393
Evaluation of plasma-deposited protective coatings for spacecraft applications p 1663 N94-21394

OXYGEN COMPOUNDS
The multicomponent lineshape of the anharmonic A(1)(TO) phonon in PbTiO3
[DE93-018995] p 1970 N94-19971

OXYGEN IONS
Local structure in oxygen-doped La2CuO(4+delta)
[DE93-040248] p 2030 N94-21768

OXYGEN ISOTOPES
Oxygen isotopic relationships between the LEW85332 carbonaceous chondrite and CR chondrites p 2083 N94-20708
Inter- and intra-crystalline oxygen isotope distribution of fassaites in Allende CAI p 2086 N94-20898

OXYGEN PRODUCTION
Production of O2 on the Moon: A lab-top demonstration of ilmenite reduction with hydrogen p 2126 N94-20821

OXYGEN SUPPLY EQUIPMENT
In-flight measurement of aircrew breathing in Navy aircraft
[AD-A271811] p 1898 N94-21154

OXYNITRIDES
Birefringence control and dispersion characteristics of silicon oxynitride optical waveguides, appendix 6 p 1989 N94-21600

OZONE
Intrusion of stratospheric ozone in the troposphere through tropopause folding and cold air droplets
[REPT-87] p 1851 N94-20154
Tropospheric chemistry of natural hydrocarbons, aldehydes, and peroxy radicals: Their connections to sulfuric acid production and climate effects
[DE93-019525] p 1855 N94-20220
Stratospheric Aerosol and Gas Experiment (SAGE 3) p 1869 N94-21644
The young Sun and photochemistry of the primitive Martian atmosphere p 2145 N94-21679
Studies in remotely sensed geophysical parameter retrieval and analysis
[NASA-CR-194768] p 1842 N94-22374
Infrared FEL photochemistry: Multiple-photon dissociation of freon gas
[DE94-000617] p 1820 N94-22585

P

P BAND
Application of Cloude's target decomposition theorem to polarimetric imaging radar data p 1724 N94-20429

P WAVES
Analysis of the effects of eurasian crustal and upper mantel structure on regional phases using broadband seismic data
[AD-A272446] p 1858 N94-21206
P-I-N JUNCTIONS
Polarized-light reflection mode p-i-n modulators with GaAs/AlGaAs multiple quantum well active layers: Design and simulation p 2023 N94-20996
P-N JUNCTIONS
Some experiences of solving 1-D semiconductor device equations on a matrix coprocessor by a domain decomposition method
[CWI-NM-R9304] p 1935 N94-21492
PACIFIC ISLANDS
Schools of the Pacific rainfall climate experiment p 1881 N94-20699
PACIFIC OCEAN
Optical climatology of the Northeast Pacific Ocean
[AD-A271671] p 1866 N94-20559
PACKET SWITCHING
A distributed reinforcement learning scheme for network routing
[AD-A270600] p 1938 N94-19845
Reduction of network cost and wiring in Ranade's butterfly routing
[CWI-CS-R9243] p 1930 N94-21023
A packet switched communications system for GRO p 1744 N94-21345
Tandem queues with deterministic service times
[CWI-BS-R9238] p 1946 N94-21577
On-board closed-loop congestion control for satellite based packet switching networks
[NASA-TM-106446] p 1656 N94-21581
IAS telecommunication infrastructure and value added network services provided by IASNET p 1744 N94-22069
A shared buffer memory switch with maximum queue and minimum allocation p 1773 N94-22119
A one-shot access scheme for a multicast switch p 1773 N94-22120
Sorting network for the partial selection problem p 1773 N94-22121
Throughput, blocking, and interference in packet radio networks p 1746 N94-22190
Buffer allocation in an ATM switch with output buffer and speed constraints p 1746 N94-22203
PACKET TRANSMISSION
Application guide for universal source encoding for space
[NASA-TP-3441] p 1741 N94-21783
A packet based, data driven telemetry system for autonomous experimental sub-orbital spacecraft
[DE94-000399] p 1657 N94-21980
CREIR: A multiaccess protocol for on-board processing satellite systems p 1780 N94-22168
PACKETS (COMMUNICATION)
A packet switched communications system for GRO p 1744 N94-21345
On-board closed-loop congestion control for satellite based packet switching networks
[NASA-TM-106446] p 1656 N94-21581
A one-shot access scheme for a multicast switch p 1773 N94-22120
Sorting network for the partial selection problem p 1773 N94-22121
Buffer allocation in an ATM switch with output buffer and speed constraints p 1746 N94-22203
PADE APPROXIMATION
Rational trigonometric approximations using Fourier series partial sums
[NASA-CR-191535] p 1959 N94-21568
The accuracy-through-order and the equivalence properties in the algebraic approximant
[DE93-040188] p 1960 N94-21946
PAINTS
An improved patch for radiative coolers
[NASA-CASE-GSC-13503-1] p 1822 N94-20127
Thermal control coatings p 1664 N94-21400
Evaluation of electroconductivity of two surface paints for spacecraft
[AD-A273063] p 1706 N94-21437
PALEOCLIMATOLOGY
Workshop on Early Mars: How Warm and How Wet?, part 1
[NASA-CR-193553] p 2142 N94-21659
Ancient Martian valley genesis and paleoclimatic inference: The present as a key to the past p 2142 N94-21661
Early Mars was wet but not warm: Erosion, fluvial features, liquid water habitats, and life below freezing p 2145 N94-21677
The Martian valley networks: Origin by nivео-fluvial processes p 2146 N94-21682
PALEOMAGNETISM
Frequency dependent electrical properties of minerals and partial-melts
[DE93-019918] p 2012 N94-19861
Two-polarity magnetization in the Manson impact breccia p 1863 N94-20789
PALEONTOLOGY
Structural evidence for reorientation of Miranda about a paleo-pole p 2098 N94-20671
PALLADIUM
The metallic bond for monolayer transition metal layers on transition metal surfaces
[DE93-019060] p 1691 N94-20313
Structure and morphology of Pd overlayers on epitaxial SnO2 films studies with the atomic force microscope
[AD-A271827] p 2028 N94-21458
PALLADIUM ALLOYS
Non-Fermi-liquid and multichannel Kondo phenomena in Y(1-x)U(x)Pd3 and related alloys
[DE93-040135] p 2015 N94-20275
Non-fermi liquid and spin-glass behavior of the Sc(1-x)U(x)Pd3 system
[DE93-040134] p 2016 N94-20335
Magnetic instability of Kondo insulators
[DE93-040064] p 1768 N94-21762
First principles calculations for analysis martensitic transformations
[DE94-000666] p 1695 N94-21964
Temperature dependence of magnetic order in single-crystalline UPdSn
[DE93-040153] p 2033 N94-21991
PANEL METHOD (FLUID DYNAMICS)
Users manual for the NASA Lewis three-dimensional ice accretion code (LEWICE 3D)
[NASA-TM-105974] p 1642 N94-21590
PAPERS
STELAR: An experiment in the electronic distribution of astronomical literature p 2049 N94-22544
PARA HYDROGEN
Theoretical phase diagrams for solid H(sub 2)
[DE94-001049] p 1684 N94-22395
PARABOLIC DIFFERENTIAL EQUATIONS
Linear and nonlinear PSE for compressible boundary layers
[NASA-CR-191537] p 1797 N94-20033
Adaptive grids for quasilinear parabolic systems in one space dimension
[ETN-93-93611] p 1954 N94-21137
Interface reflection of spherical acoustic waves in the first- and second-order rational parabolic approximations and their artifacts
[PB93-215424] p 1969 N94-22261
PARABOLOID MIRRORS
Long range fast tool servo
[AD-A271614] p 1761 N94-21257
Holographic optical elements correcting the off-axis aberrations of a parabolic mirror
[ISBN-0-315-57581-6] p 1990 N94-22411
PARADOXES
Believing in the basis of the evidence
[TR-438] p 2039 N94-20364
PARALLEL COMPUTERS
Embedded microclusters in zeolites and cluster beam sputtering: Simulation on parallel computers
[DE94-000741] p 1701 N94-20352
Measuring the effects of thread placement on the Kendall Square KSR1
[DE93-040655] p 1908 N94-20932
MGD1M: A parallel multigrid code with a fast vectorized ILU-relaxation
[CWI-NM-R9222] p 1930 N94-21077
Comparing quasi-Newton methods for solving sparse interface problems
[CWI-NM-R9303] p 1959 N94-21576
Parallelizing a highly vectorized multigrid code with zebra relaxation
[CWI-NM-R9225] p 1935 N94-21610
Numerical multigrid software (MGD5M): A parallel multigrid code with a twisted ILLU-relaxation
[CWI-NM-R9226] p 1916 N94-21611
Simulated behaviour of large scale SCI rings and tori
[DE93-040149] p 1935 N94-21745
Visualization on massively parallel computers using CM/AVS
[DE93-040151] p 1936 N94-21746
Physics Detector Simulation Facility (PDSF) architecture/utilization
[DE93-019744] p 1936 N94-21919
Scientific computing in the 1990ies: An astronomical perspective p 2057 N94-22440
PARALLEL PLATES
Method for controlling protein crystallization
[NASA-CASE-MFS-28668-1] p 2017 N94-20528
PARALLEL PROCESSING (COMPUTERS)
A parallelizing compiler based on partial evaluation
[AD-A270838] p 1898 N94-19832
Exploiting the parallelism exposed by partial evaluation
[AD-A270678] p 1928 N94-19877
A comparison of data-parallel algorithms for connected components
[AD-A270551] p 1902 N94-19918
Implementation of a portable nested data-parallel language
[AD-A270524] p 1902 N94-19932
Two-dimensional particle-in-cell simulation on transputer arrays
[DE93-017977] p 1972 N94-20181
High resolution signal processing
[AD-A271181] p 1717 N94-20215
Scientific development of a massively parallel ocean climate model
[DE93-019446] p 1855 N94-20219
Parallel band reduction and tridiagonalization
[DE93-019566] p 1951 N94-20221
Fast data parallel polygon rendering
[DE93-040157] p 1929 N94-20279
Embedded microclusters in zeolites and cluster beam sputtering: Simulation on parallel computers
[DE94-000741] p 1701 N94-20352
Massively parallel computation of RCS with finite elements p 1726 N94-20437
Time warp operating system version 2.7 internals manual
[NASA-CR-194798] p 1899 N94-20549
Design structuring and allocation optimization (Destination) prototype level 1 user's manual
[AD-A272115] p 1929 N94-20571
Algorithm/architecture study for artificial neural nets
[AD-A271820] p 1943 N94-20626
Analysis and evaluation of configuring of graphical systems on multiprocessor architectures
[ETN-93-93618] p 1930 N94-21018
A novel VLSI processor architecture for supercomputing arrays p 1758 N94-21115
Scheduling for locality in shared-memory multiprocessors
[AD-A272948] p 1930 N94-21228
Optimal repairman assignment in two maintenance models which are equivalent to routing models with early decisions
[CWI-BS-R9301] p 1930 N94-21234
The Mercury user's manual
[TR-465] p 1913 N94-21316
Analysis of multigrid methods on massively parallel computers: Architectural implications p 1938 N94-21468
Mapping robust parallel multigrid algorithms to scalable memory architectures p 1922 N94-21483
MINIFOLD: A kernel for a MANIFOLD-like coordination language
[CWI-CS-R9252] p 1915 N94-21534
A data distributed, parallel algorithm for ray-traced volume rendering
[DE93-040150] p 1935 N94-21622
Simulated behaviour of large scale SCI rings and tori
[DE93-040149] p 1935 N94-21745
Visualization on massively parallel computers using CM/AVS
[DE93-040151] p 1936 N94-21746
The transition to massively parallel computing within a production environment at a DOE access center
[DE93-019155] p 1936 N94-21828
Evaluation of DEC's GIGAswitch for distributed parallel computing
[DE94-001356] p 1936 N94-21853
Physics Detector Simulation Facility (PDSF) architecture/utilization
[DE93-019744] p 1936 N94-21919
The design of linear algebra libraries for high performance computers
[DE93-040458] p 1960 N94-21967
Impact of partitioning on parallel discrete event simulation of logic circuits p 1772 N94-22115
VLSI design of a bit serial parallel processing 4 extender chip for M-path convolutional decoding p 1775 N94-22132
VLSI design of a parallel video output interface p 1778 N94-22153
The Schur Berlekamp-Massey algorithm is parallelizable p 1784 N94-22191
Integration of parallel processing structures using a matrix approach p 1784 N94-22192
Acceleration of backpropagation learning using a parallel DSP machine p 1786 N94-22206
Image convolution using the Myrias SPS-2 parallel computer p 1786 N94-22207
Parallelizing a maximum entropy image deconvolution algorithm p 1787 N94-22208
Distributed input/output processing in data-driven multiprocessors
[DE94-000323] p 1937 N94-22378

Simulating the Euclidean time Schroedinger equations using an INTEL iPSC/860 hypercube: Application to the t-J model of high-T(sub c) superconductivity
[DE94-000489] p 2035 N94-22385
Scientific computing in the 1990ies: An astronomical perspective p 2057 N94-22440
Seeing the forest for the trees: Networked workstations as a parallel processing computer p 1938 N94-22454

PARALLEL PROGRAMMING
Multilist scheduling: A new parallel programming model
[AD-A270549] p 1929 N94-20084
Mint tutorial and user manual
[TR-452] p 1905 N94-20143
Parallel logic programming systems
[RR-891-I] p 1929 N94-20176
Scheduling for locality in shared-memory multiprocessors
[AD-A272948] p 1930 N94-21228
Behavioural semantics of parallel functional programming languages
[MEMO-INF-92-66] p 1913 N94-21313
Butcher-Kuntzmann methods for nonstiff problems on parallel computers
[CWI-NM-R9305] p 1935 N94-21493
MINIFOLD: A kernel for a MANIFOLD-like coordination language
[CWI-CS-R9252] p 1915 N94-21534
Using parallel banded linear system solvers in generalized eigenvalue problems
[NASA-CR-191540] p 1915 N94-21584
A simple modern correctness condition for a space-based high-performance multiprocessor p 1766 N94-21718
Image convolution using the Myrias SPS-2 parallel computer p 1786 N94-22207
Parallelizing a maximum entropy image deconvolution algorithm p 1787 N94-22208
Parallel functional programming in SISAL: Fictions, facts, and future
[DE93-040486] p 1937 N94-22558

PARAMETER IDENTIFICATION
Literature review of the errors-in-variables approach to the problem of system identification
[AD-A271098] p 1949 N94-19907
Parameter estimation with cost function of second order in output-error-problem
[DLR-FB-92-38] p 1964 N94-21139
A project on parameter identification in reaction kinetics
[CWI-NM-R9301] p 1682 N94-21574

PARAMETERIZATION
Adaptation of model parameters of a rail model at measured rail compliances
[ILR-MITT-274(1992)] p 1831 N94-21153
Atmospheric parameterization schemes for satellite cloud property retrieval during FIRE IFO 2 p 1874 N94-22312
Development of advanced cloud parameterizations to examine air quality, cloud properties, and cloud-radiation feedback in mesoscale models
[DE93-041164] p 1853 N94-22384

PARASITIC ELEMENTS (ANTENNAS)
Bandwidth enhancement of dielectric resonator antennas p 1734 N94-20507

PARITY
Links between N-modular redundancy and the theory of error-correcting codes p 1765 N94-21713
Likelihood analysis of parity violation in the compound nucleus
[DE94-000671] p 1977 N94-22572

PARSING ALGORITHMS
Neural data oriented parsing p 1940 N94-20248
A modular design for connectionist parsing p 1941 N94-20252

PARTIAL DIFFERENTIAL EQUATIONS
Stochastic differential equations and numerical simulation for pedestrians
[DE93-040651] p 1949 N94-20006
Linear and nonlinear PSE for compressible boundary layers
[NASA-CR-191537] p 1797 N94-20033
Dynamical systems and nonlinear partial differential equations
[AD-A271514] p 1951 N94-20545
Symmetries and conservation laws of the system: u(x)=vw(x), v(y)=uw(y), uv+w(xx)+w(yy)=0
[MEMO-1084] p 1953 N94-21046
MGD1M: A parallel multigrid code with a fast vectorized ILU-relaxation
[CWI-NM-R9222] p 1930 N94-21077
Interactive simulation package for coupled bending and torsional vibrations in flexible robot arms
[MEMO-1089] p 1944 N94-21140
A multi-level solution algorithm for steady-state Markov chains
[NASA-CR-191558] p 1914 N94-21462
MGGHAT: Elliptic PDE software with adaptive refinement, multigrid and high order finite elements p 1956 N94-21470
An automatic multigrid method for the solution of sparse linear systems p 1957 N94-21478
A semi-Lagrangian approach to the shallow water equation p 1806 N94-21480
A note on singularities caused by the hydrodynamic dispersion tensor
[CWI-NM-R9302] p 1803 N94-21575
Parallelizing a highly vectorized multigrid code with zebra relaxation
[CWI-NM-R9225] p 1935 N94-21610
Numerical multigrid software (MGD5M): A parallel multigrid code with a twisted ILLU-relaxation
[CWI-NM-R9226] p 1916 N94-21611
Universality in blow-up for non linear heat equations
[PB93-215465] p 2038 N94-22095

PARTIAL PRESSURE
High oxygen pressure synthesis of new copper oxide superconductors
[DE93-040278] p 2033 N94-21998

PARTICLE ACCELERATION
Parametric instabilities in picosecond time scales
[DE94-000384] p 1966 N94-21958
Particle acceleration in a filamentary current sheet model p 2004 N94-22659
Prompt high-energy particle acceleration during two current loops collision p 2005 N94-22661
Plasma structure in a plasma flow along a magnetic mirror field p 2005 N94-22664
Mean elemental composition and He-3 enrichments in solar energetic particles p 2006 N94-22670
Acceleration of solar-flare particles as viewed from their chemical composition p 2006 N94-22672
Particle acceleration on the Alfven surface of a plasma ejecting axisymmetric rotator p 2008 N94-22681

PARTICLE ACCELERATOR TARGETS
Development and characterization of a time-, position- and energy-resolved x ray diagnostic for PBFA 2 target experiments
[DE93-019429] p 1808 N94-20297
A high-intensity He-jet production source for radioactive beams
[DE93-040247] p 1981 N94-21767
SLAC measurement of the neutron spin structure function
[DE93-040998] p 1975 N94-21788
Studies of the deuteron at high energy and momentum transfer
[DE93-041162] p 1976 N94-21941

PARTICLE ACCELERATORS
Top search at the TEVATRON
[DE93-019392] p 1978 N94-19988
Heavy ion fusion injector experiments
[DE93-019188] p 1993 N94-20234
High current injector for heavy ion fusion
[DE93-019241] p 1979 N94-20289
B production at D0
[DE93-019250] p 1972 N94-20291
Engineering design, fabrication, installation, operation, and maintenance services in support of research on laser plasma physics
[AD-A272249] p 1994 N94-20943
Parton-parton elastic scattering and rapidity gaps at Tevatron energies
[DE93-041024] p 1974 N94-21515
Multibunch beam break-up in detuned structures
[DE93-041056] p 1981 N94-21686
Simulation and compensation of multibunch energy variation in NLC
[DE93-041057] p 1981 N94-21687
Search for excited quarks in p(-p) collisions at the square root of s = 1.8 TeV
[DE93-019910] p 1975 N94-21840
The lepton charge asymmetry in the decay of W bosons produced in p(bar p) collisions at (radical)s = 1.8 TeV
[DE93-019903] p 1976 N94-21847

PARTICLE BEAMS
Space-charge dominated beam transport in magnetic quadrupoles with large aperture ratios
[DE93-040443] p 1992 N94-20004
Heavy ion fusion injector experiments
[DE93-019188] p 1993 N94-20234
Tactical laser weapons and other directed-energy weapons
[AD-A267961] p 1816 N94-20484
Plasma lens experiments at the Final Focus Test Beam
[DE93-041081] p 1981 N94-21688
SLD results from the study of polarized Z(sup 0) produced at the SLC
[DE93-041020] p 1982 N94-21952

PARTICLE COLLISIONS
Simulating supersymmetry with ISAJET 7.0/ISASUSY 1.0
[DE93-018266] p 1969 N94-19804
A search for new gauge bosons in (bar p)p collisions at square root of s equals 1.8 TeV in the dielectron decay mode
[DE93-019901] p 1969 N94-19813
Measurements of atomic interactions and frequency stability with a cryogenic hydrogen maser
[AD-A271132] p 1814 N94-19853
Collisional processes involving atmospheric gases
[AD-A270729] p 1854 N94-19954
A study of events with the highest total transverse energy in CDF
[DE93-019904] p 1978 N94-19972
Top search at the TEVATRON
[DE93-019392] p 1978 N94-19988
New relativistic S-matrix results for scattering -- beyond the usual anomalous factors/beyond impulse approximation
[DE93-019148] p 1971 N94-20096
Jet shapes in hadron and electron colliders
[DE93-019386] p 1979 N94-20216
The cross section for the production of b(bar-b) pairs in p(bar p) collisions at the square root of s equals 1.8 TeV
[DE93-019900] p 1972 N94-20225
Detection of traveling ionospheric disturbances induced by atmospheric gravity waves using the global positioning system p 1723 N94-20425
Theoretical and numerical studies in magnetic fusion
[DE94-000536] p 1993 N94-20937
Parton-parton elastic scattering and rapidity gaps at Tevatron energies
[DE93-041024] p 1974 N94-21515
Single and double ionization of helium by high-energy photon impact
[DE94-000381] p 1975 N94-21785
Measurement of the B meson and b quark cross-section in (-p)p collisions at the square root of s = 1.8 TeV using the exclusive decays B(+) and B(exp 0) yields J/psiK*(exp 0)
[DE93-019907] p 1975 N94-21806
Search for excited quarks in p(-p) collisions at the square root of s = 1.8 TeV
[DE93-019910] p 1975 N94-21840
The lepton charge asymmetry in the decay of W bosons produced in p(bar p) collisions at (radical)s = 1.8 TeV
[DE93-019903] p 1976 N94-21847
Low p(sub T) phenomena observed in high energy nuclear collisions
[DE94-000825] p 1982 N94-21849
Recent Fermilab results on hadroproduction of heavy flavors
[DE94-000595] p 1976 N94-21867

PARTICLE DENSITY (CONCENTRATION)
A field-based technique for the longitudinal profiling of ultrarelativistic electron or positron bunches down to lengths of less than or equal to 10 microns
[DE93-040954] p 1978 N94-19873
Searching for high baryon density at the AGS with ARC
[DE93-041155] p 1975 N94-21693

PARTICLE DIFFUSION
Radial diffusion of toroidally trapped particles induced by lower hybrid and fast waves
[IPPCZ-327] p 1996 N94-21593

PARTICLE EMISSION
Electrostatic charging and secondary effects in materials submitted to radiation in space p 1661 N94-21383

PARTICLE ENERGY
Edge plasma experiments on CASTOR tokamak
[IPPCZ-332] p 1997 N94-21816

PARTICLE IMAGE VELOCIMETRY
Fluid dynamic mechanisms and interactions within separated flows
[AD-A271037] p 1797 N94-19978
Particle image velocimetry
[DE93-040657] p 1804 N94-21748

PARTICLE INTERACTIONS
Simulating supersymmetry with ISAJET 7.0/ISASUSY 1.0
[DE93-018266] p 1969 N94-19804
A study of events with the highest total transverse energy in CDF
[DE93-019904] p 1978 N94-19972
Recent Fermilab results on hadroproduction of heavy flavors
[DE94-000595] p 1976 N94-21867

PARTICLE MOTION
Aperture determination of RHIC92 from randomly generated initial coordinates
[DE93-040174] p 1978 N94-19945

PARTICLE PRECIPITATION
Importance of aggregation and small ice crystals in cirrus clouds, based on observations and an ice particle growth model p 1879 N94-22336
PARTICLE PRODUCTION
Simulating supersymmetry with ISAJET 7.0/ISASUSY 1.0
[DE93-018266] p 1969 N94-19804
A search for new gauge bosons in (bar p)p collisions at square root of s equals 1.8 TeV in the dielectron decay mode
[DE93-019901] p 1969 N94-19813
The two-jet differential cross-section at CDF
[DE93-019905] p 1978 N94-19983
The cross section for the production of b(bar-b) pairs in p(bar p) collisions at the square root of s equals 1.8 TeV
[DE93-019900] p 1972 N94-20225
B production at D0
[DE93-019250] p 1972 N94-20291
Search for excited quarks in p(-p) collisions at the square root of s = 1.8 TeV
[DE93-019910] p 1975 N94-21840
The lepton charge asymmetry in the decay of W bosons produced in p(bar p) collisions at (radical)s = 1.8 TeV
[DE93-019903] p 1976 N94-21847
Recent Fermilab results on hadroproduction of heavy flavors
[DE94-000595] p 1976 N94-21867
SLD results from the study of polarized Z(sup 0) produced at the SLC
[DE93-041020] p 1982 N94-21952
Toward a QCD analysis of jet rates in deep-inelastic Muon-Proton scattering
[DE94-000618] p 1976 N94-21962
Production, collection and utilization of very long-lived heavy charged leptons
[DE93-040867] p 1977 N94-22009
Time evolution of the quark-gluon plasma
[DE94-000804] p 1998 N94-22389
PARTICLE SIZE DISTRIBUTION
Sol-spray preparation, particulate characteristics, and sintering of alumina powders
[DE93-018577] p 1690 N94-20183
Zinc and titanium smoke: Chemical composition and physical characteristics
[FOA-C-40277-4.9] p 1680 N94-20552
Thermal conductivity measurements of particulate materials under Martian conditions p 1685 N94-20703
Coagulation of grains in static and collapsing protostellar clouds p 2085 N94-20865
Holographic measurements of ice crystals in cirrus clouds during International Cirrus Experiment ICE
[GKSS-92/E/14] p 1866 N94-21052
A documentation of icing relevant cloud physical parameters on horizontal soundings of stratiform clouds (continuation)
[DLR-MITT-92-10] p 1871 N94-22280
Spectral variation of scattering and absorption by cirrus p 1876 N94-22321
Importance of aggregation and small ice crystals in cirrus clouds, based on observations and an ice particle growth model p 1879 N94-22336
PARTICLE SPIN
A conceptual design for the STAR endcap electromagnetic calorimeter
[DE93-040801] p 1807 N94-19990
PARTICLE THEORY
Aperture determination of RHIC92 from randomly generated initial coordinates
[DE93-040174] p 1978 N94-19945
High energy physics program at Texas A/M University
[DE93-041089] p 1980 N94-20933
Recent results on top, bottom and exotic physics at the Tevatron
[DE94-000578] p 1975 N94-21786
PARTICLE TRACKS
A summary of studies of particle stability at RHIC
[DE93-040173] p 1970 N94-19868
High energy ionization in liquids: The free ion yield
[DE93-040329] p 1973 N94-20324
LREE variability in CM matrices: Another look at meteorite compaction ages p 2086 N94-20884
PARTICLE TRAJECTORIES
Modeling of particle dispersion in a stationary isotropic homogeneous turbulence by large scale numerical simulation
[ETN-93-94604] p 1801 N94-20601
Surface path lines in plane Stokes flow driven by capillarity
[DE93-041277] p 1803 N94-21651
Monte Carlo calculation of multi-electron effects on synchrotron radiation
[DE94-001259] p 1982 N94-21974
Particle acceleration in a filamentary current sheet model p 2004 N94-22659
Current loop coalescence studied by 3-D electromagnetic particle code p 2005 N94-22660
PARTICULATES
Development of a technique to determine the morphology and dynamics of agglomerates in chemically reacting flows
[AD-A271160] p 1678 N94-20000
Sol-spray preparation, particulate characteristics, and sintering of alumina powders
[DE93-018577] p 1690 N94-20183
Spiral fluid separator
[NASA-CASE-MFS-28658-1] p 1800 N94-20361
The coherent backscattering opposition effect p 1991 N94-20646
Thermal conductivity measurements of particulate materials under Martian conditions p 1685 N94-20703
PARTITIONS (MATHEMATICS)
Algorithms for Markov decision chains with partial information
[PB93-220085] p 1918 N94-22098
Impact of partitioning on parallel discrete event simulation of logic circuits p 1772 N94-22115
PARTONS
Direct photon results from CDF
[DE93-019908] p 1980 N94-20317
Parton-parton elastic scattering and rapidity gaps at Tevatron energies
[DE93-041024] p 1974 N94-21515
The lepton charge asymmetry in the decay of W bosons produced in p(bar p) collisions at (radical)s = 1.8 TeV
[DE93-019903] p 1976 N94-21847
PASCAL (PROGRAMMING LANGUAGE)
A comprehensive software engineering educational experience
[AD-A270583] p 1905 N94-20109
PASSENGER AIRCRAFT
Radiometry in commercial aircraft
[GSF-41/91] p 1892 N94-21141
PASSENGERS
Evaluation of head injury criteria
[NIAR-93-2] p 1890 N94-20190
Passenger terminal simulation model
[ISBN-0-315-61113-8] p 1652 N94-22423
PASSIVITY
ALE project
[AD-A271080] p 2014 N94-19980
The use of x ray techniques in the in situ study of corrosion
[DE93-019845] p 1690 N94-20301
PATENT POLICY
NASA patent abstracts bibliography: A continuing bibliography. Section 1: Abstracts (supplement 44)
[NASA-SP-7039(44)-SECT-1] p 2043 N94-21254
PATENTS
The official gazette of the United States Patent and Trademark Office, vol. 1145, no. 4
[PB93-202240] p 2044 N94-21449
PATHS
Neural networks for optimum routing in packet-switched communications networks p 1746 N94-22205
PATTERN METHOD (FORECASTING)
Predicting lightning events in the KSC area: A feasibility study using single station data
[AD-A271440] p 1864 N94-20088
PATTERN RECOGNITION
Recognizing 3-D objects using 2-D images
[AD-A271005] p 1983 N94-19819
Representation and recognition with algebraic invariants and geometric constraint models
[AD-A271395] p 1949 N94-19838
Robust and efficient 3D recognition by alignment
[AD-A270639] p 1904 N94-20041
Statistical object recognition
[AD-A270887] p 1962 N94-20113
New algorithm of ground track processing in high-frequency skywave over-the-horizon-B radar
[AD-A267821] p 1717 N94-20207
Generalization performance of backpropagation learning on a syllabification task p 1940 N94-20246
Multivariate statistical analysis: Principles and applications to coorbital streams of meteorite falls p 1964 N94-20881
Recognition by prototypes
[AD-A271687] p 1943 N94-20921
Efficient comparison based string matching
[CWI-CS-R9249] p 1909 N94-21028
Tight comparison bounds for the string prefix-matching problem
[CWI-CS-R9250] p 1952 N94-21029
Data and model-driven selection using parallel-line groups
[AD-A271702] p 1913 N94-21365
Mathematical theory of thermodynamics of computation
[CWI-CS-R9251] p 2038 N94-21533
Determining the 3-D structure and motion of objects using a scanning laser range sensor
[NASA-CR-194745] p 1818 N94-21817
Improvement in invariant pattern recognition with neural networks and Fourier-Mellin filters p 1780 N94-22164
A modified moment invariants technique for classification of noisy objects p 1780 N94-22165
Interference reduction using neural networks p 1783 N94-22186
An insensitive algorithm for template matching with correlation p 1793 N94-22249
STAR-1 SAR road extraction using texture analysis and mathematical morphology
[ISBN-0-315-83255-X] p 1843 N94-22429
A neural network prototyping package within IRAF p 1949 N94-22451
PATTERNS
Spatial patterns in semiconductor lasers
[DE93-040056] p 1814 N94-19865
PAYLOADS
Database of proposed payloads and instruments for SEI missions p 1811 N94-22432
PEAKS (LANDFORMS)
Morphologic classes of impact basins on Venus p 2137 N94-20883
PECULIAR STARS
What is normal among the A-type stars?
[ISBN-0-315-83947-3] p 2081 N94-22592
PEEK
Creep damage of carbon fiber reinforced PEEK
[ISBN-0-315-58962-0] p 1677 N94-22420
PENETRATION
Determination of parameters for hypervelocity dust grains encountered in near-Earth space p 2084 N94-20817
PEPTIDES
Enhancement of wound healing by biosynthetic growth factor
[AD-A272517] p 1892 N94-21415
Gamma-aminobutyric acid (GABA) and neuropeptides in neural areas mediating motion-induced emesis p 1886 N94-21902
PERCOLATION
Computerized simulations with cellular automates for cloud formation
[GKSS-92/E/22] p 1867 N94-21312
PERFLUORO COMPOUNDS
Polyimides containing amide and perfluoroisopropylidene connecting groups
[NASA-CASE-LAR-14808-1] p 1702 N94-20374
PERFORATING
A fresh look at crater scaling laws for normal and oblique hypervelocity impacts p 1666 N94-20864
PERFORMANCE PREDICTION
System performance predictions for Space Station Freedom's electric power system
[NASA-TM-106396] p 1667 N94-20062
Signal processing in the linear statistical model
[AD-A272114] p 1736 N94-20570
Mathcad computer applications predicting antenna parameters from antenna physical dimensions and ground characteristics
[AD-A272987] p 1740 N94-21264
Problem reporting management system performance simulation p 1931 N94-21328
Compatibility evaluation and research on the Computerized Adaptive Screening Test (CAST): User and programmer's guide
[AD-A273112] p 1894 N94-21510
PERFORMANCE TESTS
TCP performance analysis for wide area networks
[DE94-000449] p 1928 N94-19858
Night vision goggle model F4949 preflight adjustment/assessment procedures
[AD-A271079] p 1895 N94-19935
Efficient chip signature checking for diagnosing boundary scan systems
[RR-901-I] p 1749 N94-20166
Multiport solid-state imager characterization at variable pixel rates
[DE93-018366] p 1808 N94-20287
Performance evaluation of the JPL TOPSAR system: An across-track interferometric SAR system for topographic mapping p 1732 N94-20461
The One-Day Workshop on Batteries, Stepping Motors, and Electronic Clock Displays
[ETN-93-94632] p 1752 N94-20628
Battery tests p 1752 N94-20631
LCD display tests p 1752 N94-20635
Development and demonstration of a personal monitoring system for exposure to hydrogen fluoride
[DE93-041273] p 1891 N94-20935
Operational test and evaluation of electronic combat systems
[AD-A273093] p 1847 N94-21500

Mirror velocity sampling errors in a Michelson interferometer
[AD-A273105] p 1809 N94-21508
Performance evaluation of video on ethernet
[DE93-040696] p 1936 N94-21749
Surface acoustic wave sensing of VOC's in harsh chemical environments
[DE93-040721] p 1968 N94-21751

PERIDOTITE
Euhedral metallic-Fe-Ni grains in extraterrestrial samples p 1697 N94-20724
Basaltic magmatism on the Moon. A perspective from volcanic picritic glasses p 2114 N94-20758
Primary differentiation in the early Earth: Nd and Sr isotopic evidence from diamondiferous eclogites for both old depleted and old enriched mantle, Yakutia, Siberia p 1862 N94-20776
The carbon components in SNC meteorites of feldspathic harzburgite composition p 2086 N94-20885

PERIODIC FUNCTIONS
Stoermer-Cowell and related methods for the numerical solution of second order periodic initial value problems for ODE's 2: Numerical characteristics of the methods
[MEMO-1082] p 1953 N94-21075

PERIODIC VARIATIONS
The effects of magnetic storm phases on F-layer irregularities from auroral to equatorial latitudes
[AD-A272685] p 1857 N94-21189

PERMAFROST
Calderas produced by hydromagmatic eruptions through permafrost in northwest Alaska p 2089 N94-20385
Possible occurrence and origin of massive ice in Utopia Planitia p 2090 N94-20390
Cryoplanation terraces of interior and western Alaska p 2091 N94-20396
A formational model for the polygonal terrains of Mars: Taking a crack at the genesis of the Martian polygons p 2091 N94-20400
Interferometric detection of freeze-thaw displacements of Alaskan permafrost using ERS-1 data p 1732 N94-20460

PERMANENT MAGNETS
Measurement and correction of magnetic fields in pulsed slotted-tube microwigglers
[DE93-040100] p 1815 N94-20272
Variable-field permanent magnet dipole
[DE94-000800] p 1820 N94-22020

PERMEABILITY
High-resolution numerical methods for compressible multi-phase flow in hierarchical porous media
[DE94-000740] p 1799 N94-20351
Variable-permittivity linear inverse problem for the H(sub z)-polarized case p 1719 N94-20408

PERMITTIVITY
Numerical modeling of fringing fields and their use for complex permittivity measurements at high frequencies
[AD-A270478] p 1966 N94-19917
Variable-permittivity linear inverse problem for the H(sub z)-polarized case p 1719 N94-20408
Relating ground truth collection to model sensitivity p 1719 N94-20409
The effect of dissipative inhomogeneous medium on the statistics of the wave intensity p 1726 N94-20440
The Brewster angle effect in SAR polarimetry p 1731 N94-20456

PEROVSKITES
Ten GHz YBa2Cu3O(7-delta) superconducting ring resonators on NdGaO3 substrates p 1735 N94-20515

PERSONAL COMPUTERS
Two-dimensional particle-in-cell simulation on transputer arrays
[DE93-017977] p 1972 N94-20181
Probability of detection calculations using MATLAB
[AD-A271958] p 1736 N94-20578
Mathcad computer applications predicting antenna parameters from antenna physical dimensions and ground characteristics
[AD-A272987] p 1740 N94-21264
Application development in a PC/LAN environment p 1923 N94-22067
Crystal ball gazing p 1925 N94-22477
PCIPS 2.0: Powerful multiprofile image processing implemented on PCs p 1927 N94-22532

PERSONNEL
Activities of National Inst. for Aviation Research
[NIAR-93-16] p 2151 N94-20150

PERSONNEL DEVELOPMENT
Center for neural engineering
[AD-A271164] p 1890 N94-20185
NCCDS configuration management process improvement p 1931 N94-21327
Information and decision structure in a Japanese type of management with respect to QCC and just-in-time systems p 2046 N94-22063

PERSONNEL MANAGEMENT
Factors associated with continuance commitment to FAA matrix teams
[DOT/FAA/AM-93/18] p 2040 N94-21626

PERSONNEL SELECTION
Psychometric developments related to tests and selection
[AD-A272971] p 1894 N94-21262
Compatibility evaluation and research on the Computerized Adaptive Screening Test (CAST): User and programmer's guide
[AD-A273112] p 1894 N94-21510

PERTURBATION
Longitudinal instability of an induction linac with acceleration
[DE93-019249] p 1980 N94-20290
Direct simulation of shock-induced mixing layer
[DE93-040498] p 1803 N94-21531
Universality in blow-up for non linear heat equations
[PB93-215465] p 2038 N94-22095
Effects of magnetic field perturbations in the ATF torsatron
[DE94-000474] p 1999 N94-22568

PERTURBATION THEORY
Stability of the face-centered-cubic phase of heavy rare gas solids
[DE93-019949] p 1679 N94-20319
A theoretical and numerical study of polarimetric scattering and emission from random rough surfaces with anisotropic directional spectrum p 1730 N94-20454
Theoretical particle physics
[DE94-000538] p 1973 N94-20938
A formulation of quantum statistical mechanics based on the Feynman path centroid density 1: Equilibrium properties
[AD-A272809] p 2037 N94-21171
One- and multi-component theories of mixtures
[DE93-040543] p 1966 N94-21511
Simulating the Euclidean time Schroedinger equations using an INTEL iPSC/860 hypercube: Application to the t-J model of high-T(sub c) superconductivity
[DE94-000489] p 2035 N94-22385
Turbulization of free shear flows: 3D perturbations p 2000 N94-22626
Time variation of MHD accretion onto a black hole p 2009 N94-22692
Spiral Alfven instability in accretion disks p 2010 N94-22698

PESTICIDES
Compatibility and efficacy of biocides qualified under military specification MIL-S-53021
[AD-A271496] p 1712 N94-20551

PETN
Crystal orientation dependence of elastic precursor strength in pentaerythritol tetranitrate
[DE93-018340] p 2034 N94-22035

PETRI NETS
Interval timed coloured petri nets and their analysis
[PB93-191732] p 1903 N94-19992
Total order assumption
[PB93-191740] p 1903 N94-19993
Dependability and performability analysis
[NASA-CR-191565] p 1965 N94-21463
System level modelling using Petri nets and VHDL p 1772 N94-22113
Modeling and analysis of secure communication protocols using Petri net formalism p 1784 N94-22194
How to handle 6GBytes a night and not get swamped p 2058 N94-22444

PETROGRAPHY
Twenty-Fourth Lunar and Planetary Science Conference. Part 3: N-Z
[NASA-CR-193149] p 2092 N94-20636
Petrography of shock features in the 1953 Manson 2-A drill core p 1862 N94-20767
Petrography and origin of refractory inclusions from the Murray and Murchison C2 chondrites p 2084 N94-20770
Evaluation of lunar rocks and soils for resource utilization: Detailed image analysis of raw materials and beneficiated products p 2126 N94-20820

PETROLOGY
Twenty-Fourth Lunar and Planetary Science Conference. Part 3: N-Z
[NASA-CR-193149] p 2092 N94-20636
REE and other trace lithophiles in MAC88177, LEW88280 and LEW88763 p 2082 N94-20639
The Erevan howardite: Petrology of glassy clasts and mineral chemistry p 1684 N94-20640
Petrogenesis of Apollo 12 mare basalts. Part 1: Multiple melts and fractional crystallization to explain olivine and ilmenite basalt compositions p 1684 N94-20644
Petrogenesis of Apollo 12 mare basalts. Part 2: An open system model to explain the pigeonite basalt compositions p 1684 N94-20645
The Sm-(146,147)-Nd-(142,143) formation interval for the lunar mantle and implications for lunar evolution p 2097 N94-20663
Modelling the gravity and magnetic field anomalies of the Chicxulub crater p 1862 N94-20668
Orthopyroxenes as recorders of diogenite petrogenesis: Major and minor element systematics p 1684 N94-20670
Opaque-rich lithology in the Divnoe achondrite: Petrology and origin p 2082 N94-20680
U-Pb isotopic ages and characteristics of ancient (greater than 4.0 Ga) lunar highland rocks p 2104 N94-20700
Oxygen isotopic relationships between the LEW85332 carbonaceous chondrite and CR chondrites p 2083 N94-20708
Micrometeorite dynamic pyrometamorphism: Nonstoichiometric clinoenstatite (CLEN) p 2083 N94-20715
Lunar basalt meteorite EET 87521: Petrology of the clast population p 2083 N94-20752
Orthopyroxenes as recorders of diogenite petrogenesis: Trace element systematics p 1686 N94-20760
Geochronology and petrogenesis of the western highlands alkali suite: Radiogenic isotopic evidence from Apollo 14 p 2118 N94-20778
Magnesian anorthosites from the western highlands of the Moon: Isotope geochemistry and petrogenesis p 2118 N94-20779
Petrology and geochemistry of VLT glasses from double drive tube 79001/2 p 1687 N94-20870
Lewis Cliff 87057: A new metal-rich E3 chondrite with similarities to Mt. Egerton, Shallowater and Happy Canyon p 2086 N94-20901
Chemical composition of new Acapulcoites and Lodranites p 2086 N94-20905

PH
Analog/digital pH meter system I.C. p 1764 N94-21701

PHARMACOLOGY
Physiologically based pharmacokinetic modelling of percutaneously absorbed dibromomethane utilizing multiple dermal sub-compartments
[AD-A271106] p 1889 N94-19981

PHASE CONTROL
Phase screens for the control of the focal irradiance of the Nova laser
[DE94-001067] p 1820 N94-22401

PHASE DEMODULATORS
Phase demodulation of interferometric fiber-optic sensors
[ISBN-0-315-83425-0] p 1991 N94-22581

PHASE DIAGRAMS
Theoretical phase diagrams for solid H(sub 2)
[DE94-001049] p 1684 N94-22395
First-principles pressure-temperature phase diagrams in metals
[DE94-001056] p 1696 N94-22398

PHASE ERROR
Array Simulations Platform (ASP) predicts NASA Data Link Module (NDLM) performance p 1744 N94-21348
Effect of errors on the phase centre and pointing angle of phased array antennas p 1746 N94-22162

PHASE MODULATION
Material optimization for hard x ray Fresnel zone plates
[DE93-019569] p 1990 N94-21837
Effect of bandwidth on beam smoothing and frequency conversion at the third harmonic of the Nova laser
[DE93-019917] p 1819 N94-21920

PHASE SHIFT
Topographic slope from the SAR interferometric phase gradient p 1731 N94-20459
Four-channel HF receiving antenna array simulator
[AD-A271876] p 1732 N94-20471
Space applications of superconducting microwave electronics at NASA Lewis Research Center p 1671 N94-20513
The coherent backscattering opposition effect p 1991 N94-20646

PHASE SHIFT KEYING
Capacity comparison between direct sequence PSK and MFSK spread spectrum systems in CDMA applications p 1747 N94-22224

PHASE STABILITY (MATERIALS)
Stability of the face-centered-cubic phase of heavy rare gas solids
[DE93-019949] p 1679 N94-20319
Sintering silicon nitride
[NASA-CASE-LEW-15489-1] p 1703 N94-20529

PHASE TRANSFORMATIONS
Crystallographic phase transitions in actinide metals as a function of pressure
[DE93-040138] p 2011 N94-19827

Problems related to conservation laws: Phase transitions and viscoelasticity
[AD-A271429] p 1696 N94-19640
General introduction to microstructural evolution under cascade damage conditions
[DE93-017443] p 2012 N94-19923
Kinetics of phase transformations in glass forming systems
[NASA-CR-194270] p 1701 N94-20347
The effect of fluctuations on the electrical transport behavior in YBa2Cu3O(7-x) p 1736 N94-20519
Thermal expansion of electronic highly correlated materials
[ETN-93-93605] p 2026 N94-21135
Examinations of composition and deformation behavior of intermetallic phases on the basis of Fe3(AlSi)
[GKSS-92/E/16] p 1692 N94-21311
Static ultra-high pressure study of lanthanide and actinide metals using a diamond-anvil cell
[DE94-000369] p 1693 N94-21656
Temperature dependence of magnetic order in single-crystalline UPdSn
[DE93-040153] p 2033 N94-21991
The effect of correlated and point defects on the vortex lattice melting transition in single crystal YBa2Cu3O(7-delta)
[DE93-040277] p 2033 N94-21997
Theoretical studies of structural phase transitions in actinide metals
[DE94-000796] p 1696 N94-22388

PHASE VELOCITY
Azo polymers for optical storage 3: Effect of film thickness on net phase retardation and writing speed
[AD-A272094] p 1705 N94-21267

PHASED ARRAYS
Interinjection-locked quasioptical power combiners and phased arrays
[AD-A271178] p 2015 N94-20214
Quartz/fused silica chip carriers
[NASA-CR-194154] p 2016 N94-20340
Optical beam forming techniques for phased array antennas p 1727 N94-20442
Phased array antenna with couplers in spatial filter arrangement
[CA-PATENT-1,296,098] p 1737 N94-21031
Investigation of the effect of various oxide and fluoride additives on the microstructure, electronic properties, and phase shifting ability of Ba(1-x)Sr(x)TiO3
[AD-A271756] p 2027 N94-21303
Effect of errors on the phase centre and pointing angle of phased array antennas p 1746 N94-22162
AlGaAs laser diode FM spectrum: Phased array antenna application p 1746 N94-22196

PHENOLS
Water-enhanced solvation of organics
[DE93-040297] p 1683 N94-21947

PHONEMES
Speech synthesis with artificial neural networks p 1743 N94-20245

PHONONS
The multicomponent lineshape of the anharmonic A(1)(TO) phonon in PbTiO3
[DE93-018995] p 1970 N94-19971
Phonons and metastability in compressed nitrogen
[DE93-019913] p 2016 N94-20318
Solid-state dynamics and quantum transport in novel semiconductor nanostructures
[AD-A272955] p 2027 N94-21248
Inelastic neutron scattering of (gamma)-iron, and the determination of the elastic constants by lattice dynamics
[DE94-000694] p 1978 N94-22573

PHOSGENE
Infrared absorption spectroscopy of the weakly bonded CO-Cl2 complex
[AD-A271757] p 2027 N94-21304

PHOSPHATES
Transient studies of low temperature catalysts for methane conversion
[DE93-041232] p 1680 N94-20934
Spectroscopic studies of magnetic transitions in TbPO4
[DE94-001274] p 2035 N94-22565

PHOSPHIDES
Photoluminescence spectroscopy of zinc germanium diphosphide (ZnGeP2)
[AD-A270705] p 1678 N94-19953

PHOSPHINES
Photochemically induced transformations of transition complexes
[AD-A271112] p 2014 N94-19982

PHOSPHORUS
Core formation in the Moon: The mystery of the excess depletion of Mo, W and P p 2095 N94-20651
Polymeric nitrogen
[DE93-040544] p 1706 N94-21512
Refractive index behaviour of phosphorus-doped planar silica waveguides, appendix 7 p 1989 N94-21601

PHOTOABSORPTION
Photoabsorption and Compton scattering in ionization of helium at high photon energies
[DE94-000380] p 1974 N94-21658
Single and double ionization of helium by high-energy photon impact
[DE94-000381] p 1975 N94-21785
The effect of Compton scattering on the double to single ionization ratio in helium
[DE94-000884] p 1827 N94-22390

PHOTOCATHODES
Performance of the high brightness linac for the Advanced Free Electron Laser Initiative at Los Alamos
[DE93-040141] p 1816 N94-20277
CsI and some new photocathodes
[DE93-019387] p 1750 N94-20314
Electron quantum yields from a barium photocathode illuminated with polarized light
[DE93-019232] p 1980 N94-20475
SLD results from the study of polarized Z(sup 0) produced at the SLC
[DE93-041020] p 1982 N94-21952

PHOTOCHEMICAL REACTIONS
Laboratory studies of low temperature rate coefficients: The atmospheric chemistry of the outer planets
[NASA-CR-193485] p 1972 N94-20130
Recent developments in aromatic azo polymers research
[AD-A272966] p 1705 N94-21259
Polyimide-based electrooptic materials
[DE93-019416] p 1706 N94-21526
Requirements for the early atmosphere of Mars from nitrogen isotope ratios p 2144 N94-21669
Mars atmosphere loss and isotopic fractionation by solar-wind-induced sputtering and photochemical escape p 2144 N94-21672
Possible solutions to the problem of channel formation on early Mars p 2144 N94-21673
The young Sun and photochemistry of the primitive Martian atmosphere p 2145 N94-21679
Global emissions and models of photochemically active compounds
[DE93-040490] p 1852 N94-21969
Photochemical approaches to conversion of light to electricity or fuel
[DE94-001650] p 1849 N94-22048
Development of advanced cloud parameterizations to examine air quality, cloud properties, and cloud-radiation feedback in mesoscale models
[DE93-041164] p 1853 N94-22384
Infrared FEL photochemistry: Multiple-photon dissociation of freon gas
[DE94-000817] p 1820 N94-22585

PHOTOCONDUCTIVITY
Process to fabricate thick coplanar microwave electrode structures
[AD-D015913] p 1748 N94-19892
Photoconductive Semiconductor Switches for pulsed power applications
[DE93-019411] p 1750 N94-20294
Optically controlled current filamentation in GaAs photoconductive semiconductor switches
[DE93-019427] p 2016 N94-20296
Transport in microstructures in the microwave and millimeter-wave regime
[AD-A271875] p 2017 N94-20470
Advanced far infrared detectors
[DE93-040289] p 1988 N94-21528

PHOTOCONDUCTORS
Advanced far infrared detectors
[DE93-040289] p 1988 N94-21528

PHOTODIODES
The quantum efficiency of HgCdTe photodiodes in relation to the direction of illumination and to their geometry p 1735 N94-20512

PHOTODISSOCIATION
Ionization of H2(+) in intense laser fields
[DE93-019160] p 1818 N94-21829
Infrared FEL photochemistry: Multiple-photon dissociation of freon gas
[DE94-000817] p 1820 N94-22585

PHOTOELECTRIC EMISSION
Magnetic circular dichroism in x ray absorption and core-level photoemission
[DE93-019381] p 1688 N94-19986
Development of a numerical simulation model for a-Si:H solar cells and application to the analysis of experimentally obtained spectral characteristics
[ETN-93-95061] p 1846 N94-20151
Electron quantum yields from a barium photocathode illuminated with polarized light
[DE93-019232] p 1980 N94-20475
Photoemission and the electronic properties of heavy fermions: Limitations of the Kondo model
[DE93-040191] p 1974 N94-21553
Photoelectron holography of platinum (111)
[DE93-040856] p 1810 N94-21950

PHOTOELECTRON SPECTROSCOPY
ALE project
[AD-A271080] p 2014 N94-19980
Photoelectron spectroscopy at model boundary surfaces of energy converter semiconductors/electrolyte contacts: Adsorption, coadsorption, and triadsorption of Br2, Na, and H2O on Van der Waals surfaces of metal chalocogenide semiconductors
[ETN-93-95063] p 2015 N94-20152
Applications and source development for high-repetition rate x ray lasers
[DE93-019547] p 1815 N94-20259
Temperature dependence of 4f PES features and hole occupancy in ytterbium heavy fermions
[DE93-040131] p 1691 N94-20321
Study of the utilization of thin oxides in indium phosphides for the realisation of electron components
[ECL-92-38] p 2018 N94-20593
Alumoxanes: Rationalization of black box materials
[AD-A272805] p 1704 N94-21170
Diffraction and holography of photoelectrons and fluorescent x rays
[DE93-019240] p 1808 N94-21441
Photoemission and the electronic properties of heavy fermions: Limitations of the Kondo model
[DE93-040191] p 1974 N94-21553

PHOTOELECTRONS
Ionospheric photoelectrons measured at geosynchronous orbit
[AD-A272431] p 1857 N94-21202
Diffraction and holography of photoelectrons and fluorescent x rays
[DE93-019240] p 1808 N94-21441
Photoelectron holography of platinum (111)
[DE93-040856] p 1810 N94-21950
A Monte Carlo study of the Sudbury Neutrino Observatory small test detector experiment
[ISBN-0-315-59056-4] p 1977 N94-22416

PHOTOEXCITATION
Photochemical approaches to conversion of light to electricity or fuel
[DE94-001650] p 1849 N94-22048

PHOTOGEOLOGY
Preliminary results from Mariner 10: High resolution images of the Moon p 2107 N94-20719
Photogeological analysis of Europan tectonic features p 2129 N94-20838

PHOTOGRAMMETRY
Robust photo-topography by fusing shape-from-shading and stereo
[NASA-CR-194697] p 1806 N94-19920
Discharge rates in Ma'adim Vallis, Mars p 2128 N94-20830

PHOTOGRAPHIC TRACKING
Trajectory computations for an improved cinetheodolite tracking system p 1791 N94-22236

PHOTOGRAPHS
A comparison of some of the most current methods of image compression
[AD-A271841] p 1907 N94-20525
Debris/ice/TPS assessment and integrated photographic analysis for Shuttle Mission STS-51
[NASA-TM-109189] p 1656 N94-21884
SkiCAT: A cataloging and analysis tool for wide field imaging surveys p 2049 N94-22546

PHOTOGRAPHY
Synchrotron x ray diffraction analysis of photorefractive crystals and their gratings
[AD-A271176] p 2015 N94-20213

PHOTOINTERPRETATION
Evaluation of C-band SAR data from SAREX 1992: Tapajos study site p 1839 N94-20964

PHOTOIONIZATION
Angular distributions of high-order ATI
[DE93-019125] p 1972 N94-20230
Photopumped x ray laser research on Saturn
[DE93-019430] p 1816 N94-20298
Generation of intense ultrashort x ray pulses
[DE93-019607] p 1817 N94-21299
Photoabsorption and Compton scattering in ionization of helium at high photon energies
[DE94-000380] p 1974 N94-21658
Single and double ionization of helium by high-energy photon impact
[DE94-000381] p 1975 N94-21785
Ionization of H2(+) in intense laser fields
[DE93-019160] p 1818 N94-21829
Direct detection of atomic ions from molecular photofragmentation during nonresonant multiphoton ionization of sputtered species
[DE93-040886] p 1976 N94-21951

The effect of Compton scattering on the double to single ionization ratio in helium
[DE94-000884] p 1827 N94-22390
PHOTOLITHOGRAPHY
X ray reflection masks: Manufacturing, characterization and first tests
[BONN-IR-92-31] p 1986 N94-21043
Examination for optimization of synchrotron radiation spectrum for the x ray depth lithography
[BONN-IR-92-32] p 1987 N94-21148
PHOTOLUMINESCENCE
Effect of exciton localization and delocalization on magnetic-field-dependent photoluminescence linewidths in semiconductors
[DE93-018860] p 1748 N94-19884
Photoluminescence spectroscopy of zinc germanium diphosphide (ZnGeP2)
[AD-A270705] p 1678 N94-19953
Optically controlled current filamentation in GaAs photoconductive semiconductor switches
[DE93-019427] p 2016 N94-20296
Dephasing processes in III-V semiconductors
[AD-A271677] p 2028 N94-21362
Growth, characterization and device development in monocrystalline diamond films
[AD-A273097] p 2028 N94-21506
Implantation of carbon in GaAs and compensating native defects
[DE93-040122] p 2030 N94-21763
PHOTOLYSIS
Photochemically induced transformations of transition complexes
[AD-A271112] p 2014 N94-19982
PHOTOMAGNETIC EFFECTS
Photo- and thermal-induced antiferromagnetic interlayer coupling in Fe/(Fe-Si) superlattices
[DE93-040822] p 2031 N94-21930
PHOTOMETERS
High Speed/High Frequency Optoelectronics
[AD-A271985] p 1751 N94-20580
Silicon retina for optical tracking systems p 1755 N94-21098
Bidirectional method for optical channel waveguide attenuation measurement by detectors integrated on the wafer, appendix 3 p 1988 N94-21597
PHOTOMETRY
Sunphotometer network for monitoring aerosol properties in the Brazilian Amazon p 1839 N94-20961
PHOTCAL: The IRAF photometric calibration package p 1925 N94-22465
MOSAIC: Software for creating mosaics from collections of images p 1927 N94-22543
PHOTOMULTIPLIER TUBES
A Monte Carlo study of the Sudbury Neutrino Observatory small test detector experiment
[ISBN-0-315-59056-4] p 1977 N94-22416
PHOTON BEAMS
Target motion detecting impulse Doppler radar system
[AD-D015898] p 1717 N94-20198
PHOTON-ELECTRON INTERACTION
Photoabsorption and Compton scattering in ionization of helium at high photon energies
[DE94-000380] p 1974 N94-21658
Single and double ionization of helium by high-energy photon impact
[DE94-000381] p 1975 N94-21785
PHOTONICS
Photonics and nonlinear optics with molecular materials and polymers
[AD-A271747] p 1988 N94-21457
PHOTONS
Target motion detecting impulse Doppler radar system
[AD-D015898] p 1717 N94-20198
Direct photon results from CDF
[DE93-019908] p 1980 N94-20317
Material optimization for hard x ray Fresnel zone plates
[DE93-019589] p 1990 N94-21837
Search for excited quarks in p(-p) collisions at the square root of s = 1.8 TeV
[DE93-019910] p 1975 N94-21840
Studies of the deuteron at high energy and momentum transfer
[DE93-041162] p 1976 N94-21941
Detector noise statistics in the non-linear regime p 1748 N94-22526
PHOTONUCLEAR REACTIONS
Studies of the deuteron at high energy and momentum transfer
[DE93-041162] p 1976 N94-21941
PHOTOPRODUCTION
Direct photon results from CDF
[DE93-019908] p 1980 N94-20317
Proceedings of the 1993 DOE/NREL Hydrogen Program Review
[DE93-018207] p 1847 N94-21616
PHOTORECEPTORS
Nature's crucible: Manufacturing optical nonlinearities for high resolution, high sensitivity encoding in the compound eye of the fly, Musca domestica p 1755 N94-21095
PHOTOSPHERE
Solar imaging vector magnetograph
[NASA-CR-194729] p 1810 N94-21876
Large-scale structure of the solar plasma corona: An analysis of Yohkoh SXT images p 2004 N94-22657
PHOTOVOLTAIC CELLS
System performance predictions for Space Station Freedom's electric power system
[NASA-TM-106396] p 1667 N94-20062
Fabrication of stable large-area thin-film CdTe photovoltaic modules
[DE93-018204] p 1845 N94-20095
Self-deploying photovoltaic power system
[NASA-CASE-LEW-15308-1] p 1846 N94-20196
Building integrated photovoltaic systems analysis
[DE93-018208] p 1846 N94-21298
Annual Report, Materials Science Branch, FY 1992
[DE94-000204] p 1849 N94-22015
PHOTOVOLTAIC CONVERSION
Development of high-efficiency CdTe solar cells
[DE93-018206] p 1845 N94-19925
Growth mechanisms and characterization of hydrogenated amorphous-silicon-alloy films
[DE93-018202] p 1699 N94-20047
Power transmission by laser beam from lunar-synchronous satellite
[NASA-TM-4496] p 1669 N94-20102
Building integrated photovoltaic systems analysis
[DE93-018208] p 1846 N94-21298
Stable, high-efficiency amorphous-silicon solar cells with low hydrogen content
[DE93-018214] p 1848 N94-21826
Thin-film CdTe and CuInSe2 photovoltaic technologies
[DE93-018217] p 1848 N94-21827
Investigation on the chemically fixing technique of carbon dioxide utilizing solar energy
[DE94-714886] p 1849 N94-22043
Photochemical approaches to conversion of light to electricity or fuel
[DE94-001650] p 1849 N94-22048
Surveys on specific patterns of facility intallation of photovoltaic power generating technologies for international cooperation
[DE94-714901] p 1850 N94-22092
Research on stable, high-efficiency amorphous silicon multijunction modules
[DE93-018220] p 1850 N94-22257
PHTHALATES
Growth and morphology of crystals: Theory and observations
[PB93-221166] p 2035 N94-22273
PHYSICAL CHEMISTRY
A comparison of calculated and measured rheological properties of crystallising lavas in the field and in the laboratory p 1862 N94-20690
PHYSICAL EXAMINATIONS
Analysis of health status from preliminary physical examination of flight academy applicants
[AD-A267759] p 1889 N94-19962
PHYSICAL EXERCISE
Physiological correlates of stress-induced decrements in human perceptual performance
[DOT/FAA/AM-93/19] p 1893 N94-20081
PHYSICAL FITNESS
Maximum team lifting capacity as a function of team size
[AD-A271642] p 1892 N94-21036
PHYSICAL OPTICS
Study of electromagnetic wave scattering from characterized rough surfaces
[AD-A270931] p 1716 N94-19934
RCS Analysis of Plate Geometries, parts 1 and 2
[NASA-CR-194173] p 1717 N94-20269
High-frequency techniques for RCS prediction of plate geometries p 1717 N94-20270
FD-TD modeling of 2-D dielectric waveguides for propagation and scattering of femtosecond optical solitons p 1719 N94-20408
An optically-assisted 3-D cellular array machine
[AD-A272683] p 1987 N94-21163
PHYSICAL WORK
Apparatus and method for measuring subject work rate on an exercise device
[NASA-CASE-MSC-21752-1] p 1895 N94-20194
PHYSIOLOGICAL EFFECTS
Cosmos 2229
[NASA-CR-194734] p 1895 N94-20338
Extra-corporeal blood access, sensing, and radiation methods and apparatuses
[NASA-CASE-MSC-21775-1] p 1890 N94-20372
Studies of neural and cognitive function in subjects exposed to the marine-air interface, phases 1 and 2
[AD-A272282] p 1891 N94-20624
A proposed methodology for combustion toxicology testing of combined halon replacement agent/jet fuel interaction
[AD-A272695] p 1681 N94-21165
Physiological efficacy of a lightweight ambient air cooling unit for various applications
[AD-A272952] p 1896 N94-21247
PHYSIOLOGICAL RESPONSES
Human responses to exercise-heat stress
[AD-A272581] p 1892 N94-21209
PHYSIOLOGY
Physiologically based pharmacokinetic modelling of percutaneously absorbed dibromomethane utilizing multiple dermal sub-compartments
[AD-A271106] p 1889 N94-19981
Physiological correlates of stress-induced decrements in human perceptual performance
[DOT/FAA/AM-93/19] p 1893 N94-20081
Wind chill: The temperature feeling caused by the wind velocity
[KNMI-TR-103A] p 1890 N94-20238
Studies of neural and cognitive function in subjects exposed to the marine-air interface, phases 1 and 2
[AD-A272282] p 1891 N94-20624
PICOSECOND PULSES
Infrared FEL photochemistry: Multiple-photon dissociation of freon gas
[DE94-000817] p 1820 N94-22585
PIEZOELECTRIC GAGES
Free flight experiment with a laminar wing glove p 1639 N94-22600
PIEZOELECTRICITY
Proceedings of the 8th International Symposium on Applications of Ferroelectrics
[AD-A270679] p 1749 N94-20012
Application of change detection to dynamic contact sensing
[AD-A270523] p 1939 N94-20105
Actively controlled shaft seals for aerospace applications
[NASA-CR-194759] p 1823 N94-20538
PIEZORESISTIVE TRANSDUCERS
High accuracy die mechanical stress measurement with the ATC04 Assembly Test Chip
[DE93-019435] p 1830 N94-20477
PILOT PERFORMANCE
Perception/action: An holistic approach 2
[AD-A271822] p 1891 N94-20627
Modelling decision-making by pilots
[NASA-CR-194767] p 2040 N94-21821
PILOT TRAINING
Modelling decision-making by pilots
[NASA-CR-194767] p 2040 N94-21821
Public-sector aviation issues: Graduate research award papers, 1991-1992
[PB93-206258] p 1642 N94-22055
PILOTLESS AIRCRAFT
Low-cost, dual-use platforms for environmental sensing, phase 1
[AD-A272951] p 1646 N94-21246
PILOTS
ATC/pilot voice communications: A survey of the literature
[DOT/FAA/AM-93/20] p 1738 N94-21201
PINCH EFFECT
Research on plasma-puff initiation of high Coulomb transfer switches
[NASA-CR-194371] p 1994 N94-21289
Plasma-puff initiation of high Coulomb transfer switches p 1994 N94-21290
Characteristics of plasma-puff trigger for a inverse-pinch plasma switch p 1995 N94-21291
Characteristics of switching plasma in an inverse-pinch switch p 1995 N94-21292
Comparative study of INPIStron and spark gap p 1995 N94-21293
PINHOLES
Multisensor pinhole yawsonde
[AD-A271715] p 1808 N94-20930
PINNING
Relaxation of hysteresis loop in a single crystal of YBa2Cu4O8
[DE93-019519] p 2029 N94-21649
PIONS
Evaluation of the chemical composition of cosmic radiation in energy area of 10(exp 15) eV
[ETN-93-93682] p 2150 N94-21056
Qualitative and quantitative aspects of the QCD theory of elastic form factors
[DE93-040864] p 2038 N94-21513
Low p(sub T) phenomena observed in high energy nuclear collisions
[DE94-000825] p 1962 N94-21849

PIPELINING (COMPUTERS)
Avoiding and tolerating latency in large-scale next-generation shared-memory multiprocessors p 1753 N94-21081
Instruction set commutivity p 1766 N94-21719
Using stream interleaving to eliminate the need for interlocks in deeply pipelined processors p 1781 N94-22175

PIPES (TUBES)
Evaluation of the fabricability of advanced iron aluminide-clad austenitic stainless steel tubing [DE93-040598] p 1693 N94-21771
Fabrication of whisker-toughened alumina tubes [DE94-001012] p 1677 N94-22022

PISTONS
The flow of gas across the piston-segments-cylinder interface [ECL-92-40] p 1824 N94-20594
Vapor-delivered lubrication of steel-steel and steel-ceramic systems [PB93-202364] p 1825 N94-21451

PITCH
Segmentation and frequency domain ML pitch estimation of speech signals p 1747 N94-22212

PITOT TUBES
Free flight experiment with a laminar wing glove p 1639 N94-22600
Riblet boundary layer measurements of an A-310 fuselage with Pitot combs p 1640 N94-22605

PIVOTS
Bladder operated robotic joint [NASA-CASE-MFS-28682-1] p 1701 N94-20359

PIXELS
The roughness of the Martian surface: A scale dependent model p 2115 N94-20762
Objective determination of image end-members in spectral mixture analysis p 1686 N94-20831
Convex set and linear mixing model p 1844 N94-20888
Nature's crucible: Manufacturing optical nonlinearities for high resolution, high sensitivity encoding in the compound eye of the fly, Musca domestica p 1755 N94-21095

PLAINS
Workshop on the Martian Northern Plains: Sedimentological, Periglacial, and Paleoclimatic Evolution [NASA-CR-194831] p 2088 N94-20382
The fate of water deposited in the low-lying northern plains p 2089 N94-20387
Stratigraphy of the Martian northern plains p 2091 N94-20398
Geomorphic evidence for an eolian contribution to the formation of the Martian northern plains p 2092 N94-20402
Mars: New evidence for origin of some Vallies Marineris layered deposits p 2112 N94-20748

PLANAR STRUCTURES
High temperature superconducting planar circuit structure for high frequency applications [AD-A273083] p 2028 N94-21521
Geometric optimization [DE93-040152] p 1917 N94-21764
Time-laplace-transform-domain analysis of wave propagation in planar waveguides [PB93-215226] p 1960 N94-22096

PLANE WAVES
Variable-permittivity linear inverse problem for the H(sub z)-polarized case p 1719 N94-20408
The effect of dissipative inhomogeneous medium on the statistics of the wave intensity p 1726 N94-20440
Signal processing in the linear statistical model [AD-A272114] p 1736 N94-20570

PLANETARY ATMOSPHERES
Laboratory studies of low temperature rate coefficients: The atmospheric chemistry of the outer planets [NASA-CR-193485] p 1972 N94-20130
Remote sounding of tropospheric minor constituents [NASA-CR-194265] p 1855 N94-20132
Dynamics of large scale impacts on Venus and Earth p 2098 N94-20666
Low-energy ion implantation: Large mass fractionation of argon p 1685 N94-20697
Numerical modeling of impact erosion of atmospheres: Preliminary results p 2131 N94-20847
Core formation, wet early mantle, and H2O degassing on early Mars p 2145 N94-21674

PLANETARY BASES
Mars exploration study workshop 2 [NASA-CP-3243] p 2146 N94-21883

PLANETARY BOUNDARY LAYER
Temperature/pressure and water vapor sounding with microwave spectroscopy p 1812 N94-22436

PLANETARY COMPOSITION
Twenty-Fourth Lunar and Planetary Science Conference. Part 3: N-Z [NASA-CR-193149] p 2092 N94-20636
Detectability of crystalline ferric and ferrous minerals on Mars p 2110 N94-20730
Fine resolution chronology based on initial Sr-87/Sr-86 [CONTRIB-5230(794)] p 1686 N94-20794
Discovery Venera surface: Atmosphere geochemistry experiments mission concept p 2123 N94-20806
The x ray microprobe determination of chromium oxidation state in olivine from lunar basalt and kimberlitic diamonds p 1686 N94-20807
Geology and radiophysical properties of the Venera and Vega landing sites p 2135 N94-20867
A study of carbonates, sulfates, and phosphates using thermal emission spectroscopy p 1686 N94-20868
An attempt to comprehend Martian weathering conditions through the analysis of terrestrial palagonite samples p 2143 N94-21668
In situ identification of the Martian surface material and its interaction with the Martian atmosphere using DTA/GC p 1812 N94-22434

PLANETARY CORES
Expectations for the Martian core magnetic field p 2120 N94-20792
Core formation by giant impacts: Conditions for intact melt region formation p 1863 N94-20833
The connection between Venus' free obliquity and its CMB oblateness p 2139 N94-20896
Core formation, wet early mantle, and H2O degassing on early Mars p 2145 N94-21674

PLANETARY CRATERS
Twenty-Fourth Lunar and Planetary Science Conference. Part 3: N-Z [NASA-CR-193149] p 2092 N94-20636
Largest impact features on Venus: Non-preserved or non-recognizable? p 2096 N94-20657
Venus magmatic and tectonic evolution p 2101 N94-20683
Crater destruction on the Venusian highlands by tectonic processes p 2103 N94-20696
Kalkkop crater, Eastern Cape: A new impact crater in South Africa p 1862 N94-20714
The Manson impact crater: Estimation of the energy of formation, possible size of the impacting asteroid or comet, and ejecta volume and mass p 2083 N94-20721
Named Venusian craters p 2109 N94-20725
Venus' impact-crater database: Update to approximately 98 percent of the planet's surface p 2110 N94-20736
Searching for ancient Venus p 2111 N94-20743
The missing impact craters on Venus p 2119 N94-20782
Impact basins on Venus and some interplanetary comparisons p 2119 N94-20785
Parabolic features and the erosion rate on Venus p 2122 N94-20801
Discovery Venera surface: Atmosphere geochemistry experiments mission concept p 2123 N94-20806
Original size of the Vredefort structure, South Africa p 1863 N94-20825
Origin of the Vredefort structure, South Africa: Impact model p 1863 N94-20826
Core formation by giant impacts: Conditions for intact melt region formation p 1863 N94-20833
Is there uniformitarian or catastrophic tectonics on Venus? p 2129 N94-20839
Geology of Galileo Regio quadrangle, Ganymede p 2130 N94-20842
Elevation and igneous crater modification on Venus: Implications for magmatic volatile content p 2135 N94-20872
Large floor-fractured craters and isostatic crater modification: Implications for lithospheric thickness on Venus p 2135 N94-20873
Evolution of the global water cycle on Mars: The geological evidence p 2142 N94-21660
The early Martian environment: Clues from the cratered highlands and the Precambrian Earth p 2143 N94-21667

PLANETARY CRUSTS
Beta Regio rift system on Venus: Geologic interpretation of Magellan images p 2095 N94-20655
Formation and evolution of radial fracture systems on Venus p 2099 N94-20672
Mixing of a chemically buoyant layer at the top of a thermally convecting fluid: Implications for mantle dynamics with application to Venus p 2099 N94-20675
Ridge belt-related scarps and troughs: Compressional crustal bending on Venus p 2106 N94-20711
Geoid, topography, and convection-driven crustal deformation on Venus p 2116 N94-20769
Response of the topography and gravity field on Venus to mantle upwelling beneath a chemical boundary layer p 2117 N94-20775
Differentiation of magma oceans and the thickness of the depleted layer on Venus p 2118 N94-20780
Impact basins on Venus and some interplanetary comparisons p 2119 N94-20785
The parent magma of the Nakhla (SNC) meteorite: Reconciliation of composition estimates from magmatic inclusions and element partitioning p 2085 N94-20836
Morphologic classes of impact basins on Venus p 2137 N94-20883
Wrinkle ridges, reverse faulting, and the depth penetration of lithospheric stress in lunae planum, Mars p 2141 N94-20910
Possible flexural signatures around Olympus and Ascraeus Montes, Mars p 2142 N94-20911
The evolution of the early Martian climate and the initial emplacement of crustal H2O p 2143 N94-21665
The hydrologic response of Mars to the onset of a colder climate and to the thermal evolution of its early crust p 2143 N94-21666

PLANETARY EVOLUTION
Twenty-Fourth Lunar and Planetary Science Conference. Part 3: N-Z [NASA-CR-193149] p 2092 N94-20636
Dynamics of large scale impacts on Venus and Earth p 2098 N94-20666
Mixing of a chemically buoyant layer at the top of a thermally convecting fluid: Implications for mantle dynamics with application to Venus p 2099 N94-20675
Venus magmatic and tectonic evolution p 2101 N94-20683
Low-energy ion implantation: Large mass fractionation of argon p 1685 N94-20697
Diffusive redistribution of water vapor in the solar nebula revisited p 2113 N94-20751
Recondensation in the early solar system: Physical conditions and source material p 2085 N94-20849
Variety in planetary systems p 2086 N94-20871
The hydrologic response of Mars to the onset of a colder climate and to the thermal evolution of its early crust p 2143 N94-21666
The early Martian environment: Clues from the cratered highlands and the Precambrian Earth p 2143 N94-21667

PLANETARY GEOLOGY
Workshop on the Martian Northern Plains: Sedimentological, Periglacial, and Paleoclimatic Evolution [NASA-CR-194831] p 2088 N94-20382
A wet-geology and cold-climate Mars model: Punctuation of a slow dynamic approach to equilibrium p 2090 N94-20389
Possible occurrence and origin of massive ice in Utopia Planitia p 2090 N94-20390
Observed climatic activity pertaining to the evolution of the northern plains p 2090 N94-20392
The thumbprint terrain: What will Mars Observer tell us? p 2091 N94-20397
Stratigraphy of the Martian northern plains p 2091 N94-20398
Balloon exploration of the northern plains of Mars near and north of the Viking 2 landing site p 2092 N94-20401
Twenty-Fourth Lunar and Planetary Science Conference. Part 3: N-Z [NASA-CR-193149] p 2092 N94-20636
SO2 on Venus: IUE, HST and ground-based measurements, and the active volcanism connection p 2092 N94-20637
The Koshak section: Evidence for element fractionation and an oxidation event at the K/T boundary p 1862 N94-20641
Determination of cosmic bodies size-velocity distribution by observation of current impacts on Mars p 2082 N94-20648
Geologic mapping of Northern Atla Regio on Venus: Preliminary data p 2095 N94-20654
Beta Regio rift system on Venus: Geologic interpretation of Magellan images p 2095 N94-20655
Beta Regio - Phoebe Regio on Venus: Geologic mapping with the Magellan data p 2096 N94-20656
Largest impact features on Venus: Non-preserved or non-recognizable? p 2096 N94-20657
Dynamics of large scale impacts on Venus and Earth p 2098 N94-20666
Structural evidence for reorientation of Miranda about a paleo-pole p 2098 N94-20671
Formation and evolution of radial fracture systems on Venus p 2099 N94-20672
Thermal and rheological controls on magma migration in dikes: Examples from the east rift zone of Kilauea volcano, Hawaii p 1862 N94-20673

Constraints on the rate of discharge and duration of the Mangala Valles flood p 2099 N94-20674
Venus magmatic and tectonic evolution p 2101 N94-20683
Eruption history of the Tharsis shield volcanoes, Mars p 2102 N94-20692
Geology of Biblis Patera, Ulysses Patera, and Jovis Tholus, Mars p 2103 N94-20693
Crater destruction on the Venusian highlands by tectonic processes p 2103 N94-20696
Geologic mapping of Harmakhis and Reull Valles region, Mars: Evidence for multiple resurfacing and drainage events p 1844 N94-20705
Some deformation trends and topographic characteristics of tesserae on Venus p 2105 N94-20706
Studying Venus using a GIS database p 2105 N94-20707
Chocolate tablet aspects of cytherean Meshkenet Tessera p 2106 N94-20710
Ridge belt-related scarps and troughs: Compressional crustal bending on Venus p 2106 N94-20711
Detectability of crystalline ferric and ferrous minerals on Mars p 2110 N94-20730
Venus pancake dome formation: Morphologic effects of a cooling-induced variable viscosity during emplacement p 2110 N94-20732
Mars: New evidence for origin of some Valles Marineris layered deposits p 2112 N94-20748
Rifting at Devana Chasma, Venus: Structure and estimation of the effective thickness of the elastic lithosphere p 2113 N94-20754
Volcanic rises on Venus: Geology, formation, and sequence of evolution p 2113 N94-20755
The roughness of the Martian surface: A scale dependent model p 2115 N94-20762
GMM-1: A 50 degree and order gravitational field model for Mars p 2117 N94-20774
Differentiation of magma oceans and the thickness of the depleted layer on Venus p 2118 N94-20780
Impact basins on Venus and some interplanetary comparisons p 2119 N94-20785
Discovery Venera surface: Atmosphere geochemistry experiments mission concept p 2123 N94-20806
Extensional history of Mars' Tharsis Region p 2125 N94-20814
Complex structure of the Thaumasia region of Mars p 2125 N94-20815
Large, ancient, compressional structures on Mars p 2125 N94-20816
Tumuli and tubes: Teaching scientific techniques p 2039 N94-20818
Magellan Mission p 1652 N94-20829
Discharge rates in Ma'adim Vallis, Mars p 2128 N94-20830
Complex ridged terrain-related ridge belts on Venus: Global distribution and classification p 2129 N94-20835
Is there uniformitarian or catastrophic tectonics on Venus? p 2129 N94-20839
Geology of Galileo Regio quadrangle, Ganymede p 2130 N94-20842
Spectral analysis of chemisorbed CO2 on Mars analog materials p 2140 N94-20900
Comparison of flank modification on Ascraeus and Arsia Montes volcanoes, Mars p 2140 N94-20903
Evolution of the global water cycle on Mars: The geological evidence p 2142 N94-21660
Ancient Martian valley genesis and paleoclimatic inference: The present as a key to the past p 2142 N94-21661
A carbon dioxide/methane greenhouse atmosphere on early Mars p 2142 N94-21662
Oxidation of dissolved iron under warmer, wetter conditions on Mars: Transitions to present-day arid environments p 2143 N94-21663
Mars: Noachian hydrology by its statistics and topology p 2143 N94-21664
The evolution of the early Martian climate and the initial emplacement of crustal H2O p 2143 N94-21665
An attempt to comprehend Martian weathering conditions through the analysis of terrestrial palagonite samples p 2143 N94-21668
Fluvial valleys in the heavily cratered terrains of Mars: Evidence for paleoclimatic change? p 2144 N94-21670
Early Mars: The inextricable link between internal and external influences on valley network formation p 2146 N94-21681
The Martian valley networks: Origin by niveo-fluvial processes p 2146 N94-21682
Post-Palbozoic crustal responses to the contemporary stress field in the eastern United States [DE93-040604] p 1859 N94-22006
MSATT Workshop on Innovative Instrumentation for the In Situ Study of Atmosphere-Surface Interactions on Mars [NASA-CR-194584] p 1811 N94-22430
A Backscatter Moessbauer Spectrometer (BaMS) for use on Mars p 1811 N94-22431
Optical luminescence spectroscopy as a probe of the surface mineralogy of Mars p 1813 N94-22437

PLANETARY GRAVITATION
Largest impact features on Venus: Non-preserved or non-recognizable? p 2096 N94-20657
Magellan at Venus: Summary of science findings p 2110 N94-20734
Venus gravity: New Magellan low altitude data p 2117 N94-20772
Variety in planetary systems p 2086 N94-20871

PLANETARY IONOSPHERES
Nonthermal planetary radio emissions: Theories and observations p 2001 N94-22635

PLANETARY MAGNETIC FIELDS
Expectations for the Martian core magnetic field p 2120 N94-20792

PLANETARY MAGNETOSPHERES
Nonthermal planetary radio emissions: Theories and observations p 2001 N94-22635

PLANETARY MANTLES
Differentiation of magma oceans and the thickness of the depleted layer on Venus p 2118 N94-20780
Arcuate and circular structures in the Tharsis region: Evidence of coronae on Mars p 2134 N94-20863
The connection between Venus' free obliquity and its CMB oblateness p 2139 N94-20896
Wrinkle ridges, reverse faulting, and the depth penetration of lithospheric stress in lunae planum, Mars p 2141 N94-20910
Wet inside and out? Constraints on water in the Martian mantle and on outgassed water, based on melt inclusions in SNC meteorites p 2145 N94-21678

PLANETARY MAPPING
Stratigraphy of the Martian northern plains p 2091 N94-20398
Balloon exploration of the northern plains of Mars near and north of the Viking 2 landing site p 2092 N94-20401
Geologic mapping of Northern Atla Regio on Venus: Preliminary data p 2095 N94-20654
Beta Regio - Phoebe Regio on Venus: Geologic mapping with the Magellan data p 2096 N94-20656
MinMap: An imaging spectrometer for high resolution compositional mapping of the Moon p 1813 N94-20688
Geologic mapping of Harmakhis and Reull Valles region, Mars: Evidence for multiple resurfacing and drainage events p 1844 N94-20705
Chronology, eruption duration, and atmospheric contribution of Apollinaris Patera, Mars p 2108 N94-20720
Earth-based measurement of lunar topography using delayed radar interferometry p 2119 N94-20787
The role of CO2 in weathering reactions and the presence of S2 on Venus: Implications for the pyrite stability field p 2122 N94-20799
Complex structure of the Thaumasia region of Mars p 2125 N94-20815
Comparison of flank modification on Ascraeus and Arsia Montes volcanoes, Mars p 2140 N94-20903

PLANETARY METEOROLOGY
Observed climatic activity pertaining to the evolution of the northern plains p 2090 N94-20392

PLANETARY NEBULAE
Evaporation in equilibrium, in vacuum, and in hydrogen gas p 1684 N94-20638
AGB stars as a source of short-lived radioactive nuclei in the solar nebula p 2133 N94-20859

PLANETARY QUAKES
Seismic-triggering history of the catastrophic outflows in the Chryse region of Mars p 2091 N94-20399

PLANETARY ROTATION
The connection between Venus' free obliquity and its CMB oblateness p 2139 N94-20896

PLANETARY STRUCTURE
Differentiation of magma oceans and the thickness of the depleted layer on Venus p 2118 N94-20780
Large, ancient, compressional structures on Mars p 2125 N94-20816
Wet inside and out? Constraints on water in the Martian mantle and on outgassed water, based on melt inclusions in SNC meteorites p 2145 N94-21678

PLANETARY SURFACES
Advances in spaceborne radar remote sensing p 1723 N94-20424
Twenty-Fourth Lunar and Planetary Science Conference. Part 3: N-Z [NASA-CR-193149] p 2092 N94-20636
Largest impact features on Venus: Non-preserved or non-recognizable? p 2096 N94-20657
Goniospectrometric properties of a white standard p 1684 N94-20664
Dynamics of large scale impacts on Venus and Earth p 2098 N94-20666
Comparative hypsometric analysis of both Earth and Venus topographic distributions p 2108 N94-20722
The Clementine Mission science return at the Moon and Geographos p 1652 N94-20850

PLANETARY SYSTEMS
Variety in planetary systems p 2086 N94-20871

PLANETARY TEMPERATURE
Mars and the early Sun p 2146 N94-21683

PLANETARY WAVES
Interactions of free modes, tides, and gravity waves in the middle atmosphere [REPT-84] p 1855 N94-20155

PLANNING
Graphical interactive planning of robotic applications with support of integrated simulation [ETN-93-93793] p 1944 N94-21057
Multicriteria optimisation problem in the agricultural modelling p 1844 N94-22073

PLANTS (BOTANY)
Health effects of global warming: Problems in assessment [DE93-040323] p 1850 N94-19930

PLASMA ACCELERATION
Magnetic insulation of secondary electrons in plasma source ion implantation [DE93-040106] p 1997 N94-21988

PLASMA ARC WELDING
Impact of copper vapour contamination on argon arcs p 1994 N94-21053

PLASMA COMPOSITION
Transient thermal analysis of cryocondensation pump for JET [DE93-040372] p 1992 N94-20003

PLASMA CONDUCTIVITY
The relaxed state and entropy production due to the electric resistivity and viscosity of plasma p 2010 N94-22696

PLASMA CONTROL
Effect of limiter end loss in finite Larmor radius theory [DE93-040913] p 1992 N94-19887
Fast ion behavior during neutral beam injection in ATF [DE93-040267] p 1992 N94-20058
Beta-limiting instabilities in D3-D discharges with large bootstrap current [DE93-015476] p 1993 N94-20326
Shear flow generation by Reynolds stress and suppression of resistive g-modes [DE93-040911] p 1995 N94-21514
Parametric instabilities in picosecond time scales [DE94-000384] p 1966 N94-21958
Fusion Plasma Theory. Task 1: Magnetic confinement fusion plasma theory [DE94-000778] p 1998 N94-22019
Enhanced confinement regimes and control technology in the DIII-D tokamak [DE93-019004] p 1998 N94-22039
A spheromak ignition experiment reusing Mirror Fusion Test Facility (MFTF) equipment [DE94-001856] p 2034 N94-22050
A two-dimensional kinetic model of the scrape-off layer [DE94-001235] p 1999 N94-22562
Fluid simulations of Delta T(sub e)-driven turbulence and transport in boundary plasmas [DE94-001304] p 1999 N94-22566
Effects of magnetic field perturbations in the ATF torsatron [DE94-000474] p 1999 N94-22568
Physics of transport phenomena in magnetic confinement plasmas p 2000 N94-22628

PLASMA CURRENTS
Radiation of plasma wave wings through an electrodynamic tether satellite system with any sharp angle geometry [REPT-85] p 1993 N94-20156
Beta-limiting instabilities in D3-D discharges with large bootstrap current [DE93-015476] p 1993 N94-20326
Plasma heating in toroidal systems p 2000 N94-22629
Consequences of chaotic particle motion for the stability of space plasma current sheets p 2001 N94-22636
Current loop coalescence studied by 3-D electromagnetic particle code p 2005 N94-22660
Formation of fast magnetosonic shock waves during two current loops collision in solar flare p 2005 N94-22662
Dynamics of physical state during two current loops collision p 2005 N94-22663

PLASMA DENSITY
Measurement of mesospheric turbulence in the framework of the metal campaign and development of a sensor for static pressure free measurements of neutral and electron density
[BONN-IR-92-45] p 1857 N94-21149
On effects of a local plasma density growth due to ponderomotive forces at fast wave launching in tokamaks
[IPPCZ-328] p 1996 N94-21571
Enhanced confinement regimes and control technology in the DIII-D tokamak
[DE93-019004] p 1998 N94-22039
Effects of magnetic field perturbations in the ATF torsatron
[DE94-000474] p 1999 N94-22568
Initial operation of a large-scale plasma source ion implantation experiment
[DE94-000805] p 2036 N94-22583
Non-equilibrium ionization in an M class solar flare p 2004 N94-22653
Plasma structure in a plasma flow along a magnetic mirror field p 2005 N94-22664
On the nonlinear instability of thermal structures p 2006 N94-22668

PLASMA DIAGNOSTICS
Parametric variations of ion transport in TFTR
[DE93-012653] p 1991 N94-19883
Optical diagnostic instrument for monitoring etch uniformity during plasma etching of polysilicon in a chlorine-helium plasma
[DE93-019582] p 1993 N94-20261
Development and characterization of a time-, position- and energy-resolved x ray diagnostic for PBFA 2 target experiments
[DE93-019429] p 1808 N94-20297
Laser diagnostics of RF hydrogen plasma reactors: Application to the processing of III-V materials
[AD-A272659] p 1994 N94-21214
A new innovative instrument for space plasma instrumentation
[NASA-CR-194736] p 1666 N94-21780
On Plasma Edge Spectroscopy and Spectroscopic Studies of Impurity Densities and Impurity Transport
[IPF-92-2] p 1996 N94-21802
Plasma edge spectroscopy p 1996 N94-21803
Spectroscopic studies of impurity densities and impurity transport p 1997 N94-21804
Fusion Plasma Theory. Task 1: Magnetic confinement fusion plasma theory
[DE94-000778] p 1998 N94-22019

PLASMA DIFFUSION
Parametric variations of ion transport in TFTR
[DE93-012653] p 1991 N94-19883
Fluid simulations of Delta T(sub e)-driven turbulence and transport in boundary plasmas
[DE94-001304] p 1999 N94-22566
Double diffusion convection in a rotating spherical shell p 2006 N94-22666

PLASMA DYNAMICS
Performance potential of plasma thrusters: Arcjet and Hall thruster modeling
[AD-A271085] p 1667 N94-19847
Neoclassical kinetic theory near an X-point: Plateau regime
[DE93-019825] p 1951 N94-20224
Comparative study of INPIStron and spark gap p 1995 N94-21293
INPIStron switched pulsed power for dense plasma pinches p 1995 N94-21294
Evaluation of externally heated pulsed MPD thruster cathodes
[NASA-CR-191090] p 1670 N94-21565
MHD relaxation in magnetic loops p 2004 N94-22658

PLASMA ENGINES
Performance potential of plasma thrusters: Arcjet and Hall thruster modeling
[AD-A271085] p 1667 N94-19847

PLASMA ETCHING
Optical diagnostic instrument for monitoring etch uniformity during plasma etching of polysilicon in a chlorine-helium plasma
[DE93-019582] p 1993 N94-20261
Particle behavior in an ECR plasma etch tool
[DE93-040343] p 1996 N94-21769

PLASMA FOCUS
Research on plasma-puff initiation of high Coulomb transfer switches
[NASA-CR-194371] p 1994 N94-21289
Plasma-puff initiation of high Coulomb transfer switches p 1994 N94-21290
Characteristics of plasma-puff trigger for a inverse-pinch plasma switch p 1995 N94-21291
INPIStron switched pulsed power for dense plasma pinches p 1995 N94-21294
Plasma lens experiments at the Final Focus Test Beam
[DE93-041081] p 1981 N94-21688

PLASMA FREQUENCIES
Theory of leaked auroral kilometric radiation p 2003 N94-22649

PLASMA GENERATORS
A dc Penning surface-plasma source
[DE93-040126] p 1997 N94-21989

PLASMA HEATING
Fusion plasma theory grant. Task 3: Auxiliary radiofrequency heating of tokamaks
[DE94-000779] p 1994 N94-20940
High resolution studies of the structure of the solar atmosphere
[AD-A273084] p 2147 N94-21522
The TST: A small steady-state tokamak for integrated divertor testing
[DE94-001016] p 1998 N94-22045
Opacity measurements in shock-generated argon plasmas
[DE94-001057] p 1998 N94-22399
Plasma heating in toroidal systems p 2000 N94-22629

PLASMA INTERACTION EXPERIMENT
The angular velocity spread of REB induced by magnetic field discontinuity
[IPPCZ-331] p 1996 N94-21573

PLASMA INTERACTIONS
Two-dimensional particle-in-cell simulation on transputer arrays
[DE93-017977] p 1972 N94-20181
Modeling of the coupled magnetospheric and neutral wind dynamos
[NASA-CR-194728] p 1856 N94-20537
TROPIX plasma interactions group report
[NASA-CR-191149] p 1666 N94-21864
Consequences of plasma-maser in plasma astrophysics p 2006 N94-22669

PLASMA JETS
Jet shapes in hadron and electron colliders
[DE93-019386] p 1979 N94-20216
Impact of copper vapour contamination on argon arcs p 1994 N94-21053
Numerical simulation of magnetic reconnection associated with emerging flux in the solar atmosphere p 2004 N94-22654
X ray jets in the solar corona: Observations with Yohkoh Soft X Ray Telescope p 2004 N94-22655
Three-dimensional simulations of cosmic jets employing the smoothed particle hydrodynamics technique p 2008 N94-22685
Helical kink instability of jets from young stellar objects p 2008 N94-22686

PLASMA LAYERS
Three-wave resonant interaction in a thin layer
[AD-A272331] p 1994 N94-21039
A moving finite element model of the tokamak scrapeoff layer
[DE94-000673] p 1997 N94-21965
A two-dimensional kinetic model of the scrape-off layer
[DE94-001235] p 1999 N94-22562
Fluid simulations of Delta T(sub e)-driven turbulence and transport in boundary plasmas
[DE94-001304] p 1999 N94-22566
Electron temperature gradient driven instability in the tokamak boundary plasma
[DE94-001307] p 1999 N94-22596

PLASMA PHYSICS
Laser propagation in underdense plasmas: Scaling arguments
[DE93-040439] p 1816 N94-20480
Fusion plasma theory grant. Task 3: Auxiliary radiofrequency heating of tokamaks
[DE94-000779] p 1994 N94-20940
Engineering design, fabrication, installation, operation, and maintenance services in support of research on laser plasma physics
[AD-A272249] p 1994 N94-20943
Shock compression of low-density foams
[DE93-040545] p 1707 N94-21546
Fusion Plasma Theory. Task 1: Magnetic confinement fusion plasma theory
[DE94-000778] p 1998 N94-22019
Continuum damping of ideal toroidal Alfven eigenmodes
[DE94-001233] p 1998 N94-22560
Theory and simulation of plasma sheath waves
[DE94-001305] p 1999 N94-22567
Fourth International Toki Conference on Plasma Physics and Controlled Nuclear Fusion
[ESA-SP-351] p 2000 N94-22624
Driven reconnection and self-organization p 2000 N94-22625
Physics of transport phenomena in magnetic confinement plasmas p 2000 N94-22626
Jets associated with active galactic nuclei p 2000 N94-22631
Physical properties of dense astrophysical plasmas p 2001 N94-22637

PLASMA PINCH
Research on plasma-puff initiation of high Coulomb transfer switches
[NASA-CR-194371] p 1994 N94-21289
Plasma-puff initiation of high Coulomb transfer switches p 1994 N94-21290
Characteristics of plasma-puff trigger for a inverse-pinch plasma switch p 1995 N94-21291
Characteristics of switching plasma in an inverse-pinch switch p 1995 N94-21292
Comparative study of INPIStron and spark gap p 1995 N94-21293
INPIStron switched pulsed power for dense plasma pinches p 1995 N94-21294
The relaxed state and entropy production due to the electric resistivity and viscosity of plasma p 2010 N94-22696

PLASMA POTENTIALS
Plasma structure in a plasma flow along a magnetic mirror field p 2005 N94-22664

PLASMA PROPULSION
Evaluation of externally heated pulsed MPD thruster cathodes
[NASA-CR-191090] p 1670 N94-21565

PLASMA RESONANCE
Kinetic resonance damping rate of the toroidal ion temperature gradient mode
[DE94-001234] p 1998 N94-22561

PLASMA SHEATHS
Theoretical and numerical studies in magnetic fusion
[DE94-000536] p 1993 N94-20937
Magnetic insulation of secondary electrons in plasma source ion implantation
[DE93-040106] p 1997 N94-21988
Theory and simulation of plasma sheath waves
[DE94-001305] p 1999 N94-22567
Initial operation of a large-scale plasma source ion implantation experiment
[DE94-000805] p 2036 N94-22583

PLASMA SLABS
Three-wave resonant interaction in a thin layer
[AD-A272331] p 1994 N94-21039
Fluid simulations of Delta T(sub e)-driven turbulence and transport in boundary plasmas
[DE94-001304] p 1999 N94-22566
Theory and simulation of plasma sheath waves
[DE94-001305] p 1999 N94-22567

PLASMA SPRAYING
Turntable mechanism
[NASA-CASE-MFS-28522-1] p 1823 N94-20380
Method of fabricating a rocket engine combustion chamber
[NASA-CASE-MFS-28569-1] p 1703 N94-20541
Surface modification for corrosion resistance
[DE93-017419] p 1693 N94-21825

PLASMA TEMPERATURE
Plasma heating in toroidal systems p 2000 N94-22629
On the nonlinear instability of thermal structures p 2006 N94-22668

PLASMA TURBULENCE
Multi-CPU plasma fluid turbulence calculations on a CRAY Y-MP C90
[DE93-015425] p 1801 N94-20562
Shear flow generation by Reynolds stress and suppression of resistive g-modes
[DE93-040911] p 1995 N94-21514
Fluid simulations of Delta T(sub e)-driven turbulence and transport in boundary plasmas
[DE94-001304] p 1999 N94-22566
Dynamo driven by weak plasma turbulence: The effect of differential rotation p 2005 N94-22665
The onset and spectra of a magnetized Langmuir turbulence p 2006 N94-22673

PLASMA WAVES
A study of Saturn's E-ring particles using the Voyager 1 plasma wave instrument
[NASA-CR-194694] p 2088 N94-20048
Radiation of plasma wave wings through an electrodynamic tether satellite system with any sharp angle geometry
[REPT-85] p 1993 N94-20156
Kinetic resonance damping rate of the toroidal ion temperature gradient mode
[DE94-001234] p 1998 N94-22561
Theory and simulation of plasma sheath waves
[DE94-001305] p 1999 N94-22567

PLASMA-ELECTROMAGNETIC INTERACTION
Radiation of plasma wave wings through an electrodynamic tether satellite system with any sharp angle geometry
[REPT-85] p 1993 N94-20156
Three-wave resonant interaction in a thin layer
[AD-A272331] p 1994 N94-21039
Solar wind-magnetosphere interaction as simulated by a 3D, EM particle code p 2007 N94-22674
PLASMA-PARTICLE INTERACTIONS
Current loop coalescence studied by 3-D electromagnetic particle code p 2005 N94-22660
Dynamics of physical state during two current loops collision p 2005 N94-22663
Consequences of plasma-maser in plasma astrophysics p 2006 N94-22669
PLASMAPAUSE
Detailed analysis case studies of trapped plasmas at the Earth's magnetic equator
[AD-A272497] p 1858 N94-21432
PLASMAS (PHYSICS)
Plasma chemical vapor deposition of halide glasses
[AD-D015933] p 1701 N94-20331
Interleaved bismaleimide composites
[AD-A272233] p 1674 N94-20574
On magnetodynamic effects initiated by a high-speed impact of a large cosmic body upon the Earth's surface p 2082 N94-20647
Engineering design, fabrication, installation, operation, and maintenance services in support of research on laser plasma physics
[AD-A272249] p 1994 N94-20943
Three-wave resonant interaction in a thin layer
[AD-A272331] p 1994 N94-21039
Characteristics of switching plasma in an inverse-pinch switch p 1995 N94-21292
Radial diffusion of toroidally trapped particles induced by lower hybrid and fast waves
[IPPCZ-327] p 1996 N94-21593
Results from long conduction time plasma opening switch experiments at Sandia National Laboratories
[DE93-019063] p 1762 N94-21632
Particle behavior in an ECR plasma etch tool
[DE93-040343] p 1996 N94-21769
Plasma-chemical conversion of hydrogen sulfide into hydrogen and sulfur
[DE93-041167] p 1682 N94-21789
Edge plasma experiments on CASTOR tokamak
[IPPCZ-332] p 1997 N94-21816
Time evolution of the quark-gluon plasma
[DE94-000804] p 1998 N94-22389
A two-dimensional kinetic model of the scrape-off layer
[DE94-001235] p 1999 N94-22562
PLASMASPHERE
Ionospheric photoelectrons measured at geosynchronous orbit
[AD-A272431] p 1857 N94-21202
PLASMONS
Formation of colloidal Ag precipitates in fused silica by MeV ion implantation
[DE93-040268] p 2012 N94-19869
PLASTIC DEFORMATION
Finite element mesh generation and analysis of solder joints for fatigue life predictions
[AD-A271329] p 1829 N94-19937
PLASTIC PROPERTIES
CTH: A software family for multi-dimensional shock physics analysis
[DE93-019428] p 1904 N94-20052
Development of bioelastic material for aspects of wound repair
[AD-A272000] p 1892 N94-21503
PLASTICS
Mold bolt and means for achieving close tolerances between bolts and bolt holes
[NASA-CASE-MFS-28720-1] p 1823 N94-20379
PLATE THEORY
Improvements to a method for the geometrically nonlinear analysis of compressively loaded stiffened composite panels
[NASA-CR-194715] p 1832 N94-21814
PLATES (STRUCTURAL MEMBERS)
Three point lead screw positioning apparatus for a cavity tuning plate
[NASA-CASE-LEW-15216-1] p 1822 N94-20375
PLATES (TECTONICS)
Seafloor characterization/Galapagos propagating rift
[AD-A272001] p 1882 N94-20581
Response of the topography and gravity field on Venus to mantle upwelling beneath a chemical boundary layer p 2117 N94-20775
Post-Palbozoic crustal responses to the contemporary stress field in the eastern United States
[DE93-040604] p 1859 N94-22006
PLATING
Process to fabricate thick coplanar microwave electrode structures
[AD-D015913] p 1748 N94-19892
PLATINUM
Oxidation-reduction induced roughening of platinum (111) surface
[DE93-017408] p 1687 N94-19922
Guanidine based vehicle/binders for use with oxides, metals, and ceramics
[NASA-CASE-LEW-15314-1] p 1700 N94-20195
Observation of x ray absorption magnetic circular dichroism in well-characterized iron-cobalt-platinum multilayers
[DE94-000303] p 1684 N94-21944
Photoelectron holography of platinum (111)
[DE93-040856] p 1810 N94-21950
PLATINUM ALLOYS
Surface science and modeling studies of endothermic fuels catalysis
[AD-A272850] p 1712 N94-21192
Magnetic instability of Kondo insulators
[DE93-040064] p 1768 N94-21762
PLAYAS
Briny lakes on early Mars? Terrestrial intracrater playas and Martian candidates p 2145 N94-21675
PLOTTERS
Post-experimental plots for high speed data acquisition program
[DE94-000956] p 1918 N94-22011
PLOTTING
The IDL astronomy user's library p 2048 N94-22500
PLUGS
Disengagable adapter for an optical fiber connector
[AD-D015959] p 1822 N94-20356
PLUMES
Experimental investigation of nozzle/plume aerodynamics at hypersonic speeds
[NASA-CR-194628] p 1636 N94-20014
UVPI imaging from the LACE satellite: The Starbird rocket plume
[AD-A271981] p 1658 N94-20617
Are Plinian type eruptions possible on Venus? p 2123 N94-20803
Iterative electromagnetic Born inversion applied to earth conductivity imaging
[DE93-040668] p 1859 N94-21928
PLUTONIUM
Crystallographic phase transitions in actinide metals as a function of pressure
[DE93-040138] p 2011 N94-19827
A weighted least-squares lump correction algorithm for transmission-corrected gamma ray nondestructive assay
[DE93-018474] p 1904 N94-20049
PLUTONIUM 238
Calorimeter measurements of low wattage items
[DE93-018473] p 1807 N94-20115
POINT DEFECTS
The effect of correlated and point defects on the vortex lattice melting transition in single crystal YBa2Cu3O(7-delta)
[DE93-040277] p 2033 N94-21997
POINT SOURCES
Localization from near-source quasi-static electromagnetic fields
[DE93-040390] p 1732 N94-20479
SkICAT: A cataloging and analysis tool for wide field imaging surveys p 2049 N94-22546
POINT SPREAD FUNCTIONS
Telescope image modelling software in STSDAS p 1926 N94-22483
Deconvolution of Hubble Space Telescope images using simulated point spread functions p 2048 N94-22497
SPECFOCUS: An IRAF task for focusing spectrographs p 1965 N94-22540
POINTING CONTROL SYSTEMS
Pointing control design for autonomous space vehicle applications
[DE93-019943] p 1657 N94-19863
POISONS
Air transport of samples containing chemical warfare agents
[FFI-93/6005] p 1851 N94-21455
POISSON DENSITY FUNCTIONS
On estimation and testing in Poisson regression models with over-dispersion
[MEMO-1063] p 1963 N94-21078
Trends in software reliability modeling p 1788 N94-22214
POISSON EQUATION
F2D users manual: A two-dimensional compressible gas flow code
[DE94-000853] p 1805 N94-22386
POISSON RATIO
Molecular dynamics modeling of the mechanical behavior of metallic multilayers
[DE93-019947] p 1694 N94-21921
POLAR CAPS
Balloon exploration of the northern plains of Mars near and north of the Viking 2 landing site p 2092 N94-20401
Geology of the southern hemisphere of Triton: No polar cap p 2111 N94-20739
POLAR COORDINATES
Polar processing project
[AD-A271583] p 1739 N94-21235
POLAR REGIONS
Compositional diversity of the lunar North Pole: Preliminary analyses of Galileo SSI data p 2101 N94-20686
Linear structures on the small inner satellites of Saturn p 2121 N94-20797
POLAR WANDERING (GEOLOGY)
Estimability of polar motion using range observations to satellites
[PB93-219319] p 1842 N94-22265
POLARIMETERS
Earth observing scanning polarimeter p 1844 N94-21645
The polarization sensitivity of the liquid xenon imaging telescope p 2056 N94-22282
POLARIMETRY
A general rough-surface inversion algorithm: Theory and application to SAR data p 1719 N94-20407
Comparison of remote sensing measurements with a two-scale polarimetric emission and scattering model for sea surfaces p 1721 N94-20415
Advances in spaceborne radar remote sensing p 1723 N94-20424
Polarimetric backscattering from sea ice p 1723 N94-20426
On evaluating the accuracy of SAR sea-ice classification using multifrequency polarimetric AIRSAR data p 1724 N94-20428
Application of Cloude's target decomposition theorem to polarimetric imaging radar data p 1724 N94-20429
Retrieval of ice thickness from polarimetric SAR data p 1724 N94-20432
Radar backscattering from snow facies of the Greenland ice sheet: Results from the AIRSAR 1991 campaign p 1725 N94-20434
Polarimetric thermal emission from rough surfaces p 1727 N94-20441
Polarimetric thermal emission from periodic water surfaces p 1728 N94-20445
Symmetry in polarimetric remote sensing p 1729 N94-20449
Mapping of taiga forest units using AIRSAR data and/or optical data, and retrieval of forest parameters p 1729 N94-20452
Application of the target decomposition theorem to a polarimetric random media model p 1730 N94-20453
A theoretical and numerical study of polarimetric scattering and emission from random rough surfaces with anisotropic directional spectrum p 1730 N94-20454
Application of neural network to remote sensing of soil moisture using theoretical polarimetric backscattering coefficients p 1730 N94-20455
The Brewster angle effect in SAR polarimetry p 1731 N94-20456
Use of microwave polarimetry to enhance SAR images of the ocean surface
[AD-A271911] p 1882 N94-20489
Magellan vertical polarization radar observations p 1744 N94-20691
Earth observing scanning polarimeter p 1844 N94-21645
POLARITONS
Dephasing processes in III-V semiconductors
[AD-A271677] p 2028 N94-21362
POLARITY
Observation of reflected waves on the SABRE positive polarity inductive adder MITL
[DE93-019413] p 1980 N94-20295
Two-polarity magnetization in the Manson impact breccia p 1863 N94-20789
Reverse polarity magnetized melt rocks from the Chicxulub impact structure, Yucatan Peninsula, Mexico p 1863 N94-20843
POLARIZATION (CHARGE SEPARATION)
Femtosecond Raman-induced Kerr effect study of polar solvent dynamics: Amides
[DE93-017563] p 1678 N94-19924
Charge collectors for the omega upgrade
[DE93-019684] p 1972 N94-20264

POLARIZATION (WAVES)
Fiber optic Michelson sensor and arrays with passive elimination of polarization fading and source feedback isolation
[AD-D015944] p 1984 N94-20065
The polarization sensitivity of the liquid xenon imaging telescope p 2056 N94-22262
POLARIZED ELECTROMAGNETIC RADIATION
Magellan vertical polarization radar observations p 1744 N94-20691
POLARIZED LIGHT
Circular polarizing mirrors for high power lasers
[AD-A267820] p 1815 N94-19965
Photonic electromagnetic field sensor apparatus
[AD-D015938] p 1717 N94-20333
Photonic electromagnetic field sensor apparatus
[AD-D015939] p 1718 N94-20334
Intensity and polarization of light scattered by size distributions of randomly oriented nonspherical particles p 1721 N94-20416
Electron quantum yields from a barium photocathode illuminated with polarized light
[DE93-019232] p 1960 N94-20475
Polarized-light reflection mode p-i-n modulators with GaAs/AlGaAs multiple quantum well active layers: Design and simulation p 2023 N94-20996
Non-destructive evaluation in manufacturing using spectroscopic ellipsometry p 1828 N94-21012
Efficiency of reversible optical storage in azo polymers
[AD-A272923] p 1705 N94-21223
POLARIZED RADIATION
The coherent backscattering opposition effect p 1991 N94-20646
POLARIZERS
X ray, extreme and far ultraviolet optical thin films for space applications
[NASA-CR-194635] p 1984 N94-20128
Miniature color display, phase 4
[AD-A272920] p 1760 N94-21221
POLARONS
Spin-polaron theory of high-(Tc) superconductivity. 1: Spin polarons and high (Tc) pairing
[DE93-019196] p 2014 N94-20002
POLICIES
Use of economic models in Finnish economic policy p 2053 N94-22085
Electronic publishing and intelligent information retrieval p 2047 N94-22479
POLISHING
Variable angle spectroscopic ellipsometric characterization of surface damage in chemical-mechanical polished GaAs p 1710 N94-20986
POLLUTION CONTROL
Advanced batteries for electric vehicle applications: Nontechnical summary
[DE93-019007] p 1748 N94-19885
Alternative refrigerants and refrigeration cycles for domestic refrigerators
[DE93-040481] p 1714 N94-20099
Survey on evaluation of energy technology contributing to preservation of the global environment. 2
[DE94-714884] p 1853 N94-22051
Investigations on trends in global environment adaptive industrial technologies
[DE94-714886] p 1853 N94-22258
POLLUTION MONITORING
Manual of DRANC (release 1.1): A computer program for the Dutch risk assessment of new chemical substances
[PB93-194827] p 1851 N94-19998
The use of lidar for the evaluation of traffic-related urban pollution
[DE94-000704] p 1852 N94-22017
POLLUTION TRANSPORT
Analysis of wind observation from towers in the period 1977-1991
[KNMI-TR-148] p 1865 N94-20239
An economic analysis of transboundary air pollution between Finland and the Soviet Union
[ETLA-DISCUSSION-PAPER-335] p 1854 N94-22072
POLOIDAL FLUX
Neoclassical kinetic theory near an X-point: Plateau regime
[DE93-019825] p 1951 N94-20224
POLYAMIDE RESINS
Polyimide-based electrooptic materials
[DE93-019416] p 1706 N94-21526
POLYATOMIC MOLECULES
Ab initio potential energy surface for the H + OCS reaction
[AD-A270577] p 1696 N94-19947
POLYCARBONATES
Techniques for producing free-standing thin films on frames
[DE93-041144] p 1708 N94-21954
POLYCARBOSILANES
Chain propagation/step propagation polymerization chemistry. The preparation of solvent resistant well phase-separated thermoplastic elastomers
[AD-A271128] p 1699 N94-20016
POLYCRYSTALS
Neutral copper cluster sputtering yields: Ne(+), Ar(+) and Xe(+) bombardment
[DE93-019010] p 1690 N94-20288
Temperature-dependent ion beam mixing
[DE93-040281] p 2033 N94-21999
Interface science of controlled metal/metal and metal/ceramic interfaces prepared using ultrahigh vacuum diffusion bonding
[DE94-001066] p 1696 N94-22025
POLYESTERS
Outgassing rate of Reemay Spunbonded Polyester and DuPont Double Aluminized Mylar
[DE93-040015] p 1699 N94-19973
POLYETHYLENES
Polymer gels as precursors to high-performance materials
[AD-A270937] p 1699 N94-20046
Spatial organization of polymer chains in a crystallizable diblock polyethylene and polystyrene
[AD-A271862] p 1702 N94-20463
Development and demonstration of a personal monitoring system for exposure to hydrogen fluoride
[DE93-041273] p 1891 N94-20935
Mechanical properties and reliability of semi-crystalline polymers
[AD-A271591] p 1704 N94-20946
Column chromatographic separation of Y(3+) from Sr(2+) by polymeric ionizable crown ether resins
[DE94-000935] p 1683 N94-22021
POLYGONS
Fast data parallel polygon rendering
[DE93-040157] p 1929 N94-20279
A model for the origin of Martian polygonal terrain p 2090 N94-20393
A formational model for the polygonal terrains of Mars: Taking a crack at the genesis of the Martian polygons p 2091 N94-20400
Geometric optimization
[DE93-040152] p 1917 N94-21764
An algorithm for the interference detection among polygonal surfaces p 1791 N94-22239
Strategy for motion of a moving body of quasi-polygonal form within a polygonal space p 1792 N94-22240
POLYIMIDE RESINS
A process for preparing an assembly of an article and a soluble polyimide which resists dimensional change, delamination, and debonding when exposed to changes in temperature
[NASA-CASE-LAR-14763-1] p 1702 N94-20373
POLYIMIDES
A process for preparing an assembly of an article and a soluble polyimide which resists dimensional change, delamination, and debonding when exposed to changes in temperature
[NASA-CASE-LAR-14763-1] p 1702 N94-20373
Polyimides containing amide and perfluoroisopropylidene connecting groups
[NASA-CASE-LAR-14608-1] p 1702 N94-20374
Simulated space environmental effects on some experimental high performance polymers p 1662 N94-21385
Polyimide-based electrooptic materials
[DE93-019416] p 1706 N94-21526
POLYMER CHEMISTRY
The modification of polymer surfaces and the fabrication of submicron-scale functionalized structures by deep-UV and electron beam lithography
[AD-A265956] p 1700 N94-20328
POLYMER MATRIX COMPOSITES
Interleaved bismaleimide composites
[AD-A272233] p 1674 N94-20574
Composite materials with improved properties in compression
[AD-A272837] p 1675 N94-21176
Space environmental effects on polymer matrix composites: The UTIAS/LDEF experiment p 1660 N94-21373
Thermal stress analysis of composites in the space environment p 1661 N94-21379
Computational Methods for Failure Analysis and Life Prediction
[NASA-CP-3230] p 1833 N94-22606
Projections on structures and material strength in the computational context p 1834 N94-22610
An overview of computational simulation methods for composite structures failure and life analysis p 1835 N94-22617
POLYMERIC FILMS
Phthalonitrile prepolymer as high temperature sizing material for composite fibers
[AD-D015912] p 1672 N94-20010
Theoretical and experimental study of the winding of a thin plastic film: The role of aerodynamic effects
[ECL-93-04] p 1703 N94-20599
Electrochemical synthesis of ultrathin film composite membranes
[AD-A272721] p 1681 N94-21168
POLYMERIZATION
Chain propagation/step propagation polymerization chemistry. The preparation of solvent resistant well phase-separated thermoplastic elastomers
[AD-A271128] p 1699 N94-20016
Rotational isomers of Mo(VI) alkylidene complexes and Cis/trans polymer structure: Investigations in ring-opening metathesis polymerization
[AD-A272647] p 1704 N94-21184
Polymerization of enantiomerically pure 2,3-dicarboalkoxy norbornadienes and 5,6-disubstituted norbornenes by well-characterized molybdenum ROMP catalysts
[AD-A272649] p 1704 N94-21186
Techniques for producing free-standing thin films on frames
[DE93-041144] p 1708 N94-21954
Photochemical approaches to conversion of light to electricity or fuel
[DE94-001650] p 1849 N94-22048
POLYMERS
Aragatz project samples experiment/MAPOL (polymer materials) experiment: Postflight expert evaluation p 1660 N94-21376
Simulated space environmental effects on some experimental high performance polymers p 1662 N94-21385
Polymeric nitrogen
[DE93-040544] p 1706 N94-21512
Modeling of polymer electrolyte fuel cell systems
[DE93-041187] p 1847 N94-21774
POLYMETHYL METHACRYLATE
Millimeter-wave imaging of composite materials
[DE93-041160] p 1677 N94-21940
POLYMORPHISM
Are types needed for natural language?
[PB93-191831] p 1949 N94-19997
System at the cross-roads of functional and logic programming
[PB93-191823] p 1928 N94-20009
Nominalization, prediction and type containment
[PB93-191799] p 1898 N94-20082
POLYNOMIALS
Affine and non-affine blossoms
[RR-913-M] p 1950 N94-20200
Polynomial interpolation of real functions 1: Interpolation in an interval
[AD-A272330] p 1951 N94-20527
Graph minors: Structure theory and algorithms
[AD-A271851] p 1952 N94-20613
Orthogonal pairs and zeros of Sobolev-type orthogonal polynomials
[REPT-92-46] p 1953 N94-21059
Explicit results on gl(lambda) and sl(lambda)
[MEMO-1075] p 1953 N94-21072
Hilbert 90 for polynomial matrices
[CWI-AM-R9211] p 1954 N94-21159
Fast fourier transforms for nonequispaced data
[AD-A272687] p 1954 N94-21164
Computing solutions uniquely collapses the polynomial hierarchy
[TR-467] p 1954 N94-21314
Toward a new method of decoding algebraic codes using Groebner bases
[AD-A273089] p 1959 N94-21524
Operational equations for the five-point rectangle
[DE94-000366] p 1959 N94-21655
A mean field neural network for hierarchical module placement p 1766 N94-21720
The accuracy-through-order and the equivalence properties in the algebraic approximant
[DE93-040188] p 1960 N94-21948
Column reduced rational matrix functions with given null-pole data in the complex plane
[PB93-220531] p 1960 N94-22099
POLYPEPTIDES
Development of bioelastic material for aspects of wound repair
[AD-A267832] p 1673 N94-20208
POLYPROPYLENE
Development and demonstration of a personal monitoring system for exposure to hydrogen fluoride
[DE93-041273] p 1891 N94-20935

POLYSTYRENE
Expanded polystyrene protective barricade full-scale fire exposure test
[AD-A271450] p 1698 N94-19938
Spatial organization of polymer chains in a crystallizable diblock polyethylene and polystyrene
[AD-A271862] p 1702 N94-20463
POLYTOPES
Determining the distance to the perfect matching polytope of a bipartite graph
[RR-895-M] p 1950 N94-20161
POLYURETHANE RESINS
Characterization studies of lower and non-TDI polyurethane encapsulants
[DE93-041129] p 1698 N94-19857
Graphite/polyurethane flexible composites: Mechanical and vibration damping properties
[AD-A271608] p 1674 N94-20950
POMERONS
Parton-parton elastic scattering and rapidity gaps at Tevatron energies
[DE93-041024] p 1974 N94-21515
PONDEROMOTIVE FORCES
On effects of a local plasma density growth due to ponderomotive forces at fast wave launching in tokamaks
[IPPCZ-328] p 1996 N94-21571
POPULATIONS
Extracting galactic structure parameters from multivariated density estimation p 1964 N94-22458
POROSITY
High-resolution numerical methods for compressible multi-phase flow in hierarchical porous media
[DE94-000740] p 1799 N94-20351
Embedded microclusters in zeolites and cluster beam sputtering: Simulation on parallel computers
[DE94-000741] p 1701 N94-20352
Dynamic response of multiphase porous media
[AD-A272915] p 1831 N94-21219
Fabrication of porous ceramics by freeze-casting/freeze-drying
[PB93-202513] p 1705 N94-21425
Symposium on Microscopy and Image Analysis of Building Materials
[VTT-SYMP-136] p 1707 N94-21890
Optical air pore analysis p 1708 N94-21892
Determination of pore structure of concrete from thin sections by image analysis p 1708 N94-21895
Fabrication of whisker-toughened alumina tubes
[DE94-001012] p 1677 N94-22022
POROUS MATERIALS
Time-resolved shock compression of porous rutile: Wave dispersion in porous solids
[DE93-018848] p 1829 N94-19927
Shock response of porous Al-2 + Fe2O3 powder mixtures
[DE93-018851] p 1688 N94-19944
Silver lined ceramic vessel
[AD-D015917] p 1700 N94-20057
Antipodal fragment velocities for porous and weak targets at catastrophic impacts p 1836 N94-20891
Two-dimensional finite element analysis of porous media at multikilobar stress levels
[AD-A271540] p 1831 N94-20916
Dynamic response of multiphase porous media
[AD-A272915] p 1831 N94-21219
Fabrication of porous ceramics by freeze-casting/freeze-drying
[PB93-202513] p 1705 N94-21425
A note on singularities caused by the hydrodynamic dispersion tensor
[CWI-NM-R9302] p 1803 N94-21575
Local uniform grid refinement and brine transport in porous media with inhomogeneities
[CWI-NM-R9224] p 1803 N94-21609
PORTABLE EQUIPMENT
Downlink acquisition and tracking procedures for the ASCAMP satellite communications terminal
[AD-A272912] p 1739 N94-21244
Physiological efficacy of a lightweight ambient air cooling unit for various applications
[AD-A272952] p 1896 N94-21247
POSITION (LOCATION)
Localization from near-source quasi-static electromagnetic fields
[DE93-040390] p 1732 N94-20479
Optimization of a satellite localization and message sending system
[ETN-93-94448] p 1737 N94-20592
Characterization of the Marquez Dome buried impact crater using gravity and magnetic data
p 1863 N94-20882
POSITION ERRORS
Silicon retina for optical tracking systems
p 1755 N94-21098
A motion extraction method for synthetic aperture radars
[DLR-FB-92-31] p 1742 N94-22279
POSITION SENSING
Rotary encoding device using polygonal mirror with diffraction gratings on each facet
[NASA-CASE-GSC-13543-1] p 1985 N94-20240
Silicon retina for optical tracking systems
p 1755 N94-21098
A 3-D vision method for estimating workspace occupancy of a power-line maintenance robot
p 1770 N94-22105
Sensor integration and data fusion for object localization in robotic workcells p 1774 N94-22130
Charge integrating optical position sensor
p 1778 N94-22152
An approach to the estimation of ground structure and aircraft motion from aerial image sequences
p 1789 N94-22226
Wideband source location in two-dimensional array processing p 1747 N94-22250
Mobile robot perception in unknown and unstructured dynamic voxel environments
[ISBN-0-315-83951-1] p 1947 N94-22591
POSITIONING
The data acquisition system for the Anglo-Australian Observatory 2-degree field project p 2048 N94-22529
POSITIONING DEVICES (MACHINERY)
Counter-balanced, multiple cable construction crane
[NASA-CASE-LAR-14565-1-CU] p 1822 N94-20369
Three point lead screw positioning apparatus for a cavity tuning plate
[NASA-CASE-LEW-15216-1] p 1822 N94-20375
Turntable mechanism
[NASA-CASE-MFS-28522-1] p 1823 N94-20380
POSITIVE IONS
Low emittance 0.8A K(+) ion source for the LBL Induction Linac System Experiment (ILSE)
[DE93-019237] p 1981 N94-21439
POSITRON ANNIHILATION
Positron annihilation study of Sr Doping in La(2-x)Sr(x)CuO4
[DE94-000307] p 2036 N94-22594
POSITRONIUM
Proof of stability of the hydrogen molecule
[PB93-221026] p 1977 N94-22271
POSTFLIGHT ANALYSIS
Conversion of LDEF experiment M0003 sample observation database to MS-DOS formats
[AD-A272945] p 1681 N94-21226
POSTLAUNCH REPORTS
Debris/ice/TPS assessment and integrated photographic analysis for Shuttle Mission STS-51
[NASA-TM-109189] p 1658 N94-21884
POTABLE WATER
Atmospheric moisture collection device
[AD-D015935] p 1865 N94-20332
POTASSIUM
K, U, and Th behavior in Martian environmental conditions p 2141 N94-20908
Low emittance 0.8A K(+) ion source for the LBL Induction Linac System Experiment (ILSE)
[DE93-019237] p 1981 N94-21439
POTENTIAL ENERGY
Ab initio potential energy surface for the H + OCS reaction
[AD-A270577] p 1698 N94-19947
Computed potential energy surfaces for chemical reactions
[NASA-CR-194600] p 1679 N94-20169
POTENTIAL FLOW
Modelling stalled airfoils
[ISBN-0-315-59525-6] p 1639 N94-22382
POWDER (PARTICLES)
Sol-spray preparation, particulate characteristics, and sintering of alumina powders
[DE93-018577] p 1690 N94-20183
Improvement of the stability of the process for synthesizing chemically prepared varistor powder
[DE94-000345] p 1763 N94-21654
Sulfur-bonded thiophenes in organometallic rhenium complexes and adsorption of isocyanides on gold
[DE93-041126] p 1694 N94-21937
Effect of powder characteristics on gas-pressure sintering of Si3N4 with rare earth additives
[DE94-000330] p 1694 N94-21945
Characteristics of shock-compressed configuration of Ti and Si powder mixtures
[DE93-018857] p 1713 N94-22033
POWDERED ALUMINUM
Powdered aluminum and oxygen rocket propellants: Subscale combustion experiments
[NASA-TM-106439] p 1713 N94-21760
POWER AMPLIFIERS
Laser amplifier developments at Mercury
[DE93-040103] p 1814 N94-19867
Method for remotely powering a device such as a lunar rover
[NASA-CASE-LAR-14789-1] p 1824 N94-20587
Heterojunction bipolar transistor technology for data acquisition and communication p 1763 N94-21697
POWER CONDITIONING
Power conditioning system modelling for nuclear electric propulsion
[NASA-CR-191136] p 1846 N94-21179
POWER EFFICIENCY
Optical fiber sensor having an active core
[NASA-CASE-LAR-14607-1-SB] p 1986 N94-20586
Mixed voltage VLSI design p 1756 N94-21104
POWER FACTOR CONTROLLERS
Technical manual PCDU MT 254
[FFI-92/7020] p 1751 N94-20553
POWER GAIN
Recent activities in printed Antennas at LeRC
p 1722 N94-20422
POWER PLANTS
Design considerations for a fiber optic communications network for power systems
[DE93-018404] p 1984 N94-20179
POWER SPECTRA
Signal processing in the linear statistical model
[AD-A272114] p 1736 N94-20570
A motion extraction method for synthetic aperture radars
[DLR-FB-92-31] p 1742 N94-22279
Time variations of x rays from black hole candidates: Canonical time variations in high and low intensity states
p 2009 N94-22690
POWER SUPPLY CIRCUITS
Control and readout of the extraction septum of AmPS
[DIGEL-1993-2] p 1979 N94-20117
POWERED LIFT AIRCRAFT
Survey of lift-fan aerodynamic technology
[NASA-CR-177615] p 1646 N94-21592
PRANDTL NUMBER
Low Reynolds-number turbulent boundary layers
[AD-A272011] p 1803 N94-21459
PRASEODYMIUM COMPOUNDS
Synthesis and characterization of charge-substituted garnets YCaLnGa5O12 (Ln = Ce, Pr, Tb)
[DE93-040227] p 2033 N94-21992
PRE-MAIN SEQUENCE STARS
Pre-main sequence stars in the Chamaeleon cloud and pre-main sequence stars in the Rho Ophiuchi cloud core
[NASA-CR-194713] p 2080 N94-20337
The circumstellar environments of intermediate mass main sequence stars
[NASA-CR-189311] p 2055 N94-21498
The formation of massive stars: A 30 Mo case study
[ISBN-0-315-83944-9] p 2081 N94-22593
PREAMPLIFIERS
New preamplifiers for the SEM scanner
[DIGEL-1993-3] p 1979 N94-20118
Bundle profile monitor for AmPS
[DIGEL-1992-8] p 1979 N94-20123
PRECIPITATES
Formation of colloidal Ag precipitates in fused silica by MeV ion implantation
[DE93-040268] p 2012 N94-19869
Microstructural stability of wrought, laser and electron beam glazed NARloy-Z alloy at elevated temperatures
[NASA-TM-108431] p 1689 N94-20100
PRECIPITATION (METEOROLOGY)
Snow cover measurements and areal assessment of precipitation and soil moisture
[WMO-749] p 1841 N94-21068
Remote sensing for hydrology progress and prospects
[WMO-773] p 1841 N94-21069
A documentation of icing relevant cloud physical parameters on horizontal soundings of stratiform clouds (continuation)
[DLR-MITT-92-10] p 1871 N94-22280
PRECIPITATION HARDENING
Alloying effects on mechanical and metallurgical properties of NiAl
[DE93-040814] p 1694 N94-21948
PRECISION
Evaluation of a scanning Hartmann device for single point turning applications
[DE93-019204] p 1821 N94-19891
Calorimeter measurements of low wattage items
[DE93-018473] p 1807 N94-20115
PRECONDITIONING
Butcher-Kuntzmann methods for nonstiff problems on parallel computers
[CWI-NM-R9305] p 1935 N94-21493
PREDICTION ANALYSIS TECHNIQUES
Numerical modeling of fringing fields and their use for complex permittivity measurements at high frequencies
[AD-A270478] p 1966 N94-19917

Statistical analysis of a reciprocal translocations data base
[RR-900-I] p 1963 N94-20165
Offshore decision support system: ERS-1 pilot project WAVEWATCH
[BCRS-92-09] p 1865 N94-20532
The flow of gas across the piston-segments-cylinder interface
[ECL-92-40] p 1824 N94-20594
Psychometric developments related to tests and selection
[AD-A272971] p 1894 N94-21262
Columbus PMP Critical Technologies Program: Approach for materials life time prediction p 1664 N94-21402
Survey of lift-fan aerodynamic technology
[NASA-CR-177615] p 1646 N94-21592
Brief summary of the evolution of high-temperature creep-fatigue life prediction models for crack initiation p 1834 N94-22613
Life prediction systems for critical rotating components p 1835 N94-22615
Analysis of thermal mechanical fatigue in titanium matrix composites p 1835 N94-22618
A high temperature fatigue life prediction computer code based on the total strain version of StrainRange Partitioning (SRP) p 1835 N94-22620

PREDICTIONS
Psychometric developments related to tests and selection
[AD-A272971] p 1894 N94-21262
Mathcad computer applications predicting antenna parameters from antenna physical dimensions and ground characteristics
[AD-A272987] p 1740 N94-21264
Predicting scheduling success p 1932 N94-21334
The program system for the diagnostics of strains and fracture prediction of solids p 1836 N94-22065
NASA Langley developments in response calculations needed for failure and life prediction p 1836 N94-22621

PREDICTOR-CORRECTOR METHODS
Stoermer-Cowell and related methods for the numerical solution of second order periodic initial value problems for ODE's 2: Numerical characteristics of the methods
[MEMO-1082] p 1953 N94-21075
Users manual for the NASA Lewis three-dimensional ice accretion code (LEWICE 3D)
[NASA-TM-105974] p 1642 N94-21590
Extended range modified gradient technique for profile inversion (extended version of report Et/Em-1992-8)
[PB93-215242] p 1742 N94-22346
F2D users manual: A two-dimensional compressible gas flow code
[DE94-000653] p 1805 N94-22386

PRELAUNCH SUMMARIES
Space Shuttle Mission STS-61: Hubble Space Telescope servicing mission-01
[NASA-TM-109344] p 1653 N94-20192

PREMIXED FLAMES
Detailed structure study of an H2/N2O/Ar flame employing molecular beam mass spectrometry, laser spectroscopy, and modeling
[AD-A270720] p 1679 N94-20111

PREPARATION
Preparation of concrete specimens for microstructural image analysis studies p 1707 N94-21891

PREPOLYMERS
Phthalonitrile prepolymer as high temperature sizing material for composite fibers
[AD-D015912] p 1672 N94-20010

PREPREGS
Phthalonitrile prepolymer as high temperature sizing material for composite fibers
[AD-D015912] p 1672 N94-20010

PREPROCESSING
Segmented operations for sparse matrix computation on vector multiprocessors
[AD-A270601] p 1928 N94-19950
An optically-assisted 3-D cellular array machine
[AD-A272683] p 1987 N94-21163

PRESSURE BREATHING
In-flight measurement of aircrew breathing in Navy aircraft
[AD-A271811] p 1896 N94-21154

PRESSURE BROADENING
The young Sun and photochemistry of the primitive Martian atmosphere p 2145 N94-21679

PRESSURE DEPENDENCE
Electron reactions in nonpolar liquids: Pressure effects
[DE93-040328] p 1970 N94-19931
Magnetism in CeRu2Ge2 and CeRh2Ge2 and its pressure dependence
[DE93-040061] p 2032 N94-21987
High oxygen pressure synthesis of new copper oxide superconductors
[DE93-040278] p 2033 N94-21998
First-principles pressure-temperature phase diagrams in metals
[DE94-001056] p 1696 N94-22398

PRESSURE DISTRIBUTION
Variable-permittivity linear inverse problem for the H(sub z)-polarized case p 1719 N94-20408
A study of the compressible flow through a diffusing S-duct
[NASA-TM-106411] p 1638 N94-21591
Modelling stalled airfoils
[ISBN-0-315-59525-6] p 1639 N94-22382

PRESSURE EFFECTS
Electron reactions in nonpolar liquids: Pressure effects
[DE93-040328] p 1970 N94-19931
Lamellar olivine in the Divnoe achondrite: Evidence for high-pressure exsolution? p 1685 N94-20679
Pressure versus drag effects on crater size p 1862 N94-20742
Adhesive bonded joint with improved cyclic fatigue life for alumina-ceramic cylinders and hemispheres: Fourth generation housings
[AD-A273061] p 1831 N94-21310
First-principles pressure-temperature phase diagrams in metals
[DE94-001056] p 1696 N94-22398

PRESSURE GRADIENTS
Low Reynolds-number turbulent boundary layers
[AD-A272011] p 1803 N94-21459

PRESSURE ICE
Observation of pressure ridges in SAR images of sea ice: Scattering theory and comparison with observations p 1723 N94-20427

PRESSURE MEASUREMENT
Shock response of porous Al-2 + Fe2O3 powder mixtures
[DE93-018851] p 1668 N94-19944
Description and assessment of a new Optical Pressure Measurement System (OPMS) demonstrated in the high speed wind tunnel in Goettingen (Germany)
[DLR-FB-92-24] p 1651 N94-21280
Measurement Technology for Flight Tests
[ILR-MITT-256(1991)] p 1639 N94-22597
Free flight experiment with a laminar wing glove p 1639 N94-22600
Riblet boundary layer measurements of an A-310 fuselage with Pitot combs p 1640 N94-22605

PRESSURE OSCILLATIONS
Stability curves for a thermoacoustic prime mover
[AD-A272607] p 1968 N94-21422
Shear flow generation by Reynolds stress and suppression of resistive g-modes
[DE93-040911] p 1995 N94-21514

PRESSURE RATIO
Internal performance of a nonaxisymmetric nozzle with a rotating upper flap and a center-pivoted lower flap
[NASA-TP-3385] p 1637 N94-21569

PRESSURE REGULATORS
A novel scheme to handle highly pulsed loads with a standard helium refrigerator
[DE93-019617] p 1799 N94-20263

PRESSURE SENSORS
Description and assessment of a new Optical Pressure Measurement System (OPMS) demonstrated in the high speed wind tunnel in Goettingen (Germany)
[DLR-FB-92-24] p 1651 N94-21280
Experimental evaluation of oxygen-enriched air and emulsified fuels in a six-cylinder diesel engine
[DE94-000907] p 1811 N94-22391

PRESSURE SUITS
System test results of the Advanced Technology Anti-G Suit (ATAGS)
[AD-A271535] p 1896 N94-20914

PRESSURE VESSELS
Atom probe field ion microscopy characterizations of VVER steels
[DE93-017864] p 1689 N94-20180

PRESSURIZED WATER REACTORS
Hydrogen pickup and redistribution in alpha-annealed zircaloy-4
[DE93-018050] p 1689 N94-20182

PRESTRESSING
Process and apparatus for the release of a prestress initially applied to a mechanism such as a bearing on board a space vehicle
[CA-PATENT-APPL-SN-2,020,90] p 1824 N94-21142

PRETREATMENT
Monocrystalline germanium film on sapphire
[AD-D015925] p 2017 N94-20348

PRINTED CIRCUITS
Solder technology in the manufacturing of electronic products
[DE93-018842] p 1699 N94-19960
A comparative study between shielded and open coplanar waveguide discontinuities p 1733 N94-20501
Computer-Aided Test Equipment Graphics System (CATEGS)
[DE94-000383] p 1915 N94-21561
Process characterization and control of hand-soldered printed wiring assemblies
[DE93-041290] p 1763 N94-21652

PRINTING
Electronic publishing and intelligent information retrieval p 2047 N94-22479

PRISMS
Precision prism coupling setup applied to measure planar silica films on silicon, appendix 9 p 1989 N94-21603

PROBABILITY DENSITY FUNCTIONS
Quantification of uncertainties in the performance of smart composite structures
[NASA-TM-106335] p 1830 N94-20171
Interpolative modeling of GaAs FET S-parameter data bases for use in Monte Carlo simulations p 1767 N94-21723
Evaluation of a nonlinear method for the enhancement of tonal signal detection
[NASA-CR-191562] p 1968 N94-21741

PROBABILITY DISTRIBUTION FUNCTIONS
Current directions in the vulnerability/lethality process structure
[AD-A272836] p 1964 N94-21175
Detailed analysis case studies of trapped plasmas at the Earth's magnetic equator
[AD-A272497] p 1858 N94-21432
Mobile robot perception in unknown and unstructured dynamic voxel environments
[ISBN-0-315-83951-1] p 1947 N94-22591

PROBABILITY THEORY
Some topics in regenerative steady-state simulation
[AD-A271145] p 1902 N94-19855
Worldwide frequency of temperatures at selected altitudes
[AD-A271111] p 1864 N94-19908
SIMBAT theoretical manual
[AD-A271063] p 1882 N94-19979
Multi-disciplinary coupling effects for integrated design of propulsion systems
[NASA-TM-106349] p 1830 N94-20170
Quantification of uncertainties in the performance of smart composite structures
[NASA-TM-106335] p 1830 N94-20171
Electronic neural network for solving traveling salesman and similar global optimization problems
[NASA-CASE-NPO-17807-2-CU] p 1942 N94-20360
Believing in the basis of the evidence
[TR-438] p 2039 N94-20364
The effect of dissipative inhomogeneous medium on the statistics of the wave intensity p 1726 N94-20440
Development and testing of a reliability performance index for modular robotic systems
[AD-A271901] p 1942 N94-20488
The quantum efficiency of HgCdTe photodiodes in relation to the direction of illumination and to their geometry p 1735 N94-20512
Closure properties of stochastic languages
[TR-441] p 1907 N94-20521
Explanation closure, action closure, and the Sandewall test suite for reasoning about change
[TR-440] p 1907 N94-20522
Signal processing in the linear statistical model
[AD-A272114] p 1736 N94-20570
Probability of detection calculations using MATLAB
[AD-A271958] p 1736 N94-20578
Current directions in the vulnerability/lethality process structure
[AD-A272836] p 1964 N94-21175
Space-efficient deterministic simulation of probabilistic automata
[TR-463] p 1900 N94-21281
Threshold computation and cryptographic security
[TR-461] p 1912 N94-21285
Promises and fault-tolerant database access
[TR-447] p 2043 N94-21287
Computing with Bayesian multi-networks
[AD-A273106] p 1914 N94-21501
A methodology for quantifying uncertainty in models
[DE93-040154] p 1916 N94-21747
Probabilistic assessment of composite structures
[NASA-TM-106368] p 1832 N94-21757
A simulation model for probabilistic analysis of Space Shuttle abort modes
[NASA-TM-108432] p 1656 N94-21859

PROBES
Numerical modeling of fringing fields and their use for complex permittivity measurements at high frequencies
[AD-A270478] p 1966 N94-19917

PROBLEM SOLVING
Electronic neural network for solving traveling salesman and similar global optimization problems
[NASA-CASE-NPO-17807-2-CU] p 1942 N94-20360
Neural network studies
[AD-A271593] p 1943 N94-20947
An NP set with no co-DP sparse subset
[TR-475] p 1954 N94-21199
The combinatorial algorithms for large scale discrete optimization problems p 1923 N94-22079
On the discovery of approximate arithmetic relations by backpropagation networks p 1782 N94-22181
PROCEDURES
Air transport of samples containing chemical warfare agents
[FFI-93/6005] p 1851 N94-21455
PROCESS CONTROL (INDUSTRY)
Process characterization and control of hand-soldered printed wiring assemblies
[DE93-041290] p 1763 N94-21652
Improvement of the stability of the process for synthesizing chemically prepared varistor powder
[DE94-000345] p 1763 N94-21654
Application of the structures query language of APROS for specification of industrial processes p 1923 N94-22078
PROCUREMENT
Audit report. Navy's aircraft structural life surveillance program data recorders
[AD-A270391] p 1645 N94-20040
Using electronic data interchange to report product quality
[AD-A271843] p 1828 N94-20468
NASA procurement report, FY 1993
[NASA-TM-109393] p 2040 N94-21625
PROCUREMENT MANAGEMENT
Activities of National Inst. for Aviation Research
[NIAR-93-16] p 2151 N94-20150
NASA procurement: Planning for pilot test of new procurement procedures is adequate. Report to the Chairman, Committee on Governmental Affairs, US Senate
[GAO/NSIAD-94-67] p 2039 N94-20236
Implementing Electronic Data Interchange (EDI) with small business suppliers in the pre-award acquisition process
[AD-A271767] p 1945 N94-21305
Operational test and evaluation of electronic combat systems
[AD-A273093] p 1647 N94-21500
NASA procurement report, FY 1992
[NASA-TM-109390] p 2040 N94-21623
Summary data on all NASA procurement actions
[NASA-TM-109392] p 2040 N94-21638
PRODUCT DEVELOPMENT
Activities Report of the Institute of Applied Physics
[ETN-93-93749] p 1966 N94-21798
Electronic locking system p 1796 N94-21801
PRODUCTION COSTS
A novel VLSI processor architecture for supercomputing arrays p 1758 N94-21115
Self assembly: An approach to terascale integration
[DE93-040104] p 1769 N94-21846
An assessment of the cost of microwave sintering ceramic tiles for armor applications
[DE94-000978] p 1693 N94-21850
Investigation on construction of the database system for research and development of the global environment industry technology
[DE94-714890] p 1853 N94-22090
PRODUCTION ENGINEERING
Feature-based tolerancing for intelligent inspection process definition
[DE93-017984] p 1906 N94-20311
Modeling of glass fabrication p 1711 N94-21800
Microdynamic model of reproduction: Taxation and currency issue as regulators of economy p 2053 N94-22084
PROGRAM VERIFICATION (COMPUTERS)
Model checking, abstraction, and compositional verification
[AD-A270552] p 1902 N94-19919
Set based analysis of ML programs
[AD-A270597] p 1902 N94-19948
A methodology for formal hardware verification, with application to microprocessors
[AD-A270550] p 1898 N94-20085
PREVAIL-DM: A framework-based environment for formal hardware verification
[RR-899] p 1905 N94-20164
Test and evaluation: DOD has been slow in improving testing of software-intensive systems
[AD-A271541] p 1908 N94-20917
An assessment of the statistical and editorial output of text analysis programs
[AD-A272185] p 2042 N94-20924
Synthesis algorithm of VLSI multipliers for ASIC p 1758 N94-21116
Automated synthesis and verification of configurable DRAM blocks for ASIC's p 1759 N94-21123
The readiness growth model: A quantitative analysis of software risk
[AD-A272383] p 1910 N94-21144
Two visually meaningful correlation measures for comparing calculated and measured response histories
[AD-A273044] p 1964 N94-21322
MAYGEN: A symbolic debugger generation system
[AD-A272512] p 1913 N94-21413
Tests of logic spaces: A new strategy for certifying the accuracy of programs p 1772 N94-22116
Modeling software systems for data flow testing p 1772 N94-22117
Formal methods in the design of critical software systems p 1779 N94-22158
SPPTOOLS: Programming tools for the IRAF SPP language p 1925 N94-22474
Verification of the PROS timing analysis package p 1926 N94-22508
PROGRAMMERS
Security evaluation of Unix networks
[AD-A273076] p 1945 N94-21520
SPIKE: Application for ASTRO-D mission planning p 1926 N94-22486
PROGRAMMING (SCHEDULING)
Scheduling for locality in shared-memory multiprocessors
[AD-A272948] p 1930 N94-21228
PROGRAMMING ENVIRONMENTS
A proposed research program in information processing
[NASA-CR-194271] p 2041 N94-20134
Advanced software development workstation: Knowledge base methodology: Methodology for first Engineering Script Language (ESL) knowledge base
[NASA-CR-193643] p 1930 N94-21065
An investigation into the state of the practice of CASE tool integration
[AD-A272441] p 1912 N94-21205
The transition to massively parallel computing within a production environment at a DOE access center
[DE93-019155] p 1936 N94-21828
Development of the FITS tools package for multiple software environments p 1927 N94-22516
IRAF in the nineties p 2048 N94-22535
PROGRAMMING LANGUAGES
A comparison of data-parallel algorithms for connected components
[AD-A270551] p 1902 N94-19918
Implementation of a portable nested data-parallel language
[AD-A270524] p 1902 N94-19932
Set based analysis of ML programs
[AD-A270597] p 1902 N94-19948
Programming logic for F omega
[PB93-191781] p 1928 N94-19996
Nominalization, prediction and type containment
[PB93-191799] p 1898 N94-20082
Closure properties of stochastic languages
[TR-441] p 1907 N94-20521
GWB: Manual for the Grammar WorkBench version 1.5
[TR-92-14] p 1909 N94-21061
A simplified token bus protocol specified using LOTOS
[TR-92-15] p 1910 N94-21062
Advanced software development workstation: Knowledge base methodology: Methodology for first Engineering Script Language (ESL) knowledge base
[NASA-CR-193643] p 1930 N94-21065
MINIFOLD: A kernel for a MANIFOLD-like coordination language
[CWI-CS-R9252] p 1915 N94-21534
Changing preferences
[CWI-CS-R9310] p 1915 N94-21551
SPPTOOLS: Programming tools for the IRAF SPP language p 1925 N94-22474
The IDL astronomy user's library p 2048 N94-22500
DECONV-TOOL: An IDL based deconvolution software package p 1927 N94-22542
Parallel functional programming in SISAL: Fictions, facts, and future
[DE93-040486] p 1937 N94-22558
PROJECT MANAGEMENT
Networks Technology Conference
[NASA-CP-3241] p 1931 N94-21323
The NCC project: A quality management perspective p 1828 N94-21324
Let your fingers do the walking: The projects most invaluable tool p 1922 N94-21325
NCCDS configuration management process improvement p 1931 N94-21327
The automated ground network system p 1932 N94-21330
Issues in NASA program and project management. Special Report: 1993 conference
[NASA-SP-6101(07)] p 2039 N94-21497
Issues in NASA program and project management
[NASA-SP-6101(06)] p 2040 N94-21499
Factors associated with continuance commitment to FAA matrix teams
[DOT/FAA/AM-93/18] p 2040 N94-21626
PROJECTILE CRATERING
The Manson impact crater: Estimation of the energy of formation, possible size of the impacting asteroid or comet, and ejecta volume and mass p 2083 N94-20721
Pressure versus drag effects on crater size p 1862 N94-20742
Impactor control of central peak and peak-ring formation p 1862 N94-20744
Delimitation of terrestrial impact craters by way of pseudotachylytic rock distribution p 1863 N94-20783
Parabolic features and the erosion rate on Venus p 2122 N94-20801
Triton's cratering record and its time of capture p 2122 N94-20802
Hypervelocity impact
[AD-A272957] p 1831 N94-21249
PROJECTILES
Absolute total and one and two electron transfer cross sections for Ar(8+) on Ar as a function of energy
[DE93-040283] p 1970 N94-19870
Numerical modeling of impact erosion of atmospheres: Preliminary results p 2131 N94-20847
Geometrical analysis of the microcraters found on LDEF samples p 1666 N94-20890
Antipodal fragment velocities for porous and weak targets at catastrophic impacts p 1836 N94-20891
Multisensor pinhole yawsonde
[AD-A271715] p 1808 N94-20930
PROJECTION
On geometric and algebraic aspects of 3D affine and projective structures from perspective 2D views
[AD-A270520] p 1983 N94-19968
PROJECTIVE GEOMETRY
On geometric and algebraic aspects of 3D affine and projective structures from perspective 2D views
[AD-A270520] p 1983 N94-19968
PROJECTORS
A full-color, high-resolution laser projector for a flight simulator visual display
[AD-A270578] p 1651 N94-20108
PROLATE SPHEROIDS
Intensity and polarization of light scattered by size distributions of randomly oriented nonspherical particles p 1721 N94-20416
PROLOG (PROGRAMMING LANGUAGE)
Proving run-time properties of general programs w.r.t. constructive negation
[CWI-CS-R9245] p 1909 N94-21025
A declarative approach for first-order built-in's of PROLOG
[CWI-CS-R9246] p 1909 N94-21026
PROPAGATION VELOCITY
A Kirchhoff approach to seismic modeling and prestack depth migration
[AD-A271010] p 1854 N94-19820
PROPELLANT CHEMISTRY
A proposed methodology for combustion toxicology testing of combined halon replacement agent/jet fuel interaction
[AD-A272695] p 1681 N94-21165
Chemistry of the burning surface
[AD-A272725] p 1681 N94-21181
PROPELLANT COMBUSTION
Investigation of flame driving and flow turning in axial solid rocket instabilities
[AD-A271066] p 1667 N94-20015
Chemistry of the burning surface
[AD-A272725] p 1681 N94-21181
Electronically metastable molecules of high symmetry
[AD-A272015] p 1974 N94-21461
PROPELLANTS
Electronically metastable molecules of high symmetry
[AD-A272015] p 1974 N94-21461
PROPIONIC ACID
Water-enhanced solvation of organics
[DE93-040297] p 1683 N94-21947
PROPORTIONAL CONTROL
Proceedings of the Twentieth Annual Technologyfest p 1645 N94-20188
PROPORTIONAL COUNTERS
The laser and its applications on environment and biotechnology research
[DE94-000376] p 1820 N94-21957
VETA x ray data acquisition and control system p 2047 N94-22455

SPIKE: Application for ASTRO-D mission planning p 1926 N94-22486
An x ray archive on your desk: The Einstein CD-ROM's p 2048 N94-22519
PROPORTIONAL LIMIT
Crystal orientation dependence of elastic precursor strength in pentaerythritol tetranitrate [DE93-018340] p 2034 N94-22035
PROPULSION
Multi-disciplinary coupling effects for integrated design of propulsion systems [NASA-TM-106349] p 1830 N94-20170
Modeling of polymer electrolyte fuel cell systems [DE93-041187] p 1847 N94-21774
PROPULSION SYSTEM CONFIGURATIONS
Initiation and modification of reaction by energy addition: Kinetic and transport phenomena [AD-A271315] p 1797 N94-19936
Thrust expansion engine [AD-D015896] p 1669 N94-20121
Entry velocities at Mars and Earth for short transit times [AD-A272591] p 1665 N94-21420
Thrust augmentation options for the Beta 2 two-stage-to-orbit vehicle [NASA-TM-106448] p 1648 N94-21563
Modeling of polymer electrolyte fuel cell systems [DE93-041187] p 1847 N94-21774
Navy GTE seal development activity p 1655 N94-21794
Specialized data analysis for the Space Shuttle Main Engine and diagnostic evaluation of advanced propulsion system components [NASA-CR-194720] p 1656 N94-21813
Brayton power conversion system parametric design modelling for nuclear electric propulsion [NASA-CR-191135] p 1671 N94-21874
On the estimation algorithm used in adaptive performance optimization of turbofan engines [NASA-TM-4551] p 1649 N94-21879
Grid generation requirements at Marshall Space Flight Center p 1919 N94-22354
PROPULSION SYSTEM PERFORMANCE
Initiation and modification of reaction by energy addition: Kinetic and transport phenomena [AD-A271315] p 1797 N94-19936
Multi-disciplinary coupling effects for integrated design of propulsion systems [NASA-TM-106349] p 1830 N94-20170
Formulation of a next-generation interior ballistic code [AD-A271539] p 1801 N94-20915
Entry velocities at Mars and Earth for short transit times [AD-A272591] p 1665 N94-21420
Options for thrust augmentation for the Beta 2 two-stage-to-orbit launch vehicle [NASA-TM-106418] p 1649 N94-21759
Modeling of polymer electrolyte fuel cell systems [DE93-041187] p 1847 N94-21774
Navy GTE seal development activity p 1655 N94-21794
Specialized data analysis for the Space Shuttle Main Engine and diagnostic evaluation of advanced propulsion system components [NASA-CR-194720] p 1656 N94-21813
Brayton power conversion system parametric design modelling for nuclear electric propulsion [NASA-CR-191135] p 1671 N94-21874
On the estimation algorithm used in adaptive performance optimization of turbofan engines [NASA-TM-4551] p 1649 N94-21879
Advanced Turbine Systems (ATS). Phase 1: System scoping and feasibility studies [DE93-041130] p 1826 N94-21938
PROPULSIVE EFFICIENCY
Thrust augmentation options for the Beta 2 two-stage-to-orbit vehicle [NASA-TM-106448] p 1648 N94-21563
PROSTHETIC DEVICES
Automatic locking orthotic knee device [NASA-CASE-MFS-28633-1] p 1896 N94-20493
PROTEASE
Enhancement of wound healing by biosynthetic growth factor [AD-A272517] p 1892 N94-21415
PROTECTIVE CLOTHING
Cold-start minidiesel engine development [AD-A271064] p 1823 N94-20567
Aerospace medicine and biology: A continuing bibliography with indexes (supplement 383) [NASA-SP-7011(383)] p 1892 N94-21288
PROTECTIVE COATINGS
Thin-film hermeticity: A quantitative analysis of diamondlike carbon using variable angle spectroscopic ellipsometry p 1710 N94-20981
Oxidation resistant protective coating system for gas turbine components and process for penetration thereof [CA-PATENT-1,294,155] p 1704 N94-21143
Fifth International Symposium on Materials in a Space Environment [ISBN-2-85-428293-0] p 1659 N94-21367
Aragatz project samples experiment/MAPOL (polymer materials) experiment: Postflight expert evaluation p 1660 N94-21376
The implications of the LDEF results on Space Station Freedom power system materials p 1660 N94-21377
Evaluation of plasma-deposited protective coatings for spacecraft applications p 1663 N94-21394
Forecasting technique of variations of the optical absorptivity of thermal control coatings under different simultaneous radiations p 1664 N94-21399
Thermal control coatings p 1664 N94-21400
Study of space factors effect on materials for spacecraft external surfaces in NPO Energia programs p 1664 N94-21401
Review of corrosion behavior of ceramic heat exchanger materals: Corrosion characteristics of silicon carbide and silicon nitride [DE93-041307] p 1706 N94-21516
Performance of carbon-based hot frit substrates [DE94-000509] p 1676 N94-21754
Surface modification for corrosion resistance [DE93-017419] p 1693 N94-21825
Surface modification of Ti3Al for improved oxidation resistance [DE93-018297] p 1696 N94-22034
PROTEIN CRYSTAL GROWTH
Method for controlling protein crystallization [NASA-CASE-MFS-28688-1] p 2017 N94-20528
PROTEIN SYNTHESIS
A complex systems approach to computational molecular biology [DE93-040062] p 1884 N94-19866
PROTEINS
High resolution electron crystallography of protein molecules [DE93-040114] p 1884 N94-19826
Quinoa: An emerging new crop with potential for CELSS [NASA-TP-3422] p 1895 N94-20137
PROTOCOL (COMPUTERS)
TCP performance analysis for wide area networks [DE94-000449] p 1928 N94-19858
Robust, high-speed network design for large-scale multiprocessing [AD-A271003] p 1716 N94-19977
Total order assumption [PB93-191740] p 1903 N94-19993
Design considerations for a fiber optic communications network for power systems [DE93-018404] p 1984 N94-20179
Distributed Virtual System (DIVIRS) project [NASA-CR-194360] p 1905 N94-20228
Understanding Open Systems Interconnection (OSI) [AD-A271877] p 1929 N94-20472
Standard ML signatures for a protocol stack [AD-A272060] p 1908 N94-20622
A semi-Markov model of a home network access protocol [MEMO-INF-92-71] p 1909 N94-21045
A simplified token bus protocol specified using LOTOS [TR-92-15] p 1910 N94-21062
Government Open Systems Interconnection Profile (GOSIP) transition strategy [AD-A273005] p 1740 N94-21308
Using manufacturing message specification for monitor and control at Venus p 1932 N94-21333
Distributed intelligent control and status networking p 1932 N94-21335
A packet switched communications system for GRO p 1744 N94-21345
A lower bound on wait-free counting [CWI-CS-R9307] p 1915 N94-21537
Uniform self-stabilizing leader election. Part 1: Complete graph protocols [CWI-CS-R9308-PT-1] p 1935 N94-21549
A mechanized process algebra for verification of device synchronization protocols p 1766 N94-21716
Performance evaluation of video on ethernet [DE93-040696] p 1936 N94-21749
IAS telecommunication infrastructure and value added network services provided by IASNET p 1744 N94-22069
The conformance testing methodology to CTRON (communication and central TRON) extended OS p 1772 N94-22118
CREIR: A multiaccess protocol for on-board processing satellite systems p 1780 N94-22168
Throughput, blocking, and interference in packet radio networks p 1746 N94-22190
Specification and formal verification of the safety criterion in the alternating bit protocol p 1784 N94-22193
Modeling and analysis of secure communication protocols using Petri net formalism p 1784 N94-22194
File transfer performance in LAN interconnection through a satellite channel p 1746 N94-22209
Everything you might want to know about the Internet but are afraid to ask! [DE93-041118] p 2046 N94-22413
A structured data transfer protocol p 2047 N94-22450
The HEASARC graphical user interface p 1926 N94-22487
A generic archive protocol and an implementation p 2047 N94-22493
The Keck Task Library (KTL) p 2048 N94-22504
PROTON BEAMS
A high-intensity He-jet production source for radioactive beams [DE93-040247] p 1981 N94-21767
PROTON IRRADIATION
On modelling nuclear reactions in meteorites p 2085 N94-20844
Proton radiation testing of an 18 bit A/D converter p 1755 N94-21096
PROTONS
A study of events with the highest total transverse energy in CDF [DE93-019904] p 1978 N94-19972
The cross section for the production of b(bar-b) pairs in p(bar p) collisions at the square root of s equals 1.8 TeV [DE93-019900] p 1972 N94-20225
STRV RADMON: An integrated high-energy particle detector p 1666 N94-21086
SLAC measurement of the neutron spin structure function [DE93-040998] p 1975 N94-21788
Toward a QCD analysis of jet rates in deep-inelastic Muon-Proton scattering [DE94-000618] p 1976 N94-21962
PROTOPLANETS
Diffusive redistribution of water vapor in the solar nebula revisited p 2113 N94-20751
FE-60 and the evolution of eucrites p 2083 N94-20768
Volatile loss from accreting icy protoplanets p 2084 N94-20793
The Sm-Nd systematics of silicate inclusions in iron meteorites: Results from Caddo (IAB) [CONTRIB-5241(804)] p 2084 N94-20795
Triton's cratering record and its time of capture p 2122 N94-20802
Recondensation in the early solar system: Physical conditions and source material p 2085 N94-20849
PROTOSTARS
Helical kink instability of jets from young stellar objects p 2008 N94-22686
PROVING
Stochastic optimization by simulation: Convergence proofs for the G1/G/1 queue in steady-state [AD-A271141] p 1962 N94-19999
Formal hardware verification in Maple p 1771 N94-22112
Formal verification of an ALU p 1772 N94-22114
Tests of logic spaces: A new strategy for certifying the accuracy of programs p 1772 N94-22116
Modeling software systems for data flow testing p 1772 N94-22117
The conformance testing methodology to CTRON (communication and central TRON) extended OS p 1772 N94-22118
Satellite validation of GCM-simulated annual cycle of the Earth radiation budget and cloud forcing p 1860 N94-22287
Use of satellite data for validation of operational forecast models and operational analyses p 1861 N94-22291
PSYCHOLINGUISTICS
Modeling the human mental lexicon with self-organizing feature maps p 1743 N94-20244
An exploration of clause boundary effects in SRN representations p 1937 N94-20253
PSYCHOLOGICAL EFFECTS
Incongruity, incongruity resolution, and mental states: The measure and modification of situational awareness and control [NASA-CR-194568] p 1893 N94-20168
PSYCHOLOGICAL FACTORS
Incongruity, incongruity resolution, and mental states: The measure and modification of situational awareness and control [NASA-CR-194568] p 1893 N94-20168

PSYCHOLOGICAL TESTS
A description of psychological type at the Defense Systems Management College, 1993 edition
[AD-A271612] p 1894 N94-21237
Psychometric developments related to tests and selection
[AD-A272971] p 1894 N94-21262
Extracting information from wrong answers in computerized adaptive testing
[AD-A272832] p 1894 N94-21434
PSYCHOMETRICS
Development of the UTC-PAB normative database
[AD-A271319] p 1893 N94-20023
A description of psychological type at the Defense Systems Management College, 1993 edition
[AD-A271612] p 1894 N94-21237
Psychometric developments related to tests and selection
[AD-A272971] p 1894 N94-21262
Extracting information from wrong answers in computerized adaptive testing
[AD-A272832] p 1894 N94-21434
PSYCHOMOTOR PERFORMANCE
Development of the UTC-PAB normative database
[AD-A271319] p 1893 N94-20023
PUBLIC HEALTH
Health effects of global warming: Problems in assessment
[DE93-040323] p 1850 N94-19930
PULSAR MAGNETOSPHERES
Particle acceleration on the Alfven surface of a plasma ejecting axisymmetric rotator p 2008 N94-22681
PULSARS
High-energy astrophysics: A theoretical analysis of thermal radiation from neutron stars
[NASA-CR-194808] p 2055 N94-20952
Verification of the PROS timing analysis package p 1926 N94-22508
Gamma ray burst as a result of the explosive instability in the magnetosphere of old neutron star p 2007 N94-22675
Structure of accretion plasmas of x ray binary pulsars in MHD turbulence p 2007 N94-22679
VHE gamma ray generation by radio pulsars p 2007 N94-22680
PULSE CODE MODULATION
An adaptive, lossless data compression algorithm and VLSI implementations p 1753 N94-21080
Image detection using edge extraction algorithms
[AD-A272439] p 1911 N94-21203
PULSE COMMUNICATION
Nonlinear acoustics: Periodic waveguide, finite-amplitude propagation in a medium having a distribution of relaxation processes, and production of an isolated negative pulse in water
[AD-A270530] p 1967 N94-19894
PULSE COMPRESSION
Applications of correlator chips in radio science p 1763 N94-21695
PULSE DOPPLER RADAR
Description and availability of airborne Doppler radar data p 1722 N94-20419
CFAR processing for airborne pulse-Doppler radars p 1745 N94-22142
Space-based radar for moving target detection p 1745 N94-22143
PULSE DURATION
Effects of stimulated Raman scattering on light beam properties during high-power laser beam long-path propagation
[AD-A273109] p 1818 N94-21509
PULSE GENERATORS
Characterization of electromagnetic fields in an extended chamber at the Short Pulse Experimental Electron Device (SPEED) simulator
[AD-A265955] p 1717 N94-20329
Compact lightweight CO2 laser for SDIO application
[AD-A273010] p 1817 N94-21284
Results from long conduction time plasma opening switch experiments at Sandia National Laboratories
[DE93-019063] p 1762 N94-21632
Ultrafast gas switching experiments
[DE93-019071] p 1762 N94-21634
A FET-switched induction accelerator cell
[DE93-019604] p 1769 N94-21838
PULSE RADAR
Analysis of Ku-band cross section at low incidence angles p 1720 N94-20414
Real-time step frequency radar
[ISBN-0-315-83588-5] p 1743 N94-22576
PULSED LASER DEPOSITION
Particles on surfaces of laser ablated Y1Ba2Cu3O(7-delta) films
[DE93-040269] p 2013 N94-19929
PULSED LASERS
PVDF gauge characterization of hypervelocity-impact-generated debris clouds
[DE93-018831] p 1829 N94-19943
Applications and source development for high-repetition rate x ray lasers
[DE93-019547] p 1815 N94-20259
Ocular damage induced by ultrashort laser pulses
[AD-A271859] p 1890 N94-20462
Low-altitude cross-wind velocity measurements using pulsed visible fringe-type laser anemometry
[ISL-CO-216/92] p 1866 N94-20557
A theory for optical wavelength control in short pulse free electron laser oscillators
[AD-A271706] p 1817 N94-21353
Simulations of spectral broadening by cross-phase modulation (XPM) with chaotic light pulses
[DE93-019623] p 1819 N94-21872
Parametric instabilities in picosecond time scales
[DE94-000384] p 1966 N94-21958
PULSED RADIATION
Rough surface scattering from moving ocean surfaces as an indicator of scattering mechanisms p 1726 N94-20439
PURIFICATION
Photochemically induced transformations of transition complexes
[AD-A271112] p 2014 N94-19982
PYRAMIDS
A pyramid neural network architecture for stereo fusion p 1785 N94-22201
PYRENES
Synthesis and catalytic properties of metal and semiconductor nanoclusters
[DE93-019418] p 2028 N94-21541
PYRIDINES
Dynamics of adsorbed, swollen block copolymers
[AD-A272013] p 1706 N94-21460
PYRITES
The role of CO2 in weathering reactions and the presence of S2 on Venus: Implications for the pyrite stability field p 2122 N94-20799
PYROELECTRICITY
Proceedings of the 8th International Symposium on Applications of Ferroelectrics
[AD-A270679] p 1749 N94-20012
PYROLYSIS
Direct aromatization of methane
[DE93-040631] p 1678 N94-19890
Are the C delta light nitrogen and noble gases located in the same carrier? p 2085 N94-20846
High temperature size selective membranes
[DE93-019865] p 1709 N94-21982
Mass spectrometer-pyrolysis experiment for atmospheric and soil sample analysis on the surface of Mars p 1812 N94-22435
PYROLYTIC GRAPHITE
The optical constants and spectral specular reflectivity of Highly Oriented Pyrolytic Graphite (HOPG)
[DE93-040546] p 1709 N94-21970
PYROXENES
Petrogenesis of Apollo 12 mare basalts. Part 1: Multiple melts and fractional crystallization to explain olivine and ilmenite basalt compositions p 1684 N94-20644
Petrogenesis of Apollo 12 mare basalts. Part 2: An open system model to explain the pigeonite basalt compositions p 1684 N94-20645
Orthopyroxenes as recorders of diogenite petrogenesis: Major and minor element systematics p 1684 N94-20670
Post-igneous redistribution of components in eucrites p 1685 N94-20684
Primary differentiation in the early Earth: Nd and Sr isotopic evidence from diamondiferous eclogites for both old depleted and old enriched mantle, Yakutia, Siberia p 1862 N94-20776
The U-Th-Pb, Sm-Nd, and Ar-Ar isotopic systematics of lunar meteorite Yamato-793169 p 2084 N94-20834
Rare Earth elements in individual minerals in Shergottites p 1686 N94-20852
Diffuse reflectance spectra of orthopyroxene, olivine, and plagioclase as a function of composition and structure p 2087 N94-20906

Q

Q SWITCHED LASERS
Optics survivability support, volume 1
[DE93-019616] p 1985 N94-20262
QUADRANTS
Some practicable applications of quadtree data structures/representation in astronomy p 1927 N94-22515
QUADRATURE AMPLITUDE MODULATION
Coded 64QAM using a binary convolutional code p 1747 N94-22223
QUADRATURE PHASE SHIFT KEYING
Advanced coding and modulation schemes for TDRSS p 1744 N94-21350
The influence of lowpass filtering and the effects of fading on the group demodulation of QPSK signals p 1746 N94-22170
Quadrature biorthogonal modulation p 1747 N94-22232
QUADRATURES
Use of switched capacitor filters to implement the discrete wavelet transform p 1755 N94-21097
QUADRUPOLES
Space-charge dominated beam transport in magnetic quadrupoles with large aperture ratios
[DE93-040443] p 1992 N94-20004
High current injector for heavy ion fusion
[DE93-019241] p 1979 N94-20289
Study of possible energy upgrade for the ALS and modeling of the real lattice for the diagnosis of lattice problems
[DE93-040286] p 2016 N94-20323
Simulation studies of space-charge-dominated beam transport in large aperture ratio quadrupoles
[DE93-019238] p 1961 N94-21440
QUALIFICATIONS
Qualifying codes under software quality assurance: Two examples as guidelines for codes that are existing or under development
[DE93-040452] p 1904 N94-20097
QUALITY CONTROL
Qualifying codes under software quality assurance: Two examples as guidelines for codes that are existing or under development
[DE93-040452] p 1904 N94-20097
Using electronic data interchange to report product quality
[AD-A271843] p 1828 N94-20488
Correct CMOS IC defect models for quality testing p 1755 N94-21093
Software metrics: The key to quality software on the NCC project p 1922 N94-21326
Factors associated with continuance commitment to FAA matrix teams
[DOT/FAA/AM-93/18] p 2040 N94-21626
Process characterization and control of hand-soldered printed wiring assemblies
[DE93-041290] p 1763 N94-21652
Information and decision structure in a Japanese type of management with respect to QCC and just-in-time systems p 2045 N94-22063
Formal methods in the design of critical software systems p 1779 N94-22158
A robust quality control system for GPS navigation and kinematic positioning
[ISBN-0-315-83148-0] p 1644 N94-22427
Quality control of EUVE databases p 2047 N94-22490
SIMBAD quality-control p 2048 N94-22502
Tests of a simple data merging algorithm for the GONG project p 1927 N94-22549
QUANTITATIVE ANALYSIS
Quantitative evaluation of material composition of composites using x ray energy-dispersive NDE technique
[DE93-041157] p 1672 N94-19888
Thin-film hermeticity: A quantitative analysis of diamondlike carbon using variable angle spectroscopic ellipsometry p 1710 N94-20981
Temperature dependence of optical properties of AlAs, studied by in-situ spectroscopic ellipsometry p 2023 N94-20999
The readiness growth model: A quantitative analysis of software risk
[AD-A272383] p 1910 N94-21144
Quantitative analysis of scanning tunneling microscopy images for surface structure determination: Sulfur on Re(0001)
[DE93-019235] p 2034 N94-22041
QUANTUM CHEMISTRY
Ab initio potential energy surface for the H + OCS reaction
[AD-A270577] p 1698 N94-19947
QUANTUM CHROMODYNAMICS
A study of events with the highest total transverse energy in CDF
[DE93-019904] p 1978 N94-19972
The two-jet differential cross-section at CDF
[DE93-019905] p 1978 N94-19983
Jet shapes in hadron and electron colliders
[DE93-019386] p 1979 N94-20216
The cross section for the production of b(bar-b) pairs in p(bar p) collisions at the square root of s equals 1.8 TeV
[DE93-019900] p 1972 N94-20225

Theoretical particle physics
[DE94-000538] p 1973 N94-20938
Qualitative and quantitative aspects of the QCD theory of elastic form factors
[DE93-040864] p 2036 N94-21513
Hadronic molecules and scattering amplitudes from the nonrelativistic quark model
[DE94-000377] p 1974 N94-21657
Measurement of the inclusive jet cross section in p(bar-p) collisions at CDF
[DE94-000581] p 1982 N94-21866
New perspectives in quantum chromodynamics
[DE93-041021] p 2038 N94-21935
Toward a QCD analysis of jet rates in deep-inelastic Muon-Proton scattering
[DE94-000618] p 1976 N94-21962

QUANTUM EFFICIENCY
Cal and some new photocathodes
[DE93-019387] p 1750 N94-20314
The quantum efficiency of HgCdTe photodiodes in relation to the direction of illumination and to their geometry p 1735 N94-20512
Stable, high-efficiency amorphous-silicon solar cells with low hydrogen content
[DE93-015214] p 1848 N94-21826

QUANTUM ELECTRODYNAMICS
Dynamics of vortices in superconductors
[DE93-019535] p 2011 N94-19808

QUANTUM ELECTRONICS
Optical and transport properties of metallic and semiconductor nanostructures
[AD-A271716] p 2018 N94-20554
Solid-state dynamics and quantum transport in novel semiconductor nanostructures
[AD-A272955] p 2027 N94-21248

QUANTUM MECHANICS
On the theory of morphology-dependent resonances: Shape resonances, width formulas, and graphical representations
[AD-A272279] p 2037 N94-20945
A formulation of quantum statistical mechanics based on the Feynman path centroid density 2 dynamical properties
[AD-A272698] p 2037 N94-21166
A formulation of quantum statistical mechanics based on the Feynman path centroid density 1: Equilibrium properties
[AD-A272809] p 2037 N94-21171
Solid-state dynamics and quantum transport in novel semiconductor nanostructures
[AD-A272955] p 2027 N94-21248
The quantum structure of matter grand challenge project: Large-scale 3-D solutions in relativistic quantum dynamics
[DE94-000328] p 1960 N94-21955
On the correspondence limit of relativistic quantum mechanics
[DE93-040939] p 2038 N94-21971
Restoring locality with faster-than-light velocities
[DE93-040926] p 2038 N94-22010
Proof of stability of the hydrogen molecule
[PB93-221026] p 1977 N94-22271

QUANTUM OPTICS
A microscopic theory of quantum optics and new photon-locked bistable states
[AD-A271250] p 1983 N94-19901

QUANTUM THEORY
F-spin concept and g-bosons in the interceding boson model
[ETN-93-93607] p 1973 N94-21136
A formulation of quantum statistical mechanics based on the Feynman path centroid density 2 dynamical properties
[AD-A272698] p 2037 N94-21166
Restoring locality with faster-than-light velocities
[DE93-040926] p 2038 N94-22010
Non commutative geometry and physics
[PB93-215499] p 1961 N94-22264

QUANTUM WELL LASERS
High Speed/High Frequency Optoelectronics
[AD-A271985] p 1751 N94-20580
The n-p(p(+))-n Al(yGa)(1-y) As-GaAs-In(x)Ga(1-x) as quantum well laser with p(+)-n(+)GaAs-InGaAs tunnel contact on n GaAs
[AD-A271292] p 2030 N94-21805

QUANTUM WELLS
Investigation of quantum effects in heterostructures
[AD-A270938] p 2011 N94-19817
Theory of energy-assisted epitaxy: theory of ordered semiconductor alloys: In(1-x)Tl(x)Sb as a long-wave infrared material
[AD-A271007] p 2012 N94-19835
Common Themes and Mechanisms of Epitaxial Growth, volume 312 — Materials Research Society symposium proceedings
[AD-A270513] p 2013 N94-19967
Center for the integration of optical computing
[AD-A271874] p 1899 N94-20469
An x-band peeled HEMT amplifier
p 1732 N94-20498
Optical and transport properties of metallic and semiconductor nanostructures
[AD-A271716] p 2018 N94-20554
Investigation of heterojunctions and multiple quantum well structures using crystalline organic semiconductors
[AD-A272113] p 2018 N94-20569
Materials, Structures, and Devices for High-Speed Electronics
[NASA-CR-193177] p 2019 N94-20971
Measurement of superlattice optical properties by variable angle spectroscopic ellipsometry
p 2022 N94-20992
GaAs/AlGaAs superlattice characterization by variable angle spectroscopic ellipsometry p 2022 N94-20994
Characterization of an asymmetric triangular multiple quantum well, by variable angle spectroscopic ellipsometry p 2022 N94-20995
Polarized-light reflection mode p-i-n modulators with GaAs/AlGaAs multiple quantum well active layers: Design and simulation p 2023 N94-20996
Optical amplification and threshold behavior on InGaAs/InGaAsP multiquantum well structures
[ETN-93-94181] p 2026 N94-21151
Syntheais and properties of mismatched heterojunction/substrate interfaces
[AD-A272904] p 1760 N94-21229

QUARK MODELS
Hadronic molecules and scattering amplitudes from the nonrelativistic quark model
[DE94-000377] p 1974 N94-21657
A relativistic constituent quark model
[DE93-041085] p 1946 N94-21689

QUARKS
Top search at the TEVATRON
[DE93-019392] p 1978 N94-19988
Jet shapes in hadron and electron colliders
[DE93-019386] p 1979 N94-20216
Measurement of the strange quark distribution function in W(+) charm quark events
[DE93-018267] p 1973 N94-20474
Theoretical particle physics
[DE94-000538] p 1973 N94-20938
Recent results on top, bottom and exotic physics at the Tevatron
[DE94-000578] p 1975 N94-21786
Measurement of the B meson and b quark cross-section in (-p)p collisions at the square root of s = 1.8 TeV using the exclusive decays B(+) and B(exp 0) yields J/psiK*(exp 0)
[DE93-019907] p 1975 N94-21806
Search for excited quarks in p(-p) collisions at the square root of s = 1.8 TeV
[DE93-019910] p 1975 N94-21840
New perspectives in quantum chromodynamics
[DE93-041021] p 2038 N94-21935
Time evolution of the quark-gluon plasma
[DE94-000804] p 1998 N94-22389

QUARTZ
Characterization of amorphous material in shocked quartz by NMR spectroscopy
[DE93-019069] p 1679 N94-20307
Shock attenuation at the Slate Islands revisited
p 1863 N94-20887

QUARTZ CRYSTALS
Atomic oxygen fluence detector for Bremsat: Scientific and technical description p 1663 N94-21396
Application of an electrochemical quartz crystal microbalance to the study of electrocatalytic films
[DE93-041124] p 2029 N94-21691

QUASARS
Automated investigation of quasars at a galactic latitude of -45 deg
[ISBN-0-315-57576-X] p 2056 N94-22415
Adaptive filtering of Echelle spectra of distant Quasars
p 2072 N94-22520

QUERY LANGUAGES
Application of the structures query language of APROS for specification of industrial processes
p 1923 N94-22078
Intelligent text retrieval in the NASA astrophysics data system p 2048 N94-22499

QUEUEING THEORY
Stochastic optimization by simulation: Numerical experiments with M/M/1 queue in steady-state
[AD-A271143] p 1949 N94-19854
Large deviations behavior of counting processes and their inverses
[AD-A271142] p 1939 N94-19909
Memory contention in scalable cache-coherent multiprocessors
[TR-448] p 1929 N94-20144
Time warp operating system version 2.7 internals manual
[NASA-CR-194798] p 1899 N94-20549
The correlated M/G/1 queue
[CWI-BS-R9303] p 1943 N94-21032
On the optimality of FCFS for networks of multi-server queues
[CWI-BS-R9235] p 1944 N94-21160
Optimization of static traffic allocation policies
[CWI-BS-R9302] p 1930 N94-21161
N parallel queueing systems with server breakdown and repair
[CWI-BS-R9236] p 1944 N94-21232
Optimization of fixed time polling schemes
[CWI-BS-R9237] p 1945 N94-21233
Tandem queues with deterministic service times
[CWI-BS-R9238] p 1946 N94-21577
Algorithms for Markov decision chains with partial information
[PB93-220085] p 1918 N94-22098

R

RABBITS
Ocular damage induced by ultrashort laser pulses
[AD-A271859] p 1890 N94-20462

RADAR ANTENNAS
Probe compensation in cylindrical near-field scanning: A novel simulation methodology p 1718 N94-20404
Two microstrip arrays for interferometric SAR applications p 1722 N94-20421
Target angular motion and its effects on simulated SSAR ship images p 1745 N94-22161

RADAR CORNER REFLECTORS
RCS Analysis of Plate Geometries, parts 1 and 2
[NASA-CR-194173] p 1717 N94-20269
A physical optics/equivalent currents model for the RCS of trihedral corner reflectors p 1717 N94-20271
Modifications to the three-component classification algorithm for SAR data p 1719 N94-20410
Radar backscattering from snow facies of the Greenland ice sheet: Results from the AIRSAR 1991 campaign
p 1725 N94-20434

RADAR CROSS SECTIONS
RCS Analysis of Plate Geometries, parts 1 and 2
[NASA-CR-194173] p 1717 N94-20269
High-frequency techniques for RCS prediction of plate geometries p 1717 N94-20270
A physical optics/equivalent currents model for the RCS of trihedral corner reflectors p 1717 N94-20271
Massively parallel computation of RCS with finite elements p 1726 N94-20437
RCS of ships and aircraft at HF frequencies
p 1745 N94-22128

RADAR DATA
Modifications to the three-component classification algorithm for SAR data p 1719 N94-20410
Determination of noise equivalent sigma(0) using highly correlated repeat-pass SAR images
p 1720 N94-20411
On evaluating the accuracy of SAR sea-ice classification using multifrequency polarimetric AIRSAR data
p 1724 N94-20428
Application of Cloude's target decomposition theorem to polarimetric imaging radar data p 1724 N94-20429
Direction angle sensitivity of agricultural field backscatter with AIRSAR data p 1724 N94-20430
Mapping of taiga forest units using AIRSAR data and/or optical data, and retrieval of forest parameters
p 1729 N94-20452
NAVSPASUR sensor system digital signal processing receiver. Volume 1: Hardware and software overview
[AD-A272899] p 1738 N94-21198
NAVSPASUR sensor system digital signal processing receiver. Volume 2: Function and capabilities of hardware and software components
[AD-A272900] p 1739 N94-21218
Interpretation of Ground Penetrating Radar data at the Hanford Site, Richland, Washington
[DE93-040409] p 1743 N94-22557

RADAR DETECTION
Target motion detecting impulse Doppler radar system
[AD-D015898] p 1717 N94-20198
Analysis of Ku-band cross section at low incidence angles p 1720 N94-20414
Probability of detection calculations using MATLAB
[AD-A271958] p 1736 N94-20578

RADAR ECHOES
Magellan vertical polarization radar observations
p 1744 N94-20691

RADAR GEOLOGY
Interpretation of Ground Penetrating Radar data at the Hanford Site, Richland, Washington
[DE93-040409] p 1743 N94-22557

RADAR IMAGERY
Determination of noise equivalent sigma(0) using highly correlated repeat-pass SAR images p 1720 N94-20411
Topographic mapping using a monopulse SAR system p 1721 N94-20417
Observation of pressure ridges in SAR images of sea ice: Scattering theory and comparison with observations p 1723 N94-20427
On evaluating the accuracy of SAR sea-ice classification using multifrequency polarimetric AIRSAR data p 1724 N94-20428
Use of microwave polarimetry to enhance SAR images of the ocean surface
[AD-A271911] p 1882 N94-20489
Beta Regio rift system on Venus: Geologic interpretation of Magellan images p 2095 N94-20655
Beta Regio - Phoebe Regio on Venus: Geologic mapping with the Magellan data p 2096 N94-20656
Magellan at Venus: Summary of science findings p 2110 N94-20734
Magellan Mission p 1652 N94-20829
Neural network studies
[AD-A271593] p 1943 N94-20947
Evaluation of C-band SAR data from SAREX 1992: Tapajos study site p 1839 N94-20964
An overview of synthetic aperture radar signal processing techniques p 1745 N94-22159
Target angular motion and its effects on simulated SSAR ship images p 1745 N94-22161
Radar imaging of moving targets p 1747 N94-22238
STAR-1 SAR road extraction using texture analysis and mathematical morphology
[ISBN-0-315-83255-X] p 1843 N94-22429
RADAR MAPS
Performance evaluation of the JPL TOPSAR system: An across-track interferometric SAR system for topographic mapping p 1732 N94-20461
Beta Regio - Phoebe Regio on Venus: Geologic mapping with the Magellan data p 2096 N94-20656
RADAR MEASUREMENT
Radar backscatter measurements from simulated sea ice during CRRELEX 1990
[AD-A271034] p 1715 N94-19823
Multiple scattering effects on the Linear Depolarization Ratio (LDR) measured during CaPE by a Ka-band air-borne radar p 1728 N94-20446
Application of the target decomposition theorem to a polarimetric random media model p 1730 N94-20453
Magellan at Venus: Summary of science findings p 2110 N94-20734
Geology and radiophysical properties of the Venera and Vega landing sites p 2135 N94-20867
Obtaining surface optical properties from space-based lidar systems
[AD-A272831] p 1987 N94-21172
Lidar and radar derived cirrus microphysical properties for the 26 November 1991 case study p 1873 N94-22305
Dynamical characteristics of cirrus clouds from aircraft and radar measurements p 1878 N94-22332
RADAR RANGE
Development of a lidar for integration with the Naval Postgraduate School Infrared Search and Target Designation (NPS-IRSTD) system
[AD-A271847] p 1817 N94-20611
RADAR REFLECTORS
All-weather precision landing system for aircraft in remote areas
[AD-D015924] p 1643 N94-20197
RADAR SCATTERING
Classification of simple vegetation types using POLSAR image data p 1722 N94-20420
Observation of pressure ridges in SAR images of sea ice: Scattering theory and comparison with observations p 1723 N94-20427
Application of Cloude's target decomposition theorem to polarimetric imaging radar data p 1724 N94-20429
Direction angle sensitivity of agricultural field backscatter with AIRSAR data p 1724 N94-20430
Studies of Greenland using the SEASAT scatterometer p 1725 N94-20433
Radar backscattering from snow facies of the Greenland ice sheet: Results from the AIRSAR 1991 campaign p 1725 N94-20434
C-band radar backscatter of sea ice in the Weddell Sea, Antarctica during the austral winter of 1992 p 1725 N94-20435
Massively parallel computation of RCS with finite elements p 1726 N94-20437
Rough surface scattering from moving ocean surfaces as an indicator of scattering mechanisms p 1726 N94-20439
Application of the target decomposition theorem to a polarimetric random media model p 1730 N94-20453
Magellan vertical polarization radar observations p 1744 N94-20691
Low-power millimeter-wave radar observations of the atmosphere
[NASA-CR-194738] p 1858 N94-21811
RCS of ships and aircraft at HF frequencies p 1745 N94-22128
RADAR SIGNATURES
Polarimetric backscattering from sea ice p 1723 N94-20426
Use of the Weiss-Weinstein bound to compare the direction-finding performance of sparse arrays
[AD-A272582] p 1738 N94-21210
Progress in interpreting CO2 lidar signatures to obtain cirrus microphysical and optical properties p 1874 N94-22308
RADAR TARGETS
Target motion detecting impulse Doppler radar system
[AD-D015898] p 1717 N94-20198
Application of Cloude's target decomposition theorem to polarimetric imaging radar data p 1724 N94-20429
Calculation of a diffracted electric field with the aid of the Method of Equivalent Currents (MEC) p 1745 N94-22127
RCS of ships and aircraft at HF frequencies p 1745 N94-22128
RADAR TRACKING
New algorithm of ground track processing in high-frequency skywave over-the-horizon-B radar
[AD-A267821] p 1717 N94-20207
Probability of detection calculations using MATLAB
[AD-A271958] p 1736 N94-20578
Magellan vertical polarization radar observations p 1744 N94-20691
GMM-1: A 50 degree and order gravitational field model for Mars p 2117 N94-20774
NAVSPASUR sensor system digital signal processing receiver. Volume 1: Hardware and software overview
[AD-A272899] p 1738 N94-21198
NAVSPASUR sensor system digital signal processing receiver. Volume 2: Function and capabilities of hardware and software components
[AD-A272900] p 1739 N94-21218
Radar imaging of moving targets p 1747 N94-22238
Remote sensing of multilevel clouds during FIRE IFO 2 p 1844 N94-22303
RADIAL DISTRIBUTION
Optical diagnostic instrument for monitoring etch uniformity during plasma etching of polysilicon in a chlorine-helium plasma
[DE93-019582] p 1993 N94-20261
C2, CN and dust in Comet Wilson (1987VII) p 2083 N94-20746
Shock attenuation at the Slate Islands revisited p 1863 N94-20887
Impact of copper vapour contamination on argon arcs p 1994 N94-21053
RADIAL FLOW
Formation and evolution of radial fracture systems on Venus p 2099 N94-20672
RADIAL VELOCITY
The IRAF radial velocity analysis package p 1925 N94-22475
RADIANCE
UVPI imaging from the LACE satellite: The Starbird rocket plume
[AD-A271981] p 1658 N94-20617
Goniospectrometric properties of a white standard p 1684 N94-20664
Wavelength dependence of limb-darkening of Mars from visible and near-IR telescopic spectral imaging p 2101 N94-20685
Measurement of evapotranspiration with combined reflective and thermal infrared radiance observations
[NASA-CR-194802] p 1837 N94-20951
Intercomparison of MAS, AVIRIS, and HIS data from FIRE cirrus 2 p 1872 N94-22298
Development of methods for inferring cloud thickness and cloud-base height from satellite radiance data p 1872 N94-22301
Atmospheric parameterization schemes for satellite cloud property retrieval during FIRE IFO 2 p 1874 N94-22312
Spectral emissivity of cirrus clouds p 1876 N94-22322
Calibration of radiation codes in climate models: Comparison of calculations with observations from the SPECtral Radiation Experiment (SPECTRE) p 1879 N94-22337
SSH-2 measurements of cirrus at 18-28 micrometers from the King Air during FIRE 2 p 1880 N94-22338
Investigation of the effects of the macrophysical and microphysical properties of cirrus clouds on the retrieval of optical properties: Results for FIRE 2 p 1880 N94-22339
RADIANT COOLING
An improved patch for radiative coolers
[NASA-CASE-GSC-13503-1] p 1822 N94-20127
RADIANT FLUX DENSITY
RADCAL: A narrow-band model for radiation calculations in a combustion environment
[PB93-200889] p 1682 N94-21448
Miyun 232 MHz survey 1: Fields centered at: alpha:00(h)41(m), delta:41 deg 12 min and alpha: 07(h)00(m),delta:35 deg 00 min p 2080 N94-22554
RADIANT HEATING
Wavefront sensors for optical diagnostics in fluid mechanics: Application to heated flow, turbulence, and droplet evaporation
[DE93-040060] p 1797 N94-19974
The young Sun and photochemistry of the primitive Martian atmosphere p 2145 N94-21679
RADIATION
Radiation and scattering from printed antennas on cylindrically conformal platforms
[NASA-CR-194703] p 1741 N94-21885
RADIATION ABSORPTION
Optics survivability support, volume 2
[DE93-040310] p 1985 N94-20283
Extra-corporeal blood access, sensing, and radiation methods and apparatuses
[NASA-CASE-MSC-21775-1] p 1890 N94-20372
The quantum efficiency of HgCdTe photodiodes in relation to the direction of illumination and to their geometry p 1735 N94-20512
Examination for optimization of synchrotron radiation spectrum for the x ray depth lithography
[BONN-IR-92-32] p 1987 N94-21148
RADIATION CHEMISTRY
Chemistry and materials science
[DE94-001449] p 2152 N94-21858
RADIATION COUNTERS
Thermal information regarding the cooldown and operation of liquid argon calorimeters
[DE93-019391] p 1807 N94-19967
The GEM Silicon Tracking System
[DE93-040133] p 2016 N94-20322
STRV RADMON: An integrated high-energy particle detector p 1666 N94-21086
A High Resolution Liquid Xenon Imaging Telescope for 0.3-10 MeV Gamma Ray Astrophysics: Construction and Initial Balloon Flights
[NASA-CR-194709] p 2056 N94-22281
RADIATION DAMAGE
General introduction to microstructural evolution under cascade damage conditions
[DE93-017443] p 2012 N94-19923
Tensile and shear fracture behavior of fiber reinforced plastics at 77K irradiated by various radiation sources
[DE93-040280] p 1706 N94-21542
Tensile strength of fiber reinforced plastics at 77K irradiated by various radiation sources
[DE93-040826] p 1709 N94-22008
RADIATION DETECTORS
The NRL LACE program
[AD-A270861] p 1657 N94-19896
Top search at the TEVATRON
[DE93-019392] p 1978 N94-19988
B production at D0
[DE93-019250] p 1972 N94-20291
STRV RADMON: An integrated high-energy particle detector p 1666 N94-21086
Advanced far infrared detectors
[DE93-040289] p 1988 N94-21528
The lepton charge asymmetry in the decay of W bosons produced in p(bar p) collisions at (radical)s = 1.8 TeV
[DE93-019903] p 1976 N94-21847
VETA x ray data acquisition and control system p 2047 N94-22455
RADIATION DISTRIBUTION
Extra-corporeal blood access, sensing, and radiation methods and apparatuses
[NASA-CASE-MSC-21775-1] p 1890 N94-20372
Monte Carlo calculation of multi-electron effects on synchrotron radiation
[DE94-001259] p 1982 N94-21974
RADIATION DOSAGE
Focused-ion-beam material removal rates
[AD-A270852] p 1713 N94-19834
Extra-corporeal blood access, sensing, and radiation methods and apparatuses
[NASA-CASE-MSC-21775-1] p 1890 N94-20372
Radiometry in commercial aircraft
[GSF-41/91] p 1892 N94-21141
Spaceflight Radiation Health program at the Lyndon B. Johnson Space Center
[NASA-TM-104782] p 1893 N94-21863
Tensile strength of fiber reinforced plastics at 77K irradiated by various radiation sources
[DE93-040826] p 1709 N94-22008

RADIATION EFFECTS
General introduction to microstructural evolution under cascade damage conditions
[DE93-017443] p 2012 N94-19923
Hydrogen pickup and redistribution in alpha-annealed zircaloy-4
[DE93-018050] p 1689 N94-20182
Single-event upset testing of the performance semiconductor 1750A CMOS/SOS chip set
[AD-A271158] p 2015 N94-20184
Optics survivability support, volume 1
[DE93-019616] p 1985 N94-20262
Optics survivability support, volume 2
[DE93-040310] p 1985 N94-20283
High energy ionization in liquids: The free ion yield
[DE93-040329] p 1973 N94-20324
Extra-corporeal blood access, sensing, and radiation methods and apparatuses
[NASA-CASE-MSC-21775-1] p 1890 N94-20372
Effects of hydrodynamics and thermal radiation in the atmosphere after comet impacts p 1862 N94-20649
The Fifth NASA Symposium on VLSI Design
[NASA-CR-194644] p 1753 N94-21079
Rad-hard computer elements for space applications p 1753 N94-21082
Design of CMOS logic gates for TID radiation p 1754 N94-21083
Evaluation of radiation effects in re-oxidized nitrided oxide devices by hot carrier stressing at 77 K p 1754 N94-21084
Space qualified high speed Reed Solomon encoder p 1754 N94-21088
Proton radiation testing of an 18 bit A/D converter p 1755 N94-21096
Automated radiation hard ASIC design tool p 1759 N94-21126
Simulated space environmental effects on some experimental high performance polymers p 1662 N94-21385
Evaluation of electroconductivity of two surface paints for spacecraft
[AD-A273063] p 1706 N94-21437
Tensile and shear fracture behavior of fiber reinforced plastics at 77K irradiated by various radiation sources
[DE93-040280] p 1706 N94-21542
Temperature-dependent ion beam mixing
[DE93-040281] p 2033 N94-21999
Tensile strength of fiber reinforced plastics at 77K irradiated by various radiation sources
[DE93-040826] p 1709 N94-22008
Microstructural evolution of neutron-irradiated Fe-Cr-Ni ternary alloys at high helium generation rates
[DE93-018786] p 1696 N94-22037
Miniaturized disk-bend testing, nano-indentation, and the microstructure of ion-irradiated titanium aluminides
[DE93-040600] p 1697 N94-22559

RADIATION HARDENING
CMOS gate array characterization procedures
[AD-A269943] p 2014 N94-20029
Optics survivability support, volume 1
[DE93-019616] p 1985 N94-20262
Mongoose: Creation of a Rad-Hard MIPS R3000 p 1754 N94-21090
Fully-depleted silicon-on-sapphire and its application to advanced VLSI design p 1765 N94-21709
Design and test of field programmable gate arrays in space applications p 1765 N94-21710

RADIATION HAZARDS
VLF Harold E. Holt RADHAZ measurements
[AD-A272018] p 1737 N94-20620
Magnetic insulation of secondary electrons in plasma source ion implantation
[DE93-040106] p 1997 N94-21988

RADIATION MEASUREMENT
Thermal infrared remote sensing and Kirchhoff's law: 1. Laboratory measurements p 1685 N94-20733
Areally averaged estimates of surface heat flux from ARM field studies
[DE93-018569] p 1859 N94-22036
Applications of planar near-field measurements to electromagnetic radiation and interference problems p 1747 N94-22252
Proceedings of the Workshop on New Generation of Radiation Budget Measurements From Space and Their Use in Climate Modelling and Diagnostic Studies
[MPIM-90] p 1860 N94-22283
Satellite measurements of radiation budget parameters p 1860 N94-22284
Optical properties of cirrus derived from airborne measurements during FIRE IFO 2 p 1872 N94-22297
Ground-based passive remote sensing during FIRE IFO 2 p 1844 N94-22319

RADIATION SHIELDING
Transient thermal analysis of cryocondensation pump for JET
[DE93-040372] p 1992 N94-20003
Shielding from space radiations
[NASA-CR-194683] p 1895 N94-20063
Improved approximate formulas for flux from cylindrical and rectangular sources
[DE93-011390] p 1742 N94-22268

RADIATION SPECTRA
The NRL LACE program
[AD-A270861] p 1657 N94-19896
Diffuse reflectance spectra of orthopyroxene, olivine, and plagioclase as a function of composition and structure p 2087 N94-20906
Examination for optimization of synchrotron radiation spectrum for the x ray depth lithography
[BONN-IR-92-32] p 1987 N94-21148

RADIATION THERAPY
Numerical modeling for an electric-field hyperthermia applicator p 1729 N94-20451

RADIATION TOLERANCE
A method of measuring the thermoradiative properties of ceramic materials in a space environment p 1665 N94-21405
Single crystal diamond films
[AD-A266759] p 2028 N94-21517
Issues related to mechanical properties of neutron-irradiated ceramics
[DE93-040262] p 1707 N94-21560
Spaceflight Radiation Health program at the Lyndon B. Johnson Space Center
[NASA-TM-104782] p 1893 N94-21863

RADIATIVE HEAT TRANSFER
RADCAL: A narrow-band model for radiation calculations in a combustion environment
[PB93-200889] p 1682 N94-21448

RADIATIVE TRANSFER
Relating ground truth collection to model sensitivity p 1719 N94-20409
Simulated retrieval of land surface parameters using multichannel satellite microwave radiometry p 1727 N94-20443
Second order distorted born approximation for backscattering from a layer of discrete random medium p 1728 N94-20448
Effects of hydrodynamics and thermal radiation in the atmosphere after comet impacts p 1862 N94-20649
A retrieval error analysis technique for passive infrared atmospheric sounders
[AD-A272618] p 1867 N94-21212
Cirrus properties deduced from CO2 lidar observations of zenith-enhanced backscatter from oriented crystals p 1871 N94-22295
Bi-directional reflectance and other radiation parameters of cirrus from ER-2 observations p 1871 N94-22296
Lidar and radar derived cirrus microphysical properties for the 26 November 1991 case study p 1873 N94-22305
Comparisons of downwelling radiation to model predictions based on groundbased measurements during FIRE 1991 p 1876 N94-22320
A comparison of small and larger mesoscale latent heat and radiative fluxes: December 6 case study p 1879 N94-22335
Investigation of the effects of the macrophysical and microphysical properties of cirrus clouds on the retrieval of optical properties: Results for FIRE 2 p 1880 N94-22339
Extinction efficiencies from DDA calculations solved for finite circular cylinders and disks p 1880 N94-22340
Remote sensing estimates of cirrus particle size for tropical and midlatitude cirrus: Hexagonal crystals and ice spheres p 1880 N94-22342
An overview of the radiation component of the NASA TOGA-COARE experiment p 1881 N94-22344

RADICALS
Photochemically induced transformations of transition complexes
[AD-A271112] p 2014 N94-19982
Physical chemistry of energetic nitrogen compounds
[AD-A271819] p 1712 N94-20625
Polymerization of enantiomerically pure 2,3-dicarboalkoxy norbornadienes and 5,6-disubstituted norbornenes by well-characterized molybdenum ROMP catalysts
[AD-A272649] p 1704 N94-21186

RADIO ALTIMETERS
Analysis of Ku-band cross section at low incidence angles p 1720 N94-20414
C-band radar backscatter of sea ice in the Weddell Sea, Antarctica during the austral winter of 1992 p 1725 N94-20435

RADIO ASTRONOMY
Berne (Switzerland) solar observations: Data for April 1991 - August 1992
[REPT-59] p 2147 N94-21150
Applications of correlator chips in radio science p 1763 N94-21695
NASA SERC digital correlator projects p 1765 N94-21708
A 1 GHz sample rate, 256-channel, 1-bit quantization, CMOS, digital correlator chip p 1768 N94-21732
Circumstellar environments of Be stars at infra-red and radio wavelengths
[ISBN-0-315-83135-9] p 2081 N94-22426
Programmability in AIPS++ p 1926 N94-22482
Preliminary results of observations of solar flares with Nobeyama Radioheliograph p 2001 N94-22633

RADIO AURORAS
Preliminary results of observations of solar flares with Nobeyama Radioheliograph p 2001 N94-22633

RADIO BURSTS
Electron acceleration in and radio emission from SN1987A p 2007 N94-22677

RADIO COMMUNICATION
Ground wave emergency network. Final operational capability. Environmental assessment for south central Montana relay node, site no. RN8C925MT
[AD-A267795] p 1716 N94-19964
Four-channel HF receiving antenna array simulator
[AD-A271876] p 1732 N94-20471
High Frequency (HF) and meteor burst communications in a polar environment
[AD-A271604] p 1737 N94-20949
ATC/pilot voice communications: A survey of the literature
[DOT/FAA/AM-93/20] p 1738 N94-21201
Inclined orbits and interference to stationary service and to stationary service by satellite p 1653 N94-22188

RADIO DIRECTION FINDERS
Sporadic-E observations during LoVHF transionospheric direction finder measurements
[AD-A270619] p 1716 N94-19951

RADIO EMISSION
Radio and optical emission: Spectral shapes and breaks in GRB
[NASA-CR-194763] p 2150 N94-21781
Circumstellar environments of Be stars at infra-red and radio wavelengths
[ISBN-0-315-83135-9] p 2081 N94-22426
Radiation from solar flares p 2001 N94-22634
Nonthermal planetary radio emissions: Theories and observations p 2001 N94-22635
Electron acceleration in and radio emission from SN1987A p 2007 N94-22677
Langmuir microstructures and pulsar radio emission p 2007 N94-22678

RADIO EQUIPMENT
Optical signal processing
[AD-A271036] p 1983 N94-20013

RADIO FREQUENCIES
Study of coupled-bunch collective effects in the PEP-2 B-Factory
[DE93-040117] p 1979 N94-20274
Field emitter array RF amplifier development project, phase 1, option 1
[AD-A272567] p 1740 N94-21361
Hybrid finite element/waveguide mode analysis of passive RF devices
[AD-A273074] p 1740 N94-21518
Simulation and compensation of multibunch energy variation in NLC
[DE93-041057] p 1981 N94-21687
Particle behavior in an ECR plasma etch tool
[DE93-040343] p 1996 N94-21769
The preservation of low emittance flat beams
[DE93-040964] p 1981 N94-21773
Verification of frequency scaling laws for capacitive rf discharges using two-dimensional simulations
[DE94-001306] p 1999 N94-22595

RADIO FREQUENCY HEATING
Numerical modeling for an electric-field hyperthermia applicator p 1729 N94-20451
Fusion plasma theory grant. Task 3: Auxiliary radiofrequency heating of tokamaks
[DE94-000779] p 1994 N94-20940

RADIO FREQUENCY INTERFERENCE
The Composite Analytic and Simulation Package or RFI (CASPR) on a coded channel p 1744 N94-21339
The Automated Conflict Resolution System (ACRS) p 1744 N94-21341
Advanced coding and modulation schemes for TDRSS p 1744 N94-21350
Interference reduction using neural networks p 1783 N94-22186
Inclined orbits and interference to stationary service and to stationary service by satellite p 1653 N94-22188
Throughput, blocking, and interference in packet radio networks p 1746 N94-22190

RADIO GALAXIES
Radio galaxies and their environment
[DE93-040851] p 2150 N94-22397
CCD surface photometry of galaxies p 2058 N94-22445

RADIO JETS (ASTRONOMY)
Jets associated with active galactic nuclei
p 2000 N94-22631
RADIO NAVIGATION
FM interference in radio navigation receivers
p 1645 N94-22219
A robust quality control system for GPS navigation and kinematic positioning
[ISBN-0-315-83148-0] p 1644 N94-22427
RADIO RECEIVERS
Millimeter wave imaging technology
[AD-A271257] p 1715 N94-19912
NHK Science and Technical Research Laboratories
p 2151 N94-20342
Digital receiver for on-board FM/FSK-FM/BPSK demodulation p 1744 N94-21091
RADIO RELAY SYSTEMS
Visibility considerations in frequency sharing with low Earth orbit satellites p 1746 N94-22187
RADIO SIGNALS
Sporadic-E observations during LoVHF transionospheric direction finder measurements
[AD-A270619] p 1716 N94-19951
Four-channel HF receiving antenna array simulator
[AD-A271876] p 1732 N94-20471
The VLBA correlator: Real-time in the distributed era
p 2049 N94-22547
RADIO TELEMETRY
An in-depth analysis and modelling of the Shuttle to MILA S-band telemetry link p 1657 N94-21340
RADIO TELESCOPES
Miyun 232 MHz survey 1: Fields centered at: alpha:00(h)41(m), delta:41 deg 12 min and alpha: 07(h)00(m),delta:35 deg 00 min p 2080 N94-22554
RADIO TRANSMISSION
High Frequency (HF) and meteor burst communications in a polar environment
[AD-A271604] p 1737 N94-20949
Throughput, blocking, and interference in packet radio networks p 1746 N94-22190
RADIO TRANSMITTERS
Spread spectrum random access networks
[AD-A272280] p 1737 N94-20585
VLF Harold E. Holt RADHAZ measurements
[AD-A272018] p 1737 N94-20620
ELF communications system ecological monitoring program
[AD-A272507] p 1740 N94-21412
RADIO WAVE REFRACTION
Marine boundary layer model evaluation by using a height gain measurement technique in the interference region p 1777 N94-22145
RADIO WAVES
VLF Harold E. Holt RADHAZ measurements
[AD-A272018] p 1737 N94-20620
RADIOACTIVE AGE DETERMINATION
Dating native gold by noble gas analyses
p 1684 N94-20652
Exposure ages of carbonaceous chondrites, 1
p 2082 N94-20658
LREE variability in CM matrices: Another look at meteorite compaction ages p 2086 N94-20884
RADIOACTIVE DECAY
Simulating supersymmetry with ISAJET 7.0/ISASUSY 1.0
[DE93-018266] p 1969 N94-19804
A search for new gauge bosons in (bar p)p collisions at square root of s equals 1.8 TeV in the dielectron decay mode
[DE93-019901] p 1969 N94-19813
Measurement of the B(+) and B(0) lifetimes
[DE93-019906] p 1969 N94-19814
B production at D0
[DE93-019250] p 1972 N94-20291
Measurement of the B meson and b quark cross-section in (-p)p collisions at the square root of s = 1.8 TeV using the exclusive decays B(+) and B(exp 0) yields J/psiK*(exp 0)
[DE93-019907] p 1975 N94-21806
RADIOACTIVE ISOTOPES
Dating native gold by noble gas analyses
p 1684 N94-20652
Exposure ages of carbonaceous chondrites, 1
p 2082 N94-20658
Geochronology and petrogenesis of the western highlands alkali suite: Radiogenic isotopic evidence from Apollo 14 p 2118 N94-20778
AGB stars as a source of short-lived radioactive nuclei in the solar nebula p 2133 N94-20859
Column chromatographic separation of Y(3+) from Sr(2+) by polymeric ionizable crown ether resins
[DE94-000935] p 1683 N94-22021
RADIOACTIVE WASTES
Stochastic simulation for imaging spatial uncertainty: Comparison and evaluation of available algorithms
[DE93-040058] p 1916 N94-21761
Interpretation of Ground Penetrating Radar data at the Hanford Site, Richland, Washington
[DE93-040409] p 1743 N94-22557
RADIOACTIVITY
A high-intensity He-jet production source for radioactive beams
[DE93-040247] p 1981 N94-21767
Gamma ray spectrometry of LDEF samples: Results of 1992 analyses
[DE94-001177] p 1684 N94-22046
RADIOBIOLOGY
Extra-corporeal blood access, sensing, and radiation methods and apparatuses
[NASA-CASE-MSC-21775-1] p 1890 N94-20372
RADIOGENIC MATERIALS
Dating native gold by noble gas analyses
p 1684 N94-20652
Geochronology and petrogenesis of the western highlands alkali suite: Radiogenic isotopic evidence from Apollo 14 p 2118 N94-20778
Magnesian anorthosites from the western highlands of the Moon: Isotope geochemistry and petrogenesis
p 2118 N94-20779
RADIOGRAPHY
PVDF gauge characterization of hypervelocity-impact-generated debris clouds
[DE93-018831] p 1829 N94-19943
Experimental and numerical studies of high-velocity impact fragmentation
[DE93-040205] p 1832 N94-21557
RADIOMETERS
Low power, CMOS digital autocorrelator spectrometer for spaceborne applications p 1666 N94-21733
Satellite measurements of radiation budget parameters p 1860 N94-22284
ScaRaB and its subsystems p 1860 N94-22285
Bi-directional reflectance and other radiation parameters of cirrus from ER-2 observations p 1871 N94-22296
RADIOMETRIC CORRECTION
Topographic mapping using a monopulse SAR system
p 1721 N94-20417
RADIOMETRIC RESOLUTION
A motion extraction method for synthetic aperture radars
[DLR-FB-92-31] p 1742 N94-22279
RADOMES
Radome having integral heating and impedance matching elements
[CA-PATENT-APPL-SN-2,026,85] p 1738 N94-21049
RAIL TRANSPORTATION
Adaptation of model parameters of a rail model at measured rail compliances
[ILR-MITT-274(1992)] p 1831 N94-21153
RAIN
Modeling of interactions between biosphere and atmosphere on the global scale
[NASA-CR-193423] p 1837 N94-20205
Schools of the Pacific rainfall climate experiment
p 1881 N94-20699
A laboratory system for the investigation of rain fade compensation techniques for Ka-band satellites
[NASA-CR-191200] p 1762 N94-21566
Presenting the Rain-Sea Interaction Facility
[NASA-RP-1322] p 1884 N94-21628
Evolution of the global water cycle on Mars: The geological evidence p 2142 N94-21660
The evolution of the early Martian climate and the initial emplacement of crustal H2O p 2143 N94-21665
Observations of multi-layered clouds using K-band radar p 1874 N94-22311
RAIN FORESTS
Change detection on land use and rainforest cover at Paragominas region, Brazilian Amazon
p 1838 N94-20957
Evaluation of C-band SAR data from SAREX 1992: Tapajos study site p 1839 N94-20964
RAINDROPS
A laboratory system for the investigation of rain fade compensation techniques for Ka-band satellites
[NASA-CR-191200] p 1762 N94-21566
RAMAN SPECTRA
Femtosecond Raman-induced Kerr effect study of polar solvent dynamics: Amides
[DE93-017563] p 1678 N94-19924
The multicomponent lineshape of the anharmonic A(1)(TO) phonon in PbTiO3
[DE93-018995] p 1970 N94-19971
Phonons and metastability in compressed nitrogen
[DE93-019913] p 2016 N94-20318
Examinations of a thallium atomic vapor filter for a Raman temperature lidar
[GKSS-92/E/13] p 1857 N94-21044
Effects of stimulated Raman scattering on light beam properties during high-power laser beam long-path propagation
[AD-A273109] p 1818 N94-21509
Parametric instabilities in picosecond time scales
[DE94-000384] p 1966 N94-21958
RAMAN SPECTROSCOPY
Growth, characterization and device development in monocrystalline diamond films
[AD-A273097] p 2028 N94-21506
Materials Science and Engineering
[DE93-040497] p 1675 N94-21530
Laser Raman and x ray scattering studies of corrosion films on metals
[DE93-040243] p 1692 N94-21558
Femtosecond dynamics in hydrogen-bonded solvents
[DE93-019937] p 1683 N94-21842
RANDOM ACCESS
M-dimensional computer memory with M-1 dimensional hyperplane access
[AD-D015960] p 1898 N94-20357
Spread spectrum random access networks
[AD-A272280] p 1737 N94-20585
RANDOM ACCESS MEMORY
Proceedings of the 8th International Symposium on Applications of Ferroelectrics
[AD-A270679] p 1749 N94-20012
M-dimensional computer memory with M-1 dimensional hyperplane access
[AD-D015960] p 1898 N94-20357
Light update notification mechanism for shared data structures
[AD-D015967] p 2043 N94-21276
A DRAM compiler algorithm for high performance VLSI embedded memories p 1767 N94-21729
RANDOM NOISE
Noise filtering using multilayer feedforward neural network p 1770 N94-22104
Applications of a two-dimensional nonlinear filters to image restoration p 1789 N94-22225
RANDOM NUMBERS
Stochastic optimization by simulation: Convergence proofs for the G1/G/1 queue in steady-state
[AD-A271141] p 1962 N94-19999
On a proposed symbolic dynamics for the Henon map
[AD-A272514] p 1955 N94-21359
RANDOM VARIABLES
A methodology for quantifying uncertainty in models
[DE93-040154] p 1916 N94-21747
RANGE FINDERS
CMU very fast range-imaging system
[AD-A272057] p 1761 N94-21282
RANGEFINDING
Development of a lidar for integration with the Naval Postgraduate School Infrared Search and Target Designation (NPS-IRSTD) system
[AD-A271847] p 1817 N94-20611
CMU very fast range-imaging system
[AD-A272057] p 1761 N94-21282
Estimability of polar motion using range observations to satellites
[PB93-219319] p 1842 N94-22265
A feasibility study of a parallax-based passive missile approach warning system
[ISBN-0-315-60640-1] p 1743 N94-22410
RAPID QUENCHING (METALLURGY)
Investigation of cracking and erratic behavior of the uranium-titanium alloy
[DE93-018591] p 1688 N94-19957
RARE EARTH COMPOUNDS
Microstructural modeling and toughening of Si3N4 ceramics for high temperature engine applications
[AD-A272897] p 1704 N94-21197
RARE EARTH ELEMENTS
Rare Earth elements in individual minerals in Shergottites p 1686 N94-20652
The formation of FeO-rich pyroxene and enstatite in unequilibrated enstatite chondrites: A petrologic-trace element (SIMS) study p 2086 N94-20666
LREE variability in CM matrices: Another look at meteorite compaction ages p 2086 N94-20884
Static ultra-high pressure study of lanthanide and actinide metals using a diamond-anvil cell
[DE94-000369] p 1693 N94-21656
Theoretical studies of structural phase transitions in actinide metals
[DE94-000796] p 1696 N94-22388
RARE GASES
Design aspects and parametric characterisation of a neutral rare gas laser
[AD-A271100] p 1814 N94-19850
Stability of the face-centered-cubic phase of heavy rare gas solids
[DE93-019949] p 1679 N94-20319
On demand, non-halon, fire extinguishing systems
[AD-D015957] p 1714 N94-20355
Dating native gold by noble gas analyses
p 1684 N94-20652
A carbon and nitrogen isotope study of carbonaceous vein material in ureilite meteorites p 2083 N94-20726

The chondrite Mihonoseki: New observed fall p 2083 N94-20764
Are the C delta light nitrogen and noble gases located in the same carrier? p 2085 N94-20846
A long-term change of the AR/KR/XE fractionation in the solar corpuscular radiation p 2136 N94-20875
Evolution of the Martian atmosphere p 2146 N94-21680
The laser and its applications on environment and biotechnology research [DE94-000376] p 1820 N94-21957

RASTER SCANNING
Three dimensional ultrasonic imaging [DE93-040549] p 1968 N94-22003

RATIOMETERS
The laser and its applications on environment and biotechnology research [DE94-000376] p 1820 N94-21957

RATIONAL FUNCTIONS
Rational trigonometric approximations using Fourier series partial sums [NASA-CR-191535] p 1959 N94-21568
Column reduced rational matrix functions with given null-pole data in the complex plane [PB93-220531] p 1960 N94-22099

RATS
Relationship of area postrema to three putative measures of motion sickness p 1865 N94-21900
Conditioned taste aversion induced by motion is prevented by selective vagotomy in the rat p 1887 N94-21908
Experimental studies of gastric dysfunction in motion sickness: The effect of gastric and vestibular stimulation on the vagal and splanchnic gastric efferents p 1888 N94-21911
Role of the area postrema in three putative measures of motion sickness in the rat p 1888 N94-21912

RAWINSONDES
Overview of microphysical and state parameter measurements from FIRE 2 p 1871 N94-22293
Cloud fields derived from satellite and surface data during FIRE cirrus phase 2 p 1872 N94-22302
Breaking Kelvin-Helmholtz waves and cloud-top entrainment as revealed by K-band Doppler radar p 1874 N94-22310
Meteorological analysis of the December 4-6 FIRE cirrus-2 case p 1875 N94-22314
Meteorological analysis of the November 25 FIRE cirrus-2 case: A well-defined ridge-crest cirrus system over Oklahoma p 1877 N94-22328

RAY TRACING
A general purpose ionospheric ray tracing procedure [AD-A271058] p 1854 N94-19860
Feedback controlled optics with wavefront compensation [NASA-CASE-NPO-18194-1-CU] p 1985 N94-20305
Validation of the design of a high resolution all-reflection Michelson interferometer for atmospheric spectroscopy [AD-A272505] p 1987 N94-21410
A data distributed, parallel algorithm for ray-traced volume rendering [DE93-040150] p 1935 N94-21622
Telescope image modelling software in STSDAS p 1926 N94-22483

RAYLEIGH DISTRIBUTION
Ocean wave height transformation model using surface roller theory [AD-A272610] p 1883 N94-21423

RAYLEIGH NUMBER
A parametric study of heat transfer within a planar thermosyphon [DE93-019546] p 1799 N94-20258
Expectations for the Martian core magnetic field p 2120 N94-20792

RAYLEIGH SCATTERING
Development of a technique to determine the morphology and dynamics of agglomerates in chemically reacting flows [AD-A271160] p 1678 N94-20000
New relativistic S-matrix results for scattering – beyond the usual anomalous factors/beyond impulse approximation [DE93-019148] p 1971 N94-20096
Multiple scattering effects on the Linear Depolarization Ratio (LDR) measured during CaPE by a Ka-band air-borne radar p 1728 N94-20446
RADCAL: A narrow-band model for radiation calculations in a combustion environment [PB93-200689] p 1662 N94-21448
Laser guide star adaptive optics: Present and future [DE93-016642] p 1989 N94-21619

RC CIRCUITS
Computation of signal delays in RC networks p 1744 N94-21102

RDX
Evaluation of pre-extraction analytical holding times for nitroaromatic and nitramine explosives in water [AD-A271547] p 1712 N94-20927
Chemistry of the burning surface [AD-A272725] p 1681 N94-21181

REACTING FLOW
Development of a technique to determine the morphology and dynamics of agglomerates in chemically reacting flows [AD-A271160] p 1678 N94-20000
Reaction zone models for vortex simulation of turbulent combustion [AD-A272723] p 1681 N94-21213
Establishing the basis for validated predictions of highly non-equilibrium flows (with 9 attachments) [AD-A272918] p 1802 N94-21220
Instantaneous velocity field imaging instrument for supersonic reacting flows [NASA-CR-191162] p 1809 N94-21607
Comparison of mixing calculations for reacting and non-reacting flows in a cylindrical duct [NASA-TM-106435] p 1649 N94-21758
Simulations of diffusion-reaction equations with implications to turbulent combustion modeling [NASA-CR-191536] p 1804 N94-21861

REACTION KINETICS
Materials processing and manufacturing technologies for Diamond Substrate MultiChip Modules (DSMCM) [AD-A271011] p 2011 N94-19821
Segregation of Si to the surface of Fe-29Ni-17Co alloy [DE93-040053] p 1687 N94-19864
Initiation and modification of reaction by energy addition: Kinetic and transport phenomena [AD-A271315] p 1797 N94-19936
Ab initio potential energy surface for the H + OCS reaction [AD-A270577] p 1698 N94-19947
Encounters of H and D atoms with O2 in water: Relative diffusion and reaction rates [DE93-018587] p 1970 N94-19956
Common Themes and Mechanisms of Epitaxial Growth, volume 312 — Materials Research Society symposium proceedings [AD-A270513] p 2013 N94-19967
High performance heavy alloys by alloying and process control [AD-A271129] p 1689 N94-20019
Laboratory studies of low temperature rate coefficients: The atmospheric chemistry of the outer planets [NASA-CR-193485] p 1972 N94-20130
Computed potential energy surfaces for chemical reactions [NASA-CR-194600] p 1679 N94-20169
Surface science and modeling studies of endothermic fuels catalysis [AD-A272850] p 1712 N94-21192
Reaction zone models for vortex simulation of turbulent combustion [AD-A272723] p 1681 N94-21213
Electronically metastable molecules of high symmetry [AD-A272015] p 1974 N94-21461
A project on parameter identification in reaction kinetics [CWI-NM-R9301] p 1682 N94-21574
Modeling of outgassing and matrix decomposition in carbon-phenolic composites [NASA-CR-194741] p 1676 N94-21743
Simulations of diffusion-reaction equations with implications to turbulent combustion modeling [NASA-CR-191536] p 1804 N94-21861

REACTIVITY
Application of the reactive flux formalism to study water hydrogen bond dynamics [AD-A271824] p 1680 N94-20560
Surface states at the GaAs-germanium nitride interface p 1709 N94-20973
Surface electrochemistry of metals [AD-A272913] p 1691 N94-21245
Melt-spin processing of high (Tc) oxide superconductors [DE94-000696] p 2038 N94-22582

REACTOR CORES
Hydrogen pickup and redistribution in alpha-annealed zircaloy-4 [DE93-018050] p 1689 N94-20182

REACTOR DESIGN
In-situ spectroscopic ellipsometry in molecular beam epitaxy p 2024 N94-21005
Materials processing and manufacturing technologies for diamond substrate multichip modules [AD-A271484] p 2027 N94-21319
SPACE-R Thermionic Space Nuclear Power System: Design and Technology Demonstration Program [DE93-013969] p 1670 N94-21824
A spheromak ignition experiment reusing Mirror Fusion Test Facility (MFTF) equipment [DE94-001856] p 2034 N94-22050

REACTOR MATERIALS
Silver lined ceramic vessel [AD-D015917] p 1700 N94-20057
Hydrogen pickup and redistribution in alpha-annealed zircaloy-4 [DE93-018050] p 1689 N94-20182
Tensile and shear fracture behavior of fiber reinforced plastics at 77K irradiated by various radiation sources [DE93-040280] p 1706 N94-21542
Issues related to mechanical properties of neutron-irradiated ceramics [DE93-040262] p 1707 N94-21560
SPACE-R Thermionic Space Nuclear Power System: Design and Technology Demonstration Program [DE93-013969] p 1670 N94-21824

READ-ONLY MEMORY DEVICES
A high speed CMOS A/D converter p 1767 N94-21726

REAL GASES
An efficient numerical method for three-dimensional hypersonic flow [AD-A272506] p 1637 N94-21411

REAL TIME OPERATION
A software architecture for the construction and management of real-time virtual worlds [AD-A271465] p 1904 N94-20091
Simulated real-time intercomparison of hydrological models [WMO-779] p 1867 N94-21070
An optically-assisted 3-D cellular array machine [AD-A272683] p 1987 N94-21163
A formulation of quantum statistical mechanics based on the Feynman path centroid density 2 dynamical properties [AD-A272698] p 2037 N94-21166
Fault tolerant real-time systems [AD-A272878] p 1899 N94-21195
Real-time fault tolerant computer systems [AD-A272909] p 1899 N94-21230
Developing a space network interface simulator: The NTS approach p 1933 N94-21343
Analysis of multigrid methods on massively parallel computers: Architectural implications p 1938 N94-21468
A VLSI implementation of DCT using pass transistor technology p 1767 N94-21725
A real time correlator architecture using distributed arithmetic principles p 1768 N94-21734
Particle image velocimetry [DE93-040657] p 1804 N94-21748
Optimization and control of a small angle ion source using an adaptive neural network controller [DE93-040063] p 1946 N94-21845
The Board on Earth sciences and resources [DE94-000745] p 1859 N94-22018
A neural network approach to the maximum flow problem p 1783 N94-22183
A Hopfield neural net for discrete Fourier transform calculation p 1783 N94-22184
A real-time infrared image processing testbed p 1790 N94-22227
Second Annual Conference on Astronomical Data Analysis Software and Systems. Abstracts [NASA-TM-108245] p 2057 N94-22438
How to handle 6GBytes a night and not get swamped p 2058 N94-22444
VETA x ray data acquisition and control system p 2047 N94-22455
The data acquisition system for the Anglo-Australian Observatory 2-degree field project p 2048 N94-22529
The VLBA correlator: Real-time in the distributed era p 2049 N94-22547
Solar full-disk magnetic field image receiving system and observation software p 2079 N94-22552

RECEIVERS
An investigation into the integration of meter-level range and millimeter-level phase data using a multimode stimulation for optimal filter estimation software package [AD-A267955] p 1751 N94-20483
Spread spectrum random access networks [AD-A272280] p 1737 N94-20585
QPPM receiver for free-space laser communications [NASA-TM-106424] p 1741 N94-21567
Transient acoustic wave modeling: Higher-order WKBJ asymptotics and symbolical manipulation (revised) [PB93-215432] p 1969 N94-22262
Solar full-disk magnetic field image receiving system and observation software p 2079 N94-22552

RECEPTION DIVERSITY
Variable-permittivity linear inverse problem for the H(sub z)-polarized case p 1719 N94-20408

RECOGNITION
On geometric and algebraic aspects of 3D affine and projective structures from perspective 2D views
[AD-A270520] p 1983 N94-19968
Sensor integration and data fusion for object localization in robotic workcells p 1774 N94-22130
RECORDS MANAGEMENT
Project Records Information System (PRIS): User's manual
[DE94-001548] p 2045 N94-22047
RECRYSTALLIZATION
Fragments of ancient lunar crust: Ferroan noritic anorthosites from the descartes region of the Moon p 2096 N94-20660
Post-igneous redistribution of components in eucrites p 1685 N94-20684
Fine resolution chronology based on initial Sr-87/Sr-86
[CONTRIB-5230(794)] p 1686 N94-20794
RECTANGLES
Operational equations for the five-point rectangle
[DE94-000366] p 1959 N94-21655
RECTANGULAR PLATES
High-frequency techniques for RCS prediction of plate geometries p 1717 N94-20270
RECTANGULAR WAVEGUIDES
Formulation for numerical solution of radiation and transmission from arbitrary apertures p 1745 N94-22140
RECURSIVE FUNCTIONS
Efficient and correct translation of strict applicative programming languages
[ETN-93-95056] p 1903 N94-20020
Cascaded recursive artificial neural networks p 1780 N94-22167
Experiments with recursive estimation in astronomical image processing p 2047 N94-22457
RECYCLING
Current status of environmental, health, and safety issues of nickel metal-hydride batteries for electric vehicles
[DE93-017079] p 1748 N94-19902
Resonantly pumped, erbium-doped, GSGG, 2.8 micron, solid state laser with energy recycling and high slope efficiency
[AD-D015920] p 1815 N94-20060
RED SHIFT
Radio galaxies and their environment
[DE93-040851] p 2150 N94-22397
Visualizing the universe, part 2 p 2063 N94-22472
REDUCTION (CHEMISTRY)
Catalytic hydrogenation of carbon monoxide
[DE94-000881] p 1678 N94-20103
REDUNDANCY
Real-time fault tolerant computer systems
[AD-A272909] p 1899 N94-21230
Links between N-modular redundancy and the theory of error-correcting codes p 1765 N94-21713
REED-SOLOMON CODES
Arithmetic in large GF(2(exp n)) p 1760 N94-21131
The Composite Analytic and Simulation Package or RFI (CASPR) on a coded channel p 1744 N94-21339
Advanced coding and modulation schemes for TDRSS p 1744 N94-21350
Schematic driven layout of Reed Solomon encoders p 1766 N94-21722
Performance of RS codes in lognormally shadowed Rician channels p 1792 N94-22244
REENTRY SHIELDING
Compilation of reinforced carbon-carbon transatlantic abort landing arc jet test results
[NASA-TM-104778] p 1676 N94-21834
REENTRY TRAJECTORIES
Effects of thrust vector control on the performance of the aerobang orbital plane change maneuver
[AD-A272532] p 1646 N94-21418
REENTRY VEHICLES
Tetrahedral lander
[NASA-CASE-MSC-22082-1] p 1658 N94-20590
Reentry vehicle adaptive telemetry
[DE94-001168] p 1656 N94-21852
REFERENCE SYSTEMS
The Keck keyword layer p 1925 N94-22460
REFLECTANCE
High efficiency epitaxial optical reflector solar cells
[DE93-017115] p 1845 N94-19805
An expert system shell for inferring vegetation characteristics
[NASA-CR-189318] p 1837 N94-20284
A theoretical and numerical study of polarimetric scattering and emission from random rough surfaces with anisotropic directional spectrum p 1730 N94-20454
The coherent backscattering opposition effect p 1991 N94-20646
The role of CO2 in weathering reactions and the presence of S2 on Venus: Implications for the pyrite stability field p 2122 N94-20799
The stability of oxyamphiboles: Existence of Ferric-bearing minerals under the reducing conditions on the surface of Venus p 2122 N94-20800
A new Antarctic meteorite with chromite, orthopyroxene and metal with reference to a formation model of S asteroids p 2084 N94-20813
Objective determination of image end-members in spectral mixture analysis p 1686 N94-20831
Diffuse reflectance spectra of orthopyroxene, olivine, and plagioclase as a function of composition and structure p 2087 N94-20906
X ray reflection masks: Manufacturing, characterization and first tests
[BONN-IR-92-31] p 1986 N94-21043
Long-range laser imaging
[AD-A273020] p 1817 N94-21253
Forecasting technique of variations of the optical absorptivity of thermal control coatings under different simultaneous radiations p 1664 N94-21399
Role of surface characteristics in urban meteorology and air quality
[DE93-040929] p 1851 N94-21740
The optical constants and spectral specular reflectivity of Highly Oriented Pyrolytic Graphite (HOPG)
[DE93-040546] p 1709 N94-21970
X ray characterization of a three-element condenser system for soft x ray projection lithography
[DE93-019916] p 1990 N94-21985
A motion extraction method for synthetic aperture radars
[DLR-FB-92-31] p 1742 N94-22279
Bi-directional reflectance and other radiation parameters of cirrus from ER-2 observations p 1871 N94-22296
Estimation of cirrus cloud particle fallspeeds from vertically pointing Doppler radar p 1879 N94-22333
Surface-induced brightness temperature variations and their effects on detecting thin cirrus clouds using IR emission channels in the 8-12 micrometer region p 1880 N94-22341
Remote sensing estimates of cirrus particle size for tropical and midlatitude cirrus: Hexagonal crystals and ice spheres p 1880 N94-22342
REFLECTED WAVES
Observation of reflected waves on the SABRE positive polarity inductive adder MITL
[DE93-019413] p 1960 N94-20295
System and method for cancelling expansion waves in a wave rotor
[NASA-CASE-LEW-15218-1] p 1801 N94-20588
The coherent backscattering opposition effect p 1991 N94-20646
REFLECTING TELESCOPES
Holographic optical elements correcting the off-axis aberrations of a parabolic mirror
[ISBN-0-315-57581-6] p 1990 N94-22411
REFLECTION
Modifications to the three-component classification algorithm for SAR data p 1719 N94-20410
The Brewster angle effect in SAR polarimetry p 1731 N94-20456
Dynamics of surface thermal expansion and diffusivity using two-color reflection transient gratings
[DE93-040547] p 1990 N94-22002
REFLECTOMETERS
Center for X-Ray Optics, 1992
[DE94-000726] p 1990 N94-21868
REFLECTOR ANTENNAS
Multi-band reflector antenna with double-ring element frequency selective subreflector p 1728 N94-20447
Mobile terminal antennas for helicopters p 1731 N94-20458
A compact, portable EHF/SHF antenna for advanced SCAMP
[AD-A272614] p 1739 N94-21211
Performance of a simple circular polarization selective surface p 1746 N94-22198
REFLECTORS
An improved patch for radiative coolers
[NASA-CASE-GSC-13503-1] p 1822 N94-20127
Goniospectrometric properties of a white standard p 1684 N94-20664
X ray characterization of a three-element condenser system for soft x ray projection lithography
[DE93-019916] p 1990 N94-21985
REFLEXES
Area postrema ablations in cats: Evidence for separate neural routes for motion- and xylazine-induced CTA and emesis p 1887 N94-21906
Role of the area postrema in three putative measures of motion sickness in the rat p 1888 N94-21912
REFRACTION
Synchrotron x ray diffraction analysis of photorefractive crystals and their gratings
[AD-A271176] p 2015 N94-20213
Optical fibers and Fluorosensors having improved power efficiency and methods of producing same
[NASA-CASE-LAR-14525-1-CU] p 1986 N94-20378
REFRACTIVITY
Refractive index structure in the lower atmosphere
[AD-A270935] p 1854 N94-19899
Variable wavelength, variable angle ellipsometry including a sensitivities correlation test p 1710 N94-20978
Superlattice optical properties measured by variable angle spectroscopic ellipsometry p 2022 N94-20993
Refractive index behaviour of phosphorus-doped planar silica waveguides, appendix 7 p 1989 N94-21601
Precision prism coupling setup applied to measure planar silica films on silicon, appendix 9 p 1989 N94-21603
The optical constants and spectral specular reflectivity of Highly Oriented Pyrolytic Graphite (HOPG)
[DE93-040546] p 1709 N94-21970
Extended range modified gradient technique for profile inversion (extended version of report Et/Em-1992-8)
[PB93-215242] p 1742 N94-22346
REFRACTORIES
Tambo Quemado: Extraordinary concentrations of REE and refractory trace elements caused by artificial heating p 1684 N94-20657
REFRACTORY COATINGS
Performance of carbon-based hot frit substrates
[DE94-000509] p 1676 N94-21754
Compilation of reinforced carbon-carbon transatlantic abort landing arc jet test results
[NASA-TM-104778] p 1676 N94-21834
REFRACTORY MATERIALS
Phthalonitrile prepolymer as high temperature sizing material for composite fibers
[AD-D015912] p 1672 N94-20010
Development of improved processing and evaluation methods for high reliability structural ceramics for advanced heat engine applications, phase 1
[DE93-040528] p 1702 N94-20481
Petrography and origin of refractory inclusions from the Murray and Murchison C2 chondrites p 2084 N94-20770
Trace element compositions of spinel-rich refractory inclusions from the Murchison meteorite p 2086 N94-20897
Polyimide-based electrooptic materials
[DE93-019416] p 1706 N94-21526
REFRACTORY METAL ALLOYS
Strengthening and toughening in refractory metal alloys
[DE93-019942] p 1695 N94-21966
REFRACTORY METALS
Effects of processing history on the creep strength of Nb-1Zr
[DE93-015905] p 1689 N94-20093
REFRIGERANTS
Absorption heat pump for space applications
[NASA-CR-194693] p 1845 N94-20066
Alternative refrigerants and refrigeration cycles for domestic refrigerators
[DE93-040481] p 1714 N94-20099
EHD enhancement of pool and in-tube boiling of alternate refrigerants
[DE94-000787] p 1798 N94-20101
The laser and its applications on environment and biotechnology research
[DE94-000376] p 1820 N94-21957
REFRIGERATING
Alternative refrigerants and refrigeration cycles for domestic refrigerators
[DE93-040481] p 1714 N94-20099
EHD enhancement of pool and in-tube boiling of alternate refrigerants
[DE94-000787] p 1798 N94-20101
A novel scheme to handle highly pulsed loads with a standard helium refrigerator
[DE93-019617] p 1799 N94-20263
REFRIGERATORS
Alternative refrigerants and refrigeration cycles for domestic refrigerators
[DE93-040481] p 1714 N94-20099
A novel scheme to handle highly pulsed loads with a standard helium refrigerator
[DE93-019617] p 1799 N94-20263
REGENERATION (ENGINEERING)
Performance calculations and research direction for a water enhanced regenerative gas turbine cycle
[DE93-019666] p 1826 N94-21983
REGENERATORS
A low cost alternative to high performance PCM bit synchronizers p 1813 N94-21347

Performance calculations and research direction for a water enhanced regenerative gas turbine cycle
[DE93-019866] p 1826 N94-21983

REGIONAL PLANNING

The 7th Brazilian Remote Sensing Symposium, volume 1 p 1838 N94-20953

Application of SPOT to GIS/LIS in land capability evaluation for regional planning of JAICO semi-arid region of Piaui, Brazil p 1838 N94-20955

REGISTERS (COMPUTERS)

A 20 MHz CMOS reorder buffer for a superscalar microprocessor p 1764 N94-21700

REGOLITH

The distribution of ground ice on Mars p 2090 N94-20394

The Erevan howardite: Petrology of glassy clasts and mineral chemistry p 1684 N94-20640

The coherent backscattering opposition effect p 1991 N94-20646

Characterization of Minnesota lunar simulant for plant growth p 1897 N94-20665

Abundance and composition of solar KR in the H3-H6 chondrite ACFER111 p 1684 N94-20676

Evaluation of lunar rocks and soils for resource utilization: Detailed image analysis of raw materials and beneficiated products p 2126 N94-20820

Regolith breccia consisting of H and LL chondrite mixture p 2080 N94-20892

Oxidation of dissolved iron under warmer, wetter conditions on Mars: Transitions to present-day arid environments p 2143 N94-21663

Early Mars: The inextricable link between internal and external influences on valley network formation p 2146 N94-21681

Determination of Martian soil mineralogy and water content using the Thermal Analyzer for Planetary Soils (TAPS) p 1812 N94-22433

REGRESSION ANALYSIS

Statistical analysis of a reciprocal translocations data base
[RR-900-I] p 1963 N94-20165

Thermal diffusivity measurements by photothermal laser beam deflection (PTD): Data analysis using the Levenberg-Marquardt algorithm p 1820 N94-21006

On estimation and testing in Poisson regression models with over-dispersion
[MEMO-1083] p 1963 N94-21076

An evaluation of artificial neural network modeling for manpower analysis
[AD-A273001] p 1945 N94-21269

The European Southern Observatory-MIDAS table file system p 2048 N94-22518

REGULARITY

Large deviations behavior of counting processes and their inverses
[AD-A271142] p 1939 N94-19909

REGULATORS

Optimal control of the tip of a flexible arm p 1794 N94-22256

REINFORCED PLASTICS

A study of the structural stability of an unbalanced sandwich composite configuration
[AD-A272496] p 1675 N94-21431

Tensile and shear fracture behavior of fiber reinforced plastics at 77K irradiated by various radiation sources
[DE93-040280] p 1706 N94-21542

Tensile strength of fiber reinforced plastics at 77K irradiated by various radiation sources
[DE93-040826] p 1709 N94-22008

REINFORCEMENT (STRUCTURES)

Thermally activated retainer means utilizing shape memory alloy
[NASA-CASE-MSC-21793-1] p 1654 N94-20304

REINFORCING FIBERS

Biotechnology and composite materials
[AD-A264278] p 1673 N94-20327

Fiber reinforced thermosetting resin composition with coated fibers for improved toughness
[CA-PATENT-1,306,320] p 1674 N94-21040

Tensile and shear fracture behavior of fiber reinforced plastics at 77K irradiated by various radiation sources
[DE93-040280] p 1706 N94-21542

Tensile strength of fiber reinforced plastics at 77K irradiated by various radiation sources
[DE93-040826] p 1709 N94-22008

REINFORCING MATERIALS

Strength and toughness improvement of silicide intermetallics by nanophase and microphase reinforcements
[AD-A272914] p 1692 N94-21320

RELATIVISTIC EFFECTS

The quantum structure of matter grand challenge project: Large-scale 3-D solutions in relativistic quantum dynamics
[DE94-000328] p 1960 N94-21955

RELATIVISTIC ELECTRON BEAMS

The angular velocity spread of REB induced by magnetic field discontinuity
[IPPCZ-331] p 1996 N94-21573

Acceleration of solar-flare particles as viewed from their chemical composition p 2006 N94-22672

RELATIVISTIC PARTICLES

A field-based technique for the longitudinal profiling of ultrarelativistic electron or positron bunches down to lengths of less than or equal to 10 microns
[DE93-040954] p 1978 N94-19873

Relativistic shock spectra: A prediction
[NASA-CR-194764] p 2150 N94-21782

On the correspondence limit of relativistic quantum mechanics
[DE93-040939] p 2038 N94-21971

VHE gamma ray generation by radio pulsars p 2007 N94-22680

RELATIVISTIC PLASMAS

General relativistic winds in a black hole magnetosphere p 2002 N94-22644

Relativistically expanding pair plasmas as bursting sources of cosmic gamma rays p 2003 N94-22646

Langmuir microstructures and pulsar radio emission p 2007 N94-22678

Asymptotic structure of magnetically driven MHD wind p 2008 N94-22682

RELATIVISTIC THEORY

Relativistic calculations of the superheavy nucleus (sup 298)114
[KVI-969] p 1971 N94-20119

Relativistic shock spectra: A prediction
[NASA-CR-194764] p 2150 N94-21782

On the correspondence limit of relativistic quantum mechanics
[DE93-040939] p 2038 N94-21971

RELATIVISTIC VELOCITY

Restoring locality with faster-than-light velocities
[DE93-040926] p 2038 N94-22010

RELAXATION METHOD (MATHEMATICS)

Optimal convolution SOR acceleration of waveform relaxation with application to semiconductor device simulation p 1922 N94-21475

A multigrid method for steady Euler equations on unstructured adaptive grids p 1957 N94-21476

Multigrid solution of the Navier-Stokes equations on highly stretched grids with defect correction p 1806 N94-21481

Mapping robust parallel multigrid algorithms to scalable memory architectures p 1922 N94-21483

Parallelizing a highly vectorized multigrid code with zebra relaxation
[CWI-NM-R9225] p 1935 N94-21610

Numerical multigrid software (MGD5M): A parallel multigrid code with a twisted ILLU-relaxation
[CWI-NM-R9226] p 1916 N94-21611

RELIABILITY

Development and testing of a reliability performance index for modular robotic systems
[AD-A271901] p 1942 N94-20488

Lithium batteries: Future batteries p 1752 N94-20630

Army aircraft fire-detection systems operation and reliability
[AD-A271327] p 1641 N94-20912

Automated synthesis and verification of configurable DRAM blocks for ASIC's p 1759 N94-21123

N parallel queueing systems with server breakdown and repair
[CWI-BS-R9236] p 1944 N94-21232

RELIABILITY ANALYSIS

Handbook. Volume 3: Digital systems validation book plan
[DOT/FAA/CT-93/16-VOL-3] p 1647 N94-20053

Development and testing of a reliability performance index for modular robotic systems
[AD-A271901] p 1942 N94-20488

Trends in software reliability modeling p 1788 N94-22214

Recent advances in computational structural reliability analysis methods p 1828 N94-22616

Time-dependent reliability analysis of ceramic engine components p 1828 N94-22619

RELIABILITY ENGINEERING

Handbook. Volume 3: Digital systems validation book plan
[DOT/FAA/CT-93/16-VOL-3] p 1647 N94-20053

Intervention strategies for the management of human error
[NASA-CR-4547] p 1642 N94-22373

RELIEF MAPS

Topographic mapping using a monopulse SAR system p 1721 N94-20417

Topographic slope from the SAR interferometric phase gradient p 1731 N94-20459

Chronology, eruption duration, and atmospheric contribution of Apollinaris Patera, Mars p 2108 N94-20720

Linear structures on the small inner satellites of Saturn p 2121 N94-20797

Detecting topographical regions in digital terrain maps
[AD-A272889] p 1841 N94-21453

REMANENCE

Reverse polarity magnetized melt rocks from the Chicxulub impact structure, Yucatan Peninsula, Mexico p 1863 N94-20843

REMOTE CONTROL

Digital wireless control system
[DE93-040211] p 1714 N94-19946

Teleoperation with virtual force feedback
[DE93-019406] p 1942 N94-20293

Control vane guidance for a ducted-fan unmanned air vehicle
[AD-A271957] p 1645 N94-20561

Automating the control of robotic systems in unstructured environments
[DE93-040753] p 1946 N94-21929

REMOTE HANDLING

Automating the control of robotic systems in unstructured environments
[DE93-040753] p 1946 N94-21929

REMOTE SENSING

Radar backscatter measurements from simulated sea ice during CRRELEX 1990
[AD-A271034] p 1715 N94-19823

Ionospheric tomography using the FORTE satellite
[DE93-018545] p 1854 N94-19955

Global and regional comparative performance of linear and nonlinear satellite multichannel sea surface temperature algorithms
[AD-A270475] p 1837 N94-20028

Remote sounding of tropospheric minor constituents
[NASA-CR-194265] p 1855 N94-20132

Dynamics Explorer 2: Continued FPI and NACS instrument data analysis and associated scientific activity at the University of Michigan
[NASA-CR-194689] p 1657 N94-20173

The future of remote sensing from space: Civilian satellite systems and applications
[OTA-ISC-558] p 1837 N94-20209

An expert system shell for inferring vegetation characteristics
[NASA-CR-189318] p 1837 N94-20284

Milankovitch insulation forcing and cyclic formation of large-scale glacial, fluvial, and eolian landforms in central Alaska p 2089 N94-20386

Comparison of remote sensing measurements with a two-scale polarimetric emission and scattering model for sea surfaces p 1721 N94-20415

Integrated display of multi-sensor geophysical and electromagnetic flight data p 1721 N94-20418

Advances in spaceborne radar remote sensing p 1723 N94-20424

Observation of pressure ridges in SAR images of sea ice: Scattering theory and comparison with observations p 1723 N94-20427

On evaluating the accuracy of SAR sea-ice classification using multifrequency polarimetric AIRSAR data p 1724 N94-20428

Application of Cloude's target decomposition theorem to polarimetric imaging radar data p 1724 N94-20429

Direction angle sensitivity of agricultural field backscatter with AIRSAR data p 1724 N94-20430

Studies of Greenland using the SEASAT scatterometer p 1725 N94-20433

Radar backscattering from snow facies of the Greenland ice sheet: Results from the AIRSAR 1991 campaign p 1725 N94-20434

C-band radar backscatter of sea ice in the Weddell Sea, Antarctica during the austral winter of 1992 p 1725 N94-20435

Near grazing scattering from non-Gaussian ocean surfaces p 1726 N94-20438

Rough surface scattering from moving ocean surfaces as an indicator of scattering mechanisms p 1726 N94-20439

Polarimetric thermal emission from rough surfaces p 1727 N94-20441

Simulated retrieval of land surface parameters using multichannel satellite microwave radiometry p 1727 N94-20443

Symmetry in polarimetric remote sensing p 1729 N94-20449

Mapping of taiga forest units using AIRSAR data and/or optical data, and retrieval of forest parameters p 1729 N94-20452

A theoretical and numerical study of polarimetric scattering and emission from random rough surfaces with anisotropic directional spectrum p 1730 N94-20454

Application of neural network to remote sensing of soil moisture using theoretical polarimetric backscattering coefficients p 1730 N94-20455
Four-dimensional remote sensing of the marine boundary layer with a digital beamforming radar wind profiler
[AD-A270627] p 1882 N94-20564
The application of spaceborne synthetic aperture radar in the maritime environment
[DRA-TM(AWE)-91013] p 1737 N94-20596
Goniospectrometric properties of a white standard p 1684 N94-20664
Visible-infrared properties of controlled laboratory soils p 1685 N94-20689
Thermal infrared remote sensing and Kirchhoff's law: 1. Laboratory measurements p 1685 N94-20733
Convex set and linear mixing model p 1844 N94-20888
The 7th Brazilian Remote Sensing Symposium, volume 1 p 1838 N94-20953
The use of satellite images in Amazonian archaeology: A case study in the Upper Rio Negro Basin p 1838 N94-20954
Application of SPOT to GIS/LIS in land capability evaluation for regional planning of JAICO semi-arid region of Piaui, Brazil p 1838 N94-20955
The 7th Brazilian Remote Sensing Symposium, volume 2 p 1838 N94-20956
The 7th Brazilian Remote Sensing Symposium, volume 3 p 1839 N94-20960
Sunphotometer network for monitoring aerosol properties in the Brazilian Amazon p 1839 N94-20961
On the origin and evolution of circular forms observed in remote sensing images of the Rio de Janeiro State, Brazil p 1839 N94-20963
Evaluation of C-band SAR data from SAREX 1992: Tapajos study site p 1839 N94-20964
The 7th Brazilian Remote Sensing Symposium, volume4 p 1840 N94-20965
SIMA: An integrated environmental monitoring system p 1840 N94-20967
The development of remote sensing in Brazil and Canada: Comparative case studies p 1840 N94-20968
Rapid estimates of crop production using remote sensing: European experience p 1840 N94-20969
Using NDVI/AVHRR data for crop monitoring and forecasting in South Italy p 1841 N94-20970
Mobility of salt domes
[BCRS-92-08] p 1857 N94-21016
Ocean mapping using satellite radar altimetry
[ETN-93-93470] p 1841 N94-21017
Snow cover measurements and areal assessment of precipitation and soil moisture
[WMO-749] p 1841 N94-21068
Remote sensing for hydrology progress and prospects
[WMO-773] p 1841 N94-21069
Obtaining surface optical properties from space-based lidar systems
[AD-A272831] p 1987 N94-21172
Data format standards for civilian remote sensing satellites
[PB93-192920] p 1841 N94-21446
Earth observing scanning polarimeter p 1844 N94-21645
Orbit and sampling requirements: TRMM experience p 1870 N94-21647
Multiorder etalon sounder (MOES) development and test for balloon experiment
[NASA-CR-194730] p 1859 N94-22026
Remote sensing of multilevel clouds during FIRE IFO 2 p 1844 N94-22303
Microphysical properties of the November 26 cirrus cloud retrieved by Doppler radar/IR radiometer technique p 1873 N94-22304
CIMSS FIRE research activities p 1873 N94-22307
Atmospheric parameterization schemes for satellite cloud property retrieval during FIRE IFO 2 p 1874 N94-22312
Cloud boundaries during FIRE 2 p 1876 N94-22318
Ground-based passive remote sensing during FIRE IFO 2 p 1844 N94-22319
Surface-induced brightness temperature variations and their effects on detecting thin cirrus clouds using IR emission channels in the 8-12 micrometer region p 1880 N94-22341
Remote sensing estimates of cirrus particle size for tropical and midlatitude cirrus: Hexagonal crystals and ice spheres p 1880 N94-22342
Studies in remotely sensed geophysical parameter retrieval and analysis
[NASA-CR-194768] p 1842 N94-22374
Chromaticity analysis of LANDSAT multispectral scanner and thematic mapper imagery of Chilko Lake, British Columbia, using a theoretical optical water quality model
[ISBN-0-315-63832-X] p 1843 N94-22422

REMOTE SENSORS
Advances in spaceborne radar remote sensing p 1723 N94-20424
Predicting LANDSAT MSS endmember signatures from corresponding higher resolution TM fraction images p 1839 N94-20962
Observations of multi-layered clouds using K-band radar p 1874 N94-22311

REMOTELY PILOTED VEHICLES
Control vane guidance for a ducted-fan unmanned air vehicle
[AD-A271957] p 1645 N94-20561
Design, fabrication and test of a vertical attitude takeoff and landing unmanned air vehicle
[AD-A273003] p 1646 N94-21283
Low-cost Unmanned Air Vehicle (UAV) for oceanographic research
[AD-A273103] p 1646 N94-21507
Data link development for the archytas vertical takeoff and landing transitional flight unmanned aerial vehicle
[AD-A272499] p 1646 N94-21548

REMOVAL
Focused-ion-beam material removal rates
[AD-A270852] p 1713 N94-19834

REPORTS
Listing of approved recurring information requirements
[AD-A271673] p 2042 N94-20919

REPRESENTATIONS
Representation of spoken words in a self-organizing neural net p 1940 N94-20243
Representation of idioms in connectionist models p 1940 N94-20247
A connectionist representation for phrase structures p 1941 N94-20249
An exploration of clause boundary effects in SRN representations p 1937 N94-20253

REPUBLIC OF SOUTH AFRICA
The age of the Pretoria Saltpan impact crater, South Africa p 1863 N94-20798

REQUIREMENTS
Reference manual for a Requirements Specification Language (RSL), version 2.0
[NASA-CR-191460] p 1898 N94-20039
Listing of approved recurring information requirements
[AD-A271673] p 2042 N94-20919

RESEARCH AIRCRAFT
Experiments with a fluid deicing system for cleaning laminar wings p 1640 N94-22601

RESEARCH AND DEVELOPMENT
NASA's Education Program
[NASA-EP-297] p 2038 N94-20129
Documents on the history of aeronautical and space research in Germany, 1900 - 1970
[DLR-MITT-92-08] p 2152 N94-20543
High energy physics program at Texas A/M University
[DE93-041089] p 1960 N94-20933
Aerospace: Facts and figures, 1992-1993
[AD-A272571] p 1635 N94-21419
Index to 1992 NASA Tech Briefs, volume 16, numbers 1-12
[NASA-TM-109377] p 2053 N94-21736
Index to 1991 NASA Tech Briefs, volume 15, numbers 1-12
[NASA-TM-109376] p 2053 N94-21737
Cumulative index to NASA Tech Briefs, 1986-1990, volumes 10-14
[NASA-TM-109378] p 2054 N94-21738
Application development in a PC/LAN environment p 1923 N94-22067
NASA Propulsion Engineering Research Center, volume 1
[NASA-CR-194721-VOL-1] p 1671 N94-22428

RESEARCH FACILITIES
Activities of National Inst. for Aviation Research
[NIAR-93-16] p 2151 N94-20150
Center for neural engineering
[AD-A271164] p 1890 N94-20185
National Synchrotron Light Source user's manual: Guide to the VUV and x ray beamlines
[DE93-019564] p 2015 N94-20260
The National High Magnetic Field Laboratory, a user facility in support of research in high magnetic fields
[DE93-040145] p 1714 N94-20278
Hypervelocity impact studies at CEG: Experimental and numerical capabilities p 1684 N94-21397
A FET-switched induction accelerator cell
[DE93-019604] p 1789 N94-21838
Chemistry and materials science
[DE94-001449] p 2152 N94-21858

RESEARCH MANAGEMENT
Neural network studies
[AD-A271593] p 1943 N94-20947

RESERVOIRS
High-resolution numerical methods for compressible multi-phase flow in hierarchical porous media
[DE94-000740] p 1799 N94-20351
Current situation in developing petroleum substituting energy (the United Kingdom)
[DE94-714897] p 1713 N94-22091

RESIDUAL GAS
Outgassing rate of Reemay Spunbonded Polyester and DuPont Double Aluminized Mylar
[DE93-040015] p 1699 N94-19973
Residual atmosphere in the FRECOPA experiment and degassing of materials p 1660 N94-21374

RESIDUAL STRESS
Strengthening of NiAl matrix composites
[AD-A271491] p 1674 N94-20550
Benefits of thread rolling process to the stress corrosion cracking and fatigue resistance of high strength fasteners
[DE93-040438] p 1833 N94-22001
Analysis of thermal mechanical fatigue in titanium matrix composites p 1835 N94-22618

RESIDUES
Low-latency digital frequency synthesizer using the residue number system p 1759 N94-21121

RESINS
Column chromatographic separation of Y(3+) from Sr(2+) by polymeric ionizable crown ether resins
[DE94-000935] p 1683 N94-22021

RESISTANCE HEATING
A spheromak ignition experiment reusing Mirror Fusion Test Facility (MFTF) equipment
[DE94-001856] p 2034 N94-22050

RESOLUTION
A guide to resolving disputes over contractor delay entitlements
[AD-A272022] p 2039 N94-21444

RESONANCE
Rotational spectrum of a dark state in 2-fluoroethanol using microwave/radiofrequency-infrared multiple resonance
[AD-A272101] p 1817 N94-20583
On the theory of morphology-dependent resonances: Shape resonances, width formulas, and graphical representations
[AD-A272279] p 2037 N94-20945
Three-wave resonant interaction in a thin layer
[AD-A272331] p 1994 N94-21039
Search for excited quarks in p(-p) collisions at the square root of s = 1.8 TeV
[DE93-019910] p 1975 N94-21840
Low p(sub T) phenomena observed in high energy nuclear collisions
[DE94-000825] p 1982 N94-21849

RESONANCE SCATTERING
On the theory of morphology-dependent resonances: Shape resonances, width formulas, and graphical representations
[AD-A272279] p 2037 N94-20945

RESONANT FREQUENCIES
Measuring liquid properties with smooth and textured-surface resonators
[DE93-019433] p 1749 N94-20054
Coplanar waveguide radial line stub p 1733 N94-20503
Probabilistic assessment of composite structures
[NASA-TM-106368] p 1832 N94-21757
A vibration model for centrifugal contactors
[DE93-040645] p 1833 N94-21927
Improvement of the performance of IMPATT oscillators through appropriate modification of resonant-cap activity p 1782 N94-22179
Study of TE(1-delta) mode in open dielectric resonators by a finite difference time domain method p 1747 N94-22253
Aperture coupling of circular cylindrical dielectric resonator antenna
[ISBN-0-315-60632-0] p 1743 N94-22409

RESONANT TUNNELING
Investigation of quantum effects in heterostructures
[AD-A270938] p 2011 N94-19817
Interinjection-locked quasioptical power combiners and phased arrays
[AD-A271178] p 2015 N94-20214
Transport in microstructures in the microwave and millimeter-wave regime
[AD-A271875] p 2017 N94-20470

RESONANT VIBRATION
On the theory of morphology-dependent resonances: Shape resonances, width formulas, and graphical representations
[AD-A272279] p 2037 N94-20945

RESONATORS
Measuring liquid properties with smooth and textured-surface resonators
[DE93-019433] p 1749 N94-20054
TlCaBaCuO high Tc superconducting microstrip ring resonators designed for 12 GHz p 1735 N94-20516
Study of TE(1-delta) mode in open dielectric resonators by a finite difference time domain method p 1747 N94-22253
RESOURCE ALLOCATION
Optimal repairman assignment in two maintenance models which are equivalent to routing models with early decisions
[CWI-BS-R9301] p 1930 N94-21234
Generating and evaluating alternate schedules p 1933 N94-21336
Computer-aided design system for objects location and reservoir with dispersed resource evolution investigation p 1923 N94-22064
RESPONSE TIME (COMPUTERS)
A conceptual database design and performance analysis of the MILSATCOM requirements database
[AD-A272672] p 1658 N94-21217
RESTORATION
Restoration of HST images with missing data p 2057 N94-22439
HST image restoration: A comparison of pre- and post-servicing mission results p 1925 N94-22478
First MEM task IRMEO in IRAF p 1928 N94-22551
RETARDING
Magnetic insulation of secondary electrons in plasma source ion implantation
[DE93-040106] p 1997 N94-21988
REUSABLE HEAT SHIELDING
Thermally activated retainer means utilizing shape memory alloy
[NASA-CASE-MSC-21793-1] p 1654 N94-20304
REVERSE ENGINEERING
A proposal for reverse engineering CASE tools to support new software development
[DE93-040207] p 1906 N94-20281
REYNOLDS STRESS
Shear flow generation by Reynolds stress and suppression of resistive g-modes
[DE93-040911] p 1995 N94-21514
New results on the realizability of Reynolds stress turbulence closures
[NASA-CR-191548] p 1804 N94-21875
RHENIUM
Sulfur-bonded thiophenes in organometallic rhenium complexes and adsorption of isocyanides on gold
[DE93-041126] p 1694 N94-21937
RHENIUM COMPOUNDS
Photochemical approaches to conversion of light to electricity or fuel
[DE94-001650] p 1849 N94-22048
RHEOLOGY
Microscopic modeling of tribological and interfacial phenomena
[AD-A271864] p 1823 N94-20464
Thermal and rheological controls on magma migration in dikes: Examples from the east rift zone of Kilauea volcano, Hawaii p 1862 N94-20673
A comparison of calculated and measured rheological properties of crystallising lavas in the field and in the laboratory p 1862 N94-20690
RHODIUM ALLOYS
Magnetism in CeRu2Ge2 and CeRh2Ge2 and its pressure dependence
[DE93-040061] p 2032 N94-21987
RHYOLITE
Venus pancake dome formation: Morphologic effects of a cooling-induced variable viscosity during emplacement p 2110 N94-20732
RIBLETS
Measurement Technology for Flight Tests
[ILR-MITT-256(1991)] p 1639 N94-22597
Riblet boundary layer measurements of an A-310 fuselage with Pitot combs p 1640 N94-22605
RIEMANN MANIFOLD
Vanishing theorem on arithmetic surfaces
[PB93-215461] p 1961 N94-22263
Non commutative geometry and physics
[PB93-215499] p 1961 N94-22264
RIGID STRUCTURES
Estimability of polar motion using range observations to satellites
[PB93-219319] p 1842 N94-22265
RIMS
Characterization of the Marquez Dome buried impact crater using gravity and magnetic data p 1863 N94-20882
RING STRUCTURES
Morphologic classes of impact basins on Venus p 2137 N94-20883
RINGS
The IRAF Fabry-Perot analysis package: Ring fitting p 2048 N94-22527
RISK
Manual of DRANC (release 1.1): A computer program for the Dutch risk assessment of new chemical substances
[PB93-194827] p 1851 N94-19998
Meteoroids and debris impact risk assessment on Columbus and Hermes using a realistic geometrical analysis tool p 1662 N94-21388
MLS signal-in-space category 3 landing hazard analysis p 1644 N94-22134
ROADS
Traffic noise in a roundabout way p 1966 N94-21799
STAR-1 SAR road extraction using texture analysis and mathematical morphology
[ISBN-0-315-83255-X] p 1843 N94-22429
ROBOT ARMS
Research in lightweight elastic robotic arms
[AD-A270846] p 1821 N94-19833
Interactive simulation package for coupled bending and torsional vibrations in flexible robot arms
[MEMO-1089] p 1944 N94-21140
Optimal control of the tip of a flexible arm p 1794 N94-22256
ROBOT CONTROL
Research in lightweight elastic robotic arms
[AD-A270846] p 1821 N94-19833
Robot skill learning and the effects of basis function choice
[TR-437] p 1939 N94-20135
Self-organization via active exploration in robotic applications. Phase 2: Hybrid hardware prototype
[NASA-CR-194723] p 1939 N94-20212
Climbing robot — caterpillar design
[NASA-CASE-GSC-13442-1] p 1823 N94-20494
Internal camera calibration using rotation and geometric shapes
[AD-A272718] p 1808 N94-21167
Automating the control of robotic systems in unstructured environments
[DE93-040753] p 1946 N94-21929
An adaptive control to enable a robot to follow Cartesian trajectories p 1790 N94-22229
A robust adaptive control design for flexible joint manipulators p 1790 N94-22230
An algorithm for the interference detection among polygonal surfaces p 1791 N94-22239
Analytical representation of working articulation space of a plane manipulator in an encumbered environment p 1792 N94-22241
Control of multiple robot manipulators with optimal force distribution p 1794 N94-22255
Optimal control of the tip of a flexible arm p 1794 N94-22256
Robot link and contact surface dynamic interaction: An experimental study of contact instability
[ISBN-0-315-83439-0] p 1827 N94-22578
ROBOT DYNAMICS
Robot skill learning and the effects of basis function choice
[TR-437] p 1939 N94-20135
Climbing robot — caterpillar design
[NASA-CASE-GSC-13442-1] p 1823 N94-20494
Model-based automatic generation of grasping regions
[NASA-TM-104785] p 1946 N94-21550
An adaptive control to enable a robot to follow Cartesian trajectories p 1790 N94-22229
ROBOT SENSORS
Head-centered orientation strategies in animate vision
[TR-442] p 1894 N94-20520
Sensor integration and data fusion for object localization in robotic workcells p 1774 N94-22130
Ultrasonic sensor vision in robotics p 1775 N94-22131
ROBOTICS
Research in lightweight elastic robotic arms
[AD-A270846] p 1821 N94-19833
Robot skill learning and the effects of basis function choice
[TR-437] p 1939 N94-20135
Aviation safety research at the National Institute for Aviation Research, Wichita State University
[NIAR-93-4] p 1641 N94-20189
Self-organization via active exploration in robotic applications. Phase 2: Hybrid hardware prototype
[NASA-CR-194723] p 1939 N94-20212
Bladder operated robotic joint
[NASA-CASE-MFS-28682-1] p 1701 N94-20359
Development and testing of a reliability performance index for modular robotic systems
[AD-A271901] p 1942 N94-20488
Head-centered orientation strategies in animate vision
[TR-442] p 1894 N94-20520
Visual tracking
[AD-A271686] p 1943 N94-20920
Graphical interactive planning of robotic applications with support of integrated simulation
[ETN-93-93793] p 1944 N94-21057
Simulation of tripod gaits for a hexapod underwater walking machine
[AD-A271719] p 1945 N94-21355
NEP Early Flight program: System performance and development considerations
[NASA-TM-106415] p 1654 N94-21570
Robotic concepts for operation in barren terrain
[DE93-040539] p 1946 N94-21925
Automating the control of robotic systems in unstructured environments
[DE93-040753] p 1946 N94-21929
Canadian Conference on Electrical and Computer Engineering, volumes 1 and 2
[ISBN-0-9694170-2-0] p 1770 N94-22101
Optimal object modelling for an active-vision system p 1771 N94-22107
Ultrasonic sensor vision in robotics p 1775 N94-22131
Dynamic analyses of flexible robotic manipulators
[ISBN-0-315-59251-6] p 1827 N94-22421
Mobile robot perception in unknown and unstructured dynamic voxel environments
[ISBN-0-315-83951-1] p 1947 N94-22591
ROBOTS
Robot skill learning and the effects of basis function choice
[TR-437] p 1939 N94-20135
Climbing robot — caterpillar design
[NASA-CASE-GSC-13442-1] p 1823 N94-20494
Internal camera calibration using rotation and geometric shapes
[AD-A272718] p 1808 N94-21167
High dimension action spaces in robot skill learning
[TR-458] p 1945 N94-21317
Simulation of tripod gaits for a hexapod underwater walking machine
[AD-A271719] p 1945 N94-21355
Low energy CMOS for space applications p 1768 N94-21735
Determining the 3-D structure and motion of objects using a scanning laser range sensor
[NASA-CR-194745] p 1818 N94-21817
Robotic concepts for operation in barren terrain
[DE93-040539] p 1946 N94-21925
Sensor integration and data fusion for object localization in robotic workcells p 1774 N94-22130
An adaptive control to enable a robot to follow Cartesian trajectories p 1790 N94-22229
Control of multiple robot manipulators with optimal force distribution p 1794 N94-22255
Optimal control of the tip of a flexible arm p 1794 N94-22256
Robot link and contact surface dynamic interaction: An experimental study of contact instability
[ISBN-0-315-83439-0] p 1827 N94-22578
Mobile robot perception in unknown and unstructured dynamic voxel environments
[ISBN-0-315-83951-1] p 1947 N94-22591
ROBUSTNESS (MATHEMATICS)
Asymptotics of the GLRT for the disorder problem in diffusion processes
[INRIA-RR-1735] p 1951 N94-20227
Time-domain analysis of planar microstrip devices using a generalized Yee-algorithm based on unstructured grids p 1724 N94-20431
Numerical study of a multigrid method with four smoothing methods for the incompressible Navier-Stokes equations in general coordinates p 1806 N94-21487
A comparative robustness evaluation of feedforward neurofilters
[NASA-TM-106440] p 1650 N94-21742
A robust adaptive control design for flexible joint manipulators p 1790 N94-22230
Robust unstructured grid generation with VGRID p 1919 N94-22359
An advancing-front Delaunay-triangulation algorithm designed for robustness p 1920 N94-22362
A robust quality control system for GPS navigation and kinematic positioning
[ISBN-0-315-83148-0] p 1644 N94-22427
ROCK INTRUSIONS
Thermal and rheological controls on magma migration in dikes: Examples from the east rift zone of Kilauea volcano, Hawaii p 1862 N94-20673
ROCKET ENGINE DESIGN
Future technical directions p 1668 N94-20072
The Vulcain cryogenic engine p 1668 N94-20077
Dynamics of face seals for high speed turbomachinery p 1655 N94-21796

ROCKET ENGINES
Spacecraft Propulsion
[VKI-LS-1993-01] p 1667 N94-20068
Cryogenic propellant rocket engine problems
p 1666 N94-20076
Liquid fuel injection elements for rocket engines
[NASA-CASE-MFS-28547-1] p 1669 N94-20370
UVPI imaging from the LACE satellite: The Starbird rocket plume
[AD-A271981] p 1658 N94-20617
Dynamics of face seals for high speed turbomachinery
p 1655 N94-21796
ROCKET EXHAUST
The NRL LACE program
[AD-A270861] p 1657 N94-19896
Parameters affecting hydrogen chloride measurements
[AD-A271326] p 1851 N94-20025
Dual-beam multiple wavelength light transmittance measurement for particle sizing in rocket motor plumes
[AD-A272491] p 1670 N94-21208
ROCKET NOZZLES
A tutorial on the aero/thermodynamical design of liquid-propellant rocket engine nozzles
p 1668 N94-20074
ROCKET OXIDIZERS
Chemistry of the burning surface
[AD-A272725] p 1681 N94-21181
ROCKET THRUST
Liquid rocket propulsion. Theory p 1667 N94-20069
Space Shuttle Main Engine. Overview
p 1667 N94-20070
ROCKET VEHICLES
Rockets: Physical science teacher's guide with activities
[NASA-EP-291] p 1669 N94-20226
ROCKS
Thermal conductivity measurements of particulate materials under Martian conditions p 1685 N94-20703
Reverse polarity magnetized melt rocks from the Chicxulub impact structure, Yucatan Peninsula, Mexico
p 1863 N94-20843
Dynamic response of multiphase porous media
[AD-A272915] p 1831 N94-21219
Post-Palbozoic crustal responses to the contemporary stress field in the eastern United States
[DE93-040604] p 1859 N94-22006
RODS
Dynamic, multiaxial impact response of confined and unconfined ceramic rods
[DE93-040057] p 1829 N94-19824
ROLLING CONTACT LOADS
The causes of contact noise
[REPT-92-100] p 1822 N94-20157
ROOM TEMPERATURE
Static ultra-high pressure study of lanthanide and actinide metals using a diamond-anvil cell
[DE94-000369] p 1693 N94-21656
Test results of two high temperature superconducting sample coils
[DE94-000496] p 2035 N94-22570
ROOT-MEAN-SQUARE ERRORS
Orbit and sampling requirements: TRMM experience
p 1870 N94-21647
ROSAT MISSION
A deep x ray survey in the Lockman hole and the soft x ray log N - log S
[NASA-CR-194698] p 2054 N94-20174
X ray archeology in the Coma cluster
[NASA-CR-194799] p 2054 N94-20175
The x ray halo of Cen X-3
[NASA-CR-189309] p 2055 N94-21295
ROSAT implementation of a proposed multi-mission x ray data format p 2047 N94-22462
ROSAT data analysis with EXSAS
p 2080 N94-22555
Results from ROSAT p 2000 N94-22630
ROTARY WING AIRCRAFT
Rotorcraft low altitude IFR benefit/cost analysis: Conclusions and recommendations
[DOT/FAA/RD-93/22] p 1642 N94-20051
Rotorcraft noise: Status and recent developments
[NASA-CR-194761] p 1967 N94-20523
ROTARY WINGS
An experimental investigation of the drag mechanisms of a helicopter rotor in hovering flight
[AD-A270201] p 1636 N94-20486
Rotorcraft noise: Status and recent developments
[NASA-CR-194761] p 1967 N94-20523
The modern rotor aerodynamic limits survey: A report and data survey
[NASA-TM-4446] p 1635 N94-21490
ROTATING GENERATORS
Modeling of the coupled magnetospheric and neutral wind dynamos
[NASA-CR-194728] p 1856 N94-20537
ROTATING PLASMAS
Finite Larmor radius flute mode theory with end loss
[DE93-040914] p 1991 N94-19872
Neoclassical kinetic theory near an X-point: Plateau regime
[DE93-019825] p 1951 N94-20224
Gravitational instability of magnetized filamentary clouds. 2: Rotation p 2009 N94-22689
ROTATING SHAFTS
Rotary encoding device using polygonal mirror with diffraction gratings on each facet
[NASA-CASE-GSC-13543-1] p 1985 N94-20240
Shaft mount for data coupler system
[NASA-CASE-LAR-13805-1] p 1822 N94-20365
ROTATING SPHERES
Double diffusion convection in a rotating spherical shell p 2006 N94-22666
ROTATION
Turntable mechanism
[NASA-CASE-MFS-28522-1] p 1823 N94-20380
Liquid-phase circulation and mixing in multicomponent droplets vaporizing in a laminar convective environment
[AD-A272851] p 1802 N94-21193
Method for design rotation
[AD-A272440] p 1911 N94-21204
Relationship of area postrema to three putative measures of motion sickness p 1885 N94-21900
Motion sickness elicited by passive rotation in squirrel monkeys p 1887 N94-21905
Gravitational instability of magnetized filamentary clouds. 2: Rotation p 2009 N94-22689
ROTATIONAL STATES
High resolution infrared spectroscopy of formamide and deuterated formamide in a molecular beam
[AD-A271986] p 1973 N94-20618
ROTOR AERODYNAMICS
The fluid mechanics of vortex cutting by a blade
[AD-A270932] p 1636 N94-20043
An experimental investigation of the drag mechanisms of a helicopter rotor in hovering flight
[AD-A270201] p 1636 N94-20486
ROTOR BLADES
The fluid mechanics of vortex cutting by a blade
[AD-A270932] p 1636 N94-20043
ROTOR BLADES (TURBOMACHINERY)
Near wake measurements on a rotor model with Mie-vanes in the Delft open jet tunnel
[PB93-215382] p 1638 N94-22260
ROTORS
System and method for cancelling expansion waves in a wave rotor
[NASA-CASE-LEW-15218-1] p 1801 N94-20588
An application of the Cerebellar Model Articulation Controller for a switched reluctance rotor position estimator
[AD-A271769] p 1943 N94-20926
Brush seal bristle flexure and hard-rub characteristics
p 1654 N94-21791
Operation of a test bed axial-gap brushless dc rotor with a superconducting stator
[DE93-019167] p 1769 N94-21830
ROUTES
A distributed reinforcement learning scheme for network routing
[AD-A270600] p 1938 N94-19845
Next Generation Weather Radar (NEXRAD) Principal User Processor (PUP) Operational Test and Evaluation (OT/E)
[AD-A273075] p 1868 N94-21519
ROVING VEHICLES
Robotic concepts for operation in barren terrain
[DE93-040539] p 1946 N94-21925
RUBBER
Stress-induced cracking of fluorocarbon rubber MTL-0002 after exposure to DS-2
[AD-A271753] p 1705 N94-21302
The simulation of action of some space environment factors on Teflon and on rubber materials
p 1661 N94-21380
RUBIDIUM COMPOUNDS
Fullerene derivatives and fullerene superconductors
[DE93-019568] p 2031 N94-21871
RUN TIME (COMPUTERS)
Proving run-time properties of general programs w.r.t. constructive negation
[CWI-CS-R9245] p 1909 N94-21025
RUNGE-KUTTA METHOD
Adaptive grids for quasilinear parabolic systems in one space dimension
[ETN-93-93611] p 1954 N94-21137
Butcher-Kuntzmann methods for nonstiff problems on parallel computers
[CWI-NM-R9305] p 1935 N94-21493
Users manual for the NASA Lewis three-dimensional ice accretion code (LEWICE 3D)
[NASA-TM-105974] p 1642 N94-21590
Modelling short bent, graded index dielectric slab waveguides
[PB93-215283] p 1742 N94-22349
RUNWAYS
Notes on Antarctic aviation
[AD-A273018] p 1651 N94-21239
Parallel runway requirement analysis study. Volume 1: The analysis
[NASA-CR-191549-VOL-1] p 1644 N94-22277
Parallel runway requirement analysis study. Volume 2: Simulation manual
[NASA-CR-191549-VOL-2] p 1644 N94-22278
RUPTURING
Head-on collision of drops: A numerical investigation
[NASA-TM-106394] p 1798 N94-20167
RUTHENIUM
Photochemically induced transformations of transition complexes
[AD-A271112] p 2014 N94-19982
RUTHENIUM ALLOYS
Magnetism in CeRu2Ge2 and CeRh2Ge2 and its pressure dependence
[DE93-040061] p 2032 N94-21987
RUTILE
Time-resolved shock compression of porous rutile: Wave dispersion in porous solids
[DE93-018848] p 1829 N94-19927

S

S MATRIX THEORY
New relativistic S-matrix results for scattering -- beyond the usual anomalous factors/beyond impulse approximation
[DE93-019148] p 1971 N94-20096
SADDLE POINTS
Ab initio potential energy surface for the H + OCS reaction
[AD-A270577] p 1698 N94-19947
SAFETY
Current status of environmental, health, and safety issues of nickel metal-hydride batteries for electric vehicles
[DE93-017079] p 1748 N94-19902
Female security as a general mobility condition
[ISBN-3-79-831536-1] p 2039 N94-20153
The FY1992 survey on commercialization of Stirling engine utilization equipment
[DE94-707416] p 1849 N94-22029
SAFETY DEVICES
Evaluation of head injury criteria
[NIAR-93-2] p 1890 N94-20190
SAGE SATELLITE
Stratospheric Aerosol and Gas Experiment (SAGE 3)
p 1869 N94-21644
SALINITY
On the sources of North Atlantic deep water
[AD-A270854] p 1861 N94-19895
Briny lakes on early Mars? Terrestrial intracrater playas and Martian candidates p 2145 N94-21675
SALT BEDS
Mobility of salt domes
[BCRS-92-08] p 1857 N94-21016
SAMARIUM ISOTOPES
Examination of low level magnetic dipole intensities in the transition nuclei Sm-148, Sm-150, Sm-152 and Sm-154, with inelastic photon scattering at S-DALINAC
[ETN-93-95069] p 1971 N94-20030
The Sm-(146,147)-Nd-(142,143) formation interval for the lunar mantle and implications for lunar evolution
p 2097 N94-20663
Magnesian anorthosites from the western highlands of the Moon: Isotope geochemistry and petrogenesis
p 2118 N94-20779
The Sm-Nd systematics of silicate inclusions in iron meteorites: Results from Caddo (IAB)
[CONTRIB-5241(804)] p 2084 N94-20795
SAMPLED DATA SYSTEMS
An 18 bit 50 kHz ADC for low earth orbit
p 1764 N94-21702
SAMPLERS
Passive Cryogenic Sampler
[DE94-000918] p 1811 N94-22392
SAMPLING
A weighted least-squares lump correction algorithm for transmission-corrected gamma ray nondestructive assay
[DE93-018474] p 1904 N94-20049
Development and demonstration of a personal monitoring system for exposure to hydrogen fluoride
[DE93-041273] p 1891 N94-20935
Green Sheet project: Dye sheet evolution
[AD-A272019] p 1883 N94-21443
Orbit and sampling requirements: TRMM experience
p 1870 N94-21647

SANDS
Analysis of a sandstorm weather process-translation
[AD-A272959] p 1867 N94-21250
SANDWICH STRUCTURES
A study of the structural stability of an unbalanced sandwich composite configuration
[AD-A272496] p 1675 N94-21431
SAS
SkiCAT: A cataloging and analysis tool for wide field imaging surveys p 2049 N94-22546
SATELLITE ALTIMETRY
Scattering by Venus' surface p 2117 N94-20771
Geology and radiophysical properties of the Venera and Vega landing sites p 2135 N94-20867
Ocean mapping using satellite radar altimetry
[ETN-93-93470] p 1841 N94-21017
Estimating the rotation rate of mesoscale ocean rings from satellite altimetry
[AD-A272922] p 1883 N94-21222
Comparison of satellite-derived velocity fields in the coastal transition zone
[AD-A272565] p 1883 N94-21360
Influence of geoid model uncertainty on the determination of ocean circulation with satellite altimetry
[PB93-219301] p 1842 N94-22097
SATELLITE ATTITUDE CONTROL
Method of orienting a synchronous satellite
[CA-PATENT-1,305,772] p 1658 N94-21041
SATELLITE COMMUNICATION
Oceanic in situ Fraunhofer-line characteristics: Fraunhofer-line underwater experiment (FLUX)
[AD-A270659] p 1881 N94-19952
Optimization of a satellite localization and message sending system
[ETN-93-94448] p 1737 N94-20592
A compact, portable EHF/SHF antenna for advanced SCAMP
[AD-A272614] p 1739 N94-21211
Mission Operations Support Area (MOSA) for ground network support p 1932 N94-21331
Space network scheduling benchmark: A proof-of-concept process for technology transfer p 1932 N94-21332
The Automated Conflict Resolution System (ACRS) p 1744 N94-21341
Satellite Communication Hardware Emulation System (SCHES) p 1744 N94-21344
Military satellite communications decision support system requirements analysis and user interface design
[AD-A273047] p 1740 N94-21436
A laboratory system for the investigation of rain fade compensation techniques for Ka-band satellites
[NASA-CR-191200] p 1762 N94-21566
CREIR: A multiaccess protocol for on-board processing satellite systems p 1780 N94-22168
Timing recovery in the channel processor of a digital group demodulator p 1780 N94-22169
TDMA satellite communication systems for ISDN services p 1746 N94-22171
A consideration of the integration of terrestrial and satellite mobile systems p 1746 N94-22172
Visibility considerations in frequency sharing with low Earth orbit satellites p 1746 N94-22187
Inclined orbits and interference to stationary service and to stationary service by satellite p 1653 N94-22188
File transfer performance in LAN interconnection through a satellite channel p 1746 N94-22209
SATELLITE CONFIGURATIONS
The EXOSAT operational experience
[ESA-STM-248] p 1657 N94-20235
SATELLITE CONTROL
Analysis of the TDRS multiple access system for possible use as an attitude control system sensor p 1666 N94-21338
SATELLITE IMAGERY
The analysis of global cloud and radiation data for the study of cloud-climate interactions
[NASA-CR-193388] p 1865 N94-20535
Optical climatology of the Northeast Pacific Ocean
[AD-A271671] p 1866 N94-20559
Geology and radiophysical properties of the Venera and Vega landing sites p 2135 N94-20867
The 7th Brazilian Remote Sensing Symposium, volume 1 p 1838 N94-20953
The use of satellite images in Amazonian archaeology: A case study in the Upper Rio Negro Basin p 1838 N94-20954
Change detection on land use and rainforest cover at Paragominas region, Brazilian Amazon p 1838 N94-20957
Linear mixing model applied to AVHRR LAC data p 1838 N94-20958
The 7th Brazilian Remote Sensing Symposium, volume 3 p 1839 N94-20960
Predicting LANDSAT MSS endmember signatures from corresponding higher resolution TM fraction images p 1839 N94-20962
Evaluation of C-band SAR data from SAREX 1992: Tapajos study site p 1839 N94-20964
Comparison of radiation and cloud parameters derived from satellite and aircraft measurements during FIRE 2 cirrus IFO p 1872 N94-22299
Managing an archive of weather satellite images p 2048 N94-22525
SATELLITE INSTRUMENTS
Oceanic in situ Fraunhofer-line characteristics: Fraunhofer-line underwater experiment (FLUX)
[AD-A270659] p 1881 N94-19952
The EXOSAT operational experience
[ESA-STM-248] p 1657 N94-20235
Comparison of radiation and cloud parameters derived from satellite and aircraft measurements during FIRE 2 cirrus IFO p 1872 N94-22299
SATELLITE NETWORKS
The NCC project: A quality management perspective p 1828 N94-21324
Software metrics: The key to quality software on the NCC project p 1922 N94-21326
The Test Analysis Retrieval System (TARS): Meeting the challenges of the network's test processes p 1933 N94-21337
On-board closed-loop congestion control for satellite based packet switching networks
[NASA-TM-106446] p 1656 N94-21581
Visibility considerations in frequency sharing with low Earth orbit satellites p 1746 N94-22187
SATELLITE OBSERVATION
Ionospheric tomography using the FORTE satellite
[DE93-018545] p 1854 N94-19955
Global and regional comparative performance of linear and nonlinear satellite multichannel sea surface temperature algorithms
[AD-A270475] p 1837 N94-20028
The future of remote sensing from space: Civilian satellite systems and applications
[OTA-ISC-558] p 1837 N94-20209
Studies of Greenland using the SEASAT scatterometer p 1725 N94-20433
Interferometric detection of freeze-thaw displacements of Alaskan permafrost using ERS-1 data p 1732 N94-20460
Spatial and temporal variations of satellite microwave measurements of latent heat release in tropic cyclones due to environmental forcing obtained from a numerical model
[AD-A267947] p 1865 N94-20482
The analysis of global cloud and radiation data for the study of cloud-climate interactions
[NASA-CR-193388] p 1865 N94-20535
Comparison of satellite-derived velocity fields in the coastal transition zone
[AD-A272565] p 1883 N94-21360
Long-Term Monitoring of Global Climate Forcings and Feedbacks
[NASA-CP-3234] p 1868 N94-21639
Climsat rationale p 1869 N94-21643
Stratospheric Aerosol and Gas Experiment (SAGE 3) p 1869 N94-21644
Earth observing scanning polarimeter p 1844 N94-21645
Orbit and sampling requirements: TRMM experience p 1870 N94-21647
Satellite orbit and data sampling requirements p 1870 N94-21648
Urban applications of satellite remote sensing and GIS analysis
[PB93-202174] p 1842 N94-21855
Estimability of polar motion using range observations to satellites
[PB93-219319] p 1842 N94-22265
Proceedings of the Workshop on New Generation of Radiation Budget Measurements From Space and Their Use in Climate Modelling and Diagnostic Studies
[MPIM-90] p 1860 N94-22283
Satellite measurements of radiation budget parameters p 1860 N94-22284
ScaRaB and its subsystems p 1860 N94-22285
Use of satellite data for validation of the ECHAM models p 1861 N94-22289
Simulation of clear-sky outgoing longwave radiation over the oceans using operational analysis p 1861 N94-22290
Use of satellite data for validation of operational forecast models and operational analyses p 1861 N94-22291
Cloud fields derived from satellite and surface data during FIRE cirrus phase 2 p 1872 N94-22302
Remote sensing of multilevel clouds during FIRE IFO 2 p 1844 N94-22303
Comparison of cloud microphysical parameters derived from surface and satellite measurements during FIRE phase 2 p 1873 N94-22306
CIMSS FIRE research activities p 1873 N94-22307
Automated cloud classification with a fuzzy logic expert system p 1875 N94-22313
SATELLITE ORBITS
Satellite orbit and data sampling requirements p 1870 N94-21648
Estimability of polar motion using range observations to satellites
[PB93-219319] p 1842 N94-22265
SATELLITE ORIENTATION
Method of orienting a synchronous satellite
[CA-PATENT-1,305,772] p 1658 N94-21041
SATELLITE POWER TRANSMISSION
Power transmission by laser beam from lunar-synchronous satellite
[NASA-TM-4496] p 1669 N94-20102
Method for remotely powering a device such as a lunar rover
[NASA-CASE-LAR-14789-1] p 1824 N94-20587
SATELLITE SOUNDING
Remote sensing of multilevel clouds during FIRE IFO 2 p 1844 N94-22303
Comparison of cloud microphysical parameters derived from surface and satellite measurements during FIRE phase 2 p 1873 N94-22306
Atmospheric parameterization schemes for satellite cloud property retrieval during FIRE IFO 2 p 1874 N94-22312
SATELLITE SURFACES
Diapirs and cantaloupes: Layering and overturn of Triton's crust p 2111 N94-20738
Geology of Galileo Regio quadrangle, Ganymede p 2130 N94-20842
SATELLITE TRACKING
Downlink acquisition and tracking procedures for the ASCAMP satellite communications terminal
[AD-A272912] p 1739 N94-21244
Mathematician Wang Ju
[AD-A267882] p 1912 N94-21255
Enhanced networks operations using the X Window System p 1932 N94-21329
SATELLITE TRANSMISSION
NHK Science and Technical Research Laboratories p 2151 N94-20342
Advanced coding and modulation schemes for TDRSS p 1744 N94-21350
Network command processing system overview p 1935 N94-21351
Comparison of theoretical and simulated performance results for sloppy-slotted Aloha signaling p 1746 N94-22204
SATELLITE-BORNE INSTRUMENTS
Atomic oxygen fluence detector for Bremsat: Scientific and technical description p 1663 N94-21396
Single event phenomena: Testing and prediction p 1763 N94-21696
Low power, CMOS digital autocorrelator spectrometer for spaceborne applications p 1666 N94-21733
ScaRaB and its subsystems p 1860 N94-22285
ASpect: A new spectrum and line analysis package for IRAF p 1926 N94-22485
The application of artificial intelligence to astronomical scheduling problems p 1949 N94-22492
SATELLITE-BORNE RADAR
Ocean mapping using satellite radar altimetry
[ETN-93-93470] p 1841 N94-21017
SATURN RINGS
A study of Saturn's E-ring particles using the Voyager 1 plasma wave instrument
[NASA-CR-194694] p 2088 N94-20048
SATURN SATELLITES
Linear structures on the small inner satellites of Saturn p 2121 N94-20797
SCALE MODELS
Development and operation of the F/A-18 model control surface actuators
[AD-A271330] p 1645 N94-19914
Structural similitude and design of scaled down laminated models
[NASA-CR-194687] p 1673 N94-20172
Improved ceramic slip casting technique — application to aircraft model fabrication
[NASA-CASE-LAR-14471-1] p 1702 N94-20377
The roughness of the Martian surface: A scale dependent model p 2115 N94-20762
SCALING LAWS
Structural similitude and design of scaled down laminated models
[NASA-CR-194687] p 1673 N94-20172
A fresh look at crater scaling laws for normal and oblique hypervelocity impacts p 1666 N94-20864

Verification of frequency scaling laws for capacitive rf discharges using two-dimensional simulations
[DE94-001306] p 1999 N94-22595

SCANDIUM
Crystallographic phase transitions in actinide metals as a function of pressure
[DE93-040138] p 2011 N94-19827

SCANDIUM COMPOUNDS
Non-fermi liquid and spin-glass behavior of the Sc(1-x)U(x)Pd3 system
[DE93-040134] p 2016 N94-20335

SCANDIUM OXIDES
Properties of E-beam interactive oxide films for nanometer scale structures
[AD-A272848] p 1675 N94-21191

SCANNERS
Three dimensional ultrasonic imaging
[DE93-040549] p 1968 N94-22003

SCANNING ELECTRON MICROSCOPY
Asbestos characterization using scanning electron microscopy/light element x ray spectrometry
[AD-A271611] p 1681 N94-21241
The use of backscattered electron imaging mode to assess the effect of fine dispersions on development of superplastic microstructure in Al-Mg alloys
[AD-A272426] p 1691 N94-21258
Some experiments on using backscattered electron and energy dispersive x ray imaging in determination of portland cement clinker phase composition p 1708 N94-21893
A quantitative S.E.M. image analysis of cement paste microstructure p 1708 N94-21894

SCANNING TUNNELING MICROSCOPY
Scanning tunneling microscopy investigations of metal dichalcogenide materials
[AD-A272910] p 2027 N94-21242
Quantitative analysis of scanning tunneling microscopy images for surface structure determination: Sulfur on Re(0001)
[DE93-019235] p 2034 N94-22041

SCATTERING
A new conformal absorbing boundary condition for finite element meshes and parallelization of FEMATS
[NASA-CR-194740] p 1950 N94-20034
A comparative study of an ABC and an artificial absorber for truncating finite element meshes
[NASA-CR-194275] p 1716 N94-20160
Modifications to the three-component classification algorithm for SAR data p 1719 N94-20410
The effect of dissipative inhomogeneous medium on the statistics of the wave intensity p 1726 N94-20440
A theoretical and numerical study of polarimetric scattering and emission from random rough surfaces with anisotropic directional spectrum p 1730 N94-20454
Single and double ionization of helium by high-energy photon impact
[DE94-000381] p 1975 N94-21785
Radiation and scattering from printed antennas on cylindrically conformal platforms
[NASA-CR-194703] p 1741 N94-21885
Scattering by cavity-backed antennas on a circular cylinder p 1741 N94-21886

SCATTERING AMPLITUDE
Hadronic molecules and scattering amplitudes from the nonrelativistic quark model
[DE94-000377] p 1974 N94-21657

SCATTERING COEFFICIENTS
Symmetry in polarimetric remote sensing p 1729 N94-20449
Application of neural network to remote sensing of soil moisture using theoretical polarimetric backscattering coefficients p 1730 N94-20455
A simplified method for S-parameter calculations of metal septum waveguide filters p 1782 N94-22180

SCATTERING CROSS SECTIONS
New relativistic S-matrix results for scattering -- beyond the usual anomalous factors/beyond impulse approximation
[DE93-019148] p 1971 N94-20096
Near grazing scattering from non-Gaussian ocean surfaces p 1726 N94-20438
Parton-parton elastic scattering and rapidity gaps at Tevatron energies
[DE93-041024] p 1974 N94-21515
Inelastic electron scattering from surfaces
[DE94-001738] p 1977 N94-22049

SCATTERING FUNCTIONS
Analytical evaluation of a surface integral expressing the coupling between interior and exterior volumes in a FE-IE approach p 1722 N94-20423
Scattering by Venus' surface p 2117 N94-20771
Documentation for PCDIST, a FORTRAN subroutine to calculate Pollack-Cuzzi scattering
[AD-A273070] p 1988 N94-21491

SCATTEROMETERS
Probe compensation in cylindrical near-field scanning: A novel simulation methodology p 1718 N94-20404
ERS-1 and Seasat scatterometer measurements of ocean winds: Model functions and the directional distribution of short waves p 1720 N94-20412
Ku-band ocean radar backscatter observations during SWADE p 1720 N94-20413
Direction angle sensitivity of agricultural field backscatter with AIRSAR data p 1724 N94-20430

SCHEDULES
Predicting scheduling success p 1932 N94-21334
Generating and evaluating alternate schedules p 1933 N94-21336

SCHEDULING
Exploiting the parallelism exposed by partial evaluation
[AD-A270678] p 1928 N94-19877
Multilist scheduling: A new parallel programming model
[AD-A270549] p 1929 N94-20084
Fault tolerant real-time systems
[AD-A272878] p 1899 N94-21195
Space network scheduling benchmark: A proof-of-concept process for technology transfer p 1932 N94-21332
Predicting scheduling success p 1932 N94-21334
Generating and evaluating alternate schedules p 1933 N94-21336
The Automated Conflict Resolution System (ACRS) p 1744 N94-21341
Heuristic-based scheduling algorithm for high level synthesis p 1764 N94-21704
A statistical-based scheduling algorithm in automated data path synthesis p 1764 N94-21706
Instruction set commutivity p 1766 N94-21719
The EUVE proposal database and scheduling system p 2047 N94-22459
SPIKE: Application for ASTRO-D mission planning p 1926 N94-22486
The application of artificial intelligence to astronomical scheduling problems p 1949 N94-22492

SCHMIDT NUMBER
Combustion in turbulent jets and buoyant flames
[PB93-202372] p 1682 N94-21452

SCHOOLS
Schools of the Pacific rainfall climate experiment p 1881 N94-20699
Sparking young minds with Moon rocks and meteorites p 2039 N94-20819

SCHOTTKY DIODES
Study of mechanisms for long wavelength Schottky-barrier infrared detectors
[AD-A270538] p 1971 N94-20083
Study of the utilization of thin oxides in indium phosphides for the realisation of electron components
[ECL-92-38] p 2018 N94-20593

SCHREIBERSITE
Tambo Quemado: Extraordinary concentrations of REE and refractory trace elements caused by artificial heating p 1684 N94-20667

SCHROEDINGER EQUATION
Two-dimensional nonlinear Schrodinger equations and their properties
[AD-A272184] p 1952 N94-20923
Ionization of H2(+) in intense laser fields
[DE93-019160] p 1818 N94-21829
Simulating the Euclidean time Schroedinger equations using an INTEL iPSC/860 hypercube: Application to the t-J model of high-T(sub c) superconductivity
[DE94-000489] p 2035 N94-22385

SCIENTIFIC SATELLITES
Data analysis support for the SPREE instruments on the TSS-1 shuttle flight
[AD-A272445] p 1654 N94-21429

SCIENTIFIC VISUALIZATION
Fast data parallel polygon rendering
[DE93-040157] p 1929 N94-20279
A data distributed, parallel algorithm for ray-traced volume rendering
[DE93-040150] p 1935 N94-21622
Geometric optimization
[DE93-040152] p 1917 N94-21764
PROS: An IRAF based system for analysis of x ray data p 1925 N94-22461
The IDL astronomy user's library p 2048 N94-22500
GRO/EGRET data analysis software: An integrated system of custom and commercial software using standard interfaces p 1926 N94-22501
SKYMAP: Exploring the Universe in software p 1927 N94-22511
The European Southern Observatory-MIDAS table file system p 2048 N94-22518

SCINTILLATION
The effects of magnetic storm phases on F-layer irregularities from auroral to equatorial latitudes
[AD-A272685] p 1857 N94-21189
Temperature dependence of CsI(Tl) gamma ray excited scintillation characteristics
[DE94-000836] p 2034 N94-22028

SCORING
Extracting information from wrong answers in computerized adaptive testing
[AD-A272632] p 1894 N94-21434

SCREWS
Three point lead screw positioning apparatus for a cavity tuning plate
[NASA-CASE-LEW-15216-1] p 1822 N94-20375
Self locking set screw
[AD-D015969] p 1824 N94-21277

SEA BREEZE
Predicting lightning events in the KSC area: A feasibility study using single station data
[AD-A271440] p 1864 N94-20088
The sea breeze convergence zone and its relationship to fair weather electricity in east central Florida
[AD-A268511] p 1868 N94-21502

SEA ICE
Radar backscatter measurements from simulated sea ice during CRRELEX 1990
[AD-A271034] p 1715 N94-19823
Polarimetric backscattering from sea ice p 1723 N94-20426
Observation of pressure ridges in SAR images of sea ice: Scattering theory and comparison with observations p 1723 N94-20427
On evaluating the accuracy of SAR sea-ice classification using multifrequency polarimetric AIRSAR data p 1724 N94-20428
Retrieval of ice thickness from polarimetric SAR data p 1724 N94-20432
Studies of Greenland using the SEASAT scatterometer p 1725 N94-20433
Radar backscattering from snow facies of the Greenland ice sheet: Results from the AIRSAR 1991 campaign p 1725 N94-20434
C-band radar backscatter of sea ice in the Weddell Sea, Antarctica during the austral winter of 1992 p 1725 N94-20435

SEA SURFACE TEMPERATURE
Global and regional comparative performance of linear and nonlinear satellite multichannel sea surface temperature algorithms
[AD-A270475] p 1837 N94-20028
Use of satellite data for validation of the ECHAM models p 1861 N94-22289

SEA WATER
The application of spaceborne synthetic aperture radar in the maritime environment
[DRA-TM(AWE)-91013] p 1737 N94-20596

SEALS (STOPPERS)
Actively controlled shaft seals for aerospace applications
[NASA-CR-194759] p 1823 N94-20538
The 1992 Seals Flow Code Development Workshop
[NASA-CP-10124] p 1654 N94-21790
Navy GTE seal development activity p 1655 N94-21794
Dynamics of face seals for high speed turbomachinery p 1655 N94-21796

SEARCH RADAR
Development of a lidar for integration with the Naval Postgraduate School Infrared Search and Target Designation (NPS-IRSTD) system
[AD-A271847] p 1817 N94-20611

SEASAT SATELLITES
ERS-1 and Seasat scatterometer measurements of ocean winds: Model functions and the directional distribution of short waves p 1720 N94-20412
Studies of Greenland using the SEASAT scatterometer p 1725 N94-20433

SEATS
Aviation safety research at the National Institute for Aviation Research, Wichita State University
[NIAR-93-4] p 1641 N94-20189

SECONDARY EMISSION
New preamplifiers for the SEM scanner
[DIGEL-1993-3] p 1979 N94-20118
Effect of geostationary environment constituents on secondary electron emission rates p 1661 N94-21382

SECONDARY FLOW
Measurement and prediction of the flow through an annular turbine cascade
[AD-A272530] p 1803 N94-21417

SECURITY
Security evaluation of Unix networks
[AD-A273076] p 1945 N94-21520
Initial laboratory evaluation of color video cameras, phase 2
[DE93-040201] p 1809 N94-21556

SEDIMENTS
Workshop on the Martian Northern Plains: Sedimentological, Periglacial, and Paleoclimatic Evolution
[NASA-CR-194831] p 2088 N94-20382
A model for the origin of Martian polygonal terrain p 2090 N94-20393
Iridium in sediments containing large abundances of Australasian microtektites from DSDP hole 758B in the Eastern Indian Ocean and from DSDP hole 769A in the Sulu Sea p 2083 N94-20741
Mars: New evidence for origin of some Valles Marineris layered deposits p 2112 N94-20748
Early Mars: A regional assessment of denudation chronology p 2145 N94-21676

SEGMENTS
Segmented operations for sparse matrix computation on vector multiprocessors
[AD-A270601] p 1928 N94-19950
Segmented ion thruster
[NASA-CASE-NPO-18192-1-CU] p 1669 N94-20496

SEISMIC ENERGY
Proceedings of the 15th Annual Seismic Research Symposium
[AD-A271458] p 1855 N94-20090

SEISMIC WAVES
A Kirchhoff approach to seismic modeling and prestack depth migration
[AD-A271010] p 1854 N94-19820
Proceedings of the 15th Annual Seismic Research Symposium
[AD-A271458] p 1855 N94-20090
Inversion of gravity and bathymetry in oceanic regions for long-wavelength variations in upper mantle temperature and composition
[NASA-CR-192272] p 1882 N94-20131
Analysis of the effects of eurasian crustal and upper mantel structure on regional phases using broadband seismic data
[AD-A272446] p 1858 N94-21206
The Board on Earth sciences and resources
[DE94-000745] p 1859 N94-22018
Transient acoustic wave modeling: Higher-order WKBJ asymptotics and symbolical manipulation (revised)
[PB93-215432] p 1969 N94-22262

SEISMOLOGY
A Kirchhoff approach to seismic modeling and prestack depth migration
[AD-A271010] p 1854 N94-19820
Proceedings of the 15th Annual Seismic Research Symposium
[AD-A271458] p 1855 N94-20090
Seafloor characterization/Galapagos propagating rift
[AD-A272001] p 1882 N94-20581
Modal combination in response spectrum modal dynamic analysis
[DE94-000339] p 1833 N94-21956
Post-Palbozoic crustal responses to the contemporary stress field in the eastern United States
[DE93-040604] p 1859 N94-22006
The Board on Earth sciences and resources
[DE94-000745] p 1859 N94-22018

SELECTION
On the selection of indices in relational databases
[MEMO-INF-92-72] p 2043 N94-21071
Columbus: Materials for 30 years habitability in space p 1662 N94-21387

SELECTIVE DISSEMINATION OF INFORMATION
Security management of electronic data interchange
[AD-A272962] p 1899 N94-21252
Data management for interdisciplinary field experiments: OTTER project support
[NASA-CR-4559] p 1842 N94-22345

SELECTIVE SURFACES
Performance of a simple circular polarization selective surface p 1746 N94-22198

SELECTIVITY
Selectivity: Reductions, nondeterminism, and function classes
[TR-469] p 1912 N94-21273

SELENOLOGY
Contributions of the Clementine mission to our understanding of the processes and history of the Moon p 2119 N94-20784

SELF CONSISTENT FIELDS
An introduction to GUGA in the COLUMBUS Program System
[DE93-018994] p 1902 N94-19928
Theoretical studies of the structures and electronic properties of U(NH2)(sub 3) and Np(NH2)(sub 3)
[DE94-000768] p 2031 N94-21857
Asymptotic structure of magnetically driven MHD wind p 2008 N94-22682

SELF ERECTING DEVICES
Self-deploying photovoltaic power system
[NASA-CASE-LEW-15308-1] p 1846 N94-20196

SELF FOCUSING
Two-dimensional nonlinear Schrodinger equations and their properties
[AD-A272184] p 1952 N94-20923

SELF ORGANIZING SYSTEMS
Self-organization via active exploration in robotic applications. Phase 2: Hybrid hardware prototype
[NASA-CR-194723] p 1939 N94-20212
Representation of spoken words in a self-organizing neural net p 1940 N94-20243
Modeling the human mental lexicon with self-organizing feature maps p 1743 N94-20244
Retrieval of ice thickness from polarimetric SAR data p 1724 N94-20432
A framework of connectionist network toward speech waveform coding p 1746 N94-22211
Speaker-independent isolated-digit recognition using neural networks and hidden Markov model p 1747 N94-22213

SEMANTICS
Set based analysis of ML programs
[AD-A270597] p 1902 N94-19948
Total order assumption
[PB93-191740] p 1903 N94-19993
Bottom-up abstract interpretation of logic programs
[PB93-191773] p 1928 N94-19995
Programming logic for F omega
[PB93-191781] p 1928 N94-19996
Back and forth bisimulations on prime event structures
[RR-888-I-IMAG-124-LIFIA] p 1929 N94-20124
Causal reconstruction
[AD-A271692] p 1908 N94-20929
A declarative approach for first-order built-in's of PROLOG
[CWI-CS-R9246] p 1909 N94-21026
COCOLOG: A conditional observer and controller logic for finite machines
[INRIA-RR-1714] p 1910 N94-21063
Behavioural semantics of parallel functional programming languages
[MEMO-INF-92-66] p 1913 N94-21313
Procedural dynamic semantics, verb-phrase ellipsis, and presupposition
[CWI-CS-R9311] p 1914 N94-21495
MINIFOLD: A kernel for a MANIFOLD-like coordination language
[CWI-CS-R9252] p 1915 N94-21534
Fortran for the nineties p 1926 N94-22481

SEMICONDUCTOR DEVICES
Method for anisotropic etching in the manufacture of semiconductor devices
[NASA-CASE-MSC-21631-1] p 1993 N94-20491
Variable angle of incidence spectroscopic ellipsometric study of semiconductor multilayer structures p 2020 N94-20982
Amorphous Ta-rich Ta-Cu films as diffusion barriers between Au and GaAs p 1710 N94-20991
Solid-state dynamics and quantum transport in novel semiconductor nanostructures
[AD-A272955] p 2027 N94-21248
Some experiences of solving 1-D semiconductor device equations on a matrix coprocessor by a domain decomposition method
[CWI-NM-R9304] p 1935 N94-21492
Advanced far infrared detectors
[DE93-040289] p 1988 N94-21528
Defect motion as the origin of the 1/f conductance noise in solids
[EUT-92-E-259] p 2029 N94-21552
Semiconductor isotope engineering
[DE93-040119] p 2030 N94-21744
Particle behavior in an ECR plasma etch tool
[DE93-040343] p 1996 N94-21769

SEMICONDUCTOR DIODES
Interinjection-locked quasioptical power combiners and phased arrays
[AD-A271178] p 2015 N94-20214
High Speed/High Frequency Optoelectronics
[AD-A271985] p 1751 N94-20580
Investigation on the chemically fixing technique of carbon dioxide utilizing solar energy
[DE94-714886] p 1849 N94-22043

SEMICONDUCTOR LASERS
Spatial patterns in semiconductor lasers
[DE93-040056] p 1814 N94-19865
First results on InGaAsP separate confinement heterostructure diode lasers
[AD-A270849] p 1815 N94-19878
A full-color, high-resolution laser projector for a flight simulator visual display
[AD-A270578] p 1851 N94-20108
Optically controlled current filamentation in GaAs photoconductive semiconductor switches
[DE93-019427] p 2016 N94-20296
High Speed/High Frequency Optoelectronics
[AD-A271985] p 1751 N94-20580
Optical amplification and threshold behavior on InGaAs/InGaAsP multiquantum well structures
[ETN-93-94181] p 2026 N94-21151

SEMICONDUCTORS (MATERIALS)
Investigation of quantum effects in heterostructures
[AD-A270938] p 2011 N94-19817
Theory of energy-assisted epitaxy; theory of ordered semiconductor alloys: In(1-x)Tl(x)Sb as a long-wave infrared material
[AD-A271007] p 2012 N94-19835
Effect of exciton localization and delocalization on magnetic-field-dependent photoluminescence linewidths in semiconductors
[DE93-018860] p 1748 N94-19884
Development of high-efficiency CdTe solar cells
[DE93-018206] p 1845 N94-19925
Research on defects and transport in amorphous-silicon-based semiconductors
[DE93-017117] p 2013 N94-19939
Photoluminescence spectroscopy of zinc germanium diphosphide (ZnGeP2)
[AD-A270705] p 1678 N94-19953
ALE project
[AD-A271080] p 2014 N94-19980
Study of mechanisms for long wavelength Schottky-barrier infrared detectors
[AD-A270538] p 1971 N94-20083
Development of a numerical simulation model for a-Si:H solar cells and application to the analysis of experimentally obtained spectral characteristics
[ETN-93-95061] p 1846 N94-20151
Photoelectron spectroscopy at model boundary surfaces of energy converter semiconductors/electrolyte contacts: Adsorption, coadsorption, and triadsorption of Br2, Na, and H2O on Van der Waals surfaces of metal chalocogenide semiconductors
[ETN-93-95063] p 2015 N94-20152
Single-event upset testing of the performance semiconductor 1750A CMOS/SOS chip set
[AD-A271158] p 2015 N94-20184
Photoconductive Semiconductor Switches for pulsed power applications
[DE93-019411] p 1750 N94-20294
Optically controlled current filamentation in GaAs photoconductive semiconductor switches
[DE93-019427] p 2016 N94-20296
High current density contacts for photoconductive semiconductor switches
[DE93-018837] p 1750 N94-20312
Optical and transport properties of metallic and semiconductor nanostructures
[AD-A271716] p 2018 N94-20554
Fabrication and evaluation of superconducting and semiconducting materials
[AD-A271645] p 2018 N94-20558
High Speed/High Frequency Optoelectronics
[AD-A271985] p 1751 N94-20580
Materials, Structures, and Devices for High-Speed Electronics
[NASA-CR-193177] p 2019 N94-20971
Ellipsometric measurements of molecular-beam-epitaxy-grown semiconductor multilayer thicknesses: A comparative study p 1710 N94-20983
Comparative thickness measurements of heterojunction layers by ellipsometric, RBS, and XTEM analysis p 1710 N94-20984
Characterization of multilayer GaAs/AlGaAs transistor structures by variable angle spectroscopic ellipsometry p 1796 N94-20985
Variable angle of incidence spectroscopic ellipsometric measurement of the Franz-Keldysh effect in MODFET structures p 2021 N94-20987
Ellipsometric analysis of built-in electric fields in semiconductor heterostructures p 1796 N94-20988
Optical measurement of built-in and applied electric fields in Al(x)Ga(1-x)As/GaAs heterostructures p 1796 N94-20989
Characterization of an asymmetric triangular multiple quantum well, by variable angle spectroscopic ellipsometry p 2022 N94-20995
Polarized-light reflection mode p-i-n modulators with GaAs/AlGaAs multiple quantum well active layers: Design and simulation p 2023 N94-20996
In-situ spectroscopic ellipsometry in molecular beam epitaxy p 2024 N94-21005
Applications of variable angle spectroscopic ellipsometry in semiconductor technology p 2025 N94-21010
Fundamentals and applications of variable angle spectroscopic ellipsometry p 1687 N94-21011
Non-destructive evaluation in manufacturing using spectroscopic ellipsometry p 1828 N94-21012
In-situ and ex-situ ellipsometric characterization for semiconductor technology p 2026 N94-21013
Laser diagnostics of RF hydrogen plasma reactors: Application to the processing of III-V materials
[AD-A272659] p 1994 N94-21214

Dephasing processes in III-V semiconductors
[AD-A271677] p 2028 N94-21362
Analysis of semi-insulating bulk GaAs using glow discharge mass spectrometry
[AD-A273032] p 1682 N94-21435
Semiconductors A(III)B(VI): Translation
[AD-A273064] p 2028 N94-21438
Single crystal diamond films
[AD-A266759] p 2028 N94-21517
Advanced far infrared detectors
[DE93-040289] p 1988 N94-21528
Synthesis and catalytic properties of metal and semiconductor nanoclusters
[DE93-019418] p 2028 N94-21541
Heterojunction bipolar transistor technology for data acquisition and communication p 1763 N94-21697
Semiconductor isotope engineering
[DE93-040119] p 2030 N94-21744
High power, electron-beam induced switching in diamond
[DE93-040535] p 1768 N94-21770
Characterization of convection related defects in II-VI compound semiconductors
[NASA-CR-194704] p 2030 N94-21778
Hydrogen in compound semiconductors
[DE93-040300] p 2031 N94-21922
Lattice damage during ion implantation of semiconductors
[DE94-000335] p 2034 N94-22016

SENSITIVITY
Atmospheric sampling glow discharge ionization and triple quadrupole tandem mass spectrometry for explosives vapor detection
[DE93-040593] p 1852 N94-22004

SENSORIMOTOR PERFORMANCE
Gamma-aminobutyric acid (GABA) and neuropeptides in neural areas mediating motion-induced emesis p 1886 N94-21902

SENSORS
Optical fibers and Fluorosensors having improved power efficiency and methods of producing same
[NASA-CASE-LAR-14525-1-CU] p 1986 N94-20378

SENSORY DISCRIMINATION
Segment-based acoustic models for continuous speech recognition
[AD-A271483] p 1736 N94-20547

SENSORY STIMULATION
Susceptibility of the squirrel monkey to different motion conditions p 1885 N94-21899

SENTENCES
Neural data oriented parsing p 1940 N94-20248
A connectionist representation for phrase structures p 1941 N94-20249

SEPARATED FLOW
Fluid dynamic mechanisms and interactions within separated flows
[AD-A271037] p 1797 N94-19978
A theoretical investigation of unsteady separation phenomena related to dynamic stall
[AD-A271865] p 1636 N94-20465
Computational and analytical methods in nonlinear fluid dynamics
[AD-A272722] p 1802 N94-21169
Modelling stalled airfoils
[ISBN-0-315-59525-6] p 1639 N94-22382

SEPARATORS
Spiral fluid separator
[NASA-CASE-MFS-28658-1] p 1800 N94-20361
Development of an electrochemical hydrogen separator
[DE93-019877] p 1683 N94-21984

SEPTUM
A simplified method for S-parameter calculations of metal septum waveguide filters p 1782 N94-22180

SEQUENCING
Model checking, abstraction, and compositional verification
[AD-A270552] p 1902 N94-19919
Total order assumption
[PB93-191740] p 1903 N94-19993
A methodology for formal hardware verification, with application to microprocessors
[AD-A270550] p 1898 N94-20085
High-speed Viterbi decoding with overlapping code sequences p 1760 N94-21130
On the decomposition of synchronous state mechines using sequence invariant state machines p 1764 N94-21703
A shared buffer memory switch with maximum queue and minimum allocation p 1773 N94-22119
A one-shot access scheme for a multicast switch p 1773 N94-22120

SERIES EXPANSION
Asymptotic analysis: Basic concepts and definitions
[DE94-001000] p 1961 N94-22393

SERVICE LIFE
Ageing studies on a composite propellant containing a new organo-copper burn rate catalyst
[AD-A271060] p 1711 N94-19906
Photoconductive Semiconductor Switches for pulsed power applications
[DE93-019411] p 1750 N94-20294
The 1992 USAF structural integrity program conference
[AD-A272876] p 1635 N94-21194
Ceramic Technology Project
[DE94-001011] p 1707 N94-21822
Life prediction systems for critical rotating components p 1835 N94-22615

SERVICES
Passenger terminal level of service measurement: A utility theoretic approach
[ISBN-0-315-59037-8] p 1651 N94-22418

SERVOCONTROL
The optohydraulic servovalve: A novel device for the precise optical control of hydraulic pressure
[ISBN-0-315-83580-X] p 1827 N94-22577

SERVOMECHANISMS
Long range fast tool servo
[AD-A271614] p 1761 N94-21257
The optohydraulic servovalve: A novel device for the precise optical control of hydraulic pressure
[ISBN-0-315-83580-X] p 1827 N94-22577

SET THEORY
Set based analysis of ML programs
[AD-A270597] p 1902 N94-19948
Set theory and nominalisation, part 1
[PB93-191807-PT-1] p 1962 N94-20007
Set theory and nominalisation, part 2
[PB93-191815-PT-2] p 1962 N94-20008
Nominalization, prediction and type containment
[PB93-191799] p 1898 N94-20082
On multiflow problems
[RR-889-M] p 1950 N94-20125
Totally strong and strong graphs
[RR-902-I] p 1951 N94-20237
Half-integral flows in a planar graph with four holes
[RR-894-M] p 1951 N94-20302
Convex set and linear mixing model p 1844 N94-20888
The communication complexity of set intersection problems
[MEMO-1077] p 1738 N94-21073
The Robinson-Schensted and Schuetzenberger algorithms. Part 2: Geometric interpretations
[CWI-AM-R9209-PT-2] p 1911 N94-21157
An NP set with no co-DP sparse subset
[TR-475] p 1954 N94-21199
Advice from nonadaptive queries to NP
[TR-470] p 1911 N94-21200
Selectivity: Reductions, nondeterminism, and function classes
[TR-469] p 1912 N94-21273
Threshold computation and cryptographic security
[TR-461] p 1912 N94-21285
On the topological size of p-m-complete degrees
[TR-459] p 1965 N94-21286
Promises and fault-tolerant database access
[TR-447] p 2043 N94-21287
On the closure properties of #P in the context of PF of #P
[TR-445] p 1955 N94-21456
Modular interval spaces
[PB93-220663] p 1961 N94-22266

SEYFERT GALAXIES
Spatial distribution of near infrared line radiation in galactic nuclei measured with Fabry-Perot spectrometer FAST
[MPE-239] p 2081 N94-21138

SHAFTS (MACHINE ELEMENTS)
Actively controlled shaft seals for aerospace applications
[NASA-CR-194759] p 1823 N94-20538
Acceleration-augmented LQG control of an active magnetic bearing p 1757 N94-21112
Compliant seal development p 1655 N94-21795
Modeling bristle lift-off in idealized brush seal configurations p 1655 N94-21797

SHALLOW WATER
A survey of the impact on acoustic propagation of warm core ocean eddys
[AD-A272188] p 1883 N94-20925

SHAPE MEMORY ALLOYS
Process and apparatus for the release of a prestress initially applied to a mechanism such as a bearing on board a space vehicle
[CA-PATENT-APPL-SN-2,020,90] p 1824 N94-21142
Shape memory metals
[DE94-001373] p 1695 N94-21976

SHAPED CHARGES
PVDF gauge characterization of hypervelocity-impact-generated debris clouds
[DE93-018831] p 1829 N94-19943

SHAPES
Jet shapes in hadron and electron colliders
[DE93-019386] p 1979 N94-20216
Linear structures on the small inner satellites of Saturn p 2121 N94-20797

SHATTER CONES
Shock attenuation at the Slate Islands revisited p 1863 N94-20887

SHEAR
Light scattering studies of an electrorheological fluid
[DE93-019419] p 1700 N94-20315

SHEAR FLOW
Development of phased twin flip-flop jets
[NASA-TM-106404] p 1637 N94-20563
An analysis of pool surface deformation due to a plunging liquid jet
[AD-A272970] p 1802 N94-21261
Shear flow generation by Reynolds stress and suppression of resistive g-modes
[DE93-040911] p 1995 N94-21514
Coupling of smooth particle hydrodynamics with PRONTO
[DE93-019080] p 1915 N94-21539
New results on the realizability of Reynolds stress turbulence closures
[NASA-CR-191548] p 1804 N94-21875

SHEAR PROPERTIES
Frequency and temperature dependence of high damping elastomers
[DE93-019539] p 1697 N94-19809
Shear flow generation by Reynolds stress and suppression of resistive g-modes
[DE93-040911] p 1995 N94-21514

SHEAR STRENGTH
Coupling of smooth particle hydrodynamics with PRONTO
[DE93-019080] p 1915 N94-21539

SHEAR STRESS
Principles and applications of oil film interferometry for measuring wall friction fields in air flows
[ETN-93-95062] p 1798 N94-20147
Crystal orientation dependence of elastic precursor strength in pentaerythritol tetranitrate
[DE93-018340] p 2034 N94-22035

SHELLS (STRUCTURAL FORMS)
Response statistics of shell structures with geometrical and material nonlinearities, volume 1
[ISBN-0-315-84006-4] p 1833 N94-22590

SHERGOTTITES
Rare Earth elements in individual minerals in Shergottites p 1686 N94-20852
Equilibrium and fractional crystallization of a primitive Shergottite composition p 2085 N94-20861
Weathering features and secondary minerals in Antarctic Shergottites ALHA77005 and LEW88516 p 2086 N94-20869
The carbon components in SNC meteorites of feldspathic harzburgite composition p 2086 N94-20885
Further carbon isotope measurements of LEW 88516 p 2086 N94-20886
An attempt to comprehend Martian weathering conditions through the analysis of terrestrial palagonite samples p 2143 N94-21668

SHOCK FRONTS
Shock induced condensation in fluids of high molar specific heat: Shock structure and relaxation
[MPIS-106/1993] p 1798 N94-20145
Photopumped x ray laser research on Saturn
[DE93-019430] p 1816 N94-20298
Original size of the Vredefort structure, South Africa p 1863 N94-20825
Computer simulation of molecular response at a shock front
[DE94-001050] p 1977 N94-22396

SHOCK HEATING
Boost-phase discrimination research
[NASA-TM-109347] p 1666 N94-19818
Reverse polarity magnetized melt rocks from the Chicxulub impact structure, Yucatan Peninsula, Mexico p 1863 N94-20843
Opacity measurements in shock-generated argon plasmas
[DE94-001057] p 1998 N94-22399

SHOCK LAYERS
Experimental study of a shock accelerated thin gas layer
[DE93-018354] p 1799 N94-20286

SHOCK LOADS
An equation of state for shock in homogeneous materials and comparison to shock data
[AD-A271436] p 1829 N94-19881

Time-resolved shock compression of porous rutile: Wave dispersion in porous solids
[DE93-018848] p 1829 N94-19927
Shock response of porous Al-2 + Fe2O3 powder mixtures
[DE93-018851] p 1688 N94-19944
CTH: A software family for multi-dimensional shock physics analysis
[DE93-019428] p 1904 N94-20052
Characterization of amorphous material in shocked quartz by NMR spectroscopy
[DE93-019069] p 1679 N94-20307
Shock attenuation at the Slate Islands revisited
p 1863 N94-20887
Shock compression of low-density foams
[DE93-040545] p 1707 N94-21546
Ductile-brittle transition behavior of tungsten under shock loading conditions
[DE93-019945] p 1693 N94-21843
Disks of YBa2Cu3O7 shocked to 10 GPa pressures
[DE94-000464] p 2031 N94-21931
Characteristics of shock-compressed configuration of Ti and Si powder mixtures
[DE93-018857] p 1713 N94-22033
Crystal orientation dependence of elastic precursor strength in pentaerythritol tetranitrate
[DE93-018340] p 2034 N94-22035

SHOCK RESISTANCE
Fabrication of whisker-toughened alumina tubes
[DE94-001012] p 1677 N94-22022

SHOCK SPECTRA
Relativistic shock spectra: A prediction
[NASA-CR-194764] p 2150 N94-21782

SHOCK TESTS
Hydrodynamic compressibility of high-strength ceramics
[DE93-019424] p 1698 N94-19903

SHOCK TUNNELS
Experimental investigation of nozzle/plume aerodynamics at hypersonic speeds
[NASA-CR-194628] p 1636 N94-20014

SHOCK WAVE INTERACTION
Shock wave interactions with exothermic mixtures
[AD-A271149] p 1829 N94-19836
Experimental study of a shock accelerated thin gas layer
[DE93-018354] p 1799 N94-20286
The 2D and 3D hypersonic flows with unstructured meshes p 1920 N94-22365

SHOCK WAVE PROPAGATION
CTH: A software family for multi-dimensional shock physics analysis
[DE93-019428] p 1904 N94-20052
Photopumped x ray laser research on Saturn
[DE93-019430] p 1816 N94-20298

SHOCK WAVES
Shock wave interactions with exothermic mixtures
[AD-A271149] p 1829 N94-19836
An equation of state for shock in homogeneous materials and comparison to shock data
[AD-A271436] p 1829 N94-19881
Unlike-pair interactions at high pressure and high temperature
[DE93-019948] p 1796 N94-19916
Time-resolved shock compression of porous rutile: Wave dispersion in porous solids
[DE93-018848] p 1829 N94-19927
Shock response of porous Al-2 + Fe2O3 powder mixtures
[DE93-018851] p 1688 N94-19944
CTH: A software family for multi-dimensional shock physics analysis
[DE93-019428] p 1904 N94-20052
Proceedings of the 15th Annual Seismic Research Symposium
[AD-A271458] p 1855 N94-20090
Shape optimization governed by the Euler equations using an adjoint method
[NASA-CR-191555] p 1950 N94-20092
Determination of cosmic bodies size-velocity distribution by observation of current impacts on Mars
p 2082 N94-20648
Direct simulation of shock-induced mixing layer
[DE93-040498] p 1803 N94-21531
Shock compression of low-density foams
[DE93-040545] p 1707 N94-21546
Physics of magnetospheric boundary layers
[NASA-CR-194725] p 1858 N94-21836
Shock temperature measurements of iron to 350 GPa
[DE94-001058] p 1695 N94-22024
Computer simulation of molecular response at a shock front
[DE94-001050] p 1977 N94-22396
Transonic flow calculations: Integral method
[ISBN-0-315-83538-9] p 1639 N94-22586
Formation of fast magnetosonic shock waves during two current loops collision in solar flare
p 2005 N94-22662
Magnetic superbubbles in the galactic disk and halo
p 2009 N94-22694
Shock formation in magnetohydrodynamical accretion onto a black hole p 2010 N94-22699

SHORELINES
A marine sedimentary model for the evolution of the northern plains p 2091 N94-20395

SHORT WAVE RADIATION
The use of ERBE data for climate studies
p 1860 N94-22286

SIBERIA
Primary differentiation in the early Earth: Nd and Sr isotopic evidence from diamondiferous eclogites for both old depleted and old enriched mantle, Yakutia, Siberia
p 1862 N94-20776

SICKNESSES
Self-Motion Perception and Motion Sickness
[NASA-CR-194276] p 1885 N94-21897

SIDELOBE REDUCTION
Improvements on the design of optimum SAW filters with the Remez Exchange Algorithm
p 1773 N94-22123

SIDESLIP
Utilization of lasers for air data measurements
p 1640 N94-22603

SIGNAL ANALYSIS
Use of switched capacitor filters to implement the discrete wavelet transform p 1755 N94-21097
Estimation of AR signal patterns using competitive neural networks p 1744 N94-22102
Signal classification and noise filtering using artificial neural networks p 1744 N94-22103
Segmentation and frequency domain ML pitch estimation of speech signals p 1747 N94-22212
Experiments with recursive estimation in astronomical image processing p 2047 N94-22457
Verification of the PROS timing analysis package
p 1926 N94-22508

SIGNAL DETECTION
State-space models for multichannel detection
[AD-A270608] p 1715 N94-19816
Statistical fluctuations in lasers
[DE94-000710] p 1817 N94-20939
Evaluation of a nonlinear method for the enhancement of tonal signal detection
[NASA-CR-191562] p 1968 N94-21741
Asynchronous detection of SSB-SC data signals
p 1747 N94-22217

SIGNAL DETECTORS
Mathematical model and analysis of the Tactical Unmanned Ground Vehicle (TUGV) using computer simulation
[AD-A272258] p 1824 N94-20576
Surface acoustic wave sensing of VOC's in harsh chemical environments
[DE93-040721] p 1968 N94-21751

SIGNAL DISTORTION
Use of switched capacitor filters to implement the discrete wavelet transform p 1755 N94-21097

SIGNAL ENCODING
Design of a new squaring function for the Viterbi algorithm p 1764 N94-21699
Schematic driven layout of Reed Solomon encoders
p 1766 N94-21722
Encoding and decoding quasi-spherical signal sets
p 1747 N94-22233

SIGNAL FADING
The influence of lowpass filtering and the effects of fading on the group demodulation of QPSK signals
p 1746 N94-22170
ARQ on fading channels p 1747 N94-22242
Performance of RS codes in lognormally shadowed Rician channels p 1792 N94-22244

SIGNAL PROCESSING
A pipelined superconducting digital processor
[DE93-040852] p 1898 N94-19886
Literature review of the errors-in-variables approach to the problem of system identification
[AD-A271098] p 1949 N94-19907
Optical signal processing
[AD-A271036] p 1983 N94-20013
Proceedings of the 15th Annual Seismic Research Symposium
[AD-A271458] p 1855 N94-20090
Application of change detection to dynamic contact sensing
[AD-A270523] p 1939 N94-20105
Center for neural engineering
[AD-A271164] p 1890 N94-20185
High resolution signal processing
[AD-A271181] p 1717 N94-20215
Topographic slope from the SAR interferometric phase gradient p 1731 N94-20459
Signal processing in the linear statistical model
[AD-A272114] p 1736 N94-20570
An inverse DWT for nonorthogonal wavelets
[AD-A272064] p 1737 N94-20582
The Fifth NASA Symposium on VLSI Design
[NASA-CR-194644] p 1753 N94-21079
Adaptive analog video signal conditioner
p 1744 N94-21099
VLSI mixed signal processing system
p 1744 N94-21100
Using crosscorrelation techniques to determine the impulse response of linear systems
p 1759 N94-21122
NAVSPASUR sensor system digital signal processing receiver. Volume 1: Hardware and software overview
[AD-A272899] p 1738 N94-21198
Use of the Weiss-Weinstein bound to compare the direction-finding performance of sparse arrays
[AD-A272582] p 1738 N94-21210
NAVSPASUR sensor system digital signal processing receiver. Volume 2: Function and capabilities of hardware and software components
[AD-A272900] p 1739 N94-21218
Polar processing project
[AD-A271583] p 1739 N94-21235
Comparison of higher order moment spectrum estimation techniques
[AD-A272967] p 1967 N94-21260
QPPM receiver for free-space laser communications
[NASA-TM-106424] p 1741 N94-21567
Applications of correlator chips in radio science
p 1763 N94-21695
A real time correlator architecture using distributed arithmetic principles p 1768 N94-21734
A comparative robustness evaluation of feedforward neurofilters
[NASA-TM-106440] p 1650 N94-21742
Surface acoustic wave sensing of VOC's in harsh chemical environments
[DE93-040721] p 1968 N94-21751
Canadian Conference on Electrical and Computer Engineering, volumes 1 and 2
[ISBN-0-9694170-2-0] p 1770 N94-22101
Estimation of AR signal patterns using competitive neural networks p 1744 N94-22102
Signal classification and noise filtering using artificial neural networks p 1744 N94-22103
VLSI architectures for the new (T,L) algorithm
p 1745 N94-22110
Design of a floating point convolution processor
p 1775 N94-22133
CFAR processing for airborne pulse-Doppler radars
p 1745 N94-22142
Space-based radar for moving target detection
p 1745 N94-22143
A digital demodulation scheme for use in a high dynamic range radar system p 1745 N94-22144
An overview of synthetic aperture radar signal processing techniques p 1745 N94-22159
Timing recovery in the channel processor of a digital group demodulator p 1780 N94-22169
Interference reduction using neural networks
p 1783 N94-22186
Acceleration of backpropagation learning using a parallel DSP machine p 1786 N94-22206
Speaker-independent isolated-digit recognition using neural networks and hidden Markov model
p 1747 N94-22213
Asynchronous detection of SSB-SC data signals
p 1747 N94-22217
Encoding and decoding quasi-spherical signal sets
p 1747 N94-22233
The application of sample vector selection to adaptive nulling: Performance comparison for techniques combining Gram-Schmidt orthogonalization with averaging
p 1747 N94-22234
A four-band infrared data acquisition facility for signal processing development p 1791 N94-22235
An adaptive method for group delay compensation using switched capacitor filters p 1793 N94-22248
Wideband source location in two-dimensional array processing p 1747 N94-22250
On coefficient quantization and computational roundoff effects in frequency interpolation filter banks
p 1793 N94-22251
A feasibility study of a parallax-based passive missile approach warning system
[ISBN-0-315-60640-1] p 1743 N94-22410
A multiresolution wavelet representation in two or more dimensions p 1925 N94-22456
CCD data acquisition systems at Lick and Keck Observatories p 2047 N94-22495
The VLBA correlator: Real-time in the distributed era
p 2049 N94-22547

SIGNAL TO NOISE RATIOS
Determination of noise equivalent sigma(0) using highly correlated repeat-pass SAR images p 1720 N94-20411
Use of the Weiss-Weinstein bound to compare the direction-finding performance of sparse arrays [AD-A272582] p 1738 N94-21210
A low cost alternative to high performance PCM bit synchronizers p 1813 N94-21347
Design of a new squaring function for the Viterbi algorithm p 1764 N94-21699
Evaluation of a nonlinear method for the enhancement of tonal signal detection [NASA-CR-191562] p 1968 N94-21741
The application of sample vector selection to adaptive nulling: Performance comparison for techniques combining Gram-Schmidt orthogonalization with averaging p 1747 N94-22234

SIGNAL TRANSMISSION
Metrics for specifying and/or testing neural networks statement of government interest [AD-D015946] p 1938 N94-19843
Trellis coded multi-orthogonal modulation p 1747 N94-22231
Quadrature biorthogonal modulation p 1747 N94-22232

SIGNATURE ANALYSIS
Efficient chip signature checking for diagnosing boundary scan systems [RR-901-I] p 1749 N94-20166
Progress in interpreting CO2 lidar signatures to obtain cirrus microphysical and optical properties p 1874 N94-22308

SIGNATURES
Rough surface scattering from moving ocean surfaces as an indicator of scattering mechanisms p 1726 N94-20439
Standard ML signatures for a protocol stack [AD-A272060] p 1908 N94-20622

SILANES
Adhesive electroless metallization of fluoropolymeric substrates [AD-A271858] p 1703 N94-20526
Composite materials with improved properties in compression [AD-A272837] p 1675 N94-21176

SILICA GLASS
Formation of colloidal Ag precipitates in fused silica by MeV ion implantation [DE93-040268] p 2012 N94-19869

SILICATES
Neutron-scattering studies of Yb-bearing silicate glasses [DE93-019768] p 1700 N94-20265
The Sm-Nd systematics of silicate inclusions in iron meteorites: Results from Caddo (IAB) [CONTRIB-5241(804)] p 2084 N94-20795
Hydrothermal alteration experiments of olivine with varying Fe contents: An attempt to simulate aqueous alteration of the carbonaceous chondrites p 1686 N94-20810

SILICIDES
Photo- and thermal-induced antiferromagnetic interlayer coupling in Fe/(Fe-Si) superlattices [DE93-040822] p 2031 N94-21930
The effect of microstructural evolution on superplasticity in Ni3Si(V, Mo) [DE93-041320] p 1694 N94-21943

SILICON
Substrate recovery of Mo-Si multilayer coated optics [DE93-019610] p 1698 N94-19810
Segregation of Si to the surface of Fe-29Ni-17Co alloy [DE93-040053] p 1687 N94-19864
Photoconductive Semiconductor Switches for pulsed power applications [DE93-019411] p 1750 N94-20294
Attenuation of epsilon(sub eff) of coplanar waveguide transmission lines on silicon substrates p 1733 N94-20504
Spectroscopic ellipsometry studies of HF treated Si (100) surfaces p 1734 N94-20508
Spectroscopic ellipsometric characterization of Si/Si(1-x)Ge(x) strained-layer superlattices p 2025 N94-21009
Optical integrated structures and circuits on silicon [VTT-PUBS-106] p 1988 N94-21594
A novel semiconductor process for optoelectronic applications on silicon substrate p 1988 N94-21595
Integrated optical coupling element on silicon substrate, appendix 2 p 1988 N94-21596
Fibre pigtailed silicon based low cost passive optical components, appendix 5 p 1989 N94-21599
Localization of pellicle-induced open contacts using charge-induced voltage alteration [DE93-019407] p 1762 N94-21636
Micromachined actuator and sensor capabilities at the Microelectronics Development Laboratory [DE93-019417] p 1769 N94-21918
Acoustic, fiber optic, and silicon microelectronic microsensors research and development activities at Sandia National Laboratories [DE93-019075] p 1770 N94-22040
Silicon microelectronic field-emissive devices for advanced display technology [DE94-000397] p 1794 N94-22380

SILICON ALLOYS
Research on defects and transport in amorphous-silicon-based semiconductors [DE93-017117] p 2013 N94-19939
Fundamental studies of defect generation in amorphous silicon alloys grown by remote plasma-enhanced chemical-vapor deposition [DE93-017083] p 2029 N94-21615
Stable, high-efficiency amorphous-silicon solar cells with low hydrogen content [DE93-018214] p 1848 N94-21826

SILICON CARBIDES
Hydrodynamic compressibility of high-strength ceramics [DE93-019424] p 1698 N94-19903
Process for the homoepitaxial growth of single-crystal silicon carbide films on silicon carbide wafers [NASA-CASE-LEW-15223-1] p 2017 N94-20381
Review of corrosion behavior of ceramic heat exchanger materals: Corrosion characteristics of silicon carbide and silicon nitride [DE93-041307] p 1706 N94-21516
Fabrication of whisker-toughened alumina tubes [DE94-001012] p 1677 N94-22022

SILICON COMPOUNDS
Ellipsometric study of Si(0.5)Ge(0.5)/Si strained-layer superlattices p 1734 N94-20509
Spectroscopic ellipsometric characterization of Si/Si(1-x)Ge(x) strained-layer superlattices p 1734 N94-20510
Characteristics of shock-compressed configuration of Ti and Si powder mixtures [DE93-018857] p 1713 N94-22033

SILICON DIOXIDE
Quartz/fused silica chip carriers [NASA-CR-194154] p 2016 N94-20340
Evaporation in equilibrium, in vacuum, and in hydrogen gas p 1684 N94-20638
Analytic solutions for optimized ellipsometric measurements of interfaces and surface layers in thin film structures p 2019 N94-20977
Alumoxanes: Rationalization of black box materials [AD-A272805] p 1704 N94-21170
Dynamics of adsorbed, swollen block copolymers [AD-A272013] p 1706 N94-21460
Precision prism coupling setup applied to measure planar silica films on silicon, appendix 9 p 1989 N94-21603

SILICON FILMS
Analytic solutions for optimized ellipsometric measurements of interfaces and surface layers in thin film structures p 2019 N94-20977
Refractive index behaviour of phosphorus-doped planar silica waveguides, appendix 7 p 1989 N94-21601
Precision prism coupling setup applied to measure planar silica films on silicon, appendix 9 p 1989 N94-21603

SILICON ISOTOPES
Direct images of thermal disorder in Cl-Si and H-O-Si chemisorption bond on Si(100) [AD-A272386] p 1680 N94-21145

SILICON NITRIDES
Sintering silicon nitride [NASA-CASE-LEW-15489-1] p 1703 N94-20529
Ellipsometric studies of sputtered silicon nitride on n-GaAs p 1709 N94-20972
Multiple-wavelength angle-of-incidence ellipsometry: Application to silicon nitride-gallium arsenide structures p 2019 N94-20974
Structural and chemical analysis of a silicon nitride film on GaAs by null ellipsometry p 1709 N94-20975
Microstructural modeling and toughening of Si3N4 ceramics for high temperature engine applications [AD-A272897] p 1704 N94-21197
Review of corrosion behavior of ceramic heat exchanger materals: Corrosion characteristics of silicon carbide and silicon nitride [DE93-041307] p 1706 N94-21516
A novel semiconductor process for optoelectronic applications on silicon substrate p 1988 N94-21595
Electron holography applied to the study of ceramic materials [DE94-000329] p 1707 N94-21653
Surface and subsurface defect detection in Si3N4 components by laser scattering [DE93-040829] p 1832 N94-21772
Effect of powder characteristics on gas-pressure sintering of Si3N4 with rare earth additives [DE94-000330] p 1694 N94-21945

SILICON OXIDES
Neutron-scattering studies of Yb-bearing silicate glasses [DE93-019768] p 1700 N94-20265
Light scattering studies of an electrorheological fluid [DE93-019419] p 1700 N94-20315
Structural and chemical analysis of a silicon nitride film on GaAs by null ellipsometry p 1709 N94-20975
Properties of E-beam interactive oxide films for nanometer scale structures [AD-A272848] p 1675 N94-21191
Shock compression of low-density foams [DE93-040545] p 1707 N94-21546
Refractive index behaviour of phosphorus-doped planar silica waveguides, appendix 7 p 1989 N94-21601

SILICON POLYMERS
Optical diagnostic instrument for monitoring etch uniformity during plasma etching of polysilicon in a chlorine-helium plasma [DE93-019582] p 1993 N94-20261
Particle behavior in an ECR plasma etch tool [DE93-040343] p 1996 N94-21769

SILICON RADIATION DETECTORS
The GEM Silicon Tracking System [DE93-040133] p 2016 N94-20322

SILICONES
Laser driven hydrodynamic instability experiments [DE93-040550] p 1818 N94-21547

SILVER
The proximity effect in ultrathin granular Pb films [AD-A271094] p 2012 N94-19848
Formation of colloidal Ag precipitates in fused silica by MeV ion implantation [DE93-040268] p 2012 N94-19869
Silver lined ceramic vessel [AD-D015917] p 1700 N94-20057
Some results of the oxidation investigation of copper and silver samples flown on LDEF p 1660 N94-21375

SILVER OXIDES
Silver oxide batteries: Recent improvements and developments p 1752 N94-20629

SIMD (COMPUTERS)
Fast data parallel polygon rendering [DE93-040157] p 1929 N94-20279

SIMILARITY THEOREM
Structural similitude and design of scaled down laminated models [NASA-CR-194687] p 1673 N94-20172

SIMULATION
Evaluation of a scanning Hartmann device for single point turning applications [DE93-019204] p 1821 N94-19891
Study of regional climate change [DE93-018926] p 1850 N94-19941
A comparative study of an ABC and an artificial absorber for truncating finite element meshes [NASA-CR-194275] p 1716 N94-20160
SPH modelling of energy partitioning during impacts on Venus p 2124 N94-20809
Atmospheric breakup of a small comet in the Earth's atmosphere p 2084 N94-20824
Synoptic observations of near surface processes of an insolated ice-dust body under space conditions: The case of KOSI 9 and 10 p 2084 N94-20827
Application of a back-propagation neural network to isolated-word speech recognition [AD-A272495] p 1945 N94-21430

SIMULATORS
A breakdown model for the bipolar transistor to be used with circuit simulators [DE93-019422] p 1750 N94-20218

SINE SERIES
Operational equations for the five-point rectangle [DE94-000366] p 1959 N94-21655

SINGLE CRYSTALS
Oxidation-reduction induced roughening of platinum (111) surface [DE93-017408] p 1687 N94-19922
The multicomponent lineshape of the anharmonic A(1)(TO) phonon in PbTiO3 [DE93-018995] p 1970 N94-19971
Growth of zinc selenide single crystals by physical vapor transport in microgravity [NASA-CR-194679] p 2017 N94-20346
Monocrystalline germanium film on sapphire [AD-D015925] p 2017 N94-20348
Process for the homoepitaxial growth of single-crystal silicon carbide films on silicon carbide wafers [NASA-CASE-LEW-15223-1] p 2017 N94-20381
Interfacial properties of diamondlike amorphous carbon films on InP: Metal-insulator-semiconductor structures p 1710 N94-20980

Growth, characterization and device development in monocrystalline diamond films
[AD-A272715] p 2026 N94-21190
Techniques for the flux growth of optical materials: Growth of beta-barium borate
[AD-A272717] p 2028 N94-21505
Growth, characterization and device development in monocrystalline diamond films
[AD-A273097] p 2028 N94-21506
Single crystal diamond films
[AD-A266759] p 2028 N94-21517
Relaxation of hysteresis loop in a single crystal of YBa2Cu4O8
[DE93-019519] p 2029 N94-21649
Semiconductor isotope engineering
[DE93-040119] p 2030 N94-21744
Techniques for producing free-standing thin films on frames
[DE93-041144] p 1708 N94-21954
Temperature dependence of magnetic order in single-crystalline UPdSn
[DE93-040153] p 2033 N94-21991
The effect of correlated and point defects on the vortex lattice melting transition in single crystal YBa2Cu3O(7-delta)
[DE93-040277] p 2033 N94-21997
Temperature-dependent ion beam mixing
[DE93-040281] p 2033 N94-21999
Quantitative analysis of scanning tunneling microscopy images for surface structure determination: Sulfur on Re(0001)
[DE93-019235] p 2034 N94-22041
Inelastic neutron scattering of (gamma)-iron, and the determination of the elastic constants by lattice dynamics
[DE94-000694] p 1978 N94-22573

SINGLE EVENT UPSETS
Single-event upset testing of the performance semiconductor 1750A CMOS/SOS chip set
[AD-A271158] p 2015 N94-20184
Comparison of single event upset rates for microelectronic memory devices during interplanetary solar particle events p 1754 N94-21085
STRV RADMON: An integrated high-energy particle detector p 1666 N94-21086
Test results for SEU and SEL immune memory circuits p 1754 N94-21087
Complementary heterojunction FET technology for space application p 1755 N94-21094
Design methods for fault-tolerant finite state machines p 1758 N94-21120
Single event phenomena: Testing and prediction p 1763 N94-21696
Defect-sensitivity analysis of an SEU immune CMOS logic family p 1765 N94-21711

SINGLE SIDEBAND TRANSMISSION
Asynchronous detection of SSB-SC data signals p 1747 N94-22217

SINGULAR INTEGRAL EQUATIONS
Hypersingular integrals at a corner
[DE94-000340] p 1961 N94-22379

SINGULARITY (MATHEMATICS)
Classical and generalized solutions of time-dependent linear differential algebraic equations
[AD-A272834] p 1954 N94-21173

SINTERING
Sol-spray preparation, particulate characteristics, and sintering of alumina powders
[DE93-018577] p 1690 N94-20183
Sintering silicon nitride
[NASA-CASE-LEW-15489-1] p 1703 N94-20529
An assessment of the cost of microwave sintering ceramic tiles for armor applications
[DE94-000978] p 1693 N94-21850
Effect of powder characteristics on gas-pressure sintering of Si3N4 with rare earth additives
[DE94-000330] p 1694 N94-21945
Fabrication of whisker-toughened alumina tubes
[DE94-001012] p 1677 N94-22022

SIS (SEMICONDUCTORS)
Layered thin-edged field-emitter device
[AD-D015932] p 1751 N94-20350

SIS (SUPERCONDUCTORS)
Quantum noise studies with superconducting tunnel junction mixers
[AD-A270897] p 2012 N94-19897
Layered thin-edged field-emitter device
[AD-D015932] p 1751 N94-20350

SITE SELECTION
Ground wave emergency network. Final operational capability. Environmental assessment for south central Montana relay node, site no. RN8C925MT
[AD-A267795] p 1716 N94-19964

SIZE DISTRIBUTION
Intensity and polarization of light scattered by size distributions of randomly oriented nonspherical particles p 1721 N94-20416
Determination of cosmic bodies size-velocity distribution by observation of current impacts on Mars p 2082 N94-20648
Distribution of small volcanic cones on the surface of Venus by size and elevation: Implications for differential deposition of volcanic features p 2110 N94-20731
Size distributions and aerodynamic equivalence of metal chondrules and silicate chondrules in Acfer 059 p 2084 N94-20773
Triton's cratering record and its time of capture p 2122 N94-20802

SKIN (ANATOMY)
Physiologically based pharmacokinetic modelling of percutaneously absorbed dibromomethane utilizing multiple dermal sub-compartments
[AD-A271106] p 1889 N94-19981
Enhancement of wound healing by biosynthetic growth factor
[AD-A272517] p 1892 N94-21415

SKIN FRICTION
Principles and applications of oil film interferometry for measuring wall friction fields in air flows
[ETN-93-95062] p 1798 N94-20147

SKIN TEMPERATURE (BIOLOGY)
Physiological efficacy of a lightweight ambient air cooling unit for various applications
[AD-A272952] p 1896 N94-21247

SKY SURVEYS (ASTRONOMY)
A deep x ray survey in the Lockman hole and the soft x ray log N - log S
[NASA-CR-194698] p 2054 N94-20174
Optical and Gamma Ray Space Observations
[NASA-TM-109389] p 2149 N94-20602
Second Annual Conference on Astronomical Data Analysis Software and Systems. Abstracts
[NASA-TM-108245] p 2057 N94-22438
Deep near-infrared survey of the Southern Sky (DENIS) p 2062 N94-22467
The extreme ultraviolet explorer archive p 2047 N94-22468
Visualizing the universe, part 2 p 2063 N94-22472
Visualizing the universe, part 1 p 2064 N94-22476
Data indexing techniques for the EUVE all-sky survey p 2048 N94-22503
Guide star catalogue data retrieval software 2 p 1927 N94-22533
SkICAT: A cataloging and analysis tool for wide field imaging surveys p 2049 N94-22546
Miyun 232 MHz survey 1: Fields centered at: alpha:00(h)41(m), delta:41 deg 12 min and alpha: 07(h)00(m),delta:35 deg 00 min p 2080 N94-22554
ROSAT data analysis with EXSAS p 2080 N94-22555
Results from ROSAT p 2000 N94-22630
Compton Gamma Ray Observatory highlights of the sky survey p 2002 N94-22642

SLABS
Time-lapiace-transform-domain analysis of wave propagation in planar waveguides
[PB93-215226] p 1960 N94-22096

SLEEP
Physiological correlates of stress-induced decrements in human perceptual performance
[DOT/FAA/AM-93/19] p 1893 N94-20081

SLIDING FRICTION
Microscopic modeling of tribological and interfacial phenomena
[AD-A271864] p 1823 N94-20464
In-vacuo slip testing of materials for SSRMS friction brakes p 1661 N94-21381
Detailed study of oxidation/wear mechanism in lox turbopump bearings
[NASA-TM-108434] p 1825 N94-21580

SLIP CASTING
Improved ceramic slip casting technique — application to aircraft model fabrication
[NASA-CASE-LAR-14471-1] p 1702 N94-20377
Fabrication of whisker-toughened alumina tubes
[DE94-001012] p 1677 N94-22022

SLOPES
Resonantly pumped, erbium-doped, GSGG, 2.8 micron, solid state laser with energy recycling and high slope efficiency
[AD-D015920] p 1815 N94-20060
Topographic slope from the SAR interferometric phase gradient p 1731 N94-20459
Comparison of flank modification on Ascraeus and Arsia Montes volcanoes, Mars p 2140 N94-20903

SLOT ANTENNAS
Recent activities in printed Antennas at LeRC p 1722 N94-20422
Linearly tapered slot antenna with dielectric superstrate p 1734 N94-20505
Slot-coupled patch antenna with coplanar waveguide feed p 1734 N94-20506
Linearly tapered slot antenna circular array for mobile communications
[NASA-TM-106441] p 1769 N94-21808

SLOTS
Analysis of microstrip dipoles and slots transversely coupled to a microstrip line using the FDTD method p 1718 N94-20405
An analysis of pressure driven cross-flow through a long slot connecting two parallel channels
[DE93-040181] p 1804 N94-21765

SLURRIES
Fabrication of porous ceramics by freeze-casting/freeze-drying
[PB93-202513] p 1705 N94-21425

SMART STRUCTURES
Quantification of uncertainties in the performance of smart composite structures
[NASA-TM-106335] p 1830 N94-20171

SMITH CHART
Manual design technique for broadband passive thin-film attenuators using the Smith chart p 1782 N94-22178

SMOKE
Zinc and titanium smoke: Chemical composition and physical characteristics
[FOA-C-40277-4.9] p 1680 N94-20552

SMOKE DETECTORS
Army aircraft fire-detection systems operation and reliability
[AD-A271327] p 1641 N94-20912

SMOOTHING
Numerical study of a multigrid method with four smoothing methods for the incompressible Navier-Stokes equations in general coordinates p 1806 N94-21487
A lower bound on wait-free counting
[CWI-CS-R9307] p 1915 N94-21537

SNOW
Studies of Greenland using the SEASAT scatterometer p 1725 N94-20433
Radar backscattering from snow facies of the Greenland ice sheet: Results from the AIRSAR 1991 campaign p 1725 N94-20434
The evolution of the early Martian climate and the initial emplacement of crustal H2O p 2143 N94-21665
The Martian valley networks: Origin by niveo-fluvial processes p 2146 N94-21682
Observations of multi-layered clouds using K-band radar p 1874 N94-22311

SNOW COVER
Snow cover measurements and areal assessment of precipitation and soil moisture
[WMO-749] p 1841 N94-21068

SOAPS
Guanidine based vehicle/binders for use with oxides, metals, and ceramics
[NASA-CASE-LEW-15314-1] p 1700 N94-20195

SOBOLEV SPACE
Orthogonal pairs and zeros of Sobolev-type orthogonal polynomials
[REPT-92-46] p 1953 N94-21059

SOCIAL FACTORS
Soviet society informatization: The USSR state program p 2046 N94-22058
Microdynamic model of reproduction: Taxation and currency issue as regulators of economy p 2053 N94-22084

SOCIOLOGY
Female security as a general mobility condition
[ISBN-3-79-831536-1] p 2039 N94-20153

SODIUM
Laser guide star adaptive optics: Present and future
[DE93-018642] p 1989 N94-21619

SODIUM CHLORIDES
Swelling equilibria for cationic 2-hydroxyethyl methacrylate (HEMA)-based hydrogels
[DE94-000728] p 1707 N94-21856

SODIUM COMPOUNDS
Neutron-scattering studies of Yb-bearing silicate glasses
[DE93-019768] p 1700 N94-20265
Evaporation of a sodium tellurite melt in the jamic low gravity drop shaft p 1713 N94-20605

SODIUM HYDROXIDES
Improvement of the stability of the process for synthesizing chemically prepared varistor powder
[DE94-000345] p 1763 N94-21654

SODIUM SULFUR BATTERIES
Advanced batteries for electric vehicle applications: Nontechnical summary
[DE93-019007] p 1748 N94-19885

SOFTWARE ENGINEERING
Qualifying codes under software quality assurance: Two examples as guidelines for codes that are existing or under development
[DE93-040452] p 1904 N94-20097
Data and Analysis Center for Software
[AD-A270571] p 2041 N94-20106
A comprehensive software engineering educational experience
[AD-A270583] p 1905 N94-20109
A proposed research program in information processing
[NASA-CR-194271] p 2041 N94-20134
A proposal for reverse engineering CASE tools to support new software development
[DE93-040207] p 1906 N94-20281
Probability of detection calculations using MATLAB
[AD-A271958] p 1736 N94-20578
Advanced software development workstation: Knowledge base methodology: Methodology for first Engineering Script Language (ESL) knowledge base
[NASA-CR-193643] p 1930 N94-21065
Design of a computer assisted tool for object oriented acquisition, modeling and simulation of knowledge structure
[ETN-93-94183] p 1910 N94-21152
A practical software engineering curriculum: A pilot study
[AD-A272781] p 1911 N94-21183
An investigation into the state of the practice of CASE tool integration
[AD-A272441] p 1912 N94-21205
Development and operations of the Astrophysics Data System
[NASA-CR-194691] p 2043 N94-21270
The NCC project: A quality management perspective
p 1828 N94-21324
Let your fingers do the walking: The projects most invaluable tool p 1922 N94-21325
Software metrics: The key to quality software on the NCC project p 1922 N94-21326
Network command processing system overview
p 1935 N94-21351
MAYGEN: A symbolic debugger generation system
[AD-A272512] p 1913 N94-21413
Conversion and maintenance of Co-oP for Windows
[AD-A272513] p 1914 N94-21414
An evaluation of integration of the trace assertion method with the box structure method for coding in C++
[DE93-040480] p 1918 N94-21924
The Soviet software market: Current state and aspects of development p 1923 N94-22066
Application development in a PC/LAN environment
p 1923 N94-22067
Industry standards: Key to distributed computing
p 1938 N94-22070
Developing software to RTCA DO-178A
p 1645 N94-22155
The why, what, and how of Ada software development
p 1779 N94-22157
A software environment for the exploitation of the MAR image sensor p 1785 N94-22200
Trends in software reliability modeling
p 1788 N94-22214
Second Annual Conference on Astronomical Data Analysis Software and Systems. Abstracts
[NASA-TM-108245] p 2057 N94-22438
Scientific computing in the 1990ies: An astronomical perspective p 2057 N94-22440
Fortran for the nineties p 1926 N94-22481
Programmability in AIPS++ p 1926 N94-22482
GammaCore: The Compton Observatory research environment p 2048 N94-22509
XPI: The Xanadu Parameter Interface
p 1927 N94-22513
The ISO SWS on-line system p 1927 N94-22522
Khoros software specification format and interoperability p 1927 N94-22523
The evolution of the FIGARO data reduction system
p 2048 N94-22528

SOFTWARE RELIABILITY
Qualifying codes under software quality assurance: Two examples as guidelines for codes that are existing or under development
[DE93-040452] p 1904 N94-20097
Test and evaluation: DOD has been slow in improving testing of software-intensive systems
[AD-A271541] p 1908 N94-20917
An assessment of the statistical and editorial output of text analysis programs
[AD-A272185] p 2042 N94-20924
Fault tolerant real-time systems
[AD-A272878] p 1899 N94-21195
Real-time fault tolerant computer systems
[AD-A272909] p 1899 N94-21230
Using stream interleaving to eliminate the need for interlocks in deeply pipelined processors
p 1781 N94-22175
Trends in software reliability modeling
p 1788 N94-22214

SOFTWARE REUSE
Advanced software development workstation: Knowledge base methodology: Methodology for first Engineering Script Language (ESL) knowledge base
[NASA-CR-193643] p 1930 N94-21065

SOFTWARE TOOLS
SISSY: An example of a multi-threaded, networked, object-oriented databased application
[DE93-019742] p 2041 N94-19811
Reference manual for a Requirements Specification Language (RSL), version 2.0
[NASA-CR-191460] p 1898 N94-20039
PREVAIL-DM: A framework-based environment for formal hardware verification
[RR-899] p 1905 N94-20164
Advanced software development workstation: Knowledge base methodology: Methodology for first Engineering Script Language (ESL) knowledge base
[NASA-CR-193643] p 1930 N94-21065
Experiments on technology mapping using different cell libraries p 1758 N94-21118
Design of a computer assisted tool for object oriented acquisition, modeling and simulation of knowledge structure
[ETN-93-94183] p 1910 N94-21152
An investigation into the state of the practice of CASE tool integration
[AD-A272441] p 1912 N94-21205
Integration opportunities for computer models, methods, and GIS used in Corps planning studies
[AD-A271714] p 2044 N94-21354
Combination of on ground experiments and analysis software for the evaluation of material degradation in space (SILEX project) p 1662 N94-21389
Security evaluation of Unix networks
[AD-A273076] p 1945 N94-21520
Computer-Aided Test Equipment Graphics System (CATEGS)
[DE94-000383] p 1915 N94-21561
Analog/digital pH meter system I.C.
p 1764 N94-21701
Heuristic-based scheduling algorithm for high level synthesis p 1764 N94-21704
Model-based reasoning for power system management using KATE and the SSM/PMAD
[NASA-CR-194716] p 1671 N94-21882
Automated analysis tools for reducing spacecraft telemetry data
[DE94-000400] p 1657 N94-21981
Three original programmes for managers
p 1923 N94-22083
Method and software for decision making in public problems p 1923 N94-22087
Formal hardware verification in Maple
p 1771 N94-22112
Software systems used for unstructured grid generation at NASA Langley p 1918 N94-22351
NASA-Ames Research Center unstructured technology development p 1919 N94-22352
New IRAF stellar photometry software
p 1925 N94-22464
SPPTOOLS: Programming tools for the IRAF SPP language p 1925 N94-22474
FITS data conversion efforts at the Compton Observatory Science Support Center
p 1926 N94-22488
The IDL astronomy user's library
p 2048 N94-22500
GRO/EGRET data analysis software: An integrated system of custom and commercial software using standard interfaces p 1926 N94-22501
XPI: The Xanadu Parameter Interface
p 1927 N94-22513
Development of the FITS tools package for multiple software environments p 1927 N94-22516
Managing an archive of weather satellite images
p 2048 N94-22525
Tools for the IDL widget set within the X-windows environment p 1927 N94-22538
DECONV-TOOL: An IDL based deconvolution software package p 1927 N94-22542
The STARLINK software collection
p 1927 N94-22545

SOI (SEMICONDUCTORS)
Fully-depleted silicon-on-sapphire and its application to advanced VLSI design p 1765 N94-21709

SOIL MAPPING
Analysis of hyper-spectral AVIRIS image data over a mixed-conifer forest in Maine p 1838 N94-20959

SOIL MOISTURE
Synergism of active and passive microwave data for estimating bare surface soil moisture
p 1727 N94-20444
Application of neural network to remote sensing of soil moisture using theoretical polarimetric backscattering coefficients p 1730 N94-20455
Measurement of evapotranspiration with combined reflective and thermal infrared radiance observations
[NASA-CR-194802] p 1837 N94-20951
Snow cover measurements and areal assessment of precipitation and soil moisture
[WMO-749] p 1841 N94-21068
Areally averaged estimates of surface heat flux from ARM field studies
[DE93-018569] p 1859 N94-22036

SOIL SCIENCE
Soil temperatures
[KNMI-WR-92-05] p 1865 N94-20309
Visible-infrared properties of controlled laboratory soils
p 1685 N94-20689

SOILS
A general rough-surface inversion algorithm: Theory and application to SAR data p 1719 N94-20407
Visible-infrared properties of controlled laboratory soils
p 1685 N94-20689
Thermal infrared remote sensing and Kirchhoff's law: 1. Laboratory measurements p 1685 N94-20733
Determination of Martian soil mineralogy and water content using the Thermal Analyzer for Planetary Soils (TAPS) p 1812 N94-22433
Mass spectrometer-pyrolysis experiment for atmospheric and soil sample analysis on the surface of Mars p 1812 N94-22435

SOL-GEL PROCESSES
Preparation and properties of sol-gel derived PZT thin films for decoupling capacitor applications
[DE93-018853] p 2013 N94-19961
Photonics and nonlinear optics with molecular materials and polymers
[AD-A271747] p 1988 N94-21457

SOLAR ACTIVITY
Solar proton events from a 180 year depth profile of nitrate concentrations from the central Greenland ice sheet
[AD-A272888] p 2147 N94-21196
High resolution studies of the structure of the solar atmosphere
[AD-A273084] p 2147 N94-21522
Determination of coronal magnetic fields from vector magnetograms
[NASA-CR-194744] p 2147 N94-21877

SOLAR ACTIVITY EFFECTS
Tests of a simple data merging algorithm for the GONG project p 1927 N94-22549

SOLAR ARRAYS
Fabrication of stable large-area thin-film CdTe photovoltaic modules
[DE93-018204] p 1845 N94-20095
Self-deploying photovoltaic power system
[NASA-CASE-LEW-15308-1] p 1846 N94-20196

SOLAR ATMOSPHERE
High resolution studies of the structure of the solar atmosphere
[AD-A273084] p 2147 N94-21522
Solar imaging vector magnetograph
[NASA-CR-194729] p 1810 N94-21876

SOLAR BLANKETS
Self-deploying photovoltaic power system
[NASA-CASE-LEW-15308-1] p 1846 N94-20196

SOLAR CELLS
High efficiency epitaxial optical reflector solar cells
[DE93-017115] p 1845 N94-19805
Development of high-efficiency CdTe solar cells
[DE93-018206] p 1845 N94-19925
Development of a numerical simulation model for a-Si:H solar cells and application to the analysis of experimentally obtained spectral characteristics
[ETN-93-95061] p 1846 N94-20151
Advanced processing technology for high-efficiency thin-film CuInSe2 solar cells
[DE93-010045] p 1847 N94-21614
Fundamental studies of defect generation in amorphous silicon alloys grown by remote plasma-enhanced chemical-vapor deposition
[DE93-017083] p 2029 N94-21615
Research on polycrystalline thin-film submodules based on CuInSe2 materials
[DE93-018223] p 2029 N94-21617
Stable, high-efficiency amorphous-silicon solar cells with low hydrogen content
[DE93-018214] p 1848 N94-21826
Thin-film CdTe and CuInSe2 photovoltaic technologies
[DE93-018217] p 1848 N94-21827
Annual Report, Materials Science Branch, FY 1992
[DE94-000204] p 1849 N94-22015

Surveys on specific patterns of facility intallation of photovoltaic power generating technologies for international cooperation
[DE94-714901] p 1850 N94-22092
Research on stable, high-efficiency amorphous silicon multijunction modules
[DE93-016220] p 1850 N94-22257

SOLAR COLLECTORS
Fluid absorption solar energy receiver
[NASA-CR-194688] p 1846 N94-20229

SOLAR CORONA
High resolution studies of the structure of the solar atmosphere
[AD-A273084] p 2147 N94-21522
Determination of coronal magnetic fields from vector magnetograms
[NASA-CR-194744] p 2147 N94-21877
Highlights of Yohkoh results p 2001 N94-22632
X ray jets in the solar corona: Observations with Yohkoh Soft X Ray Telescope p 2004 N94-22655
Large-scale structure of the solar plasma corona: An analysis of Yohkoh SXT images p 2004 N94-22657
MHD relaxation in magnetic loops p 2004 N94-22658

SOLAR CORPUSCULAR RADIATION
A long-term change of the AR/KR/XE fractionation in the solar corpuscular radiation p 2136 N94-20875
Comparison of single event upset rates for microelectronic memory devices during interplanetary solar particle events p 1754 N94-21085
Mean elemental composition and He-3 enrichments in solar energetic particles p 2006 N94-22670

SOLAR DYNAMIC POWER SYSTEMS
Fluid absorption solar energy receiver
[NASA-CR-194688] p 1846 N94-20229

SOLAR ENERGY
Investigation on the chemically fixing technique of carbon dioxide utilizing solar energy
[DE94-714886] p 1849 N94-22043

SOLAR ENERGY CONVERSION
Development of high-efficiency CdTe solar cells
[DE93-018206] p 1845 N94-19925
Fluid absorption solar energy receiver
[NASA-CR-194688] p 1846 N94-20229
Proceedings of the 1993 DOE/NREL Hydrogen Program Review
[DE93-018207] p 1847 N94-21616

SOLAR FLARES
Comparison of single event upset rates for microelectronic memory devices during interplanetary solar particle events p 1754 N94-21085
Berne (Switzerland) solar observations: Data for April 1991 - August 1992
[REPT-59] p 2147 N94-21150
Development, refinement, and testing of a short term solar flare prediction algorithm
[NASA-CR-194726] p 2147 N94-21815
Development, refinement, and testing of a short term solar flare prediction algorithm
[NASA-CR-194727] p 2147 N94-21832
Solar imaging vector magnetograph
[NASA-CR-194729] p 1810 N94-21876
Highlights of Yohkoh results p 2001 N94-22632
Preliminary results of observations of solar flares with Nobeyama Radioheliograph p 2001 N94-22633
Radiation from solar flares p 2001 N94-22634
Energy release at Alfvenic fronts in solar flares p 2003 N94-22652
Non-equilibrium ionization in an M class solar flare p 2004 N94-22653
Numerical simulation of magnetic reconnection associated with emerging flux in the solar atmosphere p 2004 N94-22654
Yohkoh Gamma ray Spectral Observations (YGSO) p 2004 N94-22656
Large-scale structure of the solar plasma corona: An analysis of Yohkoh SXT images p 2004 N94-22657
MHD relaxation in magnetic loops p 2004 N94-22658
Current loop coalescence studied by 3-D electromagnetic particle code p 2005 N94-22660
Formation of fast magnetosonic shock waves during two current loops collision in solar flare p 2005 N94-22662
Acceleration of solar-flare particles as viewed from their chemical composition p 2006 N94-22672

SOLAR FLUX
Berne (Switzerland) solar observations: Data for April 1991 - August 1992
[REPT-59] p 2147 N94-21150
Requirements for the early atmosphere of Mars from nitrogen isotope ratios p 2144 N94-21669
Mars and the early Sun p 2146 N94-21683
Comparisons of downwelling radiation to model predictions based on groundbased measurements during FIRE 1991 p 1876 N94-22320

SOLAR GENERATORS
Investigation on the chemically fixing technique of carbon dioxide utilizing solar energy
[DE94-714886] p 1849 N94-22043
Surveys on specific patterns of facility intallation of photovoltaic power generating technologies for international cooperation
[DE94-714901] p 1850 N94-22092

SOLAR INSTRUMENTS
Concept report: Experimental vector magnetograph (EXVM) operational configuration balloon flight assembly
[NASA-CR-194702] p 1638 N94-21776
Solar imaging vector magnetograph
[NASA-CR-194729] p 1810 N94-21876

SOLAR MAGNETIC FIELD
Concept report: Experimental vector magnetograph (EXVM) operational configuration balloon flight assembly
[NASA-CR-194702] p 1638 N94-21776
Development, refinement, and testing of a short term solar flare prediction algorithm
[NASA-CR-194726] p 2147 N94-21815
Solar imaging vector magnetograph
[NASA-CR-194729] p 1810 N94-21876
Determination of coronal magnetic fields from vector magnetograms
[NASA-CR-194744] p 2147 N94-21877
Solar full-disk magnetic field image receiving system and observation software p 2079 N94-22552

SOLAR OBSERVATORIES
Tests of a simple data merging algorithm for the GONG project p 1927 N94-22549
Highlights of Yohkoh results p 2001 N94-22632
Yohkoh Gamma ray Spectral Observations (YGSO) p 2004 N94-22656

SOLAR OSCILLATIONS
Tests of a simple data merging algorithm for the GONG project p 1927 N94-22549

SOLAR PHYSICS
Development, refinement, and testing of a short term solar flare prediction algorithm
[NASA-CR-194727] p 2147 N94-21832
Determination of coronal magnetic fields from vector magnetograms
[NASA-CR-194744] p 2147 N94-21877

SOLAR PLANETARY INTERACTIONS
Mars and the early Sun p 2146 N94-21683

SOLAR PROTONS
Solar proton events from a 180 year depth profile of nitrate concentrations from the central Greenland ice sheet
[AD-A272888] p 2147 N94-21196
Acceleration of solar-flare particles as viewed from their chemical composition p 2006 N94-22672

SOLAR RADIATION
SCR neon and argon in Kapoeta feldspar: Evidence for an active ancient Sun p 2106 N94-20712
The simulation of action of some space environment factors on Teflon and on rubber materials p 1661 N94-21380
The energy performance of prototype holographic glazings
[DE93-040451] p 1809 N94-21545
The young Sun and photochemistry of the primitive Martian atmosphere p 2145 N94-21679
Evolution of the Martian atmosphere p 2146 N94-21680
Surveys on specific patterns of facility intallation of photovoltaic power generating technologies for international cooperation
[DE94-714901] p 1850 N94-22092
The use of ERBE data for climate studies p 1860 N94-22286

SOLAR RADIO EMISSION
Oceanic in situ Fraunhofer-line characteristics: Fraunhofer-line underwater experiment (FLUX)
[AD-A270659] p 1881 N94-19952

SOLAR REFLECTORS
High efficiency epitaxial optical reflector solar cells
[DE93-017115] p 1845 N94-19805

SOLAR SENSORS
Multisensor pinhole yawsonde
[AD-A271715] p 1808 N94-20930

SOLAR SIMULATORS
Solar simulator for solar dynamic space power system testing
[NASA-TM-106393] p 1984 N94-20140

SOLAR SPECTRA
Berne (Switzerland) solar observations: Data for April 1991 - August 1992
[REPT-59] p 2147 N94-21150

SOLAR SYSTEM EVOLUTION
FE-60 and the evolution of eucrites p 2083 N94-20768
Variety in planetary systems p 2086 N94-20871

SOLAR WIND
Modeling of the coupled magnetospheric and neutral wind dynamos
[NASA-CR-194728] p 1856 N94-20537
A long-term change of the AR/KR/XE fractionation in the solar corpuscular radiation p 2136 N94-20875
High resolution studies of the structure of the solar atmosphere
[AD-A273084] p 2147 N94-21522
Implications of Viking dayside auroral measurements
[ISBN-0-315-83273-8] p 1861 N94-22575
Laboratory relations between the solar wind dynamic pressure and the magnetospheric structures of the Earth and comets p 2003 N94-22647
Laboratory structure of the heliopause p 2003 N94-22648
Compressible MHD turbulence in the interplanetary medium p 2003 N94-22650
Tangential stress due to Kelvin-Helmholtz instability at the magnetospheric boundary p 2003 N94-22651
Solar wind-magnetosphere interaction as simulated by a 3D, EM particle code p 2007 N94-22674

SOLDERED JOINTS
Finite element mesh generation and analysis of solder joints for fatigue life predictions
[AD-A271329] p 1829 N94-19937
Process characterization and control of hand-soldered printed wiring assemblies
[DE93-041290] p 1763 N94-21652

SOLDERING
Solder technology in the manufacturing of electronic products
[DE93-018842] p 1699 N94-19960
Process characterization and control of hand-soldered printed wiring assemblies
[DE93-041290] p 1763 N94-21652

SOLDERS
Finite element mesh generation and analysis of solder joints for fatigue life predictions
[AD-A271329] p 1829 N94-19937
Solder technology in the manufacturing of electronic products
[DE93-018842] p 1699 N94-19960

SOLENOIDS
Performance of the high brightness linac for the Advanced Free Electron Laser Initiative at Los Alamos
[DE93-040141] p 1816 N94-20277

SOLID CRYOGENS
Energy storage and conversion in solid hydrogen
[AD-A271439] p 1845 N94-20086

SOLID ELECTRODES
Surface electrochemistry of metals
[AD-A272913] p 1691 N94-21245

SOLID ELECTROLYTES
Modeling of polymer electrolyte fuel cell systems
[DE93-041187] p 1847 N94-21774
The electrochemical performance of thin-electrolyte solid oxide fuel cells
[DE93-041184] p 1848 N94-21942
Survey on chemical engineering technologies for the global environmental protection
[DE94-714887] p 1852 N94-22044

SOLID MECHANICS
The program system for the diagnostics of strains and fracture prediction of solids p 1836 N94-22065

SOLID PHASES
Cooling apparatus and couplings therefor
[NASA-CASE-ARC-11921-1] p 1800 N94-20371
Some experiments on using backscattered electron and energy dispersive x ray imaging in determination of portland cement clinker phase composition p 1708 N94-21893

SOLID PROPELLANT COMBUSTION
Detailed structure study of an H2/N2O/Ar flame employing molecular beam mass spectrometry, laser spectroscopy, and modeling
[AD-A270720] p 1679 N94-20111

SOLID PROPELLANT ROCKET ENGINES
Investigation of flame driving and flow turning in axial solid rocket instabilities
[AD-A271066] p 1667 N94-20015

SOLID ROCKET PROPELLANTS
Chemistry of the burning surface
[AD-A272725] p 1681 N94-21181

SOLID SOLUTIONS
Metastable bcc phase formation in the Nb-Cr system
[DE93-018376] p 2012 N94-19926

SOLID STATE
Shock wave interactions with exothermic mixtures
[AD-A271149] p 1829 N94-19836
An equation of state for shock in homogeneous materials and comparison to shock data
[AD-A271436] p 1829 N94-19881
Solid State Technology Branch of NASA Lewis Research Center: Fifth Annual Digest
[NASA-TM-106303] p 1732 N94-20497

High power, electron-beam induced switching in diamond
[DE93-040535] p 1768 N94-21770
SOLID STATE DEVICES
Multiport solid-state imager characterization at variable pixel rates
[DE93-018366] p 1808 N94-20287
Compositional diversity of the lunar North Pole: Preliminary analyses of Galileo SSI data
p 2101 N94-20686
Compact lightweight CO2 laser for SDIO application
[AD-A273010] p 1817 N94-21284
SOLID STATE LASERS
Suppression of relaxation oscillations in flashpumped, two-micron tunable solid state lasers
[AD-D015928] p 1814 N94-19800
Resonantly pumped, erbium-doped, GSGG, 2.8 micron, solid state laser with energy recycling and high slope efficiency
[AD-D015920] p 1815 N94-20060
Simulations of spectral broadening by cross-phase modulation (XPM) with chaotic light pulses
[DE93-019623] p 1819 N94-21872
SOLID STATE PHYSICS
Spin-polaron theory of high-T(c) superconductivity. 3: Gap function and critical temperature
[DE93-019198] p 2030 N94-21831
SOLID WASTES
Environmental protection using social costing
[DE94-000492] p 1853 N94-22569
SOLID-SOLID INTERFACES
Surface treatment of InP and contribution to the optimization of the InP(p)/InP(p) regrown interfaces grown by GSMBE
[ECL-92-48] p 2018 N94-20598
SOLIDIFICATION
Microstructure evolution in the presence of constraints and implications on the properties of Mg-Li and Nb-Al constraints
[AD-A272088] p 1674 N94-20623
The incongruent melting and melt textured solidification process of Bi2Sr2CaCu3O8
[DE93-041123] p 2032 N94-21936
SOLIDIFIED GASES
Stability of the face-centered-cubic phase of heavy rare gas solids
[DE93-019949] p 1679 N94-20319
Theoretical phase diagrams for solid H(sub 2)
[DE94-001049] p 1684 N94-22395
SOLIDS
Thermal diffusivity measurements by photothermal laser beam deflection (PTD): Data analysis using the Levenberg-Marquardt algorithm p 1820 N94-21006
SOLITARY WAVES
Multidimensional solitons in fiber arrays
[DE93-019923] p 1983 N94-19862
Spatial patterns in semiconductor lasers
[DE93-040056] p 1814 N94-19865
Two-dimensional nonlinear Schrodinger equations and their properties
[AD-A272184] p 1952 N94-20923
The onset and spectra of a magnetized Langmuir turbulence p 2006 N94-22673
SOLUBILITY
High performance heavy alloys by alloying and process control
[AD-A271129] p 1689 N94-20019
The use of x ray techniques in the in situ study of corrosion
[DE93-019845] p 1690 N94-20301
Cathode materials for the molten carbonate fuel cell
[DE93-019515] p 1848 N94-21870
Water-enhanced solvation of organics
[DE93-040297] p 1683 N94-21947
SOLUTES
Water-enhanced solvation of organics
[DE93-040297] p 1683 N94-21947
SOLVATION
Water-enhanced solvation of organics
[DE93-040297] p 1683 N94-21947
SOLVENTS
Femtosecond Raman-induced Kerr effect study of polar solvent dynamics: Amides
[DE93-017563] p 1678 N94-19924
Chain propagation/step propagation polymerization chemistry. The preparation of solvent resistant well phase-separated thermoplastic elastomers
[AD-A271128] p 1699 N94-20016
Integral equation calculation of solvent activation free energies for electron and proton transfer reactions
[AD-A272665] p 1681 N94-21216
Dynamics of adsorbed, swollen block copolymers
[AD-A272013] p 1706 N94-21460
Techniques for the flux growth of optical materials: Growth of beta-barium borate
[AD-A272717] p 2028 N94-21505
Femtosecond dynamics in hydrogen-bonded solvents
[DE93-019937] p 1683 N94-21842
Water-enhanced solvation of organics
[DE93-040297] p 1683 N94-21947
SOOT
Dual-beam multiple wavelength light transmittance measurement for particle sizing in rocket motor plumes
[AD-A272491] p 1670 N94-21208
SORBENTS
A calcium oxide sorbent process for bulk separation of carbon dioxide
[DE93-019288] p 1847 N94-21540
SOS (SEMICONDUCTORS)
Single-event upset testing of the performance semiconductor 1750A CMOS/SOS chip set
[AD-A271158] p 2015 N94-20184
Fully-depleted silicon-on-sapphire and its application to advanced VLSI design p 1765 N94-21709
SOUND AMPLIFICATION
Journal of rehabilitation research and development, volume 30, number 1, 1993
[AD-A272956] p 1893 N94-21613
SOUND DETECTING AND RANGING
Mathematical model and analysis of the Tactical Unmanned Ground Vehicle (TUGV) using computer simulation
[AD-A272258] p 1824 N94-20576
SOUND GENERATORS
Acoustic monitoring of global ocean variability
[AD-A271998] p 1883 N94-21366
SOUND PRESSURE
Stability curves for a thermoacoustic prime mover
[AD-A272607] p 1968 N94-21422
Computation of the sound generated by isotropic turbulence
[NASA-CR-191543] p 1804 N94-21880
SOUND PROPAGATION
Mathematical model and analysis of the Tactical Unmanned Ground Vehicle (TUGV) using computer simulation
[AD-A272258] p 1824 N94-20576
SOUND TRANSMISSION
Acoustic monitoring of global ocean variability
[AD-A271998] p 1883 N94-21366
SOUND WAVES
Nonlinear acoustics: Periodic waveguide, finite-amplitude propagation in a medium having a distribution of relaxation processes, and production of an isolated negative pulse in water
[AD-A270530] p 1967 N94-19894
Acoustic radiation damping of flat rectangular plates subjected to subsonic flows
[NASA-TM-109382] p 1967 N94-20211
Mathematical model and analysis of the Tactical Unmanned Ground Vehicle (TUGV) using computer simulation
[AD-A272258] p 1824 N94-20576
A survey of the impact on acoustic propagation of warm core ocean eddys
[AD-A272188] p 1883 N94-20925
Comparison of higher order moment spectrum estimation techniques
[AD-A272967] p 1967 N94-21260
Approximation to sound radiation and scattering by simply supported layered cylinder
[AD-A272964] p 1967 N94-21306
Speed of sound data and related models for mixtures of natural gas constituents
[PB93-200822] p 1968 N94-21447
Surface acoustic wave sensing of VOC's in harsh chemical environments
[DE93-040721] p 1968 N94-21751
Three dimensional ultrasonic imaging
[DE93-040549] p 1968 N94-22003
Acoustic, fiber optic, and silicon microelectronic microsensors research and development activities at Sandia National Laboratories
[DE93-019075] p 1770 N94-22040
Interface reflection of spherical acoustic waves in the first- and second-order rational parabolic approximations and their artifacts
[PB93-215424] p 1969 N94-22261
Transient acoustic wave modeling: Higher-order WKBJ asymptotics and symbolical manipulation (revised)
[PB93-215432] p 1969 N94-22262
Enhanced absorption of p-modes on sunspot and plage regions p 2006 N94-22671
SOURCE PROGRAMS
A parallelizing compiler based on partial evaluation
[AD-A270838] p 1898 N94-19832
Application guide for universal source encoding for space
[NASA-TP-3441] p 1741 N94-21783
SOUTHERN SKY
Deep near-infrared survey of the Southern Sky (DENIS) p 2062 N94-22467
SPACE BASED RADAR
Space-based radar for moving target detection
p 1745 N94-22143
SPACE CHARGE
Space-charge dominated beam transport in magnetic quadrupoles with large aperture ratios
[DE93-040443] p 1992 N94-20004
Simulation studies of space-charge-dominated beam transport in large aperture ratio quadrupoles
[DE93-019238] p 1981 N94-21440
Evaluation of externally heated pulsed MPD thruster cathodes
[NASA-CR-191090] p 1670 N94-21565
SPACE COMMUNICATION
A compact, portable EHF/SHF antenna for advanced SCAMP
[AD-A272614] p 1739 N94-21211
Mission Operations Support Area (MOSA) for ground network support p 1932 N94-21331
Using manufacturing message specification for monitor and control at Venus p 1932 N94-21333
Predicting scheduling success p 1932 N94-21334
Generating and evaluating alternate schedules
p 1933 N94-21336
The Test Analysis Retrieval System (TARS): Meeting the challenges of the network's test processes
p 1933 N94-21337
SPACE DEBRIS
Space Station trash removal system
[NASA-CASE-MSC-21723-1] p 1657 N94-20367
Numerical simulations of hypervelocity impact experiments involving single Whipple bumper shields
[AD-A272123] p 1831 N94-20572
Determination of parameters for hypervelocity dust grains encountered in near-Earth space
p 2084 N94-20817
A fresh look at crater scaling laws for normal and oblique hypervelocity impacts p 1666 N94-20864
Orbital debris and micrometeoroids: LDEF and Mir data p 1659 N94-21368
The implications of the LDEF results on Space Station Freedom power system materials p 1660 N94-21377
Meteoroids and debris impact risk assessment on Columbus and Hermes using a realistic geometrical analysis tool p 1662 N94-21388
SPACE ENVIRONMENT SIMULATION
Apparatus for simulating an exoatmospheric structure
[NASA-CASE-MSC-21975-1] p 1653 N94-20339
New technique for oil backstreaming contamination measurements p 1652 N94-20511
Fifth International Symposium on Materials in a Space Environment
[ISBN-2-85-428293-0] p 1659 N94-21367
Flight and laboratory testing of materials in low Earth orbit p 1659 N94-21369
Complex-2: Low Earth orbital environment simulation facility for materials durability evaluation
p 1653 N94-21370
The simulation of action of some space environment factors on Teflon and on rubber materials
p 1661 N94-21380
Effect of geostationary environment constituents on secondary electron emission rates p 1661 N94-21382
Simulated space environmental effects on some experimental high performance polymers
p 1662 N94-21385
Durability of thermal control and environmental protective materials for the SSRMS in simulated LEO environment p 1663 N94-21392
Atomic oxygen interaction with spacecraft materials: Relationship between orbital and ground-based testing for materials certification p 1663 N94-21393
Fast oxygen atom studies related to low Earth orbit activities p 1663 N94-21395
SPACE EXPLORATION
Low energy CMOS for space applications
p 1768 N94-21735
Mars exploration study workshop 2
[NASA-CP-3243] p 2146 N94-21883
Robotic concepts for operation in barren terrain
[DE93-040539] p 1946 N94-21925
SPACE FLIGHT
Cosmos 2229
[NASA-CR-194734] p 1895 N94-20338
SPACE MAINTENANCE
Space Shuttle Mission STS-61: Hubble Space Telescope servicing mission-01
[NASA-TM-109344] p 1653 N94-20192
EVA tools and equipment reference book
[NASA-TM-109350] p 1897 N94-21812
SPACE MISSIONS
Space Shuttle Mission STS-61: Hubble Space Telescope servicing mission-01
[NASA-TM-109344] p 1653 N94-20192

NEP Early Flight program: System performance and development considerations
[NASA-TM-106415] p 1654 N94-21570
A generic archive protocol and an implementation p 2047 N94-22493

SPACE NAVIGATION
Pointing control design for autonomous space vehicle applications
[DE93-019943] p 1657 N94-19863

SPACE PERCEPTION
Why stereo vision is not always about 3D reconstruction
[AD-A270522] p 1939 N94-19893

SPACE PLASMAS
A study of Saturn's E-ring particles using the Voyager 1 plasma wave instrument
[NASA-CR-194694] p 2068 N94-20048
Ionospheric photoelectrons measured at geosynchronous orbit
[AD-A272431] p 1857 N94-21202
A new innovative instrument for space plasma instrumentation
[NASA-CR-194736] p 1666 N94-21780
Circumstellar environments of Be stars at infra-red and radio wavelengths
[ISBN-0-315-83135-9] p 2081 N94-22426
Consequences of chaotic particle motion for the stability of space plasma current sheets p 2001 N94-22636
Physical properties of dense astrophysical plasmas p 2001 N94-22637
Thermal properties and radiation processes in astrophysical plasmas p 2002 N94-22640
Pair plasmas in the galactic center region and in Nova Muscae p 2009 N94-22691

SPACE PLATFORMS
Obtaining surface optical properties from space-based lidar systems
[AD-A272831] p 1967 N94-21172

SPACE POWER REACTORS
Preliminary SP-100/Stirling heat exchanger designs
[NASA-TM-106444] p 1670 N94-21809
SPACE-R Thermionic Space Nuclear Power System: Design and Technology Demonstration Program
[DE93-013969] p 1670 N94-21824
Temperature and Doppler coefficients of various space nuclear reactors
[DE94-001368] p 1671 N94-21979

SPACE PROCESSING
Melt-spin processing of high (Tc) oxide superconductors
[DE94-000696] p 2036 N94-22582

SPACE PROGRAMS
Aerospace: Facts and figures, 1992-1993
[AD-A272571] p 1635 N94-21419

SPACE SHUTTLE BOOSTERS
Parameters affecting hydrogen chloride measurements
[AD-A271326] p 1851 N94-20025

SPACE SHUTTLE MAIN ENGINE
Space Shuttle Main Engine. Overview p 1667 N94-20070
Rocketdyne turbomachinery p 1667 N94-20071
Future technical directions p 1668 N94-20072
Entry velocities at Mars and Earth for short transit times
[AD-A272591] p 1665 N94-21420
Detailed study of oxidation/wear mechanism in lox turbopump bearings
[NASA-TM-108434] p 1825 N94-21580

SPACE SHUTTLE ORBITERS
Compilation of reinforced carbon-carbon transatlantic abort landing arc jet test results
[NASA-TM-104778] p 1676 N94-21634

SPACE SHUTTLE PAYLOADS
Space Shuttle Mission STS-61: Hubble Space Telescope servicing mission-01
[NASA-TM-109344] p 1653 N94-20192

SPACE SHUTTLES
Future technical directions p 1668 N94-20072
Space Shuttle Mission STS-61: Hubble Space Telescope servicing mission-01
[NASA-TM-109344] p 1653 N94-20192

SPACE SIMULATORS
Measurements of the dielectric properties of simulated comet material as part of the KOSI 10 experiment p 2085 N94-20841

SPACE STATION FREEDOM
System performance predictions for Space Station Freedom's electric power system
[NASA-TM-106396] p 1667 N94-20062
The International Telecommunications Satellite (INTELSAT) Solar Array Coupon (ISAC) atomic oxgyen flight experiment: Techniques, results and summary p 1662 N94-21391

SPACE STATION POWER SUPPLIES
The implications of the LDEF results on Space Station Freedom power system materials p 1660 N94-21377

SPACE STATION STRUCTURES
Spline screw payload fastening system
[NASA-CASE-GSC-13454-1] p 1821 N94-20126

SPACE STATIONS
Space Station trash removal system
[NASA-CASE-MSC-21723-1] p 1657 N94-20367
Numerical simulations of hypervelocity impact experiments involving single Whipple bumper shields
[AD-A272123] p 1831 N94-20572
Rewetting of monogroove heat pipe in Space Station radiators
[NASA-CR-194781] p 1804 N94-21820

SPACE SURVEILLANCE (GROUND BASED)
NAVSPASUR sensor system digital signal processing receiver. Volume 1: Hardware and software overview
[AD-A272899] p 1738 N94-21198
NAVSPASUR sensor system digital signal processing receiver. Volume 2: Function and capabilities of hardware and software components
[AD-A272900] p 1739 N94-21218

SPACE TOOLS
EVA tools and equipment reference book
[NASA-TM-109350] p 1897 N94-21812

SPACE TRANSPORTATION
NASA Propulsion Engineering Research Center, volume 1
[NASA-CR-194721-VOL-1] p 1671 N94-22428

SPACE TRANSPORTATION SYSTEM
A simulation model for probabilistic analysis of Space Shuttle abort modes
[NASA-TM-108432] p 1656 N94-21859
Johnson Space Center CFD grid generation requirements p 1919 N94-22355

SPACE TRANSPORTATION SYSTEM FLIGHTS
Space Shuttle Mission STS-61: Hubble Space Telescope servicing mission-01
[NASA-TM-109344] p 1653 N94-20192
Debris/ice/TPS assessment and integrated photographic analysis for Shuttle Mission STS-51
[NASA-TM-109189] p 1656 N94-21884

SPACE-TIME FUNCTIONS
Interface reflection of spherical acoustic waves in the first- and second-order rational parabolic approximations and their artifacts
[PB93-215424] p 1969 N94-22261
Non commutative geometry and physics
[PB93-215499] p 1961 N94-22264
Canonically covariant formulation of Landau's Newtonian superfluid dynamics
[PB93-221034] p 1805 N94-22272

SPACEBORNE ASTRONOMY
ASpect: A new spectrum and line analysis package for IRAF p 1926 N94-22485
SPIKE: Application for ASTRO-D mission planning p 1926 N94-22486
Quality control of EUVE databases p 2047 N94-22490
The application of artificial intelligence to astronomical scheduling problems p 1949 N94-22492

SPACEBORNE EXPERIMENTS
Stability limits and dynamics of nonaxisymmetric liquid bridges
[NASA-CR-194706] p 1797 N94-20037
Conversion of LDEF experiment M0003 sample observation database to MS-DOS formats
[AD-A272945] p 1681 N94-21226
Flight and laboratory testing of materials in low Earth orbit p 1659 N94-21369
German space experiments on Spacelab D-2 and Eureca-1 to investigate atomic oxygen interaction with materials p 1662 N94-21390
The International Telecommunications Satellite (INTELSAT) Solar Array Coupon (ISAC) atomic oxgyen flight experiment: Techniques, results and summary p 1662 N94-21391

SPACEBORNE PHOTOGRAPHY
The application of spaceborne synthetic aperture radar in the maritime environment
[DRA-TM(AWE)-91013] p 1737 N94-20596

SPACEBORNE TELESCOPES
UIT support observations archive p 2048 N94-22534

SPACECRAFT ANTENNAS
Magellan vertical polarization radar observations p 1744 N94-20691

SPACECRAFT CHARGING
Effect of geostationary environment constituents on secondary electron emission rates p 1661 N94-21382
Electrostatic charging and secondary effects in materials submitted to radiation in space p 1661 N94-21383
TROPIX plasma interactions group report
[NASA-CR-191149] p 1666 N94-21864

SPACECRAFT COMPONENTS
Clementine: An inexpensive mission to the Moon and Geographos p 1652 N94-20765
Process and apparatus for the release of a prestress initially applied to a mechanism such as a bearing on board a space vehicle
[CA-PATENT-APPL-SN-2,020,90] p 1824 N94-21142

SPACECRAFT CONSTRUCTION MATERIALS
Fifth International Symposium on Materials in a Space Environment
[ISBN-2-85-428293-0] p 1659 N94-21367
Flight and laboratory testing of materials in low Earth orbit p 1659 N94-21369
Complex-2: Low Earth orbital environment simulation facility for materials durability evaluation p 1653 N94-21370
Results of the post flight analyses on system materials for the LDEF-FRECOPA experiment p 1659 N94-21371
Integrity and testing concerns of thermostructural materials p 1661 N94-21384
Materials evaluation at ESA/ESTEC p 1662 N94-21386
Columbus: Materials for 30 years habitability in space p 1662 N94-21387
The International Telecommunications Satellite (INTELSAT) Solar Array Coupon (ISAC) atomic oxgyen flight experiment: Techniques, results and summary p 1662 N94-21391
Durability of thermal control and environmental protective materials for the SSRMS in simulated LEO environment p 1663 N94-21392
Atomic oxygen interaction with spacecraft materials: Relationship between orbital and ground-based testing for materials certification p 1663 N94-21393
Evaluation of plasma-deposited protective coatings for spacecraft applications p 1663 N94-21394
Fast oxygen atom studies related to low Earth orbit activities p 1663 N94-21395
Thermostructural material composites for space applications p 1664 N94-21398
Thermal control coatings p 1664 N94-21400
Study of space factors effect on materials for spacecraft external surfaces in NPO Energia programs p 1664 N94-21401
Columbus PMP Critical Technologies Program: Approach for materials life time prediction p 1664 N94-21402
R and D to HOPE airframe p 1665 N94-21406
Material properties and behavior during simulated atmospheric reentry p 1665 N94-21408
Outgassing data for selecting spacecraft materials
[NASA-RP-1124-REV-3] p 1676 N94-21889

SPACECRAFT CONTAMINATION
Measured space environmental effects to LDEF during retrieval p 1659 N94-21372
Residual atmosphere in the FRECOPA experiment and degassing of materials p 1660 N94-21374

SPACECRAFT CONTROL
Pointing control design for autonomous space vehicle applications
[DE93-019943] p 1657 N94-19863
Network command processing system overview p 1935 N94-21351

SPACECRAFT DESIGN
Power conditioning system modelling for nuclear electric propulsion
[NASA-CR-191136] p 1846 N94-21179
TROPIX plasma interactions group report
[NASA-CR-191149] p 1666 N94-21864

SPACECRAFT ELECTRONIC EQUIPMENT
Mongoose: Creation of a Rad-Hard MIPS R3000 p 1754 N94-21090

SPACECRAFT ENVIRONMENTS
Cosmos 2229
[NASA-CR-194734] p 1895 N94-20338
Toxicity of thermal degradation in a manned space environment p 1664 N94-21403

SPACECRAFT INSTRUMENTS
A packet switched communications system for GRO p 1744 N94-21345
Database of proposed payloads and instruments for SEI missions p 1811 N94-22432

SPACECRAFT LANDING
Tetrahedral lander
[NASA-CASE-MSC-22082-1] p 1658 N94-20590

SPACECRAFT LAUNCHING
Process and apparatus for the release of a prestress initially applied to a mechanism such as a bearing on board a space vehicle
[CA-PATENT-APPL-SN-2,020,90] p 1824 N94-21142
Specialized data analysis for the Space Shuttle Main Engine and diagnostic evaluation of advanced propulsion system components
[NASA-CR-194720] p 1656 N94-21813
Debris/ice/TPS assessment and integrated photographic analysis for Shuttle Mission STS-51
[NASA-TM-109189] p 1656 N94-21884

Spaceplane flight simulation: Project definition
[PB93-211399] p 1651 N94-22094

SPACECRAFT POWER SUPPLIES
Solar simulator for solar dynamic space power system testing
[NASA-TM-106393] p 1984 N94-20140
Power standard
[ESA-PSS-02-10-VOL-1-ISSUE-] p 1669 N94-20241
Model-based reasoning for power system management using KATE and the SSM/PMAD
[NASA-CR-194716] p 1671 N94-21882

SPACECRAFT PROPULSION
Spacecraft Propulsion
[VKI-LS-1993-01] p 1667 N94-20068
Space Shuttle Main Engine. Overview
p 1667 N94-20070
Rocketdyne turbomachinery p 1667 N94-20071
Turbine design p 1668 N94-20075
Cryogenic propellant rocket engine problems
p 1668 N94-20076
Advanced transportation system studies, technical area 3. Alternate propulsion subsystem concepts: J-2S restart study
[NASA-CR-193874] p 1670 N94-21271
NEP Early Flight program: System performance and development considerations
[NASA-TM-106415] p 1654 N94-21570
Specialized data analysis for the Space Shuttle Main Engine and diagnostic evaluation of advanced propulsion system components
[NASA-CR-194720] p 1656 N94-21813

SPACECRAFT RADIATORS
Rewetting of monogroove heat pipe in Space Station radiators
[NASA-CR-194781] p 1804 N94-21820

SPACECRAFT SHIELDING
Thermally activated retainer means utilizing shape memory alloy
[NASA-CASE-MSC-21793-1] p 1654 N94-20304
Numerical simulations of hypervelocity impact experiments involving single Whipple bumper shields
[AD-A272123] p 1831 N94-20572
Hypervelocity impact
[AD-A272957] p 1831 N94-21249
Meteoroids and debris impact risk assessment on Columbus and Hermes using a realistic geometrical analysis tool p 1662 N94-21388

SPACECRAFT STRUCTURES
Apparatus for simulating an exoatmospheric structure
[NASA-CASE-MSC-21975-1] p 1653 N94-20339

SPACECRAFT TRACKING
NAVSPASUR sensor system digital signal processing receiver. Volume 1: Hardware and software overview
[AD-A272899] p 1738 N94-21198
NAVSPASUR sensor system digital signal processing receiver. Volume 2: Function and capabilities of hardware and software components
[AD-A272900] p 1739 N94-21218

SPACECREWS
Spaceflight Radiation Health program at the Lyndon B. Johnson Space Center
[NASA-TM-104782] p 1893 N94-21863

SPACELAB
German space experiments on Spacelab D-2 and Eureca-1 to investigate atomic oxygen interaction with materials p 1662 N94-21390

SPARK GAPS
High-power gas switch with hydride electrodes
[AD-D015956] p 1751 N94-20354
Comparative study of INPIStron and spark gap
p 1995 N94-21293

SPATIAL DEPENDENCIES
Some practicable applications of quadtree data structures/representation in astronomy
p 1927 N94-22515

SPATIAL DISTRIBUTION
Spatial patterns in semiconductor lasers
[DE93-040056] p 1814 N94-19865
Spatial and temporal variations of satellite microwave measurements of latent heat release in tropic cyclones due to environmental forcing obtained from a numerical model
[AD-A267947] p 1885 N94-20482
Optical climatology of the Northeast Pacific Ocean
[AD-A271671] p 1866 N94-20559
Seafloor characterization/Galapagos propagating rift
[AD-A272001] p 1882 N94-20581

SPATIAL FILTERING
Optical signal processing
[AD-A271036] p 1983 N94-20013
Phased array antenna with couplers in spatial filter arrangement
[CA-PATENT-1,296,098] p 1737 N94-21031
Scale-space filtering and threshold hierarchy for image segmentation p 1777 N94-22149
Spatial region filtering in IRAF/PROS
p 1927 N94-22524

SPATIAL RESOLUTION
Uncertainty limited atomic position measurement using optical fields
[AD-A271013] p 1970 N94-19822
Near atomic resolution microanalysis of interfaces by analytical electron microscopy
[DE93-019437] p 1687 N94-19904
Ultrafast scanning microscopy
[DE93-040121] p 1985 N94-20320
Transport in microstructures in the microwave and millimeter-wave regime
[AD-A271875] p 2017 N94-20470
GMM-1: A 50 degree and order gravitational field model for Mars p 2117 N94-20774
Earth-based measurement of lunar topography using delayed radar interferometry p 2119 N94-20787
Linear mixing model applied to AVHRR LAC data
p 1838 N94-20958
Micro-ellipsometric measurements of strained layer structures p 2025 N94-21008
Breaking Kelvin-Helmholtz waves and cloud-top entrainment as revealed by K-band Doppler radar
p 1874 N94-22310

SPECIFIC HEAT
Shock induced condensation in fluids of high molar specific heat: Shock structure and relaxation
[MPIS-106/1993] p 1798 N94-20145
Non-Fermi-liquid and multichannel Kondo phenomena in Y(1-x)U(x)Pd3 and related alloys
[DE93-040135] p 2015 N94-20275
Non-fermi liquid and spin-glass behavior of the Sc(1-x)U(x)Pd3 system
[DE93-040134] p 2016 N94-20335
Specific heat of YBa2Cu3O7
[DE93-040640] p 2031 N94-21926
Magnetism in CeRu2Ge2 and CeRh2Ge2 and its pressure dependence
[DE93-040061] p 2032 N94-21987

SPECIFIC IMPULSE
Energy storage and conversion in solid hydrogen
[AD-A271439] p 1845 N94-20086
Optimization and performance analysis of a supersonic conical-flow waverider for a deck-launched intercept mission
[AD-A272498] p 1648 N94-21433
Powdered aluminum and oxygen rocket propellants: Subscale combustion experiments
[NASA-TM-106439] p 1713 N94-21760
Performance assessment of low pressure nuclear thermal propulsion
[NASA-TM-108433] p 1671 N94-21860

SPECIFICATIONS
Reference manual for a Requirements Specification Language (RSL), version 2.0
[NASA-CR-191460] p 1898 N94-20039
Specification and generation of Markov reward models
[MEMO-INF-92-60] p 1963 N94-21058
A simplified token bus protocol specified using LOTOS
[TR-92-15] p 1910 N94-21062
Application of the structures query language of APROS for specification of industrial processes
p 1923 N94-22078
Space Generic Open Avionics Architecture (SGOAA) standard specification
[NASA-CR-188269] p 1666 N94-22275

SPECTRA
The optical constants and spectral specular reflectivity of Highly Oriented Pyrolytic Graphite (HOPG)
[DE93-040546] p 1709 N94-21970

SPECTRAL EMISSION
Thermal infrared remote sensing and Kirchhoff's law: 1. Laboratory measurements p 1685 N94-20733
Spectral emissivity of cirrus clouds
p 1876 N94-22322

SPECTRAL ENERGY DISTRIBUTION
Comparison of higher order moment spectrum estimation techniques
[AD-A272967] p 1967 N94-21260

SPECTRAL LINE WIDTH
Effect of exciton localization and delocalization on magnetic-field-dependent photoluminescence linewidths in semiconductors
[DE93-018860] p 1748 N94-19884
Ellipsometric analysis of built-in electric fields in semiconductor heterostructures p 1796 N94-20988

SPECTRAL METHODS
On the relationship between spectral domain approach and method of lines p 1794 N94-22254

SPECTRAL REFLECTANCE
Comparison of remote sensing measurements with a two-scale polarimetric emission and scattering model for sea surfaces p 1721 N94-20415
Spectral reflectance studies of the Humorum Basin region p 2101 N94-20682
Optical effects of space weathering on lunar soils and the role of the finest fraction p 2101 N94-20687
Comparison of visible and near-infrared reflectance spectra of CM2 carbonaceous chondrites and primitive asteroids p 2085 N94-20848
Multispectral studies of selected crater- and basin-filling lunar Maria from Galileo Earth-Moon encounter 1
p 2136 N94-20876
In-situ spectroscopic ellipsometry for real time semiconductor growth monitor p 2024 N94-21003

SPECTRAL RESOLUTION
MinMap: An imaging spectrometer for high resolution compositional mapping of the Moon
p 1813 N94-20688
Analysis of hyper-spectral AVIRIS image data over a mixed-conifer forest in Maine p 1838 N94-20959
Michelson Interferometer (MINT)
p 1813 N94-21646
Multiorder etalon sounder (MOES) development and test for balloon experiment
[NASA-CR-194730] p 1859 N94-22026
Cirrus cloud retrievals from HIS observations during FIRE 2 p 1875 N94-22315
Adaptive filtering of Echelle spectra of distant Quasars
p 2072 N94-22520

SPECTRAL SENSITIVITY
On coefficient quantization and computational roundoff effects in frequency interpolation filter banks
p 1793 N94-22251

SPECTRAL SIGNATURES
A study of carbonates, sulfates, and phosphates using thermal emission spectroscopy p 1686 N94-20868
Predicting LANDSAT MSS endmember signatures from corresponding higher resolution TM fraction images
p 1839 N94-20962

SPECTROGRAMS
Comparison of higher order moment spectrum estimation techniques
[AD-A272967] p 1967 N94-21260
The cool-star spectral catalog: A uniform collection of IUE SWP-LOs p 2046 N94-22446

SPECTROGRAPHS
Writing instrument interfaces with xf/tktcl
p 1925 N94-22480
SPECFOCUS: An IRAF task for focusing spectrographs p 1965 N94-22540

SPECTROHELIOGRAPHS
Berne (Switzerland) solar observations: Data for April 1991 - August 1992
[REPT-59] p 2147 N94-21150
Preliminary results of observations of solar flares with Nobeyama Radioheliograph p 2001 N94-22633

SPECTROMETERS
Analysis of Ku-band cross section at low incidence angles p 1720 N94-20414
Rotational spectrum of a dark state in 2-fluoroethanol using microwave/radiofrequency-infrared multiple resonance
[AD-A272101] p 1817 N94-20583
Wavelength dispersive analysis with the synchrotron x ray fluorescence microprobe p 1685 N94-20717
Combined backscatter Moessbauer spectrometer/x ray fluorescence analyzer (BaMS/XRF) for extraterrestrial surfaces p 1686 N94-20761
Mirror velocity sampling errors in a Michelson interferometer
[AD-A273105] p 1809 N94-21508
Applications of correlator chips in radio science
p 1763 N94-21695
A 1 GHz sample rate, 256-channel, 1-bit quantization, CMOS, digital correlator chip p 1768 N94-21732
Low power, CMOS digital autocorrelator spectrometer for spaceborne applications p 1666 N94-21733
A Backscatter Moessbauer Spectrometer (BaMS) for use on Mars p 1811 N94-22431

SPECTROPHOTOMETRY
Comparison of visible and near-infrared reflectance spectra of CM2 carbonaceous chondrites and primitive asteroids p 2085 N94-20848

SPECTRORADIOMETERS
Intercomparison of MAS, AVIRIS, and HIS data from FIRE cirrus 2 p 1872 N94-22298

SPECTROSCOPIC ANALYSIS
Femtosecond Raman-induced Kerr effect study of polar solvent dynamics: Amides
[DE93-017563] p 1678 N94-19924
Microscopic origins of metastable effects in a-Si:H and deep defect characterization in a-Si,Ge:H alloys
[DE93-018205] p 1688 N94-19985
Magnetic properties and Moessbauer analyses of glass from the K-T boundary, Beloc, Haiti
p 1685 N94-20753
Multielement analysis of interplanetary dust particles using TOF-SIMS p 2084 N94-20790

Ellipsometric measurements of molecular-beam-epitaxy-grown semiconductor multilayer thicknesses: A comparative study p 1710 N94-20983
Comparative thickness measurements of heterojunction layers by ellipsometric, RBS, and XTEM analysis p 1710 N94-20984
Characterization of multilayer GaAs/AlGaAs transistor structures by variable angle spectroscopic ellipsometry p 1796 N94-20985
Variable angle spectroscopic ellipsometric characterization of surface damage in chemical-mechanical polished GaAs p 1710 N94-20986
Variable angle of incidence spectroscopic ellipsometric measurement of the Franz-Keldysh effect in MODFET structures p 2021 N94-20987
Ellipsometric analysis of built-in electric fields in semiconductor heterostructures p 1796 N94-20988
Optical measurement of built-in and applied electric fields in Al(x)Ga(1-x)As/GaAs heterostructures p 1796 N94-20989
Measurement of superlattice optical properties by variable angle spectroscopic ellipsometry p 2022 N94-20992
Superlattice optical properties measured by variable angle spectroscopic ellipsometry p 2022 N94-20993
GaAs/AlGaAs superlattice characterization by variable angle spectroscopic ellipsometry p 2022 N94-20994
Characterization of an asymmetric triangular multiple quantum well, by variable angle spectroscopic ellipsometry p 2022 N94-20995
GaAs(100) surface modifications at elevated temperatures, studied by in-situ spectroscopic ellipsometry p 2023 N94-20997
Ellipsometric study of GaAs(100) surface changes induced at elevated temperatures p 2023 N94-20998
Asbestos characterization using scanning electron microscopy/light element x ray spectrometry
[AD-A271611] p 1681 N94-21241
Shock compression of low-density foams
[DE93-040545] p 1707 N94-21546
An attempt to comprehend Martian weathering conditions through the analysis of terrestrial palagonite samples p 2143 N94-21668
Local structure in oxygen-doped La2CuO(4+delta)
[DE93-040248] p 2030 N94-21768
Gamma ray spectrometry of LDEF samples: Results of 1992 analyses
[DE94-001177] p 1684 N94-22046
Low temperature absorption spectra and ground state electronic structure of tetrakis(2,6-di-tert-butylphenoxide)uranium(IV)
[DE94-000774] p 2035 N94-22367

SPECTROSCOPY
Photoluminescence spectroscopy of zinc germanium diphosphide (ZnGeP2)
[AD-A270705] p 1678 N94-19953
Development of a numerical simulation model for a-Si:H solar cells and application to the analysis of experimentally obtained spectral characteristics
[ETN-93-95061] p 1846 N94-20151
Time-of-flight heavy ion backscattering spectrometry
[DE93-019067] p 1973 N94-20306
Characterization of amorphous material in shocked quartz by NMR spectroscopy
[DE93-019069] p 1679 N94-20307
Spectroscopic ellipsometry studies of HF treated Si (100) surfaces p 1734 N94-20508
Spectroscopic ellipsometric characterization of Si/Si(1-x)Ge(x) strained-layer superlattices p 1734 N94-20510
Thin-film hermeticity: A quantitative analysis of diamondlike carbon using variable angle spectroscopic ellipsometry p 1710 N94-20981
Variable angle of incidence spectroscopic ellipsometric study of semiconductor multilayer structures p 2020 N94-20982
Dielectric function of InGaAs in the visible p 2023 N94-21000
Study of InGaAs-based modulation doped field effect transistor structures using variable-angle spectroscopic ellipsometry p 1796 N94-21001
Study of concentration-dependent dielectric properties of n-type GaAs using variable angle spectroscopic ellipsometry p 2024 N94-21002
In-situ spectroscopic ellipsometry for real time semiconductor growth monitor p 2024 N94-21003
Real-time analysis of in-situ spectroscopic ellipsometric data during MBE growth of III-V semiconductors p 2024 N94-21004
In-situ spectroscopic ellipsometry in molecular beam epitaxy p 2024 N94-21005
Spectroscopic ellipsometric characterization of Si/Si(1-x)Ge(x) strained-layer superlattices p 2025 N94-21009
Applications of variable angle spectroscopic ellipsometry in semiconductor technology p 2025 N94-21010
Fundamentals and applications of variable angle spectroscopic ellipsometry p 1687 N94-21011
Non-destructive evaluation in manufacturing using spectroscopic ellipsometry p 1828 N94-21012
In-situ and ex-situ ellipsometric characterization for semiconductor technology p 2026 N94-21013
VASE (variable angle spectroscopic ellipsometry) p 1687 N94-21014
Validation of the design of a high resolution all-reflection Michelson interferometer for atmospheric spectroscopy
[AD-A272505] p 1987 N94-21410
Electronically metastable molecules of high symmetry
[AD-A272015] p 1974 N94-21461
Optical luminescence spectroscopy as a probe of the surface mineralogy of Mars p 1813 N94-22437
The spectral world coordinate systems in IRAF/NOAO p 2049 N94-22539

SPECTRUM ANALYSIS
A study of Saturn's E-ring particles using the Voyager 1 plasma wave instrument
[NASA-CR-194694] p 2088 N94-20048
High resolution signal processing
[AD-A271181] p 1717 N94-20215
Temperature dependence of 4f PES features and hole occupancy in ytterbium heavy fermions
[DE93-040131] p 1691 N94-20321
Characterization of electromagnetic fields in an extended chamber at the Short Pulse Experimental Electron Device (SPEED) simulator
[AD-A265955] p 1717 N94-20329
Analysis of Ku-band cross section at low incidence angles p 1720 N94-20414
Rotational spectrum of a dark state in 2-fluoroethanol using microwave/radiofrequency-infrared multiple resonance
[AD-A272101] p 1817 N94-20583
Spectral reflectance studies of the Humorum Basin region p 2101 N94-20682
Visible-infrared properties of controlled laboratory soils p 1685 N94-20689
Detectability of crystalline ferric and ferrous minerals on Mars p 2110 N94-20730
The stability of oxyamphiboles: Existence of Ferric-bearing minerals under the reducing conditions on the surface of Venus p 2122 N94-20800
Determining the composition of olivine on asteroidal surfaces p 1686 N94-20805
Objective determination of image end-members in spectral mixture analysis p 1686 N94-20831
Multispectral studies of selected crater- and basin-filling lunar Maria from Galilec Earth-Moon encounter 1 p 2136 N94-20876
Spectral analysis of chemisorbed CO2 on Mars analog materials p 2140 N94-20900
GaAs/AlGaAs superlattice characterization by variable angle spectroscopic ellipsometry p 2022 N94-20994
Characterization of an asymmetric triangular multiple quantum well, by variable angle spectroscopic ellipsometry p 2022 N94-20995
Comparative study of INPIStron and spark gap p 1995 N94-21293
RADCAL: A narrow-band model for radiation calculations in a combustion environment
[PB93-200889] p 1682 N94-21448
Defect motion as the origin of the 1/f conductance noise in solids
[EUT-92-E-259] p 2029 N94-21552
Radiation driven winds of hot stars: Some remarks on stationary models and spectrum synthesis in time-dependent simulations
[NASA-CR-194691] p 2081 N94-21578
Evaluation of a nonlinear method for the enhancement of tonal signal detection
[NASA-CR-191562] p 1968 N94-21741
On Plasma Edge Spectroscopy and Spectroscopic Studies of Impurity Densities and Impurity Transport
[IPF-92-2] p 1996 N94-21802
Plasma edge spectroscopy p 1996 N94-21803
Spectroscopic studies of impurity densities and impurity transport p 1997 N94-21804
Modal combination in response spectrum modal dynamic analysis
[DE94-000339] p 1833 N94-21956
Spectral variation of scattering and absorption by cirrus p 1876 N94-22321
ASpect: A new spectrum and line analysis package for IRAF p 1926 N94-22485
Interactive Spectral Analysis and Computation (ISAAC) p 1926 N94-22505
An x ray archive on your desk: The Einstein CD-ROM's p 2048 N94-22519
SPECFOCUS: An IRAF task for focusing spectrographs p 1965 N94-22540
What is normal among the A-type stars?
[ISBN-0-315-83947-3] p 2081 N94-22592

SPEECH
Segmentation and frequency domain ML pitch estimation of speech signals p 1747 N94-22212

SPEECH RECOGNITION
Representation of spoken words in a self-organizing neural net p 1940 N94-20243
Modeling the human mental lexicon with self-organizing feature maps p 1743 N94-20244
Segment-based acoustic models for continuous speech recognition
[AD-A271483] p 1736 N94-20547
Application of a back-propagation neural network to isolated-word speech recognition
[AD-A272495] p 1945 N94-21430
Recognizing hesitation phenomena in continuous, spontaneous speech p 1746 N94-22210
A framework of connectionist network toward speech waveform coding p 1748 N94-22211
Segmentation and frequency domain ML pitch estimation of speech signals p 1747 N94-22212
Speaker-independent isolated-digit recognition using neural networks and hidden Markov model p 1747 N94-22213
On coefficient quantization and computational roundoff effects in frequency interpolation filter banks p 1793 N94-22251

SPHERES
Intensity and polarization of light scattered by size distributions of randomly oriented nonspherical particles p 1721 N94-20416

SPHERICAL SHELLS
Symmetry-dictated trucation: Solutions of the spherical shell model for heavy nuclei
[DE94-000482] p 1976 N94-21961
Double diffusion convection in a rotating spherical shell p 2006 N94-22666

SPHERICAL TANKS
Pressurization and expulsion of a flightweight liquid hydrogen tank
[NASA-TM-106427] p 1799 N94-20177

SPHERICAL WAVES
Initiation and modification of reaction by energy addition: Kinetic and transport phenomena
[AD-A271315] p 1797 N94-19936
Interface reflection of spherical acoustic waves in the first- and second-order rational parabolic approximations and their artifacts
[PB93-215424] p 1969 N94-22261

SPHEROIDS
Stable Ni isotopes and Be-10 and Al-26 in metallic spheroids from Meteor Crater, Arizona p 1863 N94-20889

SPHEROMAKS
A spheromak ignition experiment reusing Mirror Fusion Test Facility (MFTF) equipment
[DE94-001856] p 2034 N94-22050

SPHERULES
First discovery of the organic materials in deep-sea iron cosmic spherule p 1685 N94-20677
Elemental depletions in Antarctic micrometeorites and Arctic cosmic spherules: Comparison and relationships p 2082 N94-20704
Research program on the Manson impact structure, Iowa p 1862 N94-20766

SPIKING
Suppression of relaxation oscillations in flashpumped, two-micron tunable solid state lasers
[AD-D015928] p 1814 N94-19800

SPIN DYNAMICS
Spin dynamics and implications for superconductivity: Some problems with the d-wave scenario
[DE94-001183] p 2032 N94-21972

SPIN EXCHANGE
Measurements of atomic interactions and frequency stability with a cryogenic hydrogen maser
[AD-A271132] p 1814 N94-19853
Encounters of H and D atoms with O2 in water: Relative diffusion and reaction rates
[DE93-018587] p 1970 N94-19956

SPIN GLASS
Study of (+-)J Ising spin glasses via multicanonical ensemble
[DE93-018269] p 2016 N94-20285
Non-fermi liquid and spin-glass behavior of the Sc(1-x)U(x)Pd3 system
[DE93-040134] p 2016 N94-20335

SPIN STABILIZATION
Apparatus for simulating an exoatmospheric structure
[NASA-CASE-MSC-21975-1] p 1653 N94-20339

SPIN-LATTICE RELAXATION
NMR studies of oxygen-doped La2CuO(4+delta)
[DE93-040756] p 2034 N94-22007

SPINEL
Trace element compositions of spinel-rich refractory inclusions from the Murchison meteorite p 2086 N94-20897
SPIRAL GALAXIES
Visualizing the universe, part 2 p 2063 N94-22472
Generation and maintenance of bisymmetric spiral magnetic fields in disk galaxies in differential rotation p 2010 N94-22695
Magnetic fields in spiral galaxies p 2010 N94-22697
SPIRALS (CONCENTRATORS)
Spiral fluid separator
[NASA-CASE-MFS-28656-1] p 1800 N94-20361
SPLASHING
Improvement of helicopter attitude stability by active control of the conventional swash plate
[NASA-CR-194786] p 1650 N94-20524
SPLINE FUNCTIONS
Development and operation of the F/A-18 model control surface actuators
[AD-A271330] p 1645 N94-19914
Affine and non-affine blossoms
[RR-913-M] p 1950 N94-20200
A geometrical process for three dimensional osteotomy planning
[ETN-93-93602] p 1892 N94-21134
Higher order Bezier circles
[NASA-CR-177633] p 1897 N94-21784
Achieving high data reduction with integral cubic B-splines
[NASA-CR-177628] p 1966 N94-21881
The quantum structure of matter grand challenge project: Large-scale 3-D solutions in relativistic quantum dynamics
[DE94-000328] p 1960 N94-21955
SPLINES
On the spline-based wavelet differentiation matrix
[NASA-CR-191557] p 1950 N94-20087
Spline screw payload fastening system
[NASA-CASE-GSC-13454-1] p 1821 N94-20126
An extended UTD analysis for the scattering and diffraction from cubic polynomial strips
[NASA-CR-194581] p 1716 N94-20139
Unstructured surface grid generation p 1920 N94-22366
SPORADIC E LAYER
Sporadic-E observations during LoVHF transionospheric direction finder measurements
[AD-A270619] p 1716 N94-19951
High Frequency (HF) and meteor burst communications in a polar environment
[AD-A271604] p 1737 N94-20949
SPRAYERS
Particle dispersion in turbulent sprays
[AD-A271314] p 1796 N94-19913
Aircraft cabin water spray disbenefits study
[NASA-CR-194750] p 1642 N94-21818
SPREAD SPECTRUM TRANSMISSION
Spread spectrum random access networks
[AD-A272280] p 1737 N94-20585
Capacity comparison between direct sequence PSK and MFSK spread spectrum systems in CDMA applications p 1747 N94-22224
SPRINGS (ELASTIC)
Shape memory metals
[DE94-001373] p 1695 N94-21976
SPUTTERING
Neutral copper cluster sputtering yields: Ne(+), Ar(+) and Xe(+) bombardment
[DE93-019010] p 1690 N94-20288
Embedded microclusters in zeolites and cluster beam sputtering: Simulation on parallel computers
[DE94-000741] p 1701 N94-20352
Fabrication and evaluation of superconducting and semiconducting materials
[AD-A271645] p 2018 N94-20558
Ellipsometric studies of sputtered silicon nitride on n-GaAs p 1709 N94-20972
Surface states at the GaAs-germanium nitride interface p 1709 N94-20973
InP MIS structures with diamondlike amorphous carbon films deposited by ion-beam sputtering and from plasma p 1710 N94-20979
Properties of E-beam interactive oxide films for nanometer scale structures
[AD-A272848] p 1675 N94-21191
Advanced processing technology for high-efficiency thin-film CuInSe2 solar cells
[DE93-010045] p 1847 N94-21614
Research on polycrystalline thin-film submodules based on CuInSe2 materials
[DE93-018223] p 2029 N94-21617
Mars atmosphere loss and isotopic fractionation by solar-wind-induced sputtering and photochemical escape p 2144 N94-21672
Observation of x ray absorption magnetic circular dichroism in well-characterized iron-cobalt-platinum multilayers
[DE94-000303] p 1694 N94-21944
Direct detection of atomic ions from molecular photofragmentation during nonresonant multiphoton ionization of sputtered species
[DE93-040886] p 1976 N94-21951
Transmission electron microscopy study of thick copper-304 stainless steel multilayers
[DE94-001045] p 1696 N94-22394
STABILITY
A summary of studies of particle stability at RHIC
[DE93-040173] p 1970 N94-19868
Study of transverse coupled bunch instabilities by using non-linear Taylor maps for the Advanced Light Source (ALS)
[DE93-040287] p 1979 N94-19969
The stability of oxyamphiboles: Existence of Ferric-bearing minerals under the reducing conditions on the surface of Venus p 2122 N94-20600
Numerical ranges and stability estimates
[TW-92-10] p 1953 N94-21060
Stability analysis of unsteady ablation fronts
[DE93-019689] p 1819 N94-21839
Proof of stability of the hydrogen molecule
[PB93-221026] p 1977 N94-22271
STABILITY AUGMENTATION
Design, fabrication and test of a vertical attitude takeoff and landing unmanned air vehicle
[AD-A273003] p 1646 N94-21283
STABILITY TESTS
Stability analysis of unsteady ablation fronts
[DE93-019689] p 1819 N94-21839
STABILIZERS (FLUID DYNAMICS)
Apparatus and method for improving spin recovery on aircraft
[NASA-CASE-LAR-14747-1] p 1650 N94-20556
STAINLESS STEELS
Thermocapillary and arc phenomena in stainless steel welds
[DE94-000518] p 1821 N94-19859
Microscopic evaluation of low-temperature embrittlement in type 308 stainless steel welds
[DE93-040266] p 1690 N94-20282
Transmission electron microscopy study of thick copper-304 stainless steel multilayers
[DE94-001045] p 1696 N94-22394
STANDARD DEVIATION
Performance evaluation of the JPL TOPSAR system: An across-track interferometric SAR system for topographic mapping p 1732 N94-20461
DECONV-TOOL: An IDL based deconvolution software package p 1927 N94-22542
STANDARDIZATION
The manager's guide to NASA graphics standards
[NHB-1430.2] p 2042 N94-20308
The electronics technology policy of the NLR Informatics Division: The NLR electronics CAE infrastructure
[NLR-TP-91001-U] p 1753 N94-21067
Government Open Systems Interconnection Profile (GOSIP) transition strategy
[AD-A273005] p 1740 N94-21308
Data format standards for civilian remote sensing satellites
[PB93-192920] p 1841 N94-21446
Operational test and evaluation of electronic combat systems
[AD-A273093] p 1647 N94-21500
Surveys on specific patterns of facility intallation of photovoltaic power generating technologies for international cooperation
[DE94-714901] p 1850 N94-22092
STANDARDS
Power standard
[ESA-PSS-02-10-VOL-1-ISSUE-] p 1669 N94-20241
Goniospectrometric properties of a white standard p 1684 N94-20664
Named Venusian craters p 2109 N94-20725
U.S. Tag for ISO/TC 43, acoustics, IEC/TC 29 electroacoustics, and ISO/TC 108/SC4 human exposure to mechanical vibration and shock: Minutes of the accredited standards committee on bioacoustics, S3
[AD-A273014] p 1897 N94-21309
Space Generic Open Avionics Architecture (SGOAA) standard specification
[NASA-CR-188269] p 1666 N94-22275
NASA data exchange standards for computational fluid dynamics p 1920 N94-22371
Electronic publishing and intelligent information retrieval p 2047 N94-22479
Fortran for the nineties p 1926 N94-22481
STAR CLUSTERS
The distribution of dark matter in the A2256 cluster
[NASA-CR-194699] p 2055 N94-21579
STAR DISTRIBUTION
The distribution of dark matter in the A2256 cluster
[NASA-CR-194699] p 2055 N94-21579
Extracting galactic structure parameters from multivariated density estimation p 1964 N94-22458
STAR FORMATION
Formation of the low-mass solar nebula p 2109 N94-20728
The formation of massive stars: A 30 Mo case study
[ISBN-0-315-83944-9] p 2081 N94-22593
Magnetohydrodynamic phenomena in star-forming processes and their environment p 2010 N94-22701
STAR TRACKERS
Charge integrating optical position sensor p 1778 N94-22152
STATE ESTIMATION
Comparison of a distributed Kalman filter versus a centralized Kalman filter with fault detection considerations
[AD-A270713] p 1903 N94-19969
STATIC LOADS
Time-dependent reliability analysis of ceramic engine components p 1828 N94-22619
STATIC THRUST
Internal performance of a nonaxisymmetric nozzle with a rotating upper flap and a center-pivoted lower flap
[NASA-TP-3385] p 1637 N94-21569
STATISTICAL ANALYSIS
Stochastic optimization by simulation: Convergence proofs for the G1/G/1 queue in steady-state
[AD-A271141] p 1962 N94-19999
VLSI design for reliability-current density
[AD-A270719] p 1749 N94-20110
Statistical object recognition
[AD-A270887] p 1962 N94-20113
Neural data oriented parsing p 1940 N94-20248
Retrieval of ice thickness from polarimetric SAR data p 1724 N94-20432
Signal processing in the linear statistical model
[AD-A272114] p 1736 N94-20570
Functional statistical data analysis and modeling
[AD-A271520] p 1963 N94-20913
Performance management systems: A statistical analysis
[AD-A272989] p 2043 N94-21266
Some evidence on determinants of fuel economy as a function of driving cycle and test type
[DE93-019511] p 1825 N94-21637
Mars: Noachian hydrology by its statistics and topology p 2143 N94-21664
A statistical-based scheduling algorithm in automated data path synthesis p 1764 N94-21706
Applications of a two-dimensional nonlinear filters to image restoration p 1789 N94-22225
GRO/EGRET data analysis software: An integrated system of custom and commercial software using standard interfaces p 1926 N94-22501
Detector noise statistics in the non-linear regime p 1748 N94-22526
STATISTICAL DISTRIBUTIONS
High resolution signal processing
[AD-A271181] p 1717 N94-20215
A formulation of quantum statistical mechanics based on the Feynman path centroid density 1: Equilibrium properties
[AD-A272809] p 2037 N94-21171
Data compression by using wavelet transforms and vector quantization
[AD-A272763] p 1738 N94-21182
Paired comparison models with time-varying parameters
[AD-A272016] p 1964 N94-21442
Stochastic simulation for imaging spatial uncertainty: Comparison and evaluation of available algorithms
[DE93-040058] p 1916 N94-21761
Experiments with recursive estimation in astronomical image processing p 2047 N94-22457
STATISTICAL MECHANICS
A formulation of quantum statistical mechanics based on the Feynman path centroid density 2 dynamical properties
[AD-A272698] p 2037 N94-21166
A formulation of quantum statistical mechanics based on the Feynman path centroid density 1: Equilibrium properties
[AD-A272809] p 2037 N94-21171
One- and multi-component theories of mixtures
[DE93-040543] p 1966 N94-21511
STATISTICAL TESTS
The European Southern Observatory-MIDAS table file system p 2048 N94-22518
STATORS
Operation of a test bed axial-gap brushless dc rotor with a superconducting stator
[DE93-019167] p 1769 N94-21830

STDN (NETWORK)
Developing a space network interface simulator: The NTS approach p 1933 N94-21343
STEADY STATE
Stochastic optimization by simulation: Numerical experiments with M/M/1 queue in steady-state [AD-A271143] p 1949 N94-19854
Some topics in regenerative steady-state simulation [AD-A271145] p 1902 N94-19855
Design of a controllable pitch underwater thruster system [AD-A271140] p 1821 N94-20021
Stability curves for a thermoacoustic prime mover [AD-A272607] p 1968 N94-21422
Stability of an uncooled segment of a high-temperature superconductor [DE94-000476] p 2032 N94-21932
The TST: A small steady-state tokamak for integrated divertor testing [DE94-001016] p 1998 N94-22045
STEELS
PVDF gauge characterization of hypervelocity-impact-generated debris clouds [DE93-018831] p 1829 N94-19943
Atom probe field ion microscopy characterizations of VVER steels [DE93-017864] p 1689 N94-20180
Lubricated wear of steel-ceramic and ceramic-ceramic systems [PB93-202356] p 1825 N94-21450
STEERING
Proceedings of the Twentieth Annual Technologyfest p 1645 N94-20188
STEFAN-BOLTZMANN LAW
Examination for optimization of synchrotron radiation spectrum for the x ray depth lithography [BONN-IR-92-32] p 1987 N94-21148
STELLAR ATMOSPHERES
Molecular equilibria and condensation sequences in carbon rich gases p 2083 N94-20756
STELLAR COMPOSITION
What is normal among the A-type stars? [ISBN-0-315-83947-3] p 2081 N94-22592
STELLAR ENVELOPES
The circumstellar environments of intermediate mass main sequence stars [NASA-CR-189311] p 2055 N94-21498
Circumstellar environments of Be stars at infra-red and radio wavelengths [ISBN-0-315-83135-9] p 2081 N94-22426
STELLAR EVOLUTION
Formation of the low-mass solar nebula p 2109 N94-20728
Variety in planetary systems p 2066 N94-20871
The circumstellar environments of intermediate mass main sequence stars [NASA-CR-189311] p 2055 N94-21498
New production mechanisms for unstable nuclei in stars, supernovae, and the big bang [DE93-018627] p 2081 N94-21618
Physical properties of dense astrophysical plasmas p 2001 N94-22637
Neutrino emission processes in dense high-temperature plasmas p 2001 N94-22638
STELLAR LUMINOSITY
Pre-main sequence stars in the Chamaeleon cloud and pre-main sequence stars in the Rho Ophiuchi cloud core [NASA-CR-194713] p 2080 N94-20337
STELLAR MAGNETIC FIELDS
Shock formation in magnetohydrodynamical accretion onto a black hole p 2010 N94-22699
Magnetohydrodynamic phenomena in star-forming processes and their environment p 2010 N94-22701
STELLAR MAGNETOSPHERES
General relativistic winds in a black hole magnetosphere p 2002 N94-22644
STELLAR MASS
Formation of the low-mass solar nebula p 2109 N94-20728
AGB stars as a source of short-lived radioactive nuclei in the solar nebula p 2133 N94-20859
The distribution of dark matter in the A2256 cluster [NASA-CR-194699] p 2055 N94-21579
Mars and the early Sun p 2146 N94-21683
STELLAR MASS ACCRETION
VVNRS: Variable phenomena in VV Cephei [NASA-CR-194731] p 2056 N94-21835
The formation of massive stars: A 30 Mo case study [ISBN-0-315-83944-9] p 2081 N94-22593
Time variation of MHD accretion onto a black hole p 2009 N94-22692
Accretion of a hot plasma onto the central black hole: Fokker-Planck formulation p 2009 N94-22693
Shock formation in magnetohydrodynamical accretion onto a black hole p 2010 N94-22699
STELLAR MASS EJECTION
Helical kink instability of jets from young stellar objects p 2008 N94-22686
STELLAR MODELS
High-energy astrophysics: A theoretical analysis of thermal radiation from neutron stars [NASA-CR-194808] p 2055 N94-20952
Mars and the early Sun p 2146 N94-21683
The cool-star spectral catalog: A uniform collection of IUE SWP-LOs p 2046 N94-22446
The formation of massive stars: A 30 Mo case study [ISBN-0-315-83944-9] p 2081 N94-22593
Magnetohydrodynamic phenomena in star-forming processes and their environment p 2010 N94-22701
STELLAR PHYSICS
New production mechanisms for unstable nuclei in stars, supernovae, and the big bang [DE93-018627] p 2081 N94-21618
VVNRS: Variable phenomena in VV Cephei [NASA-CR-194731] p 2056 N94-21835
The formation of massive stars: A 30 Mo case study [ISBN-0-315-83944-9] p 2081 N94-22593
STELLAR RADIATION
Factor analysis as a tool for spectral line component separation 21cm emission in the direction of L1780 p 1965 N94-22536
Properties of x ray emission from x ray novae p 2007 N94-22676
Time variations of x rays from black hole candidates: Canonical time variations in high and low intensity states p 2009 N94-22690
STELLAR ROTATION
Dynamo driven by weak plasma turbulence: The effect of differential rotation p 2005 N94-22665
Particle acceleration on the Alfven surface of a plasma ejecting axisymmetric rotator p 2008 N94-22681
Shock formation in magnetohydrodynamical accretion onto a black hole p 2010 N94-22699
STELLAR SPECTRA
The circumstellar environments of intermediate mass main sequence stars [NASA-CR-189311] p 2055 N94-21498
Circumstellar environments of Be stars at infra-red and radio wavelengths [ISBN-0-315-83135-9] p 2081 N94-22426
The cool-star spectral catalog: A uniform collection of IUE SWP-LOs p 2046 N94-22446
ASpect: A new spectrum and line analysis package for IRAF p 1926 N94-22485
What is normal among the A-type stars? [ISBN-0-315-83947-3] p 2081 N94-22592
STELLAR SPECTROPHOTOMETRY
New IRAF stellar photometry software p 1925 N94-22464
STELLAR STRUCTURE
Physical properties of dense astrophysical plasmas p 2001 N94-22637
STELLAR WINDS
Radiation driven winds of hot stars: Some remarks on stationary models and spectrum synthesis in time-dependent simulations [NASA-CR-194691] p 2081 N94-21578
Asymptotic structure of magnetically driven MHD wind p 2008 N94-22682
Hydrodynamical winds from an accretion disk p 2008 N94-22683
MHD flows from compact objects: Effects on magnetic field configurations p 2008 N94-22684
Magnetic fields in spiral galaxies p 2010 N94-22697
STELLARATORS
Fast ion behavior during neutral beam injection in ATF [DE93-040267] p 1992 N94-20058
Effects of magnetic field perturbations in the ATF torsatron [DE94-000474] p 1999 N94-22568
STEPPING MOTORS
The One-Day Workshop on Batteries, Stepping Motors, and Electronic Clock Displays [ETN-93-94632] p 1752 N94-20628
Lavet type stepping motors and associated controls p 1752 N94-20632
Test device for Lavet motors p 1752 N94-20633
STEREOPHOTOGRAPHY
Robust photo-topography by fusing shape-from-shading and stereo [NASA-CR-194697] p 1806 N94-19920
The High Resolution Stereo Camera (HRSC) for the Lunar Scout 1 Mission p 1813 N94-20650
STEREOSCOPIC VISION
Why stereo vision is not always about 3D reconstruction [AD-A270522] p 1939 N94-19893
Robust photo-topography by fusing shape-from-shading and stereo [NASA-CR-194697] p 1806 N94-19920
A pyramid neural network architecture for stereo fusion p 1785 N94-22201
STEREOSCOPY
The 3-D Moons: The Voyager stereo atlas of the outer solar system p 2111 N94-20740
STEROIDS
Changes in plasma vasopressin during motion sickness in cats p 1885 N94-21898
STIFFENING
Improvements to a method for the geometrically nonlinear analysis of compressively loaded stiffened composite panels [NASA-CR-194715] p 1832 N94-21814
STIFFNESS
Frequency and temperature dependence of high damping elastomers [DE93-019539] p 1697 N94-19809
Compression strength of composite primary structural components [NASA-CR-194561] p 1830 N94-20159
Graphite/polyurethane flexible composites: Mechanical and vibration damping properties [AD-A271608] p 1674 N94-20950
A vibration model for centrifugal contactors [DE93-040645] p 1833 N94-21927
STIFFNESS MATRIX
Approximation to sound radiation and scattering by simply supported layered cylinder [AD-A272964] p 1967 N94-21306
Response statistics of shell structures with geometrical and material nonlinearities, volume 1 [ISBN-0-315-84006-4] p 1833 N94-22590
STIMULATION
Recovery of the vomiting reflex following area postrema ablation in squirrel monkeys p 1886 N94-21904
Motion sickness elicited by passive rotation in squirrel monkeys p 1887 N94-21905
Immunocytochemical localization of glutamic acid decarboxylase (GAD) and substance P in neural areas mediating motion-induced emesis: Effects of vagal stimulation on GAD immunoreactivity p 1887 N94-21909
Experimental studies of gastric dysfunction in motion sickness: The effect of gastric and vestibular stimulation on the vagal and splanchnic gastric efferents p 1888 N94-21911
STIRLING CYCLE
Preliminary SP-100/Stirling heat exchanger designs [NASA-TM-106444] p 1670 N94-21809
STIRLING ENGINES
The FY1992 survey on commercialization of Stirling engine utilization equipment [DE94-707416] p 1849 N94-22029
STOCHASTIC PROCESSES
Stochastic optimization by simulation: Numerical experiments with M/M/1 queue in steady-state [AD-A271143] p 1949 N94-19854
Robust, high-speed network design for large-scale multiprocessing [AD-A271003] p 1716 N94-19977
SIMBAT theoretical manual [AD-A271063] p 1882 N94-19979
Stochastic optimization by simulation: Convergence proofs for the G1/G/1 queue in steady-state [AD-A271141] p 1962 N94-19999
Stochastic differential equations and numerical simulation for pedestrians [DE93-040651] p 1949 N94-20006
Asymptotics of the GLRT for the disorder problem in diffusion processes [INRIA-RR-1735] p 1951 N94-20227
A general rough-surface inversion algorithm: Theory and application to SAR data p 1719 N94-20407
Closure properties of stochastic languages [TR-441] p 1907 N94-20521
Segment-based acoustic models for continuous speech recognition [AD-A271483] p 1736 N94-20547
The Seventh International Symposium on Methodologies for Intelligent Systems (Poster Session) [AD-A272125] p 1942 N94-20573
Space-efficient deterministic simulation of probabilistic automata [TR-483] p 1900 N94-21281
Dependability and performability analysis [NASA-CR-191565] p 1965 N94-21483
Simulated behaviour of large scale SCI rings and tori [DE93-040149] p 1935 N94-21745
Stochastic simulation for imaging spatial uncertainty: Comparison and evaluation of available algorithms [DE93-040058] p 1916 N94-21761
Algorithmic advances in stochastic programming [DE94-001160] p 1921 N94-22406
Experiments with recursive estimation in astronomical image processing p 2047 N94-22457

STOKES FLOW
Surface path lines in plane Stokes flow driven by capillarity
[DE93-041277] p 1803 N94-21651
Mixed finite element and finite volume methods
[ISBN-0-315-63035-3] p 1805 N94-22417
STOMACH
Detection of emetic activity in the cat by monitoring venous pressure and audio signals
p 1886 N94-21903
The effects of area postrema lesions and selective vagotomy on motion-induced conditioned taste aversion
p 1888 N94-21910
STONY-IRON METEORITES
A new Antarctic meteorite with chromite, orthopyroxene and metal with reference to a formation model of S asteroids p 2084 N94-20813
Chemical zoning and diffusion of Ca, Al, Mn, and Cr in olivine of springwater pallasite p 2086 N94-20902
STORABLE PROPELLANTS
Ageing studies on a composite propellant containing a new organo-copper burn rate catalyst
[AD-A271060] p 1711 N94-19906
STORAGE BATTERIES
Surveys on specific patterns of facility intallation of photovoltaic power generating technologies for international cooperation
[DE94-714901] p 1850 N94-22092
STORAGE RINGS (PARTICLE ACCELERATORS)
Control and readout of the extraction septum of AmPS
[DIGEL-1993-2] p 1979 N94-20117
New preamplifiers for the SEM scanner
[DIGEL-1993-3] p 1979 N94-20118
Bundle profile monitor for AmPS
[DIGEL-1992-8] p 1979 N94-20123
Study of coupled-bunch collective effects in the PEP-2 B-Factory
[DE93-040117] p 1979 N94-20274
Measurement and computation of the higher order modes of the ALS 500 MHz accelerating cavities
[DE93-019256] p 1980 N94-20292
Energy and luminosity limits of hadron supercolliders
[DE93-019248] p 1980 N94-20300
Power supply and controller for the Sextupole magnet of AmPS
[DIGEL-1992-3] p 1753 N94-21064
Survey and alignment analysis for the ALS storage ring using computer spreadsheets
[DE93-019254] p 1917 N94-21917
Studies of the deuteron at high energy and momentum transfer
[DE93-041162] p 1976 N94-21941
STORAGE STABILITY
Ageing studies on a composite propellant containing a new organo-copper burn rate catalyst
[AD-A271060] p 1711 N94-19906
Evaluation of pre-extraction analytical holding times for nitroaromatic and nitramine explosives in water
[AD-A271547] p 1712 N94-20927
STORAGE TANKS
Pressurization and expulsion of a flightweight liquid hydrogen tank
[NASA-TM-106427] p 1799 N94-20177
On demand, non-halon, fire extinguishing systems
[AD-D015957] p 1714 N94-20355
STOVL AIRCRAFT
Survey of lift-fan aerodynamic technology
[NASA-CR-177615] p 1646 N94-21592
STRAIN DISTRIBUTION
Characteristics of 0.8- and 0.2-microns gate length In(x)Ga(1-x) As/In(0.52)Al(0.48)As/InP (0.53 less than or equal to x less than or equal to 0.70) modulation-doped field-effect transistors at cryogenic temperatures
p 1733 N94-20499
Wrinkle ridges, reverse faulting, and the depth penetration of lithospheric stress in lunae planum, Mars
p 2141 N94-20910
STRAIN GAGES
PVDF gauge characterization of hypervelocity-impact-generated debris clouds
[DE93-018831] p 1829 N94-19943
Apparatus and method for measuring subject work rate on an exercise device
[NASA-CASE-MSC-21752-1] p 1895 N94-20194
High accuracy die mechanical stress measurement with the ATC04 Assembly Test Chip
[DE93-019435] p 1830 N94-20477
OTDR strain gauge for smart skins
[DE93-041043] p 1810 N94-21953
Demodulation of a fiber Fabry-Perot strain rosette using white light interferometry
[ISBN-0-315-83427-7] p 1990 N94-22579
Phase demodulation of interferometric fiber-optic sensors
[ISBN-0-315-83425-0] p 1991 N94-22581
STRAIN HARDENING
Two-dimensional finite element analysis of porous media at multikilobar stress levels
[AD-A271540] p 1831 N94-20916
STRAIN MEASUREMENT
OTDR strain gauge for smart skins
[DE93-041043] p 1810 N94-21953
Phase demodulation of interferometric fiber-optic sensors
[ISBN-0-315-83425-0] p 1991 N94-22581
STRAIN RATE
Coupling of smooth particle hydrodynamics with PRONTO
[DE93-019080] p 1915 N94-21539
The effect of microstructural evolution on superplasticity in Ni3Si(V, Mo)
[DE93-041320] p 1694 N94-21943
STRANGENESS
Measurement of the strange quark distribution function in W(+) charm quark events
[DE93-018267] p 1973 N94-20474
STRATA
On the sources of North Atlantic deep water
[AD-A270854] p 1881 N94-19895
STRATIFIED FLOW
Meso-Beta scale numerical simulation studies of terrain-induced jet streak mass/momentum perturbations
[NASA-CR-194627] p 1864 N94-20138
STRATIGRAPHY
Stratigraphy of the Martian northern plains
p 2091 N94-20398
The Koshak section: Evidence for element fractionation and an oxidation event at the K/T boundary
p 1862 N94-20641
Modelling the gravity and magnetic field anomalies of the Chicxulub crater p 1862 N94-20668
Diapirs and cantaloupes: Layering and overturn of Triton's crust p 2111 N94-20738
Geology of the southern hemisphere of Triton: No polar cap p 2111 N94-20739
Iridium in sediments containing large abundances of Australasian microtektites from DSDP hole 758B in the Eastern Indian Ocean and from DSDP hole 769A in the Sulu Sea p 2083 N94-20741
Research program on the Manson impact structure, Iowa p 1862 N94-20766
STRATOCUMULUS CLOUDS
Clouds: Their prediction and simulation
[AD-A271161] p 1864 N94-19900
The analysis of global cloud and radiation data for the study of cloud-climate interactions
[NASA-CR-193388] p 1865 N94-20535
The FIRE Cirrus Science Results 1993
[NASA-CP-3238] p 1871 N94-22292
STRATOSPHERE
Intrusion of stratospheric ozone in the troposphere through tropopause folding and cold air droplets
[REPT-87] p 1851 N94-20154
Stratospheric Aerosol and Gas Experiment (SAGE 3)
p 1869 N94-21644
The 5-6 December 1991 FIRE IFO 2 jet stream cirrus case study: The influence of volcanic aerosols
p 1877 N94-22326
STRATUS CLOUDS
A documentation of icing relevant cloud physical parameters on horizontal soundings of stratiform clouds (continuation)
[DLR-MITT-92-10] p 1871 N94-22280
Breaking Kelvin-Helmholtz waves and cloud-top entrainment as revealed by K-band Doppler radar
p 1874 N94-22310
STREAK CAMERAS
Development and characterization of a time-, position- and energy-resolved x ray diagnostic for PBFA 2 target experiments
[DE93-019429] p 1808 N94-20297
STRESS (PHYSIOLOGY)
Physiological correlates of stress-induced decrements in human perceptual performance
[DOT/FAA/AM-93/19] p 1893 N94-20081
Studies of neural and cognitive function in subjects exposed to the marine-air interface, phases 1 and 2
[AD-A272282] p 1891 N94-20624
Human responses to exercise-heat stress
[AD-A272581] p 1892 N94-21209
STRESS ANALYSIS
Finite element mesh generation and analysis of solder joints for fatigue life predictions
[AD-A271329] p 1829 N94-19937
Audit report. Navy's aircraft structural life surveillance program data recorders
[AD-A270391] p 1645 N94-20040
A design optimization procedure for epicyclic gears
[MATHS-REPT-A-188] p 1822 N94-20146
Biaxial flexural testing of a carbon fiber reinforced epoxy composite
[AD-A271956] p 1674 N94-20577
Preliminary SP-100/Stirling heat exchanger designs
[NASA-TM-106444] p 1670 N94-21809
A finite element formulation and adaptive solution approach for large-scale thermomechanical problems with complex contact conditions
[DE93-019605] p 1960 N94-21996
Modeling of failure and response to laminated composites subjected to in-plane loads
p 1834 N94-22612
Life prediction systems for critical rotating components
p 1835 N94-22615
STRESS CORROSION
Benefits of thread rolling process to the stress corrosion cracking and fatigue resistance of high strength fasteners
[DE93-040438] p 1833 N94-22001
STRESS CORROSION CRACKING
Benefits of thread rolling process to the stress corrosion cracking and fatigue resistance of high strength fasteners
[DE93-040438] p 1833 N94-22001
STRESS DISTRIBUTION
Fundamental studies of stress distributions and stress relaxation in oxide scales on high temperature alloys
[DE94-001444] p 1693 N94-21854
Post-Palbozoic crustal responses to the contemporary stress field in the eastern United States
[DE93-040604] p 1859 N94-22006
STRESS MEASUREMENT
Time-resolved shock compression of porous rutile: Wave dispersion in porous solids
[DE93-018848] p 1829 N94-19927
High accuracy die mechanical stress measurement with the ATC04 Assembly Test Chip
[DE93-019435] p 1830 N94-20477
STRESS RELAXATION
Synthesis and properties of mismatched heterojunction/substrate interfaces
[AD-A272904] p 1760 N94-21229
Fundamental studies of stress distributions and stress relaxation in oxide scales on high temperature alloys
[DE94-001444] p 1693 N94-21854
STRESS RELIEVING
Process and apparatus for the release of a prestress initially applied to a mechanism such as a bearing on board a space vehicle
[CA-PATENT-APPL-SN-2,020,90] p 1824 N94-21142
STRESS WAVES
Time-resolved shock compression of porous rutile: Wave dispersion in porous solids
[DE93-018848] p 1829 N94-19927
Asteroid collisions: Target size effects and resultant velocity distributions p 2083 N94-20729
STRESS-STRAIN DIAGRAMS
Development of bioelastic material for aspects of wound repair
[AD-A267832] p 1673 N94-20208
STRESS-STRAIN RELATIONSHIPS
Two-dimensional finite element analysis of porous media at multikilobar stress levels
[AD-A271540] p 1831 N94-20916
Dynamic response of multiphase porous media
[AD-A272915] p 1831 N94-21219
Coupling of smooth particle hydrodynamics with the finite element method
[DE93-019081] p 1805 N94-22556
Life assessment of structural components using inelastic finite element analyses p 1834 N94-22614
STRESS-STRAIN-TIME RELATIONS
Brief summary of the evolution of high-temperature creep-fatigue life prediction models for crack initiation
p 1834 N94-22613
STRINGS
Tight comparison bounds for the string prefix-matching problem
[CWI-CS-R9250] p 1952 N94-21029
STRONTIUM
Column chromatographic separation of Y(3+) from Sr(2+) by polymeric ionizable crown ether resins
[DE94-000935] p 1683 N94-22021
STRONTIUM ISOTOPES
Elevated initial Sr-87/Sr-86 in ordinary chondrite metal
p 1685 N94-20695
STRONTIUM TITANATES
Investigation of the effect of various oxide and fluoride additives on the microstructure, electronic properties, and phase shifting ability of Ba(1-x)Sr(x)TiO3
[AD-A271756] p 2027 N94-21303
STRUCTURAL ANALYSIS
Femtosecond Raman-induced Kerr effect study of polar solvent dynamics: Amides
[DE93-017563] p 1678 N94-19924

The p-version of the finite element method in incremental elasto-plastic analysis
[NASA-CR-194707] p 1830 N94-20036
Total systems design analysis of high performance structures
[NASA-TP-3432] p 1653 N94-20141
Compression strength of composite primary structural components
[NASA-CR-194561] p 1830 N94-20159
Quantification of uncertainties in the performance of smart composite structures
[NASA-TM-106335] p 1830 N94-20171
Aviation safety research at the National Institute for Aviation Research, Wichita State University
[NIAR-93-4] p 1641 N94-20189
Complex structure of the Thaumasia region of Mars
p 2125 N94-20815
The 1992 USAF structural integrity program conference
[AD-A272876] p 1635 N94-21194
Adhesive bonded joint with improved cyclic fatigue life for alumina-ceramic cylinders and hemispheres: Fourth generation housings
[AD-A273061] p 1831 N94-21310
Modeling of outgassing and matrix decomposition in carbon-phenolic composites
[NASA-CR-194741] p 1676 N94-21743
Probabilistic assessment of composite structures
[NASA-TM-106368] p 1832 N94-21757
Development of BEM for ceramic composites
[NASA-CR-194718] p 1676 N94-21777
Nonlinear aerodynamics and the design of wing tips
[NASA-CR-194732] p 1638 N94-21833
Symposium on Microscopy and Image Analysis of Building Materials
[VTT-SYMP-136] p 1707 N94-21890
Microstructure in mortar: A summary of a new project of research p 1708 N94-21896
The program system for the diagnostics of strains and fracture prediction of solids p 1836 N94-22065
Life assessment of structural components using inelastic finite element analyses p 1834 N94-22614
Recent advances in computational structural reliability analysis methods p 1828 N94-22616
An overview of computational simulation methods for composite structures failure and life analysis
p 1835 N94-22617

STRUCTURAL BASINS
Evidence for an ice sheet/frozen lake in Utopia Planitia, Mars p 2089 N94-20388
Possible occurrence and origin of massive ice in Utopia Planitia p 2090 N94-20390
Ice in the northern plains: Relic of a frozen ocean?
p 2090 N94-20391
A marine sedimentary model for the evolution of the northern plains p 2091 N94-20395
Seismic-triggering history of the catastrophic outflows in the Chryse region of Mars p 2091 N94-20399
Spectral reflectance studies of the Humorum Basin region p 2101 N94-20682
Geologic mapping of Harmakhis and Reull Valles region, Mars: Evidence for multiple resurfacing and drainage events p 1844 N94-20705
Chicxulub impact basin: Gravity characteristics and implications for basin morphology and deep structure
p 1862 N94-20757
Impact basins on Venus and some interplanetary comparisons p 2119 N94-20785
Geology and deposits of the Serenitatis basin
p 2119 N94-20786
Origin of the Vredefort structure, South Africa: Impact model p 1863 N94-20826
Multispectral studies of selected crater- and basin-filling lunar Maria from Galileo Earth-Moon encounter 1
p 2136 N94-20876
Morphologic classes of impact basins on Venus
p 2137 N94-20883

STRUCTURAL DESIGN
Total systems design analysis of high performance structures
[NASA-TP-3432] p 1653 N94-20141
Structural similitude and design of scaled down laminated models
[NASA-CR-194687] p 1673 N94-20172
Design, fabrication and test of a vertical attitude takeoff and landing unmanned air vehicle
[AD-A273003] p 1646 N94-21263
Life assessment of structural components using inelastic finite element analyses p 1834 N94-22614
Recent advances in computational structural reliability analysis methods p 1828 N94-22616

STRUCTURAL FAILURE
Structural crashworthiness and failure
[AD-A270429] p 1828 N94-19815
Delamination, durability, and damage tolerance of laminated composite materials p 1678 N94-22622

STRUCTURAL PROPERTIES (GEOLOGY)
Evidence for an ice sheet/frozen lake in Utopia Planitia, Mars p 2089 N94-20388
Geologic mapping of Northern Atla Regio on Venus: Preliminary data p 2095 N94-20654
Gravity investigation of the Manson impact structure, Iowa p 2082 N94-20694
Studying Venus using a GIS database
p 2105 N94-20707
Diapirs and cantaloupes: Layering and overturn of Triton's crust p 2111 N94-20738
Geology of the southern hemisphere of Triton: No polar cap p 2111 N94-20739
The 3-D Moons: The Voyager stereo atlas of the outer solar system p 2111 N94-20740
Large, ancient, compressional structures on Mars
p 2125 N94-20816
Original size of the Vredefort structure, South Africa
p 1863 N94-20825
Origin of the Vredefort structure, South Africa: Impact model p 1863 N94-20826
Distribution and geologic history of materials excavated by the lunar crater Bullialdus p 2128 N94-20832
Geology of Galileo Regio quadrangle, Ganymede
p 2130 N94-20842

STRUCTURAL RELIABILITY
The 1992 USAF structural integrity program conference
[AD-A272876] p 1635 N94-21194
Recent advances in computational structural reliability analysis methods p 1828 N94-22616

STRUCTURAL STABILITY
A study of the structural stability of an unbalanced sandwich composite configuration
[AD-A272496] p 1675 N94-21431
Electron emission from nanometer-size metallic clusters: Electronic states and structural stability of supported Au clusters
[DE93-040184] p 1975 N94-21766

STRUCTURAL STRAIN
Structural similitude and design of scaled down laminated models
[NASA-CR-194687] p 1673 N94-20172

STRUCTURAL VIBRATION
Adaptation of model parameters of a rail model at measured rail compliances
[ILR-MITT-274(1992)] p 1831 N94-21153
The modern rotor aerodynamic limits survey: A report and data survey
[NASA-TM-4446] p 1635 N94-21490
Probabilistic assessment of composite structures
[NASA-TM-106368] p 1832 N94-21757
Aircraft noise effects on cultural resources: Recommendation and rationale for further research
[PB93-205326] p 1968 N94-22053
Aircraft noise effects on cultural resources: Annotated bibliography
[PB93-205334] p 1969 N94-22054
System identification of the Daisy large space structure emulator
[ISBN-0-315-83533-8] p 1653 N94-22588

STRUCTURAL WEIGHT
Nonlinear aerodynamics and the design of wing tips
[NASA-CR-194732] p 1638 N94-21833

STRUCTURED PROGRAMMING
Implementation of a portable nested data-parallel language
[AD-A270524] p 1902 N94-19932
A conceptual database design and performance analysis of the MILSATCOM requirements database
[AD-A272672] p 1658 N94-21217
Structured multimedia authoring
[CWI-CS-R9304] p 2044 N94-21535

STUDENTS
A comprehensive software engineering educational experience
[AD-A270583] p 1905 N94-20109
A description of psychological type at the Defense Systems Management College, 1993 edition
[AD-A271612] p 1894 N94-21237

STYRENES
Dynamics of adsorbed, swollen block copolymers
[AD-A272013] p 1706 N94-21460

SUBARCTIC REGIONS
The marine light-mixed layer experiment cruise and data report: R/V endeavor cruise EN-224, mooring deployment, 27 April-1 May 1991: Cruise EN-227, mooring recovery, 5-23 September 1991
[AD-A271175] p 1864 N94-20186

SUBDUCTION (GEOLOGY)
Subduction on the margins of coronae on Venus: Evidence from radiothermal emissivity measurements
p 2107 N94-20718
Parga and Hecate Chasmata, Venus: Structure, volcanism and models of formation
p 2121 N94-20796
Photogeological analysis of Europan tectonic features
p 2129 N94-20838

SUBLIMATION
The distribution of ground ice on Mars
p 2090 N94-20394

SUBMILLIMETER WAVES
Millimeter wave imaging technology
[AD-A271257] p 1715 N94-19912

SUBREFLECTORS
Multi-band reflector antenna with double-ring element frequency selective subreflector p 1728 N94-20447

SUBROUTINE LIBRARIES (COMPUTERS)
An object-oriented data reduction system in Fortran
p 2046 N94-22447
The IDL astronomy user's library
p 2048 N94-22500
The Keck Task Library (KTL) p 2048 N94-22504
Development of the FITS tools package for multiple software environments p 1927 N94-22516
The STARLINK software collection
p 1927 N94-22545

SUBROUTINES
Power conditioning system modelling for nuclear electric propulsion
[NASA-CR-191136] p 1846 N94-21179
NAVSPASUR sensor system digital signal processing receiver. Volume 2: Function and capabilities of hardware and software components
[AD-A272900] p 1739 N94-21218
The three-dimensional Event-Driven Graphics Environment (3D-EDGE) p 1922 N94-21342
Documentation for PCDIST, a FORTRAN subroutine to calculate Pollack-Cuzzi scattering
[AD-A273070] p 1988 N94-21491
An object-oriented data reduction system in Fortran
p 2046 N94-22447

SUBSONIC AIRCRAFT
Nonlinear and progressive failure aspects of transport composite fuselage damage tolerance
p 1834 N94-22609

SUBSONIC FLOW
Fluid dynamic mechanisms and interactions within separated flows
[AD-A271037] p 1797 N94-19978
Acoustic radiation damping of flat rectangular plates subjected to subsonic flows
[NASA-TM-109382] p 1967 N94-20211
A study of the compressible flow through a diffusing S-duct
[NASA-TM-106411] p 1638 N94-21591

SUBSTRATES
Substrate recovery of Mo-Si multilayer coated optics
[DE93-019610] p 1698 N94-19810
Quartz/fused silica chip carriers
[NASA-CR-194154] p 2016 N94-20340
Adhesive electroless metallization of fluoropolymeric substrates
[AD-A271858] p 1703 N94-20526
Thin film compositional analysis using null or fixed wavelength ellipsometry p 1709 N94-20976
Analytic solutions for optimized ellipsometric measurements of interfaces and surface layers in thin film structures p 2019 N94-20977
Growth, characterization and device development in monocrystalline diamond films
[AD-A272715] p 2026 N94-21190
Analysis of semi-insulating bulk GaAs using glow discharge mass spectrometry
[AD-A273032] p 1682 N94-21435
Growth, characterization and device development in monocrystalline diamond films
[AD-A273097] p 2028 N94-21506
The n-p(p(+))-n Al(yGa)(1-y) As-GaAs-In(x)Ga(1-x) as quantum well laser with p(+)-n(+)GaAs-InGaAs tunnel contact on n GaAs
[AD-A271292] p 2030 N94-21805
MOCVD growth and structure of PbTiO3 thin films
[DE93-040230] p 2033 N94-21994
Shock temperature measurements of iron to 350 GPa
[DE94-001058] p 1695 N94-22024

SULFATES
Impact-induced devolatilization of CaSO4 anhydrite and implications for K-T extinctions: Preliminary results
p 2085 N94-20840
Effect of copper sulphate on the rate of afferent discharge in the gastric branch of the vagus nerve in the rat p 1887 N94-21907
Experimental studies of gastric dysfunction in motion sickness: The effect of gastric and vestibular stimulation on the vagal and splanchnic gastric efferents
p 1888 N94-21911

SULFIDATION
Surface modification for corrosion resistance
[DE93-017419] p 1693 N94-21825

SULFIDES
The role of CO2 in weathering reactions and the presence of S2 on Venus: Implications for the pyrite stability field p 2122 N94-20799
Lewis Cliff 87057: A new metal-rich E3 chondrite with similarities to Mt. Egerton, Shallowater and Happy Canyon p 2086 N94-20901
SULFUR
Sulfur-bonded thiophenes in organometallic rhenium complexes and adsorption of isocyanides on gold
[DE93-041126] p 1694 N94-21937
SULFUR DIOXIDES
SO2 on Venus: IUE, HST and ground-based measurements, and the active volcanism connection p 2092 N94-20637
SULFURIC ACID
A comparison of sulfuric acid/boric acid anodize and chromic acid anodize processes
[AD-A271933] p 1703 N94-20614
Global blackout following the K/T Chicxulub impact: Results of impact and atmospheric modeling p 1854 N94-20698
Examination of the observed synoptic scale cirrus cloud environment: The December 3-6 FIRE cirrus case study p 1877 N94-22325
SUN
Mars and the early Sun p 2146 N94-21683
SUNSPOTS
Mars and the early Sun p 2146 N94-21683
Large-scale structure of the solar plasma corona: An analysis of Yohkoh SXT images p 2004 N94-22657
Enhanced absorption of p-modes on sunspot and plage regions p 2006 N94-22671
SUPERCHARGERS
Experimental evaluation of oxygen-enriched air and emulsified fuels in a six-cylinder diesel engine
[DE94-000907] p 1811 N94-22391
SUPERCOMPUTERS
Particle image velocimetry
[DE93-040657] p 1804 N94-21748
The transition to massively parallel computing within a production environment at a DOE access center
[DE93-019155] p 1936 N94-21828
Introduction to the LaRC central scientific computing complex
[NASA-TM-104092-REV-1] p 1900 N94-22100
Seeing the forest for the trees: Networked workstations as a parallel processing computer p 1938 N94-22454
SUPERCONDUCTING CAVITY RESONATORS
Space applications of superconducting microwave electronics at NASA Lewis Research Center p 1671 N94-20513
Ten GHz YBa2Cu3O(7-delta) superconducting ring resonators on NdGaO3 substrates p 1735 N94-20515
SUPERCONDUCTING DEVICES
A pipelined superconducting digital processor
[DE93-040852] p 1898 N94-19886
Quantum noise studies with superconducting tunnel junction mixers
[AD-A270897] p 2012 N94-19897
SUPERCONDUCTING FILMS
Particles on surfaces of laser ablated Y1Ba2Cu3O(7-delta) films
[DE93-040269] p 2013 N94-19929
Superconducting property measurements in tape geometry
[DE93-018943] p 2014 N94-19970
Ten GHz YBa2Cu3O(7-delta) superconducting ring resonators on NdGaO3 substrates p 1735 N94-20515
A 10 GHz Y-Ba-Cu-O/GaAs hybrid oscillator proximity coupled to a circular microstrip patch antenna p 1736 N94-20517
Microwave properties and characterization of co-evaporated BSCCO thin films p 1709 N94-20518
The effect of fluctuations on the electrical transport behavior in YBa2Cu3O(7-x) p 1736 N94-20519
Thin-film fabrication of Pb-doped BiSrCaCuO superconductor p 1781 N94-22176
SUPERCONDUCTING MAGNETS
Tensile and shear fracture behavior of fiber reinforced plastics at 77K irradiated by various radiation sources
[DE93-040280] p 1706 N94-21542
The 13th International Conference on Magnetically Levitated Systems and Linear Drives MAGLEV 1993
[DE93-040381] p 1825 N94-21544
Operation of a test bed axial-gap brushless dc rotor with a superconducting stator
[DE93-019167] p 1769 N94-21830
Stability of an uncooled segment of a high-temperature superconductor
[DE94-000476] p 2032 N94-21932
Tensile strength of fiber reinforced plastics at 77K irradiated by various radiation sources
[DE93-040826] p 1709 N94-22008
SUPERCONDUCTING SUPER COLLIDER
Energy and luminosity limits of hadron supercolliders
[DE93-019248] p 1980 N94-20300
SUPERCONDUCTIVITY
Dynamics of vortices in superconductors
[DE93-019535] p 2011 N94-19808
Spin-polaron theory of high-(Tc) superconductivity. 1: Spin polarons and high (Tc) pairing
[DE93-019196] p 2014 N94-20002
Machinable oxide ceramic
[AD-D015927] p 1699 N94-20017
Solid State Technology Branch of NASA Lewis Research Center: Fifth Annual Digest
[NASA-TM-106303] p 1732 N94-20497
Space applications of superconducting microwave electronics at NASA Lewis Research Center p 1671 N94-20513
Fabrication and evaluation of superconducting and semiconducting materials
[AD-A271645] p 2018 N94-20558
Local structure and superconductivity in La(2-x)Ba(x)CuO4 for x=0.125 and x=0.15
[DE93-040193] p 2029 N94-21555
Local structure in oxygen-doped La2CuO(4+delta)
[DE93-040248] p 2030 N94-21768
Spin-polaron theory of high-T(c) superconductivity. 3: Gap function and critical temperature
[DE93-019198] p 2030 N94-21831
Fullerene derivatives and fullerene superconductors
[DE93-019568] p 2031 N94-21871
Specific heat of YBa2Cu3O7
[DE93-040640] p 2031 N94-21926
Spin dynamics and implications for superconductivity: Some problems with the d-wave scenario
[DE94-001183] p 2032 N94-21972
NMR studies of oxygen-doped La2CuO(4+delta)
[DE93-040756] p 2034 N94-22007
SUPERCONDUCTORS
Dynamics of vortices in superconductors
[DE93-019535] p 2011 N94-19808
The proximity effect in ultrathin granular Pb films
[AD-A271094] p 2012 N94-19848
Fullerene derivatives and fullerene superconductors
[DE93-019568] p 2031 N94-21871
SUPERFLUIDITY
Acoustic microscopy and nonlinear effects in pressurized superfluid helium
[AD-A270598] p 1967 N94-19949
Canonically covariant formulation of Landau's Newtonian superfluid dynamics
[PB93-221034] p 1805 N94-22272
SUPERGIANT STARS
VVNRS: Variable phenomena in VV Cephei
[NASA-CR-194731] p 2056 N94-21835
SUPERHETERODYNE RECEIVERS
FM interference in radio navigation receivers p 1645 N94-22219
SUPERHIGH FREQUENCIES
Ku-band ocean radar backscatter observations during SWADE p 1720 N94-20413
Analysis of Ku-band cross section at low incidence angles p 1720 N94-20414
Studies of Greenland using the SEASAT scatterometer p 1725 N94-20433
Mobile antenna development at JPL p 1731 N94-20457
An in-depth analysis and modelling of the Shuttle to MILA S-band telemetry link p 1657 N94-21340
Heterojunction bipolar transistor technology for data acquisition and communication p 1763 N94-21697
Radio wave propagation studies along an Earth-space satellite link
[ISBN-0-315-60627-4] p 1742 N94-22408
SUPERLATTICES
Investigation of quantum effects in heterostructures
[AD-A270938] p 2011 N94-19817
Theory of energy-assisted epitaxy; theory of ordered semiconductor alloys: In(1-x)Tl(x)Sb as a long-wave infrared material
[AD-A271007] p 2012 N94-19835
Ellipsometric study of Si(0.5)Ge(0.5)/Si strained-layer superlattices p 1734 N94-20509
Spectroscopic ellipsometric characterization of Si/Si(1-x)Ge(x) strained-layer superlattices p 1734 N94-20510
Materials, Structures, and Devices for High-Speed Electronics
[NASA-CR-193177] p 2019 N94-20971
Characterization of multilayer GaAs/AlGaAs transistor structures by variable angle spectroscopic ellipsometry p 1796 N94-20985
Measurement of superlattice optical properties by variable angle spectroscopic ellipsometry p 2022 N94-20992
Superlattice optical properties measured by variable angle spectroscopic ellipsometry p 2022 N94-20993
GaAs/AlGaAs superlattice characterization by variable angle spectroscopic ellipsometry p 2022 N94-20994
Spectroscopic ellipsometric characterization of Si/Si(1-x)Ge(x) strained-layer superlattices p 2025 N94-21009
Semiconductor isotope engineering
[DE93-040119] p 2030 N94-21744
Photo- and thermal-induced antiferromagnetic interlayer coupling in Fe/(Fe-Si) superlattices
[DE93-040822] p 2031 N94-21930
Orientationally independent antiferromagnetic coupling in epitaxial Fe/Cr (211) and (100) superlattices
[DE94-001270] p 2035 N94-22564
SUPERNOVA 1987A
Electron acceleration in and radio emission from SN1987A p 2007 N94-22677
SUPERNOVAE
New production mechanisms for unstable nuclei in stars, supernovae, and the big bang
[DE93-018627] p 2081 N94-21618
SUPERPLASTICITY
The use of backscattered electron imaging mode to assess the effect of fine dispersions on development of superplastic microstructure in Al-Mg alloys
[AD-A272426] p 1691 N94-21258
Materials Science and Engineering
[DE93-040497] p 1675 N94-21530
The effect of microstructural evolution on superplasticity in Ni3Si(V, Mo)
[DE93-041320] p 1694 N94-21943
SUPERSONIC COMBUSTION
Instantaneous velocity field imaging instrument for supersonic reacting flows
[NASA-CR-191162] p 1809 N94-21607
SUPERSONIC COMBUSTION RAMJET ENGINES
Optimization and performance analysis of a supersonic conical-flow waverider for a deck-launched intercept mission
[AD-A272498] p 1648 N94-21433
SUPERSONIC FLOW
Fluid dynamic mechanisms and interactions within separated flows
[AD-A271037] p 1797 N94-19978
Instantaneous velocity field imaging instrument for supersonic reacting flows
[NASA-CR-191162] p 1809 N94-21607
Three-dimensional simulations of cosmic jets employing the smoothed particle hydrodynamics technique p 2008 N94-22685
SUPERSONIC JET FLOW
Instability modes excited by natural screech tones in a supersonic rectangular jet
[NASA-TM-106409] p 1638 N94-22274
SUPERSONIC SPEED
Options for thrust augmentation for the Beta 2 two-stage-to-orbit launch vehicle
[NASA-TM-106418] p 1649 N94-21759
SUPERSONIC TRANSPORTS
Proceedings of the Twentieth Annual Technologyfest p 1645 N94-20188
SUPERSYMMETRY
Simulating supersymmetry with ISAJET 7.0/ISASUSY 1.0
[DE93-018266] p 1969 N94-19804
On the twisted N=2 superconformal structure in 2d gravity coupled to matter
[DE93-628627] p 2037 N94-20178
Theoretical particle physics
[DE94-000538] p 1973 N94-20938
SUPPORT SYSTEMS
Military satellite communications decision support system requirements analysis and user interface design
[AD-A273047] p 1740 N94-21436
A comparison of IDEF1X and NIAM ISDM
[DE93-040899] p 1921 N94-22383
SUPPORTS
Shaft mount for data coupler system
[NASA-CASE-LAR-13805-1] p 1822 N94-20365
SURFACE ACOUSTIC WAVE DEVICES
Improvements on the design of optimum SAW filters with the Remez Exchange Algorithm p 1773 N94-22123
SURFACE DEFECTS
Surface and subsurface defect detection in Si3N4 components by laser scattering
[DE93-040829] p 1832 N94-21772
SURFACE DISTORTION
Principles and applications of oil film interferometry for measuring wall friction fields in air flows
[ETN-93-95062] p 1798 N94-20147
SURFACE EMITTING LASERS
Spatial patterns in semiconductor lasers
[DE93-040056] p 1814 N94-19865

SURFACE ENERGY
Measurement of evapotranspiration with combined reflective and thermal infrared radiance observations [NASA-CR-194802] p 1837 N94-20951
Role of surface characteristics in urban meteorology and air quality [DE93-040929] p 1851 N94-21740
SURFACE FINISHING
Oxidation resistant protective coating system for gas turbine components and process for penetration thereof [CA-PATENT-1,294,155] p 1704 N94-21143
Laser driven hydrodynamic instability experiments [DE93-040550] p 1818 N94-21547
Experiments with a fluid deicing system for cleaning laminar wings p 1640 N94-22601
SURFACE LAYERS
Polarimetric thermal emission from periodic water surfaces p 1728 N94-20445
A theoretical investigation of unsteady separation phenomena related to dynamic stall [AD-A271865] p 1636 N94-20485
Spectroscopic ellipsometric characterization of Si/Si(1-x)Ge(x) strained-layer superlattices p 1734 N94-20510
Analytic solutions for optimized ellipsometric measurements of interfaces and surface layers in thin film structures p 2019 N94-20977
Laser Raman and x ray scattering studies of corrosion films on metals [DE93-040243] p 1692 N94-21558
SURFACE NAVIGATION
Robotic concepts for operation in barren terrain [DE93-040539] p 1946 N94-21925
SURFACE PROPERTIES
Surface science at the solid liquid interface [AD-A271422] p 1678 N94-19839
Formation of colloidal Ag precipitates in fused silica by MeV ion implantation [DE93-040268] p 2012 N94-19869
Particles on surfaces of laser ablated Y1Ba2Cu3O(7-delta) films [DE93-040269] p 2013 N94-19929
The metallic bond for monolayer transition metal layers on transition metal surfaces [DE93-019060] p 1691 N94-20313
Direct imaging of the surface microstructure of dielectric materials using an atomic force microscope [AD-A272251] p 2018 N94-20575
Distribution of small volcanic cones on the surface of Venus by size and elevation: Implications for differential deposition of volcanic features p 2110 N94-20731
Variable angle spectroscopic ellipsometric characterization of surface damage in chemical-mechanical polished GaAs p 1710 N94-20986
GaAs(100) surface modifications at elevated temperatures, studied by in-situ spectroscopic ellipsometry p 2023 N94-20997
Ellipsometric study of GaAs(100) surface changes induced at elevated temperatures p 2023 N94-20998
Obtaining surface optical properties from space-based lidar systems [AD-A272831] p 1967 N94-21172
An analysis of pool surface deformation due to a plunging liquid jet [AD-A272970] p 1802 N94-21261
A method of measuring the thermoradiative properties of ceramic materials in a space environment p 1665 N94-21405
The early Martian environment: Clues from the cratered highlands and the Precambrian Earth p 2143 N94-21667
Role of surface characteristics in urban meteorology and air quality [DE93-040929] p 1851 N94-21740
Surface and subsurface defect detection in Si3N4 components by laser scattering [DE93-040829] p 1832 N94-21772
Spin dynamics and implications for superconductivity: Some problems with the d-wave scenario [DE94-001183] p 2032 N94-21972
Dynamics of surface thermal expansion and diffusivity using two-color reflection transient gratings [DE93-040547] p 1990 N94-22002
Areally averaged estimates of surface heat flux from ARM field studies [DE93-018569] p 1859 N94-22036
Quantitative analysis of scanning tunneling microscopy images for surface structure determination: Sulfur on Fe(0001) [DE93-019235] p 2034 N94-22041
Surface-induced brightness temperature variations and their effects on detecting thin cirrus clouds using IR emission channels in the 8-12 micrometer region p 1880 N94-22341
SURFACE REACTIONS
Materials processing and manufacturing technologies for Diamond Substrate MultiChip Modules (DSMCM) [AD-A271011] p 2011 N94-19821
Segregation of Si to the surface of Fe-29Ni-17Co alloy [DE93-040053] p 1687 N94-19864
Oxidation-reduction induced roughening of platinum (111) surface [DE93-017408] p 1687 N94-19922
The modification of polymer surfaces and the fabrication of submicron-scale functionalized structures by deep-UV and electron beam lithography [AD-A265956] p 1700 N94-20328
In-situ electrochemical surface science [AD-A265942] p 1680 N94-20330
Surface science and modeling studies of endothermic fuels catalysis [AD-A272850] p 1712 N94-21192
Model for liquid boron oxide droplet gasification in H/O/C/F combustion environments [AD-A272911] p 1682 N94-21243
Fast oxygen atom studies related to low Earth orbit activities p 1663 N94-21395
Vapor-delivered lubrication of steel-steel and steel-ceramic systems [PB93-202364] p 1825 N94-21451
Sulfur-bonded thiophenes in organometallic rhenium complexes and adsorption of isocyanides on gold [DE93-041126] p 1694 N94-21937
SURFACE ROUGHNESS
Substrate recovery of Mo-Si multilayer coated optics [DE93-019610] p 1698 N94-19810
Radar backscatter measurements from simulated sea ice during CRRELEX 1990 [AD-A271034] p 1715 N94-19823
Oxidation-reduction induced roughening of platinum (111) surface [DE93-017408] p 1687 N94-19922
Study of electromagnetic wave scattering from characterized rough surfaces [AD-A270931] p 1716 N94-19934
Growth mechanisms and characterization of hydrogenated amorphous-silicon-alloy films [DE93-018202] p 1699 N94-20047
Measuring liquid properties with smooth and textured-surface resonators [DE93-019433] p 1749 N94-20054
Analysis of Ku-band cross section at low incidence angles p 1720 N94-20414
Rough surface scattering from moving ocean surfaces as an indicator of scattering mechanisms p 1726 N94-20439
Synergism of active and passive microwave data for estimating bare surface soil moisture p 1727 N94-20444
Wavelength dependence of limb-darkening of Mars from visible and near-IR telescopic spectral imaging p 2101 N94-20685
The roughness of the Martian surface: A scale dependent model p 2115 N94-20762
Non-destructive evaluation in manufacturing using spectroscopic ellipsometry p 1826 N94-21012
In-situ and ex-situ ellipsometric characterization for semiconductor technology p 2026 N94-21013
VASE (variable angle spectroscopic ellipsometry) p 1687 N94-21014
Flow transition with 2-D roughness elements in a 3-D channel p 1806 N94-21466
Role of surface characteristics in urban meteorology and air quality [DE93-040929] p 1851 N94-21740
Experiments with a fluid deicing system for cleaning laminar wings p 1640 N94-22601
SURFACE ROUGHNESS EFFECTS
Polarimetric thermal emission from rough surfaces p 1727 N94-20441
Symmetry in polarimetric remote sensing p 1729 N94-20449
SURFACE TEMPERATURE
Soil temperatures [KNMI-WR-92-05] p 1865 N94-20309
Measurement of evapotranspiration with combined reflective and thermal infrared radiance observations [NASA-CR-194802] p 1837 N94-20951
High-energy astrophysics: A theoretical analysis of thermal radiation from neutron stars [NASA-CR-194808] p 2055 N94-20952
GaAs(100) surface modifications at elevated temperatures, studied by in-situ spectroscopic ellipsometry p 2023 N94-20997
A carbon dioxide/methane greenhouse atmosphere on early Mars p 2142 N94-21662
A model for the evolution of CO2 on Mars p 2144 N94-21671
Early Mars: The inextricable link between internal and external influences on valley network formation p 2146 N94-21681
Fluorescent microthermographic imaging [DE93-040332] p 1810 N94-22000
Dynamics of surface thermal expansion and diffusivity using two-color reflection transient gratings [DE93-040547] p 1990 N94-22002
SURFACE TREATMENT
Substrate recovery of Mo-Si multilayer coated optics [DE93-019610] p 1698 N94-19810
The modification of polymer surfaces and the fabrication of submicron-scale functionalized structures by deep-UV and electron beam lithography [AD-A265956] p 1700 N94-20328
Surface treatment of InP and contribution to the optimization of the InP(p)/InP(p) regrown interfaces grown by GSMBE [ECL-92-48] p 2018 N94-20598
A comparison of sulfuric acid/boric acid anodize and chromic acid anodize processes [AD-A271933] p 1703 N94-20614
Spectroscopic ellipsometric characterization of Si/Si(1-x)Ge(x) strained-layer superlattices p 2025 N94-21009
Surface modification for corrosion resistance [DE93-017419] p 1693 N94-21825
SURFACE WATER
Ice in the northern plains: Relic of a frozen ocean? p 2090 N94-20391
Evolution of the global water cycle on Mars: The geological evidence p 2142 N94-21660
The evolution of the early Martian climate and the initial emplacement of crustal H2O p 2143 N94-21665
SURFACE WAVES
Ku-band ocean radar backscatter observations during SWADE p 1720 N94-20413
Ocean wave height transformation model using surface roller theory [AD-A272610] p 1883 N94-21423
Theory and simulation of plasma sheath waves [DE94-001305] p 1999 N94-22567
SURFACTANTS
Thrust expansion engine [AD-D015896] p 1669 N94-20121
Non-ionic surfactants in the treatment of third degree burns [AD-A271582] p 1891 N94-21035
Synthesis and catalytic properties of metal and semiconductor nanoclusters [DE93-019418] p 2028 N94-21541
SURGERY
A geometrical process for three dimensional osteotomy planning [ETN-93-93602] p 1892 N94-21134
SURVEILLANCE
Rotorcraft low altitude IFR benefit/cost analysis: Conclusions and recommendations [DOT/FAA/RD-93/22] p 1642 N94-20051
SURVEILLANCE RADAR
State-space models for multichannel detection [AD-A270608] p 1715 N94-19816
The application of spaceborne synthetic aperture radar in the maritime environment [DRA-TM(AWE)-91013] p 1737 N94-20596
SURVEYS
Relating ground truth collection to model sensitivity p 1719 N94-20409
Performance management systems: A statistical analysis [AD-A272989] p 2043 N94-21266
Implementing Electronic Data Interchange (EDI) with small business suppliers in the pre-award acquisition process [AD-A271767] p 1945 N94-21305
Survey and alignment analysis for the ALS storage ring using computer spreadsheets [DE93-019254] p 1917 N94-21917
Current situation in developing petroleum substituting energy (the United Kingdom) [DE94-714897] p 1713 N94-22091
Surveys on specific patterns of facility intallation of photovoltaic power generating technologies for international cooperation [DE94-714901] p 1850 N94-22092
SWELLING
Swelling equilibria for cationic 2-hydroxyethyl methacrylate (HEMA)-based hydrogels [DE94-000728] p 1707 N94-21856
SWEPT FORWARD WINGS
Experimental study on interference aerodynamics of close-coupled canard configuration [AD-A267760] p 1636 N94-19963
SWEPT WINGS
Surface hot film measurements at ATTAS laminar glove p 1639 N94-22598

SWITCHES
Photoconductive Semiconductor Switches for pulsed power applications
[DE93-019411] p 1750 N94-20294
Optically controlled current filamentation in GaAs photoconductive semiconductor switches
[DE93-019427] p 2016 N94-20296
High current density contacts for photoconductive semiconductor switches
[DE93-018837] p 1750 N94-20312
High-power gas switch with hydride electrodes
[AD-D015956] p 1751 N94-20354
Two dimensional simulation of the electric arc behavior in a cut-off device
[ECL-92-41] p 1751 N94-20595
Results from long conduction time plasma opening switch experiments at Sandia National Laboratories
[DE93-019063] p 1762 N94-21632
Ultrafast gas switching experiments
[DE93-019071] p 1762 N94-21634
SWITCHING
Delivery of very high bandwidth with ATM switches and SONET
[DE93-019432] p 1899 N94-20476
An application of the Cerebellar Model Articulation Controller for a switched reluctance rotor position estimator
[AD-A271769] p 1943 N94-20926
Low-latency digital frequency synthesizer using the residue number system p 1759 N94-21121
Optimization of fixed time polling schemes
[CWI-BS-R9237] p 1945 N94-21233
Research on plasma-puff initiation of high Coulomb transfer switches
[NASA-CR-194371] p 1994 N94-21289
Plasma-puff initiation of high Coulomb transfer switches p 1994 N94-21290
Characteristics of plasma-puff trigger for a inverse-pinch plasma switch p 1995 N94-21291
Characteristics of switching plasma in an inverse-pinch switch p 1995 N94-21292
Comparative study of INPIStron and spark gap p 1995 N94-21293
INPIStron switched pulsed power for dense plasma pinches p 1995 N94-21294
Ultrafast gas switching experiments
[DE93-019071] p 1762 N94-21634
Evaluation of DEC's GIGAswitch for distributed parallel computing
[DE94-001356] p 1936 N94-21853
SWITCHING CIRCUITS
SPICE macromodel for a 1-megawatt power MOSFET switch
[DE93-019415] p 1748 N94-19844
Computational model of a magnetic modulator for copper lasers
[DE93-019603] p 1815 N94-20223
Photoconductive Semiconductor Switches for pulsed power applications
[DE93-019411] p 1750 N94-20294
Novel N x N integrated channel waveguide optical crossbars for large scale high speed non-blocking data switching
[AD-A272065] p 1986 N94-20922
High power, electron-beam induced switching in diamond
[DE93-040535] p 1768 N94-21770
A FET-switched induction accelerator cell
[DE93-019604] p 1769 N94-21838
A shared buffer memory switch with maximum queue and minimum allocation p 1773 N94-22119
An adaptive method for group delay compensation using switched capacitor filters p 1793 N94-22248
SWITCHING THEORY
Throughput and blocking in circuit-switched interconnection networks p 1784 N94-22189
Buffer allocation in an ATM switch with output buffer and speed constraints p 1746 N94-22203
SYLLABLES
Generalization performance of backpropagation learning on a syllabification task p 1940 N94-20246
SYMBOLS
Links between N-modular redundancy and the theory of error-correcting codes p 1765 N94-21713
SYMMETRY
Symmetry in polarimetric remote sensing p 1729 N94-20449
High resolution infrared spectroscopy of cyclobutane: A study of vibrational mode coupling involving large amplitude, low frequency modes
[AD-A271987] p 1973 N94-20619
Symmetries and conservation laws of the system: u(x)=vw(x), v(y)=uw(y), uv+w(xx)+w(yy)=0
[MEMO-1084] p 1953 N94-21046
Electronically metastable molecules of high symmetry
[AD-A272015] p 1974 N94-21461
Lattice gauge theory: Present status
[DE93-041154] p 2038 N94-21692
Symmetry-dictated trucation: Solutions of the spherical shell model for heavy nuclei
[DE94-000482] p 1976 N94-21961
SYNCHROCYCLOTRONS
On modelling nuclear reactions in meteorites p 2085 N94-20844
SYNCHRONISM
Structural modeling: An application framework and development process for flight simulators
[AD-A271348] p 1650 N94-19880
Time warp operating system version 2.7 internals manual
[NASA-CR-194798] p 1899 N94-20549
Avoiding and tolerating latency in large-scale next-generation shared-memory multiprocessors p 1753 N94-21081
Reliable interface design for combining asynchronous and synchronous circuits p 1758 N94-21119
Partition algebraic design of asynchronous sequential circuits p 1759 N94-21125
Structured multimedia authoring
[CWI-CS-R9304] p 2044 N94-21535
The Amsterdam hypermedia model: Extending hypertext to support real multimedia
[CWI-CS-R9306] p 2045 N94-21536
A mechanized process algebra for verification of device synchronization protocols p 1766 N94-21716
SYNCHRONOUS MOTORS
Flow and heat transfer model for a rotating cryogenic motor
[DE94-001151] p 1794 N94-22405
SYNCHROTRON RADIATION
Synchrotron x ray diffraction analysis of photorefractive crystals and their gratings
[AD-A271176] p 2015 N94-20213
Examination for optimization of synchrotron radiation spectrum for the x ray depth lithography
[BONN-IR-92-32] p 1967 N94-21148
Radio and optical emission: Spectral shapes and breaks in GRB
[NASA-CR-194763] p 2150 N94-21781
Monte Carlo calculation of multi-electron effects on synchrotron radiation
[DE94-001259] p 1982 N94-21974
SYNCHROTRONS
A summary of studies of particle stability at RHIC
[DE93-040173] p 1970 N94-19868
ALE project
[AD-A271080] p 2014 N94-19960
Synchrotron x ray diffraction analysis of photorefractive crystals and their gratings
[AD-A271176] p 2015 N94-20213
Jet shapes in hadron and electron colliders
[DE93-019386] p 1979 N94-20216
The cross section for the production of b(bar-b) pairs in p(bar p) collisions at the square root of s equals 1.8 TeV
[DE93-019900] p 1972 N94-20225
National Synchrotron Light Source user's manual: Guide to the VUV and x ray beamlines
[DE93-019564] p 2015 N94-20260
Energy and luminosity limits of hadron supercolliders
[DE93-019248] p 1980 N94-20300
Wavelength dispersive analysis with the synchrotron x ray fluorescence microprobe p 1685 N94-20717
Infrared FEL photochemistry: Multiple-photon dissociation of freon gas
[DE94-000817] p 1820 N94-22585
SYNOPTIC METEOROLOGY
The life cycles of intense cyclonic and anticyclonic circulation systems observed over oceans
[NASA-CR-194760] p 1865 N94-20353
A synoptic-scale overview of the TOGA COARE intensive observing period November 1992 to February 1993 based on analyses from US operational global data assimilation systems
[NASA-TM-104593] p 1868 N94-21605
A documentation of icing relevant cloud physical parameters on horizontal soundings of stratiform clouds (continuation)
[DLR-MITT-92-10] p 1871 N94-22280
Examination of the observed synoptic scale cirrus cloud environment: The December 3-6 FIRE cirrus case study p 1877 N94-22325
Cirrus cloud development in a mobile upper tropospheric trough: The November 26th FIRE cirrus case study p 1878 N94-22329
SYNTAX
Representation of idioms in connectionist models p 1940 N94-20247
Hopfield models as neural-network acceptors p 1941 N94-20250
Syntactic neural networks for natural language processing p 1941 N94-20254
COCOLOG: A conditional observer and controller logic for finite machines
[INRIA-RR-1714] p 1910 N94-21063
Recognizing hesitation phenomena in continuous, spontaneous speech p 1746 N94-22210
Fortran for the nineties p 1926 N94-22481
SYNTHESIS (CHEMISTRY)
Synthesis and structural characterization of new light molecular weight inorganic oxidizers and relative derivatives, volume 1
[AD-A271437] p 2012 N94-19842
Electrochemical synthesis of ultrathin film composite membranes
[AD-A272721] p 1681 N94-21168
Development of bioelastic material for aspects of wound repair
[AD-A272000] p 1892 N94-21503
Synthesis and catalytic properties of metal and semiconductor nanoclusters
[DE93-019418] p 2028 N94-21541
SYNTHETIC APERTURE RADAR
Modifications to the three-component classification algorithm for SAR data p 1719 N94-20410
Determination of noise equivalent sigma(0) using highly correlated repeat-pass SAR images p 1720 N94-20411
Topographic mapping using a monopulse SAR system p 1721 N94-20417
Classification of simple vegetation types using POLSAR image data p 1722 N94-20420
Two microstrip arrays for interferometric SAR applications p 1722 N94-20421
Observation of pressure ridges in SAR images of sea ice: Scattering theory and comparison with observations p 1723 N94-20427
On evaluating the accuracy of SAR sea-ice classification using multifrequency polarimetric AIRSAR data p 1724 N94-20426
Direction angle sensitivity of agricultural field backscatter with AIRSAR data p 1724 N94-20430
Retrieval of ice thickness from polarimetric SAR data p 1724 N94-20432
Radar backscattering from snow facies of the Greenland ice sheet: Results from the AIRSAR 1991 campaign p 1725 N94-20434
C-band radar backscatter of sea ice in the Weddell Sea, Antarctica during the austral winter of 1992 p 1725 N94-20435
Mapping of taiga forest units using AIRSAR data and/or optical data, and retrieval of forest parameters p 1729 N94-20452
The Brewster angle effect in SAR polarimetry p 1731 N94-20456
Topographic slope from the SAR interferometric phase gradient p 1731 N94-20459
Interferometric detection of freeze-thaw displacements of Alaskan permafrost using ERS-1 data p 1732 N94-20460
Performance evaluation of the JPL TOPSAR system: An across-track interferometric SAR system for topographic mapping p 1732 N94-20461
Use of microwave polarimetry to enhance SAR images of the ocean surface
[AD-A271911] p 1882 N94-20489
The application of spaceborne synthetic aperture radar in the maritime environment
[DRA-TM(AWE)-91013] p 1737 N94-20596
Beta Regio rift system on Venus: Geologic interpretation of Magellan images p 2095 N94-20655
Beta Regio - Phoebe Regio on Venus: Geologic mapping with the Magellan data p 2096 N94-20656
Magellan vertical polarization radar observations p 1744 N94-20691
Magellan Mission p 1652 N94-20829
Massachusetts Institute of Technology Lincoln Laboratory Journal volume 6, number 1, Spring 1993
[AD-A272273] p 1737 N94-20944
Neural network studies
[AD-A271593] p 1943 N94-20947
The 7th Brazilian Remote Sensing Symposium, volume 3 p 1839 N94-20960
Evaluation of C-band SAR data from SAREX 1992: Tapajos study site p 1839 N94-20964
An overview of synthetic aperture radar signal processing techniques p 1745 N94-22159
Target angular motion and its effects on simulated SSAR ship images p 1745 N94-22161
A motion extraction method for synthetic aperture radars
[DLR-FB-92-31] p 1742 N94-22279
STAR-1 SAR road extraction using texture analysis and mathematical morphology
[ISBN-0-315-83255-X] p 1843 N94-22429

SYSTEM FAILURES
Development and testing of a reliability performance index for modular robotic systems
[AD-A271901] p 1942 N94-20488
Real-time fault tolerant computer systems
[AD-A272909] p 1899 N94-21230
Reducing the cognitive workload: Trouble managing power systems
[NASA-TM-106413] p 1714 N94-21564
SYSTEM IDENTIFICATION
Literature review of the errors-in-variables approach to the problem of system identification
[AD-A271098] p 1949 N94-19907
SYSTEMS ANALYSIS
SISSY: An example of a multi-threaded, networked, object-oriented databased application
[DE93-019742] p 2041 N94-19811
Interval timed coloured petri nets and their analysis
[PB93-191732] p 1903 N94-19992
System performance predictions for Space Station Freedom's electric power system
[NASA-TM-106396] p 1667 N94-20062
Multi-disciplinary coupling effects for integrated design of propulsion systems
[NASA-TM-106349] p 1830 N94-20170
Test and evaluation: DOD has been slow in improving testing of software-intensive systems
[AD-A271541] p 1908 N94-20917
Specification and generation of Markov reward models
[MEMO-INF-92-60] p 1963 N94-21058
N parallel queueing systems with server breakdown and repair
[CWI-BS-R9236] p 1944 N94-21232
Building integrated photovoltaic systems analysis
[DE93-018208] p 1846 N94-21298
Physics Detector Simulation Facility (PDSF) architecture/utilization
[DE93-019744] p 1936 N94-21919
Mathematical modelling of economic systems
p 2050 N94-22060
Macromodel of centrally planned economy
p 2050 N94-22062
Mesoscale simulations of the November 25-26 and December 5-6 cirrus cases using the RAMS model
p 1878 N94-22331
SYSTEMS COMPATIBILITY
The conformance testing methodology to CTRON (communication and central TRON) extended OS
p 1772 N94-22118
SYSTEMS ENGINEERING
Model checking, abstraction, and compositional verification
[AD-A270552] p 1902 N94-19919
Total systems design analysis of high performance structures
[NASA-TP-3432] p 1653 N94-20141
Design considerations for a fiber optic communications network for power systems
[DE93-018404] p 1984 N94-20179
Design structuring and allocation optimization (Destination) prototype level 1 user's manual
[AD-A272115] p 1929 N94-20571
Let your fingers do the walking: The projects most invaluable tool p 1922 N94-21325
Canadian Conference on Electrical and Computer Engineering, volumes 1 and 2
[ISBN-0-9694170-2-0] p 1770 N94-22101
ScaRaB and its subsystems p 1860 N94-22285
SYSTEMS INTEGRATION
SISSY: An example of a multi-threaded, networked, object-oriented databased application
[DE93-019742] p 2041 N94-19811
A modular design for connectionist parsing
p 1941 N94-20252
Space Generic Open Avionics Architecture (SGOAA) standard specification
[NASA-CR-188269] p 1666 N94-22275
SYSTEMS MANAGEMENT
Distributed Virtual System (DIVIRS) project
[NASA-CR-194360] p 1905 N94-20228
Government Open Systems Interconnection Profile (GOSIP) transition strategy
[AD-A273005] p 1740 N94-21308
Intervention strategies for the management of human error
[NASA-CR-4547] p 1642 N94-22373
SYSTEMS SIMULATION
Model checking, abstraction, and compositional verification
[AD-A270552] p 1902 N94-19919
Back and forth bisimulations on prime event structures
[RR-888-I-IMAG-124-LIFIA] p 1929 N94-20124
Multi-disciplinary coupling effects for integrated design of propulsion systems
[NASA-TM-106349] p 1830 N94-20170
SYSTOLIC ARRAYS
The Fifth NASA Symposium on VLSI Design
[NASA-CR-194644] p 1753 N94-21079
Practical issues in implementing roving spares in VLSI systolic arrays p 1758 N94-21114
Bit-systolic arithmetic arrays using dynamic differential gallium arsenide circuits p 1767 N94-21724
A 1 GHz sample rate, 256-channel, 1-bit quantization, CMOS, digital correlator chip p 1768 N94-21732
Design of a floating point convolution processor
p 1775 N94-22133

T

T TAURI STARS
Pre-main sequence stars in the Chamaeleon cloud and pre-main sequence stars in the Rho Ophiuchi cloud core
[NASA-CR-194713] p 2080 N94-20337
TABLES (DATA)
Evaluation of RDBMS packages for use in astronomy
p 2048 N94-22514
The European Southern Observatory-MIDAS table file system p 2048 N94-22518
TACTILE DISCRIMINATION
Application of change detection to dynamic contact sensing
[AD-A270523] p 1939 N94-20105
TACTILE SENSORS (ROBOTICS)
Application of change detection to dynamic contact sensing
[AD-A270523] p 1939 N94-20105
TAIL ASSEMBLIES
Apparatus and method for improving spin recovery on aircraft
[NASA-CASE-LAR-14747-1] p 1650 N94-20556
TALKING
Recognizing hesitation phenomena in continuous, spontaneous speech p 1746 N94-22210
TANTALUM
The metallic bond for monolayer transition metal layers on transition metal surfaces
[DE93-019060] p 1691 N94-20313
Gamma ray spectrometry of LDEF samples: Results of 1992 analyses
[DE94-001177] p 1684 N94-22046
TANTALUM CARBIDES
Performance of carbon-based hot frit substrates
[DE94-000509] p 1676 N94-21754
TANTALUM COMPOUNDS
High temperature stability of amorphous Ta(x)Cu(1-x) diffusion barriers on GaAs p 2022 N94-20990
TANTALUM OXIDES
A quantitative model for interpreting nanometer scale hardness measurements of thin films
[DE93-040601] p 2034 N94-22005
TAPE RECORDERS
Recording system using multiplexed inputs to a multichannel recorder
[AD-D015971] p 1808 N94-21278
TARGET ACQUISITION
Target motion detecting impulse Doppler radar system
[AD-D015898] p 1717 N94-20198
Probability of detection calculations using MATLAB
[AD-A271958] p 1736 N94-20578
Development of a lidar for integration with the Naval Postgraduate School Infrared Search and Target Designation (NPS-IRSTD) system
[AD-A271847] p 1817 N94-20611
Current directions in the vulnerability/lethality process structure
[AD-A272836] p 1964 N94-21175
NAVSPASUR sensor system digital signal processing receiver. Volume 2: Function and capabilities of hardware and software components
[AD-A272900] p 1739 N94-21218
TARGET DRONE AIRCRAFT
AIAA Techfest 29 proceedings
[NIAR-93-1] p 1635 N94-20191
TARGET RECOGNITION
Recognition by prototypes
[AD-A271687] p 1943 N94-20921
Massachusetts Institute of Technology Lincoln Laboratory Journal volume 6, number 1, Spring 1993
[AD-A272273] p 1737 N94-20944
Improvement in invariant pattern recognition with neural networks and Fourier-Mellin filters p 1780 N94-22164
A modified moment invariants technique for classification of noisy objects p 1780 N94-22165
Signal processing and target discrimination algorithms for a rosette scan tracker p 1747 N94-22237
Radar imaging of moving targets
p 1747 N94-22238
TARGETS
Facilities for in situ ion beam studies in transmission electron microscopes
[DE93-019567] p 1979 N94-20222
Geometrical analysis of the microcraters found on LDEF samples p 1666 N94-20890
Antipodal fragment velocities for porous and weak targets at catastrophic impacts p 1836 N94-20891
TASKS
Development of the UTC-PAB normative database
[AD-A271319] p 1893 N94-20023
Multilist scheduling: A new parallel programming model
[AD-A270549] p 1929 N94-20084
TASTE
Reassessment of area postrema's role in motion sickness and conditioned taste aversion
p 1886 N94-21901
Recovery of the vomiting reflex following area postrema ablation in squirrel monkeys p 1886 N94-21904
Conditioned taste aversion induced by motion is prevented by selective vagotomy in the rat
p 1887 N94-21908
The effects of area postrema lesions and selective vagotomy on motion-induced conditioned taste aversion
p 1888 N94-21910
Role of the area postrema in three putative measures of motion sickness in the rat p 1888 N94-21912
Investigating motion sickness using the conditioned taste aversion paradigm p 1888 N94-21913
Conditioned taste aversion and motion sickness in cats and squirrel monkeys p 1888 N94-21914
TAXIING
A study of parallel pier finger airport terminal configuration
[ISBN-0-315-83128-6] p 1652 N94-22425
TDR SATELLITES
The NCC project: A quality management perspective
p 1828 N94-21324
Software metrics: The key to quality software on the NCC project p 1922 N94-21326
Problem reporting management system performance simulation p 1931 N94-21328
Enhanced networks operations using the X Window System p 1932 N94-21329
Space network scheduling benchmark: A proof-of-concept process for technology transfer
p 1932 N94-21332
Analysis of the TDRS multiple access system for possible use as an attitude control system sensor
p 1666 N94-21338
The Automated Conflict Resolution System (ACRS)
p 1744 N94-21341
Satellite Communication Hardware Emulation System (SCHES) p 1744 N94-21344
Using the USCCS for sub microsecond spacecraft clock calibration p 1813 N94-21346
Advanced coding and modulation schemes for TDRSS
p 1744 N94-21350
TEAMS
Factors associated with continuance commitment to FAA matrix teams
[DOT/FAA/AM-93/18] p 2040 N94-21626
TEARING MODES (PLASMAS)
Effects of magnetic field perturbations in the ATF torsatron
[DE94-000474] p 1999 N94-22568
TECHNICAL WRITING
An assessment of the statistical and editorial output of text analysis programs
[AD-A272185] p 2042 N94-20924
TECHNOLOGY ASSESSMENT
Statement of David E. Baldwin, Associate Director for Energy, Lawrence Livermore National Laboratory and John C. Crawford, Vice President, Sandia National Laboratories, California, to the Subcommittee on Research and Development of the Committee on Environment and Public Works, US Senate, Washington, DC, 22 March 1993
[DE93-017991] p 1844 N94-19803
Data format standards for civilian remote sensing satellites
[PB93-192920] p 1841 N94-21446
NEP Early Flight program: System performance and development considerations
[NASA-TM-106415] p 1654 N94-21570
Survey of lift-fan aerodynamic technology
[NASA-CR-177615] p 1646 N94-21592
Thin-film CdTe and CuInSe2 photovoltaic technologies
[DE93-018217] p 1848 N94-21827
Microtechnology: The key to the technical challenges of the 21st century
[DE94-000403] p 1769 N94-21959
Survey on evaluation of energy technology contributing to preservation of the global environment. 2
[DE94-714884] p 1853 N94-22051

Study on possibility of developing energy integration technology
[DE94-714903] p 1849 N94-22052
Manufacturing and information technology p 2046 N94-22082
Spaceplane flight simulation: Project definition
[PB93-211399] p 1651 N94-22094

TECHNOLOGY TRANSFER
The development of remote sensing in Brazil and Canada: Comparative case studies p 1840 N94-20968
Networks Technology Conference
[NASA-CP-3241] p 1931 N94-21323
First Biomass Conference of the Americas: Energy, Environment, Agriculture, and Industry, volume 2
[DE94-000435] p 1847 N94-21562
Index to 1992 NASA Tech Briefs, volume 16, numbers 1-12
[NASA-TM-109377] p 2053 N94-21736
Index to 1991 NASA Tech Briefs, volume 15, numbers 1-12
[NASA-TM-109376] p 2053 N94-21737
Cumulative index to NASA Tech Briefs, 1986-1990, volumes 10-14
[NASA-TM-109378] p 2054 N94-21738
Spinoff, 1992
[NASA-NP-201] p 2054 N94-21739
Microtechnology: The key to the technical challenges of the 21st century
[DE94-000403] p 1769 N94-21959

TECHNOLOGY UTILIZATION
Space applications of superconducting microwave electronics at NASA Lewis Research Center p 1671 N94-20513
Lithium batteries: Future batteries p 1752 N94-20630
Rad-hard computer elements for space applications p 1753 N94-21082
Conversion of LDEF experiment M0003 sample observation database to MS-DOS formats
[AD-A272945] p 1681 N94-21226
Index to 1992 NASA Tech Briefs, volume 16, numbers 1-12
[NASA-TM-109377] p 2053 N94-21736
Index to 1991 NASA Tech Briefs, volume 15, numbers 1-12
[NASA-TM-109376] p 2053 N94-21737
Cumulative index to NASA Tech Briefs, 1986-1990, volumes 10-14
[NASA-TM-109378] p 2054 N94-21738
Spinoff, 1992
[NASA-NP-201] p 2054 N94-21739
Acoustic, fiber optic, and silicon microelectronic microsensors research and development activities at Sandia National Laboratories
[DE93-019075] p 1770 N94-22040

TECTONICS
Beta Regio rift system on Venus: Geologic interpretation of Magellan images p 2095 N94-20655
Formation and evolution of radial fracture systems on Venus p 2099 N94-20672
Venus magmatic and tectonic evolution p 2101 N94-20683
Crater destruction on the Venusian highlands by tectonic processes p 2103 N94-20696
Strength and deformation properties of basaltic lava flows on planetary surfaces p 1862 N94-20747
Volcanic rises on Venus: Geology, formation, and sequence of evolution p 2113 N94-20755
Geoid, topography, and convection-driven crustal deformation on Venus p 2116 N94-20769
Response of the topography and gravity field on Venus to mantle upwelling beneath a chemical boundary layer p 2117 N94-20775
A tectonic resurfacing model for Venus p 2118 N94-20781
Delimitation of terrestrial impact craters by way of pseudotachylytic rock distribution p 1863 N94-20783
Parga and Hecate Chasmata, Venus: Structure, volcanism and models of formation p 2121 N94-20796
Extensional history of Mars' Tharsis Region p 2125 N94-20814
Complex structure of the Thaumasia region of Mars p 2125 N94-20815
Photogeological analysis of Europan tectonic features p 2129 N94-20838
Is there uniformitarian or catastrophic tectonics on Venus? p 2129 N94-20839
Wrinkle ridges, reverse faulting, and the depth penetration of lithospheric stress in lunae planum, Mars p 2141 N94-20910
On the origin and evolution of circular forms observed in remote sensing images of the Rio de Janeiro State, Brazil p 1839 N94-20963
Mobility of salt domes
[BCRS-92-08] p 1857 N94-21016
Post-Palbozoic crustal responses to the contemporary stress field in the eastern United States
[DE93-040604] p 1859 N94-22006

TEFLON (TRADEMARK)
Interleaved bismaleimide composites
[AD-A272233] p 1674 N94-20574
The simulation of action of some space environment factors on Teflon and on rubber materials p 1661 N94-21380

TEKTITES
Modelling the gravity and magnetic field anomalies of the Chicxulub crater p 1862 N94-20668
Iridium in sediments containing large abundances of Australasian microtektites from DSDP hole 758B in the Eastern Indian Ocean and from DSDP hole 769A in the Sulu Sea p 2083 N94-20741
Further analyses of Rio Cuarto impact glass p 1685 N94-20745
Magnetic properties and Moessbauer analyses of glass from the K-T boundary, Beloc, Haiti p 1685 N94-20753

TELECOMMUNICATION
Rotorcraft low altitude IFR benefit/cost analysis: Conclusions and recommendations
[DOT/FAA/RD-93/22] p 1642 N94-20051
Optimization of fixed time polling schemes
[CWI-BS-R9237] p 1945 N94-21233
Networks Technology Conference
[NASA-CP-3241] p 1931 N94-21323
Telecommunications services for multimedia data exchange support
[AD-A271704] p 1740 N94-21352
IAS telecommunication infrastructure and value added network services provided by IASNET p 1744 N94-22069
Everything you might want to know about the Internet but are afraid to ask!
[DE93-041118] p 2046 N94-22413

TELECONFERENCING
Performance evaluation of video on ethernet
[DE93-040696] p 1936 N94-21749

TELEMETRY
The EXOSAT operational experience
[ESA-STM-248] p 1657 N94-20235
SIMA: An integrated environmental monitoring system p 1840 N94-20967
Mission Operations Support Area (MOSA) for ground network support p 1932 N94-21331
An in-depth analysis and modelling of the Shuttle to MILA S-band telemetry link p 1657 N94-21340
Developing a space network interface simulator: The NTS approach p 1933 N94-21343
Concept report: Experimental vector magnetograph (EXVM) operational configuration balloon flight assembly
[NASA-CR-194702] p 1638 N94-21776
Reentry vehicle adaptive telemetry
[DE94-001168] p 1656 N94-21852
A packet based, data driven telemetry system for autonomous experimental sub-orbital spacecraft
[DE94-000399] p 1657 N94-21980
Automated analysis tools for reducing spacecraft telemetry data
[DE94-000400] p 1657 N94-21981

TELEOPERATORS
Teleoperation with virtual force feedback
[DE93-019406] p 1942 N94-20293

TELEPHONES
Conversion of the proprietary ROLM (tm) inter-node link from multimode to singlemode operation p 1744 N94-21349

TELEROBOTICS
Telerobotic control of a mobile coordinated robotic server, executive summary
[NASA-CR-194685] p 1821 N94-20044

TELESCOPES
Conically scanned holographic lidar telescope
[NASA-CASE-GSC-13462-1] p 1986 N94-20591
Advanced far infrared detectors
[DE93-040289] p 1988 N94-21526
Laser guide star adaptive optics: Present and future
[DE93-018642] p 1989 N94-21619
Archiving data from ground-based telescopes p 2046 N94-22442
Programmability in AIPS++ p 1926 N94-22482
Telescope image modelling software in STSDAS p 1926 N94-22483
The University of Hawaii Institute for Astronomy CCD camera control system p 1828 N94-22489
The ADAM environment and transputers p 1926 N94-22494
The VLBA correlator: Real-time in the distributed era p 2049 N94-22547
Solar full-disk magnetic field image receiving system and observation software p 2079 N94-22552

TELEVISION CAMERAS
Initial laboratory evaluation of color video cameras, phase 2
[DE93-040201] p 1809 N94-21556

TELEVISION TRANSMISSION
NHK Science and Technical Research Laboratories p 2151 N94-20342

TELLURIDES
Evaporation of a sodium tellurite melt in the jamic low gravity drop shaft p 1713 N94-20605

TEMPERATE REGIONS
Are tropical cirrus brighter than mid-latitude cirrus? p 1881 N94-22343

TEMPERATURE CONTROL
Materials processing and manufacturing technologies for diamond substrate multichip modules
[AD-A271484] p 2027 N94-21319
SPACE-R Thermionic Space Nuclear Power System: Design and Technology Demonstration Program
[DE93-013969] p 1670 N94-21824

TEMPERATURE DEPENDENCE
Frequency and temperature dependence of high damping elastomers
[DE93-019539] p 1697 N94-19809
Temperature dependence of 4f PES features and hole occupancy in ytterbium heavy fermions
[DE93-040131] p 1691 N94-20321
High energy ionization in liquids: The free ion yield
[DE93-040329] p 1973 N94-20324
Ten GHz YBa2Cu3O(7-delta) superconducting ring resonators on NdGaO3 substrates p 1735 N94-20515
Stability of an uncooled segment of a high-temperature superconductor
[DE94-000476] p 2032 N94-21932
Investigation of moisture-induced embrittlement of iron aluminides
[DE93-040841] p 1695 N94-21949
Temperature dependence of magnetic order in single-crystalline UPdSn
[DE93-040153] p 2033 N94-21991
Temperature-dependent ion beam mixing
[DE93-040281] p 2033 N94-21999
Dynamics of surface thermal expansion and diffusivity using two-color reflection transient gratings
[DE93-040547] p 1990 N94-22002
Temperature dependence of CsI(Tl) gamma ray excited scintillation characteristics
[DE94-000836] p 2034 N94-22028
Microstructural evolution of neutron-irradiated Fe-Cr-Ni ternary alloys at high helium generation rates
[DE93-018786] p 1696 N94-22037
First-principles pressure-temperature phase diagrams in metals
[DE94-001056] p 1696 N94-22398
Test results of two high temperature superconducting sample coils
[DE94-000496] p 2035 N94-22570
Alloying studies in U(1-x)Th(x)Pd2Al3 (0 (le) x (le) 1)
[DE94-000807] p 2036 N94-22584

TEMPERATURE DISTRIBUTION
Three-dimensional dynamic thermal imaging of structural flaws by dual-band infrared computed tomography
[DE93-019575] p 1906 N94-20316
Comparison of mixing calculations for reacting and non-reacting flows in a cylindrical duct
[NASA-TM-106435] p 1649 N94-21758

TEMPERATURE EFFECTS
Parametric variations of ion transport in TFTR
[DE93-012653] p 1991 N94-19883
Thermal behavior of natural zeolites
[DE93-040091] p 1699 N94-19975
Energy storage and conversion in solid hydrogen
[AD-A271439] p 1845 N94-20086
Strengthening of NiAl matrix composites
[AD-A271491] p 1674 N94-20550
Tambo Quemado: Extraordinary concentrations of REE and refractory trace elements caused by artificial heating p 1684 N94-20667
Further analyses of Rio Cuarto impact glass p 1685 N94-20745
A classification scheme for the morphology of lava flow fields p 1863 N94-20879
Chemical reaction fouling model for single-phase heat transfer
[DE93-019556] p 1802 N94-20942
Amorphous Ta-rich Ta-Cu films as diffusion barriers between Au and GaAs p 1710 N94-20991
Ellipsometric study of GaAs(100) surface changes induced at elevated temperatures p 2023 N94-20998
Human responses to exercise-heat stress
[AD-A272581] p 1892 N94-21209
Description and assessment of a new Optical Pressure Measurement System (OPMS) demonstrated in the high speed wind tunnel in Goettingen (Germany)
[DLR-FB-92-24] p 1651 N94-21280

A quantitative S.E.M. image analysis of cement paste microstructure p 1708 N94-21894
Photo- and thermal-induced antiferromagnetic interlayer coupling in Fe/(Fe-Si) superlattices
[DE93-040822] p 2031 N94-21930
First-principles pressure-temperature phase diagrams in metals
[DE94-001056] p 1696 N94-22398
Projections on structures and material strength in the computational context p 1834 N94-22610

TEMPERATURE GRADIENTS
The distribution of ground ice on Mars p 2090 N94-20394
Stability curves for a thermoacoustic prime mover
[AD-A272607] p 1968 N94-21422
Low Reynolds-number turbulent boundary layers
[AD-A272011] p 1803 N94-21459
Shock temperature measurements of iron to 350 GPa
[DE94-001058] p 1695 N94-22024
Kinetic resonance damping rate of the toroidal ion temperature gradient mode
[DE94-001234] p 1998 N94-22561
Fluid simulations of Delta T(sub e)-driven turbulence and transport in boundary plasmas
[DE94-001304] p 1999 N94-22566
Electron temperature gradient driven instability in the tokamak boundary plasma
[DE94-001307] p 1999 N94-22596

TEMPERATURE MEASUREMENT
Global and regional comparative performance of linear and nonlinear satellite multichannel sea surface temperature algorithms
[AD-A270475] p 1837 N94-20028
Acoustic monitoring of global ocean variability
[AD-A271998] p 1883 N94-21366
Fluorescent microthermographic imaging
[DE93-040332] p 1810 N94-22000
Shock temperature measurements of iron to 350 GPa
[DE94-001058] p 1695 N94-22024
Overview of microphysical and state parameter measurements from FIRE 2 p 1871 N94-22293
Alloying studies in U(1-x)Th(x)Pd2Al3 (0 (le) x (le) 1)
[DE94-000807] p 2036 N94-22584
Measurement Technology for Flight Tests
[ILR-MITT-256(1991)] p 1639 N94-22597
Surface hot film measurements at ATTAS laminar glove p 1639 N94-22598
Testing of a multisensor hot film technique in wind tunnel and free flight p 1639 N94-22599

TEMPERATURE PROFILES
Thermal characterization of thin films by photothermally induced laser beam deflection p 1710 N94-21007
Impact of copper vapour contamination on argon arcs p 1994 N94-21053
Low Reynolds-number turbulent boundary layers
[AD-A272011] p 1803 N94-21459

TEMPERATURE SENSORS
The marine light-mixed layer experiment cruise and data report: R/V endeavor cruise EN-224, mooring deployment, 27 April-1 May 1991: Cruise EN-227, mooring recovery, 5-23 September 1991
[AD-A271175] p 1864 N94-20186
On demand, non-halon, fire extinguishing systems
[AD-D015957] p 1714 N94-20355
Army aircraft fire-detection systems operation and reliability
[AD-A271327] p 1641 N94-20912

TEMPLATES
An insensitive algorithm for template matching with correlation p 1793 N94-22249

TEMPORAL DISTRIBUTION
Spatial and temporal variations of satellite microwave measurements of latent heat release in tropic cyclones due to environmental forcing obtained from a numerical model
[AD-A267947] p 1865 N94-20482

TEMPORAL RESOLUTION
Ultrafast scanning microscopy
[DE93-040121] p 1985 N94-20320
Measurement of thermal-hydraulic parameters in two-phase flow using flow visualization image analysis
[DE93-006255] p 1805 N94-22269

TENSILE PROPERTIES
Rapid heating tensile testing update: 304L stainless steel
[DE93-018770] p 1688 N94-19942
Investigation of cracking and erratic behavior of the uranium-titanium alloy
[DE93-018591] p 1688 N94-19957
Weldalite (tm) 049 (Al 2095-T8): Anisotropy effects at cryogenic conditions
[AD-A272658] p 1691 N94-21188
Applicability and performance benefits of XD (Tradename) titanium aluminides to expendable gas turbine engines
[AD-A272998] p 1648 N94-21268
Tensile and shear fracture behavior of fiber reinforced plastics at 77K irradiated by various radiation sources
[DE93-040280] p 1706 N94-21542

TENSILE STRENGTH
Strength and deformation properties of basaltic lava flows on planetary surfaces p 1862 N94-20747
Tensile strength of fiber reinforced plastics at 77K irradiated by various radiation sources
[DE93-040826] p 1709 N94-22008

TENSILE TESTS
Rapid heating tensile testing update: 304L stainless steel
[DE93-018770] p 1688 N94-19942
Stress-induced cracking of fluorocarbon rubber MTL-0002 after exposure to DS-2
[AD-A271753] p 1705 N94-21302
Tensile and shear fracture behavior of fiber reinforced plastics at 77K irradiated by various radiation sources
[DE93-040280] p 1706 N94-21542
Results of the second Round Robin on opening-load measurement conducted by ASTM Task Group E24.04.04 on crack closure measurement and analysis
[NASA-TM-109032] p 1832 N94-21624
Tensile strength of fiber reinforced plastics at 77K irradiated by various radiation sources
[DE93-040826] p 1709 N94-22008
Nonlinear and progressive failure aspects of transport composite fuselage damage tolerance p 1834 N94-22609

TERBIUM COMPOUNDS
Synthesis and characterization of charge-substituted garnets YCaLnGa5O12 (Ln = Ce, Pr, Tb)
[DE93-040227] p 2033 N94-21992
Spectroscopic studies of magnetic transitions in TbPO4
[DE94-001274] p 2035 N94-22565

TERMINAL BALLISTICS
Impactor control of central peak and peak-ring formation p 1862 N94-20744
Hypervelocity impact
[AD-A272957] p 1831 N94-21249

TERMINAL FACILITIES
Passenger terminal level of service measurement: A utility theoretic approach
[ISBN-0-315-59037-8] p 1651 N94-22418
Passenger terminal simulation model
[ISBN-0-315-61113-8] p 1652 N94-22423
A study of parallel pier finger airport terminal configuration
[ISBN-0-315-83128-6] p 1652 N94-22425

TERMINOLOGY
Qualifying codes under software quality assurance: Two examples as guidelines for codes that are existing or under development
[DE93-040452] p 1904 N94-20097
Understanding Open Systems Interconnection (OSI)
[AD-A271877] p 1929 N94-20472
The Keck keyword layer p 1925 N94-22460

TERNARY ALLOYS
Non-fermi liquid and spin-glass behavior of the Sc(1-x)U(x)Pd3 system
[DE93-040134] p 2016 N94-20335
In-situ spectroscopic ellipsometry in molecular beam epitaxy p 2024 N94-21005
Microstructural evolution of neutron-irradiated Fe-Cr-Ni ternary alloys at high helium generation rates
[DE93-018786] p 1696 N94-22037

TERRACES (LANDFORMS)
Milankovitch insulation forcing and cyclic formation of large-scale glacial, fluvial, and eolian landforms in central Alaska p 2089 N94-20386
Cryoplanation terraces of interior and western Alaska p 2091 N94-20396

TERRAIN
Meso-Beta scale numerical simulation studies of terrain-induced jet streak mass/momentum perturbations
[NASA-CR-194627] p 1864 N94-20138
A wet-geology and cold-climate Mars model: Punctuation of a slow dynamic approach to equilibrium p 2090 N94-20389
Possible occurrence and origin of massive ice in Utopia Planitia p 2090 N94-20390
A model for the origin of Martian polygonal terrain p 2090 N94-20393
The thumbprint terrain: What will Mars Observer tell us? p 2091 N94-20397
A formational model for the polygonal terrains of Mars: Taking a crack at the genesis of the Martian polygons p 2091 N94-20400
Balloon exploration of the northern plains of Mars near and north of the Viking 2 landing site p 2092 N94-20401
Geomorphic evidence for an eolian contribution to the formation of the Martian northern plains p 2092 N94-20402
Topographic mapping using a monopulse SAR system p 1721 N94-20417
Diapirs and cantaloupes: Layering and overturn of Triton's crust p 2111 N94-20738
Geology of the southern hemisphere of Triton: No polar cap p 2111 N94-20739
Complex ridged terrain-related ridge belts on Venus: Global distribution and classification p 2129 N94-20835
Early Mars: A regional assessment of denudation chronology p 2145 N94-21676
Role of surface characteristics in urban meteorology and air quality
[DE93-040929] p 1851 N94-21740

TERRAIN ANALYSIS
Application of Cloude's target decomposition theorem to polarimetric imaging radar data p 1724 N94-20429
Geology and radiophysical properties of the Venera and Vega landing sites p 2135 N94-20867
Detecting topographical regions in digital terrain maps
[AD-A272889] p 1841 N94-21453

TERRESTRIAL PLANETS
Determination of cosmic bodies size-velocity distribution by observation of current impacts on Mars p 2082 N94-20648
Largest impact features on Venus: Non-preserved or non-recognizable? p 2096 N94-20657
Numerical simulation of lava flows: Applications to the terrestrial planets p 1863 N94-20904

TEST CHAMBERS
Measurement of thermal-hydraulic parameters in two-phase flow using flow visualization image analysis
[DE93-006255] p 1805 N94-22269

TEST FACILITIES
High temperature simulation chambers. Physico-chemical and thermal effect of atmospheric reentry on ceramic materials p 1653 N94-21404
Material properties and behavior during simulated atmospheric reentry p 1665 N94-21408

TEST STANDS
Optimization and control of a small angle ion source using an adaptive neural network controller
[DE93-040063] p 1946 N94-21845
A real-time infrared image processing testbed p 1790 N94-22227

TETHERED SATELLITES
Radiation of plasma wave wings through an electrodynamic tether satellite system with any sharp angle geometry
[REPT-85] p 1993 N94-20156
Data analysis support for the SPREE instruments on the TSS-1 shuttle flight
[AD-A272445] p 1654 N94-21429

TETHERING
Data analysis support for the SPREE instruments on the TSS-1 shuttle flight
[AD-A272445] p 1654 N94-21429

TETRAHEDRONS
Tetrahedral lander
[NASA-CASE-MSC-22082-1] p 1658 N94-20590
Dynamic mesh adaption for triangular and tetrahedral grids p 1920 N94-22363

TEXTS
Speech synthesis with artificial neural networks p 1743 N94-20245
An assessment of the statistical and editorial output of text analysis programs
[AD-A272185] p 2042 N94-20924
CMIFed: A presentation environment for porta ble hypermedia documents
[CWI-CS-R9305] p 2044 N94-21494
The Amsterdam hypermedia model: Extending hypertext to support real multimedia
[CWI-CS-R9306] p 2045 N94-21536

TEXTURES
Multiplicity of chondrule heating events and the coarsening of chondrule textures p 2085 N94-20860

THALLIUM
Superconductivity Technology Program for Electric Power Systems: Proceedings
[DE93-040074] p 2011 N94-19825

THALLIUM COMPOUNDS
Theory of energy-assisted epitaxy; theory of ordered semiconductor alloys: In(1-x)Tl(x)Sb as a long-wave infrared material
[AD-A271007] p 2012 N94-19835
TlCaBaCuO high Tc superconducting microstrip ring resonators designed for 12 GHz p 1735 N94-20516

THEMATIC MAPPERS (LANDSAT)
Linear mixing model applied to AVHRR LAC data p 1838 N94-20958
The 7th Brazilian Remote Sensing Symposium, volume 3 p 1839 N94-20960
Evaluation of C-band SAR data from SAREX 1992: Tapajos study site p 1839 N94-20964

Information extraction for multispectral images using radiation interaction models
[BCRS-90-22] p 1841 N94-21015
Chromaticity analysis of LANDSAT multispectral scanner and thematic mapper imagery of Chilko Lake, British Columbia, using a theoretical optical water quality model
[ISBN-0-315-63832-X] p 1843 N94-22422
THEMATIC MAPPING
Classification of simple vegetation types using POLSAR image data p 1722 N94-20420
Geology and radiophysical properties of the Venera and Vega landing sites p 2135 N94-20867
THEOREM PROVING
COCOLOG: A conditional observer and controller logic for finite machines
[INRIA-RR-1714] p 1910 N94-21063
Partition algebraic design of asynchronous sequential circuits p 1759 N94-21125
The Robinson-Schensted and Schuetzenberger algorithms. Part 1: New combinatorial proofs
[CWI-AM-R9208-PT-1] p 1911 N94-21156
On semisimple cocommutative bialgebras
[CWI-AM-R9210] p 1954 N94-21158
Hilbert 90 for polynomial matrices
[CWI-AM-R9211] p 1954 N94-21159
An NP set with no co-DP sparse subset
[TR-475] p 1954 N94-21199
A mechanized process algebra for verification of device synchronization protocols p 1766 N94-21716
HDL to verification logic translator p 1766 N94-21717
Semi-stability and heights of cycles
[PB93-215507] p 1961 N94-22377
THEOREMS
Symmetries and conservation laws of the system: $u(x)=vw(x)$, $v(y)=uw(y)$, $uv+w(xx)+w(yy)=0$
[MEMO-1084] p 1953 N94-21046
Hilbert 90 for polynomial matrices
[CWI-AM-R9211] p 1954 N94-21159
Instruction set commutivity p 1766 N94-21719
THEORETICAL PHYSICS
Energy and luminosity limits of hadron supercolliders
[DE93-019248] p 1980 N94-20300
High energy physics program at Texas A/M University
[DE93-041089] p 1980 N94-20933
Theoretical particle physics
[DE94-000538] p 1973 N94-20938
Non commutative geometry and physics
[PB93-215499] p 1961 N94-22264
THERMAL ANALYSIS
Transient thermal analysis of cryocondensation pump for JET
[DE93-040372] p 1992 N94-20003
Three-dimensional dynamic thermal imaging of structural flaws by dual-band infrared computed tomography
[DE93-019575] p 1906 N94-20316
Kinetics of phase transformations in glass forming systems
[NASA-CR-194270] p 1701 N94-20347
A study of the induction heating of organic composites
[AD-A272657] p 1675 N94-21187
Estimating the rotation rate of mesoscale ocean rings from satellite altimetry
[AD-A272922] p 1883 N94-21222
Thermal stress analysis of composites in the space environment p 1661 N94-21379
Concept report: Experimental vector magnetograph (EXVM) operational configuration balloon flight assembly
[NASA-CR-194702] p 1638 N94-21776
Development of BEM for ceramic composites
[NASA-CR-194718] p 1676 N94-21777
Preliminary SP-100/Stirling heat exchanger designs
[NASA-TM-106444] p 1670 N94-21809
A finite element formulation and adaptive solution approach for large-scale thermomechanical problems with complex contact conditions
[DE93-019605] p 1960 N94-21996
In situ identification of the Martian surface material and its interaction with the Martian atmosphere using DTA/GC p 1812 N94-22434
THERMAL BOUNDARY LAYER
EHD enhancement of pool and in-tube boiling of alternate refrigerants
[DE94-000787] p 1798 N94-20101
THERMAL CONDUCTIVITY
A database of selected transport coefficients for combustion studies
[DE93-041278] p 1678 N94-19889
A parametric study of heat transfer within a planar thermosyphon
[DE93-019546] p 1799 N94-20258
Thermal conductivity measurements of particulate materials under Martian conditions p 1685 N94-20703
Thermal diffusivity measurements by photothermal laser beam deflection (PTD): Data analysis using the Levenberg-Marquardt algorithm p 1820 N94-21006
THERMAL CONTROL COATINGS
Calibration of a calorimeter for measuring the performance of thermal control surfaces p 1660 N94-21378
THERMAL CYCLING TESTS
Investigation of austenitic alloys for advanced heat recovery and hot gas cleanup systems
[DE93-017863] p 1687 N94-19802
The implications of the LDEF results on Space Station Freedom power system materials p 1660 N94-21377
Materials evaluation at ESA/ESTEC p 1662 N94-21386
Durability of thermal control and environmental protective materials for the SSRMS in simulated LEO environment p 1663 N94-21392
A method of measuring the thermoradiative properties of ceramic materials in a space environment p 1665 N94-21405
Analysis of thermal mechanical fatigue in titanium matrix composites p 1835 N94-22618
THERMAL DECOMPOSITION
ALE project
[AD-A271080] p 2014 N94-19980
Chemistry of the burning surface
[AD-A272725] p 1681 N94-21181
THERMAL DEGRADATION
Ageing studies on a composite propellant containing a new organo-copper burn rate catalyst
[AD-A271060] p 1711 N94-19906
Toxicity of thermal degradation in a manned space environment p 1684 N94-21403
THERMAL DIFFUSION
Hydrogen isotope separation experience at the Savannah River Site
[DE93-019832] p 1679 N94-20266
THERMAL DIFFUSIVITY
Thermal diffusivity measurements by photothermal laser beam deflection (PTD): Data analysis using the Levenberg-Marquardt algorithm p 1820 N94-21006
Thermal characterization of thin films by photothermally induced laser beam deflection p 1710 N94-21007
Dynamics of surface thermal expansion and diffusivity using two-color reflection transient gratings
[DE93-040547] p 1990 N94-22002
THERMAL EMISSION
Polarimetric thermal emission from rough surfaces p 1727 N94-20441
Polarimetric thermal emission from periodic water surfaces p 1728 N94-20445
A study of carbonates, sulfates, and phosphates using thermal emission spectroscopy p 1686 N94-20868
Michelson Interferometer (MINT) p 1813 N94-21646
THERMAL ENERGY
Effects of processing history on the creep strength of Nb-1Zr
[DE93-015905] p 1689 N94-20093
Modeling of the coupled magnetospheric and neutral wind dynamos
[NASA-CR-194728] p 1856 N94-20537
Amorphous Ta-rich Ta-Cu films as diffusion barriers between Au and GaAs p 1710 N94-20991
THERMAL EXPANSION
Thermal behavior of natural zeolites
[DE93-040091] p 1699 N94-19975
A process for preparing an assembly of an article and a soluble polyimide which resists dimensional change, delamination, and debonding when exposed to changes in temperature
[NASA-CASE-LAR-14763-1] p 1702 N94-20373
Thermal expansion of electronic highly correlated materials
[ETN-93-93605] p 2026 N94-21135
Space environmental effects on polymer matrix composites: The UTIAS/LDEF experiment p 1660 N94-21373
Integrity and testing concerns of thermostructural materials p 1661 N94-21384
High temperature size selective membranes
[DE93-019865] p 1709 N94-21982
Magnetism in CeRu2Ge2 and CeRh2Ge2 and its pressure dependence
[DE93-040061] p 2032 N94-21987
Dynamics of surface thermal expansion and diffusivity using two-color reflection transient gratings
[DE93-040547] p 1990 N94-22002
THERMAL FATIGUE
Analysis of thermal mechanical fatigue in titanium matrix composites p 1835 N94-22618
THERMAL MAPPING
Degradation sequence of young lunar craters from orbital infrared survey p 2136 N94-20874
Fluorescent microthermographic imaging
[DE93-040332] p 1810 N94-22000
THERMAL PLASMAS
On one numerical approach to Stefan problem
[IPPCZ-330] p 1996 N94-21572
THERMAL PROTECTION
Materials evaluation at ESA/ESTEC p 1662 N94-21386
Durability of thermal control and environmental protective materials for the SSRMS in simulated LEO environment p 1663 N94-21392
Forecasting technique of variations of the optical absorptivity of thermal control coatings under different simultaneous radiations p 1664 N94-21399
Thermal control coatings p 1664 N94-21400
A method of measuring the thermoradiative properties of ceramic materials in a space environment p 1665 N94-21405
R and D to HOPE airframe p 1665 N94-21406
Material properties and behavior during simulated atmospheric reentry p 1665 N94-21408
Compilation of reinforced carbon-carbon transatlantic abort landing arc jet test results
[NASA-TM-104778] p 1676 N94-21834
THERMAL RADIATION
Effects of hydrodynamics and thermal radiation in the atmosphere after comet impacts p 1862 N94-20649
Thermal infrared remote sensing and Kirchhoff's law: 1. Laboratory measurements p 1685 N94-20733
High-energy astrophysics: A theoretical analysis of thermal radiation from neutron stars
[NASA-CR-194808] p 2055 N94-20952
THERMAL SHOCK
Euhedral metallic-Fe-Ni grains in extraterrestrial samples p 1697 N94-20724
Fabrication of whisker-toughened alumina tubes
[DE94-001012] p 1677 N94-22022
THERMAL SIMULATION
High temperature simulation chambers. Physico-chemical and thermal effect of atmospheric reentry on ceramic materials p 1653 N94-21404
THERMAL STABILITY
Further examinations on the thermodynamic stability of the Mie-Gruneisen equation of state
[AD-A270526] p 2037 N94-19831
Microstructural stability of wrought, laser and electron beam glazed NARloy-Z alloy at elevated temperatures
[NASA-TM-108431] p 1689 N94-20100
N,N'-bis(4,4,4-trinitro butyryl) hydrazine
[AD-D015897] p 1712 N94-20122
Polyimides containing amide and perfluoroisopropylidene connecting groups
[NASA-CASE-LAR-14608-1] p 1702 N94-20374
High temperature stability of amorphous Ta(x)Cu(1-x) diffusion barriers on GaAs p 2022 N94-20990
Amorphous Ta-rich Ta-Cu films as diffusion barriers between Au and GaAs p 1710 N94-20991
Stability curves for a thermoacoustic prime mover
[AD-A272607] p 1968 N94-21422
Thermal stability relationships between PMR-15 resin and its composites
[NASA-TM-106285] p 1675 N94-21488
Polyimide-based electrooptic materials
[DE93-019416] p 1706 N94-21526
Fullerene derivatives and fullerene superconductors
[DE93-019568] p 2031 N94-21871
Balanced arrow Mach-Zehnder interferometer p 1789 N94-22221
Non-linear thermal instability of optical thin molecular structures p 2006 N94-22667
On the nonlinear instability of thermal structures p 2006 N94-22668
THERMAL STRESSES
Strengthening of NiAl matrix composites
[AD-A271491] p 1674 N94-20550
Thermal stress analysis of composites in the space environment p 1661 N94-21379
Improvements to a method for the geometrically nonlinear analysis of compressively loaded stiffened composite panels
[NASA-CR-194715] p 1832 N94-21814
A finite element formulation and adaptive solution approach for large-scale thermomechanical problems with complex contact conditions
[DE93-019605] p 1960 N94-21996
Analysis of thermal mechanical fatigue in titanium matrix composites p 1835 N94-22618
THERMAL VACUUM TESTS
Calibration of a calorimeter for measuring the performance of thermal control surfaces p 1660 N94-21378
THERMIONIC DIODES
Observation of reflected waves on the SABRE positive polarity inductive adder MITL
[DE93-019413] p 1980 N94-20295

THERMISTORS
Advanced far infrared detectors
[DE93-040289] p 1988 N94-21528
THERMOCHEMISTRY
Evaporation in equilibrium, in vacuum, and in hydrogen gas p 1684 N94-20638
THERMODYNAMIC CYCLES
Alternative refrigerants and refrigeration cycles for domestic refrigerators
[DE93-040481] p 1714 N94-20099
Hydrogen isotope separation experience at the Savannah River Site
[DE93-019832] p 1679 N94-20266
Advanced Turbine Systems (ATS). Phase 1: System scoping and feasibility studies
[DE93-041130] p 1826 N94-21938
Performance calculations and research direction for a water enhanced regenerative gas turbine cycle
[DE93-019866] p 1826 N94-21983
THERMODYNAMIC EFFICIENCY
Advanced Turbine Systems (ATS). Phase 1: System scoping and feasibility studies
[DE93-041130] p 1826 N94-21938
Performance calculations and research direction for a water enhanced regenerative gas turbine cycle
[DE93-019866] p 1826 N94-21983
Experimental evaluation of oxygen-enriched air and emulsified fuels in a six-cylinder diesel engine
[DE94-000907] p 1811 N94-22391
THERMODYNAMIC EQUILIBRIUM
Modeling the minimum energy state of the Earth's magnetotail
[AD-A267984] p 1856 N94-20485
THERMODYNAMIC PROPERTIES
Complex and stereoregular nonlinear optical materials
[AD-A271067] p 1983 N94-19846
Technology to prevent greenhouse effect gases
[DE94-707421] p 1850 N94-19976
Absorption heat pump for space applications
[NASA-CR-194693] p 1845 N94-20066
Catalytic hydrogenation of carbon monoxide
[DE94-000881] p 1678 N94-20103
The thermodynamic properties to 700 K of naphthalene and 2,7-dimethylnaphthalene
[DE93-000160] p 2037 N94-20473
Mathematical model and analysis of the Tactical Unmanned Ground Vehicle (TUGV) using computer simulation
[AD-A272258] p 1824 N94-20576
Analysis of cost: CVD diamond deposition
[AD-A271980] p 2018 N94-20616
Recondensation in the early solar system: Physical conditions and source material p 2085 N94-20849
Direct images of thermal disorder in the Cl-Si and H-O-Si chemisorption bond on Si(100)
[AD-A272386] p 1680 N94-21145
Chemistry of the burning surface
[AD-A272725] p 1681 N94-21181
Recent developments in aromatic azo polymers research
[AD-A272966] p 1705 N94-21259
Electron emission from nanometer-size metallic clusters: Electronic states and structural stability of supported Au clusters
[DE93-040184] p 1975 N94-21766
High power, electron-beam induced switching in diamond
[DE93-040535] p 1768 N94-21770
THERMODYNAMICS
Further examinations on the thermodynamic stability of the Mie-Gruneisen equation of state
[AD-A270526] p 2037 N94-19831
CTH: A software family for multi-dimensional shock physics analysis
[DE93-019428] p 1904 N94-20052
A parametric study of heat transfer within a planar thermosyphon
[DE93-019546] p 1799 N94-20258
Mathematical theory of thermodynamics of computation
[CWI-CS-R9251] p 2038 N94-21533
A thermodynamic theory of dynamic fragmentation
[DE93-019066] p 1833 N94-21916
Universality in blow-up for non linear heat equations
[PB93-215465] p 2038 N94-22095
A thermodynamic analysis of propagating subcritical cracks with cohesive zones p 1834 N94-22611
THERMOGRAPHY
Three-dimensional dynamic thermal imaging of structural flaws by dual-band infrared computed tomography
[DE93-019575] p 1906 N94-20316
Fluorescent microthermographic imaging
[DE93-040332] p 1810 N94-22000
THERMOGRAVIMETRY
Ageing studies on a composite propellant containing a new organo-copper burn rate catalyst
[AD-A271060] p 1711 N94-19906
THERMOLUMINESCENCE
Temperature dependence of CsI(Tl) gamma ray excited scintillation characteristics
[DE94-000836] p 2034 N94-22028
THERMOMECHANICAL TREATMENT
Effects of processing history on the creep strength of Nb-1Zr
[DE93-015905] p 1689 N94-20093
The use of backscattered electron imaging mode to assess the effect of fine dispersions on development of superplastic microstructure in Al-Mg alloys
[AD-A272426] p 1691 N94-21258
Examinations of composition and deformation behavior of intermetallic phases on the basis of Fe3(AlSi)
[GKSS-92/E/16] p 1692 N94-21311
THERMOPHYSICAL PROPERTIES
Initial development of a high-pressure crystal growth facility: Center director's discretionary fund
[NASA-TM-108430] p 2030 N94-21807
THERMOPLASTIC RESINS
Chain propagation/step propagation polymerization chemistry. The preparation of solvent resistant well phase-separated thermoplastic elastomers
[AD-A271128] p 1699 N94-20016
Graphite/polyurethane flexible composites: Mechanical and vibration damping properties
[AD-A271608] p 1674 N94-20950
A study of the induction heating of organic composites
[AD-A272657] p 1675 N94-21187
THERMOPLASTICITY
Chain propagation/step propagation polymerization chemistry. The preparation of solvent resistant well phase-separated thermoplastic elastomers
[AD-A271128] p 1699 N94-20016
A study of the induction heating of organic composites
[AD-A272657] p 1675 N94-21187
THERMOREGULATION
Human responses to exercise-heat stress
[AD-A272581] p 1892 N94-21209
THERMOSETTING RESINS
Fiber reinforced thermosetting resin composition with coated fibers for improved toughness
[CA-PATENT-1,306,320] p 1674 N94-21040
THERMOSIPHONS
A parametric study of heat transfer within a planar thermosyphon
[DE93-019546] p 1799 N94-20258
THERMOSPHERE
Validation of the design of a high resolution all-reflection Michelson interferometer for atmospheric spectroscopy
[AD-A272505] p 1987 N94-21410
Empirical wind model for the middle and lower atmosphere. Part 2: Local time variations
[NASA-TM-104592] p 1870 N94-21862
THESES
Influence of geoid model uncertainty on the determination of ocean circulation with satellite altimetry
[PB93-219301] p 1842 N94-22097
THICKNESS
Quantitative evaluation of material composition of composites using x ray energy-dispersive NDE technique
[DE93-041157] p 1672 N94-19888
Retrieval of ice thickness from polarimetric SAR data p 1724 N94-20432
Differentiation of magma oceans and the thickness of the depleted layer on Venus p 2118 N94-20780
Ellipsometric measurements of molecular-beam-epitaxy-grown semiconductor multilayer thicknesses: A comparative study p 1710 N94-20983
Comparative thickness measurements of heterojunction layers by ellipsometric, RBS, and XTEM analysis p 1710 N94-20984
Enhanced software for the GT1022 automated gaging system
[DE94-001374] p 1918 N94-21977
THIN FILMS
The proximity effect in ultrathin granular Pb films
[AD-A271094] p 2012 N94-19848
Development of high-efficiency CdTe solar cells
[DE93-018206] p 1845 N94-19925
Preparation and properties of sol-gel derived PZT thin films for decoupling capacitor applications
[DE93-018853] p 2013 N94-19961
A novel method for characterizing the electrical Priorities of lead Zirconate Titanate (PZT) ferroelectric films and memory devices
[AD-A270463] p 2013 N94-19966
Proceedings of the 8th International Symposium on Applications of Ferroelectrics
[AD-A270679] p 1749 N94-20012
Fabrication of stable large-area thin-film CdTe photovoltaic modules
[DE93-018204] p 1845 N94-20095
X ray, extreme and far ultraviolet optical thin films for space applications
[NASA-CR-194635] p 1984 N94-20128
Atom probe field ion microscopy characterizations of VVER steels
[DE93-017864] p 1689 N94-20180
Layered thin-edged field-emitter device
[AD-D015932] p 1751 N94-20350
Polyimides containing amide and perfluoroisopropylidene connecting groups
[NASA-CASE-LAR-14608-1] p 1702 N94-20374
Microwave properties and characterization of co-evaporated BSCCO thin films p 1709 N94-20518
The effect of fluctuations on the electrical transport behavior in YBa2Cu3O(7-x) p 1736 N94-20519
Development of fundamental understanding of friction and wear mechanisms by atomic-scale tribological studies of ceramic materials and multilayered thin films
[AD-A271485] p 1703 N94-20548
Study of the utilization of thin oxides in indium phosphides for the realisation of electron components
[ECL-92-38] p 2018 N94-20593
Ellipsometric studies of sputtered silicon nitride on n-GaAs p 1709 N94-20972
Multiple-wavelength angle-of-incidence ellipsometry: Application to silicon nitride-gallium arsenide structures p 2019 N94-20974
Thin film compositional analysis using null or fixed wavelength ellipsometry p 1709 N94-20976
Thin-film hermeticity: A quantitative analysis of diamondlike carbon using variable angle spectroscopic ellipsometry p 1710 N94-20981
Thermal characterization of thin films by photothermally induced laser beam deflection p 1710 N94-21007
Fundamentals and applications of variable angle spectroscopic ellipsometry p 1687 N94-21011
Electrochemical synthesis of ultrathin film composite membranes
[AD-A272721] p 1681 N94-21168
Alumoxanes: Rationalization of black box materials
[AD-A272805] p 1704 N94-21170
Efficiency of reversible optical storage in azo polymers
[AD-A272923] p 1705 N94-21223
Field emitter array RF amplifier development project, phase 1, option 1
[AD-A272567] p 1740 N94-21361
Intelligent processing of ferroelectric thin films
[AD-A272518] p 1705 N94-21416
Advanced processing technology for high-efficiency thin-film CuInSe2 solar cells
[DE93-010045] p 1847 N94-21614
Fundamental studies of defect generation in amorphous silicon alloys grown by remote plasma-enhanced chemical-vapor deposition
[DE93-017083] p 2029 N94-21615
Research on polycrystalline thin-film submodules based on CuInSe2 materials
[DE93-018223] p 2029 N94-21617
High power, electron-beam induced switching in diamond
[DE93-040535] p 1768 N94-21770
Stable, high-efficiency amorphous-silicon solar cells with low hydrogen content
[DE93-018214] p 1848 N94-21826
Thin-film CdTe and CuInSe2 photovoltaic technologies
[DE93-018217] p 1848 N94-21827
Observation of x ray absorption magnetic circular dichroism in well-characterized iron-cobalt-platinum multilayers
[DE94-000303] p 1694 N94-21944
Techniques for producing free-standing thin films on frames
[DE93-041144] p 1708 N94-21954
MOCVD growth and structure of PbTiO3 thin films
[DE93-040230] p 2033 N94-21994
Interactions of slow H, H2, and H3 with thin foils
[DE93-040263] p 1976 N94-21995
A quantitative model for interpreting nanometer scale hardness measurements of thin films
[DE93-040601] p 2034 N94-22005
Thin-film fabrication of Pb-doped BiSrCaCuO superconductor p 1781 N94-22176
Research on stable, high-efficiency amorphous silicon multijunction modules
[DE93-018220] p 1850 N94-22257
Silicon microelectronic field-emissive devices for advanced display technology
[DE94-000397] p 1794 N94-22380
THORIUM
Crystallographic phase transitions in actinide metals as a function of pressure
[DE93-040138] p 2011 N94-19827

K, U, and Th behavior in Martian environmental conditions p 2141 N94-20908

THREADS

Self locking set screw
[AD-D015969] p 1824 N94-21277

Benefits of thread rolling process to the stress corrosion cracking and fatigue resistance of high strength fasteners
[DE93-040438] p 1833 N94-22001

THREE DIMENSIONAL BODIES

Recognizing 3-D objects using 2-D images
[AD-A271005] p 1983 N94-19819

Robust and efficient 3D recognition by alignment
[AD-A270839] p 1904 N94-20041

Recognition by prototypes
[AD-A271687] p 1943 N94-20921

The local measurement and global interpretation of 3D motion field generated by several moving objects from range image sequences p 1777 N94-22146

THREE DIMENSIONAL BOUNDARY LAYER

Numerical investigation of laminar-turbulent transition in two- and three-dimensional boundary layers
[DLR-FB-92-36] p 1800 N94-20533

THREE DIMENSIONAL FLOW

Three dimensional unsteady flow calculations in radial components p 1669 N94-20080

Some practical turbulence modeling options for Reynolds-averaged full Navier-Stokes calculations of three-dimensional flows
[NASA-TM-106399] p 1637 N94-20534

Finite element numerical simulation of three dimensional turbulent flows with dispersion: Eulerian and Lagrangian approaches
[ECL-92-42] p 1801 N94-20597

An efficient numerical method for three-dimensional hypersonic flow
[AD-A272506] p 1637 N94-21411

Users manual for the NASA Lewis three-dimensional ice accretion code (LEWICE 3D)
[NASA-TM-105974] p 1642 N94-21590

Three-dimensional unstructured grid method applied to turbomachinery p 1919 N94-22360

The 3D Euler solutions using automated Cartesian grid generation p 1920 N94-22367

THREE DIMENSIONAL MODELS

Three dimensional modeling of cirrus during the 1991 FIRE IFO 2: Detailed process study p 1877 N94-22327

Robust unstructured grid generation with VGRID p 1919 N94-22359

Current loop coalescence studied by 3-D electromagnetic particle code p 2005 N94-22660

Solar wind-magnetosphere interaction as simulated by a 3D, EM particle code p 2007 N94-22674

THREE DIMENSIONAL MOTION

Visual tracking
[AD-A271686] p 1943 N94-20920

A study of the compressible flow through a diffusing S-duct
[NASA-TM-106411] p 1638 N94-21591

The local measurement and global interpretation of 3D motion field generated by several moving objects from range image sequences p 1777 N94-22146

THRESHOLD CURRENTS

First results on InGaAsP separate confinement heterostructure diode lasers
[AD-A270849] p 1815 N94-19878

Optical amplification and threshold behavior on InGaAs/InGaAsP multiquantum well structures
[ETN-93-94181] p 2026 N94-21151

THRESHOLD LOGIC

Threshold computation and cryptographic security
[TR-443] p 1907 N94-20536

THRESHOLD VOLTAGE

Evaluation of radiation effects in re-oxidized nitrided oxide devices by hot carrier stressing at 77 K p 1754 N94-21084

Low energy CMOS for space applications p 1768 N94-21735

THRUST AUGMENTATION

Thrust augmentation options for the Beta 2 two-stage-to-orbit vehicle
[NASA-TM-106448] p 1648 N94-21563

Options for thrust augmentation for the Beta 2 two-stage-to-orbit launch vehicle
[NASA-TM-106418] p 1649 N94-21759

THRUST VECTOR CONTROL

Effects of thrust vector control on the performance of the aerobang orbital plane change maneuver
[AD-A272532] p 1646 N94-21418

Internal performance of a nonaxisymmetric nozzle with a rotating upper flap and a center-pivoted lower flap
[NASA-TP-3385] p 1637 N94-21569

THRUSTORS

Segmented ion thruster
[NASA-CASE-NPO-18192-1-CU] p 1669 N94-20496

THUNDERSTORMS

Multiple scattering effects on the Linear Depolarization Ratio (LDR) measured during CaPE by a Ka-band air-borne radar p 1728 N94-20446

Localization from near-source quasi-static electromagnetic fields
[DE93-040390] p 1732 N94-20479

A parametric representation of a thunderstorm cell
[AD-A271983] p 1866 N94-20579

THYRATRONS

Computational model of a magnetic modulator for copper lasers
[DE93-019603] p 1815 N94-20223

THYRISTORS

Some experiences of solving 1-D semiconductor device equations on a matrix coprocessor by a domain decomposition method
[CWI-NM-R9304] p 1935 N94-21492

TILES

Thermally activated retainer means utilizing shape memory alloy
[NASA-CASE-MSC-21793-1] p 1654 N94-20304

An assessment of the cost of microwave sintering ceramic tiles for armor applications
[DE94-000978] p 1693 N94-21850

TIME

Paired comparison models with time-varying parameters
[AD-A272016] p 1964 N94-21442

Tandem queues with deterministic service times
[CWI-BS-R9238] p 1946 N94-21577

TIME DEPENDENCE

Neural network for processing both spatial and temporal data with time based back-propagation
[NASA-CASE-MSC-21874-1] p 1942 N94-20366

Classical and generalized solutions of time-dependent linear differential algebraic equations
[AD-A272834] p 1954 N94-21173

Finite difference methods for time-dependent, linear differential algebraic equations
[AD-A272835] p 1954 N94-21174

Characteristic based methods for the time-domain Maxwell equations
[AD-A272973] p 1802 N94-21263

Time-accurate Navier-Stokes calculations with multigrid acceleration p 1956 N94-21469

Surface path lines in plane Stokes flow driven by capillarity
[DE93-041277] p 1803 N94-21651

Monte Carlo calculation of multi-electron effects on synchrotron radiation
[DE94-001259] p 1982 N94-21974

Time-dependent reliability analysis of ceramic engine components p 1828 N94-22619

TIME DIVISION MULTIPLE ACCESS

A laboratory system for the investigation of rain fade compensation techniques for Ka-band satellites
[NASA-CR-191200] p 1762 N94-21566

TDMA satellite communication systems for ISDN services p 1746 N94-22171

TIME FUNCTIONS

A formulation of quantum statistical mechanics based on the Feynman path centroid density 2 dynamical properties
[AD-A272698] p 2037 N94-21166

TIME MARCHING

Time-domain analysis of planar microstrip devices using a generalized Yee-algorithm based on unstructured grids p 1724 N94-20431

Approximate methods for N-component solute transport and ion-exchange
[CWI-NM-R9223] p 1910 N94-21078

TIME MEASUREMENT

Using the USCCS for sub microsecond spacecraft clock calibration p 1813 N94-21346

Verification of the PROS timing analysis package p 1926 N94-22508

An x ray archive on your desk: The Einstein CD-ROM's p 2048 N94-22519

TIME OF FLIGHT SPECTROMETERS

Time-of-flight heavy ion backscattering spectrometry
[DE93-019067] p 1973 N94-20306

Multielement analysis of interplanetary dust particles using TOF-SIMS p 2084 N94-20790

TIME SERIES ANALYSIS

State-space models for multichannel detection
[AD-A270608] p 1715 N94-19816

SIMBAT theoretical manual
[AD-A271063] p 1882 N94-19979

Partial empirical autocorrelation of a vectorial chronological series
[RR-896-M] p 1963 N94-20162

Studies of Greenland using the SEASAT scatterometer p 1725 N94-20433

Signal processing in the linear statistical model
[AD-A272114] p 1736 N94-20570

Functional statistical data analysis and modeling
[AD-A271520] p 1983 N94-20913

Direct simulation of shock-induced mixing layer
[DE93-040498] p 1803 N94-21531

Registering and resampling images in STSDAS p 1927 N94-22550

TIME SIGNALS

Recording system using multiplexed inputs to a multichannel recorder
[AD-D015971] p 1808 N94-21278

Using the USCCS for sub microsecond spacecraft clock calibration p 1813 N94-21346

TIMING DEVICES

The One-Day Workshop on Batteries, Stepping Motors, and Electronic Clock Displays
[ETN-93-94632] p 1752 N94-20628

Verification of the PROS timing analysis package p 1926 N94-22508

TIN ALLOYS

Magnetic instability of Kondo insulators
[DE93-040064] p 1768 N94-21782

Temperature dependence of magnetic order in single-crystalline UPdSn
[DE93-040153] p 2033 N94-21991

TIN OXIDES

Corrosion inhibition in high temperature environment
[AD-D015910] p 1698 N94-19830

Structure and morphology of Pd overlayers on epitaxial SnO2 films studies with the atomic force microscope
[AD-A271827] p 2028 N94-21458

TIP SPEED

Near wake measurements on a rotor model with Mie-vanes in the Delft open jet tunnel
[PB93-215382] p 1638 N94-22260

TITAN

Laboratory studies of low temperature rate coefficients: The atmospheric chemistry of the outer planets
[NASA-CR-193485] p 1972 N94-20130

TITANATES

MOCVD growth and structure of PbTiO3 thin films
[DE93-040230] p 2033 N94-21994

TITANIUM

Origin of the Apollo 15 very low Ti green glass. A perspective from the compositional diversity in the very low Ti glasses p 1665 N94-20759

Shattering the myth of the resonantly photo-pumped neon-like titanium laser
[DE93-019624] p 1819 N94-21873

Analysis of thermal mechanical fatigue in titanium matrix composites p 1835 N94-22618

TITANIUM ALLOYS

On the experimental determination of low order structure factors in TiAl by energy filtered convergent beam electron diffraction
[DE93-019521] p 1667 N94-19806

Investigation of cracking and erratic behavior of the uranium-titanium alloy
[DE93-018591] p 1688 N94-19957

Production of NiAl and TiAl intermetallics by mechanical alloying
[VTT-JULK-760] p 1691 N94-20530

First principles calculations for analysis martensitic transformations
[DE94-000666] p 1695 N94-21984

Shape memory metals
[DE94-001373] p 1695 N94-21976

Interfacial reactions between titanium and borate glass
[DE93-012847] p 1683 N94-22031

Surface modification of Ti3Al for improved oxidation resistance
[DE93-018297] p 1696 N94-22034

Miniaturized disk-bend testing, nano-indentation, and the microstructure of ion-irradiated titanium aluminides
[DE93-040600] p 1697 N94-22559

TITANIUM BORIDES

Hydrodynamic compressibility of high-strength ceramics
[DE93-019424] p 1698 N94-19903

Interfacial reactions between titanium and borate glass
[DE93-012847] p 1683 N94-22031

TITANIUM CHLORIDES

Zinc and titanium smoke: Chemical composition and physical characteristics
[FOA-C-40277-4.9] p 1680 N94-20552

TITANIUM COMPOUNDS

Applicability and performance benefits of XD (Tradename) titanium aluminides to expendable gas turbine engines
[AD-A272998] p 1648 N94-21268

Characteristics of shock-compressed configuration of Ti and Si powder mixtures
[DE93-018857] p 1713 N94-22033

TITANIUM OXIDES
Ti-bearing oxide minerals in lunar meteorite Y793169 with the VLT affinity p 2084 N94-20812
Petrology and geochemistry of VLT glasses from double drive tube 79001/2 p 1687 N94-20870
Investigation of the effect of various oxide and fluoride additives on the microstructure, electronic properties, and phase shifting ability of Ba(1-x)Sr(x)TiO3 [AD-A271756] p 2027 N94-21303

TOKAMAK DEVICES
Transient thermal analysis of cryocondensation pump for JET [DE93-040372] p 1992 N94-20003
Theoretical and numerical studies in magnetic fusion [DE94-000536] p 1993 N94-20937
Fusion plasma theory grant. Task 3: Auxiliary radiofrequency heating of tokamaks [DE94-000779] p 1994 N94-20940
Shear flow generation by Reynolds stress and suppression of resistive g-modes [DE93-040911] p 1995 N94-21514
On effects of a local plasma density growth due to ponderomotive forces at fast wave launching in tokamaks [IPPCZ-328] p 1996 N94-21571
On the stability of shear-Alfven vortices [DE93-040912] p 1996 N94-21752
Edge plasma experiments on CASTOR tokamak [IPPCZ-332] p 1997 N94-21816
A moving finite element model of the tokamak scrapeoff layer [DE94-000673] p 1997 N94-21965
Fusion Plasma Theory. Task 1: Magnetic confinement fusion plasma theory [DE94-000778] p 1998 N94-22019
Enhanced confinement regimes and control technology in the DIII-D tokamak [DE93-019004] p 1998 N94-22039
The TST: A small steady-state tokamak for integrated divertor testing [DE94-001016] p 1998 N94-22045
Use of open systems for control, analysis, and data acquisition of the DIII-D tokamak [DE94-001101] p 1998 N94-22089
Continuum damping of ideal toroidal Alfven eigenmodes [DE94-001233] p 1998 N94-22560
A two-dimensional kinetic model of the scrape-off layer [DE94-001235] p 1999 N94-22562
Fluid simulations of Delta T(sub e)-driven turbulence and transport in boundary plasmas [DE94-001304] p 1999 N94-22566
Effects of magnetic field perturbations in the ATF torsatron [DE94-000474] p 1999 N94-22568
Electron temperature gradient driven instability in the tokamak boundary plasma [DE94-001307] p 1999 N94-22596
MHD instabilities of fusion oriented plasmas p 2000 N94-22627

TOLERANCES (MECHANICS)
Feature-based tolerancing for intelligent inspection process definition [DE93-017984] p 1906 N94-20311
Mold bolt and means for achieving close tolerances between bolts and bolt holes [NASA-CASE-MFS-28720-1] p 1823 N94-20379

TOMOGRAPHY
Ionospheric tomography using the FORTE satellite [DE93-018545] p 1854 N94-19955
Variable-permittivity linear inverse problem for the H(sub z)-polarized case p 1719 N94-20406
High resolution, three dimensional soft x ray imaging [DE93-018667] p 1989 N94-21630

TOOLS
Loads produced by a suited subject performing tool tasks without the use of foot restraints [NASA-TP-3424] p 1896 N94-20606
Strength capabilities and load requirements while performing torquing tasks in zero gravity [NASA-TP-3433] p 1897 N94-21627

TOPOGRAPHY
Robust photo-topography by fusing shape-from-shading and stereo [NASA-CR-194697] p 1806 N94-19920
Topographic mapping using a monopulse SAR system p 1721 N94-20417
Polarimetric backscattering from sea ice p 1723 N94-20426
Topographic slope from the SAR interferometric phase gradient p 1731 N94-20459
Interferometric detection of freeze-thaw displacements of Alaskan permafrost using ERS-1 data p 1732 N94-20460
Performance evaluation of the JPL TOPSAR system: An across-track interferometric SAR system for topographic mapping p 1732 N94-20461
Seafloor characterization/Galapagos propagating rift [AD-A272001] p 1882 N94-20581
Beta Regio rift system on Venus: Geologic interpretation of Magellan images p 2095 N94-20655
Some deformation trends and topographic characteristics of tesserae on Venus p 2105 N94-20706
Chronology, eruption duration, and atmospheric contribution of Apollinaris Patera, Mars p 2108 N94-20720
Comparative hypsometric analysis of both Earth and Venus topographic distributions p 2108 N94-20722
Distribution of small volcanic cones on the surface of Venus by size and elevation: Implications for differential deposition of volcanic features p 2110 N94-20731
Local topography of Mars and its relationship to surface weathering processes p 2111 N94-20737
The 3-D Moons: The Voyager stereo atlas of the outer solar system p 2111 N94-20740
Geoid, topography, and convection-driven crustal deformation on Venus p 2116 N94-20769
Response of the topography and gravity field on Venus to mantle upwelling beneath a chemical boundary layer p 2117 N94-20775
Contributions of the Clementine mission to our understanding of the processes and history of the Moon p 2119 N94-20784
Magellan Mission p 1652 N94-20829
Is there uniformitarian or catastrophic tectonics on Venus? p 2129 N94-20839
Possible flexural signatures around Olympus and Ascraeus Montes, Mars p 2142 N94-20911
Ocean mapping using satellite radar altimetry [ETN-93-93470] p 1841 N94-21017
Detecting topographical regions in digital terrain maps [AD-A272889] p 1841 N94-21453
Role of surface characteristics in urban meteorology and air quality [DE93-040929] p 1851 N94-21740

TOPOLOGY
On the topological size of p-m-complete degrees [TR-459] p 1965 N94-21286
Superpatch [NASA-CR-177627] p 1914 N94-21489
Mars: Noachian hydrology by its statistics and topology p 2143 N94-21664
IAS telecommunication infrastructure and value added network services provided by IASNET p 1744 N94-22069
Vanishing theorem on arithmetic surfaces [PB93-215481] p 1961 N94-22263
Non commutative geometry and physics [PB93-215499] p 1961 N94-22264
Semi-stability and heights of cycles [PB93-215507] p 1961 N94-22377

TOROIDAL PLASMAS
Transient thermal analysis of cryocondensation pump for JET [DE93-040372] p 1992 N94-20003
Continuum damping of ideal toroidal Alfven eigenmodes [DE94-001233] p 1998 N94-22560
Kinetic resonance damping rate of the toroidal ion temperature gradient mode [DE94-001234] p 1998 N94-22561
Effects of magnetic field perturbations in the ATF torsatron [DE94-000474] p 1999 N94-22568
MHD instabilities of fusion oriented plasmas p 2000 N94-22627
Physics of transport phenomena in magnetic confinement plasmas p 2000 N94-22628
Dynamo driven by weak plasma turbulence: The effect of differential rotation p 2005 N94-22665

TORQUE
FSR based force torque transducer design [AD-A271337] p 1650 N94-19879
Loads produced by a suited subject performing tool tasks without the use of foot restraints [NASA-TP-3424] p 1896 N94-20606
Strength capabilities and load requirements while performing torquing tasks in zero gravity [NASA-TP-3433] p 1897 N94-21627

TORSION
Torsion spring powered missile wing deployment system [CA-PATENT-1,306,384] p 1645 N94-21051

TORSIONAL VIBRATION
Interactive simulation package for coupled bending and torsional vibrations in flexible robot arms [MEMO-1089] p 1944 N94-21140

TOTAL QUALITY MANAGEMENT
The NCC project: A quality management perspective p 1828 N94-21324
NCCDS configuration management process improvement p 1931 N94-21327
Problem reporting management system performance simulation p 1931 N94-21328
The automated ground network system p 1932 N94-21330

TOUGHNESS
Properties and potential of high-temperature niobium beryllides [DE93-019169] p 1690 N94-20233
Weldalite (tm) 049 (Al 2095-T8): Anisotropy effects at cryogenic conditions [AD-A272658] p 1691 N94-21188

TOXICITY
Manual of DRANC (release 1.1): A computer program for the Dutch risk assessment of new chemical substances [PB93-194827] p 1851 N94-19998
Toxicity of thermal degradation in a manned space environment p 1684 N94-21403

TRACE ELEMENTS
Remote sounding of tropospheric minor constituents [NASA-CR-194265] p 1855 N94-20132
Volatility in the lunar crust: Trace element analyses of lunar minerals by PIXE proton microprobe p 2097 N94-20661
Tambo Quemado: Extraordinary concentrations of REE and refractory trace elements caused by artificial heating p 1684 N94-20667
Orthopyroxenes as recorders of diogenite petrogenesis: Major and minor element systematics p 1684 N94-20670
Origin of the Apollo 15 very low Ti green glass. A perspective from the compositional diversity in the very low Ti glasses p 1685 N94-20759
Orthopyroxenes as recorders of diogenite petrogenesis: Trace element systematics p 1686 N94-20760
The formation of FeO-rich pyroxene and enstatite in unequilibrated enstatite chondrites: A petrologic-trace element (SIMS) study p 2086 N94-20866
Trace element compositions of spinel-rich refractory inclusions from the Murchison meteorite p 2086 N94-20897
Global emissions and models of photochemically active compounds [DE93-040490] p 1852 N94-21969

TRACKING (POSITION)
A summary of studies of particle stability at RHIC [DE93-040173] p 1970 N94-19868
Aviation safety research at the National Institute for Aviation Research, Wichita State University [NIAR-93-4] p 1641 N94-20189
A flight test system design for the microwave landing system p 1645 N94-22156

TRACKING STATIONS
Enhanced networks operations using the X Window System p 1932 N94-21329
The automated ground network system p 1932 N94-21330
An in-depth analysis and modelling of the Shuttle to MILA S-band telemetry link p 1657 N94-21340

TRAFFIC
Traffic noise in a roundabout way p 1966 N94-21799

TRAFFIC CONTROL
Routing of freeway traffic: A discrete-time state space model and routing problems [CWI-BS-R9232] p 1944 N94-21033

TRAINING ANALYSIS
Modelling decision-making by pilots [NASA-CR-194767] p 2040 N94-21821

TRAINING DEVICES
Weather tutor 1: Stability basics [AD-A270758] p 1866 N94-20565
Sparking young minds with Moon rocks and meteorites p 2039 N94-20819

TRAINING EVALUATION
Mathematics B for the study direction VWO: A reconnaissance [REPT-92-80] p 1950 N94-20032

TRAJECTORIES
Development and testing of a reliability performance index for modular robotic systems [AD-A271901] p 1942 N94-20488

TRAJECTORY ANALYSIS
Trajectory computations for an improved cinetheodolite tracking system p 1791 N94-22236

TRAJECTORY PLANNING
Robot skill learning and the effects of basis function choice [TR-437] p 1939 N94-20135

Development and evaluation of a profile negotiation process for integrating aircraft and air traffic control automation
[NASA-TM-4360] p 1643 N94-21606
An adaptive control to enable a robot to follow Cartesian trajectories p 1790 N94-22229
An algorithm for the interference detection among polygonal surfaces p 1791 N94-22239
Strategy for motion of a moving body of quasi-polygonal form within a polygonal space p 1792 N94-22240
Analytical representation of working articulation space of a plane manipulator in an encumbered environment p 1792 N94-22241

TRANSDUCERS
FSR based force torque transducer design
[AD-A271337] p 1650 N94-19879
Three dimensional ultrasonic imaging
[DE93-040549] p 1968 N94-22003

TRANSFER FUNCTIONS
A theory for optical wavelength control in short pulse free electron laser oscillators
[AD-A271706] p 1817 N94-21353
Stochastic simulation for imaging spatial uncertainty: Comparison and evaluation of available algorithms
[DE93-040058] p 1916 N94-21761

TRANSFORMATIONS (MATHEMATICS)
Speech synthesis with artificial neural networks p 1743 N94-20245
Causal reconstruction
[AD-A271692] p 1908 N94-20929
Use of switched capacitor filters to implement the discrete wavelet transform p 1755 N94-21097
Classical and generalized solutions of time-dependent linear differential algebraic equations
[AD-A272834] p 1954 N94-21173
Data compression by using wavelet transforms and vector quantization
[AD-A272763] p 1738 N94-21182
Model-based automatic generation of grasping regions
[NASA-TM-104785] p 1946 N94-21550
Reduction of blocking effects for the JPEG baseline image compression standard p 1765 N94-21714
An in-place and in-order algorithm for the discrete cosine transform p 1771 N94-22111
The 3-D unstructured mesh generation using local transformations p 1919 N94-22356
Efficient transfer of images over networks p 1748 N94-22517

TRANSFORMERS
Computational model of a magnetic modulator for copper lasers
[DE93-019603] p 1815 N94-20223

TRANSIENT RESPONSE
Dynamic, multiaxial impact response of confined and unconfined ceramic rods
[DE93-040057] p 1829 N94-19824

TRANSISTOR AMPLIFIERS
Field emitter array RF amplifier development project, phase 1, option 1
[AD-A272567] p 1740 N94-21361

TRANSISTOR CIRCUITS
Delay analysis of combinations of pass transistors and classical logic gates p 1756 N94-21103
Design and implementation of GaAs HBT circuits with ACME p 1758 N94-21117
Fully-depleted silicon-on-sapphire and its application to advanced VLSI design p 1765 N94-21709
Interpolative modeling of GaAs FET S-parameter data bases for use in Monte Carlo simulations p 1767 N94-21723
A VLSI implementation of DCT using pass transistor technology p 1767 N94-21725
On fast carry select adders p 1767 N94-21728
Non-linear analysis of the electrical properties of the active circuits of high-frequency oscillators p 1785 N94-22195

TRANSISTOR LOGIC
Power optimization in logic isomers p 1756 N94-21101
Delay analysis of combinations of pass transistors and classical logic gates p 1756 N94-21103

TRANSISTORS
Characterization of multilayer GaAs/AlGaAs transistor structures by variable angle spectroscopic ellipsometry p 1796 N94-20985
Localization of pellicle-induced open contacts using charge-induced voltage alteration
[DE93-019407] p 1762 N94-21636
HDL to verification logic translator p 1766 N94-21717
A VLSI implementation of DCT using pass transistor technology p 1767 N94-21725
A high speed CMOS A/D converter p 1767 N94-21726
On fast carry select adders p 1767 N94-21728
Low energy CMOS for space applications p 1768 N94-21735
Self assembly: An approach to terascale integration
[DE93-040104] p 1769 N94-21846
Simple method to estimate MOS oxide-trap, interface-trap, and border-trap densities
[DE93-041138] p 2032 N94-21939

TRANSIT TIME
Entry velocities at Mars and Earth for short transit times
[AD-A272591] p 1665 N94-21420

TRANSITION FLIGHT
Data link development for the archytas vertical takeoff and landing transitional flight unmanned aerial vehicle
[AD-A272499] p 1646 N94-21548

TRANSITION FLOW
Flow transition with 2-D roughness elements in a 3-D channel p 1806 N94-21466

TRANSITION METALS
Photochemically induced transformations of transition complexes
[AD-A271112] p 2014 N94-19982
The metallic bond for monolayer transition metal layers on transition metal surfaces
[DE93-019060] p 1691 N94-20313
Wavelength dispersive analysis with the synchrotron x ray fluorescence microprobe p 1685 N94-20717
Theoretical studies of structural phase transitions in actinide metals
[DE94-000796] p 1696 N94-22388
First-principles pressure-temperature phase diagrams in metals
[DE94-001056] p 1696 N94-22398

TRANSITION POINTS
Ductile-brittle transition behavior of tungsten under shock loading conditions
[DE93-019945] p 1693 N94-21843

TRANSITION PROBABILITIES
Theoretical investigations of metastability and energy storage in molecular systems
[AD-A271849] p 1973 N94-20612

TRANSITION TEMPERATURE
Development of bioelastic material for aspects of wound repair
[AD-A267832] p 1673 N94-20208
Spin-polaron theory of high-T(c) superconductivity. 3: Gap function and critical temperature
[DE93-019198] p 2030 N94-21831
Spin dynamics and implications for superconductivity: Some problems with the d-wave scenario
[DE94-001183] p 2032 N94-21972
NMR studies of oxygen-doped La2CuO(4+delta)
[DE93-040756] p 2034 N94-22007
Thin-film fabrication of Pb-doped BiSrCaCuO superconductor p 1781 N94-22176

TRANSLATING
Efficient and correct translation of strict applicative programming languages
[ETN-93-95056] p 1903 N94-20020
System level modelling using Petri nets and VHDL p 1772 N94-22113

TRANSMISSION
Spread spectrum random access networks
[AD-A272280] p 1737 N94-20585

TRANSMISSION EFFICIENCY
Specification and formal verification of the safety criterion in the alternating bit protocol p 1784 N94-22193
Efficient transfer of images over networks p 1748 N94-22517

TRANSMISSION ELECTRON MICROSCOPY
Facilities for in situ ion beam studies in transmission electron microscopes
[DE93-019567] p 1979 N94-20222
Comparative thickness measurements of heterojunction layers by ellipsometric, RBS, and XTEM analysis p 1710 N94-20984
Measurement of superlattice optical properties by variable angle spectroscopic ellipsometry p 2022 N94-20992
Growth, characterization and device development in monocrystalline diamond films
[AD-A273097] p 2028 N94-21506
Electron holography applied to the study of ceramic materials
[DE94-000329] p 1707 N94-21653
Transmission electron microscopy study of thick copper-304 stainless steel multilayers
[DE94-001045] p 1696 N94-22394

TRANSMISSION LINES
Robust, high-speed network design for large-scale multiprocessing
[AD-A271003] p 1716 N94-19977
Interinjection-locked quasioptical power combiners and phased arrays
[AD-A271178] p 2015 N94-20214
Observation of reflected waves on the SABRE positive polarity inductive adder MITL
[DE93-019413] p 1960 N94-20295
Analysis of microstrip dipoles and slots transversely coupled to a microstrip line using the FDTD method p 1718 N94-20405
Solid State Technology Branch of NASA Lewis Research Center: Fifth Annual Digest
[NASA-TM-106303] p 1732 N94-20497
Attenuation of epsilon(sub eff) of coplanar waveguide transmission lines on silicon substrates p 1733 N94-20504
High temperature superconducting planar circuit structure for high frequency applications
[AD-A273083] p 2028 N94-21521
Manual design technique for broadband passive thin-film attenuators using the Smith chart p 1782 N94-22178
Electromagnetic interference and shielding: An introduction (revised version of 1991-23)
[PB93-215275] p 1742 N94-22348

TRANSMITTANCE
Dual-beam multiple wavelength light transmittance measurement for particle sizing in rocket motor plumes
[AD-A272491] p 1670 N94-21208

TRANSMITTER RECEIVERS
Automated HMC assembly
[DE93-040641] p 1749 N94-20005

TRANSMITTERS
Photoconductive Semiconductor Switches for pulsed power applications
[DE93-019411] p 1750 N94-20294
Spread spectrum random access networks
[AD-A272280] p 1737 N94-20585
Conversion of the proprietary ROLM (tm) inter-node link from multimode to singlemode operation p 1744 N94-21349

TRANSMUTATION
Semiconductor isotope engineering
[DE93-040119] p 2030 N94-21744

TRANSONIC FLOW
Transonic flow calculations: Integral method
[ISBN-0-315-83538-9] p 1639 N94-22586
Experiments with a fluid deicing system for cleaning laminar wings p 1640 N94-22601

TRANSONIC SPEED
Options for thrust augmentation for the Beta 2 two-stage-to-orbit launch vehicle
[NASA-TM-106418] p 1649 N94-21759

TRANSPARENCE
Variable wavelength, variable angle ellipsometry including a sensitivities correlation test p 1710 N94-20978
Polyimide-based electrooptic materials
[DE93-019416] p 1706 N94-21526

TRANSPORT PROPERTIES
Boost-phase discrimination research
[NASA-TM-109347] p 1666 N94-19818
Parametric variations of ion transport in TFTR
[DE93-012653] p 1991 N94-19883
A database of selected transport coefficients for combustion studies
[DE93-041278] p 1678 N94-19889
Computed potential energy surfaces for chemical reactions
[NASA-CR-194600] p 1679 N94-20169
Growth of zinc selenide single crystals by physical vapor transport in microgravity
[NASA-CR-194679] p 2017 N94-20346
Optical and transport properties of metallic and semiconductor nanostructures
[AD-A271716] p 2018 N94-20554
Establishing the basis for validated predictions of highly non-equilibrium flows (with 9 attachments)
[AD-A272918] p 1802 N94-21220
IR materials producibility
[AD-A273031] p 1987 N94-21321
Dephasing processes in III-V semiconductors
[AD-A271677] p 2028 N94-21362
Local uniform grid refinement and brine transport in porous media with inhomogeneities
[CWI-NM-R9224] p 1803 N94-21609
Fundamental studies of defect generation in amorphous silicon alloys grown by remote plasma-enhanced chemical-vapor deposition
[DE93-017083] p 2029 N94-21615

TRANSPORT THEORY
Shielding from space radiations
[NASA-CR-194663] p 1895 N94-20063
Neoclassical kinetic theory near an X-point: Plateau regime
[DE93-019825] p 1951 N94-20224

TRANSPORTATION
Multigrid approach to solving the long transportation problem on a regular grid in cost space
[AD-A272323] p 1909 N94-21038

The 13th International Conference on Magnetically Levitated Systems and Linear Drives MAGLEV 1993
[DE93-040381] p 1825 N94-21544
TRANSPORTATION ENERGY
First Biomass Conference of the Americas: Energy, Environment, Agriculture, and Industry, volume 2
[DE94-000435] p 1847 N94-21562
TRANSPUTERS
Two-dimensional particle-in-cell simulation on transputer arrays
[DE93-017977] p 1972 N94-20181
The ADAM environment and transputers
p 1926 N94-22494
TRANSVERSE LOADS
Improvements to a method for the geometrically nonlinear analysis of compressively loaded stiffened composite panels
[NASA-CR-194715] p 1832 N94-21814
TRAPPED PARTICLES
Research on defects and transport in amorphous-silicon-based semiconductors
[DE93-017117] p 2013 N94-19939
Energy storage and conversion in solid hydrogen
[AD-A271439] p 1845 N94-20086
Ionospheric photoelectrons measured at geosynchronous orbit
[AD-A272431] p 1857 N94-21202
Detailed analysis case studies of trapped plasmas at the Earth's magnetic equator
[AD-A272497] p 1858 N94-21432
Radial diffusion of toroidally trapped particles induced by lower hybrid and fast waves
[IPPCZ-327] p 1996 N94-21593
TRAPPING
Evaluation of a diffusion/trapping model for hydrogen ingress in high-strength alloys
[AD-A271328] p 1689 N94-20027
TRAPS
Simple method to estimate MOS oxide-trap, interface-trap, and border-trap densities
[DE93-041138] p 2032 N94-21939
TRAVELING IONOSPHERIC DISTURBANCES
Detection of traveling ionospheric disturbances induced by atmospheric gravity waves using the global positioning system p 1723 N94-20425
TRAVELING SALESMAN PROBLEM
Electronic neural network for solving traveling salesman and similar global optimization problems
[NASA-CASE-NPO-17807-2-CU] p 1942 N94-20360
TRAVELING WAVE AMPLIFIERS
A laboratory system for the investigation of rain fade compensation techniques for Ka-band satellites
[NASA-CR-191200] p 1762 N94-21566
TRAVELING WAVES
High Speed/High Frequency Optoelectronics
[AD-A271985] p 1751 N94-20580
Simulation of traveling-wave output structures for high power RF tubes
[DE93-041005] p 1763 N94-21685
TRAYS
Long Duration Exposure Facility (LDEF) contamination study
[AD-A272419] p 1658 N94-21147
TREADMILLS
Apparatus and method for measuring subject work rate on an exercise device
[NASA-CASE-MSC-21752-1] p 1895 N94-20194
TREES (MATHEMATICS)
Totally strong and strong graphs
[RR-902-I] p 1951 N94-20237
Graph minors: Structure theory and algorithms
[AD-A271851] p 1952 N94-20613
The combinatorics of reconstructing evolutionary trees
[CWI-BS-R9233] p 1963 N94-21022
On the core-structure of minimum cost spanning tree games
[MEMO-1085] p 1953 N94-21047
Fourier calculus on evolutionary trees
[CWI-BS-R9234] p 1954 N94-21231
A neural M-ary tree method for data compression
p 1780 N94-22166
TREES (PLANTS)
Mapping of taiga forest units using AIRSAR data and/or optical data, and retrieval of forest parameters
p 1729 N94-20452
TRELLIS CODING
Advanced coding and modulation schemes for TDRSS
p 1744 N94-21350
Design of a new squaring function for the Viterbi algorithm p 1764 N94-21699
Coded 64QAM using a binary convolutional code
p 1747 N94-22223
Trellis coded multi-orthogonal modulation
p 1747 N94-22231
TRENDS
Industry standards: Key to distributed computing
p 1938 N94-22070
Current situation in developing petroleum substituting energy (the United Kingdom)
[DE94-714897] p 1713 N94-22091
Investigations on trends in global environment adaptive industrial technologies
[DE94-714888] p 1853 N94-22258
TRIANGULATION
Geometric optimization
[DE93-040152] p 1917 N94-21764
Hierarchical surface triangulation of range data
p 1771 N94-22108
Unstructured surface grid generation
p 1920 N94-22366
Computational geometry issues p 1920 N94-22370
Surface acquisition through virtual milling
p 1920 N94-22372
TRIATOMIC MOLECULES
Electronically metastable molecules of high symmetry
[AD-A272015] p 1974 N94-21461
TRIBOLOGY
Microscopic modeling of tribological and interfacial phenomena
[AD-A271864] p 1823 N94-20464
Development of fundamental understanding of friction and wear mechanisms by atomic-scale tribological studies of ceramic materials and multilayered thin films
[AD-A271485] p 1703 N94-20548
Utilization of metals to improve the lubrication of ceramic load-bearing devices
[PB93-202448] p 1825 N94-21424
Integrity testing of brush seal in a T-700 engine
p 1654 N94-21792
TRIGGER CIRCUITS
Results from long conduction time plasma opening switch experiments at Sandia National Laboratories
[DE93-019063] p 1762 N94-21632
TRIGONOMETRIC FUNCTIONS
Fast fourier transforms for nonequispaced data
[AD-A272687] p 1954 N94-21164
Rational trigonometric approximations using Fourier series partial sums
[NASA-CR-191535] p 1959 N94-21568
TRINITRO COMPOUNDS
N,N'-bis(4,4,4-trinitro butyryl) hydrazine
[AD-D015897] p 1712 N94-20122
TRINITROTOLUENE
Evaluation of pre-extraction analytical holding times for nitroaromatic and nitramine explosives in water
[AD-A271547] p 1712 N94-20927
TRIODES
Silicon microelectronic field-emissive devices for advanced display technology
[DE94-000397] p 1794 N94-22380
TRIPODS
Simulation of tripod gaits for a hexapod underwater walking machine
[AD-A271719] p 1945 N94-21355
TRITIUM
Hydrogen isotope separation experience at the Savannah River Site
[DE93-019832] p 1679 N94-20266
TRITON
Diapirs and cantaloupes: Layering and overturn of Triton's crust p 2111 N94-20738
Geology of the southern hemisphere of Triton: No polar cap p 2111 N94-20739
TROPICAL METEOROLOGY
Spatial and temporal variations of satellite microwave measurements of latent heat release in tropic cyclones due to environmental forcing obtained from a numerical model
[AD-A267947] p 1865 N94-20482
TROPICAL REGIONS
Orbit and sampling requirements: TRMM experience
p 1870 N94-21647
Are tropical cirrus brighter than mid-latitude cirrus?
p 1881 N94-22343
TROPICAL STORMS
Spatial and temporal variations of satellite microwave measurements of latent heat release in tropic cyclones due to environmental forcing obtained from a numerical model
[AD-A267947] p 1865 N94-20482
Large-scale circulation regimes and tropical cyclone characteristics over the western pacific ocean
[AD-A273004] p 1867 N94-21307
TROPOPAUSE
Intrusion of stratospheric ozone in the troposphere through tropopause folding and cold air droplets
[REPT-87] p 1851 N94-20154
TROPOSPHERE
Tropospheric chemistry of natural hydrocarbons, aldehydes, and peroxy radicals: Their connections to sulfuric acid production and climate effects
[DE93-019525] p 1855 N94-20220
Spatial and temporal variations of satellite microwave measurements of latent heat release in tropic cyclones due to environmental forcing obtained from a numerical model
[AD-A267947] p 1865 N94-20482
Earth observing scanning polarimeter
p 1844 N94-21645
Michelson Interferometer (MINT)
p 1813 N94-21646
Global emissions and models of photochemically active compounds
[DE93-040490] p 1852 N94-21969
Breaking Kelvin-Helmholtz waves and cloud-top entrainment as revealed by K-band Doppler radar
p 1874 N94-22310
Analysis of the GOES 6.7 micrometer channel observations during FIRE 2 p 1875 N94-22316
Examination of the observed synoptic scale cirrus cloud environment: The December 3-6 FIRE cirrus case study
p 1877 N94-22325
The 5-6 December 1991 FIRE IFO 2 jet stream cirrus case study: The influence of volcanic aerosols
p 1877 N94-22326
A comparison of small and larger mesoscale latent heat and radiative fluxes: December 6 case study
p 1879 N94-22335
TROUGHS
Possible flexural signatures around Olympus and Ascraeus Montes, Mars p 2142 N94-20911
TUBES
Spiral fluid separator
[NASA-CASE-MFS-28658-1] p 1800 N94-20361
TUMORS
Calculation and optimization of electromagnetic fields in a patient by local hyperthermia utilization
[ETN-93-95059] p 1889 N94-20024
TUNABLE LASERS
Suppression of relaxation oscillations in flashpumped, two-micron tunable solid state lasers
[AD-D015928] p 1814 N94-19800
Initial performance of Los Alamos advanced free electron laser
[DE93-040158] p 1814 N94-19828
Evaluation of a single stage of the LADS filter
[AD-A271101] p 1814 N94-19851
Tunable laser frequency stabilizing system
[AD-D015904] p 1815 N94-20055
Rotational spectrum of a dark state in 2-fluoroethanol using microwave/radiofrequency-infrared multiple resonance
[AD-A272101] p 1817 N94-20583
TUNGSTEN
Core formation in the Moon: The mystery of the excess depletion of Mo, W and P p 2095 N94-20651
Electron emission from nanometer-size metallic clusters: Electronic states and structural stability of supported Au clusters
[DE93-040184] p 1975 N94-21766
Ductile-brittle transition behavior of tungsten under shock loading conditions
[DE93-019945] p 1693 N94-21843
TUNGSTEN ALLOYS
Strengthening and toughening in refractory metal alloys
[DE93-019942] p 1695 N94-21986
TUNING
A summary of studies of particle stability at RHIC
[DE93-040173] p 1970 N94-19868
Novel N x N integrated channel waveguide optical crossbars for large scale high speed non-blocking data switching
[AD-A272065] p 1986 N94-20922
Multibunch beam break-up in detuned structures
[DE93-041056] p 1981 N94-21686
TUNNEL JUNCTIONS
Quantum noise studies with superconducting tunnel junction mixers
[AD-A270897] p 2012 N94-19897
The n-p(p(+))-n Al(yGa)(1-y) As-GaAs-In(x)Ga(1-x) as quantum well laser with p(+)-n(+)GaAs-InGaAs tunnel contact on n GaAs
[AD-A271292] p 2030 N94-21805
Energy-resolving x ray detectors with charge amplification due to multiple quasiparticle tunneling
[DE93-019506] p 2031 N94-21869
Research on stable, high-efficiency amorphous silicon multijunction modules
[DE93-018220] p 1850 N94-22257
TURBIDITY
Distribution of turbidity in Australian tropical waters
[AD-A271059] p 1881 N94-19905

TURBINE BLADES
Turbine design p 1668 N94-20075
Oxidation resistant protective coating system for gas turbine components and process for penetration thereof
[CA-PATENT-1,294,155] p 1704 N94-21143
Integrity testing of brush seal in a T-700 engine p 1654 N94-21792
Recent advances in computational structural reliability analysis methods p 1828 N94-22616

TURBINE ENGINES
Integrity testing of brush seal in a T-700 engine p 1654 N94-21792
Modeling bristle lift-off in idealized brush seal configurations p 1655 N94-21797

TURBINE PUMPS
Rocketdyne turbomachinery p 1667 N94-20071
Turbine design p 1668 N94-20075
Distributed loss model: Application to a spatial turbopump inducer p 1668 N94-20078
Actively controlled shaft seals for aerospace applications
[NASA-CR-194759] p 1823 N94-20538
Detailed study of oxidation/wear mechanism in lox turbopump bearings
[NASA-TM-108434] p 1825 N94-21580
The 1992 Seals Flow Code Development Workshop
[NASA-CP-10124] p 1654 N94-21790
Dynamics of face seals for high speed turbomachinery p 1655 N94-21796

TURBINES
Turbine design p 1668 N94-20075
Measurement and prediction of the flow through an annular turbine cascade
[AD-A272530] p 1803 N94-21417

TURBOCOMPRESSORS
Experimental evaluation of oxygen-enriched air and emulsified fuels in a six-cylinder diesel engine
[DE94-000907] p 1811 N94-22391

TURBOFAN ENGINES
On the estimation algorithm used in adaptive performance optimization of turbofan engines
[NASA-TM-4551] p 1649 N94-21879

TURBOMACHINE BLADES
Blade row interaction effects on flutter and forced response
[NASA-TM-106438] p 1649 N94-21586

TURBOMACHINERY
Dynamics of face seals for high speed turbomachinery p 1655 N94-21796
Three-dimensional unstructured grid method applied to turbomachinery p 1919 N94-22360

TURBULENCE
Particle dispersion in turbulent sprays
[AD-A271314] p 1796 N94-19913
Wavefront sensors for optical diagnostics in fluid mechanics: Application to heated flow, turbulence, and droplet evaporation
[DE93-040060] p 1797 N94-19974
Some practical turbulence modeling options for Reynolds-averaged full Navier-Stokes calculations of three-dimensional flows
[NASA-TM-106399] p 1637 N94-20534
Magnetically controlled solar nebula p 2120 N94-20791
Long-range laser imaging
[AD-A273020] p 1817 N94-21253
Direct simulation of shock-induced mixing layer
[DE93-040498] p 1803 N94-21531
Turbulization of free shear flows: 3D perturbations p 2000 N94-22626

TURBULENCE EFFECTS
Coherent lidar design and performance verification
[NASA-CR-193813] p 1816 N94-20341

TURBULENCE MODELS
Turbulence modeling for high speed compressible flows
[NASA-CR-194547] p 1799 N94-20210
Some practical turbulence modeling options for Reynolds-averaged full Navier-Stokes calculations of three-dimensional flows
[NASA-TM-106399] p 1637 N94-20534
Flow interaction experiment. Volume 1: Aerothermal modeling, phase 1
[NASA-CR-189192-VOL-1] p 1648 N94-21582
Flow interaction experiment. Volume 2: Aerothermalmodeling, phase 2
[NASA-CR-189192-VOL-2] p 1648 N94-21583
New results on the realizability of Reynolds stress turbulence closures
[NASA-CR-191548] p 1804 N94-21875

TURBULENT BOUNDARY LAYER
The effect of transverse curvature on the fluctuating wall pressure and structure of boundary layer turbulence
[AD-A271868] p 1800 N94-20466
Some practical turbulence modeling options for Reynolds-averaged full Navier-Stokes calculations of three-dimensional flows
[NASA-TM-106399] p 1637 N94-20534
Investigation of the physics of the turbulent boundary layer focusing on vortex structures
[AD-A272879] p 1802 N94-21155
Computational and analytical methods in nonlinear fluid dynamics
[AD-A272722] p 1802 N94-21169
Low Reynolds-number turbulent boundary layers
[AD-A272011] p 1803 N94-21459

TURBULENT COMBUSTION
Reaction zone models for vortex simulation of turbulent combustion
[AD-A272723] p 1681 N94-21213
Simulations of diffusion-reaction equations with implications to turbulent combustion modeling
[NASA-CR-191536] p 1804 N94-21861

TURBULENT DIFFUSION
Simulations of diffusion-reaction equations with implications to turbulent combustion modeling
[NASA-CR-191536] p 1804 N94-21861

TURBULENT FLOW
Particle dispersion in turbulent sprays
[AD-A271314] p 1796 N94-19913
Wavefront sensors for optical diagnostics in fluid mechanics: Application to heated flow, turbulence, and droplet evaporation
[DE93-040060] p 1797 N94-19974
The effect of transverse curvature on the fluctuating wall pressure and structure of boundary layer turbulence
[AD-A271868] p 1800 N94-20466
Some practical turbulence modeling options for Reynolds-averaged full Navier-Stokes calculations of three-dimensional flows
[NASA-TM-106399] p 1637 N94-20534
Two-point laser Doppler velocimetry measurements of length-turbulent scales
[ECL-92-12] p 1801 N94-20542
Four-dimensional remote sensing of the marine boundary layer with a digital beamforming radar wind profiler
[AD-A270627] p 1882 N94-20564
Finite element numerical simulation of three dimensional turbulent flows with dispersion: Eulerian and Lagrangian approaches
[ECL-92-42] p 1801 N94-20597
Low Reynolds-number turbulent boundary layers
[AD-A272011] p 1803 N94-21459
Shear flow generation by Reynolds stress and suppression of resistive g-modes
[DE93-040911] p 1995 N94-21514
Consequences of plasma-maser in plasma astrophysics p 2006 N94-22669

TURBULENT JETS
Particle dispersion in turbulent sprays
[AD-A271314] p 1796 N94-19913
Combustion in turbulent jets and buoyant flames
[PB93-202372] p 1682 N94-21452
Flow interaction experiment. Volume 1: Aerothermal modeling, phase 1
[NASA-CR-189192-VOL-1] p 1648 N94-21582
Flow interaction experiment. Volume 2: Aerothermalmodeling, phase 2
[NASA-CR-189192-VOL-2] p 1648 N94-21583

TURBULENT MIXING
Turbulence modeling for high speed compressible flows
[NASA-CR-194547] p 1799 N94-20210
Simulations of diffusion-reaction equations with implications to turbulent combustion modeling
[NASA-CR-191536] p 1804 N94-21861

TURBULENT WAKES
Prediction and control of vortex-dominated and vortex-wake flows
[NASA-CR-194722] p 1637 N94-21054

TURING MACHINES
Threshold computation and cryptographic security
[TR-443] p 1907 N94-20536
COCOLOG: A conditional observer and controller logic for finite machines
[INRIA-RR-1714] p 1910 N94-21063
Design methods for fault-tolerant finite state machines p 1758 N94-21120
Advice from nonadaptive queries to NP
[TR-470] p 1911 N94-21200
Space-efficient deterministic simulation of probabilistic automata
[TR-463] p 1900 N94-21281
Threshold computation and cryptographic security
[TR-461] p 1912 N94-21285
Promises and fault-tolerant database access
[TR-447] p 2043 N94-21287
Beta(sub k)-complete problems and greediness
[TR-455] p 1913 N94-21316
On the closure properties of #P in the context of PF of #P
[TR-445] p 1955 N94-21456

TWO DIMENSIONAL BOUNDARY LAYER
Numerical investigation of laminar-turbulent transition in two- and three-dimensional boundary layers
[DLR-FB-92-36] p 1800 N94-20533

TWO DIMENSIONAL FLOW
Formulation of a next-generation interior ballistic code
[AD-A271539] p 1801 N94-20915
F2D users manual: A two-dimensional compressible gas flow code
[DE94-000653] p 1805 N94-22386

TWO DIMENSIONAL MODELS
Two-dimensional particle-in-cell simulation on transputer arrays
[DE93-017977] p 1972 N94-20181
Investigation of the effects of the macrophysical and microphysical properties of cirrus clouds on the retrieval of optical properties: Results for FIRE 2 p 1880 N94-22339
Robust unstructured grid generation with VGRID p 1919 N94-22359
A two-dimensional kinetic model of the scrape-off layer
[DE94-001235] p 1999 N94-22562
Verification of frequency scaling laws for capacitive rf discharges using two-dimensional simulations
[DE94-001306] p 1999 N94-22595

TWO FLUID MODELS
Measurement of thermal-hydraulic parameters in two-phase flow using flow visualization image analysis
[DE93-006255] p 1805 N94-22269

TWO PHASE FLOW
Formulation of a next-generation interior ballistic code
[AD-A271539] p 1801 N94-20915
Measurement of thermal-hydraulic parameters in two-phase flow using flow visualization image analysis
[DE93-006255] p 1805 N94-22269

U

U.S.S.R.
Soviet society informatization: The USSR state program p 2046 N94-22058
The Soviet software market: Current state and aspects of development p 1923 N94-22066
Models of transient processes in centrally planned economy p 2051 N94-22071

U-2 AIRCRAFT
Bi-directional reflectance and other radiation parameters of cirrus from ER-2 observations p 1871 N94-22296

UH-60A HELICOPTER
The modern rotor aerodynamic limits survey: A report and data survey
[NASA-TM-4446] p 1635 N94-21490

ULLAGE
On demand, non-halon, fire extinguishing systems
[AD-D015957] p 1714 N94-20355

ULTRAHIGH FREQUENCIES
Application of Cloude's target decomposition theorem to polarimetric imaging radar data p 1724 N94-20429
Mapping of taiga forest units using AIRSAR data and/or optical data, and retrieval of forest parameters p 1729 N94-20452
Mobile antenna development at JPL p 1731 N94-20457
Mobile terminal antennas for helicopters p 1731 N94-20458
An in-depth analysis and modelling of the Shuttle to MILA S-band telemetry link p 1657 N94-21340

ULTRAHIGH VACUUM
Fabrication and evaluation of superconducting and semiconducting materials
[AD-A271645] p 2018 N94-20558
GaAs(100) surface modifications at elevated temperatures, studied by in-situ spectroscopic ellipsometry p 2023 N94-20997
Ellipsometric study of GaAs(100) surface changes induced at elevated temperatures p 2023 N94-20998
Interface science of controlled metal/metal and metal/ceramic interfaces prepared using ultrahigh vacuum diffusion bonding
[DE94-001066] p 1696 N94-22025

ULTRASONIC SCANNERS
Ultrasonic sensor vision in robotics p 1775 N94-22131

ULTRASONIC TESTS
Three dimensional ultrasonic imaging
[DE93-040549] p 1968 N94-22003
Cold starting an alcohol-fueled engine with ultrasonic fuel atomization
[PB93-206597] p 1826 N94-22093

Strength, ultrasonic and metallurgical evaluation of diffusion bonds
[DE94-000665] p 1697 N94-22571
ULTRAVIOLET ASTRONOMY
X ray, extreme and far ultraviolet optical thin films for space applications
[NASA-CR-194635] p 1984 N94-20128
VVNRS: Variable phenomena in VV Cephei
[NASA-CR-194731] p 2056 N94-21835
UIT support observations archive
p 2048 N94-22534
ULTRAVIOLET DETECTORS
UVPI imaging from the LACE satellite: The Starbird rocket plume
[AD-A271981] p 1658 N94-20617
ULTRAVIOLET FILTERS
X ray, extreme and far ultraviolet optical thin films for space applications
[NASA-CR-194635] p 1984 N94-20128
ULTRAVIOLET LASERS
Ocular damage induced by ultrashort laser pulses
[AD-A271859] p 1890 N94-20462
Optical metrology of magnetically trapped hydrogen
[AD-A272110] p 1680 N94-20584
Demonstration of ultraviolet lasing with a low energy electron beam
[DE93-040192] p 1818 N94-21554
ULTRAVIOLET RADIATION
The modification of polymer surfaces and the fabrication of submicron-scale functionalized structures by deep-UV and electron beam lithography
[AD-A265956] p 1700 N94-20328
The implications of the LDEF results on Space Station Freedom power system materials p 1660 N94-21377
The simulation of action of some space environment factors on Teflon and on rubber materials
p 1661 N94-21380
Simulated space environmental effects on some experimental high performance polymers
p 1662 N94-21385
A carbon dioxide/methane greenhouse atmosphere on early Mars p 2142 N94-21662
UNDERGROUND EXPLOSIONS
Proceedings of the 15th Annual Seismic Research Symposium
[AD-A271458] p 1855 N94-20090
UNDERWATER ACOUSTICS
A survey of the impact on acoustic propagation of warm core ocean eddys
[AD-A272188] p 1883 N94-20925
Acoustic monitoring of global ocean variability
[AD-A271998] p 1883 N94-21366
Transient acoustic wave modeling: Higher-order WKBJ asymptotics and symbolical manipulation (revised)
[PB93-215432] p 1969 N94-22262
UNDERWATER COMMUNICATION
Oceanic in situ Fraunhofer-line characteristics: Fraunhofer-line underwater experiment (FLUX)
[AD-A270659] p 1881 N94-19952
UNDERWATER VEHICLES
Design of a controllable pitch underwater thruster system
[AD-A271140] p 1821 N94-20021
A software architecture for a small autonomous underwater vehicle navigation system
[AD-A272322] p 1643 N94-21037
Simulation of tripod gaits for a hexapod underwater walking machine
[AD-A271719] p 1945 N94-21355
UNITED KINGDOM
Current situation in developing petroleum substituting energy (the United Kingdom)
[DE94-714897] p 1713 N94-22091
UNITED STATES
Biofuels: Project summaries
[DE93-010003] p 1712 N94-19984
Post-Palbozoic crustal responses to the contemporary stress field in the eastern United States
[DE93-040604] p 1859 N94-22006
UNIVERSE
Visualizing the universe, part 1 p 2064 N94-22476
UNIVERSITIES
A comprehensive software engineering educational experience
[AD-A270583] p 1905 N94-20109
Schools of the Pacific rainfall climate experiment
p 1881 N94-20699
UNIX (OPERATING SYSTEM)
Lightweight recoverable virtual memory
[AD-A270576] p 1898 N94-20107
Security evaluation of Unix networks
[AD-A273076] p 1945 N94-21520
Database activity in the Italian Astronet: DIRA 2
p 2047 N94-22452
VETA x ray data acquisition and control system
p 2047 N94-22455
Writing instrument interfaces with xf/tktcl
p 1925 N94-22480
The University of Hawaii Institute for Astronomy CCD camera control system p 1828 N94-22489
The ADAM environment and transputers
p 1926 N94-22494
CCD data acquisition systems at Lick and Keck Observatories p 2047 N94-22495
UNSTEADY AERODYNAMICS
Blade row interaction effects on flutter and forced response
[NASA-TM-106438] p 1649 N94-21586
UNSTEADY FLOW
Transient thermal analysis of cryocondensation pump for JET
[DE93-040372] p 1992 N94-20003
Three dimensional unsteady flow calculations in radial components p 1669 N94-20080
Rotorwash wind sensor evaluation
[AD-A268987] p 1807 N94-20203
System and method for cancelling expansion waves in a wave rotor
[NASA-CASE-LEW-15218-1] p 1801 N94-20588
Computational and analytical methods in nonlinear fluid dynamics
[AD-A272722] p 1802 N94-21169
An efficient numerical method for three-dimensional hypersonic flow
[AD-A272506] p 1637 N94-21411
Active control of wake/blade-row interaction noise through the use of blade surface actuators
[NASA-CR-4556] p 1968 N94-21608
Local uniform grid refinement and brine transport in porous media with inhomogeneities
[CWI-NM-R9224] p 1803 N94-21609
Time-dependent grid adaptation for meshes of triangles and tetrahedra p 1920 N94-22369
UPWIND SCHEMES (MATHEMATICS)
Order of accuracy of QUICK and related convection-diffusion schemes
[NASA-TM-106402] p 1959 N94-21588
URANIUM
Crystallographic phase transitions in actinide metals as a function of pressure
[DE93-040138] p 2011 N94-19827
A weighted least-squares lump correction algorithm for transmission-corrected gamma ray nondestructive assay
[DE93-018474] p 1904 N94-20049
K, U, and Th behavior in Martian environmental conditions p 2141 N94-20908
URANIUM ALLOYS
Investigation of cracking and erratic behavior of the uranium-titanium alloy
[DE93-018591] p 1688 N94-19957
Non-Fermi-liquid and multichannel Kondo phenomena in Y(1-x)U(x)Pd3 and related alloys
[DE93-040135] p 2015 N94-20275
Non-fermi liquid and spin-glass behavior of the Sc(1-x)U(x)Pd3 system
[DE93-040134] p 2016 N94-20335
Temperature dependence of magnetic order in single-crystalline UPdSn
[DE93-040153] p 2033 N94-21991
URANIUM COMPOUNDS
Theoretical studies of the structures and electronic properties of U(NH2)(sub 3) and Np(NH2)(sub 3)
[DE94-000768] p 2031 N94-21857
Low temperature absorption spectra and ground state electronic structure of tetrakis(2,6-di-tert-butylphenoxide)uranium(IV)
[DE94-000774] p 2035 N94-22387
URANIUM ISOTOPES
U-Pb isotopic ages and characteristics of ancient (greater than 4.0 Ga) lunar highland rocks
p 2104 N94-20700
U-Pb provenance ages of shocked zircons from the K-T boundary, Raton Basin, Colorado p 1685 N94-20701
U-Pb isotopic systematics of ferroan anorthosite 60025 p 1685 N94-20702
URANIUM 238
A high-intensity He-jet production source for radioactive beams
[DE93-040247] p 1981 N94-21767
URANUS (PLANET)
Structural evidence for reorientation of Miranda about a paleo-pole p 2098 N94-20671
URBAN DEVELOPMENT
Urban applications of satellite remote sensing and GIS analysis
[PB93-202174] p 1842 N94-21855
URBAN PLANNING
Urban applications of satellite remote sensing and GIS analysis
[PB93-202174] p 1842 N94-21855
URBAN TRANSPORTATION
Electromechanical battery research and development at the Lawrence Livermore National Laboratory
[DE93-019159] p 1762 N94-21620
UREILITES
A carbon and nitrogen isotope study of carbonaceous vein material in ureilite meteorites p 2083 N94-20726
USER MANUALS (COMPUTER PROGRAMS)
Planning process software: A user guide for the DMCA
[AD-A271252] p 1902 N94-19911
SIMBAT theoretical manual
[AD-A271063] p 1882 N94-19979
The best of GYMNOS: A users guide
[DE93-041275] p 1992 N94-19991
Manual of DRANC (release 1.1): A computer program for the Dutch risk assessment of new chemical substances
[PB93-194827] p 1851 N94-19998
Mint tutorial and user manual
[TR-452] p 1905 N94-20143
Time warp operating system version 2.7 internals manual
[NASA-CR-194798] p 1899 N94-20549
Design structuring and allocation optimization (Destination) prototype level 1 user's manual
[AD-A272115] p 1929 N94-20571
GWB: Manual for the Grammar WorkBench version 1.5
[TR-92-14] p 1909 N94-21061
The Mercury user's manual
[TR-465] p 1913 N94-21316
The term processor Kimwitu manual and cookbook
[MEMO-INF-92-67] p 1914 N94-21454
Development of BEM for ceramic composites
[NASA-CR-194718] p 1676 N94-21777
User manual for EXCALIBUR: A FE-BI numerical laboratory for cavity-backed antennas in a circular cylinder, version 1.2 p 1741 N94-21888
Parallel runway requirement analysis study. Volume 2: Simulation manual
[NASA-CR-191549-VOL-2] p 1644 N94-22278
F2D users manual: A two-dimensional compressible gas flow code
[DE94-000653] p 1805 N94-22386
USER REQUIREMENTS
Research in image management and access
[NASA-CR-194797] p 1907 N94-20376
PEGASUS, electronic bulletin board system user's guide
[AD-A271679] p 2044 N94-21363
Software systems used for unstructured grid generation at NASA Langley p 1918 N94-22351
UTILITIES
Wind energy: Program overview, FY 1992
[DE93-000056] p 1845 N94-19921

V

V/STOL AIRCRAFT
Some VTOL head-up display drive-law problems and solutions
[NASA-TM-104027] p 1635 N94-20035
VACANCIES (CRYSTAL DEFECTS)
Crystal structure and short-range oxygen defects in La- and Nd-modified ZrO2
[DE93-040229] p 2033 N94-21993
VACUUM
Evaporation in equilibrium, in vacuum, and in hydrogen gas p 1684 N94-20638
Outgassing data for selecting spacecraft materials
[NASA-RP-1124-REV-3] p 1676 N94-21889
VACUUM APPARATUS
Turntable mechanism
[NASA-CASE-MFS-28522-1] p 1823 N94-20380
VACUUM CHAMBERS
Characterization of electromagnetic fields in an extended chamber at the Short Pulse Experimental Electron Device (SPEED) simulator
[AD-A265955] p 1717 N94-20329
New technique for oil backstreaming contamination measurements p 1652 N94-20511
GaAs(100) surface modifications at elevated temperatures, studied by in-situ spectroscopic ellipsometry p 2023 N94-20997
Ellipsometric study of GaAs(100) surface changes induced at elevated temperatures p 2023 N94-20998
Initial operation of a large-scale plasma source ion implantation experiment
[DE94-000805] p 2036 N94-22583
VACUUM DEPOSITION
Fabrication and evaluation of superconducting and semiconducting materials
[AD-A271645] p 2018 N94-20558

VACUUM EFFECTS
Surface science at the solid liquid interface
[AD-A271422] p 1678 N94-19839
VACUUM TESTS
Solar simulator for solar dynamic space power system testing
[NASA-TM-106393] p 1984 N94-20140
In-vacuo slip testing of materials for SSRMS friction brakes p 1661 N94-21381
VALENCE
The x ray microprobe determination of chromium oxidation state in olivine from lunar basalt and kimberlitic diamonds p 1686 N94-20807
Microanalysis of iron oxidation state in iron oxides using X Ray Absorption Near Edge Structure (XANES) p 1686 N94-20808
VALIDITY
Handbook. Volume 3: Digital systems validation book plan
[DOT/FAA/CT-93/16-VOL-3] p 1647 N94-20053
VALLEYS
Beta Regio rift system on Venus: Geologic interpretation of Magellan images p 2095 N94-20655
Evolution of the global water cycle on Mars: The geological evidence p 2142 N94-21660
Ancient Martian valley genesis and paleoclimatic inference: The present as a key to the past p 2142 N94-21661
Early Mars: The inextricable link between internal and external influences on valley network formation p 2146 N94-21681
The Martian valley networks: Origin by niveo-fluvial processes p 2146 N94-21682
VALUE ENGINEERING
Optimization of a satellite localization and message sending system
[ETN-93-94448] p 1737 N94-20592
VALVES
Vapor-delivered lubrication of steel-steel and steel-ceramic systems
[PB93-202364] p 1825 N94-21451
VAN DER WAALS FORCES
Investigation of heterojunctions and multiple quantum well structures using crystalline organic semiconductors
[AD-A272113] p 2018 N94-20569
One- and multi-component theories of mixtures
[DE93-040543] p 1966 N94-21511
VANADIUM
Transient studies of low temperature catalysts for methane conversion
[DE93-041232] p 1680 N94-20934
VAPOR DEPOSITION
Fabrication of stable large-area thin-film CdTe photovoltaic modules
[DE93-018204] p 1845 N94-20095
Plasma chemical vapor deposition of halide glasses
[AD-D015933] p 1701 N94-20331
Growth of zinc selenide single crystals by physical vapor transport in microgravity
[NASA-CR-194679] p 2017 N94-20346
Monocrystalline germanium film on sapphire
[AD-D015925] p 2017 N94-20348
Volatile CVD precursors based on copper alkoxides and mixed group 2A-copper alkoxides
[AD-D015930] p 1701 N94-20349
Analysis of cost: CVD diamond deposition
[AD-A271980] p 2018 N94-20616
Growth, characterization and device development in monocrystalline diamond films
[AD-A273097] p 2028 N94-21506
Fundamental studies of defect generation in amorphous silicon alloys grown by remote plasma-enhanced chemical-vapor deposition
[DE93-017083] p 2029 N94-21615
Research on polycrystalline thin-film submodules based on CuInSe2 materials
[DE93-018223] p 2029 N94-21617
Surface modification for corrosion resistance
[DE93-017419] p 1693 N94-21825
Techniques for producing free-standing thin films on frames
[DE93-041144] p 1708 N94-21954
VAPOR PHASES
Parameters affecting hydrogen chloride measurements
[AD-A271326] p 1851 N94-20025
Volatile loss from accreting icy protoplanets p 2084 N94-20793
Recondensation in the early solar system: Physical conditions and source material p 2085 N94-20849
Utilization of metals to improve the lubrication of ceramic load-bearing devices
[PB93-202448] p 1825 N94-21424
Lubricated wear of steel-ceramic and ceramic-ceramic systems
[PB93-202356] p 1825 N94-21450
Combustion in turbulent jets and buoyant flames
[PB93-202372] p 1682 N94-21452
Effect of powder characteristics on gas-pressure sintering of Si3N4 with rare earth additives
[DE94-000330] p 1694 N94-21945
VAPOR PRESSURE
Thermal behavior of natural zeolites
[DE93-040091] p 1699 N94-19975
VAPORIZING
On magnetodynamic effects initiated by a high-speed impact of a large cosmic body upon the Earth's surface p 2082 N94-20647
Stable Ni isotopes and Be-10 and Al-26 in metallic spheroids from Meteor Crater, Arizona p 1863 N94-20889
Liquid-phase circulation and mixing in multicomponent droplets vaporizing in a laminar convective environment
[AD-A272851] p 1802 N94-21193
VAPORS
Image detection using edge extraction algorithms
[AD-A272439] p 1911 N94-21203
Establishing the basis for validated predictions of highly non-equilibrium flows (with 9 attachments)
[AD-A272918] p 1802 N94-21220
Atmospheric sampling glow discharge ionization and triple quadrupole tandem mass spectrometry for explosives vapor detection
[DE93-040593] p 1852 N94-22004
VARACTOR DIODES
Millimeter wave imaging technology
[AD-A271257] p 1715 N94-19912
Non-linear analysis of the electrical properties of the active circuits of high-frequency oscillators p 1785 N94-22195
VARIABILITY
Large-scale circulation regimes and tropical cyclone characteristics over the western pacific ocean
[AD-A273004] p 1867 N94-21307
VARIABLE CYCLE ENGINES
Options for thrust augmentation for the Beta 2 two-stage-to-orbit launch vehicle
[NASA-TM-106418] p 1649 N94-21759
VARIABLE PITCH PROPELLERS
Design of a controllable pitch underwater thruster system
[AD-A271140] p 1821 N94-20021
VARIANCE (STATISTICS)
Linear programming for standard and nonstandard Markovian control problems. A survey
[PB93-191948] p 1963 N94-21066
Parameter estimation with cost function of second order in output-error-problem
[DLR-FB-92-38] p 1964 N94-21139
VARIATIONAL PRINCIPLES
Proof of stability of the hydrogen molecule
[PB93-221026] p 1977 N94-22271
VARIATIONS
Paired comparison models with time-varying parameters
[AD-A272016] p 1964 N94-21442
Surface-induced brightness temperature variations and their effects on detecting thin cirrus clouds using IR emission channels in the 8-12 micrometer region p 1880 N94-22341
VARIOMETERS
Concept report: Experimental vector magnetograph (EXVM) operational configuration balloon flight assembly
[NASA-CR-194702] p 1638 N94-21776
VARISTORS
Improvement of the stability of the process for synthesizing chemically prepared varistor powder
[DE94-000345] p 1763 N94-21654
VARNISHES
Thermal control coatings p 1664 N94-21400
VATOL AIRCRAFT
Design, fabrication and test of a vertical attitude takeoff and landing unmanned air vehicle
[AD-A273003] p 1646 N94-21283
VAX COMPUTERS
Telescope image modelling software in STSDAS p 1926 N94-22483
The evolution of the FIGARO data reduction system p 2048 N94-22528
VECTOR PROCESSING (COMPUTERS)
MGD1M: A parallel multigrid code with a fast vectorized ILU-relaxation
[CWI-NM-R9222] p 1930 N94-21077
Parallelizing a highly vectorized multigrid code with zebra relaxation
[CWI-NM-R9225] p 1935 N94-21610
Numerical multigrid software (MGD5M): A parallel multigrid code with a twisted ILLU-relaxation
[CWI-NM-R9226] p 1916 N94-21611
A low-cost vector processor boosting compute-intensive image processing operations p 1925 N94-22441
VECTOR QUANTIZATION
Low bit rate coding of Earth science images
[NASA-CR-193729] p 2041 N94-20158
Data compression by using wavelet transforms and vector quantization
[AD-A272763] p 1738 N94-21182
Some extensions of the k-means algorithm for image segmentation and pattern classification
[AD-A271691] p 1913 N94-21364
Hierarchical multirate vector quantization for image coding p 1781 N94-22174
VECTORS (MATHEMATICS)
Segmented operations for sparse matrix computation on vector multiprocessors
[AD-A270601] p 1928 N94-19950
The quantum structure of matter grand challenge project: Large-scale 3-D solutions in relativistic quantum dynamics
[DE94-000328] p 1960 N94-21955
VEGETATION
Modeling of interactions between biosphere and atmosphere on the global scale
[NASA-CR-193423] p 1837 N94-20205
An expert system shell for inferring vegetation characteristics
[NASA-CR-189318] p 1837 N94-20284
Classification of simple vegetation types using POLSAR image data p 1722 N94-20420
Application of Cloude's target decomposition theorem to polarimetric imaging radar data p 1724 N94-20429
Direction angle sensitivity of agricultural field backscatter with AIRSAR data p 1724 N94-20430
Measurement of evapotranspiration with combined reflective and thermal infrared radiance observations
[NASA-CR-194802] p 1837 N94-20951
VEGETATION GROWTH
Characterization of Minnesota lunar simulant for plant growth p 1897 N94-20665
VEGETATIVE INDEX
Change detection on land use and rainforest cover at Paragominas region, Brazilian Amazon p 1838 N94-20957
Linear mixing model applied to AVHRR LAC data p 1838 N94-20958
Analysis of hyper-spectral AVIRIS image data over a mixed-conifer forest in Maine p 1838 N94-20959
The 7th Brazilian Remote Sensing Symposium, volume4 p 1840 N94-20965
Using NDVI/AVHRR data for crop monitoring and forecasting in South Italy p 1841 N94-20970
VEINS
A carbon and nitrogen isotope study of carbonaceous vein material in ureilite meteorites p 2083 N94-20726
VELOCITY
Antipodal fragment velocities for porous and weak targets at catastrophic impacts p 1836 N94-20891
VELOCITY DISTRIBUTION
Electrode array electromagnetic velocimeter
[AD-D015950] p 1806 N94-19882
Experimental and computational results from a large low-speed centrifugal impeller
[NASA-TM-106421] p 1636 N94-20136
Kinetic theory of runaway air-breakdown
[DE93-040731] p 1750 N94-20325
An experimental investigation of the drag mechanisms of a helicopter rotor in hovering flight
[AD-A270201] p 1636 N94-20486
Determination of cosmic bodies size-velocity distribution by observation of current impacts on Mars p 2082 N94-20648
Comparison of satellite-derived velocity fields in the coastal transition zone
[AD-A272565] p 1883 N94-21360
Low Reynolds-number turbulent boundary layers
[AD-A272011] p 1803 N94-21459
A study of the compressible flow through a diffusing S-duct
[NASA-TM-106411] p 1638 N94-21591
Direct detection of atomic ions from molecular photofragmentation during nonresonant multiphoton ionization of sputtered species
[DE93-040886] p 1976 N94-21951
Solar full-disk magnetic field image receiving system and observation software p 2079 N94-22552
VELOCITY ERRORS
Mirror velocity sampling errors in a Michelson interferometer
[AD-A273105] p 1809 N94-21508
VELOCITY MEASUREMENT
Electrode array electromagnetic velocimeter
[AD-D015950] p 1806 N94-19882
Time-resolved shock compression of porous rutile: Wave dispersion in porous solids
[DE93-018848] p 1829 N94-19927

PVDF gauge characterization of hypervelocity-impact-generated debris clouds
[DE93-018831] p 1829 N94-19943
Coherent lidar design and performance verification
[NASA-CR-193613] p 1816 N94-20341
An experimental investigation of the drag mechanisms of a helicopter rotor in hovering flight
[AD-A270201] p 1636 N94-20486
Shipboard ADCP observations during RRS Charles Darwin Cruise 62
[IOS-298-1992] p 1882 N94-20531
Two-point laser Doppler velocimetry measurements of length-turbulent scales
[ECL-92-12] p 1801 N94-20542
Low-altitude cross-wind velocity measurements using pulsed visible fringe-type laser anemometry
[ISL-CO-216/92] p 1866 N94-20557
Shock compression of low-density foams
[DE93-040545] p 1707 N94-21546
Instantaneous velocity field imaging instrument for supersonic reacting flows
[NASA-CR-191162] p 1809 N94-21607
Particle image velocimetry
[DE93-040657] p 1804 N94-21748
Near wake measurements on a rotor model with Mie-vanes in the Delft open jet tunnel
[PB93-215382] p 1638 N94-22260
Breaking Kelvin-Helmholtz waves and cloud-top entrainment as revealed by K-band Doppler radar
p 1874 N94-22310
Utilization of lasers for air data measurements
p 1640 N94-22603
Hot wire anemometry: A versatile instrumentation used for predevelopment studies and flight testing of the Do-328 aircraft p 1640 N94-22604

VENUS (PLANET)
SO2 on Venus: IUE, HST and ground-based measurements, and the active volcanism connection
p 2092 N94-20637
Geologic mapping of Northern Atla Regio on Venus: Preliminary data p 2095 N94-20654
Beta Regio rift system on Venus: Geologic interpretation of Magellan images p 2095 N94-20655
Beta Regio - Phoebe Regio on Venus: Geologic mapping with the Magellan data p 2096 N94-20656
Largest impact features on Venus: Non-preserved or non-recognizable? p 2096 N94-20657
Dynamics of large scale impacts on Venus and Earth
p 2098 N94-20666
Formation and evolution of radial fracture systems on Venus p 2099 N94-20672
Mixing of a chemically buoyant layer at the top of a thermally convecting fluid: Implications for mantle dynamics with application to Venus
p 2099 N94-20675
Venus magmatic and tectonic evolution
p 2101 N94-20683
Studying Venus using a GIS database
p 2105 N94-20707
Subduction on the margins of coronae on Venus: Evidence from radiothermal emissivity measurements
p 2107 N94-20718
Comparative hypsometric analysis of both Earth and Venus topographic distributions p 2108 N94-20722
Named Venusian craters p 2109 N94-20725
Venus pancake dome formation: Morphologic effects of a cooling-induced variable viscosity during emplacement p 2110 N94-20732
Magellan at Venus: Summary of science findings
p 2110 N94-20734
Venus' impact-crater database: Update to approximately 98 percent of the planet's surface p 2110 N94-20736
Searching for ancient Venus p 2111 N94-20743
Rifting at Devana Chasma, Venus: Structure and estimation of the effective thickness of the elastic lithosphere p 2113 N94-20754
Volcanic rises on Venus: Geology, formation, and sequence of evolution p 2113 N94-20755
Geoid, topography, and convection-driven crustal deformation on Venus p 2116 N94-20769
Venus gravity: New Magellan low altitude data
p 2117 N94-20772
Response of the topography and gravity field on Venus to mantle upwelling beneath a chemical boundary layer
p 2117 N94-20775
Differentiation of magma oceans and the thickness of the depleted layer on Venus p 2118 N94-20780
A tectonic resurfacing model for Venus
p 2118 N94-20781
The missing impact craters on Venus
p 2119 N94-20782
Impact basins on Venus and some interplanetary comparisons p 2119 N94-20785
Parga and Hecate Chasmata, Venus: Structure, volcanism and models of formation
p 2121 N94-20796
The role of CO2 in weathering reactions and the presence of S2 on Venus: Implications for the pyrite stability field p 2122 N94-20799
The stability of oxyamphiboles: Existence of Ferric-bearing minerals under the reducing conditions on the surface of Venus p 2122 N94-20800
Parabolic features and the erosion rate on Venus
p 2122 N94-20801
SPH modelling of energy partitioning during impacts on Venus p 2124 N94-20809
Elevation and igneous crater modification on Venus: Implications for magmatic volatile content
p 2135 N94-20872
Large floor-fractured craters and isostatic crater modification: Implications for lithospheric thickness on Venus p 2135 N94-20873
Morphologic classes of impact basins on Venus
p 2137 N94-20883
The connection between Venus' free obliquity and its CMB oblateness p 2139 N94-20896

VENUS ATMOSPHERE
Impact disturbance of the Venus atmosphere
p 2106 N94-20709
Searching for ancient Venus p 2111 N94-20743
The role of CO2 in weathering reactions and the presence of S2 on Venus: Implications for the pyrite stability field p 2122 N94-20799
The stability of oxyamphiboles: Existence of Ferric-bearing minerals under the reducing conditions on the surface of Venus p 2122 N94-20800
Parabolic features and the erosion rate on Venus
p 2122 N94-20801
Are Plinian type eruptions possible on Venus?
p 2123 N94-20803
Discovery Venera surface: Atmosphere geochemistry experiments mission concept p 2123 N94-20806
SPH modelling of energy partitioning during impacts on Venus p 2124 N94-20809

VENUS SURFACE
SO2 on Venus: IUE, HST and ground-based measurements, and the active volcanism connection
p 2092 N94-20637
Geologic mapping of Northern Atla Regio on Venus: Preliminary data p 2095 N94-20654
Beta Regio rift system on Venus: Geologic interpretation of Magellan images p 2095 N94-20655
Beta Regio - Phoebe Regio on Venus: Geologic mapping with the Magellan data p 2096 N94-20656
Largest impact features on Venus: Non-preserved or non-recognizable? p 2096 N94-20657
Formation and evolution of radial fracture systems on Venus p 2099 N94-20672
Magellan vertical polarization radar observations
p 1744 N94-20691
Crater destruction on the Venusian highlands by tectonic processes p 2103 N94-20696
Some deformation trends and topographic characteristics of tesserae on Venus
p 2105 N94-20706
Studying Venus using a GIS database
p 2105 N94-20707
Impact disturbance of the Venus atmosphere
p 2106 N94-20709
Chocolate tablet aspects of cytherean Meshkenet Tessera p 2106 N94-20710
Ridge belt-related scarps and troughs: Compressional crustal bending on Venus p 2106 N94-20711
Comparative hypsometric analysis of both Earth and Venus topographic distributions p 2108 N94-20722
Named Venusian craters p 2109 N94-20725
Distribution of small volcanic cones on the surface of Venus by size and elevation: Implications for differential deposition of volcanic features p 2110 N94-20731
Venus pancake dome formation: Morphologic effects of a cooling-induced variable viscosity during emplacement p 2110 N94-20732
Venus' impact-crater database: Update to approximately 98 percent of the planet's surface p 2110 N94-20736
Searching for ancient Venus p 2111 N94-20743
Rifting at Devana Chasma, Venus: Structure and estimation of the effective thickness of the elastic lithosphere p 2113 N94-20754
Volcanic rises on Venus: Geology, formation, and sequence of evolution p 2113 N94-20755
Geoid, topography, and convection-driven crustal deformation on Venus p 2116 N94-20769
Scattering by Venus' surface p 2117 N94-20771
A tectonic resurfacing model for Venus
p 2118 N94-20781
The missing impact craters on Venus
p 2119 N94-20782
Impact basins on Venus and some interplanetary comparisons p 2119 N94-20785
Earth-based measurement of lunar topography using delayed radar interferometry p 2119 N94-20787
The stability of oxyamphiboles: Existence of Ferric-bearing minerals under the reducing conditions on the surface of Venus p 2122 N94-20800
Discovery Venera surface: Atmosphere geochemistry experiments mission concept p 2123 N94-20806
SPH modelling of energy partitioning during impacts on Venus p 2124 N94-20809
Magellan Mission p 1652 N94-20829
Complex ridged terrain-related ridge belts on Venus: Global distribution and classification
p 2129 N94-20835
Is there uniformitarian or catastrophic tectonics on Venus? p 2129 N94-20839
Arcuate and circular structures in the Tharsis region: Evidence of coronae on Mars p 2134 N94-20863
Geology and radiophysical properties of the Venera and Vega landing sites p 2135 N94-20867
Elevation and igneous crater modification on Venus: Implications for magmatic volatile content
p 2135 N94-20872
Large floor-fractured craters and isostatic crater modification: Implications for lithospheric thickness on Venus p 2135 N94-20873
Morphologic classes of impact basins on Venus
p 2137 N94-20883

VERBAL COMMUNICATION
ATC/pilot voice communications: A survey of the literature
[DOT/FAA/AM-93/20] p 1738 N94-21201

VERTICAL DISTRIBUTION
Meso-Beta scale numerical simulation studies of terrain-induced jet streak mass/momentum perturbations
[NASA-CR-194627] p 1864 N94-20138
Wrinkle ridges, reverse faulting, and the depth penetration of lithospheric stress in lunae planum, Mars
p 2141 N94-20910

VERTICAL FLIGHT
Optimal flight guidance for aircraft in windshear
[CA-PATENT-1,307,573] p 1650 N94-21050

VERTICAL LANDING
Design, fabrication and test of a vertical attitude takeoff and landing unmanned air vehicle
[AD-A273003] p 1646 N94-21283
Data link development for the archytas vertical takeoff and landing transitional flight unmanned aerial vehicle
[AD-A272499] p 1646 N94-21548

VERTICAL MOTION SIMULATORS
Some VTOL head-up display drive-law problems and solutions
[NASA-TM-104027] p 1635 N94-20035

VERTICAL TAKEOFF AIRCRAFT
Design, fabrication and test of a vertical attitude takeoff and landing unmanned air vehicle
[AD-A273003] p 1646 N94-21283
Data link development for the archytas vertical takeoff and landing transitional flight unmanned aerial vehicle
[AD-A272499] p 1646 N94-21548

VERY HIGH FREQUENCIES
Sporadic-E observations during LoVHF transionospheric direction finder measurements
[AD-A270619] p 1716 N94-19951

VERY LARGE SCALE INTEGRATION
VLSI design for reliability-current density
[AD-A270719] p 1749 N94-20110
The Fifth NASA Symposium on VLSI Design
[NASA-CR-194644] p 1753 N94-21079
An adaptive, lossless data compression algorithm and VLSI implementations p 1753 N94-21080
Space qualified high speed Reed Solomon encoder
p 1754 N94-21088
High performance MPEG-audio decoder IC
p 1744 N94-21092
VLSI mixed signal processing system
p 1744 N94-21100
Power optimization in logic isomers
p 1756 N94-21101
Computation of signal delays in RC networks
p 1744 N94-21102
Delay analysis of combinations of pass transistors and classical logic gates p 1756 N94-21103
Mixed voltage VLSI design p 1756 N94-21104
Bridging faults in BiCMOS circuits
p 1756 N94-21105
Test pattern generation for ILA sequential circuits
p 1757 N94-21107
Testing self-timed circuits using scan paths
p 1757 N94-21109
Detection of CMOS bridging faults using minimal stuck-at fault test sets p 1757 N94-21110
Robust neural classifier circuits using asynchronous design p 1757 N94-21111
Practical issues in implementing roving spares in VLSI systolic arrays p 1758 N94-21114
A novel VLSI processor architecture for supercomputing arrays p 1758 N94-21115

Synthesis algorithm of VLSI multipliers for ASIC
p 1758 N94-21116
Design and implementation of GaAs HBT circuits with ACME p 1758 N94-21117
Reliable interface design for combining asynchronous and synchronous circuits p 1758 N94-21119
Design methods for fault-tolerant finite state machines
p 1758 N94-21120
A unified approach to VLSI layout automation and algorithm mapping on processor arrays
p 1759 N94-21127
A fixed/variable bit-rate data compression architecture
p 1759 N94-21128
High-speed Viterbi decoding with overlapping code sequences p 1760 N94-21130
A cost-effective methodology for the design of massively-parallel VLSI functional units
p 1760 N94-21132
Behavioral model simulation studies of an image compressor p 1760 N94-21133
Polar processing project
[AD-A271583] p 1739 N94-21235
VLSI design for reliability-hot carrier effects
[AD-A271586] p 1761 N94-21256
CMU very fast range-imaging system
[AD-A272057] p 1761 N94-21282
The 1992 4th NASA SERC Symposium on VLSI Design
[NASA-CR-194591] p 1763 N94-21694
Applications of correlator chips in radio science
p 1763 N94-21695
Single event phenomena: Testing and prediction
p 1763 N94-21696
A 20 MHz CMOS reorder buffer for a superscalar microprocessor p 1764 N94-21700
Analog/digital pH meter system I.C.
p 1764 N94-21701
On the decomposition of synchronous state machines using sequence invariant state machines
p 1764 N94-21703
Heuristic-based scheduling algorithm for high level synthesis p 1764 N94-21704
NASA SERC digital correlator projects
p 1765 N94-21708
Fully-depleted silicon-on-sapphire and its application to advanced VLSI design p 1765 N94-21709
Defect-sensitivity analysis of an SEU immune CMOS logic family p 1765 N94-21711
A novel visual hardware behavioral language
p 1765 N94-21715
HDL to verification logic translator
p 1766 N94-21717
A simple modern correctness condition for a space-based high-performance multiprocessor
p 1766 N94-21718
A mean field neural network for hierarchical module placement p 1766 N94-21720
Schematic driven layout of Reed Solomon encoders
p 1766 N94-21722
Bit-systolic arithmetic arrays using dynamic differential gallium arsenide circuits p 1767 N94-21724
A VLSI implementation of DCT using pass transistor technology p 1767 N94-21725
A DRAM compiler algorithm for high performance VLSI embedded memories p 1767 N94-21729
Low power, CMOS digital autocorrelator spectrometer for spaceborne applications p 1666 N94-21733
A real time correlator architecture using distributed arithmetic principles p 1768 N94-21734
Low energy CMOS for space applications
p 1768 N94-21735
Self assembly: An approach to terascale integration
[DE93-040104] p 1769 N94-21846
The distributed CAD system for LSI/VLSI design
p 1923 N94-22068
VLSI architectures for the new (T,L) algorithm
p 1745 N94-22110
VLSI design of a bit serial parallel processing 4 extender chip for M-path convolutional decoding
p 1775 N94-22132
VLSI design of a parallel video output interface
p 1778 N94-22153
Architectures of the free space optical interconnects
p 1789 N94-22220
The VLBA correlator: Real-time in the distributed era
p 2049 N94-22547

VERY LONG BASELINE ARRAY (VLBA)
The VLBA correlator: Real-time in the distributed era
p 2049 N94-22547

VERY LOW FREQUENCIES
VLF Harold E. Holt RADHAZ measurements
[AD-A272018] p 1737 N94-20620

VIBRATION
U.S. Tag for ISO/TC 43, acoustics, IEC/TC 29 electroacoustics, and ISO/TC 108/SC4 human exposure to mechanical vibration and shock: Minutes of the accredited standards committee on bioacoustics, S3
[AD-A273014] p 1897 N94-21309
Semiconductor isotope engineering
[DE93-040119] p 2030 N94-21744
A vibration model for centrifugal contactors
[DE93-040645] p 1833 N94-21927
Modal combination in response spectrum modal dynamic analysis
[DE94-000339] p 1833 N94-21956

VIBRATION DAMPING
Study of transverse coupled bunch instabilities by using non-linear Taylor maps for the Advanced Light Source (ALS)
[DE93-040287] p 1979 N94-19989
Graphite/polyurethane flexible composites: Mechanical and vibration damping properties
[AD-A271608] p 1674 N94-20950

VIBRATION ISOLATORS
Diagnostics and methods for real-time laser microchemistry
[AD-A270871] p 1680 N94-20566

VIBRATION MODE
System identification of the Daisy large space structure emulator
[ISBN-0-315-83533-8] p 1653 N94-22588

VIBRATION TESTS
The effect of delamination on the dynamic response of composite laminates as measured by embedded fiber optic Michelson sensor
[ISBN-0-315-83534-6] p 1677 N94-22587

VIBRATIONAL SPECTRA
Rotational spectrum of a dark state in 2-fluoroethanol using microwave/radiofrequency-infrared multiple resonance
[AD-A272101] p 1817 N94-20583
Surface electrochemistry of metals
[AD-A272913] p 1691 N94-21245
Modal combination in response spectrum modal dynamic analysis
[DE94-000339] p 1833 N94-21956

VIBRATIONAL STATES
Femtosecond Raman-induced Kerr effect study of polar solvent dynamics: Amides
[DE93-017563] p 1678 N94-19924
Rotational spectrum of a dark state in 2-fluoroethanol using microwave/radiofrequency-infrared multiple resonance
[AD-A272101] p 1817 N94-20583
Theoretical investigations of metastability and energy storage in molecular systems
[AD-A271849] p 1973 N94-20612
High resolution infrared spectroscopy of formamide and deuterated formamide in a molecular beam
[AD-A271986] p 1973 N94-20618
Semiconductor isotope engineering
[DE93-040119] p 2030 N94-21744
Ionization of H2(+) in intense laser fields
[DE93-019160] p 1818 N94-21829
Non-adiabatic effects in low-energy electron-molecule scattering
[DE93-040485] p 1976 N94-21968

VIDEO COMMUNICATION
Performance evaluation of video on ethernet
[DE93-040696] p 1936 N94-21749

VIDEO DATA
The Amsterdam hypermedia model: Extending hypertext to support real multimedia
[CWI-CS-R9306] p 2045 N94-21536
Concept report: Experimental vector magnetograph (EXVM) operational configuration balloon flight assembly
[NASA-CR-194702] p 1638 N94-21776

VIDEO EQUIPMENT
Image processing as a tool in flight testing evaluation
p 1640 N94-22606

VIDEO SIGNALS
Adaptive analog video signal conditioner
p 1744 N94-21099

VIDICONS
The cool-star spectral catalog: A uniform collection of IUE SWP-LOs p 2046 N94-22446

VIKING MARS PROGRAM
Observed climatic activity pertaining to the evolution of the northern plains p 2090 N94-20392
Chronology, eruption duration, and atmospheric contribution of Apollinaris Patera, Mars
p 2108 N94-20720
GMM-1: A 50 degree and order gravitational field model for Mars p 2117 N94-20774
Mass spectrometer-pyrolysis experiment for atmospheric and soil sample analysis on the surface of Mars p 1812 N94-22435

VIRTUAL MEMORY SYSTEMS
Lightweight recoverable virtual memory
[AD-A270576] p 1898 N94-20107

VIRTUAL REALITY
A software architecture for the construction and management of real-time virtual worlds
[AD-A271465] p 1904 N94-20091

VISCOELASTICITY
Problems related to conservation laws: Phase transitions and viscoelasticity
[AD-A271429] p 1698 N94-19840

VISCOPLASTICITY
Life assessment of structural components using inelastic finite element analyses p 1834 N94-22614

VISCOSITY
A database of selected transport coefficients for combustion studies
[DE93-041278] p 1678 N94-19889
Measuring liquid properties with smooth and textured-surface resonators
[DE93-019433] p 1749 N94-20054
Venus pancake dome formation: Morphologic effects of a cooling-induced variable viscosity during emplacement p 2110 N94-20732
Experiments with a fluid deicing system for cleaning laminar wings p 1640 N94-22601
Measurement of the influence of deicing liquids on aircraft aerodynamics p 1640 N94-22602
The relaxed state and entropy production due to the electric resistivity and viscosity of plasma
p 2010 N94-22696

VISCOUS FLOW
Time-accurate Navier-Stokes calculations with multigrid acceleration p 1956 N94-21469
Multigrid schemes for viscous hypersonic flows
p 1641 N94-21473
Surface path lines in plane Stokes flow driven by capillarity
[DE93-041277] p 1803 N94-21651
Unstructured low-Mach number viscous flow solver
p 1919 N94-22358
Robust unstructured grid generation with VGRID
p 1919 N94-22359
Cartesian-cell based grid generation and adaptive mesh refinement p 1920 N94-22364

VISIBILITY
Distribution of turbidity in Australian tropical waters
[AD-A271059] p 1881 N94-19905
Visibility considerations in frequency sharing with low Earth orbit satellites p 1746 N94-22187

VISIBLE SPECTRUM
Wavelength dependence of limb-darkening of Mars from visible and near-IR telescopic spectral imaging
p 2101 N94-20685
Visible-infrared properties of controlled laboratory soils
p 1685 N94-20689

VISION
Analysis of health status from preliminary physical examination of flight academy applicants
[AD-A267759] p 1889 N94-19962
Toward a neurobiological theory of visual attention
[AD-A270724] p 1890 N94-20112
Head-centered orientation strategies in animate vision
[TR-442] p 1894 N94-20520

VISUAL ACUITY
Analysis of health status from preliminary physical examination of flight academy applicants
[AD-A267759] p 1889 N94-19962

VISUAL AIDS
The manager's guide to NASA graphics standards
[NHB-1430.2] p 2042 N94-20306

VISUAL DISCRIMINATION
The 3-D Moons: The Voyager stereo atlas of the outer solar system p 2111 N94-20740

VISUAL OBSERVATION
Cloud fields derived from satellite and surface data during FIRE cirrus phase 2 p 1872 N94-22302

VISUAL PERCEPTION
On geometric and algebraic aspects of 3D affine and projective structures from perspective 2D views
[AD-A270520] p 1983 N94-19966
Head-centered orientation strategies in animate vision
[TR-442] p 1894 N94-20520
Perception/action: An holistic approach 2
[AD-A271822] p 1891 N94-20627
A new procedure for orbit determination based on three lines of sight: Angles only
[AD-A272937] p 1652 N94-21224
Two-dimensional perception based on a laser rangefinder p 1786 N94-22202

VISUAL STIMULI
Motion sickness elicited by passive rotation in squirrel monkeys p 1887 N94-21905

VISUAL TASKS
Head-centered orientation strategies in animate vision
[TR-442] p 1894 N94-20520

Perception/action: An holistic approach 2
[AD-A271822] p 1891 N94-20627

VITERBI DECODERS
High-speed Viterbi decoding with overlapping code sequences p 1760 N94-21130
Design of a new squaring function for the Viterbi algorithm p 1764 N94-21699
Coded 64QAM using a binary convolutional code p 1747 N94-22223
Adaptive decoding of convolutional codes p 1793 N94-22246
Bidirectional algorithms for the decoding of convolutional codes over memoryless channels p 1793 N94-22247

VOCODERS
Data compression by using wavelet transforms and vector quantization
[AD-A272763] p 1738 N94-21182
Software implementation of an adaptive digital automatic level control p 1773 N94-22124

VOICE COMMUNICATION
Ground proximity warning system voice warning unit requirements study
[AD-A270541] p 1641 N94-19876
ATC/pilot voice communications: A survey of the literature
[DOT/FAA/AM-93/20] p 1738 N94-21201
Software implementation of an adaptive digital automatic level control p 1773 N94-22124

VOICE CONTROL
Representation of spoken words in a self-organizing neural net p 1940 N94-20243

VOICE DATA PROCESSING
Ground proximity warning system voice warning unit requirements study
[AD-A270541] p 1641 N94-19876
Data compression by using wavelet transforms and vector quantization
[AD-A272763] p 1738 N94-21182
Software implementation of an adaptive digital automatic level control p 1773 N94-22124

VOIDS
Experimental study of void formation during aluminum solidification in reduced gravity
[NASA-TM-106190] p 1692 N94-21604
Surface and subsurface defect detection in Si3N4 components by laser scattering
[DE93-040829] p 1832 N94-21772
Strength, ultrasonic and metallurgical evaluation of diffusion bonds
[DE94-000665] p 1697 N94-22571

VOLATILITY
Volatile CVD precursors based on copper alkoxides and mixed group 2A-copper alkoxides
[AD-D015930] p 1701 N94-20349
Volatility in the lunar crust: Trace element analyses of lunar minerals by PIXE proton microprobe p 2097 N94-20661
C-O volatiles in Apollo 15 and Apollo 17 picritic glasses p 1685 N94-20727
Volatile loss from accreting icy protoplanets p 2084 N94-20793
Impact-induced devolatilization of CaSO4 anhydrite and implications for K-T extinctions: Preliminary results p 2085 N94-20840

VOLCANOES
SO2 on Venus: IUE, HST and ground-based measurements, and the active volcanism connection p 2092 N94-20637
Geologic mapping of Northern Atla Regio on Venus: Preliminary data p 2095 N94-20654
Beta Regio rift system on Venus: Geologic interpretation of Magellan images p 2095 N94-20655
Beta Regio - Phoebe Regio on Venus: Geologic mapping with the Magellan data p 2096 N94-20656
Formation and evolution of radial fracture systems on Venus p 2099 N94-20672
Thermal and rheological controls on magma migration in dikes: Examples from the east rift zone of Kilauea volcano, Hawaii p 1862 N94-20673
Distribution of small volcanic cones on the surface of Venus by size and elevation: Implications for differential deposition of volcanic features p 2110 N94-20731
Volcanic rises on Venus: Geology, formation, and sequence of evolution p 2113 N94-20755
Basaltic magmatism on the Moon. A perspective from volcanic picritic glasses p 2114 N94-20758
Origin of the Apollo 15 very low Ti green glass. A perspective from the compositional diversity in the very low Ti glasses p 1685 N94-20759
Tumuli and tubes: Teaching scientific techniques p 2039 N94-20818
Elevation and igneous crater modification on Venus: Implications for magmatic volatile content p 2135 N94-20872
Formation of perched lava ponds on basaltic volcanoes: Interaction between cooling rate and flow geometry allows estimation of lava effusion rates p 1863 N94-20878
CO2 lidar observations of Mount Pinatubo debris: FIRE 2 and longer-term measurements p 1876 N94-22323

VOLCANOLOGY
A model for the origin of Martian polygonal terrain p 2090 N94-20393
Twenty-Fourth Lunar and Planetary Science Conference. Part 3: N-Z
[NASA-CR-193149] p 2092 N94-20636
SO2 on Venus: IUE, HST and ground-based measurements, and the active volcanism connection p 2092 N94-20637
Largest impact features on Venus: Non-preserved or non-recognizable? p 2096 N94-20657
Thermal and rheological controls on magma migration in dikes: Examples from the east rift zone of Kilauea volcano, Hawaii p 1862 N94-20673
Mixing of a chemically buoyant layer at the top of a thermally convecting fluid: Implications for mantle dynamics with application to Venus p 2099 N94-20675
Spectral reflectance studies of the Humorum Basin region p 2101 N94-20682
Venus magmatic and tectonic evolution p 2101 N94-20683
A comparison of calculated and measured rheological properties of crystallising lavas in the field and in the laboratory p 1862 N94-20690
Eruption history of the Tharsis shield volcanoes, Mars p 2102 N94-20692
Geology of Biblis Patera, Ulysses Patera, and Jovis Tholus, Mars p 2103 N94-20693
Chronology, eruption duration, and atmospheric contribution of Apollinaris Patera, Mars p 2108 N94-20720
Distribution of small volcanic cones on the surface of Venus by size and elevation: Implications for differential deposition of volcanic features p 2110 N94-20731
Venus pancake dome formation: Morphologic effects of a cooling-induced variable viscosity during emplacement p 2110 N94-20732
Volcanic rises on Venus: Geology, formation, and sequence of evolution p 2113 N94-20755
Chronology and genesis of high-Ti mare volcanism: Melting of cogenetic depleted and enriched reservoirs p 2118 N94-20777
A tectonic resurfacing model for Venus p 2118 N94-20781
Parga and Hecate Chasmata, Venus: Structure, volcanism and models of formation p 2121 N94-20796
Are Plinian type eruptions possible on Venus? p 2123 N94-20803
Elevation and igneous crater modification on Venus: Implications for magmatic volatile content p 2135 N94-20872
Multispectral studies of selected crater- and basin-filling lunar Maria from Galileo Earth-Moon encounter 1 p 2136 N94-20876
Numerical simulation of lava flows: Applications to the terrestrial planets p 1863 N94-20904

VOLTAGE GENERATORS
High current injector for heavy ion fusion
[DE93-019241] p 1979 N94-20289

VOMITING
Susceptibility of the squirrel monkey to different motion conditions p 1885 N94-21899
Reassessment of area postrema's role in motion sickness and conditioned taste aversion p 1886 N94-21901
Detection of emetic activity in the cat by monitoring venous pressure and audio signals p 1886 N94-21903
Recovery of the vomiting reflex following area postrema ablation in squirrel monkeys p 1886 N94-21904
Area postrema ablations in cats: Evidence for separate neural routes for motion- and xylazine-induced CTA and emesis p 1887 N94-21906
Immunocytochemical localization of glutamic acid decarboxylase (GAD) and substance P in neural areas mediating motion-induced emesis: Effects of vagal stimulation on GAD immunoreactivity p 1887 N94-21909
The effects of area postrema lesions and selective vagotomy on motion-induced conditioned taste aversion p 1888 N94-21910
Experimental studies of gastric dysfunction in motion sickness: The effect of gastric and vestibular stimulation on the vagal and splanchnic gastric efferents p 1888 N94-21911
Role of the area postrema in three putative measures of motion sickness in the rat p 1888 N94-21912

VORTEX ALLEVIATION
Prediction and control of vortex-dominated and vortex-wake flows
[NASA-CR-194722] p 1637 N94-21054

VORTEX BREAKDOWN
Prediction and control of vortex-dominated and vortex-wake flows
[NASA-CR-194722] p 1637 N94-21054

VORTICES
Dynamics of vortices in superconductors
[DE93-019535] p 2011 N94-19808
Particle dispersion in turbulent sprays
[AD-A271314] p 1796 N94-19913
The fluid mechanics of vortex cutting by a blade
[AD-A270932] p 1636 N94-20043
A theoretical investigation of unsteady separation phenomena related to dynamic stall
[AD-A271865] p 1636 N94-20465
Processing of climatological data for model initialization
[AD-A271878] p 1865 N94-20487
Prediction and control of vortex-dominated and vortex-wake flows
[NASA-CR-194722] p 1637 N94-21054
Investigation of the physics of the turbulent boundary layer focusing on vortex structures
[AD-A272879] p 1802 N94-21155
Reaction zone models for vortex simulation of turbulent combustion
[AD-A272723] p 1681 N94-21213
On the stability of shear-Alfven vortices
[DE93-040912] p 1996 N94-21752
The effect of correlated and point defects on the vortex lattice melting transition in single crystal YBa2Cu3O(7-delta)
[DE93-040277] p 2033 N94-21997

VORTICITY
Direct simulation of shock-induced mixing layer
[DE93-040498] p 1803 N94-21531

VOYAGER 1 SPACECRAFT
A study of Saturn's E-ring particles using the Voyager 1 plasma wave instrument
[NASA-CR-194694] p 2088 N94-20048

VULNERABILITY
Current directions in the vulnerability/lethality process structure
[AD-A272836] p 1964 N94-21175

W

WAFERS
Metal-glass composite field-emitting arrays
[AD-D015942] p 1673 N94-20064
Process for the homoepitaxial growth of single-crystal silicon carbide films on silicon carbide wafers
[NASA-CASE-LEW-15223-1] p 2017 N94-20381
Attenuation of epsilon(sub eff) of coplanar waveguide transmission lines on silicon substrates p 1733 N94-20504
Analysis of cost: CVD diamond deposition
[AD-A271980] p 2018 N94-20616
Interfacial properties of diamondlike amorphous carbon films on InP: Metal-insulator-semiconductor structures p 1710 N94-20980

WAKES
Persistent wakefields associated with waveguide damping of higher order modes
[DE93-040973] p 1715 N94-19874
Effects of hydrodynamics and thermal radiation in the atmosphere after comet impacts p 1862 N94-20649
An integro-algebraic equation for high frequency wake fields in a tube with smoothly varying radius
[DE93-040940] p 1741 N94-21684
Modelling stalled airfoils
[ISBN-0-315-59525-6] p 1639 N94-22382
Recent ONERA contributions to the development of flight test measurement techniques p 1641 N94-22607

WALKING MACHINES
Simulation of tripod gaits for a hexapod underwater walking machine
[AD-A271719] p 1945 N94-21355
Robotic concepts for operation in barren terrain
[DE93-040539] p 1946 N94-21925

WALL FLOW
Principles and applications of oil film interferometry for measuring wall friction fields in air flows
[ETN-93-95062] p 1798 N94-20147
An analysis of pressure driven cross-flow through a long slot connecting two parallel channels
[DE93-040181] p 1804 N94-21765

WALL PRESSURE
The effect of transverse curvature on the fluctuating wall pressure and structure of boundary layer turbulence
[AD-A271868] p 1800 N94-20466

WALL TEMPERATURE
Chemical reaction fouling model for single-phase heat transfer
[DE93-019556] p 1802 N94-20942
WALSH FUNCTION
Addition of decimal numbers in optical computing architecture by Walsh coded digits p 1773 N94-22122
WARFARE
Massachusetts Institute of Technology Lincoln Laboratory Journal volume 6, number 1, Spring 1993
[AD-A272273] p 1737 N94-20944
WARHEADS
N,N'-bis(4,4,4-trinitro butyryl) hydrazine
[AD-D015897] p 1712 N94-20122
WARNING SYSTEMS
Ground proximity warning system voice warning unit requirements study
[AD-A270541] p 1641 N94-19876
Evaluation of head injury criteria
[NIAR-93-2] p 1890 N94-20190
Army aircraft fire-detection systems operation and reliability
[AD-A271327] p 1641 N94-20912
Windshear detection for aircraft using temperature lapse rate
[CA-PATENT-1,295,736] p 1641 N94-21030
Initial laboratory evaluation of color video cameras, phase 2
[DE93-040201] p 1609 N94-21556
WASTE DISPOSAL
Current status of environmental, health, and safety issues of nickel metal-hydride batteries for electric vehicles
[DE93-017079] p 1748 N94-19902
Space Station trash removal system
[NASA-CASE-MSC-21723-1] p 1657 N94-20367
Automating the control of robotic systems in unstructured environments
[DE93-040753] p 1946 N94-21929
Environmental protection using social costing
[DE94-000492] p 1853 N94-22569
WASTE TREATMENT
Advanced Energy Projects, FY 1993
[DE94-000539] p 1847 N94-21755
Plasma-chemical conversion of hydrogen sulfide into hydrogen and sulfur
[DE93-041167] p 1682 N94-21789
Automating the control of robotic systems in unstructured environments
[DE93-040753] p 1946 N94-21929
WASTE UTILIZATION
First Biomass Conference of the Americas: Energy, Environment, Agriculture, and Industry, volume 2
[DE94-000435] p 1847 N94-21562
Current situation of development of petroleum substituting energies (Canada)
[DE94-707493] p 1849 N94-22014
WATER
Encounters of H and D atoms with O2 in water: Relative diffusion and reaction rates
[DE93-018587] p 1970 N94-19956
Thermal behavior of natural zeolites
[DE93-040091] p 1699 N94-19975
Monopropellant aqueous hydroxyl ammonium nitrate/fuel
[AD-D015922] p 1712 N94-20061
Atmospheric moisture collection device
[AD-D015935] p 1865 N94-20332
Hydrological consequences of ponded water on Mars p 2089 N94-20383
The fate of water deposited in the low-lying northern plains p 2089 N94-20387
Application of the reactive flux formalism to study water hydrogen bond dynamics
[AD-A271824] p 1680 N94-20560
Derivation of the midinfrared (5.0-25.0 micron) optical constants of hydrous carbonate and sulfate p 2108 N94-20723
High D/H ratios of water in magmatic amphiboles in Chassigny: Possible constraints on the isotopic composition of magmatic water on Mars p 2134 N94-20862
Evaluation of pre-extraction analytical holding times for nitroaromatic and nitramine explosives in water
[AD-A271547] p 1712 N94-20927
The hydrologic response of Mars to the onset of a colder climate and to the thermal evolution of its early crust p 2143 N94-21666
The early Martian environment: Clues from the cratered highlands and the Precambrian Earth p 2143 N94-21667
Core formation, wet early mantle, and H2O degassing on early Mars p 2145 N94-21674
Wet inside and out? Constraints on water in the Martian mantle and on outgassed water, based on melt inclusions in SNC meteorites p 2145 N94-21678
Modeling of outgassing and matrix decomposition in carbon-phenolic composites
[NASA-CR-194741] p 1676 N94-21743
Plasma-chemical conversion of hydrogen sulfide into hydrogen and sulfur
[DE93-041167] p 1682 N94-21789
Aircraft cabin water spray disbenefits study
[NASA-CR-194750] p 1642 N94-21818
Water-enhanced solvation of organics
[DE93-040297] p 1683 N94-21947
WATER COLOR
Optical climatology of the Northeast Pacific Ocean
[AD-A271671] p 1666 N94-20559
WATER DEPTH
Distribution of turbidity in Australian tropical waters
[AD-A271059] p 1881 N94-19905
A marine sedimentary model for the evolution of the northern plains p 2091 N94-20395
Discharge rates in Ma'adim Vallis, Mars p 2128 N94-20830
Green Sheet project: Dye sheet evolution
[AD-A272019] p 1883 N94-21443
WATER EROSION
Early Mars was wet but not warm: Erosion, fluvial features, liquid water habitats, and life below freezing p 2145 N94-21677
WATER FLOW
Ancient Martian valley genesis and paleoclimatic inference: The present as a key to the past p 2142 N94-21661
WATER IMMERSION
Investigation of cracking and erratic behavior of the uranium-titanium alloy
[DE93-018591] p 1686 N94-19957
WATER INJECTION
Thrust expansion engine
[AD-D015896] p 1669 N94-20121
Thrust augmentation options for the Beta 2 two-stage-to-orbit vehicle
[NASA-TM-106448] p 1648 N94-21563
Options for thrust augmentation for the Beta 2 two-stage-to-orbit launch vehicle
[NASA-TM-106418] p 1649 N94-21759
Performance calculations and research direction for a water enhanced regenerative gas turbine cycle
[DE93-019866] p 1826 N94-21983
WATER POLLUTION
Manual of DRANC (release 1.1): A computer program for the Dutch risk assessment of new chemical substances
[PB93-194827] p 1851 N94-19998
WATER QUALITY
Chromaticity analysis of LANDSAT multispectral scanner and thematic mapper imagery of Chilko Lake, British Columbia, using a theoretical optical water quality model
[ISBN-0-315-63832-X] p 1843 N94-22422
WATER RESOURCES
Integration opportunities for computer models, methods, and GIS used in Corps planning studies
[AD-A271714] p 2044 N94-21354
WATER TEMPERATURE
Early Mars was wet but not warm: Erosion, fluvial features, liquid water habitats, and life below freezing p 2145 N94-21677
WATER TREATMENT
Manual of DRANC (release 1.1): A computer program for the Dutch risk assessment of new chemical substances
[PB93-194827] p 1851 N94-19998
Plasma-chemical conversion of hydrogen sulfide into hydrogen and sulfur
[DE93-041167] p 1682 N94-21789
WATER VAPOR
Thermal behavior of natural zeolites
[DE93-040091] p 1699 N94-19975
Predicting lightning events in the KSC area: A feasibility study using single station data
[AD-A271440] p 1864 N94-20088
On demand, non-halon, fire extinguishing systems
[AD-D015957] p 1714 N94-20355
Diffusive redistribution of water vapor in the solar nebula revisited p 2113 N94-20751
Discovery Venera surface: Atmosphere geochemistry experiments mission concept p 2123 N94-20806
Analysis of the GOES 6.7 micrometer channel observations during FIRE 2 p 1875 N94-22316
Analysis of the tropospheric water distribution during FIRE 2 p 1876 N94-22324
A comparison of small and larger mesoscale latent heat and radiative fluxes: December 6 case study p 1879 N94-22335
Studies in remotely sensed geophysical parameter retrieval and analysis
[NASA-CR-194768] p 1842 N94-22374
Temperature/pressure and water vapor sounding with microwave spectroscopy p 1812 N94-22436
WATER WAVES
SIMBAT theoretical manual
[AD-A271063] p 1882 N94-19979
ERS-1 and Seasat scatterometer measurements of ocean winds: Model functions and the directional distribution of short waves p 1720 N94-20412
Analysis of Ku-band cross section at low incidence angles p 1720 N94-20414
Rough surface scattering from moving ocean surfaces as an indicator of scattering mechanisms p 1726 N94-20439
Ocean wave height transformation model using surface roller theory
[AD-A272610] p 1883 N94-21423
WAVE ATTENUATION
Relationship of attenuation in a vegetation canopy to physical parameters of the canopy p 1729 N94-20450
WAVE DIFFRACTION
Nonlinear acoustics: Periodic waveguide, finite-amplitude propagation in a medium having a distribution of relaxation processes, and production of an isolated negative pulse in water
[AD-A270530] p 1967 N94-19694
An extended UTD analysis for the scattering and diffraction from cubic polynomial strips
[NASA-CR-194581] p 1716 N94-20139
RCS Analysis of Plate Geometries, parts 1 and 2
[NASA-CR-194173] p 1717 N94-20269
High-frequency techniques for RCS prediction of plate geometries p 1717 N94-20270
A physical optics/equivalent currents model for the RCS of trihedral corner reflectors p 1717 N94-20271
WAVE DISPERSION
Time-resolved shock compression of porous rutile: Wave dispersion in porous solids
[DE93-018848] p 1829 N94-19927
Birefringence control and dispersion characteristics of silicon oxynitride optical waveguides, appendix 6 p 1989 N94-21600
First principles calculations for analysis martensitic transformations
[DE94-000666] p 1695 N94-21964
Simulating the Euclidean time Schroedinger equations using an INTEL iPSC/860 hypercube: Application to the t-J model of high-T(sub c) superconductivity
[DE94-000489] p 2035 N94-22385
ASpect: A new spectrum and line analysis package for IRAF p 1926 N94-22485
WAVE EQUATIONS
Variable-permittivity linear inverse problem for the H(sub z)-polarized case p 1719 N94-20408
Interface reflection of spherical acoustic waves in the first- and second-order rational parabolic approximations and their artifacts
[PB93-215424] p 1969 N94-22261
WAVE FRONTS
Feedback controlled optics with wavefront compensation
[NASA-CASE-NPO-18194-1-CU] p 1985 N94-20305
WAVE FUNCTIONS
An introduction to GUGA in the COLUMBUS Program System
[DE93-018^94] p 1902 N94-19928
Qualitative and quantitative aspects of the QCD theory of elastic form factors
[DE93-040864] p 2038 N94-21513
Photoabsorption and Compton scattering in ionization of helium at high photon energies
[DE94-000380] p 1974 N94-21658
Single and double ionization of helium by high-energy photon impact
[DE94-000381] p 1975 N94-21785
Simulating the Euclidean time Schroedinger equations using an INTEL iPSC/860 hypercube: Application to the t-J model of high-T(sub c) superconductivity
[DE94-000489] p 2035 N94-22385
WAVE INTERACTION
Asteroid collisions: Target size effects and resultant velocity distributions p 2083 N94-20729
WAVE PROPAGATION
Spatial patterns in semiconductor lasers
[DE93-040056] p 1814 N94-19865
Nonlinear acoustics: Periodic waveguide, finite-amplitude propagation in a medium having a distribution of relaxation processes, and production of an isolated negative pulse in water
[AD-A270530] p 1967 N94-19694
Proceedings of the 15th Annual Seismic Research Symposium
[AD-A271458] p 1855 N94-20090
High-resolution numerical methods for compressible multi-phase flow in hierarchical porous media
[DE94-000740] p 1799 N94-20351

The effect of dissipative inhomogeneous medium on the statistics of the wave intensity p 1726 N94-20440
Laser propagation in underdense plasmas: Scaling arguments
[DE93-040439] p 1816 N94-20480
Mathematical model and analysis of the Tactical Unmanned Ground Vehicle (TUGV) using computer simulation
[AD-A272258] p 1824 N94-20576
Asteroid collisions: Target size effects and resultant velocity distributions p 2083 N94-20729
Analysis of the effects of eurasian crustal and upper mantel structure on regional phases using broadband seismic data
[AD-A272446] p 1858 N94-21206
Dynamic response of multiphase porous media
[AD-A272915] p 1831 N94-21219
The Board on Earth sciences and resources
[DE94-000745] p 1859 N94-22018
Time-laplace-transform-domain analysis of wave propagation in planar waveguides
[PB93-215226] p 1960 N94-22096
Lidar and radar derived cirrus microphysical properties for the 26 November 1991 case study
p 1873 N94-22305
Observations of multi-layered clouds using K-band radar p 1874 N94-22311
Radio wave propagation studies along an Earth-space satellite link
[ISBN-0-315-60627-4] p 1742 N94-22408
Theory and simulation of plasma sheath waves
[DE94-001305] p 1999 N94-22567
Theory of leaked auroral kilometric radiation
p 2003 N94-22649
Enhanced absorption of p-modes on sunspot and plage regions p 2006 N94-22671

WAVE REFLECTION
A physical optics/equivalent currents model for the RCS of trihedral corner reflectors p 1717 N94-20271

WAVE SCATTERING
RCS Analysis of Plate Geometries, parts 1 and 2
[NASA-CR-194173] p 1717 N94-20269
A physical optics/equivalent currents model for the RCS of trihedral corner reflectors p 1717 N94-20271
FD-TD modeling of 2-D dielectric waveguides for propagation and scattering of femtosecond optical solitons p 1719 N94-20406
Hadronic molecules and scattering amplitudes from the nonrelativistic quark model
[DE94-000377] p 1974 N94-21657
Continuous-time discretized-space approach to modeling short-pulse propagation and scattering
[PB93-215259] p 1742 N94-22347

WAVEFORMS
A study of Saturn's E-ring particles using the Voyager 1 plasma wave instrument
[NASA-CR-194694] p 2088 N94-20048
Optimal convolution SOR acceleration of waveform relaxation with application to semiconductor device simulation p 1922 N94-21475
Optimization and control of a small angle ion source using an adaptive neural network controller
[DE93-040063] p 1946 N94-21845
A framework of connectionist network toward speech waveform coding p 1746 N94-22211

WAVEGUIDE ANTENNAS
Recent activities in printed Antennas at LeRC
p 1722 N94-20422
Slot-coupled patch antenna with coplanar waveguide feed p 1734 N94-20506

WAVEGUIDE FILTERS
A simplified method for S-parameter calculations of metal septum waveguide filters p 1782 N94-22180

WAVEGUIDES
Persistent wakefields associated with waveguide damping of higher order modes
[DE93-040973] p 1715 N94-19874
Process to fabricate thick coplanar microwave electrode structures
[AD-D015913] p 1748 N94-19892
Nonlinear acoustics: Periodic waveguide, finite-amplitude propagation in a medium having a distribution of relaxation processes, and production of an isolated negative pulse in water
[AD-A270530] p 1967 N94-19894
FD-TD modeling of 2-D dielectric waveguides for propagation and scattering of femtosecond optical solitons p 1719 N94-20406
A comprehensive theoretical and experimental study of coplanar waveguide shunt stubs p 1733 N94-20500
A comparative study between shielded and open coplanar waveguide discontinuities
p 1733 N94-20501
A theoretical and experimental study of coplanar waveguide shunt stubs p 1733 N94-20502
Coplanar waveguide radial line stub
p 1733 N94-20503
Attenuation of epsilon(sub eff) of coplanar waveguide transmission lines on silicon substrates
p 1733 N94-20504
Slot-coupled patch antenna with coplanar waveguide feed p 1734 N94-20506
Hybrid finite element/waveguide mode analysis of passive RF devices
[AD-A273074] p 1740 N94-21518
Polyimide-based electrooptic materials
[DE93-019416] p 1706 N94-21526
Simulation of traveling-wave output structures for high power RF tubes
[DE93-041005] p 1763 N94-21685
On the relationship between spectral domain approach and method of lines p 1794 N94-22254

WAVELENGTHS
Surface-induced brightness temperature variations and their effects on detecting thin cirrus clouds using IR emission channels in the 8-12 micrometer region
p 1880 N94-22341

WAVELET ANALYSIS
Convergence of the hermite wavelet expansion
[AD-A271435] p 1854 N94-19841
On the spline-based wavelet differentiation matrix
[NASA-CR-191557] p 1950 N94-20087
Rough surface scattering from moving ocean surfaces as an indicator of scattering mechanisms
p 1726 N94-20439
Signal processing in the linear statistical model
[AD-A272114] p 1736 N94-20570
An inverse DWT for nonorthogonal wavelets
[AD-A272064] p 1737 N94-20582
Use of switched capacitor filters to implement the discrete wavelet transform p 1755 N94-21097
Data compression by using wavelet transforms and vector quantization
[AD-A272763] p 1738 N94-21182
A multiresolution wavelet representation in two or more dimensions p 1925 N94-22456

WAVERIDERS
Optimization and performance analysis of a supersonic conical-flow waverider for a deck-launched intercept mission
[AD-A272498] p 1648 N94-21433

WEAK INTERACTIONS (FIELD THEORY)
Summary of the Hadronic Weak Interaction session
[DE94-000592] p 1975 N94-21775

WEAPON SYSTEMS
Tactical laser weapons and other directed-energy weapons
[AD-A267961] p 1816 N94-20484

WEAPONS
Chemistry and materials science
[DE94-001449] p 2152 N94-21858

WEAR
Microscopic modeling of tribological and interfacial phenomena
[AD-A271864] p 1823 N94-20464
Development of fundamental understanding of friction and wear mechanisms by atomic-scale tribological studies of ceramic materials and multilayered thin films
[AD-A271485] p 1703 N94-20548
Lubricated wear of steel-ceramic and ceramic-ceramic systems
[PB93-202356] p 1825 N94-21450
Vapor-delivered lubrication of steel-steel and steel-ceramic systems
[PB93-202364] p 1825 N94-21451
Detailed study of oxidation/wear mechanism in lox turbopump bearings
[NASA-TM-108434] p 1825 N94-21580
Brush seal bristle flexure and hard-rub characteristics
p 1654 N94-21791
Integrity testing of brush seal in a T-700 engine
p 1654 N94-21792
Dynamics of face seals for high speed turbomachinery
p 1655 N94-21796

WEAR INHIBITORS
The use of screening tests in spacecraft lubricant evaluation
[AD-A272943] p 1705 N94-21225

WEAR TESTS
Lubricated wear of steel-ceramic and ceramic-ceramic systems
[PB93-202356] p 1825 N94-21450

WEATHER
An analysis of cloud-cover reporting in the 1977 surface observation database
[AD-A271102] p 1864 N94-19852
Analysis of a sandstorm weather process-translation
[AD-A272959] p 1867 N94-21250
Parallel runway requirement analysis study. Volume 1: The analysis
[NASA-CR-191549-VOL-1] p 1644 N94-22277

WEATHER FORECASTING
Clouds: Their prediction and simulation
[AD-A271161] p 1864 N94-19900
Offshore decision support system: ERS-1 pilot project WAVEWATCH
[BCRS-92-09] p 1865 N94-20532
Weather tutor 1: Stability basics
[AD-A270758] p 1866 N94-20565
Drought early warning system for crop production
p 1840 N94-20966
Simulated real-time intercomparison of hydrological models
[WMO-779] p 1867 N94-21070
Incorporation and comparative evaluation of a non-convective cloud parameterization scheme in the Naval Research Laboratory west coast mesoscale weather prediction model
[AD-A272417] p 1867 N94-21146
A retrieval error analysis technique for passive infrared atmospheric sounders
[AD-A272618] p 1867 N94-21212
Mesoscale simulations of the November 25-26 and December 5-6 cirrus cases using the RAMS model
p 1878 N94-22331

WEATHER STATIONS
Cloud fields derived from satellite and surface data during FIRE cirrus phase 2 p 1872 N94-22302

WEATHERING
Optical effects of space weathering on lunar soils and the role of the finest fraction p 2101 N94-20687
Local topography of Mars and its relationship to surface weathering processes p 2111 N94-20737
The role of CO2 in weathering reactions and the presence of S2 on Venus: Implications for the pyrite stability field p 2122 N94-20799
Weathering features and secondary minerals in Antarctic Shergottites ALHA77005 and LEW88516
p 2086 N94-20869
K, U, and Th behavior in Martian environmental conditions p 2141 N94-20908
Oxidation of dissolved iron under warmer, wetter conditions on Mars: Transitions to present-day arid environments p 2143 N94-21663
An attempt to comprehend Martian weathering conditions through the analysis of terrestrial palagonite samples p 2143 N94-21668

WEIGHT ANALYSIS
Nonlinear aerodynamics and the design of wing tips
[NASA-CR-194732] p 1638 N94-21833

WEIGHT REDUCTION
Nonlinear aerodynamics and the design of wing tips
[NASA-CR-194732] p 1638 N94-21833

WEIGHTING FUNCTIONS
A weighted least-squares lump correction algorithm for transmission-corrected gamma ray nondestructive assay
[DE93-018474] p 1904 N94-20049
Smoothed-particle hydrodynamics and nonequilibrium molecular dynamics
[DE94-001059] p 1977 N94-22400

WEIGHTLESSNESS
Apparatus and method for measuring subject work rate on an exercise device
[NASA-CASE-MSC-21752-1] p 1895 N94-20194

WELD TESTS
Thermocapillary and arc phenomena in stainless steel welds
[DE94-000518] p 1821 N94-19859
Microscopic evaluation of low-temperature embrittlement in type 308 stainless steel welds
[DE93-040266] p 1690 N94-20282

WELDED JOINTS
Thermocapillary and arc phenomena in stainless steel welds
[DE94-000518] p 1821 N94-19859
Microscopic evaluation of low-temperature embrittlement in type 308 stainless steel welds
[DE93-040266] p 1690 N94-20282
Shape memory metals
[DE94-001373] p 1695 N94-21976
Evaluation of non-chromium-containing deoxidizers for aluminum
[DE94-001377] p 1695 N94-21978

WENTZEL-KRAMER-BRILLOUIN METHOD
Spiral Alfven instability in accretion disks
p 2010 N94-22698

WESTERN HEMISPHERE
Research program on the Manson impact structure, Iowa p 1862 N94-20766

WETTING
Experimental study of void formation during aluminum solidification in reduced gravity
[NASA-TM-106190] p 1692 N94-21604

WHISKER COMPOSITES
Deformation of an alumina-zirconia-silicon carbide-whisker reinforced composite
[DE93-040244] p 1676 N94-21559

Fabrication of whisker-toughened alumina tubes
[DE94-001012] p 1677 N94-22022

WHISPERING GALLERY MODES
An extended UTD analysis for the scattering and diffraction from cubic polynomial strips
[NASA-CR-194581] p 1716 N94-20139
Modelling short bent, graded index dielectric slab waveguides
[PB93-215283] p 1742 N94-22349

WHITE NOISE
Comparison of higher order moment spectrum estimation techniques
[AD-A272967] p 1967 N94-21260
A comparative robustness evaluation of feedforward neurofilters
[NASA-TM-106440] p 1650 N94-21742

WIDE ANGLE LENSES
Wide-angle imaging system with fiberoptic components providing angle-dependent virtual material stops
[NASA-CASE-NPO-18146-1-CU] p 1986 N94-20345
Internal camera calibration using rotation and geometric shapes
[AD-A272718] p 1808 N94-21167

WIDMANSTATTEN STRUCTURE
Tambo Quemado: Extraordinary concentrations of REE and refractory trace elements caused by artificial heating p 1684 N94-20667

WIENER HOPF EQUATIONS
A two-dimensional kinetic model of the scrape-off layer
[DE94-001235] p 1999 N94-22562

WIGGLER MAGNETS
Measurement and correction of magnetic fields in pulsed slotted-tube microwigglers
[DE93-040100] p 1815 N94-20272
Demonstration of ultraviolet lasing with a low energy electron beam
[DE93-040192] p 1818 N94-21554
Generation of harmonic radiation using the multi-cavity free-electron laser
[DE94-001261] p 1820 N94-21975

WIND (METEOROLOGY)
Dynamics Explorer 2: Continued FPI and NACS instrument data analysis and associated scientific activity at the University of Michigan
[NASA-CR-194689] p 1657 N94-20173
ERS-1 and Seasat scatterometer measurements of ocean winds: Model functions and the directional distribution of short waves p 1720 N94-20412
Offshore decision support system: ERS-1 pilot project WAVEWATCH
[BCRS-92-09] p 1865 N94-20532
Imaging radar studies of atmospheric winds and waves
[AD-A271672] p 1866 N94-20918

WIND DIRECTION
Predicting lightning events in the KSC area: A feasibility study using single station data
[AD-A271440] p 1864 N94-20088
Analysis of wind observation from towers in the period 1977-1991
[KNMI-TR-148] p 1865 N94-20239
Comparison of remote sensing measurements with a two-scale polarimetric emission and scattering model for sea surfaces p 1721 N94-20415
The sea breeze convergence zone and its relationship to fair weather electricity in east central Florida
[AD-A268511] p 1868 N94-21502

WIND EFFECTS
Wind chill: The temperature feeling caused by the wind velocity
[KNMI-TR-103A] p 1890 N94-20238

WIND EROSION
Geomorphic evidence for an eolian contribution to the formation of the Martian northern plains p 2092 N94-20402

WIND MEASUREMENT
Rotorwash wind sensor evaluation
[AD-A268987] p 1807 N94-20203
Integrated display of multi-sensor geophysical and electromagnetic flight data p 1721 N94-20418
Description and availability of airborne Doppler radar data p 1722 N94-20419
Low-altitude cross-wind velocity measurements using pulsed visible fringe-type laser anemometry
[ISL-CO-216/92] p 1866 N94-20557
Presenting the Rain-Sea Interaction Facility
[NASA-RP-1322] p 1884 N94-21628
Vertical velocity in cirrus case obtained from wind profiler p 1878 N94-22330

WIND PROFILES
Empirical wind model for the middle and lower atmosphere. Part 2: Local time variations
[NASA-TM-104592] p 1870 N94-21862
Vertical velocity in cirrus case obtained from wind profiler p 1878 N94-22330

WIND SHEAR
Coherent lidar design and performance verification
[NASA-CR-193813] p 1816 N94-20341
Integrated display of multi-sensor geophysical and electromagnetic flight data p 1721 N94-20418
Description and availability of airborne Doppler radar data p 1722 N94-20419
Windshear detection for aircraft using temperature lapse rate
[CA-PATENT-1,295,736] p 1641 N94-21030
Optimal flight guidance for aircraft in windshear
[CA-PATENT-1,307,573] p 1650 N94-21050

WIND TUNNEL MODELS
Development and operation of the F/A-18 model control surface actuators
[AD-A271330] p 1645 N94-19914
Improved ceramic slip casting technique --- application to aircraft model fabrication
[NASA-CASE-LAR-14471-1] p 1702 N94-20377

WIND TUNNEL TESTS
Development and operation of the F/A-18 model control surface actuators
[AD-A271330] p 1645 N94-19914
Description and assessment of a new Optical Pressure Measurement System (OPMS) demonstrated in the high speed wind tunnel in Goettingen (Germany)
[DLR-FB-92-24] p 1651 N94-21280
Measurement and prediction of the flow through an annular turbine cascade
[AD-A272530] p 1803 N94-21417
A study of the compressible flow through a diffusing S-duct
[NASA-TM-106411] p 1638 N94-21591
Near wake measurements on a rotor model with Mie-vanes in the Delft open jet tunnel
[PB93-215382] p 1638 N94-22260
Testing of a multisensor hot film technique in wind tunnel and free flight p 1639 N94-22599

WIND TURBINES
Wind energy: Program overview, FY 1992
[DE93-000056] p 1845 N94-19921
Derivation of a model of the exciter of a brushless synchronous machine
[EUT-92-E-258] p 1761 N94-21538
The FY1992 survey on multi-purpose dam and energy utilization system by the wind power generation eration
[DE94-707408] p 1848 N94-22012
Near wake measurements on a rotor model with Mie-vanes in the Delft open jet tunnel
[PB93-215382] p 1638 N94-22260

WIND VANES
Rotorwash wind sensor evaluation
[AD-A268987] p 1807 N94-20203

WIND VELOCITY
Rotorwash wind sensor evaluation
[AD-A268987] p 1807 N94-20203
Wind chill: The temperature feeling caused by the wind velocity
[KNMI-TR-103A] p 1890 N94-20238
Analysis of wind observation from towers in the period 1977-1991
[KNMI-TR-148] p 1865 N94-20239
ERS-1 and Seasat scatterometer measurements of ocean winds: Model functions and the directional distribution of short waves p 1720 N94-20412
Ku-band ocean radar backscatter observations during SWADE p 1720 N94-20413
Comparison of remote sensing measurements with a two-scale polarimetric emission and scattering model for sea surfaces p 1721 N94-20415
Imaging radar studies of atmospheric winds and waves
[AD-A271672] p 1866 N94-20918
Airborne surface backscattering strength measurements in the western Atlantic Ocean
[AD-A271737] p 1883 N94-21358
Vertical velocity in cirrus case obtained from wind profiler p 1878 N94-22330

WIND VELOCITY MEASUREMENT
Imaging radar studies of atmospheric winds and waves
[AD-A271672] p 1866 N94-20918

WINDING
Counter-balanced, multiple cable construction crane
[NASA-CASE-LAR-14565-1-CU] p 1822 N94-20369
Theoretical and experimental study of the winding of a thin plastic film: The role of aerodynamic effects
[ECL-93-04] p 1703 N94-20599

WINDOWS (COMPUTER PROGRAMS)
Design and implementation of a prototype PC based graphical and interactive MILSATCOM requirements database system
[AD-A272960] p 1658 N94-21251
Enhanced networks operations using the X Window System p 1932 N94-21329
Conversion and maintenance of Co-oP for Windows
[AD-A272513] p 1914 N94-21414
VETA x ray data acquisition and control system p 2047 N94-22455
Tools for the IDL widget set within the X-windows environment p 1927 N94-22538

WINDPOWER UTILIZATION
Wind energy: Program overview, FY 1992
[DE93-000056] p 1845 N94-19921
The FY1992 survey on multi-purpose dam and energy utilization system by the wind power generation eration
[DE94-707408] p 1848 N94-22012
Current situation of development of petroleum substituting energies (Canada)
[DE94-707493] p 1849 N94-22014

WINDPOWERED PUMPS
The FY1992 survey on multi-purpose dam and energy utilization system by the wind power generation eration
[DE94-707408] p 1848 N94-22012

WING TIPS
Nonlinear aerodynamics and the design of wing tips
[NASA-CR-194732] p 1638 N94-21833

WINGS
Experimental study on interference aerodynamics of close-coupled canard configuration
[AD-A267760] p 1636 N94-19963
Nonlinear aerodynamics and the design of wing tips
[NASA-CR-194732] p 1638 N94-21833
Dynamic mesh adaption for triangular and tetrahedral grids p 1920 N94-22363

WINTER
C-band radar backscatter of sea ice in the Weddell Sea, Antarctica during the austral winter of 1992 p 1725 N94-20435

WIRE
Superconductivity Technology Program for Electric Power Systems: Proceedings
[DE93-040074] p 2011 N94-19825
Automated HMC assembly
[DE93-040641] p 1749 N94-20005
Flexible heating head for induction heating
[NASA-CASE-LAR-14418-15-B] p 1718 N94-20368
Wire assembly for electrically conductive circuits
[AD-D015966] p 1761 N94-21275

WIRELESS COMMUNICATION
Digital wireless control system
[DE93-040211] p 1714 N94-19946

WORDS (LANGUAGE)
A computational theory of lexical relatedness
[TR-421] p 1904 N94-20067
Connectionism and Natural Language Processing
[MEMO-INF-92-64] p 1940 N94-20242
Representation of spoken words in a self-organizing neural net p 1940 N94-20243
An exploration of clause boundary effects in SRN representations p 1937 N94-20253
On the topological size of p-m-complete degrees
[TR-459] p 1965 N94-21286
Application of a back-propagation neural network to isolated-word speech recognition
[AD-A272495] p 1945 N94-21430
Procedural dynamic semantics, verb-phrase ellipsis, and presupposition
[CWI-CS-R9311] p 1914 N94-21495
Recognizing hesitation phenomena in continuous, spontaneous speech p 1746 N94-22210

WORK-REST CYCLE
Physiological efficacy of a lightweight ambient air cooling unit for various applications
[AD-A272952] p 1896 N94-21247

WORKING FLUIDS
EHD enhancement of pool and in-tube boiling of alternate refrigerants
[DE94-000787] p 1798 N94-20101
System and method for cancelling expansion waves in a wave rotor
[NASA-CASE-LEW-15218-1] p 1801 N94-20588

WORKLOADS (PSYCHOPHYSIOLOGY)
Cognition and the brain: A continuation of the university research initiative at New York University
[AD-A271872] p 1894 N94-20467
Reducing the cognitive workload: Trouble managing power systems
[NASA-TM-106413] p 1714 N94-21564

WORKSTATIONS
Multiple-fold clustered processor mesh array p 1757 N94-21113
Evaluation of DEC's GIGAswitch for distributed parallel computing
[DE94-001356] p 1936 N94-21853
Use of open systems for control, analysis, and data acquisition of the DIII-D tokamak
[DE94-001101] p 1998 N94-22069
Seeing the forest for the trees: Networked workstations as a parallel processing computer p 1938 N94-22454

The University of Hawaii Institute for Astronomy CCD camera control system p 1828 N94-22489
An object-oriented approach for supporting both X and terminal interfaces p 1926 N94-22491
CCD data acquisition systems at Lick and Keck Observatories p 2047 N94-22495

WOUND HEALING
Development of bioelastic material for aspects of wound repair
[AD-A267832] p 1673 N94-20208
Non-ionic surfactants in the treatment of third degree burns
[AD-A271582] p 1891 N94-21035
Enhancement of wound healing by biosynthetic growth factor
[AD-A272517] p 1892 N94-21415

WOVEN COMPOSITES
Intercalated hybrid graphite fiber composite
[NASA-CASE-LEW-15241-1] p 1673 N94-20539

WRINKLING
The effects of processing and constituent materials on compressive strength of thick composite laminates
[AD-A271912] p 1673 N94-20490
Theoretical and experimental study of the winding of a thin plastic film: The role of aerodynamic effects
[ECL-93-04] p 1703 N94-20599

WROUGHT ALLOYS
Microstructural stability of wrought, laser and electron beam glazed NARloy-Z alloy at elevated temperatures
[NASA-TM-108431] p 1689 N94-20100

X

X RAY ABSORPTION
Magnetic circular dichroism in x ray absorption and core-level photoemission
[DE93-019381] p 1688 N94-19986
The use of x ray techniques in the in situ study of corrosion
[DE93-019845] p 1690 N94-20301
The x ray microprobe determination of chromium oxidation state in olivine from lunar basalt and kimberlitic diamonds p 1686 N94-20807
Microanalysis of iron oxidation state in iron oxides using X Ray Absorption Near Edge Structure (XANES) p 1686 N94-20808
Observation of x ray absorption magnetic circular dichroism in well-characterized iron-cobalt-platinum multilayers
[DE94-000303] p 1694 N94-21944

X RAY ANALYSIS
Quantitative evaluation of material composition of composites using x ray energy-dispersive NDE technique
[DE93-041157] p 1672 N94-19888
Near atomic resolution microanalysis of interfaces by analytical electron microscopy
[DE93-019437] p 1687 N94-19904
The use of x ray techniques in the in situ study of corrosion
[DE93-019845] p 1690 N94-20301
Spatial organization of polymer chains in a crystallizable diblock polyethylene and polystyrene
[AD-A271662] p 1702 N94-20463
The x ray microprobe determination of chromium oxidation state in olivine from lunar basalt and kimberlitic diamonds p 1686 N94-20807
X ray analysis of alpha mercuric iodide crystal structure and processing effects
[DE93-017620] p 2027 N94-21296
X ray characterization of a three-element condenser system for soft x ray projection lithography
[DE93-019916] p 1990 N94-21985
PROS: An IRAF based system for analysis of x ray data p 1925 N94-22461

X RAY APPARATUS
Characterization and possible repair of defects in soft x ray projection lithography masks
[DE93-019147] p 1750 N94-20231

X RAY ASTRONOMY
X ray, extreme and far ultraviolet optical thin films for space applications
[NASA-CR-194635] p 1984 N94-20128
A deep x ray survey in the Lockman hole and the soft x ray log N - log S
[NASA-CR-194698] p 2054 N94-20174
X ray archeology in the Coma cluster
[NASA-CR-194799] p 2054 N94-20175
Pre-main sequence stars in the Chamaeleon cloud and pre-main sequence stars in the Rho Ophiuchi cloud core
[NASA-CR-194713] p 2080 N94-20337
Studies of an x ray selected sample of cataclysmic variables
[NASA-CR-194773] p 2055 N94-20344
High-energy astrophysics: A theoretical analysis of thermal radiation from neutron stars
[NASA-CR-194808] p 2055 N94-20952
Dust content of a hydrogen rich, low surface brightness galaxy and the luminosity history of 3C273
[NASA-CR-194705] p 2056 N94-21779
ROSAT implementation of a proposed multi-mission x ray data format p 2047 N94-22462
Detection of x ray sources in PROS p 2062 N94-22466
SPIKE: Application for ASTRO-D mission planning p 1926 N94-22486
ROSAT data analysis with EXSAS p 2080 N94-22555
Results from ROSAT p 2000 N94-22630
Time variations of x rays from black hole candidates: Canonical time variations in high and low intensity states p 2009 N94-22690

X RAY ASTROPHYSICS FACILITY
VETA x ray data acquisition and control system p 2047 N94-22455

X RAY BINARIES
Studies of an x ray selected sample of cataclysmic variables
[NASA-CR-194773] p 2055 N94-20344
Accretion disks in bright x ray binaries p 2002 N94-22639
Structure of accretion plasmas of x ray binary pulsars in MHD turbulence p 2007 N94-22679

X RAY DETECTORS
Quantitative evaluation of material composition of composites using x ray energy-dispersive NDE technique
[DE93-041157] p 1672 N94-19888
Energy-resolving x ray detectors with charge amplification due to multiple quasiparticle tunneling
[DE93-019506] p 2031 N94-21869
Detection of x ray sources in PROS p 2062 N94-22466

X RAY DIFFRACTION
Metastable bcc phase formation in the Nb-Cr system
[DE93-018376] p 2012 N94-19926
Synchrotron x ray diffraction analysis of photorefractive crystals and their gratings
[AD-A271176] p 2015 N94-20213
Variable angle spectroscopic ellipsometric characterization of surface damage in chemical-mechanical polished GaAs p 1710 N94-20986
Material optimization for hard x ray Fresnel zone plates
[DE93-019569] p 1990 N94-21837

X RAY FLUORESCENCE
The use of x ray techniques in the in situ study of corrosion
[DE93-019845] p 1690 N94-20301
Wavelength dispersive analysis with the synchrotron x ray fluorescence microprobe p 1685 N94-20717
Combined backscatter Moessbauer spectrometer/x ray fluorescence analyzer (BaMS/XRF) for extraterrestrial surfaces p 1686 N94-20761
Diffraction and holography of photoelectrons and fluorescent x rays
[DE93-019240] p 1808 N94-21441

X RAY IMAGERY
An assessment of COMSCAN, a Compton backscatter imaging camera, for the one-sided non-destructive inspection of aerospace components
[AD-A271331] p 1806 N94-19837
Pre-main sequence stars in the Chamaeleon cloud and pre-main sequence stars in the Rho Ophiuchi cloud core
[NASA-CR-194713] p 2080 N94-20337
High resolution, three dimensional soft x ray imaging
[DE93-018667] p 1989 N94-21630
Material optimization for hard x ray Fresnel zone plates
[DE93-019569] p 1990 N94-21837
Center for X-Ray Optics, 1992
[DE94-000726] p 1990 N94-21868
Some experiments on using backscattered electron and energy dispersive x ray imaging in determination of portland cement clinker phase composition p 1708 N94-21893
The ALEXIS data processing package: An IDL based system p 2047 N94-22453

X RAY INSPECTION
An assessment of COMSCAN, a Compton backscatter imaging camera, for the one-sided non-destructive inspection of aerospace components
[AD-A271331] p 1806 N94-19837

X RAY LASERS
PVDF gauge characterization of hypervelocity-impact-generated debris clouds
[DE93-018831] p 1829 N94-19943
Applications and source development for high-repetition rate x ray lasers
[DE93-019547] p 1815 N94-20259
Photopumped x ray laser research on Saturn
[DE93-019430] p 1816 N94-20298
Generation of intense ultrashort x ray pulses
[DE93-019607] p 1817 N94-21299
Parametric instabilities in picosecond time scales
[DE94-000384] p 1966 N94-21958

X RAY OPTICS
Center for X-Ray Optics, 1992
[DE94-000726] p 1990 N94-21868
X ray characterization of a three-element condenser system for soft x ray projection lithography
[DE93-019916] p 1990 N94-21985

X RAY SCATTERING
An assessment of COMSCAN, a Compton backscatter imaging camera, for the one-sided non-destructive inspection of aerospace components
[AD-A271331] p 1806 N94-19837
Oxidation-reduction induced roughening of platinum (111) surface
[DE93-017408] p 1687 N94-19922
Spatial organization of polymer chains in a crystallizable diblock polyethylene and polystyrene
[AD-A271662] p 1702 N94-20463
The x ray halo of Cen X-3
[NASA-CR-189309] p 2055 N94-21295
Laser Raman and x ray scattering studies of corrosion films on metals
[DE93-040243] p 1692 N94-21558

X RAY SOURCES
The x ray halo of AM Her
[NASA-CR-189310] p 2054 N94-20142
Applications and source development for high-repetition rate x ray lasers
[DE93-019547] p 1815 N94-20259
Pre-main sequence stars in the Chamaeleon cloud and pre-main sequence stars in the Rho Ophiuchi cloud core
[NASA-CR-194713] p 2080 N94-20337
Studies of an x ray selected sample of cataclysmic variables
[NASA-CR-194773] p 2055 N94-20344
The x ray halo of Cen X-3
[NASA-CR-189309] p 2055 N94-21295
Generation of intense ultrashort x ray pulses
[DE93-019607] p 1817 N94-21299
The distribution of dark matter in the A2256 cluster
[NASA-CR-194699] p 2055 N94-21579
Dust content of a hydrogen rich, low surface brightness galaxy and the luminosity history of 3C273
[NASA-CR-194705] p 2056 N94-21779
Parametric instabilities in picosecond time scales
[DE94-000384] p 1966 N94-21958
CCD surface photometry of galaxies p 2058 N94-22445
The ALEXIS data processing package: An IDL based system p 2047 N94-22453
Detection of x ray sources in PROS p 2062 N94-22466
Spatial region filtering in IRAF/PROS p 1927 N94-22524
Results from ROSAT p 2000 N94-22630
Highlights of Yohkoh results p 2001 N94-22632
Thermal properties and radiation processes in astrophysical plasmas p 2002 N94-22640

X RAY SPECTRA
SPIKE: Application for ASTRO-D mission planning p 1926 N94-22486
Pair plasmas in the central engine of active galactic nuclei p 2002 N94-22641
Vertical structure of accretion disks p 2002 N94-22645
Non-equilibrium ionization in an M class solar flare p 2004 N94-22653
Properties of x ray emission from x ray novae p 2007 N94-22676
Structure of accretion plasmas of x ray binary pulsars in MHD turbulence p 2007 N94-22679
Time variations of x rays from black hole candidates: Canonical time variations in high and low intensity states p 2009 N94-22690
Time variation of MHD accretion onto a black hole p 2009 N94-22692
Shock formation in magnetohydrodynamical accretion onto a black hole p 2010 N94-22699

X RAY SPECTROSCOPY
Alumoxanes: Rationalization of black box materials
[AD-A272805] p 1704 N94-21170
Asbestos characterization using scanning electron microscopy/light element x ray spectrometry
[AD-A271611] p 1681 N94-21241
Center for X-Ray Optics, 1992
[DE94-000726] p 1990 N94-21868

X RAY STARS
Time variations of x rays from black hole candidates: Canonical time variations in high and low intensity states p 2009 N94-22690

X RAY TELESCOPES
The ALEXIS data processing package: An IDL based system p 2047 N94-22453
Results from ROSAT p 2000 N94-22630
Highlights of Yohkoh results p 2001 N94-22632
X ray jets in the solar corona: Observations with Yohkoh Soft X Ray Telescope p 2004 N94-22655
Yohkoh Gamma ray Spectral Observations (YGSO) p 2004 N94-22656
Large-scale structure of the solar plasma corona: An analysis of Yohkoh SXT images p 2004 N94-22657

X RAYS
X ray, extreme and far ultraviolet optical thin films for space applications
[NASA-CR-194635] p 1984 N94-20128
National Synchrotron Light Source user's manual: Guide to the VUV and x ray beamlines
[DE93-019564] p 2015 N94-20260
Development and characterization of a time-, position- and energy-resolved x ray diagnostic for PBFA 2 target experiments
[DE93-019429] p 1808 N94-20297
Kinetic theory of runaway air-breakdown
[DE93-040731] p 1750 N94-20325
X ray reflection masks: Manufacturing, characterization and first tests
[BONN-IR-92-31] p 1986 N94-21043
Examination for optimization of synchrotron radiation spectrum for the x ray depth lithography
[BONN-IR-92-32] p 1987 N94-21148
Multifrequency data analysis software on STARLINK p 1925 N94-22443
VETA x ray data acquisition and control system p 2047 N94-22455
PROS: An IRAF based system for analysis of x ray data p 1925 N94-22461
ROSAT implementation of a proposed multi-mission x ray data format p 2047 N94-22462
Detection of x ray sources in PROS p 2062 N94-22466

XENON
A High Resolution Liquid Xenon Imaging Telescope for 0.3-10 MeV Gamma Ray Astrophysics: Construction and Initial Balloon Flights
[NASA-CR-194709] p 2056 N94-22281
The polarization sensitivity of the liquid xenon imaging telescope p 2056 N94-22282

Y

YAG LASERS
Development of a lidar for integration with the Naval Postgraduate School Infrared Search and Target Designation (NPS-IRSTD) system
[AD-A271847] p 1817 N94-20611

YANG-MILLS THEORY
Time evolution of the quark-gluon plasma
[DE94-000804] p 1998 N94-22389

YAW
Multisensor pinhole yawsonde
[AD-A271715] p 1808 N94-20930

YBCO SUPERCONDUCTORS
Particles on surfaces of laser ablated Y1Ba2Cu3O(7-delta) films
[DE93-040269] p 2013 N94-19929
Y-Ba-Cu-O superconducting/GaAs semiconducting hybrid circuits for microwave applications p 1735 N94-20514
Ten GHz YBa2Cu3O(7-delta) superconducting ring resonators on NdGaO3 substrates p 1735 N94-20515
A 10 GHz Y-Ba-Cu-O/GaAs hybrid oscillator proximity coupled to a circular microstrip patch antenna p 1736 N94-20517
The effect of fluctuations on the electrical transport behavior in YBa2Cu3O(7-x) p 1736 N94-20519
Relaxation of hysteresis loop in a single crystal of YBa2Cu4O8
[DE93-019519] p 2029 N94-21649
Specific heat of YBa2Cu3O7
[DE93-040640] p 2031 N94-21926
Spin dynamics and implications for superconductivity: Some problems with the d-wave scenario
[DE94-001183] p 2032 N94-21972
Melt-spin processing of high (Tc) oxide superconductors
[DE94-000696] p 2036 N94-22582

YIELD STRENGTH
Dynamic, multiaxial impact response of confined and unconfined ceramic rods
[DE93-040057] p 1829 N94-19824
Alloying effects on mechanical and metallurgical properties of NiAl
[DE93-040814] p 1694 N94-21948
Miniaturized disk-bend testing, nano-indentation, and the microstructure of ion-irradiated titanium aluminides
[DE93-040600] p 1697 N94-22559

YTTERBIUM
Temperature dependence of 4f PES features and hole occupancy in ytterbium heavy fermions
[DE93-040131] p 1691 N94-20321

YTTERBIUM COMPOUNDS
Neutron-scattering studies of Yb-bearing silicate glasses
[DE93-019768] p 1700 N94-20265
Temperature dependence of 4f PES features and hole occupancy in ytterbium heavy fermions
[DE93-040131] p 1691 N94-20321
Photoemission and the electronic properties of heavy fermions: Limitations of the Kondo model
[DE93-040191] p 1974 N94-21553

YTTRIUM
Column chromatographic separation of Y(3+) from Sr(2+) by polymeric ionizable crown ether resins
[DE94-000935] p 1683 N94-22021

YTTRIUM ALLOYS
Non-Fermi-liquid and multichannel Kondo phenomena in Y(1-x)U(x)Pd3 and related alloys
[DE93-040135] p 2015 N94-20275

YTTRIUM COMPOUNDS
Spectroscopic studies of magnetic transitions in TbPO4
[DE94-001274] p 2035 N94-22565

YTTRIUM OXIDES
Properties of E-beam interactive oxide films for nanometer scale structures
[AD-A272848] p 1675 N94-21191
Disks of YBa2Cu3O7 shocked to 10 GPa pressures
[DE94-000464] p 2031 N94-21931
Synthesis and characterization of charge-substituted garnets YCaLnGa5O12 (Ln = Ce, Pr, Tb)
[DE93-040227] p 2033 N94-21992

Z

ZENITH
Cirrus properties deduced from CO2 lidar observations of zenith-enhanced backscatter from oriented crystals p 1871 N94-22295

ZEOLITES
Thermal behavior of natural zeolites
[DE93-040091] p 1699 N94-19975
Embedded microclusters in zeolites and cluster beam sputtering: Simulation on parallel computers
[DE94-000741] p 1701 N94-20352

ZETA PINCH
Photopumped x ray laser research on Saturn
[DE93-019430] p 1816 N94-20298

ZINC
Photoluminescence spectroscopy of zinc germanium diphosphide (ZnGeP2)
[AD-A270705] p 1678 N94-19953

ZINC CHLORIDES
Zinc and titanium smoke: Chemical composition and physical characteristics
[FOA-C-40277-4.9] p 1680 N94-20552
Improvement of the stability of the process for synthesizing chemically prepared varistor powder
[DE94-000345] p 1763 N94-21654

ZINC OXIDES
Advanced processing technology for high-efficiency thin-film CuInSe2 solar cells
[DE93-010045] p 1847 N94-21614
Research on polycrystalline thin-film submodules based on CuInSe2 materials
[DE93-018223] p 2029 N94-21617

ZINC SELENIDES
Growth of zinc selenide single crystals by physical vapor transport in microgravity
[NASA-CR-194679] p 2017 N94-20346
Hydrogen in compound semiconductors
[DE93-040300] p 2031 N94-21922

ZINC-BROMIDE BATTERIES
Advanced batteries for electric vehicle applications: Nontechnical summary
[DE93-019007] p 1748 N94-19885

ZIRCALOYS (TRADEMARK)
Hydrogen pickup and redistribution in alpha-annealed zircaloy-4
[DE93-018050] p 1689 N94-20182

ZIRCONIUM ALLOYS
Using the rule of mixtures to examine the hardness of Cu/Cu-Zr multilayers
[DE94-001068] p 1697 N94-22402

ZIRCONIUM OXIDES
Guanidine based vehicle/binders for use with oxides, metals, and ceramics
[NASA-CASE-LEW-15314-1] p 1700 N94-20195
Crystal structure and short-range oxygen defects in La- and Nd-modified ZrO2
[DE93-040229] p 2033 N94-21993

ZIRCONIUM TITANATES
Preparation and properties of sol-gel derived PZT thin films for decoupling capacitor applications
[DE93-018853] p 2013 N94-19961

ZONAL FLOW (METEOROLOGY)
Interactions of free modes, tides, and gravity waves in the middle atmosphere
[REPT-84] p 1855 N94-20155
Empirical wind model for the middle and lower atmosphere. Part 2: Local time variations
[NASA-TM-104592] p 1870 N94-21882

PERSONAL AUTHOR INDEX

Typical Personal Author Index Listing

ALEXOPOULOS, JIM S. ..... p 436 N94-12023

PERSONAL AUTHOR | PAGE NUMBER | ACCESSION NUMBER

Listings in this index are arranged alphabetically by personal author. The page number helps you locate the citation in the abstract section. The accession number denotes the number by which the citation is identified.

A

AARNIO, J. ..... p 1988 N94-21595
p 1989 N94-21598
p 1989 N94-21599
p 1989 N94-21600
p 1989 N94-21602
AARNIO, JAAKKO ..... p 1988 N94-21594
p 1988 N94-21596
p 1988 N94-21597
p 1989 N94-21601
p 1989 N94-21603
AARONS, JULES ..... p 1857 N94-21189
AARTMAN, L. J. ..... p 1753 N94-21067
AARTS, HARRY ..... p 1953 N94-21047
ABDULLAEV, G. B. ..... p 2028 N94-21438
ABENS, S. ..... p 1683 N94-21984
ABID, RIDHA ..... p 1804 N94-21875
ABOLHASSAN, FERRI ..... p 1908 N94-21024
ABOWD, GREGORY D. ..... p 1650 N94-19880
ABRAHAM, M. M. ..... p 2035 N94-22565
ABROMAVAGE, M. M. ..... p 1740 N94-21412
ABUL-HAJ, N. A. ..... p 1851 N94-20025
ABUMERI, GALIB H. ..... p 1832 N94-21757
ACETO, S. C. ..... p 1992 N94-20056
p 1999 N94-22568
ACEVES, A. B. ..... p 1983 N94-19862
ACKERMAN, MARK S. ..... p 1926 N94-22507
ACKERMAN, S. A. ..... p 1873 N94-22307
p 1875 N94-22315
p 1875 N94-22316
ACKERMAN, T. ..... p 1876 N94-22320
p 1878 N94-22332
ACKERMAN, T. P. ..... p 1844 N94-22303
ACKERMAN, THOMAS ..... p 1881 N94-22344
ACKERMAN, THOMAS P. ..... p 1872 N94-22301
p 1876 N94-22318
p 1877 N94-22325
p 1878 N94-22329
ACKERMANN, M. ..... p 1748 N94-19844
ACTON, L. ..... p 2004 N94-22655
ADAMS, G. W. ..... p 1866 N94-20918
ADAMS, J. ..... p 1676 N94-21754
ADAMS, JOHN B. ..... p 2110 N94-20730
ADAMS, MARILYN J. ..... p 1894 N94-20610
ADAMS, P. W. ..... p 2012 N94-19848
ADDY, A. L. ..... p 1797 N94-19978
ADEL-HADADI, M. A. ..... p 1685 N94-20753
ADOLPHSEN, C. ..... p 1978 N94-19856
p 1981 N94-21686
ADORF, HANS-MARTIN ..... p 2057 N94-22439
p 2057 N94-22440
p 1925 N94-22441
AGER, J. W., III ..... p 2030 N94-21763
AGGARWAL, ISHWAR D. ..... p 1701 N94-20331
AGOSTINI, P. ..... p 1972 N94-20230
AGRESTI, D. G. ..... p 1686 N94-20761
p 1811 N94-22431
AHEARN, M. F. ..... p 2083 N94-20746
AHERN, F. J. ..... p 1839 N94-20964
AHLHEIM, M. C. ..... p 1825 N94-21297
AHLSTROM, DANIEL J. ..... p 1763 N94-21698
AHLUWALIA, R. ..... p 1847 N94-21774
AHMAD, M. OMAIR ..... p 1744 N94-22102
AHMED, ASHAF ..... p 1758 N94-21115
AHMED, S. ..... p 1750 N94-20257
AHRENS, E. T. ..... p 2030 N94-21768
p 2034 N94-22007
AHRENS, T. J. ..... p 2124 N94-20809
AHRENS, THOMAS J. ..... p 2098 N94-20666
p 2085 N94-20840
AHUJA, R. ..... p 2011 N94-19827
AHUJA, S. ..... p 1917 N94-21923
AIDEL, SALIH ..... p 1785 N94-22195
AIKEN, H. B. ..... p 2046 N94-22407
AKAY, HASAN U. ..... p 1829 N94-19937
AKBAR, SALIM ..... p 1994 N94-21053
AKELLA, J. ..... p 1693 N94-21656
AKERS, STEPHEN A. ..... p 1831 N94-20916
AKHUNDOV, G. A. ..... p 2028 N94-21438
AKICHIN, A. ..... p 1661 N94-21383
AL-ASSADI, WALEED K. ..... p 1757 N94-21108
p 1766 N94-21721
AL-HADDAD, K. ..... p 1790 N94-22229
ALBEE, A. L. ..... p 2085 N94-20837
ALBERT, JACQUES ..... p 1742 N94-22408
ALBRECHT, M. A. ..... p 2046 N94-22442
p 2047 N94-22469
ALBRIGHT, K. A. ..... p 1808 N94-20287
ALCOCK, C. ..... p 2058 N94-22444
ALEMAN, C. ORTIZ ..... p 1862 N94-20668
ALET, IRENEE ..... p 1659 N94-21371
ALEXANDER, C. ..... p 2086 N94-20884
ALEXANDER, D. E. ..... p 2033 N94-21999
ALEXANDER, D. J. ..... p 1690 N94-20282
ALEXANDER, J. IWAN D. ..... p 1797 N94-20037
ALEXANDER, M. L. ..... p 1712 N94-20551
ALEXANDER, W. MERLE ..... p 2084 N94-20817
ALEXANDROV, P. E. ..... p 2082 N94-20647
ALI, M. K. MEHMET ..... p 1773 N94-22120
ALI, M. MEHMET ..... p 1783 N94-22183
p 1746 N94-22205
ALIBERT, C. ..... p 2096 N94-20660
ALIYEVA, M. KH. ..... p 2028 N94-21438
ALKALAJ, LEON ..... p 1756 N94-21101
p 1756 N94-21104
p 1768 N94-21735
ALLAN, P. M. ..... p 1925 N94-22443
ALLARD, L. F. ..... p 1707 N94-21653
ALLEGRE, G. ..... p 1786 N94-22202
ALLEN, C. W. ..... p 1979 N94-20222
ALLEN, CHERYL L. ..... p 1939 N94-20089
ALLEN, DAVID H. ..... p 1834 N94-22611
ALLEN, G. D. ..... p 1984 N94-20179
ALLEN, J. ..... p 1928 N94-19812
ALLEN, M. G. ..... p 1809 N94-21607
ALLENSPACH, P. ..... p 2016 N94-20335
ALLISON, P. ..... p 1997 N94-21989
ALLSMAN, R. ..... p 2058 N94-22444
ALLTON, JUDITH H. ..... p 1812 N94-22433
ALTER, TAO D. ..... p 1904 N94-20041
ALTEROVITZ, S. A. ..... p 1734 N94-20509
p 1734 N94-20510
p 1652 N94-20511
ALTEROVITZ, SAMUEL A. ..... p 1736 N94-20519
p 1732 N94-20498
p 1733 N94-20499
p 1734 N94-20508
p 1709 N94-20972
p 2019 N94-20974
p 1709 N94-20975
p 1709 N94-20976
p 2019 N94-20977
p 1710 N94-20981
p 2020 N94-20982
p 1796 N94-20985
p 2022 N94-20990
p 1710 N94-20991
p 2022 N94-20994
p 2023 N94-21000
p 1796 N94-21001
p 2025 N94-21009
ALUMBAUGH, D. L. ..... p 1859 N94-21928
ALVAREZ, A. ..... p 1744 N94-21100
ALVAREZ, J. ..... p 1844 N94-22303
ALVAREZ, J. M. ..... p 1874 N94-22309
ALVAREZ, JOSEPH M. ..... p 1872 N94-22301
ALVES, MARIA VIRGINIA ..... p 2003 N94-22649
AMAR, FAOUZI ..... p 1719 N94-20409
AMENDT, P. ..... p 1815 N94-20259
AMMERMAN, D. J. ..... p 1829 N94-19940
ANDERSEN, VICTOR A. ..... p 1808 N94-21278
ANDERSIN, HANS ..... p 2046 N94-22059
ANDERSON, CHARLES E., JR. ..... p 1831 N94-21249
ANDERSON, D. F. ..... p 1750 N94-20314
ANDERSON, E. ..... p 1989 N94-21630
ANDERSON, J. ..... p 1825 N94-21637
ANDERSON, M. U. ..... p 1829 N94-19927
p 1688 N94-19944
ANDERSON, R. E. ..... p 1761 N94-21532
ANDERSON, R. J. ..... p 1942 N94-20293
ANDERSON, R. R. ..... p 2083 N94-20721
p 1862 N94-20766
ANDERSON, WILLIAM R. ..... p 1679 N94-20111
ANDERSSON, L. R. ..... p 1974 N94-21658
p 1975 N94-21785
ANDERSSON, PER ..... p 1688 N94-20075
ANDREOU, A. G. ..... p 1755 N94-21098
ANDRES, R. P. ..... p 1975 N94-21766
ANDREWS, A. B. ..... p 1691 N94-20321
p 1974 N94-21553
ANDREWS, J. D. ..... p 1822 N94-20146
ANGELICI, GARY ..... p 1842 N94-21585
p 1842 N94-22345
ANGELICI, GARY L. ..... p 1905 N94-20149
ANGERS, D. ..... p 1645 N94-22219
ANOLL, ROBERT K. ..... p 1642 N94-20051
ANTIPOV, KONSTANTIN A. ..... p 1923 N94-22083
ANTONIAK, Z. I. ..... p 1669 N94-20102
ANTONIK, M. D. ..... p 2028 N94-21458
ANTONIO, JOSEPH C. ..... p 1895 N94-19935
ANUPAMA, G. C. ..... p 2058 N94-22445
APON, A. W. ..... p 1908 N94-20932
APPELQUIST, G. ..... p 2042 N94-20193
APPLEGATE, JAMES H. ..... p 2055 N94-20952
APRILE, ELENA ..... p 2056 N94-22281
p 2056 N94-22282
APT, KRYSZTOF R. ..... p 1909 N94-21026
ARAI, TOMOKO ..... p 2084 N94-20812
ARAVE, K. ..... p 1754 N94-21087
ARAVE, KARI ..... p 1766 N94-21722
ARAVE, L. ..... p 1754 N94-21087
ARCHER, D. H. ..... p 1846 N94-21527
p 1826 N94-21983
ARDELL, A. J. ..... p 1697 N94-22559
ARDEN, J. W. ..... p 2083 N94-20726
ARDOUIN, JEAN-PIERRE ..... p 1791 N94-22236
ARDUINI, ROBERT ..... p 1880 N94-22342
AREZKI, HALET ..... p 1780 N94-22165
ARISKIN, A. A. ..... p 1684 N94-20640
ARKO, A. J. ..... p 1691 N94-20321
p 1974 N94-21553
ARLINO, PAULO R. A. ..... p 1840 N94-20967
ARMSTRONG-CARROLL, EILEEN
p 1674 N94-20574
ARNAL, D. ..... p 1641 N94-22607
ARNOLD, G. THOMAS ..... p 1872 N94-22298
ARNOLD, J. R. ..... p 2082 N94-20658
p 2106 N94-20713
ARNOTT, W. P. ..... p 1871 N94-22294
ARNOTT, W. PATRICK ..... p 1879 N94-22336
p 1881 N94-22343
ARONSSON, M. ..... p 2047 N94-22496
ARPE, K. ..... p 1861 N94-22289
ARRASMITH, S. R. ..... p 2036 N94-22582
ARSENAULT, RICHARD J. ..... p 1674 N94-20550
ARTEMIEV, V. I. ..... p 2082 N94-20647
ARVIDSON, R. E. ..... p 2115 N94-20762
ARYA, R. ..... p 2029 N94-21617
ARYA, VINOD K. ..... p 1834 N94-22614
ASANO, K. G. ..... p 1852 N94-22004
ASCHENBACH, B. ..... p 1926 N94-22508
ASHE, THOMAS L. ..... p 1671 N94-21874
ASSEO, ESTELLE ..... p 2007 N94-22678
ASSINK, R. A. ..... p 1679 N94-20307

ASTON, A. p 1927 N94-22538
ATHERTON, C. S. p 1852 N94-21969
ATKINS, HAROLD L. p 1956 N94-21469
ATKINSON, D. R. p 1666 N94-20864
ATTAR, G. p 1847 N94-21614
ATTAWAY, S. W. p 1915 N94-21539
p 1805 N94-22556
ATTIA, JOHN OKYERE p 1754 N94-21083
AUBERT, J. H. p 1708 N94-21954
AUDETTE, MICHEL p 1789 N94-22226
AUFDERHEIDE, M. B. p 2081 N94-21618
AURAND, J. F. p 1762 N94-21634
AUSTIN, R. H. p 1814 N94-19828
p 1816 N94-20277
AVERY, S. K. p 1870 N94-21862
AXELROD, T. p 2058 N94-22444
AYDEMIR, A. Y. p 1997 N94-21973
AYERS, JACK D. p 1673 N94-20064
AYRES, T. p 2046 N94-22446
AZEVEDO, S. p 1898 N94-19886

B

BABINEAU, DAVID p 1644 N94-22154
BABUSKA, IVO p 1951 N94-20527
BACA, A. p 2016 N94-20296
BACA, A. G. p 1750 N94-20312
BACA, R. G. p 1794 N94-22405
BADALEC, J. p 1997 N94-21816
BADAVI, FOROOZ F. p 1895 N94-20063
BADEN, A. p 1921 N94-22375
BADER, ROBERT M. p 1635 N94-21194
BADER, S. D. p 2031 N94-21930
p 2035 N94-22564
BADHWAR, GAUTAM D. p 1893 N94-21863
BADJUKOV, D. D. p 1862 N94-20641
BAER, FERDINAND p 1837 N94-20205
BAER, H. p 1969 N94-19804
BAETEN, J. C. M. p 1903 N94-19993
BAGCHI, A. p 1944 N94-21140
BAGHERZADEH, NADER p 1764 N94-21700
BAGUHL, M. p 2141 N94-20909
BAHIR, G. p 1735 N94-20512
BAI, G. p 2033 N94-21994
BAI, Y. p 1981 N94-21767
BAILEY, J. p 2046 N94-22447
p 2046 N94-22448
p 2048 N94-22529
BAILEY, J. M. p 1769 N94-21830
BAINES, K. H. p 1854 N94-20698
BAIR, EDWARD J. p 1846 N94-20229
BAJT, S. p 1685 N94-20717
p 1686 N94-20807
p 1686 N94-20808
BAJUK, MARK p 2063 N94-22472
BAKANOVA, HELEN S. p 1923 N94-22083
BAKER, C. P. p 1826 N94-22036
BAKER, G. A., JR. p 1960 N94-21946
BAKER, J. P. p 1707 N94-21856
BAKER, S. L. p 1696 N94-19810
BAKER, V. R. p 2069 N94-20383
p 2142 N94-21660
p 2144 N94-21670
BAKHTIARI, S. p 1677 N94-21940
BALACHANDRAN, U. p 1690 N94-20183
p 2031 N94-21931
BALANIS, CONSTANTINE A. p 1717 N94-20269
p 1717 N94-20270
p 1717 N94-20271
BALASUBRAMANIAN, S. p 1778 N94-22152
BALAT, M. p 1653 N94-21404
p 1665 N94-21405
BALAZS, L. G. p 1965 N94-22536
BALDIS, H. A. p 1966 N94-21958
BALDWIN, D. E. p 1844 N94-19803
p 1762 N94-21620
p 1762 N94-21621
BALDWIN, DAN p 1643 N94-20148
BALL, J. A. p 1960 N94-22099
BALL, LEWIS p 2007 N94-22677
BALLARD, DANA H. p 1894 N94-20520
BALLESTER, P. p 2047 N94-22449
BALMAIN, K. G. p 1663 N94-21394
BALOGH, A. p 2141 N94-20909
BALOUGH, D. p 1635 N94-21490
BALUJA, SHUMEET p 1942 N94-20621
BAMBERGER, J. A. p 1669 N94-20102
BAMBERGER, ROBERTO H. p 1765 N94-21714
BAME, S. J. p 2141 N94-20909
BANDEKAR, RAJENDRA p 1758 N94-21114
BANDELT, H. J. p 1961 N94-22266
BANE, K. L. F. p 1981 N94-21686
BANERJEE, P. K. p 1676 N94-21777
BANGS, A. L. p 1918 N94-21924
BANKMAN, I. p 1949 N94-22451
BANKS, BRUCE A. p 1660 N94-21377
BANKS, J. C. p 1973 N94-20306
BANSAL, B. M. p 2097 N94-20663
BANSAL, NAROTTAM P. p 1703 N94-20529
BARBASHEV, E. A. p 1661 N94-21380
BARBEE, T. W., III p 2016 N94-20318
p 1706 N94-21512
BARBEE, T. W., JR. p 1696 N94-22394
p 1697 N94-22402
BARBER, T. p 1808 N94-20297
BARBOSA, D. D. p 2088 N94-20048
BARCLAY, CATHY p 1932 N94-21332
BARFKNECHT, A. T. p 2031 N94-21869
BARKATT, A. p 1685 N94-20753
BARKER, D. p 1694 N94-21945
BARKER, E. S. p 2092 N94-20637
BARLETTA, B. p 1981 N94-21688
BARLETTA, R. p 1676 N94-21754
BARLETTA, W. A. p 1980 N94-20300
BARLOW, D. B. p 1820 N94-22020
BARLOW, N. G. p 2089 N94-20384
p 1811 N94-22432
BARNES, C. W. p 1991 N94-19883
p 1946 N94-21845
BARNES, J. W. p 1942 N94-20488
BARNES, T. p 1974 N94-21657
p 2035 N94-22385
BARNETT, JON C. p 1765 N94-21710
BARNETT, M. p 1903 N94-19959
p 1936 N94-22032
BARRACLOUGH, B. L. p 1976 N94-21995
BARRETT, P. p 2047 N94-22450
p 1926 N94-22487
p 1927 N94-22513
BARRETT, R. A. p 2087 N94-20907
BARRIOS, J. RENE p 1650 N94-21050
BARRON, ANDREW R. p 1704 N94-21170
BARRON, BILLY J. p 1907 N94-20376
BARROSO, LISIA VAMACOR p 1838 N94-20957
BARSUKOVA, L. D. p 1862 N94-20641
BARTEL, WARREN A. p 1882 N94-19979
BARTELS, D. M. p 1970 N94-19956
BARTH, TIMOTHY J. p 1919 N94-22356
BARTHOLET, BILL p 1759 N94-21126
BARTLETT, R. J. p 1827 N94-22390
BARTON, D. L. p 1916 N94-21633
p 1810 N94-22000
BARTON, J. J. p 1810 N94-21950
BARTON, J. R. L. p 1668 N94-20077
BARTSCH, R. A. p 1683 N94-22021
BASHARA, N. M. p 2019 N94-20974
p 1710 N94-20978
BASILEVSKY, A. T. p 2135 N94-20867
BASRI, RONEN p 1943 N94-20921
BASS, LEN p 1650 N94-19880
BASSIRI, SASSAN p 1723 N94-20425
BASTIAANSEN, HARRIE J. M. p 1742 N94-22349
BASTURK, NACI p 1752 N94-20634
BASU, A. p 2101 N94-20687
BATANI, N. p 1793 N94-22248
BATCHELDER, M. p 2117 N94-20772
BATES, J. M. p 1669 N94-20102
BATES, J. R. p 1806 N94-21480
BATINA, JOHN T. p 1919 N94-22361
BATON, S. p 1966 N94-21958
BAUER, ERNEST p 1858 N94-21207
BAUKMAN, DAVID p 1858 N94-21357
BAUM, BRYAN A. p 1844 N94-22303
p 1874 N94-22312
p 1875 N94-22313
BAUMANN, HEINRICH p 1664 N94-21402
BAUR, H. p 2136 N94-20875
BAUR, U. p 1973 N94-20474
BAXA, E. G. p 1722 N94-20419
BAXI, C. B. p 1992 N94-20003
BAYRAKTAROGULU, B. p 1709 N94-20972
BAZE, MARK p 1759 N94-21126
BAZELL, D. p 1949 N94-22451
BEAGLES, GRANT p 1767 N94-21724
BEASLEY, J. p 1757 N94-21106
BEATTY, DEREK I. p 1898 N94-20085
BEAUDET, ROBERT A. p 2027 N94-21304
BEAULIEU, NORMAN C. p 1788 N94-22218
BEAVEN, S. G. p 1715 N94-19823
BECCUE, S. p 1763 N94-21697
BECK, GORDON H. p 1876 N94-22322
BECKERS, JOS p 1858 N94-21206
BECKMAN, R. J. p 1916 N94-21747
BECKWITH, P. H. p 1789 N94-22222
BEDARD, J. p 1745 N94-22127
BEDSON, JANET B. p 2028 N94-21505
BEECH, MARTIN p 2081 N94-22593
BEGET, J. E. p 2089 N94-20385
p 2089 N94-20386
BEHRINGER, K. p 1996 N94-21802
p 1996 N94-21803
p 1997 N94-21804
BEIROUTI, PATRICK p 1747 N94-22242
BELAK, J. p 1694 N94-21821
p 1977 N94-22396
BELHADJHAMIDA, A. p 1689 N94-20019
BELINFANTE, AXEL p 1914 N94-21454
BELL, J. B. p 1803 N94-21531
p 2143 N94-21668
BELL, JAMES F., III p 2110 N94-20730
BELL, R. L. p 1904 N94-20052
BELLARE, A. p 1702 N94-20463
BELLONI, T. p 2080 N94-22555
BELMABROUK, HAFEDH p 1801 N94-20542
BELTON, M. p 2101 N94-20686
BELTRAN, L. p 1809 N94-21545
BELZILE, JEAN p 1773 N94-22121
p 1775 N94-22132
p 1793 N94-22247
BENACCHIO, L. p 2047 N94-22452
BENAMEUR, KAOUTHAR p 1794 N94-22256
BENBASSAT, G. p 1744 N94-21092
BENDER, BARRY A. p 1699 N94-20017
BENDER, D. A. p 1762 N94-21620
p 1762 N94-21621
BENDER, E. p 1790 N94-22227
BENDER, S. C. p 1818 N94-21554
BENGOUGH, P. A. p 1745 N94-22110
BENGTSSON, J. p 1979 N94-19989
p 1979 N94-20273
p 2016 N94-20323
BENHABIB, B. p 1771 N94-22107
p 1774 N94-22129
p 1774 N94-22130
p 1777 N94-22148
BENJAMIN, R. F. p 1799 N94-20286
BENNANI, ABDELMAJID p 1778 N94-22153
BENNETT, D. p 2058 N94-22444
BENNETT, J. p 2046 N94-22446
BENNETT, THEODORE J., JR. p 1883 N94-21222
BENNING, P. G. p 1974 N94-21553
BENOIT, P. H. p 2086 N94-20901
BENOIT, PAUL H. p 2083 N94-20750
BENSON, S. p 1968 N94-22003
BENYAMIN-SEEYAR, ANADER p 1792 N94-22245
BENZ, WILLY p 2008 N94-22685
BERDING, M. A. p 2012 N94-19835
p 1987 N94-21321
BERENJI, HAMID R. p 1947 N94-22270
BERG, BERND p 2016 N94-20285
BERG, J. M. p 2035 N94-22387
BERGELSON, V. I. p 2082 N94-20647
BERGER, M. J. p 1958 N94-21484
BERGER, MARSHA J. p 1920 N94-22367
BERGSTROM, K. A. p 1743 N94-22557
BERGSTROM, P. M., JR. p 1971 N94-20096
BERGSTROM, R. p 1876 N94-22320
BERK, H. L. p 1991 N94-19872
p 1992 N94-19887
BERKLEY, WILLIAM E. p 1895 N94-19935
BERLIN, ANDREW p 1928 N94-19877
BERMAN, N. S. p 1714 N94-21426
BERMAN, TED p 1744 N94-21339
p 1744 N94-21350
BERNARD, M. p 1808 N94-20297
BERNARD, M. A. p 1980 N94-20295
BERNHART, G. p 1665 N94-21408
BERTHEL, ROBERT O. p 1864 N94-20088
BERTON, B. p 1665 N94-21408
BERTON, E. p 1636 N94-20486
BERTSCH, D. p 1926 N94-22501
BESKIN, VASILY S. p 2002 N94-22643
BETTI, R. p 1819 N94-21839
BETZ, V. p 1747 N94-22252
BEUHLER, A. J. p 1706 N94-21526
BHARGAVA, VIJAY K. p 1747 N94-22223
p 1792 N94-22243
BHASIN, K. B. p 1671 N94-20513
p 1735 N94-20514
p 1735 N94-20515
p 1735 N94-20516
BHASIN, KUL B. p 1736 N94-20517
BHAT, A. K. p 1845 N94-19925
BHAT, B. p 1689 N94-20100
BHATTACHARYA-KODALI, INDRANI p 1681 N94-21216
BHATTACHARYA, P. K. p 2023 N94-21000
p 1796 N94-21001
BHATTACHARYA, PALLAB K. p 1733 N94-20499
BHUSHAM, BHARAT p 1703 N94-20548
BI, ZHI-QIANG p 1747 N94-22253
BI, ZHIQIANG p 1745 N94-22138
BIAGIONI, EDOARDO p 1908 N94-20622
BIANCHINI, RICARDO p 1929 N94-20144
BICKEL, T. C. p 1794 N94-22405
BICKERT, K. F. p 2150 N94-20604
BIDWELL, COLIN S. p 1642 N94-21590
BIELICK, E. p 1807 N94-19990

BIENAYME, O. p 1964 N94-22458
BILL, ROBERT C. p 1654 N94-21792
BILLINGE, S. J. L. p 2029 N94-21555
BILLS, B. G. p 2142 N94-20911
BINDIGANAVALE, SUNIL p 1741 N94-21885
BINDSCHADLER, D. L. p 2113 N94-20755
BIRCH, P. V. p 2083 N94-20746
BIRD, D. p 2019 N94-20941
BIRD, E. L. p 1688 N94-19957
BIRD, THOMAS p 2023 N94-20999
BIRDSALL, C. K. p 1999 N94-22567
p 1999 N94-22595
BIRENHEIDE, RICHARD p 2014 N94-20026
BIRKMIRE, R. p 2029 N94-21617
BIRMAN, KEN p 1912 N94-21300
BIRTCHER, ROBERT C. p 1706 N94-21542
BIRTWISTLE, G. p 1772 N94-22114
BISCHOF, C. p 1951 N94-20221
BISH, D. L. p 1699 N94-19975
BISSONNETTE, D. p 1705 N94-21267
BISWAS, RUPAK p 1920 N94-22363
BLACKBURN, J. K. p 1927 N94-22516
BLACKSTOCK, DAVID T. p 1967 N94-19894
BLAES, BRENT p 1666 N94-21086
BLAIN, M. G. p 1996 N94-21769
p 1769 N94-21918
BLAKE, MATTHEW p 1920 N94-22371
BLANCH, H. W. p 1707 N94-21856
BLANCHARD, AUGUSTE p 1790 N94-22228
BLAND-HAWTHORN, J. p 1748 N94-22526
p 2048 N94-22527
BLANFORD, G. E. p 2084 N94-20628
BLANKEN, HENK p 2043 N94-21071
BLASDELL, R. C. p 1972 N94-20187
BLAZEK, R. J. p 1749 N94-20005
BLELLOCH, GUY E. p 1902 N94-19932
p 1928 N94-19950
BLEVINS, BRUCE ALLYN p 1666 N94-21338
BLEWETT, D. T. p 2101 N94-20682
BLIGHT, DAVID C. p 1782 N94-22182
BLIVEN, LARRY F. p 1884 N94-21628
BLOCH, J. J. p 2047 N94-22453
BLOK, HANS p 1742 N94-22349
BLOSS, DAVID A. p 1946 N94-21550
BLOSSER, MAX L. p 1800 N94-20495
BLOUIN, SCOTT E. p 1831 N94-21219
BLUE, BRIAN p 1670 N94-21809
BLUM, FRANK D. p 1706 N94-21460
BLY, VINCENT T. p 1822 N94-20127
BLYTH, R. I. R. p 1691 N94-20321
p 1974 N94-21553
BOATNER, L. A. p 2035 N94-22565
BOBIN, V. p 1765 N94-21713
BOBINA, N. N. p 2095 N94-20655
p 2096 N94-20656
BOBULA, GEORGE A. p 1654 N94-21792
BOCK, G. p 1975 N94-21775
BOCKELIE, MICHAEL J. p 1918 N94-22351
BOCKER, R. P. p 1739 N94-21240
BOCKO, MARK F. p 2012 N94-19897
BODE, R. p 1759 N94-21129
BODSON, MARC p 1899 N94-21230
BOEHMER, WILLIAM p 1829 N94-19937
BOERCKER, D. B. p 1694 N94-21921
p 2032 N94-21960
BOERSMA, HIELKE FREERK p 1971 N94-20119
BOGARD, D. D. p 2106 N94-20712
p 2115 N94-20763
BOGDANOFF, DAVID W. p 1636 N94-20014
BOGOVALOV, SERGEII VLADIMIROVICH
p 2007 N94-22680
p 2008 N94-22681
BOGUSZ, MICHAEL p 1745 N94-22126
BOHM, C. p 2042 N94-20193
BOIS, G. p 1668 N94-20078
BOISVERT, ERIC p 1778 N94-22153
BOKHAREE, S. A. p 1742 N94-22268
BOLEY, C. D. p 1815 N94-20223
BOLOSKY, WILLIAM JOSEPH p 1931 N94-21272
BOLOTNIKOV, A. p 2056 N94-22282
BOLTON, P. R. p 1815 N94-20259
BOMALASKI, SUSAN H. p 1896 N94-21247
BONETTO, F. p 1802 N94-21261
BONY, SANDRINE p 1860 N94-22287
BOOTHROYD, S. A. p 1789 N94-22222
BOOZIN, A. Y. p 1923 N94-22077
BORDE, J. p 1662 N94-21388
BORDERIES, N. p 2117 N94-20772
BORGES, H. A. p 2032 N94-21987
BORGMAN, LEON E. p 1882 N94-19979
BORING, A. M. p 2011 N94-19827
p 1696 N94-22388
BORISKOVSKI, V. p 1836 N94-22065
BORMET, JOERG p 2014 N94-20018
BORNEMANN, JENS p 1782 N94-22180
BORNHOLDT, S. p 1947 N94-22563
BOROZDIN, V. K. p 2095 N94-20655
p 2096 N94-20656
BORS, DENNIS p 1675 N94-21488
BORSON, EUGENE N. p 1659 N94-21372
BORST, S. C. p 1945 N94-21233
BOSCAGLI, G. p 1744 N94-21091
BOSCH, J. H. A. p 1857 N94-21016
BOSLOUGH, M. B. p 1829 N94-19943
p 1679 N94-20307
BOSSE, H. p 1692 N94-21311
BOST, J. B. p 1961 N94-22377
BOTKIN, D. p 1985 N94-20320
BOTTCHER, C. p 1960 N94-21955
BOTTIGER, JEROLD R. p 1988 N94-21491
BOTTS, MICHAEL p 2042 N94-20268
BOUCHER, LARRY p 1744 N94-21349
BOUQUEREL, FRANCK p 1703 N94-20599
BOWEN, BARRY C. p 1656 N94-21884
BOWERS, C. p 2083 N94-20746
BOWLES, DAVID E. p 1661 N94-21379
BOWLES, KENNETH J. p 1675 N94-21488
BOWLING, P. S. p 1946 N94-21845
BOWMAN, D. p 1977 N94-22572
BOXMA, O. J. p 1943 N94-21032
p 1930 N94-21161
p 1945 N94-21233
p 1946 N94-21577
BOYAN, JUSTIN p 1938 N94-19845
BOYLE, MICHAEL E. p 1984 N94-20059
BRACALENTE, E. M. p 1721 N94-20418
p 1722 N94-20419
BRAKENRIDGE, G. R. p 2142 N94-21661
BRAND, N. p 2045 N94-22276
BRANDSTAETTER, F. p 1684 N94-20642
p 2082 N94-20643
BRANDT, J. p 1936 N94-21853
BRANDVOLD, J. B. p 1666 N94-20864
BRANNON, J. C. p 1685 N94-20695
BRASE, J. p 1989 N94-21630
BRAUER, EDGAR HANS p 1839 N94-20963
BRAUER, G. p 1689 N94-20180
BRECKENRIDGE, WILLIAM G. p 1985 N94-20305
BREEN, J. O. p 1938 N94-22454
BRENNAN, T. M. p 1814 N94-19865
BRENNER, DOUGLAS M. p 1851 N94-20025
BRESLAUER, DANY p 1909 N94-21028
p 1952 N94-21029
BRETT, M. J. p 1778 N94-22151
BRICMONT, J. p 2038 N94-22095
BRIDGEWATER, A. W. p 1745 N94-22143
BRIEL, ULRICH G. p 2054 N94-20175
p 2055 N94-21579
BRILL, THOMAS B. p 1681 N94-21181
BRILLA, J. p 1635 N94-21490
BRIMHALL, J. L. p 1690 N94-20233
BRINKKEMPER, S. p 2045 N94-22276
BRINKMANN, R. P. p 1768 N94-21770
BRISSENDEN, R. J. V. p 2047 N94-22455
BRITT, C. L., JR. p 1721 N94-20418
BRITTON, THOMAS W. p 1738 N94-21201
BRIZZEE, KENNETH R. p 1886 N94-21901
p 1886 N94-21904
p 1887 N94-21906
p 1888 N94-21914
BROADWELL, J. E. p 1682 N94-21452
BROCHARDT, GARY C. p 1908 N94-20929
BROCK, TIMOTHY L. p 1733 N94-20499
BRODSKY, S. J. p 2038 N94-21935
BROMLEY, B. C. p 1925 N94-22456
BROOKES, STEPHEN D. p 1902 N94-19919
BROOKINS, A. H. p 1883 N94-21423
BROOKS, RODNEY A. p 1939 N94-19875
BROPHY, JOHN R. p 1669 N94-20496
BROSNAHAN, JOHN W. p 1866 N94-20918
BROTZMAN, L. E. p 2049 N94-22544
BROW, R. K. p 1683 N94-22031
BROWN, A. P. p 1848 N94-21870
BROWN, ALAN W. p 1912 N94-21205
BROWN, C. M. p 1939 N94-20135
BROWN, C. W. p 1906 N94-20311
BROWN, CHRISTOPHER M. p 1945 N94-21315
BROWN, D. p 1706 N94-21523
BROWN, GAIR D. p 1822 N94-20356
BROWN, GREGORY L. p 1892 N94-21415
BROWN, I. FOSTER p 1838 N94-20957
BROWN, JAMES E. p 2014 N94-19982
BROWN, KIMBERLY R. p 1911 N94-21183
BROWN, L. L. p 2142 N94-21662
BROWN, R. C. p 1682 N94-21243
BROWN, S. E. G. p 1642 N94-22055
BROWN, S. K. p 1946 N94-21845
BROWN, THOMAS L. p 1945 N94-21520
BROWNDECOLSTOUN, F. p 1814 N94-19865
BROWNING, DAVID G. p 1883 N94-20925
BROWNLEE, D. E. p 2085 N94-20837
BRUCKER, J. P. p 1814 N94-19867
BRUEMMER, S. M. p 1690 N94-20233
BRUETSCH, R. I. p 1826 N94-22093
BRULE, MICHEL p 1775 N94-22131
BRUMMEL, CHRISTOPHER L. p 1973 N94-20618
BRUNELLE, CHRISTIAN p 1788 N94-22214
BRUNO, F. p 1989 N94-21600
BRUNS, JUERGEN p 1846 N94-20151
BRUNVAND, ERIK L. p 1757 N94-21109
p 1757 N94-21111
p 1758 N94-21119
BRYANT, CARL p 1894 N94-21237
BRYANT, CAROLYN F. p 1738 N94-21198
p 1739 N94-21218
BRYANT, D. p 1684 N94-21403
BRYANT, PHILLIP G. p 1823 N94-20379
BRYANT, RANDAL E. p 1902 N94-19919
p 1898 N94-20085
BRYMAN, D. A. p 1975 N94-21775
BU-ABBUD, GEORGE H. p 1709 N94-20972
p 2019 N94-20974
p 1709 N94-20975
p 1709 N94-20976
p 2019 N94-20977
p 1710 N94-20978
BUBENHEIM, DAVID L. p 1895 N94-20137
BUCHANAN, R. C. p 1675 N94-21191
BUCHOLTZ, ANTHONY p 1872 N94-22297
BUCK, GREGORY M. p 1702 N94-20377
BUCK, O. p 1697 N94-22571
BUDDEN, NANCY ANN p 2148 N94-21883
BUDGE, K. G. p 1916 N94-21635
BUDINGER, J. M. p 1741 N94-21567
BUECHNER, JOERG p 2001 N94-22636
BUEHLER, MARTIN p 1666 N94-21086
BUFFUM, DANIEL H. p 1649 N94-21586
BUI, T. D. p 1771 N94-22109
BUI, TRONG T. p 1637 N94-20534
BULTERMAN, DICK C. A. p 2044 N94-21494
p 2044 N94-21535
p 2045 N94-21536
BUNCH, T. E. p 1685 N94-20745
BUNEMAN, O. p 2005 N94-22660
p 2007 N94-22674
BUNKER, STEPHEN N. p 2028 N94-21517
BUNTE, STEVEN W. p 2027 N94-21304
BURBA, G. A. p 2095 N94-20654
p 2095 N94-20655
p 2096 N94-20656
BURD, WILLIAM p 2029 N94-21690
BURDESHAW, MARK D. p 1964 N94-21175
BURDETTE, DANIEL W. p 1643 N94-21629
BURG, R. p 2054 N94-20174
BURG, RICHARD p 1927 N94-22524
BURGDOERFER, J. p 1974 N94-21658
p 1975 N94-21785
BURGESS, G. p 2019 N94-20941
BURKE, KEVIN p 1862 N94-20757
BURNETT, J. W. p 1976 N94-21951
BURNS, ALAN p 1657 N94-20173
BURNS, J. p 1779 N94-22158
BURNS, PATRICIA J. p 1922 N94-21326
BURNS, R. G. p 2143 N94-21663
BURNS, ROGER G. p 2122 N94-20800
BURNS, W. K. p 1748 N94-19892
BUROSCH, GUSTAV p 1950 N94-20163
BURRELL, K. H. p 1998 N94-22039
BURROWS, C. J. p 2055 N94-20204
BURTON, R. p 2046 N94-22446
BUSDEKER, A. p 1985 N94-20262
p 1985 N94-20283
BUSHENKOV, VLADIMIR p 1923 N94-22087
BUSHIMATA, T. p 2001 N94-22633
BUSKO, I. p 2047 N94-22457
BUSS, R. J. p 1993 N94-20261
BUSSE, LYNDA E. p 1701 N94-20331
BUSSO, M. p 2133 N94-20859
BUTNER, STEVEN E. p 1900 N94-21301
BUTTLER, W. p 1852 N94-22017
BUTTRAM, M. T. p 1750 N94-20294
p 1762 N94-21634
BUTTRY, R. W. p 1687 N94-19864
BYERS, TERRY B. p 1812 N94-22433
BYRD, D. A. p 1818 N94-21554
BYRD, J. p 1979 N94-20274
BYRD, J. M. p 1980 N94-20292
BYRNE, BRIAN J. p 1945 N94-21289
BYRNE, T. p 1979 N94-20273

C

CABRAL, B. p 1917 N94-21841
CABROL, N. A. p 2143 N94-21664
CAELLI, TERRY p 1841 N94-21453
CAFFEE, M. W. p 2082 N94-20658
p 2106 N94-20713

CAHILL, P. A.	p 1706	N94-21526
CAI, JIN-YI	p 2043	N94-21287
CAI, KERRY ZHENGLIAN	p 1782	N94-22180
CAI, SUI X.	p 1700	N94-20328
CAIN, CLARENCE P.	p 1890	N94-20462
CAIN, RUSSEL P.	p 1765	N94-21710
CAINES, PETER E.	p 1910	N94-21063
CAIRNS, I. H.	p 1858	N94-21836
CALAWAY, W. F.	p 1690	N94-20288
	p 1976	N94-21951
CALCO, FRANK S.	p 1822	N94-20375
CALDERON-MORENO, J. M.	p 1676	N94-21559
CALEDONIA, G. E.	p 1663	N94-21395
CALKOEN, C. J.	p 1865	N94-20532
CALLAHAN, DEBRA A.	p 1992	N94-19915
CALLEN, J. D.	p 1998	N94-22019
CALVERT, JEFFREY M.	p 1703	N94-20526
CAMARDA, CHARLES J.	p 1800	N94-20495
CAMBIER, JEAN-LUC	p 1636	N94-20014
CAMERON, K.	p 1764	N94-21703
CAMERON, KELLY	p 1760	N94-21131
CAMISO, J. C.	p 1723	N94-20427
CAMP, K. L.	p 1807	N94-20114
	p 1807	N94-20115
CAMPBELL, A. N.	p 1761	N94-21532
CAMPBELL, BRUCE A.	p 1863	N94-20904
CAMPBELL, D. B.	p 2119	N94-20787
CAMPBELL, D. C.	p 1750	N94-20218
CAMPBELL, G. H.	p 1696	N94-22025
CAMPBELL, L.	p 1767	N94-21723
CAMPBELL, STEVE	p 1754	N94-21089
CAMPBELL, V. W.	p 1769	N94-21830
CAMPBELL, WILLIAM A., JR.	p 1676	N94-21889
CAMPILLO, FABIEN	p 1951	N94-20227
CANARIS, J.	p 1754	N94-21087
CANARIS, JOHN	p 1765	N94-21708
	p 1766	N94-21722
CANAVAN, G. H.	p 1965	N94-22403
CANFIELD, P. C.	p 1974	N94-21553
	p 2030	N94-21768
	p 2032	N94-21987
	p 2034	N94-22007
CANFIELD, RICHARD C.	p 1810	N94-21876
CANNELL, G. J.	p 1989	N94-21599
CANS, CHRISTINE	p 1963	N94-20165
CANTRELL, L.	p 1674	N94-20623
CAO, JIANSHU	p 2037	N94-21166
CAPO, R. C.	p 1686	N94-20794
CAPRON, WILLIAM R.	p 1643	N94-21629
CARD, H. C.	p 1782	N94-22181
CARD, HOWARD C.	p 1786	N94-22206
CARDON, J. G.	p 1658	N94-20617
CARLILE, JULIE A.	p 1654	N94-21791
CARLSON, BARBARA	p 1813	N94-21646
CARLSON, K. D.	p 2011	N94-19807
CARLSON, SCOTT M.	p 1967	N94-21410
CARLSSON, THOMAS	p 1708	N94-21896
CAROGLANIAN, ARMEN	p 1657	N94-21340
CARR, D.	p 1674	N94-20623
CARR, M. H.	p 2089	N94-20387
CARRE, D.	p 1705	N94-21225
CARREIRA, DANIEL J.	p 1671	N94-21882
CARRERAS, B. A.	p 1801	N94-20562
CARTER, B.	p 1805	N94-22272
CARTER, EMILY A.	p 1712	N94-21192
CARTER, TONY M.	p 1758	N94-21117
CARTLAND, HARRY E.	p 1698	N94-19947
CASACCHIA, RUGGERO	p 2130	N94-20842
CASAUS, L.	p 1749	N94-20054
CASPERS, H. H.	p 1987	N94-21236
CASSEL, GUDRUN	p 1680	N94-20552
CASTAGNA, A.	p 1695	N94-21949
CASTELLANO, DAVID R.	p 1910	N94-21144
CASTLE, KENT D.	p 1890	N94-20372
CASTNER, E. W., JR.	p 1678	N94-19924
	p 1683	N94-21842
CASTRO-ALVES, V.	p 1749	N94-20166
CASTRO, R.	p 1696	N94-22034
CATALDI, M.	p 1664	N94-21398
CATTO, P. J.	p 1999	N94-22562
CATURA, RICHARD C.	p 2054	N94-20142
	p 2055	N94-21295
CAVICCHI, R. E.	p 2028	N94-21458
CECIL, G.	p 2048	N94-22527
CEGLIO, N. M.	p 1769	N94-21959
CELATA, C. M.	p 1981	N94-21440
CELIK, TARIK	p 2016	N94-20285
CELIO, PAUL V.	p 1891	N94-20615
CEPERLEY, D. M.	p 1972	N94-20187
CERJAN, C.	p 1997	N94-21848
CERNOSEK, R. W.	p 1749	N94-20054
CERSOVSKY, DONALD D.	p 1824	N94-20576
CHA, HO-JUNG	p 1935	N94-21745
CHABALOWSKI, CARY F.	p 1698	N94-19947
CHADWICK, D. JOHN	p 2125	N94-20814
CHADWICK, DAVID J.	p 2110	N94-20736
CHAGELISHVILI, G. D.	p 2000	N94-22626
CHAI, STEVEN K.	p 1879	N94-22336
CHAIB-DRAA, B.	p 1776	N94-22141
CHAIKEN, SETH	p 1744	N94-21102
CHALIFOUX, MARTIN	p 1775	N94-22132
CHAMBERLAND, MARTIN	p 1746	N94-22196
CHAMBERS, D. M.	p 1852	N94-22004
CHAMBERS, JOHN G.	p 2126	N94-20820
CHAMIS, C. C.	p 1830	N94-20170
CHAMIS, CHRISTOS C.	p 1830	N94-20171
	p 1832	N94-21757
	p 1835	N94-22617
CHAN, C. T.	p 1695	N94-21964
CHAN, FRANCOIS	p 1793	N94-22246
CHAN, G. K.	p 1783	N94-22186
CHAN, GORDON	p 1784	N94-22191
CHAN, K. C. D.	p 1814	N94-19828
CHAN, K. D. C.	p 1816	N94-20277
CHAN, K. W.	p 1729	N94-20451
CHAN, L.	p 1789	N94-22222
CHAN, S. H.	p 1804	N94-21820
CHAN, S. K.	p 1970	N94-19971
CHANDLER, C.	p 1727	N94-20442
CHANDLER, D.	p 1680	N94-20560
CHANDRA, KUMAR	p 1666	N94-21733
CHANDRA, SURESH	p 1799	N94-20210
CHANG-RONG, MING	p 2079	N94-22552
CHANG, C.	p 1928	N94-19812
CHANG, C. KEN	p 1895	N94-20063
CHANG, CHAU-LYAN	p 1797	N94-20033
CHANG, CHEIN-I	p 1911	N94-21203
CHANG, FU-KUO	p 1834	N94-22612
CHANG, H. L. M.	p 2033	N94-21994
CHANG, JOHN W.	p 1746	N94-22187
CHANG, M.	p 1763	N94-21697
CHANG, S. K.	p 1663	N94-21392
CHANG, SUSAN	p 1744	N94-21350
CHANG, THIEL	p 2043	N94-21071
CHANG, Y. J.	p 1683	N94-21842
CHANG, YONG JOON	p 1678	N94-19924
CHANISHVILI, R. G.	p 2000	N94-22626
CHAO, TIEN-HSIN	p 1985	N94-20303
CHAOURAR, BRAHIM	p 1951	N94-20237
CHAPLA, DANIEL B.	p 1894	N94-21237
CHAPMAN, B.	p 1731	N94-20456
CHAPMAN, M. G.	p 2089	N94-20388
CHAPRON, B.	p 1720	N94-20414
CHARALAMPOPOULOS, TRYFON		
	p 1678	N94-20000
CHARGEISHVILI, BIDZINA	p 2005	N94-22661
	p 2005	N94-22663
CHASE, T. J.	p 1825	N94-21580
CHASSINDEKERGOMMEAUX, JACQUES		
	p 1929	N94-20176
CHATTERJEE, A.	p 1950	N94-20034
CHATTERJEE, SIDDHARTHA	p 1902	N94-19932
CHATTOPADHYAY, S.	p 1980	N94-20475
	p 1981	N94-21688
CHAU, D. S. C.	p 1714	N94-21426
CHAVEZ, J.	p 1737	N94-20620
CHEE, O.	p 1885	N94-21898
CHEE, SONNY HANSENG	p 1827	N94-22577
CHEMLA, D. S.	p 1985	N94-20320
CHEN, B.	p 1964	N94-22458
CHEN, C. H.	p 1820	N94-21957
CHEN, C. I.	p 1825	N94-21424
CHEN, C. J.	p 1819	N94-21872
CHEN, D.	p 2056	N94-22282
CHEN, E. I.	p 2030	N94-21805
CHEN, F. C.	p 1820	N94-21957
CHEN, H.	p 1936	N94-21853
CHEN, H. Y.	p 1928	N94-19858
CHEN, HONG-SHENG	p 2080	N94-22554
CHEN, J.	p 1852	N94-21787
CHEN, KRISTEN Q.	p 1759	N94-21125
CHEN, MU-SAN	p 1703	N94-20526
CHEN, P.	p 1981	N94-21688
CHEN, QI	p 1951	N94-20527
CHEN, QING-MING	p 1815	N94-19965
CHEN, RICHARD L.	p 1932	N94-21333
CHEN, XING	p 1773	N94-22119
	p 1773	N94-22120
CHEN, Y. J.	p 1993	N94-20234
CHEN, YASU T.	p 1896	N94-21247
CHENET, C.	p 1665	N94-21408
CHENG, A. Y.	p 2027	N94-21296
CHENG, C. C.	p 1680	N94-21145
CHENG, H. D.	p 1765	N94-21715
CHENG, KWANG-PING	p 2048	N94-22534
CHENG, YING	p 1746	N94-22211
CHEONG, S. W.	p 2030	N94-21768
	p 2034	N94-22007
CHERAY, D. L.	p 1763	N94-21652
CHERIEF, FERROUDJA	p 1929	N94-20124
CHERNIK, V. N.	p 1653	N94-21370
CHERNYKH, OLEG	p 1923	N94-22087
CHERVIN, R. M.	p 1855	N94-20219
CHEW, W. C.	p 1719	N94-20408
CHHABILDAS, L. C.	p 1829	N94-19943
CHIAN, ABRAHAM C.-L.	p 2001	N94-22635
	p 2003	N94-22649
	p 2005	N94-22665
CHIARAMONTE, FRANCIS PAUL, III		
	p 1692	N94-21604
CHIEN, LIAN	p 1818	N94-21509
CHIRICO, R. D.	p 2037	N94-20473
CHITTY, DANIEL E.	p 1831	N94-21219
CHIU, M. A.	p 1669	N94-20102
CHIZHOV, SERGEI A.	p 1923	N94-22066
CHNG, CHEW-LYE	p 1764	N94-21704
CHOCK, RICAURTE	p 1666	N94-21864
CHOENNI, SUNIL	p 2043	N94-21071
CHOI, EUN H.	p 1994	N94-21290
	p 1995	N94-21291
CHOI, K. Y.	p 2024	N94-21004
	p 2024	N94-21005
CHOI, S. H.	p 1669	N94-20102
CHOI, SANG H.	p 1995	N94-21292
CHOI, YUMI	p 1679	N94-20319
CHONG, PARKSON L.	p 1700	N94-20299
CHOREY, C. M.	p 1735	N94-20514
	p 1735	N94-20516
	p 1709	N94-20516
CHOREY, C. Z.	p 1671	N94-20513
CHOU, C. K.	p 1729	N94-20451
CHOU, H. C.	p 1845	N94-19925
CHOU, JIN	p 1897	N94-21784
CHOU, JIN J.	p 1914	N94-21489
	p 1966	N94-21881
CHOU, MAU-SONG	p 1797	N94-19936
CHOW, JOSEPH	p 1994	N94-20943
CHOYKE, W. J.	p 1680	N94-21145
CHREN, WILLIAM A., JR.	p 1759	N94-21121
CHRISS, R. M.	p 1636	N94-20136
CHRISTENSEN, P. R.	p 2091	N94-20400
	p 1685	N94-20703
	p 1686	N94-20868
CHRISTIAN, C.	p 2047	N94-22459
CHRISTIANSON, ROLLIN C.	p 1824	N94-20589
CHRISTIN, F.	p 1664	N94-21398
CHRISTY, CLIFFORD	p 1832	N94-21421
CHROSTOWSKI, J.	p 1789	N94-22221
	p 1789	N94-22222
CHRZAS, J.	p 1990	N94-21837
CHU, M. S.	p 1993	N94-20326
CHU, PONG P.	p 1656	N94-21581
CHUA, O. H.	p 1758	N94-21116
CHUN, KEN S.	p 1644	N94-22278
CHUNG, WILSON C.	p 2041	N94-20158
CHUNG, YEUNG	p 1709	N94-20973
CHUPP, W. W.	p 1979	N94-20289
	p 1981	N94-21439
CHURCH, J. R.	p 1691	N94-20478
CIARDO, GIANFRANCO	p 1965	N94-21463
CIFTAN, MIKAEL	p 1983	N94-19901
CIVCO, DANIEL L.	p 1838	N94-20955
CLANCY, R. T.	p 1812	N94-22436
CLARK, BETH E.	p 2107	N94-20719
CLARK, G.	p 1926	N94-22486
CLARK, MICHAEL J.	p 2039	N94-21444
CLARK, R. R.	p 1870	N94-21862
CLARKE, EDMUND M.	p 1902	N94-19919
CLARKE, EDMUND M., JR.	p 1898	N94-20085
CLARKE, NORMAN P.	p 1865	N94-20332
CLARKE, R. S., JR.	p 2082	N94-20681
CLARKSEAN, R.	p 1799	N94-20258
CLAY, WALLACE H.	p 1808	N94-20930
CLAYTON, R. N.	p 2082	N94-20681
	p 2083	N94-20708
CLAYTON, ROBERT N.	p 1862	N94-20776
	p 1686	N94-20855
CLERGEOT, H.	p 1786	N94-22202
CLIFFORD, S. M.	p 2091	N94-20399
	p 2143	N94-21665
	p 2143	N94-21666
CLIMIE, COLIN C.	p 1788	N94-22218
CLINARD, F. W., JR.	p 1707	N94-21560
CLINE, D.	p 1981	N94-21688
CLOTHIAUX, EUGENE	p 1872	N94-22301
CLOTHIAUX, EUGENE E.	p 1876	N94-22318
CLOTHIER, J.	p 1902	N94-19911
CLOUTMAN, L. D.	p 1678	N94-19889
COAKLEY, JAMES A., JR.	p 1872	N94-22300
COBB, S. D.	p 2030	N94-21807
CODA, S.	p 1998	N94-22039
CODISH, M.	p 1928	N94-19995
CODOGNET, PHILLIPPE	p 1929	N94-20176
COGGI, J. M.	p 1681	N94-21226
COHEN, GERALD C.	p 1898	N94-20039
	p 1937	N94-22414
COHEN, J. D.	p 1688	N94-19985
COHEN, OLIVIER	p 1963	N94-20165

COHEN, PAUL p 1789 N94-22226
COHEN, R. E. p 1702 N94-20463
COIRIER, WILLIAM J. p 1920 N94-22364
COLCHIN, R. J. p 1992 N94-20058
p 1998 N94-22045
p 1999 N94-22568
COLE, E. I., JR. p 1761 N94-21532
p 1762 N94-21636
COLE, KEVIN p 1710 N94-21007
COLE, N. C. p 1848 N94-21823
COLE, R. L. p 1811 N94-22391
COLEMAN, C. J. p 1854 N94-19860
COLEMAN, J. p 1885 N94-21899
p 1886 N94-21904
COLEMAN, MICHAEL T. p 1691 N94-21258
COLLINS, CONRAD p 1823 N94-20567
COLLINS, D. p 1662 N94-21386
COLLINS, W. p 1685 N94-20745
COLMENARES, C. A. p 1688 N94-19986
COLOZZA, ANTHONY J. p 1846 N94-20196
COLUSSI, LIVIO p 1952 N94-21029
COMBE, M. B. p 1943 N94-21032
p 1930 N94-21161
COMBS, R. J. p 1809 N94-21508
COMEAU, M. p 1784 N94-22189
COMEAU, MARC p 1746 N94-22190
COMPARINI, M. C. p 1744 N94-21091
CONDE, M. E. p 1980 N94-20475
CONDLEY, C. J. p 1737 N94-20596
CONNELL, JOHN W. p 1672 N94-20540
p 1662 N94-21385
CONNES, A. p 1961 N94-22264
CONOVER, HELEN p 2042 N94-20268
CONOVER, M. J. p 2035 N94-22564
CONRAD, A. R. p 1925 N94-22460
p 2047 N94-22495
p 2048 N94-22504
CONROY, M. p 2047 N94-22462
CONROY, M. A. p 1925 N94-22461
p 1926 N94-22508
CONSTABLE, STEFAN H. p 1896 N94-21247
CONSTANTINIDES, E. D. p 1716 N94-20139
CONWELL, PETER R. p 1757 N94-21111
COOK, A. C. p 2128 N94-20830
COOK, D. R. p 1859 N94-22036
COOK, K. p 2058 N94-22444
COOMBE, ROBERT D. p 1712 N94-20625
COOMBS, A. W. p 1696 N94-22025
COOMBS, C. R. p 1666 N94-20864
COOMES, E. P. p 1669 N94-20102
COON, S. R. p 1690 N94-20288
p 1976 N94-21951
COONEY, GERALD T. p 2024 N94-21003
p 2024 N94-21004
COOPER, A. B., III p 1959 N94-21524
COOPER, A. C. p 2031 N94-21871
COOPER, D. p 1852 N94-22017
COOPER, F. p 1998 N94-22389
COOPER, THOMAS D. p 1635 N94-21194
COOPER, W. E. p 1807 N94-19987
COPPENS, T. p 1865 N94-20532
CORBUS, D. p 1748 N94-19902
CORCORAN, M. p 2047 N94-22462
CORCORAN, MERYL LEE p 1886 N94-21901
p 1886 N94-21904
p 1887 N94-21906
p 1888 N94-21914
CORDOVA, FRANCE p 2043 N94-21055
CORLETT, J. N. p 1980 N94-20292
CORNETT, ANNETTE P. p 1909 N94-21038
CORONITI, F. C. p 2010 N94-22698
COSTARD, F. M. p 2090 N94-20390
COTE, DOMINIC p 1781 N94-22176
COTEMUNOZ, JAIRO ANTONIO p 1908 N94-21020
COTTINGAME, W. p 1852 N94-22017
COTTON, W. R. p 1864 N94-19900
COTTON, WILLIAM R. p 1878 N94-22331
COTUGNO, KRISTEN p 2121 N94-20796
COULTER, R. L. p 1859 N94-22036
COULTRIP, ROBERT H. p 1718 N94-20368
COURTOIS, B. p 1749 N94-20166
COVA, A. p 1783 N94-22184
COX, GEORGE B., JR. p 1669 N94-20370
COX, LEON p 2029 N94-21690
COX, S. K. p 1880 N94-22340
COX, STEPHEN K. p 1876 N94-22321
p 1876 N94-22322
p 1878 N94-22330
CRABTREE, G. W. p 2011 N94-19807
p 2029 N94-21649
p 2033 N94-21997
CRABTREE, MARK S. p 1893 N94-20023
CRADDOCK, R. A. p 2143 N94-21667
p 2145 N94-21676
CRADDOCK, W. p 1981 N94-21688
CRAM, LAWRENCE p 2010 N94-22697
CRAMPTON, G. p 1887 N94-21906
CRAMPTON, G. H. p 1886 N94-21901
CRANE, ROGER M. p 1674 N94-20950
CRAVEY, W. R. p 1769 N94-21838
CRAWFORD, DANIEL J. p 1643 N94-21629
CRAWFORD, J. C. p 1844 N94-19803
CRAWFORD, S. p 1988 N94-22003
CRAYTON, L. p 1642 N94-22055
CREMERS, T. L. p 1807 N94-20114
p 1807 N94-20115
CREUTZ, M. p 2038 N94-21692
CREZE, M. p 1964 N94-22458
CRISWELL, EVAN p 2042 N94-20268
CROCKETT, JOHN P. p 1883 N94-21358
CROES, G. A. p 2047 N94-22463
CROFT, S. K. p 2122 N94-20802
CROKE, E. T. p 1734 N94-20509
CRONIN-GOLOMB, MARK p 2015 N94-20213
CROSIER, RONALD B. p 1911 N94-21204
CROSS, DAVID p 1930 N94-21023
CROSS, J. p 1635 N94-21490
CROSS, JON B. p 1993 N94-20491
p 1663 N94-21393
CROTEAU, ALAIN p 1770 N94-22105
CROVELLA, MARK E. p 1929 N94-20144
CROW, J. E. p 1714 N94-20278
CROZAZ, GHISLAINE p 1686 N94-20852
CROZIER, STEWART N. p 1745 N94-22204
CUBBAGE, C. D. p 1671 N94-20513
CUHACI, M. p 1782 N94-22177
p 1782 N94-22178
p 1785 N94-22199
CUI, NING p 1789 N94-22226
CULLER, DAVID p 2029 N94-21690
CUMMINGS, WILLIAM H. p 1894 N94-21237
CUNEO, M. E. p 1980 N94-20295
CUNNINGHAM, SUSAN E. p 1835 N94-22615
CUPERMAN, VLADIMIR p 1747 N94-22213
CURLEE, T. R. p 1693 N94-21850
CURTIS, B. C. p 1801 N94-20562
CWIK, T. p 1722 N94-20423
p 1725 N94-20436
CYGAN, R. T. p 1679 N94-20307
CYR, K. p 1744 N94-21092
CZIESLA, MANFRED J. p 1712 N94-20061

D

DABROWSKI, B. p 2029 N94-21649
p 2033 N94-21998
DADA, EZEKIEL SUNDAY p 1652 N94-22425
DAELEMANS, WALTER p 1940 N94-20246
DAFERMOS, CONSTANTINE M. p 1951 N94-20545
DAGLE, J. E. p 1669 N94-20102
DAI, FAN p 1944 N94-21057
DAIDA, J. M. p 1723 N94-20427
DALICHAOUCH, Y. p 2036 N94-22564
DALLABETTA, MICHAEL J. p 1759 N94-21122
DALLENBACH, R. p 1752 N94-20629
DALRYMPLE, G. BRENT p 2084 N94-20834
DAMELIO, F. p 1886 N94-21901
p 1886 N94-21902
p 1887 N94-21909
DAMINI, A. p 1745 N94-22161
DAMODARAN, A. D. p 1690 N94-20183
DAMS, D. p 1928 N94-19995
DANDY, DAVID S. p 2011 N94-19821
DANIEL, BRADY R. p 1667 N94-20015
DANIEL, JAMES A. p 1824 N94-20589
DANIEL, R., JR. p 1935 N94-21745
DANIEL, RONALD L., JR. p 1703 N94-20541
DANIELS, E. J. p 1682 N94-21789
DANY, RAIMUND p 1987 N94-21148
DAPKUNAS, S. J. p 1706 N94-21516
DAPKUS, P. D. p 1845 N94-19805
DARGUSH, G. F. p 1676 N94-21777
DARIA, D. M. p 1685 N94-20733
DAS, N. C. p 1754 N94-21064
DAS, S. p 1693 N94-21850
DASILVA, L. B. p 1819 N94-21873
DATTA, ASIT K. p 1773 N94-22122
DAUNTON, NANCY G. p 1885 N94-21898
p 1885 N94-21899
p 1885 N94-21900
p 1886 N94-21901
p 1886 N94-21902
p 1886 N94-21903
p 1886 N94-21904
p 1887 N94-21905
p 1887 N94-21906
p 1887 N94-21907
p 1887 N94-21909
p 1888 N94-21911
p 1888 N94-21912
DAUSCH, DAVID p 1705 N94-21416
DAVENHALL, A. C. p 2048 N94-22514
DAVENPORT, J. W. p 1691 N94-20313
DAVID, J. p 1892 N94-21141
DAVID, S. A. p 1690 N94-20282
DAVIDSON, K. p 1868 N94-21356
DAVIES, M. E. p 1652 N94-20850
DAVIES, W. J. p 1739 N94-21235
DAVIS, A. M. p 2082 N94-20881
DAVIS, ANDREW M. p 1686 N94-20855
DAVIS, D. W. p 1715 N94-19816
DAVIS, J. BRADLEY p 1656 N94-21884
DAVIS, JOHN M. p 1876 N94-22321
p 1876 N94-22322
DAVIS, L. E. p 1925 N94-22464
p 1925 N94-22465
DAVIS, ROBERT F. p 2026 N94-21190
p 2026 N94-21506
DAVIS, S. J. p 1809 N94-21607
DAVIS, W. L. p 2144 N94-21671
p 2145 N94-21677
DAVISSON, C. p 1694 N94-21945
DAWSON, J. p 1998 N94-22389
DAWSON, RONALD p 1670 N94-21809
DAY, C. T. p 1921 N94-22375
DAY, DELBERT E. p 1713 N94-20605
DAY, T. p 2128 N94-20830
DAYTON, DAVID C. p 1679 N94-20111
DE, BHOLA N. p 1710 N94-20981
p 2022 N94-20992
p 2022 N94-20993
DEANGELIS, C. p 1983 N94-19862
DEARELLANO-LOPEZ, A. R. p 1676 N94-21559
DEBOISSEZON, HELENE p 1840 N94-20969
DECASTRO, ANTONIO CARLOS J. p 1839 N94-20963
DECOSTA, VLADIMIR M. p 1840 N94-20967
DEES, B. R. p 1698 N94-19938
DEGERINE, SERGE p 1963 N94-20162
DEGOUVEIADALPINO, ELISABETE M. p 2008 N94-22685
DEGROH, KIM K. p 1660 N94-21377
DEGROOT, A. J. p 1937 N94-22042
DEHON, ANDRE p 1716 N94-19977
DEHOOP, A. T. p 1969 N94-22261
p 1742 N94-22348
DEHOOP, M. V. p 1969 N94-22261
DEINES, PETER p 1862 N94-20776
DEIRMENDJIAN, G. K. p 1675 N94-21504
DEKKERS, C. p 1909 N94-21061
DELANEY, J. p 1686 N94-20808
DELDUCA, V. p 1974 N94-21515
DELGADO, JOSE G. p 1757 N94-21113
DELGENIO, ANTHONY p 1869 N94-21642
DELGIUDICE, M. p 1969 N94-21599
p 1989 N94-21600
DELGRANDE, N. K. p 1906 N94-20316
DELISLE, G. Y. p 1745 N94-22127
DELISLE, GILLES Y. p 1794 N94-22254
DELL, G. F. p 1978 N94-19945
DELNORE, V. E. p 1721 N94-20418
DELONG, D. F. p 1738 N94-21210
DELUISI, J. p 1876 N94-22320
p 1879 N94-22337
DEMIDOV, S. A. p 1653 N94-21370
DEMMEL, JOHANN p 1871 N94-22280
DEMUTH, HOWARD B. p 1759 N94-21122
DENBRAVEN, WIM p 1643 N94-21606
DENISON, G. J. p 1750 N94-20294
DENNIS, K. W. p 2036 N94-22562
DENSMORE, A. p 1731 N94-20457
DEPONTE, J. p 1925 N94-22461
p 2062 N94-22466
p 1926 N94-22508
DERKS, PETER L. p 1893 N94-20168
DEROO, F. p 1966 N94-21799
DEROOIJ, A. p 1660 N94-21375
DERVIEUX, ALAIN p 1806 N94-21471
DERZON, M. S. p 1808 N94-20297
DESHONG, BRUCE p 1813 N94-21347
DESOUZA, J. p 1760 N94-21132
DESSAINT, L. p 1790 N94-22229
DESSIATOUN, S. p 1796 N94-20101
DETWILER, RACHEL J. p 1708 N94-21894
DEUL, E. p 2062 N94-22467
DEUSER, D. A. p 1892 N94-21320
DEUTSCH, STEPHEN E. p 1894 N94-20610
DEUTSCHE, EMMANUEL p 1801 N94-20601
DEVANATHAN, R. p 1758 N94-21115
DEVEAU, DAVID M. p 1808 N94-21278
DEVENEY, M. p 1748 N94-19844
DEVILLIERS, Y. p 1745 N94-22127
DEVILLIERS, YVES p 1747 N94-22238
DEVRIES, FER-JAN p 1914 N94-21496
DEY, N. p 1674 N94-20623
DEYONG, MARK p 1757 N94-21106
DEYOUNG, R. J. p 1669 N94-20102

DEYOUNG, RUSSELL J. p 1824 N94-20587
DEZERN, JAMES F. p 1702 N94-20374
DIAMOND, P. H. p 1999 N94-22596
DIAS, LUIZ ALBERTO VIEIRA p 1838 N94-20953
p 1838 N94-20956
p 1839 N94-20960
p 1840 N94-20965
DIAZ, C. p 1761 N94-21256
DIB, NIHAD I. p 1733 N94-20500
p 1733 N94-20501
p 1733 N94-20502
DICK, ERIK p 1957 N94-21476
DICK, J. J. p 2034 N94-22035
DICK, P. p 1640 N94-22604
DICKEY, THOMAS D. p 1884 N94-20186
DICTOR, M. p 1885 N94-21898
DIDZIULIS, S. p 1705 N94-21225
DIECKMAN, S. L. p 1677 N94-21940
DIEDEN, KATHY p 2045 N94-21750
DIENST, W. p 1707 N94-21560
DIERKING, W. p 1725 N94-20435
DIMAURO, L. F. p 1972 N94-20230
DIMOS, D. p 2013 N94-19961
DIMOTAKIS, P. E. p 1682 N94-21452
DING, Y. p 1695 N94-21964
DION, DENIS p 1777 N94-22145
DION, JEAN-LUC p 1775 N94-22131
DIPESO, G. p 1999 N94-22567
p 1999 N94-22595
DIPLANETOLOGIA, REPARTO p 2130 N94-20842
DIVECHA, AMARNATH p 1700 N94-20057
DIVECHA, AMARNATH P. p 1749 N94-20120
DIVSALAR, D. p 1731 N94-20458
DIX, M. R. p 1855 N94-20256
DIXIT, S. N. p 1819 N94-21872
p 1819 N94-21920
p 1820 N94-22401
DIXON, BRIAN G. p 1963 N94-19846
DIXON, K. D. p 1807 N94-19987
DJORGOVSKI, S. G. p 2049 N94-22546
DOBSON, C. p 2048 N94-22503
DOBSON, CARL p 2047 N94-22468
DOCHAIN, DENIS p 1794 N94-22256
DOCTOR, R. D. p 1682 N94-21789
DODD, B. A. p 1761 N94-21532
DOFT, F. p 1985 N94-20262
p 1985 N94-20283
DOHERTY, MICHAEL P. p 1654 N94-21570
DOHM, JAMES M. p 2125 N94-20815
DOHNALEK, Z. p 1680 N94-21145
DOLAN, K. W. p 1906 N94-20316
DOLCE, JAMES L. p 1714 N94-21564
p 1715 N94-21589
DOLEV, SHLOMI p 1935 N94-21549
DOMANUS, H. M. p 1917 N94-21923
DOMINGUEZ-RODRIGUEZ, A. p 1676 N94-21559
DOMONKOS, MATTHEW p 1670 N94-21565
DONAHUE, D. J. p 2106 N94-20713
DONG, Y. Y. p 1871 N94-22294
DONG, YAYI p 1879 N94-22336
p 1881 N94-22343
DONGARRA, J. J. p 1960 N94-21967
DONNELLAN, THOMAS M. p 1674 N94-20574
DONOHOE, GREGORY p 1744 N94-21099
DOPKER, BERNHARD p 1834 N94-22609
DOROFEEV, Y. I. p 1661 N94-21380
DOROFEYEVA, V. A. p 2085 N94-20849
DOUGHERTY, SEAN MELBOURNE p 2081 N94-22426
DOUGHTY, G. E. p 1671 N94-21860
DOUGLAS, C. p 2086 N94-20885
p 2086 N94-20886
p 2143 N94-21668
DOUVILLE, R. p 1785 N94-22199
DOW, THOMAS A. p 1761 N94-21257
DOWDY, L. W. p 1908 N94-20932
DOWLER, CONNIE p 1655 N94-21793
DOWLING, K. p 1946 N94-21925
DOWNEY, ALAN N. p 1733 N94-20499
DOWNEY, J. p 2033 N94-21997
DOWNING, K. H. p 1884 N94-19826
DOYLE, B. L. p 1973 N94-20306
DOYLE, L. R. p 2146 N94-21683
DRACH, W. C. p 2027 N94-21303
DRAGO, RAYMOND J. p 1826 N94-21756
DRAKE, J. p 1960 N94-21955
p 2047 N94-22490
DRAKE, JEREMY J. p 2047 N94-22468
DRAYSON, S. ROLAND p 1855 N94-20132
DREFENSTEDT, REINHARD p 1930 N94-21023
DRESCHHOFF, GISELA A. p 2147 N94-21196
DRESNER, L. p 2032 N94-21932
DREW, D. A. p 1802 N94-21261
DRICOT, FABIENNE p 1684 N94-21402
DRIESSEN, THEO p 1953 N94-21047
DRINKWATER, MARK p 1725 N94-20433
DRINKWATER, MARK R. p 1724 N94-20428
p 1725 N94-20434
p 1725 N94-20435
DROLET, J. p 1775 N94-22133
DROLSHAGEN, G. p 1662 N94-21388
p 1663 N94-21396
DROOPAD, R. p 2024 N94-21004
p 2024 N94-21005
DROSSAERS, M. F. J. p 1940 N94-20242
DROSSAERS, MARC F. J. p 1941 N94-20250
DROTOS, M. N. p 1652 N94-20511
DRYER, F. L. p 1682 N94-21243
DRZEWINSKI, M. p 1702 N94-20463
DUBE, Y. p 1790 N94-22229
DUBNICKI, CEZARY p 1899 N94-21177
DUBOIS, PASCALE C. p 1724 N94-20430
DUDA, J. L. p 1825 N94-21424
p 1825 N94-21450
p 1825 N94-21451
DUDECK, M. p 1653 N94-21404
DUEMENIL, L. p 1860 N94-22283
DUFFIN, W. J. p 1689 N94-20182
DUKART, R. J. p 1808 N94-20297
DUKE, MICHAEL B. p 2146 N94-21883
DUMMEL, A. p 1684 N94-20664
DUNBAR, E. p 1713 N94-22033
DUNBAR, R. SCOTT p 1720 N94-20412
DUNLOP, JIM p 1994 N94-21214
DUNN, MICHAEL L. p 1894 N94-21510
DUNN, PAT p 1670 N94-21809
DUNN, ROBERT P. p 1812 N94-22433
DUNNET, A. p 1662 N94-21391
DUNNING, J. E. p 1652 N94-20511
DUNPHY, J. C. p 2034 N94-22041
DUONG, TUAN A. p 1942 N94-20360
DUPRE, A. p 1668 N94-20073
DUPUIS, CLEMONT p 1791 N94-22239
DUPUY, C. p 1665 N94-21405
DURAND, D. p 2047 N94-22469
DURBIN, P. F. p 1906 N94-20316
DURBIN, PAUL A. p 1804 N94-21875
DURIN, CHRISTIAN p 1659 N94-21371
DUROUCHOUX, PHILIPPE p 2009 N94-22691
DUTT, ALOK p 1954 N94-21164
DUVA, ANTHONY W. p 1824 N94-21274
DUVEL, JEAN-PHILIPPE p 1860 N94-22287
DWORAK, T. D. p 1695 N94-21976
DYACHENKO, A. I. p 1972 N94-20181
DYKHUIZEN, R. C. p 1794 N94-22405
DYNES, R. C. p 2012 N94-19848

E

EAGAN, MARY ELLEN p 1968 N94-22053
EARL, MARILYN P. p 1738 N94-21198
p 1739 N94-21218
EARLY, J. W. p 1818 N94-21554
p 1820 N94-22585
EAST, N. P. p 1747 N94-22252
EBERHARD, P. H. p 2038 N94-22010
EBERHARD, WYNN L. p 1871 N94-22295
p 1874 N94-22308
p 1877 N94-22326
EBERHARDT, SILVIO P. p 1942 N94-20360
EBERMAN, BRIAN p 1939 N94-20105
EBRAHIMI, YAGHOOB S. p 1644 N94-22277
p 1644 N94-22278
ECK, MATTHIAS p 1892 N94-21134
ECK, T. F. p 1839 N94-20961
ECKLUND, WAYNE D. p 1823 N94-20494
EDER, D. C. p 1815 N94-20259
p 1817 N94-21299
EDGERTON, V. REGGIE p 1895 N94-20338
EDMONSON, PETER J. p 1773 N94-22123
EDWARDS, B. C. p 2047 N94-22453
EDWARDS, JOHN L. p 2024 N94-21003
p 2024 N94-21004
p 2024 N94-21005
EDWARDS, KAY p 2107 N94-20719
EGALON, CLAUDIO O. p 1986 N94-20378
EGALON, CLAUDIO OLIVEIRA p 1986 N94-20586
EGAN, DONALD F. p 1828 N94-20468
EGNER, L. K. p 1689 N94-20093
EGUSA, S. p 1709 N94-22008
EGUSA, SHIGENORI p 1706 N94-21542
EHRLICH, DANIEL p 1680 N94-20566
EICHHORN, G. p 2048 N94-22499
EICHINGER, W. p 1852 N94-22017
EIMERL, D. p 1820 N94-22401
EISENHAMER, J. D. p 1925 N94-22470
p 1926 N94-22483
p 1926 N94-22485
EL-GAMAL, M. Z. p 1644 N94-22135
EL-NMEIR, RITA p 1777 N94-22147
ELACHI, C. p 1723 N94-20424
ELDIN, A. G. p 1758 N94-21116
p 1759 N94-21123
p 1767 N94-21724
p 1767 N94-21729
ELDRIDGE, C. p 1744 N94-21092
ELEMA, INA A. p 1842 N94-22097
ELFAR, S. p 1886 N94-21901
p 1886 N94-21903
p 1886 N94-21904
ELFOUHAILY, TONAS M. p 1884 N94-21628
ELGHAZZANI, E. M. p 1688 N94-20078
ELKHALFI, AHMED p 1868 N94-20600
ELLINGSON, R. G. p 1879 N94-22337
ELLINGSON, W. A. p 1832 N94-21772
ELLIOTT, JAMES R., JR. p 1822 N94-20365
ELLIOTT, W. R. p 1890 N94-20462
ELLIS, DAVID p 1641 N94-20189
ELLISON, A. J. G. p 1700 N94-20265
ELLISON, MIKE p 2110 N94-20731
ELORANTA, E. W. p 1877 N94-22326
ELRICK, M. G. p 1904 N94-20052
ELSHANI, S. p 1683 N94-22021
ELWELL, D. p 1647 N94-20343
EMERSON, J. P. p 2031 N94-21926
EMERY, WILLIAM p 1643 N94-20148
EMSLIE, BETTY p 1949 N94-19907
ENGEL, OTFRIED p 1973 N94-21136
ENGELMANN, B. E. p 1960 N94-21996
ENGLAND, A. C. p 1992 N94-20058
p 1999 N94-22568
ENGLER, R. H. p 1651 N94-21280
ENGLISH, R. E. p 1990 N94-21985
ENGRAND, C. p 2082 N94-20678
ENOME, S. p 2001 N94-22633
ENOMOTO, FRANCIS p 1914 N94-21489
ENOMOTO, FRANCIS Y. p 1920 N94-22367
ENOMOTO, KIYOSHI p 1746 N94-22171
EPPLEY, K. R. p 1763 N94-21685
EPSTEIN, S. p 2134 N94-20862
ERDEMIR, ALPER p 1738 N94-21182
ERDOES, P. L. p 1963 N94-21022
p 1954 N94-21231
ERDOGAN, S. p 1764 N94-21705
ERIKSSON, O. p 2011 N94-19827
p 1696 N94-22388
ERLANDSON, ROBERT E. p 1982 N94-21878
ERLEBACHER, GORDON p 1797 N94-20033
ERNST, D. p 1991 N94-19883
ERSKINE, D. p 1998 N94-22399
ERSKINE, FRED T. p 1883 N94-21358
ERWIN, DAN p 1802 N94-21220
ESAT, TEZER M. p 2126 N94-20822
ESHRAGHI, ARIA p 1764 N94-21699
ESKELINEN, JUHA p 1744 N94-22076
ESKRIDGE, TOM p 2029 N94-21690
ESPANA, MARTIN D. p 1649 N94-21879
ESPOSITO, L. W. p 2092 N94-20637
ESSELLE, KARU P. p 1745 N94-22139
ESTEP, P. p 1928 N94-19812
ESTEROWITZ, LEON p 1814 N94-19800
p 1815 N94-20060
ETIENNE, A. p 1926 N94-22501
EUGSTER, O. p 1684 N94-20652
EVANS, K. p 2022 N94-20992
p 2022 N94-20993
EVANS, KEITH p 2022 N94-20995
EVANS, M. S. p 1826 N94-22038
EVRIPIDOU, P. p 1937 N94-22378
EWING, J. A. p 1925 N94-22471
EWING, KENNETH J. p 1701 N94-20331
EWING, RICHARD E. p 1957 N94-21479
EYLON, S. p 1993 N94-20234
p 1979 N94-20289
p 1981 N94-21439
EZELL, CALVIN p 1911 N94-21183

F

FABES, B. D. p 2034 N94-22005
FABIETTI, L. p 1674 N94-20623
FADLEY, C. S. p 1808 N94-21441
FAEHL, R. J. p 1997 N94-21988
p 2036 N94-22583
FAENGMARK, INGRID p 1680 N94-20552
FAIGLE, ULRICH p 1738 N94-21073
FAIR, HARRY D. p 1831 N94-21249
FALABELLA, S. p 2032 N94-21960
FALCO, EMILIO E. p 2063 N94-22472
FALTENS, A. p 1981 N94-21440
FALTER, KARL J. p 1761 N94-21257
FAMINI, GEORGE R. p 1974 N94-21185
FANALE, F. P. p 2146 N94-21681
FANG, DA-GANG p 1794 N94-22254
FANNI, M. A. p 1798 N94-20101
FARAZIAN, K. p 1731 N94-20458

FARHLOUL, MOHAMED ..... p 1805 N94-22417
FARIS, J. L. ..... p 2085 N94-20858
FARNSWORTH, A. V. ..... p 1904 N94-20052
FARNUM, E. H. ..... p 1707 N94-21560
FARRELL, R. ..... p 1936 N94-21749
FARRELL, T. J. ..... p 2048 N94-22529
FARRIS, A. ..... p 2063 N94-22473
FATSIS, A. ..... p 1669 N94-20080
FAUBERT, D. ..... p 1745 N94-22142
FAUDREE, R. J. ..... p 1953 N94-21074
FAUST, CYNTHIA M. ..... p 1679 N94-20111
FAVIER, D. ..... p 1636 N94-20486
FAWLEY, W. F. ..... p 1992 N94-20004
FAWLEY, W. M. ..... p 1981 N94-21440
FAYYAD, U. M. ..... p 2049 N94-22546
FECHTIG, H. ..... p 2141 N94-20909
FEEHRER, CARL E. ..... p 1894 N94-20610
FEELEY, JOSEPH J. ..... p 1757 N94-21112
p 1763 N94-21898
FEGLEY, BRUCE, JR. ..... p 1811 N94-22430
FEIEREISEN, WILLIAM J. ..... p 1666 N94-19818
FEIGELSON, ERIC D. ..... p 2080 N94-20337
FEINGOLD, GRAHAM ..... p 1873 N94-22305
FEINGOLD, R. A. ..... p 2044 N94-21529
FELDMAN, D. W. ..... p 1818 N94-21554
FELDMAN, V. ..... p 2083 N94-20735
FENDELL, FRANCIS E. ..... p 1797 N94-19936
FENDRICH, J. ..... p 2033 N94-21997
FENG, YU ..... p 1757 N94-21107
FERANDEZ, DAMACENE V. ..... p 1867 N94-21146
FERGUSON, EUGENE M. ..... p 1808 N94-20930
FERRANDO, WILLIAM ..... p 1700 N94-20057
FERRANDO, WILLIAM A. ..... p 1749 N94-20120
FERRARI, ATTILIO ..... p 2000 N94-22631
FERRON, J. R. ..... p 1993 N94-20326
p 1998 N94-22039
FEYZI, F. ..... p 1639 N94-22599
FIELD, P. E. ..... p 1809 N94-21506
FIERRO, J. ..... p 1926 N94-22501
FIEZ, TERRI ..... p 1764 N94-21699
FIGUCIA, ROBERT J. ..... p 1739 N94-21244
FIJMA, DUCO ..... p 1913 N94-21313
FILHO, PEDRO HERNANDEZ ..... p 1839 N94-20964
FILUK, A. B. ..... p 1808 N94-20297
FINKE, REINALD G. ..... p 1665 N94-21420
FINKEL, R. C. ..... p 2082 N94-20658
p 2106 N94-20713
FINNEMORE, D. K. ..... p 2029 N94-21649
FIORINO, M. ..... p 1868 N94-21605
FISCHER, E. M. ..... p 2101 N94-20686
p 2101 N94-20687
FISCHER, RICHARD P. ..... p 1752 N94-20931
FISCHER, T. ..... p 1748 N94-19844
FISCHER, THOMAS ..... p 1764 N94-21699
FISENKO, A. V. ..... p 2085 N94-20846
FISHER, ALLAN L. ..... p 1898 N94-20085
FISHER, G. C. ..... p 1681 N94-21241
FISHER, GENE L. ..... p 1898 N94-20039
FISHER, R. A. ..... p 2031 N94-21926
FISHMAN, G. J. ..... p 2149 N94-20603
FISK, D. ..... p 1974 N94-21553
FISK, Z. ..... p 2030 N94-21768
p 2034 N94-22007
FITZPATRICK, M. ..... p 1925 N94-22474
p 1925 N94-22475
FLACH, JOHN M. ..... p 1891 N94-20627
FLAHERTY, JOSEPH ..... p 1952 N94-20568
FLAHERTY, KARLA ..... p 1641 N94-20912
FLAMANT, G. ..... p 1653 N94-21404
FLANERY, R. ..... p 1960 N94-21955
FLEETWOOD, D. M. ..... p 2032 N94-21939
FLEISCHAUER, P. ..... p 1705 N94-21225
FLEISCHMANN, H. H. ..... p 1997 N94-21988
FLEISHER, S. ..... p 1747 N94-22231
p 1747 N94-22232
FLEMING, E. L. ..... p 1870 N94-21862
FLEMING, J. G. ..... p 1769 N94-21918
FLESHLER, S. ..... p 2033 N94-21997
FLIFLET, ARNE W. ..... p 1752 N94-20931
FLUSS, M. J. ..... p 2036 N94-22594
FOEHLICH, J. ..... p 1977 N94-22271
FOEHNER, FRANK ..... p 1857 N94-21149
FOGARTY, GERARD ..... p 2015 N94-20213
FOGEL, R. A. ..... p 2086 N94-20866
FOGEL, ROBERT A. ..... p 1685 N94-20727
FOGLEBOCH, J. ..... p 2029 N94-21617
FOLEY, M. R. ..... p 1702 N94-20481
FOLKERTS, T. J. ..... p 2036 N94-22582
FOLLO, JEFFREY C. ..... p 1667 N94-20062
FONTANA, ANTONIO P. ..... p 1955 N94-21359
FOO, GRACE ..... p 1865 N94-20487
FORNEK, T. ..... p 1807 N94-19990
FORREST, STEPHEN R. ..... p 2018 N94-20589
FORSYTH, DONALD W. ..... p 1686 N94-20631
FORSYTH, R. ..... p 2141 N94-20909
FORTGANG, C. ..... p 1814 N94-19828
FORTGANG, C. M. ..... p 1815 N94-20272
p 1818 N94-21554
FORTIER, PAUL ..... p 1746 N94-22211
p 1747 N94-22233
FORTIN, ANDRE ..... p 1932 N94-21335
FOSTER, C. M. ..... p 1970 N94-19971
FOWLER, G. W. ..... p 1684 N94-20670
FOWLER, R. H. ..... p 1992 N94-20058
FOWLER, T. K. ..... p 1782 N94-21620
p 1782 N94-21621
p 2034 N94-22050
FOX, J. L. ..... p 2144 N94-21669
p 2144 N94-21672
FOX, ROBERT ..... p 1885 N94-21898
FOX, ROBERT A. ..... p 1885 N94-21897
p 1885 N94-21899
p 1885 N94-21900
p 1886 N94-21901
p 1886 N94-21902
p 1886 N94-21903
p 1886 N94-21904
p 1887 N94-21905
p 1887 N94-21906
p 1887 N94-21907
p 1887 N94-21908
p 1887 N94-21909
p 1888 N94-21910
p 1888 N94-21911
p 1888 N94-21912
p 1888 N94-21913
p 1888 N94-21914
p 1889 N94-21915
FOX, ROBERT L. ..... p 1718 N94-20368
FRALICH, RUSS ..... p 1745 N94-22137
FRANCEZ, NISSIM ..... p 1914 N94-21495
FRANCHI, I. A. ..... p 2083 N94-20726
FRANK, ANDRAS ..... p 1950 N94-20125
p 1950 N94-20161
FRANK, ARTHUR M. ..... p 1645 N94-21051
FRANK, DONALD T. ..... p 1828 N94-20468
FRANKE, S. J. ..... p 1870 N94-21862
FRANKENA, JAN F. ..... p 1953 N94-21075
FRANKLIN, D. G. ..... p 1689 N94-20182
FRANKLIN, HENRY ..... p 1760 N94-21221
FRASER, G. J. ..... p 1870 N94-21862
FRASER, H. L. ..... p 1687 N94-19806
FRAUENFELDER, ULI H. ..... p 1743 N94-20244
FREDERICK, N. V. ..... p 1968 N94-21447
FREDRIKSSON, STEN-AAKE ..... p 1680 N94-20552
FREEDMAN, JEFF ..... p 1744 N94-21339
FREEDMAN, JEFFREY ..... p 1922 N94-21342
FREEMAN, A. ..... p 1719 N94-20410
p 1721 N94-20417
p 1722 N94-20420
FREEMAN, ANTHONY ..... p 1720 N94-20411
FREHLICH, ROD ..... p 1816 N94-20341
FREILICH, MICHAEL H. ..... p 1720 N94-20412
FREIMAN, CHARLES ..... p 1751 N94-20580
FRENZEL, JAMES F. ..... p 1757 N94-21107
p 1757 N94-21110
p 1758 N94-21120
p 1765 N94-21711
p 1768 N94-21731
FRERKING, M. ..... p 1812 N94-22436
FREY, H. V. ..... p 2142 N94-20911
FREY, JEFFREY ..... p 1748 N94-19910
FRIACA, AMANACIO C. S. ..... p 2010 N94-22700
FRICKE, S. K. ..... p 2117 N94-20774
FRIEDMAN, ALEX ..... p 1992 N94-19915
FRINK, NEAL T. ..... p 1919 N94-22357
FROGGATT, M. ..... p 1662 N94-21386
FROLOVA, ALLA ..... p 1915 N94-21551
FROST, C. A. ..... p 1762 N94-21634
FRUCHTMAN, J. ..... p 1683 N94-21984
FRYE, G. C. ..... p 1749 N94-20054
FU, C. L. ..... p 1690 N94-20232
FUJII, DONALD S. ..... p 1894 N94-21237
FUJIMOTO, M. ..... p 2010 N94-22695
FUKUYAMA, ATSUSHI ..... p 2000 N94-22628
FULGHUM, STEPHEN ..... p 1817 N94-21284
FULLER, G. M. ..... p 2081 N94-21618
FULLER, W. ..... p 1915 N94-21561
FULLERTON, E. E. ..... p 2031 N94-21930
p 2035 N94-22564
FULLERTON, R. K. ..... p 1897 N94-21812
FUNG, ADRIAN K. ..... p 1719 N94-20409
FUNG, I. ..... p 1868 N94-21639
FUNSTEN, H. O. ..... p 1976 N94-21995
FUOSS, PAUL ..... p 2013 N94-19967
FURA, DAVID A. ..... p 1937 N94-22414
FURLER, R. ..... p 1809 N94-21545
FURTAK, THOMAS E. ..... p 1678 N94-19839
FUTAGAMI, TSUNEJI ..... p 1686 N94-20804

G

GABELLA, W. ..... p 1981 N94-21668
GABRIEL, ANDREW K. ..... p 1732 N94-20460
GABRIEL, CAMELIA ..... p 1988 N94-19917
GABRIEL, PETER ..... p 2150 N94-21056
GAFFNEY, J. S. ..... p 1855 N94-20220
GAGNE, SIMON ..... p 1785 N94-22201
GAIER, JAMES R. ..... p 1673 N94-20639
GAINER, J. C. ..... p 1651 N94-20108
GAINES, D. P. ..... p 1990 N94-21985
GAINES, JAMES R. ..... p 1845 N94-20088
GAJEWSKI, D. A. ..... p 2018 N94-20335
GALEA, S. C. ..... p 1675 N94-21504
GALES, J. M. ..... p 1925 N94-22471
GALIL, ZVI ..... p 1909 N94-21028
GALINDO, C. ..... p 2087 N94-20908
GALLAGHER, A. ..... p 1699 N94-20047
GALLET, DIDIER ..... p 2018 N94-20598
GALLIE, ELIZABETH ANN ..... p 1843 N94-22422
GALLIMORE, ALEC D. ..... p 1670 N94-21565
GALLINO, R. ..... p 2133 N94-20859
GAMBLES, J. ..... p 1754 N94-21087
GAMBLES, J. W. ..... p 1766 N94-21717
GAMBLES, JODY ..... p 1753 N94-21080
GAMBLES, JODY W. ..... p 1754 N94-21088
GANESH, N. ..... p 1758 N94-21115
GANN, BRIAN ..... p 1671 N94-21882
GAO, BO-CAI ..... p 1636 N94-20959
p 1872 N94-22296
p 1880 N94-22341
GAO, KEQIN ..... p 1744 N94-22102
GAO, Q. ..... p 1680 N94-21145
GAO, XIAO-PING ..... p 1680 N94-20330
GAO, Y. ..... p 2033 N94-21994
GARBER, DONALD P. ..... p 1968 N94-21741
GARBER, H. E. ..... p 1868 N94-21356
GARBEY, M. ..... p 1961 N94-22381
p 1961 N94-22393
GARBINCIUS, P. H. ..... p 1978 N94-21867
GARCIA, E. J. ..... p 1769 N94-21918
GARCIA, JOSEPH P. ..... p 1984 N94-20056
GARCIA, M. ..... p 2048 N94-22519
GARDELLA, JOSEPH A., JR. ..... p 1703 N94-20526
GARGOUR, C. S. ..... p 1793 N94-22248
GARNER, F. A. ..... p 1696 N94-22037
GARRISON, D. H. ..... p 2106 N94-20712
p 2115 N94-20763
GARRISON, J. C. ..... p 1949 N94-20006
p 1816 N94-20480
GASS, J. ..... p 2049 N94-22544
GASTAL, J. ..... p 1668 N94-20077
GATES, S. M. ..... p 2014 N94-19980
GATHMAN, S. G. ..... p 1868 N94-21356
GAUDET, S. ..... p 2047 N94-22469
GAUDIOT, J. L. ..... p 1937 N94-22378
GAUDREAU, MICHEL ..... p 1653 N94-22188
GAUDREAULT, M. ..... p 1782 N94-22177
GAULT, D. E. ..... p 1862 N94-20744
GEBAUER, LINDA ..... p 1660 N94-21377
GEBERT, C. T. ..... p 1749 N94-20054
GEBHARD, J. ..... p 2084 N94-20827
GEDDES, J. J. ..... p 1710 N94-20984
GEDNEY, STEPHEN D. ..... p 1724 N94-20431
GEER, JAMES F. ..... p 1959 N94-21588
GEERTSEMA, GERTIE ..... p 1865 N94-20239
GEIL, BRUCE ..... p 1713 N94-19834
GEISIK, C. ..... p 1997 N94-21989
GELLER, M. J. ..... p 2064 N94-22476
GEORGANAS, N. D. ..... p 1746 N94-22203
GEORGE, ALBERT R. ..... p 1967 N94-20523
GEORGE, E. P. ..... p 1694 N94-21948
GEORGE, JEFFREY A. ..... p 1654 N94-21570
GERBERICH, W. W. ..... p 1693 N94-21854
GERMAN, R. M. ..... p 1689 N94-20019
GERRISH, H. P., JR. ..... p 1671 N94-21860
GERRY, DONALD D. ..... p 1740 N94-21264
GERSTELL, M. F. ..... p 2145 N94-21679
GERSTENBERG, HEIKO ..... p 1706 N94-21542
GETTYS, JIM ..... p 1925 N94-22477
GEYER, H. K. ..... p 1847 N94-21774
GEZARI, D. Y. ..... p 1927 N94-22543
GHARAKANIAN, V. ..... p 1991 N94-20646
GHONIEM, AHMED F. ..... p 1681 N94-21213
GHOSH, M. ..... p 1850 N94-22257
GIACCONI, R. ..... p 2054 N94-20174
GIALLORENZI, THOMAS G. ..... p 1797 N94-20094
GIBBONS, FRANK L. ..... p 1812 N94-22433
GIBBONS, PAUL C. ..... p 1740 N94-21352
GIBBS, H. M. ..... p 1814 N94-19665
GIBBS, M. A. ..... p 1887 N94-21909
GIBSON, JONATHAN S. ..... p 1756 N94-21103
GIBSON, MICHAEL A. ..... p 2126 N94-20621
GIERMAN, S. M. ..... p 1814 N94-19828
p 1816 N94-20277

GIGOUX, P. p 1925 N94-22465
GILBERT, WILLIAM E. p 1964 N94-21322
GILL, M. p 1744 N94-21092
GILL, P. E. p 1950 N94-20217
GILLIES, D. C. p 2030 N94-21807
GILLIKIN, LYNN S. p 1893 N94-20168
GILLILAND, GUY D. p 2028 N94-21362
GILLILAND, KIRBY p 1893 N94-20023
GILYARD, GLENN B. p 1649 N94-21879
GIRIMAJI, SHARATH S. p 1804 N94-21861
GIROSI, FEDERICO p 1913 N94-21364
GIROUX, NATALY p 1949 N94-19854
GIUSTI-SUZOR, A. p 1818 N94-21829
GLAESER, R. M. p 1884 N94-19826
GLASS, JEFFREY T. p 2026 N94-21190
GLASSER, A. H. p 1997 N94-21965
GLENDINNING, S. G. p 1818 N94-21547
GLICKMAN, MARK E. p 1964 N94-21442
GLISH, G. L. p 1852 N94-22004
GLYNN, PETER W. p 1949 N94-19854
p 1902 N94-19855
p 1939 N94-19909
p 1962 N94-19999
GMUER, N. F. p 2015 N94-20260
GODART, C. p 2032 N94-21987
GODBEY, DAVID J. p 2017 N94-20348
GOEBEL, MARTIN p 1930 N94-21018
GOERINGER, D. E. p 1852 N94-22004
GOGINENI, S. P. p 1715 N94-19823
p 1725 N94-20435
GOGINENI, S. PRASAD p 1858 N94-21811
GOHIL, P. p 1998 N94-22039
GOITY, J. L. p 1977 N94-22009
GOLD, D. P. p 1862 N94-20767
GOLDBERG, R. K. p 1676 N94-21777
GOLDEN, D. C. p 2143 N94-21668
GOLDEN, SUSAN M. p 1712 N94-20927
GOLDSTEIN, J. p 1814 N94-19828
GOLDSTEIN, J. C. p 1818 N94-21554
GOLDSTEIN, J. L. p 2086 N94-20894
p 1683 N94-22031
GOLDSTEIN, W. H. p 1818 N94-21547
GOLIGHTLY, MICHAEL J. p 1893 N94-21863
GOLSHAN, N. p 1731 N94-20458
GONZALEZ, AVELINO J. p 1671 N94-21682
GOODING, JAMES L. p 2086 N94-20869
p 1812 N94-22433
GOODING, R. H. p 1652 N94-21224
GOORJIAN, PETER p 1719 N94-20406
GOPALAKRISHAN, GANESH p 1758 N94-21119
GOPALAKRISHNAN, G. K. p 1748 N94-19892
GOPALAKRISHNAN, SURESH K. p 1759 N94-21125
GOPALSAMI, N. p 1677 N94-21940
GORDGE, DENNIS N. p 1807 N94-20203
p 1896 N94-21154
GORDON, H. B. p 1855 N94-20256
GORDON, J. E. p 2031 N94-21926
GORDON, J. S., JR. p 2029 N94-21691
GORSLINE, D. S. p 2091 N94-20395
p 2099 N94-20674
GORVAD, M. R. p 1906 N94-20316
GOSS, SIMON p 1841 N94-21453
GOSSAGE, S. A. p 1899 N94-20476
GOSSELIN, CLEMENT p 1792 N94-22240
GOSSELIN, CLEMENT M. p 1792 N94-22241
GOTWAY, C. A. p 1916 N94-21781
GOUBRAN, RAFIK A. p 1774 N94-22125
GOUDER, T. H. p 1688 N94-19986
GOUGH, PAUL S. p 1801 N94-20915
GOURMELON, G. p 1662 N94-21386
GOW, A. p 1715 N94-19823
GOYCOCHEA, J. F. p 1739 N94-21235
GRADY, CAROL A. p 2055 N94-21498
GRADY, D. E. p 1829 N94-19824
p 1698 N94-19903
p 1832 N94-21557
p 1708 N94-21963
GRAEDEL, T. E. p 1852 N94-21969
GRAF, G. M. p 1977 N94-22271
GRAF, JOHN p 2126 N94-20820
GRAF, T. p 2032 N94-21987
GRAF, TH. p 1685 N94-20697
GRAGERT, P. K. p 1953 N94-21046
GRAHAM, R. A. p 1829 N94-19927
p 1688 N94-19944
p 1713 N94-22033
GRALA, CARL P. p 1655 N94-21794
GRAMSCH, S. A. p 2033 N94-21992
GRAND, G. p 1989 N94-21599
GRANT, B. C. p 1852 N94-22004
GRANT, CLARENCE L. p 1712 N94-20927
GRANT, KENNETH J. p 1814 N94-19850
GRAPPIN, R. p 2003 N94-22650
GRASHCHENKO, A. P. p 1664 N94-21399
GRAUDENZ, D. p 1947 N94-22563
GRAVES, SARA p 2042 N94-20268
GRAY, G. T., III p 1693 N94-21843
GRAY, HENRY F. p 1751 N94-20350
GRAY, L. J. p 1961 N94-22379
GRAYZECK, E. p 2047 N94-22496
GREELEY, R. p 2098 N94-20671
p 2101 N94-20686
p 2136 N94-20876
p 1844 N94-20888
GREEN, JOHN A. p 1648 N94-21268
GREEN, ROBERT D. p 1667 N94-20062
GREEN, STEVEN M. p 1643 N94-21606
GREEN, WILLIAM S. p 1765 N94-21710
GREENOUGH, J. A. p 1803 N94-21531
GREENWELL, D. p 1701 N94-20352
GREINER, J. p 2149 N94-20603
p 2150 N94-20604
GREINER, JOHN p 1902 N94-19918
GRENIER, D. p 1745 N94-22160
GRIBBLE, R. J. p 2036 N94-22583
GRIEST, K. p 2058 N94-22444
GRIEVE, R. A. F. p 1862 N94-20668
p 1863 N94-20887
GRIFFIN, J. C. p 2046 N94-22407
GRIFFIN, MICHAEL K. p 1880 N94-22338
GRIFFIN, THOMAS A. p 1654 N94-21792
GRIFFIN, W. L. p 2097 N94-20661
GRIMALDI, MARGARET E. p 1654 N94-20304
GRIMSDITCH, M. p 1970 N94-19971
p 2031 N94-21930
GRIMSON, W. E. p 1939 N94-19893
GRIN, E. A. p 2143 N94-21664
GRISHAM, D. L. p 1981 N94-21767
GROEBNER, R. J. p 1998 N94-22039
GROENEWALD, G. p 1960 N94-22099
GROLLMANN, THOMAS p 1855 N94-20155
GROSBOL, P. p 2048 N94-22518
GROSSHANDLER, W. L. p 1682 N94-21448
GROSSMAN, J. N. p 2085 N94-20854
GROSSMAN, L. p 2084 N94-20770
p 2086 N94-20897
GROSSMAN, R. p 1921 N94-22375
GROSSMAN, ROBERT p 1921 N94-22376
GROSSMAN, T. p 1906 N94-20276
GROSSO, ENRICO p 1894 N94-20520
GROTE, D. p 1993 N94-20234
GROVE, T. L. p 1686 N94-20853
GRUBB, J. W. p 1937 N94-22267
GRUEN, E. p 2084 N94-20827
p 2141 N94-20909
GRUMBERG, ORNA p 1902 N94-19919
GRUND, CHRISTIAN J. p 1876 N94-22323
GRUSS, ANDREW p 1761 N94-21282
GRYK, THOMAS J. p 1987 N94-21279
GU, QING p 2013 N94-19939
GUCCIONE, ROBERTO p 1653 N94-22588
GUERARD, FRANCOISE p 1664 N94-21400
GUERIN, YVES p 1752 N94-20632
GUEVENC, Z. B. p 1971 N94-20050
GUHA, JOYTI p 1705 N94-21416
GUIDRY, M. W. p 1976 N94-21961
GUILLAUMON, J. C. p 1659 N94-21369
GUILLAUMON, JEAN-CLAUDE p 1664 N94-21400
GUILLIN, J. p 1660 N94-21374
GUILLOT, MICHEL p 1792 N94-22241
GUINNESS, E. A. p 2115 N94-20762
GULICK, V. C. p 2142 N94-21660
p 2144 N94-21670
GULKIS, S. p 1812 N94-22436
GULLIVER, T. AARON p 1792 N94-22243
GULTEPE, I. p 1878 N94-22332
p 1879 N94-22335
GUMLEY, LIAM E. p 1872 N94-22298
GUNAWARDENA, J. A. p 1767 N94-21730
GUNZEL, CHARLES A., III p 1650 N94-19879
GUO, YAO-BIN p 1636 N94-19963
GUPTA, ANIL K. p 1746 N94-22203
GUPTA, ARUN P. p 1911 N94-21183
GUPTA, L. C. p 2032 N94-21987
GUREVICH, A. V. p 1750 N94-20325
GUREVICH, ALEXANDER V. p 2002 N94-22643
GURNETT, D. A. p 2088 N94-20048
GUSEYNOV, G. D. p 2028 N94-21438
GUSMAN, M. I. p 1705 N94-21425
GUYENNE, H. T. DUC p 2000 N94-22624
GYETVAY, S. R. p 1681 N94-21226

H

HAAK, K. F. I. p 1960 N94-22096
HAAN, S. W. p 1818 N94-21547
HAAS, ULRIK p 1952 N94-21042
HABBAL, SHADIA R. p 2147 N94-21522
HABER, I. p 1981 N94-21440
HABER, IRVING p 1992 N94-19915
HABERLE, R. M. p 2144 N94-21671
p 1812 N94-22436
HACCOUN, D. p 1793 N94-22247
HACCOUN, DAVID p 1773 N94-22121
p 1775 N94-22132
p 1793 N94-22246
HADIMIOGLU, B. p 1967 N94-19949
HADJ-MESSAOUD, AMMAR p 1792 N94-22241
HADZIEVSKI, L. R. p 2006 N94-22673
HAERTLING, G. p 1749 N94-20012
HAERTLING, GENE p 1705 N94-21416
HAFEZ, H. M. p 1783 N94-22188
HAGE, R. T. p 1656 N94-21859
HAGEN, DONALD E. p 1877 N94-22326
HAGEN, JOHN B. p 1763 N94-21695
HAGER, BRADFORD H. p 2116 N94-20769
HAGGERTY, JAMES J. p 2054 N94-21739
HAH, CHUNILL p 1919 N94-22360
HAHN, H. T. p 1673 N94-20490
HAHN, ROGER p 1922 N94-21342
HAIKALA, L. p 1965 N94-22536
HAJJ, GEORGE A. p 1723 N94-20425
HAJJ, I. p 1761 N94-21256
HAJJ, I. N. p 1749 N94-20110
HALFORD, GARY R. p 1834 N94-22613
p 1834 N94-22614
HALL, C. A. p 1829 N94-19943
HALL, G. S. p 1863 N94-20889
HALL, MARY-JO p 1894 N94-21237
HALL, S. A. p 1863 N94-20882
HALL, STUART A. p 1862 N94-20757
HALLER, E. E. p 1988 N94-21528
p 2030 N94-21744
p 2030 N94-21763
p 2031 N94-21922
HALLETT, J. p 1871 N94-22294
HALLETT, JOHN p 1877 N94-22326
p 1879 N94-22336
p 1881 N94-22343
HALLIDAY, ALEX N. p 1862 N94-20776
p 2118 N94-20777
p 2118 N94-20778
p 2118 N94-20779
HALZEN, F. p 1973 N94-20474
HAM, NORMAN D. p 1650 N94-20524
HAMACHER, H. p 1662 N94-21390
HAMADY, F. J. p 1826 N94-22093
HAMILTON, PAUL D. p 1779 N94-22157
HAMILTON, THOMAS T. p 2056 N94-21779
HAMILTON, VICTORIA E. p 2121 N94-20796
HAMMEL, C. J. p 1748 N94-19902
HAMMEL, P. C. p 2030 N94-21768
p 2034 N94-22007
HAMMELRATH, FRO p 1964 N94-21139
HAMMER, J. p 1640 N94-22603
HAMMOND, C. R. p 1833 N94-21956
HAMMONS, B. E. p 1814 N94-19865
HAMSHERE, B.L. p 1711 N94-19906
HAN, C. p 1847 N94-21540
HAN, KWANG S. p 1994 N94-21289
p 1994 N94-21290
p 1995 N94-21291
p 1995 N94-21292
p 1995 N94-21293
p 1995 N94-21294
HAN, P. p 1970 N94-19956
HAN, YENJO p 1907 N94-20536
p 1911 N94-21200
p 1912 N94-21285
HANAOKA, Y. p 2001 N94-22633
HANAWA, TOMOYUKI p 2008 N94-22687
p 2008 N94-22688
p 2009 N94-22689
HANCHANG, PENG p 1685 N94-20677
HANISCH, R. J. p 1925 N94-22478
HANNA, SALIM A. p 1747 N94-22212
HANNER, M. S. p 2141 N94-20909
HANNON, R. p 2033 N94-21998
HANSEN, C. p 1917 N94-21764
HANSEN, C. D. p 1929 N94-20279
p 1935 N94-21622
p 1936 N94-21746
HANSEN, J. p 1868 N94-21639
HANSEN, JAMES p 1869 N94-21641
p 1869 N94-21643
HANSEN, P. M. p 1737 N94-20620
HANSEN, V. L. p 2101 N94-20683
HANSMANN, ULRICH H. E. p 2016 N94-20285
HANSON, C. E. p 1969 N94-22054
HANSON, CARL E. p 1968 N94-22053
HANSON, D. L. p 1980 N94-20295
HANSON, F. E. p 1987 N94-21236
HANSON, J. p 1780 N94-22166
HANSON, J. S. p 1641 N94-21428
HANSON, J. V. p 1747 N94-22217
HAPKE, B. W. p 1991 N94-20646
HAPPELL, NADINE p 1932 N94-21332
HARBISON, BARRY B. p 1701 N94-20331

HARBOR, KAREN S. p 1942 N94-20573
HARDEE, H. K. p 1859 N94-22006
HARDIN, DANNY p 2042 N94-20268
HARDMAN, LYNDA p 2044 N94-21535
p 2045 N94-21536
HARDWICK, JONATHAN C. p 1902 N94-19932
HARDY, ALVA C. p 1893 N94-21863
HARELAND, W. A. p 1993 N94-20261
HARFOUSH, F. A. p 1982 N94-21934
HARINK, J. H. A. p 1945 N94-21233
HARKNESS, J. B. L. p 1682 N94-21789
HARMON, B. N. p 1695 N94-21964
HARMSEN, F. p 2045 N94-22276
HAROKOPUS, W. P., JR. p 1733 N94-20501
HARPER, ROBERT p 1908 N94-20622
HARR, PATRICK A. p 1867 N94-21307
HARRAH, S. D. p 1721 N94-20418
p 1722 N94-20419
HARRELL, LINDA p 1744 N94-21350
HARRELL, M. J. p 1734 N94-20509
HARRIGAN, R. W. p 1946 N94-21929
HARRINGTON, J. L. p 1878 N94-22331
HARRIS, C. B. p 1990 N94-22002
HARRIS, CHARLES E. p 1833 N94-22608
HARRISON, D. P. p 1847 N94-21540
HARRISON, GEORGE C. p 1905 N94-20109
HARRISON, L. p 1647 N94-20343
HARRISON, P. ANN p 1837 N94-20284
HARRISON, PATRICK R. p 1837 N94-20284
HARSHVARDHAN p 1865 N94-20535
HART, GERALD E. p 1643 N94-20197
HART, K. J. p 1852 N94-22004
HARTENSTEIN, S. p 1683 N94-22021
HARTMAN, M. C. p 1882 N94-20531
HARTMANN, K. p 1651 N94-21280
HARTNER, G. p 2054 N94-20174
HARTZ, LESLIE S. p 1654 N94-20304
HARVEY, R. P. p 2145 N94-21678
HARVEY, ROBERT LYNN p 1653 N94-20339
HARVEY, WILSON A., JR. p 1809 N94-21445
HASAN, H. p 2055 N94-20204
p 2048 N94-22497
HASHIMOTO, AKIHIKO p 1686 N94-20855
HASINGER, G. p 2054 N94-20174
HASLAM, G. E. p 1745 N94-22161
HASLAM, GEORGE p 1745 N94-22144
HASLETT, J. W. p 1778 N94-22152
HATHAWAY, M. D. p 1636 N94-20136
HATTORI, HARUMI p 1698 N94-19840
HAUGLAND, E. p 1709 N94-20972
HAVERKORT, BOUDEWIJN R. p 1963 N94-21058
HAVSTAD, M. A. p 1709 N94-21970
HAWKE, B. R. p 2101 N94-20682
HAWKE, B. RAY p 2107 N94-20719
p 2119 N94-20786
HAWKINS, CHARLES F. p 1755 N94-21093
HAWKINS, S. A. p 1769 N94-21838
HAWRYLUK, A. M. p 1750 N94-20231
HAWTHORNE, H. M. p 1661 N94-21381
HAY, P. J. p 2031 N94-21857
HAYAKAWA, JUNJI p 1713 N94-20605
HAYASHI, T. p 2000 N94-22625
HAYASHIDA, KIYOSHI p 2009 N94-22690
HAYDEN, B. J. p 1932 N94-21332
HAYDEN, S. Z. p 1833 N94-22001
HAYES, JEREMIAH F. p 1773 N94-22119
p 1773 N94-22120
HAYNES, T. E. p 2034 N94-22016
HAYS, PAUL B. p 1855 N94-20132
p 1859 N94-22026
HAZELTINE, R. D. p 1951 N94-20224
p 1999 N94-22562
HAZEWINKEL, MICHIEL p 1954 N94-21158
p 1954 N94-21159
HE, X. p 1771 N94-22107
HE, YONG-GUI p 1815 N94-19965
HE, Z. X. p 1827 N94-22390
HEAD, JAMES W. p 2099 N94-20672
p 2101 N94-20686
p 1813 N94-20688
p 2123 N94-20806
p 1863 N94-20879
HEBBALALU, K. p 1764 N94-21703
HECK, A. p 2047 N94-22479
HECK, PATRICK W. p 1872 N94-22299
p 1872 N94-22302
HEDIN, A. E. p 1870 N94-21862
HEGEDUS, S. S. p 1848 N94-21826
HEGER, D. p 1657 N94-20235
HEIDELBACH, F. p 1695 N94-21990
HEIMALA, P. p 1989 N94-21600
p 1989 N94-21602
HEIMALA, PAEIVI p 1989 N94-21601
p 1989 N94-21603
HEIMRATH, D. p 1857 N94-21044
HEIN, PAUL F. p 1876 N94-22321
HEINSTEIN, M. W. p 1915 N94-21539
p 1805 N94-22556
HEINTZE, NEVIN p 1902 N94-19948
HEIRATH, J. p 2117 N94-20772
HELALY, A. p 1746 N94-22162
HELENELUND, KURT p 1923 N94-22067
HELGESON, W. D. p 1750 N94-20294
p 2016 N94-20296
HELLMAN, CHAN M. p 2040 N94-21626
HELM, HANSPETER p 1974 N94-21461
HELMS, C. p 1748 N94-19844
HEMACHANDRA, LANE A. p 1907 N94-20536
p 2043 N94-21287
HEMASPAANDRA, LANE A. p 1912 N94-21273
p 1912 N94-21285
p 1954 N94-21314
HEMKER, P. W. p 1910 N94-21078
p 1682 N94-21574
HENAGER, C. H., JR. p 1690 N94-20233
HENDEN, A. A. p 1925 N94-22480
HENDERSON, C. L. p 1916 N94-21633
HENDRICKS, ROBERT C. p 1654 N94-21790
p 1654 N94-21791
p 1654 N94-21792
p 1655 N94-21795
HENDRZAK, GARY E. p 1933 N94-21343
HENESIAN, M. A. p 1819 N94-21872
p 1819 N94-21920
p 1820 N94-22401
HENESTROZA, E. p 1993 N94-20234
p 1981 N94-21439
HENINS, I. p 2036 N94-22583
HENKE, MICHAEL p 1889 N94-20022
HENKE, R. p 1640 N94-22601
p 1640 N94-22605
HENLINE, P. A. p 1998 N94-22089
HENRIKSEN, G. L. p 1748 N94-19885
HENRY, D. P. p 1676 N94-21777
HENRY, HUGH A. p 1740 N94-21436
HENRY, J. PATRICK p 2054 N94-20175
p 2055 N94-21579
HENSYL, J. p 1647 N94-20343
HEPNER, DAVID J. p 1808 N94-20930
HERGENROTHER, PAUL M. p 1672 N94-20540
HERMANN, MICHAEL p 1798 N94-20145
HERNANDEZ, D. p 1665 N94-21405
HEROUX, MICHAEL A. p 1928 N94-19950
HERR, JOEL L. p 1666 N94-21864
HERRERA, P. p 1991 N94-20646
HERTEL, E. S., JR. p 1904 N94-20052
HERZINGER, CRAIG M. p 2022 N94-20995
p 2023 N94-20996
HERZOG, G. F. p 1863 N94-20889
HESS, P. C. p 2099 N94-20675
HEUSER, W. RANDY p 1932 N94-21333
HEWETT, D. p 1993 N94-20234
HEWETT, D. W. p 1992 N94-19991
HEWETT, KEVIN B. p 1973 N94-20618
HEYMSFIELD, A. J. p 1878 N94-22332
p 1879 N94-22335
HEYMSFIELD, ANDREW p 1871 N94-22293
HICKEY, DAVID H. p 1646 N94-21592
HICKEY, M. H. p 1769 N94-21830
HICKMAN, R. p 1829 N94-19943
HIDALGO, JUAN CARLOS p 1744 N94-21102
HIENBICH, VO p 1861 N94-22575
HILDEBRAND, A. R. p 1862 N94-20668
HILDNER, S. S. p 1807 N94-20114
p 1807 N94-20115
HILL, CAROL M. p 1660 N94-21377
HILL, F. p 1927 N94-22549
HILL, GRANT MICHAEL p 2081 N94-22592
HILL, TIMOTHY J. p 1893 N94-20081
HILLIARD, DONALD P. p 1717 N94-20333
p 1718 N94-20334
HILTON, M. p 1705 N94-21225
HILTON, THOMAS F. p 2040 N94-21626
HIMER, J. T. p 1926 N94-22481
HIMPSEL, F. J. p 2014 N94-19980
HINEDI, S. p 1731 N94-20458
HINES, R. E. p 1918 N94-21977
HINKER, P. p 1917 N94-21764
HINKS, D. G. p 2029 N94-21649
p 2033 N94-21998
HINSEY, N. A. p 2031 N94-21931
HINTZEN, PAUL p 2048 N94-22534
HIRAYAMA, T. p 2004 N94-22655
HIROI, T. p 2085 N94-20848
HIROI, TAKAHIRO p 2084 N94-20813
HIROTANI, KOUICHI p 2009 N94-22692
HIRTH, J. P. p 1690 N94-20233
HIRVONEN, LUDWIK p 1708 N94-21893
HITTERMAN, R. L. p 2033 N94-21998
HJALMARSON, H. P. p 2016 N94-20296
p 1750 N94-20312
HJELLMING, R. M. p 1926 N94-22482
HLIVAK, R. J. p 1828 N94-22489
HO, K. M. p 1695 N94-21964
HOBAN, FRANCIS T. p 2040 N94-21499
HODD, J. p 1790 N94-22227
HODGE, P. E. p 1926 N94-22483
HODGES, JOSEPH T. p 1802 N94-21193
HODGSON, JOHN A. p 1895 N94-20338
HODSON, ROBERT F. p 1754 N94-21089
HOEHLER, G. p 1639 N94-22596
HOENE, ALBRECHT p 1912 N94-21273
HOFER, W. W. p 1768 N94-21770
HOFFMAN, E. L. p 1829 N94-19940
HOFFMAN, ED p 2039 N94-21497
HOFFMAN, RICHARD G. p 1891 N94-20624
HOFFMANN, HANS-EBERHARD p 1871 N94-22280
HOFMANN, B. p 1684 N94-20652
HOFMEISTER, GRETCHEN E. p 1704 N94-21186
HOJNICKI, JEFFREY S. p 1667 N94-20062
HOLBEN, BRENT N. p 1838 N94-20958
p 1839 N94-20961
HOLBER, W. M. p 1996 N94-21769
HOLDEMAN, J. D. p 1649 N94-21758
HOLDEN, N. E. p 1682 N94-21631
HOLLENBECK, J. L. p 1675 N94-21191
HOLMAN, G. T. p 1829 N94-19927
HOLMAN, G. T., JR. p 1688 N94-19944
HOLMANN, E. p 2117 N94-20771
HOLMES, N. C. p 1707 N94-21546
p 1695 N94-22024
HOLMES, RICHARD R. p 1703 N94-20541
HOLONYAK, N., JR. p 2030 N94-21805
HOLROYD, R. p 1973 N94-20324
HOLROYD, R. A. p 1970 N94-19931
HOLT, R. J. p 1976 N94-21941
HOLTZCLAW, K. W. p 1663 N94-21395
HOLZER, STEFAN M. p 1830 N94-20036
HONDA, M. p 2082 N94-20658
HONIG, E. M. p 1814 N94-19867
HONKANEN, S. p 1988 N94-21595
HOOPER, ROSS p 1645 N94-22155
HOOPER, STEVE p 1641 N94-20189
HOOPER, W. P. p 1868 N94-21356
HOOVER, C. G. p 1937 N94-22042
p 1977 N94-22400
HOOVER, W. G. p 1937 N94-22042
p 1977 N94-22400
HOPE, ALLEN S. p 1837 N94-20951
HOPKINS, D. A. p 1676 N94-21777
HOPKINS, DALE A. p 1833 N94-22608
HOPPE, P. p 2082 N94-20659
HOPPER, R. W. p 1803 N94-21651
HOPPIN, ANDREW p 1685 N94-20689
HORAK, J. A. p 1689 N94-20093
HORAN, D. M. p 1657 N94-19896
p 1658 N94-20617
p 1652 N94-20850
HORAN, M. F. p 2085 N94-20854
HORANYI, M. p 2141 N94-20909
HORIUCHI, R. p 2000 N94-22625
HORNSTEIN, JOHN S. p 1858 N94-21357
HORONJEFF, RICHARD D. p 1968 N94-22053
HOROWITZ, PAUL p 1897 N94-20336
HORTON, GRAHAM p 1914 N94-21462
HORTON, J. A. p 1694 N94-21948
HORTON, W. p 1995 N94-21514
p 1996 N94-21752
p 1998 N94-22561
HORWEDEL, J. E. p 1918 N94-22088
HOSHINO, MASAHIRO p 2007 N94-22679
HOSSEINMOSTAFA, R. p 1725 N94-20435
HOTALING, STEVEN P. p 1651 N94-20011
HOUSEMAN, JOHN p 1660 N94-21378
HOUSNER, JERROLD M. p 1833 N94-22608
p 1836 N94-22621
HOVANDER, B. p 2042 N94-20193
HOWARD, LARRY p 1650 N94-19880
HOWARD, STEPHEN L. p 1679 N94-20111
HOWE, HAROLD W. p 1654 N94-21792
HOWELL, R. H. p 2036 N94-22594
HSU, A. p 2084 N94-20770
p 2086 N94-20897
HSU, I. p 1981 N94-21688
HSU, J.-C. p 1926 N94-22484
HSU, SHIH-YING p 2012 N94-19848
p 2012 N94-19849
HUA, LI p 1706 N94-21437
HUANG, HO-CHUNG p 1760 N94-21178
HUANG, J. p 1928 N94-19812
p 1722 N94-20421
p 1731 N94-20457
HUANG, ZHI-SONG S. p 2027 N94-21304
HUBBARD, ARTHUR T. p 1691 N94-21245
HUCHRA, J. P. p 2064 N94-22476
HUDEC, R. p 2149 N94-20603
HUDSON, DAVID F. p 1815 N94-20055
p 1717 N94-20198

HUDSON, H. p 2004 N94-22657
HUGHES, E. p 1975 N94-21788
HUGHES, T. H. p 1697 N94-19809
HUITEMA, G. B. p 1945 N94-21233
HULBERT, S. J. p 1926 N94-22485
HUMER, K. p 1706 N94-21542
p 1709 N94-22008
HUMMEL, JOHN R. p 1987 N94-21172
HUMMEL, S. G. p 1845 N94-19805
HUMPHREYS, R. M. p 1927 N94-22512
HUNDLEY, M. F. p 2032 N94-21987
HUNG, DO-DUY p 1644 N94-22135
HUNT, JAMES J. p 2000 N94-22624
HUNT, KENNETH K. p 1717 N94-20329
HUNTER, B. A. p 2033 N94-21998
HUNTER, IAN W. p 1784 N94-22192
p 1784 N94-22193
HUNTLEY, M. p 1683 N94-22021
HUO, Q. p 2017 N94-20544
HURDLE, JOHN F. p 1757 N94-21111
p 1758 N94-21119
HURTEAU, RICHARD p 1794 N94-22256
HUSAIN, SHABU p 1744 N94-21345
HUSSAINI, M. Y. p 1804 N94-21880
HUSSAINI, M. YOUSUFF p 1797 N94-20033
HUSSEIN, ZIAD A. p 1718 N94-20404
HUTCHEON, I. p 1684 N94-20667
HUTCHEON, I. D. p 2134 N94-20862
HUTCHERSON, R. K. p 1751 N94-20354
HUTCHINGS, BRAD L. p 1758 N94-21117
HUTCHINS, J. p 1936 N94-21853
HUTCHINS, J. A. p 1928 N94-19858
HUTCHISON, MATTHEW G. p 1646 N94-21246
HUTLICKA, EVA p 1894 N94-20610
HUYNH, D. D. p 1724 N94-20432
HUYNH, H. T. p 1780 N94-22165
p 1645 N94-22219

I

IBANEZ, S. MIGUEL H. p 2006 N94-22667
p 2006 N94-22666
IBRAHIM, B. B. p 1804 N94-21748
IGA, SAYURI p 2009 N94-22690
IGUCHI, TOSHIO p 1728 N94-20446
IJAZ, NABEEL p 1757 N94-21110
ILCEWICZ, L. p 1834 N94-22609
ILIFFE, J. C. p 2128 N94-20830
IMAMURA, H. p 1638 N94-22260
IMAMURA, M. p 2082 N94-20658
INDACOCHEA, E. p 1847 N94-21650
INDACOCHEA, E. J. p 1848 N94-21870
INGERMANN, ERIK H. p 1765 N94-21711
INGRAHAM, DIANE p 1747 N94-22213
INGRAM, DAVID C. p 1710 N94-20981
p 1710 N94-20983
p 1710 N94-20984
p 2022 N94-20990
p 1710 N94-20991
INOUE, HAJIME p 2002 N94-22639
INTRIERI, J. p 1844 N94-22303
INTRIERI, JANET M. p 1872 N94-22301
p 1873 N94-22305
p 1873 N94-22306
p 1875 N94-22317
IOLLO, ANGELO p 1950 N94-20092
IRELAND, T. p 2086 N94-20884
ISAACMAN, RICHARD B. p 1925 N94-22471
ISAACS, H. S. p 1690 N94-20301
ISHIDO, Y. p 2004 N94-22655
ISHIGURO, SEIJI p 2005 N94-22664
ISLER, R. C. p 1999 N94-22568
ISOBE, SHUNKICHI p 1746 N94-22170
ISOBE, T. p 1926 N94-22486
ISRAELI, AMOS p 1935 N94-21549
ISRAELI, MOSHE p 1957 N94-21478
ISTOMIN, Y. N. p 2007 N94-22675
ITIKAWA, Y. p 2004 N94-22653
ITOH, KIMITAKA p 2000 N94-22628
ITOH, NAOKI p 2001 N94-22638
ITOH, SANAE-I. p 2000 N94-22628
ITOH, TATSUO p 2028 N94-21521
ITOI, T. p 1836 N94-20891
ITTIPIBOON, A. p 1782 N94-22178
IVANCIC, WILLIAM D. p 1656 N94-21581
IVANILOV, Y. P. p 2052 N94-22081
IVANOV, B. A. p 1854 N94-20698
p 2106 N94-20709
IWAHASHI, TSUTOMU p 1772 N94-22118
IYER, K. p 1829 N94-19836
IYER, S. S. p 2014 N94-19980
IZETT, G. p 1685 N94-20753
IZETT, G. A. p 1685 N94-20701
IZYGON, MICHEL p 1930 N94-21065
IZZO, C. p 2080 N94-22555

J

JACKSON, EUGENE D. p 1667 N94-20070
p 1667 N94-20071
p 1668 N94-20072
JACKSON, M. P. A. p 2111 N94-20738
JACOB, JONAH p 1817 N94-21284
JACOBI, S. p 1774 N94-22129
JACOBS, DAVID W. p 1983 N94-19819
JACOBS, J. W. p 1799 N94-20286
JACOBS, P. p 1926 N94-22487
p 1927 N94-22513
JACOBSEN, C. p 1989 N94-21630
JAFELICE, LUIZ C. p 2010 N94-22700
JAJODIA, SUSHIL p 1909 N94-21034
JAKOSKY, B. M. p 2090 N94-20394
p 2144 N94-21672
JAKUBKA, K. p 1997 N94-21816
JAMALI, M. p 1759 N94-21123
JAMES, J. E. p 1868 N94-21356
JAMES, J. H. p 1967 N94-21306
JAMES, P. B. p 2090 N94-20392
JAMESON, LELAND p 1950 N94-20087
JAMNEJAD, V. p 1722 N94-20423
p 1725 N94-20436
p 1731 N94-20457
JAN, Y.-J. p 1798 N94-20167
JANKE, GERD p 1798 N94-20147
JANKOWSKI, A. F. p 1694 N94-21944
JANOWITZ, JOAN p 1647 N94-20053
JANSEN, JACK p 2044 N94-21494
JANSSEN, M. A. p 1812 N94-22436
JANUSZ, PAUL E. p 1910 N94-21144
JAROSEWICH, E. p 2082 N94-20681
JASKOWIAK, MARTHA H. p 1700 N94-20195
JATA, KUMAR V. p 1691 N94-21188
JAYARAM, R. p 1689 N94-20180
JAYASUMANA, ANURA P. p 1756 N94-21105
p 1757 N94-21108
p 1766 N94-21721
p 1767 N94-21727
JAYNE, DOUGLAS p 1675 N94-21488
JEANMONOD, ROLAND W. p 1752 N94-20631
JEANMONOD, ROLAND-W. p 1752 N94-20635
JEDAMZIK, K. p 2081 N94-21618
JEFFERIES, KENT S. p 1984 N94-20140
JEHLE, ROBERT E. p 1717 N94-20198
JELINSKY, P. p 2047 N94-22459
JELLINEK, J. p 1971 N94-20050
JENKINS, D. G. p 1799 N94-20286
JENKINS, R. E. p 1755 N94-21098
JENKINS, THOMAS F. p 1712 N94-20927
JENNINGS, D. G. p 1926 N94-22488
p 2047 N94-22493
p 2048 N94-22509
JENSEN, ERIC J. p 1877 N94-22327
JEON, BYUNG WOOK p 1764 N94-21706
p 1765 N94-21707
JEONG, CHEOL-HO p 1744 N94-21099
JERDE, ERIC A. p 1662 N94-20776
p 2126 N94-20820
p 2126 N94-20821
JERMAN, G. p 1689 N94-20100
JESCHKE, CAROLA p 2039 N94-20153
JESSBERGER, E. K. p 2084 N94-20790
JEZEK, K. p 1715 N94-19823
p 1725 N94-20434
JI, XIANGMING p 1867 N94-21250
JIANG, Z. Y. p 1888 N94-21911
JIANG, ZHENG-YAO p 1887 N94-21907
JIANG, ZHI-JIAN p 1788 N94-22215
JIE, LU p 2083 N94-20750
JIM, K. T. C. p 1828 N94-22489
JIMENEZ, B. p 1664 N94-21397
JOCHEM, TODD p 1942 N94-20621
JOERG, WERNER B. p 1786 N94-22207
p 1787 N94-22208
JOHANSSON, A. p 2042 N94-20193
JOHANSSON, B. p 2011 N94-19827
JOHN, L. M. p 2047 N94-22490
JOHNSEN, BJOERN p 1851 N94-21455
JOHNSON, A. STEVE p 1893 N94-21863
JOHNSON, B. R. p 2037 N94-20945
JOHNSON, D. R. p 1707 N94-21822
JOHNSON, DEBRA STEELE p 1895 N94-21810
JOHNSON, ERIC R. p 1830 N94-20159
JOHNSON, G. W. p 1696 N94-22025
JOHNSON, J. p 2110 N94-20731
p 1926 N94-22491
JOHNSON, J. T. p 1727 N94-20441
p 1728 N94-20445
JOHNSON, PAUL T. p 2044 N94-21383
JOHNSON, R. E. p 2144 N94-21672
JOHNSON, RICHARD E. p 1646 N94-21418
JOHNSON, S. M. p 1705 N94-21425
JOHNSON, SAMUEL D. p 1718 N94-20368
JOHNSON, W. J. D. p 1814 N94-19828
JOHNSON, W. STEVEN p 1835 N94-22618
JOHNSTON, A. R. p 1984 N94-20179
JOHNSTON, DAVID L. p 1823 N94-20379
JOHNSTON, M. p 1926 N94-22486
JOHNSTON, MARK D. p 1949 N94-22492
JOHS, BLAINE p 2024 N94-21003
p 2024 N94-21004
p 2024 N94-21005
p 2026 N94-21013
JOLLY, Y. p 1773 N94-22124
JONES, DAVID p 1699 N94-20017
JONES, E. D. p 1748 N94-19884
JONES, I. P. p 1687 N94-19806
JONES, J. H. p 2085 N94-20861
JONES, JAMES R. p 1987 N94-21172
JONES, K. W. p 1685 N94-20717
JONES, M. T. p 2047 N94-22455
JONES, NORMAN p 1826 N94-19815
JONES, P. J. p 1694 N94-21945
JONES, R. p 2022 N94-20992
p 2022 N94-20993
p 2022 N94-20995
JONES, R. D. p 1946 N94-21845
JONES, ROBERT E. p 1698 N94-19830
JORDAN, J. E. p 1783 N94-22185
JORDAN, J. M. p 1926 N94-22488
p 2047 N94-22493
p 2048 N94-22509
JORDAN, THOMAS H. p 1882 N94-20131
JORGENSEN, J. D. p 2033 N94-21998
JORGENSON, PHILIP C. E. p 1919 N94-22358
JOSEPH, ROSE p 1719 N94-20406
JOSEPHSON, LUELI p 1758 N94-21119
JOSHI, C. H. p 2035 N94-22570
JOSHI, R. P. p 1768 N94-21770
JOVANOVIC, D. p 1996 N94-21752
JOYCE, J. J. p 1974 N94-21553
JUDD, M. D. p 1664 N94-21403
JUDKINS, R. R. p 1848 N94-21823
JUENEMANN, D. p 1863 N94-20889
JULES, KENOL p 1649 N94-21759
JULL, A. J. T. p 2106 N94-20713
JULLIEN, G. A. p 1771 N94-22111
JUREWICZ, A. J. G. p 2085 N94-20861
JUSLIN, KAJ p 1923 N94-22078

K

KAASHOEK, M. A. p 1960 N94-22099
KACHMAR, BRIAN A. p 1762 N94-21566
KAELLDAHL, ANDERS p 1640 N94-22606
KAHABKA, P. p 2080 N94-22555
KAHANA, S. H. p 1975 N94-21693
KAISER, J. H. p 2036 N94-22594
KAISER, KRAIG E. p 1755 N94-21097
KAITALA, VEIJO p 1854 N94-22072
KALAYCIOGLU, S. p 1794 N94-22255
KALIA, R. K. p 1701 N94-20352
KALIBJIAN, J. R. p 1657 N94-21980
KALKER, J. J. p 1822 N94-20157
KALKUR, T. S. p 1709 N94-20518
KALLEMEYN, G. W. p 2086 N94-20893
KALLENBERG, L. C. M. p 1963 N94-21066
KALOGERAS, CHRIS p 1705 N94-21225
KALRA, PARVEEN p 1827 N94-22421
KAM, D. p 1744 N94-21092
KAMAREDDINE, F. p 1949 N94-19997
p 1962 N94-20007
p 1962 N94-20008
p 1928 N94-20009
p 1898 N94-20082
KAMATH, G. p 1749 N94-20110
KAMATH, S. p 1767 N94-21725
KAMATSU, G. p 2110 N94-20731
KAMENEV, GEORGE p 1923 N94-22087
KAMMENZIND, B. F. p 1689 N94-20182
KAMODO, YASUHIDE p 2009 N94-22690
KAMOUN, FAOUZI p 1783 N94-22183
p 1746 N94-22205
KAMPAS, F. p 1850 N94-22257
KAMRA, S. p 1845 N94-19925
KANADE, TAKEO p 1761 N94-21282
KANAMORI, HIROSHI p 2126 N94-20821
KANDEL, ROBERT S. p 1860 N94-22287
KANDIL, OSAMA p 1637 N94-21054
KANG, S. p 1761 N94-21256
KANIA, D. R. p 1768 N94-21770
KAP, A. P. p 1842 N94-22265
KAPER, H. G. p 1961 N94-22381
p 1961 N94-22393
KAPLAN, MICHAEL L. p 1864 N94-20138
KAPLAN, TED p 1744 N94-21341
p 1744 N94-21344
p 1744 N94-21350

KAPOOR, V. J. p 1735 N94-20516
KAR, SUBAL p 1762 N94-22179
KARAKASHIAN, T. p 2048 N94-22499
KARAM, M. A. p 1729 N94-20450
KARAM, MOSTAFA A. p 1719 N94-20409
KARGEL, J. S. p 2090 N94-20389
p 2090 N94-20390
KARGEL, JEFFREY S. p 2088 N94-20382
KARPOV, V. G. p 1970 N94-19971
KARRAY, MOUFID p 1792 N94-22240
KARTHIKEYAN, S. p 1847 N94-21614
KARZANOV, ALEXANDER p 1950 N94-20125
KARZANOV, ALEXANDER K. p 1951 N94-20302
KARZANOV, ALEXANDER V. p 1950 N94-20161
KASCHMITTER, J. p 1898 N94-19886
KASCHMITTER, J. L. p 1768 N94-21753
KASPER, ROLF G. p 1806 N94-19882
KASSABIAN, N. C. p 1642 N94-22055
KASTING, J. p 2142 N94-21659
KASTING, J. F. p 2142 N94-21662
p 2144 N94-21673
KASVAND, T. p 1777 N94-22146
KATAN, J. R. p 1737 N94-20949
KATEHI, L. P. B. p 1733 N94-20501
KATEHI, LINDA P. B. p 1733 N94-20500
p 1733 N94-20502
KATES, RONALD E. p 1952 N94-20923
KATNIK, GREGORY N. p 1656 N94-21884
KATO, SHUZO p 1746 N94-22171
KATO, TAKAKO p 2004 N94-22653
KATO, TOMOKAZU p 2010 N94-22696
KATOEN, JOOST-PIETER p 1909 N94-21045
KATSOULEAS, T. p 1981 N94-21688
KATZ, I. p 1654 N94-21429
KATZ, J. I. p 2150 N94-21781
p 2150 N94-21782
KAUFMAN, LLOYD p 1894 N94-20467
KAUFMAN, Y. A. p 1839 N94-20961
KAUHANEN, K. p 2106 N94-20711
KAUKLER, WILLIAM F. p 1797 N94-20037
KAUP, D. J. p 1952 N94-20923
KAWASHIMA, S. p 2001 N94-22633
KAWAZOE, KATSUHIKO p 1746 N94-22171
KAY, ROBERT T. p 1907 N94-20525
KAYE, G. T. p 1881 N94-19952
KEANA, JOHN F. p 1700 N94-20328
KEARNS, RONALD G. p 1658 N94-21217
KEATING, P. p 1862 N94-20668
KEEFE, ROBERT W. p 1821 N94-20021
KEIL, K. p 2083 N94-20749
KEIL, L. p 1885 N94-21898
KELLER, JOERG p 1930 N94-21023
p 1908 N94-21024
KELLER, L. p 2027 N94-21296
KELLER, L. P. p 2097 N94-20662
p 2084 N94-20828
KELLER, R. p 1917 N94-21917
KELLER, S. p 1973 N94-20474
KELLER, TEDDY M. p 1672 N94-20010
KELLY, B. D. p 1926 N94-22494
KELLY, B. E. p 1696 N94-22025
KELLY, ERON p 1769 N94-21908
KELLY, R. J. p 1644 N94-22134
KEMBHAVI, A. K. p 2058 N94-22445
KEMP, P. R. p 1852 N94-21787
KEMPEL, LEO C. p 1741 N94-21885
p 1741 N94-21886
p 1741 N94-21887
p 1741 N94-21888
KEMPF, T. L. p 1695 N94-21978
KEMPIN, M. p 2083 N94-20746
KEMPNER, E. A. p 1673 N94-20490
KENNEDY, IAN M. p 1796 N94-19913
KEPHART, A. R. p 1833 N94-22001
KERCEL, S. W. p 1810 N94-21953
KEREKES, JOHN P. p 1867 N94-21212
KERLEY, G. I. p 1904 N94-20052
KERLEY, JAMES J. p 1823 N94-20494
KERN, WALTER p 1738 N94-21073
KERR, JAMES p 1700 N94-20057
KERSEY, ALAN D. p 1984 N94-20065
KERSLAKE, THOMAS W. p 1667 N94-20062
KERSTEN, P. H. M. p 1953 N94-21046
KERSTHOLT, J. H. p 2042 N94-20310
KESHAVARZ, A. A. p 1750 N94-20218
KESKINEN, JARI p 1691 N94-20530
KESSLER, W. J. p 1809 N94-21607
KESTER, D. J. M. p 1927 N94-22522
KEUR, MICHIEL V. D. p 1742 N94-22349
KHACHATUROV, V. R. p 1923 N94-22079
KHALATNIKOV, I. M. p 1805 N94-22272
KHALI, ABDELHAKIM p 1778 N94-22153
KHATUNCEV, I. V. p 2109 N94-20728
KHITROVA, G. p 1814 N94-19865
KHOCHE, AJAY p 1757 N94-21109
KHORASANI, K. p 1790 N94-22230
KHRUSHCH, B. I. p 1661 N94-21380
KIBERT, CHARLES J. p 1681 N94-21165
KIBINA, STANLEY J. p 1745 N94-22126
KIBRICK, R. I. p 2047 N94-22495
KIDNER, R. E. p 1656 N94-21852
KIEFER, W. S. p 2142 N94-20911
KIEFLING, LARRY p 1919 N94-22354
KIEHNE, THOMAS M. p 1831 N94-21249
KILBY, JAMES W. p 2043 N94-21266
KILGORE, ROGER T. p 2044 N94-21354
KILKENNY, J. D. p 1818 N94-21547
KILLEEN, T. L. p 1657 N94-20173
KIM, HEECHUL p 1656 N94-21581
KIM, J. p 1675 N94-21191
p 1960 N94-22099
KIM, J. H. p 1994 N94-21290
KIM, J. Y. p 1998 N94-22561
KIM, JONGMIN p 1984 N94-20128
KIM, K. p 1714 N94-21426
KIM, K. J. p 1980 N94-20475
KIM, K. W. p 2027 N94-21248
KIM, KWANG J. p 1831 N94-21219
KIM, N. p 1783 N94-22184
KIM, Y. K. p 1994 N94-21290
KIM, YUNJIN p 1726 N94-20438
p 1726 N94-20439
KIMBERLY, H. J. p 1981 N94-21767
KIMURA, M. p 2033 N94-21993
KING, G. p 1662 N94-21391
KING, KENNETH W. p 1968 N94-22053
KING, MICHAEL D. p 1872 N94-22298
KING, W. E. p 1696 N94-22025
KINGON, A. p 1749 N94-20012
KINNE, S. p 1876 N94-22320
KINNISON, J. D. p 1754 N94-21085
KINNISON, JAMES D. p 2015 N94-20184
p 1763 N94-21696
p 1765 N94-21710
KINROSS-WRIGHT, J. p 1814 N94-19828
KINROSS-WRIGHT, J. M. p 1816 N94-20277
KINSLEY, KAREN M. p 1705 N94-21302
KIPP, M. E. p 1832 N94-21557
KIRBIE, H. C. p 1769 N94-21838
KIRBY, KATE P. p 1973 N94-20612
KIRK, J. G. p 2007 N94-22677
KIRK, JERRY V. p 1648 N94-21592
KIRKENDAHL, T. p 1662 N94-21391
KIRKHAM, H. p 1984 N94-20179
KISHI, Y. p 2005 N94-22664
KISHIMOTO, Y. p 1998 N94-22561
KISHIYAMA, JENNY S. p 2039 N94-21497
KISKER, DAVID W. p 2013 N94-19967
KISSEL, J. p 2141 N94-20909
KISSEL, L. p 1971 N94-20096
KISTLER, JAMES J. p 1898 N94-20107
KITAMOTO, SHUNJI p 2007 N94-22676
p 2009 N94-22690
KJELLSEN, KNUT O. p 1708 N94-21894
KLAASEN, K. p 2101 N94-20686
KLAUS, E. E. p 1825 N94-21424
p 1825 N94-21450
p 1825 N94-21451
KLAVETTER, E. p 2028 N94-21541
KLEIMAN, J. p 1660 N94-21373
KLEIN, D. L. p 1799 N94-20286
KLEIN, E. p 1898 N94-20082
KLEIN, J. p 1863 N94-20689
KLEINMAN, R. E. p 1742 N94-22346
KLEINROCK, MARTIN C. p 1882 N94-20581
KLEINSCHMIDT, EDWARD p 1824 N94-20576
KLEPPNER, DANIEL p 1680 N94-20584
KLETECKA, P. p 1997 N94-21816
KLIEM, BERNHARD p 2004 N94-22659
KLINE, STEVE p 1802 N94-21155
KLINGLESMITH, D. A., III p 2047 N94-22496
KLINKER, E. p 1861 N94-22291
KLOECK, W. p 2084 N94-20790
KLUGER, Y. p 1998 N94-22389
KLUTE, GLENN K. p 1896 N94-20606
p 1897 N94-21627
KNAPP, J. A. p 1973 N94-20306
KNAPP, R. B. p 1809 N94-21508
KNAUSS, WOLFGANG G. p 1834 N94-22610
KNICKMEYER, ELFRIEDE T. p 1861 N94-22424
KNIGHT, SCOTT p 1788 N94-22216
KNIPMEYER, S. E. p 2037 N94-20473
KNIPP, PETER A. p 2018 N94-20554
KNOWLES, A. p 1935 N94-21745
KNUDSEN, CHRISTIAN W. p 2126 N94-20821
KNUETSON, R. O. p 1875 N94-22315
KNUTESON, R. O. p 1873 N94-22307
KOBAYASHI, K. p 2082 N94-20658
KOCH, CHRISTOF p 1890 N94-20112
KOCH, J. A. p 1819 N94-21873
KOCHAN, H. p 2084 N94-20827
p 2085 N94-20841
KOEBERL, C. p 2082 N94-20704
p 1862 N94-20714
p 1685 N94-20745
p 2086 N94-20693
KOEBERL, CHRISTIAN p 1863 N94-20796
KOEHLER, D. R. p 1769 N94-21918
KOEL, BRUCE E. p 1712 N94-21192
KOELZER, G. p 2084 N94-20827
KOIDE, G. p 1918 N94-22011
KOIDE, SHINJI p 2005 N94-22660
p 2005 N94-22662
KOJIMA, H. p 2086 N94-20693
KOJIMA, HIDEYASU p 2080 N94-20892
KOK, J. p 1682 N94-21574
KOLB, C. E. p 1682 N94-21243
KOLESKE, D. D. p 2014 N94-19980
KOLESOV, G. M. p 1862 N94-20841
KOLLE, J. J. p 1646 N94-21507
KOLLMANN, WOLFGANG p 1796 N94-19913
KOMOROWSKI, J. p 1944 N94-21162
KONG, J. A. p 1727 N94-20441
p 1728 N94-20445
p 1730 N94-20455
KONG, S. H. p 1814 N94-19828
p 1816 N94-20277
KONKINA, T. V. p 2109 N94-20728
KONONKOVA, N. N. p 2083 N94-20752
KONOPLIV, A. S. p 2117 N94-20772
KONRADI, ANDREI p 1893 N94-21863
KONTINEN, KALEVI p 2046 N94-22057
KONTOTHANASSIS, LEONIDAS p 1929 N94-20144
p 1913 N94-21316
KONYAVSKY, V. A. p 1923 N94-22068
KOOLE, GER p 1944 N94-21160
p 1930 N94-21234
KOONTZ, S. p 1662 N94-21391
KOONTZ, STEVEN L. p 1993 N94-20491
p 1663 N94-21393
KORNBERGER, M. p 1639 N94-22599
KORNBLUM, B. T. p 1906 N94-20316
KOROTAEVA, N. p 2083 N94-20735
KORPELA, ASKO p 2050 N94-22061
KOSC, T. Z. p 1706 N94-21526
KOSSENTINI, FAOUZI p 2041 N94-20158
KOSSLER, W. J. p 1977 N94-22009
KOSTER, C. H. A. p 1909 N94-21061
KOSTROUN, V. O. p 1970 N94-19870
p 1970 N94-19871
p 1974 N94-21543
KOTALIK, PAVEL p 1996 N94-21572
KOTELNIKOV, I. A. p 1991 N94-19872
p 1992 N94-19887
KOTOV, Y. D. p 2007 N94-22680
KOUSEN, KENNETH A. p 1968 N94-21608
KOUSOUM, JULIANA p 1863 N94-20904
KOUVELIOTOU, C. p 2149 N94-20803
KOVALSKY, D. p 2049 N94-22544
KOVANEN, JYRKI p 1744 N94-22076
KOVARIK, M. D. p 2035 N94-22385
KOWALCZYK, T. C. p 1706 N94-21526
KOZLOWSKI, G. C. p 1967 N94-19949
KOZUKA, Y. p 2004 N94-22657
KRAAIJ, WESSEL p 1940 N94-20247
KRAAKMAN, M. p 2045 N94-22276
KRAMER, M. J. p 2031 N94-21931
p 2036 N94-22582
KRAUS, R. H., JR. p 1820 N94-22020
KRECH, R. H. p 1663 N94-21395
KREMNEV, ROALD p 2123 N94-20806
KREMPETZ, K. J. p 1807 N94-19987
KREPLIN, H.-P. p 1639 N94-22598
KRIHA, V. p 1997 N94-21816
KRIPLANI, H. p 1749 N94-20110
KRISHNAGOPAL, S. p 1820 N94-21975
KRISHNAMAGARU, DHARMESH p 2045 N94-21865
KRISHNAN, G. S. p 1753 N94-21082
KRISHNAN, KALPAGAM p 1786 N94-22207
p 1787 N94-22208
KRIST, J. E. p 2048 N94-22497
p 1926 N94-22498
KRLIN, L. p 1998 N94-21593
KROGH, M. F. p 1935 N94-21622
p 1936 N94-21746
KROLAK, JOSEPH S. p 2044 N94-21354
KROLL, N. M. p 1715 N94-19874
KROO, ILAN p 1638 N94-21833
KROPFLI, ROBERT A. p 1873 N94-22304
p 1874 N94-22311
p 1879 N94-22333
p 1879 N94-22334
KROT, T. V. p 2141 N94-20908
KRUEGER-ELENCWAJG, H. p 1753 N94-21021
KRUMPELT, M. p 1847 N94-21650
p 1847 N94-21774
p 1848 N94-21870
KRUPP, C. p 1866 N94-21052

KRUTOV, ALEXANDER P. p 2050 N94-22062
KRYSKA, L. p 1997 N94-21816
KRZYZAK, A. p 1771 N94-22109
p 1777 N94-22146
KUB, FRANCIS J. p 1749 N94-20199
KUBINA, S. J. p 1745 N94-22128
KUBO, HIROKO p 2004 N94-22658
KUBOTA, SHUJI p 1746 N94-22171
KUCERA, G. H. p 1847 N94-21650
p 1848 N94-21870
KUDRITZKI, ROLF-PETER p 2081 N94-21578
KUECH, THOMAS p 2013 N94-19967
KUENY, J. L. p 1668 N94-20079
KUEPER, T. p 1848 N94-21942
KUFELD, R. p 1635 N94-21490
KULAK, R. F. p 1697 N94-19809
KULANDER, K. C. p 1972 N94-20230
p 1818 N94-21829
KUMAR, K. S. p 1648 N94-21268
KUMAR, PUNEET p 1898 N94-20107
KUMAR, R. p 1750 N94-20257
p 1847 N94-21774
KUMAR, S. p 2031 N94-21930
KUNC, JOSEPH p 1802 N94-21220
KUNG, SUN-YUAN p 1943 N94-20626
KUNK, J. R. p 1743 N94-22557
KUNK, M. J. p 1863 N94-20899
KUO, FAN-MING p 1968 N94-21422
KUPIAINEN, A. p 2038 N94-22095
KUPRAT, A. P. p 1997 N94-21965
KURAMOTO, K. p 2145 N94-21674
KURAT, G. p 1684 N94-20642
p 2082 N94-20643
p 2082 N94-20678
p 2082 N94-20704
KURTH, W. S. p 2088 N94-20048
KURTZ, M. J. p 2048 N94-22499
KURTZ, MICHAEL J. p 2063 N94-22472
KURTZ, S. R. p 1748 N94-19884
KUSANO, KANYA p 2000 N94-22625
p 2004 N94-22658
p 2006 N94-22666
KUSH, A. p 1683 N94-21984
KUTLALIYEV, A. H. p 1653 N94-21370
KUTOYANTS, YURII p 1951 N94-20227
KUTTINEN, R. p 1841 N94-21069
KWAK, DOCHAN p 1798 N94-20104
KWAN, HON-KEUNG p 1770 N94-22104
p 1780 N94-22167
KWAN, S. p 1750 N94-20314
KWATRA, S. C. p 1759 N94-21123
KWEI, G. H. p 2029 N94-21555
KWOK, P. p 1981 N94-21688
KWOK, R. p 1721 N94-20415
p 1723 N94-20426
p 1724 N94-20432
p 1727 N94-20441
p 1728 N94-20445
p 1729 N94-20449
p 1730 N94-20454
KWOK, W. K. p 2033 N94-21997
KWON, OH JOON p 1919 N94-22360
KWON, S. I. p 1980 N94-20475
KWOR, R. Y. p 1709 N94-20516
KY, H. DO p 1782 N94-22176
KYBURG, HENRY E., JR. p 2039 N94-20364

L

LABAUNE, C. p 1966 N94-21958
LABLANS, W. N. p 1865 N94-20309
LABONTE, BARRY J. p 2006 N94-22671
LABORDE, JEAN MARIE p 1950 N94-20183
LABOV, S. E. p 2031 N94-21869
LACHARTRE, DAVID p 1778 N94-22153
LACIS, ANDREW p 1813 N94-21646
LACOSTE, M. p 1664 N94-21398
LAD, R. J. p 2018 N94-20575
p 2028 N94-21458
LAFONTAINE, S. p 1784 N94-22192
LAFONTAINE, SERGE p 1784 N94-22193
LAHEY, RICHARD T., JR. p 1802 N94-21261
LAI, B. p 1990 N94-21837
LAI, C.-H. p 1935 N94-21492
p 1959 N94-21576
LAI, RICHARD p 1733 N94-20499
LAKE, ROBERT E. p 1807 N94-20203
LAL, N. p 1926 N94-22501
LAM, D. J. p 2033 N94-21994
LAM, S. S. p 1645 N94-19914
LAMB, JOEL D. p 1710 N94-20979
p 1710 N94-20980
LAMET, DAN p 1768 N94-21731
LAMPKIN, DERRICK J. p 1863 N94-20904
LAMPROPOULOS, G. A. p 1780 N94-22165
LAN, ESTHER H. p 1683 N94-21393
LANCTO, R. p 2027 N94-21303
LANDMAN, UZI p 1823 N94-20464
LANDSMAN, W. B. p 2048 N94-22500
p 1927 N94-22542
LANG, MICHAEL p 2026 N94-21135
LANG, ROGER H. p 1728 N94-20448
LANGDON, A. BRUCE p 1992 N94-19915
LANGER, DIETER p 1709 N94-20972
LANGER, DIETER W. p 1709 N94-20973
p 2022 N94-20992
p 2022 N94-20993
LANGFORD, JOHN S. p 1646 N94-21246
LANGHOFF, STEPHEN R. p 1666 N94-19818
LANGLOIS, MARC p 1639 N94-22586
LANGSTON, LEE S. p 1806 N94-19882
LANKARANI, HAMID M. p 1890 N94-20190
LANSING, FAIZA p 1724 N94-20431
LANTTO, ERIC S. p 1858 N94-21432
p 1993 N94-20326
LAO, L. L. p 1884 N94-19866
LAPEDES, A. p 2014 N94-19980
LAPIANO-SMITH, D. p 1666 N94-20864
LAPIN, S. L. p 1954 N94-21137
LAPPE, MATTHIAS p 1699 N94-20047
LARACUENTE, A. p 1875 N94-22314
LARE, ANDREW R. p 1877 N94-22328
LAREAU, RICHARD T. p 1682 N94-21435
LAROSE, C. p 1745 N94-22128
LAROUCHE, MARIO p 1778 N94-22153
LARSON, D. J. p 1992 N94-19991
LARUE, GEORGE p 1755 N94-21094
LASGORCEIX, P. p 1653 N94-21404
LASLETT, L. J. p 1981 N94-21440
LASSILA, D. H. p 1693 N94-21843
LASZAKOVITS, JOHN S. p 1857 N94-21202
LAU, P. p 1981 N94-21688
LAU, W. K.-M. p 1868 N94-21605
LAUBENTHAL, N. A. p 1926 N94-22501
LAUER, V. p 2087 N94-20906
LAURENDEAU, D. p 1785 N94-22200
LAURENDEAU, DENIS p 1770 N94-22105
p 1771 N94-22108
LAURENT, PIERRE-JEAN p 1950 N94-20200
LAVERGNE, CHRISTIAN p 1963 N94-20165
LAVRUKHINA, A. K. p 2085 N94-20844
LAWLESS, G. W. p 1675 N94-21187
LAWRENCE, PAUL J., JR. p 1903 N94-19969
LAWRENCE, ROBERT W. p 2028 N94-21505
LAWRENCE, WILLIAM T. p 1838 N94-20959
LAWRYSHYN, YURI ANDREW p 1827 N94-22578
LAWSON, A. C. p 2033 N94-21991
LAWSON, J. K. p 1820 N94-22401
LAXEN, MARK R. p 1740 N94-21308
LAY, THORNE p 1858 N94-21206
LAYNE, G. D. p 1686 N94-20760
LAYPUNOV, M. A. p 1972 N94-20181
LAZARUS, E. A. p 1998 N94-22039
LE, CHAU G. p 1945 N94-21430
LE, L. p 2085 N94-20861
p 2087 N94-20906
LEASKY, T. p 1676 N94-21559
LEAVITT, LAURENCE D. p 1637 N94-21569
LEBLANC, THOMAS J. p 1929 N94-20144
LEBLEBICI, Y. p 1761 N94-21256
LEBOEUF, F. p 1668 N94-20078
LEBOEUF, J. N. p 1801 N94-20562
LECHTER, WILLIAM p 2018 N94-20558
LECUYER, PIERRE p 1949 N94-19854
p 1962 N94-19999
LEDERICH, R. J. p 1692 N94-21320
LEDYANKIN, D. p 1661 N94-21383
LEE, CHI H. p 1760 N94-21178
LEE, DAVID CHUNG LIANG p 1839 N94-20964
LEE, DUNG-HAI p 1768 N94-21762
LEE, E. H. p 1694 N94-21948
LEE, E. P. p 1980 N94-20290
LEE, E. S. p 1809 N94-21545
LEE, GORDON p 1821 N94-20044
LEE, HSUE-FU p 1816 N94-20546
LEE, IN-YOUNG p 1853 N94-22384
LEE, J. H. p 1683 N94-21947
LEE, JA H. p 1824 N94-20587
p 1994 N94-21290
p 1995 N94-21291
p 1995 N94-21292
p 1995 N94-21293
p 1995 N94-21294
LEE, JOSEPH C. p 1739 N94-21211
LEE, M. W. p 1679 N94-20266
LEE, P. p 2145 N94-21675
LEE, PETER p 1908 N94-20622
LEE, R. p 1853 N94-22569
LEE, RAYMOND H. p 1828 N94-21324
LEE, RICHARD Q. p 1722 N94-20422
p 1734 N94-20505
p 1734 N94-20506
p 1734 N94-20507
p 1769 N94-21808
LEE, S. L. p 1960 N94-21966
LEE, S. R. p 2031 N94-21930
LEE, S. W. p 1728 N94-20447
LEE, SCOTT p 1662 N94-20757
LEEDOM, L. C. p 1917 N94-21841
LEEFE, SIMON p 1655 N94-21796
LEEMANS, W. p 1979 N94-20273
LEENHOUTS, JAMES M. p 2084 N94-20773
LEFEBVRE, PAUL A. p 1838 N94-20957
LEGLAND, FRANCOIS p 1951 N94-20227
LEGNER, H. H. p 1809 N94-21607
LEGNINI, D. p 1990 N94-21837
LEHN, W. H. p 1793 N94-22249
LEHOCZKY, JOHN P. p 1899 N94-21195
p 1899 N94-21230
LEHOCZKY, S. L. p 2030 N94-21807
LEIB, HARRY p 1747 N94-22242
LEJEUNE, CLAUDE p 1780 N94-22164
LEMELIN, GUYLAIN p 1990 N94-22411
LEMOINE, F. G. p 2117 N94-20774
LENELL, JOHN p 1764 N94-21700
LENSKI, JOSEPH W., JR. p 1826 N94-21756
LENZ, D. p 2046 N94-22446
LEONARD, B. P. p 1959 N94-21588
LEONARD, R. A. p 1833 N94-21927
LEONARD, R. F. p 1671 N94-20513
LEONE, STEPHEN R. p 1972 N94-20130
LEONHARDT, TODD A. p 1675 N94-21488
LEPAGE, RICHARD p 1779 N94-22163
LEPPER, M. J. p 1677 N94-21940
LEPPIHALME, M. p 1988 N94-21595
LEPPIHALME, MATTI p 1988 N94-21596
p 1988 N94-21597
LERCH, F. J. p 2117 N94-20774
LEROUX, F. G. p 1862 N94-20714
LESSARD, JEAN p 1770 N94-22105
LESTEVEN, SOIZICK p 2048 N94-22502
LESUER, D. R. p 1675 N94-21530
LETREUT, HERVE p 1860 N94-22287
LETUNOVSKIY, SERGEI V. p 1923 N94-22083
LEUNG, C. M. p 1789 N94-22225
LEUNG, K. N. p 1980 N94-20475
LEUTENEGGER, SCOTT T. p 1914 N94-21462
LEVACK, DANIEL p 1670 N94-21271
LEVADOU, F. p 1661 N94-21382
LEVAY, Z. G. p 1925 N94-22470
p 1926 N94-22485
LEVESQUE, MARTIN P. p 1790 N94-22228
LEVESQUE, R. p 1989 N94-21630
LEVESQUE, STEVE p 2056 N94-22415
LEVIN, EUGENE p 1679 N94-20169
LEVIN, K. p 2032 N94-21972
LEVINE, D. M. p 1729 N94-20450
LEVINE, STANLEY R. p 1703 N94-20529
LEVINSON, DAVID H. p 1876 N94-22323
LEVITON, DOUGLAS B. p 1985 N94-20240
LEVY, L. p 1661 N94-21382
LEWIS, J. p 2048 N94-22503
LEWIS, M. p 1898 N94-19686
LEWIS, R. S. p 2082 N94-20659
LEWKOWICZ, JAMES F. p 1855 N94-20090
LI-DEMARTEAU, Q. p 1978 N94-19988
LI, DANIAN p 1782 N94-22180
LI, F. K. p 1720 N94-20413
p 1721 N94-20415
p 1728 N94-20445
LI, H. p 1973 N94-20619
p 1825 N94-21451
LI, HARRY W. p 1759 N94-21122
LI, HON F. p 1766 N94-21718
LI, JING-YUN p 1747 N94-22250
LI, MING p 2038 N94-21533
LI, P. p 1749 N94-20110
p 1761 N94-21256
LI, S. p 1744 N94-21092
LI, XIAO-PING p 1768 N94-21762
LI, XUEQIN p 1765 N94-21715
LI, Z. p 1970 N94-19971
LI, ZIAO-PING p 1815 N94-19965
LIANG, ANITA D. p 1654 N94-21790
p 1654 N94-21791
LIBERMAN, EUGENE M. p 1714 N94-21564
p 1715 N94-21589
LIEBER, CHARLES M. p 2027 N94-21242
LIEBERMAN, EDWARD M. p 1890 N94-20045
LIEBERMAN, M. A. p 1999 N94-22595
LIEBSCHER, D.-E. p 2072 N94-22520
LIECHTI, K. M. p 1830 N94-20001
LIEVAART, ANNETTE p 1950 N94-20032
LIFKA, D. p 1921 N94-22375
LIFKA, DAVE p 1921 N94-22376
LIGHT, MARC p 1904 N94-20067
p 1911 N94-21180
LIMBER, MARK A. p 1955 N94-21465

LIN, CHUN C. p 1854 N94-19954
LIN, FREDDIE p 1987 N94-21163
LIN, M. E. p 1975 N94-21766
LIN, X. p 1715 N94-19874
LIN, XIJIAN p 1872 N94-22300
LIN, YUH-LANG p 1864 N94-20138
LINARES, IRVING p 1932 N94-21329
LINCOLN, DAN p 1754 N94-21090
LINCOLN, JOHN W. p 1635 N94-21194
LINDER, W. KELLY p 1659 N94-21372
LINDSAY, WILLARD L. p 1897 N94-20665
LINDSTROM, D. J. p 1685 N94-20684
p 1687 N94-20870
LINDSTROM, M. M. p 2086 N94-20893
LINDSTROM, MARILYN M. p 2039 N94-20819
p 2085 N94-20857
LINK, Y. Y. p 1645 N94-19914
LINNA, MIIKA p 1744 N94-22076
LINTON, R. p 1662 N94-21391
LIOEN, WALTER M. p 1935 N94-21610
LIOU, KUO-NAN p 1872 N94-22299
p 1880 N94-22342
LIPPMANN, S. I. p 1998 N94-22039
LIPSCHUTZ, M. E. p 2082 N94-20681
p 1964 N94-20881
LITHOPOULOS, E. p 1790 N94-22227
LITTLEFIELD, D. L. p 1829 N94-19943
LITTLEFIELD, R. p 1903 N94-19959
p 1936 N94-22032
LITTMAN, MICHAEL p 1938 N94-19845
LITVA, JOHN p 1745 N94-22137
p 1745 N94-22138
p 1747 N94-22253
LIU, BEDE p 1781 N94-22173
LIU, C. T. p 1694 N94-21933
p 1694 N94-21948
LIU, CHAOQUIN p 1806 N94-21466
LIU, D. p 2041 N94-19811
LIU, DAVID C. p 1709 N94-20972
p 1709 N94-20975
p 1709 N94-20976
p 1710 N94-20979
LIU, G. K. p 2035 N94-22565
LIU, J. p 1928 N94-19812
LIU, M. p 1749 N94-20012
LIU, MEILAN p 1833 N94-22590
LIU, WILLIAM T. p 1840 N94-20966
LIU, ZHEN-YUE p 1854 N94-19820
LIU, ZHINING p 1806 N94-21466
LIZANICH, P. J. p 1741 N94-21567
LJUNGBERG, M. p 2047 N94-22455
LOCKWOOD, J. F. p 2110 N94-20731
LOCKWOOD, S. J. p 2013 N94-19961
p 1763 N94-21654
LOEVE, J. A. p 1918 N94-22098
LOFTIS, J. P. p 1937 N94-22267
LOHANICK, A. p 1715 N94-19823
p 1727 N94-20441
LOHR, J. p 1998 N94-22039
LOKE, Y. p 1778 N94-22151
LOKEN, S. p 1921 N94-22375
LOMAX, CURTIS p 1800 N94-20371
LOMINADZE, JUMBER G. p 2000 N94-22626
LOMMASSON, T. p 2029 N94-21617
LONDON, R. A. p 1817 N94-21299
LONG, DAVID E. p 1902 N94-19919
LONG, DAVID G. p 1725 N94-20433
LONG, STEPHEN I. p 1900 N94-21301
LONGEROT, CARL D. p 1753 N94-21082
LONGMAN, D. E. p 1811 N94-22391
LONGSTRETH, J. p 1850 N94-19930
LONGTIN, DAVID R. p 1987 N94-21172
LOO, CHUN p 1746 N94-22170
LOOK, P. p 1744 N94-21092
LOONG, C. K. p 1700 N94-20265
p 2033 N94-21993
LOONG, C.-K. p 2035 N94-22565
LOPES, SERGIO R. p 2003 N94-22649
LOPEZ, ALFRED R. p 1737 N94-21031
p 1738 N94-21049
LORD, JOHN p 1645 N94-22155
LORD, MARK T. p 1822 N94-20365
LORD, S. J. p 1868 N94-21605
LORENZ, E. p 2084 N94-20827
LORENZ, H. p 2072 N94-22520
LORENZZETTI, JOAO ANTONIO p 1840 N94-20967
LOTOV, ALEXANDER p 1923 N94-22087
LOU, S. H. p 1720 N94-20413
LOU, Y. L. p 1725 N94-20434
LOUBRIEL, G. M. p 1750 N94-20294
p 2016 N94-20296
p 1750 N94-20312
LOUCKS, W. M. p 1772 N94-22115
LOUIS, PASCAL p 2018 N94-20593
LOUPIAS, C. p 1664 N94-21397
LOUTER-NOOL, MARGREET p 1930 N94-21077
p 1916 N94-21611
LOUTFY, RAOUF O. p 1677 N94-22022
LOVERN, M. G. p 1881 N94-19952
LOWNDES, D. H. p 2013 N94-19929
LOWREY, ALFRED H. p 1974 N94-21185
LOWRY, C. W. p 1814 N94-19865
LU, DING p 1757 N94-21108
LU, W.-S. p 1789 N94-22225
LUBASZEWSKI, M. p 1749 N94-20166
LUBELL, M. S. p 2035 N94-22570
LUCAS, B. N. p 1697 N94-22559
LUCAS, S. M. p 1941 N94-20254
LUCCHITTA, B. K. p 2090 N94-20391
LUCEY, P. G. p 2101 N94-20682
p 1652 N94-20850
LUCEY, PAUL G. p 2107 N94-20719
p 2119 N94-20784
p 2119 N94-20786
LUCOVSKY, G. p 2029 N94-21615
LUDEWIG, HANS p 1671 N94-21979
LUE, J. W. p 2035 N94-22570
LUEDTKE, JACQUELINE R. p 1635 N94-20191
LUETTGEN, ANDREA p 1993 N94-20156
LUGMAIR, G. W. p 2083 N94-20768
LUHMANN, NEVILLE p 1715 N94-19912
LUIGJES, G. p 1979 N94-20117
LUMSDEN, DOUGLAS R. p 1933 N94-21337
LUPPINO, G. A. p 1828 N94-22489
p 1814 N94-22510
LUPTON, W. F. p 1925 N94-22460
p 2048 N94-22504
LURSINSAP, CHIDCHANOK p 1764 N94-21706
p 1765 N94-21707
LUSK, E. p 1921 N94-22375
LUTON, J. N. p 2035 N94-22570
LUYTEN, JAMES p 1881 N94-19895
LUZAR, A. p 1680 N94-20560
LYCOU, PETER P. p 1824 N94-20589
LYLE, KAREN HEITMAN p 1967 N94-20211
LYMAN, J. L. p 1820 N94-22585
LYNCH, V. E. p 1801 N94-20562
LYNN, DOUGLAS p 1767 N94-21725
LYNN, J. W. p 2033 N94-21991
LYO, S. K. p 1748 N94-19884
LYTLE, D. M. p 1928 N94-22505
p 1926 N94-22506

M

MA, HAN-HUA p 1784 N94-22189
p 1746 N94-22190
MA, KWAN-LIU p 1935 N94-21622
MA, X. L. p 1873 N94-22307
p 1875 N94-22315
MAAG, CARL R. p 2084 N94-20817
p 1659 N94-21372
MABSON, G. E. p 1660 N94-21373
MACARIE, IOAN p 1907 N94-20521
MACARIE, IOAN I. p 1900 N94-21281
MACCORMACK, ROBERT W. p 1637 N94-21411
MACE, GERALD G. p 1877 N94-22325
p 1877 N94-22326
p 1878 N94-22329
MACFARLANE, J. F. p 1921 N94-22375
MACGOWAN, B. J. p 1819 N94-21873
MACHLAB, HASSANAYN p 1820 N94-21006
p 1710 N94-21007
MACII, ENRICO p 1758 N94-21118
MACINTYRE, KATHY p 1645 N94-22155
MACLAUGHLIN, D. E. p 2030 N94-21768
p 2034 N94-22007
MADANI, NAVID p 1760 N94-21133
MADHUKAR, M. p 1908 N94-20932
MADSEN, SOREN N. p 1732 N94-20461
MAEHR, S. A. p 2095 N94-20651
MAENCHEN, J. E. p 1980 N94-20295
MAES, G. J. p 1917 N94-21851
MAETHNER, SCOTT R. p 1831 N94-20572
MAGALLANES, D. p 1757 N94-21106
MAGEE, D. P. p 1826 N94-22038
MAGRUDER, R. H. p 2012 N94-19869
MAHAFFY, PAUL p 1812 N94-22435
MAHAJAN, S. M. p 1998 N94-22560
MAHDAVI, M. A. p 1998 N94-22039
MAHER, D. M. p 1687 N94-19806
MAHLMAN, JERRY D. p 1868 N94-21640
MAHMOOD, SYEDA-TANVEER F. p 1913 N94-21365
MAILHIOT, C. p 1706 N94-21512
MAILLOUX, GUY p 1777 N94-22147
MAJOR, WILLIAM M. p 1658 N94-21251
MAJUMDAR, AMITAVA p 1758 N94-21114
MAKALKIN, A. B. p 2085 N94-20849
MAKI, G. p 1785 N94-21713
MAKI, GARY K. p 1757 N94-21107
p 1759 N94-21125
MAKIHARA, MASAKI p 1713 N94-20605
MALAIYA, YASHWANT K. p 1756 N94-21105
p 1757 N94-21108
p 1766 N94-21721
p 1767 N94-21727
MALAPATI, SRINIVAS REDDY p 1890 N94-20190
MALARET, E. R. p 1658 N94-20617
MALHOTRA, MANISH p 1965 N94-21463
MALIK, MUJEEB R. p 1797 N94-20033
MALKANI, MOHAN J. p 1890 N94-20185
MALKOV, O. YU. p 1927 N94-22533
MALLET-PARET, JOHN p 1951 N94-20545
MALY, TIMOTHY p 1949 N94-19898
MANCINELLI, R. L. p 1812 N94-22434
MANDEL, ERIC p 1926 N94-22507
p 1927 N94-22524
MANDELKERN, LEO p 1704 N94-20946
MANDELL, M. J. p 1654 N94-21429
MANDERS, P. J. H. M. p 1753 N94-21067
MANDEVILLE, J. C. p 1659 N94-21368
MANDL, R. G. p 1763 N94-21652
MANDRUS, D. p 2032 N94-21987
MANES, K. R. p 1820 N94-22401
MANGANO, M. L. p 1973 N94-20474
MANGOLD, D. p 1904 N94-20097
MANHEIMER, WALLACE M. p 1752 N94-20931
MANI, T. V. p 1690 N94-20183
MANNE, L. L. p 1961 N94-22379
MANNER, DAVID B. p 1714 N94-21564
p 1715 N94-21589
MANNERMAA, KAUKO p 2053 N94-22085
MANNING, K. p 2048 N94-22519
MANNING, K. R. p 1926 N94-22508
MANSFIELD, J. p 2019 N94-20941
MANSON, A. H. p 1870 N94-21862
MANTEUFFEL, THOMAS A. p 1955 N94-21464
p 1955 N94-21465
p 1955 N94-21467
MANUKIAN, NARBIK p 1943 N94-20947
MAO, J. p 1705 N94-21223
MAPLE, M. B. p 2015 N94-20275
p 2016 N94-20335
p 2036 N94-22584
MARACAS, GEORGE N. p 2024 N94-21003
p 2024 N94-21004
p 2024 N94-21005
MARANCI, ARUTUN p 1674 N94-21040
MARANOWSKI, S. A. p 2030 N94-21805
MARBURY, G. S. p 1685 N94-20753
MARCHENKO, SERGEI p 1744 N94-22069
MARCHENKO, SERGEI V. p 1923 N94-22083
MARCHIORI, ELENA p 1909 N94-21025
p 1909 N94-21026
MARCINIAK, T. J. p 1811 N94-22391
MARCO, J. p 1659 N94-21369
MARGOLESE, D. p 2017 N94-20544
MARHEFKA, R. J. p 1716 N94-20139
MARIN, LUIS E. p 1862 N94-20757
p 1863 N94-20843
MARK, J. p 1748 N94-19902
MARK, J. E. p 1699 N94-20046
MARKATOS, EVANGELOS p 1930 N94-21228
MARLEY, N. A. p 1855 N94-20220
MARQUES, M. p 1951 N94-20221
MARQUEZ, M. p 1928 N94-19812
MARR, W. W. p 1825 N94-21297
p 1811 N94-22391
MARRA, JOHN p 1864 N94-20186
MARRIOTT, K. B. p 2011 N94-19825
MARRON, JOSEPH C. p 1817 N94-21253
MARROQUIN, JOSE L. p 1964 N94-21215
p 1913 N94-21364
MARSHALL, I. H. p 1672 N94-20031
MARSHALL, JEFFREY S. p 1636 N94-20043
MARSHALL, S. p 2058 N94-22444
MARTEL, SYLVAIN p 1784 N94-22192
p 1784 N94-22193
MARTI, K. p 1685 N94-20697
MARTIN, C. R. p 1681 N94-21168
MARTIN, FRED p 1919 N94-22355
MARTIN, J. E. p 1700 N94-20315
MARTIN, JAN p 1732 N94-20461
MARTIN, L. J. p 2090 N94-20392
MARTIN, L. R. p 1851 N94-20025
MARTIN, R. p 2083 N94-20746
MARTIN, R. L. p 2031 N94-21857
MARTIN, S. J. p 1749 N94-20054
p 1968 N94-21751
MARTIN, T. H. p 1762 N94-21634
MARTIN, T. J. p 1859 N94-22036
MARTINEZ-SANCHEZ, M. p 1667 N94-20069
MARTINEZ-SANCHEZ, MANUEL p 1667 N94-19847
MARTINEZ, A. R. p 2034 N94-22035
MARTINEZ, R. R. p 1685 N94-20684
p 1687 N94-20870
MARTINO, T. p 2028 N94-21541
MARTNER, BROOKS E. p 1874 N94-22310
p 1874 N94-22311

MARTONE, M. p 1744 N94-21091
MASAI, KUNIAKI p 2002 N94-22640
p 2004 N94-22653
MASARIK, J. p 2106 N94-20713
MASHBURN, HENRY H. p 1898 N94-20107
MASON, KEVIN T. p 1891 N94-20615
p 1891 N94-20928
MASON, THOMAS GORDON BECK
p 1991 N94-22581
MASSINK, MIEKE p 1910 N94-21062
MASUR, L. J. p 2035 N94-22570
MATHESON, LESLEY R. p 1938 N94-21488
MATHEWS, G. J. p 2081 N94-21618
MATHIJSSEN, J. E. T. p 2042 N94-20310
MATHIJSSEN, R. W. p 1753 N94-21067
MATROSOV, SERGEY p 1873 N94-22306
MATROSOV, SERGEY Y. p 1873 N94-22304
MATSUI, T. p 2145 N94-21674
MATSUI, TAKAFUMI p 2123 N94-20803
MATSUMOTO, R. p 2004 N94-22655
MATSUMOTO, TOMOAKI p 2009 N94-22689
MATSUSHITA, TADASHI p 1665 N94-21406
MATSUYAMA, HIROSHI p 1772 N94-22118
MATTA, LAWRENCE M. p 1667 N94-20015
MATTHEWS, M. J. p 2028 N94-21458
MATTILA, K. p 1965 N94-22536
MATTOX, J. p 1926 N94-22501
MATTSON, J. E. p 2031 N94-21930
p 2035 N94-22564
MAUERSBERGER, KONRAD p 1812 N94-22435
MAURASSE, F. J.-M. R. p 1685 N94-20753
MAURER, M. J. p 2117 N94-20771
MAURER, R. H. p 1754 N94-21085
MAURETTE, MICHEL p 2082 N94-20678
p 2082 N94-20704
MAVADDAT, F. p 1771 N94-22112
MAVRIPLIS, D. J. p 1958 N94-21484
p 1920 N94-22362
MAX, C. E. p 1989 N94-21619
MAXTED, A. p 1906 N94-20280
p 1906 N94-20281
MAXWELL, K. L. p 1996 N94-21769
MAXWELL, T. A. p 2143 N94-21667
p 2145 N94-21676
MAY, DOUGLAS A. p 1837 N94-20028
MAY, E. p 1921 N94-22375
MAY, EDWARD L. p 1823 N94-20494
MAY, L. p 1685 N94-20753
MAYEDA, T. K. p 2082 N94-20681
p 2083 N94-20708
MAYEDA, TOSHIKO K. p 1862 N94-20776
MAYER, S. T. p 1768 N94-21753
MAYER, THOMAS p 2015 N94-20152
MAYNARD, JULIAN D. p 2013 N94-19933
MAYOR, SHALINI p 1872 N94-22299
MAZEROLLE, TERRY MARK p 1651 N94-22419
MAZURE, MARIE-LAURENCE p 1950 N94-20200
MCALLISTER, A. p 2004 N94-22655
MCALONEY, MIKE p 1644 N94-22154
MCALOON, JEFFREY F. p 1967 N94-21260
MCCALLUM, R. W. p 2036 N94-22582
MCCARTNEY, MICHAEL p 1881 N94-19895
MCCARTY, J. P. p 1825 N94-21580
MCCARTY, R. D. p 1968 N94-21447
MCCLEESE, D. J. p 1812 N94-22436
MCCOMAS, D. J. p 1976 N94-21995
MCCONKEY, EDWIN D. p 1642 N94-20051
MCCONVILLE, DAVID H. p 1704 N94-21186
MCCORD, T. B. p 1813 N94-20688
MCCORMICK, ANTHONY W. p 1710 N94-20983
p 1710 N94-20984
MCCORMICK, M. P. p 1869 N94-21644
MCCORMICK, STEPHEN F. p 1955 N94-21465
p 1806 N94-21466
p 1806 N94-21480
MCCORMICK, STEVE F. p 1955 N94-21464
MCCOWN, A. W. p 1814 N94-19867
MCCOY, M. G. p 1936 N94-21828
MCCOY, T. J. p 2083 N94-20749
MCCRACKIN, DANIEL C. p 1781 N94-22175
MCCRAE, JACK E., JR. p 1678 N94-19953
MCCRORY, R. L. p 1819 N94-21839
MCCULLOCH, M. T. p 2096 N94-20660
MCDANIEL, CHRISTOPHER R. p 1889 N94-19981
MCDONALD, L. p 1926 N94-22501
MCDOUGAL, DAVID S. p 1871 N94-22292
MCDOUGALL, J. p 1729 N94-20451
MCDOWELL, J. p 2048 N94-22519
MCELHANON, R. W. p 1748 N94-19892
MCEWEN, A. p 2101 N94-20686
MCEWEN, A. S. p 1852 N94-20850
MCGAHAN, WILLIAM A. p 1820 N94-21006
p 1710 N94-21007
MCGAW, MICHAEL A. p 1835 N94-22620
MCGEE, W. F. p 1793 N94-22251
MCGILL, G. E. p 2090 N94-20393
MCGLAUN, J. M. p 1904 N94-20052
MCGLYNN, T. A. p 1926 N94-22488
p 2047 N94-22493
p 2048 N94-22509
MCGRATH, DANIEL T. p 1740 N94-21518
MCGRAW, J. R. p 1937 N94-22558
MCGREGOR, J. L. p 1855 N94-20256
MCGUIRE, GARY E. p 1740 N94-21361
MCGUIRE, MICHAEL p 1747 N94-22213
MCHARG, B. B., JR. p 2045 N94-22404
MCINTOSH, ROBERT E. p 1882 N94-20489
MCKAY, C. P. p 2144 N94-21671
p 2145 N94-21677
MCKAY, D. S. p 2097 N94-20662
p 2084 N94-20828
p 1887 N94-20870
MCKAY, DAVID S. p 2126 N94-20820
p 2126 N94-20821
MCKAY, M. D. p 1916 N94-21747
MCKECHNIE, T. S. p 1797 N94-19974
MCKECHNIE, TIMOTHY N. p 1703 N94-20541
MCKEEVER, J. W. p 1769 N94-21830
MCKENNA, SUSAN p 1887 N94-21908
p 1888 N94-21910
MCKENZIE, F. D. p 1671 N94-21882
MCKERRACHER, P. L. p 1754 N94-21085
MCKERRACHER, PRISCILLA L. p 1765 N94-21710
MCKINNON, G. H. p 1778 N94-22151
MCLAUGHLIN, D. L. p 1750 N94-20294
p 2016 N94-20296
p 1750 N94-20312
MCLEAN, GARNET A. p 1893 N94-20081
MCLEAN, W., II p 1709 N94-21970
MCLEOD, ROBERT D. p 1782 N94-22182
p 1788 N94-22206
MCLUCKEY, S. A. p 1852 N94-22004
MCMAHAN, A. K. p 1706 N94-21512
MCMANUS, HUGH L. p 1676 N94-21743
MCMANUS, K. R. p 1809 N94-21607
MCNALLY, B. V. p 1926 N94-22494
MCNAMARA, W. F. p 1708 N94-21954
MCNIDER, RICHARD T. p 2042 N94-20268
MCPHERSON, JAMES C. p 1891 N94-21035
MCPHETRES, JEANNE M. p 1855 N94-20090
MCSWEEN, H. Y., JR. p 2145 N94-21678
MCWHORTER, SHARYN N. p 1751 N94-20483
MEAD, JAMES B. p 1882 N94-20564
MEAD, W. C. p 1946 N94-21845
MEARS, C. A. p 2031 N94-21869
MEDDAHI, M. p 1979 N94-19989
p 2016 N94-20323
MEDINA, DAVID F. p 1831 N94-20572
MEEGAN, C. A. p 2149 N94-20603
MEEKER, LARRY J. p 1896 N94-20914
MEGARIDIS, CONSTANTINE M. p 1802 N94-21193
MEHLER, W. R. p 1887 N94-21909
MEIER, K. L. p 1814 N94-19828
MEIJER, H. G. p 1953 N94-21059
MEINHARDT, M. B. p 1706 N94-21526
MEKHTIYEV, R. F. p 2028 N94-21438
MELEEDY, D. M. p 1938 N94-22454
MELENDRES, C. A. p 1692 N94-21558
MELFI, H. p 1879 N94-22337
MELFI, S. H. p 1877 N94-22326
MELLO, F. J. p 1915 N94-21539
MELLON, M. T. p 2090 N94-20394
MELLOR, MALCOLM p 1651 N94-21239
MELLOR, PAMELA A. p 1714 N94-21564
p 1715 N94-21589
MELOSH, H. J. p 1863 N94-20833
MELROSE, DON B. p 2001 N94-22634
MELSEN, J. p 2011 N94-19827
MELSON, N. DUANE p 1955 N94-21464
p 1956 N94-21469
MELTON, JOHN E. p 1920 N94-22367
MENDEL, C. W. p 1980 N94-20295
MENDELL, W. W. p 2136 N94-20874
MENDEZ, EMILIO E. p 2011 N94-19817
MENDILLO, MICHAEL p 1857 N94-21189
MENEGHINI, ROBERT p 1728 N94-20446
MENON, RAJIV p 1890 N94-20190
MENON, SANKARAN M. p 1756 N94-21105
p 1767 N94-21727
MENSA, DEAN L. p 1717 N94-20333
p 1718 N94-20334
MENSHIKOV, IVAN p 1965 N94-22075
MENYUK, C. R. p 1819 N94-21872
MERKEL, KENNETH G. p 1796 N94-20985
p 1796 N94-20989
p 2022 N94-20992
p 2022 N94-20993
p 2022 N94-20994
p 2022 N94-20995
MERKLE, B. D. p 2036 N94-22582
MERKLE, K. L. p 2033 N94-21994
MERRIAM, MARSHAL L. p 1920 N94-22372
MERRICK, VERNON K. p 1635 N94-20035
MERRILL, WALTER p 1650 N94-21742
MESSING, FREDRIC p 1932 N94-21334
MESTAD, S. p 1928 N94-19812
MESZAROS, PETER p 2003 N94-22646
MESZAROS, S. p 1785 N94-22199
METCALF, KENNETH J. p 1846 N94-21179
METZ, T. R. p 1918 N94-22011
METZGER, M. R. p 1814 N94-22510
MEYER, B. S. p 2081 N94-21618
MEYER, DUANE p 2024 N94-21003
p 2024 N94-21004
MEYER, MAURICE p 1644 N94-22154
MEYER, MIKE L. p 1713 N94-21760
MEYER, R. E. p 1820 N94-22020
MEYERHOFF, CURTIS L. p 1807 N94-20203
MEYERS, MICHAEL P. p 1878 N94-22331
MEYERS, P. V. p 1845 N94-20095
MICHAEL, J. R. p 1687 N94-19904
MICHAEL, MAGED M. p 1912 N94-21227
MICHAELS, J. F. p 1644 N94-22136
MICHALOPOULOS, DEMETRI p 1744 N94-22103
MIDDLETON, R. p 1863 N94-20889
MIES, F. H. p 1818 N94-21829
MIGLIORI, A. p 2032 N94-21987
MIIKKULAINEN, RISTO p 1941 N94-20255
MIKIC, ZORAN p 2147 N94-21877
MIKKOLA, ARI p 1938 N94-22070
MIKULAS, MARTIN M., JR. p 1822 N94-20369
MILES, LOWELL p 1766 N94-21722
MILES, W. F. p 2046 N94-22407
MILHOAN, JAMES D. p 1676 N94-21834
MILIKH, G. M. p 1750 N94-20325
MILINCHUK, A. V. p 1661 N94-21380
MILITCH, PETER N. p 1932 N94-21330
MILLER, ARTHUR C., JR. p 1821 N94-19891
MILLER, C. C. p 1817 N94-20583
p 1973 N94-20619
MILLER, J. M. p 1829 N94-19943
MILLER, JASON B. p 2027 N94-21304
MILLER, KENT L. p 1866 N94-20918
MILLER, M. K. p 1689 N94-20180
MILLER, S. A. p 1881 N94-19952
MILLER, T. A. p 1994 N94-21214
MILLER, WARNER H. p 1753 N94-21080
p 1741 N94-21783
MILLS, G. B. p 2016 N94-20322
MILLWATER, HARRY R. p 1828 N94-22616
MILOSHEVICH, LARRY M. p 1871 N94-22293
MINAMI, SHIGEYUKI p 2003 N94-22647
p 2003 N94-22648
p 2004 N94-22657
MINCHAU, BRIAN p 1786 N94-22207
MINESHIGE, S. p 2009 N94-22694
MING, DOUGLAS W. p 1812 N94-22433
MING, JIA p 1792 N94-22245
MINK, D. J. p 1927 N94-22511
MINNIS, PATRICK p 1872 N94-22299
p 1872 N94-22301
p 1872 N94-22302
p 1873 N94-22306
p 1880 N94-22342
MINTZ, Y. p 1837 N94-20205
MIRANDA, F. A. p 1709 N94-20518
MIRDAMADI, MASSOUD p 1835 N94-22618
MIRTICH, MICHAEL J. p 1660 N94-21377
MISAWA, K. p 2086 N94-20893
MISAWA, KEJI p 2084 N94-20834
MISHCHENKO, M. I. p 1721 N94-20416
MISHIMA, HIRAKU p 1746 N94-22172
MISHRA, C. S. p 1982 N94-21934
MISHRA, S. R. p 1745 N94-22128
MISTICHELLI, MARK P. p 2044 N94-21354
MISYCHENKO, N. I. p 2084 N94-20824
MITCHELL, DAVID L. p 1879 N94-22336
p 1881 N94-22343
MITCHELL, M. A. p 1749 N94-20054
MITCHELL, T. H. p 1743 N94-22557
MITCHELL, WILLIAM F. p 1956 N94-21470
MITTLEFEHLDT, D. W. p 1685 N94-20684
MIURA, AKIRA p 2003 N94-22651
MIYAMOTO, MASAMICHI p 2124 N94-20811
MIYAMOTO, SIGENORI p 2009 N94-22690
MO, J. p 1925 N94-22478
MODI, VIJAY p 1655 N94-21797
MOE, KAREN p 1932 N94-21332
MOEHRLE, MARTIN p 2026 N94-21151
MOGHADDAM, M. p 1719 N94-20407
p 1719 N94-20408
p 1719 N94-20410
MOHAMED, GULAM p 1764 N94-21704
MOHAMED, J. H. p 1741 N94-21567
MOHEB, H. p 1745 N94-22140
p 1746 N94-22162
MOHN, W. R. p 1693 N94-21771
MOLAWANY, A. S. p 1775 N94-22133

MOLENBROEK, E. ..... p 1699 N94-20047
MOLINA, C. ..... p 1768 N94-21770
MOLL, A. J. ..... p 2030 N94-21763
MONAT, J. P. ..... p 1891 N94-20935
MONDAY, J. F. ..... p 1998 N94-22045
MONGIA, H. C. ..... p 1648 N94-21582
p 1648 N94-21583
p 1649 N94-21758
MONNIER, A. ..... p 2017 N94-20544
MONONEN, TERO ..... p 1744 N94-22076
MONTI, JOSEPH M. ..... p 1883 N94-20925
MONTMINY, BENOIT ..... p 1791 N94-22235
MONTREUIL, JEAN ..... p 1746 N94-22197
MOOPENN, ALEXANDER W. ..... p 1942 N94-20360
MOORE, C. ..... p 1684 N94-20667
MOORE, J. M. ..... p 2111 N94-20739
p 2111 N94-20740
MOORE, JEFFREY ..... p 2088 N94-20382
MOOREFIELD, G. M., II ..... p 1761 N94-21257
MORAN, J. F. ..... p 1925 N94-22461
p 1926 N94-22508
MORAN, PATRICK J. ..... p 1645 N94-20561
MORAN, SHLOMO ..... p 1915 N94-21537
p 1935 N94-21549
MORAN, STUART L. ..... p 1751 N94-20354
MORANO, ERIC ..... p 1806 N94-21471
MORCHAT, R. M. ..... p 1681 N94-21241
MOREIRA-NETO, JOAO ROBERTO
p 1742 N94-22279
MOREL, D. L. ..... p 1847 N94-21614
MORENO, J. C. ..... p 1819 N94-21873
MORGAN, A. J. ..... p 1820 N94-22401
MORGAN, E. ..... p 1926 N94-22486
MORGAN, J. W. ..... p 2085 N94-20854
MORGERA, SALVATORE D. ..... p 1747 N94-22242
MORI, MASATO ..... p 1746 N94-22172
MORI, YOSHIHARU ..... p 2086 N94-20898
MORIARTY, J. A. ..... p 1696 N94-22398
MORIKAWA, N. ..... p 2082 N94-20639
MORIKURA, MASAHIRO ..... p 1746 N94-22171
MORIN, ANDRE ..... p 1747 N94-22237
MORIN, G. A. ..... p 1746 N94-22198
MORINO, YOSHIKI ..... p 1665 N94-21406
p 1652 N94-21407
MORISON, W. D. ..... p 1660 N94-21373
MOROZ, L. V. ..... p 2141 N94-20908
MORRIS, CARL J. ..... p 1738 N94-21198
p 1739 N94-21218
MORRIS, ED ..... p 1912 N94-21205
MORRIS, R. ..... p 2087 N94-20906
MORRIS, R. V. ..... p 1686 N94-20761
p 2143 N94-21668
p 1811 N94-22431
MORRIS, ROBERT A. ..... p 1671 N94-21882
MORRISSEY, M. L. ..... p 1881 N94-20699
MORSE, J. D. ..... p 1794 N94-22380
MORSS, L. R. ..... p 2033 N94-21992
MORTENSEN, D. J. ..... p 1741 N94-21567
MORTIMER, R. G. ..... p 1641 N94-21428
MORTON, D. P. ..... p 1921 N94-22406
MOSER, SUSAN A. ..... p 1932 N94-21331
MOSHER, J. C. ..... p 1732 N94-20479
MOSLEY, W. C. ..... p 1688 N94-19942
MOSS, DON ..... p 2042 N94-20268
MOSS, WILLIAM F. ..... p 1915 N94-21584
MOSYAGIN, D. V. ..... p 2007 N94-22675
MOUGIN, ERIC ..... p 1719 N94-20409
MOUGINIS-MARK, P. ..... p 1881 N94-20699
MOUGINIS-MARK, P. J. ..... p 2106 N94-20720
p 2039 N94-20818
MOULTHROP, A. A. ..... p 1967 N94-19949
MOUNAIX, PH. ..... p 1966 N94-21958
MOUROU, GERARD A. ..... p 2017 N94-20470
MU, ZHEN ..... p 1793 N94-22249
MUELLER, JAMES L. ..... p 1866 N94-20559
MUELLER, JOHANNES ..... p 1860 N94-22285
MUELLER, KURT F. ..... p 1712 N94-20061
MUENCH, F. X. ..... p 1640 N94-22605
MUGHABGHAB, SAID F. ..... p 1671 N94-21979
MUHA, M. S. ..... p 1967 N94-19949
MUHLEMAN, D. O. ..... p 1812 N94-22436
MUKHERJEE, AMIYA K. ..... p 1694 N94-21943
MUKHERJEE, R. ..... p 2056 N94-22282
MULHALL, P. A. ..... p 1809 N94-21607
MULHEARN, P. J. ..... p 1881 N94-19905
MULHOLLAND, G. T. ..... p 1807 N94-19987
MULLENDER, K. SJOERD ..... p 2044 N94-21494
MULLER, J-P. ..... p 2128 N94-20830
MULLIN, S. A. ..... p 1829 N94-19943
MULLIS, CLIFFORD T. ..... p 1736 N94-20570
MUNDY, JOSEPH L. ..... p 1949 N94-19838
MUNK, WALTER H. ..... p 1883 N94-21366
MUNRO, R. G. ..... p 1706 N94-21516
MUNTZ, E. P. ..... p 1802 N94-21220
MURAKAMI, M. ..... p 1999 N94-22568
MURPHY, DAN ..... p 1834 N94-22609
MURPHY, LISA D. ..... p 1935 N94-21351
MURPHY, MARY C. ..... p 1675 N94-21431
MURPHY, T. C. ..... p 1854 N94-19955
MURRAY, J. B. ..... p 2128 N94-20830
MURRAY, S. S. ..... p 2043 N94-21270
p 2048 N94-22499
MURTHY, S. N. B. ..... p 1648 N94-21582
p 1648 N94-21583
MUSLINER, ANDREW ..... p 1744 N94-21341
MUSTARD, J. F. ..... p 1685 N94-20689
MUSTARD, JOHN F. ..... p 1686 N94-20831
p 2128 N94-20832
MUTHAIAH, A. ..... p 1847 N94-21614
MUTHEN, BENGT O. ..... p 1894 N94-21282
MYERS, G. B. ..... p 1929 N94-20472
MYERS, ROGER M. ..... p 1670 N94-21565
MYERS, TAMARA A. ..... p 1738 N94-21198
p 1739 N94-21218
MYERS, WILLIAM NEILL ..... p 1823 N94-20380
MYLES, K. M. ..... p 1848 N94-21870

N

NA, C. Y. ..... p 2092 N94-20637
NADOBNY, JACEK ..... p 1889 N94-20024
NAGAHARA, A. ..... p 1886 N94-21903
NAGAHARA, HIROKO ..... p 1684 N94-20638
NAGAI, H. ..... p 2082 N94-20658
NAGAI, SIRO ..... p 1686 N94-20804
NAGAMORI, HIDEO ..... p 2010 N94-22696
NAGAO, K. ..... p 2083 N94-20764
NAGASAWA, HIROSHI ..... p 2086 N94-20898
NAGEL, K. ..... p 1867 N94-21312
NAGY, L. A. ..... p 1741 N94-21567
NAGY, Z. ..... p 1687 N94-19922
NAIDIN, D. P. ..... p 1862 N94-20641
NAIK, ASHISH V. ..... p 1912 N94-21273
p 1954 N94-21314
NAIR, H. ..... p 2145 N94-21679
NAJARRO, FRANCISCO ..... p 2081 N94-21578
NAKAJIMA, HIROSHI ..... p 2001 N94-22633
NAKAMURA, FUMITAKA ..... p 2008 N94-22687
p 2008 N94-22688
p 2009 N94-22689
NAKAMURA, N. ..... p 2082 N94-20639
NAKANO, TAKENORI ..... p 2008 N94-22687
p 2008 N94-22688
NAKASHIMA, KAZUO ..... p 1666 N94-20890
NAKOTTE, H. ..... p 2033 N94-21991
NAM, SANG H. ..... p 1995 N94-21292
NAM, YON-WOO ..... p 1935 N94-21351
NAMBU, MITSUHIRO ..... p 2006 N94-22669
NANDHAKUMAR, N. ..... p 1818 N94-21817
NANDY, B. ..... p 1772 N94-22115
NANNI, M. ..... p 2047 N94-22452
NARAYAN, R. ..... p 1673 N94-20327
NARENDRAN, PALIATH ..... p 1744 N94-21102
NARTKER, T. A. ..... p 1821 N94-19833
NASH, J. K. ..... p 1818 N94-21547
NASH, T. J. ..... p 1816 N94-20298
NASTASI, M. A. ..... p 2036 N94-22583
NATANSOHN, A. ..... p 1705 N94-21223
p 1705 N94-21238
p 1705 N94-21259
p 1705 N94-21267
p 1706 N94-21523
NATESAN, K. ..... p 1693 N94-21825
NATHAN, V. ..... p 1754 N94-21084
NAUMOV, S. F. ..... p 1653 N94-21370
NAVARRE, G. ..... p 1665 N94-21408
NAZAROV, M. A. ..... p 1684 N94-20640
p 1862 N94-20641
p 1684 N94-20642
p 2082 N94-20643
p 2083 N94-20752
NEAL, CLIVE R. ..... p 1684 N94-20644
p 1684 N94-20645
NEAL, D. R. ..... p 1797 N94-19974
NEDERHOF, M.-J. ..... p 1909 N94-21061
NEGORO, HITOSHI ..... p 2009 N94-22690
NEKILI, MOHAMED ..... p 1778 N94-22153
NELLIS, W. J. ..... p 2031 N94-21931
NELSON, B. E. ..... p 1998 N94-22045
NELSON, G. C. ..... p 1687 N94-19864
NELSON, R. M. ..... p 1991 N94-20646
NEMANICH, R. J. ..... p 2026 N94-21190
NEMCHINOV, I. V. ..... p 2082 N94-20647
p 2082 N94-20648
p 1862 N94-20649
p 2084 N94-20823
p 2084 N94-20824
NEMETH, NOEL N. ..... p 1828 N94-22619
NEPSTAD, DANIEL C. ..... p 1838 N94-20957
NEREM, R. S. ..... p 2117 N94-20774
p 2142 N94-20911
NEUBERT, T. ..... p 2005 N94-22680
p 2007 N94-22674
NEUHAUS, JOSEPH ..... p 1943 N94-20947
NEUKUM, G. ..... p 1813 N94-20650
p 2101 N94-20688
p 2136 N94-20876
NEUMAN, B. CLIFFORD ..... p 1905 N94-20228
NEUMANN, G. ..... p 1720 N94-20413
NEVES, EDUARDO G. ..... p 1838 N94-20954
NEWBURN, R. L. ..... p 2047 N94-22496
NEWMAN, B. E. ..... p 1818 N94-21554
NEWMAN, ROBERT B. ..... p 1642 N94-20051
NEWNAM, B. E. ..... p 1820 N94-22585
NEWSOM, H. E. ..... p 2095 N94-20651
NEWTON, M. A. ..... p 1789 N94-21838
NG, P. ..... p 1744 N94-21092
NGHIEM, S. V. ..... p 1720 N94-20413
p 1721 N94-20415
p 1723 N94-20426
p 1724 N94-20432
p 1727 N94-20441
p 1728 N94-20445
p 1729 N94-20449
NGO, E. ..... p 2027 N94-21303
NGUYEN, A. ..... p 2037 N94-20473
NGUYEN, CUONG M. ..... p 1929 N94-20571
NGUYEN, D. C. ..... p 1814 N94-19828
p 1816 N94-20277
NGUYEN, D. T. ..... p 2047 N94-22455
NGUYEN, D. X. ..... p 1994 N94-21290
NGUYEN, J. ..... p 1950 N94-20034
NGUYEN, MINH ..... p 1775 N94-22132
NGUYEN, T. ..... p 1686 N94-20781
p 1811 N94-22431
NGUYEN, TUAN ..... p 1845 N94-20066
NICHOLLS, JENNIFER ..... p 2003 N94-22652
NICOLAIDIS, M. ..... p 1749 N94-20186
NIEDERMANN, S. ..... p 1684 N94-20652
NIEDNER, M. B. ..... p 2047 N94-22496
NIEH, BENJAMIN B. ..... p 1784 N94-22194
NIEH, T. G. ..... p 1695 N94-21986
NIELSEN, CHRISTINE ..... p 1840 N94-20968
NIEMANN, HASSO ..... p 1812 N94-22435
NIER, A. O. ..... p 2082 N94-20653
NIEUWKOOP, E. ..... p 1796 N94-21801
NIIJIMA, A. ..... p 1888 N94-21911
NIIJIMA, AKIRA ..... p 1887 N94-21907
NIJHOLT, A. ..... p 1940 N94-20242
NIKISHIN, A. M. ..... p 2095 N94-20654
p 2095 N94-20655
p 2096 N94-20656
NIKITSKIY, V. P. ..... p 1664 N94-21401
NIKJOOY, M. ..... p 1648 N94-21582
p 1648 N94-21583
NIKOLAEVA, OLGA V. ..... p 2096 N94-20657
NILSEN, J. ..... p 1819 N94-21873
NINDL, BRADLEY C. ..... p 1892 N94-21036
NIRANJAN, SHAILESH ..... p 1758 N94-21120
NISHI, YASUKI ..... p 1746 N94-22172
NISHIIZUMI, K. ..... p 2082 N94-20658
p 2106 N94-20713
NISHIKAWA, KEN-ICHI ..... p 2005 N94-22660
p 2007 N94-22674
NISHIKAWA, KYOJI ..... p 2004 N94-22658
p 2006 N94-22666
NISHIO, M. ..... p 2001 N94-22633
NITSCHE, W. ..... p 1639 N94-22597
p 1639 N94-22600
NITTA, SHIN-YA ..... p 2008 N94-22682
NITTLER, L. R. ..... p 2082 N94-20659
NJOKU, ENI G. ..... p 1727 N94-20443
p 1727 N94-20444
NOBARI, M. R. ..... p 1798 N94-20167
NOCK, K. T. ..... p 2123 N94-20806
NOEVER, DAVID A. ..... p 2017 N94-20528
NOGAMI, KENICHI ..... p 1666 N94-20890
NOLAN, J. F. ..... p 1845 N94-20095
NOLAN, P. ..... p 1926 N94-22501
NOLAN, T. A. ..... p 1707 N94-21653
NOMA, MOTOSAKU ..... p 1666 N94-20890
NOOJIN, GARY D. ..... p 1890 N94-20462
NOOR, AHMED K. ..... p 1833 N94-22606
NORDGREN, C. E. ..... p 1709 N94-20518
NORMAN, M. D. ..... p 2096 N94-20660
p 2097 N94-20661
NORMAN, M. R. ..... p 2032 N94-21972
NORMAN, MARC D. ..... p 2126 N94-20822
NORRIS, J. A. ..... p 2097 N94-20662
NORRIS, THEODORE B. ..... p 2017 N94-20470
NORTH, GERALD ..... p 1870 N94-21647
NORTHROP, LINDA ..... p 1650 N94-19880
NORTON, GILL ..... p 1862 N94-20690
NOVIKOV, L. ..... p 1661 N94-21383
NOYES, H. P. ..... p 2038 N94-21971
NOZETTE, S. ..... p 1652 N94-20850
NOZETTE, STEWART ..... p 1652 N94-20765

NSI, M. p 1636 N94-20486
NUBLING, R. p 1763 N94-21697
NULSEN, PAUL E. J. p 2055 N94-21579
NUMAO, T. p 1975 N94-21775
NUNN, S. D. p 1694 N94-21945
NURNBERGER, M. p 1950 N94-20034
NYQUIST, L. E. p 2097 N94-20663
p 2115 N94-20763

O

OBERACKER, V. E. p 1960 N94-21955
OBERREUTER, ANDREAS p 1851 N94-20154
OBERT, W. p 1992 N94-20003
OBRIEN, T. KEVIN p 1678 N94-22622
OBRYAN, M. V. p 2085 N94-20858
OCAMPO, A. C. p 1854 N94-20698
ODELL, RICHARD p 1704 N94-21186
ODER, ROBIN R. p 2126 N94-20820
ODEWAHN, S. C. p 1927 N94-22512
ODINEK, J. p 1700 N94-20315
ODONNELL, KEVIN A. p 1716 N94-19934
OECHSLE, V. L. p 1649 N94-21758
OEGMEN, HALUK p 1939 N94-20212
OEHLER, A. p 1684 N94-20664
OETTL, H. p 1721 N94-20417
OEZDEMIR, T. p 1716 N94-20160
OFFORD, BRUCE W. p 1765 N94-21709
OGDEN, PETER M. p 1883 N94-21358
OGIWARA, MITSUNORI p 1912 N94-21273
p 1954 N94-21314
p 1955 N94-21456
OGLESBY, JAMES P. p 1897 N94-20665
OGLETREE, D. F. p 2034 N94-22041
OH, JAE E. p 1710 N94-20979
p 1710 N94-20980
p 2021 N94-20987
p 1796 N94-20988
p 2022 N94-20990
p 1710 N94-20991
OHADI, M. M. p 1798 N94-20101
OHASHI, HIDEO p 1666 N94-20890
OHERN, T. J. p 1797 N94-19974
OHNUKI, S. p 1979 N94-20222
OHSAWA, YUKIHARU p 2006 N94-22670
OJARD, G. C. p 1697 N94-22571
OKADA, A. p 2083 N94-20764
OKADA, RIKA p 2008 N94-22683
OKAMOTO, MASAO p 2000 N94-22629
OKEEFE, JOHN D. p 2098 N94-20666
OKIISHI, THEODORE H. p 1638 N94-21591
OLALDE, G. p 1665 N94-21405
OLHAUSEN, JOHN H. p 1896 N94-20914
OLIVER, W. C. p 2034 N94-22005
p 1697 N94-22559
OLIVIER, S. S. p 1989 N94-21619
OLLE, RAYMOND p 1660 N94-21377
OLLIS, C. W. p 1769 N94-21838
OLLUS, MARTIN p 2046 N94-22082
OLSEN, E. p 1684 N94-20667
OLSEN, E. J. p 2082 N94-20681
OLSEN, R. p 1808 N94-20297
OLSON, C. G. p 1974 N94-21553
OLSON, E. p 2047 N94-22459
OMALLEY, M. W. p 1750 N94-20294
p 2016 N94-20296
OMELCHENKO, YU. A. p 1972 N94-20181
OMER, KHIZER FAROOQ p 1651 N94-22418
OMORI, RIE p 1666 N94-20690
ONEEL, B. p 1926 N94-22487
p 1927 N94-22513
ONEILL, J. p 1902 N94-19911
ONEILL, K. p 1727 N94-20441
ONSTOTT, R. H. p 1723 N94-20427
ORENBERG, JAMES B. p 2108 N94-20723
ORLOFF, MAI T. p 1914 N94-21414
ORLOV, SERGEI A. p 1923 N94-22083
ORLOV, V. B. p 2029 N94-21552
ORR, BRAD W. p 1873 N94-22304
p 1879 N94-22333
p 1879 N94-22334
ORSZAK, J. S. p 1925 N94-22461
ORTEGA, F. A. p 1929 N94-20279
ORZESZKO, S. p 1710 N94-20981
OSBORNE, T. A. p 1998 N94-22039
OSBORNE, T. H. p 1993 N94-20326
OSBORNE, WILLIAM P. p 1760 N94-21130
OSHAUGHNESSY, DOUGLAS p 1746 N94-22210
OSHEA, P. G. p 1818 N94-21554
OSKAM, JOHN H. p 1704 N94-21184
OSSORIO, P. G. p 2048 N94-22499
OSTENDORF, MARI p 1736 N94-20547
OSTERLE, J. F. p 1846 N94-21527
OSWALD, FRED B. p 1826 N94-21756
OTHEN, P. J. p 1689 N94-20180
OTSUKA, AKIRA p 1772 N94-22118
OTSUKI, MAYUMI p 2084 N94-20813
OTT, G. W. p 1769 N94-21830
OTTING, WILLIAM D. p 1671 N94-21874
OTTO, ANTONIUS p 2001 N94-22636
OULDBRAHIM, HAMID p 1677 N94-22420
OVERMAN, ANDREA p 1922 N94-21483
OWENS, K. C. p 1732 N94-20471
OWENS, R. E. p 1796 N94-20988
OWOCKI, STANLEY P. p 2081 N94-21578
OZAWA, M. p 2033 N94-21993

P

PACIESAS, W. S. p 2149 N94-20603
PADILLA, S. p 1849 N94-22015
PAGE, C. G. p 2048 N94-22514
PAIGE, F. E. p 1969 N94-19804
PAILLAT, O. p 1684 N94-20669
PAILLE, N. I. p 1702 N94-20481
PAILLOUS, A. p 1659 N94-21369
PAINTER, J. S. p 1935 N94-21622
PAIVADOSSANTOSFILHO, CELIO
p 1839 N94-20964
PAKKURTI, M. p 1759 N94-21123
PALAMIDESSI, CATUSCIA p 1909 N94-21026
PALMA, R. E. p 1657 N94-19896
PALME, H. p 2082 N94-20704
p 2086 N94-20905
PAMULAPATI, J. p 2023 N94-21000
p 1796 N94-21001
PAN, J. p 1928 N94-19812
PANCHAL, C. B. p 1802 N94-20942
PANDA, S. p 2037 N94-20178
PANDOLF, KENT B. p 1892 N94-21209
PANG, Y. p 1975 N94-21693
PANISSET, J. F. p 1775 N94-22133
PANTELELIS, NIKOS p 1641 N94-21472
PANTUSO, J. p 1808 N94-20297
PANWAR, RAMESH p 1756 N94-21101
p 1756 N94-21104
p 1768 N94-21735
PAO, HUA-FU p 1899 N94-21252
PAPAMICHAEL, K. p 1809 N94-21545
PAPANASTASSIOU, D. A. p 1686 N94-20794
p 2084 N94-20795
PAPIKE, J. J. p 1684 N94-20670
p 2114 N94-20758
p 1685 N94-20759
p 1686 N94-20760
PAPKE, JOERG p 1910 N94-21152
PAPPALARDO, R. p 2098 N94-20671
PAPPAS, D. P. p 1688 N94-19986
PARENT, F. p 1785 N94-22200
PARFITT, E. A. p 2099 N94-20672
p 1862 N94-20673
p 1863 N94-20878
PARIKH, PARESH p 1919 N94-22357
PARIS, CECILE L. p 2041 N94-20133
PARK, H.-S. p 2058 N94-22444
PARK, JEA p 1764 N94-21701
PARK, RANDOLPH K. p 1894 N94-21510
PARKER, F. T. p 2031 N94-21930
PARKER, JAY p 1726 N94-20437
PARKER, LINDSAY p 1880 N94-22342
PARKER, T. E. p 1809 N94-21607
PARKER, T. J. p 2091 N94-20395
p 2099 N94-20674
PARKER, TIMOTHY p 2088 N94-20382
PARKES, A. G. p 1657 N94-20235
PARKIN, D. p 1714 N94-20278
PARKS, ALLEN D. p 1898 N94-20357
PARMAR, A. N. p 2048 N94-22521
PARMENTIER, E. M. p 2099 N94-20675
PARMENTIER, E. MARC p 2117 N94-20775
PARRAVANO, ANTONIO p 2006 N94-22667
p 2006 N94-22668
PARTON, V. Z. p 1836 N94-22065
PARZEN, EMANUEL p 1963 N94-20913
PARZEN, G. p 1970 N94-19868
PASZTOR, L. p 1927 N94-22515
PATCHEN, ALLAN p 2126 N94-20820
PATE, D. p 1699 N94-19973
PATE, DANIEL B. p 1812 N94-22433
PATEL, G. B. p 2117 N94-20774
PATEL, MANOJ p 1932 N94-21335
PATRICK, NICHOLAS J. M. p 2040 N94-21821
PATTABIRAMAN, S. p 1758 N94-21115
p 1759 N94-21127
PATTERSON, P. E. p 1762 N94-21634
PAULDRACH, ADALBERT W. A. p 2081 N94-21578
PAULSSON, B. p 1842 N94-21855
PAXMAN, RICHARD G. p 1817 N94-21253
PAXSON, DANIEL E. p 1801 N94-20588
PAYDAR, NASSER H. p 1829 N94-19937
PAYNE, D. G. p 1903 N94-19959
p 1936 N94-22032
PECHANEK, GERALD G. p 1757 N94-21113
PEDERSEN, BJOERN p 1851 N94-21455
PEDRONI, A. p 1684 N94-20676
PEDRYCZ, WITOLD p 1782 N94-22182
PEERIS, KUMAR p 1930 N94-21065
PEERY, J. S. p 1916 N94-21635
PEGGION, GERMANA p 1865 N94-20487
PEICANG, XU p 1685 N94-20677
PEILIANG, GAO p 1677 N94-22587
PEINAN, JIAO p 1717 N94-20207
PEKALA, R. W. p 1768 N94-21753
PEKKARI, LARS-OLAF p 1668 N94-20074
PELLAS, P. p 1685 N94-20695
PELLAT, R. p 2010 N94-22698
PELLERANO, FERNANDO A. p 1657 N94-21340
PELLETIER, P. J. p 1702 N94-20481
PELLETIER, ROBERT V. p 1782 N94-22182
PELLIN, M. J. p 1690 N94-20288
p 1976 N94-21951
PENCE, W. p 2047 N94-22462
PENCE, W. D. p 1927 N94-22516
PENG, Y. K. p 1709 N94-20972
PENG, Y. K. M. p 1998 N94-22045
PENNER, J. E. p 1852 N94-21969
PENNINGTON, D. M. p 1819 N94-21920
p 1990 N94-22002
PEPE, FRANK R. p 1703 N94-20614
PEPIN, R. O. p 2144 N94-21672
p 2146 N94-21680
PEPPARD, L. E. p 1772 N94-22113
PEPPLER, PHILIPP W. p 1651 N94-20108
PERCIVAL, J. W. p 1748 N94-22517
PEREIRA, ALFREDO p 1839 N94-20961
PEREIRADACUNHA, ROBERTO p 1838 N94-20953
p 1838 N94-20956
p 1839 N94-20960
p 1840 N94-20965
PERELOMOVA, A. A. p 2082 N94-20648
PEREPEZKO, J. H. p 2012 N94-19926
PEREZ, L. p 1658 N94-20617
PERIYALWAR, SHALINI p 1747 N94-22231
p 1747 N94-22232
PERKEY, DONALD J. p 1842 N94-22374
PERKINS, D. E. p 1906 N94-20316
PERLMUTTER, S. p 2058 N94-22444
PERON, M. p 2048 N94-22518
PERRAM, R. E. p 1657 N94-19896
PERREAU, M. p 2082 N94-20678
PERRON, C. p 1685 N94-20695
PERRY, JAMES C. p 1898 N94-20357
PERUCCHI, N. p 1752 N94-20633
PESKOV, V. p 1750 N94-20314
PESME, D. p 1966 N94-21958
PETAEV, M. I. p 1685 N94-20679
p 2082 N94-20680
p 2082 N94-20681
PETERS, H. R. p 1689 N94-20182
PETERSEN, B. L. p 1810 N94-21950
PETERSON, C. A. p 2101 N94-20682
PETERSON, D. W. p 1830 N94-20477
PETERSON, JAMES N. p 1755 N94-21097
PETERSON, N. p 1969 N94-22054
PETITPAS, LINDA S. p 1883 N94-20925
PETNEY, S. V. p 1904 N94-20052
PETOUHOFF, N. L. p 1697 N94-22559
PETRO, ANDREW J. p 1657 N94-20367
PETRONI, M. p 1783 N94-22184
PETROV, ALEXANDER A. p 2050 N94-22060
PETRZILKA, J. p 1997 N94-21816
PETRZILKA, V. p 1996 N94-21571
PETTERSEN, KJETIL p 1751 N94-20553
PETZOLD, LINDA R. p 1949 N94-19898
PFEIFER, HANS J. p 1866 N94-20557
PFEIFER, K. B. p 1968 N94-21751
PHAM, DINH TUAN p 1905 N94-20201
PHAM, VUONG T. p 1676 N94-21834
PHILIPP, WARREN H. p 1700 N94-20195
PHILIPS, L. A. p 1817 N94-20583
PHILIPS, LAURA A. p 1973 N94-20618
p 1973 N94-20619
PHILLIPS, E. P. p 1832 N94-21624
PHILLIPS, G. p 1799 N94-20258
PHILLIPS, J. E. p 1848 N94-21826
PHILLIPS, MARY A. p 1692 N94-21525
PHILLIPS, N. E. p 2031 N94-21926
PHILLIPS, R. J. p 2101 N94-20683
PHILLIPS, W. MORRIS p 1718 N94-20368
PHINNEY, W. C. p 1685 N94-20684
PHOEBUS, P. A. p 1868 N94-21605
PHONG, LINH NGO p 1781 N94-22178
PICCOLO, M. p 1982 N94-21952
PICONE, PHILIP J. p 2028 N94-21505
PIEDBOUEUF, JEAN-CLAUDE p 1794 N94-22256
PIERAZZO, E. p 2101 N94-20685

PIERCE, S. W. p 1821 N94-19859
PIERCE, T. G. p 1937 N94-22042
PIERSON, R. p 1763 N94-21697
PIETERS, C. M. p 2101 N94-20686
p 2101 N94-20687
p 1813 N94-20688
p 1685 N94-20689
p 1652 N94-20850
PIETERS, CARLE M. p 1686 N94-20805
p 1686 N94-20831
p 2128 N94-20832
PIFFL, V. p 1996 N94-21573
PIHLMAN, M. p 1936 N94-21749
PILEWSKIE, PETER p 1872 N94-22297
p 1844 N94-22319
PILKINGTON, M. p 1862 N94-20668
PILLINGER, C. T. p 2083 N94-20726
p 2085 N94-20846
p 2086 N94-20885
p 2086 N94-20886
p 2143 N94-21668
PIMPERL, M. M. p 1686 N94-20761
p 1811 N94-22431
PINET, P. C. p 2108 N94-20722
PINHOBRASIL, CESAR, JR. p 1801 N94-20597
PINKERTON, H. p 1862 N94-20673
p 1863 N94-20879
PINKERTON, HARRY p 1862 N94-20690
PINTO, JOSEPH F. p 1814 N94-19800
PIRENNE, B. p 2047 N94-22469
PIRZADEH, SHAHYAR p 1919 N94-22357
p 1919 N94-22359
PISKUNOV, N. E. p 1927 N94-22531
p 1927 N94-22532
PITCHUMANI, VIJAY p 1766 N94-21720
PLANTZ, D. H. p 2012 N94-19926
PLATEAU, BRIGITTE p 1963 N94-20202
PLATNICK, STEVEN p 1872 N94-22297
PLAUT, J. J. p 2110 N94-20734
PLAUT, JEFFREY J. p 1744 N94-20691
PLESCIA, J. B. p 2102 N94-20692
p 2103 N94-20693
p 2082 N94-20694
PLUEDDEMANN, ALBERT J. p 1864 N94-20186
PLUMMER, D. p 2048 N94-22519
PLUTCHAK, J. p 2101 N94-20686
POCHEC, PRZEMYSLAW p 1777 N94-22150
POCZ, Z. p 1944 N94-21140
PODLESNY, R. p 2029 N94-21617
PODOSEK, F. A. p 1685 N94-20695
PODTBURG, E. R. p 2035 N94-22570
POE, CLARENCE C., JR. p 1647 N94-22623
POELLOT, M. p 1844 N94-22303
p 1878 N94-22332
POELLOT, M. R. p 1871 N94-22294
POELLOT, MICHAEL R. p 1877 N94-22326
POELSTRA, KAREN p 2086 N94-20884
POHJOLA, MATTI p 1854 N94-22072
POHN, HOWARD A. p 2103 N94-20696
POISL, W. H. p 2034 N94-22005
POLAK, DAVID R. p 1967 N94-20523
POLASKI, DENNIS A. p 1913 N94-21409
POLETTE, THOMAS M. p 1812 N94-22433
POLINER, JEFFREY p 1896 N94-20606
p 1897 N94-21627
POLKA, LESLEY A. p 1717 N94-20269
p 1717 N94-20270
POLL, E. p 1928 N94-19996
POLLACK, JAMES B. p 2108 N94-20723
POLLIZZI, J. p 2049 N94-22537
POLLIZZI, J. A. p 2049 N94-22548
POLOMSKI, ELISHA p 2047 N94-22468
POLONKA, J. p 2032 N94-21936
POLYCARPOU, ANASTASIS C. p 1717 N94-20269
p 1717 N94-20271
POMERLEAU, DEAN p 1942 N94-20621
PONCHAK, G. E. p 1733 N94-20501
PONCHAK, GEORGE E. p 1733 N94-20500
p 1733 N94-20502
PONCINO, MASSIMO p 1758 N94-21118
PONGANIS, K. V. p 1685 N94-20697
POORMAN, R. p 1689 N94-20100
POORTEMA, KLAAS p 1963 N94-21076
POPE, K. O. p 1854 N94-20698
POPOVA, M. P. p 1862 N94-20649
POPOVICI, LIDIA p 1842 N94-22345
PORTER, KENT W. p 1642 N94-21818
POSENAU, MARY-ANNE K. p 1918 N94-22350
p 1920 N94-22370
POSPELOV, I. p 2051 N94-22071
POST, G. p 1953 N94-21072
POST, MADISON J. p 1876 N94-22323
POST, R. F. p 1762 N94-21620
p 1762 N94-21621
POSTAWKO, S. E. p 1881 N94-20699
p 2146 N94-21681
POTAPCZUK, MARK G. p 1642 N94-21590
p 1919 N94-22353
POUCH, JOHN J. p 1710 N94-20981
p 2022 N94-20990
p 1710 N94-20991
POUKEY, J. W. p 1980 N94-20295
POUND, BRUCE G. p 1689 N94-20027
POUSSART, D. p 1785 N94-22200
POUSSART, DENIS p 1779 N94-22163
p 1785 N94-22201
p 1746 N94-22211
POWELL, H. T. p 1819 N94-21920
p 1820 N94-22401
POWELL, J. ANTHONY p 2017 N94-20381
POWELL, J. R. p 1676 N94-21754
POWELL, KENNETH G. p 1920 N94-22364
POWER, CHRISTOPHER A. p 1703 N94-20541
PRASAD, PARAS N. p 1988 N94-21457
PRATT, DAVID R. p 1904 N94-20091
PRATT, R. H. p 1971 N94-20096
PRATT, S. F. p 1685 N94-20689
PRAUSNITZ, J. M. p 1707 N94-21856
PRAVEC, P. p 2149 N94-20603
PREMKUMAR, A. B. p 1744 N94-21100
p 1764 N94-21705
PREMKUMAR, A. BENJAMIN p 1768 N94-21734
PREMO, W. R. p 2104 N94-20700
p 1685 N94-20701
p 1685 N94-20702
PREPPERNAU, BRYAN L. p 1994 N94-21214
PRESLEY, M. A. p 1685 N94-20703
PRESPER, T. p 2082 N94-20704
PRESPER, TH. p 2082 N94-20678
PRESTON, CHARLES S. p 1646 N94-21246
PRESTON, S. p 1661 N94-21381
PRESTWICH, A. p 2048 N94-22519
PRETTYMAN, T. H. p 1904 N94-20049
PRICE, DAVID R. p 1648 N94-21433
PRICE, KATHERINE H. p 1844 N94-20705
PRICE, L. E. p 1921 N94-22375
PRICE, MARIBETH p 2105 N94-20706
p 2105 N94-20707
PRIEBE, A. p 2072 N94-22520
PRIEST, RICHARD G. p 1858 N94-21357
PRIGGE, KARL F. p 1647 N94-20042
PRIMDAHL, K. p 1807 N94-19987
PRIMINI, F. A. p 2062 N94-22466
p 1926 N94-22508
PRINZ, M. p 2063 N94-20708
p 2086 N94-20866
p 2087 N94-20907
PRINZO, O. VERONIKA p 1738 N94-21201
PRIOR, P. T. p 1657 N94-20235
PROBST, DAVID K. p 1753 N94-21081
p 1766 N94-21718
PRONKO, PETER P. p 1710 N94-20983
p 1710 N94-20984
PROTOPOPESCU, S. D. p 1969 N94-19804
PROVALOV, A. A. p 2106 N94-20709
PTITSYN, MIKHAIL O. p 2002 N94-22643
PUGH, ROBERT D. p 2013 N94-19966
PUJARI, V. K. p 1702 N94-20481
PULKKIS, GOERAN p 2049 N94-22056
PULS, JOACHIM p 2081 N94-21578
PURDY, ANDREW p 1701 N94-20349
PURVIANCE, J. p 1767 N94-21723
PURVIANCE, JOHN E. p 1765 N94-21712
PUSHKAREV, A. N. p 1972 N94-20181

Q

QADRI, SYED B. p 2017 N94-20348
QIN, X. p 1921 N94-22375
QIN, XIAO p 1921 N94-22376
QIU, CINDY X. p 1781 N94-22176
QU, SHOU-XING p 1747 N94-22231
p 1747 N94-22232
QUAK, D. p 1742 N94-22348
QUEZADA-MUNETON, JUAN MANUEL p 1862 N94-20757
QUEZADA, JUAN MANUEL p 1863 N94-20843

R

RABIER, PATRICK J. p 1954 N94-21173
p 1954 N94-21174
RABIITZ, H. p 1682 N94-21243
RABOIN, P. J. p 1960 N94-21996
RADAR, JOCK p 1912 N94-21205
RADESPIEL, R. p 1641 N94-21473
RADTKE, PAUL H. p 2042 N94-20924
RADTKE, R. J. p 2032 N94-21972
RADYUSHKIN, A. V. p 2038 N94-21513
RAGUE, BRIAN p 1727 N94-20443
RAHMAN, H. U. p 2003 N94-22647
RAHMAT-SAMII, YAHYA p 1718 N94-20404
RAHN, STEPHEN p 1986 N94-21043
RAI, A. K. p 1710 N94-20983
p 1710 N94-20984
p 1796 N94-20985
p 2022 N94-20992
p 2022 N94-20993
RAITALA, J. p 2106 N94-20710
p 2106 N94-20711
RAITERI, C. M. p 2133 N94-20859
RAIVIO, PAULA p 1707 N94-21890
p 1707 N94-21891
RAJKUMAR, RAGUNATHAN p 1899 N94-21230
RAJULU, SUDHAKAR L. p 1896 N94-20606
RALPH, F. MARTIN p 1874 N94-22310
RAMACHANDRA, A. p 1975 N94-21766
RAMACHANDRAN, F. p 1793 N94-22248
RAMAMURTHY, HEMA p 1757 N94-21106
RAMAN, GANESH p 1637 N94-20563
p 1638 N94-22274
RAMAN, R. p 2031 N94-21931
RAMAN, RAJEEV p 2049 N94-20098
RAMOS, J. p 1636 N94-20486
RANEY, C. W. p 1750 N94-20218
RAO, M. N. p 2106 N94-20712
RAPTIS, A. C. p 1677 N94-21940
RAS, Z. W. p 1944 N94-21162
RASCHKE, E. p 1860 N94-22283
p 1860 N94-22284
RASMUSSEN, D. A. p 1999 N94-22568
RATCLIFFE, COLIN P. p 1674 N94-20950
RAUBENHEIMER, T. p 1978 N94-19856
RAUBENHEIMER, T. O. p 1981 N94-21773
RAUCH, ALAN F. p 1831 N94-21219
RAUSCH, RUSS D. p 1920 N94-22369
RAWSON, P. p 1711 N94-19906
RAY, CHANDRA S. p 1701 N94-20347
p 1713 N94-20605
RAYMOND, J. p 1745 N94-22127
RAYNAL, R. p 1661 N94-21384
RAYNE, ROY J. p 1699 N94-20017
RAZEGHI, M. p 1815 N94-19878
RE, RICHARD J. p 1637 N94-21569
REAGAN, J. A. p 1839 N94-20961
REASS, W. A. p 2036 N94-22583
REDDING, DAVID C. p 1985 N94-20305
REDDY, SURENDER D. p 1933 N94-21336
REE, F. H. p 1796 N94-19916
p 1679 N94-20319
p 1966 N94-21511
REED, JAMES J. p 2041 N94-20106
REEDY, R. C. p 2106 N94-20713
REES, M. J. p 2003 N94-22646
REES, S. p 1814 N94-19851
REGER, R. D. p 2091 N94-20396
REGLER, HANS p 1957 N94-21474
REGULLA, D. p 1892 N94-21141
REGUSH, MURRAY M. p 1817 N94-20611
REHBEIN, D. K. p 1697 N94-22571
REHN, L. E. p 2033 N94-21999
REICHE, HARALD p 1752 N94-20630
REICHELT, MARK p 1922 N94-21475
REICHERT, BRUCE A. p 1638 N94-21591
REICHERT, FREDERICK W., JR. p 1646 N94-21548
REID, A. M. p 1863 N94-20825
p 1863 N94-20826
p 1863 N94-20882
REIFENBERGER, R. p 1975 N94-21766
REILLY, RONAN p 1937 N94-20253
REIMOLD, W. U. p 1684 N94-20652
p 1862 N94-20714
p 1863 N94-20825
p 1863 N94-20826
REIMOLD, WOLF UWE p 1863 N94-20796
REINBOLDT, WERNER C. p 1954 N94-21174
REINHART, TED p 1675 N94-21187
REINHART, W. D. p 1829 N94-19943
REITZ, T. C. p 1696 N94-22025
REJ, D. J. p 1997 N94-21988
p 2036 N94-22583
REMINGTON, B. A. p 1818 N94-21547
REMPEL, GLEN p 1745 N94-22144
REN, YUHE p 1949 N94-19898
RENARD, P. p 1662 N94-21389
RENDZIO, ROBERT J. p 1641 N94-20912
RENNELS, DAVID p 1756 N94-21101
p 1756 N94-21104
RESCIGNO, T. N. p 1976 N94-21968
RESING, J. A. C. p 1946 N94-21577
RESNIK, ANDY p 1797 N94-20037
RESSEL, KLAUS p 1955 N94-21467
REULET, R. p 1661 N94-21382
REVERCOMB, H. E. p 1873 N94-22307
p 1875 N94-22315
REYES-RUIZ, M. p 2120 N94-20791

REYES, A. P. p 2030 N94-21768
p 2034 N94-22007
REYES, ROY M. p 1951 N94-20358
REYNOLDS, A. P. p 2048 N94-22521
REYNOLDS, D. C. p 2022 N94-20995
REYNOLDS, J. F. p 1852 N94-21787
REYNOLDS, R. T. p 2146 N94-21683
REYNOLDS, THOMAS L. p 1642 N94-21818
REZAEEPAZHAND, J. p 1673 N94-20172
REZEK, T. p 2149 N94-20803
RHEINBOLDT, WERNER C. p 1954 N94-21173
RICARD, CAROLINE p 1791 N94-22239
RICCO, A. J. p 1968 N94-21751
RICE, BETSY M. p 1898 N94-19947
RICE, C. L. p 1714 N94-20099
RICE, EDWARD J. p 1637 N94-20563
p 1638 N94-22274
RICE, J. W., JR. p 2146 N94-21682
RICE, VALERIE J. p 1892 N94-21036
RICHARD, J.-M. p 1977 N94-22271
RICHARD, M. A. p 1736 N94-20517
RICHARD, T. A. p 2030 N94-21805
RICHARDS, J. p 1814 N94-19851
RICHARDSON, J. W., JR. p 2033 N94-21993
RICHARDSON, MICHAEL A. p 1822 N94-20356
RICHTER, G.-M. p 2072 N94-22520
RICHTER, H. E. p 1662 N94-21390
RIECO, S. R. p 1666 N94-20864
RIELAND, M. p 1860 N94-22286
RIEMSLAGH, KRIS p 1957 N94-21478
RIESSELMANN, K. p 1973 N94-20474
RIETMEIJER, FRANS J. M. p 2083 N94-20715
p 2083 N94-20716
RIGNOT, ERIC p 1724 N94-20428
p 1724 N94-20430
p 1725 N94-20434
p 1729 N94-20452
RIHA, DAVID S. p 1828 N94-22616
RIMEY, RAYMOND D. p 1945 N94-21315
RINEHART, L. F. p 1762 N94-21634
RIORDON, J. SPRUCE p 1779 N94-22158
RIPKE, B. p 1831 N94-21153
RIPLEY, GRADY L. p 1896 N94-20914
RISEBOROUGH, P. S. p 1974 N94-21553
RITCHIE, C. E. p 1926 N94-22484
RIVERS, M. L. p 1685 N94-20717
p 1686 N94-20807
p 1686 N94-20808
RIVETTI, NATALIE p 1943 N94-20947
RIVOIRE, B. p 1653 N94-21404
RO, PAUL I. p 1781 N94-21257
ROACH, LISA K. p 1964 N94-21175
ROACH, W. P. p 1890 N94-20462
ROARK, J. H. p 2142 N94-20911
ROBERT, J. F. p 1665 N94-21405
ROBERTS, J. J. p 2012 N94-19861
ROBERTS, K. MAGEE p 1863 N94-20879
ROBERTS, M. W. p 1881 N94-19952
ROBERTS, MICHAEL L. p 1658 N94-20590
ROBERTS, THOMAS W. p 1806 N94-21485
ROBERTS, W. P. p 1925 N94-22461
ROBERTSON, GLEN A. p 1701 N94-20359
p 1800 N94-20361
ROBERTSON, M. J. p 1694 N94-21937
ROBERTSON, P. B. p 1863 N94-20887
ROBERTSON, R. p 1829 N94-19881
ROBILLARD, PIERRE-N. p 1772 N94-22116
ROBIN-JOUAN, PHILIPPE p 1751 N94-20595
ROBIN, A. p 1964 N94-22458
ROBINSON, C. A. p 2107 N94-20718
ROBINSON, M. S. p 2108 N94-20720
ROBINSON, MARK S. p 2107 N94-20719
ROBINSON, R. A. p 2033 N94-21991
ROCHE, M. p 1847 N94-21650
ROCHE, M. F. p 1848 N94-21870
ROCHON, P. p 1705 N94-21223
p 1705 N94-21259
p 1705 N94-21267
p 1706 N94-21523
RODDY, D. J. p 2083 N94-20721
p 1862 N94-20766
RODE, O. D. p 2101 N94-20687
RODEN, J. p 2049 N94-22546
RODIN, G. J. p 1830 N94-20001
RODRIGUEZ, ERNESTO p 1726 N94-20438
p 1726 N94-20439
ROECKNER, ERICH p 1860 N94-22288
ROELFSEMA, P. R. p 1927 N94-22522
ROEST, W. R. p 1862 N94-20666
ROGERS, L. H. p 1826 N94-21983
ROGERS, STUART E. p 1798 N94-20104
ROGNLIEN, T. D. p 1999 N94-22595
ROGOWSKI, ROBERT S. p 1986 N94-20378
p 1986 N94-20586
ROHATGI, A. p 1845 N94-19925
ROHLICEK, J. R. p 1736 N94-20547
ROHRER, N. J. p 1735 N94-20514
ROHRER, NORMAN J. p 1736 N94-20517
ROHWEIN, G. J. p 1762 N94-21634
ROLL, J. B., JR. p 2047 N94-22455
ROLL, JOHN p 1926 N94-22507
p 1927 N94-22524
ROLODEALMEIDA, RIONALDO p 1839 N94-20964
ROMAN, J. R. p 1715 N94-19816
ROMANOFSKY, R. R. p 1671 N94-20513
ROMANOFSKY, ROBERT R. p 1732 N94-20498
ROMANOV, G. S. p 2084 N94-20824
ROME, J. A. p 1992 N94-20058
ROMERO, V. O. p 1814 N94-19867
ROMIG, A. D., JR. p 1687 N94-19904
RONG, XING p 2079 N94-22552
RONNAU, JAMES F. p 1858 N94-21811
RONNING, ERIK p 1743 N94-22410
ROOIJAKKERS, LUC p 1910 N94-21062
ROOSE, L. D. p 1762 N94-21634
ROPER, R. G. p 1866 N94-20918
ROSE, E. A. p 1814 N94-19867
ROSE, ROBERT B. p 1716 N94-19951
ROSEN, M. D. p 1817 N94-21299
ROSEN, PAUL A. p 1731 N94-20459
ROSENAUER, D. p 1981 N94-21767
ROSENBERG, CARLA R. p 1669 N94-20226
ROSENBERGER, FRANZ p 2017 N94-20346
ROSENBLATT, P. p 2108 N94-20722
ROSENBLUTH, M. N. p 1999 N94-22596
ROSENDAHL, GLENN K. p 1786 N94-22206
ROSENFELD, D. p 1735 N94-20512
ROSENKRANZ, PHILIP W. p 1856 N94-20362
ROSENTHAL, S. E. p 1980 N94-20295
ROSS, D. p 1950 N94-20034
ROSS, M. p 1695 N94-22024
ROSS, MICHAEL D. p 1760 N94-21130
ROSSINI, PAOLO p 1841 N94-20970
ROSSOW, W. p 1868 N94-21639
ROSSOW, WILLIAM p 1870 N94-21648
ROTACIUC, VALENTIN p 2081 N94-21138
ROTHERY, D. A. p 2128 N94-20830
ROTHWARF, A. p 2029 N94-21617
ROTS, A. p 2047 N94-22450
ROTS, A. H. p 1927 N94-22523
ROTSTAYN, L. D. p 1855 N94-20256
ROUDAKOV, A. p 1668 N94-20076
ROUSH, T. L. p 2140 N94-20900
ROUSH, TED L. p 2108 N94-20723
ROUSSEL-DUPRE, R. A. p 1750 N94-20325
ROUTBORT, J. L. p 1676 N94-21559
ROY, J. E. p 1746 N94-22198
ROY, R. p 1817 N94-20939
ROY, ROLAND R. p 1895 N94-20338
ROY, S. p 2037 N94-20178
ROY, S. K. p 1782 N94-22179
ROZMUS, W. p 1966 N94-21958
RUBENCHIK, A. M. p 1983 N94-19862
RUBENSTEIN, CARL J. p 1893 N94-20081
RUBIN, ALAN E. p 1697 N94-20724
RUBIN, M. p 1809 N94-21545
RUCINSKI, R. A. p 1807 N94-19987
RUCKMAN, M. W. p 1691 N94-20313
RUDAK, L. V. p 2084 N94-20824
RUEDE, ULRICH p 1957 N94-21474
RUGE, JOHN p 1806 N94-21480
RUGGIERO, N. p 2048 N94-22509
RUGGIERO, N. G. p 1926 N94-22488
p 2047 N94-22493
RUGGLES, L. p 1816 N94-20298
RULLE, H. p 2084 N94-20790
RUMMELMANN, U. p 1640 N94-22602
RUNGE, K. J. p 1684 N94-22395
RUSCHAU, JOHN J. p 1691 N94-21188
RUSSELL, JOEL F. p 2109 N94-20725
RUSSELL, L. p 2029 N94-21617
RUSSELL, S. J. p 1816 N94-20277
RUSSELL, S. S. p 2063 N94-20726
p 2085 N94-20846
RUTH, R. D. p 1981 N94-21687
RUTHERFORD, B. M. p 1916 N94-21761
RUTHERFORD, MALCOLM J. p 1685 N94-20727
RUTKOWSKI, H. p 1993 N94-20234
RUTLEDGE, DAVID p 1715 N94-19912
RUTLEDGE, SHARON K. p 1660 N94-21377
RUTTEN, E. P. B. M. p 1915 N94-21534
RUUSKANEN, PEKKA p 1691 N94-20530
RUZMAIKINA, T. V. p 2109 N94-20728
p 2085 N94-20665
RYAN, C. G. p 2097 N94-20661
RYAN, EILEEN V. p 2083 N94-20729
RYAN, JAMES G. p 1774 N94-22125
RYBAKOV, V. A. p 2082 N94-20647
RYUTOVA, MARGARITA p 2006 N94-22671

S

SAAD, M. p 1790 N94-22229
SAATCHI, SASAN S. p 1726 N94-20440
p 1727 N94-20444
p 1728 N94-20448
p 1730 N94-20453
SABA, V. p 2048 N94-22503
SABAH, I. p 1774 N94-22130
SABLE, C. p 1660 N94-21376
SABOL, DONALD E., JR. p 2110 N94-20730
SACCOMANDO, JAMES G., JR. p 1864 N94-19852
p 1864 N94-19908
SADEH, WILLY Z. p 1897 N94-20665
SADLER, PAMELA p 1648 N94-21268
SAETRE, H. J. p 1865 N94-20532
SAFAEE-RAD, R. p 1777 N94-22148
SAFARI, A. p 1749 N94-20012
SAGHIR, HASSAN p 1824 N94-20594
SAGURTON, M. p 1827 N94-22390
SAHA, S. K. p 1683 N94-22031
SAHAGIAN, RICHARD p 2028 N94-21517
SAHAY, VISHNU p 1653 N94-22188
SAHNER, ROBIN A. p 1965 N94-21463
SAID, ABDELLATIF p 1785 N94-22195
SAIKI, KAZUTO p 2084 N94-20812
p 2084 N94-20813
SAILOR, D. J. p 1851 N94-21740
SAITO, T. p 2003 N94-22647
p 2004 N94-22657
SAKAI, JUN-ICHI p 2005 N94-22660
p 2005 N94-22661
p 2005 N94-22662
p 2005 N94-22663
SAKIMOTO, K. p 2004 N94-22653
SAKIMOTO, S. E. H. p 2110 N94-20732
SAKURAI, HIROHISA p 1666 N94-20890
SAKURAI, KUNITOMO p 2006 N94-22672
SALANT, RICHARD F. p 1823 N94-20538
SALAS, MANUEL D. p 1950 N94-20092
SALAZAR, GEORGE A. p 1907 N94-20492
SALES, L. C. p 1702 N94-20481
SALGADO, C. W. p 1976 N94-21962
SALISBURY, J. K., JR. p 1939 N94-20105
SALISBURY, J. W. p 1685 N94-20733
SALMERON, M. B. p 2034 N94-22041
SALTSMAN, JAMES F. p 1835 N94-22620
SAMAREH-ABOLHASSANI, JAMSHID p 1920 N94-22366
SAMSON, J. A. R. p 1827 N94-22390
SAMUEL, M. p 2047 N94-22459
SAND, J. R. p 1714 N94-20099
SANDERS, D. M. p 2032 N94-21960
SANDERS, WILLIAM A. p 1703 N94-20529
SANDRI, G. H. p 1854 N94-19841
SANETRIK, MARK D. p 1956 N94-21469
SANK, VICTOR J. p 1666 N94-21338
p 1813 N94-21346
SANTINI, D. J. p 1825 N94-21637
SANTOS, EUGENE, JR. p 1914 N94-21501
SAPPENFIELD, PATRICIA p 2084 N94-20817
SARKAR, S. p 1804 N94-21880
SARKER, JOGENDRA C. p 1765 N94-21712
SARKIS, MARCUS p 1957 N94-21477
SASABO, MARIA L. p 1754 N94-21083
SASSEN, KENNETH p 1877 N94-22326
p 1881 N94-22343
SASTRY, AMBATIPUDI R. p 1737 N94-20585
SASTRY, S. M. L. p 1692 N94-21320
SATO, N. p 2005 N94-22664
SATO, TETSUYA p 2000 N94-22625
p 2004 N94-22658
p 2006 N94-22666
SATYANARAYANAN, M. p 1898 N94-20107
SAUNDERS, D. S. p 1675 N94-21504
SAUNDERS, M. p 2019 N94-20941
SAUNDERS, M. A. p 1950 N94-20217
SAUNDERS, R. S. p 2110 N94-20734
SAUSA, ROSARIO C. p 1679 N94-20111
SAUSEN, TANIA MARIA p 1840 N94-20968
SAUTET, P. p 2034 N94-22041
SAVAGE, M. E. p 1762 N94-21632
SAVARIA, YVON p 1773 N94-22121
p 1775 N94-22132
p 1778 N94-22153
SAWA, TAKEYASU p 2010 N94-22695
SAWCHUK, A. A. p 1899 N94-20469
SAWKA, MICHAEL N. p 1892 N94-21209
SAXELBY, ROBERT M. p 1703 N94-20541
SAZONOVA, L. p 2083 N94-20735
SCARPETTI, R. D. p 1768 N94-21770
SCHABER, GERALD G. p 2103 N94-20696
p 2109 N94-20725
p 2110 N94-20736
SCHAEFER, M. W. p 2091 N94-20397
p 2111 N94-20737

SCHAFER, K. J. ..... p 1972 N94-20230
p 1818 N94-21829
SCHAFFNER, P. R. ..... p 1722 N94-20419
SCHARER, J. E. ..... p 1994 N94-20940
SCHARF, LOUIS L. ..... p 1736 N94-20570
SCHEERER, DIETER ..... p 1908 N94-21024
SCHENK, P. ..... p 2111 N94-20738
p 2111 N94-20739
p 2111 N94-20740
SCHIAVONE, R. C. ..... p 1673 N94-20327
SCHIFF, E. A. ..... p 2013 N94-19939
SCHILDBACH, M. A. ..... p 1709 N94-21970
SCHIRBER, J. E. ..... p 2030 N94-21768
p 2034 N94-22007
SCHLAGEL, T. J. ..... p 1975 N94-21693
SCHLEGEL, ROBERT E. ..... p 1893 N94-20023
SCHLICK, GREG ..... p 1895 N94-20137
SCHLUETER, J. A. ..... p 2031 N94-21871
SCHLUMPF, F. ..... p 1946 N94-21689
SCHLUTTER, D. J. ..... p 2082 N94-20653
SCHMIDLIN, F. J. ..... p 1870 N94-21862
SCHMIDT, D. ..... p 1925 N94-22461
SCHMIDT, DENNIS ..... p 1927 N94-22524
SCHMIDT, ELDON ..... p 1671 N94-21979
SCHMIDT, GERHARD ..... p 2083 N94-20741
SCHMIDT, M. ..... p 2054 N94-20174
SCHMIDT, R. M. ..... p 1862 N94-20742
SCHMITT, D. R. ..... p 1997 N94-21989
SCHMITT, R. C. ..... p 1917 N94-21923
SCHMITT, V. ..... p 1641 N94-22607
SCHMITZ, PAUL ..... p 1670 N94-21809
SCHNEBERK, D. J. ..... p 1906 N94-20316
SCHNEIDER-MUNTAU, H. J. ..... p 1714 N94-20278
SCHNEIDER, DEAN L. ..... p 1942 N94-20488
SCHNEIDER, E. ..... p 1759 N94-21129
SCHNEIDER, J. D. ..... p 1997 N94-21989
SCHNEIDER, J. G. ..... p 1939 N94-20135
SCHNEIDER, JEFF G. ..... p 1945 N94-21317
SCHNEIDER, WALTER T. ..... p 1761 N94-21275
SCHOEFFTER, JEAN-PIERRE ..... p 1824 N94-21142
SCHOENBACH, K. H. ..... p 1768 N94-21770
SCHOLTES, JAN C. ..... p 1940 N94-20248
SCHORR, HERBERT ..... p 2041 N94-20134
p 1905 N94-20228
SCHOWALTER, LEO J. ..... p 1971 N94-20083
SCHROBILGEN, G. J. ..... p 2012 N94-19842
SCHROCK, RICHARD R. ..... p 1704 N94-21184
p 1704 N94-21186
SCHROEDER, D. J. ..... p 2055 N94-20204
SCHUBERT, E. THOMAS ..... p 1766 N94-21716
SCHUBERT, LENHART K. ..... p 1907 N94-20522
SCHUE, CHARLES A., III ..... p 1945 N94-21355
SCHUETH, F. ..... p 2017 N94-20544
SCHULTE, WOLFRAM ..... p 1903 N94-20020
SCHULTZ, GREGORY S. ..... p 1892 N94-21415
SCHULTZ, P. ..... p 1868 N94-21427
SCHULTZ, P. H. ..... p 2135 N94-20873
SCHULTZ, PETER H. ..... p 2111 N94-20743
p 1862 N94-20744
p 1685 N94-20745
SCHULTZ, RICHARD A. ..... p 1862 N94-20747
p 2125 N94-20816
SCHULZ, HELMUT ..... p 1952 N94-21019
SCHULZ, R. ..... p 2083 N94-20746
SCHUSTER, G. L. ..... p 1669 N94-20102
SCHUSTER, GREGORY L. ..... p 1824 N94-20587
SCHUTTLER, H. B. ..... p 2032 N94-21972
SCHWAB, FREDRICK C. ..... p 1706 N94-21460
SCHWANK, J. R. ..... p 2032 N94-21939
SCHWARTZ, D. S. ..... p 1692 N94-21320
SCHWARTZ, DAVID M. ..... p 1922 N94-21342
SCHWARTZ, R. W. ..... p 2013 N94-19961
SCHWARTZ, SUSAN ..... p 1858 N94-21206
SCHWARZ, R. B. ..... p 2012 N94-19926
SCHWARZ, R. K. ..... p 2045 N94-22047
SCHWEMMER, GEARY ..... p 1986 N94-20591
SCHWENTERLY, S. W. ..... p 1769 N94-21830
p 2035 N94-22570
SCHWENTKER, O. ..... p 2060 N94-22555
SCIALDONE, JOHN J. ..... p 1676 N94-21889
SCIPIONI, B. ..... p 2041 N94-19811
p 1928 N94-19812
p 1936 N94-21919
SCOTT, D. H. ..... p 2134 N94-20863
SCOTT, DAVID H. ..... p 2112 N94-20748
SCOTT, E. R. D. ..... p 2083 N94-20749
SCOTT, KAREN P. ..... p 1658 N94-21147
SCOTT, MICHAEL L. ..... p 1912 N94-21227
SCOTT, S. D. ..... p 1991 N94-19883
SCOTTI, STEPHEN J. ..... p 1800 N94-20495
SEAGER, C. H. ..... p 1706 N94-21526
SEAMAN, C. L. ..... p 2015 N94-20275
p 2016 N94-20335
SEAMAN, R. L. ..... p 2048 N94-22525
SEARS, ANDREW S. R. ..... p 2083 N94-20750
SEARS, D. W. G. ..... p 2086 N94-20901
SEARS, DEREK W. G. ..... p 2083 N94-20750
SEARS, WILLIAM D. ..... p 2113 N94-20751
SEBAK, A. ..... p 1746 N94-22162
p 1747 N94-22252
SEBO, ANDRAS ..... p 1950 N94-20125
p 1951 N94-20237
SECORD, NORMAN ..... p 1780 N94-22169
p 1746 N94-22170
SEDLACEK, W. A. ..... p 1807 N94-20114
p 1807 N94-20115
SEDOV, V. V. ..... p 1661 N94-21380
SEE, E. ..... p 1695 N94-22024
SEGAL, H. M. ..... p 1851 N94-20948
SEGAL, I. N. ..... p 2000 N94-22626
SEGER, CARL-JOHAN H. ..... p 1898 N94-20085
SEGLETES, STEVEN B. ..... p 2037 N94-19831
SEIFERT, M. ..... p 1977 N94-22271
SEKAR, R. R. ..... p 1825 N94-21297
p 1811 N94-22391
SEKHAR, J. A. ..... p 1674 N94-20623
SEKIGUCHI, H. ..... p 2001 N94-22633
SEKIMURA, N. ..... p 1696 N94-22037
SEKULA-MOISE, P. A. ..... p 2023 N94-21000
p 1796 N94-21001
SELKOWITZ, S. ..... p 1809 N94-21545
SELMAN, ALAN L. ..... p 1912 N94-21273
p 1954 N94-21314
SEMANCIK, S. ..... p 2028 N94-21458
SEMENOVA, A. S. ..... p 2083 N94-20752
SEMTNER, A. J., JR. ..... p 1855 N94-20219
SEN, SUNIT K. ..... p 1773 N94-22122
SENFTLE, F. E. ..... p 1685 N94-20753
SENGUPTA, L. C. ..... p 2027 N94-21303
SENSKE, D. A. ..... p 2110 N94-20734
p 2113 N94-20754
p 2113 N94-20755
SERGESON, ROBERT B. ..... p 1945 N94-21305
SERLEMITSOS, T. A. ..... p 1926 N94-22488
p 2047 N94-22493
p 2048 N94-22509
SESSLER, A. M. ..... p 1820 N94-21975
SESTITO, SABRINA ..... p 1841 N94-21453
SETTI, JOSE REYNALDO ANSELMO
p 1652 N94-22423
SETZER, A. ..... p 1639 N94-20961
SEVILLANO, EVELIO ..... p 2027 N94-21319
SEVIORA, RUDOLPH E. ..... p 1788 N94-22214
SEVRUK, B. ..... p 1841 N94-21068
SEWARD, F. D. ..... p 1926 N94-22508
SEYMOUR, R. S. ..... p 1814 N94-19851
SHA, LUI ..... p 1899 N94-21230
SHADDAY, M. A., JR. ..... p 1804 N94-21765
SHAFAI, L. ..... p 1745 N94-22140
p 1746 N94-22162
p 1746 N94-22198
SHAHID, IQBAL ..... p 1834 N94-22612
SHAMA, DALE D. ..... p 1657 N94-21340
SHAMANNA, M. ..... p 1767 N94-21728
SHANANIN, A. A. ..... p 2052 N94-22074
SHANEYFELT, M. R. ..... p 2032 N94-21939
SHANG, J. S. ..... p 1802 N94-21263
SHANNON, JENIFER M. ..... p 1943 N94-20926
SHANNON, SAMUEL G. ..... p 1891 N94-20615
SHAPIRA, YAIR ..... p 1957 N94-21478
SHAPIRO, A. B. ..... p 1906 N94-20316
SHAPIRO, P. R. ..... p 2009 N94-22694
SHARAPOV, E. ..... p 1977 N94-22572
SHARKEY, AMANDA J. C. ..... p 1941 N94-20252
SHARKEY, NOEL E. ..... p 1941 N94-20252
SHARMA, P. ..... p 2082 N94-20658
SHARMAN, M. ..... p 1840 N94-20989
SHARP, C. M. ..... p 2083 N94-20756
SHARP, J. K. ..... p 1921 N94-22383
SHARP, MARILYN A. ..... p 1892 N94-21036
SHARPTON, V. L. ..... p 1863 N94-20882
SHARPTON, VIRGIL L. ..... p 1862 N94-20757
p 2119 N94-20785
p 1863 N94-20843
SHASHUA, AMNON ..... p 1983 N94-19968
SHAVER, SCOTT M. ..... p 1876 N94-22318
SHAW, M. S. ..... p 1796 N94-19829
SHAW, N. M. ..... p 1975 N94-21786
SHAW, PETER R. ..... p 1882 N94-20581
SHAW, R. A. ..... p 1926 N94-22483
p 1926 N94-22485
SHAY, KATHY ..... p 1931 N94-21327
SHEARER, C. K. ..... p 1684 N94-20670
p 2114 N94-20758
p 1685 N94-20759
p 1686 N94-20760
SHEFFIELD, R. L. ..... p 1816 N94-20277
p 1818 N94-21554
SHELFER, T. D. ..... p 1686 N94-20761
p 1811 N94-22431
SHELTON, ROBERT O. ..... p 1942 N94-20366
SHEN, JIAN ..... p 1957 N94-21479
SHEN, M. H. ..... p 1686 N94-20761
SHEN, M.-H. ..... p 1811 N94-22431
SHEN, MEIHUA ..... p 1973 N94-20618
SHEN, YING ..... p 1747 N94-22253
SHENG, N. ..... p 1763 N94-21697
SHENG, YUN-LONG ..... p 1780 N94-22164
p 1789 N94-22220
SHENSA, M. J. ..... p 1737 N94-20582
SHEPARD, H. ..... p 1998 N94-22389
SHEPARD, M. K. ..... p 2115 N94-20762
SHEPARD, R. ..... p 1902 N94-19928
SHEPARD, TERRY ..... p 1788 N94-22216
SHEPPARD, G. A. ..... p 1904 N94-20049
SHER, A. ..... p 2012 N94-19835
SHER, M. ..... p 1977 N94-22009
SHEVALIER, MAURICE THOMAS ..... p 1861 N94-22574
SHIAO, MICHAEL C. ..... p 1830 N94-20171
SHIAO, MICHAEL E. ..... p 1832 N94-21757
SHIBASAKI, K. ..... p 2001 N94-22633
SHIBATA, KAZUMARI ..... p 2004 N94-22654
p 2009 N94-22694
SHIBATA, KAZUNARI ..... p 2004 N94-22655
SHIELDS, DAVID R. ..... p 1882 N94-19979
SHIH, C.-Y. ..... p 2097 N94-20663
p 2115 N94-20763
SHIH, ISHIANG ..... p 1781 N94-22176
SHIMA, MASAKO ..... p 2083 N94-20764
SHIMABUKURO, YOSIO E. ..... p 1838 N94-20958
p 1838 N94-20959
p 1839 N94-20962
SHIMABUKURO, YOSIO EDEMIR ..... p 1839 N94-20964
SHIMIZU, N. ..... p 2086 N94-20666
SHIMIZU, T. ..... p 2004 N94-22655
SHIMURA, TOSHIYA ..... p 2002 N94-22645
SHIN, R. T. ..... p 1727 N94-20441
p 1730 N94-20455
SHINNERL, J. R. ..... p 1950 N94-20217
SHIRALAGI, K. ..... p 2024 N94-21005
SHIRALAGI, K. T. ..... p 2024 N94-21004
SHIREY, S. B. ..... p 1862 N94-20714
SHIRK, JAMES S. ..... p 1984 N94-20059
SHIVELY, J. H. ..... p 1829 N94-19881
SHOEMAKER, E. M. ..... p 2083 N94-20721
p 1862 N94-20766
p 1863 N94-20789
p 1652 N94-20850
SHOEMAKER, EUGENE M. ..... p 1652 N94-20765
SHOLL, DAVID S. ..... p 1955 N94-21465
p 1806 N94-21480
SHOOSMITH, JOHN N. ..... p 1900 N94-22100
SHOPBELL, P. L. ..... p 1748 N94-22526
p 2048 N94-22527
SHORES, D. A. ..... p 1693 N94-21854
SHORT, N. M. ..... p 1862 N94-20767
SHORTRIDGE, K. ..... p 2048 N94-22528
p 2048 N94-22529
SHUBADEEVA, L. P. ..... p 1862 N94-20649
SHUCHMAN, R. A. ..... p 1723 N94-20427
SHUI, ZHAN ..... p 1818 N94-21509
SHUKOLYUKOV, A. ..... p 2083 N94-20768
SHUKOLYUKOV, YURI A. ..... p 2085 N94-20846
SHUL, R. ..... p 1797 N94-19974
SHULER, ALBERT P. ..... p 1898 N94-20357
SHUVALOV, V. V. ..... p 2082 N94-20648
p 1862 N94-20649
SI, Q. ..... p 2032 N94-21972
SIDI, AVRAM ..... p 1957 N94-21478
SIEBES, ARNO P. J. M. ..... p 1916 N94-21587
SIEBES, GEORG ..... p 1660 N94-21378
SIEG, R. E. ..... p 2023 N94-21000
SIEG, R. M. ..... p 1734 N94-20509
p 1652 N94-20511
p 1796 N94-21001
SIGAL, I. H. ..... p 1923 N94-22079
SIGNER, P. ..... p 2136 N94-20875
SIGUIER, J.-M. ..... p 1661 N94-21382
SIGURDSSON, H. ..... p 1685 N94-20753
SILABAN, A. ..... p 1847 N94-21540
SILBER, ANDREW D. ..... p 2055 N94-20344
SILBERBERG, D. P. ..... p 2048 N94-22530
SILLING, S. A. ..... p 1904 N94-20052
SILVA, C. P. ..... p 1967 N94-19949
SILVA, M. ..... p 1636 N94-20486
SILVER, A. ..... p 1898 N94-19886
SILVER, G. L. ..... p 1959 N94-21655
SIM, BEN WEI-C. ..... p 1967 N94-20523
SIMITSES, G. J. ..... p 1673 N94-20172
SIMMONS, R. O. ..... p 1972 N94-20187
SIMMONS, S. J. ..... p 1745 N94-22110
SIMON-GILLO, J. ..... p 1982 N94-21849
SIMON, FABIENNE ..... p 1737 N94-20592
SIMON, S. B. ..... p 2084 N94-20770
p 2086 N94-20897
SIMON, WILLIAM E. ..... p 1845 N94-20066
SIMONIS, F. ..... p 1711 N94-21800
SIMONS, MARK ..... p 2116 N94-20769

SIMONS, N. R. S. p 1782 N94-22181
SIMONS, R. N. p 1733 N94-20503
SIMONS, RAINEE N. p 1722 N94-20422
p 1734 N94-20505
p 1734 N94-20506
p 1734 N94-20507
p 1769 N94-21808
SIMPSON, R. A. p 2117 N94-20771
SIMPSON, T. p 1985 N94-20282
p 1985 N94-20283
SIMPSON, W. W. p 1762 N94-21632
SIN, Y. W. p 1696 N94-22034
SINDIR, MUNIR p 1668 N94-20072
SINGER, K. D. p 1706 N94-21526
SINGER, R. B. p 2101 N94-20685
SINGER, S. p 1769 N94-21846
SINGH, A. p 1798 N94-20101
SINGH, H. P. p 1709 N94-20973
SINGH, J. p 1689 N94-20100
SINGH, P. P. p 1695 N94-22023
SINGHAL, M. K. p 1833 N94-21956
SINGHAL, S. N. p 1830 N94-20170
SINHA, BRIJNARESH p 1706 N94-21460
SINYUKOV, M. I. p 2046 N94-22058
SIPELSTEIN, JAY p 1902 N94-19932
SISK, FRANK p 1641 N94-20912
SITZMANN, MICHAEL E. p 1711 N94-19801
p 1712 N94-20122
SJOGREN, W. L. p 2117 N94-20772
SKAAR, ERIC p 1705 N94-21416
SKIBO, S. p 2029 N94-21617
SKILES, J. W. p 1905 N94-20149
p 1842 N94-21585
p 1842 N94-22345
SKINNER, WILLIAM R. p 2084 N94-20773
SKORIC, MILOS M. p 2006 N94-22673
SKURAT, V. E. p 1661 N94-21380
SLACK, D. S. p 1799 N94-20263
SLATER, TED p 2029 N94-21690
SLAUGHTER, J. p 1673 N94-20490
SLINGO, A. p 1861 N94-22290
SLIVA, RANDY p 1741 N94-21887
SLOT, H. p 1753 N94-21067
SLUITER, M. H. F. p 1695 N94-22023
SLUTSKER, I. p 1839 N94-20961
SMATHERS, H. W. p 1658 N94-20617
SMETANNIKOV, A. S. p 2064 N94-20824
SMIRNI, E. p 1908 N94-20932
SMIRNOV, O. M. p 1927 N94-22531
p 1927 N94-22532
p 1927 N94-22533
SMIRNOV, OLEG L. p 1744 N94-22069
p 1923 N94-22083
SMITH, B. K. p 1769 N94-21918
SMITH, B. W. p 2047 N94-22453
SMITH, BENGAMIN D. p 1714 N94-20355
SMITH, BRIAN p 1754 N94-21090
SMITH, D. E. p 2117 N94-20774
SMITH, DEBORAH K. p 1882 N94-20581
SMITH, EDWYN D. p 1732 N94-20498
SMITH, ERIC P. p 2048 N94-22534
SMITH, G. S. p 1693 N94-21656
SMITH, H. V., JR. p 1997 N94-21989
SMITH, J. H. p 1769 N94-21918
SMITH, J. R. p 1980 N94-20295
SMITH, J. V. p 1686 N94-20807
p 1686 N94-20808
SMITH, JAMES A. p 1839 N94-20962
SMITH, JESSE B., JR. p 2147 N94-21815
p 2147 N94-21832
SMITH, JOSEPH G., JR. p 1672 N94-20540
SMITH, K. C. p 1771 N94-22107
p 1774 N94-22130
p 1777 N94-22148
SMITH, KEVIN p 1994 N94-20943
SMITH, L. p 1980 N94-20290
SMITH, LANDGRAVE T. p 1893 N94-20081
SMITH, MARK J. T. p 2041 N94-20158
SMITH, MILES T. p 1932 N94-21330
SMITH, PETER M. p 1773 N94-22123
SMITH, PHILIP W. p 1818 N94-21817
SMITH, PHILLIP J. p 1865 N94-20353
SMITH, R. p 1714 N94-19946
SMITH, R. P. p 1715 N94-19912
SMITH, THANE p 1760 N94-21178
SMITH, VYACHESLAV Y. p 1923 N94-22083
SMITH, W. p 1879 N94-22337
SMITH, W. L. p 1873 N94-22307
p 1875 N94-22315
SMITH, WILLIAM L., JR. p 1872 N94-22301
p 1872 N94-22302
SMREKAR, S. E. p 2113 N94-20755
SMREKAR, SUZANNE E. p 2117 N94-20775
SMYTHE, W. D. p 1991 N94-20646
SNARSKI, STEPHEN R. p 1800 N94-20466
SNIDER, JACK p 1873 N94-22306
SNIDER, JACK B. p 1873 N94-22304
SNIEGOWSKI, J. J. p 1769 N94-21918
SNOOK, ALLEN DAVID p 1744 N94-21348
SNYDER, CHRISTOPHER A. p 1648 N94-21563
SNYDER, GREGORY A. p 1862 N94-20776
p 2118 N94-20777
p 2118 N94-20778
p 2118 N94-20779
SNYDER, PAUL G. p 2019 N94-20971
p 1710 N94-20979
p 1710 N94-20980
p 2020 N94-20982
p 1710 N94-20983
p 1710 N94-20984
p 1796 N94-20985
p 1710 N94-20986
p 2021 N94-20987
p 1796 N94-20988
p 1796 N94-20989
p 2022 N94-20992
p 2022 N94-20993
p 2022 N94-20994
p 2022 N94-20995
p 2023 N94-20996
p 2023 N94-20997
p 2023 N94-20998
p 2023 N94-20999
p 2023 N94-21000
p 1796 N94-21001
p 2024 N94-21002
p 2024 N94-21003
p 2025 N94-21008
p 2025 N94-21010
p 1687 N94-21011
p 1828 N94-21012
p 2026 N94-21013
p 1687 N94-21014
SOBOLEV, NICKOLAI V. p 1862 N94-20776
SOBOLEV, VLADIMIR N. p 1862 N94-20776
SOCKOL, PETER M. p 1806 N94-21481
SODEN, B. J. p 1875 N94-22316
SODEN, J. M. p 1762 N94-21636
SODEN, JERRY M. p 1755 N94-21093
SOEDERLIND, P. p 2011 N94-19827
p 1696 N94-22388
SOHNS, C. W. p 1769 N94-21830
SOLANO, E. R. p 1951 N94-20224
SOLI, GEORGE p 1666 N94-21086
SOLOMATOV, V. S. p 2118 N94-20780
SOLOMON, N. p 1642 N94-22055
SOLOMON, SEAN C. p 1882 N94-20131
p 2116 N94-20769
p 2118 N94-20781
SOLOVIEV, G. G. p 1664 N94-21399
SOLOVYEV, G. G. p 1653 N94-21370
SOLTIS, J. J. p 1771 N94-22111
SOMMARGREN, G. E. p 1990 N94-21985
SOMMEIJER, B. P. p 1935 N94-21493
SOMMER, ECKHARDT W. p 1866 N94-20557
SOMMERVILLE, T. R. p 1747 N94-22217
SONG, RAN p 1878 N94-22330
SONG, T. p 2041 N94-19811
SONNENFROH, D. p 1663 N94-21395
SONNENFROH, D. M. p 1809 N94-21607
SORRELLS, MARKUS S. p 1856 N94-20485
SOTIN, C. p 2099 N94-20675
SOUCY, MARC p 1771 N94-22108
SOUGANIDIS, PANAGIOTIS E. p 1951 N94-20545
SOULE, C. p 1961 N94-22263
SOULEN, ROBERT J., JR. p 1699 N94-20017
SOUTHON, J. p 2106 N94-20713
SOUTHON, J. R. p 2082 N94-20658
SOUZIS, ANDREW E. p 1682 N94-21435
SOWERS, C. H. p 2031 N94-21930
p 2035 N94-22564
SPADAFORA, STEPHEN J. p 1703 N94-20614
SPARGO, J. p 1898 N94-19886
SPATZ, T. L. p 2046 N94-22407
SPEIDEL, D. H. p 2119 N94-20782
SPEIER, H. J. p 1652 N94-20511
SPENCE, SCOTT E. p 1951 N94-20358
SPENCER, ROBERT H. p 1826 N94-21756
SPENCER, S. p 2010 N94-22697
SPENCER, W. A. p 2046 N94-22407
SPEZIALE, CHARLES G. p 1804 N94-21875
SPIEKER, BORIS p 1738 N94-21073
SPIELMAN, R. B. p 1816 N94-20298
SPIJKER, M. N. p 1953 N94-21060
SPILDE, M. N. p 1684 N94-20670
SPINHIME, JAMES p 1871 N94-22296
SPINHIRNE, JAMES D. p 1872 N94-22299
p 1877 N94-22326
SPINKA, H. p 1807 N94-19990
SPONDER, L. p 1806 N94-19837
SPRATT, JAMES P. p 2014 N94-20029
SPRAY, JOHN G. p 1863 N94-20783
SPRINKLE, J. K., JR. p 1904 N94-20049
SPUDIS, P. D. p 2101 N94-20682
SPUDIS, PAUL D. p 2119 N94-20784
p 2119 N94-20785
p 2119 N94-20786
SQUYRES, S. p 2142 N94-21659
SQUYRES, S. W. p 1652 N94-20850
SREEKUMAR, P. p 1926 N94-22501
SRIKANTHAN, T. p 1768 N94-21734
SRINIVASAN, VINOO N. p 1759 N94-21127
SRIRAM, G. p 1760 N94-21132
ST.CLAIR, ANNE K. p 1702 N94-20373
ST-MARTIN, JOSEPH THEODORE H. p 1743 N94-22409
STACHIW, J. D. p 1831 N94-21310
STACKHOUSE, PAUL W., JR. p 1880 N94-22339
STACY, N. J. S. p 2119 N94-20787
STAELIN, D. H. p 1727 N94-20441
STAELIN, DAVID H. p 1856 N94-20362
STAIR, KATHLEEN p 2023 N94-20999
STAMOULIS, G. p 1749 N94-20110
STAN, M. A. p 1709 N94-20518
p 1736 N94-20519
STAROMLYNSKA, J. p 1814 N94-19851
STARR, DAVID p 1875 N94-22314
p 1875 N94-22316
p 1877 N94-22326
p 1877 N94-22328
p 1878 N94-22332
p 1879 N94-22335
STASSIS, C. p 1978 N94-22573
STAUB, W. P. p 1859 N94-22006
STEARNS, D. G. p 1698 N94-19810
STECH, JOSE LUIZ p 1840 N94-20967
STECKENRIDER, J. S. p 1832 N94-21772
STEEL, M. A. p 1963 N94-21022
p 1954 N94-21231
STEELE, I. M. p 2082 N94-20681
STEELE, IAN M. p 2084 N94-20788
p 2086 N94-20902
STEELE, W. V. p 2037 N94-20473
STEERE, DAVID C. p 1898 N94-20107
STEIER, W. H. p 1899 N94-20469
STEIN, C. p 1829 N94-19881
STEIN, GIDEON P. p 1808 N94-21167
STEIN, LYNN A. p 1939 N94-19875
STEINER, M. B. p 1863 N94-20789
STEINLE, HELMUT p 2002 N94-22642
STELMASZEK, ROBERT L. p 1933 N94-21337
STELZER, J. E. p 1997 N94-21989
STENCEL, ROBERT E. p 2056 N94-21835
STEPHAN, T. p 2084 N94-20790
STEPHEN, KARL D. p 2015 N94-20214
STEPHENS, G. L. p 1864 N94-19900
STEPHENS, GRAEME L. p 1880 N94-22339
STEPINSKI, T. F. p 2120 N94-20791
STERN, C. P. p 2048 N94-22499
STERN, S. A. p 2092 N94-20637
STERNE, P. A. p 2036 N94-22594
STEVENS, CLARK D. p 1643 N94-21037
STEVENSON, D. J. p 2118 N94-20780
p 2120 N94-20792
p 2084 N94-20793
STEVENSON, MERRITT R. p 1840 N94-20967
STEWART, B. W. p 1686 N94-20794
STEWART, BRIAN W. p 2084 N94-20795
STEWART, J. M. p 1926 N94-22494
STIMETZ, C. J. p 1695 N94-21978
STOAKLEY, DIANE M. p 1702 N94-20373
STOCHL, R. J. p 1799 N94-20177
STOCKEL, J. p 1997 N94-21816
STOCKETT, MICHAEL H. p 1932 N94-21333
STOFAN, E. R. p 2110 N94-20734
p 2113 N94-20755
STOFAN, ELLEN R. p 2121 N94-20796
STOLIAROVA, H. M. p 1844 N94-22073
STOLL, FREDERICK p 1832 N94-21814
STOLOFF, N. S. p 1695 N94-21949
STOLPER, E. M. p 2134 N94-20862
STOMMEL, HENRY p 1881 N94-19895
STONEMAN, ROBERT C. p 1815 N94-20060
STONER, J. L. p 2048 N94-22499
STONER, S. L. p 1696 N94-22025
STONER, SUSAN L. p 1694 N94-21943
STONEY, ROBERT B. p 1646 N94-21283
STOOKE, PHILIP J. p 2121 N94-20797
STORM, J. H. p 1698 N94-19938
STORZER, DIETER p 1863 N94-20798
STOUGH, H. PAUL, II p 1650 N94-20556
STOUT, J. H. p 1693 N94-21854
STOVALL, JOHN R. p 1666 N94-22275
STOVER, R. J. p 2047 N94-22495
STOWELL, S. p 2027 N94-21303
STRAIT, E. J. p 1993 N94-20326
STRANGMAN, THOMAS E. p 1704 N94-21143
STRAUB, DARCY W. p 2122 N94-20799
p 2122 N94-20800

STRAUSS, WALTER ..... p 1951 N94-20545
STRAWN, ROGER ..... p 1920 N94-22363
STRAYER, M. R. ..... p 1960 N94-21955
STRAZISAR, A. J. ..... p 1636 N94-20136
STRETCHER, BAXTER ..... p 1868 N94-21519
STREY, C. G. ..... p 1868 N94-21605
STROBEL, G. L. ..... p 1817 N94-21299
STROHBEHN, K. ..... p 1755 N94-21098
STROM, R. G. ..... p 2122 N94-20802
STROM, ROBERT G. ..... p 2122 N94-20801
STRONG, K. ..... p 2004 N94-22655
STRONGIN, M. ..... p 1691 N94-20313
STUBBS, C. ..... p 2058 N94-22444
STUCHLY, STANISLAW S. ..... p 1745 N94-22139
STUCKY, G. D. ..... p 2017 N94-20544
STUHLINGER, TILMAN W. ..... p 1821 N94-19891
STUHLMANN, R. ..... p 1860 N94-22286
STUNS, I. ..... p 1989 N94-21602
STUTZ, C. E. ..... p 2022 N94-20992
p 2022 N94-20993
p 2022 N94-20995
SU, YANG ..... p 2005 N94-22665
SUAREZ, GERARDO ..... p 1862 N94-20757
SUBRAMANIAN, K. N. ..... p 1696 N94-22034
SUBRAMANYAM, G. ..... p 1735 N94-20516
SUDIBJO, ELLY RASDIANI ..... p 1843 N94-22429
SUGAMA, H. ..... p 1995 N94-21514
SUGAR, ISTVAN P. ..... p 1700 N94-20299
SUGG, A. R. ..... p 2030 N94-21805
SUGITA, SEIJI ..... p 2123 N94-20803
SUGIURA, NAOJI ..... p 1686 N94-20804
SULLIVAN, J. P. ..... p 1648 N94-21582
p 1648 N94-21583
SULLIVAN, N. S. ..... p 1714 N94-20278
SULONEN, REIJO ..... p 1744 N94-22076
SUN, JAMES ..... p 1720 N94-20411
SUN, X. ..... p 1951 N94-20221
p 1755 N94-21098
SUNCHUN, CHU ..... p 1743 N94-22576
SUNSHINE, J. M. ..... p 2101 N94-20686
p 1685 N94-20689
SUNSHINE, JESSICA M. ..... p 1686 N94-20805
SUO-ANTTILA, A. ..... p 1805 N94-22386
SUPPE, JOHN ..... p 2105 N94-20706
p 2105 N94-20707
SURATI, RAJEEV ..... p 1898 N94-19832
SURATI, RAJEEV J. ..... p 1928 N94-19877
SURH, M. P. ..... p 1684 N94-22395
SURKOV, YURI A. ..... p 2123 N94-20806
SURYANARAYANAN, R. ..... p 1692 N94-21320
SUTTLES, JOHN T. ..... p 1881 N94-22344
SUTTON, J. C. ..... p 1797 N94-19978
SUTTON, R. ..... p 1885 N94-21900
SUTTON, R. L. ..... p 1888 N94-21910
SUTTON, RICHARD L. ..... p 1888 N94-21912
SUTTON, S. R. ..... p 1685 N94-20717
p 1686 N94-20807
p 1686 N94-20808
SUWONO, FRANCIUS ..... p 1912 N94-21265
SUZUKI, YOSHIO ..... p 2004 N94-22658
SVANDRLIK, J. ..... p 1676 N94-21754
SVEDHEM, H. ..... p 2085 N94-20841
SVETSOV, V. V. ..... p 1862 N94-20649
SVOBODA, JAMES S. ..... p 1762 N94-21566
SVOBODA, ROBERT ..... p 2080 N94-20880
SVOBODA, V. ..... p 1997 N94-21816
SWAIN, D. W. ..... p 1998 N94-22045
SWAMIKANNU, A. X. ..... p 1709 N94-21982
SWAMINATHAN, S. ..... p 1687 N94-19806
SWAMY, M. N. S. ..... p 1744 N94-22102
SWANSON, R. C. ..... p 1641 N94-21473
SWEET, J. N. ..... p 1830 N94-20477
SWEGLE, J. W. ..... p 1915 N94-21539
p 1832 N94-21557
p 1805 N94-22556
SWINDEMAN, R. W. ..... p 1687 N94-19802
SY, MARIANO ..... p 1994 N94-20943
SYLVESTER, P. J. ..... p 2086 N94-20897
SYLWESTER, A. P. ..... p 2028 N94-21541
SYM, A. M. ..... p 1953 N94-21046
SYM, N. ..... p 1927 N94-22522
SYMES, L. R. ..... p 1777 N94-22149
SYMPSON, J. B. ..... p 1894 N94-21434
SYRETT, B. A. ..... p 1789 N94-22221
SZEKELY, L. A. ..... p 1963 N94-21022
p 1954 N94-21231
SZELEPCSENYI, ROBERT ..... p 1913 N94-21318
SZODRUCH, J. ..... p 1639 N94-22597
SZOFRAN, F. R. ..... p 2030 N94-21807
SZOKE, H. ..... p 1989 N94-21630
SZYMCZAK, ANDREI ..... p 1785 N94-22195

T

TAALEBINEZHAAD, M. A. ..... p 1943 N94-20920
TAASAN, SHLOMO ..... p 1950 N94-20092
TADA, SHIGEYUKI ..... p 1761 N94-21282
TAFLOVE, ALLEN ..... p 1719 N94-20406
TAGGER, MICHEL ..... p 2010 N94-22696
TAHVONEN, OLLI ..... p 1854 N94-22072
TAIJERON, SABRINA ..... p 1868 N94-21502
TAJIMA, T. ..... p 1998 N94-22561
TAKAGI, H. ..... p 2029 N94-21555
TAKAHARA, FUMIO ..... p 2002 N94-22645
p 2008 N94-22683
p 2009 N94-22693
TAKAHASHI, H. ..... p 1979 N94-20222
TAKAHASHI, MASAAKI ..... p 2008 N94-22684
p 2009 N94-22692
TAKAHASHI, T. ..... p 2004 N94-22657
TAKANO, T. ..... p 2001 N94-22633
TAKANO, YOSHIHIDE ..... p 1672 N94-22299
p 1880 N94-22342
TAKATA, T. ..... p 2124 N94-20809
TAKATORI, KOICHI ..... p 1686 N94-20810
TAKEDA, HIROSHI ..... p 1686 N94-20810
p 2124 N94-20811
p 2084 N94-20812
p 2084 N94-20813
p 2086 N94-20893
TAKESHIMA, TOSHIAKI ..... p 2007 N94-22679
TAKKEN, EDWARD H. ..... p 1858 N94-21357
TALBERT, W. L. ..... p 1981 N94-21767
TALEGHANI, BARMAC K. ..... p 1674 N94-20577
TALNYKIN, E. A. ..... p 1972 N94-20181
TAM, WESLEY ..... p 2137 N94-20883
TAMBE, MILIND ..... p 1809 N94-21445
TAMMELA, SIMO ..... p 1989 N94-21603
TAN, HAN-NGEE ..... p 1764 N94-21704
TANAKA, K. L. ..... p 2091 N94-20398
p 2091 N94-20399
TANAKA, KENNETH L. ..... p 2125 N94-20814
p 2125 N94-20815
p 2125 N94-20816
TANENBAUM, D. ..... p 1699 N94-20047
TANG, WAI-KEUNG ..... p 1974 N94-21515
TANIS, J. A. ..... p 1970 N94-19958
TANNER, WILLIAM G. ..... p 2084 N94-20817
TANRE, D. ..... p 1839 N94-20961
TARASOV, Y. I. ..... p 1653 N94-21370
TARDIO, GEMMA ..... p 1666 N94-21086
TARJAN, ROBERT E. ..... p 1938 N94-21468
TARKKA, JUHA ..... p 2053 N94-22086
TASAKI, KEIJI K. ..... p 1931 N94-21323
TATA, X. ..... p 1969 N94-19804
TATCHYN, R. ..... p 1978 N94-19873
TATEBE, OSAMU ..... p 1958 N94-21482
TATSUMOTO, M. ..... p 1685 N94-20702
p 2086 N94-20893
TATSUMOTO, MITSUNOBU ..... p 2084 N94-20834
TATSUMURA, MICHELLE J. ..... p 2039 N94-20818
TATTARI, KAI ..... p 1708 N94-21895
TAUB, S. R. ..... p 1733 N94-20503
TAUB, SUSAN R. ..... p 1733 N94-20504
p 1769 N94-21808
TAUBENFELD, GADI ..... p 1915 N94-21537
TAVARES, CARLOS M. ..... p 2043 N94-21276
TAVARES, STAFFORD E. ..... p 1784 N94-22194
TAVEAU, P. ..... p 1664 N94-21398
TAYLOR, G. J. ..... p 2101 N94-20682
p 1881 N94-20699
TAYLOR, G. JEFFREY ..... p 2039 N94-20818
TAYLOR, KEVIN B. ..... p 2039 N94-20819
TAYLOR, LAWRENCE A. ..... p 1670 N94-21208
p 1684 N94-20644
p 1684 N94-20645
p 1862 N94-20776
p 2118 N94-20777
p 2118 N94-20778
p 2118 N94-20779
p 2126 N94-20820
p 2126 N94-20821
TAYLOR, P. A. ..... p 1904 N94-20052
p 1833 N94-21916
TAYLOR, PETER R. ..... p 1804 N94-22027
TAYLOR, STUART ROSS ..... p 2126 N94-20822
TAYLOR, T. S. ..... p 1993 N94-20326
TCHOUKANOV, I. ..... p 1777 N94-22148
TEDESCO, E. F. ..... p 2085 N94-20845
TEELING, MICHAEL J. ..... p 2130 N94-20842
TEJWANI, M. J. ..... p 1734 N94-20510
p 2025 N94-21009
TELLAMBURA, CHINTHA ..... p 1747 N94-22223
TELLIER, L. ..... p 1852 N94-22017
TELSCHOW, K. L. ..... p 2014 N94-19970
TENHARMSENVANDERBEEK, A. ..... p 2045 N94-22276
TENNYSON, R. C. ..... p 1660 N94-21373
p 1663 N94-21394
TEOTIA, HARENDRA S. ..... p 1838 N94-20955
TERADA, KENTARO ..... p 2009 N94-22690
TERASHIMA, YOSHIAKI ..... p 1772 N94-22118
TERIELE, H. J. J. ..... p 1935 N94-21492
TERMINELLO, L. J. ..... p 1810 N94-21950
TERRY, P. L. ..... p 1809 N94-21556
TESAR, DELBERT ..... p 1942 N94-20488
TESTI, N. ..... p 1928 N94-19858
TETEREV, A. V. ..... p 2084 N94-20823
p 2084 N94-20824
TETU, MICHEL ..... p 1746 N94-22196
THACKER, BEN H. ..... p 1828 N94-22616
THADHANI, N. N. ..... p 1713 N94-22033
THAKOOR, ANILKUMAR P. ..... p 1942 N94-20360
THALMANN, CH. ..... p 1684 N94-20652
THAREJA, RAJIV ..... p 1920 N94-22365
THAYER, JEFF P. ..... p 1856 N94-20537
THELEN, DONALD C. ..... p 1755 N94-21096
p 1764 N94-21702
THERRIAULT, A. M. ..... p 1863 N94-20825
p 1863 N94-20826
THIBERT, J. J. ..... p 1641 N94-22607
THIEL, E. ..... p 2046 N94-22413
THIEL, K. ..... p 2084 N94-20827
THIERAUF, THOMAS ..... p 1907 N94-20536
p 1911 N94-21200
p 1912 N94-21273
p 1912 N94-21285
p 1955 N94-21456
THIFFAULT, STEVE ..... p 1775 N94-22132
THO, LE-NGOC ..... p 1780 N94-22168
p 1792 N94-22245
THOLE, JOHAN ..... p 1743 N94-20245
THOMA, D. J. ..... p 2012 N94-19926
THOMAS, C. E. ..... p 1992 N94-20058
THOMAS, E. V. ..... p 1763 N94-21654
THOMAS, G. H. ..... p 1968 N94-22003
THOMAS, GREGORY D. ..... p 1803 N94-21417
THOMAS, I. M. ..... p 1820 N94-22401
THOMAS, J. E. ..... p 1970 N94-19822
THOMAS, K. L. ..... p 2084 N94-20828
THOMAS, P. C. ..... p 1652 N94-20850
THOMAS, R. ..... p 1731 N94-20457
THOMAS, ROBIN ..... p 1952 N94-20613
THOMPSON, C. E. ..... p 1819 N94-21920
THOMPSON, CLAY M. ..... p 1806 N94-19920
THOMPSON, J. D. ..... p 1974 N94-21553
p 2030 N94-21788
p 2032 N94-21987
p 2034 N94-22007
THOMPSON, K. A. ..... p 1981 N94-21686
p 1981 N94-21687
THOMPSON, STEVEN R. ..... p 1692 N94-21525
THOMPSON, THOMAS W. ..... p 1652 N94-20829
THOMSEN, D. ..... p 1885 N94-21898
THOMSON, D. ..... p 1854 N94-19899
THOOLEN, P. M. C. ..... p 1910 N94-21078
THORN, K. S. ..... p 1685 N94-20717
THORN, M. ..... p 1744 N94-21092
THORNHILL, G. D. ..... p 2128 N94-20830
THORNTON, WILLIAM E. ..... p 1895 N94-20194
THORPE, A. N. ..... p 1685 N94-20753
THOUVENOT, E. ..... p 2108 N94-20722
THURMES, P. ..... p 1927 N94-22512
TIEGS, T. N. ..... p 1694 N94-21945
TIJHUIS, A. G. ..... p 1742 N94-22347
TIKHONCHUK, V. ..... p 1966 N94-21958
TIMMER, C. A. ..... p 1816 N94-20277
TIMOC, C. ..... p 1768 N94-21732
TIMOKHOV, A. V. ..... p 2053 N94-22084
TING, J. ..... p 1672 N94-19888
TIPTON, G. D. ..... p 1996 N94-21769
TITCOMBE, MICHELE SUSANNE ..... p 1805 N94-22580
TITLOW, J. ..... p 1844 N94-22303
TITLOW, JAMES ..... p 1874 N94-22312
TITOV, V. I. ..... p 1653 N94-21370
TJONGKIMSANG, ERIK F. ..... p 1941 N94-20249
TO, H. Y. ..... p 1735 N94-20515
TOBIAS, A. G. ..... p 1642 N94-22055
TOBIN, J. G. ..... p 1688 N94-19986
p 1694 N94-21944
TODA, SEINOSUKE ..... p 1955 N94-21456
TODD, R. J. ..... p 1699 N94-19973
TODO, YASUSHI ..... p 2008 N94-22686
TODY, D. ..... p 2048 N94-22535
TOERMAENEN, T. ..... p 2106 N94-20711
p 2129 N94-20835
TOERNES, JOHN AASULF ..... p 1851 N94-21455
TOERNWALL, TOM ..... p 2046 N94-22080
TOET, C. ..... p 1851 N94-19998
TOIDA, M. ..... p 2006 N94-22670
TOKKONEN, T. ..... p 2106 N94-20711
TOLOCHKO, SHARYN L. ..... p 1910 N94-21144
TOM, C. N. ..... p 1739 N94-21235
TOMEOKA, KAZUSHIGE ..... p 1686 N94-20810
TOMIMATSU, AKIRA ..... p 2002 N94-22644
p 2009 N94-22692
TOMPKINS, STEFANIE ..... p 1686 N94-20831
p 2128 N94-20832

TONCICH, S. S.	p 1735	N94-20514
TONG, CAROL Q.	p 1757	N94-21108
TONG, YI	p 2005	N94-22665
TONG, YIHONG	p 1829	N94-19937
TONIOLO, LAURA	p 1952	N94-21029
TONKS, W. B.	p 1863	N94-20833
TONRY, J. L.	p 1814	N94-22510
TOON, OWEN B.	p 1677	N94-22327
TOPOLSKI, M. J.	p 1693	N94-21771
TORBERT, ROY B.	p 1666	N94-21780
TORCZYNSKI, J. R.	p 1797	N94-19974
TORIGOE, N.	p 2086	N94-20893
TORIGOYE, NORIKO	p 2084	N94-20834
TORII, C.	p 2001	N94-22633
TORNG, TONY Y.	p 1828	N94-22616
TORR, DOUGLAS G.	p 1984	N94-20128
TORRES, V. M.	p 2013	N94-19961
TOTH, L. V.	p 1965	N94-22536
TOTH, LOUIS E.	p 1699	N94-20017
TOULGOAT, MYLENE	p 1747	N94-22234
TOVINKERE, V.	p 1844	N94-22303
TOVINKERE, VASANTH	p 1875	N94-22313
TOWER, LEONARD	p 1670	N94-21809
TRABELSI, CHOKRI	p 1792	N94-22244
TRABOLD, T. A.	p 1805	N94-22269
TRACEY, D. M.	p 1702	N94-20481
TRAN, T.	p 1768	N94-21732
TRANGENSTEIN, J. A.	p 1799	N94-20351
TRAVIS, L. D.	p 1721	N94-20416
TRAVIS, LARRY	p 1844	N94-21645
TRAVISANO, J. J.	p 2049	N94-22537
TREBES, J.	p 1989	N94-21630
TREECE, R. KEITH	p 1753	N94-21082
TREIMAN, A. H.	p 2085	N94-20836
	p 1813	N94-22437
TREMBLAY, BRUNO	p 1781	N94-22176
TREMBLAY, M.	p 1785	N94-22200
TREMOLIERES, MARC	p 1963	N94-20202
TRENHOLME, J. B.	p 1820	N94-22401
TRINH, MY-HANH N.	p 1929	N94-20571
TRIPATHI, RAM K.	p 1895	N94-20063
TRIPPE, T. G.	p 1972	N94-20291
TRISCHLER, HELMUTH	p 2152	N94-20543
TRITZ, B. G.	p 2002	N94-22641
TRIVEDI, KISHOR S.	p 1963	N94-21058
	p 1965	N94-21463
TROFIMENKOFF, F. N.	p 1778	N94-22152
TROMP, JOHN T.	p 1952	N94-21027
TROMPERT, RON A.	p 1803	N94-21575
	p 1803	N94-21609
TROTTER, B. C.	p 1681	N94-21226
TROUDET, TERRY	p 1650	N94-21742
TROUTMAN, R. L.	p 1801	N94-20562
TROUW, F.	p 2035	N94-22565
TROYANOVSKI, I.	p 1651	N94-21280
TRUCANO, T. G.	p 1916	N94-21635
TRUDNOWSKI, D. J.	p 1826	N94-22038
TRUEMAN, C. W.	p 1745	N94-22128
TRUEMPER, J.	p 2054	N94-20174
TRUEMPER, JOACHIM	p 2000	N94-22630
TRUMP, C. L.	p 1883	N94-21443
TRYGGVASON, G.	p 1798	N94-20167
TSANGARAKIS, NIKOS	p 1674	N94-20577
TSAO, JEFFREY	p 2013	N94-19967
TSAW, WILLIAM	p 1677	N94-22589
TSAY, SI-CHEE	p 1872	N94-22298
	p 1880	N94-22342
TSCHEGG, E. K.	p 1706	N94-21542
	p 1709	N94-22008
TSEREPI, ANGELIKI	p 1994	N94-21214
TSIEN, CHRISTINE L.	p 1913	N94-21413
TSINTIKIDIS, D.	p 2088	N94-20048
TSOU, P.	p 2085	N94-20837
TSUDA, T.	p 1870	N94-21852
TSUKIMURA, KATSUHIRO	p 1688	N94-20810
TSUNETA, SAKU	p 2001	N94-22632
	p 2004	N94-22655
	p 2004	N94-22657
TSURUTA, SACHIKO	p 2002	N94-22841
TUCCHIO, MICHAEL A.	p 1824	N94-21277
TUEV, S. V.	p 1923	N94-22064
TUFTS, B. R.	p 2129	N94-20838
TUFTS, DONALD W.	p 1717	N94-20215
TULINTSEFF, A.	p 1731	N94-20457
TULINTSEFF, A. N.	p 1718	N94-20405
TUNNELL, T.	p 1750	N94-20325
TUPPER, GEORGE H.	p 1864	N94-20186
TURCOTTE, DONALD L.	p 2129	N94-20839
TURGEON, B.	p 1927	N94-22538
TURITSYN, S. K.	p 1983	N94-19862
TURKO, B. T.	p 1808	N94-20287
TURNBULL, A. D.	p 1993	N94-20326
TURNER, ROSS M.	p 1747	N94-22234
TUTRIN, Y.	p 1661	N94-21383
TYBURCZY, J. A.	p 2012	N94-19861
TYBURCZY, JAMES A.	p 2085	N94-20840
TYLER, D.	p 2144	N94-21671
TYLER, G. L.	p 2117	N94-20771
TYRNI, ILARI	p 2046	N94-22063

U

UCHIDA, YUTAKA	p 2004	N94-22655
	p 2010	N94-22701
UCKAN, T.	p 1999	N94-22568
ULAMEC, S.	p 2085	N94-20841
ULBRICHT, KLAUS A.	p 1838	N94-20955
ULLAL, H. S.	p 1848	N94-21827
UMAR, A. S.	p 1960	N94-21955
UNALTUNA, M. KEMAL	p 1766	N94-21720
UNDERWOOD, D. G.	p 1807	N94-19990
UNDERWOOD, JAMES R., JR.	p 2130	N94-20842
UNERTL, W. N.	p 2018	N94-20575
URAL, HASAN	p 1772	N94-22117
URBIN, J. B.	p 1807	N94-19987
URRUTIA-FUCUGAUCHI, JAIME	p 1862	N94-20757
	p 1863	N94-20843
USHER, M. A.	p 1762	N94-21632
USTINOVA, G. K.	p 2085	N94-20844
UTTAL, T.	p 1844	N94-22303
	p 1878	N94-22332
UTTAL, TANEIL	p 1872	N94-22301
	p 1873	N94-22306
	p 1875	N94-22317
	p 1876	N94-22318
UUSPAEAE, PENTTI	p 2049	N94-22056
UWATOKO, Y.	p 2032	N94-21987

V

VADLAMUDI, RANI	p 1744	N94-21345
VAHEDI, V.	p 1999	N94-22567
	p 1999	N94-22595
VAIDYA, R. U.	p 1696	N94-22034
VAJTA, M.	p 1944	N94-21140
VALCO, G. J.	p 1735	N94-20514
	p 1735	N94-20515
VALCO, GEORGE J.	p 1736	N94-20517
VALCO, MARK	p 1826	N94-21756
VALDES, F.	p 2049	N94-22539
	p 1965	N94-22540
VALENTI, JOSEPH	p 1744	N94-21345
VALERO, FRANCISCO P. J.	p 1872	N94-22297
	p 1844	N94-22319
VALETTE, S.	p 1989	N94-21599
VALLES, J. M., JR.	p 2012	N94-19648
	p 2012	N94-19849
VANBEMMELEN, T.	p 1953	N94-21046
VANBENTHEM, JOHAN	p 1915	N94-21551
VANBEUZEKOM, M. G.	p 1979	N94-20123
VANBREUGEL, W.	p 2150	N94-22397
VANCURA, J.	p 1970	N94-19870
	p 1970	N94-19871
	p 1974	N94-21543
VANDALSEM, WILLIAM R.	p 1919	N94-22352
VANDEGEIJN, R.	p 1903	N94-19959
	p 1936	N94-22032
VANDEMARK, D.	p 1720	N94-20414
VANDENBERG, P. M.	p 1742	N94-22346
VANDENBOSCH, ANTAL	p 1940	N94-20246
VANDENEIJNDE, J. P. H. W.	p 1903	N94-19994
VANDENHEUVEL, J.	p 1953	N94-21048
	p 1953	N94-21074
VANDENHIJLIGENBERG, N. W.	p 1953	N94-21072
VANDERAALST, W. M. P.	p 1903	N94-19992
VANDERHOEVEN, P. C.	p 1865	N94-20309
VANDERHOUWEN, P. J.	p 1935	N94-21493
VANDERLINDEN, ERIK-JAN	p 1940	N94-20247
VANDERLUGT, A.	p 1983	N94-20013
VANDERVLUGT, A. J. M.	p 1865	N94-20532
VANDERVOORT, M. H. LEONIE	p 1916	N94-21587
VANDEVEL, M.	p 1961	N94-22266
VANDRESAR, N. T.	p 1799	N94-20177
VANEESBEEK, M.	p 1663	N94-21396
VANEIJCK, D. JAN N.	p 1914	N94-21495
	p 1914	N94-21496
VANEIJCK, JAN	p 1915	N94-21551
VANEIJK, PETER	p 1914	N94-21454
VANES, J. T.	p 1979	N94-20117
	p 1979	N94-20123
	p 1753	N94-21084
VANHILST, MIKE	p 1927	N94-22524
VANHORN, HUGH M.	p 2001	N94-22637
VANIER, P.	p 1676	N94-21754
VANLEEUWEN, MARC A. A.	p 1911	N94-21156
	p 1911	N94-21157
VANNATTA, DAVID S.	p 1931	N94-21328
VANROSENDALE, JOHN	p 1922	N94-21483
VANROSSUM, GUIDO	p 2044	N94-21494
	p 2044	N94-21535
	p 2045	N94-21536
VANSCHUPPEN, J. H.	p 1944	N94-21033
VANSTEENBERG, M. E.	p 2049	N94-22541
VANSTEENBURG, M. E.	p 2049	N94-22544
VANSUETENDAEL, N.	p 1647	N94-20343
VANT, M. R.	p 1745	N94-22159
VANTHIEL, M.	p 1796	N94-19916
VANTRIGT, J. H.	p 1979	N94-20117
	p 1753	N94-21064
VANZWOL, A.	p 1909	N94-21061
VANZYL, J. J.	p 1725	N94-20434
VANZYL, JAKOB J.	p 1724	N94-20429
	p 1724	N94-20430
	p 1730	N94-20453
VARGAS, M.	p 1816	N94-20298
VARGO, TERRENCE G.	p 1703	N94-20526
VARMA, H. K.	p 1690	N94-20183
VAROSI, F.	p 1927	N94-22542
	p 1927	N94-22543
VASHISHTA, P.	p 1701	N94-20352
VASQUEZ, PETER	p 1702	N94-20377
VASSILIADIS, STAMATIS	p 1757	N94-21113
VAUGHAN, ARTHUR H.	p 1986	N94-20345
VAUGHAN, M. A.	p 1874	N94-22309
VAUGHN, J.	p 1662	N94-21391
VAUSE, C. A.	p 1845	N94-20086
VEEDER, G. J.	p 2085	N94-20845
VEELENTURF, L. P. J.	p 1940	N94-20243
VEENSTRA, JACK E.	p 1905	N94-20143
VEITCH, LISA C.	p 1700	N94-20195
VELLI, MARCO	p 2003	N94-22650
VENABLE, DEMETRIUS D.	p 1994	N94-21289
	p 1994	N94-21290
	p 1995	N94-21291
	p 1995	N94-21292
VENBRUX, JACK	p 1753	N94-21080
	p 1759	N94-21128
VENETSANOPOULOS, A. N.	p 1781	N94-22174
VENETSANOPOULOS, ANATASIOS N.	p 1771	N94-22106
VENKATAKRISHNAN, V.	p 1958	N94-21484
VENKATARAMAN, S.	p 1758	N94-21115
VENKATESAN, R.	p 1788	N94-22215
VENKATESWARAN, N.	p 1758	N94-21115
	p 1759	N94-21127
	p 1760	N94-21132
VERCHOVSKY, A. B.	p 2085	N94-20846
VERDASCO, JUAN E.	p 2027	N94-21304
VERDERAIME, V.	p 1653	N94-20141
VERDON, C. P.	p 1819	N94-21839
VERDON, JOSEPH M.	p 1968	N94-21608
VERHEUL, E.	p 1961	N94-22266
VERHOEF, W.	p 1841	N94-21015
VERKOOIJEN, H.	p 1979	N94-20118
VERMEER, N. J.	p 1638	N94-22260
VERMOTE, E.	p 1839	N94-20961
VERNON, S. P.	p 1990	N94-21985
VERONIS, ANDREW M.	p 1744	N94-22103
VERONNEAU, PIERRE	p 1772	N94-22116
VERWEIJ, M. D.	p 1969	N94-22262
VESECKY, J. F.	p 1723	N94-20427
VESELOVSKII, V. E.	p 1923	N94-22079
VESIKARI, ERKKI	p 1708	N94-21892
VESSOT, ROBERT F.	p 1814	N94-19853
VEZIN, J. M.	p 1645	N94-22219
VIAL, F.	p 1870	N94-21862
VIANCO, P. T.	p 1699	N94-19960
VICKERS, D. B.	p 1645	N94-22156
VICKERY, A. M.	p 2131	N94-20847
VIEIRA, ANDRE CALIXTO	p 1839	N94-20963
VIEIRA, D. J.	p 1981	N94-21767
VIERECK, LESLIE	p 1729	N94-20452
VILAS, F.	p 2085	N94-20848
	p 2087	N94-20906
VILJA, JOHN	p 1670	N94-21271
VILLAEYS, J.	p 1660	N94-21376
VILLARREAL, JAMES A.	p 1942	N94-20366
VINCENT, JEAN-MARC	p 1963	N94-20202
VINCENT, PAUL	p 1764	N94-21701
VINEYARD, E. A.	p 1714	N94-20099
VINOKUR, V. M.	p 2029	N94-21649
VISSER, C. J. M.	p 1851	N94-19998
VITANYI, PAUL M. B.	p 2038	N94-21533
VITEK, J. M.	p 1690	N94-20282
VITELLO, ROBERT	p 1744	N94-21099
VITTA, SATISH	p 1736	N94-20519
VITYAZEV, A. V.	p 2085	N94-20849
VLEESHOUWERS, J. M.	p 1761	N94-21538
VOELKL, E.	p 1707	N94-21653
VOGEL, GERARD N.	p 1866	N94-20579
VOGELS, L.	p 2035	N94-22273
VOGT, GREGORY L.	p 1669	N94-20226
VOITSEKHOVICH, I.	p 1997	N94-21816
VOLAKIS, J. L.	p 1950	N94-20034
VOLAKIS, JOHN L.	p 1716	N94-20160
	p 1741	N94-21885
	p 1741	N94-21886
	p 1741	N94-21887

VOLLAN, A. p 1651 N94-21280
VONDRAN, RAYMOND F. p 1907 N94-20376
VONK, STEVEN J. p 1704 N94-21143
VONKAENEL, PETER A. p 1945 N94-21315
VONROEDERN, B. G. p 1848 N94-21827
VORDERBRUEGGE, R. W. p 1652 N94-20850
VOSS, T. J. p 1657 N94-21981
VOTH, GREGORY p 1681 N94-21216
VOTH, GREGORY A. p 2037 N94-21166
VRANISH, JOHN M. p 1821 N94-20126
VRBA, P. p 1996 N94-21573
VRCKOVNIK, G. p 1745 N94-22142
VRIDHAGIRI, A. p 1757 N94-21106
VYSKOC, JOZEF p 2043 N94-21287

W

WACKER, J. F. p 1686 N94-20851
WADDILL, G. D. p 1688 N94-19986
p 1694 N94-21944
WADE, M. R. p 1992 N94-20058
WADHWA, MEENAKSHI p 1686 N94-20852
WADSWORTH, J. p 1695 N94-21986
WAENKE, HEINRICH p 1811 N94-22430
WAGENER, KEN B. p 1699 N94-20016
WAGNER, FLAVIO RECH p 1905 N94-20164
WAGNER, J. p 1700 N94-20265
WAGNER, J. L. p 2033 N94-21998
WAGNER, MICHAEL p 1800 N94-20533
WAGNER, R. p 2136 N94-20876
WAGNER, T. D. p 1908 N94-20932
WAGNER, T. P. p 1686 N94-20853
WAHAB, A. p 1764 N94-21705
WAI, C. M. p 1683 N94-22021
WAI, P. K. A. p 1819 N94-21872
WAINER, N. p 1979 N94-20216
WAKATANI, MASAHIRO p 2000 N94-22627
WAKAYAMA, SEAN p 1638 N94-21833
WALBERT, JAMES N. p 1964 N94-21175
WALCH, STEPHEN P. p 1679 N94-20169
WALD, A. p 1685 N94-20733
WALKER, B. p 1972 N94-20230
WALKER, D. W. p 1960 N94-21967
WALKER, GILBERT H. p 1824 N94-20587
WALKER, J. D. p 1636 N94-20465
WALKER, JAMES p 1802 N94-21169
WALKER, K. p 1744 N94-21092
WALKER, R. J. p 2085 N94-20854
WALKER, R. M. p 2082 N94-20659
WALKER, TOM p 1834 N94-22609
WALL, M. A. p 1696 N94-22394
p 1697 N94-22402
WALLACE, O. J. p 1742 N94-22268
WALLACE, P. T. p 1927 N94-22545
WALLACE, R. J. p 1818 N94-21547
WALLACE, STEVE p 1764 N94-21700
WALLS, C. A. p 1694 N94-21945
WALLYN, P. p 2009 N94-22691
WALUKIEWICZ, W. p 2030 N94-21763
WAMPLER, DAVID p 1744 N94-21341
WAMPLER, DAVID L. p 1641 N94-19876
WANG, C. p 1763 N94-21697
p 1982 N94-21974
WANG, E. X. p 2027 N94-21296
WANG, FEI-LING p 1705 N94-21416
WANG, H. H. p 2011 N94-19807
p 2031 N94-21871
WANG, JIANHUA p 1686 N94-20855
WANG, JIE p 1912 N94-21273
WANG, JIN-HUA p 1815 N94-19965
WANG, JINXUE p 1855 N94-20132
WANG, JUN p 1747 N94-22224
WANG, L. p 1730 N94-20455
WANG, M.-S. p 2082 N94-20681
WANG, MICHAEL p 1986 N94-20922
WANG, NENG-GUAN p 1777 N94-22149
WANG, P. J. p 1734 N94-20510
p 2025 N94-21009
WANG, QI. p 2013 N94-19939
WANG, QIANG p 1747 N94-22223
WANG, RONGRUI p 1816 N94-20484
WANG, SHENGRUI p 1785 N94-22201
WANG, SHOU-GUAN p 2080 N94-22554
WANG, SUNING p 1910 N94-21063
WANG, TING p 1803 N94-21459
WANG, WEI-CHYUNG p 1850 N94-19941
WANG, Z. p 2033 N94-21998
WANG, ZHI-CHENG p 1780 N94-22166
WANG, ZHONG-DE p 1771 N94-22111
WANG, ZIQIANG p 1768 N94-21762
WARGOWSKI, D. A. p 1706 N94-21526
WARMACK, R. J. p 2013 N94-19929
WARNER, B. E. p 1819 N94-21844
WARNOCK, A. p 2049 N94-22544
WARNOCK, A., III p 2047 N94-22496
WARNOCK, R. L. p 1741 N94-21684
WARREN-SMITH, R. F. p 1927 N94-22545
WARREN, GARY P. p 1806 N94-21485
p 1920 N94-22368
p 1797 N94-19974
WARREN, M. E. p 2086 N94-20893
WARREN, P. H. p 2133 N94-20856
WARREN, PAUL H. p 2085 N94-20857
p 1815 N94-20272
WARREN, R. W. p 1818 N94-21554
p 1845 N94-20066
WARRIER, GOPINATH R. p 1690 N94-20183
WARRIER, K. G. K. p 1944 N94-21232
WARTENHORST, PIETER p 2085 N94-20858
WASILEWSKI, P. J. p 1684 N94-20669
WASSERBURG, G. J. p 2083 N94-20756
p 1686 N94-20794
p 2084 N94-20795
p 2133 N94-20859
WASSERMAN, M. O. p 1833 N94-21927
WASSON, JOHN T. p 2083 N94-20741
p 2085 N94-20860
WASYLENKI, L. E. p 2085 N94-20861
WATANABE, K. p 2000 N94-22625
WATANABE, OSAMU p 1954 N94-21199
p 1955 N94-21456
WATANABE, T. p 2004 N94-22653
p 2004 N94-22657
WATKINSON, A. P. p 1802 N94-20942
WATSON, J. M. p 2048 N94-22499
WATSON, L. L. p 2134 N94-20862
WATSON, R. E. p 1691 N94-20313
WATTERS, T. R. p 2134 N94-20863
WATTERSON, I. G. p 1855 N94-20256
WATTS, A. J. p 1666 N94-20864
WAY, JOBEA p 1729 N94-20452
WAYLAND, B. B. p 1678 N94-20103
WEAVER, C. F. p 1745 N94-22143
WEAVER, MICHAEL J. p 1680 N94-20330
WEBB, M. J. p 1861 N94-22290
WEBBON, BRUCE p 1800 N94-20371
WEBER, H. W. p 1706 N94-21542
p 1709 N94-22008
WEBER, P. D. p 1819 N94-21844
WEBER, S. V. p 1818 N94-21547
WEBER, WILLIAM P. p 1675 N94-21176
WEDDENDORF, BRUCE C. p 1896 N94-20493
WEGMUELLER, URS p 1727 N94-20444
WEI, XIAO-FENG p 1818 N94-21509
WEI, YUNG-CHUNG p 1736 N94-20578
WEIDENSCHILLING, S. J. p 2085 N94-20865
WEIHS, T. p 1696 N94-22394
WEIHS, T. P. p 1697 N94-22402
WEIJTERS, TON p 1743 N94-20245
WEILAND, T. L. p 1819 N94-21920
WEINAN, E. p 2011 N94-19808
WEINERT, M. p 1691 N94-20313
WEIR, N. p 2049 N94-22546
WEIR, S. T. p 1693 N94-21656
p 2031 N94-21931
WEISBERG, M. K. p 2083 N94-20708
p 2086 N94-20866
p 2087 N94-20907
WEISER, N. p 1639 N94-22600
WEISS, S. p 1985 N94-20320
WEITZ, C. M. p 2135 N94-20867
WELCH, K. M. p 1699 N94-19973
WELLBORN, STEVEN R. p 1638 N94-21591
WELLER, ROBERT A. p 1864 N94-20186
WELLS, D. C. p 2049 N94-22547
WELLS, J. C. p 1960 N94-21955
WELLS, WILLIAM M., III p 1962 N94-20113
WELP, U. p 2033 N94-21997
WEN-YING, CHEN p 1706 N94-21437
WENG, JU-YANG p 1789 N94-22226
WENGER, C. BRUCE. p 1892 N94-21209
WENGER, D. F. p 1980 N94-20295
WENRICH, M. L. p 2091 N94-20400
p 1686 N94-20868
WENSINK, G. J. p 1865 N94-20532
WENTWORTH, SUSAN J. p 2086 N94-20869
p 1687 N94-20870
WENTZ, WILLIAM H., JR. p 1641 N94-20189
p 1635 N94-20191
WENZEL, W. p 2149 N94-20603
WERNER, CHARLES L. p 1731 N94-20459
p 1732 N94-20460
WERTHEIMER, M. R. p 1663 N94-21394
WESSELING, P. p 1806 N94-21487
WESSELIUS, P. R. p 1927 N94-22522
WESSENDORF, K. O. p 1749 N94-20054
WEST, DEREK A. p 1865 N94-20482
WEST, FREDERICK R. p 2092 N94-20401
WESTBERG, KARL R. p 1851 N94-20025
WESTBROOK, S. R. p 1712 N94-20551
WESTERFIELD, P. L. p 1996 N94-21769
WESTERLUND, LAWRENCE H. p 1658 N94-21041
p 1876 N94-22324
p 1877 N94-22327
WETHERILL, GEORGE p 2086 N94-20877
WETHERILL, GEORGE W. p 2086 N94-20871
WEXLER, A. p 1793 N94-22249
WHANG, BENJAMIN p 1964 N94-21322
WHIRLEY, R. G. p 1960 N94-21996
WHITAKER, JOHN F. p 2017 N94-20470
WHITAKER, S. p 1754 N94-21087
p 1764 N94-21703
p 1765 N94-21713
p 1767 N94-21728
WHITAKER, STERLING p 1760 N94-21133
p 1766 N94-21722
p 1767 N94-21725
WHITAKER, STERLING R. p 1763 N94-21694
p 1767 N94-21726
WHITE, C. W. p 2012 N94-19869
WHITE, D. J. p 1826 N94-21938
WHITE, J. M. p 1976 N94-21951
WHITE, M. R. p 1812 N94-22434
WHITE, MIKE p 1759 N94-21126
WHITE, N. p 1926 N94-22487
p 1927 N94-22513
WHITE, R. p 2047 N94-22462
WHITE, R. L. p 1748 N94-22517
WHITE, R. S. p 2003 N94-22647
WHITE, SIMON D. M. p 2054 N94-20175
WHITEHEAD, M. C. p 2034 N94-22035
WHITELEY, S. p 1898 N94-19886
WHITMAN, P. G. p 2146 N94-21683
WHITMIRE, D. P. p 2146 N94-21683
WHITT, WARD p 1939 N94-19909
WICHMAN, R. W. p 2135 N94-20872
p 2135 N94-20873
WICK, CHARLES p 1974 N94-21185
WICZER, J. J. p 1770 N94-22040
WIECZOREK, M. A. p 2136 N94-20874
WIEDEMAN, S. p 2029 N94-21617
WIEDERSICH, H. p 2012 N94-19923
WIELER, R. p 2136 N94-20875
WIELICKI, BRUCE A. p 1880 N94-22342
WIEN, W. L. p 1696 N94-22025
WIENER, EARL L. p 1642 N94-22373
WIEPRECH, E. p 1927 N94-22522
WIERZBICKI, TOMASZ p 1828 N94-19815
WIESMANN, H. p 2097 N94-20663
p 2115 N94-20763
WILCOX, MIKE p 1755 N94-21095
WILCOXON, J. P. p 2028 N94-21541
WILD, N. p 1985 N94-20262
p 1985 N94-20283
WILENSKY, GREGG p 1943 N94-20947
WILGEN, J. B. p 1999 N94-22568
WILKENS, C. A. p 1702 N94-20481
WILKENSON, WADE F. p 1817 N94-21353
WILLIAMS, CYNTHIA p 1729 N94-20452
WILLIAMS, D. A. p 2136 N94-20876
WILLIAMS, D. B. p 2086 N94-20894
WILLIAMS, DAVID H. p 1643 N94-21606
WILLIAMS, DAVID R. p 2086 N94-20877
WILLIAMS, J. D. p 2049 N94-22548
WILLIAMS, J. M. p 2011 N94-19807
WILLIAMS, M. C. p 1846 N94-21527
WILLIAMS, M. D. p 1669 N94-20102
WILLIAMS, MICHAEL D. p 1824 N94-20587
WILLIAMS, W. E. p 1927 N94-22549
WILLIAMSON, R. L., II p 1926 N94-22483
p 1927 N94-22550
WILLIAMSON, TANIA L. p 1892 N94-21036
WILLS, E. L. p 1686 N94-20761
p 1811 N94-22431
WILLS, J. M. p 2011 N94-19827
p 1696 N94-22388
WILMINGTON, ROBERT P. p 1897 N94-21627
WILSON, B. G. p 1818 N94-21547
WILSON, D. M. p 1696 N94-22025
WILSON, J. R. p 2081 N94-21618
WILSON, L. p 1862 N94-20673
p 1863 N94-20878
p 1863 N94-20879
WILSON, M. H. p 1698 N94-19857
WILSON, M. J. p 1698 N94-19938
WILSON, P. p 1814 N94-19851
WILSON, R. B. p 2149 N94-20603
WILSON, R. V. p 1959 N94-21486
WILSON, THOMAS L. p 2080 N94-20880
WILSON, W. J. p 1728 N94-20445
WILSON, WILLIAM J. p 1666 N94-21733
WILTBERGER, N. LYN p 1798 N94-20104
WIMBERLY, R. N. p 2117 N94-20772
WIMER, J. G. p 1846 N94-21527
WINDER, H. H. p 1760 N94-21229
WINDLEY, P. p 1766 N94-21719
WINDLEY, P. J. p 1766 N94-21717

WINDLEY, PHILLIP J. p 1759 N94-21124
p 1937 N94-22414
WING, DAVID J. p 1637 N94-21569
WING, DAVID LEE p 2056 N94-22412
WINKERT, TOM p 1754 N94-21088
WINN, W. G. p 1684 N94-22046
WINTER, DIK T. p 1916 N94-21612
WINTERS, K. p 1759 N94-21129
WINTERS, KEL p 1764 N94-21699
p 1767 N94-21724
WISCOMBE, W. J. p 1879 N94-22337
p 1880 N94-22341
WISE, J. L. p 1829 N94-19824
p 1708 N94-21963
WISEMAN, D. p 1754 N94-21087
WISEMAN, DON p 1753 N94-21080
WISEMAN, DON R. p 1755 N94-21096
p 1767 N94-21726
WITHROW, J. R. p 1880 N94-22340
WITT, AUGUST F. p 2030 N94-21778
WITT, LAWRENCE ALAN p 2040 N94-21626
WITTENAUER, J. p 1695 N94-21986
WITTENBURG, PETER p 1743 N94-20244
WITTIG, CURT p 2027 N94-21304
WITTMERS, LORENTZ E., JR. p 1891 N94-20624
WITTSTRUCK, RICHARD p 1682 N94-21435
WNAG, JINXUE p 1859 N94-22026
WOLF, E. E. p 1680 N94-20934
WOLF, S. F. p 1964 N94-20881
WONG, A. M. p 1863 N94-20882
WONG, M. K. W. p 1916 N94-21635
WONG, P. B. p 2117 N94-20771
WONG, T. p 1793 N94-22248
WONGSO, J. p 1768 N94-21732
WOO, A. C. p 1772 N94-22113
WOO, K. p 1731 N94-20457
p 1731 N94-20458
WOOD, B. D. p 1714 N94-21426
WOOD, B. P. p 1997 N94-21988
p 2036 N94-22583
WOOD, CHARLES A. p 2137 N94-20883
WOOD, D. J. p 1683 N94-22021
WOOD, J. R. p 1636 N94-20136
WOOD, R. F. p 2014 N94-20002
p 2030 N94-21831
WOODALL, ROGER L. p 1938 N94-19843
WOODFIELD, B. F. p 2031 N94-21926
WOODS, B. W. p 1820 N94-22401
WOODS, DAVID D. p 1647 N94-21819
WOODS, ROBERT D. p 1932 N94-21331
WOOLLAM, J. A. p 1734 N94-20510
WOOLLAM, JOHN A. p 1734 N94-20508
p 2019 N94-20971
p 1709 N94-20972
p 1709 N94-20973
p 2019 N94-20974
p 1709 N94-20975
p 1709 N94-20976
p 2019 N94-20977
p 1710 N94-20978
p 1710 N94-20979
p 1710 N94-20980
p 1710 N94-20981
p 2020 N94-20982
p 1710 N94-20983
p 1710 N94-20984
p 1796 N94-20985
p 2021 N94-20987
p 1796 N94-20988
p 1796 N94-20989
p 2022 N94-20990
p 1710 N94-20991
p 2022 N94-20992
p 2022 N94-20993
p 2022 N94-20994
p 2022 N94-20995
p 2023 N94-20997
p 2023 N94-20998
p 2023 N94-21000
p 1796 N94-21001
p 2024 N94-21003
p 2024 N94-21004
p 2024 N94-21005
p 1820 N94-21006
p 1710 N94-21007
p 2025 N94-21009
p 2025 N94-21010
p 1687 N94-21011
p 1828 N94-21012
p 2026 N94-21013
p 1687 N94-21014
WOOLSEY, BARBARA C. p 1673 N94-20327
WOOLUM, DOROTHY S. p 2086 N94-20884
WORAMONTRI, WORANUN p 1845 N94-20066
WORONOW, ALEX p 2130 N94-20642
WOSNITZA, J. p 2011 N94-19807
WOUTERS, J. M. p 1981 N94-21767
WRAY, RICHARD B. p 1666 N94-22275
WRIGHT, D. A. p 2031 N94-21926
WRIGHT, E. M. p 1814 N94-19865
WRIGHT, FREDERICK L. p 1647 N94-21500
WRIGHT, I. P. p 2086 N94-20885
p 2086 N94-20886
p 2143 N94-21668
WRIGHT, S. I. p 1695 N94-21990
WRIGHTON, MARK S. p 1849 N94-22048
WU, CHEN p 1745 N94-22137
p 1745 N94-22138
WU, HAI-QING p 1794 N94-22254
WU, HENGNING p 2036 N94-22582
WU, I-CHEN p 1929 N94-20084
WU, J. C. p 1700 N94-20328
WU, JIAN p 1859 N94-22026
WU, KE-LI p 1745 N94-22137
p 1745 N94-22138
WU, NAILONG p 1747 N94-22253
WU, S. p 1928 N94-22551
WU, S. S. C. p 1863 N94-20687
WU, TE-KAO p 2108 N94-20720
p 1727 N94-20442
p 1728 N94-20447
p 1729 N94-20451
p 1731 N94-20458
WU, W. T. p 1825 N94-21450
WU, Y.-T. p 1828 N94-22616
WYARD, PETER p 1941 N94-20251
WYBOURNE, M. N. p 1700 N94-20328
WYGMANS, D. G. p 1833 N94-21927
WYNGAARD, J. p 1854 N94-19899

X

XI, J. p 1850 N94-22257
XIAO-WEN, HAN p 1706 N94-21437
XIAO, Y. p 1990 N94-21837
XIE, S. p 1705 N94-21223
p 1705 N94-21238
p 1705 N94-21259
p 1705 N94-21267
p 1706 N94-21523
XIONG, YI-MING p 1710 N94-20986
p 2024 N94-21002
p 2025 N94-21008
XU, MING p 2029 N94-21649
XU, P. p 1844 N94-20888
XU, X. Q. p 1999 N94-22566
p 1999 N94-22567
p 1999 N94-22596
XU, YAN p 2079 N94-22552
XUE, S. p 1863 N94-20889

Y

YAAKOBI, B. p 1972 N94-20264
YABUKI, FUMIKO p 2009 N94-22693
YAMADA, H. T. p 1828 N94-22489
YAMAKOSHI, KAZUO p 1666 N94-20890
YAN, MING-DI p 1700 N94-20328
YANAGISAWA, M. p 1836 N94-20891
YANAI, KEIZO p 2080 N94-20892
p 2086 N94-20893
YANG, BAORUI p 1972 N94-20230
YANG, BO p 1772 N94-22117
YANG, C. W. p 2086 N94-20894
YANG, DAVID p 1733 N94-20499
YANG, DONGZHEN p 1867 N94-21250
YANG, GOA p 1644 N94-22427
YANG, L. H. p 1706 N94-21512
YANG, LI-FARN p 1822 N94-20369
YANG, OLIVER W. W. p 1746 N94-22209
YANG, TRACY CHUI-HSU p 1893 N94-21863
YANG, WEN-HSING p 1744 N94-21345
YANG, XUE-DONG p 1777 N94-22149
YAO, H. p 1734 N94-20510
YAO, HUADE p 1734 N94-20508
YAO, HUADE D. p 2023 N94-20997
p 2023 N94-20998
p 2023 N94-20999
p 2023 N94-21000
p 1796 N94-21001
p 2024 N94-21003
p 2025 N94-21009
p 2026 N94-21013
YAO, XIAO-XIONG p 1746 N94-22209
YAO, YU-DONG p 1780 N94-22168
YARDENI, E. p 1928 N94-19995
YARRINGTON, L. p 1904 N94-20052
YATES, G. J. p 1808 N94-20287
YATES, J. T., JR. p 1680 N94-21145
YATES, P. D. p 2086 N94-20895
YATES, S. F. p 1709 N94-21982
YAVNEH, IRAD p 1806 N94-21480
YE, Y. Y. p 1695 N94-21964
YECKLEY, R. L. p 1702 N94-20481
p 1704 N94-21197
YEH, PEN-SHU p 1753 N94-21080
p 1759 N94-21128
p 1741 N94-21783
YETTER, R. A. p 1682 N94-21243
YEUNG, ALAN B. p 1977 N94-22416
YEUNG, WILLIAM WAIHUNG p 1639 N94-22382
YEW, CHING H. p 1833 N94-21916
YIP, PATRICK p 1747 N94-22250
YODER, C. F. p 2139 N94-20896
YOKOSAWA, MASAYOSHI p 2010 N94-22699
YOKOYAMA, TAKAAKI p 2004 N94-22654
YONEDA, S. p 2086 N94-20897
YONGACOGLU, ABBAS p 1747 N94-22224
p 1792 N94-22244
YOO, C. S. p 1695 N94-22024
YOO, M. H. p 1690 N94-20232
YOO, S. I. p 2036 N94-22582
YORK, G. W. p 1814 N94-19867
YORKEY, T. p 1989 N94-21630
YOSHIMORI, M. p 2004 N94-22656
YOSIBASH, ZOHAR p 1830 N94-20036
YOU, H. p 1687 N94-19922
YOUNG, A. T. p 1980 N94-20475
YOUNG, DAVID F. p 1872 N94-22299
p 1872 N94-22302
p 1873 N94-22306
YOUNG, K. D. p 1657 N94-19863
YOUNG, M. S. p 1891 N94-20935
YOUNG, PAUL G. p 1732 N94-20498
p 1733 N94-20504
YOUNG, R. W., SR. p 1769 N94-21830
YOUNGLOVE, B. A. p 1968 N94-21447
YU, BRIAN p 1744 N94-21099
YU, K. M. p 2030 N94-21763
YU, M. p 1750 N94-20257
YU, P. p 1781 N94-22174
YU, S. p 1993 N94-20234
p 1979 N94-20289
p 1981 N94-21439
YU, XIN-MING p 1771 N94-22109
YUAN, XIAO-DONG p 1818 N94-21509
YUEFENG, ZHANG p 1947 N94-22591
YUEH, S. H. p 1721 N94-20415
p 1723 N94-20426
p 1724 N94-20432
p 1727 N94-20441
p 1728 N94-20445
p 1729 N94-20449
p 1730 N94-20454
p 1730 N94-20455
YUEN, ERIC H. p 1676 N94-21834
YUEN, S. F. p 1789 N94-22221
YUN, W. p 1990 N94-21837
YUNG, Y. L. p 2145 N94-21679
YURIMOTO, HISAYOSHI p 2086 N94-20898
YUSUN, LU p 1706 N94-21437

Z

ZABAWSKIJ, B. p 1783 N94-22184
ZACCARIN, ANDRE p 1781 N94-22173
ZACEK, F. p 1997 N94-21816
ZACHAROV, V. G. p 2046 N94-22058
p 1923 N94-22068
ZAFAR, A. p 1847 N94-21614
ZAGHA, MARCO p 1902 N94-19932
p 1928 N94-19950
ZALUZEC, N. J. p 1687 N94-19806
ZAMORANI, G. p 2054 N94-20174
ZAMPARDI, P. p 1763 N94-21697
ZANDBERGEN, B. T. C. p 1651 N94-22094
ZANGWILL, ANDREW p 2013 N94-19967
ZANOTTI, D. p 1662 N94-21387
ZARATE, N. R. p 2049 N94-22553
ZAROWSKI, CHRISTOPHER p 1784 N94-22191
ZEBKER, HOWARD A. p 1732 N94-20461
ZEHNPFENNING, J. p 2084 N94-20790
ZEITLER, P. K. p 1863 N94-20899
ZELLER, EDWARD J. p 2147 N94-21196
ZENG, S. p 1806 N94-21487
ZENT, A. P. p 2140 N94-20900
ZEOLI, RICHARD R. p 1987 N94-21172
ZHA, Y. p 2032 N94-21972
ZHANG-MACCOY, V. p 2033 N94-21998
ZHANG, B. L. p 1695 N94-21964
ZHANG, GEN-ZAO p 1793 N94-22251
ZHANG, HONG p 1915 N94-21584
ZHANG, K. p 2029 N94-21649
ZHANG, T. X. p 2006 N94-22670
ZHANG, X.-D. p 1998 N94-22560

ZHANG, XIAO-MIN ..... p 1818 N94-21509
ZHANG, XIZ-HEN ..... p 2080 N94-22554
ZHANG, Y. ..... p 2086 N94-20901
ZHANG, Y.-Z. ..... p 1998 N94-22560
ZHAO, G. L. ..... p 1695 N94-21964
ZHAO, JIE ..... p 2005 N94-22661
p 2005 N94-22663
ZHENG, X. Y. ..... p 2013 N94-19929
ZHENG, YI-JIA ..... p 2080 N94-22554
ZHOU, D. S. ..... p 2012 N94-19869
ZHOU, FENG-QING ..... p 1815 N94-19965
ZHOU, LEI ..... p 2083 N94-20741
ZHOU, Y. ..... p 2086 N94-20902
ZHOU, ZHI-YING ..... p 1889 N94-19962
ZHOU, ZI-HENG ..... p 1771 N94-22106
ZHU, P. Y. ..... p 1777 N94-22146
ZHU, S. ..... p 2013 N94-19929
ZHU, WEIBIN ..... p 1911 N94-21183
ZIEGLER, WOLFGANG P. ..... p 1971 N94-20030
ZIELINSKI, J. J. ..... p 1999 N94-22568
ZILLIACUS, STEPHEN ..... p 1964 N94-21322
ZIMAND, MARIUS ..... p 1965 N94-21286
ZIMBELMAN, J. R. ..... p 2092 N94-20402
p 2108 N94-20720
p 2134 N94-20863
ZIMBELMAN, JAMES R. ..... p 2140 N94-20903
p 1863 N94-20904
ZIMCIK, D. G. ..... p 1663 N94-21394
ZIMMERMANN, H. U. ..... p 2080 N94-22555
ZINK, M. ..... p 1721 N94-20417
ZINN, BEN T. ..... p 1667 N94-20015
ZINNER, E. ..... p 2082 N94-20659
ZIPFEL, J. ..... p 2086 N94-20905
ZIRK, DEBORAH A. ..... p 1922 N94-21325
ZLOTOV, A. V. ..... p 1923 N94-22079
ZOLENSKY, M. E. ..... p 2085 N94-20848
p 2087 N94-20906
p 2087 N94-20907
ZOLOTOV, M. YU. ..... p 2141 N94-20908
ZOOK, H. A. ..... p 2141 N94-20909
ZOVKO, CARL T. ..... p 1669 N94-20121
ZUBER, M. T. ..... p 2110 N94-20732
p 2117 N94-20774
p 2141 N94-20910
p 2142 N94-20911
ZUCLICH, JOSEPH A. ..... p 1890 N94-20462
ZUFFADA, C. ..... p 1722 N94-20423
p 1725 N94-20436
ZUHR, R. A. ..... p 2012 N94-19869
ZUKIC, MUAMER ..... p 1984 N94-20128
ZULIANI, GARY LOUIS ..... p 1990 N94-22579
ZURAWSKI, D. ..... p 1848 N94-21942
ZUREK, A. K. ..... p 1696 N94-22034
ZUREK, R. ..... p 1812 N94-22436
ZUTAVERN, F. J. ..... p 1750 N94-20294
p 2016 N94-20296
p 1750 N94-20312
ZWART, B. ..... p 1890 N94-20238
ZWEIBEL, K. ..... p 1848 N94-21827
ZWEIFEL, TERRY L. ..... p 1641 N94-21030
p 1650 N94-21050
ZWEIGLE, GREG ..... p 1753 N94-21080
ZWEIGLE, GREGARY C. ..... p 1759 N94-21128
p 1765 N94-21714
ZYBIN, KIRILL P. ..... p 2002 N94-22643

Typical Corporate Source Index Listing

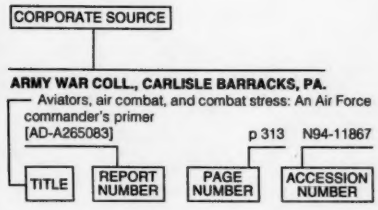

Listings in this index are arranged alphabetically by corporate source. The title of the document provides the user with a brief description of the subject matter. The report number helps to indicate the type of document cited (e.g., NASA report, translation, NASA contractor report). The accession number denotes the number by which the citation is identified. The page number helps you locate the citation in the abstract section. The titles are arranged under each corporate source in ascending accession number order.

A

ABASTUMANI ASTROPHYSICAL OBSERVATORY, GEORGIA (USSR).
Turbulization of free shear flows: 3D perturbations p 2000 N94-22626

ABCOR, INC., WILMINGTON, MA.
Development and demonstration of a personal monitoring system for exposure to hydrogen fluoride [DE93-041273] p 1891 N94-20935

ABERDEEN PROVING GROUND, MD.
Application of molecular modeling to biological processing [AD-A272612] p 1974 N94-21185
Method for design rotation [AD-A272440] p 1911 N94-21204
Mirror velocity sampling errors in a Michelson interferometer [AD-A273105] p 1609 N94-21508

ACADEMIA SINICA, BEIJING (CHINA).
Solar full-disk magnetic field image receiving system and observation software p 2079 N94-22552
Miyun 232 MHz survey 1: Fields centered at: alpha:00(h)41(m), delta:41 deg 12 min and alpha: 07(h)00(m),delta:35 deg 00 min p 2080 N94-22554
Dynamo driven by weak plasma turbulence: The effect of differential rotation p 2005 N94-22665

ACADEMY OF SCIENCES, POTSDAM (GERMAN D.R.).
Particle acceleration in a filamentary current sheet model p 2004 N94-22659

ACADEMY OF SCIENCES (USSR), MOSCOW.
The Erevan howardite: Petrology of glassy clasts and mineral chemistry p 1684 N94-20640
The Koshak section: Evidence for element fractionation and an oxidation event at the K/T boundary p 1862 N94-20641
Carbonaceous xenoliths from the Erevan howardite p 1684 N94-20642
Igneous rock from Severnyi Kolchim (H3) chondrite: Nebular origin p 2082 N94-20643
On magnetodynamic effects initiated by a high-speed impact of a large cosmic body upon the Earth's surface p 2082 N94-20647
Determination of cosmic bodies size-velocity distribution by observation of current impacts on Mars p 2082 N94-20648
Effects of hydrodynamics and thermal radiation in the atmosphere after comet impacts p 1862 N94-20649
Largest impact features on Venus: Non-preserved or non-recognizable? p 2096 N94-20657
Impact disturbance of the Venus atmosphere p 2106 N94-20709
Lunar basalt meteorite EET 87521: Petrology of the clast population p 2083 N94-20752
On modelling nuclear reactions in meteorites p 2085 N94-20844
Recondensation in the early solar system: Physical conditions and source material p 2085 N94-20849
K, U, and Th behavior in Martian environmental conditions p 2141 N94-20908
The simulation of action of some space environment factors on Teflon and on rubber materials p 1661 N94-21380
Mathematical modelling of economic systems p 2050 N94-22060
Macromodel of centrally planned economy p 2050 N94-22062
Computer-aided design system for objects location and reservoir with dispersed resource evolution investigation p 1923 N94-22064
IAS telecommunication infrastructure and value added network services provided by IASNET p 1744 N94-22069
Models of transient processes in centrally planned economy p 2051 N94-22071
Multicriteria optimisation problem in the agricultural modelling p 1844 N94-22073
Analysis of consumer demand structure by means of economic indexes p 2052 N94-22074
A model of negotiation in an extensive form game p 1965 N94-22075
APL-technology of computer simulation p 1923 N94-22077
The combinatorial algorithms for large scale discrete optimization problems p 1923 N94-22079
An expert system of econometric analysis p 2052 N94-22081
Three original programmes for managers p 1923 N94-22083
Method and software for decision making in public problems p 1923 N94-22087
A new programming metaphor for image processing procedures p 1927 N94-22531
PCIPS 2.0: Powerful multiprofile image processing implemented on PCs p 1927 N94-22532
Guide star catalogue data retrieval software 2 p 1927 N94-22533
Dark matter: Neutron star halo and the nature of gamma-bursts p 2002 N94-22643
Gamma ray burst as a result of the explosive instability in the magnetosphere of old neutron star p 2007 N94-22675

ACOUSTICAL SOCIETY OF AMERICA, NEW YORK, NY.
U.S. Tag for ISO/TC 43, acoustics, IEC/TC 29 electroacoustics, and ISO/TC 108/SC4 human exposure to mechanical vibration and shock: Minutes of the accredited standards committee on bioacoustics, S3 [AD-A273014] p 1897 N94-21309

ADMIRALTY RESEARCH ESTABLISHMENT, GOSPORT (ENGLAND).
The application of spaceborne synthetic aperture radar in the maritime environment [DRA-TM(AWE)-91013] p 1737 N94-20596

ADVANCED MATERIALS, INC., METAIRIE, LA.
Cold-start minidiesel engine development [AD-A271064] p 1823 N94-20567

ADVANCED PHOTOVOLTAIC SYSTEMS, INC., PRINCETON, NJ.
Research on stable, high-efficiency amorphous silicon multijunction modules [DE93-018220] p 1850 N94-22257

AERODYNE RESEARCH, INC., BILLERICA, MA.
Model for liquid boron oxide droplet gasification in H/O/C/F combustion environments [AD-A272911] p 1682 N94-21243

AERONAUTICAL RESEARCH LABS., MELBOURNE (AUSTRALIA).
An assessment of COMSCAN, a Compton backscatter imaging camera, for the one-sided non-destructive inspection of aerospace components [AD-A271331] p 1806 N94-19837
Literature review of the errors-in-variables approach to the problem of system identification [AD-A271098] p 1949 N94-19907
Development and operation of the F/A-18 model control surface actuators [AD-A271330] p 1645 N94-19914
Detecting topographical regions in digital terrain maps [AD-A272889] p 1841 N94-21453
Damage states around fastener holes in thick graphite/epoxy composite laminates [AD-A272613] p 1675 N94-21504

AEROSPACE CORP., EL SEGUNDO, CA.
Acoustic microscopy and nonlinear effects in pressurized superfluid helium [AD-A270568] p 1967 N94-19949
On the theory of morphology-dependent resonances: Shape resonances, width formulas, and graphical representations [AD-A272279] p 2037 N94-20945
The use of screening tests in spacecraft lubricant evaluation [AD-A272943] p 1705 N94-21225
Conversion of LDEF experiment M0003 sample observation database to MS-DOS formats [AD-A272945] p 1681 N94-21226

AEROSPACE CORP., LOS ANGELES, CA.
Parameters affecting hydrogen chloride measurements [AD-A271326] p 1851 N94-20025

AEROSPACE INDUSTRIES ASSOCIATION OF AMERICA, INC., WASHINGTON, DC.
Aerospace: Facts and figures, 1992-1993 [AD-A272571] p 1635 N94-21419

AEROSPACE MEDICAL DIV., BROOKS AFB, TX.
Physiological efficacy of a lightweight ambient air cooling unit for various applications [AD-A272952] p 1896 N94-21247

AEROSPACE MEDICAL RESEARCH LABS., BROOKS AFB, TX.
PEGASUS, electronic bulletin board system user's guide [AD-A271679] p 2044 N94-21363

AEROSPACE MEDICAL RESEARCH LABS., WRIGHT-PATTERSON AFB, OH.
System test results of the Advanced Technology Anti-G Suit (ATAGS) [AD-A271535] p 1896 N94-20914

AGENCY OF INDUSTRIAL SCIENCE AND TECHNOLOGY, TOKYO (JAPAN).
Evaporation of a sodium tellurite melt in the jamic low gravity drop shaft p 1713 N94-20605

AICHI UNIV. OF EDUCATION (JAPAN).
MHD flows from compact objects: Effects on magnetic field configurations p 2008 N94-22684
Generation and maintenance of bisymmetric spiral magnetic fields in disk galaxies in differential rotation p 2010 N94-22695

AIR FORCE AVIONICS LAB., WRIGHT-PATTERSON AFB, OH.
Surface states at the GaAs-germanium nitride interface p 1709 N94-20973

AIR FORCE ENVIRONMENTAL TECHNICAL APPLICATIONS CENTER, SCOTT AFB, IL.
An analysis of cloud-cover reporting in the 1977 surface observation database [AD-A271102] p 1864 N94-19852
Worldwide frequency of temperatures at selected altitudes [AD-A271111] p 1864 N94-19908

AIR FORCE INST. OF TECH., WRIGHT-PATTERSON AFB, OH.
Photoluminescence spectroscopy of zinc germanium diphosphide (ZnGeP2)
[AD-A270705] p 1678 N94-19953
Analysis of health status from preliminary physical examination of flight academy applicants
[AD-A267759] p 1889 N94-19962
Experimental study on interference aerodynamics of close-coupled canard configuration
[AD-A267760] p 1636 N94-19963
Circular polarizing mirrors for high power lasers
[AD-A267820] p 1815 N94-19965
A novel method for characterizing the electrical Priorities of lead Zirconate Titanate (PZT) ferroelectric films and memory devices
[AD-A270463] p 2013 N94-19966
Comparison of a distributed Kalman filter versus a centralized Kalman filter with fault detection considerations
[AD-A270713] p 1903 N94-19969
Physiologically based pharmacokinetic modelling of percutaneously absorbed dibromomethane utilizing multiple dermal sub-compartments
[AD-A271106] p 1889 N94-19981
New algorithm of ground track processing in high-frequency skywave over-the-horizon-B radar
[AD-A267821] p 1717 N94-20207
Spatial and temporal variations of satellite microwave measurements of latent heat release in tropic cyclones due to environmental forcing obtained from a numerical model
[AD-A267947] p 1865 N94-20482
An investigation into the integration of meter-level range and millimeter-level phase data using a multimode stimulation for optimal filter estimation software package
[AD-A267955] p 1751 N94-20483
Tactical laser weapons and other directed-energy weapons
[AD-A267961] p 1816 N94-20484
Modeling the minimum energy state of the Earth's magnetotail
[AD-A267984] p 1856 N94-20485
Development and testing of a reliability performance index for modular robotic systems
[AD-A271901] p 1942 N94-20488
Analysis of a sandstorm weather process-translation
[AD-A272959] p 1867 N94-21250
Mathematician Wang Ju
[AD-A267882] p 1912 N94-21255
Evaluation of electroconductivity of two surface paints for spacecraft
[AD-A273063] p 1706 N94-21437
Computing with Bayesian multi-networks
[AD-A273106] p 1914 N94-21501
The sea breeze convergence zone and its relationship to fair weather electricity in east central Florida
[AD-A268511] p 1868 N94-21502
Effects of stimulated Raman scattering on light beam properties during high-power laser beam long-path propagation
[AD-A273109] p 1818 N94-21509

AIR FORCE SYSTEMS COMMAND, BROOKS AFB, TX.
A full-color, high-resolution laser projector for a flight simulator visual display
[AD-A270578] p 1651 N94-20108

AIR FORCE SYSTEMS COMMAND, WRIGHT-PATTERSON AFB, OH.
Semiconductors A(III)B(VI): Translation
[AD-A273064] p 2028 N94-21436
Air Force brush seal programs p 1655 N94-21793

AIR UNIV., MAXWELL AFB, AL.
Operational test and evaluation of electronic combat systems
[AD-A273093] p 1647 N94-21500

AIR WEATHER SERVICE, KESSLER AFB, MS.
Weather tutor 1: Stability basics
[AD-A270758] p 1866 N94-20565

AIRBUS INDUSTRIE, TOULOUSE (FRANCE).
Utilization of lasers for air data measurements
p 1640 N94-22603

ALABAMA UNIV., HUNTSVILLE.
Stability limits and dynamics of nonaxisymmetric liquid bridges
[NASA-CR-194706] p 1797 N94-20037
X ray, extreme and far ultraviolet optical thin films for space applications
[NASA-CR-194635] p 1984 N94-20128
Development of a naming convention and data ma nagement system
[NASA-CR-193860] p 2042 N94-20268
Growth of zinc selenide single crystals by physical vapor transport in microgravity
[NASA-CR-194679] p 2017 N94-20346
Combined backscatter Moessbauer spectrometer/x ray fluorescence analyzer (BaMS/XRF) for extraterrestrial surfaces p 1686 N94-20761
Development, refinement, and testing of a short term solar flare prediction algorithm
[NASA-CR-194726] p 2147 N94-21815
Development, refinement, and testing of a short term solar flare prediction algorithm
[NASA-CR-194727] p 2147 N94-21832

ALASKA UNIV., FAIRBANKS.
Calderas produced by hydromagmatic eruptions through permafrost in northwest Alaska p 2089 N94-20385
Milankovitch insulation forcing and cyclic formation of large-scale glacial, fluvial, and eolian landforms in central Alaska p 2089 N94-20386

ALBERTA UNIV., CALGARY.
Image convolution using the Myrias SPS-2 parallel computer p 1786 N94-22207
Parallelizing a maximum entropy image deconvolution algorithm p 1787 N94-22208

ALBERTA UNIV., EDMONTON.
Silicon micromachined threshold accelerometers
p 1778 N94-22151

ALENIA SPAZIO S.P.A., ROME (ITALY).
Digital receiver for on-board FM/FSK-FM/BPSK demodulation p 1744 N94-21091

ALGORITHM CO. (RUSSIA).
The Soviet software market: Current state and aspects of development p 1923 N94-22066

ALL-UNION RESEARCH INST. ON COMPUTER AND INFORMATICS PROBLEMS, MOSCOW (RUSSIA).
Soviet society informatization: The USSR state program p 2046 N94-22058
The distributed CAD system for LSI/VLSI design
p 1923 N94-22068

ALLIED-SIGNAL AEROSPACE CANADA, TORONTO (ONTARIO).
MLS signal-in-space category 3 landing hazard analysis p 1644 N94-22134

ALLIED-SIGNAL AEROSPACE CO., COLUMBIA, MD.
A low cost alternative to high performance PCM bit synchronizers p 1813 N94-21347
Network command processing system overview
p 1935 N94-21351

ALLIED-SIGNAL AEROSPACE CO., KANSAS CITY, MO.
Characterization studies of lower and non-TDI polyurethane encapsulants
[DE93-041129] p 1698 N94-19857
Automated HMC assembly
[DE93-040641] p 1749 N94-20005
Feature-based tolerancing for intelligent inspection process definition
[DE93-017984] p 1906 N94-20311
Cratering evaluations and results
[DE93-040347] p 1691 N94-20478
Computer-Aided Test Equipment Graphics System (CATEGS)
[DE94-000383] p 1915 N94-21561
Process characterization and control of hand-soldered printed wiring assemblies
[DE93-041290] p 1763 N94-21652
Shape memory metals
[DE94-001373] p 1695 N94-21976
Enhanced software for the GT1022 automated gaging system
[DE94-001374] p 1918 N94-21977
Evaluation of non-chromium-containing deoxidizers for aluminum
[DE94-001377] p 1695 N94-21978

ALLIED-SIGNAL AEROSPACE CO., SEABROOK, MD.
Mission Operations Support Area (MOSA) for ground network support p 1932 N94-21331

ALLIED-SIGNAL CORP., DES PLAINES, IL.
High temperature size selective membranes
[DE93-019865] p 1709 N94-21982

ALLIED-SIGNAL CORP., OLATHE, KS.
Test pattern generation for ILA sequential circuits
p 1757 N94-21107

ALTAMIRA INSTRUMENTS, INC., PITTSBURGH, PA.
Direct aromatization of methane
[DE93-040631] p 1678 N94-19890

AMERICAN CYANAMID CO., STAMFORD, CT.
Fiber reinforced thermosetting resin composition with coated fibers for improved toughness
[CA-PATENT-1,306,320] p 1674 N94-21040

AMERICAN INST. FOR RESEARCH, WASHINGTON, DC.
Compatibility evaluation and research on the Computerized Adaptive Screening Test (CAST): User and programmer's guide
[AD-A273112] p 1894 N94-21510

AMERICAN MUSEUM OF NATURAL HISTORY, NEW YORK, NY.
Oxygen isotopic relationships between the LEW85332 carbonaceous chondrite and CR chondrites
p 2083 N94-20708
The formation of FeO-rich pyroxene and enstatite in unequilibrated enstatite chondrites: A petrologic-trace element (SIMS) study p 2086 N94-20866

AMERICAN NATIONAL STANDARDS INST., NEW YORK, NY.
Fortran for the nineties p 1926 N94-22481

AMERICAN SOCIETY FOR COMPOSITES, DAYTON, OH.
Biotechnology and composite materials
[AD-A264278] p 1673 N94-20327

AMES LAB., IA.
Quantitative evaluation of material composition of composites using x ray energy-dispersive NDE technique
[DE93-041157] p 1672 N94-19888
Application of an electrochemical quartz crystal microbalance to the study of electrocatalytic films
[DE93-041124] p 2029 N94-21691
Disks of YBa2Cu3O7 shocked to 10 GPa pressures
[DE94-000464] p 2031 N94-21931
Sulfur-bonded thiophenes in organometallic rhenium complexes and adsorption of isocyanides on gold
[DE93-041126] p 1694 N94-21937
First principles calculations for analysis martensitic transformations
[DE94-000666] p 1695 N94-21964
Inelastic neutron scattering of (gamma)-iron, and the determination of the elastic constants by lattice dynamics
[DE94-000694] p 1978 N94-22573

AMSTERDAM UNIV. (NETHERLANDS).
Neural data oriented parsing p 1940 N94-20248

ANALYTIC SCIENCES CORP., READING, MA.
Ocular damage induced by ultrashort laser pulses
[AD-A271859] p 1890 N94-20462

ANGLO-AUSTRALIAN OBSERVATORY, EPPING.
An object-oriented data reduction system in Fortran
p 2046 N94-22447
A self-defining hierarchical data system
p 2046 N94-22448

ANGLO-AUSTRALIAN OBSERVATORY, SYDNEY.
The evolution of the FIGARO data reduction system
p 2048 N94-22528
The data acquisition system for the Anglo-Australian Observatory 2-degree field project p 2048 N94-22529

APPLIED ANALYTICS CORP., MARKHAM (ONTARIO).
A real-time infrared image processing testbed
p 1790 N94-22227

APPLIED RESEARCH ASSOCIATES, INC., ALBUQUERQUE, NM.
Expanded polystyrene protective barricade full-scale fire exposure test
[AD-A271450] p 1698 N94-19938
Dynamic response of multiphase porous media
[AD-A272915] p 1831 N94-21219

APPLIED RESEARCH CORP., GREENBELT, MD.
An IDL-based analysis package for COBE and other skycube-formatted astronomical data
p 1925 N94-22471

APPLIED RESEARCH CORP., LANDOVER, MD.
The circumstellar environments of intermediate mass main sequence stars
[NASA-CR-189311] p 2055 N94-21498

APPLIED SCIENCE AND TECHNOLOGY, INC., WOBURN, MA.
Materials processing and manufacturing technologies for diamond substrate multichip modules
[AD-A271484] p 2027 N94-21319

ARGONNE NATIONAL LAB., IDAHO FALLS, ID.
A parametric study of heat transfer within a planar thermosyphon
[DE93-019546] p 1799 N94-20258
The 13th International Conference on Magnetically Levitated Systems and Linear Drives MAGLEV 1993
[DE93-040381] p 1825 N94-21544

ARGONNE NATIONAL LAB., IL.
On the experimental determination of low order structure factors in TiAl by energy filtered convergent beam electron diffraction
[DE93-019521] p 1687 N94-19806
Fermiology and De Haas-Van Alphen effect of beta-(ET)2IBr2
[DE93-019523] p 2011 N94-19807
Dynamics of vortices in superconductors
[DE93-019535] p 2011 N94-19808
Frequency and temperature dependence of high damping elastomers
[DE93-019539] p 1697 N94-19809
Advanced batteries for electric vehicle applications: Nontechnical summary
[DE93-019007] p 1748 N94-19885
Oxidation-reduction induced roughening of platinum (111) surface
[DE93-017408] p 1687 N94-19922
General introduction to microstructural evolution under cascade damage conditions
[DE93-017443] p 2012 N94-19923

An introduction to GUGA in the COLUMBUS Program System
[DE93-018994] p 1902 N94-19928
Encounters of H and D atoms with O2 in water: Relative diffusion and reaction rates
[DE93-018587] p 1970 N94-19956
The multicomponent lineshape of the anharmonic A(1)(TO) phonon in PbTiO3
[DE93-018995] p 1970 N94-19971
A conceptual design for the STAR endcap electromagnetic calorimeter
[DE93-040801] p 1807 N94-19990
Collisions of molecules with clusters: A quasiclassical study
[DE93-018614] p 1971 N94-20050
Sol-spray preparation, particulate characteristics, and sintering of alumina powders
[DE93-018577] p 1690 N94-20183
Neutron and PIMC determination of the longitudinal momentum distribution of HCP, BCC and normal liquid He-4
[DE93-019009] p 1972 N94-20187
Tropospheric chemistry of natural hydrocarbons, aldehydes, and peroxy radicals: Their connections to sulfuric acid production and climate effects
[DE93-019525] p 1855 N94-20220
Parallel band reduction and tridiagonalization
[DE93-019566] p 1951 N94-20221
Facilities for in situ ion beam studies in transmission electron microscopes
[DE93-019567] p 1979 N94-20222
Fuel processing requirements and techniques for fuel cell propulsion power
[DE93-019516] p 1750 N94-20257
Neutron-scattering studies of Yb-bearing silicate glasses
[DE93-019768] p 1700 N94-20265
Neutral copper cluster sputtering yields: Ne(+), Ar(+) and Xe(+) bombardment
[DE93-019010] p 1690 N94-20288
Determination of structure factors of copper by convergent beam electron diffraction
[DE93-019520] p 2019 N94-20941
Chemical reaction fouling model for single-phase heat transfer
[DE93-019556] p 1802 N94-20942
Analysis of a diesel-electric hybrid urban bus system
[DE93-019514] p 1825 N94-21297
Laser Raman and x ray scattering studies of corrosion films on metals
[DE93-040243] p 1692 N94-21558
Some evidence on determinants of fuel economy as a function of driving cycle and test type
[DE93-019511] p 1825 N94-21637
Relaxation of hysteresis loop in a single crystal of YBa2Cu4O8
[DE93-019519] p 2029 N94-21649
Research and development of alternative components at Argonne National Laboratory for molten carbonate fuel cells
[DE93-019536] p 1847 N94-21650
Surface and subsurface defect detection in Si3N4 components by laser scattering
[DE93-040829] p 1832 N94-21772
Modeling of polymer electrolyte fuel cell systems
[DE93-041187] p 1847 N94-21774
Plasma-chemical conversion of hydrogen sulfide into hydrogen and sulfur
[DE93-041167] p 1682 N94-21789
Surface modification for corrosion resistance
[DE93-017419] p 1693 N94-21825
Material optimization for hard x ray Fresnel zone plates
[DE93-019569] p 1990 N94-21837
Cathode materials for the molten carbonate fuel cell
[DE93-019515] p 1848 N94-21870
Fullerene derivatives and fullerene superconductors
[DE93-019568] p 2031 N94-21871
User's guide for the casting process simulator software CaPS-2D, version 1.0
[DE93-040398] p 1917 N94-21923
A vibration model for centrifugal contactors
[DE93-040645] p 1833 N94-21927
Photo- and thermal-induced antiferromagnetic interlayer coupling in Fe/(Fe-Si) superlattices
[DE93-040822] p 2031 N94-21930
Disks of YBa2Cu3O7 shocked to 10 GPa pressures
[DE94-000464] p 2031 N94-21931
Millimeter-wave imaging of composite materials
[DE93-041160] p 1677 N94-21940
Studies of the deuteron at high energy and momentum transfer
[DE93-041162] p 1976 N94-21941
The electrochemical performance of thin-electrolyte solid oxide fuel cells
[DE93-041184] p 1848 N94-21942
Direct detection of atomic ions from molecular photofragmentation during nonresonant multiphoton ionization of sputtered species
[DE93-040886] p 1976 N94-21951
Spin dynamics and implications for superconductivity: Some problems with the d-wave scenario
[DE94-001183] p 2032 N94-21972
Synthesis and characterization of charge-substituted garnets YCaLnGa5O12 (Ln = Ce, Pr, Tb)
[DE93-040227] p 2033 N94-21992
Crystal structure and short-range oxygen defects in La- and Nd-modified ZrO2
[DE93-040229] p 2033 N94-21993
MOCVD growth and structure of PbTiO3 thin films
[DE93-040230] p 2033 N94-21994
The effect of correlated and point defects on the vortex lattice melting transition in single crystal YBa2Cu3O(7-delta)
[DE93-040277] p 2033 N94-21997
High oxygen pressure synthesis of new copper oxide superconductors
[DE93-040278] p 2033 N94-21998
Temperature-dependent ion beam mixing
[DE93-040281] p 2033 N94-21999
Tensile strength of fiber reinforced plastics at 77K irradiated by various radiation sources
[DE93-040826] p 1709 N94-22008
Areally averaged estimates of surface heat flux from ARM field studies
[DE93-018569] p 1859 N94-22036
Asymptotic analysis. Working Note No. 2, approximation of integrals
[DE94-000433] p 1961 N94-22381
Development of advanced cloud parameterizations to examine air quality, cloud properties, and cloud-radiation feedback in mesoscale models
[DE93-041164] p 1853 N94-22384
Experimental evaluation of oxygen-enriched air and emulsified fuels in a six-cylinder diesel engine
[DE94-000907] p 1811 N94-22391
Asymptotic analysis: Basic concepts and definitions
[DE94-001000] p 1961 N94-22393
Orientationally independent antiferromagnetic coupling in epitaxial Fe/Cr (211) and (100) superlattices
[DE94-001270] p 2035 N94-22564
Spectroscopic studies of magnetic transitions in TbPO4
[DE94-001274] p 2035 N94-22565

ARIZONA STATE UNIV., TEMPE.
RCS Analysis of Plate Geometries, parts 1 and 2
[NASA-CR-194173] p 1717 N94-20269
High-frequency techniques for RCS prediction of plate geometries p 1717 N94-20270
A physical optics/equivalent currents model for the RCS of trihedral corner reflectors p 1717 N94-20271
A formational model for the polygonal terrains of Mars: Taking a crack at the genesis of the Martian polygons p 2091 N94-20400
Structural evidence for reorientation of Miranda about a paleo-pole p 2098 N94-20671
Thermal conductivity measurements of particulate materials under Martian conditions p 1685 N94-20703
Impact-induced devolatilization of CaSO4 anhydrite and implications for K-T extinctions: Preliminary results p 2085 N94-20840
A study of carbonates, sulfates, and phosphates using thermal emission spectroscopy p 1686 N94-20868
Multispectral studies of selected crater- and basin-filling lunar Maria from Galileo Earth-Moon encounter 1 p 2136 N94-20876
Convex set and linear mixing model p 1844 N94-20888
In-situ spectroscopic ellipsometry in molecular beam epitaxy p 2024 N94-21005
Heat transfer additives for absorption cooling system fluids
[PB93-202521] p 1714 N94-21426
The Martian valley networks: Origin by niveo-fluvial processes p 2146 N94-21682

ARIZONA UNIV., TUCSON.
Hydrological consequences of ponded water on Mars p 2089 N94-20383
Wavelength dependence of limb-darkening of Mars from visible and near-IR telescopic spectral imaging p 2101 N94-20685
Formation of the low-mass solar nebula p 2109 N94-20728
Diffusive redistribution of water vapor in the solar nebula revisited p 2113 N94-20751
Parabolic features and the erosion rate on Venus p 2122 N94-20801
Triton's cratering record and its time of capture p 2122 N94-20802
Core formation by giant impacts: Conditions for intact melt region formation p 1863 N94-20833
Photogeological analysis of Europan tectonic features p 2129 N94-20838
Numerical modeling of impact erosion of atmospheres: Preliminary results p 2131 N94-20847
Coagulation of grains in static and collapsing protostellar clouds p 2085 N94-20885
Long Duration Exposure Facility (LDEF) contamination study
[AD-A272419] p 1658 N94-21147
Evolution of the global water cycle on Mars: The geological evidence p 2142 N94-21660
Fluvial valleys in the heavily cratered terrains of Mars: Evidence for paleoclimatic change? p 2144 N94-21670
A quantitative model for interpreting nanometer scale hardness measurements of thin films
[DE93-040601] p 2034 N94-22005

ARKANSAS UNIV., FAYETTEVILLE.
Cathodoluminescence observations of in situ aqueous destruction of chondrules in the Murchison CM chondrite p 2083 N94-20750
Lewis Cliff 87057: A new metal-rich E3 chondrite with similarities to Mt. Egerton, Shallowater and Happy Canyon p 2086 N94-20901

ARMY AEROMEDICAL RESEARCH LAB., FORT RUCKER, AL.
Coronary angiography outcomes of US Army aircrew with the finding of coronary artery calcifications: Aviation epidemiology data register
[AD-A271968] p 1891 N94-20615
Review of using cardiac fluoroscopy in symptomatic and asymptomatic patients
[AD-A271690] p 1891 N94-20928

ARMY ARMAMENT RESEARCH, DEVELOPMENT AND ENGINEERING CENTER, PICATINNY ARSENAL, NJ.
The readiness growth model: A quantitative analysis of software risk
[AD-A272383] p 1910 N94-21144

ARMY AVIATION SYSTEMS COMMAND, MOFFETT FIELD, CA.
An experimental investigation of the drag mechanisms of a helicopter rotor in hovering flight
[AD-A270201] p 1636 N94-20486

ARMY COLD REGIONS RESEARCH AND ENGINEERING LAB., FORT WAINRIGHT, AK.
Evaluation of pre-extraction analytical holding times for nitroaromatic and nitramine explosives in water
[AD-A271547] p 1712 N94-20927

ARMY COLD REGIONS RESEARCH AND ENGINEERING LAB., HANOVER, NH.
Notes on Antarctic aviation
[AD-A273018] p 1651 N94-21239

ARMY ENGINEER WATERWAYS EXPERIMENT STATION, VICKSBURG, MS.
Two-dimensional finite element analysis of porous media at multikilobar stress levels
[AD-A271540] p 1831 N94-20916

ARMY MEDICAL CENTER, FORT GORDON, GA.
Non-ionic surfactants in the treatment of third degree burns
[AD-A271582] p 1891 N94-21035

ARMY RESEARCH INST. OF ENVIRONMENTAL MEDICINE, NATICK, MA.
Maximum team lifting capacity as a function of team size
[AD-A271642] p 1892 N94-21036
Human responses to exercise-heat stress
[AD-A272581] p 1892 N94-21209

ARMY RESEARCH LAB., ABERDEEN PROVING GROUND, MD.
Further examinations on the thermodynamic stability of the Mie-Gruneisen equation of state
[AD-A270526] p 2037 N94-19831
Ab initio potential energy surface for the H + OCS reaction
[AD-A270577] p 1698 N94-19947
Detailed structure study of an H2/N2O/Ar flame employing molecular beam mass spectrometry, laser spectroscopy, and modeling
[AD-A270720] p 1679 N94-20111
Multisensor pinhole yawsonde
[AD-A271715] p 1808 N94-20930
Current directions in the vulnerability/lethality process structure
[AD-A272836] p 1964 N94-21175
Infrared absorption spectroscopy of the weakly bonded CO-Cl2 complex
[AD-A271757] p 2027 N94-21304
Toward a new method of decoding algebraic codes using Groebner bases
[AD-A273089] p 1959 N94-21524

ARMY RESEARCH LAB., ADELPHI, MD.
Focused-ion-beam material removal rates
[AD-A270852] p 1713 N94-19834

ARMY RESEARCH LAB., FORT MONMOUTH, NJ.
Analysis of semi-insulating bulk GaAs using glow discharge mass spectrometry
[AD-A273032] p 1682 N94-21435
ARMY RESEARCH LAB., WATERTOWN, MA.
Biaxial flexural testing of a carbon fiber reinforced epoxy composite
[AD-A271956] p 1674 N94-20577
Stress-induced cracking of fluorocarbon rubber MTL-0002 after exposure to DS-2
[AD-A271753] p 1705 N94-21302
Investigation of the effect of various oxide and fluoride additives on the microstructure, electronic properties, and phase shifting ability of Ba(1-x)Sr(x)TiO3
[AD-A271756] p 2027 N94-21303
ARMY TRAINING AND DOCTRINE COMMAND, FORT MONROE, VA.
Operational Requirements Document (ORD) for the Alternating Current/Direct Current (AC/DC) clamp-on ammeter, mE-563
[AD-A271606] p 1751 N94-20555
ASTROPHYSICAL INST., POTSDAM (GERMANY).
Adaptive filtering of Echelle spectra of distant Quasars p 2072 N94-22520
ASULAB S.A., NEUCHATEL (SWITZERLAND).
Battery tests p 1752 N94-20631
Liquid crystal displays p 1752 N94-20634
LCD display tests p 1752 N94-20635
ATOMINSTITUT DER OESTERREICHISCHEN HOCHSCHULEN, VIENNA.
Tensile and shear fracture behavior of fiber reinforced plastics at 77K irradiated by various radiation sources
[DE93-040280] p 1706 N94-21542
AURORA FLIGHT SCIENCES CORP., MANASSAS, VA.
Low-cost, dual-use platforms for environmental sensing, phase 1
[AD-A272951] p 1646 N94-21246
AUSTRALIAN NATIONAL UNIV., CANBERRA.
The Mg-suite and the highland crust: An unsolved enigma p 2126 N94-20822

B

BABCOCK AND WILCOX CO., ALLIANCE, OH.
Evaluation of the fabricability of advanced iron aluminide-clad austenitic stainless steel tubing
[DE93-040598] p 1693 N94-21771
BANK OF FINLAND, HELSINKI.
Experiences of the bank of Finland's econometric simulation model p 2053 N94-22086
BATTELLE NORTHWEST LABS., RICHLAND, WA.
Aluminum-26 activities in meteorites p 1686 N94-20851
BAYLOR UNIV., WACO, TX.
Determination of parameters for hypervelocity dust grains encountered in near-Earth space p 2084 N94-20817
BEIJING NORMAL UNIV. (CHINA).
Dynamo driven by weak plasma turbulence: The effect of differential rotation p 2005 N94-22665
BELEIDSCOMMISSIE REMOTE SENSING, DELFT (NETHERLANDS).
Offshore decision support system: ERS-1 pilot project WAVEWATCH
[BCRS-92-09] p 1865 N94-20532
Information extraction for multispectral images using radiation interaction models
[BCRS-90-22] p 1841 N94-21015
Mobility of salt domes
[BCRS-92-08] p 1857 N94-21016
Ocean mapping using satellite radar altimetry
[ETN-93-93470] p 1841 N94-21017
BELL-NORTHERN RESEARCH LTD., OTTAWA (ONTARIO).
Modeling software systems for data flow testing p 1772 N94-22117
BELORUSSIAN STATE UNIV., MINSK (BELARUS).
The sand bag model of the dispersion of the cosmic body in the atmosphere p 2084 N94-20823
Atmospheric breakup of a small comet in the Earth's atmosphere p 2084 N94-20824
BERN UNIV. (SWITZERLAND).
Dating native gold by noble gas analyses p 1684 N94-20652
Berne (Switzerland) solar observations: Data for April 1991 - August 1992
[REPT-59] p 2147 N94-21150
BERTIN ET CIE., PLAISIR (FRANCE).
Optimization of a satellite localization and message sending system
[ETN-93-94448] p 1737 N94-20592
BETTIS ATOMIC POWER LAB., PITTSBURGH, PA.
Hydrogen pickup and redistribution in alpha-annealed zircaloy-4
[DE93-018050] p 1689 N94-20182
BETTIS ATOMIC POWER LAB., WEST MIFFLIN, PA.
Particle image velocimetry
[DE93-040657] p 1804 N94-21748
Improved approximate formulas for flux from cylindrical and rectangular sources
[DE93-011390] p 1742 N94-22268
BIOELASTICS RESEARCH LTD., BIRMINGHAM, AL.
Development of bioelastic material for aspects of wound repair
[AD-A267832] p 1673 N94-20208
Development of bioelastic material for aspects of wound repair
[AD-A272000] p 1892 N94-21503
BOEING COMMERCIAL AIRPLANE CO., SEATTLE, WA.
Aircraft cabin water spray disbenefits study
[NASA-CR-194750] p 1642 N94-21818
Parallel runway requirement analysis study. Volume 1: The analysis
[NASA-CR-191549-VOL-1] p 1644 N94-22277
Parallel runway requirement analysis study. Volume 2: Simulation manual
[NASA-CR-191549-VOL-2] p 1644 N94-22278
Nonlinear and progressive failure aspects of transport composite fuselage damage tolerance p 1834 N94-22609
BOEING DEFENSE AND SPACE GROUP, SEATTLE, WA.
Pressure versus drag effects on crater size p 1862 N94-20742
Complementary heterojunction FET technology for space application p 1755 N94-21094
Automated radiation hard ASIC design tool p 1759 N94-21126
Towards the formal verification of the requirements and design of a processor interface unit: HOL listings
[NASA-CR-191466] p 1937 N94-22414
BOLT, BERANEK, AND NEWMAN, INC., CAMBRIDGE, MA.
Research, Development, Training, and Evaluation (RDTE) support delivery order 1: Computational cognitive models
[AD-A271637] p 1894 N94-20610
BONN UNIV. (GERMANY).
X ray reflection masks: Manufacturing, characterization and first tests
[BONN-IR-92-31] p 1986 N94-21043
Examination for optimization of synchrotron radiation spectrum for the x ray depth lithography
[BONN-IR-92-32] p 1987 N94-21148
Measurement of mesospheric turbulence in the framework of the metal campaign and development of a sensor for static pressure free measurements of neutral and electron density
[BONN-IR-92-45] p 1857 N94-21149
BOOZ-ALLEN AND HAMILTON, INC., SEABROOK, MD.
Developing a space network interface simulator: The NTS approach p 1933 N94-21343
BOSTON UNIV., MA.
Convergence of the hermite wavelet expansion
[AD-A271435] p 1854 N94-19841
Segment-based acoustic models for continuous speech recognition
[AD-A271483] p 1736 N94-20547
The effects of magnetic storm phases on F-layer irregularities from auroral to equatorial latitudes
[AD-A272685] p 1857 N94-21189
BRIGHAM YOUNG UNIV., PROVO, UT.
Design and implementation of GaAs HBT circuits with ACME p 1758 N94-21117
Correctness properties for iterated hardware structures p 1759 N94-21124
BRITISH COLUMBIA UNIV., VANCOUVER.
Modelling stalled airfoils
[ISBN-0-315-59525-6] p 1639 N94-22382
Chromaticity analysis of LANDSAT multispectral scanner and thematic mapper imagery of Chilko Lake, British Columbia, using a theoretical optical water quality model
[ISBN-0-315-63832-X] p 1843 N94-22422
BRITISH HYDROMECHANICS RESEARCH ASSOCIATION, CRANFIELD (ENGLAND).
Dynamics of face seals for high speed turbomachinery p 1655 N94-21796
BRITISH TELECOM RESEARCH LABS., IPSWICH (ENGLAND).
A single layer higher order neural net and its application to grammar recognition p 1941 N94-20251
BROOKHAVEN NATIONAL LAB., UPTON, NY.
A summary of studies of particle stability at RHIC
[DE93-040173] p 1970 N94-19868
Femtosecond Raman-induced Kerr effect study of polar solvent dynamics: Amides
[DE93-017563] p 1678 N94-19924
Electron reactions in nonpolar liquids: Pressure effects
[DE93-040328] p 1970 N94-19931
Aperture determination of RHIC92 from randomly generated initial coordinates
[DE93-040174] p 1978 N94-19945
Outgassing rate of Reemay Spunbonded Polyester and DuPont Double Aluminized Mylar
[DE93-040015] p 1699 N94-19973
Angular distributions of high-order ATI
[DE93-019125] p 1972 N94-20230
National Synchrotron Light Source user's manual: Guide to the VUV and x ray beamlines
[DE93-019564] p 2015 N94-20260
The use of x ray techniques in the in situ study of corrosion
[DE93-019845] p 1690 N94-20301
The metallic bond for monolayer transition metal layers on transition metal surfaces
[DE93-019060] p 1691 N94-20313
High energy ionization in liquids: The free ion yield
[DE93-040329] p 1973 N94-20324
The atomic weight and isotopic composition of boron and their variation in nature
[DE93-019046] p 1682 N94-21631
Lattice gauge theory: Present status
[DE93-041154] p 2038 N94-21692
Searching for high baryon density at the AGS with ARC
[DE93-041155] p 1975 N94-21693
Performance of carbon-based hot frit substrates
[DE94-000509] p 1676 N94-21754
Femtosecond dynamics in hydrogen-bonded solvents
[DE93-019937] p 1683 N94-21842
Temperature and Doppler coefficients of various space nuclear reactors
[DE94-001388] p 1671 N94-21979
BROWN UNIV., PROVIDENCE, RI.
The proximity effect in ultrathin granular Pb films
[AD-A271094] p 2012 N94-19848
The Coulomb anomaly in strongly disordered films
[AD-A271095] p 2012 N94-19849
Dynamical systems and nonlinear partial differential equations
[AD-A271514] p 1951 N94-20545
Formation and evolution of radial fracture systems on Venus p 2099 N94-20672
Thermal and rheological controls on magma migration in dikes: Examples from the east rift zone of Kilauea volcano, Hawaii p 1862 N94-20673
Mixing of a chemically buoyant layer at the top of a thermally convecting fluid: Implications for mantle dynamics with application to Venus p 2099 N94-20675
Compositional diversity of the lunar North Pole: Preliminary analyses of Galileo SSI data p 2101 N94-20686
Optical effects of space weathering on lunar soils and the role of the finest fraction p 2101 N94-20687
MinMap: An imaging spectrometer for high resolution compositional mapping of the Moon p 1813 N94-20688
Visible-infrared properties of controlled laboratory soils p 1685 N94-20689
C-O volatiles in Apollo 15 and Apollo 17 picritic glasses p 1685 N94-20727
Searching for ancient Venus p 2111 N94-20743
Impactor control of central peak and peak-ring formation p 1862 N94-20744
Further analyses of Rio Cuarto impact glass p 1685 N94-20745
Are Plinian type eruptions possible on Venus? p 2123 N94-20803
Determining the composition of olivine on asteroidal surfaces p 1686 N94-20805
Objective determination of image end-members in spectral mixture analysis p 1686 N94-20831
Distribution and geologic history of materials excavated by the lunar crater Bullialdus p 2128 N94-20832
Formation of perched lava ponds on basaltic volcanoes: Interaction between cooling rate and flow geometry allows estimation of lava effusion rates p 1863 N94-20878
BRTRC, INC., VIENNA, VA.
RDA-PC system user's guide
[AD-A270356] p 2041 N94-20038

C

CALCUTTA UNIV. (INDIA).
Addition of decimal numbers in optical computing architecture by Walsh coded digits p 1773 N94-22122
Improvement of the performance of IMPATT oscillators through appropriate modification of resonant-cap activity p 1782 N94-22179
CALGARY UNIV. (ALBERTA).
Formal verification of an ALU p 1772 N94-22114
Charge integrating optical position sensor p 1778 N94-22152

Vector gravimetry by a combination of inertial and GPS satellite measurements
[ISBN-0-315-61980-5] p 1861 N94-22424
A study of parallel pier finger airport terminal configuration
[ISBN-0-315-83128-6] p 1652 N94-22425
Circumstellar environments of Be stars at infra-red and radio wavelengths
[ISBN-0-315-83135-9] p 2081 N94-22426
A robust quality control system for GPS navigation and kinematic positioning
[ISBN-0-315-83148-0] p 1644 N94-22427
STAR-1 SAR road extraction using texture analysis and mathematical morphology
[ISBN-0-315-83255-X] p 1843 N94-22429
A comparison of a simple model of EUV dayglow with Viking data
[ISBN-0-315-83258-4] p 1861 N94-22574
Implications of Viking dayside auroral measurements
[ISBN-0-315-83273-8] p 1861 N94-22575

CALIFORNIA INST. OF TECH., PASADENA.
Toward a neurobiological theory of visual attention
[AD-A270724] p 1890 N94-20112
Dynamics of large scale impacts on Venus and Earth
p 2098 N94-20666
Self diffusion of alkaline-Earth in Ca-Mg-aluminosilicate melts: Experimental improvements on the determination of the self-diffusion coefficients p 1684 N94-20669
Differentiation of magma oceans and the thickness of the depleted layer on Venus p 2118 N94-20780
Expectations for the Martian core magnetic field
p 2120 N94-20792
Volatile loss from accreting icy protoplanets
p 2084 N94-20793
Fine resolution chronology based on initial Sr-87/Sr-86
[CONTRIB-5230(794)] p 1686 N94-20794
The Sm-Nd systematics of silicate inclusions in iron meteorites: Results from Caddo (IAB)
[CONTRIB-5241(804)] p 2084 N94-20795
SPH modelling of energy partitioning during impacts on Venus p 2124 N94-20809
AGB stars as a source of short-lived radioactive nuclei in the solar nebula p 2133 N94-20859
High D/H ratios of water in magmatic amphiboles in Chassigny: Possible constraints on the isotopic composition of magmatic water on Mars
p 2134 N94-20862
Combustion in turbulent jets and buoyant flames
[PB93-202372] p 1682 N94-21452
The young Sun and photochemistry of the primitive Martian atmosphere p 2145 N94-21679

CALIFORNIA POLYTECHNIC STATE UNIV., SAN LUIS OBISPO.
Reference manual for a Requirements Specification Language (RSL), version 2.0
[NASA-CR-191460] p 1898 N94-20039

CALIFORNIA STATE UNIV., FULLERTON.
LREE variability in CM matrices: Another look at meteorite compaction ages p 2086 N94-20884

CALIFORNIA UNIV., BERKELEY.
Studies of an x ray selected sample of cataclysmic variables
[NASA-CR-194773] p 2055 N94-20344
Application of the reactive flux formalism to study water hydrogen bond dynamics
[AD-A271824] p 1680 N94-20560
Exposure ages of carbonaceous chondrites, 1
p 2082 N94-20658
The EUVE proposal database and scheduling system
p 2047 N94-22459
The extreme ultraviolet explorer archive
p 2047 N94-22468
Quality control of EUVE databases
p 2047 N94-22490
Data indexing techniques for the EUVE all-sky survey
p 2048 N94-22503
Fluid simulations of Delta T(sub e)-driven turbulence and transport in boundary plasmas
[DE94-001304] p 1999 N94-22566
Theory and simulation of plasma sheath waves
[DE94-001305] p 1999 N94-22567
Verification of frequency scaling laws for capacitive rf discharges using two-dimensional simulations
[DE94-001306] p 1999 N94-22595
Electron temperature gradient driven instability in the tokamak boundary plasma
[DE94-001307] p 1999 N94-22596

CALIFORNIA UNIV., BERKELEY. LAWRENCE BERKELEY LAB.
High resolution electron crystallography of protein molecules
[DE93-040114] p 1884 N94-19826
Study of transverse coupled bunch instabilities by using non-linear Taylor maps for the Advanced Light Source (ALS)
[DE93-040287] p 1979 N94-19989
Space-charge dominated beam transport in magnetic quadrupoles with large aperture ratios
[DE93-040443] p 1992 N94-20004
Qualifying codes under software quality assurance: Two examples as guidelines for codes that are existing or under development
[DE93-040452] p 1904 N94-20097
Heavy ion fusion injector experiments
[DE93-019188] p 1993 N94-20234
Emittance measurement and modeling of the ALS 50 MeV LINAC to booster line
[DE93-040116] p 1979 N94-20273
Study of coupled-bunch collective effects in the PEP-2 B-Factory
[DE93-040117] p 1979 N94-20274
High current injector for heavy ion fusion
[DE93-019241] p 1979 N94-20289
Longitudinal instability of an induction linac with acceleration
[DE93-019249] p 1980 N94-20290
B production at D0
[DE93-019250] p 1972 N94-20291
Measurement and computation of the higher order modes of the ALS 500 MHz accelerating cavities
[DE93-019256] p 1980 N94-20292
Ultrafast scanning microscopy
[DE93-040121] p 1985 N94-20320
Study of possible energy upgrade for the ALS and modeling of the real lattice for the diagnosis of lattice problems
[DE93-040286] p 2016 N94-20323
Electron quantum yields from a barium photocathode illuminated with polarized light
[DE93-019232] p 1980 N94-20475
Low emittance 0.8A K(+) ion source for the LBL Induction Linac System Experiment (ILSE)
[DE93-019237] p 1981 N94-21439
Simulation studies of space-charge-dominated beam transport in large aperture ratio quadrupoles
[DE93-019238] p 1981 N94-21440
Diffraction and holography of photoelectrons and fluorescent x rays
[DE93-019240] p 1808 N94-21441
Advanced far infrared detectors
[DE93-040289] p 1988 N94-21528
The energy performance of prototype holographic glazings
[DE93-040451] p 1809 N94-21545
Role of surface characteristics in urban meteorology and air quality
[DE93-040929] p 1851 N94-21740
Semiconductor isotope engineering
[DE93-040119] p 2030 N94-21744
Implantation of carbon in GaAs and compensating native defects
[DE93-040122] p 2030 N94-21763
Swelling equilibria for cationic 2-hydroxyethyl methacrylate (HEMA)-based hydrogels
[DE94-000728] p 1707 N94-21856
Center for X-Ray Optics, 1992
[DE94-000726] p 1990 N94-21868
Survey and alignment analysis for the ALS storage ring using computer spreadsheets
[DE93-019254] p 1917 N94-21917
Hydrogen in compound semiconductors
[DE93-040300] p 2031 N94-21922
Specific heat of YBa2Cu3O7
[DE93-040640] p 2031 N94-21926
Iterative electromagnetic Born inversion applied to earth conductivity imaging
[DE93-040668] p 1859 N94-21928
Water-enhanced solvation of organics
[DE93-040297] p 1683 N94-21947
Monte Carlo calculation of multi-electron effects on synchrotron radiation
[DE94-001259] p 1982 N94-21974
Restoring locality with faster-than-light velocities
[DE93-040926] p 2038 N94-22010
Quantitative analysis of scanning tunneling microscopy images for surface structure determination: Sulfur on Re(0001)
[DE93-019235] p 2034 N94-22041
Database computing in HEP
[NASA-CR-194791] p 1921 N94-22375
General asymmetric neural networks and structure design by genetic algorithms: A learning rule for temporal patterns
[DE94-001254] p 1947 N94-22563

CALIFORNIA UNIV., DAVIS.
Particle dispersion in turbulent sprays
[AD-A271314] p 1796 N94-19913
A mechanized process algebra for verification of device synchronization protocols p 1766 N94-21716

CALIFORNIA UNIV., FULLERTON.
Analog/digital pH meter system I.C.
p 1764 N94-21701

CALIFORNIA UNIV., LOS ANGELES.
Cosmos 2229
[NASA-CR-194734] p 1895 N94-20338
The effects of processing and constituent materials on compressive strength of thick composite laminates
[AD-A271912] p 1673 N94-20490
Euhedral metallic-Fe-Ni grains in extraterrestrial samples p 1697 N94-20724
Iridium in sediments containing large abundances of Australasian microtektites from DSDP hole 758B in the Eastern Indian Ocean and from DSDP hole 769A in the Sulu Sea p 2083 N94-20741
Limits on differentiation of melt sheets from basin-scale lunar impacts p 2133 N94-20856
Multiplicity of chondrule heating events and the coarsening of chondrule textures p 2085 N94-20860
Psychometric developments related to tests and selection
[AD-A272971] p 1894 N94-21262
High temperature superconducting planar circuit structure for high frequency applications
[AD-A273083] p 2028 N94-21521
Plasma lens experiments at the Final Focus Test Beam
[DE93-041081] p 1981 N94-21688

CALIFORNIA UNIV., SAN DIEGO, LA JOLLA.
Low-energy ion implantation: Large mass fractionation of argon p 1685 N94-20697
Theoretical particle physics
[DE94-000538] p 1973 N94-20938
Synthesis and properties of mismatched heterojunction/substrate interfaces
[AD-A272904] p 1760 N94-21229

CALIFORNIA UNIV., SANTA BARBARA.
Molecular and atomic arrays in nano- and mesoporous materials synthesis
[AD-A271500] p 2017 N94-20544
Decoupled computer architectures for very high-speed technologies
[AD-A271646] p 1900 N94-21301

CALIFORNIA UNIV., SANTA CRUZ.
Analysis of the effects of eurasian crustal and upper mantel structure on regional phases using broadband seismic data
[AD-A272446] p 1858 N94-21206

CALSPAN-STATE UNIV. OF NEW YORK JOINT VENTURE, BUFFALO, NY.
Development of BEM for ceramic composites
[NASA-CR-194718] p 1676 N94-21777

CAMBRIDGE UNIV. (ENGLAND).
Nonthermal planetary radio emissions: Theories and observations p 2001 N94-22635
Dynamo driven by weak plasma turbulence: The effect of differential rotation p 2005 N94-22665

CAPE COD RESEARCH, BUZZARDS BAY, MA.
Complex and stereoregular nonlinear optical materials
[AD-A271067] p 1983 N94-19846

CARLETON UNIV., OTTAWA (ONTARIO).
Sub-band adaptive noise cancelling
p 1774 N94-22125
Interference reduction using neural networks
p 1783 N94-22186
Segmentation and frequency domain ML pitch estimation of speech signals p 1747 N94-22212
Some best rate 1/p and rate (p-1)/p systematic quasi-cyclic codes over GF(3) and GF(4)
p 1792 N94-22243
A Monte Carlo study of the Sudbury Neutrino Observatory small test detector experiment
[ISBN-0-315-59056-4] p 1977 N94-22416
Passenger terminal level of service measurement: A utility theoretic approach
[ISBN-0-315-59037-8] p 1651 N94-22418

CARNEGIE INSTITUTION OF WASHINGTON, DC.
A tectonic resurfacing model for Venus
p 2118 N94-20781
Variety in planetary systems p 2086 N94-20871
Equilibrium models of mass distribution and collisional lifetimes of asteroids p 2086 N94-20877

CARNEGIE-MELLON UNIV., PITTSBURGH, PA.
A distributed reinforcement learning scheme for network routing
[AD-A270600] p 1938 N94-19845
Structural modeling: An application framework and development process for flight simulators
[AD-A271348] p 1650 N94-19880
A comparison of data-parallel algorithms for connected components
[AD-A270551] p 1902 N94-19918

Model checking, abstraction, and compositional verification
[AD-A270552] p 1902 N94-19919
Implementation of a portable nested data-parallel language
[AD-A270524] p 1902 N94-19932
Set based analysis of ML programs
[AD-A270597] p 1902 N94-19948
Segmented operations for sparse matrix computation on vector multiprocessors
[AD-A270601] p 1928 N94-19950
Multilist scheduling: A new parallel programming model
[AD-A270549] p 1929 N94-20084
A methodology for formal hardware verification, with application to microprocessors
[AD-A270550] p 1898 N94-20085
Lightweight recoverable virtual memory
[AD-A270576] p 1898 N94-20107
Simulating a user's preferences: Towards automated artificial evolution for computer generated images
[AD-A272058] p 1942 N94-20621
Standard ML signatures for a protocol stack
[AD-A272060] p 1908 N94-20622
Fault tolerant real-time systems
[AD-A272878] p 1899 N94-21195
An investigation into the state of the practice of CASE tool integration
[AD-A272441] p 1912 N94-21205
Real-time fault tolerant computer systems
[AD-A272909] p 1899 N94-21230
CMU very fast range-imaging system
[AD-A272057] p 1761 N94-21282
Experiments in knowledge refinement for a large rule-based system
[AD-A272055] p 1809 N94-21445

CENTER FOR ANALYSIS, NEWPORT BEACH, CA.
Seeing the forest for the trees: Networked workstations as a parallel processing computer p 1938 N94-22454

CENTER FOR MATHEMATICS AND COMPUTER SCIENCE, AMSTERDAM (NETHERLANDS).
The combinatorics of reconstructing evolutionary trees
[CWI-BS-R9233] p 1963 N94-21022
Reduction of network cost and wiring in Ranade's butterfly routing
[CWI-CS-R9243] p 1930 N94-21023
Optimal sorting in linear arrays with minimum global control
[CWI-CS-R9244] p 1908 N94-21024
Proving run-time properties of general programs w.r.t. constructive negation
[CWI-CS-R9245] p 1909 N94-21025
A declarative approach for first-order built-in's of PROLOG
[CWI-CS-R9246] p 1909 N94-21026
On Update Last schemes
[CWI-CS-R9247] p 1952 N94-21027
Efficient comparison based string matching
[CWI-CS-R9249] p 1909 N94-21028
Tight comparison bounds for the string prefix-matching problem
[CWI-CS-R9250] p 1952 N94-21029
The correlated M/G/1 queue
[CWI-BS-R9303] p 1943 N94-21032
Routing of freeway traffic: A discrete-time state space model and routing problems
[CWI-BS-R9232] p 1944 N94-21033
MGD1M: A parallel multigrid code with a fast vectorized ILU-relaxation
[CWI-NM-R9222] p 1930 N94-21077
Approximate methods for N-component solute transport and ion-exchange
[CWI-NM-R9223] p 1910 N94-21078
The Robinson-Schensted and Schuetzenberger algorithms. Part 1: New combinatorial proofs
[CWI-AM-R9208-PT-1] p 1911 N94-21156
The Robinson-Schensted and Schuetzenberger algorithms. Part 2: Geometric interpretations
[CWI-AM-R9209-PT-2] p 1911 N94-21157
On semisimple cocommutative bialgebras
[CWI-AM-R9210] p 1954 N94-21158
Hilbert 90 for polynomial matrices
[CWI-AM-R9211] p 1954 N94-21159
On the optimality of FCFS for networks of multi-server queues
[CWI-BS-R9235] p 1944 N94-21160
Optimization of static traffic allocation policies
[CWI-BS-R9302] p 1930 N94-21161
Fourier calculus on evolutionary trees
[CWI-BS-R9234] p 1954 N94-21231
N parallel queueing systems with server breakdown and repair
[CWI-BS-R9236] p 1944 N94-21232
Optimization of fixed time polling schemes
[CWI-BS-R9237] p 1945 N94-21233
Optimal repairman assignment in two maintenance models which are equivalent to routing models with early decisions
[CWI-BS-R9301] p 1930 N94-21234
Some experiences of solving 1-D semiconductor device equations on a matrix coprocessor by a domain decomposition method
[CWI-NM-R9304] p 1935 N94-21492
Butcher-Kuntzmann methods for nonstiff problems on parallel computers
[CWI-NM-R9305] p 1935 N94-21493
CMIFed: A presentation environment for porta ble hypermedia documents
[CWI-CS-R9305] p 2044 N94-21494
Procedural dynamic semantics, verb-phrase ellipsis, and presupposition
[CWI-CS-R9311] p 1914 N94-21495
Reasoning about update logic
[CWI-CS-R9312] p 1914 N94-21496
Mathematical theory of thermodynamics of computation
[CWI-CS-R9251] p 2038 N94-21533
MINIFOLD: A kernel for a MANIFOLD-like coordination language
[CWI-CS-R9252] p 1915 N94-21534
Structured multimedia authoring
[CWI-CS-R9304] p 2044 N94-21535
The Amsterdam hypermedia model: Extending hypertext to support real multimedia
[CWI-CS-R9306] p 2045 N94-21536
A lower bound on wait-free counting
[CWI-CS-R9307] p 1915 N94-21537
Uniform self-stabilizing leader election. Part 1: Complete graph protocols
[CWI-CS-R9308-PT-1] p 1935 N94-21549
Changing preferences
[CWI-CS-R9310] p 1915 N94-21551
A project on parameter identification in reaction kinetics
[CWI-NM-R9301] p 1682 N94-21574
A note on singularities caused by the hydrodynamic dispersion tensor
[CWI-NM-R9302] p 1803 N94-21575
Comparing quasi-Newton methods for solving sparse interface problems
[CWI-NM-R9303] p 1959 N94-21576
Tandem queues with deterministic service times
[CWI-BS-R9238] p 1946 N94-21577
Termination and confluence of rule execution
[CWI-CS-R9309] p 1916 N94-21587
Local uniform grid refinement and brine transport in porous media with inhomogeneities
[CWI-NM-R9224] p 1803 N94-21609
Parallelizing a highly vectorized multigrid code with zebra relaxation
[CWI-NM-R9225] p 1935 N94-21610
Numerical multigrid software (MGD5M): A parallel multigrid code with a twisted ILLU-relaxation
[CWI-NM-R9226] p 1916 N94-21611
A package for long integer arithmetic on the Cray Y-MP
[CWI-NM-R9227] p 1916 N94-21612

CENTRAL INST. OF AVIATION MOTORS, MOSCOW (RUSSIA).
Cryogenic propellant rocket engine problems p 1668 N94-20076

CENTRE D'ETUDES DE GRAMAT (FRANCE).
Hypervelocity impact studies at CEG: Experimental and numerical capabilities p 1664 N94-21397

CENTRE D'ETUDES DE LIMEIL-VALENTON, VILLENEUVE SAINT-GEORGES (FRANCE).
Molecular equilibria and condensation sequences in carbon rich gases p 2083 N94-20756

CENTRE D'ETUDES ET DE RECHERCHES, TOULOUSE (FRANCE).
Orbital debris and micrometeoroids: LDEF and Mir data p 1659 N94-21368
Aragatz project samples experiment/MAPOL (polymer materials) experiment: Postflight expert evaluation p 1660 N94-21376
Effect of geostationary environment constituents on secondary electron emission rates p 1661 N94-21382

CENTRE NATIONAL D'ETUDES SPATIALES, TOULOUSE (FRANCE).
Comparative hypsometric analysis of both Earth and Venus topographic distributions p 2108 N94-20722
Fifth International Symposium on Materials in a Space Environment
[ISBN-2-85-428293-0] p 1659 N94-21367
Flight and laboratory testing of materials in low Earth orbit p 1659 N94-21369
Results of the post flight analyses on system materials for the LDEF-FRECOPA experiment p 1659 N94-21371
Residual atmosphere in the FRECOPA experiment and degassing of materials p 1660 N94-21374
Thermal control coatings p 1664 N94-21400

CENTRE NATIONAL DE LA RECHERCHE SCIENTIFIQUE, ODEILLO (FRANCE).
High temperature simulation chambers. Physico-chemical and thermal effect of atmospheric reentry on ceramic materials p 1653 N94-21404
A method of measuring the thermoradiative properties of ceramic materials in a space environment p 1665 N94-21405

CENTRE NATIONAL DE LA RECHERCHE SCIENTIFIQUE, PARIS (FRANCE).
Two-dimensional perception based on a laser rangefinder p 1786 N94-22202

CHICAGO UNIV., IL.
Wavelength dispersive analysis with the synchrotron x ray fluorescence microprobe p 1685 N94-20717
Petrography and origin of refractory inclusions from the Murray and Murchison C2 chondrites p 2084 N94-20770
Fe/Mn in olivine of carbonaceous meteorites p 2084 N94-20788
The x ray microprobe determination of chromium oxidation state in olivine from lunar basalt and kimberlitic diamonds p 1686 N94-20807
Microanalysis of iron oxidation state in iron oxides using X Ray Absorption Near Edge Structure (XANES) p 1686 N94-20808
Diffusion-controlled magnesium isotopic fractionation of a single crystal forsterite evaporated from the solid state p 1686 N94-20855
Trace element compositions of spinel-rich refractory inclusions from the Murchison meteorite p 2086 N94-20897
Chemical zoning and diffusion of Ca, Al, Mn, and Cr in olivine of springwater pallasite p 2086 N94-20902

CHICAGO UNIV. HOSPITALS AND CLINICS, IL.
Tambo Quemado: Extraordinary concentrations of REE and refractory trace elements caused by artificial heating p 1684 N94-20667

CHINESE ACADEMY OF GEOLOGICAL SCIENCES, BEIJING.
Shock attenuation at the Slate Islands revisited p 1863 N94-20887

CHRISTOPHER NEWPORT COLL., NEWPORT NEWS, VA.
Shielding from space radiations
[NASA-CR-194683] p 1895 N94-20063
Optical and transport properties of metallic and semiconductor nanostructures
[AD-A271716] p 2018 N94-20554
An ASIC memory buffer controller for a high speed disk system p 1754 N94-21089

CINCINNATI UNIV., OH.
Polymer gels as precursors to high-performance materials
[AD-A270937] p 1699 N94-20046
Structural similitude and design of scaled down laminated models
[NASA-CR-194687] p 1673 N94-20172
Microstructure evolution in the presence of constraints and implications on the properties of Mg-Li and Nb-Al constraints
[AD-A272088] p 1674 N94-20623
Surface electrochemistry of metals
[AD-A272913] p 1691 N94-21245

CITY UNIV. OF NEW YORK, FLUSHING.
The missing impact craters on Venus p 2119 N94-20782

CIUDAD UNIV., MEXICO CITY (MEXICO).
Modelling the gravity and magnetic field anomalies of the Chicxulub crater p 1862 N94-20668

CLARKSON UNIV., POTSDAM, NY.
Two-dimensional nonlinear Schrodinger equations and their properties
[AD-A272184] p 1952 N94-20923

CLEMSON UNIV., SC.
Proceedings of the 8th International Symposium on Applications of Ferroelectrics
[AD-A270679] p 1749 N94-20012
Three-wave resonant interaction in a thin layer
[AD-A272331] p 1994 N94-21039
Intelligent processing of ferroelectric thin films
[AD-A272518] p 1705 N94-21416
Low Reynolds-number turbulent boundary layers
[AD-A272011] p 1803 N94-21459

COLLEGE OF AERONAUTICAL ENGINEERING, RISALPUR CANTT (PAKISTAN).
Impact of copper vapour contamination on argon arcs p 1994 N94-21053

COLLEGE OF WILLIAM AND MARY, WILLIAMSBURG, VA.
Incongruity, incongruity resolution, and mental states: The measure and modification of situational awareness and control
[NASA-CR-194568] p 1893 N94-20168

COLOGNE UNIV. (GERMANY).
Intrusion of stratospheric ozone in the troposphere through tropopause folding and cold air droplets
[REPT-87] p 1851 N94-20154
Interactions of free modes, tides, and gravity waves in the middle atmosphere
[REPT-84] p 1855 N94-20155
Radiation of plasma wave wings through an electrodynamic tether satellite system with any sharp angle geometry
[REPT-85] p 1993 N94-20156
Synoptic observations of near surface processes of an insolated ice-dust body under space conditions: The case of KOSI 9 and 10 p 2084 N94-20827
COLORADO SCHOOL OF MINES, GOLDEN.
A Kirchhoff approach to seismic modeling and prestack depth migration
[AD-A271010] p 1854 N94-19820
Surface science at the solid liquid interface
[AD-A271422] p 1678 N94-19839
COLORADO STATE UNIV., FORT COLLINS.
Materials processing and manufacturing technologies for Diamond Substrate MultiChip Modules (DSMCM)
[AD-A271011] p 2011 N94-19821
Clouds: Their prediction and simulation
[AD-A271161] p 1864 N94-19900
Characterization of Minnesota lunar simulant for plant growth p 1897 N94-20665
Bridging faults in BiCMOS circuits p 1756 N94-21105
Faulty behavior of asynchronous storage elements p 1757 N94-21108
Electrochemical synthesis of ultrathin film composite membranes
[AD-A272721] p 1681 N94-21168
Detection of feed-through faults in CMOS storage elements p 1766 N94-21721
Behavior of faulty double BJT BiCMOS logic gates p 1767 N94-21727
Spectral variation of scattering and absorption by cirrus p 1876 N94-22321
Spectral emissivity of cirrus clouds p 1876 N94-22322
Vertical velocity in cirrus case obtained from wind profiler p 1878 N94-22330
Mesoscale simulations of the November 25-26 and December 5-6 cirrus cases using the RAMS model p 1878 N94-22331
Investigation of the effects of the macrophysical and microphysical properties of cirrus clouds on the retrieval of optical properties: Results for FIRE 2 p 1880 N94-22339
Extinction efficiencies from DDA calculations solved for finite circular cylinders and disks p 1880 N94-22340
COLORADO UNIV., BOULDER.
Laboratory studies of low temperature rate coefficients: The atmospheric chemistry of the outer planets
[NASA-CR-193485] p 1972 N94-20130
Automatic AVHRR image navigation software
[NASA-CR-194802] p 1643 N94-20148
Coherent lidar design and performance verification
[NASA-CR-193813] p 1816 N94-20341
The distribution of ground ice on Mars p 2090 N94-20394
Signal processing in the linear statistical model
[AD-A272114] p 1736 N94-20570
Experiments on technology mapping using different cell libraries p 1758 N94-21118
Mars atmosphere loss and isotopic fractionation by solar-wind-induced sputtering and photochemical escape p 2144 N94-21672
VVNRS: Variable phenomena in VV Cephei
[NASA-CR-194731] p 2056 N94-21835
Microphysical properties of the November 26 cirrus cloud retrieved by Doppler radar/IR radiometer technique p 1873 N94-22304
Lidar and radar derived cirrus microphysical properties for the 26 November 1991 case study p 1873 N94-22305
CO2 lidar observations of Mount Pinatubo debris: FIRE 2 and longer-term measurements p 1876 N94-22323
COLORADO UNIV., COLORADO SPRINGS.
Flow transition with 2-D roughness elements in a 3-D channel p 1806 N94-21466
COLORADO UNIV., DENVER.
Optimal resolution in maximum entropy image reconstruction from projections with multigrid acceleration p 1955 N94-21465
Multilevel methods for transport equations in diffusive regimes p 1955 N94-21467
COLUMBIA UNIV., NEW YORK, NY.
High-energy astrophysics: A theoretical analysis of thermal radiation from neutron stars
[NASA-CR-194808] p 2055 N94-20952
Scanning tunneling microscopy investigations of metal dichalcogenide materials
[AD-A272910] p 2027 N94-21242
Dust content of a hydrogen rich, low surface brightness galaxy and the luminosity history of 3C273
[NASA-CR-194705] p 2056 N94-21779
Modeling bristle lift-off in idealized brush seal configurations p 1655 N94-21797
A High Resolution Liquid Xenon Imaging Telescope for 0.3-10 MeV Gamma Ray Astrophysics: Construction and Initial Balloon Flights
[NASA-CR-194709] p 2056 N94-22281
The polarization sensitivity of the liquid xenon imaging telescope p 2056 N94-22282
COMMISSARIAT A L'ENERGIE ATOMIQUE, GRENOBLE (FRANCE).
Fibre pigtailed silicon based low cost passive optical components, appendix 5 p 1989 N94-21599
COMMISSARIAT A L'ENERGIE ATOMIQUE, SACLAY (FRANCE).
Pair plasmas in the galactic center region and in Nova Muscae p 2009 N94-22691
Spiral Alfven instability in accretion disks p 2010 N94-22698
COMMONWEALTH SCIENTIFIC AND INDUSTRIAL RESEARCH ORGANIZATION, SYDNEY (AUSTRALIA).
The CSIRO 9-level atmospheric general circulation model
[CSIRO-TP-26] p 1855 N94-20256
COMMUNICATIONS RESEARCH CENTRE, OTTAWA (ONTARIO).
Software implementation of an adaptive digital automatic level control p 1773 N94-22124
Timing recovery in the channel processor of a digital group demodulator p 1780 N94-22169
The influence of lowpass filtering and the effects of fading on the group demodulation of QPSK signals p 1746 N94-22170
Characterization and modelling of extremely high frequency enclosures p 1782 N94-22177
Manual design technique for broadband passive thin-film attenuators using the Smith chart p 1782 N94-22178
MHMIC: Technology for the integration of microwave sub-assemblies p 1785 N94-22199
Comparison of theoretical and simulated performance results for sloppy-slotted Aloha signaling p 1746 N94-22204
COMMUNICATIONS SATELLITE CORP., CLARKSBURG, MD.
Method of orienting a synchronous satellite
[CA-PATENT-1,305,772] p 1658 N94-21041
Non-destructive semiconductor wafer probing system using laser pulses to generate and detect millimeter-wave signals
[CA-PATENT-APPL-SN-2,020,73] p 1760 N94-21178
COMPUTER RESOURCE MANAGEMENT, INC., PLEASANTVILLE, NJ.
Handbook. Volume 2: Digital systems validation. Chapter 18: Avionic data bus integration technology
[DOT/FAA/CT-88/10-VOL-2] p 1647 N94-20343
COMPUTER SCIENCES CORP., BELTSVILLE, MD.
Predicting scheduling success p 1932 N94-21334
Generating and evaluating alternate schedules p 1933 N94-21336
COMPUTER SCIENCES CORP., HAMPTON, VA.
Software systems used for unstructured grid generation at NASA Langley p 1918 N94-22351
Unstructured surface grid generation p 1920 N94-22366
COMPUTER SCIENCES CORP., LANHAM, MD.
The NCC project: A quality management perspective p 1828 N94-21324
Let your fingers do the walking: The projects most invaluable tool p 1922 N94-21325
Software metrics: The key to quality software on the NCC project p 1922 N94-21326
NCCDS configuration management process improvement p 1931 N94-21327
COMPUTER SCIENCES CORP., MOUNTAIN VIEW, CA.
Superpatch
[NASA-CR-177627] p 1914 N94-21489
Higher order Bezier circles
[NASA-CR-177633] p 1897 N94-21784
Achieving high data reduction with integral cubic B-splines
[NASA-CR-177628] p 1966 N94-21881
CONCORDIA UNIV., MONTREAL (QUEBEC).
Avoiding and tolerating latency in large-scale next-generation shared-memory multiprocessors p 1753 N94-21081
A simple modern correctness condition for a space-based high-performance multiprocessor p 1766 N94-21718
Estimation of AR signal patterns using competitive neural networks p 1744 N94-22102
Segmentation and fitting by residual consensus p 1771 N94-22109
A shared buffer memory switch with maximum queue and minimum allocation p 1773 N94-22119
A one-shot access scheme for a multicast switch p 1773 N94-22120
Improvements in antenna coupling path algorithms for aircraft EMC analysis p 1745 N94-22126
RCS of ships and aircraft at HF frequencies p 1745 N94-22128
The local measurement and global interpretation of 3D motion field generated by several moving objects from range image sequences p 1777 N94-22146
CREIR: A multiaccess protocol for on-board processing satellite systems p 1780 N94-22168
A neural network approach to the maximum flow problem p 1783 N94-22183
Throughput and blocking in circuit-switched interconnection networks p 1784 N94-22189
Throughput, blocking, and interference in packet radio networks p 1746 N94-22190
Neural networks for optimum routing in packet-switched communications networks p 1746 N94-22205
A robust adaptive control design for flexible joint manipulators p 1790 N94-22230
On the capacity of (T,U) permutation decoding method p 1792 N94-22245
CONTINUOUS ELECTRON BEAM ACCELERATOR FACILITY, NEWPORT NEW, VA.
Qualitative and quantitative aspects of the QCD theory of elastic form factors
[DE93-040864] p 2038 N94-21513
Production, collection and utilization of very long-lived heavy charged leptons
[DE93-040867] p 1977 N94-22009
CORNELL UNIV., ITHACA, NY.
Absolute total and one and two electron transfer cross sections for Ar(8+) on Ar as a function of energy
[DE93-040283] p 1970 N94-19870
Energy gain spectroscopic study of Ar(q+)-Ar collisions at 40 qeV
[DE93-040284] p 1970 N94-19871
Rotorcraft noise: Status and recent developments
[NASA-CR-194761] p 1967 N94-20523
Rotational spectrum of a dark state in 2-fluoroethanol using microwave/radiofrequency-infrared multiple resonance
[AD-A272101] p 1817 N94-20583
High resolution infrared spectroscopy of formamide and deuterated formamide in a molecular beam
[AD-A271986] p 1973 N94-20618
High resolution infrared spectroscopy of cyclobutane: A study of vibrational mode coupling involving large amplitude, low frequency modes
[AD-A271987] p 1973 N94-20619
Earth-based measurement of lunar topography using delayed radar interferometry p 2119 N94-20787
Is there uniformitarian or catastrophic tectonics on Venus? p 2129 N94-20839
A response to Cheriton and Skeen's criticism of casual and totally ordered communication
[AD-A271486] p 1912 N94-21300
Electron emissions in low energy Ar(q+)-Ar collisions
[DE93-040285] p 1974 N94-21543
Briny lakes on early Mars? Terrestrial intracrater playas and Martian candidates p 2145 N94-21675
Applications of correlator chips in radio science p 1763 N94-21695

D

DANISH METEOROLOGICAL INST., COPENHAGEN.
Narsarsuaq Geophysical Observatory: Magnetic results, 1985 - 1990
[DATA-REPT-93-1] p 1856 N94-20607
Magnetic results 1991: Brorfelde, Godhavn, Thule and Narsarsuaq
[DATA-REPT-92-3] p 1856 N94-20608
Thule Geophysical Observatory: Magnetic results 1985 - 1990
[DATA-REPT-92-4] p 1857 N94-20609
DARTMOUTH COLL., HANOVER, NH.
Ancient Martian valley genesis and paleoclimatic inference: The present as a key to the past p 2142 N94-21661
A multiresolution wavelet representation in two or more dimensions p 1925 N94-22456
DASSAULT AVIATION, BALGNAC (FRANCE).
Material properties and behavior during simulated atmospheric reentry p 1665 N94-21408
DAYTON UNIV., OH.
Night vision goggle model F4949 preflight adjustment/assessment procedures
[AD-A271079] p 1895 N94-19935

A study of the induction heating of organic composites
[AD-A272657] p 1675 N94-21187

DAYTON UNIV. RESEARCH INST., OH.
Weldalite (tm) 049 (Al 2095-T8): Anisotropy effects at cryogenic conditions
[AD-A272658] p 1691 N94-21188

DEFENCE RESEARCH AGENCY, FARNBOROUGH (ENGLAND).
A new procedure for orbit determination based on three lines of sight: Angles only
[AD-A272937] p 1652 N94-21224
Approximation to sound radiation and scattering by simply supported layered cylinder
[AD-A272984] p 1967 N94-21306

DEFENCE RESEARCH ESTABLISHMENT ATLANTIC, DARTMOUTH (NOVA SCOTIA).
Asbestos characterization using scanning electron microscopy/light element x ray spectrometry
[AD-A271611] p 1681 N94-21241

DEFENCE RESEARCH ESTABLISHMENT, OTTAWA (ONTARIO).
CFAR processing for airborne pulse-Doppler radars
p 1745 N94-22142
A digital demodulation scheme for use in a high dynamic range radar system p 1745 N94-22144
An overview of synthetic aperture radar signal processing techniques p 1745 N94-22159
Target angular motion and its effects on simulated SSAR ship images p 1745 N94-22161
The application of sample vector selection to adaptive nulling: Performance comparison for techniques combining Gram-Schmidt orthogonalization with averaging
p 1747 N94-22234

DEFENCE RESEARCH ESTABLISHMENT VALCARTIER (QUEBEC).
Marine boundary layer model evaluation by using a height gain measurement technique in the interference region p 1777 N94-22145
Thin-film fabrication of Pb-doped BiSrCaCuO superconductor p 1781 N94-22176
Memory based vision: A new concept
p 1790 N94-22228
A four-band infrared data acquisition facility for signal processing development p 1791 N94-22235
Trajectory computations for an improved cinetheodolite tracking system p 1791 N94-22236
Signal processing and target discrimination algorithms for a rosette scan tracker p 1747 N94-22237
Radar imaging of moving targets
p 1747 N94-22238

DEFENSE SYSTEMS MANAGEMENT SCHOOL, FORT BELVOIR, VA.
A description of psychological type at the Defense Systems Management College, 1993 edition
[AD-A271612] p 1894 N94-21237

DELAWARE UNIV., NEWARK.
Chemistry of the burning surface
[AD-A272725] p 1681 N94-21181

DENVER UNIV., CO.
Physical chemistry of energetic nitrogen compounds
[AD-A271819] p 1712 N94-20625

DEPARTMENT OF COMMUNICATIONS, OTTAWA (ONTARIO).
Visibility considerations in frequency sharing with low Earth orbit satellites p 1746 N94-22187
Inclined orbits and interference to stationary service and to stationary service by satellite p 1653 N94-22188

DEPARTMENT OF DEFENSE, ARLINGTON, VA.
Audit report. Navy's aircraft structural life surveillance program data recorders
[AD-A270391] p 1645 N94-20040

DEPARTMENT OF DEFENSE, WASHINGTON, DC.
Listing of approved recurring information requirements
[AD-A271673] p 2042 N94-20919

DEPARTMENT OF ENERGY, MORGANTOWN, WV.
Performance calculations and research direction for a water enhanced regenerative gas turbine cycle
[DE93-019866] p 1826 N94-21983

DEPARTMENT OF ENERGY, WASHINGTON, DC.
Superconductivity Technology Program for Electric Power Systems: Proceedings
[DE93-040074] p 2011 N94-19825
Research in progress: FY 1992
[DE94-000410] p 1836 N94-20936
Advanced Energy Projects, FY 1993
[DE94-000539] p 1847 N94-21755

DEPARTMENT OF THE NAVY, WASHINGTON, DC.
Suppression of relaxation oscillations in flashpumped, two-micron tunable solid state lasers
[AD-D015928] p 1814 N94-19800
High melting amino aromatic nitrate esters
[AD-D015929] p 1711 N94-19801
Corrosion inhibition in high temperature environment
[AD-D015910] p 1698 N94-19830
Metrics for specifying and/or testing neural networks statement of government interest
[AD-D015946] p 1938 N94-19843
Electrode array electromagnetic velocimeter
[AD-D015950] p 1806 N94-19882
Process to fabricate thick coplanar microwave electrode structures
[AD-D015913] p 1748 N94-19892
Phthalonitrile prepolymer as high temperature sizing material for composite fibers
[AD-D015912] p 1672 N94-20010
Machinable oxide ceramic
[AD-D015927] p 1699 N94-20017
Tunable laser frequency stabilizing system
[AD-D015904] p 1815 N94-20055
Optical encoding of imaging data
[AD-D015915] p 1984 N94-20056
Silver lined ceramic vessel
[AD-D015917] p 1700 N94-20057
Optical switching devices
[AD-D015918] p 1984 N94-20059
Resonantly pumped, erbium-doped, GSGG, 2.8 micron, solid state laser with energy recycling and high slope efficiency
[AD-D015920] p 1815 N94-20060
Monopropellant aqueous hydroxyl ammonium nitrate/fuel
[AD-D015922] p 1712 N94-20061
Metal-glass composite field-emitting arrays
[AD-D015942] p 1673 N94-20064
Fiber optic Michelson sensor and arrays with passive elimination of polarization fading and source feedback isolation
[AD-D015944] p 1984 N94-20065
Thermal dilation fiber optical flow sensor
[AD-D015926] p 1797 N94-20094
Lightweight battery electrode and method of making it
[AD-D015895] p 1749 N94-20120
Thrust expansion engine
[AD-D015896] p 1669 N94-20121
N,N'-bis(4,4,4-trinitro butyryl) hydrazine
[AD-D015897] p 1712 N94-20122
All-weather precision landing system for aircraft in remote areas
[AD-D015924] p 1643 N94-20197
Target motion detecting impulse Doppler radar system
[AD-D015898] p 1717 N94-20198
Resistive gate magnetic field sensor
[AD-D015923] p 1749 N94-20199
Plasma chemical vapor deposition of halide glasses
[AD-D015933] p 1701 N94-20331
Atmospheric moisture collection device
[AD-D015935] p 1865 N94-20332
Photonic electromagnetic field sensor apparatus
[AD-D015938] p 1717 N94-20333
Photonic electromagnetic field sensor apparatus
[AD-D015939] p 1718 N94-20334
Monocrystalline germanium film on sapphire
[AD-D015925] p 2017 N94-20348
Volatile CVD precursors based on copper alkoxides and mixed group 2A-copper alkoxides
[AD-D015930] p 1701 N94-20349
Layered thin-edged field-emitter device
[AD-D015932] p 1751 N94-20350
High-power gas switch with hydride electrodes
[AD-D015956] p 1751 N94-20354
On demand, non-halon, fire extinguishing systems
[AD-D015957] p 1714 N94-20355
Disengagable adapter for an optical fiber connector
[AD-D015959] p 1822 N94-20356
M-dimensional computer memory with M-1 dimensional hyperplane access
[AD-D015960] p 1898 N94-20357
System for solving Boolean equations using optical lookup tables
[AD-D015962] p 1951 N94-20358
Heat regenerative external combustion engine
[AD-D015965] p 1824 N94-21274
Wire assembly for electrically conductive circuits
[AD-D015966] p 1761 N94-21275
Light update notification mechanism for shared data structures
[AD-D015967] p 2043 N94-21276
Self locking set screw
[AD-D015969] p 1824 N94-21277
Recording system using multiplexed inputs to a multichannel recorder
[AD-D015971] p 1808 N94-21278
Mode transition matrix measuring system
[AD-D015973] p 1987 N94-21279

DEPARTMENT OF VETERANS AFFAIRS, WASHINGTON, DC.
Journal of rehabilitation research and development, volume 30, number 1, 1993
[AD-A272956] p 1893 N94-21613

DEPAUW UNIV., GREENCASTLE, IN.
Geologic mapping of Harmakhis and Reull Valles region, Mars: Evidence for multiple resurfacing and drainage events p 1844 N94-20705

DESERT RESEARCH INST., RENO, NV.
Cirrus microphysics observations made during FIRE 2: Small particles, high concentrations, and probe comparisons p 1871 N94-22294
Importance of aggregation and small ice crystals in cirrus clouds, based on observations and an ice particle growth model p 1879 N94-22336
Are tropical cirrus brighter than mid-latitude cirrus?
p 1881 N94-22343

DEUTSCHE AIRBUS G.M.B.H., BREMEN (GERMANY).
Experiments with a fluid deicing system for cleaning laminar wings p 1640 N94-22601
Riblet boundary layer measurements of an A-310 fuselage with Pitot combs p 1640 N94-22605

DEUTSCHE FORSCHUNGS- UND VERSUCHSANSTALT FUER LUFT- UND RAUMFAHRT, OBERPFAFFENHOFEN (GERMANY).
Goniospectrometric properties of a white standard
p 1684 N94-20664

DEUTSCHE FORSCHUNGSANSTALT FUER LUFT- UND RAUMFAHRT, BERLIN (GERMANY).
The High Resolution Stereo Camera (HRSC) for the Lunar Scout 1 Mission p 1813 N94-20650

DEUTSCHE FORSCHUNGSANSTALT FUER LUFT- UND RAUMFAHRT, BRUNSWICK (GERMANY).
Parameter estimation with cost function of second order in output-error-problem
[DLR-FB-92-38] p 1964 N94-21139

DEUTSCHE FORSCHUNGSANSTALT FUER LUFT- UND RAUMFAHRT, COLOGNE (GERMANY).
German space experiments on Spacelab D-2 and Eureca-1 to investigate atomic oxygen interaction with materials p 1662 N94-21390

DEUTSCHE FORSCHUNGSANSTALT FUER LUFT- UND RAUMFAHRT, GOETTINGEN (GERMANY).
Numerical investigation of laminar-turbulent transition in two- and three-dimensional boundary layers
[DLR-FB-92-36] p 1800 N94-20533
Description and assessment of a new Optical Pressure Measurement System (OPMS) demonstrated in the high speed wind tunnel in Goettingen (Germany)
[DLR-FB-92-24] p 1651 N94-21280
Surface hot film measurements at ATTAS laminar glove p 1639 N94-22598

DEUTSCHE FORSCHUNGSANSTALT FUER LUFT- UND RAUMFAHRT, MUNICH (GERMANY).
Documents on the history of aeronautical and space research in Germany, 1900 - 1970
[DLR-MITT-92-08] p 2152 N94-20543

DEUTSCHE FORSCHUNGSANSTALT FUER LUFT- UND RAUMFAHRT, OBERPFAFFENHOFEN (GERMANY).
A motion extraction method for synthetic aperture radars
[DLR-FB-92-31] p 1742 N94-22279
A documentation of icing relevant cloud physical parameters on horizontal soundings of stratiform clouds (continuation)
[DLR-MITT-92-10] p 1871 N94-22280

DEUTSCHE LUFTHANSA A.G., HAMBURG (GERMANY).
Measurement of the influence of deicing liquids on aircraft aerodynamics p 1640 N94-22602

DIGITAL EQUIPMENT CORP., CAMBRIDGE, MA.
Crystal ball gazing p 1925 N94-22477

DORNIER LUFTFAHRT G.M.B.H., FRIEDRICHSHAFEN (GERMANY).
Hot wire anemometry: A versatile instrumentation used for predevelopment studies and flight testing of the Do-328 aircraft p 1640 N94-22604

DUKE UNIV., DURHAM, NC.
Uncertainty limited atomic position measurement using optical fields
[AD-A271013] p 1970 N94-19822
A microscopic theory of quantum optics and new photon-locked bistable states
[AD-A271250] p 1983 N94-19901
Acoustic radiation damping of flat rectangular plates subjected to subsonic flows
[NASA-TM-109382] p 1967 N94-20211
High-resolution numerical methods for compressible multi-phase flow in hierarchical porous media
[DE94-000740] p 1799 N94-20351
Modeling the response of ecosystems to CO2 and climate change
[DE94-000748] p 1852 N94-21787

E

EAST CAROLINA UNIV., GREENVILLE, NC.
The role of axon-Schwann cell interactions in nervous system ionic homeostasis
[AD-A270936] p 1890 N94-20045

EAST CHINA INST. OF TECH., NANJING.
On the relationship between spectral domain approach and method of lines p 1794 N94-22254
ECOLE CENTRALE DE LYON (FRANCE).
Two-point laser Doppler velocimetry measurements of length-turbulent scales
[ECL-92-12] p 1801 N94-20542
Study of the utilization of thin oxides in indium phosphides for the realisation of electron components
[ECL-92-38] p 2018 N94-20593
The flow of gas across the piston-segments-cylinder interface
[ECL-92-40] p 1824 N94-20594
Two dimensional simulation of the electric arc behavior in a cut-off device
[ECL-92-41] p 1751 N94-20595
Finite element numerical simulation of three dimensional turbulent flows with dispersion: Eulerian and Lagrangian approaches
[ECL-92-42] p 1801 N94-20597
Surface treatment of InP and contribution to the optimization of the InP(p)/InP(p) regrown interfaces grown by GSMBE
[ECL-92-48] p 2018 N94-20598
Theoretical and experimental study of the winding of a thin plastic film: The role of aerodynamic effects
[ECL-93-04] p 1703 N94-20599
Hydrostatic/nonhydrostatic comparison with the MERCURE code on orographic flows
[ETN-93-94603] p 1866 N94-20600
Modeling of particle dispersion in a stationary isotropic homogeneous turbulence by large scale numerical simulation
[ETN-93-94604] p 1801 N94-20601
ECOLE NORMALE SUPERIEURE, PARIS (FRANCE).
Satellite validation of GCM-simulated annual cycle of the Earth radiation budget and cloud forcing p 1860 N94-22267
ECOLE POLYTECHNIQUE, MONTREAL (QUEBEC).
Tests of logic spaces: A new strategy for certifying the accuracy of programs p 1772 N94-22116
Sorting network for the partial selection problem p 1773 N94-22121
VLSI design of a bit serial parallel processing 4 extender chip for M-path convolutional decoding p 1775 N94-22132
VLSI design of a parallel video output interface p 1778 N94-22153
Numerical method for computing the electric field produced by a microwave beam in a stratified medium p 1746 N94-22197
An approach to the estimation of ground structure and aircraft motion from aerial image sequences p 1789 N94-22226
Adaptive decoding of convolutional codes p 1793 N94-22246
Bidirectional algorithms for the decoding of convolutional codes over memoryless channels p 1793 N94-22247
ECOLE POLYTECHNIQUE, PALAISEAU (FRANCE).
Langmuir microstructures and pulsar radio emission p 2007 N94-22678
EDGEWOOD ARSENAL, ABERDEEN PROVING GROUND, MD.
Documentation for PCDIST, a FORTRAN subroutine to calculate Pollack-Cuzzi scattering
[AD-A273070] p 1988 N94-21491
EG AND G ENERGY MEASUREMENTS, INC., IDAHO FALLS.
Superconducting property measurements in tape geometry
[DE93-018943] p 2014 N94-19970
EG AND G ENERGY MEASUREMENTS, INC., LAS VEGAS, NV.
X ray analysis of alpha mercuric iodide crystal structure and processing effects
[DE93-017620] p 2027 N94-21296
EG AND G ENERGY MEASUREMENTS, INC., LOS ALAMOS, NM.
Kinetic theory of runaway air-breakdown
[DE93-040731] p 1750 N94-20325
EG AND G ROCKY FLATS, INC., GOLDEN, CO.
Thermocapillary and arc phenomena in stainless steel welds
[DE94-000518] p 1821 N94-19859
EHRLICH ASSOCIATES, LEXINGTON, MA.
Diagnostics and methods for real-time laser microchemistry
[AD-A270871] p 1680 N94-20566
EIDGENOESSISCHE TECHNISCHE HOCHSCHULE, ZURICH (SWITZERLAND).
A long-term change of the AR/KR/XE fractionation in the solar corpuscular radiation p 2136 N94-20875
ELECTRONIC SYSTEMS DIV., HANSCOM AFB, MA.
Ground wave emergency network. Final operational capability. Environmental assessment for south central Montana relay node, site no. RN8C925MT
[AD-A267795] p 1716 N94-19964
ELECTRONICS RESEARCH LAB., SALISBURY (AUSTRALIA).
Design aspects and parametric characterisation of a neutral rare gas laser
[AD-A271100] p 1814 N94-19850
Planning process software: A user guide for the DMCA
[AD-A271252] p 1902 N94-19911
ELORET CORP., PALO ALTO, CA.
Theoretical research program to study chemical reactions in AOTV bow shock tubes
[NASA-CR-194710] p 1804 N94-22027
ELORET CORP., SUNNYVALE, CA.
Experimental investigation of nozzle/plume aerodynamics at hypersonic speeds
[NASA-CR-194628] p 1636 N94-20014
Computed potential energy surfaces for chemical reactions
[NASA-CR-194800] p 1679 N94-20169
ELSEVIER SCIENCE PUBLISHERS LTD., BARKING (ENGLAND).
Structural crashworthiness and failure
[AD-A270429] p 1828 N94-19815
The Seventh International Conference on Composite Structures, volume 25, numbers 1-4
[AD-A269961] p 1672 N94-20031
EMORY UNIV., ATLANTA, GA.
Dephasing processes in III-V semiconductors
[AD-A271677] p 2028 N94-21362
ENERGY RESEARCH CORP., DANBURY, CT.
Development of an electrochemical hydrogen separator
[DE93-019877] p 1683 N94-21984
ENGINEERING INST. OF CANADA, MONTREAL (QUEBEC).
Canadian Conference on Electrical and Computer Engineering, volumes 1 and 2
[ISBN-0-9694170-2-0] p 1770 N94-22101
ENVIRONMENTAL PROTECTION AGENCY, ANN ARBOR, MI.
Cold starting an alcohol-fueled engine with ultrasonic fuel atomization
[PB93-206597] p 1826 N94-22093
ENVIRONMENTAL RESEARCH INST. OF MICHIGAN, ANN ARBOR.
Long-range laser imaging
[AD-A273020] p 1817 N94-21253
EOETVOES LORAND UNIV., BUDAPEST (HUNGARY).
Some practicable applications of quadtree data structures/representation in astronomy p 1927 N94-22515
ERG INTERNATIONAL, INC., GOLDEN, CO.
Building integrated photovoltaic systems analysis
[DE93-018208] p 1846 N94-21298
ESSEX UNIV., COLCHESTER (ENGLAND).
Syntactic neural networks for natural language processing p 1941 N94-20254
ETA S.A., GRENCHEN (SWITZERLAND).
Lavet type stepping motors and associated controls p 1752 N94-20632
Test device for Lavet motors p 1752 N94-20633
EUROPEAN CENTRE FOR MEDIUM-RANGE WEATHER FORECASTS, READING (ENGLAND).
Use of satellite data for validation of operational forecast models and operational analyses p 1861 N94-22291
EUROPEAN SOUTHERN OBSERVATORY, GARCHING (GERMANY).
A distributed clients/distributed servers model for STARCAT p 2047 N94-22469
EUROPEAN SOUTHERN OBSERVATORY, MUNICH (GERMANY).
Restoration of HST images with missing data p 2057 N94-22439
Scientific computing in the 1990ies: An astronomical perspective p 2057 N94-22440
A low-cost vector processor boosting compute-intensive image processing operations p 1925 N94-22441
Archiving data from ground-based telescopes p 2046 N94-22442
GUIs in the MIDAS environment p 2047 N94-22449
The European Southern Observatory-MIDAS table file system p 2048 N94-22518
EUROPEAN SPACE AGENCY, PARIS (FRANCE).
Fourth International Toki Conference on Plasma Physics and Controlled Nuclear Fusion
[ESA-SP-351] p 2000 N94-22624
EUROPEAN SPACE AGENCY. EUROPEAN SPACE OPERATIONS CENTER, DARMSTADT (GERMANY).
The EXOSAT operational experience
[ESA-STM-248] p 1657 N94-20235
EUROPEAN SPACE AGENCY. EUROPEAN SPACE RESEARCH AND TECHNOLOGY CENTER, ESTEC, NOORDWIJK (NETHERLANDS).
Power standard
[ESA-PSS-02-10-VOL-1-ISSUE-] p 1669 N94-20241
Some results of the oxidation investigation of copper and silver samples flown on LDEF p 1660 N94-21375
Integrity and testing concerns of thermostructural materials p 1661 N94-21384
Materials evaluation at ESA/ESTEC p 1662 N94-21386
Columbus: Materials for 30 years habitability in space p 1662 N94-21387
Atomic oxygen fluence detector for Bremsat: Scientific and technical description p 1663 N94-21396
Toxicity of thermal degradation in a manned space environment p 1664 N94-21403
EUROPEAN SPACE RESEARCH LAB., NOORDWIJK (NETHERLANDS).
Micrometeorite pre-solar diamonds from Greenland cryoconite? p 2086 N94-20895
EUROPEAN SPACE RESEARCH ORGANIZATION, NOORDWIKJ (NETHERLANDS).
Measurements of the dielectric properties of simulated comet material as part of the KOSI 10 experiment p 2085 N94-20841
The EXOSAT database and archive p 2048 N94-22521
EVERGREEN HIGH SCHOOL, VANCOUVER, WA.
Distribution of small volcanic cones on the surface of Venus by size and elevation: Implications for differential deposition of volcanic features p 2110 N94-20731
EXETER UNIV. (ENGLAND).
A modular design for connectionist parsing p 1941 N94-20252

F

FEDERAL AVIATION ADMINISTRATION, ATLANTA, GA.
Next Generation Weather Radar (NEXRAD) Principal User Processor (PUP) Operational Test and Evaluation (OT/E)
[AD-A273075] p 1868 N94-21519
FEDERAL AVIATION ADMINISTRATION, OKLAHOMA CITY, OK.
ATC/pilot voice communications: A survey of the literature
[DOT/FAA/AM-93/20] p 1738 N94-21201
Factors associated with continuance commitment to FAA matrix teams
[DOT/FAA/AM-93/18] p 2040 N94-21626
FEDERAL AVIATION ADMINISTRATION, WASHINGTON, DC.
EDMS microcomputer pollution model for civilian airports and Air Forces bases: User's guide, supplement A
[AD-A271596] p 1851 N94-20948
FERMI NATIONAL ACCELERATOR LAB., BATAVIA, IL.
A search for new gauge bosons in (bar p)p collisions at square root of s equals 1.8 TeV in the dielectron decay mode
[DE93-019901] p 1969 N94-19813
Measurement of the B(+) and B(0) lifetimes
[DE93-019906] p 1969 N94-19814
A study of events with the highest total transverse energy in CDF
[DE93-019904] p 1978 N94-19972
The two-jet differential cross-section at CDF
[DE93-019905] p 1978 N94-19983
Thermal information regarding the cooldown and operation of liquid argon calorimeters
[DE93-019391] p 1807 N94-19987
Top search at the TEVATRON
[DE93-019392] p 1978 N94-19988
Jet shapes in hadron and electron colliders
[DE93-019386] p 1979 N94-20216
The cross section for the production of b(bar-b) pairs in p(bar p) collisions at the square root of s equals 1.8 TeV
[DE93-019900] p 1972 N94-20225
CsI and some new photocathodes
[DE93-019387] p 1750 N94-20314
Direct photon results from CDF
[DE93-019908] p 1980 N94-20317
Summary of the Hadronic Weak Interaction session
[DE94-000592] p 1975 N94-21775
Recent results on top, bottom and exotic physics at the Tevatron
[DE94-000578] p 1975 N94-21786
Measurement of the B meson and b quark cross-section in (-p)p collisions at the square root of s = 1.8 TeV using the exclusive decays B(+) and B(exp 0) yields J/psiK*(exp 0)
[DE93-019907] p 1975 N94-21806

Search for excited quarks in p(-p) collisions at the square root of s = 1.8 TeV
[DE93-019910] p 1975 N94-21840
The lepton charge asymmetry in the decay of W bosons produced in p(bar p) collisions at (radical)s = 1.8 TeV
[DE93-019903] p 1976 N94-21847
Measurement of the inclusive jet cross section in p(bar-p) collisions at CDF
[DE94-000581] p 1962 N94-21866
Recent Fermilab results on hadroproduction of heavy flavors
[DE94-000595] p 1976 N94-21867
Stability of beam in the Fermilab Main Injector
[DE94-000619] p 1982 N94-21934
Toward a QCD analysis of jet rates in deep-inelastic Muon-Proton scattering
[DE94-000618] p 1976 N94-21962

FIRST INST. OF OCEANOGRAPHY, QINGDAO (CHINA).
First discovery of the organic materials in deep-sea iron cosmic spherule p 1685 N94-20677

FLORIDA ATLANTIC UNIV., BOCA RATON.
The fluid mechanics of vortex cutting by a blade
[AD-A270932] p 1636 N94-20043

FLORIDA INST. OF TECH., MELBOURNE.
Model-based reasoning for power system management using KATE and the SSM/PMAD
[NASA-CR-194716] p 1671 N94-21882

FLORIDA STATE UNIV., TALLAHASSEE.
Simulating supersymmetry with ISAJET 7.0/ISASUSY 1.0
[DE93-018266] p 1969 N94-19804
Study of (+-)J Ising spin glasses via multicanonical ensemble
[DE93-018269] p 2016 N94-20285
Measurement of the strange quark distribution function in W(+) charm quark events
[DE93-018267] p 1973 N94-20474
Mechanical properties and reliability of semi-crystalline polymers
[AD-A271591] p 1704 N94-20946

FLORIDA UNIV., GAINESVILLE.
Chain propagation/step propagation polymerization chemistry. The preparation of solvent resistant well phase-separated thermoplastic elastomers
[AD-A271128] p 1699 N94-20016
A proposed methodology for combustion toxicology testing of combined halon replacement agent/jet fuel interaction
[AD-A272695] p 1681 N94-21165

FULL CIRCLE RESEARCH, INC., SAN MARCOS, CA.
CMOS gate array characterization procedures
[AD-A269943] p 2014 N94-20029

G

GALAXY SCIENTIFIC CORP., PLEASANTVILLE, NJ.
Handbook. Volume 3: Digital systems validation book plan
[DOT/FAA/CT-93/16-VOL-3] p 1647 N94-20053

GARRETT TURBINE ENGINE CO., PHOENIX, AZ.
Oxidation resistant protective coating system for gas turbine components and process for penetration thereof
[CA-PATENT-1,294,155] p 1704 N94-21143

GENERAL ACCOUNTING OFFICE, WASHINGTON, DC.
NASA property: Improving management of government equipment provided to contractors. Report to the Chairman, Subcommittee on Investigations and Oversight, Committee on Science, Space, and Technology, House of Representatives
[GAO/NSIAD-93-191] p 2039 N94-20206
NASA procurement: Planning for pilot test of new procurement procedures is adequate. Report to the Chairman, Committee on Governmental Affairs, US Senate
[GAO/NSIAD-94-67] p 2039 N94-20236
Test and evaluation: DOD has been slow in improving testing of software-intensive systems
[AD-A271541] p 1908 N94-20917

GENERAL ATOMIC CO., SAN DIEGO, CA.
Transient thermal analysis of cryocondensation pump for JET
[DE93-040372] p 1992 N94-20003
Beta-limiting instabilities in D3-D discharges with large bootstrap current
[DE93-015476] p 1993 N94-20326
Enhanced confinement regimes and control technology in the DIII-D tokamak
[DE93-019004] p 1998 N94-22039
Access to D3-D data located in multiple files and multiple locations
[DE94-001104] p 2045 N94-22404

GENERAL ATOMICS TECHNOLOGIES CORP., SAN DIEGO, CA.
Use of open systems for control, analysis, and data acquisition of the DIII-D tokamak
[DE94-001101] p 1998 N94-22089

GENERAL ELECTRIC CO., MOORESTOWN, NJ.
MGGHAT: Elliptic PDE software with adaptive refinement, multigrid and high order finite elements p 1956 N94-21470

GENERAL ELECTRIC CO., SCHENECTADY, NY.
Representation and recognition with algebraic invariants and geometric constraint models
[AD-A271395] p 1949 N94-19838
Benefits of thread rolling process to the stress corrosion cracking and fatigue resistance of high strength fasteners
[DE93-040438] p 1833 N94-22001
Measurement of thermal-hydraulic parameters in two-phase flow using flow visualization image analysis
[DE93-006255] p 1805 N94-22269

GENERAL MOTORS CORP., INDIANAPOLIS, IN.
Flow interaction experiment. Volume 1: Aerothermal modeling, phase 1
[NASA-CR-189192-VOL-1] p 1648 N94-21582
Flow interaction experiment. Volume 2: Aerothermalmodeling, phase 2
[NASA-CR-189192-VOL-2] p 1648 N94-21583

GEO ECO ARC RESEARCH, LA CANADA, CA.
Global blackout following the K/T Chicxulub impact: Results of impact and atmospheric modeling p 1854 N94-20698

GEOLOGICAL AND GEOPHYSICAL SURVEYS, FAIRBANKS, AK.
Cryoplanation terraces of interior and western Alaska p 2091 N94-20396

GEOLOGICAL SURVEY, DENVER, CO.
U-Pb isotopic ages and characteristics of ancient (greater than 4.0 Ga) lunar highland rocks p 2104 N94-20700
U-Pb provenance ages of shocked zircons from the K-T boundary, Raton Basin, Colorado p 1685 N94-20701
U-Pb isotopic systematics of ferroan anorthosite 60025 p 1685 N94-20702
The U-Th-Pb, Sm-Nd, and Ar-Ar isotopic systematics of lunar meteorite Yamato-793169 p 2084 N94-20834

GEOLOGICAL SURVEY, FLAGSTAFF, AZ.
Evidence for an ice sheet/frozen lake in Utopia Planitia, Mars p 2089 N94-20388
A wet-geology and cold-climate Mars model: Punctuation of a slow dynamic approach to equilibrium p 2090 N94-20389
Possible occurrence and origin of massive ice in Utopia Planitia p 2090 N94-20390
Ice in the northern plains: Relic of a frozen ocean? p 2090 N94-20391
Stratigraphy of the Martian northern plains p 2091 N94-20398
The Manson impact crater: Estimation of the energy of formation, possible size of the impacting asteroid or comet, and ejecta volume and mass p 2083 N94-20721
Named Venusian craters p 2109 N94-20725
Venus' impact-crater database: Update to approximately 98 percent of the planet's surface p 2110 N94-20736
Mars: New evidence for origin of some Valles Marineris layered deposits p 2112 N94-20748
Clementine: An inexpensive mission to the Moon and Geographos p 1652 N94-20765
Research program on the Manson impact structure, Iowa p 1862 N94-20766
Extensional history of Mars' Tharsis Region p 2125 N94-20814
Complex structure of the Thaumasia region of Mars p 2125 N94-20815
Large, ancient, compressional structures on Mars p 2125 N94-20816

GEOLOGICAL SURVEY, MENLO PARK, CA.
The fate of water deposited in the low-lying northern plains p 2089 N94-20387

GEOLOGICAL SURVEY, RESTON, VA.
Crater destruction on the Venusian highlands by tectonic processes p 2103 N94-20696

GEORGE MASON UNIV., FAIRFAX, VA.
Replica control algorithms in distributed databases
[AD-A271571] p 1909 N94-21034

GEORGIA INST. OF TECH., ATLANTA.
Development of high-efficiency CdTe solar cells
[DE93-018206] p 1845 N94-19925
Study of electromagnetic wave scattering from characterized rough surfaces
[AD-A270931] p 1716 N94-19934
Investigation of flame driving and flow turning in axial solid rocket instabilities
[AD-A271066] p 1667 N94-20015
Low bit rate coding of Earth science images
[NASA-CR-193729] p 2041 N94-20158
Microscopic modeling of tribological and interfacial phenomena
[AD-A271864] p 1823 N94-20464
Actively controlled shaft seals for aerospace applications
[NASA-CR-194759] p 1823 N94-20538
Graph minors: Structure theory and algorithms
[AD-A271851] p 1952 N94-20613
Statistical fluctuations in lasers
[DE94-000710] p 1817 N94-20939

GEORGIA SOUTHWESTERN COLL., AMERICUS.
A practical software engineering curriculum: A pilot study
[AD-A272781] p 1911 N94-21183

GEORGIA UNIV., ATHENS.
Impact glasses from the ultrafine fraction of lunar soils p 2097 N94-20662

GESELLSCHAFT FUER STRAHLEN- UND UMWELTFORSCHUNG M.B.H., MUNICH (GERMANY).
Radiometry in commercial aircraft
[GSF-41/91] p 1892 N94-21141

GHENT UNIV. (BELGIUM).
A multigrid method for steady Euler equations on unstructured adaptive grids p 1957 N94-21476

GKSS-FORSCHUNGSZENTRUM GEESTHACHT (GERMANY).
Examinations of a thallium atomic vapor filter for a Raman temperature lidar
[GKSS-92/E/13] p 1857 N94-21044
Holographic measurements of ice crystals in cirrus clouds during International Cirrus Experiment ICE
[GKSS-92/E/14] p 1866 N94-21052
Examinations of composition and deformation behavior of intermetallic phases on the basis of Fe3(AlSi)
[GKSS-92/E/16] p 1692 N94-21311
Computerized simulations with cellular automates for cloud formation
[GKSS-92/E/22] p 1867 N94-21312
Satellite measurements of radiation budget parameters p 1860 N94-22284
ScaRaB and its subsystems p 1860 N94-22285
The use of ERBE data for climate studies p 1860 N94-22286

GKY AND ASSOCIATES, INC., SPRINGFIELD, VA.
Integration opportunities for computer models, methods, and GIS used in Corps planning studies
[AD-A271714] p 2044 N94-21354

GOUGH (PAUL) ASSOCIATES, INC., PORTSMOUTH, NH.
Formulation of a next-generation interior ballistic code
[AD-A271539] p 1801 N94-20915

GOVERNMENT INDUSTRIAL RESEARCH INST., OSAKA (JAPAN).
Evaporation of a sodium tellurite melt in the jamic low gravity drop shaft p 1713 N94-20605

GRADUATE UNIV. FOR ADVANCED STUDIES (JAPAN).
Numerical simulation of magnetic reconnection associated with emerging flux in the solar atmosphere p 2004 N94-22654

GRAND VALLEY STATE COLL., ALLENDALE, MI.
Low-latency digital frequency synthesizer using the residue number system p 1759 N94-21121

GRENOBLE-1 UNIV. (FRANCE).
Back and forth bisimulations on prime event structures
[RR-888-I-IMAG-124-LIFIA] p 1929 N94-20124
On multiflow problems
[RR-889-M] p 1950 N94-20125
Determining the distance to the perfect matching polytope of a bipartite graph
[RR-895-M] p 1950 N94-20161
Partial empirical autocorrelation of a vectorial chronological series
[RR-896-M] p 1963 N94-20162
Label-connected graphs: An overview
[RR-898-M] p 1950 N94-20163
PREVAIL-DM: A framework-based environment for formal hardware verification
[RR-899] p 1905 N94-20164
Statistical analysis of a reciprocal translocations data base
[RR-900-I] p 1963 N94-20165
Efficient chip signature checking for diagnosing boundary scan systems
[RR-901-I] p 1749 N94-20166
Parallel logic programming systems
[RR-891-I] p 1929 N94-20176
Affine and non-affine blossoms
[RR-913-M] p 1950 N94-20200
Fast scalar algorithms for multivariate partial correlations and their empirical counterparts
[RR-903-M] p 1905 N94-20201
Determination of the optimal stochastic upper bound of a Markovian generator
[RR-906-I] p 1963 N94-20202
Totally strong and strong graphs
[RR-902-I] p 1951 N94-20237

Half-integral flows in a planar graph with four holes
[RR-894-M] p 1951 N94-20302

GRONINGEN RIJKSUNIV. (NETHERLANDS).
Relativistic calculations of the superheavy nucleus (sup 298)114
[KVI-969] p 1971 N94-20119
A connectionist representation for phrase structures
p 1941 N94-20249

GRUMMAN AEROSPACE CORP., BETHPAGE, NY.
Torsion spring powered missile wing deployment system
[CA-PATENT-1,306,384] p 1645 N94-21051

GTE GOVERNMENT SYSTEMS CORP., LAS CRUCES, NM.
Analysis of the TDRS multiple access system for possible use as an attitude control system sensor
p 1666 N94-21338
Conversion of the proprietary ROLM (tm) inter-node link from multimode to singlemode operation
p 1744 N94-21349

H

HAHN-MEITNER-INST. FUER KERNFORSCHUNG, BERLIN (GERMANY).
A contribution to development and parameter extraction of SPICE compatible macromodels for discrete bipolar transistors
[HMI-B-499] p 1753 N94-21021

HAMPTON UNIV., VA.
Research on plasma-puff initiation of high Coulomb transfer switches
[NASA-CR-194371] p 1994 N94-21289
Plasma-puff initiation of high Coulomb transfer switches
p 1994 N94-21290
Characteristics of plasma-puff trigger for a inverse-pinch plasma switch
p 1995 N94-21291
Comparative study of INPIStron and spark gap
p 1995 N94-21293
INPIStron switched pulsed power for dense plasma pinches
p 1995 N94-21294

HARRIS, MILLER, MILLER AND HANSON, INC., LEXINGTON, MA.
Aircraft noise effects on cultural resources: Recommendation and rationale for further research
[PB93-205326] p 1968 N94-22053
Aircraft noise effects on cultural resources: Annotated bibliography
[PB93-205334] p 1969 N94-22054

HARVARD-SMITHSONIAN CENTER FOR ASTROPHYSICS, CAMBRIDGE, MA.
Lamellar olivine in the Divnoe achondrite: Evidence for high-pressure exsolution?
p 1685 N94-20679
Opaque-rich lithology in the Divnoe achondrite: Petrology and origin
p 2082 N94-20680
Chaunskij: The most highly metamorphosed, shock-modified and metal-rich mesosiderite
p 2082 N94-20681
Subduction on the margins of coronae on Venus: Evidence from radiothermal emissivity measurements
p 2107 N94-20718

HARVARD UNIV., CAMBRIDGE, MA.
Wide-bandwidth high-resolution search for extraterrestrial intelligence
[NASA-CR-194724] p 1897 N94-20336
Alumoxanes: Rationalization of black box materials
[AD-A272805] p 1704 N94-21170
Paired comparison models with time-varying parameters
[AD-A272016] p 1964 N94-21442

HAWAII UNIV., HILO.
Preliminary results from Mariner 10: High resolution images of the Moon
p 2107 N94-20719
Chronology, eruption duration, and atmospheric contribution of Apollinaris Patera, Mars
p 2108 N94-20720

HAWAII UNIV., HONOLULU.
Fragments of ancient lunar crust: Ferroan noritic anorthosites from the descartes region of the Moon
p 2096 N94-20660
Volatility in the lunar crust: Trace element analyses of lunar minerals by PIXE proton microprobe
p 2097 N94-20661
Spectral reflectance studies of the Humorum Basin region
p 2101 N94-20682
Post-metamorphic brecciation in type 3 ordinary chondrites
p 2083 N94-20749
Tumuli and tubes: Teaching scientific techniques
p 2039 N94-20818
Solar imaging vector magnetograph
[NASA-CR-194729] p 1810 N94-21876
The University of Hawaii Institute for Astronomy CCD camera control system
p 1828 N94-22489
Enhanced absorption of p-modes on sunspot and plage regions
p 2006 N94-22671

HAWAII UNIV., MANOA.
Energy storage and conversion in solid hydrogen
[AD-A271439] p 1845 N94-20086

HAZELTINE CORP., COMMACK, NY.
Phased array antenna with couplers in spatial filter arrangement
[CA-PATENT-1,296,098] p 1737 N94-21031
Radome having integral heating and impedance matching elements
[CA-PATENT-APPL-SN-2,026,85] p 1738 N94-21049

HEALTH AND WELFARE CANADA, OTTAWA (ONTARIO).
A broadband V-antenna for pulsed field measurements: Experimental results
p 1745 N94-22139

HELSINKI UNIV. (FINLAND).
Universality in blow-up for non linear heat equations
[PB93-215465] p 2038 N94-22095
Factor analysis as a tool for spectral line component separation 21cm emission in the direction of L1780
p 1965 N94-22536

HELSINKI UNIV. OF TECHNOLOGY, ESPOO (FINLAND).
Information sciences and business enterprises
p 2046 N94-22059
An economic analysis of transboundary air pollution between Finland and the Soviet Union
[ETLA-DISCUSSION-PAPER-335] p 1854 N94-22072
Controlling multisupplier operations by intelligent EDI
p 1744 N94-22076

HEROLD (FREDRICK) AND ASSOCIATES, INC., GREENBELT, MD.
Using the USCCS for sub microsecond spacecraft clock calibration
p 1813 N94-21346

HEWLETT-PACKARD CO., CORVALLIS, OR.
Delay analysis of combinations of pass transistors and classical logic gates
p 1756 N94-21103

HIROSHIMA UNIV. (JAPAN).
MHD relaxation in magnetic loops
p 2004 N94-22658
Double diffusion convection in a rotating spherical shell
p 2006 N94-22666

HOKKAIDO INDUSTRIAL RESEARCH INST. (JAPAN).
Evaporation of a sodium tellurite melt in the jamic low gravity drop shaft
p 1713 N94-20605

HONEYWELL, INC., PHOENIX, AZ.
Windshear detection for aircraft using temperature lapse rate
[CA-PATENT-1,295,736] p 1641 N94-21030
Optimal flight guidance for aircraft in windshear
[CA-PATENT-1,307,573] p 1650 N94-21050
Miniature color display, phase 4
[AD-A272920] p 1760 N94-21221

HOPITAL DU SACRE-COEUR, MONTREAL (QUEBEC).
Segmenting the optical flow due to the motion of several rigid objects
p 1777 N94-22147

HOUSTON UNIV., TX.
Self-organization via active exploration in robotic applications. Phase 2: Hybrid hardware prototype
[NASA-CR-194723] p 1939 N94-20212
Original size of the Vredefort structure, South Africa
p 1863 N94-20825
Origin of the Vredefort structure, South Africa: Impact model
p 1863 N94-20826
Characterization of the Marquez Dome buried impact crater using gravity and magnetic data
p 1863 N94-20882
The effects of instructional sets on reactions to and performance on an intelligent tutoring system
[NASA-CR-194739] p 1895 N94-21810

HOWARD UNIV., WASHINGTON, DC.
Magnetic properties and Moessbauer analyses of glass from the K-T boundary, Beloc, Haiti
p 1685 N94-20753

HUGHES STX, INC., GREENBELT, MD.
The IDL astronomy user's library
p 2048 N94-22500
DECONV-TOOL: An IDL based deconvolution software package
p 1927 N94-22542
STELAR: An experiment in the electronic distribution of astronomical literature
p 2049 N94-22544

I

IBARAKI UNIV., MITO (JAPAN).
Shock formation in magnetohydrodynamical accretion onto a black hole
p 2010 N94-22699

IBIS ASSOCIATES, INC., WELLESLEY, MA.
Analysis of cost: CVD diamond deposition
[AD-A271980] p 2018 N94-20616

IBM WATSON RESEARCH CENTER, YORKTOWN HEIGHTS, NY.
Investigation of quantum effects in heterostructures
[AD-A270938] p 2011 N94-19817

IDAHO UNIV., MOSCOW.
Use of switched capacitor filters to implement the discrete wavelet transform
p 1755 N94-21097
Detection of CMOS bridging faults using minimal stuck-at fault test sets
p 1757 N94-21110
Acceleration-augmented LQG control of an active magnetic bearing
p 1757 N94-21112
Design methods for fault-tolerant finite state machines
p 1758 N94-21120
Using crosscorrelation techniques to determine the impulse response of linear systems
p 1759 N94-21122
A CAM-based LZ data compression IC
p 1759 N94-21129
Behavioral model simulation studies of an image compressor
p 1760 N94-21133
The 1992 4th NASA SERC Symposium on VLSI Design
[NASA-CR-194591] p 1763 N94-21694
A new eddy current model for magnetic bearing control system design
p 1763 N94-21696
An 18 bit 50 kHz ADC for low earth orbit
p 1764 N94-21702
On the decomposition of synchronous state machines using sequence invariant state machines
p 1764 N94-21703
NASA SERC digital correlator projects
p 1765 N94-21708
Defect-sensitivity analysis of an SEU immune CMOS logic family
p 1765 N94-21711
Dimension scaling effects on the yield sensitivity of HEMT digital circuits
p 1765 N94-21712
HDL to verification logic translator
p 1766 N94-21717
Instruction set commutivity
p 1766 N94-21719
Interpolative modeling of GaAs FET S-parameter data bases for use in Monte Carlo simulations
p 1767 N94-21723
A VLSI implementation of DCT using pass transistor technology
p 1767 N94-21725
On fast carry select adders
p 1767 N94-21726
A set-associative, fault-tolerant cache design
p 1768 N94-21731
Column chromatographic separation of Y(3+) from Sr(2+) by polymeric ionizable crown ether resins
[DE94-000935] p 1683 N94-22021

IIT RESEARCH INST., BARTLESVILLE, OK.
The thermodynamic properties to 700 K of naphthalene and 2,7-dimethylnaphthalene
[DE93-000160] p 2037 N94-20473

IIT RESEARCH INST., CHICAGO, IL.
ELF communications system ecological monitoring program
[AD-A272507] p 1740 N94-21412

ILLINOIS UNIV., CHICAGO.
Liquid-phase circulation and mixing in multicomponent droplets vaporizing in a laminar convective environment
[AD-A272851] p 1802 N94-21193
A proof-of-concept implementation of persistence in a hierarchical storage system
[NASA-CR-194790] p 1921 N94-22376

ILLINOIS UNIV., URBANA.
Fluid dynamic mechanisms and interactions within separated flows
[AD-A271037] p 1797 N94-19978
VLSI design for reliability-current density
[AD-A270719] p 1749 N94-20110
Properties of E-beam interactive oxide films for nanometer scale structures
[AD-A272848] p 1675 N94-21191
VLSI design for reliability-hot carrier effects
[AD-A271586] p 1761 N94-21256
The n-p(p(+))-n Al(yGa)(1-y) As-GaAs-In(x)Ga(1-x) as quantum well laser with p(+)-n(+)GaAs-InGaAs tunnel contact on n GaAs
[AD-A271292] p 2030 N94-21805

ILLINOIS UNIV., URBANA-CHAMPAIGN.
Aviation safety research. Volume 1: Literature review of sources of aviation accident and incident data and selected factors contributing to accidents
[PB93-202685] p 1641 N94-21428

IMPLANT SCIENCES CORP., WAKEFIELD, MA.
Single crystal diamond films
[AD-A266759] p 2028 N94-21517

INDIANA UNIV., BLOOMINGTON.
Fluid absorption solar energy receiver
[NASA-CR-194688] p 1846 N94-20229

INDIANA UNIV.-PURDUE UNIV., INDIANAPOLIS.
Finite element mesh generation and analysis of solder joints for fatigue life predictions
[AD-A271329] p 1829 N94-19937

INDORE UNIV. (INDIA).
Generation of harmonic radiation using the multi-cavity free-electron laser
[DE94-001261] p 1820 N94-21975

INFORMATION SCIENCE INST., MARINA DEL REY, CA.
Distributed Virtual System (DIVIRS) project
[NASA-CR-194360] p 1905 N94-20226

INSTITUT DES HAUTES ETUDES SCIENTIFIQUES, BURES-SUR-YVETTE (FRANCE).
Universality in blow-up for non linear heat equations
[PB93-215465] p 2038 N94-22095
Vanishing theorem on arithmetic surfaces
[PB93-215481] p 1961 N94-22263
Non commutative geometry and physics
[PB93-215499] p 1961 N94-22264
Proof of stability of the hydrogen molecule
[PB93-221026] p 1977 N94-22271
Canonically covariant formulation of Landau's Newtonian superfluid dynamics
[PB93-221034] p 1805 N94-22272
Semi-stability and heights of cycles
[PB93-215507] p 1961 N94-22377
INSTITUT FRANCO-ALLEMAND DE RECHERCHES, SAINT-LOUIS (FRANCE).
Low-altitude cross-wind velocity measurements using pulsed visible fringe-type laser anemometry
[ISL-CO-216/92] p 1866 N94-20557
INSTITUT NATIONAL DE RECHERCHE D'INFORMATIQUE ET D'AUTOMATIQUE, VALBONNE (FRANCE).
Asymptotics of the GLRT for the disorder problem in diffusion processes
[INRIA-RR-1735] p 1951 N94-20227
COCOLOG: A conditional observer and controller logic for finite machines
[INRIA-RR-1714] p 1910 N94-21063
INSTITUT NATIONAL POLYTECHNIQUE, GRENOBLE (FRANCE).
Cavitation modelling p 1668 N94-20079
INSTITUT ZA NUKLEARNE NAUKE BORIS KIDRIC, BELGRADE (YUGOSLAVIA).
The onset and spectra of a magnetized Langmuir turbulence p 2006 N94-22673
INSTITUTE FOR COMPUTER APPLICATIONS IN SCIENCE AND ENGINEERING, HAMPTON, VA.
Linear and nonlinear PSE for compressible boundary layers
[NASA-CR-191537] p 1797 N94-20033
On the spline-based wavelet differentiation matrix
[NASA-CR-191557] p 1950 N94-20087
Shape optimization governed by the Euler equations using an adjoint method
[NASA-CR-191555] p 1950 N94-20092
A multi-level solution algorithm for steady-state Markov chains
[NASA-CR-191558] p 1914 N94-21462
Dependability and performability analysis
[NASA-CR-191565] p 1965 N94-21463
Rational trigonometric approximations using Fourier series partial sums
[NASA-CR-191535] p 1959 N94-21568
Using parallel banded linear system solvers in generalized eigenvalue problems
[NASA-CR-191540] p 1915 N94-21584
Simulations of diffusion-reaction equations with implications to turbulent combustion modeling
[NASA-CR-191536] p 1804 N94-21861
New results on the realizability of Reynolds stress turbulence closures
[NASA-CR-191548] p 1804 N94-21875
Computation of the sound generated by isotropic turbulence
[NASA-CR-191543] p 1804 N94-21880
An advancing-front Delaunay-triangulation algorithm designed for robustness p 1920 N94-22362
INSTITUTE FOR DEFENSE ANALYSES, ALEXANDRIA, VA.
Standard atmospheres for engagement modeling
[AD-A272447] p 1858 N94-21207
Entry velocities at Mars and Earth for short transit times
[AD-A272591] p 1665 N94-21420
INSTITUTE FOR PERCEPTION RVO-TNO, SOESTERBERG (NETHERLANDS).
HERMES, a report generator for research on information processing in command posts: The effect of missing information
[IZF-1992-A-28] p 2042 N94-20310
INSTITUTE FOR SPACE AND TERRESTRIAL SCIENCE, CONCORD (ONTARIO).
Tools for the IDL widget set within the X-windows environment p 1927 N94-22538
INSTITUTE OF OCEANOGRAPHIC SCIENCES, WORMLEY (ENGLAND).
Shipboard ADCP observations during RRS Charles Darwin Cruise 62
[IOS-298-1992] p 1882 N94-20531
INSTITUTE OF PHYSICAL AND CHEMICAL RESEARCH, SAITAMA (JAPAN).
Structure of accretion plasmas of x ray binary pulsars in MHD turbulence p 2007 N94-22679
Particle acceleration on the Alfven surface of a plasma ejecting axisymmetric rotator p 2008 N94-22681
INSTITUTE OF PLASMA PHYSICS, PRAGUE (CZECHOSLOVAKIA).
On effects of a local plasma density growth due to ponderomotive forces at fast wave launching in tokamaks
[IPPCZ-328] p 1996 N94-21571
On one numerical approach to Stefan problem
[IPPCZ-330] p 1996 N94-21572
The angular velocity spread of REB induced by magnetic field discontinuity
[IPPCZ-331] p 1996 N94-21573
Radial diffusion of toroidally trapped particles induced by lower hybrid and fast waves
[IPPCZ-327] p 1996 N94-21593
Edge plasma experiments on CASTOR tokamak
[IPPCZ-332] p 1997 N94-21816
INSTITUTO BRASILEIRO DO MEIO AMBIENTE E DOS RECURSOS NATURAIS RENOVAVEIS, RIO DE JANEIRO.
Change detection on land use and rainforest cover at Paragominas region, Brazilian Amazon p 1838 N94-20957
INSTITUTO DE PESQUISAS ESPACIAIS, SAO JOSE DOS CAMPOS (BRAZIL).
The 7th Brazilian Remote Sensing Symposium, volume 1 p 1838 N94-20953
The 7th Brazilian Remote Sensing Symposium, volume 2 p 1838 N94-20956
The 7th Brazilian Remote Sensing Symposium, volume 3 p 1839 N94-20960
Evaluation of C-band SAR data from SAREX 1992: Tapajos study site p 1839 N94-20964
The 7th Brazilian Remote Sensing Symposium, volume4 p 1840 N94-20965
The development of remote sensing in Brazil and Canada: Comparative case studies p 1840 N94-20968
Experiments with recursive estimation in astronomical image processing p 2047 N94-22457
Theory of leaked auroral kilometric radiation p 2003 N94-22649
Dynamo driven by weak plasma turbulence: The effect of differential rotation p 2005 N94-22665
INTER-UNIVERSITY CENTRE FOR ASTRONOMY AND ASTROPHYSICS, PUNE (INDIA).
CCD surface photometry of galaxies p 2058 N94-22445
INTERNATIONAL BANK FOR RECONSTRUCTION AND DEVELOPMENT, WASHINGTON, DC.
Urban applications of satellite remote sensing and GIS analysis
[PB93-202174] p 1842 N94-21855
INTERNATIONAL BUSINESS MACHINES CORP., RESEARCH TRIANGLE PARK, NC.
Multiple-fold clustered processor mesh array p 1757 N94-21113
INTERNATIONAL BUSINESS MACHINES CORP., YORKTOWN HEIGHTS, NY.
ALE project
[AD-A271080] p 2014 N94-19980
INTERNATIONAL CENTRE FOR THEORETICAL PHYSICS, TRIESTE (ITALY).
On the twisted N=2 superconformal structure in 2d gravity coupled to matter
[DE93-628627] p 2037 N94-20178
IOWA STATE UNIV. OF SCIENCE AND TECHNOLOGY, AMES.
The incongruent melting and melt textured solidification process of Bi2Sr2CaCu3O8
[DE93-041123] p 2032 N94-21936
Strength, ultrasonic and metallurgical evaluation of diffusion bonds
[DE94-000665] p 1697 N94-22571
Melt-spin processing of high (Tc) oxide superconductors
[DE94-000696] p 2036 N94-22582
IOWA UNIV., IOWA CITY.
A study of Saturn's E-ring particles using the Voyager 1 plasma wave instrument
[NASA-CR-194694] p 2088 N94-20048
Physics of magnetospheric boundary layers
[NASA-CR-194725] p 1858 N94-21836
Current loop coalescence studied by 3-D electromagnetic particle code p 2005 N94-22660

J

JAPAN BROADCASTING CORP., TOKYO.
NHK Science and Technical Research Laboratories p 2151 N94-20342
JAPAN MACHINERY FEDERATION, TOKYO.
Technology to prevent greenhouse effect gases
[DE94-707421] p 1850 N94-19976
Technology to prevent greenhouse effect gases
[DE94-707420] p 1851 N94-20116
The FY1992 survey on multi-purpose dam and energy utilization system by the wind power generation eration
[DE94-707408] p 1848 N94-22012
The FY1992 survey on commercialization of Stirling engine utilization equipment
[DE94-707416] p 1849 N94-22029
JAPAN MICROGRAVITY CENTER, HOKKAIDO.
Evaporation of a sodium tellurite melt in the jamic low gravity drop shaft p 1713 N94-20605
JAPAN SPACE UTILIZATION PROMOTION CENTER, TOKYO.
Evaporation of a sodium tellurite melt in the jamic low gravity drop shaft p 1713 N94-20605
JAYCOR, SAN DIEGO, CA.
Optics survivability support, volume 1
[DE93-019616] p 1985 N94-20262
Optics survivability support, volume 2
[DE93-040310] p 1985 N94-20283
JET PROPULSION LAB., CALIFORNIA INST. OF TECH., PASADENA.
Millimeter wave imaging technology
[AD-A271257] p 1715 N94-19912
Design considerations for a fiber optic communications network for power systems
[DE93-018404] p 1984 N94-20179
Optoelectronic associative memory
[NASA-CASE-NPO-18278-1-CU] p 1985 N94-20303
Feedback controlled optics with wavefront compensation
[NASA-CASE-NPO-18194-1-CU] p 1985 N94-20305
Wide-angle imaging system with fiberoptic components providing angle-dependent virtual material stops
[NASA-CASE-NPO-18146-1-CU] p 1986 N94-20345
Electronic neural network for solving traveling salesman and similar global optimization problems
[NASA-CASE-NPO-17807-2-CU] p 1942 N94-20360
Progress in Electromagnetics Research Symposium (PIERS)
[NASA-CR-194629] p 1718 N94-20403
Probe compensation in cylindrical near-field scanning: A novel simulation methodology p 1718 N94-20404
Analysis of microstrip dipoles and slots transversely coupled to a microstrip line using the FDTD method p 1718 N94-20405
A general rough-surface inversion algorithm: Theory and application to SAR data p 1719 N94-20407
Variable-permittivity linear inverse problem for the H(sub z)-polarized case p 1719 N94-20408
Modifications to the three-component classification algorithm for SAR data p 1719 N94-20410
Determination of noise equivalent sigma(0) using highly correlated repeat-pass SAR images p 1720 N94-20411
ERS-1 and Seasat scatterometer measurements of ocean winds: Model functions and the directional distribution of short waves p 1720 N94-20412
Ku-band ocean radar backscatter observations during SWADE p 1720 N94-20413
Comparison of remote sensing measurements with a two-scale polarimetric emission and scattering model for sea surfaces p 1721 N94-20415
Topographic mapping using a monopulse SAR system p 1721 N94-20417
Classification of simple vegetation types using POLSAR image data p 1722 N94-20420
Two microstrip arrays for interferometric SAR applications p 1722 N94-20421
Analytical evaluation of a surface integral expressing the coupling between interior and exterior volumes in a FE-IE approach p 1722 N94-20423
Advances in spaceborne radar remote sensing p 1723 N94-20424
Detection of traveling ionospheric disturbances induced by atmospheric gravity waves using the global positioning system p 1723 N94-20425
Polarimetric backscattering from sea ice p 1723 N94-20426
On evaluating the accuracy of SAR sea-ice classification using multifrequency polarimetric AIRSAR data p 1724 N94-20428
Application of Cloude's target decomposition theorem to polarimetric imaging radar data p 1724 N94-20429
Direction angle sensitivity of agricultural field backscatter with AIRSAR data p 1724 N94-20430
Time-domain analysis of planar microstrip devices using a generalized Yee-algorithm based on unstructured grids p 1724 N94-20431
Retrieval of ice thickness from polarimetric SAR data p 1724 N94-20432
Studies of Greenland using the SEASAT scatterometer p 1725 N94-20433
Radar backscattering from snow facies of the Greenland ice sheet: Results from the AIRSAR 1991 campaign p 1725 N94-20434

C-band radar backscatter of sea ice in the Weddell Sea, Antarctica during the austral winter of 1992 p 1725 N94-20435
An efficient formulation of the coupled finite element-integral equation technique for solving large 3D scattering problems p 1725 N94-20436
Massively parallel computation of RCS with finite elements p 1726 N94-20437
Near grazing scattering from non-Gaussian ocean surfaces p 1726 N94-20438
Rough surface scattering from moving ocean surfaces as an indicator of scattering mechanisms p 1726 N94-20439
The effect of dissipative inhomogeneous medium on the statistics of the wave intensity p 1726 N94-20440
Polarimetric thermal emission from rough surfaces p 1727 N94-20441
Optical beam forming techniques for phased array antennas p 1727 N94-20442
Simulated retrieval of land surface parameters using multichannel satellite microwave radiometry p 1727 N94-20443
Synergism of active and passive microwave data for estimating bare surface soil moisture p 1727 N94-20444
Polarimetric thermal emission from periodic water surfaces p 1728 N94-20445
Multi-band reflector antenna with double-ring element frequency selective subreflector p 1728 N94-20447
Second order distorted born approximation for backscattering from a layer of discrete random medium p 1728 N94-20448
Symmetry in polarimetric remote sensing p 1729 N94-20449
Numerical modeling for an electric-field hyperthermia applicator p 1729 N94-20451
Mapping of taiga forest units using AIRSAR data and/or optical data, and retrieval of forest parameters p 1729 N94-20452
Application of the target decomposition theorem to a polarimetric random media model p 1730 N94-20453
A theoretical and numerical study of polarimetric scattering and emission from random rough surfaces with anisotropic directional spectrum p 1730 N94-20454
Application of neural network to remote sensing of soil moisture using theoretical polarimetric backscattering coefficients p 1730 N94-20455
The Brewster angle effect in SAR polarimetry p 1731 N94-20456
Mobile antenna development at JPL p 1731 N94-20457
Mobile terminal antennas for helicopters p 1731 N94-20458
Topographic slope from the SAR interferometric phase gradient p 1731 N94-20459
Interferometric detection of freeze-thaw displacements of Alaskan permafrost using ERS-1 data p 1732 N94-20460
Performance evaluation of the JPL TOPSAR system: An across-track interferometric SAR system for topographic mapping p 1732 N94-20461
Segmented ion thruster [NASA-CASE-NPO-18192-1-CU] p 1669 N94-20496
Time warp operating system version 2.7 internals manual [NASA-CR-194798] p 1899 N94-20549
The coherent backscattering opposition effect p 1991 N94-20646
Magellan vertical polarization radar observations p 1744 N94-20691
Eruption history of the Tharsis shield volcanoes, Mars p 2102 N94-20692
Geology of Biblis Patera, Ulysses Patera, and Jovis Tholus, Mars p 2103 N94-20693
Gravity investigation of the Manson impact structure, Iowa p 2082 N94-20694
Magellan at Venus: Summary of science findings p 2110 N94-20734
Rifting at Devana Chasma, Venus: Structure and estimation of the effective thickness of the elastic lithosphere p 2113 N94-20754
Volcanic rises on Venus: Geology, formation, and sequence of evolution p 2113 N94-20755
Venus gravity: New Magellan low altitude data p 2117 N94-20772
Response of the topography and gravity field on Venus to mantle upwelling beneath a chemical boundary layer p 2117 N94-20775
Parga and Hecate Chasmata, Venus: Structure, volcanism and models of formation p 2121 N94-20796
Discovery Venera surface: Atmosphere geochemistry experiments mission concept p 2123 N94-20806
Magellan Mission p 1652 N94-20829
Intact capture of hypervelocity particles on Shuttle p 2085 N94-20837
IMPS albedo and diameter for Asteroid 243 Ida p 2085 N94-20845
Geology and radiophysical properties of the Venera and Vega landing sites p 2135 N94-20867
The connection between Venus' free obliquity and its CMB oblateness p 2139 N94-20896
STRV RADMON: An integrated high-energy particle detector p 1666 N94-21086
Power optimization in logic isomers p 1756 N94-21101
Mixed voltage VLSI design p 1756 N94-21104
Using manufacturing message specification for monitor and control at Venus p 1932 N94-21333
Calibration of a calorimeter for measuring the performance of thermal control surfaces p 1660 N94-21378
Low power, CMOS digital autocorrelator spectrometer for spaceborne applications p 1666 N94-21733
Low energy CMOS for space applications p 1766 N94-21735
SkICAT: A cataloging and analysis tool for wide field imaging surveys p 2049 N94-22546
Projections on structures and material strength in the computational context p 1834 N94-22610

JJM SYSTEMS, INC., ARLINGTON, VA.
An expert system shell for inferring vegetation characteristics [NASA-CR-189318] p 1837 N94-20284

JOHNS HOPKINS UNIV., BALTIMORE, MD.
Venus pancake dome formation: Morphologic effects of a cooling-induced variable viscosity during emplacement p 2110 N94-20732
Thermal infrared remote sensing and Kirchhoff's law: 1. Laboratory measurements p 1685 N94-20733
Wrinkle ridges, reverse faulting, and the depth penetration of lithospheric stress in lunae planum, Mars p 2141 N94-20910

JOHNS HOPKINS UNIV., COLUMBIA, MD.
Studies of electromagnetic ion cyclotron waves using AMPTE/CCE and Dynamics Explorer [NASA-CR-194711] p 1982 N94-21878

JOHNS HOPKINS UNIV., LAUREL, MD.
Single-event upset testing of the performance semiconductor 1750A CMOS/SOS chip set [AD-A271158] p 2015 N94-20184
Comparison of single event upset rates for microelectronic memory devices during interplanetary solar particle events p 1754 N94-21085
Silicon retina for optical tracking systems p 1755 N94-21098
Single event phenomena: Testing and prediction p 1763 N94-21696
Design and test of field programmable gate arrays in space applications p 1765 N94-21710

JOHNSON CONTROLS WORLD SERVICES, CAPE CANAVERAL, FL.
Data management for support of the Oregon Transect Ecosystem Research (OTTER) project [NASA-CR-4557] p 1905 N94-20149

K

KAMAN SCIENCES CORP., UTICA, NY.
Data and Analysis Center for Software [AD-A270571] p 2041 N94-20106

KANAGAWA UNIV., YOKAHAMA (JAPAN).
Acceleration of solar-flare particles as viewed from their chemical composition p 2006 N94-22672

KANSAS STATE UNIV., MANHATTAN.
Geology of Galileo Regio quadrangle, Ganymede p 2130 N94-20842

KANSAS UNIV., LAWRENCE.
Low-power millimeter-wave radar observations of the atmosphere [NASA-CR-194738] p 1858 N94-21811

KANSAS UNIV. CENTER FOR RESEARCH, INC., LAWRENCE.
Radar backscatter measurements from simulated sea ice during CRRELEX 1990 [AD-A271034] p 1715 N94-19823
Solar proton events from a 180 year depth profile of nitrate concentrations from the central Greenland ice sheet [AD-A272888] p 2147 N94-21196

KARLSRUHE UNIV. (GERMANY).
Evaluation of the chemical composition of cosmic radiation in energy area of 10(exp 15) eV [ETN-93-93682] p 2150 N94-21056

KATHOLIEKE UNIV., NIJMEGEN (NETHERLANDS).
Growth and morphology of crystals: Theory and observations [PB93-221166] p 2035 N94-22273

KATHOLIEKE UNIV. TE LEUVEN (BELGIUM).
Properties of cryogenic liquids p 1668 N94-20073

KECK OBSERVATORY, MAUNA KEA, HI.
The Keck keyword layer p 1925 N94-22460
The Keck Task Library (KTL) p 2048 N94-22504

KINGS COLL., LONDON (ENGLAND).
Numerical modeling of fringing fields and their use for complex permittivity measurements at high frequencies [AD-A270478] p 1966 N94-19917

KITT PEAK NATIONAL OBSERVATORY, TUCSON, AZ.
New IRAF stellar photometry software p 1925 N94-22464
PHOTCAL: The IRAF photometric calibration package p 1925 N94-22465
SPPTOOLS: Programming tools for the IRAF SPP language p 1925 N94-22474
The IRAF radial velocity analysis package p 1925 N94-22475
Interactive Spectral Analysis and Computation (ISAAC) p 1926 N94-22505
The NSO FTS database program and archive (FTSDBM) p 1926 N94-22506
Managing an archive of weather satellite images p 2048 N94-22525
IRAF in the nineties p 2048 N94-22535
The spectral world coordinate systems in IRAF/NOAO p 2049 N94-22539
SPECFOCUS: An IRAF task for focusing spectrographs p 1965 N94-22540
Tests of a simple data merging algorithm for the GONG project p 1927 N94-22549

KOBE UNIV. (JAPAN).
REE and other trace lithophiles in MAC88177, LEW88280 and LEW88763 p 2082 N94-20639

KYOTO UNIV. (JAPAN).
Magnetic superbubbles in the galactic disk and halo p 2009 N94-22694

KYOTO UNIV., UJI (JAPAN).
MHD instabilities of fusion oriented plasmas p 2000 N94-22627

KYUSHU UNIV., FUKUOKA (JAPAN).
Consequences of plasma-maser in plasma astrophysics p 2006 N94-22669

L

LAMAR UNIV., BEAUMONT, TX.
Absorption heat pump for space applications [NASA-CR-194693] p 1845 N94-20066

LANCASTER UNIV. (ENGLAND).
A comparison of calculated and measured rheological properties of crystallising lavas in the field and in the laboratory p 1862 N94-20690
A classification scheme for the morphology of lava flow fields p 1863 N94-20879

LAVAL UNIV. (QUEBEC).
A 3-D vision method for estimating workspace occupancy of a power-line maintenance robot p 1770 N94-22105
Hierarchical surface triangulation of range data p 1771 N94-22108
Calculation of a diffracted electric field with the aid of the Method of Equivalent Currents (MEC) p 1745 N94-22127
Language as primary dimension of distributed AI systems activity p 1776 N94-22141
Adaptive synthesis of a ray diagram for an antenna array p 1745 N94-22160
A neural network for multiresolution edge detection p 1779 N94-22163
Improvement in invariant pattern recognition with neural networks and Fourier-Mellin filters p 1780 N94-22164
A modified moment invariants technique for classification of noisy objects p 1780 N94-22165
Coding of color quantized images p 1781 N94-22173
AlGaAs laser diode FM spectrum: Phased array antenna application p 1746 N94-22196
A software environment for the exploitation of the MAR image sensor p 1785 N94-22200
A framework of connectionist network toward speech waveform coding p 1746 N94-22211
FM interference in radio navigation receivers p 1645 N94-22219
Architectures of the free space optical interconnects p 1789 N94-22220
Encoding and decoding quasi-spherical signal sets p 1747 N94-22233
An algorithm for the interference detection among polygonal surfaces p 1791 N94-22239
Strategy for motion of a moving body of quasi-polygonal form within a polygonal space p 1792 N94-22240
Analytical representation of working articulation space of a plane manipulator in an encumbered environment p 1792 N94-22241

Holographic optical elements correcting the off-axis aberrations of a parabolic mirror
[ISBN-0-315-57561-6] p 1990 N94-22411
Automated investigation of quasars at a galactic latitude of -45 deg
[ISBN-0-315-57576-X] p 2056 N94-22415
Mixed finite element and finite volume methods
[ISBN-0-315-63035-3] p 1805 N94-22417

LAWRENCE LIVERMORE NATIONAL LAB., CA.
Substrate recovery of Mo-Si multilayer coated optics
[DE93-019610] p 1698 N94-19810
Frequency dependent electrical properties of minerals and partial-melts
[DE93-019918] p 2012 N94-19861
Multidimensional solitons in fiber arrays
[DE93-019923] p 1983 N94-19862
Pointing control design for autonomous space vehicle applications
[DE93-019943] p 1657 N94-19863
A pipelined superconducting digital processor
[DE93-040652] p 1898 N94-19886
A database of selected transport coefficients for combustion studies
[DE93-041278] p 1678 N94-19889
Longitudinal beam dynamics for heavy ion fusion using WARPrz
[DE93-019154] p 1992 N94-19915
Unlike-pair interactions at high pressure and high temperature
[DE93-019948] p 1796 N94-19916
Magnetic circular dichroism in x ray absorption and core-level photoemission
[DE93-019381] p 1688 N94-19986
The best of GYMNOS: A users guide
[DE93-041275] p 1992 N94-19991
Stochastic differential equations and numerical simulation for pedestrians
[DE93-040651] p 1949 N94-20006
New relativistic S-matrix results for scattering -- beyond the usual anomalous factors/beyond impulse approximation
[DE93-019148] p 1971 N94-20096
Two-dimensional particle-in-cell simulation on transputer arrays
[DE93-017977] p 1972 N94-20161
Computational model of a magnetic modulator for copper lasers
[DE93-019803] p 1815 N94-20223
Characterization and possible repair of defects in soft x ray projection lithography masks
[DE93-019147] p 1750 N94-20231
Applications and source development for high-repetition rate x ray lasers
[DE93-019547] p 1815 N94-20259
Optics survivability support, volume 1
[DE93-019616] p 1985 N94-20262
A novel scheme to handle highly pulsed loads with a standard helium refrigerator
[DE93-019617] p 1799 N94-20263
Optics survivability support, volume 2
[DE93-040310] p 1985 N94-20283
Energy and luminosity limits of hadron supercolliders
[DE93-019248] p 1980 N94-20300
Three-dimensional dynamic thermal imaging of structural flaws by dual-band infrared computed tomography
[DE93-019575] p 1906 N94-20316
Phonons and metastability in compressed nitrogen
[DE93-019913] p 2016 N94-20318
Stability of the face-centered-cubic phase of heavy rare gas solids
[DE93-019949] p 1679 N94-20319
Laser propagation in underdense plasmas: Scaling arguments
[DE93-040439] p 1816 N94-20480
Generation of intense ultrashort x ray pulses
[DE93-019607] p 1817 N94-21299
One- and multi-component theories of mixtures
[DE93-040543] p 1966 N94-21511
Polymeric nitrogen
[DE93-040544] p 1706 N94-21512
Electronic resources for security related information: Reference document
[DE93-040488] p 2044 N94-21529
Materials Science and Engineering
[DE93-040497] p 1675 N94-21530
Direct simulation of shock-induced mixing layer
[DE93-040498] p 1803 N94-21531
Shock compression of low-density foams
[DE93-040545] p 1707 N94-21546
Laser driven hydrodynamic instability experiments
[DE93-040550] p 1818 N94-21547
New production mechanisms for unstable nuclei in stars, supernovae, and the big bang
[DE93-018627] p 2081 N94-21618
Laser guide star adaptive optics: Present and future
[DE93-018642] p 1989 N94-21619
Electromechanical battery research and development at the Lawrence Livermore National Laboratory
[DE93-019159] p 1762 N94-21620
Electromechanical battery research and development at the Lawrence Livermore National Laboratory
[DE94-000391] p 1762 N94-21621
High resolution, three dimensional soft x ray imaging
[DE93-018667] p 1989 N94-21630
Surface path lines in plane Stokes flow driven by capillarity
[DE93-041277] p 1803 N94-21651
Static ultra-high pressure study of lanthanide and actinide metals using a diamond-anvil cell
[DE94-000369] p 1693 N94-21656
Performance evaluation of video on ethernet
[DE93-040696] p 1936 N94-21749
Assessment of the organizational structure and services of DOE National Laboratory Libraries
[DE93-040697] p 2045 N94-21750
Effects of aqueous solution compositions on Aerocapacitor energy density
[DE94-000385] p 1768 N94-21753
High power, electron-beam induced switching in diamond
[DE93-040535] p 1768 N94-21770
The transition to massively parallel computing within a production environment at a DOE access center
[DE93-019155] p 1936 N94-21828
Ionization of H2(+) in intense laser fields
[DE93-019160] p 1818 N94-21829
A FET-switched induction accelerator cell
[DE93-019604] p 1769 N94-21838
Imaging vector fields using line integral convolution
[DE93-019922] p 1917 N94-21841
Ductile-brittle transition behavior of tungsten under shock loading conditions
[DE93-019945] p 1693 N94-21843
High-power copper vapor lasers and their application to precision drilling and cutting
[DE93-019951] p 1819 N94-21844
Spectral characterization of lithographic sources
[DE93-019941] p 1997 N94-21848
Chemistry and materials science
[DE94-001449] p 2152 N94-21858
Energy-resolving x ray detectors with charge amplification due to multiple quasiparticle tunneling
[DE93-019506] p 2031 N94-21869
Simulations of spectral broadening by cross-phase modulation (XPM) with chaotic light pulses
[DE93-019823] p 1819 N94-21872
Shattering the myth of the resonantly photo-pumped neon-like titanium laser
[DE93-019824] p 1819 N94-21873
Effect of bandwidth on beam smoothing and frequency conversion at the third harmonic of the Nova laser
[DE93-019917] p 1819 N94-21920
Molecular dynamics modeling of the mechanical behavior of metallic multilayers
[DE93-019947] p 1694 N94-21921
Robotic concepts for operation in barren terrain
[DE93-040539] p 1946 N94-21925
Disks of YBa2Cu3O7 shocked to 10 GPa pressures
[DE94-000464] p 2031 N94-21931
The effect of microstructural evolution on superplasticity in Ni3Si(V, Mo)
[DE93-041320] p 1694 N94-21943
Observation of x ray absorption magnetic circular dichroism in well-characterized iron-cobalt-platinum multilayers
[DE94-000303] p 1694 N94-21944
Photoelectron holography of platinum (111)
[DE93-040856] p 1810 N94-21950
Parametric instabilities in picosecond time scales
[DE94-000384] p 1966 N94-21958
Microtechnology: The key to the technical challenges of the 21st century
[DE94-000403] p 1769 N94-21959
Fabrication of amorphous diamond films
[DE94-000404] p 2032 N94-21960
Non-adiabatic effects in low-energy electron-molecule scattering
[DE93-040485] p 1976 N94-21968
Global emissions and models of photochemically active compounds
[DE93-040490] p 1852 N94-21969
The optical constants and spectral specular reflectivity of Highly Oriented Pyrolytic Graphite (HOPG)
[DE93-040546] p 1709 N94-21970
A packet based, data driven telemetry system for autonomous experimental sub-orbital spacecraft
[DE94-000399] p 1657 N94-21980
Automated analysis tools for reducing spacecraft telemetry data
[DE94-000400] p 1657 N94-21981
X ray characterization of a three-element condenser system for soft x ray projection lithography
[DE93-019916] p 1990 N94-21985
Strengthening and toughening in refractory metal alloys
[DE93-019942] p 1695 N94-21986
A finite element formulation and adaptive solution approach for large-scale thermomechanical problems with complex contact conditions
[DE93-019605] p 1960 N94-21996
Dynamics of surface thermal expansion and diffusivity using two-color reflection transient gratings
[DE93-040547] p 1990 N94-22002
Three dimensional ultrasonic imaging
[DE93-040549] p 1968 N94-22003
Post-experimental plots for high speed data acquisition program
[DE94-000956] p 1918 N94-22011
Transferable tight-binding parameters: An application to Ni and Ni-Al alloys
[DE94-001044] p 1695 N94-22023
Shock temperature measurements of iron to 350 GPa
[DE94-001058] p 1695 N94-22024
Interface science of controlled metal/metal and metal/ceramic interfaces prepared using ultrahigh vacuum diffusion bonding
[DE94-001066] p 1696 N94-22025
Microscopic and macroscopic dynamics
[DE93-019576] p 1937 N94-22042
A spheromak ignition experiment reusing Mirror Fusion Test Facility (MFTF) equipment
[DE94-001856] p 2034 N94-22050
Silicon microelectronic field-emissive devices for advanced display technology
[DE94-000397] p 1794 N94-22380
Transmission electron microscopy study of thick copper-304 stainless steel multilayers
[DE94-001045] p 1696 N94-22394
Theoretical phase diagrams for solid H(sub 2)
[DE94-001049] p 1684 N94-22395
Computer simulation of molecular response at a shock front
[DE94-001050] p 1977 N94-22396
Radio galaxies and their environment
[DE93-040851] p 2150 N94-22397
First-principles pressure-temperature phase diagrams in metals
[DE94-001056] p 1696 N94-22398
Opacity measurements in shock-generated argon plasmas
[DE94-001057] p 1998 N94-22399
Smoothed-particle hydrodynamics and nonequilibrium molecular dynamics
[DE94-001059] p 1977 N94-22400
Phase screens for the control of the focal irradiance of the Nova laser
[DE94-001067] p 1820 N94-22401
Using the rule of mixtures to examine the hardness of Cu/Cu-Zr multilayers
[DE94-001068] p 1697 N94-22402
Everything you might want to know about the Internet but are afraid to ask!
[DE93-041118] p 2046 N94-22413
How to handle 6GBytes a night and not get swamped p 2058 N94-22444
Parallel functional programming in SISAL: Fictions, facts, and future
[DE93-040486] p 1937 N94-22558
Positron annihilation study of Sr Doping in La(2-x)Sr(x)CuO4
[DE94-000307] p 2036 N94-22594

LEHIGH UNIV., BETHLEHEM, PA.
A theoretical investigation of unsteady separation phenomena related to dynamic stall
[AD-A271865] p 1636 N94-20465
Preliminary AEM study of the microstructure and composition of metal particles in ordinary chondrites p 2086 N94-20894
Age and thermochronology of K-feldspars from the Manson Impact Structure p 1863 N94-20899
Computational and analytical methods in nonlinear fluid dynamics
[AD-A272722] p 1802 N94-21169

LEICESTER UNIV. (ENGLAND).
Evaluation of RDBMS packages for use in astronomy p 2048 N94-22514

LEIDEN UNIV. (NETHERLANDS).
Numerical ranges and stability estimates
[TW-92-10] p 1953 N94-21060
Linear programming for standard and nonstandard Markovian control problems. A survey
[PB93-191948] p 1963 N94-21066
Algorithms for Markov decision chains with partial information
[PB93-220085] p 1918 N94-22098

Deep near-infrared survey of the Southern Sky (DENIS) p 2062 N94-22467

LICK OBSERVATORY, SANTA CRUZ, CA.

CCD data acquisition systems at Lick and Keck Observatories p 2047 N94-22495

LIMBURG STATE UNIV., MAASTRICHT (NETHERLANDS).

Speech synthesis with artificial neural networks p 1743 N94-20245

LOCKHEED ENGINEERING AND SCIENCES CO., HAMPTON, VA.

Techniques used for the analysis of oculometer eye-scanning data obtained from an air traffic control display
[NASA-CR-191559] p 1643 N94-21629

Evaluation of a nonlinear method for the enhancement of tonal signal detection
[NASA-CR-191562] p 1968 N94-21741

The 2D and 3D hypersonic flows with unstructured meshes p 1920 N94-22365

LOCKHEED ENGINEERING AND SCIENCES CO., HOUSTON, TX.

Chronology of lunar granite 12033,576: Resetting of Rb-Sr and K-Ca isochrons p 2115 N94-20763

The parent magma of the Nakhla (SNC) meteorite: Reconciliation of composition estimates from magmatic inclusions and element partitioning p 2085 N94-20836

Space Generic Open Avionics Architecture (SGOAA) standard specification
[NASA-CR-188269] p 1666 N94-22275

LOCKHEED MISSILES AND SPACE CO., PALO ALTO, CA.

The x ray halo of AM Her
[NASA-CR-189310] p 2054 N94-20142

The x ray halo of Cen X-3
[NASA-CR-189309] p 2055 N94-21295

LOGICON R AND D ASSOCIATES, LOS ANGELES, CA.

Neural network studies
[AD-A271593] p 1943 N94-20947

LOGISTICS MANAGEMENT INST., BETHESDA, MD.

Using electronic data interchange to report product quality
[AD-A271843] p 1828 N94-20468

LONDON UNIV. (ENGLAND).

Survey on utilization of database for research and development of global environmental industry technology
[DE94-714891] p 1853 N94-22259

LORAL AEROSYS, SEABROOK, MD.

Array Simulations Platform (ASP) predicts NASA Data Link Module (NDLM) performance p 1744 N94-21348

LOS ALAMOS NATIONAL LAB., NM.

Statement of David E. Baldwin, Associate Director for Energy, Lawrence Livermore National Laboratory and John C. Crawford, Vice President, Sandia National Laboratories, California, to the Subcommittee on Research and Development of the Committee on Environment and Public Works, US Senate, Washington, DC, 22 March 1993
[DE93-017991] p 1844 N94-19803

Crystallographic phase transitions in actinide metals as a function of pressure
[DE93-040138] p 2011 N94-19827

Initial performance of Los Alamos advanced free electron laser
[DE93-040158] p 1814 N94-19828

Chemical equilibrium in high pressure molecular fluid mixtures
[DE93-040160] p 1796 N94-19829

A complex systems approach to computational molecular biology
[DE93-040062] p 1884 N94-19866

Laser amplifier developments at Mercury
[DE93-040103] p 1814 N94-19867

Parametric variations of ion transport in TFTR
[DE93-012653] p 1991 N94-19883

Metastable bcc phase formation in the Nb-Cr system
[DE93-018376] p 2012 N94-19926

Ionospheric tomography using the FORTE satellite
[DE93-018545] p 1854 N94-19955

Thermal behavior of natural zeolites
[DE93-040091] p 1699 N94-19975

A weighted least-squares lump correction algorithm for transmission-corrected gamma ray nondestructive assay
[DE93-018474] p 1904 N94-20049

Techniques for reducing error in the calorimetric measurement of low wattage items
[DE93-018472] p 1807 N94-20114

Calorimeter measurements of low wattage items
[DE93-018473] p 1807 N94-20115

Measurement and correction of magnetic fields in pulsed slotted-tube microwigglers
[DE93-040100] p 1815 N94-20272

Non-Fermi-liquid and multichannel Kondo phenomena in Y(1-x)U(x)Pd3 and related alloys
[DE93-040135] p 2015 N94-20275

Applying the INN model to the MaxClique
[DE93-040137] p 1906 N94-20276

Performance of the high brightness linac for the Advanced Free Electron Laser Initiative at Los Alamos
[DE93-040141] p 1816 N94-20277

The National High Magnetic Field Laboratory, a user facility in support of research in high magnetic fields
[DE93-040145] p 1714 N94-20278

Fast data parallel polygon rendering
[DE93-040157] p 1929 N94-20279

Experimental study of a shock accelerated thin gas layer
[DE93-018354] p 1799 N94-20286

Multiport solid-state imager characterization at variable pixel rates
[DE93-018366] p 1808 N94-20287

Temperature dependence of 4f PES features and hole occupancy in ytterbium heavy fermions
[DE93-040131] p 1691 N94-20321

The GEM Silicon Tracking System
[DE93-040133] p 2016 N94-20322

Non-fermi liquid and spin-glass behavior of the Sc(1-x)U(x)Pd3 system
[DE93-040134] p 2016 N94-20335

Localization from near-source quasi-static electromagnetic fields
[DE93-040390] p 1732 N94-20479

Cosmogenic-radionuclide profiles in Knyahinya: New measurements and models p 2106 N94-20713

Photoemission and the electronic properties of heavy fermions: Limitations of the Kondo model
[DE93-040191] p 1974 N94-21553

Demonstration of ultraviolet lasing with a low energy electron beam
[DE93-040192] p 1818 N94-21554

Local structure and superconductivity in La(2-x)Ba(x)CuO4 for x=0.125 and x=0.15
[DE93-040193] p 2029 N94-21555

Issues related to mechanical properties of neutron-irradiated ceramics
[DE93-040262] p 1707 N94-21560

A data distributed, parallel algorithm for ray-traced volume rendering
[DE93-040150] p 1935 N94-21622

Simulated behaviour of large scale SCI rings and tori
[DE93-040149] p 1935 N94-21745

Visualization on massively parallel computers using CM/AVS
[DE93-040151] p 1936 N94-21746

A methodology for quantifying uncertainty in models
[DE93-040154] p 1916 N94-21747

Magnetic instability of Kondo insulators
[DE93-040064] p 1768 N94-21762

Geometric optimization
[DE93-040152] p 1917 N94-21764

A high-intensity He-jet production source for radioactive beams
[DE93-040247] p 1981 N94-21767

Local structure in oxygen-doped La2CuO(4+delta)
[DE93-040248] p 2030 N94-21768

Optimization and control of a small angle ion source using an adaptive neural network controller
[DE93-040063] p 1946 N94-21845

Self assembly: An approach to terascale integration
[DE93-040104] p 1769 N94-21846

Low p(sub T) phenomena observed in high energy nuclear collisions
[DE94-000825] p 1982 N94-21849

Proceedings of the IMOG (Interagency Manufacturing Operations Group) Numerical Systems Group
[DE94-001009] p 1917 N94-21851

Theoretical studies of the structures and electronic properties of U(NH2)(sub 3) and Np(NH2)(sub 3)
[DE94-000768] p 2031 N94-21857

The accuracy-through-order and the equivalence properties in the algebraic approximant
[DE93-040188] p 1960 N94-21946

A moving finite element model of the tokamak scrapeoff layer
[DE94-000673] p 1997 N94-21965

Magnetism in CeRu2Ge2 and CeRh2Ge2 and its pressure dependence
[DE93-040061] p 2032 N94-21987

Magnetic insulation of secondary electrons in plasma source ion implantation
[DE93-040106] p 1997 N94-21988

A dc Penning surface-plasma source
[DE93-040126] p 1997 N94-21989

Microtextural characterization of annealed and deformed copper
[DE93-040144] p 1695 N94-21990

Temperature dependence of magnetic order in single-crystalline UPdSn
[DE93-040153] p 2033 N94-21991

Interactions of slow H, H2, and H3 with thin foils
[DE93-040263] p 1976 N94-21995

The use of lidar for the evaluation of traffic-related urban pollution
[DE94-000704] p 1852 N94-22017

Variable-field permanent magnet dipole
[DE94-000800] p 1820 N94-22020

Surface modification of Ti3Al for improved oxidation resistance
[DE93-018297] p 1696 N94-22034

Crystal orientation dependence of elastic precursor strength in pentaerythritol tetranitrate
[DE93-018340] p 2034 N94-22035

Low temperature absorption spectra and ground state electronic structure of tetrakis(2,6-di-tert-butylphenoxide)uranium(IV)
[DE94-000774] p 2035 N94-22387

Theoretical studies of structural phase transitions in actinide metals
[DE94-000796] p 1696 N94-22388

Time evolution of the quark-gluon plasma
[DE94-000804] p 1998 N94-22389

The effect of Compton scattering on the double to single ionization ratio in helium
[DE94-000884] p 1827 N94-22390

High-velocity interceptors for boost-phase intercepts
[DE94-001077] p 1965 N94-22403

The ALEXIS data processing package: An IDL based system p 2047 N94-22453

Likelihood analysis of parity violation in the compound nucleus
[DE94-000671] p 1977 N94-22572

Initial operation of a large-scale plasma source ion implantation experiment
[DE94-000805] p 2036 N94-22583

Alloying studies in U(1-x)Th(x)Pd2Al3 (0 (le) x (le) 1)
[DE94-000807] p 2036 N94-22584

Infrared FEL photochemistry: Multiple-photon dissociation of freon gas
[DE94-000817] p 1820 N94-22585

LOUGHBOROUGH UNIV. OF TECHNOLOGY (ENGLAND).

A design optimization procedure for epicyclic gears
[MATHS-REPT-A-188] p 1822 N94-20146

LOUISIANA STATE UNIV., BATON ROUGE.

Development of a technique to determine the morphology and dynamics of agglomerates in chemically reacting flows
[AD-A271160] p 1678 N94-20000

Embedded microclusters in zeolites and cluster beam sputtering: Simulation on parallel computers
[DE94-000741] p 1701 N94-20352

A calcium oxide sorbent process for bulk separation of carbon dioxide
[DE93-019288] p 1847 N94-21540

LOUISVILLE UNIV., KY.

Enhancement of wound healing by biosynthetic growth factor
[AD-A272517] p 1892 N94-21415

LOWELL OBSERVATORY, FLAGSTAFF, AZ.

Observed climatic activity pertaining to the evolution of the northern plains p 2090 N94-20392

LUNAR AND PLANETARY INST., HOUSTON, TX.

Workshop on the Martian Northern Plains: Sedimentological, Periglacial, and Paleoclimatic Evolution
[NASA-CR-194831] p 2088 N94-20382

Morphologic and morphometric studies of impact craters in the northern plains of Mars p 2089 N94-20384

Seismic-triggering history of the catastrophic outflows in the Chryse region of Mars p 2091 N94-20399

Twenty-Fourth Lunar and Planetary Science Conference. Part 3: N-Z
[NASA-CR-193149] p 2092 N94-20636

Diapirs and cantaloupes: Layering and overturn of Triton's crust p 2111 N94-20738

Geology of the southern hemisphere of Triton: No polar cap p 2111 N94-20739

The 3-D Moons: The Voyager stereo atlas of the outer solar system p 2111 N94-20740

Chicxulub impact basin: Gravity characteristics and implications for basin morphology and deep structure p 1862 N94-20757

Contributions of the Clementine mission to our understanding of the processes and history of the Moon p 2119 N94-20784

Impact basins on Venus and some interplanetary comparisons p 2119 N94-20785

Geology and deposits of the Serenitatis basin p 2119 N94-20786

Magnetically controlled solar nebula p 2120 N94-20791

Workshop on Early Mars: How Warm and How Wet?, part 1
[NASA-CR-193553] p 2142 N94-21659

The evolution of the early Martian climate and the initial emplacement of crustal H2O p 2143 N94-21665

The hydrologic response of Mars to the onset of a colder climate and to the thermal evolution of its early crust p 2143 N94-21666
MSATT Workshop on Innovative Instrumentation for the In Situ Study of Atmosphere-Surface Interactions on Mars
[NASA-CR-194584] p 1811 N94-22430
LUND INST. OF TECH. (SWEDEN).
Microstructure in mortar: A summary of a new project of research p 1706 N94-21896

M

MAINE UNIV., ORONO.
Direct imaging of the surface microstructure of dielectric materials using an atomic force microscope
[AD-A272251] p 2018 N94-20575
Structure and morphology of Pd overlayers on epitaxial SnO2 films studies with the atomic force microscope
[AD-A271827] p 2026 N94-21458
MANITOBA UNIV., WINNIPEG.
Formulation for numerical solution of radiation and transmission from arbitrary apertures p 1745 N94-22140
Effect of errors on the phase centre and pointing angle of phased array antennas p 1746 N94-22162
On the discovery of approximate arithmetic relations by backpropagation networks p 1782 N94-22181
Logic oriented neural networks p 1782 N94-22182
Performance of a simple circular polarization selective surface p 1746 N94-22198
Acceleration of backpropagation learning using a parallel DSP machine p 1786 N94-22206
An insensitive algorithm for template matching with correlation p 1793 N94-22249
Applications of planar near-field measurements to electromagnetic radiation and interference problems p 1747 N94-22252
MARTIN MARIETTA LABS., BALTIMORE, MD.
Applicability and performance benefits of XD (Tradename) titanium aluminides to expendable gas turbine engines
[AD-A272998] p 1648 N94-21268
MARYLAND UNIV., BALTIMORE.
Image detection using edge extraction algorithms
[AD-A272439] p 1911 N94-21203
MARYLAND UNIV., COLLEGE PARK.
Modeling failure and reliability in new-generation devices
[AD-A271150] p 1748 N94-19910
EHD enhancement of pool and in-tube boiling of alternate refrigerants
[DE94-000787] p 1798 N94-20101
Modeling of interactions between biosphere and atmosphere on the global scale
[NASA-CR-193423] p 1837 N94-20205
The thumbprint terrain: What will Mars Observer tell us? p 2091 N94-20397
Polynomial interpolation of real functions 1: Interpolation in an interval
[AD-A272330] p 1951 N94-20527
Strengthening of NiAl matrix composites
[AD-A271491] p 1674 N94-20550
Local topography of Mars and its relationship to surface weathering processes p 2111 N94-20737
C2, CN and dust in Comet Wilson (1987VII) p 2083 N94-20746
Rhenium-osmium isotope systematics of ordinary chondrites and iron meteorites p 2085 N94-20854
Calibration of radiation codes in climate models: Comparison of calculations with observations from the SPECtral Radiation Experiment (SPECTRE) p 1879 N94-22337
MARYLAND UNIV., PRINCESS ANNE.
Signal classification and noise filtering using artificial neural networks p 1744 N94-22103
MASSACHUSETTS INST. OF TECH., CAMBRIDGE.
Recognizing 3-D objects using 2-D images
[AD-A271005] p 1983 N94-19819
A parallelizing compiler based on partial evaluation
[AD-A270838] p 1898 N94-19832
Performance potential of plasma thrusters: Arcjet and Hall thruster modeling
[AD-A271085] p 1667 N94-19847
Building brains for bodies
[AD-A270531] p 1939 N94-19875
Exploiting the parallelism exposed by partial evaluation
[AD-A270678] p 1928 N94-19877
Why stereo vision is not always about 3D reconstruction
[AD-A270522] p 1939 N94-19893
Robust photo-topography by fusing shape-from-shading and stereo
[NASA-CR-194697] p 1806 N94-19920
On geometric and algebraic aspects of 3D affine and projective structures from perspective 2D views
[AD-A270520] p 1983 N94-19968
Robust, high-speed network design for large-scale multiprocessing
[AD-A271003] p 1716 N94-19977
Robust and efficient 3D recognition by alignment
[AD-A270839] p 1904 N94-20041
Liquid rocket propulsion. Theory p 1667 N94-20069
Application of change detection to dynamic contact sensing
[AD-A270523] p 1939 N94-20105
Statistical object recognition
[AD-A270887] p 1962 N94-20113
Inversion of gravity and bathymetry in oceanic regions for long-wavelength variations in upper mantle temperature and composition
[NASA-CR-192272] p 1882 N94-20131
Atmospheric infrared sounder
[NASA-CR-194814] p 1856 N94-20362
Spatial organization of polymer chains in a crystallizable diblock polyethylene and polystyrene
[AD-A271862] p 1702 N94-20463
Improvement of helicopter attitude stability by active control of the conventional swash plate
[NASA-CR-194786] p 1650 N94-20524
Optical metrology of magnetically trapped hydrogen
[AD-A272110] p 1680 N94-20584
Geoid, topography, and convection-driven crustal deformation on Venus p 2116 N94-20769
The role of CO2 in weathering reactions and the presence of S2 on Venus: Implications for the pyrite stability field p 2122 N94-20799
The stability of oxyamphiboles: Existence of Ferric-bearing minerals under the reducing conditions on the surface of Venus p 2122 N94-20800
Origin of high-Ti lunar ultramafic glasses p 1686 N94-20853
Visual tracking
[AD-A271686] p 1943 N94-20920
Recognition by prototypes
[AD-A271687] p 1943 N94-20921
Causal reconstruction
[AD-A271692] p 1906 N94-20929
Internal camera calibration using rotation and geometric shapes
[AD-A272718] p 1808 N94-21167
Rotational isomers of Mo(VI) alkylidene complexes and Cis/trans polymer structure: Investigations in ring-opening metathesis polymerization
[AD-A272647] p 1704 N94-21184
Polymerization of enantiomerically pure 2,3-dicarboalkoxy norbornadienes and 5,6-disubstituted norbornenes by well-characterized molybdenum ROMP catalysts
[AD-A272649] p 1704 N94-21186
Reaction zone models for vortex simulation of turbulent combustion
[AD-A272723] p 1681 N94-21213
Measure fields for function approximation
[AD-A272660] p 1964 N94-21215
Some extensions of the k-means algorithm for image segmentation and pattern classification
[AD-A271691] p 1913 N94-21364
Data and model-driven selection using parallel-line groups
[AD-A271702] p 1913 N94-21365
MAYGEN: A symbolic debugger generation system
[AD-A272512] p 1913 N94-21413
Optimal convolution SOR acceleration of waveform relaxation with application to semiconductor device simulation p 1922 N94-21475
Oxidation of dissolved iron under warmer, wetter conditions on Mars: Transitions to present-day arid environments p 2143 N94-21663
Modeling of outgassing and matrix decomposition in carbon-phenolic composites
[NASA-CR-194741] p 1676 N94-21743
Characterization of convection related defects in II-VI compound semiconductors
[NASA-CR-194704] p 2030 N94-21778
Modelling decision-making by pilots
[NASA-CR-194787] p 2040 N94-21821
Photochemical approaches to conversion of light to electricity or fuel
[DE94-001650] p 1849 N94-22048
SPIKE: Application for ASTRO-D mission planning p 1926 N94-22486
Wilbur: A low-cost CCD camera system for MDM Observatory p 1814 N94-22510
MASSACHUSETTS INST. OF TECH., LEXINGTON.
Massachusetts Institute of Technology Lincoln Laboratory Journal volume 6, number 1, Spring 1993
[AD-A272273] p 1737 N94-20944
Use of the Weiss-Weinstein bound to compare the direction-finding performance of sparse arrays
[AD-A272582] p 1738 N94-21210
A compact, portable EHF/SHF antenna for advanced SCAMP
[AD-A272614] p 1739 N94-21211
A retrieval error analysis technique for passive infrared atmospheric sounders
[AD-A272618] p 1867 N94-21212
Downlink acquisition and tracking procedures for the ASCAMP satellite communications terminal
[AD-A272912] p 1739 N94-21244
MASSACHUSETTS UNIV., AMHERST.
Interinjection-locked quasioptical power combiners and phased arrays
[AD-A271178] p 2015 N94-20214
A model for the origin of Martian polygonal terrain p 2090 N94-20393
Use of microwave polarimetry to enhance SAR images of the ocean surface
[AD-A271911] p 1882 N94-20489
MATERIALS AND ELECTROCHEMICAL RESEARCH CORP., TUCSON, AZ.
Fabrication of whisker-toughened alumina tubes
[DE94-001012] p 1677 N94-22022
MATERIALS RESEARCH LABS., ASCOT VALE (AUSTRALIA).
Distribution of turbidity in Australian tropical waters
[AD-A271059] p 1881 N94-19905
Ageing studies on a composite propellant containing a new organo-copper burn rate catalyst
[AD-A271060] p 1711 N94-19906
MATERIALS RESEARCH SOCIETY, PITTSBURG, PA.
Common Themes and Mechanisms of Epitaxial Growth, volume 312
[AD-A270513] p 2013 N94-19967
MATRA MARCONI SPACE, TOULOUSE (FRANCE).
Meteoroids and debris impact risk assessment on Columbus and Hermes using a realistic geometrical analysis tool p 1662 N94-21388
Combination of on ground experiments and analysis software for the evaluation of material degradation in space (SILEX project) p 1662 N94-21389
MAX-PLANCK-INST. FOR PSYCHOLINGUISTICS, NIJMEGEN (NETHERLANDS).
Modeling the human mental lexicon with self-organizing feature maps p 1743 N94-20244
MAX-PLANCK-INST. FUER CHEMIE, MAINZ (GERMANY).
Abundance and composition of solar KR in the H3-H6 chondrite ACFER111 p 1684 N94-20676
Chemical composition of new Acapulcoites and Lodranites p 2086 N94-20905
MAX-PLANCK-INST. FUER EXTRATERRESTRISCHE PHYSIK, BERLIN (GERMANY).
Consequences of chaotic particle motion for the stability of space plasma current sheets p 2001 N94-22636
MAX-PLANCK-INST. FUER EXTRATERRESTRISCHE PHYSIK, GARCHING (GERMANY).
Spatial distribution of near infrared line radiation in galactic nuclei measured with Fabry-Perot spectrometer FAST
[MPE-239] p 2081 N94-21138
ROSAT data analysis with EXSAS p 2080 N94-22555
Results from ROSAT p 2000 N94-22630
Compton Gamma Ray Observatory highlights of the sky survey p 2002 N94-22642
MAX-PLANCK-INST. FUER METEOROLOGIE, HAMBURG (GERMANY).
Proceedings of the Workshop on New Generation of Radiation Budget Measurements From Space and Their Use in Climate Modelling and Diagnostic Studies
[MPIM-90] p 1860 N94-22283
The seasonal variation of the cloud radiative forcing: Comparison of ECHAM model simulations with ERBE data p 1860 N94-22288
Use of satellite data for validation of the ECHAM models p 1861 N94-22289
MAX-PLANCK-INST. FUER PHYSIK UND ASTROPHYSIK, GARCHING (GERMANY).
A deep x ray survey in the Lockman hole and the soft x ray log N - log S
[NASA-CR-194698] p 2054 N94-20174
X ray archeology in the Coma cluster
[NASA-CR-194799] p 2054 N94-20175
Optical and Gamma Ray Space Observations
[NASA-TM-109389] p 2149 N94-20602
Gamma ray bursts from collisions of primordial small mass black holes with comets p 2150 N94-20604
Radiation driven winds of hot stars: Some remarks on stationary models and spectrum synthesis in time-dependent simulations
[NASA-CR-194691] p 2081 N94-21578
The distribution of dark matter in the A2256 cluster
[NASA-CR-194699] p 2055 N94-21579

MAX-PLANCK-INST. FUER STROEMUNGSFORSCHUNG, GOETTINGEN (GERMANY).
Shock induced condensation in fluids of high molar specific heat: Shock structure and relaxation
[MPIS-106/1993] p 1796 N94-20145

MAXWELL LABS., INC., SAN DIEGO, CA.
Data analysis support for the SPREE instruments on the TSS-1 shuttle flight
[AD-A272445] p 1654 N94-21429

MCDONNELL-DOUGLAS AEROSPACE INFORMATION SERVICES CO., SAINT LOUIS, MO.
Strength and toughness improvement of silicide intermetallics by nanophase and microphase reinforcements
[AD-A272914] p 1692 N94-21320

MCGILL UNIV., MONTREAL (QUEBEC).
Design of a floating point convolution processor p 1775 N94-22133
A Hopfield neural net for discrete Fourier transform calculation p 1783 N94-22184
Integration of parallel processing structures using a matrix approach p 1784 N94-22192
Specification and formal verification of the safety criterion in the alternating bit protocol p 1784 N94-22193
ARQ on fading channels p 1747 N94-22242

MCMASTER UNIV., HAMILTON (ONTARIO).
Synthesis and structural characterization of new light molecular weight inorganic oxidizers and relative derivatives, volume 1
[AD-A271437] p 2012 N94-19842
Improvements on the design of optimum SAW filters with the Remez Exchange Algorithm p 1773 N94-22123
Full wave numerical model of arbitrarily-shaped proximity coupled microstrip antennas p 1745 N94-22137
Modeling of coaxial-fed microstrip patch antenna by finite difference time domain method p 1745 N94-22138
Using stream interleaving to eliminate the need for interlocks in deeply pipelined processors p 1781 N94-22175
Wideband source location in two-dimensional array processing p 1747 N94-22250
Study of TE(1-delta) mode in open dielectric resonators by a finite difference time domain method p 1747 N94-22253

MEHARRY MEDICAL COLL., NASHVILLE, TN.
Lateral distribution of lipids in membranes at high pressure
[AD-A271183] p 1700 N94-20299

MEMORIAL UNIV. OF NEWFOUNDLAND, SAINT JOHNS.
A new class of multi-function two-rail totally self-checking basic building blocks p 1788 N94-22215
Dynamic analyses of flexible robotic manipulators
[ISBN-0-315-59251-6] p 1827 N94-22421

MESSERSCHMITT-BOELKOW-BLOHM G.M.B.H., BREMEN (GERMANY).
Columbus PMP Critical Technologies Program: Approach for materials life time prediction p 1664 N94-21402

METEOROLOGICAL OFFICE, BRACKNELL (ENGLAND).
Simulation of clear-sky outgoing longwave radiation over the oceans using operational analysis p 1861 N94-22290

METRAFLU, ECULLY (FRANCE).
Distributed loss model: Application to a spatial turbopump inducer p 1668 N94-20078
Finite element numerical simulation of three dimensional turbulent flows with dispersion: Eulerian and Lagrangian approaches
[ECL-92-42] p 1801 N94-20597

MIAMI UNIV., CORAL GABLES, FL.
Intervention strategies for the management of human error
[NASA-CR-4547] p 1642 N94-22373

MICHIGAN UNIV., ANN ARBOR.
A new conformal absorbing boundary condition for finite element meshes and parallelization of FEMATS
[NASA-CR-194740] p 1950 N94-20034
Remote sounding of tropospheric minor constituents
[NASA-CR-194265] p 1855 N94-20132
A comparative study of an ABC and an artificial absorber for truncating finite element meshes
[NASA-CR-194275] p 1716 N94-20160
Dynamics Explorer 2: Continued FPI and NACS instrument data analysis and associated scientific activity at the University of Michigan
[NASA-CR-194689] p 1657 N94-20173
Transport in microstructures in the microwave and millimeter-wave regime
[AD-A271875] p 2017 N94-20470
Radiation and scattering from printed antennas on cylindrically conformal platforms
[NASA-CR-194703] p 1741 N94-21885
Scattering by cavity-backed antennas on a circular cylinder p 1741 N94-21886
Radiation by cavity-backed antennas on a circular cylinder p 1741 N94-21887
User manual for EXCALIBUR: A FE-BI numerical laboratory for cavity-backed antennas in a circular cylinder, version 1.2 p 1741 N94-21888
Multiorder etalon sounder (MOES) development and test for balloon experiment
[NASA-CR-194730] p 1859 N94-22026

MICROELECTRONICS CENTER OF NORTH CAROLINA, RESEARCH TRIANGLE PARK.
Field emitter array RF amplifier development project, phase 1, option 1
[AD-A272567] p 1740 N94-21361

MICRONAV LTD., SYDNEY (NOVA SCOTIA).
MLS pointing angle error sources and effects p 1644 N94-22154
Developing software to RTCA DO-178A p 1645 N94-22155

MIDWEST RESEARCH INST., GOLDEN, CO.
High efficiency epitaxial optical reflector solar cells
[DE93-017115] p 1845 N94-19805
Current status of environmental, health, and safety issues of nickel metal-hydride batteries for electric vehicles
[DE93-017079] p 1748 N94-19902
Wind energy: Program overview, FY 1992
[DE93-000056] p 1845 N94-19921
Development of high-efficiency CdTe solar cells
[DE93-018206] p 1845 N94-19925
Research on defects and transport in amorphous-silicon-based semiconductors
[DE93-017117] p 2013 N94-19939
Biofuels: Project summaries
[DE93-010003] p 1712 N94-19984
Microscopic origins of metastable effects in a-Si:H and deep defect characterization in a-Si,Ge:H alloys
[DE93-018205] p 1688 N94-19985
Growth mechanisms and characterization of hydrogenated amorphous-silicon-alloy films
[DE93-018202] p 1699 N94-20047
Fabrication of stable large-area thin-film CdTe photovoltaic modules
[DE93-018204] p 1845 N94-20095
Building integrated photovoltaic systems analysis
[DE93-018208] p 1846 N94-21298
First Biomass Conference of the Americas: Energy, Environment, Agriculture, and Industry, volume 2
[DE94-000435] p 1847 N94-21562
Advanced processing technology for high-efficiency thin-film CuInSe2 solar cells
[DE93-010045] p 1847 N94-21614
Fundamental studies of defect generation in amorphous silicon alloys grown by remote plasma-enhanced chemical-vapor deposition
[DE93-017083] p 2029 N94-21615
Proceedings of the 1993 DOE/NREL Hydrogen Program Review
[DE93-018207] p 1847 N94-21616
Research on polycrystalline thin-film submodules based on CuInSe2 materials
[DE93-018223] p 2029 N94-21617
Stable, high-efficiency amorphous-silicon solar cells with low hydrogen content
[DE93-018214] p 1848 N94-21826
Thin-film CdTe and CuInSe2 photovoltaic technologies
[DE93-018217] p 1848 N94-21827
Annual Report, Materials Science Branch, FY 1992
[DE94-000204] p 1849 N94-22015
Research on stable, high-efficiency amorphous silicon multijunction modules
[DE93-018220] p 1850 N94-22257

MINISTRY OF FINANCE (FINLAND).
Use of economic models in Finnish economic policy p 2053 N94-22085

MINNESOTA UNIV., DULUTH.
Studies of neural and cognitive function in subjects exposed to the marine-air interface, phases 1 and 2
[AD-A272282] p 1891 N94-20624

MINNESOTA UNIV., MINNEAPOLIS.
Numerical solution of differential-algebraic equations with ill-conditioned constraints
[AD-A270934] p 1949 N94-19898
Helium in interplanetary dust particles p 2082 N94-20653
Evolution of the Martian atmosphere p 2146 N94-21680
Fundamental studies of stress distributions and stress relaxation in oxide scales on high temperature alloys
[DE94-001444] p 1693 N94-21854
STARBASE: Database software for the automated plate scanner p 1927 N94-22512

MISSION RESEARCH CORP., ALBUQUERQUE, NM.
Characterization of electromagnetic fields in an extended chamber at the Short Pulse Experimental Electron Device (SPEED) simulator
[AD-A265955] p 1717 N94-20329

MISSISSIPPI STATE UNIV., BAY SAINT LOUIS.
Design document and database specifications for the Naval Interactive Data Analysis System (NIDAS), version 1.0
[NASA-CR-194817] p 2045 N94-21885

MISSOURI UNIV., ROLLA.
Kinetics of phase transformations in glass forming systems
[NASA-CR-194270] p 1701 N94-20347
Evaporation of a sodium tellurite melt in the jamic low gravity drop shaft p 1713 N94-20605
Dynamics of adsorbed, swollen block copolymers
[AD-A272013] p 1706 N94-21460

MITSUBISHI ELECTRIC CORP., KAMAKURA (JAPAN).
The conformance testing methodology to CTRON (communication and central TRON) extended OS p 1772 N94-22118

MONTANA STATE UNIV., BOZEMAN.
Pair plasmas in the central engine of active galactic nuclei p 2002 N94-22641

MONTREAL UNIV. (QUEBEC).
Creep damage of carbon fiber reinforced PEEK
[ISBN-0-315-58962-0] p 1677 N94-22420

MORGANTOWN TECHNOLOGY CENTER, WV.
Molten carbonate fuel cell networks: Principles, analysis, and performance
[DE93-019872] p 1846 N94-21527

MOSCOW PHYSICAL-ENGINEERING INST. (RUSSIA).
VHE gamma ray generation by radio pulsars p 2007 N94-22680

MOSCOW STATE UNIV. (RUSSIA).
Geologic mapping of Northern Atla Regio on Venus: Preliminary data p 2095 N94-20654
Beta Regio rift system on Venus: Geologic interpretation of Magellan images p 2095 N94-20655
Beta Regio - Phoebe Regio on Venus: Geologic mapping with the Magellan data p 2096 N94-20656
Preliminary estimation of tagamite cooling conditions (Puchezh-Katunki Astroblema, Russia) p 2083 N94-20735
Complex-2: Low Earth orbital environment simulation facility for materials durability evaluation p 1653 N94-21370
Electrostatic charging and secondary effects in materials submitted to radiation in space p 1661 N94-21383
Forecasting technique of variations of the optical absorptivity of thermal control coatings under different simultaneous radiations p 1664 N94-21399
Microdynamic model of reproduction: Taxation and currency issue as regulators of economy p 2053 N94-22084

MOUND LAB., MIAMISBURG, OH.
Operational equations for the five-point rectangle
[DE94-000366] p 1959 N94-21655

MUENSTER UNIV. (GERMANY).
Multielement analysis of interplanetary dust particles using TOF-SIMS p 2084 N94-20790

N

NAGOYA UNIV. (JAPAN).
General relativistic winds in a black hole magnetosphere p 2002 N94-22644
Mean elemental composition and He-3 enrichments in solar energetic particles p 2006 N94-22670
Asymptotic structure of magnetically driven MHD wind p 2008 N94-22682
Fragmentation of magnetized filamentary interstellar clouds p 2008 N94-22687
Gravitational instability of magnetized filamentary clouds. 1: Helical magnetic fields p 2008 N94-22688
Gravitational instability of magnetized filamentary clouds. 2: Rotation p 2009 N94-22689
Time variation of MHD accretion onto a black hole p 2009 N94-22692

NANYANG TECHNOLOGICAL INST. (SINGAPORE).
VLSI mixed signal processing system p 1744 N94-21100
Heuristic-based scheduling algorithm for high level synthesis p 1764 N94-21704
Evaluation of floating-point sum or difference of products in carry-save domain p 1764 N94-21705
A real time correlator architecture using distributed arithmetic principles p 1768 N94-21734

NATIONAAL INST. VOOR KERNFYSICA EN HOGE ENERGIEFYSICA, AMSTERDAM (NETHERLANDS).
Control and readout of the extraction septum of AmPS
[DIGEL-1993-2] p 1979 N94-20117
New preamplifiers for the SEM scanner
[DIGEL-1993-3] p 1979 N94-20118

Bundle profile monitor for AmPS
[DIGEL-1992-8] p 1979 N94-20123
Power supply and controller for the Sextupole magnet of AmPS
[DIGEL-1992-3] p 1753 N94-21064

NATIONAL ACADEMY OF SCIENCES - NATIONAL RESEARCH COUNCIL, WASHINGTON, DC.

The Board on Earth sciences and resources
[DE94-000745] p 1859 N94-22018

NATIONAL AERONAUTICS AND SPACE ADMINISTRATION, WASHINGTON, DC.

NASA's Education Program
[NASA-EP-297] p 2038 N94-20129
Space Shuttle Mission STS-61: Hubble Space Telescope servicing mission-01
[NASA-TM-109344] p 1653 N94-20192
Rockets: Physical science teacher's guide with activities
[NASA-EP-291] p 1669 N94-20226
Aeronautical engineering: A continuing bibliography with indexes (supplement 294)
[NASA-SP-7037(294)] p 1635 N94-20267
The manager's guide to NASA graphics standards
[NHB-1430.2] p 2042 N94-20308
NASA patent abstracts bibliography: A continuing bibliography. Section 1: Abstracts (supplement 44)
[NASA-SP-7039(44)-SECT-1] p 2043 N94-21254
Aerospace medicine and biology: A continuing bibliography with indexes (supplement 383)
[NASA-SP-7011(383)] p 1892 N94-21288
Issues in NASA program and project management. Special Report: 1993 conference
[NASA-SP-6101(07)] p 2039 N94-21497
Issues in NASA program and project management
[NASA-SP-6101(06)] p 2040 N94-21499
NASA procurement report, FY 1992
[NASA-TM-109390] p 2040 N94-21623
NASA procurement report, FY 1993
[NASA-TM-109393] p 2040 N94-21625
Summary data on all NASA procurement actions
[NASA-TM-109392] p 2040 N94-21638
Index to 1992 NASA Tech Briefs, volume 16, numbers 1-12
[NASA-TM-109377] p 2053 N94-21736
Index to 1991 NASA Tech Briefs, volume 15, numbers 1-12
[NASA-TM-109376] p 2053 N94-21737
Cumulative index to NASA Tech Briefs, 1986-1990, volumes 10-14
[NASA-TM-109378] p 2054 N94-21738
Spinoff, 1992
[NASA-NP-201] p 2054 N94-21739
An overview of the radiation component of the NASA TOGA-COARE experiment p 1881 N94-22344
Second Annual Conference on Astronomical Data Analysis Software and Systems. Abstracts
[NASA-TM-108245] p 2057 N94-22438
The cool-star spectral catalog: A uniform collection of IUE SWP-LOs p 2046 N94-22446

NATIONAL AERONAUTICS AND SPACE ADMINISTRATION. AMES RESEARCH CENTER, MOFFETT FIELD, CA.

Boost-phase discrimination research
[NASA-TM-109347] p 1666 N94-19818
Some VTOL head-up display drive-law problems and solutions
[NASA-TM-104027] p 1635 N94-20035
A comparison of two incompressible Navier-Stokes algorithms for unsteady internal flow
[NASA-TM-108794] p 1798 N94-20104
Quinoa: An emerging new crop with potential for CELSS
[NASA-TP-3422] p 1895 N94-20137
Cooling apparatus and couplings therefor
[NASA-CASE-ARC-11921-1] p 1800 N94-20371
FD-TD modeling of 2-D dielectric waveguides for propagation and scattering of femtosecond optical solitons p 1719 N94-20406
Derivation of the midinfrared (5.0-25.0 micron) optical constants of hydrous carbonate and sulfate p 2108 N94-20723
Spectral analysis of chemisorbed CO2 on Mars analog materials p 2140 N94-20900
The modern rotor aerodynamic limits survey: A report and data survey
[NASA-TM-4446] p 1635 N94-21490
Survey of lift-fan aerodynamic technology
[NASA-CR-177615] p 1646 N94-21592
Development and evaluation of a profile negotiation process for integrating aircraft and air traffic control automation
[NASA-TM-4360] p 1643 N94-21606
An attempt to comprehend Martian weathering conditions through the analysis of terrestrial palagonite samples p 2143 N94-21668
A model for the evolution of CO2 on Mars p 2144 N94-21671
Early Mars was wet but not warm: Erosion, fluvial features, liquid water habitats, and life below freezing p 2145 N94-21677
Mars and the early Sun p 2146 N94-21683
Self-Motion Perception and Motion Sickness
[NASA-CR-194276] p 1885 N94-21897
Changes in plasma vasopressin during motion sickness in cats p 1885 N94-21898
Susceptibility of the squirrel monkey to different motion conditions p 1885 N94-21899
Relationship of area postrema to three putative measures of motion sickness p 1885 N94-21900
Reassessment of area postrema's role in motion sickness and conditioned taste aversion p 1886 N94-21901
Gamma-aminobutyric acid (GABA) and neuropeptides in neural areas mediating motion-induced emesis p 1886 N94-21902
Detection of emetic activity in the cat by monitoring venous pressure and audio signals p 1886 N94-21903
Recovery of the vomiting reflex following area postrema ablation in squirrel monkeys p 1886 N94-21904
Motion sickness elicited by passive rotation in squirrel monkeys p 1887 N94-21905
Area postrema ablations in cats: Evidence for separate neural routes for motion- and xylazine-induced CTA and emesis p 1887 N94-21906
Effect of copper sulphate on the rate of afferent discharge in the gastric branch of the vagus nerve in the rat p 1887 N94-21907
Conditioned taste aversion induced by motion is prevented by selective vagotomy in the rat p 1887 N94-21908
Immunocytochemical localization of glutamic acid decarboxylase (GAD) and substance P in neural areas mediating motion-induced emesis: Effects of vagal stimulation on GAD immunoreactivity p 1887 N94-21909
The effects of area postrema lesions and selective vagotomy on motion-induced conditioned taste aversion p 1888 N94-21910
Experimental studies of gastric dysfunction in motion sickness: The effect of gastric and vestibular stimulation on the vagal and splanchnic gastric efferents p 1888 N94-21911
Role of the area postrema in three putative measures of motion sickness in the rat p 1888 N94-21912
Conditioned taste aversion and motion sickness in cats and squirrel monkeys p 1888 N94-21914
Fuzzy and neural control
[NASA-TM-108753] p 1947 N94-22270
Optical properties of cirrus derived from airborne measurements during FIRE IFO 2 p 1872 N94-22297
Ground-based passive remote sensing during FIRE IFO 2 p 1844 N94-22319
Comparisons of downwelling radiation to model predictions based on groundbased measurements during FIRE 1991 p 1876 N94-22320
Analysis of the tropospheric water distribution during FIRE 2 p 1876 N94-22324
Three dimensional modeling of cirrus during the 1991 FIRE IFO 2: Detailed process study p 1877 N94-22327
NASA-Ames Research Center unstructured technology development p 1919 N94-22352
The 3-D unstructured mesh generation using local transformations p 1919 N94-22356
Dynamic mesh adaption for triangular and tetrahedral grids p 1920 N94-22363
The 3D Euler solutions using automated Cartesian grid generation p 1920 N94-22367
NASA data exchange standards for computational fluid dynamics p 1920 N94-22371
Surface acquisition through virtual milling p 1920 N94-22372
In situ identification of the Martian surface material and its interaction with the Martian atmosphere using DTA/GC p 1812 N94-22434
Temperature/pressure and water vapor sounding with microwave spectroscopy p 1812 N94-22436

NATIONAL AERONAUTICS AND SPACE ADMINISTRATION. GODDARD INST. FOR SPACE STUDIES, NEW YORK, NY.

Intensity and polarization of light scattered by size distributions of randomly oriented nonspherical particles p 1721 N94-20416
Long-Term Monitoring of Global Climate Forcings and Feedbacks
[NASA-CP-3234] p 1868 N94-21639
Climate forcings and feedbacks p 1869 N94-21641
Accuracy requirements p 1869 N94-21642
Climsat rationale p 1869 N94-21643
Earth observing scanning polarimeter p 1844 N94-21645
Michelson Interferometer (MINT) p 1813 N94-21646
Satellite orbit and data sampling requirements p 1870 N94-21648

NATIONAL AERONAUTICS AND SPACE ADMINISTRATION. GODDARD SPACE FLIGHT CENTER, GREENBELT, MD.

Spline screw payload fastening system
[NASA-CASE-GSC-13454-1] p 1821 N94-20126
An improved patch for radiative coolers
[NASA-CASE-GSC-13503-1] p 1822 N94-20127
Rotary encoding device using polygonal mirror with diffraction gratings on each facet
[NASA-CASE-GSC-13543-1] p 1985 N94-20240
The thumbprint terrain: What will Mars Observer tell us? p 2091 N94-20397
Relating ground truth collection to model sensitivity p 1719 N94-20409
Observation of pressure ridges in SAR images of sea ice: Scattering theory and comparison with observations p 1723 N94-20427
Multiple scattering effects on the Linear Depolarization Ratio (LDR) measured during CaPE by a Ka-band air-borne radar p 1728 N94-20446
Relationship of attenuation in a vegetation canopy to physical parameters of the canopy p 1729 N94-20450
Climbing robot
[NASA-CASE-GSC-13442-1] p 1823 N94-20494
Conically scanned holographic lidar telescope
[NASA-CASE-GSC-13462-1] p 1986 N94-20591
GMM-1: A 50 degree and order gravitational field model for Mars p 2117 N94-20774
Magnetic record in chondrite meteorites p 2085 N94-20858
Possible flexural signatures around Olympus and Ascraeus Montes, Mars p 2142 N94-20911
Linear mixing model applied to AVHRR LAC data p 1838 N94-20958
Sunphotometer network for monitoring aerosol properties in the Brazilian Amazon p 1839 N94-20961
Predicting LANDSAT MSS endmember signatures from corresponding higher resolution TM fraction images p 1839 N94-20962
An adaptive, lossless data compression algorithm and VLSI implementations p 1753 N94-21080
Rad-hard computer elements for space applications p 1753 N94-21082
Space qualified high speed Reed Solomon encoder p 1754 N94-21088
Mongoose: Creation of a Rad-Hard MIPS R3000 p 1754 N94-21090
A fixed/variable bit-rate data compression architecture p 1759 N94-21128
Networks Technology Conference
[NASA-CP-3241] p 1931 N94-21323
Enhanced networks operations using the X Window System p 1932 N94-21329
The automated ground network system p 1932 N94-21330
Space network scheduling benchmark: A proof-of-concept process for technology transfer p 1932 N94-21332
Distributed intelligent control and status networking p 1932 N94-21335
The Test Analysis Retrieval System (TARS): Meeting the challenges of the network's test processes p 1933 N94-21337
An in-depth analysis and modelling of the Shuttle to MILA S-band telemetry link p 1657 N94-21340
A packet switched communications system for GRO p 1744 N94-21345
A semi-Lagrangian approach to the shallow water equation p 1806 N94-21480
A synoptic-scale overview of the TOGA COARE intensive observing period November 1992 to February 1993 based on analyses from US operational global data assimilation systems
[NASA-TM-104593] p 1868 N94-21605
Application guide for universal source encoding for space
[NASA-TP-3441] p 1741 N94-21783
Empirical wind model for the middle and lower atmosphere. Part 2: Local time variations
[NASA-TM-104592] p 1870 N94-21862
Outgassing data for selecting spacecraft materials
[NASA-RP-1124-REV-3] p 1676 N94-21889
Bi-directional reflectance and other radiation parameters of cirrus from ER-2 observations p 1871 N94-22296
Intercomparison of MAS, AVIRIS, and HIS data from FIRE cirrus 2 p 1872 N94-22298
Meteorological analysis of the December 4-6 FIRE cirrus-2 case p 1875 N94-22314
Analysis of the GOES 6.7 micrometer channel observations during FIRE 2 p 1875 N94-22316

The 5-6 December 1991 FIRE IFO 2 jet stream cirrus case study: The influence of volcanic aerosols p 1877 N94-22326

Meteorological analysis of the November 25 FIRE cirrus-2 case: A well-defined ridge-crest cirrus system over Oklahoma p 1877 N94-22328

Dynamical characteristics of cirrus clouds from aircraft and radar measurements p 1878 N94-22332

A comparison of small and larger mesoscale latent heat and radiative fluxes: December 6 case study p 1879 N94-22335

Surface-induced brightness temperature variations and their effects on detecting thin cirrus clouds using IR emission channels in the 8-12 micrometer region p 1880 N94-22341

Mass spectrometer-pyrolysis experiment for atmospheric and soil sample analysis on the surface of Mars p 1812 N94-22435

A structured data transfer protocol p 2047 N94-22450

ROSAT implementation of a proposed multi-mission x ray data format p 2047 N94-22462

The HEASARC graphical user interface p 1926 N94-22487

FITS data conversion efforts at the Compton Observatory Science Support Center p 1926 N94-22488

A generic archive protocol and an implementation p 2047 N94-22493

The digital archive of the International Halley Watch p 2047 N94-22496

GRO/EGRET data analysis software: An integrated system of custom and commercial software using standard interfaces p 1926 N94-22501

GammaCore: The Compton Observatory research environment p 2048 N94-22509

XPI: The Xanadu Parameter Interface p 1927 N94-22513

Development of the FITS tools package for multiple software environments p 1927 N94-22516

Khoros software specification format and interoperability p 1927 N94-22523

UIT support observations archive p 2048 N94-22534

Recommendations for a service framework to access astronomical archives p 2049 N94-22537

NASA's astrophysics archives at the National Space Science Data Center p 2049 N94-22541

MOSAIC: Software for creating mosaics from collections of images p 1927 N94-22543

NATIONAL AERONAUTICS AND SPACE ADMINISTRATION. HUGH L. DRYDEN FLIGHT RESEARCH FACILITY, EDWARDS, CA.

On the estimation algorithm used in adaptive performance optimization of turbofan engines [NASA-TM-4551] p 1649 N94-21879

NATIONAL AERONAUTICS AND SPACE ADMINISTRATION. JOHN F. KENNEDY SPACE CENTER, COCOA BEACH, FL.

Debris/ice/TPS assessment and integrated photographic analysis for Shuttle Mission STS-51 [NASA-TM-109189] p 1656 N94-21884

NATIONAL AERONAUTICS AND SPACE ADMINISTRATION. LYNDON B. JOHNSON SPACE CENTER, HOUSTON, TX.

Apparatus and method for measuring subject work rate on an exercise device [NASA-CASE-MSC-21752-1] p 1895 N94-20194

Thermally activated retainer means utilizing shape memory alloy [NASA-CASE-MSC-21793-1] p 1654 N94-20304

Apparatus for simulating an exoatmospheric structure [NASA-CASE-MSC-21975-1] p 1653 N94-20339

Neural network for processing both spatial and temporal data with time based back-propagation [NASA-CASE-MSC-21874-1] p 1942 N94-20366

Space Station trash removal system [NASA-CASE-MSC-21723-1] p 1657 N94-20367

Extra-corporeal blood access, sensing, and radiation methods and apparatuses [NASA-CASE-MSC-21775-1] p 1890 N94-20372

Method for anisotropic etching in the manufacture of semiconductor devices [NASA-CASE-MSC-21631-1] p 1993 N94-20491

Reconfigurable fuzzy cell [NASA-CASE-MSC-21613-1] p 1907 N94-20492

High-temperature, high-pressure oxygen metering valve [NASA-CASE-MSC-21823-1] p 1824 N94-20589

Tetrahedral lander [NASA-CASE-MSC-22082-1] p 1658 N94-20590

Loads produced by a suited subject performing tool tasks without the use of foot restraints [NASA-TP-3424] p 1896 N94-20606

The Sm-(146,147)-Nd-(142,143) formation interval for the lunar mantle and implications for lunar evolution p 2097 N94-20663

Post-igneous redistribution of components in eucrites p 1685 N94-20684

SCR neon and argon in Kapoeta feldspar: Evidence for an active ancient Sun p 2106 N94-20712

A new Antarctic meteorite with chromite, orthopyroxene and metal with reference to a formation model of S asteroids p 2084 N94-20813

Sparking young minds with Moon rocks and meteorites p 2039 N94-20819

Evaluation of lunar rocks and soils for resource utilization: Detailed image analysis of raw materials and beneficiated products p 2126 N94-20820

Cometary interplanetary dust particles? An update on carbon in anhydrous IDPS p 2084 N94-20828

Comparison of visible and near-infrared reflectance spectra of CM2 carbonaceous chondrites and primitive asteroids p 2085 N94-20848

Consortium study of lunar meteorites Yamato-793169 and Asuka-881757: Geochemical evidence of mutual similarity, and dissimilarity versus other mare basalts p 2085 N94-20857

Equilibrium and fractional crystallization of a primitive Shergottite composition p 2085 N94-20861

Weathering features and secondary minerals in Antarctic Shergottites ALHA77005 and LEW88516 p 2086 N94-20869

Petrology and geochemistry of VLT glasses from double drive tube 79001/2 p 1687 N94-20870

Degradation sequence of young lunar craters from orbital infrared survey p 2136 N94-20874

CERN-derived analysis of lunar radiation backgrounds p 2080 N94-20880

Consortium reports on lunar meteorites Yamato 793169 and Asuka 881757, a new type of mare basalt p 2086 N94-20893

Diffuse reflectance spectra of orthopyroxene, olivine, and plagioclase as a function of composition and structure p 2087 N94-20906

Mineralogy of dark clasts in primitive versus differentiated meteorites p 2087 N94-20907

On dust emissions from the jovian system p 2141 N94-20909

Measured space environmental effects to LDEF during retrieval p 1659 N94-21372

The International Telecommunications Satellite (INTELSAT) Solar Array Coupon (ISAC) atomic oxygen flight experiment: Techniques, results and summary p 1662 N94-21391

Atomic oxygen interaction with spacecraft materials: Relationship between orbital and ground-based testing for materials certification p 1663 N94-21393

Model-based automatic generation of grasping regions [NASA-TM-104785] p 1946 N94-21550

Strength capabilities and load requirements while performing torquing tasks in zero gravity [NASA-TP-3433] p 1897 N94-21627

EVA tools and equipment reference book [NASA-TM-109350] p 1897 N94-21812

Compilation of reinforced carbon-carbon transatlantic abort landing arc jet test results [NASA-TM-104778] p 1676 N94-21834

Spaceflight Radiation Health program at the Lyndon B. Johnson Space Center [NASA-TM-104782] p 1893 N94-21863

Mars exploration study workshop 2 [NASA-CP-3243] p 2146 N94-21883

Johnson Space Center CFD grid generation requirements p 1919 N94-22355

A Backscatter Moessbauer Spectrometer (BaMS) for use on Mars p 1811 N94-22431

Database of proposed payloads and instruments for SEI missions p 1811 N94-22432

Determination of Martian soil mineralogy and water content using the Thermal Analyzer for Planetary Soils (TAPS) p 1812 N94-22433

Optical luminescence spectroscopy as a probe of the surface mineralogy of Mars p 1813 N94-22437

NATIONAL AERONAUTICS AND SPACE ADMINISTRATION. LANGLEY RESEARCH CENTER, HAMPTON, VA.

An expert system executive for automated assembly of large space truss structures [NASA-TM-4487] p 1939 N94-20089

Power transmission by laser beam from lunar-synchronous satellite [NASA-TM-4496] p 1669 N94-20102

Shaft mount for data coupler system [NASA-CASE-LAR-13805-1] p 1822 N94-20365

Flexible heating head for induction heating [NASA-CASE-LAR-14418-15-B] p 1718 N94-20368

Counter-balanced, multiple cable construction crane [NASA-CASE-LAR-14565-1-CU] p 1822 N94-20369

A process for preparing an assembly of an article and a soluble polyimide which resists dimensional change, delamination, and debonding when exposed to changes in temperature [NASA-CASE-LAR-14763-1] p 1702 N94-20373

Polyimides containing amide and perfluoroisopropylidene connecting groups [NASA-CASE-LAR-14608-1] p 1702 N94-20374

Improved ceramic slip casting technique [NASA-CASE-LAR-14471-1] p 1702 N94-20377

Optical fibers and Fluorosensors having improved power efficiency and methods of producing same [NASA-CASE-LAR-14525-1-CU] p 1986 N94-20378

Integrated display of multi-sensor geophysical and electromagnetic flight data p 1721 N94-20418

Description and availability of airborne Doppler radar data p 1722 N94-20419

Heat exchanger with oscillating flow [NASA-CASE-LAR-14033-2] p 1800 N94-20495

Polybenzoxazole via aromatic nucleophilic displacement [NASA-CASE-LAR-14606-1-CU] p 1672 N94-20540

Apparatus and method for improving spin recovery on aircraft [NASA-CASE-LAR-14747-1] p 1650 N94-20556

Optical fiber sensor having an active core [NASA-CASE-LAR-14607-1-SB] p 1986 N94-20586

Method for remotely powering a device such as a lunar rover [NASA-CASE-LAR-14789-1] p 1824 N94-20587

Characteristics of switching plasma in an inverse-pinch switch p 1995 N94-21292

Thermal stress analysis of composites in the space environment p 1661 N94-21379

Simulated space environmental effects on some experimental high performance polymers p 1662 N94-21385

The Sixth Copper Mountain Conference on Multigrid Methods, part 2 [NASA-CP-3224-PT-2] p 1955 N94-21464

Time-accurate Navier-Stokes calculations with multigrid acceleration p 1956 N94-21469

Looking for O(N) Navier-Stokes solutions on non-structured meshes p 1806 N94-21471

Multigrid schemes for viscous hypersonic flows p 1641 N94-21473

Mapping robust parallel multigrid algorithms to scalable memory architectures p 1922 N94-21483

Unstructured multigrid through agglomeration p 1958 N94-21484

Multigrid properties of upwind-biased data reconstructions p 1806 N94-21485

Internal performance of a nonaxisymmetric nozzle with a rotating upper flap and a center-pivoted lower flap [NASA-TP-3385] p 1637 N94-21569

Results of the second Round Robin on opening-load measurement conducted by ASTM Task Group E24.04.04 on crack closure measurement and analysis [NASA-TM-109032] p 1832 N94-21624

Stratospheric Aerosol and Gas Experiment (SAGE 3) p 1869 N94-21644

Introduction to the LaRC central scientific computing complex [NASA-TM-104092-REV-1] p 1900 N94-22100

The FIRE Cirrus Science Results 1993 [NASA-CP-3238] p 1871 N94-22292

Comparison of radiation and cloud parameters derived from satellite and aircraft measurements during FIRE 2 cirrus IFO p 1872 N94-22299

Development of methods for inferring cloud thickness and cloud-base height from satellite radiance data p 1872 N94-22301

Cloud fields derived from satellite and surface data during FIRE cirrus phase 2 p 1872 N94-22302

Remote sensing of multilevel clouds during FIRE IFO 2 p 1844 N94-22303

Comparison of cloud microphysical parameters derived from surface and satellite measurements during FIRE phase 2 p 1873 N94-22306

A numerical technique for the calculation of cloud optical extinction from lidar p 1874 N94-22309

Atmospheric parameterization schemes for satellite cloud property retrieval during FIRE IFO 2 p 1874 N94-22312

Automated cloud classification with a fuzzy logic expert system p 1875 N94-22313

Remote sensing estimates of cirrus particle size for tropical and midlatitude cirrus: Hexagonal crystals and ice spheres p 1880 N94-22342

Unstructured Grid Generation Techniques and Software [NASA-CP-10119] p 1918 N94-22350

Status of VGRID/USM3D aero analysis system p 1919 N94-22357

Development of a gridless CFD method p 1919 N94-22361

Accuracy assessment for grid adaptation
p 1920 N94-22368
Computational geometry issues p 1920 N94-22370
Computational Methods for Failure Analysis and Life Prediction
[NASA-CP-3230] p 1833 N94-22608
Analysis of thermal mechanical fatigue in titanium matrix composites p 1835 N94-22618
NASA Langley developments in response calculations needed for failure and life prediction
p 1836 N94-22621
Delamination, durability, and damage tolerance of laminated composite materials p 1678 N94-22622
Demonstrating damage tolerance of composite airframes p 1647 N94-22623

NATIONAL AERONAUTICS AND SPACE ADMINISTRATION. LEWIS RESEARCH CENTER, CLEVELAND, OH.

System performance predictions for Space Station Freedom's electric power system
[NASA-TM-106396] p 1667 N94-20062
Experimental and computational results from a large low-speed centrifugal impeller
[NASA-TM-106421] p 1636 N94-20136
Solar simulator for solar dynamic space power system testing
[NASA-TM-106393] p 1984 N94-20140
Head-on collision of drops: A numerical investigation
[NASA-TM-106394] p 1798 N94-20167
Multi-disciplinary coupling effects for integrated design of propulsion systems
[NASA-TM-106349] p 1830 N94-20170
Quantification of uncertainties in the performance of smart composite structures
[NASA-TM-106335] p 1830 N94-20171
Pressurization and expulsion of a flightweight liquid hydrogen tank
[NASA-TM-106427] p 1799 N94-20177
Guanidine based vehicle/binders for use with oxides, metals, and ceramics
[NASA-CASE-LEW-15314-1] p 1700 N94-20195
Self-deploying photovoltaic power system
[NASA-CASE-LEW-15308-1] p 1846 N94-20196
Three point lead screw positioning apparatus for a cavity tuning plate
[NASA-CASE-LEW-15216-1] p 1822 N94-20375
Process for the homoepitaxial growth of single-crystal silicon carbide films on silicon carbide wafers
[NASA-CASE-LEW-15223-1] p 2017 N94-20381
Recent activities in printed Antennas at LeRC
p 1722 N94-20422
Solid State Technology Branch of NASA Lewis Research Center: Fifth Annual Digest
[NASA-TM-106303] p 1732 N94-20497
An x-band peeled HEMT amplifier
p 1732 N94-20498
Characteristics of 0.8- and 0.2-microns gate length In(x)Ga(1-x) As/In(0.52)Al(0.48)As/InP (0.53 less than or equal to x less than or equal to 0.70) modulation-doped field-effect transistors at cryogenic temperatures
p 1733 N94-20499
A comprehensive theoretical and experimental study of coplanar waveguide shunt stubs p 1733 N94-20500
A comparative study between shielded and open coplanar waveguide discontinuities
p 1733 N94-20501
A theoretical and experimental study of coplanar waveguide shunt stubs p 1733 N94-20502
Coplanar waveguide radial line stub
p 1733 N94-20503
Attenuation of epsilon(sub eff) of coplanar waveguide transmission lines on silicon substrates
p 1733 N94-20504
Linearly tapered slot antenna with dielectric superstrate p 1734 N94-20505
Slot-coupled patch antenna with coplanar waveguide feed p 1734 N94-20506
Bandwidth enhancement of dielectric resonator antennas p 1734 N94-20507
Spectroscopic ellipsometry studies of HF treated Si (100) surfaces p 1734 N94-20508
Ellipsometric study of Si(0.5)Ge(0.5)/Si strained-layer superlattices p 1734 N94-20509
Spectroscopic ellipsometric characterization of Si/Si(1-x)Ge(x) strained-layer superlattices
p 1734 N94-20510
New technique for oil backstreaming contamination measurements p 1652 N94-20511
The quantum efficiency of HgCdTe photodiodes in relation to the direction of illumination and to their geometry p 1735 N94-20512
Space applications of superconducting microwave electronics at NASA Lewis Research Center
p 1671 N94-20513
Y-Ba-Cu-O superconducting/GaAs semiconducting hybrid circuits for microwave applications
p 1735 N94-20514
Ten GHz YBa2Cu3O(7-delta) superconducting ring resonators on NdGaO3 substrates
p 1735 N94-20515
TlCaBaCuO high Tc superconducting microstrip ring resonators designed for 12 GHz p 1735 N94-20516
A 10 GHz Y-Ba-Cu-O/GaAs hybrid oscillator proximity coupled to a circular microstrip patch antenna
p 1736 N94-20517
Microwave properties and characterization of co-evaporated BSCCO thin films p 1709 N94-20518
The effect of fluctuations on the electrical transport behavior in YBa2Cu3O(7-x) p 1736 N94-20519
Sintering silicon nitride
[NASA-CASE-LEW-15489-1] p 1703 N94-20529
Some practical turbulence modeling options for Reynolds-averaged full Navier-Stokes calculations of three-dimensional flows
[NASA-TM-106399] p 1637 N94-20534
Intercalated hybrid graphite fiber composite
[NASA-CASE-LEW-15241-1] p 1673 N94-20539
Development of phased twin flip-flop jets
[NASA-TM-106404] p 1637 N94-20563
System and method for cancelling expansion waves in a wave rotor
[NASA-CASE-LEW-15218-1] p 1801 N94-20588
Ellipsometric studies of sputtered silicon nitride on n-GaAs p 1709 N94-20972
Structural and chemical analysis of a silicon nitride film on GaAs by null ellipsometry p 1709 N94-20975
Thin film compositional analysis using null or fixed wavelength ellipsometry p 1709 N94-20976
InP MIS structures with diamondlike amorphous carbon films deposited by ion-beam sputtering and from plasma
p 1710 N94-20979
Thin-film hermeticity: A quantitative analysis of diamondlike carbon using variable angle spectroscopic ellipsometry p 1710 N94-20981
Variable angle of incidence spectroscopic ellipsometric study of semiconductor multilayer structures
p 2020 N94-20982
Characterization of multilayer GaAs/AlGaAs transistor structures by variable angle spectroscopic ellipsometry
p 1796 N94-20985
High temperature stability of amorphous Ta(x)Cu(1-x) diffusion barriers on GaAs p 2022 N94-20990
Amorphous Ta-rich Ta-Cu films as diffusion barriers between Au and GaAs p 1710 N94-20991
GaAs/AlGaAs superlattice characterization by variable angle spectroscopic ellipsometry p 2022 N94-20994
Dielectric function of InGaAs in the visible
p 2023 N94-21000
Study of InGaAs-based modulation doped field effect transistor structures using variable-angle spectroscopic ellipsometry p 1796 N94-21001
Spectroscopic ellipsometric characterization of Si/Si(1-x)Ge(x) strained-layer superlattices
p 2025 N94-21009
The implications of the LDEF results on Space Station Freedom power system materials p 1660 N94-21377
Multigrid solution of the Navier-Stokes equations on highly stretched grids with defect correction
p 1806 N94-21481
Thermal stability relationships between PMR-15 resin and its composites
[NASA-TM-106285] p 1675 N94-21488
Thrust augmentation options for the Beta 2 two-stage-to-orbit vehicle
[NASA-TM-106448] p 1648 N94-21563
Reducing the cognitive workload: Trouble managing power systems
[NASA-TM-106413] p 1714 N94-21564
QPPM receiver for free-space laser communications
[NASA-TM-106424] p 1741 N94-21567
NEP Early Flight program: System performance and development considerations
[NASA-TM-106415] p 1654 N94-21570
On-board closed-loop congestion control for satellite based packet switching networks
[NASA-TM-106446] p 1656 N94-21581
Blade row interaction effects on flutter and forced response
[NASA-TM-106438] p 1649 N94-21586
Order of accuracy of QUICK and related convection-diffusion schemes
[NASA-TM-106402] p 1959 N94-21588
Design and implementation of a status at a glance user interface for a power distribution expert system
[NASA-TM-106412] p 1715 N94-21589
Users manual for the NASA Lewis three-dimensional ice accretion code (LEWICE 3D)
[NASA-TM-105974] p 1642 N94-21590
A study of the compressible flow through a diffusing S-duct
[NASA-TM-106411] p 1638 N94-21591
Experimental study of void formation during aluminum solidification in reduced gravity
[NASA-TM-106190] p 1692 N94-21604
A comparative robustness evaluation of feedforward neurofilters
[NASA-TM-106440] p 1650 N94-21742
The relative noise levels of parallel axis gear sets with various contact ratios and gear tooth forms
[NASA-TM-106431] p 1826 N94-21756
Probabilistic assessment of composite structures
[NASA-TM-106368] p 1832 N94-21757
Comparison of mixing calculations for reacting and non-reacting flows in a cylindrical duct
[NASA-TM-106435] p 1649 N94-21758
Options for thrust augmentation for the Beta 2 two-stage-to-orbit launch vehicle
[NASA-TM-106418] p 1649 N94-21759
Powdered aluminum and oxygen rocket propellants: Subscale combustion experiments
[NASA-TM-106439] p 1713 N94-21760
The 1992 Seals Flow Code Development Workshop
[NASA-CP-10124] p 1654 N94-21790
Brush seal bristle flexure and hard-rub characteristics
p 1654 N94-21791
Integrity testing of brush seal in a T-700 engine
p 1654 N94-21792
Compliant seal development p 1655 N94-21795
Linearly tapered slot antenna circular array for mobile communications
[NASA-TM-106441] p 1769 N94-21808
Preliminary SP-100/Stirling heat exchanger designs
[NASA-TM-106444] p 1670 N94-21809
Instability modes excited by natural screech tones in a supersonic rectangular jet
[NASA-TM-106409] p 1638 N94-22274
Unstructured grid research and use at NASA Lewis Research Center p 1919 N94-22353
Unstructured low-Mach number viscous flow solver
p 1919 N94-22358
Cartesian-cell based grid generation and adaptive mesh refinement p 1920 N94-22364
Brief summary of the evolution of high-temperature creep-fatigue life prediction models for crack initiation
p 1834 N94-22613
Life assessment of structural components using inelastic finite element analyses p 1834 N94-22614
An overview of computational simulation methods for composite structures failure and life analysis
p 1835 N94-22617
Time-dependent reliability analysis of ceramic engine components p 1828 N94-22619
A high temperature fatigue life prediction computer code based on the total strain version of StrainRange Partitioning (SRP) p 1835 N94-22620

NATIONAL AERONAUTICS AND SPACE ADMINISTRATION. MARSHALL SPACE FLIGHT CENTER, HUNTSVILLE, AL.

Microstructural stability of wrought, laser and electron beam glazed NARloy-Z alloy at elevated temperatures
[NASA-TM-108431] p 1689 N94-20100
Total systems design analysis of high performance structures
[NASA-TP-3432] p 1653 N94-20141
Bladder operated robotic joint
[NASA-CASE-MFS-28682-1] p 1701 N94-20359
Spiral fluid separator
[NASA-CASE-MFS-28658-1] p 1800 N94-20361
Liquid fuel injection elements for rocket engines
[NASA-CASE-MFS-28547-1] p 1669 N94-20370
Mold bolt and means for achieving close tolerances between bolts and bolt holes
[NASA-CASE-MFS-28720-1] p 1823 N94-20379
Turntable mechanism
[NASA-CASE-MFS-28522-1] p 1823 N94-20380
Automatic locking orthotic knee device
[NASA-CASE-MFS-28633-1] p 1896 N94-20493
Method for controlling protein crystallization
[NASA-CASE-MFS-28688-1] p 2017 N94-20528
Method of fabricating a rocket engine combustion chamber
[NASA-CASE-MFS-28569-1] p 1703 N94-20541
Simultaneous optical/gamma ray observations of GRB's p 2149 N94-20603
Detailed study of oxidation/wear mechanism in lox turbopump bearings
[NASA-TM-108434] p 1825 N94-21580
Initial development of a high-pressure crystal growth facility: Center director's discretionary fund
[NASA-TM-108430] p 2030 N94-21807
A simulation model for probabilistic analysis of Space Shuttle abort modes
[NASA-TM-108432] p 1656 N94-21859

Performance assessment of low pressure nuclear thermal propulsion
[NASA-TM-108433] p 1671 N94-21860
Grid generation requirements at Marshall Space Flight Center p 1919 N94-22354

NATIONAL AERONAUTICS AND SPACE ADMINISTRATION. PASADENA OFFICE, CA.
Optoelectronic associative memory
[NASA-CASE-NPO-18278-1-CU] p 1985 N94-20303
Feedback controlled optics with wavefront compensation
[NASA-CASE-NPO-18194-1-CU] p 1985 N94-20305
Wide-angle imaging system with fiberoptic components providing angle-dependent virtual material stops
[NASA-CASE-NPO-18146-1-CU] p 1986 N94-20345
Electronic neural network for solving traveling salesman and similar global optimization problems
[NASA-CASE-NPO-17807-2-CU] p 1942 N94-20360
Segmented ion thruster
[NASA-CASE-NPO-18192-1-CU] p 1669 N94-20496

NATIONAL AERONAUTICS AND SPACE ADMINISTRATION. WALLOPS FLIGHT FACILITY, WALLOPS ISLAND, VA.
Analysis of Ku-band cross section at low incidence angles p 1720 N94-20414
Presenting the Rain-Sea Interaction Facility
[NASA-RP-1322] p 1884 N94-21628

NATIONAL AEROSPACE LAB., AMSTERDAM (NETHERLANDS).
The electronics technology policy of the NLR Informatics Division: The NLR electronics CAE infrastructure
[NLR-TP-91001-U] p 1753 N94-21067

NATIONAL AIR AND SPACE MUSEUM, WASHINGTON, DC.
Geomorphic evidence for an eolian contribution to the formation of the Martian northern plains p 2092 N94-20402
The early Martian environment: Clues from the cratered highlands and the Precambrian Earth p 2143 N94-21667
Early Mars: A regional assessment of denudation chronology p 2145 N94-21676

NATIONAL CENTER FOR ATMOSPHERIC RESEARCH, BOULDER, CO.
Overview of microphysical and state parameter measurements from FIRE 2 p 1871 N94-22293

NATIONAL DEFENCE RESEARCH ESTABLISHMENT, UMEA (SWEDEN).
Zinc and titanium smoke: Chemical composition and physical characteristics
[FOA-C-40277-4.9] p 1680 N94-20552

NATIONAL INST. FOR FUSION SCIENCE, NAGOYA (JAPAN).
Driven reconnection and self-organization p 2000 N94-22625
Physics of transport phenomena in magnetic confinement plasmas p 2000 N94-22628
Plasma heating in toroidal systems p 2000 N94-22629
Thermal properties and radiation processes in astrophysical plasmas p 2002 N94-22640
Non-equilibrium ionization in an M class solar flare p 2004 N94-22653
Helical kink instability of jets from young stellar objects p 2008 N94-22686

NATIONAL INST. OF POLAR RESEARCH, TOKYO (JAPAN).
Regolith breccia consisting of H and LL chondrite mixture p 2080 N94-20892

NATIONAL INST. OF STANDARDS AND TECHNOLOGY, BOULDER, CO.
Growth mechanisms and characterization of hydrogenated amorphous-silicon-alloy films
[DE93-018202] p 1699 N94-20047
Speed of sound data and related models for mixtures of natural gas constituents
[PB93-200822] p 1968 N94-21447

NATIONAL INST. OF STANDARDS AND TECHNOLOGY, GAITHERSBURG, MD.
RADCAL: A narrow-band model for radiation calculations in a combustion environment
[PB93-200889] p 1682 N94-21448
Review of corrosion behavior of ceramic heat exchanger materals: Corrosion characteristics of silicon carbide and silicon nitride
[DE93-041307] p 1706 N94-21516

NATIONAL MUSEUM OF NATURAL HISTORY, PARIS (FRANCE).
The age of the Pretoria Saltpan impact crater, South Africa p 1863 N94-20798

NATIONAL OCEANIC AND ATMOSPHERIC ADMINISTRATION, BOULDER, CO.
Development and tests of a cloud physics parameterization for real-time aviation and public numerical weather forecasting
[PB93-202711] p 1868 N94-21427
Cirrus properties deduced from CO2 lidar observations of zenith-enhanced backscatter from oriented crystals p 1871 N94-22295
Progress in interpreting CO2 lidar signatures to obtain cirrus microphysical and optical properties p 1874 N94-22308
Breaking Kelvin-Helmholtz waves and cloud-top entrainment as revealed by K-band Doppler radar p 1874 N94-22310
Observations of multi-layered clouds using K-band radar p 1874 N94-22311
Comparison of cloud boundaries measured with 8.6 mm radar and 10.6 micrometer lidar p 1875 N94-22317
Cloud boundaries during FIRE 2 p 1876 N94-22318
Estimation of cirrus cloud particle fallspeeds from vertically pointing Doppler radar p 1879 N94-22333
Normalized vertical ice mass flux profiles from vertically pointing 8-mm-wavelength Doppler radar p 1879 N94-22334

NATIONAL OCEANIC AND ATMOSPHERIC ADMINISTRATION, PRINCETON, NJ.
Monitoring issues from a modeling perspective p 1868 N94-21640

NATIONAL OPTICAL ASTRONOMY LAB. TUCSON, AZ.
First MEM task IRMEO in IRAF p 1928 N94-22551

NATIONAL PARK SERVICE, DENVER, CO.
Aircraft noise effects on cultural resources: Recommendation and rationale for further research
[PB93-205326] p 1968 N94-22053

NATIONAL RADIO ASTRONOMY OBSERVATORY, GREEN BANK, WV.
On AIPS++, a new astronomical information processing system p 2047 N94-22463
Programmability in AIPS++ p 1926 N94-22482
The VLBA correlator: Real-time in the distributed era p 2049 N94-22547

NATIONAL RESEARCH COUNCIL OF CANADA, OTTAWA (ONTARIO).
Experiences in airborne computing at NRC for geophysical exploration applications p 1783 N94-22185
Balanced arrow Mach-Zehnder interferometer p 1789 N94-22221
Optical processing in photorefractive media p 1789 N94-22222

NATIONAL RESEARCH COUNCIL OF CANADA, VANCOUVER (BRITISH COLUMBIA).
In-vacuo slip testing of materials for SSRMS friction brakes p 1661 N94-21381

NATIONAL SCIENCE MUSEUM, TOKYO (JAPAN).
The chondrite Mihonoseki: New observed fall p 2083 N94-20764

NATIONAL SPACE DEVELOPMENT AGENCY, TOKYO (JAPAN).
Japanese space program p 1652 N94-21407

NATIONAL TECHNICAL UNIV., ATHENS (GREECE).
The block adaptive multigrid method applied to the solution of the Euler equations p 1641 N94-21472

NATURHISTORISCHES MUSEUM, VIENNA (AUSTRIA).
Elemental depletions in Antarctic micrometeorites and Arctic cosmic spherules: Comparison and relationships p 2082 N94-20704

NAUCHNO-PROIZVODSTVENNOE OBEDINENIE ENERGIJA, KALININGRAD (USSR).
Study of space factors effect on materials for spacecraft external surfaces in NPO Energia programs p 1664 N94-21401

NAVAL ACADEMY, ANNAPOLIS, MD.
Photochemically induced transformations of transition complexes
[AD-A271112] p 2014 N94-19982
Design of a state-space controller for an advanced gas turbine engine
[AD-A270859] p 1647 N94-20042

NAVAL AIR WARFARE CENTER, INDIANAPOLIS, IN.
Ground proximity warning system voice warning unit requirements study
[AD-A270541] p 1641 N94-19876

NAVAL AIR WARFARE CENTER, PATUXENT RIVER, MD.
Rotorwash wind sensor evaluation
[AD-A268987] p 1807 N94-20203
In-flight measurement of aircrew breathing in Navy aircraft
[AD-A271811] p 1896 N94-21154

NAVAL AIR WARFARE CENTER, TRENTON, NJ.
Navy GTE seal development activity p 1655 N94-21794

NAVAL AIR WARFARE CENTER, WARMINSTER, PA.
Interleaved bismaleimide composites
[AD-A272233] p 1674 N94-20574
A comparison of sulfuric acid/boric acid anodize and chromic acid anodize processes
[AD-A271933] p 1703 N94-20614
An application of the Cerebellar Model Articulation Controller for a switched reluctance rotor position estimator
[AD-A271769] p 1943 N94-20926

NAVAL CIVIL ENGINEERING LAB., PORT HUENEME, CA.
SIMBAT theoretical manual
[AD-A271063] p 1882 N94-19979

NAVAL COMMAND, CONTROL AND OCEAN SURVEILLANCE CENTER, SAN DIEGO, CA.
Sporadic-E observations during LoVHF transionospheric direction finder measurements
[AD-A270619] p 1716 N94-19951
Oceanic in situ Fraunhofer-line characteristics: Fraunhofer-line underwater experiment (FLUX)
[AD-A270659] p 1681 N94-19952
Four-channel HF receiving antenna array simulator
[AD-A271876] p 1732 N94-20471
Understanding Open Systems Interconnection (OSI)
[AD-A271877] p 1929 N94-20472
An inverse DWT for nonorthogonal wavelets
[AD-A272064] p 1737 N94-20582
VLF Harold E. Holt RADHAZ measurements
[AD-A272018] p 1737 N94-20620
Polar processing project
[AD-A271583] p 1739 N94-21235
Optical properties of chromium and neodymium in zirconium - barium - lanthanum - aluminum fluoride glass
[AD-A271609] p 1987 N94-21236
A new matrix formulation of classical electrodynamics. Part 3: Wave propagation through a multilayer dielectric medium with planar boundaries
[AD-A271610] p 1739 N94-21240
Adhesive bonded joint with improved cyclic fatigue life for alumina-ceramic cylinders and hemispheres: Fourth generation housings
[AD-A273061] p 1831 N94-21310
NOVAM evaluation utilizing electro-optics and meteorological data from KEY-90
[AD-A271722] p 1868 N94-21356

NAVAL OCEAN SYSTEMS CENTER, SAN DIEGO, CA.
Fully-depleted silicon-on-sapphire and its application to advanced VLSI design p 1765 N94-21709

NAVAL POSTGRADUATE SCHOOL, MONTEREY, CA.
FSR based force torque transducer design
[AD-A271337] p 1650 N94-19879
A software architecture for the construction and management of real-time virtual worlds
[AD-A271465] p 1904 N94-20091
Scientific development of a massively parallel ocean climate model
[DE93-019446] p 1855 N94-20219
A comparison of some of the most current methods of image compression
[AD-A271841] p 1907 N94-20525
Control vane guidance for a ducted-fan unmanned air vehicle
[AD-A271957] p 1645 N94-20561
Mathematical model and analysis of the Tactical Unmanned Ground Vehicle (TUGV) using computer simulation
[AD-A272258] p 1824 N94-20576
Probability of detection calculations using MATLAB
[AD-A271958] p 1736 N94-20578
Development of a lidar for integration with the Naval Postgraduate School Infrared Search and Target Designation (NPS-IRSTD) system
[AD-A271847] p 1817 N94-20611
A software architecture for a small autonomous underwater vehicle navigation system
[AD-A272322] p 1643 N94-21037
Multigrid approach to solving the long transportation problem on a regular grid in cost space
[AD-A272323] p 1909 N94-21038
Incorporation and comparative evaluation of a non-convective cloud parameterization scheme in the Naval Research Laboratory west coast mesoscale weather prediction model
[AD-A272417] p 1867 N94-21146
Data compression by using wavelet transforms and vector quantization
[AD-A272763] p 1738 N94-21182
Ionospheric photoelectrons measured at geosynchronous orbit
[AD-A272431] p 1857 N94-21202
Dual-beam multiple wavelength light transmittance measurement for particle sizing in rocket motor plumes
[AD-A272491] p 1670 N94-21208
A conceptual database design and performance analysis of the MILSATCOM requirements database
[AD-A272672] p 1658 N94-21217
Design and implementation of a prototype PC based graphical and interactive MILSATCOM requirements database system
[AD-A272960] p 1658 N94-21251

Security management of electronic data interchange
[AD-A272952] p 1899 N94-21252
The use of backscattered electron imaging mode to assess the effect of fine dispersions on development of superplastic microstructure in Al-Mg alloys
[AD-A272428] p 1691 N94-21258
Comparison of higher order moment spectrum estimation techniques
[AD-A272967] p 1967 N94-21260
Mathcad computer applications predicting antenna parameters from antenna physical dimensions and ground characteristics
[AD-A272987] p 1740 N94-21264
A graphical user-interface development tool for intelligent computer-assisted instruction systems
[AD-A272988] p 1912 N94-21265
Performance management systems: A statistical analysis
[AD-A272989] p 2043 N94-21266
An evaluation of artificial neural network modeling for manpower analysis
[AD-A273001] p 1945 N94-21269
Design, fabrication and test of a vertical attitude takeoff and landing unmanned air vehicle
[AD-A273003] p 1646 N94-21283
Implementing Electronic Data Interchange (EDI) with small business suppliers in the pre-award acquisition process
[AD-A271767] p 1945 N94-21305
Large-scale circulation regimes and tropical cyclone characteristics over the western pacific ocean
[AD-A273004] p 1867 N94-21307
Government Open Systems Interconnection Profile (GOSIP) transition strategy
[AD-A273005] p 1740 N94-21308
Telecommunications services for multimedia data exchange support
[AD-A271704] p 1740 N94-21352
A theory for optical wavelength control in short pulse free electron laser oscillators
[AD-A271706] p 1817 N94-21353
Simulation of tripod gaits for a hexapod underwater walking machine
[AD-A271719] p 1945 N94-21355
On a proposed symbolic dynamics for the Henon map
[AD-A272514] p 1955 N94-21359
Use of computers in the instruction of integral calculus
[AD-A272500] p 1913 N94-21409
Validation of the design of a high resolution all-reflection Michelson interferometer for atmospheric spectroscopy
[AD-A272505] p 1987 N94-21410
Conversion and maintenance of Co-oP for Windows
[AD-A272513] p 1914 N94-21414
Measurement and prediction of the flow through an annular turbine cascade
[AD-A272530] p 1803 N94-21417
Effects of thrust vector control on the performance of the aerobang orbital plane change maneuver
[AD-A272532] p 1646 N94-21418
Numerical modeling of a propagating crack
[AD-A272604] p 1832 N94-21421
Stability curves for a thermoacoustic prime mover
[AD-A272607] p 1968 N94-21422
Ocean wave height transformation model using surface roller theory
[AD-A272610] p 1883 N94-21423
Application of a back-propagation neural network to isolated-word speech recognition
[AD-A272495] p 1945 N94-21430
A study of the structural stability of an unbalanced sandwich composite configuration
[AD-A272496] p 1675 N94-21431
Detailed analysis case studies of trapped plasmas at the Earth's magnetic equator
[AD-A272497] p 1858 N94-21432
Optimization and performance analysis of a supersonic conical-flow waverider for a deck-launched intercept mission
[AD-A272498] p 1648 N94-21433
Military satellite communications decision support system requirements analysis and user interface design
[AD-A273047] p 1740 N94-21436
Security evaluation of Unix networks
[AD-A273076] p 1945 N94-21520
Data link development for the archytas vertical takeoff and landing transitional flight unmanned aerial vehicle
[AD-A272499] p 1646 N94-21548

NAVAL RESEARCH LAB., BAY SAINT LOUIS, MS.
Global and regional comparative performance of linear and nonlinear satellite multichannel sea surface temperature algorithms
[AD-A270475] p 1837 N94-20028
Estimating the rotation rate of mesoscale ocean rings from satellite altimetry
[AD-A272922] p 1883 N94-21222

NAVAL RESEARCH LAB., WASHINGTON, DC.
The NRL LACE program
[AD-A270861] p 1657 N94-19896
A parametric representation of a thunderstorm cell
[AD-A271983] p 1866 N94-20579
UVPI imaging from the LACE satellite: The Starbird rocket plume
[AD-A271981] p 1658 N94-20617
An 85 GHz quasioptical gyroklystron experiment
[AD-A272020] p 1752 N94-20931
NAVSPASUR sensor system digital signal processing receiver. Volume 1: Hardware and software overview
[AD-A272899] p 1738 N94-21198
NAVSPASUR sensor system digital signal processing receiver. Volume 2: Function and capabilities of hardware and software components
[AD-A272900] p 1739 N94-21218
Models of refraction in the marine atmosphere surface layer
[AD-A271724] p 1858 N94-21357
Airborne surface backscattering strength measurements in the western Atlantic Ocean
[AD-A271737] p 1883 N94-21358
Green Sheet project: Dye sheet evolution
[AD-A272019] p 1883 N94-21443

NAVAL SURFACE WARFARE CENTER, BETHESDA, MD.
Graphite/polyurethane flexible composites: Mechanical and vibration damping properties
[AD-A271608] p 1674 N94-20950
Two visually meaningful correlation measures for comparing calculated and measured response histories
[AD-A273044] p 1964 N94-21322

NAVAL SURFACE WARFARE CENTER, SILVER SPRING, MD.
Design structuring and allocation optimization (Destination) prototype level 1 user's manual
[AD-A272115] p 1929 N94-20571

NAVAL UNDERSEA WARFARE CENTER, NEW LONDON, CT.
The effect of transverse curvature on the fluctuating wall pressure and structure of boundary layer turbulence
[AD-A271868] p 1800 N94-20466

NAVAL UNDERSEA WARFARE CENTER, NEWPORT, RI.
A survey of the impact on acoustic propagation of warm core ocean eddys
[AD-A272188] p 1883 N94-20925
High Frequency (HF) and meteor burst communications in a polar environment
[AD-A271604] p 1737 N94-20949

NAVY PERSONNEL RESEARCH AND DEVELOPMENT CENTER, SAN DIEGO, CA.
An assessment of the statistical and editorial output of text analysis programs
[AD-A272185] p 2042 N94-20924
Extracting information from wrong answers in computerized adaptive testing
[AD-A272832] p 1894 N94-21434

NEBRASKA UNIV., LINCOLN.
Materials, Structures, and Devices for High-Speed Electronics
[NASA-CR-193177] p 2019 N94-20971
Multiple-wavelength angle-of-incidence ellipsometry: Application to silicon nitride-gallium arsenide structures p 2019 N94-20974
Analytic solutions for optimized ellipsometric measurements of interfaces and surface layers in thin film structures p 2019 N94-20977
Variable wavelength, variable angle ellipsometry including a sensitivities correlation test p 1710 N94-20978
Interfacial properties of diamondlike amorphous carbon films on InP: Metal-insulator-semiconductor structures p 1710 N94-20980
Ellipsometric measurements of molecular-beam-epitaxy-grown semiconductor multilayer thicknesses: A comparative study p 1710 N94-20983
Comparative thickness measurements of heterojunction layers by ellipsometric, RBS, and XTEM analysis p 1710 N94-20984
Variable angle spectroscopic ellipsometric characterization of surface damage in chemical-mechanical polished GaAs p 1710 N94-20986
Variable angle of incidence spectroscopic ellipsometric measurement of the Franz-Keldysh effect in MODFET structures p 2021 N94-20987
Ellipsometric analysis of built-in electric fields in semiconductor heterostructures p 1796 N94-20988
Optical measurement of built-in and applied electric fields in Al(x)Ga(1-x)As/GaAs heterostructures p 1796 N94-20989
Measurement of superlattice optical properties by variable angle spectroscopic ellipsometry p 2022 N94-20992
Superlattice optical properties measured by variable angle spectroscopic ellipsometry p 2022 N94-20993
Characterization of an asymmetric triangular multiple quantum well, by variable angle spectroscopic ellipsometry p 2022 N94-20995
Polarized-light reflection mode p-i-n modulators with GaAs/AlGaAs multiple quantum well active layers: Design and simulation p 2023 N94-20996
GaAs(100) surface modifications at elevated temperatures, studied by in-situ spectroscopic ellipsometry p 2023 N94-20997
Ellipsometric study of GaAs(100) surface changes induced at elevated temperatures p 2023 N94-20998
Temperature dependence of optical properties of AlAs, studied by in-situ spectroscopic ellipsometry p 2023 N94-20999
Study of concentration-dependent dielectric properties of n-type GaAs using variable angle spectroscopic ellipsometry p 2024 N94-21002
Thermal diffusivity measurements by photothermal laser beam deflection (PTD): Data analysis using the Levenberg-Marquardt algorithm p 1820 N94-21006
Thermal characterization of thin films by photothermally induced laser beam deflection p 1710 N94-21007
Micro-ellipsometric measurements of strained layer structures p 2025 N94-21008
Applications of variable angle spectroscopic ellipsometry in semiconductor technology p 2025 N94-21010
Fundamentals and applications of variable angle spectroscopic ellipsometry p 1687 N94-21011
Non-destructive evaluation in manufacturing using spectroscopic ellipsometry p 1828 N94-21012
In-situ and ex-situ ellipsometric characterization for semiconductor technology p 2026 N94-21013
VASE (variable angle spectroscopic ellipsometry) p 1687 N94-21014

NEVADA UNIV., LAS VEGAS.
Research in lightweight elastic robotic arms
[AD-A270846] p 1821 N94-19833

NEVADA UNIV., RENO.
Strength and deformation properties of basaltic lava flows on planetary surfaces p 1862 N94-20747

NEW BRUNSWICK UNIV., FREDERICTON.
Delimitation of terrestrial impact craters by way of pseudotachylytic rock distribution p 1863 N94-20783
New algorithm for the detection of the orientation of a planar Lambertian surface in 3D p 1777 N94-22150
An airport economic impact study procedure for Atlantic Canada
[ISBN-0-315-59445-4] p 1651 N94-22419

NEW ENERGY AND INDUSTRIAL TECHNOLOGY DEVELOPMENT ORGANIZATION, TOKYO (JAPAN).
Current situation of development of petroleum substituting energies (USA)
[DE94-707492] p 1848 N94-22013
Current situation of development of petroleum substituting energies (Canada)
[DE94-707493] p 1849 N94-22014
Present status of developing petroleum-substituting energy (EC)
[DE94-707494] p 1849 N94-22030
Investigation on the chemically fixing technique of carbon dioxide utilizing solar energy
[DE94-714886] p 1849 N94-22043
Survey on chemical engineering technologies for the global environmental protection
[DE94-714887] p 1852 N94-22044
Survey on evaluation of energy technology contributing to preservation of the global environment. 2
[DE94-714884] p 1853 N94-22051
Study on possibility of developing energy integration technology
[DE94-714903] p 1849 N94-22052
Investigation on construction of the database system for research and development of the global environment industry technology
[DE94-714890] p 1853 N94-22090
Current situation in developing petroleum substituting energy (the United Kingdom)
[DE94-714897] p 1713 N94-22091
Surveys on specific patterns of facility intallation of photovoltaic power generating technologies for international cooperation
[DE94-714901] p 1850 N94-22092
Investigations on trends in global environment adaptive industrial technologies
[DE94-714888] p 1853 N94-22258

NEW HAMPSHIRE UNIV., DURHAM.
A new innovative instrument for space plasma instrumentation
[NASA-CR-194736] p 1666 N94-21780

NEW MEXICO STATE UNIV., LAS CRUCES.
Fault detection in digital and analog circuits using an i(DD) temporal analysis technique p 1757 N94-21106
High-speed Viterbi decoding with overlapping code sequences p 1760 N94-21130

NEW MEXICO UNIV., ALBUQUERQUE.
Core formation in the Moon: The mystery of the excess depletion of Mo, W and P p 2095 N94-20651
Orthopyroxenes as recorders of diogenite petrogenesis: Major and minor element systematics p 1684 N94-20670
Micrometeorite dynamic pyrometamorphism: Nonstoichiometric clinoenstatite (CLEN) p 2083 N94-20715
Micrometeorite dynamic pyrometamorphism: Observation of a thermal gradient in iron-nickel sulfide p 2083 N94-20716
Basaltic magmatism on the Moon. A perspective from volcanic picritic glasses p 2114 N94-20758
Origin of the Apollo 15 very low Ti green glass. A perspective from the compositional diversity in the very low Ti glasses p 1685 N94-20759
Orthopyroxenes as recorders of diogenite petrogenesis: Trace element systematics p 1686 N94-20760
The Fifth NASA Symposium on VLSI Design [NASA-CR-194644] p 1753 N94-21079
Test results for SEU and SEL immune memory circuits p 1754 N94-21087
Nature's crucible: Manufacturing optical nonlinearities for high resolution, high sensitivity encoding in the compound eye of the fly, Musca domestica p 1755 N94-21095
Proton radiation testing of an 18 bit A/D converter p 1755 N94-21096
Adaptive analog video signal conditioner p 1744 N94-21099
Partition algebraic design of asynchronous sequential circuits p 1759 N94-21125
Arithmetic in large GF(2(exp n)) p 1760 N94-21131
Links between N-modular redundancy and the theory of error-correcting codes p 1765 N94-21713
Reduction of blocking effects for the JPEG baseline image compression standard p 1765 N94-21714
Schematic driven layout of Reed Solomon encoders p 1766 N94-21722
A high speed CMOS A/D converter p 1767 N94-21726

NEW YORK UNIV., NEW YORK.
Cognition and the brain: A continuation of the university research initiative at New York University [AD-A271872] p 1894 N94-20467
Two-level Schwartz methods for nonconforming finite elements and discontinuous coefficients p 1957 N94-21477

NIJMEGEN UNIV. (NETHERLANDS).
GWB: Manual for the Grammar WorkBench version 1.5 [TR-92-14] p 1909 N94-21061
A simplified token bus protocol specified using LOTOS [TR-92-15] p 1910 N94-21062

NIPPON TELEGRAPH AND TELEPHONE PUBLIC CORP., YOKOSUKA (JAPAN).
TDMA satellite communication systems for ISDN services p 1746 N94-22171
A consideration of the integration of terrestrial and satellite mobile systems p 1746 N94-22172

NOBEYEMA SOLAR RADIO OBSERVATORY (JAPAN).
Preliminary results of observations of solar flares with Nobeyama Radioheliograph p 2001 N94-22633

NOKIA DATA, HELSINKI (FINLAND).
Application development in a PC/LAN environment p 1923 N94-22067
Industry standards: Key to distributed computing p 1938 N94-22070
Databases in distributed systems p 2046 N94-22080

NORFOLK STATE UNIV., VA.
A comprehensive software engineering educational experience [AD-A270583] p 1905 N94-20109

NORTH CAROLINA AGRICULTURAL AND TECHNICAL STATE UNIV., GREENSBORO.
Turbulence modeling for high speed compressible flows [NASA-CR-194547] p 1799 N94-20210

NORTH CAROLINA STATE UNIV., RALEIGH.
Shock wave interactions with exothermic mixtures [AD-A271149] p 1829 N94-19836
Optical signal processing [AD-A271036] p 1983 N94-20013
Telerobotic control of a mobile coordinated robotic server, executive summary [NASA-CR-194685] p 1821 N94-20044
Meso-Beta scale numerical simulation studies of terrain-induced jet streak mass/momentum perturbations [NASA-CR-194627] p 1864 N94-20138
Growth, characterization and device development in monocrystalline diamond films [AD-A272715] p 2026 N94-21190
Solid-state dynamics and quantum transport in novel semiconductor nanostructures [AD-A272955] p 2027 N94-21248
Long range fast tool servo [AD-A271614] p 1761 N94-21257
Growth, characterization and device development in monocrystalline diamond films [AD-A273097] p 2028 N94-21506
Fundamental studies of defect generation in amorphous silicon alloys grown by remote plasma-enhanced chemical-vapor deposition [DE93-017083] p 2029 N94-21615

NORTH DAKOTA UNIV., GRAND FORKS.
Elevation and igneous crater modification on Venus: Implications for magmatic volatile content p 2135 N94-20872
Large floor-fractured craters and isostatic crater modification: Implications for lithospheric thickness on Venus p 2135 N94-20873
Morphologic classes of impact basins on Venus p 2137 N94-20883

NORTHWESTERN UNIV., EVANSTON, IL.
First results on InGaAsP separate confinement heterostructure diode lasers [AD-A270849] p 1815 N94-19878

NORTON CO., NORTHBORO, MA.
Microstructural modeling and toughening of Si3N4 ceramics for high temperature engine applications [AD-A272897] p 1704 N94-21197

NORWEGIAN DEFENCE RESEARCH ESTABLISHMENT, KJELLER.
Technical manual PCDU MT 254 [FFI-92/7020] p 1751 N94-20553
Air transport of samples containing chemical warfare agents [FFI-93/6005] p 1851 N94-21455

NOTRE DAME UNIV., IN.
Petrogenesis of Apollo 12 mare basalts. Part 1: Multiple melts and fractional crystallization to explain olivine and ilmenite basalt compositions p 1684 N94-20644
Petrogenesis of Apollo 12 mare basalts. Part 2: An open system model to explain the pigeonite basalt compositions p 1684 N94-20645
Transient studies of low temperature catalysts for methane conversion [DE93-041232] p 1680 N94-20934

NOVA SCOTIA TECHNICAL COLL., HALIFAX.
Trellis coded multi-orthogonal modulation p 1747 N94-22231
Quadrature biorthogonal modulation p 1747 N94-22232

O

OAK RIDGE K-25 SITE, TN.
Project Records Information System (PRIS): User's manual [DE94-001548] p 2045 N94-22047

OAK RIDGE NATIONAL LAB., TN.
Investigation of austenitic alloys for advanced heat recovery and hot gas cleanup systems [DE93-017863] p 1687 N94-19802
Formation of colloidal Ag precipitates in fused silica by MeV ion implantation [DE93-040268] p 2012 N94-19869
Evaluation of a scanning Hartmann device for single point turning applications [DE93-019204] p 1821 N94-19891
Particles on surfaces of laser ablated Y1Ba2Cu3O(7-delta) films [DE93-040269] p 2013 N94-19929
Spin-polaron theory of high-(Tc) superconductivity. 1: Spin polarons and high (Tc) pairing [DE93-019196] p 2014 N94-20002
Fast ion behavior during neutral beam injection in ATF [DE93-040267] p 1992 N94-20058
Effects of processing history on the creep strength of Nb-1Zr [DE93-015905] p 1689 N94-20093
Alternative refrigerants and refrigeration cycles for domestic refrigerators [DE93-040481] p 1714 N94-20099
Atom probe field ion microscopy characterizations of VVER steels [DE93-017864] p 1689 N94-20180
Fundamentals of mechanical behavior in structural intermetallics: A synthesis of atomistic and continuum modeling [DE93-019166] p 1690 N94-20232
Microscopic evaluation of low-temperature embrittlement in type 308 stainless steel welds [DE93-040266] p 1690 N94-20282
Development of improved processing and evaluation methods for high reliability structural ceramics for advanced heat engine applications, phase 1 [DE93-040528] p 1702 N94-20481
Multi-CPU plasma fluid turbulence calculations on a CRAY Y-MP C90 [DE93-015425] p 1801 N94-20562
The Seventh International Symposium on Methodologies for Intelligent Systems (Poster Session) [AD-A272125] p 1942 N94-20573
Measuring the effects of thread placement on the Kendall Square KSR1 [DE93-040655] p 1908 N94-20932
Electron holography applied to the study of ceramic materials [DE94-000329] p 1707 N94-21653
Hadronic molecules and scattering amplitudes from the nonrelativistic quark model [DE94-000377] p 1974 N94-21657
Photoabsorption and Compton scattering in ionization of helium at high photon energies [DE94-000380] p 1974 N94-21658
Evaluation of the fabricability of advanced iron aluminide-clad austenitic stainless steel tubing [DE93-040598] p 1693 N94-21771
Single and double ionization of helium by high-energy photon impact [DE94-000381] p 1975 N94-21785
Ceramic Technology Project [DE94-001011] p 1707 N94-21822
Proceedings of the Seventh Annual Conference on Fossil Energy Materials [DE94-001091] p 1848 N94-21823
Operation of a test bed axial-gap brushless dc rotor with a superconducting stator [DE93-019167] p 1769 N94-21830
Spin-polaron theory of high-T(c) superconductivity. 3: Gap function and critical temperature [DE93-019198] p 2030 N94-21831
An assessment of the cost of microwave sintering ceramic tiles for armor applications [DE94-000978] p 1693 N94-21850
An evaluation of integration of the trace assertion method with the box structure method for coding in C++ [DE93-040480] p 1918 N94-21924
Stability of an uncooled segment of a high-temperature superconductor [DE94-000476] p 2032 N94-21932
Ni3Al aluminide alloys [DE94-000493] p 1694 N94-21933
Effect of powder characteristics on gas-pressure sintering of Si3N4 with rare earth additives [DE94-000330] p 1694 N94-21945
Alloying effects on mechanical and metallurgical properties of NiAl [DE93-040814] p 1694 N94-21948
Investigation of moisture-induced embrittlement of iron aluminides [DE93-040841] p 1695 N94-21949
OTDR strain gauge for smart skins [DE93-041043] p 1810 N94-21953
The quantum structure of matter grand challenge project: Large-scale 3-D solutions in relativistic quantum dynamics [DE94-000328] p 1960 N94-21955
Modal combination in response spectrum modal dynamic analysis [DE94-000339] p 1833 N94-21956
The laser and its applications on environment and biotechnology research [DE94-000376] p 1820 N94-21957
A sharp upper bound for departure from normality [DE93-040457] p 1960 N94-21966
The design of linear algebra libraries for high performance computers [DE93-040458] p 1960 N94-21967
Atmospheric sampling glow discharge ionization and triple quadrupole tandem mass spectrometry for explosives vapor detection [DE93-040593] p 1852 N94-22004
Post-Palbozoic crustal responses to the contemporary stress field in the eastern United States [DE93-040604] p 1859 N94-22006
Lattice damage during ion implantation of semiconductors [DE94-000335] p 2034 N94-22016
Fabrication of whisker-toughened alumina tubes [DE94-001012] p 1677 N94-22022
Temperature dependence of CsI(Tl) gamma ray excited scintillation characteristics [DE94-000836] p 2034 N94-22028
The TST: A small steady-state tokamak for integrated divertor testing [DE94-001016] p 1998 N94-22045

Reverse automatic differentiation of modular FORTRAN programs
[DE94-000336] p 1918 N94-22088
Distributed processing using Oracle7 and SQL*Net v2: An implementation story
[DE94-000494] p 1937 N94-22267
Hypersingular integrals at a corner
[DE94-000340] p 1961 N94-22379
Simulating the Euclidean time Schroedinger equations using an INTEL iPSC/860 hypercube: Application to the t-J model of high-T(sub c) superconductivity
[DE94-000489] p 2035 N94-22385
Miniaturized disk-bend testing, nano-indentation, and the microstructure of ion-irradiated titanium aluminides
[DE93-040600] p 1697 N94-22559
Effects of magnetic field perturbations in the ATF torsatron
[DE94-000474] p 1999 N94-22568
Environmental protection using social costing
[DE94-000492] p 1853 N94-22569
Test results of two high temperature superconducting sample coils
[DE94-000496] p 2035 N94-22570

OAK RIDGE Y-12 PLANT, TN.
Investigation of cracking and erratic behavior of the uranium-titanium alloy
[DE93-018591] p 1688 N94-19957

OBERLIN COLL., OH.
Size distributions and aerodynamic equivalence of metal chondrules and silicate chondrules in Acfer 059
p 2084 N94-20773

OBSERVATOIRE DE PARIS-MEUDON (FRANCE).
Mars: Noachian hydrology by its statistics and topology p 2143 N94-21664
Compressible MHD turbulence in the interplanetary medium p 2003 N94-22650

OBSERVATOIRE DE STRASBOURG (FRANCE).
Extracting galactic structure parameters from multivariated density estimation p 1964 N94-22458
Electronic publishing and intelligent information retrieval p 2047 N94-22479
SIMBAD quality-control p 2048 N94-22502

OFFICE NATIONAL D'ETUDES ET DE RECHERCHES AERONAUTIQUES, PARIS (FRANCE).
C/O atomic ratios in micrometer-size crushed grains from Antarctic micrometeorites and two carbonaceous meteorites p 2082 N94-20678

OFFICE NATIONAL D'ETUDES ET DE RECHERCHES AEROSPATIALES, PARIS (FRANCE).
Recent ONERA contributions to the development of flight test measurement techniques
p 1641 N94-22607

OFFICE OF TECHNOLOGY ASSESSMENT, WASHINGTON, DC.
The future of remote sensing from space: Civilian satellite systems and applications
[OTA-ISC-558] p 1837 N94-20209
Data format standards for civilian remote sensing satellites
[PB93-192920] p 1841 N94-21446

OHIO STATE UNIV., COLUMBUS.
An extended UTD analysis for the scattering and diffraction from cubic polynomial stripe
[NASA-CR-194581] p 1716 N94-20139
Development of fundamental understanding of friction and wear mechanisms by atomic-scale tribological studies of ceramic materials and multilayered thin films
[AD-A271485] p 1703 N94-20548
Laser diagnostics of RF hydrogen plasma reactors: Application to the processing of III-V materials
[AD-A272659] p 1994 N94-21214
Cognitive engineering in aerospace applications
[NASA-CR-194782] p 1647 N94-21819
Writing instrument interfaces with xf/tktcl
p 1925 N94-22480

OHIO UNIV., ATHENS.
A flight test system design for the microwave landing system p 1645 N94-22156

OKLAHOMA UNIV., NORMAN.
Schools of the Pacific rainfall climate experiment
p 1881 N94-20699
Early Mars: The inextricable link between internal and external influences on valley network formation
p 2146 N94-21681

OKLAHOMA UNIV. HEALTH SCIENCES CENTER, OKLAHOMA CITY.
Physiological correlates of stress-induced decrements in human perceptual performance
[DOT/FAA/AM-93/19] p 1893 N94-20081

OLD DOMINION UNIV., NORFOLK, VA.
Prediction and control of vortex-dominated and vortex-wake flows
[NASA-CR-194722] p 1637 N94-21054
On the prediction of multigrid efficiency through local mode analysis p 1959 N94-21486

ONAGAWA MAGNETIC OBSERVATORY (JAPAN).
Large-scale structure of the solar plasma corona: An analysis of Yohkoh SXT images p 2004 N94-22657

OPEN UNIV., MILTON (ENGLAND).
A carbon and nitrogen isotope study of carbonaceous vein material in ureilite meteorites p 2083 N94-20726
Discharge rates in Ma'adim Vallis, Mars
p 2128 N94-20830
Are the C delta light nitrogen and noble gases located in the same carrier? p 2085 N94-20846
The carbon components in SNC meteorites of feldspathic harzburgite composition
p 2086 N94-20885
Further carbon isotope measurements of LEW 88516
p 2086 N94-20886

OREGON STATE UNIV., CORVALLIS.
Cloud properties from the analysis of AVHRR observations for FIRE 2 p 1872 N94-22300

OREGON UNIV., EUGENE.
Microscopic origins of metastable effects in a-Si:H and deep defect characterization in a-Si,Ge:H alloys
[DE93-018205] p 1688 N94-19985
The modification of polymer surfaces and the fabrication of submicron-scale functionalized structures by deep-UV and electron beam lithography
[AD-A265956] p 1700 N94-20328

OSAKA CITY UNIV. (JAPAN).
Laboratory relations between the solar wind dynamic pressure and the magnetospheric structures of the Earth and comets p 2003 N94-22647
Laboratory structure of the heliopause
p 2003 N94-22648

OSAKA UNIV., TOYONAKA (JAPAN).
Properties of x ray emission from x ray novae
p 2007 N94-22676
Time variations of x rays from black hole candidates: Canonical time variations in high and low intensity states
p 2009 N94-22690

OSSERVATORIO ASTRONOMICO, TURIN (ITALY).
Jets associated with active galactic nuclei
p 2000 N94-22631

OTTAWA UNIV. (ONTARIO).
Buffer allocation in an ATM switch with output buffer and speed constraints p 1746 N94-22203
File transfer performance in LAN interconnection through a satellite channel p 1746 N94-22209
Capacity comparison between direct sequence PSK and MFSK spread spectrum systems in CDMA applications
p 1747 N94-22224
Performance of RS codes in lognormally shadowed Rician channels p 1792 N94-22244
On coefficient quantization and computational roundoff effects in frequency interpolation filter banks
p 1793 N94-22251

OULU UNIV. (FINLAND).
Chocolate tablet aspects of cytherean Meshkenet Tessera p 2106 N94-20710
Ridge belt-related scarps and troughs: Compressional crustal bending on Venus p 2106 N94-20711
Complex ridged terrain-related ridge belts on Venus: Global distribution and classification
p 2129 N94-20835

P

PACIFIC NORTHWEST LAB., RICHLAND, WA.
Health effects of global warming: Problems in assessment
[DE93-040323] p 1850 N94-19930
Global combine on mesh architectures with wormhole routing
[DE93-018792] p 1903 N94-19959
Properties and potential of high-temperature niobium beryllides
[DE93-019169] p 1690 N94-20233
Efficient communication primitives on mesh architectures with hardware routing
[DE93-018791] p 1936 N94-22032
Microstructural evolution of neutron-irradiated Fe-Cr-Ni ternary alloys at high helium generation rates
[DE93-018786] p 1696 N94-22037
Active damping of oscillations in a long compliant manipulator link
[DE93-018878] p 1826 N94-22038

PADUA UNIV. (ITALY).
Database activity in the Italian Astronet: DIRA 2
p 2047 N94-22452

PARAIBA UNIV., SAO JOSE DOS CAMPOS (BRAZIL).
SIMA: An integrated environmental monitoring system
p 1840 N94-20967

PARAMAX ELECTRONIC, INC., MONTREAL (QUEBEC).
The why, what, and how of Ada software development
p 1779 N94-22157

PATENT AND TRADEMARK OFFICE, WASHINGTON, DC.
The official gazette of the United States Patent and Trademark Office, vol. 1145, no. 4
[PB93-202240] p 2044 N94-21449

PENNSYLVANIA STATE UNIV., UNIVERSITY PARK.
Refractive index structure in the lower atmosphere
[AD-A270935] p 1854 N94-19899
Innovative acoustic technique for studying new materials and new developments in solid state physics
[AD-A270540] p 2013 N94-19933
High performance heavy alloys by alloying and process control
[AD-A271129] p 1689 N94-20019
Pre-main sequence stars in the Chamaeleon cloud and pre-main sequence stars in the Rho Ophiuchi cloud core
[NASA-CR-194713] p 2080 N94-20337
Petrography of shock features in the 1953 Manson 2-A drill core p 1862 N94-20767
Multi Wave Link: An interactive database for co-ordination of multiwavelength programs
[NASA-CR-194778] p 2043 N94-21055
Utilization of metals to improve the lubrication of ceramic load-bearing devices
[PB93-202448] p 1825 N94-21424
A guide to resolving disputes over contractor delay entitlements
[AD-A272022] p 2039 N94-21444
Lubricated wear of steel-ceramic and ceramic-ceramic systems
[PB93-202356] p 1825 N94-21450
Vapor-delivered lubrication of steel-steel and steel-ceramic systems
[PB93-202364] p 1825 N94-21451
A carbon dioxide/methane greenhouse atmosphere on early Mars p 2142 N94-21662
Possible solutions to the problem of channel formation on early Mars p 2144 N94-21673
Examination of the observed synoptic scale cirrus cloud environment: The December 3-6 FIRE cirrus case study
p 1877 N94-22325
Cirrus cloud development in a mobile upper tropospheric trough: The November 26th FIRE cirrus case study
p 1878 N94-22329
NASA Propulsion Engineering Research Center, volume 1
[NASA-CR-194721-VOL-1] p 1671 N94-22428
Relativistically expanding pair plasmas as bursting sources of cosmic gamma rays p 2003 N94-22646

PENNSYLVANIA UNIV., PHILADELPHIA.
Catalytic hydrogenation of carbon monoxide
[DE94-000881] p 1678 N94-20103
A formulation of quantum statistical mechanics based on the Feynman path centroid density 2 dynamical properties
[AD-A272698] p 2037 N94-21166
A formulation of quantum statistical mechanics based on the Feynman path centroid density 1: Equilibrium properties
[AD-A272809] p 2037 N94-21171
Integral equation calculation of solvent activation free energies for electron and proton transfer reactions
[AD-A272665] p 1681 N94-21216

PERADENIYA UNIV. (SRI LANKA).
A novel cache mechanism p 1767 N94-21730

PHILLIPS LAB., HANSCOM AFB, MA.
Predicting lightning events in the KSC area: A feasibility study using single station data
[AD-A271440] p 1864 N94-20088
Proceedings of the 15th Annual Seismic Research Symposium
[AD-A271458] p 1855 N94-20090
SSH-2 measurements of cirrus at 18-28 micrometers from the King Air during FIRE 2 p 1880 N94-22338

PHILLIPS LAB., KIRTLAND AFB, NM.
An equation of state for shock in homogeneous materials and comparison to shock data
[AD-A271436] p 1829 N94-19881
Numerical simulations of hypervelocity impact experiments involving single Whipple bumper shields
[AD-A272123] p 1831 N94-20572
Evaluation of radiation effects in re-oxidized nitrided oxide devices by hot carrier stressing at 77 K
p 1754 N94-21084

PHYSICAL OPTICS CORP., TORRANCE, CA.
Novel N x N integrated channel waveguide optical crossbars for large scale high speed non-blocking data switching
[AD-A272065] p 1986 N94-20922
An optically-assisted 3-D cellular array machine
[AD-A272683] p 1987 N94-21163

PHYSICAL SCIENCES, INC., ANDOVER, MA.
Fast oxygen atom studies related to low Earth orbit activities p 1663 N94-21395

Instantaneous velocity field imaging instrument for supersonic reacting flows
[NASA-CR-191162] p 1809 N94-21607

PITTSBURGH UNIV., PA.
Direct images of thermal disorder in the Cl-Si and H-O-Si chemisorption bond on Si(100)
[AD-A272386] p 1680 N94-21145
Classical and generalized solutions of time-dependent linear differential algebraic equations
[AD-A272834] p 1954 N94-21173
Finite difference methods for time-dependent, linear differential algebraic equations
[AD-A272835] p 1954 N94-21174

PLANETARY SCIENCE INST., TUCSON, AZ.
Asteroid collisions: Target size effects and resultant velocity distributions p 2083 N94-20729

POD ASSOCIATES, INC., ALBUQUERQUE, NM.
A fresh look at crater scaling laws for normal and oblique hypervelocity impacts p 1666 N94-20864

PRAIRIE VIEW AGRICULTURAL AND MECHANICAL COLL., TX.
Design of CMOS logic gates for TID radiation p 1754 N94-21083

PRATT AND WHITNEY AIRCRAFT, WEST PALM BEACH, FL.
Life prediction systems for critical rotating components p 1835 N94-22615

PRINCETON UNIV., NJ.
Algorithm/architecture study for artificial neural nets
[AD-A271820] p 1943 N94-20626
Some deformation trends and topographic characteristics of tesserae on Venus p 2105 N94-20706
Studying Venus using a GIS database p 2105 N94-20707
Analysis of multigrid methods on massively parallel computers: Architectural implications p 1938 N94-21468

PURDUE UNIV., WEST LAFAYETTE, IN.
In-situ electrochemical surface science
[AD-A265942] p 1680 N94-20330
The life cycles of intense cyclonic and anticyclonic circulation systems observed over oceans
[NASA-CR-194760] p 1865 N94-20353
The analysis of global cloud and radiation data for the study of cloud-climate interactions
[NASA-CR-193388] p 1865 N94-20535
Multivariate statistical analysis: Principles and applications to coorbital streams of meteorite falls p 1964 N94-20881
Electron emission from nanometer-size metallic clusters: Electronic states and structural stability of supported Au clusters
[DE93-040184] p 1975 N94-21766
Time-dependent grid adaptation for meshes of triangles and tetrahedra p 1920 N94-22369

Q

QUADRANT ENGINEERING, INC., HADLEY, MA.
Four-dimensional remote sensing of the marine boundary layer with a digital beamforming radar wind profiler
[AD-A270627] p 1882 N94-20564

QUEBEC UNIV., MONTREAL.
Ultrasonic sensor vision in robotics p 1775 N94-22131
An adaptive control to enable a robot to follow Cartesian trajectories p 1790 N94-22229
An adaptive method for group delay compensation using switched capacitor filters p 1793 N94-22248

QUEBEC UNIV., VERDUN.
Recognizing hesitation phenomena in continuous, spontaneous speech p 1746 N94-22210

QUEENS UNIV., KINGSTON (ONTARIO).
Efficiency of reversible optical storage in azo polymers
[AD-A272923] p 1705 N94-21223
The 13C-NMR spectra of poly (4-((2-(acryloyloxy) ethyl) ethyl amino)- 4-nitroazobenzene-co-methyl methacrylate)
[AD-A273016] p 1705 N94-21238
Recent developments in aromatic azo polymers research
[AD-A272966] p 1705 N94-21259
Azo polymers for optical storage 3: Effect of film thickness on net phase retardation and writing speed
[AD-A272994] p 1705 N94-21267
Optically induced birefringence in copolymers and blends containing azobenzene groups
[AD-A273085] p 1706 N94-21523
VLSI architectures for the new (T,L) algorithm p 1745 N94-22110
System level modelling using Petri nets and VHDL p 1772 N94-22113
The Schur Berlekamp-Massey algorithm is parallelizable p 1784 N94-22191
Modeling and analysis of secure communication protocols using Petri net formalism p 1784 N94-22194
Intersymbol interference effects in digital matched filters p 1788 N94-22218

QUEST INTEGRATED, INC., KENT, WA.
Low-cost Unmanned Air Vehicle (UAV) for oceanographic research
[AD-A273103] p 1646 N94-21507

R

RALSTON ENERGY SYSTEMS S.A., GENEVA (SWITZERLAND).
Silver oxide batteries: Recent improvements and developments p 1752 N94-20629

RAYTHEON CANADA LTD., WATERLOO (ONTARIO).
Space-based radar for moving target detection p 1745 N94-22143

RAYTHEON SERVICE CO., BURLINGTON, MA.
Problem reporting management system performance simulation p 1931 N94-21328

REGINA UNIV. (SASKATCHEWAN).
Scale-space filtering and threshold hierarchy for image segmentation p 1777 N94-22149

RENATA S.A., ITINGEN (SWITZERLAND).
Lithium batteries: Future batteries p 1752 N94-20630

RENDZIO (ROBERT J.), OZARK, AL.
Army aircraft fire-detection systems operation and reliability
[AD-A271327] p 1641 N94-20912

RENSSELAER POLYTECHNIC INST., TROY, NY.
Study of mechanisms for long wavelength Schottky-barrier infrared detectors
[AD-A270538] p 1971 N94-20083
Numerical methods for singularly perturbed differential equations with applications
[AD-A272112] p 1952 N94-20568
An analysis of pool surface deformation due to a plunging liquid jet
[AD-A272970] p 1802 N94-21261

REPUBLIC ELECTRONIC INDUSTRIES CORP., MELVILLE, NY.
Testing of DME/P equipment performance for complex MLS procedures p 1644 N94-22136

RESEARCH INST. FOR COMPUTING AND INFORMATION SYSTEMS, HOUSTON, TX.
Research in image management and accese
[NASA-CR-194797] p 1907 N94-20376
Advanced software development workstation: Knowledge base methodology: Methodology for first Engineering Script Language (ESL) knowledge base
[NASA-CR-193643] p 1930 N94-21065

RHODE ISLAND UNIV., KINGSTON.
High resolution signal processing
[AD-A271181] p 1717 N94-20215

RICE UNIV., HOUSTON, TX.
Detector noise statistics in the non-linear regime p 1748 N94-22526
The IRAF Fabry-Perot analysis package: Ring fitting p 2048 N94-22527

RIJKSINSTITUUT VOOR VOLKSGEZONDHEID EN MILIEUHYGIEENE, BILTHOVEN (NETHERLANDS).
Manual of DRANC (release 1.1): A computer program for the Dutch risk assessment of new chemical substances
[PB93-194827] p 1851 N94-19998

RIKKYO UNIV., TOKYO (JAPAN).
Yohkoh Gamma ray Spectral Observations (YGSO) p 2004 N94-22656

ROCHESTER UNIV., NY.
Quantum noise studies with superconducting tunnel junction mixers
[AD-A270897] p 2012 N94-19897
A computational theory of lexical relatedness
[TR-421] p 1904 N94-20067
Eliminating amortization: On data structures with guaranteed response time
[TR-439] p 2049 N94-20098
Robot skill learning and the effects of basis function choice
[TR-437] p 1939 N94-20135
Mint tutorial and user manual
[TR-452] p 1905 N94-20143
Memory contention in scalable cache-coherent multiprocessors
[TR-448] p 1929 N94-20144
Charge collectors for the omega upgrade
[DE93-019684] p 1972 N94-20264
Believing in the basis of the evidence
[TR-438] p 2039 N94-20364
Head-centered orientation strategies in animate vision
[TR-442] p 1894 N94-20520
Closure properties of stochastic languages
[TR-441] p 1907 N94-20521
Explanation closure, action closure, and the Sandewall test suite for reasoning about change
[TR-440] p 1907 N94-20522
Threshold computation and cryptographic security
[TR-443] p 1907 N94-20536
The effects of block size on the performance of coherent caches in shared-memory multiprocessors
[AD-A272838] p 1899 N94-21177
Classification in feature-based default inheritance hierarchies
[TR-473] p 1911 N94-21180
An NP set with no co-DP sparse subset
[TR-475] p 1954 N94-21199
Advice from nonadaptive queries to NP
[TR-470] p 1911 N94-21200
Fast mutual exclusion, even with contention
[AD-A272947] p 1912 N94-21227
Scheduling for locality in shared-memory multiprocessors
[AD-A272948] p 1930 N94-21228
Software coherence in multiprocessor memory systems
[NASA-CR-194696] p 1931 N94-21272
Selectivity: Reductions, nondeterminism, and function classes
[TR-469] p 1912 N94-21273
Space-efficient deterministic simulation of probabilistic automata
[TR-463] p 1900 N94-21281
Threshold computation and cryptographic security
[TR-461] p 1912 N94-21285
On the topological size of p-m-complete degrees
[TR-459] p 1965 N94-21286
Promises and fault-tolerant database access
[TR-447] p 2043 N94-21287
Computing solutions uniquely collapses the polynomial hierarchy
[TR-467] p 1954 N94-21314
Goal-oriented dynamic vision
[TR-466] p 1945 N94-21315
The Mercury user's manual
[TR-465] p 1913 N94-21316
High dimension action spaces in robot skill learning
[TR-458] p 1945 N94-21317
Beta(sub k)-complete problems and greediness
[TR-455] p 1913 N94-21318
On the closure properties of #P in the context of PF of #P
[TR-445] p 1955 N94-21456
Stability analysis of unsteady ablation fronts
[DE93-019689] p 1819 N94-21839
Physical properties of dense astrophysical plasmas p 2001 N94-22637

ROCKWELL INTERNATIONAL CORP., CANOGA PARK, CA.
Space Shuttle Main Engine. Overview p 1667 N94-20070
Rocketdyne turbomachinery p 1667 N94-20071
Future technical directions p 1668 N94-20072
Power conditioning system modelling for nuclear electric propulsion
[NASA-CR-191136] p 1846 N94-21179
Advanced transportation system studies, technical area 3. Alternate propulsion subsystem concepts: J-2S restart study
[NASA-CR-193874] p 1670 N94-21271
Brayton power conversion system parametric design modelling for nuclear electric propulsion
[NASA-CR-191135] p 1671 N94-21874

ROCKWELL INTERNATIONAL SCIENCE CENTER, THOUSAND OAKS, CA.
Spread spectrum random access networks
[AD-A272280] p 1737 N94-20565
Heterojunction bipolar transistor technology for data acquisition and communication p 1763 N94-21697

ROME LAB., GRIFFISS AFB, NY.
The aerogel mesh contamination collector
[AD-A270537] p 1651 N94-20011
Hybrid finite element/waveguide mode analysis of passive RF devices
[AD-A273074] p 1740 N94-21518

ROYAL MILITARY COLL. OF CANADA, KINGSTON (ONTARIO).
Fault tolerance for real-time multiprocessor operating systems p 1788 N94-22216
Optimal control of the tip of a flexible arm p 1794 N94-22256
Radio wave propagation studies along an Earth-space satellite link
[ISBN-0-315-60627-4] p 1742 N94-22408
Aperture coupling of circular cylindrical dielectric resonator antenna
[ISBN-0-315-60632-0] p 1743 N94-22409

A feasibility study of a parallax-based passive missile approach warning system
[ISBN-0-315-60640-1] p 1743 N94-22410
ROYAL NETHERLANDS METEOROLOGICAL INST., DE BILT.
Wind chill: The temperature feeling caused by the wind velocity
[KNMI-TR-103A] p 1890 N94-20238
Analysis of wind observation from towers in the period 1977-1991
[KNMI-TR-148] p 1865 N94-20239
Soil temperatures
[KNMI-WR-92-05] p 1865 N94-20309
ROYAL OBSERVATORY, EDINBURGH (SCOTLAND).
The ADAM environment and transputers
p 1926 N94-22494
RUTGERS UNIV., NEW BRUNSWICK, NJ.
Stable Ni isotopes and Be-10 and Al-26 in metallic spheroids from Meteor Crater, Arizona
p 1863 N94-20689
RUTHERFORD APPLETON LAB., CHILTON (ENGLAND).
Multifrequency data analysis software on STARLINK
p 1925 N94-22443

S

SAAB-SCANIA, LINKOPING (SWEDEN).
Image processing as a tool in flight testing evaluation
p 1640 N94-22606
SAHUARO HIGH SCHOOL, TUCSON, AZ.
Distribution of small volcanic cones on the surface of Venus by size and elevation: Implications for differential deposition of volcanic features p 2110 N94-20731
SAINT MARY'S UNIV., HALIFAX (NOVA SCOTIA).
Surface photometry of the shell galaxy NGC 2865
[ISBN-0-315-60441-7] p 2056 N94-22412
SAN DIEGO STATE UNIV., CA.
Optical climatology of the Northeast Pacific Ocean
[AD-A271671] p 1866 N94-20559
Measurement of evapotranspiration with combined reflective and thermal infrared radiance observations
[NASA-CR-194802] p 1837 N94-20951
SAN JOSE STATE UNIV., CA.
Investigating motion sickness using the conditioned taste aversion paradigm p 1888 N94-21913
Current status: Animal models of nausea
p 1889 N94-21915
SANDIA NATIONAL LABS., ALBUQUERQUE, NM.
Dynamic, multiaxial impact response of confined and unconfined ceramic rods
[DE93-040057] p 1829 N94-19824
SPICE macromodel for a 1-megawatt power MOSFET switch
[DE93-019415] p 1748 N94-19844
Segregation of Si to the surface of Fe-29Ni-17Co alloy
[DE93-040053] p 1687 N94-19864
Spatial patterns in semiconductor lasers
[DE93-040056] p 1814 N94-19865
Effect of exciton localization and delocalization on magnetic-field-dependent photoluminescence linewidths in semiconductors
[DE93-018860] p 1748 N94-19884
Hydrodynamic compressibility of high-strength ceramics
[DE93-019424] p 1698 N94-19903
Near atomic resolution microanalysis of interfaces by analytical electron microscopy
[DE93-019437] p 1687 N94-19904
Time-resolved shock compression of porous rutile: Wave dispersion in porous solids
[DE93-018848] p 1829 N94-19927
A benchmark study of 2D and 3D finite element calculations simulating dynamic pulse buckling tests of cylindrical shells under axial impact
[DE93-018859] p 1829 N94-19940
PVDF gauge characterization of hypervelocity-impact-generated debris clouds
[DE93-018831] p 1829 N94-19943
Shock response of porous Al-2 + Fe2O3 powder mixtures
[DE93-018851] p 1688 N94-19944
Solder technology in the manufacturing of electronic products
[DE93-018842] p 1699 N94-19960
Preparation and properties of sol-gel derived PZT thin films for decoupling capacitor applications
[DE93-018853] p 2013 N94-19961
Wavefront sensors for optical diagnostics in fluid mechanics: Application to heated flow, turbulence, and droplet evaporation
[DE93-040060] p 1797 N94-19974
CTH: A software family for multi-dimensional shock physics analysis
[DE93-019428] p 1904 N94-20052
Measuring liquid properties with smooth and textured-surface resonators
[DE93-019433] p 1749 N94-20054
A breakdown model for the bipolar transistor to be used with circuit simulators
[DE93-019422] p 1750 N94-20218
Optical diagnostic instrument for monitoring etch uniformity during plasma etching of polysilicon in a chlorine-helium plasma
[DE93-019582] p 1993 N94-20261
Object-oriented DFD models to present the functional and behavioral views
[DE93-040206] p 1906 N94-20280
A proposal for reverse engineering CASE tools to support new software development
[DE93-040207] p 1906 N94-20281
Teleoperation with virtual force feedback
[DE93-019406] p 1942 N94-20293
Photoconductive Semiconductor Switches for pulsed power applications
[DE93-019411] p 1750 N94-20294
Observation of reflected waves on the SABRE positive polarity inductive adder MITL
[DE93-019413] p 1980 N94-20295
Optically controlled current filamentation in GaAs photoconductive semiconductor switches
[DE93-019427] p 2016 N94-20296
Development and characterization of a time-, position- and energy-resolved x ray diagnostic for PBFA 2 target experiments
[DE93-019429] p 1808 N94-20297
Photopumped x ray laser research on Saturn
[DE93-019430] p 1816 N94-20298
Time-of-flight heavy ion backscattering spectrometry
[DE93-019067] p 1973 N94-20306
Characterization of amorphous material in shocked quartz by NMR spectroscopy
[DE93-019069] p 1679 N94-20307
High current density contacts for photoconductive semiconductor switches
[DE93-018837] p 1750 N94-20312
Light scattering studies of an electrorheological fluid
[DE93-019419] p 1700 N94-20315
Delivery of very high bandwidth with ATM switches and SONET
[DE93-019432] p 1899 N94-20476
High accuracy die mechanical stress measurement with the ATC04 Assembly Test Chip
[DE93-019435] p 1830 N94-20477
Correct CMOS IC defect models for quality testing
p 1755 N94-21093
Polyimide-based electrooptic materials
[DE93-019416] p 1706 N94-21526
Magnetic force microscopy/current contrast imaging: A new technique for internal current probing of IC's
[DE93-040754] p 1761 N94-21532
Coupling of smooth particle hydrodynamics with PRONTO
[DE93-019080] p 1915 N94-21539
Synthesis and catalytic properties of metal and semiconductor nanoclusters
[DE93-019418] p 2028 N94-21541
Initial laboratory evaluation of color video cameras, phase 2
[DE93-040201] p 1809 N94-21556
Experimental and numerical studies of high-velocity impact fragmentation
[DE93-040205] p 1832 N94-21557
Results from long conduction time plasma opening switch experiments at Sandia National Laboratories
[DE93-019063] p 1762 N94-21632
Advanced failure analysis laboratory equipment networking
[DE93-019070] p 1916 N94-21633
Ultrafast gas switching experiments
[DE93-019071] p 1762 N94-21634
RHALE: A 3-D MMALE code for unstructured grids
[DE93-019405] p 1916 N94-21635
Localization of pellicle-induced open contacts using charge-induced voltage alteration
[DE93-019407] p 1762 N94-21636
Improvement of the stability of the process for synthesizing chemically prepared varistor powder
[DE94-000345] p 1763 N94-21654
The Milling assistant, case-based Reasoning, and machining strategy: A report on the development of automated numerical control programming systems at New Mexico State University
[DE93-041101] p 2029 N94-21690
Surface acoustic wave sensing of VOC's in harsh chemical environments
[DE93-040721] p 1968 N94-21751
Stochastic simulation for imaging spatial uncertainty: Comparison and evaluation of available algorithms
[DE93-040058] p 1916 N94-21761
Particle behavior in an ECR plasma etch tool
[DE93-040343] p 1996 N94-21769
Reentry vehicle adaptive telemetry
[DE94-001168] p 1656 N94-21852
Evaluation of DEC's GIGAswitch for distributed parallel computing
[DE94-001356] p 1936 N94-21853
A thermodynamic theory of dynamic fragmentation
[DE93-019066] p 1833 N94-21916
Micromachined actuator and sensor capabilities at the Microelectronics Development Laboratory
[DE93-019417] p 1769 N94-21918
Automating the control of robotic systems in unstructured environments
[DE93-040753] p 1946 N94-21929
Simple method to estimate MOS oxide-trap, interface-trap, and border-trap densities
[DE93-041138] p 2032 N94-21939
Techniques for producing free-standing thin films on frames
[DE93-041144] p 1708 N94-21954
Dynamic properties of ceramic materials
[DE94-000654] p 1708 N94-21963
Fluorescent microthermographic imaging
[DE93-040332] p 1810 N94-22000
NMR studies of oxygen-doped La2CuO(4+delta)
[DE93-040756] p 2034 N94-22007
Interfacial reactions between titanium and borate glass
[DE93-012847] p 1683 N94-22031
Characteristics of shock-compressed configuration of Ti and Si powder mixtures
[DE93-018857] p 1713 N94-22033
Acoustic, fiber optic, and silicon microelectronic microsensors research and development activities at Sandia National Laboratories
[DE93-019075] p 1770 N94-22040
A comparison of IDEF1X and NIAM ISDM
[DE93-040899] p 1921 N94-22383
F2D users manual: A two-dimensional compressible gas flow code
[DE94-000653] p 1805 N94-22386
Flow and heat transfer model for a rotating cryogenic motor
[DE94-001151] p 1794 N94-22405
Coupling of smooth particle hydrodynamics with the finite element method
[DE93-019081] p 1805 N94-22556
SANDIA NATIONAL LABS., LIVERMORE, CA.
TCP performance analysis for wide area networks
[DE94-000449] p 1928 N94-19858
SANDIA NATIONAL LABS., TONOPAH, NV.
Digital wireless control system
[DE93-040211] p 1714 N94-19946
SAO PAULO UNIV. (BRAZIL).
The use of satellite images in Amazonian archaeology: A case study in the Upper Rio Negro Basin
p 1838 N94-20954
Drought early warning system for crop production
p 1840 N94-20966
Three-dimensional simulations of cosmic jets employing the smoothed particle hydrodynamics technique
p 2008 N94-22685
SCIENCE AND TECHNOLOGY AGENCY, TOKYO (JAPAN).
Evaporation of a sodium tellurite melt in the jamic low gravity drop shaft p 1713 N94-20605
SCIENCE APPLICATIONS INTERNATIONAL CORP., ALBUQUERQUE, NM.
F2D users manual: A two-dimensional compressible gas flow code
[DE94-000653] p 1805 N94-22386
SCIENCE APPLICATIONS INTERNATIONAL CORP., SAN DIEGO, CA.
Determination of coronal magnetic fields from vector magnetograms
[NASA-CR-194744] p 2147 N94-21877
SCIENCE APPLICATIONS INTERNATIONAL CORP., WASHINGTON, DC.
The Clementine Mission science return at the Moon and Geographos p 1652 N94-20850
SCIENCE RESEARCH COUNCIL, SLOUGH (ENGLAND).
The STARLINK software collection
p 1927 N94-22545
SCIENCE RESEARCH LAB., INC., SOMERVILLE, MA.
Compact lightweight CO2 laser for SDIO application
[AD-A273010] p 1817 N94-21284
SCIENTIFIC STUDIES CORP., PALM BEACH GARDENS, FL.
State-space models for multichannel detection
[AD-A270608] p 1715 N94-19816
SCRIPPS INSTITUTION OF OCEANOGRAPHY, LA JOLLA, CA.
FE-60 and the evolution of eucrites
p 2083 N94-20768

Acoustic monitoring of global ocean variability
[AD-A271998] p 1883 N94-21366

SD SCICON PUBLIC LTD. CO., CHEADLE (ENGLAND).
Formal methods in the design of critical software systems p 1779 N94-22158

SECRETARIA DE ESTADO DO MEIO AMBIENTE, PARANA (BRAZIL).
The 7th Brazilian Remote Sensing Symposium, volume 1 p 1838 N94-20953
The 7th Brazilian Remote Sensing Symposium, volume 2 p 1838 N94-20956
The 7th Brazilian Remote Sensing Symposium, volume 3 p 1839 N94-20960
The 7th Brazilian Remote Sensing Symposium, volume4 p 1840 N94-20965

SEVILLE UNIV. (SPAIN).
Deformation of an alumina-zirconia-silicon carbide-whisker reinforced composite
[DE93-040244] p 1676 N94-21559

SFA, INC., LANDOVER, MD.
Fabrication and evaluation of superconducting and semiconducting materials
[AD-A271645] p 2018 N94-20558
Engineering design, fabrication, installation, operation, and maintenance services in support of research on laser plasma physics
[AD-A272249] p 1994 N94-20943

SHERBROOKE UNIV. (QUEBEC).
A pyramid neural network architecture for stereo fusion p 1785 N94-22201

SIMON FRASER UNIV., BURNABY (BRITISH COLUMBIA).
Speaker-independent isolated-digit recognition using neural networks and hidden Markov model p 1747 N94-22213

SMITHSONIAN ASTROPHYSICAL OBSERVATORY, CAMBRIDGE, MA.
Measurements of atomic interactions and frequency stability with a cryogenic hydrogen maser
[AD-A271132] p 1814 N94-19853
Theoretical investigations of metastability and energy storage in molecular systems
[AD-A271849] p 1973 N94-20612
Development and operations of the Astrophysics Data System
[NASA-CR-194691] p 2043 N94-21270
High resolution studies of the structure of the solar atmosphere
[AD-A273084] p 2147 N94-21522
VETA x ray data acquisition and control system p 2047 N94-22455
PROS: An IRAF based system for analysis of x ray data p 1925 N94-22461
Detection of x ray sources in PROS p 2062 N94-22466
Visualizing the universe, part 1 p 2064 N94-22476
AXAF user interfaces for heterogeneous analysis environments p 1926 N94-22507
Verification of the PROS timing analysis package p 1926 N94-22508
SKYMAP: Exploring the Universe in software p 1927 N94-22511
An x ray archive on your desk: The Einstein CD-ROM's p 2048 N94-22519
Spatial region filtering in IRAF/PROS p 1927 N94-22524

SMITHSONIAN INSTITUTION, CAMBRIDGE, MA.
Visualizing the universe, part 2 p 2063 N94-22472
Intelligent text retrieval in the NASA astrophysics data system p 2048 N94-22499

SMITHSONIAN INSTITUTION, WASHINGTON, DC.
Arcuate and circular structures in the Tharsis region: Evidence of coronae on Mars p 2134 N94-20863
Comparison of flank modification on Ascraeus and Arsia Montes volcanoes, Mars p 2140 N94-20903
Numerical simulation of lava flows: Applications to the terrestrial planets p 1863 N94-20904

SOCIEDAD DE ESPECIALISTAS LATINOAMERICANOS EN PERCEPTION REMOTA (CHILE).
The 7th Brazilian Remote Sensing Symposium, volume 1 p 1838 N94-20953
The 7th Brazilian Remote Sensing Symposium, volume 2 p 1838 N94-20956
The 7th Brazilian Remote Sensing Symposium, volume 3 p 1839 N94-20960
The 7th Brazilian Remote Sensing Symposium, volume4 p 1840 N94-20965

SOCIEDADE BRASILEIRA DE CARTOGRAFIA, GEODESIA, FOTOGRAMTRIA E SENSORIAMENTO REMOTO.
The 7th Brazilian Remote Sensing Symposium, volume 1 p 1838 N94-20953
The 7th Brazilian Remote Sensing Symposium, volume 2 p 1838 N94-20956
The 7th Brazilian Remote Sensing Symposium, volume 3 p 1839 N94-20960
The 7th Brazilian Remote Sensing Symposium, volume4 p 1840 N94-20965

SOCIETE EUROPEENNE DE PROPULSION, VERNON (FRANCE).
The Vulcain cryogenic engine p 1668 N94-20077
Thermostructural material composites for space applications p 1664 N94-21398

SOCIETE NATIONALE INDUSTRIELLE AEROSPATIALE, PARIS (FRANCE).
Process and apparatus for the release of a prestress initially applied to a mechanism such as a bearing on board a space vehicle
[CA-PATENT-APPL-SN-2,020,90] p 1824 N94-21142

SOCIETE SUISSE DE CHRONOMETRIE, NEUCHATEL.
The One-Day Workshop on Batteries, Stepping Motors, and Electronic Clock Displays
[ETN-93-94632] p 1752 N94-20628

SOLAR CELLS, INC., TOLEDO, OH.
Fabrication of stable large-area thin-film CdTe photovoltaic modules
[DE93-018204] p 1845 N94-20095

SOLAR TURBINES, INC. SAN DIEGO, CA.
Advanced Turbine Systems (ATS). Phase 1: System scoping and feasibility studies
[DE93-041130] p 1826 N94-21938

SOLAREX CORP., NEWTOWN, PA.
Research on polycrystalline thin-film submodules based on CuInSe2 materials
[DE93-018223] p 2029 N94-21617

SOPHIA UNIV., TOKYO (JAPAN).
Neutrino emission processes in dense high-temperature plasmas p 2001 N94-22638

SOTEMA, RAMONVILLE SAINT-AGNE (FRANCE).
Rapid estimates of crop production using remote sensing: European experience p 1840 N94-20969

SOUTHEASTERN CENTER FOR ELECTRICAL ENGINEERING EDUCATION, INC., SAINT CLOUD, FL.
Development of the UTC-PAB normative database
[AD-A271319] p 1893 N94-20023

SOUTHWEST RESEARCH AND DEVELOPMENT CO., LAS CRUCES, NM.
SO2 on Venus: IUE, HST and ground-based measurements, and the active volcanism connection p 2092 N94-20637

SOUTHWEST RESEARCH INST., SAN ANTONIO, TX.
Recommendations resulting from the SPDS Community-Wide Workshop
[NASA-CR-194684] p 2042 N94-20363
Compatibility and efficacy of biocides qualified under military specification MIL-S-53021
[AD-A271496] p 1712 N94-20551
Recent advances in computational structural reliability analysis methods p 1828 N94-22616

SPACE POWER, INC., SAN JOSE, CA.
SPACE-R Thermionic Space Nuclear Power System: Design and Technology Demonstration Program
[DE93-013969] p 1670 N94-21824

SPACE RESEARCH ORGANIZATION NETHERLANDS, GRONINGEN.
The ISO SWS on-line system p 1927 N94-22522

SPACE TELESCOPE SCIENCE INST., BALTIMORE, MD.
Focus history of the Hubble Space Telescope: Launch to May 1993
[NASA-CR-194179] p 2055 N94-20204
A neural network prototyping package within IRAF p 1949 N94-22451
Enhancements to IRAF/STSDAS graphics p 1925 N94-22470
C++, objected-oriented programming, and astronomical data models p 2083 N94-22473
HST image restoration: A comparison of pre- and post-servicing mission results p 1925 N94-22478
Telescope image modelling software in STSDAS p 1926 N94-22483
How is WFPC flat field made p 1926 N94-22484
ASpect: A new spectrum and line analysis package for IRAF p 1926 N94-22485
An object-oriented approach for supporting both X and terminal interfaces p 1926 N94-22491
The application of artificial intelligence to astronomical scheduling problems p 1949 N94-22492
Deconvolution of Hubble Space Telescope images using simulated point spread functions p 2048 N94-22497
HST PSF simulation using Tiny Tim p 1926 N94-22498
Integrating a local database into the StarView distributed user interface p 2048 N94-22530
StarView: The object oriented design of the ST DADS user interface p 2049 N94-22548
Registering and resampling images in STSDAS p 1927 N94-22550
IRAF and STSDAS under the new ALPHA architecture p 2049 N94-22553

SPACEBORN, INC., LA CANADA, CA.
A 1 GHz sample rate, 256-channel, 1-bit quantization, CMOS, digital correlator chip p 1788 N94-21732

SPAR AEROSPACE LTD., TORONTO (ONTARIO).
Durability of thermal control and environmental protective materials for the SSRMS in simulated LEO environment p 1663 N94-21392

SPARTA, INC., LEXINGTON, MA.
Obtaining surface optical properties from space-based lidar systems
[AD-A272831] p 1987 N94-21172

SPRINGER-VERLAG G.M.B.H. AND CO. K.G., HEIDELBERG (GERMANY).
Lecture notes in artificial intelligence 689: The 7th International Symposium on Methodologies for Intelligent Symposium (ISMIS 1993)
[AD-A271768] p 1944 N94-21162

SRI INTERNATIONAL CORP., MENLO PARK, CA.
Theory of energy-assisted epitaxy; theory of ordered semiconductor alloys: In(1-x)Tl(x)Sb as a long-wave infrared material
[AD-A271007] p 2012 N94-19835
Evaluation of a diffusion/trapping model for hydrogen ingress in high-strength alloys
[AD-A271328] p 1689 N94-20027
Modeling of the coupled magnetospheric and neutral wind dynamos
[NASA-CR-194728] p 1856 N94-20537
IR materials producibility
[AD-A273031] p 1987 N94-21321
Fabrication of porous ceramics by freeze-casting/freeze-drying
[PB93-202513] p 1705 N94-21425
Electronically metastable molecules of high symmetry
[AD-A272015] p 1974 N94-21461

SRI VENKATESWARA UNIV., TIRUPATI (INDIA).
A novel VLSI processor architecture for supercomputing arrays p 1758 N94-21115
A unified approach to VLSI layout automation and algorithm mapping on processor arrays p 1759 N94-21127
A cost-effective methodology for the design of massively-parallel VLSI functional units p 1760 N94-21132

STANDARD MICROSYSTEMS, CA.
A 20 MHz CMOS reorder buffer for a superscalar microprocessor p 1764 N94-21700

STANFORD LINEAR ACCELERATOR CENTER, CA.
Method to evaluate steering and alignment algorithms for controlling emittance growth
[DE93-041004] p 1978 N94-19856
A field-based technique for the longitudinal profiling of ultrarelativistic electron or positron bunches down to lengths of less than or equal to 10 microns
[DE93-040954] p 1978 N94-19873
Persistent wakefields associated with waveguide damping of higher order modes
[DE93-040973] p 1715 N94-19874
Parton-parton elastic scattering and rapidity gaps at Tevatron energies
[DE93-041024] p 1974 N94-21515
An integro-algebraic equation for high frequency wake fields in a tube with smoothly varying radius
[DE93-040940] p 1741 N94-21684
Simulation of traveling-wave output structures for high power RF tubes
[DE93-041005] p 1763 N94-21685
Multibunch beam break-up in detuned structures
[DE93-041056] p 1981 N94-21686
Simulation and compensation of multibunch energy variation in NLC
[DE93-041057] p 1981 N94-21687
A relativistic constituent quark model
[DE93-041085] p 1946 N94-21689
The preservation of low emittance flat beams
[DE93-040964] p 1981 N94-21773
SLAC measurement of the neutron spin structure function
[DE93-040998] p 1975 N94-21788
New perspectives in quantum chromodynamics
[DE93-041021] p 2038 N94-21935
On the correspondence limit of relativistic quantum mechanics
[DE93-040939] p 2038 N94-21971

STANFORD RESEARCH INST., MENLO PARK, CA.
SLD results from the study of polarized Z(sup 0) produced at the SLC
[DE93-041020] p 1982 N94-21952

STANFORD TELECOMMUNICATIONS, INC., SEABROOK, MD.
The Composite Analytic and Simulation Package or RFI (CASPR) on a coded channel p 1744 N94-21339
The Automated Conflict Resolution System (ACRS) p 1744 N94-21341
The three-dimensional Event-Driven Graphics Environment (3D-EDGE) p 1922 N94-21342
Satellite Communication Hardware Emulation System (SCHES) p 1744 N94-21344

Advanced coding and modulation schemes for TDRSS
p 1744 N94-21350

STANFORD UNIV., CA.
Stochastic optimization by simulation: Numerical experiments with M/M/1 queue in steady-state
[AD-A271143] p 1949 N94-19854
Some topics in regenerative steady-state simulation
[AD-A271145] p 1902 N94-19855
Large deviations behavior of counting processes and their inverses
[AD-A271142] p 1939 N94-19909
Stochastic optimization by simulation: Convergence proofs for the G1/G/1 queue in steady-state
[AD-A271141] p 1962 N94-19999
On the numerical stability of quasi-definite systems
[DE93-019404] p 1950 N94-20217
Scattering by Venus' surface p 2117 N94-20771
Investigation of the physics of the turbulent boundary layer focusing on vortex structures
[AD-A272879] p 1802 N94-21155
An efficient numerical method for three-dimensional hypersonic flow
[AD-A272506] p 1637 N94-21411
Nonlinear aerodynamics and the design of wing tips
[NASA-CR-194732] p 1638 N94-21833
Algorithmic advances in stochastic programming
[DE94-001160] p 1921 N94-22406
Modeling of failure and response to laminated composites subjected to in-plane loads
p 1834 N94-22612
Solar wind-magnetosphere interaction as simulated by a 3D, EM particle code p 2007 N94-22674

STATE UNIV. OF NEW YORK, ALBANY.
Study of regional climate change
[DE93-018926] p 1850 N94-19941
Computation of signal delays in RC networks
p 1744 N94-21102
Photonics and nonlinear optics with molecular materials and polymers
[AD-A271747] p 1988 N94-21457

STATE UNIV. OF NEW YORK, BUFFALO.
Adhesive electroless metallization of fluoropolymeric substrates
[AD-A271858] p 1703 N94-20526

STATE UNIV. OF NEW YORK, STONY BROOK.
Requirements for the early atmosphere of Mars from nitrogen isotope ratios p 2144 N94-21669

STERLING SOFTWARE, INC., PALO ALTO, CA.
Publication of science data on CD-ROM: A guide and example
[NASA-CR-4560] p 1842 N94-21585
Data management for interdisciplinary field experiments: OTTER project support
[NASA-CR-4559] p 1842 N94-22345

STOCKHOLM UNIV. (SWEDEN).
A SCSI-bus data acquisition system for nuclear spectroscopy experiments
[USIP-92-03] p 2042 N94-20193

STRATEDGE CORP., SAN DIEGO, CA.
Quartz/fused silica chip carriers
[NASA-CR-194154] p 2016 N94-20340

STUTTGART UNIV. (GERMANY).
On Plasma Edge Spectroscopy and Spectroscopic Studies of Impurity Densities and Impurity Transport
[IPF-92-2] p 1996 N94-21802
Plasma edge spectroscopy p 1996 N94-21803
Spectroscopic studies of impurity densities and impurity transport p 1997 N94-21804

SUMMA TECHNOLOGY, INC., HUNTSVILLE, AL.
Specialized data analysis for the Space Shuttle Main Engine and diagnostic evaluation of advanced propulsion system components
[NASA-CR-194720] p 1656 N94-21813

SUPERCONDUCTING SUPER COLLIDER LAB., DALLAS, TX.
SISSY: An example of a multi-threaded, networked, object-oriented databased application
[DE93-019742] p 2041 N94-19811
Physics Detector Simulation Facility. Phase 2: System software description
[DE93-019745] p 1928 N94-19812
Physics Detector Simulation Facility (PDSF) architecture/utilization
[DE93-019744] p 1936 N94-21919

SURVEILLANCE RESEARCH LAB., SALISBURY (AUSTRALIA).
Evaluation of a single stage of the LADS filter
[AD-A271101] p 1814 N94-19851
A general purpose ionospheric ray tracing procedure
[AD-A271058] p 1854 N94-19860
Techniques for the flux growth of optical materials: Growth of beta-barium borate
[AD-A272717] p 2028 N94-21505

SVERDRUP TECHNOLOGY, INC., BROOK PARK, OH.
Evaluation of externally heated pulsed MPD thruster cathodes
[NASA-CR-191090] p 1670 N94-21565
A laboratory system for the investigation of rain fade compensation techniques for Ka-band satellites
[NASA-CR-191200] p 1762 N94-21566
TROPIX plasma interactions group report
[NASA-CR-191149] p 1666 N94-21864
Three-dimensional unstructured grid method applied to turbomachinery p 1919 N94-22360

SWEDISH CEMENT AND CONCRETE RESEARCH INST., STOCKHOLM.
A quantitative S.E.M. image analysis of cement paste microstructure p 1708 N94-21894

SYDNEY UNIV. (AUSTRALIA).
Radiation from solar flares p 2001 N94-22634
Energy release at Alfvenic fronts in solar flares
p 2003 N94-22652
Electron acceleration in and radio emission from SN1987A p 2007 N94-22677
Magnetic fields in spiral galaxies
p 2010 N94-22697

SYRACUSE UNIV., NY.
Research on defects and transport in amorphous-silicon-based semiconductors
[DE93-017117] p 2013 N94-19939
A mean field neural network for hierarchical module placement p 1766 N94-21720

SYSTEMS CONTROL TECHNOLOGY, INC., ARLINGTON, VA.
Rotorcraft low altitude IFR benefit/cost analysis: Conclusions and recommendations
[DOT/FAA/RD-93/22] p 1642 N94-20051

T

TAMPERE UNIV. OF TECHNOLOGY (FINLAND).
Information and decision structure in a Japanese type of management with respect to QCC and just-in-time systems p 2046 N94-22063

TECHNICAL RESEARCH CENTRE OF FINLAND, ESPOO.
Production of NiAl and TiAl intermetallics by mechanical alloying
[VTT-JULK-760] p 1691 N94-20530
Optical integrated structures and circuits on silicon
[VTT-PUBS-106] p 1988 N94-21594
A novel semiconductor process for optoelectronic applications on silicon substrate p 1988 N94-21595
Integrated optical coupling element on silicon substrate, appendix 2 p 1988 N94-21596
Bidirectional method for optical channel waveguide attenuation measurement by detectors integrated on the wafer, appendix 3 p 1988 N94-21597
An integrated-optic polarization splitter on silicon substrate, appendix 4 p 1989 N94-21598
Birefringence control and dispersion characteristics of silicon oxynitride optical waveguides, appendix 6
p 1989 N94-21600
Refractive index behaviour of phosphorus-doped planar silica waveguides, appendix 7 p 1989 N94-21601
Wide passband wavelength multi/demultiplexer at 1.3/1.55 micrometers based on etched Fresnel mirror, appendix 8 p 1989 N94-21602
Precision prism coupling setup applied to measure planar silica films on silicon, appendix 9 p 1989 N94-21603
Symposium on Microscopy and Image Analysis of Building Materials
[VTT-SYMP-136] p 1707 N94-21890
Preparation of concrete specimens for microstructural image analysis studies p 1707 N94-21891
Optical air pore analysis p 1708 N94-21892
Some experiments on using backscattered electron and energy dispersive x ray imaging in determination of portland cement clinker phase composition p 1708 N94-21893
Determination of pore structure of concrete from thin sections by image analysis p 1708 N94-21895
Information Technology and Economic Modelling
[VTT-SYMP-135] p 2049 N94-22056
AJKA: An econometric macromodel for Finland
p 2050 N94-22061
The program system for the diagnostics of strains and fracture prediction of solids p 1836 N94-22065
Application of the structures query language of APROS for specification of industrial processes
p 1923 N94-22078
Manufacturing and information technology
p 2046 N94-22082

TECHNION - ISRAEL INST. OF TECH., HAIFA.
An automatic multigrid method for the solution of sparse linear systems p 1957 N94-21478

TECHNISCHE HOCHSCHULE, AACHEN (GERMANY).
Testing of a multisensor hot film technique in wind tunnel and free flight p 1639 N94-22599

TECHNISCHE HOCHSCHULE, DARMSTADT (GERMANY).
Optically induced rotation diffusion in polymer liquid crystals: Phenomenological theory and experimental verification
[ETN-93-95068] p 2014 N94-20026
Examination of low level magnetic dipole intensities in the transition nuclei Sm-148, Sm-150, Sm-152 and Sm-154, with inelastic photon scattering at S-DALINAC
[ETN-93-95069] p 1971 N94-20030
Analysis and evaluation of configuring of graphical systems on multiprocessor architectures
[ETN-93-93618] p 1930 N94-21018
Asymptotic behavior of Fourier transform of surface measures on convex and radial hypersurfaces
[ETN-93-93790] p 1952 N94-21019
AIDA: A graphical interactive system, adapted to the user
[ETN-93-93792] p 1908 N94-21020
Graphical interactive planning of robotic applications with support of integrated simulation
[ETN-93-93793] p 1944 N94-21057
A geometrical process for three dimensional osteotomy planning
[ETN-93-93602] p 1892 N94-21134
Thermal expansion of electronic highly correlated materials
[ETN-93-93605] p 2026 N94-21135
F-spin concept and g-bosons in the interceding boson model
[ETN-93-93607] p 1973 N94-21136
Adaptive grids for quasilinear parabolic systems in one space dimension
[ETN-93-93611] p 1954 N94-21137

TECHNISCHE HOGESCHOOL, DELFT (NETHERLANDS).
Numerical study of a multigrid method with four smoothing methods for the incompressible Navier-Stokes equations in general coordinates p 1806 N94-21487

TECHNISCHE PHYSISCHE DIENST TNO-TH, DELFT (NETHERLANDS).
Activities Report of the Institute of Applied Physics
[ETN-93-93749] p 1966 N94-21798
Traffic noise in a roundabout way
p 1966 N94-21799
Modeling of glass fabrication p 1711 N94-21800
Electronic locking system p 1796 N94-21801

TECHNISCHE UNIV., BERLIN (GERMANY).
A Green function method for calculation of atomic and electronic properties of isolated adsorbate atoms
[ETN-93-95055] p 2014 N94-20018
Efficient and correct translation of strict applicative programming languages
[ETN-93-95056] p 1903 N94-20020
A concept for implementing hypermedia technology in computer aided workplaces in medicine
[ETN-93-95057] p 1889 N94-20022
Calculation and optimization of electromagnetic fields in a patient by local hyperthermia utilization
[ETN-93-95059] p 1889 N94-20024
Principles and applications of oil film interferometry for measuring wall friction fields in air flows
[ETN-93-95062] p 1798 N94-20147
Development of a numerical simulation model for a-Si:H solar cells and application to the analysis of experimentally obtained spectral characteristics
[ETN-93-95061] p 1846 N94-20151
Photoelectron spectroscopy at model boundary surfaces of energy converter semiconductors/electrolyte contacts: Adsorption, coadsorption, and triadsorption of Br2, Na, and H2O on Van der Waals surfaces of metal chalocogenide semiconductors
[ETN-93-95063] p 2015 N94-20152
Female security as a general mobility condition
[ISBN-3-79-831536-1] p 2039 N94-20153
Theoretical and numerical examinations of nonlinear parameter dependent advanced differential difference equations
[ETN-93-93681] p 1952 N94-21042
Optical amplification and threshold behavior on InGaAs/InGaAsP multiquantum well structures
[ETN-93-94181] p 2026 N94-21151
Design of a computer assisted tool for object oriented acquisition, modeling and simulation of knowledge structure
[ETN-93-94183] p 1910 N94-21152
Adaptation of model parameters of a rail model at measured rail compliances
[ILR-MITT-274(1992)] p 1831 N94-21153
Measurement Technology for Flight Tests
[ILR-MITT-256(1991)] p 1639 N94-22597
Free flight experiment with a laminar wing glove
p 1639 N94-22600

TECHNISCHE UNIV., DELFT (NETHERLANDS).
Mathematics B for the study direction VWO: A reconnaissance
[REPT-92-80] p 1950 N94-20032

The causes of contact noise
[REPT-92-100] p 1822 N94-20157
Orthogonal pairs and zeros of Sobolev-type orthogonal polynomials
[REPT-92-46] p 1953 N94-21059
Spaceplane flight simulation: Project definition
[PB93-211399] p 1651 N94-22094
Time-laplace-transform-domain analysis of wave propagation in planar waveguides
[PB93-215226] p 1960 N94-22096
Influence of geoid model uncertainty on the determination of ocean circulation with satellite altimetry
[PB93-219301] p 1842 N94-22097
Near wake measurements on a rotor model with Mie-vanes in the Delft open jet tunnel
[PB93-215382] p 1638 N94-22260
Interface reflection of spherical acoustic waves in the first- and second-order rational parabolic approximations and their artifacts
[PB93-215424] p 1969 N94-22261
Transient acoustic wave modeling: Higher-order WKBJ asymptotics and symbolical manipulation (revised)
[PB93-215432] p 1969 N94-22262
Estimability of polar motion using range observations to satellites
[PB93-219319] p 1842 N94-22265
Extended range modified gradient technique for profile inversion (extended version of report Et/Em-1992-8)
[PB93-215242] p 1742 N94-22346
Continuous-time discretized-space approach to modeling short-pulse propagation and scattering
[PB93-215259] p 1742 N94-22347
Electromagnetic interference and shielding: An introduction (revised version of 1991-23)
[PB93-215275] p 1742 N94-22348
Modelling short bent, graded index dielectric slab waveguides
[PB93-215283] p 1742 N94-22349

TECHNISCHE UNIV., EINDHOVEN (NETHERLANDS).
Interval timed coloured petri nets and their analysis
[PB93-191732] p 1903 N94-19992
Total order assumption
[PB93-191740] p 1903 N94-19993
Program derivation in acyclic graphs and related problems
[PB93-191765] p 1903 N94-19994
Bottom-up abstract interpretation of logic programs
[PB93-191773] p 1928 N94-19995
Programming logic for F omega
[PB93-191781] p 1928 N94-19996
Are types needed for natural language?
[PB93-191831] p 1949 N94-19997
Set theory and nominalisation, part 1
[PB93-191807-PT-1] p 1962 N94-20007
Set theory and nominalisation, part 2
[PB93-191815-PT-2] p 1962 N94-20008
System at the cross-roads of functional and logic programming
[PB93-191823] p 1928 N94-20009
Nominalization, prediction and type containment
[PB93-191799] p 1898 N94-20082
Derivation of a model of the exciter of a brushless synchronous machine
[EUT-92-E-258] p 1761 N94-21538
Defect motion as the origin of the 1/f conductance noise in solids
[EUT-92-E-259] p 2029 N94-21552

TECHNISCHE UNIV., MUNICH (GERMANY).
Layout optimization with algebraic multigrid methods p 1957 N94-21474

TELEDYNE BROWN ENGINEERING, HUNTSVILLE, AL.
Concept report: Experimental vector magnetograph (EXVM) operational configuration balloon flight assembly
[NASA-CR-194702] p 1638 N94-21776

TELESPAZIO S.P.A., ROME (ITALY).
Using NDVI/AVHRR data for crop monitoring and forecasting in South Italy p 1841 N94-20970

TENNESSEE UNIV., KNOXVILLE.
Primary differentiation in the early Earth: Nd and Sr isotopic evidence from diamondiferous eclogites for both old depleted and old enriched mantle, Yakutia, Siberia p 1862 N94-20776
Chronology and genesis of high-Ti mare volcanism: Melting of cogenetic depleted and enriched reservoirs p 2118 N94-20777
Geochronology and petrogenesis of the western highlands alkali suite: Radiogenic isotopic evidence from Apollo 14 p 2118 N94-20778
Magnesian anorthosites from the western highlands of the Moon: Isotope geochemistry and petrogenesis p 2118 N94-20779
Production of O2 on the Moon: A lab-top demonstration of ilmenite reduction with hydrogen p 2126 N94-20821
Wet inside and out? Constraints on water in the Martian mantle and on outgassed water, based on melt inclusions in SNC meteorites p 2145 N94-21678
Symmetry-dictated trucation: Solutions of the spherical shell model for heavy nuclei
[DE94-000482] p 1976 N94-21961
Simulating the Euclidean time Schroedinger equations using an INTEL iPSC/860 hypercube: Application to the t-J model of high-T(sub c) superconductivity
[DE94-000489] p 2035 N94-22385

TENNESSEE UNIV., NASHVILLE.
Center for neural engineering
[AD-A271164] p 1890 N94-20185

TEXAS A&M UNIV., COLLEGE STATION.
Functional statistical data analysis and modeling
[AD-A271520] p 1963 N94-20913
High energy physics program at Texas A/M University
[DE93-041089] p 1980 N94-20933
A multigrid algorithm for the cell-centered finite difference scheme p 1957 N94-21479
Orbit and sampling requirements: TRMM experience p 1870 N94-21647
A thermodynamic analysis of propagating subcritical cracks with cohesive zones p 1834 N94-22611

TEXAS INSTRUMENTS, INC., DALLAS.
High performance MPEG-audio decoder IC p 1744 N94-21092

TEXAS INSTRUMENTS, INC., LEWISVILLE.
Bit-systolic arithmetic arrays using dynamic differential gallium arsenide circuits p 1767 N94-21724

TEXAS UNIV., AUSTIN.
Finite Larmor radius flute mode theory with end loss
[DE93-040914] p 1991 N94-19872
Effect of limiter end loss in finite Larmor radius theory
[DE93-040913] p 1992 N94-19887
Nonlinear acoustics: Periodic waveguide, finite-amplitude propagation in a medium having a distribution of relaxation processes, and production of an isolated negative pulse in water
[AD-A270530] p 1967 N94-19894
Durability predictions for adhesively bonded joints in humid environments
[AD-A271177] p 1830 N94-20001
Neoclassical kinetic theory near an X-point: Plateau regime
[DE93-019825] p 1951 N94-20224
DISCERN: A distributed neural network model of script processing and memory p 1941 N94-20255
Hypervelocity impact
[AD-A272957] p 1831 N94-21249
Shear flow generation by Reynolds stress and suppression of resistive g-modes
[DE93-040911] p 1995 N94-21514
On the stability of shear-Alfven vortices
[DE93-040912] p 1996 N94-21752
A unified Monte Carlo interpretation of particle simulations and applications to nonneutral plasmas
[DE94-001231] p 1997 N94-21973
Continuum damping of ideal toroidal Alfven eigenmodes
[DE94-001233] p 1998 N94-22560
Kinetic resonance damping rate of the toroidal ion temperature gradient mode
[DE94-001234] p 1998 N94-22561

TEXAS UNIV., BASTROP.
A two-dimensional kinetic model of the scrape-off layer
[DE94-001235] p 1999 N94-22562

THOMSON-CSF SYSTEMS CANADA, INC., NEPEAN (ONTARIO).
Control of multiple robot manipulators with optimal force distribution p 1794 N94-22255

TILBURG UNIV. (NETHERLANDS).
Generalization performance of backpropagation learning on a syllabification task p 1940 N94-20246
Representation of idioms in connectionist models p 1940 N94-20247

TOHOKU UNIV., SENDAI (JAPAN).
Plasma structure in a plasma flow along a magnetic mirror field p 2005 N94-22664

TOKYO ASTRONOMICAL OBSERVATORY, MITAKA (JAPAN).
X ray jets in the solar corona: Observations with Yohkoh Soft X Ray Telescope p 2004 N94-22655

TOKYO METROPOLITAN UNIV. (JAPAN).
Vertical structure of accretion disks p 2002 N94-22645
Hydrodynamical winds from an accretion disk p 2008 N94-22683
Accretion of a hot plasma onto the central black hole: Fokker-Planck formulation p 2009 N94-22693

TOKYO UNIV. (JAPAN).
Evaporation in equilibrium, in vacuum, and in hydrogen gas p 1684 N94-20638
Implantation of nitrogen: Effects of hydrogen and implantation energy p 1686 N94-20804

Hydrothermal alteration experiments of olivine with varying Fe contents: An attempt to simulate aqueous alteration of the carbonaceous chondrites p 1686 N94-20810
Mineralogy and cooling history of magnesian lunar granulite 67415 p 2124 N94-20811
Ti-bearing oxide minerals in lunar meteorite Y793169 with the VLT affinity p 2084 N94-20812
Geometrical analysis of the microcraters found on LDEF samples p 1666 N94-20890
Antipodal fragment velocities for porous and weak targets at catastrophic impacts p 1836 N94-20891
The multigrid preconditioned conjugate gradient method p 1958 N94-21482
Core formation, wet early mantle, and H2O degassing on early Mars p 2145 N94-21674
Tangential stress due to Kelvin-Helmholtz instability at the magnetospheric boundary p 2003 N94-22651
Magnetohydrodynamic phenomena in star-forming processes and their environment p 2010 N94-22701

TOKYO UNIV., MITAKE (JAPAN).
Highlights of Yohkoh results p 2001 N94-22632

TOKYO UNIV., SAGAMIHARA (JAPAN).
Accretion disks in bright x ray binaries p 2002 N94-22639

TOLEDO UNIV., OH.
Synthesis algorithm of VLSI multipliers for ASIC p 1758 N94-21116
Automated synthesis and verification of configurable DRAM blocks for ASIC's p 1759 N94-21123
A DRAM compiler algorithm for high performance VLSI embedded memories p 1767 N94-21729

TORONTO UNIV., DOWNSVIEW (ONTARIO).
Space environmental effects on polymer matrix composites: The UTIAS/LDEF experiment p 1660 N94-21373

TORONTO UNIV. (ONTARIO).
Evaluation of plasma-deposited protective coatings for spacecraft applications p 1663 N94-21394
Directional coding of morphological pyramidal representations p 1771 N94-22106
Optimal object modelling for an active-vision system p 1771 N94-22107
The conceptual design of a short-range distance sensor p 1774 N94-22129
Sensor integration and data fusion for object localization in robotic workcells p 1774 N94-22130
Elliptical-shape parameter estimation from a set of normal lines p 1777 N94-22148
Hierarchical multirate vector quantization for image coding p 1781 N94-22174
Real-time step frequency radar
[ISBN-0-315-83588-5] p 1743 N94-22576
The optohydraulic servovalve: A novel device for the precise optical control of hydraulic pressure
[ISBN-0-315-83580-X] p 1827 N94-22577
Robot link and contact surface dynamic interaction: An experimental study of contact instability
[ISBN-0-315-83439-0] p 1827 N94-22578
Demodulation of a fiber Fabry-Perot strain rosette using white light interferometry
[ISBN-0-315-83427-7] p 1990 N94-22579
Orthogonalization method for determination of boundary layer receptivity coefficients
[ISBN-0-315-83426-9] p 1805 N94-22580
Phase demodulation of interferometric fiber-optic sensors
[ISBN-0-315-83425-0] p 1991 N94-22581
Transonic flow calculations: Integral method
[ISBN-0-315-83538-9] p 1639 N94-22586
The effect of delamination on the dynamic response of composite laminates as measured by embedded fiber optic Michelson sensor
[ISBN-0-315-83534-6] p 1677 N94-22587
System identification of the Daisy large space structure emulator
[ISBN-0-315-83533-8] p 1653 N94-22588
An embedded fibre optic for damage growth monitoring in Kevlar composites
[ISBN-0-315-83501-X] p 1677 N94-22589

TOYAMA UNIV. (JAPAN).
Prompt high-energy particle acceleration during two current loops collision p 2005 N94-22661
Formation of fast magnetosonic shock waves during two current loops collision in solar flare p 2005 N94-22662
Dynamics of physical state during two current loops collision p 2005 N94-22663

TRANSPORT CANADA, OTTAWA (ONTARIO).
Application of scattering by arrays of cylinders to MLS signal propagation error estimation p 1644 N94-22135

TRANSPORTATION RESEARCH BOARD, WASHINGTON, DC.
Public-sector aviation issues: Graduate research award papers, 1991-1992
[PB93-206258] p 1642 N94-22055
TRW, INC., REDONDO BEACH, CA.
Initiation and modification of reaction by energy addition: Kinetic and transport phenomena
[AD-A271315] p 1797 N94-19936
TSUKUBA SPACE CENTER (JAPAN).
R and D to HOPE airframe p 1665 N94-21406
TSUKUBA UNIV. (JAPAN).
Inter- and intra-crystalline oxygen isotope distribution of fassaites in Allende CAI p 2086 N94-20898
TUFTS UNIV., MEDFORD, MA.
Synchrotron x ray diffraction analysis of photorefractive crystals and their gratings
[AD-A271176] p 2015 N94-20213

U

UNION BANK OF FINLAND.
System architectures for banking applications p 2046 N94-22057
UNITED ENGINEERING TRUSTEES, INC., NEW YORK, NY.
High Speed/High Frequency Optoelectronics
[AD-A271985] p 1751 N94-20580
UNITED TECHNOLOGIES RESEARCH CENTER, EAST HARTFORD, CT.
Active control of wake/blade-row interaction noise through the use of blade surface actuators
[NASA-CR-4556] p 1968 N94-21608
UNIVERSAL ANALYTICS, INC., LOS ANGELES, CA.
Constraints on the rate of discharge and duration of the Mangala Valles flood p 2099 N94-20674
UNIVERSIDAD DE LOS ANDES, MERIDA (VENEZUELA).
Non-linear thermal instability of optical thin molecular structures p 2006 N94-22667
On the nonlinear instability of thermal structures p 2006 N94-22668
UNIVERSIDAD NACIONAL AUTONOMA DE MEXICO, COYOACAN.
Reverse polarity magnetized melt rocks from the Chicxulub impact structure, Yucatan Peninsula, Mexico p 1863 N94-20843
UNIVERSIDADE FEDERAL DE PARAIBA (BRAZIL).
Application of SPOT to GIS/LIS in land capability evaluation for regional planning of JAICO semi-arid region of Piaui, Brazil p 1838 N94-20955
UNIVERSIDADE FEDERAL DO RIO DE JANEIRO (BRAZIL).
On the origin and evolution of circular forms observed in remote sensing images of the Rio de Janeiro State, Brazil p 1839 N94-20963
UNIVERSIDADE FEDERAL DO RIO GRANDE DO NORTE, NATAL (BRAZIL).
Magnetic reconnection in emission nebulae in clusters of galaxies p 2010 N94-22700
UNIVERSITE DES SCIENCES ET DE LA TECHNOLOGIE HOUARI BOUMEDIENE, ALGIERS (ALGERIA).
Non-linear analysis of the electrical properties of the active circuits of high-frequency oscillators p 1785 N94-22195
UNIVERSITEIT TWENTE, ENSCHEDE (NETHERLANDS).
Connectionism and Natural Language Processing
[MEMO-INF-92-64] p 1940 N94-20242
Representation of spoken words in a self-organizing neural net p 1940 N94-20243
Hopfield models as neural-network acceptors p 1941 N94-20250
A semi-Markov model of a home network access protocol
[MEMO-INF-92-71] p 1909 N94-21045
Symmetries and conservation laws of the system: $u(x)=vw(x)$, $v(y)=uw(y)$, $uv+w(xx)+w(yy)=0$
[MEMO-1084] p 1953 N94-21046
On the core-structure of minimum cost spanning tree games
[MEMO-1085] p 1953 N94-21047
Long cycles in graphs containing a 2-factor with many odd components
[MEMO-1086] p 1953 N94-21048
Specification and generation of Markov reward models
[MEMO-INF-92-60] p 1963 N94-21058
On the selection of indices in relational databases
[MEMO-INF-92-72] p 2043 N94-21071
Explicit results on gl(lambda) and sl(lambda)
[MEMO-1075] p 1953 N94-21072
The communication complexity of set intersection problems
[MEMO-1077] p 1738 N94-21073
Degree sums, k-factors and Hamiltonian cycles in graphs
[MEMO-1078] p 1953 N94-21074
Stoermer-Cowell and related methods for the numerical solution of second order periodic initial value problems for ODE's 2: Numerical characteristics of the methods
[MEMO-1082] p 1953 N94-21075
On estimation and testing in Poisson regression models with over-dispersion
[MEMO-1083] p 1963 N94-21076
Interactive simulation package for coupled bending and torsional vibrations in flexible robot arms
[MEMO-1089] p 1944 N94-21140
Behavioural semantics of parallel functional programming languages
[MEMO-INF-92-66] p 1913 N94-21313
The term processor Kimwitu manual and cookbook
[MEMO-INF-92-67] p 1914 N94-21454
The logistic model: The integration of business process redesign and information systems development based on logistic principles
[MEMO-INF-92-70] p 2045 N94-22276
UNIVERSITIES SPACE RESEARCH ASSOCIATION, GREENBELT, MD.
Analysis of hyper-spectral AVIRIS image data over a mixed-conifer forest in Maine p 1838 N94-20959
UNIVERSITIES SPACE RESEARCH ASSOCIATION, HUNTSVILLE, AL.
Studies in remotely sensed geophysical parameter retrieval and analysis
[NASA-CR-194768] p 1842 N94-22374
UNIVERSITY COLL., DUBLIN (IRELAND).
An exploration of clause boundary effects in SRN representations p 1937 N94-20253
UNIVERSITY OF CENTRAL FLORIDA, ORLANDO.
Model-based reasoning for power system management using KATE and the SSM/PMAD
[NASA-CR-194716] p 1671 N94-21882
UNIVERSITY OF SOUTH FLORIDA, TAMPA.
Advanced processing technology for high-efficiency thin-film CuInSe2 solar cells
[DE93-010045] p 1847 N94-21614
UNIVERSITY OF SOUTHERN CALIFORNIA, LOS ANGELES.
High efficiency epitaxial optical reflector solar cells
[DE93-017115] p 1845 N94-19805
A proposed research program in information processing
[NASA-CR-194271] p 2041 N94-20134
A marine sedimentary model for the evolution of the northern plains p 2091 N94-20395
Center for the integration of optical computing
[AD-A271874] p 1899 N94-20469
Investigation of heterojunctions and multiple quantum well structures using crystalline organic semiconductors
[AD-A272113] p 2018 N94-20569
Composite materials with improved properties in compression
[AD-A272837] p 1675 N94-21176
Surface science and modeling studies of endothermic fuels catalysis
[AD-A272850] p 1712 N94-21192
Establishing the basis for validated predictions of highly non-equilibrium flows (with 9 attachments)
[AD-A272918] p 1802 N94-21220
Distributed input/output processing in data-driven multiprocessors
[DE94-000323] p 1937 N94-22378
UNIVERSITY OF SOUTHERN CALIFORNIA, MARINA DEL REY.
Explainable expert systems: A research program in information processing
[NASA-CR-193422] p 2041 N94-20133
UNIVERSITY OF SOUTHERN ILLINOIS, CARBONDALE.
Practical issues in implementing roving spares in VLSI systolic arrays p 1758 N94-21114
UNIVERSITY OF SOUTHERN MISSISSIPPI, HATTIESBURG.
Processing of climatological data for model initialization
[AD-A271878] p 1865 N94-20487
UNIVERSITY OF SOUTHWESTERN LOUISIANA, LAFAYETTE.
A statistical-based scheduling algorithm in automated data path synthesis p 1764 N94-21706
Micro-rollback and self-recovery synthesis p 1765 N94-21707
UNIVERSITY OF WESTERN MICHIGAN, KALAMAZOO.
Testing double ionization mechanisms with highly-charged ions
[DE93-018750] p 1970 N94-19958
UNIVERSITY OF WESTERN ONTARIO, LONDON.
Linear structures on the small inner satellites of Saturn p 2121 N94-20797
Response statistics of shell structures with geometrical and material nonlinearities, volume 1
[ISBN-0-315-84006-4] p 1833 N94-22590
Mobile robot perception in unknown and unstructured dynamic voxel environments
[ISBN-0-315-83951-1] p 1947 N94-22591
What is normal among the A-type stars?
[ISBN-0-315-83947-3] p 2081 N94-22592
The formation of massive stars: A 30 Mo case study
[ISBN-0-315-83944-9] p 2081 N94-22593
UTAH STATE UNIV., LOGAN.
Imaging radar studies of atmospheric winds and waves
[AD-A271672] p 1866 N94-20918
A novel visual hardware behavioral language p 1765 N94-21715
UTAH UNIV., SALT LAKE CITY.
Testing self-timed circuits using scan paths p 1757 N94-21109
Robust neural classifier circuits using asynchronous design p 1757 N94-21111
Reliable interface design for combining asynchronous and synchronous circuits p 1758 N94-21119

V

VICTORIA UNIV. (BRITISH COLUMBIA).
A simplified method for S-parameter calculations of metal septum waveguide filters p 1782 N94-22180
Coded 64QAM using a binary convolutional code p 1747 N94-22223
Applications of a two-dimensional nonlinear filters to image restoration p 1789 N94-22225
VIGYAN RESEARCH ASSOCIATES, INC., HAMPTON, VA.
Robust unstructured grid generation with VGRID p 1919 N94-22359
VIRGINIA POLYTECHNIC INST. AND STATE UNIV., BLACKSBURG.
Compression strength of composite primary structural components
[NASA-CR-194561] p 1830 N94-20159
Improvements to a method for the geometrically nonlinear analysis of compressively loaded stiffened composite panels
[NASA-CR-194715] p 1832 N94-21814
VIRGINIA UNIV., CHARLOTTESVILLE.
Determining the 3-D structure and motion of objects using a scanning laser range sensor
[NASA-CR-194745] p 1818 N94-21817
VOLVO FLYGMOTOR A.B., TROLLHAETTAN (SWEDEN).
A tutorial on the aero/thermodynamical design of liquid-propellant rocket engine nozzles p 1668 N94-20074
Turbine design p 1668 N94-20075
VON KARMAN INST. FOR FLUID DYNAMICS, RHODE-SAINT-GENESE (BELGIUM).
Spacecraft Propulsion
[VKI-LS-1993-01] p 1667 N94-20068
Three dimensional unsteady flow calculations in radial components p 1669 N94-20080
VRIJE UNIV., AMSTERDAM (NETHERLANDS).
Column reduced rational matrix functions with given null-pole data in the complex plane
[PB93-220531] p 1960 N94-22099
Modular interval spaces
[PB93-220663] p 1961 N94-22266

W

WASEDA UNIV., TOKYO (JAPAN).
The relaxed state and entropy production due to the electric resistivity and viscosity of plasma p 2010 N94-22696
WASHINGTON STATE UNIV., PULLMAN.
Design of a new squaring function for the Viterbi algorithm p 1764 N94-21699
WASHINGTON UNIV., SAINT LOUIS, MO.
The p-version of the finite element method in incremental elasto-plastic analysis
[NASA-CR-194707] p 1830 N94-20036
Identification of an interstellar oxide grain from the Murchison meteorite by ion imaging p 2082 N94-20659
Venus magmatic and tectonic evolution p 2101 N94-20683
Elevated initial Sr-87/Sr-86 in ordinary chondrite metal p 1685 N94-20695
The roughness of the Martian surface: A scale dependent model p 2115 N94-20762
Rare Earth elements in individual minerals in Shergottites p 1686 N94-20852
Radio and optical emission: Spectral shapes and breaks in GRB
[NASA-CR-194763] p 2150 N94-21781

Relativistic shock spectra: A prediction
[NASA-CR-194764] p 2150 N94-21782
WASHINGTON UNIV., SEATTLE.
Detectability of crystalline ferric and ferrous minerals on Mars p 2110 N94-20730
Acoustic monitoring of global ocean variability
[AD-A271998] p 1883 N94-21366
WATERLOO UNIV. (ONTARIO).
Formal hardware verification in Maple p 1771 N94-22112
Impact of partitioning on parallel discrete event simulation of logic circuits p 1772 N94-22115
A neural M-ary tree method for data compression p 1780 N94-22166
Trends in software reliability modeling p 1788 N94-22214
Asynchronous detection of SSB-SC data signals p 1747 N94-22217
Passenger terminal simulation model
[ISBN-0-315-61113-8] p 1652 N94-22423
WEST (FREDERICK R.), HANOVER, PA.
Balloon exploration of the northern plains of Mars near and north of the Viking 2 landing site p 2092 N94-20401
WEST VIRGINIA UNIV., MORGANTOWN.
Problems related to conservation laws: Phase transitions and viscoelasticity
[AD-A271429] p 1698 N94-19840
WESTINGHOUSE HANFORD CO., RICHLAND, WA.
Interpretation of Ground Penetrating Radar data at the Hanford Site, Richland, Washington
[DE93-040409] p 1743 N94-22557
WESTINGHOUSE IDAHO NUCLEAR CO., INC., IDAHO FALLS.
Passive Cryogenic Sampler
[DE94-000918] p 1811 N94-22392
WESTINGHOUSE SAVANNAH RIVER CO., AIKEN, SC.
Rapid heating tensile testing update: 304L stainless steel
[DE93-018770] p 1688 N94-19942
Hydrogen isotope separation experience at the Savannah River Site
[DE93-019832] p 1679 N94-20266
An analysis of pressure driven cross-flow through a long slot connecting two parallel channels
[DE93-040181] p 1804 N94-21765
Gamma ray spectrometry of LDEF samples: Results of 1992 analyses
[DE94-001177] p 1684 N94-22046
Implementation of a laboratory information management system for environmental regulatory analyses
[DE94-001198] p 2046 N94-22407
WICHITA STATE UNIV., KS.
Activities of National Inst. for Aviation Research
[NIAR-93-16] p 2151 N94-20150
Proceedings of the Twentieth Annual Technologyfest p 1645 N94-20188
Aviation safety research at the National Institute for Aviation Research, Wichita State University
[NIAR-93-4] p 1641 N94-20189
Evaluation of head injury criteria
[NIAR-93-2] p 1890 N94-20190
AIAA Techfest 29 proceedings
[NIAR-93-1] p 1635 N94-20191
WINDSOR UNIV. (ONTARIO).
Noise filtering using multilayer feedforward neural network p 1770 N94-22104
An in-place and in-order algorithm for the discrete cosine transform p 1771 N94-22111
Cascaded recursive artificial neural networks p 1780 N94-22167
WISCONSIN UNIV., MADISON.
Collisional processes involving atmospheric gases
[AD-A270729] p 1854 N94-19954
Fusion plasma theory grant. Task 3: Auxiliary radiofrequency heating of tokamaks
[DE94-000779] p 1994 N94-20940
Fusion Plasma Theory. Task 1: Magnetic confinement fusion plasma theory
[DE94-000778] p 1998 N94-22019
CIMSS FIRE research activities p 1873 N94-22307
Cirrus cloud retrievals from HIS observations during FIRE 2 p 1875 N94-22315
Efficient transfer of images over networks p 1748 N94-22517
WISCONSIN UNIV., MILWAUKEE.
Rewetting of monogroove heat pipe in Space Station radiators
[NASA-CR-194781] p 1804 N94-21820
Inelastic electron scattering from surfaces
[DE94-001738] p 1977 N94-22049
WITWATERSRAND UNIV., JOHANNESBURG (SOUTH AFRICA).
Kalkkop crater, Eastern Cape: A new impact crater in South Africa p 1862 N94-20714
WOODS HOLE OCEANOGRAPHIC INST., MA.
On the sources of North Atlantic deep water
[AD-A270854] p 1881 N94-19895
Design of a controllable pitch underwater thruster system
[AD-A271140] p 1821 N94-20021
The marine light-mixed layer experiment cruise and data report: R/V endeavor cruise EN-224, mooring deployment, 27 April-1 May 1991: Cruise EN-227, mooring recovery, 5-23 September 1991
[AD-A271175] p 1864 N94-20186
Comparison of satellite-derived velocity fields in the coastal transition zone
[AD-A272565] p 1883 N94-21360
WOODS HOLE RESEARCH CENTER, MA.
Seafloor characterization/Galapagos propagating rift
[AD-A272001] p 1882 N94-20581
WOOLLAM (JOHN A.) CO., LINCOLN, NE.
In-situ spectroscopic ellipsometry for real time semiconductor growth monitor p 2024 N94-21003
Real-time analysis of in-situ spectroscopic ellipsometric data during MBE growth of III-V semiconductors p 2024 N94-21004
WORLD METEOROLOGICAL ORGANIZATION, GENEVA (SWITZERLAND).
Snow cover measurements and areal assessment of precipitation and soil moisture
[WMO-749] p 1841 N94-21068
Remote sensing for hydrology progress and prospects
[WMO-773] p 1841 N94-21069
Simulated real-time intercomparison of hydrological models
[WMO-779] p 1867 N94-21070
WRIGHT LAB., WRIGHT-PATTERSON AFB, OH.
Analysis and design of weight balancing system for laser velocimetry traverse
[AD-A271171] p 1816 N94-20546
The 1992 USAF structural integrity program conference
[AD-A272876] p 1635 N94-21194
Characteristic based methods for the time-domain Maxwell equations
[AD-A272973] p 1802 N94-21263
The mechanical property data base from an Air Force/industry cooperative test program on advanced aluminum alloys: 2091 sheet, plate, and 8090 extrusion
[AD-A273091] p 1692 N94-21525
WRIGHT STATE UNIV., DAYTON, OH.
Perception/action: An holistic approach 2
[AD-A271822] p 1891 N94-20827
WYOMING UNIV., LARAMIE.
Two-polarity magnetization in the Manson impact breccia p 1863 N94-20789

Y

YALE UNIV., NEW HAVEN, CT.
Theoretical and numerical studies in magnetic fusion
[DE94-000536] p 1993 N94-20937
Fast fourier transforms for nonequispaced data
[AD-A272687] p 1954 N94-21164

Typical Contract Number Index Listing

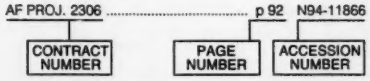

Listings in this index are arranged alphanumerically by contract number. Under each contract number the accession numbers denoting documents that have been produced as a result of research done under that contract are arranged in ascending order. The page number helps to locate the citation in the abstract section. The accession number denotes the number by which the citation is identified.

AERO-0018C ..... p 1641 N94-21472
AF PROJ. RS3-4-AS-0 ..... p 1674 N94-20574
AF PROJ. SNL-O ..... p 1831 N94-20572
AF PROJ. 1123 ..... p 1651 N94-20108
AF PROJ. 2008 ..... p 1883 N94-21222
AF PROJ. 2304 ..... p 1740 N94-21518
AF PROJ. 2307 ..... p 1637 N94-21411
AF PROJ. 2309 ..... p 1855 N94-20090
AF PROJ. 2729 ..... p 1896 N94-21247
AF PROJ. 2830 ..... p 1896 N94-20914
AF PROJ. 3487 ..... p 2018 N94-20575
AF PROJ. 6302 ..... p 1681 N94-21165
AF PROJ. 6670 ..... p 1864 N94-20088
AF-AFOSR-0029-90 ..... p 2027 N94-21242
AF-AFOSR-0042-88 ..... p 1973 N94-20612
AF-AFOSR-0065-88 ..... p 2147 N94-21196
AF-AFOSR-0069-91 ..... p 1636 N94-20465
AF-AFOSR-0075-91 ..... p 2018 N94-20569
AF-AFOSR-0090-93 ..... p 1950 N94-20087
AF-AFOSR-0117-90 ..... p 1823 N94-20484
AF-AFOSR-0122-91 ..... p 1966 N94-19917
AF-AFOSR-0133-90 ..... p 1899 N94-20469
AF-AFOSR-0135-90 ..... p 1909 N94-21034
AF-AFOSR-0160-91 ..... p 1667 N94-20015
AF-AFOSR-0170-90 ..... p 1802 N94-21220
AF-AFOSR-0187-91 ..... p 1751 N94-20580
AF-AFOSR-0194-90 ..... p 1952 N94-20568
AF-AFOSR-0214-90 ..... p 2017 N94-20470
AF-AFOSR-0221-90 ..... p 1894 N94-20467
AF-AFOSR-0231-90 ..... p 2012 N94-19897
AF-AFOSR-0244-91 ..... p 2147 N94-21522
AF-AFOSR-0256-91 ..... p 1667 N94-19847
AF-AFOSR-0258-90 ..... p 2028 N94-21458
AF-AFOSR-0259-90 ..... p 1712 N94-20625
AF-AFOSR-0269-91 ..... p 1864 N94-19900
AF-AFOSR-0281-90 ..... p 1691 N94-21245
AF-AFOSR-0282-90 ..... p 1681 N94-21168
AF-AFOSR-0282-91 ..... p 1814 N94-19853
AF-AFOSR-0293-90 ..... p 1673 N94-20327
AF-AFOSR-0296-91 ..... p 1878 N94-22331
AF-AFOSR-0308-90 ..... p 1674 N94-20623
AF-AFOSR-0324-89 ..... p 1803 N94-21459
AF-AFOSR-0331-90 ..... p 1712 N94-21192
AF-AFOSR-0364-91 ..... p 1802 N94-21155
AF-AFOSR-0487-89 ..... p 1802 N94-21169
AF-AFOSR-0501-89 ..... p 1943 N94-20626
AF-AFOSR-0521-89 ..... p 1681 N94-21181
ARPA ORDER 6356 ..... p 1900 N94-21301
ARPA ORDER 7006 ..... p 1943 N94-20947
ARPA ORDER 7330 ..... p 1929 N94-20084
ARPA ORDER 7511 ..... p 1761 N94-21282
ARPA ORDER 7597 ..... p 1902 N94-19919
p 1902 N94-19932
p 1928 N94-19950
p 1898 N94-20085
p 1898 N94-20107
ARPA ORDER 8228 ..... p 1949 N94-19838
ARPA ORDER 8313 ..... p 1902 N94-19918
p 1902 N94-19948
p 1908 N94-20622
ARPA ORDER 8557 ..... p 1987 N94-21321
ARPA ORDER 8930 ..... p 1929 N94-20144
ASI-91-RS-86 ..... p 2054 N94-20174
ASR-ME-03640247 ..... p 2005 N94-22660
p 2005 N94-22661
p 2005 N94-22662
p 2005 N94-22663
ASR-ME-04640268 ..... p 2009 N94-22692
A89/KL/309 ..... p 2042 N94-20310
CDA-90-24735 ..... p 1909 N94-21028
CEC-DG-XIII-BRA-QMIBS ..... p 1945 N94-21233
CEC-DG-XIII-BRA-QMIPS ..... p 1944 N94-21160
p 1930 N94-21161
p 1946 N94-21577
CNPQ-203133/89.7 ..... p 1838 N94-20954
CNR-89.00036.69 ..... p 1909 N94-21026
DA PROJ. R12-99 ..... p 1866 N94-20559
DA PROJ. 1L1-61102-AH-43 ..... p 1698 N94-19947
p 1679 N94-20111
p 1801 N94-20915
DA PROJ. 1L1-61102-AH-45 ..... p 1636 N94-20136
DA PROJ. 1L1-61192-SAH-43 ..... p 2027 N94-21304
DA PROJ. 1L1-6211-A-47-A ..... p 1826 N94-21756
DA PROJ. 1L1-62618-AH-80 ..... p 2037 N94-19831
p 1806 N94-20930
p 1964 N94-21175
DA PROJ. 1L1-62786-AH-98 ..... p 1823 N94-20567
DA PROJ. 1L2-63001-D-150 ..... p 1712 N94-20551
DA PROJ. 3M1-62787-A-879 ..... p 1891 N94-20928
DAAA15-91-K-0002 ..... p 1911 N94-21203
DAAA15-91-M-0073 ..... p 1801 N94-20915
DAAA21-90-D-0009 ..... p 1831 N94-21249
DAAH01-89-C-0357 ..... p 2024 N94-21003
p 2024 N94-21004
DAAH04-93-G-0044 ..... p 1815 N94-19878
DAAK60-91-C-0093 ..... p 1823 N94-20567
DAAK70-92-C-0059 ..... p 1712 N94-20551
DAAK70-92-D-0003 ..... p 2041 N94-20038
DAAL02-91-C-0053 ..... p 2014 N94-20029
DAAL03-86-D-0001 ..... p 1894 N94-21510
DAAL03-87-G-0004 ..... p 1821 N94-19833
DAAL03-88-K-0102 ..... p 1890 N94-20045
DAAL03-89-C-0034 ..... p 1963 N94-19901
DAAL03-89-C-0037 ..... p 1829 N94-19836
DAAL03-89-C-0038 ..... p 1949 N94-19898
DAAL03-89-D-0002 ..... p 1983 N94-19901
DAAL03-89-G-0088 ..... p 1698 N94-19840
DAAL03-89-G-0113 ..... p 1995 N94-21291
p 1995 N94-21292
DAAL03-89-K-0034 ..... p 2015 N94-20214
DAAL03-89-K-0103 ..... p 1699 N94-20016
DAAL03-90-C-0008 ..... p 2011 N94-19617
DAAL03-90-G-0003 ..... p 1830 N94-20001
DAAL03-90-G-0012 ..... p 1951 N94-20545
DAAL03-90-G-0021 ..... p 1797 N94-19978
DAAL03-90-G-0039 ..... p 1983 N94-20013
DAAL03-90-G-0041 ..... p 1716 N94-19934
DAAL03-90-G-0069 ..... p 1963 N94-20913
DAAL03-90-G-0106 ..... p 1717 N94-20215
DAAL03-90-G-0114 ..... p 1970 N94-19822
DAAL03-90-G-0116 ..... p 2015 N94-20213
DAAL03-90-G-0120 ..... p 1748 N94-19910
DAAL03-90-G-0131 ..... p 1699 N94-20046
DAAL03-91-G-0101 ..... p 1949 N94-19854
p 1902 N94-19855
p 1939 N94-19909
p 1962 N94-19999
DAAL03-91-G-0187 ..... p 1829 N94-19937
DAAL03-91-G-0228 ..... p 1700 N94-20299
DAAL03-91-G-0309 ..... p 1689 N94-20019
DAAL03-92-C-0030 ..... p 2028 N94-21517
DAAL03-92-G-0004 ..... p 1854 N94-19899
DAAL03-92-G-0247 ..... p 1949 N94-19898
DAAL03-92-G-0264 ..... p 2030 N94-21805
DAAL03-92-G-0277 ..... p 1636 N94-20043
DAAL04-91-C-0034 ..... p 1648 N94-21268
DAAL04-91-C-0039 ..... p 1704 N94-21197
DACA76-85-C-0010 ..... p 1904 N94-20041
p 1913 N94-21365
DACA76-92-C-0036 ..... p 1809 N94-21445
DACA88-90-D-0028-28 ..... p 1641 N94-21428
DACW72-90-D-0001 ..... p 2044 N94-21354
DAJA45-92-M-0089 ..... p 1828 N94-19815
DAJA45-93-M-0343 ..... p 1672 N94-20031
DAMD17-83-C-3194 ..... p 1893 N94-20081
DAMD17-91-C-1095 ..... p 1892 N94-21415
DARA-50-OR-9104-3 ..... p 2149 N94-20603
DARA-50-QL-8208-5 ..... p 2004 N94-22659
DE-AC02-76CH-00016 ..... p 1970 N94-19868
p 1687 N94-19922
p 1678 N94-19924
p 1970 N94-19931
p 1978 N94-19945
p 1699 N94-19973
p 1972 N94-20230
p 2015 N94-20260
p 1690 N94-20301
p 1691 N94-20313
p 1973 N94-20324
p 1685 N94-20717
p 1686 N94-20807
p 1686 N94-20808
p 1682 N94-21631
p 2038 N94-21692
p 1975 N94-21693
p 1676 N94-21754
p 1683 N94-21842
p 1671 N94-21979
DE-AC02-76CH-03000 ..... p 1969 N94-19813
p 1969 N94-19814
p 1978 N94-19972
p 1978 N94-19983
p 1807 N94-19987
p 1978 N94-19988
p 1979 N94-20216
p 1972 N94-20225
p 1750 N94-20314
p 1980 N94-20317
p 1975 N94-21775
p 1975 N94-21786
p 1975 N94-21806
p 1975 N94-21840
p 1976 N94-21847
p 1982 N94-21866
p 1976 N94-21867
p 1982 N94-21934
p 1976 N94-21962
DE-AC02-76ER-00881 ..... p 1973 N94-20474
DE-AC02-83CH-10093 ..... p 1845 N94-19805
p 1748 N94-19902
p 1845 N94-19921
p 1845 N94-19925
p 2013 N94-19939
p 1712 N94-19984
p 1688 N94-19985
p 1699 N94-20047
p 1845 N94-20095
p 1846 N94-21298
p 1847 N94-21562
p 1847 N94-21614
p 2029 N94-21615
p 1847 N94-21616
p 2029 N94-21617
p 1848 N94-21826
p 1848 N94-21827
p 1849 N94-22015
p 1850 N94-22257
DE-AC03-76SF-00098 ..... p 1884 N94-19826
p 1979 N94-19989
p 1992 N94-20004
p 1904 N94-20097
p 1993 N94-20234
p 1979 N94-20273
p 1979 N94-20274
p 1979 N94-20289
p 1980 N94-20290
p 1972 N94-20291
p 1980 N94-20292
p 1980 N94-20300
p 1985 N94-20320
p 2016 N94-20323
p 1980 N94-20475
p 1981 N94-21439
p 1981 N94-21440
p 1808 N94-21441
p 1988 N94-21528
p 1809 N94-21545

DE-AC03-76SF-00515 ..... p 1851 N94-21740
p 2030 N94-21744
p 2030 N94-21763
p 1707 N94-21856
p 1990 N94-21868
p 1917 N94-21917
p 2031 N94-21922
p 2031 N94-21926
p 1859 N94-21928
p 1683 N94-21947
p 1982 N94-21974
p 1820 N94-21975
p 1990 N94-22002
p 2038 N94-22010
p 2034 N94-22028
p 2034 N94-22041
p 1921 N94-22375
p 1947 N94-22563
p 1978 N94-19856
p 1978 N94-19873
p 1715 N94-19874
p 1974 N94-21515
p 1741 N94-21684
p 1763 N94-21685
p 1981 N94-21686
p 1981 N94-21687
p 1981 N94-21688
p 1946 N94-21689
p 1981 N94-21773
p 1975 N94-21788
p 2038 N94-21935
p 1982 N94-21952
p 2038 N94-21971
DE-AC03-89ER-51114 ..... p 1992 N94-20003
p 1993 N94-20326
p 1998 N94-22039
p 1998 N94-22089
p 2045 N94-22404
DE-AC03-92SF-19441 ..... p 1670 N94-21824
DE-AC04-76DP-00613 ..... p 1698 N94-19857
p 1749 N94-20005
p 1906 N94-20311
p 1691 N94-20478
p 1915 N94-21561
p 1763 N94-21652
p 1695 N94-21976
p 1918 N94-21977
p 1695 N94-21978
DE-AC04-76DP-00789 ..... p 1629 N94-19824
p 1748 N94-19844
p 1687 N94-19864
p 1814 N94-19865
p 1748 N94-19884
p 1698 N94-19903
p 1687 N94-19904
p 1829 N94-19927
p 1829 N94-19940
p 1829 N94-19943
p 1688 N94-19944
p 1714 N94-19946
p 1699 N94-19960
p 2013 N94-19961
p 1797 N94-19974
p 1904 N94-20052
p 1749 N94-20054
p 1750 N94-20218
p 1993 N94-20261
p 1906 N94-20280
p 1906 N94-20281
p 1942 N94-20293
p 1750 N94-20294
p 1980 N94-20295
p 2016 N94-20296
p 1808 N94-20297
p 1816 N94-20298
p 1973 N94-20306
p 1679 N94-20307
p 1750 N94-20312
p 1700 N94-20315
p 1899 N94-20476
p 1830 N94-20477
p 1755 N94-21093
p 1706 N94-21526
p 1761 N94-21532
p 1915 N94-21539
p 2028 N94-21541
p 1809 N94-21556
p 1832 N94-21557
p 1762 N94-21632
p 1916 N94-21633
p 1762 N94-21634
p 1916 N94-21635
p 1762 N94-21636
p 1763 N94-21654
p 2029 N94-21690
p 1968 N94-21751

DE-AC04-76DR-00789 ..... p 1928 N94-19858
p 1936 N94-21853
DE-AC04-88DP-43495 ..... p 1959 N94-21655
DE-AC05-76OR-00033 ..... p 2034 N94-22005
p 2034 N94-22028
p 1697 N94-22559
DE-AC05-84ER-40150 ..... p 2038 N94-21513
p 1977 N94-22009
DE-AC05-84OR-21400 ..... p 1687 N94-19802
p 2012 N94-19869
p 1821 N94-19891
p 2013 N94-19929
p 2014 N94-20002
p 1992 N94-20058
p 1689 N94-20093
p 1714 N94-20099
p 1689 N94-20180
p 1690 N94-20232
p 1690 N94-20282
p 1702 N94-20481
p 1801 N94-20562
p 1908 N94-20932
p 1707 N94-21653
p 1974 N94-21657
p 1974 N94-21658
p 1693 N94-21771
p 1975 N94-21785
p 1707 N94-21822
p 1848 N94-21823
p 1769 N94-21830
p 2030 N94-21831
p 1693 N94-21850
p 1918 N94-21924
p 2032 N94-21932
p 1694 N94-21933
p 1694 N94-21945
p 1694 N94-21948
p 1695 N94-21949
p 1810 N94-21953
p 1960 N94-21955
p 1833 N94-21956
p 1820 N94-21957
p 1976 N94-21961
p 1960 N94-21966
p 1960 N94-21967
p 1852 N94-22004
p 2034 N94-22005
p 1859 N94-22006
p 2034 N94-22016
p 1677 N94-22022
p 1998 N94-22039
p 1998 N94-22045
p 1918 N94-22088
p 1937 N94-22267
p 1961 N94-22379
p 2035 N94-22385
p 1697 N94-22559
p 2035 N94-22565
p 1999 N94-22568
p 1853 N94-22569
p 2035 N94-22570
DE-AC05-84OS-21400 ..... p 1688 N94-19957
DE-AC05-84OT-21400 ..... p 2045 N94-22047
DE-AC06-76RL-01830 ..... p 1850 N94-19930
p 1903 N94-19959
p 1690 N94-20233
p 1936 N94-22032
p 1696 N94-22037
p 1826 N94-22038
DE-AC06-87RL-10930 ..... p 1743 N94-22557
DE-AC07-76ID-01570 ..... p 2014 N94-19970
DE-AC07-84ID-12435 ..... p 1683 N94-22021
p 1811 N94-22392
DE-AC08-88NV-10617 ..... p 2027 N94-21296
DE-AC08-93NV-11265 ..... p 1750 N94-20325
DE-AC09-89SR-18035 ..... p 1688 N94-19942
p 1679 N94-20266
p 1804 N94-21765

p 1916 N94-21761
p 1996 N94-21769
p 1656 N94-21852
p 1833 N94-21916
p 1769 N94-21918
p 1946 N94-21929
p 2032 N94-21939
p 1708 N94-21954
p 1708 N94-21963
p 1810 N94-22000
p 2034 N94-22007
p 1683 N94-22031
p 1713 N94-22033
p 1770 N94-22040
p 1921 N94-22383
p 1805 N94-22386
p 1794 N94-22405
p 1805 N94-22556
p 1928 N94-19858
p 1936 N94-21853
p 1959 N94-21655
p 2034 N94-22005
p 2034 N94-22028
p 1697 N94-22559
p 2038 N94-21513
p 1977 N94-22009
p 1687 N94-19802
p 2012 N94-19869
p 1821 N94-19891
p 2013 N94-19929
p 2014 N94-20002
p 1992 N94-20058
p 1689 N94-20093
p 1714 N94-20099
p 1689 N94-20180
p 1690 N94-20232
p 1690 N94-20282
p 1702 N94-20481
p 1801 N94-20562
p 1908 N94-20932
p 1707 N94-21653
p 1974 N94-21657
p 1974 N94-21658
p 1693 N94-21771
p 1975 N94-21785
p 1707 N94-21822
p 1848 N94-21823
p 1769 N94-21830
p 2030 N94-21831
p 1693 N94-21850
p 1918 N94-21924
p 2032 N94-21932
p 1694 N94-21933
p 1694 N94-21945
p 1694 N94-21948
p 1695 N94-21949
p 1810 N94-21953
p 1960 N94-21955
p 1833 N94-21956
p 1820 N94-21957
p 1976 N94-21961
p 1960 N94-21966
p 1960 N94-21967
p 1852 N94-22004
p 2034 N94-22005
p 1859 N94-22006
p 2034 N94-22016
p 1677 N94-22022
p 1998 N94-22039
p 1998 N94-22045
p 1918 N94-22088
p 1937 N94-22267
p 1961 N94-22379
p 2035 N94-22385
p 1697 N94-22559
p 2035 N94-22565
p 1999 N94-22568
p 1853 N94-22569
p 2035 N94-22570
p 1688 N94-19957
p 2045 N94-22047
p 1850 N94-19930
p 1903 N94-19959
p 1690 N94-20233
p 1936 N94-22032
p 1696 N94-22037
p 1826 N94-22038
p 1743 N94-22557
p 2014 N94-19970
p 1683 N94-22021
p 1811 N94-22392
p 2027 N94-21296
p 1750 N94-20325
p 1688 N94-19942
p 1679 N94-20266
p 1804 N94-21765

DE-AC11-88PN-38014 ..... p 1684 N94-22046
DE-AC11-89PN-38014 ..... p 2046 N94-22407
p 1742 N94-22268
p 1689 N94-20182
p 1804 N94-21748
DE-AC12-76SN-00052 ..... p 1833 N94-22001
p 1805 N94-22269
DE-AC21-86MC-23166 ..... p 1826 N94-21938
DE-AC21-89MC-26040 ..... p 1683 N94-21984
DE-AC21-89MC-26366 ..... p 1847 N94-21540
DE-AC21-92MC-29245 ..... p 1709 N94-21982
DE-AC22-92PC-92109 ..... p 1678 N94-19890
DE-AC34-90RF-62349 ..... p 1821 N94-19859
DE-AC35-89ER-40486 ..... p 2041 N94-19811
p 1928 N94-19812
p 1936 N94-21919
DE-AI05-79ET-29372 ..... p 1984 N94-20179
DE-AI05-83ER-40112 ..... p 1992 N94-19915
DE-AI05-90ER-61074 ..... p 1876 N94-22324
DE-AI05-91ER-61224 ..... p 1855 N94-20219
DE-AI05-92ER-54177 ..... p 1992 N94-19915
p 1981 N94-21440
DE-AI06-91RL-12348 ..... p 1880 N94-22338
DE-AI22-92PC-92179 ..... p 1706 N94-21516
DE-AM03-76SF-00235 ..... p 1969 N94-19804
DE-AS05-81ER-40039 ..... p 1980 N94-20933
DE-FC03-85DP-40200 ..... p 1972 N94-20264
DE-FC03-92SF-19460 ..... p 1819 N94-21839
DE-FC05-85ER-25000 ..... p 2016 N94-20285
DE-FC22-83FE-60149 ..... p 2037 N94-20473
DE-FG02-84ER-45076 ..... p 1977 N94-22049
DE-FG02-84ER-45162 ..... p 1975 N94-21766
DE-FG02-86ER-13519 ..... p 1970 N94-19870
p 1970 N94-19871
p 1974 N94-21543
DE-FG02-86ER-13615 ..... p 1678 N94-20103
DE-FG02-86ER-53218 ..... p 1994 N94-20940
p 1998 N94-22019
DE-FG02-86ER-53240 ..... p 1993 N94-20937
DE-FG02-86NE-37969 ..... p 2034 N94-22028
DE-FG02-87ER-13778 ..... p 1970 N94-19958
DE-FG02-88ER-13914 ..... p 1849 N94-22048
DE-FG02-88ER-45337 ..... p 1693 N94-21854
DE-FG02-90ER-45427 ..... p 2036 N94-22582
DE-FG02-90ER-60970 ..... p 1876 N94-22322
p 1878 N94-22330
p 1880 N94-22340
DE-FG02-90ER-61071 ..... p 1876 N94-22318
p 1877 N94-22325
p 1878 N94-22329
DE-FG02-91CE-23810 ..... p 1798 N94-20101
DE-FG02-91ER-40672 ..... p 1982 N94-21952
p 1982 N94-21952
DE-FG02-91ER-40676 ..... p 1982 N94-21952
DE-FG02-91ER-40677 ..... p 1982 N94-21952
DE-FG02-91ER-45439 ..... p 1972 N94-20187
DE-FG02-91ER-54109 ..... p 1998 N94-22039
p 1999 N94-22562
DE-FG02-91ER-81190 ..... p 2031 N94-21869
DE-FG02-92ER-14244 ..... p 1685 N94-20717
p 1686 N94-20808
DE-FG02-92ER-25127 ..... p 1957 N94-21477
DE-FG02-92ER-25133 ..... p 1921 N94-22375
p 1921 N94-22376
DE-FG02-92ER-61369 ..... p 1850 N94-19941
DE-FG03-86ER-45230 ..... p 2015 N94-20275
p 2016 N94-20335
p 2036 N94-22584
DE-FG03-86ER-45264 ..... p 1697 N94-22559
DE-FG03-87ER-25043 ..... p 1937 N94-22378
DE-FG03-88ER-53275 ..... p 1999 N94-22596
DE-FG03-89ER-04053 ..... p 2027 N94-21304
DE-FG03-90ER-40546 ..... p 1973 N94-20938
DE-FG03-90ER-54079 ..... p 1999 N94-22566
p 1999 N94-22567
p 1999 N94-22595
p 1999 N94-22596
DE-FG03-91ER-40618 ..... p 1982 N94-21952
DE-FG03-92ER-25116 ..... p 1921 N94-22406
DE-FG03-92ER-25117 ..... p 1950 N94-20217
DE-FG03-92ER-40701 ..... p 1982 N94-21952
DE-FG05-79EV-10249 ..... p 1891 N94-20935
DE-FG05-80ET-53088 ..... p 1991 N94-19872
p 1992 N94-19887
p 1995 N94-21514
p 1996 N94-21752
p 1997 N94-21973
p 1998 N94-22560
p 1998 N94-22561
p 1999 N94-22562
p 2009 N94-22694
DE-FG05-87ER-13708 ..... p 1817 N94-20939
DE-FG05-87ER-40319 ..... p 1969 N94-19804
p 2016 N94-20285
p 1973 N94-20474
DE-FG05-88ER-53266 ..... p 1951 N94-20224

DE-FG05-88ER-53267 p 1999 N94-22562
DE-FG05-89ER-14061 p 1859 N94-22018
DE-FG05-89ER-53288 p 1951 N94-20224
DE-FG05-92ER-25143 p 1957 N94-21479
DE-FG05-92ER-25145 p 1799 N94-20351
DE-FG05-92ER-45477 p 1701 N94-20352
DE-FG05-92ER-61493 p 1852 N94-21787
DE-FG05-93ER-40770 p 1976 N94-21961
DE-FG22-92PC-92529 p 1680 N94-20934
DESY-PH-05-5S414(4) p 2149 N94-20603
DFG-EB-56/9 p 1855 N94-20155
DFG-PA-477/1-1 p 2081 N94-21578
DFG-PU-117/1-1 p 2081 N94-21578
DFG-SPA-112/1/90 p 2081 N94-21578
DLA900-88-D-0392 p 1817 N94-21253
DTFA01-87-C-00014 p 1642 N94-20051
DTFA01-92-Y-02017 p 1807 N94-20203
DTFA03-86-C-00042 p 1647 N94-20343
DTFA03-89-C-00043 p 1647 N94-20053
F040701-88-C-0089 p 2037 N94-20945
F04611-88-K-0048 p 1845 N94-20086
F04611-91-K-0004 p 2012 N94-19842
F04701-85-C-0086 p 1851 N94-20025
F04701-88-C-0089 p 1967 N94-19949
p 1705 N94-21225
p 1681 N94-21226
F08635-88-C-0067 p 1698 N94-19938
F19628-88-K-0017 p 1854 N94-19841
F19628-90-C-0002 p 1738 N94-21210
p 1739 N94-21211
p 1867 N94-21212
p 1739 N94-21244
F19628-90-C-0003 p 1650 N94-19880
p 1912 N94-21205
F19628-90-C-0133 p 1654 N94-21429
F19628-90-K-0041 p 1858 N94-21206
F19628-91-C-0093 p 1987 N94-21172
F19628-91-C-0168 p 1902 N94-19918
p 1902 N94-19948
p 1908 N94-20622
F19628-91-K-0030 p 1971 N94-20083
F29601-89-C-0014 p 1717 N94-20329
F30602-89-C-0082 p 2041 N94-20106
F30602-91-C-0010 p 1907 N94-20522
F30602-91-C-0053 p 1761 N94-21256
F30602-91-C-0054 p 1749 N94-20110
F30602-92-C-0081 p 1715 N94-19816
F33615-86-C-3015 p 1637 N94-21411
F33615-88-D-0532 p 1893 N94-20023
F33615-89-C-2921 p 1994 N94-21214
F33615-89-C-5643 p 1675 N94-21187
F33615-90-C-0005 p 1895 N94-19935
F33615-90-C-1465 p 1902 N94-19919
p 1902 N94-19932
p 1928 N94-19950
p 1898 N94-20085
p 1898 N94-20107
F33615-90-C-2007 p 1974 N94-21461
F33615-90-C-5915 p 1691 N94-21188
F33615-91-C-0534 p 1760 N94-21221
F33615-91-D-0009 p 1894 N94-20610
F33615-92-C-0017 p 1890 N94-20462
F49620-89-C-0037 p 1831 N94-21219
F49620-90-C-0021 p 1988 N94-21457
F49620-90-C-0030 p 1692 N94-21320
F49620-90-C-0070 p 1797 N94-19936
F49620-92-C-0029 p 1680 N94-20566
F49620-92-C-0076 p 1986 N94-20922
F49620-92-J-0193 p 1866 N94-20918
F49620-92-J-0318 p 1809 N94-21445
F49620-92-J-0356 p 1680 N94-20584
F49620-92-J-0376 p 1854 N94-19954
F49620-92-J-0418 p 1796 N94-19913
F49620-92-J-0445 p 1681 N94-21213
F49620-92-J-0447 p 1678 N94-20000
F49620-92-J-0454 p 1890 N94-20112
F49620-92-J-0476 p 1802 N94-21193
F49620-92-J-0511 p 1891 N94-20627
F49620-93-C-0006 p 1983 N94-19846
F49620-93-1-0173 p 1830 N94-20036
GRI-5084-238-1302 p 1825 N94-21424
p 1825 N94-21450
p 1825 N94-21451
GRI-5087-260-1467 p 1682 N94-21452
GRI-5089-260-1874 p 1714 N94-21426
GRI-5091-260-2144 p 1705 N94-21425
JPL-959193 p 2088 N94-20048
JSPS-ENGR-207 p 1955 N94-21456
MDA903-89-C-0003 p 1858 N94-21207
MDA903-90-C-0006 p 1828 N94-20468
MDA904-91-C-7054 p 1766 N94-21719
MDA972-90-C-0035 p 1929 N94-20084
MDA972-91-C-0028 p 1740 N94-21361
MDA972-91-C-0053 p 1949 N94-19838
MDA972-92-C-0019 p 1883 N94-21366
MDA972-92-C-0053 p 1967 N94-21321
MDA972-92-J-1012 p 1939 N94-20135
p 1945 N94-21315
p 1945 N94-21317
MDA972-92-J-1024 p 1905 N94-20109
MDA972-92-J-1035 p 1911 N94-21183
MIPR-NS-93-76 p 1658 N94-21251
MIPR-135-92 p 1666 N94-19818
MIPR-137-91 p 1715 N94-19912
MIPR-138-90 p 1715 N94-19912
MIPR-90-MM0544 p 1891 N94-21035
NAGW-1356 p 1671 N94-22428
NAGW-1406 p 1759 N94-21122
p 1763 N94-21698
p 1765 N94-21708
p 1765 N94-21711
p 1765 N94-21713
p 1766 N94-21717
p 1766 N94-21722
p 1767 N94-21723
p 1767 N94-21725
p 1767 N94-21726
p 1767 N94-21728
p 1768 N94-21731
NAGW-1454 p 1810 N94-21876
NAGW-1483 p 1858 N94-21836
NAGW-1522 p 2003 N94-22646
NAGW-1920 p 2043 N94-21055
NAGW-2013 p 2056 N94-22281
NAGW-2043 p 1666 N94-21780
NAGW-2208 p 2002 N94-22641
NAGW-2212 p 2108 N94-20723
NAGW-2220 p 2122 N94-20799
p 2122 N94-20800
p 2143 N94-21663
NAGW-2257 p 2090 N94-20392
NAGW-2350 p 2005 N94-22660
p 2007 N94-22674
NAGW-2438 p 1972 N94-20130
NAGW-2508 p 2054 N94-20174
NAGW-2624 p 2081 N94-21578
NAGW-2872 p 1897 N94-20336
NAGW-2898 p 1984 N94-20128
NAGW-28 p 1686 N94-20805
NAGW-2918 p 2150 N94-21781
p 2150 N94-21782
NAGW-2955 p 2039 N94-20818
NAGW-3036 p 1882 N94-20131
NAGW-3075 p 2055 N94-20952
NAGW-3150 p 1865 N94-20535
NAGW-3224 p 1643 N94-20148
NAGW-3292 p 1753 N94-21080
p 1759 N94-21128
NAGW-3293 p 1753 N94-21079
p 1757 N94-21107
p 1763 N94-21694
NAGW-3311 p 2090 N94-20392
NAGW-3508 p 1856 N94-20537
NAGW-748 p 2101 N94-20687
NAG1-1095 p 1876 N94-22318
p 1877 N94-22325
p 1878 N94-22329
NAG1-1113 p 1871 N94-22294
p 1879 N94-22336
p 1881 N94-22343
NAG1-1146 p 1876 N94-22321
p 1876 N94-22322
p 1878 N94-22330
p 1880 N94-22340
NAG1-1215 p 1832 N94-21814
NAG1-1280 p 1673 N94-20172
NAG1-1283 p 1821 N94-20044
NAG1-1287 p 1799 N94-20210
NAG1-1478 p 1741 N94-21885
NAG1-537 p 1830 N94-20159
NAG1-562 p 1717 N94-20269
NAG1-970 p 1994 N94-21289
p 1995 N94-21291
p 1995 N94-21294
NAG1-994 p 1637 N94-21054
NAG1-999 p 1877 N94-22325
p 1878 N94-22329
NAG2-513 p 1921 N94-22375
p 1921 N94-22376
NAG2-554 p 1967 N94-20523
NAG2-729 p 2040 N94-21821
NAG2-866 p 1950 N94-20034
NAG3-1014 p 1846 N94-20229
NAG3-1226 p 1732 N94-20498
NAG3-1317 p 1798 N94-20167
NAG3-1379 p 1656 N94-21581
NAG3-1381 p 1804 N94-21820
NAG3-1384 p 1797 N94-20037
NAG3-154 p 1734 N94-20508
p 1734 N94-20510
p 2019 N94-20971
NAG3-799 p 1759 N94-21123
NAG3-888 p 1676 N94-21777
NAG3-974 p 1823 N94-20538
NAG4-0751 p 1736 N94-20519
NAG5-1492 p 2147 N94-21877
NAG5-1531 p 2054 N94-20174
NAG5-1601 p 1982 N94-21878
NAG5-1635 p 1785 N94-21706
NAG5-1649 p 2054 N94-20174
NAG5-1657 p 2081 N94-21578
NAG5-1678 p 2080 N94-20337
NAG5-1789 p 2055 N94-21579
NAG5-1790 p 1864 N94-20138
NAG5-1832 p 2056 N94-21835
NAG5-2079 p 2056 N94-21779
NAG5-2187 p 2041 N94-20156
NAG5-2264 p 2042 N94-20363
NAG5-383 p 1837 N94-20205
NAG5-485 p 1657 N94-20173
NAG5-911 p 1837 N94-20951
NAG8-253 p 1816 N94-20341
NAG8-295 p 1676 N94-21743
NAG8-691 p 2055 N94-20344
NAG8-767 p 2017 N94-20346
NAG8-794 p 2054 N94-20174
NAG8-858 p 1855 N94-20132
NAG8-888 p 2147 N94-21815
p 2147 N94-21832
NAG8-898 p 1701 N94-20347
NAG8-913 p 2030 N94-21778
NAG8-915 p 1865 N94-20353
NAG8-919 p 1859 N94-22026
NAG9-104 p 1686 N94-20808
NAG9-106 p 1685 N94-20717
p 1686 N94-20807
p 1686 N94-20806
NAG9-184 p 2101 N94-20687
NAG9-337 p 1754 N94-21083
NAG9-43 p 1686 N94-20794
p 2084 N94-20795
NAG9-497 p 1684 N94-20670
p 2114 N94-20758
p 1685 N94-20759
p 1686 N94-20760
NAG9-555 p 1895 N94-21810
NAG9-613 p 1845 N94-20066
NAG9-622 p 1830 N94-20036
NAG9-81 p 2086 N94-20901
NASA ORDER A-25364-D p 1646 N94-21592
NASA ORDER H-07978-D p 1638 N94-21776
NASW-4574 p 2088 N94-20382
p 2092 N94-20636
p 2142 N94-21659
p 1811 N94-22430
NASW-4616 p 2085 N94-20865
NASW-4728 p 2147 N94-21877
NAS1-18027 p 1642 N94-21818
p 1644 N94-22277
p 1644 N94-22278
NAS1-18240 p 1797 N94-20033
NAS1-18586 p 1898 N94-20039
p 1766 N94-21716
p 1937 N94-22414
NAS1-18605 p 1797 N94-20033
p 1922 N94-21483
NAS1-19000 p 1643 N94-21629
p 1968 N94-21741
NAS1-19312 p 1806 N94-21466
NAS1-19460 p 1797 N94-20033
p 1950 N94-20087
p 1950 N94-20092
p 1914 N94-21462
p 1965 N94-21463
p 1922 N94-21483
p 1959 N94-21566
p 1915 N94-21584
p 1804 N94-21861
p 1804 N94-21875
p 1804 N94-21880
NAS1-970 p 1995 N94-21292
NAS13-564 p 2045 N94-21865
NAS2-12961 p 1914 N94-21489
p 1897 N94-21784
p 1968 N94-21881
NAS2-13210 p 1842 N94-21585
p 1842 N94-22345
NAS2-13712 p 1905 N94-20149
NAS3-24350 p 1648 N94-21582
p 1648 N94-21583
NAS3-25266 p 1637 N94-20563
p 1714 N94-21564
p 1670 N94-21565
p 1762 N94-21566
p 1715 N94-21569
p 1650 N94-21742
p 1769 N94-21808
p 1670 N94-21809

	p 1666	N94-21864
NAS3-25425	p 1968	N94-21608
NAS3-25644	p 1654	N94-21790
NAS3-25776	p 1762	N94-21566
NAS3-25808	p 1846	N94-21179
	p 1671	N94-21874
NAS3-25870	p 2016	N94-20340
NAS3-26254	p 1809	N94-21607
NAS5-26555	p 2055	N94-20204
NAS5-27772	p 1744	N94-21345
NAS5-30127	p 1837	N94-20264
NAS5-31000	p 1935	N94-21351
NAS5-31223	p 2054	N94-20142
NAS5-31352	p 1806	N94-19920
NAS5-31376	p 1856	N94-20362
NAS5-31500	p 1744	N94-21339
	p 1922	N94-21342
NAS5-31855	p 2055	N94-21295
NAS5-32059	p 2055	N94-21498
NAS7-918	p 1718	N94-20403
	p 1899	N94-20549
NAS8-37139	p 2042	N94-20268
NAS8-38089	p 1638	N94-21776
NAS8-38769	p 1842	N94-22374
NAS8-38772	p 2005	N94-22660
	p 2007	N94-22674
NAS8-39210	p 1670	N94-21271
NAS8-39385	p 1671	N94-21882
NAS8-39725	p 1656	N94-21813
NAS9-17900	p 1896	N94-20606
	p 1666	N94-22275
NATO-CRG-910415	p 2055	N94-21579
NA16RC0118-01	p 1879	N94-22336
	p 1881	N94-22343
NCA2-OR-675-801	p 1887	N94-21905
NCA2-441	p 1642	N94-22373
NCA2-839	p 1716	N94-20160
NCCW-24	p 2043	N94-21270
NCC1-160	p 1893	N94-20168
NCC1-178	p 1895	N94-20063
NCC2-1421	p 1887	N94-21908
NCC2-167	p 1885	N94-21897
NCC2-371	p 1804	N94-22027
NCC2-447	p 1650	N94-20524
NCC2-478	p 1679	N94-20169
NCC2-487	p 1636	N94-20014
NCC2-520	p 2041	N94-20133
	p 2041	N94-20134
NCC2-535	p 1895	N94-20338
NCC2-539	p 1905	N94-20228
NCC2-592	p 1647	N94-21819
NCC2-683	p 1638	N94-21833
NCC3-197	p 1735	N94-20515
NCC3-233	p 1798	N94-20167
	p 1959	N94-21588
NCC9-16	p 1907	N94-20376
	p 1930	N94-21065
NF-62-376	p 1930	N94-21023
	p 1908	N94-21024
NGT-50628	p 1858	N94-21811
NGT-51055	p 1816	N94-21817
NIH-506RR06192-02	p 1887	N94-21905
NIH-1R24RR06853	p 1894	N94-20520
NPS-CX-2000-0-0025	p 1968	N94-22053
	p 1969	N94-22054
NR PROJ. RA1-1-M-16	p 1858	N94-21357
NR PROJ. R03-5-B-03	p 1883	N94-21358
NRL PROJ. 0101	p 1837	N94-20028
NSERC-A0921	p 1766	N94-21718
NSERC-A1329	p 1910	N94-21063
NSERC-A3363	p 1753	N94-21081
	p 1766	N94-21718
NSERC-MEF-0040121	p 1753	N94-21081
NSERC-MEF0040121	p 1766	N94-21718
NSERC-OGP-046506	p 2038	N94-21533
NSF ASC-92-17041	p 1913	N94-21364
NSF ATM-89-22630	p 1858	N94-21811
NSF ATM-91-06639	p 2005	N94-22660
	p 2007	N94-22674
NSF ATM-91-21116	p 2005	N94-22660
	p 2007	N94-22674
NSF ATM-92-96165	p 2147	N94-21877
NSF CCR-89-20505	p 1938	N94-21468
NSF CCR-89-57604	p 1907	N94-20536
	p 1911	N94-21200
	p 1912	N94-21273
	p 1912	N94-21285
	p 1965	N94-21286
	p 2043	N94-21287
	p 1954	N94-21314
	p 1913	N94-21318
	p 1955	N94-21456
NSF CCR-90-02292	p 1912	N94-21273
	p 1954	N94-21314
	p 1955	N94-21456
NSF CCR-90-14605	p 1909	N94-21028
NSF CCR-90-57486	p 1907	N94-20536
	p 1912	N94-21285
	p 2043	N94-21287
NSF CCR-91-03296	p 1915	N94-21584
NSF CCR-91-08114	p 1963	N94-21058
NSF CCR-91-08899	p 1912	N94-21273
NSF CCR-92-03488	p 1954	N94-21173
	p 1954	N94-21174
NSF CCR-92-04255	p 1957	N94-21477
NSF CDA-88-22724	p 1939	N94-20135
	p 1905	N94-20143
	p 1929	N94-20144
	p 1900	N94-21281
	p 1945	N94-21315
NSF CTS-91-32140	p 1798	N94-20167
NSF DBS-92-23763	p 1838	N94-20954
NSF DMS-89-03041	p 2038	N94-22095
NSF DMS-90-12751	p 1954	N94-21164
NSF DMS-92-11820	p 1950	N94-20087
NSF EAR-89-15699	p 1685	N94-20717
	p 1686	N94-20807
	p 1686	N94-20808
NSF EAR-91-19065	p 2083	N94-20741
NSF ECS-86-57951	p 1733	N94-20500
	p 1733	N94-20501
NSF HRD-92-53013	p 1757	N94-21106
NSF INT-90-16293	p 2001	N94-22637
NSF INT-91-16781	p 1954	N94-21199
	p 1911	N94-21200
	p 1912	N94-21273
	p 1912	N94-21285
	p 2043	N94-21287
	p 1954	N94-21314
	p 1955	N94-21456
NSF IRI-89-00267	p 1939	N94-19893
	p 1913	N94-21365
NSF IRI-89-02124	p 1736	N94-20547
NSF IRI-89-20771	p 1939	N94-20135
	p 1945	N94-21315
NSF IRI-90-02659	p 2039	N94-20364
NSF IRI-90-03841	p 1907	N94-20521
NSF IRI-90-13160	p 1904	N94-20067
	p 1911	N94-21180
NSF IRI-92-14873	p 1938	N94-19845
NSF MIP-88-58764	p 1922	N94-21475
NSF MIP-89-15969	p 1761	N94-21282
NSF MIP-90-01651	p 1928	N94-19877
NSF MIP-90-47590	p 1761	N94-21282
NSF MIP-91-09618	p 1763	N94-21698
	p 1766	N94-21717
	p 1766	N94-21722
	p 1767	N94-21723
	p 1767	N94-21725
NSF MIPS-91-16683	p 1765	N94-21714
NSF RII-89-21978	p 2002	N94-22641
NSF STC-88-09648	p 2043	N94-21287
	p 1938	N94-21468
NSG-1498	p 1716	N94-20139
N00014-82-K-0193	p 2049	N94-20098
	p 1907	N94-20522
N00014-82-0280	p 1680	N94-21145
N00014-83-C-0347	p 1763	N94-21697
N00014-85-K-0124	p 1983	N94-19819
	p 1904	N94-20041
	p 1962	N94-20113
N00014-87-C-6002	p 1866	N94-20559
N00014-87-J-1185	p 1704	N94-20946
N00014-88-C-0096	p 2012	N94-19835
N00014-88-K-0317	p 1675	N94-21191
N00014-88-K-0582	p 1891	N94-20624
N00014-89-C-0257	p 1943	N94-20947
N00014-89-C-2392	p 2018	N94-20558
N00014-89-C-6007	p 1866	N94-20559
N00014-89-J-1021	p 1882	N94-20581
N00014-89-J-1070	p 1736	N94-20570
N00014-89-J-1109	p 1967	N94-19894
N00014-89-J-1456	p 1715	N94-19823
N00014-89-J-1527	p 1954	N94-21164
N00014-89-J-1653	p 1995	N94-21294
N00014-89-J-1683	p 1864	N94-20186
N00014-89-J-1754	p 1857	N94-21189
N00014-89-J-1961	p 1675	N94-21176
N00014-89-J-3120	p 2024	N94-21003
N00014-89-J-3230	p 1882	N94-20489
N00014-90-C-0162	p 1817	N94-21284
N00014-90-C-0265	p 1673	N94-20208
	p 1892	N94-21503
N00014-90-J-1025	p 1954	N94-21173
	p 1954	N94-21174
N00014-90-J-1030	p 1951	N94-20527
N00014-90-J-1159	p 2017	N94-20544
N00014-90-J-1425	p 1881	N94-19895
N00014-90-J-1508	p 1881	N94-19895
N00014-90-J-1604	p 2028	N94-21506
N00014-90-J-1808	p 1883	N94-21360
N00014-90-J-1835	p 2027	N94-21248
N00014-90-J-1971	p 1817	N94-20583
	p 1973	N94-20618
	p 1973	N94-20619
N00014-90-J-4052	p 1658	N94-21147
N00014-91-C-0080	p 2014	N94-19980
N00014-91-C-0234	p 1737	N94-20585
N00014-91-C-0263	p 1689	N94-20027
N00014-91-C-4016	p 1950	N94-20087
N00014-91-J-1005	p 1964	N94-21442
N00014-91-J-1009	p 1756	N94-21101
	p 1756	N94-21104
N00014-91-J-1045	p 1702	N94-20463
N00014-91-J-1267	p 1854	N94-19820
N00014-91-J-1270	p 1983	N94-19968
	p 1913	N94-21364
N00014-91-J-1271	p 1802	N94-21261
N00014-91-J-1274	p 1706	N94-21460
N00014-91-J-1353	p 1674	N94-20550
N00014-91-J-1372	p 1890	N94-20185
N00014-91-J-1385	p 1963	N94-21022
	p 1954	N94-21231
N00014-91-J-1409	p 1680	N94-20330
N00014-91-J-1422	p 1876	N94-22321
	p 1880	N94-22340
N00014-91-J-1463	p 1938	N94-21468
N00014-91-J-1508	p 1705	N94-21416
N00014-91-J-1651	p 2028	N94-21521
N00014-91-J-1688	p 1678	N94-19839
N00014-91-J-1698	p 1716	N94-19977
	p 1922	N94-21475
N00014-91-J-1934	p 1704	N94-21170
N00014-91-J-4038	p 1983	N94-19819
	p 1939	N94-19875
	p 1939	N94-19893
	p 1806	N94-19920
	p 1939	N94-20105
	p 1962	N94-20113
	p 1943	N94-20920
	p 1943	N94-20921
	p 1908	N94-20929
	p 1808	N94-21167
	p 1964	N94-21215
	p 1913	N94-21364
	p 1913	N94-21365
	p 1913	N94-21413
N00014-91-K-2019	p 1760	N94-21229
N00014-92-C-0225	p 1682	N94-21243
N00014-92-D-2000	p 1994	N94-20943
N00014-92-J-1186	p 2013	N94-19933
N00014-92-J-1243	p 2037	N94-21166
	p 1681	N94-21216
N00014-92-J-1344	p 2012	N94-19848
	p 2012	N94-19849
N00014-92-J-1361	p 1680	N94-20560
N00014-92-J-1412	p 1700	N94-20328
N00014-92-J-1433	p 1704	N94-21184
	p 1704	N94-21186
N00014-92-J-1474	p 1749	N94-20012
N00014-92-J-1512	p 1911	N94-21180
N00014-92-J-1524	p 1899	N94-21230
N00014-92-J-1771	p 1899	N94-21195
N00014-92-J-1778	p 1736	N94-20547
N00014-92-J-1801	p 1929	N94-20144
	p 1899	N94-21177
	p 1912	N94-21227
	p 1930	N94-21228
N00014-92-J-1814	p 1939	N94-20105
N00014-92-J-1846	p 1673	N94-20490
N00014-92-J-1866	p 1912	N94-21300
N00014-92-J-1868	p 1675	N94-21191
N00014-92-J-1879	p 1983	N94-19968
	p 1964	N94-21215
	p 1913	N94-21364
N00014-92-J-1927	p 2028	N94-21362
N00014-92-J-4082	p 1761	N94-21257
N00014-92-J-4093	p 1928	N94-19877
N00014-92-J-4097	p 1898	N94-19832
N00014-92-J-4112	p 1865	N94-20487
N00014-93-C-0021	p 1987	N94-21163
N00014-93-C-0029	p 1646	N94-21507
N00014-93-C-0037	p 1646	N94-21246
N00014-93-C-0042	p 1882	N94-20564
N00014-93-C-2026	p 2027	N94-21319
N00014-93-C-2044	p 2018	N94-20616
N00014-93-I-0437	p 2026	N94-21190
N00014-93-1-0067	p 1703	N94-20548
N00014-93-1-0140	p 2018	N94-20554
N00014-93-1-0244	p 1944	N94-21162
N00014-93-1-0325	p 1952	N94-20613
N00014-93-1-0468	p 2013	N94-19967
N00014-93-1-0615	p 1705	N94-21223
	p 1705	N94-21238
	p 1705	N94-21259
	p 1705	N94-21267
	p 1706	N94-21523
N00014-93-1-0619	p 1894	N94-21262

N00014-93-1-0806 ..... p 1942 N94-20621
N00014-93-1-2002 ..... p 2011 N94-19821
N00014-93-310058 ..... p 1703 N94-20526
N00039-88-C-0065 ..... p 1740 N94-21412
N00039-91-C-0001 ..... p 2015 N94-20184
PROJ. K-7-33 ..... p 1895 N94-20338
RF PROJ. 767386/721951 ..... p 1647 N94-21819
RICIS PROJ. IR-02 ..... p 1907 N94-20376
RTOP 199-61-12-28 ..... p 1895 N94-20137
RTOP 199-70-22-11 ..... p 2108 N94-20723
RTOP 210-02-12 ..... p 1830 N94-20171
RTOP 232-01-OA ..... p 1713 N94-21760
RTOP 235-01-04 ..... p 1656 N94-21581
RTOP 310-20-46 ..... p 1741 N94-21783
RTOP 313-00-00 ..... p 1676 N94-21889
RTOP 324-02-00 ..... p 1809 N94-21607
RTOP 460-42-90-70 ..... p 1871 N94-22292
RTOP 462-61-14 ..... p 1837 N94-20284
RTOP 474-12-10 ..... p 1667 N94-20062
RTOP 476-14-10 ..... p 1714 N94-21564
p 1715 N94-21589
RTOP 50-63-50-04 ..... p 1832 N94-21624
RTOP 505-10-01 ..... p 1798 N94-20104
RTOP 505-10-11 ..... p 1830 N94-20170
RTOP 505-59-36 ..... p 1635 N94-21490
RTOP 505-59-53-01 ..... p 1955 N94-21464
RTOP 505-60-01-01 ..... p 1900 N94-22100
RTOP 505-62-10 ..... p 1649 N94-21586
p 1826 N94-21756
RTOP 505-62-30-01 ..... p 1637 N94-21569
RTOP 505-62-52 ..... p 1637 N94-20534
p 1637 N94-20563
p 1648 N94-21582
p 1648 N94-21583
p 1638 N94-21591
p 1638 N94-22274
RTOP 505-63-50-17 ..... p 1833 N94-22608
RTOP 505-63-70-02 ..... p 1968 N94-21741
RTOP 505-64-10-07 ..... p 1898 N94-20039
p 1937 N94-22414
RTOP 505-64-13-01 ..... p 1643 N94-21629
RTOP 505-64-13 ..... p 1643 N94-21606
RTOP 505-66-41-04 ..... p 1644 N94-22277
p 1644 N94-22278
RTOP 505-68-10 ..... p 1642 N94-21590
RTOP 505-70-00 ..... p 1648 N94-21563
p 1649 N94-21759
RTOP 505-90-5K ..... p 1798 N94-20167
p 1959 N94-21588
RTOP 505-90-52-01 ..... p 1797 N94-20033
p 1950 N94-20087
p 1950 N94-20092
p 1914 N94-21462
p 1965 N94-21463
p 1959 N94-21568
p 1915 N94-21584
p 1804 N94-21861
p 1804 N94-21875
p 1804 N94-21880
RTOP 505-90-53-02 ..... p 1918 N94-22350
RTOP 506-41-41-01 ..... p 1669 N94-20102
RTOP 506-41-52 ..... p 1666 N94-21864
RTOP 506-42-31 ..... p 1670 N94-21565
RTOP 506-42-73 ..... p 1799 N94-20177
RTOP 506-44-2C ..... p 1769 N94-21808
RTOP 506-49-00 ..... p 1654 N94-21570
RTOP 506-72-1B ..... p 1732 N94-20497
RTOP 506-72-1E ..... p 1762 N94-21566
RTOP 506-72-21 ..... p 1741 N94-21567
RTOP 510-01-50 ..... p 1675 N94-21488
RTOP 510-02-12 ..... p 1832 N94-21757
RTOP 533-02-37 ..... p 1635 N94-20035
RTOP 533-02-39 ..... p 1649 N94-21879
RTOP 535-00-00 ..... p 1931 N94-21323
RTOP 535-03-10 ..... p 1968 N94-21608
RTOP 537-02-21 ..... p 1649 N94-21758
RTOP 583-02-21 ..... p 1670 N94-21809
RTOP 584-03-11 ..... p 1650 N94-21742
RTOP 585-03-21 ..... p 1984 N94-20140
RTOP 586-02-11 ..... p 1939 N94-20089
RTOP 590-21-11 ..... p 1654 N94-21790
RTOP 593-72-00 ..... p 1846 N94-21179
p 1671 N94-21874
RTOP 665-31-00-08-71 ..... p 1718 N94-20403
RTOP 674-24-05 ..... p 1692 N94-21604
SC1-CT91-0695 ..... p 2038 N94-22095
SRI PROJ. 4604 ..... p 1856 N94-20537
SWRI PROJ. 15-5659 ..... p 2042 N94-20363
W-31-109-ENG-38 ..... p 1687 N94-19806
p 2011 N94-19807
p 2011 N94-19808
p 1697 N94-19809
p 1748 N94-19885
p 1687 N94-19922
p 2012 N94-19923
p 1902 N94-19928
W-7405-ENG-36 ..... p 1970 N94-19956
p 1970 N94-19971
p 1807 N94-19990
p 1971 N94-20050
p 1690 N94-20183
p 1972 N94-20187
p 1855 N94-20220
p 1951 N94-20221
p 1979 N94-20222
p 1750 N94-20257
p 1799 N94-20258
p 1700 N94-20265
p 1690 N94-20288
p 2019 N94-20941
p 1802 N94-20942
p 1825 N94-21297
p 1706 N94-21542
p 1825 N94-21544
p 1692 N94-21558
p 1676 N94-21559
p 1825 N94-21637
p 2029 N94-21649
p 1847 N94-21650
p 1832 N94-21772
p 1847 N94-21774
p 1682 N94-21789
p 1693 N94-21825
p 1990 N94-21837
p 1848 N94-21870
p 2031 N94-21871
p 1917 N94-21923
p 1833 N94-21927
p 2031 N94-21930
p 2031 N94-21931
p 1677 N94-21940
p 1976 N94-21941
p 1848 N94-21942
p 1976 N94-21951
p 2032 N94-21972
p 2033 N94-21992
p 2033 N94-21993
p 2033 N94-21994
p 2033 N94-21997
p 2033 N94-21998
p 2033 N94-21999
p 1709 N94-22008
p 1859 N94-22036
p 1961 N94-22381
p 1853 N94-22384
p 1811 N94-22391
p 1961 N94-22393
p 2035 N94-22564
p 2035 N94-22565
p 2011 N94-19827
p 1814 N94-19828
p 1796 N94-19829
p 1884 N94-19866
p 1814 N94-19867
p 1991 N94-19883
p 2012 N94-19926
p 1854 N94-19955
p 1699 N94-19975
p 1904 N94-20049
p 1807 N94-20114
p 1807 N94-20115
p 1815 N94-20272
p 2015 N94-20275
p 1906 N94-20276
p 1816 N94-20277
p 1714 N94-20278
p 1929 N94-20279
p 1799 N94-20286
p 1808 N94-20287
p 1691 N94-20321
p 2016 N94-20322
p 2016 N94-20335
p 1732 N94-20479
p 1974 N94-21553
p 1818 N94-21554
p 2029 N94-21555
p 1707 N94-21560
p 1935 N94-21622
p 1935 N94-21745
p 1936 N94-21746
p 1916 N94-21747
p 1768 N94-21762
p 1917 N94-21764
p 1981 N94-21767
p 2030 N94-21768
p 1946 N94-21845
p 1769 N94-21846
p 1982 N94-21849
p 1917 N94-21851
p 2031 N94-21857
p 1960 N94-21946
p 1997 N94-21965
W-7405-ENG-48 ..... p 2032 N94-21967
p 1997 N94-21988
p 1997 N94-21989
p 1695 N94-21990
p 2033 N94-21991
p 1976 N94-21995
p 1968 N94-22003
p 1852 N94-22017
p 1820 N94-22020
p 1696 N94-22034
p 2034 N94-22035
p 2035 N94-22387
p 1696 N94-22388
p 1998 N94-22389
p 1827 N94-22390
p 1977 N94-22400
p 1965 N94-22403
p 1977 N94-22572
p 2036 N94-22583
p 2036 N94-22584
p 1820 N94-22585
p 1844 N94-19803
p 1698 N94-19810
p 2012 N94-19861
p 1983 N94-19862
p 1657 N94-19863
p 1898 N94-19886
p 1678 N94-19889
p 1992 N94-19915
p 1796 N94-19916
p 1688 N94-19986
p 1992 N94-19991
p 1949 N94-20006
p 1971 N94-20096
p 1972 N94-20181
p 1815 N94-20223
p 1750 N94-20231
p 1815 N94-20259
p 1985 N94-20262
p 1799 N94-20263
p 1985 N94-20283
p 1906 N94-20316
p 2016 N94-20318
p 1679 N94-20319
p 1816 N94-20480
p 1817 N94-21299
p 1966 N94-21511
p 1706 N94-21512
p 2044 N94-21529
p 1675 N94-21530
p 1803 N94-21531
p 1707 N94-21546
p 1818 N94-21547
p 2081 N94-21618
p 1989 N94-21619
p 1762 N94-21620
p 1762 N94-21621
p 1989 N94-21630
p 1803 N94-21651
p 1693 N94-21656
p 1936 N94-21749
p 2045 N94-21750
p 1766 N94-21753
p 1768 N94-21770
p 1936 N94-21828
p 1818 N94-21829
p 1769 N94-21838
p 1917 N94-21841
p 1693 N94-21843
p 1819 N94-21844
p 1997 N94-21848
p 2152 N94-21858
p 2031 N94-21869
p 1819 N94-21872
p 1819 N94-21873
p 1819 N94-21920
p 1694 N94-21921
p 1946 N94-21925
p 2031 N94-21931
p 1694 N94-21943
p 1694 N94-21944
p 1810 N94-21950
p 1966 N94-21958
p 1769 N94-21959
p 2032 N94-21960
p 1976 N94-21968
p 1852 N94-21969
p 1709 N94-21970
p 1657 N94-21980
p 1657 N94-21981
p 1990 N94-21985
p 1695 N94-21986
p 1960 N94-21996
p 1990 N94-22002
p 1918 N94-22011
p 1695 N94-22023

p 1695 N94-22024
p 1696 N94-22025
p 1937 N94-22042
p 2034 N94-22050
p 1794 N94-22380
p 1696 N94-22394
p 1684 N94-22395
p 1977 N94-22396
p 2150 N94-22397
p 1696 N94-22398
p 1998 N94-22399
p 1697 N94-22402
p 2046 N94-22413
p 1937 N94-22558
p 2036 N94-22594
p 1999 N94-22595
W-7405-ENG-82 ..... p 1672 N94-19888
p 2029 N94-21691
p 2031 N94-21931
p 2032 N94-21936
p 1694 N94-21937
p 1695 N94-21964
p 1697 N94-22571
p 1978 N94-22573
p 2036 N94-22582

Typical Report Number Index Listing

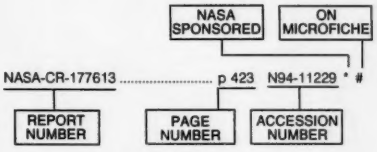

Listings in this index are arranged alphanumerically by report number. The accession number denotes the number by which the citation is identified. The page number helps to locate the citation in the abstract section. An asterisk (*) indicates that the item is a NASA report. A pound sign (#) indicates that the item is available on microfiche.

A-91183 ..... p 1635 N94-21490 * #
A-92038 ..... p 1643 N94-21606 * #
A-93090 ..... p 1635 N94-20035 * #
A-93100 ..... p 1895 N94-20137 * #
A-93106 ..... p 1646 N94-21592 * #
A-93120 ..... p 1642 N94-22373 * #
A-94007 ..... p 1798 N94-20104 * #
A-94010 ..... p 1914 N94-21489 * #
A-94011 ..... p 1966 N94-21881 * #
A-94020 ..... p 1905 N94-20149 * #
A-94023 ..... p 1842 N94-22345 * #
A-94024 ..... p 1842 N94-21585 * #
A-94040 ..... p 1897 N94-21784 * #

AD-A264278 ..... p 1673 N94-20327
AD-A265942 ..... p 1680 N94-20330
AD-A265955 ..... p 1717 N94-20329
AD-A265956 ..... p 1700 N94-20328
AD-A266759 ..... p 2028 N94-21517
AD-A267759 ..... p 1889 N94-19962 #
AD-A267760 ..... p 1636 N94-19963 #
AD-A267795 ..... p 1716 N94-19984
AD-A267820 ..... p 1815 N94-19965 #
AD-A267821 ..... p 1717 N94-20207 #
AD-A267832 ..... p 1673 N94-20208 #
AD-A267882 ..... p 1912 N94-21255
AD-A267947 ..... p 1865 N94-20482 #
AD-A267955 ..... p 1751 N94-20483 #
AD-A267961 ..... p 1816 N94-20484 #
AD-A267984 ..... p 1856 N94-20485
AD-A268511 ..... p 1868 N94-21502
AD-A268987 ..... p 1807 N94-20203 #
AD-A269943 ..... p 2014 N94-20029 #
AD-A269961 ..... p 1672 N94-20031 #
AD-A270201 ..... p 1636 N94-20486
AD-A270356 ..... p 2041 N94-20038 #
AD-A270391 ..... p 1645 N94-20040
AD-A270429 ..... p 1828 N94-19815
AD-A270463 ..... p 2013 N94-19966
AD-A270475 ..... p 1837 N94-20028 #
AD-A270478 ..... p 1966 N94-19917
AD-A270513 ..... p 2013 N94-19967
AD-A270520 ..... p 1983 N94-19968
AD-A270522 ..... p 1939 N94-19893
AD-A270523 ..... p 1939 N94-20105
AD-A270524 ..... p 1902 N94-19932
AD-A270526 ..... p 2037 N94-19831
AD-A270530 ..... p 1967 N94-19894
AD-A270531 ..... p 1939 N94-19875
AD-A270537 ..... p 1651 N94-20011
AD-A270538 ..... p 1971 N94-20083
AD-A270540 ..... p 2013 N94-19933
AD-A270541 ..... p 1641 N94-19876
AD-A270549 ..... p 1929 N94-20084
AD-A270550 ..... p 1898 N94-20085
AD-A270551 ..... p 1902 N94-19918
AD-A270552 ..... p 1902 N94-19919
AD-A270571 ..... p 2041 N94-20106
AD-A270576 ..... p 1898 N94-20107
AD-A270577 ..... p 1698 N94-19947
AD-A270578 ..... p 1651 N94-20108
AD-A270583 ..... p 1905 N94-20109
AD-A270597 ..... p 1902 N94-19948
AD-A270598 ..... p 1967 N94-19949
AD-A270600 ..... p 1938 N94-19845
AD-A270601 ..... p 1928 N94-19950
AD-A270608 ..... p 1715 N94-19816 #
AD-A270619 ..... p 1716 N94-19951
AD-A270627 ..... p 1882 N94-20564 #
AD-A270659 ..... p 1881 N94-19952
AD-A270678 ..... p 1928 N94-19877
AD-A270679 ..... p 1749 N94-20012
AD-A270705 ..... p 1678 N94-19953
AD-A270713 ..... p 1903 N94-19969
AD-A270719 ..... p 1749 N94-20110
AD-A270720 ..... p 1679 N94-20111
AD-A270724 ..... p 1890 N94-20112
AD-A270729 ..... p 1854 N94-19954
AD-A270758 ..... p 1866 N94-20565 #
AD-A270838 ..... p 1898 N94-19832 #
AD-A270839 ..... p 1904 N94-20041 #
AD-A270846 ..... p 1821 N94-19833 #
AD-A270849 ..... p 1815 N94-19878 #
AD-A270852 ..... p 1713 N94-19834 #
AD-A270854 ..... p 1881 N94-19895 #
AD-A270859 ..... p 1647 N94-20042 #
AD-A270861 ..... p 1657 N94-19896 #
AD-A270871 ..... p 1680 N94-20566 #
AD-A270885 ..... p 1806 N94-19920 *
AD-A270887 ..... p 1962 N94-20113
AD-A270897 ..... p 2012 N94-19897 #
AD-A270931 ..... p 1716 N94-19934 #
AD-A270932 ..... p 1636 N94-20043 #
AD-A270934 ..... p 1949 N94-19898 #
AD-A270935 ..... p 1854 N94-19899 #
AD-A270936 ..... p 1890 N94-20045 #
AD-A270937 ..... p 1699 N94-20046 #
AD-A270938 ..... p 2011 N94-19817 #
AD-A270939 ..... p 1666 N94-19818 * #
AD-A271003 ..... p 1716 N94-19977
AD-A271005 ..... p 1983 N94-19819
AD-A271007 ..... p 2012 N94-19835 #
AD-A271010 ..... p 1854 N94-19820
AD-A271011 ..... p 2011 N94-19821
AD-A271013 ..... p 1970 N94-19822
AD-A271034 ..... p 1715 N94-19823
AD-A271036 ..... p 1983 N94-20013
AD-A271037 ..... p 1797 N94-19978 #
AD-A271058 ..... p 1854 N94-19860 #
AD-A271059 ..... p 1881 N94-19905
AD-A271060 ..... p 1711 N94-19906 #
AD-A271063 ..... p 1882 N94-19979 #
AD-A271064 ..... p 1823 N94-20567
AD-A271066 ..... p 1667 N94-20015
AD-A271067 ..... p 1983 N94-19846
AD-A271079 ..... p 1895 N94-19935 #
AD-A271080 ..... p 2014 N94-19980 #
AD-A271085 ..... p 1667 N94-19847 #
AD-A271094 ..... p 2012 N94-19848
AD-A271095 ..... p 2012 N94-19849
AD-A271098 ..... p 1949 N94-19907
AD-A271100 ..... p 1814 N94-19850
AD-A271101 ..... p 1814 N94-19851
AD-A271102 ..... p 1864 N94-19852 #
AD-A271106 ..... p 1889 N94-19981 #
AD-A271111 ..... p 1864 N94-19908
AD-A271112 ..... p 2014 N94-19982 #
AD-A271128 ..... p 1699 N94-20016
AD-A271129 ..... p 1689 N94-20019
AD-A271132 ..... p 1814 N94-19853
AD-A271140 ..... p 1821 N94-20021
AD-A271141 ..... p 1962 N94-19999
AD-A271142 ..... p 1939 N94-19909
AD-A271143 ..... p 1949 N94-19854
AD-A271145 ..... p 1902 N94-19855
AD-A271149 ..... p 1829 N94-19836
AD-A271150 ..... p 1748 N94-19910
AD-A271158 ..... p 2015 N94-20184 #
AD-A271160 ..... p 1678 N94-20000
AD-A271161 ..... p 1864 N94-19900
AD-A271164 ..... p 1890 N94-20185 #
AD-A271171 ..... p 1816 N94-20546 #
AD-A271175 ..... p 1864 N94-20186 #
AD-A271176 ..... p 2015 N94-20213 #
AD-A271177 ..... p 1830 N94-20001
AD-A271178 ..... p 2015 N94-20214 #
AD-A271181 ..... p 1717 N94-20215 #
AD-A271183 ..... p 1700 N94-20299 #
AD-A271250 ..... p 1983 N94-19901
AD-A271252 ..... p 1902 N94-19911
AD-A271257 ..... p 1715 N94-19912 #
AD-A271292 ..... p 2030 N94-21805
AD-A271314 ..... p 1796 N94-19913
AD-A271315 ..... p 1797 N94-19936
AD-A271319 ..... p 1893 N94-20023
AD-A271326 ..... p 1851 N94-20025
AD-A271327 ..... p 1641 N94-20912
AD-A271328 ..... p 1689 N94-20027
AD-A271329 ..... p 1829 N94-19937
AD-A271330 ..... p 1645 N94-19914
AD-A271331 ..... p 1806 N94-19837
AD-A271337 ..... p 1650 N94-19879
AD-A271348 ..... p 1650 N94-19880
AD-A271395 ..... p 1949 N94-19838
AD-A271422 ..... p 1678 N94-19839
AD-A271429 ..... p 1698 N94-19840
AD-A271435 ..... p 1854 N94-19841
AD-A271436 ..... p 1829 N94-19881
AD-A271437 ..... p 2012 N94-19842
AD-A271439 ..... p 1845 N94-20086
AD-A271440 ..... p 1864 N94-20088
AD-A271450 ..... p 1698 N94-19938
AD-A271458 ..... p 1855 N94-20090
AD-A271465 ..... p 1904 N94-20091
AD-A271483 ..... p 1736 N94-20547 #
AD-A271484 ..... p 2027 N94-21319 #
AD-A271485 ..... p 1703 N94-20548 #
AD-A271486 ..... p 1912 N94-21300 #
AD-A271489 ..... p 1899 N94-20549 * #
AD-A271491 ..... p 1674 N94-20550 #
AD-A271496 ..... p 1712 N94-20551 #
AD-A271500 ..... p 2017 N94-20544 #
AD-A271514 ..... p 1951 N94-20545 #
AD-A271520 ..... p 1963 N94-20913 #
AD-A271535 ..... p 1896 N94-20914 #
AD-A271539 ..... p 1801 N94-20915 #
AD-A271540 ..... p 1831 N94-20916 #
AD-A271541 ..... p 1908 N94-20917 #
AD-A271547 ..... p 1712 N94-20827 #
AD-A271571 ..... p 1909 N94-21034 #
AD-A271582 ..... p 1891 N94-21035 #
AD-A271583 ..... p 1739 N94-21235 #
AD-A271586 ..... p 1761 N94-21256 #
AD-A271591 ..... p 1704 N94-20946 #
AD-A271593 ..... p 1943 N94-20947 #
AD-A271596 ..... p 1851 N94-20948 #
AD-A271604 ..... p 1737 N94-20949 #
AD-A271608 ..... p 1674 N94-20950 #
AD-A271609 ..... p 1987 N94-21236 #
AD-A271610 ..... p 1739 N94-21240 #
AD-A271611 ..... p 1681 N94-21241 #
AD-A271612 ..... p 1894 N94-21237 #
AD-A271614 ..... p 1761 N94-21257 #
AD-A271642 ..... p 1892 N94-21036 #
AD-A271645 ..... p 2018 N94-20558
AD-A271646 ..... p 1900 N94-21301 #
AD-A271671 ..... p 1866 N94-20559
AD-A271672 ..... p 1866 N94-20918
AD-A271673 ..... p 2042 N94-20919
AD-A271677 ..... p 2028 N94-21362 #
AD-A271679 ..... p 2044 N94-21363 #
AD-A271686 ..... p 1943 N94-20920
AD-A271687 ..... p 1943 N94-20921
AD-A271690 ..... p 1891 N94-20926
AD-A271691 ..... p 1913 N94-21364 #
AD-A271692 ..... p 1908 N94-20929
AD-A271702 ..... p 1913 N94-21365 #
AD-A271704 ..... p 1740 N94-21352 #
AD-A271706 ..... p 1817 N94-21353 #
AD-A271714 ..... p 2044 N94-21354 #
AD-A271715 ..... p 1808 N94-20930

AD-A271716 ..... p 2018 N94-20554
AD-A271719 ..... p 1945 N94-21355 #
AD-A271722 ..... p 1868 N94-21356 #
AD-A271724 ..... p 1858 N94-21357 #
AD-A271737 ..... p 1883 N94-21358 #
AD-A271747 ..... p 1988 N94-21457 #
AD-A271753 ..... p 1705 N94-21302 #
AD-A271756 ..... p 2027 N94-21303 #
AD-A271757 ..... p 2027 N94-21304 #
AD-A271767 ..... p 1945 N94-21305 #
AD-A271768 ..... p 1944 N94-21162
AD-A271769 ..... p 1943 N94-20926
AD-A271806 ..... p 1751 N94-20555
AD-A271811 ..... p 1896 N94-21154
AD-A271819 ..... p 1712 N94-20625
AD-A271820 ..... p 1943 N94-20626
AD-A271822 ..... p 1891 N94-20627
AD-A271824 ..... p 1680 N94-20560
AD-A271827 ..... p 2028 N94-21458 #
AD-A271837 ..... p 1894 N94-20610
AD-A271841 ..... p 1907 N94-20525
AD-A271843 ..... p 1828 N94-20468
AD-A271847 ..... p 1817 N94-20611 #
AD-A271849 ..... p 1973 N94-20612 #
AD-A271851 ..... p 1952 N94-20613 #
AD-A271858 ..... p 1703 N94-20526
AD-A271859 ..... p 1890 N94-20462 #
AD-A271862 ..... p 1702 N94-20463
AD-A271864 ..... p 1823 N94-20464
AD-A271865 ..... p 1636 N94-20465 #
AD-A271868 ..... p 1800 N94-20466
AD-A271872 ..... p 1894 N94-20467
AD-A271874 ..... p 1899 N94-20469
AD-A271875 ..... p 2017 N94-20470
AD-A271876 ..... p 1732 N94-20471
AD-A271877 ..... p 1929 N94-20472 #
AD-A271878 ..... p 1865 N94-20487
AD-A271901 ..... p 1942 N94-20488 #
AD-A271911 ..... p 1882 N94-20489 #
AD-A271912 ..... p 1673 N94-20490 #
AD-A271933 ..... p 1703 N94-20614 #
AD-A271956 ..... p 1674 N94-20577 #
AD-A271957 ..... p 1645 N94-20561 #
AD-A271958 ..... p 1736 N94-20578 #
AD-A271968 ..... p 1891 N94-20615 #
AD-A271980 ..... p 2018 N94-20616 #
AD-A271981 ..... p 1658 N94-20617 #
AD-A271983 ..... p 1866 N94-20579 #
AD-A271985 ..... p 1751 N94-20580 #
AD-A271986 ..... p 1973 N94-20618
AD-A271987 ..... p 1973 N94-20619 #
AD-A271998 ..... p 1883 N94-21366 #
AD-A272000 ..... p 1892 N94-21503 #
AD-A272001 ..... p 1882 N94-20581 #
AD-A272011 ..... p 1803 N94-21459 #
AD-A272013 ..... p 1706 N94-21460 #
AD-A272015 ..... p 1974 N94-21461 #
AD-A272016 ..... p 1964 N94-21442 #
AD-A272018 ..... p 1737 N94-20620 #
AD-A272019 ..... p 1883 N94-21443 #
AD-A272020 ..... p 1752 N94-20931
AD-A272022 ..... p 2039 N94-21444 #
AD-A272055 ..... p 1809 N94-21445 #
AD-A272057 ..... p 1761 N94-21282 #
AD-A272058 ..... p 1942 N94-20621 #
AD-A272060 ..... p 1908 N94-20622 #
AD-A272064 ..... p 1737 N94-20582 #
AD-A272065 ..... p 1986 N94-20922
AD-A272068 ..... p 1674 N94-20623 #
AD-A272101 ..... p 1817 N94-20583 #
AD-A272110 ..... p 1680 N94-20584 #
AD-A272112 ..... p 1952 N94-20568 #
AD-A272113 ..... p 2018 N94-20569 #
AD-A272114 ..... p 1736 N94-20570 #
AD-A272115 ..... p 1929 N94-20571 #
AD-A272123 ..... p 1831 N94-20572 #
AD-A272125 ..... p 1942 N94-20573 #
AD-A272184 ..... p 1952 N94-20923
AD-A272185 ..... p 2042 N94-20924
AD-A272188 ..... p 1883 N94-20925
AD-A272233 ..... p 1674 N94-20574 #
AD-A272249 ..... p 1994 N94-20943 #
AD-A272251 ..... p 2018 N94-20575 #
AD-A272258 ..... p 1824 N94-20576 #
AD-A272273 ..... p 1737 N94-20944 #
AD-A272279 ..... p 2037 N94-20945 #
AD-A272280 ..... p 1737 N94-20585 #
AD-A272282 ..... p 1891 N94-20624 #
AD-A272322 ..... p 1643 N94-21037 #
AD-A272323 ..... p 1909 N94-21038 #
AD-A272330 ..... p 1951 N94-20527
AD-A272331 ..... p 1994 N94-21039 #
AD-A272383 ..... p 1910 N94-21144 #
AD-A272386 ..... p 1680 N94-21145
AD-A272417 ..... p 1867 N94-21146
AD-A272419 ..... p 1658 N94-21147 #
AD-A272426 ..... p 1691 N94-21258 #
AD-A272431 ..... p 1857 N94-21202
AD-A272439 ..... p 1911 N94-21203
AD-A272440 ..... p 1911 N94-21204
AD-A272441 ..... p 1912 N94-21205 #
AD-A272445 ..... p 1654 N94-21429
AD-A272446 ..... p 1858 N94-21206
AD-A272447 ..... p 1858 N94-21207 #
AD-A272491 ..... p 1670 N94-21208 #
AD-A272495 ..... p 1945 N94-21430 #
AD-A272496 ..... p 1675 N94-21431 #
AD-A272497 ..... p 1858 N94-21432 #
AD-A272498 ..... p 1648 N94-21433 #
AD-A272499 ..... p 1646 N94-21548 #
AD-A272500 ..... p 1913 N94-21409
AD-A272505 ..... p 1987 N94-21410
AD-A272506 ..... p 1637 N94-21411 #
AD-A272507 ..... p 1740 N94-21412 #
AD-A272512 ..... p 1913 N94-21413 #
AD-A272513 ..... p 1914 N94-21414 #
AD-A272514 ..... p 1955 N94-21359 #
AD-A272517 ..... p 1892 N94-21415 #
AD-A272518 ..... p 1705 N94-21416 #
AD-A272530 ..... p 1803 N94-21417 #
AD-A272532 ..... p 1646 N94-21418 #
AD-A272565 ..... p 1883 N94-21360
AD-A272567 ..... p 1740 N94-21361
AD-A272571 ..... p 1635 N94-21419 #
AD-A272581 ..... p 1892 N94-21209 #
AD-A272582 ..... p 1738 N94-21210 #
AD-A272591 ..... p 1665 N94-21420 #
AD-A272604 ..... p 1832 N94-21421 #
AD-A272607 ..... p 1968 N94-21422 #
AD-A272610 ..... p 1883 N94-21423 #
AD-A272612 ..... p 1974 N94-21185 #
AD-A272613 ..... p 1675 N94-21504
AD-A272614 ..... p 1739 N94-21211 #
AD-A272618 ..... p 1867 N94-21212 #
AD-A272647 ..... p 1704 N94-21184 #
AD-A272649 ..... p 1704 N94-21186 #
AD-A272657 ..... p 1675 N94-21187 #
AD-A272658 ..... p 1691 N94-21188 #
AD-A272659 ..... p 1994 N94-21214 #
AD-A272660 ..... p 1964 N94-21215 #
AD-A272665 ..... p 1681 N94-21216 #
AD-A272672 ..... p 1658 N94-21217 #
AD-A272683 ..... p 1987 N94-21163 #
AD-A272685 ..... p 1857 N94-21189 #
AD-A272687 ..... p 1954 N94-21164 #
AD-A272695 ..... p 1681 N94-21165 #
AD-A272698 ..... p 2037 N94-21166 #
AD-A272715 ..... p 2026 N94-21190 #
AD-A272717 ..... p 2028 N94-21505
AD-A272718 ..... p 1808 N94-21167 #
AD-A272721 ..... p 1681 N94-21168 #
AD-A272722 ..... p 1802 N94-21169 #
AD-A272723 ..... p 1681 N94-21213 #
AD-A272725 ..... p 1681 N94-21181 #
AD-A272763 ..... p 1738 N94-21182 #
AD-A272781 ..... p 1911 N94-21183 #
AD-A272805 ..... p 1704 N94-21170 #
AD-A272809 ..... p 2037 N94-21171 #
AD-A272831 ..... p 1987 N94-21172 #
AD-A272832 ..... p 1894 N94-21434
AD-A272834 ..... p 1954 N94-21173 #
AD-A272835 ..... p 1954 N94-21174 #
AD-A272836 ..... p 1964 N94-21175 #
AD-A272837 ..... p 1675 N94-21176 #
AD-A272838 ..... p 1899 N94-21177 #
AD-A272848 ..... p 1675 N94-21191 #
AD-A272850 ..... p 1712 N94-21192 #
AD-A272851 ..... p 1802 N94-21193 #
AD-A272876 ..... p 1635 N94-21194 #
AD-A272878 ..... p 1899 N94-21195 #
AD-A272879 ..... p 1802 N94-21155 #
AD-A272888 ..... p 2147 N94-21196 #
AD-A272889 ..... p 1841 N94-21453
AD-A272897 ..... p 1704 N94-21197 #
AD-A272899 ..... p 1738 N94-21198 #
AD-A272900 ..... p 1739 N94-21218 #
AD-A272904 ..... p 1760 N94-21229 #
AD-A272909 ..... p 1899 N94-21230 #
AD-A272910 ..... p 2027 N94-21242 #
AD-A272911 ..... p 1682 N94-21243 #
AD-A272912 ..... p 1739 N94-21244 #
AD-A272913 ..... p 1691 N94-21245 #
AD-A272914 ..... p 1692 N94-21320 #
AD-A272915 ..... p 1831 N94-21219 #
AD-A272918 ..... p 1802 N94-21220 #
AD-A272920 ..... p 1760 N94-21221 #
AD-A272922 ..... p 1863 N94-21222 #
AD-A272923 ..... p 1705 N94-21223 #
AD-A272937 ..... p 1652 N94-21224 #
AD-A272943 ..... p 1705 N94-21225 #
AD-A272945 ..... p 1681 N94-21226 #
AD-A272947 ..... p 1912 N94-21227 #
AD-A272948 ..... p 1930 N94-21228 #
AD-A272951 ..... p 1646 N94-21246 #
AD-A272952 ..... p 1896 N94-21247 #
AD-A272955 ..... p 2027 N94-21248 #
AD-A272956 ..... p 1893 N94-21613 #
AD-A272957 ..... p 1831 N94-21249 #
AD-A272959 ..... p 1867 N94-21250 #
AD-A272960 ..... p 1658 N94-21251 #
AD-A272962 ..... p 1899 N94-21252 #
AD-A272964 ..... p 1967 N94-21306
AD-A272966 ..... p 1705 N94-21259 #
AD-A272967 ..... p 1967 N94-21260 #
AD-A272970 ..... p 1802 N94-21261 #
AD-A272971 ..... p 1894 N94-21262 #
AD-A272973 ..... p 1802 N94-21263 #
AD-A272987 ..... p 1740 N94-21264 #
AD-A272988 ..... p 1912 N94-21265 #
AD-A272989 ..... p 2043 N94-21266 #
AD-A272994 ..... p 1705 N94-21267 #
AD-A272998 ..... p 1648 N94-21268 #
AD-A273001 ..... p 1945 N94-21269 #
AD-A273003 ..... p 1646 N94-21283 #
AD-A273004 ..... p 1867 N94-21307
AD-A273005 ..... p 1740 N94-21308
AD-A273010 ..... p 1817 N94-21284 #
AD-A273014 ..... p 1897 N94-21309 #
AD-A273016 ..... p 1705 N94-21238 #
AD-A273018 ..... p 1651 N94-21239 #
AD-A273020 ..... p 1817 N94-21253 #
AD-A273031 ..... p 1987 N94-21321 #
AD-A273032 ..... p 1682 N94-21435
AD-A273044 ..... p 1964 N94-21322 #
AD-A273047 ..... p 1740 N94-21436
AD-A273056 ..... p 2045 N94-21865 * #
AD-A273061 ..... p 1831 N94-21310 #
AD-A273063 ..... p 1706 N94-21437 #
AD-A273064 ..... p 2028 N94-21438 #
AD-A273070 ..... p 1988 N94-21491 #
AD-A273074 ..... p 1740 N94-21518 #
AD-A273075 ..... p 1868 N94-21519 #
AD-A273076 ..... p 1945 N94-21520 #
AD-A273083 ..... p 2028 N94-21521 #
AD-A273084 ..... p 2147 N94-21522 #
AD-A273085 ..... p 1706 N94-21523 #
AD-A273089 ..... p 1959 N94-21524 #
AD-A273091 ..... p 1692 N94-21525
AD-A273093 ..... p 1647 N94-21500 #
AD-A273097 ..... p 2028 N94-21506 #
AD-A273103 ..... p 1646 N94-21507 #
AD-A273105 ..... p 1809 N94-21508 #
AD-A273106 ..... p 1914 N94-21501 #
AD-A273109 ..... p 1818 N94-21509 #
AD-A273112 ..... p 1894 N94-21510 #
AD-D015895 ..... p 1749 N94-20120
AD-D015896 ..... p 1669 N94-20121
AD-D015897 ..... p 1712 N94-20122
AD-D015898 ..... p 1717 N94-20198
AD-D015904 ..... p 1815 N94-20055
AD-D015910 ..... p 1698 N94-19830 #
AD-D015912 ..... p 1672 N94-20010 #
AD-D015913 ..... p 1748 N94-19892 #
AD-D015915 ..... p 1984 N94-20056
AD-D015917 ..... p 1700 N94-20057
AD-D015918 ..... p 1984 N94-20059
AD-D015920 ..... p 1815 N94-20060
AD-D015922 ..... p 1712 N94-20061
AD-D015923 ..... p 1749 N94-20199
AD-D015924 ..... p 1643 N94-20197
AD-D015925 ..... p 2017 N94-20348
AD-D015926 ..... p 1797 N94-20094
AD-D015927 ..... p 1699 N94-20017
AD-D015928 ..... p 1814 N94-19800
AD-D015929 ..... p 1711 N94-19801
AD-D015930 ..... p 1701 N94-20349
AD-D015932 ..... p 1751 N94-20350
AD-D015933 ..... p 1701 N94-20331
AD-D015935 ..... p 1865 N94-20332
AD-D015938 ..... p 1717 N94-20333
AD-D015939 ..... p 1718 N94-20334
AD-D015942 ..... p 1673 N94-20064
AD-D015944 ..... p 1984 N94-20065
AD-D015946 ..... p 1938 N94-19843
AD-D015950 ..... p 1806 N94-19882
AD-D015956 ..... p 1751 N94-20354
AD-D015957 ..... p 1714 N94-20355 #
AD-D015959 ..... p 1822 N94-20356 #
AD-D015960 ..... p 1898 N94-20357
AD-D015962 ..... p 1951 N94-20358 #
AD-D015965 ..... p 1824 N94-21274
AD-D015966 ..... p 1761 N94-21275
AD-D015967 ..... p 2043 N94-21276
AD-D015969 ..... p 1824 N94-21277
AD-D015971 ..... p 1808 N94-21278
AD-D015973 ..... p 1987 N94-21279

AD-E201456 ..... p 1717 N94-20329
AD-E201629 ..... p 1855 N94-20090
AD-E201663 ..... p 1829 N94-19881
AD-E201665 ..... p 1854 N94-19841
AD-E201667 ..... p 1845 N94-20086
AD-E201668 ..... p 2012 N94-19842
AD-E501719 ..... p 1665 N94-21420 #

AFESC/ESL-TR-89-23 ..... p 1851 N94-20025
AFESC/ESL-TR-91-31-SUPPL-A . p 1851 N94-20948 #
AFESC/ESL-TR-92-53 ..... p 1698 N94-19938

AFIT/CI/CIA-93-053 ..... p 1865 N94-20482 #
AFIT/CI/CIA-93-115 ..... p 1751 N94-20483 #
AFIT/CI/CIA-93-121 ..... p 1868 N94-21502
AFIT/CI/CIA-93-123 ..... p 1856 N94-20485

AFIT/DS/ENP/93-06 ..... p 2013 N94-19966

AFIT/EN/TR-93-08 ..... p 1942 N94-20488 #

AFIT/EN/TR93-10 ..... p 1914 N94-21501 #

AFIT/ENC/GEE/93S-2 ..... p 1889 N94-19981 #

AFIT/GAP/ENP/93S-01 ..... p 1678 N94-19953

AFIT/GE/ENG/93S-06 ..... p 1903 N94-19969

AFOSR-93-0249TR ..... p 1673 N94-20327
AFOSR-93-0413TR ..... p 1986 N94-20922
AFOSR-93-0753TR ..... p 1667 N94-19847 #
AFOSR-93-0757TR ..... p 1983 N94-19846
AFOSR-93-0774TR ..... p 1854 N94-19954
AFOSR-93-0775TR ..... p 1890 N94-20112
AFOSR-93-0776TR ..... p 1667 N94-20015
AFOSR-93-0778TR ..... p 1680 N94-20566 #
AFOSR-93-0779TR ..... p 2012 N94-19897 #
AFOSR-93-0780 ..... p 1814 N94-19853
AFOSR-93-0787TR ..... p 1909 N94-21034 #
AFOSR-93-0788TR ..... p 1797 N94-19936
AFOSR-93-0790TR ..... p 1864 N94-19900
AFOSR-93-0791TR ..... p 1796 N94-19913
AFOSR-93-0792TR ..... p 1678 N94-20000
AFOSR-93-0803TR ..... p 2028 N94-21458 #
AFOSR-93-0806TR ..... p 1988 N94-21457 #
AFOSR-93-0807TR ..... p 1952 N94-20568 #
AFOSR-93-0809TR ..... p 1803 N94-21459 #
AFOSR-93-0810TR ..... p 1712 N94-20625
AFOSR-93-0811TR ..... p 1943 N94-20626
AFOSR-93-0812TR ..... p 1674 N94-20623 #
AFOSR-93-0814TR ..... p 1751 N94-20580 #
AFOSR-93-0815TR ..... p 2018 N94-20569 #
AFOSR-93-0817TR ..... p 1823 N94-20464
AFOSR-93-0818TR ..... p 1894 N94-20467
AFOSR-93-0819TR ..... p 1680 N94-20584 #
AFOSR-93-0820TR ..... p 1891 N94-20627
AFOSR-93-0822TR ..... p 1636 N94-20465 #
AFOSR-93-0823TR ..... p 2018 N94-20575 #
AFOSR-93-0824TR ..... p 1973 N94-20612 #
AFOSR-93-0825TR ..... p 1866 N94-20918
AFOSR-93-0826TR ..... p 1899 N94-20469
AFOSR-93-0827TR ..... p 2017 N94-20470
AFOSR-93-0828TR ..... p 1802 N94-21193 #
AFOSR-93-0833TR ..... p 2147 N94-21522 #
AFOSR-93-0834TR ..... p 2147 N94-21196 #
AFOSR-93-0835TR ..... p 1681 N94-21213 #
AFOSR-93-0836TR ..... p 1692 N94-21320 #
AFOSR-93-0838TR ..... p 1831 N94-21219 #
AFOSR-93-0839TR ..... p 1691 N94-21245 #
AFOSR-93-0840TR ..... p 1681 N94-21181 #
AFOSR-93-0841TR ..... p 2027 N94-21242 #
AFOSR-93-0842TR ..... p 1802 N94-21220 #
AFOSR-93-0843TR ..... p 1802 N94-21155 #
AFOSR-93-0844TR ..... p 1712 N94-21192 #
AFOSR-93-0845TR ..... p 1681 N94-21168 #
AFOSR-93-0846TR ..... p 1802 N94-21169 #

AI-M-1390 ..... p 1913 N94-21364 #
AI-M-1399 ..... p 1913 N94-21365 #

AI-TR-1377 ..... p 1898 N94-19832 #
AI-TR-1398 ..... p 1962 N94-20113
AI-TR-1410 ..... p 1904 N94-20041 #
AI-TR-1411 ..... p 1806 N94-19920 *
AI-TR-1416 ..... p 1983 N94-19819
AI-TR-1429 ..... p 1913 N94-21413 #
AI-TR-1445 ..... p 1716 N94-19977

AIAA PAPER 93-1823 ..... p 1649 N94-21879 * #
AIAA PAPER 93-1966 ..... p 1799 N94-20177 * #
AIAA PAPER 93-2084 ..... p 1649 N94-21586 * #
AIAA PAPER 93-2964 ..... p 1637 N94-20534 * #
AIAA PAPER 93-4014 ..... p 1648 N94-21563 * #
AIAA PAPER 93-4321 ..... p 1638 N94-22274 * #
AIAA PAPER 93-4657 ..... p 1715 N94-21589 * #

AIAA PAPER 93-4703-CP ..... p 1714 N94-21564 * #
AIAA PAPER 94-0397 ..... p 1650 N94-21742 * #
AIAA PAPER 94-0865 ..... p 1649 N94-21758 * #
AIAA PAPER 94-0917 ..... p 1762 N94-21566 * #
AIAA PAPER 94-1062 ..... p 1656 N94-21581 * #
AIAA PAPER 94-1160 ..... p 1741 N94-21567 * #

AIM-1382 ..... p 1943 N94-20920
AIM-1391 ..... p 1943 N94-20921
AIM-1403 ..... p 1908 N94-20929
AIM-1405 ..... p 1983 N94-19968
AIM-1421 ..... p 1939 N94-20105
AIM-1435 ..... p 1939 N94-19893
AIM-1439 ..... p 1939 N94-19875

AL-TP-1993-0013 ..... p 1896 N94-21247 #

AL-TR-1992-0145 ..... p 1893 N94-20023

AL/CF-SR-1993-0009-PHASE-4 .. p 1760 N94-21221 #

AL/CF-TP-1993-0033 ..... p 1896 N94-20914 #

AL/HR-TR-1993-0072 ..... p 1894 N94-20610
AL/HR-TR-1993-0111 ..... p 1895 N94-19935 #
AL/HR-TR-1993-0120 ..... p 1651 N94-20108

AL/OE-TR-1993-0067 ..... p 2044 N94-21363 #
AL/OE-TR-1993-0068 ..... p 1968 N94-19917
AL/OE-TR-1993-0099 ..... p 1890 N94-20462 #

AL/OET-TR-1993-0047 ..... p 1681 N94-21165 #

ANL-HEP-TR-93-62 ..... p 1807 N94-19990 #

ANL-92/40 ..... p 1833 N94-21927 #
ANL-93/14 ..... p 1917 N94-21923 #

ANL/CHM/CP-79242 ..... p 2033 N94-21992 #
ANL/CHM/CP-79706 ..... p 1970 N94-19956 #
ANL/CHM/CP-79761 ..... p 1971 N94-20050 #
ANL/CHM/CP-80106 ..... p 2031 N94-21871 #
ANL/CHM/CP-80470 ..... p 1690 N94-20288 #
ANL/CHM/CP-80472 ..... p 1902 N94-19928 #
ANL/CHM/CP-80906 ..... p 2035 N94-22565 #

ANL/CHM/PP-79176 ..... p 1976 N94-21951 #

ANL/CMT/CP-79337 ..... p 1692 N94-21558 #
ANL/CMT/CP-79617 ..... p 1848 N94-21942 #
ANL/CMT/CP-79775 ..... p 1848 N94-21870
ANL/CMT/CP-79776 ..... p 1750 N94-20257 #
ANL/CMT/CP-79801 ..... p 1748 N94-19885 #
ANL/CMT/CP-80209 ..... p 1847 N94-21650 #
ANL/CMT/CP-80587 ..... p 1847 N94-21774

ANL/ER/CP-78472 ..... p 1855 N94-20220 #
ANL/ER/CP-79787 ..... p 1859 N94-22036 #
ANL/ER/CP-80454 ..... p 1853 N94-22384 #

ANL/ES/CP-78818 ..... p 1825 N94-21637 #
ANL/ES/CP-79376 ..... p 1802 N94-20942 #
ANL/ES/CP-80046 ..... p 1825 N94-21297 #
ANL/ES/CP-80089 ..... p 1682 N94-21789

ANL/ES/PROC-79713 ..... p 1825 N94-21544 #

ANL/ESD/TM-53 ..... p 1811 N94-22391 #

ANL/ET/CP-78942 ..... p 1690 N94-20183
ANL/ET/CP-79207 ..... p 2031 N94-21931 #
ANL/ET/CP-79533 ..... p 1677 N94-21940 #
ANL/ET/CP-79613 ..... p 1832 N94-21772
ANL/ET/CP-80044 ..... p 1693 N94-21825

ANL/FC/CP-78624 ..... p 1799 N94-20258 #

ANL/IPNS/CP-79265 ..... p 2033 N94-21993 #

ANL/MCS-TM-179 ..... p 1961 N94-22393 #
ANL/MCS-TM-180 ..... p 1961 N94-22381 #

ANL/MCS/CP-80512 ..... p 2011 N94-19808 #
ANL/MCS/CP-80518 ..... p 1951 N94-20221 #

ANL/MSD/CP-78121 ..... p 1970 N94-19971 #
ANL/MSD/CP-78737 ..... p 2033 N94-21999 #
ANL/MSD/CP-79238 ..... p 2033 N94-21994
ANL/MSD/CP-79440 ..... p 1709 N94-22008 #
ANL/MSD/CP-79635 ..... p 1979 N94-20222 #
ANL/MSD/CP-79636 ..... p 2011 N94-19807 #
ANL/MSD/CP-79645 ..... p 1676 N94-21559 #
ANL/MSD/CP-79655 ..... p 2029 N94-21649 #
ANL/MSD/CP-79659 ..... p 2019 N94-20941 #
ANL/MSD/CP-79660 ..... p 1687 N94-19806 #
ANL/MSD/CP-79820 ..... p 1700 N94-20265 #

ANL/MSD/CP-79906 ..... p 2035 N94-22564 #
ANL/MSD/CP-80216 ..... p 2012 N94-19923 #
ANL/MSD/CP-80232 ..... p 1687 N94-19922 #
ANL/MSD/CP-80610 ..... p 1706 N94-21542 #
ANL/MSD/CP-80634 ..... p 2033 N94-21997 #
ANL/MSD/CP-80635 ..... p 2033 N94-21996 #
ANL/MSD/CP-80646 ..... p 2031 N94-21930 #
ANL/MSD/CP-80660 ..... p 2032 N94-21972 #

ANL/PHY/CP-80703 ..... p 1976 N94-21941 #

ANL/RE/CP-78944 ..... p 1697 N94-19809 #

ANL/XFD/CP-80438 ..... p 1972 N94-20187 #
ANL/XFD/CP-80547 ..... p 1990 N94-21837 #

AR-9305 ..... p 1646 N94-21246 #

ARA-5535-3 ..... p 1831 N94-21219 #

ARC-R93-209 ..... p 2055 N94-21498 * #

ARI-RN-94-01 ..... p 1894 N94-21510 #

ARI-RR-1045 ..... p 1682 N94-21243 #

ARL-CR-61 ..... p 1648 N94-21268 #
ARL-CR-62 ..... p 1704 N94-21197 #
ARL-CR-68 ..... p 1801 N94-20915 #
ARL-CR-71 ..... p 2014 N94-20029 #

ARL-MR-114 ..... p 1713 N94-19834 #

ARL-RR-12 ..... p 1675 N94-21504

ARL-TN-29 ..... p 1645 N94-19914
ARL-TN-42 ..... p 1949 N94-19907

ARL-TR-202 ..... p 2027 N94-21304 #
ARL-TR-213 ..... p 1808 N94-20930
ARL-TR-217 ..... p 2027 N94-21303 #
ARL-TR-219 ..... p 1705 N94-21302 #
ARL-TR-221 ..... p 1674 N94-20577 #
ARL-TR-231 ..... p 1698 N94-19947
ARL-TR-232 ..... p 1679 N94-20111
ARL-TR-234 ..... p 2037 N94-19831
ARL-TR-293 ..... p 1959 N94-21524 #
ARL-TR-296 ..... p 1964 N94-21175 #
ARL-TR-318 ..... p 1826 N94-21756 * #
ARL-TR-331 ..... p 1636 N94-20136 * #
ARL-TR-34 ..... p 1806 N94-19837
ARL-TR-53 ..... p 1841 N94-21453
ARL-TR-69 ..... p 1682 N94-21435
ARL-TR-93-17 ..... p 1967 N94-19894

ARO-24960.70-MA-REP ..... p 1821 N94-19833 #
ARO-25752.10-LS ..... p 1890 N94-20045 #
ARO-26441.5-CH ..... p 1699 N94-20016
ARO-26599.7-EL ..... p 2015 N94-20214 #
ARO-27130.14-MA-SM ..... p 1698 N94-19840
ARO-27307.6-EL ..... p 1715 N94-19912 #
ARO-27315.3-EG ..... p 1830 N94-20001
ARO-27364.2-MS ..... p 1829 N94-19836
ARO-27373.10-MS ..... p 1699 N94-20046 #
ARO-27403.8-MA ..... p 1951 N94-20545 #
ARO-27424.1-PH ..... p 1983 N94-19901
ARO-27458.54-PH ..... p 2011 N94-19817 #
ARO-27469.1-EG-SDI ..... p 1666 N94-19818 * #
ARO-27485.9-GS ..... p 1716 N94-19934 #
ARO-27558.14-EG ..... p 1797 N94-19978 #
ARO-27574.16-MA ..... p 1963 N94-20913 #
ARO-27586.21-PH ..... p 1983 N94-20013
ARO-27620.13-MA ..... p 1717 N94-20215 #
ARO-27766.2-PH ..... p 1970 N94-19822
ARO-27882.1-PH ..... p 2015 N94-20213 #
ARO-28004.1-EL ..... p 1748 N94-19910
ARO-28468.8-PH ..... p 1983 N94-19901
ARO-28657.3-LS-SAH ..... p 1700 N94-20299 #
ARO-28809.14-MA-SDI ..... p 1939 N94-19909
ARO-28809.15-MA-SDI ..... p 1962 N94-19999
ARO-28809.16-MA-SDI ..... p 1949 N94-19854
ARO-29042.1-MS ..... p 1829 N94-19837
ARO-29196.1-GS ..... p 1854 N94-19899 #
ARO-29326.14-MS ..... p 1689 N94-20019
ARO-29412.2-MA-SDI ..... p 1902 N94-19855
ARO-30090.3-EL ..... p 2030 N94-21805
ARO-30168.5-EG-YIP ..... p 1636 N94-20043 #
ARO-30461.1-MS-SBI ..... p 2028 N94-21517
ARO-30980.2-MA ..... p 1949 N94-19898 #
ARO-31108.2-PH ..... p 1815 N94-19878 #

ARPAD-TR-93003 ..... p 1910 N94-21144 #

AU-ARI-92-2 ..... p 1647 N94-21500 #

AWS/ITP-93/001 ..... p 1868 N94-20585 #

B-253482 p 2039 N94-20206 #
B-254647 p 2039 N94-20236 #

BCRS-90-22 p 1841 N94-21015
BCRS-92-08 p 1857 N94-21016
BCRS-92-09 p 1865 N94-20532 #

BFLRF-282 p 1712 N94-20551 #

BN-1153 p 1951 N94-20527

BNL-48724 p 2015 N94-20260 #
BNL-49140 p 1683 N94-21842 #
BNL-49234 p 1678 N94-19924 #
BNL-49288 p 1691 N94-20313
BNL-49333 p 1682 N94-21631 #
BNL-49345 p 1699 N94-19973 #
BNL-49361 p 1660 N94-20301 #
BNL-49362 p 1972 N94-20230 #
BNL-49380 p 1978 N94-19945 #
BNL-49382 p 1970 N94-19868 #
BNL-49385 p 1676 N94-21754 #
BNL-49429 p 1970 N94-19931 #
BNL-49430 p 1973 N94-20324
BNL-49432 p 1975 N94-21693 #
BNL-49463 p 1671 N94-21979 #
BNL-49465 p 2038 N94-21692 #

BONN-IR-92-31 p 1986 N94-21043
BONN-IR-92-32 p 1987 N94-21148
BONN-IR-92-45 p 1857 N94-21149

BR317257 p 1737 N94-20596 #

CA-PATENT-APPL-SN-2,020,733 p 1760 N94-21178
CA-PATENT-APPL-SN-2,020,909 p 1824 N94-21142 #
CA-PATENT-APPL-SN-2,026,855 p 1738 N94-21049

CA-PATENT-1,294,155 p 1704 N94-21143
CA-PATENT-1,295,736 p 1641 N94-21030
CA-PATENT-1,296,098 p 1737 N94-21031
CA-PATENT-1,305,772 p 1658 N94-21041
CA-PATENT-1,306,320 p 1674 N94-21040
CA-PATENT-1,306,384 p 1645 N94-21051
CA-PATENT-1,307,573 p 1650 N94-21050

CAL-2149 p 2056 N94-21779 * #
CAL-2150 p 2056 N94-22281 * #
CAL-2151 p 2055 N94-20952 * #

CAM-9301 p 1825 N94-21451 #
CAM-9302 p 1825 N94-21424 #
CAM-9303 p 1825 N94-21450 #

CARDEROCKDIV-U-SSM-67-93/15 p 1964 N94-21322 #

CARDIVNSWC-TR-601-93/02 p 1674 N94-20950 #

CARDS-ORD-16039 p 1751 N94-20555

CASS-93-3-01 p 1866 N94-20918

CAST-TN-01-94 p 2045 N94-21865 * #

CBCI-78 p 1983 N94-19968

CEBAF-TH-93-07 p 1977 N94-22009
CEBAF-TH-93-12 p 2038 N94-21513 #

CHORS-001-93 p 1866 N94-20559

CMU-CS-93-112 p 1902 N94-19932
CMU-CS-93-143 p 1898 N94-20107
CMU-CS-93-165 p 1938 N94-19845
CMU-CS-93-170 p 1908 N94-20622 #
CMU-CS-93-173 p 1928 N94-19950
CMU-CS-93-178 p 1902 N94-19919
CMU-CS-93-179 p 1761 N94-21282 #
CMU-CS-93-184 p 1929 N94-20084
CMU-CS-93-190 p 1898 N94-20085
CMU-CS-93-191 p 1902 N94-19918
CMU-CS-93-193 p 1902 N94-19948
CMU-CS-93-195 p 1809 N94-21445 #
CMU-CS-93-198 p 1942 N94-20621 #

CMU/SEI-93-TR-14 p 1650 N94-19880
CMU/SEI-93-TR-15 p 1912 N94-21205 #

COAM-TM-2/94 p 1865 N94-20487

COMPUTING SCIENCE NOTES-92/04 p 1903 N94-19994
COMPUTING SCIENCE NOTES-92/12 p 1962 N94-20007
COMPUTING SCIENCE NOTES-92/13 p 1962 N94-20008
COMPUTING SCIENCE NOTES-92/14 p 1903 N94-19993
COMPUTING SCIENCE NOTES-92/15 p 1928 N94-20009
COMPUTING SCIENCE NOTES-92/17 p 1903 N94-19992
COMPUTING SCIENCE NOTES-92/20 p 1949 N94-19997
COMPUTING SCIENCE NOTES-92/23 p 1898 N94-20082
COMPUTING SCIENCE NOTES-92/24 p 1928 N94-19995
COMPUTING SCIENCE NOTES-92/25 p 1928 N94-19996

CONF-901221-2 p 1937 N94-22378 #
CONF-9109510-1 p 2150 N94-22397 #
CONF-9207218-1 p 1975 N94-21766
CONF-920817-2 p 2011 N94-19808 #
CONF-9208186-5 p 1971 N94-20096 #
CONF-9208188-3 p 1966 N94-21958 #
CONF-9208215-1-REV-1 p 2012 N94-19861 #
CONF-9208237-1 p 1902 N94-19928 #
CONF-9208239-1 p 1884 N94-19866 #
CONF-9208240-1 p 1917 N94-21841 #
CONF-9209239-8 p 1976 N94-21961 #
CONF-9209267-5 p 1972 N94-20187 #
CONF-9209407-1 p 2038 N94-22010 #
CONF-920948-17 p 1970 N94-19958 #
CONF-920948-18 p 1970 N94-19871 #
CONF-920948-19 p 1974 N94-21543 #
CONF-920948-20 p 1970 N94-19870 #
CONF-920970-9 p 1696 N94-22037 #
CONF-9210278-2 p 1989 N94-21630 #
CONF-9210398-1 p 2012 N94-19923 #
CONF-921077-12 p 1970 N94-19868 #
CONF-921077-13 p 1978 N94-19945 #
CONF-921101-137 p 1690 N94-20233 #
CONF-921103-6-REV-1 p 1818 N94-21547 #
CONF-9211117-11 p 1687 N94-19864 #
CONF-9211268-1 p 1694 N94-21943 #
CONF-921277-2 p 1690 N94-20301 #
CONF-930102-1 p 1984 N94-20179 #
CONF-9301107-1 p 1991 N94-19883 #
CONF-9301114-3 p 1884 N94-19826
CONF-9301119-2 p 1818 N94-21829
CONF-9301127-1 p 1989 N94-21619 #
CONF-930150-2 p 1985 N94-20320
CONF-930159-54 p 2034 N94-22041 #
CONF-930159-55 p 1819 N94-21872
CONF-930159-56 p 1819 N94-21920 #
CONF-930159-57 p 1990 N94-22002 #
CONF-930159-58 p 1820 N94-22401 #
CONF-9302103-6 p 2036 N94-22582 #
CONF-9302137-1 p 2016 N94-20285 #
CONF-9302137-2 p 2035 N94-22385 #
CONF-9302151 p 1917 N94-21851 #
CONF-930269-20 p 1992 N94-19915 #
CONF-930269-23 p 1741 N94-21684 #
CONF-9303105-2 p 1844 N94-19803 #
CONF-9303122-6 p 1859 N94-22036 #
CONF-9303126-9 p 1803 N94-21531 #
CONF-930317-2 p 1695 N94-21986 #
CONF-9303172-3 p 1979 N94-20216 #
CONF-9303172-5 p 1982 N94-21952 #
CONF-9303198-6 p 1794 N94-22380 #
CONF-9303204-1 p 1936 N94-22032 #
CONF-9303206-1 p 2027 N94-21296 #
CONF-930331-15 p 1951 N94-20221 #
CONF-930363-6 p 1972 N94-20291 #
CONF-930363-9 p 1975 N94-21788
CONF-930367-10 p 2036 N94-22594 #
CONF-930389-23 p 1975 N94-21775 #
CONF-930405-36 p 1808 N94-21441 #
CONF-930405-37 p 1688 N94-19986 #
CONF-930405-38-REV-1 p 1694 N94-21921 #
CONF-930405-39 p 2033 N94-21994
CONF-930405-40 p 2034 N94-22005 #
CONF-930405-41 p 1810 N94-21950 #
CONF-930405-42 p 1694 N94-21944 #
CONF-930405-44 p 1697 N94-22402 #
CONF-930405-45 p 1696 N94-22394 #
CONF-930405-46 p 1696 N94-22025 #
CONF-930405-5 p 1683 N94-22031 #
CONF-9304144-12 p 2013 N94-19929 #
CONF-9304159-2 p 1936 N94-21828
CONF-9304419-5 p 2032 N94-21960 #
CONF-9304191-1 p 2014 N94-20002 #
CONF-9304191-2 p 2030 N94-21831 #
CONF-9304197-1 p 2013 N94-19961 #
CONF-9304200-1 p 1903 N94-19959 #
CONF-930438-29 p 1707 N94-21653 #
CONF-930443-1 p 1852 N94-21969 #
CONF-930445-23 p 1906 N94-20316
CONF-930445-25 p 1968 N94-22003 #
CONF-930449-2 p 1978 N94-19988 #
CONF-930511-363 p 1981 N94-21440 #
CONF-930511-365 p 1980 N94-20290 #
CONF-930511-372 p 1980 N94-20292 #
CONF-930511-376 p 1980 N94-20475 #
CONF-930511-377 p 1980 N94-20300 #
CONF-930511-393 p 2016 N94-20323
CONF-930511-396 p 1979 N94-20273 #
CONF-930511-397 p 1979 N94-20274 #
CONF-930511-398 p 1979 N94-19989 #
CONF-930511-406 p 1981 N94-21773
CONF-930511-419 p 1978 N94-19873 #
CONF-930511-429 p 1715 N94-19874 #
CONF-930511-432 p 1981 N94-21688 #
CONF-930511-435 p 1763 N94-21685 #
CONF-930511-436 p 1978 N94-19856 #
CONF-930511-478 p 1981 N94-21686 #
CONF-930511-479 p 1981 N94-21687 #
CONF-930511-489 p 1982 N94-21934 #
CONF-9305134-2 p 2014 N94-19970 #
CONF-9305135-6 p 1687 N94-19802 #
CONF-9305135 p 1848 N94-21823 #
CONF-9305136-14 p 1993 N94-20234 #
CONF-9305136-6 p 1981 N94-21439 #
CONF-9305136-9 p 1979 N94-20289 #
CONF-9305141-2 p 1693 N94-21843 #
CONF-9305157-1 p 1971 N94-20050 #
CONF-9305159-4 p 1750 N94-20231 #
CONF-9305159-7 p 1698 N94-19810 #
CONF-9305159-8 p 1997 N94-21848
CONF-9305159-9 p 1990 N94-21985 #
CONF-9305168-6 p 1936 N94-21746 #
CONF-9305210-3 p 1992 N94-20058 #
CONF-9305210-6 p 1999 N94-22568 #
CONF-9305235-4 p 1977 N94-22572 #
CONF-9305254-1 p 1970 N94-19956 #
CONF-9305266 p 1847 N94-21616 #
CONF-9305267-1 p 2016 N94-20322
CONF-9305268-1 p 1916 N94-21761
CONF-9305270-1 p 1683 N94-21842 #
CONF-9305282-1 p 2038 N94-21935 #
CONF-9305283-1 p 1708 N94-21954 #
CONF-9305284-1 p 2044 N94-21529 #
CONF-9305285-1 p 1918 N94-22088 #
CONF-9305290-1 p 1811 N94-22392 #
CONF-930534-4 p 2081 N94-21618 #
CONF-930534-7 p 1981 N94-21767
CONF-930537-100 p 1936 N94-21919 #
CONF-930537-101 p 2041 N94-19811 #
CONF-930537-99 p 1928 N94-19812 #
CONF-930550 p 1825 N94-21544 #
CONF-930571-12-REV-1 p 1768 N94-21753 #
CONF-9306100-5 p 1699 N94-19975 #
CONF-9306125-3 p 1972 N94-20230 #
CONF-9306134-1 p 2038 N94-21692 #
CONF-9306134-2 p 1974 N94-21657 #
CONF-9306134-3 p 1976 N94-21867 #
CONF-9306148-19 p 1709 N94-21982 #
CONF-9306148-24 p 1683 N94-21984 #
CONF-9306148-5 p 1847 N94-21540 #
CONF-930616-22 p 1750 N94-20312
CONF-930616-23 p 1699 N94-19960 #
CONF-930616-28 p 1762 N94-21634 #
CONF-930616-29 p 2016 N94-20296 #
CONF-930616-30 p 1980 N94-20295 #
CONF-930616-31 p 1750 N94-20294 #
CONF-930616-32 p 1762 N94-21632 #
CONF-930616-34 p 1769 N94-21838 #
CONF-930616-35 p 1815 N94-20223 #
CONF-930616-36 p 1814 N94-19867 #
CONF-930616-37 p 1768 N94-21770
CONF-9306176-3 p 1969 N94-19804 #
CONF-9306176-6 p 1975 N94-21786 #
CONF-9306176-7 p 1976 N94-21962 #
CONF-9306188-2 p 1750 N94-20314
CONF-9306204-2-REV-1 p 1762 N94-21621 #
CONF-9306205-2 p 1749 N94-20054 #
CONF-9306209-1 p 1906 N94-20311
CONF-9306221-2 p 1974 N94-21515 #
CONF-9306223-1 p 2028 N94-21541 #
CONF-9306224-1 p 1700 N94-20315
CONF-9306235-1 p 1988 N94-21528 #
CONF-9306246-1 p 1693 N94-21825
CONF-9306247-1 p 1678 N94-19924 #
CONF-9306248-1 p 1687 N94-19922 #
CONF-9306250-1 p 1937 N94-22558 #
CONF-9306255-1 p 2038 N94-21971 #
CONF-930636-1 p 1975 N94-21693 #
CONF-930636-3 p 1982 N94-21849 #
CONF-930655-1 p 1998 N94-22039 #
CONF-930656-1 p 1850 N94-19930 #
CONF-930676-23 p 2034 N94-22035 #
CONF-930676-34 p 1679 N94-20307 #
CONF-930676-36 p 1713 N94-22033 #
CONF-930676-38 p 1829 N94-19943 #
CONF-930676-40 p 1829 N94-19927 #
CONF-930676-41 p 1688 N94-19944 #

CONF-930676-42 ..... p 1679 N94-20319
CONF-930676-43 ..... p 2016 N94-20318
CONF-930676-45 ..... p 1829 N94-19824 #
CONF-930676-47 ..... p 1796 N94-19829 #
CONF-930676-48 ..... p 1966 N94-21511 #
CONF-930676-49 ..... p 1707 N94-21546 #
CONF-930676-50-REV-2 ..... p 1706 N94-21512 #
CONF-930676-52 ..... p 1693 N94-21656 #
CONF-930676-53 ..... p 2031 N94-21931 #
CONF-930676-54 ..... p 1695 N94-22024 #
CONF-930676-55 ..... p 1696 N94-22398 #
CONF-930676-56 ..... p 1998 N94-22399 #
CONF-930676-57 ..... p 1978 N94-22573 #
CONF-930676-58 ..... p 1684 N94-22395 #
CONF-930676-60 ..... p 1977 N94-22396 #
CONF-930703-21 ..... p 1769 N94-21830
CONF-930703-22 ..... p 1807 N94-19987 #
CONF-930703-26 ..... p 1799 N94-20263 #
CONF-930703-31 ..... p 1714 N94-20278 #
CONF-930703-32 ..... p 1706 N94-21542 #
CONF-930703-33 ..... p 1992 N94-20003 #
CONF-930703-35 ..... p 2032 N94-21932 #
CONF-930703-36 ..... p 2035 N94-22570 #
CONF-930709-1 ..... p 1973 N94-20306 #
CONF-930710-1 ..... p 2033 N94-21998 #
CONF-930710-2 ..... p 2031 N94-21926 #
CONF-930710-3 ..... p 2032 N94-21972 #
CONF-930711-12 ..... p 1974 N94-21658 #
CONF-930711-3 ..... p 1975 N94-21785 #
CONF-9307115-1 ..... p 1689 N94-20182 #
CONF-9307118-1 ..... p 1688 N94-19957 #
CONF-9307118-2 ..... p 1690 N94-20282 #
CONF-930712-3 ..... p 1690 N94-20288 #
CONF-930712-5 ..... p 1976 N94-21995 #
CONF-9307120 ..... p 2011 N94-19825 #
CONF-9307121-1 ..... p 1688 N94-19942 #
CONF-9307123-1 ..... p 2031 N94-21871 #
CONF-9307124-2 ..... p 2030 N94-21763 #
CONF-9307126-1 ..... p 1826 N94-22038
CONF-930713-23 ..... p 1796 N94-19916 #
CONF-9307139-1 ..... p 2031 N94-21922 #
CONF-9307142-1 ..... p 1695 N94-21964 #
CONF-9307145-1 ..... p 1976 N94-21941 #
CONF-9307171-1 ..... p 1976 N94-21968 #
CONF-930720-10 ..... p 1993 N94-20326 #
CONF-930722-18 ..... p 1808 N94-20287 #
CONF-930722-21 ..... p 1821 N94-19891 #
CONF-930722-24 ..... p 1808 N94-20297 #
CONF-930722-25 ..... p 1816 N94-20298 #
CONF-930722-26 ..... p 1990 N94-21837 #
CONF-930722-28 ..... p 1706 N94-21526
CONF-930722-29 ..... p 1817 N94-21299 #
CONF-930722-30 ..... p 1815 N94-20259 #
CONF-930722-31 ..... p 1819 N94-21873
CONF-930722-35 ..... p 1797 N94-19974 #
CONF-930722-44 ..... p 1982 N94-21974 #
CONF-930722-46 ..... p 1852 N94-22017
CONF-930749-58 ..... p 1807 N94-20115 #
CONF-930749-59 ..... p 1807 N94-20114 #
CONF-930749-60 ..... p 1904 N94-20049 #
CONF-930759-1 ..... p.1691 N94-20313
CONF-930759-2 ..... p 1695 N94-22023 #
CONF-930781-2 ..... p 1657 N94-19863 #
CONF-930785-3 ..... p 1960 N94-21996 #
CONF-930788-2 ..... p 1799 N94-20286 #
CONF-930788-3 ..... p 1904 N94-20052 #
CONF-930796-4 ..... p 1820 N94-21957 #
CONF-930796-5 ..... p 1853 N94-22569 #
CONF-930801-10 ..... p 2011 N94-19807 #
CONF-930801-12 ..... p 2033 N94-21997 #
CONF-930801-9 ..... p 2029 N94-21649 #
CONF-930802-11 ..... p 1848 N94-21870
CONF-930802-13 ..... p 1748 N94-19885 #
CONF-930802-9 ..... p 1750 N94-20257 #
CONF-930803-16 ..... p 1829 N94-19940 #
CONF-930803-22 ..... p 1697 N94-19809 #
CONF-930804-16 ..... p 1855 N94-20220 #
CONF-930804-18 ..... p 1826 N94-21983 #
CONF-930804-19 ..... p 1846 N94-21527 #
CONF-9308106-VOL-2 ..... p 1847 N94-21562 #
CONF-9308122-2 ..... p 1690 N94-20183
CONF-9308122-3 ..... p 1979 N94-20222 #
CONF-9308122-4 ..... p 2033 N94-21999 #
CONF-9308122-5 ..... p 2012 N94-19869 #
CONF-9308122-6 ..... p 2034 N94-22016 #
CONF-9308122-8 ..... p 1694 N94-21945 #
CONF-9308133-3 ..... p 1698 N94-19903 #
CONF-9308136-3 ..... p 1946 N94-21845 #
CONF-9308136-5 ..... p 1997 N94-21989 #
CONF-9308138-2 ..... p 1769 N94-21846 #
CONF-9308140-1 ..... p 2012 N94-19926 #
CONF-9308143-3 ..... p 1825 N94-21637 #
CONF-9308143-4 ..... p 1825 N94-21297 #
CONF-9308144-1 ..... p 1847 N94-21650 #
CONF-9308146-1 ..... p 1916 N94-21633 #
CONF-9308148-2 ..... p 1682 N94-21631 #
CONF-9308150-6 ..... p 1898 N94-19857 #
CONF-9308151-1 ..... p 1996 N94-21769
CONF-9308156-1 ..... p 1997 N94-21988 #
CONF-9308156-2 ..... p 2036 N94-22583 #
CONF-9308161-1 ..... p 1805 N94-22556 #
CONF-9308164-2 ..... p 1946 N94-21689
CONF-9308167-2 ..... p 1832 N94-21772
CONF-9308167-3 ..... p 1677 N94-21940 #
CONF-9308168-2 ..... p 1769 N94-21959 #
CONF-9308171-1 ..... p 1946 N94-21929 #
CONF-9308173-1 ..... p 2034 N94-22007 #
CONF-9308173-3 ..... p 2036 N94-22584 #
CONF-9308175-1 ..... p 2031 N94-21930 #
CONF-9308176-1 ..... p 1961 N94-22379 #
CONF-9308181-1 ..... p 1998 N94-22389 #
CONF-930822-7 ..... p 2019 N94-20941 #
CONF-930822-8 ..... p 1687 N94-19606 #
CONF-930823-10 ..... p 1980 N94-20317
CONF-930823-11 ..... p 1982 N94-21866 #
CONF-930823-1 ..... p 1978 N94-19983 #
CONF-930823-2 ..... p 1969 N94-19814 #
CONF-930823-3 ..... p 1978 N94-19972 #
CONF-930823-4 ..... p 1972 N94-20225 #
CONF-930823-5 ..... p 1969 N94-19813 #
CONF-930823-6 ..... p 1976 N94-21847 #
CONF-930823-8 ..... p 1975 N94-21806 #
CONF-930823-9 ..... p 1975 N94-21840 #
CONF-930825-3 ..... p 1689 N94-20180 #
CONF-930825-5 ..... p 1833 N94-22001 #
CONF-930830-11-REV-1 ..... p 1709 N94-21970 #
CONF-930830-25 ..... p 1802 N94-20942 #
CONF-930830-28 ..... p 1799 N94-20258 #
CONF-930830-29 ..... p 1804 N94-21765
CONF-930831-2 ..... p 1748 N94-19884 #
CONF-930838-1 ..... p 1848 N94-21827 #
CONF-930852-1 ..... p 1970 N94-19971 #
CONF-930854-2 ..... p 1750 N94-20218 #
CONF-930854-3 ..... p 1748 N94-19844 #
CONF-930855-1 ..... p 1816 N94-20277 #
CONF-930855-2 ..... p 1815 N94-20272 #
CONF-930855-3 ..... p 1814 N94-19828 #
CONF-930855-4 ..... p 1818 N94-21554 #
CONF-930855-7 ..... p 1820 N94-21975 #
CONF-930855-8 ..... p 1820 N94-22585 #
CONF-930863-1 ..... p 2031 N94-21869
CONF-930863-2 ..... p 1898 N94-19686 #
CONF-930865-10 ..... p 1691 N94-20321
CONF-930865-2 ..... p 2032 N94-21987 #
CONF-930865-3 ..... p 1788 N94-21762
CONF-930865-5 ..... p 2016 N94-20335 #
CONF-930865-6 ..... p 2015 N94-20275 #
CONF-930865-7 ..... p 2030 N94-21766
CONF-930865-8 ..... p 1974 N94-21553 #
CONF-930865-9 ..... p 2029 N94-21555 #
CONF-930905-12 ..... p 2031 N94-21857 #
CONF-930905-16 ..... p 2035 N94-22387 #
CONF-930905-2 ..... p 2011 N94-19827 #
CONF-930905-3 ..... p 1696 N94-22388 #
CONF-9309130-1 ..... p 1761 N94-21532 #
CONF-9309142-1 ..... p 1700 N94-20265 #
CONF-9309142-3 ..... p 2033 N94-21993 #
CONF-9309142-4 ..... p 2033 N94-21992 #
CONF-9309150-6 ..... p 1692 N94-21558 #
CONF-9309199-2 ..... p 1942 N94-20293 #
CONF-9309204-2 ..... p 1917 N94-21917
CONF-9309207-1 ..... p 1687 N94-19904 #
CONF-9309215-1 ..... p 1916 N94-21747 #
CONF-9309227-1 ..... p 1960 N94-21946 #
CONF-9309231-1 ..... p 1695 N94-21990 #
CONF-9309238-1 ..... p 1921 N94-22383 #
CONF-9309246-1 ..... p 1937 N94-22267 #
CONF-930926-5 ..... p 1820 N94-22020 #
CONF-930927-2 ..... p 1676 N94-21559 #
CONF-930928-2 ..... p 1707 N94-21560 #
CONF-930928-5 ..... p 1709 N94-22008 #
CONF-930937-2 ..... p 1679 N94-20266 #
CONF-930964-1 ..... p 1782 N94-21620 #
CONF-930993-1 ..... p 1973 N94-20324
CONF-930993-2 ..... p 1970 N94-19931 #
CONF-930997-4 ..... p 1690 N94-20232 #
CONF-930997-5 ..... p 1697 N94-22559 #
CONF-930997-6 ..... p 1694 N94-21933 #
CONF-931009-2 ..... p 1696 N94-22034 #
CONF-9310102-17 ..... p 1859 N94-22006 #
CONF-9310102-21 ..... p 1833 N94-21956 #
CONF-9310131-2 ..... p 1899 N94-20476 #
CONF-9310131-3 ..... p 1657 N94-21981 #
CONF-9310131-6 ..... p 1657 N94-21980 #
CONF-9310146-1 ..... p 1770 N94-22040 #
CONF-9310147-1 ..... p 1830 N94-20477 #
CONF-9310153-1 ..... p 1935 N94-21622 #
CONF-9310154-1 ..... p 1906 N94-20276 #
CONF-9310156-1 ..... p 2030 N94-21744 #
CONF-9310160-1 ..... p 1743 N94-22557 #
CONF-9310161-1 ..... p 1937 N94-22042 #
CONF-9310169-1 ..... p 1847 N94-21774
CONF-9310171-1 ..... p 1682 N94-21789
CONF-9310173-2 ..... p 1853 N94-22384 #
CONF-931018-18 ..... p 2045 N94-22404 #
CONF-931018-9 ..... p 1998 N94-22089 #
CONF-9310190-1 ..... p 1827 N94-22390 #
CONF-931024-3 ..... p 1848 N94-21942 #
CONF-931057-1 ..... p 1983 N94-19862 #
CONF-931070-1 ..... p 1997 N94-21966 #
CONF-931080-4 ..... p 1917 N94-21764
CONF-931081-1 ..... p 2048 N94-22407 #
CONF-931103-1 ..... p 1689 N94-20093 #
CONF-9311101-1 ..... p 1769 N94-21918 #
CONF-931115-11 ..... p 1929 N94-20279 #
CONF-931115-12 ..... p 1960 N94-21955 #
CONF-931115-6 ..... p 1801 N94-20562 #
CONF-931115-8 ..... p 1972 N94-20181 #
CONF-931121-17 ..... p 1915 N94-21539 #
CONF-931121-18 ..... p 1833 N94-21916 #
CONF-931121-19 ..... p 1916 N94-21635 #
CONF-931121-24 ..... p 1697 N94-22571 #
CONF-931121-25 ..... p 1977 N94-22400 #
CONF-931133-1 ..... p 2033 N94-21991 #
CONF-931133-2 ..... p 2035 N94-22565 #
CONF-931133-3 ..... p 2035 N94-22564 #
CONF-931191-1 ..... p 1762 N94-21636 #
CONF-931191-3 ..... p 1810 N94-22000 #
CONF-931196-1 ..... p 1854 N94-19955 #
CONF-931197-1 ..... p 1814 N94-19865 #
CONF-931197-2 ..... p 1819 N94-21844 #
CONF-931220-2 ..... p 1935 N94-21745 #
CONF-931226-1 ..... p 2032 N94-21939 #

CONTRIB-5230(794) ..... p 1686 N94-20794 * #
CONTRIB-5241(804) ..... p 2084 N94-20795 * #

CRREL-93-14 ..... p 1651 N94-21239 #

CSIRO-TP-26 ..... p 1855 N94-20256

CTN-93-60639 ..... p 1641 N94-21030
CTN-93-60666 ..... p 1737 N94-21031
CTN-93-60667 ..... p 1760 N94-21178
CTN-93-60669 ..... p 1824 N94-21142 #
CTN-93-60672 ..... p 1704 N94-21143
CTN-93-60679 ..... p 1738 N94-21049
CTN-93-60686 ..... p 1650 N94-21050
CTN-93-60687 ..... p 1645 N94-21051
CTN-93-60688 ..... p 1674 N94-21040
CTN-93-60690 ..... p 1658 N94-21041
CTN-94-60867 ..... p 1770 N94-22101
CTN-94-60877 ..... p 1742 N94-22408
CTN-94-60878 ..... p 1743 N94-22409
CTN-94-60879 ..... p 1743 N94-22410
CTN-94-60880 ..... p 1990 N94-22411
CTN-94-60881 ..... p 2056 N94-22412
CTN-94-60882 ..... p 2056 N94-22415
CTN-94-60883 ..... p 1977 N94-22416
CTN-94-60884 ..... p 1805 N94-22417
CTN-94-60885 ..... p 1651 N94-22418
CTN-94-60886 ..... p 1651 N94-22419
CTN-94-60887 ..... p 1677 N94-22420
CTN-94-60888 ..... p 1827 N94-22421
CTN-94-60889 ..... p 1843 N94-22422
CTN-94-60890 ..... p 1652 N94-22423
CTN-94-60891 ..... p 1639 N94-22382
CTN-94-60892 ..... p 1861 N94-22424
CTN-94-60936 ..... p 1652 N94-22425
CTN-94-60937 ..... p 2061 N94-22426
CTN-94-60938 ..... p 1644 N94-22427
CTN-94-60939 ..... p 1843 N94-22429
CTN-94-60940 ..... p 1861 N94-22574
CTN-94-60941 ..... p 1861 N94-22575
CTN-94-60942 ..... p 1743 N94-22576
CTN-94-60943 ..... p 1827 N94-22577
CTN-94-60948 ..... p 1639 N94-22586
CTN-94-60949 ..... p 1677 N94-22587
CTN-94-60950 ..... p 1653 N94-22588
CTN-94-60951 ..... p 1677 N94-22589
CTN-94-60952 ..... p 1827 N94-22578
CTN-94-60953 ..... p 1990 N94-22579
CTN-94-60954 ..... p 1805 N94-22580
CTN-94-60955 ..... p 1991 N94-22581
CTN-94-60960 ..... p 1833 N94-22590
CTN-94-60961 ..... p 1947 N94-22591
CTN-94-60962 ..... p 2061 N94-22592
CTN-94-60963 ..... p 2061 N94-22593

CU-CSD-TR-93-1390 ..... p 1912 N94-21300 #

CWI-AM-R9206-PT-1 ..... p 1911 N94-21156 #
CWI-AM-R9209-PT-2 ..... p 1911 N94-21157 #
CWI-AM-R9210 ..... p 1954 N94-21158
CWI-AM-R9211 ..... p 1954 N94-21159 #

CWI-BS-R9232 ..... p 1944 N94-21033 #
CWI-BS-R9233 ..... p 1963 N94-21022 #

CWI-BS-R9234 ..... p 1954 N94-21231 #
CWI-BS-R9235 ..... p 1944 N94-21160 #
CWI-BS-R9236 ..... p 1944 N94-21232 #
CWI-BS-R9237 ..... p 1945 N94-21233 #
CWI-BS-R9238 ..... p 1946 N94-21577 #
CWI-BS-R9301 ..... p 1930 N94-21234 #
CWI-BS-R9302 ..... p 1930 N94-21161
CWI-BS-R9303 ..... p 1943 N94-21032 #

CWI-CS-R9243 ..... p 1930 N94-21023
CWI-CS-R9244 ..... p 1908 N94-21024
CWI-CS-R9245 ..... p 1909 N94-21025 #
CWI-CS-R9246 ..... p 1909 N94-21026 #
CWI-CS-R9247 ..... p 1952 N94-21027
CWI-CS-R9249 ..... p 1909 N94-21028
CWI-CS-R9250 ..... p 1952 N94-21029
CWI-CS-R9251 ..... p 2038 N94-21533
CWI-CS-R9252 ..... p 1915 N94-21534
CWI-CS-R9304 ..... p 2044 N94-21535
CWI-CS-R9305 ..... p 2044 N94-21494
CWI-CS-R9306 ..... p 2045 N94-21536
CWI-CS-R9307 ..... p 1915 N94-21537
CWI-CS-R9308-PT-1 ..... p 1935 N94-21549 #
CWI-CS-R9309 ..... p 1916 N94-21587
CWI-CS-R9310 ..... p 1915 N94-21551
CWI-CS-R9311 ..... p 1914 N94-21495
CWI-CS-R9312 ..... p 1914 N94-21496

CWI-NM-R9222 ..... p 1930 N94-21077
CWI-NM-R9223 ..... p 1910 N94-21078
CWI-NM-R9224 ..... p 1903 N94-21609
CWI-NM-R9225 ..... p 1935 N94-21610
CWI-NM-R9226 ..... p 1916 N94-21611 #
CWI-NM-R9227 ..... p 1916 N94-21612 #
CWI-NM-R9301 ..... p 1682 N94-21574 #
CWI-NM-R9302 ..... p 1803 N94-21575 #
CWI-NM-R9303 ..... p 1959 N94-21576 #
CWI-NM-R9304 ..... p 1935 N94-21492 #
CWI-NM-R9305 ..... p 1935 N94-21493 #

C931033-U-2R00 ..... p 1837 N94-20284 * #

DARPA-BAA-92-20 ..... p 2027 N94-21319 #

DATA-REPT-92-3 ..... p 1856 N94-20608
DATA-REPT-92-4 ..... p 1857 N94-20609
DATA-REPT-93-1 ..... p 1856 N94-20607

DCN-1-1-PP-02147 ..... p 1670 N94-21271 * #

DE93-000056 ..... p 1845 N94-19921 #
DE93-000160 ..... p 2037 N94-20473 #
DE93-006255 ..... p 1805 N94-22269 #
DE93-010003 ..... p 1712 N94-19984 #
DE93-010045 ..... p 1847 N94-21614 #
DE93-011390 ..... p 1742 N94-22268 #
DE93-012653 ..... p 1991 N94-19883 #
DE93-012847 ..... p 1683 N94-22031 #
DE93-013969 ..... p 1670 N94-21824 #
DE93-015425 ..... p 1801 N94-20562 #
DE93-015476 ..... p 1993 N94-20326 #
DE93-015905 ..... p 1689 N94-20093 #
DE93-017079 ..... p 1748 N94-19902 #
DE93-017083 ..... p 2029 N94-21615 #
DE93-017115 ..... p 1845 N94-19805 #
DE93-017117 ..... p 2013 N94-19939 #
DE93-017408 ..... p 1687 N94-19922 #
DE93-017419 ..... p 1693 N94-21825
DE93-017443 ..... p 2012 N94-19923 #
DE93-017563 ..... p 1678 N94-19924 #
DE93-017620 ..... p 2027 N94-21296 #
DE93-017863 ..... p 1687 N94-19802 #
DE93-017864 ..... p 1689 N94-20180 #
DE93-017977 ..... p 1972 N94-20181 #
DE93-017984 ..... p 1906 N94-20311
DE93-017991 ..... p 1844 N94-19803 #
DE93-018050 ..... p 1689 N94-20182 #
DE93-018202 ..... p 1699 N94-20047 #
DE93-018204 ..... p 1845 N94-20095 #
DE93-018205 ..... p 1688 N94-19985 #
DE93-018206 ..... p 1845 N94-19925 #
DE93-018207 ..... p 1847 N94-21616 #
DE93-018208 ..... p 1846 N94-21296 #
DE93-018214 ..... p 1848 N94-21826 #
DE93-018217 ..... p 1848 N94-21827 #
DE93-018220 ..... p 1850 N94-22257 #
DE93-018223 ..... p 2029 N94-21617 #
DE93-018266 ..... p 1969 N94-19804 #
DE93-018267 ..... p 1973 N94-20474 #
DE93-018269 ..... p 2016 N94-20285 #
DE93-018297 ..... p 1696 N94-22034 #
DE93-018340 ..... p 2034 N94-22035 #
DE93-018354 ..... p 1799 N94-20286 #
DE93-018366 ..... p 1808 N94-20287 #
DE93-018376 ..... p 2012 N94-19926 #
DE93-018404 ..... p 1964 N94-20179 #
DE93-018472 ..... p 1807 N94-20114 #
DE93-018473 ..... p 1807 N94-20115 #
DE93-018474 ..... p 1904 N94-20049 #
DE93-018545 ..... p 1854 N94-19955 #
DE93-018569 ..... p 1859 N94-22036 #
DE93-018577 ..... p 1690 N94-20183
DE93-018587 ..... p 1970 N94-19956 #
DE93-018591 ..... p 1688 N94-19957 #
DE93-018614 ..... p 1971 N94-20050 #
DE93-018627 ..... p 2081 N94-21618 #
DE93-018642 ..... p 1989 N94-21619 #
DE93-018667 ..... p 1989 N94-21630 #
DE93-018750 ..... p 1970 N94-19958 #
DE93-018770 ..... p 1688 N94-19942 #
DE93-018786 ..... p 1696 N94-22037 #
DE93-018791 ..... p 1936 N94-22032 #
DE93-018792 ..... p 1903 N94-19959 #
DE93-018831 ..... p 1829 N94-19943 #
DE93-018837 ..... p 1750 N94-20312
DE93-018842 ..... p 1699 N94-19960 #
DE93-018848 ..... p 1829 N94-19927 #
DE93-018851 ..... p 1688 N94-19944 #
DE93-018853 ..... p 2013 N94-19961 #
DE93-018857 ..... p 1713 N94-22033 #
DE93-018859 ..... p 1829 N94-19940 #
DE93-018860 ..... p 1748 N94-19884 #
DE93-018878 ..... p 1826 N94-22038
DE93-018926 ..... p 1850 N94-19941 #
DE93-018943 ..... p 2014 N94-19970 #
DE93-018994 ..... p 1902 N94-19928 #
DE93-018995 ..... p 1970 N94-19971 #
DE93-019004 ..... p 1998 N94-22039 #
DE93-019007 ..... p 1748 N94-19885 #
DE93-019009 ..... p 1972 N94-20187 #
DE93-019010 ..... p 1690 N94-20288 #
DE93-019048 ..... p 1682 N94-21631 #
DE93-019060 ..... p 1691 N94-20313
DE93-019063 ..... p 1762 N94-21632 #
DE93-019066 ..... p 1833 N94-21916 #
DE93-019067 ..... p 1973 N94-20306 #
DE93-019069 ..... p 1679 N94-20307 #
DE93-019070 ..... p 1916 N94-21633 #
DE93-019071 ..... p 1762 N94-21634 #
DE93-019075 ..... p 1770 N94-22040 #
DE93-019080 ..... p 1915 N94-21539 #
DE93-019081 ..... p 1805 N94-22556 #
DE93-019125 ..... p 1972 N94-20230 #
DE93-019147 ..... p 1750 N94-20231 #
DE93-019148 ..... p 1971 N94-20096 #
DE93-019154 ..... p 1992 N94-19915 #
DE93-019155 ..... p 1936 N94-21828
DE93-019159 ..... p 1762 N94-21620 #
DE93-019160 ..... p 1818 N94-21829
DE93-019166 ..... p 1690 N94-20232 #
DE93-019167 ..... p 1769 N94-21830
DE93-019169 ..... p 1690 N94-20233 #
DE93-019188 ..... p 1993 N94-20234 #
DE93-019196 ..... p 2014 N94-20002 #
DE93-019198 ..... p 2030 N94-21831 #
DE93-019204 ..... p 1821 N94-19891 #
DE93-019232 ..... p 1980 N94-20475 #
DE93-019235 ..... p 2034 N94-22041 #
DE93-019237 ..... p 1981 N94-21439 #
DE93-019238 ..... p 1981 N94-21440 #
DE93-019240 ..... p 1808 N94-21441 #
DE93-019241 ..... p 1979 N94-20289 #
DE93-019248 ..... p 1980 N94-20300 #
DE93-019249 ..... p 1980 N94-20290 #
DE93-019250 ..... p 1972 N94-20291 #
DE93-019254 ..... p 1917 N94-21917
DE93-019256 ..... p 1980 N94-20292 #
DE93-019288 ..... p 1847 N94-21540 #
DE93-019381 ..... p 1688 N94-19986 #
DE93-019386 ..... p 1979 N94-20216 #
DE93-019387 ..... p 1750 N94-20314
DE93-019391 ..... p 1807 N94-19987 #
DE93-019392 ..... p 1978 N94-19988 #
DE93-019404 ..... p 1950 N94-20217 #
DE93-019405 ..... p 1916 N94-21635 #
DE93-019406 ..... p 1942 N94-20293 #
DE93-019407 ..... p 1762 N94-21636 #
DE93-019411 ..... p 1750 N94-20294 #
DE93-019413 ..... p 1980 N94-20295 #
DE93-019415 ..... p 1748 N94-19844 #
DE93-019416 ..... p 1706 N94-21526
DE93-019417 ..... p 1769 N94-21918 #
DE93-019418 ..... p 2028 N94-21541 #
DE93-019419 ..... p 1700 N94-20315
DE93-019422 ..... p 1750 N94-20218 #
DE93-019424 ..... p 1698 N94-19903 #
DE93-019427 ..... p 2016 N94-20296 #
DE93-019428 ..... p 1904 N94-20052 #
DE93-019429 ..... p 1808 N94-20297 #
DE93-019430 ..... p 1816 N94-20298 #
DE93-019432 ..... p 1899 N94-20476 #
DE93-019433 ..... p 1749 N94-20054 #
DE93-019435 ..... p 1830 N94-20477 #
DE93-019437 ..... p 1687 N94-19904 #
DE93-019446 ..... p 1855 N94-20219 #
DE93-019506 ..... p 2031 N94-21869
DE93-019511 ..... p 1825 N94-21637 #
DE93-019514 ..... p 1825 N94-21297 #
DE93-019515 ..... p 1848 N94-21870
DE93-019516 ..... p 1750 N94-20257 #
DE93-019519 ..... p 2029 N94-21649 #
DE93-019520 ..... p 2019 N94-20941 #
DE93-019521 ..... p 1687 N94-19806 #
DE93-019523 ..... p 2011 N94-19807 #
DE93-019525 ..... p 1855 N94-20220 #
DE93-019535 ..... p 2011 N94-19808 #
DE93-019536 ..... p 1847 N94-21650 #
DE93-019539 ..... p 1697 N94-19809 #
DE93-019546 ..... p 1799 N94-20258 #
DE93-019547 ..... p 1815 N94-20259 #
DE93-019556 ..... p 1802 N94-20942 #
DE93-019564 ..... p 2015 N94-20260 #
DE93-019566 ..... p 1951 N94-20221 #
DE93-019567 ..... p 1979 N94-20222 #
DE93-019568 ..... p 2031 N94-21871 #
DE93-019569 ..... p 1990 N94-21837 #
DE93-019575 ..... p 1906 N94-20316
DE93-019576 ..... p 1937 N94-22042 #
DE93-019582 ..... p 1993 N94-20261 #
DE93-019603 ..... p 1815 N94-20223 #
DE93-019604 ..... p 1769 N94-21838 #
DE93-019605 ..... p 1960 N94-21996 #
DE93-019607 ..... p 1817 N94-21299 #
DE93-019610 ..... p 1698 N94-19810 #
DE93-019616 ..... p 1985 N94-20262 #
DE93-019617 ..... p 1799 N94-20263 #
DE93-019623 ..... p 1819 N94-21872
DE93-019624 ..... p 1819 N94-21873
DE93-019684 ..... p 1972 N94-20264 #
DE93-019689 ..... p 1819 N94-21839 #
DE93-019742 ..... p 2041 N94-19811 #
DE93-019744 ..... p 1936 N94-21919 #
DE93-019745 ..... p 1928 N94-19812 #
DE93-019768 ..... p 1700 N94-20265 #
DE93-019825 ..... p 1951 N94-20224 #
DE93-019832 ..... p 1679 N94-20266 #
DE93-019845 ..... p 1690 N94-20301 #
DE93-019865 ..... p 1709 N94-21982 #
DE93-019866 ..... p 1826 N94-21983 #
DE93-019872 ..... p 1846 N94-21527 #
DE93-019877 ..... p 1683 N94-21984 #
DE93-019900 ..... p 1972 N94-20225 #
DE93-019901 ..... p 1969 N94-19813 #
DE93-019903 ..... p 1976 N94-21847 #
DE93-019904 ..... p 1978 N94-19972 #
DE93-019905 ..... p 1978 N94-19983 #
DE93-019906 ..... p 1969 N94-19814 #
DE93-019907 ..... p 1975 N94-21806 #
DE93-019908 ..... p 1980 N94-20317
DE93-019910 ..... p 1975 N94-21840 #
DE93-019913 ..... p 2016 N94-20318
DE93-019916 ..... p 1990 N94-21985 #
DE93-019917 ..... p 1819 N94-21920 #
DE93-019918 ..... p 2012 N94-19861 #
DE93-019922 ..... p 1917 N94-21841 #
DE93-019923 ..... p 1983 N94-19862 #
DE93-019937 ..... p 1683 N94-21842 #
DE93-019941 ..... p 1997 N94-21848
DE93-019942 ..... p 1695 N94-21986 #
DE93-019943 ..... p 1657 N94-19863 #
DE93-019945 ..... p 1693 N94-21843 #
DE93-019947 ..... p 1694 N94-21921 #
DE93-019948 ..... p 1796 N94-19916 #
DE93-019949 ..... p 1679 N94-20319
DE93-019951 ..... p 1819 N94-21844 #
DE93-040015 ..... p 1699 N94-19973 #
DE93-040053 ..... p 1687 N94-19864 #
DE93-040056 ..... p 1814 N94-19865 #
DE93-040057 ..... p 1829 N94-19624 #
DE93-040058 ..... p 1916 N94-21761
DE93-040060 ..... p 1797 N94-19974 #
DE93-040061 ..... p 2032 N94-21987 #
DE93-040062 ..... p 1884 N94-19866 #
DE93-040063 ..... p 1946 N94-21845 #
DE93-040064 ..... p 1768 N94-21762
DE93-040074 ..... p 2011 N94-19825 #
DE93-040091 ..... p 1699 N94-19975 #
DE93-040100 ..... p 1815 N94-20272 #
DE93-040103 ..... p 1814 N94-19867 #
DE93-040104 ..... p 1769 N94-21846 #
DE93-040106 ..... p 1997 N94-21988 #
DE93-040114 ..... p 1884 N94-19826
DE93-040116 ..... p 1979 N94-20273 #
DE93-040117 ..... p 1979 N94-20274 #
DE93-040119 ..... p 2030 N94-21744 #
DE93-040121 ..... p 1985 N94-20320
DE93-040122 ..... p 2030 N94-21763 #
DE93-040126 ..... p 1997 N94-21989 #

DE93-040131 ..... p 1691 N94-20321
DE93-040133 ..... p 2016 N94-20322
DE93-040134 ..... p 2016 N94-20335 #
DE93-040135 ..... p 2015 N94-20275 #
DE93-040137 ..... p 1906 N94-20276 #
DE93-040138 ..... p 2011 N94-19827 #
DE93-040141 ..... p 1816 N94-20277 #
DE93-040144 ..... p 1695 N94-21990 #
DE93-040145 ..... p 1714 N94-20278 #
DE93-040149 ..... p 1935 N94-21745 #
DE93-040150 ..... p 1935 N94-21622 #
DE93-040151 ..... p 1936 N94-21746 #
DE93-040152 ..... p 1917 N94-21784
DE93-040153 ..... p 2033 N94-21991 #
DE93-040154 ..... p 1916 N94-21747 #
DE93-040157 ..... p 1929 N94-20279 #
DE93-040158 ..... p 1814 N94-19828 #
DE93-040160 ..... p 1796 N94-19829 #
DE93-040173 ..... p 1970 N94-19868 #
DE93-040174 ..... p 1978 N94-19945 #
DE93-040181 ..... p 1804 N94-21765
DE93-040184 ..... p 1975 N94-21766
DE93-040188 ..... p 1960 N94-21946 #
DE93-040191 ..... p 1974 N94-21553 #
DE93-040192 ..... p 1818 N94-21554 #
DE93-040193 ..... p 2029 N94-21555 #
DE93-040201 ..... p 1809 N94-21556 #
DE93-040205 ..... p 1832 N94-21557 #
DE93-040206 ..... p 1906 N94-20280 #
DE93-040207 ..... p 1908 N94-20281 #
DE93-040211 ..... p 1714 N94-19946 #
DE93-040227 ..... p 2033 N94-21992 #
DE93-040229 ..... p 2033 N94-21993 #
DE93-040230 ..... p 2033 N94-21994
DE93-040243 ..... p 1692 N94-21558 #
DE93-040244 ..... p 1676 N94-21559 #
DE93-040247 ..... p 1981 N94-21767
DE93-040248 ..... p 2030 N94-21768
DE93-040262 ..... p 1707 N94-21560 #
DE93-040263 ..... p 1976 N94-21995 #
DE93-040266 ..... p 1690 N94-20282 #
DE93-040267 ..... p 1992 N94-20058 #
DE93-040268 ..... p 2012 N94-19869 #
DE93-040269 ..... p 2013 N94-19929 #
DE93-040277 ..... p 2033 N94-21997 #
DE93-040278 ..... p 2033 N94-21998 #
DE93-040280 ..... p 1706 N94-21542 #
DE93-040281 ..... p 2033 N94-21999 #
DE93-040283 ..... p 1970 N94-19870 #
DE93-040284 ..... p 1970 N94-19871 #
DE93-040285 ..... p 1974 N94-21543 #
DE93-040286 ..... p 2016 N94-20323
DE93-040287 ..... p 1979 N94-19989 #
DE93-040289 ..... p 1988 N94-21528 #
DE93-040297 ..... p 1683 N94-21947 #
DE93-040300 ..... p 2031 N94-21922 #
DE93-040310 ..... p 1985 N94-20283 #
DE93-040323 ..... p 1850 N94-19930 #
DE93-040328 ..... p 1970 N94-19931 #
DE93-040329 ..... p 1973 N94-20324
DE93-040332 ..... p 1810 N94-22000 #
DE93-040343 ..... p 1996 N94-21769
DE93-040347 ..... p 1691 N94-20478 #
DE93-040372 ..... p 1992 N94-20003 #
DE93-040381 ..... p 1825 N94-21544 #
DE93-040390 ..... p 1732 N94-20479 #
DE93-040398 ..... p 1917 N94-21923 #
DE93-040409 ..... p 1743 N94-22557 #
DE93-040438 ..... p 1833 N94-22001 #
DE93-040439 ..... p 1816 N94-20480 #
DE93-040443 ..... p 1992 N94-20004 #
DE93-040451 ..... p 1809 N94-21545 #
DE93-040452 ..... p 1904 N94-20097 #
DE93-040457 ..... p 1960 N94-21966
DE93-040458 ..... p 1960 N94-21967 #
DE93-040480 ..... p 1918 N94-21924 #
DE93-040481 ..... p 1714 N94-20099 #
DE93-040485 ..... p 1976 N94-21968 #
DE93-040486 ..... p 1937 N94-22558 #
DE93-040488 ..... p 2044 N94-21529 #
DE93-040490 ..... p 1852 N94-21969 #
DE93-040497 ..... p 1675 N94-21530 #
DE93-040498 ..... p 1803 N94-21531 #
DE93-040528 ..... p 1702 N94-20481 #
DE93-040535 ..... p 1768 N94-21770
DE93-040539 ..... p 1946 N94-21925 #
DE93-040543 ..... p 1966 N94-21511 #
DE93-040544 ..... p 1706 N94-21512 #
DE93-040545 ..... p 1707 N94-21546 #
DE93-040546 ..... p 1709 N94-21970 #
DE93-040547 ..... p 1990 N94-22002 #
DE93-040549 ..... p 1968 N94-22003 #
DE93-040550 ..... p 1818 N94-21547 #
DE93-040593 ..... p 1852 N94-22004 #
DE93-040598 ..... p 1693 N94-21771
DE93-040600 ..... p 1697 N94-22559 #
DE93-040601 ..... p 2034 N94-22005 #
DE93-040604 ..... p 1859 N94-22006 #
DE93-040631 ..... p 1678 N94-19890 #
DE93-040640 ..... p 2031 N94-21926 #
DE93-040641 ..... p 1749 N94-20005 #
DE93-040645 ..... p 1833 N94-21927 #
DE93-040651 ..... p 1949 N94-20006 #
DE93-040655 ..... p 1908 N94-20932 #
DE93-040657 ..... p 1804 N94-21748 #
DE93-040668 ..... p 1859 N94-21928 #
DE93-040696 ..... p 1936 N94-21749 #
DE93-040697 ..... p 2045 N94-21750 #
DE93-040721 ..... p 1968 N94-21751 #
DE93-040731 ..... p 1750 N94-20325
DE93-040753 ..... p 1946 N94-21929 #
DE93-040754 ..... p 1761 N94-21532 #
DE93-040756 ..... p 2034 N94-22007 #
DE93-040801 ..... p 1807 N94-19990 #
DE93-040814 ..... p 1694 N94-21948 #
DE93-040822 ..... p 2031 N94-21930 #
DE93-040826 ..... p 1709 N94-22008 #
DE93-040829 ..... p 1832 N94-21772
DE93-040841 ..... p 1695 N94-21949 #
DE93-040851 ..... p 2150 N94-22397 #
DE93-040852 ..... p 1898 N94-19886 #
DE93-040856 ..... p 1810 N94-21950 #
DE93-040864 ..... p 2038 N94-21513 #
DE93-040867 ..... p 1977 N94-22009
DE93-040886 ..... p 1976 N94-21951 #
DE93-040899 ..... p 1921 N94-22383 #
DE93-040911 ..... p 1995 N94-21514 #
DE93-040912 ..... p 1996 N94-21752 #
DE93-040913 ..... p 1992 N94-19887 #
DE93-040914 ..... p 1991 N94-19872 #
DE93-040926 ..... p 2038 N94-22010 #
DE93-040929 ..... p 1851 N94-21740 #
DE93-040939 ..... p 2038 N94-21971 #
DE93-040940 ..... p 1741 N94-21684 #
DE93-040954 ..... p 1978 N94-19873 #
DE93-040964 ..... p 1981 N94-21773
DE93-040973 ..... p 1715 N94-19874 #
DE93-040998 ..... p 1975 N94-21788
DE93-041004 ..... p 1978 N94-19856 #
DE93-041005 ..... p 1763 N94-21685 #
DE93-041020 ..... p 1982 N94-21952 #
DE93-041021 ..... p 2038 N94-21935 #
DE93-041024 ..... p 1974 N94-21515 #
DE93-041043 ..... p 1810 N94-21953 #
DE93-041056 ..... p 1981 N94-21686 #
DE93-041057 ..... p 1981 N94-21687 #
DE93-041081 ..... p 1981 N94-21688 #
DE93-041085 ..... p 1946 N94-21689
DE93-041089 ..... p 1980 N94-20933 #
DE93-041101 ..... p 2029 N94-21690 #
DE93-041118 ..... p 2046 N94-22413 #
DE93-041123 ..... p 2032 N94-21936 #
DE93-041124 ..... p 2029 N94-21691
DE93-041126 ..... p 1694 N94-21937 #
DE93-041129 ..... p 1698 N94-19857 #
DE93-041130 ..... p 1826 N94-21938 #
DE93-041138 ..... p 2032 N94-21939 #
DE93-041144 ..... p 1708 N94-21954 #
DE93-041154 ..... p 2038 N94-21692 #
DE93-041155 ..... p 1975 N94-21693 #
DE93-041157 ..... p 1672 N94-19888 #
DE93-041160 ..... p 1677 N94-21940 #
DE93-041162 ..... p 1976 N94-21941 #
DE93-041164 ..... p 1853 N94-22384 #
DE93-041167 ..... p 1682 N94-21789
DE93-041184 ..... p 1848 N94-21942 #
DE93-041187 ..... p 1847 N94-21774
DE93-041232 ..... p 1680 N94-20934 #
DE93-041273 ..... p 1891 N94-20935 #
DE93-041275 ..... p 1992 N94-19991 #
DE93-041277 ..... p 1803 N94-21651 #
DE93-041278 ..... p 1678 N94-19889 #
DE93-041290 ..... p 1763 N94-21652 #
DE93-041307 ..... p 1706 N94-21516 #
DE93-041320 ..... p 1694 N94-21943 #
DE93-628627 ..... p 2037 N94-20178
DE94-000204 ..... p 1849 N94-22015 #
DE94-000303 ..... p 1694 N94-21944 #
DE94-000307 ..... p 2036 N94-22594 #
DE94-000323 ..... p 1937 N94-22378 #
DE94-000328 ..... p 1960 N94-21955 #
DE94-000329 ..... p 1707 N94-21653 #
DE94-000330 ..... p 1694 N94-21945 #
DE94-000335 ..... p 2034 N94-22016 #
DE94-000336 ..... p 1918 N94-22088 #
DE94-000339 ..... p 1833 N94-21956 #
DE94-000340 ..... p 1961 N94-22379 #
DE94-000345 ..... p 1763 N94-21654 #
DE94-000366 ..... p 1959 N94-21655 #
DE94-000369 ..... p 1693 N94-21656 #
DE94-000376 ..... p 1820 N94-21957 #
DE94-000377 ..... p 1974 N94-21657 #
DE94-000380 ..... p 1974 N94-21658 #
DE94-000381 ..... p 1975 N94-21785 #
DE94-000383 ..... p 1915 N94-21561 #
DE94-000384 ..... p 1966 N94-21958 #
DE94-000385 ..... p 1768 N94-21753 #
DE94-000391 ..... p 1762 N94-21621 #
DE94-000397 ..... p 1794 N94-22380 #
DE94-000399 ..... p 1657 N94-21980 #
DE94-000400 ..... p 1657 N94-21981 #
DE94-000403 ..... p 1769 N94-21959 #
DE94-000404 ..... p 2032 N94-21960 #
DE94-000410 ..... p 1836 N94-20936 #
DE94-000433 ..... p 1961 N94-22381 #
DE94-000435 ..... p 1847 N94-21562 #
DE94-000449 ..... p 1928 N94-19858 #
DE94-000464 ..... p 2031 N94-21931 #
DE94-000474 ..... p 1999 N94-22566 #
DE94-000476 ..... p 2032 N94-21932 #
DE94-000482 ..... p 1976 N94-21961 #
DE94-000489 ..... p 2035 N94-22385 #
DE94-000492 ..... p 1853 N94-22569 #
DE94-000493 ..... p 1694 N94-21933 #
DE94-000494 ..... p 1937 N94-22267 #
DE94-000496 ..... p 2035 N94-22570 #
DE94-000509 ..... p 1676 N94-21754 #
DE94-000518 ..... p 1821 N94-19859 #
DE94-000536 ..... p 1993 N94-20937 #
DE94-000538 ..... p 1973 N94-20938 #
DE94-000539 ..... p 1847 N94-21755 #
DE94-000578 ..... p 1975 N94-21786 #
DE94-000581 ..... p 1982 N94-21866 #
DE94-000592 ..... p 1975 N94-21775 #
DE94-000595 ..... p 1976 N94-21867 #
DE94-000618 ..... p 1976 N94-21962 #
DE94-000619 ..... p 1982 N94-21934 #
DE94-000653 ..... p 1805 N94-22386 #
DE94-000654 ..... p 1708 N94-21963 #
DE94-000665 ..... p 1697 N94-22571 #
DE94-000666 ..... p 1695 N94-21964 #
DE94-000671 ..... p 1977 N94-22572 #
DE94-000673 ..... p 1997 N94-21965 #
DE94-000694 ..... p 1978 N94-22573 #
DE94-000696 ..... p 2036 N94-22582 #
DE94-000704 ..... p 1852 N94-22017
DE94-000710 ..... p 1817 N94-20939 #
DE94-000726 ..... p 1990 N94-21868 #
DE94-000728 ..... p 1707 N94-21856 #
DE94-000740 ..... p 1799 N94-20351
DE94-000741 ..... p 1701 N94-20352
DE94-000745 ..... p 1859 N94-22018 #
DE94-000748 ..... p 1852 N94-21787 #
DE94-000768 ..... p 2031 N94-21857 #
DE94-000774 ..... p 2035 N94-22387 #
DE94-000778 ..... p 1998 N94-22019 #
DE94-000779 ..... p 1994 N94-20940 #
DE94-000787 ..... p 1798 N94-20101 #
DE94-000796 ..... p 1696 N94-22388 #
DE94-000800 ..... p 1820 N94-22020 #
DE94-000804 ..... p 1998 N94-22389 #
DE94-000805 ..... p 2036 N94-22583 #
DE94-000807 ..... p 2036 N94-22584 #
DE94-000817 ..... p 1820 N94-22585 #
DE94-000825 ..... p 1982 N94-21849 #
DE94-000836 ..... p 2034 N94-22028 #
DE94-000881 ..... p 1678 N94-20103 #
DE94-000884 ..... p 1827 N94-22390 #
DE94-000907 ..... p 1811 N94-22391 #
DE94-000918 ..... p 1811 N94-22392 #
DE94-000935 ..... p 1683 N94-22021 #
DE94-000956 ..... p 1918 N94-22011 #
DE94-000978 ..... p 1693 N94-21850
DE94-001000 ..... p 1961 N94-22393 #
DE94-001009 ..... p 1917 N94-21851 #
DE94-001011 ..... p 1707 N94-21822 #
DE94-001012 ..... p 1677 N94-22022 #
DE94-001016 ..... p 1998 N94-22045 #
DE94-001044 ..... p 1695 N94-22023 #
DE94-001045 ..... p 1696 N94-22394 #
DE94-001049 ..... p 1684 N94-22395 #
DE94-001050 ..... p 1977 N94-22396 #
DE94-001056 ..... p 1696 N94-22398 #
DE94-001057 ..... p 1998 N94-22399 #
DE94-001058 ..... p 1695 N94-22024 #
DE94-001059 ..... p 1977 N94-22400 #
DE94-001066 ..... p 1696 N94-22025 #
DE94-001067 ..... p 1820 N94-22401 #
DE94-001068 ..... p 1697 N94-22402 #
DE94-001077 ..... p 1965 N94-22403 #
DE94-001091 ..... p 1848 N94-21823 #
DE94-001101 ..... p 1998 N94-22069 #
DE94-001104 ..... p 2045 N94-22404 #
DE94-001151 ..... p 1794 N94-22405 #
DE94-001160 ..... p 1921 N94-22406 #
DE94-001168 ..... p 1656 N94-21852 #
DE94-001177 ..... p 1684 N94-22046 #
DE94-001183 ..... p 2032 N94-21972 #

DE94-001198 ..... p 2046 N94-22407 #
DE94-001231 ..... p 1997 N94-21973 #
DE94-001233 ..... p 1998 N94-22580 #
DE94-001234 ..... p 1998 N94-22561 #
DE94-001235 ..... p 1999 N94-22562 #
DE94-001254 ..... p 1947 N94-22563 #
DE94-001259 ..... p 1982 N94-21974 #
DE94-001261 ..... p 1820 N94-21975 #
DE94-001270 ..... p 2035 N94-22564 #
DE94-001274 ..... p 2035 N94-22565 #
DE94-001304 ..... p 1999 N94-22566 #
DE94-001305 ..... p 1999 N94-22567 #
DE94-001306 ..... p 1999 N94-22595 #
DE94-001307 ..... p 1999 N94-22596 #
DE94-001356 ..... p 1936 N94-21853 #
DE94-001373 ..... p 1695 N94-21976 #
DE94-001374 ..... p 1918 N94-21977 #
DE94-001377 ..... p 1695 N94-21978 #
DE94-001388 ..... p 1671 N94-21979 #
DE94-001444 ..... p 1693 N94-21854 #
DE94-001449 ..... p 2152 N94-21858 #
DE94-001548 ..... p 2045 N94-22047 #
DE94-001650 ..... p 1849 N94-22048 #
DE94-001738 ..... p 1977 N94-22049 #
DE94-001856 ..... p 2034 N94-22050 #
DE94-707408 ..... p 1848 N94-22012 #
DE94-707416 ..... p 1849 N94-22029 #
DE94-707420 ..... p 1851 N94-20116 #
DE94-707421 ..... p 1850 N94-19976 #
DE94-707492 ..... p 1848 N94-22013 #
DE94-707493 ..... p 1849 N94-22014 #
DE94-707494 ..... p 1849 N94-22030 #
DE94-714884 ..... p 1853 N94-22051 #
DE94-714886 ..... p 1849 N94-22043 #
DE94-714887 ..... p 1852 N94-22044 #
DE94-714888 ..... p 1853 N94-22258 #
DE94-714890 ..... p 1853 N94-22090 #
DE94-714891 ..... p 1853 N94-22259 #
DE94-714897 ..... p 1713 N94-22091 #
DE94-714901 ..... p 1850 N94-22092 #
DE94-714903 ..... p 1849 N94-22052

DIGEL-1979-5 ..... p 1979 N94-20118 #
DIGEL-1992-3 ..... p 1753 N94-21064
DIGEL-1992-8 ..... p 1979 N94-20123 #
DIGEL-1993-2 ..... p 1979 N94-20117 #
DIGEL-1993-3 ..... p 1979 N94-20118 #

DLR-FB-92-24 ..... p 1651 N94-21260 #
DLR-FB-92-31 ..... p 1742 N94-22279
DLR-FB-92-36 ..... p 1800 N94-20533 #
DLR-FB-92-38 ..... p 1964 N94-21139

DLR-MITT-92-08 ..... p 2152 N94-20543 #
DLR-MITT-92-10 ..... p 1871 N94-22280

DOD-8910.1-L ..... p 2042 N94-20919

DODA-AR-008-673 ..... p 1675 N94-21504
DODA-AR-008-156 ..... p 2028 N94-21505
DODA-AR-008-171 ..... p 1854 N94-19860 #
DODA-AR-008-232 ..... p 1711 N94-19906 #
DODA-AR-008-262 ..... p 1881 N94-19905
DODA-AR-008-345 ..... p 1645 N94-19914
DODA-AR-008-346 ..... p 1806 N94-19837
DODA-AR-008-387 ..... p 1841 N94-21453
DODA-AR-008-489 ..... p 1902 N94-19911

DODA-007-097 ..... p 1949 N94-19907
DODA-008-107 ..... p 1814 N94-19851
DODA-008-148 ..... p 1814 N94-19850

DOE/CE-23810/17 ..... p 1798 N94-20101 #

DOE/CH-10093/191 ..... p 1845 N94-19921 #
DOE/CH-10093/213 ..... p 1712 N94-19984 #

DOE/DP-40200-265 ..... p 1819 N94-21839 #
DOE/DP-40200/267 ..... p 1972 N94-20264 #

DOE/EE-0005 ..... p 2011 N94-19825 #

DOE/ER-0592(08-93) ..... p 1836 N94-20936 #
DOE/ER-0596T ..... p 1847 N94-21755 #
DOE/ER-13615/7 ..... p 1678 N94-20103 #
DOE/ER-13708/1 ..... p 1817 N94-20939 #
DOE/ER-13914/16 ..... p 1849 N94-22048 #
DOE/ER-14061/2 ..... p 1859 N94-22018 #
DOE/ER-25145/1 ..... p 1799 N94-20351
DOE/ER-40039/99 ..... p 1980 N94-20933 #
DOE/ER-40150/238 ..... p 1977 N94-22009
DOE/ER-40150/242 ..... p 2038 N94-21513 #
DOE/ER-40546/2 ..... p 1973 N94-20938 #
DOE/ER-45076/3 ..... p 1977 N94-22049 #
DOE/ER-45337/T5 ..... p 1693 N94-21854 #
DOE/ER-45477/1 ..... p 1701 N94-20352

DOE/ER-53218/22 ..... p 1998 N94-22019 #
DOE/ER-53218/23 ..... p 1994 N94-20940 #
DOE/ER-53240/5 ..... p 1993 N94-20937 #
DOE/ER-53266/45 ..... p 1951 N94-20224 #
DOE/ER-61224/2 ..... p 1855 N94-20219 #
DOE/ER-61369/2 ..... p 1850 N94-19941 #
DOE/ER-61493/1 ..... p 1852 N94-21787 #

DOE/ET-53088/602 ..... p 1997 N94-21973 #
DOE/ET-53088/617 ..... p 1995 N94-21514 #
DOE/ET-53088/618 ..... p 1996 N94-21752 #
DOE/ET-53088/619 ..... p 1992 N94-19887 #
DOE/ET-53088/620 ..... p 1991 N94-19872 #
DOE/ET-53088/621 ..... p 1998 N94-22560 #
DOE/ET-53088/623 ..... p 1998 N94-22561 #
DOE/ET-53088/626 ..... p 1999 N94-22562 #

DOE/EV-10249/T1 ..... p 1891 N94-20935 #

DOE/MC-23166/3414 ..... p 1826 N94-21938 #
DOE/MC-26040/93/C0220 ..... p 1683 N94-21984 #
DOE/MC-26366/93/C0194 ..... p 1847 N94-21540 #
DOE/MC-29245/93/C0205 ..... p 1709 N94-21982 #

DOE/METC-C/93/7097 ..... p 1826 N94-21983 #
DOE/METC-C/93/7100 ..... p 1846 N94-21527 #

DOE/OR-00033/T542 ..... p 2034 N94-22028 #

DOE/PC-92109/T1 ..... p 1678 N94-19890 #
DOE/PC-92179/T1 ..... p 1706 N94-21516 #
DOE/PC-92529/T3 ..... p 1680 N94-20934 #

DOE/SF-19441/T4 ..... p 1670 N94-21824 #

DOT/FAA/AM-93/18 ..... p 2040 N94-21626 #
DOT/FAA/AM-93/19 ..... p 1893 N94-20081 #
DOT/FAA/AM-93/20 ..... p 1738 N94-21201 #

DOT/FAA/CT-TN93/36 ..... p 1868 N94-21519 #

DOT/FAA/CT-88/10-VOL-2 ..... p 1647 N94-20343 #
DOT/FAA/CT-92/6 ..... p 1642 N94-21818 * #
DOT/FAA/CT-93/16-VOL-3 ..... p 1647 N94-20053 #

DOT/FAA/DS-89/11 ..... p 1642 N94-20051 #

DOT/FAA/EE-91-3-SUPPL-A ..... p 1851 N94-20948 #

DOT/FAA/RD-93/10 ..... p 1807 N94-20203 #
DOT/FAA/RD-93/22 ..... p 1642 N94-20051 #

DP-9 ..... p 1842 N94-21855

DRA-TM(AWE)-91013 ..... p 1737 N94-20596 #

DRA-TM(USGR)93339 ..... p 1967 N94-21306

DRA-TR-93004 ..... p 1652 N94-21224 #

DREA-TM-93/206 ..... p 1681 N94-21241 #

E-7520-1 ..... p 1692 N94-21604 * #
E-7609 ..... p 1637 N94-20563 * #
E-7847 ..... p 1642 N94-21590 * #
E-8004 ..... p 1732 N94-20497 * #
E-8023 ..... p 1675 N94-21488 * #
E-8102 ..... p 1830 N94-20171 * #
E-8125 ..... p 1830 N94-20170 * #
E-8131 ..... p 1809 N94-21607 * #
E-8169 ..... p 1666 N94-21864 * #
E-8172 ..... p 1654 N94-21790 * #
E-8173 ..... p 1832 N94-21757 * #
E-8177-VOL-1 ..... p 1648 N94-21582 * #
E-8180-VOL-2 ..... p 1648 N94-21583 * #
E-8186 ..... p 1762 N94-21566 * #
E-8188 ..... p 1769 N94-21808 * #
E-8218 ..... p 1984 N94-20140 * #
E-8219 ..... p 1798 N94-20167 * #
E-8221 ..... p 1667 N94-20062 * #
E-8227 ..... p 1968 N94-21608 * #
E-8231 ..... p 1637 N94-20534 * #
E-8236 ..... p 1959 N94-21588 * #
E-8246 ..... p 1638 N94-22274 * #
E-8247 ..... p 1638 N94-21591 * #
E-8248 ..... p 1715 N94-21589 * #
E-8249 ..... p 1714 N94-21564 * #
E-8252 ..... p 1654 N94-21570 * #
E-8255 ..... p 1649 N94-21759 * #
E-8258 ..... p 1636 N94-20136 * #
E-8265 ..... p 1741 N94-21567 * #
E-8269 ..... p 1799 N94-20177 * #
E-8273 ..... p 1826 N94-21756 * #
E-8277 ..... p 1649 N94-21758 * #
E-8280 ..... p 1649 N94-21586 * #
E-8281 ..... p 1713 N94-21760 * #

E-8282 ..... p 1650 N94-21742 * #
E-8288 ..... p 1670 N94-21809 * #
E-8292 ..... p 1656 N94-21581 * #
E-8293 ..... p 1670 N94-21565 * #
E-8301 ..... p 1648 N94-21563 * #

ECE-93-19 ..... p 1900 N94-21301 #

ECL-92-12 ..... p 1801 N94-20542 #
ECL-92-38 ..... p 2018 N94-20593 #
ECL-92-40 ..... p 1824 N94-20594 #
ECL-92-41 ..... p 1751 N94-20595 #
ECL-92-42 ..... p 1801 N94-20597 #
ECL-92-48 ..... p 2018 N94-20598 #
ECL-93-04 ..... p 1703 N94-20599 #

EDR-16026 ..... p 1648 N94-21582 * #
EDR-16026 ..... p 1648 N94-21583 * #

EGG-M-93181 ..... p 2014 N94-19970 #

EGG-10617-2184 ..... p 2027 N94-21296 #
EGG-11265-5007 ..... p 1750 N94-20325

EMRL-93-10 ..... p 1830 N94-20001

ENAEC-TS-CR-93096 ..... p 1712 N94-20927 #

EPA/AA/TDG-93/02A ..... p 1826 N94-22093

ERDEC-TR-029 ..... p 1974 N94-21185 #
ERDEC-TR-085 ..... p 1988 N94-21491 #
ERDEC-TR-099 ..... p 1911 N94-21204
ERDEC-TR-106 ..... p 1809 N94-21508 #

ERIM-246830-9-F ..... p 1817 N94-21253 #

ERL-0703-GD ..... p 1814 N94-19850
ERL-0718-GD ..... p 1902 N94-19911

ERP-1114 ..... p 1864 N94-20088
ERP-1125 ..... p 1855 N94-20090

ESA-PSS-02-10-VOL-1-ISSUE-1 .. p 1669 N94-20241 #

ESA-SP-351 ..... p 2000 N94-22624 #

ESA-STM-248 ..... p 1657 N94-20235 #

ESC-TR-92-204 ..... p 1867 N94-21212 #
ESC-TR-93-192 ..... p 1650 N94-19880
ESC-TR-93-192 ..... p 1912 N94-21205 #
ESC-TR-93-211 ..... p 1739 N94-21211 #
ESC-TR-93-236 ..... p 1739 N94-21244 #
ESC-TR-93-244 ..... p 1738 N94-21210 #

ESG-218 ..... p 2016 N94-20323
ESG-219 ..... p 1979 N94-19989 #
ESG-230 ..... p 1979 N94-20274 #
ESG-233 ..... p 1980 N94-20292 #
ESG-236 ..... p 1980 N94-20475 #

ET/EM-1992-17 ..... p 1969 N94-22261 #
ET/EM-1992-18 ..... p 1969 N94-22262 #
ET/EM-1992-19 ..... p 1742 N94-22349
ET/EM-1992-20 ..... p 1742 N94-22348
ET/EM-1992-22 ..... p 1742 N94-22347
ET/EM-1992-26 ..... p 1742 N94-22346
ET/EM-1992-28 ..... p 1960 N94-22096

ETDE/JP-MF-94707408 ..... p 1848 N94-22012 #
ETDE/JP-MF-94707416 ..... p 1849 N94-22029 #
ETDE/JP-MF-94707420 ..... p 1851 N94-20116 #
ETDE/JP-MF-94707421 ..... p 1850 N94-19976 #

ETLA-DISCUSSION-PAPER-335 .. p 1854 N94-22072 #

ETN-0924-2953 ..... p 1911 N94-21156 #
ETN-93-93306 ..... p 1753 N94-21064
ETN-93-93312 ..... p 1841 N94-21015
ETN-93-93316 ..... p 1857 N94-21016
ETN-93-93458 ..... p 1892 N94-21141
ETN-93-93470 ..... p 1841 N94-21017
ETN-93-93602 ..... p 1892 N94-21134
ETN-93-93605 ..... p 2026 N94-21135
ETN-93-93607 ..... p 1973 N94-21136
ETN-93-93611 ..... p 1954 N94-21137
ETN-93-93618 ..... p 1930 N94-21018
ETN-93-93680 ..... p 2081 N94-21138
ETN-93-93681 ..... p 1952 N94-21042
ETN-93-93682 ..... p 2150 N94-21056
ETN-93-93749 ..... p 1966 N94-21798 #
ETN-93-93759 ..... p 1680 N94-20552 #
ETN-93-93769 ..... p 1751 N94-20553 #
ETN-93-93790 ..... p 1952 N94-21019
ETN-93-93792 ..... p 1908 N94-21020

ETN-93-93793 ..... p 1944 N94-21057
ETN-93-93808 ..... p 1753 N94-21021
ETN-93-93809 ..... p 1986 N94-21043
ETN-93-93810 ..... p 1987 N94-21148
ETN-93-93811 ..... p 1857 N94-21149
ETN-93-93838 ..... p 1963 N94-21058
ETN-93-93856 ..... p 1953 N94-21059
ETN-93-93866 ..... p 1953 N94-21060
ETN-93-93868 ..... p 1909 N94-21061
ETN-93-93869 ..... p 1910 N94-21062
ETN-93-93881 ..... p 2147 N94-21150
ETN-93-93913 ..... p 1910 N94-21063
ETN-93-94108 ..... p 1913 N94-21313
ETN-93-94109 ..... p 1914 N94-21454
ETN-93-94112 ..... p 2045 N94-22276
ETN-93-94113 ..... p 1909 N94-21045
ETN-93-94114 ..... p 2043 N94-21071
ETN-93-94116 ..... p 1953 N94-21072
ETN-93-94117 ..... p 1738 N94-21073
ETN-93-94118 ..... p 1953 N94-21074
ETN-93-94122 ..... p 1953 N94-21075
ETN-93-94123 ..... p 1963 N94-21076
ETN-93-94124 ..... p 1953 N94-21046
ETN-93-94125 ..... p 1953 N94-21047
ETN-93-94126 ..... p 1953 N94-21048
ETN-93-94129 ..... p 1944 N94-21140
ETN-93-94174 ..... p 1831 N94-21153
ETN-93-94181 ..... p 2026 N94-21151
ETN-93-94183 ..... p 1910 N94-21152
ETN-93-94184 ..... p 1857 N94-21044
ETN-93-94185 ..... p 1866 N94-21052
ETN-93-94186 ..... p 1692 N94-21311
ETN-93-94187 ..... p 1867 N94-21312
ETN-93-94207 ..... p 1996 N94-21802 #
ETN-93-94273 ..... p 1950 N94-20032 #
ETN-93-94289 ..... p 1822 N94-20157
ETN-93-94335 ..... p 1753 N94-21067 #
ETN-93-94412 ..... p 1801 N94-20542 #
ETN-93-94435 ..... p 1951 N94-20227 #
ETN-93-94444 ..... p 1667 N94-20068 #
ETN-93-94448 ..... p 1737 N94-20592 #
ETN-93-94456 ..... p 1742 N94-22279
ETN-93-94457 ..... p 1964 N94-21139
ETN-93-94458 ..... p 1871 N94-22280
ETN-93-94468 ..... p 1691 N94-20530 #
ETN-93-94480 ..... p 1988 N94-21594 #
ETN-93-94486 ..... p 2049 N94-22056 #
ETN-93-94528 ..... p 1940 N94-20242 #
ETN-93-94561 ..... p 1882 N94-20531 #
ETN-93-94595 ..... p 2018 N94-20593 #
ETN-93-94596 ..... p 1824 N94-20594 #
ETN-93-94597 ..... p 1751 N94-20595 #
ETN-93-94598 ..... p 1801 N94-20597 #
ETN-93-94599 ..... p 2018 N94-20598 #
ETN-93-94602 ..... p 1703 N94-20599 #
ETN-93-94603 ..... p 1866 N94-20600 #
ETN-93-94604 ..... p 1801 N94-20601
ETN-93-94623 ..... p 1979 N94-20117 #
ETN-93-94624 ..... p 1979 N94-20118 #
ETN-93-94632 ..... p 1752 N94-20628 #
ETN-93-94697 ..... p 1930 N94-21077
ETN-93-94818 ..... p 1971 N94-20119 #
ETN-93-94820 ..... p 1865 N94-20532 #
ETN-93-94839 ..... p 1798 N94-20145 #
ETN-93-94841 ..... p 1841 N94-21068 #
ETN-93-94842 ..... p 1841 N94-21069 #
ETN-93-94843 ..... p 1867 N94-21070 #
ETN-93-94846 ..... p 2042 N94-20193 #
ETN-93-94864 ..... p 2152 N94-20543 #
ETN-93-94868 ..... p 1651 N94-21280 #
ETN-93-94870 ..... p 1800 N94-20533 #
ETN-93-94879 ..... p 1657 N94-20235 #
ETN-93-94881 ..... p 1669 N94-20241 #
ETN-93-94889 ..... p 1851 N94-21455
ETN-93-94903 ..... p 1979 N94-20123 #
ETN-93-94906 ..... p 1822 N94-20146 #
ETN-93-94914 ..... p 2081 N94-21578 * #
ETN-93-94916 ..... p 2054 N94-20174 * #
ETN-93-94922 ..... p 2055 N94-21579 * #
ETN-93-94923 ..... p 2054 N94-20175 * #
ETN-93-94970 ..... p 1737 N94-20596 #
ETN-93-94980 ..... p 1929 N94-20124 #
ETN-93-94981 ..... p 1950 N94-20125 #
ETN-93-94982 ..... p 1929 N94-20176 #
ETN-93-94985 ..... p 1951 N94-20302 #
ETN-93-94986 ..... p 1950 N94-20161 #
ETN-93-94987 ..... p 1963 N94-20162 #
ETN-93-94988 ..... p 1950 N94-20163 #
ETN-93-94989 ..... p 1905 N94-20164 #
ETN-93-94990 ..... p 1963 N94-20165 #
ETN-93-94991 ..... p 1749 N94-20166 #
ETN-93-94992 ..... p 1951 N94-20237 #
ETN-93-94993 ..... p 1950 N94-20200 #
ETN-93-94994 ..... p 1905 N94-20201 #
ETN-93-94995 ..... p 1963 N94-20202 #
ETN-93-95055 ..... p 2014 N94-20018 #
ETN-93-95056 ..... p 1903 N94-20020 #
ETN-93-95057 ..... p 1889 N94-20022 #
ETN-93-95059 ..... p 1889 N94-20024
ETN-93-95061 ..... p 1846 N94-20151
ETN-93-95062 ..... p 1798 N94-20147
ETN-93-95063 ..... p 2015 N94-20152
ETN-93-95064 ..... p 2039 N94-20153
ETN-93-95065 ..... p 1851 N94-20154
ETN-93-95066 ..... p 1855 N94-20155
ETN-93-95067 ..... p 1993 N94-20156
ETN-93-95068 ..... p 2014 N94-20026 #
ETN-93-95069 ..... p 1971 N94-20030 #
ETN-94-93802 ..... p 1860 N94-22283 #
ETN-94-94530 ..... p 1890 N94-20238
ETN-94-94533 ..... p 1865 N94-20239
ETN-94-94537 ..... p 1865 N94-20309
ETN-94-94698 ..... p 1910 N94-21078
ETN-94-94699 ..... p 1803 N94-21609
ETN-94-94700 ..... p 1935 N94-21610
ETN-94-94701 ..... p 1916 N94-21611 #
ETN-94-94702 ..... p 1916 N94-21612 #
ETN-94-94703 ..... p 1682 N94-21574 #
ETN-94-94704 ..... p 1803 N94-21575 #
ETN-94-94705 ..... p 1959 N94-21576 #
ETN-94-94706 ..... p 1935 N94-21492 #
ETN-94-94707 ..... p 1935 N94-21493 #
ETN-94-94709 ..... p 1911 N94-21157 #
ETN-94-94710 ..... p 1954 N94-21158
ETN-94-94711 ..... p 1954 N94-21159 #
ETN-94-94713 ..... p 1944 N94-21160 #
ETN-94-94714 ..... p 1954 N94-21231 #
ETN-94-94715 ..... p 1944 N94-21232 #
ETN-94-94716 ..... p 1945 N94-21233 #
ETN-94-94717 ..... p 1946 N94-21577 #
ETN-94-94718 ..... p 1930 N94-21234 #
ETN-94-94719 ..... p 1930 N94-21161
ETN-94-94720 ..... p 1943 N94-21032 #
ETN-94-94721 ..... p 1944 N94-21033 #
ETN-94-94722 ..... p 1963 N94-21022 #
ETN-94-94723 ..... p 1930 N94-21023
ETN-94-94724 ..... p 1908 N94-21024
ETN-94-94725 ..... p 1909 N94-21025 #
ETN-94-94726 ..... p 1909 N94-21026 #
ETN-94-94727 ..... p 1952 N94-21027
ETN-94-94729 ..... p 1909 N94-21028
ETN-94-94730 ..... p 1952 N94-21029
ETN-94-94731 ..... p 2038 N94-21533
ETN-94-94732 ..... p 1915 N94-21534
ETN-94-94733 ..... p 2044 N94-21535
ETN-94-94734 ..... p 2044 N94-21494
ETN-94-94735 ..... p 2045 N94-21536
ETN-94-94736 ..... p 1915 N94-21537
ETN-94-94737 ..... p 1935 N94-21549 #
ETN-94-94738 ..... p 1916 N94-21587
ETN-94-94739 ..... p 1915 N94-21551
ETN-94-94740 ..... p 1914 N94-21495
ETN-94-94741 ..... p 1914 N94-21496
ETN-94-94765 ..... p 1761 N94-21538
ETN-94-94766 ..... p 2029 N94-21552
ETN-94-94861 ..... p 2000 N94-22624 #
ETN-94-94925 ..... p 2042 N94-20310
ETN-94-94965 ..... p 1856 N94-20607
ETN-94-94966 ..... p 1856 N94-20608
ETN-94-94967 ..... p 1857 N94-20609
ETN-94-94968 ..... p 1659 N94-21367
ETN-94-95076 ..... p 1639 N94-22597 #
ETN-94-95125 ..... p 1866 N94-20557
ETN-94-95245 ..... p 1707 N94-21890 #

EUT-92-E-258 ..... p 1761 N94-21538
EUT-92-E-259 ..... p 2029 N94-21552

E25-666 ..... p 1823 N94-20538 * #

FASTC-ID(RS)T-0100-93 ..... p 1818 N94-21509 #
FASTC-ID(RS)T-0101-93 ..... p 1815 N94-19965 #
FASTC-ID(RS)T-0124-93 ..... p 1816 N94-20484 #
FASTC-ID(RS)T-0331-93 ..... p 1867 N94-21250 #
FASTC-ID(RS)T-0560-93 ..... p 1706 N94-21437 #
FASTC-ID(RS)T-0579-93 ..... p 2028 N94-21438 #
FASTC-ID(RS)T-0730-92 ..... p 1636 N94-19963 #
FASTC-ID(RS)T-0732-92 ..... p 1889 N94-19962 #
FASTC-ID(RS)T-0831-92 ..... p 1912 N94-21255
FASTC-ID(RS)T-0853-92 ..... p 1717 N94-20207 #

FFI-92/7020 ..... p 1751 N94-20553 #
FFI-93/6005 ..... p 1851 N94-21455

FIA-92-19 ..... p 1947 N94-22270 * #

FNAL/C-93/122-E ..... p 1979 N94-20216 #
FNAL/C-93/128 ..... p 1750 N94-20314
FNAL/C-93/197 ..... p 1975 N94-21775 #
FNAL/C-93/198-E ..... p 1969 N94-19814 #
FNAL/C-93/199-E ..... p 1972 N94-20225 #
FNAL/C-93/200-E ..... p 1975 N94-21806 #
FNAL/C-93/201-E ..... p 1978 N94-19983 #
FNAL/C-93/202-E ..... p 1980 N94-20317
FNAL/C-93/204-E ..... p 1982 N94-21866 #
FNAL/C-93/205-E ..... p 1975 N94-21840 #
FNAL/C-93/208-E ..... p 1978 N94-19972 #
FNAL/C-93/209-E ..... p 1976 N94-21847 #
FNAL/C-93/211-E ..... p 1969 N94-19813 #
FNAL/C-93/222 ..... p 1807 N94-19987 #
FNAL/C-93/223 ..... p 1978 N94-19988 #
FNAL/C-93/229 ..... p 1982 N94-21934 #
FNAL/C-93/238 ..... p 1976 N94-21867 #
FNAL/C-93/251 ..... p 1976 N94-21962 #
FNAL/C-93/263-E ..... p 1975 N94-21786 #

FOA-C-40277-4.9 ..... p 1680 N94-20552 #

FRCR-436 ..... p 1951 N94-20224 #

FSU-HEP-930329 ..... p 1969 N94-19804 #
FSU-HEP-930608 ..... p 1973 N94-20474 #

FSU-SCRI-93-31 ..... p 2016 N94-20285 #

GA-A-20941 ..... p 1992 N94-20003 #
GA-A-21301 ..... p 1993 N94-20326 #
GA-A-21342 ..... p 1998 N94-22039 #
GA-A-21403 ..... p 1998 N94-22089 #
GA-A-21404 ..... p 2045 N94-22404 #

GAO/NSIAD-93-191 ..... p 2039 N94-20206 #
GAO/NSIAD-93-198 ..... p 1908 N94-20917 #
GAO/NSIAD-94-67 ..... p 2039 N94-20236 #

GKSS-92/E/13 ..... p 1857 N94-21044
GKSS-92/E/14 ..... p 1866 N94-21052
GKSS-92/E/16 ..... p 1692 N94-21311
GKSS-92/E/22 ..... p 1867 N94-21312

GRI-93/0047 ..... p 1825 N94-21451 #
GRI-93/0048 ..... p 1825 N94-21424 #
GRI-93/0049 ..... p 1825 N94-21450 #
GRI-93/0108 ..... p 1682 N94-21452 #
GRI-93/0149 ..... p 1714 N94-21426
GRI-93/0176 ..... p 1705 N94-21425 #

GSF-41/91 ..... p 1892 N94-21141

H-1908 ..... p 1649 N94-21879 * #

HD-THEP-93-26 ..... p 1947 N94-22563 #

HIFAN-566 ..... p 1981 N94-21440 #
HIFAN-573 ..... p 1980 N94-20290 #
HIFAN-581 ..... p 1981 N94-21439 #
HIFAN-585 ..... p 1979 N94-20289 #
HIFAN-614 ..... p 1992 N94-20004 #

HMI-B-499 ..... p 1753 N94-21021

HMMH-290940.04-2 ..... p 1968 N94-22053
HMMH-290940.04-3 ..... p 1969 N94-22054

IAT.R-0023 ..... p 1831 N94-21249 #

IC-93/81 ..... p 2037 N94-20178

ICASE-93-68 ..... p 1959 N94-21568 * #
ICASE-93-69 ..... p 1804 N94-21861 * #
ICASE-93-70 ..... p 1797 N94-20033 * #
ICASE-93-71 ..... p 1915 N94-21584 * #
ICASE-93-74 ..... p 1804 N94-21880 * #
ICASE-93-76 ..... p 1804 N94-21875 * #
ICASE-93-78 ..... p 1950 N94-20092 * #
ICASE-93-80 ..... p 1950 N94-20087 * #
ICASE-93-81 ..... p 1914 N94-21462 * #
ICASE-93-85 ..... p 1965 N94-21463 * #

ICMA-93-183 ..... p 1954 N94-21173 #
ICMA-93-184 ..... p 1954 N94-21174 #

ICOMP-93-45 ..... p 1798 N94-20167 * #
ICOMP-93-47 ..... p 1959 N94-21586 * #

IDA-D-1197 ..... p 1858 N94-21207 #

IDA-P-2602 ..... p 1865 N94-21420 #

IDA/HQ-91-37961 ..... p 1665 N94-21420 #
IDA/HQ-92-42146 ..... p 1858 N94-21207 #

IEPC-93-084 ..... p 1654 N94-21570 * #

IFSR-602 ..... p 1997 N94-21973 #
IFSR-617 ..... p 1995 N94-21514 #
IFSR-618 ..... p 1996 N94-21752 #
IFSR-619 ..... p 1992 N94-19887 #

IFSR-620 ..... p 1991 N94-19872 #
IFSR-621 ..... p 1998 N94-22560 #
IFSR-623 ..... p 1998 N94-22561 #
IFSR-626 ..... p 1999 N94-22562 #

IG/DCD-93-022 ..... p 1645 N94-20040

IHES/M-93/31 ..... p 1961 N94-22377 #
IHES/M-93/32 ..... p 1961 N94-22264 #
IHES/M-93/34 ..... p 1961 N94-22263 #

IHES/P-93/30 ..... p 2038 N94-22095

IHES/P/93/23 ..... p 1977 N94-22271
IHES/P/93/24 ..... p 1805 N94-22272

IITRI-D06200-3 ..... p 1740 N94-21412 #

ILR-MITT-256(1991) ..... p 1639 N94-22597 #
ILR-MITT-274(1992) ..... p 1631 N94-21153

INRIA-RR-1714 ..... p 1910 N94-21063
INRIA-RR-1735 ..... p 1951 N94-20227 #

INS-241 ..... p 1952 N94-20923

INT-PATENT-CLASS-A61F-5/00 . p 1896 N94-20493 *
INT-PATENT-CLASS-A61M-1/03 p 1890 N94-20372 *
INT-PATENT-CLASS-A63B-22/02 p 1895 N94-20194 *
INT-PATENT-CLASS-A63B-71/00 p 1895 N94-20194 *

INT-PATENT-CLASS-B01D-21/26 p 1800 N94-20361 *
INT-PATENT-CLASS-B05C-13/00 p 1823 N94-20380 *
INT-PATENT-CLASS-B05D-1/00 . p 1702 N94-20373 *
INT-PATENT-CLASS-B05D-5/00 . p 1700 N94-20195 *
INT-PATENT-CLASS-B05D-5/06 . p 1702 N94-20373 *
INT-PATENT-CLASS-B05D-5/12 . p 1702 N94-20373 *
INT-PATENT-CLASS-B23P-15/00 p 1703 N94-20541 *
INT-PATENT-CLASS-B25J-5/00 .. p 1823 N94-20494 * #
INT-PATENT-CLASS-B32B-15/01 p 1704 N94-21143
INT-PATENT-CLASS-B62D-57/024 p 1823 N94-20494 * #
INT-PATENT-CLASS-B64C-13/16 p 1650 N94-21050
INT-PATENT-CLASS-B64C-3/58 . p 1645 N94-21051
INT-PATENT-CLASS-B64C-9/02 . p 1650 N94-20556 *
INT-PATENT-CLASS-B64G-1/10 . p 1824 N94-20587 *
INT-PATENT-CLASS-B64G-1/10 . p 1658 N94-21041
INT-PATENT-CLASS-B64G-1/22 . p 1657 N94-20367 *
INT-PATENT-CLASS-B66C-23/76 p 1822 N94-20369 *

INT-PATENT-CLASS-C04B-33/28 p 1702 N94-20377 *
INT-PATENT-CLASS-C04B-35/58 p 1703 N94-20529 *
INT-PATENT-CLASS-C08G-59/50 p 1674 N94-21040
INT-PATENT-CLASS-C08G-69/32 p 1702 N94-20374 *
INT-PATENT-CLASS-C08G-73/10 p 1702 N94-20374 *
INT-PATENT-CLASS-C08J-5/06 .. p 1674 N94-21040
INT-PATENT-CLASS-C22C-19/05 p 1704 N94-21143
INT-PATENT-CLASS-C23C-30/00 p 1704 N94-21143
INT-PATENT-CLASS-C30B-7/02 . p 2017 N94-20528 *

INT-PATENT-CLASS-F02C-3/02 . p 1801 N94-20588 *
INT-PATENT-CLASS-F02K-9/00 . p 1669 N94-20370 *
INT-PATENT-CLASS-F16B-3/06 . p 1822 N94-20365 *
INT-PATENT-CLASS-F16B-39/00 p 1823 N94-20379 *
INT-PATENT-CLASS-F16B-39/02 p 1823 N94-20379 *
INT-PATENT-CLASS-F16C-23/00 p 1824 N94-21142 #
INT-PATENT-CLASS-F16K-5/04 . p 1824 N94-20589 *
INT-PATENT-CLASS-F25B-23/00 p 1822 N94-20127 *
INT-PATENT-CLASS-F28D-20/00 p 1800 N94-20371 *
INT-PATENT-CLASS-F42B-10/18 p 1645 N94-21051

INT-PATENT-CLASS-G01C-3/08 . p 1986 N94-20591 *
INT-PATENT-CLASS-G01D-5/34 . p 1985 N94-20240 *
INT-PATENT-CLASS-G01N-21/00 p 1986 N94-20378 *
INT-PATENT-CLASS-G01R-31/28 p 1780 N94-21178
INT-PATENT-CLASS-G02B-5/10 . p 1985 N94-20305 *
INT-PATENT-CLASS-G02B-5/32 . p 1986 N94-20591 *
INT-PATENT-CLASS-G05B-13/00 p 1907 N94-20492 *
INT-PATENT-CLASS-G06F-15/18 p 1942 N94-20366 *
INT-PATENT-CLASS-G06F-15/46 p 1942 N94-20360 *
INT-PATENT-CLASS-G06F-9/44 . p 1907 N94-20492 *
INT-PATENT-CLASS-G06G-7/12 p 1942 N94-20360 *
INT-PATENT-CLASS-G08B-31/00 p 1641 N94-21030
INT-PATENT-CLASS-G09B-9/08 . p 1653 N94-20339 *
INT-PATENT-CLASS-G11C-15/00 p 1985 N94-20303 *

INT-PATENT-CLASS-H01J-5/16 .. p 1986 N94-20345 *
INT-PATENT-CLASS-H01L-31/45 p 1846 N94-20196 *
INT-PATENT-CLASS-H01P-7/06 . p 1822 N94-20375 *
INT-PATENT-CLASS-H01Q-1/42 . p 1738 N94-21049
INT-PATENT-CLASS-H01Q-3/34 . p 1737 N94-21031
INT-PATENT-CLASS-H01R-13/00 p 1821 N94-20126 *
INT-PATENT-CLASS-H05B-6/36 . p 1718 N94-20368 *
INT-PATENT-CLASS-H05H-1/00 . p 1669 N94-20496 *

IOS-296-1992 ..... p 1682 N94-20531 #

IPF-92-2 ..... p 1996 N94-21802 #

IPPCZ-327 ..... p 1996 N94-21593 #
IPPCZ-328 ..... p 1996 N94-21571 #
IPPCZ-330 ..... p 1996 N94-21572 #
IPPCZ-331 ..... p 1996 N94-21573 #
IPPCZ-332 ..... p 1997 N94-21816 #

IS-M-761 ..... p 1695 N94-21964 #
IS-M-762 ..... p 1697 N94-22571 #
IS-M-765 ..... p 1978 N94-22573 #
IS-M-766 ..... p 2036 N94-22582 #

IS-T-1640 ..... p 1672 N94-19888 #
IS-T-1645 ..... p 1694 N94-21937 #
IS-T-1665 ..... p 2032 N94-21936 #
IS-T-1670 ..... p 2029 N94-21691

ISBN-0-16-038211-4 ..... p 2054 N94-21739 *
ISBN-0-16-041884-4 ..... p 1837 N94-20209 #
ISBN-0-315-57576-X ..... p 2056 N94-22415
ISBN-0-315-57581-6 ..... p 1990 N94-22411
ISBN-0-315-58962-0 ..... p 1677 N94-22420
ISBN-0-315-59037-8 ..... p 1651 N94-22418
ISBN-0-315-59056-4 ..... p 1977 N94-22416
ISBN-0-315-59251-6 ..... p 1827 N94-22421
ISBN-0-315-59445-4 ..... p 1651 N94-22419
ISBN-0-315-59525-6 ..... p 1639 N94-22382
ISBN-0-315-60441-7 ..... p 2056 N94-22412
ISBN-0-315-60627-4 ..... p 1742 N94-22408
ISBN-0-315-60632-0 ..... p 1743 N94-22409
ISBN-0-315-60640-1 ..... p 1743 N94-22410
ISBN-0-315-61113-8 ..... p 1652 N94-22423
ISBN-0-315-61980-5 ..... p 1861 N94-22424
ISBN-0-315-63035-3 ..... p 1805 N94-22417
ISBN-0-315-63832-X ..... p 1843 N94-22422
ISBN-0-315-83128-6 ..... p 1652 N94-22425
ISBN-0-315-83135-9 ..... p 2061 N94-22426
ISBN-0-315-83148-0 ..... p 1644 N94-22427
ISBN-0-315-83255-X ..... p 1843 N94-22429
ISBN-0-315-83258-4 ..... p 1861 N94-22574
ISBN-0-315-83273-8 ..... p 1861 N94-22575
ISBN-0-315-83425-0 ..... p 1991 N94-22581
ISBN-0-315-83426-9 ..... p 1805 N94-22580
ISBN-0-315-83427-7 ..... p 1990 N94-22579
ISBN-0-315-83439-0 ..... p 1827 N94-22578
ISBN-0-315-83501-X ..... p 1677 N94-22589
ISBN-0-315-83533-8 ..... p 1653 N94-22588
ISBN-0-315-83534-6 ..... p 1677 N94-22587
ISBN-0-315-83538-9 ..... p 1639 N94-22586
ISBN-0-315-83580-X ..... p 1827 N94-22577
ISBN-0-315-83588-5 ..... p 1743 N94-22576
ISBN-0-315-83944-9 ..... p 2081 N94-22593
ISBN-0-315-83947-3 ..... p 2081 N94-22592
ISBN-0-315-83951-1 ..... p 1947 N94-22591
ISBN-0-315-84006-4 ..... p 1833 N94-22590
ISBN-0-643-05250-X ..... p 1855 N94-20256
ISBN-0-9694170-2-0 ..... p 1770 N94-22101
ISBN-2-85-428293-0 ..... p 1659 N94-21367
ISBN-3-79-831536-1 ..... p 2039 N94-20153
ISBN-9-03-692025-6 ..... p 1865 N94-20309
ISBN-9-05-411046-5 ..... p 1857 N94-21016
ISBN-9-05-411047-3 ..... p 1865 N94-20532 #
ISBN-9-05-411052-X ..... p 1841 N94-21015
ISBN-9-06-144258-3 ..... p 1761 N94-21538
ISBN-9-06-144259-1 ..... p 2029 N94-21552
ISBN-9-26-310749-1 ..... p 1841 N94-21068 #
ISBN-9-26-310773-9 ..... p 1841 N94-21069 #
ISBN-9-26-310779-3 ..... p 1867 N94-21070 #
ISBN-9-51-384224-X ..... p 1988 N94-21594 #
ISBN-90-369-2027-2 ..... p 1865 N94-20239
ISBN-90-369-2029-9 ..... p 1890 N94-20238
ISBN-90-9003857-4 ..... p 2035 N94-22273
ISBN-92-9092-246-X ..... p 2000 N94-22624 #
ISBN-92-9092-357-1 ..... p 1657 N94-20235 #
ISBN-95-1384-086-7 ..... p 2049 N94-22056 #
ISBN-951-38-4087-5 ..... p 1707 N94-21890 #
ISBN-951-38-4106-1 ..... p 1691 N94-20530 #

ISL-CO-216/92 ..... p 1866 N94-20557

IW-92052R ..... p 1638 N94-22260 #

IWR-93-R-5 ..... p 2044 N94-21354 #

IZF-1992-A-28 ..... p 2042 N94-20310

J-204-93-0052/2789-VOL-2 ..... p 1985 N94-20283 #

JHU/APL-TG-1384 ..... p 2015 N94-20184 #

JPL-D-9516 ..... p 1899 N94-20549 * #

JPL-PUBL-93-17 ..... p 1718 N94-20403 * #

JSC-20466-REV-B ..... p 1897 N94-21812 * #

K/CSD/TM-93-REV-2 ..... p 2045 N94-22047 #

KAPL-4739 ..... p 1805 N94-22269 #
KAPL-4759 ..... p 1833 N94-22001 #

KCP-613-5079 ..... p 1749 N94-20005 #
KCP-613-5111 ..... p 1691 N94-20478 #
KCP-613-5153 ..... p 1918 N94-21977 #
KCP-613-5155 ..... p 1915 N94-21561 #
KCP-613-5215 ..... p 1695 N94-21976 #
KCP-613-5255 ..... p 1695 N94-21978 #
KCP-613-5258 ..... p 1763 N94-21652 #
KCP-613-5260 ..... p 1906 N94-20311
KCP-613-5282 ..... p 1698 N94-19857 #

KNMI-TR-103A ..... p 1890 N94-20238
KNMI-TR-148 ..... p 1865 N94-20239

KNMI-WR-74-14 ..... p 1865 N94-20309
KNMI-WR-92-05 ..... p 1865 N94-20309

KVI-969 ..... p 1971 N94-20119 #

L-17189 ..... p 1939 N94-20089 * #
L-17235 ..... p 1637 N94-21569 * #
L-17243 ..... p 1669 N94-20102 * #
L-17275-PT-2 ..... p 1955 N94-21464 * #
L-17321 ..... p 1833 N94-22608 * #
L-17365 ..... p 1871 N94-22292 * #

LA-UR-93-1255 ..... p 1991 N94-19883 #
LA-UR-93-2343 ..... p 2034 N94-22035 #
LA-UR-93-2449 ..... p 1799 N94-20286 #
LA-UR-93-2500 ..... p 2012 N94-19926 #
LA-UR-93-2545 ..... p 1808 N94-20287 #
LA-UR-93-2601 ..... p 1854 N94-19955 #
LA-UR-93-2632 ..... p 1904 N94-20049 #
LA-UR-93-2637 ..... p 1807 N94-20115 #
LA-UR-93-2638 ..... p 1807 N94-20114 #
LA-UR-93-2686 ..... p 1696 N94-22034 #
LA-UR-93-2759 ..... p 1981 N94-21767
LA-UR-93-2790 ..... p 1976 N94-21995 #
LA-UR-93-2820 ..... p 1707 N94-21560 #
LA-UR-93-2879 ..... p 2030 N94-21768
LA-UR-93-2879 ..... p 2034 N94-22007 #
LA-UR-93-2881 ..... p 1699 N94-19975 #
LA-UR-93-2888 ..... p 1768 N94-21762
LA-UR-93-2908 ..... p 1946 N94-21845 #
LA-UR-93-2909 ..... p 1884 N94-19866 #
LA-UR-93-2919 ..... p 2032 N94-21987 #
LA-UR-93-2924 ..... p 1815 N94-20272 #
LA-UR-93-2950 ..... p 1997 N94-21988 #
LA-UR-93-2957 ..... p 1769 N94-21846 #
LA-UR-93-2961 ..... p 1814 N94-19867 #
LA-UR-93-2990 ..... p 1997 N94-21989 #
LA-UR-93-3014 ..... p 1691 N94-20321
LA-UR-93-3022 ..... p 2016 N94-20322
LA-UR-93-3024 ..... p 2016 N94-20335 #
LA-UR-93-3025 ..... p 2015 N94-20275 #
LA-UR-93-3039 ..... p 1818 N94-21554 #
LA-UR-93-3041 ..... p 1974 N94-21553 #
LA-UR-93-3072 ..... p 1960 N94-21946 #
LA-UR-93-3082 ..... p 1906 N94-20276 #
LA-UR-93-3086 ..... p 2011 N94-19827 #
LA-UR-93-3101 ..... p 1816 N94-20277 #
LA-UR-93-3115 ..... p 1695 N94-21990 #
LA-UR-93-3120 ..... p 1714 N94-20278 #
LA-UR-93-3137 ..... p 1935 N94-21745 #
LA-UR-93-3138 ..... p 1935 N94-21622 #
LA-UR-93-3139 ..... p 1936 N94-21746 #
LA-UR-93-3140 ..... p 1917 N94-21764
LA-UR-93-3143 ..... p 2036 N94-22584 #
LA-UR-93-3155 ..... p 2033 N94-21991 #
LA-UR-93-3160 ..... p 1916 N94-21747 #
LA-UR-93-3173 ..... p 1929 N94-20279 #
LA-UR-93-3175 ..... p 1814 N94-19828 #
LA-UR-93-3185 ..... p 1796 N94-19829 #
LA-UR-93-3194 ..... p 2029 N94-21555 #
LA-UR-93-3216 ..... p 2036 N94-22583 #
LA-UR-93-3227 ..... p 1998 N94-22389 #
LA-UR-93-3237 ..... p 1820 N94-22020 #
LA-UR-93-3249 ..... p 1696 N94-22388 #
LA-UR-93-3333 ..... p 2035 N94-22387 #
LA-UR-93-3375 ..... p 2031 N94-21857 #
LA-UR-93-3419 ..... p 1820 N94-22585 #
LA-UR-93-3426 ..... p 1827 N94-22390 #
LA-UR-93-3429 ..... p 1982 N94-21849 #
LA-UR-93-3437 ..... p 1852 N94-22017
LA-UR-93-3502 ..... p 1997 N94-21965 #
LA-UR-93-3516 ..... p 1977 N94-22572 #

LA-12300-MS ..... p 1965 N94-22403 #
LA-12622-T ..... p 1732 N94-20479 #
LA-12646-C ..... p 1917 N94-21851 #

LBL-33225 ..... p 2016 N94-20323

LBL-33226 ..... p 1979 N94-19989 #
LBL-33272 ..... p 1979 N94-20274 #
LBL-33278 ..... p 1980 N94-20292 #
LBL-33282 ..... p 1981 N94-21440 #
LBL-33288 ..... p 1980 N94-20290 #
LBL-33303 ..... p 1980 N94-20475 #
LBL-33309 ..... p 1979 N94-20273 #
LBL-33355 ..... p 1982 N94-21974 #
LBL-33575 ..... p 1988 N94-21528 #
LBL-33608 ..... p 1992 N94-20004 #
LBL-33786 ..... p 2034 N94-22041 #
LBL-33801 ..... p 1993 N94-20234 #
LBL-33802 ..... p 1981 N94-21439 #
LBL-33806 ..... p 1979 N94-20289 #
LBL-34015 ..... p 1820 N94-21975 #
LBL-34068 ..... p 1980 N94-20300 #
LBL-34224 ..... p 1884 N94-19826
LBL-34261 ..... p 1985 N94-20320
LBL-34278 ..... p 2030 N94-21763 #
LBL-34279 ..... p 2030 N94-21744 #
LBL-34294 ..... p 1972 N94-20291 #
LBL-34335 ..... p 1917 N94-21917
LBL-34367 ..... p 1809 N94-21545 #
LBL-34374 ..... p 1808 N94-21441 #
LBL-34384 ..... p 1947 N94-22563 #
LBL-34395 ..... p 2031 N94-21922 #
LBL-34410 ..... p 1683 N94-21947 #
LBL-34423 ..... p 1904 N94-20097 #
LBL-34450 ..... p 1707 N94-21856 #
LBL-34459 ..... p 1851 N94-21740 #
LBL-34462 ..... p 1990 N94-21868 #
LBL-34523 ..... p 2031 N94-21926 #
LBL-34553 ..... p 1859 N94-21928 #
LBL-34575 ..... p 2038 N94-22010 #

LESC-30354-B ..... p 1666 N94-22275 * #

LMI-DL207R1 ..... p 1828 N94-20468

LPI-TR-93-03-PT-1 ..... p 2142 N94-21859 * #
LPI-TR-93-04-PT-1 ..... p 2088 N94-20382 * #

LPI/TR-92-07-PT-1 ..... p 1811 N94-22430 * #

LSGN-143 ..... p 1917 N94-21917

LTR93-004 ..... p 1987 N94-21172 #

M-661 ..... p 1651 N94-22094
M-733 ..... p 1653 N94-20141 * #

MATHS-REPT-A-188 ..... p 1822 N94-20146 #

MDC-93B0465 ..... p 1692 N94-21320 #

MEMO-INF-92-60 ..... p 1963 N94-21058
MEMO-INF-92-64 ..... p 1940 N94-20242 #
MEMO-INF-92-66 ..... p 1913 N94-21313
MEMO-INF-92-67 ..... p 1914 N94-21454
MEMO-INF-92-70 ..... p 2045 N94-22276
MEMO-INF-92-71 ..... p 1909 N94-21045
MEMO-INF-92-72 ..... p 2043 N94-21071

MEMO-1075 ..... p 1953 N94-21072
MEMO-1077 ..... p 1738 N94-21073
MEMO-1078 ..... p 1953 N94-21074
MEMO-1082 ..... p 1953 N94-21075
MEMO-1083 ..... p 1963 N94-21076
MEMO-1084 ..... p 1953 N94-21046
MEMO-1085 ..... p 1953 N94-21047
MEMO-1086 ..... p 1953 N94-21048
MEMO-1089 ..... p 1944 N94-21140

MIT-AI-TR-1426 ..... p 1608 N94-21167 #

MIT-AIM-1433 ..... p 1964 N94-21215 #

MLM-3787 ..... p 1959 N94-21655 #

MML-TR-93-09 ..... p 1648 N94-21268 #

MML-1993-1 ..... p 1674 N94-20550 #

MP-93-078 ..... p 1974 N94-21461 #

MPA-707 ..... p 2081 N94-21578 * #

MPE-PREPRINT-235 ..... p 2149 N94-20602 * #
MPE-PREPRINT-238 ..... p 2054 N94-20174 * #
MPE-PREPRINT-242 ..... p 2055 N94-21579 * #
MPE-PREPRINT-246 ..... p 2054 N94-20175 * #

MPE-239 ..... p 2081 N94-21138

MPIM-90 ..... p 1860 N94-22283 #

MPIS-106/1993 ..... p 1798 N94-20145 #

MRL-TN-627 ..... p 1711 N94-19906 #
MRL-TN-688 ..... p 1881 N94-19905

NAS 1.15:104027 ..... p 1635 N94-20035 * #
NAS 1.15:104092-REV-1 ..... p 1900 N94-22100 * #
NAS 1.15:104592 ..... p 1870 N94-21862 * #
NAS 1.15:104593 ..... p 1868 N94-21605 * #
NAS 1.15:104778 ..... p 1676 N94-21834 * #
NAS 1.15:104782 ..... p 1893 N94-21863 * #
NAS 1.15:104785 ..... p 1946 N94-21550 * #
NAS 1.15:105974 ..... p 1642 N94-21590 * #
NAS 1.15:106190 ..... p 1692 N94-21604 * #
NAS 1.15:106285 ..... p 1675 N94-21488 * #
NAS 1.15:106303 ..... p 1732 N94-20497 * #
NAS 1.15:106335 ..... p 1830 N94-20171 * #
NAS 1.15:106349 ..... p 1830 N94-20170 * #
NAS 1.15:106368 ..... p 1832 N94-21757 * #
NAS 1.15:106393 ..... p 1984 N94-20140 * #
NAS 1.15:106394 ..... p 1798 N94-20167 * #
NAS 1.15:106396 ..... p 1667 N94-20062 * #
NAS 1.15:106399 ..... p 1637 N94-20534 * #
NAS 1.15:106402 ..... p 1959 N94-21588 * #
NAS 1.15:106404 ..... p 1637 N94-20563 * #
NAS 1.15:106409 ..... p 1638 N94-22274 * #
NAS 1.15:106411 ..... p 1638 N94-21591 * #
NAS 1.15:106412 ..... p 1715 N94-21589 * #
NAS 1.15:106413 ..... p 1714 N94-21564 * #
NAS 1.15:106415 ..... p 1654 N94-21570 * #
NAS 1.15:106418 ..... p 1649 N94-21759 * #
NAS 1.15:106421 ..... p 1636 N94-20136 * #
NAS 1.15:106424 ..... p 1741 N94-21567 * #
NAS 1.15:106427 ..... p 1799 N94-20177 * #
NAS 1.15:106431 ..... p 1826 N94-21756 * #
NAS 1.15:106435 ..... p 1649 N94-21758 * #
NAS 1.15:106438 ..... p 1649 N94-21586 * #
NAS 1.15:106439 ..... p 1713 N94-21760 * #
NAS 1.15:106440 ..... p 1650 N94-21742 * #
NAS 1.15:106441 ..... p 1769 N94-21808 * #
NAS 1.15:106444 ..... p 1670 N94-21809 * #
NAS 1.15:106446 ..... p 1656 N94-21581 * #
NAS 1.15:106448 ..... p 1648 N94-21563 * #
NAS 1.15:108245 ..... p 2057 N94-22438 * #
NAS 1.15:108430 ..... p 2030 N94-21807 * #
NAS 1.15:108431 ..... p 1689 N94-20100 * #
NAS 1.15:108432 ..... p 1656 N94-21859 * #
NAS 1.15:108433 ..... p 1671 N94-21860 * #
NAS 1.15:108434 ..... p 1825 N94-21580 * #
NAS 1.15:108753 ..... p 1947 N94-22270 * #
NAS 1.15:108794 ..... p 1798 N94-20104 * #
NAS 1.15:109032 ..... p 1832 N94-21624 * #
NAS 1.15:109189 ..... p 1656 N94-21884 * #
NAS 1.15:109344 ..... p 1653 N94-20192 * #
NAS 1.15:109347 ..... p 1666 N94-19818 * #
NAS 1.15:109350 ..... p 1897 N94-21812 * #
NAS 1.15:109377 ..... p 2053 N94-21736 *
NAS 1.15:109378 ..... p 2054 N94-21738 *
NAS 1.15:109382 ..... p 1967 N94-20211 * #
NAS 1.15:109389 ..... p 2149 N94-20602 * #
NAS 1.15:109390 ..... p 2040 N94-21623 * #
NAS 1.15:109392 ..... p 2040 N94-21638 * #
NAS 1.15:109393 ..... p 2040 N94-21625 * #
NAS 1.15:4360 ..... p 1643 N94-21606 * #
NAS 1.15:4446 ..... p 1635 N94-21490 * #
NAS 1.15:4487 ..... p 1939 N94-20089 * #
NAS 1.15:4496 ..... p 1669 N94-20102 * #
NAS 1.15:4551 ..... p 1649 N94-21879 * #
NAS 1.18:1430.2 ..... p 2042 N94-20308 * #
NAS 1.19:291 ..... p 1669 N94-20226 * #
NAS 1.19:297 ..... p 2038 N94-20129 * #
NAS 1.21:6101(06) ..... p 2040 N94-21499 * #
NAS 1.21:6101(07) ..... p 2039 N94-21497 * #
NAS 1.21:7011(383) ..... p 1892 N94-21288 *
NAS 1.21:7037(294) ..... p 1635 N94-20267 *
NAS 1.21:7039(44)-SECT-1 ..... p 2043 N94-21254 *
NAS 1.26:109376 ..... p 2053 N94-21737 *
NAS 1.26:177615 ..... p 1646 N94-21592 * #
NAS 1.26:177627 ..... p 1914 N94-21489 * #
NAS 1.26:177628 ..... p 1966 N94-21881 * #
NAS 1.26:177633 ..... p 1897 N94-21784 * #
NAS 1.26:188269 ..... p 1666 N94-22275 * #
NAS 1.26:189192-VOL-1 ..... p 1648 N94-21582 * #
NAS 1.26:189192-VOL-2 ..... p 1648 N94-21583 * #
NAS 1.26:189309 ..... p 2055 N94-21295 * #
NAS 1.26:189310 ..... p 2054 N94-20142 * #
NAS 1.26:189311 ..... p 2055 N94-21498 * #
NAS 1.26:189318 ..... p 1837 N94-20284 * #
NAS 1.26:191090 ..... p 1670 N94-21565 * #
NAS 1.26:191135 ..... p 1671 N94-21874 * #
NAS 1.26:191136 ..... p 1846 N94-21179 * #
NAS 1.26:191149 ..... p 1666 N94-21864 * #
NAS 1.26:191162 ..... p 1809 N94-21607 * #
NAS 1.26:191200 ..... p 1762 N94-21566 * #
NAS 1.26:191460 ..... p 1698 N94-20039 * #
NAS 1.26:191466 ..... p 1937 N94-22414 * #
NAS 1.26:191535 ..... p 1959 N94-21568 * #
NAS 1.26:191536 ..... p 1804 N94-21861 * #
NAS 1.26:191537 ..... p 1797 N94-20033 * #
NAS 1.26:191540 ..... p 1915 N94-21584 * #
NAS 1.26:191543 ..... p 1804 N94-21880 * #
NAS 1.26:191549 ..... p 1804 N94-21875 * #
NAS 1.26:191549-VOL-1 ..... p 1644 N94-22277 * #
NAS 1.26:191549-VOL-2 ..... p 1644 N94-22278 * #
NAS 1.26:191555 ..... p 1950 N94-20092 * #
NAS 1.26:191557 ..... p 1950 N94-20057 * #
NAS 1.26:191558 ..... p 1914 N94-21403 * #
NAS 1.26:191559 ..... p 1643 N94-21629 * #
NAS 1.26:191562 ..... p 1968 N94-21741 * #
NAS 1.26:191565 ..... p 1965 N94-21463 * #
NAS 1.26:192272 ..... p 1882 N94-20131 * #
NAS 1.26:193149 ..... p 2092 N94-20636 * #
NAS 1.26:193177 ..... p 2019 N94-20971 * #
NAS 1.26:193388 ..... p 1865 N94-20535 * #
NAS 1.26:193422 ..... p 2041 N94-20133 * #
NAS 1.26:193423 ..... p 1837 N94-20205 * #
NAS 1.26:193485 ..... p 1972 N94-20130 * #
NAS 1.26:193553 ..... p 2142 N94-21659 * #
NAS 1.26:193643 ..... p 1930 N94-21065 * #
NAS 1.26:193729 ..... p 2041 N94-20158 * #
NAS 1.26:193813 ..... p 1816 N94-20341 * #
NAS 1.26:193860 ..... p 2042 N94-20268 * #
NAS 1.26:193874 ..... p 1670 N94-21271 * #
NAS 1.26:194154 ..... p 2016 N94-20340 * #
NAS 1.26:194173 ..... p 1717 N94-20269 * #
NAS 1.26:194179 ..... p 2055 N94-20204 * #
NAS 1.26:194265 ..... p 1855 N94-20132 * #
NAS 1.26:194270 ..... p 1701 N94-20347 * #
NAS 1.26:194271 ..... p 2041 N94-20134 * #
NAS 1.26:194275 ..... p 1716 N94-20160 * #
NAS 1.26:194276 ..... p 1885 N94-21897 * #
NAS 1.26:194360 ..... p 1905 N94-20228 * #
NAS 1.26:194371 ..... p 1994 N94-21289 * #
NAS 1.26:194547 ..... p 1799 N94-20210 * #
NAS 1.26:194561 ..... p 1830 N94-20159 * #
NAS 1.26:194568 ..... p 1893 N94-20168 * #
NAS 1.26:194581 ..... p 1716 N94-20139 * #
NAS 1.26:194584 ..... p 1811 N94-22430 * #
NAS 1.26:194591 ..... p 1763 N94-21694 * #
NAS 1.26:194600 ..... p 1679 N94-20169 * #
NAS 1.26:194602 ..... p 1643 N94-20148 * #
NAS 1.26:194627 ..... p 1864 N94-20138 * #
NAS 1.26:194628 ..... p 1636 N94-20014 * #
NAS 1.26:194629 ..... p 1718 N94-20403 * #
NAS 1.26:194635 ..... p 1984 N94-20128 * #
NAS 1.26:194644 ..... p 1753 N94-21079 * #
NAS 1.26:194679 ..... p 2017 N94-20346 * #
NAS 1.26:194683 ..... p 1895 N94-20063 * #
NAS 1.26:194684 ..... p 2042 N94-20363 * #
NAS 1.26:194685 ..... p 1821 N94-20044 * #
NAS 1.26:194687 ..... p 1673 N94-20172 * #
NAS 1.26:194688 ..... p 1846 N94-20229 * #
NAS 1.26:194689 ..... p 1657 N94-20173 * #
NAS 1.26:194691 ..... p 2043 N94-21270 * #
NAS 1.26:194692 ..... p 2081 N94-21578 * #
NAS 1.26:194693 ..... p 1845 N94-20066 * #
NAS 1.26:194694 ..... p 2088 N94-20048 * #
NAS 1.26:194696 ..... p 1931 N94-21272 * #
NAS 1.26:194697 ..... p 1806 N94-19920 *
NAS 1.26:194698 ..... p 2054 N94-20174 * #
NAS 1.26:194699 ..... p 2055 N94-21579 * #
NAS 1.26:194702 ..... p 1638 N94-21776 * #
NAS 1.26:194703 ..... p 1741 N94-21885 * #
NAS 1.26:194704 ..... p 2030 N94-21778 * #
NAS 1.26:194705 ..... p 2056 N94-21779 * #
NAS 1.26:194706 ..... p 1797 N94-20037 * #
NAS 1.26:194707 ..... p 1830 N94-20036 * #
NAS 1.26:194709 ..... p 2056 N94-22281 * #
NAS 1.26:194710 ..... p 1804 N94-22027 * #
NAS 1.26:194711 ..... p 1982 N94-21878 * #
NAS 1.26:194713 ..... p 2080 N94-20337 * #
NAS 1.26:194715 ..... p 1832 N94-21814 * #
NAS 1.26:194716 ..... p 1671 N94-21882 * #
NAS 1.26:194718 ..... p 1676 N94-21777 * #
NAS 1.26:194720 ..... p 1656 N94-21813 * #
NAS 1.26:194721-VOL-1 ..... p 1671 N94-22428 * #
NAS 1.26:194722 ..... p 1637 N94-21054 * #
NAS 1.26:194723 ..... p 1939 N94-20212 * #
NAS 1.26:194724 ..... p 1897 N94-20336 * #
NAS 1.26:194725 ..... p 1858 N94-21836 * #
NAS 1.26:194726 ..... p 2147 N94-21815 * #
NAS 1.26:194727 ..... p 2147 N94-21832 * #
NAS 1.26:194728 ..... p 1856 N94-20537 * #
NAS 1.26:194729 ..... p 1810 N94-21876 * #
NAS 1.26:194730 ..... p 1859 N94-22026 * #
NAS 1.26:194731 ..... p 2056 N94-21835 * #
NAS 1.26:194732 ..... p 1638 N94-21833 * #
NAS 1.26:194734 ..... p 1895 N94-20338 * #
NAS 1.26:194736 ..... p 1666 N94-21780 * #
NAS 1.26:194738 ..... p 1858 N94-21811 * #
NAS 1.26:194739 ..... p 1895 N94-21810 * #
NAS 1.26:194740 ..... p 1950 N94-20034 * #

NAS 1.26:194741 ..... p 1676 N94-21743 * #
NAS 1.26:194744 ..... p 2147 N94-21877 * #
NAS 1.26:194745 ..... p 1818 N94-21817 * #
NAS 1.26:194750 ..... p 1642 N94-21818 * #
NAS 1.26:194759 ..... p 1823 N94-20538 * #
NAS 1.26:194760 ..... p 1865 N94-20353 * #
NAS 1.26:194761 ..... p 1967 N94-20523 * #
NAS 1.26:194763 ..... p 2150 N94-21781 * #
NAS 1.26:194764 ..... p 2150 N94-21782 * #
NAS 1.26:194767 ..... p 2040 N94-21821 * #
NAS 1.26:194768 ..... p 1842 N94-22374 * #
NAS 1.26:194773 ..... p 2055 N94-20344 * #
NAS 1.26:194778 ..... p 2043 N94-21055 * #
NAS 1.26:194781 ..... p 1804 N94-21820 * #
NAS 1.26:194782 ..... p 1647 N94-21819 * #
NAS 1.26:194786 ..... p 1650 N94-20524 * #
NAS 1.26:194790 ..... p 1921 N94-22376 * #
NAS 1.26:194791 ..... p 1921 N94-22375 * #
NAS 1.26:194797 ..... p 1907 N94-20376 * #
NAS 1.26:194798 ..... p 1899 N94-20549 * #
NAS 1.26:194799 ..... p 2054 N94-20175 * #
NAS 1.26:194802 ..... p 1837 N94-20951 * #
NAS 1.26:194808 ..... p 2055 N94-20952 * #
NAS 1.26:194814 ..... p 1856 N94-20362 * #
NAS 1.26:194817 ..... p 2045 N94-21865 * #
NAS 1.26:194831 ..... p 2088 N94-20382 * #
NAS 1.26:4547 ..... p 1642 N94-22373 * #
NAS 1.26:4556 ..... p 1968 N94-21608 * #
NAS 1.26:4557 ..... p 1905 N94-20149 * #
NAS 1.26:4559 ..... p 1842 N94-22345 * #
NAS 1.26:4560 ..... p 1842 N94-21585 * #
NAS 1.55:10119 ..... p 1918 N94-22350 * #
NAS 1.55:10124 ..... p 1654 N94-21790 * #
NAS 1.55:3224-PT-2 ..... p 1955 N94-21464 * #
NAS 1.55:3230 ..... p 1833 N94-22608 * #
NAS 1.55:3234 ..... p 1868 N94-21639 * #
NAS 1.55:3238 ..... p 1871 N94-22292 * #
NAS 1.55:3241 ..... p 1931 N94-21323 * #
NAS 1.55:3243 ..... p 2146 N94-21883 * #
NAS 1.60:3385 ..... p 1637 N94-21569 * #
NAS 1.60:3422 ..... p 1895 N94-20137 * #
NAS 1.60:3424 ..... p 1896 N94-20606 * #
NAS 1.60:3432 ..... p 1653 N94-20141 * #
NAS 1.60:3433 ..... p 1897 N94-21627 * #
NAS 1.60:3441 ..... p 1741 N94-21783 * #
NAS 1.61:1124-REV-3 ..... p 1676 N94-21889 * #
NAS 1.61:1322 ..... p 1884 N94-21628 * #
NAS 1.83:201 ..... p 2054 N94-21739 *

NASA-CASE-ARC-11921-1 ..... p 1800 N94-20371 *

NASA-CASE-GSC-13442-1 ..... p 1823 N94-20494 * #
NASA-CASE-GSC-13454-1 ..... p 1821 N94-20126 *
NASA-CASE-GSC-13462-1 ..... p 1986 N94-20591 *
NASA-CASE-GSC-13503-1 ..... p 1822 N94-20127 *
NASA-CASE-GSC-13543-1 ..... p 1985 N94-20240 *

NASA-CASE-LAR-13805-1 ..... p 1822 N94-20365 *
NASA-CASE-LAR-14033-2 ..... p 1800 N94-20495 *
NASA-CASE-LAR-14418-15-B ..... p 1718 N94-20368 *
NASA-CASE-LAR-14471-1 ..... p 1702 N94-20377 *
NASA-CASE-LAR-14525-1-CU ..... p 1986 N94-20378 *
NASA-CASE-LAR-14565-1-CU ..... p 1822 N94-20369 *
NASA-CASE-LAR-14606-1-CU ..... p 1672 N94-20540 *
NASA-CASE-LAR-14607-1-SB ..... p 1986 N94-20586 *
NASA-CASE-LAR-14608-1 ..... p 1702 N94-20374 *
NASA-CASE-LAR-14747-1 ..... p 1650 N94-20556 *
NASA-CASE-LAR-14763-1 ..... p 1702 N94-20373 *
NASA-CASE-LAR-14789-1 ..... p 1824 N94-20587 *

NASA-CASE-LEW-15216-1 ..... p 1822 N94-20375 *
NASA-CASE-LEW-15218-1 ..... p 1801 N94-20588 *
NASA-CASE-LEW-15223-1 ..... p 2017 N94-20381 *
NASA-CASE-LEW-15241-1 ..... p 1673 N94-20539 *
NASA-CASE-LEW-15308-1 ..... p 1846 N94-20196 *
NASA-CASE-LEW-15314-1 ..... p 1700 N94-20195 *
NASA-CASE-LEW-15489-1 ..... p 1703 N94-20529 *

NASA-CASE-MFS-28522-1 ..... p 1823 N94-20380 *
NASA-CASE-MFS-28547-1 ..... p 1669 N94-20370 *
NASA-CASE-MFS-28569-1 ..... p 1703 N94-20541 *
NASA-CASE-MFS-28633-1 ..... p 1896 N94-20493 *
NASA-CASE-MFS-28658-1 ..... p 1800 N94-20361 *
NASA-CASE-MFS-28682-1 ..... p 1701 N94-20359 *
NASA-CASE-MFS-28688-1 ..... p 2017 N94-20528 *
NASA-CASE-MFS-28720-1 ..... p 1823 N94-20379 *

NASA-CASE-MSC-21613-1 ..... p 1907 N94-20492 *
NASA-CASE-MSC-21631-1 ..... p 1993 N94-20491 *
NASA-CASE-MSC-21723-1 ..... p 1657 N94-20367 *
NASA-CASE-MSC-21752-1 ..... p 1895 N94-20194 *
NASA-CASE-MSC-21775-1 ..... p 1890 N94-20372 *
NASA-CASE-MSC-21793-1 ..... p 1654 N94-20304 *
NASA-CASE-MSC-21823-1 ..... p 1824 N94-20589 *
NASA-CASE-MSC-21874-1 ..... p 1942 N94-20366 *
NASA-CASE-MSC-21975-1 ..... p 1653 N94-20339 *
NASA-CASE-MSC-22082-1 ..... p 1658 N94-20590 *

NASA-CASE-NPO-17807-2-CU ..... p 1942 N94-20360 *
NASA-CASE-NPO-18146-1-CU ..... p 1986 N94-20345 *
NASA-CASE-NPO-18192-1-CU ..... p 1669 N94-20496 *
NASA-CASE-NPO-18194-1-CU ..... p 1985 N94-20305 *
NASA-CASE-NPO-18278-1-CU ..... p 1985 N94-20303 *

NASA-CP-10119 ..... p 1918 N94-22350 * #
NASA-CP-10124 ..... p 1654 N94-21790 * #
NASA-CP-3224-PT-2 ..... p 1955 N94-21464 * #
NASA-CP-3230 ..... p 1833 N94-22608 * #
NASA-CP-3234 ..... p 1868 N94-21639 * #
NASA-CP-3238 ..... p 1871 N94-22292 * #
NASA-CP-3241 ..... p 1931 N94-21323 * #
NASA-CP-3243 ..... p 2146 N94-21883 * #

NASA-CR-177615 ..... p 1646 N94-21592 * #
NASA-CR-177627 ..... p 1914 N94-21489 * #
NASA-CR-177628 ..... p 1966 N94-21881 * #
NASA-CR-177633 ..... p 1897 N94-21784 * #
NASA-CR-188269 ..... p 1666 N94-22275 * #
NASA-CR-189192-VOL-1 ..... p 1648 N94-21582 * #
NASA-CR-189192-VOL-2 ..... p 1648 N94-21583 * #
NASA-CR-189309 ..... p 2055 N94-21295 * #
NASA-CR-189310 ..... p 2054 N94-20142 * #
NASA-CR-189311 ..... p 2055 N94-21498 * #
NASA-CR-189318 ..... p 1837 N94-20284 * #
NASA-CR-191090 ..... p 1670 N94-21565 * #
NASA-CR-191135 ..... p 1671 N94-21874 * #
NASA-CR-191136 ..... p 1846 N94-21179 * #
NASA-CR-191149 ..... p 1666 N94-21864 * #
NASA-CR-191162 ..... p 1809 N94-21607 * #
NASA-CR-191200 ..... p 1762 N94-21566 * #
NASA-CR-191460 ..... p 1898 N94-20039 * #
NASA-CR-191466 ..... p 1937 N94-22414 * #
NASA-CR-191535 ..... p 1959 N94-21568 * #
NASA-CR-191536 ..... p 1804 N94-21861 * #
NASA-CR-191537 ..... p 1797 N94-20033 * #
NASA-CR-191540 ..... p 1915 N94-21584 * #
NASA-CR-191543 ..... p 1804 N94-21880 * #
NASA-CR-191548 ..... p 1804 N94-21875 * #
NASA-CR-191549-VOL-1 ..... p 1644 N94-22277 * #
NASA-CR-191549-VOL-2 ..... p 1644 N94-22278 * #
NASA-CR-191555 ..... p 1950 N94-20092 * #
NASA-CR-191557 ..... p 1950 N94-20087 * #
NASA-CR-191558 ..... p 1914 N94-21462 * #
NASA-CR-191559 ..... p 1643 N94-21629 * #
NASA-CR-191562 ..... p 1968 N94-21741 * #
NASA-CR-191565 ..... p 1965 N94-21463 * #
NASA-CR-192272 ..... p 1882 N94-20131 * #
NASA-CR-193149 ..... p 2092 N94-20636 * #
NASA-CR-193177 ..... p 2019 N94-20971 * #
NASA-CR-193388 ..... p 1865 N94-20535 * #
NASA-CR-193422 ..... p 2041 N94-20133 * #
NASA-CR-193423 ..... p 1837 N94-20205 * #
NASA-CR-193485 ..... p 1972 N94-20130 * #
NASA-CR-193553 ..... p 2142 N94-21659 * #
NASA-CR-193643 ..... p 1930 N94-21065 * #
NASA-CR-193729 ..... p 2041 N94-20158 * #
NASA-CR-193813 ..... p 1816 N94-20341 * #
NASA-CR-193860 ..... p 2042 N94-20268 * #
NASA-CR-193874 ..... p 1670 N94-21271 * #
NASA-CR-194154 ..... p 2016 N94-20340 * #
NASA-CR-194173 ..... p 1717 N94-20269 * #
NASA-CR-194179 ..... p 2055 N94-20204 * #
NASA-CR-194265 ..... p 1855 N94-20132 * #
NASA-CR-194270 ..... p 1701 N94-20347 * #
NASA-CR-194271 ..... p 2041 N94-20134 * #
NASA-CR-194275 ..... p 1716 N94-20160 * #
NASA-CR-194276 ..... p 1885 N94-21897 * #
NASA-CR-194360 ..... p 1905 N94-20228 * #
NASA-CR-194371 ..... p 1994 N94-21289 * #
NASA-CR-194547 ..... p 1799 N94-20210 * #
NASA-CR-194561 ..... p 1830 N94-20159 * #
NASA-CR-194566 ..... p 1893 N94-20168 * #
NASA-CR-194581 ..... p 1716 N94-20139 * #
NASA-CR-194584 ..... p 1811 N94-22430 * #
NASA-CR-194591 ..... p 1763 N94-21694 * #
NASA-CR-194600 ..... p 1679 N94-20169 * #
NASA-CR-194602 ..... p 1643 N94-20148 * #
NASA-CR-194627 ..... p 1864 N94-20138 * #
NASA-CR-194628 ..... p 1636 N94-20014 * #
NASA-CR-194629 ..... p 1718 N94-20403 * #
NASA-CR-194635 ..... p 1984 N94-20128 * #
NASA-CR-194644 ..... p 1753 N94-21079 * #
NASA-CR-194679 ..... p 2017 N94-20346 * #
NASA-CR-194683 ..... p 1895 N94-20063 * #
NASA-CR-194684 ..... p 2042 N94-20363 * #
NASA-CR-194685 ..... p 1821 N94-20044 * #
NASA-CR-194687 ..... p 1673 N94-20172 * #
NASA-CR-194688 ..... p 1846 N94-20229 * #
NASA-CR-194689 ..... p 1657 N94-20173 * #
NASA-CR-194691 ..... p 2043 N94-21270 * #
NASA-CR-194691 ..... p 2081 N94-21578 * #
NASA-CR-194693 ..... p 1845 N94-20066 * #
NASA-CR-194694 ..... p 2088 N94-20048 * #
NASA-CR-194696 ..... p 1931 N94-21272 * #
NASA-CR-194697 ..... p 1806 N94-19920 *
NASA-CR-194698 ..... p 2054 N94-20174 * #
NASA-CR-194699 ..... p 2055 N94-21579 * #
NASA-CR-194702 ..... p 1638 N94-21776 * #
NASA-CR-194703 ..... p 1741 N94-21885 * #
NASA-CR-194704 ..... p 2030 N94-21778 * #
NASA-CR-194705 ..... p 2056 N94-21779 * #
NASA-CR-194706 ..... p 1797 N94-20037 * #
NASA-CR-194707 ..... p 1830 N94-20036 * #
NASA-CR-194709 ..... p 2056 N94-22261 * #
NASA-CR-194710 ..... p 1804 N94-22027 * #
NASA-CR-194711 ..... p 1982 N94-21878 * #
NASA-CR-194713 ..... p 2080 N94-20337 * #
NASA-CR-194715 ..... p 1832 N94-21814 * #
NASA-CR-194716 ..... p 1671 N94-21882 * #
NASA-CR-194718 ..... p 1676 N94-21777 * #
NASA-CR-194720 ..... p 1656 N94-21813 * #
NASA-CR-194721-VOL-1 ..... p 1671 N94-22428 * #
NASA-CR-194722 ..... p 1637 N94-21054 * #
NASA-CR-194723 ..... p 1939 N94-20212 * #
NASA-CR-194724 ..... p 1897 N94-20336 * #
NASA-CR-194725 ..... p 1858 N94-21836 * #
NASA-CR-194726 ..... p 2147 N94-21815 * #
NASA-CR-194727 ..... p 2147 N94-21832 * #
NASA-CR-194728 ..... p 1856 N94-20537 * #
NASA-CR-194729 ..... p 1810 N94-21876 * #
NASA-CR-194730 ..... p 1859 N94-22026 * #
NASA-CR-194731 ..... p 2056 N94-21835 * #
NASA-CR-194732 ..... p 1638 N94-21833 * #
NASA-CR-194734 ..... p 1895 N94-20338 * #
NASA-CR-194736 ..... p 1666 N94-21780 * #
NASA-CR-194738 ..... p 1858 N94-21811 * #
NASA-CR-194739 ..... p 1895 N94-21810 * #
NASA-CR-194740 ..... p 1950 N94-20034 * #
NASA-CR-194741 ..... p 1676 N94-21743 * #
NASA-CR-194744 ..... p 2147 N94-21877 * #
NASA-CR-194745 ..... p 1818 N94-21817 * #
NASA-CR-194750 ..... p 1642 N94-21818 * #
NASA-CR-194759 ..... p 1823 N94-20538 * #
NASA-CR-194760 ..... p 1865 N94-20353 * #
NASA-CR-194761 ..... p 1967 N94-20523 * #
NASA-CR-194763 ..... p 2150 N94-21781 * #
NASA-CR-194764 ..... p 2150 N94-21782 * #
NASA-CR-194767 ..... p 2040 N94-21821 * #
NASA-CR-194768 ..... p 1842 N94-22374 * #
NASA-CR-194773 ..... p 2055 N94-20344 * #
NASA-CR-194778 ..... p 2043 N94-21055 * #
NASA-CR-194781 ..... p 1804 N94-21820 * #
NASA-CR-194782 ..... p 1647 N94-21819 * #
NASA-CR-194786 ..... p 1650 N94-20524 * #
NASA-CR-194790 ..... p 1921 N94-22376 * #
NASA-CR-194791 ..... p 1921 N94-22375 * #
NASA-CR-194797 ..... p 1907 N94-20376 * #
NASA-CR-194798 ..... p 1899 N94-20549 * #
NASA-CR-194799 ..... p 2054 N94-20175 * #
NASA-CR-194802 ..... p 1837 N94-20951 * #
NASA-CR-194808 ..... p 2055 N94-20952 * #
NASA-CR-194814 ..... p 1856 N94-20362 * #
NASA-CR-194817 ..... p 2045 N94-21865 * #
NASA-CR-194831 ..... p 2088 N94-20382 * #
NASA-CR-4547 ..... p 1642 N94-22373 * #
NASA-CR-4556 ..... p 1968 N94-21608 * #
NASA-CR-4557 ..... p 1905 N94-20149 * #
NASA-CR-4559 ..... p 1842 N94-22345 * #
NASA-CR-4560 ..... p 1842 N94-21585 * #

NASA-EP-291 ..... p 1669 N94-20226 * #
NASA-EP-297 ..... p 2038 N94-20129 * #

NASA-NP-201 ..... p 2054 N94-21739 *

NASA-RP-1014 ..... p 1676 N94-21889 * #
NASA-RP-1124-REV-2 ..... p 1676 N94-21889 * #
NASA-RP-1124-REV-3 ..... p 1676 N94-21889 * #
NASA-RP-1322 ..... p 1884 N94-21628 * #

NASA-SP-6101(06) ..... p 2040 N94-21499 * #
NASA-SP-6101(07) ..... p 2039 N94-21497 * #
NASA-SP-7011(383) ..... p 1892 N94-21288 *
NASA-SP-7037(294) ..... p 1635 N94-20267 *
NASA-SP-7039(44)-SECT-1 ..... p 2043 N94-21254 *

NASA-TM-104027 ..... p 1635 N94-20035 * #
NASA-TM-104092-REV-1 ..... p 1900 N94-22100 * #
NASA-TM-104592 ..... p 1870 N94-21862 * #
NASA-TM-104593 ..... p 1868 N94-21605 * #
NASA-TM-104778 ..... p 1676 N94-21834 * #
NASA-TM-104782 ..... p 1893 N94-21863 * #
NASA-TM-104785 ..... p 1946 N94-21550 * #
NASA-TM-105974 ..... p 1642 N94-21590 * #
NASA-TM-106190 ..... p 1692 N94-21604 * #
NASA-TM-106285 ..... p 1675 N94-21488 * #
NASA-TM-106303 ..... p 1732 N94-20497 * #
NASA-TM-106335 ..... p 1830 N94-20171 * #

NASA-TM-106349 ..... p 1830 N94-20170 * #
NASA-TM-106368 ..... p 1832 N94-21757 * #
NASA-TM-106393 ..... p 1984 N94-20140 * #
NASA-TM-106394 ..... p 1798 N94-20167 * #
NASA-TM-106396 ..... p 1667 N94-20062 * #
NASA-TM-106399 ..... p 1637 N94-20534 * #
NASA-TM-106402 ..... p 1959 N94-21588 * #
NASA-TM-106404 ..... p 1637 N94-20563 * #
NASA-TM-106409 ..... p 1638 N94-22274 * #
NASA-TM-106411 ..... p 1638 N94-21591 * #
NASA-TM-106412 ..... p 1715 N94-21589 * #
NASA-TM-106413 ..... p 1714 N94-21564 * #
NASA-TM-106415 ..... p 1654 N94-21570 * #
NASA-TM-106418 ..... p 1649 N94-21759 * #
NASA-TM-106421 ..... p 1636 N94-20136 * #
NASA-TM-106424 ..... p 1741 N94-21567 * #
NASA-TM-106427 ..... p 1799 N94-20177 * #
NASA-TM-106431 ..... p 1826 N94-21756 * #
NASA-TM-106435 ..... p 1649 N94-21758 * #
NASA-TM-106438 ..... p 1649 N94-21586 * #
NASA-TM-106439 ..... p 1713 N94-21760 * #
NASA-TM-106440 ..... p 1650 N94-21742 * #
NASA-TM-106441 ..... p 1769 N94-21808 * #
NASA-TM-106444 ..... p 1670 N94-21809 * #
NASA-TM-106446 ..... p 1656 N94-21581 * #
NASA-TM-106448 ..... p 1648 N94-21563 * #
NASA-TM-108245 ..... p 2057 N94-22438 * #
NASA-TM-108430 ..... p 2030 N94-21807 * #
NASA-TM-108431 ..... p 1689 N94-20100 * #
NASA-TM-108432 ..... p 1656 N94-21859 * #
NASA-TM-108433 ..... p 1671 N94-21860 * #
NASA-TM-108434 ..... p 1825 N94-21580 * #
NASA-TM-108753 ..... p 1947 N94-22270 * #
NASA-TM-108794 ..... p 1798 N94-20104 * #
NASA-TM-109032 ..... p 1832 N94-21624 * #
NASA-TM-109189 ..... p 1656 N94-21884 * #
NASA-TM-109344 ..... p 1653 N94-20192 * #
NASA-TM-109347 ..... p 1666 N94-19818 * #
NASA-TM-109350 ..... p 1897 N94-21812 * #
NASA-TM-109376 ..... p 2053 N94-21737 *
NASA-TM-109377 ..... p 2053 N94-21736 *
NASA-TM-109378 ..... p 2054 N94-21738 *
NASA-TM-109382 ..... p 1967 N94-20211 * #
NASA-TM-109389 ..... p 2149 N94-20602 * #
NASA-TM-109390 ..... p 2040 N94-21623 * #
NASA-TM-109392 ..... p 2040 N94-21638 * #
NASA-TM-109393 ..... p 2040 N94-21625 * #
NASA-TM-4360 ..... p 1643 N94-21606 * #
NASA-TM-4446 ..... p 1635 N94-21490 * #
NASA-TM-4487 ..... p 1939 N94-20089 * #
NASA-TM-4496 ..... p 1669 N94-20102 * #
NASA-TM-4551 ..... p 1649 N94-21879 * #

NASA-TN-D-7362 ..... p 1676 N94-21889 * #
NASA-TN-D-8008 ..... p 1676 N94-21889 * #

NASA-TP-3385 ..... p 1637 N94-21569 * #
NASA-TP-3422 ..... p 1895 N94-20137 * #
NASA-TP-3424 ..... p 1896 N94-20606 * #
NASA-TP-3432 ..... p 1653 N94-20141 * #
NASA-TP-3433 ..... p 1897 N94-21627 * #
NASA-TP-3441 ..... p 1741 N94-21783 * #

NATICK-TR-93/039 ..... p 1823 N94-20567

NAVY-CASE-73073 ..... p 1938 N94-19843
NAVY-CASE-73185 ..... p 1806 N94-19882
NAVY-CASE-74654 ..... p 1748 N94-19892 #
NAVY-CASE-74791 ..... p 1672 N94-20010 #
NAVY-CASE-75029 ..... p 1822 N94-20356 #
NAVY-CASE-75053 ..... p 1698 N94-19830 #
NAVY-CASE-75238 ..... p 1714 N94-20355 #

NAWCADIND-TR-2481 ..... p 1641 N94-19876

NAWCADPAX-TM-93-59-SY ..... p 1896 N94-21154

NAWCADWAR-92102-60 ..... p 1674 N94-20574 #
NAWCADWAR-93041-60 ..... p 1943 N94-20926
NAWCADWAR-93042-60 ..... p 1703 N94-20614 #

NCCOSC/RDT/E-TD-2499 ..... p 1929 N94-20472 #
NCCOSC/RDT/E-TD-2551 ..... p 1732 N94-20471
NCCOSC/RDT/E-TD-2565 ..... p 1739 N94-21235 #
NCCOSC/RDT/E-TD-2569-PT-3 .. p 1739 N94-21240 #

NCCOSC/RDT/E-TR-1553 ..... p 1881 N94-19952
NCCOSC/RDT/E-TR-1587 ..... p 1831 N94-21310 #
NCCOSC/RDT/E-TR-1617 ..... p 1737 N94-20620 #
NCCOSC/RDT/E-TR-1621 ..... p 1737 N94-20582 #
NCCOSC/RDT/E-TR-1623 ..... p 1987 N94-21236 #

NCEL-TR-941 ..... p 1882 N94-19979 #

NEDO-GET-9205 ..... p 1853 N94-22051 #
NEDO-GET-9208 ..... p 1849 N94-22043 #
NEDO-GET-9209 ..... p 1852 N94-22044 #
NEDO-GET-9210-1 ..... p 1853 N94-22258 #
NEDO-GET-9210-5 ..... p 1853 N94-22090 #
NEDO-GET-9213 ..... p 1853 N94-22259 #

NEDO-P-9201 ..... p 1848 N94-22013 #
NEDO-P-9202 ..... p 1849 N94-22014 #
NEDO-P-9203 ..... p 1713 N94-22091 #
NEDO-P-9204 ..... p 1849 N94-22030 #
NEDO-P-9218 ..... p 1850 N94-22092 #
NEDO-P-9220 ..... p 1849 N94-22052

NHB-1430.2 ..... p 2042 N94-20308 * #

NIAR-93-16 ..... p 2151 N94-20150 #
NIAR-93-1 ..... p 1635 N94-20191 #
NIAR-93-2 ..... p 1890 N94-20190 #
NIAR-93-4 ..... p 1641 N94-20189 #

NIPER-678 ..... p 2037 N94-20473 #

NIST/MONO-178 ..... p 1968 N94-21447

NIST/TN-1402 ..... p 1682 N94-21448 #

NLR-TP-90243-U ..... p 1841 N94-21015
NLR-TP-91001-U ..... p 1753 N94-21067 #

NOAA-TM-ERL-FSL-6 ..... p 1868 N94-21427 #

NPRDC-TN-94-1 ..... p 1894 N94-21434
NPRDC-TN-94-6 ..... p 2042 N94-20924

NRAD-TR-1608 ..... p 1868 N94-21356 #

NREL/CP-200-5768-VOL-2 ..... p 1847 N94-21562 #
NREL/CP-470-5777 ..... p 1847 N94-21616 #

NREL/TP-411-5749 ..... p 1699 N94-20047 #
NREL/TP-411-5760 ..... p 1850 N94-22257 #
NREL/TP-413-5740 ..... p 1845 N94-20095 #
NREL/TP-413-5752 ..... p 1848 N94-21827 #
NREL/TP-413-5759 ..... p 2029 N94-21617 #
NREL/TP-451-5452 ..... p 2029 N94-21615 #
NREL/TP-451-5591 ..... p 1845 N94-19805 #
NREL/TP-451-5650 ..... p 1845 N94-19925 #
NREL/TP-451-5651 ..... p 2013 N94-19939 #
NREL/TP-451-5653 ..... p 1847 N94-21614 #
NREL/TP-451-5733 ..... p 1849 N94-22015 #
NREL/TP-451-5737 ..... p 1688 N94-19985 #
NREL/TP-451-5758 ..... p 1848 N94-21826 #
NREL/TP-463-5475 ..... p 1748 N94-19902 #
NREL/TP-472-5539 ..... p 1846 N94-21298 #

NRL-CR/7410-93-0004 ..... p 1866 N94-20559

NRL/FR/7142-93-9563 ..... p 1883 N94-21358 #
NRL/FR/7227-93-9547 ..... p 1858 N94-21357 #
NRL/FR/7322-93-9443 ..... p 1883 N94-21222 #
NRL/FR/8105-93-9546 ..... p 1658 N94-20617 #
NRL/FR/8121-93-9565 ..... p 1657 N94-19896 #
NRL/FR/8154-93-9577-VOL-1 ..... p 1738 N94-21198 #
NRL/FR/8154-93-9578-VOL-2 ..... p 1739 N94-21218 #

NRL/MR/6793-93-7387 ..... p 1752 N94-20931
NRL/MR/7240-93-7049 ..... p 1837 N94-20028 #
NRL/MR/7340-93-7402 ..... p 1883 N94-21443 #
NRL/MR/7543-93-7209 ..... p 1866 N94-20579 #

NSWCDD/TR-92/372 ..... p 1929 N94-20571 #

NUSW-NPT-TD-10451 ..... p 1883 N94-20925

NUWC-NPT-TD-10375 ..... p 1737 N94-20949 #
NUWC-NPT-TD-10459 ..... p 1800 N94-20466

OHR-35 ..... p 1841 N94-21068 #
OHR-36 ..... p 1841 N94-21069 #
OHR-38 ..... p 1867 N94-21070 #

ORNL-TM-12375 ..... p 1942 N94-20573 #

ORNL/FMP-93/1 ..... p 1848 N94-21823 #

ORNL/M-2270 ..... p 1714 N94-20099 #

ORNL/SUB-86-SE793C ..... p 1677 N94-22022 #
ORNL/SUB-88-SB775/03 ..... p 1693 N94-21771
ORNL/SUB-89-SB182/1 ..... p 1702 N94-20481 #
ORNL/SUB-90-SF521/01 ..... p 1695 N94-21949 #

ORNL/TM-12200 ..... p 1694 N94-21948 #
ORNL/TM-12216 ..... p 1998 N94-22045 #
ORNL/TM-12363 ..... p 1707 N94-21822 #
ORNL/TM-12383 ..... p 1810 N94-21953 #
ORNL/TM-12404 ..... p 1960 N94-21967 #
ORNL/TM-12423 ..... p 1693 N94-21850
ORNL/TM-12426 ..... p 1960 N94-21966
ORNL/TM-12434 ..... p 1852 N94-22004 #
ORNL/TM-12439 ..... p 1918 N94-21924 #
ORNL/TM-12462 ..... p 1908 N94-20932 #

OTA-ISC-558 ..... p 1837 N94-20209 #

PAPER-C18 ..... p 1636 N94-20486

PB93-191732 ..... p 1903 N94-19992
PB93-191740 ..... p 1903 N94-19993
PB93-191765 ..... p 1903 N94-19994
PB93-191773 ..... p 1928 N94-19995
PB93-191781 ..... p 1928 N94-19996
PB93-191799 ..... p 1896 N94-20062
PB93-191807-PT-1 ..... p 1962 N94-20007
PB93-191815-PT-2 ..... p 1962 N94-20008
PB93-191823 ..... p 1928 N94-20009
PB93-191831 ..... p 1949 N94-19997
PB93-191948 ..... p 1963 N94-21066
PB93-192920 ..... p 1841 N94-21446
PB93-194827 ..... p 1851 N94-19998
PB93-200822 ..... p 1968 N94-21447
PB93-200889 ..... p 1682 N94-21448 #
PB93-202174 ..... p 1842 N94-21855
PB93-202240 ..... p 2044 N94-21449 #
PB93-202356 ..... p 1825 N94-21450 #
PB93-202364 ..... p 1825 N94-21451 #
PB93-202372 ..... p 1682 N94-21452 #
PB93-202448 ..... p 1825 N94-21424 #
PB93-202513 ..... p 1705 N94-21425 #
PB93-202521 ..... p 1714 N94-21426
PB93-202711 ..... p 1868 N94-21427 #
PB93-202885 ..... p 1641 N94-21428
PB93-205326 ..... p 1968 N94-22053
PB93-205334 ..... p 1969 N94-22054
PB93-206258 ..... p 1642 N94-22055
PB93-206597 ..... p 1826 N94-22093
PB93-211399 ..... p 1651 N94-22094
PB93-215226 ..... p 1960 N94-22096
PB93-215242 ..... p 1742 N94-22346
PB93-215259 ..... p 1742 N94-22347
PB93-215275 ..... p 1742 N94-22348
PB93-215283 ..... p 1742 N94-22349
PB93-215382 ..... p 1638 N94-22260 #
PB93-215424 ..... p 1969 N94-22261 #
PB93-215432 ..... p 1969 N94-22262 #
PB93-215465 ..... p 2038 N94-22095
PB93-215481 ..... p 1961 N94-22263 #
PB93-215499 ..... p 1961 N94-22264 #
PB93-215507 ..... p 1961 N94-22377 #
PB93-219301 ..... p 1842 N94-22097
PB93-219319 ..... p 1842 N94-22265
PB93-220085 ..... p 1918 N94-22098
PB93-220531 ..... p 1960 N94-22099
PB93-220663 ..... p 1961 N94-22266
PB93-221026 ..... p 1977 N94-22271
PB93-221034 ..... p 1805 N94-22272
PB93-221166 ..... p 2035 N94-22273

PGA-TR-91-3 ..... p 1801 N94-20915 #

PL-TR-92-1060 ..... p 1829 N94-19881
PL-TR-92-1065 ..... p 1717 N94-20329
PL-TR-92-2325 ..... p 1854 N94-19841
PL-TR-92-2333 ..... p 1864 N94-20068
PL-TR-92-3019 ..... p 1845 N94-20086
PL-TR-93-1027 ..... p 1831 N94-20572 #
PL-TR-93-2081 ..... p 1987 N94-21172 #
PL-TR-93-2131 ..... p 1858 N94-21206
PL-TR-93-2160 ..... p 1855 N94-20090
PL-TR-93-2180 ..... p 1654 N94-21429
PL-TR-93-3007-VOL-1 ..... p 2012 N94-19842

PNL-SA-20214 ..... p 1696 N94-22037 #
PNL-SA-21290 ..... p 1690 N94-20233 #
PNL-SA-22001 ..... p 1936 N94-22032 #
PNL-SA-22002 ..... p 1903 N94-19959 #
PNL-SA-22414 ..... p 1826 N94-22036
PNL-SA-22711 ..... p 1850 N94-19930 #

R/D-6917-AN-02 ..... p 1828 N94-19815
R/D-7145-AN-02 ..... p 1672 N94-20031 #

RDA-TR-43-0005-001 ..... p 1943 N94-20947 #

REPT-026845-910719 ..... p 2017 N94-20470
REPT-53-2380 ..... p 1681 N94-21168 #
REPT-59 ..... p 2147 N94-21150
REPT-725311-2 ..... p 1716 N94-20139 * #
REPT-84 ..... p 1855 N94-20155
REPT-85 ..... p 1993 N94-20156
REPT-87 ..... p 1851 N94-20154
REPT-92-100 ..... p 1822 N94-20157
REPT-92-46 ..... p 1953 N94-21059

REPT-92-80 ..... p 1950 N94-20032 #
REPT-93-24 ..... p 1712 N94-20927 #
REPT-93E02369 ..... p 1868 N94-21639 * #
REPT-93E02432 ..... p 1676 N94-21889 * #
REPT-93RC-010143 ..... p 1671 N94-21874 * #
REPT-94B00005 ..... p 1870 N94-21862 * #
REPT-94B00011 ..... p 1931 N94-21323 * #
REPT-94B00012 ..... p 1884 N94-21628 * #
REPT-94B00015 ..... p 1868 N94-21605 * #

RFP-4768 ..... p 1821 N94-19859 #

RIVM-679102010 ..... p 1851 N94-19998

RL-TR-93-129 ..... p 1749 N94-20110
RL-TR-93-130 ..... p 1740 N94-21518 #
RL-TR-93-135 ..... p 1971 N94-20083
RL-TR-93-146 ..... p 1715 N94-19816 #
RL-TR-93-148 ..... p 1651 N94-20011
RL-TR-93-163 ..... p 2041 N94-20106
RL-TR-93-25 ..... p 1761 N94-21256 #

RR-888-I-IMAG-124-LIFIA ..... p 1929 N94-20124 #
RR-889-M ..... p 1950 N94-20125 #
RR-891-I ..... p 1929 N94-20176 #
RR-894-M ..... p 1951 N94-20302 #
RR-895-M ..... p 1950 N94-20161 #
RR-896-M ..... p 1963 N94-20162 #
RR-898-M ..... p 1950 N94-20163 #
RR-899 ..... p 1905 N94-20164 #
RR-900-I ..... p 1963 N94-20165 #
RR-901-I ..... p 1749 N94-20166 #
RR-902-I ..... p 1951 N94-20237 #
RR-903-M ..... p 1905 N94-20201 #
RR-906-I ..... p 1963 N94-20202 #
RR-913-M ..... p 1950 N94-20200 #

RSL-TR-8243-2 ..... p 1715 N94-19823
RSL-TR-8750-1 ..... p 1858 N94-21811 * #
RSL-TR-8920-1 ..... p 1858 N94-21811 * #

S-735 ..... p 1676 N94-21834 * #
S-742 ..... p 1893 N94-21863 * #
S-744 ..... p 1896 N94-20606 * #
S-745 ..... p 1946 N94-21550 * #
S-750 ..... p 2146 N94-21883 * #
S-751 ..... p 1897 N94-21627 * #

SAFETY RESEARCH-93-1-VOL-1 p 1641 N94-21428

SAIC-93/1224-APPAT-158 ..... p 2147 N94-21877 * #

SAND-91-2579/2 ..... p 1809 N94-21556 #
SAND-92-1986 ..... p 1763 N94-21654 #
SAND-92-2089C ..... p 1904 N94-20052 #
SAND-92-2754C ..... p 1808 N94-20297 #
SAND-92-2779C ..... p 1683 N94-22031 #
SAND-92-2812C ..... p 1980 N94-20295 #
SAND-92-7343 ..... p 1805 N94-22386 #
SAND-93-0070 ..... p 1968 N94-21751 #
SAND-93-0114C ..... p 1762 N94-21634 #
SAND-93-0153C ..... p 1762 N94-21632 #
SAND-93-0178C ..... p 1916 N94-21635 #
SAND-93-0241C ..... p 1750 N94-20218 #
SAND-93-0298C ..... p 1748 N94-19844 #
SAND-93-0305C ..... p 1797 N94-19974 #
SAND-93-0336C ..... p 1706 N94-21526
SAND-93-0397C ..... p 1829 N94-19943 #
SAND-93-0406C ..... p 1829 N94-19927 #
SAND-93-0422C ..... p 1688 N94-19944 #
SAND-93-0438C ..... p 1916 N94-21761
SAND-93-0441C ..... p 1679 N94-20307 #
SAND-93-0455 ..... p 1993 N94-20261 #
SAND-93-0456C ..... p 1762 N94-21636 #
SAND-93-0510C ..... p 1713 N94-22033 #
SAND-93-0610 ..... p 1708 N94-21963 #
SAND-93-0641C ..... p 1829 N94-19940 #
SAND-93-0773 ..... p 1832 N94-21557 #
SAND-93-0785C ..... p 1973 N94-20306 #
SAND-93-0816C ..... p 1769 N94-21918 #
SAND-93-0832C ..... p 1748 N94-19884 #
SAND-93-0887C ..... p 1833 N94-21916 #
SAND-93-0940 ..... p 1906 N94-20280 #
SAND-93-0941 ..... p 1906 N94-20281 #
SAND-93-0998C ..... p 1708 N94-21954 #
SAND-93-1430 ..... p 2029 N94-21690 #
SAND-93-1468C ..... p 1946 N94-21929 #
SAND-93-1474C ..... p 1750 N94-20312
SAND-93-1564C ..... p 1770 N94-22040 #
SAND-93-1565C ..... p 1749 N94-20054 #
SAND-93-1588 ..... p 1794 N94-22405 #
SAND-93-1604C ..... p 1699 N94-19960 #
SAND-93-1612 ..... p 1714 N94-19946 #
SAND-93-1629C ..... p 2016 N94-20296 #
SAND-93-1630C ..... p 1750 N94-20294 #
SAND-93-1639C ..... p 1816 N94-20298 #
SAND-93-1640C ..... p 1698 N94-19903 #
SAND-93-1652C ..... p 2013 N94-19961 #
SAND-93-1686C ..... p 1899 N94-20476 #
SAND-93-1703C ..... p 1829 N94-19824 #
SAND-93-1748C ..... p 1916 N94-21633 #
SAND-93-1756C ..... p 1687 N94-19904 #
SAND-93-1781C ..... p 1915 N94-21539 #
SAND-93-1808C ..... p 1805 N94-22556 #
SAND-93-1837C ..... p 1830 N94-20477 #
SAND-93-1844C ..... p 1700 N94-20315
SAND-93-1846C ..... p 2028 N94-21541 #
SAND-93-1847C ..... p 1814 N94-19865 #
SAND-93-1874C ..... p 1810 N94-22000 #
SAND-93-1881C ..... p 1761 N94-21532 #
SAND-93-1911C ..... p 1687 N94-19864 #
SAND-93-1914C ..... p 1942 N94-20293 #
SAND-93-1927C ..... p 2032 N94-21939 #
SAND-93-1979C ..... p 2034 N94-22007 #
SAND-93-1981C ..... p 1996 N94-21769
SAND-93-1985 ..... p 1656 N94-21852 #
SAND-93-2130C ..... p 1921 N94-22383 #
SAND-93-8013 ..... p 1936 N94-21853 #
SAND-93-8243 ..... p 1928 N94-19858 #

SCT-92RR-8 ..... p 1642 N94-20051 #

SFA-93/003 ..... p 2018 N94-20558
SFA-93/005 ..... p 1994 N94-20943 #

SLAC-PUB-6105 ..... p 1978 N94-19873 #
SLAC-PUB-6144 ..... p 1715 N94-19874 #
SLAC-PUB-6233 ..... p 1978 N94-19858 #

SLAC/SSRL-0019 ..... p 1978 N94-19873 #

SMC-TR-93-50 ..... p 1705 N94-21225 #
SMC-TR-93-54 ..... p 2037 N94-20945 #
SMC-TR-93-55 ..... p 1681 N94-21226 #

SR-5 ..... p 1987 N94-21172 #
SR-93-R-5278-115 ..... p 1826 N94-21938 #

SRI-PROJ.-2399 ..... p 1705 N94-21425 #

SRL-0109-TR ..... p 1814 N94-19851
SRL-0116-RN ..... p 2028 N94-21505
SRL-0131-TR ..... p 1854 N94-19860 #
SRL-12-F-1993 ..... p 1817 N94-21284 #

SSC-TR-93-02 ..... p 1715 N94-19816 #

SSCL-PREPRINT-321 ..... p 2041 N94-19811 #
SSCL-PREPRINT-322 ..... p 1928 N94-19812 #
SSCL-PREPRINT-324 ..... p 1936 N94-21919 #

SSS-DRF-93-14180 ..... p 1654 N94-21429

SU-SLAC-PUB-6010 ..... p 2038 N94-21971 #
SU-SLAC-PUB-6038 ..... p 1741 N94-21684 #
SU-SLAC-PUB-6117 ..... p 1981 N94-21773
SU-SLAC-PUB-6153 ..... p 1981 N94-21686 #
SU-SLAC-PUB-6154 ..... p 1981 N94-21687 #
SU-SLAC-PUB-6195 ..... p 1981 N94-21688 #
SU-SLAC-PUB-6217 ..... p 1975 N94-21788
SU-SLAC-PUB-6234 ..... p 1763 N94-21685 #
SU-SLAC-PUB-6285 ..... p 1982 N94-21952 #
SU-SLAC-PUB-6304 ..... p 2038 N94-21935 #
SU-SLAC-PUB-6310 ..... p 1974 N94-21515 #
SU-SLAC-PUB-6335 ..... p 1946 N94-21689

SU-SOL-93-4 ..... p 1950 N94-20217 #
SU-SOL-93-6 ..... p 1921 N94-22406 #

SU-TR-93-12 ..... p 1962 N94-19999
SU-TR-93-13 ..... p 1949 N94-19854
SU-TR-93-5 ..... p 1902 N94-19855
SU-TR-93-7 ..... p 1939 N94-19909

53/368 ..... p 1897 N94-21309 #

TD-92-2290 ..... p 2042 N94-20310

TIOS-92-27 ..... p 1963 N94-21058
TIOS-92/28 ..... p 1914 N94-21454
TIOS-92/29 ..... p 1909 N94-21045

TP042-121493-MS ..... p 1656 N94-21813 * #

TR-ONR-C-14 ..... p 1964 N94-21442 #

TR-0091(6925-02)-1 ..... p 1967 N94-19949
TR-10-ONR ..... p 1817 N94-20583 #
TR-11 ..... p 1973 N94-20619 #
TR-137 ..... p 1680 N94-20330
TR-1 ..... p 1705 N94-21259 #
TR-22 ..... p 1704 N94-21186 #
TR-3 ..... p 1680 N94-20560
TR-3 ..... p 1681 N94-21216 #
TR-3 ..... p 1705 N94-21238 #
TR-421 ..... p 1904 N94-20067 #
TR-437 ..... p 1939 N94-20135 #
TR-438 ..... p 2039 N94-20364 #
TR-439 ..... p 2049 N94-20096 #
TR-440 ..... p 1907 N94-20522 #
TR-441 ..... p 1907 N94-20521 #
TR-442 ..... p 1894 N94-20520 #
TR-443 ..... p 1907 N94-20536 #
TR-445 ..... p 1955 N94-21456 #
TR-447 ..... p 2043 N94-21287 #
TR-448 ..... p 1929 N94-20144 #
TR-452 ..... p 1905 N94-20143 #
TR-455 ..... p 1913 N94-21318 #
TR-456 ..... p 1931 N94-21272 * #
TR-457 ..... p 1930 N94-21228 #
TR-458 ..... p 1945 N94-21317 #
TR-459 ..... p 1965 N94-21286 #
TR-460 ..... p 1912 N94-21227 #
TR-461 ..... p 1912 N94-21285 #
TR-462-ONR ..... p 1899 N94-21177 #
TR-463 ..... p 1900 N94-21281 #
TR-465 ..... p 1913 N94-21316 #
TR-466 ..... p 1945 N94-21315 #
TR-467 ..... p 1954 N94-21314 #
TR-469 ..... p 1912 N94-21273 #
TR-470 ..... p 1911 N94-21200 #
TR-473 ..... p 1911 N94-21180 #
TR-475 ..... p 1954 N94-21199 #
TR-4 ..... p 1705 N94-21223 #
TR-5-ONR ..... p 1705 N94-21267 #
TR-59 ..... p 1680 N94-21145
TR-6 ..... p 1706 N94-21523 #
TR-92(2940)-3 ..... p 2037 N94-20945 #
TR-92-14 ..... p 1909 N94-21061
TR-92-15 ..... p 1910 N94-21062
TR-93(3935)-16 ..... p 1681 N94-21226 #
TR-93(3935)-6 ..... p 1705 N94-21225 #
TR-93-59 ..... p 1949 N94-19898 #
TR-978 ..... p 1867 N94-21212 #
TR-981 ..... p 1739 N94-21211 #
TR-982 ..... p 1738 N94-21210 #
TR-9 ..... p 1973 N94-20618

TRB/TRR-1379, ... p 1642 N94-22055

TRC-EM-CAB-9306-PT-1/2 ..... p 1717 N94-20269 * #

TRI-PP-93-68 ..... p 1975 N94-21775 #

TW-92-10 ..... p 1953 N94-21060
TW-92-12 ..... p 1963 N94-21066
TW-92-14 ..... p 1918 N94-22098

U-OF-IOWA-93-19 ..... p 2088 N94-20048 * #

UCB/ERL-M-92/145 ..... p 1999 N94-22596 #
UCB/ERL-M-92/146 ..... p 1999 N94-22595 #
UCB/ERL-M-92/147 ..... p 1999 N94-22566 #
UCB/ERL-M-92/148 ..... p 1999 N94-22567 #

UCID-20622-93-1 ..... p 2152 N94-21858 #

UCRL-CR-114855 ..... p 1946 N94-21925 #
UCRL-CR-114992-VOL-1 ..... p 1985 N94-20262 #
UCRL-CR-114992-VOL-2 ..... p 1985 N94-20283 #

UCRL-ID-110499 ..... p 1992 N94-19991 #
UCRL-ID-112775-REV-1 ..... p 1675 N94-21530 #
UCRL-ID-114069 ..... p 2045 N94-21750 #
UCRL-ID-114105 ..... p 1803 N94-21651 #
UCRL-ID-114297 ..... p 1816 N94-20480 #
UCRL-ID-114696 ..... p 2034 N94-22050 #
UCRL-ID-114808 ..... p 1918 N94-22011 #
UCRL-ID-114856 ..... p 1949 N94-20006 #
UCRL-ID-115050 ..... p 1678 N94-19889 #
UCRL-ID-115116 ..... p 1936 N94-21749 #

UCRL-JC-110049-REV-2 ..... p 1706 N94-21512 #
UCRL-JC-111286-REV-1 ..... p 1818 N94-21547 #
UCRL-JC-111288 ..... p 1990 N94-22002 #
UCRL-JC-111340-REV-1 ..... p 2012 N94-19881 #
UCRL-JC-111445 ..... p 1820 N94-22401 #
UCRL-JC-111524 ..... p 1796 N94-19916 #
UCRL-JC-111593 ..... p 1819 N94-21920 #
UCRL-JC-111938 ..... p 1815 N94-20223 #
UCRL-JC-111960 ..... p 2032 N94-21960 #
UCRL-JC-111969-REV-1 ..... p 1709 N94-21970 #
UCRL-JC-112023 ..... p 1768 N94-21770
UCRL-JC-112045 ..... p 2036 N94-22594 #
UCRL-JC-112054 ..... p 1696 N94-22394 #
UCRL-JC-112108 ..... p 1694 N94-21943 #
UCRL-JC-112177-REV-1 ..... p 1768 N94-21753 #
UCRL-JC-112208 ..... p 1803 N94-21531 #

UCRL-JC-112247 ..... p 1992 N94-19915 #
UCRL-JC-112273 ..... p 1852 N94-21969 #
UCRL-JC-112347-REV-1 ..... p 1694 N94-21921 #
UCRL-JC-112349 ..... p 1998 N94-22399 #
UCRL-JC-112492 ..... p 1817 N94-21299 #
UCRL-JC-112493 ..... p 1815 N94-20259 #
UCRL-JC-112510 ..... p 1769 N94-21838 #
UCRL-JC-112554 ..... p 1819 N94-21873
UCRL-JC-112596 ..... p 1960 N94-21996 #
UCRL-JC-112599 ..... p 1799 N94-20263 #
UCRL-JC-112636 ..... p 1657 N94-21980 #
UCRL-JC-112639 ..... p 1657 N94-21981 #
UCRL-JC-112742 ..... p 1819 N94-21872
UCRL-JC-112766 ..... p 1693 N94-21843 #
UCRL-JC-112935 ..... p 1917 N94-21841 #
UCRL-JC-113183 ..... p 1819 N94-21844 #
UCRL-JC-113296 ..... p 1679 N94-20319
UCRL-JC-113300 ..... p 1696 N94-22398 #
UCRL-JC-113366 ..... p 1688 N94-19986 #
UCRL-JC-113400 ..... p 1977 N94-22396 #
UCRL-JC-113401 ..... p 2016 N94-20318
UCRL-JC-113403 ..... p 1684 N94-22395 #
UCRL-JC-113406 ..... p 1695 N94-22024 #
UCRL-JC-113413 ..... p 2031 N94-21931 #
UCRL-JC-113429 ..... p 1989 N94-21630 #
UCRL-JC-113437 ..... p 1968 N94-22003 #
UCRL-JC-113444 ..... p 1989 N94-21619 #
UCRL-JC-113458 ..... p 1657 N94-19863 #
UCRL-JC-113483 ..... p 1794 N94-22380 #
UCRL-JC-113505 ..... p 1966 N94-21958 #
UCRL-JC-113506 ..... p 1936 N94-21828
UCRL-JC-113664 ..... p 1844 N94-19803 #
UCRL-JC-113744 ..... p 1906 N94-20316
UCRL-JC-113765 ..... p 1966 N94-21511 #
UCRL-JC-113766 ..... p 1707 N94-21546 #
UCRL-JC-113778 ..... p 1694 N94-21944 #
UCRL-JC-113779 ..... p 1696 N94-22025 #
UCRL-JC-113795 ..... p 1695 N94-21986 #
UCRL-JC-113802 ..... p 1810 N94-21950 #
UCRL-JC-113823 ..... p 1972 N94-20181 #
UCRL-JC-113857 ..... p 2044 N94-21529 #
UCRL-JC-113895 ..... p 1937 N94-22042 #
UCRL-JC-113905-REV-1 ..... p 1762 N94-21621 #
UCRL-JC-113905 ..... p 1762 N94-21620 #
UCRL-JC-114023 ..... p 1818 N94-21829
UCRL-JC-114072 ..... p 1997 N94-21848
UCRL-JC-114074 ..... p 1990 N94-21985 #
UCRL-JC-114077 ..... p 2081 N94-21618 #
UCRL-JC-114087 ..... p 1698 N94-19810 #
UCRL-JC-114095 ..... p 2150 N94-22397 #
UCRL-JC-114157 ..... p 1697 N94-22402 #
UCRL-JC-114166 ..... p 1693 N94-21656 #
UCRL-JC-114285 ..... p 2031 N94-21869
UCRL-JC-114311 ..... p 1977 N94-22400 #
UCRL-JC-114340 ..... p 1976 N94-21968 #
UCRL-JC-114360 ..... p 1937 N94-22558 #
UCRL-JC-114416 ..... p 1750 N94-20231 #
UCRL-JC-114583 ..... p 1971 N94-20096 #
UCRL-JC-114594 ..... p 1898 N94-19886 #
UCRL-JC-114779 ..... p 1695 N94-22023 #
UCRL-JC-114989 ..... p 1983 N94-19862 #
UCRL-JC-115147 ..... p 1769 N94-21959 #

UCRL-MA-115210 ..... p 2046 N94-22413 #

UCSD-916904R ..... p 1973 N94-20938 #
UCSD-92-1070 ..... p 1883 N94-21366 #

UDR-TR-92-146 ..... p 1675 N94-21187 #
UDR-TR-93-69 ..... p 1691 N94-21188 #

UG-3/93 ..... p 2037 N94-20178

UH-511-764-93 ..... p 1969 N94-19804 #

UILU-ENG-93-4019 ..... p 1797 N94-19978 #

UM-030601-3-T ..... p 1741 N94-21885 * #

UMICH-031155-1-T ..... p 1950 N94-20034 * #
UMICH-031173-1-T ..... p 1716 N94-20160 * #

UMR-FDB-32 ..... p 1706 N94-21460 #

UO-JFWK-MNW-05 ..... p 1700 N94-20328

UOP-93-4 ..... p 1864 N94-20186 #

US-PATENT-APPL-SN-008427 ..... p 1822 N94-20127 *
US-PATENT-APPL-SN-009908 ..... p 1703 N94-20541 *
US-PATENT-APPL-SN-009909 ..... p 1823 N94-20379 *
US-PATENT-APPL-SN-010037 ..... p 1669 N94-20370 *
US-PATENT-APPL-SN-012837 ..... p 1824 N94-21277
US-PATENT-APPL-SN-012839 ..... p 1658 N94-20590 *
US-PATENT-APPL-SN-018844 ..... p 1653 N94-20339 *
US-PATENT-APPL-SN-033223 ..... p 1822 N94-20356 #
US-PATENT-APPL-SN-033225 ..... p 1938 N94-19843
US-PATENT-APPL-SN-035867 ..... p 1824 N94-21274
US-PATENT-APPL-SN-038598 ..... p 1806 N94-19882
US-PATENT-APPL-SN-049648 ..... p 1654 N94-20304 *
US-PATENT-APPL-SN-077903 ..... p 1748 N94-19892 #
US-PATENT-APPL-SN-082640 ..... p 1698 N94-19830 #
US-PATENT-APPL-SN-082645 ..... p 1672 N94-20010 #
US-PATENT-APPL-SN-083403 ..... p 1714 N94-20355 #
US-PATENT-APPL-SN-470664 ..... p 1942 N94-20360 *
US-PATENT-APPL-SN-501909 ..... p 1800 N94-20495 *
US-PATENT-APPL-SN-531720 ..... p 2017 N94-20348
US-PATENT-APPL-SN-535612 ..... p 1751 N94-20350
US-PATENT-APPL-SN-543132 ..... p 1699 N94-20017
US-PATENT-APPL-SN-551103 ..... p 1898 N94-20357
US-PATENT-APPL-SN-553058 ..... p 1984 N94-20056
US-PATENT-APPL-SN-556606 ..... p 1643 N94-20197
US-PATENT-APPL-SN-636348 ..... p 1749 N94-20199
US-PATENT-APPL-SN-700379 ..... p 1985 N94-20305 *
US-PATENT-APPL-SN-703649 ..... p 1800 N94-20371 *
US-PATENT-APPL-SN-718314 ..... p 2017 N94-20381 *
US-PATENT-APPL-SN-722447 ..... p 1701 N94-20331
US-PATENT-APPL-SN-728915 ..... p 1749 N94-20120
US-PATENT-APPL-SN-729107 ..... p 1993 N94-20491 *
US-PATENT-APPL-SN-731829 ..... p 1654 N94-20304 *
US-PATENT-APPL-SN-736667 ..... p 1702 N94-20373 *
US-PATENT-APPL-SN-747059 ..... p 1985 N94-20303 *
US-PATENT-APPL-SN-752246 ..... p 1702 N94-20374 *
US-PATENT-APPL-SN-758143 ..... p 1984 N94-20059
US-PATENT-APPL-SN-760633 ..... p 1890 N94-20372 *
US-PATENT-APPL-SN-761198 ..... p 1986 N94-20378 *
US-PATENT-APPL-SN-761198 ..... p 1986 N94-20586 *
US-PATENT-APPL-SN-761566 ..... p 1907 N94-20492 *
US-PATENT-APPL-SN-767189 ..... p 1797 N94-20094
US-PATENT-APPL-SN-770207 ..... p 2043 N94-21276
US-PATENT-APPL-SN-770509 ..... p 1822 N94-20365 *
US-PATENT-APPL-SN-772186 ..... p 1808 N94-21278
US-PATENT-APPL-SN-775404 ..... p 1895 N94-20194 *
US-PATENT-APPL-SN-786618 ..... p 1986 N94-20345 *
US-PATENT-APPL-SN-788660 ..... p 1751 N94-20354
US-PATENT-APPL-SN-789567 ..... p 1942 N94-20360 *
US-PATENT-APPL-SN-790723 ..... p 1718 N94-20368 *
US-PATENT-APPL-SN-793974 ..... p 1822 N94-20369 *
US-PATENT-APPL-SN-798464 ..... p 1673 N94-20539 *
US-PATENT-APPL-SN-804558 ..... p 1673 N94-20064
US-PATENT-APPL-SN-812567 ..... p 1712 N94-20061
US-PATENT-APPL-SN-813556 ..... p 1942 N94-20366 *
US-PATENT-APPL-SN-813629 ..... p 1896 N94-20493 *
US-PATENT-APPL-SN-822457 ..... p 1824 N94-20587 *
US-PATENT-APPL-SN-826547 ..... p 1822 N94-20375 *
US-PATENT-APPL-SN-828612 ..... p 1823 N94-20380 *
US-PATENT-APPL-SN-829634 ..... p 1701 N94-20349
US-PATENT-APPL-SN-829145 ..... p 1814 N94-19800
US-PATENT-APPL-SN-838635 ..... p 1700 N94-20057
US-PATENT-APPL-SN-841105 ..... p 1987 N94-21279
US-PATENT-APPL-SN-842313 ..... p 1700 N94-20195 *
US-PATENT-APPL-SN-843653 ..... p 1800 N94-20495 *
US-PATENT-APPL-SN-843861 ..... p 1823 N94-20494 * #
US-PATENT-APPL-SN-848685 ..... p 1986 N94-20591 *
US-PATENT-APPL-SN-849866 ..... p 1865 N94-20332
US-PATENT-APPL-SN-855363 ..... p 1986 N94-20586 *
US-PATENT-APPL-SN-857536 ..... p 1717 N94-20198
US-PATENT-APPL-SN-862113 ..... p 1846 N94-20196 *
US-PATENT-APPL-SN-866921 ..... p 1761 N94-21275
US-PATENT-APPL-SN-867864 ..... p 1672 N94-20540 *
US-PATENT-APPL-SN-883336 ..... p 1815 N94-20060
US-PATENT-APPL-SN-887001 ..... p 1657 N94-20367 *
US-PATENT-APPL-SN-888996 ..... p 1815 N94-20055
US-PATENT-APPL-SN-889003 ..... p 1801 N94-20588 *
US-PATENT-APPL-SN-891027 ..... p 1669 N94-20121
US-PATENT-APPL-SN-901618 ..... p 1711 N94-19801
US-PATENT-APPL-SN-901620 ..... p 1712 N94-20122
US-PATENT-APPL-SN-912401 ..... p 1701 N94-20359 *
US-PATENT-APPL-SN-929552 ..... p 1824 N94-20589 *
US-PATENT-APPL-SN-932271 ..... p 1718 N94-20334
US-PATENT-APPL-SN-934988 ..... p 1669 N94-20496 *
US-PATENT-APPL-SN-936376 ..... p 2017 N94-20528 *
US-PATENT-APPL-SN-937782 ..... p 1984 N94-20065
US-PATENT-APPL-SN-939229 ..... p 1951 N94-20358 #
US-PATENT-APPL-SN-947612 ..... p 1821 N94-20126 *
US-PATENT-APPL-SN-948057 ..... p 1650 N94-20556 *
US-PATENT-APPL-SN-950580 ..... p 1702 N94-20377 *
US-PATENT-APPL-SN-958404 ..... p 1717 N94-20333
US-PATENT-APPL-SN-958843 ..... p 1800 N94-20361 *
US-PATENT-APPL-SN-971035 ..... p 1985 N94-20240 *
US-PATENT-APPL-SN-982535 ..... p 1703 N94-20529 *

US-PATENT-CLASS-114-20.2 ..... p 1669 N94-20121
US-PATENT-CLASS-118-500 ..... p 1823 N94-20380 *
US-PATENT-CLASS-118-728 ..... p 1823 N94-20380 *
US-PATENT-CLASS-118-730 ..... p 1823 N94-20380 *
US-PATENT-CLASS-136-245 ..... p 1846 N94-20196 *
US-PATENT-CLASS-136-292 ..... p 1846 N94-20196 *
US-PATENT-CLASS-137-625.47 .. p 1824 N94-20589 *
US-PATENT-CLASS-137-853 ..... p 1669 N94-20370 *
US-PATENT-CLASS-137-855 ..... p 1669 N94-20370 *
US-PATENT-CLASS-137-876 ..... p 1824 N94-20589 *
US-PATENT-CLASS-148-DIG.148 p 2017 N94-20381 *
US-PATENT-CLASS-148-33.3 ..... p 2017 N94-20348
US-PATENT-CLASS-148-33 ..... p 2017 N94-20381 *
US-PATENT-CLASS-149-45 ..... p 1712 N94-20061
US-PATENT-CLASS-156-DIG.64 . p 2017 N94-20381 *
US-PATENT-CLASS-156-272.2 .... p 1718 N94-20368 *
US-PATENT-CLASS-156-272.4 .... p 1718 N94-20368 *
US-PATENT-CLASS-156-600 ..... p 2017 N94-20528 *
US-PATENT-CLASS-156-612 ..... p 2017 N94-20381 *
US-PATENT-CLASS-156-621 ..... p 2017 N94-20528 *
US-PATENT-CLASS-156-622 ..... p 2017 N94-20528 *
US-PATENT-CLASS-156-643 ..... p 1993 N94-20491 *
US-PATENT-CLASS-156-645 ..... p 2017 N94-20381 *
US-PATENT-CLASS-156-646 ..... p 2017 N94-20381 *
US-PATENT-CLASS-156-646 ..... p 1993 N94-20491 *
US-PATENT-CLASS-156-662 ..... p 2017 N94-20381 *
US-PATENT-CLASS-156-662 ..... p 1993 N94-20491 *
US-PATENT-CLASS-156-668 ..... p 1993 N94-20491 *
US-PATENT-CLASS-165-104.17 .. p 1800 N94-20371 *
US-PATENT-CLASS-165-104.31 .. p 1800 N94-20495 *
US-PATENT-CLASS-165-109.1 .... p 1800 N94-20495 *
US-PATENT-CLASS-165-10 ..... p 1800 N94-20371 *
US-PATENT-CLASS-165-110 ..... p 1800 N94-20495 *
US-PATENT-CLASS-165-41 ..... p 1822 N94-20127 *
US-PATENT-CLASS-165-78 ..... p 1800 N94-20371 *
US-PATENT-CLASS-165-903 ..... p 1800 N94-20495 *
US-PATENT-CLASS-165-904 ..... p 1822 N94-20127 *
US-PATENT-CLASS-165-913 ..... p 1800 N94-20495 *
US-PATENT-CLASS-165-97 ..... p 1800 N94-20495 *
US-PATENT-CLASS-174-36 ..... p 1761 N94-21275
US-PATENT-CLASS-180-7.1 ..... p 1823 N94-20494 * #
US-PATENT-CLASS-200-144 ..... p 1751 N94-20354
US-PATENT-CLASS-209-144 ..... p 1800 N94-20361 *
US-PATENT-CLASS-209-211 ..... p 1800 N94-20361 *
US-PATENT-CLASS-210-512.1 .... p 1800 N94-20361 *
US-PATENT-CLASS-210-787 ..... p 1800 N94-20361 *
US-PATENT-CLASS-212-148 ..... p 1822 N94-20369 *
US-PATENT-CLASS-212-196 ..... p 1822 N94-20369 *
US-PATENT-CLASS-212-262 ..... p 1822 N94-20369 *
US-PATENT-CLASS-219-10.75 .... p 1718 N94-20368 *
US-PATENT-CLASS-219-10.77 .... p 1718 N94-20368 *
US-PATENT-CLASS-219-10.79 .... p 1718 N94-20368 *
US-PATENT-CLASS-219-200 ..... p 1654 N94-20304 *
US-PATENT-CLASS-219-9.5 ..... p 1718 N94-20368 *
US-PATENT-CLASS-23-295R ..... p 2017 N94-20528 *
US-PATENT-CLASS-239-410 ..... p 1669 N94-20370 *
US-PATENT-CLASS-239-533.2 .... p 1669 N94-20370 *
US-PATENT-CLASS-244-1A ..... p 1673 N94-20539 *
US-PATENT-CLASS-244-1R ..... p 1824 N94-20587 *
US-PATENT-CLASS-244-100A .... p 1658 N94-20590 *
US-PATENT-CLASS-244-110D .... p 1658 N94-20590 *
US-PATENT-CLASS-244-113 ..... p 1658 N94-20590 *
US-PATENT-CLASS-244-121 ..... p 1654 N94-20304 *
US-PATENT-CLASS-244-138A .... p 1658 N94-20590 *
US-PATENT-CLASS-244-138R .... p 1658 N94-20590 *
US-PATENT-CLASS-244-158A .... p 1822 N94-20127 *
US-PATENT-CLASS-244-158A .... p 1654 N94-20304 *
US-PATENT-CLASS-244-158A .... p 1658 N94-20590 *
US-PATENT-CLASS-244-158R .... p 1822 N94-20127 *
US-PATENT-CLASS-244-158R .... p 1657 N94-20367 *
US-PATENT-CLASS-244-160 ..... p 1657 N94-20367 *
US-PATENT-CLASS-244-160 ..... p 1658 N94-20590 *
US-PATENT-CLASS-244-163 ..... p 1822 N94-20127 *
US-PATENT-CLASS-244-75R ..... p 1650 N94-20556 *
US-PATENT-CLASS-244-87 ..... p 1650 N94-20558 *
US-PATENT-CLASS-250-201.1 .... p 1985 N94-20305 *
US-PATENT-CLASS-250-201.9 .... p 1985 N94-20305 *
US-PATENT-CLASS-250-206.2 .... p 1718 N94-20334
US-PATENT-CLASS-250-227.14 .. p 1986 N94-20378 *
US-PATENT-CLASS-250-227.17 .. p 1717 N94-20333
US-PATENT-CLASS-250-227.2 .... p 1986 N94-20345 *
US-PATENT-CLASS-250-231.18 .. p 1985 N94-20240 *
US-PATENT-CLASS-250-237G .... p 1985 N94-20240 *
US-PATENT-CLASS-250-251 ..... p 1993 N94-20491 *
US-PATENT-CLASS-250-423P .... p 1993 N94-20491 *
US-PATENT-CLASS-250-423R .... p 1993 N94-20491 *
US-PATENT-CLASS-251-214 ..... p 1824 N94-20589 *
US-PATENT-CLASS-257-421 ..... p 1749 N94-20199
US-PATENT-CLASS-264-221 ..... p 1702 N94-20377 *
US-PATENT-CLASS-264-86 ..... p 1702 N94-20377 *
US-PATENT-CLASS-269-71 ..... p 1823 N94-20380 *
US-PATENT-CLASS-29-2 ..... p 1749 N94-20120
US-PATENT-CLASS-29-890.01 .... p 1703 N94-20541 *
US-PATENT-CLASS-294-119.3 .... p 1701 N94-20359 *
US-PATENT-CLASS-313-309 ..... p 1673 N94-20064
US-PATENT-CLASS-313-355 ..... p 1751 N94-20350
US-PATENT-CLASS-315-5.54 ..... p 1822 N94-20375 *
US-PATENT-CLASS-322-2R ..... p 1824 N94-20587 *
US-PATENT-CLASS-333-233 ..... p 1822 N94-20375 *
US-PATENT-CLASS-342-21 ..... p 1717 N94-20198
US-PATENT-CLASS-356-345 ..... p 1797 N94-20094
US-PATENT-CLASS-356-5 ..... p 1986 N94-20591 *
US-PATENT-CLASS-356-73.1 ..... p 1987 N94-21279
US-PATENT-CLASS-358-448 ..... p 1984 N94-20056
US-PATENT-CLASS-359-107 ..... p 1951 N94-20358 #
US-PATENT-CLASS-359-17 ..... p 1986 N94-20591 *

US-PATENT-CLASS-359-18 ..... p 1986 N94-20591 *
US-PATENT-CLASS-359-243 ..... p 1984 N94-20059
US-PATENT-CLASS-359-561 ..... p 1985 N94-20303 *
US-PATENT-CLASS-359-849 ..... p 1985 N94-20305 *
US-PATENT-CLASS-359-896 ..... p 1986 N94-20345 *
US-PATENT-CLASS-360-32 ..... p 1808 N94-21278
US-PATENT-CLASS-361-218 ..... p 1673 N94-20539 *
US-PATENT-CLASS-364-148 ..... p 1985 N94-20305 *
US-PATENT-CLASS-364-525 ..... p 1985 N94-20305 *
US-PATENT-CLASS-364-559 ..... p 1985 N94-20305 *
US-PATENT-CLASS-365-215 ..... p 1985 N94-20303 *
US-PATENT-CLASS-365-49 ..... p 1985 N94-20303 *
US-PATENT-CLASS-372-20 ..... p 1814 N94-19800
US-PATENT-CLASS-372-32 ..... p 1815 N94-20055
US-PATENT-CLASS-372-43 ..... p 1824 N94-20587 *
US-PATENT-CLASS-372-6 ..... p 1986 N94-20586 *
US-PATENT-CLASS-372-71 ..... p 1815 N94-20060
US-PATENT-CLASS-382-42 ..... p 1985 N94-20303 *
US-PATENT-CLASS-385-123 ..... p 1986 N94-20586 *
US-PATENT-CLASS-385-126 ..... p 1986 N94-20586 *
US-PATENT-CLASS-385-127 ..... p 1986 N94-20586 *
US-PATENT-CLASS-385-128 ..... p 1986 N94-20586 *
US-PATENT-CLASS-385-12 ..... p 1986 N94-20378 *
US-PATENT-CLASS-385-142 ..... p 1986 N94-20586 *
US-PATENT-CLASS-385-24 ..... p 1984 N94-20065
US-PATENT-CLASS-395-23 ..... p 1942 N94-20366 *
US-PATENT-CLASS-395-24 ..... p 1942 N94-20360 *
US-PATENT-CLASS-395-24 ..... p 1942 N94-20366 *
US-PATENT-CLASS-395-27 ..... p 1942 N94-20360 *
US-PATENT-CLASS-395-3 ..... p 1907 N94-20492 *
US-PATENT-CLASS-395-400 ..... p 1898 N94-20357
US-PATENT-CLASS-395-61 ..... p 1907 N94-20492 *
US-PATENT-CLASS-395-700 ..... p 2043 N94-21276
US-PATENT-CLASS-395-900 ..... p 1907 N94-20492 *
US-PATENT-CLASS-403-24 ..... p 1822 N94-20365 *
US-PATENT-CLASS-403-27 ..... p 1822 N94-20365 *
US-PATENT-CLASS-403-344 ..... p 1822 N94-20365 *
US-PATENT-CLASS-403-404 ..... p 1654 N94-20304 *
US-PATENT-CLASS-403-408.1 .... p 1654 N94-20304 *
US-PATENT-CLASS-403-6 ..... p 1822 N94-20365 *
US-PATENT-CLASS-411-258 ..... p 1823 N94-20379 *
US-PATENT-CLASS-411-271 ..... p 1824 N94-21277
US-PATENT-CLASS-411-82 ..... p 1823 N94-20379 *
US-PATENT-CLASS-411-909 ..... p 1654 N94-20304 *
US-PATENT-CLASS-411-930 ..... p 1823 N94-20379 *
US-PATENT-CLASS-416-61 ..... p 1822 N94-20365 *
US-PATENT-CLASS-417-64 ..... p 1801 N94-20588 *
US-PATENT-CLASS-422-241 ..... p 1700 N94-20057
US-PATENT-CLASS-422-245 ..... p 2017 N94-20528 *
US-PATENT-CLASS-425-129.1 .... p 1823 N94-20379 *
US-PATENT-CLASS-427-163 ..... p 1702 N94-20373 *
US-PATENT-CLASS-427-236 ..... p 1703 N94-20541 *
US-PATENT-CLASS-427-248.1 .... p 1701 N94-20349
US-PATENT-CLASS-427-270 ..... p 1703 N94-20541 *
US-PATENT-CLASS-427-374.2 .... p 1700 N94-20195 *
US-PATENT-CLASS-427-383.1 .... p 1700 N94-20195 *
US-PATENT-CLASS-427-383.3 .... p 1700 N94-20195 *
US-PATENT-CLASS-427-383.5 .... p 1700 N94-20195 *
US-PATENT-CLASS-427-384 ..... p 1700 N94-20195 *
US-PATENT-CLASS-427-385.5 .... p 1702 N94-20373 *
US-PATENT-CLASS-427-388.1 .... p 1702 N94-20373 *
US-PATENT-CLASS-427-455 ..... p 1703 N94-20541 *
US-PATENT-CLASS-427-96 ..... p 1702 N94-20373 *
US-PATENT-CLASS-428-257 ..... p 1673 N94-20539 *
US-PATENT-CLASS-428-260 ..... p 1673 N94-20539 *
US-PATENT-CLASS-428-288 ..... p 1673 N94-20539 *
US-PATENT-CLASS-428-289 ..... p 1673 N94-20539 *
US-PATENT-CLASS-428-334 ..... p 1673 N94-20539 *
US-PATENT-CLASS-434-34 ..... p 1653 N94-20339 *
US-PATENT-CLASS-439-362 ..... p 1821 N94-20126 *
US-PATENT-CLASS-482-54 ..... p 1895 N94-20194 *
US-PATENT-CLASS-482-8 ..... p 1895 N94-20194 *
US-PATENT-CLASS-501-96 ..... p 1703 N94-20529 *
US-PATENT-CLASS-501-97 ..... p 1703 N94-20529 *
US-PATENT-CLASS-505-1 ..... p 1699 N94-20017
US-PATENT-CLASS-528-125 ..... p 1672 N94-20540 *
US-PATENT-CLASS-528-126 ..... p 1672 N94-20540 *
US-PATENT-CLASS-528-128 ..... p 1672 N94-20540 *
US-PATENT-CLASS-528-167 ..... p 1672 N94-20540 *
US-PATENT-CLASS-528-171 ..... p 1672 N94-20540 *
US-PATENT-CLASS-528-172 ..... p 1672 N94-20540 *
US-PATENT-CLASS-528-174 ..... p 1672 N94-20540 *
US-PATENT-CLASS-528-28 ..... p 1702 N94-20374 *
US-PATENT-CLASS-528-310 ..... p 1702 N94-20374 *
US-PATENT-CLASS-528-331 ..... p 1702 N94-20374 *
US-PATENT-CLASS-528-353 ..... p 1702 N94-20374 *
US-PATENT-CLASS-528-41 ..... p 1702 N94-20374 *
US-PATENT-CLASS-55-459.1 .... p 1800 N94-20361 *
US-PATENT-CLASS-558-482 ..... p 1711 N94-19801
US-PATENT-CLASS-564-151 ..... p 1712 N94-20122
US-PATENT-CLASS-60-202 ..... p 1669 N94-20496 *
US-PATENT-CLASS-60-258 ..... p 1669 N94-20370 *
US-PATENT-CLASS-60-39.45 .... p 1801 N94-20588 *
US-PATENT-CLASS-60-39.462 ... p 1824 N94-21274
US-PATENT-CLASS-60-741 ..... p 1669 N94-20370 *
US-PATENT-CLASS-602-16 ..... p 1896 N94-20493 *
US-PATENT-CLASS-602-26 ..... p 1896 N94-20493 *
US-PATENT-CLASS-604-26 ..... p 1890 N94-20372 *
US-PATENT-CLASS-604-4 ..... p 1890 N94-20372 *
US-PATENT-CLASS-62-259.3 ..... p 1800 N94-20371 *
US-PATENT-CLASS-62-271 ..... p 1865 N94-20332
US-PATENT-CLASS-62-299 ..... p 1800 N94-20371 *
US-PATENT-CLASS-62-467 ..... p 1822 N94-20127 *
US-PATENT-CLASS-62-59 ..... p 1800 N94-20371 *
US-PATENT-CLASS-623-26 ..... p 1701 N94-20359 *
US-PATENT-CLASS-623-43 ..... p 1896 N94-20493 *
US-PATENT-CLASS-623-44 ..... p 1896 N94-20493 *
US-PATENT-CLASS-65-3.12 ..... p 1701 N94-20331
US-PATENT-CLASS-73-379.01 .... p 1895 N94-20194 *
US-PATENT-CLASS-74-479B ..... p 1701 N94-20359 *
US-PATENT-CLASS-901-1 ..... p 1823 N94-20494 * #
US-PATENT-CLASS-901-22 ..... p 1701 N94-20359 *
US-PATENT-CLASS-901-37 ..... p 1701 N94-20359 *
US-PATENT-CLASS-92-48 ..... p 1701 N94-20359 *
US-PATENT-CLASS-92-92 ..... p 1701 N94-20359 *

US-PATENT-5,183,938 ..... p 1712 N94-20122
US-PATENT-5,193,475 ..... p 1669 N94-20121
US-PATENT-5,194,659 ..... p 1711 N94-19801
US-PATENT-5,197,993 ..... p 1749 N94-20120
US-PATENT-5,200,966 ..... p 1815 N94-20060
US-PATENT-5,202,802 ..... p 1673 N94-20064
US-PATENT-5,202,786 ..... p 1984 N94-20059
US-PATENT-5,205,871 ..... p 2017 N94-20348
US-PATENT-5,205,996 ..... p 1700 N94-20057
US-PATENT-5,206,867 ..... p 1814 N94-19800
US-PATENT-5,206,924 ..... p 1984 N94-20065
US-PATENT-5,206,477 ..... p 1749 N94-20199
US-PATENT-5,208,801 ..... p 1643 N94-20197
US-PATENT-5,208,650 ..... p 1797 N94-20094
US-PATENT-5,211,731 ..... p 1701 N94-20331
US-PATENT-5,213,844 ..... p 1701 N94-20349
US-PATENT-5,214,347 ..... p 1751 N94-20350
US-PATENT-5,215,961 ..... p 1699 N94-20017
US-PATENT-5,220,328 ..... p 1717 N94-20198
US-PATENT-5,223,057 ..... p 1712 N94-20061
US-PATENT-5,224,110 ..... p 1815 N94-20055
US-PATENT-5,225,668 ..... p 1718 N94-20334
US-PATENT-5,233,143 ..... p 1751 N94-20354
US-PATENT-5,233,440 ..... p 1984 N94-20056
US-PATENT-5,233,843 ..... p 1865 N94-20332
US-PATENT-5,238,056 ..... p 1800 N94-20495 *
US-PATENT-5,241,836 ..... p 1822 N94-20127 *
US-PATENT-5,242,134 ..... p 1657 N94-20367 *
US-PATENT-5,242,339 ..... p 1895 N94-20194 *
US-PATENT-5,243,023 ..... p 1702 N94-20374 *
US-PATENT-5,243,186 ..... p 1717 N94-20333
US-PATENT-5,243,310 ..... p 1822 N94-20375 *
US-PATENT-5,244,323 ..... p 1824 N94-21277
US-PATENT-5,244,406 ..... p 1821 N94-20126 *
US-PATENT-5,244,508 ..... p 1846 N94-20196 *
US-PATENT-5,245,885 ..... p 1701 N94-20359 *
US-PATENT-5,247,630 ..... p 1896 N94-20357
US-PATENT-5,247,684 ..... p 2043 N94-21273
US-PATENT-5,248,385 ..... p 2017 N94-20381 *
US-PATENT-5,248,421 ..... p 1800 N94-20361 *
US-PATENT-5,248,519 ..... p 1702 N94-20373 *
US-PATENT-5,249,085 ..... p 1808 N94-21278
US-PATENT-5,249,251 ..... p 1986 N94-20586 *
US-PATENT-5,249,357 ..... p 1703 N94-20541 *
US-PATENT-5,250,753 ..... p 1761 N94-21275
US-PATENT-5,251,002 ..... p 1987 N94-21279
US-PATENT-5,251,052 ..... p 1951 N94-20358 #
US-PATENT-5,251,663 ..... p 1824 N94-20589 *
US-PATENT-5,253,329 ..... p 1942 N94-20366 *
US-PATENT-5,253,473 ..... p 1824 N94-21274
US-PATENT-5,253,771 ..... p 1822 N94-20369 *
US-PATENT-5,254,173 ..... p 1823 N94-20380 *
US-PATENT-5,254,837 ..... p 1654 N94-20304 *
US-PATENT-5,255,065 ..... p 1986 N94-20591 *
US-PATENT-5,255,349 ..... p 1942 N94-20360 *
US-PATENT-5,256,241 ..... p 2017 N94-20528 *
US-PATENT-5,256,451 ..... p 1700 N94-20195 *
US-PATENT-5,256,610 ..... p 1703 N94-20529 *
US-PATENT-5,257,669 ..... p 1823 N94-20494 * #
US-PATENT-5,259,063 ..... p 1907 N94-20492 *
US-PATENT-5,259,573 ..... p 1650 N94-20556 *
US-PATENT-5,260,124 ..... p 1673 N94-20539 *
US-PATENT-5,260,639 ..... p 1824 N94-20587 *
US-PATENT-5,261,482 ..... p 1800 N94-20371 *
US-PATENT-5,261,757 ..... p 1822 N94-20365 *
US-PATENT-5,261,819 ..... p 1653 N94-20339 *
US-PATENT-5,261,874 ..... p 1890 N94-20372 *
US-PATENT-5,262,638 ..... p 1986 N94-20378 *
US-PATENT-5,262,979 ..... p 1985 N94-20303 *
US-PATENT-5,265,034 ..... p 1985 N94-20305 *
US-PATENT-5,265,415 ..... p 1669 N94-20370 *
US-PATENT-5,265,829 ..... p 1658 N94-20590 *
US-PATENT-5,265,994 ..... p 1823 N94-20379 *
US-PATENT-5,266,252 ..... p 1702 N94-20377 *
US-PATENT-5,266,764 ..... p 1718 N94-20368 *
US-PATENT-5,266,795 ..... p 1986 N94-20345 *
US-PATENT-5,266,796 ..... p 1985 N94-20240 *
US-PATENT-5,267,432 ..... p 1801 N94-20588 *
US-PATENT-5,267,950 ..... p 1896 N94-20493 *
US-PATENT-5,269,131 ..... p 1669 N94-20496 *
US-PATENT-5,270,432 ..... p 1672 N94-20540 *
US-PATENT-5,271,800 ..... p 1993 N94-20491 *

USAARL-93-28 ..... p 1891 N94-20615 #
USAARL-93-29 ..... p 1891 N94-20928

USAFETAC/PR-93/002 ..... p 1864 N94-19852 #
USAFETAC/PR-93/003 ..... p 1864 N94-19908

USARIEM-TR-T94-3 ..... p 1892 N94-21209 #

USARIEM-T94-2 ..... p 1892 N94-21036 #

USIP-92-03 ..... p 2042 N94-20193 #

USNA-TSPR-200 ..... p 2014 N94-19982 #
USNA-TSPR-207 ..... p 1647 N94-20042 #

UVA/528476/EE94/101 ..... p 1818 N94-21817 * #

VKI-LS-1993-01 ..... p 1667 N94-20068 #

VTL-TR-198-6 ..... p 1650 N94-20524 * #

VTT-JULK-760 ..... p 1691 N94-20530 #

VTT-PUBS-106 ..... p 1988 N94-21594 #

VTT-SYMP-135 ..... p 2049 N94-22056 #
VTT-SYMP-136 ..... p 1707 N94-21890 #

WAPD-T-3010 ..... p 1689 N94-20182 #

WAPD-TM-1623 ..... p 1742 N94-22268 #
WAPD-TM-1629 ..... p 1804 N94-21748 #

WES/TR/SL-93-16 ..... p 1831 N94-20916 #

WHC-SA-2018 ..... p 1743 N94-22557 #

WHOI-CONTRIB-7943 ..... p 1881 N94-19895 #

WHOI-93-33 ..... p 1864 N94-20186 #

WINCO-11955 ..... p 1811 N94-22392 #
WINCO-11973 ..... p 1683 N94-22021 #

WL-TM-93-307 ..... p 1816 N94-20546 #

WL-TR-93-2046 ..... p 1994 N94-21214 #
WL-TR-93-2079 ..... p 1974 N94-21461 #
WL-TR-93-3012 ..... p 1637 N94-21411 #
WL-TR-93-3080 ..... p 1802 N94-21263 #
WL-TR-93-4032 ..... p 1675 N94-21187 #
WL-TR-93-4076 ..... p 1692 N94-21525
WL-TR-93-4080 ..... p 1635 N94-21194 #

WL/ML-TR-93-4096 ..... p 1691 N94-21188 #

WMO-749 ..... p 1841 N94-21068 #
WMO-773 ..... p 1841 N94-21069 #
WMO-779 ..... p 1867 N94-21070 #

WS-402 ..... p 1960 N94-22099
WS-404 ..... p 1961 N94-22266

WSRC-MS-92-306 ..... p 1804 N94-21765
WSRC-MS-93-255 ..... p 1679 N94-20266 #
WSRC-MS-93-390 ..... p 2046 N94-22407 #
WSRC-MS-93-404 ..... p 1688 N94-19942 #

WSRC-TR-93-430 ..... p 1684 N94-22046 #

WSU/TR/662238-39 ..... p 1891 N94-20627

WU/CCM-93/4 ..... p 1830 N94-20036 * #

Y/DV-1227 ..... p 1688 N94-19957 #

94B00028 ..... p 1741 N94-21783 * #

APPENDIX

NASA SCIENTIFIC AND TECHNICAL INFORMATION PROGRAM PRODUCTS AND SERVICES

The NASA Scientific and Technical Information (STI) Program provides for the collection and announcement of aerospace-related reports and literature obtained worldwide through agreements and exchanges. The result of the collection is the comprehensive NASA STI Database that covers aeronautics, space, and supporting disciplines.

The STI Database, documents generated or obtained by NASA, and products and services derived from or supporting the database are made available to the NASA research community and to the public. Descriptions and sources of these items are presented in the following pages.

Scientific and Technical Aerospace Reports (STAR) is an abstract journal, listing citations with abstracts for aerospace-related reports obtained from worldwide sources. *STAR* is issued on the first of each month, and announces current documents that have been entered into the NASA STI Database during the previous month. The reports are of the following types:

- NASA, NASA contractor, and NASA grantee reports;
- Reports issued by other U.S. Government agencies, domestic and foreign institutions, universities, and private firms;
- Translations in report form;
- NASA-owned patents and patent applications
- Other U.S. Government agency and foreign patents and patent applications
- Domestic and foreign dissertations and theses.

Journal, book, and conference literature, journal translations, and certain foreign dissertations having the same subject scope as *STAR* are announced in a companion journal, *NASA Open Volumes on Aerospace (NOVA). NOVA* is issued on the 15th of each month and is available from the NASA Center for AeroSpace Information, at the address below.

ELIGIBILITY AND REGISTRATION FOR NASA STI PRODUCTS AND SERVICES

Organizations of the type listed below that have registered with NASA can receive products and services.

- NASA offices and installations, contractors, subcontractors, grantees, and consultants;
- Other U.S. Government agencies and their contractors;
- Libraries in the United States that have arrangements with NASA to maintain collections of NASA documents for public reference;
- Other organizations in the United States having a need for NASA documents in work related to aeronautics and space research;
- Organizations abroad that have established reciprocal documents exchange arrangements with NASA.

The central service points—central points of document acquisition and control within qualified organizations—or individuals are eligible to register for NASA STI products and services. Domestic organizations or individuals may be eligible to receive various classes of NASA publications and services and should address their requests for registration or further information to:

ATTN: Registration Services
NASA Center for AeroSpace Information
800 Elkridge Landing Road
Linthicum Heights, MD 21090-2934
301-621-0390

Organizations abroad should direct requests to:

National Aeronautics and Space Administration
Scientific and Technical Information Program (JTT)
International STI Program
Washington, DC 20546-0001
USA
703-271-5640

SUBJECT SCOPE

The subject scope of *STAR* and *NOVA* includes all aspects of aeronautics and space research and development, supporting basic and applied research, and applications. Aerospace aspects of Earth resources, energy development, conservation, oceanography, environmental protection, urban transportation, and other topics of high national priority are also covered.

HOW TO USE *STAR* SUBJECT CATEGORIES

Abstracts in *STAR* are categorized by 10 major subject divisions that are divided further into 76 specific subject categories. The subject divisions and categories are listed in the Table of Contents together with a note for each that defines its scope and provides any cross-references. For example:

16 SPACE TRANSPORTATION

Includes passenger and cargo space transportation, e.g., shuttle operations; and space rescue techniques. For related information see also *03 Air Transportation and Safety* and *18 Spacecraft Design, Testing and Performance*. For space suits see *54 Man/System Technology and Life Support*.

CROSS-REFERENCES

Individual *STAR* abstracts are not ordinarily cross-referenced, except for certain conference reports or book translations that have had separate abstracts written for their component papers or chapters. Citations and abstracts of the components follow immediately after those of the parent document. When the subject content of a component differs sufficiently from the general content of the parent, a cross-reference citation also is printed at the end of the category to which it normally would have been assigned if it were independent.

DOCUMENTS ON MICROFICHE

Documents available on microfiche are designated by a pound sign (#) following the accession number.

LIMITED REPRODUCIBILITY

A note of limited reproducibility appears in the citation, if there are factors affecting the reproducibility of more than 20% of the document. These factors include faint or broken type, color photographs, black and white photographs, foldouts, dot matrix print, or some other factor that limits the reproducibility of the document. This notation also appears on the microfiche header.

COLOR COPIES

An increasing number of NASA scientific and technical reports are being produced with color graphs, charts, illustrations, and photographs. An indication that a document has color pages follows the source and pricing (SAP) information in the *STAR* citation.

Registered users of the NASA Scientific and Technical Information Program will receive ordered documents with color at no additional cost, as long as stock copies of the document are available. Otherwise, an additional fee of $2.00 per color page will be charged. The NASA Center for AeroSpace Information staff will contact registered users to determine individual user's needs.

NASA PATENTS AND PATENT APPLICATIONS

Patents and patent applications owned by NASA are announced in *STAR* under appropriate subject categories and are referenced in the *STAR* indexes. In the Report Number Index, patents are indexed by the NASA Case Number, and the U.S. Patent Class. Patent applications are indexed by the NASA Case Number and the U.S. Patent Application Serial Number.

Printed copies of patents (which are not microfiched) are available for purchase from the U.S. Patent and Trademark Office.

When ordering patents, the U.S. Patent Number should be used, and payment must be remitted in advance, by money order or check payable to the Commissioner of Patents and Trademarks. Prepaid purchase coupons for ordering are also available from the U.S. Patent and Trademark Office.

NASA patent application specifications are sold in both paper copy and microfiche by the NASA Center for AeroSpace Information (CASI). The N accession number should be used in ordering either paper copy or microfiche from CASI.

The patents and patent applications announced in *STAR* are owned by NASA and are available for royalty-free licensing. Requests for licensing terms and further information should be addressed to:

National Aeronautics and Space Administration
Associate General Counsel for Intellectual Property
Code GP
Washington, DC 20546-0001

SOURCES FOR DOCUMENTS

One or more sources from which a document announced in *STAR* is available to the public is ordinarily given on the last line of the citation. The most commonly indicated sources and their acronyms or abbreviations are listed below, and their addresses are listed on page A-6. If the publication is available from a source other than those listed, the publisher and his address will be displayed on the availability line or in combination with the corporate source line.

Avail: CASI. Sold by the NASA Center for AeroSpace Information. Prices for hard copy (HC) and microfiche (MF) are indicated by a price code following the letters HC or MF in the *STAR* citation. Current values for the price codes are given in the tables on page A-7.

NOTE ON ORDERING DOCUMENTS: When ordering publications from CASI, use the N accession number or other report number. It is also advisable to cite the title and other bibliographic identification.

Avail: SOD (or GPO). Sold by the Superintendent of Documents, U.S. Government Printing Office, in hard copy.

Avail: BLL (formerly NLL): British Library Lending Division, Boston Spa, Wetherby, Yorkshire, England. Photocopies available from this organization at the price shown. (If none is given, inquiry should be addressed to the BLL.)

Avail: DOE Depository Libraries. Organizations in U.S. cities and abroad that maintain collections of Department of Energy reports, usually in microfiche form, are listed in *Energy Research Abstracts*. Services available from the DOE and its depositories are described in a booklet, *DOE Technical Information Center - Its Functions and Services* (TID-4660), which may be obtained without charge from the DOE Technical Information Center.

Avail: ESDU. Pricing information on specific data, computer programs, and details on Engineering Sciences Data Unit (ESDU) topic categories can be obtained from ESDU International Ltd. Requesters in North America should use the Virginia address while all other requesters should use the London address, both of which are on page A-6.

Avail: Fachinformationszentrum Karlsruhe. Gesellschaft für wissenschaftlich-technische Information mbH 76344 Eggenstein-Leopoldshafen, Germany.

Avail: HMSO. Publications of Her Majesty's Stationery Office are sold in the U.S. by Pendragon House, Inc. (PHI), Redwood City, CA. The U.S. price (including a service and mailing charge) is given, or a conversion table may be obtained from PHI.

Avail: Issuing Activity, or Corporate Author, or no indication of availability. Inquiries as to the availability of these documents should be addressed to the organization shown in the citation as the corporate author of the document.

Avail: NASA Public Document Rooms. Documents so indicated may be examined at or purchased from the National Aeronautics and Space Administration (JBD-4), Public Documents Room (Room 1H23), Washington, DC 20546-0001, or public document rooms located at NASA installations, and the NASA Pasadena Office at the Jet Propulsion Laboratory.

Avail: NTIS. Sold by the National Technical Information Service. Initially distributed microfiche under the NTIS SRIM (Selected Research in Microfiche) are available. For information concerning this service, consult the NTIS Subscription Section, Springfield, VA 22161.

Avail: Univ. Microfilms. Documents so indicated are dissertations selected from *Dissertation Abstracts* and are sold by University Microfilms as xerographic copy (HC) and microfilm. All requests should cite the author and the Order Number as they appear in the citation.

Avail: US Patent and Trademark Office. Sold by Commissioner of Patents and Trademarks, U.S. Patent and Trademark Office, at the standard price of $1.50 each, postage free. (See discussion of NASA patents and patent applications on page A-3.)

Avail: (US Sales Only). These foreign documents are available to users within the United States from the National Technical Information Service (NTIS). They are available to users outside the United States through the International Nuclear Information Service (INIS) representative in their country, or by applying directly to the issuing organization.

Avail: USGS. Originals of many reports from the U.S. Geological Survey, which may contain color illustrations, or otherwise may not have the quality of illustrations preserved in the microfiche or facsimile reproduction, may be examined by the public at the libraries of the USGS field offices whose addresses are listed on page A-6. The libraries may be queried concerning the availability of specific documents and the possible utilization of local copying services, such as color reproduction.

FEDERAL DEPOSITORY LIBRARY PROGRAM

In order to provide the general public with greater access to U.S. Government publications, Congress established the Federal Depository Library Program under the Government Printing Office (GPO), with 53 regional depositories responsible for permanent retention of material, inter-library loan, and reference services. At least one copy of nearly every NASA and NASA-sponsored publication, either in printed or microfiche format, is received and retained by the 53 regional depositories. A list of the regional GPO libraries, arranged alphabetically by state, appears on page A-8. These libraries are *not* sales outlets. A local library can contact a regional depository to help locate specific reports, or direct contact may be made by an individual.

PUBLIC COLLECTION OF NASA DOCUMENTS

An extensive collection of NASA and NASA-sponsored publications is maintained by the British Library Lending Division, Boston Spa, Wetherby, Yorkshire, England for public access. The British Library Lending Division also has available many of the non-NASA publications cited in *STAR*. European requesters may purchase facsimile copy or microfiche of NASA and NASA-sponsored documents, those identified by both the symbols # and * from ESA — Information Retrieval Service European Space Agency, 8-10 rue Mario-Nikis, 75738 CEDEX 15, France.

SUBMITTING DOCUMENTS

All users of this abstract service are urged to forward reports to be considered for announcement in *STAR*. This will aid NASA in its efforts to provide the fullest possible coverage of all scientific and technical publications that might support aeronautics and space research and development. If you have prepared relevant reports (other than those you will transmit to NASA, DOD, or DOE through the usual contract- or grant-reporting channels), please send them for consideration to the NASA Center for AeroSpace Information, 800 Elkridge Landing Road, Linthicum Heights, MD 21090-2934.

Reprints of journal articles, book chapters, and conference papers are also welcome. These will be considered for announcement in *STAR's* companion journal, *NOVA*.

You may specify a particular source to be included in a report announcement if you wish; otherwise the report will be placed on a public sale at the NASA Center for AeroSpace Information. Copyrighted publications will be announced but not distributed or sold.

PURCHASE OF *STAR*

STAR is publicly available on annual subscription from the NASA Center for AeroSpace Information (CASI) at $94.00/domestic, $117.00/foreign. Single copy prices: $33.00/domestic, $41.00/foreign.

An annual, cumulative *STAR Index* is also available at $54.00/domestic, $65.00/foreign.

STAR is available to registered users on annual subscription from the NASA Center for AeroSpace Information, ATTN: Registration Services, 800 Elkridge Landing Road, Linthicum Heights, MD 21090-2934.

ADDRESSES OF ORGANIZATIONS

British Library Lending Division
Boston Spa, Wetherby, Yorkshire
England

Commissioner of Patents and Trademarks
U.S. Patent and Trademark Office
Washington, DC 20231

Department of Energy
Technical Information Center
P.O. Box 62
Oak Ridge, TN 37830

European Space Agency-
Information Retrieval Service ESRIN
Via Galileo Galilei
00044 Frascati (Rome) Italy

Engineering Sciences Data Unit International
P.O. Box 1633
Manassas, VA 22110

Engineering Sciences Data Unit
International, Ltd.
251-259 Regent Street
London, W1R 7AD, England

Fachinformationszentrum Karlsruhe
Gesellschaft für wissenschaftlich-technische
Information mbH
76344 Eggenstein-Leopoldshafen, Germany

Her Majesty's Stationery Office
P.O. Box 569, S.E. 1
London, England

NASA Center for AeroSpace Information
800 Elkridge Landing Road
Linthicum Heights, MD 21090-2934

National Aeronautics and Space Administration
Scientific and Technical Information Program
(JTT)
Washington, DC 20546-0001

National Technical Information Service
5285 Port Royal Road
Springfield, VA 22161

Pendragon House, Inc.
899 Broadway Avenue
Redwood City, CA 94063

Superintendent of Documents
U.S. Government Printing Office
Washington, DC 20402

University Microfilms
A Xerox Company
300 North Zeeb Road
Ann Arbor, MI 48106

University Microfilms, Ltd.
Tylers Green
London, England

U.S. Geological Survey Library National Center
MS 950
12201 Sunrise Valley Drive
Reston, VA 22092

U.S. Geological Survey Library
2255 North Gemini Drive
Flagstaff, AZ 86001

U.S. Geological Survey
345 Middlefield Road
Menlo Park, CA 94025

U.S. Geological Survey Library
Box 25046
Denver Federal Center, MS914
Denver, CO 80225

CASI PRICE TABLES

(Effective August 1, 1993)

STANDARD PRICE DOCUMENTS

PRICE CODE	NORTH AMERICAN PRICE	FOREIGN PRICE
A01	$ 9.00	$ 18.00
A02	12.50	25.00
A03	17.50	35.00
A04-A05	19.50	39.00
A06-A09	27.00	54.00
A10-A13	36.50	73.00
A14-A17	44.50	89.00
A18-A21	52.00	104.00
A22-A25	61.00	122.00
A99	Call For Price	Call For Price

MICROFICHE

PRICE CODE	NORTH AMERICAN PRICE	FOREIGN PRICE
A01	$ 9.00	$ 18.00
A02	12.50	25.00
A03	17.50	35.00
A04	19.50	39.00
A06	27.00	54.00
A10	36.50	73.00

IMPORTANT NOTICE

CASI Shipping and Handling Charges
U.S.—ADD $3.00 per TOTAL ORDER
Canada and Mexico—ADD $3.50 per TOTAL ORDER
All Other Countries—ADD $7.50 per TOTAL ORDER
Does NOT apply to orders
requesting CASI RUSH HANDLING.
CASI accepts most credit/charge cards.

NASA Center for AeroSpace Information
800 Elkridge Landing Road
Linthicum Heights, MD 21090-2934
Telephone: (301) 621-0390
E-mail: help@sti.nasa.gov
Fax: (301) 621-0134

FEDERAL REGIONAL DEPOSITORY LIBRARIES

ALABAMA

AUBURN UNIV. AT MONTGOMERY LIBRARY
Documents Dept.
7300 University Dr.
Montgomery, AL 36117-3596
(205) 244-3650 Fax: (205) 244-0678

UNIV. OF ALABAMA
Amelia Gayle Gorgas Library
Govt. Documents
Box 870266
Tuscaloosa, AL 35487-0266
(205) 348-6046 Fax: (205) 348-8833

ARIZONA

DEPT. OF LIBRARY, ARCHIVES, AND PUBLIC RECORDS
Federal Documents
Third Floor State Capitol
1700 West Washington
Phoenix, AZ 85007
(602) 542-4121 Fax: (602) 542-4400, 542-4500

ARKANSAS

ARKANSAS STATE LIBRARY
State Library Services
One Capitol Mall
Little Rock, AR 72201
(501) 682-2869

CALIFORNIA

CALIFORNIA STATE LIBRARY
Govt. Publications Section
914 Capitol Mall - P.O. Box 942837
Sacramento, CA 94237-0001
(916) 322-4572 Fax: (916) 324-8120

COLORADO

UNIV. OF COLORADO - BOULDER
Norlin Library
Govt. Publications
Campus Box 184
Boulder, CO 80309-0184
(303) 492-8834 Fax: (303) 492-2185

DENVER PUBLIC LIBRARY
Govt. Publications Dept. BS/GPD
1357 Broadway
Denver, CO 80203
(303) 571-2135

CONNECTICUT

CONNECTICUT STATE LIBRARY
231 Capitol Avenue
Hartford, CT 06106
(203) 566-4971 Fax: (203) 566-3322

FLORIDA

UNIV. OF FLORIDA LIBRARIES
Documents Dept.
Library West
Gainesville, FL 32611-2048
(904) 392-0366 Fax: (904) 392-7251

GEORGIA

UNIV. OF GEORGIA LIBRARIES
Govt. Documents Dept.
Jackson Street
Athens, GA 30602
(404) 542-8949 Fax: (404) 542-6522

HAWAII

UNIV. OF HAWAII
Hamilton Library
Govt. Documents Collection
2550 The Mall
Honolulu, HI 96822
(808) 948-8230 Fax: (808) 956-5968

IDAHO

UNIV. OF IDAHO LIBRARY
Documents Section
Moscow, ID 83843
(208) 885-6344 Fax: (208) 885-6817

ILLINOIS

ILLINOIS STATE LIBRARY
Reference Dept.
300 South Second
Springfield, IL 62701-1796
(217) 782-7596 Fax: (217) 524-0041

INDIANA

INDIANA STATE LIBRARY
Serials/Documents Section
140 North Senate Avenue
Indianapolis, IN 46204
(317) 232-3678 Fax: (317) 232-3728

IOWA

UNIV. OF IOWA LIBRARIES
Govt. Publications Dept.
Washington & Madison Streets
Iowa City, IA 52242
(319) 335-5926 Fax: (319) 335-5830

KANSAS

UNIV. OF KANSAS
Govt. Documents & Map Library
6001 Malott Hall
Lawrence, KS 66045-2800
(913) 864-4660 Fax: (913) 864-5380

KENTUCKY

UNIV. OF KENTUCKY LIBRARIES
Govt. Publications/Maps Dept.
Lexington, KY 40506-0039
(606) 257-3139 Fax: (606) 257-1563, 257-8379

LOUISIANA

LOUISIANA STATE UNIV.
Middleton Library
Govt. Documents Dept.
Baton Rouge, LA 70803
(504) 388-2570 Fax: (504) 388-6992

LOUISIANA TECHNICAL UNIV.
Prescott Memorial Library
Govt. Documents Dept.
305 Wisteria Street
Ruston, LA 71270-9985
(318) 257-4962 Fax: (318) 257-2447

MAINE

TRI-STATE DOCUMENTS DEPOS.
Raymond H. Fogler Library
Govt. Documents & Microforms Dept.
Univ. of Maine
Orono, ME 04469
(207) 581-1680

MARYLAND

UNIV. OF MARYLAND
Hornbake Library
Govt. Documents/Maps Unit
College Park, MD 20742
(301) 454-3034 Fax: (301) 454-4985

MASSACHUSETTS

BOSTON PUBLIC LIBRARY
Govt. Documents Dept.
666 Boylston Street
Boston, MA 02117
(617) 536-5400 ext. 226
Fax: (617) 267-8273, 267-8248

MICHIGAN

DETROIT PUBLIC LIBRARY
5201 Woodward Avenue
Detroit, MI 48202-4093
(313) 833-1440, 833-1409
Fax: (313) 833-5039

LIBRARY OF MICHIGAN
Govt. Documents Unit
P.O. Box 30007
Lansing, MI 48909
(517) 373-0640 Fax: (517) 373-3381

MINNESOTA

UNIV. OF MINNESOTA
Wilson Library
Govt. Publications Library
309 19th Avenue South
Minneapolis, MN 55455
(612) 624-5073 Fax: (612) 626-9353

MISSISSIPPI

UNIV. OF MISSISSIPPI
J.D. Williams Library
Federal Documents Dept.
106 Old Gym Bldg.
University, MS 38677
(601) 232-5857 Fax: (601) 232-5453

MISSOURI

UNIV. OF MISSOURI - COLUMBIA
Ellis Library
Govt. Documents
Columbia, MO 65201
(314) 882-6733 Fax: (314) 882-8044

MONTANA

UNIV. OF MONTANA
Maureen & Mike Mansfield Library
Documents Div.
Missoula, MT 59812-1195
(406)243-6700 Fax: (406) 243-2060

NEBRASKA

UNIV. OF NEBRASKA - LINCOLN
D.L. Love Memorial Library
Documents Dept.
Lincoln, NE 68588
(402) 472-2562

NEVADA

UNIV. OF NEVADA
Reno Library
Govt. Publications Dept.
Reno, NV 89557
(702) 784-6579 Fax: (702) 784-1751

NEW JERSEY

NEWARK PUBLIC LIBRARY
U.S. Documents Div.
5 Washington Street - P.O. Box 630
Newark, NJ 07101-0630
(201) 733-7812 Fax: (201) 733-5648

NEW MEXICO

UNIV. OF NEW MEXICO
General Library
Govt. Publications Dept.
Albuquerque, NM 87131-1466
(505) 277-5441 Fax: (505) 277-6019

NEW MEXICO STATE LIBRARY
325 Don Gaspar Avenue
Santa Fe, NM 87503
(505) 827-3826 Fax: (505) 827-3820

NEW YORK

NEW YORK STATE LIBRARY
Documents/Gift & Exchange Section
Federal Depository Program
Cultural Education Center
Albany, NY 12230
(518) 474-5563 Fax: (518) 474-5786

NORTH CAROLINA

UNIV. OF NORTH CAROLINA - CHAPEL HILL
CB#3912, Davis Library
BA/SS Dept. - Documents
Chapel Hill, NC 27599
(919) 962-1151 Fax: (919) 962-0484

NORTH DAKOTA

NORTH DAKOTA STATE UNIV. LIB.
Documents Office
Fargo, ND 58105
(701) 237-8886 Fax: (701) 237-7138
In cooperation with Univ. of North Dakota, Chester Fritz Library
Grand Forks

OHIO

STATE LIBRARY OF OHIO
Documents Dept.
65 South Front Street
Columbus, OH 43266
(614) 644-7051 Fax: (614) 752-9178

OKLAHOMA

OKLAHOMA DEPT. OF LIBRARIES
U.S. Govt. Information Div.
200 NE 18th Street
Oklahoma City, OK 73105-3298
(405) 521-2502, ext. 252, 253
Fax: (405) 525-7804

OKLAHOMA STATE UNIV.
Edmon Low Library
Documents Dept.
Stillwater, OK 74078
(405) 744-6546 Fax: (405) 744-5183

OREGON

PORTLAND STATE UNIV.
Millar Library
934 SW Harrison - P.O. Box 1151
Portland, OR 97207
(503) 725-3673 Fax: (503) 725-4527

PENNSYLVANIA

STATE LIBRARY OF PENN.
Govt. Publications Section
Walnut St. & Commonwealth Ave. - P.O. Box 1601
Harrisburg, PA 17105
(717) 787-3752

SOUTH CAROLINA

CLEMSON UNIV.
Cooper Library
Public Documents Unit
Clemson, SC 29634-3001
(803) 656-5174 Fax: (803) 656-3025
In cooperation with Univ. of South Carolina, Thomas Cooper Library, Columbia

TENNESSEE

MEMPHIS STATE UNIV. LIBRARIES
Govt. Documents
Memphis, TN 38152
(901) 678-2586 Fax: (901) 678-2511

TEXAS

TEXAS STATE LIBRARY
United States Documents
P.O. Box 12927 - 1201 Brazos
Austin, TX 78711
(512) 463-5455 Fax: (512) 463-5436

TEXAS TECH. UNIV. LIBRARY
Documents Dept.
Lubbock, TX 79409
(806) 742-2268 Fax: (806) 742-1920

UTAH

UTAH STATE UNIV.
Merrill Library & Learning Resources Center, UMC-3000
Documents Dept.
Logan, UT 84322-3000
(801) 750-2684 Fax: (801) 750-2677

VIRGINIA

UNIV. OF VIRGINIA
Alderrman Library
Govt. Documents
Charlottesville, VA 22903-2498
(804) 824-3133 Fax: (804) 924-4337

WASHINGTON

WASHINGTON STATE LIBRARY
Document Section
MS AJ-11
Olympia, WA 98504-0111
(206) 753-4027 Fax: (206) 753-3546

WEST VIRGINIA

WEST VIRGINIA UNIV. LIBRARY
Govt. Documents Section
P.O. Box 6069
Morgantown, WV 26506
(304) 293-3640

WISCONSIN

ST. HIST. SOC. OF WISCONSIN LIBRARY
Govt. Publications Section
816 State Street
Madison, WI 53706
(608) 262-2781 Fax: (608) 262-4711
In cooperation with Univ. of Wisconsin - Madison, Memorial Library

MILWAUKEE PUBLIC LIBRARY
Documents Div.
814 West Wisconsin Avenue
Milwaukee, WI 53233
(414) 278-2167 Fax: (414) 278-2137

*U.S. GOVERNMENT PRINTING OFFICE:1994-301-249/00004

POSTMASTER
Address Correction Requested
(Sections 137 and 159 Post Manual)

National Aeronautics and
Space Administration
Code JTT
Washington, DC 20546-0001

Official Business
Penalty for Private Use, $300

BULK RATE
POSTAGE & FEES PAID
NASA
PERMIT No. G-27

NASA

POSTMASTER: If Undeliverable (Section 158
Postal Manual) Do Not Return

Please circulate this publication to other colleagues within your organization.

NASA STI PROGRAM
SCIENTIFIC &
TECHNICAL
INFORMATION